JFIC2015

PROCEEDINGS OF THE

JOINT FEDERAL INTERAGENCY CONFERENCE 2015

Proceedings of papers of the
5th Federal Interagency Hydrologic Modeling Conference
and the 10th Federal Interagency Sedimentation
Conference
Reno, NV, April 19 – 23, 2015

The first Federal Interagency Sedimentation Conference (FISC) was held in 1947. Since then, they have been sponsored by the ACWI Subcommittee on Sedimentation (SOS) and held in 1963, 1976, 1986, 1991, 1996, 2001, 2006, and 2010. The Subcommittee on Hydrology (SOH) held their first Federal Interagency Workshop, "Hydrologic Modeling Demands for the 90s" in Fort Collins, Colorado, in 1993. That workshop was limited to Federal participants. Subsequent to that workshop, the SOH decided to hold a broader series of conferences and to open them to all interested parties. Federal Interagency Hydrologic Modeling Conferences were held in 1998, 2002, 2006, and 2010, and covered models addressing surface water quality and quantity issues.

These conferences have been well-attended, and together have produced over 2,100 technical papers. Combined, the Joint Conferences provide engineers and scientists the opportunity to discuss recent accomplishments in the physical, chemical, and biological aspects of sedimentation, and the development and use of hydrologic models addressing surface water quality and quantity issues. As a continuation of these conferences, SEDHYD again provides an interdisciplinary mix of scientists and managers from government agencies, academia, and the business community to present their recent accomplishments and progress in research and on technical developments related to sedimentation processes and the impact of sediment on the environment.

The Joint Conference follows a mixed set of formats including formal technical presentations, poster sessions, field trips, short courses, and model demonstrations. The Joint Conference is also hosting a ***student*** paper competition for cash prizes.

The Joint Conference is being held at the Peppermill Hotel and Resort, Reno, Nevada, USA. Reno is situated in a high desert just east of the beautiful Sierra Nevada. It lies on the western edge of the Great Basin, at an elevation of about 4,400 feet (1,300 m) above sea level. The downtown area (along with Sparks) occupies a valley informally known as Truckee Meadows. The area offers spectacular desert landscapes and ecosystems, as well as numerous indoor and outdoor recreational opportunities.

Joint Federal Interagency Conference

Joint Conference Chair:	G. Douglas Glysson, US Geological Survey (ret.)
Operations Chair:	Paula Makar, US Bureau of Reclamation
Technical Program Coordinator:	Jerry Bernard, USDA NRCS (ret.)
Proceedings Coordinator:	Mark Strudley, NOAA National Weather Service
Poster/Demo Coordinator:	Jennifer Bountry, US Bureau of Reclamation
Registration:	Darren Nezamfar, US Army Corps of Engineers
Exhibits:	Mark Landers, US Geological Survey
Short Course Coordinator:	Jeff Bradley, ASCE
Computer-A/V Coordinator:	Jeff Harris, US Army Corps of Engineers (ret.)
Field Trip Coordinator:	Victor Hom, NOAA
Student Program:	Amanda Cox, Saint Louis University
ACWI-SOS Chair:	Amanda Cox, Saint Louis University
ACWI-SOH Chair:	Victor Hom, NOAA

10th FISC

Chair:	Tim Randle, US Bureau of Reclamation
Technical Program Chair:	Marie Garsjo, US Geological Survey (ret.)

5th FIHMC

Chair:	Jerry Webb, US Army Corps of Engineers
Technical Program Chair:	Claudia Hoeft, USDA NRCS

The Federal Interagency Subcommittees on Hydrology (SOH) and Sedimentation (SOS), under the Advisory Committee on Water Information (ACWI).

Subcommittee Organizations

American Forests
American Society of Civil Engineers (ASCE)
Association of State Floodplain Managers
Bureau of Land Management (BLM)
Bureau of Reclamation (USBR)
Colorado Water Resources Research Institute CWRRI)
Defenders of Property Rights
U.S. Army Corps of Engineers (USACE)
Electric Power Research Institute (EPRI)
Federal Emergency Management Agency (FEMA)
Federal Energy Regulatory Commission (FERC)
Federal Highway Administration (FHwA)
National Aeronautics and Space Administration (NASA)
National Hydrologic Warning Council
National Park Service (NPS)
National Science Foundation (NSF)
NOAA-National Weather Service (NWS)
Office of Surface Mining (OSM)
U.S. Environmental Protection Agency (USEPA)
U.S. Geological Survey (USGS)
Universities Council on Water Research (UCOWR)
USDA-Agricultural Research Service (ARS)
USDA-Forest Service (FS)
USDA-Natural Resources Conservation Service (NRCS)

Suggested Citation:
In Proceedings of the 3rd Joint Federal Interagency Conference (10th Federal Interagency Sedimentation Conference and 5th Federal Interagency Hydrologic Modeling Conference), April 19 – 23, 2015, Reno, Nevada.

JFIC2015

TABLE OF CONTENTS

1D Stream Restoration 1

1E Climate Change, Variability, and Impact 1

1F Flood Hydrology 1

2A Sediment Yield and Transport Modeling 2

2B Surrogates of Sediment, Optical

2C Physical Measurement and Modeling 1

Release of the USGS Sediment Data Portal
Casey Lee and Meredith Warren

Electronic Notes Application for On-Site Recording and Storage of U.S. Geological Survey Fluvial-Sediment Data
Julio A. Oms, Dianne Lopez-Trujillo, John R. Gray, Kenneth A. Skach, and Francisco Granado-Santos

Characterizing and Simulating Sediment Loads and Transport in the Lower Part of the San Antonio River Basin
J. Ryan Banta, Darwin J. Ockerman, Cassi L. Crow, and Stephen P. Opsahl

2D Stream Restoration 2

Development of a Velocity-Based Quantitative Design Methodology for Bendway Weirs
Nathan Holste

Performance of Log Crib Walls for Bluff Stabilization
Ben Lee, Marty Melchior, Andy Selle, and Ben Swanson

Rock Check Structures for Restoration of Headwaters
Jon Fripp and Richard Weber

Riparian and Channel Changes Along the Trinity River Below Lewiston Dam, California, 1980 to 2011
Jennifer Curtis

2E Climate Change, Variability, and Impact 2

Reservoir Sustainability: Evaluation of Climate Change and Sedimentation Impacts to Reservoir Water Management Operations at Coralville Dam, Iowa
Kevin J. Landwehr and Gregory S. Karlovits

Using an Integrated Surface Water-Groundwater Flow Model for Evaluating the Hydrologic Impacts of Historic and Potential Future Dry Periods on Simulated Water Budgets in the Santa Rosa Plain Watershed, Northern California
Joseph A. Hevesi, Linda R. Woolfenden, and Tracy Nishikawa

Collaboration on Climate Change Analysis in the Pacific Northwest
James D. Barton

ADHydro: Quasi-3D HIgh Performance Hydrological Model
Fred L. Ogden, Wencong Lai, and Robert C. Steinke

2F Flood Hydrology 2

SToRM: A Model for 2D Environmental Hydraulics
Francisco J.M. Simões

Hydraulic Modeling of Truckee Canal Alluvial Fans using SRH-2D
Rebecca Kallio, Joseph Wright, and Victoria Sankovich-Bhals

Model Integration for Real-Time Flood Forecasting Inundation Mapping for Nashville Tributaries *
William Charley

Evaluating Physical Models of Dam Removal Against Results from Condit, Marmot, and Elwha for Process Driven Sediment Transport and Channel Bed Response
Joanna Crowe Curran

3A Sediment Yield and Transport Modeling 3

Mount St. Helens Update: Recent Trends, Understandings and Projects to Manage Debris Avalanche Sediments
Chris Nygaard and Paul Sclafani

Forecasting Long-Term Sediment Yield from the Upper North Fork Toutle River, Mount St. Helens, Washington State
Tim Meadows, Colin Thorne, Nick Mount, and Tom Coulthard

Mount St. Helens Long Term Sediment Management Alternative Analysis
Paul Sclafani and Chris Nygaard

Two Dimensional Numerical Modelling of Hyperconcentrated Flows
Jianchun Huang, Yong Lai, and Kuowei Wu

3B Surrogates of Sediment 1

Sediment-Generated Noise (SGN): Comparison with Physical Bedload Measurements in a Small Semi-arid Watershed
James R. Rigby, Roger A. Kuhnle, Bradley T. Goodwiller, Mary H. Nichols, Wayne O. Carpenter, Daniel G. Wren, and James P. Chambers

Sediment-Generated Noise (SGN): Laboratory Determination of Measurement Volume
Daniel G. Wren, Bradley T. Goodwiller, J. R. Rigby, Wayne O. Carpenter, Roger A. Kuhnle, and James P. Chambers

Design and Implementation of a Field Deployable Passive Acoustic Bedload-Monitoring Surrogate
Bradley T. Goodwiller, Daniel G. Wren, J. R. Rigby, Wayne O. Carpenter, James P. Chambers, Roger A. Kuhnle, and Robert C. Hilldale

Continuous Bedload Measurement on the Elwha River Using Impact Plates: Installation and Calibration
Robert C. Hilldale

3C Physical Measurement and Modeling 2

USGS Training of Sediment Data Collection Techniques
Gary P. Johnson, John R. Gray, Kurt Spicer, and Mark Landers

3D Stream Restoration 3

3E Restoring and Sustaining River Environments 1

3F Flood Hydrology 3

Performance of Suspended Sediment Concentration in Two Distinctive Lower Mississippi River Hydrographs
Tzenge-huey (Jerry) Shih and Dave Ramirez

4A Sediment Yield and Transport Modeling 4

Sediment Modeling on the Lower Yellowstone River at Intake Dam
Curtis J. Miller, Daniel B. Pridal, and Christopher J. Svendsen

Sedimentation Analysis of the Yellowstone River at Intake Diversion Dam
Mike Sixta, Blair Greimann, and Kent Collins

Inaccuracies in Sediment Budgets Arising from Estimations of Tributary Sediment Inputs: An Example from a Monitoring Network on the Southern Colorado Plateau
Ronald E. Griffiths and David J. Topping

User-interactive Sediment Budgets in a Browser: A Web Application for River Science and Management
David Sibley, David J. Topping, Megan Hines, and Bradley Garner

4B Surrogates of Bedload 2

Update on ISSDOTv2 Method of Measuring Bedload Transport Using Time Sequenced Bathymetric Data
David Abraham, Tate McAlpin, David May, Thad Pratt, and John Shelley

Distinguishing Bed-load and Bed-material-load Fluxes with Repeat Bathymetric Data
Brandon McElroy and David Abraham

Using Hydrophones as a Surrogate Sediment Monitoring Technique to Detect Temporal and Spatial Variability in Bedload Sediment Transport
Mathieu Marineau, J. Toby Minear, and Scott Wright

Evaluation of Multiple-Frequency, Active and Passive Acoustics as Surrogates for Bedload Transport
Molly Wood, Ryan Fosness, Greg Pachman, Mark Lorang, and Diego Tonolla

4C Physical Measurement and Modeling 3

Bed Sediment Characterization of the Mississippi River, Grafton, Illinois to Head of Passes, November 2013
Roger Gaines and Anthony M. Priestas

Drought, Low Water, and Dredging of the Middle Mississippi River in 2012
David C. Gordon and Michael T. Rodgers

Missouri River 2011 Extreme Flood – Channel Response Evaluation and Observations
Chris Svendsen and Daniel Pridal

4D Stream Restoration 4

Rapid, Quantitative Analysis of the Cost Effectiveness of Streambank Protection Measures Using the Bank-Stability and Toe Erosion Model (BSTEM)
Natasha Bankhead and Andrew Simon

Streambank Erosion: Developing Recession Rates Based on Condition Class and Flow Stage Characteristics
W. Barry Southerland and Lisa J. French

Vegetation Calibration in a Sediment Transport Model of the Middle Rio Grande
David Varyu and Lisa Fotherby

Removing Invasive Plants from the Mojave River, An Erosive Inland Desert River System in Southern California
Gregory Norris and Julia Grim

4E Restoring and Sustaining River Environments 2

Estimation of Suspended Sediment and Total Mercury Loads and Application of Flow-Adjusted Trend Analyses to Assess Floodplain Restoration, Carson River, Nevada
Carl E. Thodal, Eric Morway, and Karen A. Thomas

Missouri River Habitat Project Design, Performance, and Aspects of the 2011 Flood
Daniel Pridal

Evaluation of Levee Setbacks as a Sustainable Solution Along the Missouri River
Tony D. Krause, Kelly Baxter, David J. Crane, and Randall L. Behm

PIANC Working with Nature Concept: Development of the 3 Meter Navigation Channel on the Middle Mississippi River *
Robert Davinroy

4F Hydroecological Modeling 1

Hydrodynamic Modeling to Evaluate the Influence of Constructed Side-Channel Habitat on Larval Drift of Pallid Sturgeon in the Lower Missouri River
Susannah O. Erwin and Robert B. Jacobson

Impact of Precipitation Uncertainty on SWAT Model Performance
Milo Anderson, Yongping Yuan, and Ronald L. Bingner

Modeling Interactions of Flow and Vegetation for Improved Riverine System Management
Daniel Dombroski, Blair Greimann, Yong Lai, Victor Huang, Lisa Fotherby, Mark Stone and Li Chen

5A Sediment Yield and Transport Modeling 5

Sand Bar Volume Model: Improving Modeled Sand Bar Response in Marble Canyon
David Varyu, Blair Greimann, Nate Bradley, and Kendra Russell

Processes Limiting Depth of Arroyo Incision: Examples from the Rio Puerco, New Mexico
Eleanor Griffin and Jonathan Friedman

Estimating Flow Concentration and Sediment Redistribution in Shrub-Dominated Rangeland Communities
Sayjro Kossi Nouwakpo, Mark Weltz, Kenneth McGwire, and Colleen G. Rossi

Temperature Simulation of a Reach of the Methow River near Winthrop, Washington
Jianchun Huang and Jennifer Bountry

5B Surrogates of Sediment, Acoustics 1

Physically Based Method for Measuring Suspended-Sediment Concentration and Grain Size Using Multi-Frequency Arrays of Single-Frequency Acoustic-Doppler Profilers
David J. Topping, Scott A. Wright, Ronald E. Griffiths, and David J. Dean

Research and Methods Development in the Sediment Acoustic Leadership Team *
Mark Landers

Surrogate Analysis and Index Development (SAID) and Real-Time Dissemination
Marian Domanski, Timothy Straub, Molly Wood, Mark Landers, Gary Wall, and Steven Brady

5C Physical Measurement and Modeling 4

Effective Particle Sizes of Cohesive Sediment in a North Mississippi Stream
Roger Kuhnle and Daniel Wren

Suspended-Sediment Concentrations, Loads, Total Suspended Solids and Particle-Size Fractions in Minnesota, 2007-2011
Christopher A. Ellison, Brett E. Savage, and Gregory D. Johnson

Coarse Particulate Organic Matter Transport in Two Rocky Mountain Streams: Measurements, Transport Dynamics, Annual loads, and Yields
Kristin Bunte, Kurt W. Swingle, Jens M. Turowski, Steven R. Abt, and Daniel A. Cenderelli

Sediment Budgets, Transport, and Depositional Trends in a Large Tidal Delta
Tara L. Morgan-King and Scott A. Wright

5D Fluvial Geomorphology 1

The Study of Most Probable Mean Daily Bankfull Runoff Volumes in Small Watersheds dominated by Convective/Frontal Channel-Forming Events and the Co-incident Inner Berm Channel
Thomas J. Garday

5E Post Fire Analyses and Restoration 1

5F Hydroecological Modeling 2

6A Sediment Yield and Transport Modeling 6

The Upper Bound of Abutment Scour Defined by Selected Laboratory and Field Data
Stephen T. Benedict

Baffle-Post Structures for Flow and Bed-Sediment Control in Open Channels
Caroline Ubing, Robert Ettema, and Christopher Thornton

6B Surrogates of Sediment, Acoustics 2

Suspended-Sediment Transport and Storage: a Demonstration of Acoustic Methods in the Evaluation of Reservoir Management Strategies for a Small Water-Supply Reservoir in Western Colorado
Cory A. Williams, Rodney J. Richards, and Kent Collins

Ultrasonic Measurements of Suspended Sediment Concentrations at Harris Bayou
Wayne Carpenter, Daniel Wren, Bradley Goodwiller, James Chambers, Thomas Kajdan, Cristiane Surbeck, and Roger Kuhnle

Studying Surrogates to Estimate Suspended Sediment Concentrations on the Missouri River at Nebraska City, NE
Jon F. Nania

Hydroacoustic Signatures of Colorado Riverbed Sediments in Marble and Grand Canyons Using Multibeam Sonar
Daniel Buscombe, Paul E. Grams, Matt A. Kaplinski, Robert Tusso, and David M. Rubin

6C Physical Measurement and Modeling 5

Application of Cross-Plot Analysis on Francis Levee Site Using Time Lapse SRT and ERT
Leti Wodajo, Craig Hickey, and Chung Song

A Simplified Bathymetric Survey System Using a Modified Sounder GPS
Theodore L. Huscher and David Griffith

Subsurface Hydrologic Effects on Sediment Deposition
Zhaoxia Li, Sayjro Nouwakpo, and Chi-hua Huang

Representativeness of Soil Samples Collected to Assess Mining-Related Contamination of Flood Plains in Southeast Kansas
Kyle Juracek

6D Fluvial Geomorphology 2

Morphological Evolution of Fluvial and Estuarine Segment Flows
Geraldo Wilson Junior and Mario Grüne de Souza e Silva

Flow Energy and Bedload-Transport Efficiency: The Froude Number as a Metric for Bedload Transport Rates
Andrew Simon and Michael Singer

Effects of Upstream Sediment Supply and Flow Rate on the Initiation and Topographic Evolution of Sandbars in Laboratory and Numerical Channels
Paul J. Kinzel, Brandy L. Logan, and Jonathan M. Nelson

Reconciliation of Flux-based and Morphologic-based Sediment Budgets
Paul E. Grams, Daniel Buscombe, David J. Topping, Joseph E. Hazel, Jr., and Matt Kaplinski

6E Post Fire Analyses and Restoration 2

Predicting and Comparing Measured Bulking and Peak Discharge Using Multiple Methods for Post-Fire Hydrologic and Sedimentation Analysis on the "Dump Fire" in Saratoga Springs, Utah
Nathaniel Todea

Stream Restoration Within a Confined Space : A Case Study on the Middle Rio Grande
Jonathan AuBuchon and Chi Bui

The Application of WARSSS for a Watershed-Based Sediment Budget and Post-Fire Stream Restoration: The Hayman Fire, Trail Creek Watershed, Colorado
David Rosgen, Darcie Frantila Geenen, and Brandon Rosgen

6F Hydroecological Modeling 3

Hybrid Hydraulic Modeling of River-Training Structures in Sinuous Channels
S. Michael Scurlock, Amanda L. Cox, Drew C. Baird, Christopher I. Thornton, and Steven R. Abt

Modeling Flow Complexity with In-Stream Structures: A Semi-Automatic Approach *
Yong Lai

Space-Time Substitution in a Stream Evolution Model Integrating Habitat and Ecosystem Benefits
Brian Cluer and Colin Thorne

Composite Modeling of the Halfway Wash Fish Barrier
Mike Sixta, Kendra Russell, and Leslie Hanna

7A Sediment Yield and Transport Modeling 7

Coupled Sediment Yield and Sediment Transport Modeling to support Waterway Navigation Planning in Northeast Brazil
Calvin T. Creech, Rafael Brito Siquiera, James P. Selegean, Carol Miller, and Pedro Cunha

Sediment Dynamics on River Networks: Incorporating Sources, Stores, and Sinks from a Sediment Budget into a Network-Modeling Framework
Jonathan A. Czuba, Efi Foufoula-Georgiou, Karen B. Gran, Patrick Belmont, and Peter Wilcock

Constructing a Near-Continuous Suspended-Sediment Budget Using Acoustic Instrumentation on the Rio Grande in Big Bend National Park, USA
David J. Dean, David J. Topping, Ronald Griffiths, Thomas A. Sabol, John C. Schmidt, and Jeffrey Bennett

Development and Analysis of Suspended Sediment Rating Curves for the Kalamazoo River from Marshall to Morrow Dam, Michigan
David T. Soong, Christopher J. Hoard, Faith A. Fitzpatrick, and Ronald B. Zelt

7B Surrogates of Sediment

From Mobile ADCP to High-Res SSC: A Cross-Section Calibration Tool
Justin A. Boldt

Densimetric Measurements as a Surrogate for Suspended-Sediment Concentration in the Rio Puerco, New Mexico
Jeb E. Brown, John R. Gray, and Nancy J. Hornewer

Large River Bed Sediment Characterization with Low-Cost Sidescan Sonar: Case Studies from Two Settings in the Colorado (Arizona) and Penobscot Rivers (Maine)
Daniel Buscombe, Paul E. Grams, Theodore S. Melis, and Sean M.C. Smith

7C Reservoir Sedimentation and Sustainability 1

Reservoir Sustainability Workshop
Timothy J. Randle, Sean Kimbrel, and Kent L. Collins

Progress Toward Developing a National, Dynamic Reservoir-Sedimentation Database
John R. Gray

USACE Reservoir Sedimentation Survey Database (RESSED) Oracle conversion
Deborah Cooper

Reservoir Sedimentation and Sustainability in USACE: Status Report
Meg Jonas

7D Fluvial Geomorphology 3

An Analysis of an Extreme Flood Properties to 2-D Model Outputs
Rebecca Kallio and Jeanne Godaire

Setting the Stage for Change: Geomorphic Response of a Secondary Channel on the Rio Grande
Jonathan AuBuchon and Mark S. Nemeth

Bank Erosion Modeling with SRH-2D on the Rio Grande, New Mexico
Yong G. Lai

Complex Geomorphic Responses to Base Level Fluctuations: A Case Study on the Rio Grande Upstream of Elephant Butte Reservoir
Nathan Holste

7E Post Fire Analyses and Restoration 3

Restoring Alluvial Fan Function as Part of Post-Wildfire Restoration Efforts
David Rosgen and Brandon Rosgen

The Automated Geospatial Watershed Assessment Tool (AGWA): Using Raingage, Radar and Streamflow Records from Burned Watersheds to Evaluate and Improve Parameter Estimations
B. Scott Sheppard, I. Shea Burns, Gabriel Sidman, D. Phillip Guertin, and David C. Goodrich

Combining Fire and Erosion Modeling to Target Forest Management Activities
William J. Elliot, Mary Ellen Miller, and Nic Enstice

Climate Change Impacts and Mitigation/Adaptation: Coping with Weather Extremes from an Engineering Student's Viewpoint
Brittany R. Bennett

7F Sediment Impacts on Wildlife and Habitat

Downstream Sediment Impacts of Breaching the Elwha Dam and Glines Dam WA on Aquatic Habitat, Fish Restoration, River Dynamics, and Flood Plain Development
Frank Reckendorf and Barry Southerland

Sandbar Growth and Decay on the Missouri River during the High Flows of 2010 and the Historic 2011 Flood
Jake Gusman, Vicki Tripolitis, Cameron Jenkins, Christopher Svendsen, and Daniel Pridal

San Joaquin River Spawning Habitat Suitability Study
Elaina Gordon and Blair Greimann

Early Warnings and Long-Term Changes: Application of Continuous Turbidity Monitoring to Protect an Endangered Fish Species During Construction of a Large-Scale Flood-Reduction Effort
John D. Jastram, Douglas L. Moyer, and Kenneth E. Hyer

8A Sediment Yield and Transport Modeling 8

Shortcomings of Two-parameter Power Functions for Fitting Bedload Rating Curves
David Gaeuman

A Definitive Method for the Selection of Sediment Transport Relations
David T. Williams

Two-Dimensional Poissonian Homogeneous Model for Suspended Sediment and Pollutant Movements in Open-Channel Flow
Geraldo Wilson Junior and Cid da Silva Garcia Monteiro

Estimation of Suspended-Sediment and Nutrient Fluxes and Associated Trends Across the Chesapeake Bay Watershed
Douglas L. Moyer, Jeffrey G. Chanat, Kenneth E. Hyer, Michael J. Langland, and Joel D. Blomquist

8B Surrogates of Sediment

8C Reservoir Sedimentation and Sustainability 2

Developing Guidelines for Formulating Reservoir Sustainability Plans
Sean Kimbrel, Kent Collins, and Tim Randle

An Inventory of Sedimentation in Hawaii's Reservoirs Using Mixed Methods
Kim Falinski and David Penn

Simulations of Lake Mills Drawdown Experiment Using SRH2D Model
Jennifer G. Duan, Lei Liu, and Chunshui Yu

Numerical Modeling of Isleta Diversion Dam Gate Operation Hydraulics to Minimize Sediment Effects
Drew Baird and Michael Sixta

8D Fluvial Geomorphology 4

Geomorphic Change in the Limitrophe Reach of the Colorado River in Response to the 2014 Delta Pulse Flow, United States and Mexico
Erich R. Mueller, John C. Schmidt, David J. Topping, and Paul E. Grams

Basin-Scale Geomorphology and Sediment Transport Analysis for the Mouse/Souris River Enhanced Flood Protection Plan
Peter Hinck, Benjamin Sheets, Miguel Wong, and Amy Anderson

Suspended Sediment Transport Through a Large Fluvial-Tidal Channel Network
Scott A. Wright and Tara L. Morgan

Bedload Database and Prediction Performance
Rollin H. Hotchkiss and Darren D. Hinton

8E Modeling of Major River Systems 1

The Analysis of Modeled and Satellite Great Lakes Snow Water Equivalent Data and Incorporating Near Real-Time Estimates into Water Level Forecasting
James W. Lewis, Carrie M. Vuyovich, and Steven F. Daly

Hydraulic Modeling and Mapping of the Yellowstone River to Support Cumulative Effects Assessment
Laurel J. Hamilton, Kevin K. Adams, Megan A. Splattstoesser, and Roger L. Kay

The Colorado River Basin Water Supply and Demand Study: Modeling to Support a Robust Planning Framework
Alan Butler, Carly Jerla, Ken Nowak, Jim Prairie, Bill Oakley, Neil Wilson, and Edie Zagona

Truckee-Carson RiverWare© Planning Model Description and Applications
Heather Gacek, Thomas Scott, and Shane Coors

8F Management and Decision-Making Models 1

Real-Time Water Control Decision Support with CWMS 3.0 *
William Charley

Utilizing Probabilistic Forecasts for Colorado River Reservoir Operations: Decision Making and Risk Management
Anthony Powell, Daniel Bunk, Shana Tighi, Katrina Grantz, and Shane Coors

Pipeline Stream Crossings – a Risk-Based Approach to Minimize Aquatic Impacts
Janine Castro, Anne MacDonald, Erin Lynch, and Colin Thorne

Multi-Objective Modeling in RiverWare for USACE-SWD
John Daylor, David Neumann, Edith Zagona, and Jennifer Steffen

9A Sediment Yield and Transport Modeling 9

Channel and Bank Stability of the Burnett River in the Aftermath of the 2011 and 2013 Floods: Implications for Sediment Delivery to the Great Barrier Reef
Andrew Simon, Natasha Bankhead, and Peter Wilson

Sediment Diversion Efficiency, Lessons from Mississippi River Models
Ronald Heath, Gary Brown, and Jeremy Sharp

Preliminary Results for Calculating Salinity and Sediment Loading for Runoff in the Upper Colorado River Basin
Erik Cadaret, Robert Blank, Kenneth McGwire, Sayjro K. Nouwakpo, Colleen G. Rossi, Mark Weltz, Todd Adams, Alice Boizet, Sandra Li, Tye Morgan, and Jacob Phillips

Continuous Vertical Sorting Model in a One-Dimensional Sediment Transport Model, SRH-1D
Sean Kimbrel, Blair Greimann, and Victor Huang

9B Dam Removal/Rehabilitation 1

Bankfull Width Controls on Riffle-Pool Morphology Under Conditions of Increased Sediment Supply Field Observations During the Elwha River Dam Removal Project
Andrew K. Brew, Jacob A. Morgan, and Peter A. Nelson

Scour and Subsequent Repair at Lock and Dam 25
Timothy Lauth, David Gordon, Matthew Rector, and William Moeller

Geomorphic Adjustments on the Upper Missouri River in Response to Dam Management and Flooding
Katherine Skalak, Edward Schenk, Adam Benthem, Cliff Hupp, Joel Galloway, and Rochelle Nustad

Elwha PlaneCam, Affordable Near-Real-Time Orthoimagery and Digital Elevation Models in Support of Adaptive Sediment Management and Modeling During Elwha and Glines Canyon Dam Removal
Andrew Ritchie, Jennifer A. Bountry, and Timothy J. Randle

9C Reservoir Sedimentation and Sustainability 3

Collection and Interpretation of Reservoir Data to Support Sustainable Use
Gregory L. Morris

Unsteady Flow and Sediment Modeling in a Large Reservoir Using HEC-RAS 5.0
John Shelley, Stanford Gibson, and Aaron Williams

Developing a Sediment Management Plan for Paonia Reservoir
Kent Collins and Sean Kimbrel

Rio Grande and Cochiti Reservoir Sedimentation Issues: Are There Sustainable Solutions?
Charles M. Davis, C. Bahner, Darrel E. Eidson, and Stanford Gibson

9D Fluvial Geomorphology 5

Proposed Diversion Works in Rivers that Show Significantly Less Morphodynamic Activity Than Expected *
Miguel Wong

A Review of the Lower Mississippi River Potamology Program
David S. Biedenharn, John H. Brooks, Roger A. Gaines, Barbara A. Kleiss, Charles F. Pinkard, and Wayne A. Stroupe

Gravel Deposits on Lower Mississippi River Sandbars
Richard McComas and C. Fred Pinkard

Sediment and Carbon Sequestration in the Atchafalaya River Basin, Louisiana
Cliff R. Hupp, Daniel E. Kroes, Edward R. Schenk, and Gregory B. Noe

9E Modeling of Major River Systems 2

Mississippi River Model
Edmund M. Howe

Current and Historical Sediment Loads in the Lower Mississippi River
Colin Thorne, Kevin Knuuti, Oliver Harmar, Chester Watson, Nick Clifford, and David Biedenharn

Saint-Venant Modeling for Large River Basins – Challenges and Data Needs
Ben R. Hodges, Frank Liu, and Alfredo Hijar

Synthetic Bathymetry Method Development, Validation and Application to five Pacific Northwest Rivers
Zachary P. Corum, Travis D. Ball, and Matthew J. Hubbard

9F Management and Decision-Making Models 2

Problems and Prospects of SWAT Model Application on an Arid/Semi-arid Watershed in Arizona
Yongping Yuan, Wenming Nie, and Emily Sanders

The KINEROS2 – AGWA Suite of Modeling Tools
David C. Goodrich, Carl L. Unkrich, Yoganand Korgaonkar, Shea Burns, Jeff Kennedy, Gabriel Sidman, Brian Scott Sheppard, Mariano Hernandez, Phil Guertin, Scott N. Miller, William Kepner, Phil Heilman, and Mark Nearing

Representing Green Infrastructure Management Techniques in Arid and Semi-arid Regions: Software Implementation and Demonstration Using the AGWA/KINEROS2 Watershed Model
Yoganand Korgaonkar, I. Shea Burns, Jane Barlow, D. Phillip Guertin, Carl Unkrich, David C. Goodrich, and William Kepner

Integrated Modeling Approach for Fate and Transport of Submerged Oil and Oil-Particle Aggregates in a Freshwater Riverine Environment
Faith A. Fitzpatrick, Rex Johnson, Zhenduo Zhu, David Waterman, Richard D. McCulloch, Earl J. Hayter, Marcelo H. Garcia, Michel Boufadel, Timothy Dekker, Jacob S. Hassan, and Kenneth Lee

Models/Demos

2D Hydrologic Modeling using the Gridded Surface Subsurface Hydrologic Analysis (GSSHA) model and the Watershed Modeling System (WMS) *
Christopher Smemoe

Demonstration of the Capabilities of the KINEROS2 – AGWA 3.0 Suite of Modeling Tools
I. Shea Burns, Carl L. Unkrich, David C. Goodrich, Yoganand Korgaonkar, Jeff Kennedy, Gabriel Sidman, Brian Scott Sheppard, Mariano Hernandez, Phil Guertin, William Kepner, Phil Heilman, and Mark Nearing

Demonstration of the Water Erosion Prediction Project (WEPP) Internet Interfaces and Web Services
Jim Frankenberger, Dennis Flanaga, Bill Elliot, and Eric Theller

Hydrologic Modeling System (HEC-HMS) Model Demonstration *
William Scharffenberg

Modeling of a Non-Physical Fish Barrier, Demonstration
Marcela Politano, Ezequiel martin, Yong Lai, Merlynn Bender, and Dave Smith

River Analysis System (HEC-RAS) Model Demonstration *
Gary W. Brunner

RiverWare Demonstration
David Neumann and Edie Zagona

RVR Meander – A Toolbox for River Meander Planform Design and Evaluation
Eddy J. Langendoen, Davide Motta, Jorge D. Abad, Marcelo H. Garcia, Roberto Fernandez, and Nils Oberg

WinDAM B & C Earthen Embankment Overtopping and Internal Erosion Analysis Software Computer Demonstration
Karl Visser, Ronald D. Tejral, and Mitchell L. Neilsen

WinTR-20 Software Computer Demonstration
Quan D. Quan, William H. Merkel, and Helen Fox Moody

Posters

2011 Morganza Control Structure Tail Bay Scour Development and Sediiment Distribution
Tzenge-huey Shih and Suchen Chien

An Approximation of the Sediment Budget for the Tombigbee River and the Mobile River Basins
John J. Ramirez-Avila, William McAnally, and Sandra L. Ortega-Achury

Analyzing Streambank Erosion Using LIDAR *
Gary Trent Snellings

Assessment of Fire Impacts on Hydrology and Erosion Using Field Experiments and the Rangeland Hydrology and Erosion Model *
C. Jason Williams

Computation of Continuous Suspended-Sediment Concentration Records related to a Short-Term Drawdown of Fall Creek Lake, Upper Willamette Basin, Oregon *
Heather Bragg

Continuous Loosening and Transport of Sediment Deposition *
Yannick Ratke

Continuous Turbidity Monitoring as a Tool for Evaluating Suspended Sediment Loading in the Middle Truskee River and Tributaries, Placer and Nevada Counties, California
Brian Hastings, David Shaw, Stefan Schuster, and Beth Christman

Creation and Maintenance of Dynamic Channels: Lessons Learned from the Large-Scale Restoration of a Regulated River *
Susannah Erwin

Effects of Bedload Sampler Netting Properties on Hydraulic and Sampling Efficiency
Kristin Bunte, Kurt W. Swingle, Steven R. Abt, and Daniel A. Cenderelli

Estimating Sediment Yield on Disturbed Rangeland Using the Rangeland Hydrology and Erosion Model (RHEM) *
Osama Al-Hamdan

Evaluation of Surrogate Technology to Determine the Sediment Transport in the Raulerson Brothers Canal, Everglades National Park, Florida *
Carrie Boudreau

Measures of Sediment in Minnesota
Greg Johnson and Bill Thompson

New Insights into the Effectiveness of a Lower Mississippi River Sediment Diversion Using a Decade of Field Observations and Morphological Modeling *
Brendan Yuill

Online Modeling Tools Assist in Evaluating Postfire Flooding and Erosion Risk
Peter Robichaud, William Elliot, Erin Brooks, Marianna Dobre, Dennis Flanagan, and James Frankenburger

POTAMOD – Mobile-Bed Sediment-Transport Modeling Application for Use with SIAM and HEC-RAS
Amanda L. Cox, David S. Biedenharn, Chester C. Watson, and Michelle Martin

Quantifying and Modeling Sediment Loads from Streambank Erosion along the Headwaters of Town Creek in Mississippi
John J. Ramirez-Avila, Eddy J. Langendoen, William McAnally, James L. Martin, Sandra L. Ortega-Achury, and Ron Bingner

Sediment and Nutrient Trapping on the Morganza Spillway During the 2011 Mississippi River Flood
Daniel E. Kroes, Edward R. Schenk, Gregory B. Noe, and Adam J. Benthem

Sediment Characteristics and Sediment Transport Modeling for the Saginaw River Navigation Channel
John Barkach, Carol J. Miller, James Selegean, and Fatemeh Babakhani

Sediment Chemistry Results from Sediment Cores Collected from the Escalante and San Juan River Deltas in Lake Powell, UT, in 2010-2011
Nancy Hornewer and Robert J. Hart

Sediment Fingerprinting to Delineate Sources of Sediment in an Urban Sub-Watershed Within the Chesapeake Bay Watershed
Anna C. Baker, A.C. Gellis, L.G. Sanisaca, and G.B. Noe

Sediment Transport on Cape Sable, Everglades National Park, Florida *
Carrie Boudreau

Simulating Salinity Concentration at the Colorado River Basin Scale
James Prairie, David Neumann, Nicholas Williams, and Edith Zagona

State of the Practice of Sediment Management in Reservoirs: Minimizing Sedimentation and Removing Deposits
Kathleen M. Healy, Amanda L. Cox, Daniel M. Hanes, and Lisa G. Chambers

Surrogate Analysis and Index Development (SAID) and Real-Time Dissemination
Marian Domanski, Timothy Straub, Molly Wood, Mark Landers, Gary Wall, Steven Brady

The Influence of Sampling Technique on Bedload Prediction

Darren D. Hinton and Rollin H. Hotchkiss

Using Acoustic Surrogates to Monitor Discharge, Sediment and Nutrient Supply to Texas Bays and Estuaries*
Michael Lee

Utilizing GIS to Identify Sediment Fluctuations in Nambe Falls Reservoir, NM *
Joel Murray

Web-based Rangeland Hydrology and Erosion Model
Mariano Hernandez, Mark Nearing, Jeffry Stone, Gerardo Armendariz, Fred Pierson, Osama Al-Hamdan, C. Jason Williams, Ken Spaeth, Mark Weltz, Haiyan Wei, Phil Heilman, and Dave Goodrich

10A Sediment Transport and Fingerprinting

Numerical Modeling of Laboratory Flume Experiments for Tracking Unsteady Sediment Transport Using Colored Particles
Mustafa S. Altinakar, Reza Marsooli, and Zhaosong Qu

Scaling Relations for Exponents and Coefficients of Bedload Transport and Flow Competence Curves in Coarse-Bedded Streams with Channel Gradient, Runoff Yield, Basin Area, and Subsurface Fines
Kristin Bunte, Steven R. Abt, Kurt W. Swingle, Daniel A. Cenderelli, Dieter Rickenmann, and Dave Gaeuman

Evaluation of the HSR Model as a River Engineering Tool *
Edward Brauer

Identifying Sediment Sources in the Sediment TMDL Process
Allen C. Gellis, F.A. Fitzpatrick, J.P. Schubauer-Berigan, R.B. Landy, and L. Gorman-Sanisaca

10B Dam Removal/Rehabilitation 2

Progress on Dam Removal Analysis Guidelines for Sediment
Timothy Randle and Jennifer Bountry

Example Applications of the Dam Removal Analysis Guidelines for Sediment *
Jennifer Bountry

Role of Adaptive Sediment Management in Elwha Dam Removal
Jennifer Bountry, Patrick Crain, Josh Chenowith, Timothy Randle, and Andrew Ritchie

Elwha River Restoration: Reservoir Sediment Modeling in a GIS Framework
Timothy J. Randle, Jennifer Bountry, and Kurt B. Wille

10C Reservoir Sedimentation and Sustainability 4

Negotiating Hydrologic Uncertainty in Long Term Reservoir Sediment Models: Simulating Arghandab Reservoir Deposition with HEC-RAS
Stanford Gibson and D. Pridal

10D Regional Watershed Management 1

10E GIS and Water Resources Management

10F Management and Decision-Making Models 3

TAPER: A Real-time Decision Support Tool for Balanced Flood Operation of the Arkansas River in Tulsa District
Jennifer Steffen, Jody Stringer, John Daylor, David Neumann, and Edith Zagona

Integrating Hydrologic and River Operations Modeling with Explicit Simulation of Groundwater and Surface-Water Exchange
Eric D. Morway, Richard G. Niswonger, and Enrique Triana

11A Earth Embankment Erosion Prediction

WinDAM C Earthen Embankment Internal Erosion Analysis Software
Karl K. Visser, Ronald D. Tejral, and Mitchell L. Neilsen

Changes in the Acoustic Response of Soils as a Function of Grass Cover
Blake Armstrong, Craig Hickey, and Zhiqu Lu

Comparing Process-Based Breach Models for Earthen Embankments Subjected to Internal Erosion
Ronald D. Tejral and Sherry L. Hunt

11D Regional Watershed Management 2

Effectiveness of Channel Improvement Work on the Mississippi River
Richard McComas and C. Fred Pinkard, Jr.

Simulation of Streamflow and Sediment Mobility in the Missouri River near Bismarck, North Dakota *
Rochelle Nustad

Developing a New Stream Metric for Comparing Stream Function Using a Bank-Floodplain Sediment Budget: a Case Study of Three Piedmont Streams
Edward R. Schenk, Cliff R. Hupp, Allen Gellis, and Greg Noe

Automated Updates to 2D Hydrologic Models for Open-pit Mining
Christopher M. Smemoe and Clark Barlow

11F Management and Decision-Making Models 4

Low Water Planning in the Columbia River Basin
Thomas Chisholm

River Engineering Research Needs in the Corps of Engineers
Meg Jonas and John Remus

Modelling Extreme Flood Hydrology for Grand Coulee Dam through Collaboration with Multiple Government Agencies, Universities, and the Private Sector
Frank Dworak, John Englund, Marketa Elsner, and Ralph Klinger

Development and Validation of a 2D Dam Break Process Model

Yafei Jia and Sherry Hunt

Instructions:
To view a paper, click on the corresponding title. Titles marked with an asterisk (*) denote presentations for which full-length manuscripts were not submitted by the respective authors.

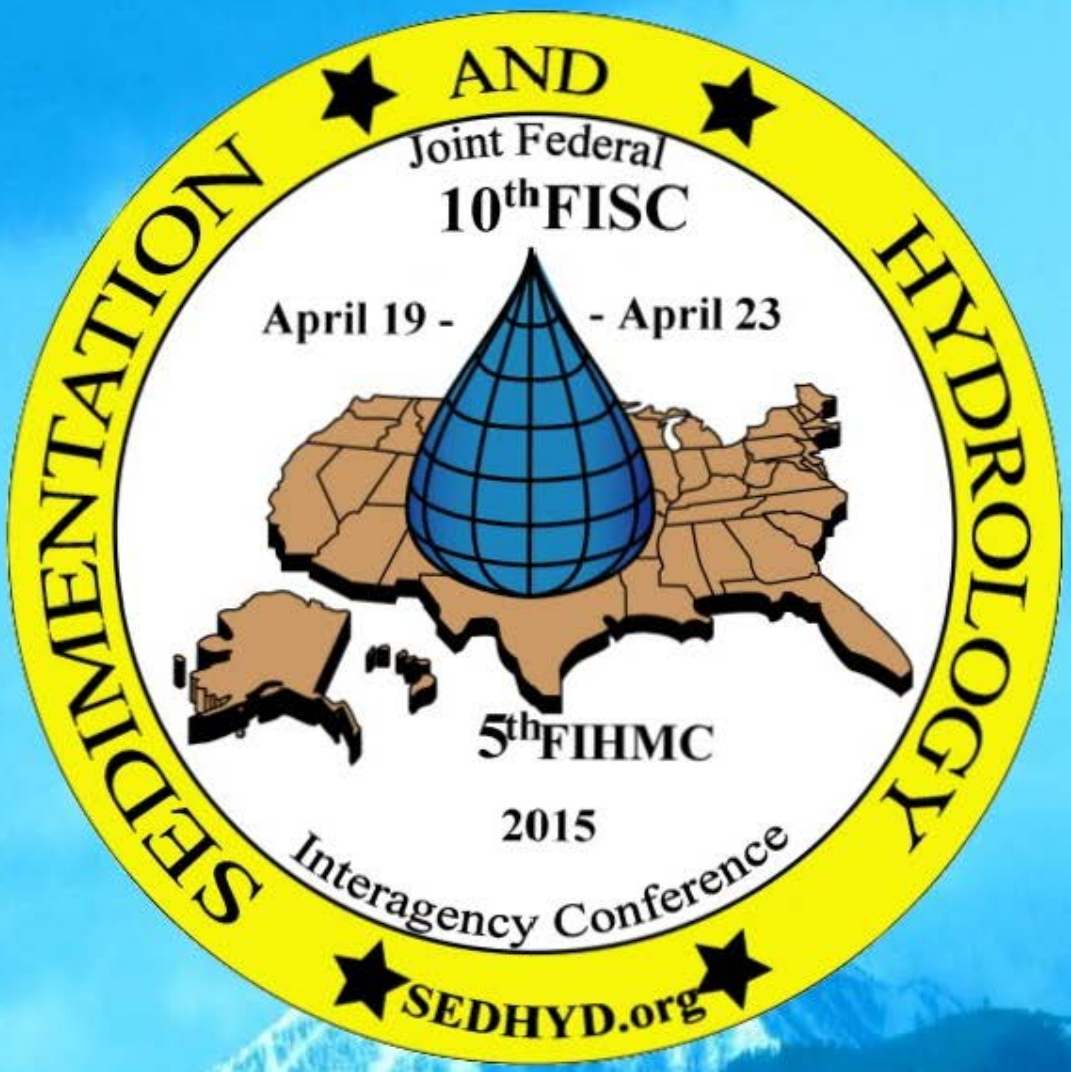
SEDIMENTATION
AND
HYDROLOGY
Joint Federal
10thFISC
April 19 -
- April 23
5thFIHMC
2015
Interagency Conference
SEDHYD.org

A PHYSICALLY-BASED CHANNEL-MODELING FRAMEWORK INTEGRATING HEC-RAS SEDIMENT TRANSPORT CAPABILITIES AND THE USDA-ARS BANK-STABILITY AND TOE-EROSION MODEL (BSTEM)

Gibson, Stanford, Research Hydraulic Engineer Hydrologic Engineering Center Davis, CA
stanford.gibson@usace.army.mil
Simon, Andrew, Senior Consultant/Geomorphologist Cardno, Oxford, MS andrew.simon@cardno.com
Langendoen Eddy, Research Hydraulic Engineer Agricultural Research Service Oxford, MS
eddy.langendoen@ars.usda.gov
Bankhead, Natasha, Senior Project Scientist Cardno Entrix Oxford, MS, natasha.bankhead@cardno.com
Shelley, John, Senior Hydraulic Engineer, US Army Corps of Engineers - Kansas City District
john.shelley@usace.army.mil

Abstract: One-dimensional sediment-transport models historically simulate vertical channel adjustment, raising or lowering cross-section node elevations to simulate erosion or deposition. This approach does not account for bank erosion processes including toe scour and mass failure. In many systems lateral channel adjustments can be as important – or more important – than vertical bed changes. There is also important feedback between incision, deposition, toe scour, and bank-failure processes. Each process can depend on the others. Additionally, bank-derived sediments can affect downstream processes and impact downstream projects, depositing in flood damage reduction channels, silting natural or engineered spawning substrates, or filling downstream reservoirs. Therefore, to account for these processes and feedback between them, the USDA-ARS Bank Stability and Toe Erosion Model (BSTEM) has been integrated with the sediment transport methods in HEC-RAS 5.0.

BSTEM is a physically based bank-erosion model that accounts for hydraulic, toe erosion and bank-failure processes in homogeneous or layered banks. It computes toe-erosion by subdividing flow segments in the near bank zone to compute a vertical distribution of boundary shear stresses and calculates a critical failure plane through layered bank sediments, failing the bank and adjusting the cross section when driving forces exceed resisting forces.

Because of their complementary features, river modelers often run HEC-RAS and BSTEM iteratively, in tandem, simulating toe scour and bank failure with BSTEM and computing water surface elevations, simulating bed change and routing bed and bank-derived sediment with HEC-RAS. To provide a more efficient, integrated modeling framework and continuous simulation of potential bed and bank-erosion loadings, HEC-RAS and BSTEM have been coupled, automating the feedbacks between hydraulic, bed, toe, and bank processes. BSTEM uses HEC-RAS hydraulics to determine water surface elevations and to compute the vertical distribution of shear stresses along the bank surface, and evaluates if cross section deposition or erosion simulated by HEC-RAS sediment transport exacerbates or improves bank stability. If BSTEM computes failure, HEC-RAS updates the cross section to reflect the new bank geometry and adds the sediment mass of the failed layers (by particle-size class) to the transport model, routing it downstream. This paper will describe the model integration, and present an example application and model validation.

Keywords: Sediment modeling, Bank Failure, Toe Erosion, HEC-RAS, BSTEM

INTRODUCTION

The USDA ARS – Bank Stability and Toe Erosion Model (BSTEM) simulates two major stream bank erosion processes:

1. Bank Failure: A geotechnical model that evaluates bank stability by computing failure planes through the bank to determine if the driving forces exceed the resisting forces, and selecting the 'critical failure plane,' with the lowest factor of safety.

2. Toe Scour: A lateral erosion model that computes a shear distribution between the water surface and bank toe and simulates lateral hydraulic scour in this zone.

HEC-RAS sediment transport simulates a third processes:

3. Channel Erosion or Deposition: Vertical adjustment of the channel portion of the cross section in response to erosion or deposition.

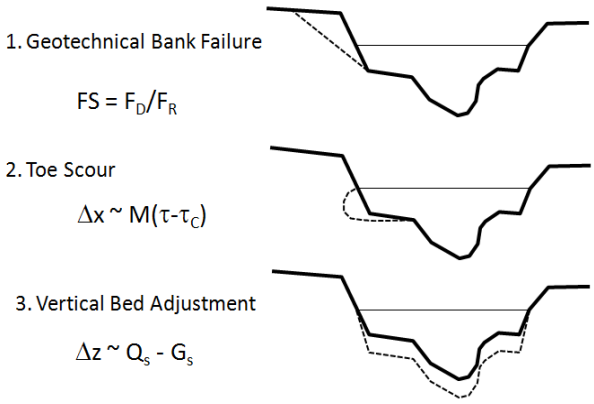

Figure 1 The three processes coupled in the integration of the USDA-ARS BSTEM model and HEC-RAS, including bank and toe-erosion processes from BSTEM and vertical adjustment (and sediment routing) from HEC-RAS, where FS=factor of safety, F_D=driving forces, F_R=resisting forces, Δx=lateral bank change, M=erodibility, τ=shear stress, τ_c=critical shear stress, Δz=vertical bed change, Q_s=sediment supply, and G_s=sediment capacity.

However, these three processes interact. Vertical change can stabilize toes or steepen banks, accelerating or preventing bank failures. Bank scour and failure add sediment to the stream, affecting sediment continuity and downstream deposition or erosion while decreasing available shear stress for a given discharge. To simulate these processes simultaneously, and to capture the interactions and feedbacks between them, USDA-ARS BSTEM algorithms were incorporated into the HEC-RAS sediment-transport algorithms.

METHODOLOGY

Exhaustive presentation of the processes, equations and algorithms that compose USDA-ARS BSTEM and HEC-RAS sediment transport are outside of the scope of this paper. A separate document accompanies the HEC-RAS 5.0 (USACE, 2015), documenting the methodology in detail. However, it is important to summarize the model approach to the three main processes:

1. Bank Failure Methods

The USDA-ARS Bank Stability and Toe Erosion Model (BSTEM) computes the critical linear failure plane through layered bank materials. It uses either the method of slices (Langendoen and Simon, 2008) or the horizontal layer method (Simon et al., 2000) to compute a factor of safety for multiple failure planes, starting at several elevations along the bank and extending through the bank at multiple angles. At each time step specified, a "bracket and Brent" optimization algorithm (Teukolsky et al., 2007) converges on the critical failure-plane angle at each bank intersection point within a few iterations and

selects the failure plane with the lowest factor of safety as the 'critical failure plane'. If BSTEM computes a factor of safety less than 1.0, HEC-RAS fails the bank, introducing the failure block mass into the sediment routing model as a sediment source. HEC-RAS also updates the cross section to compute future hydraulics based on the new, wider, cross-section geometry. The geotechnical model can compute failure planes through homogeneous banks or 'soil layers,' stratified materials with distinct vertical variation in soil properties. The method of slices can also compute tension cracks, which decrease failure plane length, usually removing more resisting forces than driving forces, decreasing the factor of safety and increasing bank-failure frequency.

The geotechnical algorithms are very sensitive to pore-water pressure. Positive and negative pore-water pressures are computed from groundwater elevation and the relation between hydrostatic pressures in the bank and the confining hydrostatic forces from the water in the channel. Groundwater elevation can be specified in HEC-RAS or computed dynamically, in response to rising and falling water-surface elevations in the channel, with a simple 'bank reservoir' groundwater model.

2. Toe Scour Methods

The BSTEM toe erosion model (Simon et al., 2011) moved specified cross section nodes normal to the bank surface. HEC-RAS moves nodes laterally to keep nodes from eroding below the bed elevation. The toe scour methods use cohesive equations if ≥20% (an adjustable threshold) of the layer is silt and clay and cohesionless methods if the fine content is lower than the threshold. Cohesive scour uses a simple excess shear equation emphasizing site specific soil parameters (critical shear stress and erodibility [k in cm^3/N-s or ft^3/lbf-s]). However, neither laboratory nor field methods reliably measure cohesionless erodibilities, so the cohesionless methods apply transport functions. Applying bed transport equations to well graded (poorly sorted) bank sediment (especially with substantial silt or clay content, but not enough to trigger the cohesive equations) can pose sorting problems and often over predicts scour. Bed sorting algorithms and theory (Gibson and Piper, 2007) are not directly applicable. The development team is experimenting with alternate bank sorting methodologies to model these processes.

Both cohesive and cohesionless toe scour methods compute lateral adjustment based on local bank shear at each cross section node. HEC-RAS is a one-dimensional model, which computes a single, cross section average bed shear for each time step. Bank shear stress is maximum at the bed, decreasing up the bank towards the water surface, so applying the average bed shear to all bank nodes overpredicts scour. BSTEM accounts for this, computing shear at each inundated bank node with a radial shear distribution, based on the ratio of the hydraulic radius of the local radial flow zone to the hydraulic radius of the bank (Simon et al., 2011).

Unlike stand alone, USDA-ARS versions of BSTEM (Simon et al., 2011), toe scour algorithms in HEC-RAS cannot currently simulate overhanging banks. If a node scours past the node above it, which is common since shear stress is higher at deeper nodes or material is more erodible, HEC-RAS shears the bank vertically, scouring the higher node to match station of the node below it. This is a technical limitation (HEC-RAS requires monotonically increasing cross section stations) but translates into the physical assumption that cantilever failure will make overhanging banks vertical.

3. Bed Change Methods

HEC-RAS added sediment transport calculations in version 4.0, (Gibson et al., 2006), applying sediment transport functions, bed mixing algorithms, and temporal limiters to compute a sediment balance at each control volume, then adjusting wetted cross section nodes vertically, raising them in response to erosion and dropping them in response to deposition. These capabilities leveraged the full suite of steady flow hydraulic analysis in those earlier versions of HEC-RAS (e.g. ineffective flow areas, inline structures,

flow dependent roughness, etc…) and HEC-RAS 5.0 integrates sediment transport capabilities with unsteady flow (Gibson and Boyd, 2014, Shelley et al. 2015) and powerful features associated with that modeling environment (e.g. lateral structures, flow splits, operational rules).

MODEL INTEGRATION

HEC-RAS 5.0 includes the USDA-ARS Bank Stability and Toe Erosion Model (BSTEM) interface as an optional third tab in the sediment editor (Figure 2). The model requires users to designate the 'bank' portion of the cross section, the nodes that can scour laterally and the zone where failures can start, between the bank 'toe' and 'edge' stations. It also requires a ground water elevation which will either remain static for the entire simulation or initializes the dynamic groundwater model. Finally, BSTEM requires soil properties for each bank layer.

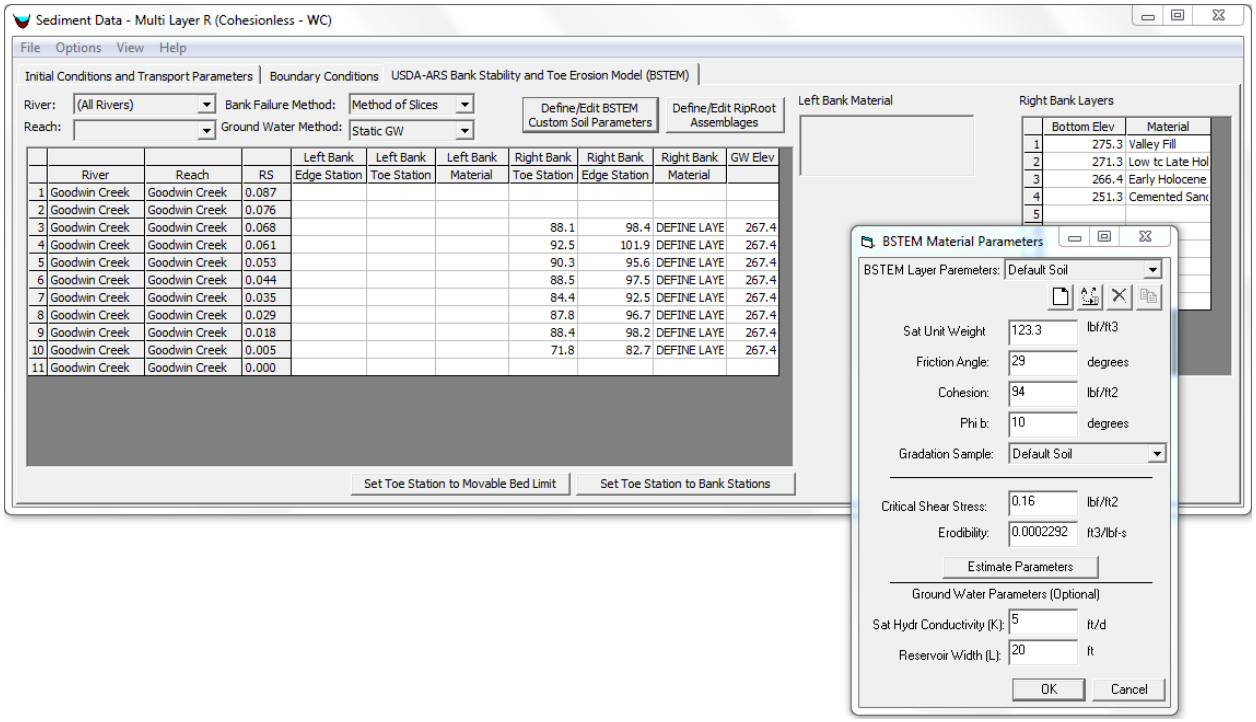

Figure 2 USDA-ARS Bank Stability and Toe Erosion Model (BSTEM) interface in HEC-RAS including the soil parameter interface and an example of soil layer definition.

Defining soil parameters is the most data intensive part of using the BSTEM algorithms. Each soil layer requires classical geotechnical parameters (unit weight, friction angle, cohesion, and bulk unit weight), ϕ^b (representing the rate of increasing apparent cohesion with increasing matric suction), and hydraulic scour parameters (critical shear and erodibility). The model can be very sensitive to these parameters, particularly *k* where values can span orders of magnitude, making them highly site specific. Therefore, HEC-RAS included three methods of increasing complexity, to specify soil properties and negotiate the trade-off between data collection costs and parameter uncertainty. First, HEC-RAS included 16 default parameters from the BSTEM database, regression estimates based on decades of USDA-ARS measurements and modeling. Computing bank erosion in an HEC-RAS sediment model can be as simple as defining bank toe and edge stations, defining a groundwater elevation, and selecting the closest soil type from a default drop down list. However, because these parameters are so site specific, defining customized soil parameters (Figure 2) is recommended. HEC-RAS populates the soil type drop down list with customized soils as well as the default types. Finally, users can specify soil stratigraphy, selecting

the layer contact elevation and either a default or customized soil type for each layer (the method used in Figure 2 and the example application below).

The model can also be sensitive to the toe station parameter. The USDA-ARS BSTEM toe station and the HEC-RAS movable bed limits should generally be the same node, to avoid immobile cross section nodes or double counting scour. HEC-RAS includes a button to copy the movable bed limits to the BSTEM toes, to keep them consistent. If these nodes coincide, channel nodes move vertically and bank nodes move laterally, with the toe/movable bed limit node tracking both degrees of freedom. HEC-RAS also includes an option that deposits (but doesn't erode) outside the movable bed limits, allowing bank stations to move laterally and vertically in one direction.

Bank failure computations can increase sediment simulation run times by as much as an order of magnitude if BSTEM runs for both banks of every cross section at every computation increment. However, HEC-RAS only computes bank processes for banks with BSTEM data, allowing users to analyze particular reaches or stretches. Additionally, the model computes bank failure at every computational increment by default, but can often provide the same results computing on a coarser temporal scale. Users can reduce run times by increasing the number of time steps between bank computations, reducing run times dramatically. HEC is actively working on methods to optimize searches, detect and skip unnecessary computations, and find other opportunities to reduce run times further.

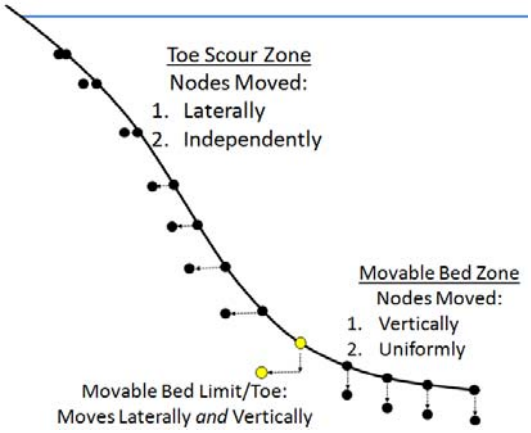

Figure 3 Differences between toe scour and bed change node updates in the coupled HEC-RAS/BSTEM model.

BSTEM algorithms are tied to the sediment transport module in HEC-RAS, requiring a sediment model to perform a dynamic bank-migration analysis. However, bank mechanics can be isolated from bed mechanics by defining the sediment transport parameters but setting the cross section(s) to 'pass through nodes.' A pass through cross section with BSTEM parameters will only adjust the cross section according to the BSTEM processes.

EXAMPLE APPLICATION

The USDA-ARS bank-process models are often tested and validated on Goodwin Creek (Simon et al., 2000; Langendoen and Simon, 2008; Lai et al., 2014), a carefully instrumented research reach in northern Mississippi with detailed hydrologic, groundwater and bank migration time-series data. ARS has measured flow on both major reach tributaries continuously since October 1981, recording flow each time stage changes by a small increment, providing a reliable, high resolution, upstream boundary condition. Up to eleven fixed cross sections were surveyed 51 times, between February 1996, and a bank stabilization project in 2007 (as well as six times since the project), recording up to 8 m of bank migration (Simon et al., 2000; 2008; 2011). The reach also has distinct stratigraphy, with four easily distinguished soil layers, each with detailed soil parameter and erodibility data from extensive borehole shear and jet tests. The soil property measurements, the temporal resolution of the boundary condition and bank migration time series, and the magnitude of the lateral bank scour and failure make Goodwin Creek an ideal site to test the coupled HEC-RAS/BSTEM model.

The initial, 1996 cross sections were used to build the HEC-RAS model and three customized soils were entered in the HEC-RAS Soil Property data base. Cross section "Toe" and "Top of Bank" nodes were

carefully identified and the "Define Layers" option (Figure 2) was selected for each cross section, populating each with the same four-soil-stratigraphy: a cemented sand and gravel conglomerate on the bottom, an early Holocene cohesive soil, a late Holocene cohesive soil, covered with valley fill.

Validation is a wrought concept with unhelpfully broad semantic range in model development (Oreskes et al, 1994; Rykiel, 1996; Gibson, 2013). In this case, 'validation' simply means an exercise to increase user confidence that the algorithms in the HEC-RAS/BSTEM coupling behave as designed by comparing them to field data and other models.

Since this was a model validation, rather than a project calibration, we adopted the parameters from the successful CONCEPTS model in Langendoen and Simon (2008) without adjustment. Langendoen and Simon (2008) adjusted the erodibility and critical shear of the toe material at the outside of a bend to compensate increased shear stresses produced by the three-dimensional flow that the 1D model ignores. The HEC-RAS validation adopted this approach and these parameters.

The toe material in Goodwin Creek is a cemented conglomerate, which controls the stream morphology and the rate of bank recession. The conglomerate has a relatively low fine content (1.4% finer than 63 μm) but has cohesive properties, amenable to jet tests and cohesive erodibity equations. However, since BSTEM uses cohesionless equations, by default, if the layer is less than 20% fine-grained material, the model was run with both the cohesionless approach and with the cohesive, erodibility approach used in Langendoen and Simon (2008) (by dropping the "% fine for cohesionless approach" factor to zero).

The Goodwin Creek analysis was run through the period (Mar 1996 – Feb 2001) replicated by Langendoen and Simon (2008) and then extended to include subsequent migration until the banks were modified as part of a bank-stabilization project in March 2006.

RESULTS

Cohesive model results are plotted with seven, measured, right-bank surveys for two representative, cross sections on Goodwin Creek in Figure 4 (XS6 and XS7, two mid-reach cross sections from Langendoen and Simon, 2008) . The location and shape of the final model cross section approximately matched the observations, estimating total bank migration and computing tension cracks where observed. The tension cracks in the prototype are longer than those the model computed. Langendoen and Simon (2008) customized the tension crack, specifying the observed crack length, but customized crack length is not available in HEC-RAS 5.0. Despite these minor differences, the results suggest the following: First, they represent a code verification step for the HEC-RAS/BSTEM model, demonstrating that it replicates prototype behavior and other model results. Second, results validate the Langendoen and Simon (2008) calibration (based on 1996-2001 measurements), demonstrating that their parameterization performed well outside of its calibrated time window (e.g. 2001-2007).

Select cross sections are plotted in Figure 4. Including all 51 repeated cross-sections would make the plot too dense to evaluate model results. It is still useful to evaluate the model against all measured data, however. Therefore all prototype measurements were plotted with the model results by interpolating the lateral migration time series at five reference elevations in Figure 5. The cross-section stations for lower elevations migrate more gradually in both the prototype and the model, as the toe consistently scours. Bank-failure events expand the higher elevations more episodically. The high bank processes track the observed stations better than the toe scour processes for both cross sections. The model also simulates more retreat at XS6 early in the time series and less later, matching the final migration but not matching intermediate steps. However, given the complexity of the processes and the uncertainty in the data, the spatial and temporal agreement for XS7 is excellent and XS6 is acceptable for most purposes.

Finally, the relative contribution of bank sediment is plotted in Figure 6, differentiating between hydraulic (toe scour) and geotechnical (mass failure) processes. Bank failure contributes almost an order of magnitude more sediment (205.6 tonnes) than toe scour (25.6 tonnes), but the rate of the former is correlated with the rate of hydraulic toe erosion, as expected. Both processes slow as the simulation progresses (a phenomenon also observed in the prototype data in Figure 5). Flows in the first two years were higher than the rest of the simulation, but model results also indicate process feedbacks. Widening cross sections and depositing upstream sediment decrease boundary shear stress and, therefore slow toe erosion and consequently, bank failure rates and overall migration.

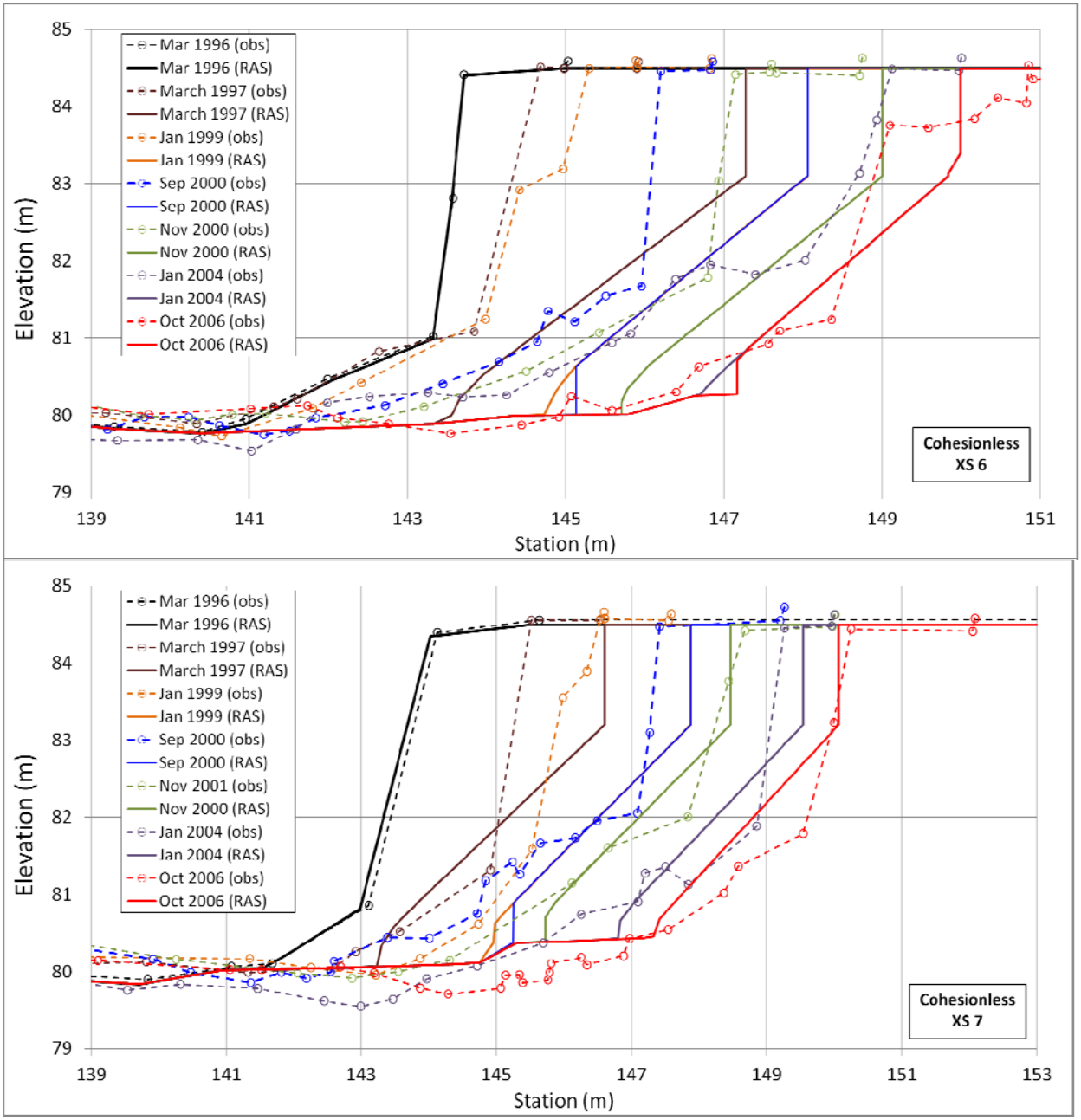

Figure 4 Select Goodwin Creek repeated right bank surveys at the two central cross sections with HEC-RAS/BSTEM cross section migration.

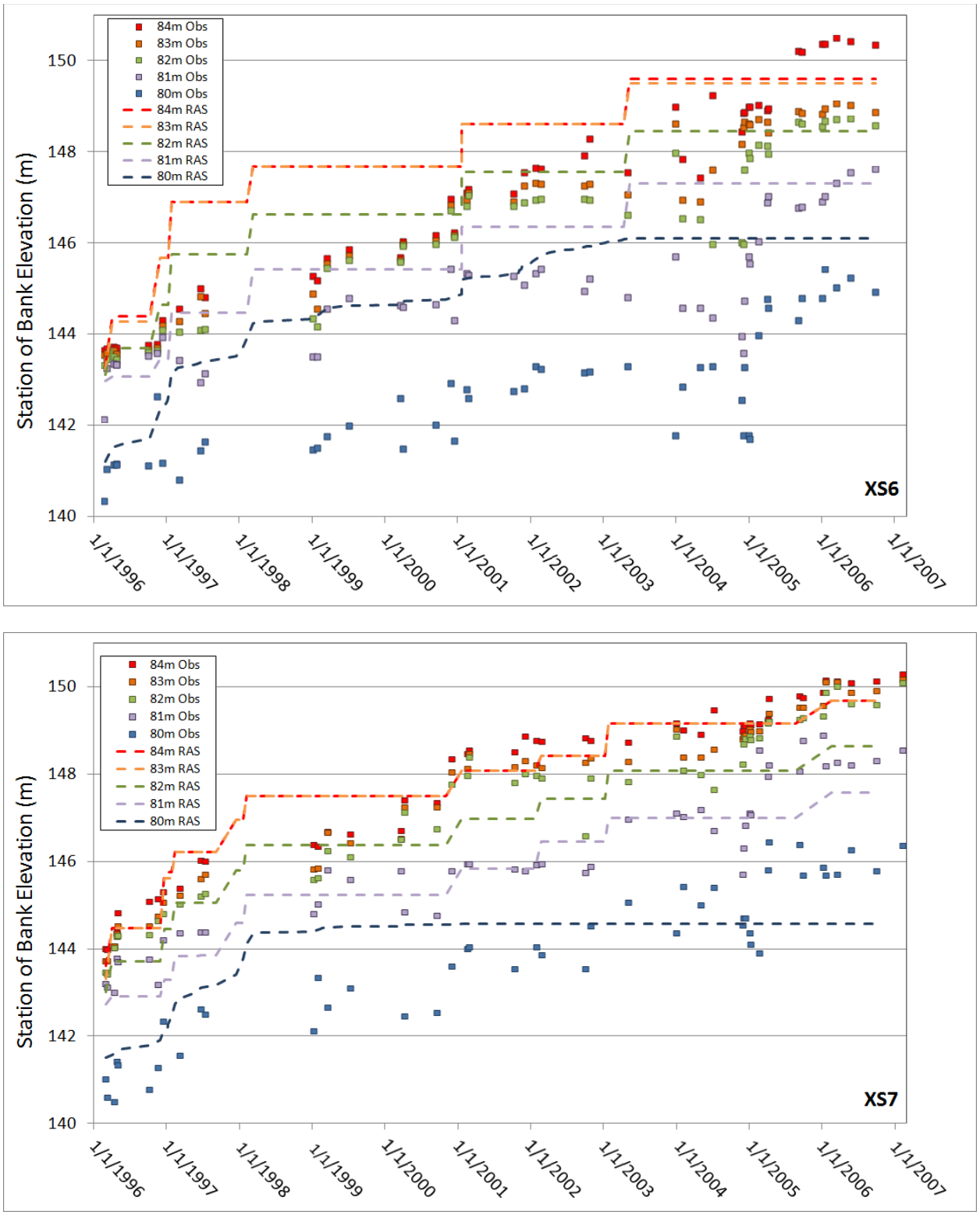

Figure 5 The lateral migration of the right bank of cross sections 6 and 7 (from Figure 4) at five different elevations. The HEC-RAS/BSTEM continuous simulation results are plotted with stations interpolated at the five elevations from all surveys between March 1996 and October 2006.

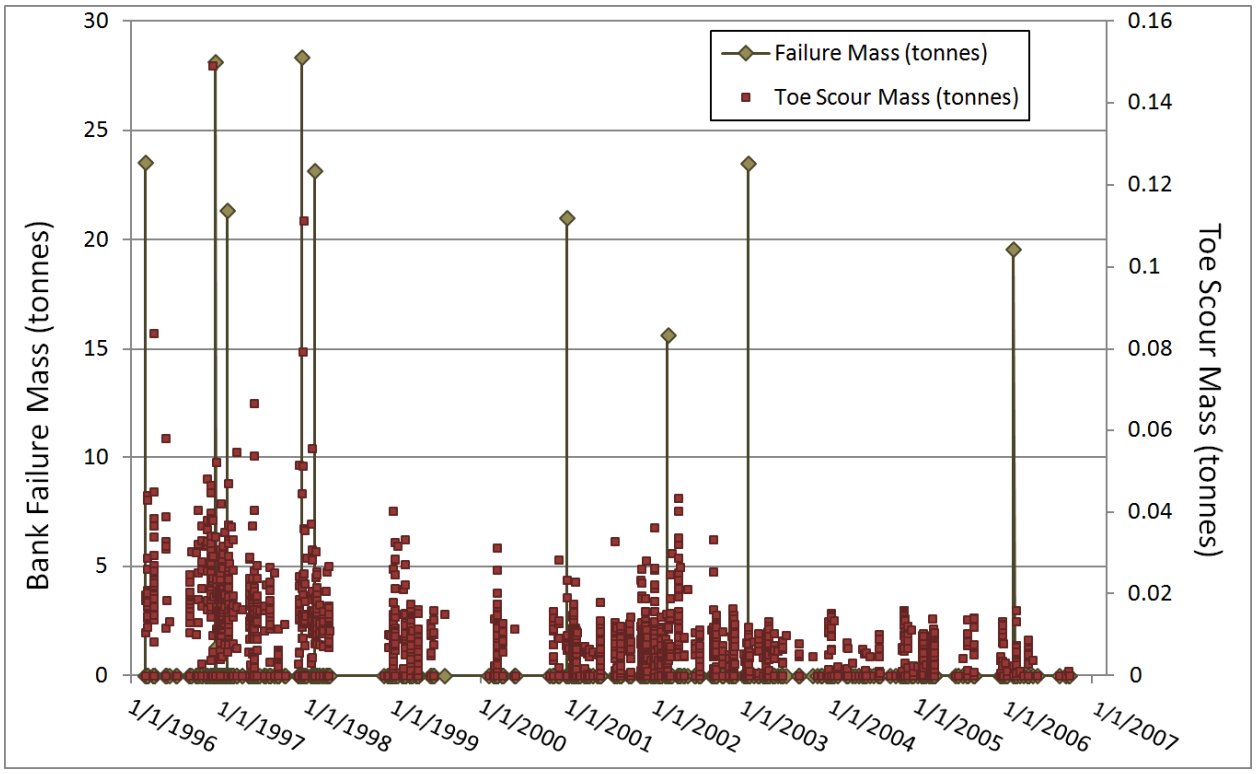

Figure 6 Time series of toe scour and bank failure contributions from the cohesive simulation for XS7 above. The toe scour contribution dropped over time as the channel widened and the ten failures contributed almost an order of magnitude more sediment over the simulation.

The cohesive model results reported above were based on excellent soil and flow data and model parameters that are not only based on copious, careful measurements, but already calibrated by Langendoen and Simon (2008). The cohesionless toe scour prediction in the coupled HEC-RAS/BSTEM code with the transport equations have over predicted scour in most model applications to date, often dramatically. Hundreds of feet of bank migration are not uncommon with some transport functions. Therefore, whether the data-driven cohesive or equation-driven cohesionless method is used, calibration (e.g. comparison to repeated cross sections or historic aerial photographs) is still essential. Additionally, the authors are experimenting with bank 'mixing algorithms' that apply transport-capacity calculations to clast-sized bank materials.

Despite these limitations, the cohesionless methods successfully bracketed prototype migration. Wilcock and Crowe (2003) seemed the most appropriate transport function *a priori*, with its surficial transport formulation (building mixing processes into the equation) and its bimodal flexibility. This method under predicted migration by 30 to 50%, (Figure 7) indicating that the transport equation performed as intended, mainly missing cementation effects in the toe conglomerate, which it was not designed to capture. Alternately, Engelund and Hansen (1972) over predicted bank migration by 50 to 100% (Figure 8). The range of results between the best fit equations underlines the importance of site specific data, but the cohesionless methods bounded the results.

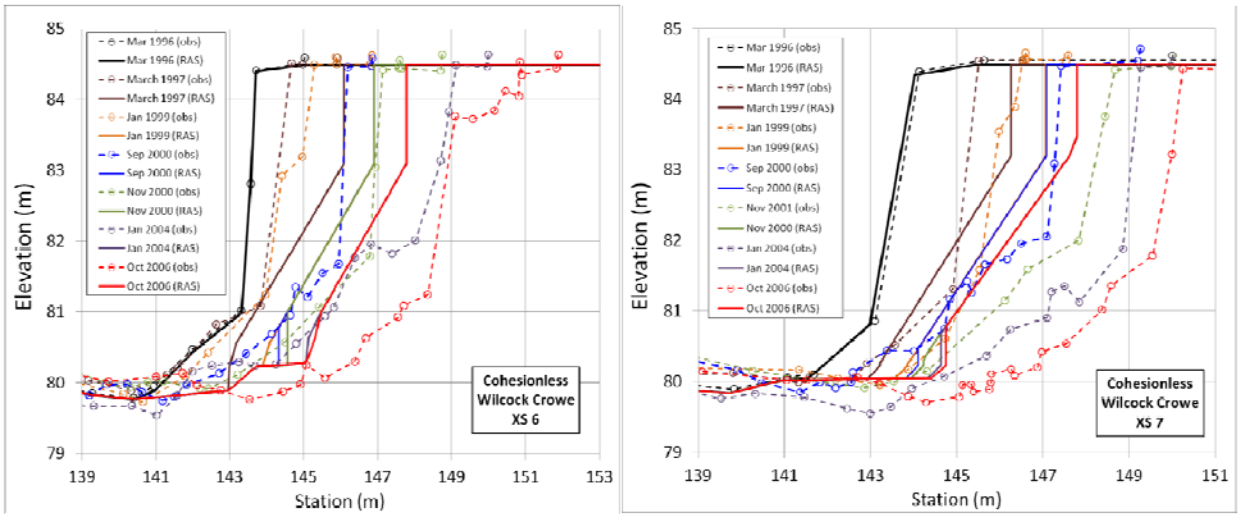

Figure 7 Measured cross sections from Figure 3 and simulated cross sections, computed with cohesionless methods base on the Wilcock and Crowe (2003) transport equation.

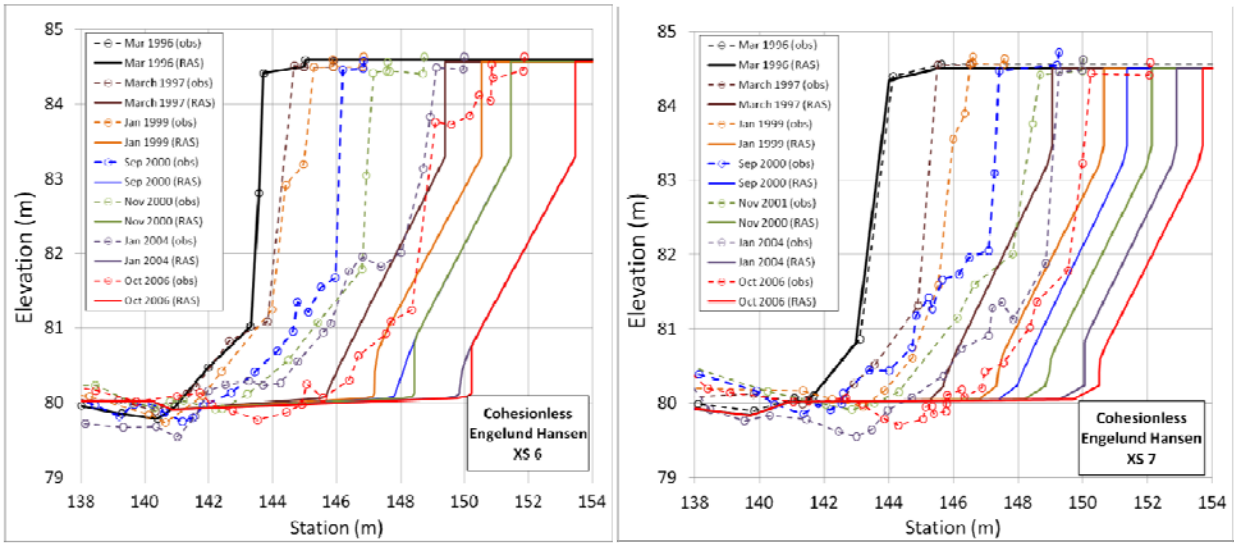

Figure 8 Measured cross sections from Figure 3 and simulated cross sections, computed with cohesionless methods base on the Engelund Hansen transport equation.

CONCLUSION

The USDA-ARS Bank Stability and Toe Erosion Model (BSTEM) has been integrated into HEC-RAS. The joint model simulates coupled bed and bank processes, and the feedbacks between vertical bed erosion and deposition, lateral toe scour, and geotechnical bank stability. Bank migration at Goodwin Creek, Mississippi was simulated with the coupled model using the parameters and benchmarks in Langendoen and Simon (2008), and then continued for five years beyond. The coupled HEC-RAS/BSTEM model performed well, replicating the calibration and demonstrating its subsequent robustness. HEC-RAS 5.0 includes these capabilities, making them broadly available.

Acknowledgements: The integration of HEC-RAS and the USDA-ARS Bank Stability and Toe Erosion Model (BSTEM) has been a substantial undertaking including multiple contributors in the USACE, the private sector, other Federal agencies, and international interests. Andrew Simon (PhD - Cardno, formerly of USDA-ARS) partnered with HEC to initiate, envision and facilitate the integration. Eddy Langendoen (PhD - USDA-ARS) provided essential technical support and advice throughout the process. The integration utilized code developed by Andrea Curini, (MSc. - URS, formerly of USDA-ARS), Robert Thomas (PhD - University of Leeds, formerly of University of Tennessee) and Yong Lai (PhD - USBR), funded by the Bureau of Reclamation and the Taiwanese Water Resources Agency, with input from Yavuz Ozeren (PhD - University of Mississippi). John Shelly (PhD – USACE-Kansas City) and Paul Boyd (PhD - USACE-Omaha) provided District guidance and feedback on the development. Stanford Gibson (PhD - HEC) and Steve Piper (RMA) worked on the integrated HEC-RAS code. Funding for the development, troubleshooting, and documentation of the integrated HEC-RAS/BSTEM product has come from multiple sources including two USACE R&D Programs (Regional Sediment Management and Flood & Coastal Storm Damage Reduction), the Australian Rivers Institute, and the Missouri River Recovery Program. Imaan Taghavi (UC Davis) tested the combined code, running simulations and analyzing the results plotted in this paper.

REFERENCES

Engelund, F., and Hansen, E. (1972). A Monograph on Sediment Transport in Alluvial Streams, Teknisk Forlag, Copenhagen.

Gibson, S. and Boyd, P. (2014). "Modeling Long Term Alternatives for Sustainable Sediment Management Using Operational Sediment Transport Rules," *Reservoir Sedimentation* –Scheiss et al. (eds), 229-236.

Gibson, S. (2013). Comparing Depth and Velocity Grids Computed With One- and Two-Dimensional Models at Ecohydraulic Scales, UC Davis Thesis, 267 p.

Gibson, S. and Piper, S. (2007). "Sensitivity and Applicability of Bed Mixing Algorithms" World Environmental and Water Resources Congress – 2007, American Society of Civil Engineers.

Gibson, S., Brunner, G., Piper, S., and Jensen, M. (2006). "Sediment Transport Computations in HEC-RAS." Eighth Federal Interagency Sedimentation Conference (8thFISC), Reno, NV, 57-64.

Lai, Y. G., Thomas, R. E., Ozeren, Y., Simon, A., Greimann, B. P., and Wu. K. (2014). Modeling of multilayer cohesive bank erosion with a coupled bank stability and mobile-bed model. Geomorphology, doi: 10.1016/j.geomorph.2014.07.017.

Langendoen, E.J. and Simon, A. (2008). Modeling the evolution of incised streams, II: Streambank erosion. Journal of Hydraulic Engineering, 134(7): 905-915.

Shelley, J., Gibson, S., and Williams, A. (2015). "Unsteady Flow and Sediment Modeling in a Large Reservoir Using HEC-RAS 5.0" *Federal Interagency Sediment Conference.*

Simon, A., Curini, A., Darby, S.E., and Langendoen, E.J., (2000). Bank and near-bank processes in an incised channel. Geomorphology, 35: 193-217.

Simon, A., Derrick, D., Alonso, C.V., and Bankhead, N.L. (2008). Application of a deterministic bank-stability model to design a reach-scale restoration project. Proc. ASCE-EWRI, World Environmental Water Resources Congress, Honolulu, Hawaii, 10 p. (on CD).

Simon, A., Pollen-Bankhead, N., and Thomas, R.E. (2011). Development and application of a deterministic bank stability and toe-erosion model for stream restoration. In Stream Restoration in Dynamic Fluvial Systems: Scientific Approaches, Analyses, and Tools. A. Simon, S.J. Bennett, and J.M. Castro (Eds.), Geophysical Monograph Series, 194, 500 p. ISBN 978-0-87590-483-2, Washington, DC.

Teukolsky, S.A., Vetterling, W.T., and Flannery, B.P. (2007). *Numerical Recipies: The Art of Scientific Computing*, Cambridge University Press; 3 edition, 1256 p.

Oreskes, N., Shrader-Frechette, K., and Belitz, K. (1994). Verification, Validation, and Confirmation of Numerical Models in the Earth Sciences, Science, 263(5147), 641-646.

Rykiel, E. (1996). Testing ecological models: the meaning of validation., Ecological Modeling, 90(229-244).

Wilcock, P.R. and Crowe, J.C. (2003). Surface-based transport model for mixed-size sediment, Journal of Hydraulic Engineering, 129, 120-128.

HEC-RAS Sediment Transport Simulation of Three Reservoirs in the Lower Susquehanna River Basin, Pennsylvania and Maryland

Michael Langland, Hydrologist, US Geological Survey, Pennsylvania Water Science Center, New Cumberland, PA, langland@usgs.gov

Abstract

The U.S. Environmental Protection Agency (USEPA) recently (2010) listed the nation's largest estuary, the Chesapeake Bay, as impaired and established sediment and nutrient load allocations for the six states and the District of Columbia waters draining into the Bay. The Susquehanna River is the largest tributary to the Chesapeake Bay and transports about one-half of the freshwater and substantial amounts of sediment, nitrogen, and phosphorus. The loads transported by the Susquehanna River to the Bay are affected by the deposition of sediment and nutrients behind three large hydroelectric dams on the Lower Susquehanna River in Pennsylvania and Maryland. The three consecutive reservoirs (Lake Clarke, Lake Aldred, and Conowingo Reservoir) formed behind the three dams (Safe Harbor, Holtwood, and Conowingo) involve nearly 32 miles of the river and have a combined design capacity of 510,000 acre-feet at their normal pool elevations.

Previous studies by Ott and others (1991), Hainly and others, (1995), Reed and Hoffman (1996), Langland and Hainly (1997), Langland (2009), Hirsch (2012) and Gomez and Sullivan (2012) have indicated the two upstream reservoirs have minimal sediment storage capacity and have been in a "dynamic equilibrium" with respect to sediment transport since the 1950's. The most downstream reservoir (Conowingo) is nearly at sediment storage capacity and transitioning to a "dynamic equilibrium" state. Dynamic equilibrium implies there will be no change in long-term (decades) sediment retention resulting from the loss of storage capacity, however short-term (years) deposition and erosion cycles will continue. When capacity is reached, increased flow velocities through the reservoirs will result in less time for transported sediments to deposit resulting in increased sediment loads to receiving waters, including the Chesapeake Bay.

In order to simulate the sediment transport out of the reservoir system and into the lower Susquehanna (2008-11), the U.S. Geological Survey (USGS), in cooperation with the U.S. Army Corps of Engineers (USCOE) and the Lower Susquehanna River Watershed Assessment Team (LSWA, a consortium of Federal, State, and private organizations), completed the development of a one-dimensional (1-D) model (HEC-RAS). The USGS constructed new geometric and hydraulic boundaries to align with previous bathymetric cross sections. USGS also constructed sediment transport curves and utilized historical bathymetric data, existing sediment core samples, particle–size and sheer stress data, and current (2008-2011) hydrology and load information to help calibrate the model.

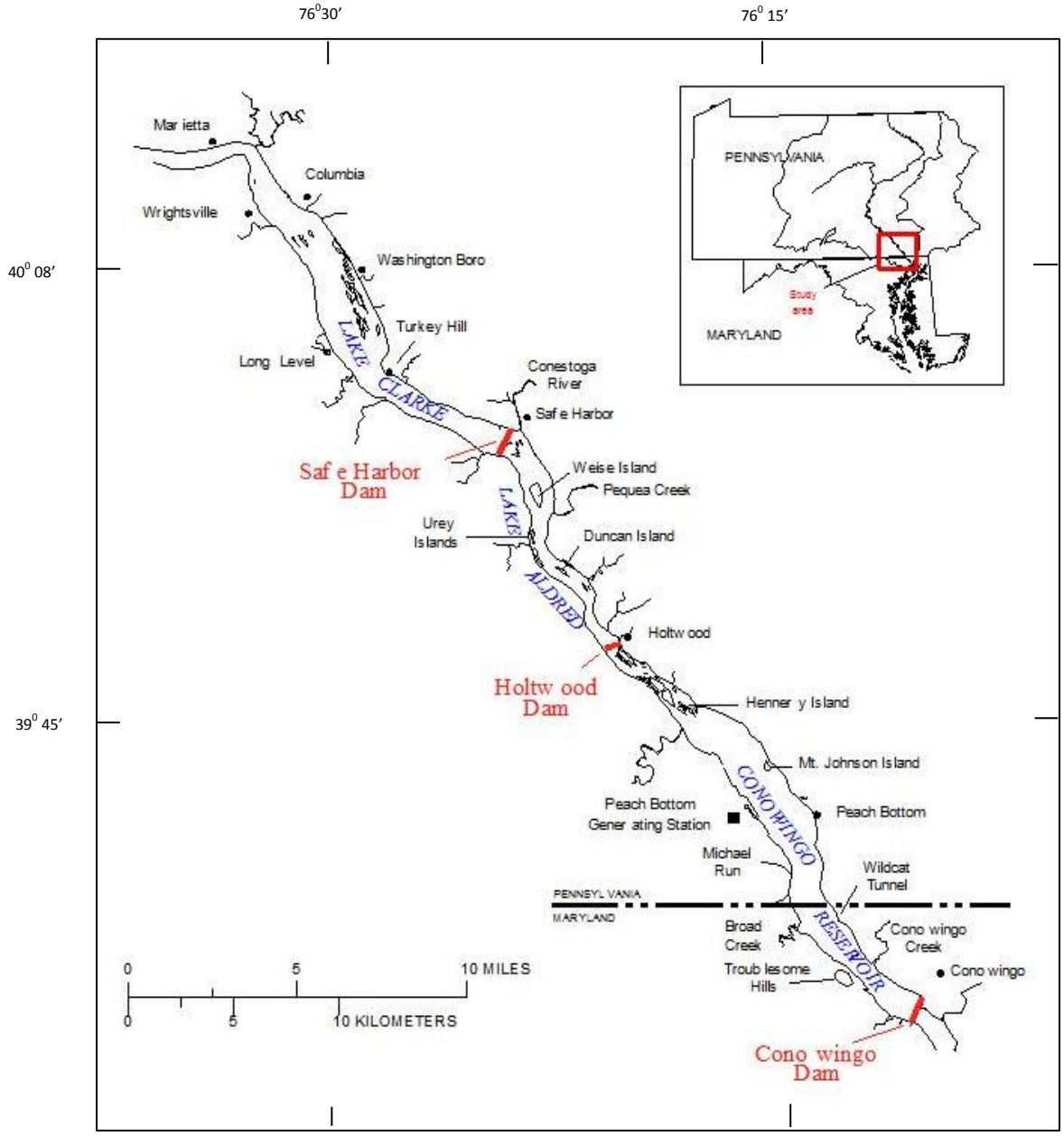

Figure 1 Location of three Hydroelectric Dams and associated reservoirs in the Lower Susquehanna River, Pennsylvania.

The 4-year simulation period was generally normal (10 percent above or below the long-term mean streamflow) for 2 of the 4 years, and above and below normal the other 2 years. In addition, a flood event that produced the second highest daily mean streamflow since 1968 occurred in September 2011. Numerous model iterations of the model were performed and checked to determine bed movement, bed shear, estimated sediment loads, particle size transport, and energy dispersion. During model development, it became apparent that the HEC-RAS model

did moderately well at simulating reservoir deposition over the 4-year simulation period (figure 2A) but did not represent the increased sediment loads from scour during the large storm event that occurred during the simulation period (September 2011). To simulate erosion (scour), two model parameters (fall velocity and bed sorting method) were changed to predict increased sediment loads from larger storm events (figure 2B).

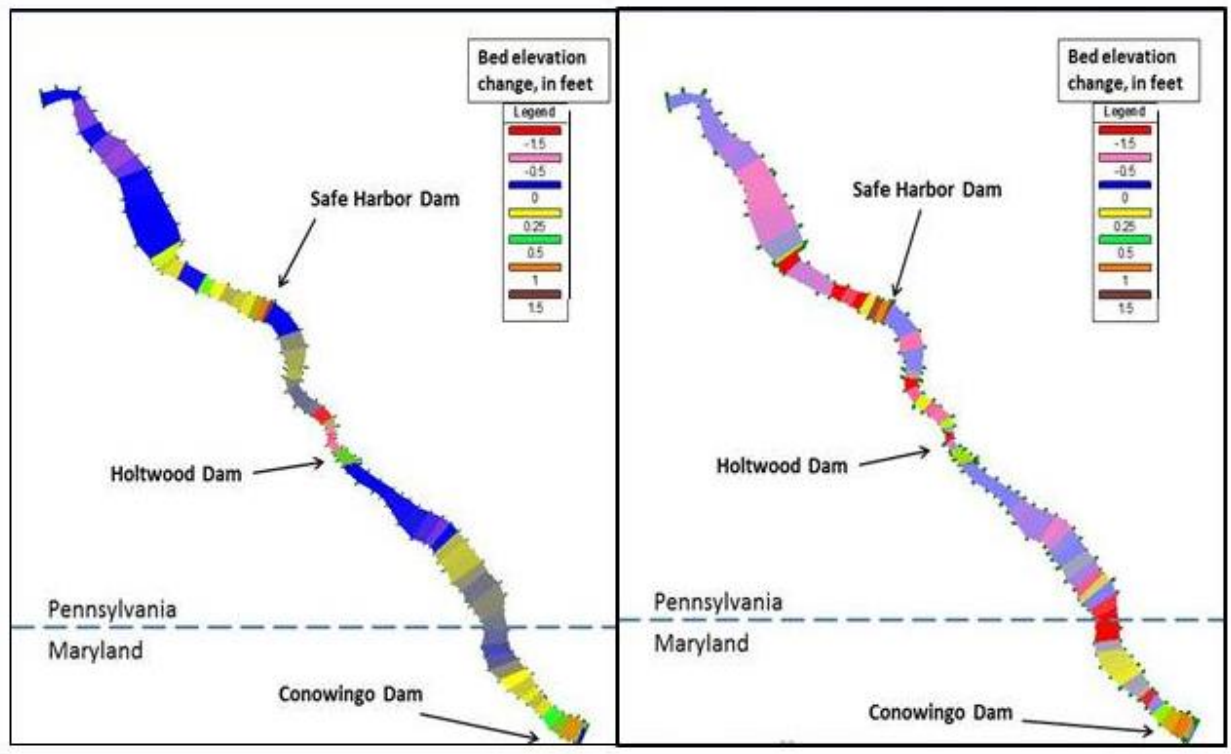

Figure 2 Changes in bed elevation using a HEC-RAS depositional model (A-left), and changes in bed elevation using a HEC-RAS scour model (B-right) for simulation period 2008-2011.

Overall, the two models (deposition and scour) allowed for a range in uncertainty and generally simulated the deposition or scour to about one-half of the expected sediment when compared to estimates from bathymetric change and load results. Lower than expected load estimates were attributed to three likely reasons. First, the HEC-RAC model is limited to simulating either sediment deposition or removal, not both, along a single transect. Comparisons of the 2008 and 2011 bathymetry data showed within individual transects where sediment was both deposited and removed. Second, the modeled "fall velocity" of the fines was about two times lower than literature values and 2-D model runs performed by the USACE. Third, the 1-D model allows one shear stress value when laboratory stress studies on the sediment core data indicate an eight-fold range in variability.

REFERENCES

Gomez and Sullivan Engineers, 2012, 2011 Conowingo pond bathymetric survey, appendix F *of* Final study report, Sediment introduction and transport study, Conowingo hydroelectric project: Exelon Report RSP 3.15, 129 p.

Hainly, R.A., Reed, L.A., Flippo, H.N., Jr., and Barton, G.J., 1995, Deposition and simulation of sediment transport in the Lower Susquehanna River reservoir system: U.S. Geological Survey Water-Resources Investigations Report 95–4122, 39 p.

Hirsch, R.M., 2012, Flux of nitrogen, phosphorus, and suspended sediment from the Susquehanna River Basin to the Chesapeake Bay during Tropical Storm Lee, September 2011, as an indicator of the effects of reservoir sedimentation on water quality: U.S. Geological Survey Scientific Investigations Report 2012–5185, 17 p. [Also available at *http://pubs.usgs.gov/sir/2012/5185/*.]

Langland, M.J., and Hainly, R.A., 1997, Changes in bottom-surface elevations in three reservoirs on the Lower Susquehanna River, Pennsylvania and Maryland, following the January 1996 flood—Implications for nutrient and sediment loads to the Chesapeake Bay: U.S. Geological Survey, Water-Resources Investigations Report 97–4138, 34 p.

Langland, Michael J. 2009. Bathymetry and sediment-storage capacity change in three reservoirs on the Lower Susquehanna River, 1996-2008: U.S. Geological Survey Scientific Investigations Report 2009-5110, 21 p. (Also available at *http://pubs.usgs.gov/sir/2009/5110/*.)

Ott, A.N., C.S. Takita, R.E. Edwards, and S.W. Bollinger. 1991. Loads and yields of nutrients and suspended sediment transported in the Susquehanna River Basin, 1985-89: Susquehanna River Basin Commission Publication no. 136, 253 p.

Reed, L.A. and S.A. Hoffman. 1996. Sediment deposition in Lake Clarke, Lake Aldred, and Conowingo Reservoir, Pennsylvania and Maryland, 1910-93: U.S. Geological Survey Water-Resources Investigations Report 96-4048, 14 p.

EVALUATING SUSTAINABLE SEDIMENT MANAGEMENT ALTERNATIVES FOR LEWIS AND CLARK LAKE

Paul M. Boyd, Ph.D. P.E, Hydraulic Engineer, U.S. Army Corps of Engineers, Omaha, NE, paul.m.boyd@usace.army.mil; Stanford Gibson Ph.D., Hydraulic Engineer, U.S. Army Corps of Engineers, Hydrologic Engineering Center, Davis. CA, Stanford.gibson@usace.army.mil

Abstract

The Missouri River Recovery Program initiated the Lewis and Clark Lake Sediment Management Study (LCLSMS) to evaluate sediment flushing scenarios at Lewis and Clark Lake/Gavins Point Dam near Yankton, South Dakota. Phase I of the report examined large discharges for short durations, and was published in April 2013. Phase II utilized new features in HEC-RAS (e.g. unsteady sediment transport and bank erosion modeling) to develop an updated reservoir model to examine additional scenarios. The second phase considered in-channel discharges of varying durations to estimate delta progression, evaluate dam and spillway modifications, and predict sediment delivery through Gavins Point Dam.

This paper describes the application of these new tools to the reservoir model and a downstream model to assess impacts of the predicted sediment discharge. Results of the modeled scenarios are summarized and conclusions made about the effectiveness of using HEC-RAS for reservoir modeling.

INTRODUCTION

The deposition of hydraulically transported sediments occurs in all flow impoundments, whether they are constructed or naturally occurring. Sedimentation occurs when flow velocities drop below the threshold required for transport. This deposition can cause an impediment to flow and an eventually redirection of flow. This usually occurs when the impoundment is completely or nearly full of sediment. If left in the current flow regime, Lewis and Clark Lake will eventually fill with sediment, albeit more than 150 years in the future according to current projections.

Lewis and Clark Lake is impounded by Gavins Point Dam on the Missouri River. Its existing uses would be severely compromised if the reservoir is allowed to fill with sediment. The reservoir is operated for flood risk reduction, hydropower, navigation, recreation, water supply, water quality, fish and wildlife, and irrigation. The Lewis and Clark Lake Sediment Management Study is evaluating a wide variety of scenarios for managing the reservoir and the sediment within it to continue to provide the intended benefits.

Lewis and Clark Lake

Lewis and Clark Lake was formed by the closure of Gavins Point Dam in 1955. The dam is located at river mile 811.1 (RM 811.1), approximately five miles upstream of Yankton, South Dakota, on the Missouri River as shown in Figure 1. Gavins Point Dam is one of six mainstem dams on the upper Missouri that are operated by the Northwestern Division of the U.S. Army Corps of Engineers. The Missouri River dams and reservoirs provide significant benefits to the nearly 15 million people that reside in the states through which it flows.

Figure 1 Lewis and Clark Lake behind Gavins Point Dam

Lewis and Clark Lake reached its full water surface elevation of 1208 feet (NGVD 1929) in early 1957 and has been managed with water elevations between 1206 feet and 1210 feet (NGVD 1929) ever since. When closed, the lake extended to approximately RM 836, creating an open-water lake that was approximately 25 miles long.

Since closure, sediment surveys have been performed approximately every decade to determine the amount of sediment deposition and changes in the reservoir's storage capacity. These surveys have indicated that approximately 2,600 acre-feet of sediment have been deposited per year below elevation 1210 feet (NGVD 1929) through the 2011 surveys (USACE, 2013a). In the reach between Gavins Point Dam and Fort Randall Dam at RM 880, sediment is delivered from tributaries including the Niobrara River, Ponca Creek, and Bazile Creek, as well as from the banks and bed of the river upstream. Figure 2 shows the two largest deltas in the river reach. Additional sediments are deposited in the overbanks of the river and in the Niobrara River delta at RM 844, yielding a total sediment input into the reach in excess of the volume below the 1210-foot threshold.

Figure 2 Niobrara River Delta (left) and Lewis and Clark Lake Delta (right)

The deposition of sediments in the Lewis and Clark Lake delta has effectively shortened the length of the lake over the past 50 years. Currently, the open reach of the lake extends to near RM 826, a distance of 15 miles of open lake. The migration of the delta appears from visual observations to be approximately 500 to 600 feet per year, although the deposition rate has remained fairly constant over the past 50 years (USACE, 2011).

The migration of the delta both up- and down-river reduces the storage capacity of the reservoir. The initial capacity of the lake was 575,000 acre-feet below the 1210-foot elevation, and the 1995 capacity was 470,000 acre-feet, which is a storage loss of approximately 18.5 percent. Storage loss was updated with the 2011 surveys for this project. These surveys indicated the total storage loss at the 1210-foot elevation was 26 percent (USACE, 2013).

THE LEWIS AND CLARK LAKE SEDIMENT MANAGEMENT STUDY (LCLSMS)

The LCLSMS was developed to examine the engineering viability of moving the sediments deposited behind Gavins Point Dam into the river downstream of the reservoir. In the 2003 amended Biological Opinion (BiOp) for the Missouri River, the U.S. Fish and Wildlife Service stated *"The Corps shall research and develop a way to restore the dynamic equilibrium of sediment transport and associated turbidity in river reaches downstream of Fort Peck, Garrison, Ft. Randall, and Gavins Point Dams. Sediment bypass around large dams is feasible (Singh and Durgunoglu, 1991). Bed degradation below dams and head cutting at the mouths of tributaries might be addressed with grade control structures. Weir notches at grade control structures would allow for fish passage to the tributaries. Because of the large sediment deposition zone at the upper end of Lewis and Clark Lake and its proximity to Gavins Point Dam, Gavins Point may provide the best opportunity for a pilot study (USFWS 2003)."*

Initial consideration of using flows through the reservoir to transport sediment was not strongly supported. Additional research on the reservoir system in the Lewis and Clark Lake reach showed that there is the possibility that sediments can be transported through Lewis and Clark Lake (Engineering and Hydrosystems, 2002). A number of different flow and stage

scenarios have been suggested by this research. With the recommendation for a study at Gavins Point Dam through the BiOp, and proof of concept provided by the 2002 study by E&H, the LCLSMS was initiated in 2005.

Project Goals

The LCLSMS is an engineering viability study. As defined, the study will deal only with the physical processes of hydraulic flow, and sediment erosion, transport, and deposition. Environmental, economic, political, and quality of life issues will not be considered in the scope of this study. The project goals are to:

- Determine the hydraulic capacity to transport sediment in and below Lewis and Clark Lake
- Develop estimated final reservoir geometries as a result of flow alternatives
- Determine downstream sediment transport capacity and possible deposition zones
- Develop a test flow to mimic the hydraulic alternative most likely to result in the desired outcome
- Protect existing project infrastructure

Since the study began, it has grown to include two modeling phases to evaluate hydraulic drawdown flushing, a modeling effort to examine the future depletion of available sediments below the dam, and a cost analysis of dredging alternatives.

LCLSMS Activities

Phase I – Using GSTARS-HTC to Examine High Flow Single Events

The LCLSMS project began with the development of the project plan and scope of work for modifying GSTARS3 by Colorado State University's Hydroscience and Training Center (HTC) in 2005. Award of the work to develop GSTARS-HTC signaled the beginning of the project in late 2005. This effort was considered Phase I, and was completed in 2012.

Phase II – Using HEC-RAS to Examine Repeated Flow Events

Based on the results of Phase I and stakeholder feedback, the Missouri River Recovery Program (MRRP) chose to continue the study by expanding it to include more flow scenarios and examine the impacts of repeated events into the future. This phase also included the transition to the HEC-RAS one-dimensional model for analysis (HEC-RAS v.5.0). This phase began in latter 2011 and is expected to be completed by the fall of 2015.

Projection of Future Conditions below Gavins Point Dam

In coordination with the Emergent Sandbar Habitat (ESH) Program, the LCLSMS expanded the study to include an analysis of future sediment availability in the reach below Gavins Point Dam in 2012. It is expected to be completed in the fall of 2015.

Cost Analysis of Dredging Alternatives for Lewis and Clark Lake

Dredging is a common management action for rivers, lakes, and harbors. Many stakeholders have inquired about the Corps' ability to dredge Lewis and Clark Lake and the magnitude of the effort needed to maintain the current reservoir capacity. The study has teamed with the Corps of Engineers Research and Development Centers (ERDC) Dredging Operations Technical Support

Program (DOTS) (http://el.erdc.usace.army.mil/dots/) to consider three dredging configurations for Lewis and Clark Lake. The dredging alternatives study was begun in mid-2013 and is expected to be completed by the fall of 2015.

ANALYSIS AND RESULTS

Phase I Results

Two numerical sediment transport models were developed to predict the movement of sediment through and below Gavins Point Dam. The Lewis and Clark Lake Model used the GSTARS-HTC (USACE, 2013b) code to predict sediment transport through the Missouri River delta and past the spillway at Gavins Point Dam. The model extends from Fort Randall Dam (RM 880) to Gavins Point Dam (RM 811). The model for the reach from Gavins Point Dam to Sioux City, Iowa (RM 730) used HEC-RAS to route the flow and sediment output from the reservoir model through the recreational river reach below the dam, and deliver it to the downstream navigation channel.

Five flushing scenarios were developed based on guidance from a flushing-reconnaissance report (Engineering and Hydrosystems Inc, 2002) that recommended very high river flows for short durations. Flow scenarios varied from 88,000 to 176,000 cfs, with the peak flow lasting up to seven days.

The largest event was also simulated with a section of the Gavins Point Dam spillway lowered by ten feet to increase the energy available to move sediment. For the study analysis, all flows were released through the spillway at Gavins Point Dam to avoid sending sediment through the powerhouse. All the scenarios included draining Lewis and Clark Lake (to increase effectiveness), increasing discharge at Fort Randall Dam upstream to the peak flow, maintaining the flow for the flush duration, and reducing the flow as the reservoir refills.

All the flushing scenarios predicted transport of silt and clay size particles through the dam. In the cases of the high flow and modified spillway, the model predicted very high sediment concentrations and total mass of sediment transported. Each scenario also predicted the redistribution of sand-size particles throughout the delta and bottom of Lewis and Clark Lake. However, due to the length of the reservoir and the location of the spillway gates, which are 20 feet above the lake bottom, almost no sand passed through the spillway for any scenario. Only the flushing scenario with 176,000 cfs and the modified spillway gates, when sediment concentrations were the highest, predicted 0.07% of the mass of sediment passing the spillway as sand; the remaining 99.93% was silt and clay (USACE, 2013c).

While these high-flow, short-duration scenarios did not predict the delivery of enough sand to support sandbar habitat below the dam, a number of conclusions indicate that there may be scenarios not modeled in this study that would hold promise. Study results are summarized as:

- All the modeled scenarios showed erosion of delta deposits and redistribution of sand within the reservoir, with much of the sand settling in the deepest area of the lake. Repeated flushing events may result in better sediment transport to the downstream channel once the deeper areas are filled in.

- Modifying the spillway resulted in a significant increase in sediment transport. The modification of the spillway or inclusion of low-elevation outlets in the dam structure could greatly increase flushing efficiency.
- The spillway crest elevation above the reservoir bottom prevents complete draining of the reservoir through the spillway, resulting in a sediment trap at the face of the dam. As the delta migrates closer to the dam, transport of sand to the face of the dam will increase during any flushing event. Therefore, flushing effectiveness will increase in the future.
- The downstream model predicted minor aggradation of the channel only with the highest sediment discharge from the dam. Since the sediment in the dam discharge was comprised of silts and clays, most were transported through the reach and into the navigation channel.

These conclusions directly led to the development of Phase II and the inclusion of longer and more varied management scenarios. All the documents associated with the Phase I and Phase II modeling studies are available at http://moriverrecovery.usace.army.mil/mrrp/f?p=136:155:2604171657024::NO::PIS_ID:28.

Phase II Analysis - Using HEC-RAS to Examine Repeated Flow Events

Stakeholder feedback and additional questions from other Federal agencies prompted the MRRP to expand the LCLSMS study to include flushing scenarios that limited flow to the bank-full condition coupled with a long term view to sediment management.

Table 1 Gavin's Point Dam and Lewis and Clark Lake Advantages and Challenges to Alternative Sediment Management (USACE, 2015)

Advantages	Challenges
Gavins Point is the most downstream dam of the Missouri cascade and immediately upstream of the target reach to increase sand load.	Eighteen miles of open water between the current sediment delta and the dam.
Relatively small reservoir for the Missouri River.	The dam has no low-level outlets. So even when drained, the reservoir has a standing pool and multiple miles of open water between the delta and the structure.
Niobrara River delivers a substantial sand load 33 miles upstream of the dam.	There are social and policy constraints on the releases that can be made from Gavins Point dam.
Fort Randall Dam allows managers the flexibility to specify an optimal inflowing hydrograph with unusual precision.	
The impoundment volume of the upstream Missouri cascade removes the standard refilling uncertainties associated with sediment management draw downs in other systems.	

Morris and Fan (1998) defined the classical taxonomy of passive reservoir sediment management alternatives, including: flushing, sluicing, bypass, and turbidity currents. It is still very difficult to predict, model, or manage turbidity currents, and bypass solutions that are not part of the

original design are almost always prohibitively expensive, making flushing and sluicing the two main passive options.

The reservoir model was constructed using a developmental version of HEC-RAS 5.0. HEC-RAS was selected primarily for institutional and transparency reasons. Since the Omaha District has constructed 1D hydraulic models of this system with HEC-RAS, it was advantageous to use HEC-RAS for the sediment modeling. Keeping the sediment model in the same modeling platform as the hydraulic analyses leverages District data and expertise. However, Omaha and HEC identified several limitations of the release version of HEC-RAS 4.1 that complicated flushing analyses in this system. Therefore, this analysis integrated project modeling with software development to implement new methods in HEC-RAS and apply them to the Lewis and Clark Lake analysis.

The scenarios to be modeled were vetted through stakeholder and local and Federal agency feedback. While the list is not all-inclusive, it does cover most of the commonly considered management modifications for reservoir flushing. Many of these scenarios would require significant investment in the project infrastructure. However, any cost comparisons should include the cost of lost benefits due to sedimentation. Table 2 summarizes the scenarios modeled in the HEC-RAS Lewis and Clark Lake model.

Table 2 Phase II HEC-RAS Model Flow Scenarios

Scenario	Flushing Flow (cfs)	Flushing Duration	Other
II-1	None	None	No Action – 53 year projection to determine delta progression through 2064
II-2	60,000	7 days	Base alternative – single drawdown flushing event
II-3	60,000	7 days	Scenario II-2 with 2064 geometry
II-4	60,000	7 days	Seven spillway gate inverts lowered to 1,170 feet
II-5	30,000	7 days	Half magnitude version of II-2
II-6a	60,000	7 days	Low Elevation Tunnels (invert 1,157 feet)
II-6b	30,000	7 days	Low Elevation Tunnels (invert 1,157 feet)
II-7a	180,000	~8 days	Repeat of Scenario I-1 from Phase I
II-7b	88,000	~10 days	Repeat of Scenario I-2 from Phase I
II-8	30,000	7 day repeating	Annual flushing event through 2064
II-9	30,000	7 day repeating	Annual flushing event with longitudinal revetment through 2064
II-10	30,000	7 days	Annual flushing event with dredging 675 tons per day during flush through 2064

The model was calibrated from 1955-2012 to water surface profiles, bed volume change, and grain size distributions. All the scenarios were run in HEC-RAS 5.0, and a short summary of results follows.

Scenarios II-1 and II-3 were compared to determine if there would be an increase in flushing efficiency if the delta were closer to the dam. While results showed that sediment delivery during the event was higher with the future delta conditions, it was not appreciably so.

The highest increases in sediment delivery downstream of Gavin Point Dam were seen in scenarios where physical modifications were made to the dam or reservoir infrastructure. Figure 3 shows the five low-level tunnels simulated in scenario II-6. They are placed below the spillway gates and would allow for nearly complete dewatering of the reservoir to a run-of-river condition, which is ideal for drawdown flushing.

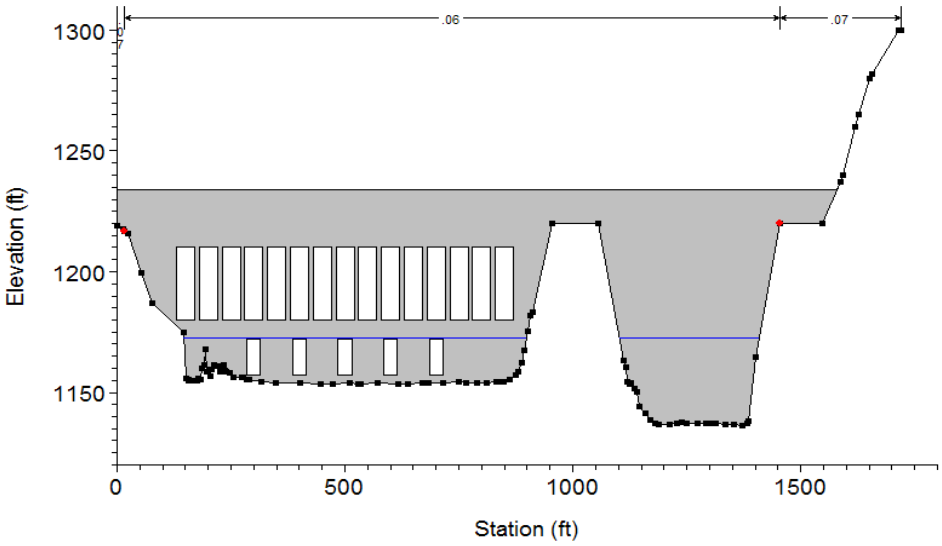

Figure 3 Low level outlets added to Gavin's Point Dam for Scenario II-6.

In both cases (II-6a and 6b) the low level outlets drained the reservoir more effectively, which reduced the total event duration by decreasing the draining time and almost eliminating the transition phase required to reach an equilibrium run-of-river flow. Local bed change was computed for Scenario II-6a and 6b and is shown in figure 4.

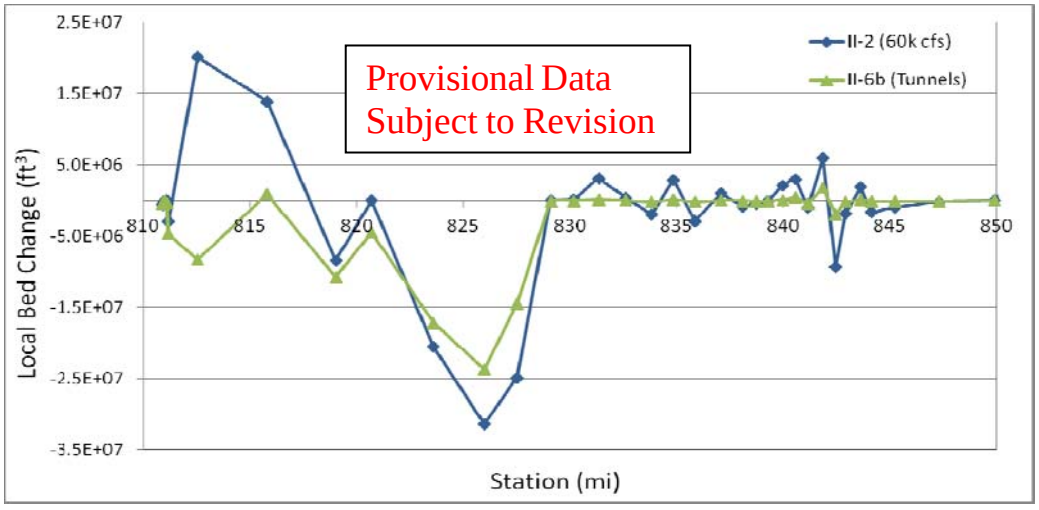

Figure 4 Seven day, 60,000 cfs sluicing event with and without low-level outlet tunnels.

The low level gates flush sediment because they decreased trap efficiency (or increased pass thorough efficiency). In both cases, the low-level outlet models passed most or all of the sediment scoured from the delta and even scoured some pool deposits on the way to the outlets. Scenario II-6 flushes more sediment of every size class than the other scenarios. But more importantly, it flushes sand. In fact, the 30,000 cfs version of Scenario II-6 releases more than half of the 60,000 cfs volume of each size class and orders of magnitude more sand than any of the other higher flow scenarios.

Scenario II-9 included an underwater revetment that would be approximately 15 feet below the water surface at full pool. It would be exposed during drawdown to channelize flows on the south bank of the reservoir, increasing flow velocity and transporting sand-size sediments to the spillway. Figure 5 lays out the approximate location of the revetment.

Figure 5 Approximate alignment of modeled revetment.

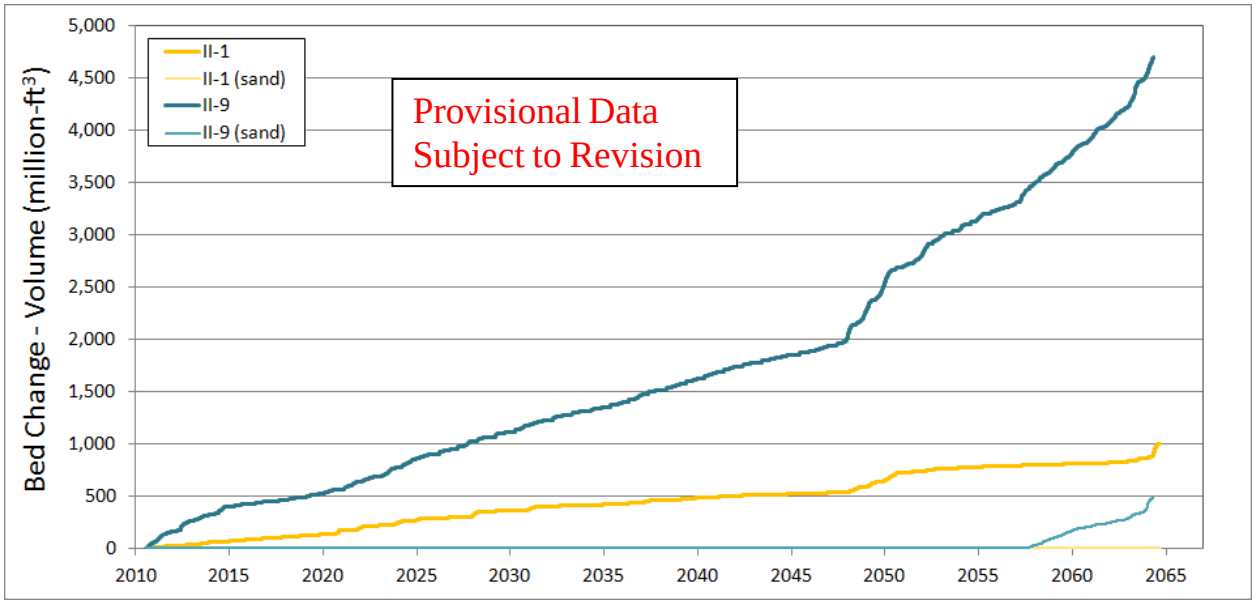

Figure 6 Time series of sediment released from Gavin's Point dam for Scenario II-1 (no action) and II-9 (revetment and flush), including total release and the sand component.

Figure 6 shows a comparison of scenarios II-1 and II-9. Scenario II-9 included two management alternatives, a drawdown flush and the revetment. A sensitivity analysis suggests that most of the value in this alternative comes from the revetment and that the reservoir may start passing sand before 2065 with just the revetment.

Modeling a Drawdown Flush on the Niobrara River

In August 2014, USACE Omaha and HEC began a joint project to model a scheduled drawdown flushing event at Spencer Dam on the Niobrara River. This project is intended to determine the uncertainty associated with using HEC-RAS to model a reservoir drawdown flush in a sand-bed river system. The results will be used to improve the LCLSMS Phase II reservoir model. The Spencer Dam flush study is supported by the Corps' Regional Sediment Management (RSM) Program.

Projection of Future Conditions Below Gavins Point Dam

The reach of the Missouri River directly below Gavins Point Dam has been historically significant as nesting habitat for the Interior Least Tern and Piping Plover. These shore birds rely on bare sandbars to forage and provide clear lines of sight to identify predators.

The construction of dams on the Missouri River has resulted in the loss of nearly 100% of the sediment load from the upper river into this reach. Without sufficient sediment load, the bed and banks of the river have degraded, resulting in channel armoring, bank erosion, and the loss of emergent sandbar habitat for these and other birds.

The question has often been raised as to when, under the current management regime, the reach will effective run out of available sand in the bed and banks. This would seriously inhibit the ability to build sandbars through any means, whether with designed flows or through traditional construction methods.

USACE Omaha is developing a HEC-RAS 5.0 model with WEST Consultants, Inc. to examine future sediment erosion and project bed armoring and bank erosion over the next 100 years. In addition, the model will test the threshold for the projected sediment loads required to prevent future degradation. Finally, the model will be tested with varying discharges to observe what sandbar building can be expected in the future. The analysis and the completed report are expected by the end of 2015.

Cost Analysis of Dredging Alternatives for Lewis and Clark Lake

Coker et al. (2009) suggested a sediment management plan for Lewis and Clark Lake that includes yet undeveloped autonomous vehicles for material movement. While the Corps does not current have any technology of this design, the agency has considerable experience in traditional sediment movement methods including mechanical movement and hydraulic dredging.

The LCLSMS has teamed with ERDC and the Corps' New Orleans District to develop practical cost estimates for three systems for moving sediment from the Lewis and Clark Lake delta to the Missouri River directly below Gavins Point Dam. These three systems are:

- Mechanical excavation with barge transport
- Staged dredging
- Single line dredging with booster pump

Each of these systems is being analyzed with production rates varying from 10,000 to 30,000 tons per day of sediment delivered.

The ability to discharge sediment below the dam is dependent upon the river's ability to transport this sediment without incurring significant aggradation. To address this concern the number of days per season where discharge is above thresholds is being evaluated. The cost analysis is ongoing, and a report is expected with the release of the Phase II modeling reports.

FUTURE ACTIVITES

There are four ongoing research efforts within the greater LCLSMS. Each of these will add to the original, single-event drawdown flushing analysis in phase I, and give a more complete view of possible management actions that could be considered in the future. However, these studies all deal with the existing sediment in the system and do not examine ways to reduce sediment delivery to the reservoir. While sediment delivery from upstream on the Missouri River has been significantly reduced due to the mainstem dam system, tributaries, primarily the Niobrara River, continue to be the major contributor to the delta sediments at Lewis and Clark Lake. The influence of the tributary sediment delivery warrants further examination.

The results presented in this paper should be considered provisional and subject to change. Once the Spencer Dam flushing model and analysis are complete, minor modifications may be made to the Lewis and Clark Lake model before publication.

However, there are some actions that clearly result in increased sediment transport when compared to the current infrastructure and management regime. These include lowering of spillway gates, low-level tunnels, and prioritizing flow to improve flushing efficiency. These are all techniques that have been included in dam designs over the past half century, but not originally included in the design of Gavins Point Dam.

The Corps intends to complete the LCLSMS in 2015 and provide all the associated reports via the MRRP website page at: http://moriverrecovery.usace.army.mil/mrrp/f?p=136:155:2604171657024::NO::PIS_ID:28.

REFERENCES

Coker, E. Howard, Rollin H. Hotchkiss, and Dennis A. Johnson (2009). Conversion of a Sustainable Missouri River Dam and Reservoir to a Sustainable System: Sediment Management. Journal of the American Water Resources Association. Vol. 45, No. 4.

Engineering and Hydrosystems Inc. (2002). Conceptual analysis of sedimentation issues on the Niobrara and Missouri Rivers, South Dakota and Nebraska: Omaha, NE, US Army Corps of Engineers.

Morris, Gregory L. and Jiahua Fan (1998). Reservoir Sedimentation Handbook, McGraw-Hill Book Co., New York.

Singh, K. P., and A. Durgunoglu (1991). Remedies for sediment buildup, Hydro Review: 90-95.

U.S. Fish and Wildlife Service (2003). Amendment to the 2000 Biological Opinion on the operation of the Missouri River main stem Reservoir system, operation and maintenance of the Missouri River bank stabilization and navigation project, and operation of the Kansas River reservoir system: Minneapolis, MN. U.S. Fish and Wildlife Service, 318 p.

USACE (2011). Office Report: Lewis and Clark Lake, History of Delta Growth. Reconnaissance Assessment, Omaha District.

USACE (2013a). Sedimentation Conditions at Lewis and Clark Lake. Omaha District, U.S. Army Corps of Engineers. Missouri River Basin Report MRB 29.

USACE (2013b). Lewis and Clark Lake Sediment Management Study (LSLCMS). Part I: Summary Report on Evaluation Hydraulic Transport of Missouri River Delta Sediments. Omaha District, U.S. Army Corps of Engineers.
http://moriverrecovery.usace.army.mil/mrrp/f?p=136:155:2604171657024::NO::PIS_ID:28

USACE (2013c). Lewis and Clark Lake Sediment Management Study (LSLCMS). Part II: Sediment Transport and Flow Analysis with GSTARS4. Omaha District, U.S. Army Corps of Engineers.
http://moriverrecovery.usace.army.mil/mrrp/f?p=136:155:2604171657024::NO::PIS_ID:28

USACE (2015). Lewis and Clark Lake Sediment Management Study (LSLCMS) Phase II. Part II: Sediment Transport and Flow Analysis through Lewis and Clark Lake using the HEC-RAS Reservoir Model. Omaha District and Hydrologic Engineering Center, U.S. Army Corps of Engineers. In Review – expected publication in 2015.

MODELING BED DEGRADATION OF A LARGE, SAND-BED RIVER WITH IN-CHANNEL MINING WITH HEC-RAS 5.0

John Shelley, Ph.D., P.E., U.S. Army Corps of Engineers, Kansas City District, john.shelley@usace.army.mil; Stanford Gibson, Ph.D., U.S. Army Corps of Engineers, Hydrologic Engineering Center, stanford.gibson@usace.army.mil.

INTRODUCTION

The Missouri River is a large, regulated, sand-bed river. Over the past several decades, large stretches of the lower Missouri River have degraded with bed elevations dropping as much as 7 ft (USACE, 2009a). Bed degradation on the lower Missouri River has already cost Federal, State, and local entities over a hundred million dollars in emergency slope protection, bridge pier stabilization, and water intake retrofitting. To analyze and find solutions to this problem, the U.S. Army Corps of Engineers, with support from local stakeholders, developed a one-dimensional mobile-bed hydraulic/sediment model for 165 miles of the lower Missouri River using HEC-RAS 5.0. The modeling effort utilized features new to HEC-RAS 5.0, including specification of sediment load and gradation via a DSS file and new commercial dredging features. The model calibrated, reproducing historic bed volume changes, water surface elevations and channel velocities. This paper documents novel aspects of this modeling effort. More information on the full range of model inputs and choices can be found in USACE (2014).

MODEL OVERVIEW

USACE engineers developed a one-dimensional, quasi-unsteady HEC-RAS 5.0 sediment model (USACE, 2015, Gibson et al., 2006) to predict future degradation and to screen and evaluate potential solutions. The model starts ten miles upstream from the St. Joseph, Missouri USGS gaging station and ends near the Waverly, Missouri USGS gaging station. The downstream boundary is a historically stable location on the river. The model contains 303 cross-sections which span approximately 165 river miles of the Missouri River, with six to twelve cross-sections per river bend. The model was built with 1994 bathymetry and run forward to November of 2011. Figure 1 provides a schematic of the model network with river miles, major tributaries, channel cross-sections, and USGS gages located.

Channel roughness was assigned as Manning ‘n’ values in four horizontally-varied regions: the active channel, the channel with sill influence, the channel with dike influence, and the floodplain. At very high flows, the roughness for the active bed decreases as the bed transitions from dunes to plane bed. Bedform amplitude changes were verified using multi-beam bathymetric surveys, as seen in Figure 2. Dunes which dominate normal flows (67,000 cfs on May 27, 2010) transition to a planar transport regime at higher flows (196,000 cfs on June 28, 2011) during the 2011 flood.

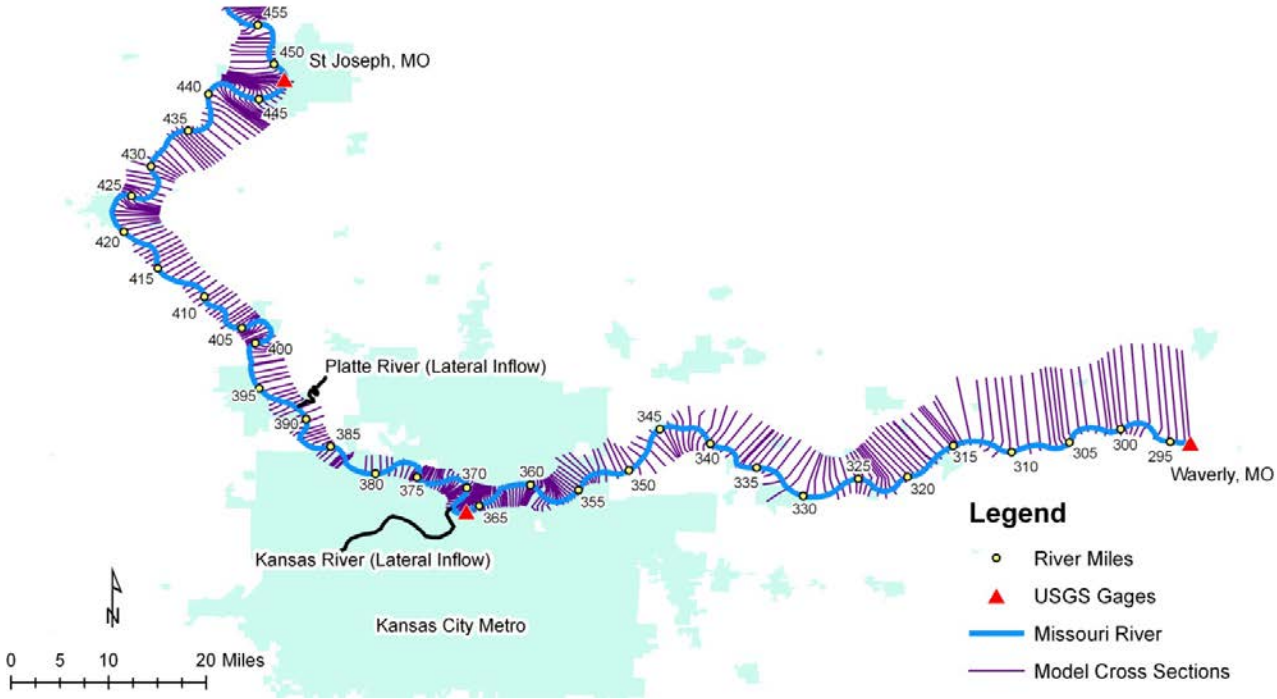

Figure 1 Model Schematic.

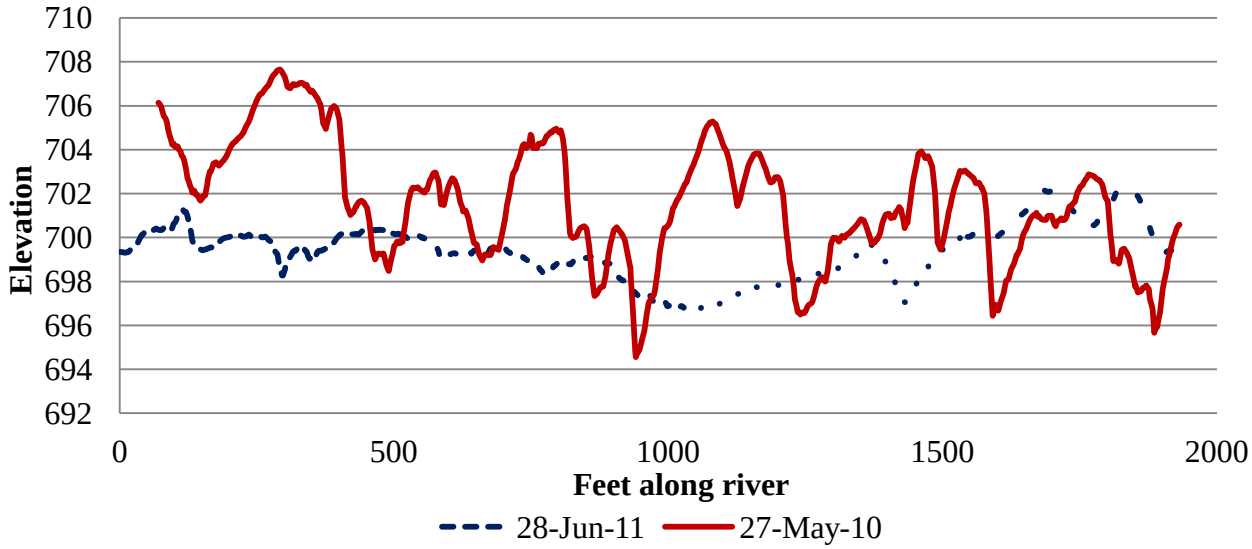

Figure 2 Flatter bedforms during flood flows just upstream of the Kansas River confluence.

The Brownlie bed roughness predictor (Brownlie, 1983), a new feature included in HEC-RAS 5.0 (Gibson, 2013) was evaluated for use in this model. Although this roughness predictor was developed for large sand rivers with bed forms that shift regimes, it over predicted roughness at high flows and under predicted roughness at low flows at the Kansas City gage. An 'n' value of 0.028 calibrated well with observed stages at the Kansas City gage for moderate and high flows,

but the highest flows calibrated to a lower 'n' value. This flow dependence was modeled using the flow-roughness factor in HEC-RAS.

NEW HEC-RAS FEATURES

DSS-TIME SERIES FOR SEDIMENT

HEC-RAS 4.1 included three sediment load options at upstream model boundaries: Equilibrium Load, Rating Curves, and Sediment Load Series. None of these options provided sufficient flexibility to specify loads with gradations that vary over time. On the Missouri River, a second flow-load-gradation relationship was required to model the unique supply-limited sediment loading of the historic 2011 flood. During the 2011 flood, the mainstem dams released tremendous volumes of relatively clear water while the watershed downstream from the dams contributed very little due to drought conditions.

HEC-RAS 5.0 includes a fourth sediment load option, Sediment Load Series by DSS, which was flexible enough to accommodate non-stationary loads and gradations with some pre-processing. HEC-Data Storage System (DSS) is the base that HEC-RAS and other HEC models use for input, and output time series, and to pass data between models (USACE, 2009b). In HEC-RAS 5.0, the DSS Sediment Load Series boundary condition reads a DSS sediment mass time series for each grain class.

In the degradation model, the sediment load series for each grain class were computed in Excel using the following formula:

$$Qs_i = Qbed * Pbed_i + Qsus * Psus_i$$

where Qs_i = the daily sediment load input for grain class size i, in tons

Qbed = the daily bed material load, in tons

$Pbed_i$ = the proportion of bed material corresponding to grain size i

Qsus = the daily suspended sediment load, in tons

$Psus_i$ = the proportion of suspended sediment load corresponding to grain size i

The suspended sediment load was computed from two separate flow-load curves based on USGS water quality data. The first flow-load curve applied from 1994 through March 2011. The second, supply-limited flood curve applied from April 2011 through November 2011. Gradations for the suspended sediment load were computed from USGS water quality samples.

The bedload portion of the sediment load was computed from a bedload rating curve for the Missouri River just upstream of the confluence of the Kansas River. This bedload rating curve was computed by using successive multi-beam bathymetric surveys (Abraham et al., 2011) with the time correction suggested in Shelley et al. (2013) and is provided in Figure 3.

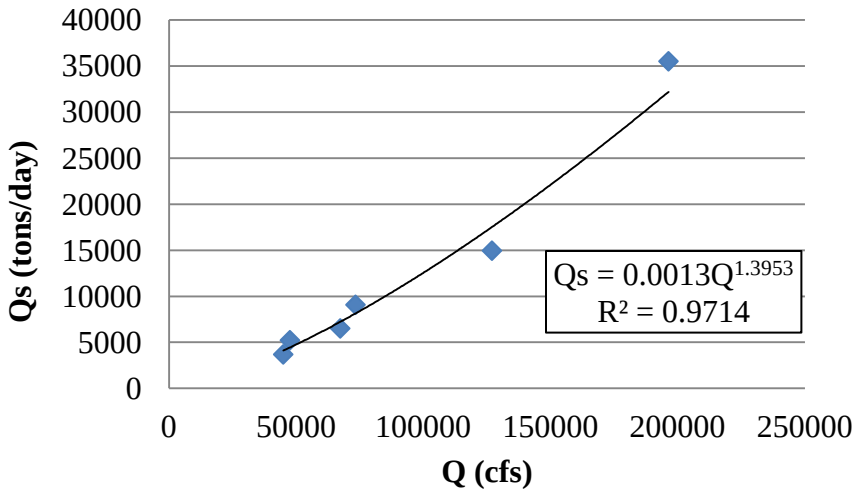

Figure 3 Missouri River Bedload Rating Curve at Kansas City (above Kansas River Confluence).

The gradation of the incoming total sediment load is a function of the relative contributions from bed load and suspended load, which varies by flow and shifts during the 2011 flood. From these, daily load series for each grain class were compiled in a DSS file using HEC-DSSVue 2.0 (USACE, 2009b) with the Period Cumulative (PER-CUM) data type, and a 'SEDIMENT' parameter (the required C: segment of the DSS path name) HEC-RAS 5.0 read the DSS file and matched the size specific load series with the corresponding grain classes.

Sediment rating curves at two major tributaries—the Platte River and the Kansas River—were included in the model as flow-load boundary conditions with the Rating Curve option, with loads and gradations estimated from USGS measurements.

DREDGING

HEC-RAS 4.1 includes algorithms to simulate navigation dredging. The Navigation dreding feature removes the material instantly, at a specified time, down to the specified template elevation. Dredging on the Missouri River is commercial dredging (sand and gravel mining), which differs from typical navigation dredging in several important respects. On the Missouri River, bed material is extracted and sold as aggregate for construction purposes. There is no target elevation, but rather a reported (or permitted) tonnage. On the Missouri River, commercial dredging takes are recorded as a daily location and tonnage. The navigation dredging features, with instantaneous, *a priori* dredge depths, in HEC-RAS 4.1 could not adequately reproduce this process.

HEC-RAS 5.0 includes new features better suited for modeling commercial dredging of river beds. First, a dredging start and end time can be specified so that dredging occurs gradually over time, not instantly. Second, the dredging can be specified as a target tonnage instead of a target elevation, allowing the cross section shape to respond to the mass removal. Third, the cross-section maintains the natural shape of the river bottom as material is removed, rather than the flat bottom channel the navigational dredging algorithms produce.

Dredging was included in the Missouri River degradation model as monthly tonnages at each cross-section with the start date the first day of the month and the end date the last day of the month. The model calibration used the standard "flat bottom" dredging algorithm, as the "natural bottom" routine was not yet available. The impact of dredging was restricted to the actual dredging tonnage, i.e. one ton of material extracted lowers the bed by a volume equivalent to one ton. Potential dredging effects due to bed disturbance and destruction of the armor layer were not explicitly modeled.

CALIBRATION AND VERIFICATION

The calibration/verification period runs from Aug 1, 1994 to Nov 30, 2011, with an intermediate calibration point Sep 30, 2009. The principal parameters which were varied to achieve calibration were the Manning 'n' values, the flow-based 'n' adjustment factors, the level of smoothing of the gradation data, and the sediment loading from the Kansas River. Channel geometry, moveable bed extents, incoming sediment load and gradation at the upstream model boundary, sediment transport function coefficients, and dredging were not used as calibration parameters.

EARLY HYDRAULIC CALIBRATION

A major high-flow event occurred within a year of the model start. Figure 4 compares model results to the water surface elevation at the USGS Missouri River gage at Kansas City. The computed water surface elevations are from the mobile-bed model run and therefore include slight bed changes over the course of the first year. However, as these changes are relatively small, Figure 4 is an indication of the ability of the model to reproduce channel hydraulics, more than the ability of the model to reproduce sediment fluxes.

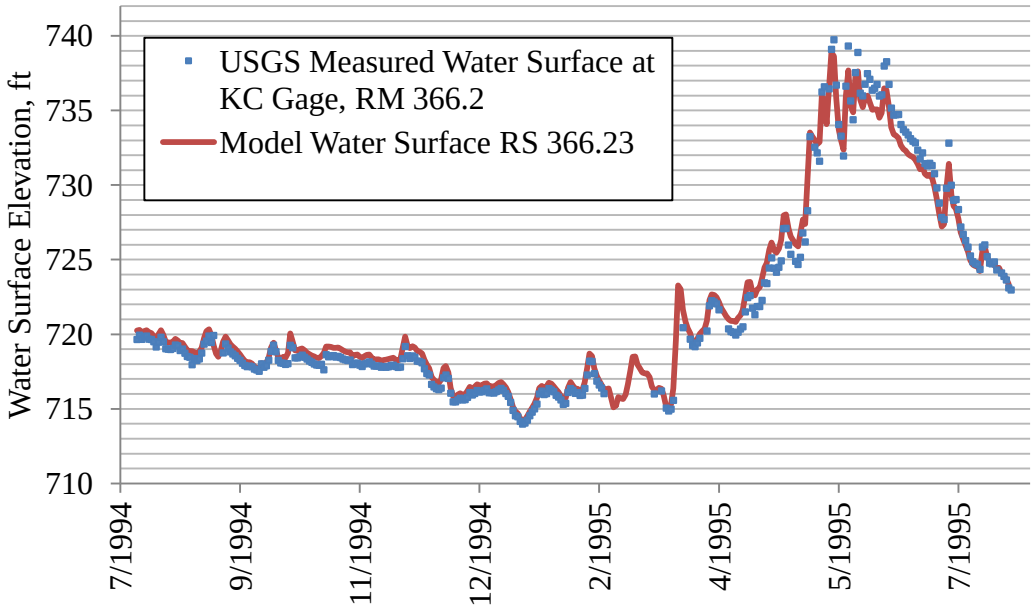

Figure 4 Water surface at Kansas City gage during first year of calibration period.

The average absolute difference between measured and modeled water surfaces is 0.67 ft. Agreement is better for steadily increasing and decreasing flows than rapidly fluctuating flows. In this particular event, input from the Kansas River and overbank storage issues were not reflected well in the model and causes rapid fluctuations near the peak. Notwithstanding this limitation, the model reproduces channel hydraulics reasonably well.

LONG-TERM HYDRAULIC CALIBRATION

Model water surface elevation agreement over the full calibration time period verified the temporal fidelity of bed change in the model. The model reproduced water surface elevations at the Kansas City gage with an average absolute error of 1.3 ft over the duration of the calibration period. For low flows less than 30 kcfs, the average absolute error is 1.0 ft.

VELOCITY CALIBRATION

Channel velocities were measured during and after the 2011 flood via ADCP. Figure 5 shows that the model channel velocities match measured velocities reasonably well for both a high flood discharge (153 to 225 kcfs) and a more moderate discharge (58 to 64 kcfs).

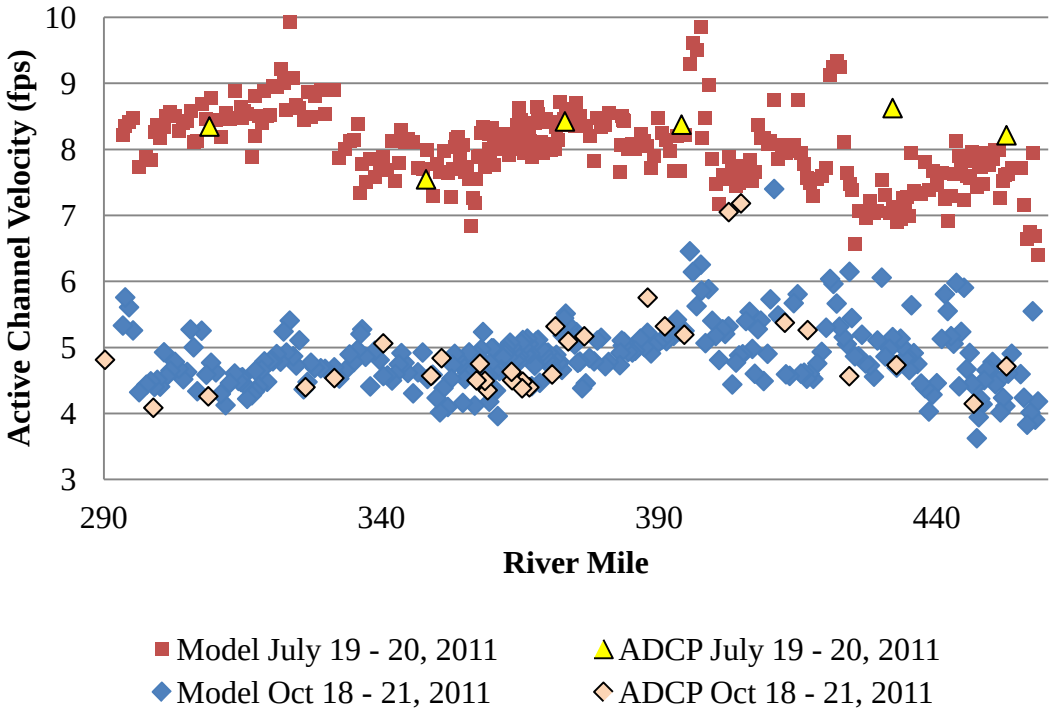

Figure 5 Velocity Comparisons.

SEDIMENT MASS CALIBRATION

The calibrated model simulates the magnitude and location of measured bed sediment change from 1994 to 2009 and 1994 to 2011, as indicated in Figure 6.

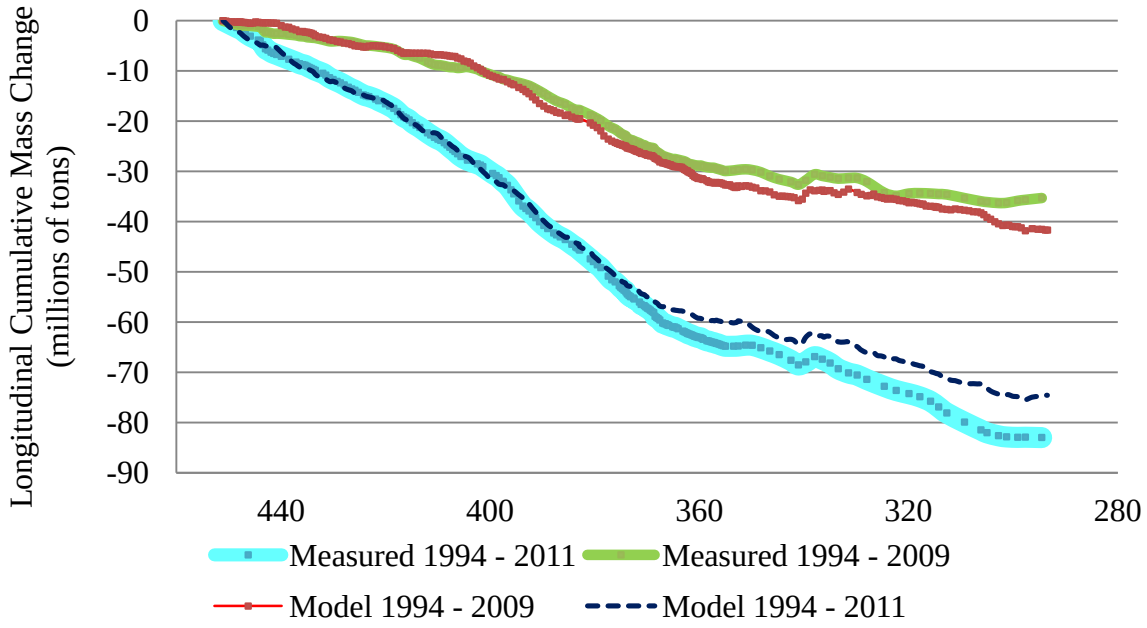

Figure 6 Mass Calibration.

The model outputs for water surface, mass change, and velocity over the calibration period approximate the prototype using realistic initial conditions and boundary conditions and appropriate model parameters.

CONCLUSION

This paper described the development of a one-dimensional HEC-RAS 5.0 mobile-bed model to simulate and predict degradation on the lower Missouri River. This model utilizes new sediment input and dredging features in HEC-RAS 5.0. Simulated water surface elevations, channel velocity, and sediment mass change, over the calibration period approximate the prototype using realistic initial conditions and boundary conditions and appropriate model parameters. This model demonstrates the utility of HEC-RAS 5.0 for bed degradation analysis in large, complex river systems with in-channel mining.

REFERENCES

Abraham, D., Kuhnle, R., and Odgaard, A. J., (2011). "Validation of Bed Load Transport Measurements with Time-Sequenced Bathymetric Data." J. Hydr. Engrg., ASCE, 137(7), 723-728.

Brownlie, W.R. (1983). "Flow Depth in Sand-Bed Channels," Journal of Hydraulic Engineering, ASCE, 109(7), 959-990.

Gibson, S., Brunner, G., Piper, S., and Jensen, M. (2006). "Sediment Transport Computations in HEC-RAS." *Eighth Federal Interagency Sedimentation Conference* (8th FISC), Reno, Nevada, 57-64.

Gibson, S. (2013). Sacramento River HEC-6T Model Conversion and Additional HEC-RAS Sediment Features, 56p.

Shelley, J., Abraham, D., and McAlpin, T. (2013). "Removing Systemic Bias in Bed-Load Transport Measurements in Large Sand-Bed Rivers." J. Hydraul. Eng., 0.1061/(ASCE)HY.1943-7900.0000760 (Mar. 22, 2013). http://ascelibrary.org/doi/abs/10.1061/(ASCE)HY.1943-7900.0000760

USACE (2014). Missouri River Bed Degradation Study Mobile Bed Model Calibration Report. February 2014. Kansas City District, U.S. Army Corps of Engineers. Kansas City, Missouri.

USACE (1994). Missouri River Hydrographic Survey: Rulo, Nebraska to the Mouth. U.S. Army Corps of Engineers, Kansas City District. Kansas City, Missouri.

USACE (2009a). Missouri River Bed Degradation Reconnaissance Study Section 905(b) (Water Resources Development Act of 1986) Analysis. U.S. Army Corps of Engineers, Kansas City District. Kansas City, Missouri.

USACE (2009b). HEC-DSSVue HEC Data Storage System Visual Utility Engine, Version 2.0, Hydrologic Engineering Center User Manual, CPD-79.

USACE (2015). HEC-RAS River Analysis System, Version 5.0, Hydrologic Engineering Center User Manual.

GULLY ANNEALING BY FLUVIALLY-SOURCED AEOLIAN SAND: REMOTE SENSING INVESTIGATIONS OF CONNECTIVITY ALONG THE FLUVIAL-AEOLIAN-HILLSLOPE CONTINUUM ON THE COLORADO RIVER

EXTENDED ABSTRACT

Joel B. Sankey, Research Geologist, U.S. Geological Survey, Southwest Biological Science Center, Grand Canyon Monitoring and Research Center, Flagstaff, AZ, jsankey@usgs.gov; Amy E. East, Research Geologist, U.S. Geological Survey, Pacific Coastal and Marine Science Center, Santa Cruz, CA, aeast@usgs.gov; Brian D. Collins, Research Civil Engineer, U.S. Geological Survey, Geology Minerals Energy and Geophysics Science Center, Menlo Park, CA, bcollins@usgs.gov; Joshua Caster, Geographer, U.S. Geological Survey, Southwest Biological Science Center, Grand Canyon Monitoring and Research Center, Flagstaff, AZ, jcaster@usgs.gov

INTRODUCTION

Processes contributing to development of ephemeral gully channels are of great importance to landscapes worldwide, and particularly in dryland regions where soil loss and land degradation from gully erosion pose long-term, land-management problems. Whereas gully formation has been relatively well studied, much less is known of the processes that anneal gullies and impede their growth. This work investigates gully annealing by aeolian sediment, along the Colorado River downstream of Glen Canyon Dam in Glen, Marble, and Grand Canyons, Arizona, USA (Figure 1).

In this segment of the Colorado River, gully erosion potentially affects the stability and preservation of archaeological sites that are located within valley margins. Gully erosion occurs as a function of ephemeral, rainfall-induced overland flow associated with intense episodes of seasonal precipitation. Measurements of sediment transport and topographic change have demonstrated that fluvial sand in some locations is transported inland and upslope by aeolian processes to areas affected by gully erosion, and aeolian sediment activity can be locally effective at counteracting gully erosion (Draut, 2012; Collins and others, 2009, 2012; Sankey and Draut, 2014). The degree to which specific locations are affected by upslope wind redistribution of sand from active channel sandbars to higher elevation valley margins is termed "connectivity". Connectivity is controlled spatially throughout the river by (1) the presence of upwind sources of fluvial sand within the contemporary active river channel (e.g., sandbars), and (2) bio-physical barriers that include vegetation and topography that might impede aeolian sediment transport. The primary hypothesis of this work is that high degrees of connectivity lead to less gullying potential.

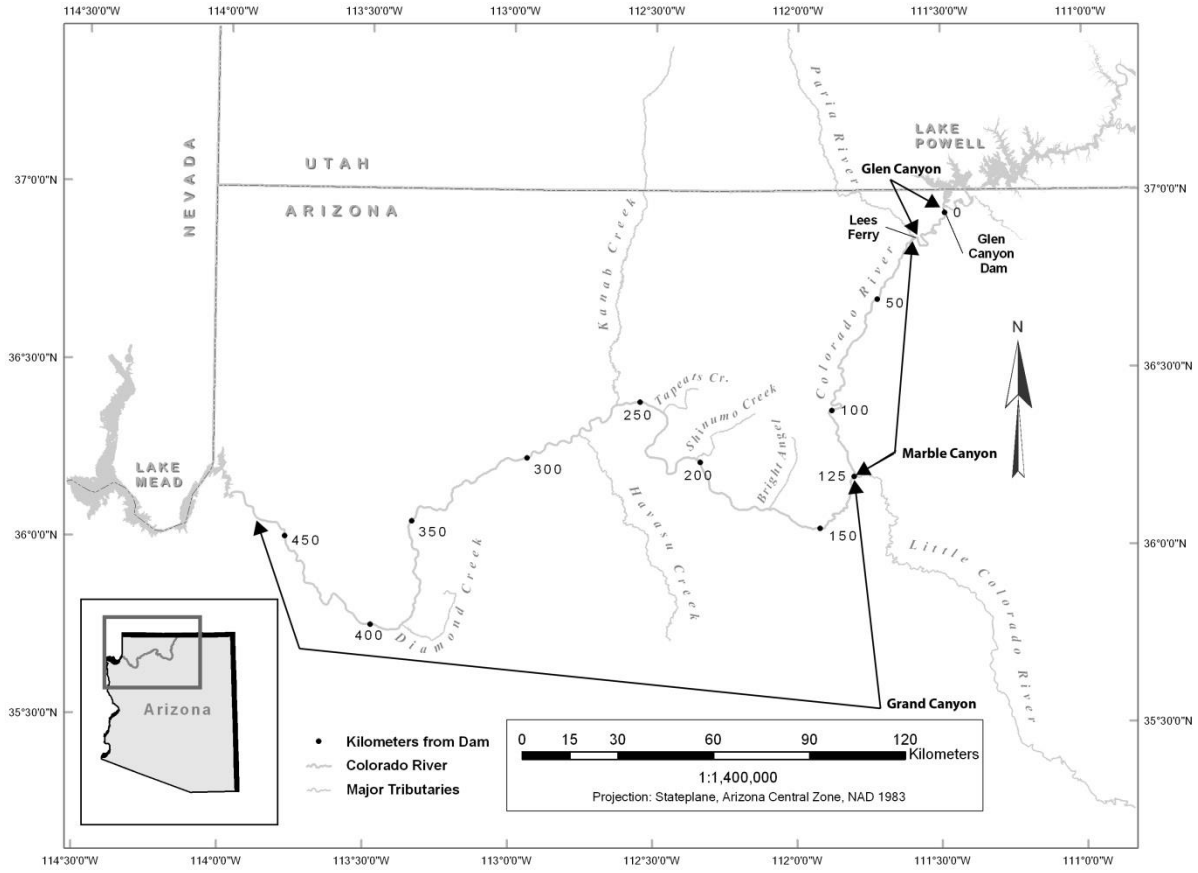

Figure 1 Map of the Colorado River downstream of Glen Canyon Dam, Arizona, USA.

METHODS

We have used a variety of remote sensing and field methods to map the distribution of fluvially-sourced aeolian sand within gullied valley margins above the active river channel (Draut, 2012; Collins and others, 2009, 2012; Sankey and Draut, 2014). We define the active channel as the area below the 1,270 m^3/s flood shoreline; 1,270 m^3/s is the approximate magnitude of recent controlled floods of the Colorado River from Glen Canyon Dam that have been conducted episodically since 1996. We have used remote sensing observations, including topographic modelling with high resolution automated digital photogrammetry and topographic change detection with lidar (light detection and ranging), to map and measure changes in gullies and fluvially-sourced aeolian surfaces (Collins and others, 2009, 2012; Sankey and Draut, 2014). Topographic change detection with repeat ground-based lidar surveys was conducted periodically from 2006 to 2010 at a total of 13 study sites (Collins and others, 2009, 2012).

In addition to high resolution change detection at sample locations, the spatial distribution of fluvially-sourced aeolian sand located above the active river channel has been mapped for six reaches of the river (Draut, 2012; Sankey and Draut, 2014). Mapping was completed in the field on high resolution imagery (22 cm-resolution). Fluvially-sourced sand units were identified as either active or inactive with respect to contemporary aeolian transport (Draut, 2012). Draut (2012) and Sankey and Draut (2014) showed that there is substantially less active sand area than inactive sand area throughout the river valley.

To investigate the effect of fluvially-sourced aeolian sand on gully development within these reaches, identification of potential gullies was conducted with high resolution digital elevation data (1-m grid cell resolution). Potential gullies were defined topographically as hillslope flowpaths with concave across-slope shape with potential to channel overland flow. Potential gullies were detected using a novel combination of overland-flow accumulation and topographic modelling procedures commonly available in GIS and remote sensing software. Methods for the identification of potential gullies are described in detail in Sankey and Draut (2014).

RESULTS

Sediment volume changes that were previously mapped with ground-based lidar and attributed to aeolian deposition (Collins and others, 2009, 2012) were summarized for three types of sites as a function of connectivity. The types were: 1) sites with recent Colorado River controlled flood sediment deposited upwind, and with a connected aeolian pathway from the active channel flood deposit to the site (where change detection was conducted); 2) sites with recent controlled flood sediment deposited upwind, but with reduced connectivity due to vegetation or topography that interrupted the aeolian pathway between the active channel flood deposit and the site; or 3) sites without a recent, upwind active channel controlled flood sediment deposit. Results are based on a small sample size, yet suggest that influx of fluvially-sourced aeolian sand is larger in valley margin landscape positions that have greater connectivity (Figure 2). Sediment volume changes were similar for type 1 and 2 sites, which was somewhat unexpected. A larger sample of sites could be studied in the future to either confirm this finding, or test whether changes in sediment volume vary as a function of transport barrier types (i.e, vegetation or topography) and characteristics (e.g. size, roughness, porosity).

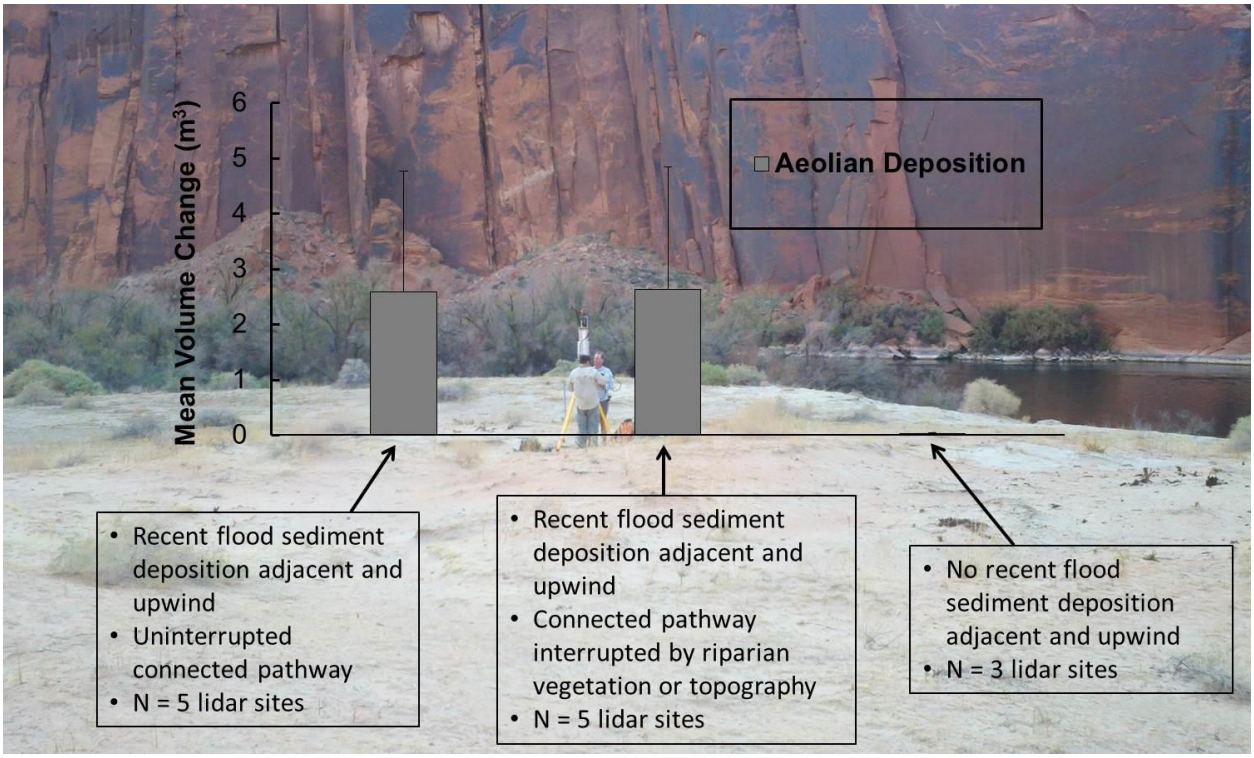

Figure 2 Volumetric surface change measured with ground-based lidar. Only volumetric changes attributed to aeolian deposition of fluvially-sourced sand are shown. Lidar study sites were located in valley margins above the contemporary active Colorado River channel and are prone to gully erosion. Individual site change data are from Collins and others (2009, 2012). Site change data are summarized by presence/absence of: 1) an upwind flood sediment source (sandbar); and 2) a topographic or vegetation barrier that might interrupt the connected pathway for aeolian transport of fluvially-sourced sediment to the higher elevation study site. Changes were determined at 1-3 year intervals for 13 sites between 2006 and 2010. Error bars show the standard error of the mean for n sites.

Figure 3 shows an example of the relative distribution of river-derived sediment above the active river channel for one reach of the river (70.8–98.2 km downstream of Glen Canyon Dam and within Grand Canyon National Park). In this reach, river-derived sediment that is active with respect to aeolian transport (showing evidence of contemporary aeolian sand transport) is located closer to the active river channel. This suggests that the degree to which valley margins are comprised of river-derived, active aeolian sand is influenced by connectivity, and specifically the length of the connected pathway to the active river channel and controlled flood sandbar deposits.

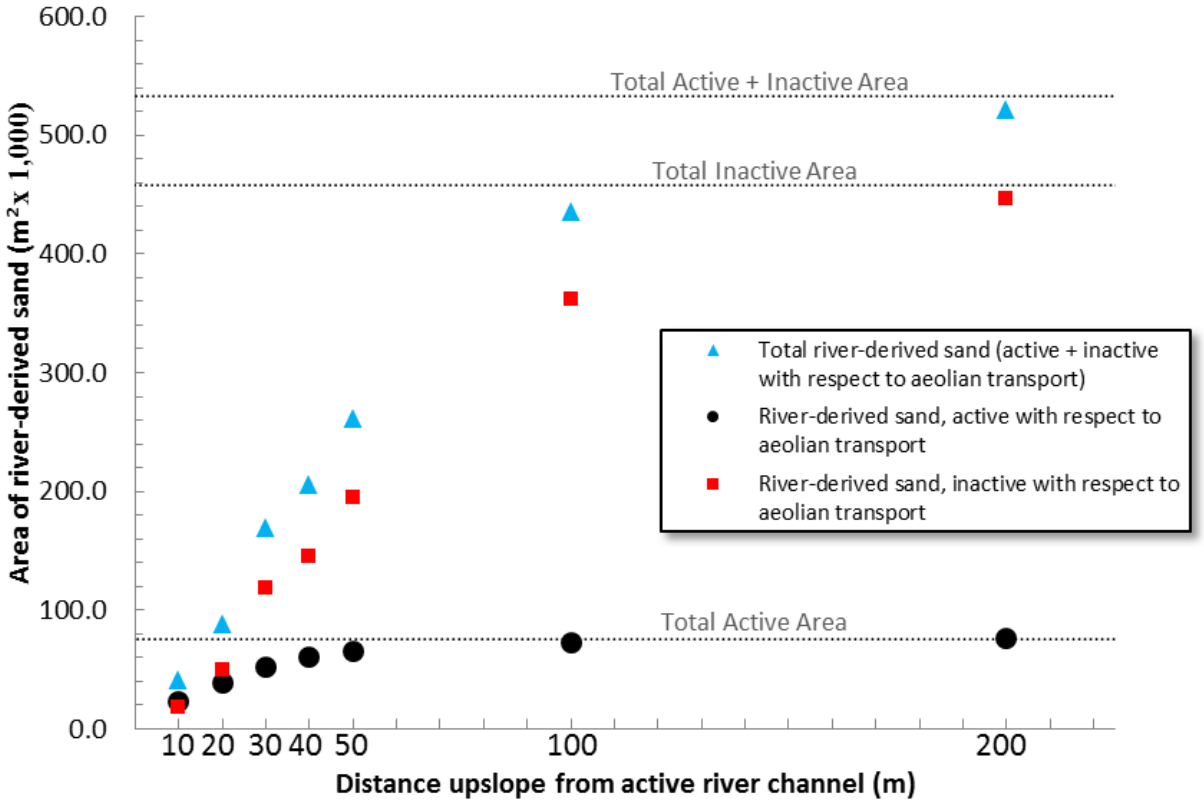

Figure 3 Distribution of river-derived sand that is active and/or inactive with respect to aeolian transport as a function of proximity to the contemporary active Colorado River channel. The active channel is defined as the area below the 1,270 m^3/s maximum controlled flood shoreline. Results are shown for a reach of the river (70.8–98.2 km downstream of Glen Canyon Dam) within Grand Canyon National Park.

The spatial intersection of mapped fluvially-sourced aeolian sand and potential gullies identified with digital topographic modelling indicate that gullies are less prevalent in areas where surficial sediment undergoes active aeolian transport (Figure 4). Potential gullies also have a greater tendency to terminate in fluvially-sourced sand that is active as opposed to inactive with respect to aeolian transport (Sankey and Draut, 2014). Although not common, examples exist in the records of historical imagery of gullies that underwent infilling by aeolian sediment in past decades and evidently were effectively annealed (Sankey and Draut, 2014).

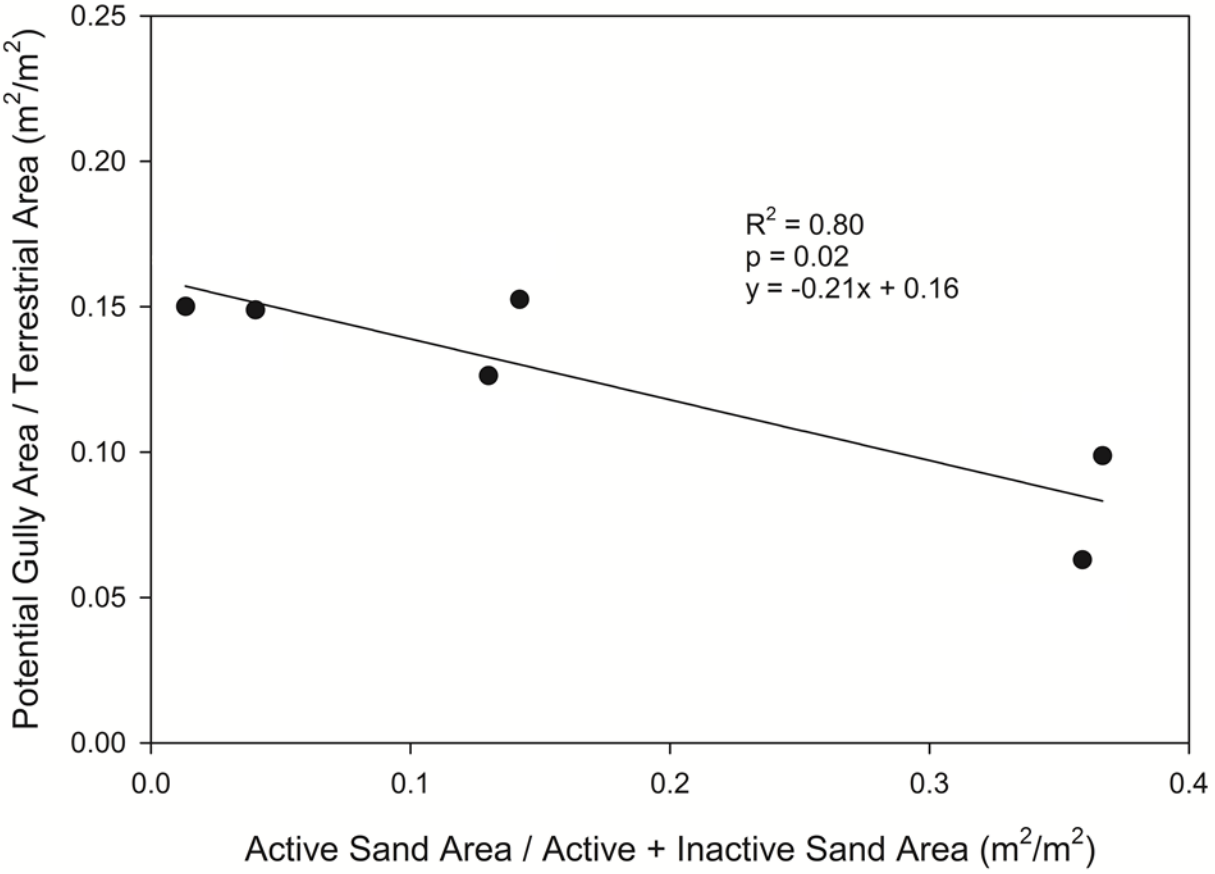

Figure 4 Relationship of area of potential gullies and active sand among six study reaches of the Colorado River in Glen, Marble, and Grand Canyons. Gullies are less prevalent in valley margins above the active river channel where river-derived sediment undergoes active aeolian transport. Figure is modified from Sankey and Draut (2014).

DISCUSSION and CONCLUSION

Connectivity is an important control on the distribution of fluvially-sourced sand in valley margins above the active channel of the Colorado River in Glen, Marble, and Grand Canyons. The distribution of fluvially-sourced sand can in turn influence the prevalence and extent of gullying in valley margins through annealing (e.g., infilling) mechanisms. The degree of connectivity between the active river channel and valley margins can therefore have an important influence on the potential for hillslope erosion in upland landscapes of the canyon-bound river. These investigations provide new evidence for an interaction of aeolian–hillslope–fluvial processes that can affect dryland regions substantially in ways not widely recognized. Continuation of this and related research will provide a basis for studies of natural and anthropogenic landscape change in the Colorado River and along similar river margins.

ACKNOWLEDGEMENTS

This study was supported by the U.S. Bureau of Reclamation through the Glen Canyon Dam Adaptive Management Program, with logistical and managerial support from the U.S. Geological Survey Grand Canyon Monitoring and Research Center. The authors thank the National Park Service and the Hualapai Tribe's Department of Cultural Resources for permission to conduct the field research.

REFERENCES

Collins, B.D., Minasian, D., and Kayen, R. (2009). "Topographic Change Detection at Select Archaeological Sites in Grand Canyon National Park, Arizona, 2006-2007: U.S. Geological Survey, Scientific Investigations Report 2009-5116," 97 p., [http://pubs.usgs.gov/sir/2009/5116/].

Collins, B.D., Corbett, S., Fairley, H., Minasian, D., Kayen, R., Dealy, T.P., and Bedford, D.R. (2012). "Topographic Change Detection at Select Archeological Sites in Grand Canyon National Park, Arizona, 2007-2010: U.S. Geological Survey, Scientific Investigations Report 2012-5133," 150pg; (http://pubs.usgs.gov/sir/2012/5133/).

Draut, A., 2012, Effects of river regulation on aeolian landscapes, Colorado River, southwestern USA: Journal of Geophysical Research – Earth Surface, v. 117, F2, doi:10.1029/2011JF002329.

Sankey, J.B., and Draut, A.E. (2014). "Gully annealing by aeolian sediment: Field and remote-sensing investigation of aeolian-hillslope-fluvial interactions, Colorado River corridor, Arizona, USA," Geomorphology 220, pp 68-80, doi: 10.1016/j.geomorph.2014.05.028

VAN DEEMTER'S STEADY STATE ANALYSIS OF DRAINAGE IN AN INFINITELY DEEP HOMOGENEOUS SOIL PROFILE

M.J.M. Römkens (Ret.), USDA-ARS- Nat'l Sedimentation Lab, Oxford, Mississippi, matt.romkens@ars.usda.gov

INTRODUCTION

The rapid development of sophisticated numerical techniques aided by highly sophisticated digital computer technology has led to the usage of numerical schemes in preference to analytical approaches in seeking solutions to groundwater flow problems. While numerical schemes can address more conveniently saturated as well as unsaturated complex geometric flow regions, analytical approaches may offer more insight in the physics of the problem. This is particular true if one deals with two-dimensional geometrically simple saturated flow regimes. For this class of problems potential theory may offer elegant, but also mathematically difficult to obtain solutions. One of the earliest work of solving two-dimensional groundwater flow problem for steady state flow using potential theory was by Muskat and Wyckoff (1937) who solved problems of horizontal flow into wells or vertical flow under sheet piles in dams. Since that time, the subject matter has been of interest in steady state gravity flow problems involving seepage to groundwater tables or through earthen dams, into ditches, etc.

Interestingly, solution approaches using potential flow theory of the conformal type to solve drainage problems in agricultural land did never find much acceptance among agricultural engineers even though the conditions for which this approach could be used were very amenable to this technique when it concerned low lying bottomland areas in need of drainage. The exception is perhaps the work by van Deemter (1950), a mathematician who under the leadership of S. Hooghoudt addressed the need to account for radial flow resistances in fields with closely spaced drains as opposed to the case with widely spaced drains with a Dupuit-Forcheimer flow regime. His work (van Deemter, 1950) did not receive the attention it should have had. Van Deemter was far ahead in his time, but the mathematical complexity was not conducive for adoption by most practically oriented or applied drainage engineers. In this article, the author discusses in rudimentary manner van Deemter's work by bringing out highlights of his approach and to relate the relevance of this work in the context of erosion problem from upland areas. For details of his work, the author refers the reader to the dissertation itself or to a summary discussion of selected aspects of this work with a relevant derivation for a particular flow regime by Römkens (2013)

PRINCIPLES OF SOLUTION TECHNIQUE

The principle of the conformal solution technique is to describe the flow region in two representations: (1) the complex gravitational geometric field or the z-plane ($z = x + iy$), and (2) the potentials in the z-field or the ω-plane consisting of pressure $\varphi = \varphi(x,y)$ and stream potentials $\psi = \psi(x,y)$ or $\omega(x,y) = \varphi(x,y) + i\,\psi(x,y)$. Each point $z(x, y)$ in the flow field has a unique set of values for the potential function (φ) and the streaming potential (ψ). The objective is to determine the relationship $\omega = f(z)$. The common approach is to transform both the spatial geometric flow region or z-plane and the potential field or ω-plane of this flow region onto a common complex

field, say the t-plane in a 1:1 correspondence. Depending on the complexity of the flow field geometry and the potential field several successive transformation may be involved. The simplest case is for the flow field to have straight vertical or horizontal boundaries. Likewise for the flow potential field to consist of straight pressure and flow potential lines as boundaries of which the intersections are the vertices that are used in the transformations. The boundary conditions of the potential field may be open or closed and irregular posing challenges on finding the appropriate mathematical descriptions for the flow region. In practice, one may have to seek a simplification of the flow field geometry that closely approximates the real situation if this technique is to be successfully used. Also, the flow field may have sinks (drains or ditches) and sources (rainfall, infiltration points). Two special techniques, that often must be employed in the analysis are the Schwarz-Christoffel transformation that allows a polygonal surface to be projected on a half-plane and the Hodograph method which method describes the flow field in terms of a complex velocity field $W = - d\omega(z)/dz = u + iv$ and which is commonly used when dealing with an open nonlinear boundary such as a groundwater table receiving rain. In that case, the boundary is represented by a streamline where water may enter the flow region (rain) and the potential function $\Phi = (y + p/(\rho g)$ with $\varphi = K \cdot \Phi$ where p assumes the value p = 0 at the open boundary or air-water interface. It can be shown, using the Cauchy-Riemann equations in this Laplacian flow field that the complex velocity at points on this surface can be described by a circle:

$$W = -\frac{(K+N)}{2} \cdot \sin 2\alpha - i \cdot \frac{(K+N)}{2} \cdot \cos 2\alpha + i \cdot \frac{(K-N)}{2} \qquad (1)$$

where u and v are the component flow velocities in the x and y directions, respectively, α is defined by the relationship; $\cot g\alpha = v/\mu$. N is rainfall intensity and K is the soil hydraulic conductivity. More detailed descriptions of the methodology can be obtained from the source (van Deemter, 1950) or from a recent publication about this work by Römkens, (2013).

An example of how the conformal methodology approach was used for a simple case of rainfall on a bottomland incised by a drain or ditch with an impervious layer at a finite depth was given by Römkens (2009). His study concerned a homogeneous isotropic soil profile below the soil surface having a hydraulic conductivity value K and receiving a rainfall intensity N. In that study, seepage losses from a bottomland area with a border-zone of varying width were calculated. Van Deemter (1950) presented a generalized model for 6 combinations of drainage, deep drainage, seepage, evaporation and infiltration. Figure 1 summarizes schematically these combinations. In his analysis, he assumed that the soil profile or aquifer was infinitely deep, and therefore the streamlines were vertical at that depth. This condition appreciably simplified the conformal analysis. The flow adjoining flow regions stood in symmetry to the flow region under consideration and therefore the analysis became mathematically feasible. The flow region surface boundary was open and therefore water fluxes at this boundary consisted of either rainfall or evaporation. The sink/source P in this schematic was represented by a point which in the analysis was either a water supply pipe or a drain of finite size or a ditch. While the geometric region was similar for the different flow regimes, the type solutions obtained were of course flow regime-dependent.

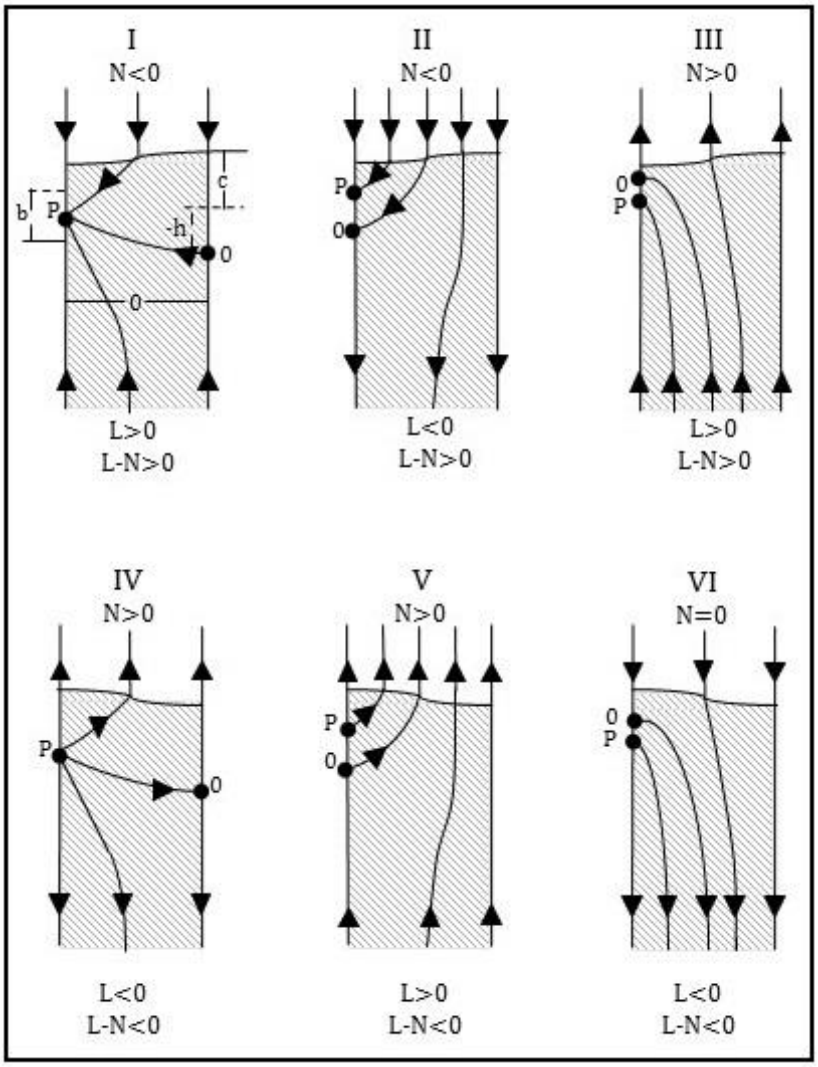

Figure 1 Groundwater flow regimes considered in the analysis by van Deemter: Drainage cases in I, II, III and infiltration cases IV, V, and VI. N = precipitation (rainfall) or evaporation expressed as an intensity and L = the deep drainage or seepage, also expressed as an intensity.

INFILTRATION AND DRAINAGE (CASE II)

The specific case considered in this article (Case II) concerns infiltration (N < 0)) with drainage and deep drainage (L < 0). In case I with seepage, the flow regime differs in that both rainfall and seepage contributes to drainage. The difference between these two flow regimes in otherwise the same geometric area is consequential when this technique is used to assess water quality issues. When different parts of the surface or of groundwater contribute different amounts of pollutant to the drains. A schematic of the flow region is shown in Figure 2.

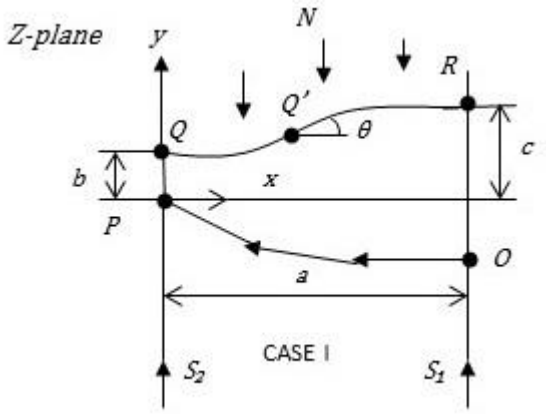

Figure 2 A schematic representation of the flow regime for infiltration, drainage, and deep drainage (Case II).

The boundary conditions for this flow region in terms of φ and ψ with the corresponding values of the vertices P, Q, R, S, in the z-plane are:

$$\begin{aligned} &\text{PQ (streamline):} && \psi = 0, \text{ with } z(P) = 0 \text{ and } z(Q) = i\cdot b \\ &\text{QR (phreatic surface)} && \varphi = K\cdot y \\ & && \psi = N\cdot x \\ &\text{RS (streamline):} && \psi = N\cdot a \text{ with } z(R) = a + i\cdot c \text{ and } z(S) = a - i\cdot\infty \\ &\text{SP (streamline):} && \psi = (N - L)\cdot a \text{ with } z(S) = -i\cdot\infty \text{ and } z(P) = 0 \end{aligned} \tag{2}$$

From these values, the boundary conditions in the Ω - plane defined by the relationship (3)

$$\Omega = \omega - i\cdot Nz = \varphi + Ny + i\cdot(\psi - N\cdot x) \tag{3}$$

can be determined. The flow region in the Ω-plane turns out to be, fortuitously, an infinitely long strip of finite depth (L-N)·a where the vertices are:

$$\begin{aligned} &\Omega(P) = -\infty \quad \text{and} \quad -\infty - i\cdot(L-N)\cdot a \\ &\Omega(S) = +\infty \quad \text{and} \quad +\infty - i\cdot(L-N)\cdot a \\ &\Omega(Q) = (K+N)\cdot b \\ &\Omega(R) = (K+N)\cdot c \end{aligned} \tag{4}$$

The product N·a represents the total amount of rainfall, while (N - L)·a represents the total amount of drainage in which rainfall was adjusted for seepage or deep drainage. For seepage (L > 0). Drainage constitutes the total amount of rainfall plus the amount of seepage, while for the case with deep drainage (L < 0) the amount of drainage equals the total amount of rainfall less the amount of deep drainage.

The spatial location of the open boundary is not defined but must be derived. An important parameter on this boundary is the point of inflection of the water table given by the angle θ. The flow velocity is defined by Eq. (1) and is -i·N at the vertices Q and R, which are the endpoints of the open boundary. At the vertices S the flow velocity is defined as −i·L, which is the seepage or deep drainage rate. From Eq. (1) the location of the center and the radius are determined on the hodograph W (see Fig. 3), which describes in effect the component velocities at all points of the open boundary including that at the inflection point Q'. At Q" the vertical velocity by virtue of Eq. (1) equals i·K.

In seeking the solution ω = f(z) for this flow regimes a common plane is sought onto which the geometric flow region and the potential field within this space are transformed so that a 1: 1 correspondence is obtained. The transformation equations can be obtained by mutual substitution. Figure 3 summarizes a series of conformal transformations of the flow field in the z-plane and ω-plane for Case II of van Deemter. From these transformations a number of parameter were identified to make a 1:1 correspondence possible. Those are:

$$\frac{\lambda^2 - 1}{2\lambda} = tg(\theta)$$

$$\frac{\mu^2 - 1}{2\mu} = (1 + \gamma) \cdot tg(\theta) = \frac{(K + L)}{(L - N)} \cdot tg(\theta) \tag{5}$$

$$\frac{\nu^2 - 1}{2\nu} = -\frac{K}{N} \cdot tg(\theta)$$

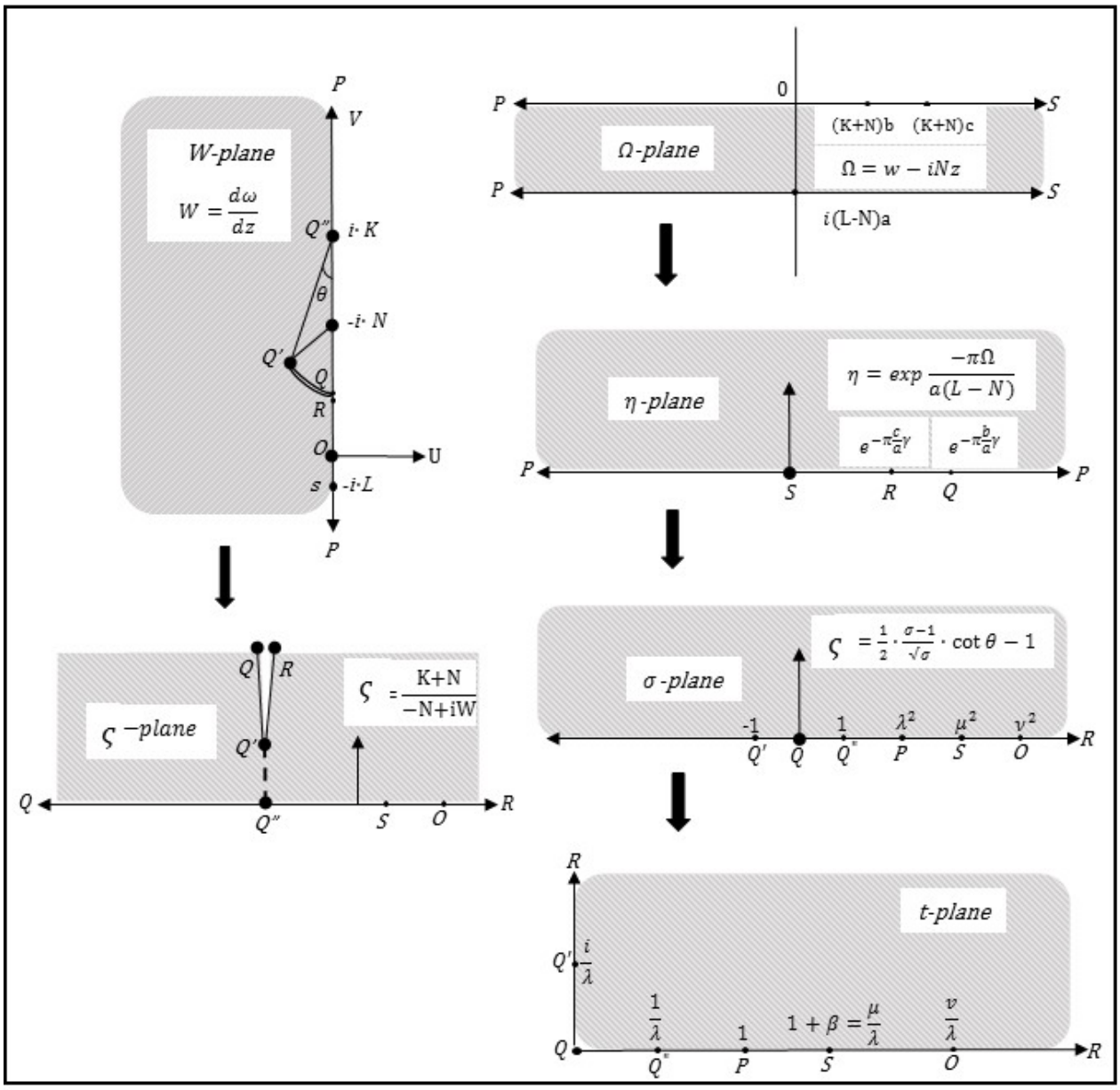

Figure 3 Conformal Transformations of the z-plane and W-plane onto the common plane t.

The fractional linear transformation between points on the upper half planes of η and σ yields the relationship:

$$\eta = \frac{(\sigma - \mu^2)}{(\sigma - \lambda^2)} \cdot \exp\left(-\pi\gamma\frac{c}{a}\right) \tag{6}$$

from which the identity:

$$(1+\beta)=\frac{\mu}{\lambda}=\exp\left(\pi\gamma\frac{c-b}{2a}\right)>1 \tag{7}$$

can be obtained with $\gamma = (K+N)/(L-N)$. Since the hodograph was presented in terms of the differential equation $d\omega/dz$, one must perform an integration to be able to obtain expressions for ω and z in terms of common independent variable. This is done by introducing the variable t so that $t = \frac{1}{\lambda}\sqrt{\sigma}$. The t-plane, shown in Figure 4, has as vertices: $t(R) = \infty$ and $i\cdot\infty$; $t(Q') = i/\lambda$; $t(Q) = 0$; $t(Q'') = 1/\lambda$; $t(P) = 1$; $t(S) = \mu|\lambda = 1+\beta$; $t(O) = \nu|\lambda$. It shows how the upper half of the σ-plane is projected on the first quadrant of the t-plane with the vertices located on the positive real and imaginary axes. By substituting in a systematic manner the t variable in a reverse order into the sequence of transformations one can now obtain expressions for z(t) and ω(t). These expressions are:

$$z=a+ic+i\frac{a}{\pi}\cdot\left[ln\frac{t-1-\beta}{t+1+\beta}+\frac{2}{\gamma}\cdot ln\frac{t+1}{t+1+\beta}\right] \tag{8}$$

$$\omega=K\cdot c+i\cdot Na+\frac{a}{\pi}\cdot\left[\begin{array}{c}(L-N)\cdot ln(t-1)-L\cdot ln(t-1-\beta)+N\cdot ln(t+1+\beta)+\\ (L-N)\cdot\frac{(K-N)}{(K+N)}\cdot ln\left(\frac{t+1}{t+1+\beta}\right)\end{array}\right] \tag{9}$$

with $\gamma = (K + N)/((L-N)$ and $1+ \beta = \mu/\lambda$. The veracity of these relationships can be verified upon substitution of selected t-values (for the vertices, see Figure 2). For instance from Eq. (8): $t = t(Q) = 0$ will yield $z = i\cdot b$; $t = t(S) = 1+\beta$ yields $z = -i\cdot\infty$ and $z=a -I\cdot\infty$; and $t(R) = \infty$ yields $z = a + i\cdot c$. Actually, the latter result was used as input to determine the integration constant. Similarly, from Eq. (9): $t = t(P) = 1$ one obtains $\varphi = -\infty$ and $\psi = i\cdot(N-L)\cdot a$; for $t = t(Q) = 0$ one obtains $\varphi = K\cdot b$ and $\psi = 0$; and for $t = t(R) = \infty$ one obtains $\varphi = K\cdot c$ and $\psi = N\cdot a$.

With the solutions of z and ω in terms of t it should now be possible, barring algebraic complexities, to calculate in principle at any point in the flow region the corresponding values of the potential function φ and stream function ψ. Of particular interest would be the groundwater table above the sink (P) and midway between sinks assuming mirror images of adjacent flow regions. Note that in calculating these values the t-parameter has a real value for points on the QR line segment in the t-plane of Figure 3.

From the spatial relationship, Eq. (7). The groundwater table can be determined by substituting in Eq. (7) $t = i\cdot s$ where s is a real number. Then the groundwater surface, which is the imaginary axis of the t-plane (Figure 3) is given by the relationships:

$$\frac{x}{a} = \frac{2}{\pi}\left[\frac{1+\gamma}{\gamma} \cdot arctg\,\frac{s}{(1+\beta)} - \frac{1}{\gamma} \cdot arctg \cdot s\right] \tag{10}$$

and

$$\frac{y}{a} = \frac{c}{a} + \frac{1}{\pi\gamma} \cdot ln\,\frac{(s^2+1)}{(s^2+(1+\beta)^2)} \tag{11}$$

The distance c midway point between two adjacent symmetrical flow regions and the point b directly above the drain, can be determined and are respectively:

$$\frac{\pi c}{a} = ln\left(1+\frac{2}{\beta}\right) + \frac{2}{\gamma} \cdot ln\left(1+\frac{\beta}{2}\right) \tag{12}$$

and

$$\frac{\pi b}{a} = ln\left(1+\frac{2}{\beta}\right) + \frac{2}{\gamma} \cdot ln\frac{\left(1+\frac{\beta}{2}\right)}{(1+\beta)} \tag{13}$$

The total flow rate into or out of the aquifer is determined by; (1) the pressure difference between the groundwater table level and the water level in the in the ditch or open water body to which the flow region is connected, (2) the size of the soil/surface water area through which the flow region drains or supplies water, and (3) the geometric configuration of the flow region. It is to be expected that the location of the groundwater table adjusts dependent on the amount of incoming (rain) or evaporation and to changes in the deep drainage or seepage rates. The effect of these changes are expressed in the parameter γ. In this treatise, the drain or supply line have a spherical perimeter. However, the flow regime in the aquiver is asymmetric and therefore the aquipotential functions away from a circular drain or supply line are not concentric. Adjustments must be made in selecting the locations of the sink or source to ensure a constant value for the aquipotential function around the drain circumference if an accurate value of water fluxes out (drainage) or into (infiltration) is to be obtained. In his work, van Deemter (1950) indicated that for small drains in relation to the flow region the aquipotential coincides with the drain water in the drain lines. On the other hand, Römkens (2009) shifted the location of the sink within the drain in an iterative manner such that the circumference was closely aligned with an aquipotential. At that point, the calculated flow rate and flow gradients at the perimeter are the correct ones. Having accurate values are important from both a hydrological standpoint of knowing how much water is discharged or must be supplied in a watershed, but also from an environmental standpoint of knowing the sources and amounts of pollutants in the flow region. In the van Deemter approach discussed here in which a drain with radius r_o, the aquipotential at the drain circumference is defined as:

$$\varphi_0 = K \cdot \left(\frac{P_0}{\delta g} - \mathrm{r}_0\right) \tag{14}$$

where p_o is the pressure at the drain and h_o is the equivalent water column height. The point on the drain perimeter below the center P is given in his analysis as $z_o = -i \cdot r_o$ in the z-plane and as $t_o = 1 + \delta$ in the t-plane, then δ can be determined using Eq. (8), which yields:

$$\frac{\pi r_0}{a} = ln\frac{\beta}{\beta-\delta} + \frac{(2+\gamma)}{\gamma}\cdot ln\frac{(2+\beta+\delta)}{(2+\beta)} - \frac{2}{\gamma}\cdot \ln\left(1+\frac{\delta}{a}\right) \tag{15}$$

Also, the aquipotential line at the bottom of the drain perimeter can be obtained from Eq. (7) yielding:

$$\varphi_0 = K\cdot c + \frac{a}{\pi}\cdot\left[(L-N)\cdot ln\,\delta - L\cdot ln(\beta-\delta) + N\cdot ln(2+\beta+\delta) + (L-N)\cdot\frac{(K-N)}{(K+N)}\cdot ln\frac{(2+\delta)}{(2+\beta+\delta)}\right] \tag{16}$$

From the above relationships, β and δ can be determined given known values for K, L, N, ho, and r_o.

Another point of interest is the location of vertice z(O), which is the confluence of the flow originating at the groundwater surface and the flow emanating at great depth of the aquifer. In that case, z(O) becomes t(O) = ν\λ in the t-plane. Then:

$$z(O) = a + i\cdot c + i\cdot\frac{a}{K}\cdot\left[ln\frac{\left(\frac{\nu}{\lambda}-1-\beta\right)}{\left(\frac{\nu}{\lambda}+1+\beta\right)} + \frac{2}{\gamma}\cdot ln\frac{\left(\frac{\nu}{\lambda}+1\right)}{\left(\frac{\nu}{\lambda}+1+\beta\right)}\right] \tag{17}$$

From Eq. (4) one can determine λ and ν for a known β and the value of h for z(O) = a + i·h.

INFILTRATION

The analyses for cases IV, V, and VI, representing sub-irrigation are very similar to those described for drainage in I, II, and III. In fact, the same formulae apply.

Drainage by incised ditches The analysis of drainage through cylindrical shaped drains was facilitated by the geometric simplicity. On the other hand, drainage of bottomland often takes place through incised ditches. Van Deemter addressed that problem as well and presented an analysis for two ditch geometries; (1) A rectangular incised ditch, kept water free but with a saturated bottom and aside wall that was also partially saturated (Figure 4), and (2) an incised ditch in which the side wall was impervious (Figure 5). In both cases the flow region was infinitely deep.

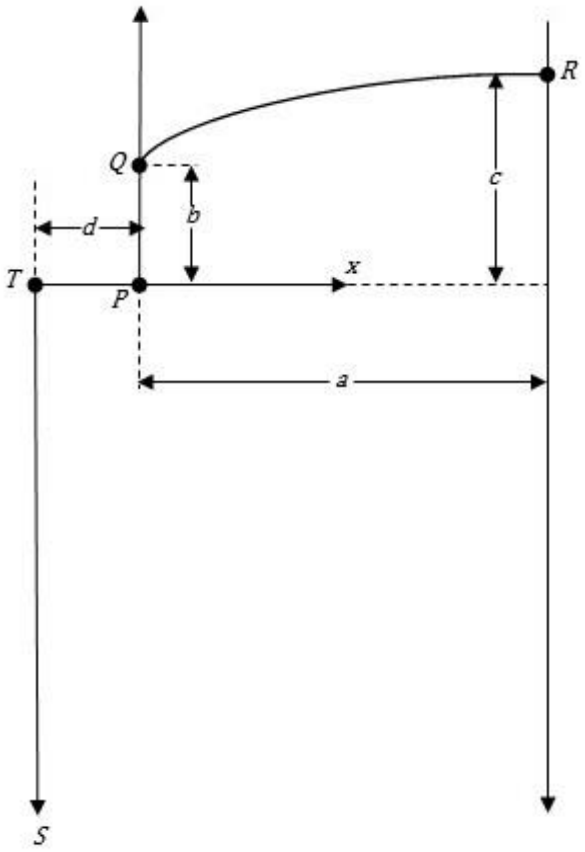

Figure 4

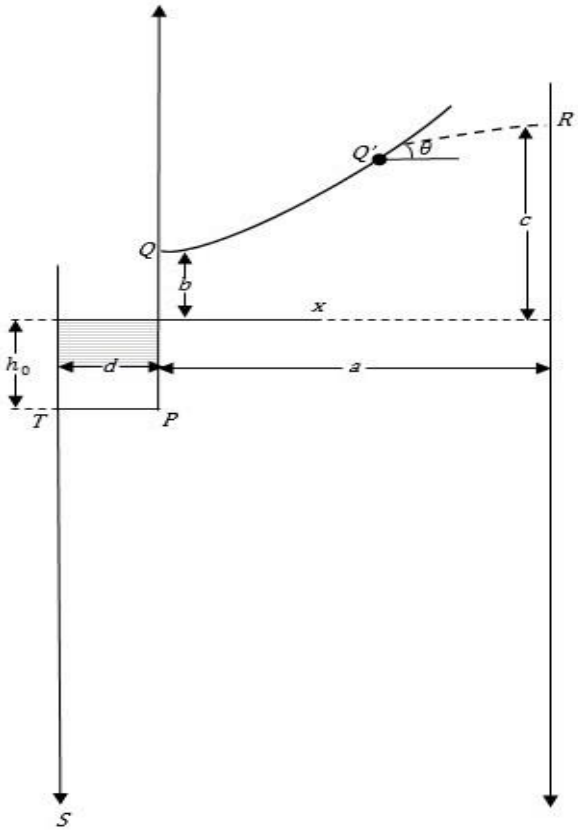

Figure 5

Again the solution approach was by conformal analysis and different mathematical expressions were obtained.

CONCLUDING REMARKS

The advanced analysis by van Deemter, done more than 65 years ago, represented a major breakthrough and achievement at that time. Yet, it never received the recognition it deserved. While the models and analysis described represented idealized situations void of geometric complexities and heterogeneity by layering and/or soil permeability variations., this technology as old as it is may be very useful in water management problems at the field and watershed scale of bottomland areas with drainage and irrigation needs.. From the erosion perspective, the analysis allows the calculation of seepage gradients at the soil profile-surface water interface and the determination of aequipotential surfaces in bank stability problems near ditches and channels. These calculations are the subject of further studies.

LITERATURE CITED

Muskat, M. and R.D. Wickoff. 1937. The flow of homogeneous fluids through porous media. McGraw-Hill Book Company, Inc. 1st. Edition. New York and London.

van Deemter, J.J. 1950.Theoretical and numerical treatment of flow problems connected with drainage and irrigation. Verslagen van Landbouwkundige Onderzoekingen. No 576. Dutch Ministery of Agriculture, Fisheries, and Food supplies... The Hague, Netherlands. (In Dutch).

Römkens, M.J.M. 2013. A theoretical treatise of drainage and seepage in bottomland areas adjacent to incised channels: The J.J. van Deemter analysis. Advances in River Sediment Research-Fukuoka et al. (Eds). Taylor and Francis Group, London, ISBN 978-1-138-00062-9

Römkens, M.J.M. 2009.Estimating seepage and hydraulic potentials near incised ditches in a homogeneous isotropic aquifer. Earth Surface Processes and Landforms. 34: 1903-1914.

ORIGIN OF TILL RIDGES IN A NORTHEASTERN VERMONT VALLEY

John S. Moore, Retired National Geologist, Natural Resources Conservation Service (NRCS), United States Department of Agriculture (USDA)
Home: 7723 Modisto Lane, Springfield, VA 22153 (johnniednm@hotmail.com)

INTRODUCTION

Background: Since 2008 the author discovered several previously unreported till ridge sets in a northeastern Vermont (VT) valley. The question arose as to their mode of origin. To answer this question, the author selected one set for detailed field study, called Study Area 001 (figures 1 and 2). It is located along a northwest to southeast trending, a three-kilometer long segment of the Harvey-Symes valley (HSV) between Roy Mountain Wildlife Management Area and Lower Symes Pond near Ryegate, VT. The set contains no fewer than 90 ridges and mounds along both sides of the valley. Individual ridges are similar in composition of the boulder-size clasts, range in grain size distribution, and in shape, height, length, spacing (where clustered) and position on the landscape. Some ridges appear to have cross-valley counterparts. Study Areas 002 and 003 (figures 1 and 2) in Maine (ME) were control sites of known origin to contrast with conditions in Study Area 001 in VT.

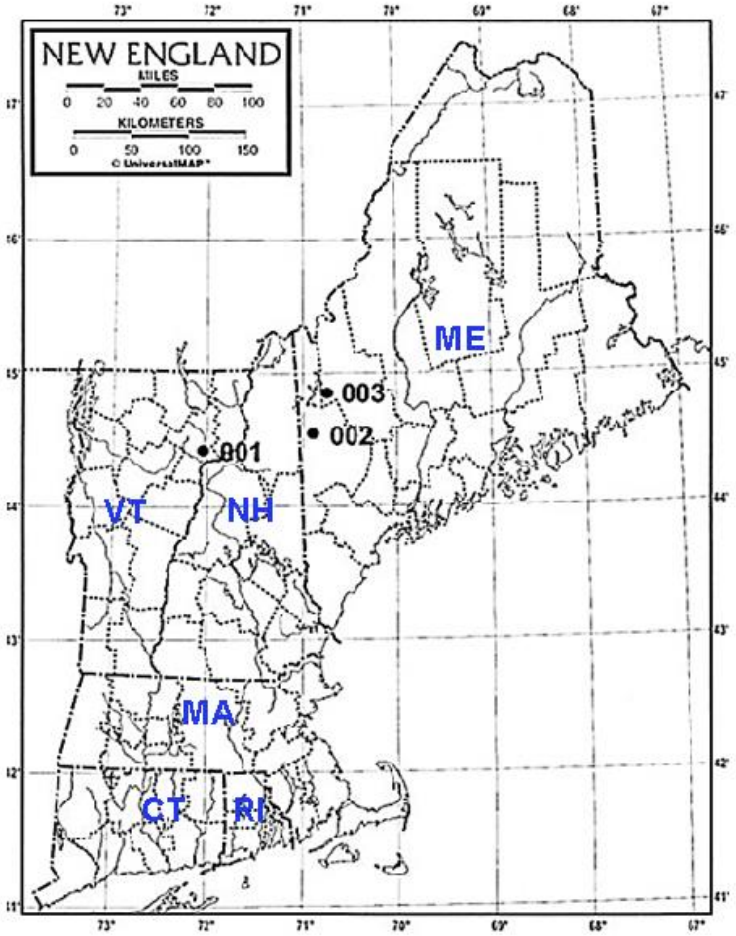

Figure 1 Regional map showing location of study areas (National Geographic Map of New England).

Purpose of Study: The purpose was to develop a classification system based on field criteria to determine the probable origin of the till ridge set in Study Area 001 and similar sets in this region. The classification would also

serve to improve reconstruction of late glacial history and post-glacial geomorphic events in northern New England, and may contribute to the understanding of global climate changes.

During fieldwork, the author considered two diametrically opposed hypotheses, erosion versus deposition. One hypothesis contends the ridges in a given set are interfluves formed by erosion, specifically, post-glacial dissection of a hillside till sheet by gullying and associated mass wasting processes. The other argues they are moraine ridges or ice-marginal deposits formed by periodic deposition of detritus released near the receding margin of the Laurentide Ice Sheet in New England. The author conducted two reconnaissance surveys in ME to serve as control sites because their origin is known to be erosional. Study Area 002 near Newry, ME (figures 1 and 2) is considered the largest known cluster of interfluvial ridges formed by post-glacial gullying of a till sheet in the region (Woodrow Thompson, Maine Geological Survey, personal communication, 2012). Study Area 003 is on the south flank of nearby Elephant Peak, ME (figures 1 and 2). This site offers a small analog of the Newry site that exemplifies active gullying and rilling on a well-exposed, unvegetated till sheet near a recently cut logging road. The study results provided field evidence to develop a classification to differentiate origin by either erosion or deposition. The classification addresses five physical parameters: swale morphology, swale soils, ridge morphology, drainage pattern and hydrology, and fate of eroded materials.

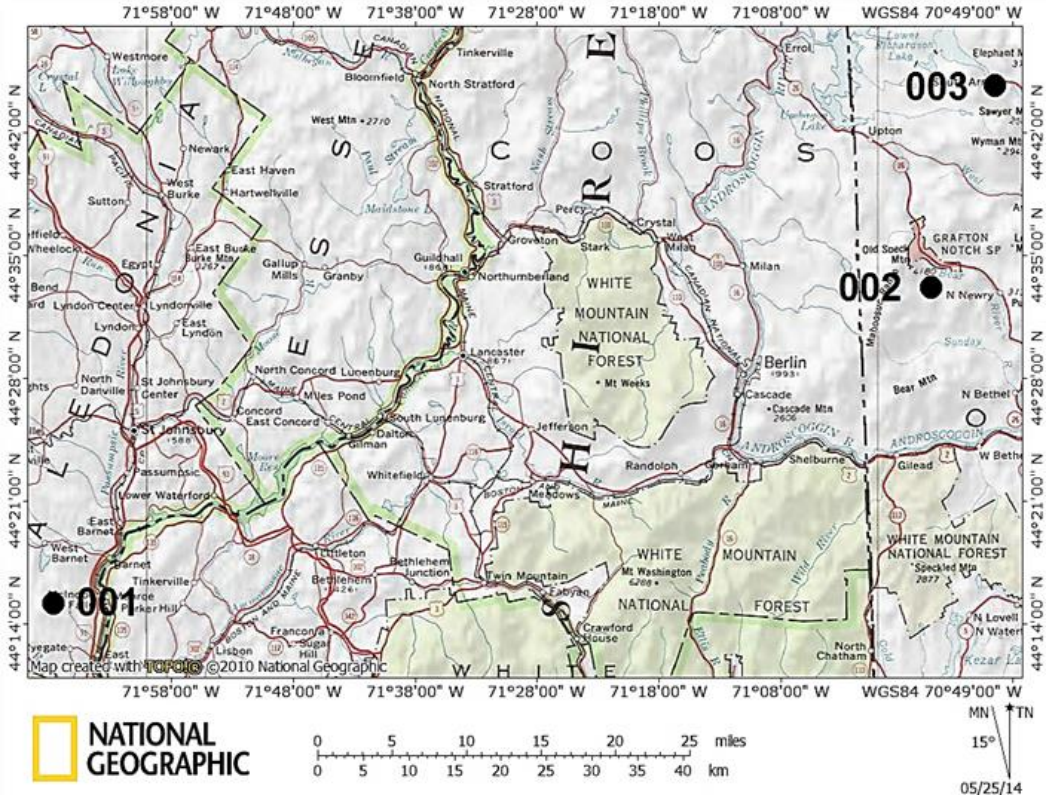

Figure 2 Shaded relief location map of Study Areas 001, 002, and 003, based on National Geographic Maps.

Definition of Moraine Ridge: Glacial geologists have not agreed upon a single definition or a classification scheme for moraine ridges. Moraine ridges that occur in sets have been variously termed ribbed moraine, washboard moraine, ridged moraine, corrugated ground moraine, recessional moraine, and other terms. For examples, refer to studies by Benn and Lukas (2006), Bennett and Glasser (2009), Hart and Boulton (1991), Hart and Rose (2001), Hättestrand and Kleman (1999), Koteff and Pessl (1981), Stewart, Bryant, and Sweat (1988), and Lundqvist (1969). Moore (1974) referred to them simply as recessional moraines. The fact remains, multivariate processes can construct a host of different landforms on various scales that manifest similar morphology and sedimentological characteristics. This paper applies the definition of moraine ridge used by Thompson (1999): *"A single-crested ridge of glacial sediment inferred to have been deposited at or near the ice margin and parallel to it"*. A swale is the low ground between adjacent ridges and is usually concave upwards in cross-section.

Definition of Interfluvial Till Ridge: This paper defines an interfluvial ridge or the broader, flat and uneroded area between adjacent gullies, as "*The high ground separating adjacent gullies flowing in the same direction and which were formed or are forming by fluvial and associated mass wasting processes that occur on the gully notch side slopes"* (Glossary of Geology, 1997). Interfluvial ridges tend to be oriented parallel with the fall line of the slope. Gully erosion on a till sheet produces consequent, ephemeral or intermittent streams that tend to form a dendritic drainage pattern.

Field Methods: Material and mass properties of soil and rock were described according standardized definitions of terms and field practices given in Moore (2001a, and 2001b) and ASTM D2488, "Standard practice for description and identification of soils (Visual-Manual Procedure)", also called the Unified Soil Classification System (USCS).

Base maps are seamlessly joined, 7.5-minute, US Geological Survey (USGS) topographic quadrangles available from the National Geographic's commercial software for computer-assisted drawings. The software also was used for track-recording and field navigation by a hand-held, Global Positioning System unit. Because some of the USGS maps use metric units and others use English units for contour elevations (six meters or 20 feet) and scales (kilometers and miles), both units are provided in the paper. Ridges that are less than six meters high are poorly discernible on these maps. Small ridges and isolated masses were not mapped. Due to innate ground irregularities, linear measurements were estimated by pacing and dead reckoning. The heights of features were measured by altimeters or by dead reckoning.

FINDINGS

Study Area 001: The till ridge set in Study Area 001 is a portion of a larger complex of hundreds of ridges and mounds that are mostly within the Roy Mountain Wildlife Management Area along the unnamed valley, herein referred to as Harvey-Symes Valley (HSV) between W. Barnet and Ryegate, Caledonia County, VT (figures 2 and 3). The black rectangle in figure 3 encloses the four-kilometer square study area which the HSV bisects longitudinally and follows the wet bottom. The northern margin of the study area is located at a valley bottom divide blocked by thick, hummocky till that effectively redirects perennial flow of Jewett Brook north to Harveys Lake. Streams south of the till divide flow into HSV to discharge into the Connecticut (CT) River at E. Ryegate, VT. The southern limit of Study Area 001 is near Lower Symes Pond.

Subsequent area surveys on nearby hills outside of Study Area 001 revealed small till ridges that partially wrap around upper sections of north facing hill slopes. These suggest nunatak formation and ice margin moraine deposition by retreating active ice. These ridges and numerous others in the vicinity are still under field study and are not shown on figure 3.

Numerous locally derived, angular to sub-rounded boulders up to 200 cubic meters in volume litter the surfaces of ridges and inter-ridge areas. Ridge lengths vary between several tens of meters and 200 meters. Average crest spacing on the both sides of HSV is approximately 60 meters. Ridge heights vary between three and 25 meters, but most are between four and six meters. Ridges tend to be straight and oriented between 60° (pointed down-valley) to perpendicular to the valley walls. The majority occur in declining fashion below the 318-meter (1040-foot) contour elevation. Frontal and distal side slopes of most ridges range between 25° and 35° and are nearly symmetrical in cross-section. Distal slopes are generally a few degrees steeper than frontal. Where angular, large boulders and cobbles are abundant in the till, slopes range between 35° and 45°. These ranges are consistent with angles of repose for unconsolidated, uncompacted, granular soils. Figures 5 and 6 illustrate a typical ridge in cross-section and in profile, respectively. Field assessment tests of unconfined compressive strength of numerous till boulders composed of foliated rock material ranged between 12.5 and 100 megapascals (MPa). Hammer blows perpendicular to schistosity gave higher values than parallel with it. Granite, gneiss, and quartzite boulders had values between 100 and 250 MPa. Angularity of edges and planar faces of large clasts were between sub-angular and sub-rounded, with sub-angular dominating. Large clasts showed no signs of weathering other than superficial iron oxide staining.

Grain-size gradation in till is variable from place to place and tends to be gap-graded. It consists of a coarse fraction ($\geq$ 3.0 inches) of cobbles through extremely large boulders that account for up to 80 % of till volume. The matrix varies between 10 and 25 % micaceous, fine sandy silt (ML), silty fine sand (SM), and non-plastic silt (ML). The clay fraction is low, ranging between 0 and 10 %. The gap accounts for less than 10 % of the till and consists of material between the coarse sand and coarse gravel range (approximately 10 to 40 millimeters).

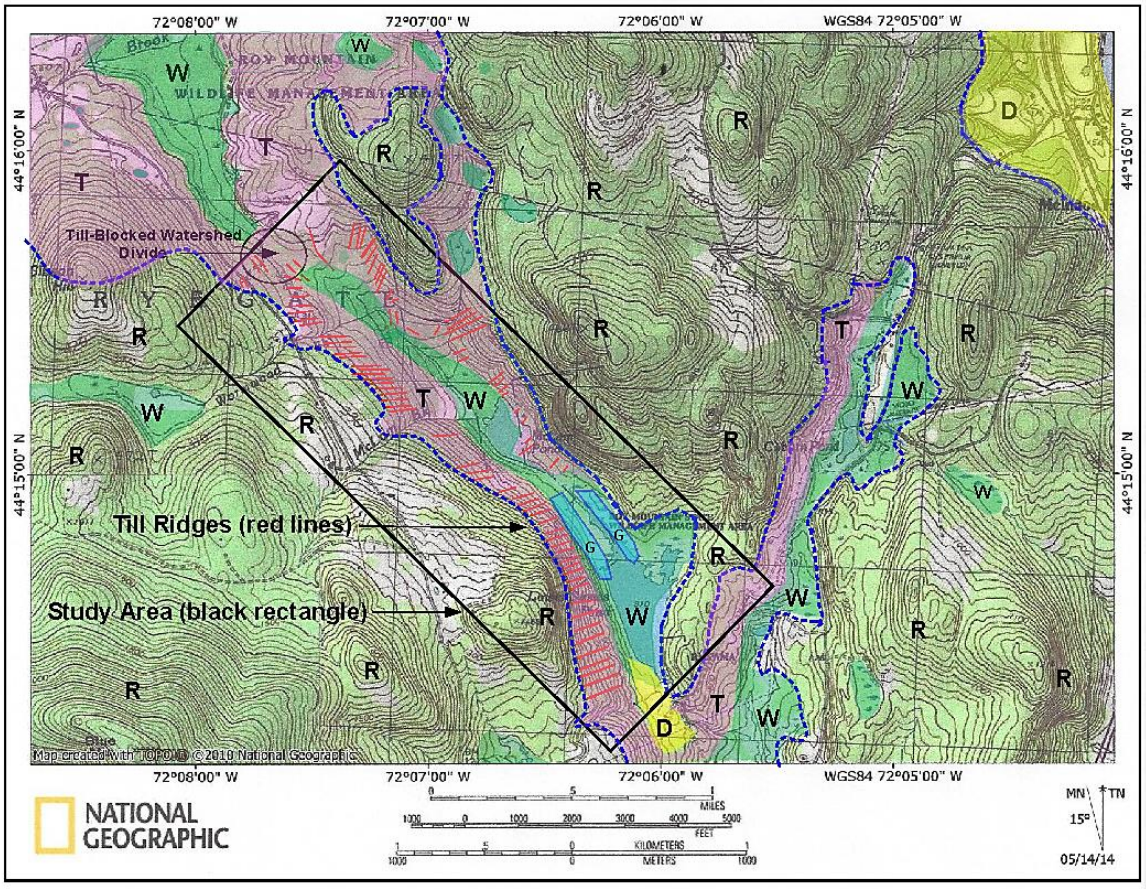

Figure 3 Generalized surficial geologic map of Study Area 001 drawn on integrated, National Geographic maps of USGS 7.5-minute topographic quadrangles. Contour interval is 20 feet (6 meters).

KEY TO SYMBOLS AND COLORS

R ***Dashed Blue Lines*****:** Inferred margins of areas of bedrock outcrop or thin till mantle above rock.

T ***Pink Overlay*****:** Areas of thick till, till ridges, and mounds. Red lines indicate till ridge crests within study area. Crest orientations are within +/- 10°. Ridges outside study area are not shown.

D ***Yellow Overlay*****:** Deltaic sediments in the sand- through cobble- size range, and undifferentiated lake sediments associated with proglacial Lake Hitchcock (not shown).

O ***Blue Overlay*****:** Small areas of glacial outwash (coarse gravels to large cobbles).

W ***Green Overlay*****:** Areas of natural ponds, wetlands, marshes, and wet floodplains. Those in valley bottoms were glacial meltwater channels. Those on higher ground were kettle holes or glacially scoured bedrock depressions that are now marshes or wetlands. Faded green is forested areas depicted on USGS base maps.

Figure 4 Explanation of symbols and colors used in figure 3.

The Natural Resources Conservation Service (NRCS), US Department of Agriculture (USDA), conducts county-wide soil surveys and classifies soils to a depth of 1.5 meters according to the texture-based, USDA Soil Classification System (Soil Survey Staff, 1999). The Caledonia County, VT soil survey (Gourley, 2007) indicates the USDA classification of soils on the ridges and in swale bottoms in Study Area 001 correlate well with the USCS. Cobbles and boulders are derived from local bedrock. Matrix fines are largely derived from local, foliated bedrock.

The material strength of foliated bedrock is inherently low and thus afforded little resistance to glacial erosion, abrasion, and percussion. Therefore, the rock readily disintegrated into non-plastic, fine particles.

In Study Area 001, swale drainage areas vary from a fraction of a hectare to approximately 10 hectares. There is no alluvium in the swale bottoms. They are perennially wet due to thin, poorly drained soils and organic-rich muck that cover dense till. Swales support denser and more water-tolerant ground vegetation than ridge sides and tops. Most swales have an ephemeral or intermittent stream channel that carries runoff from the nearby hills or from small, rock-fracture springs. Between rainfalls or during dry spells, intermittent stream channels are recharged by connate water seepage along the bases of till ridges. For example, after one flow event, a channel at the head of a swale was flowing one liter per minute. At its lower end, the stream was flowing five liters per minute. If clean, permeable alluvium were to occur in a swale bottom, stream discharge would decrease downstream due to infiltration into the alluvium. To check for Holocene alluvium, the author dug into 17 swales with a hand pick and never encountered fluvial sediment. In every case, bottom material consisted of a veneer of wet, organic-rich, silty muck overlying dense, slowly permeable till. Near surface water in swales is perched above and within poorly drained till and silty muck.

Figure 5 Cross-section of typical ridge viewed looking up axis. Ridge crest is crowned and varies between five and 10 meters in width. Height is three to five meters, and axis is approximately 150 meters long. Photo by author.

Figure 6 Profile view of ridge and swale near Lower Symes Pond. Photo by author.

Study Area 002: The site is on the southwest side of the Bear River valley, near Newry, ME (figures 1 and 2). It is the state's largest known interfluvial till ridge set. The set consists of at least 50 interfluvial ridges demarcated by adjacent gullies. The set is discernable on the topographic map (figure 7) and the aerial photo (figure 8).

The author traversed the entire site in July 2012 and made the following observations. The surface of the till sheet slopes between 10 and 30 % to the northeast. Gully incision depths vary between three and 25 meters. Because no bedrock is exposed in gullies, these depths provide an estimate for minimum till sheet thickness on this hillslope. All gullies in their upper reaches are V-notched. Large gullies widen downstream and present trapezoidal cross sections where small floodplains have developed. These floodplains have ephemeral or intermittent stream channels incised to a depth of 0.3 to 1.2 meters. During dry weather in July 2012, stream discharge in the lower reaches of large trunk gullies was no more than a few liters per minute. Discharges modestly increased downstream due to vadose water contribution from interfluves. Every gully channel has knickpoints in various places along its profile. During headcut advancement knickpoints migrate upstream or become erased by fluvial processes.

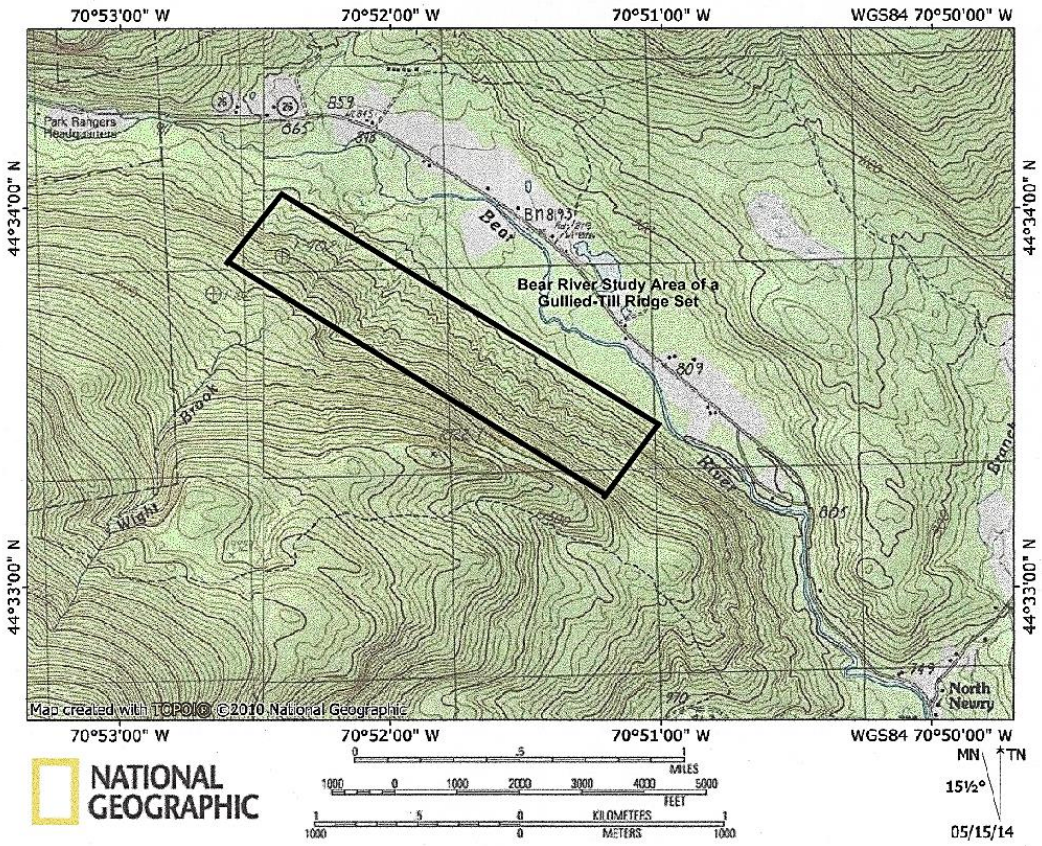

Figure 7 Topographic map of Study Area 002 near Bear River, Newry, ME. Contour interval is six meters.

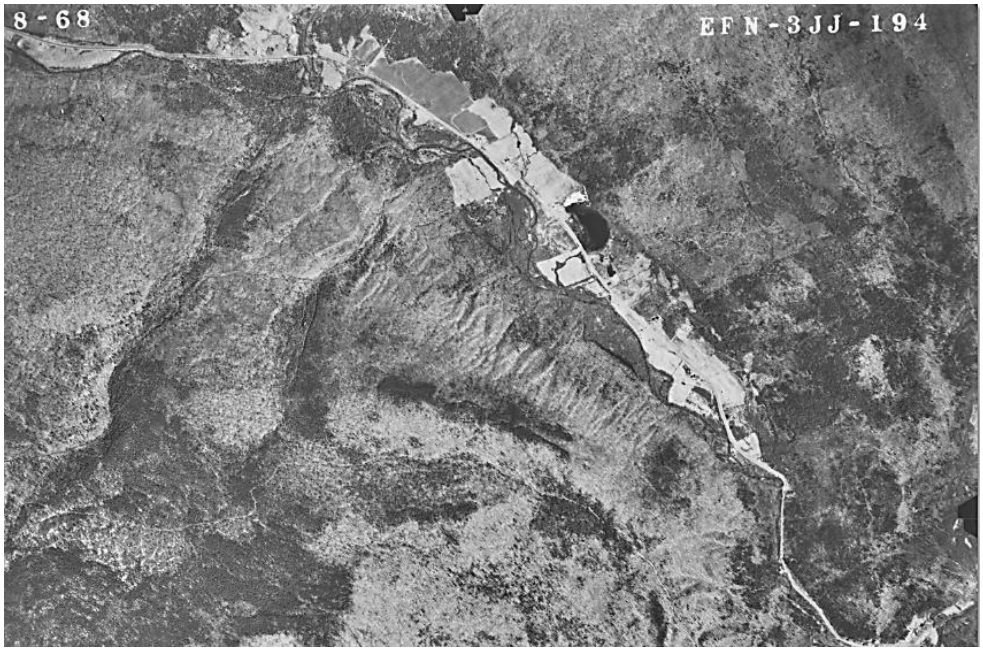

Figure 8 Vertical, aerial photo of figure 7, same scale. In center of photo, interfluvial ridges are well-exposed. Several trunk gullies branch into dendritic drainage patterns. Photo by USDA, Farm Services Agency.

Gully sidewalls are generally steep and irregular where mass wasting has occurred. Nevertheless, most reaches appeared stable with vegetated sidewalls, and the author could climb up or down them with little slippage. When slumps occur they form blockages that reroute the stream flows against the base of the walls. This intermittent process de-stabilizes the gully wall and induces additional mass wasting, which in turn, widens the gully. Individual boulders and cobbles can also perturb the flows with similar effect. All gully bottoms are covered by materials in the coarse gravel to boulder size range, with cobbles predominating.

The gullies are not regularly spaced (figure 8). Some adjacent gullies formed narrow interfluvial ridges. Flat, uneroded areas are well over 100 meters wide and reflect the original surface of the till sheet. Gully drainage areas vary between 5 and 50 hectares. The lengths of gullies in this cluster are similar because their upper ends, as well as the undissected portions of the till sheet, terminate against steep to vertical granite outcrops that trend NW-SE near hill 1822. Talus boulders at the base of the outcrop are not part of the till sheet. The boulders range between six and 20 cubic meters in volume.

The grain size distribution of the till is gap-graded. The matrix consists of non-plastic fines (ML and SM) through very fine sands (SW and SM) that collectively account for 20 to 30 % of the till volume. Clay content is minimal. Clasts larger than three inches (7.6 centimeters) account for 70 to 80 % of the volume. Large clasts vary between 0.020 and several cubic meters in size. The gradation gap occurs between the coarse sand through coarse gravel range. Basal ice comminution of local, foliated bedrock formations produce mostly fines. Crystalline rocks tend to yield clasts that reflect the spacing of discontinuities in the source rock mass. Size and shape of cobbles and boulders are usually functions of discontinuity patterns of the rock mass source area. Clast size may be further diminished by post-glacial weathering (mechanical disintegration or chemical dissolution), or by mechanical breakage and percussion during fluvial transport. Weathering may yield coarse sand through coarse gravel sizes provided the mineral constituents are similarly textured. In this area, most cobbles and boulders are sub-rounded, a characteristic that indicates reworking either by fluvial processes or by basal ice comminution near the end of the last glaciation.

Study Area 003: On Elephant Peak, ME, there is a small analog of the Bear River gully site. The site is a machine-cut slope adjacent to a new logging road ditch cut into till. Figure 9 shows the sharp break between the ditch side slope (30°) and the flatter (10°) slope above the ditch. The grain size distribution is similar to till in Study Area 002. The upper slope is analogous to unvegetated conditions that immediately follow ice recession when the till is well-exposed to rill and gully erosion (figure 9). Although spacing and depth of gullies and rills vary, they are roughly parallel to the slope. Headcut advance and dissection progress up through the flatter slope. Some gullies are branched. Slopes of undissected, interfluvial areas are essentially undisturbed, although rain has removed some fines to produce stone pedestals (figure 10).

Figure 9 A recently constructed logging road on Elephant Peak, ME. The side ditch that was excavated into a till sheet illustrates an unvegetated, sloping surface that is undergoing gully and rill erosion. Photo by author.

Figure 10 Close-up view showing how lag cobbles and boulders cause channel flows to impinge on the gully or rill side slopes. The side slopes become subject to mass wasting, and the channel widens, deepens, or changes direction. Photo by author.

DISCUSSION OF TILL RIDGE ORIGIN

Assessment of bedrock as it occurs regionally and locally is fundamental to reconstructing late glacial events in New England. Rock masses differ in composition, areal distribution, material and mass strength, and geologic structure. These factors collectively affect regional physiography, landscape form, and drainage patterns. During ice ages, near surface bedrock conditions can influence basal ice flow direction and determine the composition of glacial deposits.

An essential requirement for development of moraine and other ice-marginal deposits is a nearby, easily comminuted source of detritus. Study Area 001 follows a lineament formed by a mixed contact zone that measures 12 kilometers long by up to four kilometers wide in this region. The lineament trends through the long axis of Harveys Lake, the entire HSV, and lower Manchester Brook Valley (MBV). Its orientation aligns well with known flow directions of continental glaciers. The zone occurs along the margin of the Knox Mountain granite pluton that invaded foliated rocks of the Waits River and Gile Mountain formations. The mixed zone consist of unaltered xenoliths of foliated rock fragments embedded in granite, and a complex system of dikes and sills injected along cleavage and fractures of stratified units. The dike complex and inclusions in the granite indicate disruption and shattering near the border of the pluton (Hall, 1959; White and Billings, 1951; and Konig, 1961). During glacial advances, the buttresses afforded by Roy and Harvey Mountains and the steep, bedrock valley walls along HSV

steered basal ice south and southeast toward the Connecticut River valley. During recession, the outlet valley glacier in the HSV therefore had access to abundant, erodible rock material to form moraine.

An active glacier carries the bulk of ice-eroded debris within the lower few meters of its base. Koteff and Pessl (1981) stated that most till in New England was transported no more than 1.5 kilometers from its bedrock source. Throughout Study Area 001, ubiquitous, surface-exposed, large boulders express low to moderate edge and face rounding. These conditions, plus the composition of till components, including boulders and matrix alike, inarguably reflect local provenance. Koteff and Pessl (1981) considered end moraines as *prima face* evidence of stalled margins of active ice.

For the till ridge set in Study Area 001, the hypothesis of origin by Holocene erosion is not supported by field evidence. Severe summer storms that damaged VT in the past few years produced virtually no out-of-channel sediment in swales in Study Area 001. Furthermore, no alluvium occurs in swale bottoms that would have resulted from immediate, post-glacial erosion. Field evidence collectively indicates the predominant hydrogeology of swale bottoms is perched water above and within poorly drained till and organic-rich muck. Swales provide the primary outlet for connate water that slowly seeps from the toes of ridges. If swale bottoms contained permeable alluvial deposits, they would act as French drains where surface waters infiltrate into the alluvium, move downhill, and outlet into HSV River or Upper and Lower Symes Ponds. Stream discharges in swales would thus diminish downslope. The fact that the swales are perennially wet and mucky is clear evidence that the swale soils are slowly permeable.

Local topography indicates the HSV served as the primary flume for local glacial meltwater. The lower ends of ridges next to Upper and Lower Symes Ponds appear truncated along a common line parallel to a presumed hydraulic gradient during times of high meltwater discharge. The line of truncation is approximately three to five meters above current pond elevation. Meltwater also was likely responsible for breaching cross-valley moraines. Heyman and Hättestrand (2006) described these ridges as valley-side moraines. They defined them as "*sub-horizontal, relatively straight ridges situated on valley sides and formed at the margins of outlet glaciers during deglaciation of an ice sheet"*. They based this definition on morphology and topographic setting.

There are many significant factors that preclude the hypothesis that the ridges are interfluves formed by hydraulic erosion. (1) The drainage areas of all the swales are far too small to provide sufficient hydrodynamic energy to erode sediment larger than medium gravel. The enormous body of research on erosion and sedimentation unquestionably indicates that the hydrology of such small watersheds cannot enable the entrainment and transport of clasts greater than coarse gravel, even on bare surfaces (Yang and Huang, 2001). According to classic literature, the most erodible grain size range is 0.10 to 0.50 millimeter (modified Hjulstrom curve *in* Sundborg, 1956; and Shields Diagram *in* Vanoni, 1975). Thus, streams that flow through erodible materials quickly become turbid during the rising stage of a hydrograph. The fine fraction continues to move throughout the entire runoff event. At the end of a flow event suspended and bedload sediments drop out and become available for subsequent events. (2) The erodible size range accounts for only 20 % of the till volume. The remaining 80 % is therefore not erodible and would remain *in situ*. (3) The erosion hypothesis does not account for isolated ridges or ridges that are not parallel the fall line of the slope. (4) The volume of the space between all ridges in the set is conservatively estimated to be five million cubic meters. There is no evidence of any of this material down valley. The obvious site of deposition would be the MBV located just below the bedrock outlet of Lower Symes Pond. During the time of continental ice recession in this area, the MBV was an isolated arm of proglacial Lake Hitchcock. According to glacial rebound studies of the CT River valley by Koteff et al. (1993), Lake Hitchcock's surface elevation at this latitude was 246 meters (808 feet), the same elevation as today's Lower Symes Pond. Below the junction of HSV and MBV, the MBV is approximate one-half kilometer wide by four kilometers long above where Manchester Brook discharges into the CT River near E. Ryegate, VT. Except for trivial amounts of Holocene floodplain sediments, no fluvial, glaciofluvial, or lacustrine sediments occur in the MBV.

The field work in the three study areas provided sufficient evidence to develop a classification system (table 1) to identify the probable origin of till ridges as either depositional or erosional. The system uses five physical parameters: swale/gully morphology, swale/gully soils, ridge morphology, drainage pattern and hydrology, and fate of the eroded materials. No doubt other factors could serve as identifying parameters, but these five are adequate for field identification.

Table 1 Field classification criteria for determining origin of till ridge sets in VT.

PARAMETER	ORIGIN BY EROSION (Gullying and Mass Wasting)	ORIGIN BY DEPOSITION (Moraine/Ice-Marginal)
Swale/Gully Morphology	1. Cross-sections of gullies are steeply V-notched or trapezoidal. 2. Mass wasting occurs on steep gully sides and is initiated primarily by stream impingement at base of slope. 3. Gully bottom deposits consist of alluvium and reworked mass wasting debris. 4. Gullies always contain ephemeral or intermittent stream channels, some of which may have small flood-plains developed in alluvium. 5. Main stem gully may be branched with headcutting tributaries.	1. Swales may have small, ephemeral or intermittent stream channels till. 2. There is little to no fluvial sediment in swales. 3. In dry weather, intermittent streams are gaining due to connate water seepage from toes of adjacent ridges. 4. Cross-sections of swales are broad, and are concave upwards.
Swale/Gully Soils	1. Gully bottoms are covered by sorted alluvium as well as mass wasting debris released from sidewalls.	1. Alluvium is trivial to non-existent. 2. Swale bottom material is dense, slowly permeable till commonly covered with organic-rich, wet, silty muck.
Ridge Morphology	1. All interfluves and interfluvial areas are sub-parallel with ground slope. 2. Ridge tops and interfluvial surfaces reflect original slope of till sheet. 3. Margins along axis of interfluvial ridge tops are irregular due to headcutting tributaries of master gullies.	1. Orientation of ridges is not necessarily parallel to hill slope. 2. Ridges may occur in regularly spaced sets, or in-line clustered mounds. 3. Ridges may occur isolated from others. 4. Axes may be linear, curvilinear, or align with ridges on opposite side of valley. 5. Ridge sides rarely cut by gullies.
Drainage Area and Hydrology	1. Gullies expand by headcut advance-ment and tend to form consequent, dendritic drainage patterns over time. 2. As gully drainage area increases, the gully network produces greater discharges for similar runoff events. Greater discharges and flow depths directly increase hydraulic energy that can erode and transport larger particles. 3. Slumped boulders and detritus perturb stream flows and may initiate gully sidewall instability by changing meander patterns, developing micro-stream piracy, or forming new headcuts.	1. There is no headcutting at upper end of swales, thus swale drainage areas remain constant. 2. Drainage areas of swales are too small to provide adequate hydrodynamic energy to erode most constituents of till materials in swales. 3. Boulders in swale bottoms are *in-situ*, and may occur on top of or partially embedded in ground.
Fate of Eroded Materials	1. Gully-eroded sediments form alluvial fans at outlet of gully or discharge into the lower, major trunk stream. 2. High energy flows of major trunk valley stream may erode alluvial fans.	1. Fluvial erosion in swales or on ridges is minimal to non-existent. 2. There are no sediment deposits down-valley to account for the large volume of materials required for voiding by erosion between ridges.

CONCLUSIONS

The author conducted on-ground reconnaissance surveys of surficial deposits in Northeastern VT between 2008 and 2014 and encountered several till ridge sets along some valley slopes. The question arose as to the origin of these ridges. One 90-ridge set (Study Area 001) was evaluated to address two diametrically opposed hypotheses for ridge origin. One hypothesis contends the ridges in a given set are interfluves formed by erosion, specifically by Holocene gullying and associated mass wasting processes that dissect a hillside till sheet. The other hypothesis argues they are moraine ridges or ice-marginal deposits formed by periodic deposition of detritus released near the receding margin of the Laurentide ice sheet in New England. Two ridge sets in ME (Study Areas 002 and 003) were selected as control sites because they are clearly interfluvial ridges formed by erosion. Diagnostic field evidence gleaned from these two sites was contrasted with the VT set's physical characteristics.

The body of field evidence demonstrably supports the hypothesis that the VT till ridge set was formed as recessional moraines deposited by active, receding ice in the HSV during waning phases of the Laurentide ice sheet in this part New England. The following facts support this conclusion. (1) All swale drainage areas in Study Area 001 are far too small to generate streams with sufficient hydraulic energy to entrain and transport sediment larger than medium-sized gravel (approximately 10 to 40 millimeters). Given that up to 80 % of the local till consists of material greater than coarse gravel size, it is impossible for hydraulic erosion to create the inter-ridge voids. (2) There are no lag deposits or alluvial sediments in the swale bottoms to indicate that erosion processes have occurred. (3) If streams were competent to erode and transport all available grain sizes and in the volumes represented by inter-ridge voids, the question arises as to the fate of this material. The most logical sediment trap would have been the MBV just below the HSV, yet there is no appreciable sediment to be found. In fact, thorough field checking between the HSV and the CT River valley did not reveal any meaningful volumes of alluvial fan, stream alluvium, or lacustrine deposits (associated with proglacial Lake Hitchcock) to account for the material. (4) Cross sections of swales and ridges are gently rounded, concave and convex, respectively. These configurations are not consistent with small-scale valley development formed by stream erosion and concomitant mass wasting (Bloom, 1969). (5) In obvious contrast, cross-sections of gullies and interfluves in Study Areas 002 and 003 are more sharply defined than swales in Study Area 001. Gullies are V-notched where narrow, and trapezoidal in the downstream, wider reaches. Drainage patterns are sub-dendritic formed by consequent gullies that advanced by headcutting into a till sheet. (6) In Study Areas 002 and 003, the occurrence of gully bottom alluvium and evidence of mass wasting on gully sidewalls obviously indicate the interfluvial ridges formed by classic gully erosion.

Observations at the three study areas led to the development of a classification system to differentiate the two modes of till ridge origin. The classification uses five physical parameters: swale/gully morphology, swale/gully soils, ridge morphology, drainage pattern and hydrology, and fate of the eroded materials. Each parameter is identified by criteria to support each mode of origin. The field classification system will readily assist the field worker in determining the origin of till ridges by either erosional or depositional processes. When higher resolution imagery, such as Lidar, becomes more widely available, more glacial features undoubtedly will be discovered that cannot be discerned on USGS topographic quadrangle maps. Because the origin of newly discovered features should be ground-truthed, it is hoped the classification will serve to improve reconstruction of late glacial history and post-glacial geomorphic events in northeastern VT and in other similar regions.

ACKNOWLEDGMENTS

I thank David G. Johnson for his interest, time, and stimulating discussions, and for providing numerous constructive and thorough peer reviews of the manuscript. David accompanied me in the field on many occasions and offered a wealth of valuable ideas and useful critique throughout this study. I appreciate Jeffrey Noyes for his helpful discussions and ideas. I thank my wife Christine Moore for her critical editorial review of the manuscript. I thank Claudia Hoeft for providing substantive, editorial and technical review of the final manuscript.

REFERENCES

ASTM Standard D2488. (2009). Standard practice for description and identification of soils (Visual-Manual Procedure). ASTM International, West Conshohocken, PA 19428.

Bennett, M.R., and Glasser, N.F. (2009). Glacial Geology: Ice Sheets and Landforms. Second edition, Wiley-Blackwell, 385 p.

Bloom, A.L. (1969). The Surface of the Earth. Foundations of Earth Science Series. Prentice-Hall, 152 p.

Doll, C.G. (compiler and editor). (1970). Surficial geologic map of VT, scale 1:250,000, Geology by D.P. Stewart, and MacClintock, P.. VT Geol. Surv., Waterbury, VT 05671-2420.

Gourley, S.H. (2007). Soil Survey of Caledonia County, VT. NRCS, USDA, Burlington, VT 05401.

Hall, L.M. (1959). Geology of St. Johnsbury Quad, (15-min.), VT and NH. VT Geol. Surv. Bull. 13, 105 p.

Hart, R., and Boulton, G.S. (1991). Interrelationship between glaciotectonic deformation and glaciodeposition. Quaternary Science Reviews, vol. 10, pp. 335-350.

Hart, R., and Rose, J. (2001). Approaches to the study of glacial bed deformation. Quat. Intl., vol. 86, pp. 45-58.

Hättestrand, C., and Kleman, J. (1999). Ribbed moraine formation. Quat. Sci. Rev., vol. 18, pp. 43-61.

Homer, J.W. (1999). Soil Survey of Grafton Co. Area, NH. NRCS, USDA, in cooperation with UNH, Agricultural Experiment Station.

Jackson, J.A. (editor) (1997). Glossary of Geology, Fourth edition. American Geological Institute, Alexandria, VA 22302.

Koteff, C., and Pessl, F. (1981). Systematic ice retreat in New England. USGS Prof. Paper 1179, 20 p.

Koteff, C., Robinson, G.R., Goldsmith, R., and Thompson, W.B. (1993). Delayed postglacial uplift and synglacial sea levels in coastal central New England. Quaternary Research, vol. 40, p. 46-54.

Konig, R.H. (1961). Geology of the Plainfield 15-min. Quad (15-min.), VT. VT Geol. Surv. Bull. 16, 86 p.

Lundqvist, J. (1969). Problems of the so-called Rogen moraine. Sverges Geologiska Undersökning C, 648, 32 p.

Moore, J.S. (1974). Origin and geolimnology of Joes Pond, VT. Unpublished MS thesis, Dept. Geol., UVM, 80 p.

Moore. (2001a, revised). Field procedures guide for the headcut erodibility index. NEH-628-52, NRCS, USDA, Washington, DC 20013, 31 p.

Moore. (2001b). Rock material field classification system. NEH-12-631, Geology. NRCS, USDA, Washington, D.C. 20013, 12 p.

Soil Survey Staff. (1999). Soil taxonomy: A basic system of soil classification for making and interpreting soil surveys. Second ed. Natural Resources Conservation Service. U.S. Department of Agriculture Handbook 436.

Stewart, D.P. and MacClintock, P. (1969). Surficial geology and Pleistocene history of VT. VT Geol. Surv. Bull. 31, 251 p.

Stewart, R.A., Bryant, D., and Sweat, M.J. (1988). Nature and origin of corrugated ground moraine of the Des Moines lobe, Story County, IA. Geomorphology, vol. 1, issue 2, pp. 111-130.

Thompson W.B. (1999). History of research on glaciation in the White Mountains, NH. Geographie Physique et Quaternaire, vol. 53 (1), pp. 7-24.

White, W.S., and Billings, M.P. (1951). Geology of Woodsville Quad (15-min.), VT – NH. Bull. Geol. Soc. Am., vol. 62, pp. 647-696.

ESTIMATING CONCENTRATIONS OF FINE-GRAINED AND TOTAL SUSPENDED SEDIMENT FROM CLOSE-RANGE REMOTE SENSING IMAGERY

Adam R. Mosbrucker, Kurt R. Spicer, Tami S. Christianson, and Mark A. Uhrich,
U.S. Geological Survey, Cascades Volcano Observatory, Vancouver, Wash., amosbrucker@usgs.gov

INTRODUCTION

Fluvial sediment, a vital surface water resource, is hazardous in excess. Suspended sediment, the most prevalent source of impairment of river systems, can adversely affect flood control, navigation, fisheries and aquatic ecosystems, recreation, and water supply (e.g., Rasmussen et al., 2009; Qu, 2014). Monitoring programs typically focus on suspended-sediment concentration (SSC) and discharge (SSQ). These time-series data are used to study changes to basin hydrology, geomorphology, and ecology caused by disturbances. The U.S. Geological Survey (USGS) has traditionally used physical sediment sample-based methods (Edwards and Glysson, 1999; Nolan et al., 2005; Gray et al., 2008) to compute SSC and SSQ from continuous streamflow data using a sediment transport-curve (e.g., Walling, 1977) or hydrologic interpretation (Porterfield, 1972). Accuracy of these data is typically constrained by the resources required to collect and analyze intermittent physical samples.

Quantifying SSC using continuous instream turbidity is rapidly becoming common practice among sediment monitoring programs. Estimations of SSC and SSQ are modeled from linear regression analysis of concurrent turbidity and physical samples. Sediment-surrogate technologies such as turbidity promise near real-time information, increased accuracy, and reduced cost compared to traditional physical sample-based methods (Walling, 1977; Uhrich and Bragg, 2003; Gray and Gartner, 2009; Rasmussen et al., 2009; Landers et al., 2012; Landers and Sturm, 2013; Uhrich et al., 2014). Statistical comparisons among SSQ computation methods show that turbidity-SSC regression models can have much less uncertainty than streamflow-based sediment transport-curves or hydrologic interpretation (Walling, 1977; Lewis, 1996; Glysson et al., 2001; Lee et al., 2008). However, computation of SSC and SSQ records from continuous instream turbidity data is not without challenges; some of these include environmental fouling, calibration, and data range among sensors. Of greatest interest to many programs is a hysteresis in the relationship between turbidity and SSC, attributed to temporal variation of particle size distribution (Landers and Sturm, 2013; Uhrich et al., 2014). This phenomenon causes increased uncertainty in regression-estimated values of SSC, due to changes in nephelometric reflectance off the varying grain sizes in suspension (Uhrich et al., 2014).

Here, we assess the feasibility and application of close-range remote sensing to quantify SSC and particle size distribution of a disturbed, and highly-turbid, river system. We use a consumer-grade digital camera to acquire imagery of the river surface and a depth-integrating sampler to collect concurrent suspended-sediment samples. We then develop two empirical linear regression models to relate image spectral information to concentrations of fine sediment (clay to silt) and total suspended sediment. Before presenting our regression model development, we briefly summarize each data-acquisition method.

RIVER REMOTE SENSING

Remote sensing is a rapidly growing subdiscipline in river science due to its ability to answer complex spatial and temporal questions; cost-effective data acquisition, processing and analysis; and the increasing adoption of geospatial technology by hydrologists (Marcus and Fonstad, 2010). River remote sensing has become a broad field. Active (e.g., lidar) and passive optical (e.g., photogrammetry) remote sensing provide precise topographic measurements to assess geomorphic characteristics and sediment transport of river environments. Spectral analyses of reflected electromagnetic (EM) radiation recorded by satellite-based optical sensors have been successfully used to estimate turbidity and SSC of large rivers over a broad range of time-scales and from low to medium concentrations (e.g., Curran and Novo, 1988; Mertes et al., 1993; Islam et al., 2001; Wang et al., 2009; Wang and Lu, 2010; Wang et al., 2010; Qu, 2014).

SATELLITE SENSORS

Satellite imagery provides retrospective and spatial information about a river system. Spectral analyses of satellite imagery are based on the measurement of reflected EM solar radiation. Material properties produce unique signatures, or curves, depending on reflection and absorption of different wavelengths (λ); sensors commonly record data in the

visible to short-wave-infrared spectra. Multispectral data are recorded as pixel unit values within a multilayer array, or raster image file. Each layer, or band, is sensitive to a unique wavelength range, commonly rendered as red, green, and blue (RGB), though imagery may contain dozens of bands.

In satellite remote sensing, pixel values, generally referred to as digital numbers (DNs), are calibrated into physically meaningful units of radiance (i.e., watts per unit area). Surface reflectance spectra, derived from atmospheric correction of radiance imagery, are then used to quantify features within an image. Maximum reflectance sensitivity of clear water is near the blue end of the spectrum (λ<500 nm), reflectance decreases as wavelength increases. Turbid water, with greater SSC, has increased sensitivity toward the red end of the spectrum (λ>600 nm), accounting for its brownish appearance.

The relationship between reflectance and SSC is affected by suspended material composition, water depth, SSC variation over depth, and view geometry (Qu, 2014). Empirically-developed models relating spectra to SSC in riverine and laboratory environments use linear, second-order polynomial, and logarithmic equations (Table 1). While most utilize the near-infrared (NIR) spectrum (λ>700 nm), of interest to our study is Islam et al. (2001) who used the blue spectrum of MODIS satellite imagery (Band 3, λ=459–479 nm) to estimate SSC in the Ganges and Brahmaputra Rivers (about 400–1,800 mg/L) (Table 1). Peak response of our consumer-grade sensor is 470 nm.

Table 1 Selected empirical models predicting river suspended-sediment concentration (SSC) from satellite imagery and laboratory measurements. The values of the surface reflectance of the water at the given wavelengths (r_i) are explanatory variables in these equations (*ith* band of a given sensor). Table modified from Qu (2014).

Sensor Platform	Wavelength λ (nm)	Spatial Resolution (m)	Location	Model	R^2	Samples (n)	Reference
MODIS satellite	841-876, 1230-1250	250-500	Yangtze River (China)	$SSC = -23.03 + 60.25(r_2 - r_5) - 23.03$	0.73	153	Wang et al., 2010
		250-500	Yangtze River (China)	$ln(SSC) = 4.117 + 0.262(r_2 - r_5)$	0.78	35	Wang and Lu, 2010
Landsat satellite	760-900	30	Yangtze River (China)	$ln(SSC) = -1.40060 + 3.18263 ln(r_4)$	0.88	24	Wang et al., 2009
MODIS satellite	459-479	500	Ganges and Brahmaputra Rivers (Bangladesh)	$SSC = -201 + 69.39 r_3$	0.98	10	Islam et al., 2001
Laboratory spectrometer	852	--	Lab, silt	$SSC = -23.367 + 116.869 r_{852} + 24.04 r^2_{852}$	0.99	10	Lodhi et al., 1997
	852	--	Lab, clay	$SSC = -23.367 + 116.869 r_{852} + 24.04 r^2_{852}$	0.96	10	Lodhi et al., 1997
	555, 754	--	Lab, clay (organic)	$SSC = -0.31 + 12.32(r_{555}/r_{754})$	0.92	7	Gin et al., 2003

CONSUMER-GRADE DIGITAL CAMERA SENSORS

We expand upon previous laboratory and satellite image analyses by evaluating the feasibility of using imagery acquired with a consumer-grade digital camera at a distance <10 m above a river surface to estimate SSC. Compared to satellite-based platforms, close-range remote sensing can measure smaller streams at similar wavelengths with as much as 1,000 times greater spatial resolution, and algorithms for spectral mixing and atmospheric correction are not needed (Mertes et al., 1993; Qu, 2014). The primary differences between industrial- and consumer-grade sensors are the characteristics of individual bands (Table 2). Whereas each band of satellite imagery is sensitive to radiation within a narrow and discrete bandwidth (e.g., 20–80 nm), consumer-grade sensors have a broadband response (e.g., 200–300 nm) with significant overlap among only three bands (Table 2).

Consumer-grade sensors are sensitive to wavelengths between 200 and 1,300 nm. However, manufacturers use ultraviolet (UV) and NIR interference filters to restrict recorded EM radiation to the visible spectrum (400–700 nm) in order to more precisely focus light rays onto a single plane (Figure 1). These filters, located in front of the sensor, can be removed to restore the full spectral range of the native sensor. Apparent brightness and color measurements are typically recorded in 8-bit integer (i.e., values 0–255) Joint Photographic Experts Group (JPEG) file format, which have a defined color space, or coordinate system (e.g., sRGB, Adobe RGB, ProPhoto RGB). File format type, bit depth, and color space determine the degree of signal processing, precision, and range of data.

Table 2 Spectral response characteristics for selected satellite and consumer-grade sensors (band λ in nm). Lighter grey area is native (unfiltered) response of a Nikon D800E sensor. Where known, peak response is given in white font. A Forest Technology Systems (FTS) DTS-12 turbidity sensor (emitted λ) is included for reference purposes.

Platform	Sensor	Band No.	Range (λ, nm)	Bandwidth (λ, nm)	UV Light 300	Visible Light 400 500 600	NIR Light 700 800 900 1000 1100 1200
Terrestrial	D800E	1	380-620	240		470	
		2	380-620	240		540	
		3	380-680	300		590	
Satellite	Landsat TM[1]	1	450-520	70		510	
		2	520-600	80		590	
		3	630-690	60		650	
		4	760-900	140			880
Satellite	MODIS[2]	1	620-670	50		650	
		2	841-876	35			880
		3	459-479	20		470	
		4	545-565	20		550	
		5	1230-125	20			1250
In situ	DTS-12	1	780-900	120			880

[1]The Landsat TM sensor has three additional middle- to thermal-infrared bands (band 5–7, λ=1,550–12,500 nm). [2] The MODIS sensor has 31 additional bands (λ=450–14,385 nm). Abbreviations: ultraviolet (UV); near infrared (NIR).

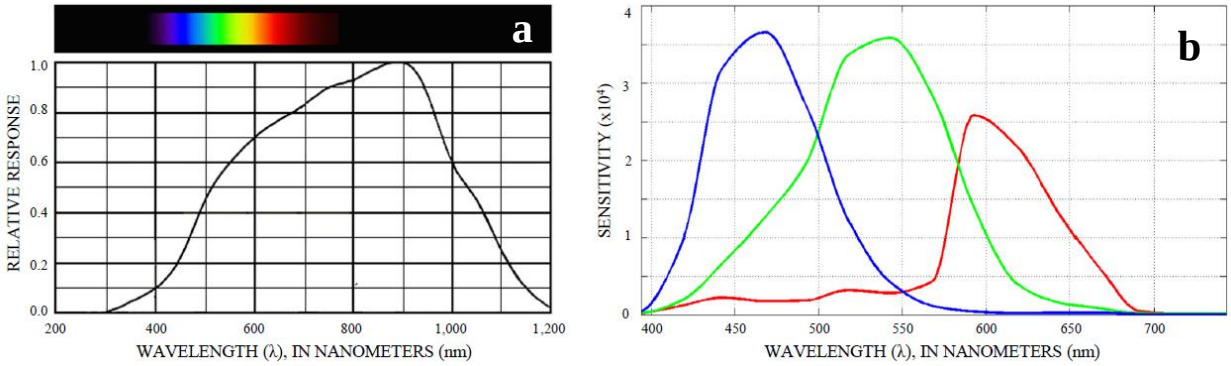

Figure 1 Spectral response curves of (a) native and (b) filtered sensor used in a Nikon D800E digital single-lens reflex (DSLR) camera. Response curves for sensors used in consumer-grade digital cameras from other manufacturers are similar. Figure modified from Profilocolore Sri (2013).

STUDY AREA

The May 18, 1980, eruption of Mount St. Helens consisted of a 2.5 km^3 debris avalanche followed by a blast density current, pyroclastic flows, lahars, and tephra falls (e.g., Lipman and Mullineaux, 1981). These disturbances severely altered the hydrogeomorphic regime of the upper North Fork Toutle River, whose 450 km^2 basin includes the north flank of the volcano. Our investigation was conducted at an existing USGS surface water discharge and suspended-sediment monitoring station, 13 river km downstream of the toe of the debris avalanche deposit (primary sediment source), and 2 river km below a sediment retention structure near Kid Valley, Washington (14240525). More than three decades after the eruption, the river continues to transport an average of 3 million tonnes (or megagrams, Mg) of suspended sediment per year; daily average SSC is 31–79,800 mg/L (water years 2007–2013). A significant portion of the annual SSQ is transported during infrequent high-streamflow events. Suspended particle sizes range from clay to sand; material is commonly 50–80% fines (i.e., <63 µm). Fines are well distributed in cross section and vertical profile. Bed material is dominantly sand. Annual mean water discharge at the station is 22.3 m^3/s (water years 1990–2013).

DATA COLLECTION AND ANALYSIS METHODS

To evaluate the feasibility of estimating suspended-sediment characteristics from close-range multispectral imagery, we developed a simple, reproducible, and effective methodology for image acquisition, sample collection, and analysis. Concurrent pairs of suspended-sediment samples and imagery were acquired during routine site visits between January and June, 2014. Data were collected over a range of hydrologic conditions and turbidity, with an emphasis on capturing high-flow events. In total, 716 photographs and 100 samples were acquired during this 6-month period. A calibration data pair consists of a series of normalized imagery and associated suspended-sediment samples.

SUSPENDED-SEDIMENT SAMPLES

Standard USGS field and laboratory methods were used for suspended-sediment sample collection and analyses (Guy, 1969; Edwards and Glysson, 1999). Suspended-sediment samples were collected using a D-74 depth-integrating sampler with a 0.48-cm-diameter brass nozzle (Edwards and Glysson, 1999; Davis et al., 2005) deployed from a bank-operated cableway. Primary samples used in the calibration dataset were collected at a single station within the camera's field of view. Secondary cross-section samples were collected using an equal discharge increment (EDI) method for future relation of results to cross-sectional mean concentrations. We collected full-depth and near-surface samples (i.e., 7 cm below the river surface), usually in two sets to assess variability (Topping et al., 2011).

Sediment analyses were performed at the USGS Cascades Volcano Observatory in Vancouver, Washington. SSC data were computed using the dry weight of all sediment from a sampled volume. Particle diameter was measured with a sieve and sedigraph. Primary samples (n=39) have wide variation in SSC (262–7339 mg/L) and particle size distribution (28–94% <63 µm; 10–33% <4 µm; 4–24% <2 µm). Root-mean-square error (RMSE) of lab results is about 4% (USGS, 2014), but sample data show a moderate to high degree of spatial and temporal variability. SSC for full-depth samples is typically <10% greater than near-surface samples and occasionally as much as 40% (due to sand in suspension near the streambed). Samples taken within a few minutes of each other in the same location have SSC values that differ by ≤25%. Particle size data show 9–30% less sand near the river surface.

CLOSE-RANGE MULTISPECTAL IMAGERY

CAMERA SYSTEM

One of the first tasks of our study was to select a camera system and develop a consistent procedure for data acquisition and analysis. We used the same camera system and configuration throughout the study. Camera sensor and lens (i.e., camera system) selection focused on optimizing spatial and spectral resolution, ability to calibrate white balance, automate exposure compensation, produce RAW image files (which have 64–256 times more brightness levels than a standard 8-bit JPEG files), select color space, and use a configuration file. Spatial resolution is a function of the sensor and the lens. Higher resolution sensors, commonly measured in megapixels (MP), combined with fixed focal length lenses (generally 35–85 mm) produce the greatest resolution; optical aberrations of lenses can have a significant impact on resolution.

Although data are widely available for spatial resolution and other image-quality parameters of consumer-grade digital camera systems, the spectral response of a specific sensor is difficult to obtain. DxO Labs, an imaging solution and standardization company, publishes image quality lab test results of digital image capture devices through their website (*http://dxomark.com*). DxOMark quantifies image quality using three resolution-normalized metrics: dynamic range, color sensitivity, and noise levels. For our purposes, we sought to maximize dynamic range and color sensitivity (or color bit-depth), while minimizing noise in an affordable off-the-shelf consumer-grade camera.

On the basis of these criteria, we chose a Nikon D800E digital single-lens reflex camera (DSLR) with a 70–300 mm focal length lens to provide flexibility. According to DxOMark lab results, this system has similar image quality to others costing as much as 10 times more. The camera uses a 864 mm^2 Sony IMX094AQP CMOS image sensor, which has 36.56 MP (4.8 µm each), a 14-bit non-linear analogue-to-digital converter (for 14.3 exposure values (EV) of dynamic range), 25.6 bits of color depth, and an ISO of 2979. The broadband sensor has a native spectral response range of 300–1250 nm, reduced to about 380–680 nm after passing through UV-NIR interference filters (Figure 1). The system allows JPEG files to be spectrally normalized through custom white balance calibration.

IMAGE ACQUISITION AND ANALYSIS

Immediately before, during, or after collecting suspended-sediment samples, we acquired multispectral imagery of the water surface at a camera station collocated at the sampling site. The camera was mounted to a handrail <5 m above the water surface at a 45° angle to maximize water surface penetration (Figure 2). The rail was marked to facilitate precise relocation of the mount. The same 70 mm focal length was used for all imagery; field of view was 28.8° horizontal and 19.5° vertical, imaging an ~8.9 m^2 frame, depending on river stage. This represents a nominal water surface sampling distance of 0.5 mm per pixel (i.e., medium- to course-sand) at the center of the field of view, which was set to the sample location, 1.5–2.1 m from the left bank (Figure 2).

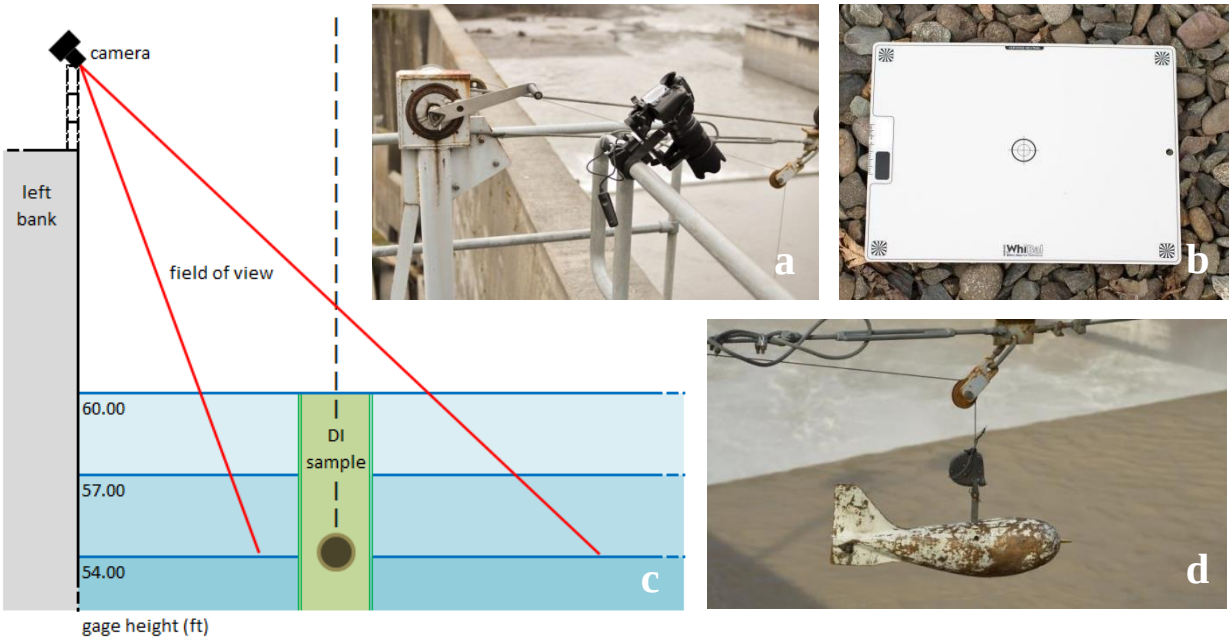

Figure 2 Field data collection panel showing (a) the camera system mounted on handrail near bank-operated cableway, (b) white balance calibration card, (c) relationship of camera field of view to suspended-sediment sample location, and (d) D-74 depth-integrated sampler deployed from the cableway. Views are downstream from left bank.

Initial methodology focused on maximizing the information capacity of each dataset, because we did not know what would prove to be most useful. Datasets consisted of three sequences of nine exposure-bracketed images (0.3–1.0 EV intervals) at a high frame rate (Figure 3). Each sequence used a different glass lens filter (clear, ultraviolet, polarized) to modify the water surface reflectance prior to sensor detection. To account for changing ambient lighting conditions, each sequence was normalized by a calibrated white balance target (Figure 2b). Camera settings optimized image quality at the expense of file size and shutter speed; a configuration file was used to ensure consistent in-camera processing settings. Consistent image acquisition proved challenging in some conditions, such as rapidly changing ambient light or presence of woody debris (drift) within the field of view. These were mitigated by acquiring additional bracketing sequences at wider EV intervals to prevent limited dynamic range from clipping the sensor output values. Sand boils on the river surface, which cause irregular dark patches, were common and could not be avoided.

A total of 15 datasets were collected during our initial investigation (Table 3). The limited scope of this study prevented comprehensive image analysis; we explored only a few spectral indices, file format conversions, and signal processing filters (e.g., low-pass). We sought to evaluate the use of a standard-precision file format (8-bit JPEG), medium-resolution color space (Adobe RGB), normal EV, and test the sensitivity among lens filters.

Each image file is comprised of three spectral bands within the visible spectrum; RGB (Red, 380–680 nm; Green, 380–680 nm; Blue, 380–620 nm). Due to the broadband response of the sensor, we focused our analysis on the peak of the response curve for each band (Red, 590 nm; Green, 540 nm; Blue, 470 nm). Descriptive statistic were computed

from uncalibrated, but spectrally normalized, DNs (pixel values) for each band as well as the average of all three bands; statistics included minimum, maximum, mean, standard deviation (1-sigma), and covariance.

Figure 3 Typical 10-frame dataset showing white balance reference card (WB) and -4 to +4 exposure value (EV) bracketing sequence. This example was acquired during diffuse (overcast) ambient lighting conditions.

CALIBRATION DATASET

A calibration dataset compiled image statistics and sample lab results. Imagery and suspended-sediment samples were paired by time of acquisition; time differences between images and physical samples were limited to ≤30 minutes for all pairs. Mean time difference for the dataset is 11 minutes. Samples were then grouped by near-surface, full-depth, and combined sample depths. All samples were analyzed for SSC and a subset for particle size distribution. We selected three representative size classes (<63 µm, <4 µm, and <2 µm) and computed mass concentrations from total SSC.

Table 3 Calibration dataset summary table. Sample total suspended-sediment concentration (SSC) is given as well as concentration of material finer than 63 µm (SSC_{fines}). Six SSC samples were excluded due to significantly different times (i.e., >30 minutes) between image acquisition and sample collection.

Date	Dataset	Imagery		Suspended Sediment Samples			Turbidity		Streamflow (m^3/s)
		(n)	EV[1]	(n)	SSC (mg/L)	SSC_{fines} (mg/L)	Trend[2]	FNU[3]	
1/6/2014	1	27	8.0	3	368	220	Fall	73	16.4
	2	27	8.0	1	262	192	Fall	62	16.8
1/11/2014	3	54	8.0	3	4664	2955	Rise	890	69.1
	4	54	8.0	2	5424	3713	Rise	1840	73.6
	5	27	2.6	2	6535	4905	Peak	3380*	72.8
2/12/2014	6	54	8.0	2	2325	1415	Peak	870	53.8
	7	74	8.0	1	1989	1357	Fall	820	53.8
	8	99	8.0	4	1668	942	Fall	570	51.0
3/6/2014	9	54	2.6	4	6765	3520	Trough	3840*	91.2
	10	36	2.6	2	6885	6183	Rise	4170*	92.3
	11	54	2.6	4	6661	6027	Fall	4160*	97.7
3/7/2014	12	54	5.4	4	5154	4409	Fall	2520	78.4
4/22/2014	13	27	5.4	3	929	338	Trough	66	33.1
	14	18	5.4	1	1182	329	Rise	78	32.0
6/6/2014	15	57	5.4	3	367	256	Fall	140	13.5

[1]Exposure value (EV) is the range of illuminance, as referenced to the camera exposure meter. For instance, a dataset with an exposure-bracketed sequence of -4 to +4 EV has a range of 8 EV. [2]Trend of turbidity is based on 15-minute unit values whereas sample collection took <5 minutes. [3]Turbidity is recorded using a Forest Technology Systems DTS-12 sensor in Formazin Nephelometric Units (FNU) (Anderson, 2005). Values exceeding the sensor maximum (1,850 FNU, denoted by an * in the table) are recorded from a Hach Solitax sensor in Formazin Backscatter Ratio Units (FBRU).

EMPIRICAL REGRESSION MODELS

Relationships between imagery, suspended-sediment concentration, and particle size were investigated using ordinary least squares regression. We used simple linear regression (SLR) to describe the covariability of these variables and evaluate the ability to predict suspended-sediment information from spectral measurements of a river surface. Statistical methods described in Helsel and Hirsch (2002) were used to develop and evaluate our models.

We began investigating the relationship between possible explanatory (x) and response (y) variables by generating a correlation matrix for our entire calibration dataset. From these results, we modeled the most highly correlated variables to evaluate the quality of fit and significance of the relationship. More specifically, we checked for non-linearity, heteroscedasticity (i.e., non-constant variability of residuals), and the coefficient of determination (R^2). Full-depth and near-surface samples were evaluated both individually and combined. From these exploratory data analyses, we found the explanatory variable B_{max} (maximum DN, or pixel value, of the blue band) using a clear lens filter to be most related to *SSC* and particle size response variables. Concentration of material smaller than sand (<63 µm, SSC_{fines}) was of greatest interest; other particle size classes were weakly correlated. We developed two SLR models: one for total *SSC* and another for SSC_{fines} response variables based on the B_{max} explanatory variable using combined full-depth and near-surface samples. Both models benefited from base-10 logarithmic transformation to achieve linearity, homoscedasticity, and normality of residuals (Helsel and Hirsch, 2002). Base-10 transformation, or equivalent power function regression, is common among turbidity-*SSC* regression and streamflow-*SSC* transport curves (e.g., Glysson, 1987; Curtis et al., 2006; Rasmussen et al., 2009; Uhrich et al., 2014).

CORRELATION OF IMAGERY TO SUSPENDED-SEDIMENT CONCENTRATION

Our final SLR model predicting *SSC* from B_{max} DN shows a statistically significant relationship between the two variables (t-statistic and p-value at 95% confidence interval; Figure 4 and Table 4). The model explains 90% of the variability in sampled SSC (R^2; Table 4). Probability plot correlation coefficient (PPCC, R^2=0.87) indicates that residuals have a homoscedastic pattern and near-normal distribution (Helsel and Hirsch, 2002; Rasmussen et al., 2009). The $\log_{10}$-transformed model is:

$$\log_{10}(SSC) = 12.707 - 4.225\log_{10}(B_{max}), \quad (1)$$

where

SSC is suspended-sediment concentration (mg/L), and
B_{max} is the maximum uncalibrated pixel value, in DN (8-bit, $0<x<255$).

The $\log_{10}$-transformated SLR model (equation 1) can be retransformed and corrected for associated bias, resulting in:

$$SSC = (5.0933 \times 10^{12})(B_{max}^{-4.225}) \times BCF, \quad (2)$$

where

BCF is a nonparametric bias correction factor.

It should be noted that Duan's smearing bias correction factor (*BCF*) (Duan, 1983) is a best estimate of the bias introduced by retransforming regression estimates to the original units (e.g., *SSC* in mg/L), computed using the average of residuals (e.g., Uhrich and Bragg, 2003; Rasmussen et al., 2009; Uhrich et al., 2014). The bias correction factor for equation 2 was determined to be 1.0461, yielding a final SLR model:

$$SSC = (5.3281 \times 10^{12})(B_{max}^{-4.225}). \quad (3)$$

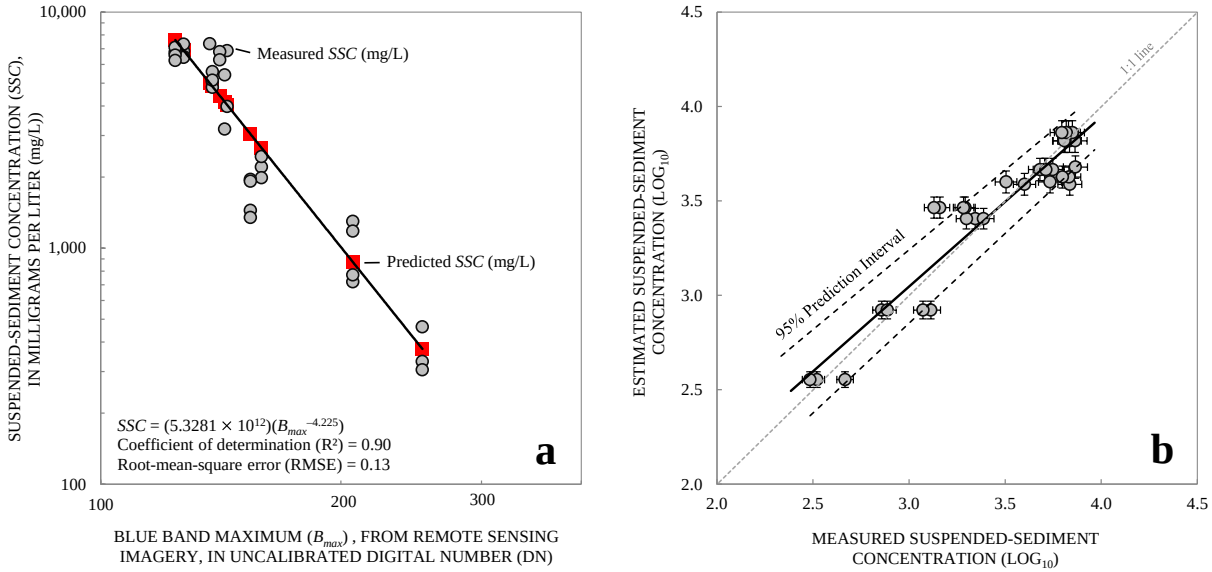

Figure 4 Results of simple linear regression (SLR) analysis using $\log_{10}$-transformed data for (a) spectra and suspended-sediment concentration (SSC) data, and (b) comparison of measured and estimated SSC in log space with 95% prediction interval and 5% error bars on measured concentration. Standard errors of intercept and slope are 0.560 and 0.256 respectively.

Table 4 Regression model summary with statistical diagnostics and analysis of variance (ANOVA). A multivariate regression model for the North Fork Toutle River station is shown for comparison purposes (Uhrich et al., 2014).

Response (y)	Explanatory (x)		Model	Obs. (n)	Conc. (mg/L)	R^2	RMSE	MSPE	Coefficient		
									SE	t-statistic	p-value
SSC	B_{max}		$\log_{10}(SSC) = 12.707 - 4.225\log_{10}(B_{max})$	33	305–7339	0.90	0.133	26.4–35.8	0.256	- 16.53	6.29E-17
SSC_{fines}	B_{max}		$\log_{10}(SSC_{fines}) = 14.484 - 5.111\log_{10}(B_{max})$	33	250–6438	0.90	0.163	31.3–45.6	0.314	- 16.29	9.43E-17
SSC			$\log_t(SSC) = -0.8054 + 0.1854\log_t T +$	653	30–10100	0.81	0.228				
	T	turbidity	$0.3545\log_t Tlag + 0.8952\log_t Q$						0.2882	0.64	0.52
	Q	discharge							0.2897	1.22	0.221
	$Tlag$	lag T value							0.04497	19.91	0.
	t	15-minute interval time									

Abbreviations: Coefficient of determination (R^2); model standard percentage error (MSPE); coefficient standard error (SE).

CORRELATION OF IMAGERY TO CONCENTRATION OF SUSPENDED OF FINES

The final SLR model predicting concentration of fine material in suspension (<63 µm) shows a statistically significant relationship that explains 90% of the concentration variability (R^2; Figure 5 and Table 4). Normality of residuals was significantly improved by logarithmic transformation (PPCC, R^2=0.90). The $\log_{10}$-transformed model is:

$$\log_{10}(SSC_{fines}) = 14.484 - 5.111\log_{10}(B_{max}), \quad (4)$$

where

SSC_{fines} is concentration of fine material (<63 µm) in suspension.

Retransformation of equation 4 with an associated *BCF* of 1.0675 yields a final SLR model in exponential form:

$$SSC_{fines} = (3.2540 \times 10^{14})(B_{max}^{-5.111}). \quad (5)$$

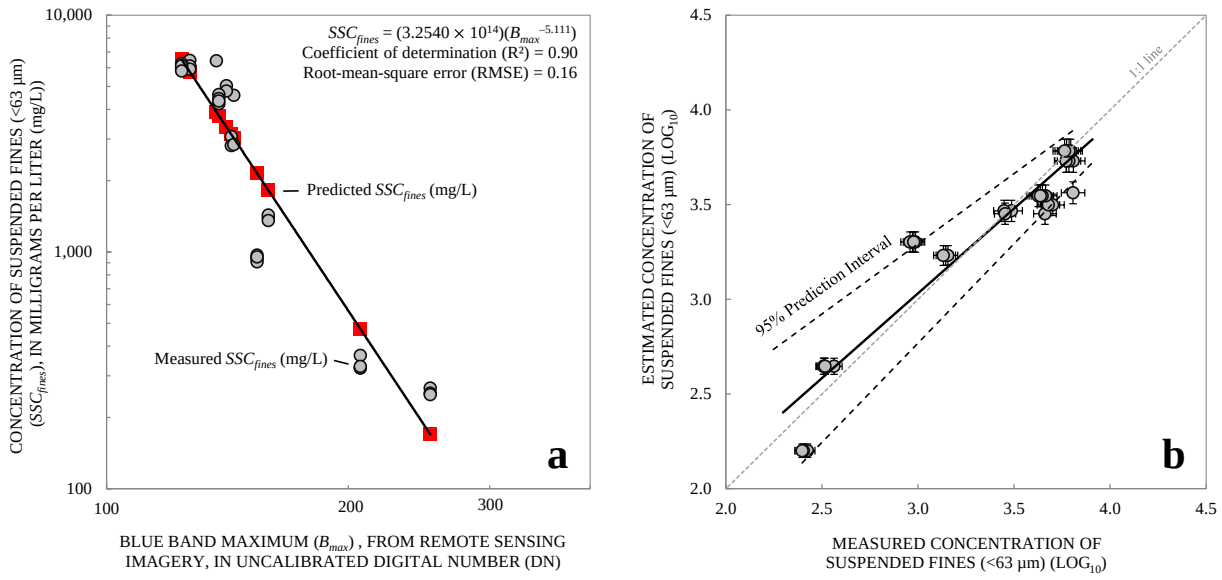

Figure 5 Results of simple linear regression (SLR) analysis using $\log_{10}$-transformed data for (a) spectra and concentration of suspended fines (SSC_{fines}) data, and (b) comparison of measured and estimated SSC_{fines} in log space with 95% prediction interval and 5% error bars on measured concentration. Standard errors of intercept and slope are 0.687 and 0.314 respectively.

DISCUSSION AND FUTURE STUDIES

Our results show that uncalibrated DNs (pixel values) extracted from RGB imagery of a river surface can be used as the explanatory variable in a SLR model to predict *SSC* (R^2=0.90). Modeled SSC values are -126% to 41% different than sampled SSC, with a mean error of -10%. The satellite-based spectral reflectance signature of turbid water is well established, with a positive correlation of the near-infrared (NIR) spectrum (λ>700 nm) to SSC. Because unmodified consumer-grade digital camera sensors are weakly sensitive to red and near-infrared wavelengths, we use the peak response of the UV-blue end of the spectrum (B_{max}, λ=470 nm), which yields a negative correlation (i.e., negative slope of regression line). Our finding makes logical sense; color saturation of a river's opaque brownish appearance increases as SSC in the river increases. In this situation, the response near the red spectra increases while the blue spectra decreases.

Expanding upon this result, we show that the same SLR explanatory variable (B_{max}) can be used to predict SSC_{fines} (R^2=0.90). This is not surprising, given that the response variables *SSC* and SSC_{fines} are strongly correlated (i.e., $SSC_{fines} \propto SSC$) for our data (fines average 3,204 mg/L or 72% of total suspended mass). Modeled SSC_{fines} error is -136% to 39% with a mean of -15%. Like the previous model, the regression line has a negative slope; opacity of water is largely a function of fines concentration. Given that the absorption of EM energy by water is the weakest in the blue spectra (i.e., greatest depth penetration), we expected B_{max} to be better correlated to SSC_{fines} than *SSC*. Our results show the SSC model is slightly better than the SSC_{fines} model.

Both models are less sensitive at concentrations above about 4,000 mg/L, despite the greatest error occurring below 2,000 mg/L. As the response of the blue spectra decreases, large changes to concentrations produce small changes to DN. Qu (2014) suggests that a weaker linear relation with increasing SSC is attributed to absorption by suspended sediments; the river surface appears darker and more opaque at greater concentrations. There may be several solutions to increase model effectiveness at greater concentrations. One possible solution is to use RAW to TIF conversions with greater DN range and precision (e.g., >8-bit JPEG). Another solution may be to acquire imagery in the near-infrared spectrum, accomplished with a NIR glass filter (e.g., interference <720 nm) or permanent removal of the UV-NIR interference filters in front of a DSLR sensor.

These results warrant continued investigation and refinement of our methods. Due to the nature of regression analysis, our empirical models are likely applicable only to waters with similar characteristics such as sediment composition.

Future work will investigate the applicability of our method to other river reaches and basins, as well as to additional camera systems. Deployment of a stationary time-lapse camera is a logical advancement to our initial feasibility study as this would provide time-series information and test the system in an operational environment. These methods may provide opportunities for rapid deployment of remote camera systems at sites not suitable for in situ equipment. If paired with concurrent turbidity data, automated processing of time-lapse imagery could feed a simple piecewise defined function, to select among turbidity-SSC regressions tuned to particle size classes. Such tuning could significantly increase the accuracy of record computation at sites known to experience hysteresis in the relationship between turbidity and SSC.

CONCLUSION

Our 6-month-long study evaluated the feasibility of estimating the concentration of fine sediment (clay to silt) and total suspended sediment using close-range remote sensing imagery of a river surface acquired with an off-the-shelf consumer-grade camera system. Two empirical simple linear regression models were developed from three-band imagery and concurrent physical sample pairs (n=33, 250–7339 mg/L). Results show statistically significant relationships (90% of variability explained) between the maximum pixel value (i.e., uncalibrated digital number) of the blue band (peak response at 470 nm) and suspended-sediment concentration response variables with mean errors of 10–15%.

Standard USGS sample-based methods of generating time-series records of suspended-sediment concentration and discharge can be time- and cost-prohibitive for some studies. Although near real-time application of turbidity-based regression models may overcome these restrictions, temporal variability in suspended particle size (fines in particular) can increase uncertainty due to hysteresis. The non-contact approach we present here can mitigate some of this uncertainty by providing near real-time estimates of fines in suspension. In addition, our method can directly estimate total suspended concentration without subjecting the sensor to environmental fouling, burial, or damage during high-streamflow events.

Integration of multiple geospatial tools is becoming commonplace in river science. Despite the limited scope of this study, our results make a significant contribution in the field of river remote sensing. This method provides a consistent and straightforward procedure to quantify suspended sediment in a river using a consumer-grade digital camera. Upon further investigation and refinement, imagery-based regression models could increase the accuracy of real-time estimates of concentration, which are vital to sediment-program cooperators dependent on these data.

ACKNOWLEDGEMENTS

The USGS Volcano Hazards Program and the Federal Interagency Sediment Project supported this study. We thank Mark Landers and Kate Norton for their insightful manuscript reviews. Use of trade names in this manuscript is for identification purposes only and does not constitute endorsement by the U.S. Geological Survey.

REFERENCES

Anderson, C.W. (2005). "Turbidity (ver. 2.1)," U.S. Geological Survey Techniques of Water-Resources Investigations, book 9, chap. A6, section 6.7, 64 p.

Curran, P.J., and Novo, E.M.M. (1988). "The relationship between suspended sediment concentration and remotely sensed spectral radiance: a review," Journal of Coastal Research, 4(3), pp 351–368.

Curtis, J.A., Flint, L.E., Alpers, C.N., Wright, S.A., and Snyder, N.P. (2006). "Use of sediment rating curves and optical backscatter data to characterize sediment transport in the upper Yuba River watershed, California, 2001–03," U.S. Geological Survey Scientific Investigations Report 2005–5246, 74 p.

Davis, B.E. (2005). "A guide to the proper selection and use of Federally approved sediment and water-quality samplers," U.S. Geological Survey Open-File Report 2005–1087, 20 p.

Duan, N. (1983). "Smearing estimate: A non-parametric retransformation method," Journal of the American Statistical Association, 78(383), pp 605–610.

Edwards, T.K., and Glysson, G.D. (1999). "Field methods for measurement of fluvial sediment," U.S. Geological Survey Techniques of Water-Resources Investigations, book 3, chap. C2, 89 p.

Gin, K.Y.H., Koh, S.T., and Lin I.I. (2003). "Spectral irradiance profiles of suspended marine clay for the estimation of suspended sediment concentration in tropical waters," International Journal of Remote Sensing, 24(16), pp 3,235–3,245.

Glysson, G.D. (1987). "Sediment transport curves," U.S. Geological Survey Open-File Report 87–218, 53 p.

Gray, J.R., Glysson, G.D., and Edwards, T.E. (2008). "Suspended-sediment samplers and sampling methods," in Garcia, Marcelo, ed., Sedimentation engineering – Processes, measurements, modeling, and practice, American Society Civil Engineers Manual 110, chap. 5.3, pp 320–339.

Gray, J.R., and Gartner, J.W. (2009). "Technological advances in suspended-sediment surrogate monitoring," Water Resources Research, 45(4), 20 p.

Guy, H.P. (1969). "Laboratory theory and methods for sediment analysis," U.S. Geological Survey Techniques of Water-Resources Investigations, book 5, chap. C1, 64 p.

Helsel, D.R., and Hirsch, R.M. (2002). "Statistical methods in water resources: hydrologic analysis and interpretation," U.S. Geological Survey Techniques of Water-Resources Investigations, book 4, chap. A3, 510 p.

Islam, M.R., Yamaguchi, Y., and Ogawa, K. (2001). "Suspended sediment in the Ganges and Brahmaputra River in Bangladesh: observation from TM and AVHRR data," Hydrological Processes, 15(3), pp 493–509.

Landers, M.N., Arrigo, J., and Gray, J.R. (2012). "Advancing hydroacoustic technologies for sedimentology research and monitoring," Eos Transactions American Geophysical Union, 93(26), p 244.

Landers, M.N., and Sturm, T.W. (2013). "Hysteresis in suspended sediment to turbidity relations due to changing particle size distributions," Water Resources Research, 49(9), pp 5,487–5,500.

Lee, C.J., Rasmussen, P.P., and Ziegler, A.C. (2008). "Characterization of suspended-sediment loading to and from John Redmond Reservoir, east-central Kansas, 2007–08," U.S. Geological Survey Scientific Investigations Report 2008–5123, 25 p.

Lewis, J. (1996). "Turbidity-controlled suspended sediment sampling for runoff-event load estimation," Water Resources Research, 32(7), pp 2,299–2,310.

Lipman, P.W., and Mullineaux, D.R., eds. (1981). "The 1980 eruptions of Mount St. Helens, Washington," U.S. Geological Survey Professional Paper 1250, 844 p.

Lodhi, M.A., Rundquist, D.C., Han, L., and Kuzila, M.S. (1997). "The potential for remote sensing of loess soils suspended in surface waters," Journal of the American Water Resources Association, 33(1), pp 111–117.

Marcus, W.A., and Fonstad, M.A. (2010). "Remote sensing of rivers: the emergence of a subdiscipline in the river sciences," Earth Surface Processes and Landforms, 35(15), pp 1867–1872.

Mertes, L.A.K., Smith, M.O., and Adams, J.B. (1993). "Estimating suspended sediment concentrations in surface waters of the Amazon River wetlands from Landsat images," Remote Sensing of the Environment, 43, pp 281–301.

Nolan, K.M., Gray, J.R., and Glysson, G.D. (2005). "Introduction to suspended-sediment sampling," U.S. Geological Survey Scientific Investigations Report 2005–5077, CD-ROM.

Porterfield, G. (1972). "Computation of fluvial-sediment discharge," U.S. Geological Survey Techniques of Water Resources Investigations, book 3, chap. C3, 66 p.

Profilocolore Sri (2013). "Variant full range on Nikon cameras: hardware and software make the system measure reflectance and spectra," Nikon experience, website accessed August 2014 at *http://www.profilocolore.com/pubblicazioni-2*

Qu, L. (2014). "Remote sensing suspended sediment concentration in the Yellow River," Ph.D. dissertation paper 383, University of Connecticut, website accessed December 2014 at *http://digitalcommons.uconn.edu/dissertations/383/*.

Rasmussen, P.P., Gray, J.R., Glysson, G.D., and Ziegler, A.C. (2009). "Guidelines and procedures for computing time-series suspended-sediment concentrations and loads from in-stream turbitiy-sensor and streamflow data," U.S. Geological Survey Techniques and Methods, book 3, chap. C4, 53 p., http://pubs.usgs.gov/tm/tm3c4/

Topping, D.J., Rubin, D.M., Wright, S.A., and Melis, T.S. (2011). "Field evaluation of the error arising from inadequate time averaging in the standard use of depth-integrating suspended-sediment samplers," U.S. Geological Survey Professional Paper 1774, 95 p.

Uhrich, M.A., and Bragg, H.M. (2003). "Monitoring in-stream turbidity to estimate continuous suspended-sediment loads and yields and clay-water volumes in the Upper North Santiam River Basin, Oregon, 1998–2000," U.S. Geological Survey Water-Resources Investigations Report 03–4098, 43 p.

Uhrich, M.A., Kolasinac, J., Booth, P.L., Fountain, R.L., Spicer, K.R., and Mosbrucker, A.R. (2014). "Correlations of turbidity to suspended-sediment concentration in the Toutle River basin, near Mount St. Helens, WA, 2010–11," U.S. Geological Survey Open-File Report 2014–1204, 30 p.

U.S. Geological Survey (2014). Branch of Quality Systems: Sediment Laboratory Quality Assurance Project, website accessed October 2014 at *https://bqs.usgs.gov/slqa/index.html*.

Walling, D.E. (1977). "Assessing the accuracy of suspended sediment rating curves for a small basin," Water Resources Research, 13(3), pp 531–538.

Wang, J.J., and Lu, X.X. (2010). "Estimation of suspended sediment concentrations using Terra MODIS: an example from the Lower Yangtze River, China," Science of the Total Environment, 408(5), pp 1,131–1,138.

Wang, J.J., Lu, X.X., Liew, S.C., and Zhou, Y. (2010). "Remote sensing of suspended sediment concentrations of large rivers using multi-temporal MODIS images: an example in the Middle and Lower Yangtze River, China," International Journal of Remote Sensing, 31(4), pp 1,103–1,111.

Wang, J.J., Lu, X.X., Liew, S.C., and Zhou, Y. (2009). "Retrieval of suspended sediment concentrations in large turbid rivers using Landsat ETM+: an example from the Yangtze River, China," Earth Surface Processes and Landforms, 34(8), pp 1,082–1,092.

USING OBLIQUE DIGITAL PHOTOGRAPHY FOR ALLUVIAL SANDBAR MONITORING AND LOW-COST CHANGE DETECTION

EXTENDED ABSTRACT

Robert B. Tusso, Hydrologist, US Geological Survey, Southwest Biological Science Center, Grand Canyon Monitoring and Research Center, Flagstaff, AZ, rtusso@usgs.gov;
Daniel Buscombe, Research Geologist, US Geological Survey, Southwest Biological Science Center, Grand Canyon Monitoring and Research Center, Flagstaff, AZ, dbuscombe@usgs.gov;
Paul E. Grams, Research Hydrologist, US Geological Survey, Southwest Biological Science Center, Grand Canyon Monitoring and Research Center, Flagstaff, AZ, pgrams@usgs.gov

Abstract The maintenance of alluvial sandbars is a longstanding management interest along the Colorado River in Grand Canyon. Resource managers are interested in both the long-term trend in sandbar condition and the short-term response to management actions, such as intentional controlled floods released from Glen Canyon Dam. Long-term monitoring is accomplished at a range of scales, by a combination of annual topographic survey at selected sites, daily collection of images from those sites using novel, autonomously operating, digital camera systems (hereafter referred to as 'remote cameras'), and quadrennial remote sensing of sandbars canyon-wide. In this paper, we present results from the remote camera images for daily changes in sandbar topography.

Figure 1 Typical setup of a remote camera system, at river mile (RM) 145.9, Grand Canyon. Visible is the waterproof box containing camera and electronics, and the 20W solar panel.

Beginning in the early 1990s, 35 mm film cameras were deployed at selected sites in the canyon to take photos daily at many of the long-term sandbar monitoring sites (Dexter et al., 1995). In 2008, higher-resolution digital cameras capable of taking multiple photos daily were installed at many of these sites, enabling rapid and low-cost analyses of sandbar response to geomorphic events. By 2014, all of the analog cameras had been replaced as well as additional cameras added

to the monitoring network for a total of 45 cameras. These camera systems are completely autonomous and can be left for months to years without maintenance. Each system (Figure 1) consists of a digital SLR camera controlled by a datalogger programmed with an intervalometer script that triggers the shutter release on the camera to take images at prescribed times. Solar panels are used for power, and the datalogger regulates and minimizes power usage by the camera such that batteries do not drain significantly, even in shaded locations. More details can be found in Bogle et al. (2012).

Controlled flood experiments have been periodically conducted to rebuild subaerial sandbars along the river, and the camera imagery is playing an increasing role in the evaluation of the floods' effects. Post-flood images are compared to pre-flood images taken at the same discharge, and qualitatively analyzed for change in sandbar size by visual inspection. Because of the unique geometry at each site, a particular sandbar may be more likely to change in either area or height (though not necessarily both), thus necessitating use of the general term "size." Each sandbar is manually classified as having undergone major negative size change (lost more than 15%, assigned a rating of "-2"), minor negative size change (-15% to -3%, "-1"), negligible size change (-2% to +2%, "0"), minor positive size change (+3% to +15%, 1"), or major positive size change (gained more than 15%, "2"). Examples are shown in figure 2. For a 2008 flood, 22 sites had three sets of topographic surveys corresponding with the photos. The surveys provided area and volume measurements for each site. To address the "size" conundrum described above, a composite change value was derived from these measurements. The visual analysis agreed with the composite topographic survey change values at 78% of the sites, and disagreed at 2%. Surveyed change was not visually recognized at 15% of the sites, and at 6%, surveys indicated that no change occurred where visual analysis indicated it had.

A 2012 flood was evaluated primarily by photo analysis, and a smaller subset of five surveyed sites was in 100% agreement with the outcomes. Of the 33 sites photographed, this flood produced positive change at 51%, negligible change at 39%, and negative change at 9%. Six months later, 28% of the sites were still larger, while 47% showed negligible change, and 24% were smaller. A 2013 flood, with 42 sites photographed, resulted in enlarged sandbars at 50% of the sites, negligible change at 38%, and negative change at 12%. Six months later, 27% were still enlarged, 50% had negligible change, and 17% were smaller. The two floods resulted in the same type of response at 61% of the sites, while 33% had a recognized change from one flood and negligible change from the other. Six percent showed responses of differing sign. These data show that, overall, the 2012 and 2013 floods were successful in building sandbars in the short term, but that long term results are only marginally improved. Resource managers can use these data (along with sediment budget data) to help design aspects of future controlled flood events, such as duration, peak flow, time of year, and up-ramp/down-ramp rates.

Figure 2 Photos of before and after the November 2012 controlled flood, at two monitoring sites on the Colorado River. The score on the lower right is the qualitative assessment of how much the sandbar changed in size - major negative size change (-2), minor negative size change (-1), negligible size change (0), minor positive size change (1), or major positive size change (2). Both sites in this example saw an increase in size, though to differing degrees.

While this method of photo analysis is based on qualitative assessment, it has been demonstrated to provide a rapid and fairly accurate metric for assessing the immediate downstream effects of controlled floods on bars. Results of controlled floods on sandbar maintenance were available to resource managers within two weeks of the flood events in 2012 and 2013. As well as their primary use in examining sandbar dynamics, these photo datasets can also been used for monitoring other aspects of the river corridor, including vegetation encroachment, spring discharge, endangered species habitat, archeological site protection, and recreational use patterns.

In order to provide a more accurate and quantitative assessment of how sandbar areas are changing with time, photos from the large (and ever-growing) archive of imagery are now being orthorectified using a network of surveyed ground control points at each site. An automated computer process extracts georeferenced shorelines from the orthorectified photos, and calculates an area value for the bar (Figure 3).

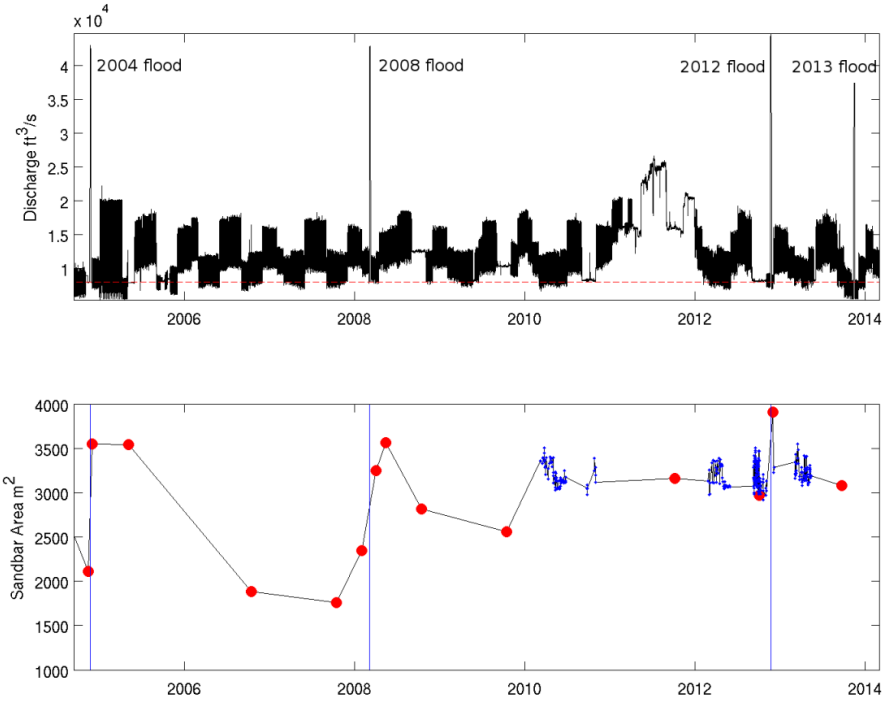

Figure 3 Top panel: the hydrograph at RM 30 in Upper Marble Canyon from summer 2004 to early 2014. The four controlled floods during this period are labelled. Bottom panel: the sandbar area at the RM 30.7 site, at a river discharge of 8000 ft^3/s, prior to the 2013 controlled flood. Red dots are from annual total station surveys. Blue dots are derived from remote camera images and show the short-term variability not captured by infrequent conventional monitoring.

Examining the changes in sandbar area for a given period can yield clues about the effects of different flow patterns on sandbar area and stability. The sandbar at river mile (RM) 30.7, for example, increased in area 33% as a result of the 2012 controlled flood (topographic surveys are in agreement). The next topographic survey, conducted 11 months later, shows the bar back to within 5% of its pre-flood size. Areas derived from the orthorectified photos, however, show that the bar had shrunk to this size within three months of the flood, and then maintained a mostly steady area for the following eight months (Figure 3). In the summer of 2011, for another example, flows were elevated (though not as high as during controlled floods) to equalize the amount of water in upstream and downstream reservoirs (Figure 3). Area calculations for the sandbar at RM 22.0 show the potential bar-building effects of these moderately elevated flows: this sandbar attained its largest area since the 2008 flood, including after the 2012 and 2013 floods.

A weakness of this method is the inability to recognize positive size change in sandbars that aggrade significantly while showing little change in area. To better derive a comprehensive calculation of size change, efforts are underway to extract 3D topographic data from image sets, thus potentially providing a means to estimate sandbar volumes. This process is facilitated by the dam-controlled diurnal stage fluctuations on this section of the Colorado River. Cameras are programmed to take hourly photos, and traces of the water's edge on the sandbar (hereafter

referred to as "shorelines") are extracted from rectified images using the same methods as above (Figure 4).

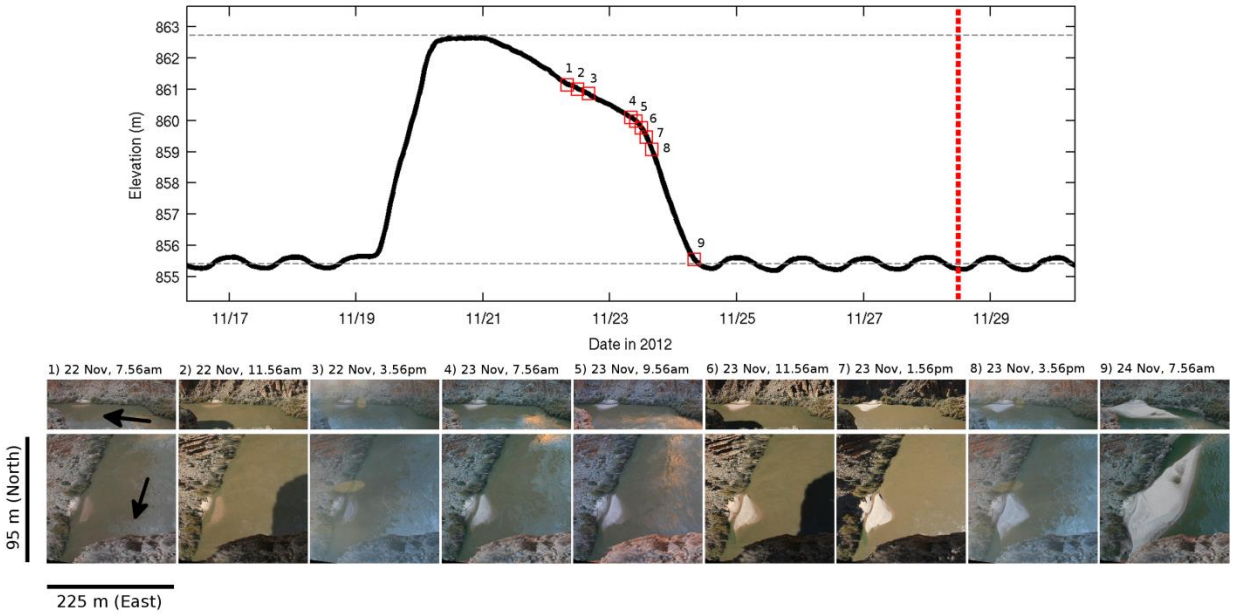

Figure 4 Top panel: the 2012 controlled flood hydrograph at RM 30. The dashed line shows the time when a conventional total station survey was carried out after the flood. The markers indicate the times an image was taken with the remote camera system at RM 30.7. Bottom panel: a time-series of those images, and orthorectified images, from which shoreline locations and elevations are extracted. The arrows in the first panels show the direction of river flow.

These shorelines essentially become contour lines if the stage at the time of the photo is known. A pressure transducer deployed at the site provides the river stage, and thus elevation of the shoreline at the time the photo was taken. Grouping several of these extracted shorelines over a diurnal stage fluctuation will constitute a contour map of the wetted portion of the bar. The process is schematized in Figure 5. The contour model made from the sequences of images in Figure 4 is shown overlain onto the rectified image, in Figure 6.

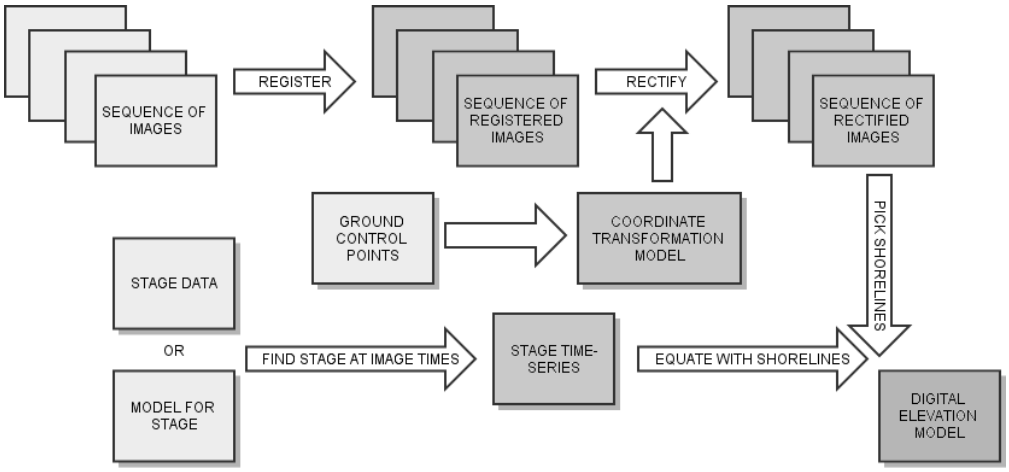

Figure 5 Schematic of the stages required to build a 3D digital elevation model (DEM) of a sandbar using a time-series of sandbar images which have been registered and rectified, and a known stage elevation or stage-discharge relation used to map shoreline elevations.

Figure 6 A colored DEM with contours of the RM 30.7 sandbar, overlain onto an orthorectified image of the bar after the 2012 controlled flood. This DEM was computed from the sequence of images taken during the flood shown in Figure 4, and associated stage elevations, following the methods summarized in Figure 4.

Change in pre- and post-event digital elevation models derived from the contour sets will allow estimates of volumetric changes to be made, and provide quantifiable topographic data that can be processed quickly and without the need to repeatedly send survey crews into the field. Such data provide valuable insight into sandbar changes during times between ongoing annual topographic surveys, especially for sandbars that don't change much in area, but may significantly aggrade - a characteristic that can be difficult to recognize with area calculations

and visual inspection methods. Knowing the sign of sandbar volume change can also be used to corroborate suspended-sediment transport data collected along the river by the USGS (Griffiths et al., 2012). During a flood event, for example, river reaches shown to have a negative sediment mass balance should also show sandbars that decreased in volume. While still in its developmental stages, this technique has the potential to provide high-resolution, low-cost topographic data to help resource managers better understand sandbar dynamics, in the short-term and the long-term, as a result of river management actions.

REFERENCES

Bogle, R., Velasco, M., and Vogel, J. (2012). "An Automated Digital Imaging System for Environmental Monitoring Applications," U.S. Geological Survey Open-File Report 2012-1271, 18 p.

Dexter, L.R., Cluer, B.L., and Manone, M. (1995). "Using land based photogrammetry to monitor sandbar stability in Grand Canyon on a daily time scale," in Van Riper, C., III, ed., Proceedings of the Second Biennnial Conference of Research in Colorado Plateau National Parks, Transactions and Proceedings Series, National Park Service, p. 67-86.

Griffiths, R.E., Topping, D.J., Andrews, T., Bennett, G.E., Sabol, T.A., and Melis, T.S. (2012). "Design and maintenance of a network for collecting high-resolution suspended-sediment data at remote locations on rivers, with examples from the Colorado River" U.S. Geological Survey Techniques and Methods, book 8, chapter C2, 44 p.

LONG-TERM MONITORING OF SANDBARS ON THE COLORADO RIVER IN GRAND CANYON USING REMOTE SENSING

Robert P. Ross, Hydrologist, U. S. Geological Survey, Grand Canyon Monitoring and Research Center, 2255 N. Gemini Dr., Flagstaff, AZ 86001, rross@usgs.gov
Paul E. Grams, Research Hydrologist, U. S. Geological Survey, Grand Canyon Monitoring and Research Center, 2255 N. Gemini Dr., Flagstaff, AZ 86001, pgrams@usgs.gov

INTRODUCTION

Closure of Glen Canyon Dam in 1963 dramatically changed discharge and sediment supply to the downstream Colorado River in Marble and Grand Canyons. Magnitudes of seasonal flow variation have been suppressed, while daily fluctuations have increased because of hydropower generation. Lake Powell, the upstream reservoir, traps all sediment, leaving the Paria and Little Colorado Rivers as the main suppliers of fine sediment to the system below Glen Canyon Dam. The reduction in sediment supply, along with changes in discharge, have resulted in fine-sediment deficit (Topping et al., 2000), leading to a decrease in the size and number of alluvial sandbars (Schmidt and Graf, 1990; Schmidt et al., 2004). However, the understanding of these important spatial and temporal changes in sandbars located along the banks of the river have been limited to infrequent measurements mostly made by direct visitation and topographic surveying (Hazel et al., 2010).

Aerial photographs are the only data available from which it is possible to evaluate changes in alluvial deposits at a large number of sites and compare recent conditions with those that existed prior to the initiation of ground-based monitoring in the early 1990s. Previous studies have evaluated the effects of Glen Canyon Dam on sandbars by analysis of comprehensive maps of surficial geology that are based on seven sets of aerial imagery taken between 1935 and 1996 for selected reaches in the first 120 km downstream from Lees Ferry, Arizona (Figure 1). These studies showed that the area of exposed sand in eddy-deposition zones was less in the post-dam period than in the pre-dam period (Leschin and Schmidt, 1995; Schmidt et al., 1999b; Sondossi, 2001, Sondossi and Schmidt, 2001, Schmidt et al., 2004).

In this study, we extend these analyses to encompass a 74-year period by including maps of sand deposits visible in aerial imagery taken in 2002, 2005, and 2009 for the same reaches that were mapped in the earlier studies. Results are analyzed for two post-dam periods, based on the implementation of the first controlled flood in March 1996. The period from 1965 to March 1996 is the pre-controlled flood period and was dominated by flows that fluctuated up to the maximum capacity of the Glen Canyon Dam powerplant. Beginning in 1991, fluctuations were constrained such that maximum daily flows were typically less than 65 percent of powerplant capacity. Thus, the pre-controlled flood period also includes five years of restricted dam operations. This period also included unplanned spills from the reservoir in 1983, 1984, and 1986. We refer to the period from April 1996 to 2009 as the controlled-flood period. This period consisted entirely of restricted dam operations and included three controlled floods conducted as sandbar-building experiments. We show that the areal extent of exposed sand was greater in the images taken in the controlled-flood period than in the pre-controlled flood period. We also show that in the controlled-flood period, the area of exposed sand is negatively correlated with the elapsed time

since the most recent controlled flood.

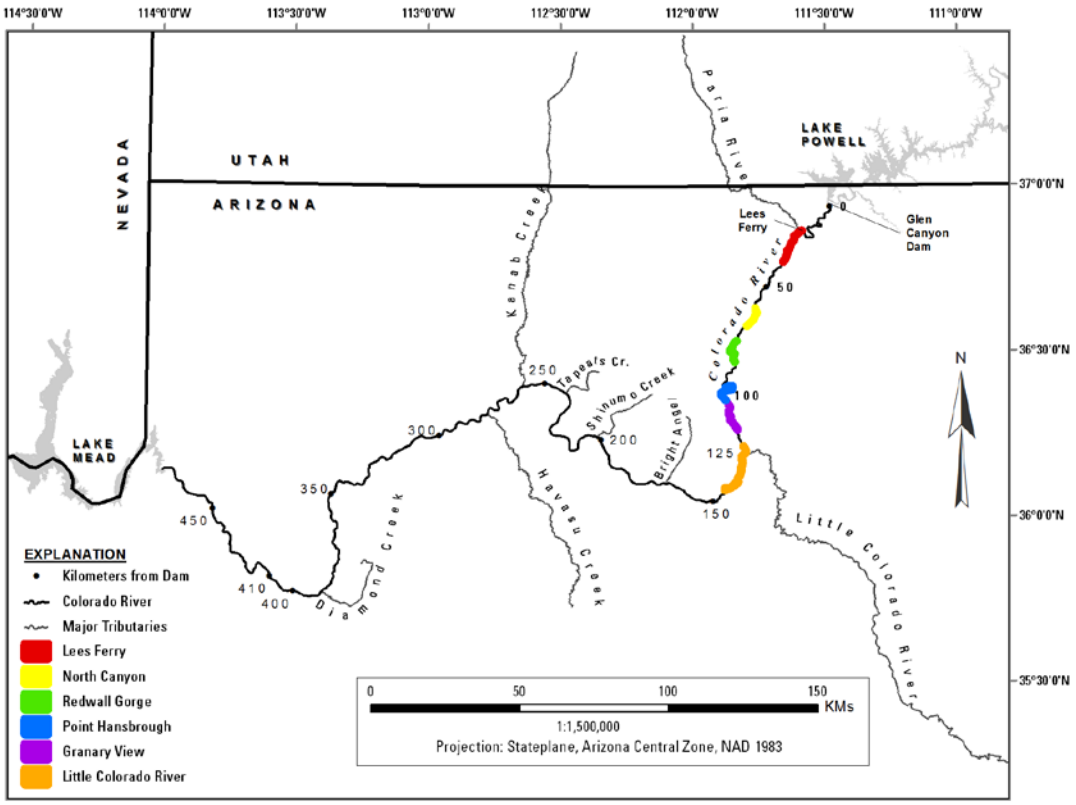

Figure 1 Location map of study area, showing Colorado River, major tributaries, and study reaches. The study reaches are informally named and range in length from 7.5 km to 20.3 km. The numbers show distance downstream from Glen Canyon Dam along the river centerline.

METHODS

We used high-resolution (25-centimeter pixel size) aerial imagery collected by fixed wing aircraft in May 2002, May 2005, and May 2009 to map the extent of exposed sand in each of the reaches examined by Schmidt et al. (2004). Each set of images was acquired during a steady dam release of approximately 227 m^3/s (8,000 ft^3/s), enabling a direct comparison of the area of deposits exposed above the water surface without introducing bias caused by difference in water surface elevation. Thus, we use the water surface elevation associated with 227 m^3/s as a reference elevation. The shoreline in each reach was determined by automated image classification of the water that was visually inspected for accuracy (Davis et al., 2012). We intersected the 227 m^3/s shoreline with the sand deposits mapped from the April 1996 images to create revised maps for the same sand deposits for 2002, 2005, and 2009 (Figure 2). Areas mapped as sand in 1996 and classified as water in the recent images were interpreted to have eroded. Conversely, areas that were below the water surface in 1996 and above the water surface in the recent images were interpreted to have aggraded. Eroded areas were subtracted from the 1996 maps and aggraded areas were added to produce the final maps of exposed sand deposits for 2002, 2005, and 2009.

We use the eddy-deposition zone (EDZ) accounting unit as defined by Schmidt et al. (2004) to track changes in sandbar area. The EDZ is the sum of all sand deposits that occur in an eddy that is downstream or immediately upstream from a channel constriction created by a debris fan (Figure 2). In this study, we report only on EDZs larger than 1000 m^2, consistent with the approach of Schmidt et al. (2004).

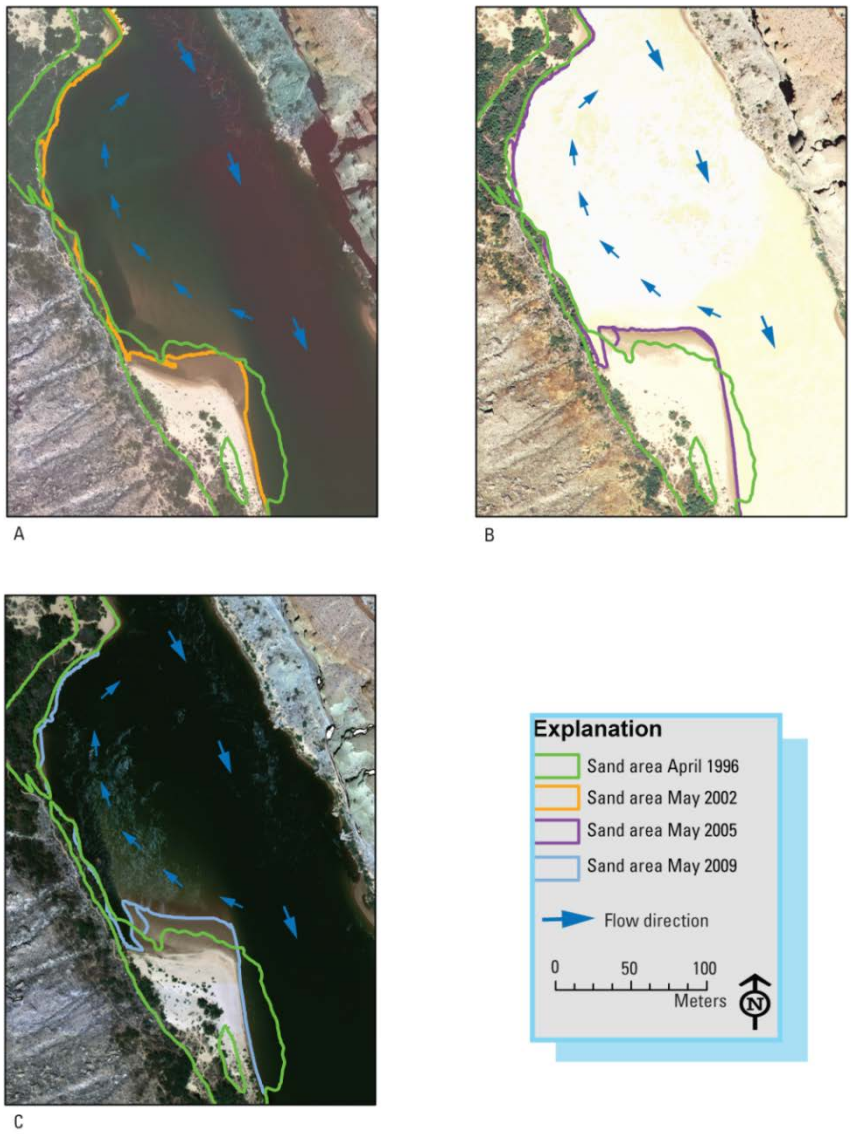

Figure 2 Aerial images at Saddle Canyon show comparisons of sand area mapped in April 1996 with sand area mapped in recent images. (A) Sand area in April 1996 and May 2002 on May 2002 image, (B) Sand area in April 1996 and May 2005 on May 2005 image, and (C) Sand area in April 1996 and May 2009 on May 2009 image. Blue arrows indicate flow direction. Debris fan constriction is in upper left area of images. Imagery from Grand Canyon Monitoring and Research Center archives.

Because the study reaches are of different lengths, ranging from 7.5 to 20.3 kilometers (km), we report the measurements of sand area as the total sand area within EDZs for each reach normalized by the reach length (m^2/km). Standard error was calculated for each reach by dividing the standard deviation of the area of exposed sand deposit per reach length by the square root of the number of sand deposits per reach length. Changes in exposed sand area greater than the standard error were considered significant. We also report on the eddy fill ratios, which are the ratio of exposed sand within each EDZ boundary to the area of the EDZ boundary. Thus, an eddy fill ratio of 1.0 would indicate the sandbar completely filled the eddy deposition zone. We compare eddy fill ratios from the 1935 images (the only set of pre-dam aerial photography that includes all reaches) with the average eddy fill ratio for the pre-controlled flood period and the average eddy fill ratio for the controlled flood period for each reach. We averaged the eddy fill ratio for each EDZ over the range of years of imagery common to all reaches, and then used the average value of the eddy fill ratios for all EDZs to determine the time period average. We chose these three time periods because they represent the pre-dam period of unregulated flows and two post-dam periods before and after controlled floods (Figure 3).

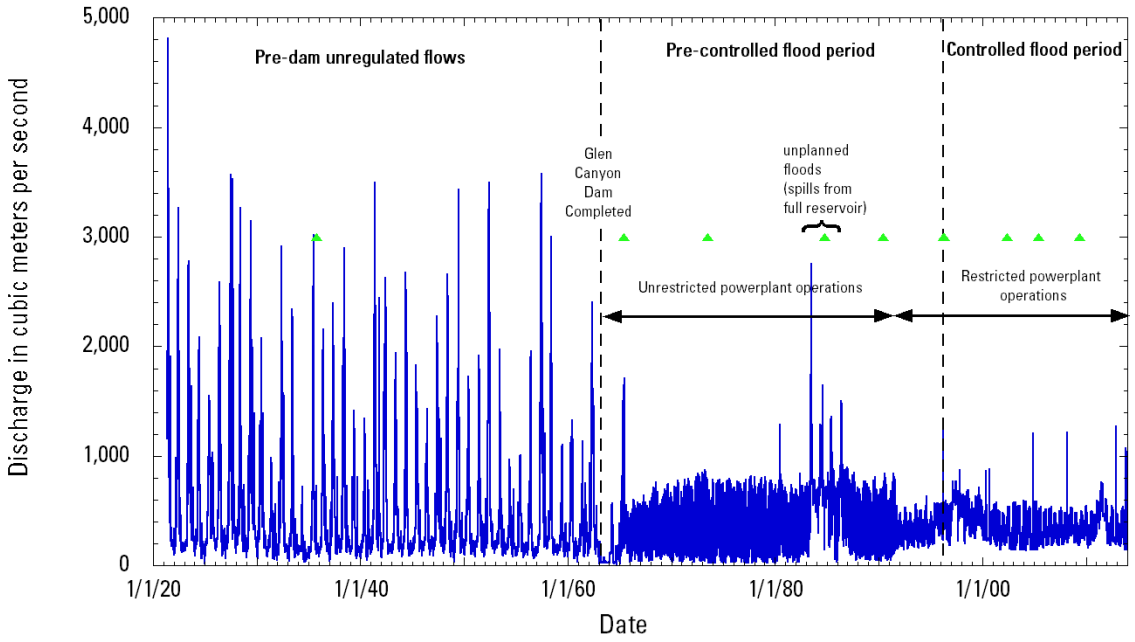

Figure 3 Discharge of the Colorado River at Lees Ferry, Arizona (USGS gage 09380000), 1922 to 2012. The pre-controlled flood period consists of unrestricted powerplant operations, restricted powerplant operations, and unplanned floods. The controlled-flood period consists of restricted powerplant operations and periodic controlled floods. Horizontal arrows show periods of unrestricted powerplant operations and restricted powerplant operations. Aerial imagery collection dates are marked with green triangles.

The first 26 years of the pre-controlled flood period consisted primarily of flows which fluctuated on a daily basis for hydroelectric power generation from daily low flows of about 140 m^3/s (5,000 ft^3/s) to daily high flows of about 850 m^3/s (30,000 ft^3/s). This period also included unplanned floods in 1983-86 that were spills from Lake Powell during years of large upper

Colorado River basin runoff. Beginning in 1991, the range of daily fluctuations was restricted such that daily low flows were about 200 m^3/s (7,000 ft^3/s) or higher and highs were 570 m^3/s (20,000 ft^3/s) or lower. The controlled-flood period consisted entirely of these restricted dam operations and included three dam releases above power-plant capacity (31,500 ft^3/s). Short-duration (less than 96 hour) controlled floods were released in April 1996, November 2004, and March 2008 to evaluate the use of dam releases for building sandbars (Webb et al., 1999; Melis, 2011; Schmidt and Grams, 2011).

We evaluated uncertainty by comparing the area of exposed sand we measured from the images to sand area measured by total station survey at 15 long-term monitoring sites for coincident dates in 2002, 2005, and 2009 (Hazel et al., 2010). To minimize the chance that deposits eroded or aggraded between comparisons, we only utilized total station surveys made within 2 weeks of aerial imagery collection. Analysis of the root-mean square error about the residuals indicates a 3,838 m^2 error between the sum of sand area from all 36 aerial photo measurements and the sum of total station measurements for all 15 sites, representing about 2 percent of the total sum of sand area (190,055 m^2) observed in all 15 EDZs as measured by total station (Figure 4). Error between the average of these 36 aerial photo measurements and the coincident total station surveys is 640 m^2, also about 2 percent of the average sand area (31,676 m^2) for the 15 sites.

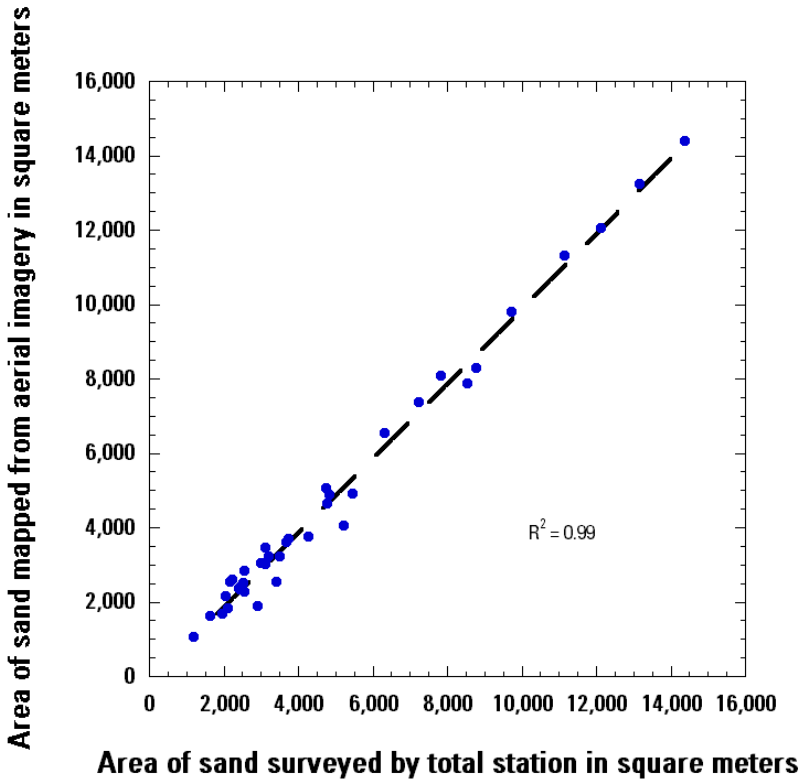

Figure 4 Comparison of change in sand area from aerial imagery to change in sand area measured by conventional total station survey of long-term monitoring sites. Line fit by least-squares regression shows a near perfect 1:1 correspondence between sand area surveyed by total station and sand area measured by analysis of aerial photographs.

RESULTS

In all reaches, sand area was less in 1965 than in 1935, supporting the conclusion previously reported by Schmidt et al. (2004). From 1965 to 1973, sand area decreased in all reaches (Figure 5). Between 1973 and 1984, sand area increased in all reaches. These increases are the result of deposition that occurred during the 1983 and 1984 reservoir spills (Schmidt and Graf, 1990). Sand area decreased from 1984 to 1990 in all reaches, except Granary View, which was not mapped from the 1990 images. From 1990 to March 1996, sand area increased in all reaches (except Granary View). During the 1996 controlled flood, bracketed by the March 1996 and April 1996 image collections, sand area increased in the Lees Ferry, North Canyon, Redwall Gorge, Point Hansbrough, and the Little Colorado River reaches, and decreased in the Granary View reach. These changes are consistent with the findings of Hazel et al. (1999) that many sandbars increased in elevation during the 1996 controlled flood without increasing in area. Sand area decreased from April 1996 to 2002 in the Lees Ferry, North Canyon, Redwall Gorge, and Little Colorado River reaches, and increased in the Point Hansbrough and Granary View reaches. From 2002 to 2005, sand area increased in all reaches. Between 2005 and 2009, sand area decreased in the Point Hansbrough and Little Colorado River reaches; no change occurred in the other reaches. In all comparison intervals described above, the reported changes are larger than the standard error of the population of all EDZs for each date and reach, respectively.

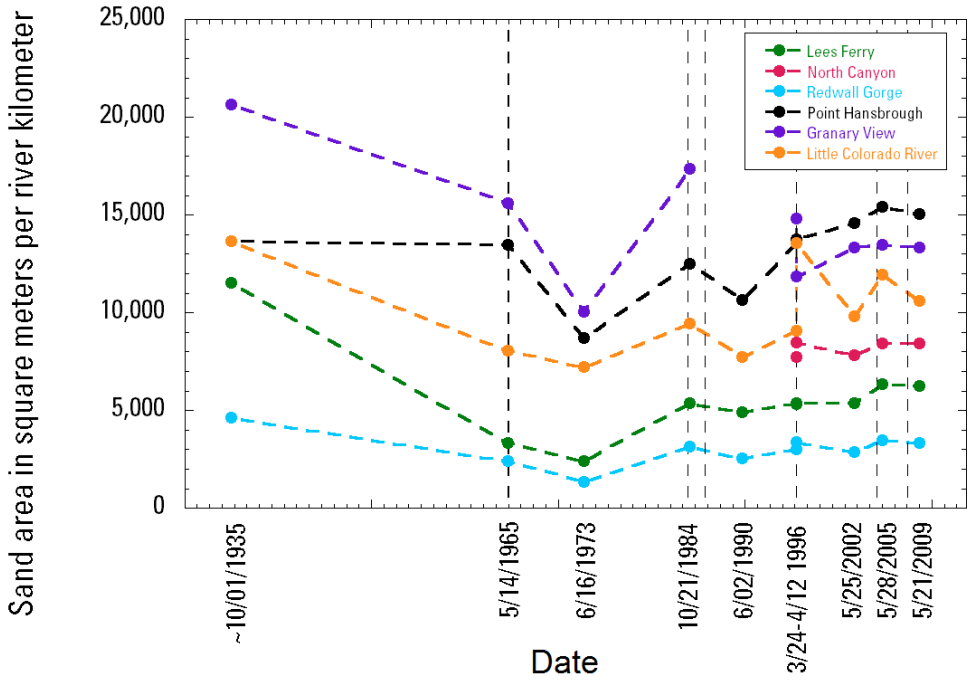

Figure 5 Total sand area within eddy deposition zones larger than 1000 m^2 per river kilometer (m^2/km) for all study reaches for 1935 through 2009, showing change between imagery collection dates. Vertical dashed lines indicate last flood event prior to imagery dates.

Median eddy fill ratios decreased from 1935 to the pre-controlled flood period, and then increased from the pre-controlled flood period to the controlled-flood period in three of five

reaches (Figure 6). Only in the Granary View reach did the median eddy fill ratio continue to decrease in the controlled-flood period. The Lees Ferry reach showed only a slight increase in eddy fill ratio value from the pre-controlled flood period to the controlled-flood period.

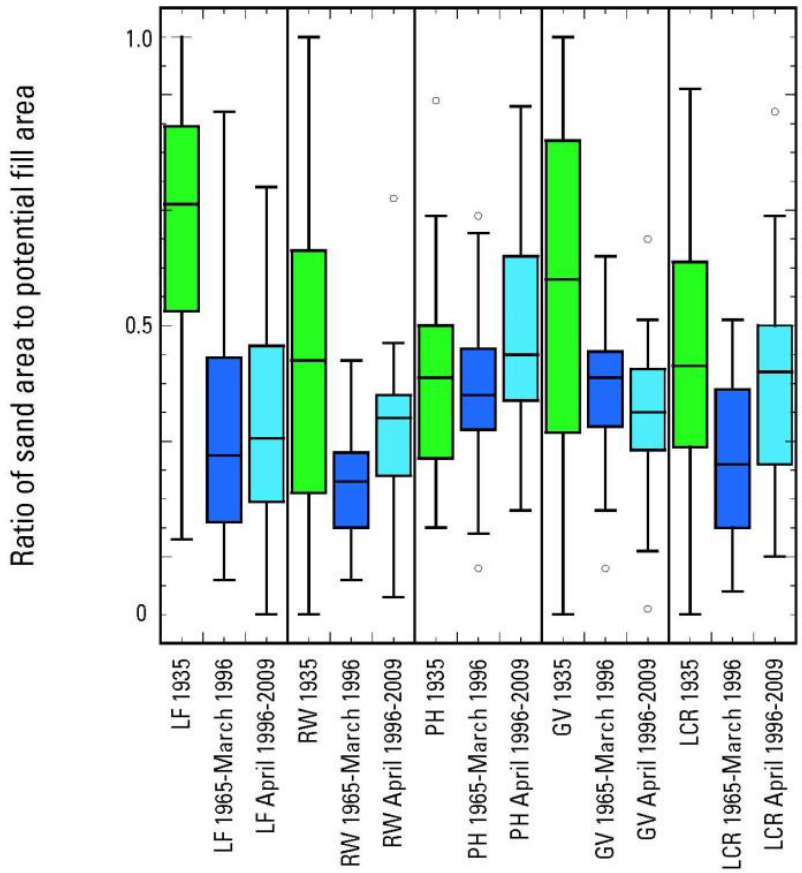

Figure 6 Box and whisker plots of the average eddy fill ratio (ratio of sand area to area of eddy deposition zone) for the pre-dam period, the pre-controlled flood period (1965 to March 1996), and the controlled-flood period (April 1996 to 2009). The median value is marked as the hingeline, the first and second quartiles are the boxes on either side of the median hingeline, the third and fourth quartiles are plotted as whiskers on either side of the boxes, and outliers are plotted as hollow circles.

We examined the effect of flow regime (Figure 3) on measured sandbar area by evaluating the relation between exposed sandbar area and elapsed time since the most recent flood event. Flood events were defined as releases of 1,161 m^3/s (41,000 ft^3/s) or more. The images from the pre-controlled flood period were collected between 1 week and almost 10 years following the previous flood. The images from the controlled-flood period were collected between 2 weeks and nearly 6 years following the most recent controlled flood. For the controlled-flood period, there is a strong correlation between measured sandbar area and elapsed time since the previous controlled flood (Figure 7). In this period, sandbar area was largest in April 1996, 0.5 months after the 1996 controlled flood; and sandbar area was smallest in 2002, 72 months after the 1996 controlled flood. The measurements of sandbar area in the pre-controlled flood period are not

strongly correlated with elapsed time since the most recent flood event.

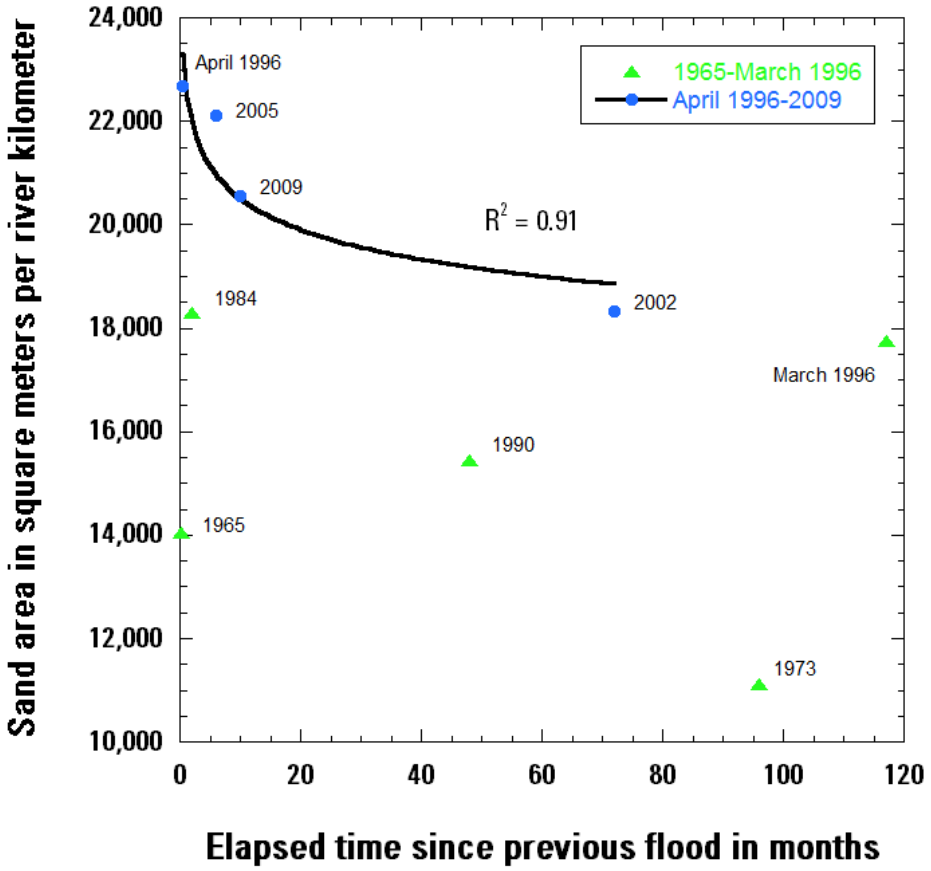

Figure 7 Post-dam reach area plotted against time elapsed since previous flood of 1,161 m^3/s (41,000 ft^3/s) in months. Power trendline fit to data from the controlled-flood period shows clear relationship with an R^2 value of 0.91, while no significant trend was observed in the data from the pre-controlled flood period.

DISCUSSION AND CONCLUSIONS

Previous analyses of aerial imagery concluded that the sandbar area in the post-dam photographs from the period before the first controlled flood was less than in the pre-dam era (Schmidt and Graf, 1990; Schmidt et al., 2004). Our analysis of more recent (2002 – 2009) post-dam imagery shows that sandbars in 2009 were still smaller than in the pre-dam period. There are, however, substantial differences in sandbar size between images collected in the periods with and without controlled floods. The relative proportion of EDZs occupied by exposed sand deposits was greater, on average, in the controlled-flood period than in the period preceding controlled floods. Only in the Granary View reach was the median sandbar size less in the images collected in the controlled-flood period than in the period preceding the first controlled flood, although some sandbars in this reach did increase in size. Importantly, the presence and absence of controlled floods are not the only differences between these two periods. The pre-controlled flood period consisted primarily of unrestricted fluctuating flows while the controlled-flood period consisted entirely of restricted fluctuating flows. Thus, the combination of controlled floods and restricted

powerplant operations is most likely responsible for the observed increases in sandbar size.

The strong correlation between sandbar area and elapsed time since the most recent controlled flood is consistent with previous studies of sandbar deposition and subsequent erosion of flood-formed bars (Hazel et al., 1999; Hazel et al., 2010; Grams et al., 2010). The negative correlation also illustrates that the mean among a set of images is sensitive to the timing of image collection. The image collection dates are neither a systematic nor a random sample. Thus, the average responses shown in Figure 6 only show the average among the image collection dates and are not necessarily representative for the time period. Because of this sensitivity to time of image acquisition and because all images were collected at different intervals relative to the most recent controlled flood, it is not possible to identify a trend in sandbar area with time between 2002 and 2009. The apparent trend between 2002 and 2009 shown in Figure 5 is most likely attributable to the shorter elapsed time between the 2008 controlled flood and the 2009 images.

Because the volume of sand above the reference discharge of 227 m^3/s is only a small fraction of the sand in storage (Hazel et al., 2006; Grams et al., 2015), changes in sandbar area determined from analysis of aerial images cannot be interpreted to reflect changes in total sand storage. Thus, although the images showed larger sandbars in the post-dam period with controlled floods than in the post-dam period before controlled floods, this does not mean that there was more sand in the system during this period.

This study involves only a subset of the reaches that comprise the entire length of the Colorado River in Marble and Grand Canyons, downstream from Glen Canyon Dam. These findings may not, therefore, be representative of the entire system. Ongoing work includes classification of the area of exposed sand for all of Marble and Grand Canyons using the same 2002 and 2009 images used in this analysis, and supplemented with images collected in 2013. This analysis will report on changes in sand area for approximately 1,400 EDZs between Glen Canyon Dam and Lake Mead, located 275 miles downstream.

REFERENCES

Davis, P. A. (2012). “Airborne digital-image data for monitoring the Colorado River corridor below Glen Canyon Dam, Arizona, 2009 – Image-mosaic production and comparison with 2002 and 2005 image mosaics,” U. S. Geological Survey Open-File Report 2012-1139, 82 p.

Grams, P. E., Schmidt, J. C., and Andersen, M. A. (2010). “2008 High-Flow Experiment at Glen Canyon Dam: Morphologic response of eddy-deposited sandbars and associated aquatic backwater habitats along the Colorado River in Grand Canyon National Park,” U. S. Geological Survey Open-File Report 2010-1032, 73 p.

Grams, P. E., Buscombe, D., Topping, D. J., Kaplinski, M. A., and Hazel, J. E., Jr. (2015). “Use of flux and morphologic sediment budgets for sandbar monitoring on the Colorado River in Marble Canyon, Arizona,” Proc. of the 3rd Joint Federal Interagency Conference, Reno, Nevada, April 19-23, 2015.

Hazel, J. E. Jr., Kaplinski, M. A, Parnell, R. A., Manone, M. F., and Dale, A. (1999). “Topographic and bathymetric changes at thirty-three long-term study sites:” in Webb, R. H., Schmidt, J. C., Marzolf, G. R., and Valdez, R. A., eds., The Controlled Flood in Grand Canyon. Washington D. C., American Geophysical Union, Geophysical Monograph 110: p.

161-183.

Hazel, J. E. Jr., Topping, D. J., Schmidt, J. C., and Kaplinski, M. A. (2006). "Influence of a dam on fine-sediment storage in a canyon river," Journal of Geophysical Research, AGU, 111(F01025), p 1-16.

Hazel, J. E. Jr., Grams, P. E., Schmidt, J. C., and Kaplinski, M. A. (2010). "Sandbar response in Marble and Grand Canyons, Arizona, following the 2008 high-flow experiment on the Colorado River," U. S. Geological Survey Scientific Investigations Report 2010-5015, 52 p.

Leschin, M. F., and Schmidt, J. C. (1995). "Description of map units to accompany maps showing surficial geology and geomorphology of the Point Hansbrough and Little Colorado River confluence reaches of the Colorado River, Grand Canyon National Park, Arizona," Flagstaff, Bureau of Reclamation Glen Canyon Environmental Studies report, 6 p. and plates.

Melis, T. S, ed. (2011). "Effects of three high-flow experiments on the Colorado River ecosystem downstream from Glen Canyon Dam, Arizona," U. S. Geological Survey Circular 1366, 147 p.

Schmidt, J. C, and Graf, J. B. (1990). "Aggradation and degradation of alluvial sand deposits, 1965-1986, Colorado River, Grand Canyon National Park, Arizona," U. S. Geological Survey Professional Paper 1493, 74 p.

Schmidt, J. C., Grams, P. E., and Leschin, M. F. (1999b). "Variation in the magnitude and style of deposition and erosion in three long (8-12 km) reaches as determined by photographic analysis:" in, Webb, R. H., Schmidt, J. C., Marzolf, G. R., and Valdez, R. A., eds., The Controlled Flood in Grand Canyon. Washington, D. C., American Geophysical Union, Geophysical Monograph 110: p. 185-203.

Schmidt, J. C., Topping, D. J., Grams, P. E., and Hazel, J. E. (2004). "System-wide changes in the distribution of fine sediment in the Colorado River corridor between Glen Canyon Dam and Bright Angel Creek, Arizona," final report submitted to U. S. Geological Survey, Grand Canyon Monitoring and Research Center, under cooperative agreement no. 1425-98-FC-40-22640, 107 p.

Schmidt, J. C., and Grams, P. E. (2011). "The High Flows – Physical Science Results," in: Melis, T. S., ed. (2011). "Effects of three high-flow experiments on the Colorado River ecosystem downstream from Glen Canyon Dam, Arizona," U. S. Geological Survey Circular 1366, p. 53-92.

Sondossi, H. A. (2001). "Historical analysis of the geomorphology of sand bars along the Colorado River in Upper Marble Canyon, Arizona," Unpublished MS thesis, Utah State University, Department of Geography and Earth Sciences, 138 p.

Sondossi, H. A., and Schmidt, J. C. (2001). "GIS as a tool for studying the geomorphology of fine-grained deposits in the Colorado River in Grand Canyon National Park," final report in partial fulfillment of contract 1425-98-FC-40-22640, 45 p.

Topping, D. J., Rubin, D. M., Vierra Jr., L. E. (2000). "Colorado River sediment transport—1. Natural sediment supply limitation and the influence of Glen Canyon Dam," Water Resources Research, AGU, 36(2), p. 515-542.

U. S. Department of the Interior (1995). "Operation of Glen Canyon Dam final environmental impact statement, Colorado River Storage Project, Coconino County, Arizona." Salt Lake City, Utah, U. S. Bureau of Reclamation, Upper Colorado Regional Office, 337 p.

U. S. Department of the Interior (2011). "Environmental assessment, development and implementation of a protocol for High-Flow Experimental Releases from Glen Canyon

Dam, Arizona, 2011 through 2020." Salt Lake City, Utah, U. S. Bureau of Reclamation, Upper Colorado Regional Office, 150 p.

Webb, R. H., Schmidt, J. C., Marzolf, G. R., and Valdez, R. A., eds. (1999). The Controlled Flood in Grand Canyon. Washington, D. C., American Geophysical Union, Geophysical Monograph 110, 367 p.

DETERMINATION OF RIVER MAINTENANCE NEED AT INDIVIDUAL SITES AND REACHES ON THE MIDDLE RIO GRANDE

Robert Padilla, P.E. [1], Paula Makar, P.E. [2], and Joseph Maestas, P.E.[3]

[1]River Analysis Group, Albuquerque Area Office, Bureau of Reclamation, Department of the Interior; 555 Broadway Ave. NE, Ste 100, Albuquerque, NM, 87102-2352; PH (505) 462-3626; email: rpadilla@usbr.gov
[2]Sedimentation and River Hydraulics Group, Technical Service Center, Bureau of Reclamation, Department of the Interior; PO Box 25007 (86-68240), 80225-0007; PH (303) 445-2555; email: pmakar@usbr.gov
[3]Technical Services Division, Albuquerque Area Office, Bureau of Reclamation, Department of the Interior: 555 Broadway Ave. NE, Ste 100, Albuquerque, NM, 87102-2352; PH (505) 462-3615; email: jmmaestas@usbr.gov

ABSTRACT

The channel of the Middle Rio Grande (MRG) has been confined to a narrow corridor by riverside infrastructure and geology. It is actively evolving in most locations in response to reduced sediment loads and managed flow regimes due to reservoirs and diversions. In support of the Bureau of Reclamation's (Reclamation) responsibility for MRG Project river maintenance, river work identification and planning follows a systematic process involving: 1) monitoring and analysis: 2) need assessment; 3) work classification; 4) documentation of results (for 1-3); and 5) programmatic project and work planning.

This paper describes the methodology for step 2; determine the relative *Need* for river maintenance. The *Need* for river maintenance relies on both the *Value* of the maintenance and the *Likelihood* of the necessity for maintenance. In the described methodology, *Value* and *Likelihood* are rated by water resources professionals using technical factors associated with river conditions, public interests, and water delivery. Each factor has individual criteria which are updated as state-of-the-practice river hydraulic, geomorphic, and ecological monitoring and assessment improve. The final relative *Need* for river maintenance is the product of the *Value* and *Likelihood* ratings at each location. *Need*, *Value*, and *Likelihood* are terminology specific to this report and assessment methodology that describe the importance, benefit, and potential conditions for river maintenance work.

In applying the rating criteria to the MRG, the *Need* for river maintenance was calculated for 86 sites and 11 reaches for the value-based technical factors of Public Health and Safety and Water Delivery. Rating results from the application were consistent with professional and experiential judgment, and objectively reflected the significance of the sites and reaches for the technical factors. The next steps for *Need* for river maintenance are the development of ecologic and cultural resource ratings.

INTRODUCTION

The MRG Project purposes include performing channel maintenance, ensuring effective water delivery through the middle valley downstream to Elephant Butte Reservoir, reducing the risk of flooding, bankline erosion protection, as well as meeting international treaty water delivery obligations to the Republic of Mexico. These needs and services remain important in the present and are joined by newer considerations for habitat improvement to enhance the ecological function of the system within the Project's congressional authorization. Reclamation has responsibility for sound environmental stewardship with the National Environmental Policy Act of 1973, and the Endangered Species Act of 1973 for listed species and their critical habitats.

River maintenance can be divided into two general types for project development:

- Individual sites - These are projects designed to meet immediate and local river maintenance at specific locations.
- Reach-level strategies – The strategies are designed to holistically address large-scale, observed, geomorphic trends, on a proactive basis. Implementation of projects considers the entire reach is intended to work with the river's underlying governing processes along with enhancing river functions like providing habitat and water delivery.

The Middle Rio Grande River Maintenance Comprehensive Plan and Guide (Maintenance Plan and Guide) (Reclamation, 2012) discusses the MRGP Program, reaches, and strategies in more detail.

The MRG Project river maintenance work identification and planning follows a systematic process involving five main steps. They are:

1) Monitor, analyze, and document channel and floodplain conditions and changes – performed continuously.
2) Identify, evaluate, and rate sites and reaches to determine the relative *Need* for river maintenance – performed annually and as needed.
3) Assign a Maintenance Classification utilizing the following designations for each site or reach – performed annually and as needed. These classifications are patterned after the Review of Operations and Maintenance (Reclamation, 1991) process, recognizing that the river is not a facility but a system. Professional judgment and experience combined with information obtained during the *Need* for River Maintenance assessment are used to assign classes.
    - Class 1 – Maintenance is required in the short term (typically before the next high flow event or could be required immediately) because there is a high likelihood of substantial consequences if no action is taken. Work can be described as interim and unanticipated projects are commonly individual sites.
    - Class 2 – Maintenance can be planned in advance but the consequences of no action could be substantial in the near term (the next normal spring runoff or within the next few years). The class includes the majority of ongoing or normal river maintenance work at existing and new sites.
    - Class 3a – Maintenance can be planned in advance and the consequences of no action are less likely to be substantial in the near term (the next normal spring runoff or within the next few years). It is work that can be described as preventative maintenance and also includes habitat enhancement.
    - Class 3b – Maintenance can be planned and the consequences of no action are less likely to be substantial in the near term (the next normal spring runoff or within the next few years). Data collection and/or analysis are required to determine if preventative or normal maintenance (including habitat enhancement) is needed.
    - Class 4 – Maintenance is not anticipated to be needed in the near term (the next normal spring runoff or within the next few years) because change appears to be occurring at a slow rate. Work can be described as monitoring for potential changes that could accelerate the need for maintenance to the near term. This class also includes monitoring of completed projects.
    - Class 5 – Maintenance may be needed but is not within Reclamation's authority. Responsible parties will be notified if it appears that the consequences of no action could be substantial in the near term.
4) Document assessment results for each location in an individual Site or Reach Report and summarize Relative *Need* for River Maintenance results in a report.
5) Plan maintenance projects and work – annually and as needed. Information from Steps 1 through 4 above, plus programmatic considerations like resource management, policy, budgeting, and stakeholder collaboration are utilized for planning projects and scheduling. Scheduling may require adjustment given the uncertainties in predicting hydrology, geomorphic trends, modeling, etc. on an alluvial river.

This process follows Chapters 3-5 of the Best Practices in Dam and Levee Safety Risk Analysis (Reclamation and USACE, 2012) and the Maintenance Plan and Guide.

This report details the methodology developed for Step 2-Identify, Evaluate, and Rate the Need for river maintenance. *Need* is identified where conditions are causing or may lead to: impacts to public health and safety (e.g. flooding of homes and businesses); damage to riverside infrastructure (e.g. river erodes into a levee, heading, or canal); and reduced effectiveness of water deliveries (e.g. aggradation causes the loss of a competent channel).

The *Need* for River Maintenance relies on the combination of *Value* of the maintenance and the *Likelihood* of the necessity for maintenance. The technical factors of *Value* and *Likelihood* are rated by engineering, geomorphic, ecologic and cultural resources professionals. The technical factors are explained in more detail below. It should be noted that *Value*, *Likelihood*, and *Need* of river maintenance are not specific quantitative consequence, probability, or risk determinations resulting from conventional risk analysis approaches. The *Value*, *Likelihood*, and *Need* ratings are intended for comparative analysis amongst a group of sites or reaches. Step 2 is a screening tool for work identification and prioritization.

SITE AND REACH MAINTENANCE NEEDS

Site Identification:

Individual sites needing river maintenance are currently identified based on meeting any or all of the following general criteria (Reclamation, 2012; Maestas and Padilla, 2011; Smith, 2005):

- The continuation of current trends of channel migration or morphology will likely result in damage to riverside infrastructure within the near term
- Similar conditions have historically resulted in failures or near failures at flows less than the two-year flood
- Existing conditions could cause significant economic loss, danger to public health and safety, or loss of water

River conditions at sites that meet the above criteria are evaluated through ongoing monitoring, evaluation of historical trends, geomorphic analyses, and numerical modeling to help understand the middle Rio Grande system as referenced in Step 1. These same criteria also apply when determining the need for implementation of reach-based strategies. Additionally, habitat value and enhancement opportunities at a site or reach will be included as part of the identification of sites or reaches benefiting from river maintenance. (At the time of this report submission, work is in progress to develop the ecologic and cultural resource *Need* ratings). The benefit of habitat enhancement is primarily a function of the habitat needs of threatened and endangered species.

The evolving river morphology – as it responds to the variable drivers of change (e.g. hydrology and sediment loads) and the controls of change (e.g. bed and bank stability, base level control, floodplain connectivity, floodplain lateral confinement) – is the fundamental cause of river maintenance needs. The combination of Steps 1 and 2 reflects this linkage between the river's morphology and the need for maintenance. Evaluation of the *Need* for maintenance requires characterizing geomorphic processes and current conditions for each reach and site, then estimating the likely future conditions.

Maintenance Need (Likelihood and Value) Technical Factors:

Technical Factors and criteria associated with river conditions, public interests, and water delivery infrastructure are presented below. The technical factors are structured to allow for the site and reach criteria to be updated with advancements in river engineering and ecosystem understanding, and measurement and analysis techniques.

T

he criteria are only guidelines and experienced engineers should use professional judgment and the understanding of local conditions and fluvial processes during the ratings as well.

Likelihood-based Technical Factors

The *Likelihood* is a semi-quantitative estimate of the relative probability that conditions are causing or may lead to damage or impairment without future maintenance. When the damage or function impairment is imminent or has already occurred (e.g. levee failure or degraded habitat), the *Need* for river maintenance has been established so the *Likelihood* rating is simply the highest possible and thus the *Likelihood* Factors do not need to be rated.

1. Percent of Reach Length with Sites (Rating from 1 to 5)

This factor applies only to reach assessments and reflects how the evolving channel and floodplain fit within the lateral constraints of riverside infrastructure and geology. The number of identified maintenance sites is considered as well as the levee condition. Individual local sites are assumed to be ½ mile in length at a minimum; the total actual length for a reach scale project is also used when known. The total length of sites is divided by the reach length to get a normalized percentage of sites by reach.

- **Very low** – Sites occupy less than 5 percent of the reach length.
- **Low** – Sites occupy 5 - 15% percent of the reach length.
- **Moderate** – Sites occupy 15 – 25 percent of the reach length.
- **High** – Sites occupy 25 – 50 percent of the reach length. Downstream of San Acacia the levees rate as high or very high depending on condition.
- **Very high** – Sites occupy more than 50% percent of the reach length. Downstream of San Acacia the levees rate as high or very high depending on condition.

2. Bed and Slope Instability (Rating from 2 to 4)

A key criterion is the comparison of sediment transport capacity to sediment supply. The Maintenance Plan and Guide report provides information on the extent of imbalance as estimated by slope stability. Trends in bed material size, bed elevation and channel width are also important, but not all criteria need to be met for a rating. Local conditions may be used when known.

- **Low** – The reach slope is near the stable slope, bed material is stable, and bed elevation and widths are not changing
- **Moderate** – The reach slope is near the stable slope, local bed material and width changes are occurring, bed elevation may or may not be changing
- **High** – The reach slope is not near the stable slope, local bed material is not stable, and/or widths are narrowing and bed elevations are changing

3. Planform Instability (Rating from 1 to 5)

The main criteria are the current planform stage, the balance between sediment transport capacity and supply, and the degree of vegetation encroachment. Figure 1 shows the stages used below. More information can be found in Massong et al. (2010).

Planform changes are evaluated based upon likely conditions in the near term (< 5 years). Below are the descriptions of the classes:

- **Very low** – Planform is stage 1, A6, or M8 and sediment transport capacity is near supply, with no vegetation encroachment
- **Low** – Planform is stage 2, 3, or M5 and sediment transport capacity is near supply, with little or no vegetation encroachment
- **Moderate** – Planform is stage A4, M4, or M7 and sediment transport capacity is near supply, with little vegetation encroachment, or stage 3 with some vegetation encroachment
- **High** – Planform is stage A4, M4 or M5 and sediment transport capacity is not near supply, with vegetation encroachment present
- **Very high** - Planform is stage A5 or M6-M7 and sediment transport capacity is not near supply, with vegetation encroachment present

4. Bank Susceptibility to Erosion (Rating from 1 to 5)

The main criteria are the erosive susceptibility of the bank and the angle of attack. The erosive susceptibility of the bank includes the type of bank material, the type of river bed material, and the amount of vegetation. BSTEM (Simon et al., 2013) or meander evaluations may be used instead of the qualitative evaluation below. For reaches the same criteria are used and consider the majority of the reach length plus the sinuosity. Below are the descriptions of the classes for rating:

- **Very low** - mostly cohesive bank and/or dense root mass and/or gravel, very dense understory (have to crawl through), no incision, and a very low angle of attack (less than 20^o)
- **Low** - some cohesion and/or root mass, dense understory but can still walk, low level incision, low angle of attack (20^o to 30^o)
- **Moderate** - cohesionless banks (sand), sand bed with small amount of gravel, some understory, some open areas but can still drive, moderate level of incision, moderate angle of attack (30^o to 40^o), minor opposite bar and meander pattern
- **High** - cohesionless banks (sand), some gravel bed material, sparse vegetation (majority of area between bank and levee is open, minimal understory), high incision, high angle of attack (40^o to 60^o), opposite bar and meander pattern
- **Very High** - cohesionless banks (sand), very sparse vegetation (little to none), very highly incised, very high angle of attack (60^o to 90^o), strong opposite bar and/or meander pattern

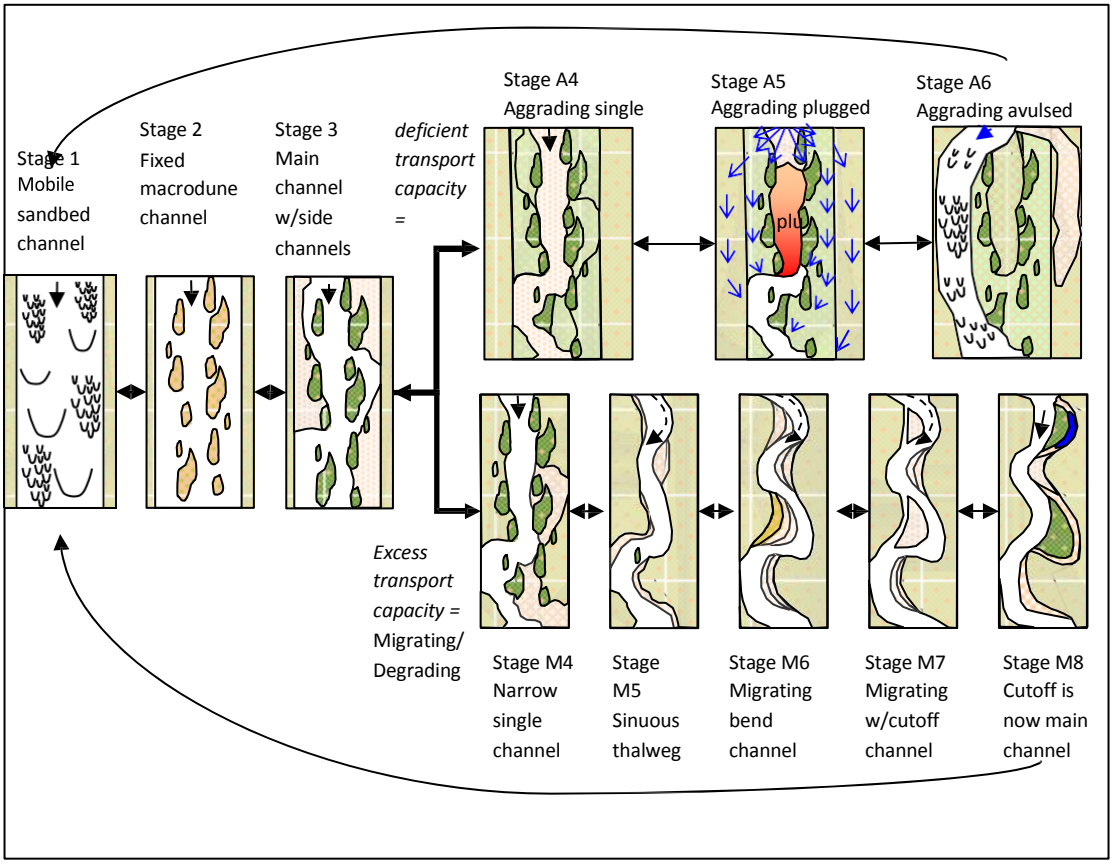

Figure 1 Planform cycles identified on the Rio Grande (Massong et al., 2010)

5. Proximity of infra-structure to river (e.g. levee toe or edge of facility) (Rating from 1 to 5)

The main criterion is the distance between the riverbank and the edge of the structure for river maintenance sites. For reach evaluations, the percent of the reach length where the meander belt width fits between the lateral constraints should be used as well as the percent of the area available between the constraints used by the meander belt width. The class descriptions are as follows:

- **Very Low -** greater than 200 feet. For reaches, the meander belt fits along 100 percent of the reach length and it uses less than 25 percent of the available area.
- **Low –** 150 to 200 feet. For reaches, the meander belt fits along a least 90 percent of the reach length and it uses less than 50 percent of the available area.
- **Moderate –** 100 to 150 feet. For reaches, the meander belt fits along less than 90 percent of the reach length and it uses less than 50 percent of the available area.
- **High -** 50 to l00 feet. For reaches, the meander belt fits along less than 90 percent of the reach length and it uses less than 75 percent of the available area.
- **Very High -** less than 50 feet. For reaches, the meander belt fits along less than 90 percent of the reach length and it uses more than 75 percent of the available area.

6. Past rate of lateral movement (Rating from 1 to 5)

The main criterion for this factor is the average rate of bank erosion and migration toward infrastructure. Typically, this average rate over several years will be based on aerial photography; unless the site is heavily monitored in which case it may be based on physical measurements. When known, the maximum rate of movement during one season should be considered. For reaches, professional judgment as to whether the average rate of movement for the reach as a whole is qualitatively very low to very high should be used to assign a rating class, but may be modified by consideration of the highest rate at a single location in that reach. Hydrology during the measurement period shouldalso be considered in the rating. For example, if flows have been low for several years and the rate of lateral

movement is low, it may be useful to look at rates of movement during periods of higher flows as well. Classes are:

- **Very Low** - channel is gradually moving toward the riverside facility, <5 ft/yr.
- **Low** - channel is slowly moving toward the riverside facility, 5 - 10 ft/yr.
- **Moderate** - channel is migrating at a moderate rate toward the riverside facility, 10 - 20 ft/yr.
- **High** - channel is migrating rapidly toward the riverside facility, 20 - 30 ft/yr.
- **Very High** - channel is migrating very rapidly toward the riverside facility, >30 ft/yr.

7. Channel and Floodplain Capacity Compared to MRGP Authorization (Rating from 2 to 4)

These criteria are used to evaluate the likelihood of flooding or other effects due to inadequate safe channel capacity. Capacity is reduced by sediment deposition that isn't mobilized by later flows. For example, this may be due to large grain sizes (e.g. coarse material supplied by arroyos), large sediment volume events (e.g. significant fires in the watershed), or vegetation encroachment with sediment trapping and stabilization. The time frame is the next few years. Middle Rio Grande Project authorization provides for Reclamation to maintain a channel capacity of not less than 5,000 cfs or the equivalent two-year return flow of the reach. Channel capacity is assessed through hydraulic modeling. When assessing floodplain and levee capacity with hydraulic modeling, an extra two to three feet of freeboard should be added in a perched system.

- **Low** - Capacity exceeds standards
- **Moderate** - Capacity meets standards
- **High** - Capacity is less than standards

8. Possibility of Channel Capacity Loss (Rating from 1 to 5)

Current trends are examined to determine expectations of a reduction, little change, or an increase in channel capacity. Hydraulic geometry trends should be used when available. The classes are:

- **Very Low** – channel capacity is increasing
- **Low** – channel capacity is generally constant, little or no channel narrowing
- **Moderate** – channel capacity is expected to slightly reduce every few years; with minimal levee raising, channel dredging, and minor channel narrowing and vegetation encroachment
- **High** – channel capacity is expected to reduce, continued levee raising or channel dredging are required, some channel narrowing and vegetation encroachment is occurring
- **Very High** – channel capacity is significantly reduced, levees need considerable raising or the channel needs considerable dredging year after year, significant channel narrowing and vegetation encroachment is occurring, plugs have occurred in past, bank heights are less than two to three feet.

9. Possibility of Levee or Embankment Failure (Rating from 1 to 5)

There are three main modes of levee failure: piping and internal erosion from flows against the levee, overtopping of the levee, and bank erosion into the levee. Only the first mode is assessed through this Factor.

- Water against Levee is of sufficient depth to cause failure through erosion or piping
  - **Very low** – no water against levee
  - **Low** - Engineered levee; water remains for few days; no sand boils; no longitudinal or lateral cracking; no sloughing; no extensive burrow holes; not an avulsion or plug prone area
  - **Moderate** - Engineered levee; water remains for several days; no sand boils; no longitudinal and lateral cracking; no sloughing; no extensive burrow holes; not an avulsion and plug prone area
  - **High** – Spoil levee; water remains for a few days; no sand boils; no longitudinal and lateral cracking; no sloughing; no extensive burrow holes; avulsion and plug prone area
  - **Very High** – Engineered or spoil levee; water remains for several days; sand boils, longitudinal and lateral cracking, sloughing, or extensive burrow holes present; avulsion and plug prone area
- Levee Overtopping – this is a failure mode, its condition is assessed through Factors related to channel capacity
- Bank erosion into levee – this is a failure mode, its condition is assessed through Factors related to bank erosion

10. Degree of Perching (Rating from 1 to 5)

The historical aggrading nature of, and the historic levees on, the Rio Grande have resulted in a channel bed that

may be perched above the local floodplain between the levees and may also be perched above the area outside the levees as shown in Figure 2. The average of the ratings from inside and outside the levee will apply in most cases. For reaches, the greatest percentage of cross sections in a reach determines the rating.

- **Very low** – Channel bed substantially below overbank elevation and/or outside of the levee system
- **Low** - Channel bed below overbank elevation and/or outside of the levee system
- **Moderate** - Channel bed near overbank elevation and/or outside of the levee system
- **High** - Channel bed higher than overbank elevation and/or outside of the levee system
- **Very High** – Channel bed substantially higher than overbank elevation and/or outside the levee system

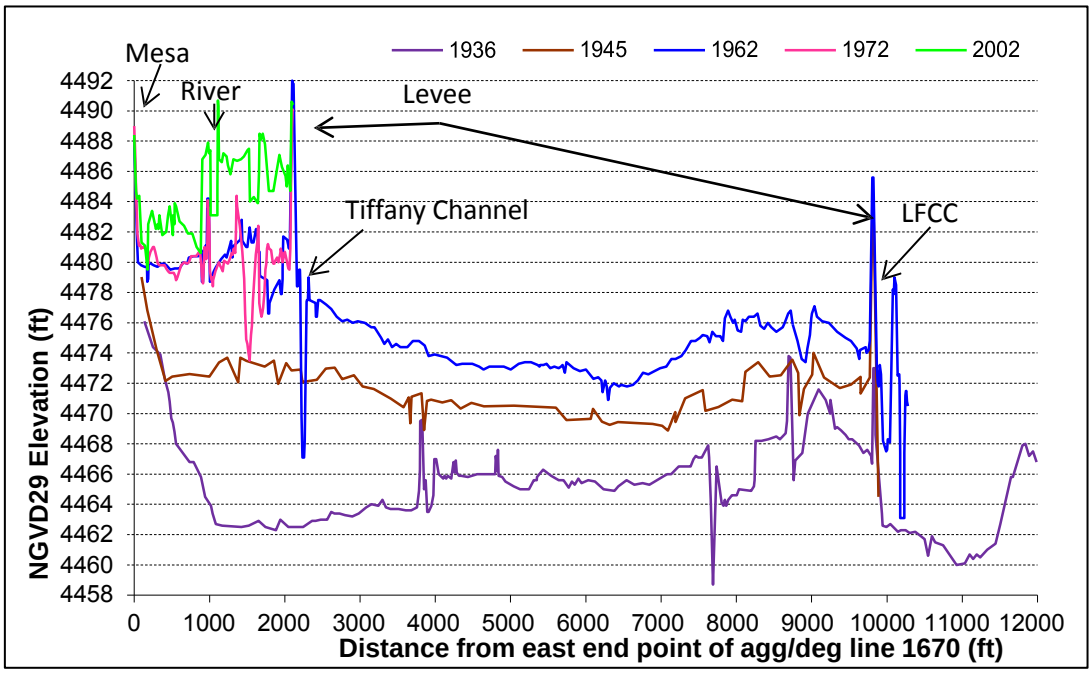

Figure 2 Agg/Deg Line 1670 where river is perched above floodplain and above valley

Value-based Technical Factors

Two factors (Public Health and Safety and Water Delivery) are used to estimate the *Value* or derived benefit of performing river maintenance at a site or reach from an authorized mission and public trust responsibility. *Value* of river maintenance from an ecological function and/or cultural resources viewpoint is not presented in this paper and is in development. Evaluation of the *Value* of performing river maintenance at a site or reach from an ecological function and/or cultural resources viewpoint could bring the number of *Value* factors to four. It is important to note the *Value* factors are rated linearly (i.e. 1-5) while the effects to the river system associated with any impacts (by the *Likelihood* factors) on these factors may be nonlinear.

1. Public Health and Safety (Rating from 1 to 5)

These criteria are used to evaluate the *Value* impact of no river maintenance and take into consideration the population concentration, the proximity of population to flooding (groundwater wells, septic systems, roads, homes, etc.) and the potential outcome of that flooding. Considerations include public infrastructure such as railroads, roads, and sewer lift stations. Rating descriptions were adapted from Smith (2005) and the Truckee Canal Issue Evaluation Report of Findings (2011):

- **Very low** –- Non-Populated Areas – No significant effects to the local population other than temporary minor flooding of roads or land
- **Low** – Sparsely Populated Areas – Minor property and environmental damage may occur. Damage is possible to sewer outfalls, recreation areas, rural roads, and bridges in low-lying areas. Direct loss of life is unlikely.

- **Moderate** – Moderately Populated Areas – Impacts could include moderate property and environmental damage. Damage to permanently occupied structures, recreation areas, local paved roads and bridges in low lying areas is possible. Terrain suggests direct loss of life is possible related primarily to difficulties in warning and evacuating recreationists/travelers and small population centers.
- **High** – Densely Populated Areas – Impacts could include extensive damage to permanently occupied structures, secondary roadways and bridges, and sewer lift stations. Terrain suggests direct loss of life is possible, related primarily to difficulties in warning and evacuating smaller population centers, or difficulties evacuating large population centers with significant warning time.
- **Very High** – Large Population affected – Impacts could include extensive damage to permanently occupied structures, primary roadways, bridges, and railroads, or regional effects such as contamination of Elephant Butte or Cochiti reservoirs. Terrain suggests direct loss of life could be high due to limited warning for large population centers and/or limited evacuation routes.

2. Water Delivery (Rating from 1 to 5)

These criteria are used to evaluate the *Value* impact on water delivery and riverside irrigation infrastructure of no maintenance. Consideration includes both impacts at specific sites (e.g. diversions) and downstream effects. Descriptive classes for infrastructure/function effects:

- **Very low –-** Little change to Water Delivery
- **Low** – Minor change to Water Delivery – impacts to drains for one to two miles,
- **Moderate** – Medium change to Water Delivery – impacts on secondary canals, irrigation/laterals (drains) for two to ten miles
- **High** – Major change to Water Delivery – impacts to main canals or multiple miles of damage to drains/canals (greater than ten miles),
- **Very high** – Regional change to Water Delivery – regional impacts on water delivery

CALCULATION OF SITE AND REACH NEED FOR MAINTENANCE

The steps to calculate the estimated Relative *Need* for River Maintenance are shown in Figure 3. As discussed earlier, the *Need* for River Maintenance is a function of the *Likelihood* of *Need* for River Maintenance and the *Value* of River Maintenance. The sources of change that lead to the *Likelihood* of *Need* for River Maintenance at a site or reach on the Middle Rio Grande can be grouped into three physical processes/ mechanisms: instability of channel bed, slope and planform; bank erosion leading to damage; and aggradation and/or island and bar growth leading to inadequate channel capacity. The 10 *Likelihood* Technical Factors (LTF) are therefore grouped into Potential for Channel Instability (LTF 1, 2, and 3), Potential for Bank Erosion (LTF 4, 5, and 6), and Potential for Loss of Channel Capacity(LTF 7, 8, 9, and 10), the geometric mean is calculated for each grouping. The Potentials for Channel Instability and Bank erosion are combined by calculating their geometric mean. The Potentials for Inadequate Channel Capacity and Channel Instability are also combined by calculating their geometric mean. These combinations provide both the Likelihood for Bank Erosion and Inadequate Channel Capacity Effects. Lastly, these Likelihoods are combined by taking their geometric mean to determine a composite Likelihood of Need for River Maintenance.

The *Value* Technical Factors (VTF) are then directly assessed through the criteria listed above. The Relative *Need* for River Maintenance of a reach or site is calculated by multiplying the *Likelihood* of *Need* for River Maintenance by each of the two presented *Values* (Public Health and Safety, Water Delivery) of River Maintenance. An overall *Need* for river maintenance is not calculated because each *Value* (Public Health and Safety and Water Delivery) can vary in importance due to programmatic considerations.

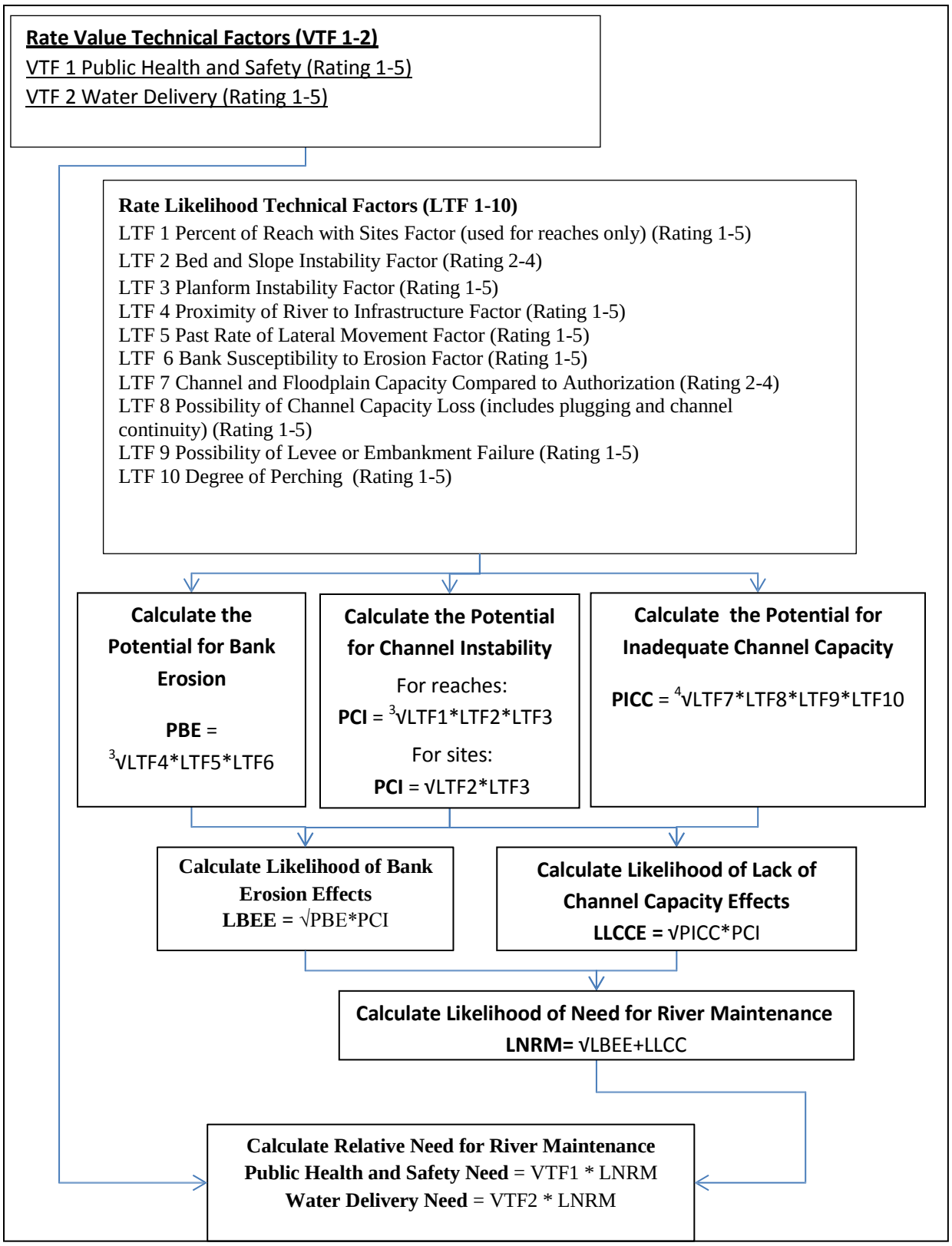

Figure 3 Flowchart of Relative Need for River Maintenance Determination

SITE AND REACH MAINTENANCE NEEDS RESULTS

Eighty six sites and eleven reaches were evaluated at current conditions. Final rating results for Likelihoods of Bank Erosion Effects, Channel Capacity Effects, Need for River Maintenance, and the Relative Needs for River Maintenance are presented in Reclamation (2014). Figures 4 and 5 below show the results of Need determination for the individual sites (only 17 shown, 86 rated total) and all eleven of the geomorphic reaches.

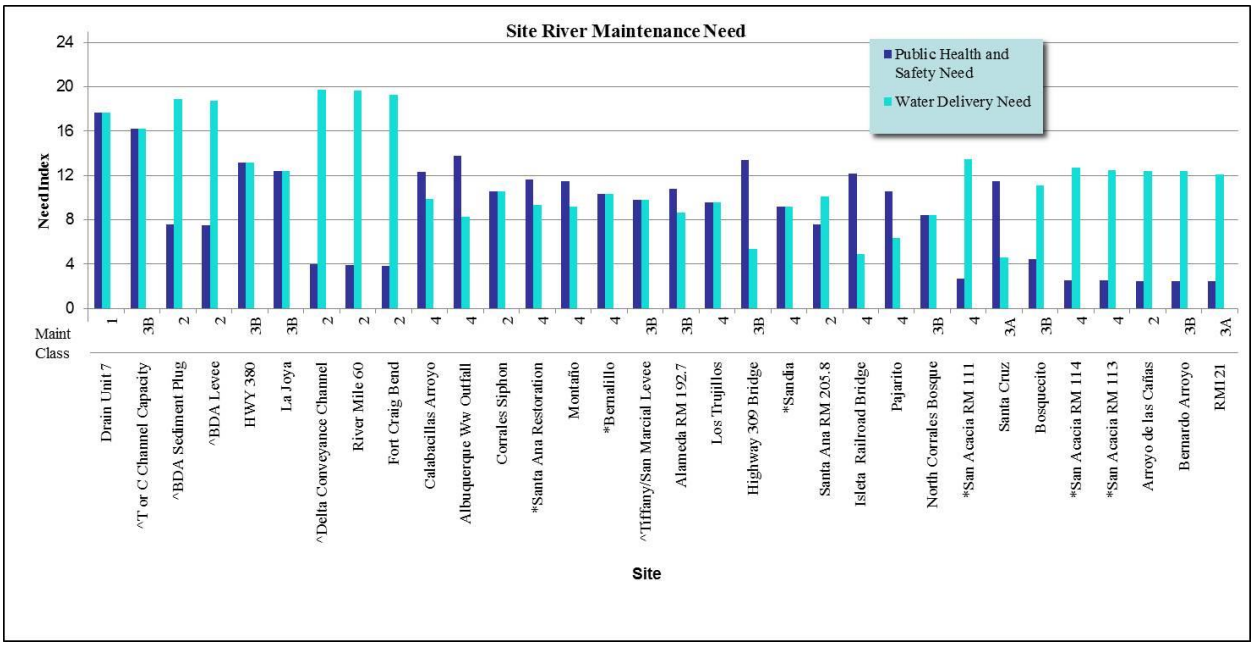

Figure 4 Site River Maintenance Need Results for Public Health and Safety; Water Delivery

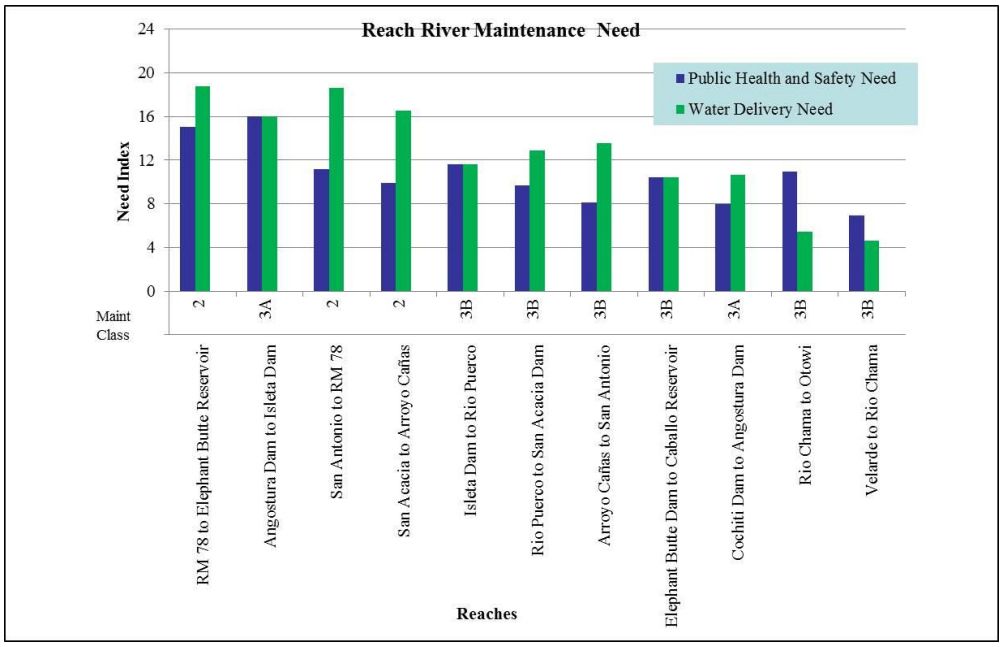

Figure 5 – Reach River Maintenance Need Results for Public Health and Safety; Water Delivery

These ratings provide semi-quantitative technical decision-making guidance for project planning. The assessment of the *Need* for river maintenance and assignment of a Maintenance Class occurred during a May 2014 workshop setting that best utilized the expertise of knowledgeable and experienced engineers, geomorphologists, biologists, and other professionals. The results of this workshop were documented for future reference related to maintenance need identification for the River Maintenance Program. Future updates to the ratings should be conducted and documented in similar workshops (with the best available tools/criteria for the Likelihood and Value Factors) as a part of the normal annual river review.

The Best Practices in Dam and Levee Safety Risk Analysis (2012) provides guidance on documenting or "making the case" for the Need for river maintenance. Chapters 3 and 4 are especially pertinent for further consideration. Other considerations in the final decisions on river maintenance work planning are the real-time circumstance and humanistic-based operational decisions that are made in regards to maintenance activities. Such considerations may include but are not limited to: area office priorities, scheduling, proximity to other sites, and if there is a potential for increased maintenance resulting from other non-Reclamation river projects. These considerations allow effective planning of river maintenance activities and may result in lower Class projects being undertaken concurrently with higher Class projects. The end result is anticipated to maximize the benefits from river maintenance. It is important to note that the Maintenance Class designations identified in Step 3 on page 2 of this report rely heavily on professional/experiential judgment and understanding the historic and real time dynamic river conditions.

The Maintenance Class Designations (1, 2, 3a, 3b, 4, and 5) indicate the recommended *Urgency* and corresponding level of response by the River Maintenance Program to the identified relative maintenance *Need*. There is not a simple correspondence of the factor ratings to Class Designations because the criteria do not directly evaluate the *Urgency*. *Urgency* for river maintenance reflects the apparent response time before further impacts occur to the identified *Values*. The *Urgency* is strongly dependent on professional judgment and experiential considerations derived from observing and monitoring the river system. Urgency can further be analyzed by defining the hydrologic loadings/triggers that drive river response to create a *Need*. These loadings include single events and also long term river flow trends involving frequency, magnitude, and duration. The *Likelihood*, *Value*, and *Need* ratings help inform the Maintenance Class designation. Since Technical Factors and criteria to rate the Ecological Function *Value* of river maintenance are not available at this time, it should be noted that the Maintenance Classes may be adjusted or a separate class structure for habitat restoration added after development of those Technical Factors and criteria.

Overall, this tool helps to systematically evaluate all sites and reaches with consistent Factors for *Likelihood* and *Value* to arrive at a relative *Need* determination for the two *Values* of Public Health and Safety and Water Delivery. This methodology is intended to be a rapid assessment tool to be applied at least annually in response to the dynamic river and hydrologic conditions on the Middle Rio Grande. It should be noted that even though the Potential for Channel Instability, the Potential for Inadequate Channel Capacity, and the Potential for Bank Erosion along with the Values of Public Health and Safety and Water Delivery are rated for the sites and reaches, not all potential effects to the river system are explicitly accounted for. This is due to the non-linear relationships in the rating Factors for predicting channel response and associated impacts; their scale (localized and reach level effects); their spatial variability (varying geomorphic conditions in each reach); and the temporal nature of effects occurring from a progression of physical processes due to specific hydrologic events or long term trends.

REFERENCES

Holste, N. (2013). Geomorphic Assessment of the Rio Grande Upstream of Elephant Butte Reservoir. U.S. Department of the Interior, Bureau of Reclamation, Upper Colorado Region, Albuquerque Area Office, Technical Services Division, Albuquerque, New Mexico.

Maestas, J.M. and Padilla, R.S. (2011). Leadership Team Strategic Plan, Final Report: Lessons Learned on Planning and Scheduling River Maintenance and Restoration Projects. U.S.Department of the Interior, Bureau of Reclamation, Upper Colorado Region, Albuquerque Area Office, Technical Services Division, Albuquerque, NM.

Makar, P. and AuBuchon, J. (2012). Channel Conditions and Dynamics on the Middle Rio Grande. Department of the Interior, Bureau of Reclamation, Upper Colorado Region, Albuquerque Area Office, Technical Services Division, Albuquerque, NM.

Massong, T., Makar, P., Bauer, T. (2010). Planform Evolution Model for the Middle Rio Grande, NM , Proceedings of the 2nd Joint Federal Interagency Conference, Las Vegas, NV, June 27 - July 1, 2010

Reclamation, (2014). Determination of River Maintenance Need at Individual Sites and Reaches on the Middle Rio Grande, NM. Department of the Interior, Bureau of Reclamation, Upper Colorado Region, Albuquerque Area Office, Determination of River Maintenance Need Team, Albuquerque, NM.

Reclamation and USACE. (2012). Best Practices in Dam and Levee Safety Risk Analysis. U.S. Department of the Interior, Bureau of Reclamation, Dam Safety Office, Denver, CO.

Reclamation. (2012). Middle Rio Grande River Maintenance Program Comprehensive Plan and Guide, U.S. Department of the Interior, Bureau of Reclamation, Upper Colorado Region, Albuquerque Area Office, Technical Services Division, Albuquerque, NM.

Reclamation. (2011). Truckee Canal Issue Evaluation Report of Findings. U.S. Department of the Interior, Bureau of Reclamation, Technical Service Center, Geotechnical Services Division, Denver, CO.

Reclamation. (1991). Review of Operation and Maintenance Program Field Examination Guidelines. U.S. Department of the Interior, Bureau of Reclamation, Technical Service Center, Denver, CO.

Simon, A., Pollen-Bankhead, N., and Thomas, R. E. (2013). Development and Application of a Deterministic Bank Stability and Toe Erosion Model for Stream Restoration, *in* Stream Restoration in Dynamic Fluvial Systems (eds A. Simon, S. J. Bennett and J. M. Castro), American Geophysical Union, Washington, D.C.

Smith K.I. (2005). Determination of the Overall Recommended Action. U.S. Department of the Interior, Bureau of Reclamation, Upper Colorado Region, Albuquerque Area Office, Technical Services Division, Albuquerque, NM.

MORPHOLOGICAL IMPACT OF A REHABILITATION PROJECT: SRH-2D MODELING ASSESSMENT

Yong G. Lai, Technical Service Center, U.S. Bureau of Reclamation, Denver, Colorado, ylai@urbr.gov; David Gaeuman and David J. Bandrowski, Trinity River Restoration Program, U.S. Bureau of Reclamation, Weaverville, California, dgaeuman@usbr.gov, dbandrowski@usbr.gov

Abstract. Geofluvial modeling is carried out using a coupled morpho-dynamic and bank erosion model referred to as SRH-2D. This model is used to predict the geomorphic impact of the Upper Junction City (UJC) rehabilitation project located on the Trinity River in Northern California. This geofluvial model was developed for the study and consists of two components: (1) a 2D mobile-bed model (SRH-2D) for vertical stream bed changes and hydraulic forces acting on bank toes; and (2) a bank retreat model for lateral bank erosions. The geofluvial model is first calibrated between a "pre-erosion" baseline condition from April 2009 and a measured "post- erosion" condition from August 2011. The model was found to be capable of predicting vertical bed changes and lateral bank erosion. The calibrated model is then applied to assess the potential future impacts of the river rehabilitation project on channel morphology under two scenarios: a 2011 "post-erosion" condition and a 2012 "design construction" condition. A comparison of the two provides necessary data with which to evaluate the potential design impact of the UJC project over a hypothetical evolution scenario.

INTRODUCTION

Stream bank erosion is a natural geomorphic process occurring in all alluvial channels. It is an important mechanism by which a channel adjusts its size, shape, and slope to convey the supply of both water and sediment. In recent years, both one-dimensional (1D) and two-dimensional (2D) numerical models have been used to predict channel responses, but most either ignore bank failure mechanisms or implement only simple ad hoc methods. Not accounting for stream bank failures in mobile-bed simulations may result in biased or erroneous predictions of degradation, aggradation, equilibrium channel geometry, and sediment loadings.

Most river restoration and rehabilitation projects are carried out without performing a quantitative geofluvial assessment. Physical analyses are usually restricted to hydraulic simulations only, due to the limited amount of practical and reliable geofluvial models available. A number of mobile-bed sediment transport models are available, such as HEC-RAS, SRH-1D, CONCEPTS, CCHE2D, and SRH-2D. They are versatile and offer extensive capabilities and choices in modeling the vertical changes in stream bed elevations. However, most of them do not take lateral bank erosion into consideration, except for CONCEPTS and SRH-2D, and cannot be used to predict lateral stream changes.

Recently, SRH-2D has been extended to include a bank erosion module, which is the motivation behind the present study. In this study, we investigate how the geofluvial SRH-2D model performs when tested against a field case at the Upper Junction City (UJC) rehabilitation project on the Trinity River in Northern California. Further, we demonstrate how a 2D geofluvial model like SRH-2D may be used to assess the impact of a proposed river rehabilitation project design on local channel morphology.

NUMERICAL MODEL AND MODELING DETAILS

SRH-2D Model Description SRH-2D is a 2D, depth-averaged, hydraulic and sediment transport model for river systems under development at the Bureau of Reclamation. The hydraulic flow model, documented by Lai (2008; 2010), has been widely utilized by internal and external users. The sediment transport module is used to predict vertical stream-bed changes and has been described by Lai and Greimann (2008; 2010) and Lai et al. (2011). The sediment module tracks multi-size, non-equilibrium sediment transport of suspended, mixed, or bed load for both cohesive and non-cohesive materials. The effects of gravity and secondary flows are accounted for by displacing the direction of the sediment transport vector from that of the local depth-averaged flow vector.

Recently, SRH-2D has been expanded for geofluvial modeling by developing and incorporating a number of bank modules (Lai et al., 2012; Lai and Wu, 2013; Lai et al., 2015). The simultaneous vertical and lateral modeling capability, i.e., geofluvial modeling, has been reviewed and summarized by Lai (2014). With the latest SRH-2D model, main channel fluvial processes may be solved with the regular 2D depth-averaged mobile-bed module, while the lateral bank erosion processes are solved with bank modules. In this study, the latest geofluival SRH-2D model is used.

Modeling Steps and Scenarios SRH-2D modeling, in general, includes the following steps: (1) selection of the solution domain; (2) mesh generation and definition of boundary conditions; (3) assigning topography, flow roughness and bed sediment gradations; (4) model calibration; and (5) model applications. The first three steps are discussed herein; the remaining two steps are reported later.

Two sets of modeling scenarios are carried out at the UJC project reach. The first set of model runs is for model calibration and validation using the 2009 "Pre-erosion" baseline condition (named "*Pre_E*"). The *Pre_E* runs use the 2009 terrain as the initial bathymetry and the 2009- 2011 three-year hydrograph is simulated. The predicted 2011 topography is compared to the measured 2011 terrain data. The second set of runs applies the calibrated model for assessing the impact of design construction on stream morphology. Two scenarios are simulated: the 2011 "post-erosion" condition (named "*Post_E*") and the 2012 "Proposed Design" condition (named "*Design*"). The *Post_E* runs utilize the 2011 terrain as the initial bathymetry while the *Design* runs adopt the design condition topography of the UJC river rehabilitation project as the initial bathymetry. The morphological changes under *Post_E* and *Design* conditions are simulated with the same three-year hydrograph as the *Pre_E* condition. Since the topography of the proposed design condition was close to the 2011 terrain, and all model parameters are the same, a comparison of the *Pre_E* and *Design* modeling results provides the necessary data to assess the impact of the proposed design condition on future channel morphology. Note that only a three-year hydrograph is used so prediction of the form of the long-term equilibrium channel has not been attempted. Also note, the actual "As-built" or "constructed" topography was not evaluated for this study.

Solution Domain, Mesh and Initial Terrain The solution domain and one of the meshes developed for the present study are shown in Figure 1a. The solution domain is about 4,000 feet in channel length and averages 700 feet in width. The meshes are generated using Surface-water Modeling System (SMS) software. Two meshes are generated corresponding to the calibration and application modeling runs. The same mesh is used with *Post_E* and *Design* scenarios so that the differences of the model results are due mainly to the *modifications* introduced by the design condition. Meshes consist of mixed quadrilaterals and triangles with a total of 18,414 and 19,119 cells, respectively, for the *Pre_E* and *Post_E/Design* scenarios. There are three initial terrains for all modeling runs: the 2009 pre-erosion (*Pre_E*); the 2011 post-erosion (*Post_E*); and the proposed 2012 design condition (*Design*) scenarios. A 3D perspective view of the initial terrain for the *Design* scenario is shown in Figure 1b.

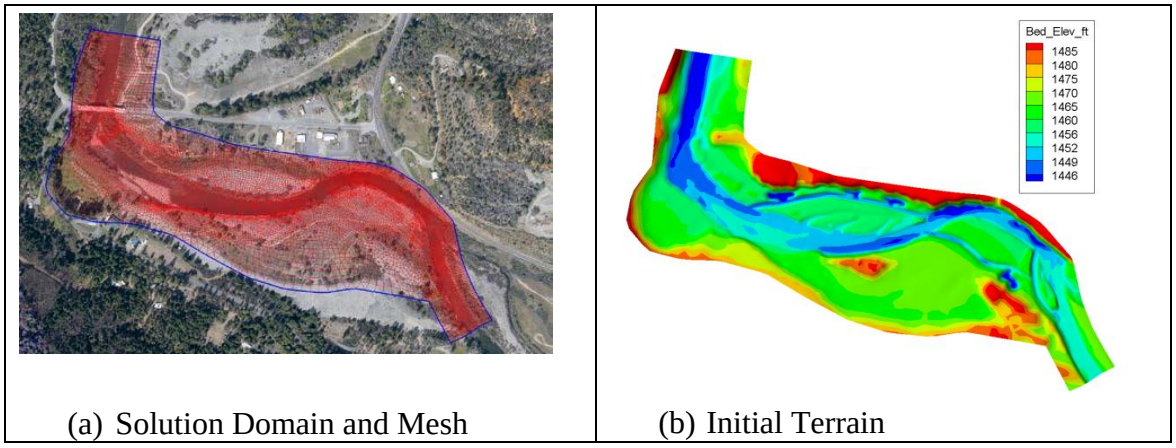

(a) Solution Domain and Mesh (b) Initial Terrain

Figure 1 Solution domain (blue) and the mesh (red) for scenario PB, and 3D perspective view of initial terrain for *Design* scenario. The aerial photo was taken in August 2011

Flow Resistance and Bed Gradation The flow resistance and initial bed/subsurface sediment gradation are the two major inputs to the model. The flow resistance is computed with the Manning's roughness equation. In this study, the Manning's coefficient (*n*) is based on estimation from previous studies on the Trinity River. The solution domain is divided into three zones (Figure 2) and *n* for each zone is assigned as: 0.035 for the main channel and the bare floodplain, and 0.085 for the vegetation zone. The bed and subsurface sediments in the main channel are based on field survey data and divided into two layers. The surface layer has a thickness of 0.65 ft and the subsurface layer has an infinite thickness. The gradations of the two layers are similar, with a medium diameter about 29 mm (Figure 3a). The bare floodplain is assumed to be uniform with a sediment gradation as the subsurface layer of the main channel. Only deposition is allowed in the vegetation, so no bed gradation is needed.

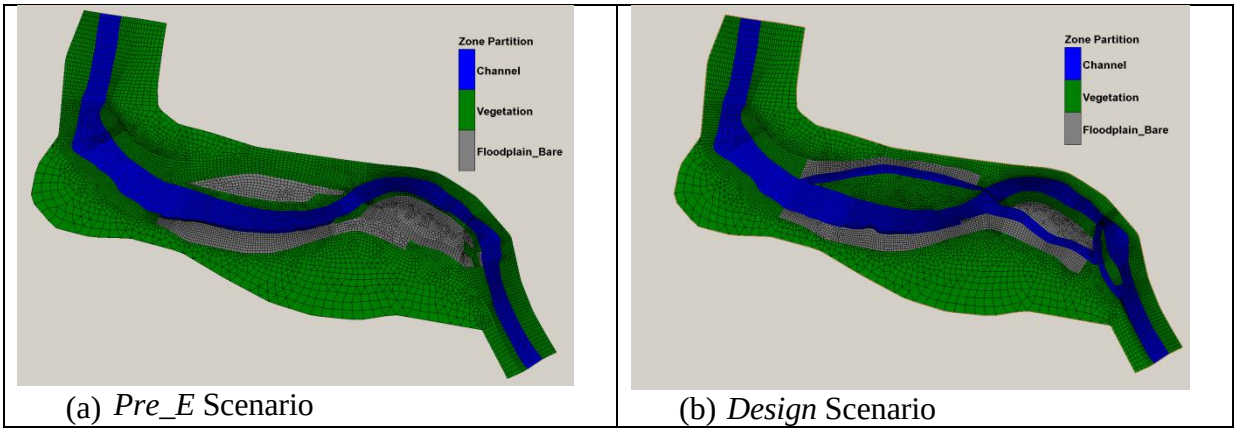

(a) *Pre_E* Scenario (b) *Design* Scenario

Figure 2 Zonal partition of the solution domain for both roughness assignment and bed gradation representation

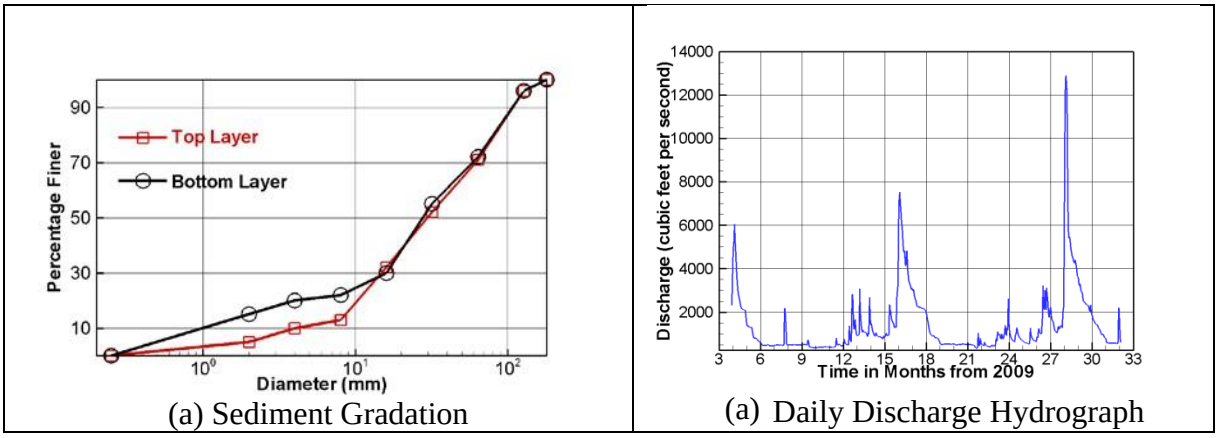

(a) Sediment Gradation (a) Daily Discharge Hydrograph

Figure 3 Bed and subsurface sediment gradation in the main channel and daily flow discharges from April 29, 2009 to September 3, 2011 at the Upper Junction City site

Boundary Conditions and Other Model Inputs Time-accurate unsteady simulations are carried out using the daily mean flow hydrograph from April 29, 2009 to September 3, 2011 (USGS gaging station 11526250), which includes three spring runoff events (Figure 3b). This hydrograph is used as the upstream flow boundary condition for all model runs. Sediment load is needed as another upstream boundary condition. Sediment rating curves developed by the Trinity River Restoration Program, based on the 2006-2007 sediment data at the Douglas City site of the Trinity River, are used. Water surface elevation (stage) is needed as the downstream boundary condition. A stage-discharge rating curve is developed using HEC-RAS modeling results for a much larger reach and is used as the boundary condition.

A total of nine sediment size classes are used to represent bed materials ranging from 0.25 to 181 mm in size. The Trinity sediment transport capacity equation developed by Gaeuman et al. (2009) is used as the equilibrium rate. The Trinity capacity equation is a modified version of the equation developed by Wilcock and Crowe (2003). For a sediment size class *k*, it may be expressed as:

$$\frac{q_{t,k}^{*} g(s-1)}{(\tau_b / \rho_w)^{1.5}} = p_{ak} G(\phi_k); \qquad \phi_k = \frac{\theta_k}{\theta_r}\left(\frac{d_k}{d_{50}}\right)^{\alpha_k} \tag{1}$$

where $q_{t,k}^{*}$ is the volumetric sediment transport rate per unit width, p_{ak} is the volumetric fraction of sediment size class *k* on the bed surface, $s = \rho_S / \rho_w$, ρ_w and ρ_S are the water and sediment density, respectively, *g* is the gravitational acceleration, τ_b is the bed shear stress, $\theta_k = \tau_b / [\rho_w g(s-1)d_k]$ is the Shield's parameter of sediment size class *k*; θ_r is the reference Shield's parameter, d_k is the diameter of sediment size class *k*, and d_{50} is the median diameter of the sediment mixture in bed. The function in the transport equation is expressed as:

$$G(\phi) = \begin{cases} 14.0(1 - 0.894/\phi^{0.5})^{4.5} & \phi \geq 1.35 \\ 0.002\phi^{7.5} & \phi < 1.35 \end{cases} \quad (2)$$

Two parameters must be defined to apply the above equation: θ_r and α_k. The parameter θ_r is a reference value above which sediment is mobilized and α_k is the exposure or hiding factor to account for reduction in critical shear stress for larger particles and increase in critical shear stress for smaller particles The standard Trinity equation used the following values:

$$\theta_r = 0.021 + 0.0155\exp(-20F_s) \quad (3a)$$

$$\alpha_k = 1 - \frac{0.7}{1 + \exp(1.9 - d_k / 3d_{50})} \quad (3b)$$

where F_s is the fraction of sand on the bed surface (the cutoff diameter of the "sand" may range from 1 to 4 mm). In this study, a constant reference value $\theta_r = 0.035$ was used. As a comparison, the Wilcock-Crowe (2003) equation used the following default values:

$$\theta_r = 0.021 + 0.015\exp(-20F_s) \quad (4a)$$

$$\alpha_k = 1 - \frac{0.67}{1 + \exp(1.5 - d_k / d_{50})} \quad (4b)$$

Other model inputs included the following. The time step is five seconds, mainly for numerical stability control. The active layer thickness is 0.15 ft, about five times d_{50} and 1.5 times d_{90}. The bedload adaptation length is based on the work of Lai (2013) derived from Seminara et al. (2002); other runs used a constant adaptation length of 80 meters.

Bank Module Inputs Additional input parameters are related to the bank properties for a coupled morpho-dynamic and bank erosion modeling. A section of the river left bank is selected for bank retreat modeling (Figure 4a) with sixteen bank cross sections simulated over six-hour time steps (Figure 4b). Field data collected by Cardno ENTRIX (2012) showed that the selected bank section consisted of essentially uniform and non-cohesive materials. A linear retreat bank module for non-cohesive materials, therefore, is used for the model, and the key input parameters are the critical shear stress and erodibility of each bank. In this study, both the critical stress and erodibility were estimated by Cardno ENTRIX (2012), and no attempt is made to improve the model prediction of bank retreat by changing either parameter.

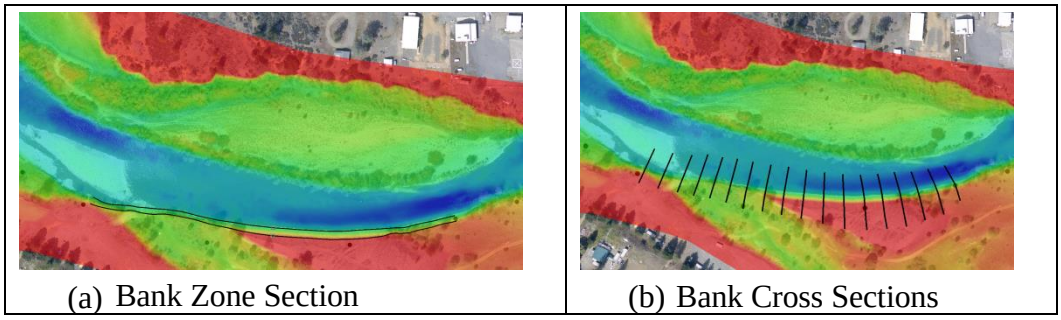

(a) Bank Zone Section (b) Bank Cross Sections

Figure 4 The bank zone section (left) and bank cross sections (right) selected for bank retreat modeling under the *Pre_E* scenario (black lines on the left figure show the bank toe and top)

RESULTS OF CALIBRATION STUDY

Model runs, with and without bank erosion modeling, are made under the *Pre_E* condition for model calibration and validation. The predicted net erosion and deposition depth during the 2009-2011 time period is shown in Figure 5 and is compared with the measured data (left three figures). The survey data suggested that three pools, marked as "Pool 1," "Pool 2" and "Pool 3," were subject to deposition while a section of the left bank, marked as "Bank Erosion," experienced significant bank erosion. The zoom-in views of the same plots are displayed on the three right figures. In addition, the predicted bed elevation changes at the deepest points of Pool 1 and Pool 2 are plotted in Figure 6.

The results show that erosion on the left bank cannot be predicted without using the bank module, but is predicted reasonably well when the bank module is used. The model predicts that the eroded bank sediments are deposited in the stream near the bank and are not transported very far downstream. More than 50% of the eroded bank sediments are large gravels and small cobbles that are difficult to entrain once deposited in the stream. Therefore, the impact of the eroded bank sediments on the downstream half of the reach is relatively small. Upstream of the bank erosion zone, the with- and without- bank model runs produce similar results. Therefore, the without-bank run may also be used to assess the model capability to predict the riffle-pool

processes at this site.

Two major discrepancies are identified between the model predictions and measured sediment. First, the model predicts much more deposition than the measured data in three pools. Second, the riffle erosion downstream of Pool 2 is not predicted by the model. The predicted bed elevation changes at the deepest points of the first two pools are plotted in Figure 6. A total of five and eight feet of deposition are predicted in Pool 1 and 2, respectively; the corresponding measured depositions are approximately 2.2 and 3.2 feet. The over-prediction of the pool filling process is a consistent problem with any depth-averaged numerical models because such models do not take the horizontal vortices into consideration (Logan et al., 2010). 3D models may have the potential to improve the predictions; but this is yet to be proven. Other factors might contribute to the over-prediction of the pool filling process. High uncertainty in the initial bed gradation specification of the riffle areas is one of them. Over-prediction of erosion at riffles might lead to increased deposition in the downstream pool. The sediment transport capacity equation may also be the cause of the poor predictions, as most existing equations are based on reach-averaged or depth-averaged variables.

Model results show that riffle erosion downstream of Pool 2 is predicted after the 2009 and 2010 runoff seasons; the area, however, changes to depositional after the 2011 runoff. The reason for the failure of the numerical model to predict the riffle erosion in the area is unclear. Possible causes include potential inaccuracy in the initial bathymetry and/or bed gradations, neglecting the impact of bank vegetation, or overestimating of the upstream sediment supply at high discharges. We speculate that the most likely cause is the mature vegetation along the nearby right bank which was inundated only during high discharges in 2011 but not represented by the model.

Downstream of the bank erosion zone, model results are less accurate because of uncertainty in the accuracy of the stage-discharge rating curved used to define the downstream boundary condition.

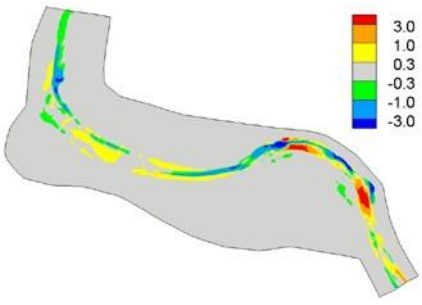

(a) Predicted without Bank Modeling

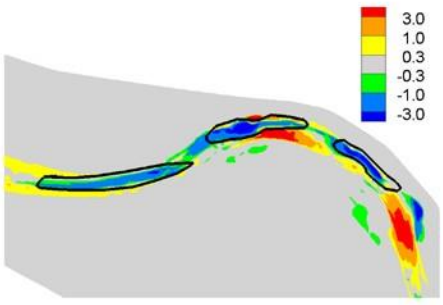

(d) Predicted without Bank Modeling

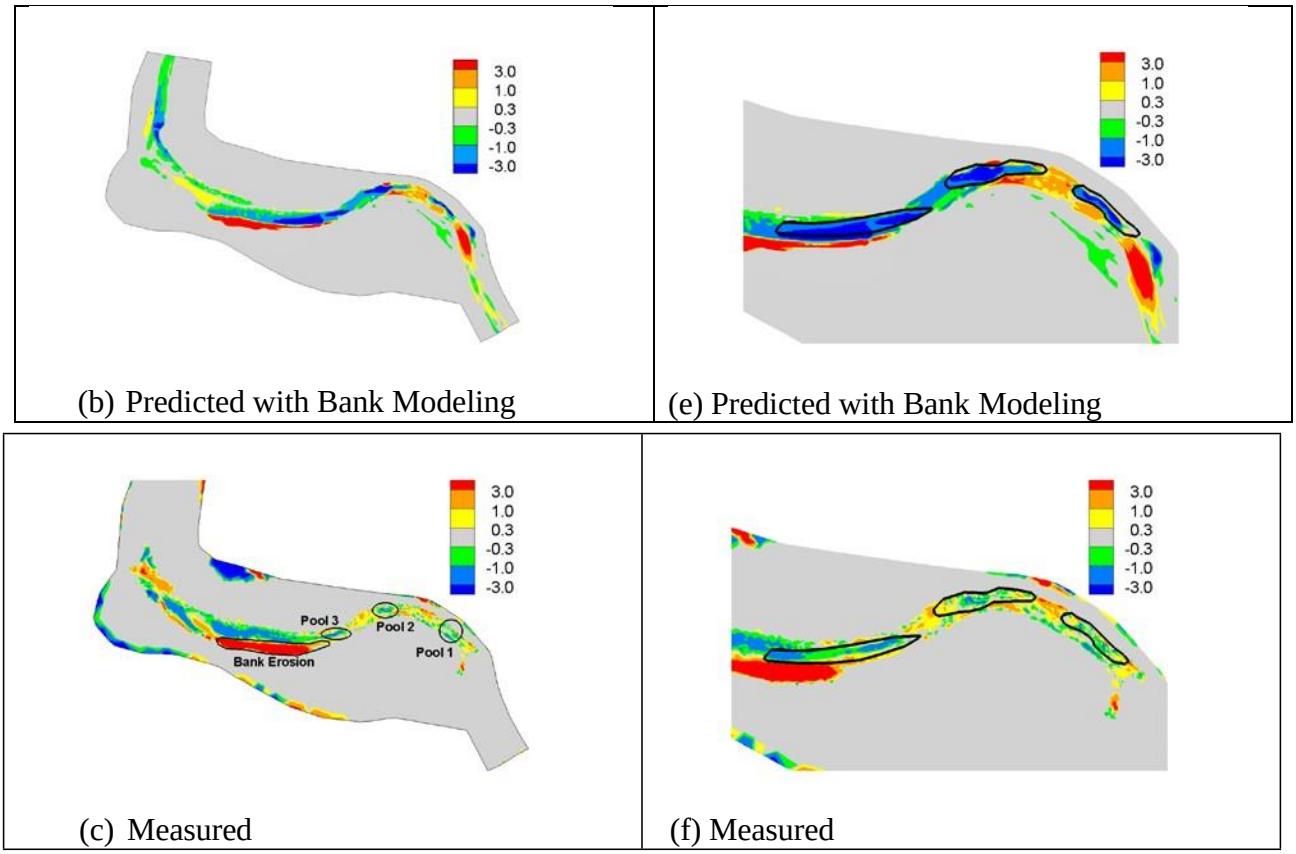

Figure 5 Predicted and measured depth of net erosion (positive) and deposition (negative) in feet, with the *Pre_E* scenario runs (Left); and pool filling after 2009-2011 three-year runoff events (Right)

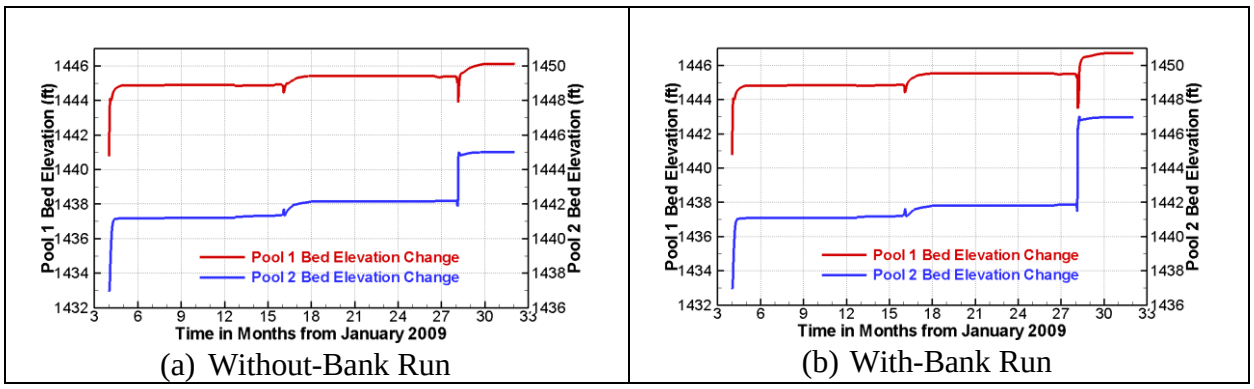

Figure 6 Predicted bed elevation variations in time at the deepest points of Pool 1 and Pool 2

ASSESSMENT OF PROJECT IMPACT

Description of Project Impact Assessment Runs The calibrated model is next applied to assess the impact of the rehabilitation project on stream morphology at the UJC site. It is expected that the pool-filling processes would not be well predicted but processes such as bank erosion; the side channel filling with coarser sediments; and vertical stream bed change downstream of the

pools would be predicted reasonably well. Two scenarios are simulated: the 2011 post-erosion condition (*Post_E*) and the 2012 design (*Design*) condition. The two use the same model inputs except for the initial terrain. Therefore, the differences of results between the two are due to the modification for the design topography at the UJC rehabilitation project.

Summary Findings The predicted net erosion and deposition during 2009 through 2011 for the two scenarios are compared in Figure 7, and Figure 8b shows a zoomed-in view of the *Design* run. The differences of the predicted net erosion and deposition between the two runs are plotted in Figure 9b. Positive depth in Figure 9b means that the bed elevation of the *Design* scenario is lower than that of the *Post_E* scenario. The following conclusions may be drawn based on the model results (for location terminology, refer to Figure 8a):

- Deposition was predicted in both the left and right side channels, as seen in Figure 7b. The model results after 2009 and 2010 runoffs are further plotted in Figure 9a. A comparison of the predicted deposition in the two side channels between Figure 9and Figure 7b shows that the predicted deposition occurred mainly during the 2011 runoff event. The peak discharge is 6,040 cfs and 7,520 cfs, respectively, in 2009 and 2010; while the peak is 12,900 cfs in 2011. Therefore, the predicted side channel deposition is mainly due to flows higher than 12,000 cfs.
- The only side channel deposition that might be of concern for the project is the entrance zone of the downstream right side channel. Increased deposition is expected with flows higher than 12,000 cfs.
- The predicted side channel deposition may not be a concern for other locations in the two side channels. With regard to the upstream left side channel, the entrance to the side channel is predicted to erode (Figure 8b) if the initial bed materials in the entrance are the same as the main channel (d_{50}=29 mm). However, much coarser sediments were used in this area when the project was built in 2012. Slight deposition is predicted downstream of the entrance zone in the left side channel (including the pool). However, only fine sediments, less than 10 mm, are deposited. For the downstream right side channel, deposition is limited to the entrance and three side channel pools. Again, only fine sediment deposition is predicted, and they are not considered to be of concern.
- A major potential impact of the design condition (*Design*), based on the model results, is that the main channel downstream of the designed island could experience deposition in some areas and erosion in others (see Figure 9b). However, the left bank zone is not predicted to experience higher rate of lateral erosion than the 2011 post-erosion condition due to the design condition (compare results in Figure 7). On the contrary, the *Design* is predicted to lead to slightly less bank erosion. Less deposition in the stream near the bank erosion zone is probably due to less bank erosion predicted with the *Design* scenario. Note that the model does not consider other bank sections.
- The model predicts some deposition in the channel to the left of the designed island and erosion in the channel to the right. In view that the 2011 *Post_E* scenario is predicted to be erosional in the same area, erosion in the right spilt channel may not be a concern. The deposition on the left split channel might be an important risk to consider since the deposited sediment sizes are not small. The model predicts that sediment deposited in the left split channel will have a d_{50} of around 15 to 17 mm.

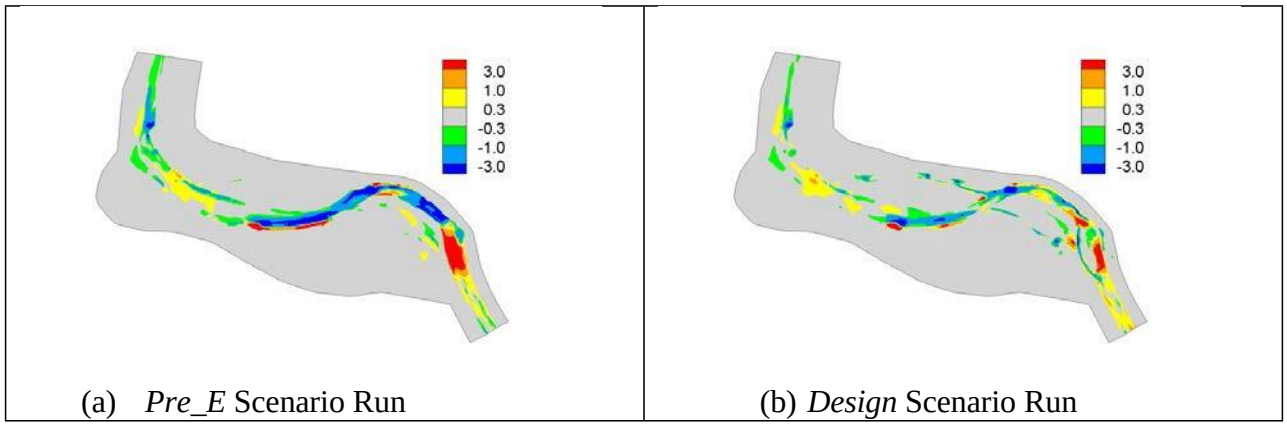

(a) *Pre_E* Scenario Run (b) *Design* Scenario Run

Figure 7 Predicted net erosion (positive) and deposition (negative) depth in feet with the two scenarios

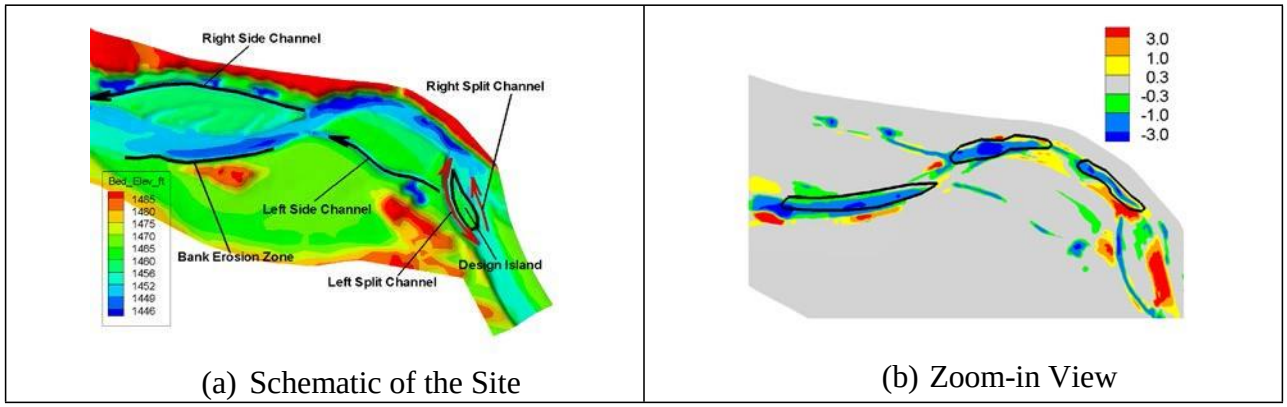

(a) Schematic of the Site (b) Zoom-in View

Figure 8 Schematic showing the terminology used to identify different features of the design construction (Left); and a zoom-in view of the predicted net erosion (positive) and deposition (negative) depth in feet with the *Design* scenario (Right)

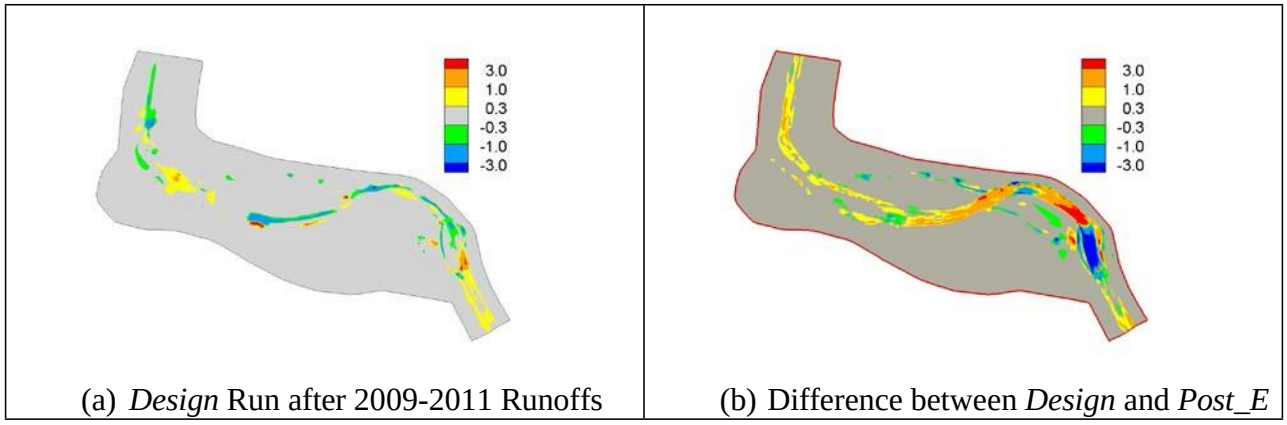

(a) *Design* Run after 2009-2011 Runoffs (b) Difference between *Design* and *Post_E*

Figure 9 Predicted net erosion (positive) and deposition (negative) depth in feet with the *Design* scenario after 2009 and 2010 runoffs (Left); and the differences of the predicted depth of erosion and deposition in feet between *Design* and *Post_E* scenarios (Right)

CONCLUDING REMARKS

A coupled morpho-dynamic and bank erosion model is carried out for the Upper Junction City (UJC) rehabilitation project on the Trinity River. The objectives of the study are twofold. First, the study is to test SRH-2D geofluvial modeling capabilities and verify whether the bank erosion module can correctly simulate observed bank erosion in study area. Second, after model calibration, SRH-2D is applied to assess the impact of the UJC rehabilitation project on channel morphology.

Calibration and validation modeling runs are carried out by comparing the 2011 measured terrain data with predicted topography obtained by simulating changes to the 2009 pre-erosion baseline (PB) condition caused by 2009 through 2011 hydrology. The necessary bank erosion model inputs, mainly the critical shear stress and erodibility, are estimated from the field measurements. The geofluvial SRH-2D model is shown to be capable of predicting bank erosion and bed level changes. The model can predict pool-filling processes only qualitatively.

The SRH-2D is also applied to assess the impact of the rehabilitation project on channel morphology. Due to potential uncertainties of numerical models, only a relative comparison can be made between the two scenarios. Relative comparisons are often more accurate than the absolute prediction with channel morphology changes. The model results have led to a number of important conclusions with regard to the impacts of the design on stream morphology.

ACKNOWLEDGEMENT

The authors acknowledge the peer review provided by Blair Greimann at the Bureau of Reclamation.

REFERENCES

Cardno ENTRIX. (2012). Bank-Stability Analysis of the Upper Junction City Reach Trinity River, California, Project Report by Cardno Entrix, Project 30088130, December, 2012.

aeuman, D., Andrews, E.D., Krause, A., and Smith, W. (2009). "Predicting fractional bed load transport rates: Application of the Wilcock-Crowe equations to a regulated gravel bed river," Water Resour. Res., 45, W06409, doi:10.1029/2008WR007320.

Lai, Y.G. (2008). *SRH-2D Theory and User's Manual version 2.0,* Technical Service Center, Bureau of Reclamation, Denver, Colorado.

Lai, Y.G. and Greimann, B.P. (2008). "Modeling of erosion and deposition at meandering channels," World Environmental & Water Resources Congress, ASCE, May 12-16, 2008, Honolulu, Hawaii.

Lai, Y.G. and Greimann, B.P. (2010). "Predicting contraction scour with a two-dimensional depth-averaged model." J. Hydraulic Research, IAHR, 48(3), 383-387.

Lai, Y.G. (2010). "Two-Dimensional Depth-Averaged Flow Modeling with an Unstructured Hybrid Mesh." J. Hydraul. Eng., ASCE, 136(1): 12-23.

Lai, Y.G., Greimann, B.P., and Wu, K. (2011). "Soft bedrock erosion modeling with a two-dimensional depth-averaged model," J. Hydraul. Eng., ASCE, 137(8): 804-814.

Lai, Y.G., Greimann, B.P. and Wu, K. (2012). "Modelling Bank Erosion in Fluvial Channels." River Flow 2012, International Conference on Fluvial Hydraulics, Sept. 5-7, San Jose, Costa Rica.

Lai, Y.G., and Wu, K. (2013). "Modeling of Vertical and Lateral Erosion on the Chosui River, Taiwan." ASCE World Environmental and Water Resources Congress, Cincinnati, Ohio, May 19-23.

Lai, Y.G. (2014). "Chapter 9. Advances in Geofluvial Modeling: Methodologies and Applications." Advances in Water Resources Engineering, Handbook of Environmental Engineering, C.T.Yang and L.K.Wang (eds). Springer New York. pp.407-470.

Lai, Y.G., Thomas, R., Ozeren, Y., Simon, A., Greimann, B.P., and Wu, K. (2015). "Modeling of multi-layer cohesive bank erosion with a coupled bank stability and mobile-bed model." To appear in Geomorphology.

Logan, B., Nelson, J., McDonald, R., and Wright, S. (2010). "Mechanics and Modeling of Flow, Sediment Transport and Morphologic Change in Riverine Lateral Separation Zones," 2nd Joint Federal Interagency Conference, Las Vegas, Nevada, June 27 - July 1, 2010.

Seminara, G., Solari, L., and Parker, G. (2002). "Bed load at low Shields stress on arbitrarily sloping beds: Failure of the Bagnold hypothesis," Water Resources Research, 38(11), 1249, doi:10.1029/2001WR000681.

Wilcock, P.R. and Crowe, J.C. (2003). "Surface-Based Transport Model for Mixed-Size Sediment," J. Hydraulic Engineering, 129: 120-128.

BATTLE CREEK: LESSONS LEARNED FROM TINKERING AT A CONFLUENCE

Steven E. Yochum, Hydrologist, US Forest Service, National Stream & Aquatic Ecology Center, Fort Collins, CO, steveneyochum@fs.fed.us

prepared for the 10th Federal Interagency Sedimentation Conference
April 19-23, 2015, Peppermill Hotel, Reno, Nevada, USA

Abstract

In the Autumn of 2008 a stream restoration project was constructed in Battle Creek just above the confluence with the Little Snake River, on the border between Colorado and Wyoming. Relevant structures were cross vanes and stream barbs, with the objectives apparently being bank stabilization and habitat enhancement for game fish. After construction, floods occurred in 2009, 2010, and 2011, including a 100-year flood in the Little Snake. With this flooding, a substantial volume of sediment was deposited in the vicinity of the Battle Creek cross vanes, forcing a channel avulsion and rapid bank erosion along multiple reaches. A review was performed to determine the likely causes of this problem. Based on a site assessment, an evaluation of historic aerial imagery, and a hydraulic model, it was concluded that the installed structures did not cause the sediment deposition and resulting bank erosion. Decreased sediment transport capacity due to backwater effects imposed by the Little Snake flooding was most likely the cause of the deposition, with the problem compounded by riparian grazing reducing the quality of the vegetative condition. Structural measures should not have been installed on Battle Creek in the vicinity of the confluence due to periodic aggradation induced by Little Snake River flooding. While these structures likely did not worsen the aggradation problem, they also provided little benefit since bank destabilization is primarily the result of backwater-induced sediment deposition and insufficient vegetative cover. Instead, riparian fencing and grazing management should have been the focus, to encourage robust riparian vegetation growth that can resist destabilization induced by the periodic sediment deposition. This project illustrates an example where livestock management should have been the core approach used in riparian restoration, rather than an engineered approach; more detailed analysis and planning by a stream-focused group of specialists was needed early in this project.

INTRODUCTION

Of particular need in the stream restoration community is enhanced understanding of where structural bank stabilization measures are needed versus where livestock grazing management alone is instead adequate to address instability issues. To help inform a discussion of this issue, this case study of a bank stabilization project constructed in 2008 on Battle Creek, in Northwest Colorado, was developed. This reach of Battle Creek is immediately upstream of its confluence with the Little Snake River. Key project features were two cross vanes constructed in Battle Creek; one stream barb constructed in Battle Creek; and one additional cross vane constructed on the Little Snake downstream of the confluence. Riparian grazing management was not included as a part of this project. Following construction, floods occurred in 2009, 2010 and 2011, including a 100-year flood in the Little Snake. With this flooding, a substantial amount of sediment was deposited on and just upstream of the upper cross vane installed on Battle Creek, which forced a stream channel avulsion and rapid bank erosion. An additional bar was deposited downstream of this location, on the west bank between the two cross canes, with a second

rapidly-eroding bank on the opposite bank. An investigation was performed to develop an understanding of how this problem could have been avoided. This paper provides an overview of the condition of this stream reach, as well as a historical and analytical assessment of dominant fluvial geomorphological processes that led to the resulting undesired state. From this postmortem assessment, conclusions are drawn to reduce the chances that such a result will be repeated in similar future situations.

ASSESSMENT METHODS

The stream condition was assessed and a forensic analysis was performed using a combination of methods, including a visual assessment of current geomorphic and hydraulic condition, identification and elevation measurements of high flow indicators, a flow frequency analysis, historic aerial photo interpretation, a greenline vegetation assessment, topographic surveying, and hydraulic modeling.

The flow frequency analysis for the Little Snake was performed using a logPearson analysis of streamgage records. For Battle Creek, a regional regression approach was implemented (Capesius and Stephens, 2009), through the Streamstats web application. Historic aerial photos were downloaded from the U.S. Geological Survey's Earth Explorer (http://earthexplorer.usgs.gov) and orthorectified in ArcGIS. The Greenline vegetation assessment was performed using the methods presented in Burton et al. (2011). Topographic surveying was performed using Trimble survey-grade GPS, with an Online Positioning User Service (OPUS) solution used to establish the benchmark.

The hydraulic analysis was performed using 1-dimensional gradually-varied flow modeling, using HEC-RAS. To assess the impacts of backwater effects on sediment transport, stream power and shear stress were computed within the reach of interest in Battle Creek. The sediment transport rate is directly proportional to stream power and shear stress, with reductions in these variables reflecting decreased sediment transport capacity and the potential for sediment deposition. This deposition causes channel aggradation and bank instability. Stream power is computed as $\Omega = \gamma Q S_f$, where Q is the discharge, γ is the specific weight of water, and S_f is the friction slope. Average boundary shear stress is computed as $\tau = \gamma R S_f$, where τ is the shear stress and R is the hydraulic radius. Backwater effects cause a reduction in energy slope, which reduces stream power and shear stress. This in turn reduces the sediment transport rate, causing deposition and aggradation. Channel flow resistance, as Manning's n, was estimated using photographic guidance (Barnes, 1967; Aldridge and Garrett, 1973) as well as through the use of a quantitative approach (Jarrett, 1984).

STREAM CONDITION

On-the-ground conditions were documented in April and June of 2012. With a drainage area of 302 mi^2 at the Battle Creek confluence, the Little Snake River is a snowmelt-dominated stream that drains portions of Northern Colorado and Southern Wyoming. Average annual precipitation varies from 19 to 55 inches (from PRISM; Daly et al., 2008). Battle Creek, at its confluence with the Little Snake, has a drainage area of 83.3 mi^2 and average annual precipitation that also varies from 19 to 55 inches. Both streams carry a substantial quantity of sediment load, with frequent bars within the channels (Figure 1 and 2). Both the Little Snake and Battle Creek have a mature

cottonwood gallery. Battle Creek enters the Little Snake with an atypical upstream orientation. Substantial sediment deposition is evident in Battle Creek just above the confluence (Figure 2). Combined with the impacts of grazing practices on riparian vegetation, this deposition resulted in rapid bank erosion rates that are problematic for the landowner.

In the Autumn of 2008 a project was constructed in Battle Creek and the Little Snake River, in vicinity of the confluence. The objectives of this project were unclear in the project documentation, but apparently the principle objectives were streambank protection and fish habitat enhancement. The project consisted of a series of cross vanes, J-hook vanes and other barbs, and minor channel realignments. Key features relevant to Battle Creek are: two cross vanes constructed in Battle Creek and one stream barb constructed in Battle Creek, armoring the channel with a continued upstream confluence orientation; one cross vane constructed on the Little Snake downstream of the confluence (Figure 2), and a few willow clump transplants along Battle Creek. During the next three years, out-of-bank flow occurred each year.

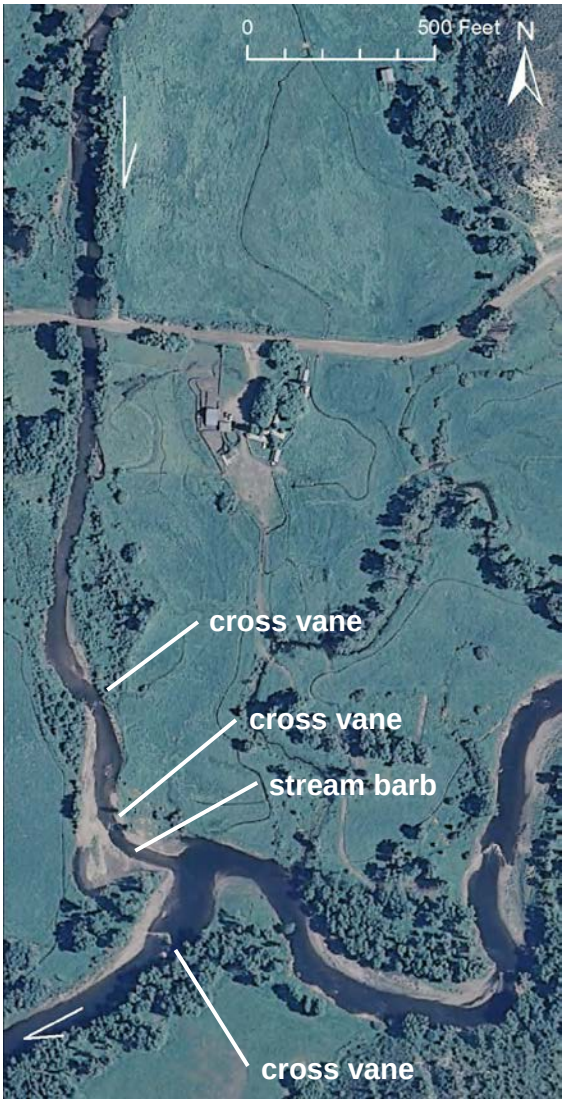

Figure 1: Battle Creek at the Little Snake River confluence (7/23/2009).

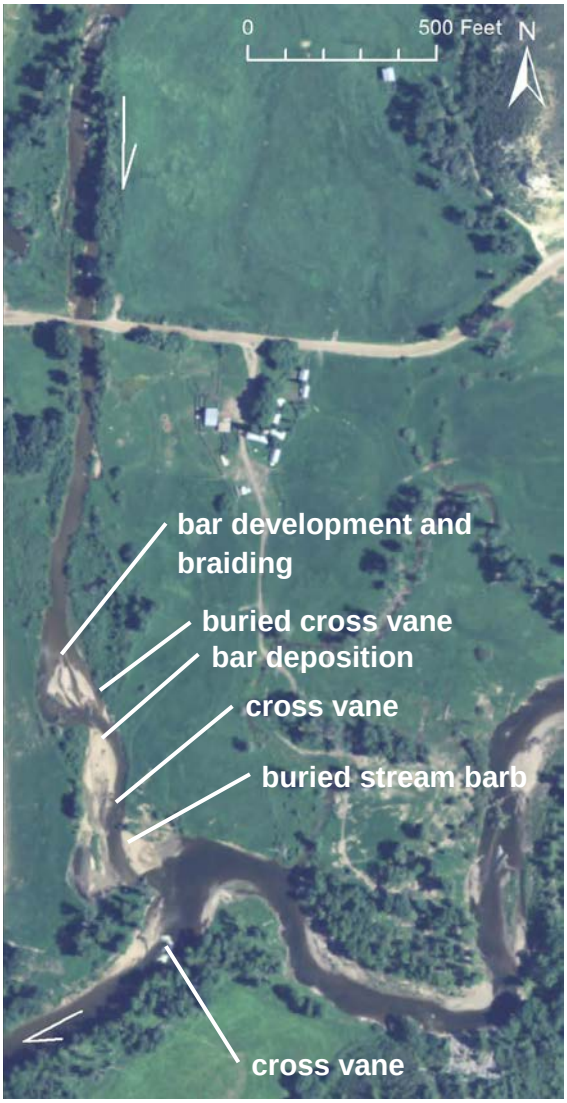

Figure 2: Battle Creek at the Little Snake River confluence (7/23/2011).

A substantial amount of sediment was deposited on and just upstream of the upper cross vane installed on Battle Creek (Figures 2 and 3). This local aggradation extends for a length of about 200 feet. This deposition forced an avulsion of the stream channel to the west of its previous location (Figure 1). The channel has a braided form within this short extent, with the preferential flow channel currently on the west edge of this depositional bar. A meander bend and point bar is forming to the east of this channel. In the vicinity of this depositional bar, both sides of the channel have willows along much of the banks, but coverage is patchy with grazing apparent on both banks, negatively impacting willow- and sedge-induced bank stability. The streambank on the west side of the depositional bar, adjacent to the principal flow channel, is actively eroding (Figure 4). A few of the patchy willows that were once present along this bank were laying in the channel. The fenceline and aerial imagery indicate rapid bank erosion rates.

An additional bar has been deposited downstream of this location, on the west bank between the two cross canes (Figures 2 and 5). Opposite this point bar, a second rapidly-eroding bank is present (Figures 5) as the stream attempts to increase its meander planform. A cross vane that appears to be functioning properly is located just downstream of this eroding bank. No willows are present on this bank. The aerial imagery (Figures 1 and 2) indicate that this bank is not eroding as quickly as the upstream bank. Heavy grazing was apparent along this bank, along with indications of additional feeding in this pasture.

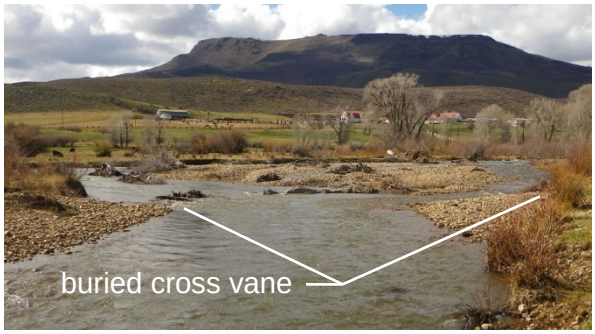

Figure 3: Upper cross vane, with sediment deposition and braiding just upstream.

Figure 4: Rapidly-eroding streambank adjacent to depositional bar.

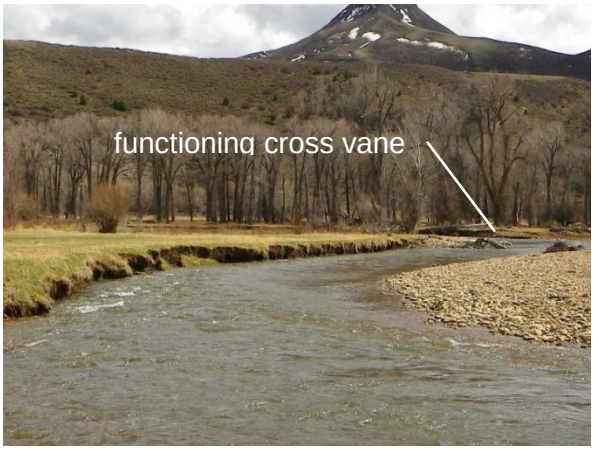

Figure 5: Rapidly-eroding streambank, opposite of an additional depositional bar.

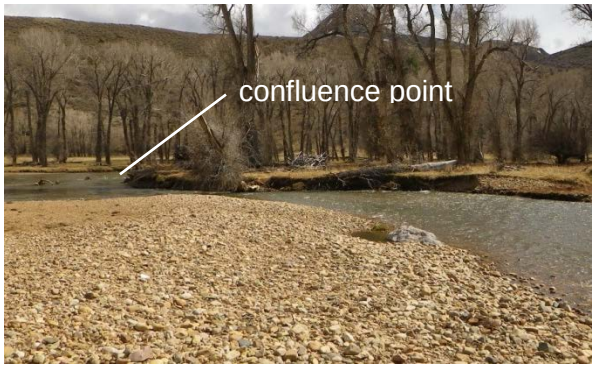

Figure 6: Confluence bar, with variable bed material size.

The third and final depositional bar is at the confluence (Figures 2 and 6), with the bar extending from north to south across the constructed channel location. This bar consists of multiple sediment sizes, with coarse material deposited on fines. A portion of a stream barb can be seen protruding from the bar (Figure 6). The growth of this bar mirrors the erosion of 20 to 30 feet of the confluence point between 2009 and 2011. Alongside this erosion the pool in the Little Snake just upstream of the confluence has been reported to have filled substantially. Additionally, flood debris is present on the fenceline on the west side of Battle Creek, showing the approximate high flow elevation for the Little Snake in 2011.

RESULTS AND DISCUSSION

Flood-Frequency Analysis

On the Little Snake, a streamgage (USGS 09253000, Little Snake near Slater, CO) is located approximately 5 miles upstream of the confluence, measuring discharge from 253 mi^2 (compared to 302 mi^2 at the confluence). With 65 years of record, the results of the log-Pearson flow-frequency analysis are provided (Table 1). A 1.5-year event, which is likely similar in magnitude to the bankfull discharge, is about 1700 cfs. Peak flow typically occurs from mid-May through early June. In 2011, peak flow of 4890 cfs occurred on June 6th. This was a ~100-year flood. In 2010, peak flow of 3230 cfs occurred on 5/29/2010, which is between a 5- and 10-year flood. In 2009, peak flow of 2710 cfs occurred on 6/3/2009, which is between a 2- and 5-year flood.

Flow frequency results for Battle Creek, from Streamstats, are provided (Table 1). With prediction errors ranging from 74 percent (100-year) to 110 percent (2-year) and application of the StreamStats equations to the Little Snake streamgage indicating accurate estimates of frequent events and substantially underestimated infrequent events, confidence in these estimates is moderate throughout the return interval range. Extrapolated from these estimates, a 1.5-year event is about 600 cfs. Rick Dornfeld, of River Fixer LLC, estimated bankfull flow to be about 500 cfs (Dornfeld, 2008). A streamgage was operated on Battle Creek (USGS 09253400, Battle Creek near Encampment, WY) approximately 15 miles upstream of the confluence. It measured discharge from only 13 mi^2 of the total 83.3 mi^2 catchment. This gage was operated from 1956 to 1963 and 1985 to 1988. While not relevant for computing flow frequency at this site, these data do indicate that peak flow timing occurs from mid May through early June, similar to the Little Snake. Local SNOTEL snowpack monitoring sites (Battle Mountain, 317; Sandstone RS, 732) indicate that Battle Creek peaked a bit later than average in 2011 and a bit earlier than average in 2010.

Table 1: Flow-frequency estimates for Battle Creek and the Little Snake River.

Return Interval (years)	Battle Creek (cfs)	Little Snake River (cfs)	Peak Flow Years in Range
1.25	----	1490	
2	660	2200	
5	1030	3090	
10	1260	3610	1943, 1952, 1957, 1958, 1997, 2008, 2010
25	1610	4210	1974, 1995, 1996
50	1850	4610	1983 (~25-year flood)
100	2140	4980	1984, 2011

Historic Aerial Photography

An important component of an assessment is an understanding of the historical range of variability; understanding the range of variability of past conditions can provide insight on what future conditions can be expected. Aerial imagery from 1953 to 2004 is illustrated (Figure 7 to 10). Throughout this 58 year record Battle Creek and the Little Snake have fairly consistent morphology but some interesting cycles and shifts in form are observable.

Over this period, the aerial images indicate cyclic sediment deposition and vegetative colonization along the last 1000 feet of Battle Creek upstream of the confluence. In 1953 (Figure 7), an upper depositional bar is apparent in Battle Creek (orange oval). This bar is in a similar location as the bar deposed in 2010 and 2011. A couple of small unvegetated bars are also visible in the lowest portion of Battle Creek (red circle). By 1968 (Figure 8) the upper depositional bar (orange oval) has become well vegetated though an avulsion across the bar is visible. Flow appears to be split at this point in time. The lower depositional bar has enlarged a bit, with a short series of exaggerated meanders at the confluence. Between 1968 and 1980 (Figure 9) the (streamwise) left channel has filled in the formerly unvegetated upper bar (orange oval) and Battle Creek flows in a single, relatively strait channel through this upper reach. This portion of the floodplain appears to be well vegetated. The increasing meandering form indicated in 1953 and 1957 straitened in 1968 and maintained this form in 1980. The lower depositional bar (red circle) has again increased in size and maintained little vegetative growth, with a growing point

Figure 7: Aerial image (8/23/1953).

Figure 9: Aerial image (7/28/1980).

Figure 8: Aerial image (9/1/1968).

Figure 10: Aerial image (8/4/2004).

bar and increasing meander extent along the well-vegetated confluence point (green oval). In 2004 (Figure 10), the upper reach in Battle Creek is again increasing its meander form while the meander at the lower reach (red circle) is becoming tortuous, as Battle Creek attempts to flank the dense stand of vegetation at the confluence point. Side bars are apparent in the upper reach. Following the flood events of 2010 and 2011, the 2011 image (Figure 2) shows Battle Creek above the confluence to be once again increasing its meander form and depositing substantial quantities of sediment in similar locations as those indicated in 1953 (upper depositional bar) and 1968 and 1980 (lower depositional bar). Some of the vegetated confluence point has eroded, despite the armoring provided by the dense vegetation. The cyclical sediment deposition, vegetative colonization, and erosion is likely due to decreased velocities, shear stress and stream power from backwater effects induced by the Little Snake, with the location varying due to relative peak flow timing, flood magnitude, and flood duration. This bar material is subsequently colonized by vegetation, with a slightly sinuous form repeatedly initiating and straightening.

Vegetation Assessment

A green line assessment (Winward, 2000) of the last ~1000 feet of Battle Creek, at the confluence with the Little Snake River, was completed on June 19, 2012. Plant communities were identified and quantified in three separate, 343 feet transects (two on the east bank, one on the west bank). Approximately 20% of the footage surveyed on the east side of Battle Creek consisted almost entirely of introduced cool season grasses, as part of a pasture. Upstream of this area, seedlings and young saplings of narrow leaf cottonwood, coyote willow, and other woody species, and herbaceous wetland plants (Carex spp. primarily), were encountered much more frequently. The west bank of Battle Creek included a large expanse of cobble and sand, and willow seedlings or sprouts, along with introduced cool season grasses. Some narrow leaf cottonwood sprouts/saplings and a few other mature woody species (shrubs) were also present in this area.

Percent composition of each community type was determined for the reach, and each community was assigned a stability class and index. A stability index of the reach was calculated. Overall, the stability of this reach is rated as moderate to poor. The plant communities were also assigned a successional rating, and a percent late seral type was calculated based on the capability group value of this stream type. Approximately 11 percent of the identified plant communities are classified as late seral, and the successional status of the reach was determined to be very early seral to early seral.

A woody species regeneration assessment was also completed by evaluating numbers of seedlings, sprouts, mature, decadent, and dead woody species in each of the two transects on the east bank of Battle Creek, just upstream of the confluence with the Little Snake. Numerous seedlings and young saplings (123 or 75% of total number of individuals) of narrow leaf cottonwood and coyote willow were found, primarily upstream of the pasture area. Several moderately to severely grazed individuals of these species were also found. A few dead individuals were noted. Approximately 41% of all individuals were browsed, which is considered moderate grazing pressure. The woody plant community of the area upstream of the pasture is healthy in that numerous seedlings and saplings were found, but grazing pressure, if continued, could slow recovery. Few woody plants were found adjacent to the pasture area.

The cottonwood gallery along the Little Snake at the confluence with Battle Creek was not quantified, but observed. It appears to consist of numerous seedlings, sprouts, and young trees, several large mature trees, and a few dead trees. This community appears healthy.

Hydraulic Modeling

For this assessment, a relatively-simple model was created for Battle Creek from the bridge to the confluence for ~bankfull flow, as well as the 10-year and 100-year flows. Eighteen cross sections were implemented. The downstream boundary condition was assumed to be the peak water surface elevation in the Little Snake, as indicated by flood debris. This elevation was 6694.5 feet. The estimated Manning's *n* values for this reach are provided (Table 2).

Table 2: Battle Creek channel Manning's *n* estimates. Implemented *n* = 0.040.

	Manning's *n*
Barnes 1967	0.045
Aldridge and Garrett 1973	0.040
Jarrett 1984	0.025
Average:	0.037

Modeled stream power and shear stress for the ~bankfull, 10-year, and 100-year flows in Battle Creek are illustrated (Figure 11 through 13). In all tested cases, stream power and shear stress decrease substantially at the point where deposition in the stream channel occurred in 2010 and 2011. Since sediment transport capacity is directly proportional to stream power, the modeling results indicate that the sediment deposition (and subsequent bank instability) is the result of backwater effects from the Little Snake reducing flow velocity and sediment transport capacity.

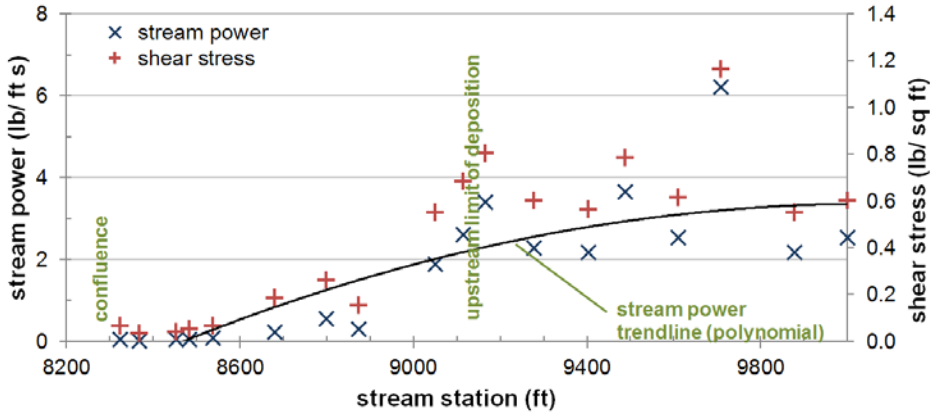

Figure 11: Modeled stream power and shear stress, ~bankfull flow in Battle Creek.

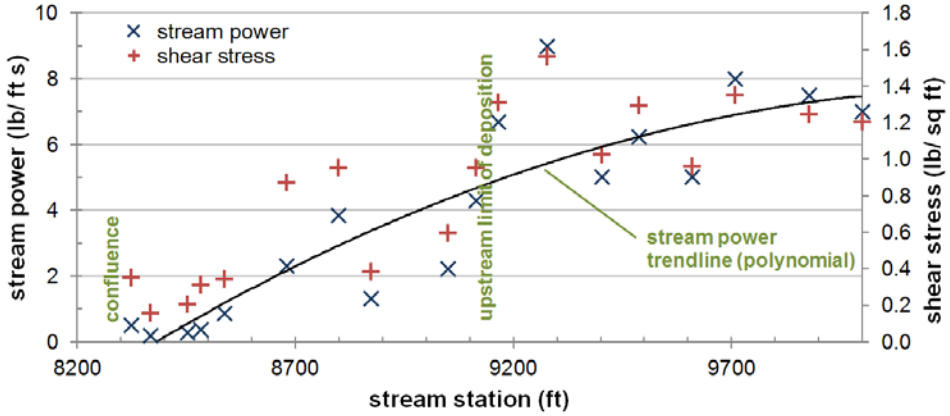

Figure 12: Modeled stream power and shear stress, 10-year flow in Battle Creek.

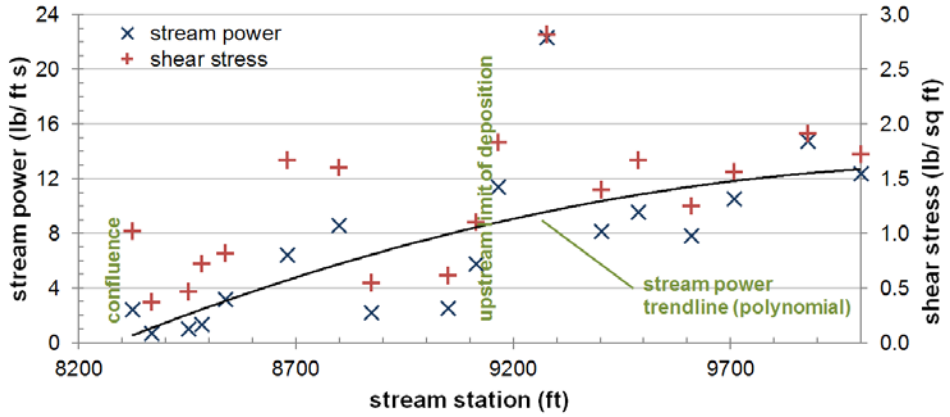

Figure 13: Modeled stream power and shear stress, 100-year flow in Battle Creek.

Interpretation of Dominant Mechanisms

Observations of current conditions, a historic aerial photography interpretation, and hydraulic modeling indicate that the Battle Creek aggradation problem and resulting bank instability that occurred since the structural stabilization measures were installed in 2008 are likely the result of backwater effects from high flow on the Little Snake River. Specifically, during high flow increased water surface elevations in the Little Snake result in increased flow depths and decreased velocities, shear stress, and stream power for the portion of Battle Creek immediately above the confluence. In turn, this results in reduced sediment conveyance capability and bedload deposition throughout the reach of concern. This deposition then encourages channel bank erosion, as new flow paths form through the deposited material. Bank erosion is facilitated by grazing practices that have discouraged robust and diverse vegetative growth along portions of the reach. The upstream-oriented confluence and Little Snake cross vane both cause increased water surface elevations at the confluence, worsening the problem.

Structural measures should not have been installed on Battle Creek in the vicinity of the confluence. While these structures likely did not worsen the aggradation problem, they also provided little benefit since bank destabilization is primarily the result of backwater-induced sediment deposition and insufficient vegetative cover. Instead, riparian fencing and grazing management should have been the focus of the Battle Creek portion of this project, to encourage robust vegetation growth that can resist destabilization induced by the periodic sedimentation. Additionally, a much more substantial revegetation component should have been included in the project.

Review of historic aerial imagery and development of hydraulic modeling prior to the project implementation would have indicated the problematic nature of stream work on Battle Creek just above the confluence. Review of the recent aerial imagery would have also shown that the channel had been recently relocated. This work should have been performed by qualified staff during the planning phase of the project. The lack of such planning resulted in the needless use of limited restoration funding, highlighting the importance of proper planning by staff with the expertise to understand fluvial processes and riparian vegetation.

CONCLUSIONS

A postmortem was performed on a failed streambank stabilization project, to assess the most likely causes. Using the results of a site assessment, a greenline vegetation assessment, an evaluation of historic aerial imagery, and hydraulic modeling, it was found that the installed project did not address the cause of the bank instabilities. These structural features on lower Battle Creek should not have been installed, due to periodic aggradation induced by backwater effects from the Little Snake during flood flow. Instead, riparian fencing and grazing management, combined with a revegetation component, should have been the focus of the project within this reach. Proper project planning by qualified staff could have identified the most appropriate strategy for addressing the landowners resource concerns prior to project implementation; this project illustrates the need for specialists to be available for the proper implementation of stream projects, to reduce the inefficient use of government funds.

ACKNOWLEDGEMENTS

David Levinson is appreciated for reviewing this manuscript. Theresa McGovern and Lori Jazwick performed the greenline assessment of vegetative condition; their efforts and Theresa's included summary was a valuable addition to this report. Field assistance was provided by Adam Dossett, Joe Messina, Clay Thompson, Megan Vasquez, and Justin Robbins. Their assistance was appreciated. Chris Gauthier, Vance Fulton, and Robert Molacek also contributed onsite insights to the stream condition. Additionally, coordination by Mark Shirley and Lori Jazwick was helpful.

REFERENCES

Aldridge, B. N., and J. M. Garrett (1973). "Roughness Coefficients for Stream Channels in Arizona," U.S. Geological Survey Open-File Report, Tucson, Arizona.

Barnes, H.H. (1967). "Roughness Characteristics of Natural Channels," U. S. Geological Survey Water-Supply Paper 1849.

Burton, T.A., Smith, S.J., and Cowley, E.R. (2011). "Multiple Indicator Monitoring (MIM) of Stream Channels and Streamside Vegetation," U.S. Department of the interior, Bureau of Land Management, Technical Reference 1737-23.

Capesius, J.P., and Stephens, V.C. (2009). "Regional Regression Equations for Estimation of Natural Streamflow Statistics in Colorado," U.S. Geological Survey Scientific Investigations Report 2009–5136, 46 p.

Daly, C., Halbleib, M., Smith, J.I., Gibson, W.P., Doggett, M.K., Taylor, G.H., Curtis, J., and Pasteris, P.A. (2008). "Physiographically-sensitive mapping of temperature and precipitation across the conterminous United States," International Journal of Climatology, 28: 2031-2064.

Dornfeld, R. (2008). "Battle Creek Restoration at the Fran Marsh Diversion," River Fixer LLC, Lakewood, CO.

Jarrett, R.D. (1984). "Hydraulics of High-Gradient Streams," Journal of Hydraulic Engineering 110 (11), 1519–1539.

Winward, A.H. (2000). "Monitoring the Vegetation Resources in Riparian Areas," U.S. Department of Agriculture, Forest Service, Rocky Mountain Research Station, RMRS-GTR-47.

ASSESSMENT, REVIEW, AND PLANNING FOR RESERVOIR SEDIMENTATION INFORMATION UPDATES FOR GLOBAL CHANGE SUSTAINABILITY

Martin J. Teal, Vice President, WEST Consultants, San Diego, CA, mteal@westconsultants.com
Paul M. Boyd, Hydraulic Engineer, U.S. Army Corps of Engineers, Omaha District, Omaha, NE, paul.m.boyd@usace.army.mil
Vicki Tripolitis, Hydraulic Engineer, WEST Consultants, San Diego, CA, vtripolitis@westconsultants.com
Daniel B. Pridal, Chief, Sedimentation and Channel Stabilization Section, U.S. Army Corps of Engineers, Omaha District, Omaha, NE, daniel.b.pridal@usace.army.mil
John I. Remus, Chief, Hydrologic Engineering Branch, U.S. Army Corps of Engineers, Omaha District, Omaha, NE, john.i.remus@usace.army.mil

Abstract: Global and climate changes, in addition to local land use changes, are altering hydrology that affects runoff and sedimentation. The U.S. Army Corps of Engineers (USACE) wishes to evaluate the effects of these changes to its project performance and reservoir storage capacity by updating reservoir sedimentation information (RSI, including sedimentation surveys, sediment load measurements, and other investigations related to sedimentation) to account for global and climate change. The goals of the current study are to assess the state of existing RSI, review and update existing methods and policies to support updated RSI, develop a strategy to update RSI, make broad estimations of the associated costs to update RSI, and prioritize needs for RSI updates.

Current RSI status was reviewed for five USACE districts using a list of specific RSI needs identified by the team of experienced engineers. Available RSI data were investigated and cataloged through interviews, site visits and conference calls with the selected districts. Costs were estimated to update RSI for the five districts and then extrapolated to the entire U.S. Army Corps of Engineers yields portfolio. This estimated amount would fill current data gaps, but does not include funding for ongoing RSI updates, which should also be considered. This amount also does not include any funds directed specifically at addressing impacts of global climate change on reservoir sedimentation, an issue which has not been considered in a significant way to date.

Additionally, a strategy was developed to update RSI that reflects new and changing conditions that impact the ability of RSI to meet intended objectives.

INTRODUCTION

Global and climate changes are altering hydrology that manifests as changes in the form (snow vs. rain), intensity (peak, seasonal, average), and duration of precipitation. In addition, ground state (frozen, saturated, unsaturated), evapotranspiration, and other factors have a significant effect on runoff. These changes may lead to and/or exacerbate modification of land use and land cover – including changing agricultural practices – that are major contributors to sedimentation in U.S. Army Corps of Engineers (USACE) reservoirs. The monitoring of sedimentation in USACE reservoirs is a vital part of a sustainable management plan for these projects. It is

essential that USACE establish baseline information on reservoir sediment levels and remaining storage capacity, and determine how future global and climate changes will impact sedimentation.

In 1981, USACE published Engineer Regulation (ER) 1110-2-4001, *Notes on Sedimentation Activities*. This regulation provides policy and guidance for the preparation of an annual report on sedimentation activities, including sedimentation surveys, sediment load measurements, and other investigations related to sedimentation. In 1989, USACE published Engineer Manual (EM) 1110-2-4000, *Sedimentation Investigations of Rivers and Reservoirs*, which provides details on the annual sediment report and also describes the Sediment Studies Work Plan (SSWP). The changes that have occurred over the intervening 30 years since the publication of ER 1110-2-4001 – especially changes in land use and land cover driving runoff and erosion – make it imperative that USACE update its understanding of the current state of reservoir sedimentation to support sustainable water management. Prioritizing reservoir sedimentation information (RSI) data gaps, and filling those gaps, is essential in developing a sustainable path forward while continually evaluating and adapting to future sedimentation impacts at all USACE reservoirs. Development of a RSI update and collection strategy will be vital to minimizing reservoir vulnerability to sedimentation impacts.

REVIEW AND ANALYSIS OF RSI

RSI Data Types: RSI study team members reviewed the current status of RSI within the five districts and analyzed the types of RSI, storage methods and organization. A team brainstorming session identified the types of RSI describing past or current conditions in district reservoirs. During this brainstorming session, the group identified a list of RSI datasets, shown in Table 1. The first four items on the list are considered the most important RSI items to fill district RSI data gaps and have the highest priority when funding requests are made. The other items have different levels of importance that depend on the authorized purposes of the district reservoirs, sedimentation issues, and overall RSI needs.

The RSI list was used as a guide during site visits and phone interviews with the districts. The following sections describe the RSI data collection methods and current RSI status by district.

RSI Data Collection Methods: During the initial review process, team members discussed RSI needs and a few districts provided a summary of their RSI status. The information was used to create RSI spreadsheet templates to be filled-in by district managers or staff participating in the study. The goal of the spreadsheets was to help account for and catalogue the RSI data for each district (including documenting the existence of sedimentation surveys, sediment load measurements, etc.) as well as present the information from various districts in a standard format. Apart from the data collection spreadsheets, interviews were conducted with five districts. During these interviews, the list of specific RSI needs (see Table 1) was used as a guide to help collect and characterize the state of the RSI.

Table 1 District Specific RSI Needs

Most important	1.	Topographic and/or Hydrographic Sedimentation Surveys – how collected, when, datum
	2.	Area-capacity analysis, changes with time
	3.	Aerial imagery/photography
	4.	Sediment samples/characteristics – cores vs. surface samples
	5.	Studies that include climate change
	6.	Sediment chemistry/quality
	7.	Project information (pools, authorized purposes, water control)
	8.	Anecdotal evidence/observations
	9.	Measured sediment load, inflow
	10.	Sediment rating curves
	11.	Gage/sediment gage locations, information
	12.	Sediment management activities (e.g., dredging, flushing, sluicing, etc.)
	13.	Past sediment studies
	14.	Sediment models
	15.	Volume depletion at different pools
	16.	Original design information
	17.	Funding over time, sources (especially alternative sources)
	18.	Sediment Studies Work Plan (SSWP)
	19.	Environmental factors driving data collection
	20.	Operational impacts, e.g., stage-frequency shifts, reallocation of pools/storage
	21.	Water surface profiles

RSI Spreadsheet Templates: Two types of spreadsheets were prepared for each district: (1) a Project Summary Form and (2) a set of individual project forms. The number of individual project forms matched the number of reservoir projects within a particular district (e.g., if a district has 35 reservoirs, then the set of forms contained 35 sheets). The following sections present a brief summary of the RSI spreadsheet templates.

Project Summary Form. The project summary form is designed to be a brief synopsis of all district projects. Table 2 describes some of the data fields included in the form while Figure 1 shows an example of the form (truncated).

A space is included at the bottom of each sheet to list any annual sedimentation reports, such as Notes on Sedimentation Activities, Sediment Studies Work Plan – SSWP, etc.

Table 2 Summary of RSI Spreadsheet Project Summary Form Fields

Data Type Field	Field Information
Authorized Project Purpose(s):	▪ Project authorized and/or operational purposes
Sediment Survey:	▪ Date of the latest and previous sediment surveys ▪ Survey method
Reservoir Pool and Spillway Information:	▪ Original reservoir storage ▪ Reservoir storage calculated from the most recent survey ▪ Volume lost between the original and most recent surveys ▪ Percentage loss between the original and most recent surveys
Permanent/Dead Storage:	▪ Permanent or dead storage volume (if applicable)
Sediment Allowance:	▪ Reservoir sediment allowance in years - number of years until reservoir is expected to be full of sediment and no longer operational

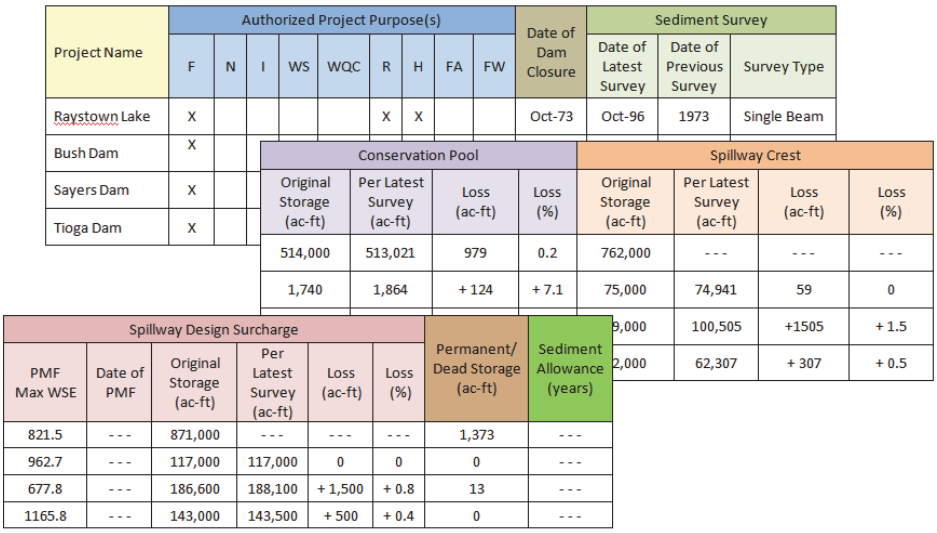

Project Name	Authorized Project Purpose(s)									Date of Dam Closure	Sediment Survey		
	F	N	I	WS	WQC	R	H	FA	FW		Date of Latest Survey	Date of Previous Survey	Survey Type
Raystown Lake	X					X	X			Oct-73	Oct-96	1973	Single Beam
Bush Dam	X												
Sayers Dam	X												
Tioga Dam	X												

Conservation Pool				Spillway Crest			
Original Storage (ac-ft)	Per Latest Survey (ac-ft)	Loss (ac-ft)	Loss (%)	Original Storage (ac-ft)	Per Latest Survey (ac-ft)	Loss (ac-ft)	Loss (%)
514,000	513,021	979	0.2	762,000	---	---	---
1,740	1,864	+ 124	+ 7.1	75,000	74,941	59	0
				9,000	100,505	+1505	+ 1.5
				2,000	62,307	+ 307	+ 0.5

Spillway Design Surcharge						Permanent/ Dead Storage (ac-ft)	Sediment Allowance (years)
PMF Max WSE	Date of PMF	Original Storage (ac-ft)	Per Latest Survey (ac-ft)	Loss (ac-ft)	Loss (%)		
821.5	---	871,000	---	---	---	1,373	---
962.7	---	117,000	117,000	0	0	0	---
677.8	---	186,600	188,100	+ 1,500	+ 0.8	13	---
1165.8	---	143,000	143,500	+ 500	+ 0.4	0	---

Figure 1 Project Summary Form Spreadsheet Example (truncated)

Individual Project Forms. Individual project forms were created for each project within a district and the files were named for that project. The forms are meant to include a more detailed summary of the RSI data for the project, including the data collection year, methods, and format in which the data are stored. There are two tabs within each individual project spreadsheet: (1) Project Information and (2) Data Types. Each of these sheets is described below.

(1) Project Information: The Project Information sheet includes a brief summary of the project. An example of the data sheet form is shown in Table 3. At the bottom of the form is space to list any data gaps, sources of funding, and an estimate of funding required to fill the gaps.

Table 3 Project Information Spreadsheet Example

Project Name:	Coldbrook							
Location of Reservoir/Dam								
Latitude:	43° 27' 14" N (Google Earth)							
Longitude:	103° 29' 21" W							
City, State, County:	Hot Springs, South Dakota, Fall River County							
Basin:	Missouri River/Cold Brook							
District:	Omaha – NWO							
Division:	Northwestern – NWD							
Dam Description								
Date of Dam Closure:	1953							
Type of Dam:	Rolled Earthfill							
Dam Length:	925 ft							
Top of Dam Elevation:	3675.0 ft (NGVD29)							
Drainage Area:	70.5 sq. miles							
Reservoir Surface Area:	(1972) 279 acres at elevation 3667.2 ft (NGVD29)							
Spillway Length:	200 ft							
Reservoir Pool Elevation	Main reservoir pools and maximum elevations (NGVD29)							
Flood Surcharge:	3667.2 ft							
Flood Control:	3651.4 ft							
Multipurpose:	3585.0 ft							
Spillway Pool:	Not applicable							
Storage Capacity	Storage capacity per latest survey (based on 1972 survey)							
Flood Surcharge:	10,898 acre-ft							
Flood Control:	7,250 acre-ft							
Multipurpose:	520 acre-ft							
Spillway Pool:	Not applicable							
Sediment Gage(s):	No sediment gages							
Authorized Project Purpose:	Flood Control	Navigation	Water Supply	Water Quality Control	Recreation	Hydropower	Flow Augmentation	Fish & Wildlife
	X				x			x
List data gaps: (1) There are no sediment data of any type or water surface profile data for this project. (2) Area & capacity tables for early survey years cannot be located. Tables for these years need to be recalculated. (3) Elevation data are presented in vertical datum NGVD 29. This data should be converted to NAVD 88 per USACE standards.								
Describe sources of funding, and provide an estimate of additional funding required to fill in the data gaps: Funding sources include O&M Base Line, O&M Non-Routine, and O&M End-Of-Year Reprogrammed Funds.								
Additional information (e.g. sediment management activities):								

(2) Data Types: The Data Types sheet includes a more detailed description of the RSI data for each project. The Year of Data Collection is included with a time sequenced history of sediment surveys and other RSI data. In addition to identifying the year of data collection and method, the type of format the data are stored in is also included, such as DSS, PDF, Excel, paper, etc. Data

fields included in the Data Types sheet are Topography & Survey, Aerial Imagery/Photography, Sediment Measurement and Sediment Chemistry/Quality. At the bottom of the each Data Types form is a list of relevant sediment reports and any related sediment models. An example spreadsheet is shown in Table 4.

DATA GAP SUMMARY

A review of the current status of District RSI was completed for five of the six districts participating in this study. The purpose of this phase of the study was to investigate and catalog the available RSI data through interviews, site visits and conference calls with the selected districts. A summary of findings by RSI category is provided in this section.

Summary by RSI Category. In general, the districts indicated that there has not been funding to support critical RSI needs or even to maintain a routine sediment survey schedule. None of the Districts interviewed have ever prepared a SSWP as outlined in EM 1110-2-4000 (1989). The original purpose of preparing a SSWP was to document and identify potential sediment problems, including reservoir sedimentation. These work plans were meant to be used at the district level to include cost estimates to complete routine sediment surveys or any other sediment study. Although SSWPs have not been prepared by the five districts interviewed, most prepare an annual report of sedimentation activities that is sent to the respective USACE division office. In general, these reports identify sediment activities for the year, and describe RSI needs for the upcoming year. The reports typically include associated costs for the critical RSI needs, or the estimates are included in the Operations and Maintenance Work Request in which RSI updates are prioritized by need for the upcoming year.

Sediment Surveys: Overall, districts have not had the funding to update topographic or bathymetric surveys (or both) on a regularly scheduled basis to estimate sedimentation rates as suggested in EM 1110-2-4000. However, over the last few years, the Omaha District has received funds from multiple business lines to update all the mainstem project surveys and about half of the tributary projects. The Baltimore District receives funding for sediment surveys from federal and local sponsors. All their permanent pool reservoirs were resurveyed in 1996-2000. The surveys included both bathymetric and topographic surveys. Since this time, five of the wet dams were resurveyed by boat between 2010 and 2012. The Los Angeles District has only been able to survey about half of the reservoirs over the last 10 years. The District has all dry dams, except for one wet dam. Survey methods for the past 10-12 years have primarily been photogrammetry and LiDAR for the dry dams, and single-beam hydrographic surveys for the wet dams. A few of the dams in the District have not been surveyed in more than 40 years.

Hydrographic single-beam surveys are used for the Fort Worth and Huntington Districts. For Fort Worth, there are nine reservoirs requiring new surveys. Some of these are not meeting the terms of their water supply contracts to be resurveyed every 15 years. The Huntington District has been able to fund several sediment surveys over the last few years, but there are still 13 reservoirs that have not been resurveyed within the past 10 years, and require updates.

Table 4 Data Types Spreadsheet Example

Data Type	Year of Data Collection					
	1958	1960	1962	1964	1968	1973
TOPOGRAPHY & SURVEY						
Pre-dam Topography	N/A					
Hydrographic Survey	P/R/E/SB	P/R/E/SB	P/R/E/SB	P/R/E/SB	C/R/E/SB	C/R/E/SB
Datum	NGVD29	NGVD29	NGVD29	NGVD29	NGVD29	NGVD29
Area-Capacity Analysis	E				E	E
LiDAR						
Photogrammetry						
AERIAL IMAGERY/ PHOTOGRAPHY						
Vintage Black/White Film						
Color (film or digital)						
SEDIMENT MEASUREMENT						
Sediment Sampling Method(s)						
Surface Samples		E		E	E	
Core Samples						
Sediment Analysis						
Grain Size Distribution		E		E	E	
Density Analysis						
Sediment Transport						
Measured Sediment Load (Inflow)						
Sediment Rating Curve						
SEDIMENT CHEMISTRY/ QUALITY						
Metals						
Solids						
pH, Temperature, DO						
ADDITIONAL DATA						
Water Surface Profiles		E	E	E		E
Datum		NGVD29	NGVD29	NGVD29		NGVD29

Datum: In general, most of the Districts use the 1929 vertical datum to store data. However, the Los Angeles District indicated that there have been some datum issues. Original surveys may have been done using MSL, NGVD29, NAVD88, or some local datum. The elevations used in the District's area-capacity tables have been converted to NGVD29 datum in order for all dams to have consistent vertical datums.

Sediment Studies and Models: In general, sediment studies have not been conducted, unless project based. There have been no studies related to climate change apart from a Garrison Dam study that included some climate change data. Also, districts indicated that models have not been used for sediment management activities or to dictate management decisions.

Area-capacity Analysis: In general, area-capacity or elevation-capacity curves are updated once a survey has been completed, unless funding is unavailable. Curve data since the 1990s are stored in electronic format for all districts. The Fort Worth and Los Angeles Districts use DSS to store the data, while the other districts use Excel. Most districts also store the data in water control manuals, sedimentation survey reports and/or binders set-up for each project. Historic area-capacity data or pre-1990s data are mostly in paper format – apart for the Los Angeles District where all storage data has been transferred to DSS. Several districts also indicated that much of the original area-capacity data or historic data have been lost or misplaced. For example, most area-capacity and survey information for the Baltimore District prior to 1993 was lost after an office move. The Omaha District has historic area-capacity data still in microfiche or paper format.

Water Surface Profiles (WSP): Data for WSP have only been collected at the Omaha and Huntington Districts. The Omaha District collects most WSP data in-house, but occasionally uses WSP data collected by the U.S. Geological Survey (USGS) or an outside contractor. The Huntington District collected WSP data as part of original reservoir design, but have not been updated since that time.

Sediment Sampling: Sediment cores and bed material samples are no longer collected in-house by any of the districts. The only districts that once collected sediment data on a routine basis were Omaha and Fort Worth. Omaha stopped collecting in-house suspended sediment samples and density measurements in the 1980s. Suspended sediment data for the District are now collected by the USGS at six sediment gages. The District collects bed material under contract when funding permits. Fort Worth collected sediment data until the early 1990s. The other districts have collected little or no sediment data.

Sediment Management Activities: Sediment management activities are generally reflected in O&M records for project maintenance. Shoaling and dredging operations have occurred at some of the Omaha District projects. Operations management requests money through "non-routine funding," then issues a request for proposal before contracting out the work. Fort Worth indicated that dredging is done only to keep intakes open for water supply – not for regaining storage capacity. Studies showed that removing sediment was ineffective based upon the cost to dredge versus the amount of storage gained. Erosion at banks is an issue with some of the Fort Worth reservoirs. Although the eroded areas provide more storage in the flood pools, volume is lost in the conservation pools. The only other district surveyed where dredging has been used is in Baltimore, at Hammond Lake for boat access. The Baltimore District indicated that other management activities included raising the normal water level about 5 feet due to sediment issues at Almond Lake. There has been some discussion that the water surface elevation may need to be raised again. Los Angeles District reservoir gates are checked and cleaned annually. There are also some gravel removal activities that take place, but this is not a routine activity. The District also indicated that there are some sediment issues with seasonal flooding.

Huntington District indicated there are no current or past dredging activities. Dillon Lake, however, has lost most of its conservation pool to sediment, but this only affects recreation – not flood control. Another sediment issue occurs at Beach City Lake (completed 1936) where the reservoir is full of sediment.

RSI Data Gaps and Funding Sources: Overall, the districts identified routine execution of sediment surveys to be the main RSI need. Other needs are sediment gages and funding to support topographic studies to supplement bathymetric surveys. Most districts identified O&M as the main source of funding. The Baltimore and Fort Worth Districts indicated that there has also been some project-based sponsorship from state or local sources. An overall cost of approximately $7.5 million was estimated to fill high priority data gaps.

Scaling of Findings. One of the goals of the current study is to scale these findings to the whole of USACE and make estimations of the data gaps. This is a challenging task, as those USACE commands with major reservoir responsibilities have a wide array of geographic, climatic, operational, and political differences. Nevertheless, the five districts from which detailed RSI information was gathered form the basis for our projections.

The inventory of USACE dams shows 704 structures at 556 projects. Out of the 556 dam projects, it appears that about 409 are for traditional impoundment rather than navigation or other purposes (about 75% of inventory). The five districts providing detailed RSI data have 119 dams collectively, and therefore represent about 30% of the total.

There are some items specific to certain districts that need to be considered when trying to extrapolate findings USACE-wide. For example, Omaha District has some of the largest dams, located on one of the largest rivers in the country (Missouri River). Los Angeles District has mostly dry dams. Fort Worth District is concerned with losses in the conservation pool due to water supply obligations.

Based on the study results to date and WEST Consultants past work with multiple other USACE districts, our judgment is that the five surveyed districts are probably above average with regards to collection and management of RSI.

Taking the above into account, and applying it to the $7.5 million needed to close the RSI gap for the five districts and their 119 dams, our estimate is that $25 million would be needed to fill current RSI data gaps USACE-wide. This estimated amount would fill current gaps but does not include funding for ongoing RSI updates, which should be part of the conversation. This amount also does not include any funds directed specifically at addressing impacts of global climate change on reservoir sedimentation, an issue which has apparently not been considered in a significant way to date.

RSI UPDATE STRATEGY

Working together the project team developed a strategy to prioritize and update RSI that reflects new and changing conditions that impact the ability of RSI to meet intended objectives. The strategy includes a characterization of classes of projects that may require similar level of effort

to update, characterization of changes on a regional or national basis that may apply to groups of projects, development of methods and processes to assist in updates, and required new policy and guidance updates (mainly USACE Engineer Regulations [ER] and Engineer Manuals [EM]).

The update strategy is built around a three-tier decision tree that builds from (a) baseline data, (b) data needs for purpose, geography, and size; and (c) possible future data needs based on climate change.

a. The review of the current status of RSI was used to support the update strategy. RSI common to all reservoirs was identified as the baseline data required for each project.

b. Commonalities in collected data associated with the project purposes were identified. Datasets were then classified in a manner to support the specific project purposes. Geography, reservoir size, and environmental issues and constraints were also considered when identifying data to collect.

c. Because a goal of the overall project is to consider reservoir response to climate change, data that may be needed in the future but is not currently collected was also addressed. This may not be a specific data set but the type of data necessary.

The update strategy identifies data collection methods, resolution, and frequency that need to be considered for the update of the USACE Sedimentation EM (1110-2-4000) and writing a new ER that will address collecting reservoir data.

Individual Project Data Needs. In addition to a baseline data set, each project may require additional RSI data specific to the project purpose(s), geographic location, reservoir size, etc. The project purpose impacts both the type of RSI collected and frequency of data collection while the other considerations have more of an effect on frequency and methods of data collection. For example, 3 of the 15 projects within the Baltimore District have an authorized project purpose of water supply. The District indicated that these projects have been made the highest priority for data updates in order to monitor the amount of storage loss due to sediment deposition and the resulting storage available for water supply. Specific data collection needs may be based project authorizations such as Navigation, Flood Risk Management, Ecosystem/Water Quality/Fish & Wildlife, Hydropower, Recreation, and Water Supply/Irrigation and were identified as part of the study. A decision tree was developed to cover the range of project uses with RSI data needs defined based on those uses. All USACE projects have an authorized purpose of flood risk management. Therefore, the minimum baseline RSI should include two topographic/bathymetric surveys and area-capacity computations to determine the total volume occupied by sediment, sedimentation patterns, and the shift in the stage-area and stage-storage curves. Ideally, the first survey will have occurred before filling of the reservoir, and the second at a point in time that will allow estimation of deposition rates, identification of spatial and temporal deposition patterns, and recognition of potential sedimentation issues. Guidance on reservoir sedimentation investigations is given in EM 1110-2-4000 (USACE, 1989).

Workplan and Sediment Management Strategies. The project team recognized that RSI feeds into development of a sediment work plan, including management strategy, as shown in Figure 2.

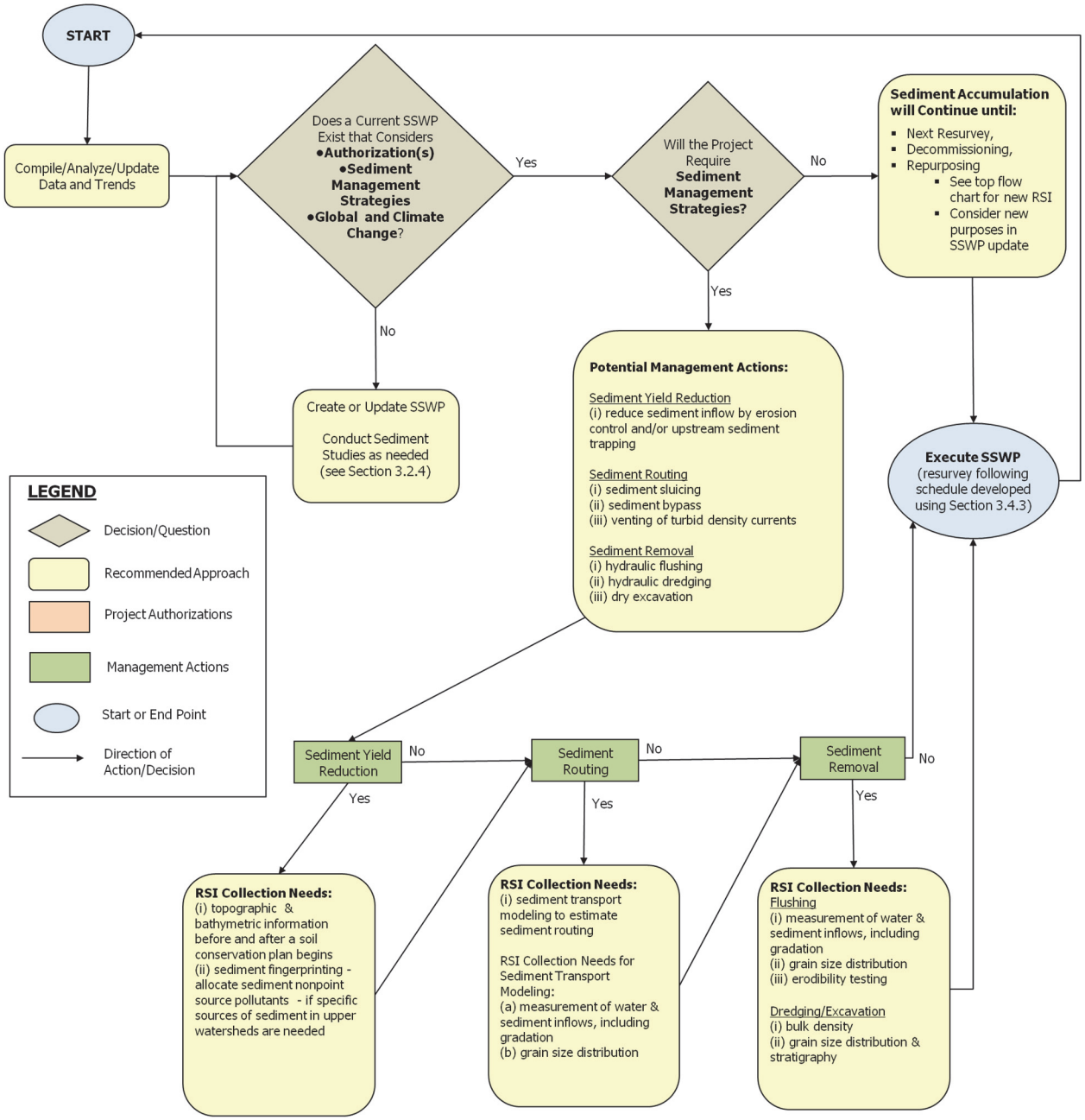

Figure 2 Workplan and Strategy Development

Sediment Studies Work Plan. EM 1110-2-4000 describes the purpose of the SSWP. Potential sediment problems and opportunities should be identified in a project SSWP. Any problems identified in the document become the basis for developing and organizing a sediment investigation. The SSWP should consider project authorizations, sediment management strategies, and global and climate changes; if not, the SSWP should be updated and any needed

sediment studies should be conducted. Reservoir sustainability should also be addressed within the SSWP. Sustainability planning should be conducted in accordance with ER 1110-2-8153 (USACE, 1995) using a staged approach. Sustainability planning may involve consideration of sediment management activities (and the RSI necessary to carry these out) or, if no feasible sustainable actions are identified, planning for reoperation or decommissioning.

Sediment Management Strategies. Different strategies for management of reservoir sedimentation are abundant in the literature. Selection of the best management strategy or action is not always straightforward, even in the present. However, given the physical characteristics of a reservoir or system and projected future conditions (e.g. future with hydrology and sediment inputs identical to the past, or future with the same affected by climate change, etc.) it may be possible to identify one or more potential future management strategies.

Sediment management methods may be broadly separated into three categories:

1. Sediment Yield Reduction – reduce sediment inflow to the reservoir
2. Sediment Routing – pass sediment around or through the reservoir
3. Sediment Removal – remove deposited sediment via hydraulic or mechanical means

Further subcategories are defined based on timing, location, and details of individual measures.

If none of the above actions are feasible or will not result in a sustainable reservoir, other management options should be considered, such as reservoir reoperation, repurposing, dam removal, or returning the dam to a run-of-river system. Most USACE dams are used for multiple purposes. As the different reservoir zones begin to fill, management practices in the future may change to account for the lost storage. For example, managers of a multipurpose reservoir with little conservation pool left may be able to increase the capacity by decreasing the capacity of another, higher, zone, or by raising the dam. Another example is a reservoir commissioned for purposes of water supply and flood risk management may be reauthorized for ecosystem management, changing from a multi-purpose to single-use reservoir. A reservoir that is reauthorized to serve a different purpose will also have new RSI needs. If a reservoir no longer serves a useful purpose, removal should be considered to restore the river to its natural pre-dam condition to the extent possible. In cases where the dam is not removed, managers may let a reservoir fill, which would eventually allow more sediment to pass over the spillway and lead to increased sediment loading to downstream reaches, including any downstream reservoirs.

REFERENCES

USACE (1981). *Notes on Sedimentation Activities,* Engineer Regulation 1110-2-4001, Washington, DC.

USACE (1989). *Sedimentation Investigations of Rivers and Reservoirs* Engineer Manual 1110-2-4000, Washington, DC (including Change 1, October 1995).

USACE (1995). *Sedimentation Investigations,* Engineer Regulation 1110-2-8153, Washington, DC.

CLIMATE CHANGE: NATURAL VARIABILITY IS A BIG DEAL TOO!

David C. Curtis, Ph.D., Vice President, WEST Consultants, Inc., Folsom, CA, dcurtis@westconsultants.com, Om Prakash, Ph.D., PE, Project Manager, WEST Consultants, Inc., Folsom, CA, oprakash@westconsultants.com

Abstract: Climate changes. That's what climate does. It is a natural and dynamic process. The National Weather Service (NWS) recognizes on-going climate change by publishing new figures for average climate every ten years. Climate averages for precipitation, temperature, and other weather parameters are computed on a 30-year basis but only updated once per decade.
With all of the discussion about anthropogenic (i.e. man-made) climate change, it is easy to overlook just how variable our natural climate can be in the relatively short-term. Our climate can and does vary by significant amounts within one human lifetime and well within the design lifetime of our water infrastructure. Sometimes this fact gets lost in the noise of the climate change debate. Part of the reason is the relatively short records of our key meteorologic and hydrologic parameters.

Here's an example. Sacramento, CA, has one of the longest rainfall records in the western US. Annual rainfall totals are available from 1850 to present. Over the 164 year record from 1850-2014, the average annual rainfall was 18.34 inches. However, the 30-year moving average rainfall varies from 20.42 inches in 1896 down to 14.51 inches in 1937 and up again to 20.47 inches by 2007. That's 30-40% swing of 30-year average rainfall in a single lifetime. (Human lifetime, not geologic time!) Most of our short records completely miss that signal. Recent streamflow reconstructions of Sacramento River flows using tree ring data show this signal repeatedly over the past 1100 years. That such significant changes can occur relatively fast has major implications for water resources infrastructure design. That such significant changes can occur relatively fast has major implications for water resources infrastructure design.

This presents explores and presents findings regarding rapid variation of "climate averages" in northern California and Oregon using long-term rainfall records. It also emphasizes the importance selecting climate models that replicate this multi-decadal signal when analyzing impacts of climate change. These results suggest that not only is stationarity dead, it likely wasn't really alive in the first place. We simply assumed it was.

INTRODUCTION

Climate changes. That's what climate does. It is a natural and dynamic process. The National Weather Service (NWS) recognizes on-going climate change by publishing new figures for average climate every ten years. Climate averages for precipitation, temperature, and other weather parameters are computed on a 30-year basis but only updated once per decade.

With all of the discussion about anthropogenic (i.e. man-made) climate change, it is easy to overlook just how variable our natural climate can be in the relatively short-term. Our climate can and does vary by significant amounts within one human lifetime and well within the design lifetime of our water infrastructure. Sometimes this fact gets lost in the noise of the climate change debate. Part of the reason is the relatively short records of our key meteorologic and hydrologic parameters.

This paper explores findings regarding rapid variation of "climate averages" in northern California using long-term rainfall records and insights from paleoclimatological proxies. It also emphasizes the importance selecting climate models that replicate this multi-decadal signal when analyzing impacts of climate change. These results suggest that not only is stationarity dead, it likely wasn't really alive in the first place. We simply assumed it was

RECENT OBSERVATIONS

In the western US, most precipitation and stream gages were installed in the latter half of the 20th Century. As such, 50-80 year records are considered long. Only a handful of gages date back to the 1800s. Sacramento, CA, has one of the longest rainfall records in the western US. Annual rainfall totals are available from 1850 to present. Figure 1 shows the highly variable annual Sacramento rainfall from 1850. The average annual rainfall for the past 164 years is a little more than 18 inches. The rainfall trend over the entire period of record, shown in Figure 2, indicates just a very slight downward trend.

The linear rainfall trend shown in Figure 2 suggests that, overall, rainfall amounts in Sacramento have been stable over the past century and a half. However, that is not the whole story.

The US National Weather Service reports climate averages on a 30-year basis. These averages are updated once per decade. In addition to being a standard reporting interval for climate averages, the 30-year time frame is similar to the time horizons used in common planning studies for civil infrastructure.

A much more dynamic picture emerges by shifting the trend analysis for the full Sacramento record to a shorter trend on the same scale as planning studies. As Figure 3 suggests, the 30-year moving average rainfall ranges from a peak of more than 20 inches annually in the 1890s to a minimum of less than 15 inches before recovering to more than 20 inches again by the 1990s. Overall, that's a 30-40% swing of 30-year average rainfall in a single lifetime. (Human lifetime, not geologic time!) Most rainfall records completely miss that signal. What these rainfall records do capture is a precipitation regime with a strong upward trend over the last 60-70 years of the 20th Century.

The California Department of Water Resources (DWR) monitors precipitation at 8 locations in a 15,700 square mile area in the northern Sierra Nevada Mountains (Roos, 2009). DWR has maintained the Northern Sierra 8 Station Index since 1921. Figure 4 presents a scatterplot of Sacramento's annual precipitation versus the Northern Sierra 8 Station Index during the overlapping period of record, 1921-2013. Sacramento's annual rainfall and the Northern Sierra 8 Station Index are highly correlated. Using the linear trend line shown on Figure 4, Sacramento's annual precipitation explains about 77% of the variance in the 92 year record on 8 Station Index values.

Such strong correspondence between the annual rainfall in Sacramento and conditions in the Northern Sierra since 1921 suggests that the Sacramento annual rainfall is a reasonable indicator of conditions throughout the Northern Sierra. Given this strong correspondence, it is likely that the Northern Sierra was relatively wet during the last half of the 19th century and became increasingly dry during the first half of the 20th century before rebounding to a relatively wet condition over the last 70 years.

LOOKING FURTHER BACK

Tree ring data are also useful indicators of past climate, when direct observations of rainfall or streamflow are unavailable. The California Department of Water Resources (DWR) recently commissioned a research project to reconstruct hydroclimates for the Klamath, San Joaquin, and Sacramento River basins from tree ring data. (Meko et al, 2014) The project reconstructed unimpaired streamflows in the Sacramento River basin for 1100 years, 900-2010 A.D. (See Figure 5)

The 30-year trailing average annual streamflow volume is plotted on Figure 5 as the heavy black line. Throughout the 1100 year record, Sacramento streamflow drifted back and forth from wet regimes to dry and back to wet again. The 30-year trailing average of reconstructed Sacramento River annual volumes over the last half of the 19th Century and through the 20th Century follows a pattern that is very similar to the 30-year trailing average of Sacramento's annual precipitation. This result is not unexpected as one would expect streamflow volumes to follow persistent precipitation patterns.

Looking again at the long-term trends in streamflow volumes (30-year trailing averages in Figure 5), repeated wet/dry cycles appear throughout 1100 year reconstructed record. The 30-year trailing average annual streamflow volume maxima is often 25-50% greater than preceding minima. Repeatedly the transition from a hydroclimate maximum to a hydroclimate minimum occurs relatively quickly; on the order of 3-4 decades.

Evidence that a warming atmosphere is already impacting the region comes from Salzar et al. (2009). Salzar examined tree ring widths from three locations in western North America near the tree line. Growth behavior at the tree line may be a sensitive indicator of a changing atmosphere. More hospitable conditions (i.e. warmer) may promote growth. Less hospitable or colder conditions may inhibit growth. Figure 6, using data from Salzar, shows recent growth rates unseen for more than 3,500 years. The authors suggest that dramatic environmental changes, most likely linked to increased temperature, promoted accelerated tree ring growth.

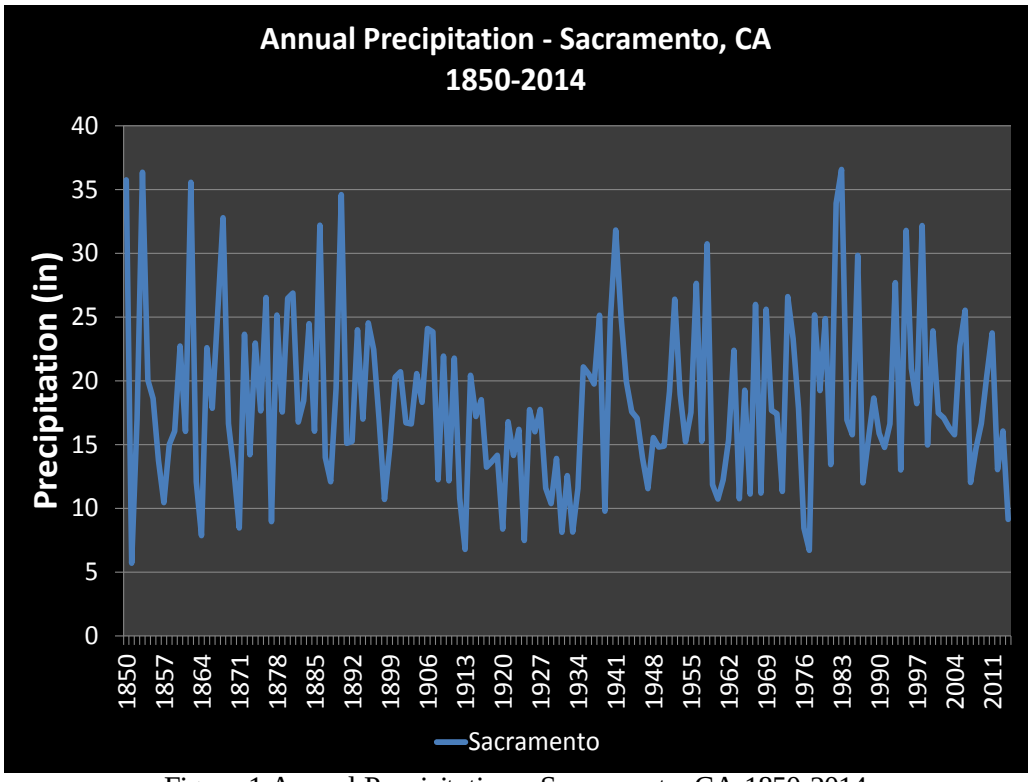

Figure 1 Annual Precipitation - Sacramento, CA 1850-2014

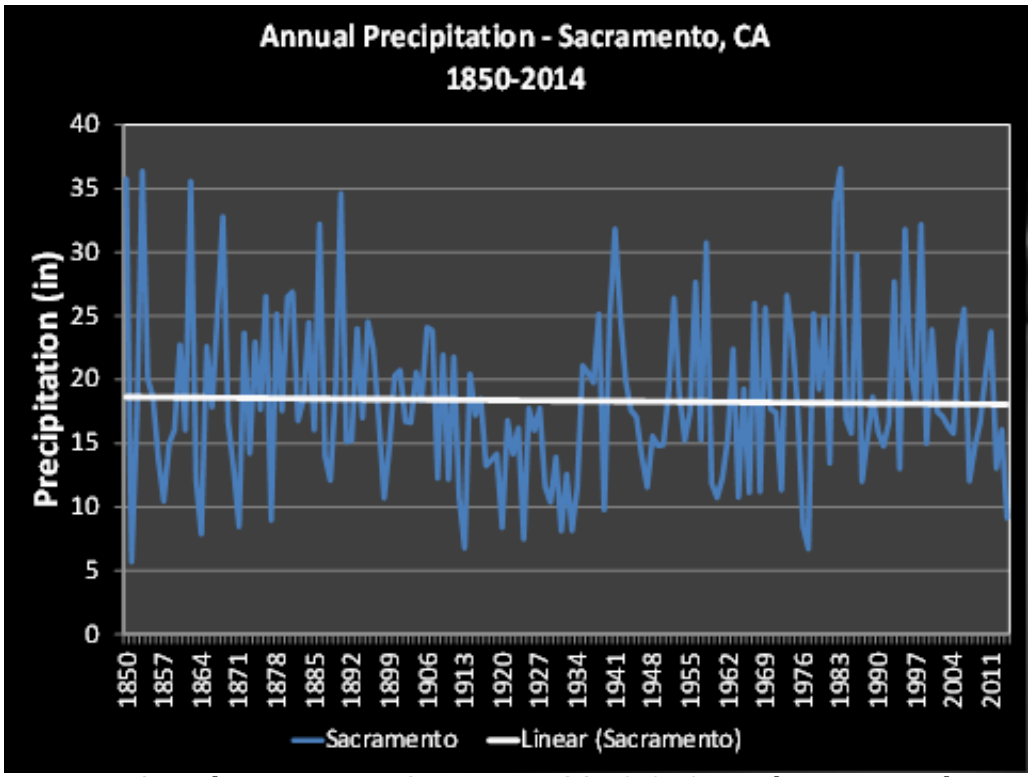

Figure 2 Annual Precipitation - Sacramento, CA 1850-2014 with Linear Trend Line

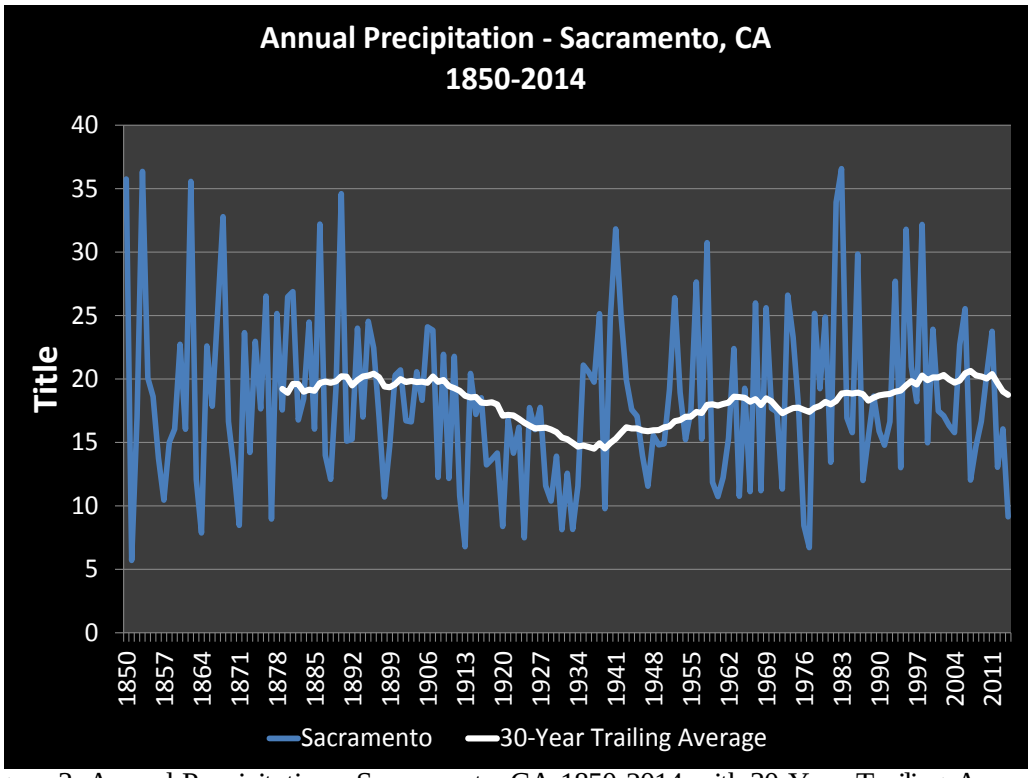

Figure 3 Annual Precipitation - Sacramento, CA 1850-2014 with 30-Year Trailing Average

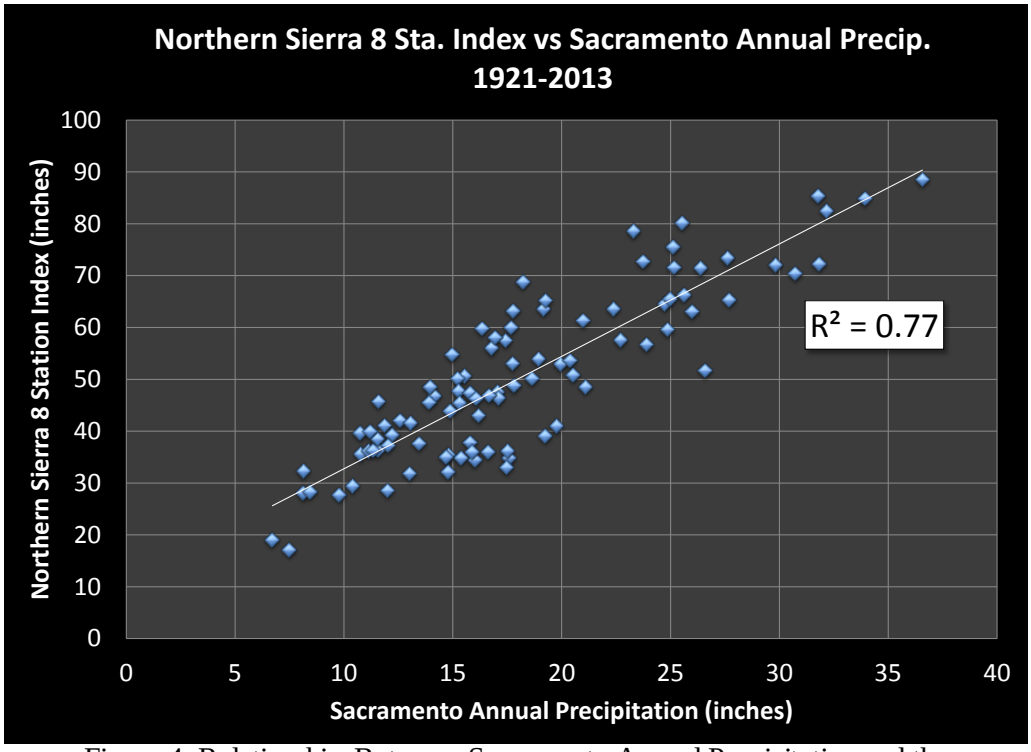

Figure 4 Relationship Between Sacramento Annual Precipitation and the Northern Sierra 8 Station Index.

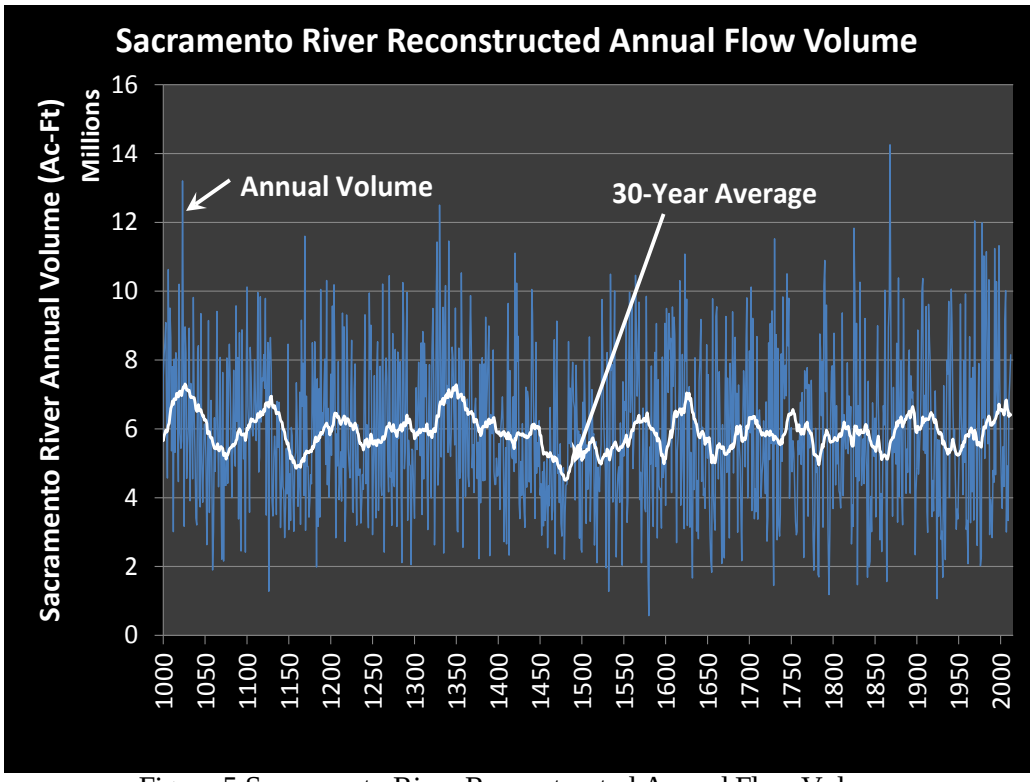

Figure 5 Sacramento River Reconstructed Annual Flow Volume

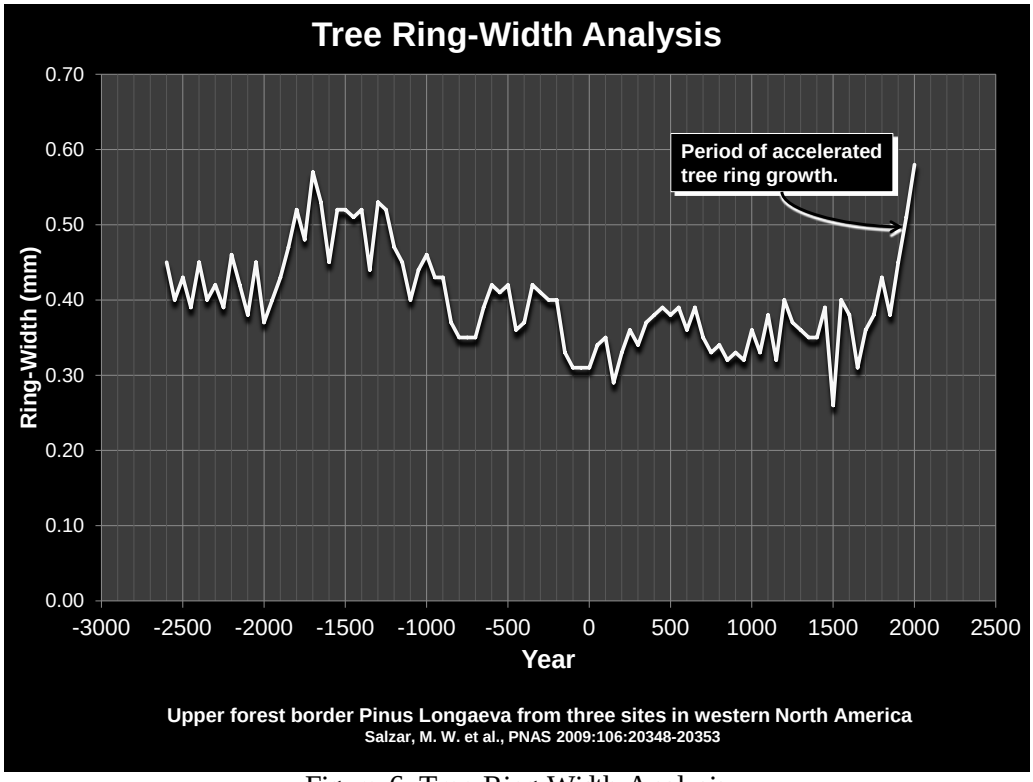

Figure 6 Tree Ring-Width Analysis

LOOKING AHEAD

Recent observations of precipitation in California and examination of paleo proxies for precipitation show that natural variability is an important feature of California's climate; a feature present long before the industrial age. Furthermore, Hawkins and Sutton (2011) suggest that natural variability will be the dominant source of total precipitation uncertainty over the next 10-30 years. Since this time frame is in line with time horizons of many water resources planning efforts, understanding and accounting for natural variability is imperative.

Changes in temperature and precipitation patterns have interrelated impacts on water resources. While natural variability will likely dominate California's precipitation uncertainty for the next several decades, it's clear that anthropogenicly driven temperature impacts such changing the rain/snow mix during winter months and earlier snowmelt may already be strongly present and can't be ignored.

Recognizing that there is a strong signal of natural variability emphasizes the importance selecting climate models that replicate this multi-decadal feature when analyzing impacts of future climate change. California's natural climate variability can either amplify or mitigate decadal scale anthropogenic climate change impacts.

Looking ahead, California water managers face a two-fold challenge. First, natural variability is a critical component to understand. Secondly, anthropogenic changes add an additional layer to California's climate complexity. Planning for California's water future must recognize and address a robustly dynamic climate now impacted by human activities of the post industrial age; impacts that we are just beginning to understand.

REFERENCES

Hawkins, Ed and Rowan Sutton, (2011), "The potential to narrow uncertainty in projections of regional precipitation change," Climate Dynamic, , Volume 37, Issue 1-2, pp 407-418

Meko, David M., Connie A. Woodhouse, and Ramzi Touchan, (2014) "Klamath/San Joaquin/Sacramento Hydroclimate Reconstructions," Draft Final Report to California Department of Water Resources, Agreement 4600008850, February 7, 2014

Roos, Maurice,(2009), "Evaluation of 9 Years of CPC Long Range Precipitation Forecasts in the Northern Sierra Nevada of California", Science and Technology Infusion Climate Bulletin, NOAA National Weather Service, 34th NOAA Annual Climate Diagnostics and Prediction Workshop, Monterey, CA, 26-30, October 2009

Salzer MW, Hughes MK, Bunn AG, Kipfmueller KF (2009) "Recent Unprecedented Tree-Ring Growth in Bristlecone Pine at the Highest Elevations and Possible Causes," Proceedings US National Academy of Science 106:20348–20353

ICE JAM PROCESSES AS INFLUENCED BY CLIMATIC VARIABILITY AND HYDROPOWER OPERATIONS: LOUP RIVER

Roger Kay, P.E., Hydraulic Engineer, U.S. Army Corps of Engineers, Omaha, NE, Roger.L.Kay@usace.army.mil

Abstract: The Loup River is the largest tributary of the Platte River and drains approximately 15,200 square miles in the State of Nebraska. Like many rivers in the region, the basin is subject to flow regime changes due to reservoirs and diversions for irrigation and hydropower. The Loup Power District operates one such hydropower plant, with flows diverted from the Loup River near Fullerton, NE, through a 35-mile canal with return flows to the Platte River downstream of the Loup River confluence. Approximately 69-percent of the annual Loup River flow is diverted for hydropower purposes in an average year.

Operational experience dictates canal flows cease when the river carries any quantity of floating ice during cold periods, to allow the canal to form a smooth ice cover and prevent entrainment of ice floes which would reduce the canal's conveyance capacity. During such periods, all flow is allowed to pass downstream through the natural river channel, carrying large quantities of ice. This operational constraint has led to the perception among local residents that these operations lead to an increased flood risk due to ice jam formation. During a recent relicensing process, FERC asked the Loup Power District to demonstrate what impact their operations may have on downstream interests, including ice processes.

Loup Power District asked the U.S. Army Corps of Engineers, Omaha District, to evaluate the impact of project hydropower (Project) operations on ice jam flooding due to any changes in hydrology, sediment transport and channel morphology on the Loup and lower Platte Rivers related to the operation of the hydropower plant. The methodology utilized included a review of flood histories, a statistical overview of climatic data, and hydraulic modeling of the study area. The statistical overview of climatic data included evaluation of temperature, snowfall, snow depth and precipitation for multiple weather stations within the study area covering a period in excess of 110 years. The climatic data was evaluated for accumulated freezing degree days (AFDD) to assess initiation of ice processes, formation of intact ice cover, thickness and quantity of ice prior to breakup and any correlation to history of ice jam flooding. Temporal trends and variability in AFDD were also assessed, as well as any correlation between snowfall depths and rainfall with occurrence of ice jams. Results of the flood history and statistical analyses of climatic data were utilized to assist in appropriate parameters for one-dimensional (1-D) hydraulic modeling of ice jam formation during freezeup and breakup periods. Two-dimensional (2-D) hydraulic modeling utilizing DynaRICE validated many of the results of the 1-D hydraulic modeling.

Results of the analyses and hydraulic modeling indicate that hydropower operations have not significantly changed the ice regime of the Loup River, nor contributed to an increased risk of

damaging ice jam flooding. The results also indicate that subtle trends in climatic variability and floodplain development may lead to an increased flood risk due to ice jams over time.

INTRODUCTION

Goals and Objectives: The goal of the study of ice jam flooding on the Loup River was to evaluate the impact of Project operations on ice jam flooding on the Loup and Platte Rivers between Fullerton, Nebraska, and North Bend, Nebraska. The study also was to develop an ice jam and/or breakup predictive model (limited to examination of Project effects), as well as identify operational or structural measures to mitigate or minimize Project effects on ice jam formation and subsequent flooding, if it was demonstrated that operation of the Project materially impacts ice jam formation on the Loup and Platte Rivers (Kay, et al, 2011).

Study Area: The study area includes the Loup River from Fullerton (approximately 7 miles upstream of the Loup Power Canal Headworks) to the confluence with the Platte River (the Loup River bypass reach), the Platte River from just upstream of the confluence of the Loup and Platte rivers to North Bend, and the Loup Power Canal from the Headworks to the Tailrace Canal confluence with the Platte River below the Loup-Platte confluence (Figure 1).

Figure 1 Study Area near Columbus, NE.

Methodology: Several methods were employed to determine if the operation of the Loup Power Canal contributes materially to the formation of ice jams along the study reach. These methods included a review of flood history, a statistical overview of meteorological data, and hydraulic modeling of the study area.

DATA COLLECTED

Flood History: A review of all available records was conducted to determine when significant flood events occurred along the study reach. The flood history was heavily influenced by Nance County Journal articles, which were some of the only records of floods before the 1930's.

Significant Floods in Lower Loup Basin: Significant floods were defined as those that resulted in loss of life and/or significant property damage. Significant floods were noted as occurring in March of either 1848 or 1849, March 1881, May 1904, February 1905, February 1907, March 1910, June 1923, April 1935, March 1936, February 1941, June 1947, February 1948, March 1960, August 1966, March 1969, February 1971 and March 1993. The 1904, 1923, 1935, 1947,

and 1966 floods were not ice-affected however. The 1960 event is not documented as being ice-affected on the Loup River, but was a significant ice-affected flood on the Platte and Elkhorn Rivers in Nebraska. For purposes of this paper, the March 1960 event is not considered an ice jam event on the Loup River.

Other Ice Related Floods: Other ice-affected floods were those that were noted as either causing low-land flooding in various records or as noted in USGS records as stage readings influenced by backwater caused by ice. There were 17 separate ice-affected flood events noted in records. USGS gaging station at Genoa indicated 32 years where the peak stage was due to backwater caused by ice; however, records prior to 1962 did not indicate the cause of backwater-influenced peak stages, so there may be as many as 10 additional years where the peak stage was influenced by ice. It was noted, however, that not all ice-affected peak stages resulted in flood stage being exceeded (Kay, et al, 2011).

Flow and Ice Thickness Measurements: The USGS maintains a network of stage-discharge gages throughout the Loup River basin. Data from two stations, listed in Table 1 below, were compiled for flow data.

Table 1 USGS Gaging Stations with Flow Data, Loup River.

Station ID	Station Name	Period of Record
06792500	Loup River Power Canal near Genoa, Nebr.	December 1936 – Present
06793000	Loup River near Genoa, Nebr.	August 1928 – June 1932, October 1943 – Present[1]

[1] Monthly Data Only, October 1953 – April 1955

Thirty sets of ice thickness measurements covering 60 years at four stations (North Loup River at St. Paul, NE; Middle Loup River at St. Paul, NE; Loup River at Genoa, NE; and Loup River at Columbus, NE) were provided by the USGS. Most ice thickness measurements were from years with below average air temperatures.

Meteorological Data: Applicable meteorological information near the study area was used, with data gathered from NOAA's National Climatic Data Center (NCDC). Temperature, snowfall, snow depth and precipitation data were collected for five stations listed in Table 2. Columbus and Genoa were selected as the primary stations for data computations, as both stations are at similar latitudes, and both have the same number of complete water year observations. Although within the study basin, St. Paul was a secondary station as its latitude is south of Columbus and Genoa, and the station has a shorter period of record. Madison and David City records were used primarily to synthesize missing daily temperature data at the two primary and one secondary station through use of multiple regression techniques.

Table 2 Climate Data Stations.

Climate Station	Period of Record
Columbus 3NE, NE	1894 – 2010
Genoa 2W, NE	1893 – 2010
St. Paul 4N, NE	1900 – 2009
Madison, NE	1895 – 1994
David City, NE	1897 – 2010

Bathymetric Data: Bathymetric surveys were collected between bank lines at 110 georeferenced cross-sections located from just downstream of the Loup Power Canal Headworks to just upstream of the Union Pacific Railroad (UPRR) bridge west of Columbus. These cross-sections were then overlain on a digital elevation model (DEM) and extended in ArcGIS to include potential overbank flow areas. HEC-GeoRAS was used to cut new cross-sections based on the extended cross-section alignments, and the surveyed cross-sections were then merged into the newly cut cross-sections and saved to a new geometry in HEC-RAS. The HEC-RAS geometry with the combined surveyed and extended cross-sections were then merged with an existing georeferenced hydraulic model geometry extending from approximately one mile downstream of the Platte-Loup confluence to upstream of the UPRR bridge west of Columbus to create a geometry extending from the Platte River at the Loup Canal Tailrace upstream to the Loup River at the Loup Power Canal Headworks Diversion. The bathymetric data, in conjunction with the DEM was also used to create a two-dimensional grid for modeling ice transport and jamming processes near the Loup Power Canal Headworks and near Columbus.

ANALYSIS

Statistical Analysis of Climatic Data: Freezing degree days (FDD) are a measure of daily average air temperature departure from freezing (32°F/0°C), with temperatures below freezing resulting in a positive FDD value and temperatures above freezing resulting in a negative FDD value. FDD can be cumulatively summed through the winter season, providing accumulated freezing degree days (AFDD), which can be used as a measure of a winter's severity. Statistical analysis of AFDD, coupled with physical measurements of ice, snow and rain, were performed to determine if the frequency and/or severity of ice jam formation has changed since commencement of Project operations.

Statistical Analysis of AFDD: The Project must cease diversions through the canal when moving ice is present on the Loup River, so the AFDD required to initiate ice production (and hence movement) in the Loup River were computed based on dates when Project flows, as recorded by USGS at Station 06792500, dropped to near zero. The AFDD required to form a stable ice cover on the Loup River (hence cessation of ice movement and resumption of Project operations) was also determined and was based on dates when Project flows returned to near normal. The annual peak AFDD value ($AFDD_{max}$), changes in AFDD during the months of January, February and post-February (referred to as $AFDD_{month}$), the change in AFDD in the 21 days preceding $AFDD_{max}$ ($AFDD_{-21}$), and the change in AFDD in the 7 days following $AFDD_{max}$ (MDD_{+7}, or melting degree days), as well as relationship between $AFDD_{max}$ and increases in Loup River discharge following $AFDD_{max}$ were all compiled as well.

Temporal Trends in AFDD: Trend analyses were performed to determine if AFDD data has changed over time, looking at annual $AFDD_{max}$ values, annual $AFDD_{month}$ values, cyclical changes in $AFDD_{max}$ over periods of 5, 10 and 30 years, annual $AFDD_{-21}$ values, annual MDD_{+7} values, and the change and variability in the Julian date of $AFDD_{max}$ (JD_{max}, where JD=1, or JD_1, is October 1 of each Water Year).

Ice Thickness Computations: Measured ice thicknesses and AFDD data from the nearest climate station were used to back-compute the coefficient for the modified Stefan equation.

Estimate Ice Thickness for Historic Ice Jams: Ice thickness values for each year just prior to breakup were estimated based on the $AFDD_{max}$ for each year, as well as a range in modified Stefan equation coefficients as determined from the statistical review of actual ice measurements.

Relationship Between Snow Cover and/or Rain and Ice Jams: Snow depth (measured on-ground depth) and snow accumulation (accumulated seasonal snowfall depth) data at Genoa and Columbus were compiled, and temporal relationships between snow cover and temperatures were analyzed, as well as any relationships between snow accumulations and $AFDD_{-21}$ and MDD_{+7} (limited to years with documented ice jams).

HEC-RAS Modeling: The HEC-RAS model was calibrated to the most recent rating curve at the Genoa gage for open water flows up to 3,000 cfs to determine the channel n-value. Higher flows were then used to calibrate overbank n-values to the Genoa gage rating curve. Flows for with- and without project hydrology were provided from the Loup Power study report (Loup River Public Power District, 2012).

Ice Formation and Freezeup Jam Formation: Flows representing the 10-, 25-, 50-, 75-, and 90% by duration flows for the months of November, December, and January (typical months for an ice cover to form) were modeled in conjunction with an ice cover. The ice n-value and thickness varied with channel velocity based on previous observations by the author and experience. Multiple iterations were needed to evaluate velocities and adjust ice n-values and thicknesses to achieve a stable ice cover consistent with velocity results.

The ice cover geometry was then adjusted to allow jamming at all cross-sections with the 10% exceedance flow to identify the most likely locations for freezeup jams to form based on available channel flow area, ice thickness, profile increase and constrictions and bends in the river. Nine potential jam locations were identified in this manner. Areas that consistently had velocities too high to allow stable ice cover formation were identified as well.

Ice Breakup and Breakup Jam formation: In order to model breakup ice jams accurately, an estimate of the volume of ice in the river prior to breakup must be known. Two single layer ice thicknesses were modeled, based on results of AFDD computations with the modified Stefan equation for average AFDD and 1-standard deviation above average AFDD at breakup to determine the initial volume of ice available at initiation of breakup. Ice jams were allowed to form at the previously identified 9 locations, with 4 locations adjusted either upstream or downstream to allow for more realistic ice jam shape and size. The upstream extent of each ice

jam was determined based on the volumes of ice previously computed and reduced by 50% to allow for broken ice pieces that are pushed into overbanks and ice that melts during transport into the jam location. Flows modeled for breakup jams were the 0.5-, 0.2-, 0.1-, 0.05-, and 0.02% ACE event assuming both current operations and no canal diversions allowed.

DynaRICE Modeling: Modeling the transport of ice floes is beyond the capabilities of a one-dimensional model such as HEC-RAS. Therefore, the two-dimensional DynaRICE ice-hydraulic numerical model was used to simulate ice transport in the Loup River, as well as ice jam initiation. The primary purpose of the DynaRICE modeling was to determine if there were any differences in ice formation and ice jamming processes with and without diversions into the Loup Power Canal. The model was calibrated against UGSG data and highwater marks from the 1993 flood near Columbus.

Two flow conditions representing 3,400 and 2,000 cfs (flows exceeded 25% and 50% of the time during freezeup conditions) were modeled for freezeup conditions near the headworks; lower flows were not modeled as the bathymetry was too coarse to accurately model shallower flows. Two historic breakup ice jams, 1969 and 1993, were simulated at Columbus as well.

RESULTS OF ANALYSES

Some of the more significant results are summarized in the following section. A more complete record of results may be found in Kay, et al (2011).

Frequency and Severity of Flooding: The record indicates 12 significant ice jam related floods and 6 open water floods along the Loup River between Genoa and Columbus between 1848 and 2010. However, records prior to the late 1800's are inconsistent, and it is possible that there are undocumented flood events during this period. Table 3 below compares the number of floods during the known period of record, including pre-Project and post-Project operations.

Table 3 Occurrence of Documented Significant Floods Before and After 1937.

Period of Record	Number of Documented:		Annual Probability of:	
	Ice Jam Floods	*Open Water Floods*	*Ice Jam Floods*	*Open Water Floods*
1848 – 1936 (88 years)	7	3	0.0795	0.0341
1893 – 1936 (43 years)	5	3	0.1163	0.0698
1937 – 2010 (73 years)	5	3	0.0685	0.0411

As can be seen, the annual probability of ice jam related flooding appears to be higher in the years preceding Project operations. The decrease in probability of ice jams cannot be credited towards Project operations, but it does discount the idea that Project operations have increased the frequency of significant ice jams. It is notable that in every year that a significant Loup River ice jam has occurred since Project operations commenced, one or more significant ice jams occurred on other Nebraska streams of similar characteristics, such as the Platte and Elkhorn Rivers. This tends to support the occurrence of ice jams as regular natural process, given the right set of ice and meteorological conditions preceding the ice jam event, irrespective of Project operations.

The occurrence of ice jams relative to meteorological conditions was also examined. Although an $AFDD_{max}$ of 1000 has about a 20% annual chance of occurrence (see Figure 2), 70% of the documented ice jams since 1905 occurred in years with $AFDD_{max}$ exceeding 1000. However, the flood of 1907, which caused four fatalities in Columbus, occurred in a year with near average $AFDD_{max}$. An $AFDD_{max}$ exceeding 1000 does not constitute a certainty of having an ice jam; less than one-third of years with $AFDD_{max}$ exceeding 1000 experienced a significant ice jam. It is noted that $AFDD_{max}$ is consistently greater at Columbus than the other stations. Since ice growth and thickness is directly correlated to FDD, it is possible that ice thickness is greatest at Columbus, which may lead to a greater risk of breakup ice jam formation at Columbus, as greater force would be required to lift, break up and transport a thicker intact ice cover.

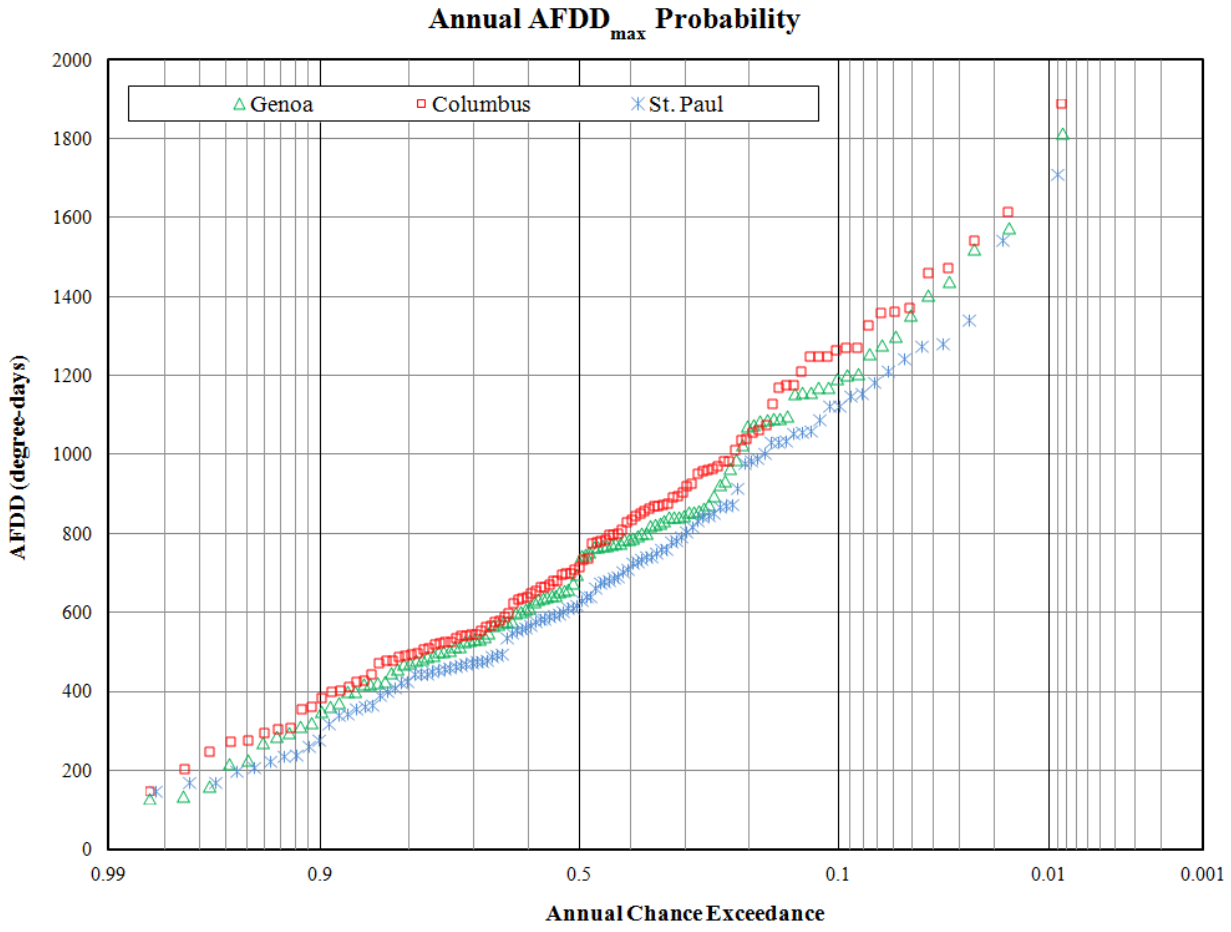

Figure 2 Annual $AFDD_{max}$ Probability at Genoa, Columbus and St. Paul.

The $AFDD_{-21}$ values may be an indicator of ice jam occurrence. Kay (2007) notes that more MDD are needed to initiate ice cover breakup on the Platte River in years with higher $AFDD_{-21}$ values. This is presumably due to greater ice growth (and hence less ice deterioration) immediately preceding ice breakup, leading to an ice cover with greater strength and therefore higher probability of resulting in jam formation. Sixty percent of the documented significant ice jams occurred in years with above average $AFDD_{-21}$. When the occurrence of $AFDD_{max}$ is

coupled with above average $AFDD_{-21}$, only 2 years, 1918 and 1893, had no documented significant flood; all other years with this combination of $AFDD_{max}$ and $AFDD_{-21}$ had significant ice jam flooding.

Likewise, higher values of MDD_{+7} may also indicate a greater likelihood of ice jam formation. White and Kay (1996) discuss that thawing degree days may be indicative of the rapidity of snowmelt but was weakly correlated with stage (i.e., severity of flooding) on the Platte River in Nebraska. Kay (2007) notes that MDD_{+7} is correlated with the increase in discharge in the 2 days preceding the peak discharge associated with an ice breakup event on the Platte River at North Bend, Nebraska. For the Loup River, 70% of the documented significant ice jams occurred in years with above average MDD_{+7}. A combination of $AFDD_{max}$ exceeding 1000 and above average MDD_{+7} results in a 50% chance of significant ice jam formation.

A review of precipitation data indicates that years with a high snow accumulation generally correlate with high discharges on the Loup River, although there was no correlation between snow accumulation and discharge with the occurrence of ice jams. However, it was noted that 80% of ice jams occurred in years with above average snowfall, and 60% of the significant ice jams occurred with snowfall in the 20^{th} percentile or higher. Only 1 significant ice jam formed in a year with a below average $AFDD_{max}$, and that was due to a rainfall event occurring on top of an existing snowpack, which indicates that rainfall may increase the probability of ice jam formation.

Although no factors point to Project operations contributing to ice jam severity, floodplain development may be a significant contributor to the severity of ice jam flooding along the lower Loup River. Floodplain development at Columbus that may impact stages include a levee along the left bank of the Loup River, highway and railroad embankments crossing the right overbank, as well as a residential development in the right overbank surrounded by a ring levee. Notable backwater under ice-affected conditions in the vicinity of the residential development and Highway 81 road crossing were noted by USACE (1994), as well as a reduction in floodplain conveyance due to these right overbank developments (USACE, 1996).

Temporal Climatic Trends: Trend analyses were performed on $AFDD_{max}$, $AFDD_{-21}$, MDD_{+7} and $AFDD_{month}$ at each of the three climate sites. It is noted that the value in any particular year is random, as a year with low $AFDD_{max}$ may be followed by a year with high $AFDD_{max}$. None of the data shows an obvious trend when looking at the entire record, as each data set exhibits a very low correlation coefficient due to the year-to-year variability. The trends over the period of record for the various parameters noted above are shown in Table 4.

Table 4 Annual Rate of Change of Key Climate Data Related to Ice Jam Formation.

Parameter	Annual Change in Value over Period of Record at:		
	Columbus	*Genoa*	*St. Paul*
$AFDD_{max}$	-0.34	-1.21	-0.24
$AFDD_{-21}$	-0.69	-0.32	-0.30
MDD_{+7}	+0.01	-0.04	-0.10
$AFDD_{Jan}$	+0.21	-0.13	-0.01
$AFDD_{Feb}$	-0.86	-1.15	-0.81
$AFDD_{Mar}$	+0.06	+0.07	+0.27

The general trend in data points to slight warming with time, although the magnitude of this increase varies with parameter and location. Two of the strongest trends are in $AFDD_{-21}$ and $AFDD_{Feb}$; both of these are significant in regards to ice breakup, as ice breakup tends to occur in late February or early March, so both $AFDD_{-21}$ and $AFDD_{Feb}$ would be indicative of ice growth just prior to breakup. The warming trend shown for both $AFDD_{-21}$ and $AFDD_{Feb}$ would indicate that breakup ice jams in the future may be less severe on average, as the ice would tend to be slightly thinner and weaker with less AFDD prior to $AFDD_{max}$ occurring. It may also indicate, however, that the ice cover will break up more readily, leading to more frequent ice jams. This may also indicate that the average ice breakup date may occur earlier on average; however, this may be offset by the slight cooling shown for $AFDD_{Mar}$ and MDD_{+7}. $AFDD_{max}$ also shows a downward trend at all three sites, which would also tend to indicate that ice jams may become slightly less severe in the future, as ice thickness would be slightly reduced, on average.

$AFDD_{max}$ does not just exhibit a downward trend, as a review of 5-, 10-, and 30-year averages of $AFDD_{max}$ indicate a cyclical nature with $AFDD_{max}$ trending up and down on a 25-35 year cycle. The Figure 3 below shows the 5-, 10- and 30-Year $AFDD_{max}$ averages at Columbus over the period of record. Similar trends were noted at both Genoa and St. Paul, although the cyclical nature of the data is not as pronounced at St. Paul. It is likely that the cyclical nature of the data will continue into the future, which would indicate that the next 10 years should likely be a period of higher $AFDD_{max}$.

A comparison of the 30-year average in $AFDD_{max}$ with the occurrence of significant ice jams can be seen in Table 5. It appears from this data that the occurrence of significant ice jams is decreasing in frequency. This data also indicates that ice jams are twice as likely to occur, on average, during periods of higher $AFDD_{max}$ than periods of lower $AFDD_{max}$. This is likely due to the high $AFDD_{max}$ periods having about a 30% probability of $AFDD_{max}$ greater than 1000, while the low $AFDD_{max}$ periods have about a 10% probability of $AFDD_{max}$ greater than 1000. This would indicate that ice jams should occur about three times more frequently during periods of high $AFDD_{max}$ as opposed to low $AFDD_{max}$, if $AFDD_{max}$ greater than 1000 was the sole indicator of ice jam formation. Since the record seems to indicate that periods of high $AFDD_{max}$ are only twice as likely to have ice jams than periods of low $AFDD_{max}$, it is apparent that there are factors other than high AFDD that determine the likelihood of an ice jam occurring.

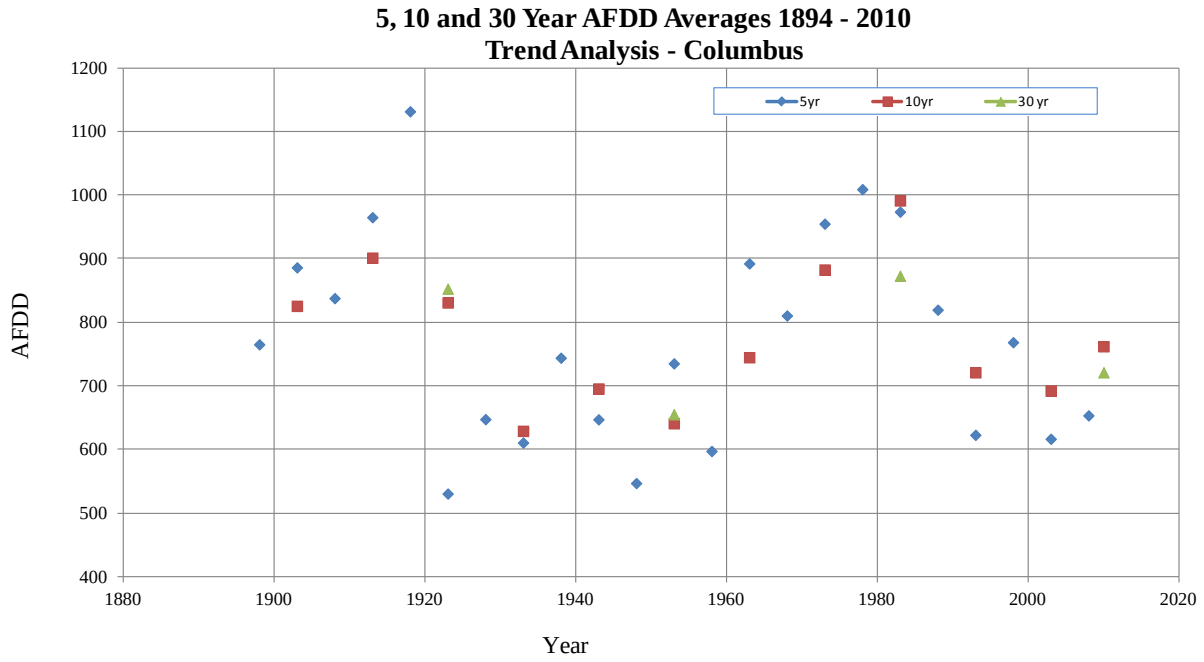

Figure 3 Average $AFDD_{max}$ Over Various Periods of Time.

Table 5 30-Year Average $AFDD_{max}$ and Ice Jam Occurrence.

	Genoa	Columbus	St. Paul	Number of Significant Ice Jams
1894 – 1923	822	853	-	4
1924 – 1953	656	655	614	3
1954 – 1983	831	872	809	2
1984 - 2010	636	721	600	1

A final trend analyzed was the Julian Date of $AFDD_{max}$ (JD_{max}), assuming JD_1 corresponded with the start of the water year on October 1, JD_2 with October 2, etc. Generally, the date of $AFDD_{max}$ is a good precursor to determining when the river ice will breakup, although in some years, most noticeably 1993, the breakup occurred prior to $AFDD_{max}$ being achieved. A review of JD_{max} over the period of record indicates that JD_{max} is occurring between 0.8 to 1.4 days earlier per decade, depending on location. This is consistent with the trends shown in Table 4 as well, as warmer temperatures will on average lead to $AFDD_{max}$ being reached at an earlier date. When the JD_{max} and $AFDD_{max}$ are averaged by decade, both show the same general cyclical trends noted in Figure 3 and shown in Table 6. However, the standard deviation of JD_{max} shows a marked increase during the past 20 years, while standard deviation of $AFDD_{max}$ does not. The reason for this significant increase in variability in JD_{max} is not readily apparent. However, it may be indicative of a more variable weather pattern with more sustained warming periods, generally occurring earlier, which would be consistent with the inter-decadal change in JD_{max} occurring earlier, as well as the decreases in $AFDD_{-21}$ and $AFDD_{Feb}$ noted earlier in this paper.

Table 6 Trends in $AFDD_{max}$ and Julian Date of $AFDD_{max}$ (JD_{max}) by Decade.

	Genoa				**Columbus**				**St. Paul**			
	Average:		*St. Dev.*		*Average:*		*St. Dev.*		*Average:*		*St. Dev.*	
	JD	*AFDD*	*JD*	*AFDD*	*JD*	*AFDD*	*JD*	*AFDD*	*JD*	*AFDD*	*JD*	*AFDD*
1890s	164	929	14.3	268	161	842	13.2	365	n/a	n/a	n/a	n/a
1900s	146	793	11.9	308	146	841	11.7	336	146	634	11.9	284
1910s	157	875	14.3	389	158	987	11.5	412	157	803	14.3	331
1920s	138	624	16.8	229	141	647	15.7	237	136	649	24.1	264
1930s	144	668	16.6	436	143	641	16.0	418	138	626	21.6	393
1940s	163	643	12.2	267	153	648	19.7	251	157	573	17.1	264
1950s	151	682	18.0	250	147	662	17.1	248	141	671	21.0	252
1960s	153	816	14.6	279	154	863	13.8	266	154	824	14.5	273
1970s	147	967	14.9	398	147	1036	14.1	400	146	988	14.6	425
1980s	141	704	14.5	329	142	759	15.6	329	142	759	15.6	329
1990s	136	597	32.9	329	136	652	37.8	317	134	638	38.0	338
2000s	141	628	22.0	313	149	766	15.5	335	139	539	23.6	261

Hydraulic Modeling: Results of the HEC-RAS modeling indicate 9 locations where freezeup jams are most likely to occur between Columbus and the Loup Power Canal Headworks. These results also show that stages are higher in the Loup River when all flows are passed down the Loup River; however, this is due strictly to the higher flows, rather than any change in ice regime. Perhaps somewhat surprisingly, there was no difference between no-diversion and diversion flows in producing stretches of river where velocities are too great to sustain a stable ice cover (except via upstream progression of a downstream ice cover increasing dynamically from upstream ice transport). This indicates that regardless of Project operation, there are certain reaches of the river that can, under the right circumstances, produce significant volumes of frazil ice, which would materially impact the potential for ice jams to occur, as the volume of the ice cover can greatly increase.

The HEC-RAS modeling also indicates 8 locations where breakup jams are most likely to form, all of which correlate with historic accounts of various ice jams of varying severity. There was one historic location, however, that the HEC-RAS model did not predict as forming an ice jam, which was just downstream of the Highway 81 bridge at Columbus, where the 1969 and 1993 ice jams formed. This may be due to a lack of detailed channel bathymetry in this location, rather than an issue with the HEC-RAS ice routine.

The DynaRICE modeling showed a freezeup jam occurring in the bend just downstream of the Genoa gage, with a thin ice cover progressing upstream towards the Canal Headworks with Loup River flows of 2000 cfs or greater, which correlated very closely with ice jam locations predicted in the HEC-RAS modeling for similar discharges. Although HEC-RAS cannot presently simulate the dynamic growth of an ice cover or ice jam, the DynaRICE modeling appears to validate the location of ice jam formation selected by the HEC-RAS modeling. The results of both modeling efforts seem to indicate slightly greater volumes of ice produced in the Loup River between the Canal Headworks and Columbus, although this slight increase in volume does not appear to contribute to a significant stage increase during ice cover formation, nor does it contribute significantly to the volume of ice available at breakup to form an ice jam.

CONCLUSIONS

A review of flood history shows that the occurrence of significant ice jam flooding has not increased since the Loup Power Canal commenced operations. A lack of historical data precludes a similar comparison of minor ice-affected flooding; however, a thorough review of climatological data and use of hydraulic models does not show a difference in the occurrence of minor ice-affected flooding due to operation of the Loup Power Canal. Other factors, such as climatic variability and floodplain developments may lead to an increased flood risk during an ice jam; however, as these factors are often subtle over time, they may be overlooked as a cause of increased flood risk. It is the opinion of the author that the Loup Power Canal has not significantly changed the ice regime of the Loup River between the Headworks and its confluence with the Platte, nor has it increased the risk of significant ice jam flooding.

REFERENCES

Kay, R.L. (2007). Ice Jam Predictive Model for Platte River at North Bend (unpublished).

Kay, R.L, Brown, J.M., Flanigan, A.J., Hamilton, L.J., and Vohl, N.W. (2011). Study 12.0, Ice Jam Flooding on the Loup River, Loup River Hydroelectric Project, FERC Project No. 1256.

Loup River Public Power District (2012). Final License Application, Volume 3 – Final Study Report, Loup River Hydroelectric Project, FERC Project No. 1256.

U.S. Army Corps of Engineers (1994). Lower Platte River Ice Jam Flooding. U.S. Army Corps of Engineers, Omaha, NE.

U.S. Army Corps of Engineers (1996). Lower Platte River and Tributaries, Nebraska. U.S. Army Corps of Engineers, Omaha, NE.

White, K.D. and Kay, R.L. (1996). Ice Jam Flooding and Mitigation: Lower Platte River Basin, Nebraska, Special Report 96-1. U.S. Army Corps of Engineers, Cold Regions Research and Engineering Laboratory, Hanover, NH.

CLIMATE CHANGE, WATER SUPPLY, AND RAINFALL-RUNOFF RELATIONSHIPS FOR SMALL INTERMITTENT STREAMS IN SOUTHERN CALIFORNIA

Peter M. Wohlgemuth, Hydrologist, USDA Forest Service, Pacific Southwest Research Station, Riverside, California pwohlgemuth@fs.fed.us

Abstract: Changing climates and altered hydrologic regimes have made future southern California water supplies uncertain. Coupled with the enormous expense and potential unreliability of large water conveyance projects, these uncertainties have led to a renewed interest in developing local water sources. Southern California is an area where water resources are scarce yet critical to support both agriculture and burgeoning population centers. The San Dimas Experimental Forest (SDEF), located in the San Gabriel Mountains about 45 km northeast of Los Angeles, experiences a Mediterranean climate with cool wet winters and hot dry summers. Multiple small watersheds 15 to 40 ha in size have been monitored for precipitation and runoff since the mid-1930s in the Bell Canyon study area. Vegetation type strongly controls water yield, presumably reflecting the rooting depth and the water demand of the different vegetation classes. Generally, higher rainfall years produce more runoff than drier years, as expected. However, runoff is also influenced by inter-annular antecedent conditions and the distribution of precipitation throughout the rainy season. An understanding of the rainfall-runoff relationships in these small intermittent streams may help guide the prospects of developing a local water source in southern California.

INTRODUCTION

If the model projections are correct, climate change will profoundly affect global weather patterns. Although there is considerable variability among the many models, the general consensus is that temperatures will increase and precipitation will decrease in most continental areas (Cayan et al., 2008). This will alter the local hydrologic cycle (the disposition of rain and snow, evaporation, transpiration, the timing of snowmelt, water storage) that will in turn affect water supplies. In southern California, the Mediterranean pattern of wet winters and dry summers is projected to continue. However, some models predict that the area could experience periods of up to 30 years where annual rainfall is more than 10 percent below historical levels (Cayan et al., 2008), and the annual precipitation could decrease by 20 to 40 percent by the year 2100 (EPA, 2013).

Water is already a scarce commodity in southern California. Most of the water for agriculture, industry, and domestic use must travel hundreds of kilometers from northern California and the Colorado River in large conveyance projects. However, these engineered water systems are currently at capacity and may be unreliable in the future, as they face issues of aging infrastructure and legal restraints for environmental concerns (Meisen and Phares, 2011). Meanwhile, demand for water is expected to remain high.

Prior to the advent of the large engineering projects that supply water to southern California, local sources had to suffice. However, interest in local supplies declined once the conveyance projects were completed and satisfied most of the regional demand (Freeman, 2008). The disturbing prospects of most climate change scenarios coupled with the potential problems and

expense of large conveyance projects have made future water supplies for southern California uncertain. These uncertainties have led to a renewed interest in developing local water sources. Nearly 40 percent of the current demand for water in southern California is still produced from local aquifers (Freeman, 2008). Moreover, developing local supplies through storm water management, using reclaimed wastewater, and groundwater management is seen as the best new source of water for future southern California needs (Nelson, 2012).

One possible source of water not currently being exploited is the intermittent streamflow from the hundreds of canyons in the mountains that ring the coastal plains and valleys of southern California. While some of this water recharges the groundwater reservoir, both naturally and by being directed into spreading grounds, much of the stormflow is quickly routed by flood control structures to the ocean. Perhaps some of this water could instead be harvested for local water supply.

The USDA Forest Service has been monitoring rainfall and stream discharge in the canyons of the San Gabriel Mountains since the 1930s. This paper explores the lessons learned from these extensive rainfall-runoff relationships that could perhaps help guide the prospects of using intermittent streams from mountainous canyons as a potential local water supply. The objectives of this study are as follows: 1) to synthesize long-term rainfall and runoff records from the San Dimas Experimental Forest; and 2) to determine the influence of rainfall distribution, antecedent conditions, and vegetation type on runoff quantity.

STUDY AREA

The San Dimas Experimental Forest (SDEF) is a nearly 7000 ha research preserve administered by the USDA Forest Service, Pacific Southwest Research Station, and has been the site of extensive hydrologic monitoring for over 80 years (Dunn et al., 1988). The SDEF was originally established in 1933 to document and quantify the hydrologic cycle in semiarid uplands with intermittent headwater streams. With its headquarters at Tanbark Flat (34^o 12' N latitude, 117^o 46' W longitude), the SDEF is located in the San Gabriel Mountains, about 45 km northeast of Los Angeles, California (Figure 1).

Elevations in the Bell Canyon study area range from 750 to 1050 m and topography consists of a highly dissected mountain block with steep hillside slopes and steep channel gradients. Bedrock geology is dominated by Precambrian metamorphics and Mesozoic granitics that produce shallow, azonal, coarse-textured soils (Dunn et al., 1988). The region experiences a Mediterranean-type climate, characterized by hot, dry summers and cool, moist winters. Temperatures range from -8^o C to 40^o C. Mean annual precipitation, falling almost exclusively as rain, is 715 mm in the SDEF (80-year record), but rain during individual years can range from 252 to 1848 mm.

Native vegetation in Bell Canyon consists primarily of mixed chaparral. Plant cover on south-facing slopes ranges from dense stands of chamise (*Adenostoma fasciculatum*) and ceanothus (*Ceanothus* spp.) to more open stands of chamise and black sage (*Salvia mellifera*). North-facing hillsides are dominated by scrub oak (*Quercus berberidifolia*) and ceanothus, with occasional

hardwood trees – live oak (*Quercus agrifolia*) and California laurel (*Umbellularia californica*) – occurring on moister shaded slopes and along the riparian corridors (Wohlgemuth, 2006).

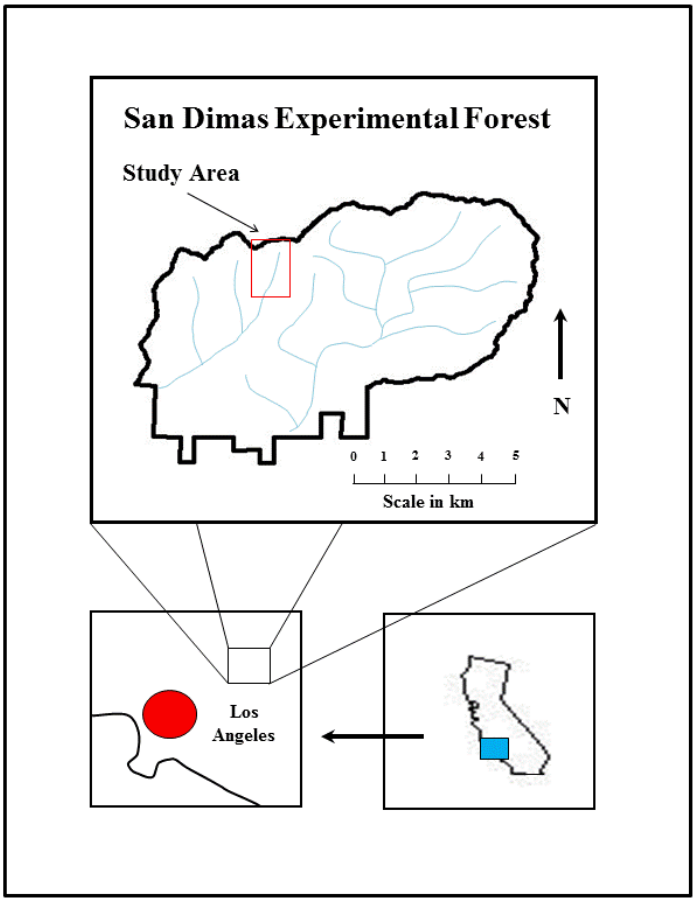

Figure 1 Location map of the San Dimas Experimental Forest.

One of the management treatments following a wildfire in 1960 involved type-converting the native chaparral vegetation in some watersheds to a mixture of perennial grasses. It was thought that type-conversion would aid in future fire control and would enhance water yield by replacing deep-rooted shrubs with shallow-rooted grasses (Rice et al., 1965). These perennials included a variety of wheatgrass species (*Agropyron* spp.), Harding grass (*Phalaris tuberosa* var. *stenoptera*), big bluegrass (*Poa ampla*), smilo grass (*Piptatherum miliaceum*), and blando brome (*Bromus hordaceous*) (Corbett and Green, 1965). Since 1960, many of the seeded grass species have disappeared from the sites and substantial amounts of buckwheat (*Eriogonum fasciculatum*) and black sage have established on the type-converted watersheds.

METHODS

Four small watersheds were selected for study in Bell Canyon (Figures 1 and 2): two in type-converted grass vegetation – Bell1 (32 ha) and Bell2 (41 ha) – and two in native chaparral –

Bell3 (25 ha) and Bell4 (15 ha). Two raingages monitored precipitation inputs across the study watersheds, one at the headwaters and one at the outlets (Figure 2). Although rainfall was very similar between these two gages, total annual rain was computed as the area-weighted average of the two stations. In addition to annual totals, rainfall is also characterized by the amount received during the highest three-month period, or quarter, describing the timing of major rain events throughout the year. Rain was assumed to be spatially uniform across the landscape and was computed as cubic meters based on watershed area.

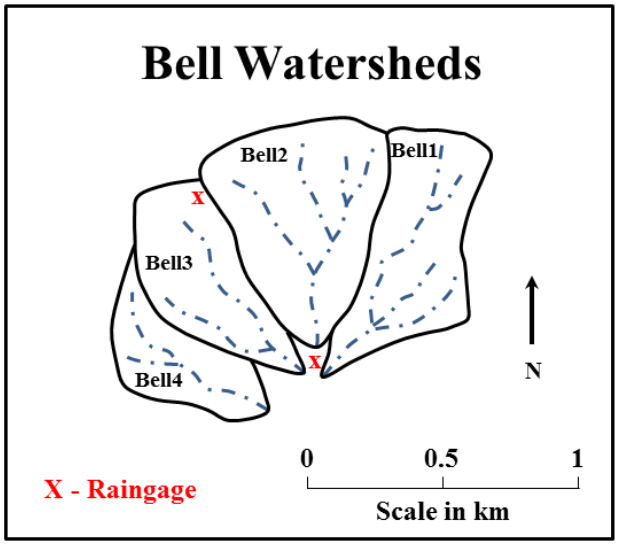

Figure 2 Bell study watersheds.

Prior to 1969, stream discharge for all watersheds was measured in small 90° v-notch weirs for low flows (<50 l s^{-1}) and 0.91 m (3-foot) flumes for higher flows. Following the 1969 floods that destroyed most of the low-flow gaging equipment, all streamflow was monitored in large 120° v-notch weirs in Bell1, Bell2, and Bell3. However, a reconstructed 90° v-notch weir and flume arrangement continued to measure flow in Bell4. Stage height for each instrument was measured in a stilling well by a float-operated recorder to produce a paper chart. In the office, stage heights were manually read from the stream charts at 6 hour intervals and at inflection points during storm events. Discharge was computed from stage height using rating curves developed for each instrument and summed over the time intervals to get an annual water yield in cubic meters. Partial-year records resulting from equipment failure or missing charts were not used in any subsequent analyses.

RESULTS AND DISCUSSION

Rainfall and stream runoff values for each of the Bell study watersheds from hydrologic years (October to September) 1960 to 2000 are arrayed in Table 1. While continuous precipitation records are available from the two raingages over the period of study, stream discharge measurement was sporadic. A wildfire in 1960 and subsequent debris-laden flows prevented continuous stream gaging for three years following the fire. A large flood destroyed the low-flow gaging equipment in all watersheds in 1969. Stream charts are missing for Bell4 from the

Table 1 Rainfall and stream runoff values for the Bell watersheds for hydrologic years 1960 to 2000. First quarter – Oct. to Dec. Second quarter – Jan. to Mar. Third quarter – Apr. to June. Fourth quarter – July to Sep. TC – type converted grass vegetation. NC – native chaparral vegetation. Runoff Ratio = Annual Streamflow/Annual Rainfall. (.) – full-year records not available because of equipment failure or missing stream charts.

			Watershed							
	Rainfall		Bell1 (TC)		Bell2 (TC)		Bell3 (NC)		Bell4 (NC)	
Year	Total (mm)	Highest Quarter (mm)	Runoff $m^3\ ha^{-1}$	Runoff Ratio	Runoff $m^3\ ha^{-1}$	Runoff Ratio	Runoff $m^3\ ha^{-1}$	Runoff Ratio	Runoff $m^3\ ha^{-1}$	Runoff Ratio
1960	377	2nd (215)	0.2	0.01	75.1	0.02	5.9	0.01	.	.
1961	279	1st (175)	.	.	.	.	.	.	.	.
1962	784	2nd (566)	.	.	.	.	.	.	.	.
1963	460	2nd (283)	.	.	.	.	.	.	.	.
1964	410	2nd (188)	370.7	0.09	379.7	0.09	52.0	0.01	.	.
1965	565	3rd (294)	1173.3	0.21	996.3	0.18	181.3	0.03	.	.
1966	859	1st (744)	5230.9	0.61	.	.	2528.1	0.29	.	.
1967	1176	1st (577)	.	.	8846.6	0.75	4632.0	0.39	.	.
1968	510	1st (261)	1207.4	0.24	1242.4	0.24	601.0	0.12	.	.
1969	1617	2nd (1539)	.	.	.	.	.	.	.	.
1970	471	2nd (375)	.	.	1071.4	0.23	620.0	0.13	460.6	0.10
1971	509	1st (340)	.	.	1113.6	0.22	401.7	0.08	297.7	0.06
1972	326	1st (293)	.	.	534.6	0.16	195.1	0.06	81.6	0.03
1973	858	2nd (658)	.	.	.	.	.	.	.	.
1974	563	2nd (436)	.	.	.	.	550.1	0.10	408.9	0.07
1975	518	1st (138)	.	.	609.2	0.12	253.2	0.05	110.7	0.02
1976	525	2nd (304)	.	.	549.8	0.10	131.0	0.02	6.1	0.01
1977	499	2nd (254)	.	.	.	.	140.6	0.03	18.5	0.01
1978	1614	2nd (1220)	.	.	.	.	.	.	7085.8	0.44
1979	744	2nd (548)	.	.	.	.	1219.9	0.16	1070.2	0.14
1980	1379	2nd (1251)	.	.	.	.	6899.7	0.50	5072.0	0.37
1981	378	2nd (289)	.	.	.	.	315.0	0.08	218.5	0.06
1982	839	2nd (266)	.	.	1832.9	0.22	836.0	0.10	809.3	0.10
1983	1463	2nd (798)	.	.	7060.2	0.48	.	.	5179.0	0.35
1984	415	1st (324)	176.0	0.04	718.3	0.17	485.5	0.12	.	.
1985	603	1st (424)	508.6	0.08	725.1	0.12	.	.	.	.
1986	846	2nd (515)	1144.0	0.14	1340.7	0.16	.	.	.	.
1987	285	2nd (190)	88.3	0.03	121.3	0.04	.	.	.	.
1988	759	1st (336)	.	.	432.6	0.06	218.4	0.03	284.9	0.04
1989	531	1st (271)	327.8	0.06	437.8	0.08	183.3	0.03	132.0	0.02
1990	374	2nd (261)	59.6	0.02	53.2	0.01	.	.	30.6	0.01
1991	618	2nd (593)	.	.	709.3	0.11	358.1	0.06	522.8	0.08
1992	800	2nd (792)	.	.	.	.	.	.	.	.
1993	1566	2nd (1215)	.	.	.	.	.	.	.	.
1994	408	2nd (277)	148.0	0.04	.	.	132.0	0.03	.	.
1995	1284	2nd (1128)	4848.1	0.38	.	.	3272.6	0.25	4659.4	0.36
1996	689	2nd (632)	1553.8	0.23	1407.9	0.20	930.2	0.13	906.7	0.13

Table 1 (cont).

			Watershed							
	Rainfall		Bell1 (TC)		Bell2 (TC)		Bell3 (NC)		Bell4 (NC)	
Year	Total (mm)	Highest Quarter (mm)	Runoff $m^3\ ha^{-1}$	Runoff Ratio	Runoff $m^3\ ha^{-1}$	Runoff Ratio	Runoff $m^3\ ha^{-1}$	Runoff Ratio	Runoff $m^3\ ha^{-1}$	Runoff Ratio
1997	718	1st (408)	.	.	.	.	.	.	.	.
1998	1427	2nd (841)	.	.	5981.2	0.42	.	.	.	.
1999	347	2nd (144)	143.2	0.04	244.5	0.07	259.0	0.07	141.0	0.04
2000	511	2nd (382)	.	.	289.2	0.06	177.5	0.03	.	.

1960s and from Bell1 from the 1970s. Miscellaneous missing charts and equipment failures (pen problems, clock stoppages, and float problems) have created additional data gaps for all watersheds throughout the study period. Thus, only half the runoff years were available for analysis.

Average annual rainfall over the study period was 750 mm, slightly more than the mean for the 80-year record on the SDEF. For subsequent comparisons, annual rainfall was divided into three categories: high (> 150 percent of average or 1130 mm; n=8); low (< 50 percent of average or 380 mm; n=7); and normal (between 380 mm and 1130 mm; n=26).

Because of the disparity in watershed size, stream runoff was normalized by area for meaningful comparisons (Table 1). Additionally, the runoff ratio (Ratzlaff, 1994), or the percentage of rainfall that leaves the watershed as streamflow, was calculated. A runoff ratio is a commonly used metric in hydrologic studies to describe basic watershed behavior. For this study, runoff ratios ranged from 1 percent to 75 percent for all watersheds and all years, with an average of 14 percent. These values correspond well with other published runoff ratios for southern California watersheds (Burke et al., 2013; Kinoshita and Hogue, 2015).

There was a distinct difference in stream discharge associated with vegetation type. Both the normalized runoff and the runoff ratio were similar within the vegetation classes of type-converted grass (Bell1 and Bell2) and native chaparral (Bell3 and Bell4). However, considerably more water flowed from the grass watersheds than the chaparral (Table 1; Figure 3). This general trend confirms earlier studies at the SDEF and from similar areas in California and Arizona (Hill and Rice, 1963; Hibbert, 1971; Rich and Gottfried, 1976; Pitt et al., 1978) and supports the rationale for replacing deep-rooted shrub species with shallow-rooted grass to increase water yield (Rice et al., 1965). Higher water yield from grass-dominated watersheds suggests that extensive type conversion of southern California shrubland to grasses could substantially increase local water supplies. However, apart from the wholesale ecosystem changes and effects on native fauna, previous studies have shown that there are serious environmental consequences of type conversion, including increased erosion in the form of soil slips and slope failures (Rice et al., 1969) and degraded water quality (Riggan et al., 1985).

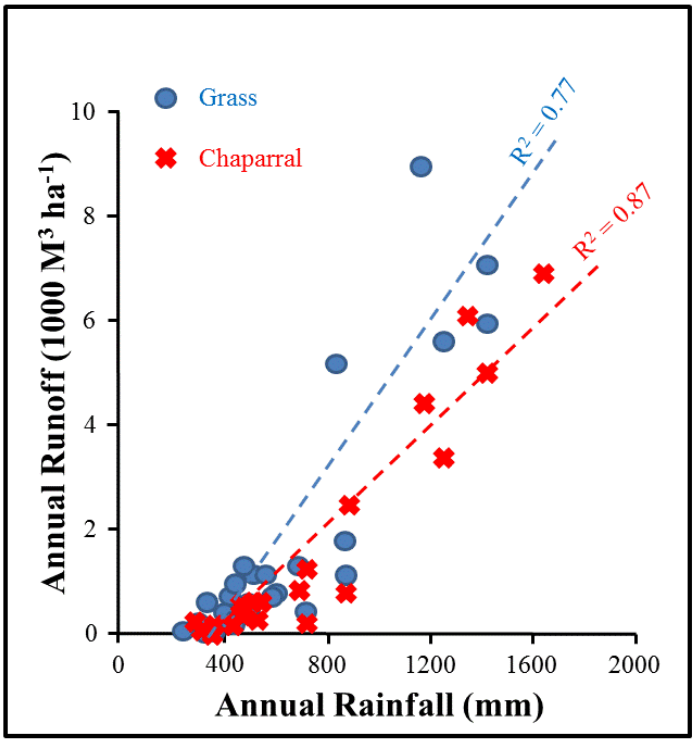

Figure 3 Runoff as a function of rainfall by vegetation type in the Bell Watersheds.

There is a good correlation between stream runoff and precipitation for both vegetation types (Figure 3). However, for the intermittent streams in Bell Canyon, heavy and protracted rainfall can produce streamflow throughout the entire year. In this case, rain from one year could continue to generate surface flow into the following year. This poses a problem with the runoff ratio (Table 1) in that flow is also affected by inter-annular antecedent conditions. So in Bell Canyon, when a high rainfall year is followed by a normal or even a low rainfall year, more runoff is produced in that following year than would otherwise be expected (in Table 1, compare 1968 with 1975 or 1976; compare 1981 or 1999 with 1987 or 1990). In contrast, a high rainfall year is always associated with high runoff, no matter what the prior conditions (1978 or 1995). Therefore, there is a lag in stream discharge from a previous high rainfall year that can enhance flow in the subsequent year.

Another factor that may affect streamflow is the distribution of rain storms throughout the year. Except under the high rainfall lag condition mentioned above, intermittent streams require early season storms to saturate the soil mantle before flow is generated by later storm events. Rainfall amounts for the highest three-month period for each year in Bell Canyon are shown in Table 1. Of the 41 hydrologic years of record, the greatest rain was received 28 times in the second quarter (Jan. to Mar.), 12 times in the first quarter (Oct. to Dec.), and once in the third quarter (Apr. to June). For low rainfall years, low runoff was produced no matter when the rain fell. Similarly, for high rainfall years, the distribution of rain was not a factor in generating the high flows. However, for more average rainfall conditions, those years that had wet second quarters generally produced higher amounts of runoff compared to those years with wet first quarters (in

Table 1, compare 1974, 1976, 1982, and 1991 with 1971, 1975, 1985, 1988, and 1989). Therefore, in normal rainfall years, the timing of storms can affect the amount of streamflow.

SUMMARY

The prospects of reduced rainfall resulting from global climate change and the potential unreliability of large conveyance projects have made future water supplies in southern California uncertain, prompting a renewed interest in developing local sources. One potential source is the intermittent streamflow from the canyons of the local mountains. Long-term research from the San Dimas Experimental Forest in the San Gabriel Mountains shows that stream runoff is strongly correlated with rainfall amounts and that this flow is mildly enhanced when major storms occur later in the rainy season. Streamflow is also greater than expected the year following heavy rains, as a lag component of the high rainfall carries over to the subsequent year. More water is produced from catchments that have been type-converted to grasses than from native chaparral shrublands, presumably reflecting the rooting depth and water demand of the different vegetation classes. While it is tempting to recommend future type-conversion to increase water yield, this must be balanced by the wholesale ecosystem changes and the negative environmental consequences associated with this method of vegetation change.

REFERENCES

Burke, M.P., Hogue, T.S., Kinoshita, A.M., Barco, J., Wessel, C., and Stein, E.D. (2013). "Pre- and post-fire pollutant loads in an urban fringe watershed in southern California," Environmental Monitoring and Assessment, 185(12), pp. 10131-10145.

Cayan, D.R., Maurer, C.P., Dettinger, M.D., Tyree, M., and Hayhoe, K. (2008). "Climate change scenarios for the California region," Climatic Change, 87(Supplement 1), pp. S21-S42.

Corbett, E.S., and Green, L.R. (1965). "Emergency revegetation to rehabilitate burned watersheds in southern California," Research Paper PSW-22, USDA Forest Service, Berkeley, CA.

Dunn, P.H., Barro, S.C., Wells, W.G., II, Poth, M.A., Wohlgemuth, P.M., and Colver, C.G. (1988). "The San Dimas Experimental Forest: 50 years of research," General Technical Report PSW-104, USDA Forest Service, Berkeley, CA.

Environmental Protection Agency. (2013). "Climate impacts in the Southwest," http://www.epa.gov/climatechange/impacts-adaptation/southwest.html.

Freeman, G. (2008). "Securing reliable water supplies," Los Angeles County Economic Development Corporation. 19 p.

Hibbert, A.R. (1971). Increases in streamflow after converting chaparral to grass," Water Resources Research, 7(1), pp. 71-80.

Hill, L.W. and Rice, R.M. (1963). "Converting from brush to grass increases water yield in southern California," Journal of Range Management, 16(6), pp. 300-305.

Kinoshita, A.M. and Hogue, T.S. (2015). "Increased dry season water yield in burned watersheds in southern California," Environmental Research Letters, 10(1) DOI 10.1088/1748-9326/10/1/014003.

Meisen, P. and Phares, N. (2011). "Impacts of climate change on California's water supply," Global Energy Network Institute. 47 p.

Nelson, B. (2012). "Southern California's new wave of local water supplies," http://switchboard.nrdc.org/blogs/bnelson.

Pitt, M.D., Burgey, R.H., and Heady, H.F. (1978). "Influences of brush conversion and weather patterns on runoff from a northern California watershed," Journal of Range Management, 31(1), pp. 23-27.

Ratzlaff, J.R. (1994). "Mean annual precipitation, runoff, and runoff ratio for Kansas, 1971-1990," Transactions of the Kansas Academy of Science, 97, pp 94-101.

Rice, R.M., Corbett, E.S., and Bailey, R.G. (1969). "Soil slips related to vegetation, topography, and soil in southern California," Water Resources Research, 5(3), pp. 647-659.

Rice, R.M., Crouse, R.P., and Corbett, E.S. (1965). "Emergency measures to control erosion after a fire on the San Dimas Experimental Forest," U.S. Department of Agriculture, Miscellaneous Publication 970, pp 123-130.

Rich, L.R. and Gottfried, G.F. (1976). "Water yields resulting from treatments on the Workman Creek experimental watersheds in central Arizona," Water Resources Research, 12(6), pp. 1053-1060.

Riggan, P.J., Lockwood, R.N., and Lopez, E.N. (1985). "Deposition and processing of airborne nitrogen pollutants in Mediterranean-type ecosystems in southern California," Environmental Science and Technology, 19(9), pp. 781-789.

Wohlgemuth, P.M. (2006). "Hillslope erosion and small watershed sediment yield following a wildfire on the San Dimas Experimental Forest, southern California," Proceedings of the 8th Federal Interagency Sedimentation Conference, Reno, NV, Interagency Advisory Committee on Water Data, Subcommittee on Sedimentation, Washington, D.C.

JUSTIFYING INFLOW DESIGN FLOOD FOR DAM HYDROLOGIC SAFETY: HOLISTIC COMPARISON OF METHODS

S. Samuel Lin, Civil Engineer, FERC, Washington, D.C., Shyangchin.Lin@FERC.gov

Abstract: The approach of selecting adequate inflow design floods (IDFs) is critical to verifying the existing or implementing designing acceptable hydrologic safety for dams. The purpose of this paper is to present state-of-the-methods for selecting an IDF in a technically defensible fashion by way of: (1) Clarifying the hypothetical dam failure scenarios between both hazard-classification based preliminary IDF determination and the more refined potential failure modes (PFMs) based IDF determination; (2) Discerning the iterative process needed for an optimal IDF determined from the refined incremental consequence approach (ICA); and (3) Recognizing the merits of the refined risk-informed decision making (RIDM) approach as a more advanced method and its challenges as well. Two example application cases are provided to illustrate and compare the IDF selection processes of those methods which are addressed in this paper.

Note: The opinions and views offered here are those of the author, and are not necessarily those of the Federal Energy Regulatory Commission, individual Commissioners, or other members of the Commission's staff.

BACKGROUND INFORMATION

Federal and State agencies bring commitment to public safety. The Federal Emergency Management Agency (FEMA) published the P-94 guidance document entitled, "Selecting and Accommodating Inflow Design Floods for Dams" in August 2013. It provides updated guidance for the analysis, evaluation, and assessment of the hydrologic safety for new and existing dams. Its release was intended to provide a flexible framework within which both federal and state agencies can develop and update guidelines according to their varied goals and resources. To be consistent and stable over time, the basic philosophy and principles are described, but not all procedures provided, in order to adequately manage the hydrologic safety risk to dams by passing a required minimum magnitude flood flow for the sake of public safety.

The methodologies of both deterministic and probabilistic approaches, shown in Fig. 1 Methodologies of IDF Selection: Deterministic vs. Probabilistic Methodology, are correctly being used to facilitate dam safety risk management for evaluating hydrologic safety of dams. The deterministic approach includes the prescriptive approach based solely on a dam's hazard potential class, and the ICA is based on the incremental upstream/downstream inundation situations. The more advanced probabilistic approach is a quantitative risk oriented RIDM process to meet a defined tolerable risk level.

To illustrate the merits and shortcomings of the deterministic and probabilistic approaches as described, two case studies are presented as examples (for reference only) to demonstrate an optimal hydrologic safety protection for a dam. Non-structural solutions to IDF issues such as considering the effectiveness of Emergency Action Plan (EAP) execution on dam failure consequences, removing dam, land acquisition, structure abandonment, etc. are not discussed in this paper.

IDF BASED HYDROLOGIC SAFETY STRATEGY

Prescriptive method, ICA method and RIDM approach are available techniques to develop a quantified hydrologic safety strategy for dams to accommodate the wide variety of situations, available resources, and conditions. The IDF analysis starts from hypothetical dam failure assumptions under various flood loading conditions for dam failure potential consequence magnitude estimations. The PFMs of a dam system including dam and appurtenant structures can be identified through a PFM analysis (PFMA) exercise. In practice, the dam breach assumptions are evaluated to use the most conservative parameters resulting in a worst downstream inundation scenario for the relatively simpler prescriptive approach but more realistic, physically based PFMs parameters are used for the refined ICA and RIDM approaches. Thus, the prescriptive method's assumed parameters are often greater than the ICA/RIDM methods'. The subsequent consequence (life and property losses, environmental damage, etc.) are estimated basically based on dam failure-induced flood flow inundation levels at the downstream impact areas.

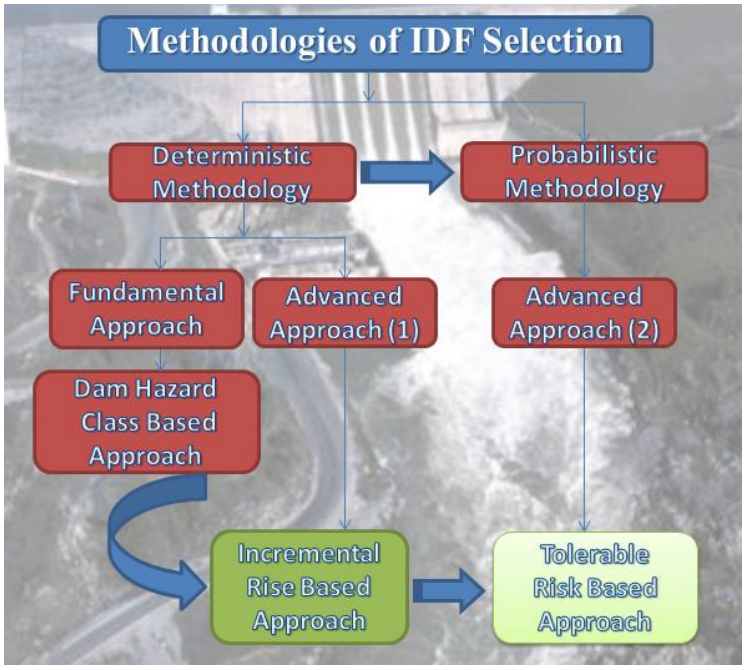

Fig. 1 Methodologies of Inflow Design Flood Selection: Deterministic vs. Probabilistic Methodology

In general, a PFM is defined as a process (i.e., dynamic mechanism) in which the dam could reasonably and logically be expected to fail under a certain adversarial condition equal to or greater than its failure threshold. The most common hydrologic PFMs include overtopping erosion of embankments/abutments, erosion and back-cutting of earthen channel spillways,

cavitation of chute channels, internal erosion (seepage and piping), dam overturning/sliding, and overstressing of the structural components of the dam, all of which may be caused by high reservoir levels due to extreme hydrological events. To attempt to avoid these PFMs, spillways are designed to safely pass the justified IDF based on the analysis results of any of the above mentioned alternative approaches.

Guiding Definitions of IDF: An IDF can technically be defined in three ways. The first is by the dam hazard class based prescriptive IDF. The second is the flood flow above which the incremental increase in downstream inundation water surface elevation due to failure of a dam is no longer considered to present an unacceptable additional downstream threat. The first and second definitions are based on deterministic approach results. The third is probability based and the IDF is the flood flow above which the consequence risk due to failure of a dam does not exceed a given level of "tolerable risk". For instance, some agencies using two tolerable risk indices to justify the IDF selection such as averaged annual failure probability (AFP) of a dam and a resulting averaged annual life loss (ALL).

Inundation Loss Rating Factors: For an IDF study, it is required to perform and provide a precise assessment of the downstream adverse impact potentials as the consequences of upstream dam failure caused by various hydrologic loading conditions. In assessing the consequences, the likelihood of loss of human life and property damage must be evaluated using dam failure analysis results and sound engineering judgment. Two rating factors commonly used to determine such likelihood are inundation depth and associated flow velocity. The references of theoretical and experimental data for building vulnerability (from Karvonen et al., 2000) and on humans and monoliths (after Lind/Hartford, 2000) can be used as a judgment basis for harmful rating factors.

Vital Importance of Implementation of the IDF Requirement: The IDF is utilized as the flood hydrograph entering a reservoir that is used as a basis to design and/or modify a specific dam and its appurtenant works; particularly for such as sizing the spillway and outlet works, and for determining the maximum flood overtopping prevention height of a dam, freeboard, and flood storage requirements. Thus, appropriate selection of the IDF is the first step in evaluating or designing a specific dam to address hydrologic PFMs and reduce risks to the public to an acceptable degree of hydrologic safety. As a result, seeking such an IDF for a dam is important to balance the risks due to its potential hydrologic failure with resulting downstream consequences and the benefits derived from the dam.

SUITABLE HYPOTHETICAL DAM FAILURES FOR HAZARD CLASSIFICATION AND REFINED IDF APPROACHES

The prescriptive approach is the method for a planned or existing dam to be evaluated for a prescribed standard, based on the hazard potential classification of the dam. This method's IDF criteria are intended to be conservative through a more conservative hypothetical dam failure scenario. It is a relatively simpler approach than other two refined approaches. But it is not

intended to assure that there is an economical marginal benefit from designing for such a conservative IDF. For some cases, specifically, this approach's IDF may be just a preliminary value and could be further reduced by the PFMs based refined ICA or RIDM approaches as shown in Fig. 2 Methodologies of IDF Selection: Preliminary Study vs. Refined Study. The basic cause is due to different dam failure assumptions as addressed below.

Failure assumptions for Hazard Classification Based Preliminary IDF Determination: The hazard potential classification of the dam is performed with the philosophical idea that is all about a dam's hypothetical worst failure case scenario. Namely, the existing dam conditions are not considered. A dam must be assumed to fail by any magnitude flood event for the purpose of evaluating its associated worst hazard potential. Thus, a hypothetical dam failure is estimated using worst dam breach parameters which are not necessarily based on the dam's PFMs. Table 1 Recommended Prescriptive Approach IDF Requirements for Dams under Flood Loadings illustrates the IDF requirements using the prescriptive approach.

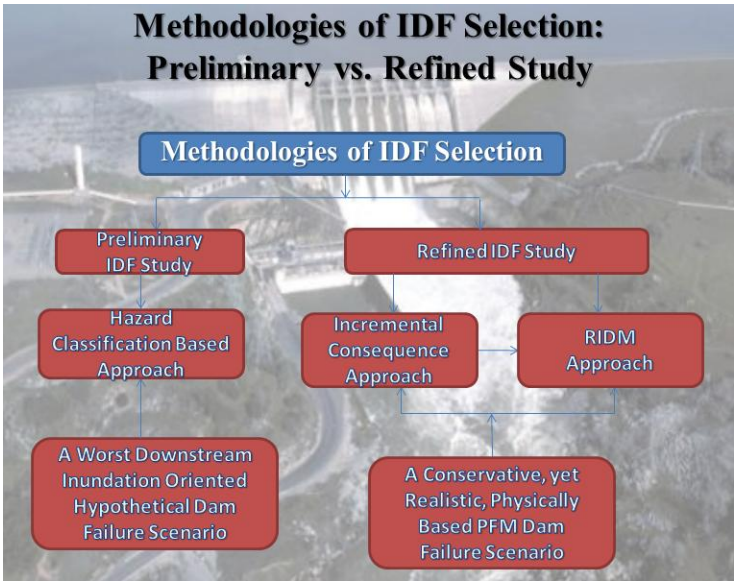

Fig. 2 Methodologies of Inflow Design Flood Selection: Preliminary Study vs. Refined Study

Table 1 Recommended Prescriptive Approach Inflow Design Flood Requirements for Dams under Flood Loadings

Hazard Potential Classification	Definition of Hazard Potential Classification	Inflow Design Flood (IDF)
High	Probable loss of life due to dam failure or misoperation (economic loss, environmental damage, or disruption of lifeline facilities may also be probable, but are not necessary for this classification)	PMF
Significant	No probable loss of human life but can cause economic loss, environmental damage, or disruption of lifeline facilities due to dam failure or misoperation	0.1% Annual Chance Exceedance Flood (1,000-year Flood)

Low	No probable loss of human life and low economic and/or environmental losses due to dam failure or misoperation	1% Annual Chance Exceedance Flood (i.e. 100-year flood) or a Smaller Flood Justified by Rationale

Failure assumptions for PFMs Based Refined IDF Determination: The philosophical idea and engineering concepts for refined IDF approaches are a direct contrast to dam hazard classification based IDF approach. The philosophical idea is about a dam's realistic capability to safely pass a required flood event given the existing dam conditions. Whether or not a dam is assumed to fail depends upon its PFMs under extreme hydrologic loading conditions. The engineering concept is that a hypothetical dam failure should be estimated using reasonably conservative, realistic, physically based dam breach parameters related to the dam conditions.

A Hybrid Case of Hazard Classification and PFM Based Failures: In dam hazard classification studies, only the most severe dam failure scenario is assumed. However, the most likely mode of dam failure for the selection of IDF is not always the most severe. For example, the concrete portion of a composite dam system (e.g., composed of concrete and embankment dams) is assumed to fail to produce the largest uncontrolled flow downstream to classify the dam's hazard potential. On the contrary, for a refined IDF analysis, the PFM of the embankment portion should be considered since it is most likely to fail during a critical overtopping event.

ICA METHOD'S ITERATIVE PROCESS TO OPTIMIZE IDF

Conceptual Scheme: As indicated above, the IDF selection using ICA is the flood above which there is a negligible increase in downstream inundation depth, flow velocity, and/or consequences due to failure of the dam when compared to the same flood without dam failure. Figure 3 Schematic Illustration of ICA for the selection of IDF presents a schematic of such a comparison. This process is continued until the flood of greatest magnitude that causes incremental consequences is identified.

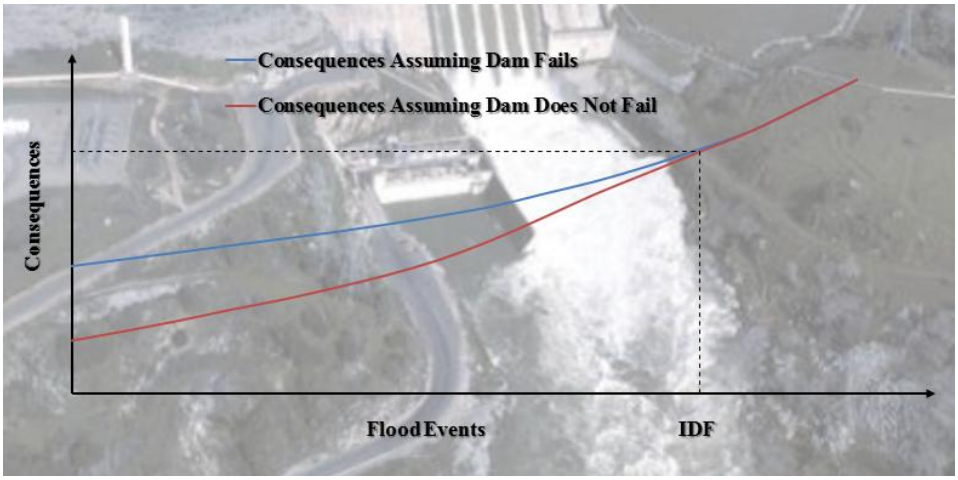

Figure 3. Schematic Illustration of Incremental Consequence Approach for the selection of IDF

Good Engineering Practices (GEPs): The GEPs consist of proven and accepted engineering methods, procedures, and practices that provide appropriate, cost-effective, and well-documented

solutions to meet user-requirements and compliance with applicable regulations. In GEPs, an appropriate measure needs to be studied to modify a dam to increase its conveyance capacity to safely pass the derived initial IDF value. For some cases, moreover, it must go through an iterative process as shown in Fig. 4 Incremental Consequence Approach: A Complete Iterative Process to Further Refine the Initial IDF's flow chart. The resulting IDF can be further refined by taking into account the hypothetically added spillway capacity. Thus, a comprehensive measure to modify a dam to increase its conveyance capacity to safely pass an adequate IDF must go through such an iterative process. The Case 1 example provided later illustrates the process of repeating the analysis until convergence to attain a minimum acceptable IDF.

Potential New Adverse Impacts: In the iterative process for the IDF selection and implementation, several hydraulically advantageous measures may be utilized to improve the spillway capacity to meet requirements while some disadvantages described below could also exist which should be identified and avoided by performing a supplemental PFMA (SPFMA) exercise:

- Raising the crest of dam: It can increase the downstream consequences should the dam fail by creating a larger dam breach flood wave or it may increase upstream inundation consequence during extreme flood events.
- Widening the spillway, or lowering the crest of the spillway and installing crest gates: It may actually increase the risk to the downstream public by increasing the spillway flows during hydrologic events that occur more often.
- The above measures could also introduce new PFMs, thus increasing dam failure risk.

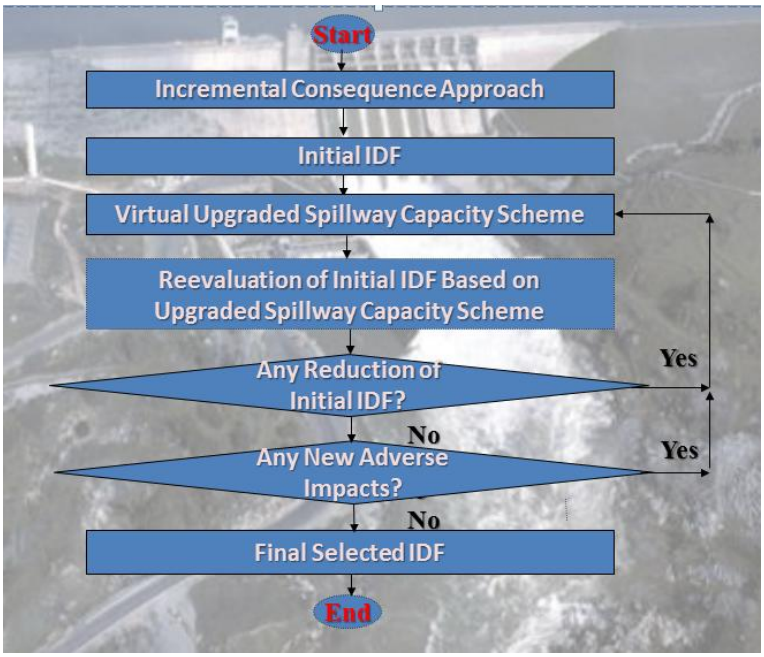

Fig. 4 Incremental Consequence Approach: A Complete Iterative Process to Further Refine the Initial Inflow Design Flood

PROBABILISTIC APPROACH TO SELECTING IDF

Risky Society toward a New Modernity: We live in a contemporary "high risk society" in which risk is everywhere. We may estimate either the cost-effectiveness between the well-being and risk or the risks to compare with tolerable risk levels by means of probabilistic risk assessment (PRA). The pursuit of absolute safety or zero risk is impractical, and self-deception. A risk assessment is not the sole basis for a decision, but rather it provides a systematic way of understanding a dam's PFMs, quantitative probabilities of loadings and structural failures, and the potential consequences and associated uncertainties. Current complementary use of the probabilistic method of RIDM approach to the deterministic method can be significantly expanded by state-of-art risk-based analysis for more realistic dam hazard potential assessment. Such a RIDM process provides a defensible basis for making decisions and helps to identify the greatest risks and prioritize efforts to minimize to a tolerable risk level or even eliminate them if it is possible.

Risk-informed Process: The RIDM approach in a risk-based system synthesizes the ICA with risk estimation through using information and reports available for the dam under study, historical performance of comparable dams, and experience based engineering judgment, etc. Specifically, RIDM is a decision making process to decide on a course of action for dam safety improvement. Qualitative and quantitative information about dam safety risks are considered along with other project-specific information. Risk-informed hydrologic hazard analysis includes a site-specific evaluation of the probabilities of a full range of extreme hydrological events and performance of the dam during those events, and evaluates in more detail the social, economic, and environmental consequences of failure. In short, RIDM is a tool for evaluating hydrologic events in a risk-based context and the level of effort is proportion to safety issues.

Quantitative Risk Indexes: Risk can be expressed in terms of life-safety and economic consequences on an annualized basis. The units of measure for dam safety risk are such as loss-of-life per year for life-safety, and costs (dollars) per year for property damages and economic losses. For instance, the RIDM process can include specifically assessing individual incremental life safety risk using probability of loss of life, societal incremental life safety risk expressed as a probability distribution of potential life loss (See F-N Chart of Fig. 5 A commonly recognized standard for life loss tolerable risk), and societal incremental life safety risk expressed as an averaged ALL. As an example, some agencies use two major tolerable risk indices to justify the IDF selection including averaged AFP of a dam (e.g., AFP $\leq 1.0 \times 10^{-4}$/year), and a resulting ALL (e.g., ALL $\leq 1.0 \times 10^{-4}$ lives/year). As examples, some merits of RIDM approach compared to the ICA method are illustrated in Table 2 Examples of Advantages of RIDM Approach over ICA Method from a practical perspective on how this approach works more realistically for an advanced IDF study.

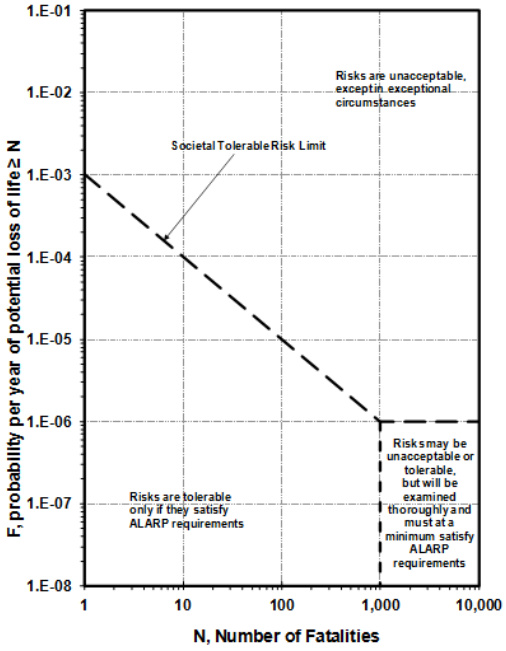

Fig. 5 A commonly recognized standard for life loss tolerable risk ("ALARP": As Low As Reasonably Practical" - the residual risks can be cost effectively reduced further)

Table 2.1 One Example of Advantages of RIDM Approach over Incremental Consequence Approach Method

ITEM	RIDM APPROACH	ICA METHOD
Dam Failure Mechanism Rationalization		
Consideration and evaluation of dam PFMs on critical uncertain sequential factors	More realistically sequential occurrence probabilities estimated as needed based on a flood event tree risk model in which loading, response and consequence of dam failure are represented by levels of branching	Subjective, conservative overall assumptions usually made on one single PFM without specifically describing the failure mode's sequential physical process
Measurement of a PFM parameter's variation	The variation considered by an uncertainty analysis (i.e., risk analysis)	A deterministic way used through sensitivity analyses
Judgment on likelihoods of PFMs occurrence	Numerical engineering judgment by quantified risk analysis based on reasonable representation of probabilities of "System Response Probability (SRP)"	Best engineering judgment on likelihoods of PFM categories I/II (most or considered but not most significant PFMs) but lacking consistency without clear criteria
Assumption on dam overtopping failure depth (i.e. the "threshold inflow flood" depth) based on factors of duration, down-stream slope protection, flow velocity, etc.	Assuming several most likely overflow depths with varied probabilities to fail the dam matching various flood magnitudes of the rising limb of a flood hydrograph regardless its frequency magnitude	Assuming a single flood frequency based conservative overtopping flow depth, some even overly conservatively assuming at a reservoir peak level

Dam breach size	Varied cases of multiple assumed sizes with individual probabilities while actual size remains uncertain	A method simplified as one single size causing a worst inundation scenario through a sensitivity analysis which may be overly conservative
Uncertainties on structural component functions	Gate reliability, spillway debris plugging, etc. driven by probabilities based on historical records	Dam structural component functions usually assumed as designed without flexibility

Table 2.2 Three Examples of Advantages of RIDM Approach over Incremental Consequence Approach Method

ITEM	RIDM APPROACH	ICA METHOD
Consequence Estimation		
Consequence model of life and property loss estimates in terms of downstream structures	Life and property loss estimates associated with each end node of the probability based event trees	Life and property loss estimates as a lump sum figure
Life loss estimation	Uniform ALL risk basis	One life loss considered equivalent to significant life loss consequence
Justification of IDF		
Risk reduction decision making basis for a selected IDF	Quantitative risk reduction measurements allowing uncertainties judgment and flexibility of IDF by ALARP principle	No overtopping allowed for IDF
Final justified solution	Tolerable risk levels of such as APF/ALL to be satisfied	Analysis result of insignificant inundation incremental rise
Sensitivity analyses for structural and non-structural measures to reduce dam failure hazard potential	Exploring the effects of modifying dam structure and adjusting the evacuation effectiveness	Exploring the effects of adjusting parameters of dam structure breach rather than including evacuation effectiveness
Solutions for Achieving Required IDF		
Justification solutions to an inadequate spillway system	Both structural/non-structural measures such as improving evacuation effectiveness	Structural measures only as a common approach
Risk reduction assessment for acceptable life and property safety risks	Using ALARP principle to evaluate the strength (i.e., adequacy and degree) of justification of risk reduction options (e.g., USBR uses increasing justification to reduce the APF)	Only the required IDF based spillway capacity upgrading as the solution

CASE STUDIES ON SELECTING IDF

Case I study on Incremental Consequence Approach: The ICA initial IDF could be reduced by taking into account the hypothetically added spillway capacity through an iterative process.

Refer to the paper by D. Steines, etc. (2003), which discusses the case of Otter Rapids Dam (Fig. 6 Otter Rapids Dam Built in 1908). The dam was classified as a high hazard potential impounding structure so the prescriptive approach resulting IDF was the PMF of 35,600 cfs. The

reason for a selected relatively smaller IDF than an initial one is that the iterative process of ICA was used to reevaluate the IDF. The IDF is influenced by routing extreme flood events through a hypothetical upgraded total spillway capacity, and vice versa the determined new spillway design is dependent on the reexamined IDF.

In this specific case by adding spillway capacity, through lowering the crest, the reservoir storage would be reduced and the discharge increased for a given flood magnitude. The reduced storage would result in lower reservoir elevations. The increased discharge would result in higher downstream river stages. The differential head between the reservoir and the tailwater would be reduced significantly. Therefore, the incremental rise in the downstream flood elevation due to a dam failure would be reduced. As summarized in Table 3 Example of a Selected IDF through an Iterative Refined Process, the adopted converged IDF is reduced 50% or 13.2% from 35,600 cfs or 20,500 cfs to 17,800 cfs, respectively. Lowering the spillway in this case would not increase the risk to the public by more frequent flooding events.

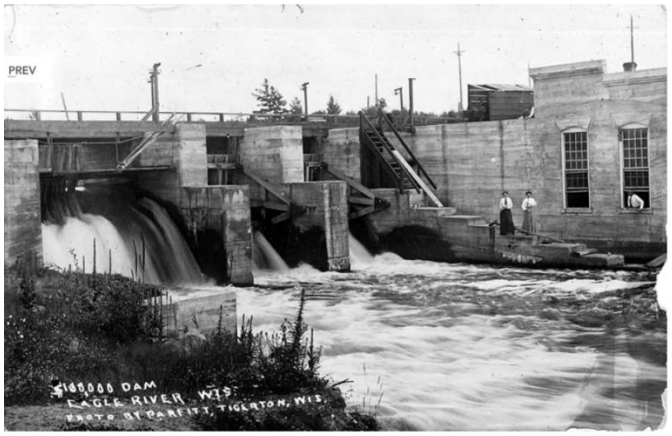

Figure 6. Otter Rapids Dam Built in 1908

Table 3. Example of a Selected Inflow Design Flood through an Iterative Refined Process

Hazard Classification Based Preliminary IDF (i.e. PMF) (cfs)	ICA's Refined Initial IDF (cfs)	Selected Converged IDF (cfs)	Reduction (%) by Selected Converged IDF	
			Preliminary IDF	Refined Initial IDF
35,600	20, 500	17,800	50.0	13.2

Case II study on RIDM Approach: The PFM based probabilistic consequence driven risk assessment is applied as a tool for the selection of IDF.

Refer to the paper by J. Hedien (2013), which discusses the case of two concrete core-wall earth embankments on the same river (Fig. 7 Upstream and Downstream Tandem Dams A & B Located on a Same River) which have insufficient spillway capacities to pass the preliminary IDFs of PMFs without overtopping and failing the dams. By applying the ICA, a key result in

Table 4 shows the comparison of determined IDFs between based on hypothetical dam failures occurring at dam crest overtopping depths of 10 feet (i.e. at the reservoir peak level) and two feet (best judgment). Another key result shows the comparison of selected IDFs between the ICA and the RIDM method.

The RIDM approach assesses both the probability of the flood loading and the probability of the resulting adverse response to evaluate AFP of each dam. The estimated total risk is the summation of risk from the identified PFMs. Based on the noted acceptable tolerance risk standards in the table, the IDFs of 60,000 cfs and 65,000 cfs were selected for the upstream and downstream dams, respectively. A 99% evacuation effectiveness was assumed (i.e. 1% not evacuated). Reductions from the prescriptive method's to the ICA's and RIDM approach's IDFs are 53% and 71%, respectively as shown in Table 4 IDF Study Results by ICA and RIDM Process for Two Tandem Dams.

Figure 7. Upstream and Downstream Tandem Dams A & B Located on a Same River

Table 4. Inflow Design Flood Study Results by Incremental Consequence Approach and RIDM Process for Two Tandem Dams (IDF unit: 10^3 cfs)

Tandem Dams	**Preliminary IDF by Prescriptive Method: Governing PMF (Cool Season)**	**ICA Refined IDF: Assumed Overtopping Failure Depths**		**RIDM Approach Refined IDF to Meet Tolerable Risk Levels***	**Final Adopted IDFs**	***For this example, the accepted **Tolerable Risk Levels** set by an agency and a foreign country committee : AFP ≤ 1.0 x 10^{-4}/year (BOR) & ALL ≤ 1.0 x 10^{-4} lives/year (ANCOLD)
		10 feet at Peak Reservoir level	Two Feet			
U/S Dam A	223	129	70	60	60	
D/S Dam B	230	230	135	53	65	

ADVANTAGES AND CHALLENGES OF IDF SELECTION METHODS

The FEMA P-94 guidance document (2013) should be utilized for the appropriateness and applicability of hydrologic safety design criteria for dams. The basic philosophy and principles are described in sufficient detail to promote a compatible approach among state and federal agencies in the design and evaluation of dams from the standpoint of hydrologic safety. Considering many engineering analyses are based on limited information, estimation results may not be fixed but inherently will have a margin of uncertainty and are subject to change as new information is obtained. Whichever IDF selection approach is applied needs to include a periodic review of information such as dam conditions, present and reasonably anticipated future upstream and/or downstream developments for hydrologic characteristics/regime and potential hazard changes, etc. to ensure the validity of the conducted IDF analysis results.

Either a deterministic or probabilistic approach can be used to effectively select the IDF to accommodate a wide variety of situations, available resources, and conditions which might be encountered in practice for a specific dam. For the purpose of comparison, three IDF selection approaches' advantages and challenges are summarized below:

Prescriptive Method: The conventional prescriptive approach is well understood in the dam safety community as a simple and efficient approach intended to be conservative to allow for effectiveness of resource utilization while providing reasonable assurance of the public safety.

Advantages: The intent of this method is to provide straightforward definitions that can be applied uniformly by all federal and state dam safety agencies and can be readily understood and easily accepted by the public for its conservative result. When other two methods described below are costly, risky and challenging to analyze and tackle challenges in a manner outside the normal convention, the prescriptive IDF criteria are recommended.

Challenges: Dam failure assumptions are not based on physical conditions but a worst downstream inundation scenario. As a result, it may be cost prohibitive to design for an overly conservative IDF. The required IDFs in Table 1 are not suitable for the sunny-day failure governed hazard classification cases so that adequate IDFs should be separately studied.

ICA Method: An incremental procedure can provide a framework for evaluating the benefits of mitigating hazards presented by hydrologic deficiencies by routing a wide range of extreme flood magnitudes through the dam. When warranted, engineers can perform additional investigations using advanced analytical tools and methods to more precisely evaluate incremental consequences.

Advantages: This information can be used to select an IDF that reduces risk to the public without spending limited resources on conservative designs that result in marginal reduction of flood risk.

Challenges: A comprehensive iterative process is not usually performed. In addition, the uncertainty associated with the analysis is not quantified, so the resulting IDF is usually more conservative than further realistically based RIDM result.

RIDM Process Method: The risk driven resulting IDF is often determined using a sliding scale between a lower threshold flood event and the maximum theoretical event.

Advantages: Applying this method is an unconventional approach to assess how safe a dam is and is also able to compare with other public safety risks in an understandable, consistent fashion. The uncertainty associated with the analysis is specifically reflected as a probability based consideration and analysis of information rather than conservative unquantified assumptions. Thus, the RIDM selected IDF is often smaller than the other two methods. The computed risks for various hydrologic loading conditions are compared against tolerable risk guidelines. The objective is to reduce risks below a tolerable risk limit. Better data would enable to reduce subjectivity significantly in risk analysis and decision-making. The consequence risk may be more reliably estimated considering the potential inundated structure has been evacuated before the failure of a dam by assuming a certain evacuation effectiveness.

Challenges: Although the present trend appears to be in such a direction of practice, major challenges of RIDM approach include below:
(1) Technical Challenges: Many agencies have to overcome the deterministic mindset and may not have the resources or training necessary to conduct or review such a comprehensive probable flood hazard analysis (PFHA); opposite to data based statistical objective probability, quantitative risk is largely subjective and almost entirely a matter of judgment by limited experts; reliable data on dams, dam components, and operations are generally not available to meet specific needs of risk assessments for individual dams or even components of dam systems;
(2) Difficult to Administer: The considerable variety in risk-based analysis criteria will complicate any precise comparisons between criteria used by different agencies. It will also result in a variation or imbalance of risk tolerances with regards to dam safety throughout the country. Thus, widely acceptable, defensible guidelines for consistent methods and uniform risk tolerance need to be established. Moreover, because risk may change with time, reevaluating risk on a periodic basis is needed; and
(3) Resources Consuming: The staff, cost and time resources required are much more than the other two IDF study methods.

CONCLUSIONS AND SUGGESTIONS

- Each of three IDF selection methods has its individual concepts, principles, merits and disadvantages. However, if the IDF value resulting from the ICA method may have a potential to be significantly reduced from the prescriptive method, then an iterative process needs to be completed, or a full range of risks based RIDM method can be used, in order to ensure an optimal IDF value.
- Each agency has a unique authority, mission, and management practice. The FEMA P-94 guidance points to individual agency processes for agency specific guidance on the definition of IDF based on incremental consequences and how to use risks to inform decisions. However, the consistency and uniformity of guidance between them is needed in the long run for a same standard of dam safety risk management across the nation.
- RIDM based on qualitative and quantitative risk assessments is the process of using information about risk to assist in decision-making with regards to a wide variety of dam safety activities. This would include decisions regarding a variety of actions such as: IDF selection; frequency of inspection; need for increased instrumentation; need for additional technical studies; assessment of how uncertainties affect the level of risk; sufficiency of evidence to support the need for remedial action; selection of a remedial action to address an

identified deficiency; prioritization of projects or actions; the sequence in which remedial actions are taken at a given dam or group of dams, etc.

- Risk is all about uncertainties, so all sources of uncertainty should be considered. Risk assessment should be unbiased and risk reduction should make economic sense or life loss reduction ALARP. The application of RIDM is a technical challenge but also an opportunity to deliberate more realistic conditions for obtaining a more refined IDF value. A requirement for acceptance of the estimated IDF should include provisions for the dam owner to engage an independent peer review or review board consisting of experts in this area of study to oversee the study and approve the analyses and final results.
- There are certain principles that are held in common for consistency and correctness about the urgency of completing required dam safety actions which should be commensurate with the level of risk for varied safety aspects such as adequate interim risk reductions before upgrading existing spillways to accommodate required IDFs. However, what the defined level is needs collaborative efforts between agencies. (Available references: the USACE – DSAC (Dam Safety Action Classification) and USBR – DSPR (Dam Safety Priority Rating)).
- Hazard potential classification is based on consequences of dam failure irrespective the cause of failure. The FEMA P-94 document's Table 2, "IDF Requirements for Dams Using a Prescriptive Approach" and its foot notes indicate required and recommended minimum IDFs. The notes can clarify that this table is based on flood scenarios, not sunny-day failures. Or the table title can be clarified as "under Flood Loadings" like Table 1 in this paper.
- Some agencies use the term "spillway design flood" (SDF) as IDF. In application, both terminologies can mean differently for some cases. For instance, if the derived IDF for an existing or planned dam is smaller or greater than the flood used for the design of spillway capacity, then the used design flood should be appropriately called SDF rather than IDF.
- Climate change concerns are addressed in the P-94 document. Experts argue that engineers can improve climate change resiliency incrementally by making small changes with minimal additional investment to the projects they are already planning or constructing. In addition, because the effects of climate change won't be the same in all areas and funding for infrastructure projects is limited, it would be advisable to determine the areas of highest risk to critical infrastructure when deciding how to allocate adaptation and mitigation spending.

ACKNOWLEDGEMENTS

My heartfelt gratitude is extended to both FERC's Division of Dam Safety and Inspections management, particularly Director, William Allerton for the opportunity to be a Steering Committee member to provide inputs/comments for the FEMA P-94 document and those for their helpful suggestions on this paper. Furthermore, I appreciate the primary contributors and other committee members for their dedicated work and perspectives and insights and other experts' additional contributions that make the P-94 document substantially benefit the users.

REFERENCES

Schweiger, Paul, etc. (2014). "Selecting and Accommodating IDFs for Dams: A Behind-the-Scenes Look at Updating Federal Guidance", The 34th USSD Annual Meeting and Conference, San Francisco.

Snorteland, Nathan (2014). "Federal Guidelines for Dam Safety Risk Management", 2014 ASDSO Annual Conference, San Diego, CA

Wilcox, Kevin (2014). "Planning for Climate Change", Civil Engineering Magazine, ASCE, September, 2014.

FEMA 94 (2013). "Selecting and Accommodating Inflow Design Floods for Dams"NRC (2013). "Workshop on Probabilistic Flood Hazard Assessment (PFHA)", Rockville, Maryland

FEMA (2012). "Hydrologic Design of Dams in the US: Past, Present & Future", Rockville, Maryland

Steines, D., etc. (2003). "Reducing the IDF by Increasing Spillway Capacity", Waterpower XIII, HCI Publications, 2003

Hedien, J. E. (2013). "RIDM Approach for IDF Selection and Accomodation for Dams: A Practical Application Case Study", NRC Probabilistic Flood Hazard Assessment Workshop, January 2013

Steines, D. S., & W. Bloczynski. (2003). Reducing the IDF by Increasing Spillway Capacity. Waterpower XIII. Buffalo, NY

DESIGN RAINFALL DISTRIBUTIONS BASED ON NOAA ATLAS 14 RAINFALL DEPTHS AND DURATIONS

William H. Merkel, Hydraulic Engineer, USDA-NRCS, Beltsville, MD,
William.Merkel@wdc.usda.gov,
Helen Fox Moody, Hydraulic Engineer, USDA-NRCS, Beltsville, MD,
Helen.Moody@wdc.usda.gov,
Quan D. Quan, Hydraulic Engineer, USDA-NRCS, Beltsville, MD,
Quan.Quan@wdc.usda.gov

Abstract

For hydrologic design purposes, the Natural Resources Conservation Service (NRCS) has historically used rainfall distributions derived from rainfall-frequency data. The rainfall distribution represents the cumulative rainfall from the beginning to the end of the design storm. The rainfall distribution is non-dimensional, and begins at a value of zero and ends at a value of 1.0. The Type I, Type IA, Type II, and Type III rainfall distributions are in general use throughout the United States. NRCS hydrologic models including Engineering Field Handbook Chapter 2 EFH-2, USDA (2014), WinTR-55 Small Watershed Hydrology, USDA (2010) and WinTR-20 Project Formulation Hydrology, USDA (2010) make use of these rainfall distributions.

The Type I, Type II, and Type III rainfall distributions were developed from rainfall-frequency data contained in the United States (US) Department of Commerce publications US Weather Bureau Technical Paper 40 (1961) and National Weather Service (NWS) Hydro-35 (1977). USDA NRCS Technical Paper 149 (1973) describes the way in which the Type I and Type II distributions were developed and shows plots of rainfall versus duration at several locations. These legacy rainfall distributions are being replaced with rainfall distributions developed from data contained in the NWS National Oceanic and Atmospheric Administration (NOAA) Atlas 14. Volumes 1 (2006) through 9 (2013) have been released and cover 37 states, Puerto Rico, US Virgin Islands, and selected Pacific Islands.

The standard design rainfall distributions are based on nesting the high intensity short durations within the longer lower intensity durations. For example, the maximum rainfall in 5 minutes is assumed to be within the maximum 10-minute rainfall, which is within the maximum 15-minute rainfall. This process is continued until the 24-hour duration is reached. The non-dimensional aspect of the rainfall distribution is that the durations from 5 minutes through 12 hours are represented as a ratio of that duration rainfall to the 24-hour rainfall.

Maps of these rainfall ratios were developed using Geographic Information System (GIS) technology. The goal was to identify regions of similar rainfall distribution. A map of a multi-state area with a group of regional rainfall distributions was developed along with 24-hour rainfall tables for use in hydrologic models.

Site-specific rainfall distributions based on NOAA Atlas 14 rainfall-duration-frequency data for a location may be developed. This approach preserves the intensities within a rainfall distribution with minimum error. A computer program was written to use NOAA Atlas 14 partial duration rainfall-frequency data at a specific site to develop a set of rainfall distributions for WinTR-20. A unique rainfall distribution may be developed for each return period from 1 year (100% chance) through 500 years (0.2% chance). When developing these rainfall distributions, rainfall at durations of 5, 10, 15, and 30 minutes and 2, 3, 6, and 12 hours are smoothed in order to make sure

the rainfall distribution and resulting runoff hydrographs are smooth. The 60 minute and 24 hour values are not changed in the smoothing process.

INTRODUCTION

The four components of the NRCS hydrologic model are 1) runoff curve number, 2) time of concentration, 3) dimensionless unit hydrograph, and 4) rainfall magnitude and distribution. Each of these has been the subject of many technical papers by authors within the government and private sectors. As research and new data have become available, analysis techniques for these components have been improved individually. The authors' opinion is that if each of these components is analyzed according to the best available data and research, collectively they will produce the most accurate estimate of hydrologic response from a watershed. This concept is important because so many applications of the NRCS hydrologic model are for ungaged watersheds. In the case of gaged watersheds, the input data for each model component may be calibrated. This paper describes significant updates to both the rainfall magnitude and distribution as proposed for use in the NRCS hydrologic models (Engineering Field Handbook Chapter 2 (EFH-2), WinTR-55, and WinTR-20). Before the publication of NOAA Atlas 14 Volumes 1 through 9, NRCS used rainfall data from Weather Bureau Technical Paper 40 and NOAA Atlas 2 (in western states) for evaluation and design of engineering projects. The rainfall data and design rainfall distributions based on these data were used for so many years by NRCS and engineers in the general public that their use been considered standard operating procedures. The publication of NOAA Atlas 14 has caused serious consideration as to how to move forward in this age of highly advanced computers, GIS data, and software. Implementing such changes has taken significant time and work with respect to both developing technical procedures, and informing and training engineers within the government and private sectors.

Traditional principles and new technology and data have been combined to produce the rainfall data and rainfall distributions to replace the legacy rainfall data and rainfall distributions used for so many years.

This paper describes the treatment of NOAA Atlas 14 data after it is acquired for a given project site. The two major concepts explained are data smoothing and development of the design rainfall distribution. These methods are described in USDA-NRCS NEH Part 630 Chapter 4 Storm Rainfall Depth and Distribution (2014 draft).

DATA SMOOTHING

Since precipitation durations were analyzed independently in NOAA Atlas 14, there are cases when the precipitation intensity between successive durations does not uniformly decrease as duration increases. In developing a design rainfall distribution, this factor is of critical importance.

Several mathematical techniques were investigated to develop a procedure which is computationally efficient, accurate, practical, stable, and robust. The relationship of rainfall intensity (inches/hour) and duration is smoothed since the generated hydrograph is primarily dependent on the relationship of precipitation intensity with duration.

The relationship of intensity and duration is based on a factor called incremental intensity. Incremental intensity is defined as the difference in precipitation divided by the difference in duration. The incremental intensity for the 5-minute duration is equal to the 5-minute precipitation divided by 1/12 in inches per hour. The incremental intensity for the 10-minute duration is the 10-minute precipitation minus the 5-minute precipitation divided by 1/12 (the difference between 5 and 10 minutes in units of hours). Incremental intensity is calculated and smoothed for each return period independently. Plotting this relationship on a log-log scale, it may be a straight line, have slight curvature, or have several dips or waves. An example of plot of original data is shown in figure 1.

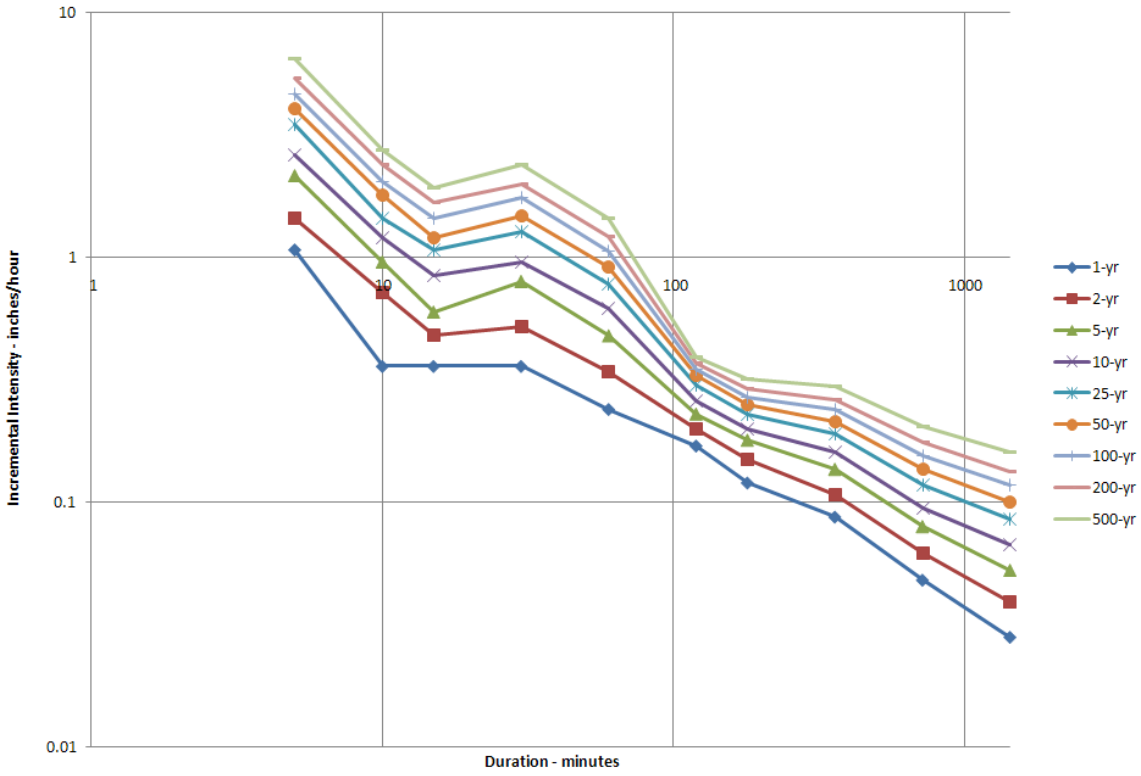

Figure 1 Incremental Intensity plot for original data for Sun City California, not smooth between 10 minutes and 6 hours.

The smoothing procedure keeps the 60-minute and 24-hour precipitation unchanged from the original NOAA Atlas 14 partial duration values. The 5-, 10-, 15-, 30-minute, and the 2-, 3-, 6-, and 12-hour values are open to adjustment. The smoothing procedure computes a straight line on the log-log plot which extends from 5-minute to 60-minute durations. The line is placed such that the squared difference between the smoothed 5-, 10-, 15-, and 30-minute incremental intensity values and the original values is minimized and the 60-minute precipitation is equal to the original value. A second straight-line segment is computed on the log-log plot that extends from the 60-minute value to the 24-hour value. This line is placed such that the incremental intensity for 60-minute duration is the same as calculated for the first line segment and the 60-minute and 24-hour precipitation values are unchanged. Calculating the adjusted values of precipitation involves a trial and error optimization procedure. An example of data smoothing is shown in figure 2.

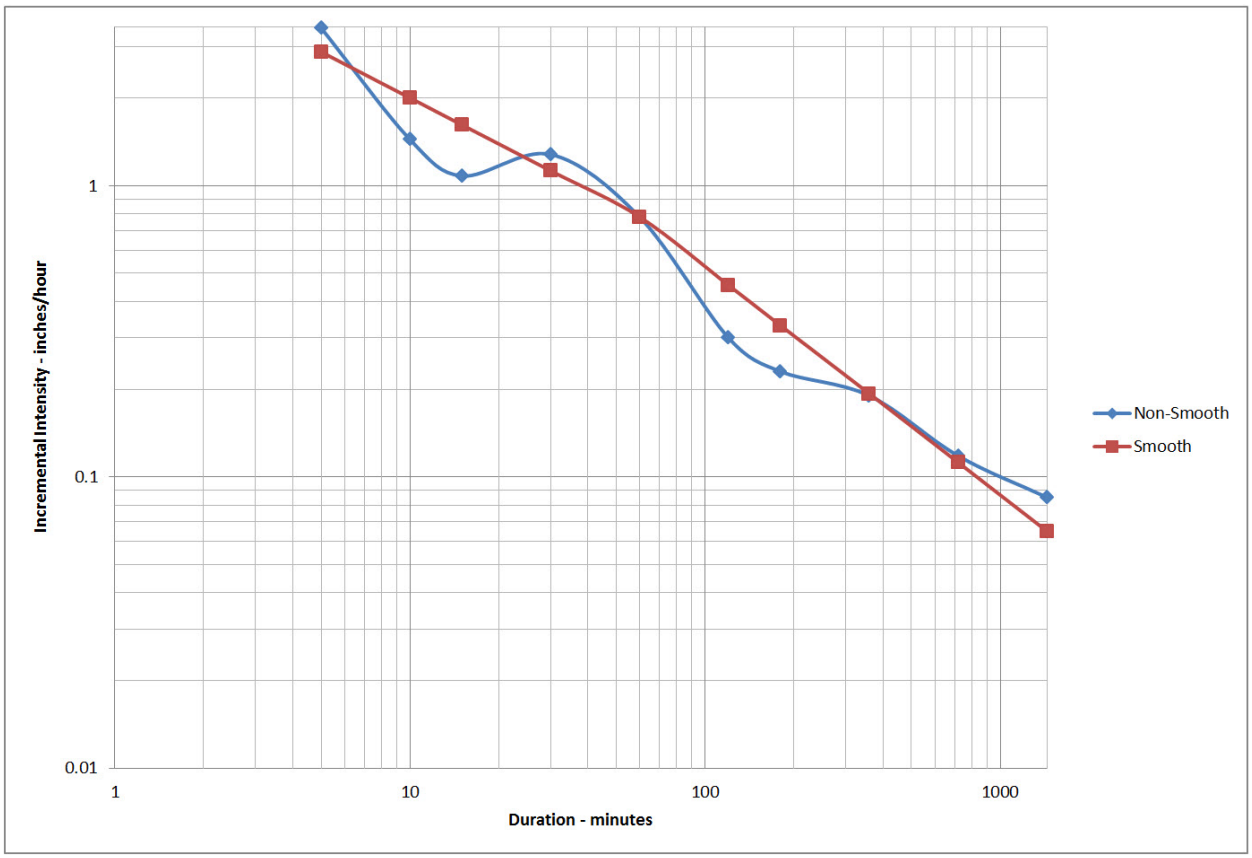

Figure 2 Plot of 25-year (4% chance) smoothed and non-smoothed incremental intensity at Sun City, California.

TEMPORAL DISTRIBUTION

A procedure has been developed that will derive rainfall distributions to cover the wide range of climatic conditions from tropical to arctic that occur in the US (Merkel, 2006).

The method used to construct the 24-hour rainfall distribution insures that the maximum rainfall of any duration less than 24 hours is included in the distribution. One of the principles of hydrology is that the peak discharge for a watershed is determined primarily by rain falling in a duration that equals the time of concentration (see USDA NEH Part 630 Chapter 15, 2010). The 24-hour rainfall distribution has the maximum 5-minute rainfall occurring at 12 hours. The maximum 10-minute rainfall is centered around 12 hours, and includes the maximum 5-minute rainfall, and so on. In this way, a single rainfall distribution for 24 hours may be used for any watershed with time of concentration less than 24 hours.

Input to the method consists of a set of rainfall values at durations of 5, 10, 15, 30 and 60 minutes and 2, 3, 6, 12, and 24 hours. These data may be original or smoothed. Naturally, the smoothness of the rainfall distribution depends on the smoothness of the relationship of duration and incremental intensity as shown in figure 2. The plot of the smooth rainfall distribution based on data in figure 2 is shown in figure 3.

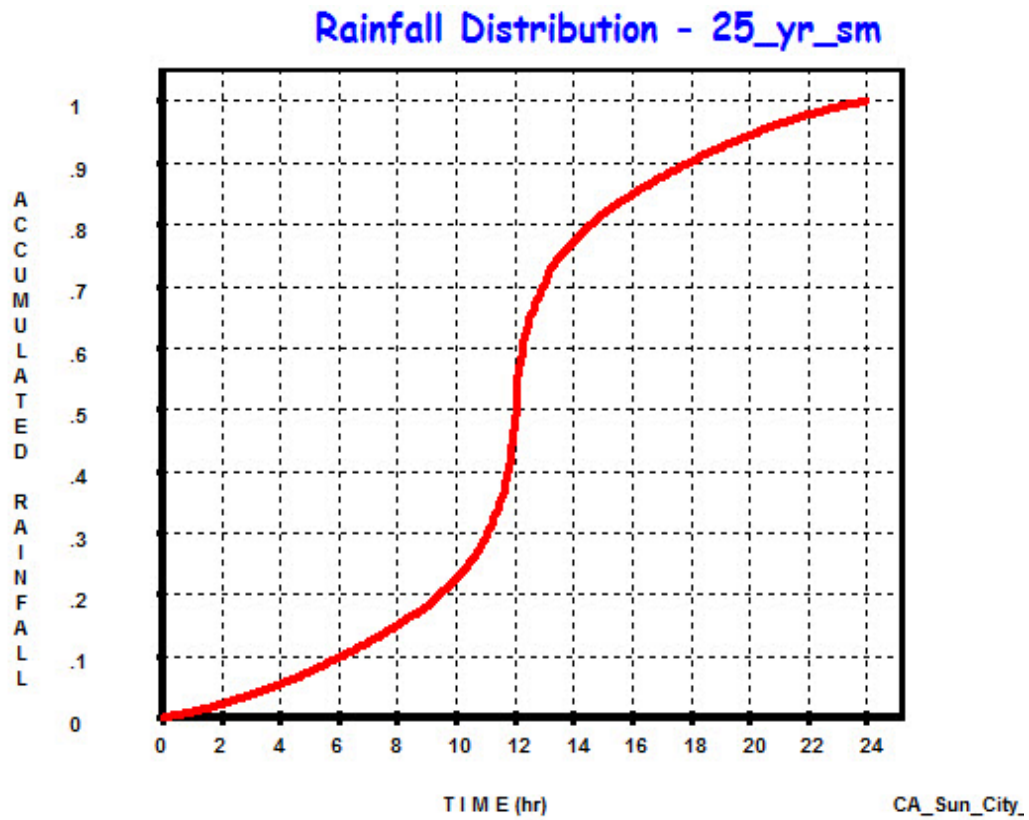

Figure 3 25-year (4% chance), 24-hour rainfall distribution for Sun City, California based on smooth data.

REGIONAL RAINFALL DISTRIBUTIONS

Figure 4 shows where to apply the regional rainfall distributions developed for the Ohio Valley and neighboring states and designated as A, B, C, and D.

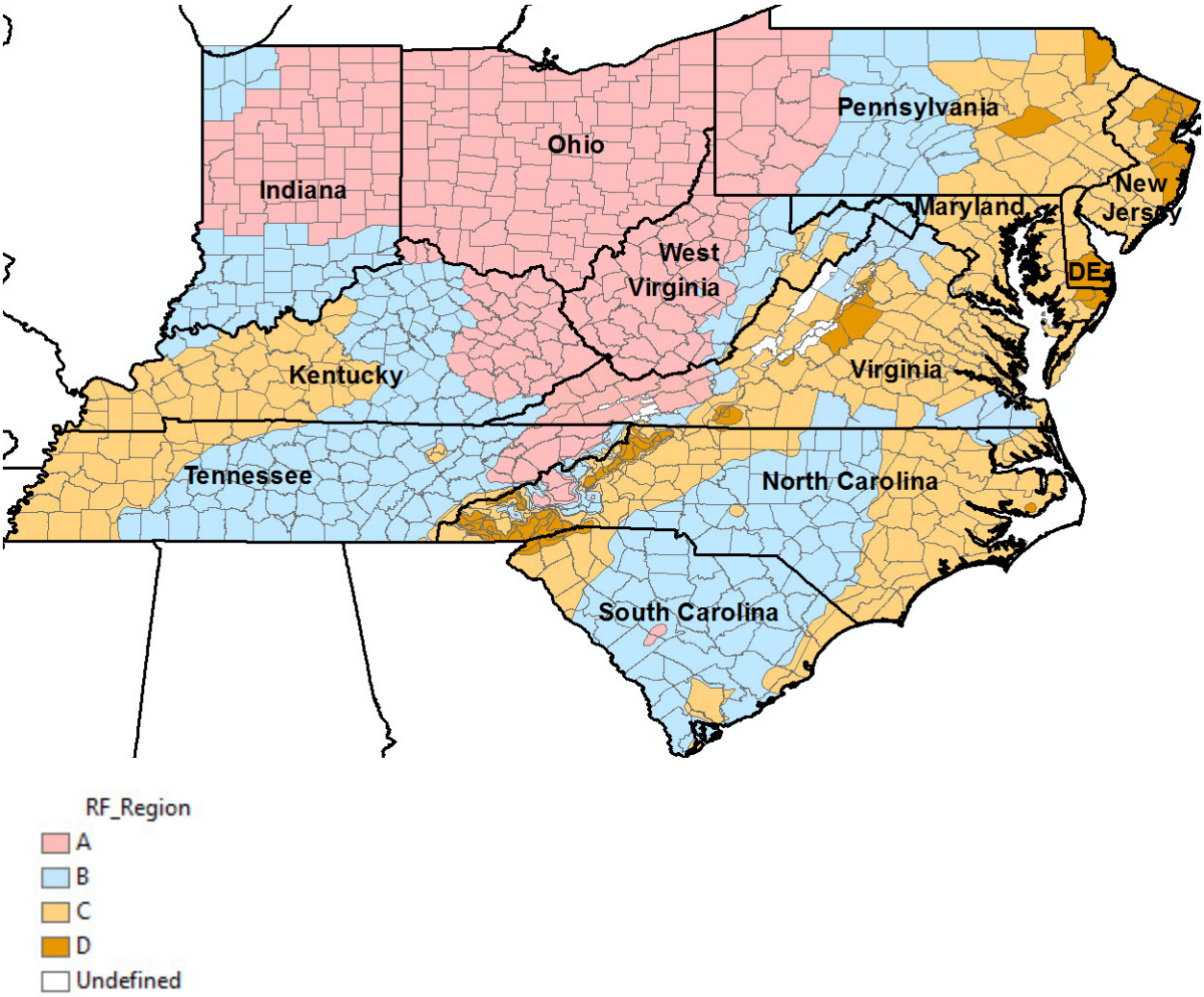

Figure 4 Regional rainfall distributions for the Ohio Valley and neighboring states.

Regional rainfall distributions were also developed from NOAA Atlas 14 data for California, Nevada, and 17 midwestern and southeastern states. Documentation and maps for these are available from the NRCS West National Technical Support Center at http://go.usa.gov/rXYw and clicking on "Technical Information".

The boundaries of the rainfall distribution regions are based on the ratio of the 25-year (4% chance), 60-minute rainfall to the 25-year (4% chance), 24-hour rainfall. Areas with a ratio greater than 0.48 are assigned rainfall distribution A. This is the most intense rainfall distribution. Areas with a ratio between 0.43 and 0.48 are assigned rainfall distribution B. Areas with a ratio between 0.38 and 0.43 are assigned rainfall distribution C. Areas with a ratio less than 0.38 are assigned rainfall distribution D. This is the least intense rainfall distribution. Once the boundaries were determined, the average ratio for each duration was determined based on the 25-year (4% chance) return period. These included the ratios of the 5, 10, 15, 30, and 60 minute to 24-hour ratio; and the 2, 3, 6, and 12 hour to 24-hour ratio. These average ratios were used to develop the 24-hour rainfall distribution for each of the four regions as shown in figure 5.

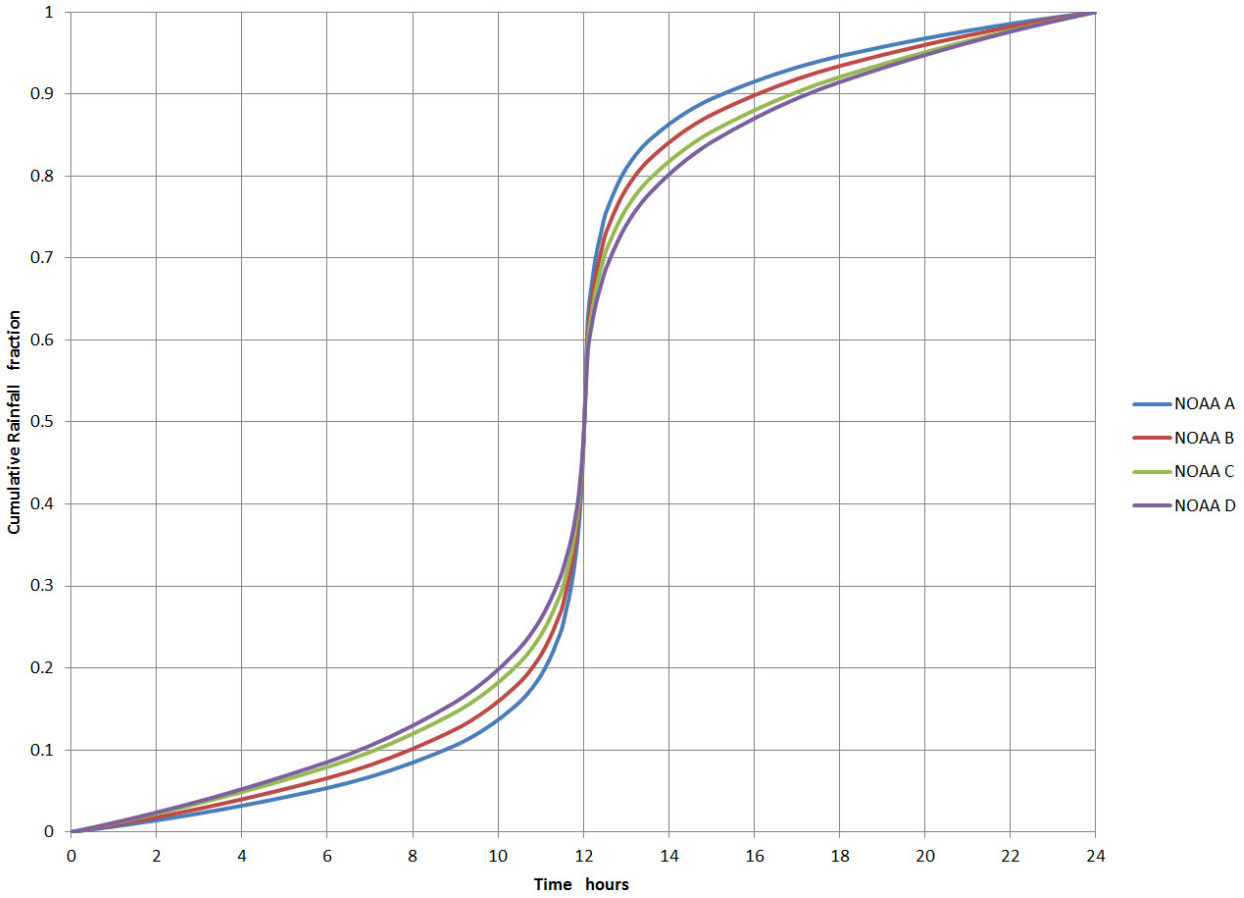

Figure 5 Plot of A, B, C, and D 24-hour rainfall distributions for the Ohio Valley and neighboring states.

These tables are available at a 0.1-hour time interval in the WinTR-20 User Documentation and WinTR-20 software.

SUMMARY

NRCS is replacing the use of its legacy rainfall distributions (Type I, Type IA, Type II, and Type III) with rainfall distributions based on NOAA Atlas 14 precipitation-frequency data. Regional rainfall distributions are being developed for use in the Engineering Field Handbook Chapter 2 computer program (EFH-2), Small Watershed Hydrology computer program (WinTR-55), and Project Formulation Hydrology computer program (WinTR-20). Site-specific rainfall distributions may also be developed using the WinTR-20 computer program.

These rainfall distributions are based on the 5-minute through 24-hour rainfall depths for a specific return period. Unique rainfall distributions may be developed for the 1-year (100% chance) through 500-year (0.2% chance) storms. Before the rainfall distribution is developed, the user has the opportunity to smooth the 5-minute through 24-hour rainfalls.

By developing new rainfall distributions using NOAA Atlas 14 data, the rainfall distributions will reflect the rainfall depth versus duration data at the project location more accurately. This will lead to more accurate estimates of peak discharges and hydrographs for design of projects.

REFERENCES

Merkel W.H., Fox Moody H., Quan Q. D. (2006). United States Department of Agriculture, Natural Resources Conservation Service. 2006. Rainfall Distribution for States Covered by NOAA Atlas 14 Volumes 1 and 2, NRCS internal publication (available upon request).

U. S. Department of Agriculture, Natural Resources Conservation Service. (2010). NEH Part 630, Chapter 5 Time of Concentration. Washington, D. C.

USDA NRCS. (2010). WinTR-55 Small Watershed Hydrology, version 1.00.10, Washington, D. C.

USDA NRCS. (2014). Engineering Field Handbook Chapter 2, EFH-2, Estimating Runoff. version 1.1.2, Washington, D. C.

USDA NRCS. (2014). Draft. NEH Part 630, Chapter 4 Storm Rainfall Depth and Distribution. Washington, D. C.

USDA NRCS. (2014). Draft WinTR–20 computer program for project formulation hydrology User Guide. Washington, D. C.

USDA NRCS. (2014). Draft WinTR–20 computer program for project formulation hydrology User Documentation. Washington, D. C.

USDA NRCS. (2015). WinTR–20 computer program for project formulation hydrology, version 3.10, Washington, D. C.

U.S. Department of Commerce, NOAA Atlas 2. (1973). Precipitation Atlas of the Western United States, volumes 1-11. Silver Spring, Maryland

U.S. Department of Commerce, NOAA Atlas 14, Precipitation-Frequency Atlas of the United States. (2004, rev 2006). Volume 1 Version 4.0: Semiarid Southwest. Silver Spring, MD.

U.S. Department of Commerce NOAA Atlas 14 Precipitation-Frequency Atlas of the United States. (2004, rev 2006). Volume 2 Version 3.0: Delaware, District of Columbia, Illinois, Indiana, Kentucky, Maryland, New Jersey, North Carolina, Ohio, Pennsylvania, South Carolina, Tennessee, Virginia, West Virginia. Silver Spring, Maryland.

U.S. Department of Commerce NOAA Atlas 14 Precipitation-Frequency Atlas of the United States. (2006). Volume 3, Version 4.0 Puerto Rico and the U.S. Virgin Islands. Silver Spring, MD.

U.S. Department of Commerce NOAA Atlas 14 Precipitation-Frequency Atlas of the United States. (2009, rev. 2011). Volume 4 Version 3: Hawaiian Islands. Silver Spring, MD.

U.S. Department of Commerce NOAA Atlas 14 Precipitation-Frequency Atlas of the United States. (2009, rev. 2011). Volume 5 Version 3.0: Selected Pacific Islands. Silver Spring, MD.

U.S. Department of Commerce NOAA Atlas 14 Precipitation-Frequency Atlas of the United States. (2011). Volume 6 Version 2.0 California. Silver Spring, MD.

U.S. Department of Commerce NOAA Atlas 14 Precipitation-Frequency Atlas of the United States. (2012). Volume 7 Version 1.0 Alaska. Silver Spring, MD.

U.S. Department of Commerce NOAA Atlas 14, Precipitation-Frequency Atlas of the United States. (2013). Volume 8 Version 2.0 Midwestern States. Silver Spring, MD.

U.S. Department of Commerce NOAA Atlas 14, Precipitation-Frequency Atlas of the United States. (2013). Volume 9 Version 2.0 Southeastern States. Silver Spring, MD.

U.S. Department of Commerce, U. S. Weather Bureau. (1961). Rainfall Frequency Atlas of the United States, Technical Paper No. 40. Washington, D.C.

AN INNOVATIVE APPROACH TO EVALUATE DOWNSTREAM FLOOD IMPACT FROM MODIFIED DAM OPERATIONS CONSIDERING EFFECTS OF STORM PATTERN AND TIMING

Henry Hu, Sr. Project Manager, WEST Consultants, Inc., Bellevue, WA, hhu@westconsultants.com; James Hathorn, Chief, Water Management Section, Mobile District, U.S. Army Corps of Engineers, Mobile, AL, james.e.hathorn.jr@usace.army.mil; Beth Faber, Hydraulic Engineer, Hydrologic Engineering Center , U.S. Army Corps of Engineers, Davis, CA, beth.a.faber@usace.army.mil

West Point Dam is one of the critical elements in the Apalachicola-Chattahoochee-Flint (ACF) Rivers system. It officially operates for flood control to reduce flood damages along the reach of the Chattahoochee River between West Point Dam and Columbus. The U.S. Army Corps of Engineers evaluated two flood operation alternatives at West Point Dam, an Early Refill condition and a Fall Stepped-down condition. Because the flood operation guide curve determines available flood storages, which affects the peak and volume of reservoir releases during flood operations, any modification to the guide curve may have some direct impacts on flood conditions downstream. For the Chattahoochee River between West Point and Columbus, the flood damage site is at Columbus. A flood operation alternative is acceptable only if it does not significantly increase the flood frequency curves at Columbus. This paper presents an innovative approach used to evaluate the flood impacts of modified flood operations at West point Dam on the flood conditions at Columbus.

The flow in the Chattahoochee River at Columbus is regulated. The magnitude of flood discharge at Columbus is primarily influenced by the magnitude of storms, which have two distinct types. One is general cyclonic storms typically occurring in winter and spring months. The other is intense tropical storms typically occurring between the summer and fall seasons. As a result, large flood events do show seasonal distributions and variations in hydrograph shapes. At the same time, due to flow regulation, it is also affected by flood operations at West Point Dam and the upstream dams, which typically vary month to month. Therefore, the combined regulated flood frequency relationship at Columbus is a function of two variables, storm and month. For each month, a regulated flood frequency relationship was developed by applying a series of hypothetical flow hydrographs with different shapes and different exceedance probabilities to a reservoir model and by associating the resulting regulated peak flows at Columbus with the exceedance probabilities of the input hypothetical hydrographs. The monthly regulated flood frequency curves was then combined to produce a combined regulated flood frequency curve at Columbus using the total probability theorem. Combined regulated flood frequency curves at Columbus were developed for the baseline and proposed conditions, and were used to evaluate potential impacts from the modified dam operations.

UNCERTAINTY ANALYSIS USING MONTE CARLO TECHNIQUES IN THE HYDROLOGIC MODELING SYSTEM (HEC-HMS)

William Scharffenberg, HEC-HMS Lead Developer, U.S. Army Corps of Engineers Institute for Water Resources, Hydrologic Engineering Center, Davis, CA, William.A.Scharffenberg@usace.army.mil; Angela Duren, Hydraulic Engineer, U.S. Army Corps of Engineers, Portland District, Portland, OR 97204; Matthew Fleming, U.S. Army Corps of Engineers Institute for Water Resources, Hydrologic Engineering Center, Davis, CA, Matthew.J.Fleming@usace.army.mil

INTRODUCTION

Traditional hydrologic simulation has focused on developing algorithms to represent each of the components of the hydrologic cycle. A great deal of effort has been dedicated to developing physically appropriate process representations and parameter estimation techniques. The Hydrologic Modeling System (HEC-HMS) is one modeling framework that takes this approach with components for precipitation, snowmelt, transpiration, infiltration, runoff, and channel flow among others. An automatic parameter estimation tool is also available.

The modern hydrologic simulation approach is often limited by knowledge uncertainty and natural variability. Knowledge uncertainty describes both our inability to fully understand hydrologic processes and the situation where we lack the observational data necessary to parameterize models. Natural variability describes inherent unpredictability in boundary conditions such as climate or initial conditions like soil moisture. Due to the nonlinear nature of the mathematical models that represent natural systems, the uncertainties due strictly to boundary conditions, initial conditions, and model parameters are difficult to distinguish and therefore quantify. However, to the capture these uncertainties together, a Monte Carlo-based uncertainty analysis tool has been added to HEC-HMS to quantify both knowledge uncertainty and natural variability. It includes the ability to statistically sample model parameters using analytical distributions, with an option for the distribution to be a function of the month of the year. It also can link a dependent parameter to a previously sampled parameter through a relationship that includes an error term.

OVERVIEW OF NEW HEC-HMS CAPABILITIES

The hydrologic modeling software, HEC-HMS, is used for dam and levee safety studies, flood damage reduction studies, real-time operations, and general planning studies. The latest version of HEC-HMS now has an integrated uncertainty assessment capability to allow for the development of probabilistic results for key metrics such as total runoff volume or maximum reservoir pool elevation.

The HEC-HMS uncertainty analysis features the ability to assign probability distributions to hydrologic model parameters such as soil loss rates, unit hydrographs, baseflow, and channel routing. Current available analytical distributions that can be assigned to parameters include beta, exponential, gamma, log normal, normal, triangular, and Weibull. Random numbers are generated using the Well19937c generator (Panneton, L'Ecuyer, and Matsumoto, 2006). Output includes the sampled parameters, key metrics, and selected time-series. As an example, the key

metrics can be processed to obtain histograms (Figure 1) or estimate the 90 percent non-exceedance value.

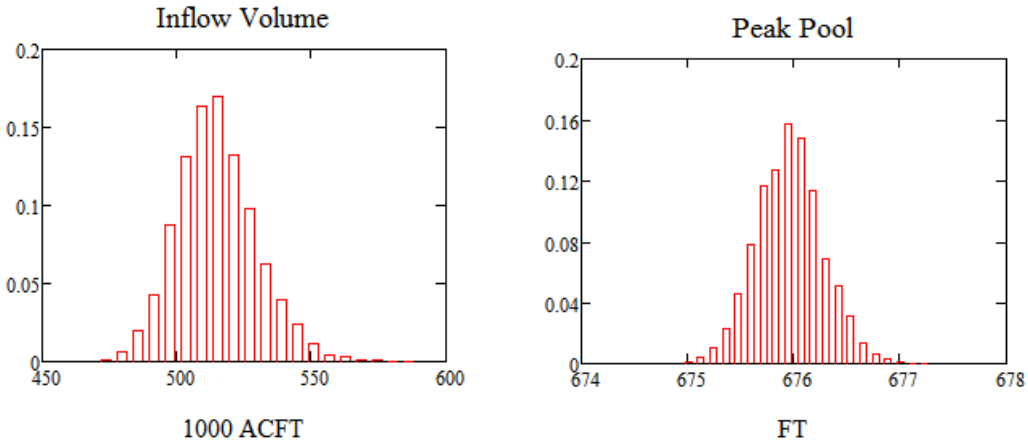

Figure 1 Example of Distribution of Inflow Volume or Peak Pool Results

IMPACT OF STOCHASTIC ANALYSIS ON POOL STAGE FREQUENCY

A study was conducted to compare a deterministic estimate of a reservoir pool stage frequency curve to an estimate generated from the new uncertainty assessment feature in HEC-HMS. The deterministic case assumed fixed parameters for loss rates while the uncertainty assessment used probability distributions estimated from calibration data. The minimum, mean, and maximum pool stage frequency curves from the uncertainty analysis are shown in Figure 2, along with the deterministic estimate. This case shows the deterministic estimate above the mean, notably so in the lower probability range which is an area of interest when performing a risk assessment for dams. Although the deterministic estimate is within the confidence limits computed from the minimum and maximum of the uncertainty analysis, the difference between the deterministic and mean stochastic estimates was profound in this study. The loss rates used in the deterministic model lie in the 'less probable' (and low soil loss) region of the estimate for the soil loss uncertainty distribution. By incorporating the estimated distribution of loss rates into the final pool stage frequency curve, a wider range of soil loss is sampled, thereby reducing the amount of runoff and peak pool stage.

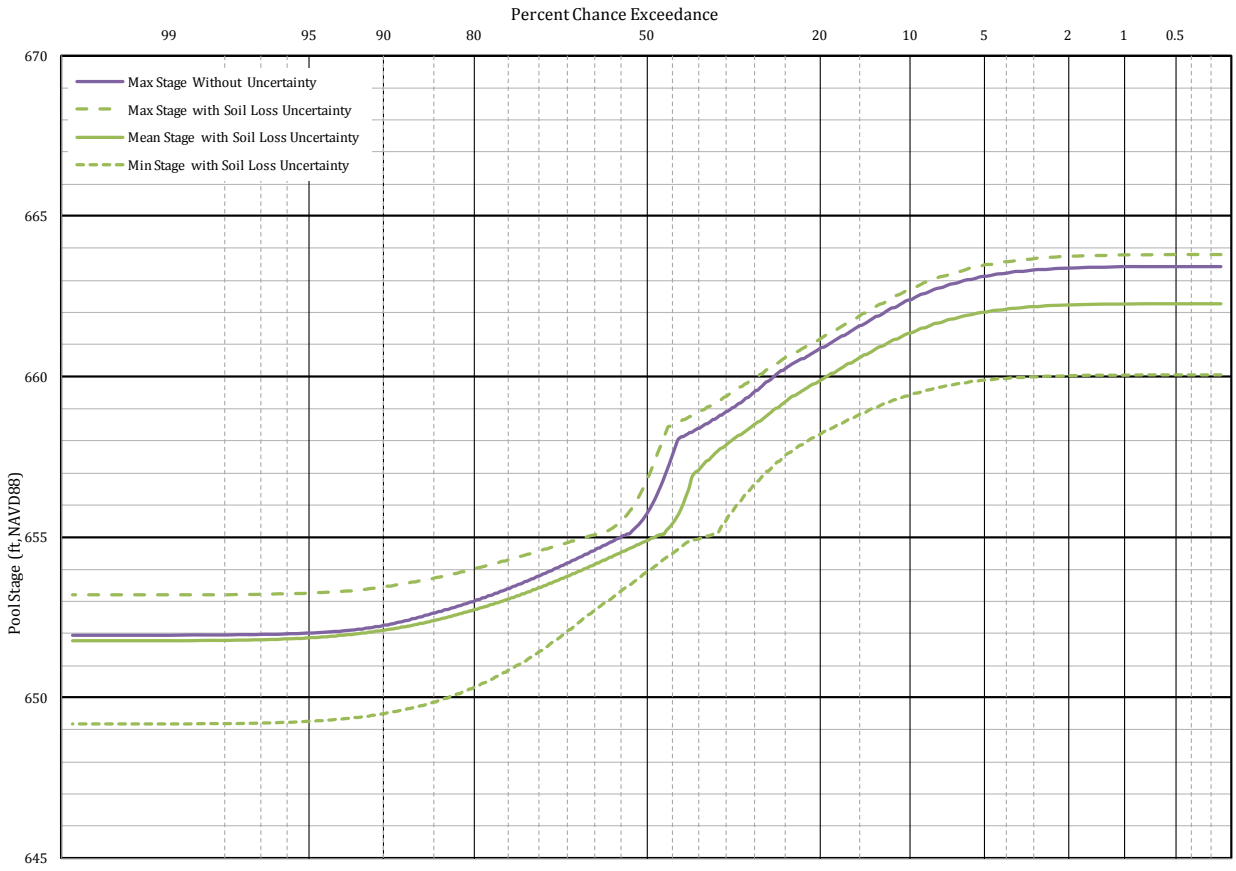

Figure 2 Pool Stage Frequency Example

EVOLUTION OF PROBABILITY DISTRIBUTIONS FOR HYDROLOGIC MODELING PARAMETERS

The most critical requirement for capturing knowledge uncertainty and natural variability in pool stage frequency curves or inflow volume is having the tools to account for the uncertainties in the parameters and having the probability distributions of the parameters themselves. Little work has been done to capture the probability distributions in hydrologic modeling parameters such as soil loss rates or unit hydrographs. Perhaps one reason this work has not been done is that up until now there has been a lack of tools that can integrate the information into the simulation process. The availability of uncertainty assessment capability in a commonly used and widely available tool such as HEC-HMS will hopefully serve as a catalyst for deeper study on expected or reasonable probability distributions of hydrologic modeling parameters in various regions around the world.

REFERENCES

Panneton, L'Ecuyer, & Matsumoto. (2006). "Improved long-period generators based upon linear resources recurrences modulo 2." *ACM Transactions on Mathematical Software (TOMS)*, vol 32, no 1.

SENSITIVITY ANALYSIS FOR SEDIMENT TRANSPORT IN THE HYDROLOGIC MODELING SYSTEM (HEC-HMS)

By Jang Pak, Ph.D., P.E.[1], Kervi Ramos[2], Matthew Fleming, P.E.[3], William Scharffenberg, Ph.D.[4], and Stanford Gibson, Ph.D.[5]

[1] Sr. Research Hydraulic Engineer, U.S. Army Corps of Engineers, Institute For Water Resources, Hydrologic Engineering Center, 609 Second Street, Davis, CA 95616; PH (530) 756-1104; FAX (530) 756-8250; email: Jay.H.Pak@usace.army.mil.
[2] Student Intern, U.S. Army Corps of Engineers, Institute For Water Resources, Hydrologic Engineering Center, 609 Second Street, Davis, CA 95616; email: Kervi.Ramos@usace.army.mil.
[3] Chief, Hydrology & Hydraulics Technology Division, U.S. Army Corps of Engineers, Institute For Water Resources, Hydrologic Engineering Center, 609 Second Street, Davis, CA 95616.
[4] HEC-HMS Lead Developer, U.S. Army Corps of Engineers, Institute For Water Resources, Hydrologic Engineering Center, 609 Second Street, Davis, CA 95616.
[5] Sr. Research Hydraulic Engineer, U.S. Army Corps of Engineers, Institute For Water Resources, Hydrologic Engineering Center, 609 Second Street, Davis, CA 95616.

Abstract

Watershed models are evaluated through calibration and validation processes. However, sediment model parameters and observed data for calibration are often expensive and difficult to collect. Where sediment data is limited, sensitivity analysis can identify the most influential parameters in the model. Identifying sensitive input parameters is critical for model development and application. This paper aims to improve understanding of the sensitivity of the sediment input parameters in the Hydrologic Engineering Center's Hydrologic Modeling System (HEC-HMS 4.0).

Historically, HEC-HMS was focused on modeling rainfall-runoff processes using a full range of components for meteorology, canopy, soil, surface runoff, baseflow, channel routing, reservoirs, and diversions. Recently, components have been added for representing land surface erosion, channel erosion and transport, and lake turbulent settling. A sensitivity analysis evaluated model parameters required by these new sediment capabilities. Sensitivity analysis results were then compared with observed data to identify sensitive parameters and their relative influence. These results can support HEC-HMS sediment model development in locations with little to no observed data.

INTRODUCTION

The Hydrologic Engineering Center's Hydrologic Modeling System (HEC-HMS) sediment transport module (STM), including surface erosion, in-stream sediment routing, and reservoir sediment routing modeling capabilities was released in December 2013 (USACE 2013). The STM was designed based on applicable knowledge of geomorphology, hydrology, hydraulics, and concepts of surface and sediment transport.

In addition to the implementation of the new STM into HEC-HMS, the HEC-HMS team conducted a detailed sensitivity analysis of the HEC-HMS sediment model to assess the overall influence of sediment input parameters on the computed total cumulated sediment loads. Sensitivity analysis evaluates the relative model response as a function to changes in model input

parameters (Nearing et al. 1990). The evaluation process includes three steps according to Nearing et al. (1990):

- Calibration and validation of the model to measured data
- Sensitivity analysis of the model response to input parameters
- Evaluation of confidence limits for the model prediction

Sensitivity analysis was conducted on selected input parameters of the three main elements (sub-basin, reach, and reservoir) of the HEC-HMS sediment model. The sensitivity analysis used a calibrated and validated HEC-HMS model that consisted of a two-year simulation period (1 January 1995 through 31 December 1996).

HYDROLOGY AND SEDIMENT MODEL OVERVIEW

The study site selected for the sensitivity analysis consists of a 921 km^2 (356 mi^2) watershed called the Upper North Bosque River. The Upper North Bosque River Watershed (UNBRW) is located in Central Texas (Figure 1). UNBRW is a headwater watershed in the North Bosque River basin. Elevation in the watershed ranges from 299 m to 495 m (981 ft to 1624 ft) above sea level. The mean annual precipitation is 750 mm and dominant soil type is fine sandy loams with sandy clay subsoil, calcareous clay, and clay loams in the watershed (Saleh and Du 2004). The HEC-HMS model included 68-subbasin, 40-reservoir, and 84-reach elements based on five gage locations, land use, soil, and topographic information (USACE 2014).

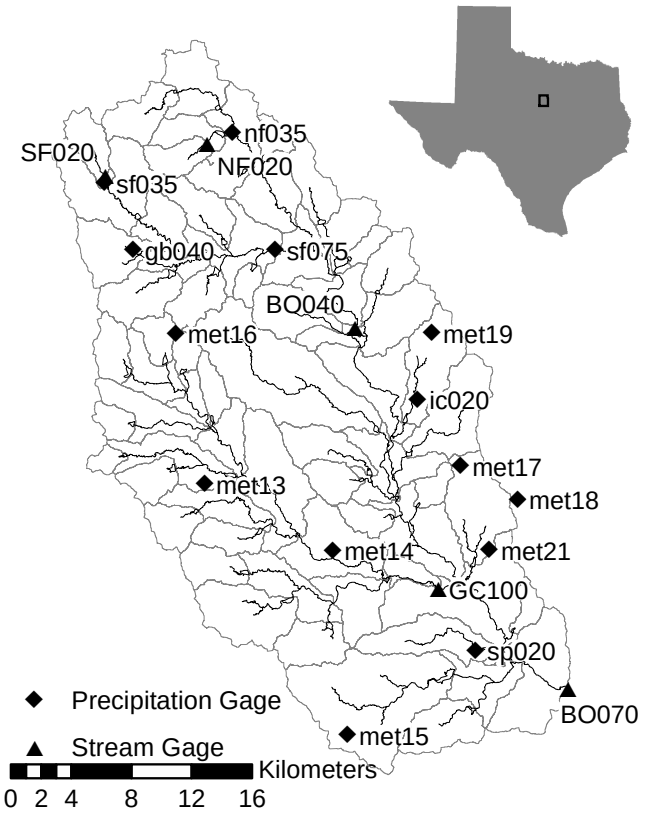

Figure 1 Project Location map including gauged locations for UNBRW

The selection of modeling methods and initial input parameters relied heavily on the data available and appropriateness for hydrology and sediment models. The model was calibrated to observed hydrologic and sediment data from 1 January 1995 to 31 December 1996 by adjusting model parameters to minimize the difference in computed and measured flow and sediment at five gage locations (NF020, SF020, BO040, GC100, and BO070) as shown in Table 1. Unlike the calibration period, the validation of the model required observed data from 1 January 1997 to 31 December 1998 (USACE 2014). Using the calibrated and validated hydrology/sediment model, a sensitivity analysis was conducted by changing one of the selected sediment model parameters or methods and fixing others as based values during the calibration period.

Table 1 Measured and computed results of daily flow and TSS loading.

		Calibration Period (01Jan1995 to 31Dec1996)					
		Hydrology (ft^3/s)			Sediment (tons)		
		Mean	Standard Deviation	Mean Error	Mean	Standard Deviation	Mean Error
NF020	Measured	1.06	4.94	N/A	2.66	23.12	N/A
	HMS	1.41	6.36	0.35	2.67	32.24	0.01
SF020	Measured	1.41	7.77	N/A	1.32	15.00	N/A
	HMS	1.77	9.89	0.35	1.32	12.79	-0.01
BO40	Measured	33.90	99.23	N/A	24.68	190.17	N/A
	HMS	32.49	123.95	-1.06	24.61	180.16	-0.07
GC100	Measured	30.72	92.88	N/A	1.32	15.00	N/A
	HMS	31.43	127.49	0.71	22.74	181.57	0.07
BO070	Measured	102.06	303.00	N/A	99.69	799.16	N/A
	HMS	108.06	423.07	6.00	100.03	890.15	0.33

METHODOLOGY

A linear sensitivity model was selected for sensitivity testing of HEC-HMS sediment model. The sensitivity parameter (S) is computed using equation (1).

$$S = \frac{\left(\frac{O_2 - O_1}{O_{12}}\right)}{\left(\frac{I_2 - I_1}{I_{12}}\right)} \quad (1)$$

Where;
I_1: the least value of input parameter
I_2: the greatest value of input parameter
I_{12}: the average value of I_1 and I_2
O_1: the output value of I_1
O_2: the output value of I_2
O_{12}: the average value of O_1 and O_2

The dimensionless sensitivity parameter (S) quantifies the sensitivity of the input parameter by comparing the relative normalized output change to a normalized input change. McCuen and

Snyder (1983) discuss limitations of the linear sensitivity analysis used in this paper. One of the biggest limitations of the linear sensitivity equation (1) above is that, equation 1 yields a single sensitivity parameter value instead of a distribution of outputs as a function of the input parameter distribution. Describing the sensitivity parameter as a distribution instead of a single value will better describe sensitivity of the parameters.

In this sensitivity analysis, wide ranges of input parameters were selected for the subbasin, reach, and reservoir elements (Table 2). Generally, one selected parameter was varied and other parameters were fixed as base values.

Table 2 Parameters and method selected for Sensitivity Analysis

Element	Parameter/Method
Subbasin Element	Enrichment Ratio
	Sand
	Silt
	Clay
	MUSLE (Cover Factor)
Reach Element	Fraction of Gravel
	Channel Width
	Active Layer Factor
Reservoir Element	Fall Velocity Method

SENTIVITY TO SEDIMENT METHODS AND PARAMETERS

The particle size distribution of source material in the subbasin (on the land surface) is generally much coarser than the stream channel sediment at the basin outlet due to changing hydrodynamic forces as water flows over the land surface and concentrates within streams and channels. The clay and silt enrichment in the suspended sediment is largely the result of preferential deposition of the courser fraction during the transport and delivery of sediment from its source to basin outlet (USACE 2014). The enrichment ratios for each particle class converted the watershed particle-size distribution to an outlet particle-size distribution: The enrichment ratio is defined in equation (2) below.

$$ER = \frac{\%\ sediment\ in\ a\ given\ size\ class\ in\ outlet}{\%\ sediment\ in\ a\ given\ size\ class\ in\ watershed} \quad (2)$$

Where, ER is the enrichment ratio. The numerator, % sediment in a given size class at the outlet, can be determined from a suspended sediment sample near the subbasin outlet. The denominator, % sediment in a given size class in watershed, comes from the SSURGO soil data. The ER was a calibration factor in the original model.

The ERs were computed by varying enrichment ratios ~ ±15% from calibrated values, for each grain class (sand, silt and clay) while fixing the base values for other parameters. The differences of sediment yields from calibrated model results, at each computation point are shown in Figures 2 through 4 for sand, silt, and clay respectively.

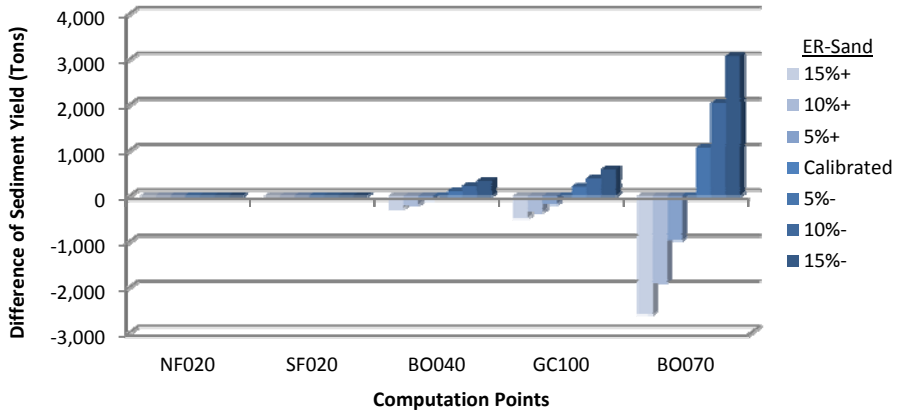

Figure 2 Impact of six selected enrichment ratios of sand on simulated sediment yield for the calibration period (1 January 1995 through 31 December 1996)

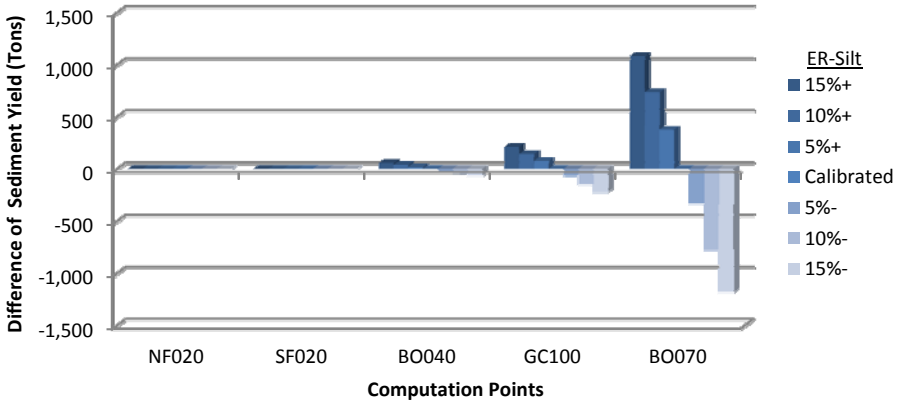

Figure 3 Impact of six selected enrichment ratios of silt on simulated sediment yield for the calibration period (1 January 1995 through 31 December 1996)

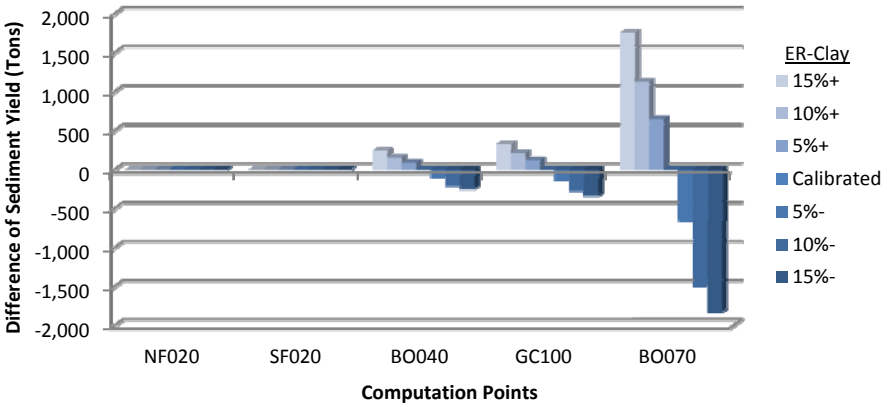

Figure 4 Impact of six selected enrichment ratios of clay on simulated sediment yield for the calibration period (1 January 1995 through 31 December 1996)

MUSLE cover factor sensitivity was determined by varying the cover factor ~ ±50%, relative to the calibrated parameter. The simulation results, in terms of the differences of sediment yields from calibrated model results at each computation point, are shown in Figure 5.

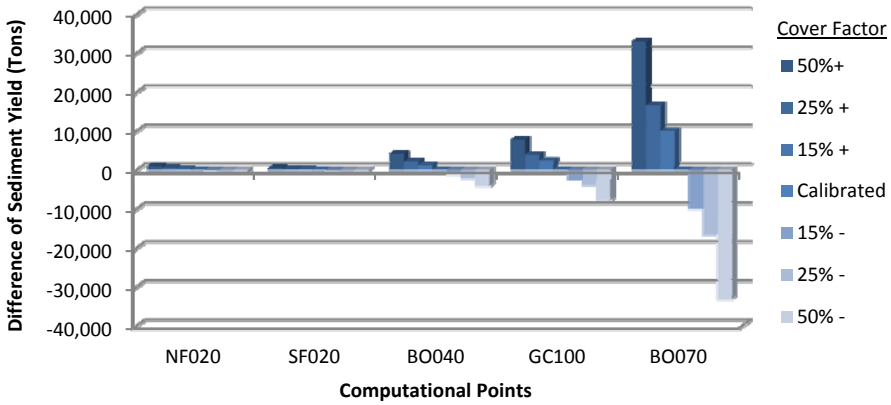

Figure 5 Impact of six selected MUSLE cover factors on simulated sediment yield for the calibration period (1 January 1995 through 31 December 1996)

Sensitivities to the fraction of gravel in the channel bed were determined by varying the gravel fraction from -1% to ~ -25% of the calibrated model parameter, using fixed base values for other parameters. The differences of sediment yields from calibrated model results for these simulations, at each computation point are shown in Figure 6.

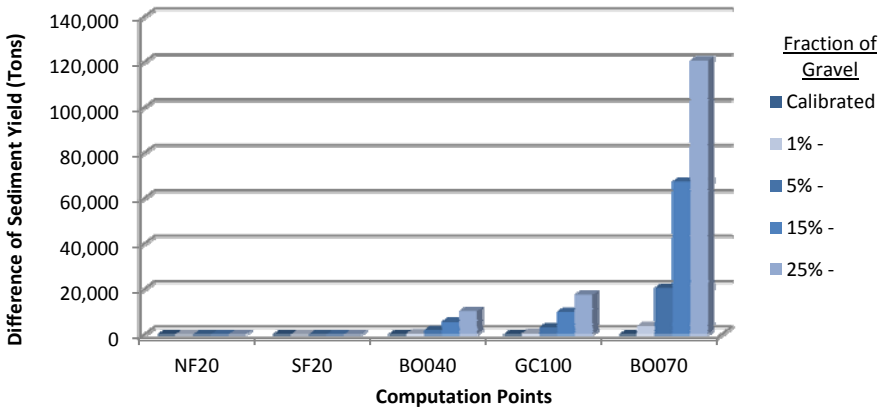

Figure 6 Impact of four selected fraction of gravel for channel gradation simulated sediment yield for the calibration period (1 January 1995 through 31 December 1996)

The channel bed widths were adjusted ~±50% of the calibrated values to test sensitivity to this routing parameter. Simulation results at each computation point are included in Figure 7.

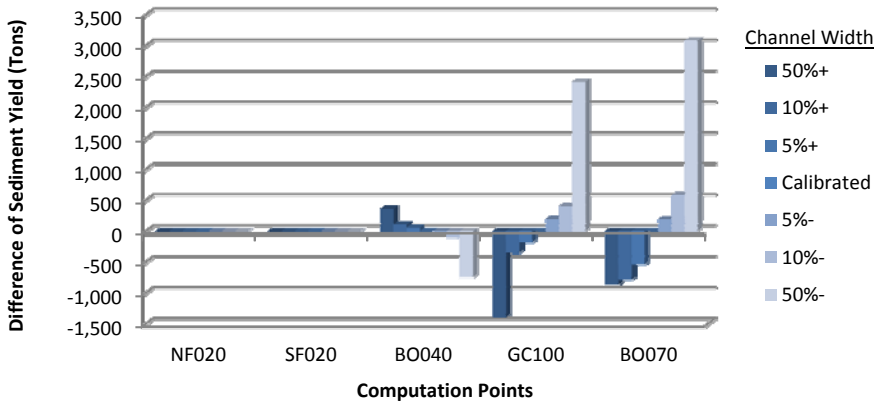

Figure 7 Impact of six selected widths of channel on simulated sediment yield for the calibration period (1 January 1995 through 31 December 1996)

Active layer factor (the thickness of the reach element active layer in multiples of d_{90}) was adjusted from 1 to 3, bracketing the calibrated value of 2. As with the other analyses, the calibration parameters were fixed for all other model variables. Simulation results, in terms of the differences of sediment yields from calibrated model results at each computation point, are shown in Figure 8. Stations NF20 and SF20 results are not sensitive to channel width, gravel content, or active layer thickness because these are directly downstream of a specific subbasin element. There are no reach elements upstream of them for the routing parameters to influence the results.

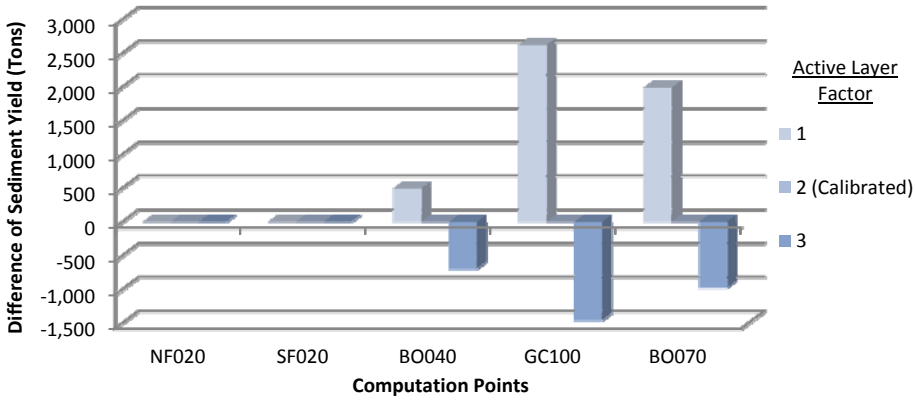

Figure 8 Impact of two selected active layer factors on simulated sediment yield for the calibration period (1 January 1995 through 31 December 1996)

Reservoir fall velocity method sensitivity was evaluated by running the model with all four options available. Results at each computation point are included in Figure 9.

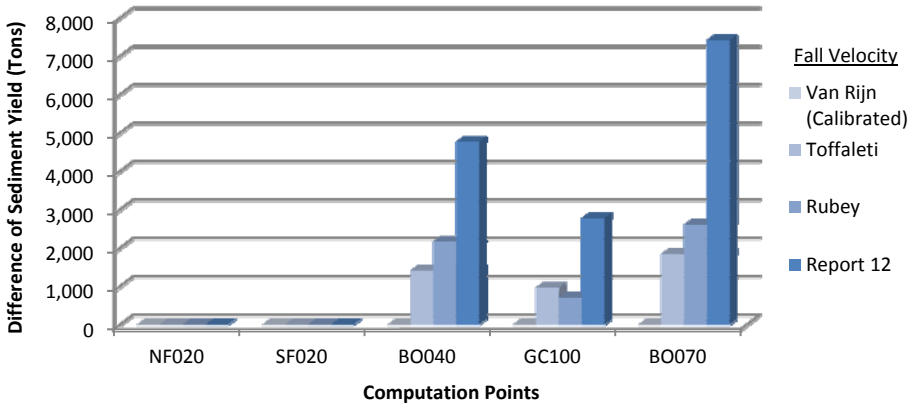

Figure 9 Impact of three selected fall velocity methods on simulated sediment yield for the calibration period (1 January 1995 through 31 December 1996)

RESULTS OF SENSITIVITY ANALYSIS

The parameters tested are listed in Table 3 and include units, base values from calibration, input values, and calculated sensitivity parameter (S) values and rank. Input 1 and Input 2 are the minimum and maximum values, respectively, from the sensitivity analysis. Total accumulated sediment yield was most sensitive to the channel gravel fraction for reach elements and the other two channel parameters (channel width and active layer thickness) were relatively insensitive. The MUSLE cover factor and Sand Enrichment Ratio were sensitive parameters for the subbasin elements. The fall velocity method (especially, Report 12) for the reservoir elements also had some influence on the outlet sediment yields.

Table 3 Summary of Sediment Model Parameters and method used for Sensitivity Analysis

Parameters	Units	Base	Input 1	Input 2	(S)	Rank
Subbasin Element						
Enrichment Ratio[1]						
Sand	Unitless	57.97	54.35	61.04	-0.67	3
Silt	Unitless	29.92	26.69	32.86	0.15	5
Clay	Unitless	12.12	10.55	13.62	0.19	4
MUSLE (Cover Factor) [1]	Unitless	0.011	0.005	0.016	0.91	2
Reach Element						
Fraction of Gravel[2]	Unitless	0.92	0.69	0.91	-3.13	1
Channel Width[2]	(ft)	30.90	15.50	46.40	-0.05	6
Active Layer	Unitless	2.00	1.00	3.00	-0.04	7

[1] – The area weighted average values were used to calculate the sensitivity parameter (S).
[2] – The length weighted average values were used to calculate the sensitivity parameter (S).

SUMMARY AND CONCLUSIONS

This paper presents a sensitivity analysis of the new sediment transport module available in HEC-HMS Version 4.0. The new sediment modeling tool allows the use of HEC-HMS for the assessment of watershed sediment transport. Eight sensitivity tests were developed to evaluate the HEC-HMS watershed sediment model parameters and identify those particularly important to calibrate a sediment model.

The output from an HEC-HMS model with a single perturbed parameter was compared to the calibrated model. This sensitivity analysis indicates the level of sensitivity for each selected parameters and provides guidance to modelers developing watershed surface erosion models with little to no observe data. While this work can inform other studies, sensitivity analysis can be site specific and sensitive parameters in other watersheds may diverge from those identified in the UNBRW study area.

REFERENCES

McCuen, R. H., and W. M. Snyder. (1993). Hydrologic Modeling: Statistical Methods and Applications. Englewood Cliffs, N.J.: Prentice-Hall.

Nearing, M. A., L. Deer-Ascough, and J.M. Laflen. (1990). "Sensitivity Analysis Of The WEEP Hillslope Profile Erosion Model." Transactions of the ASAE, 33(3): 839-849.

Saleh, A., and Du, B. (2004). "Evaluation Of SWAT And HSPF Within Basins Program For The Upper North Bosque River Watershed In Central Texas." Transactions of the ASAE, 47(4): 1039-1049.

U. S. Army Corps of Engineers. (2013). Hydrologic Modeling System HEC-HMS: User's Manual. Hydrologic Engineering Center, Davis, CA.

U. S. Army Corps of Engineers. (2014). Hydrologic Modeling System HEC-HMS: Applications Guide. Hydrologic Engineering Center, Davis, CA.

APPLICATION OF SURFACE EROSION AND SEDIMENT ROUTING CAPABILITIES OF THE HEC-HMS TO FORT HOOD, TEXAS

EXTENDED ABSTRACT

By Simon Evans, P.E[1], Jang Pak, Ph.D., P.E.[2], and Matt Fleming, P.E.[3]

[1] Hydraulic Engineer, Los Angeles District, U.S Army Corps of Engineers, 915 Wilshire Blvd, Suite 930, Los Angeles, California 90017. Simon.C.Evans@usace.army.mil
[2]Sr. Research Hydraulic Engineer, U.S. Army Corps of Engineers, Institute For Water Resources, Hydrologic Engineering Center, 609 Second Street, Davis, California 95616.
[3]Chief, Hydrology and Hydraulics Technology Division, U.S. Army Corps of Engineers, Institute For Water Resources, Hydrologic Engineering Center, 609 Second Street, Davis, California 95616.

The Hydrologic Engineering Center's Hydrologic Modeling System (HEC-HMS) is a software program used to simulate the hydrologic processes of watersheds. Surface erosion and sediment routing capabilities have recently been added to HEC-HMS version 4.0 (Scharffenberg and Fleming, 2013). These components expand the functionality of HEC-HMS and allow for more diverse applications of the program. This paper demonstrates how the sediment transport capabilities in HEC-HMS version 4.0 can be applied to develop an initial surface erosion and sediment routing model quickly, easily, and cheaply with limited observed data and resources.

The watershed used to demonstrate these capabilities was the House Creek Watershed in Fort Hood, Texas. Fort Hood is an ideal application for the newly released HEC-HMS soil erosion and sediment modeling capabilities. The extensive vehicle maneuver training grounds combined with the installation's highly erodible soils result in impaired lands and degradation of water resources. The project area is approximately 54 square miles and is a sub-watershed of the Cowhouse Watershed. There are two monitoring locations in the main watershed (FH08 and FH01) with an additional monitoring station on Clear Creek, a tributary of House Creek (FH07). The three gages record 15 minute flow data and sediment concentration data for only a few flood events that occurred at irregular intervals.

The HEC-HMS sediment model was developed using a variety of readily available data. Soil Survey Geographic Data Base (SSURGO) data, land use data from the National Land Cover Database 2011, and the USGS 10m DEM were the main data sources for the model. The meteorological model relied on hourly precipitation estimates developed from WSR-88D NEXRAD by the West Gulf River Forecast Center. An analysis period from 1996 to 2001 was established based on the availability of precipitation data, observed flow data, and observed sediment concentration data. Over this period the hydrologic model was roughly calibrated to the limited observed flow data. The surface erosion and sediment routing model was parameterized using SSURGO data, terrain and land use data, and representative soil gradations in order to apply the Modified Universal Soil Loss Equation (MUSLE) to each subbasin (Kelsey and Johnson, 2003). Channel soil gradations from the Upper North Bosque River Watershed were used as representative soil gradations in the Fort Hood model because of the proximity of the watershed and similar soil types. The sediment load output from the model was converted to a sediment concentration, and adjusted to match sediment concentration data observed at FH01, FH07 and FH08.

The limited availability of observed data prevented the traditional approach of calibration followed by a validation period. Instead, the hydrologic model was partially calibrated to two separate time periods that contained significant observed data. The two periods were then evaluated on how closely they reflected observed peak sediment concentrations. The observed sediment concentrations were not continuous data sets, therefore statistics on calibration were not calculated. However, the sedigraphs produced by the HEC-HMS model did provide a reasonable approximation of the observed sediment concentrations. Particularly during the storm event of June 2000 at gage FH01 shown in Figure 4, the peak sediment concentration produced by the HEC-HMS model corresponded with the observed sediment concentration peak. The sedigraphs developed by the HEC-HMS model at gage FH07 shown in Figures 2 and 5 overestimated the sediment concentration compared to the observed data for larger events. This may be due to the fact that the hourly precipitation estimates developed from WSR-88 NEXRAD used in the model have a coarse resolution, and may not accurately define the exact location of high intensity precipitation events in a small watershed like House Creek.

The Fort Hood HEC-HMS surface erosion and sediment transport model confirms that HEC-HMS can be used as a tool to develop a time series of sediment loads in a watershed. In the absence of other sources of data, these sediment loads can be applied as boundary conditions to detailed hydraulic models (Gibson et al., 2010). Often sediment load boundary conditions are estimated through the Universal Soil Loss Equation (USLE) or MUSLE, but this approach requires a separate runoff model and calculation for each event (Gee and MacArthur, 1996). The HEC-HMS sediment transport model provides time series sediment boundary conditions, and may prove computationally faster than other approaches. The HEC-HMS Fort Hood model could be improved by the addition of more observed data. A system of precipitation gages in the watershed would improve the hydrological model by providing detailed, site-specific data. Improved simulation of the precipitation and runoff would improve the accuracy of the soil erosion model. Soil gradations from the channel bed, sediment concentration samples, and additional stream flow gages would all refine the model and allow for more accurate calibration of the sediment transport and hydrologic modeling.

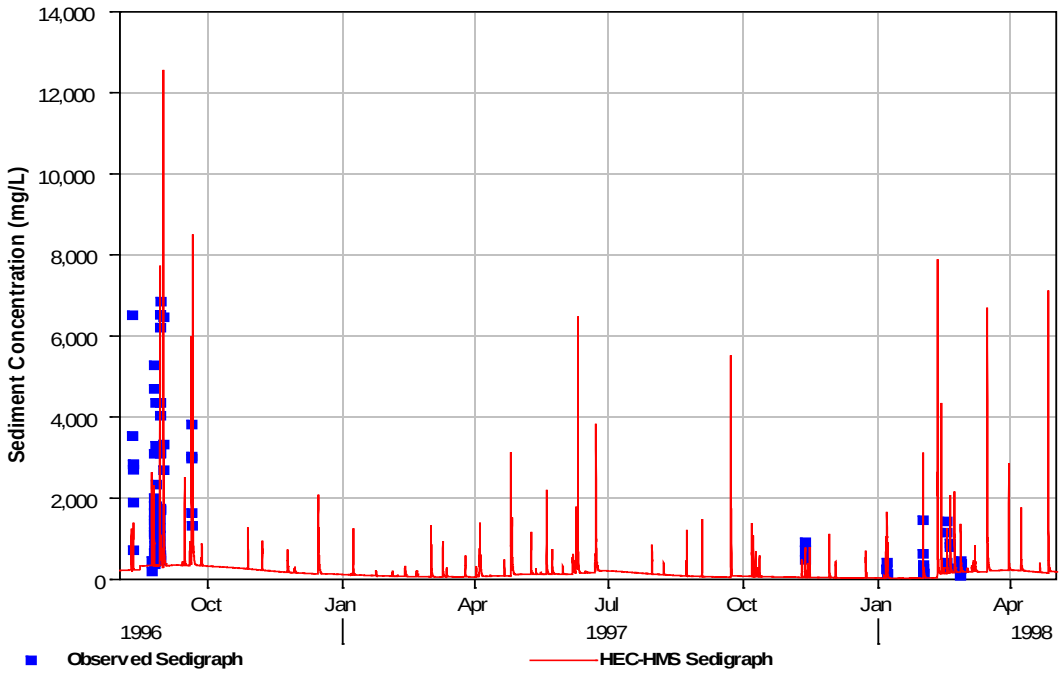

Figure 1 Sediment Concentrations at Gage FH01 for 1996-1998.

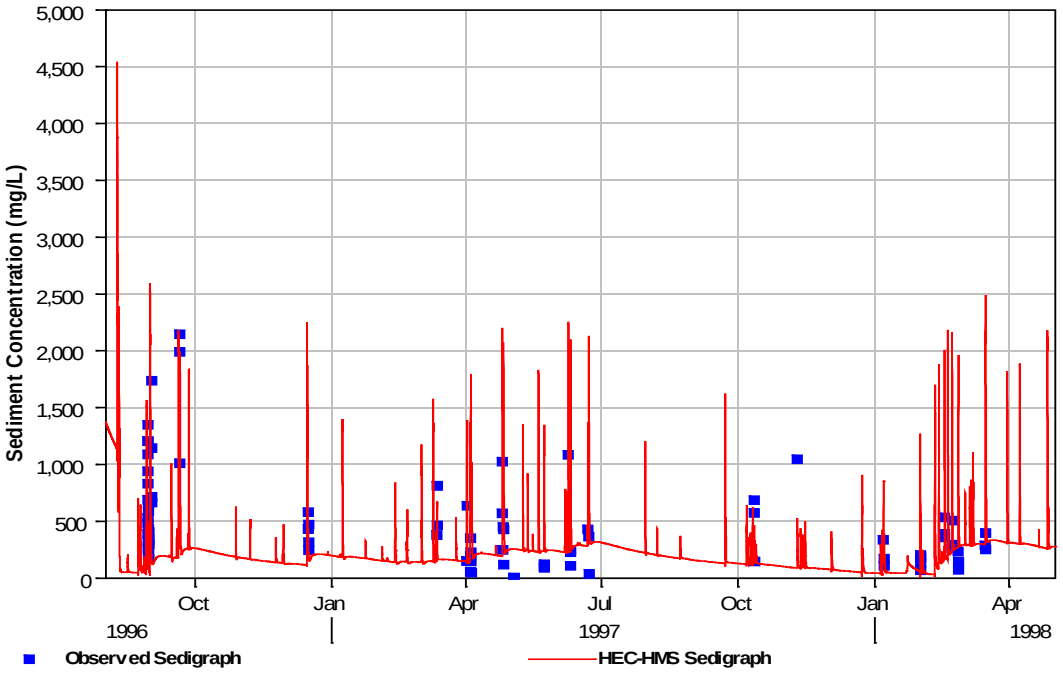

Figure 2 Sediment Concentrations at Gage FH07 for 1996-1998.

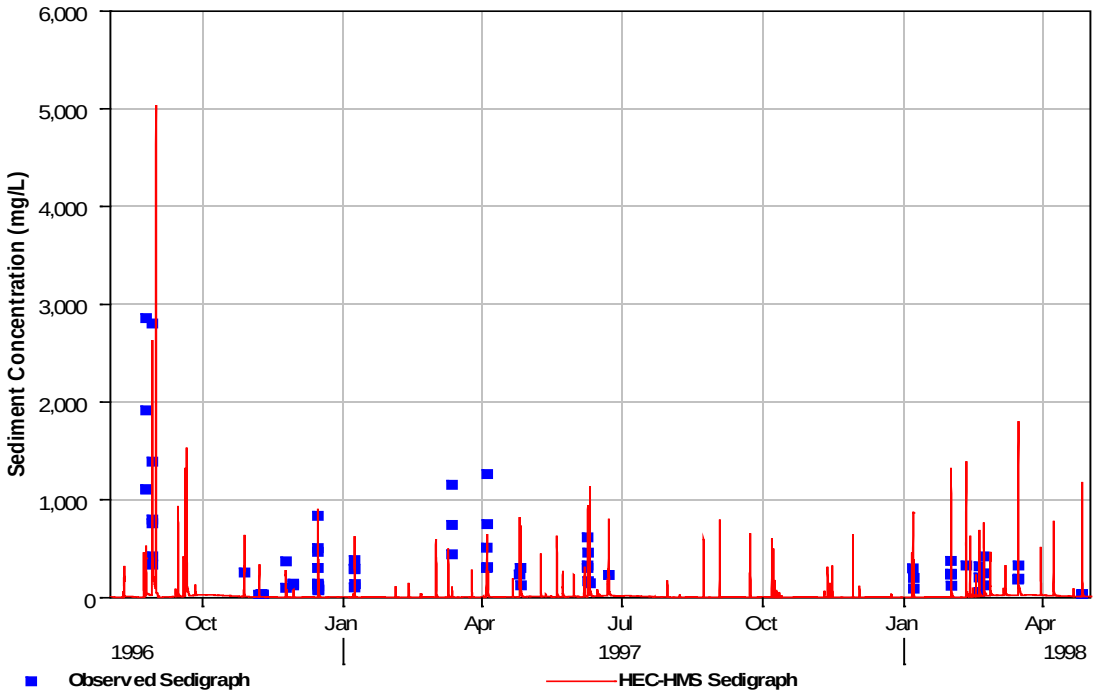

Figure 3 Sediment Concentrations at Gage FH08 for 1996-1998.

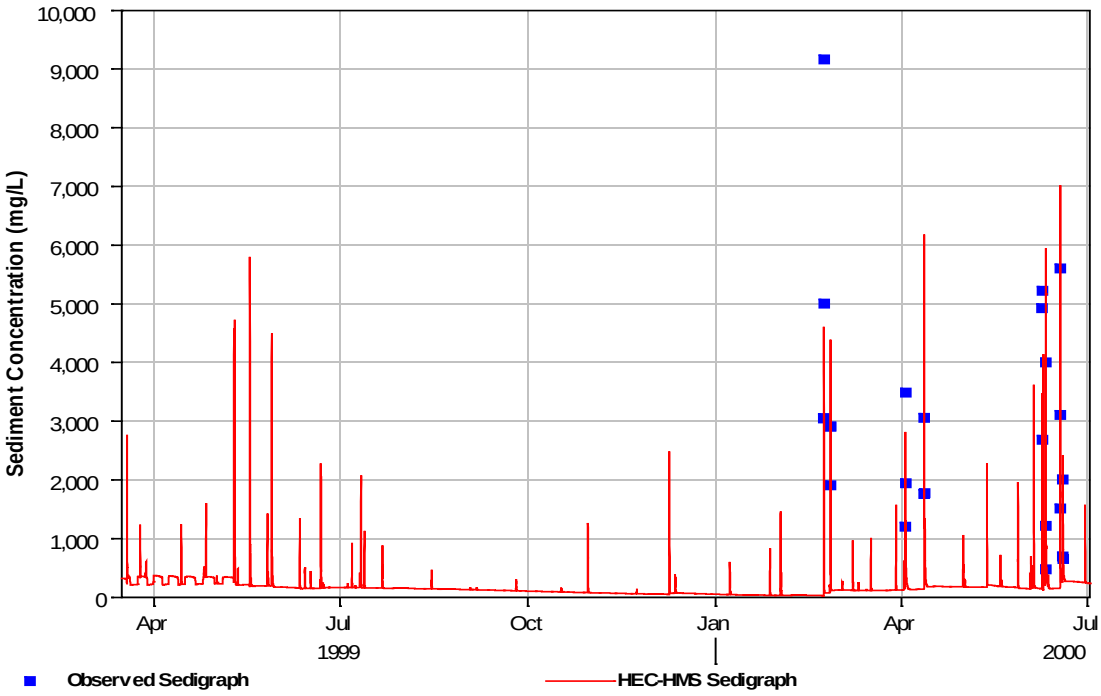

Figure 4 Sediment Concentrations at Gage FH01 for 1999-2000.

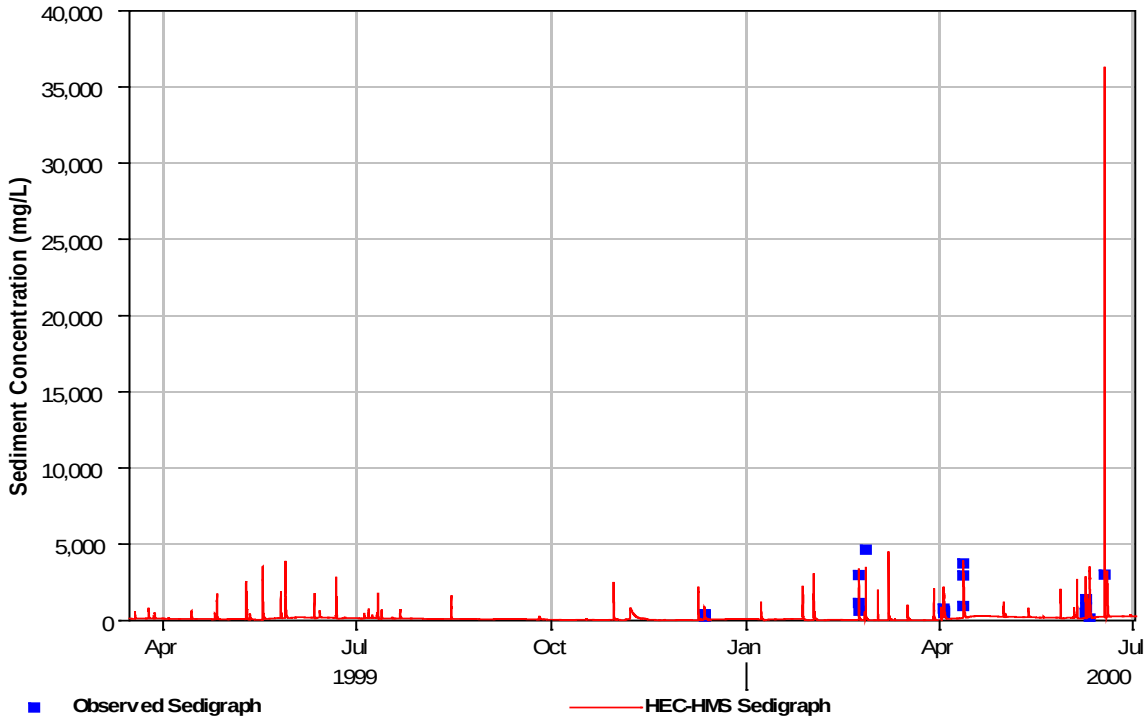

Figure 5 Sediment Concentrations at Gage FH07 for 1999-2000.

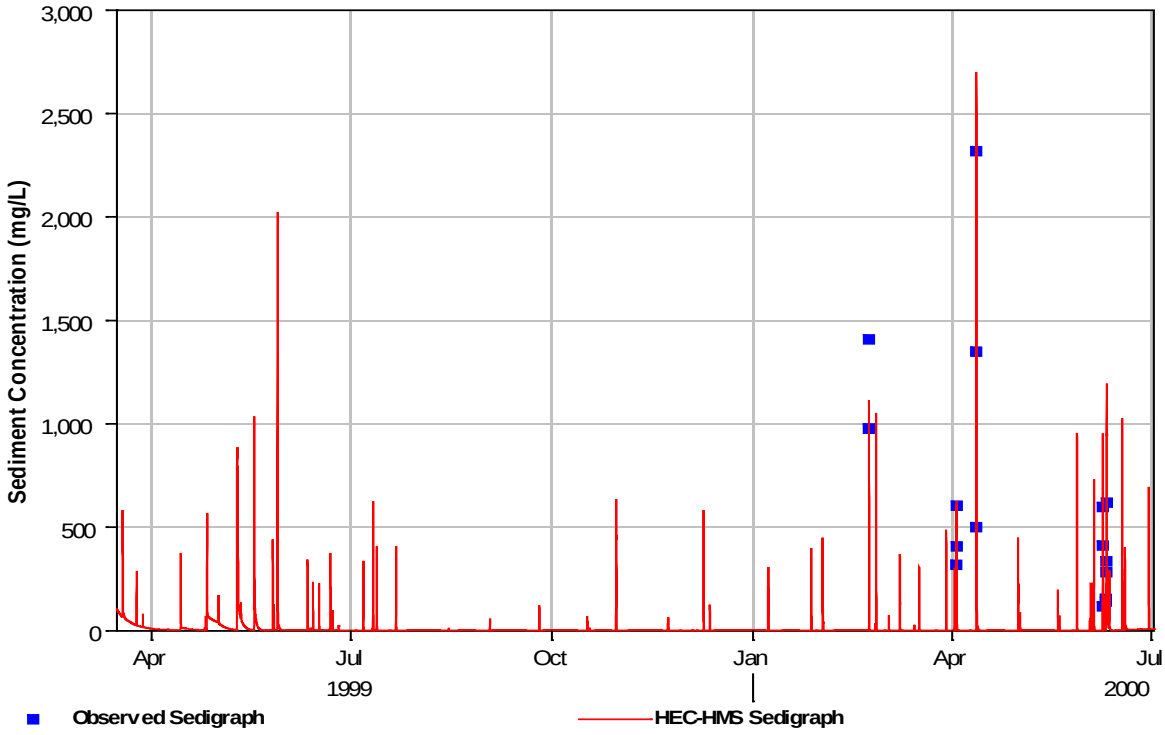

Figure 6 Sediment Concentrations at Gage FH08 for 1999-2000.

REFERENCES

Gee, D.M., and MacArthur, R.C. (1996). *TP-152 use of land surface erosion techniques with stream channel sedimentation tools.* Hydrologic Engineering Center, Davis, California.

Gibson, S.A., Pak, J.H., and Fleming, M.J. (2010). "Modeling watershed and riverine sediment processes with HEC-HMS and HEC-RAS," Watershed Management Conference, pp 1340-1349.

Kelsey, K. and Johnson, Tony. (2003). "Determining cover management values (C factors) for surface cover best management practices (BMPs)," Proceedings of the International Erosion Control Association's Conference, pp 319-328.

Scharffenberg, W.A., and Fleming, M.J. (2013). Hydrologic Modeling System HEC-HMS: User's Manual. US Army Corps of Engineers, Hydrologic Engineering Center, Davis, California.

HURRICANES, HYDROLOGY, AND SEDIMENT: BUILDING AN HMS MODEL OF SEDIMENT YIELD FROM HURRICANES FOR ST. CROIX, U.S.V.I.

Travis A. Dahl, Research Hydraulic Engineer, ERDC Coastal & Hydraulics Laboratory, Vicksburg, MS, Travis.A.Dahl@usace.army.mil; James P. Selegean, Hydraulic Engineer, USACE Detroit District, James.P.Selegean@usace.army.mil; Calvin T. Creech, Hydraulic Engineer, USACE Mobile District, Calvin.T.Creech@usace.army.mil; Jesse E. McNinch, Research Oceanographer, ERDC Coastal & Hydraulics Laboratory, Jesse.McNinch@usace.army.mil

Abstract

St. Croix, U.S. Virgin Islands, has been impacted by 46 hurricanes or tropical storms in the last 141 years. During that time, the island was hit by hurricane force winds every 7.4 years, on average. These large storm events have had a disproportionate impact on the sediment yield of the island, especially on the drier, eastern end. As part of a larger study of hurricane patterns, sediment cores were collected at two lagoons on the eastern end of the island, South Gate Pond and Great Salt Pond. In order to confirm that layers of coarse sediment contained in these cores were from hurricanes, several HMS models were developed. This development included implementation of the newly developed sediment yield routines in HMS. The annual average sediment yield from the HMS model was compared to the volumes of sediment estimated from the sediment cores and showed a good match. Finally, sediment yields were modeled for three hurricanes in the late 1990s: Lenny (1999), Georges (1998), and Mitch (1998). Based on these three events, sediment delivery to the lagoons can contribute almost half of the annual sediment yield in the span of only a few days.

INTRODUCTION

St. Croix is the largest of the U.S. Virgin Islands at 214.7 km^2. It is located at 17° 45' N 64° 45 W. Precipitation varies longitudinally across the island, with the West end being relatively wet and the East end receiving less rain. Due to its location, St. Croix has averaged one hurricane every seven to eight years since the late 19^{th} century.

As part of a larger project to study long-term trends in hurricane frequency, sediment cores were collected in two lagoons on the eastern end of St. Croix. South Gate Pond is located on the north side of the island and Great Salt Pond is located on the south side. Both of these ponds are depositional lagoons that act as sediment sinks and may preserve records of sediment delivery due to hurricanes.

METHODS

This study focused on the creation of models for the South Gate Pond and Great Salt Pond watersheds on St. Croix. Neither of these watersheds, however, contains a USGS gage with a long-term record. In order to ensure that the relevant parameters of the hydrology models were realistic, a third model was also created for the Jolly Hill watershed. This watershed contains the only USGS gage on the island with a significant record length. USGS Gage #50345000 (Jolly Hill Gut at Jolly Hill) has continuous 15-minute data available from 1986 through 2006 and was used for calibration. The locations of all three watersheds, as well as the USGS gage, are shown in Figure 1.

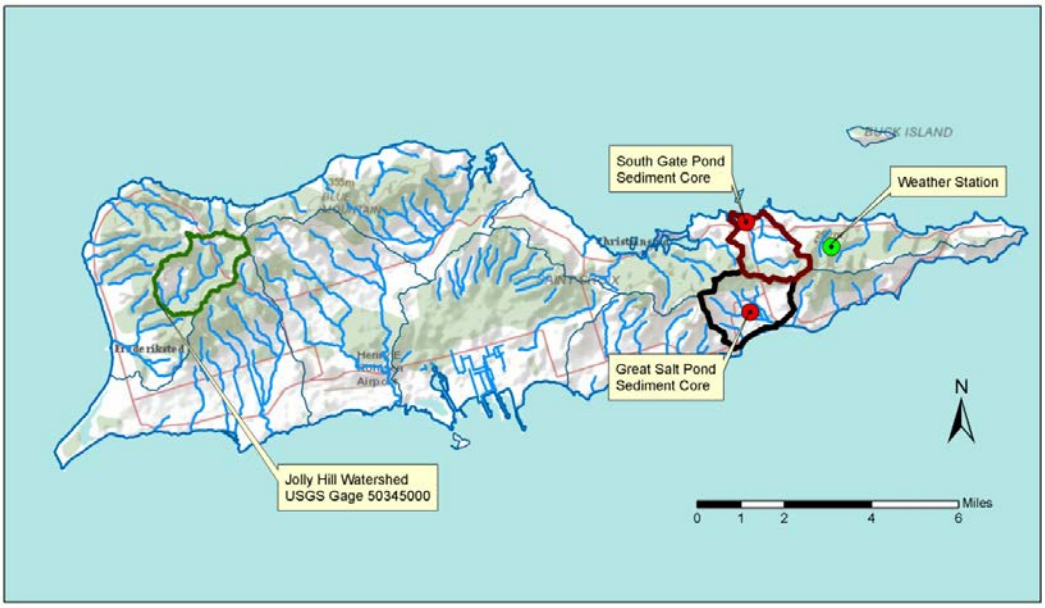

Figure 1 Watershed and time series data locations

HEC-HMS 4.0 Alpha was selected for use in modeling the target watersheds. This decision was based on balancing data requirements, ease of model setup, and the implementation of sediment yield routines in the model.

Data gathered for use in the model included the USGS gage flows, topography, soils, and weather information. The soils in the target watersheds are very coarse, primarily gravelly loam. The primary source of meteorological data was a weather station (Christiansted Station; GHCND #VQW00011624) just east of the Great Salt and South Gate Ponds. The weather station records included precipitation data from 1953 to present.

The hydrology model for Jolly Hill on the west side of St. Croix was developed first in order to take advantage of its 20-year flow record. Hydrology models can be very sensitive to certain variables, such as the percentage of impervious surface area and infiltration. For the Jolly Hill watershed model (see Figure 4), calibration was obtained only when a percolation loss of 0.07 $m^3/s/1000\ m^2$ was used, which represents a losing stream condition. Prior to adding the percolation rate the modeled stream overpredicted flow under very small precipitation events.

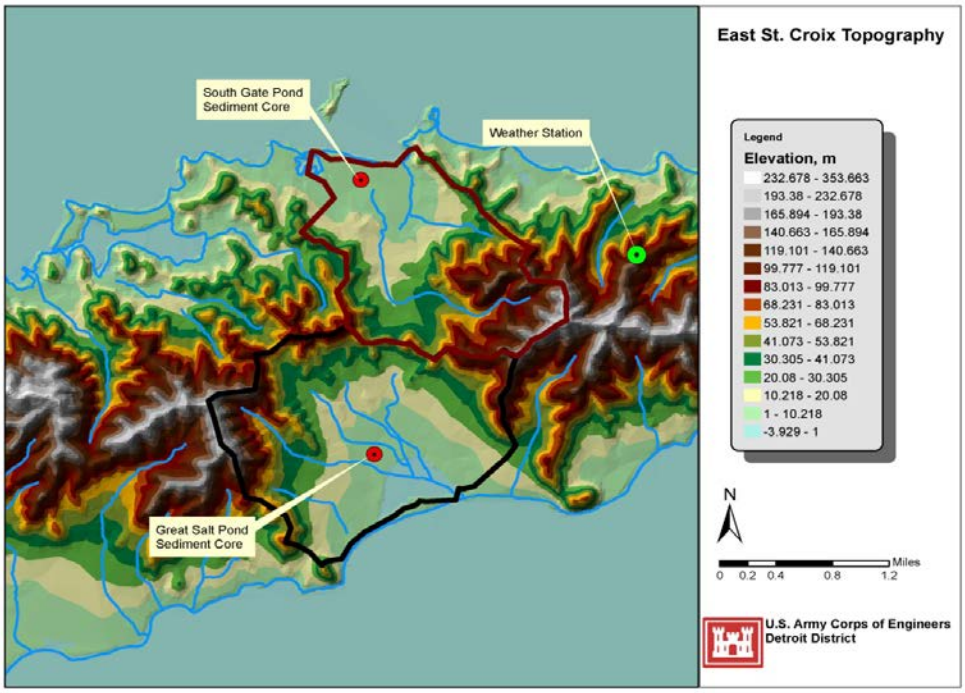

Figure 2 Eastern St. Croix Topography

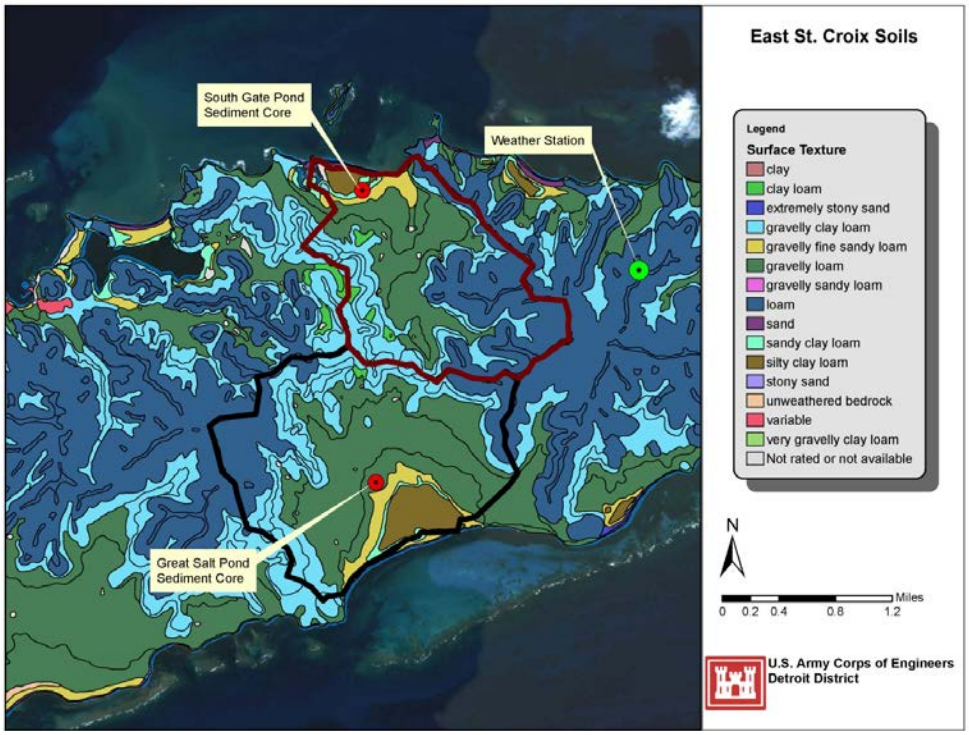

Figure 3 Eastern St. Croix Soils

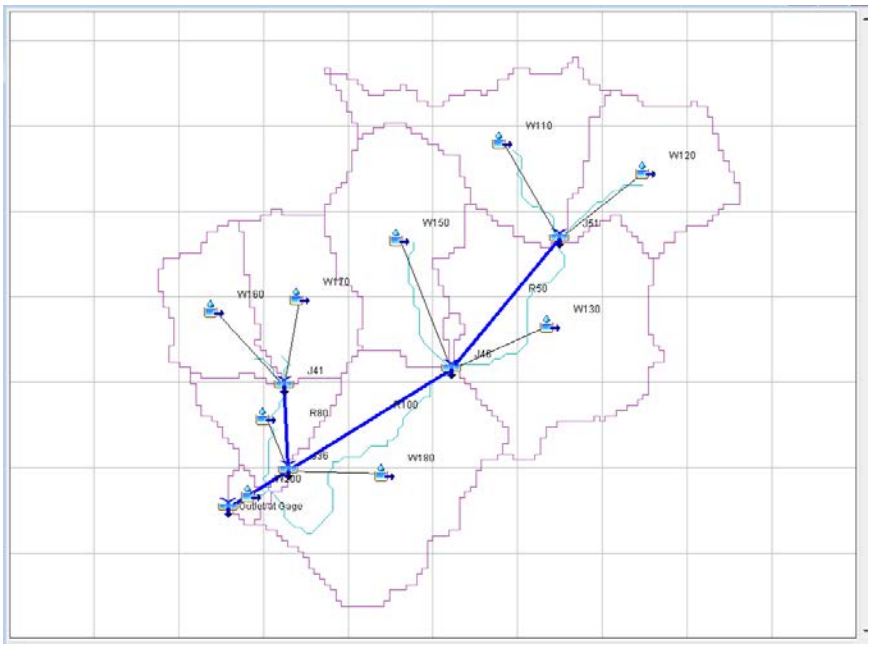

Figure 4 HEC-HMS Model Schematic for Jolly Hill (USGS Gage 50345000)

The year 2001 was selected for calibration of the Jolly Hill model. This year had extreme, moderate, and small events, as well as a complete flow and precipitation record. Figure 5 shows the output of the calibrated hydrology model for this basin.

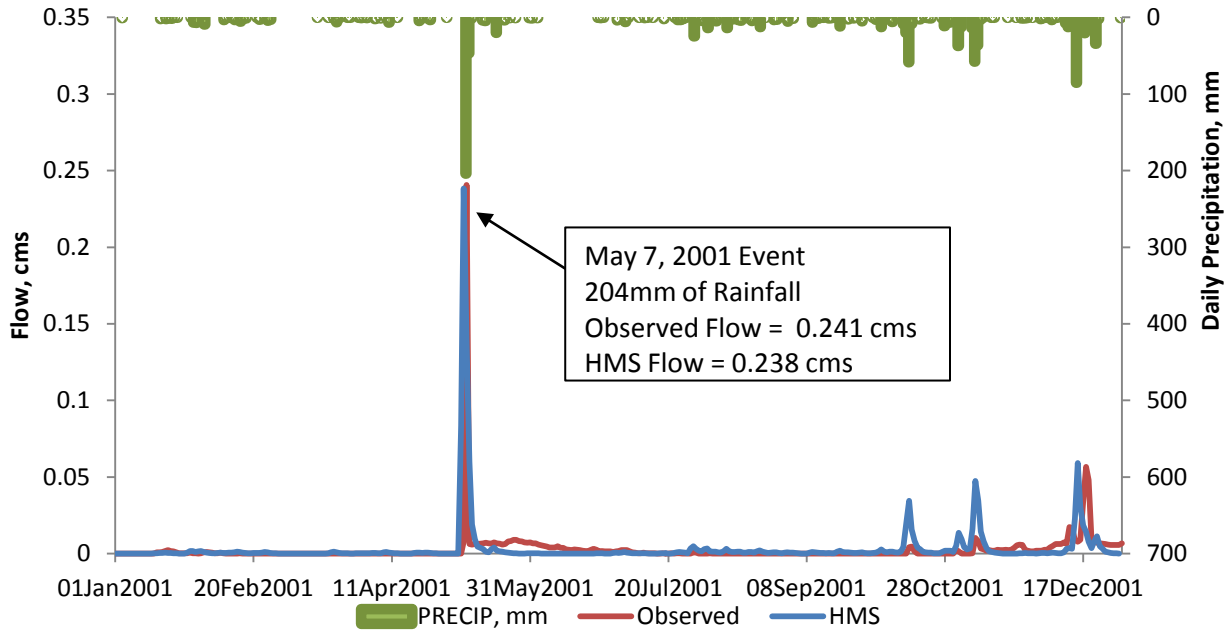

Figure 5 Calibrated Hydrology Model of Jolly Hill Watershed (USGS Gage 50345000)

The calibrated hydrologic parameters from Jolly Hill were then used in the development of sediment yield models in an Alpha version of HEC-HMS 4.0. The Great Salt Pond and South Gate Pond watersheds were both modeled for hydrology and sediment yield/delivery dynamics. The calibration parameters for the hydrology of the Jolly Hill watershed were used due to its proximity and similarity of the topography, geology, and soil types. The HEC-HMS model layouts for Great Salt Pond and South Gate Pond are shown in Figures 6 and 7, respectively.

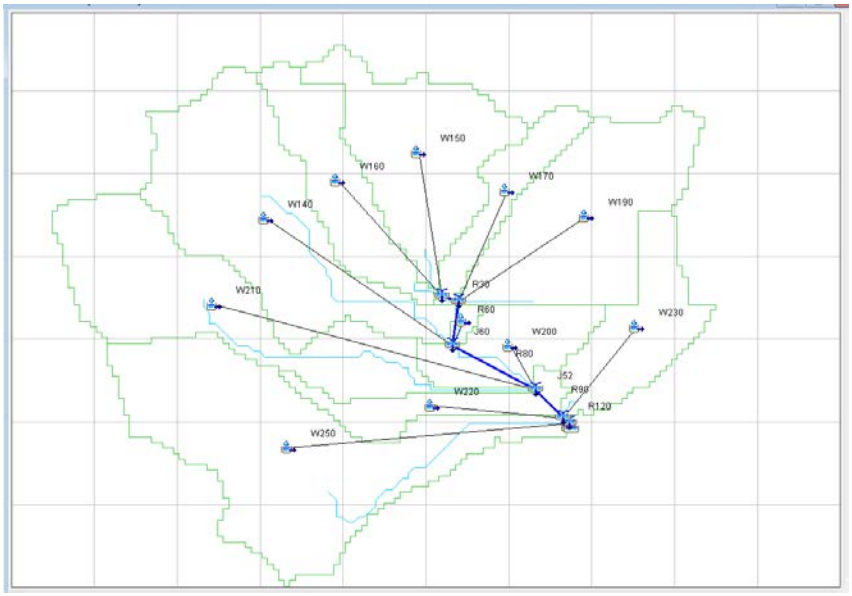

Figure 6 HMS Model Schematic for the Great Salt Pond Watershed

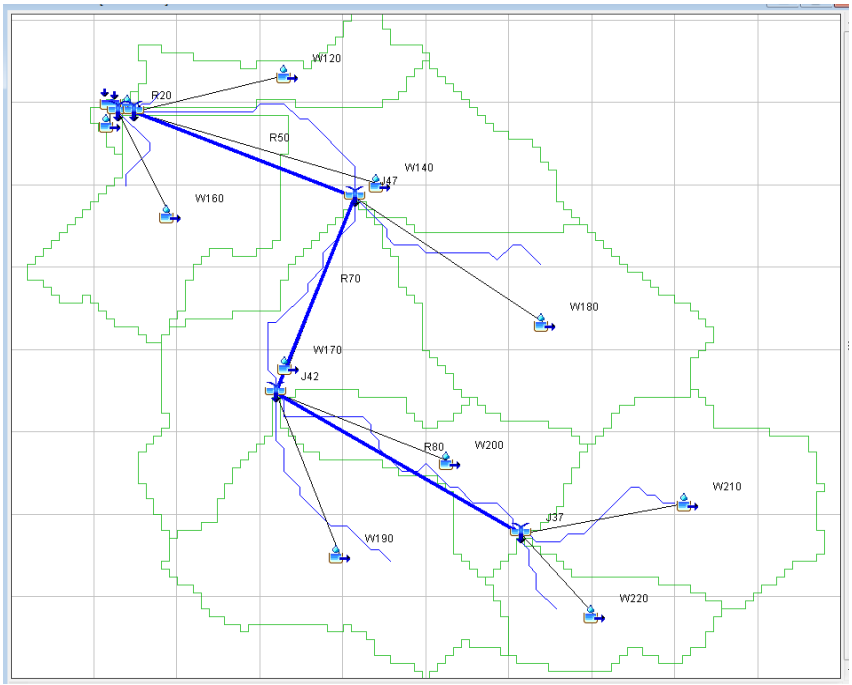

Figure 7 HMS Model Schematic for the South Gate Pond Watershed

The sediment calibration was based on long-term sediment accumulation rates obtained from the sediment cores collected in each lagoon. The physical variables associated with the annual sediment delivery to each lagoon are summarized in Table 1, below.

Table 1 Sediment Calibration Data

	Great Salt Pond	South Gate Pond
Lagoon Area	275,000 m^2	131,000 m^2
Annual Vertical Sediment Accumulation Rate (from Cores)	0.33 cm/yr	0.38 cm/yr
Annual Sediment Accumulation (Volume)	907 m^3/yr	498 m^3/yr
Porosity of Sediment (Assumed)	0.53	0.53
Calculated Annual Sediment Yield	1,274 tonnes/yr	699 tonnes/yr

The Great Salt Pond and South Gate Pond HEC-HMS model were divided into 17 annual models from 1986-2005. Calendar years 1989, 1990, and 1994 were excluded from the modeling effort due to insufficient precipitation data. Several other years also had a few days of missing data, although they were not excluded from the modeling. All missing precipitation data were assumed to be 0 mm. The annual sediment yields from the HEC-HMS model are summarized in Table 2.

The average modeled sediment delivery to Great Salt Pond over the 17 selected years was 1,385 tonnes per year. This closely approximates the sediment delivery calculated from the cores of 1,274 tonnes per year. The modeled sediment delivery to South Gate Pond of 542 tonnes per year was comparable to the 699 tonnes per year estimate based on the sediment cores. The sediment yield models for both watersheds were determined to be calibrated based on these results.

Four modern hurricanes were specifically identified as likely signatures in the sediment core record:

1. Hurricane Marilyn – September 14-15, 1995
2. Hurricane Georges – September 19-23, 1998
3. Hurricane Mitch – October 22-23, 1998
4. Hurricane Lenny – November 17, 1999

Upon investigation of the available data for each of these storms, only Hurricane Lenny, Georges, and Mitch were modeled. During Hurricane Marilyn the precipitation gage appears to have malfunctioned and the record does not contain any precipitation. This also leads to an underestimation of the sediment yield associated with the year 1995 in Table 2.

Table 2 Sediment Delivery to Great Salt Pond based on HEC-HMS Sediment Model

Year	Christiansted Precipitation, mm	Great Salt Pond Sediment Yield, tonnes	South Gate Pond Sediment Yield, tonnes
1986	919.7	1,361	530
1987	1,280.8	1,643	638
1988	1,151.3	1,032	411
1989		*Insufficient Precip Data*	*Insufficient Precip Data*
1990		*Insufficient Precip Data*	*Insufficient Precip Data*
1991	625.8	618	237
1992	957.5	1,443	563
1993	937.6	1,042	407
1994		*Insufficient Precip Data*	*Insufficient Precip Data*
1995	860.3	1,462	568
1996	1,353.2	2,782	1108
1997	809.6	1,089	422
1998	1,080.7	1,363	534
1999	1,029.7	1,568	615
2000	773.8	937	367
2001	1,068.5	1,905	747
2002	550.3	489	191
2003	1,428.2	2,283	895
2004	989.5	1,375	531
2005	897.3	1,150	447
Average	**983.2**	**1,385**	**542**

RESULTS

The HEC-HMS models were run separately for each of the three selected hurricanes: Lenny, Georges, and Mitch. The sediment yields resulting from these events, as well as the annual sediment yield for the corresponding year of the calibration runs, are shown in Tables 3 and 4.

Table 3 Sediment Modeling Results for Great Salt Lagoon for Selected Hurricanes

Hurricane	Year	Annual Sediment Yield, tons	Hurricane Precipitation, mm	Hurricane Sediment Yield, tons	Percent of Total Annual Sediment Yield
Georges	1998	1,363	100.1	209	15.3%
Mitch	1998	1,363	158.8	499	36.6%
Lenny	1999	1,568	186.9	667	43.0%

Table 4 Sediment Modeling Results for South Gate for Selected Hurricanes

Hurricane	Year	Annual Sediment Yield, tons	Hurricane Precipitation, mm	Hurricane Sediment Yield, tons	Percent of Total Annual Sediment Yield
Georges	1998	534	100.1	82.2	15.4%
Mitch	1998	534	158.8	195.3	36.6%
Lenny	1999	615	186.9	264	43.0%

Since Hurricanes Georges and Mitch occurred approximately one month apart, it is likely difficult to isolate these as two separate events in the sediment record of the cores. Instead, these combined storms may be viewed as yielding 51.9% of the total sediment in calendar year 1998 for both ponds. Figures 8 and 9 show the continuous sediment yield record from the HEC-HMS model for calendar years 1998 and 1999, respectively for the Great Salt Pond. Figures 10 and 11 show the continuous sediment yield record for the South Gate Pond for years 1998 and 1999, respectively.

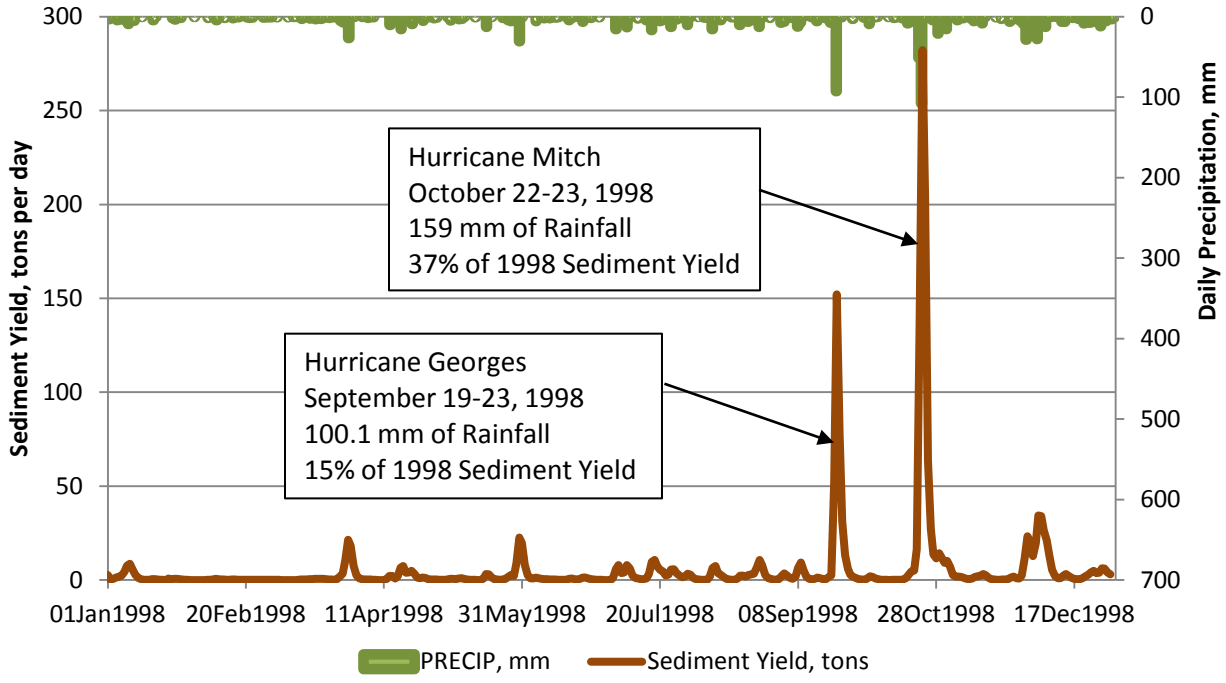

Figure 8 Great Salt Pond- Calibrated HMS Sediment Yield (1998)

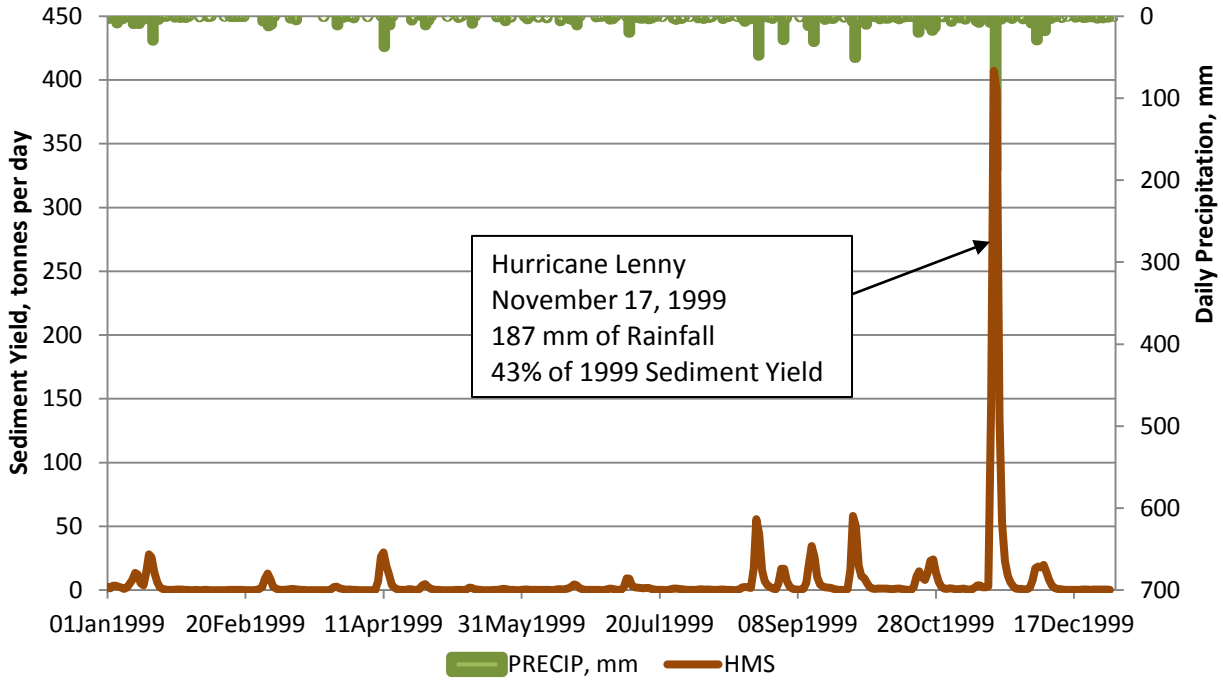

Figure 9 Great Salt Pond- Calibrated HMS Sediment Yield (1999)

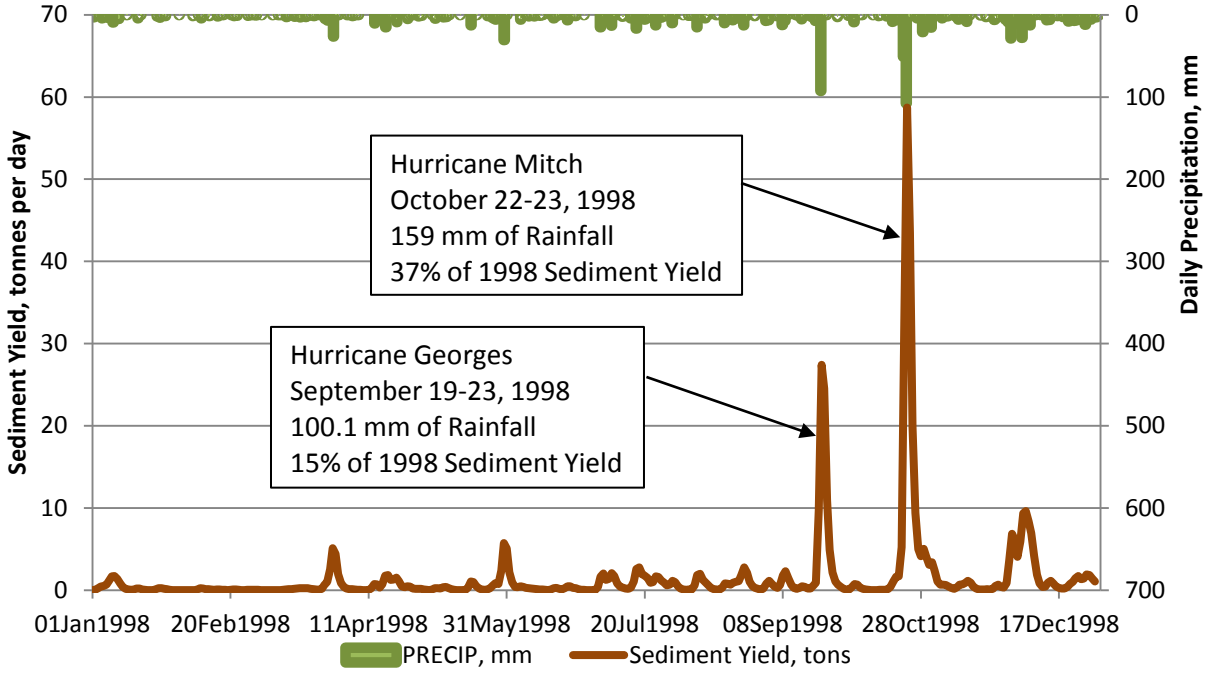

Figure 10 South Gate Pond- Calibrated HMS Sediment Yield (1998)

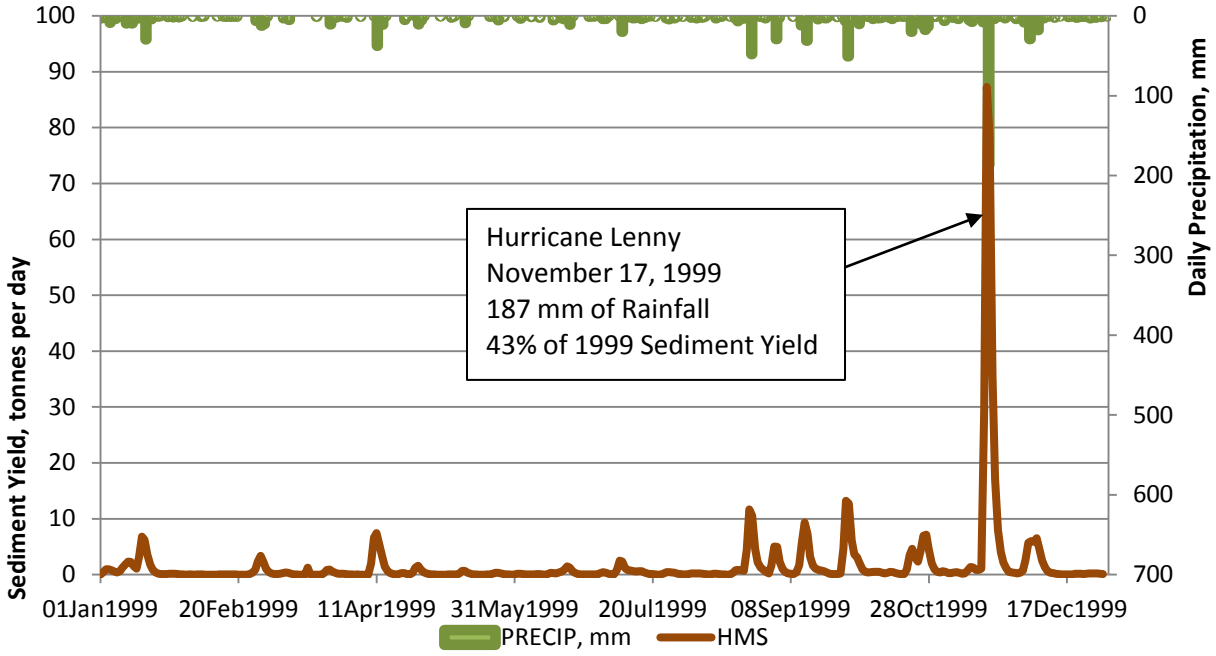

Figure 11 South Gate Pond - Calibrated HMS Sediment Yield (1999)

It should be noted that years with high sediment loads did not necessarily have hurricanes passing directly over the island. In 1996, for instance, Hurricane Hortense did not pass directly over the island but the rainfall generated by the storm still produced a significant portion of the sediment for that year. In 2001, however, a storm in May resulted in a large sediment load. Roughly a third of the modeled years with above average sediment were not the result of hurricanes.

In the sediment yield/sediment routing model, an assumed gradation was provided. The gradation included silts, sands, and gravels. Figure 12 shows the output of the cumulative sediment deposition in the Great Salt Pond by grain class.

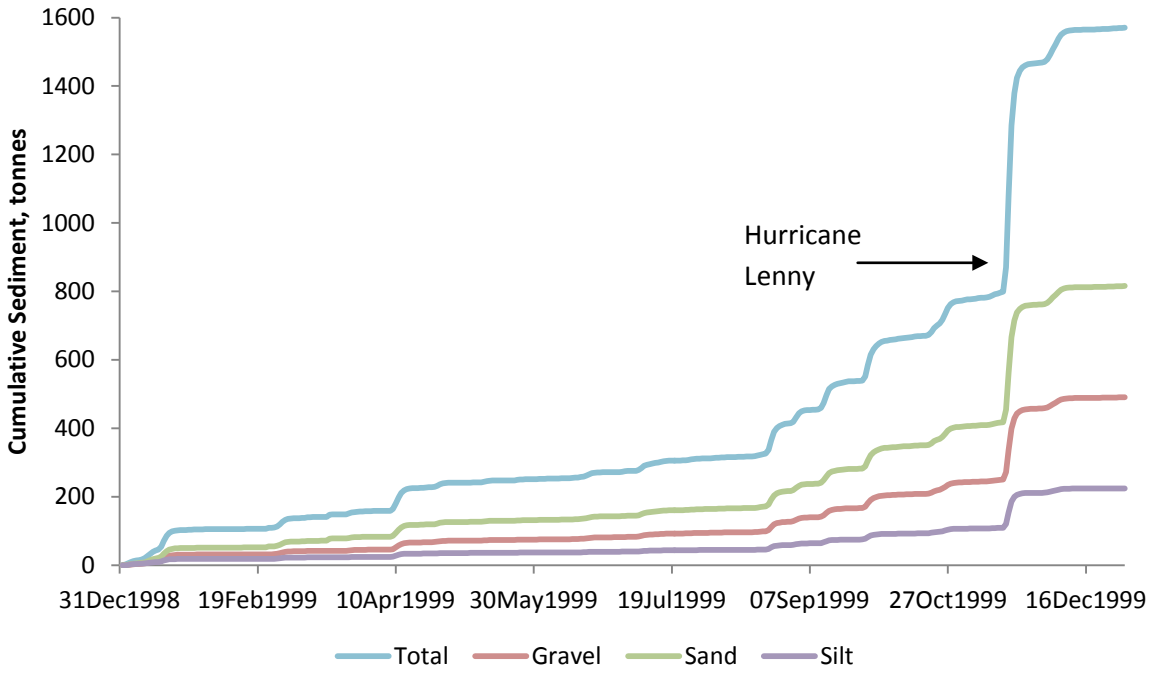

Figure 12 Cumulative Sediment Yield in Great Salt Pond Watershed by Grain Size for the 1999 Hurricane Season

Figure 13 shows the output of the cumulative sediment deposition in the South Gate Pond by grain class. Based on the model, there is approximately an equivalent amount of sediment load for the sand, silt, and gravel grain sizes, although there is slightly more sand (approximately 40% sand, 31% silt, and 29% gravel). This is a finer gradation than the Great Salt Pond, even though the same assumed gradation was supplied to the model for the channel bed and parent material in the watershed. This observation (finer sediment in the South Gate Pond) is consistent with observations of the sediment cores at the two lagoons.

Figures 12 and 13 both show the dramatic increase in sediment due to the impact of a hurricane on St. Croix. These sharp changes in sedimentation should be visible in cores taken from the lagoons.

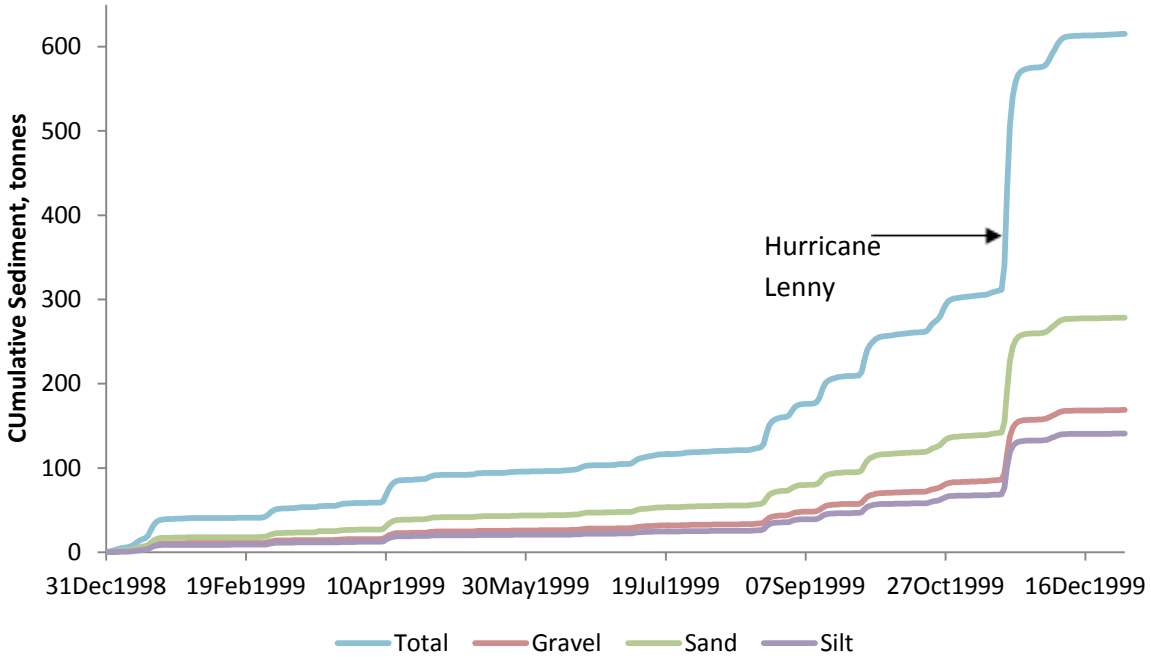

Figure 13 Cumulative Sediment Yield in South Gate Pond Watershed by Grain Size for the 1999 Hurricane Season

CONCLUSIONS

The modeling for the St. Croix watersheds yielded calibrated results for both flow and annual sediment yields in Great Salt Pond and South Gate Pond. It was found from the three hurricanes modeled that the sediment yields associated with a single named storm can contribute almost 50% of the annual sediment yield in that year. In these cases, sediment signatures associated with individual hurricane events may be extracted from sediment cores. Of the sediment that is delivered to the Lagoons, the majority (approximately half) is classified as sand, although the uncertainty associated with this conclusion is relatively high due to lack of sediment gradation data in the stream and in the watershed. The calibrated hydrology and sediment yield model can now be used to answer specific sediment loading questions from other design storms, output from climate change models, or other historic hurricane events. This modeling study demonstrates that the presence of sizeable, distinct layers in cores extracted from Great Salt Pond and South Gate Pond may be good indicators of hurricanes impacting St. Croix.

Extending WEPP Technology to Predict Fine Sediment and Phosphorus Delivery from Forested Hillslopes

William Elliot, Research Engineer, USDA Forest Service, Moscow, Idaho, welliot@fs.fed.us
Erin Brooks, Research Support Scientist, Dept. of Biological and Agricultural Engineering, University of Idaho, Moscow, Idaho, ebrooks@uidaho.edu
Drea Em Traeumer, Hydrologist, Nez Perce-ClearwaterNational Forest, USDA Forest Service, Kooskia, Idaho, atraeumer@fs.fed.us
Mariana Dobre, Post Doc. Fellow, Dept. of Biological and Agricultural Engineering, University of Idaho, Moscow, Idaho, mdobre@uidaho.edu

Abstract: In many watersheds, including the Great Lakes and Lake Tahoe Basins, two basins where the land cover is dominated by forests, the pollutants of concern are fine sediments and phosphorus. Forest runoff is generally low in nitrogen, and coarse sediment does not adversely impact the quality of lake waters. Predictive tools are needed to estimate not simply sediment, but fine sediment ($\leq$10 μm) and phosphorus delivery from forested hillslopes. We have been developing methods for making such predictions with the Water Erosion Prediction Project (WEPP) model. WEPP is a physically-based hydrology and erosion model that runs on a daily time step, with sub-daily runoff, erosion and sediment delivery predictions. The fine sediment delivery for forested hillslopes is relatively easy to estimate because WEPP provides a breakdown of primary particles (clay, silt and sand) and aggregates (silt size aggregates (30 μm) and sand size aggregates (300 μm)). The size distribution of eroded sediment is disaggregated to determine the amount of fine sediment below a user-specified size in each of the particle classes. Phosphorus transport is complex, as research has shown that in steeper forested watersheds, the dominant hydrologic flow paths are lateral flow and base flow. Surface runoff and sediment delivery are generally minimal unless the site has been disturbed by logging or fire, or the soil layer is thin (shallow to impermeable bedrock). Thus, in an undisturbed forest, the main phosphorus pathway will likely be in subsurface lateral flow as soluble reactive phosphorus (*SRP*), whereas in a disturbed forest, the dominant pathway may be in surface runoff as *SRP*, or as particulate phosphorus adsorbed to eroded sediment. Prediction is further complicated as research has shown that the *SRP* concentration in the soil water may be higher in undisturbed forests than in burned or harvested forests. Delivered sediment also is complicated in that preferential particle size sorting may occur, increasing the content of clay and organic matter in delivered sediment and thereby increasing the phosphorus concentration in delivered sediment above that in the forest. We have developed a way to use the current predictions within the WEPP technology to estimate not only the surface runoff and sediment delivery, but also delivery of fine sediment below a user-specified threshold, and phosphorus through both surface and subsurface lateral flow pathways.

BACKGROUND

In recent years, watershed managers have been challenged to determine the role of forest watersheds in generating phosphorus. Recent examples where watersheds with a significant fraction of the area in forests have concerns about phosphorus delivery include: Lake Tahoe (EPA, 2014), the Great Lakes (EPA, 2012), Big Bear Lake, CA (EPA, 2007), and Cascade Reservoir, ID (Idaho Division of Environmental Quality, 1996). In all of these cases, watershed managers were unable to evaluate the role of forests and forest management on phosphorus

delivery from the forested parts of the watershed. Within the Lake Tahoe Basin we have received funding for three projects to develop phosphorus management tools to address these concerns. This paper focuses on the development of those tools for the Lake Tahoe Basin, but the principles can be applied to forested watersheds anywhere.

Phosphorus pathways in agricultural watersheds are associated mainly with surface runoff, detached sediments, lateral flow and tile drainage water (Sharpley et al., 1994). The dominant pathway in most cases is associated with detached sediments, while phosphorus dissolved in surface runoff and tile drainage are usually lesser important. Agricultural phosphorus delivery models have tended to focus on how management practices such as manure spreading, application of chemical fertilizers and minimum tillage affect the availability of soluble reactive phosphorus (*SRP*) for runoff, and the concentration of phosphorus adsorbed to soil aggregates and particles (particulate phosphorus, *PP*) (Sharpley et al., 1994). The concentrations of phosphorus in eroded sediments, surface runoff, and drain tile flows are then used in runoff and erosion models to predict phosphorus delivery (Withers and Jarvie, 2008).

In forested watersheds, surface runoff and erosion are frequently minimal, and generally are associated with wildfire. In the absence of wildfire, the dominant flow paths for water entering streams are either subsurface lateral flow or base flow (Elliot, 2013; Srivistava et al., 2013). Phosphorus concentrations in forest soils are usually much lower than in agricultural settings. Recent research has found that the concentration of *SRP* in the upper layers of soil water that are the source of shallow lateral flow are much greater than is measured in surface runoff (Miller et al., 2005). These observations suggest that a phosphorus delivery model is needed for forest watersheds that can include the current surface runoff and sediment delivery vectors, as well as delivery from shallow subsurface lateral flow.

In order to develop a model that can predict phosphorus delivery with lateral flow, a hydrologic model that includes shallow lateral flow as well as surface runoff and sediment delivery is needed. The Water Erosion Prediction Project (WEPP) model has such a capability (Dun et al., 2009; Srivistava et al., 2013). WEPP is a physically-based distributed hydrology and erosion model, and it uses a daily time step to predict evapotranspiration, plant growth, residue accumulation and decomposition, deep seepage, and shallow lateral flow. Whenever there is a runoff event from precipitation and/or snowmelt, WEPP predicts infiltration, runoff, sediment detachment and delivery (Flanagan and Nearing, 1995). WEPP has both a hillslope version and a watershed version. In recent years, the predicted deep seepage has been used to estimate groundwater base flow (Elliot et al., 2010, Srivastava et al., 2013), further increasing the model's hydrologic capabilities.

In addition to phosphorus, stakeholders in the Lake Tahoe Basin also are concerned about fine sediment delivery (Coats, 2004). In this context, "fine sediment" is generally considered to be sediment particles and aggregates less than 10 - 20 μm in diameter. Such particles can remain suspended in lakes for a considerable period of time as vertical currents due to surface wind shear and temperature gradients are sufficient to prevent the particles from settling (Coats, 2004). It is these small particles combined with increased algal growth due to phosphorus enrichment that have caused the lake to lose some of its clarity in recent decades.

This paper describes research and development activities that are ongoing to develop phosphorus and fine sediment prediction capabilities from forested watersheds using the WEPP model.

THE WEPP MODEL

The WEPP model was originally developed to predict surface runoff, upland erosion and sediment delivery from agricultural, forest and rangeland hillslopes and small watersheds (Laflen et al., 1997. Inputs for the model include daily climate, soil, topographic, and management or vegetation information. Within the model, WEPP completes a water balance at the end of every day by considering infiltration, runoff, deep seepage, subsurface lateral flow, evapotranspiration, and soil depth and horizon properties. Surface runoff is estimated on a sub-daily time step using an input hyetograph based on the daily precipitation depth, duration, and peak intensity and the soil water content, using a Green and Ampt Mein Larson infiltration algorithm (Flanagan and Nearing, 1995; Dun et al., 2009). The deep seepage is estimated when the soil exceeds field capacity for multiple soil layers, if desired, using Darcy's law. Evapotranspiration is estimated using either a Penman method or Ritchie's model. The lateral flow is estimated for layers that exceed field capacity using Darcy's law for unsaturated conditions as downslope conditions may not be saturated (Dun et al., 2009; Boll et al., 2015). Duration of surface runoff is dependent on storm duration and surface roughness (Flanagan and Nearing, 1995) and lateral flow duration is assumed to be 24 h on days when lateral flow is estimated. If requested by the user, WEPP generates a daily "water" file that contains modeled precipitation and snow melt, surface runoff, lateral flow, deep seepage, and soil water content (Flanagan and Livingston, 1995).

Table 1 shows part of the water file for the Tahoe City, CA climate for Julian days 70-78 (March 11-19). On day 70, precipitation (*P*) was all rain, with no snowmelt; on day 71 rainfall combined with melting snow, and days 77 and 78 were snowmelt only days. Daily runoff (*Q*) occurred only on day 78, while lateral flow occurred every day. The soil exceeded field capacity on day 72 so that deep percolation (*Dp*) began. During these 9 days, the total precipitation was 32 mm, total surface runoff was 15 mm, lateral flow was 19 mm, deep percolation was 0.1 mm, the soil water

Table 1 Example of information in the WEPP water output file. The climate is for Tahoe City, CA.

Day	*P*	*RM*	*Q*	*Ep*	*Es*	*Dp*	*latqcc*	*Total-Soil*	*frozwt*	*SWE*
	mm	mm	mm	mm	mm	mm	mm	*Water*(mm)	mm	mm
70	8.4	8.4	0.00	0	2.05	0	0.28	129.73	0	258.79
71	2	42.68	0.00	0	3.09	0	0.88	168.43	0	218.12
72	0.3	17.74	0.00	0	3.2	0.01	1.89	181.08	0	200.67
73	6.9	30.09	0.00	0	2.35	0.02	2.77	206.03	0	177.49
74	13.7	4.57	0.00	0	2.08	0.02	2.77	205.69	0.04	186.62
75	0.3	0	0.00	0	1.27	0.02	2.54	201.89	0	186.92
76	0	0	0.00	0	3.52	0.02	2.26	196.09	0	186.92
77	0	11.48	0.00	0	1.73	0.02	2.77	203.06	0	175.44
78	0	22.69	14.73	0	1.12	0.02	2.77	207.11	0	152.75

Day=julian day; P= precipitation; RM=rainfall +snowmelt; Q=daily runoff; Ep=plant transpiration; Es=soil evaporation; Dp=deep percolation; latqcc=lateral subsurface flow; Total-Soil Water=unfrozen water in soil profile; frozwt=frozen water in soil profile; SWE=snow water equivalent on the surface

content increased by 77.38 mm and the snow water equivalent on the surface decreased by 106 mm. Development is ongoing to add the deep seepage to a temporary groundwater reservoir, and from that to use a linear reservoir model to predict base flow from a sub-watershed as a fraction of the volume of that reservoir (Elliot et al., 2010; Srivastava et al., 2013).

WEPP predicts delivered sediment in five classes: primary clay, silt and sand particles, small aggregates made up of clay, silt and organic matter, and larger aggregates consisting of all three primary particles and organic matter. The sediment size classes and properties are summarized in Table 2 for a coarse sandy loam soil that is widespread in the Lake Tahoe Basin. The fraction of sediment in each size class delivered from a hillslope or a watershed is presented by WEPP. In addition, WEPP calculates a specific surface enrichment ratio (*SSR*), which is the ratio of the sediment surface area in the clay and organic matter fraction in the delivered sediment divided by this value for the soil on the hillslope. This ratio was intended to be used to assist water quality modelers in determining the increase in concentration of a pollutant in the delivered sediment compared to the sediment on the hillslope (Sharpley et al., 1994). For example, if the phosphorus content in the soil was 500 mg kg^{-1} and the enrichment ratio was 2.2, the concentration of phosphorus in the delivered sediment would be 1100 mg kg^{-1}.

THE LAKE TAHOE BASIN

Figure 1 is a map of the Lake Tahoe Basin showing the dominant geologic influences. The largest tributary is the Upper Truckee River flowing into the lake from the south. The overflow for the lake is in the northwest corner, where the Truckee River routes the overflow north, and then east toward Reno, NV. The dominant geologic processes in the basin were volcanic in the north and west, and decomposing granite in the south and east. There are also significant areas of exposed rock outcrops, particularly in the southern part of the basin. Some of the lower elevation lower gradient segments of the stream tributaries are alluvial. The lake has 63 tributaries, and the lake itself accounts for 38 percent of the total watershed area (Coats, 2004). Forests cover 57 percent of the watersheds, and shrubs 31 percent (Greenburg et al, 2006).

ESTIMATING PHOSPHORUS CONCENTRATIONS

Phosphorus delivery from a hillslope either will be adsorbed to eroded sediment (particulate phosphorus, or *PP*) or will be dissolved in surface runoff, subsurface lateral flow, or base flow (soluble reactive phosphorus, or *SRP*). Concentration of phosphorus in sediment depends on the

Table 2 For a forest sandy loam soil, properties of sediment size classes in eroded sediments estimated by the WEPP model.

Class	Mean Diameter (mm)	Specific Gravity	Particle Composition (%)			
			Sand	Silt	Clay	Organic Matter
1	0.002	2.60	0.0	0.0	100.0	250.0
2	0.010	2.65	0.0	100.0	0.0	0.0
3	0.030	1.80	0.0	80.0	20.0	50.0
4	0.300	1.60	85.4	7.1	7.5	18.8
5	0.200	2.65	100.0	0.0	0.0	0.0

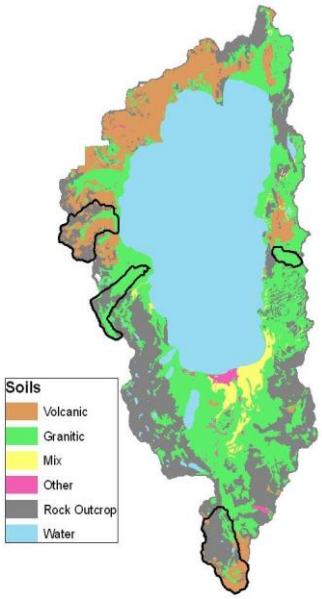

Figure 1 Major geologic categories within the Tahoe Basin.

mineralogy and particle size of the soil. Phosphorus dissolved in solution depends on the geology and the flow pathways (surface, lateral or base flow) that water follows.

For this paper, we focused on developing PP and SRP concentrations that are typical of the Lake Tahoe Basin. A similar procedure can be applied to other watersheds. Within the Lake Tahoe Basin, there is a long history of measuring total phosphorus (TP), SRP and suspended sediment concentration (SSC) in streams discharging to the lake. The number of water quality samples collected from the 13 major streams that flow into Lake Tahoe between 1989 and 2003 range from 129 samples collected from Trout Creek to 1414 at Incline Creek (Figure 2). The largest stream, the Upper Truckee, was sampled at multiple points within the watershed, and Incline Creek has two sample sites within its watershed (Figure 2) whereas the other streams were only sampled near their outlets. The analyses are available from the USGS (http://waterdata.usgs.gov/nwis/rt). Using observed TP (mg L^{-1}), SRP (mg L^{-1}) and SSC (mg L^{-1}) concentrations we calculated the Concentration of phosphorus sorbed to the suspended sediment (mg kg^{-1}) using equation 1.

$$\text{Concentration} = \frac{\text{TP}-\text{SRP}}{\text{SSC}} 10^6 \qquad (1)$$

As seen in Figure 2, the median Concentration from each of the major stream in the Lake Tahoe Basin have a distinct regional pattern with Concentrations ranging from 1000 mg kg^{-1} in the wetter, western streams in the basin to ~1500 mg kg^{-1} delivered from the northern streams, to 1850 mg kg^{-1} from the high elevation streams in the southern setcion of the basin. These regional trends are likely associated with the underlying geology and the characteristics of the delivered sediment.

In order to capture seasonal trends in SRP delivered from Lake Tahoe streams, we applied a USGS model, LOADEST (Runkel et al., 2004), to the observed SRP data. The LOADEST model transforms point data into continuous time series of P loading and concentration as a function of stream flow and time using regression techniques. As seen in Figure 3, the SRP concentrations in Lake Tahoe streams vary seasonally with the highest concentrations (~0.022 mg L^{-1}) during low flow conditions in the fall and lowest concentrations (~0.015 mg L^{-1}) in the late spring during snowmelt. The LOADEST model was able to match these monthly trends fairly well (Figure 3).

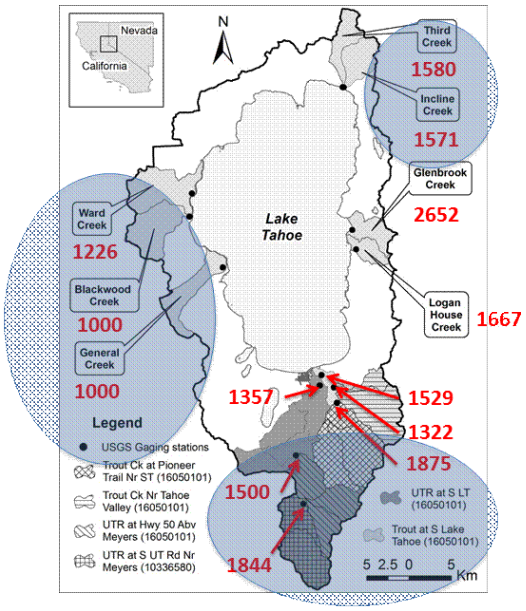

Figure 2 Concentration of phosphorus (mg kg^{-1}) adsorbed to delivered sediment from watersheds within the Lake Tahoe Basin shown in red. The concentrations tended to break down into three distinctive sets as shown by the gray circles, with the granitic soils in the Upper Truckee Basin having the larger concentrations, whereas the volcanic watersheds on the western side had lower concentrations of adsorbed *P*.

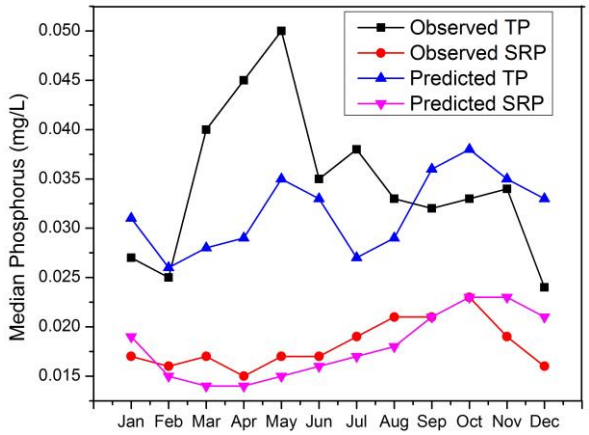

Figure 3 Observed and predicted phosphorus concentrations averaged across all years and all watersheds.

We also attempted to predict monthly TP concentrations with the LOADEST model; however the agreement was quite poor. Since the LOADEST model was not developed to use SSC as an independent variable in the regression analysis, but rather attempted to predict TP based on flow and time, it was not surprising the monthly TP concentrations simulated by LOADEST did not agree with observed patterns. This suggests that the TP concentration is largely influenced by the PP in the delivered sediment.

In addition to the sample concentrations we also generated daily hydrographs for each of the sampled streams. Figure 4 is a hydrograph for Blackwood Creek in which we have estimated the relative contribution of each of the flow paths (surface, lateral and base) using the WEPP model water file coupled to a linear groundwater flow model. Figure 4 shows that the base flow is the dominant flow path from July until snowmelt the following April, that surface runoff occurs only at times of peak flow rates, and that lateral flow is the dominant flow path during higher stream

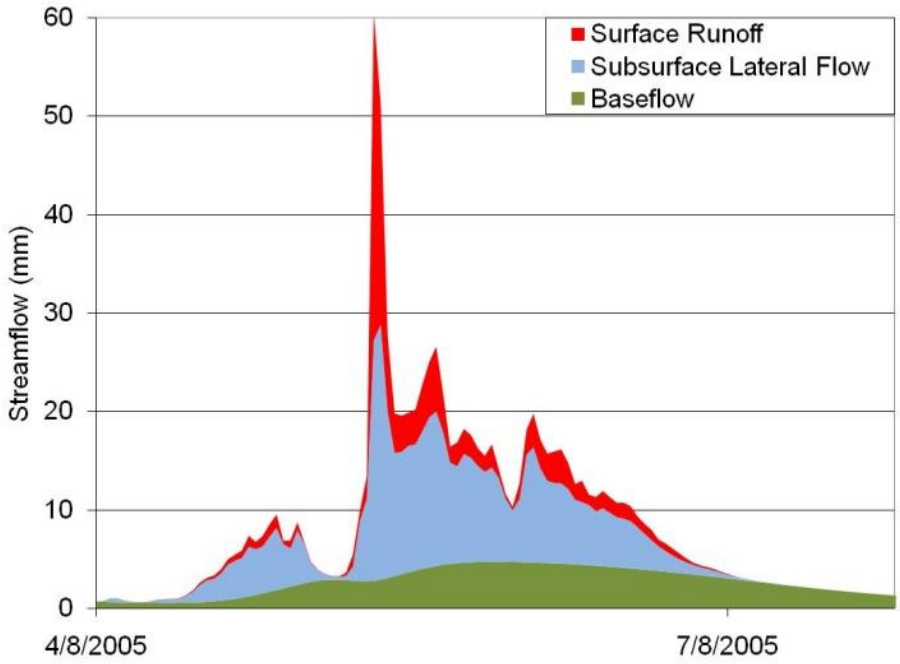

Figure 4 Example hydrograph based on WEPP hydrology for Blackwood Creek (Elliot et al., 2010).

flow rates in the late spring. Combining this information with the results shown in Figure 3, it is apparent that the SRP in surface runoff is likely less than 0.01 mg L^{-1}, whereas SRP concentrations in lateral flow and base flow are likely to be around 0.02 mg L^{-1}. Concentrations are the lowest during March and April when surface runoff is contributing to runoff and diluting lateral and base flow, but higher from June onward when lateral flow and base flow are the main sources of water in the stream system. Total phosphorus delivered, however, is likely to be the highest during the peak flow times associated with snow melt in April and May, which coincides with the greatest sediment transport as well.

ESTIMATING FINE SEDIMENT DELIVERY

The distribution of particle size delivery from hillslopes or watersheds given in the WEPP model output file can be parsed to determine the amount of each textural fraction in each particle size category by summing the delivery of a given size primary particle with the fraction of that particle contained in the aggregates. In WEPP, clay primary particles are ≤ 4 μm diameter, and silt particles are 4 - 62.5 μm diameter. To simplify modeling, we assumed that within the silt textural category the distribution of particle sizes was linear. Thus if the user needed to know the amount of sediment ≤ 10 μm, the number could be determined by adding all of the clay fraction as primary particles and in aggregates to the (10-4)/(62.5-4) fraction of the silt delivered as primary particles and in aggregates.

INTERFACES

In order to make this technology useful to managers, an interface was developed similar to the Forest Service Disturbed WEPP online interface for the WEPP model (Elliot, 2004). Figure 5

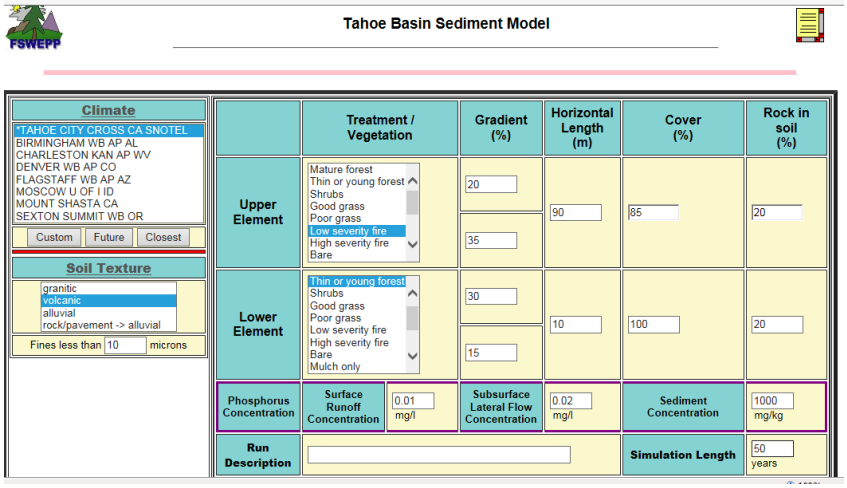

Figure 5a Input screen for the Tahoe Basin Sediment Model using a SNOTEL station from within the Lake Tahoe Basin for the weather and phosphorus concentrations from Figures 2 and 3.

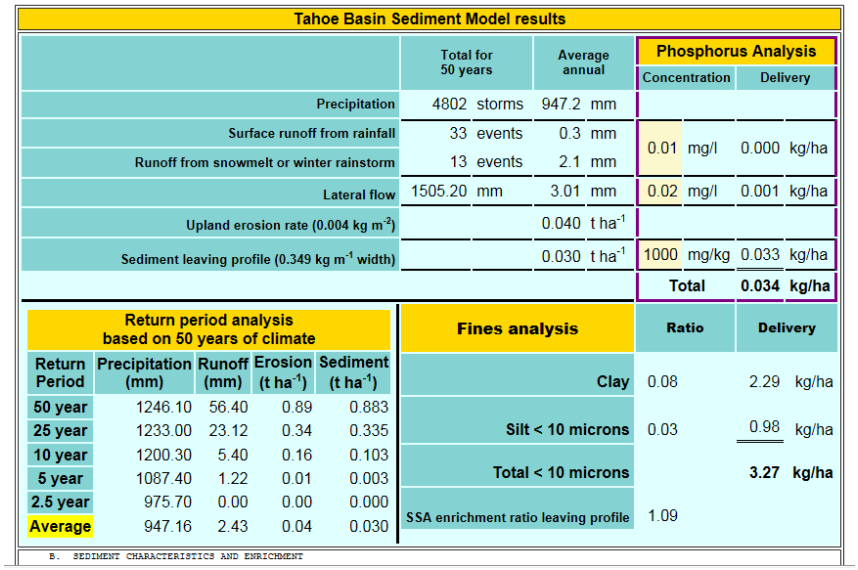

Figure 5b Output screen for the Tahoe Basin Sediment Model.

shows the input and output screens for the Tahoe Basin Sediment Model (TBSM, http://forest.moscowfsl.wsu.edu/fswepp). The user is asked to select a climate, dominant geology, vegetation conditions for the upper or treated part of a hill, and lower or stream side buffer part of the hill. In the case of an undisturbed condition, or a post-wildfire condition, the upper and lower portions of the hill may have the same vegetation.

The climate database for the TBSM includes one NOAA station within the Lake Tahoe Basin as well as five nearby weather stations. In addition, climate statistics have been added to the database for seven NRCS Snow Telemetry (SNOTEL) stations located within the Basin. Another feature unique to the TBSM interface is that future climate scenarios are available for the seven SNOTEL stations and the one NOAA station within the Basin.

The user is asked to provide the phosphorus concentrations in the surface runoff, lateral flow, and sediment. Earlier versions of the interface were designed for the user to enter the phosphorus concentration in the soil, and the model would then adjust this value using the specific surface enrichment ratio from the WEPP output. We found, however, that it was easier to obtain the concentration of total and soluble reactive phosphorus from in-stream monitoring rather than

concentrations of phosphorus in the soils themselves, so the current interface is designed to use the concentrations shown in Figure 2 based on in-stream data. The interface could be altered for other applications where on-site particulate phosphorus concentrations are readily available and be designed to use delivered sediment with a delivery ratio as previously discussed.

Figure 5b shows the output screen for the TBSM. Each phosphorus path (sediment, surface runoff and lateral flow) is presented so that users will be able to determine the dominant pathway for the condition they are modeling. In the example shown in Figure 5b for a prescribed burn with a buffer, the greatest source of phosphorus is in the delivered sediment. This is often the case in disturbed forests (Stednick, 2010). In undisturbed forests, the greatest source of SRP is likely to be in the shallow subsurface lateral flow (Miller et al., 2005).

The fine sediment category between 4–62.5 μm is specified on the input page (Figure 5a) and the total delivery per unit area is calculated from the predicted sediment delivery, and presented on the output page.

DISCUSSION

This approach to modeling phosphorus and fine sediment delivery was developed for the Lake Tahoe Basin. The principles that are described here for estimating delivery of phosphorus can be applied to any condition where the input variables are known. For conditions where P concentrations are not known, sampling of a streams may be necessary to estimate the PP and SRP concentrations and their variability to apply this tool. The Tahoe Basin Sediment Model (TBSM) interface assumes a particulate phosphorus (PP) concentration attached to stream sediment. In other conditions, it may be more appropriate to link the PP concentration to the onsite concentration, and apply a specific surface enrichment ratio to the delivered sediment. With this interface, using the large PP concentrations in stream sediments (1000 – 2500 mg/kg), we may be over-predicting the delivery of PP to the stream. Elliot et al. (2012) reported onsite concentrations of 4–22 mg/kg and concentrations on coarse sediments collected from rainfall simulation of 160–475 mg/kg. The increasing concentrations of PP from soil to upland eroded sediments to stream sediments is due to the specific surface enrichment, and further work on the interface may be necessary to make sure the high instream concentrations are linked to the delivery of clay-size material. In the Tahoe basin, clay generally accounts for around 2 percent of the soil fraction.

An interesting hydrologic feature of coarse forest soils is that unless the soils are highly disturbed, there is little surface runoff. Comparing the hydrograph in Figure 4 to the SRP concentration variability in Figure 3 suggests that when surface runoff does occur, SRP concentrations are low, but when lateral flow or subsurface flow dominate the runoff, SRP concentrations increase. The net effect of integrating the runoff and concentration values in these two figures suggests that total SRP delivery is the greatest when runoff is the greatest. It also suggests an interesting twist to managers: if managers seek to minimize surface runoff, subsurface lateral flow is likely to increase (Srivastava, 2013), and so will the concentration of SRP leaving the hillslope. Surface runoff itself will deliver less SRP, but it will also be the mechanism that delivers sediment, so that PP will likely dominate the total phosphorus (TP) budget when there is surface runoff.

The TBSM does not consider channel processes. In steep forest watersheds, stream channels and banks tend to be coarse, minimally adsorbing or desorbing TP. Forests with finer textured or higher organic materials in stream beds or banks are more likely to influence TP delivery, adding to SRP during times of low stream SRP concentration and reducing SRP during times of high concentration (Withers and Jarvie, 2008).

The interface clearly shows the link between sediment delivery and TP delivery. Past watershed research has shown that sediment budgets from forest watersheds are dominated by wildfire, with sediment delivery following wildfire being as much as 100 times greater than that associated with undisturbed forests (Elliot, 2013). Such sediment pulses will likely dominate delivery of phosphorus in the same way as they dominate the sediment budget. Managers need to consider the effects of forest practices not only on immediate phosphorus delivery, but also on the effects that forest practices may have on phosphorus delivery following wildfire (Elliot, 2013).

If applying this tool to other basins, users need to be aware of several features of this interface that were customized for the basin. The soil categories, granitic, volcanic, alluvial and rock/pavement would correspond to coarse sandy loam, sandy loam, loam and rock/pavement in other watersheds. The PP concentrations were for sediment transported by suspension through the Tahoe Basin stream system, and not necessarily the concentration of eroded sediment leaving a hillslope. Careful thought needs to be given to decide whether to use the approach described here for suspended sediment, or to use the PP concentration in the field, and apply the specific surface enrichment ratio is PP concentrations of the soil are available. In impaired watersheds, however, it is often easier to obtain TP and SSC than it is upland soil concentrations and therefore use the interface in its current form.

CONCLUSIONS

We have described an approach to using the WEPP model to aid in predicting phosphorus and fine sediment delivery from steep forested watersheds. The approach is limited to hillslope processes, and does not consider channel impacts on phosphorus delivery. The tool that was developed, however, can be useful in aiding forest managers in evaluating the effects of forest management, including wildfire, on delivery of fine sediments and phosphorus.

REFERENCES

Boll, J., Brooks, E.S., Crabtree, B., and Dun, S. (2015). "Incorporation of variable source area hydrology in WEPP", Journal of the American Water Resources Association. In Press.

Coats, R. (2004). "Nutrient and sediment transport in streams of the Lake Tahoe Basin: A 30-year retrospective" General Technical Report PSW-GTR-193. Albany, CA: USDA Forest Service, Pacific Southwest Research Station, pp 143-147.

Dun, S., Wu, J.Q., Elliot, W.J., Robichaud, P.R., Flanagan, D.C., Frankenberger, J.R., Brown, R.E., and Xu, A.D. (2009). "Adapting the Water Erosion Prediction Project (WEPP) model for forest applications," Journal of Hydrology, 336(1-4) pp 45-54.

Elliot, W.J. (2004) "WEPP Internet interfaces for forest erosion prediction," Journal of the American Water Resources Association, 40, pp 299–309.

Elliot, W.J. (2013). "Erosion processes and prediction with WEPP technology in forests in the Northwestern U.S.," Transactions of the American Society of Agricultural and Biological Engineers, 56(2), pp 563-579.

Elliot, W., Brooks, E., Link, T., and Miller, S. (2010). "Incorporating groundwater flow into the WEPP model," Proceedings of the 2nd Joint Federal Interagency Conference, 17 June – 1 July, Las Vegas, Nevada. 12 p.

Elliot, W., Brooks, E., Traeumer, D., and Bruner, E. (2012). "Predicting phosphorus from forested areas in the Tahoe Basin," Conference on Environmental Restoration in a Changing Climate, Tahoe Science Conference, 22–24 May, Incline Village, Nevada.

Environmental Protection Agency (EPA). (2007). "TMDL document for Big Bear Lake nutrients (phosphorus)," Online at < http://iaspub.epa.gov/tmdl/attains_impaired_waters.tmdl_report?p_tmdl_id=33765&p_report_type= >. Accessed December 2014.

Environmental Protection Agency (EPA). (2012). "The Great Lakes today: Concerns," Online at <http://www.epa.gov/greatlakes/atlas/glat-ch4.html>. Accessed December 2014.

Environmental Protection Agency (EPA). (2014). "Watershed priorities: Lake Tahoe, California and Nevada." Online at <http://www.epa.gov/region9/water/watershed/tahoe>. Accessed December 2014.

Flanagan, D.C., and Livingston, S.J. (editors). (1995). WEPP User Summary NSERL Report No. 11. West Lafayette, Indiana: USDA Agricultural Research Service, National Soil Erosion Research Laboratory, 131 p.

Flanagan D.C., and Nearing, M.A. (1995). USDA – Water Erosion Prediction Project: Hillslope profile and watershed model documentation. NSERL Report No. 10. West Lafayette, Indiana: USDA Agricultural Research Service, National Soil Erosion Research Laboratory.

Greenberg, J.A., Dobrowski, S.Z., Ramierez, C.M., Tuil, J.L., Ustin, S.L. (2006). "A bottom-up approach to vegetation mapping of the Lake Tahoe Basin using hyperspatial image analysis", Photogrammetric Engineering & Remote Sensing 72(5), pp 581-589.

Idaho Division of Environmental Quality. (1996). Cascade Reservoir Phase 1 Watershed Management Plan Online at < http://www.epa.gov/waters/tmdldocs/Cascade%20Reservoir%20Phase%20I%20TMDL%20-%20Main%20Report.pdf >. Accessed December 2014. 97 p.

Laflen, J.M., Elliot, W.J., Flanagan, D.C., Meyer, C.R., and Nearing, M.A. (1997). "WEPP – predicting water erosion using a process-based model," Journal of Soil and Water Conservation, 52(2), pp 96-102.

Miller, W.W., Johnson, D.W., Denton, C., Verburg, P.S.J., Dana, G.L., and Walker, R.F. (2005). "Inconspicuous nutrient laden surface runoff from mature forest Sierran watersheds," Water, Air and Soil Pollution, 163, pp 3-17.

Runkel, R.L., Crawford, C.G., and Cohn, T.A. (2004). "Load Estimator (LOADEST): A FORTRAN program for estimating constituent loads in streams and rivers," Chapter A5 in U.S. Geological Survey Techniques and Methods Book 4, 69 p.

Sharpley, A.N., Chapra, S.C., Wedepohl, R., Sims, J.T., Daniel, T.C., and Reddy, K.R. (1994). "Managing agricultural phosphorus for protection of surface waters: Issues and options," Journal of Environmental Quality, 23(3), pp 437-451.

Srivastava, A. (2013). Modeling of hydrological processes in three mountainous watersheds in the U.S. Pacific Northwest. PhD Dissertation. Pullman, Washington: Washington State University. 170 p.

Srivastava, A., Dobre, M., Wu, J., Elliot, W., Bruner, E., Dun, S., Brooks, E., and Miller, I. (2013). "Modifying WEPP to improve streamflow simulation in a Pacific Northwest watershed," Transactions of the American Society of Agricultural and Biological Engineers, 56(2), pp 603-611.

Stednick, J.D. (2010.) "Effects of fuel management practices on water quality," Chapter 8 in Elliot, W.J., Miller, I.S., and Audin, L. (eds.). "Cumulative Watershed Effects of Fuel Management in the Western U.S.," General Technical Report RMRS-GTR-231. Fort Collins, Colorado: USDA Forest Service, Rocky Mountain Research Station, pp 149-163.

Withers, P.J.A., and Jarvie, H.P. (2008). "Delivery and cycling of phosphorus in rivers: A review," Science of the Total Environment, 400, pp 379-395.

POTENTIAL INSIGHTS INTO PHYSICAL CHARACTERISTICS OF SEDIMENT FROM SIMULTANEOUS OPTICAL SIDE SCATTER AND BACK SCATTER TURBIDITY MEASUREMENTS

Barbra Utley, Ph.D., Application Specialist, Campbell Scientific Inc., Logan, Utah, barb.utley@campellsci.com; Boyd Bringhurst, Water Resources Market Manager, Campbell Scientific Inc., Logan, Utah, boyd@campbellsci.com

Abstract: Turbidity is one of the most common surrogate measurements for suspended sediment concentrations (SSC) in natural systems. One weakness of turbidity measurements is that the data collected provide no information regarding the size or shape of the particles. The Campbell Scientific OBS500 measures both side scatter and back scatter simultaneously. Normally side scatter (SS) measurements are considered more accurate at lower turbidities (0.4-1000 TU) while back scatter (BS) measurements are regularly calibrated from 0.4-4000 TU and possibly up to 10000 TU in the future. Campbell Scientific Inc. (CSI) has noticed at multiple testing locations that SS and BS measurements often track closely both in magnitude and relative change, while in other systems the measurements track with regards to relative change but are offset by 10-30 turbidity units.

CSI hypothesized that the difference in measurement magnitude is tied to size, shape, color, absorption, biological matter or other physical attributes of the water. CSI paired a controlled laboratory study with field data from two deployment locations (Spring Creek near Mendon, UT and the Wilmington River near Priest's Landing, GA) to determine the impact of mineralogy on the SS and BS measurements. Sediment samples from both field sites will be analyzed for mineralogy and morphology by DCM Sciences in Denver, CO.

The controlled laboratory study completed simultaneous SS and BS measurements at multiple concentrations over the shared calibration range of the SS and BS sensors (0-1000 TU). Six different mineral suspensions were tested at each of the six concentrations (0, 10, 100, 250, 500, and 1000 mg/L). The mineral suspension included multiple size fractions – mineral combinations of kaolinite, bentonite, quartz, feldspar, mica, and anthracite (Mica 700, Mica 2400, Mica 4000, 200 Mesh Feldspar, 325 Mesh Feldspar, Bentonite, Calcined Kaolinite, Georgia Kaolinite, Natural Brown Sand, Utah Coal, and Wyoming Coal). Also quartz suspensions at the six concentration levels were created from sieved art sand. The colors tested included white, blue, red, green, and black to determine if SS, BS, or their interaction were significantly different for the same mineral and particle size but different colors. In total SS and BS data were collected for 96 suspensions by three OBS500 sensors. A total of 600 data points were collected per treatment level.

The data collected during the laboratory study were used to develop a multivariate, linear regression model to predict concentration (mg/L) as a function of SS, BS, and particle size. This model was then tested with an independent set of laboratory data. The verification test was completed using known concentrations of natural sediments from the Spring Creek field site near Mendon, UT. Five concentrations were chosen randomly over the modeled concentration range of 0-1000 mg/L. The prediction model was also tested with the long-term turbidity data collected at the two field sites and their sediment mineralogy and morphology.

EVALUATING TURBIDITY AND SUSPENDED-SEDIMENT CONCENTRATION RELATIONS FROM THE NORTH FORK TOUTLE RIVER BASIN NEAR MOUNT ST. HELENS, WASHINGTON: ANNUAL, SEASONAL, EVENT, AND PARTICLE SIZE VARIATIONS - A PRELIMINARY ANALYSIS

Mark A. Uhrich, Kurt R. Spicer, Adam R. Mosbrucker, and Tami S. Christianson,
U.S. Geological Survey, Cascades Volcano Observatory, Vancouver, Wash.,
krspicer@usgs.gov

INTRODUCTION

Regression of in-stream turbidity with concurrent sample-based suspended-sediment concentration (SSC) has become an accepted method for producing unit-value time series of inferred SSC (Rasmussen et al., 2009). Turbidity-SSC regression models are increasingly used to generate suspended-sediment records for Pacific Northwest rivers (e.g., Curran et al., 2014; Schenk and Bragg, 2014; Uhrich and Bragg, 2003). Recent work developing turbidity-SSC models for the North Fork Toutle River in southwestern Washington (Uhrich et al., 2014), as well as other studies (Landers and Sturm, 2013; Merten et al., 2014), suggests that models derived from annual or greater datasets may not adequately reflect shorter term changes in turbidity-SSC relations, warranting closer inspection of such relations.

In-stream turbidity measurements and suspended-sediment samples have been collected from the North Fork Toutle River since 2010. The study site, U.S. Geological Survey (USGS) streamgage 14240525 near Kid Valley, Washington, is 13 river km downstream of the debris avalanche emplaced by the 1980 eruption of Mount St. Helens (Lipman and Mullineaux, 1981), and 2 river km downstream of the large sediment retention structure (SRS) built from 1987–1989 to mitigate the associated sediment hazard. The debris avalanche extends roughly 25 km down valley from the edifice of the volcano and is the primary source of suspended sediment moving past the streamgage (NF Toutle-SRS). Other significant sources are debris flow events and sand deposits upstream of the SRS, which are periodically remobilized and transported downstream. Also, finer material often is derived from the clay-rich original debris avalanche deposit, while coarser material can derive from areas such as fluvially reworked terraces.

Data Collection, Sampling, and Processing: Unit value (15-minute interval) turbidity values were collected and processed according to established USGS procedures (Wagner et al., 2006), using a Forest Technology Systems DTS-12 sensor oriented vertically in a standpipe on the left bank of the river. Sensors were calibrated in standards (i.e., solutions of known turbidity) before and after deployment periods. Data corrections were applied based on the calibration results. All turbidity sensors have a maximum threshold recording level. For the DTS-12 the threshold is approximately 2,500 Formazin Nephelometric Units (FNU). Turbidity values above the DTS-12 maximum in water year (October to September) 2013 were estimated from a Hach Solitax sensor located adjacent to the DTS-12. Solitax sensor values are measured in Formazin Backscatter Ratio Units (FBRU) up to a maximum value of about 20,000 FBRU; observed values were reasonably consistent with DTS-12 values below about 2,500 FNU. Turbidity data from sensors reporting in different units should not be used interchangeably (Anderson, 2005). Solitax FBRU data in water year 2013 were used only as a visual guide to estimate discrete values of DTS-12

turbidity in FNU for the SSC samples collected above the DTS-12 threshold. Also for water year 2012, some turbidity values above the sensor threshold were estimated by extending the slope of the DTS-12 rise and fall graph line and interpolating the appropriate turbidity value at the time of the sample.

Manual cross-sectional depth-integrated and bankside automated-pumping samples were collected using standard USGS samplers and methods. The manual method used was the Equal Discharge Increment method or EDI, in which a separate sample of the same volume is collected from each centroid in the cross-section. Each centroid has a calculated percentage of flow whose locations are determined by a discharge measurement (Edwards and Glysson, 1999). Samples were analyzed for SSC and many for particle size distribution (Guy, 1977). Sediment particle size is defined by the diameter, such that a diameter smaller than 0.062 millimeters (mm) is considered fine-grained sediment. Coefficients, calculated from a concentration ratio, were applied to correct pump samples to the manual cross-section mean SSC. For example, if an SSC from a manual sample was 120 milligrams per liter (mg/L) and the pump samples collected directly before and after the manual sample were each 100 mg/L, the pump SSCs would be multiplied by 1.2 to obtain a corrected value.

REGRESSION ANALYSIS

Datasets of the sample SSC, concurrent in-stream turbidity, and percentage of fine sediment were compiled for 2010–2013 water years. Datasets were then divided by year, season, and specific high-turbidity events. Regression models were developed from these subsets and results were compared from year-to-year and season-to-season, along with evaluations for groups of high-turbidity events. Models were also developed by categorizing the data by specific groups of particle size distribution, or percentage of fine-grained sediment. Samples were categorized in two groups: less than or greater than 60 percent fines. Regression equations and model results were evaluated for each category.

The regression analysis used the power equation form, such that SSC is equal to a x Turbidity ^{b}, where a is the y-intercept and b is the slope. The coefficient of determination (R^2) and sum of squares error of prediction (SSE) values, shown on most figures, are statistical and comparative diagnostics used in regression modeling to evaluate accuracy (Helsel and Hirsch, 2002; Uhrich et al., 2014). In general, the higher the R^2 the better the model fits the data, although there are exceptions and the R^2 should be evaluated with other model statistics and plots of the residual values. The SSE is a measure of variation in the model or its deviation from the mean, hence the lower the SSE the less the variation and tighter fit of the model.

Annual Regressions: Annual turbidity-SSC models can provide adequate results for most Pacific Northwest streams (Bragg et al., 2007) but might not be suitable for the North Fork Toutle basin near Mount St. Helens due to its variable sediment sources and erosional conditions. The analysis of North Fork Toutle River turbidity and SSC data, under varying time scales, reveals how a single turbidity value can have varying SSC and/or sediment-size fraction values associated with it.

Annual data were grouped by water year. The 2010 dataset, a partial year from May to September, was combined with the 2011 water year. The number of samples collected for the 2010–2011, 2012, and 2013 datasets were 653, 509, 408, respectively, totaling 1,570 turbidity-SSC pairs available for analysis (figure 1). Ordinary least-squares regression models, developed for each water year, yielded an equation to estimate SSC from turbidity (Helsel and Hirsch, 2002; Uhrich et al. 2014). SSC was first computed using the 2010–2011 regression equation, for a range in turbidity values from 100 to 2,000 FNU. This turbidity range was the most common amongst all years in matched turbidity with sample SSC, although in 2013 the paired turbidity with SSC was higher, due to the use of the Solitax sensor. The 2010–2011 computed SSC, for the selected turbidity range values, had a percent difference of 5 to 32 percent higher than the 2012 equation estimates, for the same range of turbidity values, with a 54 to 65 percent difference higher than the 2013 equation estimates. For example, a turbidity value of 100 FNU equated to 835 mg/L for the 2010–2011 model. The same turbidity value equated to 795 mg/L and 385 mg/L for the 2012 and 2013 models, respectively. A turbidity value of 1,600 FNU equated to 7,360 mg/L for 2010–2011. The same value equated to 5,150 and 2,630 for 2012 and 2013, respectively. Turbidity values above 2,000 FNU, which were associated with the SSC samples, occurred in 2013 and exhibited slightly greater differences in SSC.

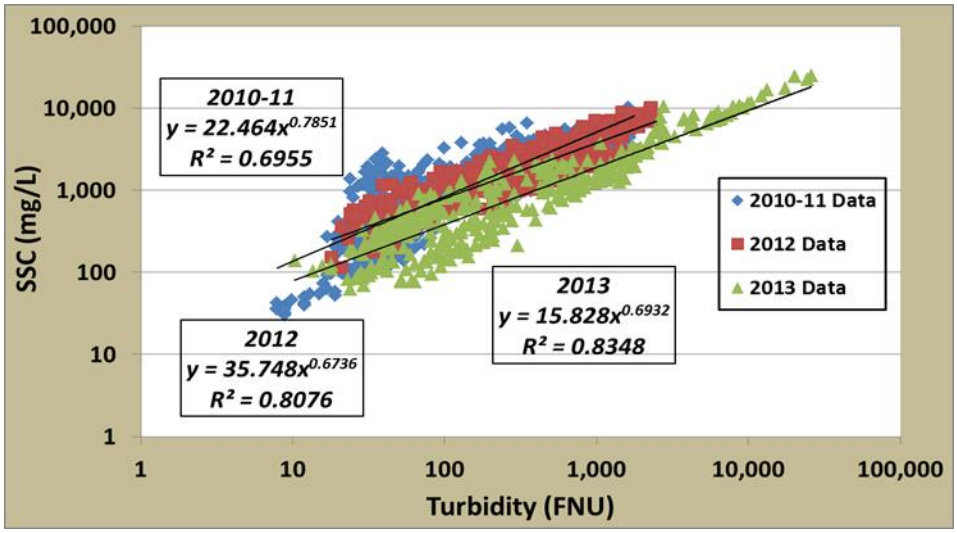

Figure 1 Ordinary least-squares regressions of turbidity and SSC for the USGS streamgage 14240525 North Fork Toutle River below SRS near Kid Valley, Washington, using 2010–2013 turbidity and SSC data pairs.

The large differences between 2013 and the other water years were largely caused by the reconstruction of the SRS spillway, about 2 km upstream from the streamgage. The spillway was raised by over 2 m in October 2012, thereby impounding greater amounts of suspended sediment and limiting downstream transport. Also in 2012, as a precursor to the spillway raise, grade-building structures and diversion channels were placed upstream of the SRS to impede and trap sediment movement. Hence, there was a significant change to turbidity-SSC relations from 2010–2011 and 2012 water years to the 2013 water year. This demonstrates that annual turbidity-SSC models for the North Fork Toutle River must be checked year-to-year as changes are

inevitable in this basin due to the ubiquitous and dynamic nature of a natural and managed sediment regime.

Seasonal Regressions: Seasonal differences are also evident. Seasons were differentiated into 4 groups comprising 3 months each: October-December, January-March, April-June, and July-September. These monthly groupings were further simplified to fall, winter, spring and summer, respectively. Regression equations were generated for each season in each year (figure 2).

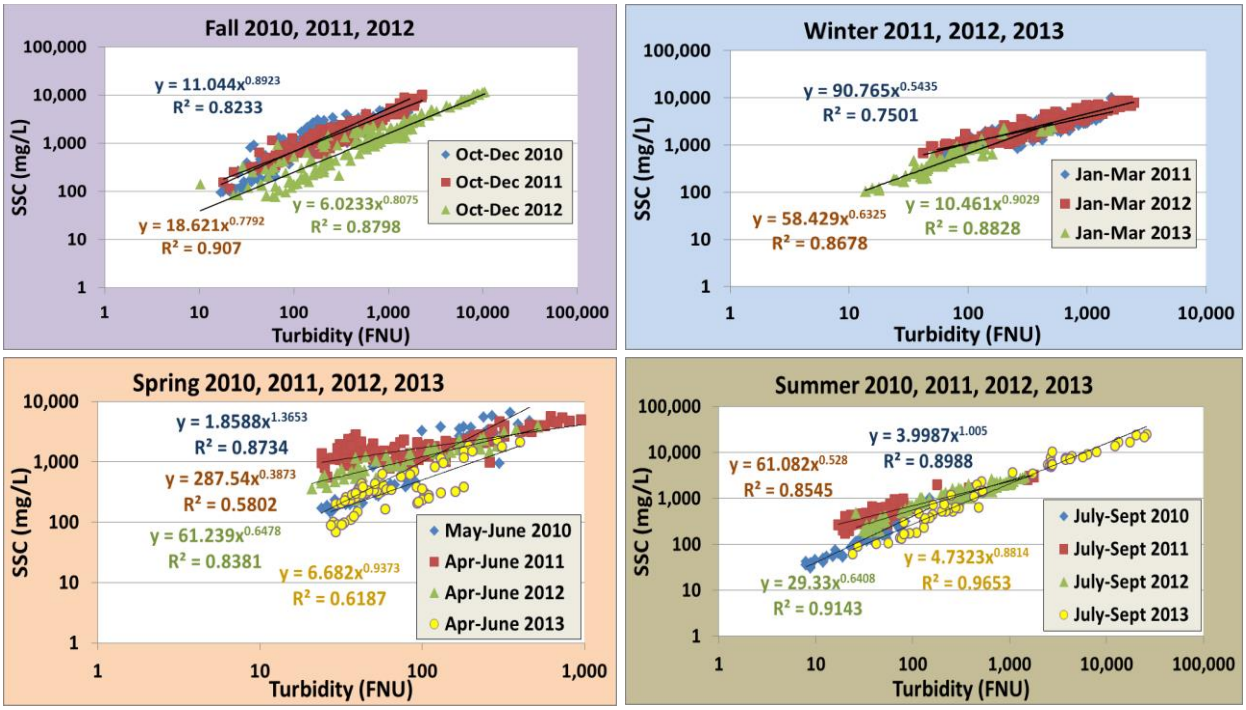

Figure 2 Seasonal regression models for the NF Toutle-SRS streamgage using 2010–2013 data.

Similar to the annual computational method, a range of turbidity values from 100 to 2,000 FNU was used to estimate seasonal SSC. The regression analysis showed that a low turbidity of less than 200 FNU with a relatively low estimated SSC occurred in the seasons of summer 2010 and 2013 and fall 2012. Seasons with high turbidity, greater than 1,200 FNU, having a low estimated SSC also occurred in fall 2012 and summer 2011, 2012, and 2013. The seasons of fall 2012 and summer 2013 had low SSC despite the turbidity level (table 1). Hence, low turbidity in the North Fork Toutle basin with a relative low SSC are indicative of late summer and early fall low flow conditions, where sediment transport is minimal. High turbidity with low SSC can result when the sediment supply is limited and may also occur in conjunction with the low flow, and low turbidity-SSC condition.

A low turbidity less than 200 FNU having a relative high SSC occurred in the two adjoining seasons winter and spring in the years 2011, 2012 (table 1). Also, spring 2010 had low turbidity with a high SSC. There was no data available for winter 2010 to determine if this year followed a similar trend as 2011 and 2012. A season having high turbidity with a high estimated SSC occurred in the 3 adjoining seasons: Spring, summer, and fall 2010. Also, there was a relative

high SSC for a high turbidity for fall 2011, and the 2 adjoining seasons of winter and spring in 2012 and 2013.

Table 1 Seasonal regression computed SSC for selected turbidity values.

Turbidity 100 to 2,000 FNU	Low SSC	High SSC
Low Turbidity (*less than 200 FNU*)	Summer 2010 Fall 2012 Summer 2013	Spring 2010 Winter 2011 Spring 2011 Winter 2012 Spring 2012
High Turbidity (*greater than 1200 FNU*)	Summer 2011 Summer 2012 Fall 2012 Summer 2013	Spring 2010 Summer 2010 Fall 2010 Fall 2011 Winter 2012 Spring 2012 Winter 2013 Spring 2013

Some high SSC conditions may be sediment-transport capacity limited, such that the sediment supply is abundant but the capacity to transport it is restricted. Low turbidity and high relative SSC conditions are indicative of high flow, and/or high sediment-transport conditions and often occur in conjunction with high turbidity-SSC seasons. Overall though, each of the seasonal differences can be attributed to a variety of sediment source, erosion, and streamflow conditions, as well as sediment-particle size, and can shift back-and-forth from a sediment supply limited to sediment-transport capacity limited system.

The seasons with the highest slope and lowest y-intercept were the two adjoining seasons spring 2010 and summer 2010. The seasons with the lowest slope and highest y-intercept were the two adjoining seasons winter 2011 and spring 2011. This shows there was a significant shift in turbidity-SSC relations from 2010 to 2011, although all data from 2010 were not available. These seasonal differences document how suspended-sediment transport can shift within a specific year and how one season can vary from another, and from the same season in different years. Hence, for the highest accuracy, turbidity-SSC model development in the North Fork Toutle basin should follow more seasonal than annual time scales.

Event Regressions: There were several events during the 2010–2011 to 2013 water years that had a distinct turbidity-SSC signature. Twenty-one major events were selected for analysis, which were determined by a rise in streamflow and/or turbidity that increased by at least 100 percent from its previous level, and with an event duration of less than 8 days. There may have been several peaks in streamflow or turbidity during a particular event period. A turbidity-SSC regression model was generated for each of the 21 events. These were categorized into 4 main event groups (A, B, C, D) based on a given turbidity, from a 100 to 2,000 FNU range of values, and a computed SSC from the regression models that was within an average 30 percent

difference for all groups. Each event group also had a similar slope and y-intercept within a 30 percent range. A second regression model was then generated for each of the 4 groups (figure 3).

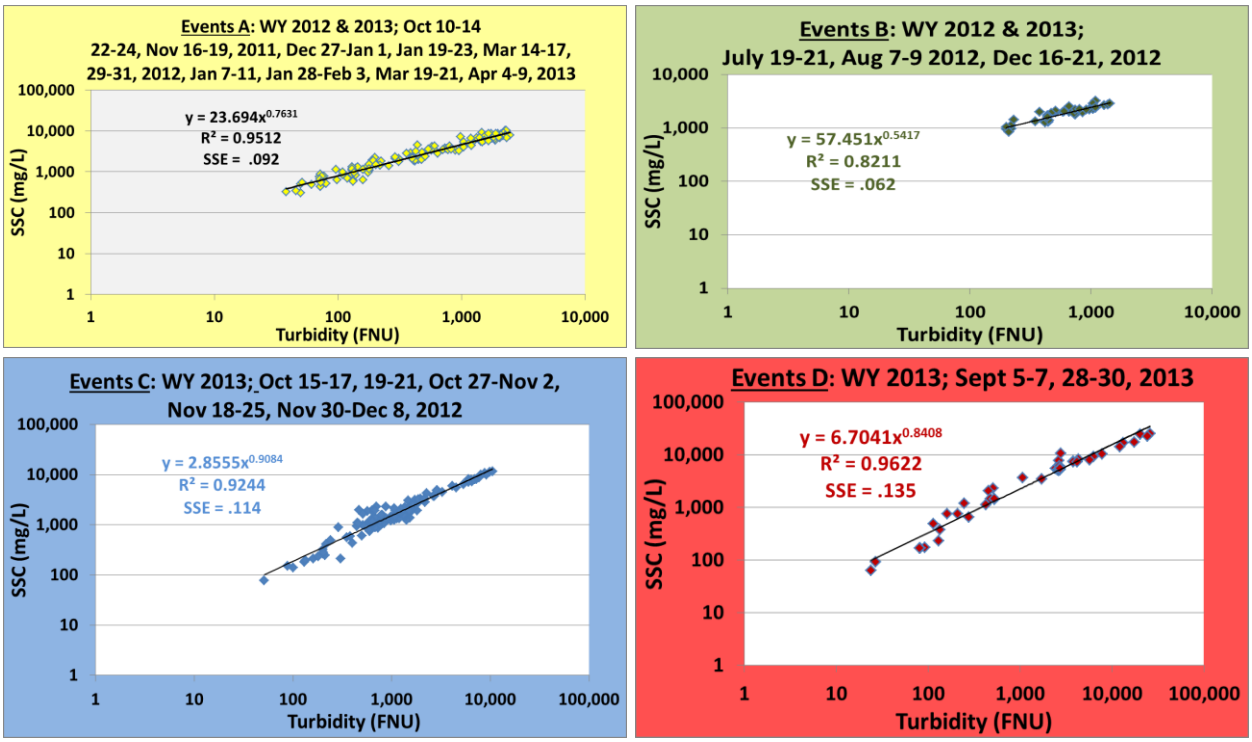

Figure 3 Event regression models for the NF-Toutle-SRS streamgage.

Event group B had the lowest slope and highest y-intercept, which was indicative of low flow, summertime conditions and first-flush autumn events where, in this case, the turbidity peaks precede the streamflow peaks. Event group C had the highest slope and lowest y-intercept, which occurred entirely during the fall of 2012 where the turbidity peaks lagged the streamflow peaks. Event group A was wedged between groups B and C and had a wide-range of events extending through several time spans, occurring primarily from November to March. This is reasonable considering most sediment transport is a combination of both conditions in groups B and C, and in slope and y-intercept. Event group D is comprised of two abnormally large peaks in September, normally the driest month of the year.

Creating separate event models enabled a more accurate SSC estimate for these periods, as compared to the annual and seasonal models, as reflected by the high R^2 and low SSE values in figure 3. Hence, it is possible to fine-tune regression models to smaller time scales for specific events in order to more appropriately approximate an SSC from turbidity for these periods.

Particle-Size Regressions: There were 317 samples available with particle size data for the entire 2010–2011, 2012, and 2013 datasets. As with the previous regression models the turbidity and SSC data with particle-size data were assembled as one dataset. The data points were then separated into two groups by particle size distribution. One group consisted of all samples with 60 percent of total material smaller than sand (<0.062 mm in diameter); the other group had 60

percent of total material larger than sand. Within each group, EDI cross-section samples and pump samples were differentiated.

Similar to the annual and seasonal regressions, a range of different turbidity values from 100 to 2,000 FNU was input to each of the particle-size equations for each year (figure 4). Comparisons were made within each year and from year-to-year for the EDI and pump groups of 60 percent finer than sand. The comparisons between years showed that average particle size decreased from 2010-11 to 2013. The 2010-11 pump sample group greater than 60 percent fines (mostly fine material) showed higher SSC by an average 63 percent difference as compared to 2013 for the turbidity values input to equations.

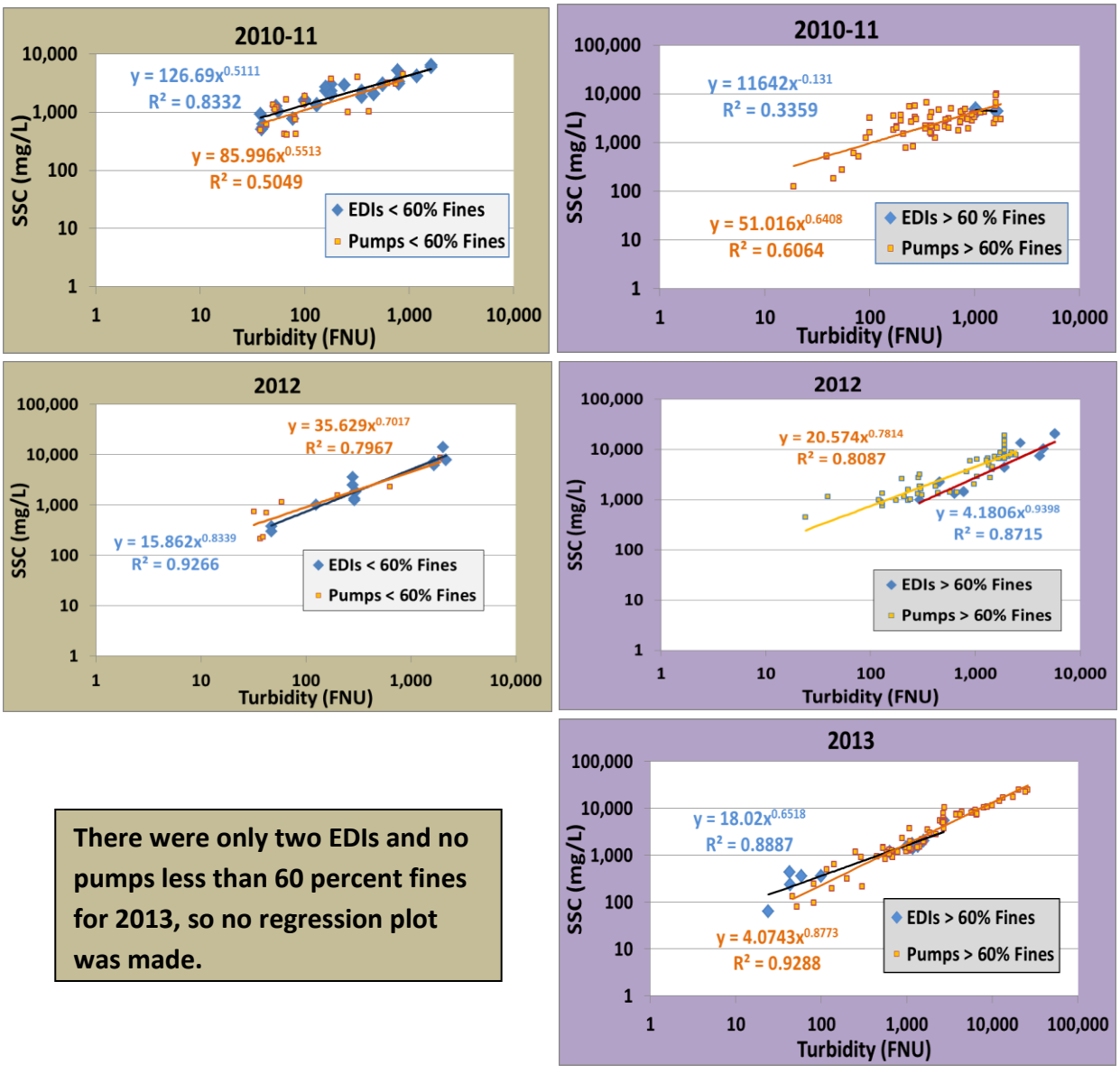

There were only two EDIs and no pumps less than 60 percent fines for 2013, so no regression plot was made.

Figure 4 NF Toutle-SRS particle-size regressions for 2010-11, 2012, and 2013.

There were no EDI samples in 2010-11 that were greater than 60 percent fines, although from 2012 to 2013, in this greater than 60 percent fines category (mostly fine material), the EDI and pump concentrations, estimated from the range of turbidity values, decreased an average 26 and 64 percent difference, respectively. Hence, the concentration of fine material for a given in-stream turbidity, transported downstream past the SRS, was lower in 2013 than 2012. Also in 2012, the EDI particle-size concentrations that were less than 60 percent sand (mostly coarse material), for the 100-2,000 range in turbidity, were all higher than the 2012 greater than 60 percent finer than sand group (mostly fine material) by an average 48 percent difference. Hence, all EDI suspended-sediment concentrations in 2012 were primarily SSCs with coarser-grained sediment than in 2013. The pump samples in 2012 did not have as much or as consistent a difference.

There also were differences between EDI and pump estimates based on particle size. In 2010-11 the EDI concentrations for a given turbidity in the less than 60 percent fines group (coarser material) had an average 12 percent difference higher than the pump concentration for the same group. Yet in 2012 the EDI concentrations were much lower than pump concentrations, especially for samples grouped as greater than 60 percent fine material, which averaged a 56 percent difference lower. For coarse material, less than 60 percent fines, the concentrations of EDIs and pumps varied in 2012, such that at low turbidity pump SSCs were higher and at high turbidity the EDIs SSCs were higher.

The 2013 estimated SSCs, for the range in turbidity values, also varied between the EDIs and pumps, although the reverse occurred in 2013 such that, at low turbidity the EDI SSCs were higher and at high turbidity the pump SSCs were higher. In 2013, there were only values for EDI and pump samples that were greater than 60 percent fines (mostly fine material), with no values for less than 60 percent fines (mostly coarse material), so no comparisons could be made for the coarser material. Hence, the EDI finer-grained SSCs for a given turbidity were usually lower than the pump SSCs, particularly in 2012. The EDI and pump differences may be due to the mechanics of pumping sediment up a stream bank, through a hose to a sampler, as opposed to directly collecting into a sampler by manual cross-sectional methods, through the water column, and at the same velocity as the stream. Auto-pump samplers tend to collect more fine sediment than coarse particles due to these restrictions, so even though the pump concentrations can be corrected to the EDIs the particle size distribution cannot. These discrepancies should be considered in deciding which samples to select for developing turbidity-SSC regression models, especially in any type of particle-size analysis.

DISCUSSION

These analyses are not the final regression equations, but were developed to demonstrate the general turbidity-SSC relations in the North Fork Toutle River basin. Also no bias correction factors were applied to the regression equations, which are used to correct for any shift in converting log values back to linear space (Helsel and Hirsch, 2002; Uhrich et al., 2014). The bias correction factors usually alter the equations only slightly so were not considered in presenting preliminary turbidity and SSC relationships. Also, the Solitax high-end turbidity sensor was used as a guide to fill in missing flat-line DTS-12 threshold periods for the 2013 data.

The estimated data was applied from the start to the stop point of the flat-line DTS-12 threshold period.

The logical next step with this preliminary analysis is to develop final regression equations, incorporating a suite of elements to fine tune the models, such as bias correction factors, and developing a separate Solitax to DTS-12 regression. Also, multiple regression models for the North Fork Toutle basin have been shown to more accurately predict SSC from turbidity by using streamflow and a lag of turbidity as added explanatory variables (Uhrich et al., 2014). The final test would be to compute a sediment record using the regression-model approach and compare the results to the conventional sample-based approach.

Fine- and coarse-grain sediment will have fluctuating turbidity and SSC, based on seasonal and rise/fall periods, which can be grouped into defined categories. Model R^2 and SSE values will usually improve with concentrations having finer particle sizes. Hence, suspended-sediment discharge can be differentiated by particle-size distribution. Defining these hysteresis effects improves resource planners' and stakeholders' understanding of fluvial sediment transport and subsequent deposition in the studied lower basins. In the lower Toutle and Cowlitz River channels, aggradation of coarse-grain sediment has significant effects on flood inundation risk to surrounding communities, and in the Columbia River it affects river navigation and shipping commerce by large deep-draft, commercial ocean-going vessels.

SUMMARY

Annual regression models are used for many Pacific Northwest streams to estimate SSC from turbidity. For the North Fork Toutle River an annual time span may not be appropriate, as episodic erosional events and changing sediment sources require shorter time scale models to accurately predict SSC from turbidity. Evaluating sediment transport using seasonal time frames is one method in which this could be achieved, as precipitation patterns in the Pacific Northwest lend themselves to predictable occurrences during certain times of the year. Although seasonal approaches offer improved accuracy over annual models the time scale may not capture shorter-term events that can occur within each season. Shorter-term models for specific events and time scales provide improved accuracy over longer-term turbidity-SSC models. Monitoring of turbidity and sediment transport can vary by particle size. The selection of samples as EDI or auto-pump is important as there can be distinct differences between the collection methods. Once representative samples are selected, it is possible to develop regression models based on sediment-size data from the sample analysis. These particle-size models can be used to predict not only the concentration but also the type of sediment in transport.

ACKNOWLEDGMENTS

The U.S. Army Corps of Engineers supported this study. Use of trade names in this manuscript is for identification purposes only and does not constitute endorsement by the U.S. Geological Survey.

REFERENCES

Anderson, C.W., 2005, Turbidity (ver. 2.1): U.S. Geological Survey Techniques of Water-Resources Investigations, book 9, chap. A6, section 6.7, 64 p., accessed December 18, 2014, at *http://water.usgs.gov/owq/FieldManual/Chapter6/6.7_contents.html*.

Bragg, H.M., Sobieszczyk, Steven, Uhrich, M.A., and Piatt, D.R., 2007, Suspended-sediment loads and yields in the North Santiam River Basin, Oregon, 1999–2004: U.S. Geological Survey Scientific Investigations Report 2007-5187, 26 p., access December 18, 2014, at *http://pubs.usgs.gov/sir/2007/5187/*

Curran, C.A., Magirl, C.S., and Duda, J.J., 2014, Suspended-sediment concentration during dam decommissioning in the Elwha River, Washington, September 2011 to September 2013: U.S. Geological Survey Data Set, accessed December 18, 2014, at *http://wa.water.usgs.gov/pubs/misc/elwha/ssc/pdf/elwhasscV2_2014.pdf*

Edwards, T.K., and Glysson, G.D., 1999, Field methods for measurement of fluvial sediment: U.S. Geological Survey Techniques of Water-Resources Investigations, book 3, chap. C2, 89 p., accessed December 18, 2014, at *http://pubs.usgs.gov/twri/twri3-c2/*.

Guy, H.P., 1977, Laboratory theory and methods for sediment analysis: U.S. Geological Survey Techniques of Water-Resources Investigations, book 5, chap. C1, accessed December 18, 2014, at *http://pubs.usgs.gov/twri/twri5c1/html/pdf.html*.

Helsel, D.R., and Hirsch, R.M., 2002, Statistical methods in water resources: U.S. Geological Survey Techniques of Water-Resources Investigations, book 4, chap. C3, p. 221–263, accessed December 18, 2014, at *http://pubs.usgs.gov/twri/twri4a3/*.

Landers, M.N., and Sturm, T.W., 2013, Hysteresis in suspended sediment to turbidity relations due to changing particle size distributions, Water Resources Research, Volume 49, Issue 9, pp. 5487-5500.

Lipman, P.W., and Mullineaux, D.R., 1981, The 1980 eruptions of Mount St. Helens, Washington 1981, U.S. Geological Survey Professional Paper: 1250, p. 844, accessed December 18, 2014, at *http://pubs.er.usgs.gov/publication/pp1250*.

Merten, G.H., Capel, P.D., Minella, J.P.G., 2014, Effects of suspended sediment concentration and grain size on three optical turbidity sensors, Journal of Soils and Sediments, July 2014, Volume 14, Issue 7, pp. 1235-1241.

Rasmussen, P.P., Gray, J.R., Glysson, G.D., and Ziegler, A.C., 2009, Guidelines and procedures for computing time-series suspended-sediment concentrations and loads from in-stream turbidity-sensor and streamflow data: U.S. Geological Survey Techniques and Methods, book 3, chap. 4, 53 p., accessed December 18, 2014, at *http://pubs.usgs.gov/tm/tm3c4/*.

Schenk, L.N., and Bragg, H.M., 2014, Assessment of suspended-sediment transport, bedload, and dissolved oxygen during a short-term drawdown of Fall Creek Lake, Oregon, winter 2012–13: U.S. Geological Survey Open-File Report 2014–1114, 80 p., accessed December 18, 2014 at, *http://dx.doi.org/10.3133/ofr20141114*.

Uhrich, M.A., and Bragg, H.M., 2003, Monitoring instream turbidity to estimate continuous suspended-sediment loads and yields and clay-water volumes in the upper North Santiam River Basin, Oregon, 1998–2000: U.S. Geological Survey Water-Resources Investigations Report 03-4098, accessed December 18, 2014, at, *http://pubs.usgs.gov/wri/WRI03-4098/*.

Uhrich, M.A., Kolasinac, Jasna, Booth, P.L., Fountain, R.L., Spicer, K.R., and Mosbrucker, A.R., 2014, Correlations of turbidity to suspended-sediment concentration in the Toutle River Basin, near Mount St. Helens, Washington, 2010–11: U.S. Geological Survey Open-File Report 2014-1204, 30 p., *http://dx.doi.org/10.3133/ofr20141204*.

Wagner, R.J., Boulger, R.W., Jr., Oblinger, C.J., and Smith, B.A., 2006, Guidelines and standard procedure for continuous water-quality monitors—Station operation, record computation, and data reporting: U.S. Geological Survey Techniques and Methods, book 1, chap. D3, 51 p., plus 8 attachments, accessed December 18, 2014, at http://pubs.usgs.gov/tm/2006/tm1D3/.

EVALUATION AND APPLICATION OF REGIONAL TURBIDITY-SEDIMENT REGRESSION MODELS IN VIRGINIA

EXTENDED ABSTRACT

Kenneth Hyer, Hydrologist, USGS, Richmond, VA, kenhyer@usgs.gov; John Jastram, Hydrologist, USGS, Richmond, VA, jdjastra@usgs.gov; Douglas Moyer, Hydrologist, USGS, Richmond, VA, dlmoyer@usgs.gov; James Webber, Hydrologist, USGS, Richmond, VA, jwebber@usgs.gov; Jeff Chanat, Hydrologist, USGS, Richmond, VA, jchanat@usgs.gov

INTRODUCTION

Conventional thinking has long held that turbidity-sediment surrogate-regression equations are site specific and that regression equations developed at a single monitoring station should not be applied to another station; however, few studies have evaluated this issue in a rigorous manner. If robust regional turbidity-sediment models can be developed successfully, their applications could greatly expand the usage of these methods. Suspended sediment load estimation could occur as soon as flow and turbidity monitoring commence at a site, suspended sediment sampling frequencies for various projects potentially could be reduced, and special-project applications (sediment monitoring following dam removal, for example) could be significantly enhanced.

The objective of this effort was to investigate the turbidity-suspended sediment concentration (SSC) relations at all available USGS monitoring sites within Virginia to determine whether meaningful turbidity-sediment regression models can be developed by combining the data from multiple monitoring stations into a single model, known as a “regional” model. Following the development of the regional model, additional objectives included a comparison of predicted SSCs between the regional models and commonly used site-specific models, as well as an evaluation of why specific monitoring stations did not fit the regional model.

METHODS

All USGS Virginia Water Science Center monitoring stations with paired turbidity (measured with a YSI 6136 sensor) and SSC data were retrieved from the USGS National Water Information System database and considered for this analysis. Data from 64 stations were initially retrieved; however, the data were filtered to ensure that only sites with sufficient observations and only sites with sampling over an extended range of hydrologic conditions were considered. A total of 29 stations met the project-assigned criteria of (1) at least 24 paired turbidity-suspended sediment concentration measurements, and (2) water-quality sampling over most of the observed range of hydrologic conditions (Table 1).

Table 1 Turbidity monitoring station identifiers, names, and watershed areas.

Station identifier	Station name	Watershed area (mi^2)
02042500	Chickahominy River near Providence Forge, VA	251
02041650	Appomattox River at Matoaca, VA	1,342
01627500	South River at Harriston, VA	212
01634000	NF Shenandoah River near Strasburg, VA	770
01631000	SF Shenandoah River at Front Royal, VA	1,634
01668000	Rappahannock River near Fredericksburg, VA	1,595
01632900	Smith Creek near New Market, VA	94
01626000	South River near Waynesboro, VA	127
02035000	James River at Cartersville, VA	6,252
02037618	James River at Boulevard Bridge at Richmond, VA	6,776
01621050	Muddy Creek at Mount Clinton, VA	14.32
01671020	North Anna River at Hart Corner near Doswell, VA	462
02024752	James River at Blue Ridge Pkwy near Big Island, VA	3,076
02054750	Roanoke River at Route 117 at Roanoke, VA	352
01667500	Rapidan River near Culpeper, VA	468
03524740	Clinch River at Route 65 at Dungannon, VA	820
0165389480	Accotink Creek Below Old Lee Hwy at Fairfax, VA	4.87
02055080	Roanoke River at Thirteenth St Bridge at Roanoke, VA	390
01654000	Accotink Creek near Annandale, VA	23.87
01673000	Pamunkey River near Hanover, VA	1,078
01646305	Dead Run at Whann Avenue near Mclean, VA	2.05
01646000	Difficult Run near Great Falls, VA	58
01656903	Flatlick Branch above Frog Branch at Chantilly, VA	4.20
01645762	SF Little Difficult Run above Mouth near Vienna, VA	2.71
01654500	Long Branch near Annandale, VA	3.72
01645704	Difficult Run above Fox Lake near Fairfax, VA	5.49
01674500	Mattaponi River near Beulahville, VA	602
02034000	Rivanna River at Palmyra, VA	663
01658500	SF Quantico Creek near Independent Hill, VA	7.62

This collection of 29 stations represents a diverse group of sites (Figure 1) that provide a range of watershed areas (from 2.05-6,776 sq miles) and locations throughout the state, which allows for a reasonable investigation of whether a regional model can be developed for the state of Virginia.

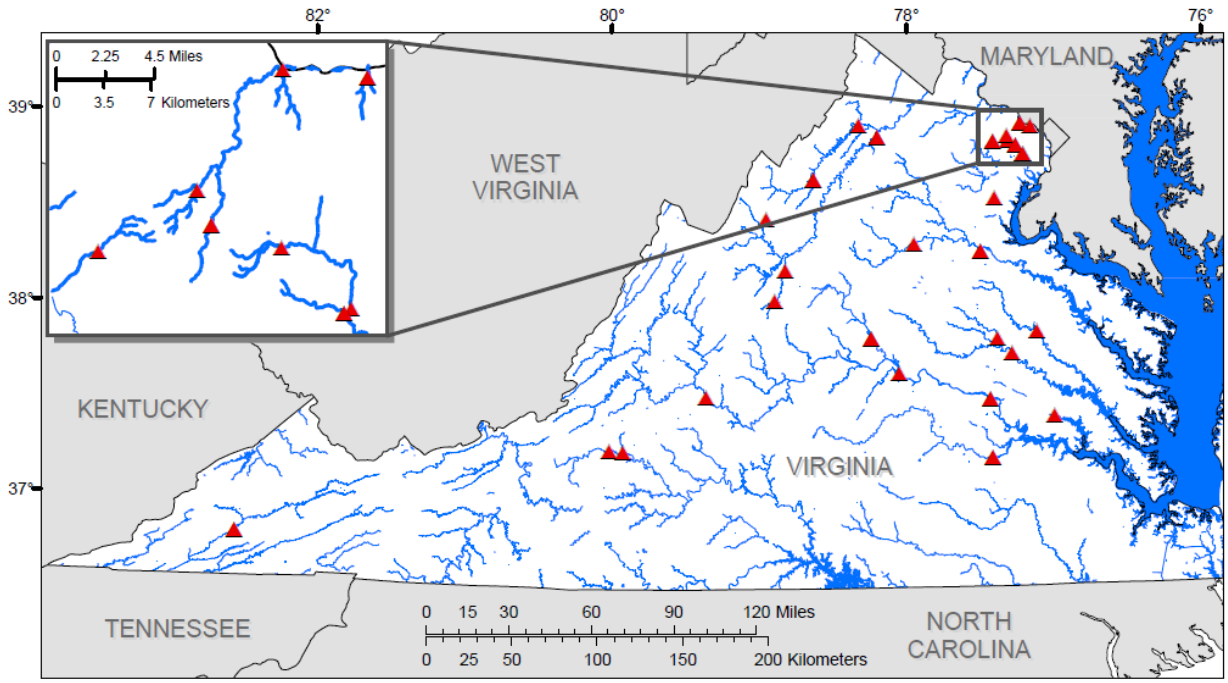

Figure 1 Map of turbidity-monitoring stations included in the study analysis.

For all 29 sites, simple linear regression models to predict SSC from turbidity were developed following standard methods for the development of regression models (Helsel and Hirsch, 2002; Jastram and others, 2009). Because of skewed distributions, both the turbidity and SSC variables were natural log transformed prior to the development of the regression models. All developed models were inspected to ensure they met the assumptions of simple linear regression.

RESULTS

Statistically significant, site-specific regression models were developed for all 29 stations (Figure 2); regression strength and quality varied among regression models. Most coefficients of determination (R^2) ranged from 0.80 to 0.95, with greater and lesser values being observed for some stations. Particularly low R-squared values were noted for station 02042500, Chickahominy River near Providence Forge, VA, and station 02041650, Appomattox River at Matoaca, VA. The Chickahominy River is a typical Coastal Plain blackwater river, with an extremely low river gradient, a broad floodplain, and extensive wetlands that yield low, and relatively uniform turbidity levels and SSCs. The Appomattox River station is located 2.2 miles downstream of a major dam, which likely acts as a sink for sediment, and causes a highly variable turbidity-sediment response.

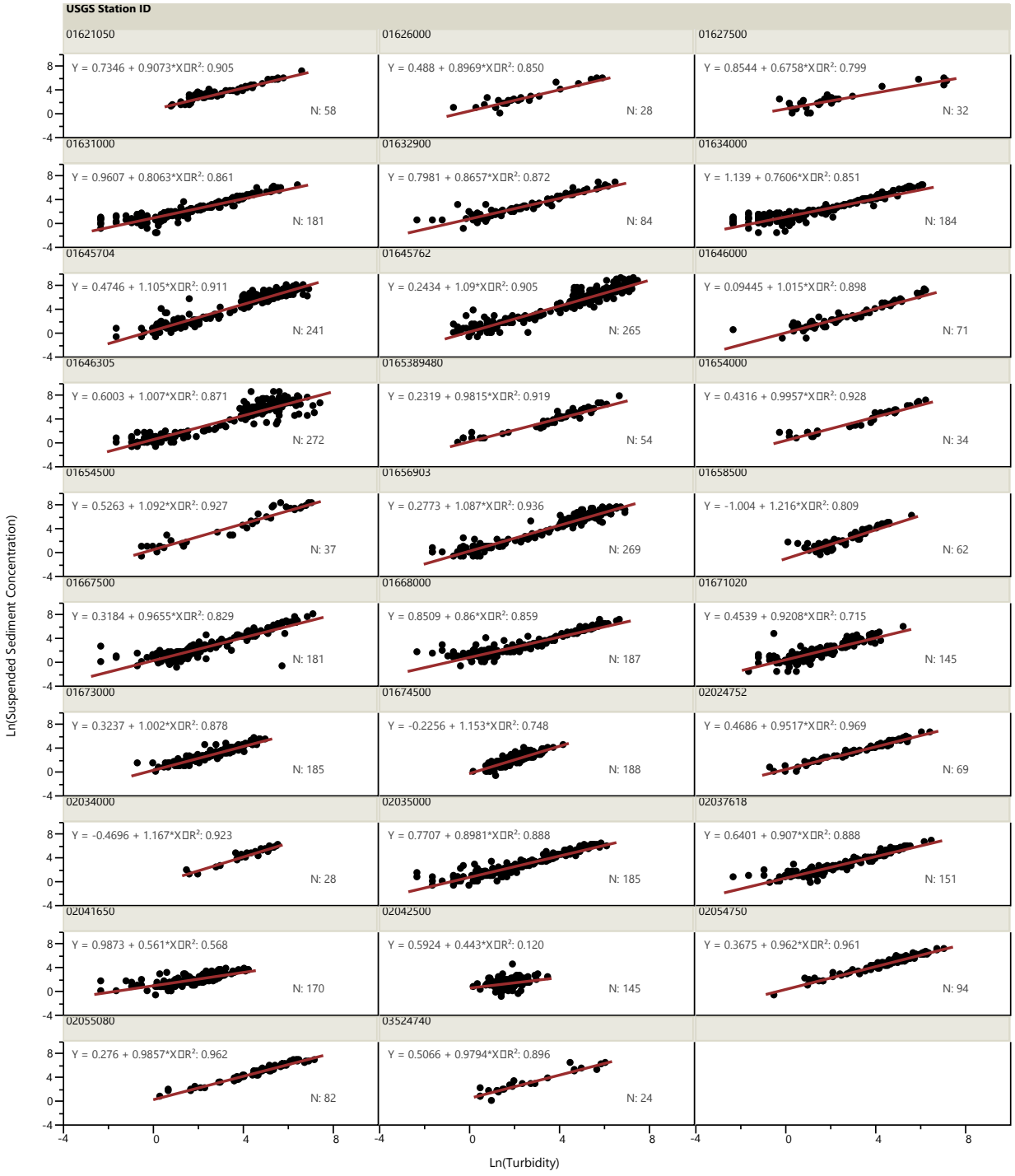

Figure 2 Site-specific turbidity-sediment regression equations for 29 monitoring stations, including model equation, the coefficient of determination (R^2) for each model, and the number of observations (N).

A single robust regional model was desired for the group of site-specific regression models that had relatively similar slope and intercept terms, so a comparison of these terms for all 29 stations was performed. The 99-percent confidence interval (CI) for the slope and intercept for each site-specific model was compared to the 99-percent CIs of the overall mean slope and intercept values for the collection of the 29 site-specific models (Figure 3). Sites where both the slope and intercept CIs of the site-specific model intersected the CIs of the overall mean slope and intercept were deemed not significantly different from the overall mean – effectively an analysis of covariance – and were included in the computation of a new regional turbidity-SSC model. A total of 19 monitoring stations (colored red in Figure 3) were included in the regional turbidity-SSC regression model for the combined data set from all 19 sites. A statistically significant regional model was developed, having an R^2 of 0.89 (Figure 4). Overall, the regional model demonstrates a strong correlation between turbidity and SSC for a diverse range of monitoring stations, however, subsequent comparisons between the regional- and site-specific models were performed.

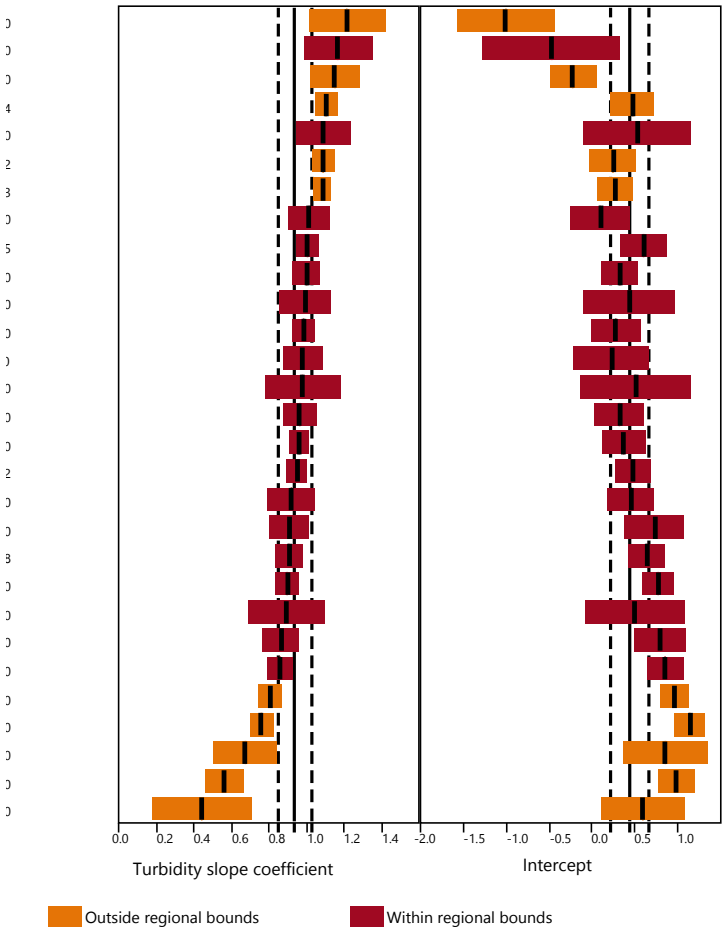

Figure 3 Site-specific model slope and intercept coefficients with 99-percent confidence intervals for 29 stations evaluated, and overall mean slope and intercept (solid line) and 99-percent confidence intervals (dashed lines).

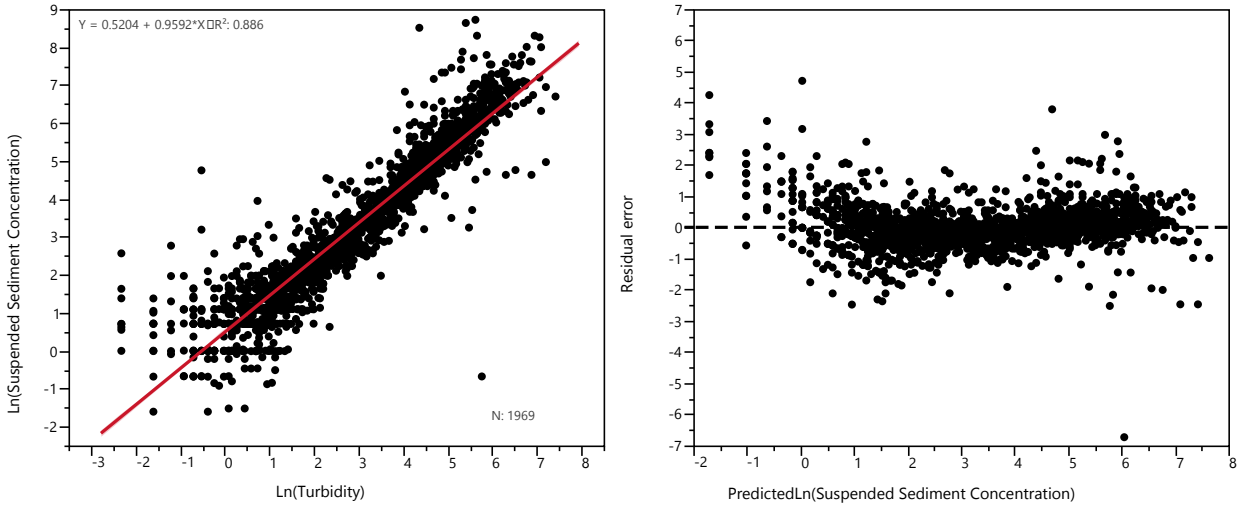

Figure 4 The regional turbidity-suspended sediment model and residuals, based on the combined datasets from 19 monitoring sites.

Direct comparisons of the predicted values between the regional- and site-specific regression models demonstrate good agreement between both models (Figure 5). Comparison of model errors demonstrates that while the regional model has slightly higher mean square error (MSE) in a few cases, overall the MSEs are comparable, regardless of model used (Figure 6).

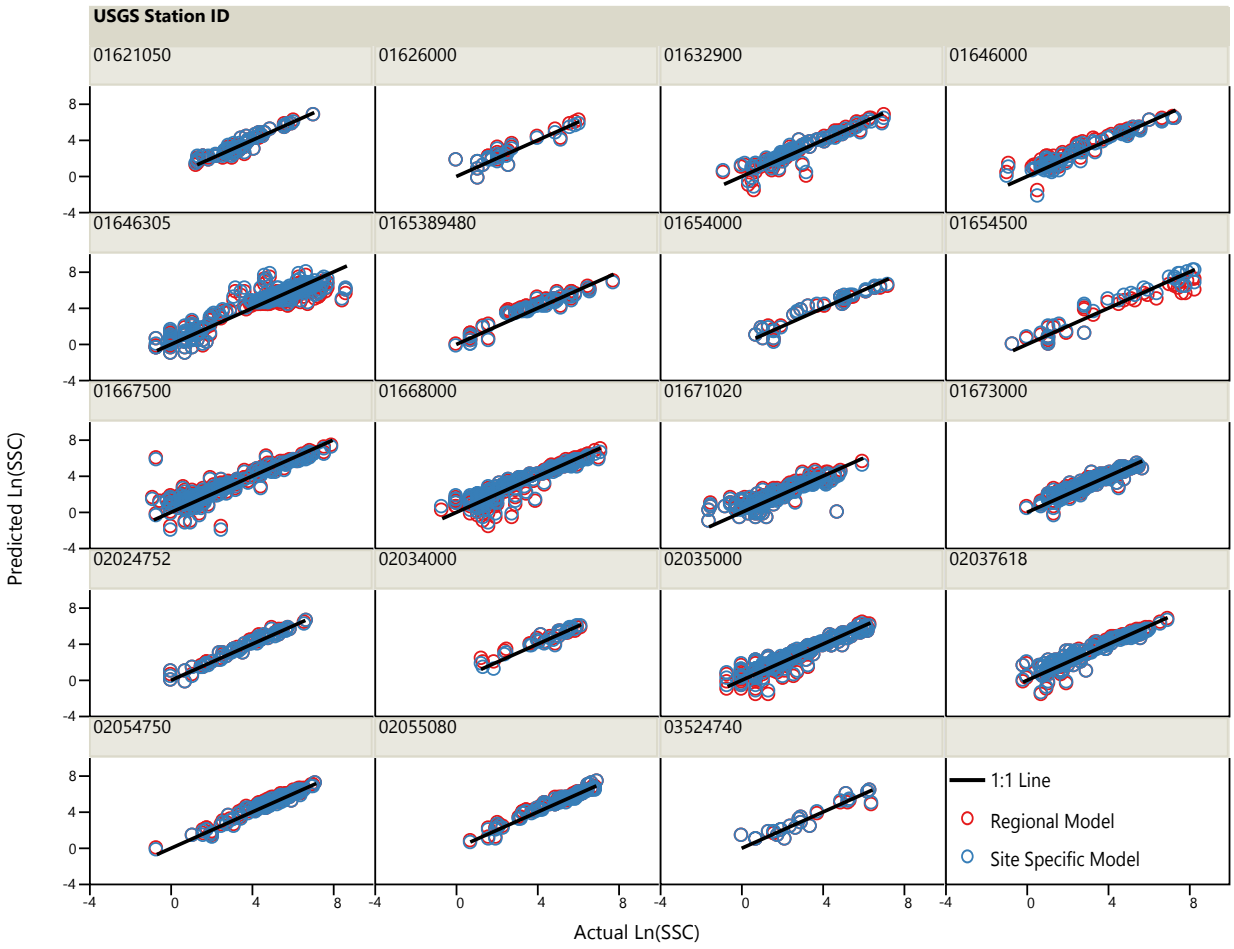

Figure 5 A comparison of actual and predicted values between the site-specific and regional models.

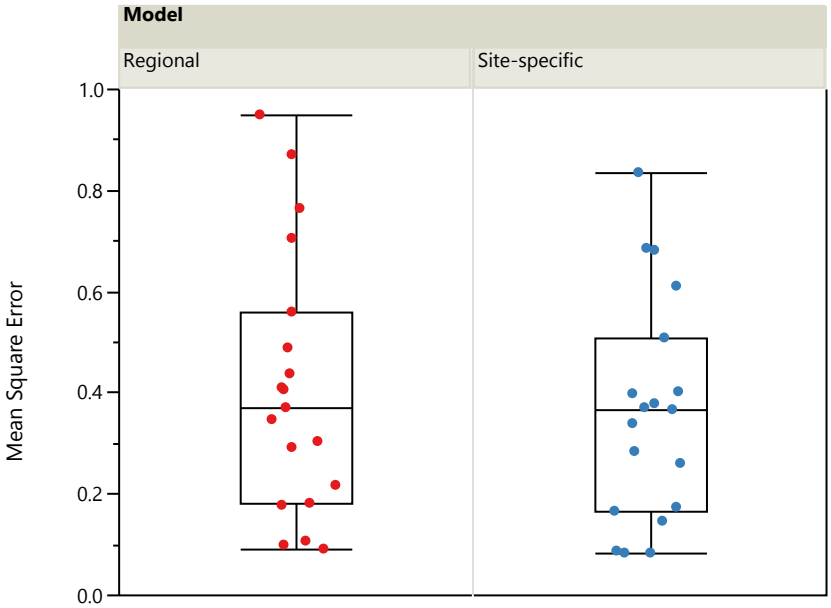

Figure 6 A comparison of the mean square errors between the site-specific and regional turbidity-sediment models.

Ten stations were not included in the regional model because their site-specific regression models were significantly different from the overall mean of the slope and intercept coefficients. The reasons for these differences are still under investigation, but are generally believed to be related to transport processes and physical characteristics of the available sediments, which may be further related to, and modeled by, watershed characteristics such as soil type, basin slope, and land-use. Overall, the sites with elevated slope coefficients generally had smaller intercept values (see the sites at the top of Figure 3) than sites with lesser slopes. These elevated slopes indicate that such streams are moving relatively more sediment per unit of turbidity than the regional model, which would be indicative of higher gradient streams, with greater energy for entrainment of sediments, flowing through more erodible soils or soils with physical characteristics that impart less turbidity per unit mass (coarse particles). The smaller intercepts of these models indicate that these are clear waters with little to no suspended material present at the low end of the turbidity range. Conversely, the sites with smaller slope coefficients had larger intercept values (see the sites at the bottom of Figure 3). These smaller slopes are indicative of streams which are moving relatively less sediment per unit of turbidity than the regional model and the greater intercepts indicate that there is some amount of fine suspended material or other turbidity-causing substance, such as organic matter, present at the low end of the turbidity range. Such streams would be expected to have lower gradients, with less energy for entrainment of sediments, to be flowing through soils less available for entrainment or that impart greater turbidity per unit mass (fine particles), or have controls on sediment transport such

as dams. Both the Chickahominy River and the Appomattox River, the sites with the poorest turbidity-sediment model fit, are in this category, and both generally move less sediment than other rivers included in the regional model. Future work will continue to explore, in more detail, how improved models could be developed to regionally model these 10 stations that were not included in the initial regional model.

SUMMARY

A robust regional turbidity-SSC regression model has been developed from data collected from 19 diverse watersheds across Virginia, supporting the idea that regional turbidity-SSC models can be developed in many areas. Subsequent investigations are planned to explore why some sites did not fit the regional model, and whether a regional model can be expanded beyond Virginia, perhaps to the entire Chesapeake Bay Watershed. Potential future applications of the regional turbidity-SSC regression model are promising, given that most of the existing streamgages within Virginia do not currently have continuous turbidity monitors or suspended sediment sampling. As sediment management strategies are implemented and regulators require reduced sediment loadings to major rivers, more efficient sediment monitoring and load estimation techniques are required to track progress towards these goals, and the use of regional turbidity-SSC models could both increase the efficiency and decrease the cost of such efforts.

REFERENCES

Helsel, D.R., and Hirsch, R.M., 2002. Statistical Methods in water resources: U.S. Geological survey Techniques of Water-Resources Investigations., book 4, chap. A3, 523 p.

Jastram, J.D., Moyer, D.L., and Hyer, K.E., 2009. A comparison of turbidity-based and streamflow-based estimates of suspended sediment concentrations in three Chesapeake Bay tributaries: U.S. Geological Survey Scientific Investigations Report 2009-5165, 37 p.

IN-STREAM LASER DIFFRACTION FOR MEASUREMENT OF SUSPENDED-SEDIMENT CONCENTRATION AND PARTICLE-SIZE DISTRIBUTION IN RIVERS

EXTENDED ABSTRACT

Jonathan A. Czuba, Department of Civil, Environmental, and Geo- Engineering and St. Anthony Falls Laboratory, University of Minnesota, Minneapolis, Minnesota, czuba004@umn.edu;
Timothy D. Straub, U.S. Geological Survey, Illinois Water Science Center, Urbana, Illinois;
Christopher A. Curran, U.S. Geological Survey, Washington Water Science Center, Tacoma, Washington;
Mark N. Landers, U.S. Geological Survey, Georgia Water Science Center, Norcross, Georgia;
Marian M. Domanski, U.S. Geological Survey, Illinois Water Science Center, Urbana, Illinois;
Eric E. Grossman, U.S. Geological Survey, Pacific Coastal and Marine Science Center, Santa Cruz, California

Laser-diffraction technology has recently been adapted for in-stream measurement of fluvial suspended sediment concentrations (SSCs) and particle-size distributions (PSDs) as a streamlined (SL), isokinetic version of the Laser In-Situ Scattering and Transmissometry (LISST). The LISST-SL instrument is capable of at-a-point measurements of volumetric SSC and PSD ranging from 1.8–415 μm in 32 log-spaced size classes at a temporal resolution of 2 seconds.

As with any new sediment-measurement or sediment-surrogate technology, the LISST-SL must be rigorously tested with respect to accuracy and reliability in different physiographic environments, and its performance must be compared to concurrent measurements using traditional methods to identify and minimize bias and changes in precision between the old and new technologies (Gray and Gartner, 2009). To this end, we have collected 22 datasets of sediment and streamflow measured concurrently by using a physical sampler, LISST-SL, and acoustic Doppler current profiler (262 samples in all) during 2010–2012 at 16 U.S. Geological Survey streamflow-gaging stations in Washington and Illinois with basin areas ranging from 38 to 69,264 km^2. A detailed description of the methods, results, and discussion of this comparative study has been published by Czuba et al. (2015); herein the major findings are summarized and potential future work is discussed.

As laser diffraction measures volumetric SSC, these measurements must be converted to mass SSC measurements before they can be compared to the data from physical measurements. The conversion from volumetric SSC to mass SSC requires a measurement or assumption of the sample effective density. For fully dispersed quartz grains, the effective density is typically around 2.65 g/mL and for 23 of the physical samples, the effective density varied from 2.56–2.87 g/mL with an average of 2.67 g/mL. In contrast, an unrealistically low computed effective density (mass SSC/volumetric SSC) of 1.24 g/mL (95% confidence interval: 1.05–1.45 g/mL) provided the best-fit value (R^2 = 0.95; RMSE = 143 mg/L) for accurately converting volumetric

SSC to mass SSC for over two orders of magnitude of SSC (12–2,170 mg/L measured by the physical sampler; covering a substantial range of SSC that can be measured by the LISST-SL). These unrealistically low values for the computed effective density suggest something systemic is happening where the LISST-SL is overestimating the volumetric SSC. Explanations for such a low computed effective density have typically pointed to flocculation. However, PSD measured by the LISST-SL and in physical samples (which are dispersed before analysis) were similar, thus ruling out particle flocculation as a major factor.

For now, obtaining accurate mass SSC measurements with a LISST-SL in the fluvial environment requires applying an effective density much less than the density of the sediment particles. Either a best-fit effective density of 1.24 g/mL can be applied, or mass SSC measurements can be made to compute a site-specific effective density for converting volumetric SSC to mass SSC.

The results (Czuba et al., 2015) suggest that the most likely issue is the shortcoming of the laser-diffraction method in only being able to account for irregular particles through the irregular particle kernel matrix (Agrawal et al., 2008). Irregular particles are defined here, following the definition by Agrawal et al. (2008), as rounded or angular particles with particle axes approximately equal. The term "irregular" is used to denote a difference in particle shape from that of spheres but this definition does not include particles that are elongated or flaky. This definition is used because these were the shapes of particles used by Agrawal et al. (2008) in developing the irregular particle kernel matrix. The irregular particle kernel matrix is used to convert "raw" laser-diffraction measurements into concentrations of particles in different size classes. Any elongated (e.g., feldspar) or flaky (e.g., mica) particles present in suspension can create a strong bias in SSC without such an effect on PSD when applying the irregular particle kernel matrix to these particles (Felix et al., 2013). This suggests that a new "fluvial particle kernel matrix" may need to be developed that can account for elongated and flaky particles that may be present in suspension, although more research is needed to confirm that this is the causative factor.

Future work should focus on assessing the suitability of the irregular particle kernel matrix (Agrawal et al., 2008) for actual suspended fluvial material by obtaining suspended material directly from the river and considering the full distribution of fine and coarse material to assess if a different particle kernel matrix would better represent what the LISST-SL is measuring in the fluvial environment. More detailed analysis of the suspended material should be performed using a microscope to assess particle shape and surface characteristics. The characteristics of any organic material should also be assessed as well as the water chemistry affecting potential flocculation. These more detailed measurements at a few sites should provide further insight into the causative factor or factors responsible for the unrealistically low computed effective densities. If this is the case then it will be possible to reprocess all 262 LISST-SL measurements from this study to verify that any new kernel matrix is suitable for the fluvial environment.

REFERENCES

Agrawal, Y.C., Whitmire, A., Mikkelsen, O.A., and Pottsmith, H.C. (2008). "Light scattering by random shaped particles and consequences on measuring suspended sediments by laser diffraction," J. Geophys. Res., 113, C04023, doi:10.1029/2007JC004403.

Czuba, J.A., Straub, T.D., Curran, C.A., Landers, M.N., and Domanski, M.M. (2015). "Comparison of fluvial suspended-sediment concentrations and particle-size distributions measured with in-stream laser diffraction and in physical samples," Water Resour. Res., doi:10.1002/2014WR015697.

Felix, D., Albayrak, I., and Boes, R.M. (2013). "Laboratory investigation on measuring suspended sediment by portable laser diffractometer (LISST) focusing on particle shape," Geo-Mar. Lett., 33(6), pp 485-498, doi:10.1007/s00367-013-0343-1.

Gray, J.R., and Gartner, J.W. (2009). "Technological advances in suspended-sediment surrogate monitoring," Water Resour. Res., 45, W00D29, doi:10.1029/2008WR007063.

HISTORY OF THE FEDERAL INTERAGENCY SEDIMENTATION PROJECT, PART V

J.R. Gray, Scientist Emeritus, U.S. Geological Survey, Reston, Virginia, graysedimentology@gmail.com, and
M.N. Landers, Chief, Federal Interagency Sedimentation Project, U.S. Geological Survey, Atlanta, Georgia, landers@usgs.gov

Abstract: In the late 19th and early 20th centuries, sediment-sampling activities in the United States increased rapidly to support the civil-works programs of several Federal agencies. These agencies and other domestic and foreign investigators developed and used physical samplers of suspended sediment, bedload, and bed material to collect data needed for specific elements of their missions. Most instruments were designed with limited attention to, or knowledge of, sediment-transport concepts or the influence of the equipment on the local flow pattern. As a result, data obtained by different investigators before the 1940s were neither comparable nor could their accuracy be evaluated.

The Federal Interagency Sedimentation Project (FISP) was created in 1939 to unify and standardize fluvial sediment-data-collection instruments and methods used by several Federal agencies. The priorities and thrusts of the FISP have evolved throughout its history in the wake of its accomplishments and in response to the needs of the Federal community for the quantifiably accurate characterization of fluvial sediment concentrations, size distributions, and fluxes. The FISP conducts and supports applied research in topics covering the range of its mission, which includes physical-sampler design, testing, quality assurance, and supply; field methods; computational methods; laboratory analytical methods; and indirect (surrogate) methods.

The priorities of the FISP, along with oversight of its activities, are provided by a Technical Committee comprised of representatives from the supporting Federal agencies. The results of applied research conducted by the FISP appear in over 60 FISP reports, industry standards, and many related journal articles, agency reports, and proceedings papers such as this.

This paper uses and expands upon summaries of the FISP published in 1950, 1963, 1965, 1976, 1979, and 1989 to describe the origins of the FISP, and its six principal phases from 1939-2014. Mission-specific endeavors and their products are highlighted, and potential future research endeavors are summarized.

INTRODUCTION

When the Federal Interagency Sedimentation Project (FISP) was formed in 1939, the objective(s) of most fluvial-sediment measurements focused on the potential for or presence of sediment deposition in reservoirs and in navigation and irrigation channels. The list of sediment-related concerns subsequently has expanded to include bridge scour, erosion of agricultural lands, turbidity-induced aquatic ecosystem degradation, loss of spawning substrate due to fine-grained sediment infilling, reduction in primary productivity, decreases in biotic diversity, and effects from sediment-associated chemical constituents (Larsen et al., 2010). Even reduced sediment-transport rates are now recognized as having deleterious morphologic and economic consequences associated with some of the world's impounded rivers, receiving estuaries, and coastal systems starved of their natural/historical fluvial-sand supplies (Collier et al., 1996; Osterkamp and Gray, 2003).

In 2010, the physical, chemical, and biological damages attributable to fluvial sediment in North America were estimated to range from $20 billion to $50 billion annually (Larsen et al., 2010). Because effective remediation of sediment damages is predicated on the availability of demonstrably credible statistics describing rates of fluvial-sediment transport and deposition, the need for reliable, temporally and spatially consistent sediment data today is paramount. Additionally, a 21st century renaissance in sediment-surrogate technologies is revolutionizing the acquisition of fluvial-sediment data (Rasmussen,

2008; Gray and Gartner, 2009 and 2010a, b; Gray et al., 2010; Voichick and Topping, 2014; Gray and Landers, 2014). Hence, the importance of the FISP's mission – to unify and standardize fluvial-sediment research and development activities of participating Federal agencies – arguably has never been greater.

Skinner's (1989) "History of the Federal Interagency Sedimentation Project," organized into three phases, followed – but did not list as references – at least five previous historical perspectives on the FISP, to wit:

- Nelson and Benedict (1950), "Measurement and Analysis of Suspended Sediment Loads in Streams."
- FISP (1963), "A Summary of the Work of the Inter-Agency Sedimentation Project."
- Witzigman (1965), "A Summary of the Work of the Inter-Agency Sedimentation Project."
- Holeman (1976), "History of the Sedimentation Committee."
- Benedict (1979), "Equipment for Investigations of Fluvial Sediment."

Nelson and Benedict (1950) is the first-such summary of the entity now known as the FISP. Witzigman (1965) is identically titled to, and evidently based on FISP (1963). Thus, Witzigman (1965), which lists four FISP phases, and FISP (1963) together are construed to be the second FISP history. Holeman (1976) is less a historical perspective than a snapshot of the functions and activities of the FISP. Because it was deemed by the authors to add little in the way of historical perspective, it was excluded from this list of FISP histories. Thus, Benedict's (1979) and Skinner's (1989) contributions are considered to be the third and fourth histories of the FISP, respectively – all to the best knowledge of the authors.

This fifth installment weaves information gleaned from the aforementioned publications with other cited sources and contemporary recollections. The latter include contributions from co-author and current FISP Chief Mark N. Landers; perspectives shared by former FISP Chief C. Wayne O'Neal; and those of the principal author based on his 36-year association with the FISP as a customer, contributor, and former U.S. Geological Survey (USGS) representative to and twice-Chairman of the Technical Committee that provides oversight, guidance and programmatic priorities to the FISP.

The intent of this contribution is threefold: Summarize and expand on some of the information contained in the contributions of Nelson and Benedict (1950), FISP (1963), Witzigman (1965), Holeman (1976), Benedict (1979), and Skinner (1989); describe FISP endeavors and accomplishments from 1989-2014; and "peer into the crystal ball" as intrepid soothsayers in an attempt to identify potential future challenges for and directions of the FISP.

BACKGROUND, FORMATION, LOCATION, LEADERSHIP, AND OVERSIGHT

In the late 19th and early 20th centuries, sediment-sampling activities increased rapidly to support civil-works programs in several agencies of the United States (U.S.) Government. These agencies and other domestic and foreign investigators developed and used physical samplers of suspended sediment, bedload, and bed material (FISP, 1940a; b) to collect data needed for specific elements of their missions. Most instruments were designed with limited attention to, or knowledge of, sediment-transport concepts or the influence of the equipment on the local flow pattern (Glysson 1989). Consequently, data obtained by different investigators before the 1940s were neither comparable nor could their accuracy be verified.

By the late 1930s, Federal managers realized that, "…the accuracy of sediment data was affected by lack of standardization in equipment and techniques" (Skinner, 1989). This led to a proposal by G.A. Hathaway of the U.S. Army Corps of Engineers (Corps) and E.W. Lane of the Iowa Institute of Hydraulic Research to form, "a[n interagency] project…to remedy the situation" (Skinner, 1989). The proposal was endorsed by the U.S. Geological Survey, U.S. Department of Agriculture, Bureau of Reclamation, Office of Indian Affairs, Tennessee Valley Authority, and the Corps, and led to the formation of an Intergovernmental Committee under the general supervision of E.W. Lane of (and at) the University of Iowa's Institute of Hydraulic Research in 1939 (Nelson and Benedict, 1950; Brown, 1965; Benedict, 1979). This committee was charged with sponsoring, "an exhaustive study of all problems encountered in collecting sediment data and, eventually, to standardize accepted methods and equipment" (Nelson and Benedict, 1950).

In April 1946, the "activities and functions of the committee were transferred to the Subcommittee on Sedimentation of the Federal Inter-Agency River Basin Committee…which [coordinates] hydrologic activities of the Federal Departments through the assistance of several subcommittees" (Witzigman, 1965). In June 1948 the project was transferred to the St. Anthony Falls Hydraulic Laboratory of the University of Minnesota under the leadership of the Corps' Byrnon C. Colby (Holeman, 1976).

In 1956, the Subcommittee on Sedimentation reorganized the project and named it the Federal Inter-Agency Sedimentation Project, a title – minus the hyphen and either referred to as "the project" or identified by the acronym "FISP" – that remains today. Since 1956, the project has been overseen and sponsored by a Technical Committee comprised of representatives from FISP-member agencies (see the attachment, "A brief history of the Federal Inter-Agency Sedimentation Project").

The USGS's John V. Skinner succeeded Byrnon Colby as project chief and served in this capacity until his 1992 retirement. That year, the project was transferred to the Corps' Waterways Experimentation Station in Vicksburg, Mississippi. The USGS's Dallas Childers led the project in an acting capacity after John Skinner's retirement until C. Wayne O'Neal became FISP Chief by or before 1994.

About two years prior to O'Neal's 2005 retirement, the project's inventory and functions to procure, quality assure, supply, and repair physical sediment samplers and supporting instrumentation were transferred to the USGS's Hydrological Instrumentation Facility (2015) in Bay St. Louis, Mississippi, where those FISP functions continue to be successfully performed today. The project retained its in-house instrument development role. However, by then a sea change in the capabilities and means for acquiring fluvial-sediment data was well underway, to wit: From routine, periodic and/or episodic collection of physical samples, to continuous in situ monitoring of selected sedimentary characteristics using surrogate technologies field-calibrated with FISP physical samplers and sampling techniques.

Upon C. Wayne O'Neal's 2005 retirement, the USGS's Broderick C. Davis became project chief and led the project until his 2012 retirement. By the time the USGS's Mark N. Landers became project chief in 2012, the FISP business model of in-house research and development lasting seven decades had largely yielded to a proposal-driven business model that took advantage of the broad-based experience and expertise in surrogate means for monitoring suspended sediment, bed material, and bedload.

The above-cited sources contain information that resolves a 2-decade-old "chicken-or-the-egg" controversy among FISP personnel and then-members of both the Technical Committee and Subcommittee on Sedimentation that included more than a modicum of jingoism: Which came first, the FISP (and Technical Committee), or the Subcommittee on Sedimentation?

A sedimentation project was formed in 1939 and managed until April 1946 by an "Interdepartmental Committee." That year, oversight authority of the project was transferred to the Subcommittee on Sedimentation of the Federal Inter-Agency River Basin Committee.

In 1956 this Subcommittee, which today is known as the Subcommittee on Sedimentation of the Advisory Council on Water Information (2015), "reorganized the project and called it the Federal Inter-Agency Sedimentation Project" (Witzigman, 1965). Since 1956, the project has been overseen and sponsored by a Technical Committee comprised of representatives from FISP-member agencies.

Thusly is the "chicken-or-the-egg" controversy answered: The Federal Interagency Sedimentation Project was so named, and the Technical committee formed, in 1956. This was at least a decade after the project was referred to as the Subcommittee on Sedimentation.

However, the FISP's mission and operational perspectives can be summarized by its 1939 formative charge which remains more-or-less relevant today, "to study problems in collecting sediment data and to develop, improve, and standardize methods and equipment for determining the quantity and character of sediment carried by streams" (Witzigman, 1965). It is referred to as "the project" in virtually all historical writings. Undoubtedly the aforementioned "basic purpose" of the FISP extends continuously from its

inception to the present, regardless of its title or that of its oversight committee. Ergo, save for any gain or loss of bragging rights, the chicken-or-the-egg question is rendered an immaterial historical footnote.

An epilogue to this story occurred in 2004 when the Subcommittee on Sedimentation was reorganized under the Advisory Committee on Water Information, a public-private entity governed by the Federal Advisory Committee Act. The expectation – subsequently borne out – that non-Federal organizations would join the Subcommittee raised the potential of non-funding organizations to exert influence on the FISP's mission and priorities. This concern, coupled with other factors, resulted in the Subcommittee's decision to formally sever its linkage with the FISP. The FISP's stand-alone status with oversight by the Technical Committee remains extant today.

SIX PHASES OF THE FEDERAL INTERAGENCY SEDIMENTATION PROJECT

With due consideration to the contributions by Nelson and Benedict (1950), FISP (1963), Witzigman (1965), Benedict (1979), and Skinner (1989), the authors determined that the history of the FISP can be summarized as occurring in six phases: Developing,

I. Manual Samplers for Collection of Physical Sediment Samples
II. Sediment-Analytical Instruments
III. Automatic Samplers
IV. Automatic Sediment Gages
V. Manual Samplers for Collection of Trace-Element Water-Quality Samples
VI. Sediment-Surrogate Technologies

Although summaries of all six phases follow, the reader is directed to Nelson and Benedict (1950), FISP (1963), Witzigman (1965), Benedict (1979), and Skinner (1989), for more in-depth descriptions of phases I-IV. Emphases in the ensuing summaries are placed on successes or lack thereof, expressed in terms of knowledge gained, and the instruments and/or methodologies approved and rendered publically available.

Phase I: Manual Samplers for Collection of Physical Sediment Samples, 1939-1980s* Phase I addressed two challenges: An insufficient understanding of the physics of the motion and distribution of sediment particles in suspension and as bedload, and a lack of standardization of samplers and sampling techniques. Research on sedimentary physics in the early years of the FISP led to the recognition of the need for, design, and development of isokinetic samplers and sampling procedures to address deficiencies associated with surface-grab or weighted-bottle samplers. An outstanding body of FISP literature on this topic is available at the FISP web site (water.usgs.gov/fisp) as part of FISP report Nos. 1-14 and A-TT.

Research and development efforts focused on samplers and sampling techniques for collection of representative sediment samples for subsequent laboratory analyses in three categories: In suspension (suspended sediment); rolling, sliding, or saltating on the bed (bedload); and stationary (bed material). Davis (2005) lists most of the FISP samplers described in the following sections. Edwards and Glysson (1999), Nolan et al. (2005), Gray and Landers (2014) and Gray and O'Halloran (2015) describe FISP- and USGS-approved sampler-deployment techniques. Three of the samplers developed as part of Phase I appear in figure 1.

Selected Rigid-Bottle Samplers Developed During FISP Phase I

US DH-48

US DH-59

US D-74

Figure 1 Examples of suspended-sediment samplers developed during Phase I of FISP.

Today there are 16 models of suspended-sediment samplers (table 1 and figures 1 and 2), including those also capable of sampling for trace elements (figure 2); two models of bedload samplers (table 2); four models of bed-material samplers (table 3); and a suite of passive single-stage suspended-sediment samplers developed as part of Phase I. These samplers are described in detail on the FISP web site catalog along with their specifications, operational limits, and links to operator's manuals. The nomenclature for FISP sediment-sampling instruments (tables 1, 2, and 3) denotes the series, type, and year that sampler development started (Davis, 2005). All are available for purchase through the FISP or authorized private-sector firms.

FISP samplers not only are used by several Federal agencies and other organizations in the U.S., but in a number of countries around the world on every continent except Antarctica (Gray and Demas, in press). The simplicity and minimal moving parts of FISP isokinetic samplers, strong theoretical underpinnings supported by laboratory and field-based research, and still-water calibrations impart general confidence in the representativeness of the samples produced.

*The US P-6 point-integrating suspended-sediment sampler (figure 2), which was designed to replace the US P-61, was approved by the Technical Committee in 2012. It cannot be used to collect contamination-free samples for trace-element analyses.

Phase II: Sediment-Analytical Instruments, 1940s-70s Witzigman (1965) and Benedict (1979) describe several laboratory-analytical instruments, some of which remain in use by USGS and other sediment laboratories. Several reports on this subject can be found at FISP (2015).

The bottom-withdrawal tube was developed to determine the size distribution of material up to 0.7 millimeters in diameter in suspended-sediment samples. Only the USGS Louisiana Water Science Center sediment laboratory continues to use this instrument, and only for samples submitted by the Corps' New Orleans District (Cheryl Joseph, USGS written commun., 2015).

The visual-accumulation tube method was developed to determine the size distribution of sand-size material in suspended-sediment, bed-, and beach-material samples. This method remains in use in several USGS fluvial-sediment laboratories.

Investigations into the use of X-rays to quantify particle-size distributions resulted in the development and commercial availability of the Sedigraph in or about 1967. Only one USGS production sediment laboratory – located at the Cascades Volcano Observatory in Vancouver, Washington – continues to use a Sedigraph (Dan Gooding and Julie Nason, USGS, written commun., 2015).

At least two other sediment-analyzing methodologies were investigated: Turbidity and ultrasonics. Turbidity is an optical water-quality characteristic affected by several factors including the color and size of the sediments and the color of the fluid in which they are suspended, in addition to sediment concentration. The ultrasonic method was developed to determine concentrations and size distributions of sediments ranging from 0.040-1.0 millimeters. A laboratory instrument was considered to operate well, but was not considered "competitive" with existing laboratory equipment. No contemporary USGS production sediment laboratory uses ultrasonics to analyze sediment samples.

Phase III: Automatic Samplers, 1940s-60s The FISP developed and produced two types of automatic samplers after the midpoint of the 20th century: Passive single-stage samplers, and the US PS-69 pumping sampler. As designed, both types of samplers drew water from a fixed point in the stream (in the case of the US PS-69, with or without a strainer affixed to the intake orifice).

Table 1 Designations for and Characteristics of FISP Manually Operated Isokinetic Suspended-Sediment Samplers (Davis, 2005; Gray et al., 2008; Gray and Landers, 2014).

Sampler Designation[1]	Nozzle Inner Diameter, cm (in)	Container Type and Capacity	Mode of Suspension	Maximum Depth, m (ft)	Min Isokinetic Velocity, m/s (ft/s)	Max Recommended Velocity[2] m/s (ft/s)	Unsampled Zone, cm (in)	Mass, kg (weight, lbs)
US DH-48	0.48 (3/16), 0.64 (¼)	Rigid bottle 0.47 L (pint)	Wading Rod	2.7 (9)	0.5 (1.5)	2.7 (8.9)	8.9 (3.5)	2 (4)
US DH-59	0.48 (3/16)		Handline or Cable Reel	4.6 (15)		1.5 (5.0)	11 (4.5)	10 (22)
US DH-59	0.64 (¼)			2.7 (9)				
US DH-76	0.48 (3/16), 0.64 (¼)	Rigid bottle 0.95 L		4.6 (15)		2.0 (6.6)	8.1 (3.2)	11 (25)
US DH-81	0.48 (3/16)	Rigid bottle 1 L	Wading Rod	2.7 (9)	0.6 (2.0)	1.9 (6.2)	10 (4.0)	0.5 (1)
US DH-81	0.64 (¼)					2.3 (7.6)		
US DH-81	0.79 (5/16)					2.1 (7.0)		
US DH-95	0.48 (3/16)		Handline or Cable Reel	4.6 (15)	0.6 (2.1)	1.9 (6.2)	12 (4.8)	13 (29)
US DH-95	0.64 (¼)				0.5 (1.7)	2.1 (7.0)		
US DH-95	0.79 (5/16)				0.6 (2.1)	2.3 (7.4)		
US DH-2	0.48 (3/16)	Flexible 1-L bag		11 (35)	0.6 (2.0)	1.8 (6.0)	8.9 (3.5)	14 (30)
US DH-2	0.64 (¼)			6.1 (20)				
US DH-2	0.79 (5/16)			4.0 (13)				
US D-74	0.48 (3/16)	Rigid bottle 0.47 L (pint) or 0.95 L (quart)	Cable Reel	4.6 (15)	0.5 (1.5)	2.0 (6.6)	10 (4.1)	28 (62)
US D-74	0.64 (¼)			2.7 (9) pint 4.6 (15) quart				
US D-74AL	0.48 (3/16)			4.6 (15)		1.8 (5.9)		19 (42)
US D-74AL	0.64 (¼)			2.7 (9) pint 4.6 (15), quart				
US D-95	0.48 (3/16)	Rigid bottle 1 L		4.6 (15)	0.5 (1.7)	1.9 (6.2)	12 (4.8)	29 (64)
US D-95	0.64 (¼)				0.6 (2.0)	2.0 (6.7)		
US D-95	0.79 (5/16)							
US D-96	0.48 (3/16)[3]	Flexible 3-L bag		34 (110)	0.9 (3.0)	3.8 (12.5)	10 (4.0)	60 (132)
US D-96	0.64 (¼)			18 (60)				
US D-96	0.79 (5/16)			12 (39)				
US D-96-A1	0.48 (3/16)[3]			34 (110)		1.8 (6.0)		36 (80)
US D-96-A1	0.64 (¼)			18 (60)				
US D-96-A1	0.79 (5/16)			12 (39)				
US D-99	0.48 (3/16)[3]	Flexible 6-L bag		67 (220)	1.22 (4.0)	4.6 (15.0)	24 (9.5)	125 (275)
US D-99	0.64 (¼)	Flexible 6- or 3-L bag		37 (120)	1.13 (3.7) or 0.91 (3.0)[4]			
US D-99	0.79 (5/16)			24 (78)				
US P-61-A1	0.48 (3/16)	Rigid bottle 0.47 L or 0.95 L		55 (180), pint 37 (120), quart	0.5 (1.5)	3.0 (10.0)	11 (4.3)	48 (105)
US P-63	0.48 (3/16)					4.6 (15.0)	15 (5.9)	91 (200)
US P-72	0.48 (3/16)			22 (72), pint 16 (51), quart		1.6 (5.3)	11 (4.3)	19 (41)
US P-6	0.48 (3/16)	Rigid bottle 0.95 L		49 (160), quart	0.5 (1.5)	4.0 (13)	8.9 (3.5)	45 (100)

[1]Samplers designated in *italics* may also be used for collection of trace-element samples as described in the USGS National Field Manual for the Collection of Water Quality-Data (USGS, 2014).

[2] For rigid-bottle samplers, the maximum recommended velocity for sampler deployment is based either on measured isokinetic limitations or on the maximum velocities used in isokinetic and stability tests. Bag samplers were determined to retain isokinetic characteristics at the highest velocities tested.

[3]The 3/16-inch-diameter nozzle is more sensitive to velocity and temperature effects than larger-diameter nozzles, and only should be used when necessary to sample greater depths with these bag samplers.

[4] The minimum isokinetic velocities for the US D-99 sampler at water temperatures greater than 10°C and less than 10°C are 0.91 m/s (3.0 ft/s) and 1.1 m/s (3.7 ft/s), respectively, unless the 0.48-mm (3/16-in) nozzle is used, in which case it is 1.22 m/s (4.0 ft/s).

Table 2 Designations for and Characteristics of FISP Manually Operated Bed-Material Samplers (Davis, 2005).

Sampler Designation	Description	Sampler Weight (pounds)	Maxi-mum Sampler Pene-tration (inches)	Maxi-mum Sample Volume (cubic inches)
US BMH-53	Hand-held, 2-inch diameter, piston-type bed-material sampler.	7.5	8	25
US BM-54	Cable-suspended, spring-loaded scoop, bed-material sampler	100	2	18
US BMH-60	Cable-suspended, spring-loaded scoop, bed-material sampler	32	1.7	11
US RBMH-80	Hand-held rotary-scoop bed-material sampler	8	1.8	15

Table 3 Designations for and Characteristics of FISP Manually Operated Bedload Samplers (Davis, 2005).

Sampler Designation	Description	Sampler Weight (pounds)	Nozzle Width X Height (inches)	Maximum Velocity (feet per second)
US BL-84	Cable-suspended, mesh bag bedload sampler	32	3 x 3	9
US BLH-84	Hand-held, mesh bag bedload sampler	10	3 x 3	**
Bed Load Trap	Portable mesh bag, fixed location bedload sampler	32	12 x 8	variable

**rod-deployed either by wading or from above the stream; maximum velocity is probably 9 ft/s.

A U-series single-stage sampler (FISP, 1963; Witzigman, 1965; Benedict, 1979; FISP, 2015) collects samples of near-surface water on the rising hydrograph. They are typically deployed in a series of samplers affixed at different elevations to a pier, wingwall, or other stable structure. When the total head incident on the intake orifice results in water cresting inside the intake-tube weir, stream water siphons into a sample bottle and the displaced air vents through an exhaust tube. When the sample rises to the elevation of the exhaust pipe's orifice inside the bottle, an airlock forms and sample collection should cease. However, in practice, sample recirculation sometimes occurs, preferentially enriching the sedimentary content of the sample. Additional unreliability could result from a presumed inability to representatively capture sand-size material. In spite of these drawbacks, the FISP U-series samplers and other types of passive automatic samplers that they inspired, including a design by Gray and Fisk (1991) that precludes the potential for sample recirculation, remain in use at some field sites.

Skinner (1989) describes the PS-69 pumping sampler, which the FISP developed and produced to collect fixed-point samples at gaging stations on relatively "flashy" streams and at those that could not be adequately sampled by an observer. FISP-produced prototypes include the PS-62, PS-66, and PS-67 pumping samplers, which, along with the PS-69, were field tested in the 1960s in Maryland (Yorke, 1976). Desirable features of the PS-69 included a 12-volt power system; sample rack that held 72 quart-size containers; and an intake-line backflush system using an in-gage reservoir that was refilled after each backflush cycle. Its drawbacks included its large size and power requirements, complexity with many moving parts, and lack of reliability in the challenging field environment. The FISP ceased to supply and support the PS-69 samplers some years after the first commercial pumping samplers made by Manning Environmental Corporation, and ISCO Corporation became available by the early 1980s.

Phase IV: Automatic Sediment Gages, 1950s-80s FISP (1963), Skinner and Beverage (1976), and Skinner (1989) summarized FISP endeavors to automate the collection of suspended-sediment data in the field and laboratory. They describe investigations in radiant energy (acoustic and electromagnetic, including gamma rays), applied forces (a densimetric technique), a vibratory technique as part of a U-tube, and electrical conduction. The latter takes advantage of a disparity in the conductivity of river water to that of the entrained sediments. In retrospect, the FISP was ahead of its time in this pre-microcomputer age. None of these efforts resulted in the wide-scale field-deployment of "automated sediment gages."

Phase V: Manual Samplers for Collection of Trace-Element Water-Quality Samples, 1990s-2006 In the 1980s, a need for trace-element data at parts-per-billion-level concentrations (as opposed to the parts-per-million-level concentrations measurements for suspended sediment and many chemical constituents including nutrients and common ions) presented the prospect of contamination from the sampling apparatus, particularly for samples collected for trace-metal analyses. A decision to simply coat FISP suspended-sediment samplers used to collect trace-element samples with white marine epoxy paint proved disastrous from a data-quality perspective. Much of the derived dissolved trace-element data were rendered unreliable due to contamination from the sampler in spite of the epoxy coating (USGS, 1991).

Rigid-Bottle Samplers Developed During FISP Phase V		
		
US DH-81	US D-95	US P-6
Bag-Type Samplers Developed During FISP Phase V		
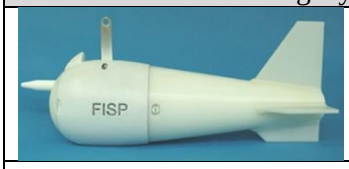	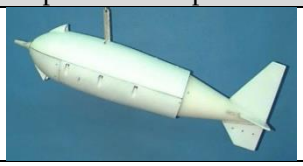	
US DH-2	US D-96	US D-99

Figure 2 Examples of suspended-sediment samplers developed during Phase V of FISP (the US P-6 cannot be used to collect samples for trace-element analyses).

Phase VI: Developing Sediment-Surrogate Technologies, approximately 2004-present By the arrival of the third millennium, the availability of hardware and relatively robust software that postdated FISP's Phase III automated sediment gage-development efforts were being exploited by a number of researchers and some private-sector firms to develop surrogate means for measurements of suspended-sediment concentrations and size distributions, bedload-transport rates, and bed-material size distributions. Their primary focus was on bulk-optic, laser-optic, acoustic, and pressure-differential surrogate metrics capable of providing high-temporal – and in some cases also high-spatial – resolution time-series data (Gray and Gartner, 2009). When calibrated to sediment characteristics using concurrently collected physical samples, these surrogate methods provide substantial improvements in the acquisition and accuracy of the data produced, primarily due to the temporal continuity afforded by in situ surrogate instruments. Moreover, these surrogate methodologies promise to lower monitoring costs in the medium-to-long term.

By 2004, after its successful decade-long, primary focus on development of trace-element samplers, the FISP found itself in need of expertise and momentum if it hoped to take on a leadership role in the burgeoning field of sediment-surrogate technologies. By then, bulk optics (turbidity) had matured as a surrogate metric for suspended-sediment concentration and was being integrated into selected operational programs (Rasmussen et al., 2008). With the publication of the USGS-produced and -sanctioned technique for converting continuous turbidity measurements to mass-concentration values (Rasmussen et

al., 2009), the FISP subsequently refrained from supporting turbidity research projects in lieu of other compelling but inadequately resolved sediment-surrogate technologies.

The initial Phase VI surrogate technology to be evaluated by the FISP was laser scattering (Gray and Gartner, 2009). Laser scattering provides at-a-point values for volumetric concentrations back-calculated from the sum of particles measured volumetrically in 32 size classes. The FISP has funded research projects to evaluate the LISST-SL, an isokinetic laser-scattering instrument (Czuba et al., 2015). This research led to the FISP's sanctioning laser-diffraction analyzers for environmental volumetric measurements for both suspended-sediment concentrations and particle-size distributions, albeit with important caveats (FISP, 2013).

FISP is currently funding sediment-acoustic research. Sediment acoustics was deemed by Gray and Gartner (2009) to be the most promising for meeting the needs of large-scale fluvial-sediment monitoring programs, a contention reiterated by the authors today. The use of manually deployed or in situ acoustic Doppler current (ADCP) meters, in particular, shows considerable potential as a surrogate technology for suspended-sediment concentration and possibly also to quantify particle-size classes, to wit:

1. ADCPs already are used extensively for streamflow monitoring and provide river-velocity data,
2. A direct measure of the cross-sectional variability in sediment concentrations is provided,
3. The technology is not as susceptible to biofouling as other surrogate technologies, such as turbidity sensors,
4. The technology measures a larger volume than other surrogate technologies, and
5. Acquisition of sediment-size information is possible using multiple acoustic frequencies.

FISP continues to fund evaluations of a densimetric technology that exploits the differences in the pressures simultaneously sensed by precision pressure transducers at two in situ orifices separated by a fixed distance in a water column. The technology's performance theoretically improves with increasing suspended-sediment concentrations exceeding some 10-20 grams per liter. The densimetric technology was evaluated by the USGS in Puerto Rico, Arizona, and, most recently and successfully, at New Mexico's Rio Puerco, a tributary of the middle Rio Grande renowned for conveying highly sediment-laden flows (Brown et al., 2015).

FUTURE CHALLENGES AND DIRECTIONS

The purpose of the FISP continues to be driven by the need for reliable sediment-monitoring equipment and methods in a world where the relevance of sediment information continues to increase. The future directions of the FISP – in response to known and emerging challenges – involve a growing knowledge of and improved methods for physical sampling and for continuous sediment monitoring using surrogate technologies. Primary focus areas and concomitant challenges for the FISP in the foreseeable future may include the following:

- Develop and improve operational instrumentation and methods to monitor suspended-sediment characteristics (concentrations, loads, particle-size distributions) using acoustic backscatter at high-temporal and/or high-spatial resolution.
- Develop and improve operational instrumentation and methods to monitor bedload using acoustic and other surrogates at high-temporal and/or high-spatial resolution.
- Obtain improved understanding and characterization (including sampling accuracy) of physical sediment samplers, particularly bag-type samplers, using computational fluid dynamic modeling and field verification.
- Evaluate and improve instruments and methods for physical bedload sampling.
- Continued evaluation and development of new technologies including those based on laser-diffraction and densimetric principals.
- Evaluate technologically advanced methods for fluvial-sediment laboratory analyses and records processing.

The foci and thrusts of the FISP have changed in response to member-agency needs and evolving capabilities over its ¾-century existence. The authors hope to read a "FISP History Part VI" before the cessation of their respective dotages – perhaps to commemorate the FISP's centennial in 2039.

ACKNOWLEDGEMENTS

The veracity and content of this contribution benefited considerably from peer reviews provided by Jerry Bernard (retired) and Marie Garsjo (retired), Natural Resources Conservation Service; C. Wayne O'Neal (retired), FISP; and Robert Hilldale, Bureau of Reclamation. The artistic prowess of the USGS's Annette Goode toward formatting of the tables and figures in this manuscript was greatly appreciated.

REFERENCES CITED

Benedict, P.C. (1979). Equipment for investigations of fluvial sediment. Proceedings of the American Society of Civil Engineers, Journal of the Hydraulics Division, Vol. 105, No. HY3, March, 1979, p. 163-170; http://cedb.asce.org/cgi/WWWdisplay.cgi?8619.

Brown, C.B. (1965). Reflections on the first Federal Sedimentation Conference: Proceedings of the [Second] Federal Inter-Agency Sedimentation Conference 1963, Jackson, Mississippi, January 28-February 1: U.S. Department of Agriculture Miscellaneous Publication No. 970, Agricultural Research Service, p. 1-4; http://acwi.gov/sos/pubs/2ndFISC/2Fiscopn.pdf.

Brown, J.E., Gray, J.R., and Hornewer, N.J. (2015). In situ densimetric measurements of suspended sediments at the Rio Puerco, New Mexico: Proceedings of the 10th Federal Interagency Sedimentation Conference, April 19-23, 2015, Reno, Nevada, 12 p.

Collier, Michael, Webb, R.H., and Schmidt, J.C. (1996). Dams and rivers – a primer on the downstream effects of dams: U.S. Geological Survey Circular 1126, 94 p.; http://pubs.usgs.gov/circ/1996/1126/report.pdf.

Czuba, J. A., Straub, T.D., Curran, C. A., Landers, M.N., and Domanski, M.M. (2015), Comparison of fluvial suspended-sediment concentrations and particle-size distributions measured with in-stream laser diffraction and in physical samples: Water Resources. Research, 51, doi:10.1002/2014WR015697; http://onlinelibrary.wiley.com/doi/10.1002/2014WR015697/abstract?campaign=agupersonalchoice.

Edwards, T.E., and Glysson, G.D. (1999). Field methods for measurement of fluvial sediment: U.S. Geological Survey Techniques of Water-Resources Investigations, Book 3, chapter C2, 89 p. http://water.usgs.gov/osw/techniques/sedimentpubs.html.

Federal Interagency Sedimentation Project. (1940a). Field practice and equipment: Report No. 1, 175 p.; http://water.usgs.gov/fisp/docs/Report_1.pdf.

Federal Interagency Sedimentation Project. (1940b). Equipment used for sampling bed-load and bed material: Report No. 2, 56 p.; http://water.usgs.gov/fisp/docs/Report_2.pdf.

Federal Interagency Sedimentation Project. (1963). A summary of the work of the Federal Inter-Agency Sedimentation Project: FISP Report S, 29 p.; http://water.usgs.gov/fisp/docs/Report_S.pdf.

Federal Interagency Sedimentation Project. (2013). FISP approval of the use of field-deployed LISST-series laser diffraction analyzers for volumetric concentration and particle-size data: Technical Memorandum 2013.02, 6 p.; http://water.usgs.gov/fisp/docs/FISP_Tech_Memo_2013.02.pdf.

Federal Interagency Sedimentation Project (2015). Home page; http://water.usgs.gov/fisp/.

Glysson, G.D. (1989).100 years of sedimentation study by the USGS: Proceedings of the International Symposium, Sediment Transport Modeling , Sam Y. Wang, ed., American Society of Civil Engineers, Reston, Virginia, p. 260-265.

Gray, J.R., and Demas, C.R. (in press). Measuring sediment transport in large rivers, D.E. Walling, ed: Chapter 4.2.2 in a compendium inspired by the1st International Conference on the Status and Future of the World's Large Rivers, Vienna, Austria, April 11-14, 2011, full volume edited by Helmut Habersack, 15 p.; see authors for manuscript.

Gray, J.R., and Fisk, G.G., 1992, Monitoring radionuclide and suspended-sediment transport in the Little Colorado River basin, Arizona and New Mexico, USA, *in*, Bogen, J., Walling, D.E., and Day, T.J., eds, Erosion and Sediment Transport Monitoring Programmes in River Basins, Proceedings: International Association of Hydrological Sciences Publication No. 210, p. 505-516; http://ks360352.kimsufi.com/redbooks/a210/iahs_210_0505.pdf.

Gray, J.R., and Gartner, J.W. (2009). Technological advances in suspended-sediment surrogate monitoring: Water Resources Research, 45, W00D29; http://water.usgs.gov/osw/techniques/2008WR007063.pdf.

Gray, J.R., and Gartner, J.W. (2010). Surrogate technologies for monitoring suspended-sediment transport in rivers, *in*, Poleto, Cristiano, and Charlesworth, Susanne, eds., Sedimentology of Aqueous Systems, London: Wiley-Blackwell, Chapter 1, p. 3-45; http://water.usgs.gov/osw/techniques/sed_aq_sys_chap_1_pdf_from_wb_3_16_2010.pdf.

Gray, J.R., and Gartner, J.W. (2010). Surrogate technologies for monitoring bed-load transport in rivers, *in*, Poleto, Cristiano, and Charlesworth, Susanne, eds., Sedimentology of Aqueous Systems, London: Wiley-Blackwell, Chapter 2, p. 45-79; http://water.usgs.gov/osw/techniques/sed_aq_sys_chap_2_pdf_from_wb_3_16_2010.pdf.

Gray, J.R., Laronne, J.B., Marr, J.D.G. (2010). Bedload-surrogate monitoring technologies: U.S. Geological Survey Scientific Investigations Report 2010–5091, 37 p.; http://pubs.usgs.gov/sir/2010/5091 [The papers listed in table 2 are available only online at: http://pubs.usgs.gov/sir/2010/5091/papers/listofpapers.html].

Gray, J.R., and Landers M.N. (2014). Measuring suspended sediment, in: Ahuja S. (ed.) Comprehensive Water Quality and Purification: United States of America, Elsevier, Vol. 1, p. 157-204; http:// water.usgs.gov/osw/techniques/sediment/gray_landers_elsevier_chapter_12_10_17_2013.pdf.

Gray J.R., and O'Halloran, Denis (2015). Maximizing the reliability and cost-effectiveness of your suspended-sediment data: Proceedings of the 10th Federal Interagency Sedimentation Conference, April 19-23, 2015, Reno, Nevada, 14 p.

Holeman, J.N. (1976). Prologue, history of the sedimentation committee: Proceedings of the Third Federal Inter-Agency Sedimentation Conference, May 22-25, 1976, Denver, Colorado, p. IX-XIV.

Larsen, M.C., Gellis, A.C., Glysson, G.D., Gray, J.R., and Horowitz, A.J. (2010). Fluvial sediment in the environment – a national challenge: Proceedings of the 9th Federal Interagency Sedimentation Conference, June 27–July 1, Las Vegas, Nevada, 15 p.; http://acwi.gov/sos/pubs/2ndJFIC/Contents/OS_Larsen_9fisc_sediment_vision_3_4_2010.pdf.

Nelson, M.E. and Benedict, P.C. (1950). Measurement and analysis of suspended sediment loads in streams: American Society of Civil Engineers, Transactions, Proceedings-Separate No. 31, p. 891-918.

Nolan, K.M., Gray, J.R., and Glysson, G.D. (2005). Introduction to suspended-sediment sampling: U.S. Geological Survey Scientific Investigations Report 2005-5077. On CD-ROM and at: http://pubs.er.usgs.gov/pubs/sir/sir20055077.

Osterkamp, W.R., and Gray, J.R. (2003). Hazard mitigation related to water and sediment fluxes in the Yellow River basin, China, based on comparable basins of the United States: Proceedings of the 1st International Yellow River Forum on River Basin Management, October 21-24, 2003, Zhengzhou, Henan Province, China, the Yellow River Conservancy Publishing House, Vol. II, p. 465-473; http://www.irtces.org/isi/isi_document/wro_jrg_yellow_river.pdf or http://pubs.er.usgs.gov/publication/70120294.

Rasmussen, T.J., Lee, C.J., and Ziegler, A.C. (2008), Estimation of constituent concentrations, loads, and yields in streams of Johnson County, northeast Kansas, using continuous water-quality monitoring and regression models, October 2002 - December 2006: U.S. Geological Survey Scientific Investigations Report 2008–5014, 103 p.; http://pubs.usgs.gov/sir/2008/5014/.

Rasmussen, P.P., Gray, J.R., Glysson, G.D., and Ziegler, A.C. (2009). Guidelines and procedures for computing time-series suspended-sediment concentrations and loads from in-stream turbidity-sensor and streamflow data: U.S. Geological Survey Techniques and Methods Book 3, Chapter C4, 53 p.; http://pubs.usgs.gov/tm/tm3c4/.

Skinner, J.V. (1989). History of the Federal Interagency Sedimentation Project, *in*, Proceedings of the International Symposium, Sediment Transport Modeling, edited by Sam S.Y. Wang, American Society of Civil Engineers, New Orleans, Louisiana, 14-18 August, p. 266-271; http://water.usgs.gov/fisp/docs/FISP_history_1989.pdf.

Skinner, J.V. and Beverage, J.P. (1976). Automatic collection of sediment data: Proceedings of the Third Federal Inter-Agency Sedimentation Conference, May 22-25, 1976, Denver, Colorado, p. 7-1 to 7-16; http://acwi.gov/sos/pubs/3rdFISC/3Fisc-7.pdf.

Subcommittee on Sedimentation of the Advisory Committee on Water Information (2015). Home page: http://acwi.gov/sos/.

U.S. Geological Survey (1991). Contamination of dissolved trace-element data: present understanding, ramifications, and issues that require resolution: Office of Water Quality Technical Memorandum 91.10; http://water.usgs.gov/admin/memo/QW/qw91.10.html.

U.S. Geological Survey (2014). National field manual for collection of water-quality data: Techniques of Water-Resources Investigations Book 9, Nine Chapters, variously paged and dated; http://water.usgs.gov/owq/FieldManual/.

U.S. Geological Survey (2015). Hydrological Instrumentation Facility: Home Page; http://water.usgs.gov/hif/.

Voichick, N., and Topping, D.J. (2014). Extending the turbidity record – making additional use of continuous data from turbidity, acoustic-Doppler, and laser diffraction instruments and suspended-sediment samples in the Colorado River in Grand Canyon: U.S. Geological Survey Scientific Investigations Report 2014–5097, 31 p.; http://dx.doi.org/10.3133/sir20145097.

Witzigman, F.S. (1965). A summary of the work of the Inter-Agency Sedimentation Project: Proceedings of the [Second] Federal Inter-Agency Sedimentation Conference 1963, January 28-February 1, 1963, Jackson, Mississippi: U.S. Department of Agriculture, Miscellaneous Publication No. 970, Agricultural Research Service, Paper No. 25, p. 166-177; http://acwi.gov/sos/pubs/2ndFISC/2Fisc-1.pdf.

Yorke, T.H. (1976). Ten years of experience with automatic pumping-sediment samplers: Proceedings of the Third Federal Inter-Agency Sedimentation Conference, May 22-25, 1976, Denver, Colorado, p. 7-54 to 7-64; http://acwi.gov/sos/pubs/3rdFISC/3Fisc-7.pdf.

ATTACHMENT

A BRIEF HISTORY OF THE FEDERAL INTER-AGENCY SEDIMENTATION PROJECT*

(unattributed and undated, inferred from content to have been written in or after 1956)

In 1939, representatives of several Federal Agencies met to discuss ways of improving methods for measuring the quantity and characteristics of sediment that is transported in rivers. These representatives organized an Interdepartmental Committee to standardize methods and equipment for collecting sediment data. The following agencies supported the standardization effort: Corps of Engineers of the Department of the Army; Flood Control Coordinating Committee of the Department of Agriculture; U.S. Geological Survey; Bureau of Reclamation; Office of Indian Affairs of the Department of Interior; and the Tennessee Valley Authority. The Iowa Institute of Hydraulic Research cooperated in the work which was performed at the Hydraulic Laboratory, State University of Iowa, Iowa City, Iowa.

From 1939 to 1942 the project was under the general supervision of Professor E. W. Lane. From July 1942 to July 1945, the project was supervised by M. E. Nelson, Army Corps of Engineers, and L. C. Crawford, Geological Survey; the research work was conducted by personnel from both agencies.

In April 1946, the Interdepartmental Committee transferred its authority the Subcommittee on Sedimentation of the Federal Inter-Agency River Basin Committee. The River Basin Committee was composed of representatives from the Department of the Army, Department of the Interior, Department of Agriculture, Department of Commerce, Tennessee Valley Authority, and Federal Power Commission. The main objective of the Committee was to coordinate all Federally sponsored hydrologic studies.

In June 1948, the Subcommittee on Sedimentation moved the project from the Iowa Institute of Hydraulic Research to the St. Anthony Falls Hydraulic Laboratory at the University of Minnesota in Minneapolis, Minnesota. From 1946 to 1955, project activities were under the general supervision of M. E. Nelson, Army Corps of Engineers, and P. C. Benedict, U.S. Geological Survey. Mr. B. C. Colby directed the research work.

In 1956, the Subcommittee reorganized the project and called it the Federal Inter-Agency Sedimentation Project. The Subcommittee also adopted a formal Guidance Memorandum that described the project's objectives and organization.

Since 1956, the project has been sponsored by a Technical Committee composed of representatives from Federal Agencies that are involved in sediment studies. Major policies that affect the project are made by the Sedimentation Committee of the Interagency Advisory Committee on Water Data of the Water Resources Council. The project's staff conducts basic and applied research and also develops, tests, and calibrates sediment equipment.

Currently, agencies represented on the Technical Committee are: Army Corps of Engineers, U.S. Geological Survey, Bureau of Reclamation, Agricultural Research Service, U.S. Forest Service, Federal Highway Administration, and the Bureau of Land Management.

**This title and ensuing text reflects verbatim the contents of an unattributed, undated 2-page FISP "history" discovered by John R. Gray (USGS Scientist Emeritus) when G. Douglas Glysson (USGS, retired) cleaned the last USGS office that Glysson occupied on the 5th floor of the USGS National Center, Reston, Virginia, in late 2014. The file was scanned by Annette Goode, USGS Office of Surface Water, in December 2014. It was subsequently reformatted to fit on one page as it appears above.*

Although the veracity of this "history" has not been unequivocally verified, some parts are undoubtedly correct based on Gray's knowledge of the Project, and on histories published by Witzigman (1965) and Skinner (1989). Coupled with the circumstances under which it was found, there is little doubt that it is authentic and reliable. Thus it is hereby included as part of the permanent FISP record by John R. Gray, 2015

ONE-STOP SHOPPING FOR FLUVIAL-SEDIMENT DATA: THE USGS SEDIMENT-DATA PORTAL

EXTENDED ABSTRACT

Casey Lee, U.S. Geological Survey National Water Quality Assessment Program; 4821 Quail Crest Place, Lawrence, KS; cjlee@usgs.gov
Meredith Warren, U.S. Geological Survey Center for Data Analytics; 8505 Research Way Middleton, WI; mwarren@usgs.gov

Since the first samples on the Rio Grande in 1889, the U.S. Geological Survey (USGS) has been collecting information on sediment transport in streams and rivers across the United States. Although the USGS maintains an extensive database of sediment and related data through the National Water Information System (NWIS), these data can be difficult to utilize because:

1. It can be challenging to ascertain where and when suspended-sediment data have been collected.
2. It can be difficult to determine if non-representative sampling methods have left suspended-sediment and associated data are prone to bias.
3. There has been limited aggregation of information needed to interpret sediment data, such as information on sediment grain size, streamflow, and landscape conditions.

In 2013, the USGS National Water Quality Assessment Program (NAWQA) took an initial step toward minimizing these problems through release of the USGS Sediment Data Portal (Figure 1). The portal improves the utility and accessibility of USGS suspended-sediment data by providing tools to visualize, filter, and download discrete and daily suspended-sediment data and sampling site characteristics.

Data served through the portal represent the best available compendium of suspended-sediment data for streams and rivers in the United States, serving results from more than 600,000 discrete sediment samples and more than 10,000 years of daily sediment data. An accompanying USGS Data Series Report, "Compilation, Quality Control, Analysis, and Summary of Discrete Suspended-Sediment and Ancillary Data in the United States, 1901-2010" describes methods used to recover and quality control existing USGS suspended-sediment data, and summarizes suspended-sediment and selected ancillary data across the United States with respect to time, streamflow, and landscape condition.

The USGS Sediment Data Portal can be accessed at: http://cida.usgs.gov/sediment.

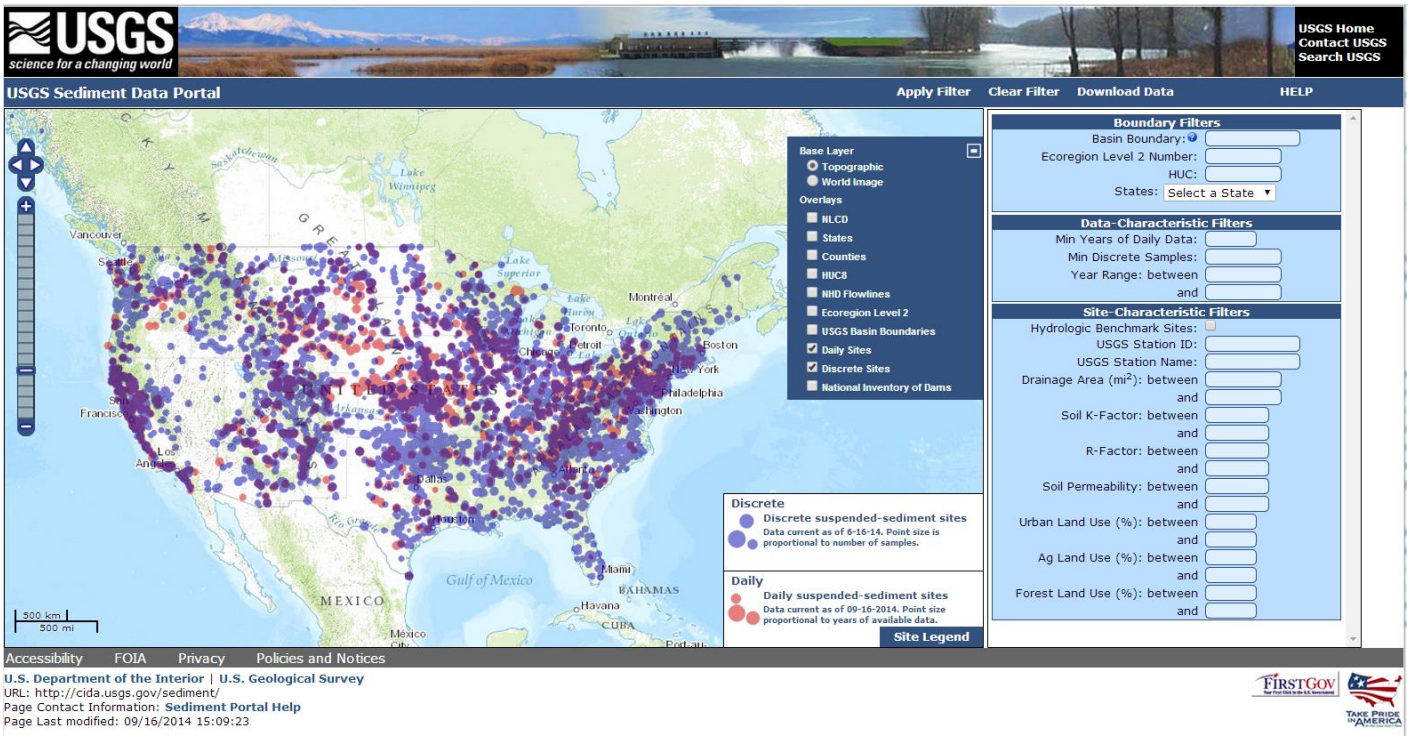

Figure 1. The USGS Sediment Data Portal

ELECTRONIC NOTES APPLICATION FOR ON-SITE RECORDING AND STORAGE OF U.S. GEOLOGICAL SURVEY FLUVIAL-SEDIMENT DATA

Julio A. Oms, Hydrologic Technician, U.S. Geological Survey, Guaynabo, Puerto Rico, omsjulio@hotmail.com
Dianne López-Trujillo, Information Technology Specialist, U.S. Geological Survey, Guaynabo, Puerto Rico, dlopez@usgs.gov
John R. Gray, U. S. Geological Survey, Scientist Emeritus, Reston, Virginia, graysedimentology@gmail.com
Kenneth A. Skach, Computer Specialist, U.S. Geological Survey, Portland, Oregon, kaskach@usgs.gov Francisco Granado-Santos, Student, U.S. Geological Survey, Guaynabo, Puerto Rico, fgranado-santos@usgs.gov

Abstract The fully electronic Sediment Data and Information Web-based (SEDWE) application enables use of a range of hand-held platforms to efficiently and accurately record U. S. Geological Survey (USGS) fluvial-sediment sample and ancillary data before departing the sediment-monitoring site. The field data are subsequently transferred to the USGS National Water Information System (NWIS) and USGS Sediment Laboratory Environmental Database System (SLEDS) via the USGS Sediment-sample LOGIN (SedLOGIN) application. The ensuing permanent NWIS record includes all relevant field data conveyed via SEDWE and sample-analytical results conveyed via SLEDS.

SEDWE provides a standardized paperless alternative for documenting fluvial-sediment data collected in the field, while retaining relevant metadata. The application, which functions on smart phones, tablets, and personal computers, is anticipated to become a standard tool for use by the USGS to capture, store, and share a more useful and explanatory record of fluvial-sediment sample and ancillary data.

INTRODUCTION

The U.S. Geological Survey (USGS) Sediment Data and Information Web-based Application (SEDWE) enables field-data collectors to efficiently and accurately record and store USGS fluvial-sediment and related ancillary data at a sediment-monitoring site (hereafter referred to as a "USGS sediment station"). These data are recorded on a hand-held electronic device in the field, and subsequently uploaded to the USGS National Water Information System (NWIS) (USGS, 2015) through the intermediary Sediment-sample LOGIN (SedLOGIN) application (USGS, 2010). The ensuing permanent NWIS record includes all relevant field data conveyed via SEDWE and sample analytical results conveyed via SLEDS.

The fully electronic SEDWE application was designed to increase the efficiency, completeness, and accuracy of field-data collection and subsequent storage in USGS databases. For storage of fluvial-sediment data collected as part of a larger suite of water-quality samples, USGS personnel are encouraged to continue to use the Personal Computer Field Form (PCFF) (Wilde, 2008). The use of the SEDWE and PCFF applications is preferred over paper-based field notes. SEDWE is anticipated to become a standard tool for use by the USGS to document a more useful and explanatory set of ancillary data associated with collection of fluvial-sediment samples.

Background Sediment-discharge measurements in the U.S. began in 1938 when Captain Talcott sampled the Mississippi River (Skinner, 1989). The formation of the Federal Interagency Sedimentation Project (FISP, 2015; Gray and Landers, 2015) in 1939 led to the development of quality-assured fluvial-sediment data-collection instruments and methods that remain in use today (Diplas and others, 2008). FISP instruments and methods are widely used for collecting fluvial-sediment data by most Federal agencies; many Tribes, States, and local governments;

and many countries around the world (Gray and Demas, in press). Sediment data produced by the USGS are collected, analyzed, and stored following guidelines and policies described by Porterfield (1972), Johnson (1997), Edwards and Glysson (1999), Nolan and others (2005), Koltun and others (2006), Diplas and others (2008), and Gray and Landers (2014), and Gray and O'Halloran (2015).

Until 2010, the only formal requirement for storage of data associated with USGS sediment stations included mean-daily values of streamflow, time-weighted suspended-sediment concentration, and suspended-sediment discharge, along with discrete particle-size data (if analyzed). In 2010, the USGS issued mandatory guidelines for storing a larger suite of discrete fluvial-sediment data and associated ancillary information. In addition to water-sediment samples collected manually or automatically in the field, ancillary parameters required by the SedLOGIN application include information on water temperature, sampler type, and method of deployment (USGS, 2010).

The SedLOGIN application was released in February 2010 as part of USGS policy to facilitate recording and storage of discrete sediment and ancillary data collected at USGS sediment stations. Its purpose is to assist USGS field personnel with database entry of fluvial-sediment sample information.

Once data are entered in SedLOGIN, a Sediment Laboratory Analytical Request (SLAR) form is automatically generated, printed, and included with the samples shipped to the sediment laboratory. The sample data and associated field parameters are automatically transferred from SedLOGIN to both the Sediment Laboratory Environmental Database Systems (SLEDS), and QWDX (the water-quality data transfer system). Results of sample analyses are also transferred by the laboratory into QWDX, from which the sample-associated data are transferred to the QWDATA module of the NWIS.

All new data derived from fluvial-sediment (discrete suspended-sediment, bedload, and bottom-material) samples collected must be stored in QWDATA using methods described by Johnson (1997), Edwards and Glysson (1999), Nolan and others (2005), Diplas and others (2008), and Gray and Landers (2014), and selected metadata as described by the USGS (2010). These storage requirements also include results of analyses of replicate samples identified by appropriate medium codes as environmental and/or quality-control samples. Data associated with physical samples collected by hydrographers, observers, and by automated means are also stored.

Entry of selected ancillary data to QWDATA prior to the aforementioned 2010 mandate was encouraged but not compulsory. Until the development of SEDWE, a limiting factor had been that SedLOGIN (or direct entry of data into QWDATA) required manual data entry using an office computer with appropriate USGS-access rights. In the past, paper forms or non-standardized electronic notes were used to record information in the field for subsequent largely manual transcription to standardized electronic media upon return to the office (Figure 1).

Figure 1 Schematic of procedure for collecting and recording fluvial-sediment data prior to the availability of the SEDWE application.

ATTRIBUTES OF SEDWE ELECTRONIC FIELD NOTES

SEDWE enables one-time electronic recording of fluvial-sediment and ancillary data for subsequent entry to the SedLOGIN application (Figure 2). The use of SEDWE has advantages over paper-based record keeping, including:

1. a reduction in arithmetic and recording errors,
2. elimination of the need to produce and archive paper notes,
3. improved consistency in, and more complete capture of field observations,
4. decreased project costs by reducing time spent on data entry and management, and
5. an increase in the overall quality and reliability of the sediment-station records concomitant with a decrease in the requisite time and effort to produce the records.

SEDWE enables USGS field hydrographers and sediment-station observers to accurately enter, view, modify, submit and print ancillary data associated with fluvial-sediment samples in accordance with USGS data-collection, management, and storage protocols (Porterfield, 1972; Koltun and others, 2006; USGS, 2010). SEDWE guides the user through a step-by-step process to complete all data entry successfully. SEDWE is secure, available any time, and can help expedite the sharing of USGS data.

SEDWE can be used in "offline mode" when the recording platform is not connected to the Internet, allowing the user to view and edit the recorded fluvial-sediment and ancillary data before submission. The available features, while on offline mode, include recording of fluvial-sediment sample data, and some tutorial information. External links and upload functionality are enabled when Internet access is restored.

Figure 2 Schematic of steps for collecting and recording sediment data using SEDWE.

SEDWE User Environment SEDWE is a field- and web-based system which operates on a variety of devices such as a PC, tablet, or smartphone. The application provides an independent platform for field-client operations. It was developed using Hypertext Markup Language 5 (HTML), jQuery mobile, Cascading Style Sheets (CSS) and PHP programming languages. USGS users can access SEDWE using any of the following browsers: Mozilla Firefox®, Apple Safari®, and Google Chrome® (use of firm or brand names is for information only and does not constitute endorsement by the U.S. Government).

Overview of SEDWE Interfaces The SEDWE application consists of three interfaces selectable based on the type of user: Observer, Hydrographer, and Administrator. The Observer Interface only is accessible to USGS sediment-station observers. The Hydrographer Interface only is accessible to USGS personnel who collect and process fluvial-sediment data, or their designees. These interfaces are used for recording pertinent data before departing the USGS sediment station. The Administrator Interface is accessible by any registered USGS Hydrographer who has access rights in QWDX/SedLOGIN. It is used for configuring the SEDWE users and their designated USGS sediment stations. Hydrographers who access the Administrator Interface will share the same access rights as the SEDWE Administrator within the Administrator Interface at the USGS Water Science Center level.

Hydrographer and Observer Interface The Observer and Hydrographer interfaces require USGS user authentication. The application will display the corresponding USGS sediment stations assigned to a particular user. The assigned stations are registered and set by a USGS administrator in the Administrator Interface. Observers and Hydrographers are able to add, modify, and delete records prior to submitting the data via an email containing the XML data file to a designated reviewer (QWDX-authorized user). Once reviewed, the XML file can be imported into SedLOGIN. Until further notice, the XML file will be delivered by email for later processing into SedLOGIN.

The Open XML option allows the user to view data stored in an XML file generated by other users. When the data stored in the local cache of the device are cleared, the user can open a previously generated XML file. Once the data are loaded into SEDWE, the user can either review or continue editing the data.

The Observer and Hydrographer Interfaces include three links or tabs, which are referred to as Shipments Manager, Manage Images, and Tutorials (Figure 3). Depending on the type of user (either Observer or Hydrographer), the corresponding form for recording sediment-sample data is shown. In each category the user enters the sediment data into a custom-designed electronic spreadsheet for each set or group of samples until all metadata are entered for later processing.

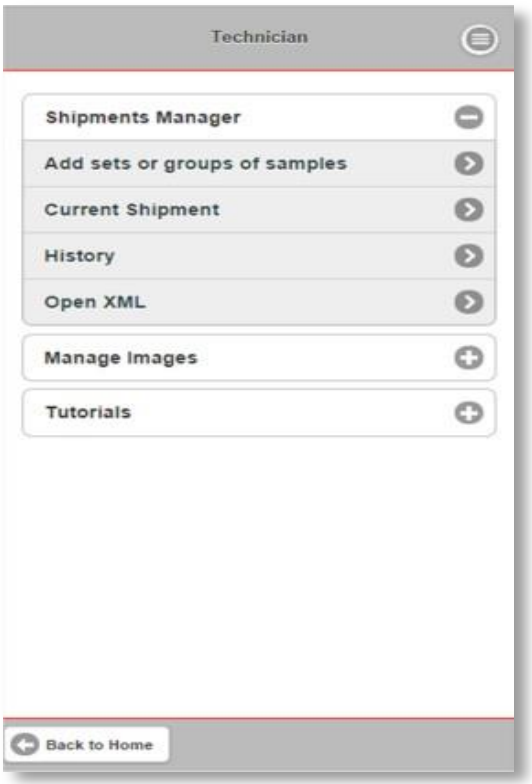

Figure 3 SEDWE main menu screen for the Observer and Hydrographer Interfaces.

The Shipments Manager tab allows the user to record data by selecting the "Add sets or groups of samples" button, and to edit or review the recorded data with the "Current Shipment" button, both of which use the same Data Recording screen (Figure 4).

The Manage Images screen (Figure 5) allows the user to send an image of field conditions at the sediment station to the designated hydrographer by selecting it from the device picture gallery or by taking the picture using a camera-equipped device. The Tutorial includes a user's manual and helpful links, videos, and educational resources about field sediment-sampling protocols and procedures.

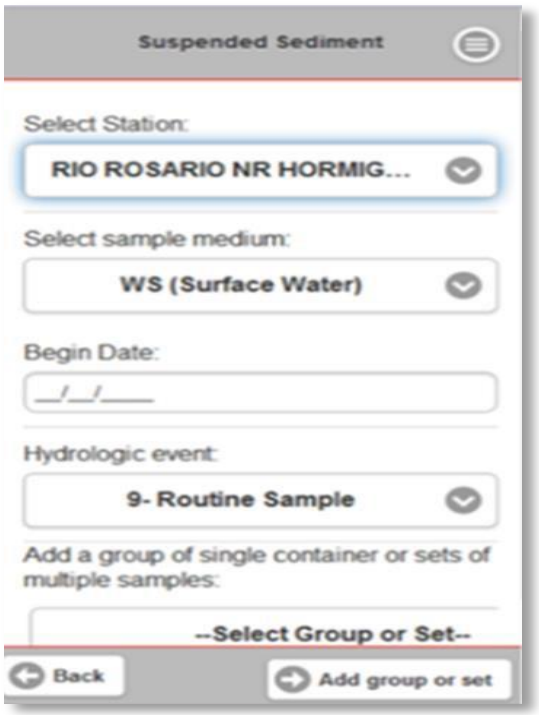

Figure 4 SEDWE Data Recording screen.

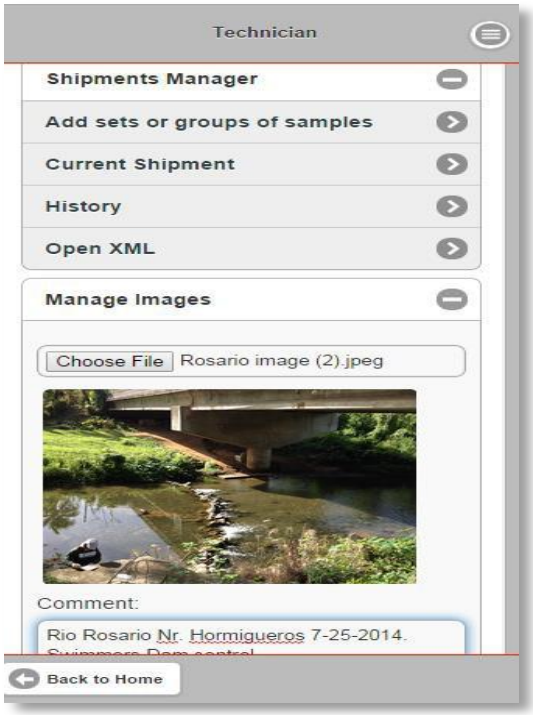

Figure 5 SEDWE Manage Images screen.

Administrator Interface The SEDWE Administrator Interface stores information related to users and stations for use by the SEDWE application. The SEDWE Administrator Interface consists of three main screens: Users, Stations, and Import from SedLOGIN. The Users and Stations screens allow the Administrator and the registered Hydrographer to query the Users and Stations stored in the SEDWE database, and to add a new user or station. The Users and Stations functionalities include:

1. add a new user or station,
2. modify an existing user or station, and
3. delete an existing user or station.

The Import from SedLOGIN screen allows a user to specify project(s) in SedLOGIN from which to import one or both of the project's stations or the project's users into the SEDWE database.

Connecting to SedLOGIN Programing codes, parameters, and validation in SEDWE prevents errors because the same codes, parameters, and validation are used by SedLOGIN. Hydrographers must log into SedLOGIN to import the XML file from SEDWE, and can import SEDWE data into any SedLOGIN project that the hydrographer is authorized to access. SedLOGIN will enforce data validation if there are any missing required parameters. Hydrographers can review and edit an XML file before importing the file into SedLOGIN by using the "Open XML" option in SEDWE.

SUMMARY

The SEDWE application serves as a standardized USGS resource to document ancillary data associated with fluvial-sediment sample collection prior to departing a USGS sediment station. SEDWE was designed to interface with other USGS sediment software to accomplish efficient transfer and accurate storage of these data. A range of electronic, hand-held platforms are supported to record and store USGS data associated with fluvial-sediment samples. The data subsequently can be transferred to the NWIS database, and to the USGS SLEDS application through the SedLOGIN application, and ultimately to the QWDATA database of the NWIS. SEDWE electronic forms serve to standardize and facilitate capture of ancillary data associated with fluvial-sediment sample collection. Benefits of using SEDWE include reductions in transcription errors due to one-time data entry; elimination of the need to archive paper records; improved data consistency and capture; decreased project costs; and an overall increase in the quality and reliability of USGS sediment-station records.

REFERENCES

Diplas, P., Kuhnle, R., Gray, J.R., Glysson, G.D., and Edwards, T.E. (2008). Sediment Transport Measurements: Chapter 5. Sedimentation engineering - processes, measurements, modeling, and practice. American Society of Civil Engineers Manual 110, p. 307-353. http://ascelibrary.org/doi/abs/10.1061/9780784408148.ch05 or http://water.usgs.gov/osw/techniques/Diplas_Kuhnle_others.pdf.

Edwards, T.E., and Glysson, G.D. (1999). Field methods for collection of fluvial sediment. U.S. Geological Survey Techniques of Water-Resources Investigations Book 3, Chapter C2. 89 p. http://water.usgs.gov/osw/techniques/Edwards-TWRI.pdf.

Federal Interagency Sedimentation Project. (2015). http://water.usgs.gov/fisp/.

Gray, J.R., and Demas, C.R. (in press). Measuring sediment transport in large rivers, D.E. Walling, ed: Chapter 4.2.2 in a compendium inspired by the1st International Conference on the Status and Future of the World's Large Rivers, Vienna, Austria, April 11-14, 2011, full volume edited by Helmut Habersack, 15 p.; see authors for manuscript.

Gray, J.R., and Landers, M.N. (2014). Measuring suspended sediment. in: Ahuja S. (ed.) Comprehensive Water Quality and Purification, Vol. 1, p. 157-204. http://water.usgs.gov/osw/techniques/sediment/gray_landers_elsevier_chapter_12_10_17_2013.pdf.

Gray, J.R., and Landers M.N. (2015). History of the Federal Interagency Sedimentation Project, Part III. Proceedings of the 10th Federal Interagency Sedimentation Conference, April 19-23, 2015, Reno, Nevada, 13 p.

Gray J.R., and O'Halloran, Denis (2015). Maximizing the reliability and cost-effectiveness of your suspended-sediment data. Proceedings of the 10th Federal Interagency Sedimentation Conference, April 19-23, 2015, Reno, Nevada, 14 p.

Johnson, G.P. (1997). Instruction manual for U.S. Geological Survey sediment observers. U.S. Geological Survey Open-File Report 96-431, 33 p. http://pubs.er.usgs.gov/publication/ofr96431.

Koltun, G.F., Eberle, Michael, Gray, J.R., and Glysson, G.D. (2006). User's manual for the Graphical Constituent Loading Analysis System (GCLAS). U.S. Geological Survey Techniques and Methods, Book 4, chap. C1, 51 p. http://water.usgs.gov/software/GCLAS/

Nolan, K.M., Gray, J.R., and Glysson, G.D. (2005). Introduction to suspended-sediment sampling. U.S. Geological Survey Scientific Investigations Report 2005-5077. http://pubs.er.usgs.gov/pubs/sir/sir20055077.

Porterfield, G. (1972). Computation of fluvial-sediment discharge. U.S. Geological Survey Techniques of Water-Resources Investigations of the United States Geological Survey, Book 3, Chapter C2, 66 p. http://pubs.usgs.gov/twri/twri3-c3/pdf/twri_3-C3_b.pdf.

Skinner, J.V. (1989). History of the Federal Interagency Sedimentation Project. Sediment Transport Modeling Proceedings, International Symposium, Hydraulic Division, American Society of Civil Engineers, New Orleans, Louisiana, August 14-18, p. 266-271 http://water.usgs.gov/fisp/docs/FISP_history_1989.pdf.

U.S. Geological Survey. (2015). National Water Information System. http://waterdata.usgs.gov/nwis.

U.S. Geological Survey. (2010). Office of Surface Water Technical Memorandum 2010.03 and Office of Water Quality Technical Memorandum 2010.05. Policy for the mandatory storage of discrete sediment data and selected metadata in the National Water Information System, and availability of SedLOGIN software to assist in data entry. http:\\water.usgs.gov\\admin\\memo\\SW\\sw10.03.pdf.

Wilde, F.D. (2008). Guidelines for field-measured water-quality properties. U.S. Geological Survey Techniques of Water Resources Book 9, Chapter 6.0.1.A. http://water.usgs.gov/owq/FieldManual/Chapter6/Chapter6.0v2.pdf.

CHARACTERIZING AND SIMULATING SEDIMENT LOADS AND TRANSPORT IN THE LOWER PART OF THE SAN ANTONIO RIVER BASIN EXTENDED ABSTRACT

J. Ryan Banta, jbanta@usgs.gov; **Darwin J. Ockerman**, ockerman@usgs.gov; **Cassi L. Crow**, ccrow@usgs.gov; and **Stephen P. Opsahl**, sopsahl@usgs.gov.
U.S. Geological Survey, 5563 De Zavala Suite 290, San Antonio, TX.

INTRODUCTION

This extended abstract is based on the U.S. Geological Survey Scientific Investigations Reports by Crow et al. (2013) and Banta and Ockerman (2014). Suspended sediment in rivers and streams can play an important role in ecological health of rivers and estuaries and consequently is an important issue for water-resource managers. The quantity and type of suspended sediment can affect the biological communities (Wood and Armitage, 1997), the concentration and movement of natural constituents and anthropogenic contaminants (Moran and others, 2012), and the amount of sediment deposition in coastal environments (Milliman and Meade, 1983). To better understand suspended-sediment characteristics in the San Antonio River Basin, the U.S. Geological Survey (USGS), in cooperation with the San Antonio River Authority and Texas Water Development Board, conducted a two-phase study to (1) collect and analyze sediment data to characterize sediment conditions in the San Antonio River downstream of San Antonio, Texas, and (2) develop and calibrate a watershed model to simulate hydrologic conditions and suspended-sediment loads for four watersheds in the San Antonio River Basin, downstream from San Antonio, Texas.

METHODS

Sediment Characterization: The study area consists of approximately 2,150 square miles. The upstream boundary of the study area coincides with USGS streamflow-gaging station 08181800 San Antonio River near Elmendorf, Tex. (hereinafter referred to as the "SAR Elmendorf gage") and USGS streamflow-gaging station 08185000 Cibolo Creek at Selma, Tex. (hereinafter referred to as the "Cibolo Selma gage"). The downstream boundary of the study area is the confluence with the Guadalupe River. During 2011–13, suspended-sediment samples were collected at 10 sites for the analysis of suspended-sediment concentration and particle size distribution. In addition, samples of bedload material were collected at six sites for the analysis of bedload mass and particle-size distribution. Samples were collected over a variety of hydrologic conditions ranging from a minimum streamflow of 1.9 cubic feet per second (ft^3/s) at the Cibolo Selma gage on September 17, 2012, to a maximum streamflow of 10,600 ft^3/s at the same site on May 25, 2013. To estimate suspended-sediment loads, log-linear regressions were developed to estimate suspended-sediment concentration based on streamflow at five sites for which sufficient data (including historically collected data) were available (see Figure 1 for example). The suspended-sediment concentrations were used in conjunction with streamflow to calculate estimated suspended-sediment loads.

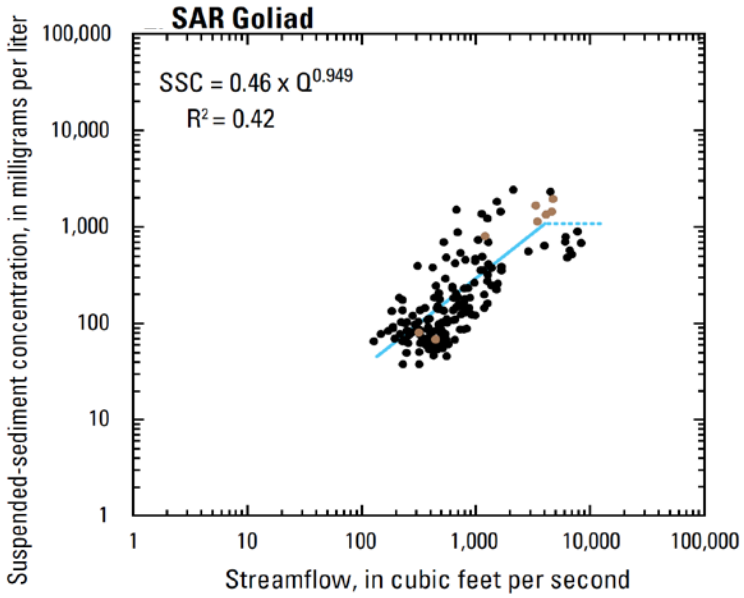

Figure 1. Example of relation between suspended-sediment concentration and streamflow at the SAR Goliad gage (USGS station 08188500 San Antonio River at Goliad, Tex.) (Modified from Figure 5 in Crow and others, 2013).

HSPF Model Development: In 2010, the U.S. Geological Survey (USGS), in cooperation with the San Antonio River Authority, the Evergreen Underground Water Conservation District, and the Goliad County Groundwater Conservation District, developed a Hydrological Simulation Program – FORTRAN (HSPF) model for the San Antonio River Basin to simulate hydrology only (hereinafter referred to as the "USGS–2010 model") (Lizarraga and Ockerman, 2010). In 2012, URS Corporation developed an updated version of the San Antonio River Basin HSPF model (hereinafter referred to as the "URS–2012 model"), which was based on the USGS–2010 model. For this study, the USGS developed an updated version of the HSPF model, based on the URS–2012 model, to simulate hydrologic conditions and suspended-sediment loads in the San Antonio River Basin during 2000–12 (hereinafter referred to as the "USGS–2014 model").

Because of the large size, the study area in the San Antonio River Basin was divided into four watershed models: (1) San Antonio River upstream from Cibolo Creek, (2) Cibolo Creek, (3) Ecleto Creek, and (4) San Antonio River downstream from Cibolo Creek. Input data for the HSPF model included spatial and time-series data. Spatial data included geology, soils, land-cover, topography, and drainage characteristics such as subwatershed boundaries and stream-reach length and cross-section data. Time-series data included meteorological data (rainfall and potential evapotranspiration), streamflow data, and suspended-sediment load data. The ranges of expected soil erosion rates were used as guidance for establishing targets for model simulation of sediment yields for different land-cover types. Sediment-related HSPF model parameters were adjusted so that simulated soil erosion rates approximated the reported soil erosion rates by land-cover type.

RESULTS AND CONCLUSIONS

Sediment Characterization: The samples collected during 2011–13 represent a wide range of SSCs, including some of the largest concentrations ever collected at some of the sites. Suspended-sediment concentrations (SSCs) in 67 samples collected during 2011–13 ranged from 14 milligrams per liter (mg/L) during base-flow conditions at USGS streamflow-gaging station 08183500 San Antonio River near Falls City, Tex. (hereinafter referred to as the "SAR Falls City gage") on August 19, 2011, to 4,480 mg/L during a stormflow event at the same site on January 26, 2012. The instantaneous suspended-sediment loads (SSLs) computed from 67 SSC samples collected during 2011–12 ranged from 0.36 tons per day at the Cibolo Selma site during base-flow conditions on September 17, 2012, to 47,800 tons per day at the SAR Elmendorf site during a stormflow event on January 25, 2012. These SSLs were used as either inputs to the HSPF model or as calibration targets for simulated model loads.

HSPF Model: The calibrated model of the study area in the San Antonio River Basin was used to simulate hydrologic conditions and suspended-sediment loads for 2000–12, as well as to simulate sediment production by various land types within the study area. Taking into consideration the model-fit statistics and graphical comparisons (Moriasi and others, 2007; Donigian, 2002; U.S. Environmental Protection Agency, 2000 and 2006), the watershed models simulated the observed streamflow within the "good" to "very good" categories during the calibration period (2006–12), with the exception of the Ecleto model. The calibration process also included a separate, post-calibration test of the model fit during 2000–2005. Simulations during the testing period had similar model-fit statistics as during the calibration period, with the exception of the USGS streamflow-gaging station 08186000 Cibolo Creek near Falls City, Tex. (hereinafter referred to as the "Cibolo Falls City gage"). One possible reason for weaker testing results (compared with calibration results) is the quality of available rainfall data for 2000–2005. During the entire 2000–12 simulation period, the model-fit statistics at each of the four primary calibration gages indicate "good" to "very good" fits (Banta and Ockerman, 2014).

Similar to the hydrology calibration, the suspended-sediment load model-fit statistics also were evaluated during the testing period at the SAR Falls City, Cibolo Falls City, and USGS streamflow-gaging station 08188500 San Antonio River at Goliad, Tex. (hereinafter referred to as the "SAR Goliad gage"), resulting in "good" to "very good" fits (Banta and Ockerman, 2014). Overall, model-fit statistics and graphic evaluations from the calibration and testing periods, provided multiple lines of evidence indicating the USGS–2014 model simulations of suspended-sediment conditions were mostly "good" to "very good," except for Ecleto Runge, which is considered unsatisfactory to fair (Banta and Ockerman, 2014).

The daily mean estimated suspended-sediment loads were 737 tons per day (tons/d) and 22 tons/d, respectively, at the SAR Elmendorf and Cibolo Selma gages during 2006–12 (Figure 2). At the outlet of the study area, the confluence of the San Antonio River with the Guadalupe River, the simulated daily mean suspended-sediment load during 2006–12 was 1,230 tons/d (Figure 2). These model results indicate that 759 of the 1,230 tons/d (approximately 62 percent) of the suspended sediment being delivered to the Guadalupe River originated upstream from the study area, mostly upstream from the SAR Elmendorf gage. Sample analyses and model results indicate that most of the suspended-sediment load in the study area consists of silt- and clay-

sized particles (less than 0.0625 millimeters). At the confluence of the San Antonio River with the Guadalupe River, approximately 98 percent of the total simulated suspended-sediment load was composed of silt and clay.

The Cibolo Creek watershed was the largest contributor of suspended sediment from the study area. The higher suspended-sediment yields in the Cibolo Creek watershed are likely because of steeper topography, more developed and cropland land cover, and more runoff than the other watersheds. For the entire study area, open/developed land and cropland exhibited the highest simulated soil erosion rates; however, the largest sources of sediment from the study area (by land-cover type) were pasture and forest/rangeland/shrubland, which account for about 80 percent of the study area and contributed about 70 percent of the suspended-sediment load.

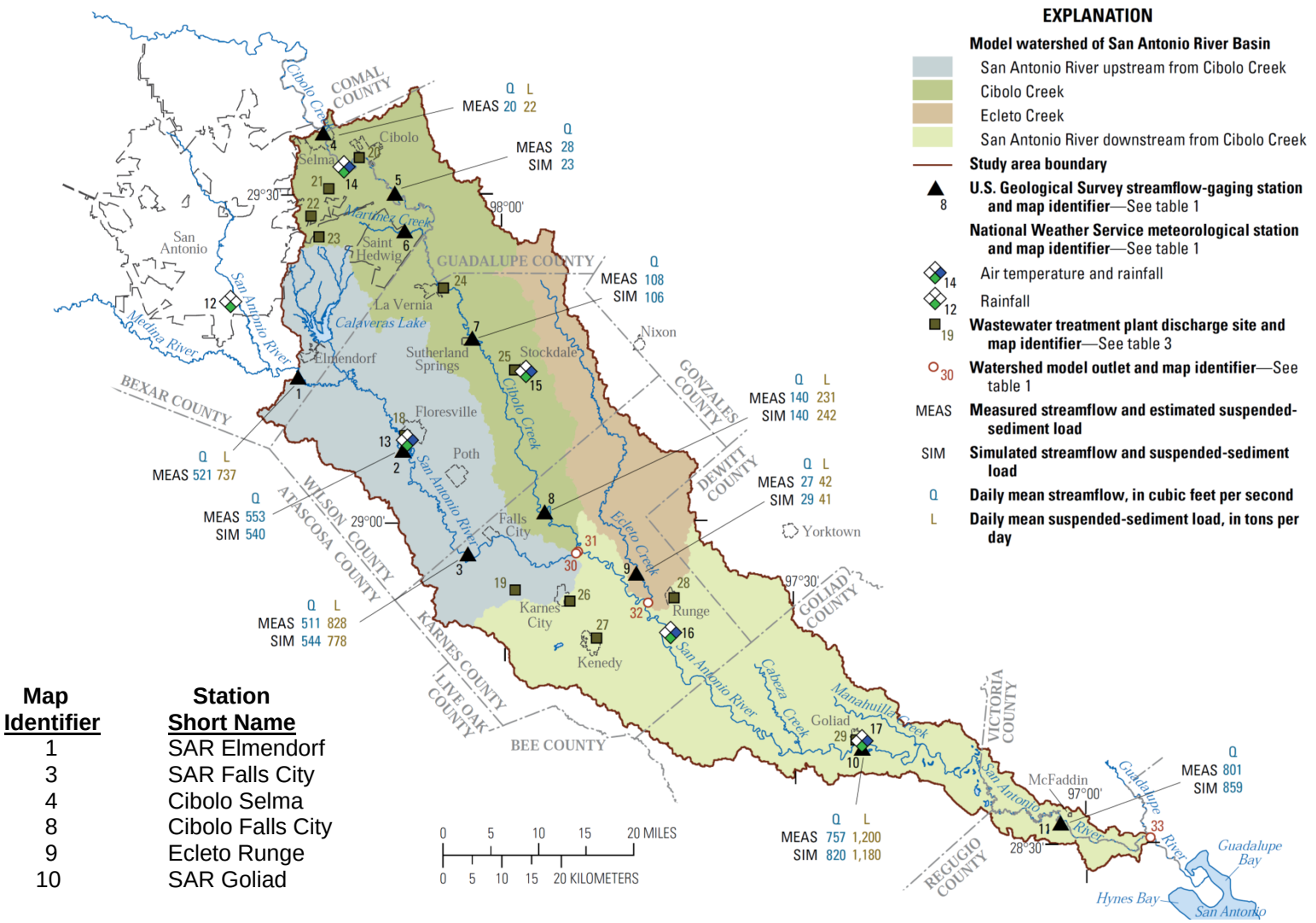

Map Identifier	Station Short Name
1	SAR Elmendorf
3	SAR Falls City
4	Cibolo Selma
8	Cibolo Falls City
9	Ecleto Runge
10	SAR Goliad

Figure 2. Measured and simulated daily mean streamflow and daily mean suspended-sediment loads at selected sites in the study area, San Antonio River Basin downstream from San Antonio, Texas, 2006–12 (Modified from Figure 13 in Banta and Ockerman, 2014).

REFERENCES

Banta, J.R., and Ockerman, D.J. (2014). Simulation of hydrologic conditions and suspended-sediment loads in the San Antonio River Basin downstream from San Antonio, Texas, 2000–12: U.S. Geological Survey Scientific Investigations Report 2014–5182, 46 p., http://dx.doi.org/10.3133/sir20145182.

Crow, C.L., Banta, J.R., and Opsahl, S.P. (2013). Sediment characteristics in the San Antonio River Basin downstream from San Antonio, Texas, and at a site on the Guadalupe River downstream from the San Antonio River Basin, 1966–2013: U.S. Geological Survey Scientific Investigations Report 2014–5048, 33 p., http://dx.doi.org/10.3133/sir20145048

Donigian, A.S., Jr. (2002). Watershed model calibration and validation—The HSPF experience, in Conference on National TMDL Science and Policy 2002, Phoenix, Ariz., November 13–16, 2002, Proceedings: Alexandria, Va., Water Environment Federation, p. 44–73.

Lizárraga, J.S., and Ockerman, D.J. (2010). Simulation of streamflow, evapotranspiration, and groundwater recharge in the lower San Antonio River watershed, south-central Texas, 2000–2007: U.S. Geological Survey Scientific Investigations Report 2010–5027, 41 p.

Milliman, J.D., and Meade, R.H. (1983). World-wide delivery of river sediment to the oceans: Journal of Geology, v. 91, p. 1–21.

Moran, P.W., Calhoun, D.L., Nowell, L.H., Kemble, N.E., Ingersoll, C.G., Hladik, M.L., Kuivila, K.M., Falcone, J.A., and Gilliom, R.J., (2012). Contaminants in stream sediments from seven U.S. metropolitan areas—Data summary of a National Pilot Study: U.S. Geological Survey Scientific Investigations Report 2011–5092, 66 p.

Moriasi, D.N., Arnold, J.G., Van Liew, M.W., Bingner, R.L., Harmel, R.D., and Veith, T.L. (2007). Model evaluation guidelines for systematic quantification of accuracy in watershed simulation: Transaction of American Society of Agricultural and Biological Engineers, v. 50, no. 3, p. 885–900.

U.S. Environmental Protection Agency (2000). Estimating hydrology and hydraulic parameters for HSPF: U.S. Environmental Protection Agency Better Assessment Science Integrating Point and Nonpoint Sources Technical Note 6, 34 p.

U.S. Environmental Protection Agency (2006). Sediment parameter and calibration guidance for HSPF: U.S. Environmental Protection Agency Better Assessment Science Integrating Point and Nonpoint Sources Technical Note 8, 43 p.

Wood, P.J., and Armitage, P.D. (1997). Biological effects of fine sediment in the lotic environment: Environmental Management, v. 21, no. 2, p. 203–217.

DEVELOPMENT OF A VELOCITY-BASED QUANTITATIVE DESIGN METHODOLOGY FOR BENDWAY WEIRS

Nathan Holste, Hydraulic Engineer, Bureau of Reclamation, Denver, CO, nholste@usbr.gov

INTRODUCTION

Transverse features such as bendway weirs have become a popular alternative to traditional bank protection methods in recent years because they offer more environmental benefits and often have a lower cost. Bendway weirs are river training structures that redirect flow and energy throughout a channel bendway while moving the thalweg and most severe hydraulic forces away from the outer bank. Installation consists of a discontinuous field of multiple transverse structures placed in series and angled into the flow. A flat crest slope and low crest elevation distinguish bendway weirs from other transverse features such as spur dikes (flat, high crest elevation near top of bank) and vanes (upward sloping crest from low instream tip elevation to near top of bank). Scour at the weir tips due to flow acceleration shifts the thalweg toward the channel center. Eddies between the weirs may encourage variable depth, velocity, and sediment deposition that is favorable to aquatic species. Geometric based design guidelines are available in the existing literature such as HEC-23 (Lagasse et al., 2009) and NCHRP 544 (McCullah and Gray, 2005); however, no methodology exists to quantify the effects of bendway weirs on channel hydraulics.

A new method is presented that supplements existing geometric guidelines with an equation to predict velocity at inner, center, and outer channel locations as a function of bendway weir geometry. This equation was developed by researchers at Colorado State University (CSU) (funded by the Bureau of Reclamation) from data collected during a series of laboratory physical model tests. A group of physically significant terms was analyzed to develop the empirical, statistically-derived velocity ratio equation. The proposed method is illustrated with a design example for a project constructed in 2013 on the Rio Grande north of Albuquerque, New Mexico. Bendway weirs were implemented at this site to restore habitat in an incised river while stabilizing the eroding outer bank. A floodplain bench was also designed and constructed within the weir field to provide riparian habitat with energy dissipation at high flows. The combination of bendway weirs and a floodplain bench provides increased lotic and riparian habitat diversity and complexity at multiple flow stages while reducing hydraulic forces at the outer bank.

INITIAL ASSESSMENTS

Prior to beginning a detailed bendway weir design, an interdisciplinary project team should be assembled. Purpose, need, goals, and objectives must be well thought out, and a list of several alternatives should be developed and assessed. Typical considerations include fluvial geomorphology, engineering, ecology, economics, and constructability. A project that addresses the causes of channel instability and is compatible with the desired river form and function will be the most effective. The selected alternative is the option that best accomplishes the project team's goals within the identified constraints. The remainder of this paper assumes that bendway weirs have been selected as the preferred alternative, although some of the initial assessments described below should be completed during the alternatives evaluation.

Conduct Geomorphic Analysis: It is important and often difficult to distinguish local instability from system instability. A dynamically stable system will still exhibit local adjustments such as channel lengthening through bank erosion in growing meander bends that is offset by cutoffs at other bends. Local instability exists where there are adjustments at individual locations, while reach-averaged parameters such as hydraulic geometry and slope remain steady. Conversely, system instability propagates throughout a stream network as a result of water and sediment discontinuity, changes to downstream base level, and land use changes. System instability is visible through reach-wide aggradation, degradation, or

planform metamorphosis (Watson et al., 2007). Transverse features such as bendway weirs may not be appropriate or effective if reach-wide instability exists.

For the Rio Grande project site, it was determined that the eroding bank was not the result of system instability, thus suggesting that goals could be achieved through a local project without being jeopardized by reach-scale factors. Historical aerial photos were used to calculate reach sinuosity over time compared to the local sinuosity trends. Cross section surveys, longitudinal profiles, and a low flow specific gage analysis (i.e., stage vs. specific discharge at a nearby gaging station) showed that the reach bed elevation had been relatively stable over time. Other important geomorphic factors that were considered include hydrology, sediment supply, bed and bank material, channel width, and slope.

Determine Hydraulic Conditions: Hydraulic modeling is recommended as a component of a robust bendway weir design methodology. Depending on project goals, risks, and resources, multi-dimensional modeling can provide significant benefits when evaluating hydraulics associated with transverse features. However, 1-D models have the advantage of less intensive data requirements and can be set up and run relatively quickly. Executing a hydraulic model requires the selection of flow rates that are important for the design and analysis. The design flow will depend on individual project conditions and is typically specified with a return period or frequency. Appropriate design flows for bendway weirs often have a return period between five and twenty-five years. The following hydraulic conditions at the design flow should be determined for use in the CSU velocity ratio equation: (1) bend-averaged, cross section averaged channel velocity, (2) bend-averaged channel top width, (3) bend-averaged maximum channel depth, (4) bend-averaged water surface elevation, and (5) bend-averaged channel cross-sectional flow area. Main channel values should be used instead of the entire cross section values because bendway weir performance is primarily affected by main channel hydraulics, and the CSU physical model was not constructed to include a floodplain. The mean annual peak flow and base flow, and their associated water surface elevation and depth, are also needed for the geometric design guidelines.

Determine Rock Size: Transverse, discontinuous features are subject to more direct and severe hydraulic forces than longitudinal, continuous methods of protection such as traditional riprap revetments. A comprehensive, quantitative method for determining rock size of transverse features is not available in the existing literature. However, de Almeida and Martin-Vide (2009) performed an experimental study to compare riprap stability for transverse, longitudinal, and continuous protection methods. They tested a transverse bed sill structure and proposed a range of discontinuity factors to increase riprap size based on protrusion height above the bed and length of protection. The discontinuity factor allows riprap sizing results from the Maynord equation (Maynord et al., 1989) to be converted to a transverse rock size. For the Rio Grande project site, a bendway weir D_{50} rock size of 24 inches was determined by applying a discontinuity factor of 2.5 to a calculated riprap revetment size of 9.6 inches.

It should also be noted that NRCS (2007) recommends that the riprap size of stream barbs should be twice the size determined from standard riprap sizing criteria. NCHRP 568 (Lagasse et al., 2006) evaluated seven of the most commonly used revetment riprap sizing equations and recommended the EM 1601 equation (USACE, 1994) on the basis of discriminating between stable or failed riprap, bank and bend correction factors, and the reasonableness of safety/stability factors. The EM 1601 equation is similar to the Maynord 1989 equation with additional safety and correction factors.

Estimate Scour Depth: Properly estimating and designing for scour is an important element of any stream erosion countermeasure project. Transverse features such as bendway weirs typically experience the largest scour (depth and volume) near the tip or nose of the structure. Scour holes that form adjacent to or underneath bendway weirs will cause riprap from the structures to launch into the scour holes, potentially leading to failure. The goal of this design component is to provide enough riprap volume so that the bendway weirs can adjust to any scour without compromising their function. More specifically,

the crest elevation and tip location should be maintained after some of the sacrificial riprap falls into the scour hole. Bendway weirs can be keyed into the bed if practicable to account for scour, but this is difficult unless construction occurs in dry conditions.

An extensive, but not exhaustive, review of scour equations was conducted to identify several methods that would be appropriate for the Rio Grande project site. The selected scour equations can be categorized as a mean velocity equation, regime equations, bend equations, and a transverse structure equation. Table 1 presents the calculated scour results along with notes describing specific methods. The equations are generally empirical and were developed from lab or river measurements for a given set of conditions. Most of the equations represent a best-fit curve, although the USACE (1994) method is an upper envelope curve designed to overpredict scour for about 95 percent of the data.

Table 1 Scour equation results (at design flow of 14,200 cfs).

		Regime Equations[1]			Bend Equations			
	Mean Velocity[1]	Neill (1973)	Lacey (1930)	Blench (1969)	Maynord[2] (1996)	Zeller[2] (1981)	USACE[3] (1994)	Blench[4] (1957)
Total Scour[5]	5.43	5.61	3.88	4.31	5.21	7.57	9.67	5.65
Total Scour (w/SF = 1.1 if applicable)	5.97	6.17	4.27	4.74	5.21	7.57	9.67	6.21
Average = 6.23 ft		Median = 6.07 ft		**Design Scour Depth = 7 ft**				

[1]Reference: Pemberton and Lara (1984)
[2]Developed for sand bed rivers, assumed conservative for gravel bed (no safety factor)
[3]Upper envelope curve (no safety factor)
[4]Cox (2005) compared 10 equations to lab bendway weir results and found that the Blench (1957) equation had the best prediction of observed scour depths
[5]Includes general, bend, and thalweg scour components. No long term scour component was included because of reach bed stability.

The design scour depth can be used to estimate the riprap volume needed to protect bendway weirs from failure due to scour. As a means of simplifying the analysis of a complex three-dimensional process, the scour pattern was examined within the context of a typical cross section view of the bendway weir tip. It is assumed that riprap will launch into the scour hole at the angle of repose and form a type of revetment that is similar to longitudinal, continuous bank protection. USACE (1994) and NCHRP 568 (Lagasse et al., 2006) recommend a revetment thickness of $1.5*D_{50}$ or D_{100}, whichever is greater. The D_{100} is largest for the example project, resulting in a 4-ft revetment thickness. At the angle of repose, a simplified parallelogram representing the launched riprap has a top and bottom width of 6 ft, resulting in an area of 42 ft^2 at the design scour depth. Incorporating a safety factor of 1.5 to account for uncertainties during the launching process yields a cross-sectional area of 63 ft^2 at the tip that should be available for scour. This is in addition to the area required to maintain the design crest elevation and tip location, which can be calculated based on a minimum a crest width of at least $1* D_{50}$ (2 ft) after scouring occurs. The cross-sectional area is a function of the crest width, weir height, and side slope angle. (Bottom width is also governed by crest width, weir height, and side slope.) The constructed bendway weir cross section side slopes were set at 1.5H:1V (34°), which is slightly flatter than the riprap angle of repose for increased stability.

INITIAL GEOMETRIC DESIGN

After completing the initial assessments, the next phase of the proposed design methodology is to incorporate established geometric design guidelines for bendway weirs. The most important geometric parameters that govern bendway weir function and effectiveness are length, planform angle, spacing, and

crest elevation (height). Other bendway weir variables that must be specified in the design include top width and key length. HEC-23 (Lagasse et al., 2009) and NCHRP 544 (McCullah and Gray, 2005) provide recommendations for determining these geometric components. A range of values is determined for each geometric parameter and the CSU velocity ratio equation is subsequently used for optimization.

Sketch Desired Thalweg and Bank Line Location: An important conceptual factor when designing a bendway weir field is the location of the bendway weir tips. Derrick (2012) recommends laying out the desired thalweg relocation throughout the bend and then placing the stream ends of the bendway weirs just short of the anticipated thalweg realignment. Smooth upstream and downstream transitions should be included, and different attack angles at a variety of flow stages should be considered. If a floodplain bench is included such as for the Rio Grande example project, this alignment should be determined as well. Historical aerial photos provide a useful tool for laying out the thalweg and floodplain bench location, and a previously observed stable channel alignment may be a helpful template for the new alignment.

Determine Key Length: Bendway weirs must be keyed into the bank to prevent the structures from being flanked if lateral erosion continues at the site. The Rio Grande bendway weir design is slightly unusual because a majority of the total bendway weir length is buried within the floodplain bench, which can be considered as part of the key. GIS was used to draw the alignment of the key terminus using the following two methods, and the most conservative length was selected at each bendway weir location.

(1) Assuming that all of the floodplain bench fill material is eroded, HEC-23 states that the key length should not be less than 1.5 times the total bank height. For a nominal bank height of 10 ft the required key length is 15 ft, so the existing top of bank was offset by this distance.
(2) The maximum probable erosion based on historical aerial photographs was estimated to be 85 ft, so the floodplain bench bank line was offset by this distance.

It should be noted that HEC-23 also provides a method to estimate key length as a function of weir length and spacing, and this result should be compared to the above methods after the final geometry is determined.

Determine Weir Crest Width: HEC-23 and NCHRP 544 both recommend a crest width of (2 to 3)*D_{100}. Therefore, a range of recommended crest widths between 8 and 12 ft corresponds to the selected riprap size (D_{100} of 4 ft). A crest width of 8 ft was chosen for the portion of the weir buried within the floodplain bench and 12 ft was selected for the weir tip exposed to the flow to accommodate the required scour volume.

Determine Weir Length: Bendway weir length can be defined as the length along the crest axis, measured horizontally from water's edge at the design flow. (Effective length is a different parameter that also incorporates planform angle and is measured perpendicular to the bank tangent.) Both HEC-23 and NCHRP 544 recommend a minimum and maximum weir length as a function of stream width as shown in Table 2. The bend-averaged channel top width is 202 ft, which was calculated by averaging the bank-to-bank widths at cross sections within the bend. A range of bendway weir lengths between 20 ft and 100 ft was considered when analyzing geometry effects with the CSU equation.

Table 2 Recommended bendway weir length.

Design Guideline	Minimum	Maximum
HEC-23	Tw/10 = 20 ft	Tw/3 = 67 ft
NCHRP 544	Tw/3 = 67 ft	Tw/2 = 101 ft

Determine Weir Planform Angle: Bendway weirs are angled upstream so that flows over the top of the structure are redirected away from the outside bank and toward the channel centerline. HEC-23 states that

the angle of projection between the bendway weir axis and the upstream bankline tangent typically varies from 60 to 80 degrees. The NCHRP 544 planview diagram shows potential angles ranging from 45 to 90 degrees measured from the upstream bankline tangent. NCHRP 544 states that the most common and preferred angles are between 70 and 80 degrees. Therefore, angles from 60 to 80 degrees were considered for the Rio Grande bendway weir design.

Determine Weir Spacing: Bendway weir spacing is the distance between the centerline axes of two consecutive weirs as measured along the bankline. Spacing is determined by the radius of the bend and the length of the bendway weirs. HEC-23 provides two equations (S_1 and S_2) that establish a range of feasible weir spacing values and a third equation (S_{max}) to calculate the maximum spacing. All three equations are a function of weir length so results are dependent on whether the maximum or minimum length is used. NCHRP 544 outlines a simpler approach where only one recommended equation is provided to calculate spacing as a multiple of weir length. All of these equations and the calculated results are summarized in Table 3. The spacing values considered for additional analysis with the CSU equation varied between 85 ft and 190 ft for the Rio Grande project. Given the length of the bend to be protected (~760 ft), the total number of weirs could be as many as 9 (spacing ~85 ft) or as few as 4 (spacing ~190 ft). Increasing the number of weirs to 10 or more results in only small changes in spacing for each additional weir and was not cost effective.

Table 3 Recommended bendway weir spacing.

Design Guideline	Minimum*	Maximum†
HEC-23	$S_1 = 1.5L\left(\frac{R_c}{T_w}\right)^{0.8}\left(\frac{L}{T_w}\right)^{0.3} = 24ft$ $S_2 = (4\ to\ 5)L = 81ft$ $S_{max} = R_c\left(1-\left(1-\frac{L}{R_c}\right)^2\right)^{0.5} = 119ft$	$S_1 = 1.5L\left(\frac{R_c}{T_w}\right)^{0.8}\left(\frac{L}{T_w}\right)^{0.3} = 115ft$ $S_2 = (4\ to\ 5)L = 337ft$ $S_{max} = R_c\left(1-\left(1-\frac{L}{R_c}\right)^2\right)^{0.5} = 210ft$
NCHRP 544	$S = 1.5L = 101ft$	$S = 1.5L = 152ft$

*from HEC-23 (L_{min} = 20 ft) and NCHRP 544 (L_{min} = 67 ft) minimum lengths
†from HEC-23 (L_{max} = 67 ft) and NCHRP 544 (L_{max} = 101 ft) maximum lengths

Determine Weir Height: As discussed, bendway weirs are low elevation structures where the crest must be overtopped to work as designed. Weir height is not clearly defined in the existing literature because all typical cross section schematics show a flat riverbed. In field applications, the riverbed undulates significantly in both the transverse and longitudinal directions. For this reason it is easier to define a weir crest elevation rather than a weir height. Therefore, the existing height recommendations should be converted to a difference between the crest elevation and water surface, rather than a height above the bed.

HEC-23 recommends that weir height should be 30 to 50 percent of the depth at the mean annual high water level. It is not clear if the depth at mean annual high water level is the maximum depth (thalweg depth) or average depth (hydraulic depth). The suggested interpretation of this guideline is that the weir crest elevation should be the water surface at the mean annual peak flow minus 70 to 50 percent of the bend-averaged maximum channel depth. It is assumed that HEC-23 refers to maximum depth because it also states that bendway weirs should cross the stream thalweg. NCHRP 544 shows that the crest elevation should be within (+/–) 1 ft of the typical base flow water surface elevation. Table 4 presents the results as interpreted from HEC-23 and NCHRP 544 and converted to a crest elevation. Crest elevations between 5505 ft and 5510 ft were analyzed for the Rio Grande site. The crest elevation of 5510 ft was

included based on the alternate HEC-23 interpretation using hydraulic depth, which results in recommended elevations that are about 2.5 ft higher than what is shown in the table for HEC-23.

Table 4 Recommended bendway weir crest elevation.

Design Guideline	Minimum	Maximum
HEC-23	(0.3H) → $WSE_{m.a.p.} - 0.7 \times D_{m.a.p.} = 5505.4\ ft$	(0.5H) → $WSE_{m.a.p.} - 0.5 \times D_{m.a.p.} = 5507.5\ ft$
NCHRP 544	$WSE_{base} - 1ft = 5507ft$	$WSE_{base} + 1ft = 5509ft$

FINAL VELOCITY-BASED DESIGN

The goal of a bendway weir field for bank protection projects is to minimize lateral erosion by reducing velocity and shear stress along the outer bank. Over the course of several years, CSU performed physical modeling of transverse structures in a trapezoidal, rigid bed channel as detailed by Heintz (2002), Darrow (2004), and Schmidt (2005). The model includes two distinct channel bends and was constructed at an undistorted, 1:12 Froude scale based on geometry of the Rio Grande. Scurlock et al. (2012) performed a statistical regression analysis of hydraulic results from 130 unique tests to develop predictive equations for maximum velocity ratio (MVR) and average velocity ratio (AVR). Channel planform zones were delineated as outer (o), center (c), and inner (i) locations throughout the bend so that MVR and AVR equations could be developed for each of the three locations. MVR is defined as the maximum velocity for a given channel location with structures installed divided by the bend-averaged velocity without structures ($MVR = Vmax_{structures}/Vavg_{baseline}$). AVR is defined as the average velocity for a given channel location with structures installed divided by the bend-averaged velocity without structures ($AVR = Vavg_{structures}/Vavg_{baseline}$).

The CSU velocity ratio equation is robust, but is also affected by significant limitations. The equation is generalized for all transverse features rather than being specific to bendway weir hydraulics. Spur dikes and vanes are included in the database because there were not enough bendway weir tests to generate a valid regression equation. Important elements of natural geometry and topography such as the pool depth ratio and cross-sectional transverse bed slope are also neglected because the modeled channel is prismatic. Therefore, it is not surprising that the trapezoidal equations have been found to underpredict outer bank maximum velocity for a channel with natural topography (Baird, 2014). Scurlock et al. (2012) also note that "maximum velocity data are difficult to capture spatiotemporally, and may behave erratically; therefore, the concept of AVR may represent a more reliable predictive method." There are currently a limited number of native bed model runs with bendway weirs, and the data are insufficient to develop a new regression equation. Equation 1 and Table 5 present the regression coefficients used to predict velocity values for the Rio Grande design project. Scurlock et al. (2014) have since revised the coefficients based on a new statistical regression that excludes certain outlier points from the original dataset. The velocity ratio equation is comprised of dimensionless terms that represent the following parameters: an area contraction ratio, a spacing ratio, a channel curvature ratio, a lateral contraction ratio, a submergence ratio, and a planimetric angle ratio.

$$MVR, AVR = a_1(A^*)^{a_2}\left(\frac{L_{arc}}{T_w}\right)^{a_3}\left(\frac{R_c}{T_w}\right)^{a_4}\left(\frac{L_{w-Proj}}{T_w}\right)^{a_5}\left(\frac{D_B}{D_B-\Delta Z}\right)^{a_6}\left(\frac{\theta}{90}\right)^{a_7} \quad (1)$$

where:

$a_1, \ldots, a_7$ = regression coefficients

A^* = percent of baseline channel cross-sectional flow area blocked by transverse structure [percent]

L_{arc} = arc length (spacing) between centerline of structures, measured along bankline [ft]

T_w = bend-averaged baseline channel top width [ft]

R_c = centerline radius of curvature of channel bend [ft]
$L_{w\text{-}Proj}$ = projected length of structure into channel, measured horizontally from water's edge along perpendicular channel cross section at design flow [ft]
D_B = bend-averaged maximum cross-section baseline flow depth [ft]
Δz = elevation difference between water surface and structure crest at the tip [ft]
θ = structure planview angle, measured from upstream line tangent to bank [degrees]

Table 5 Coefficients for MVR and AVR regression equations (all data) (Scurlock et al., 2012).

Ratio Location	R^2	*MA%E*	a_1	a_2	a_3	a_4	a_5	a_6	a_7
MVRo	0.8429	20.8533	0.0068	0.0000	0.5546	0.3846	–2.1431	0.7003	0.3824
MVRc	0.8011	4.3100	0.3773	0.2695	0.0000	0.1973	–0.1563	0.0467	0.1155
MVRi	0.6087	4.4433	0.3400	0.3404	–0.1116	0.1065	–0.2084	0.0445	0.1580
AVRo	0.4861	40.7230	0.0138	0.0000	0.5917	0.7439	–1.1451	0.4629	0.5996
AVRc	0.7255	4.0327	0.3615	0.2710	–0.0739	0.1850	–0.1412	0.0536	0.1158
AVRi	0.7530	3.9452	0.1315	0.4894	–0.1308	0.1770	–0.4098	0.1170	0.1266

Determine Permissible Velocity: In order to use MVR and AVR to predict the physical effects of bendway weirs, the ratios must be analyzed within the context of existing baseline velocity and permissible velocity. Once the baseline velocity, MVR, and AVR are known, the predicted velocities with bendway weirs can be compared to the permissible velocities to determine if erosion is expected to continue at the site. Permissible velocity is primarily a function of the bed and bank material in addition to vegetation characteristics. It is expected that bank erosion would be greatly reduced if the predicted maximum and average velocities with bendway weirs are less than the permissible velocities along the outer bank. Channel centerline and inner bank velocities are important to the river conditions downstream of the protected bend and to the point bar across from the bendway weirs. As flow velocity is reduced along the outer bank due to bendway weir installation, it is likely that velocity will increase along the channel centerline and inner bank. This may cause erosion of the point bar and increased velocity downstream. Table 6 summarizes the maximum and average permissible velocity ratios at the outer, center, and inner channel locations for the Rio Grande example project. The bend-averaged baseline velocity at the design flow (5.81 ft/s) was used to convert permissible velocities to corresponding velocity ratios. Several references such as Kilgore and Cotton (2005) and Fischenich (2001) provide methods to determine permissible velocity as a function of soil and vegetation characteristics. Rock stability at the weir tips is a consideration when selecting center permissible velocity, and the inner permissible velocity will depend on the desired point bar characteristics and historical lateral migration. Downstream effects should also be considered when selecting inner and center velocities. Average velocities can be set at an appropriate ratio of maximum permissible velocities (e.g., 75 percent) based on local conditions.

Table 6 Permissible velocity ratios for Rio Grande bendway weir design.

MVRo = 0.34	AVRo = 0.26
MVRc = 1.72	AVRc = 1.29
MVRi = 2.07	AVRi = 1.55

Use Velocity Equation to Iterate Range of Geometric Parameters: A median or most recommended value should be selected for each of the primary geometric parameters in addition to the range described above. The median value for three of the parameters can be held constant while varying the fourth parameter over the complete range determined from the geometric guidelines. These predicted velocity results should then be plotted and compared to the permissible velocity to examine the sensitivity and effect of each parameter. Figure 1 shows the results from the Rio Grande design project. The y-axis is percent difference compared to the permissible velocity, and the x-axis is the value of the geometric

parameter that is being adjusted. A negative percent difference means that the predicted velocity with bendway weirs is less than the permissible velocity. A positive percent difference means that the predicted velocity is greater than the permissible velocity and erosion would be expected. All of the recommended geometric parameters from HEC-23 and NCHRP 544 yield acceptable velocities for this example, except for very short weir lengths (less than about 38 ft). It should be noted that weir lengths less than about 30 ft for this site fall outside the bounds of configurations tested in the laboratory. The weir angle results are somewhat counterintuitive because of the relationship between angle and projected length. After completing the graphs, the desired velocity reduction and safety factor should then be used to select a narrowed range of parameter values for final analysis. This narrowed range is represented by vertical lines in the plots shown below.

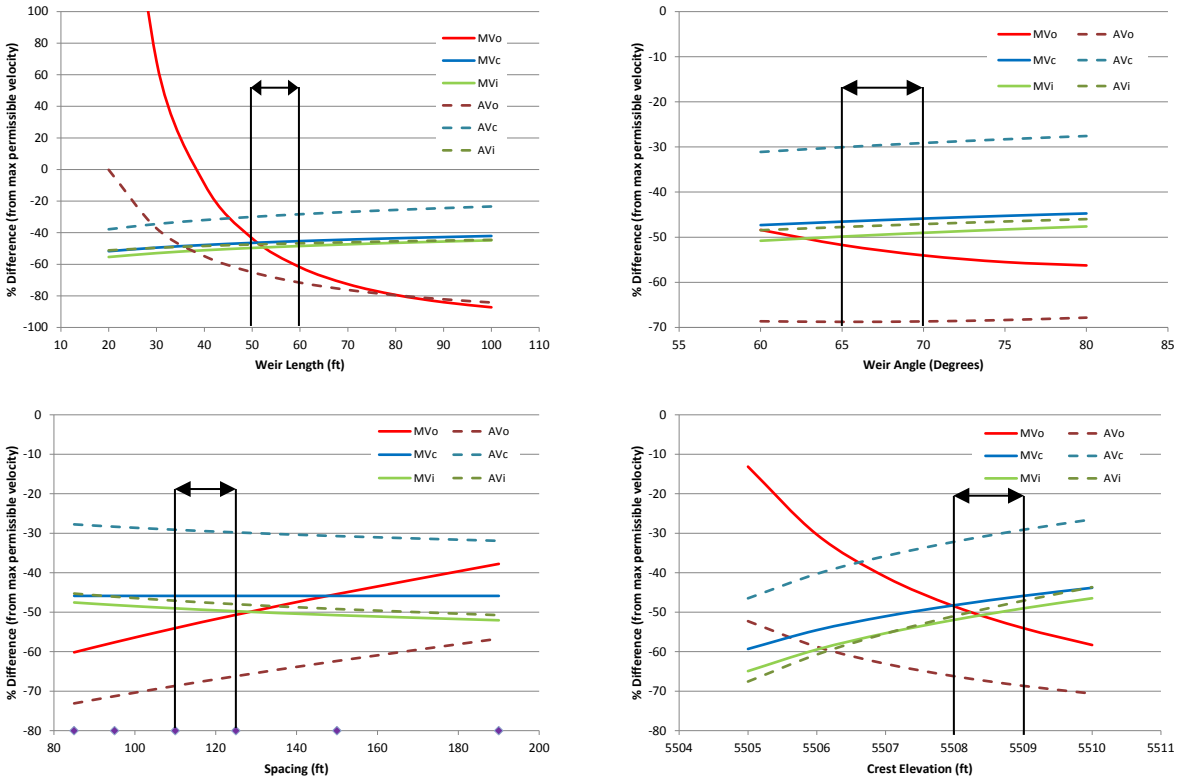

Figure 1 Velocity comparison as a function of weir length, angle, spacing, and height.

Finalize Bendway Weir Geometry: A matrix of potential final geometric values should be developed from a narrowed range based on the initial velocity calculations. The construction precision should also be accounted for, such as specifying elevation to the nearest 0.5 ft or 1 ft and specifying angles to the nearest 5°. For the Rio Grande project, the matrix consisted of 24 possible combinations based on 3 length values, 2 angle values, 2 spacing values, and 2 height values. The predicted velocities were then recalculated for every combination and plotted on a new graph. This is different than the initial iterations where only one geometric parameter was changed at a time. The selected values result in predicted maximum outer bank velocities that vary from 28 to 62 percent below the maximum permissible outer bank velocity. MVc, MVi, AVc, and AVi all remain fairly constant, but increase slightly as MVo and AVo are reduced. The final design is summarized in Table 7 and was selected based on: (1) a predicted MVo at least 50 percent smaller than the permissible MVo, (2) a balance of MVo reduction without an excessive increase in MVc and MVi, and (3) compatibility with existing bendway weirs installed further downstream in 2007. There is a balance between obtaining the greatest outer bank velocity reduction

while minimizing the amount of rock that is used for construction. Specifying a predicted MVo that is 50 percent less than the permissible MVo is similar to a safety factor of 2, although the difference in raw velocity values is only 1 ft/s.

Table 7 Design summary of final bendway weir geometric parameters.

	Exposed (active) Length*	Buried (key) Length	Total Weir Length	Angle	Spacing	Crest Elevation†	Top Width
Weir #1	37 ft	94 ft	131 ft	70°	105 ft	5509 ft	12 ft (exposed section); 8 ft (buried section)
Weir #2		98 ft	135 ft				
Weir #3		98 ft	135 ft				
Weir #4		123 ft	160 ft				
Weir #5		107 ft	144 ft				
Weir #6		90 ft	127 ft				
Weir #7		90 ft	127 ft				

*Original design length of 55 ft was modified to allow for placement of additional floodplain bench material so that final cut and fill volumes are balanced (see next section)

†On average, the modeled WSE drops about 0.6 ft between Weir #1 and Weir #7

Design Complementary Project Features: Bendway weir function and performance can be greatly improved with the addition of other compatible project features. Three additional components were included for the Rio Grande design example: point bar excavation, floodplain bench construction, and willow pole planting. Other features that should be considered are longitudinal stone toe, bioengineering, and locked logs. It may also be possible to retrofit existing projects with bendway weirs to improve aquatic habitat, relocate the thalweg, and manage energy throughout the bend. Although bendway weirs are low elevation structures, they block a portion of the main channel flow area and could reduce the effective channel width so excavating from the inner bend prevents channel narrowing. Maintaining sufficient channel width is important because a wider, shallower channel results in lower velocity and shear stress than a deep and narrow channel. Excavating the point bar at two different depths provides effective water and sediment transport with variable habitat over a range of flows. For the Rio Grande project, the upper point bar surface was also set at an elevation that promotes wetland establishment.

Creating an inset floodplain bench accomplishes the dual purpose of providing a cost effective method of disposing of the excavated material while offering significant hydraulic and environmental benefits. Reestablishing a floodplain surface allows higher flows to spread out at a shallower depth, thereby reducing velocity. Also, eddies that occur between the bendway weirs will cause scalloping of the floodplain bench rather than eroding the existing bankline. Figure 2 and Figure 3 illustrate the final design for the Rio Grande example project. An iterative process was used to design the floodplain bench and bar excavation elevation and alignment. The primary considerations while determining the floodplain bench elevation included depth to groundwater, typical inundation duration, and locations of existing willows near the site. A Reclamation biologist helped evaluate these factors and an average elevation of 5510.5 ft was selected for the floodplain bench. This is about 2.5 ft above the assumed groundwater table (base flow elevation) and corresponds to a river discharge of 3,500 cfs (1.25-yr return period). Balancing cut and fill volumes required a wider floodplain bench than originally estimated, thereby shortening the bendway weir length protruding into the flow. A final iteration was performed with the CSU velocity equations to refine the bendway weir layout based on the final floodplain bench design. A grid of coyote willows is included on the floodplain bench to stabilize the soil and create additional habitat. Vegetation provides increased hydraulic roughness to further reduce flow velocity and potentially encourage sediment deposition. Planting the willows in a grid pattern ensures that the technique will be effective regardless of flow rate and direction. It is essential that willow poles reach and maintain contact with groundwater to provide the best opportunity for survival.

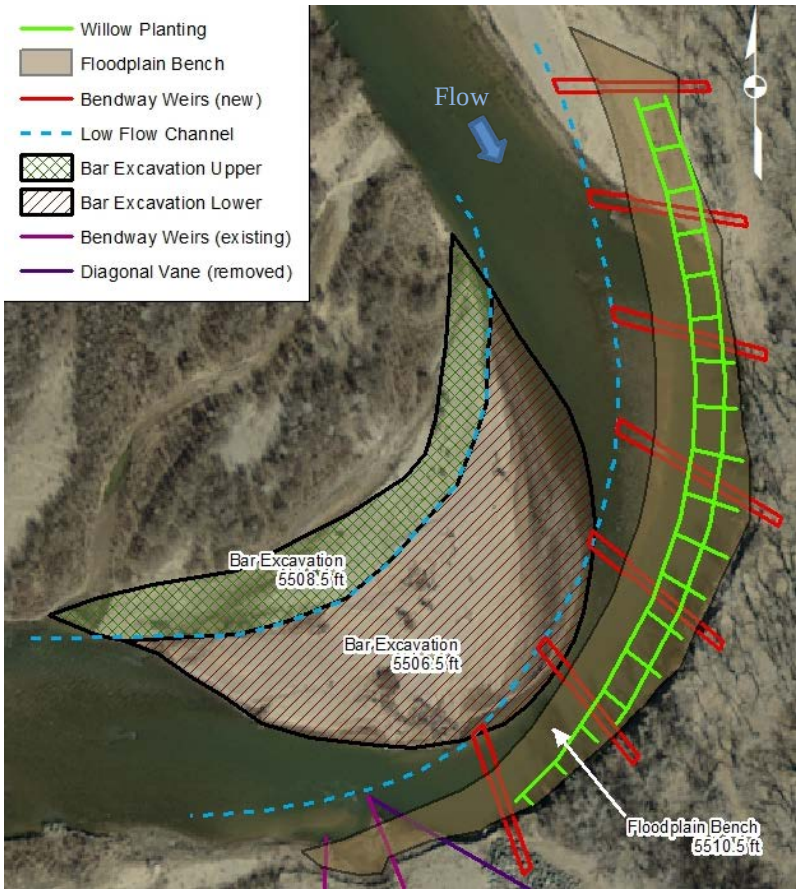

Figure 2 Site Plan with final location of project features.

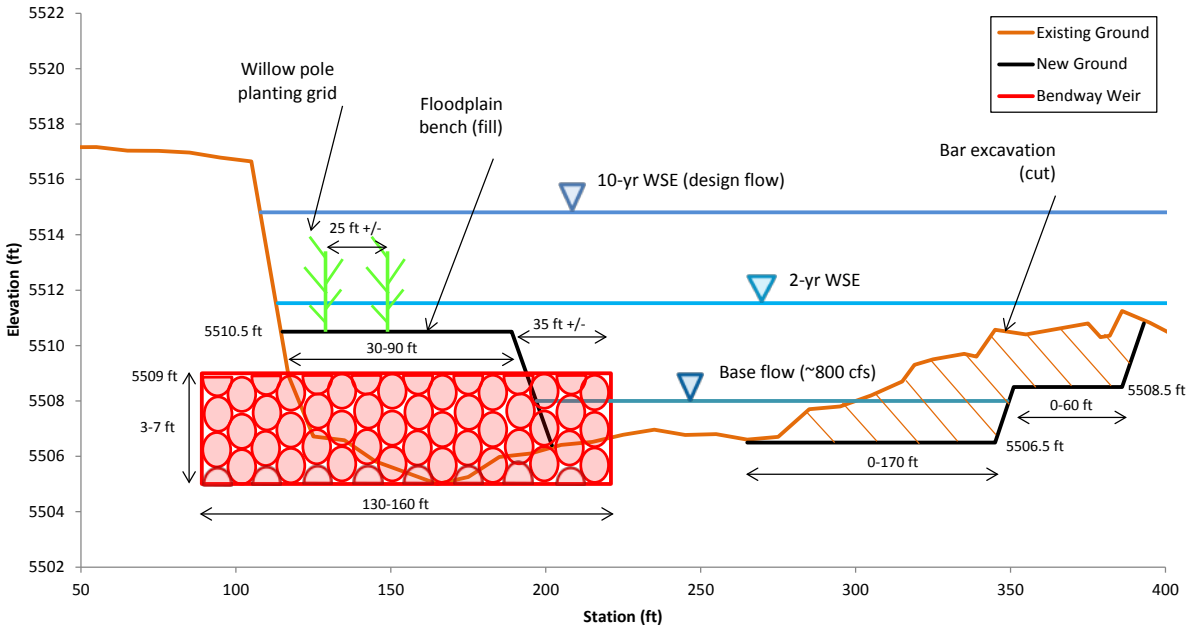

Figure 3 Typical cross section (looking downstream) with dimensions.

Summary and Recommendations: A bendway weir design methodology was described and illustrated with an example project that was constructed in 2013 on the Rio Grande north of Albuquerque, New Mexico. This project has only experienced two low spring runoff years since construction, but there have been a few high flow monsoon events. Sediment has been deposited along the bendway weirs and on the floodplain bench, indicating that the project has been effective so far. Existing guidelines were used near the beginning of the design process to establish a framework of feasible values for important geometric parameters. The existing guidelines do not quantify the effect of bendway weirs on channel hydraulics. However, they are based on field experience and designs of previous projects and should not be discounted. The CSU velocity ratio equation allows channel velocity to be predicted as a function of different bendway weir configurations. Comparing predicted velocities to the permissible velocity provides a method to estimate if the bendway weirs will be effective in preventing future bank erosion. Scurlock et al. (2012 and 2014) should be reviewed for a more detailed description of the velocity ratio equation including the range of applicability. This is an area of ongoing research by CSU for the Bureau of Reclamation, which includes the development of a 3-D numerical model.

It is recommended that an as-built survey be completed soon after construction to document field conditions of completed projects. This is important regardless of the design methodology and provides a reference for evaluating future adjustments. Bendway weir projects should be monitored for performance over time, particularly during and after high flow events. The level of monitoring can range from visual observations to more sophisticated data collection techniques. Surveys of the river channel and banks can be compared to as-built data to evaluate erosion and deposition patterns. Monitoring bendway weir tip location, crest elevation, and crest width will indicate if the riprap has been mobilized and if the structures are still functioning as intended. Measuring velocity and water surface elevation throughout the bend during high flow events will provide valuable hydraulic information that can be used to evaluate the CSU equations and the effects of bendway weirs on the flow.

REFERENCES

Baird, D.C. (2014). Bendway Weir Physical Model Re-Evaluation and Future Modeling Recommendations to Complete Design Guidelines. Bureau of Reclamation, Technical Service Center, Denver, Colorado, 39 pp.

Blench, T. (1957). Regime Behaviour of Canals and Rivers. Butterworths Scientific Publications, London, 138 pp.

Cox, A.L. (2005). A Study of In-Stream Rehabilitation Structures in Sand-Bed Channels. M.S. Thesis, Colorado State University, Fort Collins, Colorado, 462 pp.

Darrow, J.M. (2004). Effects of Bendway Weir Characteristics on Resulting Flow Conditions. M.S. Thesis, Colorado State University, Fort Collins, Colorado, 265 pp.

de Almeida, G.A., and Martin-Vide J.P. (2009). "Riprap Stability: Transverse and Longitudinal versus Continuous Protections," Journal of Hydraulic Engineering, ASCE, 135(6), pp 447–456.

Derrick, D. (2012). Streambank Erosion and Protection Training Course. U.S. Army Corps of Engineers, Vicksburg, Mississippi.

Fischenich, C. (2001). Stability Thresholds for Stream Restoration Materials, EMRRP Technical Notes Collection (ERDC TN-EMRRP-SR-29). U.S. Army Engineer Research and Development Center, Vicksburg, Mississippi.

Heintz, M.L. (2002). Investigation of Bendway Weir Spacing. M.S. Thesis, Colorado State University, Fort Collins, Colorado, 225 pp.

Lagasse, P. F., Clopper, P.E., Pagan-Ortiz, J.E., Zevenbergen, L.W., Arneson, L.A., Schall, J.D., and Girard, L.G. (2009). Bridge Scour and Stream Instability Countermeasures: Experience, Selection, and Design Guidance, Third Edition, Volume 2, Hydraulic Engineering Circular No. 23. Federal Highway Administration, Washington, DC.

Kilgore, R.T., and Cotton, G.K. (2005). Design of Roadside Channels with Flexible Linings, Hydraulic Engineering Circular No. 15, Third Edition. Federal Highway Administration, Washington, DC.

Lagasse, P.F., Clopper, P.E, Zevenbergen, L.W., and Ruff, J.F. (2006). Riprap Design Criteria, Recommended Specifications and Quality Control, National Cooperative Highway Research Program Report 568. Transportation Research Board, National Academies of Science, Washington, DC.

Maynord, S.T. (1996). "Toe-Scour Estimation in Stabilized Bendways," Journal of Hydraulic Engineering, ASCE, 122(8), pp 460–464.

Maynord, S.T., Ruff, J.F., and Abt, S.R. (1989). "Riprap Design," Journal of Hydraulic Engineering, ASCE, 115(7), pp 937–949.

McCullah, J., and Gray, D. (2005). Environmentally Sensitive Channel- and Bank-Protection Measures. National Cooperative Highway Research Program NCHRP Report 544 and Project 24-19, Transportation Research Board, National Academies of Science, Washington, DC.

NRCS (Natural Resources Conservation Service), (2007). Part 654 National Engineering Handbook – Stream Restoration Design.

Pemberton, E.L., and Lara, J.M. (1984). Computing Degradation and Local Scour, Technical Guideline for Bureau of Reclamation. U.S. Bureau of Reclamation, Denver, Colorado, 48 pp.

Schmidt, P.G. (2005). Effects of Bendway Weir Field Geometric Characteristics on Channel Flow Conditions. M.S. Thesis, Colorado State University, Fort Collins, Colorado, 364 pp.

Scurlock, S.M., Cox, A.L., Thornton, C.I., and Abt S.R. (2012). "Middle Rio Grande physical modeling – Transverse instream structure analysis: Maximum and average velocity ratios within the prismatic channel," Colorado State University, Department of Civil Engineering, Fort Collins, Colorado, 31 pp.

Scurlock, S.M., Thornton, C.I., and Abt S.R. (2014). Middle Rio Grande physical modeling – Quantification of Hydraulic Effects from Transverse Instream Structures in Channel Bends. Colorado State University, Department of Civil Engineering, Fort Collins, Colorado, 159 pp.

USACE (U.S. Army Corps of Engineers), (1994). Hydraulic Design of Flood Control Channels, Engineer Manual No. 1110-2-1601. Department of the Army, Washington, DC.

Watson, C.C., Biedenharn, D.S., and Thorne C.R. (2007). Stream Rehabilitation, Version 2.0. Cottonwood Research, LLC. Fort Collins, Colorado, 240 pp.

Zeller, M.E. (1981). Scour Depth Formula for Estimation of Toe Protection Against General Scour. Pima County Department of Transportation and Flood Control District, Tucson, Arizona.

PERFORMANCE OF LOG CRIBS FOR BLUFF STABILIZATION

Ben Lee, Hydraulic E.I.T.,' Inter-Fluve, Madison, Wisconsin, blee@interfluve.com; Marty Melchior, Regional Director, Inter-Fluve, Madison, Wisconsin, mmelchior@interfluve.com; Andy Selle, Hydraulic Engineer and Fisheries Biologist, Inter-Fluve, Madison, Wisconsin, aselle@interfluve.com; Ben Swanson, Ph.D, Fluvial Geomorphologist, Inter-Fluve, Madison, Wisconsin, bswanson@interfluve.com

INTRODUCTION

Erosion of valley walls and terraces associated with channel migration often produce high, steep erosional features, known as bluffs, along channels. In some rivers and streams, bluff erosion can add a disproportionate volume of sediment to the overall load, creating a host of ecological and sediment conveyance problems (Fitzpatrick et al., 1999; Belmont et al., 2011). A range of stabilization techniques are applied to bluffs with various levels of success. An approach that targets the toe of the bluff using natural log materials, often available on site, appears to be a low cost and effective approach to stabilization.

The technique involves constructing a log crib that mimics natural wood accumulation and provides the foundation for a floodplain bench at the toe of the bluff. The wood forms a rigid, structural treatment while also providing organic material and complexity similar to habitat features in natural streams. The creation of a floodplain bench above the wood impedes rotational failure of the upper bluff and allows recruitment of vegetation that will provide long-term stabilization. The bench also catches material that erodes from the untreated upper bluff. The approach is being applied to streams in the Midwest as (1) the benefits of woody material in streams have been shown to improve aquatic and riparian habitat (Flebbe, 1999; Zorn and Nuhfer, 2007; Kratzer and Warren, 2013), (2) it works with a natural process whereby eroding bluffs in forested watersheds contribute woody debris that impedes further erosion of the toe, and (3) the method is relatively cost effective as materials can be locally sourced and the upper bluff is not directly stabilized.

The installation and performance of the log crib and bench approach has not been well documented. While the log crib approach has been used in the past, it has been primarily used for stabilizing eroding banks rather than higher terraces or bluffs (Krymer and Robert, 2013). Furthermore, these designs have been based on a symmetrical form rather than one that mimics natural debris accumulations. We have developed an approach using log cribs with a bench that is based on more natural wood recruitment patterns to improve fish habitat while also providing bluff stabilization.

Clark Creek is a small, step-pool and plane-bed stream that meanders through glacial sands and gravels. The channel contains cold water and provides habitat for native brook trout (*Fontinalis salvelinus*). Avulsion and channel migration during floods in recent decades have resulted in stream migration toward bluffs at the edge of the valley, creating sedimentation problems and impacting aquatic and riparian habitat. To address these problems while improving aquatic habitat, we have installed log cribs and monitored their performance. Construction occurred in October, 2013, and subsequent surveys continue to provide information on the performance of the design.

REGIONAL SETTING

Clark Creek lies along the north-facing slope of the Baraboo Hills in south-central Wisconsin. The headwaters of the stream consist of hillslope debris overlying Baraboo Hills quartzite bedrock (Clayton and Attig, 1990). The middle of the watershed is located in a glacial ice-margin lake basin that filled a valley within the Baraboo Hills as the Green Bay Lobe of the Wisconsin Glaciation prevented drainage to the north. The lower watershed is located in glacial till (Clayton and Attig, 1990). Sediments throughout the middle and lower part of the watershed are primarily sand with some gravels, cobbles and localized varved clay deposits.

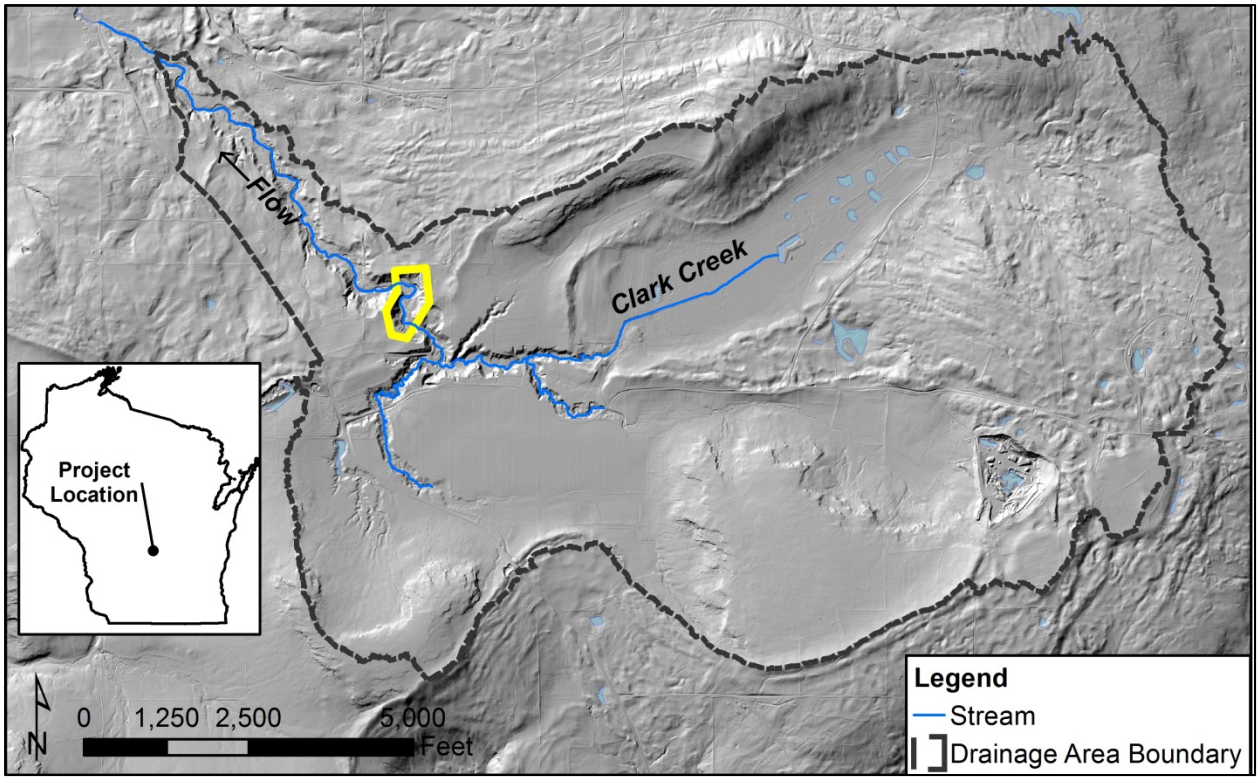

Figure 1 Clark Creek location, watershed topography and perennial flow reaches (blue lines).

GEOMORPHIC HISTORY

Clark Creek runs through a relatively confined valley in the transitional area between the glacial ice-margin lake and tills. Valley widths through the site average 150 feet. Longitudinal valley slopes are 1-2%.

Large flood events in 1993 and 2008 initiated incision and channel avulsion (Figure 3). The 1993 flood was estimated to have a recurrence interval of 500 years and the 2008 flood was estimated to have a recurrence interval of 100 years (Montgomery Associates, 2011). Based on evidence from former channel locations and an abandoned culvert, bed elevations dropped three to five feet. Incision was greatest in the eroded bluff reach due to the removal of riparian vegetation within the last century. In less disturbed reaches, riparian vegetation and other roughness features provided natural resiliency that impeded further incision.

In 2013, channel slopes varied depending on location relative to the bluffs. Adjacent to the eroding bluffs, the channel had a step-pool morphology with slopes up to 7%. Between the bluffs, the channel had a plane-bed morphology with gradients around 1-2%. The steeper slopes developed as cobbles and boulders in the glacial till comprising the bluffs deposited at the toe. This larger material, lag, was immobile and allowed the grade to steepen as fine sediment transported downstream. Despite the coarse material contributed to the channel by the bluffs, the majority of the material in the bluffs consists of sand (see Figure 2).

Reaches downstream of the eroding bluff reach did not experience the same depth of incision. The bankfull channel appeared to be adjusted to recent discharge and sediment supply regimes. Relatively low benches had formed adjacent to the channel which supported vegetation at least three years old and some minor sand deposition. The average width of the channel in this reach was around 16 ft with a depth of 1.5 ft.

Figure 2 Photo of Bluff 1 in April, 2013 (looking upstream). Note the coarse lag material deposited in the channel and bluff toe that has formed steps. Exposed sediments along the inside of the bend are from the 2008 flood.

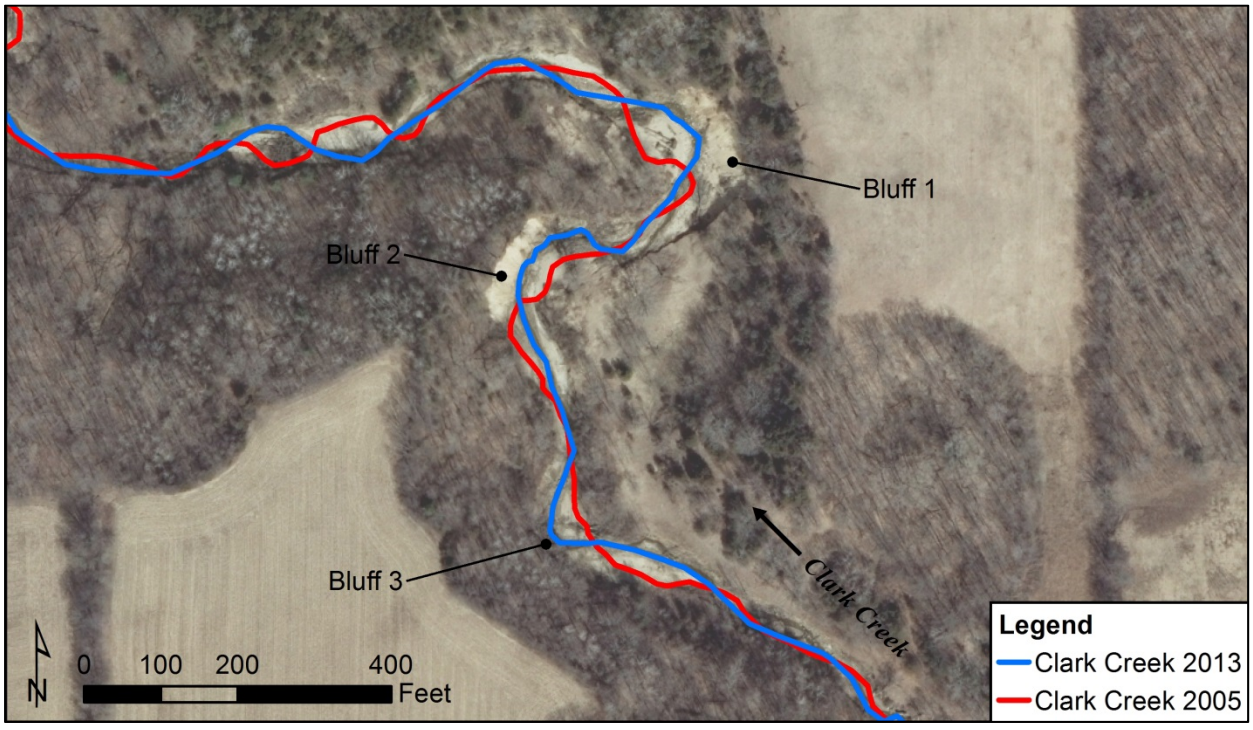

Figure 3 Channel alignments in 2013 and in 2005 before the 2008 flood event that created multiple avulsions.

PROJECT DESIGN

Stabilization of the bluffs involved three major design components: (1) re-aligning the channel away from the bluff toe, (2) building a log crib as the foundation for a floodplain bench at the toe of the bluffs, and (3) re-building the channel with native stone.

Channel Design

The channel was re-located away from each bluff toe to accommodate the log crib and bench (Figure 4). The width of the bankfull channel was based on the 16 ft average width observed along the downstream reference reach. The design called for a bank height along the log crib side of the channel of 3 ft; however, this value varied at Bluffs 2 and 3 where heights around 5 and 4 ft were constructed, respectively. The higher banks were due to the larger diameters of logs available to construct the cribs. Opposite the bluffs, channel bank heights were 1.5 ft, similar to the downstream reference reach.

Log Crib Design

Log cribs were constructed to impede erosion of the banks near the bluffs and provide a framework to contain soil for the constructed bench at the bluff toe. The benches were designed to (1) catch eroded material from the upper bluff, (2) create an area for vegetation establishment, and (3) resist rotational failure of the bluff. Constructed bench widths were approximately 23 ft at Bluff 1, 18 ft at Bluff 2, and 14 ft at Bluff 3. Each log crib was built at least 3 ft deeper than the channel bed elevation to account for local scour and additional minor incision that could occur in the future (Figure 4).

The cribs were comprised of four to five layers of logs. The angle of the logs in each layer was varied to provide habitat complexity and to better replicate the configuration of a natural log jam. Slash was incorporated into the jams to provide smaller interstitial spaces and additional organic substrate for macroinvertebrates and small fishes. Logs were sourced from nearby uplands and varied in diameter from 1 to 3 ft with lengths between 20 and 35 ft.

Channel Substrate Design

Stone from the original channel, supplemented with rock from nearby farm fields, was utilized for construction of the new channel. The median grain size of the existing channel bed material was 0.16 ft in plane-bed reaches and most stones in the step-pool reaches had diameters between 1 and 2 ft. The incipient grain size for the designed channel was 0.8 ft during the 100-year flood (Bathurst, 1987), thus imported stone had diameters between 1 and 2.5 ft to ensure stability. Natural steps in step-pool channels were replicated with the imported rocks. The stones were also extended laterally into the floodplain opposite each log crib to provide resistant material should the channel migrate. The constructed channel slope was 4.1% at Bluff 1, 3.0% at Bluff 2, and 2.5% at Bluff 3. Distances between the steps averaged 15 ft at Bluff 1, 19 ft at Bluff 2, and 22 ft at Bluff 3. These distances were consistent with the existing channel and other comparable streams (Chin et al., 2009).

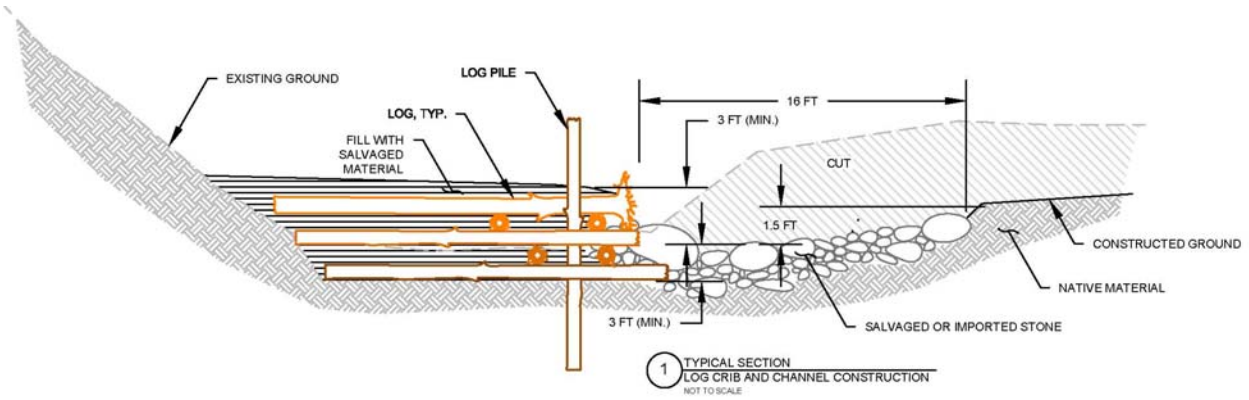

Figure 4 Typical cross section detailing the dimensions and materials used for construction of the log cribs, benches and channel.

Figure 5 Upstream view of Bluff 1 in November, 2013, immediately after construction. Logs with root wads form one side of the channel and steps and pools were constructed in the channel.

MONITORING METHODS

The topography of the bluffs and channel were surveyed at each of the three sites with a survey grade real time kinematic global positioning system. An as-built survey was completed in November, 2013, immediately after

construction. In June, 2014, a post-construction survey was completed to document changes following a six month period that included a flood with a 2.5-year recurrence interval. A final survey was completed in November, 2014, one year after construction. The final survey did not include complete coverage of Bluff 1 as snowfall inhibited characterization of the site.

Each survey included sufficient detail to construct a three dimensional surface model of the sites. The surveys included all breaks in grade along the channel, banks, adjacent floodplain, and the crib bench. With these data, triangulated irregular network (TIN) surface models were built in AutoCAD® Civil 3D®. Geomorphic changes between each survey were analyzed by creating volumetric TIN models that subtracted one survey from the previous. Geomorphic units were delineated in the models to quantify erosion and deposition patterns.

RESULTS

Bluff 1 experienced the greatest geomorphic change between November, 2013 and June, 2014 with about 60 cubic yards of material eroded from the left floodplain (Figure 6). The sandy sediments from the un-vegetated floodplain transported downstream during the 2.5-year flood and a new side channel formed. The eroded and designed channels conveyed water during base flow conditions in June. The extension of the rock steps into the left floodplain limited further downcutting into the floodplain. Within the main channel, 13 cubic yards of material deposited in pools while 18 cubic yards of material was eroded as the left bank adjusted. The bench above the crib experienced 36 cubic yards of deposition and 31 cubic yards of erosion. The erosion was likely a result of fill material settling after construction and the freeze-thaw cycle during the winter. Deposited material originated from erosion of the upper bluff.

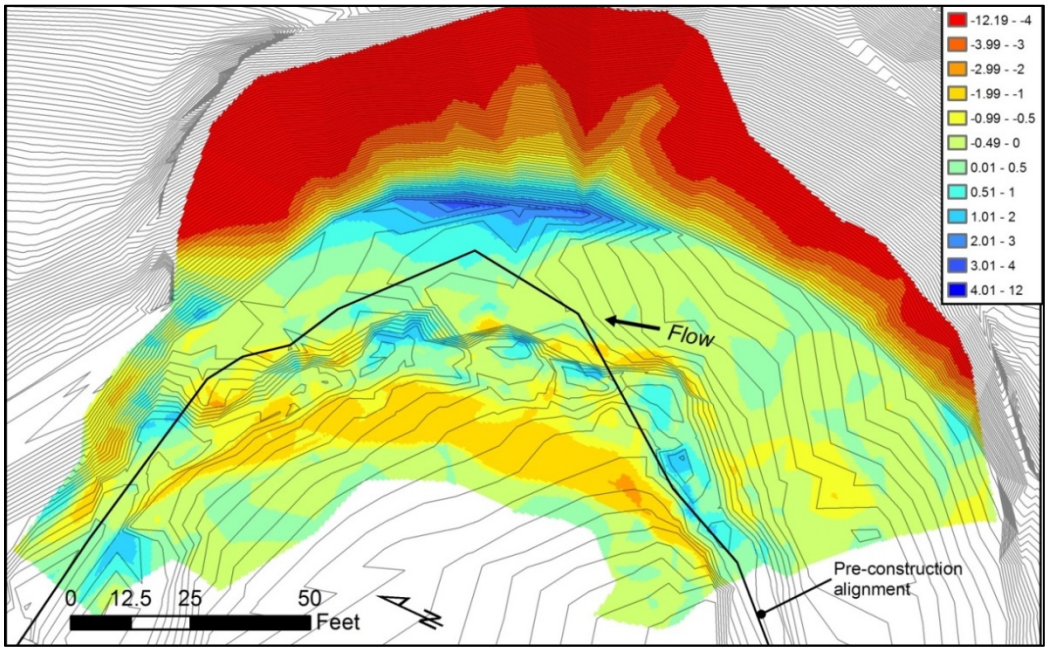

Figure 6 Erosion (red) and deposition (blue) at Bluff 1 between November, 2013, and June, 2014 (in feet). The 0.5 ft contours (gray lines) represent the November, 2013 topography integrated with LiDAR data. Note the erosion of the deposition of eroded upper bluff material on the bench. Deposition is also evident in the channel pools. Along the inside of the bend, up to 3 ft of erosion occurred.

At Bluff 2, 25 cubic yards of sediment filled the pools in the channel between November, 2013 and June, 2014 (Figure 7), and 22 cubic yards of material eroded from the channel as the right bank adjusted. Along the log crib toe,

11 cubic yards of deposition occurred. The constructed bench experienced 19 cubic yards of erosion and 12 cubic yards of deposition. The right floodplain had 58 cubic yards of erosion and 3 cubic yards of deposition.

A total of 35 cubic yards eroded from the site and 86 cubic yards deposited between June, 2014 and November, 2014. The bench at the bluff toe experienced 39 cubic yards of deposition, the channel experienced 11 cubic yards, and the right floodplain experienced 26 cubic yards.

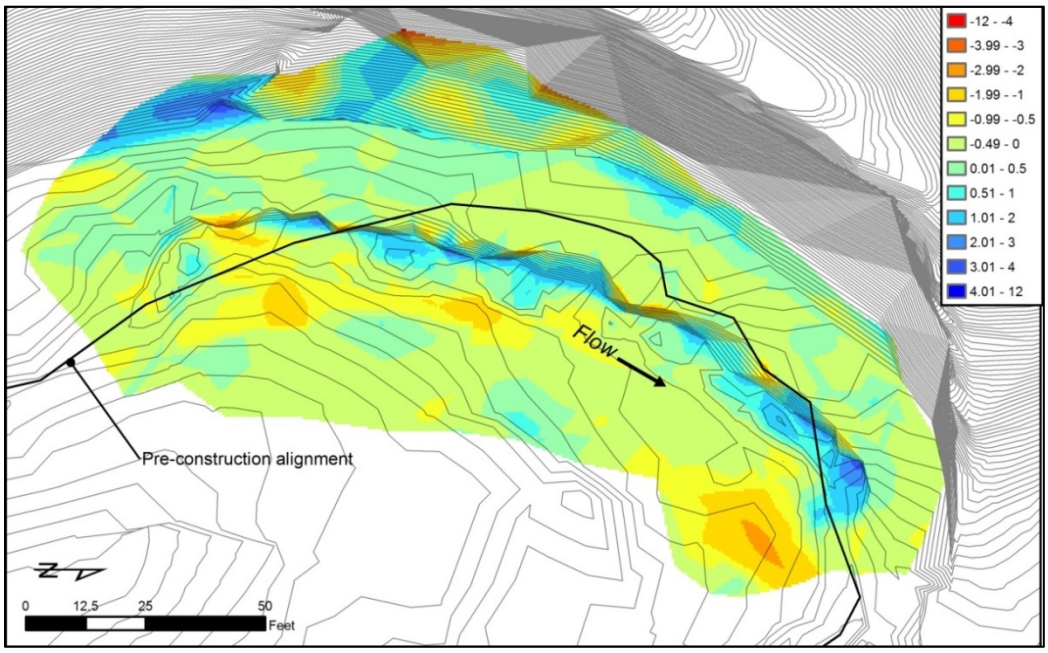

Figure 7 Erosion (red) and deposition (blue) at Bluff 2 between November, 2013 and June, 2014 (in feet). The 0.5 ft contours (gray lines) represent the November, 2013 topography integrated with LiDAR data. Sediment deposited in the channel pools and at the toe of the log crib. Erosion occurred along the inside bend floodplain.

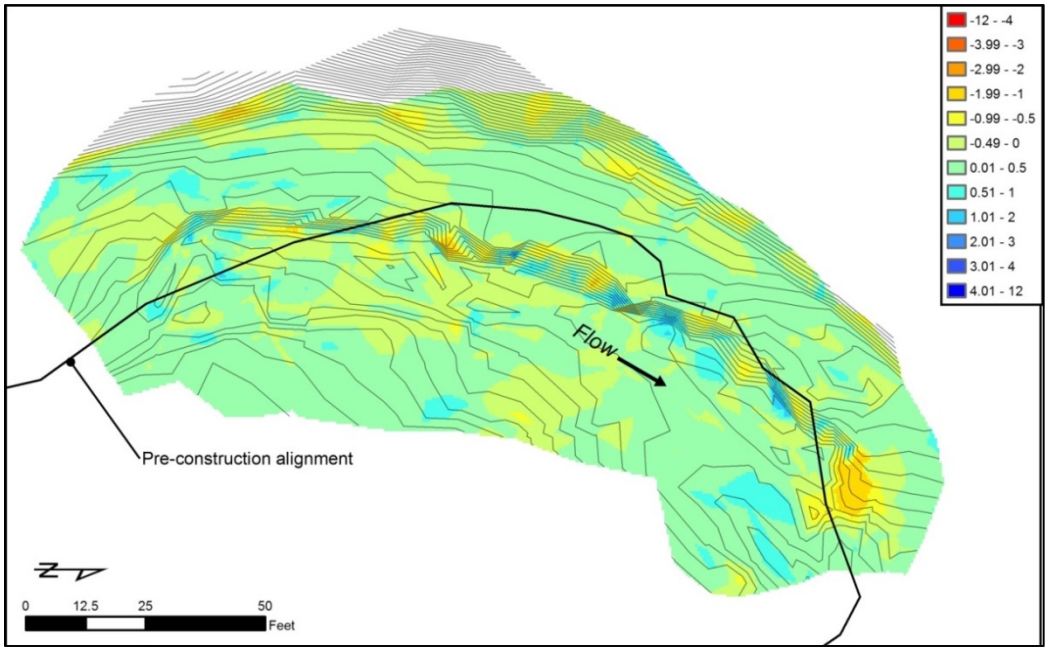

Figure 8 Erosion (red) and deposition (blue) at Bluff 2 between June, 2014 and November, 2014. The 0.5 ft contours (gray lines) represent the June, 2014 topography. Relatively little erosion and deposition took place during this time period compared to the previous 6 months.

At Bluff 3, pools in the channel and the log crib toe experienced 25 cubic yards of deposition between November, 2013 and June, 2014. Some erosion occurred just upstream of the log crib along the channel banks. The right floodplain generally degraded during this time period except for the furthest upstream area. Three logs were placed on the floodplain at this location to provide roughness and to impede avulsion.

Between June, 2014, and November, 2014, the channel accumulated 15 cubic yards of sediment and the right floodplain accumulated 30 cubic yards of sediment.

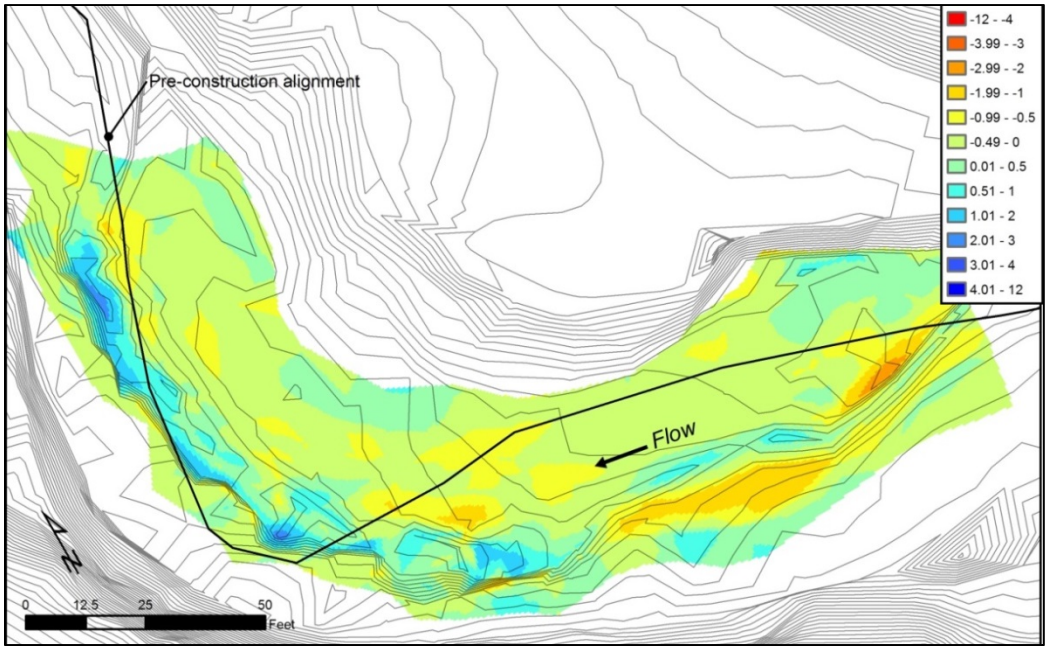

Figure 9 Erosion (red) and deposition (blue) at Bluff 3 between November, 2013 and June, 2014. The 0.5 ft contours (gray lines) represent the November, 2013 topography integrated with LiDAR data. Sediment deposited in the channel pools and at the toe of the log crib.

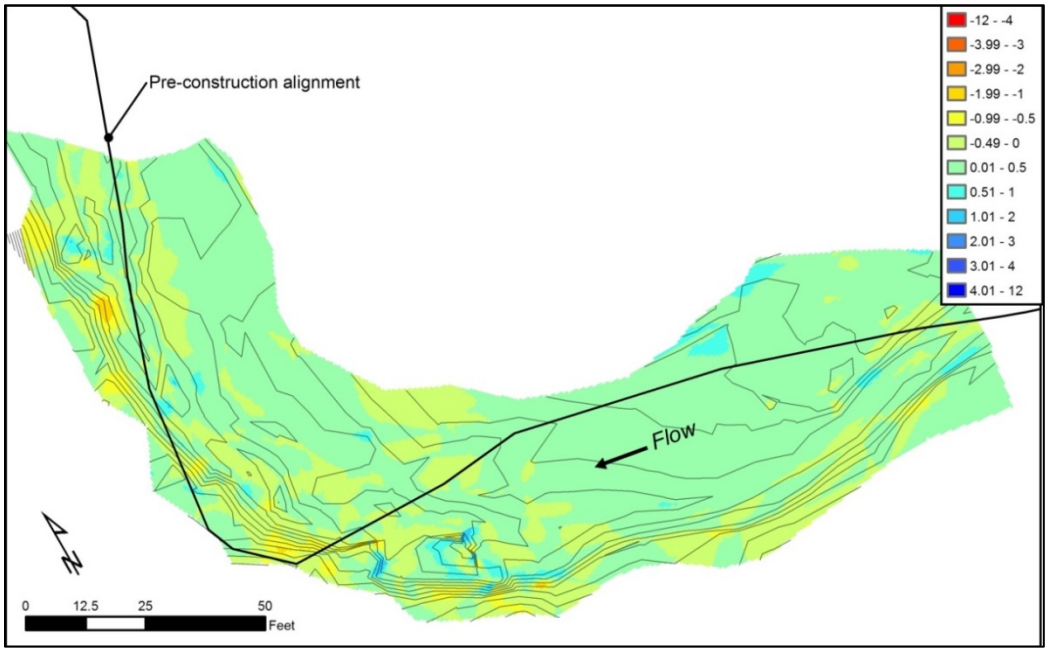

Figure 10 Erosion (red) and deposition (blue) at Bluff 3 between June, 2014 and November, 2014. The 0.5 ft contours (gray lines) represent the June, 2014 topography.

DISCUSSION

The log cribs and benches performed as designed during the first year after construction. Material eroded from the upper bluffs was deposited on the benches (Figure 12). Most of the geomorphic change occurred between November, 2013 and June, 2014 indicating that more material eroded from the upper bluff during spring thaw rather

than precipitation-induced erosion in the summer. Similarly, we noted active erosion at all of the bluff sites the previous year in April, 2013.

Soil contained in the log crib remained in place and provided resistance against channel migration. In addition, the roughness provided by the logs and root wads promoted some deposition around the toe of the structure.

The quantities and locations of erosion and deposition varied between the bluff sites. The bench at Bluff 1 experienced the greatest accumulation of sediment. This was probably due to the larger exposed area and the greater bluff height compared to Bluffs 2 and 3.

Vegetation on the benches grew closer to the channel bank where deposition did not occur (Figure 12). Additional monitoring will continue to provide information on the sustainability of vegetation in this depositional area.

Figure 11 Photo of the Bluff 1 immediately after construction in October, 2013 (looking downstream).

Figure 12 Photo of Bluff 1 in June, 2014 from the same location as Figure 11. Note the deposition on top of the bench and the secondary channel along the inside of the bend.

Channel change was relatively rapid within the first six months of construction. Sand filled in pools and deposited at the toe of the logs. Pool deposition was expected as they were over-excavated to ensure larger, immobile bed material would not limit depths. Nevertheless, the filling of the pools probably reduced the habitat available for macroinvertebrates by creating unstable substrates and for fish by concealing boulders that provided cover. Deposition around the log banks also filled in areas of habitat complexity. The sediment accumulations did not appear to be systemic as the reaches up- and downstream did not have noticeable changes. Instead, the channel form adjusted to match local hydraulics.

The lack of vegetation cover on the floodplain opposite the log cribs contributed to instability. Late autumn construction did not provide sufficient time for vegetation growth. Funds for construction and worker availability were limited to this time frame, however. The deposition surrounding the logs on the floodplain at the upstream end of Bluff 3 provides a useful reference for stabilization in these situations. Additional placement of logs throughout the floodplain would impede erosion until vegetation establishes to provide erosion resistance during floods.

CONCLUSIONS

The log cribs and benches have performed as designed after one year of construction. The benches provide a trap for sediment falling from the upper bluff while also providing an area for vegetation to establish and provide long-term lateral stability for the channel. The log cribs have impeded channel migration into the bluffs during a flood with a 2.5-year recurrence interval. The project, however, has not been tested by a significant flood event and performance measures are ongoing.

Channel adjustments have suggested improvements to the design. Placement of logs throughout the floodplain would impede erosion and maintain primary flow in the constructed channel. It is also possible that occluding some flow on the floodplain with the logs would force larger pools in the channel to minimize localized aggradation. Creating a relatively stable channel is important for bluff stability in Clark Creek. Avulsion instigated bluff erosion during the floods of 1993 and 2008. An unstable floodplain in the years immediately following construction could

lead to the initiation of bluff erosion in other areas should a large flood occur. In addition, part of the reason for utilizing a log crib was to improve aquatic habitat. Creating a channel that maximizes the habitat potential should therefore be considered an important part of the design.

Acknowledgements

Project design and construction was funded by Sauk County, Wisconsin. The Wisconsin Department of Natural Resources contributed equipment and workers for the project construction.

REFERENCES

Bathurst, J.C. (1987). "Critical conditions for bed material movement in steep, boulder-bed streams," Proc. Erosion and Sedimentation in the Pacific Rim, IAHS Publication No. 165, Corvallis, Oregon.

Belmont, P., Gran, K.B., Schottler, S.P., Wilcock, P.R., Day, S.S., Jennings, C., Lauer, J.W., Viparelli, E., Willenbring, J.K., Engstrom, D.R., and Parker, G. (2011). "Large shift in source of fine sediment in the Upper Mississippi River," Environmental Science & Technology, 45: 8804-8810, dx.doi.org/10.1021/es2019109.

Chin, A., Anderson, S., Collison, A., Ellis-Sugai, B.J., Haltiner, J.P., Hogervorst, J.B., Kondolf, G.M., O'Hirok, L.S, Purcell, A.H., Riley, A.L., and Wohl, E. (2009). "Linking theory and practice for restoration of step-pool streams," Environmental Management, 43, pp 645-661, DOI 10.1007/s00267-008-9171-x.

Clayton, L., and Attig, J.W. (1990). "Geology of Sauk County, Wisconsin," Wisconsin Geological and Natural History Survey, Information Circular 67, Madison, Wisconsin.

Fitzpatrick, F.A., Knox, J.C., and Whitman, H.E.. (1999). "Effects of historical land-cover changes on flooding and sedimentation, North Fish Creek, Wisconsin," USGS Water-Resources Investigations Report 99-4083, Middleton, Wisconsin.

Flebbe, P.A. (1999). "Trout use of woody debris and habitat in Wine Spring Creek, North Carolina," Forest Ecology and Management, 114, pp 367-376.

Kratzer, J.F., and Warren, D.R. (2013). "Factors limiting brook trout biomass in Northesatern Vermont streams," North American Journal of Fisheries Management, 33(1), pp 130-139.

Krymer, V., and Robert, A. (2013). "Stream restoration and cribwall performance: a case study of cribwall monitoring in Southern Ontario," River Research and Applications, DOI: 10.1002/rra.2684.

Montgomery Associates. (2011). Clark Creek Watershed Study, Prepared for: Sauk County, Wisconsin Land Conservation Department, Cottage Grove, Wisconsin.

Zorn, T.G., and Nuhfer, A.J. (2007). "Influences of brown trout and brook trout population dynamics in a Michigan River," Transactions of the American Fisheries Society, 136(3), pp 691-705.

ROCK CHECK STRUCTURES FOR RESTORATION OF HEADWATERS

Jon Fripp, Civil Engineer - Stream Mechanics, USDA—NRCS, National Design, Construction, and Soil Mechanics Center, Fort Worth, Texas, jon.fripp@ftw.usda.gov, Richard Weber, Civil Engineer - Wetlands, USDA—NRCS, Central National Technology Service Center, Fort Worth, Texas, richard.weber@ftw.usda.gov

ABSTRACT

Stream degradation often has its roots in problems found in the upper watershed. These areas can be degraded by gully erosion, by the prior installation of surface drainage ditches, or by the formation of a defined channel on a site that was previously vegetated with no channel. The resultant lowering of the hydraulic grade line causes a lowering of the local groundwater table, reduced flood connectivity, and, in some cases, the loss of wetland hydrology. On sites where gully erosion is still active, the channel may be actively degrading with an advancing headcut. In other cases, the gully may have reached a state of stability, but the site has lost its original hydrologic functions. Excess sediments are supplied to lower areas in the watershed and base flows are reduced. If these upper areas are not adequately addressed, the benefits of restoration efforts in the lower portions of the watershed can be limited. A stream corridor approach is needed.

The presentation will discuss the use of a systematic approach to applying vegetation and low-head structures to restore these areas. This approach results in raising the groundwater table, increasing the frequency and extent of surface inundation, increasing upland sediment deposition, and stabilizing advancing headcuts. This low impact and cost effective approach has been applied in some wetland restoration projects but has seldom been effectively applied as part of a stream restoration. The presentation will discuss benefits, design issues, construction and maintenance. Example applications will be addressed.

ESTIMATING CHANGES IN RIPARIAN AND CHANNEL FEATURES ALONG THE TRINITY RIVER DOWNSTREAM OF LEWISTON DAM, CALIFORNIA, 1980 TO 2011

Jennifer Curtis, Geomorphologist, U.S. Geological Survey, Eureka, CA, jacurtis@usgs.gov

Abstract: The Trinity River Restoration Program, one of the nation's largest adaptively managed river restoration programs, requires periodic assessments to determine the effectiveness of management actions in restoring channel dynamics and habitat features. This study documents the evolution of the intensively managed 65-km restoration reach downstream of Lewiston Dam, California during the period spanning 1980 to 2011. The nature and extent of riparian and channel changes were characterized using a series of geomorphic feature maps constructed from orthorectified photography acquired at low flow conditions in 1980, 1997, 2001, 2006, 2009, and 2011. Since 1980 there has been a general conversion of riparian to channel features and expansion of the active channel area. The primary mechanism for expansion of the active channel area was bank erosion from 1980 to 1997 with channel widening being well distributed longitudinally throughout the study reach. The primary period of bar accretion occurred from 1997 to 2001 and was followed by slightly higher rates of bar scour from 2001 to 2006. In comparison, post-2006 bank and bar changes were spatially limited to reaches with sufficient local transport capacity or sediment supply supported by gravel augmentation, mechanical channel rehabilitation, and tributary contributions to flow and sediment supply. A series of tributary floods in 1997, 1998 and 2006 were the primary factors leading to documented increases in channel complexity and floodplain connectivity. During the post-2006 period managed flow releases, gravel augmentation and mechanical restoration caused localized increases in sediment supply and transport capacity, which led to small but measurable increases in channel complexity and floodplain connectivity. Significant channel widening and muted geomorphic response of channel rehabilitation sites to post-2006 management highlights the need for continued monitoring and assessment of the magnitude, duration, and timing of prescriptive gravel augmentation, flow releases, and associated geomorphic objectives.

INTRODUCTION

Completion of the Trinity River Diversion in 1964 enabled the transfer of 75 to 90 percent of the upper Trinity River flows into the upper Sacramento River. Subsequent declines in salmon and steelhead populations prompted a series of studies (Trinity River Taskforce, 1970; USFWS, 1980; USFWS and HVT, 1999) that culminated in the Record of Decision (USDOI, 2000) and organization of the multi-agency Trinity River Restoration Program (TRRP). The Record of Decision (ROD) authorized management actions to restore salmon and steelhead populations to pre-dam levels downstream of Lewiston Dam, California. The TRRP, a collaborative partnership, is responsible for implementing ROD-mandated restoration and adaptive management for one of the largest river restoration programs in the nation.

The Trinity River is the largest tributary to Northern California's Klamath River. The study reach extends 65 kilometers along the upper main stem from Lewiston Dam downstream to the confluence with the North Fork Trinity River (Figure 1). The restoration reach is a partially confined gravel-bed river with a nearly constant bedrock-controlled slope of 0.002. The channel pattern is primarily single-thread and the dominant channel type is pool-riffle with intermittent

plane-bed and bedrock-controlled canyon reaches. Restoration efforts began in the 1970s and included: construction of spawning beds, side channels and channel complexity features, as well as riparian berm removal and re-contouring of channel margins, pool dredging, bridge replacement, installation of engineered log dams, and prescriptive gravel augmentation and flow releases.

The goal of this study was to quantify ecologically significant measures of geomorphic change, relevant to Trinity River fisheries restoration, and to evaluate the cumulative effects of natural and managed drivers of change during the period spanning 1980 to 2011.

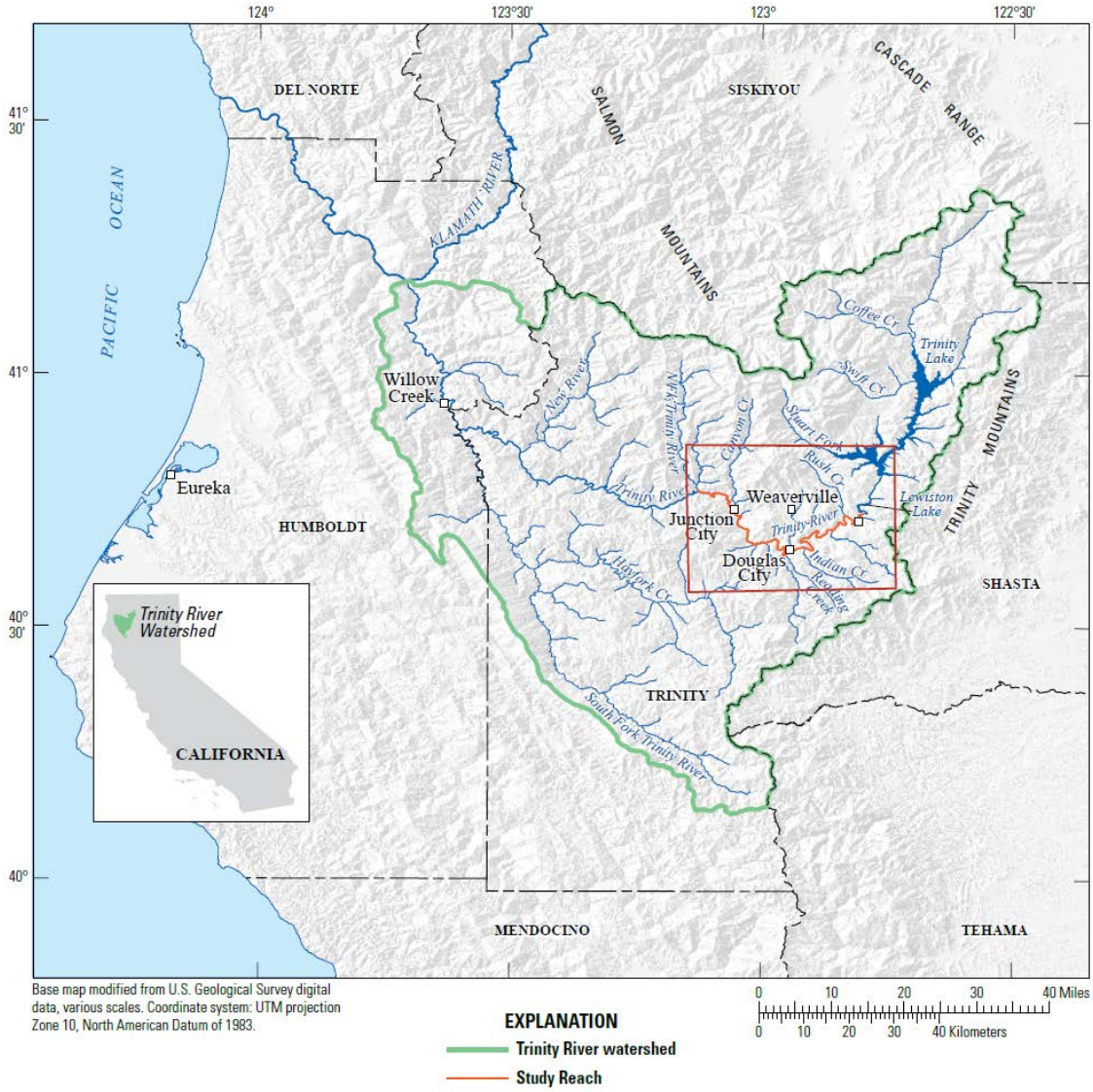

Figure 1. Map showing study area with the 65-km study reach shown in red located along the Trinity River downstream of Lewiston Dam, California.

METHODS

Six discrete geomorphic maps were created from rectified orthophotographs (1980, 1997, 2001, 2006, 2009, and 2011). Riparian and channel features larger than 30 m^2 were digitized at a scale of 1:1,000 into an ARCMap (v.10.0) geodatabase (Curtis and Guerrero, pending approval). Channel features included: the primary baseflow wetted channel, secondary water features (alcoves, wetlands, side-channels and split-flow channels), active and stable alluvial bars, and bedrock outcrops. Riparian features included: islands, wetlands and three floodplain types. Floodplain types included: a relatively continuous high-elevation pre-dam floodplain, a series of mid-elevation floodplains constructed by mechanical surface lowering, and lower elevation post-dam topographic benches composed of coalesced bars that were stabilized by 1975. The geomorphic maps were used to estimate spatial and temporal changes in ecologically significant riparian and channel features relevant to Trinity River fisheries restoration (Curtis and others, pending approval). The study reach is divided into upper, central, and lower river segments and sub-divided further into thirteen geomorphic reaches for the presentation of results. The upper river includes geomorphic reaches 1 to 5, the central river includes reaches 6 to 8, and the lower river includes reaches 9 to 13.

RESULTS

Since 1980 the general trajectory of change within the study area has been the conversion of riparian to channel features and expansion of the active channel area, which includes the baseflow wetted channel and morphologically active channel margins characterized by bedload transport. The primary mechanism for active channel area expansion was bank erosion from 1980 to 1997 (Figure 2B). The primary period of bar accretion from 1997 to 2001 was followed by slightly higher cumulative bar scour from 2001 to 2006 (Figure 3A). In comparison, smaller post-2006 bank and bar changes were spatially limited to reaches with sufficient local transport capacity or sediment supply supported by post-ROD gravel augmentation (upper river only), mechanical channel rehabilitation, and tributary contributions to flow and sediment supply (Figures 2 and 3).

Scour and deposition produced by tributary floods in 1997, 1998 and 2006 (Figure 4) were the primary factors leading to increases in the active channel area, channel complexity and floodplain connectivity. Channel complexity was characterized by the areal extent of secondary water features (alcoves, side-channels, split-flow channels and wetlands) and active alluvial bars. Increases in floodplain connectivity were characterized by the areal extent of constructed floodplains. Managed flow releases after 2006, in the absence of tributary flooding, combined with gravel augmentation and mechanical restoration caused localized increases in sediment supply and transport capacity. This led to additional increases in the active channel area, channel complexity and floodplain connectivity.

In 1980 the diversity of channel features was greatest in the upper and central river (Figure 5) where channel complexity features (active alluvial bars and secondary water features) represented approximately 12 percent of the active channel area. From 1980 to 2001 the active channel area increased by 20 percent. By 2001 channel complexity features comprised 17 percent of the active channel area. From 2001 to 2011 the active channel area increased by about

5 percent and in 2011 channel complexity features again occupied 17 percent of the active channel area.

In 1980 post-dam topographic benches comprised 94 percent of the riparian environment (Figure 6). By 2001 floodplain construction had increased riparian diversity and the proportion of post-dam benches declined to 86 percent. By the end of the study period in 2011, the relative proportions of post-dam benches, constructed floodplains, and stabilized bars were 60, 27, and 10 percent respectively.

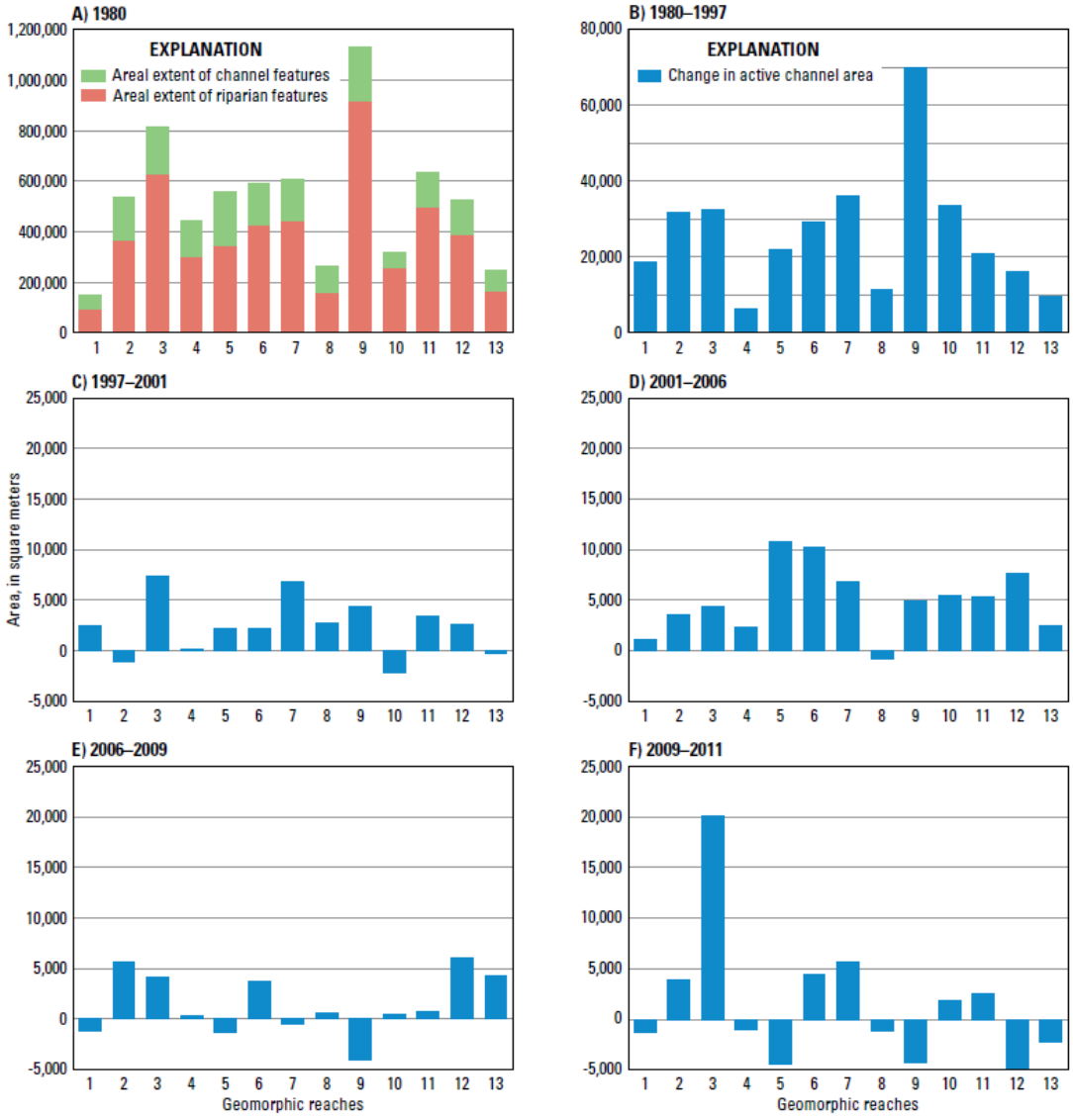

Figure 2. Graphs showing areal extent of riparian and channel features within thirteen geomorphic reaches along the Trinity River downstream from Lewiston Dam, California, A) in 1980, and change in active channel area for five periods from B) 1980 to 1997, C) 1997 to 2001, D) 2001 to 2006, E) 2006 to 2009, F) 2009 to 2011. Note the change in scale.

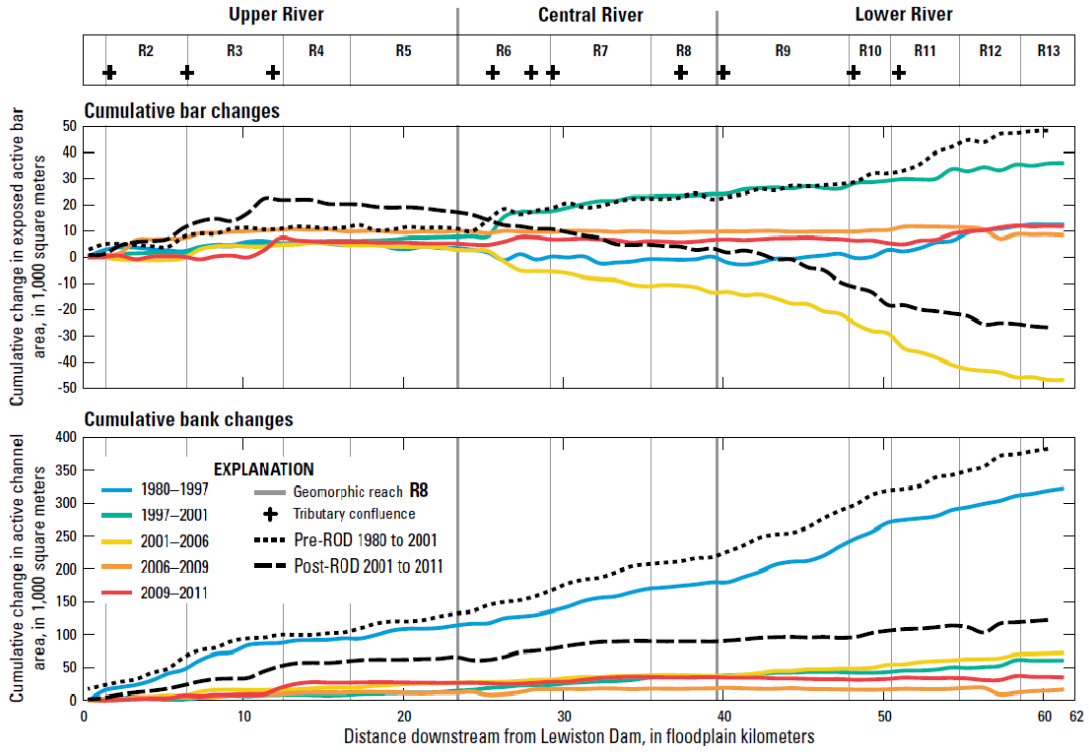

Figure 3. Cumulative longitudinal changes in A) exposed active bar area and B) active channel area estimated for five time periods spanning 1980 to 2011 along the Trinity River downstream of Lewiston Dam, California.

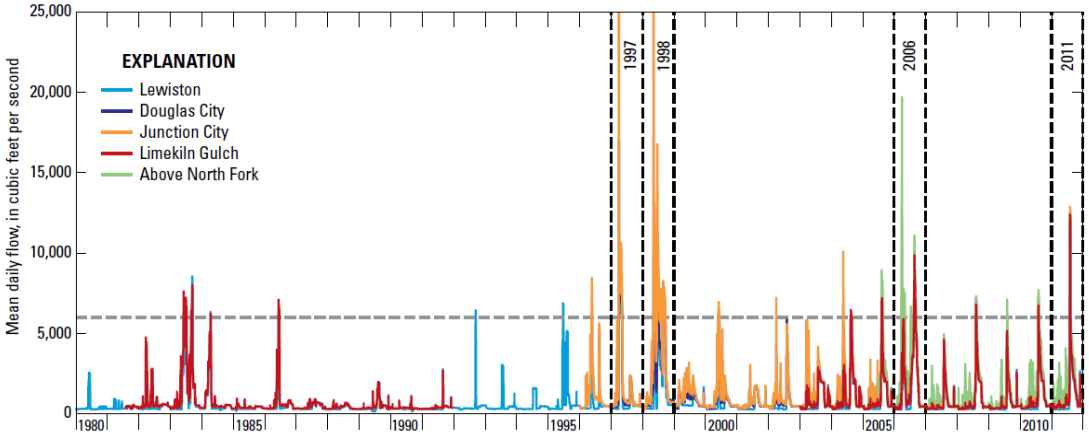

Figure 4. Mean daily flows measured at five mainstem gaging stations located along the Trinity River downstream of Lewiston Dam, California. Comparison of Lewiston flows with downstream gage data indicates tributary contributions to mainstem flow. The largest mean daily flows occurred at Junction City gage in 1997 (27,150 ft^3/s) and 1998 (25,150 ft^3/s). Dashed horizontal line denotes a managed flow release threshold of 6,000 ft^3/s

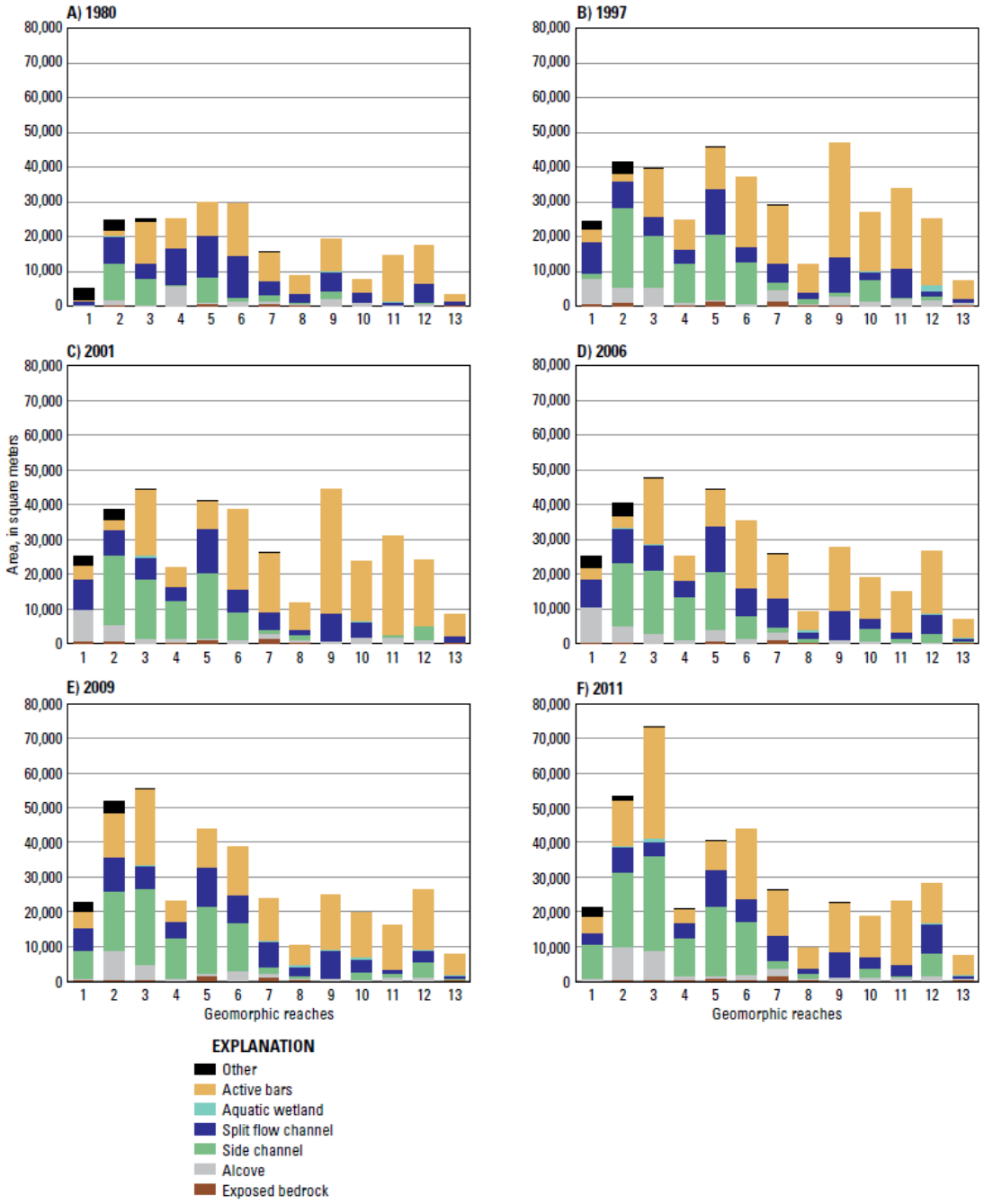

Figure 5. Areal extent of channel complexity features within thirteen geomorphic reaches located along the Trinity River downstream of Lewiston Dam, California in A) 1980 B) 1997 C) 2001 D) 2006 E) 2009 F) 2011.

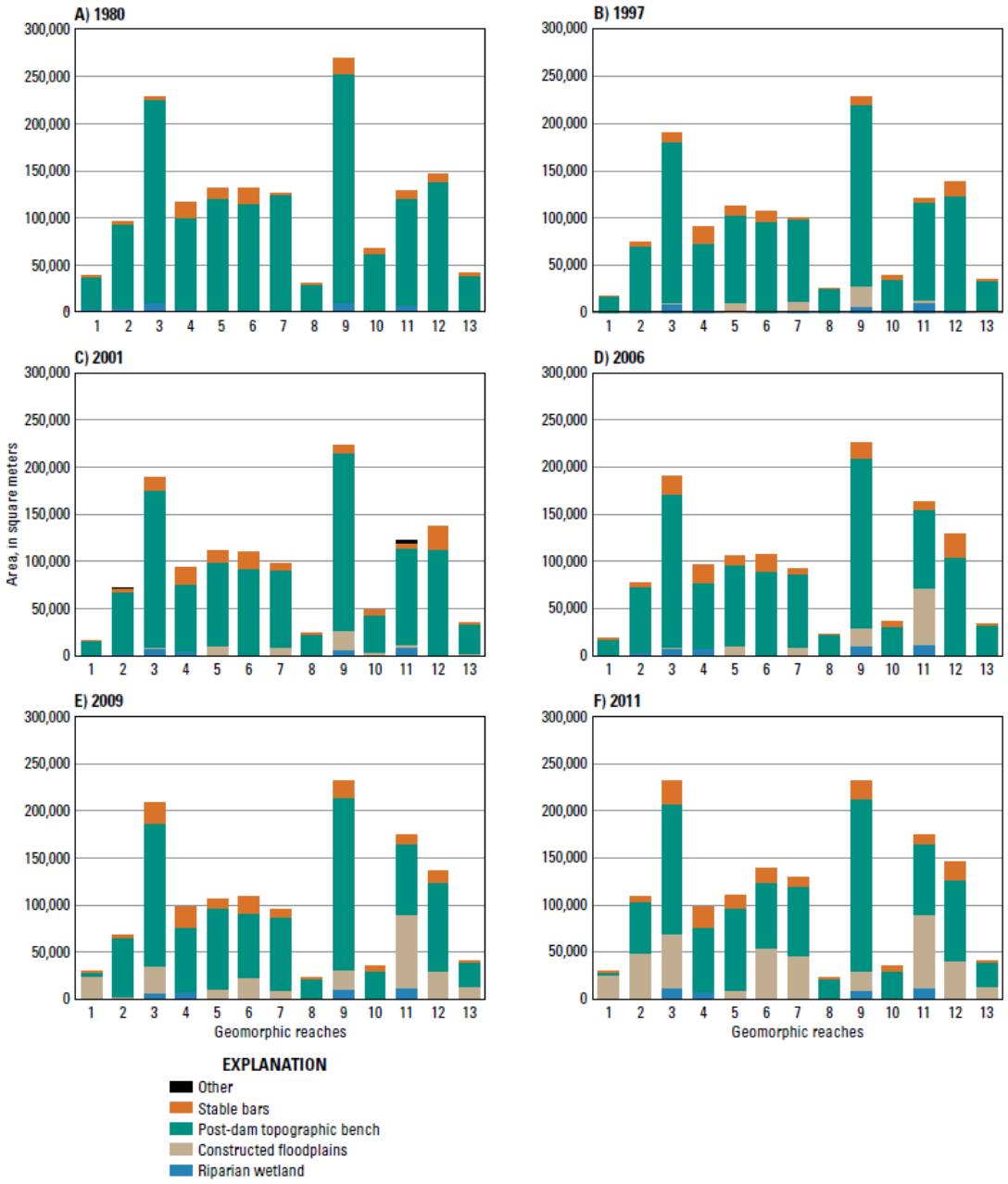

Figure 6. Areal extent of lower elevation riparian features within thirteen geomorphic reaches located along the Trinity River below Lewiston Dam, California in A) 1980 B) 1997 C) 2001 D) 2006 E) 2009 F) 2011.

CONCLUSIONS

Intrinsically the upper river has a low potential for change because dam construction and flow diversions decreased the transport capacity and sediment supply. Numerous management actions were implemented during the study period to resolve the lack of capacity for maintaining a

dynamic alluvial river with desirable habitat features. These management actions included channel rehabilitation, gravel augmentation and alterations in the size and timing of prescriptive flow releases.

In 1980 the study reach possessed a static channel form but the tendency toward stable alluvial features was disrupted by the 1997, 1998, and 2006 tributary floods. Channel widening from 1980 to 1997 represented a system-wide threshold disturbance that was followed by bar accretion (1997 to 2001) and bar scour (2001 to 2006). The geomorphic effectiveness of the post-2006 prescriptive flows and gravel augmentation was small in comparison to pre-2006 precipitation-driven tributary flows that generated higher and longer duration main stream flows (Curtis and others, pending approval). Pre-1997 studies determined that 80 percent of the low-flow channel margin was mobilized during a peak flow release of 6,000 ft^3/s (TRA, 1993; Wilcock and others, 1995; MT, 1997). More recent studies (HVT and others, 2011) indicate prescriptive flows did not produce expected scour, mobility, or channel maintenance targets at many rehabilitated sites. These observations suggest that channel widening could have altered local hydraulics such that prescriptive flows may need to be increased to achieve the TRRP's restoration goals. The muted geomorphic response of channel rehabilitation sites to the post-2006 flows highlights the need for continued monitoring and assessment of the magnitude, duration, and timing of prescriptive gravel augmentation, flow releases and associated objective for channel scour, mobility, and maintenance. Achieving the TRRP goal of a downscaled dynamic river may come with the unexpected consequence of a larger active channel area that requires larger maintenance flows.

ACKNOWLEDGEMENTS

The author acknowledges input from Bureau of Reclamation staff (Dave Gaeuman, Andreas Krause, and Eric Peterson), members of the TRRP Physical Workgroup, and U.S. Geological Survey staff (Jim O'Connor, Amy East, Lorrie Flint, Tim Guerrero, Paul Grams, Jim Howle, MacKenzie Keith, Toby Minear, Rose Wallick, and Scott Wright).

REFERENCES

Curtis, J.A., and Guerrero, T.M. (pending approval). Geomorphic Mapping to Support River Restoration along the Trinity River downstream of Lewiston Dam, California, 1980 to 2011: U.S. Geological Survey Open File Report, OFR-XXXX.

Curtis, J.A., Wright, S.A., Minear, J.T., and Flint, L.E. (pending approval). Assessing Geomorphic Change along the Trinity River downstream of Lewiston Dam, California, 1980 to 2011: U.S. Geological Survey Scientific Investigation Report, SIR-XXXX.

Hoopa Valley Tribe (HVT), U.S. Fish and Wildlife Service (USFWS) and Yurok Tribe (YT) (2011). Integrated Habitat Assessment of the Upper Trinity River, 2009, Draft Report: Prepared for the Trinity River Restoration Program, Hoopa, CA 336 pp.

McBain & Trush, Inc. (MT) (1997). Trinity River Maintenance Flow Study - Final Report: Prepared for the Hoopa Valley Tribe, McBain and Trush, Inc., Arcata, CA, 482 pp.

Trinity Restoration Associates (TRA) Inc. (1993). Trinity River maintenance flow report: evaluation of the 6000 cfs release, Report to Hoopa Valley Indian Tribe Fisheries Department, 140 pp.

Trinity River Taskforce (1970). Task Force Findings and Recommendations on Sediment Problems in the Trinity River near Lewiston and a Summary of the Watershed Investigation, State of California: The Resources Agency, 29 pp.

U.S. Department of the Interior (USDOI) (2000). Record of Decision: Trinity River Mainstem Fishery Restoration Final Environmental Impact Statement/Environmental Impact Report. 43 pp.

U.S. Fish and Wildlife Service (USFWS) (1980). Environmental Impact Statement on the Management of River Flows to Mitigate the Loss of the Anadromous Fishery of the Trinity River, California. Volume I, U.S. Fish and Wildlife Service, Division of Ecological Services. Sacramento, CA, 229 pp.

U.S. Fish and Wildlife Service (USFWS) and Hoopa Valley Tribe (HVT) (1999) Trinity River Flow Evaluation Final Report: U.S. Fish and Wildlife Service, Arcata Fish and Wildlife Office, Arcata, CA and Hoopa, CA, 310 pp.

Wilcock, P.R., Kondolf, G.M., Barta, A.F., Matthews, W.V.G. and Shea, C.C. (1995). Spawning gravel flushing during trial reservoir releases on the Trinity River: Field observations and recommendations for sediment maintenance flushing flows. Prepared for the U.S. Fish Wildlife Service, Sacramento, CA. 96 pp.

RESERVOIR SUSTAINABILITY: EVALUATION OF CLIMATE CHANGE IMPACTS TO RESERVOIR MANAGEMENT OPERATIONS AT CORALVILLE DAM, IOWA

Kevin J. Landwehr, P.E. D.WRE, Chief Hydrology and Hydraulics Branch, Corps of Engineers, Rock Island District, Rock Island, Illinois. kevin.j.landwehr@usace.army.mil
Gregory S. Karlovits, P.E., CFM, Hydraulic Engineer, Corps of Engineers, Risk Management Center, Denver, Colorado. gregory.s.karlovits@usace.army.mil

INTRODUCTION

This study evaluates the use of future climate projections to assess the potential impacts of climate change on the operation of a USACE multipurpose reservoir in east-central Iowa. The Coralville Reservoir, on the Iowa River just above Iowa City, IA, has been in operation since 1958. The two largest floods during the period of operation have occurred in the last 25 years, with the largest occurring during the Midwest Flood of 2008.

Climate conditions in the Iowa River basin have changed significantly since the reservoir was placed into operation. Analysis of historical precipitation and flow data demonstrate increased reservoir inflow volumes compared to pre-project conditions upon which the project was originally designed. Observed changes in reservoir inflow have resulted in periodic modifications to the water control plan; however, the threat of continued climate change in the future, and the uncertainty associated with those changes, has the potential to result in increased future risks to meeting project purposes.

Using a calibrated hydrologic model of the Iowa River basin and dynamically-downscaled climate data, the risk to the reservoir system associated with future climate scenarios was analyzed. Reservoir operations for a number of future climate scenarios were simulated in order to test the robustness of the reservoir system to potential climate change effects and to identify potential adaptation strategies.

The study concludes that the numerous limitations associated with climate and hydrologic modeling makes it difficult to fully assess the risks for a project due to climate change using modeling tools alone. A project-based resilience-robustness approach that considers the vulnerabilities of the project to changes in climate, such as the approach by Brown et al. [2011], gives a better picture of the climatic risk for a project. Specific to reservoir management, this study concludes that long-term reservoir planning is not as valuable a tool to meeting the missions of a reservoir as short-term weather forecasting and a framework that allows for real-time, risk-based, decision making for reservoir operations.

BACKGROUND

Study Area: Coralville Dam (Figure 1) is a 1,400 ft long, 100 ft high rolled earthfill dam impounding Coralville Reservoir on the Iowa River located 83.3 miles above its confluence with the Mississippi River and 5 miles above Iowa City, IA. There are 3,115 mi^2 of mainly row-cropped agricultural land draining into the Iowa River above the dam. An additional 9,400 mi^2 of uncontrolled drainage (below Coralville Reservoir) flows from the Iowa-Cedar watershed to the Mississippi River.

Figure 1 Coralville Dam During Midwest Flood of 2008

The primary purpose authorized by Congress (PL 75-761) is flood risk management for areas below the lake on the Iowa and Upper Mississippi Rivers. Other congressionally

authorized purposes include low flow augmentation, fish and wildlife management (PL 85-624), and recreation (PL 78-534). Construction on the dam began in July 1949 but was delayed by the Korean Conflict. The reservoir began operation in September 1958.

The reservoir is regulated by a gated conduit outlet with a discharge capacity of 20,000 cubic feet per second (cfs) at full flood control pool (712 ft NGVD). At pool elevations above full flood control pool the emergency spillway is activated and uncontrolled release begins. The 500 ft long uncontrolled concrete chute spillway has a discharge capacity of 244,000 cfs. The spillway has been activated twice in the history of the project, once each during the 1993 and 2008 floods.

During normal (non-flood or drought) operations the reservoir is regulated to maintain a seasonal conservation pool elevation (see table 1). During flood operations, the release schedule for the reservoir changes based upon forecasted pool elevations (i.e., storage utilized) and downstream constraints to control flooding. When the pool elevation is forecast to exceed elevation 707 ft (NGVD) major flood operations are initiated, and flows are regulated to maximize use of the remaining storage. During non-major flood operations, maximum releases are controlled by downstream constraints, including seasonal constraints due to agricultural production and river stage control points on the Iowa River (at Lone Tree, IA, and Wapello, IA) and the Mississippi River (at Burlington, IA). Additionally, releases are temporarily reduced in order to manage flash flood flows at Iowa City.

When reservoir inflows fall below minimum conservation releases, the reservoirs drought contingency plan is activated providing for low-flow augmentation of releases with the highest priority given to meeting downstream water supply requirements.

Table 1 Coralville Lake Seasonal Conservation Pool Elevations

Date	Regulation (Elevation ft NGVD)	Action Purpose
15 Feb – 20 Mar	Lower from 683 to 679	Increase storage for spring snowmelt
20 Mar – 20 May	Hold elevation 679	Duration of spring snowmelt period
20 May – 15 Sep	Hold 683	Storage for low-flow augmentation
15 Sep – 15 Dec	Hold 683-686	Increase in lake area for migratory waterfowl
15 Dec – 15 Feb	Hold 683	Storage for low-flow augmentation

Current Climate: Iowa City, just downstream of Coralville Dam, has a mean annual temperature of 50 °F and averages about 34.9 inches of precipitation per year [cumulative data since 1893 from Iowa Environmental Mesonet AgClimate data]. Near the headwaters of the Iowa River basin is Northwood, IA, which has a mean annual temperature of 44 °F and averages about 32.2 inches of rainfall per year. The climate across the basin is generally homogeneous as it lacks significant topography to affect precipitation and temperature patterns. The basin has a humid continental climate, which is characterized by large seasonal temperature differences including hot, humid summers and cold, sometimes frigid, winters.

Average annual temperature, total annual precipitation, and the number of days per year with precipitation have increased in Iowa from the late 19th to the early 21st century, and at the Iowa City gauge within the Iowa River basin, these trends are statistically significant at 95% confidence. Since 1893, mean annual temperature has been rising at an average rate of 0.32°F per decade at Iowa City. Prior to 1960, only 6 years out of 67 (9%) measured a mean annual temperature at or over 52 °F, but 1960 and later, 24 of 52 years (46%) have met or exceeded that threshold.

In Iowa, the biggest changes in temperature are due to wintertime and nighttime temperature increases. There are more frost-free days per year (about 5 more at the start of the 21st century than in the mid 20th century, and about 8-9 more than beginning of the 20th century). Warmer temperatures increase the length of the growing season, due to fewer days of frost. There is also earlier seasonal snowmelt, and lakes and streams remain frozen for less time. There has been a decrease in the number of extreme high temperature events (days above 100°F). Increased summer precipitation and soil moisture have suppressed surface heating and reduced daytime summer maximum daytime temperatures. From the Climate Change Impacts on Iowa 2010 report:

> *If Iowa were to experience a severe drought, as has occurred frequently in the past, the slow and steady rise in statewide annual mean temperature, now masked in summer by moist surface*

conditions, could lead to an abrupt switch to extreme summer heat comparable to the summers of 1983 or 1988.

On average, annual total precipitation has been rising by 0.43 inches per decade. There has been an increase in year-to-year variation in annual total precipitation as well, with an increase in 30-year coefficient of variation (CV) in annual precipitation from around 0.11-0.17 in the early 20th century to around 0.19-0.24 in the early 21st century.

On average, there has been one more rainy day per year every 6.4 years. While currently there are not as many rainy days as the late 1940s, total annual precipitation has increased steadily, which is due to a combination of more rainy days and increased frequency of moderate to intense rainfall.

Streamflow is largely driven by rainfall, although for any one event antecedent conditions play an important part in runoff-generating processes. Over time there has been an increase in average annual streamflow volume on the Iowa River as well as an increase in annual peak discharge. The 15-day peak discharge past Marengo is an important inflow metric for operations at Coralville Reservoir on the Iowa River, and its trend is shown in Figure 2. There is a clear increase in the average annual 15-day maximum flow, as well as an increase in the interannual variation for that parameter.

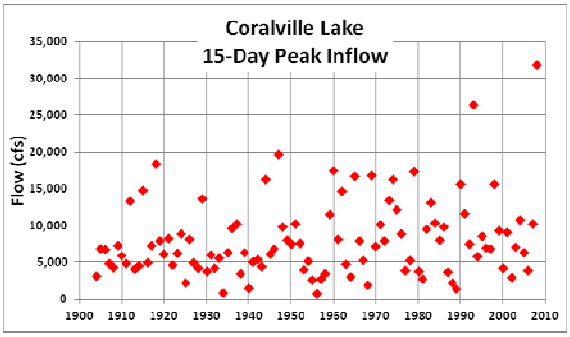

Figure 2 15-day Peak Discharge, Iowa River at Marengo

Current Problem/Concern: Historical Iowa River flows into Coralville Lake show an increase in the mean and variance of annual 15-day peak discharge between the design period (pre-reservoir streamflow records) and the period over which the reservoir has been in operation (1959-present). Of particular significance are the Floods of 1993 and 2008, which both exceeding the largest historical event upon which the original water control plan was developed. The largest historical floods available in the record at the time of project design were predominately spring snowmelt (or rain on snow) driven events, whereas the record flooding in 1993 and 2008 resulted from persistent late spring and summer thunderstorms occurring over a heavily saturated watershed. Increased total precipitation has led to higher soil moisture content, which has runoff implications both through affecting antecedent conditions preventing infiltration, and an increase in the installation of agricultural tile drains.

The floods of 1993 and 2008, coupled with significant flooding in 2010, raised questions regarding the operation of Coralville Reservoir and (from the public's perspective) whether the reservoir was giving adequate weight to the risk of urban flooding from major flooding versus favoring protection to downstream agricultural areas during minor flood events. Public and community interest led the State of Iowa's Governor to formally request that the Corps of Engineers conduct a re-evaluation of the water regulation procedures at each of the four large flood risk management reservoirs operated by the U.S. Army Corps of Engineers within Iowa. Uncertainty in future climate conditions has the potential to be a major risk driver in the evaluation of alternative water management strategies to better manage future flood risk in the Iowa River Basin.

Purpose and Scope: The study is concentrating on the following central question: "How do we incorporate climate change considerations into reservoir operating policies that will be robust and adaptive to potential climate changes in the interest of long term management of risks to project operating purposes?"

Previous Studies: This pilot study is the first attempt at evaluating the potential effects of climate change on the operation of Coralville Lake or on hydrology in the Iowa River basin. However, other studies have been completed that evaluate the regulation plan for the lake in response to past floods. In 1997, a Section 216 (Review of Completed Works) study was completed for Coralville Lake and its regulation plan. Several alternative initiatives were proposed in order to enhance benefits at the lake, but none garnered a Federal interest.

Methodology and Approach: The study utilized the following approach*:*

1) Investigate original design assumptions for the dam and determine which metrics are sensitive to climate change
   a) Evaluate changes in meteorology from historical to potential future

   b) Examine possible bias or error in GCM/RCM results
2) Obtain downscaled climate data for the Iowa River basin, the area of interest
3) Run observed meteorology and downscaled climate scenarios through a calibrated hydrologic model to obtain flow information at critical locations for a variety of scenarios
4) Use post-processing tools to learn more about the effects of changes in climate and hydrology
   a) Reservoir sedimentation model – how is storage in the reservoir changing due to sedimentation?
   b) Flow routing model – how are the operational conditions for the dam changing?
   c) Reservoir operations model – how much influence does operation have on the possible changes at the reservoir?

The first step in evaluating the potential impacts of climate change for the reservoir was to understand the design parameters and assumptions upon which the original project design and water control plan were based. Using the design documentation and regulation manuals for the project, critical design parameters and assumptions were tabulated (see table 2). These parameters serve as guidance on whether or not the project is currently functioning as intended, and if these assumptions might be violated in the future due to climate change. Tools were developed to answer the question of whether or not these parameters might be sensitive to changes in climate in the future.

Table 2 Design Parameter Matrix

Design parameter	Original Design Assumption	Observation During Operations
Frequency of uncontrolled release over emergency spillway	Uncontrolled release would occur about once in 30 years	2 spillway events since 1958 (~54 years, about 27 year average interval)
Sedimentation/loss of storage space in reservoir	Loss of storage would occur at a rate of about 750-1,200 ac-ft/yr	Average yearly loss of approximately 1,700 ac-ft
Timing/mechanism of annual flood flows	Heaviest floods would occur due to spring snowmelt and flood magnitude would be related to amount of snowpack	Largest floods occurred during the late spring or early summer due to persistent and intense thunderstorm events (e.g. 1993, 2008)
Spillway Design Flood/Dam Safety	The dam was designed with freeboard above a probable maximum flood computed from the transposition of a historical storm during worst case operational conditions, with a peak inflow of 326,000 cfs (top of dam elevation NGVD 743')	Dam has never been overtopped; max pool elevation ~717' (~26' freeboard)
Conservation pool storage volume	Maintain minimum discharge of 150 cfs at Iowa City and Lone Tree from 07/01 – 02/28 (243 days) with strong drought conditions; equating to a volume of 17,000 acre-ft	Due to sedimentation, the elevation of the conservation pool has been increased in order to maintain design volume

Climate change is highly visible in its impacts on hydrology. Changing climate conditions affect the water balance by directly changing the amount of evapotranspiration and precipitation, and timing and type of precipitation that occur. In order to assess these impacts quantitatively, the climate simulations were coupled with a hydrologic model of the study area.

Hydrologic Model: The hydrologic analysis was performed using a quasi-distributed continuous hydrologic model, the Soil and Water Assessment Tool (SWAT) [Neitsch et al. 2009]. It was forced using observed meteorological data and RCM-downscaled results from GCMs. No land use change scenarios were tested for the future cases. The minimum inputs to run SWAT include a digital elevation model, landuse/land cover, soil type and meteorology.

Table 3 Iowa River SWAT Model Input Sources

Input	Source
Land use/land cover	NLCD 2006 (MRLC)
DEM	1 Arc second NED (~30m resolution)
Soil coverage	STATSGO data for the United States included with SWAT model

Meteorology inputs for the model came from a variety of sources in order to have a long enough record of all required forcing variables to calibrate the model. Observed meteorology was necessary in order to calibrate the model to observed streamflow. Once the model was calibrated to match historical rainfall-runoff responses the model was run with downscaled climate data to evaluate the effect of climate change on hydrology.

USDA-ARS SWAT format meteorological data were used in calibration and observed meteorology runs. The data provided from this source were daily maximum and minimum temperature and daily total precipitation. These data span 1/1950-10/2009. Relative humidity, solar radiation and wind speed, in addition to temperature and precipitation, were from Iowa Environmental Mesonet data available over the time period 1/1998-12/2010.

The model was first calibrated for daily discharge at the Marengo, IA gage using historical observed meteorological data. Observed flow and meteorological data are at a daily timestep, and thus the model was run at a daily timestep.

Table 4 SWAT Model Calibration Results

Event	Location	Nash-Sutcliffe	Volume Error	R^2
Calibration (1999-2001)	Marengo	0.85	+5.7%	0.87
Validation (2006-2008)	Marengo	0.80	-7.9%	0.84
Validation (2003-2005)	Marengo	0.64	-0.51%	0.75

While achieving relatively good scores on the selected calibration metrics, one significant weakness of the model is in estimating the highest peak flow values. The model was unable to capture the most extreme flows and the relatively large variance in observed daily streamflow. Baseflow recession and the timing of peak flows were generally well-matched to observed hydrographs; however, the volume error grew with overestimation of baseflow contribution and underestimation of the most extreme peak flows. Additionally, some peak flow events were missed within the simulations (and some existed in model results without corresponding observed peaks) because of the coverage of precipitation gauges.

The daily discharge simulated by SWAT was used in three post-processing routines to gain information about dam sedimentation and reservoir operations.

Sediment Accumulation in Reservoir: Although SWAT has sediment modeling methods included in the model (based on the universal soil loss equation), sparse information for calibration and other factors made it difficult to set up and calibrate the model for sedimentation. An alternative, approximate approach was favored in order to estimate sedimentation rates in the reservoir. A power law relationship between sediment discharge and streamflow modified from USBR [1987] was established using observations at the Marshalltown gauge, upstream of Marengo on the Iowa River. The Marshalltown gauge recorded sediment loading for a short period (less than 10 years). The curve was applied to discharges at Marengo to compute a total sediment inflow to Coralville Lake. A sediment trap efficiency for the dam based on the reservoir capacity and the inflow [Brune 1953, Dendy 1974] was applied to the Coralville inflow hydrograph to compute the amount of sediment accumulating in the reservoir. The results of this method when compared to historical sediment survey results is acceptable for computing an estimate of annual average sediment accumulation.

Flow Routing (Inflow-Pool Elevation-Release Rate Computation): An Excel spreadsheet was created that routes reservoir inflow based on the water control plan in the current regulation manual (January 2001 revision). The model first attempts to discharge enough storage to achieve the seasonal conservation pool elevation, based on the pool elevation of the previous timestep and the inflow to the reservoir. The formal rules for maximum release are checked, including seasonal rules for maximum release (growing vs. non-growing season) and flow at control points downstream on the Iowa River. The action is first checked if informal rules regarding changes in pool elevation and release are being broken, but major flood and drought conditions override any informal rules.

The model gives good results for events where reservoir regulation stayed true to the manual. Some aspects of the water control plan occur variably from year-to-year based on communication with project stakeholders. The spring drawdown and the fall pool raise are variable, so the model acted on the middle date of the available range of dates in the regulation manual. In other historical cases, the reservoir was operated under a temporary deviation to store more water and avoid downstream flooding. Additionally the model could not account for the downstream flow constraints on the Mississippi River, where river stages may dictate a short-term (seven day) reduction in releases from Coralville to reduce peak Mississippi River flooding.

Climate Change Scenarios: The climate data used for the evaluations in this study came from the North American Regional Climate Change Assessment Program (NARCCAP) dataset [Mearns et al. 2007, updated 2012]. The data were processed and exported in SWAT format by Dr Christopher Anderson of Iowa State University.

Emissions Scenario: The greenhouse gas emissions scenario used to force the GCMs in the NARCCAP datasets is the A2 scenario. The A2 emissions scenario is a high-emission Special Report on Emissions Scenarios [SRES; Nakicenovic and Swart 2000] greenhouse gas (GHG) scenario family. It projects vastly increased GHG emissions throughout the 21st century, fueled by continuously increasing human population, an economic (as opposed to environmental) policy focus, and independent, regionally-focused nations. Although the A2 scenario (along with the A1FI and A1B scenarios) is near the highest projected rate of GHG emissions for the early 21st century (according to the SRES), there is evidence that global GHG emissions exceed those scenarios thus far this century [Raupach et al. 2007] The emissions scenario makes up the foundational assumption about the rest of the future climate simulations. It is the driving force behind the GCM simulation and has the greatest influence on the resulting simulations. For this study, A2 was a reasonable "worst case" assumption available at the time.

Global Climate Models: A general circulation model (GCM) is a model that simulates Earth systems, generally the coupled oceanic-atmospheric processes (AOGCM) that most characterize climate. The coupled circulation models for atmosphere, land, ocean, ice, etc. are referred to as Global Climate Models.

In this study two GCMs were used for projections, the CGCM and CCSM models. CGCM is the Meteorological Service of Canada of Environment Canada coupled atmosphere-ocean climate model from the Canadian Centre for Climate Modelling and Analysis (CCCma) Climate Research Branch. CCSM (Community Climate System Model) is the National Center for Atmospheric Research (NCAR) coupled climate model that incorporates four separate climatological models for atmosphere, ice, land and ocean. The version used for the runs in this study is CCSM3, which have since been superseded by CCSM4 as part of the Community Earth System Model.

GCMs are generally run at a coarse scale spatially (on the order of 2°-5° resolution) and temporally (monthly) because of computational limitations. These results are not as useful on a local scale, especially for investigations of climate change impacts on regional or local hydrology, so a method to disaggregate these results needs to be used. Thus the GCM results are downscaled to a finer resolution, in the case of this study ~50km resolution with a daily timestep.

Downscaling Method: The downscaling method in use for the NARCCAP data is dynamic downscaling (not a delta or statistical downscaling method). Here regional climate models (RCMs) are forced by the GCMs to produce finer-scale results. RCMs are higher-resolution numerical weather prediction models that are nested within a GCM, so that the GCM acts as a boundary condition over a focused area. This allows a higher-resolution simulation of local weather process that are often of most interest in understanding regional climate.

For the NARCCAP data, RCM runs are also forced with NCEP reanalysis data for atmospheric conditions for the late 20th century which give an estimate of the best simulation that each RCM can produce. The reanalysis data have the same fluxes and states that GCMs would produce but are based on data assimilation and atmospheric modeling over the 20th century. The data incorporate observed historical data to make a best estimate simulation of atmospheric conditions. Thus the NCEP reanalysis data are a good proxy for actual atmospheric conditions that can be used to force the RCM, which in turn gives a good estimate of the performance of the RCM over the particular application area.

The RCM runs can also produce time series of other fluxes and states (other than temperature and precipitation) that are of interest for modeling. For example, the SWAT model also needs solar radiation, wind speed, and humidity (dew point or relative humidity) data, which are readily available outputs from many RCMs. The regional climate models used for downscaling the GCM outputs in this report are the WRFG and CRCM models.

WRFG (developed by NCAR) is the Weather Research and Forecasting model, using the Grell parameterization scheme (superseding the WRFP, PNNL scheme). CRCM is the Canadian Regional Climate Model developed at the Université du Québec en Montreal.

Downscaled climate simulation results are gridded, so for the purposes of hydrologic modeling the centers of the RCM grid cells were used as gauge stations. Because different RCMs have different grid schemes, the number of gauges used to cover the basin varied between RCMs but there were generally at least six gauges over the basin. The RCM grids are at about 50km resolution. All six forcing variables (T_{max}, T_{min}, P, RH, R_s, W) were read by the model from the downscaled RCM data.

It is important to keep in mind that the resulting downscaled climate data sets are highly experimental and come with their own major limitations and caveats. This study attempted to investigate the utility of these downscaled data as applied to the Coralville project.

RESULTS

Physical System/Climate Findings:

Climate Data and Observed Meteorology: The initial analysis of the downscaled climate outputs revealed some shortcomings in the regional climate model representation of local meteorology. Using the RCM-downscaled NCEP reanalysis data, the precipitation results were compared to observed precipitation using long-term averages. As the reanalysis data acts as a proxy for observed data in place of a GCM, this analysis demonstrates the RCM's best ability to generate local meteorology.

WRFG generally reproduced how precipitation occurs in the study region – the temporal distribution throughout the year was accurate, and it produced storm events consistent with those in the region. It was, however, very dry compared to observation, being low by about 7 in of rain per year while producing about the same number of rain events (see table 5). It appears that the model reduces the amount of moderate precipitation events that occur, resulting in frequent very light or heavy events, with few events of a more moderate intensity.

CRCM performed poorly at simulating local meteorology. CRCM precipitation results were more like Seattle, with most rain coming early in the year and the annual total precipitation coming as a result of a large number of small precipitation events. Intense events were very infrequent, and the annual maximum precipitation was close to constant between years of simulation. CRCM split the precipitation over about 200 days of precipitation a year, where 100-120 is a more reasonable number. The total water balance for CRCM was much closer than WRFG, being slightly wet by about 1 inch per year on average. Brochu and Laprise [2007] similarly documented the observed precipitation biases of the CRCM model over the Mississippi River basin and show a wet bias, as well as a misdistribution of rainfall toward the earlier part of the year.

Table 5 Comparison of Annual Rainfall Statistics for RCMs Forced with Reanalysis Data

	Average Rainy Days Per Year	Annual Average Precipitation	Average Date of 50% Rainfall Accumulation
Observed	109	32.1 in	7/9
WRFG-NCEP	108	25.7 in	7/7
CRCM-NCEP	199	33.1 in	6/24

Future Climate Scenarios: In general, the shift from an RCM-GCM pair from historical emissions to future emissions scenario was not producing changes in extreme precipitation consistent with expectations of climate change in the Midwest. This is likely due to a combination of factors, namely the limitation of the RCMs noted above, as well as the short simulation periods. It is unreasonable to expect to sample events with average recurrence intervals longer than 50 or 100 years in a 25-30 year sample. The resulting data are heavily sampled out of the middle of the distribution of results, which results in very few extreme scenarios (flood or drought) that we are most concerned about.

The underlying biases in the RCMs heavily influence the output results. The WRFG-downscaled GCM results reflect the overall dryness of WRFG, and CRCM-downscaled results have the above noted wet bias and temporal misdistribution of precipitation. Overall the performance of WRFG was limited only by the dry bias; however, CRCM was producing results wholly inappropriate for the region.

The additional limitation of the hydrologic model in simulating the highest peak events meant that climate data representing the middle of the distribution of data was being processed by a model that under-predicted variance and extremes, resulting in rather average-looking flows. This limits the ability to test the operation of the reservoir under events of the most interest (extreme flood and drought). Figure 3 shows the flow-frequency curves for 15-day peak flows for the four future scenarios when compared to observed streamflow. The reduction in variance in the streamflow results creates the reduced frequency of events observed on the tails of the inflow frequency curves. The reduction in variance is due to the forcing climate data and the spatial and temporal resolution of the data used in the hydrologic model.

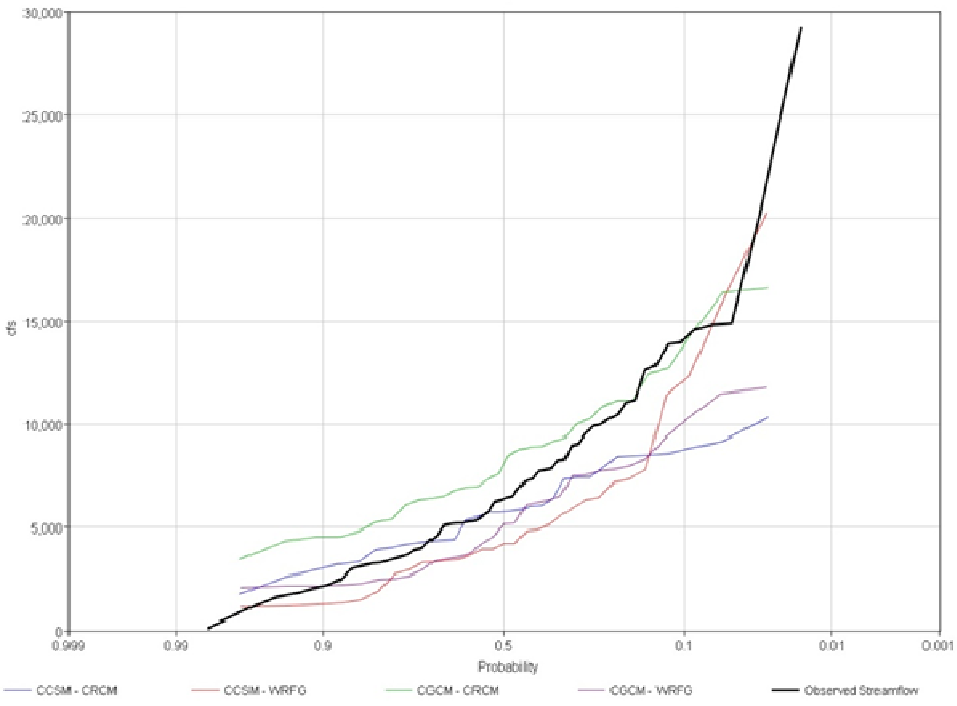

Figure 3 Annual Maximum 15-day Average Flow Past Marengo, Observed and Future Model Projections

Table 6 summarizes the output from the sediment post-processing (annual average sedimentation rate) and the reservoir routing post-processing (amount of time in flood, amount of time in drought, number of spillway events.) Spillway events are classified as being any event where water goes over the spillway, even if this amount is trivial. (This designation has the habit of including some events where the elevation of the pool would likely be very close to going over without any flow being passed by the spillway.)

Table 6 Post-Processed Hydrologic Model Results

RCM	Forcing	Time Period	Years	Average Daily Discharge (cfs)	Average Sed Rate (ac-ft/yr)	% Major Flood	% Drought	Spillway Events	Years With Major Flood
Observed Operations		09/17/1958-12/31/2010	52.3	2055	~1200			2	
Observed Meteorology		01/01/1999-10/30/2009	10.8	2171	1350	0.76%	0.00%	1	1
CRCM	NCEP	01/01/1981-11/30/2003	22.9	2641	1561	2.77%	0.00%	0	5
CRCM	CCSM	01/01/1969-11/16/1999	30.9	1825	909	0.24%	0.00%	0	2
CRCM	CCSM	01/01/2039-11/16/2070	31.9	1856	947	0.00%	0.01%	0	0
CRCM	CGCM	01/01/1969-11/16/1999	30.9	2737	1887	1.15%	0.02%	1	11
CRCM	CGCM	01/01/2039-11/16/2070	31.9	2700	1745	1.83%	0.03%	1	12
WRFG	NCEP	01/01/1981-12/25/2004	24.0	1318	596	0.45%	0.00%	0	2
WRFG	CCSM	01/01/1969-11/16/1999	30.9	1289	663	0.55%	0.00%	0	4
WRFG	CCSM	01/01/2039-11/16/2070	31.9	1282	711	0.34%	0.05%	1	4
WRFG	CGCM	01/01/1969-11/16/1999	30.9	1146	455	0.00%	0.03%	0	0
WRFG	CGCM	01/01/2039-11/16/2069	31.9	1813	991	1.26%	0.00%	0	5

The resulting simulations did not point toward one clear consensus for the future of inflows to Coralville Lake. When examining the difference between the mid-21st century and 20th century simulations for an RCM-GCM pair, there is no clear picture of the future for the system. The results for the same GCM but different RCM agreed somewhat; the CGCM results forecast an increased flood risk (increase in percent of time in major flood, and total years entering major flood operations) while the CCSM results show a slight decrease in time in major flood but also an additional spillway event.

Table 7 Changes in Hydrologic Modeling Results Due to GCM-RCM Pair

Model pair	Mean discharge	% Major flood	% Drought	Spillway events	Years with major flood
CRCM-CCSM	+31cfs	-0.24%	+0.01%	NC*	-2
CRCM-CGCM	-37cfs	+0.68%	+0.01%	NC	+1
WRFG-CCSM	-7cfs	-0.21%	+0.05%	+1	NC
WRFG-CGCM	+667cfs	+1.26%	-0.03%	NC	+5

NC=No Change

If we consider the result of the simulations without taking into account the limitations in the data and the hydrologic model it appears that modifications to the regulation plan would be sufficient to handle projected climate change. This is not a prudent lesson to take from the study, as the limitations associated with the climate data and the hydrologic model drive the overall results so much as to say the climate data offer us very little with which to try to test adaptation strategies. Thus, caution in the approach of data with such limitations is very important.

Method or Process Used: The methodology used in the study was based largely on what we viewed as a traditional type of climate change impacts analysis for hydrology, in which downscaled climate data were run through a calibrated hydrologic model for a watershed. These runs were done under existing basin conditions, and the resulting climate change scenario results were compared to historical runs and observed hydrology in order to assess the impacts that climate change could potentially have on the hydrology of a watershed. The resulting climate change scenario runs were not as useful for testing the reservoir system's response as we had hoped initially.

We did not observe any emergent processes in the climate change simulations. The streamflow results show about what is expected in terms of increased winter rainfall resulting in streamflow, and reduced spring snowmelt floods. Snowmelt flooding, which dominated the early period of record, has become less prevalent in the Iowa River basin with the largest floods on record (1993 and 2008) resulting from later spring and early summer rains. The simulated increase in flow due to spring and summer storms is consistent with observations during the operational period of the reservoir.

Implications for Future Reservoir Management:

Large Flood Operations: The current water control plan for Coralville Lake is similar to other reservoir projects within the Rock Island District in that the release schedule limits downstream flows to safe discharges (no or minimal damage with limits tied to seasonal agricultural production) until such time that a significant portion of the flood control storage has been utilized. At this point, releases are quickly ramped up to reduce the likelihood of higher, uncontrolled releases that would result when the unregulated spillway is overtopped. The major flood release schedule contained in the current water control plan is based upon an optimization of available reservoir storage to the largest flood that had occurred prior to construction of Coralville Dam.

As observed during the 1993 and 2008 major flood events, flood volumes in excess of the historically observed maximum can and will occur again in the future. The current water control plan, which emphasized optimization of flood volumes to historic events, does not necessarily optimized flood risk reduction during future major floods. In evaluating future climate change scenarios, it was anticipated that additional major flood events would be represented in the model simulations to evaluate alternative water control plans that would improve the risk performance of the reservoir across a wide range of large flood events. As discussed above, the future climate scenarios evaluated failed to produce events at the extremes of the inflow volume-duration-frequency distribution. As a result, the mid-century future climate scenarios evaluated do not provide a basis for defining a new optimized release schedule for future major flood events.

The inability of the future climate scenarios to provide such a basis points to the importance of short term climate forecasts and the need to develop tools capable of informing water managers with risk-based decision criteria to evaluate operational scenarios during major flood events. The required decision support system needs to be capable of incorporating modern forecast information into a risk-based decision tool. Such a system requires a clear set of risk-based criteria, consistent with project authorities, upon which water management decisions will ultimately be made. Further required are tools capable of incorporating the hydrologic, hydraulic, economic, and public health and safety factors into the decision process. The USACE proposed CWMS National Implementation Plan would substantially develop many of these critical tools.

Drought/Low Flow Augmentation: Consistent with the major flood operations discussion, the future climate scenarios evaluated failed to produce events at the extremes of the inflow volume-duration-frequency distribution such that a range of severe drought conditions could be evaluated to identify improvements to the water control plan to improve the robustness of the project to meet future drought conditions. Historically, the greatest threat to being able to meet future conservation needs has been sedimentation of the reservoir. The future climate scenarios indicate (with one exception) that sedimentation rates are likely to increase over historical rates consistent with projected increases in precipitation and stream flow. Historically, the Rock Island District has conducted pool raises to offset anticipated sedimentation and periodically conducts surveys to re-evaluate reservoir storage. Increases in future sedimentation will likely force decisions regarding future conservation pool raises (and the corresponding reduction in available flood storage) earlier than anticipated based upon historical sedimentation rates.

Dam Safety: Increases in temperatures and precipitation patterns from future climate change has the potential to increase maximum probable extreme event precipitation. This has major implications for dam safety if climate

change results in increased probable maximum precipitation estimates. Due to the extreme nature of these design events (having an expected recurrence of approximately once every 10,000 to 100,000 years), it was not unexpected that the 30-year blocks of future climate information do not support a direct analysis of climate change on the adequacy of the project's spillway design flood to meet future climate conditions. Continued monitoring of the trends in extreme precipitation is critical in order to detect changes in the intensity and frequency of heavy rainfall events.

LESSONS LEARNED

Lessons Related to the Physical System and Climate:

Lesson: The dynamically-downscaled NARCCAP dataset was limited in its representation of hydrologic extremes (major flood or drought). This may be due to sampling error (limitation of using 30 years blocks of future climate data to evaluate extreme events having a frequency of significantly greater than once every 30 years), or limitations in the datasets resulting from climate model biases that under represent precipitation variability. The expectation of this kind of climatic shift comes from literature and observed changes in the Midwest; however, we found that the NARCCAP dataset was insufficient for us to test these shifts in our system.

Lesson: It was observed that regional climate models may not adequately represent the local meteorology. The WRFG model performed better in terms of timing and frequency of precipitation, but overall the results were biased on the dry side. The results from CRCM were not at all similar to local weather. We found that screening the RCMs prior to use would have helped guide dataset selection and allowed us to use RCMs more "in tune" with local meteorology if they were available.

Lessons Related to the Methodology and Process Used:

Lesson: The original plan for the study was based on the expectation of greater precipitation and corresponding greater future flood risk (i.e., assumed direction of change). Consequently, the analysis was designed to answer questions specifically related to the expected outcome. We found our questions regarding climate vulnerabilities were too specific, and that more broad questions about these vulnerabilities are warranted. Asking, "How do I deal with greater and more frequent extremes?" is too specific and is biased by expectations about what the climate data will indicate; a broader question to ask is, "What vulnerabilities exist with my project related to future climate variability and how can those vulnerabilities be managed?"

Lesson: Understanding the limitations and biases of downscaled climate data would have changed the path of our study. In addition to broadening the questions that are asked of the climate data, we discovered that the approach to analyzing the climate data would be determined best by first understanding the project's sensitivity and vulnerability to climatic variation and then formulating alternatives to reduce the climate sensitivity (increase robustness) of the project.

Lesson: Hydrologic models as tools for assessing climate change impacts have significant weaknesses, even if calibrated to the system being analyzed. The inability for the hydrologic model used in this study to simulate high peak flows made even the largest precipitation events result in moderate or moderately-high flows. However, a hydrologic model calibrated to simulating peak discharge events will not be able to capture long-term flow parameters important for other reservoir management considerations, such as sedimentation and drought.

Lesson: The inability of the dynamically downscaled climate data to provide a basis for developing regulation procedures to reduce risk in future major flood events emphasizes the importance of short term climate forecasts and the need to develop tools capable of informing water managers with risk-based decision criteria to evaluate operational scenarios during an event. While this implies a level of flexibility in future water management operations that traditionally has not been built into water control plans, any such implementation would need to clearly establish the criteria by which water management decisions will be made. This is consistent with the current USACE national effort to fully develop and deploy the CWMS National Implementation Plan.

ACKNOWLEDGEMENTS

We wish to thank the North American Regional Climate Change Assessment Program (NARCCAP) for providing the data used in this paper. NARCCAP is funded by the National Science Foundation (NSF), the U.S. Department of Energy (DoE), the National Oceanic and Atmospheric Administration (NOAA), and the U.S. Environmental Protection Agency Office of Research and Development (EPA).

REFERENCES

Brochu, R and R Laprise (2007). Surface water and energy budgets over the Mississippi and Columbia River basins as simulated by two generations of the Canadian regional climate model, Atmostphere-Ocean, 45:1, 19-25

Brune, GM (1953). Trap efficiency of reservoirs. Transactions, American Geophysical Union, Volume 34 No 3, p. 407-418.

Dendy, FE (1974). Sediment trap efficiency of small reservoirs. Transactions of the ASAE, Volume 17, No 5, p. 898-908.

Elsner, M.M., L. Cuo, N. Voisin, J. Deems, A.F. Hamlet, J.A. Vano, K.E.B. Mickelson, S.Y. Lee, and D.P. Lettenmaier. 2010. Implications of 21st century climate change for the hydrology of Washington State. *Climatic Change* 102(1-2): 225-260, doi: 10.1007/s10584-010-9855-0.

Iowa Climate Change Advisory Council (2010). Climate Change Impacts on Iowa 2010. Report. http://www.iowadnr.gov/portals/idnr/uploads/air/environment/climatechange/complete_report.pdf?amp;tabid=1077Iowa Environmental Mesonet (accessed 2011): *Iowa State Agclimate Automated Weather Station data.* http://mesonet.agron.iastate.edu/agclimate/hist/dailyRequest.php

Kalnay, E et al (1996). *The NCEP/NCAR 40-year reanalysis project.* BAMS, volume 21, p. 437-471.

Mearns, L.O., et al., 2007, updated 2011. *The North American Regional Climate Change Assessment Program dataset*, National Center for Atmospheric Research Earth System Grid data portal, Boulder, CO. Data downloaded 2012-08-21. [doi:10.5065/D6RN35ST]

Nakicenovic, N and R Swart (eds.) (2000). Special report on emissions scenarios. A special report of Working Group III of the Intergovernmental Panel on Climate Change. Cambridge University Press, Cambridge, United Kingdom and New York, NY, USA.

Neitsch, S; J Arnold, JR Kiniry and J Williams (2009). Soil and water assessment tool theoretical documentation version 2009.Raupach, MR, G Marland, P Ciais, C Lequere, JG Canadell, G Klepper and CB Field (2007): Global and regional drivers of accelerating CO2 emissions. PNAS, Volume 104, No 24, p. 10288-10293.

USACE Rock Island District (2001). Coralville Lake Water Control Manual. Rock Island District, U.S. Army Corps of Engineers. Rock Island, IL.

USBR (1987). Design of Small Dams (3rd ed).

USDA-ARS (2010). SWAT format climate data for the US - Jan 1, 1950-Dec 31, 2010. http://www.ars.usda.gov/Research/docs.htm?docid=19388

USING AN INTEGRATED SURFACE WATER-GROUNDWATER FLOW MODEL FOR EVALUATING THE HYDROLOGIC IMPACTS OF HISTORIC AND POTENTIAL FUTURE DRY PERIODS ON SIMULATED WATER BUDGETS IN THE SANTA ROSA PLAIN WATERSHED, NORTHERN CALIFORNIA.

Joseph A. Hevesi, Research Hydrologist, U.S.G.S., Sacramento, CA, jhevesi@usgs.gov; Linda R. Woolfenden, Research Hydrologist, U.S.G.S., Sacramento, CA, lrwoolfe@usgs.gov; Tracy Nishikawa, Research Hydrologist, U.S.G.S., San Diego, CA, tnish@usgs.gov

Communities in the Santa Rosa Plain watershed (SRPW), Sonoma County, California are experiencing population growth and increasing demand for limited water resources. Streamflow in the SRPW is runoff dominated; however, groundwater also is an important resource in the basin. The watershed has an area of 262 square miles that includes natural, agricultural, and urban land uses. To evaluate the SRPW hydrologic system, an integrated hydrologic model was developed using the U.S. Geological Survey coupled groundwater and surface-water flow model, GSFLOW. The model uses a daily time step and a grid-based discretization of the SRPW to simulate all water budget components of the surface and subsurface hydrologic system, including components of streamflow, recharge, evapotranspiration, unsaturated and saturated groundwater flow, and changes in groundwater storage. Model results were analyzed to assess the effects of historic dry periods on the hydrology of the SRPW. Simulation results indicate significant effects on streamflow and recharge in response to the below-average precipitation that occurred during the dry periods. Although some results for the historic dry periods are similar, differences in the location of gaining and losing stream reaches have changed between earlier and more recent dry periods due to streamflow capture by groundwater pumping that has increased significantly between the two time periods.

The recharge and streamflow distributions simulated for historic dry periods were compared to future dry periods projected from 2 General Circulation Models (GCMs) and two CO_2 forcing scenarios for the 21st century. Decreases in recharge and streamflow or many of the projected dry periods were greater than for the historic dry periods due to a combination of lower precipitation and increases in simulated evapotranspiration for the warmer 21st century climates projected by the GCM realizations. The greatest effect on streamflow for both historic and projected future dry periods is the diminished baseflow simulated for the dry season, from late spring to early fall, with an increase in the percentage of intermittent and dry stream reaches. The results indicate that the coupled model is a useful tool for water managers to better understand the sensitivity of spatially and temporally distributed streamflow and other components of the water budget to potential future dry periods and groundwater pumping.

REFERENCES

Woolfenden, L.R., and Nishikawa, Tracy, eds., 2014, Simulation of groundwater and surface-water resources of the Santa Rosa Plain watershed, Sonoma County, California: U.S. Geological Survey Scientific Investigations Report 2014–5052, 258 p., http://dx.doi.org/10.3133/sir20145052

COLLABORATION ON CLIMATE CHANGE ANALYSIS IN THE PACIFIC NORTHWEST

James D. Barton, P.E., D.WRE, Chief of Columbia Basin Water Management Division, Corps of Engineers Northwestern Division, Portland, OR, james.d.barton@usace.army.mil

ABSTRACT

Climate change is likely to have a significant effect on the future of water management in the Pacific Northwest. Because many dams in this region such as those on the Columbia River are operated as a system and involve many different owners and operators, regional coordination among the various entities is extremely important. This is particularly true on issues like climate change, where the effects may vary considerably in different parts of the region.

In collaboration with the U.S. Bureau of Reclamation, Bonneville Power Administration, and other entities in the region, the U.S. Army Corps of Engineers Northwestern Division recently completed efforts to analyze the effects of climate change on water supply and water management activities in the Pacific Northwest using a regional approach. One of the major goals of this effort was to develop a common set of data, models, and tools that can be used by entities throughout the region to analyze climate change. This information was based on climate projections from the Intergovernmental Panel on Climate Change (IPCC) Fourth Assessment Report produced in 2007. Subsequent to this effort, the IPCC issued their Fifth Assessment Report, and work is now underway by this regional group to update the analysis of the effects of climate change on water management activities. These coordinated efforts are focused on reducing the potential for duplication, overlap, and conflicting results on climate change activities undertaken by the various entities, while at the same time improving regional collaboration and coordination.

The overall approach used in this effort involved the following two main phases of work that will be described in further detail: (1) selection and adoption of future climate and hydrology data that was evaluated and then used to develop water supply forecasts to reflect future hydrologic and climate conditions; (2) simulation of expected future reservoir operations using long-term reservoir models to analyze potential changes in water management planning and operations.

The climate and hydrologic data used in the first phase of this effort was developed by the University of Washington Climate Impacts Group (UW CIG). They produced "downscaled" climate data that was incorporated into a regional hydrology model that was used to produce a set of river flows for locations throughout the Columbia River Basin and associated subbasins. The "downscaling" effort involved refining global climate data into smaller geographic areas, providing usable data that better captured the highly varied mountain and valley regions of the Pacific Northwest. Two future time periods were studied and included the 30-year period surrounding the 2020s (2010 to 2039) and the 30-year period surrounding the 2040s (2030 to 2059).

The study results suggested that the Columbia River Basin annual air temperatures will rise from 1 to 3 degrees Fahrenheit above the historical reference period by the 2020 period and from 2 to

5 degrees Fahrenheit by the 2040 period. This change would affect Columbia River Basin precipitation and snowpack patterns (more rain, less snow), seasonal river flows, hydroelectric generation, demand for electricity, and other key areas. Water temperature was not a part of this study, but may be included in future analysis. Overall, yearly precipitation changes in the study were minimal, averaging a 1 to 2 percent increase. All of the climate change scenarios analyzed exhibited a seasonal shift of higher flows in the winter and lower flows in the summer. This seasonal shift is due in part to more winter precipitation in the form of rain instead of snow and increased snowmelt earlier in the year due to warmer temperatures.

The results of the second phase of this effort that involved simulation of expected future reservoir operations varied depending on the basin or subbasin that was being evaluated. For example, for the overall Columbia River Basin, during the winter-early spring period (January to April) the runoff amounts for the 2020s ranged from 108 to 150 percent of normal for the unregulated flows at The Dalles Dam on the lower Columbia River just upstream of Portland, Oregon. For the 2040s, the runoff amounts for this same period ranged from 95 to 170 percent of normal for unregulated flows. In contrast, during the summer period of June to August, the runoff amounts for the 2020s ranged from 80 to 95 percent of normal for unregulated flows at the Dalles Dam. For the 2040s, the runoff amounts varied from 65 to 95 percent of normal for unregulated flows.

Based on the analysis of the affect of climate change on reservoir operation, it is anticipated that some changes may be needed in reservoir operations. For example, flood risk management procedures will need to account for a projected shift in the timing of the spring runoff, with the average monthly peak runoff shifting from June to May. Related to this, earlier releases of water may be needed from flood risk management projects to capture the early runoff. Also, impacts to the timing of federal hydropower system operations could also impact other operational objectives in the spring and summer such as for fish and wildlife. The increase in the spring flows could results in higher power generation and increased spill of water at many dams. The additional spill could increase total dissolved gas levels, which could negatively impact fish.

ADHydro: QUASI-3D HIGH PERFORMANCE HYDROLOGICAL MODEL

Fred L. Ogden, Professor, fogden@uwyo.edu; Wencong Lai, Post-doctoral Associate, wlai@uwyo.edu; Robert C. Steinke, Research Scientist, rsteinke@uwyo.edu

Abstract: In recent decades, computational models have been developed to solve point-scale process models using physics-based or conceptual approaches. The integration of these processes across space-time has been limited by computational power to either high-resolution over small spatial domains, or coarse resolution over large spatial domains. These modeling approaches have lead to improved understanding at both small and large scales, but have required parameterization of important phenomenon, and the corresponding lack of model sensitivity to changes and uncertainties in parameter values. The CI-WATER project, a cooperative agreement between the US National Science Foundation EPSCoR program and the Utah and Wyoming Ph.D.-granting universities, is developing tools to cross the digital divide that impedes application of high performance computing (HPC) to solve hydrological science, engineering, and management problems. We are developing software tools to ease simulations using HPC resources. These tools include web-aware model setup and visualization tools that will interact with dedicated HPC systems or cloud systems, workflows for model setup, and web services for data provisioning. These tools are being developed with generality in mind, supporting a range of HPC-aware models, including the US Army Corps of Engineers Gridded Surface/Subsurface Analysis (GSSHA) model, and an unstructured mesh high-resolution physics-based hydrological model, called ADHydro. The ultimate objective of ADHydro development is perform multi-decadal simulations of large watersheds such as the Upper Colorado River above Lake Powell (288,000 km^2) in the contexts of land use, water use, and climate changes. We are cooperating with the US Army Corps of Engineers, Engineering Research and Development Center, Coastal and Hydraulics Laboratory, and the National Center for Atmospheric Research, Research Applications Laboratory in linking with their HPC hydrological and atmospheric models. This presentation will showcase our software tools under development.

INTRODUCTION

Physically-based, spatially distributed hydrologic models have been widely used in hydrologic modeling and watershed management, such as SWAT (Arnold et al., 1993), MIKE SHE (Refsgaard and Storm, 1995), and GSSHA (Downer and Ogden, 2004). Applications of such hydrologic models for large watersheds typically use coarse spatial and temporal resolution. Detailed simulation of larger watersheds with hyperresolution hydrological prediction is a grand challenge because significant computational resources and data are required (Wood et al., 2011).

In recent years, a growing number of distributed hydrological models have been developed in parallel computing environments with the advent of high performance computing (Apostolopoulos and Georgakakos, 1997; Cui et al., 2005; Wang et al., 2011; Vivoni et al., 2011; Hwang et al., 2014). HPC hydrological models coupled with meteorological models are capable to model high-resolution long term simulation in large watersheds in order to evaluate the impact of climate and land use changes. HPC hydrological models can be classified into two categories according to their parallel algorithm. One category of such models, for example ParFlow(Ashby and algout, 1996; Kollet and Maxwell, 2006), PFLOTRAN (Mills et al., 2007), PHGS (Hwang et al., 2014), utilize pre-developed HPC packages or libraries for parallel preconditioner and solver.

The other category of models adopt spatial domain decomposition with either sub-basin based (Li et al, 2011; Vivoni et al., 201; Wu et al., 2013) or unit based message passing (Cheng et al., 2005; Liu et al., 2014).

Parallelization of hydrologic models can be implemented using parallel programming standards such as Open Multi-Processing (OpenMP), Message Passing Interface (MPI), grid computing, and other parallel programming toolkit. The PHGS (Hwang et al., 2007) applied OpenMP in the HydroGeoSphere model using parallel matrix solver. The FSDHM model was parallelized using OpenMP by dividing simulation units into hydrologic independent layers (Liu et al., 2014). However, OpenMP only works in shared memory machines. Yalew et al. (2013) parallelized the SWAT watershed model using the distributed grid computing by splitting large scale model into small scale components. As MPI can distribute computing loads and converge results through message transfer and communication between processors, it is the most used technology in parallel hydrologic models for domain decomposition (Li et al, 2011; Vivoni et al., 2011; Wang et al., 2011; Wu et al., 2013). However, using the MPI library for data partitioning and communication is not straightforward. The pWASH123D model (Cheng et al., 2005) utilizes the DBuilder (Hunter and Cheng, 2005) parallel data management toolkit, which hides the MPI scheme for map generating, sending, and receiving between meshes with simple Application Programming Interfaces (API) and embedded ParMETIS partitioner library (Karypis et al., 1997).

The development of the ADHydro model is presented here. The ADHydro model is a high-resolution physics-based distributed hydrological model developed in parallel computing environment. The merits of the model comparing with other HPC hydrologic models include: an innovative method for modeling vadose zone dynamics, a water management module considering reservoirs, diversions and irrigation, a coupled strategy to estimate interception evaporation, and snow processes through the community Noah land surface model with mutiparameterization options (Noah-MP) and the capability to ingest downscaled atmospheric forcing from the Weather Research and Forecasting (WRF) meteorologic model using the CHARM++ parallel programming environment.

GEOSPATIAL DATA AND ATMOSPSHERIC FORCING

The Upper Colorado River Basin above Lake Powell has a watershed area of approximately 288,000 km^2, and total length of streams of 467,000 km. It's located in one of the 21 major geographic regions defined by the USGS hydrologic unit code (Seaber et al., 1987) in the US. In the pre-processing step, topographic base map data were acquired from National Elevation Dataset (NED) 1/3 arc-second Digital Elevation Models (DEMs), and USGS National Hydrography Dataset (NHD) (http://viewer.nationalmap.gov/viewer/). Land cover and land use data were obtained through the 30-meter resolution, 16-class land cover classification National Land Cover Database 2011 (NLCD 2011) (http://www.mrlc.gov/). Soil texture types were aggregated from the NRCS county level Soil Survey Geographic Database (SSURGO) and state-wide State Soil Geographic Database (STATSGO) (http://www.nrcs.usda.gov/wps/portal/nrcs/main/soils/survey/geo/).

The TauDEM tools (http://hydrology.usu.edu/taudem/taudem5/) were used to extract channel

network from NED DEMs. The resulting channel network and NHD were analyzed and processed by ArcGIS to produce shapefiles and steam network connectivity that includes lakes and reservoirs. The shapefiles were used to generate high resolution unstructured 2D triangular mesh using Triangle (http://www.cs.cmu.edu/~quake/triangle.html). A 1D channel network model with mesh size of 100 meters was also generated. River hydraulic geometry were described in the form of power functions of discharge, which scales with drainage area.

Atmospheric forcing for different scenarios was generated using the Weather Research and Forecasting meteorologic model (Michalakes et al., 2004). The WRF model is a mesoscale numerical weather prediction system design to both atmospheric research and operational forecasting needs. Simulation results from WRF, including precipitation, air temperature, air pressure, wind speed, short and long wave radiation and vapor pressure, were used as atmospheric forcing input for ADHydro. The 4 km resolution WRF outputs were downscaled to the high-resolution meshes.

ADHYDRO QUASI 3-D DISTRIBUTED HYDROLOGIC MODEL

The ADHydro is a high-resolution multi-physics distributed model for hydrological and water resources modeling. Major hydrologic processes are considered, including precipitation and infiltration, snowfall and snowmelt in complex terrain, vegetation and evapotranspiration, soil heat flux and freezing, overland flow, channel flow, groundwater flow and water management. These hydrologic components are described below.

The ADHydro model uses the explicit finite volume method to solve conservation laws for overland flow and saturated groundwater flow coupled to river flow. The model has a quasi-3D formulation that couples 2D overland flow and 2D saturated groundwater flow using the 1D Talbot-Ogden finite water-content infiltration and redistribution method (Talbot and Ogden, 2008). This eliminates difficulties in solving the highly nonlinear 3D Richards' equation, while the finite volume Talbot-Ogden infiltration method is computationally efficient, mass conservative, and allows simulation of the effect of shallow groundwater tables on runoff generation.

Interception, Evapotranspiration and Snow Melt: Interception, evapotranspiration and snow melt processes are simulated using the Noah-MP model (Niu et al., 2011; Yang et al., 2011). The Noah-MP model considers biophysical processes such as interactive vegetation canopy, multilayer snow pack and soil, overland runoff, and unconfined aquifer for groundwater storage with a dynamic water table. Its major components include 1-layer canopy, 3-layer snow, and 4-layer soil. In Noah-MP, partitioning precipitation into rainfall and snowfall use surface air temperature as a criterion, the canopy water scheme simulates the canopy water interception and evaporation, and the “semitile” subgrid scheme calculates the skin temperature of the canopy and snow/soil surface separately using an interactive energy balance method. Snow and soil layer temperatures are used to asses the energy for melting and freezing for the snow and soil layers. Noah-MP model input includes static input data (e.g. vegetation and soil data, latitude and longitude) and atmospheric forcing data (e.g. precipitation, air temperature, humidity, radiation).

Overland Flow Routing: The shallow overland flow can be simulated using dynamic wave or

diffusive wave Shallow Water Equations (SWE). The depth-averaged 2D shallow water equations are derived by integrating the Navier-Stokes equations in the vertical direction under the assumptions of hydrostatic pressure distribution and uniform velocity profiles in the vertical direction. The dynamic wave SWE can be written as (Ying et al., 2009):

$$\begin{aligned} \frac{\partial h}{\partial t} + \frac{\partial hu}{\partial x} + \frac{\partial hv}{\partial y} &= q_s \\ \frac{\partial hu}{\partial t} + \frac{\partial hu^2}{\partial x} + \frac{\partial huv}{\partial y} &= g\,h\left(-\frac{\partial Z}{\partial x} - S_{fx}\right) \\ \frac{\partial hv}{\partial t} + \frac{\partial huv}{\partial x} + \frac{\partial hv^2}{\partial y} &= g\,h\left(-\frac{\partial Z}{\partial y} - S_{fy}\right) \end{aligned} \tag{1}$$

where h is water depth, q_s is source/sink term, u and v are flow velocities in x and y directions, respectively, $Z = h + z_g$ is water surface elevation, z_g is surface ground elevation, and S_{fx} and S_{fy} are friction slopes.

Further under the diffusion wave approximation where inertia is not important (Akan and Yen, 1981), the diffusive wave SWE is given as:

$$\frac{\partial h}{\partial t} = \frac{\partial}{\partial x}\left(hk\frac{\partial Z}{\partial x}\right) + \frac{\partial}{\partial y}\left(hk\frac{\partial Z}{\partial y}\right) + q_s \tag{2}$$

where the diffusion coefficient:

$$k = \frac{h^{2/3}}{n}\frac{1}{\left(\partial Z/\partial s\right)^{1/2}} \tag{3}$$

with s is the maximum slope direction, and n is Manning's roughness coefficient. The diffusive wave approximation neglects the local acceleration term and convective acceleration term in the momentum equations, and it is applicable in situations where Froude number is small.

Channel Flow Routing: The dynamic wave governing equations (Saint-Venant equations) for one-dimensional flows in natural rivers include the continuity equation and momentum equation:

$$\begin{aligned} \frac{\partial A}{\partial t} + \frac{\partial Q}{\partial x} &= q_s \\ \frac{\partial Q}{\partial t} + \frac{\partial Q^2/A}{\partial x} &= -gA\frac{\partial Z}{\partial x} - gAS_f \end{aligned} \tag{4}$$

where A is cross section area of the channel, and Q is volumetric flow rate. The dynamic wave equations can also be simplified under diffusive wave assumption:

$$\frac{\partial A}{\partial t} - \frac{\partial}{\partial x}\left(\frac{A R^{2/3}}{n}\frac{\partial Z/\partial x}{\sqrt{|\partial Z/\partial x|}}\right) = 0 \tag{5}$$

Level pool routing method is used for lakes and reservoirs:

$$\frac{dS}{dt} = I - O + R - E - S_p + O_l \tag{6}$$

where S is volume of storage in the reservoir, I is inflow, O is outflow, R is rainfall, E is evaporation, S_p is seepage, and O_l is lateral overland flow. Cross-section properties come from empirically-derived scaling relations for the 2-year flow coupled with bankfull cross-section estimators.

Coupling 1D Channel and 2D Overland Flow: A source term based lateral connection between 1D channel and 2D overland flow domain is used. The broad-crested weir discharge is calculated as (Blade et al., 2012):

$$Q_L = \begin{cases} K\,L(z_1 - z_w)\sqrt{2\,g(z_1 - z_w)}, & \frac{2}{3}(z_1 - z_w) \geq (z_2 - z_w) \\ 2.6\,K\,L(z_2 - z_w)\sqrt{2\,g(z_1 - z_w)}, & \frac{2}{3}(z_1 - z_w) < (z_2 - z_w) \end{cases} \tag{7}$$

where z_1 is headwater surface elevation, z_2 is tailwater elevation, and z_w is weir crest elevation, L is the length of 1D channel element in contact with 2D mesh edge, and K is a constant (generally $0.3 < K < 0.6$).

Unsaturated Vadose Zone Flow: The 1D infiltration and redistribution method in the discretized moisture content domain (Ogden et al. 2015b, Talbot and Ogden, 2008), and an optional approximation (Lai et al., 2015) are used to simulate vadose zone flow. The T-O method assumes homogeneous soil, and the water moisture content is discretized into hypothetically interacting bins. The soil moisture characteristic and unsaturated hydraulic conductivity curves are required to discretize the T-O domain. These curves can be described using soil characteristic models such as Brooks-Corey model (1966) or van Genuchten model (1980).

In T-O method, the movement of surface water and groundwater in each bin is simulated, followed by the process of redistribution. The infiltration advancement of surface wetting front in a bin k due to capillary and gravitational forces is given as:

$$\frac{dZ_j}{dt} = \frac{K(\theta_d) - K(\theta_i)}{\theta_d - \theta_i}\left(1 + \frac{|h(\theta_d)| + h_p}{Z_j}\right) \tag{8}$$

where Z_j is position of surface wetting front of bin j, θ_i is initial water content or the water content of the first bin that is not fully saturated from the groundwater table to the surface, θ_d is the water content of the right-most bin in the surface wetting front that contains water, $K(\theta_i)$ and $K(\theta_d)$ are the unsaturated hydraulic conductivity of the θ_i and θ_d bins respectively, h_p is depth of surface ponding, and $h(\theta_d)$ is the capillary pressure of θ_d bin. While the movement of a groundwater wetting front is given as (Ogden et al. 2015a):

$$\frac{dZ_j}{dt} = \frac{K(\theta_j) - K(\theta_i)}{\theta_j - \theta_i}\left(1 - \frac{|h'(\theta_j)|}{D_j}\right) \tag{9}$$

where the hydrostatic capillary height considering a constant surface influx $q_{in} < K_s$:

$$|h'(\theta)| = \frac{|h_b|}{1 - \frac{q_{in}}{K_s}} + \frac{|h(\theta)| - |h_b|}{1 - \frac{q_{in}}{2K(\theta)} - \frac{q_{in}}{2K_s}} \tag{10}$$

The redistribution process sorts the bin depths from deepest to shallowest going from left to right for both the surface wetting fronts and the groundwater wetting fronts. This redistribution scheme moves water at the same elevation laterally, and is similar to the game "Tetris™", but operating horizontally. After redistribution, the length of both surface wetting front and groundwater front decreases monotonically from high capillary suction to low capillary suction.

Saturated Groundwater Flow: The ADhydro model simulates groundwater flow using a quasi-3D unsaturated/saturated flow scheme. Flow in the vadose zone is modeled using the 1D infiltration and redistribution method, and flow in the saturated zone is simulated using the 2D Boussinesq equation. The Boussinesq equation for saturated 2D groundwater flow in unconfined aquifer is given by:

$$S_y \frac{\partial h}{\partial t} = \frac{\partial}{\partial x}\left(K_x h \frac{\partial H}{\partial x}\right) + \frac{\partial}{\partial y}\left(K_y h \frac{\partial H}{\partial y}\right) + R \tag{11}$$

where H is total groundwater hydraulic head, h is groundwater depth, K_x are Ky hydraulic conductivity, R is the vertical recharge rate to the saturated surface, and S_y is the specific yield.

Since the amount of water recharge to saturated zone ($W = R\Delta t$) is calculated using the 1D infiltration and redistribution method, to have a more consistent way coupling unsaturated-saturated zone, the saturated flow rate (R') into an element is calculated:

$$R' = \frac{\partial}{\partial x}\left(K_x h \frac{\partial H}{\partial x}\right) + \frac{\partial}{\partial y}\left(K_y h \frac{\partial H}{\partial y}\right) \tag{12}$$

This also allows the saturated flow and unsaturated flow calculated using different time steps. Then the change of groundwater depth can be written as:

$$\Delta h = \frac{R'\Delta t + W}{S_y} \tag{13}$$

The position of groundwater table is used as boundary condition for 1D unsaturated flow. For example, if the total recharge to saturated groundwater is positive ($R'\Delta t + W > 0$), the water table moves upward, the 1D moisture curve should move upward as well using available water from the total recharge.

Coupling 1D Channel and 2D Groundwater Flow: Lateral flow between channel and groundwater is a function of river water surface elevation and groundwater head. The specific flow rate from channel to groundwater can be calculated as (Gunduz and Aral, 2005):

$$q_L = \begin{cases} K_r w_r \dfrac{Z_r - H}{\Delta z_b}, & H > z_b - \Delta z_b \\ K_r w_r \dfrac{h + \Delta z_b}{\Delta z_b}, & H \le z_b - \Delta z_b \end{cases} \tag{14}$$

where K_r is river bottom sediment conductivity, w_r is river bed wetted perimeter, Δz_b is the river bed thickness, Z_r is river water surface elevation, H is groundwater head.

Water Management: A water management model is developed for the Upper Colorado River Basin. Emphasis are placed on the engineered aspects of water management and use, where storage reservoirs, diversions, and irrigation are simulated. Statistical based method and operation rules based optimization method are used. Operational water management rules are explored for the major reservoirs and irrigation districts in the Upper Colorado River Basin from Bureau of Reclamation (http://www.usbr.gov/uc/water/). Typical constrains and rules include maximum and minimum elevations, target elevations for wet and drought seasons, maximum and minimum releases, and contractual, legal, and institutional obligations (Yeh, 1985). The simulation/optimization model determines release decisions for different planning purposes. Interactions between reservoirs and river/aquifer system are also considered.

CHARM++ Parallelization: The ADHydro implementation uses the Charm++ parallel programming system. Charm++ is based on location transparent message passing between migrateable C++ objects. Each object represents an entity in the model such as a mesh element. These objects can be migrated between processors or serialized to disk allowing the Charm++ system to automatically provide capabilities such as load balancing and checkpointing. Objects interact with each other by passing messages that the Charm++ system routes to the correct destination object regardless of its current location.

REFERENCES

Akan, A. O., and Yen, B. C. (1981). "Diffusion-wave flood routing in channel networks," Journal of the Hydraulics Division, 17(6), pp 719-732.

Apostolopoulos, T. K., and Georgakakos, K. P. (1997). "Parallel computation for streamflow prediction with distributed hydrologic models," Journal of Hydrology, 197(1-4), pp 1-24.

Arnold J. G., Allen, P. M., and Bernhardt, G. (1993). "A comprehensive surface-groundwater flow model," Journal of Hydrology, 142(1-4), pp 47-69.

Ashby, S. F., and Falgout, R. D. (1996). "A parallel multigrid preconditioned conjugate gradient algorithm for groundwater flow," Nuclear Science and Engineering, 124(1), pp 145-159.

Blade et al.,(2012). "Integration of 1D and 2D finite volume schemes for computations of water flow in natural channels," Advances in Water Resources, 42, pp 17-29.

Brooks, R. H., and Corey, A. T. (1966). "Properties of porous media affecting fluid flow," Journal of the Irrigation and Drainage Division, Proceeding of the American Society of Civil Engineers, 92(IR2), pp 61-88.

Cheng, J. R. C., Hunter, R. M., Cheng, H., Richards, D. R., and Yeh G. T. (2005). "Parallelization of a watershed model-Phase III: Coupled 1-dimensional channel, 2-dimensional overland, and 3-dimensional subsurface flows," Computational Methods in Water Resources XVI, Copenhagen, Denmark, CMWR CD-ROM, paper 64, pp 19-22.

Cui, Z., Vieux, B. E., Neeman, H., and Moreda, F. (2005). "Parallelisation of a distributed hydrologic model," Int'l. J. Computer Applications in Technology, 22(1), pp 42-52.

Downer, C. W., and Ogden F. L. (2004). "GSSHA: Model to simulate diverse stream flow producing process," Journal of Hydrological Engineering, 9(3), pp 161-174.

Gunduz, O., and Aral, M. M. (2005). "River networks and groundwater flow: a simultaneous solution of a coupled system," Journal of Hydrology, 301(1-4), pp 216-234.

Hunter, R. M., and Cheng, J. R. C. (2005). "Dbuilder: A parallel data management toolkit for scientific applications," Proceedings of the 2005 International Conference on Parallel and Distributed Processing Techniques and Applications, pp 825-831.

Hwang, H.-T., Park, Y.-J., Sudicky, E. A., and Forsyth, P. A. (2014). "A parallel computational framework to solve flow and transport in integrated surface-subsurface hydrologic systems," Environmental Modelling & Software, 61, pp 39-58.

Karypis, G., Schloegel, K., and Kumar, V. (1997). "Parmetis: Parallel graph partitioning and sparse matrix ordering library," Version 1.0, Department of Computer Science, University of Minnesota.

Kollet, S. J., and Maxwell, R. M. (2006). "Integrated surface-groudwater flow modeling: A free-surface overland flow boundary condition in a parallel groundwater flow model," Advances in Water Resources, 29(7), pp 945-958.

Lai, W., F.L. Ogden, R.C. Steinke, and C.A. Talbot, (2015). An efficient and guaranteed stable numerical method for continuous modeling of infiltration and redistribution with a shallow dynamic water table, *Water Resour. Res*., in press.

Li, T., Wang, G., Chen, J., and Wang, H. (2011). "Dynamic parallelization of hydrological model simulation," Environmental Modelling & Software, 26(12), pp 1736-1746.

Liu, J., Zhu, A., Liu, Y., Zhu, T., and Qin, C. (2014). "A layered approach to parallel computing for spatially distributed hydrological modeling," Environmental Modelling & Software, 51, pp 221-227.

Michalakes, J., Dudhia, J., Gill, D., Henderson, T., Klemp, J., Skamarock, W., & Wang, W.

(2004). "The weather research and forecast model: software architecture and performance," In Proceedings of the 11th ECMWF Workshop on the Use of High Performance Computing In Meteorology, 25, pp 29.

Mills, R. T., Lu, C., Lichtner, P. C., and Hammond, G. E. (2007). "Simulating subsurface flow and transport on ultrascale computers using PFLOTRAN," In Journal of Physics: Coference Series, 78(1), IOP Publishing.

Niu G. Y., et al. (2011). "The community Noah land surface model with muliparameterization options (Noah-MP): 1. Model description and evaluation with local-scale measurements," Journal of Geophysical Research, 116, D12109, doi:10.1029/2010JD015139.

Ogden, F.L., W. Lai, R.C. Steinke, and J. Zhu, (2015a), Validation of finite water-content vadose zone dynamics method using column experiment with a moving water table and applied surface flux. *Water Resour. Res*., in press.

Ogden, F.L., W. Lai, R.C. Steinke, J. Zhu, C.A. Talbot, and J.L. Wilson, (2015b). "An ordinary differential equation alternative to the 1-D Richards' Equation in the Unsaturated Zone". *Water Resour. Res.*, in review.

Refsgaard, J. C., and Storm, B. (1995). MIKE SHE. In: Singh, V. P. (Ed), Computer Models of Watershed Hydrology. Water Resources Publications, pp 809-846.

Seaber, P. R., Kapinos, F. P., and Knapp, G. L. (1987). Hydrologic Unit Map. US Government Printing Office.

Talbot, C. A., and Ogden, F. L. (2008). "A method for computing infiltration and redistribution in a discretized moisture content domain," Water Resources Research, 44(8), W08453, DOI: 10.1029/2008WR006815.

Van Genuchten, M. T. (1980). "A closed-from equation for predicting the hydraulic conductivity of unsaturated soils," Soil Science Society of America Journal, 44(5), pp 892-898.

Vivoni, E. R., et al. (2011). "Real-world hydrologic assessment of a fully-distributed hydrological model in a parallel computing environment," Journal of Hydrology, 409(1-2), pp 483-496.

Wang H., Fu, X., Wang, G., Li, T., and Gao, J. (2011). "A common parallel computing framework for modeling hydrological processes of river basins," Parallel Computing, 37, pp 302-315.

Wood et al. (2011). "Hyperresolution global land surface modeling: Meeting a grand challenge for monitoring Earth's terrestrial water," Water Resources Research, 47, W05301, doi:10.1029/2010WR010090.

Wu, Y., Li, T., Sun, L., and Chen, J. (2013). "Parallelization of a hydrological model using the message passing interface," Environmental Modelling & Software, 43, pp 1240131.

Yalew, S, van Griensven, A., Ray, N. Kokoszkiewicz, L, and Betrie, G. D. (2013). "Distributed computation of large scale SWAT models on the Grid," Environmental Modelling & Software, 41, pp 223-230.

Yang Z. L., et al. (2011). "The community Noah land surface model with muliparameterization options (Noah-MP): 2. Evaluation over global river basins," Journal of Geophysical Research, 116, D12110, doi:10.1029/2010JD01540.

Yeh, W. W-G. (1985). "Reservoir management and operations models: A state-of-the-art review." Water Resources Research, 21(12), 1797-1818.

Ying, X., Jorgeson, J., and Wang, S. (2009). "Modeling dam-break flows using finite volume method on unstructured grid," Engineering Applications of Computational Fluid Mechanics, 3(2), pp 184-194.

STORM: A MODEL FOR 2D ENVIRONMENTAL HYDRAULICS

Francisco J.M. Simões, US Geological Survey, Geomorphology and Sediment Transport Laboratory, Golden, CO 80403, frsimoes@usgs.gov

Abstract: A two-dimensional (depth-averaged) finite volume Godunov-type shallow water model developed for flow over complex topography is presented. The model, SToRM, is based on an unstructured cell-centered finite volume formulation and on nonlinear strong stability preserving Runge-Kutta time stepping schemes. The numerical discretization is founded on the classical and well established shallow water equations in hyperbolic conservative form, but the convective fluxes are calculated using auto-switching Riemann and diffusive numerical fluxes. Computational efficiency is achieved through a parallel implementation based on the OpenMP standard and the Fortran programming language. SToRM's implementation within a graphical user interface is discussed. Field application of SToRM is illustrated by utilizing it to estimate peak flow discharges in a flooding event of the St. Vrain Creek in Colorado, U.S.A., in 2013, which reached 850 m^3/s (~30,000 f^3/s) at the location of this study.

INTRODUCTION

Current climate change science and research predictions, such as those identified in the recent Intergovernmental Panel on Climate Change report (IPCC, 2014), indicate the hazards of flooding and their detrimental impacts are becoming more frequent and likely to increase. The need to cope with flooding effects—such as floodplain regulations, insurance, mitigation engineering works, and emergency preparedness—requires tools that can be used to provide accurate predictions of flood timing, duration, and extent. A numerical flow model that solves the shallow water equations (SWEs) and simulates the hydrodynamics of a wide variety of surface flows will be a significant asset in the gamut of tools available to engineers, managers, and decision makers involved in floodplain management. Such a model needs to be accurate, robust, efficient, and be available in a computer environment that facilitates data processing and analysis to reduce project turnaround time.

Moreover, the increased availability of high accuracy digital terrain models (DTMs) over large extents (tens to hundreds of square miles, or more) have created the demand for models that can be used to address inundation events at those scales. These DTMs are often created using remotely sensed terrain data (e.g., Light Detection and Ranging (LiDAR) or interferometric Synthetic Aperture Radar (ifSAR)) with typical horizontal resolutions of 1 m that retain very detailed features, such as individual buildings and roads. Simulating surface flow with this type of spatial accuracy can only be done at high computational cost, requiring computer systems that can accommodate the vast amounts of data in memory and that have fast numerical processors.

In the past decade, Godunov-type schemes using a finite volume formulation have become popular for solving the SWEs (Toro and Garcia-Navarro, 2007; Vazquez-Cendon et al., 2013). This can be attributed to the ability of these schemes to deal with the most complicated shallow water phenomena, such as hydraulic jumps, flow regime change, and the wet-dry interfaces encountered in fast moving catastrophic flooding flows. SToRM (System for Transport and River Modeling) is a model that employs these techniques in two-dimensional (2D) unstructured grids (Simões, 2011), and that is contained in a graphical user environment that provides a number of tools to expedite its use by trained operators.

The purpose of this article is to provide a brief presentation of the computer model SToRM and to explore the use of parallelism to improve computational efficiency in the setting of a desktop workstation. The following sections will present the governing equations and computation methods used to develop the numerical model; how parallelism is employed to move from a single- to a multi-threaded computing environment; and SToRM's implementation in a graphical user interface. Finally, to illustrate the methods in a problem of practical and recent significance, SToRM is applied to estimate peak flood flow rates in a section of the historic flooding that occurred in St. Vrain Creek, Colorado, in September of 2013.

MODEL FORMULATION

SToRM is based on the classical SWEs written in the conservative form (Chaudhry, 1993):

$$\frac{\partial \mathbf{U}}{\partial t}+\frac{\partial \mathbf{F}(\mathbf{U})}{\partial x}+\frac{\partial \mathbf{G}(\mathbf{U})}{\partial y}=\mathbf{S(U)} \tag{1}$$

$$\mathbf{U}=\begin{bmatrix} h \\ hu \\ hv \end{bmatrix},\quad \mathbf{F}=\begin{bmatrix} hu \\ hu^2+gh^2/2 \\ huv \end{bmatrix},\quad \mathbf{G}=\begin{bmatrix} hv \\ huv \\ hv^2+gh^2/2 \end{bmatrix},\quad \mathbf{S}=\begin{bmatrix} 0 \\ gh\left(S_{0x}-S_{fx}\right) \\ gh\left(S_{0y}-S_{fy}\right) \end{bmatrix}$$

where t is time, h is the water depth, g is the acceleration due to gravity, u and v are the depth-averaged flow velocities in the x and y Cartesian directions, S_0 is the bed slope, and S_f is the bottom friction. Integrating equation (1) over a standard control volume Ω and applying the divergence theorem results in

$$\frac{\partial}{\partial t}\int_{\Omega}\mathbf{U}d\Omega+\oint_{\partial\Omega}\left(\mathbf{E}\cdot\mathbf{n}\right)ds=\int_{\Omega}\mathbf{S}d\Omega \tag{2}$$

where $\mathbf{E} = (\mathbf{F},\mathbf{G})^{\mathrm{T}}$ and $\mathbf{n}$ is the outward-pointing unit vector normal to the control volume boundary $\partial\Omega$. SToRM is based on the numerical integration of equation (2) over cell-centered, non-overlapping triangles:

$$\frac{\partial \Omega_i \mathbf{U}_i}{\partial t}=\sum_{k=1}^{3}\mathbf{E}_{ik}\Delta l_{ik}+\mathbf{S}_i\Omega_i \tag{3}$$

In equation (3), $\mathbf{U}_i$ are the average values of the conserved variables over triangle i, $\mathbf{E}_{ik}$ are the inviscid fluxes through triangle edge k, Δl_{ik} is the length of edge k, $\mathbf{S}_i$ contains the source terms, and Ω_i is the triangle's area.

Following the principles of Godunov-type methods, the inviscid fluxes $\mathbf{E}_{ik}$ are numerical fluxes arising from a local Riemann problem at each triangle edge. Here, $\mathbf{E}_{ik}$ are computed using Roe's flux function at those edges (Roe, 1981):

$$\mathbf{E}_{ik}=\frac{1}{2}\left[\left(\mathbf{E}_{ik}^{+}+\mathbf{E}_{ik}^{-}\right)-\mathbf{\Gamma}\left(\mathbf{U}_{ik}^{+}-\mathbf{U}_{ik}^{-}\right)\right]$$

where the '+' quantities are reconstructed at the midpoint of the edge k using data from control volume i and the '-' quantities are reconstructed using data from the adjacent control volume. In SToRM, the up-winding factor $\mathbf{\Gamma}$ can be computed in one of two manners: (1) as in the algorithm of Alcrudo and Garcia-Navarro (1993) or (2) by using Rusanov's (1961) numerical flux. The first approach is more computational demanding (i.e., it requires more computer number crunching), but it has the shock capturing properties needed to compute the flow at discontinuities such as hydraulic jumps and wet-dry fronts, whereas the latter is computationally much simpler and less demanding, but may introduce spurious numerical diffusion into the solution. The decision of which to use is done at each triangle edge: if $|h^{+}-h^{-}|/\mathrm{Max}\{h^{+},h^{-}\} > \delta_s$ then Alcrudo and Garcia-Navarro's method is used, otherwise Rusanov's method is used. A threshold value, δ_s, is used to detect discontinuity across element edges and is usually set to 0.1%, a value found by numerical experimentation.

Second-order accuracy is achieved using a piecewise linear model for the cell variables with the usual MUSCL (Monotonic Upstream-Centered Scheme for Conservation Laws) reconstruction, with limiting to enforce monotonicity near sharp gradients and discontinuities of the dependent variables. The continuously differentiable limiter by Venkatakrishnan (1995) is chosen because it avoids introducing discontinuities to the computation of the reconstructed function and, consequently, to the fluxes, therefore improving the convergence properties of the solver over other commonly used discontinuous limiters. Computation of the gradients is accomplished with a second-order-accurate least-squares technique conditioned by the use of inverse distance weighting.

The friction terms are discretized in a semi-implicit manner:

$$q_{xi}^n = \frac{\underline{q}_{xi}^n}{1 + g\Delta t \underline{S}_{fxi}^n / \underline{u}_i^n}, \quad q_{yi}^n = \frac{\underline{q}_{yi}^n}{1 + g\Delta t \underline{S}_{fyi}^n / \underline{v}_i^n} \tag{4}$$

where $q_x = hu$ and $q_y = hv$ are the components of the unit discharge, the superscript n refers to the time step, and the underlined variables are frictionless-computed quantities. This discretization avoids numerical oscillations in regions of high friction and low water depth, such as in wet-dry fronts, and impacts positively the conditional stability limits of the time-stepping method mentioned in the next paragraph.

The solution is advanced explicitly in time using nonlinear Strong Stability Preserving Runge-Kutta (SSPRK) schemes, also known as Total Variation Diminishing (TVD) Runge-Kutta schemes (Gottlieb et al., 2001). This is done by first rewriting the governing equations, equation (3), as a coupled system of ordinary differential equations:

$$\Omega_i \frac{\partial q_i}{\partial t} = R_i(u, v; t), \qquad i = 1, 2, 3 \tag{5}$$

where R_i is called the residual. Here, a simplified form of the SSPRK schemes is used, in which a m-stage SSPRK method for equation (5) is written in the form

$$\begin{cases} u^{(0)} = u^n \\ u^{(i)} = \sum_{j=0}^{i-1} \alpha_{ij} u^{(j)} + \beta_i \frac{\Delta t}{\Omega_i} R\left(u^{(i-1)}\right), \qquad \alpha_{ij} \geq 0, i = 1, \ldots, m \\ u^{n+1} = u^{(m)} \end{cases} \tag{6}$$

where Δt is the time step size, the superscripts n and $n + 1$ denote the time level, and the parenthetic superscripts denote the Runge-Kutta level. The coefficients α and β are chosen to meet desired criteria. SToRM implements three optimal (in the sense of the Courant-Friedrichs-Lewy CFL stability coefficient θ) SSPRK schemes: first order (m = 1), second-order (m = 2), and third-order (m = 3). Note that these schemes are all subjected to the same stability criterion and have an upper bound for θ.

Boundary conditions are applied at the edges of the model grid using Riemann invariants, i.e., the boundary fluxes are also computed by solving a Riemann problem between the interior states and the "ghost" states outside the computational domain. These "ghost" states are introduced in order to compute the boundary fluxes in a similar and consistent way to the interior fluxes. Here, an approach identical to that of Anastasiou and Chan (1997) is used for solid walls, inflow, and outflow boundaries. However, wetting and drying fronts require a separate treatment.

Wetting and drying occurs not only during the propagation of floods, but also at the edges of any body of water. Thus, the dry-wet front constitutes not only a propagation problem, but also a static boundary condition problem, because it defines the shoreline. It is not easy to include these effects in a straightforward manner in a numerical code and most researchers resort to different degrees of approximation. Advancing wet-dry fronts are treated with the method of Brufau et al. (2002), which uses a numerical flux that can be applied to zero-depth cells and that maintains the C-property[1]. The key concept is that the fluxes at the advancing front must be determined from the wet side of the front: the velocity at the cell boundaries separating wet and dry states is determined from the wet side, and the interface flux only uses the information coming from the wet side. This procedure allows including wetting and drying fronts in the ordinary cell flux computations without requiring the artificial wetting of dry cells. Drying fronts pose the additional problem that, during a drying time step, negative water depths may be reached. Mass conservation requires that the time step should be restricted to the value that corresponds to the time that takes the cell to dry out, i.e., to reach h_i = 0. SToRM performs additional checks and adjustments to ensure that mass is conserved at every time step without imposing these constraints to the time step size. These checks and adjustments are presented with greater detail in Simões (2011).

[1] A numerical scheme that preserves exactly initial solutions of a steady state lake at rest is said to verify the C-property.

The shoreline treatment is different from the two preceding cases. A shoreline is defined when all the surrounding dry triangles of a partially or fully wet control volume have a mean bed elevation higher than the stage at the centroid of the triangle. Under this circumstance the shoreline is defined at the control volume edges and is also subjected to a special treatment. Partially wet triangles have corrections applied to their wetted area and water depth. The treatment is different whether drying or wetting is occurring. The interested reader is referred to Simões (2011), where detailed descriptions and validations of the methods are presented.

PARALLEL IMPLEMENTATION

SToRM was developed using the programming language Fortran 90/95 using the traditional instruction-driven SISD (Single Instruction, Single Data) computing model, where a single processor executes one instruction stream that operates on data stored in the same memory as the instructions. The algorithms and techniques used were essentially sequential in nature. The programming style, however, was modular and the use of a code profiler (Intel® Parallel Studio XE 2013 was used) permitted to clearly identify regions of the program that consumed the most central processing unit (CPU) run times and, from those, the sections of the code that were the best candidates for parallelization. These sections were then targeted for treatment, with two development criteria: (1) the parallel code must give identical results to its sequential version, and (2) there must be a reduction in computing run time over the original code.

The hardware tools available for the development of this project consisted of a desktop computer with dual Intel® Xenon® E5-2630 v2 CPUs running at 2.60 GHz, 16 GB of RAM, and using the Microsoft® Windows® 8.1 64-bit operating system. Each of the CPUs contains 6 cores and 12 threads, making a total of 24 threads available to the user. The graphics capabilities were provided by a NVIDIA® Quadro® K600 graphics processing unit (GPU) with 1 GB of memory and 192 CUDA[2] cores. The GPU supports several graphics and compute APIs (Application Program Interfaces), such as OpenGL 4.4, DirectX 11, CUDA, and OpenCL. The software tools used consisted in the group of programming applications available in the Intel® Parallel Studio XE 2013 software package (see https://softare.intel.com for the latest version available).

Parallelism can be achieved in a number of ways, but this project was restricted by the hardware described above and by keeping the code development efforts limited to relatively short times. Furthermore, there was the desire to use standard, high-level programming tools to achieve maximum portability to different hardware platforms and operating systems. Given the possibility of using the programmable graphics hardware as a general-purpose computing machine, both the GPU and the CPU can be used to reach these goals.

GPUs provide an attractive platform for parallel application development because most modern computers include programmable GPUs that have a floating point computational power that typically is more than one order of magnitude higher than comparable CPUs. Additionally, because GPUs have a more scalable architecture, their power is expected to grow considerably faster than the computational power of CPUs. Hagen et al. (2005) have developed a GPU-based numerical model of the SWEs with explicit time marching schemes. They achieved a speedup of more than one order of magnitude over using the CPU alone, and showed that the GPU can be used as an inexpensive alternative to high-performance computers. Interestingly, the number 2 system in the Top500 supercomputers (TOP500 Supercomputing Sites, available at http://www.top500.org/, accessed January 2015) in November 2014, which was the latest published list at the writing of this article, uses NVIDIA GPUs to accelerate computation. Unfortunately, GPUs are based on the SIMD (Single Instruction, Multiple Data) computing model, which is significantly different from the SISD model used in SToRM. In the SIMD model, the processor is first configured with the instructions that will be executed, and then the data stream is processed. In other words, SToRM was developed based on an instruction driven model, while GPU programming requires a stream processing model. These differences require substantial changes to the fundamental algorithms already developed and implemented in SToRM and place an onerous burden in code redevelopment and debugging.

There are other more attractive approaches to parallelism that maintain the same SISD programming paradigm and that constitute established standards and, therefore, are portable across a large spectrum of machines. Two established

[2] CUDA stands for Compute Unified Device Architecture. It is a parallel computing architecture developed by NVIDIA.

standards supported in the Intel® Parallel Studio XE 2013 application development environment are Intel® MPI (Message Passing Interface) and OpenMP (Open Multi-Processing). MPI is a distributed memory multi-processor system in which each processor has its own private memory. The processors are interconnected and can communicate among themselves, therefore the efficiency of communication is very important for good performance. An important realization of such a system is given by computer clusters that may contain hundreds or thousands of individual computational nodes. At the time of this writing, the number 1 system in the Top500 supercomputers list is a cluster of 3,120,000 Intel® Xeon® E5-2692 CPUs, with a peak computing of near 55,000 TeraFLOPS (floating-point operations per second). Sanders et al. (2010) have presented a parallel flow model for flood inundation computations on unstructured grids. They used several different sized clusters and achieved high rates of efficiency in all. Their approach, however, depends on load balancing to a high degree, i.e., on the manner in which the computational grid is partitioned among the multiple nodes of the cluster. The key to achieve a good partitioning is to subdivide the grid into subdomains with equal computation workload while sharing the least amount of data. Alas, partitioning is a computationally expensive task and is typically done only once and at the start of the computer run. Flooding, however, is an intrinsically transient phenomenon, therefore a dynamic load balancing—where all cluster nodes have to process the same number of wet and dry cells during the flooding event—is required to maintain an optimum balance. A very efficient algorithm is needed in order to minimize the computational overhead associated with recomputing the load balance and retransmitting the appropriate data to all the cluster nodes during the flooding process. Developing such an algorithm is very difficult and time consuming, and was outside of the scope of the current project.

The MPI paradigm described above is an example of coarse-grain parallelism, where parallelism in a program is achieved by decomposing the target domain into a set of subdomains that are distributed over the different processors of the machine. OpenMP, on the other hand, is an example of fine-grain parallelism, in which parallelism in a program is achieved by distributing the work of the DO-loops among the different processors, such that each processor computes only a portion of the loop iterations. Given that the most computationally-intensive segments of the code in SToRM are done in DO-loops, OpenMP was chosen as the most suitable choice of technique to achieve the desired goals.

OpenMP is an API for writing multithreaded (MT) applications that consists of a set of compiler directives, library routines, and environment variables. It greatly simplifies the development of MT applications in Fortran, C, and C++. It assumes the hardware provides a shared memory workspace with equal-time access for each process (thread), and that the OS treats every process the same way: it is a SMP, or Symmetrical Multiprocessor architecture. OpenMP, however, also provides a way to directly access the cache associated with each thread, allowing the user to take advantage of this faster type of memory when developing parallel code. This type of system architecture is very similar to the hardware configuration of modern Intel® CPUs, which can be a significant advantage for the OpenMP user.

The approach followed to add parallelism to the computer code SToRM was to use the code profiling tools in Intel® Parallel Studio XE 2013 to identify the segments of the code that consumed the most computer resources (i.e., those which were responsible for the largest portions of the total computer run times) and target them for parallelization using OpenMP. Figure 1 shows a schematic flow chart of the tasks in SToRM and provides a synoptic view of the regions that were parallelized.

Some sections of the code were straightforward to parallelize using OpenMP. These included variable interpolations and computations of the numerical gradients, operations which essentially are dot products and have no data dependencies. Computing the source/sink terms and friction terms was also an easy task, but some algorithmic changes had to be made in order to use thread cache more effectively. Dealing with the computation of the fluxes at cell edges involved the most work. SToRM uses an edge-based data structure which potentially leads to codes with reduced CPU and memory access overhead when compared to codes that use a more traditional element-based structure. However, in multithreaded programs that share the same variables simultaneously, race conditions may appear[3]. Thread synchronization must be used to avoid race conditions. Thread synchronization facilitates organized and disciplined access to shared data at the expense of overall code performance, therefore it must be used with caution and algorithms must be well designed to minimize the synchronization that must be done.

[3] Race conditions are situations where one thread updates a variable needed by another thread before the second thread has a chance to use it.

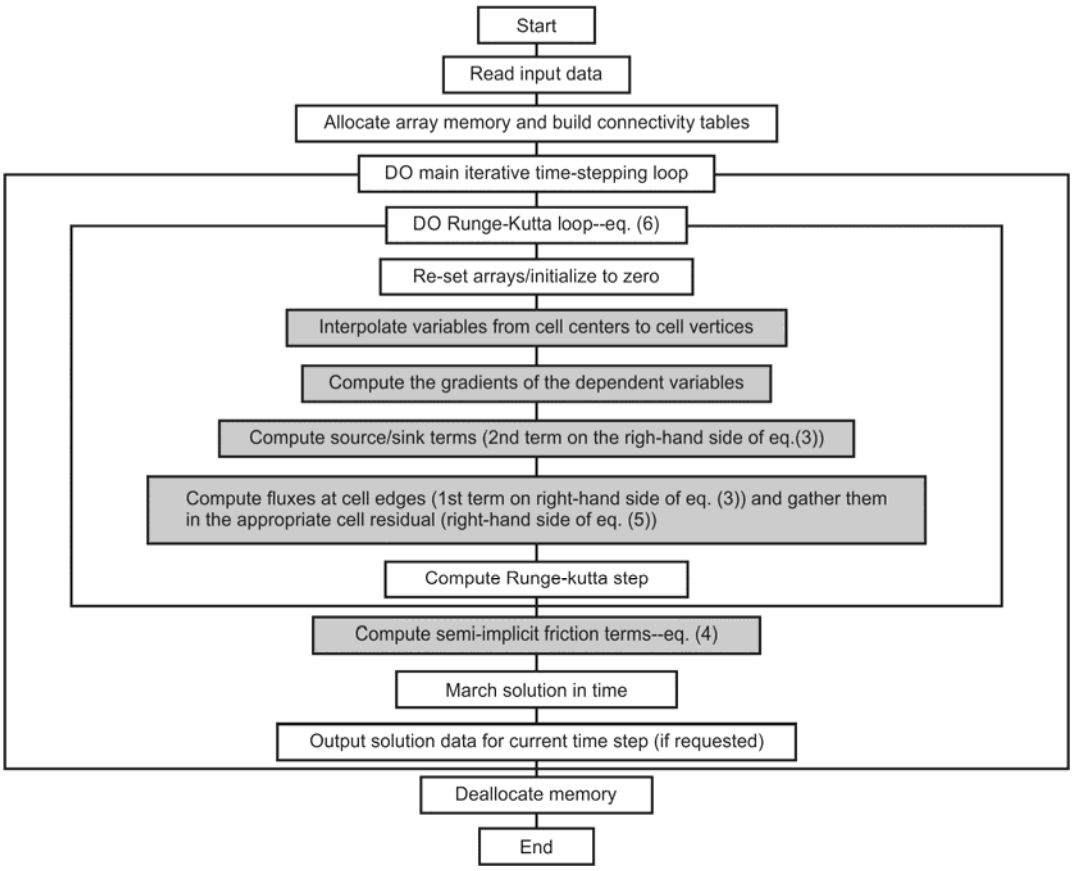

Figure 1 Flow chart of SToRM. Areas in gray represent parallel code. Operation flow is from top to bottom.

In SToRM, different types of edges are classified and distributed to different, independent computational loops (dry edges, fully wet edges, partially wet edges, solid boundary edges, inflow and outflow edges, advancing front edges, receding front edges, and bank shoreline edges). The main solution cycles over the edges and the residuals are summed by scattering (anti-symmetrically) the fluxes to the control volumes sharing the edge. The use of different cycles for different types of edges allows elimination of data dependencies and results in highly optimized code in vector-parallel computers.

At the writing of this paper, certain parts of the code remain to be parallelized. These concern sections that are more complex algorithmically, or that are treated directly by the Fortran language. An example of the latter case is initialization of arrays to zero: in Fortran, a multidimensional array is initialized to zero by the simple construct "`AnArray = 0`", where `AnArray` is an arbitrary user-defined array. The details of how this type of memory initialization is done are privy to the compiler and hidden from the user, but an analysis of the code efficiency has shown that this command does not seem to parallelize under the known compiler directives available to the user. Further investigation is needed to address these issues. Sections dealing with data input and solution output have not been parallelized.

GRAPHICAL USER INTERFACE

Integration of a numerical model within a graphical framework allows bridging the gap between model development and model use, and encourages model dissemination and application. SToRM has been integrated in iRIC (International River Interface Cooperative), a graphical user interface (GUI) framework developed specifically for environmental flow modeling (http://i-ric.org/en/). The iRIC framework provides operational facilities that are model independent, such as data input and output (multiple formats are supported), automatic grid generation (provided by the two-dimensional grid generator and Delaunay triangulation package of Shewchuk, 2002), interactive visualization

and editing of model input and output, ability to work with ancillary data sets for model calibration, and device-independent plotting.

A schematic view of how the SToRM model is integrated in the iRIC graphical framework is given in Figure 2. The graphical user interface is used to receive user input and to plot data, communicating with SToRM through a device-independent file using a format that has become a standard in many applications of computational fluid dynamics (CGNS, see http://cgns.sourceforge.net/). SToRM runtime information can also be displayed in a console window. The parameter definitions needed to customize the GUI to the specific requirements of a particular numerical model are coded in a flat file in XML format (http://www.w3.org/XML/). This file defines custom entry screens that allow the user to enter not only general numerical quantities (such as input file names, time step size, and number of time steps, for example), but also unique parameters required by SToRM, such as the threshold δ_s to detect discontinuities across element edges. The GUI can read data in a multitude of formats commonly used in hydraulics and other digital elevation modeling applications. Entire SToRM set-ups, including computational grids, boundary condition data, parameter definitions, and complete model simulation solutions obtained at multiple simulation times, can be saved in single data files for later use, and for transmission and archival.

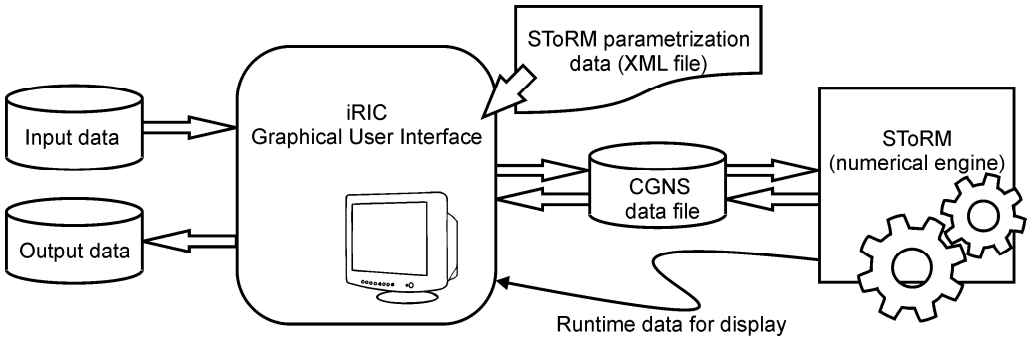

Figure 2 Schematic outline of the integration of SToRM in the iRIC modeling framework.

SToRM is implemented within the iRIC GUI and can be freely downloaded from the official iRIC Project Web Site cited above. The calculations presented in this work were obtained using version 2.3 of the iRIC distribution package.

APPLICATION: ESTIMATING PEAK FLOODING FLOWS

In the week of September 9–15 of 2013, a slow-moving cold front clashed with warm monsoonal air over Colorado, causing unusually heavy rain that resulted in catastrophic flooding along a large extent of Colorado's Front Range. Flooding conditions occurred along streams from Fort Collins in the north, to Colorado Springs in the south over an area that extended for approximately 320 km (200 miles). Nearly 19,000 homes were damaged, with over 1,500 destroyed, and more than 11,000 people had to be evacuated, with eight dead and two more missing and presumed dead. It is estimated that at least 30 state highway bridges were destroyed and an additional 20 seriously damaged, with many miles of roads and freight and passenger rail lines significantly damaged or altogether washed out. Estimates of economic losses have surpassed $2 billion USD (Novey, 2013).

Due to the high discharges and water depths that occurred in many of the affected streams, some of the US Geological Survey gaging stations were submerged or completely destroyed, precluding direct measurement of river stage at those locations. Such was the case at the confluence of the St. Vrain Creek and Boulder Creek near the city of Longmont, northwest of Denver, CO. The recurrence interval of this flood for the Boulder Creek watershed ranged mostly between 4% (25-year) and 2% (50-year) annual chance event (CH2M HILL, 2014), and between 1% (100-year) and 0.2% (500-year) annual chance event for the St. Vrain Watershed (JACOBS, 2014). As a result of high flows, the USGS Gaging Station 06725450 (http://waterdata.usgs.gov/co/nwis/uv/?site_no=06725450), located at St. Vrain Creek at Highway 119 (HWY 119) below Longmont, was destroyed and failed to record the stage at the peak of the flood. No high water marks were collected at this location during the later forensic work related to this flood, therefore preventing the realization of an indirect measurement of the peak flow. A replacement gaging station (06730525) St. Vrain Creek below Boulder Creek at HWY 119 near Longmont (http://waterdata.usgs.gov/co/nwis/uv/?site_no=06730525), was installed near the same location as the destroyed gage (Mark Smith, USGS, Personal

Comm., March 2014). This section describes the application of SToRM to estimate the peak discharge passing at the gaging station and over HWY 119, which had a section over 1.7 km (1 mile) under water.

The data sets available for this work consist of topographic data and flood delineation data. The topography was taken from USDA Geospatial Data Gateway (http://datagateway.nrcs.usda.gov/), which is from pre-flood (2008) USGS national elevation data (NED) at 1/9 arc-second resolution, i.e., with a spatial resolution of 3 meters. There was no post-flood LiDAR data for the site at the time of this study. The topographic data were used to generate a DTM for use by SToRM. Flood delineation data were obtained from remote sensing and were available as breaklines containing the discretized delineation of the flood extents in the area of interest (Chris Cole, USGS, Personal Comm., April 23, 2014). The model was set up to represent an area of 5 km (3.1 miles, east to west) by 4.5 km (2.8 miles, north to south) centered at the USGS Gaging Station 06730525, placing the model's inflow boundaries about 2.5 km (1.6 miles) upstream from the gaging station, and the outflow boundary 2.5 km (1.6 miles) downstream from it, as illustrated in Figure 3. This design places these boundaries away from the area of interest, therefore insulating it from imprecisions due to approximate representation of the water surface elevation at the downstream end, and of synthesized velocity distributions at the upstream boundaries. The outflow boundary was set at St. Vrain Creek at Interstate 25, because it is known that Interstate 25 was not flooded, and knowing that the flow was contained within the bridge opening permitted setting the boundary condition (i.e., water-surface elevation under the bridge) close to that of the actual flood, which is near the invert of the bridge.

Figure 3 Aerial photograph of the modeled region. The limits of the computational grid are given by the yellow polygon shown. Note the inflowing tributaries at the south (Boulder Creek) and southwest (St. Vrain Creek) and the outflow boundary at the northeast (St. Vrain Creek). The circle marks the location of the USGS Gaging Station. (Photo source: USDA Geospatial Data Gateway.)

Surface roughness was approximated by judging the type of land use based on the analysis of aerial photography. There are many land uses in the modeled region, including residential, commercial, agricultural, gravel mining, and open space. Different roughness values were used to represent each, assigned from previous experience using SToRM in similar land surface textures. Using aerial imagery, the computational domain was divided in areas of agricultural land use (Manning's $n = 0.045$), residential ($n = 0.055$), wooded areas in the riparian corridor ($n = 0.065$), ponds and reservoirs ($n = 0.015$), and all other surfaces ($n = 0.035$).

To determine the value of the flow discharge at St. Vrain and Boulder Creeks, which is the objective of this study, a series of runs of SToRM were carried out, each using an estimate of the flow rates for Boulder and St. Vrain Creeks. In practice, a series of discharge guesses that under- and over-predict the answer were used to perform model runs. The results of the model runs were compared to the known flood delineation contours and saved. A series of successive trials gradually honed the answer to the pair of discharges that provided the best possible agreement between the model predictions and the observations.

All model runs were carried out using the same spatial discretization. SToRM uses a spatial discretization based on triangles and the user interface iRIC provides an automatic grid generator that takes into account user input. User input is used to define grid shape and cell size, and is especially important in ensuring that topographic features of hydraulic relevance are discretized with the appropriate accuracy for model representation. Several discretizations using different grid resolutions were tried and the coarsest grid that provided the best computational performance without degrading the quality of the computed flood extents contained 57,055 points (113,140 triangles), representing a grid of triangles with a maximum area of 173.2 m^2 (1864 ft^2) each. The grid was selectively refined in certain regions, such as near the gaging station, and break lines were used to capture a number of significant terrain features.

Each run was started from an initial state in which there was little or no flooding taking place: the water was mostly confined within channel banks and the discharge was low, with an initial discharge of about 8–10 m^3/s (282.5–353 ft^3/s) for each creek. The model run progressed in an unsteady manner, where the inflows at St. Vrain and Boulder Creek were ramped to the estimated values and the computational domain was allowed to flood as if a flooding event was taking place. Similarly, the many ponds present in the computational domain (clearly visible in Figure 3) were started from a dry state and allowed to fill during the ramping of the hydrograph. Once the hydrograph attained the desired high inflow discharges, the run was sustained until steady state conditions were reached. This process does not represent the rate of flooding accurately, because the inflow hydrographs used do not represent the actual flooding event well, but it allows for the model to compute the actual flood extents without the need for any preconceived ideas about what the flood stages should be. In this study, the combination of values that provided the best agreement consisted of a discharge of 600 m^3/s (~21,000 ft^3/s) for St. Vrain Creek and a discharge of 250 m^3/s (~9,000 ft^3/s) for Boulder Creek, resulting in an estimated 850 m^3/s (~30,000 ft^3/s) passing through USGS Gaging Station 06730525 at HWY 119. The final results comparing model simulation and known flood delineation contours are shown in Figure 4.

Naturally, the predicted values of the previous paragraph are dependent on the accuracy of the data used: (1) the DTM data used by the model were sourced from USGS NED with a RMSE of 0.05–0.2 m in elevation (0.154–0.656 ft), and was 5 ½ years old at the time the flooding occurred; and (2) the flood delineation contours are subject to uncertainties in areas of visual complexity and the source images must be obtained at peak flow, which may be an unknown by itself. Finally, the comparison between model predictions and field measurements was done by visual inspection, which introduces undesired operator ambiguity and underlines the need for the development of mathematical criteria that produce objective goodness-of-fit measures and that can be implemented in an automated computational procedure.

The computational approach described above is very demanding in computer resources, because of the number of triangles in the spatial discretization and because of the small time step used (Δt = 0.01 s in equation (6)), which required many time steps for full flooding to occur. Additionally, many computer runs of the same case, albeit with different boundary conditions, had to be carried out, prolonging even further the time needed to reach the final solution. Therefore, this application of SToRM constitutes the ideal problem for testing and applying the numerical optimization techniques described in the previous sections.

To evaluate the efficiency of the parallel algorithms in SToRM, multiple runs of the same case—i.e., of the flooding simulation set-up described in the previous paragraphs—were carried out, first without parallelism to set the base run time T_1, then with multiple threads to determine the code speedup performance, T_1/T_N (where T_N is the run time taken when using N threads). The timing function provided by OpenMP, `OMP_get_wtime()`, was used to determine the value of T_N, but only the parallel regions of the code were timed. T_1 was determined by using only one thread (`OMP_set_num_threads(1)` in OpenMP syntax). The results of using a varied number of threads are shown in Figure 5 (default scheduling, the line with square markers). A run using a single thread took approximately 21 hours of CPU time in the desktop system described in a previous section.

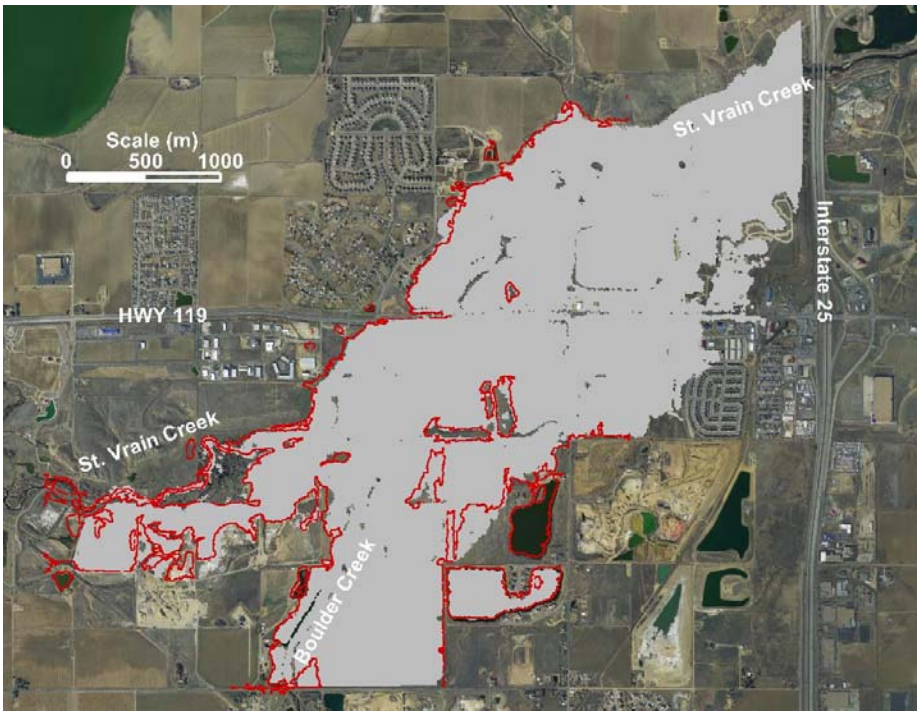

Figure 4 Comparison between observed flood delineation (red line) and predicted flooded area (gray area) on the same background image of Figure 3. Note that the observed flood delineation contour does not extend all the way to the eastern part of the computational domain due to the absence of data.

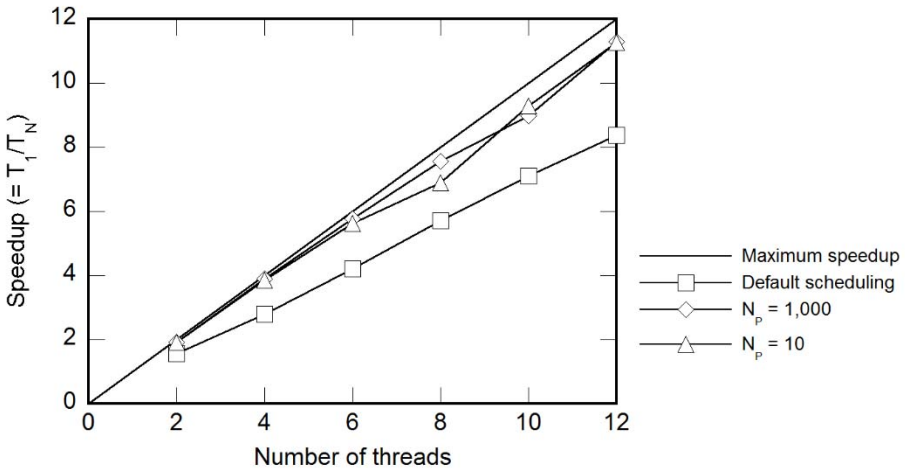

Figure 5 Speedup gain by SToRM's parallel implementation.

The initial results were satisfactory and possessed good scalability[4], but showed a somewhat lower than expected speedup, as seen in the "Default scheduling" data of Figure 5. Scheduling sets the way the iterations of a DO-loop are distributed among the several threads. OpenMP's default scheduling divides each DO-loop in N equal blocks (N = number of threads), each block with an identical number of DO-loop iterations, and assigns one to each thread. During the initial stages of flooding, however, there are many regions of the computational grid that are dry. These regions are included in all the computational DO-loops of the code, but are cycled over without using CPU time because the

[4] Scalability refers to the ability of a parallel system to increase performance when extra processors are added to it.

governing equations are not solved in dry areas. By distributing the cycles of the DO-loops equally among threads, there are some threads that may have very little to do (those with many dry areas), while others have to do much more work because they end up with larger portions of the wetted domain. As a result, the former threads finish their calculations first and must remain idle while waiting for the occupied threads to finish their computations. All the threads must finish their work before the flow of operations is able to proceed along the remainder of the code to the next DO-loop. This idle thread time may result in performance degradation, which may be minimal if the computational region is mostly wet, but that may be substantial when large dry areas exist. This is the reason for the less-than-ideal performance gain observed for the default scheduling in Figure 5.

To overcome the above limitations, a more dynamic type of scheduling scheme was tried, where work may be distributed unevenly among threads to minimize the idle thread time. This is accomplished by dividing the DO-loop iterations into blocks of smaller size, each containing N_P iterations: a DO-loop with 1,000 iterations, for example, would be divided into 5 smaller blocks with 200 iterations each if $N_p = 200$; the same DO-loop would be divided into 100 blocks of 10 iterations each if $N_P = 10$. The blocks are continuously fed to the threads, one block at a time. When a thread finishes its piece of work it gets a new block. This means that, if a thread gets a block of the DO-loop with an unusually high number of dry cells and finishes its work very quickly, it is immediately fed another block of work without having to wait for other threads to complete theirs. This dynamic type of scheduling, hopefully, balances the work out more evenly among the available threads, but comes with a limiting factor: the cost of larger overhead at runtime. This overhead is the added computational time taken by the system. It results from the additional work that must be done to divide the DO-loops and continuously assign the blocks to the processors: more blocks are more onerous to manage than fewer blocks and, consequently, this superior management effort consumes more computational resources. If the blocks are very small, increasing the size of the blocks (i.e., larger N_P) might, therefore, benefit overall code speedup by reducing overhead, but can also cause imbalance if one is not careful—the exact same imbalance that one is trying to avoid by using dynamic scheduling.

Scheduling is problem dependent and is a function of the workload. Workload may vary differently for each case and even for different simulations of the same case. Several block sizes were tried and, for the simulations carried out for the present study, a good value of N_P was found to be N_P =1,000. The results of the speedup obtained with N_P = 1,000 and with N_P = 10 are shown in Figure 5. It can be seen that using dynamic scheduling resulted in a substantial performance gain over the initial results using the default (static) scheduling. Using N_P = 10 did not provide significant differences in speedup gain over using N_P = 1,000. Taking into account that the present run was carried out in a computational grid with 57,055 points and 170,194 edges[5] (recall that SToRM uses an edge-based data structure, therefore many of the most computationally intensive DO-loops are carried over the edges), a rule of thumb for this size problems in desktop computers may be to use a value of N_P that is three orders of magnitude smaller than the number of edges in the computational grid.

CONCLUSION

A depth-averaged, two-dimensional model (SToRM) that solves the SWEs in unstructured triangular grids within the framework of the Godunov-type, cell-centered finite volume method, was briefly presented. The model was developed with the purpose of calculating unsteady flow over complex topography with wetting and drying moving fronts, such as those occurring in catastrophic flooding, and was applied to the estimation of the peak flow discharge passing at the USGS Gaging Station 06725450, near the city of Longmont, northwest of Denver, CO, during the historic flood event of September 2013.

Application of SToRM to problems that extend over large geographic areas, resulting in increasing memory and computational requirements, have created a need for an improvement in code efficiency. This was addressed by using OpenMP to parallelize some of the most computationally-intensive segments of the original code. These initial efforts have resulted in achieving substantial performance gains over the original implementation of SToRM, which was based on sequential algorithms written in Fortran 90/95.

[5] The number of edges in an unstructured grid can be found by using a modification of Euler's formula: $n_T + 1 = n_E - n_V + 2$, where n_T is the number of triangles, n_E is the number of edges, and n_V is the number of vertices (points) in the grid.

The dynamic nature of flooding problems helped identifying bottlenecks in speedup performance gains of parallel algorithms due to the potential presence of large dry regions in the computational domain. These dry areas may become inundated and dry again during the course of a simulation and cannot be ignored, posing a challenge to the computational load balancing and to the optimal use of any multiprocessing computing environment. This difficulty was addressed in SToRM and solved efficiently with the use of dynamic scheduling. A scheduling parameter N_P was proposed, with a suggested value in the order of one thousandth of the number of edges of the computational grid used in the computer simulation runs. This value is, however, problem dependent and user care must be used when selecting it.

Estimation of the peak discharge for the St. Vrain gaging site was accomplished by comparing the computed flood delineation contours with those obtained from remote sensed images. It was found that a close match was obtained when using a discharge of 600 m^3/s (~21,000 ft^3/s) for St. Vrain Creek and of 250 m^3/s (~9,000 ft^3/s) for Boulder Creek.

Disclaimer: any use of trade, product, or firm names in this document is for descriptive purposes only and does not imply endorsement by the U.S. Geological Survey or by the U.S. Government.

REFERENCES

Alcrudo, F., Garcia-Navarro, P. (1993). "A high-resolution Godunov-type scheme in finite volumes in 2D shallow water equations," Int. J. Num. Meth. Fluids, Vol. 16, pp 489-505.

Anastasiou, K., Chan, C.T. (1997). "Solution of the 2D shallow water equations using the finite volume method on unstructured triangular meshes," Int. J. Num. Meth. Fluids, Vol. 24, pp 1225-1245.

Brufau, P., Vázquez-Cendón, M.E., Garcia-Navarro, P. (2002). "A numerical model for the flooding and drying of irregular domains," Int. J. Num. Meth. Fluids, Vol. 39, pp 247-275.

CH2M HILL (2014). Boulder Creek Hydrologic Analysis, Final Report. Prepared for the Colorado Department of Transportation by CH2M HILL, 9191 S. Jamaica Street, Englewood, CO 80112, August 2014.

Chaudhry, M.H. (1993). Open-Channel Flow. Prentice Hall, Englewood Cliffs, New Jersey.

Gottlieb, S., Shu, C.-W., Tadmor, E. (2001). "Strong stability-preserving high-order time discretization methods," SIAM Review, Vol. 43, No. 1, pp 89-112.

Hagen, T., Hjelmervik, J., Lie, K.-A., Natvig, J., and Henriksen, M. (2005). "Visual simulation of shallow water waves," Simulation Modelling Practice and Theory, Vol. 13, No. 8, pp 716-726.

IPCC (2014). Climate Change 2014: Impacts, Adaptation, and Vulnerability. Intergovernmental Panel on Climate Change, http://www.ipcc.ch/report/ar5/wg2/. (Last accessed January 2015.)

JACOBS (2014). Hydrologic Evaluation of the St. Vrain Watershed, Post September 2013 Flood Event. Report prepared for the Colorado Department of Transportation by JACOBS, 707 17th Street, Suite 2400, Denver, CO 80202, August 2014.

Novey, M. (2013). "CDOT assessing 'millions and millions' in road, bridge damage," The Coloradoan, September 15, 2013.

Roe, P.L. (1981). "Approximate Riemann solvers, parameter vectors, and difference schemes," J. Comput. Phys., Vol. 43, pp 357-372.

Rusanov, V.V. (1961). "Calculation of intersection of non-steady shock waves with obstacles," J. Comput. Math. Phys. USSR, Vol. 1, pp 267-279.

Sanders, B., Schubert, J., and Detwiler, R. (2010). "ParBreZo: a parallel, unstructured grid, Godunov-type, shallow water code for high-resolution flood inundation modeling at the regional scale," Adv. Water Res., Vol. 33, pp 1456-1467.

Shewchuk, J.R. (2002). "Delaunay refinement algorithms for triangular mesh generation," Computational Geometry: Theory and Applications, Vol. 22, No. 1-3, pp 21-74.

Simões, F.J.M. (2011). "Finite volume model for two-dimensional shallow environmental flow," J. Hydr. Eng., ASCE, Vol. 137, No. 2, pp. 173-182.

Toro, E.F., and Garcia-Navarro, P. (2007). "Godunov-type methods for free-surface shallow flows: A review," J. of Hydr. Research, Vol. 45, No. 6, pp. 736-751.

Vázquez-Cendón, E., Hidalgo, A., Garcia-Navarro, P., and Cea, L. (2013). Numerical Methods for Hyperbolic Equations, CRC Press, Taylor & Francis Group, London, UK.

Venkatakrishnan, V. (1995). "Convergence to steady state solutions of the Euler equations on unstructured grids with limiters," J. Comput. Phys., Vol. 118, pp 120-130.

HYDRAULIC MODELING OF TRUCKEE CANAL ALLUVIAL FANS USING SRH-2D

Rebecca Kallio, Hydraulic Engineer, US Bureau of Reclamation, Denver, CO, rkallio@usbr.gov, Joseph Wright, Hydraulic Engineer, US Bureau of Reclamation, Denver, CO, jmwright@usbr.gov, Victoria Sankovich-Bhals, Meteorologist, US Bureau of Reclamation, vsankovich@usbr.gov

Abstract: Alluvial fans are gently sloping, fan-shaped landforms created over time by the deposition of sediment. Their gentle slope near mountainous regions attracts development in these flood-prone areas. The flow paths of flood events can change with each event, placing development at risk (National Research Council (NRC), 1996). Because of the uncertainty of flow paths and flood extent, many studies have been performed on alluvial fans in the arid west. Most of these studies focus on the flood elevations inside the alluvial fan and mitigation against such events. This study, however, is not focused on the flood elevations inside the alluvial fan; rather it is focused on the effect the alluvial fan has on the flood wave passing through and into a canal.

The Truckee Canal is located in western Nevada, approximately 35 miles east of Reno, Nevada, and adjacent to the City of Fernley. The areas adjacent to the canal are seven alluvial fans emanating from foothills to the west and southwest. The alluvial fans have complex networks of distributary channels that are constantly changing with each flood event as new sediment gets deposited. Infiltration and channel form within alluvial fans drastically varies longitudinally and laterally. These characteristics make flow modeling complex and requires two-dimensional flow modeling.

A two-dimensional hydraulic model SRH-2D (Lai Y., 2008) was used to model the 10-, 25-, 50-, and 100-year unsteady flow through the seven alluvial fans in the Truckee canal basin. SHR-2D has an unstructured hybrid mixed element mesh, which is based on the arbitrarily shared element method for geometric representation (Lai Y. , 2000). Mesh generation flexibility allows complex alluvial network of incised channels to be modeled in greater detail. SRH-2D applies gridded infiltration to model the losses within the alluvial fans. SRH-2D adopts very robust and stable numerical schemes with a seamless wetting-drying algorithm. Finally, SRH-2D uses a finite volume approach where mass balance accounting was performed to determine the validity of model results.

The model results indicated that basins with spares developed attenuate peak discharge and volume; however, the net effect of flow attenuation is lower than expected for developed alluvial fans. Development within the alluvial fans, however seemingly small, can affect the flow attenuation. The historic channels have been either preserved as they pass through developments, or new channels have been formed by road cuts. The result of this development has concentrated the flows so that the flood hydrograph passes through the alluvial fan before it has time to infiltrate into the soils.

INTRODUCTION

A team evaluating the flooding risk of the Truckee canal wanted to determine the hydrologic loadings for the 10-, 25-, 50-, and 100-year events. The loadings were achieved by coupling a one-dimensional rainfall-runoff modeled with a two-dimensional hydraulic model to simulate lateral inflow along the Truckee canal. A two dimensional hydraulic model was necessary to capture the flow dynamics of alluvial fans that have complex channel geometries and varying infiltration.

Project Location and Basin Description: The Truckee Canal is located in western Nevada, approximately 35 miles east of Reno, Nevada, and adjacent to the City of Fernley (Figure 1). The areas adjacent to the canal are seven alluvial fans emanating from foothills to the west and southwest. The alluvial fans have complex networks of distributary channels that are constantly changing with each flood event as new sediment gets deposited. Infiltration and channel form within alluvial fans drastically varies longitudinally and laterally. These characteristics make flow modeling complex and requires 2-D flow modeling.

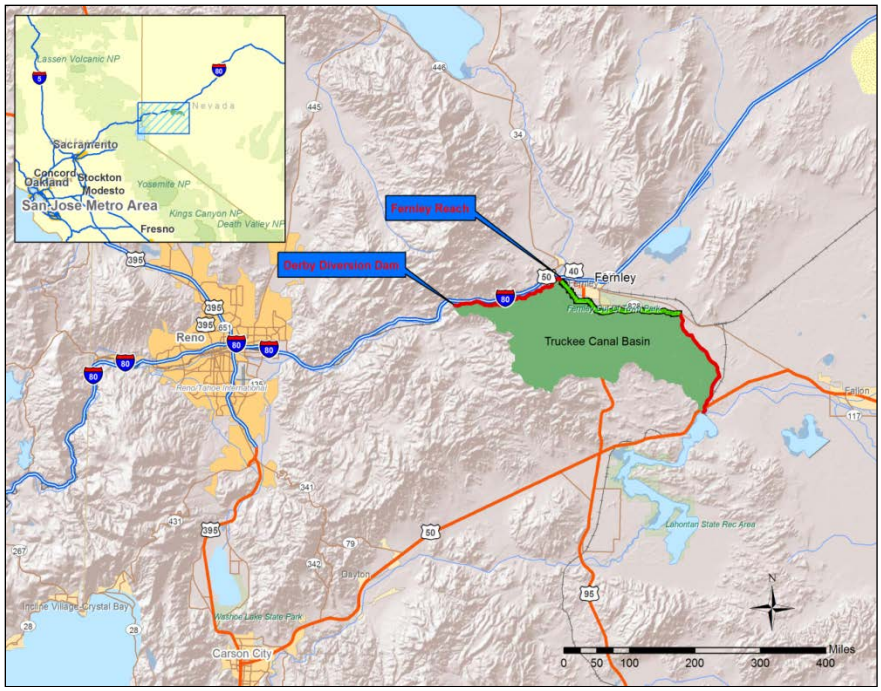

Figure 1 Vicinity map showing the location of the Truckee Canal drainage basin.

The basin area contributing to the Truckee Canal is mostly foothills draining from the south to the north. The Fernley area receives 5.91 inches of annual precipitation. Only the areas to the south of the canal contribute to the flood flows. The overall contributing area along the Truckee canal is approximately 100 mi^2. The alluvial fans are adjacent to the canal emanating from foothills to the west and southwest. The alluvial fans have complex network of distributary channels who's flow paths are in constant flux from sediment deposition. Alluvial fans have mid slopes around 0.016 ft/ft. Small washes inset into Holocene alluvial fans ranging from early to late Holocene in area. A broad distributary network of small incised channels can be found in the alluvial fan consisting of younger Holocene deposits. Alluvial fan channel beds at higher elevations contain predominately gravels and fine moving towards the fan mouth.

Model Selection: The one-dimensional hydrologic model HEC-1, Hydrological Engineering Center 1 (HEC-1) (U.S. Army Corps of Engineers, 1990) was used to model the tributary basins that provide the inflow hydrographs into the alluvial fans. HEC-1 simulates basin surface response to precipitation through a series of interconnect hydrologic and hydraulic components. USACE has superseded HEC-1 with Hydrologic Modeling System (HMS); however, this study chose HEC-1 because of the ability to automate the model and process multiple model runs. Additionally, the HEC-1 model can easily transform Reclamation dimensionless unit hydrographs (Cudworth, 1989). The Reclamation unit hydrograph converts dimensionless hydrographs into a unit hydrograph by three steps. First the basin area is calculated and the lag time is determined. Second, incremental rainfall is converted into incremental runoff while incorporating for losses due to soil infiltration. Third, incremental runoff is transformed into a flood hydrograph. The HEC-1 model simplifies the basin's response to rainfall by lumping parameters. HEC-1 model accurately captures the rainfall response for well-defined basins with incised channels such as those found in the Truckee Canal drainage basin.

The two-dimensional hydraulic model Sediment and River Hydraulics- 2D (SRH-2D) was selected to model the hydraulics within the alluvial fan. SRH2D is a two-dimensional (2D) fixed-bed depth averaged hydraulic model specifically focused on the flow hydraulics of river systems. SRH-2D adopts a zonal approach for coupled modeling of channels and floodplains; a river system is broken down into modeling zones (delineated based on natural features such as topography, vegetation, and bed roughness), each with unique parameters such as flow resistance. One of the major features of SRH-2D is the adoption of an unstructured hybrid mixed element mesh, which is based on the arbitrarily shared element method of Lai (Lai, 2000) for geometric representation. This meshing strategy is flexible enough to facilitate the implementation of the zonal modeling concept; it allows for greater modeling detail in areas of interest, and ultimately leads to increased modeling efficiency through a compromise between solution

accuracy and computing demand. The SRH-2D model is a Reclamation-developed model. The flexibility of the mesh generation allowed the complex alluvial network of incised channels to be modeled in greater detail. Because SRH-2D was developed at Reclamation, custom modifications were easily made to the source code to allow for losses in the alluvial fans.

DATA COLLECTION

Meteorology and Precipitation:

Precipitation Frequency Analysis: Precipitation magnitudes with an associated frequency of occurrence are used as input into the rainfall-runoff model to estimate flood frequency. To compute the precipitation frequency curve for the Truckee Canal watershed, the L-moments regional statistical analysis method was used (Hosking & Wallis, 1997). In regional analyses, it is assumed that additional information in space can account for lack of information in time. In other words, precipitation regional analyses allow for the user to substitute rain gauge observations from within a statistically (and climatically) homogeneous region for precipitation observations at a specific site (i.e., a rain gauge along the Truckee Canal). From this substitution, the user will obtain hundreds to thousands of observations as opposed to the approximate hundred observations (at best) available at-site.

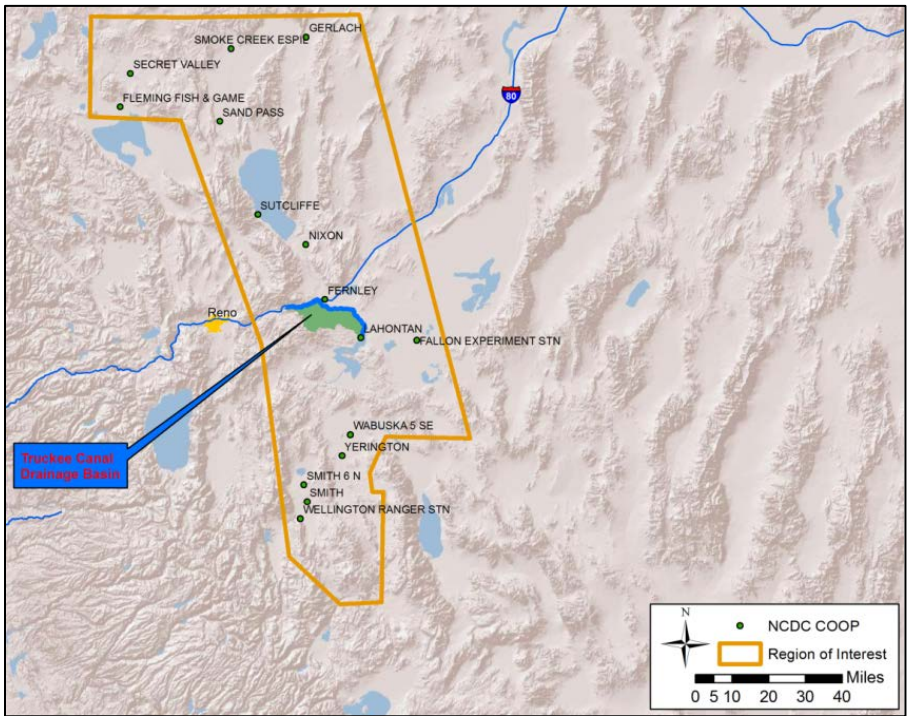

Figure 2 Fifteen NCDC COOP rain gauges with in the Truckee Canal drainage.

Climatically and Statistically Homogeneous Region: 15 NCDC COOP gauges were deemed climatically and statistically homogeneous and were used in the precipitation frequency analysis (Figure 2). These observations amounted to approximately 547 years of station data. The 24-hour annual maxima precipitation observations exhibit low variability of the L-moment ratios (i.e. L-Cv, L-skewness, and L-kurtosis; Table 1). Heterogeneity measures H1 and H2 were computed to assess the variability of station values of L-Cv and L-skewness, respectively. Measures of H1 and H2 (H1=-2.61 and H2=-0.97) confirmed that the chosen region was acceptably homogeneous.

Regional Growth Curve: For the Truckee Canal watershed, the Generalized Logistic (GLO) distribution, a unique form of the Kappa distribution, best describes the regional distribution of the 24-hour annual maxima precipitation dataset. The GLO distribution most closely represents the spread within the cloud of L-skewness and L-kurtosis pairs for the 15 gauges. The regional L-skewness and L-kurtosis estimates further suggest that the GLO distribution is the best-fit three-parameter probability distribution based on L-moment goodness-of-fit tests.

Table 1 L-moments for the 15 gauges in the homogeneous region, where L1 is the location (mean) and t3 is the skewness.

Location	ST	COOP	L1	L-Cv	t3
FLEMING FISH & GAME	CA	043087	1.08	0.1898	0.4341
SECRET VALLEY	CA	048074	0.97	0.2349	0.1384
FALLON EXPERIMENT STN	NV	262780	0.68	0.2137	0.1512
FERNLEY	NV	262840	0.90	0.2025	0.1755
GERLACH	NV	263090	0.86	0.2130	0.3258
LAHONTAN	NV	264349	0.73	0.2293	0.1871
NIXON	NV	265605	0.88	0.2118	0.1679
SAND PASS	NV	267261	0.97	0.2081	0.1832
SMITH	NV	267609	0.93	0.2392	0.2138
SMITH 6 N	NV	267612	0.86	0.2245	0.2199
SMOKE CREEK ESPIL	NV	267618	0.89	0.2544	0.2308
SUTCLIFFE	NV	267953	0.96	0.2350	0.4119
WABUSKA 5 SE	NV	268822	0.72	0.2323	0.1292
WELLINGTON RANGER STN	NV	268977	1.24	0.2259	0.3233
YERLINGTON	NV	269229	0.81	0.2375	0.2167

At-Site Precipitation-Frequency Relationship: The regional growth curve is next scaled by the mean of the 24-hour basin-average point (10 mi^2) precipitation (hereafter, referred to as the basin-average mean) to obtain a 24-hour basin-average point precipitation-frequency curve. This curve is representative of point precipitation with a common annual exceedance probability occurring throughout the watershed. The 24-hour basin-average mean for the contributing area of the Truckee Canal watershed is 0.96 inches.

The following equation is used to scale the regional growth curve by the basin-average mean to produce a site-specific precipitation-frequency relationship (Hosking and Wallis, 1997):

$$Q_i(F) = \hat{\mu}_i q(F) \quad (1)$$

Where Q_i is the at-site precipitation-frequency relationship, $\hat{\mu}_i$ is the at-site mean, and q(F) is the regional growth curve.

24-hour Basin-Average Precipitation Frequency: A fixed areal reduction factor (ARF) is applied throughout the frequency range to the 24-hour basin-average 10 mi^2 precipitation frequency relationship to obtain the basin-average precipitation frequency curve. Fixed ARFs were derived in NOAA Atlas 2 for Nevada for multiple area sizes and durations (Miller, Frederick, & Tracey, 1973). For the area size of the contributing portion of the Truckee Canal watershed (approximately 100 mi^2) at 24-hours, the scaling factor is 93.5%. Table 2 presents the precipitation estimates corresponding to these basin-average frequency curves at select return periods.

Table 2 Basin-average precipitation frequency estimates at select return periods.

1/AEP	All Season 24-hr Basin Average Precipitation (in)
5	1.281
10	1.536
25	1.913
50	2.245
100	2.628

Terrain: Watershed Sciences, Inc. (WS) collected Light Detection and Ranging (LiDAR) data for the alluvial areas on March 9, 2012. The data were combined with previously acquired LiDAR data in 2008 to ensure complete capture of the alluvial basins. The resulting Digital Terrain Model (DTM) achieved a resolution of 0.72 points per ft^2 with a vertical accuracy of 0.08 feet (Woolpert, Inc., 2012).

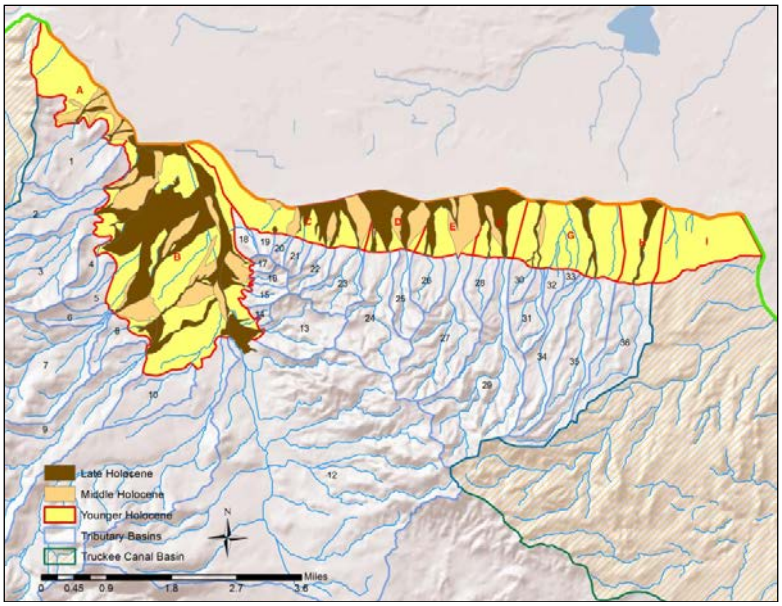

Figure 3 Geology of alluvial fans within the Truckee Canal drainage basin

Alluvial Fan Geology: The bedrock and surficial geology for the Truckee Canal drainage basin has been mapped at a 1:24,000 scale (Faulds & Ramelli, 2009; Faulds, J. E.; Ramelli, A. R.; Herny, C. D., 2008; Faulds, J. E.; Ramelli, A. R., 2005). The alluvial fan basins are comprised of three materials: Lake Lahontan deposits (younger Holocene), middle Holocene alluvial deposits, and old Holocene deposits. The Lake Lahontan deposits consist of gravel beach deposits, gravel deposits, silt deposits, tufa deposits, and silicified sands. In some locations the alluvial deposits may overlay the Lake Lahontan deposits. Locations of these deposits are shown in Figure 3. Because the alluvial deposits are the youngest material on the basin, it was assumed that these represent the locations of flow paths within the basins. When comparing the LiDAR data with the geologic map, the location of alluvial deposits were the same as locations of incised channels. The incised channel locations were also confirmed with a site visit. The channel areas of each sub-basin correlated to the alluvial deposits, and the out-of-bank floodplain areas correlated to Lake Lahontan deposits.

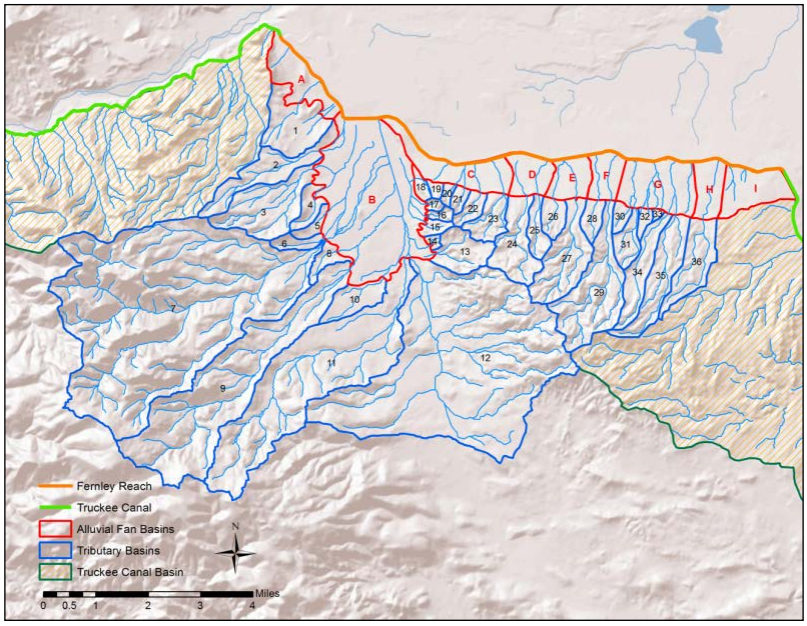

Figure 4 Tributary basins in the Truckee Canal drainage basin.

HEC-1 MODEL INPUTS

Sub-basin Delineation and Characteristics: The individual basins for the apexes of the alluvial fans along the Fernley Reach were determined initially using the national hydrology database (USGS, 2012) and further refined using 30m USGS DEM data (USGS, 2012). This method identified 36 tributary basins and is presented in Figure 3. The lag time was estimated for each sub-basin using methods outlined by the Reclamation Flood Hydrology Manual (Cudworth, 1989) and was calculated using the following equation.

$$Lag\ Time\ = C_t \left(\frac{L \times L_{ca}}{\sqrt{S}}\right)^{0.33} \quad (2)$$

Where L is the watercourse length (feet); L_{ca} is the length along the watercourse to a point opposite of the centroid of the basin (feet); S is the basin slope (feet per mile); and C_t is a constant. The length and slope parameters were estimated using ArcGIS (Environmental Systems Research Insitute (ESRI), 2011)). The value used for the constant, C_t, value of 2.6, corresponding to a Manning's roughness of about 0.1 (Chow, 1959).

Tributary Basin Loss Rates: The computation of loss rates requires consideration of many factors such as historic data, soils information, vegetation, and season. Near the end of a big storm, after the depressions have been filled and the soils within the watershed have been saturated, the difference between rainfall and runoff closely represents the minimum infiltration rate. For this study, the initial loss was assumed to be 0.5 in.

Hydrologic soil groups for each tributary basin were identified from NRCS county-level SSURGO database (Soil Survey Staff, Natural Resources Conservation Service). National Engineering Handbook Part 630 Chapter 7 (NEH) (Natural Resources Concervation Service, 2007) provides range of loss rates for each hydrologic soil group. Table 2 provides the NEH recommend soil loss rates and provides the loss rates selected in this study. The majority of tributary basins were comprised of more than one soil group type; therefore, losses rate of basins were calculated through area weighted method.

Table 3 Estimated soil loss rates for each hydrologic soil group.

Hydrologic Soil Group	Loss Rate (in/hr)		
	Low	High	Used in study
A	0.39	0.3	0.45
B	0.24	0.15	0.3
C	0.11	0.05	0.15
D	0.05	0.00	0.05

The majority of soils in the tributary basins in the Fernley reach are T*ype C* (moderately high potential runoff when thoroughly wet) and *Type D* (high runoff potential when thoroughly wet). Areas of *Type B* (moderately low runoff potential when thoroughly wet) can be found along some of the incised channel areas in basins 7 through 12 and more so in basins 18 through 33. Basins 1 through 6 are reported by NRCS to have exclusively *Type A* (low runoff potential when thoroughly wet), which appears to be a mistake in the NRCS soils reporting. The southern boundary for the *Type A* soils appears to follow a political boundary. Furthermore, the state-level NRCS STATSGO database notes this area as being generally *Type D* (NRCS, 2012).

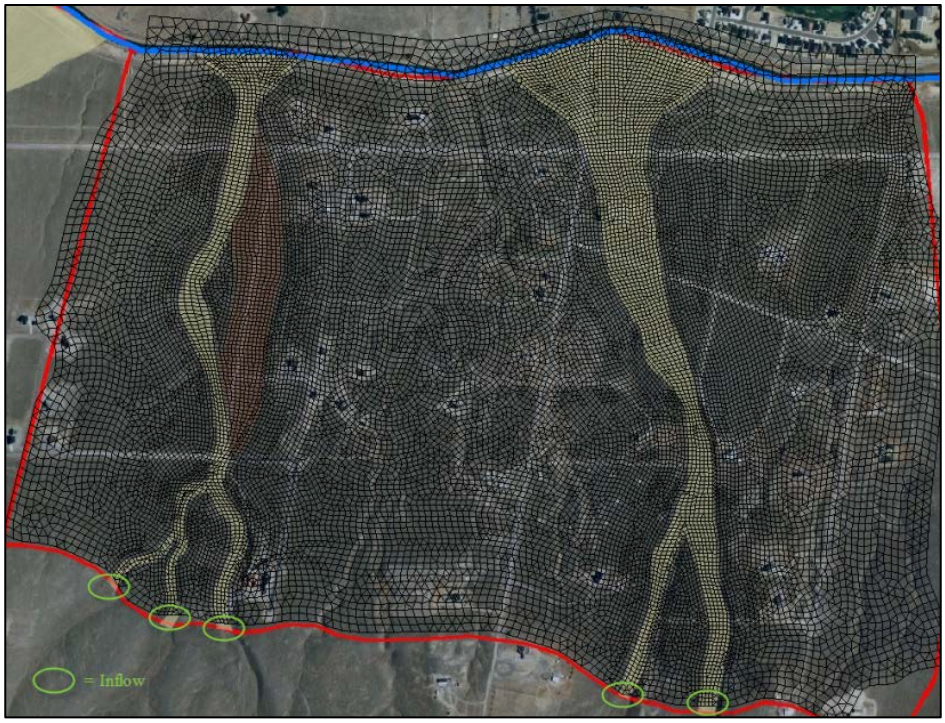

Figure 5 A typical mesh used for the alluvial fan basins. Quadrilaterals were used for younger alluvial channel materials whereas triangles were used from the older area. Alluvial fan basin G is depicted.

SRH-2D MODEL

Each alluvial fan sub-basin was modeled independently of one another. This occurred since terrain data was so robust and demanded large computational resources.

Mesh: Meshes were developed for each alluvial fan sub-basin using Surface Water Modeling Solution (SMS) version 10.1 (Aquaveo, Inc., 2012). The geologic map was imported into SMS to differentiate between in channel locations and out of channel locations. These boundaries were traced to form feature objects. For each feature object, the geologic material type was entered. For each identified identify a Manning's n roughness coefficient. The alluvial channel had no vegetation, so a manning's n of 0.045 was used. Outside of the channel areas were highly vegetated with greasewood and sagebrush; therefore, a Manning's n of 0.1 was used (Chow, 1959). The mesh types where selected for each feature object. The alluvial channels were assigned a quadrilateral mesh type, and the Lake Lahontan deposits were assigned a triangular mesh type. Quadrilateral meshes are used when flow is oriented in a general direction like river channels. Figure 5 illustrates a typical mesh used for this study. Table 4 summarizes the SRH-2D meshes used for alluvial fan basins B through H.

Table 4 SRH2D Alluvial fan mesh summary.

Alluvial Fan Basin	Number of quadrilateral elements	Area (ft^2)		Number of triangular elements	Area (ft^2)	
		Low	High		Low	High
B	19254	1089	24881	6580	613	8373
C	46645	290	19072	9114	110	5155
D	12791	560	1903	2374	191	5334
E	38783	139	263	9942	19	12547
F	16282	1044	2502	5508	137	1253
G	17195	905	8810	7541	1097	2864
H	7932	527	708	3235	237	60406

Infiltration: SRH-2D was modified for this study to account for soil losses in the alluvial areas. SRH2D subtracts a given water depth at the end of each time step using a constant loss rate. The majority of alluvial basins contain

hydrologic soil group *Type B* which has a loss rate between 0.15- to 0.45 in/hr. A loss rate of 0.27 in/hr was applied throughout the alluvial areas. A limitation of the SRH2D model is its inability to model rainfall. This means that rain fall over top of the alluvial fans could not be numerically modeled. The majority of contributing flow into the Truckee Canal Fernley Reach comes from the tributary basins; therefore, rainfall occurring over the alluvial areas was not considered to significantly affect the flood inflows. However, it was assumed that all rainfall would be absorbed in the initial losses which would account for the rainfall on the alluvial fans.

Hydrographs: Hydrographs developed from the HEC-1 model were used as inflow into the SRH2D models apex of the alluvial fans. The unsteady inflow condition was placed at the apex of each alluvial fan.

Boundary Conditions: There were no measurements of flow at the outlet of the alluvial fans to develop a rating curve for the boundary conditions. Therefore critical exits were selected as the downstream boundary conditions for the 7 alluvial fan models. This allowed the simulation of the flow across the alluvial fan with unknown water depth conditions on the downstream end. This was accomplished by artificially creating a 2:1 sloped edge along the downstream boundary. To prevent the effect of model instabilities that occur near critical flow boundaries, the boundary was placed approximately 400 ft from the canal bank.

RESULTS

HEC-1 Results: The peak discharge results of the 1-dimensional modeling for the 36 tributary basins along the Fernley Reach are presented in Table 4. The runoff response remains low for events ranging to the 100-yr events for these basins. Because of the low runoff, these basins were omitted in the 2-dimensional model due to their likelihood to create numerical instabilities from low water depths. Tributary basins 7, 9, 11 and 12 are the largest contributors along the Fernley Reach, accounting for about 50 percent of the volume for the extreme events. Alluvial fan basin I does not respond to the 100-yr or more common rainfall events because the loss rate (0.27 in/hr) is greater than the largest 100-yr incremental rainfall amount modeled for this study.

Table 5 Summary of 24-hour peak discharges from the tributary basins along the Truckee Canal Basin, Fernley Reach.

Tributary Basin	Area (mi^2)	24hr Peak Discharge (ft^3/s)			
		10-yr	25-yr	50-yr	100-yr
1	1.15	29	51	70	92
2	1.09	23	42	59	79
3	1.49	32	57	80	107
4	0.32	9	15	20	27
5	0.18	5	8	11	15
6	0.23	3	8	11	16
7	12.62	143	308	473	666
8	0.25	10	15	19	24
9	5.05	0	40	95	167
10	0.57	5	14	23	33
11	5.55	85	163	237	323
12	10.67	181	339	488	661
13	0.72	32	46	59	73
14	0.07	3	5	6	7
15	0.16	8	11	13	16
16	0.10	5	7	9	11
17	0.07	4	5	6	8
18	0.14	0	0	0	2
19	0.08	0	0	0	0
20	0.09	0	0	0	0
21	0.14	0	0	0	1
22	0.25	0	4	8	13
23	0.50	2	10	18	28
24	1.00	12	28	44	62
25	0.34	3	9	14	21
26	0.32	0	0	0	2
27	1.28	27	49	69	93
28	0.27	0	0	1	6
29	1.89	53	84	112	145
30	0.16	0	0	0	0
31	0.38	9	16	23	30
32	0.12	0	0	0	0
33	0.04	0	0	0	0
34	0.77	24	37	50	64
35	1.13	40	60	78	98
36	0.92	35	52	67	84
I	0.92	0	0	0	0

SRH-2D Results: Table 5, Table 6, Table 7, and Table 8 summarize the hydrograph peak discharges and volumes from the alluvial fans along the Fernley Reach for the 10-, 25-, 50-, and 100-yr return periods, respectively. A mass balance was computed for each model simulation. The percent error, summarized in Tables 5 through 8 was calculated by:

$$Percent\ Error = \frac{V_i - (V_o + V_{lost} + V_{surface})}{V_i} \times 100 \quad (3)$$

The overall error calculated by volume for SRH-2D was below 2 percent for all return periods. The percent error in the mass balance is one measure of the model error. The total percent mass balance error is the summation of the volume differences divided by the total inflow volume. All of the outflows listed in Tables 5 through 8 are lateral inflows along the Fernley Reach. Alluvial basin A (pour point 7) was not modeled because of the assumed 100-yr flood mitigation from the developed sub-division, which would result in no canal inflows. Alluvial basin I was not modeled in SRH-2D because it has no upstream contributing flows; therefore, it was modeled in HEC-1 similar to the tributary basins.

Table 6 10-year hydrologic event for alluvial fans long the Fernley reach.

Alluvial Basin	Peak Discharge (ft^3/s)		48-hr Volume (ac-ft)				Difference (V_{in}-(V_o+V_i+V_s))	Percent Error
	Inflow (Q_i)	Outflow (Q_o)	Inflow (V_{in})	Outflow (V_o)	Loss (V_i)	Surface (V_s)		
B	474	221	169	50	109	13	-3.66	-2.17%
C	3	N/A	N/A	N/A	N/A	N/A	N/A	N/A
D	15	9	3	1	2	0	0.24	7.96%
E	27	6	7	0.2	6.9	0.6	-0.61	-8.66%
F	53	25	19	5	12	1	1.68	8.69%
G	73	55	25	13	10	0	1.45	5.91%
H	35	20	12	4	7	1	1.07	8.99%
TOTAL			235				0.17	0.07%

Table 7 25-year hydrologic event for the alluvial fans long the Fernley reach

Alluvial Basin	Peak Discharge (ft^3/s)		60-hr Volume (ac-ft)				Difference (V_{in}-(V_{out}+V_i+V_s))	Percent Error
	Inflow (Q_i)	Outflow (Q_o)	Inflow (V_{in})	Outflow (V_{out})	Loss (V_i)	Surface (V_s)		
B	981	707	441	221	201	14	5.06	1.15%
C	14	6	3	1	2	0	-0.24	-9.60%
D	37	23	10	5	5	0	0.57	5.55%
E	49	19	18	12.6	12.6	6.0	-13.57	-76.87%
F	84	69	38	16	18	2	2.14	5.65%
G	113	94	49	30	15	0	3.76	7.72%
H	52	40	23	11	10	1	1.14	5.00%
Total			**581**				**-1.14**	**-0.20%**

Table 8 50-year hydrologic event for the alluvial fans long the Fernley reach.

Alluvial Basin	Peak Discharge (ft^3/s)		60-hr Volume (ac-ft)				Difference (V_{in}-(V_{out}+V_i+V_s))	Percent Error
	Inflow (Q_i)	Outflow (Q_o)	Inflow (V_{in})	Outflow (V_{out})	Loss (V_i)	Surface (V_s)		
B	1487	1191	778	476	278	16	8.00	1.03%
C	26	15	7	3	4	2	-2.10	-29.09%
D	58	38	21	11	8	1	1.08	5.24%
E	69	51	29	6.4	16.2	2.5	4.40	14.92%
F	113	86	59	31	24	2	2.73	4.60%
G	149	133	77	54	20	0	3.20	4.15%
H	67	54	36	19	13	1	2.38	6.62%
Total			**1008**				**19.68**	**1.95%**

Table 9 100-year hydrologic event for the alluvial fans long the Fernley reach.

Alluvial Basin	Peak Discharge (ft^3/s)		60-hr Volume (ac-ft)				Difference (V_{in}-(V_{out}+V_i+V_s))	Percent Error
	Inflow (Q_i)	Outflow (Q_o)	Inflow (V_{in})	Outflow (V_{out})	Loss (V_i)	Surface (V_s)		
B	2089	1790	1209	841	340	18	10.31	0.85%
C	41	24	14	7	7	5	-5.54	-39.68%
D	83	54	35	21	12	1	1.64	4.67%
E	93	73	44	17.3	18.4	3.9	4.62	10.45%
F	148	120	91	52	33	2	3.80	4.20%
G	191	172	117	86	27	0	3.42	2.93%
H	84	75	55	33	18	1	2.82	5.16%
Total			**1564**				**21.06**	**1.35%**

DISCUSSION

Alluvial fan flows can lose large amounts of water due to the flow spreading out and infiltrating into the ground over the mouth of the alluvial fan. This flow mechanism occurs in all of the alluvial fans to some extent; however, the net effect of flow attenuation is lower than expected for undeveloped alluvial fans. Development within the alluvial they pass through developments, or new channels have been formed by road cuts. The result of this development has concentrated the flows so that the flood hydrograph passes through the alluvial fan before it has time to infiltrate into the soils.

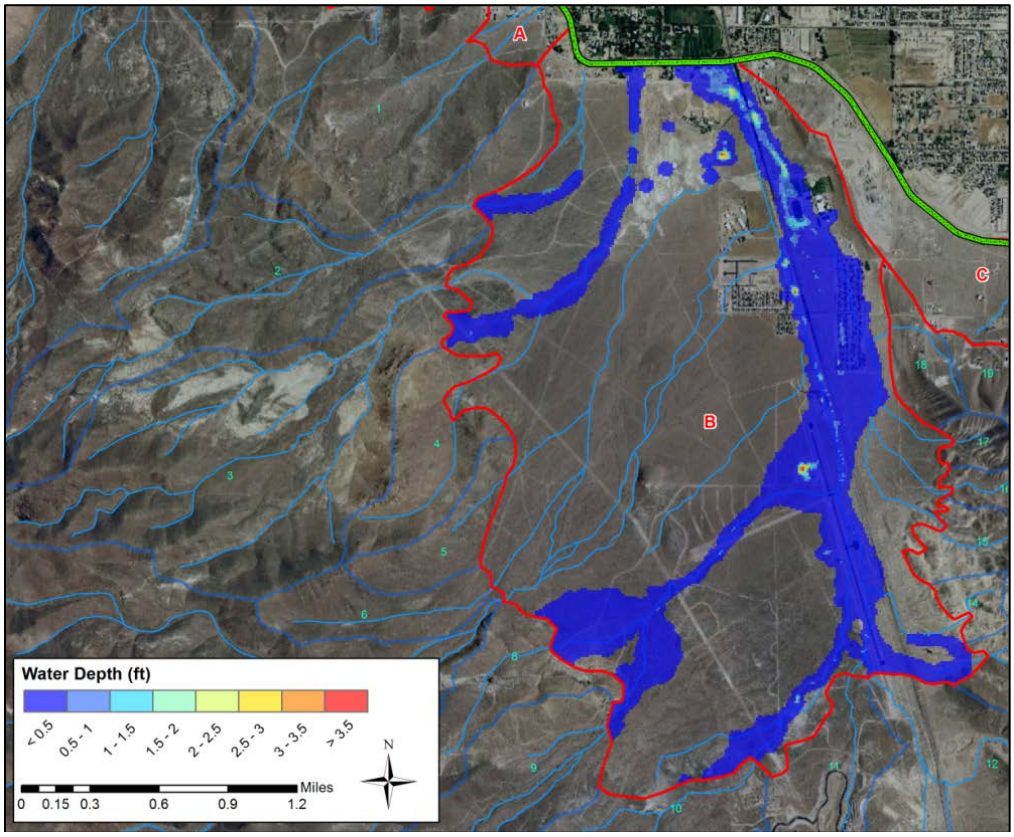

Figure 6 Alluvial basin B water depth got 100-year event at time t=10 hours.

Alluvial basin B is by far the largest flood contributor along the Fernley Reach and also the Truckee Canal. A total of 38.74 mi^2 contributes to 12 significant apexes identified along the apex boundary of alluvial basin B. Highway 95 bisects the basin from north to south providing a conduit for concentrated flow. This becomes apparent in viewing

the 100-yr event at hour 10, the peak of the water depths within the basin (Figure 6**.**). Aerial photographs of the basin also indicate dirt roads are within the historic incised channels to the west of Highway 95. Other development within the basin includes an airport and 2 subdivisions. Although seemingly insignificant in size, they contribute to the concentrated flows. These developments may provide an explanation why large floods have not been noticed in the past, because the recent developments have only recently increased the probability of larger magnitude floods into the Fernley Reach.

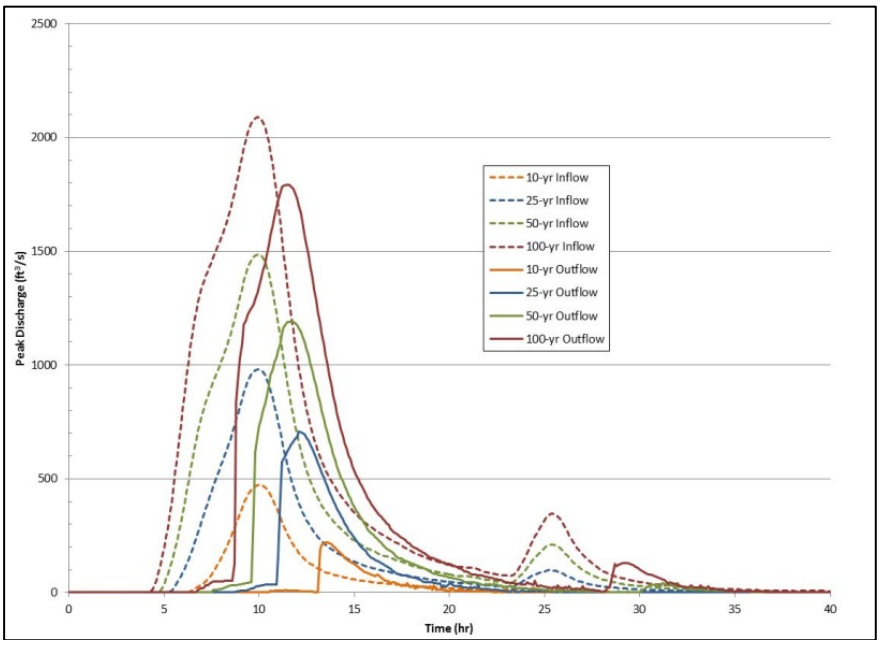

Figure 7 Flood Hydrographs attenuation for 10-, 25-, 50-, and 100-year events in alluvial basin B.

Despite the concentrated flow, a significant amount of the flood hydrograph is lost to water infiltrating into the soil. Figure 6 illustrates that some floods do not flow into the canal at all. Figure 7 illustrates the reduction of the peak inflow into alluvial basin B and the outflow into the right bank of the Fernley Reach. The peak discharge for alluvial basin B is reduced by 14% and 21% for the 100-yr and 50-yr flood events, respectively.

Alluvial basins C through H also show flood hydrograph attenuation, although not as much as expected in undeveloped alluvial channels. The more frequent events, however, did show an increasing amount of attenuation and losses. This is most likely due to less flow concentration within the alluvial fan area resulting in higher losses.

The ponded areas along the right bank in the Fernley Reach are representative of the ground topography in 2008. Material removed from the canal for cleaning since 2008 has changed the topography along the banks. The additional material would affect the amount of ponded water upstream of the canal and could cause additional losses into the soil to occur.

Minor numerical instabilities were noticed in the 2-dimensional model for the lower flow alluvial basins C through H. These instabilities were due to problems associated with SRH-2D when switching between wet and dry elements. Such instabilities are considered to be insignificant and did not affect the overall performance of the model.

CONCLUSION

It had been hypothesized that peak flooding flows within the Truckee canal basin were attenuated due to the adjacent alluvial fans. Classic one-dimensional hydrologic modeling is unable to capture the infiltration losses experience in alluvial fans since the surfaces are dynamic. To better understand the hydrology of the basin, a one-dimensional hydrologic model was coupled with a two-dimensional hydrologic model to simulate the 10-, 25-, 50-, and 100-year flows. This model was un-calibrated since there was no available data to calibrate toward. The model

uncertainty was determined through a mass balance analyses. It was found that only a 2% error in mass balance between the flows entering and leaving the two-dimensional model.

BIBLIOGRAPHY

Aquaveo. (2013). Surface-water Modeling System. Provo, Utah.

Bonnin, G. M., Martin, L. B., Parzybok, T., Yekta, M., & Riley, D. (2004). *Precipitation-Frequency Atlas of the United States, NOAA Atlas 14 Volume 1 Version 4.0: Semiarid Southwest.* Silver Spring, MD: National Weather Service.

Chow, V. T. (1959). *Open-Channel Hydraulics.* New York: McGraw - Hill Book Co.

Cudworth, A. G. (1989). *Flood Hydrology Manual.* Denver, CO: US Buearu of Reclamation.

Environmental Systems Research Insitute (ESRI). (2011). ArcGIS Desktop: Release 10. Redlands, CA: Environmental Systems Research Institute.

Faulds, J. E., & Ramelli, A. R. (2009). *Preliminary geologic map of west half of the Hazen Quardangle, Lyon, and Chruchill Counties, Nevada.* Nevada Bureau of Miles and Geology.

Faulds, J. E.; Ramelli, A. R. (2005). *Preliminary geologic map of Fernley East Quadrangle, Lyon and Washoe Counties, Nevada.* Nevada Bureau of Mines and Geology.

Faulds, J. E.; Ramelli, A. R.; Herny, C. D. (2008). *Preliminary geologic map of the Fernley West Quardangle, Lyon, Storey, and Washoe Counties, Nevada.* Nevada Bureau of Mines and Grology.

Hosking, J. M., & Wallis, J. R. (1997). *Regional Frequency Analysis- An Approach Based on L-Moments.* Cambridge University Press.

Lai, Y. (2000). Unstructure grid arbitrarily shaped element method for fluid Flow simulation. *AIAA Journal, 38*(12), 2246-2252.

Lai, Y. (2008). *Therory and User's Manual, Sedimentaion and River Hydraulics Two-Dimensional River Flow Modeling.* Denver, CO: US Bureau of Reclamation, Technical Service Center.

National Research Councle (NRC). (1996). *Alluvial Fan Flooding, Committee on Alluvial Fan Flooding, Water Science and Technology Board.* Comission on Geosciences, Environment, and Resources.

Natural Resources Concervation Service. (2007). *National Engineering Handbook Part 630 Hydrology: Chapter 7 - Hydrologic Soil Groups.* US Department of Agriculture.

Soil Survey Staff, Natural Resources Conservation Service. (n.d.). Soil Survey Geographic (SSURGO) Database. United States Department of Agriculture.

U.S. Army Corps of Engineers. (1990). HEC-1 Flood Hydrograph Package Compurer Program 723-X6-L2010 Version 4.0. Davis, CA, US Army Corps of Engineers.

USGS. (2012). *National Hydrogrpahic Dataset*. Retrieved May 2012, from http://ndh.usgs.gov

Woolpert, Inc. (2012). LiDAR Remoste Sensing Truckee Alluvial Fans, Nevada. *Final Report delivery to Reclamation*. Englewood, Colorado: Woolpert, Inc.

EVALUATING PHYSICAL MODELS OF DAM REMOVAL AGAINST RESULTS FROM CONDIT, MARMOT, AND ELWHA FOR PROCESS DRIVEN SEDIMENT TRANSPORT AND CHANNEL BED RESPONSE

Joanna Crowe Curran, Ph.D., Senior Geomorphologist / River Engineer, Northwest Hydraulic Consultants, 13600 Christensen Road, Suite 350, Seattle, WA 98188, jcurran@nhcweb.com

As dam removals have become more frequent in recent decades, the interest in and research on the downstream impacts of releasing large amounts of formerly impounded sediment on the downstream channel morphology have been investigated. A series of recently completed flume experiments evaluated the downstream effects of dam removal sequencing, impounded sediment grain size distribution, and channel flow rate on sediment transport rates and channel morphology during and following dam removal. Recent dam removals have provided data from field scale experiments in sediment transport and downstream morphologic adjustments following dam removal from situations with a variety of independent driving variables. These provide the data necessary to evaluate the physical modeling results.

Through physical modeling, 5 different dam deconstruction sequences were tested against 2 flow rates and 3 sediment mixtures to evaluate the 30 different combinations of channel and dam type. The dam deconstruction sequencing scenarios simulated were chosen to replicate current dam removal practices and included: removal in horizontal layers from the top down; removal in vertical sections with the first section removed from the middle of the dam; removal in vertical sections where the first section removed is adjacent to the channel edge; notched removal where the sides of the dam remain in place, and complete dam removal in a single step. Each removal scenario was repeated using flow rates designed to simulate low (Froude number =0.2) and high flow (Froude number = 0.6) conditions. Sediment transport was monitored throughout each stage of each dam removal and the bed surface was scanned using a laser displacement scanner after each removal stage. Digital Elevation Models (DEMs) of each bed surface were created from the bed surface laser scans and by differencing these DEMS, the spatial distribution of preferential deposition and erosion downstream of the dam removal was identified and quantified. A bed load monitoring system (BLMS) collected real-time data on the movement of the sediment through the flume channel during the experiments. BLMS data enabled re-creation of the sediment transport rates following each stage of a dam removal. Together these data provided a means of evaluating the impact of each removal type on the rate and volume of sediment movement as well as the short and long term impacts on the bed surface around the dam removal site and downstream.

This talk will present a comparison of results from flume runs against those from recent dam removals. The Marmot Dam removal from the Sandy River, OR is compared to a flume run where the dam was removed in one step, flow was moderate, and the sediment was a gravel and sand mixture. The Condit Dam removal from the White Salmon River, WA is compared to a flume run where the dam was removed in one step, flow was high, and the sediment was a mixture dominated by sand and silt, but with a small gravel fraction. Dam removals from the Elwha River, WA are compared to a flume run where the dam was removed in a sequence of horizontal stages and the sediment was a mixture dominated by sand and silt, but with a small gravel fraction. The comparisons between laboratory and field were evaluated for the representativeness of the flume

results and the information gained from both flume and field measurements. Additional information gained from the lab included measurements of real time estimates of deposition and erosion over the downstream channel reach while the field supplied information on broad scale planform channel changes. Similarities between flume and field results indicate a potential for improving predictive abilities related to sediment transport rates through and changes to the downstream channel over a range of channel and dam removal scenarios.

Research results seek to identify relationships between dam deconstruction sequencing, channel and impounded sediment sizes, and flow rate during removal so that the impact of sediment release with dam removal on the downstream channel morphology can be predicted. Many aging dams are not removed due to the economic expense of dredging impounded sediment prior to deconstruction and fears of ecosystem damage if the sediment is released. By quantifying sediment movement associated with different dam deconstruction sequencing, the effect of dam removal on the downstream channel morphology can be better predicted and impounded sediment can be released and transported downstream in a way that benefits, rather than harms, the downstream ecosystem and protects downstream infrastructure. The experimental results can aid in planning a dam removal to address specific goals related to impounded sediment movement and impact to the downstream channel.

MOUNT ST. HELENS UPDATE: RECENT TRENDS, UNDERSTANDINGS AND PROJECTS TO MANAGE DEBRIS AVALANCHE SEDIMENTS

Chris Nygaard, PE, Portland District US Army Corps of Engineers, Portland, Oregon, christopher.j.nygaard@usace.army.mil; Paul Sclafani, PE, Portland District US Army Corps of Engineers, Portland, Oregon, paul.sclafani@usace.army.mil

Abstract: Since the eruption of Mount St. Helens (MSH) in 1980, the US Army Corps of Engineers has been actively managing debris avalanche sediment in the Toutle River and lower Cowlitz Rivers in southwest Washington State. The Sediment Retention Structure (SRS), a 125 foot tall sediment trap constructed in 1987, is the primary long-term sediment management action. The SRS was designed to trap sediment high in the watershed and prevent problematic deposition in the lower reaches where floodplain development has occurred. The SRS has been effective at trapping sediment since construction and continues trap on the order of 30% of inflowing sediment 27 years after construction.

Since 2006 however, sediment has begun passing the SRS in sufficient quantities such that deposition in the leveed and populated downstream reaches has become a concern. USACE has responded to this change in trends by initiating multiple technical and planning studies as well as management actions. The primary purpose of the studies was to establish a sediment management plan through the current planning period that would be cost effective and responsive to the current economic and environmental landscape. The sediment management actions were designed to reduce flood risk to affected communities in the lower basin. This presentation will provide an update of recent trends, studies, actions and environmental concerns.

Forecasts for large scale and uncertain trends such as sediment load from the MSH debris avalanche are necessarily simplified to express the overall average volumes or rates of decay. Observed data is rarely so well behaved. In the case of MSH sediment load up to two orders of magnitude of annual variation are observed. Downstream deposition is complicated by the non-linear relationship between flow, load and erosion. While overall load from the mountain is lower than predicted in 1985, peak sediment events have deposited large amounts of material which persist for multiple years without physical removal.

Two new studies predicting sediment load from MSH have been received by USACE; a 2012 study by USDA prepared by Simon and Klimetz and a 2014 University of Nottingham Ph.D. thesis by T. Meadows. Using different methodologies for predicting future loads, the two studies come to significantly different conclusions. Simon argues for significant and persistent near term decay in load while Meadows argues for decreased overall load with mild decay into the next century. With continued uncertainty about the future sediment load trends, let alone peak sediment, USACE has prioritized flexibility in its management approach.

In addition to the planning effort that re-evaluated the long term sediment management plan, USACE has responded to increased deposition in the lower Cowlitz River with several actions: 2008 Castle Rock Levee Improvements, 2010 Pilot Grade Building Structures and the 2012 SRS Crest Raise. Purpose, effectiveness, and morphological response to each action will be discussed. Features of the project designed to comply with Endangered Species Act (ESA)

listings will be described. Additional sediment related ESA concerns within the management area will be introduced.

Simon, A. and D. Klimetz. January 2012. Empirical Analysis of Long-Term Sediment Loadings from the Upper North Fork Toutle River System, Mount St. Helens, Washington. U.S. Department of Agriculture, Agricultural Research Service, National Sedimentation Laboratory Technical Report, Watershed Physical Process Research Unit.

Meadows, Tim. May 2014. Forecasting Long-Term Sediment Yield from the Upper North Fork Toutle River, Mount St. Helens, USA. Ph.D. Thesis. University of Nottingham: U.K.

FORECASTING LONG-TERM SEDIMENT YIELD FROM THE UPPER NORTH FORK TOUTLE RIVER, MOUNT ST HELENS

EXTENDED ABSTRACT

Tim Meadows, Senior Hydromorphologist, SEPA, Edinburgh, UK, tim.meadows@sepa.org.uk; Colin Thorne, Professor, University of Nottingham, UK; Nick Mount, Associate Professor, University of Nottingham, UK; Tom Coulthard, Professor, University of Hull, UK.

INTRODUCTION

The disturbance of otherwise stable fluvial systems by heavy sediment loading is a common phenomenon, particularly in mountainous areas (Pitlick, 1993; Rathburn *et al*., 2013), and may result from both natural and anthropogenic processes (Gran and Montgomery, 2005). Post-disturbance sediment yields are often significantly elevated above background levels as a result of increased availability of source material and hydrological changes that result in higher peak floods. Some of the highest specific sediment yields have been recorded in mountain rivers disturbed by explosive volcanic eruptions, with transport rates that exceed the 99th percentile of historic sediment yields reported in undisturbed catchments (Korup, 2012). However, longer-term trends in sediment yields following disturbance are poorly understood, principally due to a lack of documentation, but also because recovery trajectories of disturbed fluvial systems are influenced by a broad range of general and local controls (Manville and Wilson, 2004; Pierson and Major, 2014).

Where long-term recovery trends from explosive eruptions have been monitored, the results often indicate that sediment yields can remain elevated for decades, centuries or even millennia (e.g. James, 1989; Manville and Wilson, 2004; Gran and Montgomery, 2005; Korup, 2005; Koi *et al*., 2008; Manville *et al*., 2009; Pierson *et al*., 2011; Pierson and Major, 2014). Given the potentially damaging socio-economic consequences of persistently high sediment yields, generating projections of long-term sediment yield from disturbed fluvial systems is essential for the development of sustainable sediment management options. However, conventional tools available to fluvial geomorphologists and river engineers, such as reductionist numerical models and empirical analyses, are not ideally suited to the task, making this challenge difficult to address. Recent advances in numerical modelling techniques, however, offer new opportunities to develop quantitative, physically-based predictions of fluvial system recovery following landscape disturbance.

Specifically, reduced complexity, landscape evolution models, which are explicitly designed to operate at low computational cost over long temporal- and large spatial-scales, have the potential to play a significant role in efforts to understand, explain and predict the long-term response of fluvial systems to disturbance. Landscape evolution models attempt to simulate the three-dimensional development of landscapes through time (Kirkby, 1971; Ahnert, 1976), and hence permit the effect of multiple geomorphic processes that contribute to the redistribution of sediment within a catchment to be integrated together over complex topographic surfaces and extended periods of time (Pazzaglia, 2003; Martin and Church, 2004). Such models therefore aim to represent the principal erosion processes operating within a catchment, including those affecting hillslopes and those operating in stream channels. In some cases, bedrock weathering and flexural isostatic uplift in response to denudation are also included.

THE 1980 ERUPTION OF MOUNT ST HELENS

The hydrogeomorphic effects of the catastrophic 1980 eruption of Mount St Helens, Washington State, USA, remain the most thoroughly studied record of long-term landscape impact following a voluminous explosive eruption (e.g. Pearson, 1984; Meyer and Dodge, 1987; Meyer and Martinson, 1989; Simon and Thorne, 1996; Simon, 1999; Major *et al*., 2000; Major, 2004; Major and Mark, 2006; Zheng *et al*., 2014). The Toutle-Cowlitz River system (Figure 1) experienced particularly dramatic landscape disturbance during this event, principally through the emplacement of by a 2.5 km^3 debris avalanche, which buried the upper 60 km^2 of the North Fork Toutle River catchment to an average depth of 45 m and obliterated the pre-eruption drainage network (Lipman and Mullineaux, 1981).

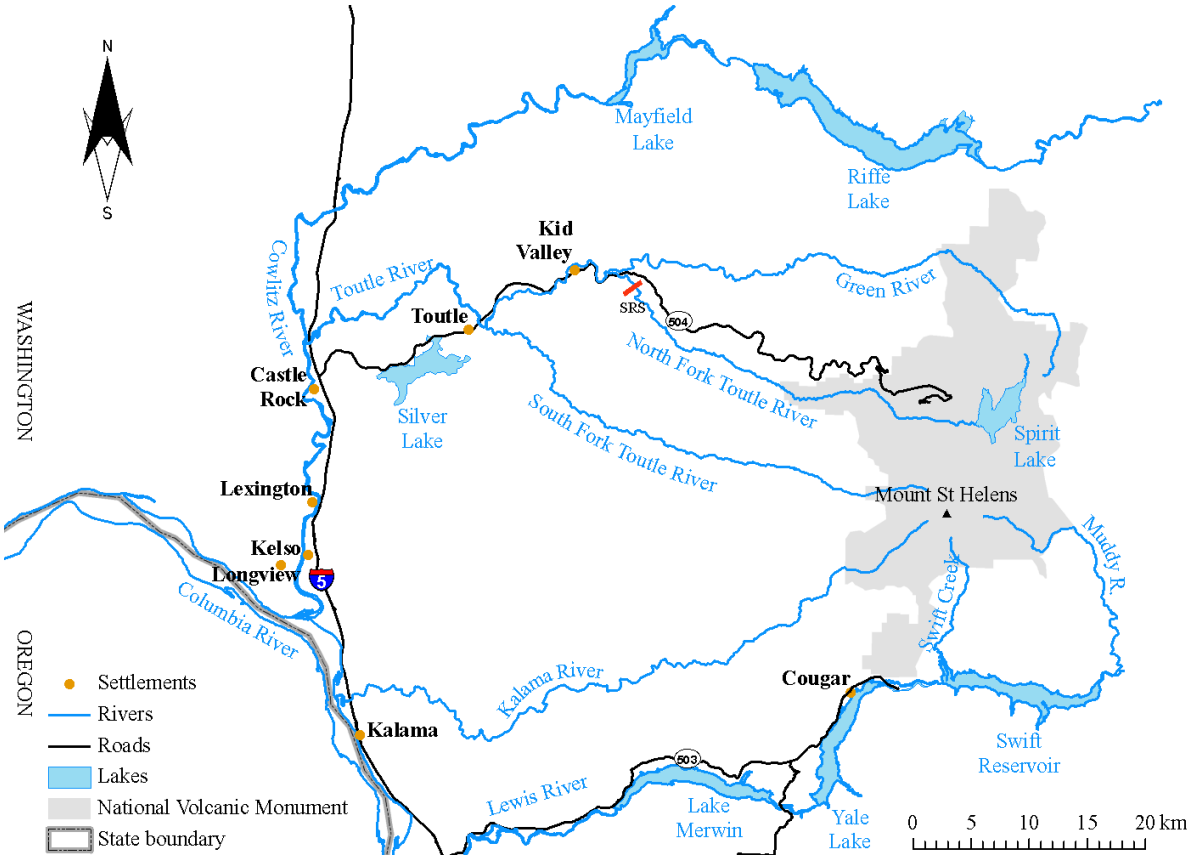

Figure 1 Map of Toutle-Cowlitz River system.

Subsequent channel response on the debris avalanche, dominated by incision and widening, has delivered significant quantities of sediment to downstream reaches of the Cowlitz River, where resultant deposition has reduced channel capacity and increased flood risk unacceptably. Over the 30+ years since the eruption, significant efforts have been made to protect vulnerable communities and to understand trends and mechanisms of sediment yield from the affected catchments. However, despite more than three decades of intensive monitoring at Mount St Helens, the recovery trajectory remains contested and future trends are clouded by uncertainty. Moreover, existing infrastructure designed to reduce downstream sediment-related flood risk may be unable to store sufficient sediment to continue to meet flood risk reduction standards over the long term. Options for future sediment management are therefore currently being assessed (USACE, 2010, 2012) but divergence in predictions of

long-term sediment yield reported in previous studies make option appraisal and decision-making difficult.

CAESAR-LISFLOOD LANDSCAPE EVOLUTION MODEL: BACKGROUND AND APPLICATON

This paper describes the use of a numerical, landscape evolution model (CAESAR-Lisflood (C-L)) to generate long-term forecasts of sediment yield from the upper North Fork Toutle River catchment. The computational efficiency of C-L enables multiple physically-based simulations to be run over long time periods (>100 years) and at the scale of whole river basins. In comparison to other contemporary reduced complexity, landscape evolution models, C-L includes the most sophisticated representation of flow hydraulics (using the LISFLOOD-FP equations of Bates *et al*. (2010), the most detailed model of fluvial erosion and deposition (including multiple grain sizes, lateral erosion and suspended sediment) and the most comprehensive representation of catchment hydrology. Importantly, the model allows for dynamic terrain adjustments and has been shown to demonstrate the complex, non-linear behaviour typical of disturbed fluvial systems (e.g. Coulthard *et al*., 1998; Coulthard and Van De Wiel, 2007) that plays an important role in long-term landscape development.

C-L model parameters were calibrated during a period of model hindcasting in which the fitness-for-purpose of the model was also assessed. During this process, values for key parameters that could not be specified on the basis of empirical data, *a priori* knowledge or pre-existing, recommended values were varied across well-constrained and feasible ranges. Model outputs were then compared to observations using four physically-meaningful evaluation criteria, specifically: total catchment sediment yield; sub-catchment sediment yield; change in cross-sectional area; and change in thalweg elevation. This multi-scale approach facilitated both volumes and mechanisms of modelled sediment yield to be evaluated, which allowed for a comprehensive assessment of model performance to be undertaken. Within the range of variations in model outputs, two model configurations were identified as providing good fits to the observed data for all four of the evaluation criteria, while also accounting for uncertainty associated with the definition of the model parameter that controls the lateral mobility of river channels.

The two selected model configurations were implemented in ensembles with runoff forecasts developed as part of the Columbia Basin Climate Change Scenarios Project (CBCCSP) undertaken by the Climate Impacts Group (CIG) at the University of Washington (Hamlet *et al*., 2010). The runoff forecasts selected from the CBCCSP represented three different global climate model (GCM) simulations and two scenarios for greenhouse gas (GHG) emissions and, therefore, encapsulated the majority of variability associated with uncertainty in predicting the future hydrological regime of the catchment. A total of 36, 91-year forecasting runs were undertaken, along with two, more speculative, 182-year simulations that produced extended forecasts for the 22nd century.

RESULTS

The forecast sediment yields fall into a band with a width of +/-20% of the mean that lies between previous estimates derived principally from the extrapolation of post-eruption trends (Biedenharn Group, 2010; Simon and Klimetz, 2012) (Figure 2). It must be noted that neither the WEST nor Biedenharn Group studies provided estimates of sediment yield beyond the year 2035. However, for comparison with the predictions based on C-L modelling, their

estimates were extrapolated from 2036 to 2100 and plotted in Figure 2. The range of sediment yields forecast by C-L is very well constrained despite conscious efforts throughout the study to maximise the difference between selected model configurations and future hydrological scenarios.

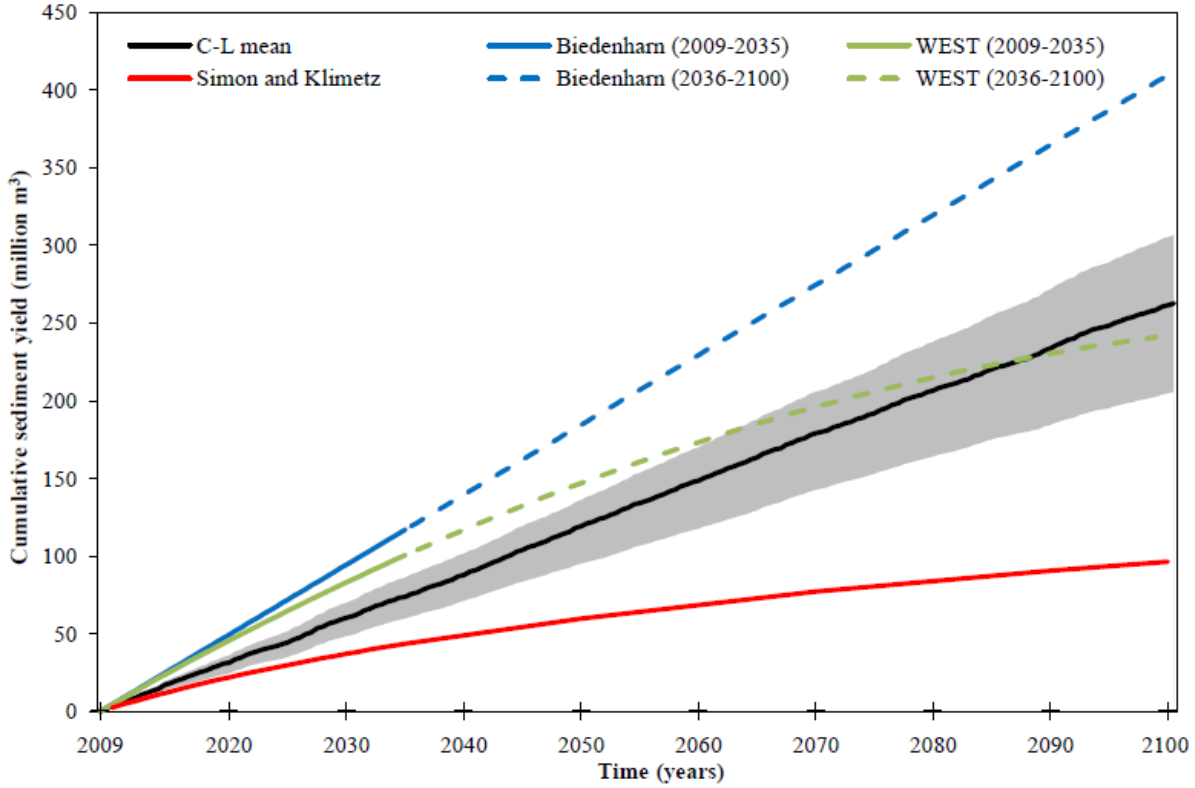

Figure 2 Projections of cumulative catchment sediment yield from the upper North Fork Toutle River from 2009 to 2100. The upper and lower bounds of the shaded area are the maximum and minimum of the C-L forecasts.

Importantly, forecast trends in future annual sediment yields are predominantly linear, and decline in future yields is limited even in forecasts produced by runs in which the parameter defining the lateral mobility of the channel is lower. As a result, the extended forecasts suggest that elevated rates of sediment production may persist into the 22nd century. The predominantly linear trend in cumulative sediment yield modelled by C-L suggests that negative exponential decay functions based on a rate law (Graf, 1977) are inappropriate for predicting sediment yields from the upper North Fork Toutle River catchment. Although the rate law can be used to describe changes in bed elevation and adjustments to the channel long profile, C-L model results reveal that it is *lateral erosion* caused by fluvial undercutting and slumping of high, steep banks, that drives long-term trends in sediment yield, rather than bed scour.

CONCLUSIONS

The C-L forecasts presented in this paper suggest that it may not be possible to maintain flood risk reduction benefits to vulnerable communities on the lower Cowlitz River solely by trapping sediment upstream of a sediment retention structure (SRS) on the North Fork Toutle

River. For example, it has been estimated that the two methods of improving the trap efficiency of the SRS proposed by the USACE (a 13 m dam raise or incremental raises of the spillway combined with grade-building structures) would be effective only until the 2040s if C-L forecasts are realised. This prospect implies that alternative strategies capable of managing sediment-related flood risk in the Toutle-Cowlitz River system into the next century in ways that are economically, environmentally and ecologically sustainable should be investigated. It may be necessary, for instance, to relocate and/or raise vulnerable communities such as Castle Rock, where risks to life and property posed by flooding are particularly high due to its position close to the mouth of the Toutle River and location on the floodplain at the inside of a tight meander bend.

The research reported in this paper also demonstrates the utility of reduced complexity, landscape evolution modelling for long-term forecasting of catchment-scale sediment yield. Although modelling based on cellular automata has often been criticised by proponents of reductionist, 'physics-based' models, in the context of the upper North Fork Toutle River it has been shown to be a powerful tool that can and should be used to explore landscape evolution and response to disturbance. It also has the potential to help inform long-term, catchment-scale planning and sustainable management of environmental hazards associated with, for example, elevated sediment yields. Moreover, the comparison between the results obtained using C-L and those derived from other modelling approaches, such as empirical extrapolation, provides important insights into the relative strengths and weaknesses of these different techniques.

ACKNOWLEDGEMENTS

The research reported herein was performed while the first author was a doctoral student at the University of Nottingham, supervised by the second and third authors and advised by the fourth. The research was funded by a studentship from the School of Geography. It could not have been undertaken without the support of the US Geological Survey, Cascades Volcano Observatory and the Portland District, US Army Corps of Engineers. In this regard, the authors would particularly like to thank Jon Major, Kurt Spicer and Adam Mosbrucker (USGS) and Chris Nygaard and Paul Sclafani (USACE). The research also benefited from input from Dr Andrew Simon, whose advice is gratefully acknowledged.

REFERENCES

Ahnert, F. (1976). Brief description of a comprehensive three-dimensional model of landform development. *Zeitschrift fur Geomorphologie Supplement Band* 25, 29-49.

Bates, P.D., Horritt, M.S. and Fewtrell, T.J. (2010). A simple inertial formulation of the shallow water equations for efficient two-dimensional flood inundation modelling. *Journal of Hydrology* 387, 33-45.

Biedenharn Group (2010). *Toutle-Cowlitz River sediment budget.* Portland, OR: US Army Corps of Engineers Portland District.

Coulthard, T.J. and Van De Wiel, M.J. (2007). Quantifying fluvial non linearity and finding self organised criticality? Insights from simulations of river basin evolution. *Geomorphology* 91, 216-235.

Coulthard, T.J., Kirkby, M.J. and Macklin, M.G. (1998). Non-linearity and spatial resolution in a cellular automaton model of a small upland basin. *Hydrology and Earth System Sciences* 2(2-3), 257-264.

Graf, W.L. (1977). The rate law in fluvial geomorphology. *American Journal of Science* 277(2), 178-191.

Gran, K.B. and Montgomery, D.R. (2005). Spatial and temporal patterns in fluvial recovery following volcanic eruptions: Channel response to basin-wide sediment loading at Mount Pinatubo, Philippines. *Geological Society of America Bulletin* 117, 195-211.

Hamlet, A.F., Carrasco, J., Deems, J., Elsner, M.M., Kamstra, T., Lee, C., Lee, S.-Y., Mauger, G., Salathe, I., Tohver, I.M. and Whitely Binder, L. (2010). Final project report for the Columbia Basin Climate Change Scenarios Project.

James, L.A. (1989). Sustained storage and transport of hydraulic gold mining sediment in the Bear River, California. *Annals of the Association of American Geographers* 79(4), 570-592.

Kirkby, M.J. (1971). Hillslope process-response models based on the continuity equation. In: Brunsden, D. (Eds.) *Slopes - form and process. Institute of British Geographers Special Publication 3*, pp. 15-30.

Koi, T., Hotta, N., Ishigaki, I., Matuzaki, N., Uchiyama, Y. and Suzuki, M. (2008). Prolonged impact of earthquake-induced landslides on sediment yield in a mountain watershed: the Tanzawa region, Japan. *Geomorphology* 101(4), 692-702.

Korup, O. (2005). Large landslides and their effect on sediment flux in South Westland, New Zealand. *Earth Surface Processes and Landforms* 30(3), 305-323.

Korup, O. (2012). Earth's portfolio of extreme sediment transport events. *Earth-Science Reviews* 112(3), 115-125.

Lipman, P.W. and Mullineaux, D.R. (Eds.) (1981). *The 1980 Eruptions of Mount St Helens, Washington: US Geological Survey Professional Paper 1250*. Washington, D.C.: US Government Printing Office.

Major, J.J. (2004). Posteruption suspended sediment transport at Mount St Helens: Decadal-scale relationships with landscape adjustments and river discharges. *Journal of Geophysical Research* 109, 1-22.

Major, J.J. and Mark, L.E. (2006). Peak flow responses to landscape disturbances caused by the cataclysmic 1980 eruption of Mount St Helens, Washington. *Geological Society of America Bulletin* 118, 938-958.

Major, J.J., Pierson, T.C., Dinehart, R.L. and Costa, J.E. (2000). Sediment yield following severe volcanic disturbance - a two-decade perspective from Mount St Helens. *Geology* 28, 819-822.

Manville, V. and Wilson, C.J. (2004). The 26.5 ka Oruanui eruption, New Zealand: A review of the roles of volcanism and climate in the post- eruptive sedimentary response. *New Zealand Journal of Geology and Geophysics* 47(3), 525-547.

Manville, V., Segschneider, B., Newton, E., White, J., Houghton, B. and Wilson, C. (2009). Environmental impact of the 1.8 ka Taupo eruption, New Zealand: Landscape responses to a large-scale explosive rhyolite eruption. *Sedimentary Geology* 220(3), 318-336.

Martin, Y. and Church, M. (2004). Numerical modelling of landscape evolution: geomorphological perspectives. *Progress in Physical Geography* 28, 317-339.

Meyer, D. and Dodge, J.E. (1987). *Post-eruption changes in channel geometry of streams in the Toutle River drainage basin, 1983-85, Mount St Helens, Washington: US Geological Survey Open-File Report 87-549*. Vancouver, WA: US Geological Survey.

Meyer, D. and Martinson, H. (1989). Rates and processes of channel development and recovery following the 1980 eruption of Mount St Helens, Washington. *Hydrological Sciences Journal* 34, 115-127.

Pazzaglia, F. (2003). Landscape evolution models. *Developments in Quaternary Science* 1, 247-274.

Pearson, M.L. (1984). *Geomorphological analysis of the North Fork, Toutle River Washington: 1980-1984. US Army Corps of Engineers Technical Report GL-94-7*. Vicksburg, MS: US Army Corps of Engineers.

Pierson, T.C. and Major, J.J. (2014). Hydrogeomorphic effects of explosive volcanic eruptions on drainage basins. *Annual Review of Earth and Planetary Sciences* 42, 469-507.

Pierson, T.C., Pringle, P.T. and Cameron, K.A. (2011). Magnitude and timing of downstream channel aggradation and degradation in response to a dome-building eruption at Mount Hood, Oregon. *Geological Society of America Bulletin* 123(1-2), 3-20.

Pitlick, J. (1993). Response and recovery of a subalpine stream following a catastrophic flood. *Geological Society of America Bulletin* 105(5), 657-670.

Rathburn, S.L., Rubin, Z.K. and Wohl, E.E. (2013). Evaluating channel response to an extreme sedimentation event in the context of historical range of variability: Upper Colorado River, USA. *Earth Surface Processes and Landforms* 38(4), 391-406.

Simon, A. (1999). *Channel and drainage-basin response of the Toutle River system in the aftermath of the 1980 eruption of Mount St Helens, Washington: US Geological Survey Open File Report 96-633*. Vancouver, WA: US Geological Survey.

Simon, A. and Thorne, C.R. (1996). Channel adjustment of an unstable coarse-grained stream: opposing trends of boundary and critical shear stress, and the applicability of extremal hypotheses. *Earth Surface Processes and Landforms* 21, 155-180.

Simon, A. and Klimetz, D. (2012). *Analysis of long-term sediment loadings from the upper North Fork Toutle River system, Mount St Helens, Washington. US Department of Agriculture, Agricultural Research Service, National Sedimentation Laboratory Technical Report Number 77.* Portland, OR.

USACE (2010). *Mount St Helens long-term sediment management plan for flood risk reduction: progress report*. Portland, OR: US Army Corps of Engineers Portland District.

USACE (2012). *Sediment retention structure (SRS) spillway raise project. Mount St Helens sediment management for flood risk reduction. Final environmental assessment.* Portland, OR: US Army Corps of Engineers Portland District.

Zheng, S., Wu, B., Thorne, C.R. and Simon, A. (2014). Morphological evolution of the North Fork Toutle River following the eruption of Mount St Helens, Washington. *Geomorphology* 208, 102-116.

MOUNT ST. HELENS LONG TERM SEDIMENT MANAGEMENT ALTERNATIVE ANALYSIS

Paul Sclafani, Hydraulic Engineer, U.S. Army Corps of Engineers, Portland Oregon, paul.sclafani@usace.army.mil; Chris Nygaard, U.S. Army Corps of Engineers, Portland, Oregon, Christopher.j.nygaard@usace.army.mil

Abstract: Thirty-three years after the eruption of Mount St. Helens, erosion from the debris avalanche into the Toutle River continues to produce a problematic quantity of sediment for downriver communities. For the past five years the U.S. Army Corps of Engineers has been revisiting the long term sediment management strategy originally developed in 1985 to determine if there are better ways to meet flood protection goals while minimizing both harm to the environment and project costs.

Long term sediment records collected by the USGS Volcanic Observatory coupled with LiDAR and field surveys were used to create a sediment budget for the Toutle River basin. A complete sediment budget was developed from 1980 to 2007. Annual sediment loads for the period from 1999 to 2007 were stochastically sampled to create a predicted sediment record for the project life, extending out to 2035. Within these sampling years the annual sediment load from the Mount St. Helens debris avalanche ranges from 0.6 to 26 million tons. This natural variability of sediment erosion from the debris avalanche provides a reasonable representation of possible future loads to be expected in the basin. Once created, this forecasted sediment load was used as input to the modeling scheme chosen for the project.

A modeling scheme was selected to numerically represent the complexity of the Toutle River basin from the debris avalanche to the mouth of the Cowlitz River. The basin can be considered as a combination of sources and sinks placed in series. The debris avalanche represents the most significant source, the erosion of which is represented by the sediment budget. The highly braided network of streams downstream of the debris avalanche was modeled using Mike 21-C; HEC-RAS was used to develop the rating curve through the sediment retention structure (SRS). Sediment/bed interaction within the Toutle River downstream of the SRS was largely ignored as it was considered a transport reach that terminates at the Toutle River's confluence with the Cowlitz River. A mobile-bed HEC-RAS model was utilized in the lower 20 miles of the Cowlitz River to evaluate the long term sediment transport potential in this reach. Output from the upstream Mike-21C model was used for the upstream sediment load input into HEC-RAS. The water surface profiles from the RAS models were used in conjunction with HEC-FDA to compute the Level of Protection (LOP) provided by the levees located on the Lower Cowlitz Rivers. Flow- frequency and levee-fragility curves were developed to support this LOP computation.

Uncertainty/variability was incorporated into this analysis through the available period of flow records, uncertainty in levee performance, variability in bedform, and incoming the sediment load. Model uncertainty was also incorporated into the FDA model through sensitivity of key hydraulic parameters such as the roughness and contraction/expansion coefficients.

The resulting LOP estimates for each levee represent the frequency of an event that reflects a 90 percent probability of levee failure.

With the modeling scheme developed and the predicted sediment loads created for the project out years, a trend in LOP for the levees was computed for the project life. Specific authorizing language dictates that the Corps maintains LOP at a specified level. It was demonstrated that, for the "do-nothing" alternative, the LOP violates the authorization within five years. Based on this trend, a study was initiated to evaluate alternatives that would result in fulfilling the congressional authorization. Initial phases of this analysis identified the 16 measures as potential measures for evaluation. Using two rounds of screening, each measure was evaluated as to the degree to which it:

- Reduces flood risk on the Cowlitz River;
- Is low-cost based on preliminary cost estimates;
- Minimizes impacts to the environment;
- Is reliable;
- Is adaptable to changing conditions; and
- Is acceptable to the public.

After the two rounds of screening, six measures were forwarded for continued scrutiny. Of these, two were considered primary measures in that they have the potential to be employed as stand-alone measures. The rest were secondary measures that may be used to enhance the performance of the primary measures.

This short list was carried forward for further analysis during development of the long term sediment management plan, and each measure was thoroughly evaluated. The remaining four measures were grouped to form three action alternatives carried forward for further evaluation:

- Cowlitz River dredging only;
- SRS dam raise only; and
- Phased-construction (SRS spillway crest raise and GBS with as-needed dredging).

Within the model construct developed for the "do-nothing" alternative, each of the final alternatives was modeled and evaluated. Each alternative has been determined to meet the overall sediment management needs and are deemed relatively efficient, effective, complete, and they will allow for the management of the significant uncertainty in future sediment deposition.

In the evaluation of the final alternatives, it became clear that each alternative provided a specific benefit and contained unique drawbacks. For example, the dredging-only option, which involves dredging the lower 20 miles of the Cowlitz River, is highly adaptable to changing conditions, however placement of dredge material is problematic in terms of logistics and considering environmental concerns. The SRS-raise option has a high degree of certainty of trapping sediment, however, it is not adaptable to changing conditions and requires high up-front costs. The phased-construction approach combines the adaptability of the dredging only plan and the effectiveness of the SRS raise. The phased construction plan is currently the preferred alternative.

The preferred alternative attempts to incorporate the high level of uncertainty in the basin through an adaptive management plan that only implements actions when the monitoring efforts show a need. The three components of the plan include gaining additional sediment capacity by raising the spillway crest and adding structures within the sediment plain to promote the depositional grade. The final component is emergency dredging in the Lower Cowlitz River to maintain the ability to react to unexpected extreme sediment loads. Inherent in an adaptable plan is a monitoring effort that quantifies sediment deposition in the Sediment plain and in the Lower Cowlitz.

In the case of the Toutle Basin, identification of the need is tied to the annual evaluation of the LOP. Evaluation of the LOP requires that sediment load measurements, survey data, and field observations be collected annually. A decision matrix has been put together that identifies the appropriate annual monitoring activities, decision criteria to implement a sediment control measure, and decision criteria for what type of sediment control measure is necessary. Specifics of these decision criteria will be part of the annual operation plan for the phased construction approach.

TWO-DIMENSIONAL NUMERICAL MODELLING OF HYPERCONCENTRATED FLOWS

Jianchun Huang, Ph.D., P.E., Hydraulic Engineer, Bureau of Reclamation, Denver, CO, yhuang@usbr.gov; Yong Lai, Ph.D., Hydraulic Engineer, Bureau of Reclamation, Denver CO, ylai@usbr.gov; and Kuowei Wu, Water Resources Planning Institute, Water Resources Agency, Wu-Fong, Taichung, Taiwan, kuowei@wrap.gov.tw

Abstract: SRH-2D, a two-dimensional sediment transport model developed at the U.S. Bureau of Reclamation, is extended to simulate hyperconcentrated flows by considering the effect of sediment concentration on the the sediment fall velocity, sediment capacity and sediment erosion and deposition. The governing equations for shallow water equations are modified to be suitable for two dimensional unsteady hyperconcentrated flow modeling. Density variance and sediment exchanges between flow and bed are incorporated. The revised model is tested and verified using two cases: an idealized transient flow and sediment process due to a dam-break flow over a horizontal bed and a more complex dam-break flow with a sudden width enlargement. The model results show that the numerical model can predict the water surface elevation with reasonable accuracy. The results also show that the extra terms related to the density gradient and the terms related to the exchange between the flow and the erodible bed are important for hyperconcentrated flow. They increase the water front speed and wave height during a dam break.

INTRODUCTION

Hyperconcentrated flow can occur in high-discharge flows of water and sediment. The definition of hyperconcentrated flow varies among different researchers. Pierson (2005) defines hyperconcentrated flows to be between two extremes. At the low extreme, water transports sediment in such quantities that the sediment has negligible effect on flow behavior and the fluid remains Newtonian. At the other extreme, high-discharge debris flows and mudflows transport much more sediment than water can carry. For such cases sediment concentrations are often in excess of 60% by volume and 80% by weight. For debris and mud flows sediment plays a very important role in flow behaviors and mechanics (Wan and Wang, 1994; Coussot and Piau, 1994). Some researchers refer the debris flows and mudflows also as hyperconcentrated flow (NRC, 1982; O'Brien and Julien, 1985; and Julien and Paris, 2010).

One dimensional (1D) numerical modelling has often been used to simulate hyperconcentrated sediment-laden flows. For example, Zhang et al. (2001) presented a 1D unsteady numerical model for hyperconcentrated sediment-laden flows and applied it to the Lower Yellow River with a length of 394km. A semi-empirical equation of sediment transport capacity was used. Cao et al. (2004 and 2006) presented a 1D numerical model for a hyperconcentrted sediment laden flow. They used a second-order TVD method in conjunction with the HLLC Riemann solver and the SUPERBEE limiter. The extra terms related to the mixture density were included in the momentum equation, but not in the mass conservation equation. The exchange between the flow and the erodible bed was included in the mass and momentum equations. Wu and Wang (2007) presented a 1D hyperconcentrated model for dam-break flow over movable beds. The mass and momentum equations included the contribution of the sediment erosion and deposition. Guo et al. (2008) presented a hyper-concentrated sediment transport model for the lower Yellow River. The model considered the effect of high concentration on the flow density and sediment settling velocity. The variation of the mixture density and the exchange between the flow and the erodible bed were not included in the mass and momentum equations. Mouri et al. (2011) simulated an extreme flood and sediment flux in a mountain stream with a 1D numerical model. The mass and momentum equations considered no contribution of the sediment erosion and deposition. Abderrezzak and Paquier (2011) investigated sediment transport capacity formulas in dam-break flows. He et al. (2012) simulated unsteady hyperconcentrated sediment-laden flow in the Yellow River, China. They incorporated the extra terms related to the density of turbid flow into mass and momentum conservation equations, but not the contribution of sediment exchange between the flow and the bed.

Kim and Lee (2012) presented a 1D and 2D finite volume method for a hyperconcentrated sediment laden flow in a Cartesian coordinate system. They pointed out that the contribution of density should not be ignored in a hyperconcentrated sediment laden flow. Shallow water equations (SWE) with variable density were solved and the

sediment erosion and deposition terms were taken account in the depth-averaged continuity and momentum equations.

In this paper, we develop a 2D hyper-concentrated flow and sediment model based on the existing SRH-2D model and previous 1D model studies. .

DESCRIPTION OF THE NUMERICAL MODELS

The governing equations for 2D, unsteady, hyperconcentrated sediment-laden flow were revised from shallow water equation to include the density variance and sediment exchanges between flow and bed. The governing equations include mass and momentum conservation equations for the water-sediment mixture, the mass conservation equations for each sediment class carried in the flow, and the bed morphological change equation.

$$\frac{\partial(h)}{\partial t}+\frac{\partial(hU)}{\partial x}+\frac{\partial(hV)}{\partial y}=\frac{(E-D)}{1-P} \tag{1}$$

$$\frac{\partial(hU)}{\partial t}+\frac{\partial(hU^2)}{\partial x}+\frac{\partial(hUV)}{\partial y}=-gh\frac{\partial z_s}{\partial x}-\frac{\tau_{bx}}{\rho}-\frac{\rho_s-\rho_m}{2\rho_s}gh^2\frac{\partial S_v}{\partial x}-\frac{\rho_b-\rho_m}{\rho_m}\frac{(E-D)U}{1-P} \tag{2}$$

$$\frac{\partial(hV)}{\partial t}+\frac{\partial(hUV)}{\partial x}+\frac{\partial(hV^2)}{\partial y}=-gh\frac{\partial z_s}{\partial y}-\frac{\tau_{by}}{\rho}-\frac{\rho_s-\rho_m}{2\rho_s}gh^2\frac{\partial S_v}{\partial y}-\frac{\rho_b-\rho_m}{\rho_m}\frac{(E-D)V}{1-P} \tag{3}$$

$$\frac{\partial(hS_k)}{\partial t}+\frac{\partial(hUS_k)}{\partial x}+\frac{\partial(hVS_k)}{\partial y}=E_k-D_k \tag{4}$$

$$(1-p)\frac{\partial z}{\partial t}=\sum_k(D_k-E_k) \tag{5}$$

where t = time (s); x and y=horizontal Cartesian coordinates (m); h = water depth (m); U and V = depth-averaged velocity components (m/s) in x and y directions, respectively; g = gravitational acceleration; z_s is water surface elevation (m); z is bed elevation (m); $\rho_m = \rho_0(1-S_v)+\rho_s S_v$=density of the water-sediment mixture (kg/m^3); $\rho_b = \rho_0 p+\rho_s(1-p)$=density of the saturated bed (kg/m^3); ρ_0 and ρ_s= densities of water and sediment (kg/m^3); respectively; S_v=$\sum S_k$= total volumetric sediment concentration; S_k = volumetric sediment concentration of size class k; p = bed sediment porosity; E and D = total sediment entrainment and deposition fluxes (m/s) across the bottom boundary of flow, representing the sediment exchange between the water column and the bed. E_k and D_k = sediment entrainment and deposition fluxes of size class k; and bed friction is calculated using the Manning's roughness equation as follows:

$$\begin{pmatrix}\tau_{bx}\\ \tau_{by}\end{pmatrix}=\rho C_f\begin{pmatrix}U\\ V\end{pmatrix}\sqrt{U^2+V^2};\qquad C_f=\frac{gn^2}{h^{\frac{1}{3}}} \tag{6}$$

where n is the Manning's roughness coefficient.

There are two ways to calculate sediment erosion and deposition for superconcentrated flows.

Cao et al. (2004 and 2006) presented sediment erosion and deposition for superconcentrated flows as,

$$D=\alpha c\omega_0(1-\alpha c)^m \tag{7}$$

$$E=\begin{cases}\varphi(\theta-\theta_c)uh^{-1}d^{-0.2} & \text{if } \theta\geq\theta_c\\ 0 & \text{else}\end{cases} \tag{8}$$

where D, E=sediment deposition and entrainment fluxes across the bottom boundary of flow (m/s), representing the sediment exchange between the water column and bed; ω_0= settling velocity in clear water (m/s), α is specified empirically by $\alpha = \min[2, \frac{1-p}{c}]$; m = exponent=2.0; h = flow depth (m); d = sediment particle diameter (m) of size class k; p = bed sediment porosity (-) =0.4; $R = \sqrt{sgd}d/\nu$; $s = \frac{\rho_s}{\rho_0} - 1$; ν = kinematic viscosity of water = 1.2E-6 m^2/s; and θ = Shields parameter=$U_*^2/(sgd)$; θ_c = critical Shields parameter for initiation of sediment movement = 0.045; and U_*=shear velocity (m/s);c is depth-averaged volumetric sediment concentration; and φ=0.015[m$^{1.2}$].

Another method is to estimate the sediment deposition and erosion the same way as in other low concentration sediment transport numerical models. The sediment transport capacity for hyperconcentrated flow is presented in the previous section. Sediment erosion and deposition for the kth-sized sediment group were calculated based on sediment transport capacity $S_{*,k}$ and volumetric sediment concentration S_k, respectively.

$$D = \alpha\omega_{s,k}S_k \tag{9}$$

$$E = \alpha\omega_{s,k}S_{*,k} \tag{10}$$

where α=recovery coefficient which ranges from 0.001 in the case of continuous deposition to 1.0 for severe erosion; $\omega_{s,k}$= settling velocity for kth-sized sediment group (m/s). Compared with Eqs. () and (), it is found that the recovery coefficient α is the ratio between the bottom and average concentrations.

Many equations have been proposed to calculate the sediment transport capacity (Zhang and Zhang, 1992; Guo et al., 1995; Yang et al., 1996; Ni et al., 2004; He et al., 2012, and Taiwan Water Resources Agency, 2012). Due to space limit, only two sediment transport capacity equations are presented here which are used in the second test case.

Wu and Long (1993) presented suspended sediment transport capacity, written as

$$S_{*k} = k\left[\frac{\rho_m}{\rho_s - \rho_m}\frac{u^3}{gh\omega_m}\right]^{\mathrm{M}}\Delta P_{*k} \tag{11}$$

where S_{*k}= suspended sediment concentration of class k (kg/m^3); k and M are two empirical parameters, k = 0.452kg/m^3 and M = 0.762; h and u = averaged depth (m) and velocity (m/s) in a cross section, respectively; ω_m = group settling velocity = $\left(\sum_{k=1}^{N_s}\Delta P_{*k}\omega_{sk}^M\right)^{1/M}$; ω_{sk} = settling velocity of sediment size k; ΔP_{*k} = percentage of suspended sediment transport capacity for the k-th class = $(\Delta P_{bk}/\omega_{sk})^\phi / \sum_{k=1}^{N_s}(\Delta P_{bk}/\omega_{sk})^\phi$; ΔP_{bk} =bed material size fraction for the k-th class; ϕ is an empirical coefficient = 0.8; ρ_s and ρ_m are sediment and flow sediment mixture densities (kg/m^3), respectively; g = gravitational acceleration.

A formula proposed by Dou et al. (1999) can be used to determine the bed-load transport capacity, which is written as

$$q_{\mathrm{b}k} = \frac{K_b}{C_0^2}\frac{\rho_s\rho_m}{\rho_s - \rho_m}(u - u_{ck})\frac{u^3}{g\omega_m}\Delta P_{bk} \tag{12}$$

where $q_{\mathrm{b}k}$ = bed-load transport capacity per unit width for the k th grain size fraction (kg/ms); K_b = empirical coefficient (=0.1 calibrated by experiment); C_0 = dimensionless Chezy coefficient = $C\sqrt{g}$ in which $C = h^{1/6}/n$ and n = Manning's coefficient; and u_{ck} = incipient velocity (m/s) of the k-th bed-load fraction; calculated by

$$u_{ck} = \left(\frac{h}{d_k}\right)^{0.14}\sqrt{17.6\frac{\rho_s - \rho_0}{\rho_0}d + 6.05\times10^{-7}\times\frac{10+h}{d_k^{0.72}}} \tag{13}$$

where h = water depth (m); d_k = grain diameter (m) of class k; ρ_s and ρ_o are sediment and clear water densities (kg/m^3), respectively.

The 2D flow and sediment transport model, SRH-2D, is updated to include the extra terms related to the density gradient and the exchange between the flow and the erodible bed in the mass and momentum equations (Eqs. through). In the mass conservation equation (Eq.), the RHS represents the mass exchange between the flow and the erodible bed, which might be potentially signification in a hyperconcentrated flow which large erosion or deposition. The 3rd terms in the RHS of Eqs. (and) represent the effect of density variations, which makes the current hyperbolic system differ from the traditional shallow water equation in which the sediment concentration has no impact on the flow. The 4th terms in the RHS of Eqs. () and () represent the momentum transfer due to sediment exchange between the water and the erodible bed.

MODEL TESTS AND VERIFICATIONS

Simulation of a Dam-break Flow in a Mobile Channel: The numerical model is used to simulate an idealized transient process due to a dam-break flow over a horizontal bed. The channel length is set to be 50km, and the dam is initially located at the middle of the channel (x=25 km). The initial water depths upstream and downstream of the dam are h1=40 m and h2=2 m, respectively. Uniform sediment of size d=4 mm is used and the Manning's roughness of n=0.03 is presumed.

To simulate the 1D problem, three cells are used in the transversal direction and symmetric boundary condition is used for the two side boundaries. The simulation is focused on the transient process due to dam-break, rather than process driven by unsteady hydrographs, thus the wall boundary condition is adopted for the upstream and downstream boundaries. A spatial step of $\Delta x = 10$ m and a time step of 0.1 s are used. Initial sediment concentration was unknown in the original paper by Cao et al. (2004), and zero initial sediment concentration is chosen here.

Figure 1 shows a comparison of the free surface and bed profiles simulate by SRH-2D with and without those extra terms associated with hyperconcentrated flows and in Cao et al. (2004). The following are observed.

Bed erosion occurs during dam break near the location of dam. Bed erosion is a combined effect of sediment eroded from the bed and deposited on the bed. SRH-2D obtained similar bed erosion with Cao et al. (2004). The location of the maximum erosion originally occurs at the dam, and then moves upstream.

Ignoring the extra terms related to the density gradient and the terms related to the exchange between the flow and the erodible bed increases the bed erosion during a dam break problem. It can be understood that the extra term from the sediment eroded from the bed would slow down the momentum of the flow, thus reduce the capability of the flow to erode bed. However, this observation is only valid in a horizontal channel without slope. The increased sediment density could increase the channel's capacity to erode bed in a sloped channel.

The extra terms related to the density gradient and the terms related to the exchange between the flow and the erodible bed in hyperconcentrated flow increase the wave front speed and height.

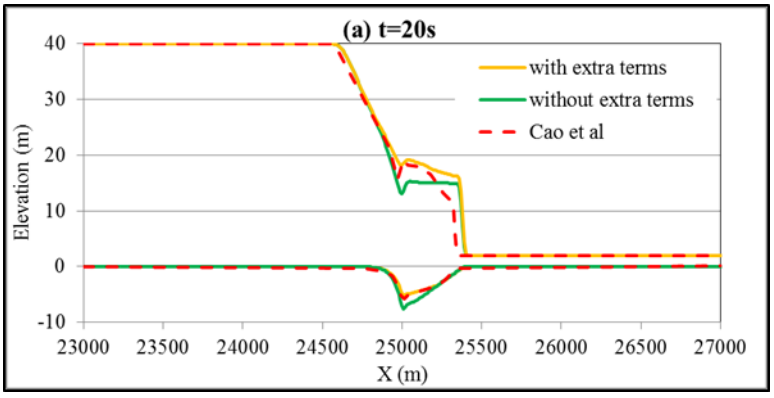

Figure 1 Evolution of water surface and bed profiles

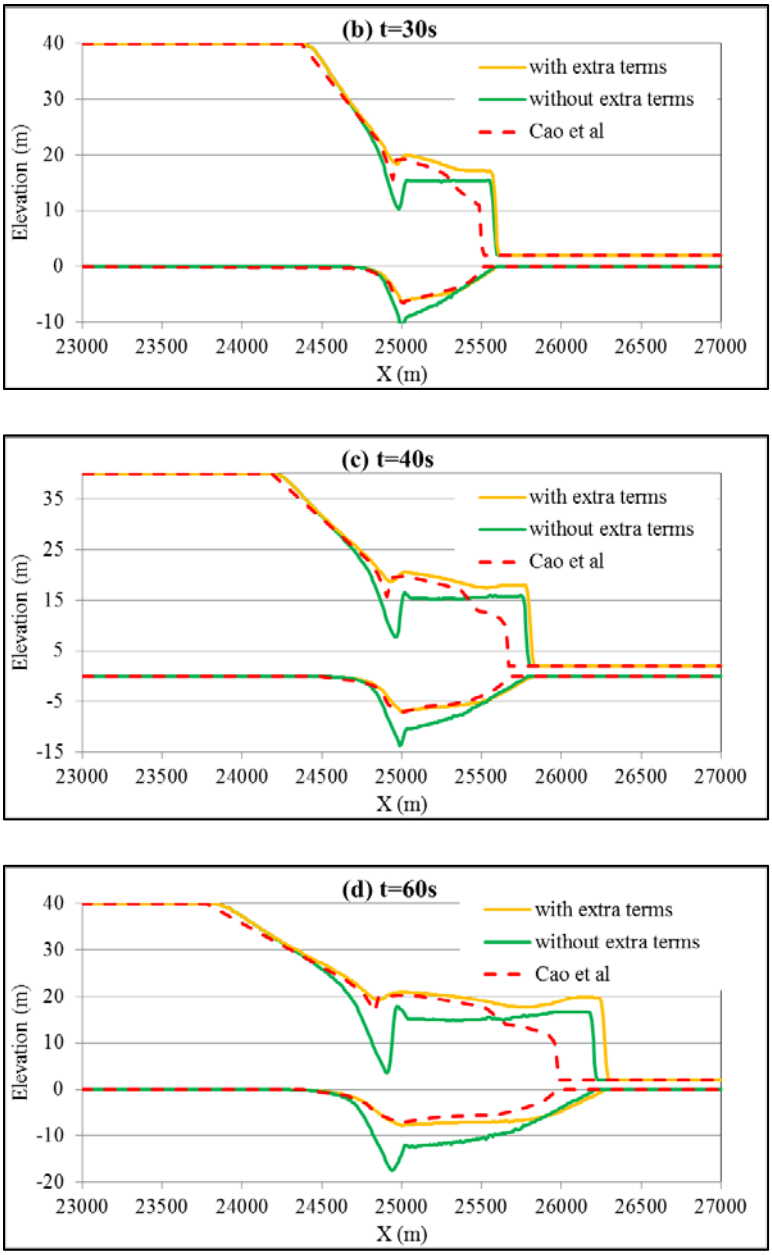

Figure 1 Continued

Simulation of a Dam-break Flow in a Mobile Channel with a Sudden Enlargement: Dam break experiments over mobile beds were performed at the Civil Engineering laboratory of the Université Catholique de Louvain, Belgium (Zech et al., 2008; Spinewine and Zech, 2007; and Palumbo et al., 2008) and was simulated by Xia et al. (2010).

The experiment was conducted in a 6m long flume with a non-symmetrical sudden enlargement from 0.25 m to 0.5 m width located 1 m downstream for the gate at x=3 m. The dam break was simulated by a rapid downwards movement of a thin gate at the middle of the flume to reach initial test conditions that approach as much as possible the idealization of an instantaneous dam collapse while minimizing perturbations to the sediment and water during gate removal. The sediment used was uniform coarse sand ranging from 1.2 to 2.4 mm with d_{50}=1.82 mm and a density of 2680 kg/m^3. Before bed profiling, the sand was compacted in place to reach a reproducible solid packing of concentration 53% (47% porosity). The initial conditions included 0.1 m sand thickness over the whole flume

and an initial clear water depth of 0.25 m upstream of the gate and dry bed downstream of the bed. A Manning's coefficient of 0.026 was used for the simulation.

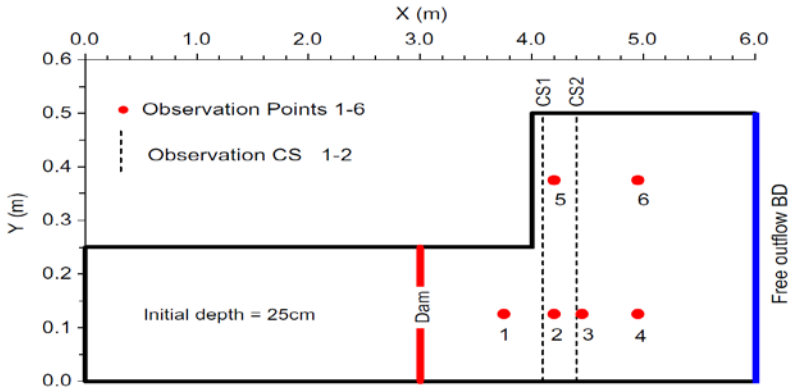

Figure 2 Sketch of a dam-break flow experiment over a mobile bed (Source: Xia et al., 2010)

Figure 3 shows measure and simulated water surface elevation time series, Xia et al. (2010) simulated, and SRH-2D simulated at locations P1 (3.7, 0.125), P2 (4.2,0.125), P3 (4.45,0.125), P4 (5.0, 0.125), P5 (4.2, 0.375), and P6 (5.0, 0.375). It can be seen that the current numerical model predicts the water surface elevation well in both the magnitude and timing.

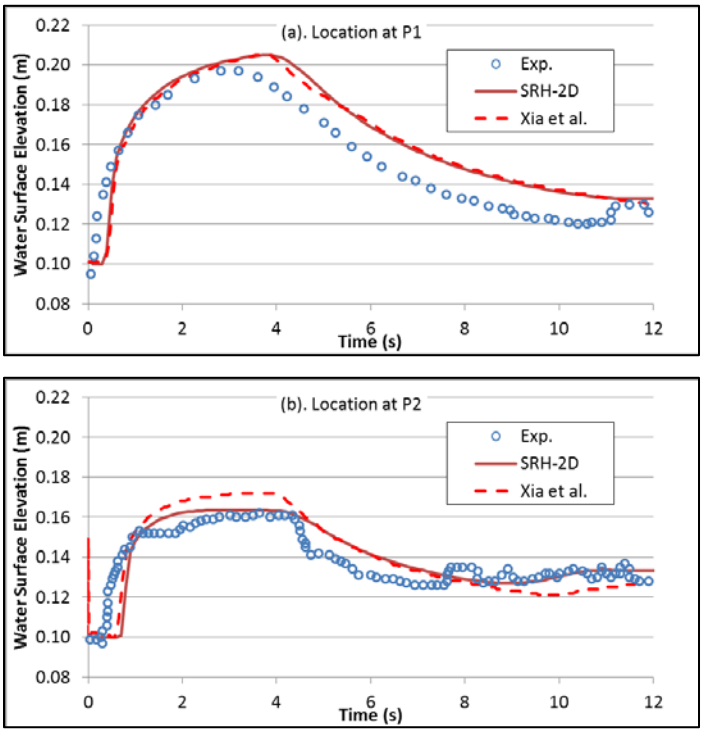

Figure 3 Comparisons between the observed, Xia et al. (2010) calculated, and current SRH-2D calculated water surface elevations

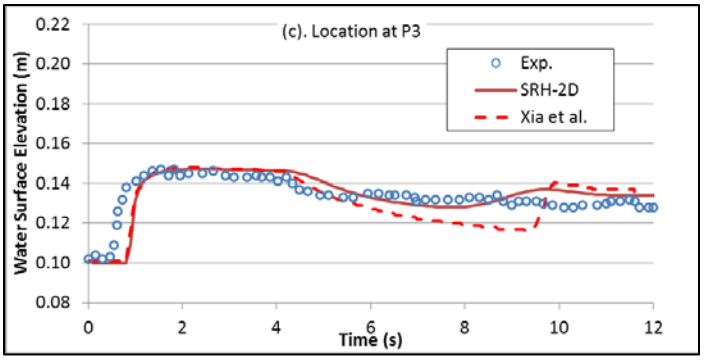

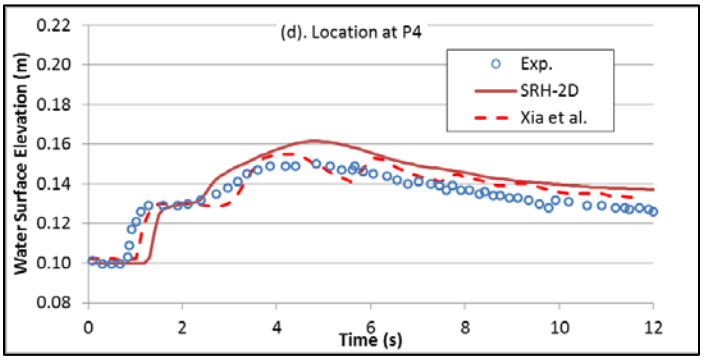

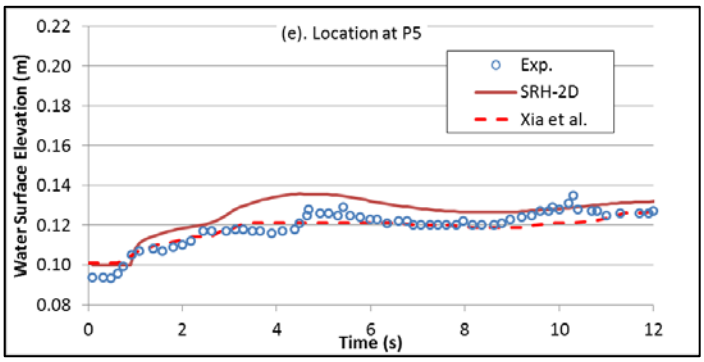

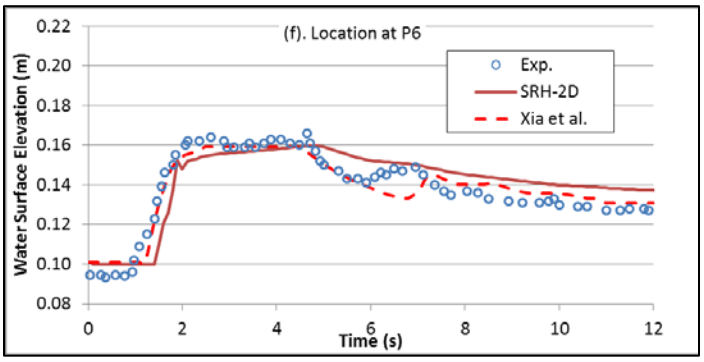

Figure 3 Continued

Figure 4 shows the comparisons of the bed profiles observed in laboratory, simulated by Xia et al. (2010), and simulated by SRH-2D. The SRH-2D simulation includes the discussed extra terms related to hyperconcentrated

flow. The sediment erosion and deposition were simulated using the sediment transport capacity functions of Wu and Long (1993) for suspended load and Dou et al. (1999) for bed load. At CS1 (x=4.1 m), the maximum bed scouring depth was predicted well, however, the model under-predicted the deposition on the left side of the channel after expansion. At CS2 (x=4.4), the model over-predicted the channel erosion and under-predicted channel deposition. A circulation zone is created by the channel expansion, and the deposition rate is closely related to the size of the circulation zone and the turbulence within it.

The test case was also simulated using the erosion and deposition equations for hyperconcentrated flow of Cao et al. (2004 and 2006, and Eqs. and) and the sediment transport capacity function of Engelund and Hansen (1966). Cao et al.'s equations over-predicted channel erosion by one order of magnitude and Engelund and Hansen's equation under-predicted the erosion by one order of magnitude. Both of these equations are intended for rivers, but the Engelund and Hansen formula was not developed for hyperconcentrated flows.

The following conclusion can be drawn from this testcase:

- The numerical model predicts the water surface elevation with high accuracy in a suddenly expanded channel.
- The numerical model reproduces the channel erosion well, however with less accuracy compared with the simulation of water surface elevation. The numerical model under-predicts the sediment deposition in the circulation zone.
- The sediment erosion and deposition rate can be calculated directly from corresponding equations or indirectly from sediment transport capacities. The correct simulation of the channel bed depends on the correct selection of these equations and model calibration.

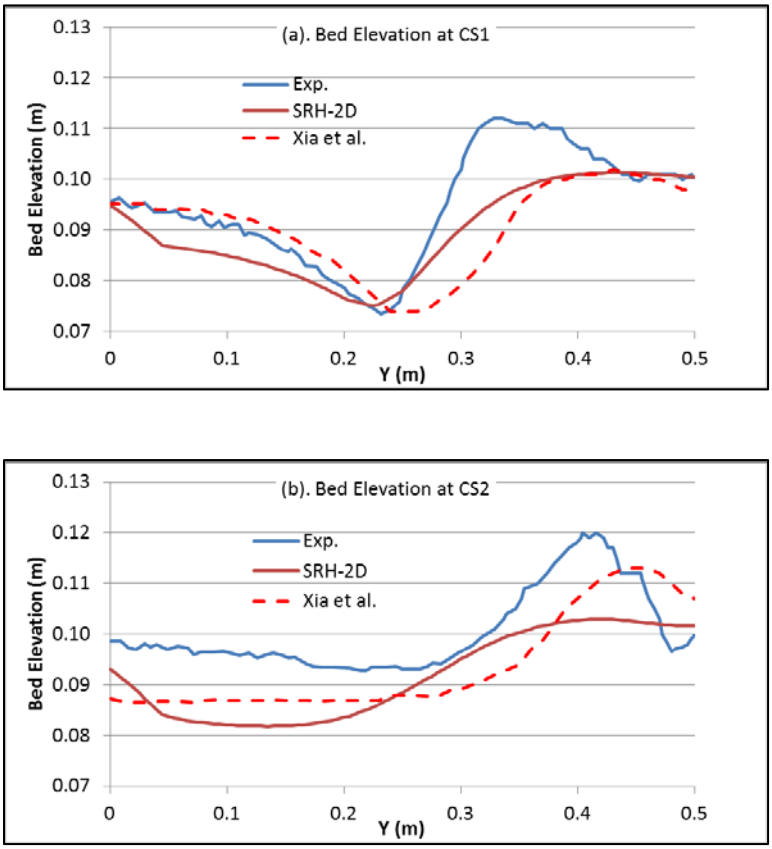

Figure 4 Comparisons between the observed, Xia et al. (2010) calculated, and current SRH-2D calculated water surface elevations

Summary

The current SRH-2D model developed at Bureau of Reclamation is extended to include the effect of sediment concentration on sediment fall velocity, sediment erosion and deposition, density variance in the momentum equation, and the exchange of flow and bed in the mass and momentum equations. The numerical model is tested and validated using two cases : an idealized transient flow and sediment process due to a dam-break flow over a horizontal bed and a more complex dam-break flow with a sudden enlargement. It is shown that the modifications are necessary for hyper-concentrated flow simulation. Also, the new model is validated and is found to predict the observed water surface elevation fairly well.

The study also finds that hyperconcentrated sediment-laden flow alters the flow density and the particle fall velocity. Currently equations for sediment erosion and deposition rates for a hyperconcentrated flow are based on laboratory data or are site specific. They should be examined before they can be applied to actual field conditions.

The extra terms related to the density gradient and the terms related to the exchange between the flow and the erodible bed in hyperconcentrated flow increase the water front speed and wave height during a dam break.

REFERENCES

Abderrezzak, K. E. K., and Paquier, A. (2011). "Applicability of Sediment Transport Capacity Formulas to Dam-Break Flows over Movable Beds." Journal of Hydraulic Engineering, Vol.137(2), 209-221.

Cao, Z. X., Pender, G., and Carling, P. (2006). "Adv. Water Resour." Shallow water hydrodynamic models for hyperconcentrated sediment-laden floods over erodible bed, Vol.29(4), 546–557.

Cao, Z., Pender, G., Wallis, S., and Carling, P. (2004). "Computational dam-break hydraulics over mobile sediment bed." Journal of Hydraulic Engineering, Vol.130(7), 689–703.

Coussot, P., and Piau, J. M. (1994). "On the behavior of fine mud suspensions." Rheologica Acta, Vol.33(3), 175-184.

Dou, X. P., Li, T.L., and R., D. G. (1999). "Numerical model of total sediment transport in the." Chinese Ocean Engineering, Vol.13(3), 277–286.

Engelund, F., and Hansen, H. (1966). "Hydraulic resistance in alluvial streams." ASCE Journal of the Hydraulics Division, Vol.92(2), 315-326.

Guo, Q. C., He, M. M., and Han, Q. W. (1995). "Analysis on Scour and Siltation in Sanmenxia Reservoir." Journal of Sediment Research, Vol.1, 48–57, (in Chinese).

Guo, Q., Hu, C., Takeuchi, K., Ishidaira, H., Cao, W., and Mao, J. (2008). "Numerical modeling of hyper-concentrated sediment transport in the lower Yellow River." Journal of Hydraulic Research, Vol.46(5), 659–667.

He, L., Duan, J. G., Wang, G., and Fu, X. (2012). "Numerical Simulation of Unsteady Hyperconcentrated Sediment-Laden Flow in the Yellow River." Journal of Hydraulic Engineering, Vol.138(11), 958-969.

Julien, P. Y., and Paris, A. (2010). "Mean velocity of mudflows and debris flows." Journal of hydraulic engineering , Vol.136(9), 676-679.

Kim, D., and Lee, S. O. (2012). "Stable Numerical Model for Transcritical Flow and Sediment Transport on Uneven Bathymetry." Journal of Hydraulic Engineering, Vol.138(1), 46-56.

Mouri, G., Shiiba, M., Hori, T., and Oki, T. (2011). "Modeling reservoir sedimentation associated with an extreme flood and sediment flux in a mountainous granitoid catchment, Japan." Geomorphology, Vol.125, 263–270.

Ni, J. R., Zhang, H. W., Xue, A., Wieprecht, S., and Borthwick, A. G. L. (2004). "Modeling of hyperconcentrated sediment-laden floods in lower Yellow river." Journal of Hydraulic Engineering, Vol.130(10), 1025–1032.

NRC. (1982). Selecting a methodology for delineating mudslide hazard areas for the National Flood Insurance Program. Committee on Methodologies for Predicting Mudflow Areas, National Research Council, National Academy Press, Washington, D.C.

O'Brien, J. S., and Julien, P. Y. (1985). "Physical properties and mechanics of hyperconcentrated sediment flows." Proc., Specialty Conf. on Delineation of Landslides, Flash Flood and Debris Flow Hazards in Utah, Utah Water Research Laboratory, Utah State Univ., Logan,Utah 260–279.

Palumbo, A., Soares-Frazao, S., Goutière, L., Pianese, D., and Zech, Y. (2008). "Dam-break flow on mobile bed in a channel with a sudden enlargement." Proceedings of the River Flow 2008 Conference.

Pierson, T. C. (2005). Hyperconcentrated flow—transitional process between water flow and debris flow. Edited by Debris-flow hazards and related phenomena (159-202). Springer Berlin Heidelberg.

Spinewine, B., and Zech, Y. (2007). "Small-scale laboratory dam-break waves on movable beds." Journal of Hydraulic Research, Vol.45(sup1), 73-86.

Taiwan Water Resources Agency. (2012). Simulation and Experiment Studies for Bed Evolution in Hyper-concentrated Flow River (2/3). Water Resources Planning Institute, Taiwan Water Resources Agency, (In Chinese).

Wan, Z., and Wang, Z. (1994). Hyperconcentrated Flow. IAHR Monograph, A.A. Balkema, RotterDam, and Brookfield.

Wu, B. S., and Long, Y. Q. (1993). "Corrections for the formula of sediment transport capacity in the Yellow River." Yellow River, Vol. (7), 1-4, (In Chinese).

Wu, W. M., and Wang, S. S. Y. (2007). "One-dimensional modeling of dam-break flow over movable beds." Journal of Hydraulic Engineering, Vol.133(1), 48–58.

Xia, J., Lin, B., Falconer, R. A., and Wang, G. (2010). "Modelling dam-break flows over mobile beds using a 2D coupled approach." Advances in Water Resources, Vol.33(2), 171-183.

Yang, C. T., Molinas, A., and Wu, B. (1996). "Sediment transport in the Yellow River." Journal of Hydraulic Engineering, Vol.122(5), 237-244.

Zech, Y., Soares-Frazão, S., Spinewine, B., and Le Grelle, N. (2008). "Dam-break induced sediment movement: Experimental approaches and numerical modelling." Journal of Hydraulic research, Vol.46(2), 176-190.

Zhang, H., and Zhang, Q. (1992). "The formula of sediment carrying capacity for the flow in the Yellow River." Journal of Yellow River, Vol.1.

Zhang, H., Huang, Y., and Zhao, L. (2001). "A Mathematical Model for Unsteady Sediment Transport in the Lower Yellow River." International Journal of Sediment Research, Vol.16(2), 150-158.

SEDIMENT-GENERATED NOISE (SGN): COMPARISON WITH PHYSICAL BED LOAD MEASUREMENTS IN A SMALL SEMI-ARID WATERSHED

J.R. Rigby, Research Hydrologist, USDA-ARS, Oxford, MS, JR.Rigby@ars.usda.gov; Roger A. Kuhnle, Research Hydraulic Engineer, USDA-ARS, Oxford, MS, Roger.Kuhnle@ars.usda.gov; Bradley T. Goodwiller, R&D Engineer, University of Mississippi National Center for Physical Acoustics, University, MS, btgoodwi@olemiss.edu; Mary H. Nichols, Research Hydraulic Engineer, USDA-ARS, Tucson, AZ, Mary.Nichols@ars.usda.gov; Wayne O. Carpenter, R&D Engineer II, University of Mississippi National Center for Physical Acoustics, University, MS, wocarpen@olemiss.edu; Daniel G. Wren, Research Hydraulic Engineer, USDA-ARS, Oxford, MS, Daniel.Wren@ars.usda.gov; James P. Chambers, Senior Scientist, University of Mississippi National Center for Physical Acoustics, University, MS, chambers@olemiss.edu

Abstract: Passive acoustic techniques for the measurement of Sediment-Generated Noise (SGN) in gravel-bed rivers present a promising alternative to traditional bedload measurement techniques. Where traditional methods are often prohibitively costly, particularly in labor requirements, and produce point-scale measurements in time and space under highly heterogeneous conditions, acoustic techniques offer the potential to inexpensively monitor gravel movement quasi-continuously over larger spatial scales. While acoustic methods show great potential, significant work is required to provide a general relationship between acoustic signals and physical bedload sampling under field conditions. We addressed this problem by deploying hydrophones for monitoring SGN in the Lucky Hills subwatershed of the USDA-ARS Walnut Gulch Experimental Watershed for the 2014 runoff season (July-September). Bedload was collected using a pit sampler attached to a supercritical Santa Rita-style measuring flume at the catchment outlet. Results of the comparison of physical measurements with SGN monitoring are shown for three runoff events. The field results are compared with expectations derived from theory and laboratory experiments to suggest improvements and new directions for future SGN investigations.

INTRODUCTION

Conventional measurements of bed load are difficult, time consuming, often of unknown accuracy, and expensive. Consequently, data on the rate of bed load transport of most streams is lacking. There is an ongoing need for low-cost instrumentation that can be deployed to work autonomously in remote locations. One promising technology that has been used as a surrogate for bedload in the past is recording sound made by particles transported by flow, which will be referred to as Sediment Generated Noise (SGN), and converting the acoustic energy into a transport rate (Gray et al. 2010). The equipment needed for the recording is relatively inexpensive and is amenable to customization into a self-contained unit. Previous work has examined sound propagation in shallow natural environments (Forrest et al. 1993; Forrest 1994) and the potential for SGN monitoring in large rivers (Barton 2006). A key need for the advancement of SGN work is a broader database of acoustic signal in different hydraulic settings and the development of data analysis techniques. For this information to be useful, the acoustic data needs supporting independent sediment load measurements that can be used in the

interpretation of the acoustic data. Our work was supported by the Federal Interagency Sedimentation Project and represents an effort to improve the techniques used to convert SGN to rates of bed load transport. Here, we describe a field test in a natural channel within the Walnut Gulch Experimental Watershed, near Tombstone, Arizona. The results include a detailed analysis of the frequency content of the acoustic signal and correlation of load with specific acoustic bandwidths.

METHODOLOGY

Data were collected in the Lucky Hills watershed, a 9.1 acre subwatershed of the United States Department of Agriculture (USDA), Agriculture Research Service (ARS) Walnut Gulch Experimental Watershed near Tombstone, Arizona. Average annual precipitation for the watershed over the period 1961-2013 was 356 mm yr^{-1} with approximately two-thirds of annual precipitation occurring during the summer monsoon season (July-September). Soils in the watershed are primarily sandy loam with a large fraction of coarse material composed of fragmented rock. Figure 1 shows the particle size distribution of bed material taken near the outlet of the Lucky Hills watershed. Further characterization of the study area is available in Ritchie et al. 2005.

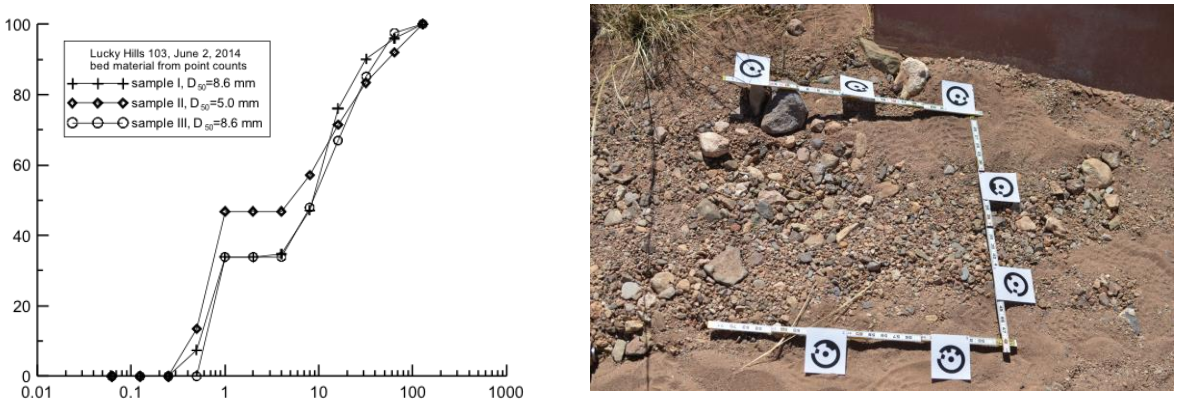

Figure 1 Left: Particle size distribution (mm) from three samples taken along the Lucky Hills watershed main channel. Large fractions of sandy loam and coarse angular material resulted in a bimodal size distribution. Right: Photo of typical coarse sediment deposits along the ephemeral channel.

Two hydrophones were deployed in the watershed immediately upstream of the Santa Rita style measuring flume at the watershed outlet (Figure 2). Due to the low flow depths anticipated during runoff events, the hydrophone housing was installed within 2 cm of the bed oriented in a downstream direction. Each hydrophone was deployed in a PVC housing affording moderate directionality in the measured acoustic signal. Hydrophones and amplifiers from Teledyne Reson were used to record sound at a rate of 25 kHz, using a computer with a multi-channel data acquisition card. The hydrophones were manually activated at the onset of precipitation prior to the appearance of runoff and sampled through the entire hydrograph.

Figure 2 Left: The Santa Rita style flume at the outlet of Lucky Hills subwatershed. This view faces upstream from the outfall (where the pit sampler was later placed) toward the hydrophone mount (post seen in the upstream channel). Right: Photo of the PVC housing of the downstream hydrophone (mounting post visible in center of left photo).

Coarse sediment was collected at the outflow of the measuring flume using a 75cm deep rectangular pit sampler. The walls of the sampler were constructed with 3 mm perforated sheet steel to allow water and finer particles to pass through during a runoff event. After each event the bulk load was removed from the pit trap, dried, and sieved into four size classes using ½", 16 mm, 32 mm, and 64 mm sieves. The size range for coarse sediment collection was chosen based in part on both the particle size characteristics of the site and on expected acoustic emissions from particles based on earlier studies. The particle size distributions derived from channel sediments shown in Figure 1 show a bimodal distribution with very little mass occurring in the 1-10 mm range. Thorne (1985, 1986) found that peak emission frequency and equivalent spherical diameters of natural marine sediments approximately followed the relationship

$$f_{peak} = 209/D^{0.88} \quad (1)$$

where the frequency, *f*, is given in Hz and diameter, *D*, in meters. Accordingly the expected peak emission frequency for a 10 mm particle should be approximately 12 kHz which is very near the resolving limit of our 25 kHz sample rate.

RESULTS

Seven runoff events were monitored between August 1 and September 8, 2014 (Figure 3). The total coarse sediment load (>12mm) for each event ranged from 0.13 kg to 444 kg, peak stage from 1.5 cm to 26 cm, and runoff duration from 28 minutes to 5.25 hours (Table 1). The size distribution of the coarse sediment load for each event is summarized in Figure 4 and Table 1. In each of the larger events, the intermediate coarse fractions (16-64 mm) represented the majority of the sampled mass.

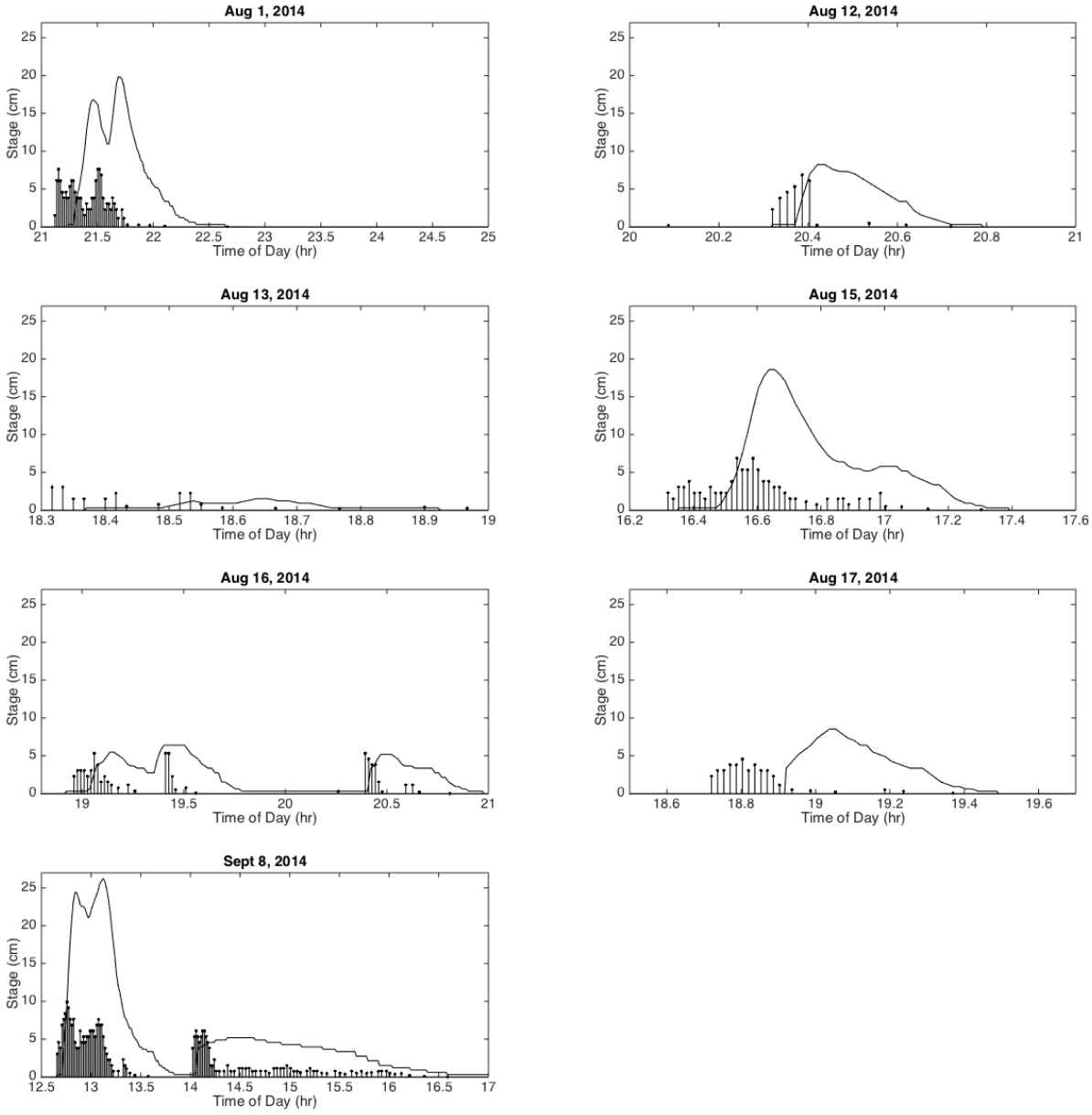

Figure 3 Hydrographs of the seven runoff events from Lucky Hills subwatershed monitored in August-September 2014. The stem plots overlaid show the occurrence of precipitation (heights shown are 1/10 of rain rate in mm/hr) at Rain Gage 83 near the center of the watershed.

Figure 5 shows a sample hydrograph from the flow event on August 15. The acoustic data for these events is also shown, represented by the integrated acoustic signal (volts) over one minute bins. There is an initial peak in the acoustic data associated with flow-induced noise around the instrument housing as the hydrophones were submerged (at ~8cm stage) followed by a period of elevated acoustic activity during the peak of the hydrograph until the stage again falls below the submergence level of the instrument. Three of the events (August 1, August 15, and September 8) reached depths significantly above 8cm which provided the target acoustic data with the hydrophone fully submerged.

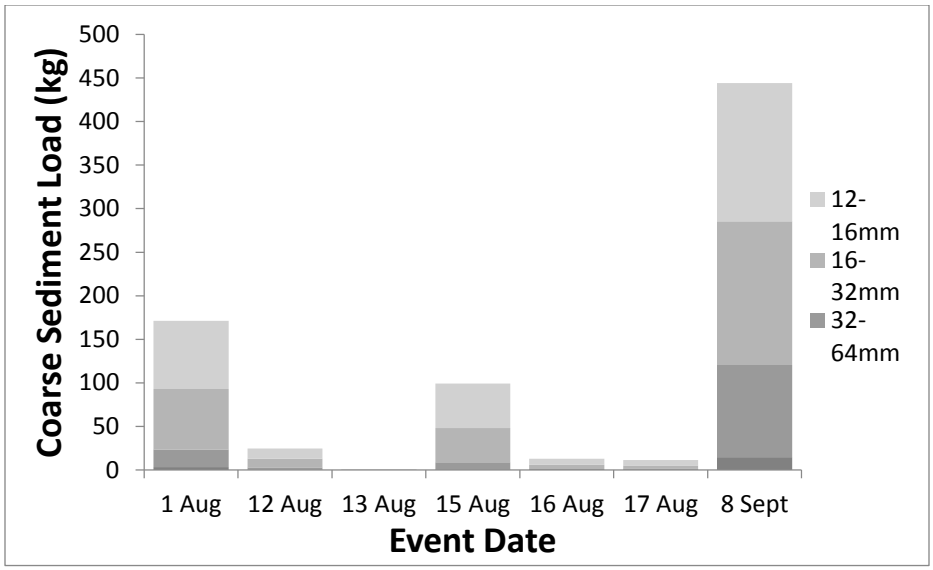

Figure 4 Coarse sediment load by size fraction for the seven runoff events monitored in 2014 in the Lucky Hills subwatershed. Coarse sediment was collected in a pit trap below the outlet flume and sieved for size fractions.

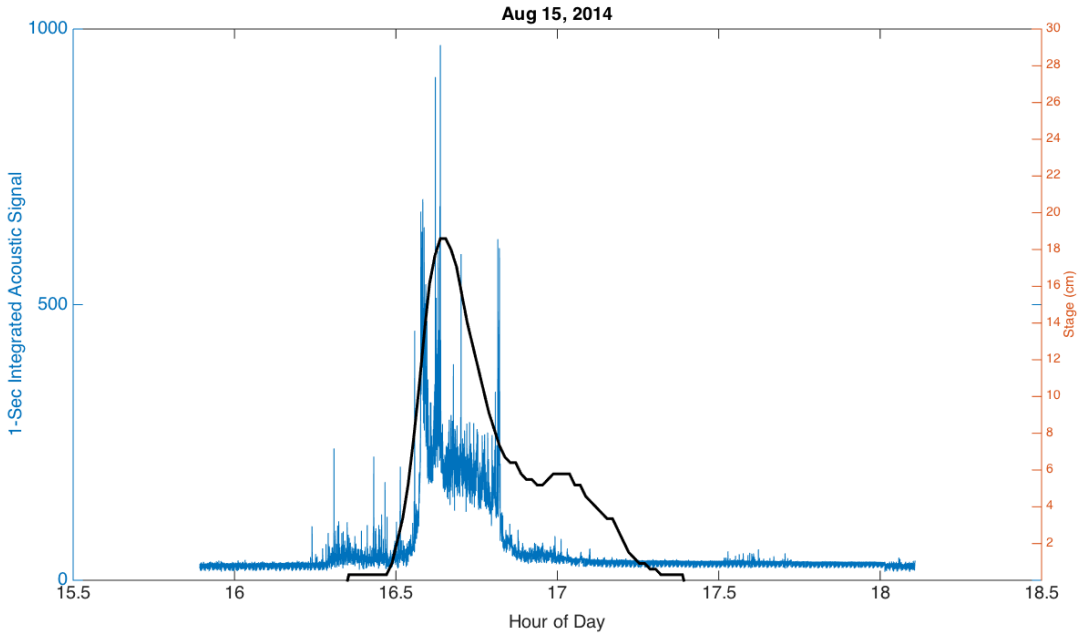

Figure 5 Hydrograph (black) and concurrent rectified acoustic signal (25kHz sampled voltage summed over one-second bins) for the August 15, 2014 runoff event. Note the rain noise prior to the rise in the hydrograph, and spikes in acoustic signal around stages of 8-10cm as the instrument was submerged and later reemerged associated with flow noise generated by the instrument housing.

The acoustic signal recorded over the course of the hydrograph is a composite of: (1) rain drop noise striking the instrument before it was submerged and the water surface after submergence; (2) elevated flow noise near the time of submergence when the water surface was at the hydrophone; (3) flow noise around the instrument housing while the instrument was submerged; and (4) acoustic emissions from particle collisions. Bjorno (1994) studied the acoustic spectra of rain splash on a free water surface and found that the acoustic energy peaked near 15 kHz with a minimum near 5 kHz. Flow noise around the instrument housing was recognizable by ear during and after submergence and displayed characteristic frequencies in the 0-2 kHz band. With these observations suggesting a window of opportunity where noise generated by particle impact would not be mixed with sound from other sources, we focused analysis on frequencies in the range 3 kHz – 11 kHz. Figure 6 shows the correlation over the three largest events between the coarse sediment load and the integrated acoustic signal in each of eight 1-kHz frequency bands beginning at 3 kHz. Each data point in Figure 6 is the correlation over three events between sediment load and SGN amplitude for a frequency band. In all cases the correlations are high, but the larger size fractions show both higher correlations and more structure as a function of frequency band with a peak near 5-6 kHz. Employing Thorne's relationship for peak emission frequency (equation 1), this would correspond to a particle size of approximately 24 mm which is notably near the median of the coarse fraction in Figure 1. The lack of frequency dependence in the correlation in the 12-16 mm particle size class suggests that the signal was made up of a combination of particle impact other flow-generated noise. It is logical that SGN and 12-16 mm load are still well-correlated, but the greater energy generated by the impacts of larger particles provide a better picture of how transport changed with passage of the hydrograph. Finally, while three events make a sparse data set, the overall high correlations in Figure 6 as well as the linear relationship shown in Figure 7 show a very promising relationship between coarse sediment load and integrated acoustic signal in the 5-6 kHz band for the three events.

Table 1 Coarse sediment load and runoff statistics for the seven monitored events.

Event	**Runoff**		**Coarse Sediment Load** (kg)				
Date	Duration (hr)	Peak Stage (cm)	>64mm	32-64mm	16-32mm	12-16mm	Total
Aug 1	1.4	19.8	3.31	20.27	69.45	78.07	171.1
Aug 12	0.47	8.2	0.42	2.62	9.82	11.73	24.59
Aug 13	0.55	1.5	0	0	0.05	0.08	0.13
Aug 15	1.03	18.6	0.81	8.04	39.29	50.9	99.04
Aug 16	2.05	6.4	0	1.08	4.8	7.13	13.01
Aug 17	0.57	8.5	0.66	1.06	3.53	6.32	11.57
Sept 8	5.25	26	14.64	105.86	165.05	158.7	444.25

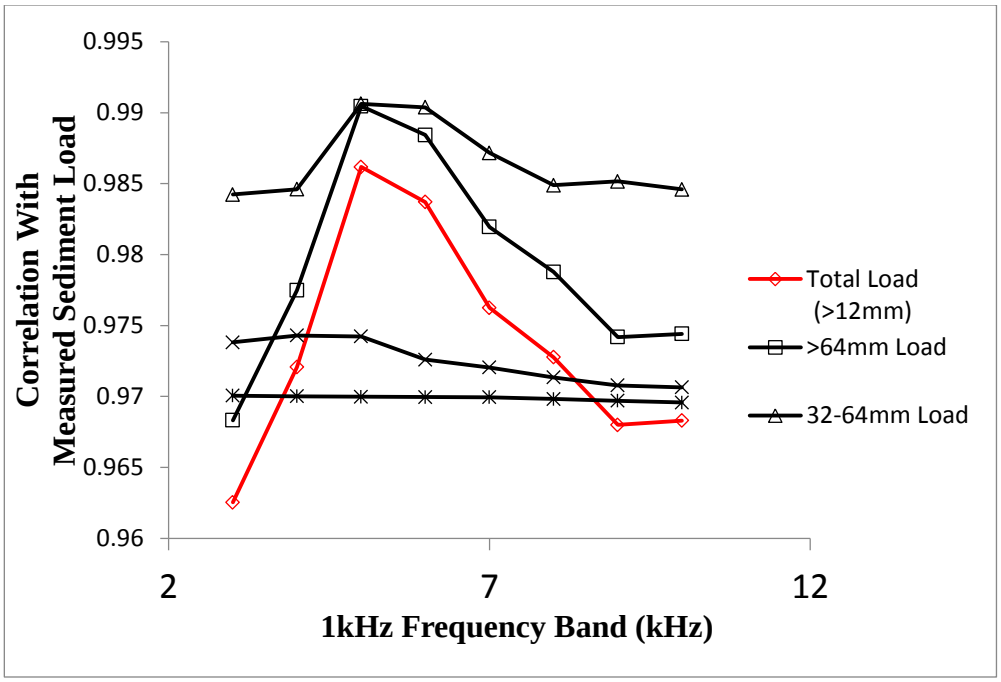

Figure 6 Correlation between coarse sediment load data and integrated acoustic signal for three runoff events (Aug 1, Aug 15, Sept 8). The power spectra of the acoustic data were integrated in 1 kHz bands from 3 kHz to 10 kHz to examine correlation with each size class of total sediment load. Correlation for the coarsest fractions is strongest in the 5-6 kHz frequency range.

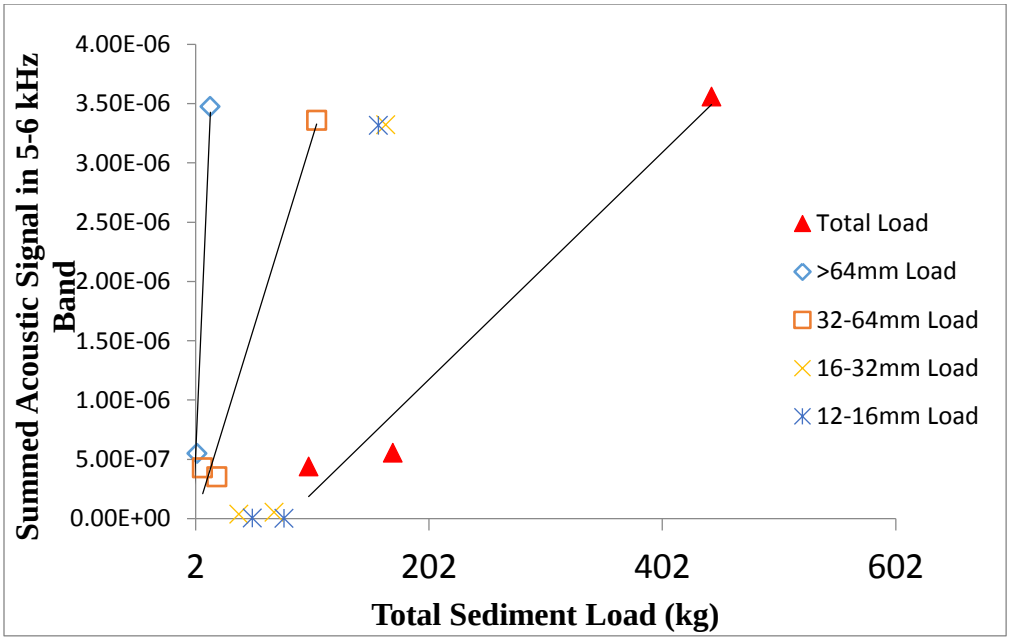

Figure 7 Relationship between integrated acoustic signal in the 5-6 kHz band versus coarse sediment load for the three largest runoff events.

CONCLUSION

We deployed hydrophones in a flashy ephemeral watershed in southeast Arizona to evaluate the potential for using passive acoustic measurements to monitor coarse sediment transport in streams. This location provided discrete flow events during which the entire coarse sediment load of the stream could be captured for analysis and characterization. While shallow flows reduced the number of events that completely submerged the hydrophone, the results of the three large flow events shown in Figures 6-7 are a high quality acoustic data set with known sediment loads. In particular, the frequency range 3 kHz-11 kHz provides a useful window that is below the peak frequencies of rain splash but above the dominant frequencies of flow noise. Correlation between total sediment load and integrated acoustic signal was high for all size classes across the frequency range of interest with a peak for the large size classes in the 5-6 kHz band.

This study has implications for future efforts to use SGN as a surrogate for bedload in flashy streams.

- Development of hydrodynamic housings for hydrophone deployment would further reduce flow noise around the instrument and simplify data analysis.
- Further study of the frequency content of acoustic phenomena such as raindrop impact may help in the separation of SGN from sound generated from other sources.
- It may be possible to use the low frequency data from the hydrophone system as an indication of flow strength, increasing the usefulness of data collected in remote deployments.

REFERENCES

Barton, J.S., (2006). Passive acoustic monitoring of bedload in mountain streams: University Park, PA, The Pennsylvania State University, Ph.D., 107 p.

Bjorno, L. (1994). Underwater rain noise : sources, spectra and interpretations. Journal de Physique IV, 04 (C5), pp.C5-1023-C5-1030.

Forrest, T. G. (1994). From sender to receiver: propagation and environmental effects on acoustic signals. Amer. Zool., 34:644-654.

Forrest, T. G., Miller, G. L., and Zagar, J. R. (1993). Sound propagation in shallow water: Implications for acoustic communication by aquatic animals. Bioacoustics 4:259-270.

Gray, J.R., Laronne, J.B., and Marr, J.D.G. (2010). Bedload-surrogate monitoring technologies: U.S. Geological Survey Scientific Investigations Report 2010–5091, 37 p.

Ritchie, J.C., Nearing, M.A., Nichols, M.H., and Ritchie, C.A. (2005). Patterns of soil erosion and redeposition on Lucky Hills watershed, Walnut Gulch Experimental Watershed, Arizona. Catena 61:122-130.

Thorne, P. D., (1985). The measurement of acoustic noise generated by moving artificial sediments. J. Acoust. Soc. Am., 78(3): 1013-1023.

Thorne, P. D., (1986). Laboratory and marine measurements on the acoustic detection of sediment transport. J. Acoust. Soc. Am., 80(3): 899-910.

SEDIMENT-GENERATED NOISE (SGN): LABORATORY DETERMINATION OF MEASUREMENT VOLUME

Daniel G. Wren, Research Hydraulic Engineer, USDA-ARS, Oxford, MS, Daniel.Wren@ars.usda.gov;
Bradley T. Goodwiller, R&D Engineer, University of Mississippi National Center for Physical Acoustics, University, MS, btgoodwi@olemiss.edu;
J.R. Rigby, Research Hydrologist, USDA-ARS, Oxford, MS, JR.Rigby@ars.usda.gov;
Wayne O. Carpenter, R&D Engineer II, University of Mississippi National Center for Physical Acoustics, University, MS, wocarpen@olemiss.edu;
Roger A. Kuhnle, Research Hydraulic Engineer, USDA-ARS, Oxford, MS, Roger.Kuhnle@ars.usda.gov;
James P. Chambers, Senior Scientist, University of Mississippi National Center for Physical Acoustics, University, MS, chambers@olemiss.edu

Abstract: Passive acoustic technology has the potential to allow continuous measurement of bedload moving through streams by recording Sediment-Generated Noise (SGN) from interactions between coarse bedload particles. The technology is relatively economical and is amenable to automated operation. While the magnitude of recorded sound has been shown to be well-correlated with bedload transport, substantial work is still needed before the technique is ready for broad deployment. A key need is a quantitative understanding of the measurement volume from which sounds are received so that field sites may be properly instrumented and data properly analyzed to estimate bed material flux. The propagation of sound in an acoustic waveguide, limited propagation of lower frequencies in shallow streams, and the effect of bed roughness on sound propagation are examples of specific areas in need of experimental research. Towards this end, a series of experiments was initiated, in collaboration with the University of Mississippi National Center for Physical Acoustics, in a flume at the National Sedimentation Laboratory in Oxford, Mississippi. The results of sound propagation testing in an empty tank, over a gravel bed, over a bed of cobbles and gravel, and over a cobble bed will be presented, along with a relationship for determining transmission loss for the different bed types.

INTRODUCTION

During efforts to develop methods for quantifying bedload transport using Sediment-Generated Noise (SGN), very little information on sound propagation in shallow water with rough boundaries was found. Most acoustic propagation research has been in marine environments (e.g., Thorne 1985 and 1986), where there is nearly infinite lateral extent and where shallow refers to depths of tens of meters. The characteristics of sound propagation over boundaries composed of gravel, cobbles, or boulders has not been documented. Without this knowledge, it is not possible to arrive at a reasonable estimate of the measurement volume of a hydrophone submerged in a stream. The development of more general calibrations for SGN conversion, which do not depend on the specific characteristics of the stream reach used for calibration, has been stymied by the lack of a technique for obtaining an estimate of the distance or volume from which SGN can be detected. There are several reasons why an estimate of the measurement volume is important in SGN measurement: (1) as a step towards development of a general approach to converting SGN data into bedload flux; (2) to determine how much of a stream is being monitored (needed for proper

scaling of bedload estimates); (3) for planning number of instruments to place in channel; and (4) for quantification of uncertainty and data quality.

Even though high amplitude sounds originating from a long range can produce the same amplitude at a receiver as low amplitude sounds originating from a short range, sound propagation characteristics and instrument parameters may be used to establish a maximum range from which sounds can be received. There are limits to the amplitude of sound generated by particle collision, and these will be a related to the bed material size distribution. By starting with an estimate of maximum likely amplitudes, a sound propagation model, and instrument parameters, an estimate of the measurement footprint can be made. Some of the parameters that will affect the size of the measurement volume include: characteristics of the sound field, bed material size distribution, water depth, bed roughness, hydrophone parameters, and recording system.

Sound pressure levels (SPL) are generally reported in the decibel (dB) scale: $SPL=20 \log(P_e/P_{ref})$ where P_e is the measured amplitude of the sound wave and P_{ref} is the reference amplitude (Urick, 1975). The decay of acoustic amplitude with range (R), caused by the spreading of sound waves in an unbounded medium (spherical spreading), is: $TL=20 \log(R)$, where TL is transmission loss. Spreading in a medium with two parallel reflecting boundaries (cylindrical spreading) is: $TL=10 \log(R)$ (Urick, 1975). For a stream bed that is covered with sand, gravel, and cobbles, it is not clear how TL should be calculated, especially since the environment often has complex and variable cross-sectional geometry. The work described here addresses the need for establishing the correct TL model for sound in a rectangular channel with one rough boundary.

METHODOLOGY

Data were collected in a rectangular cross-section with three realistic roughnesses: gravel (D_{50}≈35 mm), cobbles (D_{50}≈150 mm) and a mixture of the two, made by filling the pores of the cobble bed with gravel. The Root Mean Square (RMS) roughness of each bed was measured using a commercially available laser scanner (Figure 1). The flume section was 8.5 m long by 1.2 m wide and was lined with 3 layers of redwood lattice. For the frequencies of interest, roughly 1-10 kHz, the redwood did not provide anechoic conditions; however, the signal amplitude over distance had drastically fewer large amplitude excursions, caused by modal interference, than were observed with bare flume walls and bed. Four hydrophones were spaced at 1, 2, 4, and 8 m from the origin (Figure 2). The hydrophone positions were not changed; the sound source was moved 4 meters from the origin in 25 cm increments to provide smaller range increments. Sounds were recorded at three different depths (≈25, 30, and 35 cm), but the effect of depth for the frequencies and depths of these experiments was small.

A.

B.

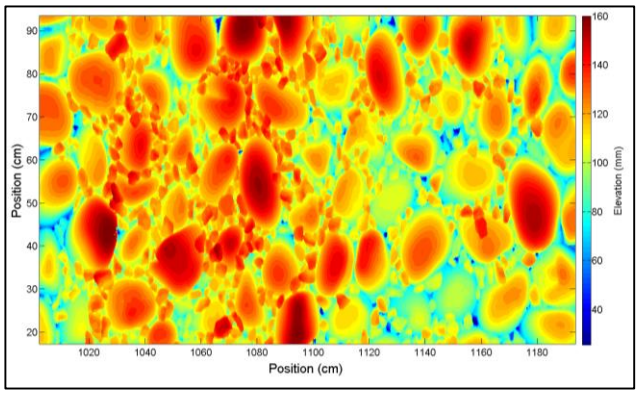

Figure 1 (A) Line laser scanner used to define RMS roughness values. (B) Laser scan data from mixed gravel/cobble roughness.

Figure 2 Hydrophones deployed over the cobble bed.

Hydrophones and amplifiers from Teledyne Reson were used to record sound at a rate of 50 kHz, using a computer with a multi-channel data acquisition card. A mechanical sound source was constructed, using a pneumatic cylinder that could be remotely activated (Figure 3). The sound produced by the impact of the steel puck on the aluminum barrier was an impulse followed by a brief ring down, resulting in a short signal without a clearly defined frequency spectrum. The signal was well-suited to the needs of this work, since it minimized the effect of water-depth related attenuation of low frequencies.

Figure 3 Mechanical sound source

RESULTS

Figure 4 shows that the transmission loss did not follow either the cylindrical or spherical models; however, there are clear patterns of transmission loss with range and increasing bed roughness. The rms roughness height of the bed materials is: gravel ≈ 13 mm, cobbles ≈ 31 mm, cobbles+gravel ≈ 18 mm, and redwood lattice ≈ 8 mm. Based on the acoustic amplitude and bed roughness measurements, transmission loss equations can be found from Figure 5. For example, transmission loss in the gravel case is estimated by substituting its rms roughness (13 mm) into $Y=0.22X+17$, yielding TL ≈20 log (R). As can been seen in Figure 5, TL increases rapidly with increasing roughness, and the intermediate case of cobbles+gravel shows a transmission loss between the cobble and gravel cases. The increase in TL with increasing roughness can be attributed to sound scattering, which reduced the amplitude of the signal propagating to the hydrophones. Another contributing effect is multiple contacts with the sides and bottom of the flume and the water surface. Each contact resulted in a loss of amplitude, although the scattering effects of bottom contacts likely resulted in the greatest losses.

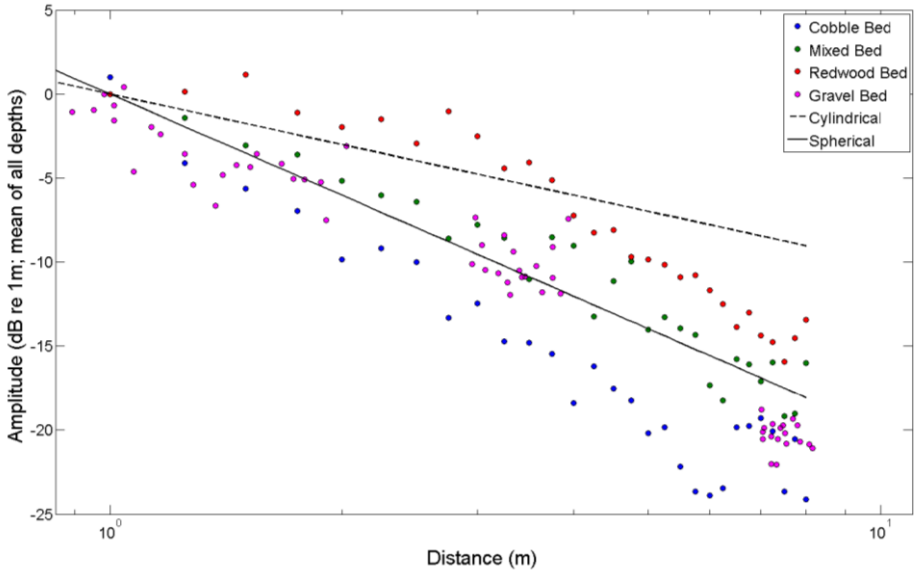

Figure 4 Results from propagation experiments.

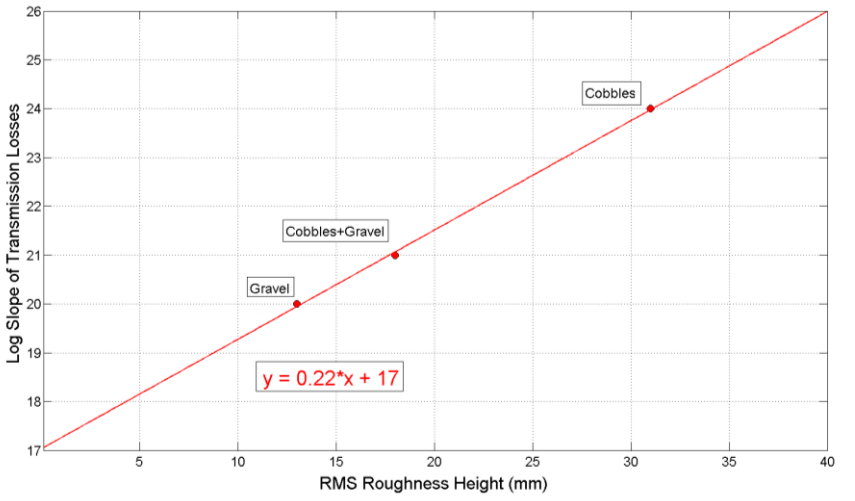

Figure 5 Transmission loss multipliers for a range of bottom roughness. The equation can be used to estimate the transmission loss based on measured RMS bottom roughness.

CONCLUSION

The results shown in Figures 4 & 5 represent an important step towards a more comprehensive picture of sound propagation in a shallow-water waveguide with rough boundaries. The propagation of sound generated by mechanical impact was measured over gravel, cobbles+gravel, and cobble beds, yielding a relationship that can be used to estimate the transmission loss for each

of the beds. Future work on this topic should include a field component, since the rectangular cross-section of the flume does not represent the geometry found in most stream channels. Field experiments will make use of the same mechanical sound source and instrumentation that was used in the laboratory. In addition, at least two of the hydrophones will be located at a small fixed distance from one another, allowing for the coherence of the sound field to be evaluated. This is another key step towards a general understanding of the sound field in a wave-guide with rough boundaries and will be affected by both the roughness of the bed and the wedge shape on the sides of the channel.

REFERENCES

Thorne, P. D., 1985. The measurement of acoustic noise generated by moving artificial sediments. J. Acoust. Soc. Am., 78(3): 1013-1023.

Thorne, P. D., 1986. Laboratory and marine measurements on the acoustic detection of sediment transport. J. Acoust. Soc. Am., 80(3): 899-910.

Urick, R. J., (1975) Principles of underwater sound. McGraw Hill, New York.

DESIGN AND IMPLEMENTATION OF A FIELD DEPLOYABLE PASSIVE ACOUSTIC BEDLOAD-MONITORING SURROGATE

Bradley T. Goodwiller, R&D Engineer, University of Mississippi National Center for Physical Acoustics, University, MS, btgoodwi@olemiss.edu. Daniel G. Wren, Research Hydraulic Engineer, USDA-ARS, Oxford, MS, Daniel.Wren@ars.usda.gov. J.R. Rigby, Research Hydrologist, USDA-ARS, Oxford, MS, JR.Rigby@ars.usda.gov. Wayne O. Carpenter, R&D Engineer II, University of Mississippi National Center for Physical Acoustics, University, MS, wocarpen@olemiss.edu. James P. Chambers, Senior Scientist, University of Mississippi National Center for Physical Acoustics, University, MS, chambers@olemiss.edu. Roger A. Kuhnle, Research Hydraulic Engineer, USDA-ARS, Oxford, MS, Roger.Kuhnle@ars.usda.gov. Robert C. Hilldale, U.S. Bureau of Reclamation, Technical Service Center, Denver, CO, rhilldale@usbr.gov

ABSTRACT

Various methods of employing passive acoustics to monitor bedload transport have been explored in both the lab and field. Expanding upon this research, a hydrophone-based passive acoustic bedload-monitoring system was designed, tested and deployed by researchers at the University of Mississippi and the National Sedimentation Laboratory in Oxford, MS. Several field studies have been conducted at various sites: the Elwha River in Port Angeles, WA; the Trinity River in Weaverville, CA; Bear Creek in Denver, CO; and the Walnut Gulch Watershed in Tombstone, AZ. At each field study, acoustic data was collected alongside physical measurements of bedload transport. Preliminary results correlating sediment transport with the measured sediment generated noise will be presented. In addition, the design and fabrication of an improved prototype system is underway. The new system is designed to be more easily deployed and operable by non-experts. This will greatly expand the range of available testing environments. Results from this effort will be presented alongside any available calibration data taken with the new system.

EXTENDED ABSTRACT

The prospect of using passive acoustic methods to monitor bedload transport has been investigated in various facets. The acoustic properties of impacting gravel particles were investigated (Thorne 1985) in a laboratory setting. Preliminary work was done on the Trinity River (Barton et al. 2010) which showed that using hydrophones to detect gravel movement showed promise. To continue this research, a passive acoustic system comprising of equipment already owned by researchers at the National Center for Physical Acoustics was assembled and tested. The system was tested at four different field sites shown in Figure 1: the Trinity River in Weaverville, Ca; the Elwha River in Port Angeles, CA; the Walnut Gulch Watershed near Tombstone, AZ at the Lucky Hills sub-watershed; and Bear Creek in Denver, CO.

Figure 1 Top Left: Photograph of the first iteration of the passive acoustic bed load monitoring system, deployed at Douglas City on the Trinity River, CA. Top Right: Installation of three hydrophones at the Elwha River, WA. Bottom Left: Installation of two hydrophones at the Lucky Hills subwatershed near Tombstone, AZ. Bottom Right: Installation at the Bear Creek, near Denver, CO

Figure 2 shows positive correlation between acoustic root-mean-square (rms) and bedload discharge at the Trinity River. The discharge was determined from concurrent physical samples taken by Graham Matthews and Associates. Although there were physical samples taken at the Elwha River, they were designed to calibrate the impact plates also being tested at the time. The physical samples were repeated at individual locations, and were thus unusable as a 'total discharge' measurement. Therefore, an attempt was made to correlate the acoustic data with the data collected from the impact plates spanning the river. Figure 3 shows that the overall trends between acoustic rms and bedload discharge are positively correlated. The data from Walnut Gulch in still in analysis as of this writing. All of these tests indicate the usefulness of acoustic surrogates. For this reason, the researchers at the NCPA began a project to redesign the system to make it much more portable, robust and user-friendly.

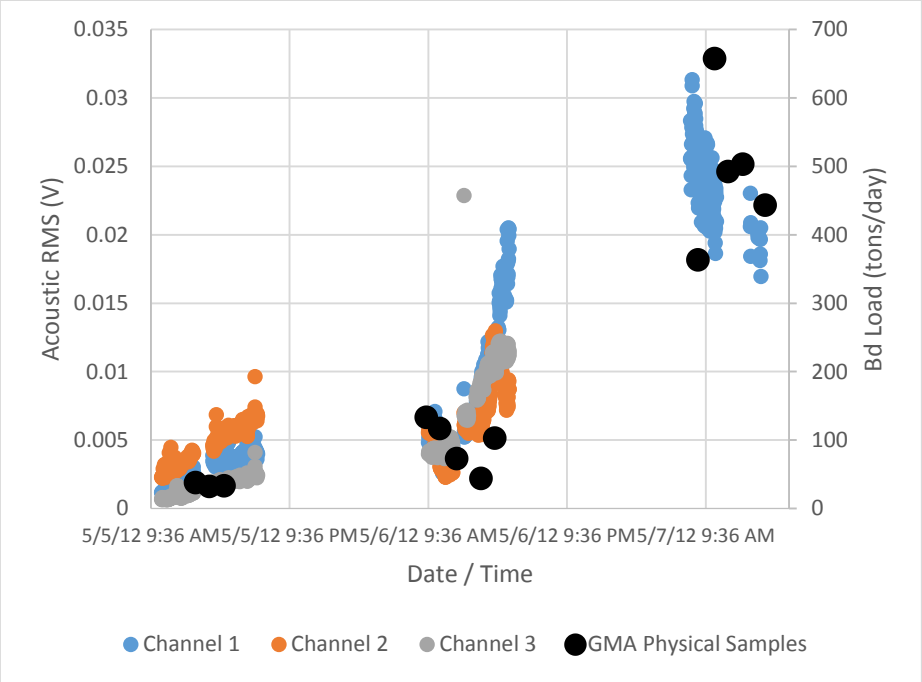

Figure 2 Acoustic data shown with physical measurements of bed load at the Douglas City site on the Trinity River, CA. Graham Matthews and Associates collected the physical bed load measurements

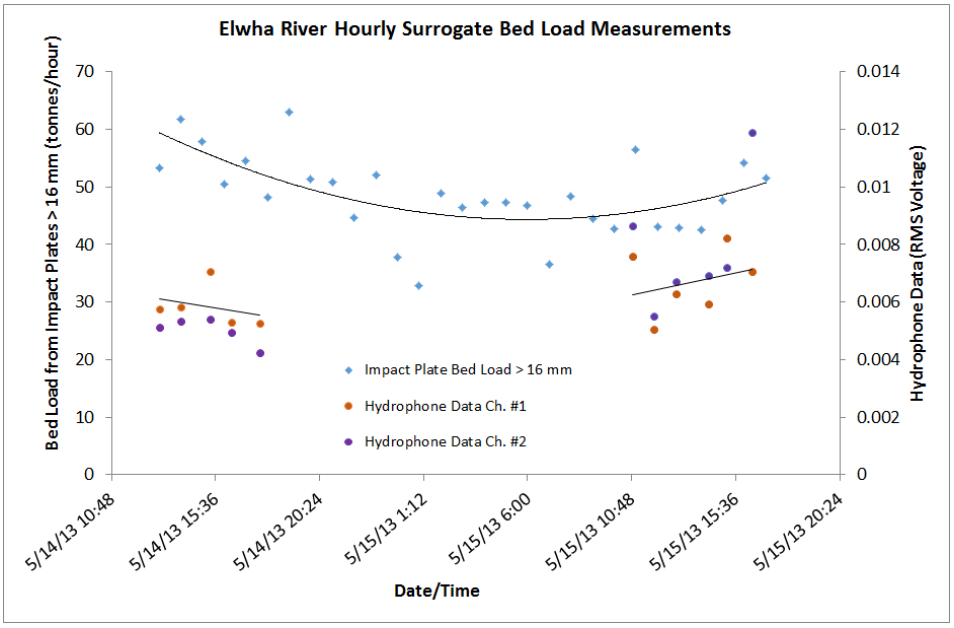

Figure 3 Comparison of bed load transport measured with the Elwha bed load impact plate system using a preliminary calibration and data from two hydrophones deployed approximately 70 meters upstream. Data shown are hourly averages of both systems

The system as it was deployed in the aforementioned field studies was comprised entirely of laboratory-grade equipment. As such, many of the components were delicate and unwieldy. Every aspect of the data collection process was investigated for improvements. The improvement process began with researching and testing alternate hydrophone options. The RESON TC-4013 hydrophones used in the field studies are delicate and far more sensitive than is necessary for the project. After testing three alternatives, the HTI 96-MIN Exportable hydrophone was chosen. This hydrophone is suitably sensitive at the audio range, and has a built-in amplifier. This eliminates the need for the external amplifiers required by the RESON hydrophones. In addition, the HTI hydrophones are sturdy and robust. A casing and mounting system for this hydrophone are currently in design. The casing will be designed to reduce flow noise around the hydrophone as much as possible, and it will also provide protection from debris. Other areas of the system including data recording, power requirements, and duration of operation are still under investigation as of this writing.

REFERENCES

Barton, J. S., Slingerland, R. L. , Pittman, S., and Bagrielson, T.B. (2010). Monitoring Course Bedload Transport with Passive Acoustic Instrumentation: A Field Study. U.S. Geological Survey Scientific Investigations Report.

Thorne, P. D. (1985). The Measurement of Acoustic Noise Generated by Moving Artificial Sediments. Journal of the Acoustical Society of America 78(3):1013-1023.

CONTINUOUS BED LOAD MEASUREMENT WITH IMPACT PLATES ON THE ELWHA RIVER, WASHINGTON

Robert C. Hilldale, Hydraulic Engineer, Sedimentation and River Hydraulics Group, Bureau of Reclamation, Denver, CO, rhilldale@usbr.gov

Abstract: A bed load impact plate system has been installed on the Elwha River for the purpose of continuously measuring coarse bed load during and after the removal of two large dams. The surrogate bed load measurement system consists of 72 instrumented stainless steel plates spanning approximately 38 meters across the channel and is currently capable of quantifying coarse bed load ≥16 mm. Each plate is instrumented with either a geophone (46 plates) or an accelerometer (26 plates). To date, a preliminary calibration of the geophone impact plates has been obtained using 16 data points, achieving an r^2 value of 0.796. Each data point is a temporal average of 8 - 10 physical bed load measurements correlated to the impulses measured with the geophones. The most recent calibration data and calibration procedures are presented herein. Observations of temporal and spatial variability in coarse bed load transport during and after dam removal are discussed.

INTRODUCTION

The use of indirect or surrogate technologies for quantifying fluvial sediment transport is a rapidly expanding field, providing the ability to continuously monitor sediment transport with high resolution. In an effort to provide continuous, high resolution measurement of coarse bed load transport on the Elwha River during and after the removal of Elwha and Glines Canyon Dams, a system of instrumented, stainless steel, bed load impact plates was installed in 2008 and 2009 at river kilometer 5 (measured upstream from the mouth, Figure 1). The Elwha impact plate system was patterned after the Swiss geophone impact plate system (Bänziger and Burch 1990; Rickenmann and McArdell 2007) installed at several locations throughout Switzerland, Austria, and Israel (Rickenmann et al. 2014). The Elwha impact plate system differs from the Swiss system by installing accelerometers on 26 of the 72 instrumented steel plates, with 46 plates instrumented with a geophone. Additionally, the dimensions of the Elwha impact plates vary slightly from the Swiss system. A thorough review of surrogate methods for quantifying bed load transport is given in Gray et al. (2010), Rickenmann et al. (2012), and Tsakiris et al. (2014). This manuscript will discuss the installation, preliminary calibration, and observations of bed load transport with respect to spatial and temporal variability. Observations of continuously measured bed load transport on the Elwha are presented and discussed.

The decision to construct a series of impact plates was based on the following: (1) maturity of the Swiss impact plate system (Rickenmann et al. 2012, 2014); (2) the ability to continuously collect bed-load data without operating personnel; (3) robust construction and demonstrated longevity (>10 years); (4) limited maintenance requirements for the physical system; (5) ability to measure bed load with a 0.5-m resolution across the stream; and (6) nonintrusive and compatible with an ecologically sensitive river (Hilldale et al. 2014). The primary drawback of the Elwha impact plate system is its inability to register a response to particles < 16 mm on the geophone plates and particles < 8 mm on the accelerometer plates. The impact plate system on the Elwha River was installed in conjunction with a previously planned concrete weir for the purpose of surface water diversion.

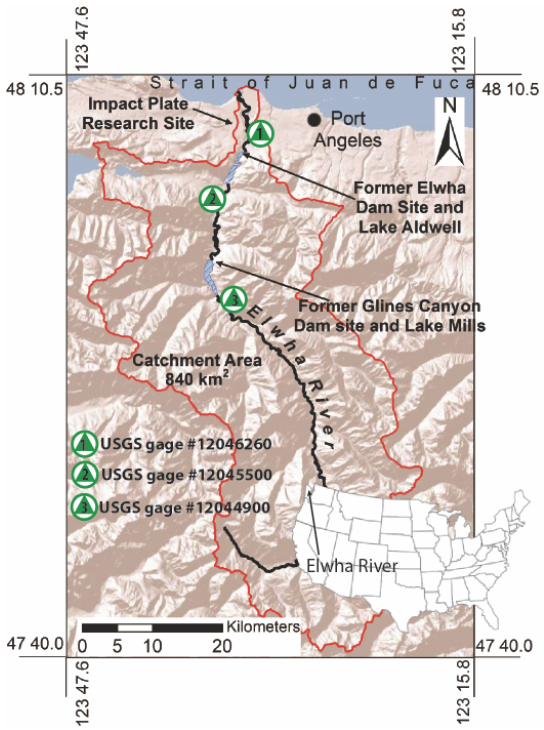

Figure 1 Location map of the Elwha River, Washington

The Elwha River: The Elwha River flows north from the Olympic Mountain range of Washington State, USA and terminates at the Strait of Juan de Fuca (Figure 1), which connects Puget Sound with the Pacific Ocean. The catchment is largely within the protected lands of Olympic National Park, consisting mostly of forested land, much of it pristine wilderness. The Elwha River is supplied with varying contributions of snowmelt, rainfall, and groundwater discharge and has a maritime climate with relatively wet, mild winters and dry, cool summers (Curran et al. 2009). Annual precipitation in the basin ranges from 560 cm in the upper basin (elevation 1,350 m) to 140 cm near the mouth (elevation 0 m) (Munn et al. 1998). The U.S. Geological Survey has operated the McDonald Bridge gage (USGS streamflow-gaging station #12045500) since 1918. The mean annual discharge is 42.8 m^3/s (Magirl et al. 2014). The 2-year, 10-year, and 100-year recurrence interval floods are 400 m^3/s, 752 m^3/s, and 1,240 m^3/s, respectively (Duda et al. 2011).

Elwha and Glines Canyon Dams: The removal of Elwha and Glines Canyon Dams on the Elwha River in Washington State is the largest dam removal project in U.S. history to date (Duda et al 2011). A total of 21 million m^3 of sediment was stored behind both dams; including an estimated 2.5 million m^3 of gravel and cobble sized sediment. Elwha Dam (32 m high, located at river kilometer 7.9) constructed in 1913, and Glines Canyon Dam (64 m high, located at river kilometer 21.6) constructed in 1927 (Figure 1) began concurrent removal beginning in September 2011. The removal of Elwha Dam was completed in May 2012, and the final portion of Glines Canyon Dam was removed in September 2014. Detailed information on the Elwha River's response to dam removal during the first two years can be found in East et al. (2014) and Magirl et al. (2014).

The Elwha Impact Plate System: The Elwha impact plate system was installed in two phases. During the first phase plates 1-12 were installed on river right. Plate numbers 1, 3, 5, 7, 9, 11 and 12 are instrumented with geophones and plates 2, 4, 6, 8, and 10 are instrumented with accelerometers. Wiring was installed in 2008 for the entire system and the wiring to be used for plates 13-72 was stored in a temporary wooden channel constructed in place of the impact plate housing to be built the following year (Figure 2). In 2009 the remaining impact plates and instrumentation were installed (Figure 2B). Plate numbers 13 – 72 are instrumented with a repeating pattern of one accelerometer plate and two geophone plates for the remainder of the cross section (e.g. plate # 13 = accelerometer,

plate # 14 and #15 = geophones, plate # 16 = accelerometer…). All wiring was routed through two conduits to the computer cabinet on the right bank and was labeled for later installation of the streamside computer monitoring system in 2011. Details on the computer hardware and software can be found in Hilldale et al. (2014).

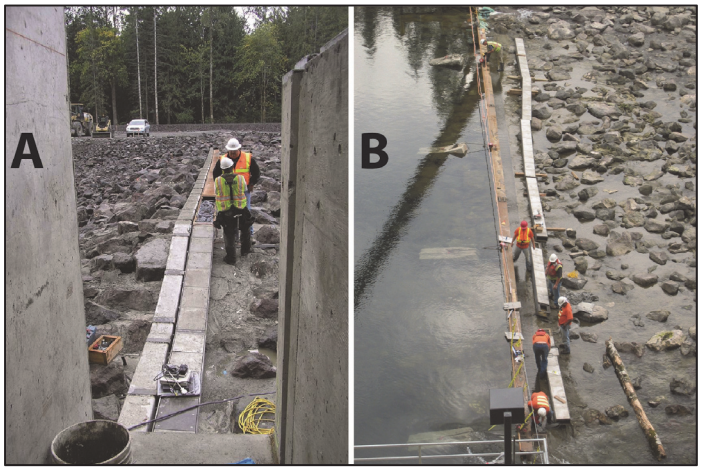

Figure 2 (A) 2008 installation of impact plates and sensors (#1 – #12) on river right, and wiring for the entire system. (B) 2009 installation of remaining impact plates (#13 – #72).

The stainless steel impact plates are 15.9 mm thick, 349 mm in the longitudinal (flow) direction, and 517 mm in the lateral dimension. The plates are mounted with their short sides adjacent to each other on a steel housing that is mounted to the downstream side of a channel spanning concrete weir. Figure 3 shows the configuration of the weir, which is at the crest of an engineered riffle with a slope of 0.015 m/m. Wiring for each instrument is routed to the stream bank through conduit contained within the housing. A low flow notch has been constructed to force low discharges against the intake structure (Figure 4). Additional details about the impact plate system can be found in Hilldale et al. 2014).

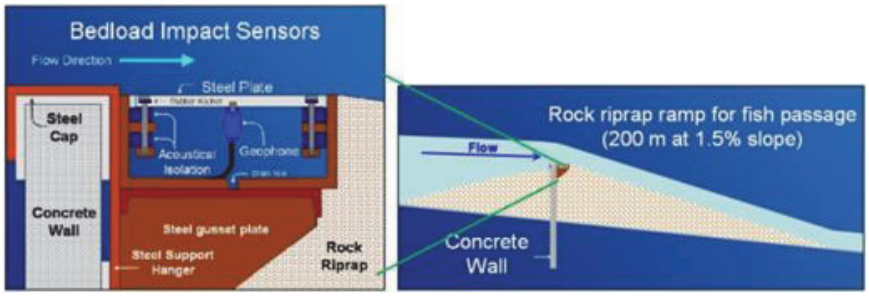

Figure 3 Drawing of the longitudinal view of the Elwha impact plate system.

A geophone induces a small voltage when a particle with sufficient mass and velocity causes the plate to deform. The voltage is sent to one of three monitoring computers, where the induced voltage is compared to the predetermined threshold value, 0.1 volts. If the voltage surpasses the threshold value, the computer program registers an impulse. The system samples at 20 kHz, accumulating impulses from individual plates for 1 minute. The software then stops collection for 19 seconds to provide limited post processing and write the data to an ASCII file for each plate.

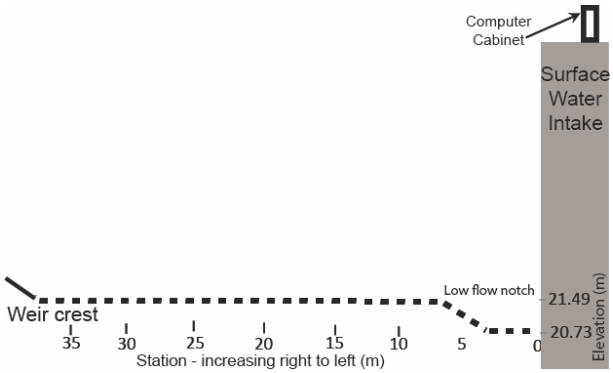

Figure 4 Cross section drawing (looking downstream) of the measurement weir.

SYSTEM TESTING AND CALIBRATION

In situ testing prior to dam removal indicated that the geophone impact plates are able to detect particles > 16 mm, and the accelerometer plates are capable of detecting particles > 8 mm. Physical bed load measurements for calibration of the geophone plates have been underway since November 2012, shortly after a major release of delta sediment the previous month from Lake Mills during the removal of Glines Canyon Dam. All references to system calibration in this manuscript refer only to those plates instrumented with a geophone. Calibration of the accelerometer plates requires further signal processing prior to in situ calibration. Flume testing is currently underway to determine an appropriate correlation between the accelerometer signals and measured bed load.

Field measurements of bed load for the purpose of system calibration were made using a TR-2 bed load sampler (Hubble et al 1985) with a 2 mm mesh bag. The TR-2 was deployed using a crane and winch mounted to a 6.4 m long cataraft that was tethered to a tag line across the channel (Figure 5). Five separate bed load sampling trips were made in November 2012, March 2013, May 2013, June 2013, and April 2014.

Figure 5 Photographs of the TR-2 (left) and the cataraft (right) used to measure bed load on the Elwha River

In November 2012 bed load transport consisted almost entirely of particles finer than 2 mm resulting in no meaningful bed load measurement due to clogging of the 2 mm mesh bag. By March 2013 bed load had coarsened significantly (Figure 6) and obtaining a correlation between measured bed load and registered impulses on the impact plates was possible. However, scatter in the individual surrogate measurements and the physical measurements using very short sample times (1 minute for the impact plate data, < 10 seconds for the physical samples) was significant enough to warrant a different approach to calibration.

A new methodology used for calibrating the geophone impact plates was employed beginning with May 2013 bed load measurements and uses both temporal and spatial averaging. The spatial average covers a 2 meter lateral distance (1 meter on either side of the TR-2), which will include two or three plates depending on the sampler location relative to the spatial arrangement of the geophone and accelerometer plates. It is assumed that bed load transport across this distance is uniform, which is consistent with USGS bed load measurement protocol outlined in Edwards and Glysson (1999). The temporal averaging uses a 30 minute sample time to obtain a reliable mean, where the TR-2 is deployed at the same station for 30 minutes, typically resulting in 8 - 10 physical measurements. The period of 30 minutes was chosen based on a temporal analysis of several arbitrarily chosen geophone plates, where the cumulative mean and standard deviation of impulses per minute arrived at a steady value in less than 30 minutes under steady flow conditions. This finding is consistent with those from a field study by Kang (1982) and a flume study by Kuhnle and Southard (1988). All measured bed load values are temporally averaged and correlated with a temporal and spatial average of the surrogate measurement from corresponding geophone impact plates. This correlation provides the necessary information with which to perform a field calibration of the impact plate system. Additional details regarding the sampling protocol can be found in Hilldale et al. 2014).

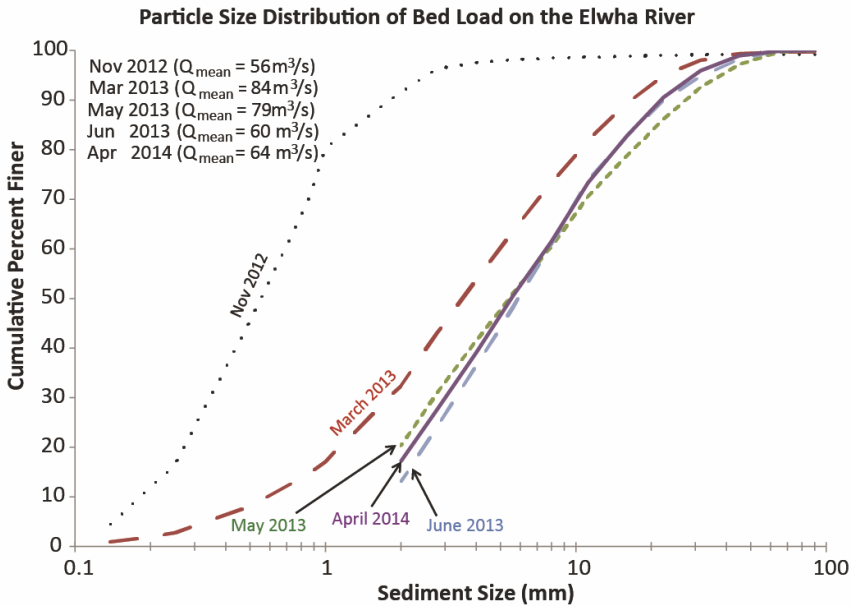

Figure 6 Grain size distribution of bed load collected with the TR-2 during system calibration.

Calibration of the Swiss geophone impact plate system using physical measurements of bed load has been shown to be best represented with a linear regression (Rickenmann et al. 2014). Based on the similarity of the impact plate systems and for comparative purposes, a linear regression has been used for the Elwha impact plate system shown in Equation 1 (Rickenmann et al. 2012):

$$IMP = k_b M \tag{1}$$

Where *IMP* represents the number of registered impulses by the geophone plate(s), *M* is the mass of sediment, and k_b is the calibration coefficient. The most recent calibration of the Elwha geophone impact plates is shown in Figure 7, indicating that k_b = 1.562x + 9.51 with a coefficient of determination (r^2) of 0.796. This calibration factor is considered to be preliminary and may change somewhat with additional data. The k_b value reported here benefits from nine additional calibration points compared to that reported by Hilldale et al. (2014). It should be noted that bed load measurements in June 2013 were not able to be used for calibration due to the malfunction of the computer monitoring system.

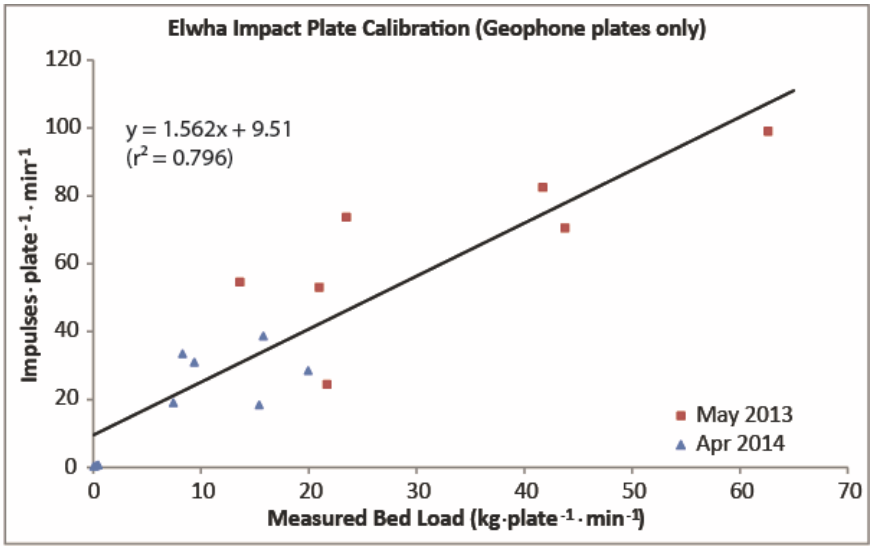

Figure 7 Plot of geophone calibration data for the Elwha impact plate system.

BED LOAD MEASUREMENT DURING DAM REMOVAL

Perhaps the most important data obtained from the impact plate system is the measurement of bed load over time. Past research has shown that correlations of bed load transport (Q_s) and discharge (Q) are poor (Habersack 2008) using a power law relationship:

$$BL = aQ^b \tag{2}$$

where BL = bed load in units of mass, Q = discharge in m^3 s^{-1}, a, and b are coefficients. Data from the Elwha bed load impact sensors also indicate that discharge is a poor predictor of bed load transport throughout the year. Figure 8 indicates a wide variability of both the coefficient (a) and exponent (b), varying throughout the year. Exponents nearly span an order of magnitude in this small sample set.

Given the unsatisfying accuracies of quantifying bed load using stage-discharge relationships or transport equations (Bunte 1990, Reid et al. 1985, Habersack et al. 2008, Kuhnle 1992), measurement of bed load presents itself as the better alternative. However, classic means of bed load measurement using pressure difference samplers present other challenges, namely poor temporal resolution, uncertainty related to involuntary particle entrainment (Bunte et al. 2008) and flow disturbance (Habersack et al. 2012). These measurements are difficult and costly to make, and potentially dangerous, on medium to large rivers during peak flows. Additionally, deployment of personnel and equipment to measure bed load during flood events is often logistically prohibitive. The use of surrogate methods for bed load measurement provides a means to eliminate many, if not all, of the challenges regarding physical measurement of bed load (aside from in-situ calibration). Surrogate bed load measurement stands to improve upon the resolution and timeliness of bed load measurement, the accuracy of which being highly dependent upon the in-situ calibration.

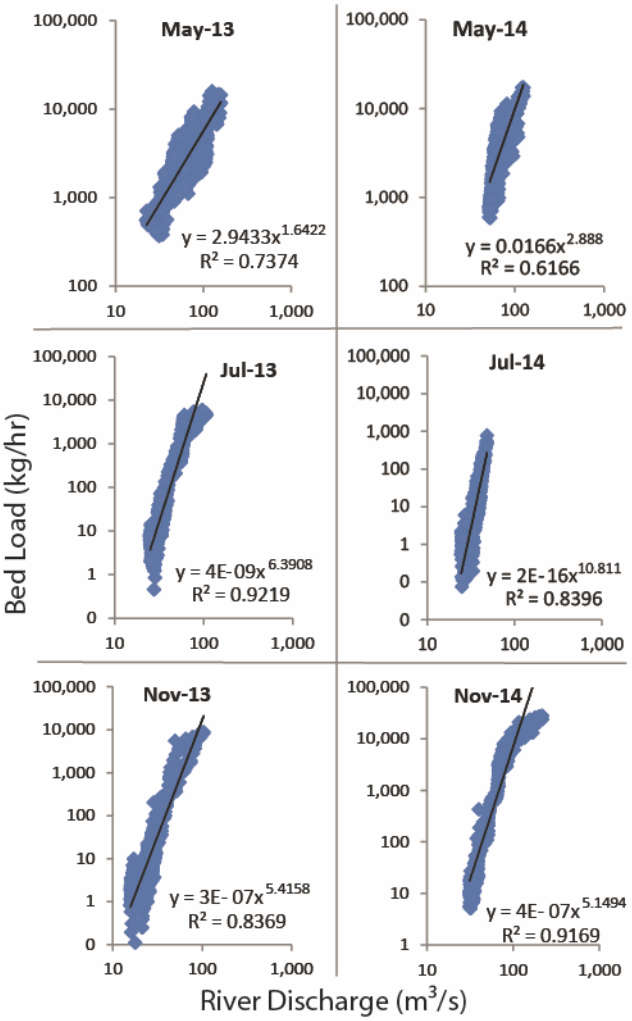

Figure 8 Plots of bed load versus discharge for selected months. November 2014 data reflects only the latter half of the month due to a brief malfunction of the data collection system.

Bed load transport > 16 mm on the Elwha River was quantified over the first two years (September 2011 through September 2013) of the incremental removal of Elwha and Glines Canyon dams using the impact plate system and a preliminary calibration of the geophone impact plates (Figure 9, Magirl et al. 2014). Geophone threshold values during most of year-one were set in such a way as to preclude the application of a bed load-to-surrogate relation. Using the standard deviation of the relative error for the preliminary calibration data (Hilldale 2014), uncertainty of the surrogate measured bed load > 16 mm is ± 52% (Magirl et al. 2014).

Because there is interest in the total bed load transported during dam removal, bed load from 2–16 mm was estimated using the ratio of coarse-grained (> 16 mm) to finer-grained (2–16 mm) material from the measured bed load samples (Figure 6) and by linearly interpolating between sample periods. The sediment-size distributions from sampled data were used to determine monthly proportions of the two size ranges, providing monthly bed load transport estimates (Figure 9). Uncertainty for bed load between 2 and 16 mm is estimated to be ± 80% (Magirl et al. 2014). For the purpose of this discussion bed load is considered to consist of particles > 2 mm. Readers are referred to Magirl et al. (2014) for additional information regarding sediment loads on the Elwha River during the first two years of dam removal.

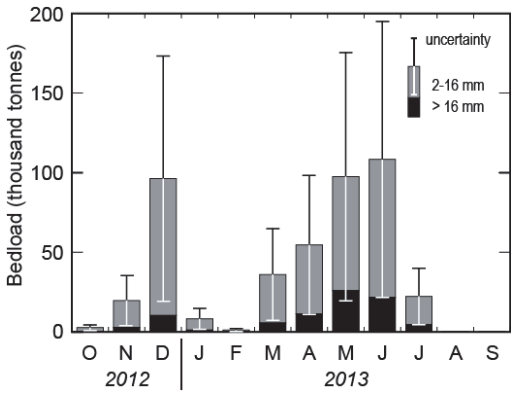

Figure 9 Monthly bed load plot for particles > 16 mm and particles between 2 and 16 mm (from Magirl et al. 2014).

BED LOAD TRANSPORT FLUCTUATIONS

Temporal and spatial variation of bed load transport has been documented in both flume (Kuhnle and Southard 1988) and field studies (Kang 1982, Reid et al. 1985, Bunte 1990, Habersack et al. 2001, Habersack et al. 2008, Habersack et al. 2012). Observations of coarse bed load transport on the Elwha present marked temporal and spatial fluctuations over more than three years of observation.

Lateral Variability: Monthly bed load data from November 2012, 2013, and 2014 (Figure 10) indicates significant variability in bed load transport (> 16 mm) across the channel. In November 2012 and November 2014 the greatest proportion of bed load transport is at river right against the surface water intake. During November 2013 bed load transport is primarily focused at stations 9.6 m to 11.7 m (Figure 10). A consistent drop in sediment transport exists at station 6.6 m, where the weir transitions from the low flow notch at river right to the flat portion across the remainder of the channel (see Figure 4). Additionally, coarse bed load transport is consistently very low or non-existent beyond station 32.5 m.

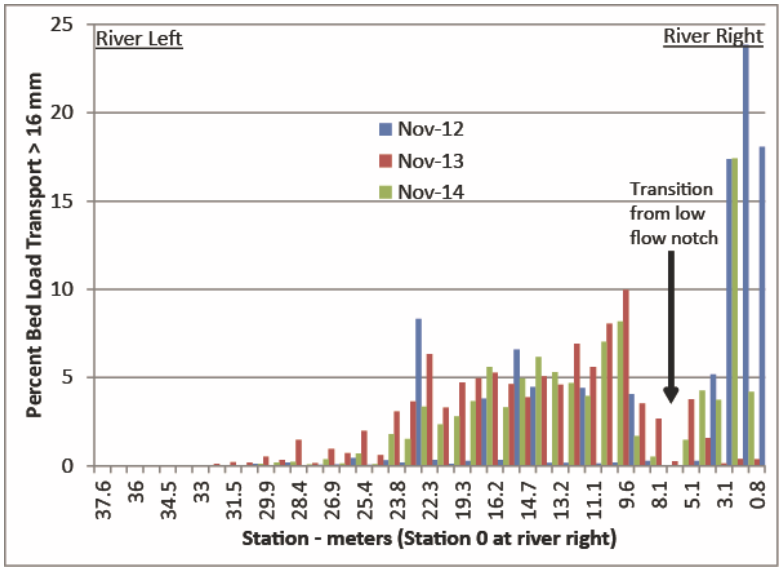

Figure 10 Graph showing the proportion of bed load transported across the channel using impact data from each geophone in the Elwha impact plate system. The transition from the low flow notch to the flat portion of the weir is shown in figure 4.

Temporal Variability: Short term and long term fluctuations of coarse bed load transport can be examined in detail using 1 minute continuous bed load data. Observations shown in Figure 11 are at a single plate (#18, station 10.1 m) over a selected day of steady flow on May 28, 2013 and May 3, 2014. Plate #18 was chosen because it is within an active portion of the cross section, and the month of May was chosen because it coincides with spring runoff, a period of typically high bed load transport. Upon examination, the periodicity of peak transport typically occurs between 15 and 35minutes, with a mean fluctuation of approximately 26 and 29 minutes in May 2013 and 2014, respectively.

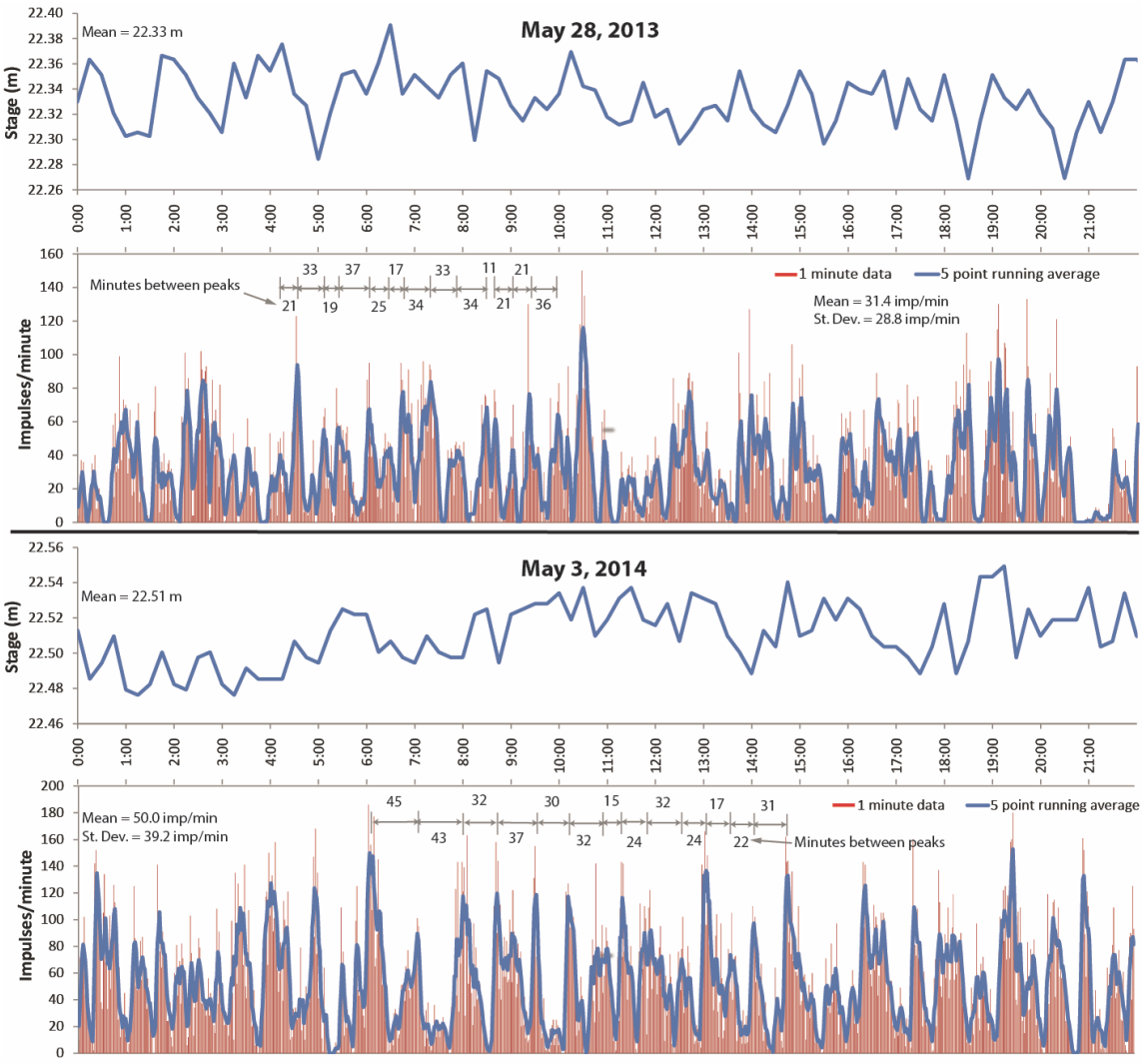

Figure 11 Plot of 1-minute bed load data during steady flow periods, May 28, 2013 and May 3, 2014.

DISCUSSION

The temporal variability in bed load measured with the Elwha impact plate system shows similarities to that measured by Habersack et al. (2008, 2012) on the River Drau, which is a perennial river similarly sized to the Elwha. Bed load measurements by Habersack et al. (2012) were accomplished with; a large Helley-Smith sampler, a bedload trap, and geophone impact plates. Habersack (2012) collected several bed load measurements at a single station using the large Helley-Smith sampler, while high temporal resolution was obtained using the bedload traps and geophone impact plates. All three methods indicate a periodicity of bed load peaks ranging from 15 – 35 minutes, very similar to that found on the Elwha River (Figure 11). Short term temporal variations in bed load have

been attributed to the stochastic nature of sediment supply and the passage of dunes or migrating sheets of bed load (Habersack et al. 2008).

Flume experiments by Kuhnle and Southard (1988) also indicated measurable bed load periodicity. The researchers attributed the short term (4 – 16 minutes) fluctuations to long, low amplitude bed load sheets, while the cause for longer term fluctuations (~ 25 minutes) was not conclusively determined. However, Kuhnle and Southard (1988) indicated that a possible cause for the longer term periodicity was related to the formation and subsequent destruction of large clasts, or gravel clusters, on the bed.

Although Figure 11 seems to indicate a quasi-periodicity similar to that found by other researchers (Kuhnle and Southard 1988, Habersack et al 2012), a Fourier analysis of the Elwha impact plate data indicates no dominant frequency for peaks of bed load transport. Kuhnle and Southard (1988) report a similar finding for particles > 16 mm. Results from their flume experiments indicate a significant difference in temporal variability for the largest size class in transport, 16-32 mm, when compared to smaller particles. Kuhnle and Southard's (1988) largest size class (16-32 mm) corresponds to what is measured on the Elwha River with the impact plate system, where 16 mm is the minimum detectable size.

Because the bed load measurements made with the Elwha bed load impact plate system were made during and shortly after dam removal, it is presumed that the Elwha River is oversupplied with sediment, resulting in a transport limited system. Measurements of bed load transport on the Elwha River during this time period indicate an ample supply of sand, disproportionately large soon after the release of large volumes of sediment from Lake Mills in October 2013. Visual observations were made of a point bar repetitively migrating up and downstream 150 m over the course of several hours, also indicative of an oversupply of sediment.

Based on previous studies (e.g. Reid et al. 1985, Kuhnle and Southard 1988, Habersack et al. 2008, Kuhnle 1992 Strom et al 2004) and data provided by the Elwha bed load impact system, temporal fluctuations of coarse bed load transport can be attributed to gravel bed forms and the stochastic nature of bedload transport, especially for the largest particles in motion. Gravel bed forms are generally limited to gravel sheets and clusters. It has been determined (Proffitt and Sutherland 1983, Dietrich et al. 1989, Hassan and Church 2000, Papanicolaou et al. 2003, and Strom et al. 2004) that gravel cluster bed forms develop under low sediment availability, which is certainly not the condition under which the Elwha bed load observations have been made thus far. This points to the presence of bed load sheets (or a kinematic wave claimed by Reid and Frostick 1986) as the primary explanation of the temporal fluctuations and apparent periodicity observed on the Elwha River. Many researchers indicate a strikingly consistent temporal fluctuation of bed load transport in the range of 15 – 35 minutes, similar to the findings of the Elwha bed load impact system. These fluctuations, or pulses, occur both in natural streams (Kang 1982, Reid and Frostick 1986, Habersack et al. 2012) and flumes (Kuhnle and Southard 1988, Strom et al 2004) under a variety of hydraulic conditions and sediment supply.

The spatial variability at the measurement cross section on the Elwha River (Figure 10) can be attributed to three major factors. 1) The geometry of the measurement weir affects flow patterns in and near the low flow notch influencing bed load transport. 2) Approximately 160 meters upstream of the measurement weir the Elwha River makes a 90 degree turn to the left, forcing flow to river right against bedrock. This forms a point bar at the bend which, at times of very high sediment supply, has extended downstream to the measurement weir on river left. 3) The presence of a wing wall on river right (17-23 m upstream of the measurement weir) focuses high velocity in the center-right portion of the cross section (approximately stations 9 – 12 m). However, these geometrical features do not explain why the highest proportion of bed load transport has changed location throughout the observation period. The temporal fluctuation of the highest concentration of bed load transport is the result of changing bed geometry upstream of the measurement weir during and after dam removal, which can be attributed to the oversupply of sediment. During bed load measurements with a TR-2 in November 2012, shortly after the large release of sediment from Lake Mills, bed elevation was measured at a single station documenting two dune cycles with a period of 12

and 15 minutes and an amplitude of 0.2 m. For three consecutive days in March 2013, depth measurements taken during discharge measurements indicated the position of the thalweg at stations 16.4, 14.4, and 7.4 meters on March 13, 14, and 15, respectively. With such shifting bed conditions it is expected that the location of the highest concentration of bed load transport will be very dynamic.

Power law relationships of coarse bed load to river discharge (Figure 8) indicate a broad range of coefficient *a* and exponent *b* (Eq. 2). Arriving at definitive conclusions regarding the relationship between river discharge and bed load transport on the Elwha River may be premature due to the changing conditions of sediment supply during and after dam removal, but there appears to be a seasonal consistency thus far, with spring snow melt run-off providing the lowest exponent (*b*) in the power law relationship (Eq. 2). The nature of the hydrograph and antecedent conditions likely plays a role in the intra-annual variability of the coefficient and exponent of the power law relationship. Continuous bed load data from the Elwha impact plate system will provide valuable insight into various bed load transport predictors.

CONCLUSIONS AND OUTLOOK

The Elwha impact plate system is in a state of preliminary calibration of the geophone plates, while the accelerometer plates are currently being tested in the flume. The calibration of the geophone impact plates will improve with additional bed load measurements and calibration data. However, it remains to be seen if the calibration will change significantly with the coarsening grain size distribution and decrease in sediment supply as the Elwha River works toward equilibrium transport conditions. Turowski and Rickenmann (2009) have shown that a cover effect plays a role in the calibration of an impact plate system, where increased sand loads dampen the impact of gravel particles on a plate. This occurrence will be evaluated as the calibration moves forward.

The method of system calibration described in this paper, using spatial and temporal averaging with multiple physical measurements over a 30-miute period, provides a reliable mean bed load transport rate with which to calibrate the impact plate system. It is acknowledged that pressure difference samplers are intrusive (Habersack et al. 2012) and sampling efficiency varies widely depending on the sampler characteristics (Johnson et al. 1977, Beschta 1981, O'Leary and Beschta 1981, Bunte et al. 2008). Every effort was made to insure, to the extent possible, that involuntary entrainment did not take occur upon placement on the bed and that the TR-2 did not scoop sediment upon retrieval during bed load measurements collected for calibration of the Elwha impact plate system. Sampler characteristics and deployment methodology remained constant throughout bed load measurements for system calibration. Given the limitations of physical bed load measurement at the measurement weir, using a pressure difference sampler (e.g. TR-2) deployed from a tethered raft is the only feasible option. Based on the findings of this study and by Kuhnle and Southard (1988), a 30-minute temporal average at a single station appears sufficient to capture the temporal variability in bed load transport, greatly improving the accuracy of the measurement and therefore improving the calibration of the Elwha impact plate system. It is acknowledged that Bunte et al. (2004) concluded that it may take up to 1 hour to sample the largest particles in transport using Dietrich and Whiting's (1989) proposed method for estimating minimum sampling time. Because physical bed load measurements are being collected for several hours for system calibration, it is presumed that the largest particles in transport are being measured and included in the calibration.

Reid and Frostick (1986) claimed that "the predictive modeling of bed load transport in alluvial rivers has made faltering progress over the past 50 years". This statement was made some 30 years ago and the performance of bed load formulas remains poor (Habersack et al. 2008). Certainly, the inability to obtain quality bed load measurements with sufficient temporal and spatial density can be blamed for the lack of progress, as well as the fact that bed load transport is a complex process. Kleinhans and van Rijn (2002) note that the hiding and exposure function in bed load transport equations is the primary uncertainty for predicting fractional bed load transport, which is consistent with temporal variability demonstrated here. Similarly, Kuhnle (1992) concludes that the formation and destruction of bed forms and the presence of bed load sheets are responsible for short term temporal variability in bed load

transport. The uncoupled relationship of bed load transport with stage, giving rise to event based and in some cases annual hysteresis is another cause of unsteadiness in bed load flux. The details mentioned here are poorly understood, but given the recent advancements in and implementation of continuous bed load measurement, our understanding of bed load transport stands to improve in the coming decades.

The Elwha impact plate system shows great promise for future evaluation of bed load transport in a moderately sized, perennial, gravel bed river. It will be possible to examine the intricacies of coarse bed load transport with high resolution data from a Eularian perspective. Equally as important will be the knowledge gained from continuous bed load measurement over a period of many years during and after the removal of two large dams. Furthermore, continuous measurement of bed load can be combined with continuous suspended load measurements on the Elwha River through collaboration with the USGS (Magirl et al. 2014), who are continuously measuring suspended sediment concentration using turbidity and acoustic backscatter at the measurement weir containing the bed load impact plates.

ACKNOWLEDGEMENTS

This project has been funded by the Bureau of Reclamation's Science and Technology research program, project numbers 0115, 9562, and 6499. Dr. James Chambers, Wayne Carpenter, and Bradley Goodwiller of The National Center for Physical Acoustics at the University of Mississippi have provided (and continue to provide) outstanding assistance with signal processing along with set-up, installation, and maintenance of the computer monitoring system. Many thanks to Smokey Pittman and the crew at Graham Matthews and Associates for their professionalism and unparalleled expertise in sediment measurement during calibration efforts.

REFERENCES

Bänziger, R., Burch, H. (1990). "Acoustic sensors (hydrophones) as indicators for bed load transport in a Mountain Torrent." *Hydrology in mountain streams. I—Hydrological measurements; The water cycle*, H. Lang and A. Musy, eds., International Association of Hydrological Sciences, Wallingford, U.K., 207–214.

Beschta, R. L. (1981). "Increased bag size improves Helley-Smith bed load sampler for use in streams with high sand and organic matter transport." *Erosion and sediment transport measurement*, International Association of Hydrological Sciences, 17–25.

Bunte, K. (1990). "Experiences and results from using a big-frame bed load sampler for coarse material bed load", *Hydrology in Mountainous Regions I – Hydrological Measurements, the Water Cycle*, Proceedings of two Lausanne Symposia, August, IAHS Publ. no. 193.

Bunte, K., Abt, S. R., Potyondy, J. P., and Swingle, K. W. (2008). "A comparison of coarse bedload transport measured with bedload traps and Helley-Smith samplers." *Geodinamica Acta*, 21(1–2), 53–68.

Curran, C.A., Konrad, C.P., Higgins, J.L., and Bryant, M.K. (2009). "Estimates of sediment load prior to dam removal in the Elwha River, Clallam County, Washington", US Geological Survey Scientific Investigations Report 2009-5221, Reston, VA, 18pp.

Dietrich, W.E., Kirchner, J.W., Ikeda, H., Iseya, F. (1989). "Sediment supply and the development of the coarse surface layer in gravel-bedded rivers", *Nature* (London), vol. 340, pp. 215-217.

Dietrich, W. E., and Whiting, P. (1989). ''Boundary shear stress and sediment transport in river meanders of sand and gravels.'' *River Meandering*, S. Ikeda and G. Parker, eds., Water Resource Monograph 12, American Geophysical Union, Washington, D.C., 1–50.

Duda, J.J., Warrick, J.A., Magirl, C.S., 2011. Coastal and lower Elwha River, Washington, prior to dam removal—History, status, and defining characteristics. In Duda, J.J., Warrick, J.A., and Magirl, C.S., eds., Coastal habitats of the Elwha River, Washington—Biological and physical patterns and processes prior to dam removal. U.S. Geological Survey Scientific Investigations Report 2011-5120, 1-26 pp.

East, A.E., Pess, G.R., Bountry, J.A., Magirl, C.S., Ritchie, A.C., Logan, J.B., Randle, T.J., Mastin, M.C., Minear, J.T., Duda, J.J., Liermann, M.C., McHenry, M.L., Beechie, T.J., and Shafroth, P.B., 2015, Large-scale dam removal on the Elwha River, Washington, USA: River channel and floodplain geomorphic change. *Geomorphology*, v. 228, p. 765–786, DOI:10.1016/j.geomorph.2014.08.028.

Edwards, T. K., and Glysson, G. D. (1999). "Field methods for measurement of fluvial sediment." Techniques of water-resources investigations, U.S. Geological Survey, Denver, CO.

Gray, J.R., Laronne, J.B., Marr, J.D.G. (2010). Bedload surrogate monitoring technologies, US Geological Survey Scientific Investigations Report 2010-5091. US Geological Survey, Reston, VA. http://pubs.usgs.gov/sir/2010/5091/ (Accessed Jan 5, 2015).

Habersack, H.M., Nachtnebel, H.P., Laronne, J.B. (2001). "The continuous measurement of bedload discharge a large alpine gravel bed river", *Journal of Hydraulic Research*, 39:2, 125-133, DOI:10.1080/00221680109499813.

Habersack, H. M., Seitz, H., and Laronne, J. B. (2008). "Spatio-temporal variability of bedload transport rate: Analysis and 2D modeling approach." *Geodinamica Acta*, 21(1–2), 67–79.

Habersack, H., Kreisler, A., Aigner, J., Leiderman, M., Seitz, H. (2012). "Spatio-temporal variability of bedload transport", in: River Flow 2012, Murillo (Ed)., pp. 423-430, Taylor and Francis Group, London.

Hassan, M. A., Church, M. (2000). "Experiments on surface structure and partial sediment transport on a gravel bed", Water Resources Research, 36(7), pp. 1885-1895.

Hilldale, R.C., Carpenter, W.O., Goodwiller, B., Chambers, J.P., Randle, T.J. (2014). "Installation of Impact Plates to Continuously Measure Bed Load: Elwha River, Washington, USA", *Journal of Hydraulic Engineering*, DOI:10.1061/(ASCE)HY.1943-7900 published on line 11/19/2014 http://ascelibrary.org/doi/abs/10.1061/(ASCE)HY.1943-7900.0000975.

Hubble, D. W., Stevens, H. H., Skinner, J. V., and Beverage, J. P. (1985). "New approach to calibrating bed load samplers." *J. Hydraul. Eng*., 10.1061/(ASCE)0733-9429(1985)111:4(677), 677–694.

Johnson, C. W., Engleman, R. L., Smith, J. P., and Hansen, C. L. (1977). "Helley-Smith bed load samplers." *J. Hydraul. Div*., 103(10), 1217–1221.

Kang, S. (1982). "Sediment transport in a small glacial stream: Hilda Creek, Alberta", M.S. Thesis, 265 pp., Univ. of Illinois at Chicago.

Kleinhans, M.G., van Rijn, L.C. (2002). "Stochastic prediction of sediment transport in sand-gravel bed rivers", *Journal of Hydraulic Engineering*, vol. 128, no. 4, pp. 412-425.

Kuhnle, R.A. and Southard, J.B. (1988). "Bed load transport fluctuations in a gravel bed laboratory channel", *Water Resources Research*, vol. 24, no. 2, February, pp. 247-160.

Kuhnle, R.A. (1992). Bed load transport during rising and falling stages on two small streams", *Earth Surface Processes and Landforms*, vol. 17, pp. 191-197.

Magirl, C.S., Hilldale, R.C., Curran, C.A., Duda, J.J., Straub, T.D., Damanski, M., Foreman, J.R. (2014). "Large-scale dam removal on the Elwha River, Washington, USA: Fluvial sediment load", *Geomorphology*, DOI:10.1016/j.geomorph.2014.12.032. published online 12/26/14, http://www.sciencedirect.com/science/article/pii/S0169555X14006369.

Munn, M.D., Black, R.W., Haggland, A.L., Hummling, M.A., and Huffman, R.L. (1998). "An assessment of stream habitat and nutrients in the Elwha River basin – Implications for restoration", US Geological Survey Water Investigations Report 98-4223, Tacoma, WA, 38p.

O'Leary, S. J., and Beschta, R. L. (1981). "Bed load transport in an Oregon Coast Range stream." *J. Am. Water Resour. Assoc*., 17(5), 886–894.

Papanicolaou, A.N., Strom, K., Schuyler, A., Talebbeydokhti, N. (2003). "The role of sediment specific gravity and availability on cluster evolution", *Earth Surface Processes and Landforms*, vol. 28, pp. 69-86.

Proffitt, G.T., Southerland, A.J. (1983). "Transport of non-uniform sediments", *Journal of Hydraulic Research*, 21(1), pp. 33-43.

Reid, I., Frostick, L.E., Layman, J.T. (1985). "The incidence and nature of bedload transport during floods in coarse-grained alluvial channels", *Earth Surface Process and Landforms*, vol. 10, pp. 33-44.

Reid, I., and Frostick, L.E. (1986). "Dynamics of bedload transport in Turkey Brook, a coarse-grained alluvial channel", *Earth Surface Processes and Landforms*, vol. 11, pp. 143-155.

Rickenmann, D. and McArdell, B.W. (2007). "Continuous measurement of sediment transport in the Erlenbach stream using piezoelectric bedload impact sensors", *Earth Surface Processes and Landforms*, **32**, 1362 – 1378.

Rickenmann, D., Turowski, J. M., Fritschi, B., Klaiber, A., and Ludwig, A. (2012). "Bedload transport measurements at the Erlenbach stream with geophones and automated basket samplers." *Earth Surf. Processes Landforms*, 37(9), 1000–1011.

Rickenmann, D., Turowski, J.M., Fritschi, B., Wyss, C., Laronne, J., Barzilai, R., Reid, I., Kreisler, A., Aigner, J., Seitz, H., Habersack, H. (2014). "Bedload transport measurements with impact plate geophones: Comparison of sensor calibration in different gravel-bed streams." *Earth Surf. Process. Landforms,* 39(7), 928–942.

Strom, K., Papanicolaou, A.N., Evangelopoulos, N., Odeh, M. (2004). "Microforms in gravel bed rivers: Formation, disintegration, and effects on bedload transport", *Journal of Hydraulic Engineering*, vol. 130, no. 6, pp. 554-567.

Tsakiris, A.G., Papanicolaou, A.N., Lauth, T.J. (2014). "Signature of bedload particle transport mode on the acoustic signal of a geophone", *Journal of Hydraulic Research*, vol. 52, no. 2, pp. 185-205, DOI:10.1080/00221686.2013.876454.

Turowski, J. M., and Rickenmann, D. (2009). "Tools and cover effects in bedload transport observations in the Pitzbach, Austria." *Earth Surf. Processes Landforms*, 34, 26–37.

USGS TRAINING OF SEDIMENT DATA COLLECTION TECHNIQUES

By Gary P. Johnson[1], John R. Gray[2], Kurt Spicer[3], and Mark Landers[4]

Sediment Data Collection Techniques is a USGS sponsored training course, held annually in the early spring in the Pacific Northwest area near Mount St. Helens. About half of the course is classroom instruction, and the other half is devoted to "hands-on" field experience using a variety of samplers and techniques on bridges and wading in west-central Washington streams including those draining the Mount St. Helens region. This training course is intended to provide instruction in:

- Basic fluvial-sediment concepts
- Sediment sampler characteristics
- Field techniques (including Safety concepts) for sampling
- Laboratory analyses of sediment samples
- Overview of computation of sediment-discharge records
- Selected methods for estimating sediment properties from surrogate technologies
- Overview of a records computation protocol using continuous turbidity
- Physical bedload samplers, and
- Quality-assurance procedures

A course website containing all presentations and a plethora of other information germane to sediment-data collection and analysis techniques is provided before the training session. Students have the option of downloading each presentation or printing hard-copies to bring to the class. The website also provides the agenda, maps, lodging details, and other links of interest.

The course is designed for:

- Those actively engaged in/or supervising individuals engaged in sediment or water-quality data-collection activities, or who plan to become involved in these activities.
- Those interested in sediment-surrogate technologies for suspended-sediment-, bed-material-, and bedload-data collection.
- Those who are or will be actively involved in the collection of data for Surface-Water Toxic Waste, NAWQA or NASQAN Programs, coal hydrology studies, geomorphic assessments that require fluvial-sediment data, science-supported activities for stream restoration, and other monitoring or research endeavors involving fluvial sediment.

1/ Hydrologist, U.S. Geological Survey, Urbana, IL
2/ Hydrologist (Emeritus), U.S. Geological Survey, Reston, VA
3/ Hydrologic Technician, U.S. Geological Survey, Vancouver, WA
4/ Hydrologist, U.S. Geological Survey, Norcross, GA

MAXIMIZING THE RELIABILITY AND COST-EFFECTIVENESS OF YOUR SUSPENDED-SEDIMENT DATA

J.R. Gray, Scientist Emeritus, U.S. Geological Survey, Reston, Virginia, graysedimentology@gmail.com, and Denis O'Halloran, Hydrologic Technician, U.S. Geological Survey, Sacramento, California, dohall@usgs.gov

Abstract An annual record of daily suspended-sediment discharges produced for a U.S. Geological Survey (USGS) streamgage requires suspended-sediment data that are representative of the flow past a river cross section. Depth-integrated isokinetic sampling by a hydrographer at appropriately selected, multiple cross-stream interval centroids by either or both of the Equal-Discharge-Increment (EWI) or Equal-Width-Increment (EDI) methods provide physical samples for subsequent laboratory analyses and use in computation of the daily sediment record. The expertise and attentiveness of the hydrographer, coupled with the sampling scheme used, can have a considerable and consequential influence on the reliability and cost-effectiveness of the derived sediment record.

An evaluation of largely controllable technical and cost factors supports the preferential use of the EDI method, with separate concentration analyses on each sample, for at least one of the two required depth-integrated cross-section sample sets. This conclusion stems from two primary considerations: The value of visually comparing the contents of individual samples to identify and discard bad samples, thus preempting their submission for laboratory analysis; and identifying concentration trends in the cross-section that, in concert with the information from the second sample set, represents a second opportunity to ferret out bad data.

The cost of individual concentration analyses for a single EDI set of six samples is about double that for a six-sample EWI composite-concentration analysis. However, the additional cost of the individually analyzed EDI sample set over that for an EWI composite-concentration analysis – about 1.3 percent – pales in comparison to the annual funding requirements for producing a daily sediment record.

Preventing erroneous sample data from degrading the quality of the sediment record – and permanent storage in the USGS National Water Information System – is desirable for the sake of the accuracy of the records produced, database integrity, and return on investment. The combined cost of composite analyses on two cross-section sample sets as a percentage of total station costs is not substantially less than that for one sample-set composite analysis plus one EDI sample set analyzed to produce concentration values for each sample. Coupled with enhanced data reliability, the added cost of the latter approach is readily justifiable as a cost-effective "sediment-data quality-assurance policy."

INTRODUCTION

Production of an annual record of daily suspended-sediment discharges by the U.S. Geological Survey (USGS) is a time- and resource-intensive undertaking that requires considerable experience and expertise. Requirements for a demonstrably reliable and accurate sediment record include:

- Collection of suitable suspended-sediment samples using appropriate sampling equipment and methods,
- Analyses of the samples by a certified fluvial-sediment laboratory,
- Derivation of a suspended-sediment concentration (SSC) time-series dataset for each day, with continuity between days, for merging with the concomitant water-discharge time series to compute mean daily suspended-sediment discharges and mean time-weighted SSCs, after the
- Judicious application of correction coefficients relating data collected at a relatively high frequency, such as by an observer (Johnson, 1997), autosampler, or surrogate technology (Gray and Gartner, 2009), to mean SSC values for the river derived from periodic and/or episodic sample sets collected by a hydrographer.

The overall quality of these records is, at best, difficult to quantify. A number of factors and potential sources of error can increase the variance of, or introduce bias in a computed record. These include:

- Failure to adequately account for the temporal and spatial variability inherent in the sediment-transport process (Topping et al., 2011),
- Potential inaccuracies or outright errors introduced by sampler selection, performance, and/or deployment; and sample processing, shipment, and/or storage at the sediment laboratory prior to analysis,
- Potential, albeit rare, sediment laboratory-related errors, and
- The incorrect application of, or failure to apply, the aforementioned correction coefficients.

Production of a reliable daily sediment record at a USGS streamgage presupposes that none of the several links in the sediment data-collection and -analysis chain will fail. This evaluation focuses on one of those links: Selection and use of the cross-section sampling method(s) used by the hydrographer, and the laboratory methods requested to process and analyze the sample sets. The evaluation's objective is to identify demonstrably reliable and cost-effective approaches available to the hydrographer for obtaining the field-calibration data for computing daily suspended-sediment records and permanent storage in the USGS National Water Information System (NWIS). The expertise and attentiveness of the field hydrographer coupled with the selected sampling scheme can have a considerable and consequential influence on the reliability and cost-effectiveness of the derived sediment record.

COLLECTION AND COMPUTATION OF SUSPENDED-SEDIMENT-DISCHARGE RECORDS

Numerous methods are available for the computation or estimation of suspended-sediment discharges in open-channel flows (Gray and Simões, 2008). The USGS sanctions two such methods for storage of daily values of suspended-sediment discharge, time-weighted suspended-sediment concentration (SSC), and water discharge in the NWIS:

1. A method that interpolates and, when necessary, extrapolates from SSC data derived from periodic or intermittent physical samples to develop a continuous SSC time series. The SSC time series is merged with a concomitant water-discharge time-series dataset to produce the daily sediment records (Porterfield, 1972; Koltun et al., 2006); and
2. Continuously monitored turbidity as an SSC surrogate (Rasmussen et al., 2009).

Other suspended-sediment surrogate technologies including those based on hydroacoustic, densimetric, and laser technologies have been or are being evaluated (Gray and Gartner, 2009). Some are incorporated in operational programs (Rasmussen et al., 2008; Voichick and Topping, 2014).

Regardless of the monitoring technique or technology selected for operation of a daily sediment station, the reliable measurement and computation of fluvial-sediment loads fundamentally depends on collection and analyses of representative water-sediment samples that integrate variations in the velocities and sediments suspended in the stream cross section. Historically, analytical results from these cross-section discharge-integrated samples were the sole SSC data used to develop the temporal SSC trace (for the most part limited to the Nation's larger rivers), or to adjust SSCs derived from samples collected on a relatively frequent basis by an observer or autosampler to be representative of the mean SSC value in the cross section (Porterfield, 1972; Johnson, 1997; Koltun et al., 2006). More recently, samples representative of the flow past the cross section are being used to calibrate an SSC surrogate time-series (Rasmussen, et al., 2009; Gray and Gartner, 2009; Voichick and Topping, 2014).

Edwards and Glysson (1999), Nolan et al. (2005), Gray et al. (2008), and Gray and Landers (2014) describe methods approved by the Federal Interagency Sedimentation Project (FISP) and USGS for collecting suspended-sediment samples for subsequent laboratory analyses. For physical sampling in all but the shallowest or most sluggish flows (generally, with cross-section depths less than about 0.3 meter and/or mean flow velocities less than about 0.5 meters/second), two USGS-approved methods for deploying an isokinetic sampler in a single vertical are available: point-integration and depth-integration. Contemporary use of the point-integration method is rare because it is relatively costly and time-intensive, and depth-integrating bag samplers developed since the mid-1990s for use in rivers with depths exceeding about 4.5 meters are available (FISP, 2015; Gray and Landers, 2015). Ergo, the point-integration sampling technique is ignored hereafter. Non-isokinetic sampling techniques are also ignored. However, the potential relevance of these sampling techniques may be inferred by the reader in the ensuing discourse.

Approved USGS sampling techniques rely on the use of an appropriate isokinetic sampler developed by the FISP (2015). A list of FISP isokinetic samplers, their physical characteristics and deployment limitations is available from Davis (2005), Gray et al. (2008), and Gray and Landers (2014; 2015). When a mean value for SSC (or SSC and particle-size distributions, PSDs) representative of the flow-weighted cross section is sought, such as for subsequent use in computation of a daily suspended-sediment record, FISP isokinetic samplers are deployed using either the Equal-Width Increment (EWI) and/or Equal-Discharge Increment (EDI) methods (Edwards and Glysson, 1999; Nolan et al., 2005; Gray et al., 2008; and Gray and Landers, 2014). The data-quality and economic ramifications related to the selection and use of either or both of these sampling methods constitute the focus of the ensuing discourse.

Description and Requirements for Use of the EWI and EDI Methods

Characteristics Common to the EWI and EDI Methods: Both the EWI and EDI methods entail collecting depth-integrated samples in a river cross section. The cross section is computationally segregated into intervals. An isokinetic sampler appropriate for the ambient depth and flow velocities in the cross section is lowered at a constant rate in a water column (vertical) located at the centroid of each interval. After the briefest contact with the bed, the sampler is retrieved at a constant rate. This is repeated at each vertical, changing sample containers as appropriate.

In larger rivers, some hydrographers retrieve the sampler at the 0.90 or 0.95 depth (i.e., without contacting the bed) to minimize the risk of snagging a submerged object, or to preclude the inadvertent collection of bed material by gouging the sampler nozzle into the relatively soft lee face of a dune or infirm bed (Gray and Landers, 2014). This approach can result in an abnormally large unsampled zone between the bed and the nadir of the deployed sampler. If a vertical SSC gradient exists, this partial-depth sampling approach may produce biased samples, usually toward underrepresentation of SSC. Hence the quest for safer sampling and avoidance of sample contamination is potentially countered by the collection of biased data.

During the course of a sampling transect, each sample container (a glass or plastic bottle, or collapsible bag) either must be replaced before overfilling, or the contents decanted to a compositing vessel for subsequent subsampling, such as with a USGS churn splitter, or by pouring through a sub-sampling device, such as a USGS cone splitter (Capel and Larsen, 1996). Subsampling, while more or less a routine step for collecting chemical-quality data, is discouraged for suspended-sediment data collection. This stems from recognition of potential subsampling vagaries that include both a potential for an increase in data variance, and introduction of bias.

At least two sets of cross-section samples are collected per site visit (Nolan et al., 2005; Topping et al., 2011; FISP, 2013; Gray and Landers, 2014). Samples are analyzed to enable comparisons of mean SSCs and PSDs derived for each sample set.

Sampler-transit rates exceeding 0.4 multiplied by the mean stream velocity ("four-tenths rule") are impermissible. Maximum transit rates for some samplers are less than the four-tenths rule (Edwards and Glysson, 1999).

Overfilling the sample container invalidates a sample. Overfilled samples must be discarded and the sampler re-deployed in the interval(s) that contributed to the overfilled sample.

Each sample should be examined closely for comparisons of the relative estimated SSCs in the sample set (after visually compensating for unequal sample volumes). Of particular interest is the quantity and size of sand-size particles that quickly settle to the bottom of the container. With rare exception, analyses of samples adulterated during the sampling process yield spuriously large SSCs, and inordinately coarse PSDs.

The photograph in figure 1 shows two near-equal volume samples collected from the same vertical on December 11, 2014, as part of a 2-set EDI measurement on the Toutle River at Tower Road near Silver Lake, Washington (USGS station 14242580). The photograph was taken less than a minute after the samples were swirled. Disparities in the quantity, and possibly also the coarseness of the accumulated sediments, are readily apparent. Collecting, examining, and, if needed, analyzing additional samples from this vertical may have been warranted.

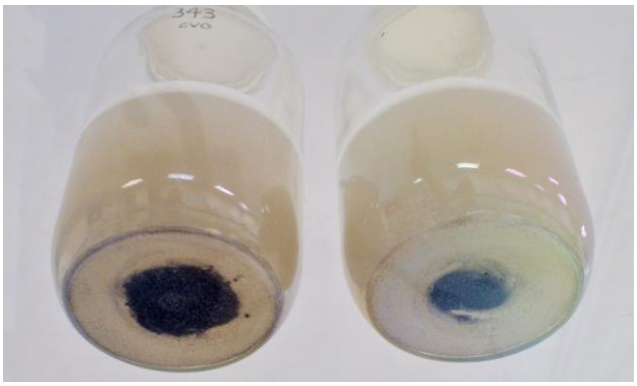

Figure 1 Photograph of two near-equal volume samples collected from the same vertical in the Toutle River at Tower Road near Silver Lake, Washington, on December 11, 2014, showing different accumulations of sediment.

The importance of examining each sample upon collection, or at least before departing the site, is hard to overstate. Ignoring this crucial step may result in retaining a sample that provides biased data due to operator error or inadvertent sample adulteration. Unreliable data generated by a hydrographer, as opposed to an observer or by automated means, are particularly counterproductive for at least four reasons:

1. The data are illegitimately ascribed the highest degree of confidence due to the employment status and presumed expertise of the collector(s), and well-documented validity of the sample-collection methods,
2. Hydrographers are correctly admonished to be generally disinclined to discard analytical results of samples, and of hydrographer-collected samples in particular,
3. The results are counterproductive from record-computation, time, and cost-effectiveness perspectives, and
4. If the spurious data represent an influential part of the streamflow hydrograph, they also may deleteriously influence the accuracy of records computed for other periods.

If the hydrographer fails to recognize a potentially bad sample on-site and does not resample the vertical(s), and/or otherwise fails to sleuth the problem – or if a bad sample received by a laboratory is analyzed but the data are neither flagged nor discarded as part of the routine dataset evaluation – the unreliable data will unknowingly compromise the quality of the computed suspended-sediment discharge record. This represents not only a failure to provide the reliable daily-value sediment record expected in return for the allocated funds, but also may compromise the effectiveness of management decisions based on the erroneous record.

Characteristics Specific to the EWI and EDI Methods

Equal-Width-Increment Method: An EWI measurement entails division of a river cross-section into equal-width intervals. Typically 10-20 verticals are sampled. The hydrographer deploys an appropriate isokinetic sampler in the centroid of the width of each interval. The sampler transit rate must be constant and equal in both the downward and upward directions – and in all sampling intervals – to ensure collection of a representative sample.

Because of its uniform transit rate, use of the EWI method allows retention of samples collected from multiple verticals into a sample container. Although sample containers can be changed after each EWI vertical is sampled, it is seldom done. This is due to the added data-collection effort; extra laboratory expense; and the availability of a generally less-costly but demonstrably superior means for obtaining data describing the cross-section SSC and PSD variability as described in the next sections.

Use of the EWI method requires knowledge of the river width at the sampling cross section. Additionally, before collecting an EWI sample set, a careful hydrographer will identify a vertical at which the product of width and mean velocity likely is at a maxima. Selection of a proper combination of a transit rate and nozzle diameter will preclude overfilling the sample container at this vertical. Absent this precautionary measure, a previously empty container may overfill while sampling in a single vertical, compelling the hydrographer to discard that and all other samples collected as part of the in-progress EWI transect. The next attempt at EWI sample collection either must include a more rapid transit rate and/or use of a smaller-diameter nozzle.

The magnitude of the water discharge is required for subsequent suspended-sediment discharge computations. However, knowledge of the lateral distribution of water discharge is not a prerequisite for EWI sample collection.

An analysis of a laboratory-produced EWI composite sample yields a single mean SSC value, and, if requested, one PSD. The same is true for an appropriately derived aliquot of a composite sample produced by a sample-splitting device, if such subsampling is necessary (Capel and Larsen, 1996).

Equal-Discharge-Increment Method: An EDI measurement entails the computational segregation of a river cross-section into intervals of equal discharge. Usually 4-10 verticals are sampled. The hydrographer deploys an appropriate isokinetic sampler in the centroid of each interval of water discharge at a constant downward rate and retrieves it at a constant rate. However, unlike the EWI transit rate which must be uniform in both vertical directions, the downward and upward EDI transit rates for an EDI vertical – and the rates used at each vertical – need not be equal. The contents of an overfilled sample container simply are discarded and that vertical resampled, usually with a briefer time-of-immersion. The vertical can be sampled multiple times to obtain the desired sample volume without changing the sample container.

Use of the EDI method requires knowledge of the distribution of water discharge in the cross section. This can be derived from an antecedent discharge measurement made with a mechanical current meter or acoustic Doppler current profiler (USGS, 2015). Alternately, if the channel is relatively stable, a discharge-width relation based on previous discharge measurements can be developed. This relation delineates the stage-dependent location of each

sampling centroid based on percentages of the total water discharge on each side of a vertical. Figure 2 shows a relation developed for EDI sampling at the Cowlitz River at Castle Rock, Washington (USGS station 14243000).

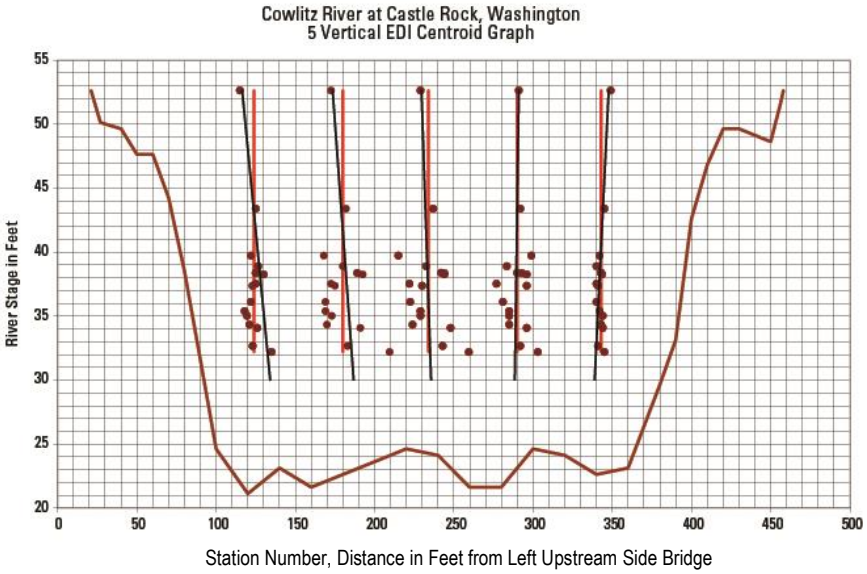

Figure 2 Graph depicting a water discharge centroid location versus stage relation developed from discharge measurements for the Cowlitz River at Castle Rock, Washington. The graph was developed to select verticals for collection of 5-vertical EDI sample sets at this site. Regression lines are black. Vertical red lines were hand-derived.

As each EDI sample is independent and discharge-weighted, the samples can be analyzed individually. Alternately, if all EDI sample volumes are more or less equal (in practice, each sample volume should be within about five percent of the mean sample-set volume), an EDI composite analysis can be performed. Individual-sample analyses as part of at least one EDI cross-section sample set are recommended, as described in the ensuing sections.

If an EDI composite analysis is sought, the extra attention and effort required to obtain a set of near-equal-volume samples is hard to justify compared to use of the EWI sampling method. The same cross-section-averaged data, more or less, are produced by either technique. Hence, the challenge to produce a set of near-equal-volume samples for an EDI composite analysis can be avoided theoretically without change in data quality by using the EWI method.

TECHNICAL CONSIDERATIONS FOR USE OF THE EWI AND EDI METHODS

Use of an appropriate sampler deployed by either the EWI or EDI method – with proper on-site and subsequent quality-control steps – will provide representative data for sediments and other constituents in suspension. However, inevitably, some adulterated samples that go unrecognized are received and analyzed by sediment laboratories. These can include bad samples in hydrographer sample sets as well as those collected by observers or autosamplers. Even valid samples can be adulterated as part of the sample handling, shipping, and storage continuum. The authors, who have reviewed scores of daily USGS sediment records from dozens of USGS Water Science Centers, have ample reason to believe that this problem occurs at a frequency worthy of concern.

Without proper screening, analytical results from composite analyses adulterated by a bad sample(s) collected at one or more verticals will be factored into the ensuing computation of the mean SSC value. With rare exception, the resulting composite SSC value is biased toward higher values. The degree of the bias can be a function of a number of factors, but can range up to an order-of-magnitude or so.

Such an outcome is more prevalent in lower-SSC streamflows where even a few grains of bed material inadvertently introduced to a sample can substantially influence the derived SSC value. Acceptance and use of spuriously variant mean-SSC values (and concomitant PSDs) result in the proportional derivation of erroneous instantaneous sediment-discharge data in addition to any subsequently derived statistics that are based on the bad data.

The hydrographer's challenge is to understand the potential for this problem and to implement procedures to preempt its occurrence. In addition to examining each sample upon collection for the presence of an inordinate

amount and/or coarseness of sand, use of the EDI method and individual-sample SSC analyses provide results that, with rare exception, enable the hydrographer to identify and discard bad SSC values.

A benefit of having each sample from an EDI cross section analyzed for SSC is exemplified by results of concurrent EDI and EWI sample sets collected on March 24, 2014, as part of field-based instruction for the USGS training course, "Sediment Data-Collection Techniques" (Johnson et al., 2015). The sample sets were collected from the bridge at the aforementioned Cowlitz River streamgage by students under the close supervision of course instructors with some three centuries of cumulative experience in sedimentology (Gary P. Johnson, USGS, written communication, 2015). SSC plots that include percentages of sand-size material are shown for the EWI (figure 3) and EDI (figure 4) cross-section sample sets. For instructional purposes, SSC and sand-fine split analyses were performed on individual EWI samples. Likewise, sand-fine splits in addition to the usual SSC analyses were performed on each EDI sample. Normally a laboratory-derived composite sample would have resulted in production of a single SSC value for the 12-bottle EWI sample set. Instead, the mean EWI SSC value was computed as the cumulative mass of sediment divided by the sum of the sample volumes. A mean EDI SSC value was calculated by the routine method of summing the individual SSC values and dividing by the number of EDI samples – five.

The mean SSC value of 262 mg/L from the EWI 12-sample set exceeds the 71 mg/L value for the concurrently collected EDI 5-sample set by a factor of 3.7. This is an inordinately large mean-SSC differential, and one that should invite skepticism from a competent record analyst.

Examination of the EWI SSC data indicates the presence of at least one outlier. The SSC value for station 140 is about double the SSC average for the other stations excluding that for station 330. The percent fines at station 140 is the maximum for this sample set, ergo, the percentage of sand-size material is at a minimum. Although the reference to "cracked bottle" gives the analyst more ammunition to question the validity of the station 140 SSC value, for present purposes this value was retained and attention directed to the more-egregious station 330 outlier.

The SSC value of 2,947 mg/L at station 330 is some 90 times larger than the average SSC of the other 11 EWI samples. The 2-percent fines value for this outlier is at odds with the average value of 43-percent fines determined from the four cross section sample sets, which ranged from about 30-80 percent fines. With little if any doubt, the inconsistent and inordinately influential station 330 SSC and PSD data are bad. Although it is possible that the sampler was incorrectly deployed – perhaps left on the bed for more than an instant before being retrieved – it is more likely that the sampler nozzle gouged the soft lee face of a sand dune at the nadir of the sampler's deployment, inadvertently adding bed material to the suspended-sediment sample.

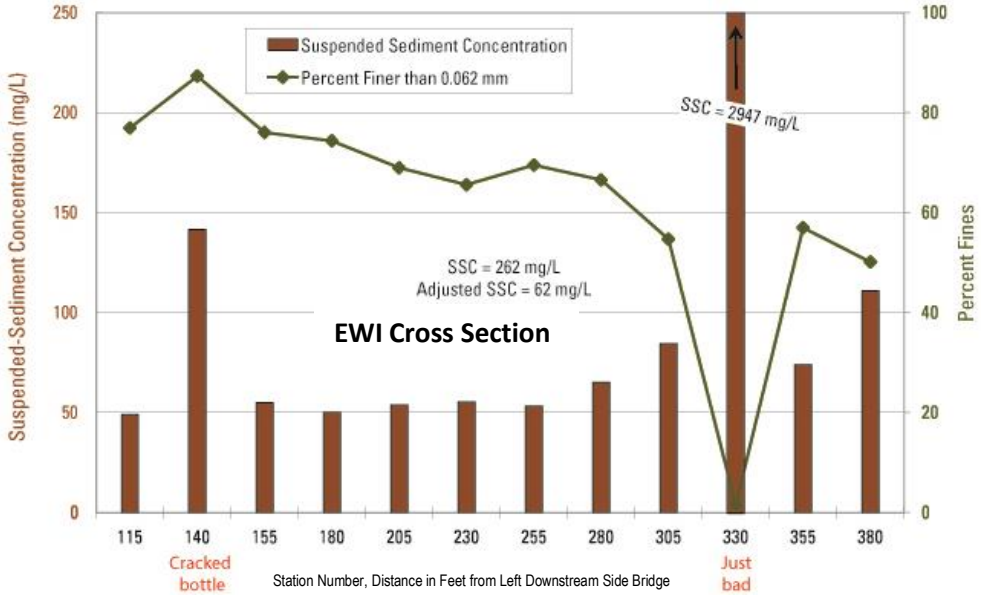

Figure 3 Graph showing SSCs and percent of material finer than 0.062 millimeters for samples collected using a US DH-76 suspended-sediment sampler and the EWI method (the EDI sample set depicted in figure 4 was collected concurrently at the USGS Cowlitz River at Castle Rock, Washington, streamgage on March 24, 2014, as part of the USGS training course, "Sediment Data-Collection Techniques"). References to "Cracked bottle" and "Just bad" were noted by the sample collectors. Sand-fine split and individual-sample SSC analyses were performed on the EWI sample set for instructional purposes.

If an inexperienced and/or inattentive hydrographer failed to notice the comparatively large mass of sand in the station 330 EWI sample and submitted it as part of the EWI sample set for a composite analysis, the resulting spuriously large SSC value of 262 mg/L and inordinately small percentage of fine material would become part of the station record as a relatively muted but still substantial composite-sample outlier. If the record analyst failed to identify and discard this composite-sample outlier in the ensuing analysis, suspended-sediment discharges computed for any part of the record influenced by this composite outlier will be inflated, perhaps by a factor of about 3.7. It is worth noting that USGS record analysts are instructed to be reluctant to discard hydrographer-collected data based on the premise, "if our own data cannot be trusted, what data can be trusted?"

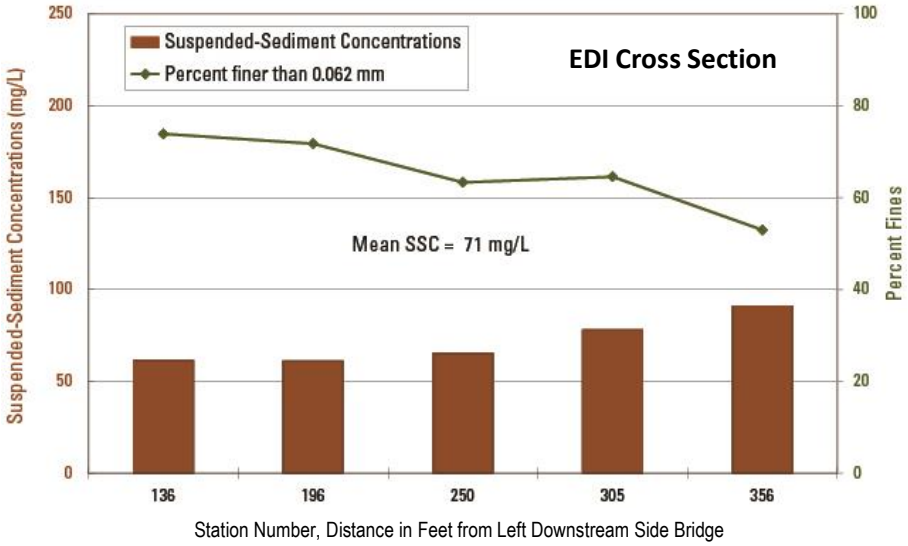

Figure 4 Graph showing SSCs and percent finer than 0.062 millimeters values for samples collected using a US DH-95 suspended-sediment sampler and the EDI method (the EWI sample set depicted in figure 3 was collected concurrently at the USGS Cowlitz River at Castle Rock, Washington, streamgage on March 24, 2014, as part of the USGS training course, "Sediment Data-Collection Techniques").

If, on the other hand, the EWI station 330 sample was inspected, suspected, disrespected, and duly discarded in the field after one or more unbiased duplicate samples were collected, the correct composite SSC value would be derived, assuming that the true station 330 SSC value was consistent with those for adjacent sections. Alternately, if the record analyst, upon receipt of these data, rightly deduced that the concurrent EDI SSC and sand-fine split values were internally reasonable and consistent, as were all individual EWI sample results other than the station 330 outlier (and perhaps also that for station 140), the EWI outlier(s) could and should be discarded.

If a composite analysis had been performed on the EWI sample set (figure 3), the perceptive record analyst would deduce that "something's wrong" with the EWI composite SSC and percent finer than sand values. After carefully evaluating all relevant information, the analyst should feel compelled to discard those data. In this case, only the values from the EDI sample set would be reported and used in record computations. This, of course, would achieve the desired technical outcome – production and use of reliable data – even if the time, effort, and funds associated with collection and analysis of the EWI sample set ultimately were wasted.

An EDI sample set can also include one or more samples with spuriously large SSC(s). However – unless, or perhaps even if an egregiously careless job was done at the sampling site – it is typically and imminently clear from results of separately analyzed EDI samples if an SSC value is unreliable. In this case, unlike in the preceding discourse that centered on the EWI composite outlier, all is not lost. An outlier in the EDI sample set simply can be mathematically eliminated from the mean-SSC computation. Alternately, an experienced analyst may discern a lateral SSC trend in the EDI data and, presupposing a high degree of confidence, estimate a replacement SSC. In this case, the estimated value is used only in the computation of the mean EDI SSC, but not stored as a discrete value.

The thrust of the previous discourse can be summarized as follows: For suspended-sediment studies, the EDI method provides both more, and more readily verifiable information than the EWI method. A composite EWI SSC value that contains the water-sediment contribution from one or more undetected anomalous sample(s) cannot be corrected. It is a bad value – the production of which cost time and money – upon being analyzed and forevermore.

On the other hand, the EDI method provides more detailed cross-section information and thus enables a more informed evaluation of the dataset. This in turn enables the analyst to revise the mean SSC value if bad data are identified and discarded.

Thus, routine use of the EDI method with individual SSC analyses as part of suspended-sediment data collection can be considered to be a "sediment-data quality-assurance policy" of sorts. However, as with the benefits accrued from ownership of a health or life insurance policy, use of the EDI method with individual sample analyses comes at a cost. This observation led to the following economic analysis performed to answer the following questions: "What is the magnitude of additional costs of the EDI method with individual sample analyses compared to those for the EWI or EDI composite method," and "Does the additional cost of the EDI method justify its use from data-quality and knowledge-gain perspectives?"

ECONOMIC CONSIDERATIONS FOR USE OF THE EWI AND EDI METHODS

With rare exception, program managers seeking cost savings select the least-expensive data-collection and -analysis scheme for operation of a daily sediment station or sediment-monitoring network. The degree to which cost reductions might affect data quality is difficult to determine, and may not be adequately considered when selecting a data-collection scheme. The ensuing analysis was performed to ascertain if the costs associated with the routine use of the EDI method with SSC analyses performed on individual samples – as part of at least one of the two cross-section sample sets collected per site visit – are reasonable as compared to those for the more prevalent dual EWI samples set (or for a single EWI sample set, contrary to USGS policy for collection of suspended-sediment data). The evaluation inevitably mixes subjective and objective factors that include but are not limited to the following considerations, each of which should be addressed in the design and operation of a daily sediment station:

- Factors associated with data production,
- The data-quantity and -quality expectations of the funding organization(s),
- The value of demonstrably good data, and
- The arguably insidious nature of unidentified bad data that degrade the quality of the sediment record, waste relatively and typically limited resources, and may result in incorrect management decisions.

A practical economic analysis was performed primarily to define and compare sediment-laboratory processing costs associated with use of the EDI method; the EWI methods; and as a combination of the two. The evaluation focused on analytical costs of hydrographer cross-section sample sets. Other sediment-related costs, such as for analyses of partial-section samples collected manually or by an autosampler, are largely independent of the hydrographer-collected samples. Likewise, the sampling scheme selected has little if any effect on the capital, travel, and labor costs associated with sediment-station operations.

Ergo, the economic analysis focused on data-analysis costs of cross-section sample sets collected as part of hydrographer station visits. The economic analysis performed was cognizant and appreciative of the perpetual competition between the quest to maximize data quality and the oft-limited resources for production of the record.

A survey of production sediment laboratories located in six USGS Science Centers, all using methods described by Guy (1961), and Knott et al., (1992; 1993), was conducted in 2014 to ascertain the costs to perform the following selected analyses:

- Suspended-sediment concentrations (SSC) analyses only,
- SSC and sand-fine break (S/F; percent finer than 0.062 millimeters in median diameter) analysis, and
- SSC and full size (FS; percentages from 0.002–2.0 millimeters in median diameter).

Table 1 lists the average analytical costs for three types of sediment-laboratory analyses. They are based on cost information from USGS production laboratories in Water Science Centers located in California, Iowa, Missouri, Kentucky-Indiana, New Mexico, and the Cascades Volcano Observatory, Washington.

Table 1 Average costs for laboratory analyses, from information provided by six USGS Science Centers in 2014.

Sediment Laboratory Analysis Type	Average Cost Per Analysis
Suspended-Sediment Concentration (SSC)	$17.00
SSC and Sand/Fine (SSC + S/F)	$40.00
SSC and Full Size (SSC + FS)	$170.00
Each Additional Container, Composite Analysis	$8.30

A second 2014 survey was conducted to determine the range of costs charged by the USGS for operating a daily sediment station (considered herein to exclude the concurrent collection of streamflow data) in tandem with a continuous-record streamgage for streamflow data (hereafter referred to as a "sediment streamgage"). The cost data in table 2 were provided by all but one first-survey respondent are included in the second survey. The Wyoming-Montana Water Science Center cost data were used in lieu of a second-survey response from Kentucky-Indiana.

Table 2 Average annual costs to operate a USGS Daily Suspended-Sediment Station (without streamflow data) and a Sediment Streamgage (with streamflow data), based on data provided by six USGS Science Centers in 2014.

Type of Data Produced by a USGS Gaging Station	Average Annual Cost
Daily-Record Sediment Station (sediment data only)	$32,700
Daily-Record Streamflow Station (streamflow data only)	$17,500
Daily-Record Sediment and Streamflow ("Sediment Streamgage")	$50,200

Operation of a sediment streamgage results in production of three sets of daily values that are computed, reviewed, permanently stored, and available to the public: Suspended-sediment discharge; mean time-weighted SSC; and water discharge; along with selected ancillary data. Table 2 lists the average annual costs for operating a sediment streamgage, and the costs of collection of the sediment records versus those for the combined sediment and the streamflow records. Because production of a daily sediment record requires continuous streamflow data, essentially all USGS sediment stations are operated as sediment streamgages that collect continuous streamflow records selected regardless of the funding source(s).

Cost comparisons for selected EDI and EWI sampling-event options are listed in Table 3. These options include costs for collecting one of the two required cross-section sample sets per site visit (referred to as a "sampling event"); collecting either four, six, or nine bottles in each cross-section set (a range that encompasses the number of bottles routinely collected as part of a sample set); and requesting the desired laboratory analyses (Table 1). In all sample-analysis options proposed other than the minimalist dual-EWI sampling method, individual samples collected as part of an EDI sample set are analyzed to identify SSC values for each vertical sampled.

Particle-size analyses–either sand-fine splits or full-size analyses–can be performed as part of either an EWI or EDI composite sample set. Size analyses performed on an unbiased, composite sample set have the advantages of being based on a demonstrably representative sample while providing a sufficient mass of sediment for a full-size analysis.

Although individual size analyses on samples from an EDI sample set would add information useful for better understanding transport characteristics per sediment-size fraction in the cross section, and for the ensuing sediment-record analysis, the relatively substantial added cost would be prohibitive. Additionally, the mass of sediment in individual EDI samples may be insufficient for a full size analysis. The authors are unaware of routine size analyses being performed on most or all suspended-sediment samples submitted to any USGS Water Mission Area sediment laboratory. At least one other USGS sediment laboratory routinely uses optically based analyses to produce concurrent sand-gradation and SSC data on each suspended-sediment sample. Routine production of particle-size data from each sample is highly desirable from the perspectives of the data analyst and data user, albeit substantially more expensive than if only SSC data are produced. These and perhaps other data produced by technologically advanced means may be sanctioned for storage and public release given compliance with USGS (2004) policy, to wit: "All data stored in publicly accessible USGS databases (the NWIS, and other publicly accessible files) must be collected and analyzed using approved collection and analytical protocols."

The combination of options listed in Table 3, factoring in sampling and analytical costs, are but some of the many sample-analysis options available. The authors consider these to represent realistic options for many sediment-monitoring planning purposes. They also might be used as a starting point in the quest to optimize the available resources with the data, and data-quality needs for collection of a daily sediment record – a quest that should include contingency plans for adequately characterizing the suspended-sediment SSCs and PSD of floods that may occur during the monitoring period.

A protocol for an annual sediment-station sampling program that presupposes ten sampling events (hydrographer site visits to collect a suite of physical samples for subsequent laboratory analyses plus a measurement of water discharge if required) was selected as a comparison of annual stations costs using the EDI, EWI, and a hybrid combination of the two methods (FISP, 2013). The hybrid composite sample set is collected using either the EWI or

EDI method (table 4). Options for three types of laboratory analyses–SSC, sand-fine split, and a full-size–were included. The actual number of sampling events in a given year might vary due to a number of factors including the frequency, timing, and magnitude of medium and higher flows at the station.

Table 3 USGS laboratory analysis cost comparisons for selected EWI and EDI single cross-section sampling event options. Laboratory costs are average values for each analytical type as shown in table 1.

Options for analyses of individual EDI subsamples, and for composite EWI or EDI analyses

EWI # of Sample Containers/X-S for Composite Analyses	SSC only Composite Analysis*	SSC + Sand/Fine Composite Analysis	SSC +Full Size Composite Analysis
4	$42	$65	$195
6	$58	$83	$212
9	$84	$106	$236

EDI # of Sample Containers/X-S for Individual Analyses	SSC Individual Analyses	SSC + Sand/Fine Composite analysis	SSC + Full Size Composite Analysis
4	$68	$65	$195
6	$102	$83	$212
9	$153	$106	$236

*The cost of an EDI composite SSC analysis is equal to that for an EWI composite analysis regardless of the number of samples collected and analyzed.

The program covers a year of sampling over a presumed range of flows: three low-flow site visits where only SSC analyses are requested (in part because a dearth in sediment mass in samples collected during lower flows often precludes accurate size analyses), and seven low-to-high flow site visits where SSC and particle-size analyses (sand-fine or full-size analyses) are sought.

Table 4 uses data from tables 1 and 3 to compare costs of sole use of the EDI method, sole use of the EWI method, or in a hybrid combination of the two. They describe cost scenarios for consistent submitting for analysis four, or six, or nine samples per cross-section, with two sample sets obtained per site visit, and ten hydrographer visits per year. Numerous permutations of these analytical options could be developed; regardless, the authors contend that no operational sampling scheme used by a credible hydrographer– given the analytical costs and frequency of site visits–would result in substantially reduced annual analytical costs than the minimum of $1,261 for dual EWI cross sections with four samples collected per cross section, and composite analyses performed on both sample sets.

The analytical cost for the minimalist dual-EWI sample set is the least costly method evaluated for a given number of samples collected per cross section, ranging from 21-33 percent (for samples sets of four and nine samples, respectively) less expensive than a dual-sample set that includes one EDI individually analyzed sample set. However, as previously noted, sole use of the EWI method tends to increase the risk of inadvertently acquiring unreliable data. For example, if analyses of one or both composite sample sets included bed material gouged from any of the 10-20 EWI verticals typically sampled in a single cross section, the composite value will not be representative of the stream conditions. The two marginally more costly methods, on the other hand, each provide at least one cross-section sample set analyzed individually for SSCs–a substantial advantage over the dual-EWI sample-set approach.

Table 4 Cost comparison for the EDI, EWI, and hybrid methods with an annual protocol of ten sampling events and four, six, or nine samples collected as part of each of two cross sections. All individual EDI samples are analyzed solely for SSC. All EWI and EDI composite sample sets are analyzed for SSCs and in some cases also for PSDs.

Sampling-Event Approach with Two Cross Sections/Event	**Number of Sampling Events, Types of Laboratory Analyses, and Costs**				
Sampling Event Cost Scenarios X-S is Cross Section	**3 Low-Flow EDI Individual SSC Analyses**	**1 Low-Flow SSC and Sand-Fine Split Composite**	**4 Medium-Flow SSC and Sand-Fine Split Composites**	**2 High-Flow SSC and 2 Full-Size Analysis Composites**	**Sum of Costs, Ten Sampling Events**
Four Containers/X-S					
Approach I: EDI Individual + Composite	$330	$133	$532	$526	$1,521
Approach II: Two EWI Composites	$252	$107	$428	$474	$1,261
Approach III: Hybrid of EDI Individual SSC + EWI or EDI Composite for Size Analysis	$330	$133	$532	$526	$1,521
Six Containers/X-S					
Approach I: EDI Individual + Composite	$480	$185	$740	$628	$2,033
Approach II: Two EWI Composites	$348	$141	$564	$540	$1,593
Approach III: Hybrid of EDI Individual SSC + EWI or EDI Composite for Size Analysis	$480	$185	$740	$628	$2,033
Nine Containers/X-S					
Approach I: EDI Individual + Composite	$711	$259	$1,036	$778	$2,784
Approach II: Two EWI Composites	$504	$190	$760	$638	$2,092
Approach III: Hybrid of EDI Individual SSC + EWI or EDI Composite for Size Analysis	$711	$259	$1,036	$778	$2,784

Table 5 summarizes annual absolute and relative costs for sediment-station operation for each of three sampling approaches: The cost-identical dual-EDI and hybrid approaches (approaches I and II), and the minimalist dual-EWI approach (III).

Table 5 Annual absolute and percent costs for the hydrographer-collected 6-sample set option shown in table 4 in comparison with total costs of a daily sediment station and a sediment streamgage (sediment and streamgage).

Station Type	**Average Annual Cost (see Table 2)**	**Approach I (Dual EDI) or Approach II (Hybrid) Cost (see Table 4)**	**Approach III Dual EWI Composites Cost**	**Added Annual Station Costs as Percent: Either Dual EDI (I) or Hybrid (II) minus Dual EWI Composites (III)**
I: Daily Sediment Station	$32,700	$2,033 6.2%	$1,593 4.9%	1.3%
II: Sediment Streamgage	$50,200	$2,033 4.0%	$1,593 2.8%	1.2%

The dual-EDI sampling approach is functionally and economically identical to the FISP (2013) hybrid approach; the only difference is submittal of an EDI sample set instead of one collected by the EWI method for a composite analysis. Their marginally higher cost is more than balanced by the dual benefits of individual EDI SSC values and with the cost savings associated with a single analysis on the composite sample set. If the composite analysis results are deemed unreliable compared to individual EDI sample-set results, discarding the EWI results is unfortunate, but all is not lost; the mathematically averaged EDI SSC results – after a careful evaluation – provide a mean SSC value for subsequent record computations. Additionally, the time spent in record analysis ultimately is reduced.

Following are observations gleaned from table 5, which relied on information from the previous four tables:

- One should expect the need to allocate about 5-7 percent of the annual daily sediment station cost toward laboratory analyses of sample sets collected by hydrographers. For the sediment streamgage, that range might fall to about 3-4 percent.
- To attain an a minimally acceptable level of confidence in hydrographer-produced data, one should be reticent to allocate much less than about six percent of the annual cost of a daily sediment station for laboratory analyses, or about four percent of sediment streamgage costs.
- The allocation of an additional 1-2 percent of funding to the total operating costs of a sediment streamgage enables use of the reliable hybrid or dual-EDI methods (table 5, approaches I and II) in lieu of the comparatively risky (from a data-quality perspective) sole use of the dual-EWI method (approach III).
- This cost evaluation does not include de facto increases in the percentage of analytical costs versus total-station costs if any bad data collected by the hydrographer must be discarded.
- Conversely, the added monetary value of enhanced data quality due to the exclusion of bad data may be substantial albeit unquantified and perhaps unquantifiable. Regardless, these de facto cost benefits are quite real and should be recognized as such when considering the cost of the sediment record.

SUMMARY AND CONCLUSIONS

The technical and economic consequences of sole use of a dual-EWI as opposed to a dual-EDI, or a hybrid of the two methods – based on practical considerations related to data quality versus the resources to collect and analyze the samples for computation of an annual sediment record – have been described in the previous sections and can be summarized thusly: The expertise and attentiveness of the field hydrographer coupled with the selected sampling scheme can have a considerable and consequential influence on the reliability and cost-effectiveness of the derived sediment record.

Factors germane to this conclusion follow:

1. **HYDROGRAPHER, EXAMINE THY SAMPLES**: At the risk of being pedantic, it is difficult to overstate that the single most important activity available to the hydrographer is to minimize the potential for collecting bad data at a site by routinely examining the volume and quantity of accumulated sediments of each sample upon or soon after collection. Samples with anomalous quantities and/or sizes are the first and foremost tip-off that something may be amiss. The wise and conscientious hydrographer will not depart the site without resampling the vertical(s) that contributed to the potentially anomalous water-sediment mixture. The hydrographer must ascertain if the visual observations are likely to reflect the sedimentary conditions at the sampled verticals, or if results of the sample analyses are likely to contribute to the desk-bound analyst's headaches when trying to deduce what might have gone awry at the sampling site.
2. **BAD DATA HAPPEN**: Some data that unequivocally are at odds with the preponderance of those used to produce a sediment record appear in the large majority these datasets. Although some of these outliers defy logical explanation, a careful review of field notes, laboratory reports, and other information usually infer with a high degree of confidence that the outliers originated as bad samples. The authors have ample reason to believe that this problem occurs at a frequency worthy of concern to those producing or using the data.
3. **BAD DATA ARE...BAD**: Without proper screening, analytical results from composite analyses adulterated by bad subsamples from one or more verticals will be factored into the computation of the mean SSC value. With rare exception, the resulting composite SSC value is biased toward higher values.
4. **ADDED COST FOR "BEST JOB" IS REASONABLE**: The annual station-operation costs for an increased number of analyses of hydrographer-collected samples listed in (one EDI sample set with individual-sample SSC analyses plus a second sample set composite analysis; table 5, approaches I or II; see FISP, 2013) exceed the minimalist dual-composite approach (approach III) by a paltry1-2 percent.

5. **AND YOU GET A BIGGER BANG-FOR-BUCK**: The hybrid or dual-EDI sample-set options have the added benefit of minimizing the risk of unknowingly including bad data in the permanent record. This is a consequence of the availability of spatially detailed SSC data from the individually analyzed EDI sample set that is both internally (within-set) comparable, and externally comparable to the results from the companion cross-section sample set. Additionally, the time spent in record analysis ultimately is reduced.
6. **A COST-EFFECTIVE QUALITY-ASSURANCE POLICY FOR YOUR SEDIMENT DATA**: To summarize the preceding observations: An EDI sample set with SSC analyses performed on each sample provides useful information on the cross-sectional SSC distribution. Also desirable, albeit rarely produced and generally cost-prohibitive, are size analyses on individual EDI samples. These data provide a "sediment-data quality-assurance policy" of sorts that enables the hydrographer to identify and discard unreliable EDI single-vertical SSC values, and/or to ascertain if the concurrent composite SSC value is consistent and reasonable with that for the EDI SSC value. This, in turn, either substantially increases the likelihood that hydrographer-collected data are demonstrably reliable, or enables the hydrographer to discard unreliable data. Conversely, this benefit is lost when using the dual-EWI composite approach.
7. **ERGO, AN ENDORSEMENT:** The authors unequivocally endorse the FISP (2013) hybrid option – or using that approach but substituting the EWI composite analysis with a composite EDI analysis – for the cost-effective and comparatively reliable derivation of hydrographer-collected SSC and PSD data. This endorsement is particularly germane to sediment-record computations for periods of medium-and-higher flows that are most influential in suspended-sediment transport.

ACKNOWLEDGEMENTS

The quality of this manuscript was improved substantially by reviews provided by Larry Freeman (retired), Kurt Spicer, Louis Cannarozzi, and Jim Kolva of the USGS; and Marie Garsjo (retired) and Jerry Bernard (retired), Natural Resources Conservation Service. The economic analysis relied on and benefited from information provided by the USGS Cascades Volcano Observatory Science Center, and the California, Iowa, Missouri, Kentucky-Indiana, New Mexico, Washington, and Wyoming-Montana USGS Water Science Centers. The artistic prowess of the USGS's Annette Goode in the production or alteration of the schematics in this manuscript was greatly appreciated.

REFERENCES CITED

Capel, P.D., and Larsen, S.J. (1996). Evaluation of selected information on splitting devices for water samples: U.S. Geological Survey Water-Resources Investigations Report 95-4141, 103 p. http://pubs.usgs.gov/wri/1995/4141/report.pdf.

Davis, B.E. (2005). A guide to the proper selection and use of Federally approved sediment and water-quality samplers: U. S. Geological Survey. Open-File Report 2005-1087, 20 p. http://pubs.usgs.gov/of/2005/1087/.

Edwards, T.E., and Glysson, G.D. (1999). Field methods for measurement of fluvial sediment: U.S. Geological Survey Techniques of Water-Resources Investigations, Book 3, Chapter C2, 89 p. http://water.usgs.gov/osw/techniques/sedimentpubs.html.

Federal Interagency Sedimentation Project. (2013). Recommendation for collecting at least two depth-integrations per vertical to reduce uncertainty as part of cross-section sampling with FISP depth-integrating suspended-sediment samplers: FISP Memorandum 2013.03. http://water.usgs.gov/fisp/docs/FISP_Tech_Memo_2013.03v2.pdf.

Federal Interagency Sedimentation Project. (2015). Home Page. http://water.usgs.gov/fisp/.

Gray, J.R., and Simões, F.J.M. (2008). Estimating sediment discharge, *in* Marcelo Garcia, ed., Sedimentation Engineering – Processes, Measurements, Modeling, and Practice: American Society of Civil Engineers Manual 110, Appendix D, p. 1067-1088. http://water.usgs.gov/osw/techniques/Gray_Simoes.pdf.

Gray, J.R., and Gartner, J.W. (2009). Technological advances in suspended-sediment surrogate monitoring: Water Resources Research, 45, W00D29. http://water.usgs.gov/osw/techniques/2008WR007063.pdf.

Gray, J.R., and Gartner, J.W. (2010). Surrogate technologies for monitoring suspended-sediment transport in rivers, *in* Poleto, C., and Charlesworth, S., eds., Sedimentology of Aqueous Systems, London: Wiley-Blackwell, Chapter 1, p. 3-45. http://water.usgs.gov/osw/techniques/sed_aq_sys_chap_1_pdf_from_wb_3_16_2010.pdf.

Gray, J.R., Glysson, G.D., and Edwards, T.E. (2008). Suspended-sediment samplers and sampling methods, *in* Sediment transport measurements, *in*, Marcelo Garcia, ed., Sedimentation Engineering – Processes, Measurements, Modeling, and Practice: American Society of Civil Engineers Manual 110, Chapter 5.3, p. 318-337. http://water.usgs.gov/osw/techniques/Diplas_Kuhnle_others.pdf.

Gray, J.R., and Landers M.N. (2014). Measuring suspended sediment, *in* Ahuja S. (ed.) Comprehensive Water Quality and Purification: United States of America, Elsevier, vol. 1, p. 157-204. http://water.usgs.gov/osw/techniques/sediment/gray_landers_elsevier_chapter_12_10_17_2013.pdf.

Gray, J.R., and Landers M.N. (2015). History of the Federal Interagency Sedimentation Project, Part V: Proceedings of the 10th Federal Interagency Sedimentation Conference, April 19-23, 2015, Reno, Nevada, 13 p.

Gray, J.R., and Simões, F.J.M. (2008). Estimating sediment discharge, *in*: Sedimentation Engineering – Processes, Measurements, Modeling, and Practice: Manual 110, edited by M. Garcia, American Society of Civil Engineers, p. 1067-1088. http://water.usgs.gov/osw/techniques/Gray_Simoes.pdf.

Guy, H.P. (1969). Laboratory Theory and Methods for Sediment Analysis: U.S. Geological Survey Techniques of Water-Resources Investigations, Book 5, Chapter C1, 58 p.; http://pubs.usgs.gov/twri/twri5c1/.

Johnson, G.P. (1997). Instruction manual for U.S. Geological Survey sediment observers: U.S. Geological Survey Open-File Report 96-431, 35 p. http://il.water.usgs.gov/pubs/ofr96_431.pdf.

Johnson, G.P., Gray, J.R., Spicer, K.R., and Landers, M.N. (2015). USGS training in Sediment Data Collection Techniques: Proceedings of the 10th Federal Interagency Sedimentation Conference, April 19-23, 2015, Reno, Nevada, 1 p.

Knott, J.M., Glysson, G.D., Malo, B.A., and Schroder, L.J. (1993). Quality assurance plan for the collection and processing of sediment data by the U.S. Geological Survey, Water Resources Division: U.S. Geological Survey Open-File Report 92-499, 18 p. http://pubs.usgs.gov/of/1992/0499/report.pdf.

Knott, J.M., Sholar, C.J., and Matthes, W.J. (1992). Quality assurance guidelines for the analysis of sediment concentration by U.S. Geological Survey sediment laboratories: U.S. Geological Survey Open-File Report 92-33, 30 p. http://pubs.usgs.gov/of/1992/0033/report.pdf.

Koltun, G.F., Eberle, Eberle, Gray, J. R., and Glysson, G.D. (2006). User's Manual for the Graphical Constituent Loading Analysis System (GCLAS): U.S. Geological Survey Techniques and Methods Book 4, Chapter C1, 50 p. http://pubs.er.usgs.gov/usgspubs/tm/tm4C1.

Larsen, M.C., Gellis, A. C., Glysson, G.D., Gray, J.R., and Horowitz, A.J. (2010). Fluvial sediment in the environment – a national challenge: Proceedings of the Joint Federal Interagency (9th Sedimentation, and 4th Hydrologic Modeling) Conferences, June 27–July 1, Las Vegas, NV, 15 p. http://acwi.gov/sos/pubs/2ndJFIC/Contents/OS_Larsen_9fisc_sediment_vision_3_4_2010.pdf.

Nolan, K.M., Gray, J.R., and Glysson, G.D. (2005). Introduction to suspended-sediment sampling: U.S. Geological Survey Scientific Investigations Report 2005-5077. On CD-ROM and at: http://pubs.er.usgs.gov/pubs/sir/sir20055077.

Porterfield, George. (1972). Computation of fluvial-sediment discharge: U.S. Geological Survey Techniques of Water-Resource Investigations Book 3, Chapter C3, 66 p. http://water.usgs.gov/pubs/twri/twri3-c3/.

Rasmussen, T.J., Lee, C.J., and Ziegler, A.C. (2008). Estimation of constituent concentrations, loads, and yields in streams of Johnson County, northeast Kansas, using continuous water-quality monitoring and regression models, October 2002 - December 2006: U.S. Geological Survey Scientific Investigations Report 2008–5014, 103 p. http://pubs.usgs.gov/sir/2008/5014/.

Rasmussen, P.P., Gray, J.R., Glysson, G.D., and Ziegler, A.C. (2009). Guidelines and procedures for computing time-series suspended-sediment concentrations and loads from in-stream turbidity-sensor and streamflow data: U.S. Geological Survey Techniques and Methods Book 3, Chapter C4, 53 p. http://pubs.usgs.gov/tm/tm3c4/.

Topping, D.J., Rubin, D.M., Wright, S.A., and Melis, T.S. (2011). Field evaluation of the error arising from inadequate time averaging in the standard use of depth-integrating suspended-sediment samplers: U.S. Geological Survey Professional Paper 1774, 95 p. http://pubs.usgs.gov/pp/1774/.

U.S. Geological Survey (2004). Water Resources Discipline policy on storage and publication of fluvial-sediment data with updated method codes: Office of Surface Water Technical Memorandum 2004.01. http://water.usgs.gov/admin/memo/SW/sw04.01.html

U.S. Geological Survey (2015). Office of Surface Water, hydroacoustics, equal-discharge-increment. http://hydroacoustics.usgs.gov/movingboat/EDI1.shtml.

Voichick, Nicholas, and Topping, D.J. (2014). Extending the turbidity record—making additional use of continuous data from turbidity, acoustic-Doppler, and laser diffraction instruments and suspended-sediment samples in the Colorado River in Grand Canyon: U.S. Geological Survey Scientific Investigations Report 2014–5097, 31 p. http://dx.doi.org/10.3133/sir20145097.

COLLECTING A BETTER WATER-QUALITY SAMPLE: REDUCING VERTICAL STRATIFICATION BIAS IN OPEN AND CLOSED CHANNELS

William R. Selbig
Research Hydrologist
U.S. Geological Survey
8505 Research Way
Middleton, WI 53562
wrselbig@usgs.gov

Abstract

Collection of water-quality samples that accurately characterize average particle concentrations and distributions in channels can be complicated by large sources of variability. The U.S. Geological Survey (USGS) developed a fully automated Depth-Integrated Sample Arm (DISA) as a way to reduce bias and improve accuracy in water-quality concentration data. The DISA was designed to integrate with existing autosampler configurations commonly used for the collection of water-quality samples in vertical profile thereby providing a better representation of average suspended sediment and sediment-associated pollutant concentrations and distributions than traditional fixed-point samplers. In controlled laboratory experiments, known concentrations of suspended sediment ranging from 596 to 1,189 mg/L were injected into a 3 foot diameter closed channel (circular pipe) with regulated flows ranging from 1.4 to 27.8 ft^3/s. Median suspended sediment concentrations in water-quality samples collected using the DISA were within 7 percent of the known, injected value compared to 96 percent for traditional fixed-point samplers. Field evaluation of this technology in open channel fluvial systems showed median differences between paired DISA and fixed-point samples to be within 3 percent. The range of particle size measured in the open channel was generally that of clay and silt. Differences between the concentration and distribution measured between the two sampler configurations could potentially be much larger in open channels that transport larger particles, such as sand.

INTRODUCTION

Collection of representative water-quality samples in fluvial systems can be complicated by large sources of variability, both temporal and spatial. For example, Horowitz (1995) found both horizontal and vertical concentrations of suspended sediment in a stream or river tend to increase with increasing distance from stream banks and depth. These increases were associated with greater concentrations of sand-size particles. This is especially notable with very fine to coarse sand-sized particles, in that suspended concentrations may be considerably higher within 3 feet of the channel bed (Guy, 1970). The stratification of solids in a flowing water column may result in biased concentration data collected from open channels.

Watershed managers depend on assessment and monitoring of water quality and flow data to help target pollutant reductions, identify the most important sources of pollutants, and evaluate the benefits of select stormwater management practices. One of the most common uses of water-quality data is to calibrate and verify urban pollutant models. Sediment concentrations and particle size distributions are especially important to assure the models provide useful results because studies have shown concentrations of urban pollutants generally increase with decreasing particle size, yet the majority of mass lies in coarse particles (Evans et al., 1999; Sansalone and Buchberger, 1997; Characklis and Wiesner, 1997; Waschbusch et al., 1999; Li et al., 2005). Once tested, models can be one of the only cost effective approaches to developing watershed plans in urban areas when confronted with the high cost of monitoring all potential sources of runoff and the stormwater management practices used to treat it. For example, the Wisconsin Department

of Natural Resources (WDNR) has promulgated a series of stormwater performance standards that will require qualifying cities to reduce the annual total suspended solids (TSS) load in urban runoff by 20 percent (Wisconsin Administrative Code NR 151, 2002). Models are used by both the WDNR and permitted entities to help determine if the goal is achieved. Another example is the development of total maximum daily loads (TMDL) for impaired waters under section 303(d) of the Clean Water Act (U.S Environmental Protection Agency, 2011). Urban areas around the country are subject to development of TMDLs that require the calculation of the maximum amount of a pollutant a waterbody can receive. Without accurate flow and pollutant concentration data to calibrate and verify models used to determine TMDLs, they could generate erroneous results that could significantly reduce the effectiveness of watershed planning. Millions of dollars are spent annually by environmental managers, engineering consultants, and others to mitigate, control, and prevent sediment and sediment-associated pollution in our nation's waterways. Accurate concentration data are vital to their decision-making process.

To help reduce uncertainty, the use of surrogate technology has been explored as a means to estimate time-varying sediment concentration (Wood and Teasdale, 2013). While this approach has been successful, it is generally focused on sediment and does not address the wide range of pollutants commonly imposed on the regulated community. To obtain reliable and representative data, Bent and others (2000) suggest the automatic sampler intake should be placed near the point at which the concentration approximates the mean sediment concentration for the channel cross-section over a full range of flows. This concept for intake placement has great merit, but the mean cross-section concentration is constantly changing as flow conditions vary (Edwards and Glysson, 1999). It is unlikely that specific guidelines for locating a sample intake for flow conditions at one water level would produce the same intake location relative to the flow conditions at a different water level. To resolve this, the USGS recommends use of equal-width-increment (EWI) samples to develop a cross-sectional coefficient to be applied to fixed-point sample concentrations (Edwards and Glysson, 1999). However, collecting depth- and width-integrated samples over a range of conditions may not be possible for a number of reasons, such as brief duration of runoff, limited access, hazardous conditions, and rapidly varying flows, especially in urban streams (Harmel et al., 2010). These techniques are also impractical for most closed systems used to convey urban stormwater. Furthermore, traditional fixed-point samplers can artificially bias sediment concentration in a water sample, especially in flashy or ephemeral streams where the zone between bed and suspended load may vary depending on water depth. Ideally, the location of the sample intake should be adjusted to reflect changing water depths.

To address this concern, the USGS – Wisconsin Water Science Center has developed a fully automated Depth-Integrated Sample Arm (DISA). The DISA was designed to integrate with existing autosampler configurations for collection of water-quality samples in vertical profile thereby providing a better representation of average sediment and sediment-associated pollutant concentrations and distributions than traditional fixed intake samplers.

The primary objective of this study was to determine whether the DISA can collect water-quality samples from both open and closed channels over varying hydraulic conditions that are more representative of the average conditions in a water column, in terms of suspended-sediment concentration (SSC) and particle size distribution (PSD), than a traditional fixed-point sampler.

METHODS

The general field of application of the DISA was originally developed in 2008 for closed conduits used to convey stormwater runoff in urban environments, such as storm sewers. As such, its design was optimized for collection of a water sample in vertical profile from the center of a circular pipe or culvert. Operation of the DISA made use of a linear actuator with position sensing capabilities to drive a rotary sample arm assembly attached to the ceiling of a closed conduit. The actuator was controlled via datalogger to move forward or retract to one or more desired positions in the water column. Once in

position, the DISA intake remained in place until the autosampler completed its normal purge/withdraw cycle. A detailed description of the device can be found in Selbig and Bannerman (2011).

Evaluation of the DISA in a closed conduit was done in 2011 at Colorado State University's hydraulics laboratory (figure 1). The DISA was programmed to collect water-quality samples at four points spaced vertically from a flowing water column of known discharge. For example, if the depth of water to be sampled was 1 foot, the DISA was programmed to take the first sub-sample at 0 percent depth (bottom of pipe), 25 percent depth (0.25 foot above the pipe floor), 50 percent depth (0.50 foot above the pipe floor), and 75 percent depth (0.75 foot above the pipe floor). Although the depth of water varied during laboratory tests, the percentages remained the same. A pre-mixed manufactured sand with particle diameters ranging from 53 to 425 μm was injected at calibrated rates to create known concentrations ranging from 596 to 1,189 mg/L. Calibrated flows rates ranged from 1.4 to 27.8 ft^3/s. Full details of the experimental design can be found in Selbig et al. (2012).

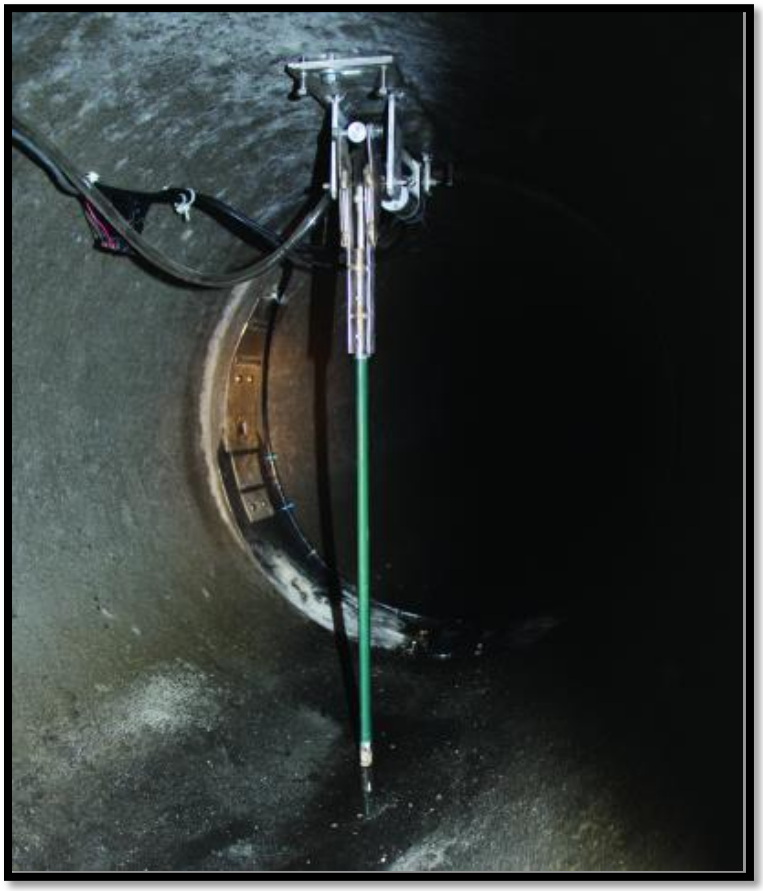

Figure 1 Image of the DISA in a closed conduit (storm sewer) with the sample arm extended in the vertical position. When at rest, the arm lies in the horizontal position near the pipe ceiling with the end of the intake pointing in the direction of flow. The sample arm (identified as green in this photo) can be sized to fit various conduit diameters. Photo by USGS.

In 2013, the DISA was modified and updated for use in open channels. Instead of being mounted to the ceiling of a closed conduit, the updated DISA is fully submersible and is anchored to the channel bed. The updated DISA includes a linear actuator with a variable rate of travel. In other words, when coupled with the static pumping rate of an autosampler, the DISA can move slower in shallow water and faster as the depth increases in order to keep the volume of water captured in each sample container consistent. Any

debris that may have accumulated on the sample arm assembly while acquiring a sample is cleared away by water discharging past as it retracts into the horizontal position

The first field-level evaluation of the DISA was done at Underwood Creek, an urban stream in Milwaukee, Wisconsin. The sampler was installed near the USGS streamgage on Underwood Creek in a section of restored channel that had its concrete lining removed in 2009. The channel was approximately 8 feet wide with a baseflow depth of approximately 2 feet and a streambed that consisted of sand, gravel and cobble. Inspection of the drainage basin revealed several large wet detention ponds intercepting stormwater runoff prior to drainage into the Underwood Creek. The DISA was attached to an aluminum frame that was anchored to the streambed using 0.75-inch steel rod. A fiberglass fairing was fabricated to shield the DISA from any debris as well as prevent the device from becoming buried in silt or organic detritus (figure 2). The sample intake was oriented in the downstream direction and was attached to an autosampler on the bank (figure 2). A second sample line was installed adjacent to the DISA similar to what would be used for a fixed-point intake associated with an autosampler (Edwards and Glysson,1999). The intake of the second sampler was located at a fixed depth of approximately 0.7 foot above the streambed. Each sampler was programmed to take a 1 liter sample for every 0.3 foot increase and 0.5 foot decrease in water level on the rise and recession limb of the hydrograph, respectively. Upon completion of each sub-sample, the DISA would return to a horizontal position near the streambed which cleared away any accumulated debris. Comparison of SSC and PSD were made between samples collected by the DISA and the fixed-point sampler. Additionally, EWI samples were periodically taken coincident with the DISA and fixed-point samples to represent a discharge-weighted concentration of the channel cross section. The coincident sampling was done in July and August, 2013 that included 3 stormwater runoff events where flows ranged from 7 to 817 ft^3/s

Figure 2 Image of the DISA in an open channel setting. The body is anchored to the streambed with the sample arm oriented in the downstream direction. Photo by USGS.

RESULTS AND DISCUSSION

Closed Conduits

In the 2011 laboratory experiments for closed conduits, the DISA was shown to improve the accuracy of sediment concentration and distribution by reducing stratification bias inherent in stormwater runoff in urban storm sewers. The results described herein are a digest of a paper previously published in the *Journal of Environmental Monitoring* and have been adapted from Selbig et al. (2012) with permission from The Royal Society of Chemistry.

For each trial flow rate, all four sub-samples collected by the DISA were combined to represent a single, average SSC. The resulting concentration was then compared to the injected concentration for assessment of sampling accuracy. A similar comparison was made for the fixed-point sampler. Although both samplers tend to overestimate SSCs in the water, the DISA had better agreement with injected concentration. Mean and median SSCs measured by the DISA came within 13 and 7 percent of the injected value, respectively, compared to 166 and 96 percent for the fixed-point sampler (table 1). An analysis of paired samples using the Wilcoxon signed-rank test confirmed that fixed-point concentrations were statistically greater than the DISA concentrations at the 5 percent significance level. The summary statistics detailed in table 1 suggest that as more of the water column is captured in a sample, a more accurate representation of the actual concentration will result. Increasing the number of collection points spaced vertically through the water column can also reduce variability through better averaging of the dynamic exchange of solids between stratified zones. The DISA demonstrates reduced variability as indicated by a lower coefficient of variation in table 1.

Table 1 Summary statistics of the percent of actual SSCs measured from the DISA (7 samples with sub-samples at 0, 25, 50, and 75 percent of water depth) and fixed-point (10 samples) samplers. A value of 100 represents perfect equality. A value greater than 100 indicates overestimation. Adapted from Selbig et al. (2012) with permission from The Royal Society of Chemistry.

Statistic	FIXED	DISA
Minimum	37	92
Maximum	795	135
Median	196	107
Mean	266	113
Standard Deviation	238	15
Coefficient of Variation	0.9	0.1

Slight changes in the distribution of particles in a sample could result in modest changes in the overall SSC of a sample. Larger particles would carry more mass resulting in a larger mass concentration. Therefore, larger sediment concentrations measured in the fixed-point samples are likely due to the over-sampling of coarse particles that tend to accumulate near the bottom of the water column. This solids stratification concept was illustrated in one laboratory test after comparing the average concentration, by particle size, between the DISA and fixed-point samplers to the actual, injected value (figure 3). Both DISA and fixed-point particle concentrations showed relatively close agreement to the actual value for particle diameters less than 106 μm; however, differences become greater as particle diameters increase. In this particular laboratory test, the fixed-point sampler overestimated actual concentrations by 33

percent for particles less than 53 μm to 185 percent for particles between 212-300 μm (figure 3). The DISA was better able to represent the full range of particles, limiting the oversampling of particles between 212-300 μm to just 47 percent greater than the actual value (figure 3).

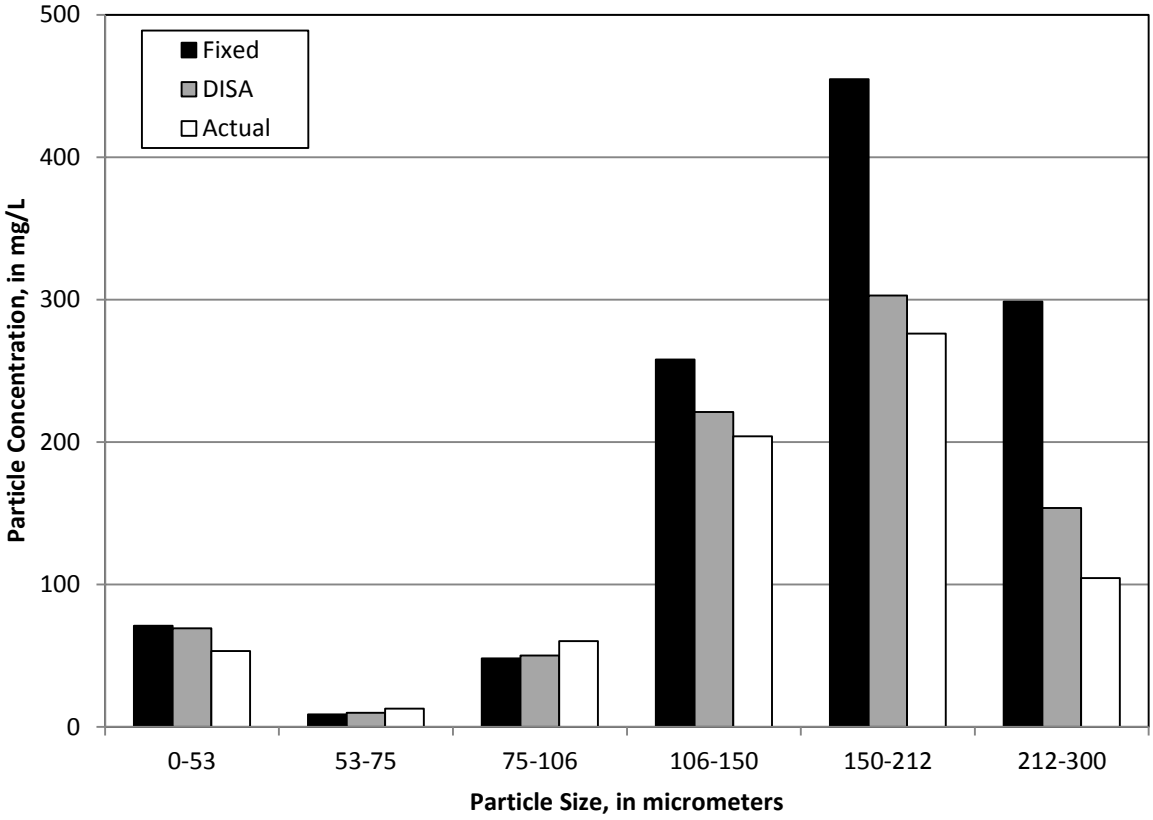

Figure 3 Comparison of the concentration of particles, by size, measured in the DISA and fixed-point samplers to the actual, injected concentration for one laboratory test in a closed conduit, 2011. Reproduced from Selbig et al. (2012) with permission from The Royal Society of Chemistry.

Open Channels

Based on the proven efficiency of the DISA in a closed conduit, it was assumed that when installed in the open channel of Underwood Creek, the DISA would yield a SSC and PSD more representative of the average condition than a fixed-point sampler. Overall, there was close agreement in SSCs between the DISA and fixed-point sampler over a range of flow conditions (figure 4). Examination of SSCs in both DISA and fixed-point datasets revealed a highly skewed distribution. Therefore, the median is a more appropriate representation of the population center than the mean (Ott and Longnecker, 2001). The median difference in SSC between paired samples was 3 percent greater in the DISA than the fixed-point sampler. While this difference is small it is statistically significant. Hypothesis testing by use of the Wilcoxon signed-rank test (Helsel and Hirsch, 1992) showed the DISA to be statistically greater than the fixed-point ($p > 0.05$). This is likely the result of only a few samples where differences in SSC between the two sample collection methods were large.

Of the 32 samples collected, only 6 showed any significant departure from a line of equality. These 6 samples (identified as red in figure 4) were all collected during the same July 21, 2013 storm event near

the peak of the hydrograph. Of the two EWI samples collected during this event, SSCs in the corresponding DISA samples were 79 and 95 percent larger and the fixed-point 43 and 57 percent lower (figure 5). It is unclear why both samplers differed from the concurrent EWI samples or why SSCs in the DISA sampler were much larger than those in the fixed-point while the vast majority of other samples collected during this and other events show close agreement. One explanation could be the proximity of the DISA intake to the channel bed. Since the DISA begins its sample collection approximately 2 inches above the streambed, sediment transporting as bedload could have been collected by the DISA and thus elevate resulting SSCs, especially for this particular event. This zone of sediment transport would have been precluded from both the EWI (minimum of 4 inches above the bed when using a DH-81) and fixed-point samplers (set at 8 inches above the bed). However, if the DISA were, in fact, sampling a portion of bedload, the majority of resulting SSCs should have been larger than those in corresponding fixed-point samples for all sampled events. Another explanation may be a large amount of organic debris found entangled around the fixed-point sampler during the July 21 event (figure 6). This may have resulted in lower SSCs by preventing exposure to the full range of suspended particles in the water column. The DISA, by design, is self-cleaning and therefore did not experience a similar problem. In either case, a simple adjustment to the DISA can prevent future sampling of bedload whereas preventing debris from accumulating on a fixed-point sampler is more challenging. The majority of data (with exception of the 6 samples from the July 21 event) suggest concentrations of sediment in both the DISA and fixed-point samplers were similar in an open channel setting, but generally greater than those measured by the EWI samples (figures 4 and 5).

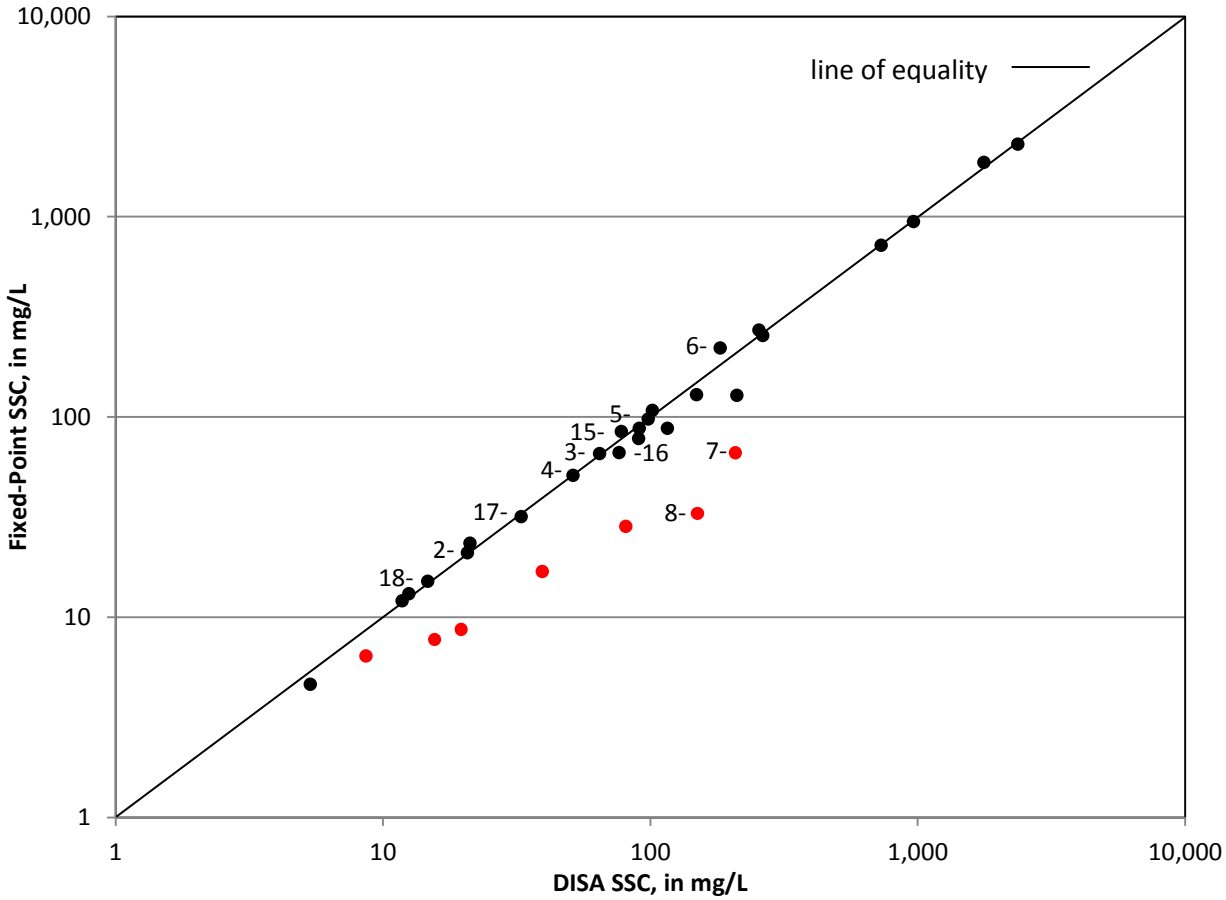

Figure 4 Concentration of suspended sediment in paired samples using the DISA and fixed-point collection methods. Red dots represent samples with the greatest departure from the line of equality, all of

which were collected during a single storm event. Labels refer to the corresponding EWI sample number detailed in figure 5.

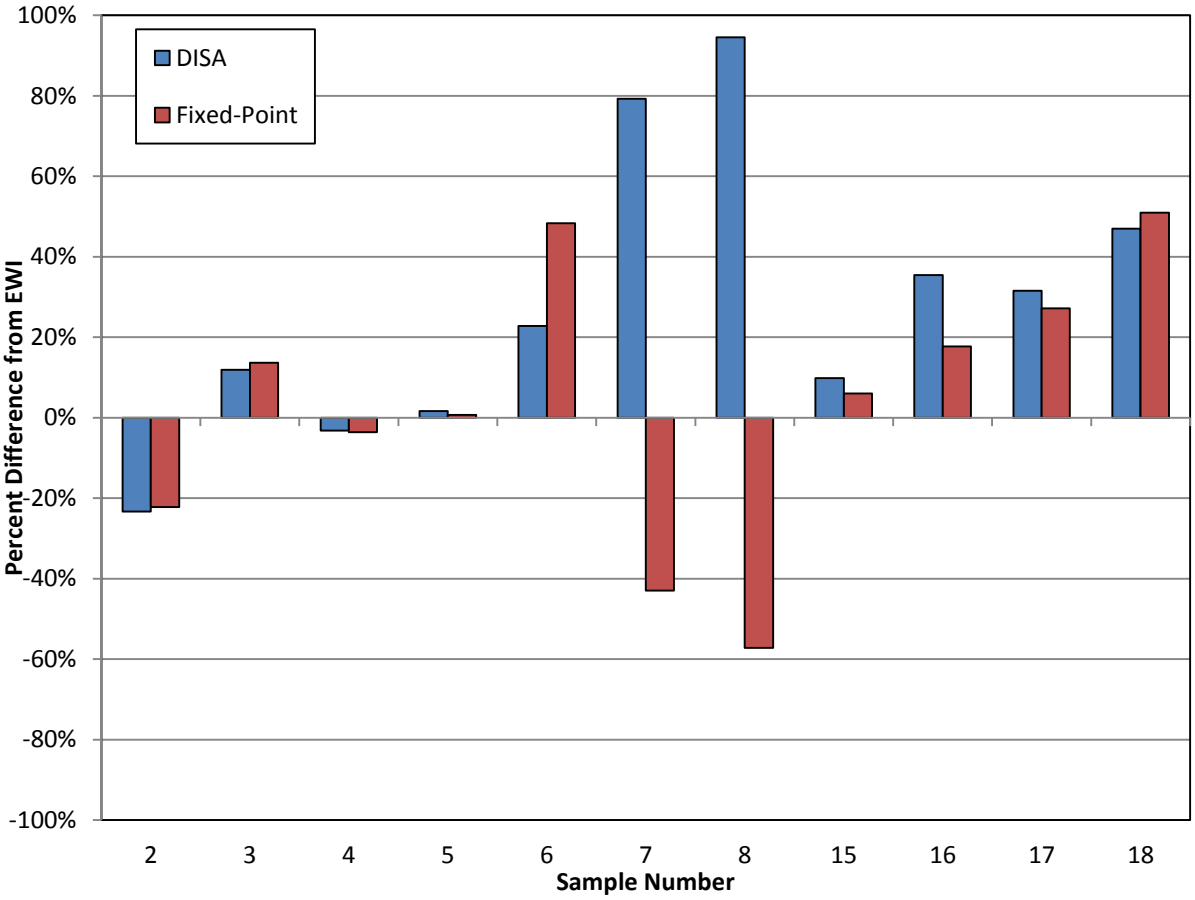

Figure 5 Percent difference in suspended sediment concentration measured in the DISA and fixed-point samplers to those measured in the EWI sampler.

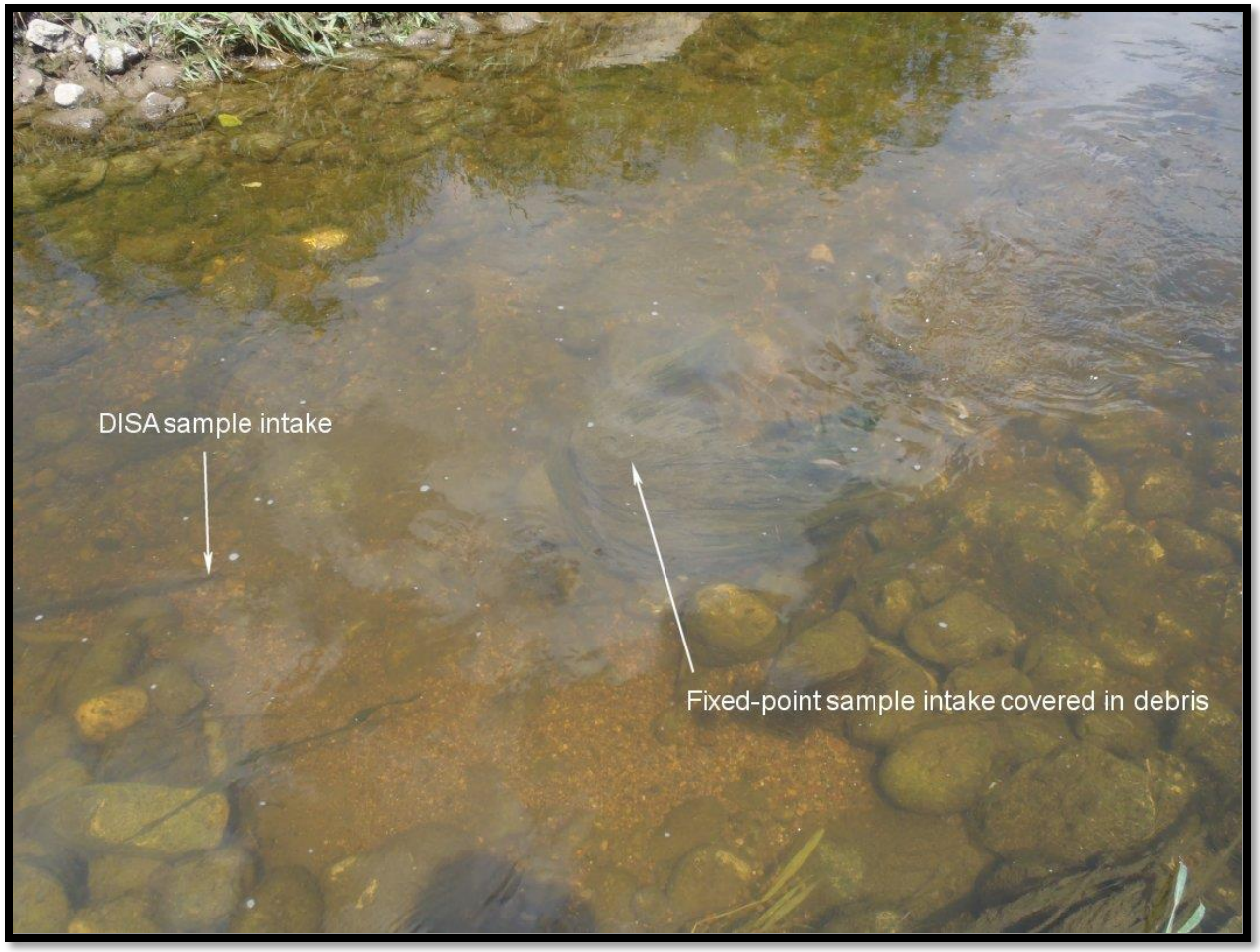

Figure 6 A large amount of organic debris covering the fixed-point sampler may have caused resulting SSCs to be much lower than corresponding DISA samples. Photo by USGS.

The DISA is designed to collect a vertical composite of the entire water column, rather than a single, fixed point thereby reducing any stratification bias caused by the presence of sand (>63 μm). A larger fraction of sand moving through a water column would likely increase heterogeneity which could increase the variability of resulting concentration data dependent on where a sample was acquired. If the water column were well mixed, differences between the DISA and fixed-point sampler would be minimal, as was the case in this study. Inspection of the PSD in DISA, fixed-point, and EWI samples showed median particle diameters (d_{50}) to be primarily that of clay and silt (<63 μm) (figure 7). Smaller particles are more easily mixed throughout the water column rendering placement of the sampler intake of less importance. Figure 7 also illustrates a general departure from equality between the d_{50} measured by the fixed-point and DISA samplers. Both sampler types show similar median particle diameters up to approximately 40μm at which point the d_{50} in the fixed-point and EWI samplers tend to remain the same while the DISA continues to increase. It is unclear whether this pattern would continue with increasing particle diameters. Additional testing in a controlled laboratory setting would help test the DISA's ability to accurately sample a wide range of particle concentrations and distributions.

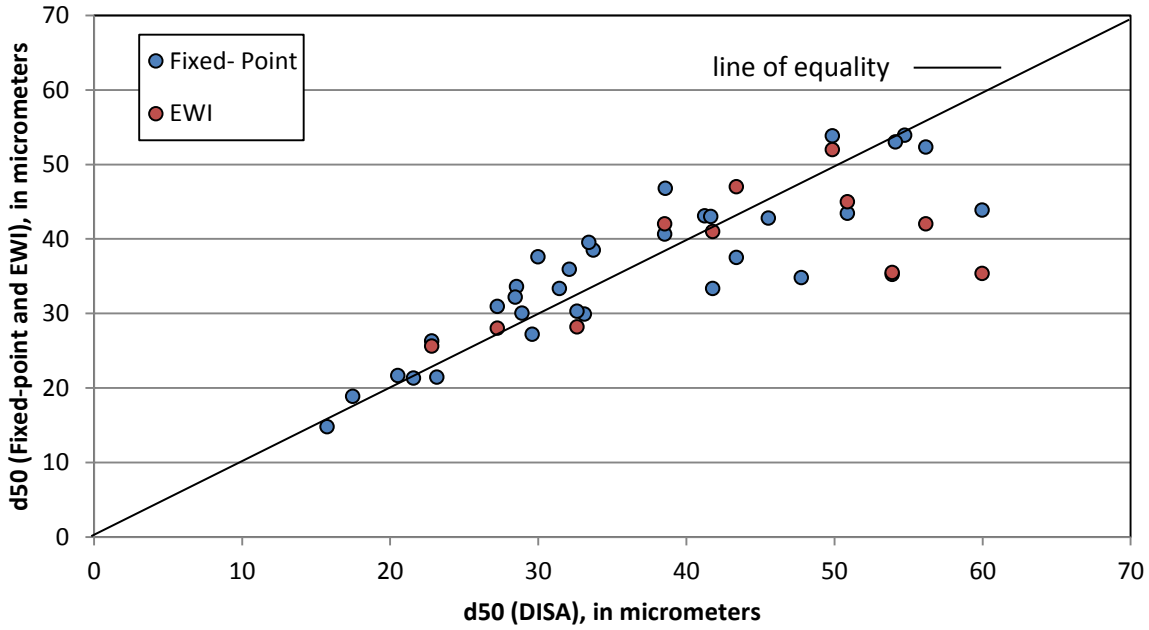

Figure 7 Median particle diameters in paired samples collected by the DISA, fixed-point and EWI samplers.

CONCLUSION

Stratification of particles in a flowing water column can be a source of bias and variability in sediment concentrations and distributions. In closed conduits, such as storm sewers, use of the DISA has shown that integrating samples from the entire water column, rather than from a single, fixed point, can result in a more accurate representation of sediment concentration and distribution, especially as the stratification of solids becomes more apparent with an increased presence of sand. When tested in an open channel, the DISA showed no marked improvement to the accuracy of sediment concentration or distribution compared to fixed-point and EWI sample collection methods. The small amount of sand measured in the water column at the open channel field site rendered placement of the sample intake of less importance. Differences between the median particle size and SSCs measured between the two sampler configurations could potentially be much greater in a fluvial setting with coarser sediment transport. An assessment of channel characteristics prior to sample collection can help determine if water-quality concentration data could benefit from the DISA sample collection method.

The DISA can improve water-quality datasets by reducing bias and variability in concentration and distribution of solids caused by stratification. In turn, environmental managers have greater confidence as they develop plans and policies to improve the quality of our Nation's waters.

REFERENCES

Bent, G.C., Gray, J.R., Smith, K.P., and Glysson, G.D. (2000). A Synopsis of Technical Issues for Monitoring Sediment in Highway and Urban Runoff. U.S. Geological Survey Open-File Report 00–497, 51 p.

Characklis, G.W., and Wiesner, M.R. (1997). Particles, metals, and water quality in runoff from large urban watershed, Journal of Environmental Engineering, 123(8), pp. 753 – 759.

Edwards, T.K., Glysson, G.D. (1999). Field methods for measurement of fluvial sediment, Techniques of Water-Resources Investigations of the U.S. Geological Survey, Book 3, Chap. 2, 23 p.

Evans, K.M., Gill, R.A., and Robotham, P.W.J. (1990). The PAH and organic content of sediment particle size fractions, Water, Air, and Soil Pollution, 51, pp. 13-31.

Guy, H.P. (1970). Fluvial sediment concepts: Techniques of Water-Resources Investigations of the U. S. Geological Survey, Chapter C1, Book 3 Applications of Hydraulics, 55 p.

Harmel, R.D., Slade Jr, R.M., and Haney, R.L. (2010). Impact of sampling techniques on measured stormwater quality data for small streams, Journal of Environmental Quality 39, pp. 1734 – 1742.

Helsel, D.R., and Hirsch, R.M. (1992). Statistical methods in water resources: New York, Elsevier, 522 p.

Horowitz, A.J. (1995). The use of suspended sediment and associated trace elements in water quality studies, International Association of Hydrological Sciences Special Publication No 4, 58 p.

Li, Y.X., Lau, S.L., Kayhanian, M., and Stenstrom, M.K. (2005). Particle size distribution in highway runoff, Journal of Environmental Engineering, 131(9), pp. 1267 – 1276.

Sansalone, J.J., and Buchberger, S. G. (1997). Characterization of solid and metal element distributions in urban highway stormwater, Water Science and Technology, 36 (8-9), pp. 155-160.

Selbig, W.R., and Bannerman, R.T. (2011). Development of a depth-integrated sampler arm (DISA) to reduce solids stratification bias in stormwater sampling, Water Environment Research, 83(4), pp. 347-357.

Selbig, W.R., Cox, A., and Bannerman, R.T. (2012). Verification of a depth-integrated sample arm as a means to reduce solids stratification bias in urban stormwater sampling, Journal of Environmental Monitoring, 14(4), pp. 1137-1143

Ott, L.R., and Longnecker, M. (2001). An introduction to statistical methods and data analysis, Fifth edition. Wadsworth Group, Pacific grove, Calif. [variously paginated].

Wisconsin Administrative Code, Wisconsin Department of Natural Resources—Runoff management: Chap. NR 151 (2002). [variously paginated].

Office of Water, U.S. Environmental Protection Agency. Total Maximum Daily Load Program: December 13, 2011; http:// water.epa.gov/lawsregs/lawsguidance/cwa/tmdl/.

Waschbusch, R.J., Selbig, W.R., and Bannerman, R.T. (1999). Sources of Phosphorus in Stormwater and Street Dirt from Two Urban Basins in Madison, Wisconsin, 1994-95, U.S. Geological Survey Water-Resources Investigations Report 99-4021, 47 p.

Wood, M.S., and Teasdale, G.N. (2013). Use of surrogate technologies to estimate suspended sediment in the Clearwater River, Idaho, and Snake River, Washington, 2008-10, U.S. Geological Survey Scientific Investigations Report 2013-5052, 40 p.

NEW INFORMATION AND GUIDANCE FOR COLLAPSIBLE BAG-TYPE SEDIMENT SAMPLERS

Authors: **Mark Landers, U.S. Geological Survey (USGS), Federal Interagency Sedimentation Project, Atlanta, GA, landers@usgs.gov; Thomas Sabol, USGS, Southwest Biological Science Center, Flagstaff, AZ, tsabol@usgs.gov; Michael Manning, USGS, Lower Mississippi-Gulf Water Science Center, Jackson, MS, mmanning@usgs.gov; Jessica Anderson, USGS, Geological Survey, Arizona Water Science Center, Flagstaff, AZ, jranderson@usgs.gov; Corey Sannes, Jr, USGS, Geological Survey, Arizona Water Science Center, Flagstaff, AZ, csannes@usgs.gov**

INTRODUCTION

Answers for many critical water-related issues require solid-phase water-quality data that are representative, accurate, and consistent. Collection of suspended sediment samples for subsequent analyses of solid-phase constituents that represent water-column sediment concentrations requires use of appropriate isokinetic samplers and sampling techniques (Davis, 2005a). Recent review of field and laboratory data indicates that the Federal Interagency Sedimentation Project (FISP) collapsible bag-type sediment samplers may not function isokinetically under certain low velocity and/or low temperature conditions. Updated guidance and operational limits for FISP bag-type samplers were issued in FISP Memorandum 2013.01 (2013). This paper describes new information and guidance for operation of FISP bag-type samplers and ongoing efforts to further characterize the factors that influence bag-type sampler efficiency.

Suspended sediment concentration (SSC) and sediment-associated water-quality constituent concentrations can be highly variable in stream cross sections, particularly when sand-size particles ($\geq$ 0.0625 millimeters (mm)) are suspended in appreciable quantities. Consequently, samples representative of the flow throughout the cross section must be collected using depth- and width-integrated methods and isokinetic samplers (Edwards and Glysson, 1999; Nolan et al., 2005; Gray et al., 2008). Isokinetic sampling means that water enters the nozzle of a sampler without accelerating or decelerating relative to streamflow velocity (ambient velocity) at the locus of the sampler nozzle opening. The measure of isokinetic sampling is the intake efficiency (IE), which is defined as the ratio of the velocity through the nozzle entrance (Vn) to the ambient stream velocity (V); IE = Vn/V, where Vn and V are averaged over the sample collection time and depth for each specific sample. Before a bag sampler is released for field use, the IE is confirmed to be within $0.9<IE<1.1$ at velocities of 3–4 feet per second (ft/s) at laboratory water temperature by flume tests conducted at the U.S. Geological Survey Hydrologic Instrumentation Facility (HIF), Stennis Space Center, Mississippi.

The importance of isokinetic sampler function on sampled SSC is illustrated in Figure 1 (Gray et al., 2008). The study on SSC bias with IE was performed in early FISP research using empirical methods and reported in FISP Report No. 5 (1941). These early FISP findings have been validated in preliminary results from new FISP-sponsored research in 2014-15 using computational fluid dynamic modeling. If flow decelerates as it enters the nozzle (IE < 1, sub-isokinetic), the sample SSC will tend to be biased high; conversely, if flow accelerates as it enters the nozzle, and the sample SSC will be biased low. The bias in SSC for the coarsest grade of sand (0.45mm) shown in Figure 1 is approximately +10% for IE=0.75, at a velocity of 5 ft/s. For a theoretical suspended-sediment sample made up of 25% of each of the size classes shown

in Figure 1 (0.01mm, 0.06mm, 0.15mm, 0.45mm) collected in a stream velocity of 5 ft/s, the overall bias for an IE 0.80, 0.75, and 0.50 is 3.5%, 4.9%, and 13.1%, respectively. The errors associated with SSC measurements due to measurement plus analytical error sources vary with concentration and grain-size distribution as well as site conditions at the time of sample collection. However, based on replicate samples, at concentrations above 20 milligrams per liter, differences of +/- 10% are common (Horowitz 2008, Edwards and Glysson, 1999). Although bias error due to non-isokinetic sampling conditions should always be considered and minimized, overall bias errors of less than 5% are much less than the typical SSC uncertainty. Under some field and deployment conditions it may not be possible to collect a sample with 0.75<IE<1.25; in which case it is particularly important to document the IE so that potential bias in sand SSCs can be considered by users of the reported data. For particles finer than sand size (≥ 0.0625 mm) the bias is less than 10%, even at extreme non-isokinetic conditions (see purple– and blue–dashed lines in figure 1). Thus, it is acceptable to sample under non-isokinetic conditions if the sand percentage of SSC has been shown to be negligible in prior analyses of samples collected at that site under similar conditions. In any case, Vn and V should be recorded and the IE calculated with each environmental sampling effort.

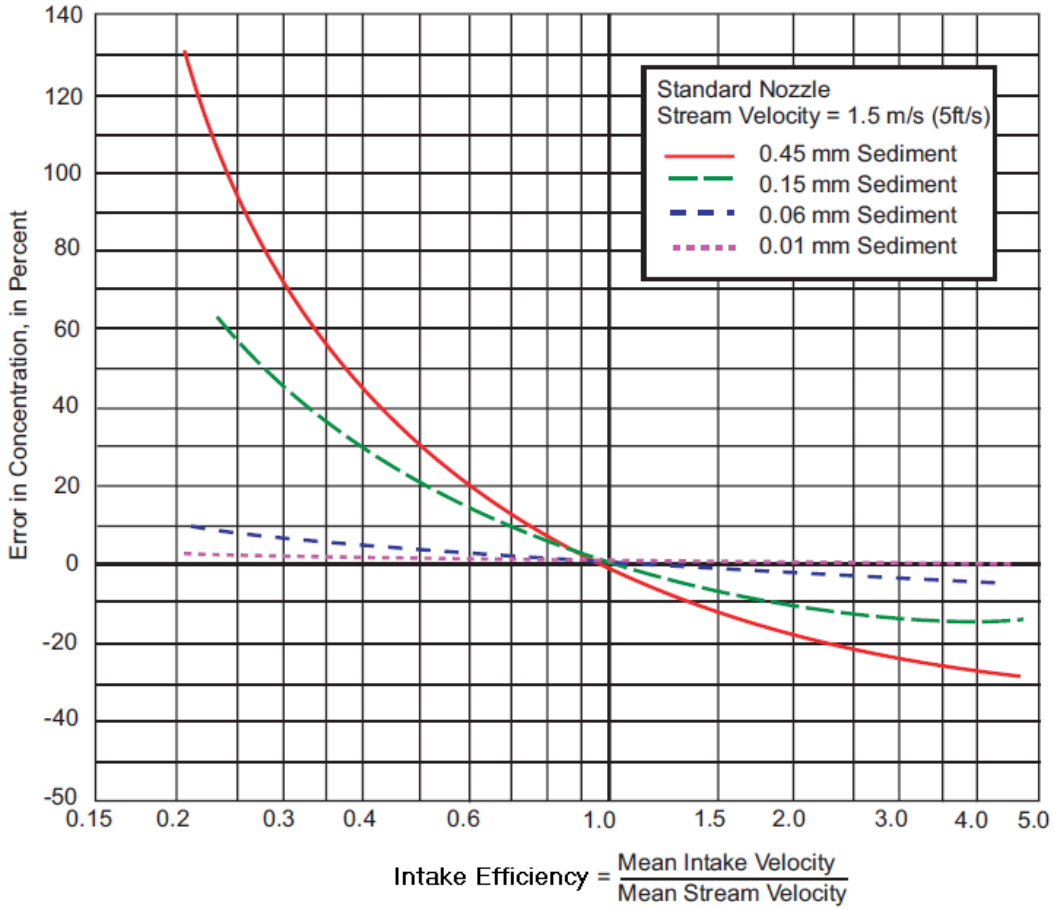

Figure 1 Errors in SSC under variable non-isokinetic sampling conditions for four sediment sizes (0.01mm, 0.06mm, 0.15mm, 0.45mm). Mean velocity of flow in the flume of 5 ft/s was maintained during data collection. Figure from Gray et al. (2008), based on data from FISP Report No. 5 (1941).

Factors that affect the IE of isokinetic samplers include sampler type and nozzle size, ambient stream velocity, water temperature, sampler orientation relative to the flow, and the volume of water collected relative to that of the sample container. IE in bag-type samplers tends to decrease rapidly as stream velocities decrease from about 4 to 2 ft/s, depending on the type of sampler, nozzle size, and stream temperature (Davis, 2001; McGregor 2006; Sabol and Topping, 2013). Because bag-type samplers require ambient velocity in order to fill, the effects of all other IE-related factors tend to increase as velocities approach the minimum recommended operating velocities. Substantial concentrations of sand are not typically in suspension for velocities less than the minimum operational limits of bag-type samplers, and this may mitigate the influence of non-isokinetic sampling on the accuracy of SSCs and sediment-associated water-quality constituent concentrations. Sample volumes should never exceed maximum sample container capacities or IE will decline very rapidly as described by Szalona (1982). Sampling up to full bag capacity did not affect IE in tests conducted in extensive laboratory tests at warm temperatures and in limited field tests in larger rivers (Davis, 2001).

RECENT STUDIES

Recent field studies have indicated problems with intake efficiencies of the US D-96 bag-type sampler. Sabol and Topping (2013) conducted an extensive study of sampling efficiencies of the US D-96 and US D-77 bag-type samplers in the Colorado River within Grand Canyon National Park. The US D-77 bag-type sampler was removed from the list of recommended samplers in 2002 (USGS OWQ Technical Memorandum 2002.09); however the US D-77 bag-type sampler results of Sabol and Topping (2013) are useful in evaluating historical sample data. Selected primary findings of Sabol and Topping (2013, page 64) are:

- Although both the US D-77 and US D-96 bag-type samplers have been proven to sample isokinetically in flumes, typically both sampled sub-isokinetically in field tests on the Colorado River.
- The US D-96 sampler performed closer to isokinetic conditions than the US D-77 bag-type sampler.
- Water temperatures in the field test environment are colder than in FISP laboratory test environment, and affect the sub-isokinetic performance of the samplers; but this is not the dominant effect.
- Intake efficiencies of the US D-77 and US D-96 bag-type samplers are time dependent. IEs decrease over time as sampling duration (and thus sample volume) increases. Intake efficiencies of rigid-container samplers in this environment were found to be constant with time, when recommended procedures were used.
- Analyses of paired, concurrent samples collected in the Colorado River using the US D-96 sampler and two rigid-container samples (tested to be isokinetic) indicate that the US D-96 samples have a positive bias error of +5 to +6 percent in the concentration of particles $\geq$ 0.0625mm, and this observed bias error is consistent with the observed sub-efficiency of the sampler according to the results from FISP Report No. 5 results shown in Figure 1.

Sabol and Topping (2013) hypothesized that the "most likely physical mechanism responsible for the large time-dependent decreases in intake efficiency observed in the Colorado River tests of both the US D-77 bag-type and US D-96-type samplers is the improper venting of the rear of the sampler cavity." They experimented with increasing the sampler venting by modifying the sampler tray from the standard FISP tray length (16.75 inches (in) long) to a shorter tray length (15.5 in long) and found slight but significant improvements in the US D-96 IE when the shorter tray length was used. In late-February 2013, the FISP tested the standard and shortened trays on a new US D-96 sampler and on a US D-96-A1 sampler that had been used in the field study of Sabol and Topping. The D-96-A1 is dimensionally identical to, but weighs 52 pounds less than, the D-96. The tests were conducted in a 6-foot (ft.) wide by 3-ft. deep, 250-ft. long tilting flume at a stream velocity of 3.31 ft/s (+/- 2%) and water temperatures of 20-22 °C (68-72 °F) at the USGS HIF hydraulics laboratory. A 3-liter (L) sample bag was used in the field and lab studies. While the FISP lab study indicates decreasing IE with increasing sample duration and volume, the IE is within the range of 0.9 to 1.15 for the 5/16 and ¼ in. nozzle sizes; and within 0.85 to 1.0 for the 3/16 in. nozzle size (Figure 2). Comparing the shortened versus the standard tray length, there was no notable difference for the 5/16 in. and ¼ in. nozzle sizes and slight improvement was noted with the shorter tray for the 3/16 in. nozzle (Figure 2). Moreover, the 2013 FISP test results agreed very closely with those from the FISP US D-96 sampler development data (Davis, 2001). Thus, the results of Sabol and Topping (2013) appear to be associated with field conditions that are not being replicated in the laboratory flume environment and may or may not be due to sample cavity venting in those conditions.

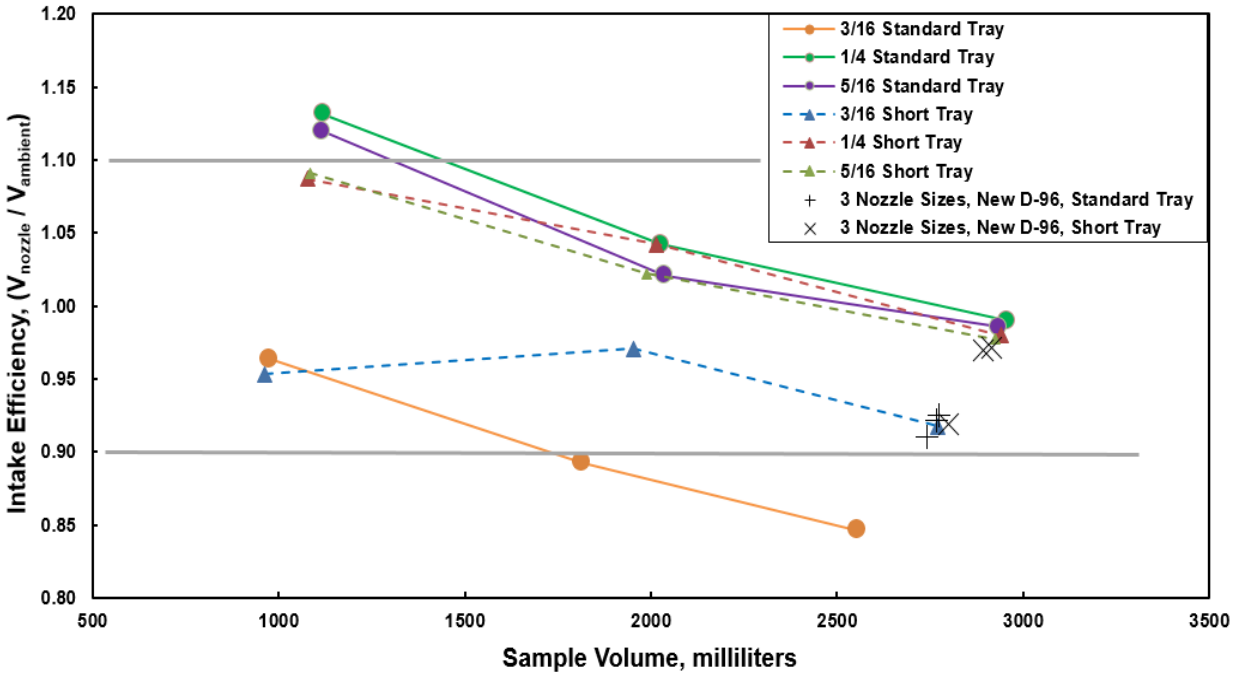

Figure 2 Intake efficiency results for US D-96 bag-type sampler conducted during February, 2013 in the tilting flume located at the USGS Hydrologic Instrumentation Facility. Tests run using standard FISP tray (16.75 in. long) and shortened tray (15.5 in. long) and available nozzle sizes (in inch fractions). For all tests the water velocity is 3.31 ft/s and the temperature is 20-22 C. Each point represents an mean of 5 to 10 measurements.

Additional field studies are being conducted to evaluate the IE of FISP bag-type samplers. An extensive study of depth-integrated sampling methods was conducted by the USGS Mississippi Water Science Center (Heather Welch, Mike Manning, and Claire Rose, personal communication). Over 240 samples, including replicates for each sampling vertical, were collected on the Mississippi River at Vicksburg, MS during 8 field trips from April 2013 to August 2013, at water temperatures ranging from 13 to 28 ^{o}C (55 to 82 ^{o}F). Velocity was measured concurrently with sample collection using an acoustic Doppler current profiler along with high-accuracy marine GPS technology to control boat movement during sampling. Velocities during normal flows in the sampled reach of the Mississippi River can surge by 1-2 ft/s within a range of 3-9 ft/s over the duration of a sample. The ADCP velocity data, concurrent with each sample, were extensively examined to obtain as accurate a concurrent sample velocity as possible. Both ¼ and 3/16 in. nozzle sizes were used. The mean IE from this data set of 240 samples was 0.81 with a standard deviation of 0.12 and IE was not significantly correlated with sample duration or volume, nozzle size, nor with stream velocity.

Field studies were conducted by the USGS, Arizona Water Science Center (Jessica Anderson and Corey Sannes, personal communication) in Water Year 2014 using US D-96-A1 (3 liter bag), and DH-2 (1 liter bag) samplers on the Colorado River at Lees Ferry, AZ. This study evaluated methods to increase the accuracy of the IE test results by limiting possible errors introduced in the field measurements. A Price-AA meter was mounted atop a D-96A1 sampler and velocity was measured concurrently with an ADCP mounted on a boat next to the sampler for the duration that the sampler was under the water surface. Two of the questions posed in the study design were: (1) Does the method by which the velocity is measured affect the intake efficiency results? and (2) Is there a directional bias either by the meter or the sampler when performing a depth-integrated sample? Tests conducted with the US D-96A1 sampler transiting through the vertical (depth-integrated samples) resulted in a mean IE of 0.70 for nine tests using a Price-AA meter; and a mean IE of 0.63 for thirty-two tests performed using an ADCP to measure velocity. Tests conducted holding the sampler at fixed locations at 2- and 10-foot depths with a ¼ in. nozzle resulted in a mean IE of 0.69 for nineteen tests using a Price-AA meter and an IE of 0.78 for nineteen tests using an ADCP to measure velocity. Tests conducted holding the D-96-A1 sampler at fixed locations at 2- and 10-foot depths with a 5/16 in. nozzle resulted in a mean IE of 0.62 for nine tests using a Price-AA meter and an IE of 0.69 for eleven tests using an ADCP to measure velocity. Velocities measured using the Price-AA (presumed to be more representative of ambient velocity at the locus of the sample nozzle) resulted in lower IE values for these tests; but sample durations did not have a significant effect on the IE results. The DH-2 had a mean IE of 0.89 with a 3/16 in. nozzle and a mean IE of 0.88 with a 1/4 in. nozzle. From all of the tests performed at this site, it was determined that the major variables that seem to affect the IE results in the field are the sampler type and nozzle size. More data needs to be collected with both samplers and with each nozzle size to determine if there is directional bias.

IE is determined, in the field or the laboratory, from measurements of ambient stream velocity (ideally at the locus of the sampler nozzle) and nozzle velocity determined from known nozzle intake area and measured sample volume and duration of sample collection. Any component measurement errors translate directly to errors in the computed IE. In the laboratory these factors

are measured with high accuracy. In field studies, the greatest source of measurement error typically is the stream velocity; and this can be more difficult when measuring from a boat. However, velocity measurement errors are not the likely cause of indicated IE in these field studies because they used detailed and careful evaluation of the velocity measurements and other measured factors. It is also noteworthy that field testing in large rivers and towed-sampler IE tests conducted during development FISP bag-type samplers do not indicate sub-isokinetic performance. The reaches of the Colorado River sampled in the above sited studies are much steeper than those in the large river test areas and in the Mississippi River, resulting in greater shear stress, turbulence, and velocity gradients. These are the likely environmental conditions, in addition to colder temperatures, that result in the sub-isokinetic performance of the bag-type samplers tested, as stated by Sabol and Topping (2013). The sub-isokinetic performance in the above noted studies appear to be due to conditions that do not occur in laboratory testing nor in all riverine conditions.

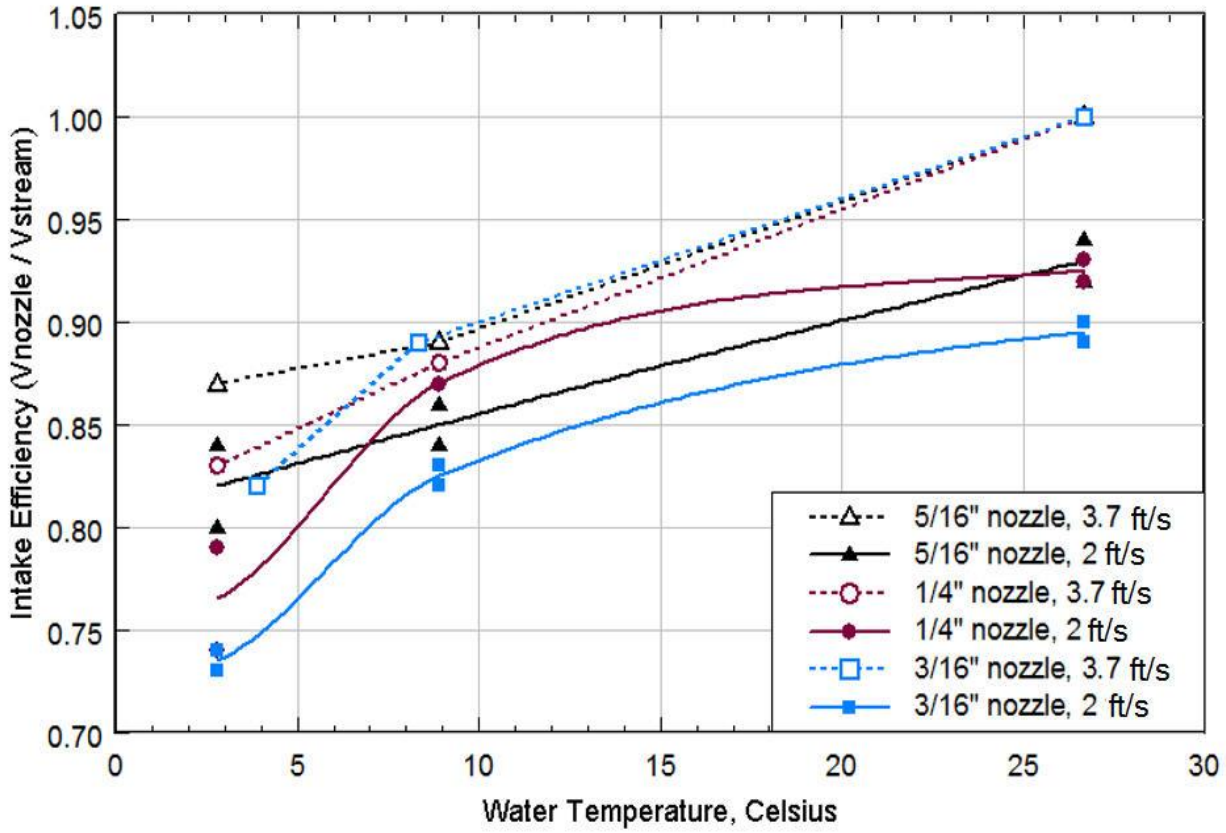

Figure 3 Changes in IE (intake efficiency) with temperature and fitted curves for the FISP US D-96 bag-type sampler at three water temperatures, and nozzle sizes, and two velocities, from data in Davis, 2001.

TEMPERATURE EFFECTS

Decreasing stream temperatures tend to cause decreasing sampler IEs because friction losses increase through the sampler nozzle as fluid viscosity increases. This effect becomes more

pronounced at lower velocities as shown in Figure 3 (from data in Davis, 2001). Tests of FISP samplers are typically conducted at water temperatures between about 24ºC–29ºC (75º–85ºF), in the warmer range of most field sampling conditions. Cold–water tests indicate that the US D-96 functions sub-isokinetically (IE < 0.9) at temperatures less than about 10ºC (50°F) at velocities less than about 3.7 ft/s for all nozzle sizes (Davis, 2001). A theoretical and empirical evaluation of temperature effects also was conducted by Sabol and Topping (2013) for US D-96 bag-type samplers in the Colorado River in Arizona. These data and subsequent review of FISP bag-sampler calibration data prompted revision by FISP of previous temperature-indexed minimum operational velocity limits; the revised limits are shown in Table 1.

RECOMMENDATIONS AND SUMMARY

FISP Memorandum 2013.01 (2013) supplements the FISP reports and operation manuals for the FISP US-series DH-2, D-96, D-96A1, and D-99 bag-type samplers (Davis 2001 and 2005a and b; McGregor, 2006) with the following recommendations to users of FISP bag-type samplers:

- Obtain quality-assurance field measurements of IE before each set of samples is collected during site visits using care to measure the stream velocity at the sample location as concurrently as possible.
- Incorporate the revised, temperature-indexed minimum stream velocities (Table 1) for bag-type samplers into data-collection practices where possible.
- If measured IE clearly indicates sub-isokinetic performance, evaluate potential bias in reported concentrations, based on percent of sand-sized material (≥ 0.0625 mm) in the sample using the chart in Figure 1 and evaluate the significance of this bias to the overall sample concentration accuracy and the purpose of the sampling effort.

The memorandum gives step-by-step instructions for field measurement and computation of IE, and provides a spreadsheet template to facilitate the computations for user-specified nozzle sizes. Revised minimum operational velocities for FISP bag-type samplers where sand-size (≥0.0625 mm) material may be in suspension are shown in Table 1. The new minimum velocity guidance is indexed to water temperature for specific nozzle sizes. The minimum-velocity requirement remains unchanged for temperatures greater than 27ºC (80°F) for all nozzle sizes, and for temperatures greater than 10ºC (50°F) for ¼- and 5/16-in. nozzle sizes. Field tests of IE are particularly important when sampling near these operational limits. Recent studies have demonstrated that the samplers do not operate isokinetically in some riverine environments, even within these limits.

In summary, recent, detailed studies have found that the FISP US D-96 and D-96A1 bag-type samplers operates sub-isokinetically (IE<0.9) in some field conditions. FISP test results in a laboratory tilting flume have not replicated these field results; and have confirmed the original results from sampler development and sampler operational guidance. Moreover, field IE testing does not uniformly indicate sub-isokinetic sampler performance. Colder water temperatures are a known cause of lower IE and revised, temperature-indexed minimum velocity guidance has been issued by the FISP in view of this effect. Colder water temperatures cannot, however, explain the magnitude of observed sub-isokinetic performance in the some of the recent studies; and the actual contributing causes and their relative influence on low IE remains uncertain. It is likely

that the effects of turbulence (at different scales) and transit through relatively high velocity gradients are important factors, as stated by Sabol and Topping (2013). FISP now recommends field IE measurements during each sampling effort and recording of this quality-assurance data with sample analytical data. If any non-isokinetic sample performance is documented, then the potential concentration bias should be evaluated based on the results of FISP Report No. 5 (1941) summarized in Figure 1. While it is essential to recognize and evaluate any source of potential bias in sample results; the bias effect should not be overstated. The significance of any IE-caused bias should be evaluated based on particle size distribution of the sediment, the significance of the bias to specific particle size classes, the overall accuracy of the analyzed sample concentration, and the accuracy needed to address the purposes of the sampling effort.

Table 1 Characteristics and operational ranges for FISP bag-type samplers.

FISP Sampler	Con-tainer type and capa-city	Wei ght, pou -nds	Mode of Suspen-sion	Un-samp-led Zone, in	Max Velo-city [1], ft/s	Nozzle Inner Dia-meter [2], in.	Maxi-mum Depth [3], ft	Minimum Isokinetic Velocity [4], ft/s for Temperature (T) °C		
								T <10°	10< T <27°	T >27°
US DH-2	Flexible 1-L bag	30	Handline or Cable Reel	3.5	6	3/16	35	3.7	3.7	2
						1/4	20	3.7	2	2
						5/16	13	3.7	2	2
US D-96	Flexible 3-L bag	132	Cable Reel	4.0	12	3/16	110	3.7	3.7	2
						1/4	60	3.7	2	2
						5/16	39	3.7	2	2
US D-96-A1	Flexible 3-L bag	80			6	3/16	110	3.7	3.7	2
						1/4	60	3.7	2	2
						5/16	39	3.7	2	2
US D-99	Flexible 3-L or 6-L bag	285	Cable Reel, Heavy	9.5	15	3/16	220	4	4	4
						1/4	120	3.7	3	3
						5/16	78	3.7	3	3

[1]The maximum recommended velocity for bag-type sampler deployment is based on maximum drift angle of the suspension cable (25–30 degrees). Actual maximum velocity should be determined based on this maximum drift angle and field safety considerations.

[2] The 3/16 in. nozzle is more sensitive to velocity and temperature effects and should only be used when necessary to sample maximum depths.

[3] The maximum theoretical depth is based on a maximum transit rate of 0.4 times the mean flow velocity in the sampled vertical and the sample bag capacity (6 L for the US D-99 sampler).

[4]Test results are not available for temperatures <10ºC (50°F). In colder water it is particularly important to test and record intake efficiency with each sample data set.

REFERENCES

Davis, B.E. (2001). The US D-96: An isokinetic suspended-sediment/water-quality collapsible-bag sampler: Federal Interagency Sedimentation Project Report PP, 37 p. (http://water.usgs.gov/fisp/docs/Report_PP,_US_D-96_011114_.pdf).

Davis, B.E. (2005a). A guide to the proper selection and use of Federally approved sediment and water-quality samplers, U. S. Geological Survey. Open-File Report 2005-1087, 20 pp. (http://pubs.usgs.gov/of/2005/1087/)

Davis, B.E. (2005b). The US DH-2: A one-liter hand-line isokinetic suspended-sediment/water-quality collapsible-bag sampler: Federal Interagency Sedimentation Project Report SS, 19 p. (http://water.usgs.gov/fisp/docs/Report_SS_050720_DH-2_.pdf).

Edwards, T.K., and Glysson, G.D. (1999). Field methods for measurement of fluvial sediment: Techniques of Water-Resources Investigations of the U.S. Geological Survey, Book 3, Chapter C2, 89 p. (http://pubs.usgs.gov/twri/twri3-c2/pdf/TWRI_3-C2.pdf).

Federal Interagency Sedimentation Project (1941). Laboratory investigation of suspended-sediment samplers: Iowa City, Iowa University Hydraulics Laboratory, Interagency report No. 5, 99 p. (http://water.usgs.gov/fisp/docs/Report_5.pdf).

Federal Interagency Sedimentation Project Technical Memorandum 2013.01, Best Practices for FISP Bag Sampler Intake Efficiency Tests and Operational Velocities, May 6, 2013 (http://water.usgs.gov/fisp/docs/FISP_Tech_Memo_2013.01.pdf)

Gray, J.R., Glysson, J.D., and Edwards, D.T. (2008). Suspended-sediment samplers and sampling methods, *in* Garcia, M., ed., Sedimentation Engineering, Processes, Measurements, Modeling, and Practice: ASCE Manuals and Reports on Engineering Practice No. 110, p. 320-339

Horowitz, A. J. (2008). Determining annual suspended sediment and sediment-associated trace element and nutrient fluxes. Science of the Total Environment, 400, 315–343

McGregor, J. (2006). The US D-99: An isokinetic depth-integrating collapsible-bag suspended-sediment sampler: Federal Interagency Sedimentation Project Report RR, 19 p. (http://water.usgs.gov/fisp/docs/Report_RR.pdf).

Nolan, K.M., Gray, J.R., and Glysson, G.D. (2005). Introduction to suspended-sediment sampling: U.S. Geological Survey Scientific Investigations Report, 2005 – 5077 (http://pubs.er.usgs.gov/pubs/sir/sir20055077).

Sabol, T.A., and Topping, D.J. (2013). Evaluation of intake efficiencies and associated sediment-concentration errors in US D-77 bag-type and US D-96-

type depth-integrating suspended-sediment samplers: U.S. Geological Survey Scientific Investigations Report 2012-5208, 111 p. (http://pubs.usgs.gov/sir/2012/5208/pdf/sir2012-5208.pdf)

Szalona, J.J. (1982). Development of a bag-type suspended-sediment sampler, A study of methods used in measurement and analysis of sediment loads in streams: FISP Report Y: Minneapolis, Minnesota, Federal Interagency Sedimentation Project, St. Anthony Falls Hydraulic Laboratory, 32 p. (http://water.usgs.gov/fisp/docs/Report_Y.pdf).

U.S. Geological Survey, Office of Water Quality (OWQ) Technical Memorandum 2002.09, 2002, "Water-Quality Field Methods phaseout of US D-77 and frame-type samplers," 1 p. (http://water.usgs.gov/admin/memo/QW/qw02.09.html).

CONVECTIVE ACCELERATION EFFECTS FROM TRANSVERSE IN-STREAM STRUCTURE INSTALLATIONS

S. Michael Scurlock, Ph.D, Post-Doctoral Fellow, Colorado State University, Fort Collins, Colorado, scurlock@engr.colostate.edu; Christopher I. Thornton, Ph.D; Associate Professor, Director Engineering Research Center, Colorado State University, thornton@engr.colostate.edu; Steven R. Abt, Ph.D; Senior Research Scientist/Scholar, Colorado State University, sabt@engr.colostate.edu; Drew C. Baird, Ph.D, Hydraulic Engineer, United States Bureau of Reclamation, dbaird@usbr.gov

Abstract: Transverse instream structures are rapidly gaining popularity in stream restoration and bank stability applications, yet are implemented with an incomplete knowledge of induced structure hydraulics. Transverse structures extend laterally from the channel bank into the flow field, serving to redirect conveyance away from the outer bank of the channel for navigation and erosion objectives. Three types of instream structures, the spur dike, vane, and bendway weir, were constructed and evaluated within a physical model representation of a natural channel. High-resolution mean-flow and turbulent velocity data were collected from similar planimetric structure configurations with a focus upon convective acceleration and turbulence at the structure tips. The zone of influence at the structure tip is critical for design considerations due to implications for sediment mobility and structural integrity. This research presents specifics of flow effects at the tips of the three structure classifications, provides comparisons between structure types, and gives implications for design procedures and sediment mobility.

INTRODUCTION

An emphasis on alternative methods for bank stabilization and river restoration in meandering systems has gained momentum in recent years. Transverse in-stream structures have been utilized in channel bend stabilization projects as a means of diverting erosive forces away from the outer bank of a migrating river. Bendway weirs, spur dikes, and bank-attached vanes are specific types of in-stream structures, identical planimetrically, yet different in their cross-sectional geometries and intended hydraulic effects. Planimetric and cross-section schematics of in-stream structures are provided in Figure 1, detailing differences between structure classifications in the cross-sectional view. In a general hydraulic sense, bendway weirs redirect flows over the top of the crests, spur dikes shift flows around the structure tip, and bank-attached vanes combine both crest overtopping and redirection around the tip to the channel center. Typical geometric parameters of interest for instream-structure design are the structure width, W, length, L, spacing, S, elevation difference between the water-surface elevation and structure crest elevation, Δz, planform angle, θ, and crest-slope angle, φ. Guidelines for the construction and installation of instream structures in channel bends as functions of the geometric parameters exist, yet are largely anecdotal.

Bendway weirs were initially developed by the U.S. Army Corps of Engineers to improve navigation in bends of the Mississippi River (Derrick et al., 1994). Structures are typically placed in series along the outside of a channel bend, are angled upstream, and have a submerged crest elevation at design flow. Flows encountering the crest are redirected to the channel center over the structure axis. Three primary sources for documentation and interpretation of bendway-

weir design and construction guidance were identified as McCullah and Gray (2005), Lagasse et al. (2009), and Julien and Duncan (2003). Currently, design guidelines for bendway-weir configurations are anecdotal, and have largely been developed on the basis of expert judgment (Rhoads, 2003).

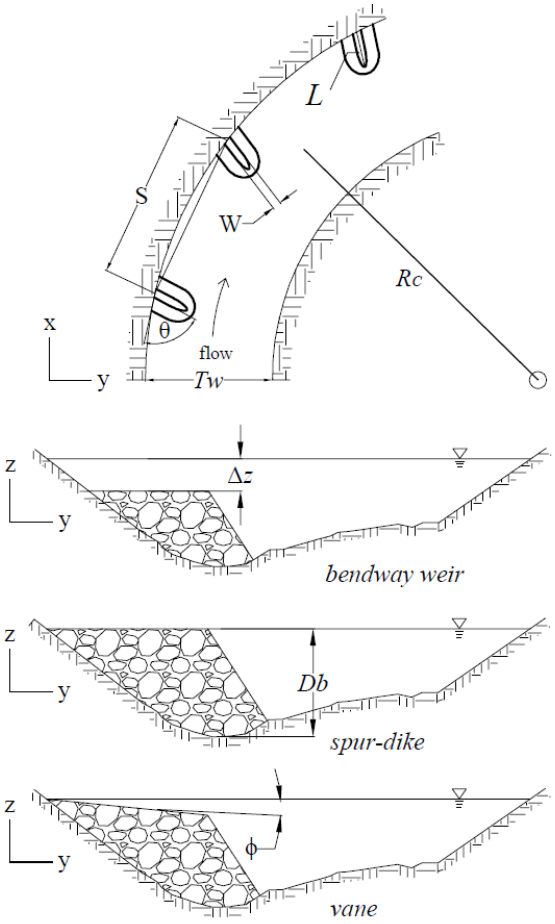

Figure 1 Instream structure geometric parameter definitions

Spur dikes, also referred to as groynes or jetties, extend from the outer bank to the channel center. They are placed in series throughout a channel bend, and are set either perpendicular or angled to the stream flow direction. In contrast to bendway weirs, spur-dike crest elevations are constructed at the design water-surface elevation and no conveyance is meant to overtop the structure crest. Spur-dike hydraulics encourage sedimentation within the structure grouping, or field, and provide outer-bank erosion protection (Radspinner et al., 2010). Current design guidelines for spur dikes are summarized by the Federal Highway Admninistration publications of Brown (1985) and Lagasse et al. (2009).

Bank-attached vanes, also known as barbs, represent a hybrid between the bendway weir and spur dike. Sturctures are constructed with a crest elevation at the design discharge water-surface elevation at the outer bank and extend into the channel at a downward angle. Vanes allow an increasing level of flow to pass over the structure crest moving into the channel center. Similar to the other transverse in-stream structure types, vanes are constructed in series and set either

perpendicular or angled upstream to the flow direction. Unique publications of geometric design criteria, including summarizations from Rosgen (2001), McCullah and Gray (2005), Brown and Johnson (1999), and others, are found in NRCS (2005), Johnson et al. (2001), and Maryland (2000).

Transverse instream structures are designed to deflect outer-bank conveyance to the channel-center, increase flow resistance near the base of the outer bank, and inhibit helical motion and redistribution of momentum near the outer bank (Derrick, 1997). Field data from studies such as Scott et al. (2011), Rhoads (2003), Smith and Wittler (1998), and Wardman and Papanicolaou (2006) for bendway weirs, and Dahle (2009) for vanes, have confirmed that transverse instream-structure configurations are typically effective at redirecting bulk channel conveyance to the central channel. Investigations into specific flow patterns associated with single structures and configuration fields have been conducted utilizing physical and numerical modeling. Hydraulics associated with transverse instream structures have been reported as three-dimensional and complex, yet the literature indicates specific and recurring trends of flow behavior across independent sources.

Abad et al. (2008) coupled surveyed field data with a three-dimensional numerical model to emulate flow characteristics at various flow depths around a bendway-weir configuration installed in an Illinois meander bend. Key insights from the study included areas of convective acceleration and high boundary shear-stress at the tips of the structures, increased velocity and shear stress over the crest of the structure at the bankline, and locally increased bed shear downstream of the crest due to plunging flows. At the lowest flow evaluated in the study, the modeled bendway weirs did not experience overtopping flows, therefore behaving as spur dikes. Acceleration and increased boundary shear stress at the structure tips, over the structure crest at the bankline, and at the overtopping jet and bed interface were noted.

Jia et al. (2002, 2005, 2011) investigated the efficacy of bendway weirs to disrupt the helical secondary current in channel bends and documented flow patterns using numerical and physical modeling on a single structure angled 70º upstream. Acceleration of the flow velocity over the weir crest and around the structure tip, and a recirculation zone directly behind the structure were reported.

McCoy et al. (2007) detailed numerical modeling results of flow encountering submerged, bendway-weir like structures angled perpendicular to the approaching flow. Evaluated structures had abrupt, blunt noses instead of being gradually angled into the channel center. Authors noted significant convective acceleration over the structure crest and around the blunt structure tip. Flow encountering the structure separated at a stagnation velocity zone at the structure face, and was redirected over and around the obstruction. Recirculation zones, or eddys, were observed to form behind the structures and between adjacent structures. Streamlines were not shown to exhibit substantial planimetric circulation in the upper water column and the effects of the structure field diminished within two structure lengths of the downstream crest. Conveyance was observed to shift to the inner channel, away from the increased roughness of the modeled structure series.

Duan (2009) performed laboratory physical modeling on a spur dike installed in a straight, mobile-bed channel under clear-water conditions. Results of the study included documentation of flow separation downstream of the structure, strong planimetric recirculation in the upper water-column which decayed moving deeper into the flow, induced cross-sectional rotation, and high tip velocities. Flow interaction with the spur dike shifted the conveyance and bulk mean kinetic energy to the outside of the tip of the structure and incited circulation and increased turbulent kinetic energy downstream and behind the structure crest.

Jamieson et al. (2013) installed vanes constructed from scaled riprap in a mobile-bed, trapezoidal laboratory channel bend and collected bathymetry and velocity data. Vanes were imbricated in series and constructed according to NRCS (2005) guidelines. Planimetric velocity measurements illustrated an effective conveyance shift from the outer bank at baseline conditions to the channel center with the installed structure configurations. Authors noted scouring downstream of the vane crests which was attributed to the combination of plunging crest flow and local acceleration around the vane tip. When vanes were constructed with the bank key-in point below the water surface, increased outer-bank erosion was noted, similar to bankline flow acceleration noted for bendway weirs (McCoy et al., 2007, Abad et al., 2008). Varying degrees of disruption of the secondary current was noted for the vane configurations and was attributed to the strength of plunging flow over the vane crest.

Studies from the literature indicated a recurring set of hydraulic trends associated with the installation of transverse in-stream structures. The bulk flow conveyance is shifted towards the channel-center, acceleration occurs around the structure tip, and acceleration is observed along the outer bank at the bankline key in for submerged crests. This proceeding focuses upon the quantification of the convective tip acceleration that occurs for bendway weirs, spur dikes, and bank-attached vanes. Comparable physical models of the three structure types were constructed and resulting hydraulics were quantified. Tip velocities were isolated and information pertaining to maximum tip velocities for structure design was obtained.

PHYSICAL MODELING

The Middle Rio Grande River between Cochiti Dam and Elephant Butte Reservoir in New Mexico has been the focus of extensive river restoration work since the upstream Cochiti Dam construction in 1975. The dam effectively disconnected the sediment continuity to the downstream reach, resulting in a geomorphic shift from a historically braided channel to a slightly sinuous, incising system. The United States Bureau of Reclamation, as the responsible agency for management of the river, jointly launched an investigative study on the performance of transverse in-stream structures with Colorado State University. A physical model was constructed at a 1:12 Froude scale representing two surveyed bends from the Middle Rio Grande. A model schematic and topographic representation of the flume is presented in Figure 2 and an image of the completed downstream bend of the model is presented in Figure 3. The downstream bend of this physical model was selected to investigate tip velocity effects between the three structure types, and comparable physical model structure configurations were designed.

Physical models of bendway-weirs, spur dikes, and bank-attached vanes were designed according to slightly different methodologies. However, each configuration was constructed to

have the largest amount of direct comparability between structure types. Spacing, structure width, and orientation angle were identical. Quantified design parameters are summarized in Table 1. The process of bendway-weir design included available guidelines to ensure applicability to the current state of knowledge. Thornton et al. (2011) evaluated four spur-dike configurations in the same physical model as the current study. Methodologies reported by Thornton et al. (2011) describe spur-dike geometric parameter determination by a variation of projected length to match a desired cross-sectional area blocked percentage (A*). Following these methods, the spur-dike configuration was designed to match a desired A* value of 19.4. The lower crest height of the bendway weirs made alterating A* to match that of the spur dikes impractical. The vane configuration kept the same length of the spur dikes and incorporated a 10% sloped crest.

Hydraulic parameters such as the channel top width and design flow depth are integral parts of instream-structure design; however, parameters vary with longitudinal distance along naturally-formed channel bends due to pool and riffle sequencing and erosional processes. It was assumed for the purposes of the instream-structure design that such parameters are bend-averaged at a bankfull, or approximately two-year return interval, scaled prototype discharge of 6,000 ft^3/s (12 ft^3/s model scale). Top-width for the model was found by bend-averaging surveyed waterlines at the bankfull flow condition across the representative channel-bend cross sections. The hydraulic flow depth (D) was determined as the most representative parameter for instream-structure design criteria and was calculated from each cross-sectional T_W and flow area (A) using $D = A/T_W$ and were averaged across the downstream bend. Cross-sectional flow area was calculated from numerical integration of surveyed bathymetric data.

Bendway-weir crest length was specified as the distance from the intersection of the weir crest and the channel bankline to the weir tip, not including the transition slope from the crest to the channel bottom (Lagasse et al., 2009). Also, the weir should be long enough to cross the stream thalweg (Lagasse et al., 2009). Setting the crest length at $T_W/3$ for the downstream bend resulted in structures which adhered to ranges of L from the literature and generally crossed the stream thalweg. For each spur-dike structure, a projected cross-sectional bathymetry and area blocked was determined. Starting with a crest height at the bank waterline and specifying a tie-in slope of 1V:1H, the projected crest length was adjusted such that the total cumulative weir blockage was 19.4% of the baseline cross-sectional flow area. Vanes were designed such that the $L_{W\text{-}PROJ}$ at each structure was the same as the spur-dike configuration. Crest lengths for the spur dike and vane configurations ranged from $T_W/4$ to $T_W/3$. The calculated range of $L_{W\text{-}PROJ}$ for impermeable spur dikes exceeded the maximum design from Lagasse et al. (2009); however, vane crest lengths fell within specified ranges found in the literature.

Crest elevations were determined based upon the intended hydraulic effects of the structures. Spur dikes and vanes have crest elevations which are set at the design flow water-surface elevation at the bankline tie in. Bendway-weir crest height was set at one-third of the bend-averaged bankfull hydraulic flow depth, or two-thirds of the hydraulic flow depth below the water surface.

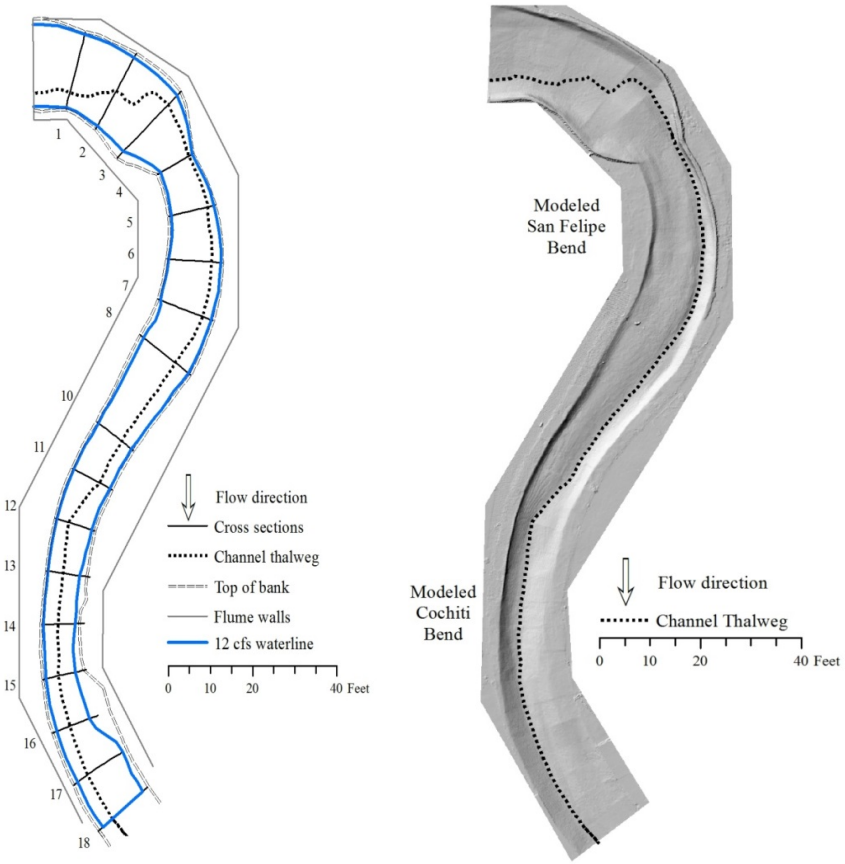

Figure 2 Native topography plan view schematic and constructed surface

Crest orientation angle was established at 60º, measured clockwise from the bankline tangent. The orientation angle coincides with design recommendations for bendway weirs, yet violates spur dike and vane recommendations (Lagasse et al., 2009; NRCS, 2005). Crest widths were constructed from approximately 0.3 ft to 0.5 ft angular rock, corroborating with design guidelines specifying instream structure crest widths of $d_{100} - 3d_{100}$, where d_{100} is the diameter of the largest grain size implemented in construction. Additionally, crest widths were set at a prototype 12 ft, allowing construction equipment to traverse the structure during installation. Each transverse instream structure was constructed from a plywood for centered in the crest and angular rocks were placed to form the required dimensions. The completed structures were impermeable to interstitial flows due to the plywood template. Topographic representations of the structures from LiDAR data, flume schematics, surveyed waterlines, and velocity data-collection locations are presented in Figure 4.

Mean-flow and turbulent velocity characteristics were obtained using two acoustic Doppler velocimeters (ADV). A SonTek® ADV of ±1% measured accuracy, and a Nortek Vectrino® ADV of ±0.5% accuracy were both utilized. ADV data have been collected in laboratory and field applications, and further details may be found in Voulgaris and Trowbridge (1998), Wahl (2000), McLelland and Nicholas (2000), Strom and Papanicolau (2007), and many others. ADV instruments operate at a high frequency (≥ 25 Hz) and allow for the determination of mean and fluctuating velocity components over the course of a sampled time period. A minimum of 1500

velocity data were obtained at each data-collection location. Data were processed using WinADV as detailed by Wahl (2000), and data used for instream-structure analyses typically had percentage-good scores greater than 70%, correlation values greater than 70, and signal-to-noise values greater than 15.

Figure 3 Completed native-topography downstream bed surface

Table 1 Instream structure configuration parameter design and values

Design parameters

Configuration	*Length*	*Height*	*Top width*	*Spacing*	θ
BW05	$T_W/4$	0.333 D	$2d_{100}$ - $3d_{100}$	2.69L	-
V05, SD05	$T_W/3$ - $T_W/4$	D *	$2d_{100}$ - $3d_{100}$	2.69L - 4.79L	-

* V05 has sloping crest at 7%

Design values

Configuration	*Length (ft)*	*Height (ft)*	*Top width (ft)*	*Spacing (ft)*	θ *(°)*
BW05	3.554	0.247	1.0	9.30	60
V05, SD05	variable	variable	1.0	9.30	60

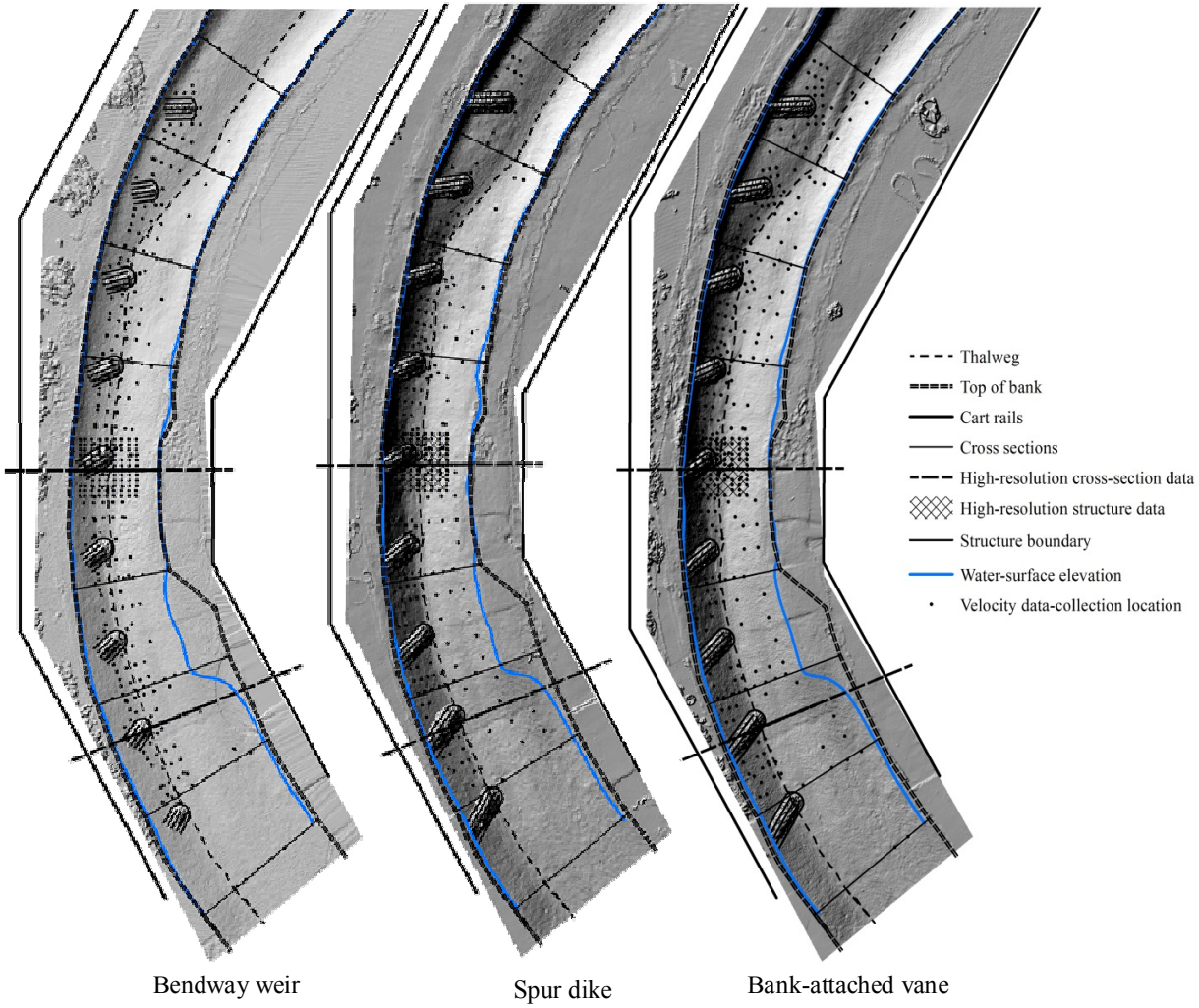

Figure 4 Constructed in-stream structure configurations and data-collection points

IN-STREAM STRUCTURE DATA RESULTS

Velocity data collected at each of the data-collection locations were processed and tabulated. Data at 60% flow depth measured below the water surface elevation were extracted as a surrogate for the depth-averaged flow. Velocities were normalized by the bend-averaged baseline cross-sectional velocity, computed through flow area and volumetric flow rate. The normalization value was found to be 1.702 ft/s at bankfull, normal-depth flow conditions. In general, all evaluated structure configurations exhibited velocities lower than the baseline velocity at the outer bank of the channel, and shifted the conveyance to the channel-center and inner-bank where all configurations showed velocities higher than baseline conditions. Normalized velocity values range from approximately zero to two for all configurations, corresponding to full velocity reduction or velocity doubling from baseline conditions, respectively.

Figure 5 depicts interpolated normalized velocity distributions for the evaluated in-stream structure configurations. Blue shades indicate velocities slower than the normalization condition, or less than unity, and red shades indicate velocities faster than normalization conditions, or greater than unity. For all structures, a strong gradient occurred between reduced and accelerated velocities, illustrated by the rapid transitions in the velocity distributions. The location of the shear gradient was found in the vicinity to the outer bank of the structure tips. Highest velocities were noted at the inner-bank vicinity of the structure tips.

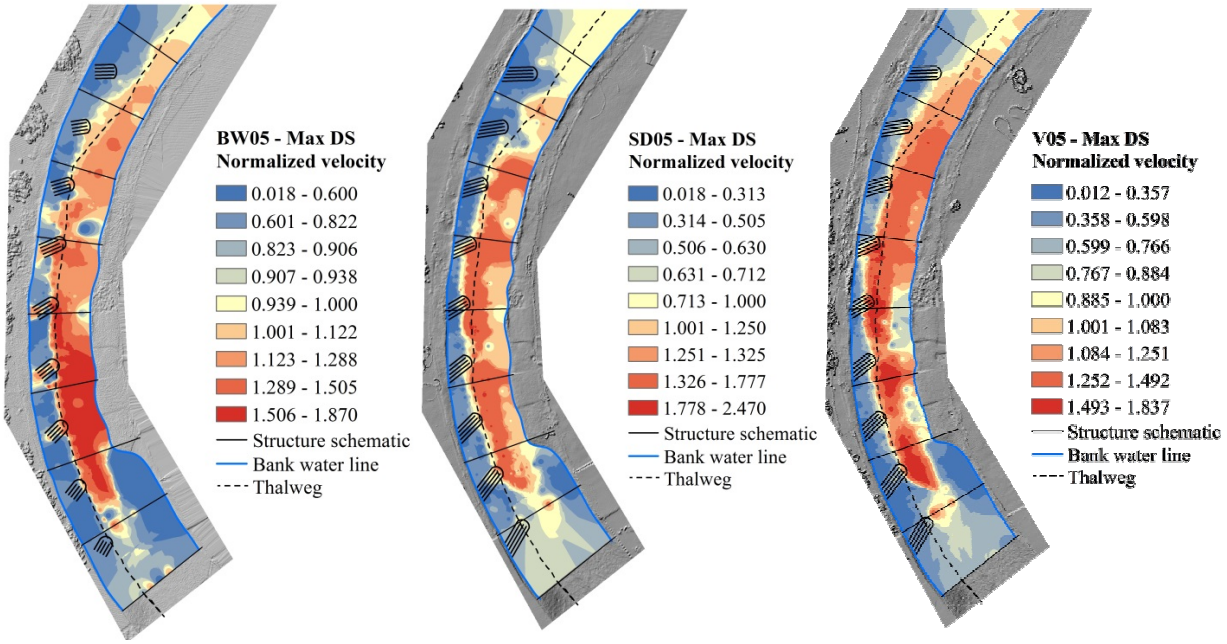

Figure 5 Normalized velocity fields (BW, SD, V = bendway weir, spur dike, vane, respectively)

Flow encountering the in-stream structures was observed to have specific features depending on the structure type. The bendway weir redirected flow over the top of the structure crest to the channel center, yet also split the conveyance to the outer bank. A localized region of higher velocity was noted at the outer-most bank region for the bendway weirs, coinciding with results reported by Lyn and Cunningham (2010) and McCoy et al. (2007). A strong degree of turbulence was noted for the bendway weirs as a function of the vertical induced currents. Velocity vectors recorded around a bendway weir are displayed in Figure 6 where flow redirection, vertical acceleration, and plunging flow are visualized. Spur dikes with no crest overflow exhibited strong planimetric recirculation zones between structures similar to those reported by Yossef and de Vriend (2011). This flow pattern was not observed for bendway weirs and to a much lesser degree in the bank-attached vane configuration. Strong recirculation zones may lead to scalloping of the bank and eventual flanking. The vanes did not exhibit outer-bank split conveyance or strong planimetric recirculation zones. A common hydraulic trait for all structures was the convective acceleration around the tip of the structure crest. Visualized in Figure 6, flow is redirected around a stagnation velocity point at the structure interface, spatially accelerating around the tip of the structure. As noted in Koken and Constantinescu (2014) and Minor et al. (2007), the tip of transverse in-stream structures is the focal point for initiation of sediment mobility. Laboratory results indicated that the tip of the structures experience the

highest velocities in the channel. Crest-tip velocities were isolated from the full dataset and analyzed for each structure type.

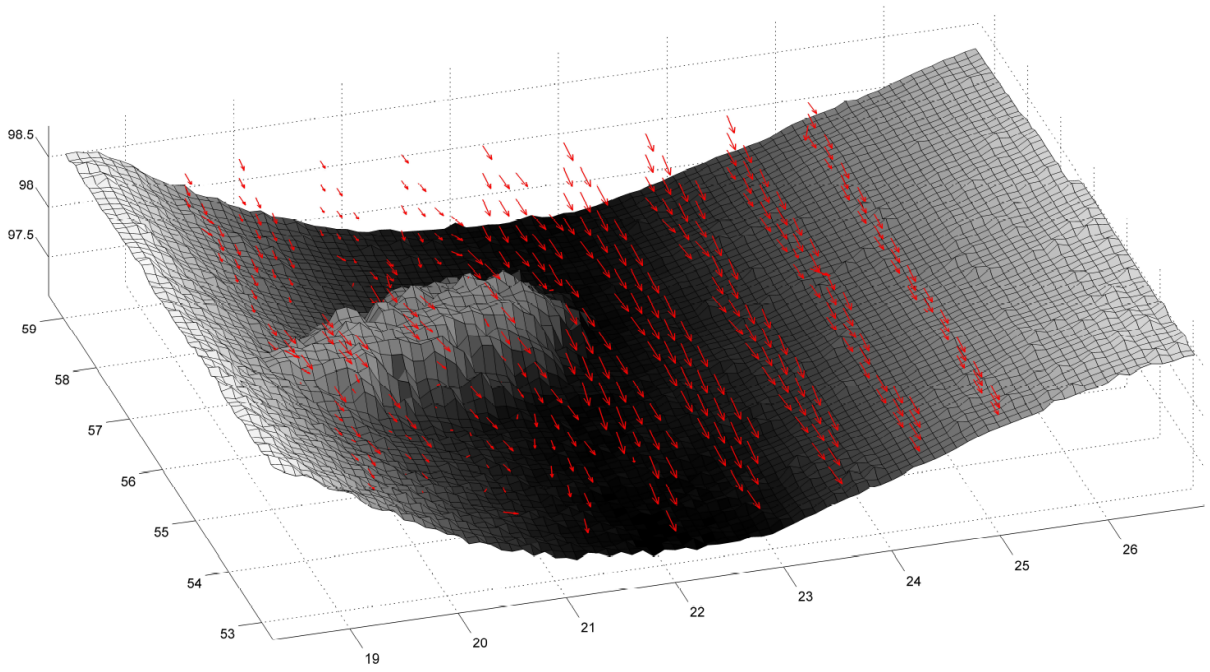

Figure 6 Velocity vectors (red) recorded around a bendway-weir structure (looking upstream)

STRUCTURE CREST TIP VELOCITY ANALYSIS

Increased velocity at the structure tip is directly related to the convective acceleration imposed by the structure boundary. Quantification of the velocity increase is important for structure stability through correct rock sizing and construction methods. Data located at the tip of the structures and in the near vicinity were isolated from the full data-collection location set illustrated in Figure 4. Values were normalized by the bend-averaged baseline flow condition and the maximum value and mean value were extracted from the dataset. Table 2 summarizes the maximum and average velocity and normalized values for each configuration. Maximum normalized velocity (*MVR*) values ranged from approximately 1.6 to 1.7 with the bank-attached vanes producing the smallest values and the spur dikes the largest. On average, normalized velocity values (*AVR*) range from approximately 1.3 to 1.6, with the bendway-weir configuration producing the smallest values and the spur dike the largest.

Table 2 Structure tip velocity summary

Configuration	Max vel. (ft/s)	*MVR*	Avg. vel. (ft/s)	*AVR*
Bendway weir	2.898	1.703	2.238	1.315
Spur dike	2.933	1.724	2.721	1.599
Bank-attached vane	2.692	1.582	2.437	1.432

Results adhere to physical intuition of the flow field. A larger channel obstruction decreases the cross-sectional flow area and increases flow acceleration. Spur dikes were the largest structure, followed by vanes, then bendway weirs which corresponds to the normalized average tip velocity magnitudes. The maximum observed velocity for the spur dike was also the largest recorded during testing. Bendway weirs produced a higher maximum velocity than the bank-attached vanes. The flow field for the bendway-weir configuration was more erratic and turbulent than the other structures. Observed hydraulics and high maximum velocities indicate that the bendway-weir structure type in particular should be evaluated further to fully understand hydraulic mechanisms.

SUMMARY AND CONCLUSIONS

Transverse in-stream structures are being installed to mitigate outer-bank erosion and stabilize migrating river channels. A physical model study of bendway weirs, spur dikes, and bank-attached vanes was undertaken in order to facilitate investigation of specific hydraulics associated with the structures and the differences between them. One configuration of each structure classification was installed according to recommended design guidelines from the literature and the desire for structure comparability. Models were evaluated under bankfull, design flow conditions and comprehensive velocity data were collected throughout the flow field.

Velocity distributions indicated that the tips of the structures were highly susceptible to the strongest hydraulics in the channel. Structure stability requires that rock sizing be appropriately scaled to expected velocities. Tip velocities for the structures were isolated and normalized by the baseline velocity averaged throughout the bend. It was found that on average, spur dikes had the highest tip velocities, followed by bank-attached vanes and bendway weirs. Maximum tip velocity analysis indicated that structure installations increased velocities up to 1.72 times the baseline average velocity. From the results of this study, it is recommended that rock sizing methods based upon flow velocity include a factor of safety of two times the baseline bend-average velocity.

REFERENCES

Abad, J.D., Rhoads, B.L., Guneralp, I., and Garcia, M.H. (2008). "Flow structure at different stages in a meander-bend with bendway weirs." *Journal of Hydraulic Engineering.* 134:8. 1052-1063.

Brown, S.A. (1985). "Design of spur-type streambank stabilization structures." Federal Highway Administration. FHWA/RD-84/101.

Brown, S.A. and Johnson, P.A. (1999). "Maryland's guidelines to waterway construction." Maryland Department of the Environment. Baltimore, Massechusets.

Dahle, B.P. (2009). "Evaluating shallow-flow rock structures as scour countermeasures at bridges." Brigham Young University. Dept. of Civil and Environmental Engineering. Technical Report. Prepared for Utah Dept. of Transportation Research Division.

Derrick, D.L. (1997). "Bendway weirs redirect rivers flow to protect highway bank abutments." U.S. Army Corps of Engineers Waterways Experiment Station, Vicksburg, M.S.

Derrick, D.L., Pokrefke, T.J., Boyd, M.B., Crutchfield, J.P., and Henderson, R.R. (1994). "Design and development of bendway-weirs for the Dogtooth Bend Reach, Mississippi River." U.S. Army Corps of Engineers.

Duan, J.G. (2009). "Mean flow and turbulence around a laboratory spur dike." *Journal of Hydraulic Engineering*.. 135(10). 803-811.

Jamieson, E.C., Rennie, C.D., and Townsend, R.D. (2013). "3D flow and sediment dynamics in a laboratory channel bend with and without stream barbs." *Journal of Hydraulic Engineering*.. 139(2). 154-166.

Jia, Y., Scott, S., Xu, Y., Huang, S., and Wang, S.Y. (2005). "Three-dimensional numerical simulation and analysis of flows around a submerged weir in a channel bendway." Journal of Hydraulic Engineering. 131:8. 682-693.

Jia, Y., Wang, S. Y. Y., and Xu, Y. (2002). "Validation and application of a 2D model to channels with complex geometry." Int. J. Comput. Eng. Sci., 3(1). 57–71.

Jia, Y., Zhu, T., and Scott, S. (2011). "Turbulent flow around submerged bendway weirs and its influence on channel navigation." Hydrodynamics - Optimizing methods and tools, Prof. Harry Schulz (Ed.), ISBN: 978-953-307-712-3, InTech.

Julien, Pierre, Y. and Duncan, Josh R. 2003. "Optimal design criteria of bendway weirs from numerical simulations and physical model studies." Colorado State University, Department of Civil Engineering. Fort Collins, Colorado.

Johnson, P.A., Hey, R.D., Tessier, M., and Rosgen, D.L. (2001). "Use of vanes for control of scour at vertical wall abutments." *Journal of Hydraulic Engineering*. 127(9). 772-778.

Koken, M., and Constantinescu, G. (2014). "Flow and turbulence structure around abutments with sloped sidewalls." *Journal of Hydraulic Engineering*. DOI: 10.1061/(ASCD)HY.1943-7900.0000876.

Lagasse, P.F., Clopper, P.E., Pagan-Ortiz, J.E., Zevenbergen, L.W., Arneson, L.A., Schall, J.D., and Girard, L.G. (2009). "Bridge scour and stream instability countermeasures: experience, selection, and design guidance." 3rd ed. HEC-23. Federal Highway Administration. FHWA-NHI-09-111.

Maryland Department of the Environment (2000). "Maryland's waterway construction guidelines." Water Management Administration.

McCullah, J.A. and Gray, D., (2005). "Environmentally Sensitive Channel- and Bank-Protection Measures," NCHRP Report 544, Transportation Research Board, National Academies of Science, Washington, D.C.

McCoy, A., Constantinescu, G., and Weber, L. (2007). "Hydrodynamics of flow in a channel with two lateral submerged groynes." ASCE. World Environmental and Water Resources Congress 2007.

McLelland, S.J. and Nicholas, A.P. (2000). "A new method for evaluating errors in high-frequency ADV measurements." *Hydrological processes*. (14). 351-366.

Minor, B., Jamieson, E., Rennie., C.D., and Townsend, R.D. (2007). "Three-dimensional flow in a barb field." *River Basin Management IV*. 104. 371-380.

Natural Resource Conservation Service (2005). "Design of stream barbs." *Tech. note 23.* Department of Agriculture. Portland, Oregon.

Radspinner, R.R., Diplas, P., Lightbody, A.F., and Sotoropoulis, F. (2010). "River training and ecologic enhancement potential using in-stream structures." *Journal of Hydraulic Engineering.* 136(12). 967-980.

Rhoads, B.L. (2003). "Protocols for geomorphic characterization of meander bends in Illinois." University of Illinois at Urbana-Champaign. Urbana, Illinois.

Rosgen, D. L. (2001). "The cross-vane, w-weir, and j-hook structures... their description, design, and application for stream stabilization and restoration." ASCE River and Wetland Restoration Conference.

Scott, S. H., Jai, Y., Wang, S.S.Y, and Xu, Y. (2001). "Analysis of near-field hydrodynamics of submerged weirs." United States Army Corps of Engineers. ERDC/EHL CHETN-VII-1.

Smith, S.P., and Wittler, R.J. (1998). "Bendway weirs and highway protection in Colorado: A case study on the Blue River." International Water Resources Engineering. 465-470.

Strom, K.B., and Papanicolaou, A.N. (2007). "ADV measurements around a cluster microform in a shallow mountain stream." *Journal of Hydraulic Engineering.* 133(12). 1379-1389.

Voulgaris, G., and Trowbridge, J.H. (1998). "Evaluation of the Acoustic Doppler Velocimeter (ADV) for turbulence measurements." *J. Atmos. and Oceanic Tech.* 15. 272-289.

Thornton, C.I., Cox, A.L, Ursic, M.E., and Youngblood, N.A. (2011). "Data report for completed bendway-weir configurations within the native topography model." Colorado State University, Department of Civil Engineering. Fort Collins, Colorado.

Wahl, T.L. (2000). "Analyzing ADV data using WinADV." *ASCE. Water Resources 2000.*

Wardman, B.G. and Papanicolaou, A.N. (2006). "Flow around submerged barbs in the Racoon River Iowa." *ASCE. World Environmental and Water Resources Congress 2006*.

Yossef, M.F.M., and de Vriend, H.J. (2011). "Flow details near river groynes: experimental investigation." *Journal of Hydraulic Engineering*. 137(5). 504-516.

ONE-DIMENSIONAL SEDIMENT MODELING OF LEVEE SETBACK AND FLOODPLAIN GRAVEL PIT CAPTURE ON THE YAKIMA RIVER, WA

Peter C. Brooks, P.E., Senior Engineer, Northwest Hydraulic Consultants, 13600 Christensen Road, Suite 350, Seattle, WA 98188, pbrooks@nhcweb.com; Dave McLean, Ph.D., P.E., Principal, Northwest Hydraulic Consultants, 405 - 495 Dunsmuir Street, Nanaimo, BC V9R 6B9 Canada, dmclean@nhcweb.com; Andrew Nelson, Geomorphologist, Northwest Hydraulic Consultants, 13600 Christensen Road, Suite 350, Seattle, WA 98188, anelson@nhcweb.com; Karen Hodges, Natural Resource Specialist\Project Manager, Water Resources Division, Yakima County Public Services, 128 N. 2nd St., Yakima, WA 98901, karen.hodges@co.yakima.wa.us

EXTENDED ABSTRACT

The Yakima River in eastern Washington State has been confined due to the construction of numerous levees over the past century. Although providing valuable flood protection, levee confinement has interrupted natural morphologic processes resulting in reduced channel complexity and habitat. As part of a plan to reactivate the Yakima River floodplain to reduce flood elevations and velocities as well as increase access to back channel habitat, the Yakima County Flood Control District has undertaken a Section 1135 Environmental Restoration Feasibility Study with the Seattle District U.S. Army Corps of Engineers for a levee setback project on the Yakima River, within the City of Yakima, WA.

However, the area is the site of former gravel mining and three large gravel pits are currently located landward of the existing levee. These pits would be vulnerable to capture through channel avulsion were the levee to be setback. Gravel pit capture poses threats to channel stability by disruption of sediment transport continuity and upstream headcut migration. An existing SRH1D model was used to evaluate possible effects of gravel pit capture on upstream and downstream channel adjustment. Computational analyses were complemented by a geomorphic assessment and review of case studies of previous gravel pit capture episodes on the Yakima River and elsewhere. Findings were used to assess risks to morphologic stability, channel habitat, and surrounding infrastructure, including several Federal flood protection levees still located on the reach.

Eco-Hydraulic Modeling to Support Levee Setback and Floodplain Design

Blair Greimann, Hydraulic Engineer, Bureau of Reclamation, Denver, CO, bgreimann@usbr.gov; Rebecca Kallio, Hydraulic Engineer, Bureau of Reclamation, Denver, CO, rkallio@usbr.gov

EXTENDED ABSTRACT

The San Joaquin River Restoration Project (SJRRP) is located below Friant Dam near Fresno, California. The project is a direct result of a Settlement reached in September 2006 on an 18-year lawsuit to provide sufficient Chinook salmon habitat by the U.S. Departments of the Interior and Commerce, the Natural Resources Defense Council (NRDC), and the Friant Water Users Authority (FWUA). The Settlement received Federal court approval in October 2006. Federal legislation was passed in March 2009 authorizing Federal agencies to implement the Settlement.

The Settlement is based on two goals: (1) Restoration : To restore and maintain fish populations in "good condition" in the main stem of the San Joaquin River below Friant Dam to the confluence of the Merced River, including naturally reproducing and self-sustaining populations of salmon and other fish; (2) Water Management: To reduce or avoid adverse water supply impacts to all of the Friant Division long-term contractors that may result from the Interim Flows and Restoration Flows provided for in the Settlement.

One of the major requirements of sustaining fish populations will be the creation of a sufficient amount of floodplain habitat for juvenile salmon rearing. The river is constrained by levees in many reaches and it is necessary to setback the levees to contain the restoration flows and to create floodplain habitat. Because the setback requires the purchase of valuable agricultural land in the Central Valley of California, the floodplain design should be carefully designed in order to maximize the benefit of this expensive resource.

The existing floodplain habitat for the SJRRP was first quantified using a two-dimensional hydraulic model (SRH-2D, Lai, 2008). The depth and velocity over approximately 100 miles of the San Joaquin River was computed. The reach was divided into several separate models to decrease computational time and make the terrain datasets more manageable. Habitat Suitability Indices (HSI) were applied to depth and velocity output from the model and then cover suitability was estimated using vegetation mapping of the river corridor. The required floodplain area was based upon estimation of the assumed territory size required to meet a sustainable population.

Once the required suitable floodplain was estimated a levee setback was proposed and the designs for the floodplain grading and revegetation were developed to meet the required habitat objective. The hydraulic and sediment transport conditions were simulated using one- and two-dimensional hydraulic and sediment transport models (Huang and Greimann, 2010; Lai, 2008). The floodplain design incorporated the expected channel evolution into the design. The revegetation strategy is based upon results from the one and two-dimensional hydraulic and sediment transport models that were linked to vegetation modules that simulate the interactions

between riparian vegetation, flow and sediment. The models simulate the effect of vegetation on hydraulic roughness, as well as the effect of hydraulics on the establishment and mortality due to desiccation, scour, and inundation.

REFERENCES

Huang, V.H., Greimann, B. (2012). Sedimentation and River Hydraulics – One Dimension, Version 3.0, Technical Service Center, Bureau of Reclamation, Denver, CO.

Lai, Y.G. (2008). SRH-2D version 2: Theory and User's Manual. Sedimentation and River Hydraulics – Two-Dimensional River Flow Modeling, Technical Service Center, Bureau of Reclamation, , Denver, CO.

SEDIMENT TRANSPORT IN STREAM CHANNEL DESIGN

Peter Wilcock, Professor, Water Sciences Department, Utah State University, Logan, Utah, wilcock@usu.edu

ABSTRACT

Stream channel design has been strongly yoked to the concept of equilibrium channel geometry, building on regime theory and hydraulic geometry over the past century. Although plausible at a cursory level, equilibrium methods are unsatisfactory for a variety of reasons. They say nothing about the nature and duration of adjustment. They provide no quantitative basis for incorporating uncertainty. They generally make little or no distinction between channels with similar flow and vastly different sediment supply.

All agree that stream channel dimensions and dynamics depend on the supply of water and sediment. Here, we link water and sediment supply to specified behavior of the channel as a complete strategy for incorporating sediment transport in stream channel design. The approach builds on the classic concepts of threshold and alluvial channels. A threshold channel is one for which the bed material is immobile at a specified discharge. An alluvial channel is one whose transport capacity must be balanced against the rate of sediment supply. It is useful to define a third type of channel that combines the first two – over-capacity threshold – in which transport capacity exceeds supply but design flows do not exceed threshold limits for channel erosion. This type of channel is more common than often realized and is, in fact, unintentionally designed in many cases. Using these three channel types, we develop a basis for evaluating the significance of sediment supply to the performance of a design channel. At small sediment supply rates, channel performance is relatively insensitive to uncertainty in sediment supply and may be designed following threshold channel principles of stream competence. At large sediment supply rates, the potential for storing or evacuating channel-changing quantities of sediment is much larger. Design options include (i) active channel shifting {requiring acquisition of sufficient riparian corridor}, (ii) an over-capacity threshold channel {if sufficient slope is available}, or (iii) an alluvial channel that balances sediment supply and capacity {which may require additional investment for adequate estimates of potentially large rates of sediment transport}.

With specified values of water and sediment supply and a designated channel behavior, basic relations for hydraulics and sediment transport are solved to provide a suite of channel design choices. At this point, characteristic values of, for example, channel width can be drawn from hydraulic geometry relations or local experience in order to select among the range of possible design options. All three design strategies are placed on a common basis to allow effective and complete evaluation of design options under uncertainty. For useful application, it is not sufficient to merely characterize uncertainty. That uncertainty must be incorporated in the analysis and design of stream channels. A computational tool for estimating uncertainty will be presented within a strategy for incorporating sediment transport in channel design.

RESTORING ANDSUSTAINING RIVER ENVIRONMENTS USING AN IN-STREAM TRAINING METHOD

Chi Bui, Hydraulic Engineer, Albuquerque, New Mexico, cbui@usbr.gov

BACKGROUND

Historically, the Rio Grande at San Felipe used to be a braided river with a sand bed channel and a very high sediment load. Through channelization from 1932 to 1960s, the channel was straightened. As Cochiti Reservoir was built and began to impound water for flood and sediment control in 1975 which caused the reduction in flood peaks and sediment load, the channel generally became narrow and incised, and the bed material became coarser (Harvey, 2007; Shah-Fairbank et al., 2010). The reservoir traps approximately 99% of the current sediment supply to the downstream reach (Shah-Fairbank et al., 2010). The primary sediment supply to the downstream reach is from channel erosion and tributary inputs. Consequently the channel bed material size has become coarser over time, transitioning from sand to gravel, and the channel longitudinal profile has been lowered about four feet on average after the construction of the dam. The bed profile of the reach has been reasonably stable since 1992, an indication that the bed could have been armored under the post-dam flow regime. Sediment transport models suggest that significant bed mobilization would not occur at flows less than the 100-year peak of 10,000 cfs (Harvey, 2007). The reach immediately below the dam has incised and river meander bends have developed. In some areas the incision has dropped below the root zone, eroding banklines with mature cottonwood trees, and threatening infrastructure adjacent to the waterway. One specific location on the Rio Grande where this condition has occurred is immediately upstream from Angostura Diversion Dam. This location is about 21 miles downstream of Cochiti Dam. There are two meander bends where bank erosion has become a concern at three locations, RM 210.0, RM 210.1, and RM 210.3 as illustrated in Figure 1, threatening irrigation drains that border each side of the river.

In 2011, a multi-disciplinary project team was formed, including Tetra Tech, the Pueblo of San Felipe, and Bureau of Reclamation (Reclamation) staff, to initiate a process of providing bank protection at these three sites that included an initial site visit, development feasible alternatives to address the river maintenance concern at each site, selection of a preferred alternative at each site based on engineering effectiveness, ecosystem function, ease of compliance, and Pueblo preference. While individual alternative concepts were evaluated for each of the sites, the close proximity of the three sites on two consecutive bends for the downstream sites made the combination into one comprehensive project more palatable to the project team. This combination also facilitated the evaluation of adverse impacts between sites for the final design. The final design was a combination of longitudinal fill stone toe protection (LFSTP) and bendway weirs coupled with removal and/or lowering of bars.

1-DIMENSIONAL HYDRAULIC MODEL

The design of the bendway weirs and LFSTP requires inputs such as velocities, width, depth, energy slope, etc. which can be acquired from a one-dimensional (1-D) HEC-RAS hydraulic model. The outputs of the design are the ranges of bendway weir length, planform angle,

spacing, and height, and the fixed values of the LFSTP crest width and height. Different combinations of bendway weir configurations can slightly change the hydraulic conditions around the weirs that cannot be modeled by a 1-D HEC-RAS model. Therefore, a two-dimensional (2-D) hydraulic model with SRH-2D was used to assist in the process to optimize the final bendway weir configurations.

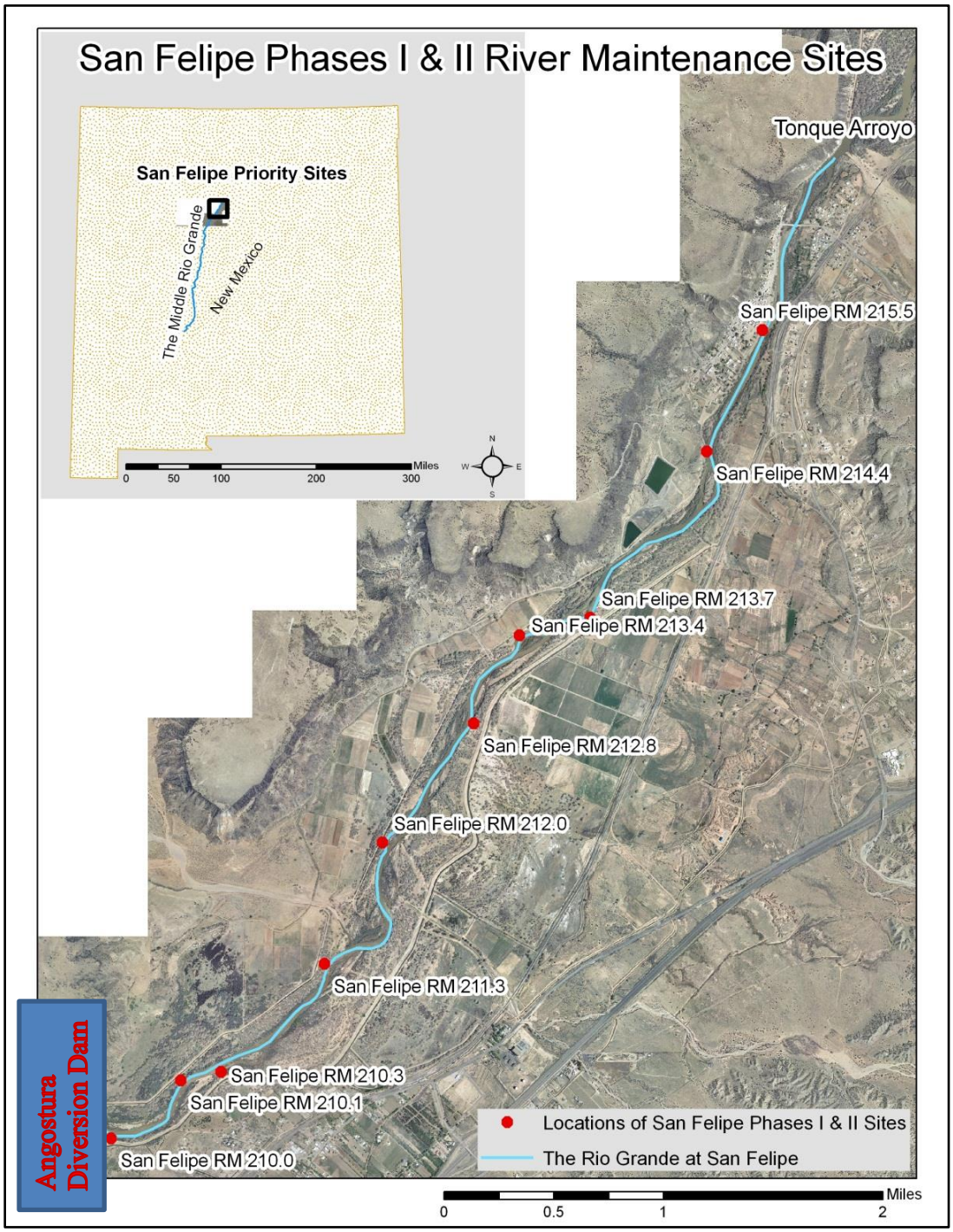

Figure 1 Map of ten priority sites along the Rio Grande at San Felipe.

There was a 1-D HEC-RAS model developed in 2007 using cross sections surveyed in 2007 to model the ten (10) priority sites illustrated in Figure 1. The floodplain elevation of the 2007 model was based on a digital terrain model (DTM) created from the 2002 photogrammetrically derived aggradation-degradation elevation. The downstream end of the model stopped just upstream from the Angostura Diversion Dam. The model was calibrated with Manning's n values gradually decreasing from upstream to downstream because the bed material is coarser upstream and becomes finer as it gets closer to the Angostura Diversion Dam. Photography of subsequent years after the model was compared with the 2007 photography and did not show denser vegetation encroachment into the channel. Therefore, it was assumed that the original Manning's n values were applicable to the updated 1-D HEC-RAS model built in 2012. The boundary of the 2012 HEC-RAS model covered from the priority site at RM 212.0 to just past the Angostura Diversion Dam.

Ineffective flow areas and obstructions were used in the geometry to model bendway weirs, areas in between weirs, and the LFSTP. Since the design of bendway weir spacing was in the range from 70 feet to 80 feet and the spacing of cross sections ranged from 150 feet to 500 feet, interpolated cross sections were required to model 12-foot wide bendway weirs. It is likely that errors inherent from the difference in bed elevation of the interpolated model and the actual river channel are present. The bendway weirs and LFSTP were modeled as obstruction objects. Areas of recirculation flow between weirs were modeled as ineffective flow areas (Sclafani et al., 2012).

In the process of riprap sizing, maximum velocities of the design flow at cross sections were required. However, this parameter cannot be obtained accurately from a 1-D hydraulic model. Instead of using a 2-D model at an early design stage that required a lot of effort, flow distribution was used to run the 1-D model to provide velocities for sub-sections of a channel cross section. These velocities are not the true 2-D velocity field, but they are interpolated velocities based on channel depth values of those sub-sections.

The pre-project 1-D simulation provided the hydraulic parameters for scour calculation, riprap sizing, and the design of the bendway weirs and LFSTP. The post-project 1-D simulation was performed for one design configuration. Then it was decided that it was more efficient to adjust design parameters using AutoCAD Civil 3D and GIS and to analyze results using a 2-D hydraulic model, so different design configuration combinations were tested with a 2-D model.

DESIGN CALCULATIONS

Immediately upstream of the Angostura Diversion Dam, the bend on the right side of the river is referred to as the upstream bend, and the bend on the left side of the river is referred to as the downstream bend in this report. The priority site RM 210.3 is immediately upstream from the upstream bend and on the opposite bank. The upstream bend passes through RM 210.1. RM 210.0 is located at the downstream end of the downstream bend.

Scour Computations: Expected scour depth was estimated as the first step of the analysis. An extensive, but not exhaustive, review of scour equations was conducted to identify a number of methods that would be appropriate for the project site. Long-term scour computation used

Yang's, Shields', Lane's, and Peter-Myer-Mueller's approaches, and competent velocity method. The selected scour equations for general and bend scour can be categorized as mean velocity equations, regime equations, and bend equations. The bend equations are based on the degree of tightness of a bend that is responsible for a transverse bed slope with significantly increased depth near the outer bank. The total scour depths developed under the 100 year-return flow of 10,000 cfs for two (2) bends are summarized in Table 1.

Table 1 Calculations of total scour

Scour Components		Velocity Equations			Regime Equations			Bend Equations		
		Limiting Velocity	Mean Velocity	Zeller[1] (1989)	Neill (1973)	Lacey (1930)	Blench (1969)	Maynord[1] (1996)	Zeller[1] (1989)	Thorne (1997)
General	Upstream	included	incl.	incl.	incl.	incl.	incl.	incl.	1.7	incl.
	Downstream								2.2	
Bend	Upstream	included	incl.	0.0	incl.	incl.	incl.	incl.	incl.	incl.
	Downstream			0.0						
Thalweg Formation	Upstream	included	incl.	1.0	incl.	incl.	incl.	incl.	1.0	incl.
	Downstream			1.0					1.0	
Long term scour	Upstream	0.04	0.04	0.04	0.04	0.04	0.04	0.04	0.04	0.04
	Downstream	0.18	0.18	0.18	0.18	0.18	0.18	0.18	0.18	0.18
Average Total Scour	Upstream	5.9	6.1	2.7	6.5	6.2	6.6	6.6	2.7	8.1
	Downstream	0.7	3.7	3.3	5.1	2.0	5.7	5.4	3.3	7.5
Avg Total Scour with	Upstream	6.5	6.7	3.0	7.2	6.8	7.2	7.2	3.0	8.9
Factor of Safety = 1.1	Downstream	0.8	4.0	3.7	5.7	2.2	6.3	5.9	3.7	8.3
Design Scour Depth for Upstream Bend =			7.0 ft		(Max =	8.9 ft		Min =	3.0 ft)	
Design Scour Depth for Downstream Bend =			5.0 ft		(Max =	8.3 ft		Min =	0.8 ft)	

[1]Developed for sand bed rivers, assumed conservative for gravel bed

Riprap Sizing: There are many approaches that are used in the professional engineering practice for sizing revetment riprap. NCHRP 568 (Lagasse, 2006) evaluated seven of the most commonly used revetment riprap sizing equations and recommended the EM 1601 equation (USACE, 1994) on the basis of discriminating between stable or failed riprap, bank and bend correction factors, and the reasonableness of safety/stability factors. The EM 1601 calculated D_{50} size can be used as the first approximation of the minimum riprap size needed for the design of the LFSTP at the upstream bend which is 12 inches. This riprap size ensures the longitudinal structure stability for discharges up to 100-year return flow of 10,000 cfs. The proposed correction factor for cross-stream features recommended by de Almeida and Martin-Vide (de Almeida and Martín-Vide, 2009) is about 2, which results in a transverse D_{50} size of 24 inches for both the upstream and the downstream bends to withstand the 100-year return flow of 10,000 cfs.

Design of Longitudinal Fill Stone Toe Protection (LFSTP): LFSTP is continuous riprap revetment with a trapezoidal cross section placed along the toe of a bankline to increase the roughness at the toe of the bank against erosion forces from incoming sustained high flows and to adapt to scour holes near the outer bank developed under sustained high flow conditions (Martin-Vide et al., 2010). Additional critical functional elements of the LFSTP are the keys and

tie-backs buried in the floodplain to prevent high flows from flanking the structure (McCullah and Gray, 2005). The LFSTP crest elevation was designed to be approximately 0.5 ft higher than the point bar at the upstream bend so that the hydraulically rougher stone toe will protect the toe of the outer bank until the hydraulic pressure is released as water overtops the high point of the opposite point bar. The width of the LFSTP was designed to provide rock that would self-launch into scour holes developed under sustained high flows along the toe of the stone structure which consequently protects the right bankline (Martin-Vide et al., 2010). As rock self-launches to the estimated scour depth, the crest width of the LFSTP is reduced to the minimum width of $2*D_{100}$ which is 4 ft (Derrick, 2011) keeping the original crest height unchanged. Since there is uncertainty in how the rock self-launches, a factor of 1.5 was added to the quantity of the self-launching rock that lands in potential scour holes (Derrick, 2011; Maynord et al., 1989). Tie-backs and keys are the LFSTP components that extend from the bankline into the floodplain. Keys are oriented perpendicular to the bankline while tie-backs are located at the upstream and downstream ends of the LFSTP and oriented at an angle from 20^o to 30^o with the bankline (Derrick, 2011). Assessing this area to be relatively, it is necessary to key the stone structure into the stable ground beyond the 1935-1962 channel boundaries, which gives the key length of 100 feet and a tie-back length as 600 feet.

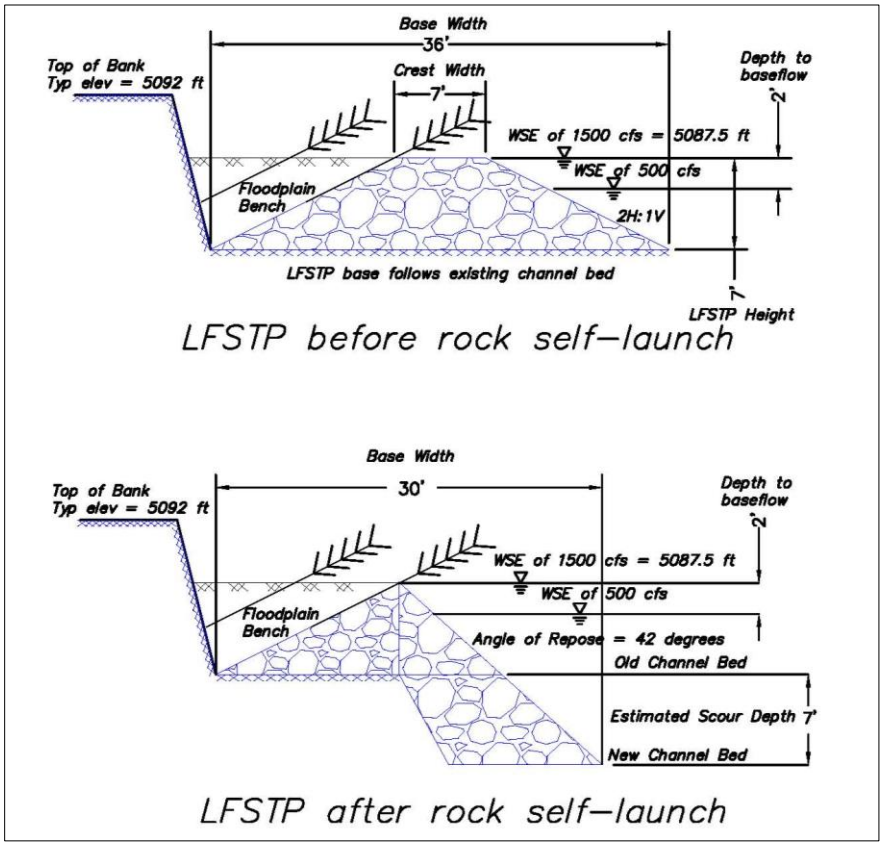

Figure 1 Process of LFSTP riprap launching into scour holes

Design of Bendway Weirs: Bendway weirs are low and upstream angled rock in-stream structures that help to lower velocities along a bankline and redirect the thalweg path away from the bankline (Kinzli and Thornton, 2010). The design references for bendway weirs are HEC-23

(FHWA, 2011), NCHRP 544 Report (McCullah and Gray, 2005), and Reclamation's modeling recommendations for transverse features such as spur dikes and vanes (Scurlock et al., 2012). From literature (FHWA, 2011; McCullah and Gray, 2005) the entire ranges of recommended bendway weir design parameters were derived. These ranges were narrowed down to a reasonable set of weir length, height, spacing, and planform angle. This was done based on literature documentation that cautioned against certain combinations (FHWA, 2011; Jia et al., 2005; Kinzli and Thornton, 2010). The narrowed ranges of the design parameters were combined into 18 combinations for the upstream bend and 37 combinations for the downstream bend. These sensitivity tests were used to determine the sensitivities of design parameters to velocities at the outer bank and at the centerline of the channel. After the sensitivity test, three design combinations were selected for each bend and a 2-dimensional (2-D) model was developed to test the post-weir baseline design parameters scenarios with the three design combinations at each bend. The scenarios modeled with a 2-D model are summarized in Table 2.

Table 2 Design parameters matrix tested with a 2-D model

Weir Parameters	Simulation ID	Weir Length (ft)	Weir Angle (degree)	Weir Spacing (ft)	Crest Elevation (ft)
Upstream Bend	Post-weir Baseline Design Parameters	65	60	85	5085
	MOD 2	65	60	85	5085.5
	MOD 3	60	70	80	5085
	MOD 4	70	70	90	5085
Downstream Bend	Post-weir Baseline Design Parameters	70	60	70	5084
	MOD 2	70	60	70	5084.5
	MOD 3	70	60	70	5083.5
	MOD 4	70	60	70	5083

FINALIZE DESIGN WITH A 2-D MODEL

SRH 2-D was selected as the hydraulic modeling software for this analysis because it was written and has been maintained by Reclamation so that the design team could get prompt technical support from Reclamation's current software developer.

As the 2-D model required very dense terrain data and there were no surveyed channel data points within areas in between the surveyed cross sections, the reach elevation was interpolated with cross sections six feet apart in HEC-RAS and exported to GIS to build the terrain for the 2-D model. As the 2-D model would be used to visually compare velocity distributions of different combinations of weir design parameters, the systematic errors caused by the interpolation of the terrain were thought to be similar for all tested bendway weir parameter combinations at the design discharge (2-year return, 5,600 cfs), which should not affect the overall final design selection. Values of WSE, velocities, shear stresses, etc. from the 2-D model would not be used specifically in the design process but rather to finalize a preferred design. Therefore, when it was assumed that the terrain systematic errors were constant for all combination simulations, the 2-D

model could assist the process to finalize the bendway weir design parameters. All 2-D simulation runs were performed with the assumption of a fixed bed and bank.

The post-weir baseline design parameters in Table 2 were initially considered to be the final parameter selection because they had a good balance between moderately reducing the outer bank maximum velocities and moderately increasing the centerline and inner bank average velocities. Therefore, they served as the post-weir design parameter baselines so that other parameter modifications should be compared to them. MOD 2 slightly changed the baseline condition by increasing all bendway weir height by 0.5 ft to investigate how higher weirs would benefit the project areas. MOD 3 has a different combination of weir design parameters at the upstream bend and a lower weir crest elevation with all other parameters unchanged at the downstream bend. MOD 4 tested another combination of bendway weir design parameters at the upstream bend as well as another lower weir crest elevation at the downstream bend with all other parameters unchanged. As the crests of the bendway weirs at the downstream bend were lowered to 5083 ft for MOD 4, the elevation of the bar near the southern end was excavated to 5082 ft, 1 ft lower than the bendway weir crest elevation at the downstream bend to release some hydraulic pressure from the high velocity field along the water intake structure. For all other modifications and baseline simulations, this bar elevation (5083 ft) was always lower than the bendway weir field at the downstream end. After the first four simulations, it was determined that MOD 3 was the best option for the upstream bend because it created a more distinct thalweg path immediately off the tips of the bendway weirs. Also the post-weir baseline simulation had the best combination for the downstream bend from the sensitivity analysis while other combinations did not show any significant difference in reducing near bank velocities. Besides it was found that lowering the bar at the southern end to 5082 feet would help to release the hydraulic pressure against the water intake structure. Therefore, this bar lowering feature was added to MOD 3 for the upstream bend and to the post-weir design parameter baseline for the downstream bend as the final weir design parameters that are summarized in Table 3.

Table 3: Final bendway weir design parameters

Weir Parameters	Bar Elevation (ft)	Weir Length (ft)	Weir Angle (degrees)	Weir Spacing (ft)	Crest Elevation (ft)
Upstream Bend	5082	60	70	80	5085
Downstream Bend	5082	70	60	70	5084

EXPECTED RESPONSE

The post-design 2-D model results showed that the velocities against the outer bank along the weirs at a bend were significantly reduced while area with higher velocities were moved to the tops of the weirs and toward the opposite point bank as in Figure 4. The model also showed that areas in between weirs had a variety of low to moderate velocities as in Figure 4. The primary hydraulic benefits of this project design are the relocation of the erosive force away from the bankline so that the river can still effectively deliver water and dissipate energy through its bends under high flow conditions within a confined space. The project's geomorphic benefits include the development of variable depth environments as the river scours along weir tips and opposite

point bars and deposits sediment in between weirs as in Figure 5. This provides bank protection, while still maintaining the current channel width and allows some geomorphic adjustments in a confined environment. The environmental benefits are potential establishment of vegetation in deposited areas between weirs and behind the LFSTP, plus a variable velocity and depth environment as in Figure 6 that potentially increases the opportunity for aquatic habitat. Therefore, it is hoped that this in-stream river training method will restore and sustain the ability of the reach to transport water and sediment, protect infrastructure along the waterway, and encourage ecosystem diversity within a confined and altered fluvial environment.

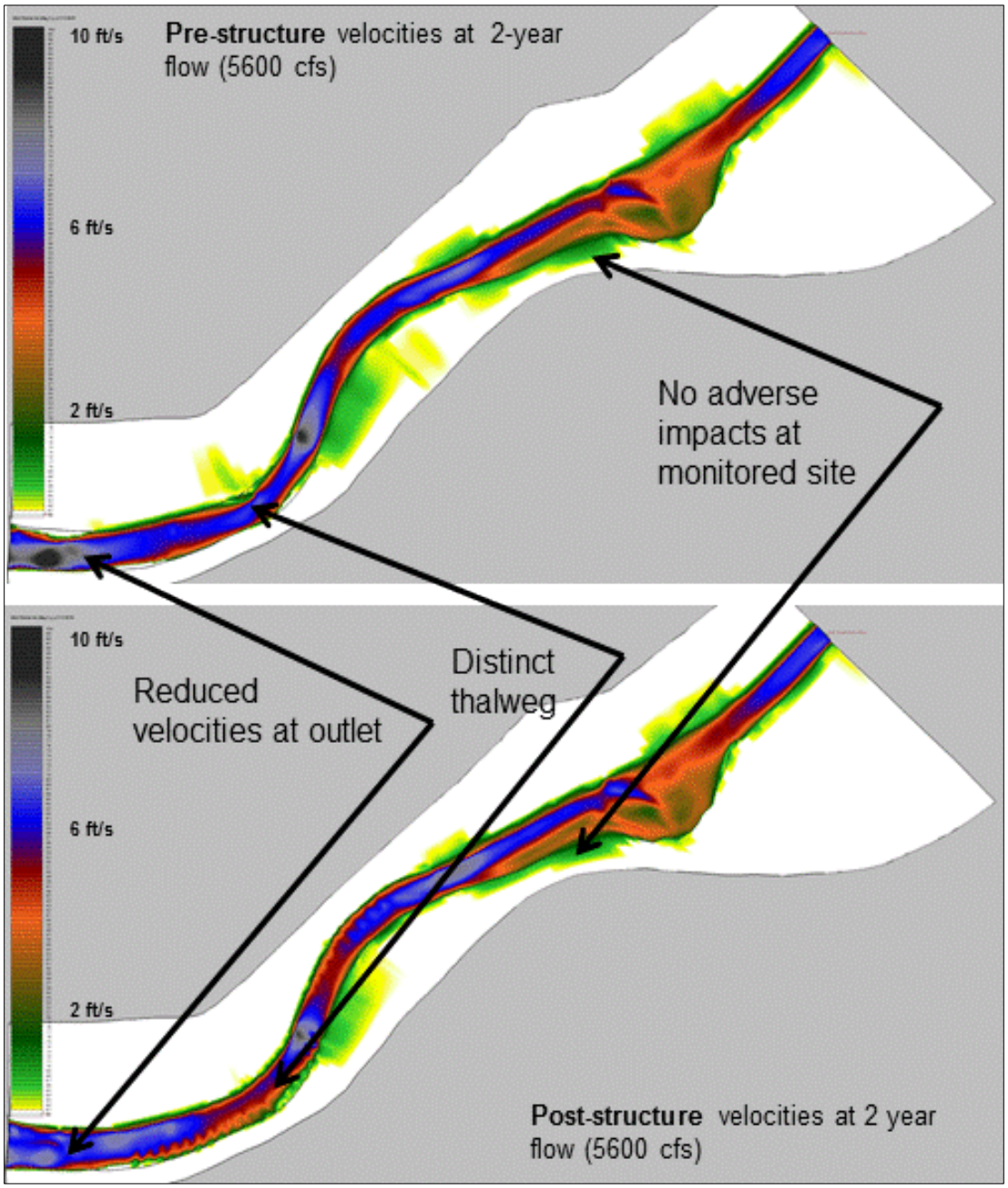

Figure 4 Hydraulic effects of in-stream structures

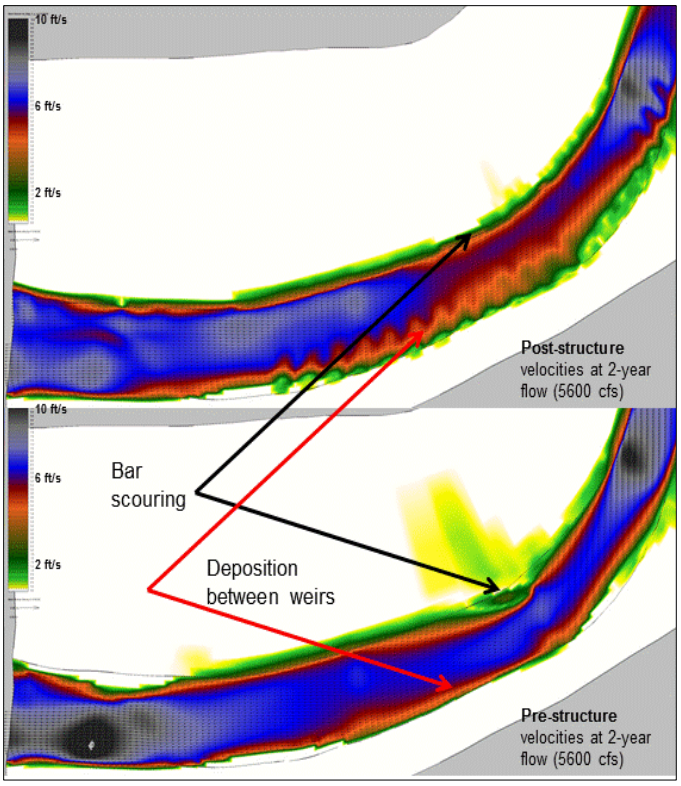

Figure 5 Geomorphic effects of in-stream structures

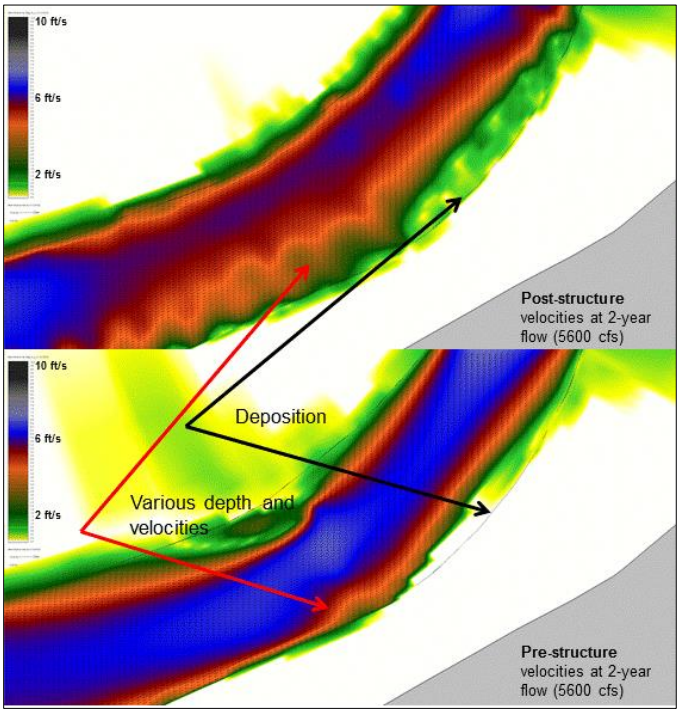

Figure 6 Environmental Effects of In-stream Structures

REFERENCES

De Almeida, G.A.M., and Martín-Vide, J.P. (2009). "Riprap Stability : Transverse and Longitudinal versus Continuous Protections." Journal of Hydraulic Engineering, 135(June), 447–456.

Derrick, D. (2011). "Longitudinal Peaked Stone Toe Protection (LPSTP) and Longitudinal Fill Stone Toe Protection (LFSTP)." The Army Corps of Engineers, <http://www.powershow.com/view/26d09c-NGY5N/Longitudinal_Peaked_Stone_Toe_Protection_LPSTP_powerpoint_ppt_presentation>.

FHWA. (2011). Design Guideline 1 - Bendway Weirs/Stream Barbs.

Harvey, M.D. (2007). San Felipe Geomorphic Assessment.

Jia, Y., Scott, S., Xu, Y., and Wang, S.S.Y. (2005). "Three-Dimensional Numerical Simulation and Analysis of Flows around a Submerged Weir in a Channel Bendway." Journal of Hydraulic Engineering, 131(8), 682–693.

Kinzli, K., and Thornton, C. (2010). "Predicting Velocity in Bendway Weir Eddy Fields." River Research and Applications, 26(7), 823–834.

Lagasse, P. (2006). NCHRP Report 568: Riprap Desgin Criteria, Recommended Specifications, and Quality Control.

Martin-Vide, J.P., Roca, M., and Alvarado-Ancieta, C.A. (2010). "Bend scour protection using riprap." Institution of Civil Engineers, 489–197.

Maynord, S. T., Ruff, J.F., and Abt, S.R. (1989). "Riprap Design." Journal of Hydraulic Engineering, 115(7), 937–949.

McCullah, J., and Gray, D. (2005). NCHRP Report 544: Environmentally Sensitive Channel and Bank Protection Measures.

Sclafani, P., Thornton, C.I., Cox, A.L., and Abt, S.R. (2012). Methodology for Predicting Maximum Velocity and Shear Stress in a Sinuous Channel with Bendway Weirs using 1-D HEC-RAS Modeling Results. 1–313.

Scurlock, S.M., Cox, A.L., Thornton, C.I., and Abt, S.R. (2012). Middle Rio Grande Physical Modelling, Transverse Instream Structure Analysis: Maximum and Average Velocity Ratios within the Prismatic Channel. Ft. Collins, CO.

Shah-Fairbank, S.C., Hanegan, K., Benally, Q., Beckman, N., and Julien, P. (2010). San Felipe Reach Arroyo Tonque to Angostura Diversion Dam Hydraulic Modeling Analysis.

USACE. (1994). EM 1110-2-1601 Chapter 3: Riprap Protection.

MODELING THE WEST BRANCH PLEASANT RIVER SYSTEM, ADDISON, MAINE FOR RESTORED TIDAL FUNCTION

Ecosystem Restoration Feasibility Study

EXTENDED ABSTRACT

US Army Corps of Engineers
New England District
Rhonda Needham Anderson & Heather Rausch

Table of Contents

1.0 INTRODUCTION.

Ridge Road crosses the mouth of the West Branch of the Pleasant River in Addison Maine (Washington County). The town of Addison is located at the confluence of the Pleasant River and the West Branch of the Pleasant River, approximately 53 miles southeast of Bangor, Maine. The study area extends upstream from the mouth of the West Branch of the Pleasant River for approximately one mile until the river, and its tributaries, intersect Route 1. Up to approximately 470 acres of fresh water wetlands could be tidally restored in the towns of Addison and Columbia, Maine.

The purpose of the West Branch Pleasant River Ecosystem Restoration Feasibility Study is to develop and evaluate tidally restored salt marsh habitat alternatives for the West Branch of the Pleasant River (West Branch); with the goal of recommending a State and Federally preferred plan for development. The Federally preferred plan must also meet Maine Department of Environmental Protection (MEDOT) transportation needs.

The Maine Department of Transportation (MEDOT) requested the U.S. Army Corps of Engineers' (Corps) assistance in restoring the fresh water marsh upstream of Ridge Road to a salt marsh. MEDOT owns, and is responsible for, the tide gates and roadway embankment at Ridge Road that are currently in disrepair and need to be replaced. The tide gates consist of six culverts with one way flapper gates that open toward the sea when the tide is low. This allows the river waters to discharge from the West Branch while seawater is blocked from entering the West Branch marsh. As a consequence, there has been inconsequential tidal influence upstream of Ridge Road since 1940 when an old bridge was replaced with the current road works.

This hydrologic and hydraulic analysis evaluated several alternatives to replace the existing gated structure at Ridge Road as well as culverts located upstream along the West Branch and several tributaries to reintroduce tidal exchange and ultimately restore the salt marsh.

2.0 SITE HYDROLOGY

a. Climate and Principle Flood Sources.

The climate of Addison is coastal, with moderately warm summers and cold winters. The average annual temperature of Addison is 45 degrees Fahrenheit (F) ranging from an average minimum temperature of approximately 12 degrees F in January to an average maximum temperature of approximately 77 degrees F in July. Surrounding bodies of water tend to temper extreme climate conditions. The mean annual precipitation is approximately 41 inches and is fairly uniformly distributed throughout the year.

The town of Addison is subject to coastal flooding caused by nor'easters and hurricanes. Nor'easters are the more frequent type of storm in this area. They can occur any time of the year, but are more prevalent in the winter months. Hurricanes, which are relatively rare, occur in the later summer and early fall months; however, they historically have not produced significant flooding in this area.

b. Tidal Regime.

In the study area, tides are semi-diurnal, with two high and low waters occurring during each lunar day (approximately 24 hours and 50 minutes). The resulting astronomic tide range varies constantly in response to relative positions of the earth, moon, and sun; the moon having the primary tide producing effect. Maximum tide ranges occur when the orbital cycles of these bodies are in phase. A complete sequence of astronomic tide ranges is approximately repeated over an interval of 19 years, known as a tidal epoch. Coastal storms and hurricanes can cause tides to be much higher than astronomically predicted. Although exact information of tidal characteristics are presently lacking at the site, approximate characteristics were developed from historical tide data (1931 to present).

c. Tidal Analysis.

The West Branch Pleasant River confluence with the Pleasant River is approximately one mile upstream from Pleasant Bay, which extends approximately eight miles downstream before discharging into the Gulf of Maine at Dyer Island. Tide elevations, heights and ranges are most accurately recorded locally and at NOAA gage stations.

The nearest NOAA gage station to the West Branch study area is in Millbridge, Maine, on the Narraguagus Bay, which also discharges to Pleasant Bay, approximately 10 miles south of Addison, Maine. Tide elevations increase as the tide travels from the open ocean, through Pleasant Bay, and up the Pleasant River due to the narrowing of the river channel. Since tide elevations published in the USACE Tide Profiles often represent the open ocean, this is not considered an accurate reference for tide elevations at the West Branch.

In order to analyze the impact of tides along the West Branch, tide elevations were established for various tidal occurrences and datums, as shown in Table 1. Since a NOAA tide gage is not available at this study area, recorded tide data collected by David Burdick as part of the 2009 Evaluation of Pre-Restoration Conditions in the West Branch of the Pleasant River, Maine were correlated to the Millbridge, Maine NOAA tide. This allows various tide events, recorded in 6-minutes intervals to be evaluated at the West Branch study area.

During storm conditions, nor'easters and hurricanes cause the tides to increase. Due to the duration of nor'easters, they often last through one or more tide cycles. The combination of sustained onshore winds and high tide causes significant elevation increases. This is known as storm surge. In Addison, the greatest storm surge is caused by winds from the southeast quadrant. The FEMA FIS also includes the wave height analysis. The coastline along the Pleasant River, on the west side of the community has a limited fetch and thus a wave height of only 3-feet and a wave period of 2.8 seconds. The fetch includes the distance waves can be generated without intersecting a land mass. (Reference 1)

TABLE 1
Estimated Tide Elevations at West Branch Pleasant River, Addison, Maine
(Estimated from interpolating NOAA recorded tides at Milbridge, Maine
and tide data recorded at the Addison, Maine pier in 2005[4].)

	Elevation NAVD88 (ft)
FEMA Zone AE Elev	11.3
100-yr Frequency Flood Event	10.8
50-yr Frequency Flood Event	10.5
10-yr Frequency Flood Event	9.8
2-yr Frequency Flood Event	9.4
1-yr Frequency Flood Event	9.0
Maximum Predicted Astronomic High Water	8.5
Mean High Water Spring (MSHW)	7.5
Mean Higher High Water (MHHW)	6.6
Mean High Water (MHW)	6.2
National Atlantic Vertical Datum (NAVD88)	0
Mean Sea Level (MSL)	-0.2
Mean Tide Level (MTL)	-0.4
National Geodetic Vertical Datum (NGVD29)	-0.7
Mean Low Water (MLW)	-6.0
Mean Lower Low Water (MLLW)	-6.3

d. Freshwater Drainage Area.

The West Branch has a total drainage area of 11.0 square miles. The drainage area extends to the foothills of Columbia and Columbia Falls. The topography of Addison ranges from moderately sloped in some area to relatively flat in other areas. Soil cover of the area is generally shallow and rock outcroppings are common. Vegetation consists primarily of softwood forests and hay field meadows.

The West Branch drainage area does not include United States Geological Survey (USGS) continuously recorded streamflow monitoring to provide real-time flow data. Additionally, the 1991 Addison Maine FEMA FIS does not include a streamflow analysis of the West Branch (reference 2). Other USGS streamflow gages

located in Washington County with watershed characteristics similar to the West Branch were investigated for comparison purposes. Although USGS Gage 01021470 Libby Brook near Northfield, Maine (DA 7.79 square miles) and USGS Gage 01021480 Old Stream near Wesley, Maine (DA 29.1 square miles) have potentially similar watershed characteristics, both only include seven years of record which is not enough to develop of streamflow analysis. Additionally, neither of these towns have a flood insurance study with a streamflow analysis for reference. USGS Gage 01022500 Narraguagus River at Cherryfield, Maine (227 square miles) is considered too large for comparison with the West Branch Pleasant River; however, the Cherryfield, Maine flood insurance study does include a streamflow analysis of the West Branch Narraguagus River (79.6 square miles). Although still considerably larger than the West Branch Pleasant River, it was referenced for comparison with the hydrologic analysis conducted for this study.

e. Hydrologic Modeling.

The Corps of Engineers Hydrologic Engineering Center Hydrologic Modeling System (HEC-HMS) was used to simulate the rainfall runoff in the West Branch. Since the West Branch does not have real-time streamflow data to compute 2-yr, 10-yr, and 100-yr flows from actual precipitation events, the U.S. Weather Bureau Technical Paper, No. 40 (TP-40) synthetic precipitation data was utilized to develop these relationships within the HEC-HMS model. The HEC-HMS model utilized similar methodology as the flow analysis conducted by the Natural Resources Conservation Service (NRCS) in their 2003 and 2007 report (reference 3).

The HEC-HMS model is comprised of two components, first the rainfall data necessary to calculate the storm event as provided by TP-40 as presented in Table 3. Secondly, the topography regime represented by the Soil Conservation Service (SCS) dimensionless unit hydrographs, based on the time of concentration, percent impervious, loss rates known as the curve number (CN) and initial abstraction (Ia) that includes all losses prior to runoff as presented in Table 4 (reference 1). Additionally, the West Branch watershed was delineated into three sub-watersheds representing Bells Brook (5.0 square miles), Branch Brook (4.4 square miles) and the unnamed tributary with Water and Point Streets (1.6 square miles).

This study also includes a flooding analysis of properties located adjacent to the West Branch, the peak flows were generated to represent wet, spring season soil conditions also referred to as a High Antecedent Moisture Condition (AMC). Therefore, these peak flows will simulate a worst case flooding analysis, see Section 3.0 Site Hydraulics. Comparison of the HEC-HMS model with the peak flows computed in the NRCS 2003/2007 reports concludes very similar results, which was expected since both analyses utilized similar computational methodologies. A comparison of these results is presented in Table 5.

Table 2
U.S. Weather Bureau Technical Paper, No. 40 (TP-40)
(Rainfall Depth in inches)

Time (hrs)	2yr/12 hr	10yr/12 hr	100yr/24 hr
1	.85	1.45	2.0
2	1.25	2.0	2.8
3	1.5	2.3	3.3
6	1.9	2.8	4.2
12	2.5	3.5	5.2
24	-	-	6.0

Table 3
Sub-Watershed Hydrologic Landuse Characteristics
Antecedent Moisture Condition (AMC) High

Watershed Area (Sq.Mi.)	Curve No. (CN)	Tc (min)	Initial Abstraction (Ia)	% Impervious
11.0	35-65	30-75	0.2-0.4	5

Table 4
Baseflow by Month (cfs)

Baseflow (cfs)												
Month	Jan	Feb	Mar	Apr	May	June	Jul	Aug	Sep	Oct	Nov	Dec
Q (cfs)	28	28	61	63	22	16	11	9	10	16	24	34

Table 5
USACE New England District HEC-HMS Peak Flows
Compared with the NRCS 2003/2007 Report Peak Flows

Sub-Basin Location	Drainage Area (sq.miles)	Peak Flows (cfs)		
		2-Yr	10-Yr	100-Yr
Ridge Road HEC-HMS	11.0	420	945	2580
Ridge Road NRCS Report	11.0	350	1170	2650

3.0 SITE HYDRAULICS

a. General.

This section discusses the hydraulic methods and assumptions used to simulate tidal flow to study marsh restoration as well as estimates of flood elevations for selected recurrence intervals. It is noted that flood elevations shown on the Flood Insurance Rate Map (FIRM) represent rounded whole-foot elevations and may not exactly reflect the elevations computed for flood profiling, such as this. Flood elevations shown on the FIRM are primarily intended for flood insurance rating purposes. For construction and/or floodplain management purposes, users are encouraged to use the detailed flood elevation data computed in conjunction with elevations shown on the FIRM.

The existing river channel, culvert crossings and flood plain were hydraulically modeled for several different tide and storm recurrences. Alternatives consist of nine primary alternatives for Ridge Road each modeled with secondary alternatives for various flow conditions and upstream culvert modifications to determine corresponding water elevations, velocities, and acres restored. The results of each alternative were evaluated to compute the total restoration area, impacts of flooding to adjacent properties, flow velocities at roadway crossings, sedimentation and sea level rise (SLR).

The Ridge Road alternatives evaluated with the HEC-GeoRAS model are as follows:

A. No Action.
B. Six 5ft x 2.5ft Box Culverts at Ridge Rd.
C. Six 5ft x 5ft Box Culverts at Ridge Rd.
D. New Bridge at Ridge Road (150ft span/ existing upstream culverts)
E. New Bridge at Ridge Road (150ft span/enlarged culverts at Addison Road & flap gate at Water Street.)
F. New Bridge at Ridge Road (150ft span/enlarged culverts at Addison Road, Point Street and Water Street.)
G. New Culvert at Ridge Road (45ft x 12ft, or equivalent area, with existing upstream culverts.)
H. New Culvert at Ridge Road (45ft x 12ft, or equivalent area, and enlarged culverts at Addison Road, Point Street and Water Street.)
I. New Culvert at Ridge Road (45ft x 12ft, or equivalent area, and enlarged culverts at Addison Road and flap gates at Water Street.

b. Elevation Data and Datums.

Study area ground survey was obtained from Light Detection and Ranging (LIDAR) topography collected in 2012 and is available through NOAA Coastal Services Center. This data was processed, using the HEC-GeoRAS

geographical information system (GIS) arc-map processor, into cross-sections that follow the West Branch channel, tributaries and floodplain.

Photogrammetric topographic mapping was collected by James W. Sewall Company in 2004 with detailed 1-5 foot contour mapping at 1:40 scale. This topography included area at and below elevation 12.0 ft NGVD with elevations being converted to NAVD88. Additionally, this data included 201 spot elevations within the wetlands and limited ground field survey conducted on 20-21 August 2005 along Ridge Road, Water Street and Addison Road to validate the given elevations. (Reference 4). Culvert and bridge elevations were obtained from the NRCS report for culverts located at the following roadway crossings: Ridge Road, Addison Road, Water Street, Point Street, Ingersoll Brook and Route 1. (Reference 3).

All topographic and water elevations shown in this study are referenced to NAVD88 datum. It is important to note that prior studies/reports, including the Addison Maine FIS reference the NGVD29 datum. Ground, structure and water elevations may be compared and/or referenced to NGVD29 by applying a standard conversion factor. The conversion from NGVD29 to NAVD88 is -0.7 feet and from NAVD88 to NGVD29 is +0.7 feet.

c. HEC-RAS Development.

The Corp's one-dimensional Hydrologic Engineering Center's River Analysis System (HEC-RAS) computer model was used to conduct unsteady flow analyses. The HEC-RAS model calculates the water surface elevations (WSE) along a river channel using backwater analysis through a network of open channels. This model was used to simulate the WSE along the West Branch under conditions representing different culvert and bridge alternatives during the spring, 2-yr and 100-yr tide events. The model has the capability to accurately model culverts and bridges. Input for the model included boundary conditions, flow regimes, loss coefficients, structure characteristics, and LIDAR topography that was processed into cross-sections. Outputs from the model include computed water surface elevations, channel velocities, acres restored and floodplain mapping.

The Hydrologic Engineering Center's River Analysis System ArcGIS extension, HEC-GeoRAS, was used to layout cross sections and reaches based on topography (LiDAR). The existing marsh was divided into five reaches: Branch Brook, Bells Brook, Ingersoll Brook, Point Street marsh and West Branch. All reaches, cross sections, banks, and bridge/culvert alignments were georeferenced and their elevations extracted from the LiDAR data with HEC-GeoRAS for use in HEC-RAS. In HEC-RAS, water surface elevations were dynamically calculated to fluctuate with the tide and culverts were modeled both with their existing geometries (see Table 6) and proposed alternative configurations.

Table 6
Existing Culvert and Roadway Geometry
(Referenced from 2007 NRCS Culvert Survey)

Roadway	Existing Culvert Size (ft)	Top of Roadway Elev (ft NAVD88)	Downstream Culvert Inv. (ft NAVD88)	Upstream Culvert Inv. (ft NAVD88)
Ridge Road	(6) 5'x5'	13.0/11.3	-4.5	-4.0
Addison Road	(2) 6'Dia.	9.8	-4.7	-4.8
Water Street	4'Dia. & 2'Dia.	8.7	-4.5 & 2.2	-3.5 & 2.4
Point Street	4'Dia	6.1	0.4	0.6
Route 1 (Branch Bk)	10.5	NA	3.0	3.3
Route 1 (Bells Bk)	10.0	NA	7.0	7.5
Ingersoll Brook	6'Dia.	NA	13.5	14.0

d. Model Calibration.

Due to the West Branch Pleasant River being restricted to tidal flow by the roadway embankment and tide gates; calibration of the model relied on evaluation of historical documentation and photos of the tidal floodplain preceding the 1940 bridge construction. For calibration, the model was simulated with mean spring high water (MWHW) hydrographs through a channel opening representing the historic, pre-bridge conditions.

Roughness coefficients (Manning's "n") used in the hydraulic computations were determined by engineering judgment and were based on field conditions of the channel and floodplain areas. These values as well as minor modifications to the channel cross-sections were considered calibrated when the MSHW tide elevations reached the historic marsh floodplain footprint. The calibrated "n" values are presented in Table 7.

The hydraulic analysis was based on unobstructed flow. The flood elevations shown on the profiles are thus considered valid only if hydraulic structures remain unobstructed and do not fail.

Table 7

Calibrated Manning "n" values

Tributary Name	Main Channel "n" values	Right Overbank "n" values	Left Overbank "n" values
West Branch Reach 1	.035-0.05	.03-0.12	.03-0.12
West Branch Reach 2	.035-0.05	.05-0.12	.035-0.12
East Swamp Reach 1	0.035-0.05	0.03-0.05	0.03-0.12
East Swamp Reach 2	0.05-0.07	0.05-0.12	0.03-0.12
East Swamp Reach 3 – d/culvert	0.10-0.12	0.10-0.12	0.10-0.12
East Swamp Reach 3 – u/culvert	0.03-0.05	0.03-0.05	0.03-0.05
East Swamp Reach 4	0.10-0.12	0.10-0.12	0.10-0.12
East Swamp Trib.	0.05-0.12	0.05-0.12	0.05-0.12
Point Street Trib.	0.25-0.30	0.25-0.30	0.25-0.30
Water Street Trib.	0.05-0.12	0.03-0.12	0.05-0.12
Branch Brook	0.05-0.12	0.05-0.12	0.10-0.12
Bells Brook Reach 1	0.10	0.05-0.12	0.10-0.12
Bells Brook Reach 2	0.15-0.20	0.15-0.20	0.12-0.20
Bells Brook Reach 3	0.30	0.20-0.30	0.20-0.30
Bells Brook Reach 4	0.12-0.30	0.035-0.30	0.12-0.30
Bells Brook Reach 5	0.12-0.20	0.12-0.20	0.12-0.20
Bells Brook West Trib.	0.12-0.30	0.12-0.30	0.15-0.30
Bells Brook East Trib.	0.20-0.30	0.12-0.30	0.20-0.30
Bells Brook North Trib.	0.20-0.30	0.12-0.30	0.20-0.30
Ingersoll Brook	0.20-0.30	0.20-0.30	0.20-0.30

e.West Branch Restoration Analysis.

The intent of modeling the West Branch was to evaluate the nine primary alternatives presented in Section 3.0 and the correlating tidal exchange to restore the salt marsh, without adversely affecting adjacent properties, roadways, or infrastructure.

i. Alternative A, Alternative B & Alternative C. Alternative A represents a 'no action' alternative, therefore, changes in either tidal or freshwater flow under this scenario is considered null. The model simulated Alternative B and alternative C, which include six box culverts of 5ft x 2.5ft and 5ft x 5ft, respectively, with neither alternative including flap gates. Alternative B culverts equal a 75 square foot opening that is equivalent to

half the existing six culverts and the Alternative C culverts equal a 150 square foot opening – the existing configuration. Additionally, Alternative B included no upstream culvert improvements while Alternative C included improvements at both Point Street and Water Street from 4-ft diameter to 5-ft diameter culverts to increase tidal exchange into the marshes upstream of these roadways. Increasing the culverts to 5-ft does not require the roadways to be raised.

The spring MHW reached at both Addison Road and Water Street is only 5.2 ft NAVD and 6.1 ft NAVD for Alternative B and Alternative C, respectively, while the spring MHW at Point Street is only 4.7 ft NAVD and 5.1 ft NAVD, respectively. These spring tide elevations are considerably lower than the spring tide elevation of Pleasant River (7.5 ft NAVD) and the marsh elevations adjacent to the channel. Therefore, a total 132 acres and 260 acres, respectively, would be restored under these scenarios out of the potential 470 acres.

Stormwater runoff hydrographs evaluated in Section 2.c and presented in Table 5 were simulated in the HEC-RAS model during spring tide conditions. Stormwater runoff increases the peak water surface elevation in the marsh but does not impact either Addison Road or Water Street. Increased water elevations at Point Street would encroach on the top of road surface during a spring tide/10-yr rain event and potentially overtop the roadway by 12-inches during a spring tide/100-yr rain event. Local observations indicate the roadway at Point Street currently experiences annual overtopping from stormwater particularly during saturated snowmelt conditions due to overgrown channel and flat gradient causing backwater effects. Therefore channel improvements in combination with an enlarged culvert may alleviate stormwater flooding in this area.

Tide hydrographs representing the 2-yr, 10-yr and 100-yr tide events were simulated in HEC-RAS to compute the expected peak water surface elevation in the marsh. Both Alternative B and Alternative C indicate increases in water elevation, although significantly lower than the correlating peak tide predicted in the Pleasant River downstream of Ridge Road. This is due to the 75 square foot and 150 square foot opening restriction at Ridge Road. Impacts to upstream roadways include no encroachment at Addison Road, encroachment at Water Street during the 10-yr flood and overtopping at Point Street of 0.6-ft to 1.6-ft during the 10yr to 100-yr tide events.

ii. Alternative D, Alternative E & Alternative F. Each of these alternatives includes replacing the existing Ridge Road causeway's six 5ft x 5ft culverts with a 150-ft open span bridge. Alternative D includes no upstream culvert improvements while Alternative E includes culvert improvements at Addison Road, Point Street and Water Street to increase tidal exchange into the marshes upstream of these roadways. Alternative F includes a culvert improvements at Addison Road only and a flap gate at Water Street to restrict tidal flow exchange upstream of Water Street into the Point Street swamps but will allow stormwater draining upstream of Water Street to discharge to the West Branch during periods of low tide. It is important to note, that stormwater will discharge through the flap gate when the tide begins to recede.

Increasing the Ridge Road opening to a 150-foot open bridge increases the tidal exchange to the West Branch marsh and significantly with the spring high water at Addison Road increasing to 1.5-1.8 feet greater than Alternative B and 0.6-0.9 feet greater than Alternative C. Similarly at Water Street, spring high water increases by 0.7-1.0 feet and 1.7-2.0 feet. The Point Street spring tide elevations increase by only 0.6 feet with the existing culvert size at Water Street (Alternative D) but increase by 2.2 feet when the Water Street Culvert is increased to a 12'x5' box (Alternative E). Alternative F includes a flap gate at the Water Street Culvert; therefore, tidal exchange is not introduced upstream of this point under this scenario. A total acres restored were computed as 349 acres, 385 acres and 314 acres, respectively, out of the potential 470 acres. It is interesting to note that the flap gate at Water Street reduces the total acres restores; however, Alternative F does include a respectable increase in total acres restored over Alternatives B and C. This is due to the increased volume of tidal flow entering the 150-foot bridge distributing across the West Branch flood plain.

The stormwater analysis evaluated in conjunction with a spring tide condition for Alternatives D, E and F determined no impact to the top of roadway at either Addison Road or Water Street, as also determined in Alternatives B and C. However, the increased volume of tidal flow entering the West Branch during these alternatives with the 12ft x 12ft box culvert at Water Street and Point Street significantly increases the flood

elevations at Point Street. Flooding at Point Street could be in excess of nearly 1-foot during a 2-yr frequency rain event coupled with peak spring tide.

Tide hydrographs representing the 2-yr, 10-yr and 100-yr tide events were simulated in HEC-RAS to compute the expected peak water surface elevation in the marsh for Alternatives D, E and F. Impacts to upstream roadways include encroachment at Addison Road during a 100-yr tide only, encroachment at Water Street during the 10-yr, 50-yr flood and 100-yr tides, and significant inundation at Point Street during each of these tide events.

iii. Alternative G, Alternative H & Alternative I. These alternatives include replacing the existing Ridge Road causeway with six 5ft x 5ft culverts with a 45ft x 12ft (or equivalent) culvert and include similar upstream culvert scenarios as Alternatives D, E and F. Alternative G includes no upstream culvert improvements while Alternative H includes culvert improvements at Addison Road, Point Street and Water Street to increase tidal exchange into the marshes upstream of these roadways. Alternative I includes a culvert improvements at Addison Road only and a flap gate at Water Street to restrict tidal flow exchange upstream of Water Street into the Point Street swamps but will allow stormwater draining upstream of Water Street to discharge to the West Branch during periods of low tide. As was noted for Alternative F, the stormwater will discharge through the flap gate when the tide begins to recede.

Increasing the Ridge Road opening to a 45ft x 12ft box culvert (or equivalent – realistic culvert dimensions will be determined during cost estimation) computed nearly identical spring tide elevations as Alternatives D, E and F with the 150-ft open bridge at each of the roadway crossings, Addison Road, Water Street and Point Street. The astronomical high water elevations for the 45ft x 12ft culvert alternatives were only 0.1-0.2 ft below those achieved in 150-ft open bridge alternatives. Total acres restored were computed as 346 acres, 377 acres and 309 acres, which was very similar to the total acres restored in Alternatives D, E and F. Again, the acres restored are reduced due to the flap gate at Water Street however some of this restricted tidal flow is distributed across the West Branch floodplain.

As expected, water elevations computed for both the stormwater analysis and tidal analysis were very similar to those computed in Alternatives D, E and F. This is due to the similar flow volume entering the marsh for the 150-ft span open bridge and 45ft x 12ft culvert opening as well as identical upstream culvert scenarios. The greatest impacts are seen at Point Street due to the low lying roadway and adjacent floodplain.

f. Channel Velocities and Sedimentation.

According to the American Society of Civil Engineers publication, Sedimentation Engineering, published in 1977, the critical water velocity for a median grain size of 0.4mm ranges between 0.45 feet per second (fps) and 0.84 fps with 0.82 fps being the critical velocity, indicating a small amount of movement, or sedimentation will occur. The critical water velocity represents the point at which the grain is suspended.

The velocities of the existing channel, computed by the model, ranged between 0.26 fps and 1.64 fps during the mean high spring water tide cycle and 0.46 fps and 1.79 fps during the 1-yr storm event. The model computed lower velocities for the 100-yr storm event because the WSE will inundate the channel and marsh. The velocity will be determined at critical locations for the alternatives that remain after the first round of feasibility selection. These velocities will be used to size rip-rap and potentially model scour/erosion/sedimentation for the selected alternative(s).

g. Sea Level Rise.

Sea level rise (SLR) was evaluated to predict the sea level change (SLC) at the West Branch and how this may impact the study area. The SLR analysis was conducted as directed in the USACE guidance, EC 1165-2-212, dated 1 October 2011. This EC requires a multiple scenario approach for three sea level rise scenarios, with each being considered equally plausible. These curves are; the historic rate of SLC at the project area, an intermediate SLC curve (modified NRC Curve I), and a high SLC curve (modified NRC Curve III). Formulation of the NRC curves from a defined starting date, and for localized su subsidence was also provided in the EC which allows from SLC to be calculated for specific project time frames and for specific geographic areas. This is critical since

SLC along the coast varies due to local subsidence, uplift, water body movement, etc. The three scenarios proposed by the NRC result in global eustatic sea-level rise values, by the year 2100, of 0.5 meters, 1.0 meters, and 1.5 meters. Adjusting the equation to include the historic Global mean sea level (GMSL) change rate of 1.7 mm/year and the start date of 1992 (which corresponds to the midpoint of the current National Tidal Datum Epoch of 1983-2001), results in updated values represented as the constant, b, in the SLC equation.

Using the SLC equation below, which is equation (3) from the EC, and a spreadsheet provided by the USACE ERDC, Figure 1 was developed for Bar Harbor, Maine. Bar Harbor was used since it is the closest NOAA station to the project site and includes historic SLC information required for this analysis.

$$E(t2) - E(t1) = 0.0017(t2-t1) + b(t22-t12)$$

Where:
t1 = is the time between the project's construction date and 1992
t2 = is the time between a future date at which one wants an estimate for sea level rise and 1992
b = 2.71 E-5 for modified NRC Curve I (low, 0.5 meter rise)
b = 7.00 E-5 for modified NRC Curve II (intermediate, 1.0 meter rise)
b = 1.13 E-4 for modified NRC Curve III (high, 1.5 meter rise)

As can be seen in both Figures 1 and 2, the historical rate (0.2 meter curve) would result in a rise of only 0.27 feet (0.04 meter) or 3.2 inches over the first 50 years. However, the level of SLR increases for each of the NRC curves as specified for use in the EC. As shown in Figure 1, the low curve (0.5 meter curve) predicts a rise of 0.4 feet (0.12 meter) or 4.8 inches, the intermediate curve a rise of 0.6 feet (0.18 meter) or 7.2 inches, and the high curve a rise of 0.81 feet (0.32 meter)or 9.7 inches.

4.0 SUMMARY

A final decision has not yet been made. The alternatives are going through cost estimation and additional, more detailed modeling, will be done on those that appear financially feasible, constructable and socially and environmentally acceptable. Additional modeling might include a sensitivity analysis of the bridge modeling approach and scour analysis, particularly for piers. Sedimentation/erosion analysis is also being considered, depending on the selected plan. Other factors will undoubtedly affect the final decision as well, and this report will be expanded.

5.0 REFERENCES

1. Natural Resources Conservation Service (NRCS), Soil Survey of Washington County, Maine.
2. 1991 FEMA Flood Insurance Study, Addison, Maine.
3. 2003/2007, NRCS Report.
4. 2006, EA Engineering, Science and Technology, Inc. "Vegetation Cover Type and Substrate Summary Report for the Pleasant River Marsh Restoration Project, Addison, Maine'.
5. 2007, Cowle, Bonnie. 'Background and Considerations of the Federal Emergency Management Agency's National Flood Insurance Program & Local Floodplain Management Regulations As They Relate to the Study of Restoring Tidal Flow to the West Branch of the Pleasant River, Addison, Maine.".
6. 2007, Cowle, Bonnie. 'Background and Considerations of Shoreland Zoning Rules and Regulations As They Relate to the Study of Restoring Tidal Flow To the West Branch of the Pleasant River'.
7. 2009, Burdick, David, Lovit, Marilee, Vincent, Robert, Eberhardt, Alyson, Peter, Chris, 'Evaluation of Pre-Restoration Conditions in the West Branch of the Pleasant River, Maine, Final Report'.
8. 2009, Robinson Resources, LLC. "Final Report: West Branch Pleasant River Restoration Feasibility Project, Addison, Maine."

COMPLICATIONS ASSOCIATED WITH MAINTAINING AUTHORIZED CHANNEL DIMENSIONS DURING LOW WATER PERIODS

Michael Rodgers, P.E., Project Manager, US Army Corps of Engineers – St. Louis District, St. Louis, Missouri, Michael.T.Rodgers@usace.army.mil

INTRODUCTION

The St. Louis District is responsible for maintaining a safe and dependable navigation channel on 300 miles of the Mississippi River between Saverton, Missouri and Cairo, Illinois. The southernmost 195 mile section of the Mississippi River in the St. Louis District, located between the confluences of the Missouri River and the Ohio River, is referred to as the Middle Mississippi River (MMR). The MMR is a vital artery in the inland navigation system and vital to the nation's safety and economy. There are two locations (Grand Tower, Illinois river miles 80-79 and Thebes, Illinois river miles 46-38) on the MMR where the river crosses a sedimentary rock outcrop. Previous attempts to remove portions of the rock outcrop were successful (as recent as the late 1980s); but, remnants of the rock outcrop still exist and pose a hazard to commercial river navigation at low river stages. These remnants are termed "pinnacles" due to their shape and size. The task of maintaining authorized channel dimension for commercial navigation on the MMR is a highly visible, politically sensitive, and extremely complex endeavor. While always a challenge, maintaining a safe and dependable navigation channel was made far more challenging during the summer, fall and winter of 2012 – 2103 due to extreme low water conditions on the MMR.

PROJECT DESCRIPTION

The drought of 2012 was equal to or exceeded any drought or low water period experienced on the MMR within the past five decades. Water levels in the MMR reached record lows, which posed a significant risk to commercial navigation traffic due to shallow channel crossings, reduced channel widths, and the rock pinnacles located along the channel bottom at Grand Tower and Thebes Illinois. The St. Louis District (MVS) was required to operate in an environment of competing demands for scarce water resources including; agriculture, recreation, environmental programs, energy production, and commercial navigation. MVS relied heavily upon diverse USACE core competencies and resources. Additionally, unique expertise was sought from other federal agencies (United States Coast Guard (USCG), United States Fish & Wildlife Service (USFWS), United States Department of Agriculture (USDA), Federal (Department of Transportation (DOT)) as this mission crossed organizational boundaries.

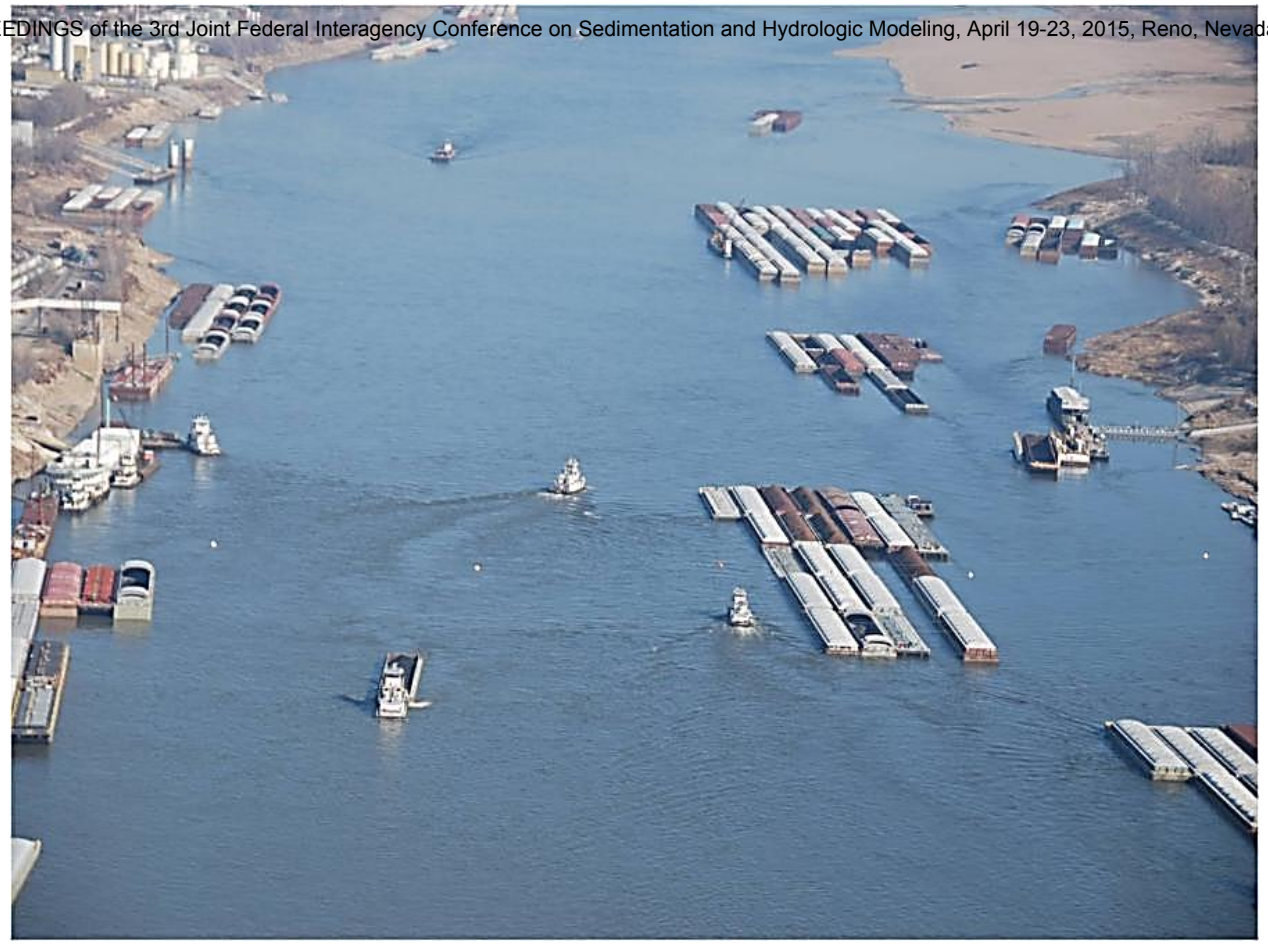

Figure 1: Low water conditions within St. Louis Harbor meant that space for fleeting is limited

The St. Louis District is responsible for planning and overseeing all aspects of providing a safe and dependable navigation channel at these record low river stages. This included (1) identifying critical specialties and disciplines required for the mission while balancing against competing demands; (2) determining and resourcing the needs of the team while maintaining cost, time, and quality assurance objectives; (3) extensive coordination with project stakeholders including (but not limited to) the River Industry Action Committee (RIAC), the River Industry Executive Task Force (RIETF), the United States Coast Guard (USCG), and the United States Fish and Wildlife Service (USFWS); (4) compliance with all relevant environmental regulations (National Environmental Policy Act (NEPA) and Fish and Wildlife Coordination Act (FWCA)); (5) managing pool and reservoir elevations; (6) forecasting river levels; (7) removing underwater rock pinnacles; (8) dredging shoals; (9) providing and utilizing a nearly continuous flow of channel and rock pinnacle surveys. Water management PDT members constantly collected water data, monitoring a number of hydrological and meteorological factors to forecast river conditions the rest of the Nation relied upon. Additionally, extensive coordination with the Kansas City District of the Northwest Division was a daily occurrence as the Missouri River releases were closely monitored. The complexity and significance of the rock removal component of the mission cannot be overstated. This work required integrated and coordinated management along with the application of innovative technology and tools / removal methodologies. Risks associated with barge tow collisions with rock pinnacles were high from a fiscal perspective as well as from an environmental perspective. Current and future river construction contract needs were adjusted in order to fund the rock removal project. River engineering projects were reprioritized to allow for detailed plans and specifications to be

produced to accommodate a tight project schedule. Removal of the pinnacles involved advanced surveying techniques coupled with innovative removal methodologies. Work locations within the rock removal areas were prioritized to get the most dangerous (highest elevation) rock removed first, with a secondary focus on providing optimal channel widths. The Project Management Plan (PMP) for the Regulating Works Project on the Middle Mississippi River includes a cost estimate, the project schedule, and all performance objectives and key assumptions. MVS was able to not only meet, but exceed the requirements outlined in the PMP through effective partnering and collaboration. During this low water event, due to the exhaustive efforts of MVS and partnering agencies, there were no accidents, groundings or unplanned closures of the Middle Mississippi River. This performance is unprecedented given that a similar drought in the late 1980's featured numerous groundings, accidents, channel closures, restrictions and a generally unreliable channel. With all eyes on the Middle Mississippi River – the White House, Congress, River Industry, and the US and international media – MVS efficiently and effectively coordinated all phases of the mission, exceeded expectations, and delivered what was promised.

Figure 2: A 20 barge tow transits upbound through the Thebes, Illinois rock removal reach

PROJECT RESULTS

Prior to the drought conditions reaching critical levels, MVS was carefully planning and preparing for strategic low water operations by identifying key problematic locations and putting into place the designs and resources to act when called upon. This foresight enabled the MVS to act quickly once critical levels were imminent and allowed USACE to provide authorized navigation channel dimensions during periods of extremely low water. The project consisted of maintaining the authorized channel dimensions in the Middle Mississippi River from St. Louis to Cairo, IL from July 2012 through February 2013 while monitoring 195 miles of river bed obstructions and moving river sediments that would have otherwise impeded navigation.

Highly specialized survey crews used the latest multi-beam technology to differentiate between sand and rock, enabling them to identify small but hazardous rock pinnacles in the navigation channel. As water levels continued to fall, the river bed material was transported and additional critical rock pinnacles were identified for removal. Expedited rock removal was required in several areas containing dense limestone to safely allow barge traffic to continue without groundings or accidents. This was accomplished using unique drilling and blasting as well as mechanical (hydro hammer) techniques. The minimum authorized channel dimensions were achieved in 30 days (approximately 30 days ahead of schedule) from award of the contracts with minimal channel closures that were coordinated with contractors, the USCG, and navigation industry. Contracts needs were adapted in order to fulfill the most critical low water needs as the drought progressed. The composition of the team responsible for the success of this project consists of many members including specialists such as engineers, technicians, project managers, construction and dredging specialists, skilled laborers, surveyors, GIS specialists, construction contractors, public affairs, barge industry representatives (port captains), towboat pilots, biologists, contracting officers, safety officers, meteorologists, and the U.S. Coast Guard. Several Corps elements throughout the U.S. provided team members in these fields. The contractual mechanisms and logistics plan were implemented as part of the strategic first step. Implementing an effective communication plan within MVS assisted project coordination and increased the efficiency of handling stakeholder concerns locally, regionally, and nationally. The effective and detailed project communication overall stakeholder collaboration nullified many coordination complexities. Dredge surveys and channel patrols surveys were posted to the district's website. Navigation channel status reports were sent out weekly. Rock pinnacle information (electronic chart overlays, surveys, rock locations, slides, etc.) were posted to a dedicated webpage. The successful completion of the Urgent and Compelling Rock Removal Project of 2012 has help restore America's faith in USACE and has established lifelong partnerships across Federal, State and Local agencies.

Figure 3: Mike Rodgers Project Manager for the Rock Removal Project departs survey vessels with Senator Durbin Representative Enyart and USACE Major General Peabody in Thebes, Illinois, January 7, 2013.

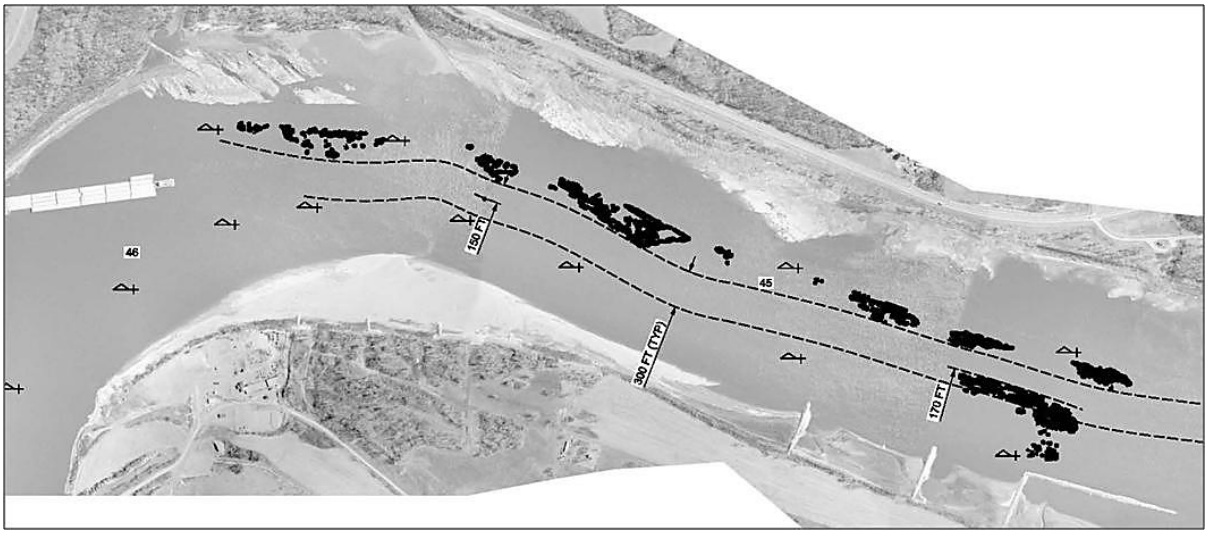

Figure 4: The plan view illustrates the pinnacle rock locations and how the encroach upon the 300' (hatch line) minimally authorized channel width from river miles 46 to 44 near Thebes, Illinois

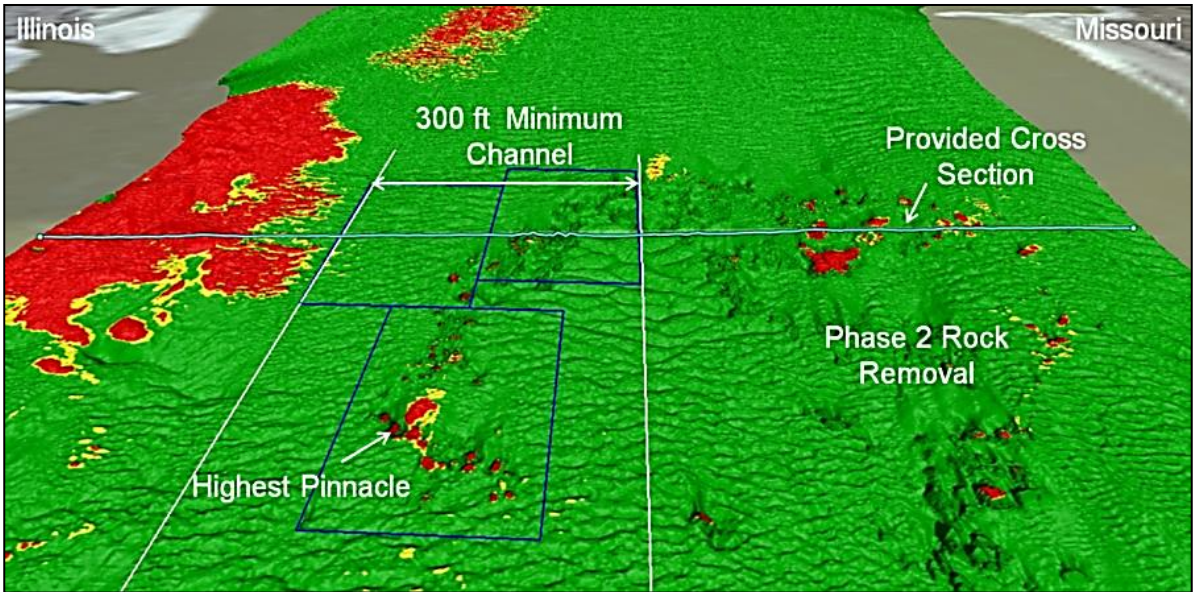

Figure 5: Prior to rock removal, a high density multi-beam survey of the river bed at Thebes (river mile 38.5) shows hazardous rock outcroppings (red) intermixed with large sandwaves (green)

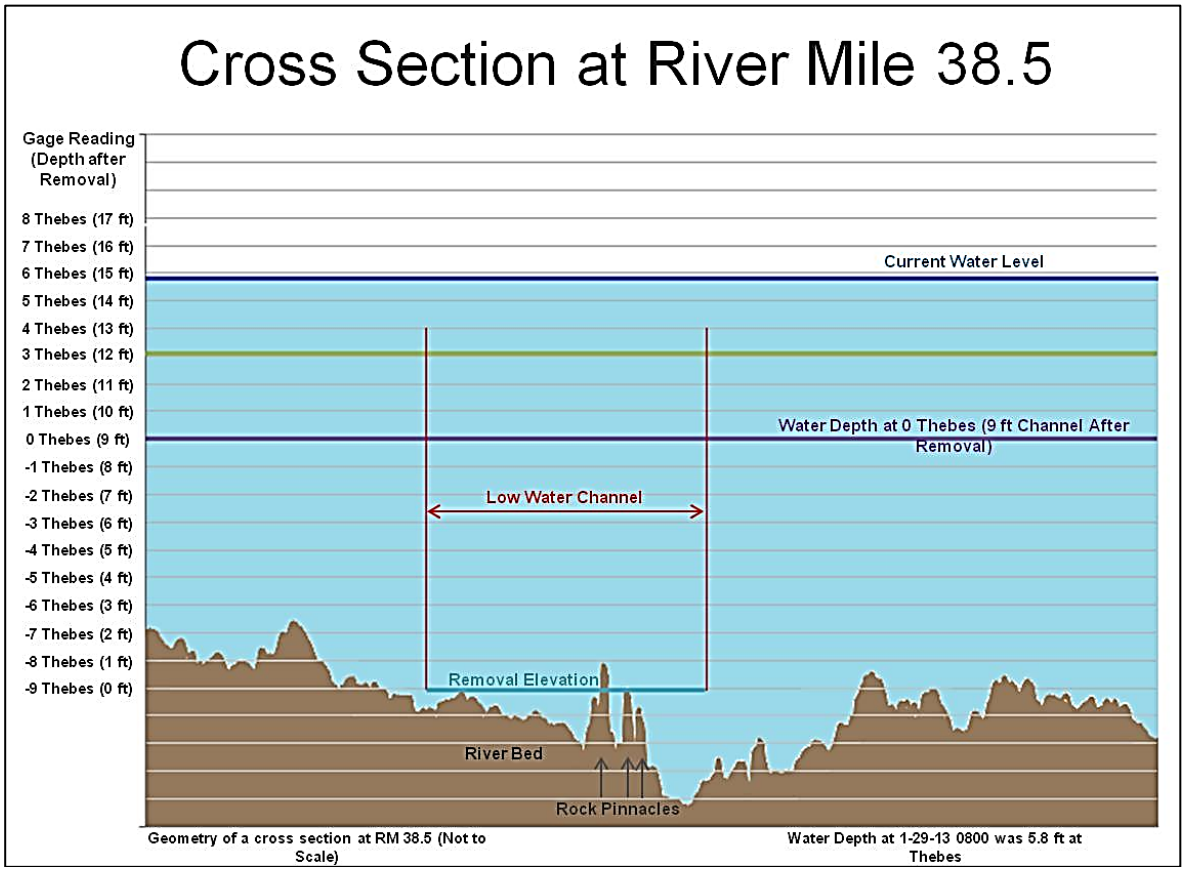

Figure 6: A cross section at river mile 38.5 identifies the low water channel and rock pinnacles needing to be removed

Figure 7: Rock was removed from the navigation channel using various means such as hydro-hammering excavating grappling and blasting

ESTIMATING FLOOD MAGNITUDE AND FREQUENCY FOR URBAN AND SMALL, RURAL STREAMS IN GEORGIA, SOUTH CAROLINA, AND NORTH CAROLINA

Toby Feaster, Hydrologist, U.S. Geological Survey, Clemson, SC, tfeaster@usgs.gov;
Anthony Gotvald, Hydrologist, U.S. Geological Survey, Atlanta, GA, agotvald@usgs.gov;
Curtis Weaver, Hydrologist, U.S. Geological Survey, Raleigh, NC, jcweaver@usgs.gov

Abstract: Reliable estimates of the magnitude and frequency of floods are essential for such things as the design of transportation and water-conveyance structures, Flood Insurance Studies, and flood-plain management. The flood-frequency estimates are particularly important in densely populated urban areas. A multistate approach was used to update methods for determining the magnitude and frequency of floods in urban and small, rural streams that are not substantially affected by regulation or tidal fluctuations in Georgia, South Carolina, and North Carolina. The multistate approach has the advantage over a single state approach of increasing the number of stations available for analysis, expanding the geographical coverage that would allow for application of regional regression equations across state boundaries, and building on a previous flood-frequency investigation of rural streamflow-gaging stations (streamgages) in the Southeastern United States. In addition, streamgages from the inner Coastal Plain of New Jersey were included in the analysis.

Generalized least-squares (GLS) regression techniques were used to generate predictive equations for estimating the 50-, 20-, 10-, 4-, 2-, 1-, 0.5-, and 0.2-percent annual exceedance probability flows (also referred to as the 2-, 5-, 10-, 25-, 50-, 100-, 200-, and 500-year recurrence interval flows) for urban and small, rural ungaged basins for three hydrologic regions: the Piedmont-Ridge and Valley, Sand Hills, and Coastal Plain. The GLS regression included 116 urban streamgages and 372 rural streamgages of which 32 came from small, rural basins draining less than 1 square mile. Incorporation of urban streamgages from New Jersey allowed for the expansion of the applicability of the predictive equations in the Coastal Plain from 2.1 to 53.5 square miles. Explanatory variables in the regression equations included drainage area (DA) and percent of impervious area (IA) for the Piedmont-Ridge and Valley region; DA and percent of developed land for the Sand Hills; and DA, IA, and 24-hour, 50-year maximum precipitation for the Coastal Plain. An application spreadsheet also was developed that can be used to compute the flood-frequency estimates along with the 95-percent prediction intervals for an ungaged location.

INTRODUCTION

Building on the success of a multistate approach for developing regional flood-frequency equations to estimate the magnitude and frequency of floods at ungaged rural streams in the Southeast, (Feaster and others, 2009; Gotvald and others, 2009; Weaver and others, 2009), a similar approach was applied to urban and small, rural streams (Feaster and others, 2014). For this investigation, Southeast refers specifically to Georgia, South Carolina, and North Carolina. The analytical techniques used incorporate both urban and rural streamgages and, therefore, can be applied to urban and small, rural streams. The lower limit of drainage area for basins included in the Southeast rural flood-frequency study was 1 square mile (mi^2). The lower limit of drainage area for rural basins included in this investigation was 0.1 mi^2. Consequently, in this study, small, rural streams refer to those with drainage areas less than 1 mi^2. Some of the

benefits of including both urban and rural streamgages in the regression analysis are (1) smoother transition between urban and rural flood-frequency estimates, (2) larger database than would be available with urban streamgages alone, and (3) larger geographical coverage in the hydrologic regions, which will represent a broader range of hydrologic conditions likely to occur at ungaged locations. More details on this investigation can be found in Feaster and others (2014).

DESCRIPTION OF STUDY AREA

The study area includes all of Georgia, South Carolina, and North Carolina with the exception of the Blue Ridge ecoregion, which lacks a sufficient number of urban streamgages to allow for a regional regression analysis, and the tidally influenced regions of the Coastal Plain. Georgia, South Carolina, and North Carolina encompass seven U.S. Environmental Protection Agency (USEPA) level III ecoregions—Southwestern Appalachians, Blue Ridge, Ridge and Valley, Piedmont, Southeastern Plains, Southern Coastal Plain, and Middle Atlantic Coastal Plain (fig. 1; U.S. Environmental Protection Agency, 2007a). The ecoregions represent areas of general similarity in ecosystems and in the type, quality, and quantity of environmental resources. The ecoregions provide a spatial framework for the research, assessment, management, and monitoring of ecosystems and ecosystem components. The ecoregions were determined from an analysis of the spatial patterns and the composition of biotic and abiotic phenomena that include geology, physiography, vegetation, climate, soils, land use, wildlife, and hydrology (Griffith and others, 2002). The Fall Line separates the higher elevation Southwestern Appalachians, Blue Ridge, Ridge and Valley, and Piedmont ecoregions from the low-lying Southeastern Plains, Southern Coastal Plain, and Middle Atlantic Coastal Plain ecoregions.

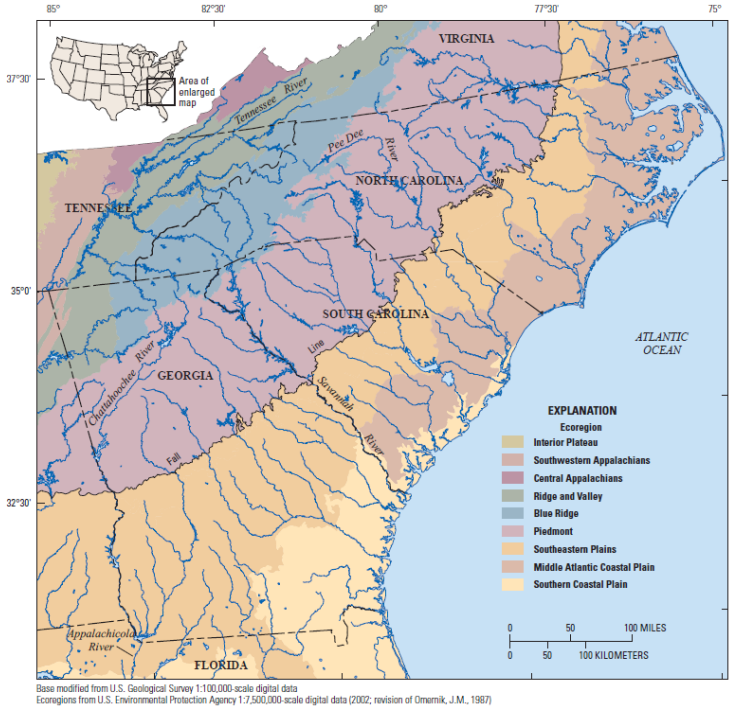

Figure 1 Study area and ecoregions in Georgia, South Carolina, North Carolina, and surrounding States.

DATA COMPILATION

For this investigation, urban and small, rural streamgages with 10 or more years of annual peak-flow record were considered for inclusion in the analysis. Additional rural flood-frequency data included in the study were based on a subset of the stations previously included in the Southeast rural flood-frequency investigation by Gotvald and others (2009), Weaver and others (2009), and Feaster and others (2009), which included annual peak-flow data for rural stations through water year 2006. Generally, the data from those studies selected for inclusion in the current study were based on the upper limits of the drainage area size for the urban streamgages. This was done to maintain some level of uniformity with respect to the range of drainage area sizes for the urban and rural basins. In the Sand Hills, which has the fewest number of streamgages in the hydrologic regions analyzed, all of the streamgages from the Southeast rural flood-frequency investigation were included.

After compiling the peak-flow data for the urban stations, quality assurance and quality control (QAQC) methods were used to assess homogeneity of the annual peak-flow data for the period being analyzed and to assess other potential issues. The QAQC methods used to review the rural streamgages previously included in the Southeast rural flood-frequency study can be found in the reports by Gotvald and others (2009), Weaver and others (2009), and Feaster and others (2009). Similar QAQC methods also were used for the urban streamgages included in this investigation. Kendall's tau was chosen to assess the significance of temporal trends in the peak-flow record for each streamgage (Helsel and Hirsch, 1992). For the urban streamgages in South Carolina and North Carolina, historical aerial photographs from Google Earth were reviewed to assess stable periods of urbanization. Along with the aerial photographs, plots of the annual peak flows also were reviewed. If the Kendall's tau analysis indicated a trend, all of the available information was used to determine whether there was a sufficient period of record available that indicated a relatively stable period of urbanization. If so, that period of record was used in the at-site flood-frequency analysis. Otherwise, the station was excluded from the analysis. For the Georgia urban stations, Gotvald and Knaak (2011) also reviewed historical information to determine periods of relatively stable urbanization.

Peak-Flow Data: Streamgages were used in the analysis only if 10 or more years of annual peak-flow data were available and if peak flows at the streamgages were not affected substantially by dam regulation, flood-retarding reservoirs, channelization, or tides. Based on results from the QAQC reviews, peak-flow data from 340 rural stations, of which 336 were previously published as part of the USGS Southeast rural flood-frequency investigation, 32 small, rural stations, and 116 urban stations were included in the analysis (fig. 2).

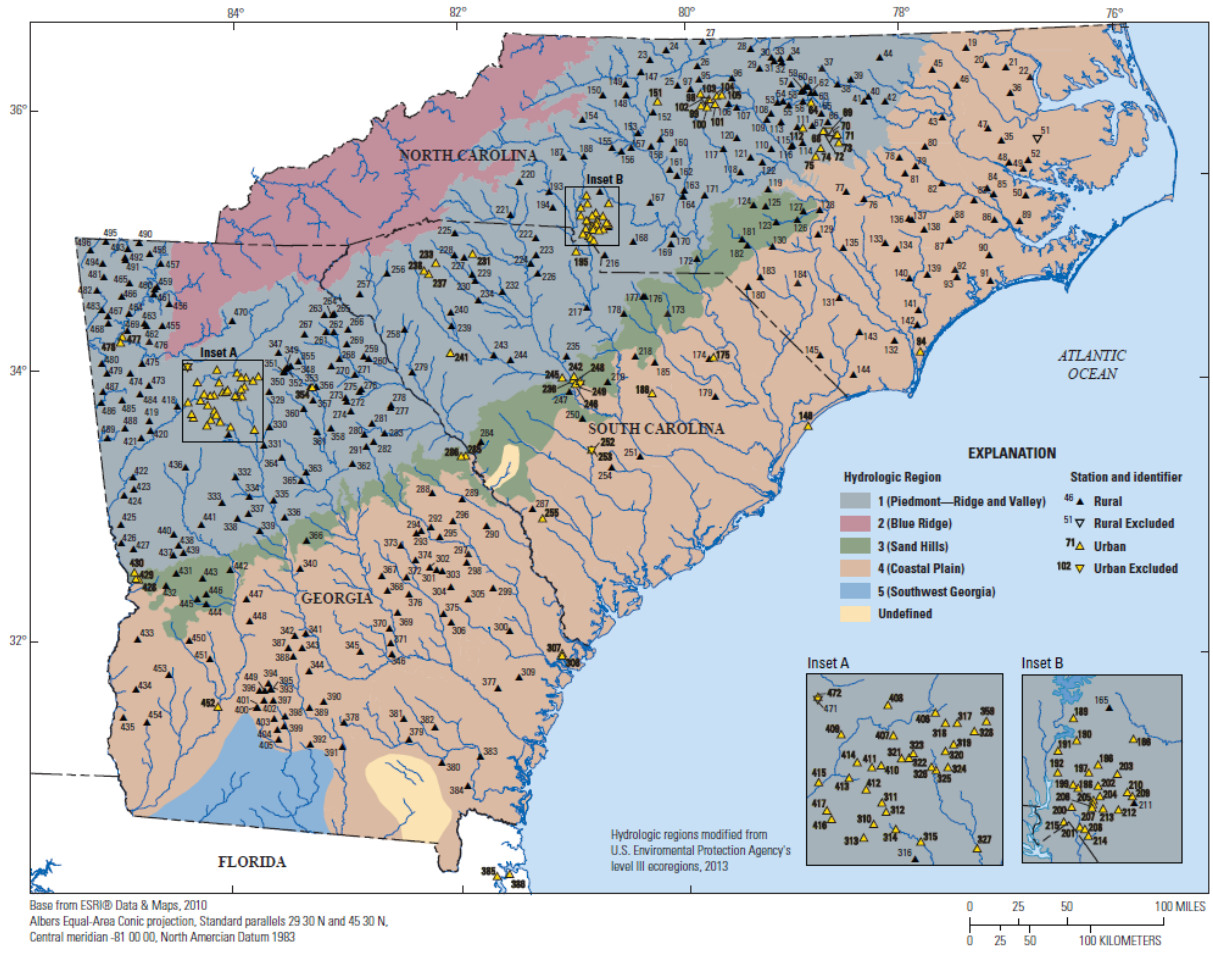

Figure 2 Locations of hydrologic regions and U.S. Geological Survey streamgages with 10 or more years of record that were included in the Southeast regional-regression analysis for urban and small, rural streams.

In an effort to increase the range of drainage basin area for the urban streamgages in the Coastal Plain, USGS flood-frequency reports from other States along the Atlantic Coastal Plain (fig. 3) were reviewed in an effort to find additional urban streamgages to include in the regression analysis. In order to verify that the Coastal Plain flood-frequency characteristics were similar to those in Georgia, South Carolina, and North Carolina, the published 1-percent annual exceedance probability (AEP) flows for rural basins in Virginia (Austin and others, 2011), Maryland (Ries and Dillow, 2006), Delaware (Ries and Dillow, 2006), and New Jersey (Watson and Schopp, 2009) were graphically compared with published 1-percent AEP flows from the Southeast rural flood-frequency study (Feaster and others, 2009; fig. 4A and 4B). As shown in figure 4B, the New Jersey inner Coastal Plain (ICP) 1-percent AEP flows are well within the dataset of the Southeast Coastal Plain streamgages whereas the New Jersey outer Coastal Plain data fall either below or on the lower edge of the Southeast data as do much of the Delaware Coastal Plain data. The Virginia and Maryland Coastal Plain data also plot well within the Southeast Coastal Plain data. Because the New Jersey ICP rural data were comparable to the Southeast rural Coastal Plain data, it was concluded that the urban streamgages from the Coastal

Plain in Virginia and Maryland as well as the New Jersey ICP would be appropriate to include in the Southeast urban flood-frequency analysis. This conclusion assumes that with respect to streamflow, the effect of urbanization in the Virginia, Maryland, and the New Jersey ICP is similar to that in the Southeast Coastal Plain. From a review of previously published peak-flow data for urban streamgages in the Coastal Plain regions of Virginia, Maryland, and the New Jersey ICP, it was determined that only New Jersey had sufficient measured urban peak-flow data that could be included in the Southeast study. Similar QAQC reviews were done for the New Jersey ICP urban streamgages as were done for the Southeast urban streamgages. Consequently, peak-flow data from 16 urban and 2 rural stations from the New Jersey ICP also were included in the analysis. Incorporation of urban streamgages from the New Jersey ICP allowed for an increase in the range of drainage area size from 2.1 to 53.5 mi^2 for which the predictive equations for the Southeast Coastal Plain are applicable.

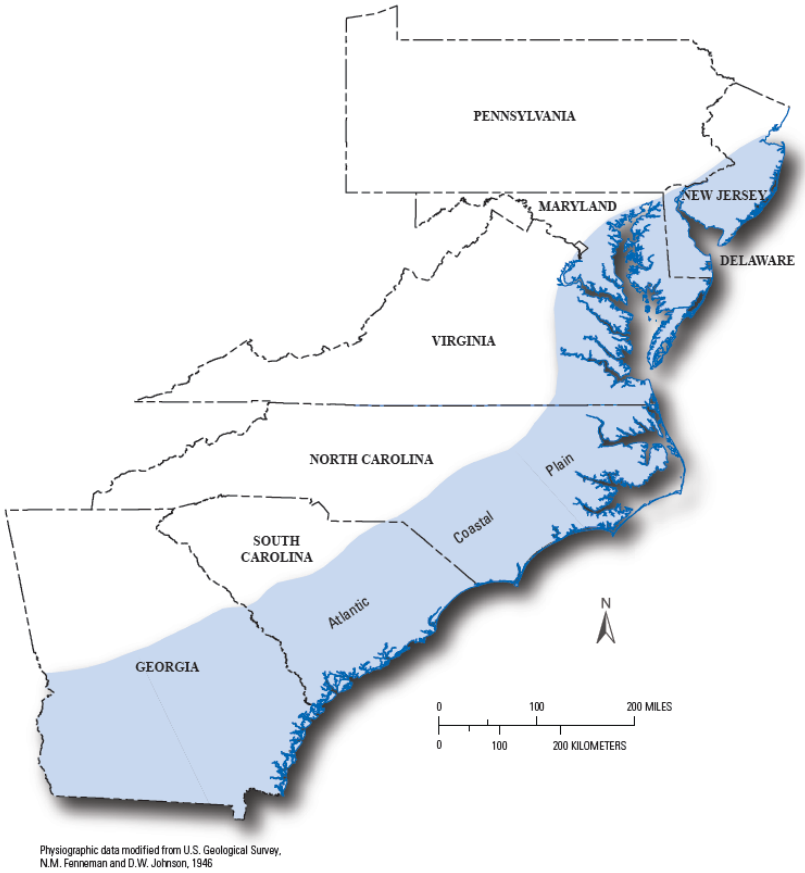

Figure 3 The Atlantic Coastal Plain from Georgia to New Jersey.

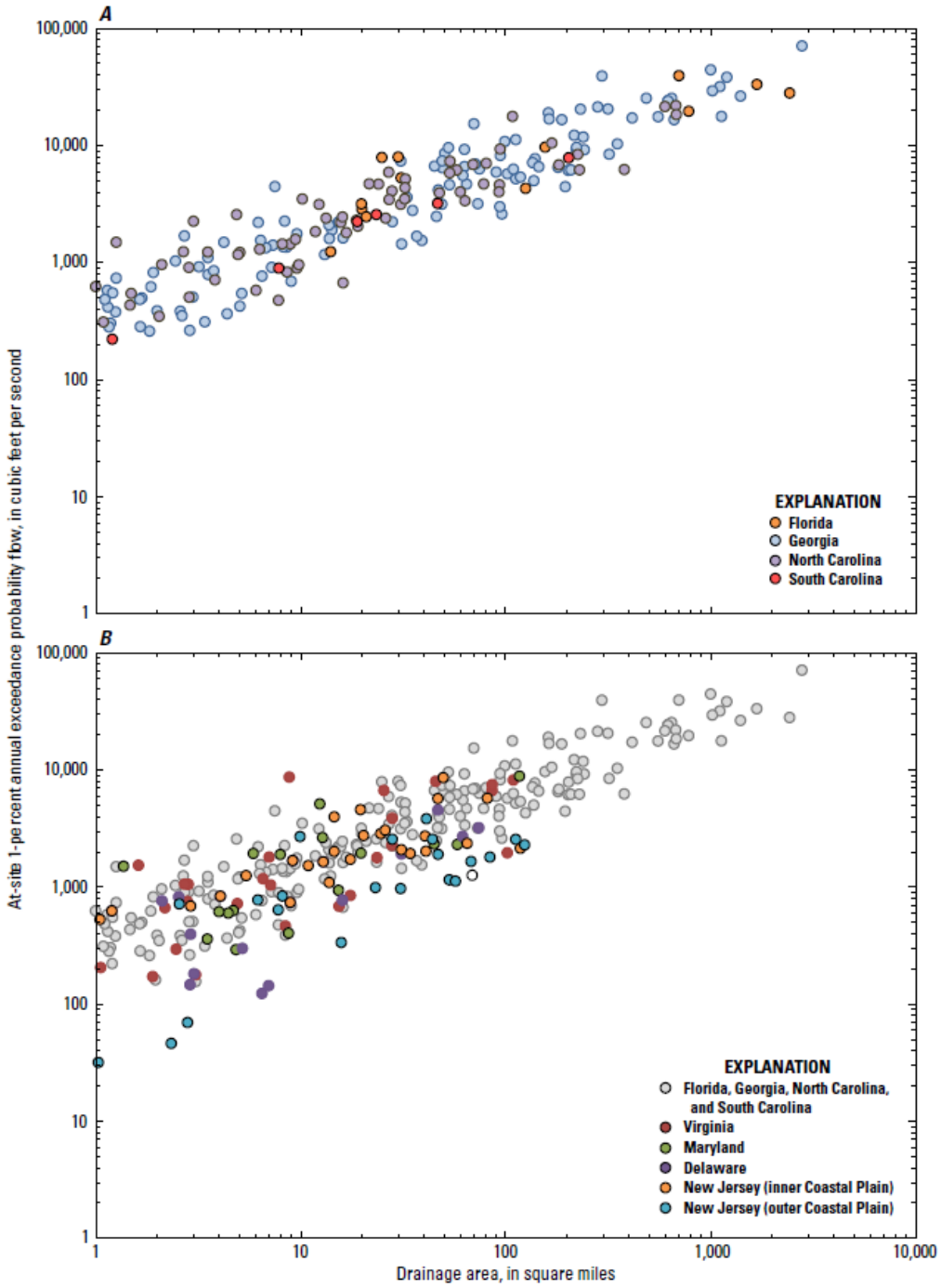

Figure 4 At-site 1-percent annual exceedance probability flow and drainage area for (A) U.S. Geological Survey rural streamflow-gaging stations (streamgages) in Florida, Georgia, South Carolina, and North Carolina that were included in the Southeast rural flood-frequency investigation (Feaster and others, 2009) and (B) rural streamgages from Virginia, Maryland, Delaware, and New Jersey (Austin and others, 2011; Ries and Dillow, 2006; and Watson and Schopp, 2009).

Physical and Climatic Basin Characteristics: The frequency and magnitude of floods can be estimated at ungaged sites through multiple regression analysis, which relates streamflow characteristics such as the 1-percent AEP flow, (also often referred to as the 100-year flood), to selected physical and climatic basin characteristics for gaged drainage basins. Physical and climatic basin characteristics were selected for use as potential explanatory variables in the regression analyses on the basis of the conceptual relation to flood flows and the ability to measure the basin characteristics using digital datasets and Geographic Information System (GIS) technology. The following 23 basin characteristics were determined for each streamgage included in the analysis: drainage area, main channel length, basin perimeter, main channel slope, mean basin slope, basin shape factor, mean basin elevation, maximum basin elevation, minimum basin elevation, percentage of impervious area, percentage of developed land, percentage of forested land, percentage of storage, mean annual precipitation, maximum 24-hour precipitation with recurrence intervals of 2-, 10-, 25-, 50-, and 100-years, soil drainage index, hydrologic soil index, drainage density, and population density.

FLOOD-FREQUENCY ANALYSIS AT URBAN AND SMALL, RURAL STREAMGAGES

A frequency analysis of annual peak-flow data at a streamgage provides an estimate of the flood magnitude and frequency for that specific stream site. Flood-frequency estimates for streamgages are computed by fitting the series of annual peak flows to a known statistical distribution. Flood-frequency estimates for streamgages included in this study were computed by fitting logarithms (base 10) of the annual peak flows to a Pearson Type III distribution. This method follows the guidelines and computational methods described in Bulletin 17B of the Hydrology Subcommittee of the Interagency Advisory Committee on Water Data (1982), which has been the standard methodology for flod-frequency analysis in the United States since 1981. However, the authors of Bulletin 17B noted that the guide was designed to *"...meet a current, ever-pressing demand that the Federal Government develop a coherent set of procedures for accurately defining flood potentials..."* but that additional studies were needed to address a number of items identified in Bulletin 17B as "Future Studies". On the basis of studies made in response to those recommendations, adoption of the expected moments algorithm (EMA) is among the changes that have been suggested (Cohn and others, 1997, 2001; Tim Cohn, U.S. Geological Survey, written commun., September 27, 2012) and are starting to be applied in USGS flood-frequency studies (Gotvald and others, 2012; Zarriello and others, 2012; Kessler and others, 2013). The flood-frequency estimates for the urban streamgages were completed using a modified version of the methods described in Bulletin 17B, by including the EMA, which allows for a more generalized approach to representing observed annual peak-flow information by using an interval range as compared to the conventional method of using point data (Cohn and others, 1997). In addition, a generalized Grubbs-Becks test, which allows for the detection of multiple potentially influential low outliers (Cohn and others, 2013), also was used.

For the rural streamgages in Georgia, South Carolina, and North Carolina, the flood-frequency estimates were obtained from those previously published in the Southeast rural flood-frequency investigation (Feaster and others, 2009; Gotvald and others, 2009; Weaver and others, 2009). In addition, the flood-frequency estimates for the Georgia urban and small, rural streamgages

included in Gotvald and Knaak (2011) were updated by including additional data collected through September 2011. Updating the flood-frequency analyses for the Georgia urban and small, rural streamgages allowed for the inclusion of the historic floods that occurred in northern Georgia during September 2009 (McCallum and Gotvald, 2010). For the streamgages included from the New Jersey inner Coastal Plain, the flood-frequency estimates were updated in consultation with USGS New Jersey Water Science Center hydrologists and also included peak-flow data through September 2011.

ESTIMATION OF FLOOD MAGNITUDE AND FREQUENCY AT UNGAGED URBAN AND SMALL, RURAL SITES

A regional regression analysis was used to develop a set of equations for use in estimating the magnitude and frequency of floods for ungaged urban and small, rural sites in Georgia, South Carolina, and North Carolina. These equations relate the 50-, 20-, 10-, 4-, 2-, 1-, 0.5-, and 0.2-percent AEP flows (also referred to as the 2-, 5-, 10-, 25-, 50-, 100-, 200-, and 500-year recurrence interval flows) computed from available peak-flow records for streamgages to measured physical and climatic basin characteristics of the associated drainage basins. For the initial analysis, the upper limit for the drainage area of the rural streamgages included in the regression analysis was established based on the upper limit of the drainage area for the urban streamgages in each hydrologic region (HR; fig. 2) so that reasonable representation of basin characteristics for both urban and rural streamgages would be included in the analysis. Additionally, only the Southeast rural streamgages that drained 100 percent from a single HR were included in the regression analysis (all the urban streamgages drained 100 percent from individual HRs). Some of the benefits of including urban and rural streamgages together in the regression analysis are (1) smoother transition between urban and rural flood-frequency estimates, (2) larger database than would be available with urban streamgages alone, and (3) larger geographical coverage in the HRs, which will represent a broader range of hydrologic conditions likely to occur at ungaged locations (fig. 2).

Regression Analysis: Selection of the explanatory variables for each hydrologic region was based on all-possible-subsets (APS) regression methods (Neter and others, 1985). The final explanatory variables for each hydrologic region were selected on the basis of several factors, including standard error of the estimate, Mallow's *Cp* statistic, statistical significance of the explanatory variables, coefficient of determination (r^2), and ease of measurement of explanatory variables. Multicollinearity, a situation in which two or more explanatory variables in a multiple regression model are highly correlated, in the candidate exploratory variables also was assessed by the variance inflation factor (VIF) and the correlation between explanatory variables. Generalized least-squares regression methods, as described by Stedinger and Tasker (1985), were used to determine the final regional P-percent chance exceedance flow regression equations, using the USGS computer program GLSNET (Tasker and Stedinger, 1989; G.D. Tasker, K.M. Flynn, A.M. Lumb, and W.O. Thomas, Jr., U.S. Geological Survey, written commun., 1995). As was done for the rural streamgages included in the Southeast rural flood-frequency investigation by Gotvald and others (2009), Weaver and others (2009) and Feaster and others (2009), the urban streamgages were assessed for redundancy. Redundancy occurs when the drainage basins of two streamgages are nested, which is when one basin is contained inside the other basin and most or all of the peak-flow data at the two streamgages are concurrent. In

order to remove the redundancy from the GLS regression analysis associated with streamgages that represent the same basin, two streamgages on the same stream where the percentage change in drainage area from one station to the second was within 50 percent were considered redundant pair streamgages. If the peak-flow record of the station with the shorter period of record was predominantly captured within the record of the station with the longer period of record and the urbanization characteristics of the two streamgages were relatively similar, the station with the shorter period of record was omitted from the analysis. Based on that criteria, three streamgages were excluded from the regional regression analysis due to redundancy.

Generalized least squares (GLS) regression methods, as described by Stedinger and Tasker (1985), were used to determine the final regional regression equations with the use of the weighted-multiple-linear regression (WREG) program version 1.06 (Julie Kiang, U.S. Geological Survey, written commun., May 2013; Eng and others, 2009). The GLS regression analysis included flood-frequency estimates generated for 488 USGS streamgages: 340 rural; 32 small, rural; and 116 urban. The regional-regression analysis resulted in predictive equations that can be used to estimate the 50-, 20-, 10-, 4-, 2-, 1-, 0.5-, and 0.2-percent AEP flows at urban and small, rural ungaged locations in the Southeast (table 1). Explanatory variables included in the equations are as follows: HR1, drainage area (DA) and percentage of impervious area (IA); HR3, DA and percentage of developed land; and HR4, DA, IA, and the 24-hour, 50-year maximum precipitation (fig. 2, table 1). Average standard error of prediction for the predictive equations, which is a measure of the average accuracy of the regression equations when predicting flood estimates for ungaged sites, ranged from 25 percent for the 10-percent AEP regression equation for the Piedmont--Ridge and Valley region to 73 percent for the 0.2-percent AEP regression equation for the Sand Hills region. An application spreadsheet also was developed that can be used to compute the flood-frequency estimates along with the 95-percent prediction intervals for an ungaged location and is available at http://pubs.usgs.gov/sir/2014/5030/.

Table 1. Regional flood-frequency equations for ungaged urban and small, rural streams in Georgia, South Carolina, and North Carolina

[mi^2, square miles; DRNAREA, drainage area, mi^2; IMPNLCD06, percentage of impervious area from the 2006 National Land Cover Dataset, in percent; DEVNLCD06, percentage of developed land from the 2006 National Land Cover Dataset; I24H50Y, 24-hour, 50-year maximum precipitation, in inches]

Percent annual exceedance probability	Hydrologic Region (shown in fig. 1)		
	1		3
	0.10 mi^2≤DRNAREA≤3mi^2	**3 mi^2<DRNAREA≤436 mi^2**	**0.22 mi^2≤DRNAREA≤459 mi^2**
50	$163(DRNAREA)^{0.7089}10^{(0.0133*IMPNLCD06)}$	$198(DRNAREA)^{0.5735}10^{(0.0101*IMPNLCD06)}$	$30.0(DRNAREA)^{0.6605}10^{(0.0122*DEVNLCD06)}$
20	$284(DRNAREA)^{0.7351}10^{(0.0096*IMPNLCD06)}$	$359(DRNAREA)^{0.5605}10^{(0.0074*IMPNLCD06)}$	$51.4(DRNAREA)^{0.6535}10^{(0.0109*DEVNLCD06)}$
10	$381(DRNAREA)^{0.7536}10^{(0.0076*IMPNLCD06)}$	$484(DRNAREA)^{0.5539}10^{(0.0060*IMPNLCD06)}$	$68.4(DRNAREA)^{0.6507}10^{(0.0102*DEVNLCD06)}$
4	$518(DRNAREA)^{0.7752}10^{(0.0053*IMPNLCD06)}$	$657(DRNAREA)^{0.5470}10^{(0.0046*IMPNLCD06)}$	$93.3(DRNAREA)^{0.6472}10^{(0.0095*DEVNLCD06)}$
2	$632(DRNAREA)^{0.7903}10^{(0.0037*IMPNLCD06)}$	$794(DRNAREA)^{0.5428}10^{(0.0037*IMPNLCD06)}$	$114(DRNAREA)^{0.6451}10^{(0.0090*DEVNLCD06)}$
1	$753(DRNAREA)^{0.8038}10^{(0.0024*IMPNLCD06)}$	$941(DRNAREA)^{0.5386}10^{(0.0028*IMPNLCD06)}$	$138(DRNAREA)^{0.6430}10^{(0.0086*DEVNLCD06)}$
0.5	$884(DRNAREA)^{0.8181}10^{(0.0011*IMPNLCD06)}$	$1096(DRNAREA)^{0.5351}10^{(0.0021*IMPNLCD06)}$	$163(DRNAREA)^{0.6413}10^{(0.0082*DEVNLCD06)}$
0.2	$1045(DRNAREA)^{0.8160}$	$1319(DRNAREA)^{0.5305}10^{(0.0011*IMPNLCD06)}$	$201(DRNAREA)^{0.6386}10^{(0.0077*DEVNLCD06)}$

Percent annual exceedance probability	Hydrologic Region (shown in fig. 1)	
	4	*5
	0.10 mi^2≤DRNAREA≤53.5mi^2	**0.20 mi^2<DRNAREA≤10 mi^2**
50	$26.3(DRNAREA)^{0.5908}10^{(0.0173*IMPNLCD06)}10^{(0.0515*I24H50Y)}$	$165(DRNAREA)^{0.537}$
20	$40.6(DRNAREA)^{0.5958}10^{(0.0125*IMPNLCD06)}10^{(0.0623*I24H50Y)}$	$265(DRNAREA)^{0.583}$
10	$51.8(DRNAREA)^{0.6004}10^{(0.0101*IMPNLCD06)}10^{(0.0666*I24H50Y)}$	$349(DRNAREA)^{0.600}$
4	$67.1(DRNAREA)^{0.6067}10^{(0.0075*IMPNLCD06)}10^{(0.0708*I24H50Y)}$	$473(DRNAREA)^{0.615}$
2	$78.4(DRNAREA)^{0.6111}10^{(0.0058*IMPNLCD06)}10^{(0.0738*I24H50Y)}$	$574(DRNAREA)^{0.624}$
1	$90.5(DRNAREA)^{0.6154}10^{(0.0043*IMPNLCD06)}10^{(0.0762*I24H50Y)}$	$684(DRNAREA)^{0.632}$
0.5	$103(DRNAREA)^{0.6201}10^{(0.0029*IMPNLCD06)}10^{(0.0785*I24H50Y)}$	$804(DRNAREA)^{0.639}$
0.2	$119(DRNAREA)^{0.6261}10^{(0.0012*IMPNLCD06)}10^{(0.0813*I24H50Y)}$	$971(DRNAREA)^{0.649}$

*From Gotvald and Knaak, 2011.

SUMMARY

This paper presents methods for determining the magnitude and frequency of floods at urban and small, rural streams in the Southeast United States, which for this investigation includes Georgia, South Carolina, and North Carolina. The regional regression analysis for the investigation includes at-site flood-frequency estimates for 488 streamgages: 340 rural; 32 small, rural; and 116 urban. The at-site flood-frequency analyses for 336 of the 340 rural streamgages were previously published as part of a U.S. Geological Survey (USGS) Southeast rural flood-frequency investigation, which included annual peak-flow data through water year 2006. The at-site flood-frequency analyses for the remaining 152 urban, rural, and small, rural streamgages were completed using annual peak-flow data through water year 2011 and was done using a modified version of the Bulletin 17B procedures by including the expected moments algorithm and a generalized Grubbs-Becks test that allows for the detection of multiple potentially influential low outliers.

In order to expand the range of the drainage area sizes for which the Coastal Plain regression equations would be applicable, 16 urban and 2 rural streamgages were included from the inner Coastal Plain of New Jersey. Analyses comparing rural flood-frequency estimates for streamgages in Virginia, Maryland, Delaware, and New Jersey with streamgages included in the Southeast rural flood-frequency investigation indicated that the 1-percent chance annual exceedance probability (AEP) flows from Virginia, Maryland, and the inner Coastal Plain of New Jersey respond similarly to the 1-percent AEP flows from the Southeast. Consequently, it seemed reasonable to assume that the 1-percent AEP flows from the urban basins in these States also would have characteristics similar to urban basins in the Southeast. However, only the inner Coastal Plain of New Jersey had streamgages with sufficient measured annual peak-flow data to be included in the regression analysis. Including the New Jersey urban streamgages allowed the upper range of the applicable drainage area size for the urban streamgage regression equations to be increased from 2.1 to 53.5 square miles.

The regional regression analysis was completed using generalized least squares regression. The regional-regression analysis resulted in predictive equations that can be used to estimate the 50-, 20-, 10-, 4-, 2-, 1-, 0.5-, and 0.2-percent AEP flows (also referred to as the 2-, 5-, 10-, 25-, 50-, 100-, 200-, and 500-year recurrence interval flows) at urban and small, rural ungaged locations in three hydrologic regions (HR) of South Carolina, North Carolina, and Georgia: HR1, Piedmont--Ridge and Valley; HR3, Sand Hills; and HR4, Coastal Plain. In addition, similar predictive equations for urban and small, rural ungaged locations in HR5, Southwest Georgia, which were published in 2011 in a USGS flood-frequency investigation of urban and small, rural basins in Georgia, were included in this report. There was not a sufficient number of urban streamgages from the Blue Ridge region to allow for generation of urban and small, rural predictive equations. Average standard error of prediction for the predictive equations, which is a measure of the average accuracy of the regression equations when predicting flood estimates for ungaged sites, range from 25.0 percent for the 10-percent AEP regression equation for the Piedmont--Ridge and Valley region to 73.3 percent for the 0.2-percent AEP regression equation for the Sand Hills region.

REFERENCES

Austin, S.H., Krstolic, J.L., and Wiegand, Ute, 2011, Peak-flow characteristics of Virginia streams: U.S. Geological Survey Scientific Investigations Report 2011-5144, 106 p. +3 tables and 2 appendices on CD.

Cohn, T.A., England, J.F., Berenbrock, C.E., Mason, R.R., Stedinger, J.R., and Lamontagne, J.R., 2013, A generalized Grubbs-Beck test statistic for detecting multiple potentially-influential low outliers in flood series: Water Resources Research, v. 49, no. 8, p. 5047-5058, doi: 10.1002/wrcr.20392.

Cohn, T.A., Lane, W.L., and Baier, W.G., 1997, An algorithm for computing moments-based flood quantile estimates when historical flood information is available: Water Resources Research, v. 33, no. 9, p. 2089-2096.

Cohn, T.A., Lane, W.L., and Stedinger, J.R., 2001, Confidence intervals for Expected Moments Algorithm flood quantile estimates: Water Resources Research, v. 37, no. 6, p. 1695–1706.

Feaster, T.D., Gotvald, A.J., and Weaver, J.C., 2014, Methods for estimating the magnitude and frequency of floods for urban and small, rural streams in Georgia, South Carolina, and North Carolina, 2011 (ver. 1.1, March 2014): U.S. Geological Survey Scientific Investigations Report 2014-5030, 104 p., available online at http://pubs.usgs.gov/sir/2014/5030/.

Feaster, T.D., Gotvald, A.J., and Weaver, J.C., 2009, Magnitude and frequency of rural floods in the southeastern United States, 2006—Volume 3, South Carolina: U.S. Geological Survey Scientific Investigations Report 2009-5156, 226 p., available online at http://pubs.usgs.gov/sir/2009/5156/

Gotvald, A.J., Barth, N.A., Veilleux, A.G., and Parrett, Charles, 2012, Methods for determining magnitude and frequency of floods in California, based on data through water year 2006: U.S. Geological Survey Scientific Investigations Report 2012-5113, 38 p., 1 pl., available online only at http://pubs.usgs.gov/sir/2012/5113/.

Gotvald, A.J., Feaster, T.D., and Weaver, J.C., 2009, Magnitude and frequency of rural floods in the southeastern United States, 2006—Volume 1, Georgia: U.S. Geological Survey Scientific Investigations Report 2009-5043, 120 p., available online at http://pubs.usgs.gov/sir/2009/5043/.

Gotvald, A.J, and Knaak, A.E., 2011, Magnitude and frequency of floods for urban and small rural streams in Georgia: U.S. Geological Survey Scientific Investigations Report 2011-5042, 39 p.

Griffith, G.E., Omernik, J.M., Comstock, J.A., Schafale, M.P., McNab, W.H., Lenat, D.R., MacPherson, T.F., Glover, J.B., and Shelburne, V.B., 2002, Ecoregions of North Carolina and South Carolina: U.S. Geological Survey color poster with map, scale 1:1,500,00.

Gruber, A.M., Reis, D.S., and Stedinger, J.R., 2007, Models of regional skew based on Bayesian GLS Regression, *in* Kabbes, K.C., ed., World Environmental & Water Resources Conference—Restoring our Natural Habitat, Paper 40927-3285, May 15–18, 2007, Tampa, Florida.

Helsel, D.R., and Hirsch, R.M., 1992, Statistical methods in water resources: New York, Elsevier, p. 326.

Interagency Advisory Committee on Water Data, 1982, Guidelines for determining flood flow frequency: Bulletin 17B of the Hydrology Subcommittee, U.S. Geological Survey, Office of Water Data Coordination, 28 p., 14 app., 1 pl.

Kessler, E.W., Lorenz, D.L., and Sanocki, C.A., 2013, Methods and results of peak-flow frequency analyses for streamgages in and bordering Minnesota, through water year 2011: U.S. Geological Survey Investigations Report 2013-5110, 43 p., http://pubs.usgs.gov/sir/2013/5110/.

Martins, E.S., and Stedinger, J.R., 2002, Cross-correlation among estimators of shape: Water Resources Research, v. 38, no. 11, 7 p.

McCallum, B.E., and Gotvald, A.J., 2010, Historic flooding in northern Georgia, September 16-22, 2009: U.S. Geological Survey Fact Sheet 2010-3061, 4 p.

Neter, J., Wasserman, W., and Kutner, M.H., 1985, Applied linear statistical models: Homewood, IL, Richard D. Irwin, 1127 p.

Ries, K.G., III, and Dillow, J.J.A., 2006, Magnitude and frequency of floods on nontidal streams in Delaware: U.S. Geological Survey Scientific Investigations Report 2006-5146, 59 p.

Reis, D.S., Jr., Stedinger, J.R., and Martins, E.S., 2005, Bayesian generalized least squares regression with application to log Pearson type 3 regional skew estimation: Water Resources Research, v. 41, W10419.

Stedinger, J.R., and Tasker, G.D., 1985, Regional hydrologic analysis, 1, ordinary, weighted and generalized least squares compared: Water Resources Research, v. 21, no. 9, p. 1421–1432 [with correction in Stedinger and Tasker, 1986, Water Resources Research, v. 22, no. 5, p. 844].

Tasker, G.D., and Stedinger, J.R., 1989, An operational GLS model for hydrologic regression: Journal of Hydrology, v. 111, p. 361–375.

U.S. Environmental Protection Agency, 2007, Level 3 ecoregions of the United States, accessed July 24, 2008 at http://www.epa.gov/bioindicators/html/lv3-eco.html

Watson, K.M., and Schopp, R.D., 2009, Methodology for estimation of flood magnitude and frequency for New Jersey streams: U.S. Geological Survey Scientific Investigations Report 2009-5167, 51 p.

Weaver, J.C., Feaster, T.D., and Gotvald, A.J., 2009, Magnitude and frequency of rural floods in the southeastern United States, 2006—Volume 2, North Carolina: U.S. Geological Survey Scientific Investigations Report 2009-5043, 111 p., available online at http://pubs.usgs.gov/sir/2009/5158/.

Zarriello, P.J., Ahearn, E.A., and Levin, S.B., 2012, Magnitude of flood flows of selected annual exceedance probabilities in Rhode Island through 2010 (ver. 1.2, revised March 2013): U.S. Geological Survey Scientific Investigations Report 2012-5109, 81 p. (Also available at http://pubs.usgs.gov/sir/2012/5109.)

IMPACTS OF ARTIFICIAL SNOWMAKING ON THE HYDROLOGY OF A SMALL STREAM

Travis A. Dahl, Research Hydraulic Engineer, ERDC Coastal & Hydraulics Laboratory, Vicksburg, MS, Travis.A.Dahl@usace.army.mil; James P. Selegean, Hydraulic Engineer, USACE Detroit District, Detroit, MI,, James.P.Selegean@usace.army.mil

Abstract: Ski areas often turn to artificial snowmaking, in an effort to provide a consistent and desirable product for their customers. This additional snow increases the water that contributes to spring runoff events, but the magnitude of the impact is not always clear. In this paper, we will discuss the hydrologic impacts of artificial snowmaking on Knowlton Creek, a small (~5km^2) watershed in Duluth, MN. Spirit Mountain Recreation Authority (SMRA) is a ski area that occupies 5% of the watershed (~0.25km^2) and relies extensively on artificial snowmaking. Increasing the potential impact on hydrology, the entirety of the water used for artificial snowmaking at this site is imported from outside of the watershed. We will discuss the development of a Hydrologic Modeling System (HEC-HMS) model for the watershed that has been used to compare the impacts of the artificial snowmaking on both the winter snowpack of the watershed and the spring runoff. We will also compare the magnitude of these impacts to those of common design storms.

INTRODUCTION

Knowlton Creek is a tributary to the St. Louis River, which drains to Lake Superior through the St. Louis River and Duluth-Superior Harbor in Duluth, MN and Superior, WI. Large portions of the watershed are within the City of Duluth and the entire watershed is in St. Louis County. Figure 1 shows the location of the watershed.

There has been significant sedimentation at the mouth of Knowlton Creek, behind Tallas Island, since the early 1960s. The timeframe for the increased sedimentation roughly coincides with the opening of a ski area (Spirit Mountain Recreation Authority, SMRA) in the watershed and the use of artificial snowmaking for the ski runs. The snow at SMRA is produced using treated City of Duluth water that is brought in from outside of the Knowlton Creek watershed.

The Knowlton Creek watershed is 5 km^2 (1.94 miles^2), while an additional 1.1 km^2 (0.4 miles^2) contributes to the same area of the St. Louis River Estuary, immediately behind Tallas Island. The majority of the watershed is forested. The exceptions are the ski runs at SMRA and associated buildings and parking lots; the I-35 corridor; and some light residential areas scattered throughout the watershed. The ski runs at SMRA account for approximately 0.25 km^2 (0.10 miles^2) or 5.0% of the Knowlton Creek watershed and 0.33km^2 (0.13 miles^2) or 5.4% of the entire area contributing to the region behind Tallas Island. The Knowlton Creek watershed and the adjacent contributing watersheds are shown in Figure 2.

The topography of the watershed can be roughly split into three categories. The uppermost portions of the watershed consist of rolling hills. The middle section of the watershed, where the ski area is located, is very steep with some areas approaching 25% slopes. The lowest portions of the watershed are relatively flat. The maximum elevation difference from the top of the watershed to Tallas Island is 232.9 m. Soils consist primarily of glacial tills with areas of exposed bedrock along Knowlton Creek.

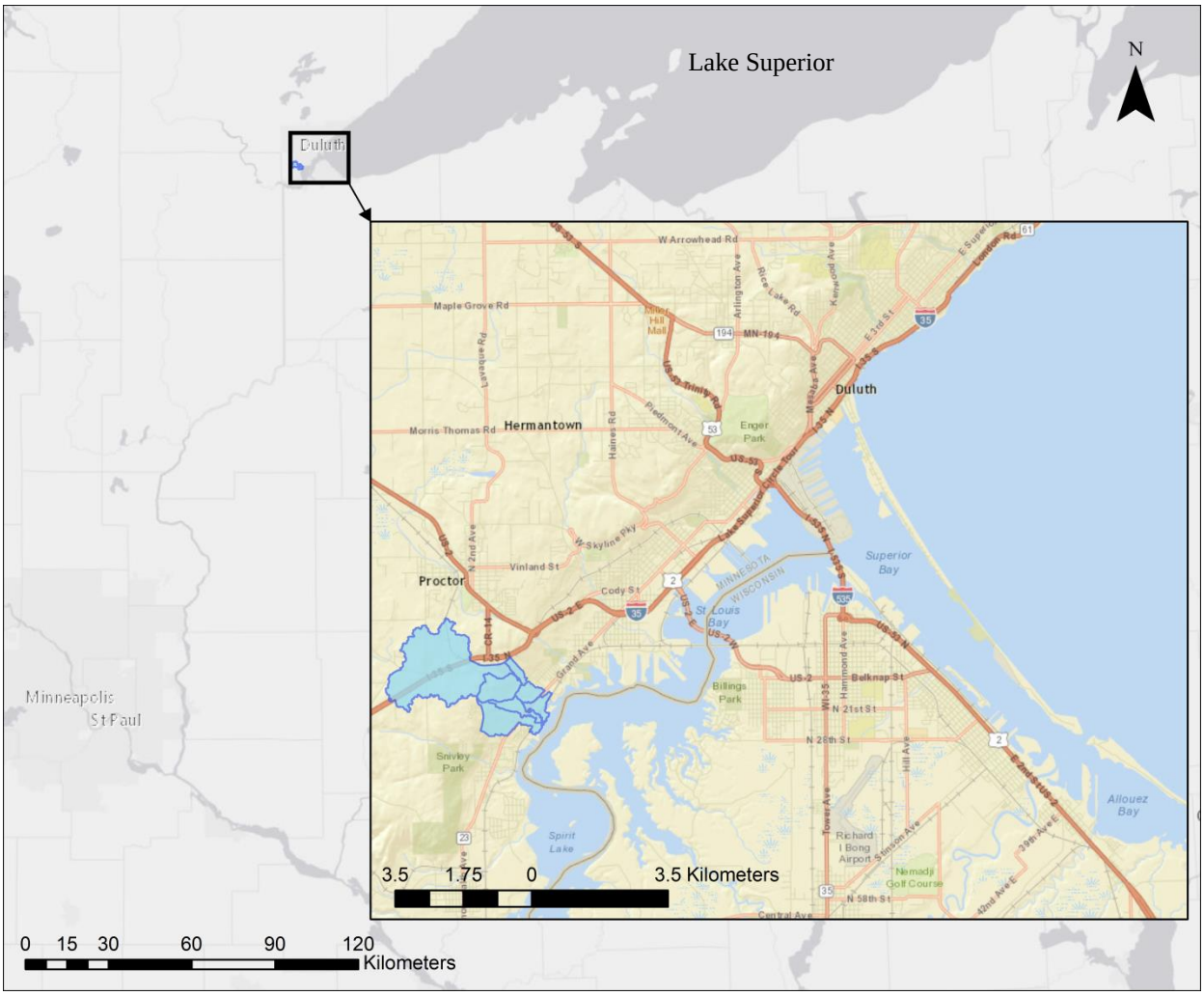

Figure 1 Location map of the Knowlton Creek watershed.

METHODS

In order to estimate the impacts of runoff and snowmaking activities, a hydrologic model was developed using the Hydrologic Engineering Center's Hydrologic Modeling System (HEC-HMS) Version 4.0 (Scharffenberg, 2013). HEC-HMS is a process-based, lumped parameter hydrology model designed to simulate rainfall-runoff processes.

Two cross-sections were surveyed on 4-Nov-2010 as part of a separate, regional bank erosion study. One of the cross-sections was located on the mainstem of Knowlton Creek and one on the eastern tributary. Onset Hobo water level loggers, model U20-001-04, were installed at both cross-sections on 3-Jun-2011 (Figure 2). An additional logger was attached to a tree in the floodplain, approximately 30 m upstream of the mainstem gage, to record atmospheric pressure. The loggers recorded at five minute intervals from 3-Jun-2011 to 17-Aug-2011 and 17-Oct-2011 to 4-Nov-2011. Data were logged at 15 minute intervals from 4-Nov-2011 to 8-Jun-2012. The stage and water temperature data are shown in Figure 3. Water level data between 2-Dec-2011 and 19-Mar-2012 were considered unreliable, since the measured water temperature was 0°C, indicating frozen water. Additionally, the total volume of streamflow estimated for the snowmelt event was greater

than the combined water that was used for snowmaking and the winter precipitation from the entire contributing area. This problem was likely due to the presence of snow and ice in the channel.

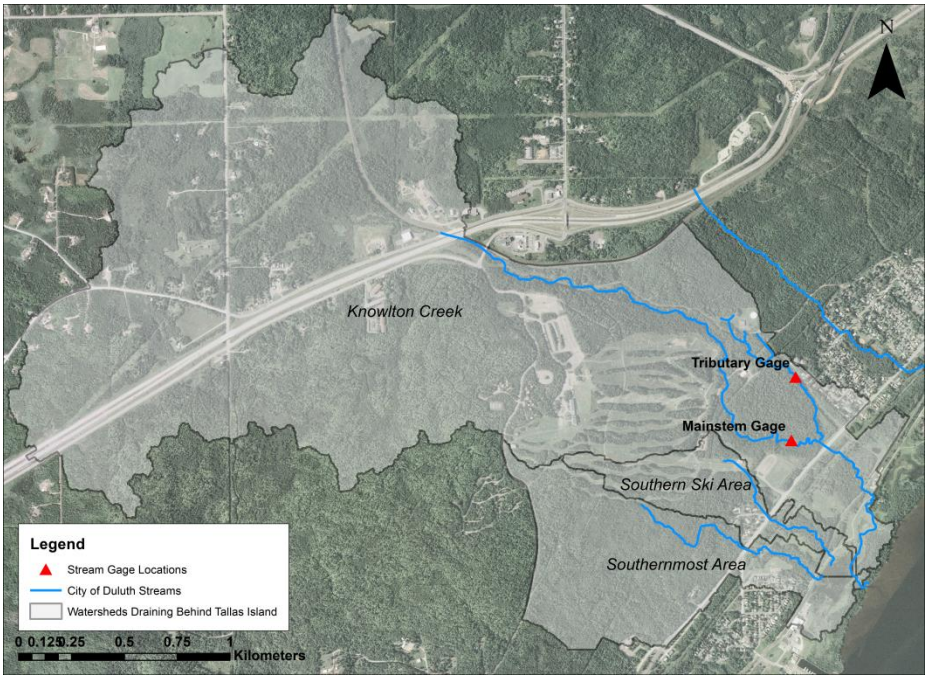

Figure 2 Aerial photo of Knowlton Creek and adjacent watersheds draining to the region behind Tallas Island. The largest watershed, to the north, is Knowlton Creek. The two watersheds on the south side of the aerial photo also drain portions of the Spirit Mountain ski area the same vicinity. The ski runs are visible as the East-West stripes in this picture. Stream gage locations are indicated by red triangles.

Flow measurements were made using a Sontek FlowTracker handheld ADV. Flows were measured on 17-Oct-2011, 19-Oct-2011, 4-Nov-2011, 7-Jun-2012, and 8-Jun-2012. Due to the small size of the watershed and the lead time necessary to reach the site, it was not possible to measure a high flow event. In order to convert the water levels to flows at each site, the collected data were used to estimate a roughness coefficient for Manning's Equation (Chow, 1959). Manning's Equation was then applied to the remainder of the water level data to generate a time series of streamflow. The resulting flows can be seen in Figure 4.

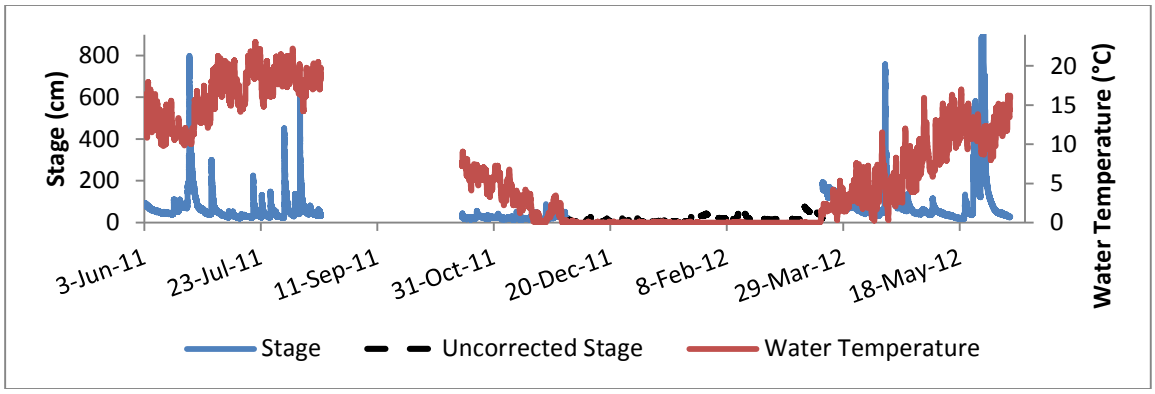

Figure 3 Stage and water temperature observations at the Knowlton Mainstem Gage. The uncorrected stage (black dashed line) indicates the portion of gage record that was not used due to concerns about its reliability.

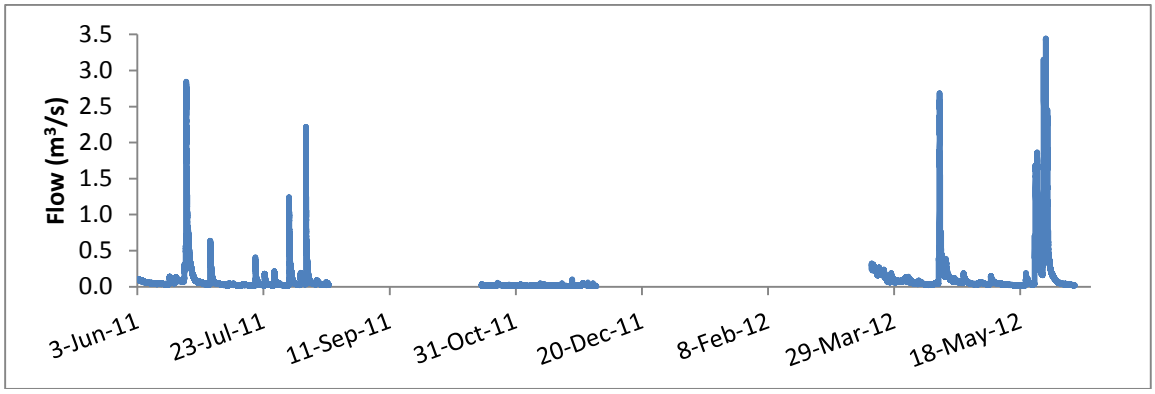

Figure 4 Flow at the Knowlton Mainstem Gage calculated from the level logger stage.

A number of data sets were collected for use in developing the HEC-HMS model. A high resolution LIDAR digital elevation model (DEM), collected in 2011, was obtained from the Minnesota Department of Natural Resources, as was a 2009 aerial photo. A shapefile of the stream network in and around Knowlton Creek was provided by the City of Duluth. SSURGO soils data were acquired from the U.S. Department of Agriculture.

In order to estimate the primary physical characteristics of the watershed, data were processed using the Geospatial Hydrologic Modeling Extension (GeoHMS, version 2010 EAP) for ArcGIS 10 (ESRI, 2011). The stream network from the City of Duluth was modified to include the section of stream extending up to the City of Cloquet pump station. This modified stream shapefile was then "burned" into the digital elevation model (DEM), in order to ensure that water would move along the known flowpaths. The DEM Reconditioning in GeoHMS was iterated several times in order to arrive at a stream network that matched the aerial photo data.

Several of the smaller subwatersheds were combined for modeling purposes. The final watershed map is shown in Figure 5 and the HMS schematic is displayed in Figure 6.

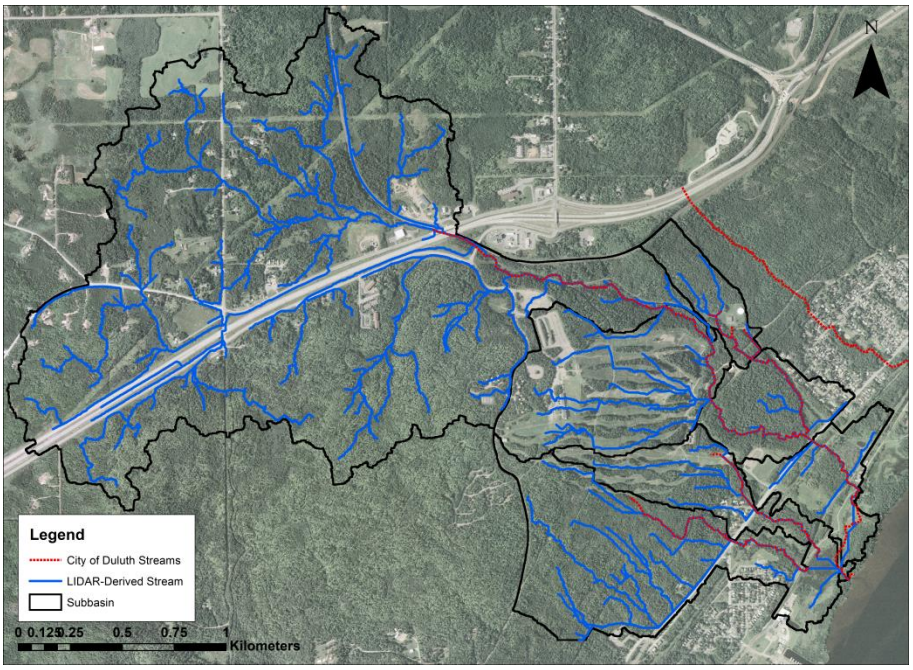

Figure 5 Modeled subwatersheds are outlined in black. The dashed red lines are the stream network provided by the City of Duluth. The blue lines indicate the LIDAR-derived stream network.

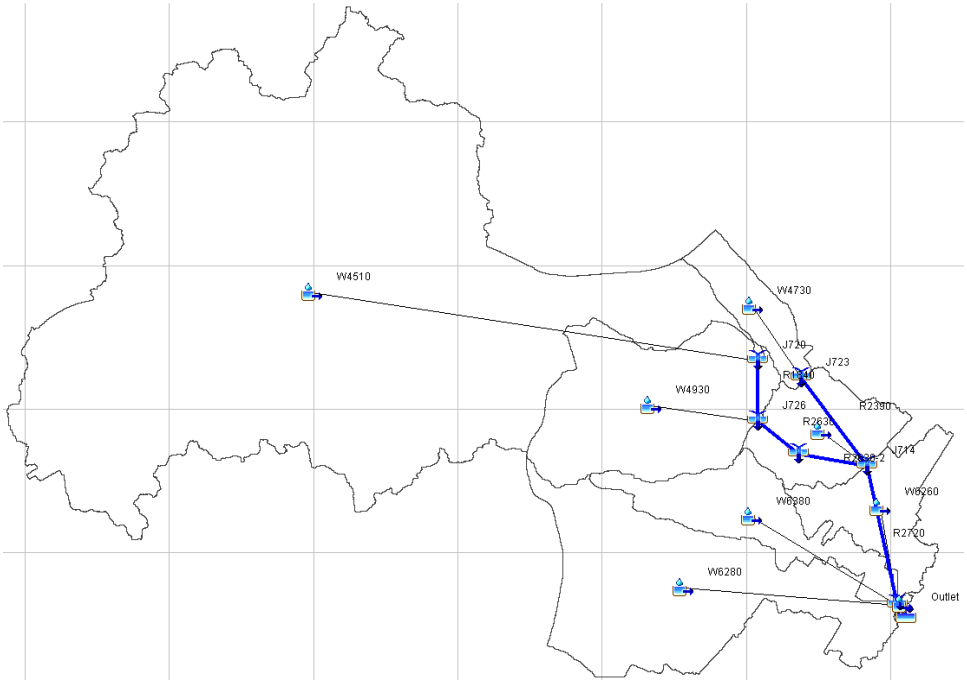

Figure 6 Schematic of the HMS model showing the relation to the modeled subwatersheds.

Precipitation and temperature data were obtained from the National Climatic Data Center (NCDC) for both Duluth International Airport (Duluth, MN) and Richard I. Bong Airport (Superior, WI). In conversations, Spirit Mountain personnel indicated that the precipitation measured at Duluth International Airport tends to be much higher than what is received at the ski area. It was decided to use the precipitation data from the Richard I. Bong Airport for the entire watershed.

HMS subwatersheds were set up with the Soil Moisture Accounting loss method. Clark Unit Hydrograph was chosen as the transform method to calculate runoff timing. The Simple Canopy and Simple Surface methods were also used. Baseflow was set to the Linear Reservoir method and the initial baseflow discharge was calculated by dividing the low flow in Knowlton Creek by the contributing watershed area.

The Kinematic Wave method was used for routing in the reach elements, due to the steep slopes (up to 6%) in the area. Channel parameters were estimated using the survey data and LIDAR-derived DEM.

The model was calibrated at the mainstem gage for the time period 24-Apr-2012 to 4-Jun-2012, since this included both a dry period and a large rain event. Calibration parameters included the Clark Unit Hydrograph time of concentration and storage coefficients, the maximum canopy and surface storages, and the Manning's roughness coefficient of the reaches. The results from the final calibration can be seen in Figure 7. After calibration, the Nash-Sutcliffe efficiency (Nash and Sutcliffe, 1970), a measure of how well the modeled values match the observed data, was 0.89. Nash-Sutcliffe efficiencies can range from $-\infty$ to 1, with 1 indicating a perfect fit of the observed data. A Nash-Sutcliffe efficiency above 0.5 is considered necessary for a good model (Moriasi et al., 2007).

The parameters from the subwatersheds upstream of the mainstem gage, including those associated with the Clark Unit Hydrograph and Soil Moisture Accounting methods, were translated to the other subwatersheds by scaling relative to the longest centroidal flowpath. The calibrated model was then run for the 2-year SCS Type 2 24-hour storm as an example of a common rainfall-driven event that would be likely to move significant sediment and could be compared to snowmelt events.

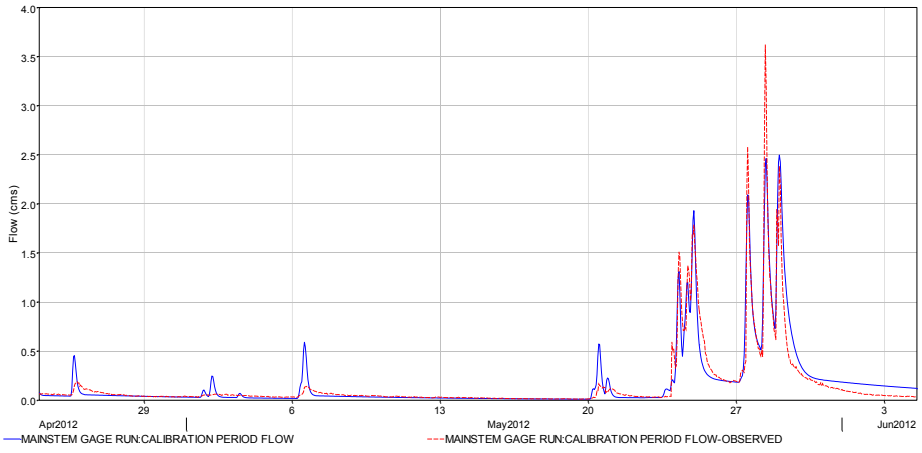

Figure 7 Calibration of the HMS model. The red line is the gaged data while the blue line is the output from the HMS model.

According to SMRA's records, provided by Johnson Controls, the ski area used an average of 238,073 m^3 of water per season between the winter of 1999-2000 and the winter of 2011-2012. It was applied at an average rate of 0.09 m^3/s. In order to determine the impacts of these snowmaking activities on the hydrology of Knowlton Creek, the HMS model was modified to calculate snow accumulation and melt. This version of the model was then run both with and without the additional water applied during snowmaking.

The accumulation and melt of snow were handled by using the Temperature Index snowmelt routine in HMS (Daly et al., 2000). To simulate the effects of frozen ground, the maximum infiltration rates for all of the watersheds were decreased. The lack of valid winter streamflow data prevented calibration of the snowmelt modeling. Instead, two sets of simulations were conducted in order to provide a range of values that would likely contain the actual snowpack and flows. The first set used typical values for the temperature index model parameters (Scharffenberg, 2013; Steve Daly, personal communication) and is referred to as the "Base" snowmelt model in this document. The second set used the high end of the suggested parameter ranges, in order to produce greater snowpack and melt. This set of parameters is called the "Peaked" snowmelt scenario. Due to the uncertainties regarding infiltration and frozen ground under the snowpack, each set of simulations was run for three different infiltration conditions: 100%, 10%, and 0% of the unfrozen infiltration.

According to SMRA, snowmaking operations run 24-hours per day during the entire snowmaking period. It was assumed that the water was applied equally to all of the ski runs maintained by SMRA. The precipitation equivalent of the snowmaking was calculated by dividing the total amount of water used by the hours of snowmaking for each season and then divided by the total area of all of the ski runs.

The ski runs are spread across three different subwatersheds in the model. HEC-HMS is a lumped parameter model and the watersheds were defined to include both ski run and non-ski run areas, so the water used for snowmaking was apportioned to each subwatershed based on the percentage of ski run area they contained. For example, 23.37% of the Southern Ski Area receives artificial snowmaking, so the hourly precipitation for the entire subwatershed was increased by multiplying the average amount of water used for snowmaking on all ski runs (as a depth in mm) by 23.37%, during the entire snowmaking period. This is illustrated graphically in Figure 8. This precipitation equivalent was calculated for each subwatershed and added to the precipitation applied using HEC-DSSVue. The area of each subwatershed, the area of ski runs, and the percentage of watershed area occupied by ski runs are summarized in Table 1.

While the magnitude of the streamflows collected during the snowmelt event in 2012 were not considered valid, the timing of both the onset of flow and the peak indicated by the gage data matched those from the simulation to within a day.

Table 1 Information used in calculating the contribution of snowmaking water to each subwatershed.

	Watershed Area (m^2)	Ski Run Area in Watershed (m^2)	% of Watershed occupied by Ski Runs	% of Total Snowmaking Water	Average Increase in Winter Precip (2007-2012)
Main Ski Area	605,740	249,866	41.25%	75.0%	326%
Southern Ski Area	292,010	68,235	23.37%	20.5%	50%
Southernmost Area	792,900	14,905	1.88%	4.5%	1%

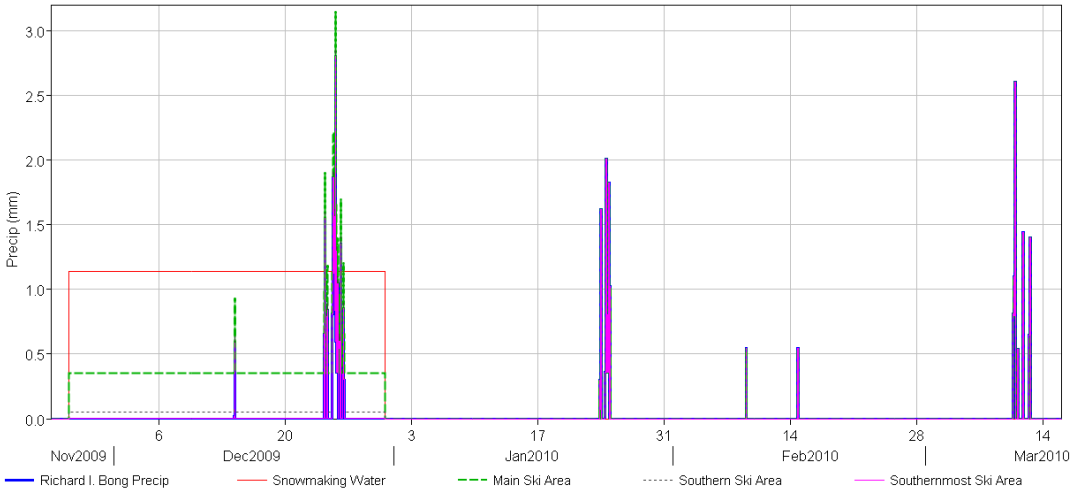

Figure 8 Example of snowmaking precipitation, for the winter of 2009-2010. The blue line is the background precipitation at Richard I. Bong Airport. The red line is the average rate of water applied for snowmaking. The dashed green line is the precipitation applied to the Main Ski Area subwatershed. Outside of the dates of snowmaking, all of the lines are identical.

The HMS model was run for five different winters (1-Oct to 1-May) between 2007 and 2012. The results were then examined and the dates of the snowmelt event, the time period that represents the conversion of the majority of the snowpack to runoff, for each winter were determined by looking at the air temperature records. The snowmelt event was started a few days before the temperature first reached 0 °C and was extended until after all of the snow had melted in the model. The same date range was used to summarize the output for each scenario covering that winter. The dates used for the modeled winters are listed in Table 2.

Table 2 Dates used to summarize the snowmelt event for each simulated winter.

Winter	Snow Melt Dates
2007-2008	30-Mar – 11-Apr-2008
2008-2009	15-Mar – 17-Apr-2009
2009-2010	7-Mar – 20-Mar-2010
2010-2011	15-Feb – 9-Apr-2011
2011-2012	11-Mar – 19-Mar-2012

RESULTS

Peak flow and volume were both reported, in order to better understand the hydrology and potential impact on sediment transport in Knowlton Creek. Figure 9 displays the locations where flow was summarized for this report. Table 3 shows the five-year average peak flow and Table 4 gives the average outflow volume results for all of the snowmelt simulations. These two tables also report the results for the simulation of the 2-year storm event. The Base and Peaked simulations produced nearly identical peak flows, but differed in the volume of the snowmelt event. On average, snowmaking increased the peak flow at the mainstem gage location by 0.2 – 0.3 m^3/s, or 27 - 66% (assuming the same infiltration conditions). The average volume of water in the snowmelt event at this location increased by 124,400 - 152,100 m^3, or 230 - 307%, on average (with identical infiltration conditions). The total volume of water delivered to the area behind Tallas Island increased by 149,300 – 208,500 m^3 (253 - 296%) and the five-year average peak flow at this point increased by 0.3 – 0.5 m^3/s (35 - 76%), assuming unchanged infiltration.

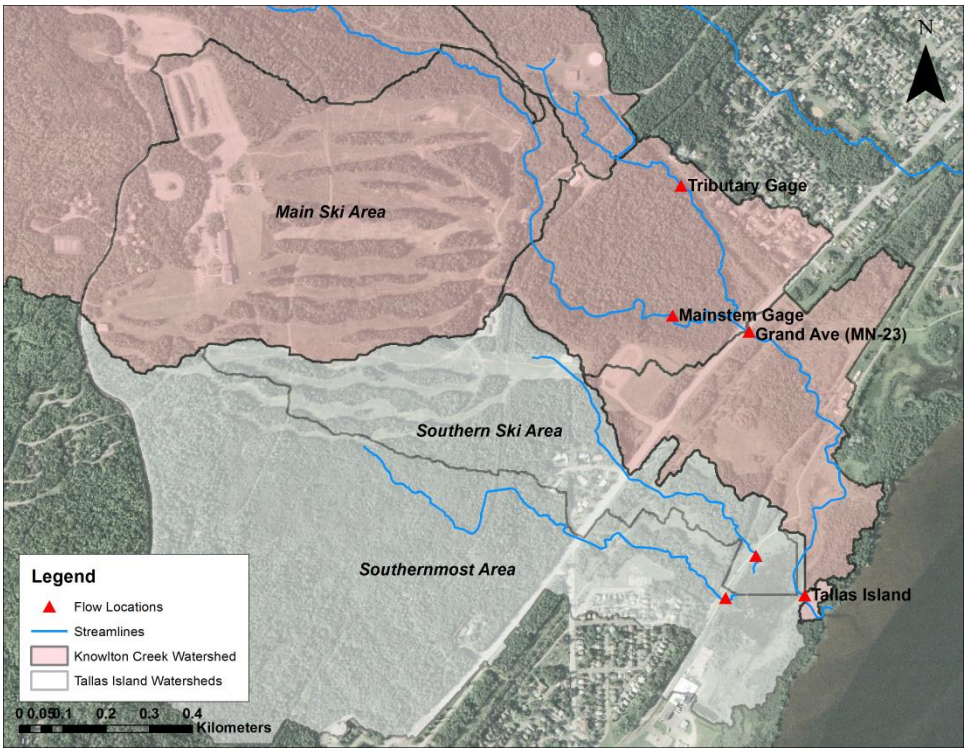

Figure 9 Map showing flow locations and watersheds where Maximum SWE was reported. The Tallas Watershed includes the shaded areas of both colors.

During the course of the winter, the accumulation of snowpack, measured as Snow Water Equivalent (SWE), is also calculated by the model. Figure 9 shows the watersheds where the snowpack was calculated for this report. Table 5 contains the five year average of maximum SWE that occurred for each scenario. Changing the infiltration did not affect the peak SWE, so only one set of results is reported for each combination of snowmaking and snowmelt parameters. The numbers shown for "Knowlton Watershed" and "Tallas Watershed" are area-weighted averages of all the component subwatersheds. This table shows that the peak SWE of the Knowlton Creek watershed increased by 40.9 - 45.3 mm while the peak SWE for the entire area contributing to the flow by Tallas Island increased by 41.4 – 47.3 mm due to snowmaking. The peak snowpack volumes (SWE) in the subwatersheds where the snowmaking took place were affected even more dramatically. The most extreme example of this is the "Main Ski Area" watershed that contains most of SMRA's ski runs. This area experienced an increase in peak SWE of over 340 mm due to snowmaking, during an average winter.

Table 3 Peak flow due to snowmelt (average of winters 2007-2012, m^3/s) and the 2-year design storm

	Snow-making	Infiltration	Mainstem Gage	Grand Ave (MN-23)	Southern Ski Area	Southernmost Area	Tallas Island
Base Snowmelt	No	100%	0.4	0.4	0.0	0.1	0.5
		10%	0.6	0.6	0.0	0.1	0.6
		0%	1.1	1.2	0.1	0.1	1.3
	Yes	100%	0.6	0.6	0.1	0.1	0.7
		10%	0.9	0.9	0.2	0.1	1.0
		0%	1.5	1.5	0.2	0.2	1.8
Peaked Snowmelt	No	100%	0.4	0.4	0.0	0.1	0.4
		10%	0.5	0.5	0.0	0.1	0.5
		0%	1.1	1.1	0.1	0.2	1.3
	Yes	100%	0.6	0.6	0.1	0.1	0.8
		10%	0.8	0.8	0.2	0.1	1.0
		0%	1.4	1.4	0.2	0.2	1.8
2-Year Storm		100%	5.8	5.9	0.5	1	7.2

Table 4 Runoff volume due to snowmelt (average of winters 2007-2012, 1000 m^3) and the 2-year design storm

	Snow-making	Infiltration	Mainstem Gage	Grand Ave (MN-23)	Southern Ski Area	Southernmost Area	Tallas Island
Base Snowmelt	No	100%	47.7	48.9	1.2	3.8	54.8
		10%	47.6	49.0	1.4	3.8	55.1
		0%	47.6	50.5	2.4	6.7	61.5
	Yes	100%	172.2	173.3	24.9	5.2	204.1
		10%	173.8	175.1	26.3	5.2	208.1
		0%	193.7	196.6	41.9	9.9	252.7
Peaked Snowmelt	No	100%	55.3	56.6	1.2	4.5	63.2
		10%	55.1	56.6	1.4	4.5	63.5
		0%	55.0	58.1	2.4	8.0	70.5
	Yes	100%	182.4	183.6	32.2	6.9	223.3
		10%	185.7	187.1	34.5	6.9	229.0
		0%	207.1	210.2	54.1	13.3	279.0
2-Year Storm		100%	309.9	329.5	11.3	29.2	379.1

Table 5 Peak Snow Water Equivalent (SWE) (average of winters 2007-2012, mm of water).

	Snow-making	Main Ski Area	Southern Ski Area	Southernmost Area	Upland Watershed	Knowlton Watershed	Tallas Island
Base Snowmelt	No	6.2	0.5	3.0	7.7	6.7	5.9
	Yes	346.3	153.5	7.2	7.7	47.6	47.4
Peaked Snowmelt	No	8.4	0.8	5.9	9.7	8.6	7.9
	Yes	385.6	194.5	11.3	9.7	53.9	55.1

CONCLUSIONS

Snowmaking activities by SMRA have increased the peak flow in the mainstem of Knowlton Creek from the annual snowmelt event by up to one half, on average. Sediment transport is a non-linear function of the flow in a stream, meaning that the ability of the stream to move sediment has likely increased by even more than that amount during these events.

It is important, however, to view these increased snowmelt flows in the context of those resulting from less frequent storm events. This can be done by comparing the values in Table 3 with those in Table 6. The typical snowmelt event resulting from snowmaking activities over 2007-2012 had a peak flow that is less than one-fifth the flow from a 2-year design storm at the Mainstem Gage location. In a well-functioning forested watershed, it is often assumed that the flow most responsible for forming the shape of the stream channel, and the one that will carry the majority of sediment over long periods of time, occurs every one to two years (Leopold et al., 1964). Therefore, it can reasonably be hypothesized that the flow increase above the background

snowmelt caused by snowmaking would play only a minor role in the sediment transport and geomorphic adjustment of Knowlton Creek.

A literature search for studies of snowmaking impacts turned up very little work. Wemple et al. (2007) studied a ski area in Vermont that used water from within its watershed for snowmaking. They found that water yield increased by 18-36%, a much smaller increase than the snowmelt volume in the Knowlton Creek model. In the Vermont study, this resulted in a 2.5-fold increase in suspended sediment yield. The suspended sediment yield typically consists of silts and clays while larger material will move as bed load, except in extreme events. Unfortunately, no estimates of changes to bed load sediment transport or overall sediment yield were given by the Wemple et al. study.

It should also be noted that another significant hydrologic impact of the ski area has likely been the clearing of the ski runs themselves. Historically, the entire hillside of Spirit Mountain was completely covered by forest, which tends to reduce both overland flow and sediment yield. The effects of tree removal and other mechanical activity in the ski area, as well as the addition of impervious surface area across the watershed were not examined in this study.

It may be advisable to reduce the effects of runoff from the snowmelt events caused by artificial snowmaking, even though this impact is likely not large enough to drive the observed changes in the mainstem of the Knowlton Creek channel. If this reduction is done by the use of runoff control on and at the base of the ski slopes, it would also partially mitigate the effects of the land cleared of forest to create the ski area.

REFERENCES

Chow V.T. (1959). *Open-Channel Hydraulics*, McGraw-Hill, New York, NY. xviii + 680 pp.

Daly S.F., Davis R., Ochs E., Pangburn T. (2000). An approach to spatially distributed snow modelling of the Sacramento and San Joaquin basins, California. *Hydrological Processes* 14, 3257-3271.

ESRI (2011). ArcGIS Desktop: Release 10. Redlands, CA: Environmental Systems Research Institute.

Leopold L., Wolman M., and Miller J. (1964). *Fluvial Processes in Geomorphology*, W.H. Freeman and Company.

Moriasi D. N., Arnold J. G., Van Liew M. W. Bingner R. L., Harmel R. D., Veith T. L. (2007). Model Evaluation Guidelines for Systematic Quantification of Accuracy in Watershed Simulations. *Transactions of the ASABE* 50(3):885-900.

Nash J. E., Sutcliffe J. V. (1970). River flow forecasting through conceptual models: Part 1. A discussion of principles. *Journal of Hydrology* 10(3): 282-290.

Scharffenberg W. A. (2013). *Hydrologic Modeling System HEC-HMS User's Manual*, U.S. Army Corps of Engineers, Institute for Water Resources, Hydrologic Engineering Center, Davis, CA.

Wemple B., Shanley J., Denner J., Ross D., and Mills K. (2007). Hydrology and water quality in two mountain basins of the northeastern US: assessing baseline conditions and effects of ski area development. *Hydrological Processes* 21, 1639-1650.

COLORADO FRONT RANGE FLOOD OF 2013: PEAK FLOWS AND FLOOD FREQUENCIES

Steven E. Yochum, Hydrologist, US Forest Service, National Stream & Aquatic Ecology Center, Fort Collins, CO, steveneyochum@fs.fed.us

prepared for the 5th Federal Interagency Hydrologic Modeling Conference
April 19-23, 2015, Peppermill Hotel, Reno, Nevada, USA

Abstract: In September of 2013, the Colorado Front Range foothills experienced an extensive period of rainfall that culminated in a major flood that peaked in many streams on Friday, the 13th. Rainfall depths of up to 18 inches were recorded over a 10 day period, with a large proportion of the rainfall falling over a 36 hour period. These foothill locations on average receive between 17 and 19 inches of precipitation annually; this event delivered an average year of rainfall at some locations. In response, many streams in the South Platte and Arkansas River basins flooded. To quantify the magnitude of the flood peaks, several entities implemented forensic hydrology methods to develop peak flow estimates, including the NRCS, USGS, and retired USGS hydrologist Bob Jarrett. Peak discharges of up to 60,000 cfs were quantified. Peak flow unit discharges varied by catchment size, as would be expected. Unit discharges as large as 1340 cfs/mi^2 were measured. For locations with streamgages, revised flow frequency estimates were developed using the logPearson methodology as presented in Bulletin 17B. The 2013 peaks were included in this analysis. For the larger streams impacted by the flooding, this flood had return intervals ranging from a 5- to 25-year flood (Fountain Creek), 25- to 50-year flood (Cache la Poudre River, South Platte River), 100-year flood (Big Thompson River), 100- to 200-year flood (Boulder Creek, Coal Creek), and greater than the 200-year flood (Lefthand Creek, Saint Vrain Creek, Fish Creek).

INTRODUCTION

In September of 2013, large portions of the Colorado Front Range foothills (Figure 1) received an unusual amount of rainfall, with up to 18 inches falling in 10 days. Raingage data over the most severely-impacted foothills indicate up to 15 inches fell in Larimer County, 18 inches fell in Boulder County, and 16 inches fell in El Paso County, the three counties most impacted by the flooding. The highest measured rainfall depths are similar to the average annual rainfall for these areas. The majority of the precipitation fell during 36 hours, on September 11th and 12th. These rainfall data were collected in settled areas and primarily within valley bottoms in many portions of the flood extent; rainfall depths and intensities may have been even greater on some mountain slopes (driven by orographic lift) and in remote areas that were void of ground-based data collection.

As a result, large floods occurred in the South Platte and Arkansas basins, in the Cache la Poudre, Little Thompson, Big Thompson, and South Platte Rivers, and in the Saint Vrain, Left Hand, Boulder, Coal, and Fountain Creeks (Figure 1). Peak flow estimates were developed using forensic hydrology methodologies in these and their contributing streams. Using these peak flow estimates, revised flood discharge relationships were developed at streamgage locations. This report provides a summary of peak flow estimates developed primarily by the Natural Resources

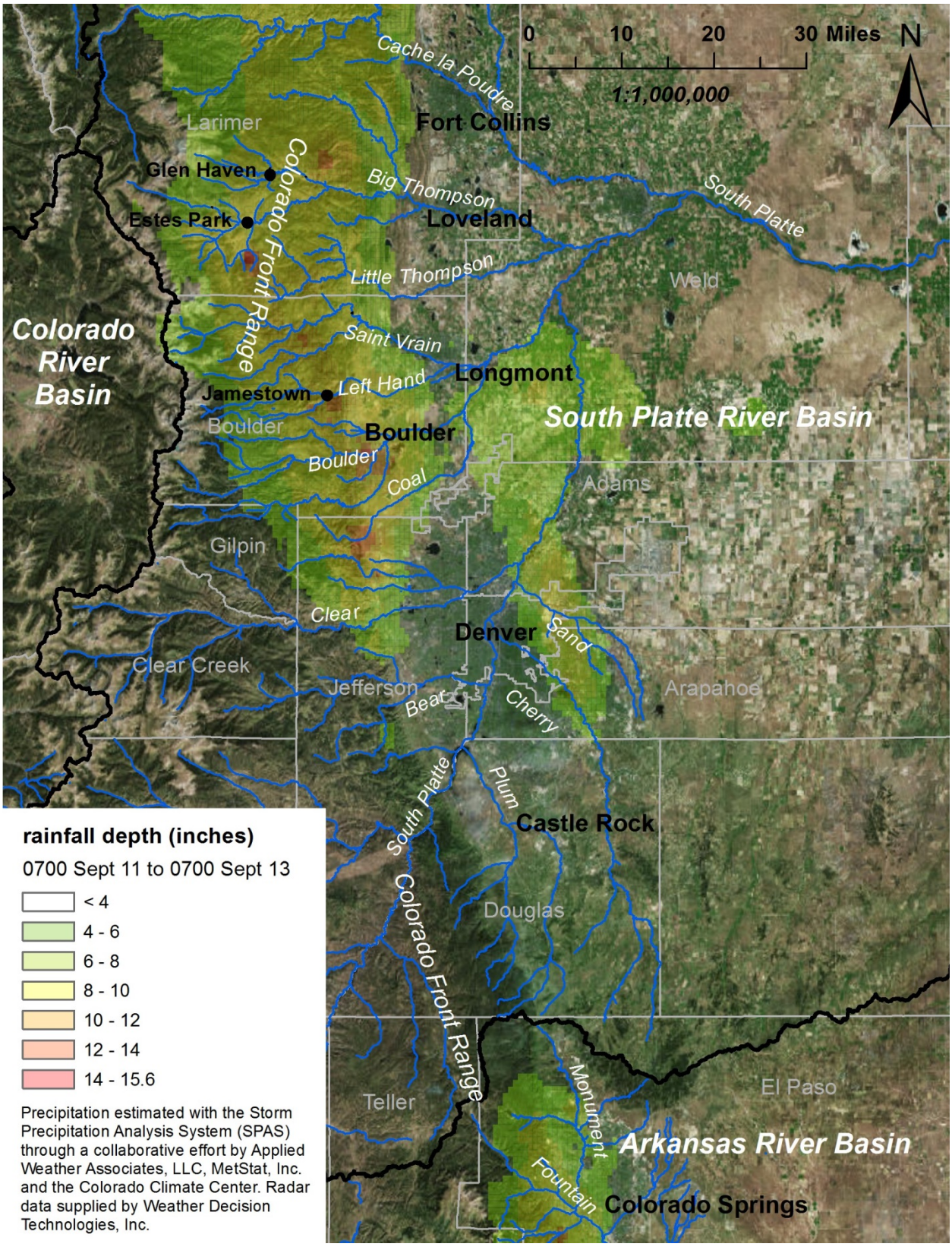

Figure 1 Rainfall depths and streams impacted by the 2013 Colorado Front Range Flood.

Conservation Service (NRCS), the U.S. Geological Survey (USGS) and by Bob Jarrett, a retired USGS research hydrologist. Unit discharges are also presented. Based on updated streamgage analyses, return intervals of the flood peaks are provided.

METHODS

Peak Flow Estimation

Data collection efforts were performed by the NRCS (Steven Yochum and Dan Moore), the USGS, and Bob Jarrett. Peak flow estimates were developed using several methods, including the slope-conveyance, step-backwater, and critical depth methods. Two-dimensional computational modeling was also performed for one site (St. Vrain Creek in Lyons). The slope-conveyance method assumes uniform flow and applies the Manning's equation to cross sectional data. This method requires a Manning's *n* estimate, which is problematic since *n* varies by stage and debris loading (Limerinos, 1970; Bathurst, 1985; Lee and Ferguson, 2002; Wilcox and Wohl, 2006; Reid and Hickin, 2008; Ferguson, 2010; Yochum et al. 2012), and since little field-based data has been collected during large floods for informing the computations. The step-backwater method implements a series of cross sections and 1-dimensional gradually-varied flow computations using such software as HEC-RAS. Discharge is varied until a series of high water marks are matched by the simulated water surface. This method also relies upon uncertain Manning's *n* estimates. The critical depth method assumes critical flow at a control cross section, such as at a constriction or drop off of a channel, or assumes critical flow in a high gradient channel. For slopes over 1 percent, it has been found that a critical depth assumption, with 3 to 6 replicate estimates from multiple cross sections within the reach of interest, can obtain estimates within $\pm 15\%$ of discharges measured with current meters (Jarrett and Tomlinson 2000; Webb and Jarrett 2002; Jarrett and England 2002). This method avoids estimation errors imposed by unknown Manning's *n* coefficients for large flood events, but is instead reliant upon the critical depth assumption and is sensitive to such conditions as backwater and localized supercritical flow. A more detailed discussion of each method is provided in Webb and Jarrett (2002).

Peak flow data were obtained from Jarrett (2014) – Applied Weather Associates, Yochum and Moore (2013) – NRCS, from Kimbrough (2014) – USGS, and from the USGS's National Water Information System (NWIS, http://waterdata.usgs.gov/co/nwis/sw). The majority of the estimates (NRCS, Jarrett) were developed using the critical depth method, in higher-gradient channels (> 1 percent). (The USGS primarily relied upon the slope-conveyance and step-backwater methods.) Using the critical-depth method, peak flow estimates are made using a single cross section, implementing high water marks at each location. Replicate measurements (separate flow estimates developed for several adjacent cross sections) were made for each reach of interest, to assess the reliability of the overall estimate. During floods, higher-gradient channels can flow at or near critical depth, where the Froude number (*Fr*) is unity and the following equation is applied to each cross section:

$$Fr = 1 = \frac{V}{\sqrt{gD}} \qquad (1)$$

where, V is the average cross section velocity, D is the average flow depth ($D = A/T_w$), A is the

flow area, T_w is the top width, and g is the acceleration due to gravity. Using the continuity equation, $Q = VA$, the Froude number equation can be reformulated to obtain flow rate:

$$Q = A\sqrt{\frac{gA}{T_w}} \quad (2)$$

where Q is the discharge in cubic feet per second (cfs).

Flood-Frequency Analysis

The flood frequency analyses at streamgages where 2013 flood peaks are available were performed using logPearson frequency analyses as described in Bulletin 17B (Interagency Advisory Committee on Water Data, 1982), with the assumptions of independence and stationarity. The Expected Moments Algorithm (EMA) method, to be presented in Bulletin 17C, was not implemented. 2013 peak flows were included in the analyses. Record lengths varied from 131 to 10 years, with an average of 45 years. All of these streamgage records are affected by flow regulation (stream diversions and reservoirs). Weighted generalized skews were implemented for streamgages that had a sufficient number of similar watersheds for grouping, to adjust results for stream gages with a shorter record length. Flagged outliers were typically retained, unless they were confirmed as high outliers associated with significant dam failures. The historic peak algorithm was implemented for records that included historic peaks. Peak flow values for the remainder of the periods of record were obtained from the USGS NWIS system (http://waterdata.usgs.gov/co/nwis/sw), and the Colorado Division of Water Resources (http://www.dwr.state.co.us/Surfacewater/default.aspx).

RESULTS AND DISCUSSION

Peak flow estimates of up to 60,000 cfs (S. Platte River at Fort Morgan) were computed (Appendix A), with the highest discharges measured in the St. Vrain, Left Hand, Boulder, Little Thompson, and Big Thompson watersheds (Figure 1, Table 2), as well as the S. Platte River into which all of these streams drain. Detailed figures illustrating peak flow measurement points, as well as unit discharges and return intervals, are provided (Figures 3 through 6). In some of these streams, this peak flow was the flood of record (St. Vrain, 122 years of record; Left Hand, 17 years; Little Thompson, 18 years), while other impacted streams have higher flows in their streamgage records (Big Thompson River, 1976; Boulder Creek, 1921; S. Platte River, 1935).

Table 1 Peak flow unit discharges by watershed size.

Watshed Size (mi^2)	< 4	4 to 25	25 to 200	> 200
Maximum Unit Discharge (cfs/mi^2)	1340	480	320	114

Unit discharges of up to 1340 cfs/mi^2 were computed, with these unit discharges varying by watershed size (Table 1). The variation by scale illustrates the variation in precipitation depth and intensity by area, with some local areas, such as mountain slopes, receiving substantially more rainfall than other areas through such a mechanism as orographic forcing. The locations with the highest unit discharges were oftentimes associated with the most severe damages, such as the Glen Haven, Fish Creek, upper Little Thompson, and Jamestown areas (Figures 3 and 4), as well as the foothills immediately adjacent to Boulder (Figure 4). Traditionally, it is often assumed that high-intensity rain events are limited to elevations below 7500 feet in the Colorado

Front Range. However, large unit discharges were computed at some locations with higher elevations (upper Little Thompson, Estes Park, Glen Haven areas); relevant catchments with >95 percent of their area above 7500 feet are marked by the red circles (Figure 3).

The peak flow and unit discharge data indicate that available raingage data appear to have missed some of the key watersheds impacted by the flooding. These raingage data are often biased towards valley bottoms, usually do not include rainfall intensity data but rather provide daily depths (CoCoRaHS data), and are absent in many large areas where public land is dominant. Calibrated radar data have also missed some of these locations (Figure 1), though localized extreme rainfall intensity could be a complicating factor. Examples of where large peak flow estimates (and observed damages) differ from precipitation data include Glen Haven (Figures 1 and 2) and the upper Little Thompson (Figure 1).

Table 2 Peak flow and flood frequency estimates for the 2013 Colorado Front Range Floods.

ID	Description	Area (mi^2)	Peak Flow (cfs)	Return Interval (non-regulatory)	Years of Record
06751150	N. F. Cache la Poudre River, blw Halligan Res.	354	1,050	5- to 10-year	15
06751490	N. F. Cache la Poudre River, at Livermore	538	4,510	25- to 50-year	27
06752000	Cache la Poudre River at Canyon Mouth	1,054	9,730	25- to 50-year	131
06752260	Cache la Poudre River at Fort Collins	1,128	8,140	25- to 50-year	39
06752280	Cache la Poudre River above Boxelder Creek	1,244	7,010	10- to 25-year	34
06752500	Cache la Poudre River near Greeley	1,879	3,770	10- to 25-year	95
06734500	Fish Creek near Estes Park	16	6,900	>200-year	49
06735500	Big Thompson River near Estes Park	155	----	>200-year	67
06736000	N. F. Big Thompson River at Drake	85	----	>100-year	52
06738000	Big Thompson River at Canyon Mouth	305	16,200	~100-year	90
06739500	Buckhorn Creek near Masonville	136	11,000	25- to 50-year[2]	30
06741510	Big Thompson River at Loveland	531	19,000	~100-year	35
06721500	N. St. Vrain Creek near Allens Park	33	----	~2-year	17
06724000	St. Vrain Creek at Lyons	216	24,700[1]	>200-year	122
06725400	Left Hand Creek near Boulder	52	----	>200-year	17
06725000	Left Hand Creek at Mouth	73	----	>200-year	19
06727500	Fourmile Creek at Orodell	24	2,510	50- to 100-year	22
06727000	Boulder Creek near Orodell	102	2,020	100- to 200-year	106
06730200	Boulder Creek, at N. 75th St., near Boulder	307	8,400	100- to 200-year	27
06729500	S. Boulder Creek, near Eldorado Springs	109	2,120	50-year	120
06730300	Coal Creek near Plainview	15	----	100- to 200-year	43
06719505	Clear Creek at Golden	394	1,530	5-year	39
06713500	Cherry Creek at Denver	410	1,410	2- to 5-year	61
06710150	Big Dry Creek, below C-470	11	527	5- to 10-year	10
06709000	Plum Creek near Sedalia	275	1,260	5- to 10-year	28
06708800	E. Plum Creek, near Castle Rock	116	930	5- to 10-year	14
06711565	S. Platte River at Englewood	3,391	1,140	< 2-year	31
06714215	S. Platte River at 64th Ave, Commerce City	3,895	5,220	< 2-year	32
06721000	S. Platte River at Fort Lupton	5,043	10,300	~25-year	40
06759500	S. Platte River at Fort Morgan	14,648	60,000	25- to 50-year	28
07103700	Fountain Creek near Colorado Springs	102	1,540	10- to 25-year	56
07103703	Camp Creek at Garden of the Gods	9	339	10- to 25-year	22
07105000	Bear Creek near Colorado Springs	7	222	25- to 50-year	22
07103800	W. Monument Creek at Air Force Academy	15	151	25- to 50-year	44
07104905	Monument Creet at Bijou St, at CO Springs	235	6,150	5- to 10-year	11
07105490	Cheyenne Creek at Evans Ave, at CO Springs	22	1,470	~50-year	22
07105500	Fountain Creek at CO Springs	392	8,670	10- to 25-year	38
07105530	Fountain Creek below Janitell Road	413	10,300	5- to 10-year	24
07105800	Fountain Creek at Security	500	12,600	5- to 10-year	49
07106000	Fountain Creek near Fountain	681	15,300	~25-year	46
07106300	Fountain Creek near Pinon	865	11,800	10- to 25-year	41
07106500	Fountain Creek at Pueblo	925	11,800	5- to 10-year	74

----: data withheld due to contractual obligations

(1): provisional data (2): problematic flood-frequency statistical analysis

The results of the flood frequency analyses where peak flow data are available at the current and historic streamgages operated by the USGS and the Colorado Division of Water Resources (CDWR) are provided (Table 2, Figures 3 through 6). Record lengths varied from 131 to 10 years, with four gages having more than 100 years of record available and the primary impacted streamgages (≥50 year flood) having at least 22 years of data available. Return intervals ranged from <2 years (>50 percent chance of occurrence in any given year) to >200 year flood (<0.5 percent chance of occurrence). Importantly, these results do not refer to regulatory flows but are instead the results of updated statistical analyses of the streamgage records.

In terms of these streamgage analyses, the most severely impacted watersheds were the Big Thompson (16,200 cfs at canyon mouth, ~100-year flood), the St. Vrain (24,700 cfs in Lyons, >200-year flood), Left Hand Creek (>200-year flood), Boulder Creek (8400 cfs just downstream of Boulder, 100- to 200-year flood), and Coal Creek (100- to 200-year flood). The Little Thompson watershed was also severely impacted, though insufficient data were available for the frequency analysis. Few streamgages exist on streams within the foothills; the only higher-elevation gages in this analysis were in the upper Big Thompson and St. Vrain watersheds. The return intervals of most of the peak flows estimated on smaller foothills streams cannot be easily associated within the context of a frequency analysis, due to the lack of annual peak flow data, though comparison with pre-flood regional regressions (Capesius and Stephens, 2009) indicates high return intervals in the most severely-impacted streams (Yochum and Moore, 2013).

The primary watersheds impacted by this rain event drain into the South Platte River. Just downstream of Chatfield Reservoir, the flow was measured to peak at only 552 cfs (1.05- to 1.25-year). Downstream of Denver, the flow increased to 5220 cfs (~ 2-year) before increasing to 10,300 cfs at Fort Lupton (~25-year), upstream of St. Vrain, Big Thompson, and Cache la Poudre confluences, and 60,000 cfs at Fort Morgan (25- to 50-year), downstream of the major runoff inputs. Lesser impacted watersheds include the Cache la Poudre (peak of 9730 cfs, 25- to 50-year), and Monument Creek, in the Arkansas River basin (peak of 15,300 cfs, ~25-year).

Figure 2 Flood damage in Glen Haven, along West Creek (photograph taken on 10/16/2013).

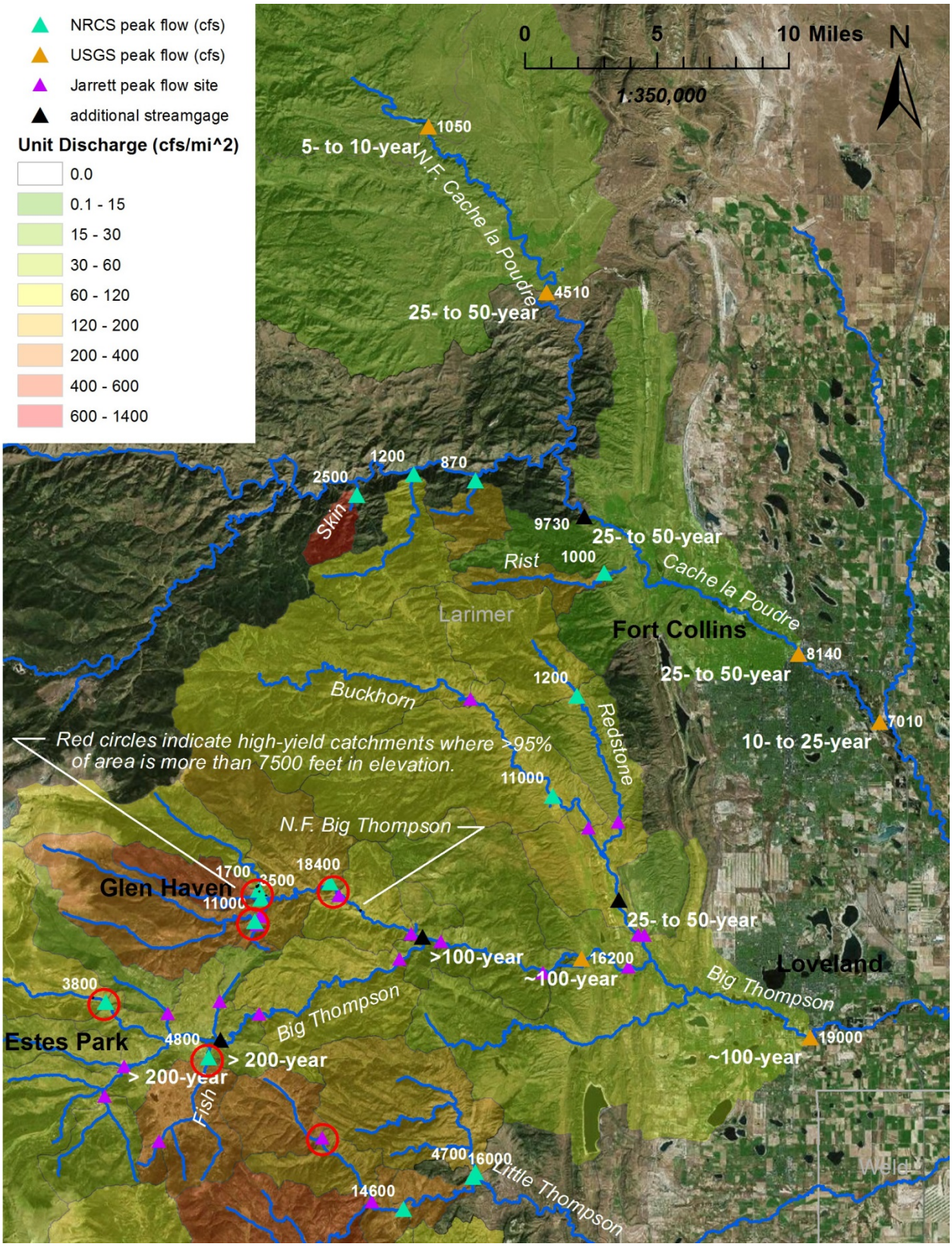

Figure 3 Peak flow estimates, unit discharges, and flood frequencies, northern portion of flood-impacted area.

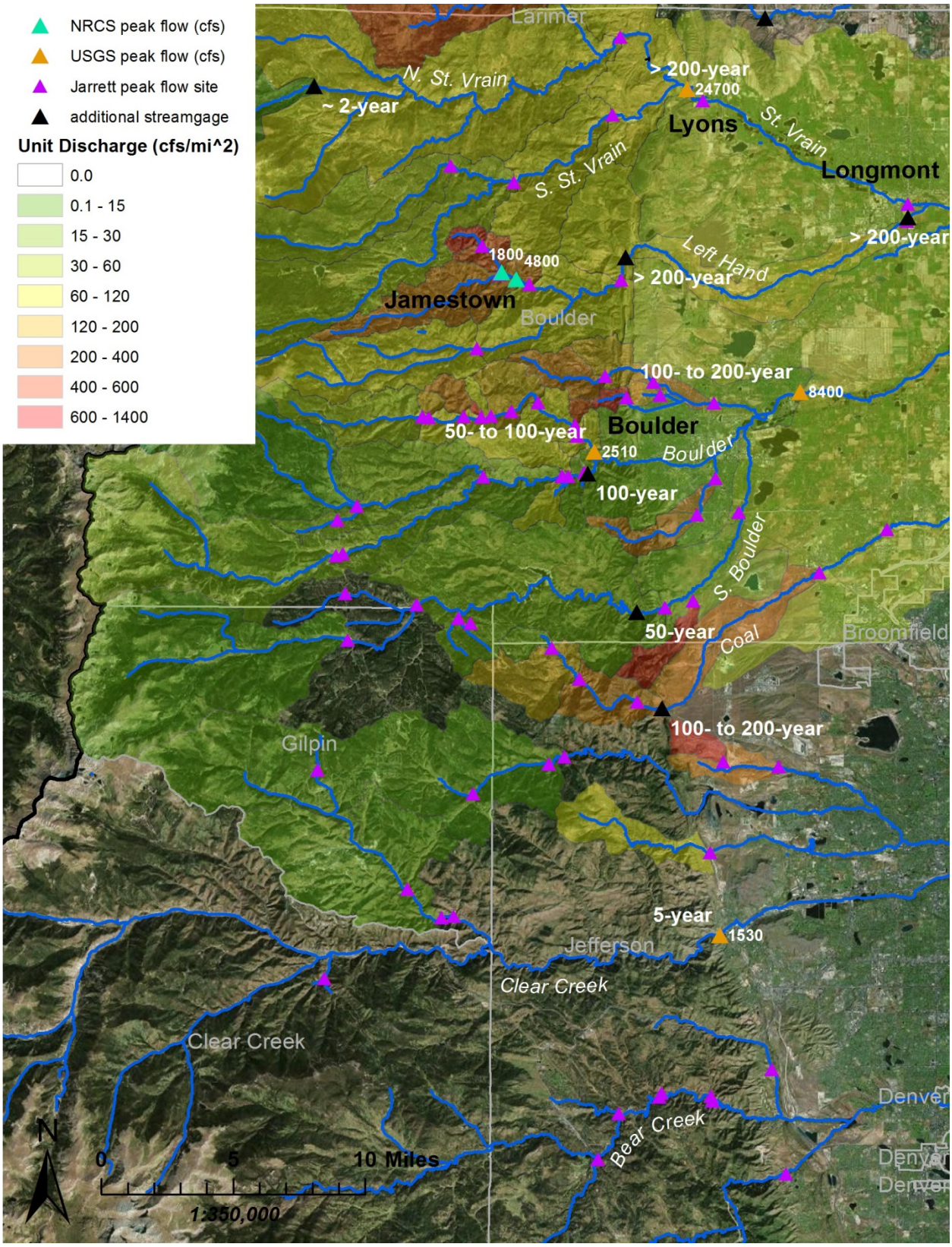

Figure 4 Peak flow estimates, unit discharges, and flood frequencies, central portion of flood-impacted area.

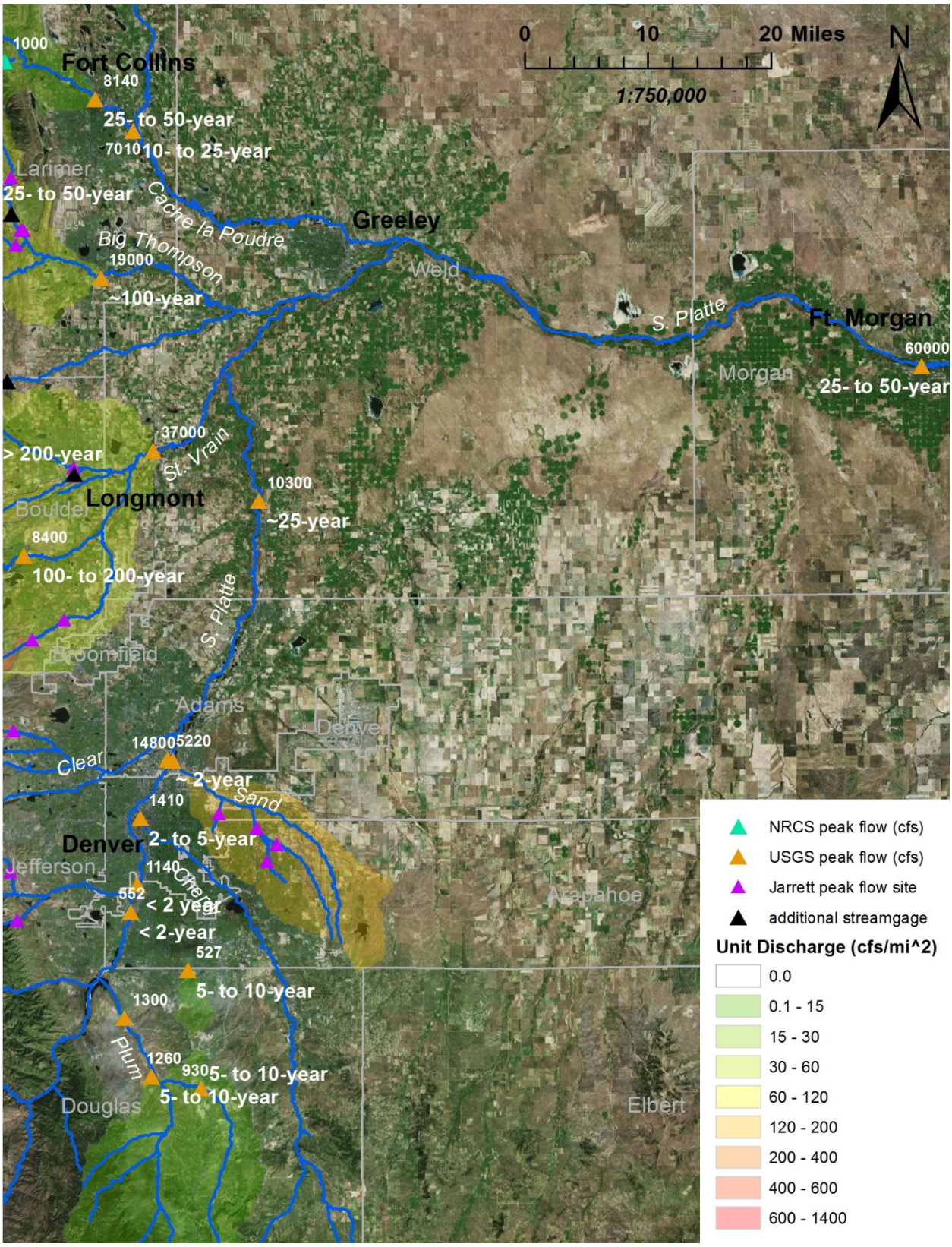

Figure 5 Peak flow estimates, unit discharges, and flood frequencies, S. Platte portion of flood-impacted area.

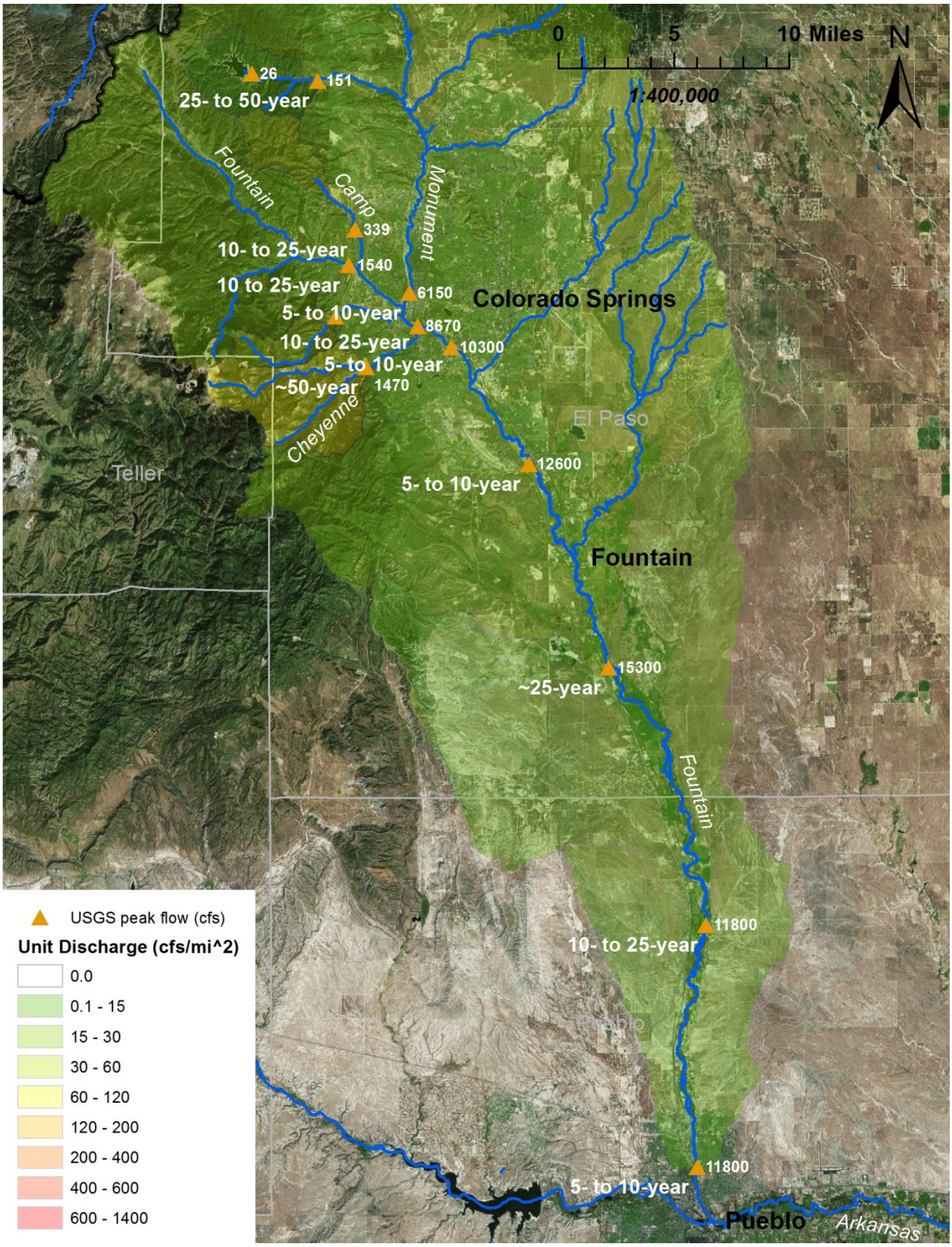

Figure 6 Peak flow estimates, unit discharges, and flood frequencies, southern portion of flood-impacted area.

CONCLUSIONS

Peak flows, peak unit discharges, and flood frequencies have been provided for the spatial extent of the September 2013 Colorado Front Range Flood. Peak flows of up to 60,000 cfs were estimated, with documented unit discharges of up to 1340 cfs/mi^2 (in foothills immediately adjacent to Boulder) and return intervals ≥100-year flood in the most heavily-impacted primary streams draining the rainfall area (Big Thompson, Little Thompson, St. Vrain, Left Hand, Boulder, and Coal). Not addressed in this paper are flood duration values; this event had substantial flood durations, which increased damages.

ACKNOWLEDGEMENTS

Bob Jarrett is appreciated for the great deal of fieldwork and computation time spent collecting the majority of the peak flow estimates from the flood. Appreciation is also expressed for Dan Moore, for data collection and peak flow computations for many of the NRCS peak flow estimates. The hydrologists and hydraulic engineers with the USGS and the Colorado Division of Water Resources are valued for the streamgaging efforts, providing the annual peak flow data required to perform the flood frequency analyses. David Levinson and Marie Garsjo are appreciated for reviewing this manuscript.

REFERENCES

Bathurst, J.C. (1985). "Flow resistance estimation in mountain rivers," Journal of Hydraulic Engineering 111(4), 625–643.

Capesius, J.P., and Stephens, V.C. (2009). Regional Regression Equations for Estimation of Natural Streamflow Statistics in Colorado U.S. Department of Interior, U.S. Geological Survey, Scientific Inv. Rpt. 2009-5136.

Ferguson, R. (2010). "Time to abandon the Manning equation?," Earth Surface Processes and Landforms 35, 1873-1876. doi:10.1002/esp.2091.

Interagency Advisory Committee on Water Data (1982). Flood Flow Frequency: Bulletin #17B of the Hydrology Subcommittee. U.S. Department of Interior, Geological Survey, Office of Water Data Coordination.

Jarrett, R.D. 2014, written communication, Applied Weather Associates.

Jarrett, R.D., and England, J.F. (2002). "Reliability of paleostage indicators for paleoflood studies," In Ancient Floods, Modern Hazards: Principles and Applications of Paleoflood Hydrology. Ed. by P.K. House, R.H. Webb, V.R. Baker, and D.R. Levish. American Geophysical Union, Water Science and Application Volume 5, 91-109.

Jarrett, R.D., and Tomlinson, E.M. (2000). "Regional interdisciplinary paleoflood approach to assess extreme flood potential," Water Resources Research 23(10), 2957-2984.

Kimbrough, R. 2014, written communication, U.S. Geological Survey.

Lee, A.J., Ferguson, R.I. (2002). "Velocity and flow resistance in step-pool streams," Geomorphology 46, 59–71.

Limerinos, J.T. (1970). "Determination of the Manning Coefficient from Measured Bed Roughness in Natural Channels," U.S. Geological Survey Water-Supply Paper 1898-B.

Reid, D. E., and Hickin, E.J. (2008). "Flow resistance in steep mountain streams," Earth Surface Processes Landforms 33, 2211–2240.

Webb, R.H., and Jarrett, R.D. (2002). "One-dimensional estimation techniques for discharges of paleofloods and historical floods," Ancient Floods, Modern Hazards: Principles and Applications of Paleoflood Hydrology. Edited by P.K. House, R.H. Webb, V.R. Baker, and D.R. Levish. American Geophysical Union, Water Science and Application Vol 5, pp 111-125.

Wilcox, A.C., and Wohl, E.E. (2006). "Flow resistance dynamics in step-pool stream channels: 1. large woody debris and controls on total resistance," Water Resources Research 42, W05418. doi:10.1029/2005WR004277.

Yochum, S.E., and Moore, D.S. (2013), Colorado Front Range Flood of 2013: Peak flow estimates at selected mountain stream locations. U.S. Department of Agriculture, Natural Resources Conservation Service, Colorado State Office, doi:10.13140/2.1.2593.0242.

Yochum, S.E., Bledsoe, B.P., David, G.C.L., and Wohl, E. (2012). "Velocity prediction in high-gradient channels," Journal of Hydrology 424-425, 84-98.

APPENDIX A: SELECTED PEAK FLOW ESTIMATES

Stream	Peak Flow Estimate (cfs)	Unit Discharge (cfs/mi^2)	Location (UTM 13) X (meters)	Y (meters)	Source
Skin Gulch	2,500	720	467155	4502854	NRCS
Hill Gulch	870	159	474406	4503735	NRCS
Young Gulch	1,200	79	470621	4504133	NRCS
Rist Canyon	1,000	182	482260	4498095	NRCS
Redstone Creek	1,200	69	480579	4490599	NRCS
Buckhorn Creek	11,000	125	479119	4484520	NRCS
West Creek	11,000	477	460948	4476858	NRCS
Fox Creek	3,500	486	461339	4478250	NRCS
Upper N.F. Big Thompson	1,700	93	461188	4478801	NRCS
N. F. Big Thompson	18,400	260	465534	4479229	NRCS
Fall River	3,800	104	451855	4471941	NRCS
Fish Creek	4,800	442	458121	4468575	NRCS
Little Thompson at Pinewood Springs	14,600	315	469999	4459309	NRCS
Little Thompson	16,000	316	474247	4461270	NRCS
N. F. Little Thompson	4,700	178	474382	4461560	NRCS
Little James Creek	1,800	579	466539	4440820	NRCS
James Creek	4,800	350	467412	4440397	NRCS
N. F. Cache la Poudre River	1,050	3.0	471518	4525304	USGS
N. F. Cache la Poudre River	4,510	8.4	478721	4515197	USGS
Cache la Poudre River at Canyon Mth.	9,730	9.2	481027	4501541	CDWR
Cache la Poudre River at Fort Collins	8,140	7.2	494102	4493153	USGS
Cache la Poudre River abv. Boxelder	7,010	5.6	499038	4489019	USGS
Big Thompson River at Canyon Mouth	16,200	53	480844	4474578	USGS
Big Thompson River at Loveland	19,000	36	494814	4469781	USGS
St. Vrain Creek at Lyons (**provisional**)	24,700	160	477835	4451976	USGS
Boulder Creek at N 75th St., nr. Boulder	8,400	27	484742	4433505	USGS
Fourmile Creek at Orodell	2,510	104	472162	4429872	USGS
St. Vrain Creek at I-25	37,000	42	501650	4447225	USGS
S. Platte River at Ft. Morgan	60,000	4.1	602082	4458260	USGS
S. Platte River at Ft. Lupton	10,300	2.0	515460	4440658	USGS
S. Platte River at Commerce City	5,220	1.3	503568	4406916	USGS
Sand Creek at mouth, Commerce City	14,800	79	504234	4406669	USGS
Clear Creek at Golden	1,530	3.9	479845	4400375	USGS
Cherry Creek at Denver	1,410	3.4	500001	4399176	USGS
Big Dry Creek below C-470	527	47	506206	4379294	USGS
Plum Creek at Titan Road near Louviers	1,300	4.1	497900	4373096	USGS
Plum Creek near Sedalia	1,260	4.6	501460	4365420	USGS
E. Plum Creek below Haskins Gulch	930	8.0	507916	4363882	USGS
W. Monument Creek at A. F. Academy	151	10	508424	4313513	USGS
Camp Creek at Garden of the Gods	339	36	511037	4303128	USGS
Fountain Creek near CO Springs	1,540	15	510583	4300661	USGS
Monument Creek at Bijou St	6,150	26	514804	4298726	USGS
Bear Creek near Colorado Springs	222	32	509671	4297084	USGS
Fountain Creek at Colorado Springs	8,670	22	515388	4296416	USGS
Fountain Creek below Janitell Rd.	10,300	25	517730	4294941	USGS
Cheyenne Creek at Evans Ave	1,470	68	511799	4293543	USGS
Fountain Creek at Security	12,600	25	523133	4286786	USGS
Fountain Creek near Fountain	15,300	23	528713	4272626	USGS
Fountain Creek near Pinon	11,800	14	535468	4254683	USGS
Fountain Creek at Pueblo	11,800	13	534887	4237821	USGS

PERFORMANCE OF SUSPENDED SEDIMENT CONCENTRATION IN TWO DISTINCTIVE LOWER MISSISSIPPI RIVER HYDROGRAPHS

T. (Jerry) Shih, Ph.D., P.E., U.S. Army Corps of Engineers, New Orleans, Louisiana,
Tzenge-Huey.Shih@usace.army.mil
Dave Ramirez, P.E., D.WRE, U.S. Army Corps of Engineers, New Orleans, Louisiana,
David.A.Ramirez@usace.army.mil

Abstract: The U.S. Army Corps of Engineers used to trace soils eroded by rainfall and surface runoff occuring in the Mississippi River frequently. When sediments travelled to the Mississippi River's outfall delta, the suspended sediments settled according to their density as the flow velocity decreased. Approximately 40 percent of the U.S. continental landmass is located in the Mississippi River basin, and much of these suspended sediments empty into the Gulf of Mexico via two Louisiana outlets.

The "LCA Medium Diversion at White Ditch" project plans to divert up to 35,000 cfs of freshwater and sediments from the Mississippi River to the Brent Sound Basin, Plaquemines Parish, Louisiana. Since the sediment concentration is a key factor to the sediment quantity that is ultimately diverted, seeking locations with high sediment concentrations that will optimize sediment delivery becomes extremely important to the project. While at the Feasibility Study phase, the project evaluated five potential sediment intake locations. When the project proceeded to the design phase, the team members decided to perform both hydrodynamic numerical modeling and physical sediment sampling to confirm the tentatively selected location. As for physical sampling, two trips were planned and meant to be executed at high water events. A total of 280 respective samples were collected from eight river mile sites, with five water columns per site, and seven nominal depths per water column in each trip. The targeted sampling depths ranged from -16.0 feet (shallow water) to -40.0 feet (deeper water).

When sampling in the river, many challenges such as logistics, sampling duration, reverse current, objects obstruction, etc. needed to be overcome. Often, the crew members needed to make quick decisions to compromise with the field conditions.

According to the investigation, it could be concluded that high suspended sediment concentrations are directly proportional to high flow rate. High sand concentration could be related to high flow rate as well. Location 3, a location at RM 60.0 which was recommended by the Feasibility Study as the tentatively selected plan (TSP), is not supported by either sampling analysis or numerical modeling. Location 1, a location at River Mile (RM) 69.0 which was not selected by the Feasibility Study, turns out to be the most favorable location based on physical sampling and laboratory analysis performed for two distinctive Mississippi River hydrographs. This location is supported by a hydrodynamic numerical model, Flow-3D, as well. The numerical model predicts the location will have Sediment Water Ratios (SWRs) greater than 1.0, i.e. sediment concentration is higher than that is occurring in the River. This conclusion is also supported by a sediment rating curve prepared for Belle Chase, located at RM 76. One lesson learned from the levels of suspended sediment concentration in two distinctive lower Mississippi River hydrographs is that seeking locations with high sediment concentrations needs to be a primary consideration when planning and designing a sediment diversion project.

INTRODUCTION

Louisiana coastal wetlands are a significant national environmental and economic resource. The erosion of wetlands has threatened the long-term stability of humans, fish, wildlife, and other resources in Louisiana. A report to Congress submitted by the Secretary of the Interior dated March 1994 stated that "from 1900 to 1978, Louisiana lost about 20 percent (901,200 acres) of its coastal wetlands, with 3.17 million acres remaining in 1978. Conservatively, an additional 300,000 acres have been lost since then. Current loss rates are estimated to be about 0.75 percent per year." [1]

Authorized by the 2007 Water Resources Development Act, the Louisiana Coastal Area (LCA) Program was immediately formed for the coastal restoration effort. Identified by the program, the 35,000 cubic feet per second "Medium Diversion at White Ditch" was selected as a near-term project and needed to transition from planning to design after a Feasibility Study. Goals and objectives of this diversion project were to provide river sediment, freshwater, and nutrients to the River aux Chenes sub-basin and other nearby portions of the upper Breton Sound Basin in order to restore and protect marsh soils, vegetation, and maintain a functional salinity regime.

The Feasibility Study was completed in 2009 and a Chief Report was presented to Congress in December 2010. The study was meant to reproduce two successful freshwater diversion structure experiences, Davis Pond (commissioned in July 2002) and Caernarvon (commissioned in August 1991), which had intake channel inverts at elevations of -11.3 feet and -12.3 feet NAVD88, respectively. The study investigated five potential sites, which all are located at the River's left descending bank for a TSP. They were Locations 1, 2, 3, 4, and 5 located at River Mile (RM) 69.0, 64.2, 60, 57.8, and 52.2, respectively. Among these five locations, Location 3 was recommended by the Study as the TSP. Presented in Figure 1 is the project vicinity map.

Figure 1 Medium Diversion at White Ditch

As shown in the figure, all except a reach between Locations 2 and 3 have a back levee in this 16.8 mile stretch. The back levee prevents the outfall channel flows from passing into the marsh. An outlet structure would need to be designed and constructed through in back levee.

Restricted by time, the study did not evaluate the River's sediment source and its distribution profile. The investigation was meant to be postponed before the pre-construction (design) phase. Led by the U.S. Army Corps of Engineers (USACE) New Orleans District (MVN), a project delivery team (PDT) was formed to take the project from planning to design, and continued to construction and operation. The pre-construction PDT members decided both numerical modeling and physical sampling needed to be performed so as to support the recommended TSP. The investigation also extended its scope of work by seeking rich sediments down to a depth of -40.0 feet NAVD88.

PHYSICAL SAMPLING PLAN

Scope of Work: Three additional sampling sites, located at the vicinity of Location 3, were added to the sediment sampling plan to support the TSP and to maximize the sediment diversion effort. They were at RMs 63.0, 61.5, and 59.5. The sampling plan had two independent trips and was meant to take samples at the high River flow rates. Suspended sediment (SS) samples were taken from eight RM sites per trip, with five water columns (WC) per site, and seven nominal depths per water column (WC), for a total of 280 total samples in each trip. Samples were taken from each RM site whose WCs were intended to be at the River cross section that was perpendicular to the flow line. The WCs were numbered in sequence starting from the left descending bank to the right descending bank. The first and the fifth WCs were to target shallow depth at -16.0 feet NAVD88. The second and the fourth WCs were to target deeper depth at -40.0 feet NAVD88. The third WC was at the center of the River. Each WC had its own designated longitude and latitude coordinates. The eight RM sampling sites are presented in Figure 2.

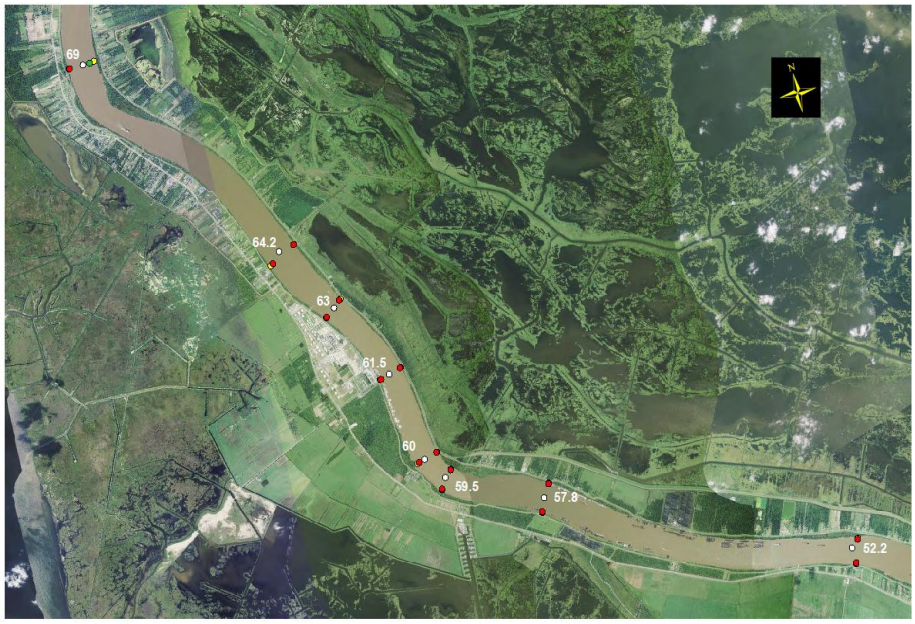

Figure 2 Suspended Sediment Sampling Sites

Boat Trip Observation: The USGS Louisiana Water Science Center in Baton Rouge performed sediment sampling and analysis for both April 23, 2012 and May 13, 2013 trips. To ensure samples were taken from the specified locations, the locations were programmed by a GPS navigator in advance. Sampling boats equipped with Acoustic Doppler current profiler (ADCP) for depth measurement is presented in Figure 3. The Global Positioning System (GPS) navigator used to locate the sampling sites is presented in Figure 4.

Figure 3 Boat Rim Mounted ADCP

Since the river hydrograph is very dynamic, USGS decided to send two crews to complete the field work within a day to minimize sampling deviation.

A few lessons were learned from sampling sediments in the River as follows:

1. Even though sampling locations were mapped by the GPS navigator, the current could carry the boat away. Therefore, samples taken at different normalized water depths may come from a different WC.
2. A slow reverse current can interfere with the sampling work, during which only very little sample volume could be collected in the same duration.
3. The designated sampling location can be occupied by barges or other vessels, which can force the crew to take samples from different places.
4. Always bring extra sampling bottles and labels because pre-labeled bottles can be accidentally broken.
5. The sampler's 12V batteries need to be fully charged for the trip, as the normalized water depth needs to be programmed by battery power.

Figure 4 GPS Navigator Used to Map Sampling Locations

Flow Rate & Stage Adjustments: Since water depths and flow rates constantly change, and the USGS could only provide samples from different normalized water depths, the actual flow rates and stages had to be interpolated from other recorded databases. Flow rates recorded by the USGS Mississippi River station 07374523, located at RM 76.0 (Belle Chasse, Louisiana), were used to interpolate the corresponding flow rates at the time when sampling took place.

Three databases were used to adjust stage readings for eight sampling sites. They were USGS Mississippi River station 07374523 located at RM 76.0, USACE Alliance station located at RM 62.5, and USACE West Point a la Hache station located at RM 48.7.

Two Distinctive Hydrographs: Sampling on April 23, 2012 occurred at the peak of the last hydrograph of that high water season, and was lower than the average flow rate for 82 year period of record for that specific day. The highest and the lowest flow rates recorded at the Belle Chasse, LA, for the first trip were 485,000 cfs and 415,000 cfs, respectively. Stages were also low as well, which were 3.36 feet at RM 69 and 2.92 feet at RM 52.2 for an elevation difference of 0.44 feet. The hydraulic slopes between referenced RM locations varied from 0.02 to 0.08 percent, which were considered very mild. Since the flow rate was so low, brackish water intrusion coming from the Gulf of Mexico could be detected at Belle Chasse (RM 76).

Sampling on May 13, 2013 occurred at the peak of the last hydrograph of that high water season, and was higher than the flow rate averaged for 83 years recorded for that specific day. The highest and the lowest flow rates recorded at Belle Chasse for the second trip were 1,080,000 cfs and 825,000 cfs, respectively. Stages were high as well, which were 8.54 feet at RM 69 and 6.76 feet at RM 52.2 for an elevation difference of 1.78 feet. The hydraulic slopes between referenced RM locations varied from 0.14 to 0.22 percent, which were steeper than the 2011 trip.

SUSPENDED SEDIMENT CONCENTRATIONS

Physical Sampling: Samples collected from the Mississippi River were analyzed for sand and fine categories. Samples collected during April 23, 2012 had very little sand, and almost all samples had fine material only. Total Suspended Sediment (TSS) concentrations were plotted for each WC as an illustration of TSS concentration profile. Five WC profiles were plotted in the same figure for each sampled RM site. Location 4 and RM 61.5 had the highest and lowest TSS concentration for the targeted depths at the lower descending bank, respectively. The second best location was at Location 1 and is presented in Figure 5. TSS concentrations collected at Location 3 are presented in Figure 6, which does not strongly support it as the TSP.

However, at a much higher flow rate, sand and fine materials were found in almost all samples collected from the May 13, 2013 trip. Location 1 and RM 61.5 had the highest and lowest TSS concentrations, respectively. Location 3 had neither the most nor the least TSS concentration; a similar conclusion was obtained during the 2012 trip. Presented in Figure 7 are TSS concentrations collected at Location 1. Presented in Figure 8 are suspended sand concentrations collected at Location 1. Presented in Figure 9 are TSS concentrations collected at Location 3.

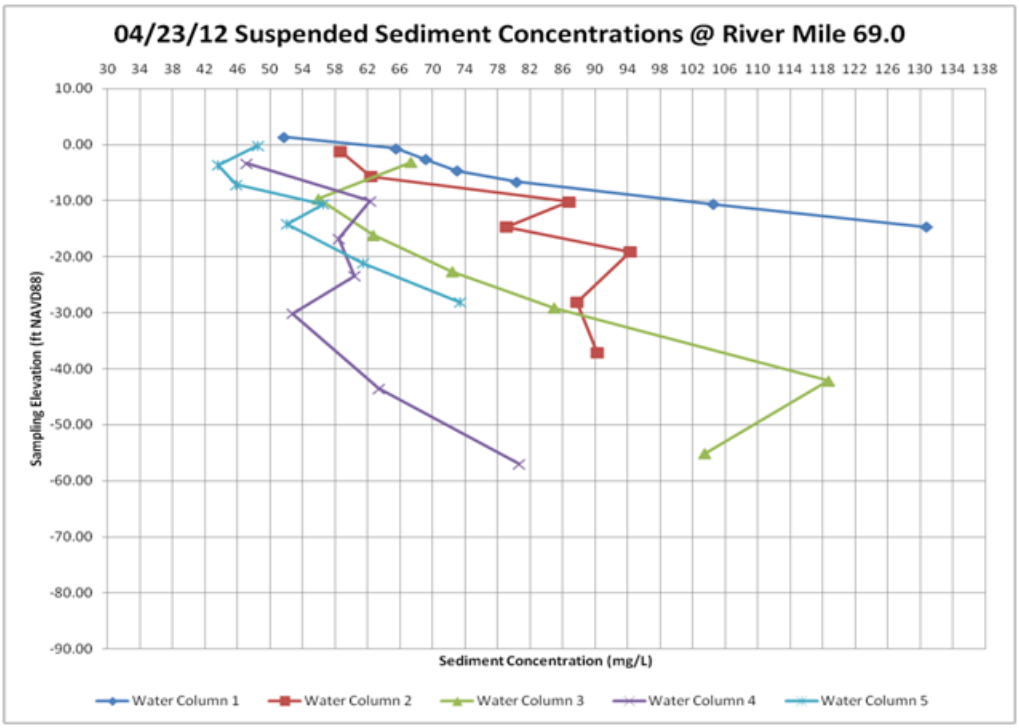

Figure 5 TSS Concentrations Collected in Location 1 from the 1st Trip

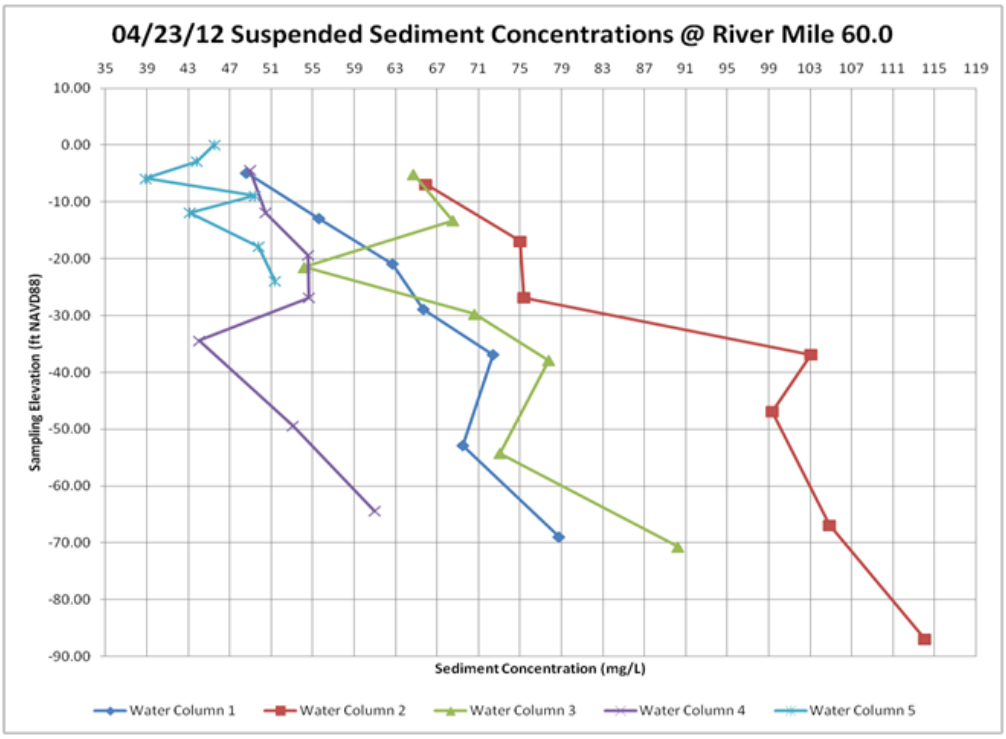

Figure 6 TSS Concentrations Collected in Location 3 from the 1st Trip

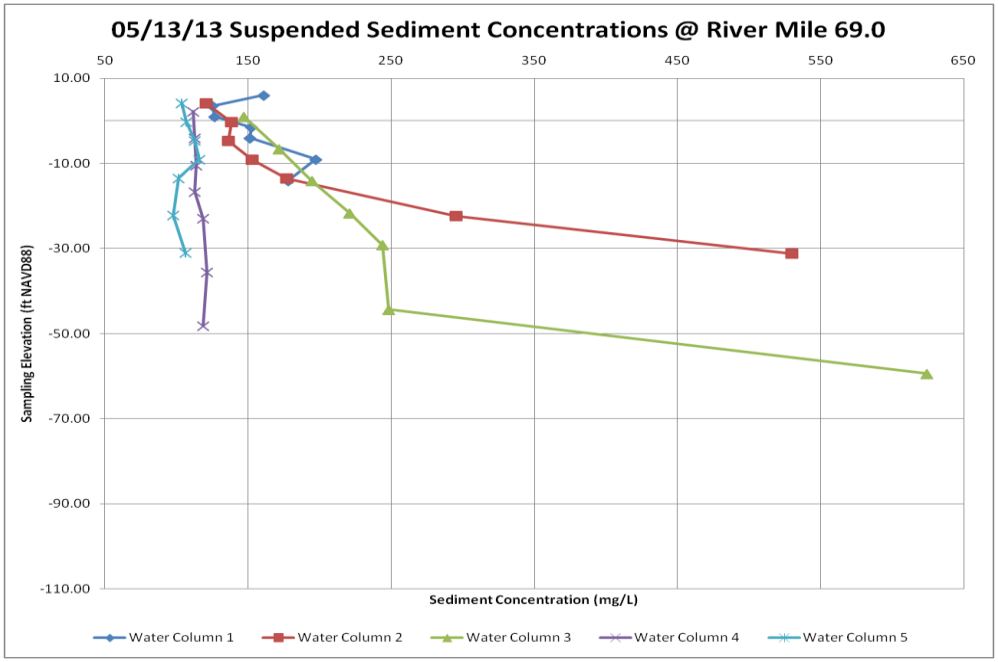

Figure 7 TSS Concentrations Collected in Location 1 from the 2nd Trip

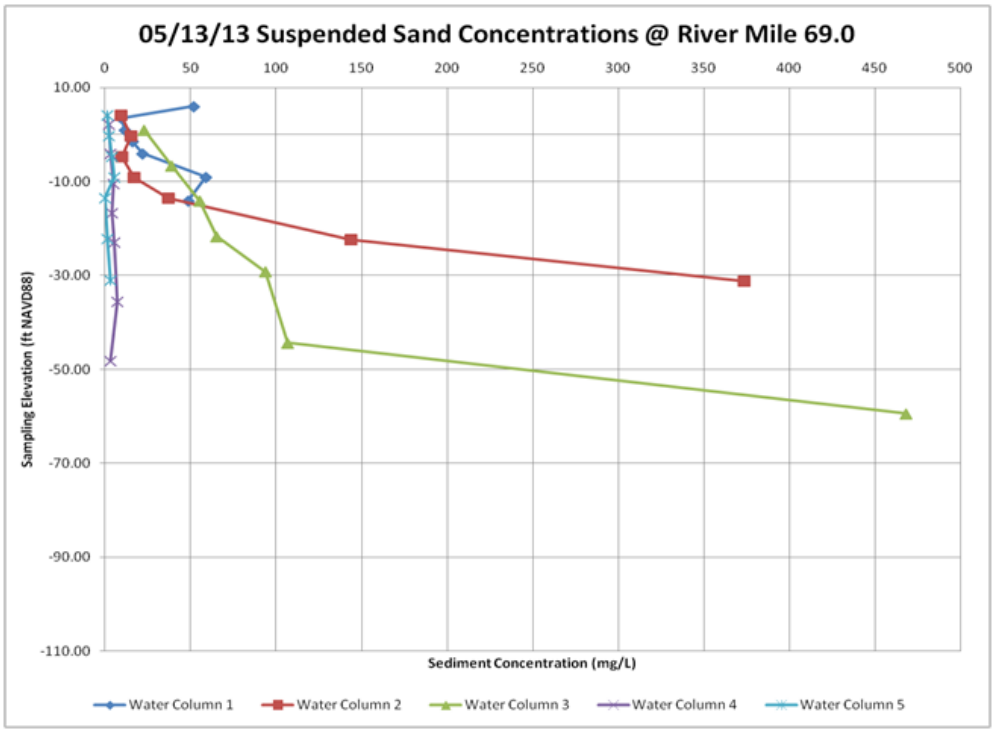

Figure 8 Sand Concentrations Collected in Location 1 from the 2nd Trip

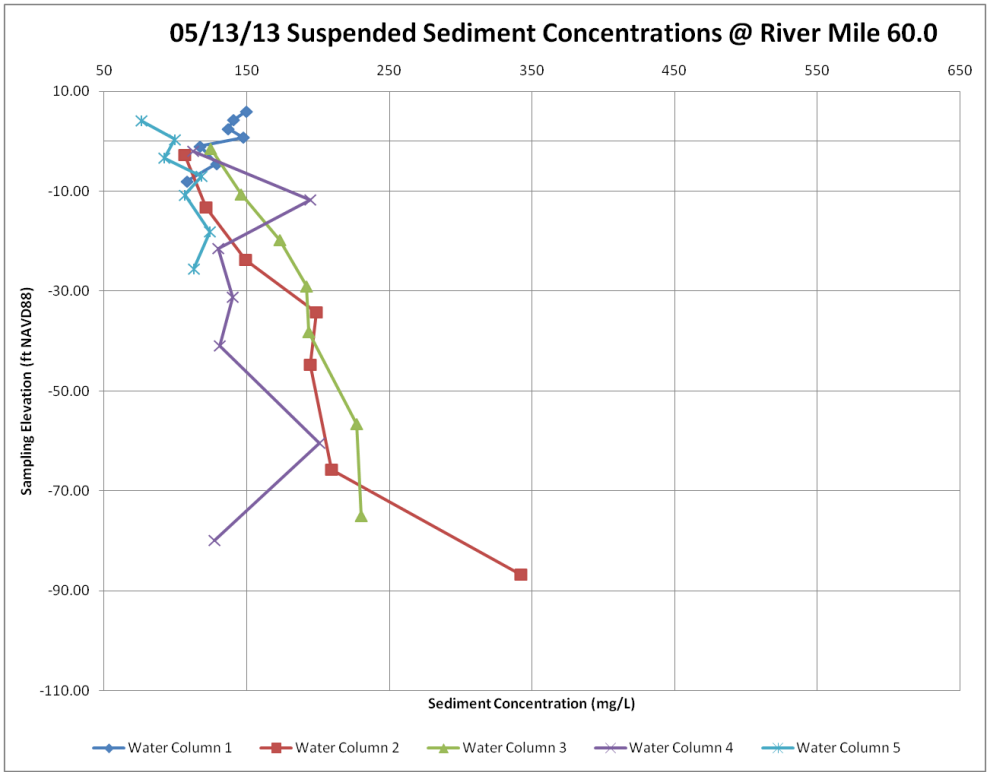

Figure 9 TSS Concentrations Collected in Location 3 from the 2nd Trip

Flow-3D Hydrodynamic Model: Other than the physical sediment sampling, MVN awarded ARCADIS U.S., Inc. to perform hydrodynamic and sediment transport modeling using Flow-3D model for site confirmation and optimization in August 2012. The investigation report was finalized in December 2013.

The study results reached the following conclusions:

1. A diversion at Location 1 or Location 4 would capture the greatest amount of sediment, with Location 1 demonstrating the greatest project benefit.
2. Location 1 is positioned in a river bend where flow patterns carry sediment into the entrance of the diversion structure; and
3. At Location 1, particularly for large material, Sediment Water Ratios (SWRs) are greater than 1.0, i.e. sediment concentration that is higher than that presented in the River will be diverted to the inflow channel by the project.
4. The investigation discouraged Location 3 as the favored sediment diversion location recommended by the Feasibility Study.

RIVER SEDIMENT QUANTITY THEORIES

Sediment Rating Curve: The "Sediment Rating Curve for Mississippi River Diversions: Caernarvon and Davis Pond," prepared by Dr. Jarrell Smith of the USACE's Engineer Research and Development Center (ERDC), dated November 19, 2010 is considered the latest research on prediction of sediment concentration presented in the lower Mississippi River. [2]

Four prediction equations were developed based on two-month long depth-integrated samples collected at the Caernarvon Diversion Structure in St. Bernard Parish, LA. The USGS-ERDC1 equation is favored by Dr. Smith because it has a comparable low bias value and RMS error number and convenience. The USGS-ERDC1 sediment rating curve equation was found to be compatible with the USGS SAND model as well. The USGS-ERDC1 equation is listed as follows:

$$L = 5.5713 \times 10^{-7} Q^{2.007} \quad (1)$$

Where,
L is the sediment load in tons/day, and
Q is the river flow rate in cfs

Sediment quantities corresponding to different river flow rates and their equivalent concentrations are presented in Figure 10.

Based on the USGS-ERDC1 equation, the sediment concentration corresponding to an 83-year averaged Mississippi River flow rate, 700,000 cfs could be 155 mg/L. The same for the average flow rate recorded at the 2012 sampling trip was 450,000 cfs, which could have an average sediment concentration 102 mg/L. The average flow rate recorded for the 2013 sampling trip was 880,000 cfs, which could have an average sediment concentration 200 mg/L.

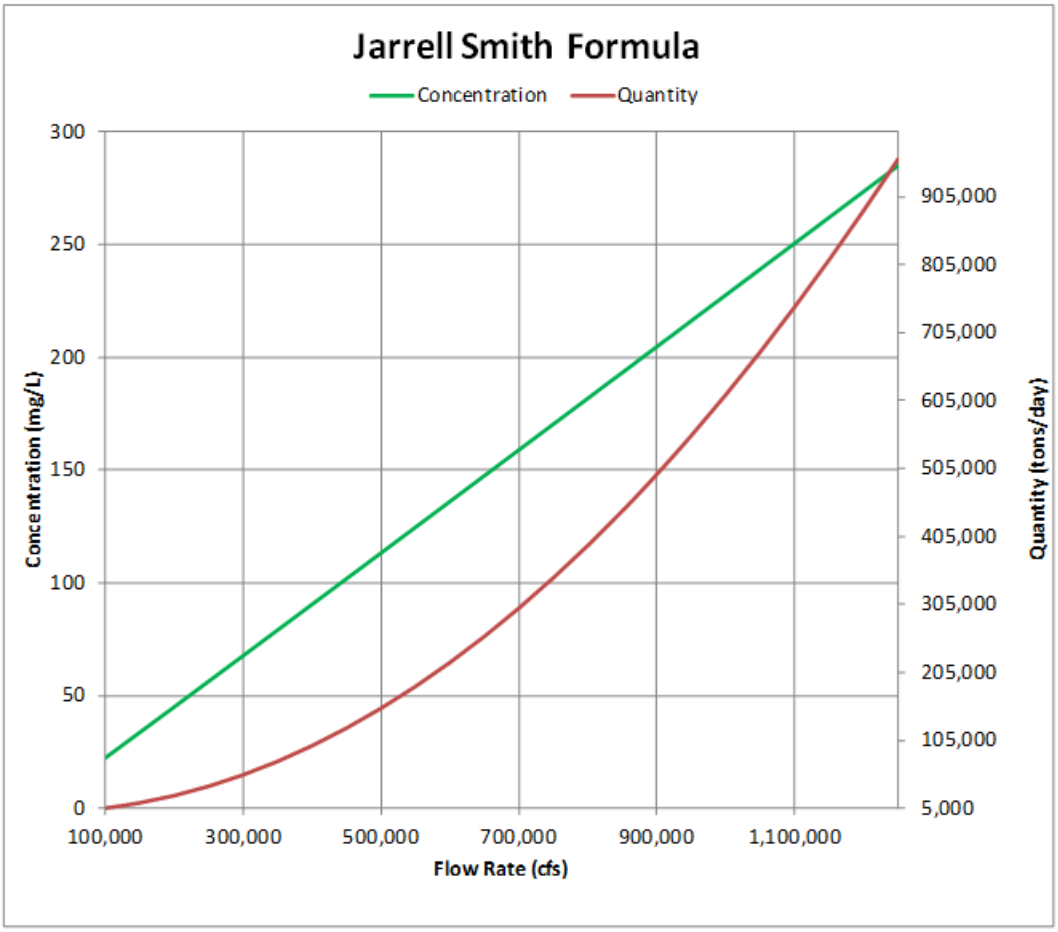

Figure 10 Dr. Smith's Sediment Quantities & Concentration Rating Curve

The 2012 trip showed that, for the targeted depths (-16 feet to -40 feet NAVD88), Location 4's left descending bank (Water Columns 1 and 2) had sediment concentrations ranging from 118 to 152 mg/L, which were higher than the value predicted by the USGS-ERDC1 equation (102 mg/L). Location 1 had concentrations ranging from 90 to 130 mg/L, which were slightly better than the sediment rating curve predicted value. The remaining locations had concentration ranges that were lower than the USGS-ERDC1 predicted value.

The 2013 trip showed that, for the targeted depths, Location 1's left descending bank had sediment concentrations ranging from 178 to 530 mg/L, which were much higher than the value predicted by the USGS-ERDC1 equation (200 mg/L). Location 4 had concentrations ranging from 136 to 359 mg/L, which were also better than the sediment rating curve predicted value. The remaining locations had sediment concentrations whose ranges were lower than the USGS-ERDC1 predicted value. It is to be noted that Location 1's left descending bank had sand concentrations ranging from 49 to 374 mg/L, which were higher than the value predicted by the USGS-ERDC1 equation.

Samples taken from both low and high hydrographs strongly support Location 1 as a favored sediment diversion location.

Other Theories: Other theories, such as impacts of rising and falling hydrographs, frequency of previous high waters, inorganic and organic sediment particle distribution, etc. also contributed to the sediment quantities presented in the river water. However, all have their significant conditions and presumptions.

CONCLUSIONS

According to the above investigation, we may be able to conclude a few highlights as follows. High suspended sediment concentrations could be related to high flow rates in the Mississippi River. High sand concentration could be related to high flow rate as well. Location 1 (RM 69) is the most favorable location based on suspended sediment concentrations, followed by Location 4 (RM 57.8). Location 3 had neither the best nor the worst suspended sediment concentrations measured at both high and low flow rates. The sampling analysis supports location selection simulated by a Flow-3D hydrodynamic modeling.

One lesson learned from the levels of suspended sediment concentration in two distinctive lower Mississippi River hydrographs is that seeking locations with high sediment concentrations needs to be a primary consideration when planning and designing a sediment diversion project.

Although Location 1 proved to be the most favorable sediment diversion location, there were still unfinished tasks, such as optimizing the geometry for the inflow channel to catch rich sediments and to minimize shoaling when the structure is not in operation. Also, sites have back levees that are normally flood-protected areas. Such sites will increase additional costs in building a back levee crossing culverts and sluice gates, rerouting highways, and acquiring costly right-of-way.

REFERENCES

U.S. Department of the Interior (1994). "The Impact of Federal Programs on Wetlands, Vol. II," A Report to Congress by the Secretary of the Interior, Washington, DC, Page 144.

Smith, Jarrell (2010). Sediment Rating Curve for Mississippi River Diversions: Caernarvon and Davis Pond (Draft). U.S. Army Corps of Engineers Engineer Research and Development Center, Vicksburg, Mississippi.

ACKNOWLEDGMENTS

Authors want to acknowledge the following agencies and people who encouraged and supported the suspended sediment concentration investigation, making the future LCA Medium Diversion at White Ditch possible: MRC, MVD, CPRA, USGS-Baton Rouge office (especially Mr. Todd E. Baumann, P.E.), Dr. Jarrell Smith of ERDC, LCA Medium Diversion at White Ditch project PDT members, ARCADIS U.S., Inc., and many others.

SEDIMENT MODELING ON THE LOWER YELLOWSTONE RIVER AT INTAKE DAM, MONTANA

Curtis J. Miller, P.E., Hydraulic Engineer, USACE Omaha District, Omaha, Nebraska, curtis.j.miller@usace.army.mil; Daniel B. Pridal, P.E., Hydraulic Engineer, USACE Omaha District, Omaha, Nebraska, daniel.b.pridal@usace.army.mil; Christopher J. Svendsen, P.E., Hydraulic Engineer, USACE Omaha District, Omaha, Nebraska, christopher.j.svendsen@usace.army.mil.

The views expressed in this paper are those of the authors and do not necessarily reflect the official policy or position of the United States Army Corps of Engineers, the Department of the Army, Department of Defense, or the United States Government.

Abstract: The Lower Yellowstone Project at Intake is a Bureau of Reclamation (BoR) irrigation project located on the Yellowstone River. The low head dam, constructed in 1906, presents a barrier to fish passage. A bypass channel in eastern Montana is proposed to improve upstream and downstream fish passage for the endangered pallid sturgeon and other native fish. The proposed bypass channel has a bottom width of 40 feet (ft) with side slopes varying from 1V:8H (one vertical to eight horizontal) to 1V:4H. With a length of approximately 11,150 ft and cut depths ranging from 4 to 20 ft, the total excavation quantity is approximately 950,000 cubic yards.

Hydraulic and sediment modeling using the Hydrologic Engineering Center's River Analysis System (HEC-RAS) and Adaptive Hydraulics (ADH) has been conducted by the U.S. Army Corps of Engineers (USACE). Additionally, the BoR's Technical Service Center used Sedimentation and River Hydraulics – Two-Dimensional (SRH-2D) to analyze hydraulics and sediment. The intent of the hydraulics analysis was to evaluate depths and velocities throughout the bypass channel with respect to fish passage. The primary goal of the sediment modeling was to evaluate sediment continuity throughout both the main and bypass channels. Coordination between USACE and BoR began with use of the same topographic and hydrographic surface data. Comparison of similarities and differences in model results allowed for better definition of natural and modeling uncertainties.

The focus of this paper is on HEC-RAS sediment modeling of the proposed bypass channel along with associated sensitivity analyses.

INTRODUCTION

Numerous sediment transport runs were completed with HEC-RAS, version 4.2.0 Beta, July 2013. Geometries representing both the main channel of the Yellowstone River and the proposed bypass channel were evaluated. Results presented herein focus on the proposed bypass channel. Figure 1 shows the project location; Figure 2 shows a general overview of the proposed project.

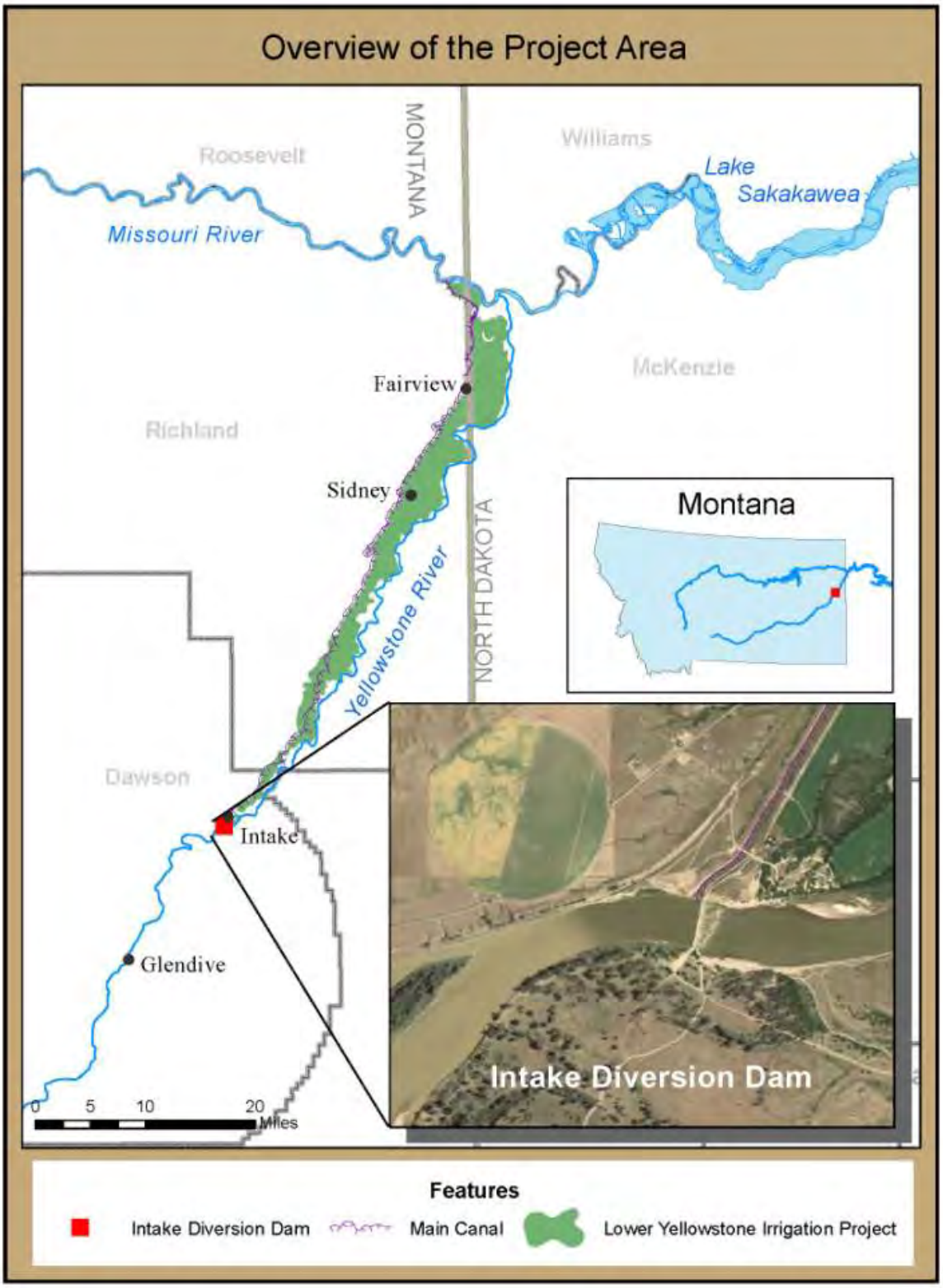

Figure 1 Project location map

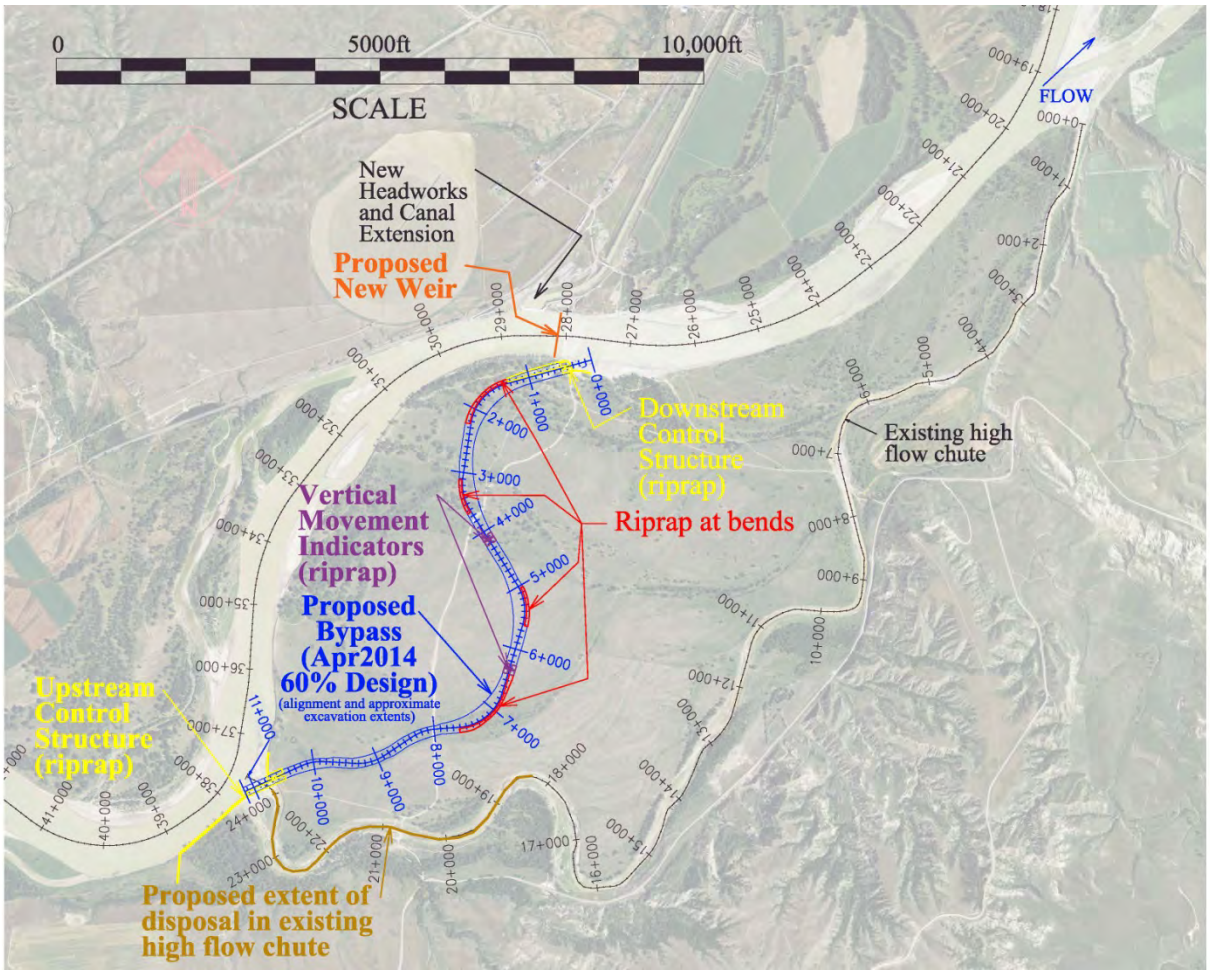

Figure 2 General overview

Because no calibration data are available for the proposed bypass channel, sensitivity runs on multiple sediment loading values, incoming gradation, bed gradation, transport functions, sorting methods, discharges and channel slopes were completed.

Historic flows from USGS gage at Sidney, Montana (approximately 42 miles downstream) were used to evaluate long-term trends. Additionally, constant flows representing the approximate channel-forming discharge were evaluated. Split flow modeling of the 50% annual chance of exceedance (50% ACE, commonly referred to as the two-year discharge) results in approximately 6,500 cfs in the bypass channel; this flow was selected as the channel-forming discharge used to evaluate channel stability. Once a relatively stable channel configuration was selected, model analysis was performed with the post-Yellowtail Dam period of record flows (1967-2014) from the Sidney gage. The maximum flow through the bypass during this analysis was limited to the approximate bankfull discharge, 9,000 cfs (equivalent to 60,000 cfs total Yellowstone flow) due to model instabilities when larger discharges were used. Similar instabilities occur in the main channel when modeling large flows, indicating that model limitations (rather than actual geometry or sediment loading) are the cause. Future evaluation will further investigate modeling of extreme Yellowstone River flows, mainly with 2-D

modeling where overland flows can be modeled with sediment (at the current time, HEC-RAS cannot model more than one reach with sediment).

BASE CONDITIONS

The proposed bypass channel characteristics are summarized below:

- Length ≈ 11,150 ft
- Base cross section shape: 40 ft bottom width, side slopes go from 1V:8H to 1V:6H to 1V:4H
- Channel slope = 0.0007 ft/ft
- Excavation quantity ≈ 950,000 yd^3

Base data used in the sediment transport analysis include the following:

- Median incoming load from the Sidney gage data (USGS Gage #06329500) was used to develop a suspended sediment loading curve for the bypass channel based on the estimated flow split. Figure 3 shows the load in tons/day and compares measured data from the Intake site to the gage data. The load was converted to a concentration which was then used to determine the load in the bypass channel.
- Gradation of incoming suspended load based on estimated median of Sidney gage data. Figure 4 shows the Sidney data as well as the selected load curves for use in HEC-RAS.
- Estimated bedload of approximately 5% of suspended load (varies from 0.5-7% depending on flow) with gradation based on 2008 bar samples (grab samples taken with shovel) collected by USACE and analyzed by USGS. Maximum incoming material size was limited to medium gravel (8-16 mm). Figure 5 shows combined suspended load/bedload as entered into HEC-RAS.
- Transport function used for base is Laursen-Copeland (Copeland 1989 and Laursen 1958), a total load function that was generalized by Copeland for gravel transport so the equation could be used for graded beds.
- Bed gradation was based on Wolman (Wolman 1954) counts collected in 2008. The design includes a processed armor layer in the bypass invert to minimize post-construction degradation. The processed armor layer includes materials greater than one inch diameter screened from the excavation. Figure 6 shows several bed gradations. The Wolman count gradation is coarser than the bar samples or test pits, but is expected to be representative of the processed armor layer after construction.

Figure 7 shows the results of the "base" run using both a constant discharge of 6,500 cfs (between 45,000 and 50,000 cfs in the main channel) and using the gaging record discharges from the post-Yellowtail Dam period (1967-2014). Bypass geometry for the base run does not include natural channel elements that are included in final design. Natural channel elements in the final design include variable cross section shapes and invert elevations representing a pool/riffle sequence (as opposed to the uniform cross section shape and channel slope used in the base run). Design of the natural channel elements generally followed guidance presented in ERDC/CHL CR-01-1 (Soar 2001).

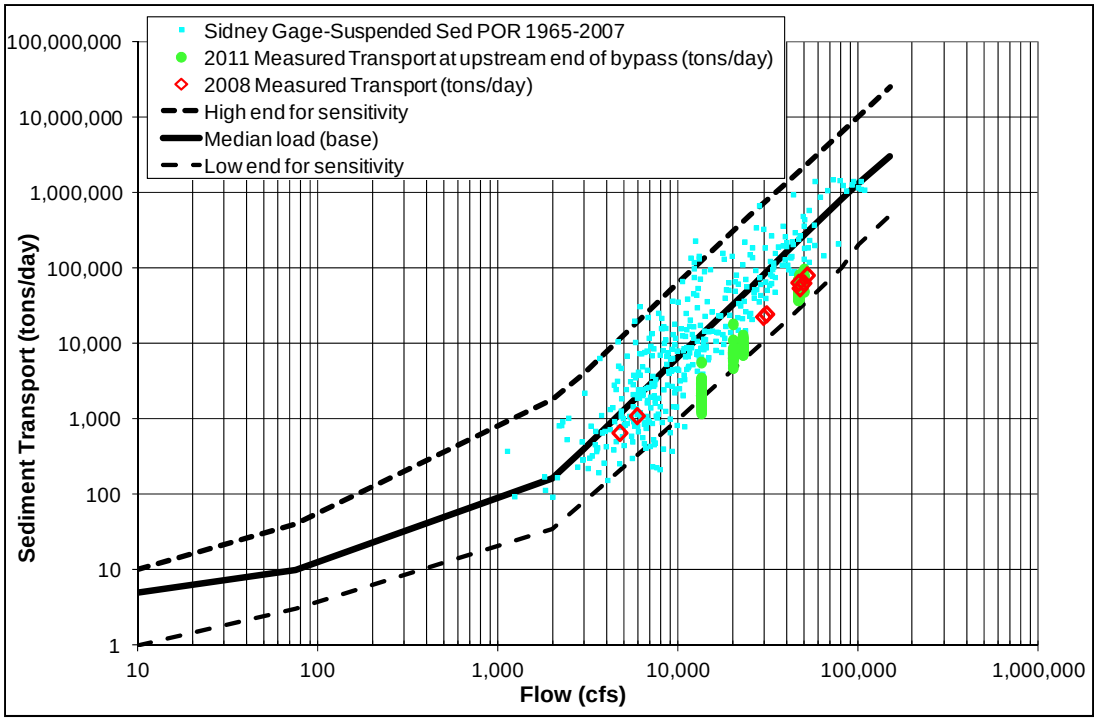

Figure 3 Incoming load data

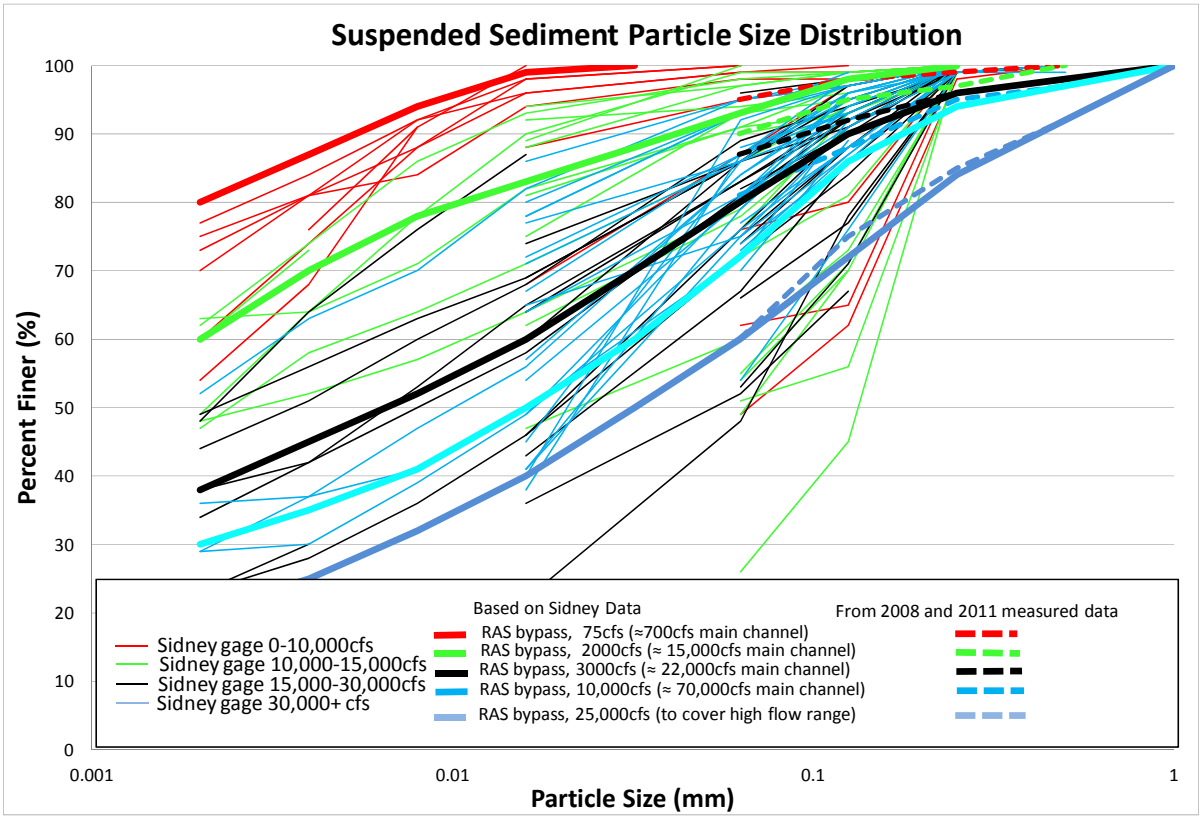

Figure 4 Suspended load gradations

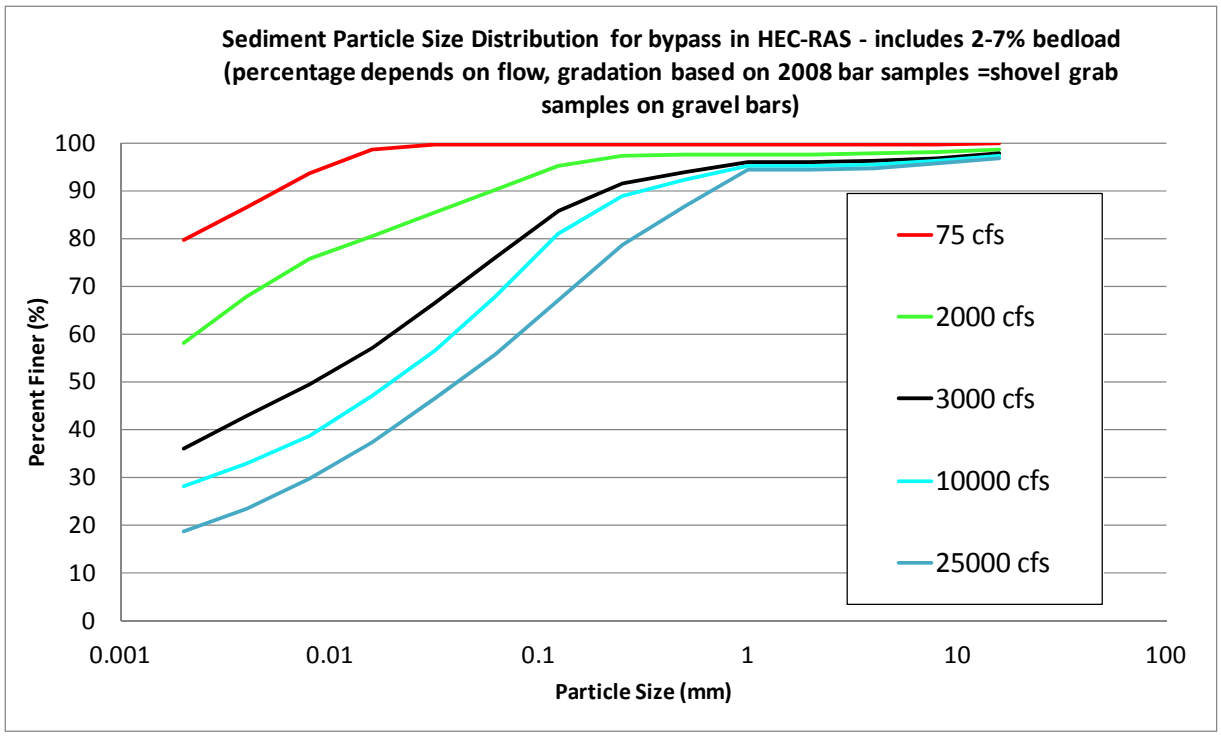

Figure 5 Combined suspended/bedload used in HEC-RAS for bypass channel

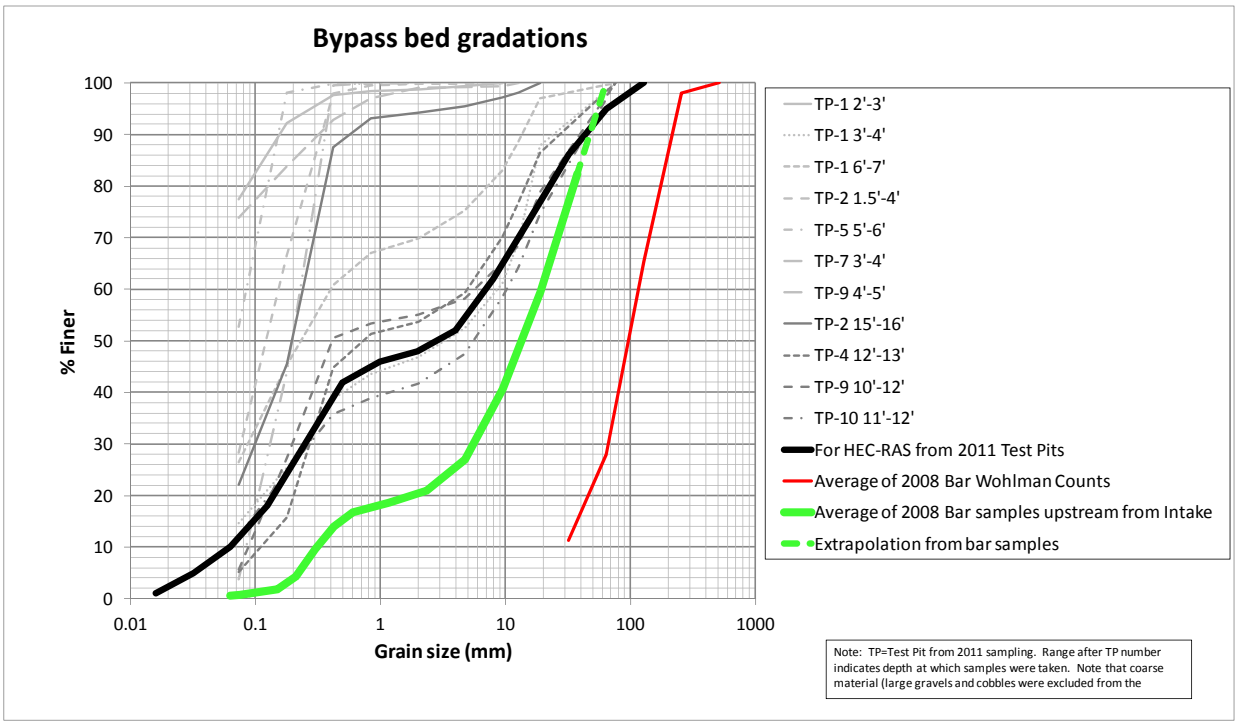

Figure 6 Bypass bed gradations

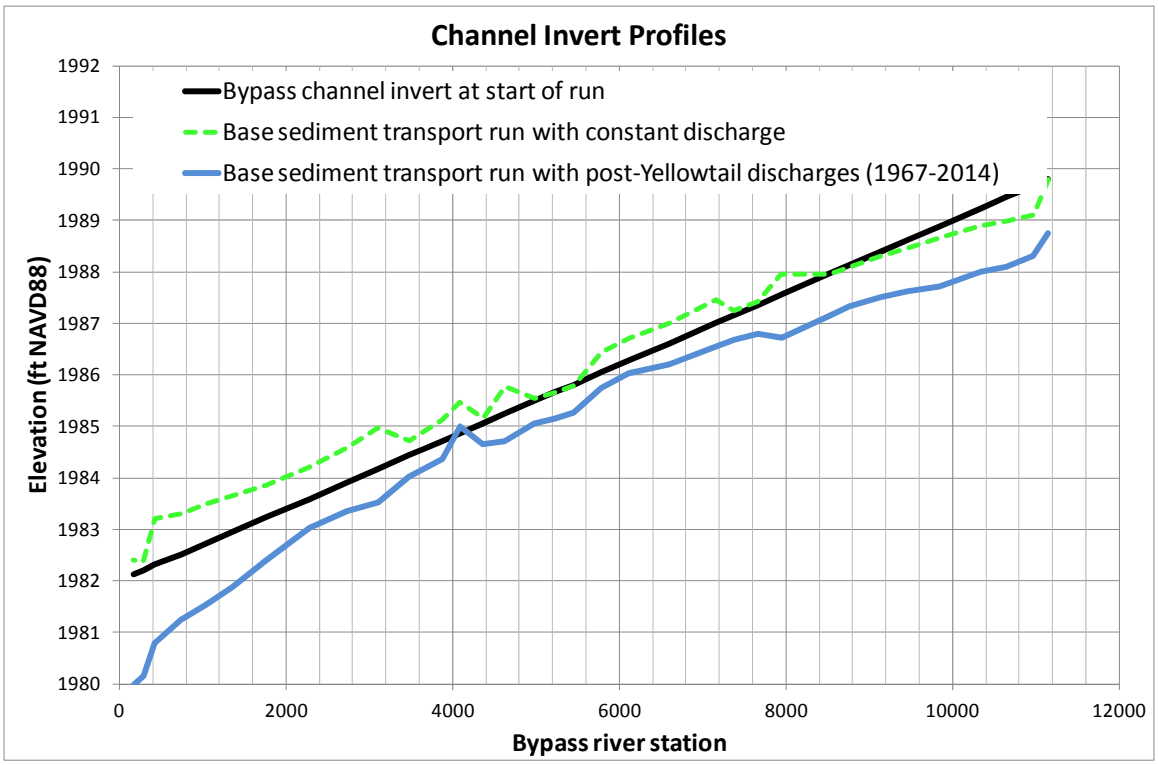

Figure 7 Invert Comparison – Base Runs

SENSITIVITIES

Numerous sensitivity analyses were run on the proposed bypass channel. Sensitivity runs on multiple sediment loading values, incoming gradation, bed gradation, transport functions, sorting methods, discharges and channel slopes were completed.

In general, the model shows high sensitivity to the incoming gradation and transport function; moderate sensitivity to the incoming load, bed gradation, discharge, and sorting method; and low to moderate sensitivity to the channel slope within the ranges considered.

The model shows particularly high sensitivity to the largest size of the incoming material, especially for certain transport functions. In addition to Laursen (Copeland), Yang (1973, 1984), Toffaleti (1968), and Ackers-White (1973) transport functions were used. When using medium gravel (8-16 mm) as the largest incoming material, Yang, Toffaleti, and Ackers-White showed unrealistic aggradation (on the order of 100+ ft). However, when the maximum size of incoming material was limited to very coarse sand (1-2 mm), results with the alternative transport functions were much more realistic. This trend was similar with the main channel of the Yellowstone River, indicating that limitations of the various transport functions are the cause rather than actual physical predictions of extreme aggradation. Figure 8 shows results from multiple runs using various transport functions and maximum incoming material size.

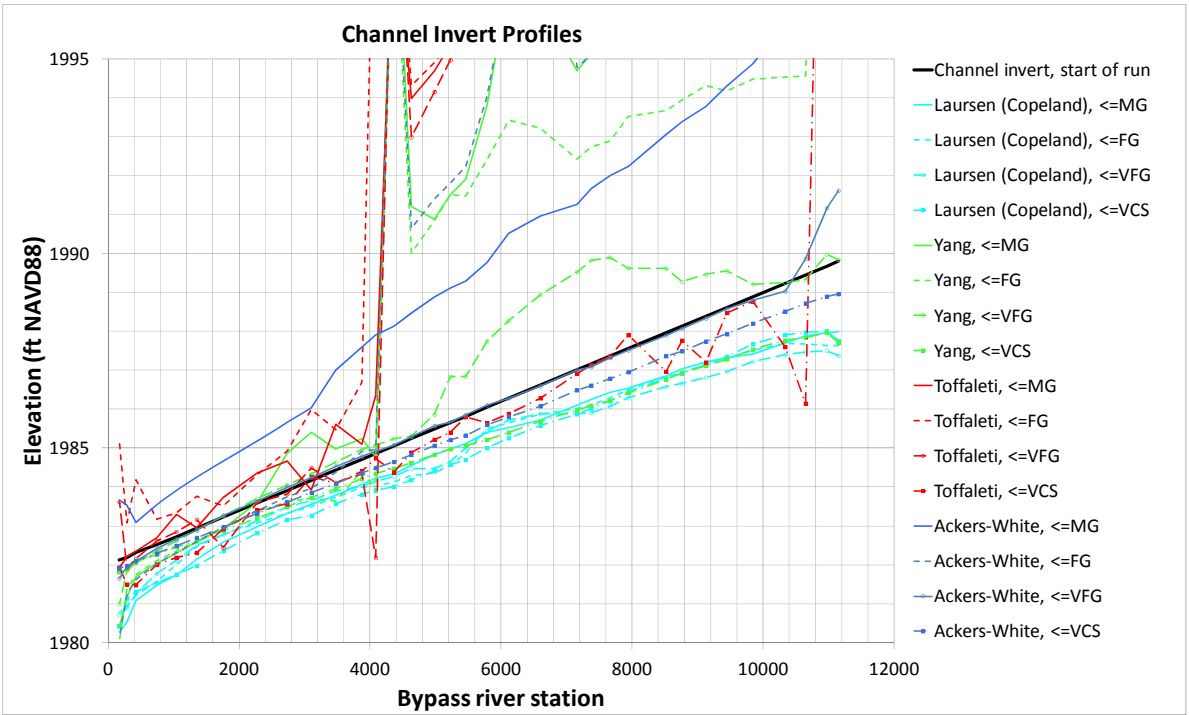

Figure 8 Transport Function and Incoming Gradation Sensitivity (s=0.0007ft/ft)

Figure 8 shows the bypass channel bed invert following the post-Yellowtail Dam flow record (47 years, 1967-2014) limited to a bypass flow of 9,000 cfs. For all runs, the initial channel slope was 0.0007 ft/ft and bed gradation is the Wolman count gradation described above. The legend in the figure indicates which transport function was used, along with the maximum material size of the incoming load (i.e. <=MG indicates the maximum size was medium gravel; FG=Fine Gravel, VFG=Very Fine Gravel, and VCS=Very Coarse Sand).

Figure 9 shows the base runs for slopes of 0.0006 ft/ft and 0.0007 ft/ft. The model shows low sensitivity to the channel slope in this range.

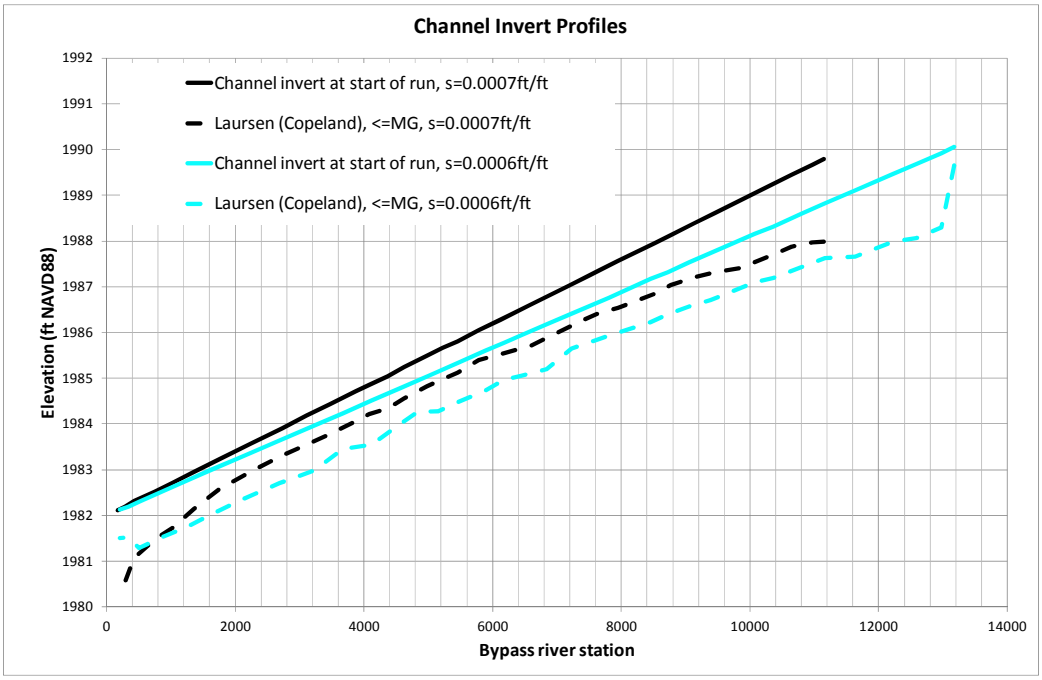

Figure 9 Slope Sensitivity

Sensitivity to the incoming load was evaluated by running the model using the high and low end loads shown in Figure 3. Results of the sensitivity analysis are shown in Figure 10. Unrealistic aggradation at the upstream end of the bypass occurs with the high incoming sediment load which is approximately nine times greater than the base load. This unrealistic aggradation also occurs in the main channel model, indicating that limitations of the transport functions, rather than physical processes are the cause. As shown in Figure 10, a second run was executed with an incoming load of approximately three times the base load.

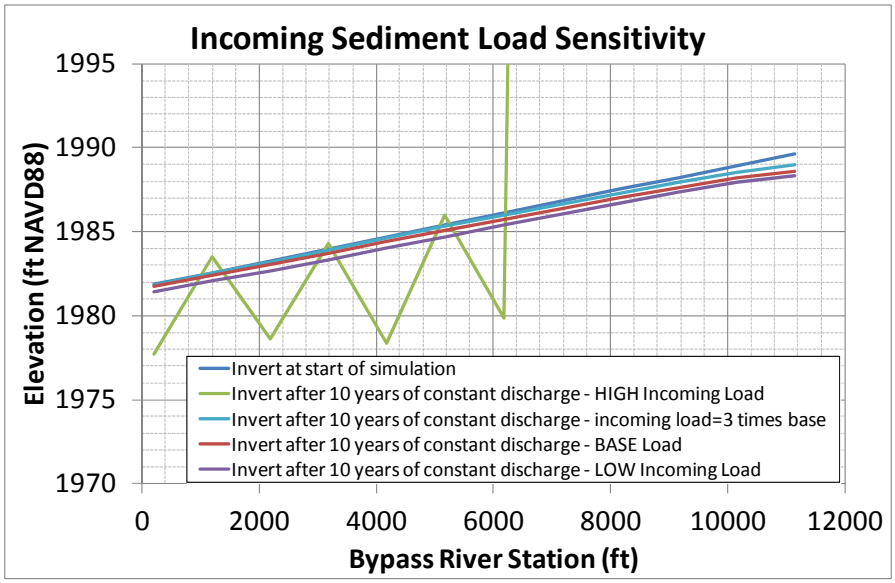

Figure 10 Incoming Sediment Load Sensitivity

Sensitivity to selected sorting method was evaluated by running the model with all three available sorting methods (Brunner 2010): Thomas (Ex5), Active Layer, and Copeland (Ex7). Results of the sensitivity analysis are shown in Figure 11. Runs using the Thomas (Ex5) and Copeland (Ex7) sorting methods produce similar results. The Active Layer method run produced unrealistic aggradation (on the order of 130 ft). Again, this unrealistic aggradation also occurs in the main channel model, indicating that limitations of the sorting method, rather than physical processes are the cause.

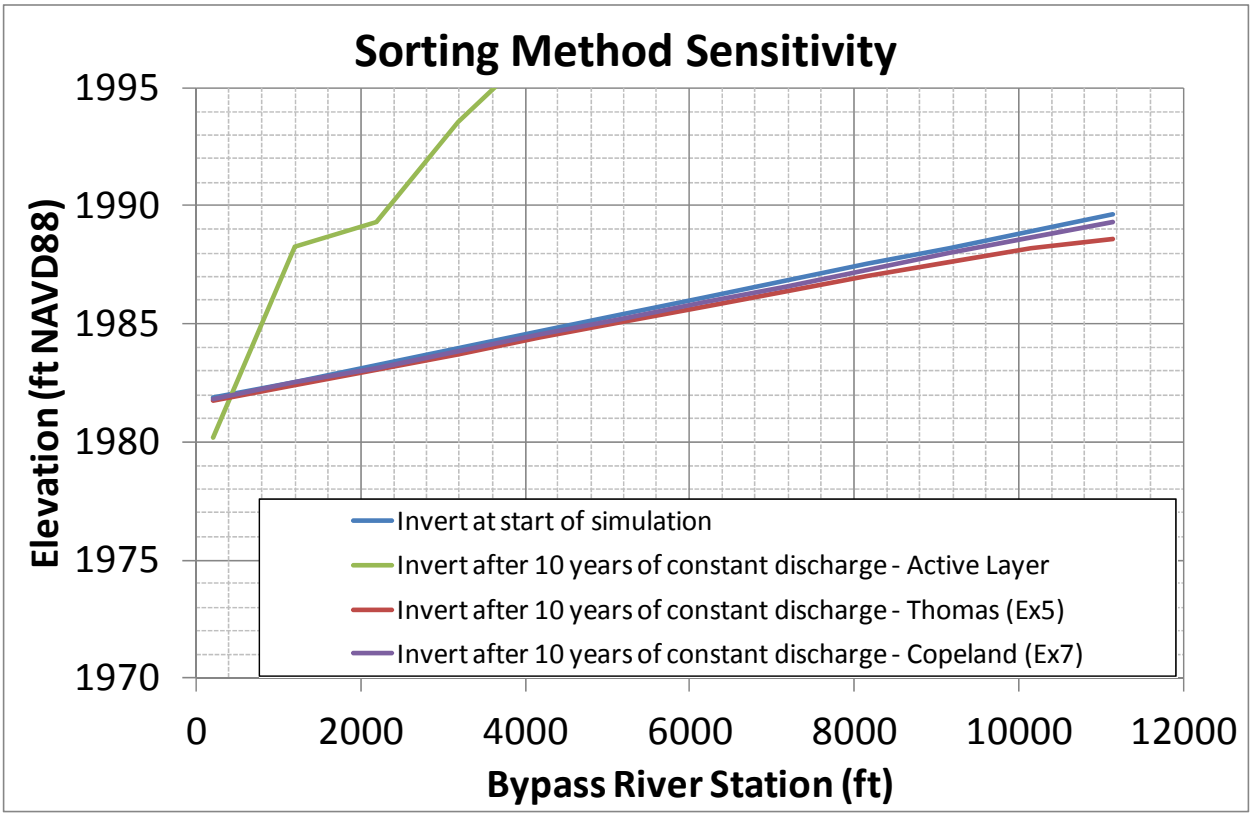

Figure 11 Sorting Method Sensitivity

Because of the large number of alternatives considered, initial sediment runs used uniform cross section shapes and channel slopes. However, the final design includes natural channel elements (varied cross section shapes and inverts). Once the final geometry was selected, the base sediment data were run to evaluate response to the proposed natural channel elements. Figure 12 compares results of the uniform channel vs. the "natural" channel. Figure 13 further compares the results shown in Figure 12. While the general trend of degradation is similar between the uniform and varied channel, HEC-RAS results indicate that some of the pool cross sections may tend to be slightly depositional.

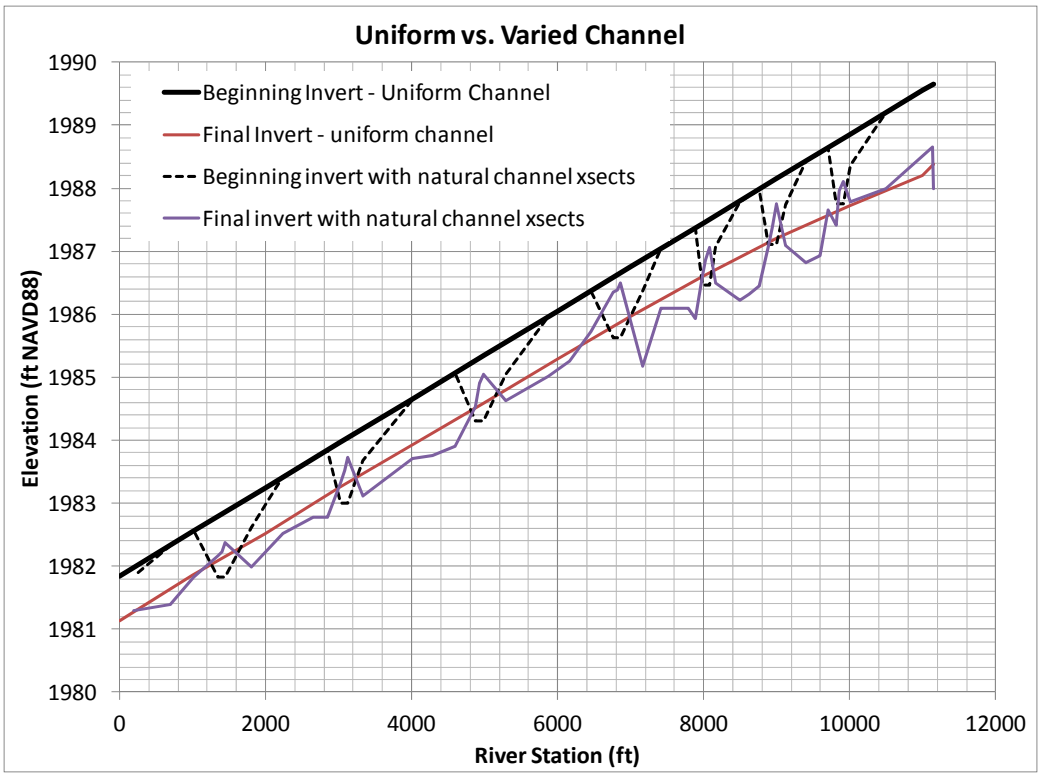

Figure 12 Uniform vs. Varied Channel

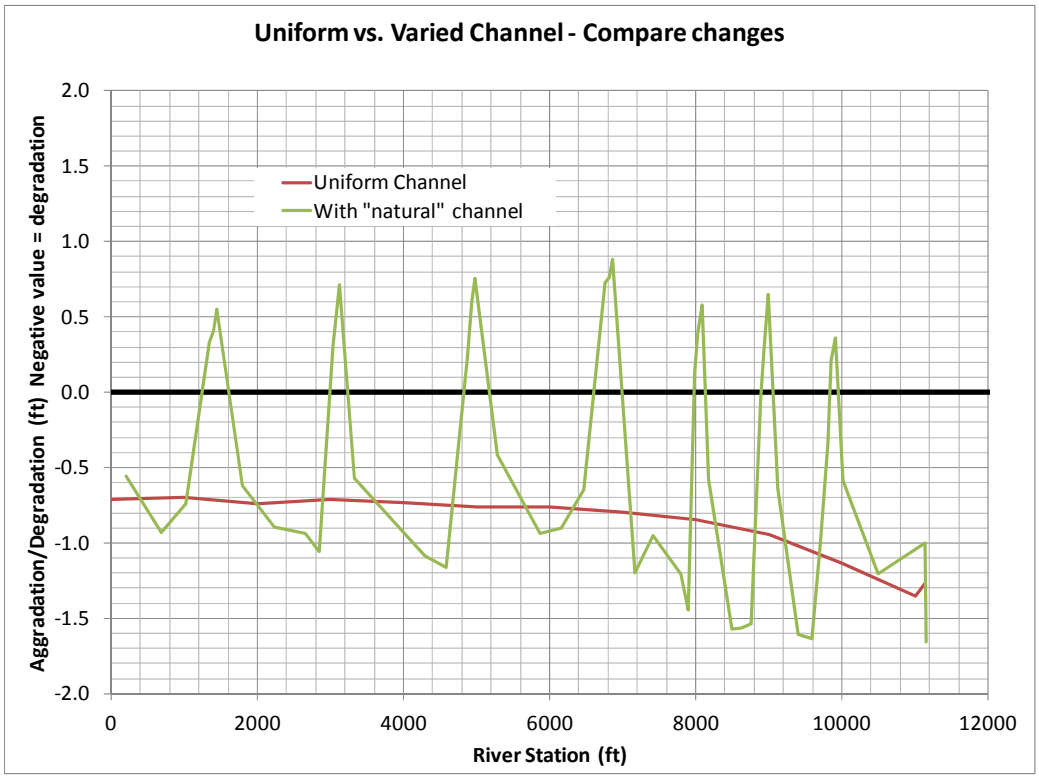

Figure 13 Comparison of Aggradation/Degradation Between Uniform and Varied Channel

SUMMARY AND CONCLUSIONS

Sediment modeling was completed with HEC-RAS to evaluate long term stability of a proposed bypass channel at Intake Dam on the Yellowstone River. Because no calibration data is available, multiple sensitivity analyses were completed to reduce uncertainty.

In general, the model shows high sensitivity to the incoming gradation and transport function; moderate sensitivity to the incoming load, bed gradation, discharge, and sorting method; and low to moderate sensitivity to the channel slope within the ranges considered.

REFERENCES

Ackers, P., and White, W.R. (1973). "Sediment Transport: New Approach and Analysis," Journal of the Hydraulics Division, American Society of Civil Engineers, Vol. 99, No. HY 11, pp. 2040-2060.

Brunner, Gary W. (2010). HEC-RAS River Analysis System, Hydraulic Reference Manual, Version 4.1, January 2010.

Copeland, R.R. and W.A. Thomas (1989). Corte Madera Creek Sedimentation Study. Numerical Model Investigation. U.S. Army Engineer Waterways Experiment Station, Vicksburg, MS. TR-HL-89-6.

Laursen, E.M. (1958). "Total sediment load of streams," Journal of the Hydraulics Division, ASCE, 84(HY1), 1530-1 to 1530-36.

Soar, Philip J. and Thorne, Colin R. (2001). Channel Restoration Design for Meandering Rivers. ERDC/CHL CR-01-1.

Toffaleti, F.B. (1968). Technical Report No. 5. "A Procedure for Computation of Total River Sand Discharge and Detailed Distribution, Bed to Surface," Committee on Channel Stabilization, U.S. Army Corps of Engineers, November, 1968.

Wolman, M.G. (1954). "A Method of Sampling Coarse River-bed Material," Transactions, American Geophysical Union 35(6):951-956.

Yang, C.T. (1973). "Incipient Motion and Sediment Transport," Journal of the Hydraulics Division, American Society of Civil Engineers, Vol. 99, No. HY10, October 1973, pp 1679-1704.

Yang, C.T. (1984). "Unit Stream Power Equation for Gravel," Journal of the Hydraulics Division, American Society of Civil Engineers, Vol. 110, No. 12, December 1984, pp 1783-1797.

SEDIMENTATION ANALYSIS OF THE YELLOWSTONE RIVER AT INTAKE DIVERSION DAM, MONTANA

Mike Sixta, M.S., P.E., Hydraulic Engineer, U.S. Bureau of Reclamation, Denver, CO, msixta@usbr.gov; Blair Greimann, Ph.D., P.E., Hydraulic Engineer, U.S. Bureau of Reclamation, Denver, CO, bgreimann@usbr.gov; Kent Collins, P.E., Hydraulic Engineer, U.S. Bureau of Reclamation, Denver, CO, kcollins@usbr.gov

BACKGROUND

The Lower Yellowstone Project is a Bureau of Reclamation (Reclamation) irrigation project built in 1908 under the Reclamation Act of 1902. It is located on the Yellowstone River in eastern Montana approximately 70 miles upstream from the confluence with the Missouri River, and 15 miles northeast of Glendive. The project consists of a low-head diversion dam, a diversion headworks structure, and an irrigation canal system that delivers water to approximately 53,000 acres in eastern Montana and western North Dakota. The diversion dam has become a known barrier to native fish migration including the endangered pallid sturgeon. In addition, the canal has been documented to entrain hundreds of thousands of fish annually during diversion operations occurring from April through September. This entrainment issue was recently addressed through the construction in the spring of 2012 of a new screened headworks structure immediately upstream of the old headworks structure.

Reclamation has an obligation, under the Endangered Species Act, to modify the structure of this facility to address pallid sturgeon concerns raised by the Fish and Wildlife Service and the Montana Department of Fish, Wildlife, and Parks. The U.S. Army Corps of Engineers (USACE) received authority to proceed with the design of the Lower Yellowstone Project. Technical staff from both Reclamation and the USACE were brought together to form a multi-agency team tasked with the development and analysis of designs that would address the recovery goals for both agencies.

INTRODUCTION

The proposed Yellowstone River Intake (YRI) Diversion Dam Modification Project includes the design of a large bypass channel around the diversion dam with the intent of improving upstream and downstream fish passage for adult pallid sturgeon and other native fish. The bypass channel will convey a significant portion of the river flow and sediment. Subsequently, the bed geometry of the reach may change as a result of the project. Reclamation conducted a sediment transport analysis utilizing a two-dimensional mobile bed hydraulics numerical model (SRH-2D; Lai, 2008) on a 5.5-mile reach of the Yellowstone River centered on the intake diversion dam and including the bypass channel. Figure 1 shows a project location map. This evaluation predicted the changes in bed elevations and stream geometry that would result from this project. The sedimentation analysis was further utilized to evaluate one of the other main goals of the proposed design; to minimize the operations and maintenance burden on the local irrigation district.

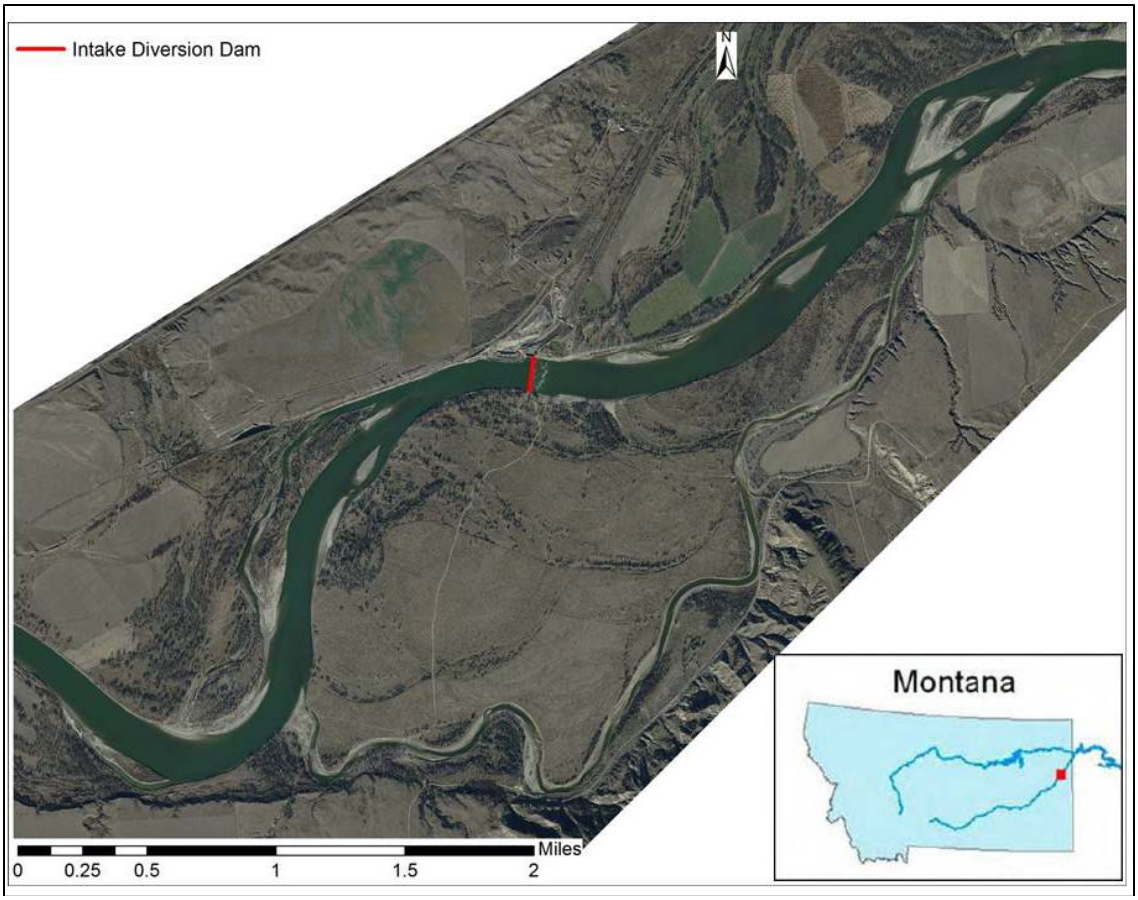

Figure 1 Lower Yellowstone Project location map (flow is from left-to-right).

DESIGN ALTERNATIVES

Reclamation has, to date, numerically modeled and evaluated two (2) iterative bypass channel design alternatives that were at a 30% and 60% completion level. Several bypass channel alignments were evaluated by the USACE before choosing a preferred one for the 30% design. Model results of the 30% design showed low velocities and the potential for sediment deposition at the downstream end of the bypass channel, largely due to backwater effects from the main channel of the Yellowstone River. To compound the issue, the bypass channel was not capturing enough flow from the main stem. These observations prompted the design of a revised bypass channel alignment and geometry, which was included in the 60% design alternative. The 60% alignment had a reduced length that precluded the use of the existing high flow channel. The proposed 60% alignment takes advantage of existing swales and cut-off channels where feasible. In addition, changes in the entrance/exit angles to the Yellowstone River were included to alter the flow direction in these critical locations for both channel stability and fish passage. The proposed 60% bypass channel design is approximately 11,150 feet long with an average channel slope of 0.0007 feet/feet, and bottom and top width of 40 feet and 150-250 feet, respectively. Approximately 900,000 cubic yards of material will need to be excavated to construct the channel (USACE, 2014).

MODELING METHODOLOGY

The model domain spans roughly 5.5 river miles on the Yellowstone River, centered on the intake diversion dam. The main goal of this project was to improve upstream and downstream fish passage for adult pallid sturgeon and other native fish by constructing a bypass channel around the diversion dam. A two-dimensional hydraulics and sediment transport mobile bed model was developed to assess the bypass channel functionality and stability as well as its effect on the main stem of the Yellowstone River. Model results were used to inform and iteratively refine project design concepts at various stages of development. Baseline hydraulic parameters, sediment transport rates, and amounts of erosion/deposition were compared through the design process.

Initially, hydraulic conditions with static channel geometry were simulated to calibrate the flow roughness, compute the quantity of flow entering the bypass, and assess mesh density sensitivity. Modeling of the mobile bed channel dynamics and sediment transport commenced after a satisfactory hydraulics model was constructed and calibrated. Model inputs, which are discussed in detail in this section, included a mesh with topographic information, bed material gradations, and flow-roughness parameters. Model boundary conditions included discharge hydrographs and sediment loads for the upstream domain boundary, while a rating curve specifying the water surface elevations over the range of modeled discharges was used at the downstream boundary.

Model Selection: All numerical models require simplifying assumptions and thus have limitations. The choice of model is often governed by time and budget constraints, knowledge of and access to existing models, and the availability of enough data with which to develop the model. It is important to understand the formulation of the selected model, recognize the model limitations, and apply the model in a manner that takes advantage of its strengths. Numerical model predictions will always include some uncertainty because the physical processes being modeled are not completely represented in the governing equations used in the model.

The numerical models utilized for this study were HEC-RAS (v 4.1.0) and SRH-2D (v 3.0). HEC-RAS is a one-dimensional (1D) step-backwater hydraulic model developed by the USACE. This model was utilized to simulate cross-section averaged river hydraulics for a series of steady flows. The basic computational procedure utilized in this model is based on the solution of the one-dimensional energy equation. Energy losses are represented through friction (Manning's equation) and contraction/expansion (coefficient multiplied by the change in velocity head). The USACE utilized HEC-RAS to develop design criteria, while Reclamation utilized it mainly to set the downstream boundary condition for the SRH-2D model simulations, which consisted of the development of a water surface elevation as a function of flow rate.

SRH-2D is a two-dimensional (2D) mobile-bed hydraulics and sediment transport model for river systems developed by Reclamation at the Technical Service Center in Denver, Colorado (Lai, 2008). SRH-2D solves the depth-averaged dynamic wave equations with a parabolic turbulence model using a finite-volume numerical scheme. The model adopts a zonal approach for coupled modeling of channels and floodplains; a river system is broken down into modeling zones (delineated based on natural features such as topography, vegetation, and bed roughness), each with unique parameters such as flow resistance. One of the major features of SRH-2D is the

adoption of an unstructured hybrid mixed element mesh, which is based on the arbitrarily shaped element method of Lai (2000) for geometric representation. This meshing strategy is flexible enough to facilitate the implementation of the zonal modeling concept; it allows for greater modeling detail in areas of interest that ultimately leads to increased modeling efficiency through a compromise between solution accuracy and computing demand.

Model Topography: To represent the model terrains, a multi-resolution three-dimensional surface was generated in a Geographic Information System (GIS) using a Triangulated Irregular Network (TIN). Topographic representations of the existing and proposed 30% and 60% design conditions were constructed. This was accomplished using a combination of bathymetric and land survey data collected through a joint effort between Reclamation and the USACE, along with Light Detection and Ranging (LiDAR) data. The type of LiDAR acquisition used does not have the ability to penetrate through water. Therefore, bathymetric survey data replaced the LiDAR data in wetted areas. Proposed design condition contours were generated by the USACE in AutoCAD that were subsequently brought into GIS for surface building. An example area from the model domain of the resulting terrain for the 60% design is shown in Figure 2.

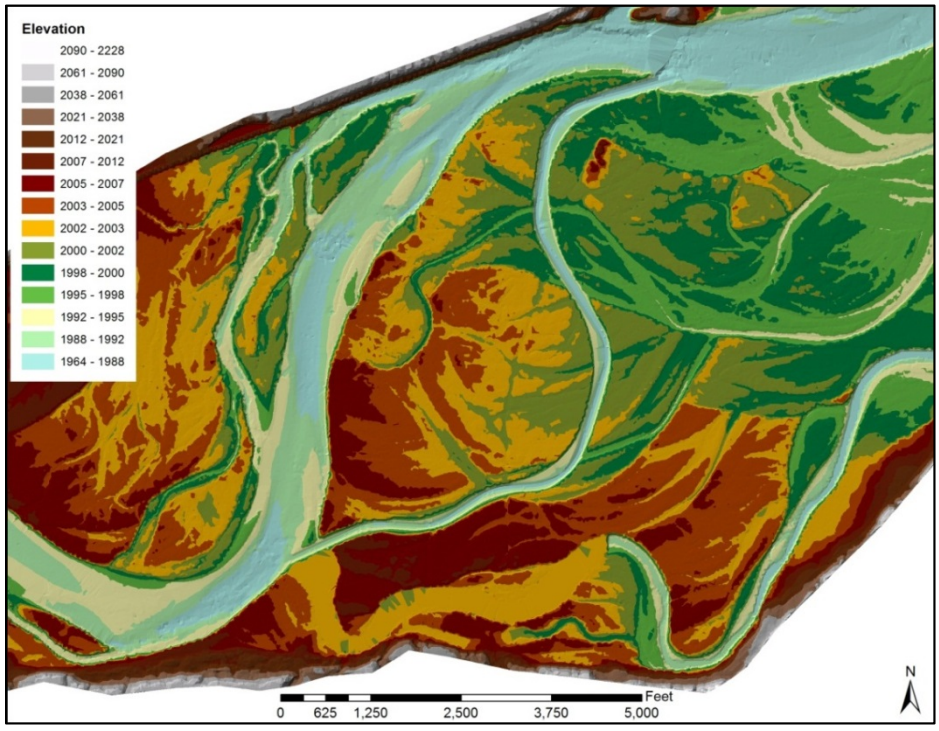

Figure 2 Example area showing the 60% design conditions surface used as input to the model. Elevation values are in feet.

Model Mesh: A 2D mesh defines the SRH-2D model topography and solution spacing. The mesh (nodes) stores ground elevation information from the model surface and consists of quadrilateral and triangular shaped elements. Surface-water Modeling System (SMS) software was used to construct flexible mixed element meshes that allowed for increased definition near areas of interest by using finer mesh cells. Coarser mesh cells were used elsewhere. A hydraulics only (fixed bed) module of SRH-2D was utilized to compare a relatively dense mesh (103,125

elements) to a much coarser mesh (25,350 elements) representing the existing conditions. This comparison was conducted using hydraulic outputs and showed the differences between the computed depths to be minimal. A coarser mesh relative to a fixed bed hydraulics model is needed for mobile bed simulations with sediment transport. This is due to the practical limitations of the number of mesh elements (and nodes) for the computationally intensive calculations in an effort to balance run time with model resolution. SMS was also utilized to delineate model roughness areas and assign model boundary conditions.

Each set of modeled design conditions (existing, 30%, and 60%) had its own computational mesh. The meshes consisted primarily of quadrilateral elements within channel areas and triangular elements in the floodplain/overbank areas. The element size varied based on location. In the main channel, the size of the quadrilateral elements was, on average, 65 feet in the lateral (cross stream) direction and 100 feet in the longitudinal (downstream) direction. The shorter dimension in the lateral direction was used to capture the more rapidly changing topography transverse to the stream flow with respect to horizontal distance. The triangular elements in the floodplain areas increased in coarseness as the model approached the domain boundary to a maximum size of 120 feet. An approximate total of 25,350 elements were used in the model domain to represent the existing topographic conditions. An increased mesh density along the proposed bypass channel alignments was incorporated into the preferred alternative meshes as it was a feature of focus. The 30% design bypass channel had an average element size of 25 by 35 feet while the 60% design bypass channel had an average element size of 20 by 35 feet. As a result the total number of mesh elements representing the proposed conditions model domain increased to roughly 30,450 for the 30% design and 39,000 for the 60% design. An example area of the model mesh for the 60% design conditions is shown in Figure 3.

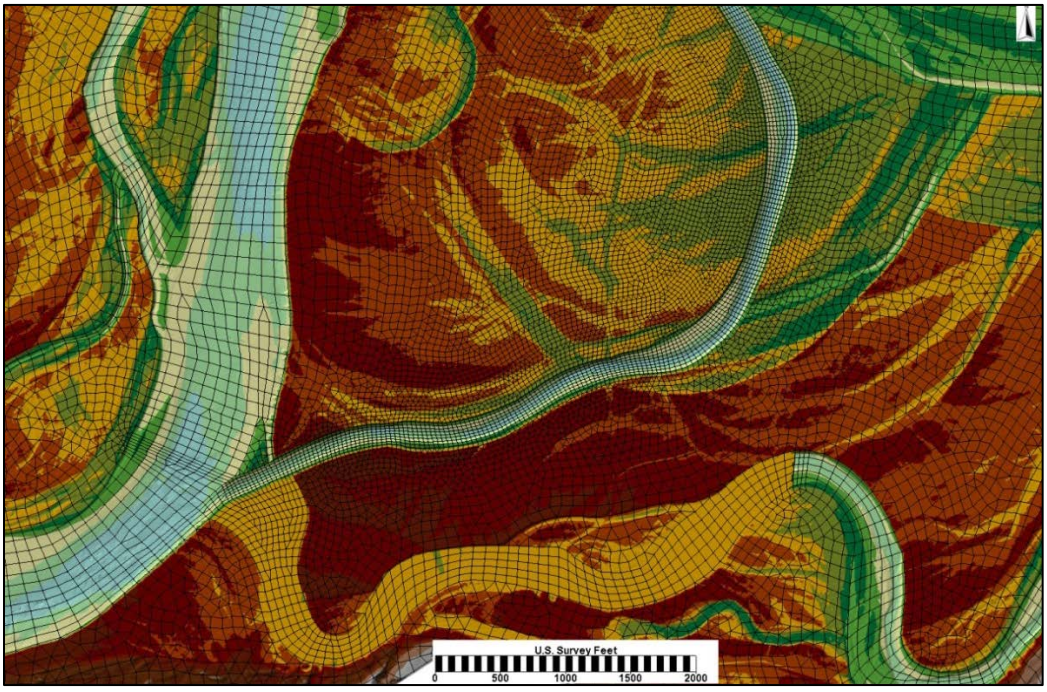

Figure 3 Example area of model mesh for 60% design conditions.

Model Boundary Conditions: Boundary conditions for the SRH-2D model were specified at the upstream and downstream model domain. The upstream boundary condition required both hydrologic (flow) and sediment data as inputs. Two average daily flow hydrographs representing particular events of interest were used for the flow input, while a rating curve relating flow to sediment discharge fluxes according to grain size was used for the sediment input. Another rating curve assigning a water surface elevation to the full range of flows from both hydrographs was used for the downstream boundary condition.

Upstream Boundary Condition – Hydrology: The closest USGS gages to the intake diversion dam are the Yellowstone River at Glendive MT Gage (06327500) which is located roughly 18 miles upstream, and the Yellowstone River near Sidney MT Gage (06329500) located roughly 36 miles downstream. For the SRH-2D sediment modeling, discharge data from only the Glendive Gage was used as it was upstream of the project site and closer in proximity. Average daily data representing two distinct hydrographs were selected to try and represent a range of flow conditions that the project design could encounter. A 2008 hydrograph was chosen as it appeared to roughly represent a typical wet year when looking at the most recent ten years of gage record. This hydrograph spans 107 days (5/19/08 - 9/2/08) with a peak flow of 63,200 cfs, which is roughly equivalent to the 5-year recurrence interval event according a flow frequency analysis conducted by the USACE (USACE, 2012). The other hydrograph used was from 2011 as it contains the flood of record. This hydrograph spans 206 days (3/1/11 - 9/22/11) and peaks at 122,000 cfs, which corresponds to a value above the 500-year event. The 2008 hydrograph is shown in Figure 4.

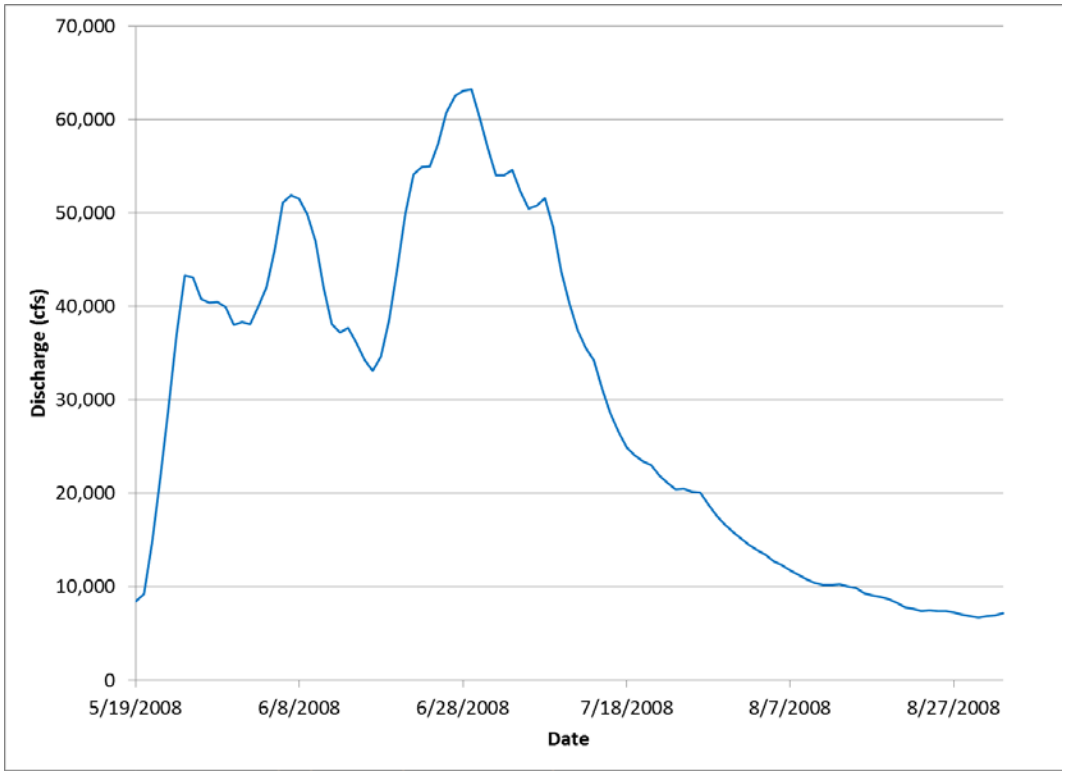

Figure 4 2008 input hydrograph.

Upstream Boundary Condition – Sediment Loads: The Yellowstone River has a mixed sand and gravel bed. Therefore, the consideration of bed load and suspended load sediment transport is necessary to quantify the passage of the total sediment load through the system. For the numerical sediment modeling, the relationship of total sediment load to the inflowing discharge is a necessary input.

To derive this total incoming sediment load relationship, Reclamation's in-house program SRH-Capacity (Huang and Bountry, 2009) was used. This model computes the sediment transport capacity using a specified transport equation for a given set of hydraulics and flow values. The required inputs for SRH-Capacity include 1D (cross section based) hydraulics, particle size gradation data, and hydrology data.

To compute the 1D hydraulics, Reclamation modified a HEC-RAS hydraulics model previously developed by the USACE. Additional cross sections were added to the HEC-RAS model to capture the pool-riffle sequence present in the morphology of the Yellowstone River channel. The geometry of the modified HEC-RAS model was then updated with the new topographic data collected in August 2012 by Reclamation and USACE staff.

Particle size gradation data were derived from gravel bar and bank sediment data collected by the USACE in August 2008 (USACE, 2008). The average of three and four grain size distributions was used in the model to represent the channel areas upstream and downstream of the intake diversion dam, respectively. These average distributions were binned into six different sediment size classes, two representing sand and the remaining four representing gravel.

Given the above input, the incoming sediment loads were calculated using the following three sediment transport equations, which are commonly used for rivers with both sand- and gravel-sized sediments:

1. Parker's (1990) bed load transport capacity equation combined with Engelund and Hansen (E/H, 1972), where the transport capacity of particle sizes greater than 2mm are computed with Parker, and the transport capacity of particle sizes less than 2mm are computed with E/H.
2. Wilcock and Crowe's (W/C, 2003) bed load transport capacity equation combined with Engelund and Hansen (E/H, 1972), where the transport capacity of particle sizes greater than 2mm are computed with W/C, and the transport capacity of particle sizes less than 2mm are computed with E/H.
3. Wu et al. (2000) total load sediment transport equation.

Downstream Boundary Condition: The downstream boundary condition consisted of a water surface elevation versus discharge rating curve. Discharge values encompassed both hydrographs. The associated water surface elevations were derived from the updated USACE HEC-RAS hydraulics model at a cross section whose location was at the downstream model domain boundary.

MODEL RESULTS DISCUSSION

The main objective of the YRI hydraulics and sediment transport model was to evaluate the stability and effect of a proposed bypass channel around the intake diversion dam by quantitatively evaluating short term and long term changes in bed elevations. 2D sediment model runs were performed using topographic representations of the currently existing conditions along with the proposed 30% and 60% project designs. Erosion/deposition results from the 30% design showed the lower half of the bypass channel (downstream of the channel split) experiencing deposition. This led to a complete re-design of the bypass channel for the 60% design. Conversely, the 60% design showed small amounts of erosion throughout the bypass channel. Given the model uncertainties however, this was viewed as being in general equilibrium. A side-by-side comparison of the erosion/deposition results from the 2008 hydrograph for the 30% and 60% designs is shown in Figure 5.

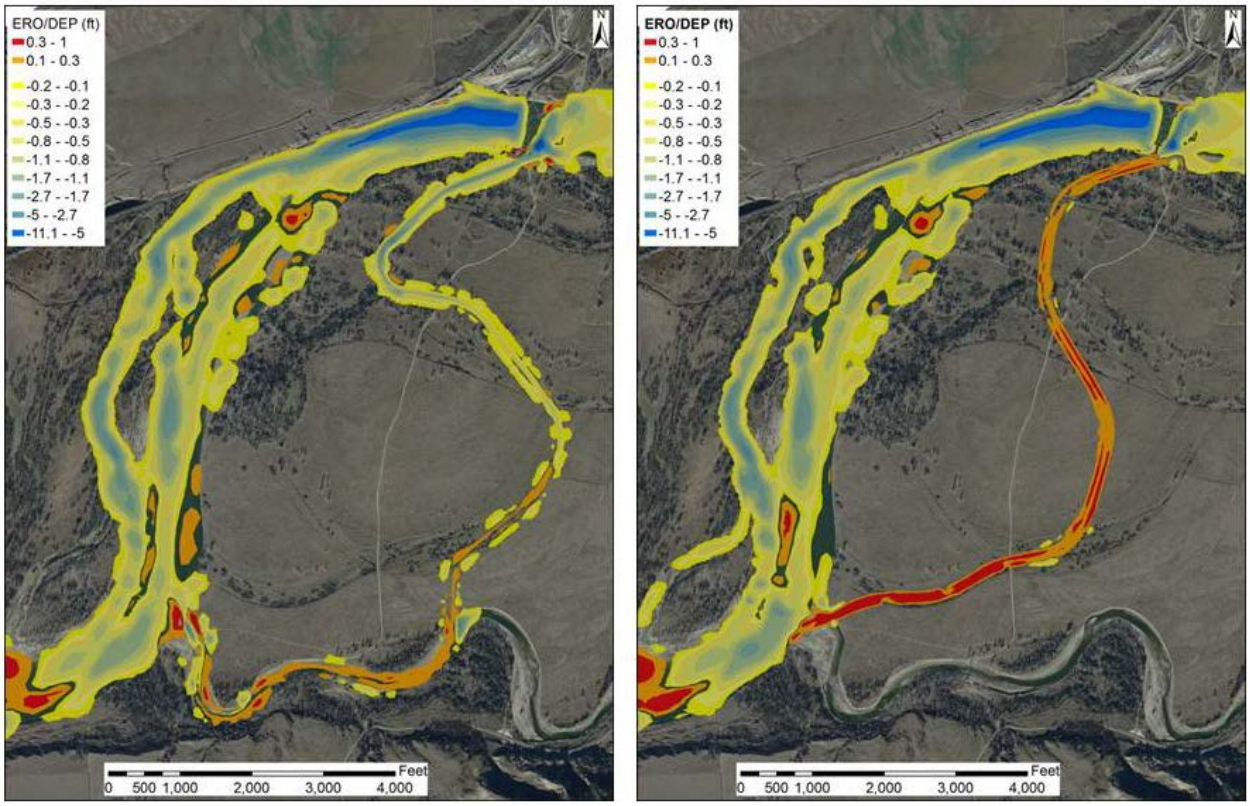

Figure 5 Erosion/Deposition results for the 2008 hydrograph using the Parker and E/H formulation for the 30% design (left) and 60% design (right). A positive (+) value indicates erosion while a negative (-) value indicates deposition.

In addition to evaluating erosion/deposition, monitoring lines were set up at areas of interest throughout the main and bypass channels to track sediment loads during the simulations. Sediment flux was measured at the upstream and downstream ends of both the main and bypass channels under all three modeled scenarios (existing conditions, 30% design, and 60% design).

Results showed the Parker, and Wilcock and Crowe formulations to be comparable, while the Wu formulation yielded noticeably lower sediment transport amounts. The average amount of main channel sediment captured by the bypass channel was roughly 8.5 to 9% for the 30% design and 11.5 to 12% for the 60% design. The relative amount of sediment being deposited in the 30% designed bypass channel is more than the amount of sediment being eroded in the 60% designed bypass channel. According to the Parker and Wilcock and Crowe formulations, an average of 12% and 17% of the incoming sediment load to the 30% design bypass channel is being deposited during the 2008 and 2011 hydrographs, respectively. Conversely, an average of 6% and 2% of the incoming sediment load to the 60% design bypass channel is being eroded during the 2008 and 2011 hydrographs, respectively. These results further indicate that the 60% design bypass channel is more stable with regards to sediment equilibrium during higher flow events. Lastly, sediment flux results showed that neither bypass channel design had a significant effect on the overall sediment balance in the reach. A sample set of sediment flux results are shown graphically in Figure 6 for the 60% design with the 2008 hydrograph that shows some of the above trends.

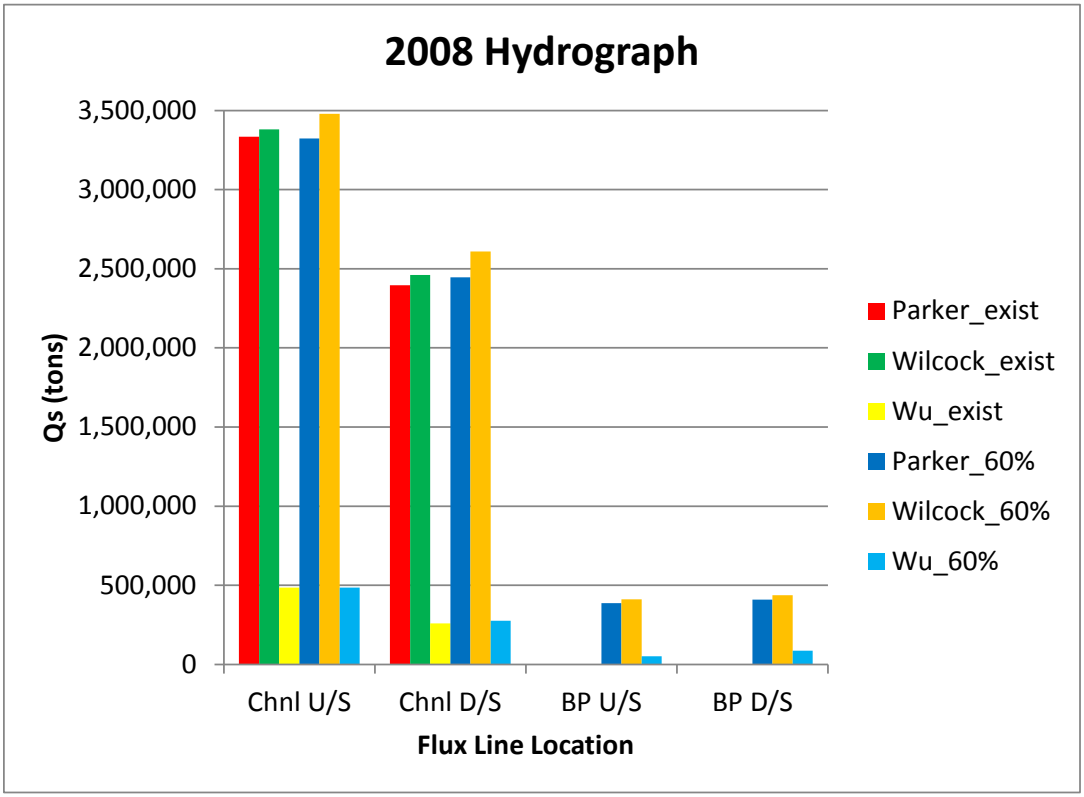

Figure 6 Sediment flux results for the 60% design under the 2008 hydrograph. (Chnl – Main Channel; BP – Bypass Channel)

SUMMARY AND CONCLUSIONS

The Lower Yellowstone Project consists, in part, of a diversion dam that has become a known barrier to migration of native fish, including the endangered pallid sturgeon. To address this, a diversion dam modification project is under design that includes a large bypass channel around the structure to improve the upstream and downstream fish passage. Reclamation evaluated the existing conditions as compared to the 30% and 60% proposed design through conducting a sediment transport analysis utilizing a two-dimensional hydraulics and sediment transport mobile bed model (SRH-2D) on the 5.5 miles of the Yellowstone River centering on the diversion dam and inclusive of the bypass channel. Model results were used iteratively through the design process, aiding the direction of future designs. The evaluation predicted the changes in bed elevations that would result from this project by looking at amounts of erosion/deposition along with overall reach affects.

Model results of the 30% design showed low velocities and corresponding deposition on the lower half of the bypass channel. As a result, the bypass channel was re-redesigned (60% design), which conversely showed small amounts of erosion throughout, but was deemed as being in approximate equilibrium. A sediment flux analysis revealed a significant difference between the Wu sediment transport formula as compared with the Parker, and Wilcock and Crowe formulations. The 30% design captured approximately 9% of the main channel sediment, while the 60% design captured roughly 12% during the 2008 hydrograph. The relative amount of sediment that was shown being deposited in the 30% bypass design was more than the amount of sediment being eroded in the 60% design. Lastly, neither bypass channel design was shown to have a significant effect on the overall sediment balance in the reach.

REFERENCES

Engelund, F., and Hansen, E. (1972). *A monograph on sediment transport in alluvial streams.* Teknish Forlag, Technical Press, Copenhagen, Denmark.

Huang, J.V. and Bountry, J. (2009). SRH-Capacity User Manual, Version 1.37. U.S. Department of Interior, Bureau of Reclamation, Technical Service Center, Denver, Colorado.

Lai, Y.G. (2000). "Unstructured grid arbitrarily shaped element method for fluid flow simulation." *AIAA Journal*. 38(12), 2246-2252.

Lai, Y.G. (2008). SRH-2D version 2: Theory and User's Manual. Sedimentation and River Hydraulics – Two-Dimensional River Flow Modeling. U.S. Department of the Interior, Bureau of Reclamation, Technical Service Center, Denver, CO.

Parker, G. (1990). "Surface based bedload transport relationship for gravel rivers." *Journal of Hydraulic Research*, Vol. 28(4), 417–436.

USACE. (2008). Bar Sample Trip Report 26-28 August 2008. U.S. Army Corps of Engineers, Omaha District. Omaha, Nebraska.

USACE. (2012). Intake Diversion Dam Modification Lower Yellowstone Project, Montana. Bypass Channel 30% Design Documentation Report. U.S. Army Corps of Engineers, Omaha District. DRAFT. December 2012. Appendix A – Hydraulics.

USACE. (2014). Intake Diversion Dam Modification Lower Yellowstone Project, Montana. Bypass Channel 60% Design – May 2014 Interim Progress Report Hydraulics. U.S. Army Corps of Engineers, Omaha District. Hydrologic Engineering Branch. DRAFT May 2014.

Wilcock, P.R., and Crowe J.C. (2003). "Surface-Based Transport Model for Mixed-Size Sediment," *Journal of Hydraulic Engineering*, ASCE, 129(2):120-128.

Wu, W., Wang, S.S.Y., and Jia, Y. (2000). "Nonuniform sediment transport in alluvial rivers." *Journal of Hydraulic Research*, Vol. 38(6):427-434.

INACCURACIES IN SEDIMENT BUDGETS ARISING FROM ESTIMATIONS OF TRIBUTARY SEDIMENT INPUTS: AN EXAMPLE FROM A MONITORING NETWORK ON THE SOUTHERN COLORADO PLATEAU

Ronald E. Griffiths, Hydrologist, U.S. Geological Survey, Flagstaff, Arizona, rgriffiths@usgs.gov;
David J. Topping, Research Hydrologist, U.S. Geological Survey, Flagstaff, Arizona, dtopping@usgs.gov

Abstract Sediment budgets are an important tool for understanding how riverine ecosystems respond to perturbations. Changes in the quantity and grain-size distribution of sediment within river systems affect the channel morphology and related habitat resources. It is therefore important for resource managers to know if a channel reach is in a state of sediment accumulation, deficit or stasis. Many studies have estimated sediment loads from ungaged tributaries using regional sediment-yield equations or other similar techniques. While these approaches may be valid in regions where rainfall and geology are uniform over large areas, use of sediment-yield equations may lead to poor estimations of sediment loads in semi-arid climates, where rainfall events, contributing geology, and vegetation have large spatial variability.

Previous estimates of the annual sediment load from the ungaged tributaries to the Colorado River downstream from Glen Canyon Dam vary by an order of magnitude; this range in sediment loads has resulted in different researchers reaching opposite conclusions on the sign (accumulation or deficit) of the sediment budget in the Colorado River. To better estimate the supply of fine sediment (sand, silt, and clay) from these tributaries to the Colorado River, eight gages have been established on previously ungaged lesser tributaries in Glen, Marble, and Grand canyons. The remote locations of these streams and short duration of floods make it prohibitively expensive, if not impossible, to directly measure streamflow or to use conventional depth-integrating suspended-sediment samplers. Discharges are therefore calculated using a stage-discharge relation developed from a series of modeled flows and a stage record measured by a downward looking sonic ranging sensor. Flows are modeled using surveyed high-water marks, surveyed channel topography, and Z_0 bed roughness constrained by pebble counts. Suspended-sediment measurements are made with passive US U-59 samplers and, at some tributary gages, stage-triggered pump samplers. During floods with a sufficient number of suspended-sediment samples, loads are calculated by interpolating sediment concentrations between the physical samples. When few or no physical samples are collected for a given flood event, regression relations between discharge and sediment concentrations are used if the relations are statistically significant. For gages with no significant relation between discharge and sediment concentrations, mean sediment concentrations – averaged over the period of record – are used. Using these methods, suspended-silt-and-clay and suspended-sand loads transported past each of the lesser-tributary gages are calculated.

Results from this sediment-monitoring network show that previous estimates of annual sediment load from the tributaries were too high, and that the sediment budget for the Colorado River below Glen Canyon Dam is in greater deficit than previously concluded by most researchers. In addition, we found that floods of the same magnitude may have different source areas, resulting in large differences in sediment loads between equal magnitude flows. Because sediment loads do not necessarily correlate with drainage size, and cumulative sediment loads may vary by two orders of magnitude on an annual basis, using techniques such as sediment-yield equations to estimate sediment loads from ungaged tributaries may lead to large errors in sediment budgets.

INTRODUCTION

The calculation of accurate sediment budgets can be sensitive to the sediment supplied from ungaged tributaries. Studies have calculated sediment loads from ungaged tributaries using a number of methods, including: mass-balance calculations assuming quasi-equilibrium (Howard and Dolan 1981; Andrews, 1986), regional sediment-yield equations (Webb and et al., 2000), sediment-rating curves (Sutherland and Bryan, 1990) and peak discharge to total sediment-load relations (Rankl, 2002). The above methods can lead to errors when estimating annual sediment loads from semi-arid streams. Depending on the local geology, topography, and vegetation, floods in semi-arid regions can have large (10x) differences in sediment concentrations between equal magnitude flows as the result of locally intense rainfall events with footprints smaller than the receiving basin.

The Colorado River below Glen Canyon Dam is an example of a river reach where quantifying the supply of fine sediment from tributaries could be essential for calculating accurate sediment budgets. The Colorado River below Glen Canyon Dam is currently the focus of a major river restoration program (Campbell and others, 2010); one of the major goals of this program is the restoration of eddy sandbars in the Colorado River in Marble and Grand Canyons. Fine sediment is supplied to this reach from the Paria and Little Colorado Rivers as well as a number of smaller, herein referred to as lesser, tributaries. Sediment budgets calculated using estimates of cumulative sediment load from the lesser tributaries have been used to inform flow alternatives from Glen Canyon Dam with the objective of restoring sandbars (U.S. Department of the Interior, 1995). Over a factor of 5 variation exists in previous studies' estimates of the annual sediment load from the lesser tributaries to the Colorado River in Marble Canyon (BOR, 1956; BOR, 1958; Howard and Dolan, 1981; Randle and Pemberton, 1987; Webb et al., 2000). This large variation in estimated sediment load is large enough to have the effect of changing the sign of sediment budgets in the Colorado River in Marble and Grand canyons under certain conditions. The magnitude of the variation in these estimates and the fact that no direct measurements of lesser-tributary flood hydrographs or sediment transport were used in these estimates were the prime motivators of this study.

To better estimate the sediment supplied from the lesser tributaries to the Colorado River in Glen and Marble canyons, the U.S. Geological Survey (USGS) Grand Canyon Monitoring and Research Center established gages on previously ungaged lesser tributaries for measuring stage and suspended-sediment. This network of lesser-tributary gages was established in late 2000; most of the gages in the network now have over 13 years of data. At these gages, stage is recorded every 15 minutes during dry, or baseflow, periods and every minute during floods. Suspended-sediment measurements are made using US U-59 samplers (Edwards and Glysson, 1999), automatic-pump samplers, and rare dip samples. Channel topography and high-water marks are surveyed for subsequent flow modeling. High-water marks are modeled to determine flow; several sets of high-water marks are used to create a stage-discharge relation (Griffiths, 2010). This indirect method of determining discharge was chosen because of the remote location of the lesser-tributary gages and the short duration of floods. In this paper, we focus on the results from the ephemeral tributaries that discharge into the Colorado River in upper Marble Canyon. Upper Marble Canyon is herein defined as the reach of river from Lees Ferry to the formerly proposed Marble Canyon dam site at river mile 32.5 (by convention, river miles in Marble and Grand canyons begin at Lees Ferry and progress downstream).

PREVIOUS ESTIMATIONS OF LESSER-TRIBUTARY SEDIMENT SUPPLIES

A number of researchers have investigated the sediment supplied to the Colorado River from its lesser tributaries. The first studies were completed by the U.S. Department of the Interior, Bureau of Reclamation (BOR) in preparation for the proposed construction of Marble Canyon Dam (BOR, 1956; 1958). The initial 1956 BOR study estimated the mean-annual sediment load from the lesser tributaries

using the area of ungaged tributaries and the sediment yield from the "roughly similar" San Juan River. This study concluded that the mean-annual sediment load from the lesser tributaries between the Paria River and the proposed dam site was approximately 2.8 million metric tons. A second study by the BOR (1958), based on field observations of geology, geomorphology, vegetation, and sedimentation in stock tanks, concluded that the mean-annual sediment load from the lesser tributaries was approximately 740,000 metric tons (including gravel). In 1981, Howard and Dolan (1981) estimated the mean-annual sediment load from all lesser tributaries upstream from the Grand Canyon gage (USGS 09402500 Colorado River near Grand Canyon, AZ) to be 34 % of the combined mean-annual load from the Paria and Little Colorado rivers, or ~4 million metric tons. Randle and Pemberton (1987) using a regional sediment-yield regression to calculate lesser-tributary sediment loads, estimated that the mean-annual sediment load from the lesser tributaries in Marble Canyon to be ~910,000 metric tons. Of this total, they estimated that the mean-annual sand load from these Marble Canyon tributaries was ~140,000 metric tons (i.e., 15% of the load was sand). Sediment yields are reported in units of mass per unit area-time, whereas annual or cumulative sediment loads (i.e., sediment supplies) are reported in units of mass. A similar regional sediment-yield regression approach was used by Webb et al. (2000), who, in addition, employed a flood-frequency rating-curve method and results from a reservoir-sedimentation study combined with a runoff model to calculate three estimates of mean-annual sediment load from the lesser tributaries; the mean-annual sediment load from all lesser tributaries in Marble Canyon was estimated to be 460,000-610,000 metric tons. Of this total, they calculated the mean-annual sand load (assumed to be 15-75% of total sediment) ranged from 70,000-460,000 metric tons.

The majority of the previous studies reported mean-annual sediment loads calculated on the basis of sediment-yield equations derived for drainages with substantially different geologic and climatic conditions. No direct measurements of sediment transport in the lesser tributaries were used. In addition, the time-averaged nature of the sediment loads reported by the previous studies make these mean-annual loads poorly suited for calculation of sediment budgets over shorter time frames.

In the sections below, we will investigate in more depth some of the methods used in the previous studies. The two BOR studies estimated sediment yields and sediment supplied to the upper Marble Canyon Reach. The remaining studies estimated sediment yields and resulting sediment supplies to longer reaches of the river than the upper Marble Canyon Reach. To allow comparison with the previous study results, and between previous studies, we converted yield values from the disparate studies using drainage area in combination with published bulk sediment density estimates to generate estimates of mean-annual sediment loads from the lesser tributaries to upper Marble Canyon (Table 1).

Table 1 Summary of previous estimations of summed lesser-tributary mean-annual sediment loads to the Colorado River corrected and apportioned to the upper Marble Canyon Reach.

Study	Total sediment (metric tons)	Sand (metric tons)
Reclamation (1956)	1,900,000	No value estimated
Reclamation (1958)	760,000[a]	No value estimated
Howard and Dolan (1981)	1,800,000	No value estimated
Randle and Pemberton (1987)	680,000	100,000[b]
Webb and others (2000)	520,000	78,000-390,000[c]

[a]Includes gravel
[b]Sand assumed to be 15% of total sediment
[c]Sand assumed to be 15-75% of total sediment

The study by BOR (1956) estimated a lesser-tributary sediment yield of 714 m^3/km^2-yr. This initial estimation of sediment yield in combination with the lesser-tributary area of upper Marble Canyon (2,319 km^2) from Webb et al. (2000) and the sediment density of 1,153 kg/m^3 used by Randle and Pemberton (1987) results in a mean-annual sediment load of ~1.9 million metric tons (Table 1). Because of errors

made by BOR (1956) in determining the lesser-tributary area from the 1:500,000-scale map used, this mean-annual sediment load is less than the original study predicted. Because no grain-size distributions are reported by BOR (1956) for the lesser-tributary sediment load, no subdivision of predicted total sediment load into silt and clay supply and sand supply is possible.

The more-comprehensive BOR (1958) study conducted individual investigations in each of the "more-important" lesser tributaries and divided the lesser-tributary area between Glen Canyon Dam and the proposed Marble Canyon dam into 12 sediment-yield units. Correcting the BOR (1958) total drainage area by that reported in Webb et al. (2000) and using the Randle and Pemberton (1987) sediment density, the 1958 BOR study predicts the mean-annual sediment load from all upper Marble Canyon lesser tributaries of 760,000 metric tons of total sediment (Table 1).

Howard and Dolan (1981) estimated the sediment yield from the lesser tributaries to the Colorado River between Lees Ferry and the Grand Canyon gage (USGS 09402500 Colorado River near Grand Canyon, AZ) based on a pre-dam sediment mass balance and the assumption of the bathymetric changes observed at one cross section was representative of all geomorphic changes in this 140-km-long reach. By this approach, they estimated the sediment yield from the lesser tributaries to be approximately 34% of the combined annual sediment load from the Paria and Little Colorado Rivers, or ~780 metric tons/km^2-yr. This sediment yield in combination with the tributary drainage-basin areas from Webb et al. (2000) results in mean-annual sediment load from all upper Marble Canyon lesser tributaries of ~1.8 million metric tons (Table 1). As with BOR (1956, 1958), because no grain-size distributions are reported by Howard and Dolan (1981) for the lesser-tributary sediment yield, no subdivision of predicted total sediment load into silt and clay supply and sand loads is possible.

Applying the sediment yield from Marble Canyon (293 metric tons/km^2-yr) of Randle and Pemberton (1987) to the lesser-tributary area of upper Marble Canyon results in ~680,000 metric tons of sediment. Randle and Pemberton (1987) assumed sand comprised 15% of the total sediment, using this figure we calculate a mean-annual sand load from the lesser tributaries of ~100,000 metric tons.

Webb et al. (2000) used three methods for determining sediment yield from the lesser tributary areas. Because the results from the three methods were similar, they presented the results of the simplest method, the regional data regression. Using their sediment yield equation ($351 \cdot A^{0.88}$ where A is tributary drainage area in km^2) and the individual tributary drainage areas, we calculated the mean-annual sediment load from the lesser tributaries to upper Marble Canyon. In addition to the tributaries listed for Marble Canyon, they estimated an extra 120 km^2 of area that was not included in the list of tributaries. We divided this extra area by river miles and applied the resultant extra 62 km^2 to the upper Marble Canyon Reach. When determining sediment load from each tributary, we assumed this extra area was comprised of small drainages (1 km^2 each) and added the sediment loads to the total load for upper Marble Canyon. Using the Webb et al. (2000) methods, we thus calculated a mean-annual sediment load from the lesser tributaries of ~520,000 metric tons. Using their estimate of 15-75% sand results in ~78,000-390,000 metric tons of sand (Table 1).

LESSER-TRIBUTARY GAGES

There are currently eight gages on the lesser tributaries of the Colorado River in lower Glen, Marble, and Grand canyons where stage and suspended sediment are automatically measured (Figure 1). This monitoring network was established in 2000 and expanded in 2006 to include Bright Angel Creek (Griffiths et al., 2014). In this network, stage, suspended-silt and clay concentration, suspended-sand concentration, and suspended-sand grain-size measurements are made on lesser tributaries representing approximately 69% of the previously ungaged drainage area of upper Marble Canyon. All of the lesser-tributary gages, except for those in Water Holes Canyon and on Bright Angel Creek, monitor streams that

drain into upper Marble Canyon. This paper will focus on the lesser tributaries that flow into upper Marble Canyon, putting aside the gages in Water Holes Canyon and on Bright Angel Creek.

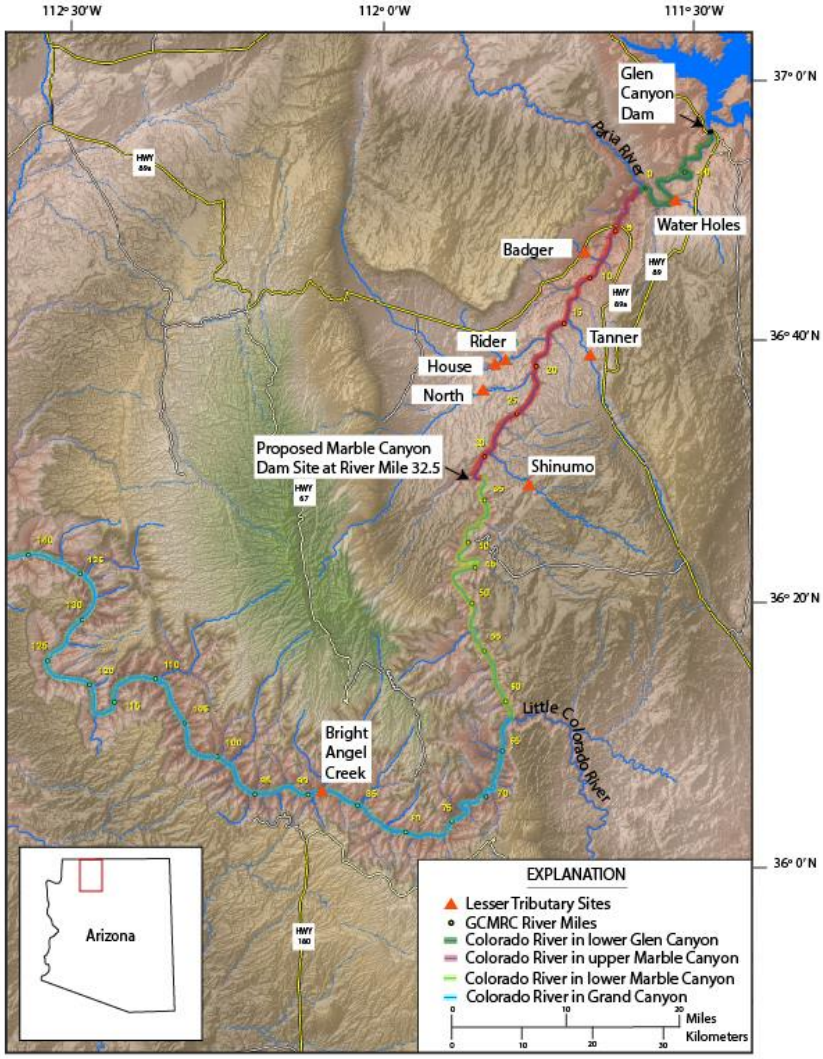

Figure 1 Digital elevation map showing the lesser-tributary gages. Lesser-tributary gages: Water Holes Canyon (Water Holes), Badger Creek (Badger), Tanner Wash (Tanner), House Rock Wash above Emmett Wash (House), House Rock Wash in Rider Canyon (Rider), North Canyon (North), Shinumo Wash (Shinumo), and Bright Angel Creek.

Geology of the lesser-tributary drainage basins can be broadly categorized into areas with higher potential fine-sediment yield associated with Mesozoic sandstones, and areas with lower potential fine-sediment yield associated with Paleozoic limestone. Four gages are located on higher potential fine-sediment yield lesser tributaries that drain into upper Marble Canyon: (1) Badger Creek, (2) Tanner Wash, (3) House Rock Wash above Emmett Wash (herein referred to as House Rock Wash), and (4) House Rock Wash in Rider Canyon (herein referred to as Rider Canyon). At the gage: the streambed of Badger Creek is composed of sand and gravel, the streambed of Tanner wash is composed of gravel and sand, the streambed of House Rock Wash is composed of sand and fine gravel, and the streambed of Rider Canyon is composed of patches of sand and gravel on bedrock. The House Rock Wash gage is located upstream, in the same drainage, as the Rider Canyon gage. The Rider Canyon gage has the most comprehensive

suspended-sediment record of the lesser-tributary gages; at this gage, suspended-sediment measurements are made using arrays of US U-59 samplers and an automatic pump sampler.

North Canyon and Shinumo Wash drain areas that consist primarily of Paleozoic limestone and have lower potential fine-sediment yields. These two tributaries have streambeds that are almost exclusively angular limestone gravel with only minor amounts of interstitial sand. Vegetation at all the gages consists primarily of sparse, low-lying bushes and grasses, with little or no vegetation in the active channel.

METHODS

Discharge calculations The remote location of the lesser-tributary gages coupled with the extremely short duration of flash floods makes it difficult and expensive to measure the discharge of water directly. Calculation of discharge at the lesser-tributary monitoring sites therefore requires the development of a stage-discharge relation constrained by modeled peak discharges from multiple floods. Peak discharges are modeled using the USGS National Research Program multi-dimensional surface water modeling system – now named international river interface cooperative – and the "quasi-three-dimensional flow and sediment transport with morphological evolution of channels solver" (McDonald et al., 2005). The approach used is to:

(1) Select a suitable reach for modeling and complete a base topographic survey. A suitable channel reach is stable and relatively straight, with simple channel geometry that will result in an easier flow-modeling process. Survey the position of the stage sensor and any suspended-sediment sampler intakes. Survey cross sections every 2-3 meters along the channel, depending on channel complexity, and generate a topographic map and model grid of the stream channel from survey data.
(2) Survey multiple sets of high-water marks within the reach corresponding to floods with different peak stages. A wide range of high-water marks allows the development of a comprehensive stage-discharge relation.
(3) Perform successive 2-D model runs varying the discharge and Z_0 (Z_0 roughness values are constrained by pebble count data) to minimize the root-mean-square error between the surveyed high-water marks and the modeled water surface.
(4) Attempt to hold the established Z_0 constant in the model, and model the discharge associated with different high-water marks to develop stage-discharge relations (Griffiths et al., 2010).
(5) Only allow Z_0 to increase with increasing peak flood stage if there is physical evidence that the roughness characteristics of the bed changes with increasing stage, as described below.

The Nikuradse (1933) Z_0 bed roughness parameter is used for flow modeling. This roughness parameter was chosen instead of the more commonly used Manning's n because, unlike the Manning's n roughness parameter, Z_0 does not depend on stage and only depends on the characteristics of the streambed. As discharge increases in gravel-bedded rivers Z_0 should remain constant unless the gravel bed becomes fully mobile or rougher areas of the streambed and banks become inundated. As either vegetated or formerly dry rougher areas of the streambed, banks, and canyon walls become inundated and are added to the model grid, Z_0 may increase. For an immobile gravel bed, Z_0 is approximately equal to $0.1 \cdot D_{84}$ (Whiting and Dietrich, 1989; Wiberg and Smith, 1991), where D_{84} is the 84th percentile grain size of the gravel. As the gravel bed becomes fully mobile, Z_0 increases to approximately equal $0.5 \cdot D_{84}$ (Pitlick, 1992)

Modeled flows are combined with corresponding recorded stages to develop a stage-discharge relation for the gage. This stage-discharge relation is used for all subsequent floods unless major changes in the channel geometry or hydraulic control are observed. If large channel changes occur, a new stage discharge relation must be developed using the steps above. Where an insufficient number or diversity of flood peaks have been modeled to develop a stage-discharge relation, any high-water marks observed

during maintenance visits to the gage are flagged for later survey. The stage-discharge relation and stage record are used to calculate the discharge record for each gage.

Sediment-transport calculations At each lesser-tributary gage, cumulative sediment load is calculated using the discharge record and a combination of physical-sample sediment-concentration data and averaged sediment concentrations or a regression relationship developed between log-transformed discharge and log-transformed sediment concentrations. Logarithmic transformation is used to reduce heteroscedasticity in the data. Samples collected by the US U-59s or the automatic pump samplers are analyzed for silt and clay concentration, sand concentration, and sand grain-size distribution. On the basis of analyses conducted on the Paria River (a similarly steep, sandy river, with similarly high sediment concentrations), the sediment concentrations measured in these "point" samples are assumed to be representative of the sediment concentrations in the entire cross section. The automatic pump samplers record the date and time the samples were collected. The US U-59 samples are assigned a date and time of sampling based on the date they were recovered, the preceding hydrograph, and the surveyed elevations of the sampler intakes. Once the date and time of collection is known for each of the samples and the laboratory analyses are completed, an F-test is preformed to determine if any significant dependence of log-transformed concentration on log-transformed discharge is present (Figure 2). Because of the large variability in suspended-sediment concentrations observed during individual flood events and between different floods, many of the gages do not exhibit significant "stable" relations between discharge and silt and clay concentration and between discharge and sand concentration. However, most sites do show a significant positive relation between discharge and suspended-sand D_{50}.

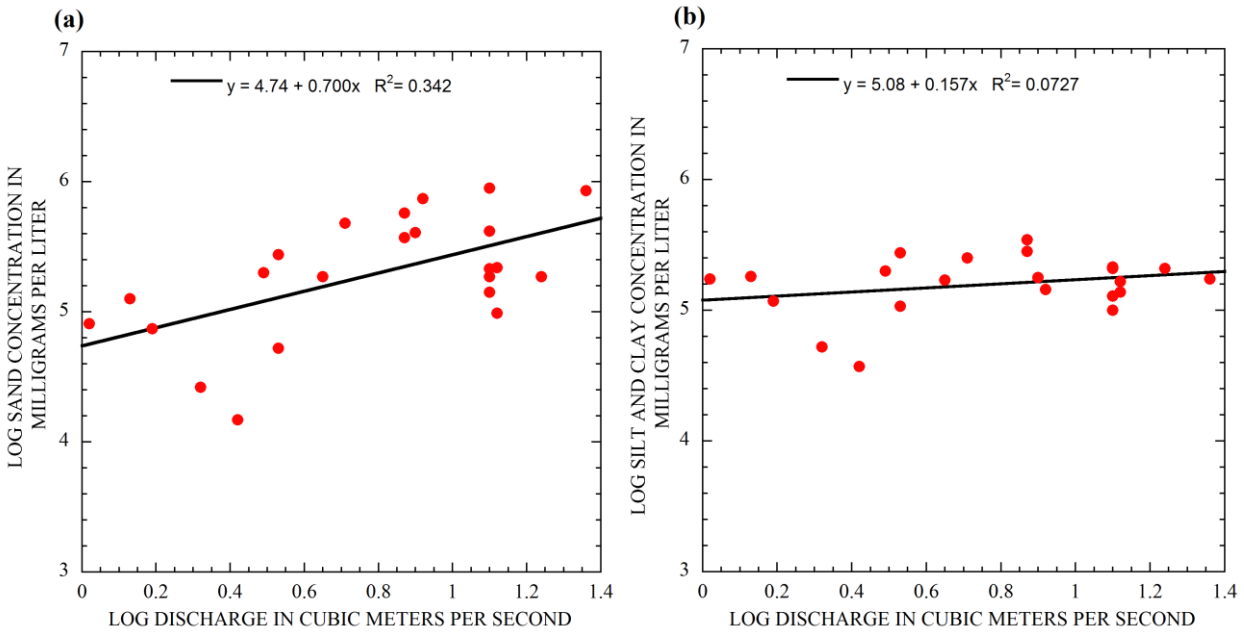

Figure 2 Log-log plots of concentration of sand (a) and silt and clay (b) vs discharge for the Badger Creek gage. Results from F-tests indicate that the linear fit is significant for the relation between log-transformed discharge and log-transformed sand concentration ($p < 0.05$), but not for the relation between log-transformed discharge and log-transformed silt and clay concentration.

For many of the lesser tributaries, suspended-sediment concentration does not correlate well with discharge. Using a F-test, log-transformed suspended silt and clay concentrations were significantly related ($p < 0.05$) to log-transformed discharge in only the Shimumo Wash drainage, while log-transformed sand concentrations are significantly related to log-transformed discharge in two of the five

drainages (Badger Creek and Shimumo Wash). Poor correlation between discharge and suspended-sediment concentration is independent of sampling method; at the Rider Canyon gage, all sampling methods yield similar poor correlations between log-transformed discharge and suspended-sand concentration (Figure 3).

Sediment concentration and discharge are combined to calculate instantaneous loads; these loads are then integrated over the entire hydrograph to calculate the cumulative loads of suspended-sediment transported past each of the lesser-tributary gages. If samples were collected during a flood event, the concentrations from those samples are used for a half hour window surrounding the sample collection time. If no samples were collected during a flood, or not collected within a half hour of a calculated discharge, mean sediment sample concentrations from the entire dataset at that gage are used; gages with significant discharge-concentration relations use these relations in the place of mean concentrations. Silt and clay loads and sand loads are calculated using the same techniques.

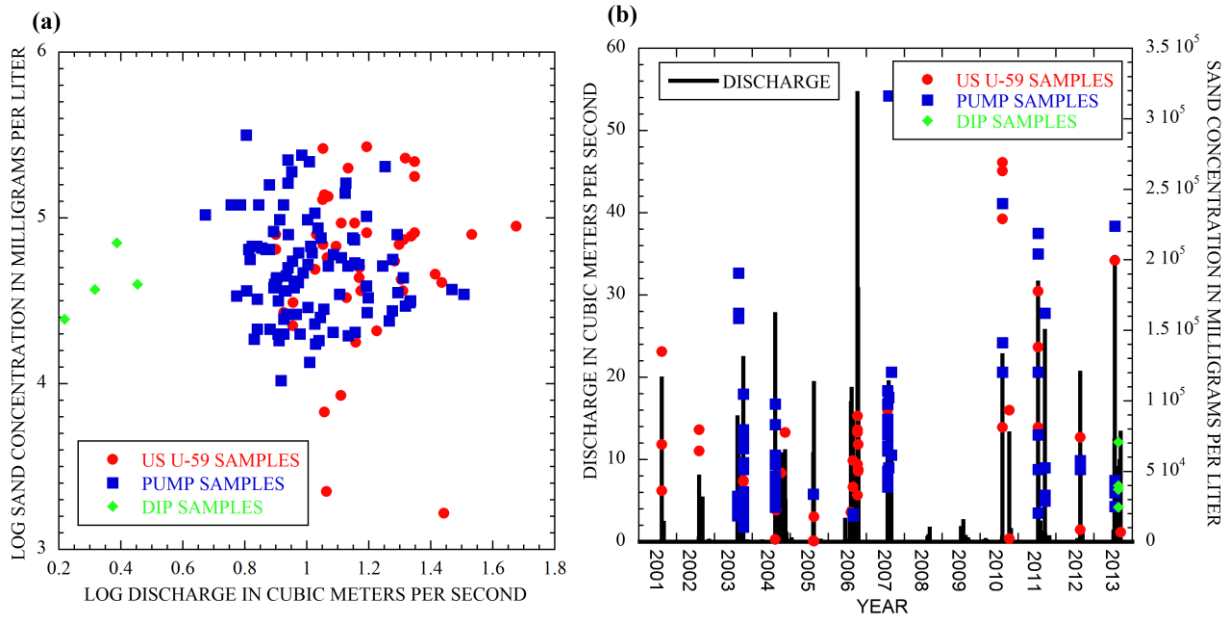

Figure 3 Log-log plot of sand concentration vs discharge for the Rider Canyon gage showing the three sampling methods (a), sand concentration and discharge for the entire period of study (b).

RESULTS AND DISCUSSION

Results from this study We estimate total sediment load from the lesser tributaries to the Colorado River in upper Marble Canyon by applying the mean-annual measured cumulative loads of the gaged tributaries, 69% of the total lesser-tributary area of upper Marble Canyon, to the remaining ungaged 31%. The ungaged area is divided into potentially higher and lower sediment yields based on drainage basin geology and similarity to other, gaged, lesser tributaries. Using this classification, only 25% of the higher-potential-yield tributaries remain ungaged; sediment yield from this ungaged area is estimated based on the annual yield of the three gaged higher-potential-yield tributaries. Ungaged tributaries draining the lower-potential-yield area represent 40% of the total lower-potential-yield tributaries; the sediment yield from this area is estimated from the annual yield of the lower-potential-yield tributaries.

Over the 13 years of this study, annual sediment load from the lesser tributaries to the Colorado River in upper Marble Canyon was found to vary two orders of magnitude from ~1,800 to 340,000 metric tons of

sand and from ~2,900 to 370,000 metric tons of silt and clay (Table 2). The mean-annual sand and silt-and-clay loads in the lesser tributaries were ~72,000 metric tons of sand and ~96,000 metric tons of silt and clay. This is equivalent to ~10% of the measured mean-annual sand load and ~8% of measured mean-annual silt-and-clay load in the Paria River over the same period (Table 2). Although the lesser tributary mean-annual sand load is 10% of the Paria River, the annual sand load of the lesser tributaries as a percent of the Paria River sand load ranges from ~1.6-49% during individual years.

The vast majority of the sediment entering Marble Canyon from the lesser tributaries is supplied from the 57% of the tributary area with higher potential sediment yield. The three gaged higher-potential-yield tributaries, Badger Creek, Rider Canyon, and Tanner Wash, contribute approximately 73% of the total sand and 65% of the total silt and clay to the upper Marble Canyon Reach.

Table 2 Measured annual sediment loads in metric tons (t) from the higher- and lower-potential-sediment-yield lesser tributaries to the Colorado River, the summed annual lesser-tributary sediment loads to upper Marble Canyon including estimates from the remaining ungaged area, and the measured Paria River annual sediment loads.

Year	Higher-Yield Tributaries		Lower-Yield Tributaries		Upper Marble Canyon		Paria River	
	Sand (t)	Silt (t)	Sand (t)	Silt (t)	Sand (t)	Silt (t)	Sand (t)	Silt (t)
2001	8,400	8,000	0	0	11,000	11,000	88,700	399,000
2002	28,000	28,000	62	720	38,000	38,000	78,100	468,000
2003	19,000	30,000	380	3,600	26,000	48,000	341,000	780,000
2004	47,000	59,000	970	6,200	64,000	89,000	676,000	1,530,000
2005	54,000	54,000	3,900	32,000	79,000	130,000	976,000	1,280,000
2006	260,000	270,000	350	5,200	340,000	370,000	1,590,000	2,080,000
2007	57,000	67,000	32	1,100	76,000	90,000	829,000	1,580,000
2008	8,400	7,400	27	550	11,000	11,000	305,000	685,000
2009	1,400	2,100	3	34	1,800	2,900	116,000	520,000
2010	72,000	63,000	310	3,500	97,000	89,000	1,460,000	2,170,000
2011	35,000	35,000	500	3,700	47,000	53,000	144,000	325,000
2012	13,000	22,000	170	1,400	17,000	32,000	706,000	1,270,000
2013	76,000	98,000	12,000	34,000	120,000	190,000	1,950,000	2,150,000
Mean	**52,000**	**58,000**	**1,400**	**710**	**72,000**	**96,000**	**712,000**	**1,170,000**

Annual sediment loads from the lesser tributaries vary greatly between drainages and from year to year (Table 2, Figure 3). Drainages have diverse geology and topography, storm cells that produce locally heavy rain may have a footprint much smaller than the size of the receiving drainage basin. While regional precipitation events do occur, precipitation events are typically more spatially variable with many higher-discharge events recorded in one tributary not present in the discharge record of other, nearby, tributaries (Figure 3a). In addition, a tributary may experience several large floods within days followed by years of quiescence. Over the course of this study, three of the gaged tributaries, Tanner Wash, Shinumo Wash, and North Canyon, have cumulative discharges that are approximately the same; however, the observed sediment loads, as well as the timing of events, differ dramatically (Figure 3). Both North Canyon and Shinumo Wash contributed very little sediment (combined less than 2% of the total sand and approximately 8% of the silt and clay), while Tanner Wash alone contributed approximately 28% of the sand and 18% of the silt and clay.

The ratio of suspended sand to suspended silt and clay varies considerably even among drainages of similar geology. Higher-potential-yield tributaries average approximately 47% sand and 53% silt and clay while the lower-potential-yield tributaries average only 17% sand. Because the higher-potential-yield tributaries contribute much more sediment than do the other tributaries, sand comprises, on average, approximately 45% of the sediment supplied to the entire Marble Canyon Reach by the lesser tributaries. Sediment yield varies within drainages as well as between different tributaries. A drainage representing

approximately 25% of the total drainage area enters between the House Rock Wash gage and the Rider Canyon gage (these gages are located on the same drainage, with House Rock Wash being the upstream gage). This drainage, which is similar to Badger Creek in geology and topographic relief, is responsible for approximately 53% of the sand passing the Rider Canyon gage, but only 22% of the silt and clay.

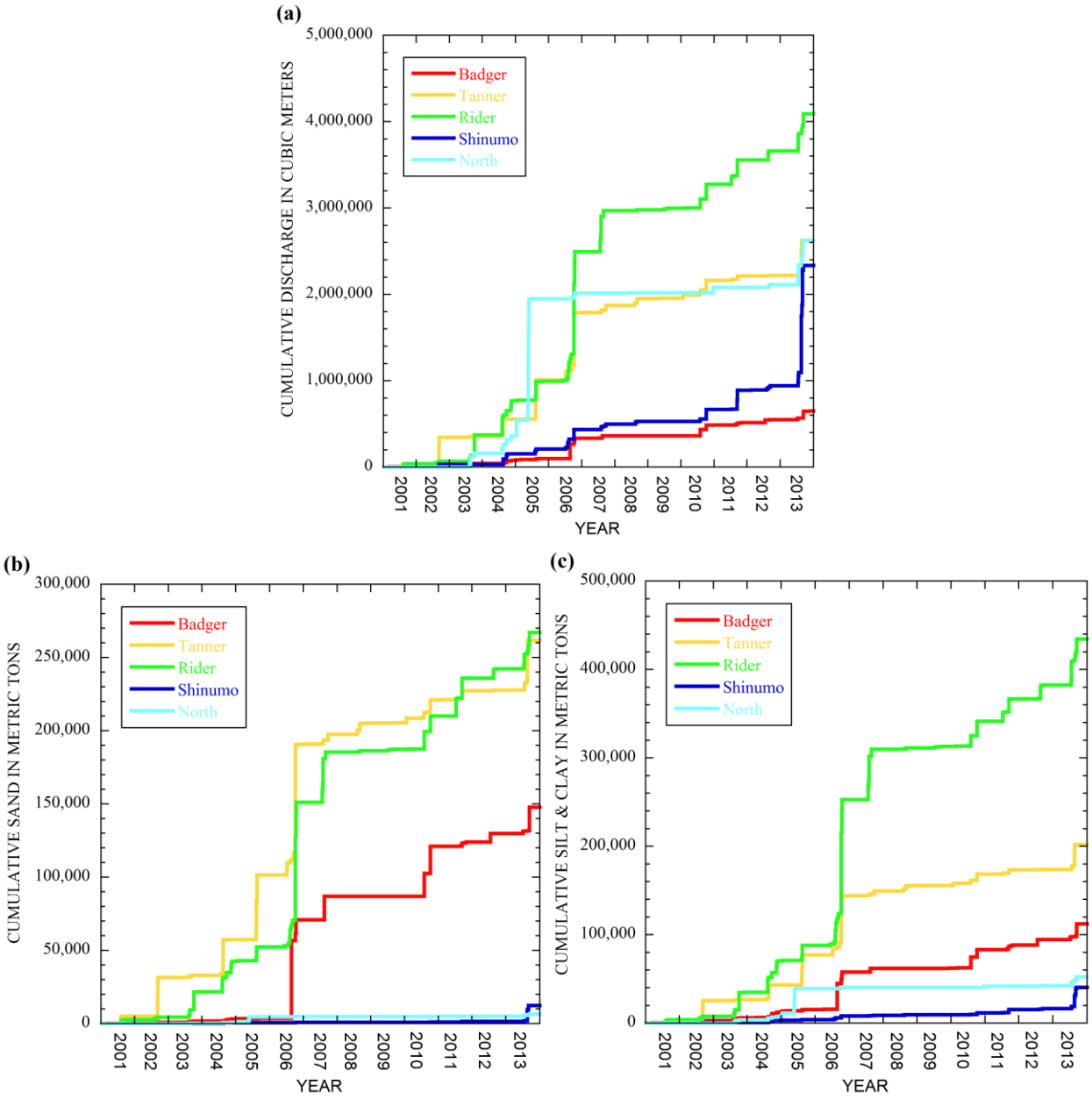

Figure 3 Cumulative water discharges in cubic meters (a) sand loads in metric tons (b) and silt and clay loads in metric tons (c) for the gaged lesser tributaries in upper Marble Canyon.

Comparison with previous work The results from this study show that previous studies all over-estimated the sediment supply from the lesser tributaries to the Colorado River in Marble Canyon (Table 1, Table 2). Two of the previous studies, BOR (1956) and Howard and Dolan (1981), overestimated the quantity of total sediment entering from the lesser tributaries by an order of magnitude. The other three

previous studies estimated mean-annual lesser-tributary sediment loads ranging from ~520,000 to 760,000 metric tons. Our study measured a mean-annual lesser-tributary sediment supply of ~170,000 metric tons, a factor of 3.1-4.5 lower than the previous estimates. Previous studies also greatly overestimated the amount of lesser-tributary sand supplied to the Colorado River in upper Marble Canyon. Only the low-end estimates of lesser-tributary sand load from Webb et al. (2000) seemingly agree with our measurements of lesser-tributary sand load; this apparent agreement is, however, misleading as Webb et al.'s (2000) low-end estimates assumed that only 15% of the total sediment load was sand. Our suspended-sediment measurements show that this estimate of percent sand is too low, the measured value is actually much larger at ~45% sand. If Webb et al. (2000) had used a more-correct higher percentage of sand, their lowest estimate of lesser-tributary sand supply would have been roughly 3.3 times larger than the values calculated in our study.

The differences in lesser tributaries sediment loads between previous studies and our study can be attributed to previous studies not using direct measurements of stage, discharge, or sediment concentrations, but relying on relations from drainage basins that do not accurately reflect the local geology, climate and vegetation. Additionally, previous studies, using older established sediment-yield relations, are based on data that do not reflect current climatic conditions. Lastly, previous studies present mean-annual results that do not capture the year-to-year variation in sediment loads measured in our study.

SUMMARY

Relying on indirect methods to estimate the cumulative sediment load from ungaged tributaries and close sediment budgets may result in substantial errors in these budgets. This study found that previous, indirect, methods that used no actual measurements of sediment transport greatly overestimated the amount of sand and the amount of silt and clay supplied by the lesser tributaries to the Colorado River in upper Marble Canyon. Because large variation exists in annual tributary sediment loads, additional error will be introduced into shorter-term sediment budgets (with durations of several years or less) even when measured mean-annual lesser-tributary sediment loads are used in these budgets; sediment supply to the Colorado River in upper Marble Canyon from the lesser tributaries was found to vary over a factor of 100 on an annual basis. For sediment budgets that vary greatly as a function of the sediment supplied from tributaries, direct measurement of the sediment loads in these tributaries may be necessary to accurately close sediment budgets, and provide valid recommendations to resource managers.

REFERENCES

Andrews, E.D. (1986). "Downstream effects of Flaming Gorge Reservoir on the Green River, Colorado and Utah," Geol. Soc. of Amer. Bull., vol. 97, pp. 1012-1023.

Campbell, D., Durst, S., Kantola, A.T., Kubly, D.M., Muth, R.T., Swett, J., and Whitmore, S. (2010). "Overview of the Colorado River Basin collaborative management programs," *in* Melis, T.S., Hamill, J.F., Bennett, G.E., Coggins, L.G., Jr., Grams, P.E., Kennedy, T.A., Kubly, D.M., and Ralston, B.E. eds., Proceedings of the Colorado River Basin Science and Resource Management Symposium, November 18-20, 2008, Scottsdale, Arizona: U.S. Geological Survey Scientific Investigations Report 2010-5135, pp.15-42. [http://pubs.usgs.gov/sir/2010/5135/]

Edwards, T.K., and Glysson, G.D. (1999). "Field methods for measurement of fluvial sediment" U.S. Geological Survey Techniques of Water-Resources Investigations, book 3, chap. C2, 89 pp. [http://pubs.usgs.gov/twri/twri3-c2/.]

Griffiths, R.E., Topping, D.J., McDonald, R.R., and Sabol, T.A. (2010). "The use of the multidimensional surface-water modeling system (MD_SWMS) in calculating discharge and sediment transport in remote ephemeral streams," Proc. of the 2nd Joint Federal Interagency Conference, Las Vegas, Nevada, June 27-July 1, 2010.

Griffiths, R.E., Topping, D.J., Anderson, R.S., Hancock, G.S., and Melis, T.S. (2014). "Design of a sediment-monitoring gaging network on ephemeral tributaries of the Colorado River in Glen, Marble, and Grand Canyons, Arizona," U.S. Geological Survey Open File Report 2014–1137, 21 pp., [http://dx.doi.org/10.3133/ofr20141137]

Howard, A.D., and Dolan, R. (1981). "Geomorphology of the Colorado River in the Grand Canyon" Journal of Geology, v. 89, pp. 269–298.

McDonald, R.R., Nelson, J.M., and Bennett, J.P. (2005). "Multi-dimensional surface-water modeling system user's guide," U.S. Geological Survey Techniques and Methods, 6-B2,136 pp.

Nikuradse, J. (1933). "Laws of flow in rough pipes," VDI-Forschungsheft, no. 361. [In German, translation NACA Tech Memo, no. 1292, 62 pp.]

Pitlick, J. (1992). "Flow resistance under conditions of intense gravel transport," Water Resources Research, 28(3), pp 891-903. doi:10.1029/91WR02932. [http://www.agu.org/journals/wr/v028/i003/91WR02932]

Randle, T.J., and Pemberton, E.L. (1987). "Results and analysis of STARS modeling efforts of the Colorado River in Grand Canyon," Glen Canyon Environmental Studies Report, 41 pp.

Rankl, J.G., (2002). "Relations between total-sediment load and peak discharge for rainstorm runoff on five ephemeral streams in Wyoming," U.S. Geological Survey Water-Resources Investigations Report 02-4150, 12 pp.

Sutherland, R.A., and Bryan, K.B. (1990). "Runoff and erosion from a small semiarid catchment, Baringo district, Kenya," Applied Geography, v. 10, pp. 91–109.

Webb, R.H., Griffiths, P.G., Melis, T.S., and Hartley, D.R. (2000). "Sediment delivery by ungaged tributaries of the Colorado River in Grand Canyon," U.S. Geological Survey Water-Resources Investigations Report 00-4055, 67 pp. [http://wwwpaztcn.wr.usgs.gov/webb_pdf/wrir00-4055.pdf]

Whiting, P.J., and Dietrich, W.E. (1989). "The roughness of alluvial surfaces, an empirical examination of the influence of size heterogeneity and natural packing," EOS, Transactions of the American Geophysical Union, 70(43), pp. 1109.

Wiberg, P.L., and Smith, J.D. (1991). "Velocity distribution and bed roughness in high-gradient streams," Water Resources Research, 27(5), pp. 825-838, doi:10.1029/90WR02770. [http://www.agu.org/pubs/crossref/1991/90WR02770.shtml]

U.S. Department of the Interior (1995). Operation of Glen Canyon Dam, final environmental impact statement, Bureau of Reclamation, Salt Lake City, Utah, 337 pp.

U.S. Department of the Interior, Bureau of Reclamation (1956). Office Memorandum from K.E. Snelson to W.M. Borland, September 10, 1956.

U.S. Department of the Interior, Bureau of Reclamation (1958). Office Memorandum from W.V Turner and S.H. Robeson, September 16, 1958.

USER-INTERACTIVE SEDIMENT BUDGETS IN A BROWSER: A WEB APPLICATION FOR RIVER SCIENCE AND MANAGEMENT

David Sibley, Computer Scientist, U.S. Geological Survey, Center for Integrated Data Analytics, 8505 Research Way, Middleton, WI 53562 - dmsibley@usgs.gov - 608-821-3895
David J. Topping, Research Hydrologist, U.S. Geological Survey, Grand Canyon Monitoring Research Center, 2255 North Gemini Dr, Flagstaff, AZ 86001 - dtopping@usgs.gov - 928-556-7396
Megan Hines, Scientist III, U.S. Geological Survey, Center for Integrated Data Analytics, 8505 Research Way, Middleton, WI 53562 - mhines@usgs.gov - 608-821-3917
Bradley Garner, Hydrologist, U.S. Geological Survey, Arizona Water Science Center, 2255 North Gemini Dr, Flagstaff, AZ 86001 - bdgarner@usgs.gov - 928-556-7331

Keywords: sediment budgeting, rivers, monitoring, management

Abstract: Decision-support tools providing accurate, near-real-time data and user-friendly interactive visualizations are of critical value to resource managers tasked with planning and carrying out management programs in their domain. Creating a system to continuously aggregate datasets and recompute derived values is difficult and error-prone when attempted by hand. To address this need for river managers in support of sediment budgeting, we have created a web-based, open source suite of tools and processes that 1) continually aggregate data of interest, 2) recompute derived values based upon latest available data, and 3) update visualizations on-demand, providing simple front-end tools available to resource managers and the public. For the first time, engineers and scientists can access these tools freely over the web to assist them with planning and adaptive management decisions.

INTRODUCTION

Fine sediment (sand, silt, and clay) forms the template for riverine ecosystems in many rivers with naturally large sediment loads in the western United States. By disrupting the natural transport of fine sediment, the construction of dams and subsequent regulation of flows has dramatically affected the aquatic and riparian ecosystems in many western rivers (Schmidt and Wilcock, 2008). Depending on the locations of the sources of water and sediment in a watershed relative to the location of a dam, and depending on how that dam is managed, the reaches downstream from a dam may undergo sediment evacuation or accumulation (Topping et al., 2000a,b; Grams et al., 2007; Dean and Schmidt, 2011). Substantial changes in the mass balance of sediment downstream from a dam may have important environmental consequences that may require flow remediation (e.g., U.S. Department of the Interior, 2012). The development of environmental flows for ecosystem management in rivers with naturally high sediment loads that are perturbed by upstream water development thus requires the ability to manage sediment. The preferred scientific tool for such management is the sediment budget (e.g., Erwin et al., 2012; Grams et al., 2013).

Accurate sediment budgets require differencing accurate measurements of the amount of sediment entering and leaving a river reach (e.g., Topping et al., 2010). In rivers dominated by suspended-sediment transport, the amount of sediment entering or leaving a reach is determined through integration of the product of water discharge and suspended-sediment concentration (Porterfield, 1972). Both discharge and sediment concentrations are subject to potential biases that accumulate over time. Uncertainty in a sediment budget cannot be accurately quantified without propagating the biases through the calculations (Topping et al., 2000a, 2010).

To assist river science and management in Grand Canyon National Park, Big Bend National Park, Dinosaur National Monument, and Canyonlands National Park (Figure 1), the U.S. Geological Survey's (USGS)

Grand Canyon Monitoring and Research Center (GCMRC) in partnership with the USGS Center for Integrated Data Analytics (CIDA) have designed and built a database and web application for serving, and operating on, time-series measurements of those key water discharge and suspended-sediment concentration values. This web application is the Discharge, Sediment, and Water Quality Monitoring web application, hereinafter referred to as the "GCMRC web application."

Figure 1 The current geographic scope for the GCMRC web application.

The GCMRC web application consists broadly of two subparts: the GCMRC Data And Workflow System (GDAWS) data warehouse (including its associated data collection and computation processes, and the services that provide that data on request); and the web application itself, which consists of back-end services that perform real-time computation on datasets, and a highly capable browser-based client presented to the user in their web browser.

The GCMRC web application is a decisive advance in the state of the art for sediment budget work. The benefits, however, are differently distributed between administrative, scientific, and technological areas of interest.

Administrative benefits: In terms of budgets and operations, the GCMRC web application's most important characteristic is its 100 percent open source implementation. This resolves to both short-term and long-term cost containment advantages. In brief: nobody is paying for licenses; more importantly, nobody's hands are tied by restrictive covenants, nondisclosure agreements, et cetera; more important still, open source projects are future- proofed against withdrawal of licensing permissions (unlike proprietary software whose terms and conditions may change); and perhaps most important, open source technologies have an inherent network effect (software with obvious value is supported and thrives) that reduces concerns about ongoing staffing for extension and maintenance.

Another significant administrative benefit of the GCMRC web application is its standards-based nature. The programming code powering the application consists of well-documented and accepted protocols and methods to deliver and visualize information. This is not a single purpose solution that is useful only in Grand Canyon, Big Bend, Dinosaur, and Canyonlands. It is readily adaptable, at no licensing cost and reasonable scope of project effort, to sediment-budgeting requirements in other reaches on other rivers. The custom programming code and open source frameworks supporting the application are provided as public

domain software via the USGS GitHub instance online at https://github.com/USGS-CIDA. While the software currently serves river science and management within the scope of the GCMRC project areas, the same code base and architecture could be used to support data integration, data services and online applications and visualizations in other domains.

Scientific benefits: The scientifically interesting aspects of the GCMRC web application are 1) the unprecedented combination of sediment/streamflow data and computation in a single real-time-capable application, and 2) the flexibly expanding suite of visualization and analysis capabilities of the client.

GDAWS handles unit-value time-series of gage height, discharge, water-quality, and sediment-transport data. These data are available for download using the same services that provide data to the web client.

In addition to building user-interactive tools for visualizing these data within a web browser, we continue to design tools for operating on multiple datasets. The first of these is a user-interactive tool that constructs sediment budgets (with propagated uncertainty) for various river reaches in these national parks.

The user-interactive sediment budgets calculated and displayed by the application are always improving in accuracy as they incorporate the latest data. Calculations performed behind the scenes are recomputed with a constant flow of near-real-time data, providing increasingly accurate outputs, allowing management decisions to be made using the most complete and accurate data.

Technological benefits: It is worth noting that GDAWS is, from a technological standpoint, fairly standard (data warehouse design, implementation, and provisioning are well-understood disciplines; there was no need to reinvent them). The interesting technological accomplishments embodied in the GCMRC web application are the clean division between service and client responsibilities, and the implementation of powerful clientside visualization and analysis without recourse to any proprietary software libraries whatsoever. The most interesting aspect of the GCMRC web application from a software developer's point of view is probably the use of clientside open source libraries to achieve remarkable visualization and real-time analysis, and overcoming the challenges of delivering attractive, responsive visualizations built on real-time data as requested by the user in their browser.

DATA AND METHODS

For the sediment budgeting application presented here, the main data types for this project include 1) continuous time-series data and 2) discrete episodically collected suspended- and bed-sediment data. These data, whether collected via automated sensors or human observations, or computed post-collection, are maintained in a single database. The web application is directly driven by that database; integrity and provenance of the data are thus easily confirmed.

The continuous time-series data are typically spaced at 15-minute intervals and include gage height, discharge, water temperature, specific conductance, dissolved oxygen, turbidity, and acoustic measurements of suspended-silt-and-clay concentration, suspended-sand concentration, and suspended-sand median grain size (Griffiths et al., 2012, 2014; Topping et al., 2003, 2007, 2015; Voichick, 2008; Voichick and Topping, 2010, 2014; Voichick and Wright, 2007).

The discrete sample data include equal-discharge-increment (EDI), equal-width-increment (EWI), single-vertical, and calibrated-pump suspended-sediment measurements, and bed-sediment measurements (Edwards and Glysson, 1999).

All of these data are collected using standard USGS methods and other peer-reviewed methods. 95-percent-confidence-level field and laboratory-processing errors for the EDI and EWI measurements are calculated using the methods of Topping et al. (2010, 2011); similar errors for the calibrated-pump measurements are calculated using unpublished analyses based on the methods of Topping et al. (2011). These errors are depicted in the user-interactive plots in the GCMRC web application.

In order to construct the visualization and modeling capabilities displayed within the GCMRC web application, the different datasets are aggregated, and derived-values calculations are performed and stored on new incoming data. The flow of this process is depicted in Figure 2.

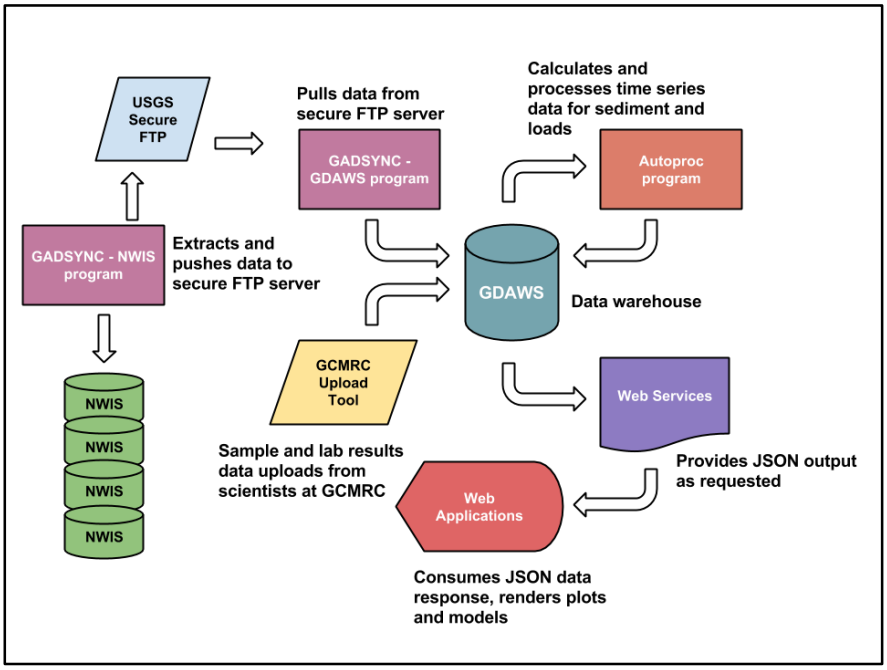

Figure 2 Data flow diagram depicting the movement of data from raw form to client-side visualization.

- GDAWS is a single database organized with the star schema typical in data warehousing. It is implemented on an Oracle database server.
- Time-series data about our stations of interest from the U.S. Geological Survey's National Water Information System (NWIS) database (USGS NWIS, 2014) are extracted twice daily and placed on a secure USGS File Transfer Protocol (FTP) site by a Python program called GADSYNC-NWIS.
- Twice daily, a C# program called GADSYNC-GDAWS retrieves the data placed on the secure FTP site, lightly processes them, and inserts their data into GDAWS. Time-series data not included in NWIS, and discrete sample data, are manually uploaded into GDAWS periodically using a custom web application (the GCMRC Upload Tool) that extracts, transforms and loads the comma-separated data values. To date, the data warehouse contains over 92 million time-series measurements from 57 sites throughout the aforementioned networks. The discrete sample data are critical for calibrating and verifying the acoustic suspended-sediment data and for calculating sediment loads.
- A C# program called Autoproc runs daily, calculating both instantaneous and cumulative sediment loads from the aggregated discharge, acoustic suspended-sediment time-series, and discrete suspended-sediment-sample information in GDAWS. Autoproc extracts data from the GDAWS database, processes parameter values based on the latest time-series data, and re-inserts the newly calculated values back into the database.

Computation of concentrations: major rivers: On the Little Snake, Yampa, Green, and Colorado rivers, and the Rio Grande, suspended-sediment concentrations and grain-size distributions are measured using a combination of 15-minute acoustic data and episodic discrete EDI, EWI, and calibrated-pump sample measurements. The discrete sample measurements are used to both calibrate the acoustic data and then subsequently the acoustic calibrations using the methods of Topping et al. (2007, 2015).

Computation of concentrations: major tributaries: On major tributary rivers where the suspended-sediment concentrations exceed the upper limit where acoustic measurements are possible, suspended-sediment concentrations are computed using a two-step process. First, suspended-silt-and-clay and suspended-sand concentrations are estimated using either physically based model curves (Topping, 1997) or statistically based curves (Topping et al., 2010). Second, these initial sediment-concentration estimates are adjusted to agree with EDI, EWI, single-vertical, and calibrated-pump measured sediment-concentrations as samples get processed through the laboratory, a time-consuming process (Topping et al., 2010). As more samples are incorporated, and the initial estimates become bona fide measurements of suspended-sediment concentration, the uncertainties applied to the tributary suspended-sediment data decrease in the web application.

Computation of concentrations: minor tributaries: The suspended-sediment concentrations in smaller, less important tributary streams are determined using a combination of measurements (Griffiths et al., 2010, 2014, 2015) and indirect estimates (Topping et al., 2010). The uncertainties assigned to the sediment loads in these streams are much larger (typically 50 to 100 percent), but because the loads in these streams are much smaller than the loads in either the mainstem rivers or major tributaries, these large uncertainties do not generally affect the sediment-budget results.

Computation of sediment loads: Sediment loads are calculated using 15-minute discharge and suspended-sediment-concentration data using the method of Porterfield (1972). Because sand, and silt and clay serve different physical and ecological purposes, sand loads and silt and clay loads are calculated independently. This approach allows construction of separate user-interactive mass-balance sand budgets and silt and clay budgets in the GCMRC web application. Construction of these mass-balance sediment budgets require sediment loads to be known on the mainstem rivers, major tributaries, and lesser tributaries, all with assigned uncertainties that are propagated through the budgets.

Computation of mass-balance sediment budgets: The mass-balance sediment budgets for each river reach are calculated using the methods described in Topping et al. (2010) and Grams et al. (2013).

Computed uncertainty: Uncertainties are applied to all sediment loads used in these budgets. The default uncertainties in the web application are chosen such that they represent the largest potential persistent bias in the computed loads at each site. The user can modify these default uncertainties to explore their effect on the uncertainties in the sediment budgets. These bias-type uncertainties result largely from instrumentation bias and include the greatest likely persistent bias in both the discharge of water and the suspended-sediment concentration, and are constrained by consistent measured differences in either discharge or sediment concentration at adjacent cross sections (Topping et al., 2010). Because no difference in either water discharge or sediment concentration occur between these closely spaced cross sections, the differences in the measurements between these cross sections represent biases (generally < 5 percent) in how acoustic-Doppler current profilers, current meters, and suspended-sediment samplers perform in slightly different cross sections. As there is no way to independently know which measurement in which cross section is correct, there is no way to know the “true” value. Thus, uncertainties that represent the greatest likely magnitude of these persistent differences are assigned to each load value. Because these uncertainties are biases, they accumulate over time, resulting in mass-balance sediment budgets in the GCMRC web application with uncertainty that gets larger over time.

Service/browser interaction in handling of computed data: To serve the aggregated and calculated sediment data for use in the front end application, the system organizes requested data into JavaScript Object Notation (JSON) responses. In order to allow the user to adjust the above-described load uncertainties in real-time on their computer, the browser requires all the data be delivered as separate pieces in the JSON response. Usually, the required data are two to five 15-minute time series that need to be transferred to the browser, which can be roughly a million values for an example span of six years. However, in order to accommodate the spectrum of browser memory capacities and variety of internet connection speeds, the application filters the plotted data to windowed local minimums and maximums on requests of periods of that length. The number of values that make it to the browser for the six-year example would therefore be reduced to a few hundred thousand. Because the application attempts to serve the truest visual representation of the data, it is set up to scale the windowed filtering based on the amount of data the user requests.

THE GCMRC DISCHARGE/QW/SEDIMENT WEB APPLICATION: USER EXPERIENCE

When the GCMRC web application at http://www.gcmrc.gov/discharge_qw_sediment/ is visited, the user has a choice of selecting between the monitoring networks for the four national parks, and selecting whether to visit the gateway web page to the time-series data at the monitoring stations or the gateway web page for the user-interactive sediment budgets. These gateway web pages provide a map and list of either the monitoring stations or the sediment-budget reaches.

The map views are supported by an open source mapping library called OpenLayers (http://openlayers.org/). Interactive sediment budget geographic feature layers are represented as shapefile data stored in an open source geospatial server called GeoServer (http://geoserver.org/). GeoServer allows for the management and support of standards-compliant services which can be consumed by many standards-supporting mapping frameworks. The GCMRC web application pulls data from GeoServer into the OpenLayers maps using the Open Geospatial Consortium's (OGC) Web Mapping Service (WMS) Standard (Open Geospatial Consortium, 2006); see also http://docs.geoserver.org/latest/en/user/services/wms/reference.html).

If the user navigates in the GCMRC web application to the monitoring station gateway and selects a specific monitoring station, a new page appears with a photograph of the river at the station, an overview map, and the list of parameters available to plot and download for that station. Within the parameter explorer on this station page, a user may select one or more classes of data (e.g., gage height, discharge amount, or water temperature) and select a date range across which the parameter values are graphed or downloaded. Once the server has returned the JSON response called by the browser and the user's request, dynamic charts consume the response contents and display returned data. To power the dynamic graphs, a JavaScript, open source graphing and charting library called Dygraphs (http://www.dygraphs.com/) is employed (see example Figure 3). Once the graphs are produced in the browser, the user can further refine the time-series displayed by adjusting its related slider to a specific time period, or get more details by hovering over the display to highlight and call out specific point in time values. The download function on each station page allows downloading of any of the time-series data with time stamps in any user-defined format. This function also allows downloading of the full laboratory-processed suspended- and bed-sediment datasets (including all ancillary data fields).

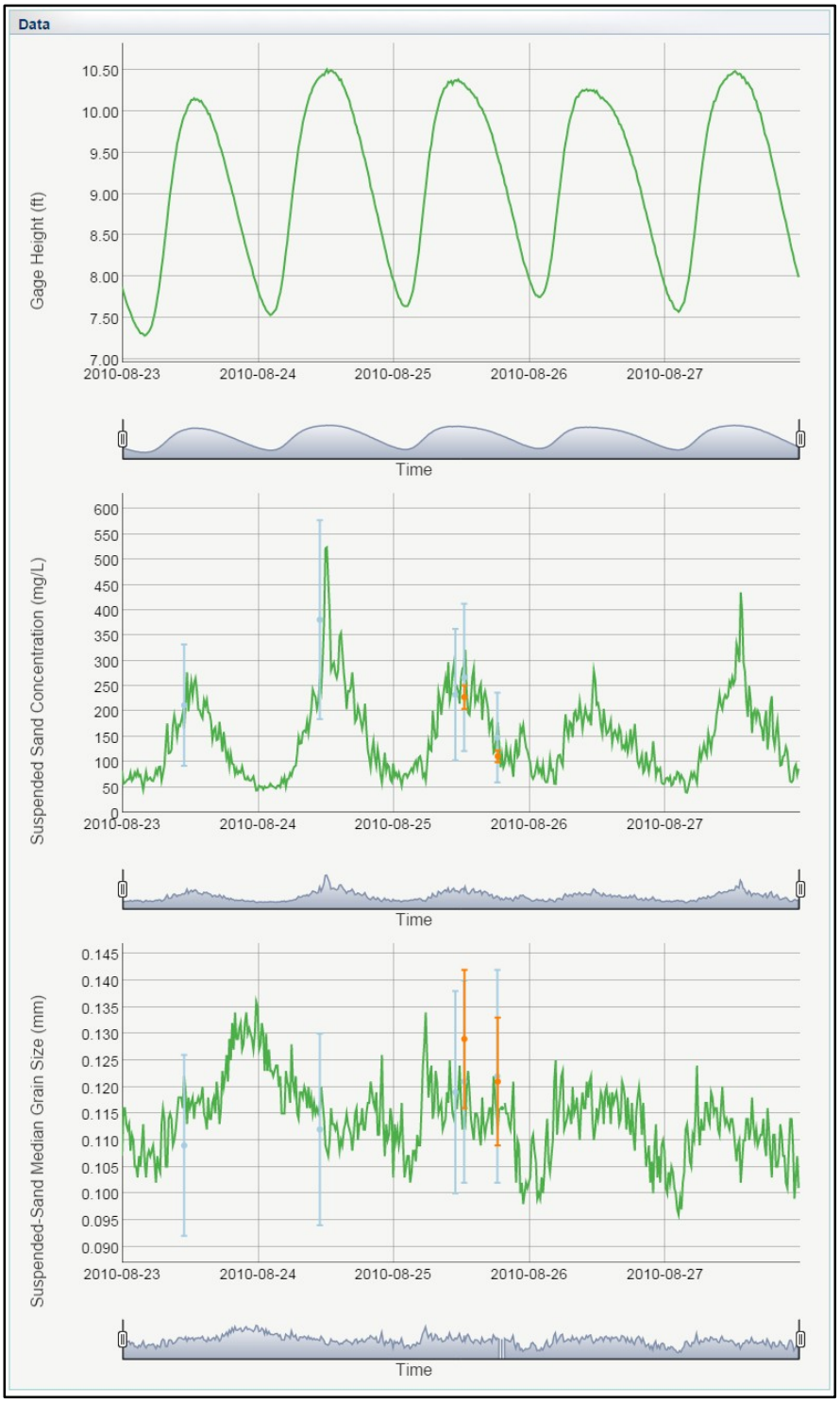

Figure 3 Example of plots of discharge, suspended-sand concentration, and suspended-sand median grain size at the Colorado River near Grand Canyon, AZ, 09402500 gaging station. Acoustic measurements of suspended-sand concentration and median grain size are depicted in green in the lower two plots. Orange points are EDI measurements, light blue points are calibrated-pump measurements. Error bars are 95%-confidence-level errors.

In addition to exploring specific stations' stacked parameter plots, scientists and managers can enter the sediment-budget gateway web pages and select a reach for construction of a mass-balance sediment budget. For any selected reach, the user has the option of setting the time period, modifying the uncertainties (i.e., possible persistent biases) in the various sediment-load time-series used to construct the budget, and modifying the bedload coefficient used to account for bedload in the river, in addition to the measured suspended-sediment load. For all reaches, default values of the possible persistent biases and bedload coefficients based on the best-available scientific information (e.g., Rubin et al., 2001) are pre-selected. An example of a mass-balance sand budget is provided in Figure 4.

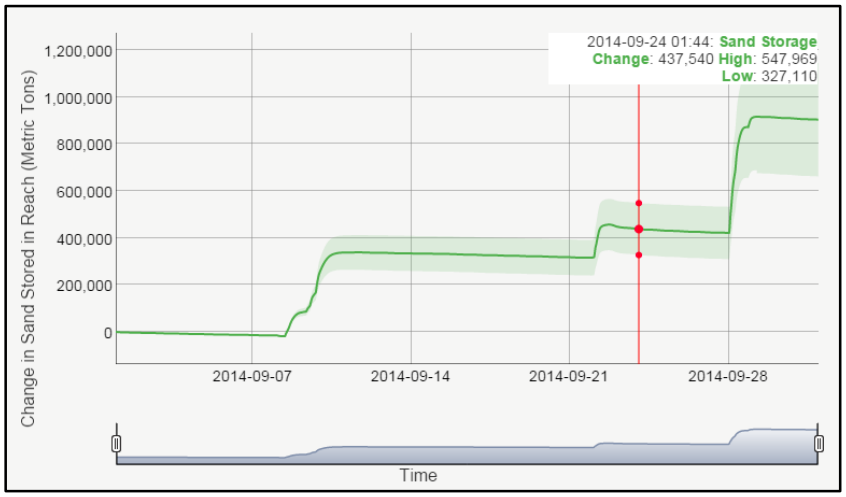

Figure 4 Example of Dygraphs plot of sand storage in the Upper Marble Canyon reach in Grand Canyon National Park.

The zero-bias value is plotted as the solid green line; the green shaded region indicates the region of uncertainty about the zero-bias value. Moving the red slider across the budget allows the user to see the zero-bias, upper, and lower bounds (given the chosen uncertainties) of the change in sediment mass for the selected time period. The ability of modifying the uncertainties in the loads is important because it allows river managers to evaluate "how well the sediment budgets need to be known" in their decision-making process.

RESULTS AND DISCUSSION

When viewing data, a user needs more than mere numerical accuracy. Meaningful conceptual and spatial presentations are essential for grasping the meaning of data. This is particularly crucial in decision-support uses of datasets. The GCMRC web application allows the user, whether a scientist, manager, or member of the lay public, easy access to user-interactive visualizations of discharge, water quality, and sediment data.

The advantage of open web applications—that they require no tools beyond a modern web browser for access and use—needs no elaboration. The GCMRC web application is built with open source components running against a standard relational database interface, making the cost of enhancements and extensions predictable and moderate. The use of web services to provide the data on request allows external users to integrate GDAWS data into other applications or models. The combination of open web services and the open browser application client allows the user easy, verifiable, and clearly comprehensible access to complicated datasets at essentially no cost.

An unprecedented resource: The user-interactive sediment-budgeting tools provided in the GCMRC web application are unique in the world. We have, for the first time, made well-established sediment-budgeting methods available on demand.

Using this tool, river scientists and managers can create a new sediment budget for a selected river reach for any time period of interest (limited only by data availability) with different levels of uncertainty within a matter of minutes. Prior to the development of this tool, the construction of a mass-balance sediment budget was a tedious process that required hours of data downloading, manual data entry, data manipulation, and mathematical operations (all the time running the risks of mistakes because these procedures were not automated in a repeatable workflow). This work was primarily done only by scientists and then presented to managers. Now, managers and members of the lay public can create sediment budgets on their own, on demand, and in real-time using the most up-to-date data available.

The real thing: The GCMRC web application is a working system in production use by multiple teams and programs. It is not a temporary proof of concept. The user-interactive sediment-budgeting tools are being used by river managers and science teams in multiple programs.

First and foremost, these tools are being used on a monthly basis by engineers in the Bureau of Reclamation working within the Glen Canyon Dam Adaptive Management Program (GCDAMP) to plan and implement the release of controlled floods from Glen Canyon Dam to rebuild sandbar habitat in Grand Canyon National Park when downstream sand conditions warrant (U.S. Department of the Interior, 2012). The sediment-budgeting tools are also being used in GCDAMP to evaluate the sediment response to these controlled floods and to evaluate the effects of hydropower operations at Glen Canyon Dam on the sand resources in multiple reaches of the Colorado River in Grand Canyon National Park and Lake Mead National Recreation Area. National Park Service managers also employ the sediment-budgeting tool to seasonally evaluate the effects of flows released from Flaming Gorge Dam on the Green River in combination with natural flood flows from the Yampa River on the sediment resources in Dinosaur National Monument (e.g., Mueller et al., 2014a,b). Finally, the sediment-budgeting tool is being used by scientists to evaluate the effects of upstream Mexican dam releases and local tributary floods on channel and floodplain evolution in the Rio Grande in Big Bend National Park (Dean et al., 2015).

Still generating useful new capabilities: Additional user-interactive functions are being developed for the GCMRC web application over the next few years to continue to improve access to managers and the lay public of tools previously only available to scientists. Some of these may prove as powerful as the sediment-budgeting tools described in this paper. Chief among these new additions will be the development of a duration-curve tool that will allow the user to plot the time equaled or exceeded for any parameter served via the GCMRC web application.

More information about the loosely coupled architecture described and all of the open source components developed for the GCMRC web application are available in a USGS-supported GitHub repository (https://github.com/USGS-CIDA). Anyone interested in expanding the work is welcome to fork the main repository and contribute their own ideas and working code to the project.

REFERENCES

Dean, D.J., and Schmidt, J.C. (2011). The role of feedback mechanisms in historic channel changes of the lower Rio Grande in the Big Bend region: Geomorphology, v. 126, p. 333-349, doi:10.1016/j.geomorph.2010.03.009.

Dean, D.J., Topping, D.J., Griffiths, R.E., Sabol, T.A., Schmidt, J.C., Bennett, J. (2015). Using acoustic data to analyze near-continuous suspended-sediment dynamics on the Rio Grande in Big Bend National Park, USA: Proceedings of the Third Joint Federal Interagency Conference on Sedimentation and Hydrologic Modeling.

Edwards, T.K., and Glysson, G.D. (1999). Field methods for measurement of fluvial sediment: Techniques of Water-Resources Investigations of the U.S. Geological Survey, book 3, chap. C2, 89 pp.

Erwin, S.O., Schmidt, J.C., Wheaton, J.M., and Wilcock, P.R. (2012). Closing a sediment budget for a reconfigured reach of the Provo River, Utah, United States: Water Resources Research, v. 48, W10512, 13 pp., doi:10.1029/2011WR011035.

Grams, P. E., Schmidt, J.C., and Topping, D.J. (2007). The rate and pattern of bed incision and bank adjustment on the Colorado River in Glen Canyon downstream from Glen Canyon Dam, 1956–2000: Geological Society of America Bulletin, v. 119, n. 5/6, p. 556–575.

Grams P.E., Topping, D.J., Schmidt, J.C., Hazel, J.E., Jr., and Kaplinski, M. (2013). Linking morphodynamic response with sediment mass balance on the Colorado River in Marble Canyon: Issues of scale, geomorphic setting, and sampling design, Journal of Geophysical Research: Earth Surface, v. 118, p. 1-21, doi:10.1002/jgrf.20050.

Griffiths, R.E., Topping, D.J., McDonald, R.R., and Sabol, T.A. (2010). The use of the multi-dimensional surface-water modeling system (MD_SWMS) in calculating discharge and sediment transport in remote ephemeral streams: Proceedings of the Joint Federal Interagency Conference on Sedimentation and Hydrologic Modeling, June 27- July 1, 2010, Riviera Hotel, Las Vegas, Nevada, http://acwi.gov/sos/pubs/2ndJFIC/Contents/P40_Griffiths_paper.pdf.

Griffiths, R.E., Topping, D.J., Andrews, Timothy, Bennett, G.E., Sabol, T.A., and Melis, T.S. (2012). Design and maintenance of a network for collecting high-resolution suspended-sediment data at remote locations on rivers, with examples from the Colorado River: U.S. Geological Survey Techniques and Methods, book 8, chapter C2, 44 p., http://pubs.usgs.gov/tm/tm8c2/

Griffiths, R.E., Topping, D.J., Anderson, R.S., Hancock, G.S., and Melis, T.S. (2014). Design of a sediment-monitoring gaging network on ephemeral tributaries of the Colorado River in Glen, Marble, and Grand Canyons, Arizona: U.S. Geological Survey Open File Report 2014-1137, 21 p.

Griffiths, R.E., and Topping, D.J. (2015). Inaccuracies in sediment budgets arising from estimations of tributary sediment inputs: An example from a monitoring network on the southern Colorado Plateau: Proceedings of the Third Joint Federal Interagency Conference on Sedimentation and Hydrologic Modeling.

Mueller, E.R., Grams, P.E., Schmidt, J.C., Hazel, J.E., Jr., Kaplinski, M., Alexander, J.S., and Kohl, K. (2014a). Monitoring and research to describe geomorphic effects of the 2011 controlled flood on the Green River in the Canyon of Lodore, Dinosaur National Monument, Colorado and Utah: U.S. Geological Survey Scientific Investigations Report 2014-5022, 66 p., http://dx.doi.org/10.3133/sir20145022.

Mueller, E.R., Grams, P.E., Schmidt, J.C., Hazel, J.E., Jr., Alexander, J.S., and Kaplinski, M. (2014b). The influence of controlled floods on fine sediment storage in debris fan-affected canyons of the Colorado River basin: Geomorphology, v. 226, p. 65-75, doi: 10.1016/j.geomorph.2014.07.029.

Open Geospatial Consortium, Inc., (2006). OpenGIS Web Map Service Implementation Specification: accessed November 3, 2014, at http://www.opengeospatial.org/standards/wms.

Porterfield, G. (1972). Computation of fluvial sediment discharge: U.S. Geological Survey Techniques of Water- Resources Investigations, book 3, chapter C3, 66 pp.

Rubin, D.M., Tate, G.M., Topping, D.J., and Anima, R.A. (2001). Use of rotating side-scan sonar to measure bedload: Proceedings of the 7th Inter-Agency Sedimentation Conference, v. 1, p. III-139 through III-143.

Schmidt, J.C., and Wilcock, P.R. (2008). Metrics for assessing the downstream effects of dams: Water Resources Research, v. 44, W04404, 19 pp., doi:10.1029/2006WR005092.

Topping, D.J., Rubin, D.M., and Vierra, L.E., Jr. (2000a). Colorado River sediment transport 1. Natural sediment supply limitation and the influence of Glen Canyon Dam: Water Resources Research, v. 36, p. 515-542.

Topping, D.J., Rubin, D.M., Nelson, J.M., Kinzel, P.J., III, and Corson, I.C. (2000b). Colorado River sediment transport 2. Systematic bed-elevation and grain-size effects of sand supply limitation: Water Resources Research, v. 36, p. 543-570.

Topping, D.J., Schmidt, J.C., and Vierra, L.E. Jr. (2003). Computation and Analysis of the Instantaneous-Discharge Record for the Colorado River at Lees Ferry, Arizona—May 8, 1921, through September 30, 2000: U.S. Geological Survey Professional Paper 1677, 118 p.

Topping, D.J., Wright, S.A., Melis, T.S., and Rubin, D.M. (2007). High-resolution measurements of suspended-sediment concentration and grain size in the Colorado River in Grand Canyon using a multi-frequency acoustic system: Tenth International Symposium on River Sedimentation, Moscow, Russia, August 1–4, 2007, Proceedings, pp. 330–339, ISBN 978-5-89575-124-4, 978-5-89575-127-5.

Topping, D.J., Rubin, D.M., Grams, P.E., Griffiths, R.E., Sabol, T.A., Voichick, N., Tusso, R.B., Vanaman, K.M., and McDonald, R.R. (2010). Sediment transport during three controlled-flood experiments on the Colorado River downstream from Glen Canyon Dam, with implications for eddy-sandbar deposition in Grand Canyon National Park: U.S. Geological Survey Open-File Report 2010-1128, 111 pp.

Topping, D.J., Rubin, D.M., Wright, S.A., and Melis, T.S. (2011). Field evaluation of the error arising from inadequate time averaging in the standard use of depth-integrating suspended-sediment samplers: U.S. Geological Survey Professional Paper 1774, 95 p.

Topping, D.J., Wright, S.A., Griffiths, R.E., and Dean, D.J. (2015). Physically based method for measuring suspended-sediment concentration and grain size using multi-frequency arrays of acoustic-Doppler profilers: Proceedings of the Third Joint Federal Interagency Conference on Sedimentation and Hydrologic Modeling.

U.S. Department of the Interior. (2012). Environmental Assessment: Development and Implementation of a Protocol for High-Flow Experimental Releases from Glen Canyon Dam, Arizona, 2011 through 2020, Bureau of Reclamation, Salt Lake City, Utah, 546 p, http://www.usbr.gov/uc/envdocs/ea/gc/HFEProtocol/index.html.

U.S. Geological Survey. (2014). National Water Information System data available on the World Wide Web (USGS Water Data for the Nation), accessed November 3, 2014, at http://waterdata.usgs.gov/nwis/.

Voichick, N. (2008). Specific conductance in the Colorado River between Glen Canyon Dam and Diamond Creek, northern Arizona, 1988–2007: U.S. Geological Survey Data Series 364, 16 p.

Voichick, N., and Topping, D.J. (2010). Use of specific conductance in estimating salinity and as a natural tracer of water parcels in the Colorado River between Glen Canyon Dam and Diamond Creek, northern Arizona, in Melis, T.S., Hamill, J.F., Bennett, G.E., Coggins, L.G., Jr., Grams, P.E., Kennedy, T.A., Kubly, D.M., and Ralston, B.E., eds., Proceedings of the Colorado River Basin Science and Resource Management Symposium, November 18–20, 2008, Scottsdale, Arizona: U.S. Geological Survey Scientific Investigations Report 2010–5135, p. 357-362.

Voichick, N., and Topping, D.J. (2014). Extending the turbidity record: Making additional use of continuous data from turbidity, acoustic-Doppler, and laser diffraction instruments, and suspended-sediment samples in the Colorado River in Grand Canyon: U.S. Geological Survey Scientific Investigations Report 2014-5097, 31 pp.

Voichick, N., and Wright, S.A. (2007). Water-temperature data for the Colorado River and tributaries between Glen Canyon Dam and Spencer Canyon, northern Arizona, 1988–2005: U.S. Geological Survey Data Series 251, 24 p.

UPDATE ON ISSDOTv2 METHOD FOR MEASURING BED-LOAD TRANSPORT WITH TIME SEQUENCED BATHYMETRIC DATA

David Abraham, Research Hydraulic Engineer, David.D.Abraham@erdc.dren.mil, Tate McAlpin, Research Physicist, Tate.O.McAlpin@erdc.dren.mil, David May, Research Hydraulic Engineer, David.P.May@erdc.dren.mil, Thad Pratt, Research Physicist, Thad.C.Pratt@erdc.dren.mil, USACE-ERDC-CHL, Vicksburg, MS, and John Shelley, Civil Engineer, John.Shelley@usace.army.mil, USACE-Kansas City District, Kansas City

Introduction

The ISSDOTv2 (Integrated Section Surface Difference Over Time version 2) method to compute bed-load transport has been employed in the field for several years. This method utilizes difference plots of time-sequenced three-dimensional bathymetric data to calculate bed-load transport. Scour volumes determined from the difference plots are related to the average transport in a sand wave. The method is described in Abraham et al. (2011) and Shelley et al. (2013).

Purpose

The need to quantify bed-load sediments moving along the bottom of large sand bed rivers varies depending on agency perspective. Sands moving in the bed of a river are no longer viewed simply as a nuisance or problem related to dredging requirements, but as a ***resource***. River engineers and managers are now asked on a regular basis to allocate bed sediment resources to a variety of competing purposes and interests. Critical issues must be addressed such as land-building in the Louisiana Coastal Areas (LCA) and commercial sand mining in many locations throughout the country. With regards to environmental concerns related to the Endangered Species Act (ESA) and Environmental Impact Statements (EIS), managers must assess the availability of sand to maintain ecological habitat features of rivers such as islands and bars. These concerns must be addressed in addition to the requirements of maintaining adequate draft depths in the navigation channels and functionality of locks and dams. In order to adequately address the varied interests, river managers must have some idea of how much bed material is available, which is directly related to its rate of movement through a river system. If the mass transport rate can be determined and related to changes in river flow, a bed-load rating curve can be produced which provides a quantitative management tool for those tasked with allocating the river's sand resources.

With regards to dredging needs, dredging records have in the past provided an estimate of future dredging requirements. However, they are only applicable to that location. Dredging records also do not provide information about the rate at which the bed-load sediments are moving. If a bed-load rating curve is produced as mentioned above, a yearly average hydrograph can be used with the bed-load rating curve to produce a bed-load transport curve for the year. Integrating under this curve provides the total mass (or volume) of bed-load sediments that moved through a reach during that year.

Theoretical Basis

By way of review and for those who are reading about this method for the first time, a brief discussion of the theoretical basis is presented here. With the new bathymetric imaging and mapping techniques developed in the mid-1990's, the ability to accurately measure the bed surface of water bodies in three dimensions became a reality. The equipment and processing of the bathymetric data were of sufficient quality that the individual features of river bottoms such as dune fields could be adequately resolved to the sub-dune scale. For the duration of this paper the terms sand waves and dunes are used interchangeably and all bed-load transport values are reported in US tons per day (1 US ton/day = 0.907 metric tons/day). Figure 1 shows a swath of bed elevation data obtained from the Mississippi River at Red-Eye-Crossing, just south of Baton Rouge, Louisiana. The dune lengths varied from about 21 to 46 meters (~70 to 150 ft), with their direction of travel being from the top of the figure to the bottom. When the same area is surveyed a second time, the two sequential data sets can be subtracted to obtain a difference plot. In such a plot, the eroding portion of any dune will be noted by a decrease in surface elevation from time 1 to time 2, while the depositional side of the dune will show an increase in elevation. These differences can be plotted as positive and negative values using two colors to show areas of scour and deposition. Such a plot is shown in figure 2 where scour is plotted as red and deposition as blue. The lateral extent of the scour occurring on any dune as well as its depth of scour is available in the difference plot. Thus the volume of scoured bed material can be determined for any individual dune or for any selected group of dunes.

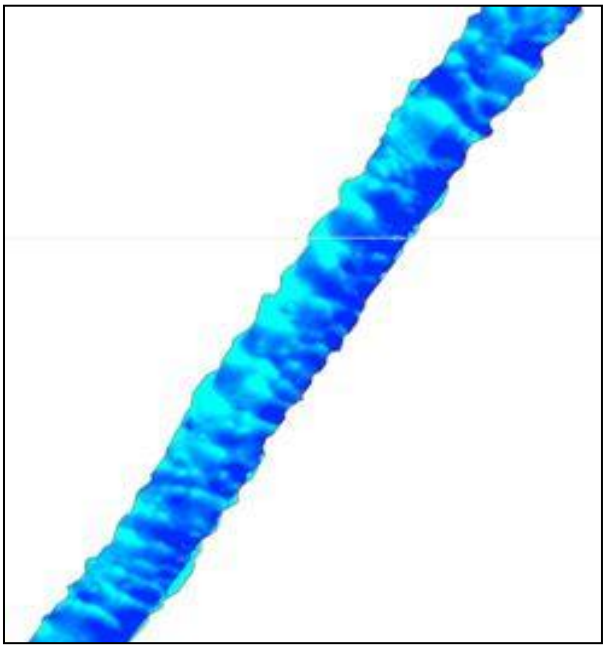

Figure 1 Plotted bathymetric data clearly delineating the individual dunes.

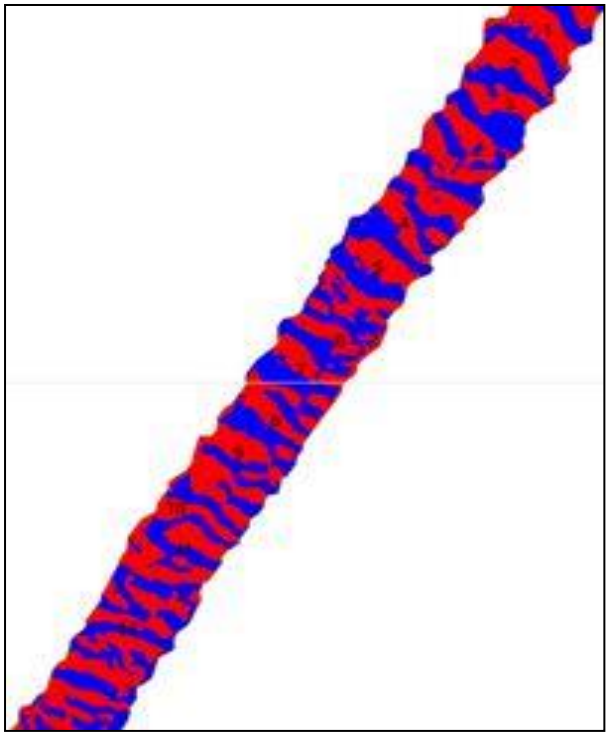

Figure 2 Bathymetric differences showing scour (red) and deposition (blue).

The relationship between the rate of scour on the eroding side of the dune and the average transport rate of the same dune is explained in Abraham et al (2011). The equation developed to quantify this relationship is shown in Equation 1

$$q_{sbi} = \frac{\rho(1-p)V}{2\Delta t} \quad (1)$$

where q_{sbi} is the bed-material load moving in the sand wave computed by the ISSDOTv2 method, ρ is the density of the submerged sand, p is the porosity of the sand, Δt is the time difference between measurements, and V is the scoured volume during the time interval Δt. Equation 1 is mathematically equivalent and dimensionally homogenous to the equation developed by Simons and Richardson (1965), provided in Equation 2.

$$q_{sb} = \frac{\rho(1-p)c\eta}{2} \quad (2)$$

where q_{sb} is the bed-material load moving in the sand wave, ρ and p are as above, c is the dune speed, and η is the dune height.

Equation 1 for the ISSDOTv2, or scour volume method, was applied to flume data [56 data sets representing 6 different flow rates varying from 0.203 cms (7.17 cfs) to 0.426 cms (15.04 cfs)] for which actual transport values were measured in a clear water scour

condition. This implies the volume of eroded bed-material on the upstream side of the dune should be equal to the volume deposited on the downstream side of the same dune. The results are shown in figure 3, which is more completely described in Abraham et al (2011). Significant to note is that assumptions of uniform wave velocity and minimal wave deformation were made in analyzing these flume data. These are conditions associated with steady uniform flow maintained during these flume experiments. The comparisons in figure 3 illustrate both the validity of those assumptions and the ability of the equation to accurately measure bed-load transport.

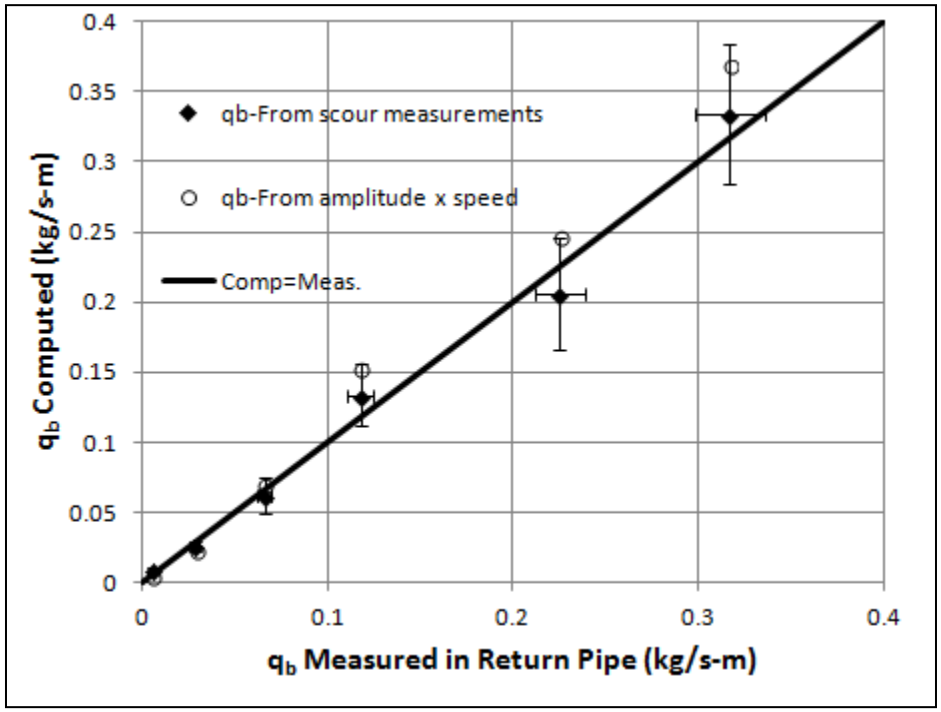

Figure 3 ISSDOTv2 computed versus measured bed-load transport in a flume study (Figure from Abraham et al. 2011).

The aforementioned discussion and results were presented in order to show that the method is founded on a sound theoretical basis that was substantiated with a large quantity of measured flume data. However, in river field applications, such ideal conditions rarely exist and present additional challenges for applying the scour volume method.

Practical Application of the Method

The high shear stresses and turbulent nature of natural channels result in a sizeable amount of the bed-material load moving in suspension. The unsteady nature of gradually varied flow also means that the rate of suspension or deposition can change significantly with time over a given river reach. In the aforementioned flume experiments, there were no suspended sediments, and therefore the assumption of the scoured volume moving to the depositional side of the same wave was a valid assumption. In a natural meandering

channel one cannot expect scoured volume to be equal to depositional volume. Some of the scoured bed-material does go into suspension and can travel far enough that it is not deposited on the dune from which it originated, thus adding depositional volume to other dune(s). The result is that for a given dune, and/or for a large dune field, the assumption of scour volume being equal to deposition volume is violated. It was noticed early on that this is often the case in natural rivers. How does this affect the computations? If, for example, 30% of the scoured volume went into suspension and was carried to some other dune, then that same 30% volume was not deposited on the same dune and thus did not participate in the dune movement. Thus the computed value of bed load transport could be in error by calculating 30% more transport in the dune than actually occurred. Based on these considerations, comparing the scour-deposition ratio should be a way to avoid data sets in which the river was excessively erosional or depositional. Such events could be caused by a rising or falling limb of a hydrograph. For ISSDOTv2 computations, scour-deposition ratios are computed for all difference plots. Those with values from 0.8 to 1.2 are retained while plots with values outside this range are deemed unsuitable for this method.

Another necessary correction occurs as a systematic bias inherent in the methodology. Figure 4 shows a translating wave form. The volumes of triangles C and D do not show up in the difference plots. These values get increasingly large as Δt gets larger and thus the 'missed' volumes result in smaller and smaller computed values of transport. So when Δt is very small, this systematic error is small, and when Δt is large, the corresponding error is large. This error was kept small in the flume study by using small time differences. In field conditions, however, this is seldom possible when surveying multiple swaths at a given river section. The later surveys could be hours apart. Shelley at al. (2013) details a procedure to correct for this systemic bias, which allows the longer time differences to still be used to obtain an accurate estimation of the true dune transport value.

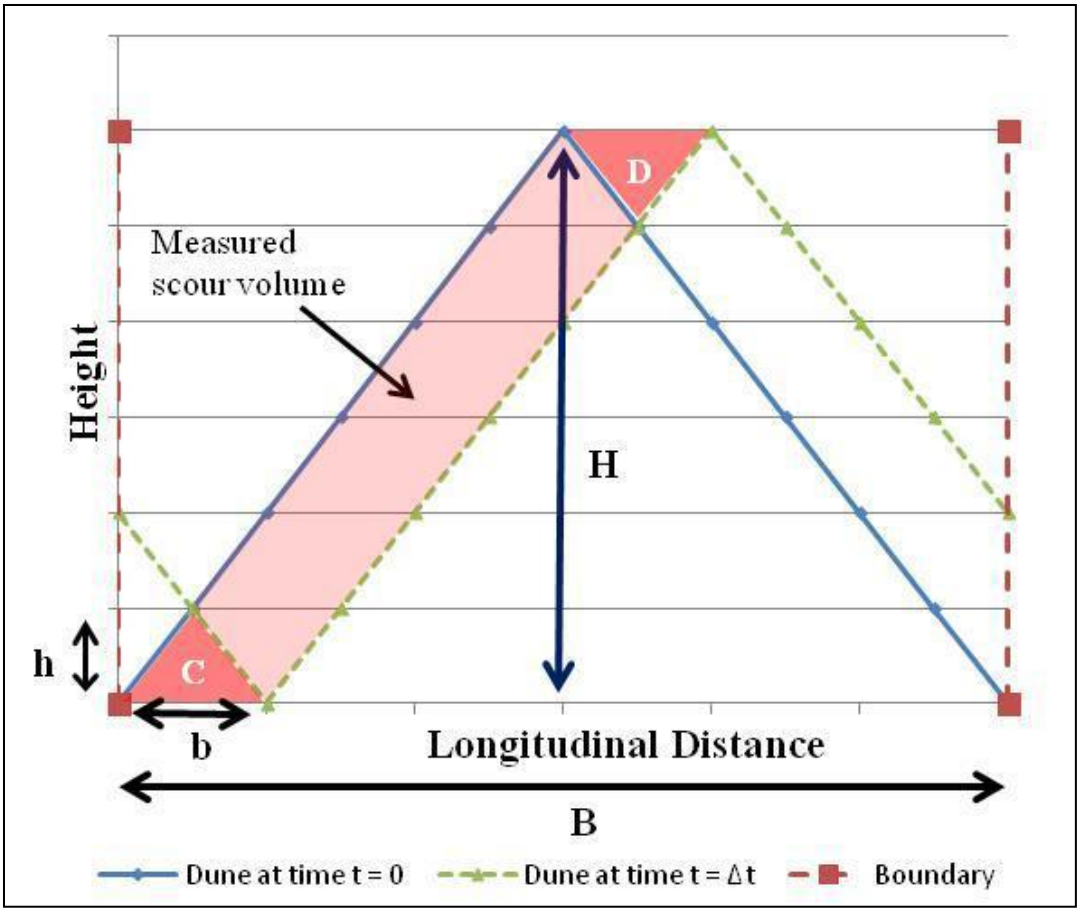

Figure 4 Schematic showing a systematic error due to lost volumes.

Example

When the two quality control procedures mentioned above are applied to the ISSDOTv2 computational method for a single bathymetric swath location, for which several repetitions were made, (temporally sequential), a transport value can be computed for that portion of the river. When multiple swaths cover a river from bank to bank, the values for each swath can be summed to provide the total bed-load transport at a river section. Figure 5 shows an example of such computations on the Ohio River near Mound City, IL. Additional information on the particular project methods and procedures are available in Abraham, Clifton and Vessels (2014).

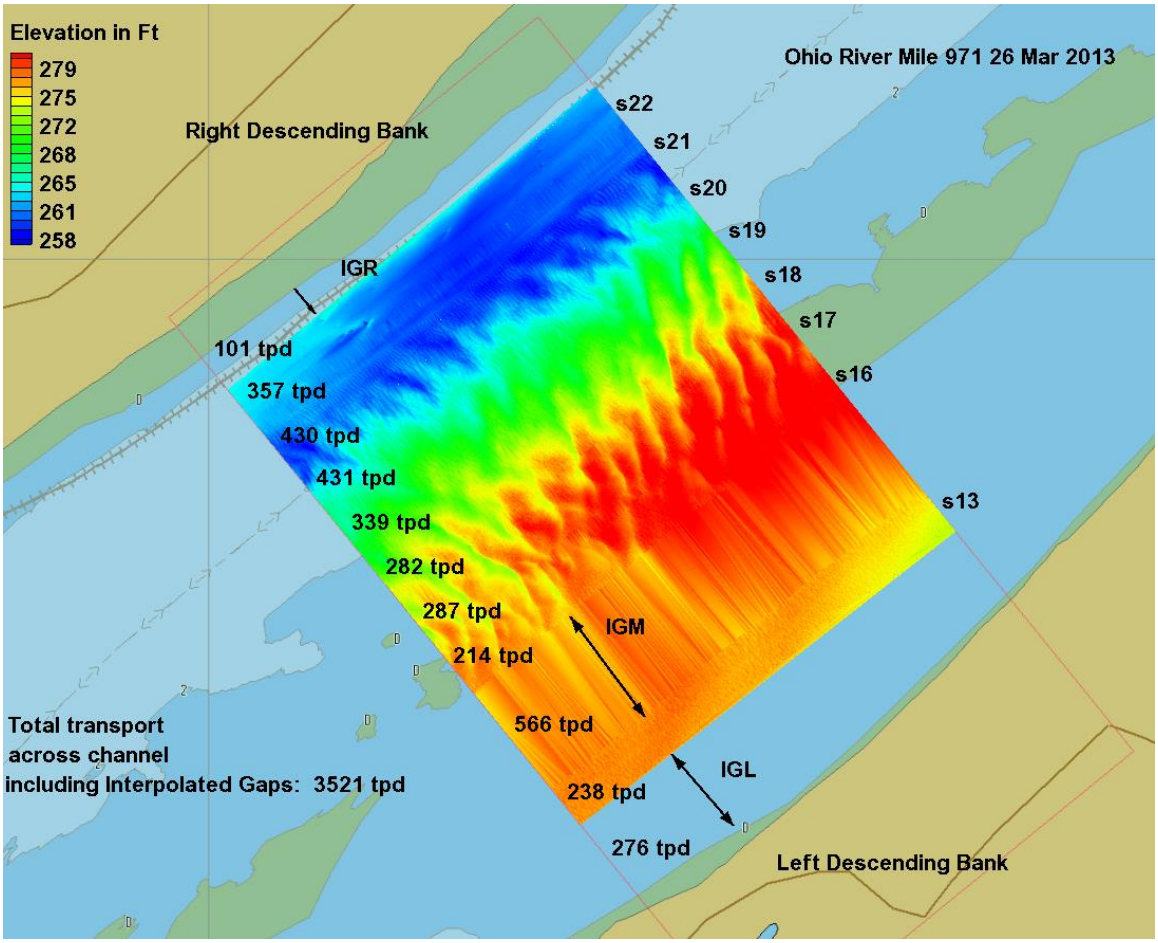

Figure 5 Multiple swaths and computed transport across a river section.

A MATLAB code has been created to calculate the transport for each swath. For this location each swath was divided into 1.524 m (5 ft) wide sections with the transport being calculated in each section using Equation 3

$$transport(tons/day) = \frac{43.2 * \rho(1-\mathrm{p}) * \mathrm{V}(ft^3)}{1.82 * \Delta t(\mathrm{sec}) * (\#waves)} \tag{3}$$

where 43.2 is a conversion from kg/s to tons/day and 1.82 is a parameter that accounts for the non-triangular shape of the dunes. The total transport for a given swath is then determined by integrating across the width of the swath. After determining the transport for various difference data sets (and different time steps), the previously discussed systematic bias was removed to obtain an accurate bed load transport value for each swath.

In figure 5, flow is from top to bottom. Swath numbers are at the top of each swath, and the computed bed load is at the bottom. The entire section was not covered, so linear interpolation was used for the gaps identified in the figure as IGR, IGM and IGL (values

of 0 were assumed for the bed-load transport at the left and right banks). They stand for Interpolated Gap Right, Interpolated Gap Middle and Interpolated Gap Left respectively. The total transport across the channel section was computed as 3,521 US tons per day including the interpolated gaps.

Field-data results from other large sand-bed rivers (Mississippi, Missouri, and Snake) have also been taken from 2011 to 2014. The measurements include bed-load transport values for various flow rates and river locations as well as suspended sediment concentrations and bed gradations. These data allow for the separation of wash load from bed-material load and also to compare total bed-material load (suspended bed material + bed load) to the ISSDOTv2 calculated bed load. In figure 6, data are plotted for a site on the Mississippi River just downstream of the Old River Control Complex (ORCC). The red square data points are the computed bed-load values (the sand moving in the dunes). As expected this value increases with increasing flow, and does so in a linear fashion as seen at this site and in most others that have been measured with three or more different flow rates. The blue diamond data points represent the bed load as a percentage of the total bed-material load. This is not a constant value and at this site varies from a low of about 10 % to a high value of over 45%.

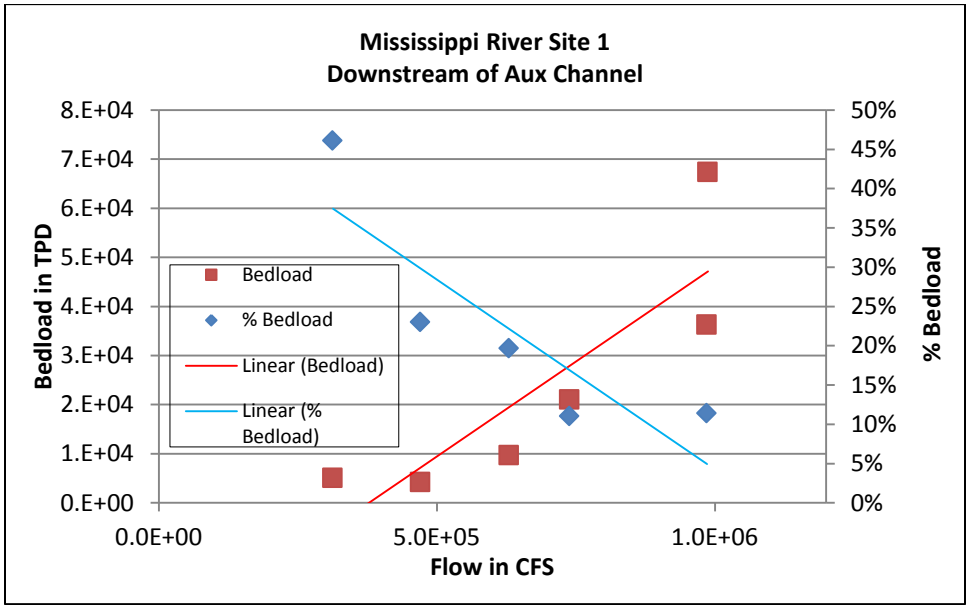

Figure 6 Bed load and % Bed load vs Flow rate on the Mississippi River.

In addition to Site 1 near the ORCC, whose data are plotted in figure 6, three other sites were measured during the same time periods, all of which were on the main channel of the Mississippi River. The bed-load computed values from all four sites (in total 22 independent data points) are plotted in figure 7. They show the same linear trend over a range of flows varying from 8,496 cms (300,000 cfs) to about 48,145 cms (1,700,000 cfs). By visual observation of the graph one can still make the case (similar to site 1) for a linear relationship between flow and bed load, with the R-squared value of 0.82 lending mathematical support to that conclusion.

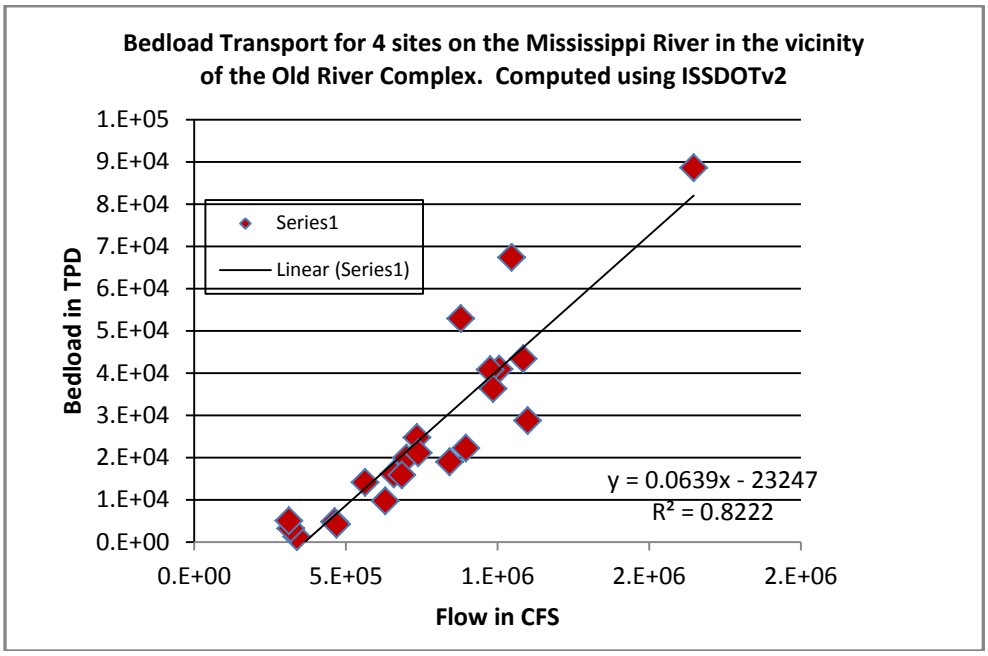

Figure 7 Mississippi River rating curve for flow versus bed-load transport.

Conclusions and Recommendations

Some of the more important conclusions noted to date are:

- The method clearly captures the lateral variability of the bed load transported in the moving sand waves for each swath, and when summed across the section provides the total bed-load transport for that river cross section.
- With sufficient measurements a bed-load rating curve can be developed.
- A bed-load rating curve can be very helpful to U.S. Army Corp of Engineers (USACE) District personnel in helping meet congressionally mandated sediment distributions as in the case of the Old River Control Complex.
- Using a bed-load rating curve and a yearly hydrograph, the net annual bed load moving through a river section can be approximated.
- Initial results on the Mississippi River indicate that bed load increases with increasing flow in a linear manner.
- Bed load is *not* a set percentage of total bed-material load, but can vary considerably depending on flow.
- Bed load *as a percentage* of bed-material load decreases with increasing flow.

The ORCC data shown here are representative of that collected and processed for 8 USACE Districts. They are St. Paul, Rock Island, Kansas City, Omaha, New Orleans, Vicksburg, Walla Walla, and Louisville, and they represent four major US Rivers; the Mississippi, Missouri, Ohio and Snake.

Corps Districts and other Federal Agencies want to know more about the method and the possibility of applying it themselves. To this end the authors have presented several workshops in the last year. An estimate of uncertainty must also be assigned to the computational results. Several proposals have been put forth for funding, including both flume and in-river studies. If funding can be secured for either case, the uncertainty of the measurements can be reduced and quantified with greater fidelity than is presently being done.

References

Abraham, D., Clifton, N., Vessels, B., (2014) 'Numerical Sedimentation Study of Shoaling on the Ohio River near Mound City, Illinois'. ERDC-CHL Technical Report (in review).

Abraham D., Kuhnle, R. Odgaard, A. J., (2011), 'Validation of Bed Load Transport Measurements with Time Sequenced Bathymetric Data' , ASCE Journal of Hydraulic Engineering, Vol 137, No. 7, pp723-728.

Shelley, J., Abraham, D., McAlpin, T., (2013), 'Removing Systemic Bias in Bed-Load Transport Measurements in Large Sand-Bed Rivers', ASCE Journal of Hydraulic Engineering, Vol 139, No 10, pp 1107-1111 .

Simons, D. B., Richardson, E. V., Nordin, C. F. Jr. (1965). 'Bed-load equation for ripples and dunes.' U. S. Geological Survey Professional Paper 462-H.

DISTINGUISHING BED-LOAD AND BED-MATERIAL-LOAD FLUXES WITH REPEAT BATHYMETRIC DATA

Brandon McElroy, Assistant Professor, University of Wyoming, Laramie, Wyoming, bmcelroy@uwyo.edu; David Abraham, US Army Corps of Engineers, Engineer Research and Development Center, Vicksburg, Mississippi david.d.abraham@erdc.dren.mil

ABSTRACT

Quantitative understanding of bed-load and bed-material-load fluxes in sandy rivers would afford greater understanding and prediction of channel form, river behavior, and habitats of river corridor biota. However, practical difficulties and cost ineffectiveness often exclude bed-sediment measurements from studies and monitoring efforts aimed at estimating sediment loads in rivers. An alternative to direct sampling is through the measurement of evolution of bed topography constrained by sediment-mass conservation. Historically, the topographic-evolution approach has been limited to systems with negligible transport of sand in suspension. We show that by loosening the constraint on mass conservation (that is, allowing divergence of sediment flux to vary temporally when averaged over a bed form length) bed load and bed-material load can be distinguished by their effects on the evolution of bed topography. As was shown decades ago, pure bed load transport is responsible for the mean migration of trains of bed forms when no sediment is exchanged between individual bed forms. In contrast, the component of bed-material load that moves in suspension is responsible for changes in the size, shape, and spacing of evolving bed forms; collectively this is called deformation. The sum of the effects of deformation and translation on bed topography reflects the total movement of bed material. Similarly, the difference between bed-load flux and bed-material-load flux equals the flux of suspended bed material. This approach is demonstrated using a set of repeat multibeam sonar bathymetric surveys coupled with point-integrated suspended-sediment profiles and acoustic Doppler velocimetry.

USING HYDROPHONES AS A SURROGATE MONITORING TECHNIQUE TO DETECT TEMPORAL AND SPATIAL VARIABILITY IN BEDLOAD TRANSPORT

Mathieu Marineau, Hydrologist, USGS, Sacramento, CA, mmarineau@usgs.gov
J. Toby Minear, Research Hydrologist, USGS, Golden, CO, jminear@usgs.gov
Scott Wright, Research Hydrologist, USGS, Sacramento, CA, sawright@usgs.gov

Abstract Collecting physical bedload measurements is an expensive and time-consuming endeavor that rarely captures the spatial and temporal variability of sediment transport. Technological advances can improve monitoring of sediment transport by filling in temporal gaps between physical sampling periods. We have developed a low-cost hydrophone recording system designed to record the sediment-generated noise (SGN) resulting from collisions of coarse particles (generally larger than 4 mm) in gravel-bedded rivers. The sound level of the signal recorded by the hydrophone is assumed to be proportional to the magnitude of bedload transport as long as the acoustic frequency of the SGN is known, the grain-size distribution of the bedload is assumed constant, and the frequency band of the ambient noise is known and can be excluded from the analysis. Each system has two hydrophone heads and samples at half-hour intervals. Ten systems were deployed on the San Joaquin River, California, and its tributaries for ten months during water year 2014, and two systems were deployed during a flood event on the Gunnison River, Colorado in 2014. A mobile hydrophone system was also tested at both locations to collect longitudinal profiles of SGN. Physical samples of bedload were not collected in this study. In lieu of physical measurements, several audio recordings from each site were aurally reviewed to confirm the presence or absence of SGN, and hydraulic data were compared to historical measurements of bedload transport or transport capacity estimates to verify if hydraulic conditions during the study would likely produce bedload transport. At one site on the San Joaquin River, the threshold of movement was estimated to have occurred around 30 m^3/s based on SGN data. During the Gunnison River flood event, continuous data showed clockwise hysteresis, indicating that bedload transport was generally less at any given streamflow discharge during the recession limb of the hydrograph. Spatial variability in transport was also detected in the longitudinal profiles audibly and using signal processing algorithms. These experiments demonstrate the ability of hydrophone technology to capture the temporal and spatial variability of sediment transport, which may be missed when samples are collected using conventional methods.

INTRODUCTION

Estimating bedload transport rates and determining the timing of incipient motion is desired for a variety of ecological and engineering purposes. High-quality data, however, are often unavailable or collected too infrequently (Gomez, 2006) due to the time and expense associated with collecting physical bedload samples (Gomez, 1989, Gray et al., 2010). Sediment transport is driven by a variety of mechanisms at a range of spatial and temporal scales (Hoey, 1992). Many practitioners use empirical relations between streamflow discharge and sediment discharge rates to predict transport during unmeasured periods (Gray and Simoes, 2008). Infrequent sampling will often fail to capture temporal variability, and therefore transport relations developed from these data may not adequately predict transport rates. An example of this is provided in Figure 1. A regression equation was developed from a simple discharge-bedload relation using physical measurements of bedload between 2010 and 2013 on the San Joaquin River (Figure 1A). The predicted bedload is shown during a 2011 flood event (Figure 1B) with the physical measurements of bedload overlaid. When compared to the physical measurements of bedload, the regression equation in this example will often either underpredict or overpredict bedload (from -70 percent to 310 percent,). The cause of such error in bedload transport prediction may be attributed to one of two (or both) sources: sampling error or temporal variations in bedload transport (Gomez and Troutman, 1997). To improve estimates of sediment transport, a low-cost surrogate technique could be used to fill in the temporal gaps between physical measurements or aid in identifying erroneous samples. This is analogous to using continuous measurements from a turbidity sensor calibrated to measurements of suspended sediment concentration to calculate sediment transport rates. Hydrophones are one example of such technology which can be used for coarse bedload transport.

Hydrophones were first used to listen to sediment-generated noise (SGN) in the 1930s (Bedeus and Invicsics, 1963). Since that time, others have conducted lab and field experiments to attempt to correlate the acoustic signal to particle size and transport rates (e.g. Thorne, 1986; Rouse, 1994, Barton et al., 2010). Several surrogate sediment monitoring technologies currently exist, each with their own advantages and disadvantages (Gray et al. 2010). Advantages of

hydrophones include: (a) low cost, (b) ease of deployment (c) minimal interference with the bed, and (d) they provide a spatially-weighted average of transport over the detection area. Disadvantages include: (a) hydrophones may detect unwanted noises in addition to SGN, (b) the precise detection area is not known and may change during a flood event, and (c) the relation between particle size and sound transmission loss is also not well understood.

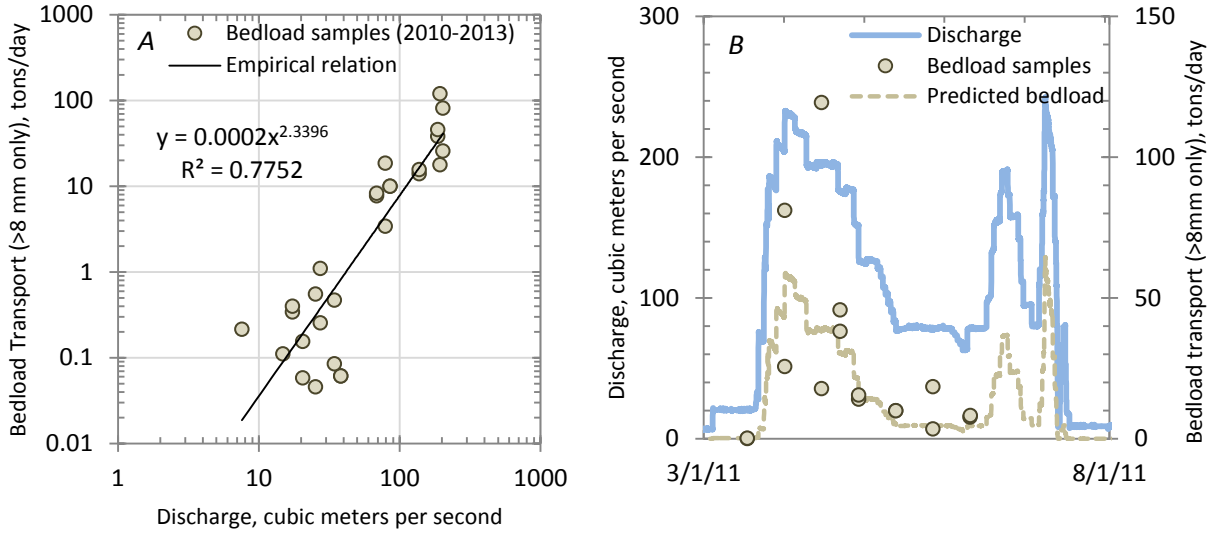

Figure 1 Example of temporal variability of bedload discharge in the San Joaquin River at Hwy 145 (USGS Site Number 11252975). Bedload measurements are plotted as a function of streamflow discharge to obtain a power law regression equation (A). The hydrograph during a 2011 flood event is shown with bedload measurements and predicted bedload discharge based on the empirical regression equation (B).

The general principle behind using hydrophones as a surrogate bedload monitoring technique is that they detect the rigid body radiations (i.e. sounds) generated by the collisions of sediment particles as the particles roll and saltate along the bed (Thorne, 2014). The sounds produced by the sediment collisions are often referred to as *sediment-generated noise* (SGN). The hydrophone uses a piezoelectric element to convert the sound pressure waves to an electrical signal. The electrical signal is proportional to the pressure acting on the piezoelectric element which is assumed to be proportional to the magnitude of bedload transport occurring near the hydrophone.

Our recent work has focused on developing a low-cost, long-term monitoring system to collect and record underwater sounds to supplement physical bedload measurements and to identify the timing of incipient motion. In addition, we developed an experimental mobile hydrophone recording system intended to measure relative spatial variability of SGN on a reach scale.

STUDY AREA

The majority of the hydrophone monitoring work was conducted on the San Joaquin River in California as part of the San Joaquin River Restoration Program (SJRRP). SJRRP is a multi-agency effort to increase populations of Chinook salmon (*Oncorhynchus tschawytscha*) in the San Joaquin River downstream of Friant Dam. This reach of the San Joaquin River consists largely of deep pools with gravel-bedded riffle clusters. There are only two major tributaries to this reach: Cottonwood Creek and Little Dry Creek. Both of these creeks are unregulated ephemeral streams. No measurable discharge occurred on the tributaries during WY 2014. Discharge on the mainstem San Joaquin River in the study area is regulated by Friant Dam. Particle-size distribution of the bed-material was measured in the San Joaquin River at hydrophone monitoring sites (using Wolman pebble counts). Median particle size (D_{50}) ranged between 26 and 80 mm on the mainstem and between 2 and 23 mm on the tributaries (which were generally a mix of sand and cobbles). Figure 2A shows the hydrophone monitoring sites on the San Joaquin River as well as the start and stop locations of the mobile hydrophone longitudinal profiles. The hydrophones were also tested on the Gunnison River, Colorado, during a spring flood event in 2014. The Gunnison River is a tributary to the Colorado River. Discharge on the Gunnison River was primarily regulated by the Blue Mesa Dam. Pitlick et al.

(1999) conducted particle-size distribution measurements at several locations along the Gunnison River. Our study reach was nearest to RM 55.6 which was measured by Pitlick et al. (1999) to have a surface D_{50} of 59 mm, and a subsurface D_{50} of 29 mm. Figure 2B shows the location of one of the hydrophone monitoring stations on the Gunnison River, as well as the start and end locations of the mobile hydrophone longitudinal profiles.

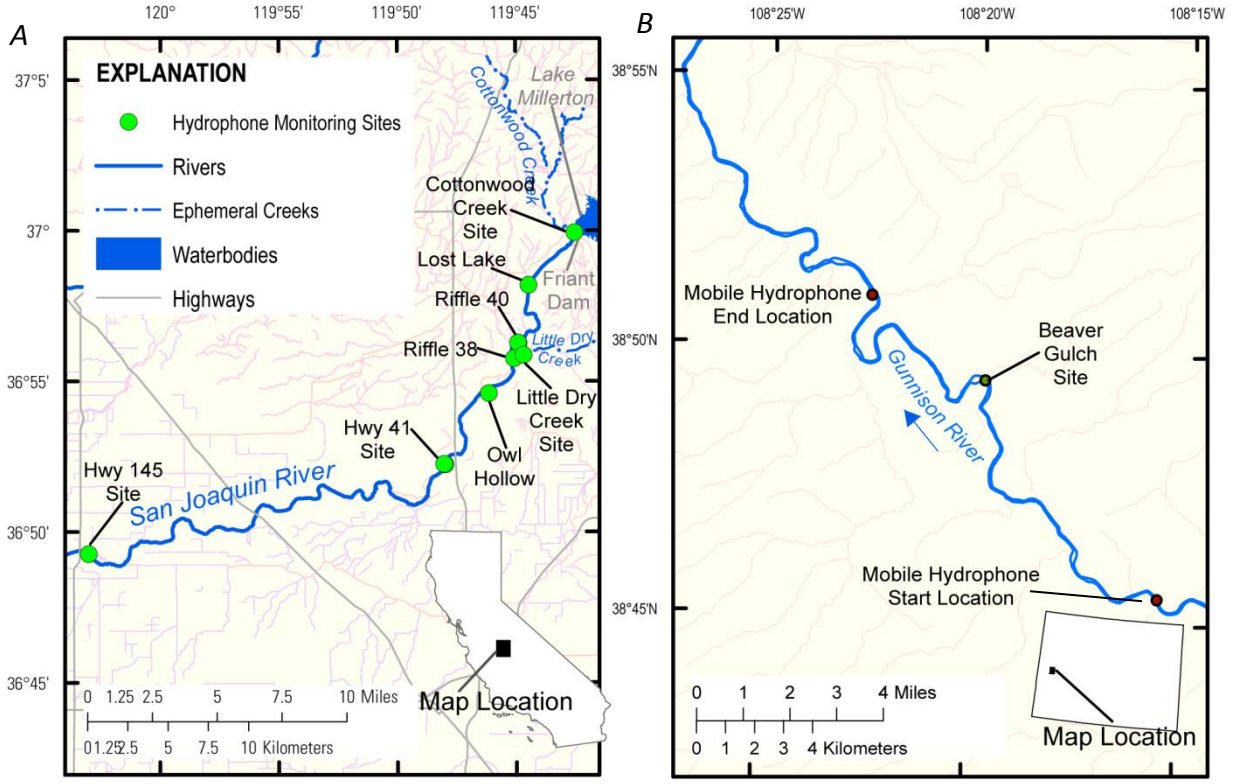

Figure 2 Study area map showing long-term hydrophone monitoring sites along the San Joaquin River, California (a), and testing locations for stationary and mobile hydrophones in the Gunnison River, Colorado (b)

METHODS

Data Collection Each hydrophone monitoring station consisted of two Aquarian H1a hydrophones and one recording system. The hydrophone recording systems were programmed to collect a 1-minute audio recording at a preset sample interval. Typically the sampling interval was set to 30 minutes; however, at the flashier tributary creeks the sampling interval was set to 20 minutes. The recording system was contained in a Pelican case and secured to the bank. The systems were capable of operating continuously for four to five weeks before they required routine servicing. Routine servicing involved downloading data and replacing batteries. At that time, the hydrophone heads were inspected (when conditions were wadable) and any debris found was removed. A pressure transducer was also installed nearby at each site to record water levels. The sensitivity of the H1a hydrophones is -190 dB re 1V/uPa (+/- 4 dB) (Aquarian Audio, 2013). The preamplifier gain was set to 14 dB, which provided a clear overall signal without clipping higher amplitude sounds.

At each site, the hydrophones were installed in the river by attaching them to a vertical piece of steel rebar approximately 30 cm above the bed. Prior to attaching the hydrophone, the rebar was driven into the bed 45-60 cm. A second piece of rebar was installed approximately 30 cm directly upstream to block debris which may otherwise accumulate on the hydrophone and result in sound transmission loss (Figure 3B). The audio cable was routed through a flexible polyvinyl chloride (PVC) conduit which was buried in a shallow trench. The PVC conduit was also secured in place using several pieces of u-shaped rebar which were driven into the bed.

Ten hydrophone recording systems were deployed across eight California sites in November 2013 (Figure 2a). Two of ten system were deployed in the tributary creeks. In addition, at two sites (Hwy 41, and Riffle 40) a hydrophone monitoring station was installed on each bank of the river in an attempt to collect a better spatial average of SGN. Due to the multi-year drought in California, peak flow during the study period was only about 37 m^3/s on the San Joaquin River, which is relatively low with minimal bed movement. In an effort to field test the hydrophone systems under a range of flow conditions, two systems were deployed on the Gunnison River, during a late-spring flood event.

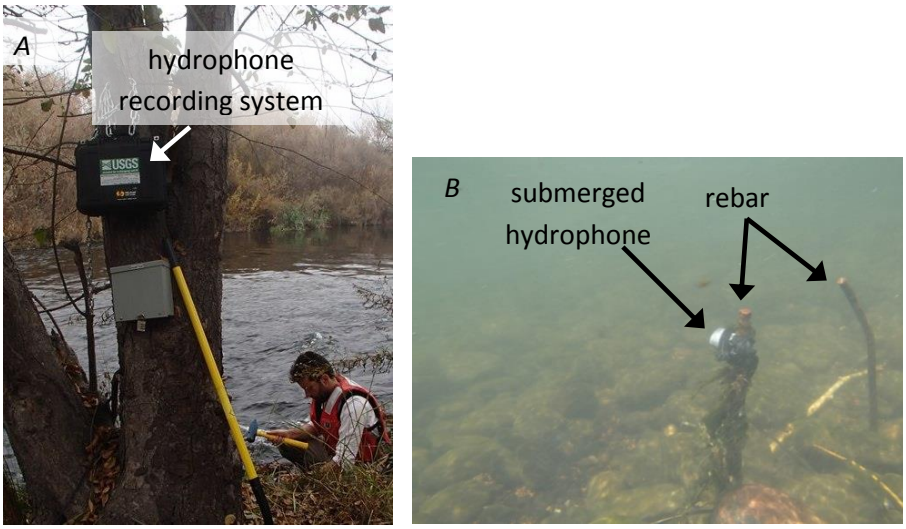

Figure 3 Photo of hydrophone recording system installed at the Owl Hollow Site (A), and photo of submerged hydrophone with additional piece of rebar installed upstream to deflect debris (B).

A mobile hydrophone system was used to record a longitudinal profile using one hydrophone mounted to a hard-shell kayak. Audio data were recorded on a portable tablet computer. Location, depth and streamflow velocity were measured using a real-time kinematics global-positioning system (RTK-GPS) and a StreamPro acoustic Doppler current profiler (ADCP). At the time of publication, GPS data were not fully processed, therefore "distance downstream" on any plots shown are approximate, and were calculated using the assumption that boat speed was constant throughout data collection. Three longitudinal profiles of underwater sounds at three different flows (303 m^3/s, 234 m^3/s, 48 m^3/s) were collected on the Gunnison River, and one longitudinal profile (at 37 m^3/s) was collected at two reaches on the San Joaquin River.

Discrimination of Sediment-Generated Noise and Ambient Noise Previous work (Jonys, 1976; Millard, 1976; Thorne, 1985; Thorne, 1986) has shown an inverse relation between the acoustic frequency of SGN and the particle size. Thorne (1986) proposed an empirical equation using those data to relate the resonance frequency of SGN and particle size (shown in Figure 4). Thorne's equation was based on particles from 0.2 mm to 43 mm. More recently, Belleudy et al. (2010) conducted experiments to measure the SGN of larger sized particles (15 to 110 mm). The hydrophones are most suited for applications in gravel-bedded rivers (Gray et al., 2010). Therefore, results from coarser particles are of particular interest, and we present a revised equation (Equation 1) using only experimental results for particles coarser than 4 mm (which includes pebbles, gravels and cobbles) (Figure 4). The following is the revised equation which provides a better approximation of experimental data for the larger sizes.

$$f_r \approx 55/D^{1.16}\ Hz \tag{1}$$

where f_r is the resonance frequency, and D is the particle diameter in meters. Assuming those results are transferable to particles in motion in a streambed, the intensity, or level, of sound in these ranges should correlate with SGN of bedload particles in transport.

Ambient noise (e.g. water motion, wind, and/or biological), however, may still overlap the same frequency range as SGN. Tonella et al. (2009), for example, found that underwater noise related to turbulence and bubble formation were most pronounced between 125 Hz and 2 kHz. Zakarauskas (1986) noted that wind noise can occur between 50

Hz and 10 kHz, but maximum wind noise is generated between 100 Hz to 1000 Hz. Therefore it is important to determine if ambient noise is present in audio recordings as well as the likely frequency range of such noise. Aural listening (i.e. listening through the ear) is particularly useful at distinguishing various sources of noise in the audible range (Camp, 1970). Aural review was combined with automated signal processing tools to analyze the audio recordings and identify if there were periods in which either ambient noise or SGN noise was dominant.

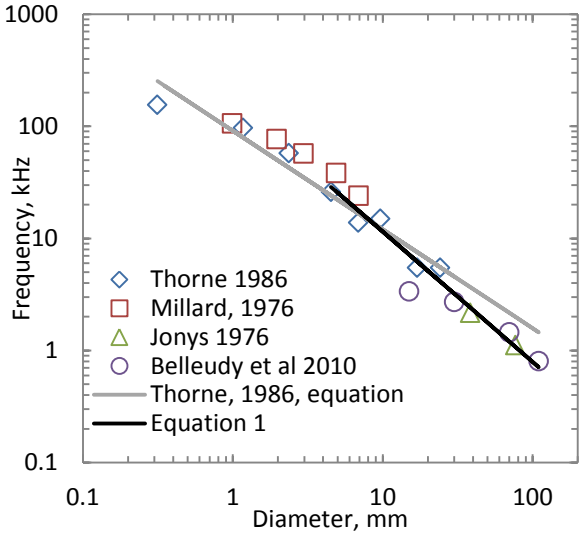

Figure 4 Measurements of acoustic frequency of sediment-generated noise (SGN) as a function of particle size. Thorne 1986 empirical equation, and Equation 1 of this study are also shown.

Signal Analysis The audio recordings were processed in MATLAB by first transforming the signals from the time domain to the frequency domain using a short-time Fourier transform to obtain the power spectral density (PSD). A spectrogram is a convenient way to display the PSD of an audio recording. Time is displayed on the x-axis, frequency on the y-axis, and the sound level for any given frequency and time is represented by color. The sound level for the recordings were averaged over a 1-minute time period. Marineau et al. (2010) found that a 1-minute sample was sufficient to average short-term temporal variability of SGN (such as a loud shock in very close proximity of the hydrophone). For the mobile hydrophone systems, however, a 1-minute time period may not be appropriate. For example, a 1-minute averaged sample may smooth over a local peak of SGN while traveling through a riffle. Therefore, the mobile audio data was split into 15-second time periods for analysis.

Hydrophones are typically calibrated in a specialized underwater-acoustics facility which involves measuring the precise voltage response of the electrical signal output to a given sound pressure at a specific frequency. Low-cost hydrophones (such as the ones used in this study) are generally not calibrated. Therefore, it is not possible to determine the exact sound pressure level from the measured voltage signal output. Sound level is generally referred to in decibels (dB), and sometimes more specifically as decibels of sound pressure level (dB SPL) where 0 dB SPL is the lower threshold of human hearing. The decibel scale is a logarithmic scale and is used because sound pressure can vary by many orders of magnitude. Since the hydrophones used in this study were not calibrated, sound levels are expressed in *dB* rather than *dB SPL*. This means that 0 dB does not necessarily correspond to the lower threshold of human hearing and also that any two hydrophones may have slightly different levels of sensitivity. Though the hydrophones are not calibrated, they can still provide useful information regarding the relative magnitude of underwater sounds. For each 1-minute sample recorded at a hydrophone monitoring station (or 15-second subsample of the mobile hydrophone recording), decibels were calculated using the following equation (Erbe, 2011) assuming cylindrical spreading sound due to shallow water (e.g. Urick, 1983):

$$dB = 10*\log(dv/FS) - M - G - S \quad (2)$$

where dv = digital values in the .wav file, FS = full scale value (for 16-bit floating point, FS is 1), M is the digital gain of the pre-amplifier, I = hydrophone sensitivity level, expressed in dB re 1V/uPa, G = preamplifier gain setting

(in dB). Each spectrogram was calculated in MATLAB using a Hamming window, with a 1 second (44,100 sample) window size, 50 percent window overlap, and fast-Fourier transform (FFT) length of 4410.

RESULTS

Temporal Variability During WY2014, streamflow on the San Joaquin River was generally not sufficient to mobilize coarse sediment at most sites. This was evidenced by audio recordings from several sites and bedload samples collected by the California Department of Water Resources (CADWR) at four sites (Matt Meyers, CADWR, written communication). Of the monitoring sites along the San Joaquin River, the most downstream site, Hwy 145 (Figure 2A), had the smallest bed-material size (D_{50} of 26 mm) and the hydrophone monitoring station at this site detected higher levels of SGN than any other site. During a portion of the deployment, streamflow was very low (4.2 m^3/s) and the hydrophone sensors were at or just above the water surface. Figure 5 shows a spectrogram (5A) and time series of average sound levels for 1.3 to 6.7 kHz frequency range (5B). Data from only one of the two hydrophones is shown in this figure. The frequency range was calculated using Equation 1 with particle diameters of 16 to 64 mm (approximately 70 percent of the bed-material was within this size range). The data includes the period when the hydrophones were out of the water and periods when the water level was at the hydrophone. Releases from Friant Dam were increased starting in early May and held steady during most of the summer. An aural review of several audio recordings revealed that during early low-flow (4.2-11.3 m^3/s) period, the dominant noise sources was water motion. Ambient noise associated with water motion was generally below 2 kHz, but at times was as high as 5 kHz. During period of higher stage, the noise associated with water motion could not be heard in any audio recordings; therefore we concluded that the average sound levels calculated during these periods was primarily SGN. The time series data was refined to exclude low-flow periods which were dominated by ambient noise (Figures 5B and 5C). The ambient noise was easily identified by ear, but could not be discerned from SGN using the signal analysis methods employed in this study. The data from the 5-month period with sustained 36.8 m^3/s flows show some temporal variability in transport; however the elevated sound levels measured during the months of data collection prior to the reservoir releases were from ambient noise, not SGN. In the absence of physical bedload measurements, an aural review of the audio recordings was helpful in distinguishing the SGN from noise originating from other sources. Based on SGN data, coarse bedload was found to generally start and stop at this site when streamflow was around 30 m^3/s.

The hydrophone monitoring station at the Beaver Gulch Site on the Gunnison River (Figure 2B) recorded audio data during the peak of a 10-year flood event. Since the hydrophones were installed in the bank during the rising limb of the flood event, as the streamflow decreased, they were no longer submerged and thus were repositioned to continue data collection. Figure 6B shows the hydrograph with the average sound-level time series overlaid. Figures 6C and 6D show scatter plots of sound level vs discharge. The colors indicate the date starting around June 1 and ending June 10. This figure shows clockwise hysteresis in the sound level. Assuming the SGN was directly proportional to the sediment discharge, these results indicate a decrease in transport which suggests a reduction in sediment supply, bed armoring, or perhaps that the geometry of the channel changed such that sound transmission decreased with time.

Spatial Variability Two longitudinal profiles of SGN were collected in two separate reaches of the San Joaquin River during a discharge of 36.8 m^3/s. Only results from the downstream-most 2.5 km are reported (Figure 7). The spectrogram (Figure 7A) indicates that near-continuous noise was present in the lower frequencies through the entire profile. Aural review of the audio recordings suggested that the source was water noise, likely generated by either the kayak or the paddle movement. The two black rectangles in Figure 7A highlight areas where SGN was audibly detected. Figure 7B shows a time series of the average sound levels for two different frequency ranges. The lower frequency range (1.3 to 6.7 kHz) overlaps with the boat/paddler-generated noise; therefore a time-series calculated from the average sound levels in this range does little to elucidate locations of bedload transport. In the mobile recordings, however, water motion noise was detected in the slower-moving pools (during which the operator was using the paddle to propel the kayak downstream), and this noise was generally limited to less than 4 kHz. The second frequency range shown in Figure 7B (4.5 to 6.7 kHz), however, excludes most of the ambient noise, and two potential riffle clusters with SGN are easily identified in the time series (black rectangles in Figure 7B). The last figure (7C) shows longitudinal profiles of depth, velocity, and water-surface elevation for the same reach. Two sections with increased water-surface slope correspond roughly to the potential riffles identified in Figure 7B. The downstream riffle is a known riffle at the Hwy 145 Site.

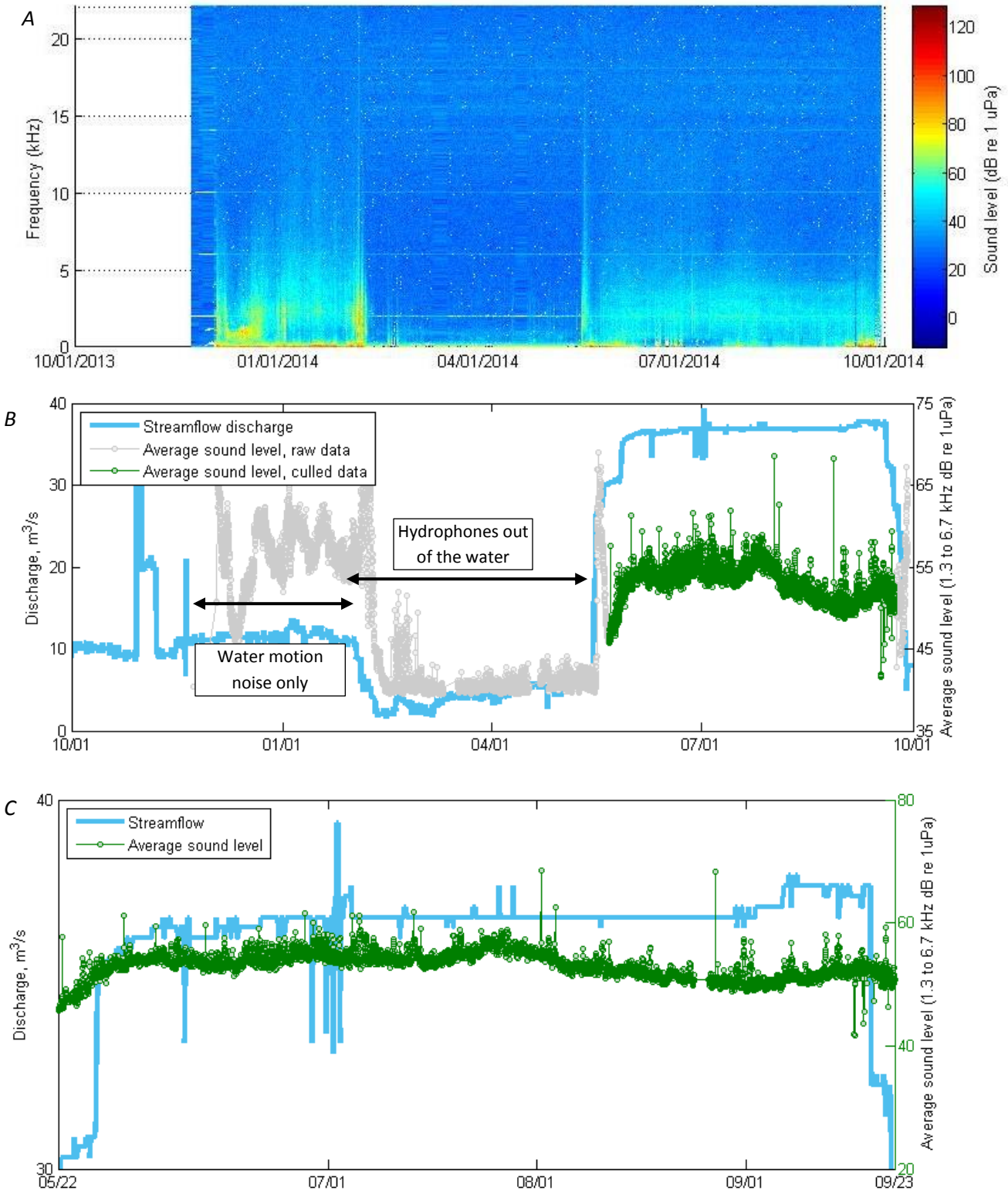

Figure 5 Spectrogram (A) and time-series of raw and refined data overlaid on the hydrograph (B) recorded in the San Joaquin River, California at Hwy 145 monitoring site, WY2014. A close-up of the period when sediment-generated noise was detected is also shown (C).

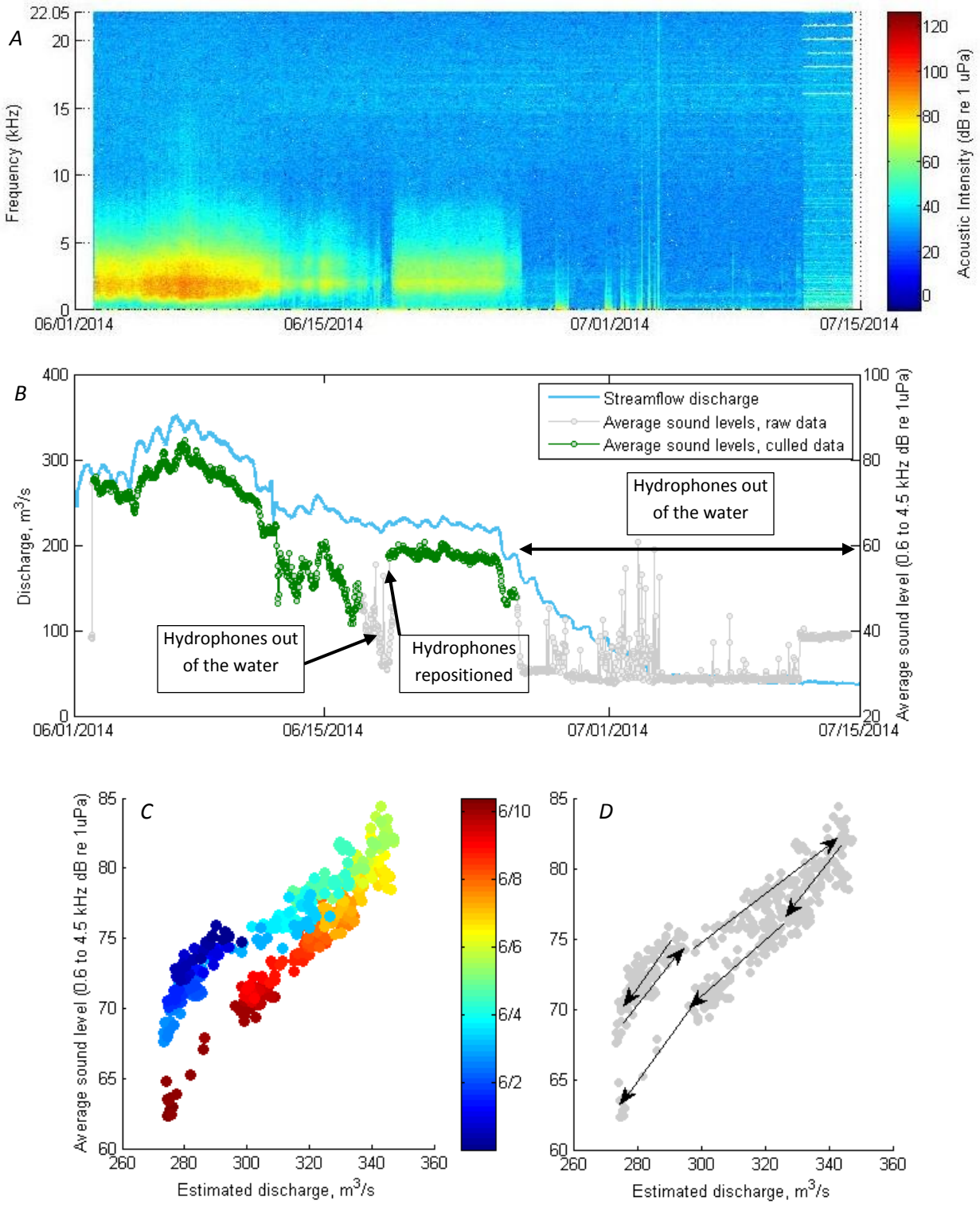

Figure 6 Spectrogram (A) and time-series (B) of 1-minute averaged sound level (0.6-4.5 kHz) in the Gunnison River, CO, Beaver Gulch Site. Scatterplot (C, D) of days 1-10 showing clockwise hysteresis of sediment-generated noise

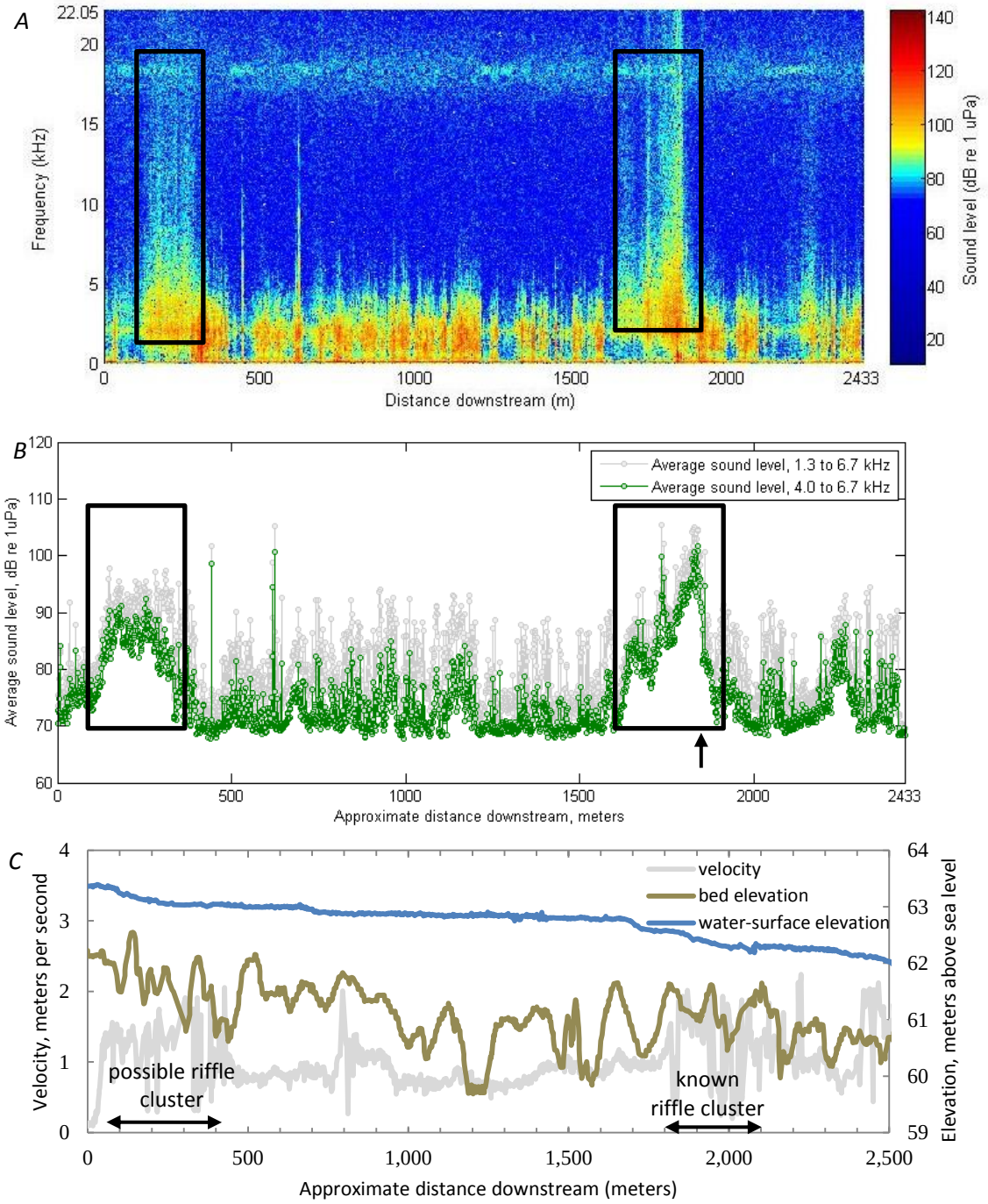

Figure 7 Longitudinal profile of San Joaquin River, California (2.5 km reach near Hwy 145) shown as spectrogram (A), time-series of average sound level for two different frequency ranges (B), and bed elevation, water velocity, and water-surface elevation (C). Boxes indicate periods in which bedload was audibly detected. Vertical arrow indicates approximate location of hydrophone monitoring station at the Hwy 145 Site.

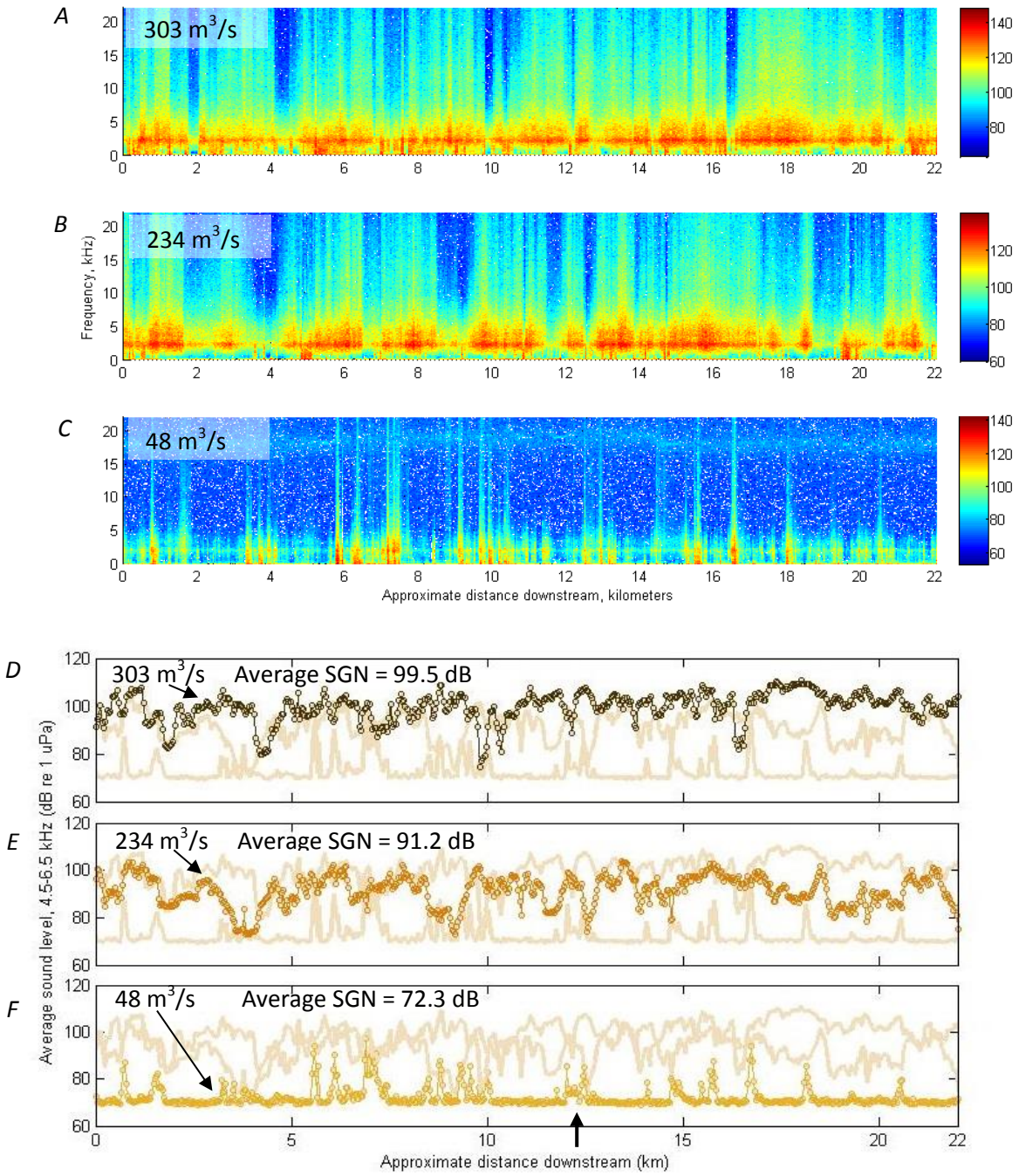

Figure 8 Spectrograms (A-C) and fifteen-second averaged sound level (D-E) recorded from mobile hydrophone system at three different flows: 303 m^3/s, 234 m^3/s, and 48 m^3/s Gunnison River, Colorado. Vertical arrow indicates approximate location of hydrophone monitoring station at the Beaver Gulch Site.

Longitudinal profiles of audio recordings were collected in the Gunnison River at three flows: 303 m^3/s, 234 m^3/s, 48 m^3/s (Figure 8). These time-series were calculated from the same frequency range as the San Joaquin River time series to reduce any potential influence of boat/paddle noise. During the higher flows, elevated sound levels were recorded over most of the reach, suggesting that most or all of the bed was at least partially mobilized. During the lowest flow, only discrete sections of the river had transport occurring. Between these sections were quiescent pools which have an ambient noise floor of about 70 dB.

Statistical information of the longitudinal profiles is also shown in Figure 8D-8F. Generally, average sound levels of SGN decreased with lower flows, however, there was still a high degree of spatial variability at all flows. Critical discharge (i.e. discharge that initiates bedload transport) in this reach, was estimated to be between 195 m^3/s and 269 m^3/s (Pitlick et al., 1999).

CONCLUSIONS

The results from this first year of data collection demonstrate that the hydrophone recording system can be used to collect high-resolution surrogate sediment data in gravel-bedded rivers. The sound level of the signal recorded by the hydrophone is assumed to be proportional to the magnitude of bedload transport as long as the acoustic frequency of the sediment-generated noise (SGN) is known, the grain-size distribution of the bedload is assumed constant, and the frequency band of the ambient noise is known and can be excluded from the analysis. These data can be calibrated and used to fill temporal gaps between physical bedload measurements or as a stand-alone qualitative measure of the timing and variability of transport. At one site on the San Joaquin River, the threshold of movement was estimated to have occurred around 30 m^3/s based on SGN data. The results from the Gunnison River show a clockwise hysteresis during a flood event, which may not be detected using traditional physical sampling at typical sampling return intervals. Previous research has found that gravel transport can occur in waves at different temporal and spatial scales. Pairing physical samples with high-resolution surrogate data may provide a method to determine if a particular sample was collected at high or low point of a sediment wave, and reduce error in estimates of sediment transport. These data may be calibrated to physical samples to obtain a continuous, quantitative estimate of bedload transport. Previous attempts (e.g. Barton et al., 2010) have attempted to relate the average acoustic intensity over a large frequency range to bedload flux. Future work should compare the acoustic signal of SGN in known mixtures from laboratory or field experiments.

The initial testing of the mobile hydrophone system shows that it could be a useful tool to identify fine-scale spatial variability in sediment transport over large reaches, something that is not possible using conventional sampling techniques. This type of qualitative information may be applicable for verifying localized transport in a hydraulic or sediment transport model. Quantifying the transport rate occurring in any particular place, however, has additional challenges; primarily that changes in depth and channel geometry will affect sound transmission and spatial variability in bedload particle-size distributions will change the acoustic signature of the SGN.

Finally, for both the stationary and mobile hydrophone systems, methods are needed to identify and reduce noise from non-sediment sources. Noise reduction may be achieved physically (e.g. changes in the hydrophone mount configuration, hydrophone placement), or through various signal processing tools. In this study, the relative magnitude of transport was quantified by calculating the average sound level over certain frequency ranges. By adjusting these (as was done for the mobile hydrophone data on the San Joaquin River), ambient noise can be excluded from the final results. In the case of the hydrophone monitoring station at the Hwy 145 Site on the San Joaquin River, the selected frequency ranges span bedload noise as well as background noise from water motion. At this site, a different mount style or site may reduce unwanted noise. Future work will consider alternative hydrophone locations and mount configurations to determine which combination will provide optimal performance.

ACKNOWLEDGEMENTS

The authors would like to thank John Franco Saraceno, and Richard Snyder for electrical engineering and development contributions; David Yancy for software coding; Amber Powell, Robert Castagna, and Joan Lopez, for field assistance. Any use of trade, product, or firm names in this paper is for descriptive purposes only and does not imply endorsement by the U.S. Government.

REFERENCES

Aquarian Audio. (2013). “Aquarian Audio Products H1a Hydrophone User’s Guide”, Available at http://www.aquarianaudio.com/AqAudDocs/H1a_manual.pdf, downloaded Feb 2013

Bedeus, K., and Ivicsics, L. (1964). “Observation of the noise of bed load,” Proc. of General Assembly, Commission on Hydrometry, Berkeley, CA, USA, International Association of Hydrological Sciences, pp 384-390.

Barton, J.S., Slingerland, R.L., Pittman, S., and Gabrielson, T.B. (2010). “Monitoring Coarse Bedload Transport with Passive Acoustic Instrumentation: A Field Study,” in Gray, J.R., Laronne, J.B., and Marr, J.D.G.,

Bedload-surrogate monitoring technologies: U.S. Geological Survey Scientific Investigations Report 2010-5091.

Belleudy, P., Valette, A., and Graff, B. (2010). "Passive Hydrophone Monitoring of Bedload in River Beds: First Trials of Signal Spectral Analysis," in Gray, J.R., Laronne, J.B., and Marr, J.D.G., Bedload-surrogate monitoring technologies: U.S. Geological Survey Scientific Investigations Report 2010-5091.

Camp, L. (1970). Underwater Acoustics. John Wiley and Sons Inc., New York. 308 p

Erbe, C. (2011). Underwater Acoustics: Noise and Effects on Marine Mammals, A Pocket Handbook, Jasco Applied Sciences, online, available at: http://oalib.hlsresearch.com/PocketBook%203rd%20ed.pdf

Gomez, B., Naff, R.L., and Hubbell, D.W. (1989). "Temporal Variations in Bedload Transport Rates Associated with the Migration of Bedforms," Earth Surface Processes and Landforms, 14(2), pp. 135-156.

Gomez, B. (2006). "The potential rate of bed-load transport," Proc. of the National Academy of Sciences, 103(46), pp 17170-17173.

Gomez, B. and Troutman, B.M. (1997). "Evaluation of process errors in bed load sampling using a dune model," Water Resources Research. 33(10). p 2387-2398.

Gray, J.R., Laronne, J.D., and Marr, J.D.G. (2010). "Bedload-surrogate monitoring technologies," U.S. Geological Survey Scientific Investigations Report 2010-5091, 37p.

Gray, J.R., and Simões, F.J.M. (2008). "Estimating sediment discharge", in Garcia, M., ed., Sedimentation Engineering, Processes, Measurements, Modeling, and Practice: ASCE Manuals and Reports on Engineering Practice No. 110, p 1067-1088.

Hoey, T. (1992). "Temporal variations in bedload transport rates and sediment storage in gravel-bedded rivers" Progress in Physical Geography, 16(3), pp 319-338.

Jonys, C.J. (1976). Acoustic measurement of sediment transport. Scientific Series No. 66. Department of Fisheries and the Environment, Inland Waters Directorate, C.C.I.W. Branch, Burlington, Ontario, Canada, 118 p.

Marineau, M.D., Gendaszek, A, Magirl, C., Czuba, J., and Czuba, C. (2012). "Surrogate Bedload Monitoring Using Hydrophones in the Gravel-Bedded Cedar River, Washington," Proc. Hydraulic Measurements and Experimental Methods Conference, Snowbird, Utah, pp. 1–6.

Millard, N.W. (1976). "Noise generated by moving sediments," Proc. of Conference on Recent Developments in Underwater Acoustics, held at A.U.W.E, Isle of Portland, England, 31st March and 1st April 1976.

Pitlick, J., Steeter, M.V., Barkett, B., Cress, R., Franseen, M. (1999). Geomorphology and Hydrology of the Colorado and Gunnison Rivers and Implications for Habitats Used by Endangered Species, Final Report, Prepared for US Fish and Wildlife Service. 66 p.

Rouse, H.L. (1994). "Measurement of bedload gravel transport: The calibration of a self-generated noise system," Earth Surface Processes and Landforms, 19(9), pp 789-800.

Thorne, P.D. (1985). "The measurement of acoustic noise generated by moving artificial sediments," Journal of the Acoustical Society of America, 78(3), pp 977-987.

Thorne, P.D. (1986). "Laboratory and marine measurements on the acoustic detection of sediment transport," Journal of the Acoustical Society of America. 80(3). pp 899-910.

Urick, R.J. (1983). "Principles of underwater sounds". 3rd edition, Peninsula Publishing, Los Altos, CA. 423 p.

Wysocki, L.E., Amoser, S., Ladich, F. (2007). "Diversity in ambient noise in European freshwater habitats: Noise levels, spectral profiles, and impact on fishes," Journal of the Acoustical Society of America, 121(5), pp 2559-2566.

Zakarauskas, P. (1986). "Ambient noise in shallow water: a literature review," Canadian Acoustics, 14(3), pp 3-17.

EVALUATION OF MULTIPLE-FREQUENCY, ACTIVE AND PASSIVE ACOUSTICS AS SURROGATES FOR BEDLOAD TRANSPORT

Molly Wood, Hydraulic Engineer, U.S. Geological Survey, Boise, ID, mswood@usgs.gov;
Ryan Fosness, Hydraulic Engineer, U.S. Geological Survey, Boise, ID;
Greg Pachman, Hydrologic Technician, U.S. Geological Survey, Boise, ID;
Mark Lorang, Assoc. Professor, Univ. of Montana Flathead Lake Biological Station, Polson, MT;
Diego Tonolla, Faculty Affiliate, Univ. of Montana Flathead Lake Biological Station, Polson, MT

Abstract: The use of multiple-frequency, active acoustics through deployment of acoustic Doppler current profilers (ADCPs) shows potential for estimating bedload in selected grain size categories. The U.S. Geological Survey (USGS), in cooperation with the University of Montana (UM), evaluated the use of multiple-frequency, active and passive acoustics as surrogates for bedload transport during a pilot study on the Kootenai River, Idaho, May 17-18, 2012. Four ADCPs with frequencies ranging from 600 to 2000 kHz were used to measure apparent moving bed velocities at 20 stations across the river in conjunction with physical bedload samples. Additionally, UM scientists measured the sound frequencies of moving particles with two hydrophones, considered passive acoustics, along longitudinal transects in the study reach. Some patterns emerged in the preliminary analysis which show promise for future studies. Statistically significant relations were successfully developed between apparent moving bed velocities measured by ADCPs with frequencies 1000 and 1200 kHz and bedload in 0.5 to 2.0 mm grain size categories. The 600 kHz ADCP seemed somewhat sensitive to the movement of gravel bedload in the size range 8.0 to 31.5 mm, but the relation was not statistically significant. The passive hydrophone surveys corroborated the sample results and could be used to map spatial variability in bedload transport and to select a measurement cross section with moving bedload for active acoustic surveys and physical samples.

INTRODUCTION

Background: Active acoustics, through deployment of acoustic Doppler current profilers (ADCPs), have been tested as a surrogate for bedload transport in Canada's Fraser River (Rennie and others, 2002) and the United States' Trinity River (Gaeuman and Pittman, 2007) and lower Missouri River (Gaeuman and Jacobson, 2006). However, little work has been done to evaluate the performance of multiple frequency ADCPs outside a laboratory environment and whether the response of the various frequencies can help identify types and thicknesses of bedload based on differences in perceived velocities of the moving layer and water depths.

One feature of an ADCP is that it transmits a sound wave, called a bottom track pulse, to keep track of its position as it moves across a stream (Gordon, 1996). If material is moving along the bed at a particular site, the ADCP will falsely appear to move upstream, which introduces bias in a streamflow measurement unless it is corrected (Mueller and others, 2013). If the specific location of the ADCP is known (by fixing its position or by connecting it to a differential global positioning system (DGPS)), and the apparent or false movement of the ADCP is measured over time, an apparent moving bed velocity can be inferred. Bedload transport rate can be estimated based on the apparent moving bed velocity and empirical parameters or through correlations between near-simultaneous measurements of apparent moving bed velocity and bedload samples.

The average velocity of the bedload layer depends on the various sizes and velocities of the particles. Apparent moving bed velocity should be representative of the average surface velocity within the volume measured by the ADCP; however, the measurement is influenced by the frequency of the instrument and the size of the particles. An ADCP preferentially measures reflections from particles with a diameter equal to or greater than the wavelength of the instrument's sound wave (Thorne and others, 1995). For example, a 1200 kHz ADCP should be most sensitive to particles with diameters equal to or greater than 0.8 mm, and the weighting of these particles in the apparent moving bed velocity should be greater. The use of multiple ADCPs with different frequencies should theoretically allow the computation of apparent moving bed velocities for different grain sizes. As a result, relations between bedload and apparent moving bed velocity may be developed separately for various grain size categories.

Passive acoustics, through deployment of hydrophones, have been tested as a surrogate for bedload transport in the United States' Trinity River (Barton and others, 2007) and Middle Fork Flathead River (Lorang and Tonolla, 2014) and France's Isère River (Belleudy and others, 2007). Most research with hydrophones has been focused on measuring

coarse gravel transport, and little work has been done to evaluate the ability of hydrophones to detect a wider range of bedload grain sizes. Additionally, research is needed to determine whether passive acoustics could be used in conjunction with active acoustics to optimize sampling design and development of surrogate relations.

STUDY SITE AND METHODS

The U.S. Geological Survey (USGS) has operated a sediment monitoring and hydrodynamic modeling project in the Kootenai River basin (fig. 1) since 2003 as part of the Kootenai River White Sturgeon Recovery Plan. Recovery efforts for the endangered Kootenai River population of white sturgeon require an understanding of the characteristics and transport of suspended and bedload sediment which have an effect on egg suffocation and mortality rates in the critical habitat reach of the river (fig. 1) as described in Fosness and Williams (2009). The pilot study site, Kootenai River at Crossport near Bonners Ferry, ID (USGS 12308500; fig. 1), is near the upstream end of the Kootenai River white sturgeon critical habitat. The site was selected for the pilot study based on observed conditions in 2010-12: consistent bedload at streamflows greater than 30,000 ft^3/s, a mixture of sand and gravel in bedload samples, and apparent moving bed velocities greater than 0.04 ft/s detected by ADCPs used to measure streamflow.

Field data collection for the pilot study was conducted May 17-18, 2012, during a controlled release of about 14,800 ft^3/s from Libby Dam (fig. 1) and fairly steady streamflow around 38,000 ft^3/s at the study site. All sampling and ADCP equipment were deployed from a jet boat. Four ADCPs with frequencies ranging from 600 to 2000 kHz (fig. 2) were used to measure apparent moving bed velocities and streamflow depths at 20 stations across the river:

- Teledyne RD Instruments (TRDI) 600 kHz Rio Grande
- TRDI 1200 kHz Rio Grande
- TRDI 2000 kHz StreamPro
- SonTek/Xylem multi-frequency RiverSurveyor M9 (1000 kHz beams used)

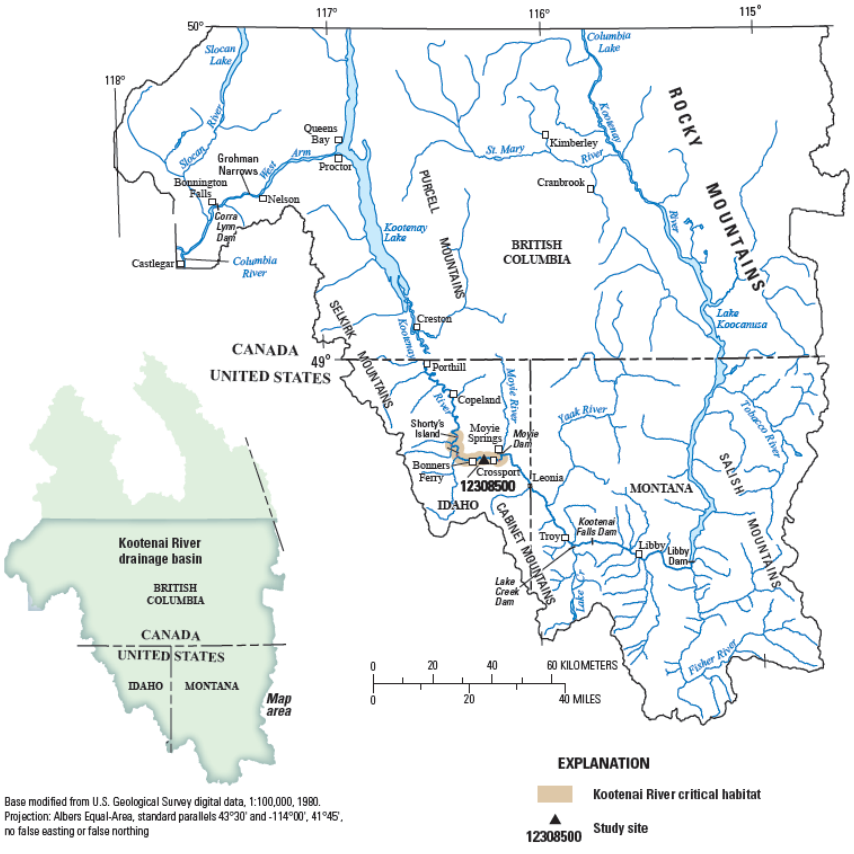

Figure 1 Map showing location of pilot study site, Kootenai River at Crossport near Bonners Ferry, Idaho (USGS 12308500).

Figure 2 Mounting configuration for ADCPs used to measure apparent moving bed velocities in the Kootenai River at Crossport near Bonners Ferry, Idaho (USGS 12308500), May 17-18, 2012. ADCPs are (from left to right): TRDI StreamPro, TRDI 600 kHz Rio Grande, TRDI 1200 kHz Rio Grande, and SonTek/Xylem RiverSurveyor M9.

All ADCPs except the TRDI StreamPro were equipped with DGPS equipment. Use of a DGPS requires a compass within the ADCP. For the TRDI StreamPro, the compass is contained within the electronics housing, which is separate from the ADCP transducer. The electronics housing must be aligned in a specific way relative to the transducer if the compass is to be used, which was not possible during the study. The compasses in all other ADCPs that were used were calibrated according to manufacturer recommendations and USGS policies in Mueller and others (2013) prior to further data collection.

The ADCPs were deployed to collect stationary moving bed tests for 5 minutes at each station. USGS personnel were unable to anchor the boat during ADCP data collection because of safety considerations and difficulty in attaching the anchor in the cobble substrate. The boat was held as stationary as possible during each moving bed test but some movement was unavoidable. Apparent moving bed velocities were calculated by determining the apparent distance moved upstream according to the ADCP's bottom track pulse. Apparent moving bed velocities for the TRDI StreamPro were taken directly from the stationary moving bed tests assuming boat position was held relatively steady (no "real" upstream movement). For all other ADCPs, the apparent moving bed velocities were calculated relative to actual boat movement determined from DGPS (equation 1):

$$V_{mb} = \frac{DU_{BT} - DU_{DGPS}}{T} \quad (1)$$

Where

V_{mb} is the apparent moving bed velocity in ft/sec,
DU_{BT} is the distance the ADCP appears to move upstream in ft when referenced to bottom track,
DU_{DGPS} is the distance the ADCP moves upstream in ft when referenced to DGPS, and
T is the duration of the test in seconds.

For all ADCPs equipped with DGPS, the National Marine Electronics Association (NMEA) "Global Positioning System Fix" (GGA) string was selected over the "Track Made Good and Ground Speed" (VTG) string as the best DGPS reference.

Immediately before or after ADCP data collection, bedload samples were collected at each of the 20 stations using an Elwha US-ER1 sampler with a 0.5 mm bag mesh size. Additionally, an underwater video camera was attached to the bedload sampler to monitor its orientation and performance at four stations. Samples were collected utilizing USGS methods for single equal width increment (SEWI) samples (Edwards and Glysson, 1999), but samples were not composited. Each station's sample was separately analyzed for mass in 12 grain size categories from 0.063 mm to 128 mm. Bedload was calculated according to equation (2) adapted from Edwards and Glysson (1999):

$$Q_b = K\left(\frac{W_t}{T_t}\right)M_t \quad (2)$$

Where

Q_b is the bedload in tons/day,
K is a conversion factor calculated as 86,400 sec/day x (1 ton/907,200 g) x (1 ft/N_w), where N_w is the width of the sampler opening in ft, or 0.67 ft,
W_t is the width of the stream represented by each station in ft, or about 23 ft on average,
T_t is the total time the sampler rests on the bed at each station in seconds, or 60 s, and
M_t is the mass of sample from each station in grams.

Sampling was repeated on May 18 at three stations that were measured on May 17 that had the highest apparent moving bed velocities and most bedload collected. Overall, 23 samples were attempted, but because no material was present in one sample collected near the left bank, data from 22 samples were available for analysis. USGS personnel intended to repeat sampling at all 20 stations but were unable to do so within the short time frame of the controlled release out of Libby Dam.

Simultaneous with the sample and ADCP data collection, UM scientists measured the sound frequencies (0.020−20 kHz; then combined in 10 octave bands from 0.0315 to 16 kHz) of moving particles with a pair of co-located Brüel and Kjaer 8103 hydrophones, amplified and connected to a digital recorder, along longitudinal transects in the study reach. The hydrophones were mounted parallel to each other at about 1 ft depth below water on the frame of a jet boat (a separate boat from the one used to collect bedload samples and ADCP data).

RESULTS AND DISCUSSION

Bedload Characteristics: Total bedload from the composite of all stations contained 3 percent sand and 97 percent gravels, with less than 0.5 percent organics. Sand was considered to include sediment retained on 0.063 to 1 mm sieves, and gravel was considered to include sediment retained on 2 mm and larger sieves, according to the Wentworth scale (Wentworth, 1922). Throughout this paper, bedload is referenced by how much material was retained on that sieve size (for example, "2 mm bedload" is bedload comprised of grain sizes passing through the 4 mm sieve but retained on the 2 mm sieve).

The most sand bedload at any station was measured at station 7, about 160 ft from the right bank (fig. 3). About 20 percent of the total bedload in the sample collected at station 7 was sand. The most gravel bedload was measured at stations 8 and 9, 180 to 203 ft from the right bank. Overall, nearly all the measured bedload was in the right 35 to 45 percent of the cross-section. The gravel bedload measured at station 1 is suspected to be the result of the sampler scooping bed (non-moving) gravel because (1) sampler control was difficult because of turbulence caused by a

submerged tree, and (2) the gravel sizes measured (16.0-31.5 mm) are unlikely to be transported by the low stream velocities observed at station 1.

Overall, bedload size distribution was unimodal and contained a much higher percent of gravel than expected. The largest sediment mass was observed in the grain size categories of 8.0 and 16 mm. Fairly equal proportions of sands were measured in the 0.5 and 1.0 mm size categories. Any sands less than 0.5 mm were assumed to be attached to other particles or were present in the bag due to occlusion of the 0.5 mm mesh openings from other particles. As a result, sand particles smaller than 0.5 mm were not considered in relations with acoustic data. None of the samples contained sediment in the 63 and 128 mm (gravel) grain size categories.

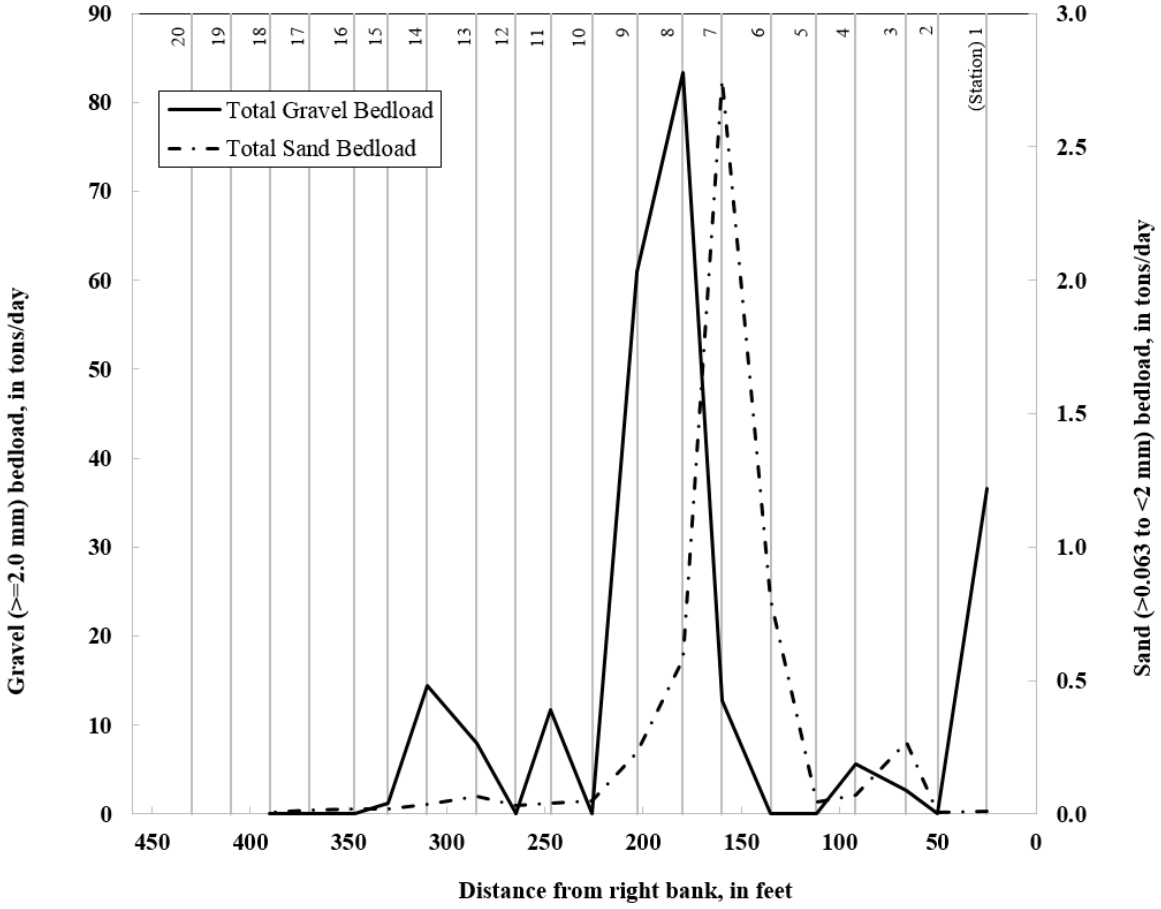

Figure 3 Total gravel and sand bedload at each station measured in the Kootenai River at Crossport near Bonners Ferry, Idaho (USGS 12308500), May 17, 2012.

Bedload Sampler Performance: Underwater video camera reconnaissance of the bedload sampler, attempted at stations 1-4, showed that the sampler often turned sideways or backwards when deployed, which raises concerns about sampler performance. The camera and accessory cable were tested in different configurations (fig. 4) in an attempt to reduce their hydraulic drag and resulting effect on sampler orientation. After several attempts the camera was removed because a proper sampler orientation could not be attained and meaningful bedload samples could not be collected. After camera removal, collected bedload samples made sense based on observed substrate and velocity distribution in the cross-section, which suggests that the sampler oriented correctly without the presence of the camera. Post-study consultation with other bedload sampling experts revealed that the weight distribution of the sampler may not have been ideal to handle the added weight and hydraulic disturbance due to the video camera (Smokey Pittman, Graham Matthews and Associates, written commun., 2013). The video reconnaissance of the bedload sampler showed some concerning behavior, which could be further verified through controlled experiments in a laboratory flume or in a river where water clarity allows direct observation of the sampler on the bed.

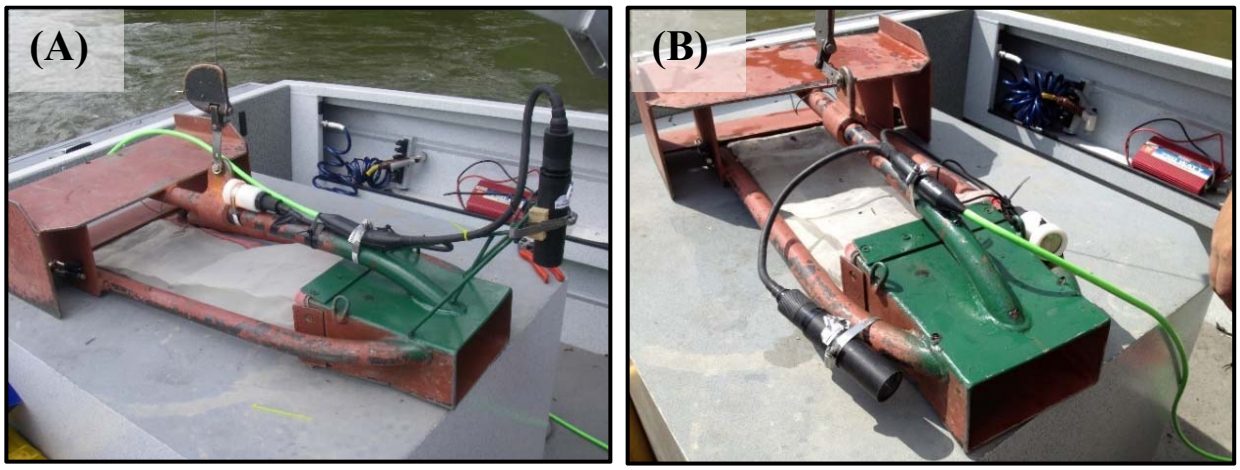

Figure 4 Elwha US-ER1 sampler used to measure bedload in the Kootenai River at Crossport near Bonners Ferry, Idaho (USGS 12308500), May 17-18, 2012. An underwater video camera was temporarily attached to the sampler, (A) looking down on the sampler opening and (B) attached to the lateral sampler supports, to evaluate sampler performance and orientation.

Active Acoustic Relations: Apparent moving bed velocities were low (0.001-0.064 ft/sec) during the selected sampling event due to the unforeseen low percentage of sands in the total bedload. In theory, sand should be more detectable by the ADCPs than gravels for the frequencies tested. Apparent moving bed velocities greater than 0.04 ft/sec were measured at only 5 stations. An apparent moving bed velocity of 0.04 ft/s is used as an uncertainty threshold for correcting ADCP streamflow measurements for moving bed using a loop correction described in Mueller and others (2013). Average apparent moving bed velocity among all instruments and sampling stations was 0.013 ft/s. As a result, uncertainty was high in identified relations between bedload and apparent moving bed velocities for all ADCPs. However, some patterns emerged in the relations that show promise for future studies.

Apparent moving bed velocities measured by the 1200 kHz ADCP had the best statistically significant, though scattered, linear relations with sands in the 0.5 – 1.0 mm size categories and very fine gravels in the 2.0 mm size category (table 1, fig. 5). The 1000 kHz ADCP showed similar, though slightly more scattered, relations with sands and very fine gravels. The 2000 kHz ADCP showed statistically significant relations with individual bedload grain size categories 0.5 and 1.0 mm but not 2.0 mm and larger. No statistically significant relations were found between bedload transport for gravels 4.0 mm and larger and apparent moving bed velocities measured by any ADCP, which was expected. However, apparent moving bed velocities measured by the 600 kHz ADCP related better to gravels in the 8.0 to 31.5 mm grain size categories than the other ADCPs (correlation = 0.46, $R^2 = 0.21$; p-value = 0.11 (table 1)). Otherwise, use of a range of frequencies did not improve the ability to define relations for individual bedload size categories.

Apparent moving bed velocities measured by the 1200 kHz ADCP had the best relations with sand and very fine gravel bedload of all tested ADCPs. The highest apparent moving bed velocities were measured by the 1200 kHz ADCP at 4 stations located 135-203 ft from the right bank. Samples collected from these stations contained 89 percent of the total sand and very fine gravel bedload measured in the cross-section.

Relations between apparent moving bed velocities measured by ADCPs with frequencies in the 1000-1200 kHz range and sand and very fine gravel bedload transport show promise for future work, but further testing is needed during an event when total bedload consists of a greater percentage of transport in these size categories and apparent moving bed velocities are consistently higher than 0.04 ft/sec.

Table 1 Regression statistics of selected relations between apparent moving bed velocities measured by acoustic Doppler current profilers and bedload in various grain-size categories in the Kootenai River at Crossport near Bonners Ferry, Idaho (USGS 12308500), May 17-18, 2012.

[A table entry of "--" indicates the regression was not statistically significant at a significance level of 0.10. The regression model between the 600 kHz Rio Grande and gravel bedload is shown because it is noteworthy and discussed in the text, even though it is not statistically significant at a significance level of 0.10. Regression model form developed in all cases is log(bedload) = m(log(V_{mb}))+b, where m is the regression slope and b is the regression constant. Abbreviations: V_{mb}, apparent moving bed velocity; kHz, kiloHertz; mm, millimeter; n, number of samples used in regression; R^2, coefficient of determination; SE, standard error; p, statistical significance or probability that the two compared variables are linearly related by chance]

Bedload grain size classification (Wentworth, 1922)	Bedload grain size (mm)	Acoustic Doppler current profiler															
		600 kHz Rio Grande				1000 kHz RiverSurveyor M9				1200 kHz Rio Grande				2000 kHz StreamPro			
		n	R^2	SE	p	n	R^2	SE	p	n	R^2	SE	p	n	R^2	SE	p
Coarse sand	0.5	--	--	--	--	22	0.35	4.6	0.004	22	0.41	4.3	0.001	[1]15	0.24	5.3	0.066
Very coarse sand	1.0	--	--	--	--	22	0.28	4.6	0.012	22	0.36	4.2	0.003	[1]15	0.22	5.3	0.077
Very fine gravel	2.0	--	--	--	--	[2]21	0.16	5.8	0.071	[2]21	0.35	4.6	0.005	--	--	--	--
Fine gravel	4.0	--	--	--	--	--	--	--	--	--	--	--	--	--	--	--	--
Medium gravel	8.0	--	--	--	--	--	--	--	--	--	--	--	--	--	--	--	--
Coarse gravel	16	--	--	--	--	--	--	--	--	--	--	--	--	--	--	--	--
Very coarse gravel	31.5	--	--	--	--	--	--	--	--	--	--	--	--	--	--	--	--
Coarse to very coarse sand	0.5 to 1.0	--	--	--	--	22	0.31	4.7	0.007	22	0.39	4.3	0.002	[1]15	0.24	5.3	0.066
Coarse sand to very fine gravel	0.5 to 2.0	--	--	--	--	22	0.30	5.1	0.008	22	0.38	4.6	0.002	[1]15	0.22	6.0	0.074
Medium to coarse gravel	8.0 to 31.5	[3]13	0.21	5.4	0.11	--	--	--	--	--	--	--	--	--	--	--	--

[1]Some data points were removed from the regression with the 2000 kHz StreamPro because the StreamPro reported downstream instead of upstream movement at those stations.
[2]Bedload in the 2.0 mm grain size category was not present in one sample.
[3]Bedload in the 8.0 to 31.5 mm grain size categories was not present in nine samples.

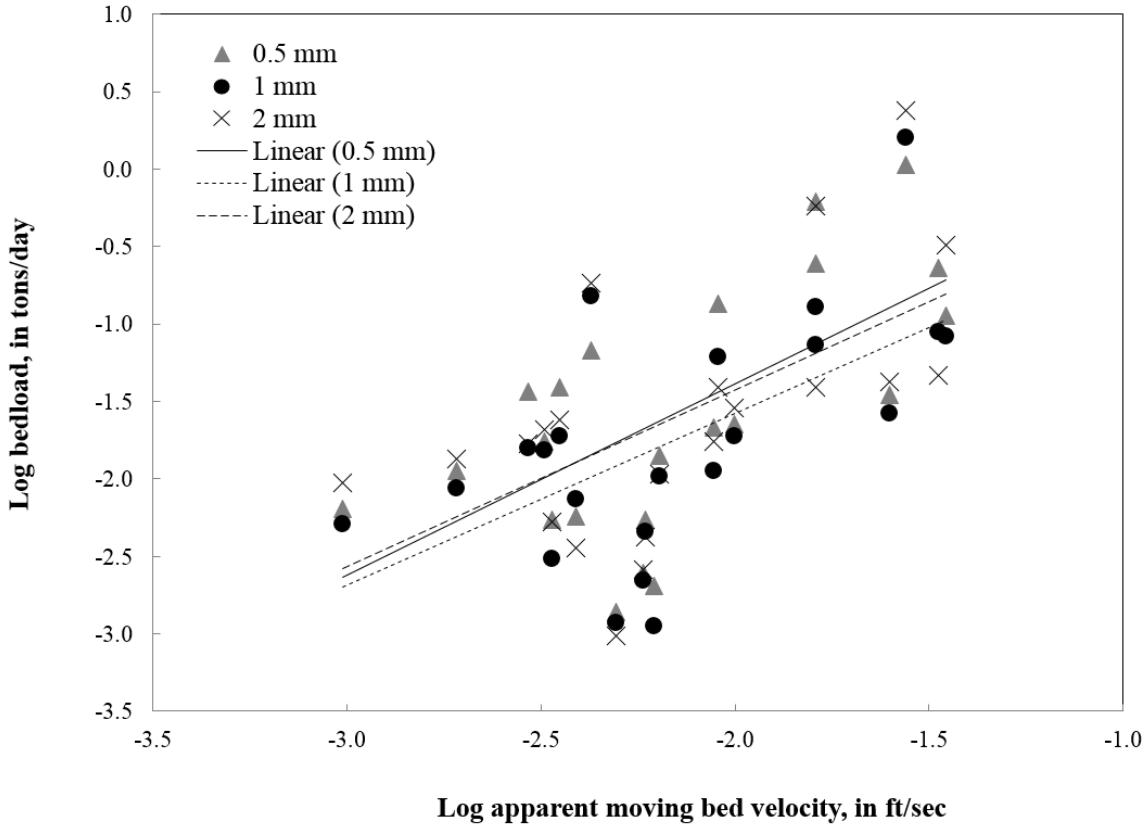

Figure 5 Selected linear relations between apparent moving bed velocities measured by the 1200 kHz TRDI Rio Grande ADCP and bedload at individual stations sampled in the Kootenai River at Crossport near Bonners Ferry, Idaho (USGS 12308500), May 17-18, 2012.

Active Acoustic Depth Differences: Streamflow depth readings from each ADCP were compared at each station, and an overall cross-sectional area was calculated based on each ADCP's depth readings using the USGS AreaComp2 program (Lant and Mueller, 2012). Differences in depth and area readings among ADCPs were examined for patterns in an attempt to determine thickness of bedload layers in various size categories. Safe anchoring was not possible during the pilot study, and, as a result, considerable uncertainty exists when comparing average depths among ADCPs because of movement of the boat. Additionally, each ADCP measured depth in a slightly different ensonified area due to their mounting configuration on the boat (fig. 2) and differences in beam angle and diameter.

Depths measured by the 600 kHz ADCP resulted in the largest cross-sectional area, which was expected because the acoustic signal strength of the 600 kHz ADCP is higher than the other ADCPs and is able to penetrate finer material moving near the bed. No clear patterns were observed between cross-sectional area and the other ADCP frequencies. Overall, the coefficient of variation among cross-sectional areas calculated from the various ADCP depths was 0.6 percent, which is small compared to the uncertainties mentioned above. Future testing would benefit by selecting a site where anchoring could be ensured; however, the other mentioned uncertainties would likely still exist.

Passive Acoustic Surveys: Selected results of the passive acoustic hydrophone surveys along longitudinal transects in the study reach are presented here as they relate to the active acoustic (ADCP) and bedload sample data in the pilot study cross-section. Further details on the results of the hydrophone surveys are presented in Lorang and Tonolla (2014).

In general, the hydrophone surveys corroborated the bedload sample results and apparent moving bed velocities measured by the ADCPs. Lorang and Tonolla (2014) state that frequency responses from 2 to 8 kHz probably correspond with gravel bedload transport and 8 to 16 kHz correspond with sand bedload transport. The hydrophones recorded highest response in the expected frequency range for gravels (2-8 kHz) where the highest gravel transport was sampled about 180-200 ft from the right bank (3rd panel from top, fig. 6) and highest response in the expected frequency range for sand (8–16 kHz) where the highest sand transport was sampled about 160 ft from the right bank (2nd panel from top, fig. 6). The hydrophones also recorded a high response in the 2-6 kHz frequency range about 300-350 ft from the right bank at the sampling cross-section (3rd panel from bottom, fig. 6) that seems to correspond with an increase in gravel transport measured in the bedload samples at station 14 (fig. 3). All of the ADCPs reported lower than average apparent moving bed velocities in this area. In the future, passive acoustic surveys could be used to measure spatial variability of bedload in a river reach and could aid in selecting locations with moving bed for sample and active acoustic data collection.

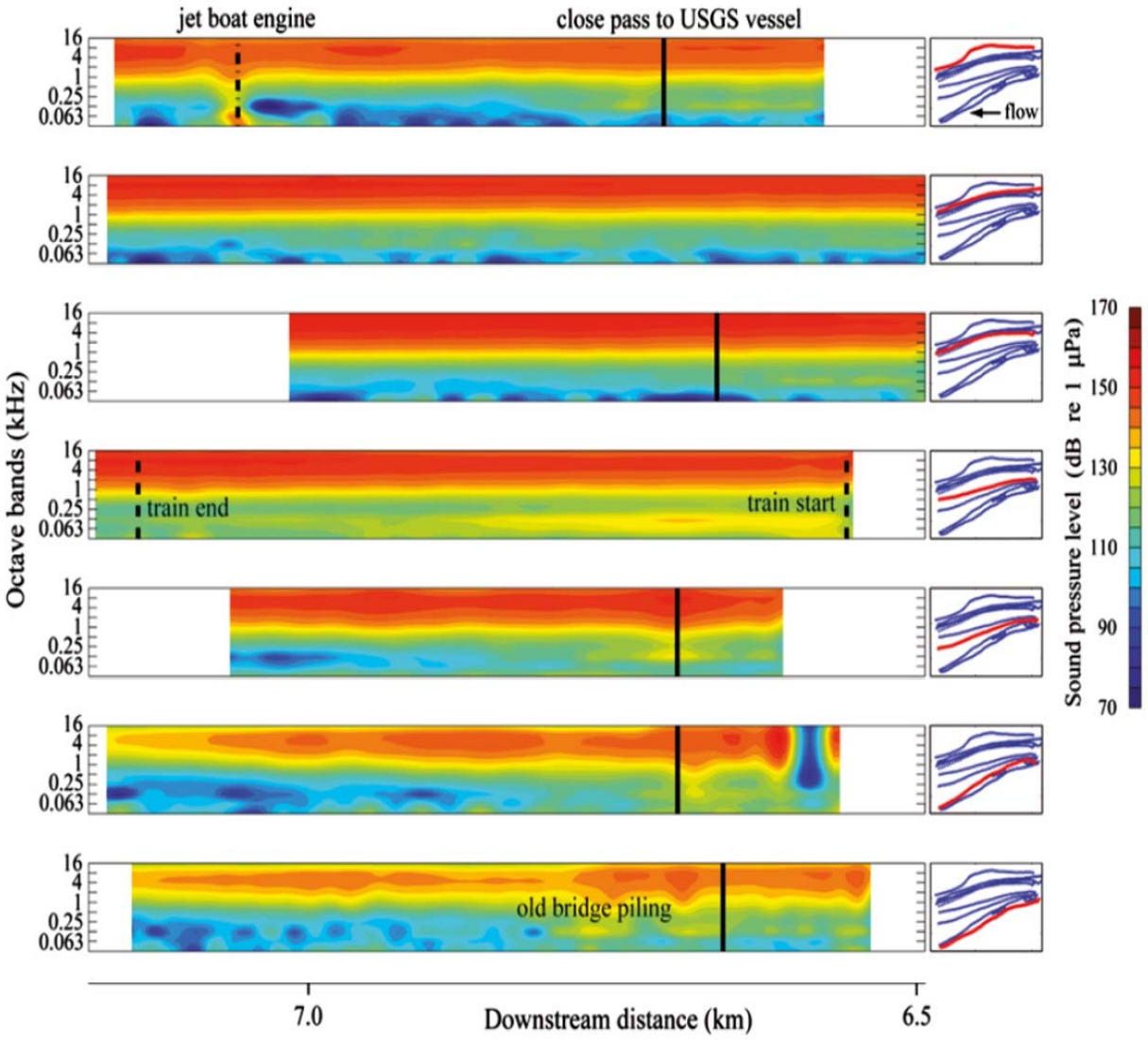

Figure 6 Lateral variation in sound moving from river left to right of the Kootenai River with vertical bars indicating the occurrence of noise from engines, nearby boats and a passing train. Panels at right show position in the river relative to bank with red line corresponding to the sound plot to the left. The solid vertical black bars generally indicate the location of the USGS cross-section for sample and ADCP data collection at Crossport near Bonners Ferry, Idaho (USGS 12308500), May 17-18, 2012. Reproduced with permission from Lorang and Tonolla (2014), www.schweizerbart.de.

SUMMARY

The USGS, in cooperation with UM scientists, evaluated the use of multiple-frequency, active and passive acoustics as surrogates for bedload transport during a pilot study in the Kootenai River at Crossport near Bonners Ferry, Idaho (USGS 12308500), on May 17-18, 2012. Four ADCPs with frequencies ranging from 600 to 2000 kHz were used to measure apparent moving bed velocities at 20 stations across the river. Bedload samples were collected at each station with an Elwha US-ER1 sampler immediately before or after the ADCP data collection. At four sampling stations, an underwater video camera was used to monitor performance of the bedload sampler. Additionally, UM scientists measured the sound frequencies (0.020−20 kHz; then combined in 10 octave bands from 0.0315 to 16 kHz) of moving particles with a pair of co-located hydrophones along longitudinal transects in the study reach. USGS scientists attempted to correlate apparent moving bed velocities measured by the active acoustics (ADCPs) and qualitatively compare frequency response from the passive acoustics (hydrophones) with the sample data at each station to determine whether surrogate relations could be developed for various bedload grain-size categories.

Some patterns emerged in the preliminary analysis which show promise for future studies. Apparent moving bed velocities were much lower than expected (average less than 0.04 ft/sec), and 97 percent of the total bedload was gravel, which in general was too large to be detected in most of the ADCP measurements but was detected by the hydrophones. Apparent moving bed velocities measured by the 1200 kHz ADCP had the best statistically significant, though scattered, linear relation with sands and very fine gravels in the 0.5-2 mm size range (highest $R^2 = 0.41$). Apparent moving bed velocities measured by the 600 kHz ADCP had a positive correlation (+0.46) and weak linear relation ($R^2 = 0.21$) with gravels in the 8.0 to 31.5 mm size range, but the p-value of the regression (0.11) was just above the threshold for statistical significance (0.10) selected for this study. Significant relations could not be developed between apparent moving bed velocities for any ADCP and sample data in individual bedload size categories of 4.0-31.5 mm. Relations between apparent moving bed velocities measured by ADCPs with frequencies in the 1000-1200 kHz range and bedload transport of sands and very fine gravels show promise for future work, but further testing is needed during an event when total bedload transport consists of a greater percentage of sands and apparent moving bed velocities are consistently higher than 0.04 ft/sec.

The passive hydrophone surveys generally corroborated the sample results. The hydrophones recorded highest response in the expected frequency range for gravels (2-8 kHz) and sand (8-16 kHz) where the most gravel and sand transport, respectively, was measured in the cross-section. In the future, active and passive acoustics used together show promise for bedload characterization. Passive acoustics could be used to characterize types and location of bedload transport in a river reach and to select an appropriate cross-section for collection of active acoustic and physical sample data, possibly resulting in development of surrogate relations, particularly for the sand fraction of bedload transport.

Underwater video reconnaissance of the bedload sampler showed that the sampler often turned sideways or backwards when deployed, which raises concerns about sampler performance. The camera was attached to the sampler in several different configurations in an attempt to reduce the camera's hydraulic drag. After several attempts, the camera was removed because it likely altered the hydraulic characteristics of the sampler, preventing proper alignment with streamflow. However, questions remain about the true performance and orientation of the sampler, which could be answered through controlled experiments in a laboratory flume or in a river where water clarity allows direct observation of the sampler on the bed.

REFERENCES

Barton, J.S., Slingerland, R.L., Pittman, S., and Gabrielson, T.B. (2007). "Monitoring coarse bedload transport with passive acoustic instrumentation: a field study," *in* Gray, J.R., Laronne, J.B., and Marr, J.D.G., "Bedload-surrogate monitoring technologies," U.S. Geological Survey Scientific Investigations Report 2010-5091, p. 266-282, available only online from http://pubs.usgs.gov/sir/2010/5091/papers/listofpapers.html.

Belleudy, P., Valette, A., and Graff, B. (2007). "Passive hydrophone monitoring of bedload in river beds: first trials of signal spectral analyses," *in* Gray, J.R., Laronne, J.B., and Marr, J.D.G., "Bedload-surrogate monitoring technologies," U.S. Geological Survey Scientific Investigations Report 2010-5091, p. 266-282, available only online from http://pubs.usgs.gov/sir/2010/5091/papers/listofpapers.html.

Edwards, T.E., and Glysson, G.D. (1999). "Field methods for collection of fluvial sediment," U.S. Geological Survey Techniques of Water-Resources Investigations Book 3, Chapter C2, 89 p. http://water.usgs.gov/osw/techniques/Edwards-TWRI.pdf.

Fosness, R.L., and Williams, M.L. (2009). "Sediment characteristics and transport in the Kootenai River white sturgeon critical habitat near Bonners Ferry, Idaho," U.S. Geological Survey Scientific Investigations Report 2009-5228, 40 p.

Gaeuman, D., and Jacobson, R.B. (2006). "Acoustic bed velocity and bedload dynamics in a large sand-bed river," J. Geophys. Res., 111, F02005.

Gaeuman, D., and Pittman, S. (2007). "Relative contributions of sand and gravel bedload transport to acoustic Doppler bed-velocity magnitudes in the Trinity River, California, in Bedload-Surrogate Monitoring," in, Gray, J.R., Laronne, J.B., and Marr, J.D.G., eds, Proceedings of the International Bedload-Surrogate Monitoring Workshop, April 11-14, 2007, Minneapolis, Minnesota.

Gordon, R.L (1996). Acoustic Doppler Current Profiler Principles of Operation: A Practical Primer. RD Instruments, San Diego, California.

Lant, J., and Mueller, D.S. (2012). "Stage area rating application – AreaComp2," U.S. Geological Survey software user's guide, accessed February 22, 2013 at http://hydroacoustics.usgs.gov/software/AreaComp2_Users_Guide.pdf.

Lorang, M.S., and Tonolla, D. (2014). "Combining active and passive hydroacoustic techniques during flood events for rapid spatial mapping of bedload transport patterns in gravel-bed rivers," Fundam. of Appl. Limnol., 184(3), p 231-246, www.schweizerbart.de.

Mueller, D.S., Wagner, C.R., Rehmel, M.S., Oberg, K.A., and Rainville, F. (2013). "Measuring discharge with acoustic Doppler current profilers from a moving boat", ver. 2.0, December 2013, U.S. Geological Survey Techniques and Methods, book 3, chap. A22, 95 p.

Rennie, C.D., Millar, R.G., and Church, M.A. (2002). "Measurement of bed load velocity using an acoustic Doppler current profiler," J. Hydraul. Eng., 128(5), 473–483.

Thorne, P.D., Waters, K.R., and Brudner, T.J. (1995). "Acoustic measurements of scattering by objects of irregular shape," J. Acoust. Soc. Am. 97(1), 242-251.

Wentworth, C.K. (1922). "A scale of grade and class terms for clastic sediments," Journal of Geology, v. 30, p. 377-392.

BED SEDIMENT CHARACTERIZATION OF THE MISSISSIPPI RIVER, GRAFTON, ILLINOIS TO HEAD OF PASSES, LOUISIANA, NOVEMBER 2013

Roger A. Gaines, U.S. Army Corps of Engineers, Memphis District, 167 North Main Street, Memphis, Tennessee 38103 roger.a.gaines@usace.army.mil
Anthony M. Priestas, U.S. Army Engineer Research and Development Center, Coastal and Hydraulic Laboratory, 3909 Halls Ferry Road, Vicksburg, Mississippi 39180 anthony.m.priestas@usace.army.mil

ABSTRACT

Changes in Mississippi River bed material gradations between Cairo, Illinois and Head of Passes, Louisiana have been previously determined. In November 2013, bed material samples were collected from the thalweg and across the channel width along a reach extending from Grafton, IL, to Head of Passes, LA. In all, 754 samples were collected at 496 locations. Results were compared to the earlier 1932 and 1989 sampling programs. Since 1932, after the completion of the Mississippi River cut-off program, there has been a general reduction in very fine materials (clay, silt, very fine sand) and very coarse materials (very coarse sand and gravel), replaced by fine to coarse sand fractions. On average the median grain size in 2013 (0.43 mm) is about 50% less than that of 1932 (0.96 mm), but little change in median grain size has occurred since 1989 (0.46 mm). In general, very little change has occurred since the 1989 sampling program.

INTRODUCTION

In 1932 and again in 1989 the U.S. Army Corps of Engineers (USACE) sponsored efforts to collect and analyze data to investigate bed sediments from the Mississippi River channel thalweg along a 1,070-mile reach between Cairo, Illinois and the Head of Passes, Louisiana. The 1932 data are reported in the 1935 Waterways Experiment Station Paper Number 17, "Studies of River Bed Material and Their Movement with Special Reference to the Lower Mississippi River" (WES, 1935). The 1989 data are reported in the Lower Mississippi Valley Division Potamology Program Report 7, "Particle Size Distributions of Bed Sediments along the Thalweg of the Mississippi River, Cairo, Illinois, to Head of Passes, September 1989" (Nordin and Queen, 1992).

The many changes that occurred on the Mississippi River between 1932 and 1989 were considered a significant reason for investigating changes in the river bed sediments for that period of time. The three predominant changes were construction of dams on the Missouri River, shortening of the river by cutoffs and channel realignment, and construction of bank revetments and training works. Since 1989 there has been a continued effort to construct bank revetments and training works, but there have been no additional reservoirs or cutoffs. Comparatively, the magnitude of changes in the Mississippi River that have occurred between 1989 and 2013 are not significant. Yet, recent data and studies indicate that the Mississippi River continues to adjust in response to earlier and on-going construction works (USACE, 2007). Recent studies involving the update of the Low Water Reference Plane in 2007 indicate continued adjustment in the river profile. The profile adjustments along with field observations signify continued change in bed material composition throughout the lower Mississippi River channel. There have been unsubstantiated claims that the bed is finer within the New Orleans District reach than in previous sampling programs. It was also conjectured that the bed has further coarsened in the upper reaches of the Memphis District.

In 2013, the Corps of Engineers determined to undertake a sampling program to duplicate as closely as possible the previous sampling programs from 1932 and 1989. The concerns with volume and gradation of sediments moving through the Mississippi River identified a need to also assess sources of sediment in the upper reaches of the basin. Historically the Missouri River was a predominant contributor of these sediments and was altered by construction of major flood control reservoirs on its main channel (Meade et al., 2009). For this reason the sampling program was extended to include the Upper Mississippi River to Grafton, Illinois.

SAMPLE LOCATIONS

The 2013 study collected 754 samples between Grafton, IL and Head of Passes, LA. Sample locations were sited to coincide with locations previously sampled by WES (1935) and Nordin and Queen (1992). Additional sites were added to capture cross channel variations and to acquire data needed for specific model studies. In addition to sampling the Mississippi River downstream of Cairo, a base line sampling was completed for the Upper Mississippi River between Grafton and Cairo. General sample locations are shown in Figure 1; red markers denote upper Mississippi River sites and green markers denote lower Mississippi River sites. The additional cross-channel samples were collected at every 10th sample location or as required for specific sediment modeling studies. The 1989 sampling program only documented three locations where multiple samples were taken across the channel.

Where transect locations were indicated, a total of five samples were collected— one at the thalweg and the other 4 equally distributed across the remaining open water subject to safe boat access. In some cases, it was not possible to obtain a total of five samples because of water levels or other situations that limited access. A few samples on sand bars were obtained from land where access permitted.

Transect sample names were appended A through E; 'A' indicated the right descending bank and 'E' the left descending bank (Figure 2).

Figure 1 Location map of thalweg samples taken November 2013. The upper Mississippi River samples are denoted by red markers.

SAMPLE ACQUISITION AND LAB ANALYSIS

The bed samples were taken by field parties on two research vessels from Engineering Research and Development Center (ERDC). Field parties on each vessel were comprised of a core staff of ERDC researchers, a representative from the USGS, and USACE District staff. Each District was responsible for providing support staff to sample their respective areas of responsibility. Each vessel covered approximately 50-60 river miles per day, for a combined 100 river miles. Table 1 shows the dates when the various portions of the river were traversed along with the number of samples obtained for each District.

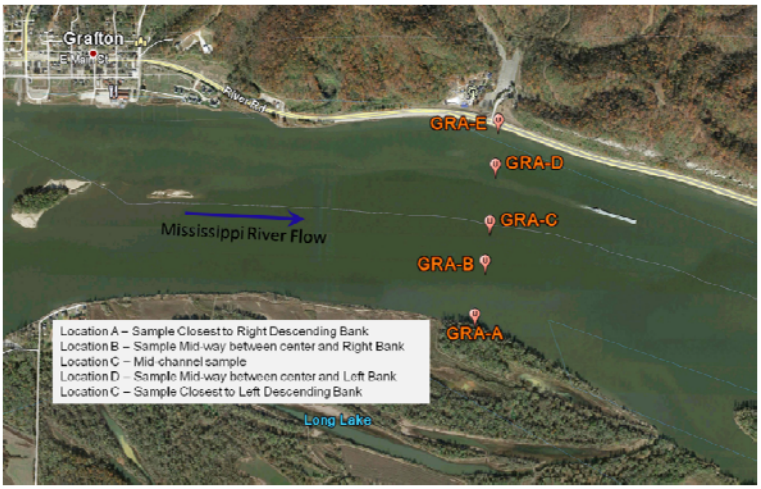

Figure 2 Multiple sample locations taken across channel.

Table 1 Samples of Bed Material of Mississippi River and Tributaries

River	USACE District	River Mile[1]	Number of Samples	Sampling Dates
Upper/Middle Mississippi	St. Louis	5 – 218 Above mouth of Ohio River (Mouth Ohio River = 953.8 AHP)	110	Nov 7-8, 2013
Mississippi	Memphis	595.6 – 958.8 AHP	291	Nov 9-11, 2013
Mississippi	Vicksburg	321.1 – 592.1 AHP	183	Nov 12-13, 2013
Mississippi	New Orleans	0 – 316 AHP	170	Nov 14-15, 2013
[1] AHP refers to river miles Above Head of Passes, Louisiana				

The sampling device used was the same WES drag sampler design used in 1932 and again in 1989, which consists of a four-inch inside diameter steel pipe four feet long closed at one end and flared to eight inches diameter at the other end (Figure 3). The sampler is lifted by use of a crab-pot puller mounted to the base of a boom arm that extends over the side of the boat (Figure 4).

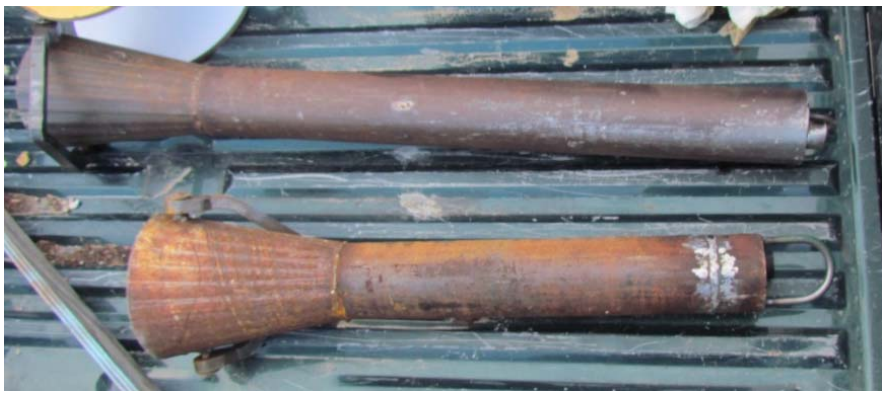

Figure 3 WES drag samplers: Original 4-ft long sampler (top); Sampler shortened by 11-inches (bottom).

Figure 4 Crab pot puller and boom after retrieving sampler.

Collected field samples were shipped to the sediment laboratory at ERDC for analyses. Initially, samples were analyzed using standard ASTM sieve techniques for non-cohesive materials larger than 1mm and laser diffraction (LD) techniques for material 1mm and smaller. Malvern (2013), Stojanovic and Markovic (2012), Wedd (2003), Ma et al. (2000), Loizeau et al. (1994), Wanogho et al. (1987), and McCave et al. (1986) describe particle size analysis using LD. Maximum particle sizes for samples containing outlying coarse grains that would bias the weighted percent grain size distribution were separated (Figure 5). Maximum sizes for these grains were determined by direct measurement. These grains were not included in the grain-size distribution data.

Figure 5a Well sorted sample, no D_{max}

Figure 5b Moderately sorted sample, 1 D_{max}

Figure 5c Poorly sorted sample, 3 D_{max}

An independent check of ERDC lab analysis was included in the original study scope. This check included duplicate analysis of ten percent of samples by the USGS Kentucky Water Science Center Sediment Laboratory. The quality control samples were selected from two pools of samples that were processed at the ERDC lab. Selection was done by random selection from each of the pools. Original sample material was split using standard ASTM splitting techniques. One part was processed using ERDC facilities and techniques. The remaining part was shipped to the USGS sediment lab in Kentucky for analysis using conventional sieve-pipet (SP) procedures for analysis of particle size distributions. Shreve and Downs (2005) provide a description of laboratory procedures at the USGS Kentucky Sediment Lab. Stevens and Hubbell (1986) give methods for calculating particle size distributions.

Once results from the USGS laboratory became available they were compared with the ERDC results. Comparison of sieve results indicated that percentage finer values were in good agreement for particle sizes 1.0 mm and larger. However, distributions for particles finer than 1.0 mm did not agree. Figure 11 shows the QC results between the ERDC and the USGS laboratories. Investigation into why the percent finer values 1.0 mm and smaller differed between the two methods pointed to differences between conventional sieving techniques employed by the USGS and the ERDC laboratory techniques, which used a combination of sieving (64 mm to 1 mm) and laser diffraction (< 1 mm). Previous literature (Eshel, et al., 2004) indicates that laser diffraction results, which are dependent on particle shape, would typically yield coarser sizes than would be obtained with conventional sieve analysis. In other words, sieving biases toward a minimum particle diameter whereas laser diffraction biases toward a maximum diameter. As a result, there is good agreement for sieved QC samples (dashed oval, Figure 6) but significant divergence for percent finer values less than 1 mm obtained by laser diffraction. This trend was verified across all QC samples evaluated in this study.

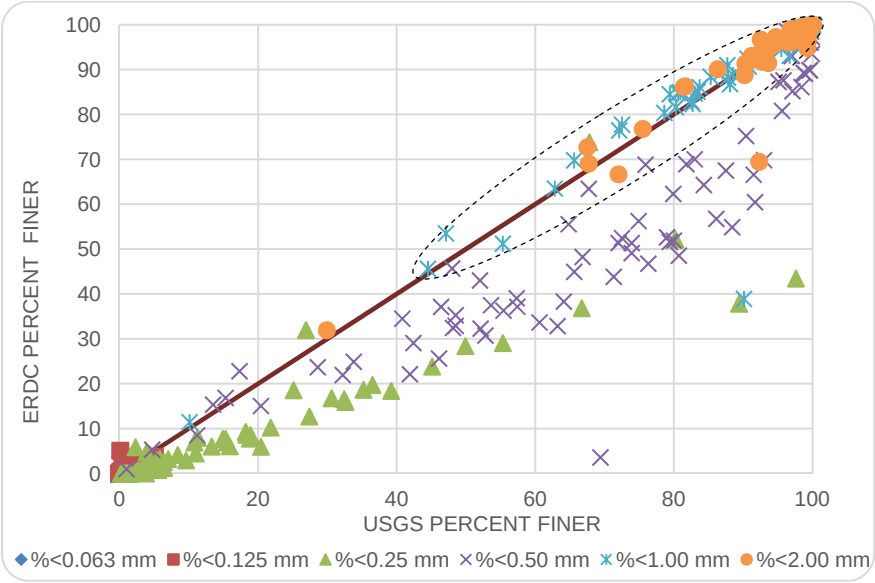

Figure 6 Comparison of size fraction results for quality control samples (particle sizes less than 2.00 mm to less than 0.063 mm). QC results show good agreement for sieve-only samples (dashed oval).

Differences between results obtained using the Sieve-Pipet (SP) method or Laser Diffraction (LD) method identified a need to review variability within the two methods. To assess variability a series of ten replicate analyses using both methods was run using a single sample as the source of material. The primary focus of the assessment was for finer particle sizes because standard sieve analysis was used to determine weights for larger particle sizes.

The average results from replicate analysis shown in Figure 7 provided two significant findings. First, as expected, the LD method consistently produced coarser particle size distributions than the SP method; similar results are reported in the literature (Eshel, et al., 2004). However, a combination of wet sieving with LD produced results similar to the SP method. Second, the SP method estimates greater percentage of very fine silt and clay fractions relative to LD due to prolonged settling times of those particles.

Because a critical component of this study included comparing bed material particle size distributions with the WES (1935) and Nordin and Queen (1992) data, it was necessary to rerun the ERDC samples using sieve analysis for material 0.063 mm and larger.

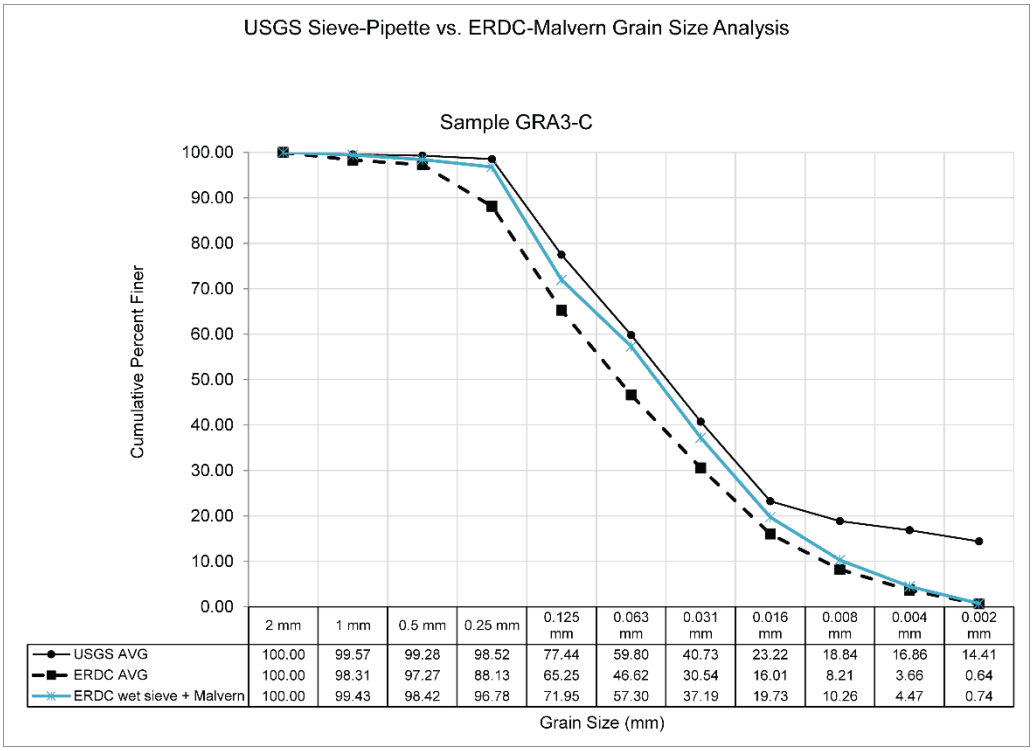

	2 mm	1 mm	0.5 mm	0.25 mm	0.125 mm	0.063 mm	0.031 mm	0.016 mm	0.008 mm	0.004 mm	0.002 mm
USGS AVG	100.00	99.57	99.28	98.52	77.44	59.80	40.73	23.22	18.84	16.86	14.41
ERDC AVG	100.00	98.31	97.27	88.13	65.25	46.62	30.54	16.01	8.21	3.66	0.64
ERDC wet sieve + Malvern	100.00	99.43	98.42	96.78	71.95	57.30	37.19	19.73	10.26	4.47	0.74

Figure 7 Comparison of Particle Size Analysis using Pipet (USGS) and Laser Diffraction (ERDC) Methods.

RESULTS

Grain size distributions for 2013 samples are given in Gaines and Priestas (2014, submitted). The first reach presented is defined as the upper Mississippi River and extends from Grafton to Cairo, Illinois. Grain size distributions for this reach are shown in Figure 8. Sediments of the upper Mississippi River are composed of coarser sand sizes and gravels ranging between 0.5 and 3.5 mm.

The second reach, the lower Mississippi River, extends from Cairo, Illinois to Head of Passes, Louisiana. Grain-size distributions for this reach are shown in Figure 9, and show relatively coarse materials dominating the upper 500 river miles and relatively finer materials dominating the lower 500. The lower Mississippi River sampling locations coincide with reaches sampled in 1932 and 1989. A decreasing trend in median particle size is shown in the downstream direction (Figure 10). This trend is typical of deltaic rivers.

The 2013 sediments were generally finer, more uniform and less variable than sediments collected in 1932 and 1989, though few changes occurred between 1989 and 2013 (Table 2, Table 3, WES, 1935, Nordin and Queen, 1992, and Gaines and Priestas, 2014).

As shown in Table 2 and Figure 11 the relative fractions of gravel and very coarse sand decreased in the upper reaches (above RM 500) since 1932, while the relative fractions of clay, silt and very fine sand have decreased throughout the entire length of the lower Mississippi River, mostly downstream of Baton Rouge (RM 200). These size fractions have been replaced by fine, medium and coarse sands. Essentially, bed materials have fined upstream of RM 500 and coarsened below RM 500. Based on sorting coefficient calculation results given in Table 3 (also see Gaines and Priestas, 2014), the 2013 data have less variability than either the 1989 or 1932 data for all particle size ranges.

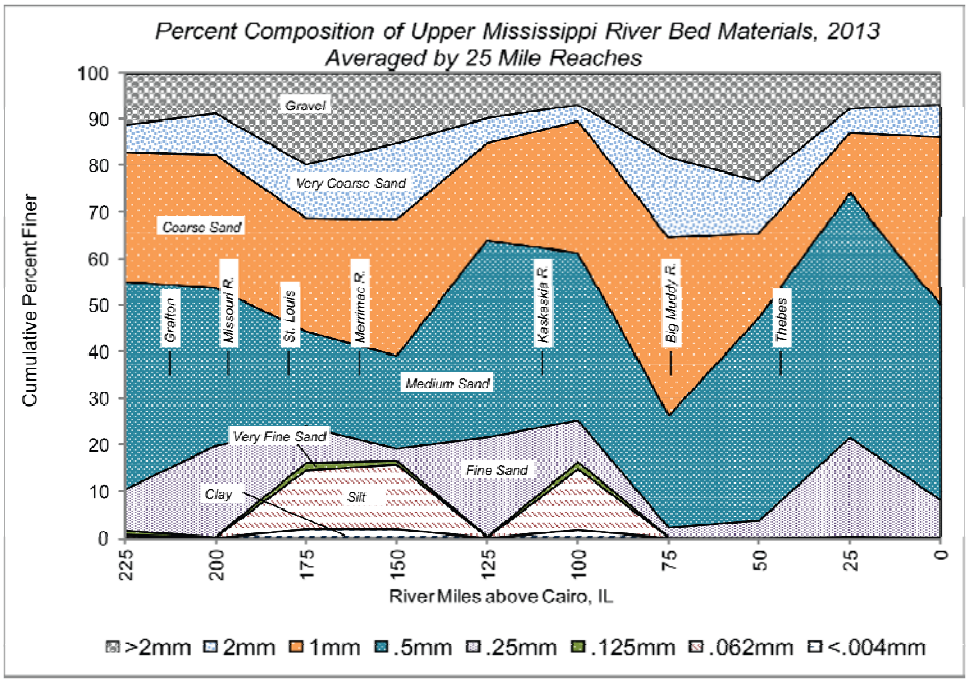

Figure 8 Composition of 2013 Thalweg Bed Material Averaged by 25 Mile Reaches, Upper Mississippi River: Grafton to Cairo, Illinois

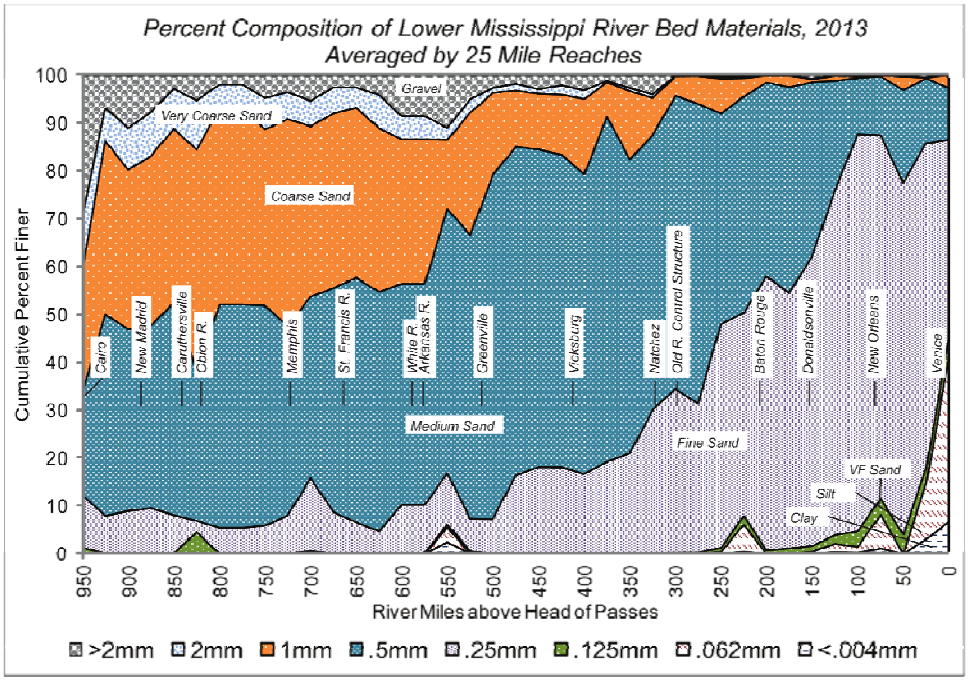

Figure 9 Composition of the 2013 Thalweg Bed Material Averaged by 25 Mile Reaches, Lower Mississippi River: Cairo, Illinois to Head of Passes, Louisiana

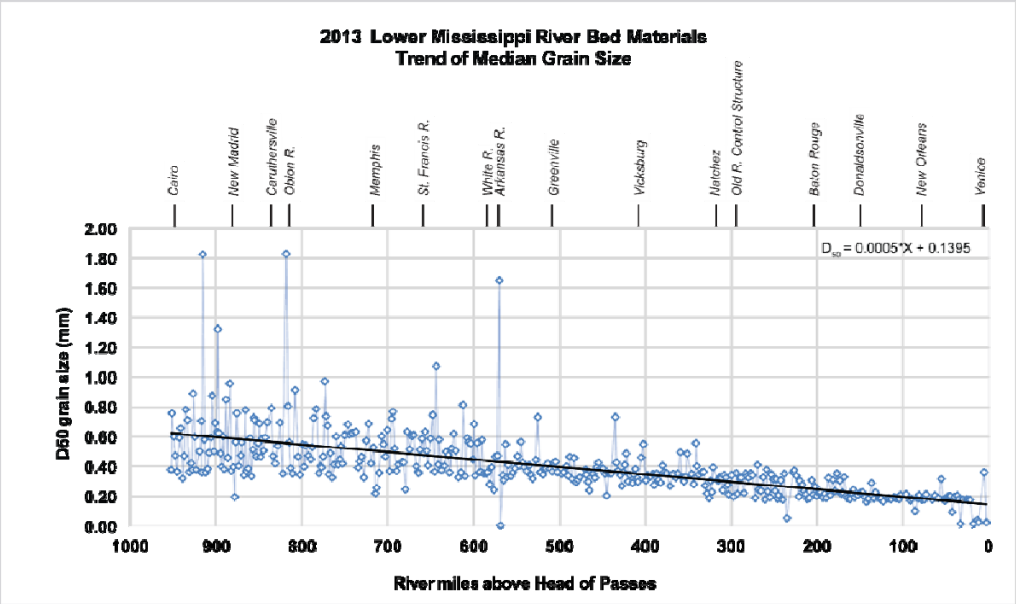

Figure 10 Trend of the Median Grain Size of Mississippi River Bed Materials, Cairo, Illinois to Head of Passes, Louisiana.

Gravel (>2.0 mm) In 1932, bed materials greater than 2.0 mm were prevalent in relative abundance along the lower Mississippi River, averaging from 18% near Cairo, IL to 5% near RM 250. When averaged between Cairo, IL and RM 750, gravel content decreased to 9% by 1989 and 7% by 2013. Between RM 750 and RM 500, average gravel content changed from 9% in 1932 to 4% in 1989 then increased slightly to 6% by 2013, although the percentage of gravel near the confluence of the White and Arkansas Rivers (near RM 550) changed little. Between RM 500 and RM 250, average gravel content changed from 8% in 1932 to 2% by 1989 with no change since.

Very coarse sand (1.0 – 2.0 mm) The magnitude and spatial extent of very coarse sand has changed little since 1932, aside from a slight reduction from 12% to 9% between Cairo, IL and RM 750 with little change since 1989.

Coarse sand (0.5 – 1.0 mm) The coarse sand fraction, present only to RM 150 in 1932, advanced to Head of Passes by 1989 and continued to represent a small percentage in 2013. Upstream of RM 500, coarse sand decreased slightly by a few percent between 1932 and 1989 but exceeded 1932 values by 4-5% in 2013.

Medium sand (0.25 – 0.50 mm) A pronounced increase in medium sand content occurred since 1932, especially within the reaches RM 950 – 750 (29% to 40%), and RM 500 – 250 (47% to 63%). However, a small, 2% reduction occurred in the lower reaches (RM 250 – 0) from 1932 to 1989 and an additional 1% drop since 1989.

Fine sand (0.125 – 0.25 mm) Upstream of RM 500 fine sand abundances increased from 4-9% in 1932 to 9-14% in 1989. Below RM 500 the increases are more dramatic; a near doubling of fine sand abundance occurred between RM 500 – 250 (15% to 28%), while the reach below RM 250 increased from 33% to 54%. Since 1989, the abundance within the reach RM 500 – 250 decreased slightly from 28% to 23% while there was a corresponding increase below RM 250 from 54% to 63%. It is conjectured that this may indicate migration of these materials downstream during episodic flood events. Further studies should evaluate progressive downstream translation of sediment classes through time.

Very fine sand (0.062 – 0.125 mm) Most significant is the marked reduction in very fine sand content throughout the lower Mississippi River, especially downstream of RM 250 where these materials were replaced by fine sands. Between 1932 and 1989, very fine sand content had reduced to near zero values between RM 950 and RM 400 with a small exception at RM 600; this pattern continued to 2013. Below RM 250 very fine sand decreased from an average of 26% in 1932 to 6% and 2% in 1989 and 2013, respectively.

Silt and clay (<0.062 mm) The 1935 WES report did not separate the <0.062 mm fraction into silt and clay sizes; therefore, comparisons of clay abundance are only made between 1989 and 2013. Very little to no change occurred in the silt and clay fractions above RM 500 between 1932 and 2013. Below RM 250, however, silt and clay reduced from an average of 10% in 1932 to 8% in 1989 and finally to 5% in 2013. Between RM 25 and RM 0 the silt and clay fractions have displaced the very fine sand present in 1989.

Table 2 Percent composition of Mississippi River bed materials averaged across reach indicated, Cairo, Illinois to Head of Passes, Louisiana.

Study year	Reach (Miles above HOP)	Silt & Clay	VF Sand	F Sand	MD Sand	C Sand	VC Sand	Gravel
1932	950 - 750	0%	3%	4%	29%	33%	12%	18%
	750 - 500	1%	5%	9%	44%	27%	5%	9%
	500 - 250	3%	11%	15%	47%	16%	2%	8%
	250 - 0	10%	26%	33%	30%	1%	0%	0%
1989	950 - 750	0%	0%	9%	42%	31%	9%	9%
	750 - 500	2%	1%	14%	51%	25%	4%	4%
	500 - 250	1%	1%	28%	54%	12%	1%	2%
	250 - 0	8%	6%	54%	28%	2%	0%	0%
2013	950 - 750	0%	1%	7%	40%	38%	8%	7%
	750 - 500	1%	0%	9%	49%	31%	5%	6%
	500 - 250	0%	0%	23%	63%	10%	1%	2%
	250 - 0	5%	2%	63%	27%	2%	0%	0%

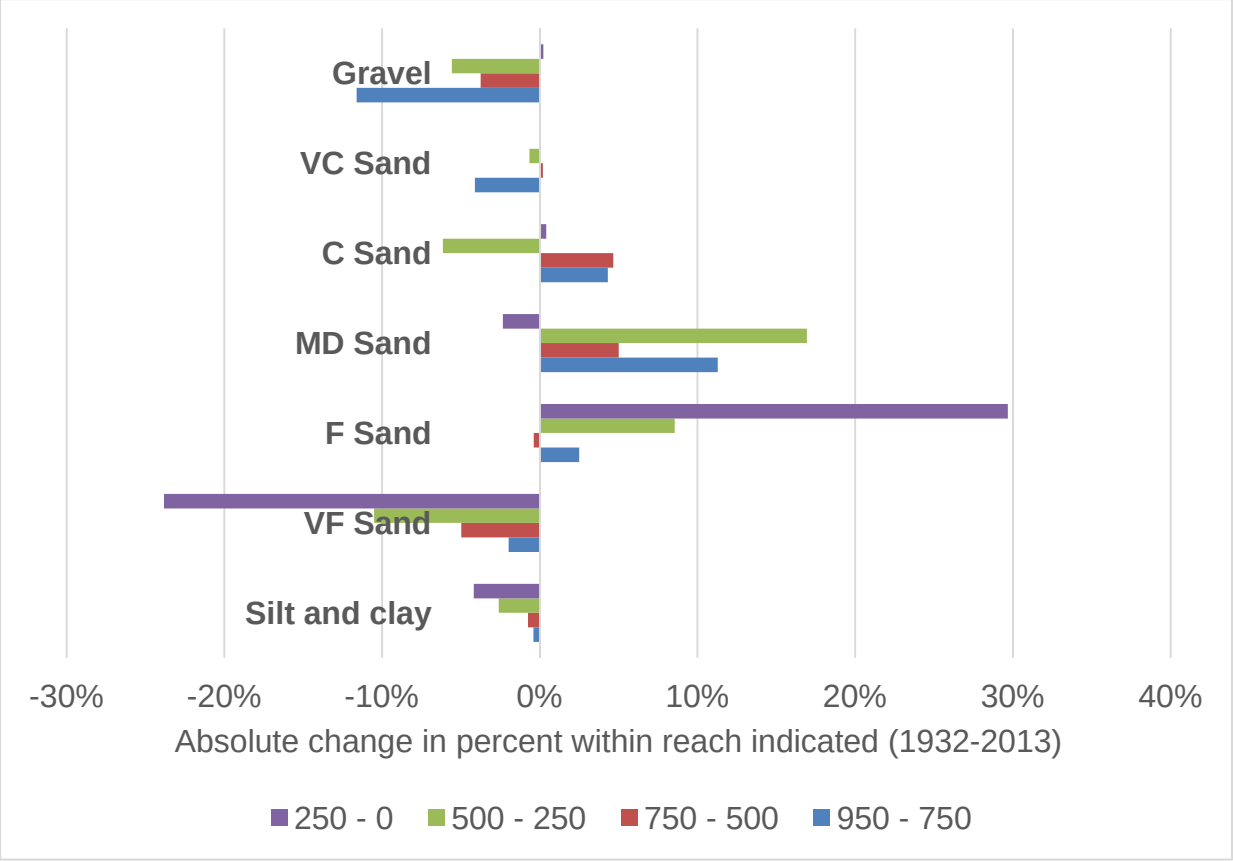

Figure 11 Relative changes in Mississippi River bed compositions from 1932 to 2013 along reach indicated.

Table 3 Calculated Sample Statistics, averaged across the lower Mississippi River reach

	Calculated Statistic				
Year	***D_{84} (mm)***	***D_{50} (mm)***	***D_{16} (mm)***	***Mean (mm)***	***Sorting***
2013	0.99	0.43	0.25	0.74	1.88
1989	0.98	0.46	0.27	0.75	2.90
1932	2.25	0.96	0.44	1.67	2.74

D_{84}, D_{50}, and D_{16} are sizes for the 84th, 50th, and 16th percentiles of the sediment grain size distribution

Sorting Coefficient, $\sigma = \frac{(D_{84}/D_{50}+D_{50}/D_{16})}{2}$

SUMMARY AND CONCLUSIONS

A total of 754 samples were collected during November 2013 between Grafton and Head of Passes. Samples were collected using the same four-inch pipe dredge and sampling techniques used by previous investigators in 1932 and again in 1989.
Particle size distributions of sands and coarser material were determined by standard sieve analysis. Particle size distributions of finer sediments were determined by Laser Diffraction with quality control of randomly selected samples by pipet analysis.

The main conclusions of this investigation are as follows:

1. The 2013 samples were significantly finer relative to 1932 (Table 3). On average the median grain size in 2013 (0.43 mm) is about 50% less than that of 1932 (0.96 mm), but little change in median grain size has occurred since 1989 (0.46 mm).

2. The 2013 samples were more uniform relative to 1932 and 1989, demonstrated by reductions in the sorting coefficient and standard deviation values (Table 3; Gaines and Priestas, 2014).

3. Since 1932, upstream of RM 500 there were marked declines in the percentage of gravel and very coarse sand, replaced by fine, medium and coarse sand. In contrast, below RM 500 there were marked declines in the clay, silt and very fine fractions, replaced by fine and medium sands. Thus, the river is becoming coarser downstream and fining upstream.

4. The 2013 samples contained less gravel than the 1932 and 1989 samples except between RM 650 to RM 575.

5. Laser Diffraction methods produce slightly different results from sieve-pipet methods. LD results trend toward coarser particle sizes than yielded from SP analysis. Pipet analysis may overestimate particle sizes < 0.063 mm due to Brownian motion and inter-particle forces which can influence the settling characteristics of the sediment.

REFERENCES

Eshel, G., Levy, G.J., Mingelgrin, U., and Singer, M.J. (2004). Critical Evaluation of the Use of Laser Diffraction for Particle-Size Distribution Analysis, Journal 68:736-743, Soil Science Society of America, Madison, Wisconsin.

Gaines, R.A. and Priestas, A.M. (2014). Particle Size Distributions of Bed Sediments along the Mississippi River, Grafton, Illinois to Head of Passes, November 2013, MRG&P Report (awaiting publication), Mississippi Valley Division, US Army Corps of Engineers, Vicksburg, Mississippi.

Loizeau, J.L., Arbouille, D., Santiago, S. and Vernet, J.P. (1994). Evaluation of a Wide Range Laser Diffraction Grain Size Analyzer for Use with Sediments, Volume 41, Issue 2, Sedimentology, International Association of Sedimentologists, pp 353-361.

Malvern (2013). Mastersizer 3000 Basic Guide, User Manual, Issue 21, Malvern Instruments, Ltd. Worchestershire, UK, On-line access at www.malvern.com on 24 Aug 2014.

McCave, I.N., Bryant, H.F., Cook, H.F. and Coughanowr, C.A. (1986). Evaluation of a Laser-Diffraction-Size Analyzer for Use with Natural Sediments: Research Method Paper, Vol. 56, No. 4 Journal of Sedimentary Petrology, pp 561-564.

Meade, R.H. and Moody, J.A. (2009). Causes for the decline of suspended-sediment discharge in the Mississippi River system, 1940-2007, Hydrological Processes, Vol 24, (www.interscience.wiley.com; DOI: 10.1002/hyp.7477).

Nordin, D.F. and Queen, B.S. (1992). Particle Size Distributions of Bed Sediments Along the Thalweg of the Mississippi River, Cairo, Illinois to Head of Passes, September 1989, Report 7, Potamology Program (P-1), Lower Mississippi Valley Division, USACE, Vicksburg, Mississippi.

Shreve, E.A. and Downs, A.C. (2005). Quality-Assurance Plan for the Analysis of Fluvial Sediment by the U.S. Geological Survey Kentucky Water Science Center Sediment Laboratory, Open-File Report 2005-1230, U.S. Geologic Survey, Reston, Virginia.

Stevens, H.H and Hubbell, D.W. (1986). Computer programs for computing particle-size statistics of fluvial sediments: U.S. Geological Survey Water-Resources Investigations Report 86-4141, US Geological Survey, Reston, Virginia.

Stojanovic, Z. and Markovic, S. (2012). Determination of Particle Size Distributions by Laser Diffraction, Vol 21, Technics-New Materials, UK.

USACE (2007). Low Water Reference Plane Update, Internal report to Mississippi Valley Division, Memphis District, US Army Corps of Engineers, Memphis, Tennessee.

Wanogho, S., Gettinby, G., and Caddy, B. (1987). Particle-Size Distribution Analysis of Soils Using Laser Diffraction, Forensic Science International, Vol 33, No. 2, Glasgow, UK, pp 117-128.

Waterways Experiment Station, (1935). Studies of River Bed Materials and Their Movement, with Special Reference to the Lower Mississippi River, US Army Waterways Experiment Station, USACE, Vicksburg, Mississippi, 161p.

Wedd, M.W. (2003). Determination of Particle Size Distributions Using Laser Diffraction, 032Q-Wedd, Education Resources for Particle Technology, http://www.erpt.org/032Q/Wedd-00.htm.

DROUGHT, LOW WATER, AND DREDGING OF THE MIDDLE MISSISSIPPI RIVER IN 2012

David C. Gordon, P.E., Chief, Hydraulic Design Section, U.S. Army Corps of Engineers – St. Louis District, St. Louis, Missouri, david.gordon@usace.army.mil
Michael T. Rodgers, P.E., Project Manager, U.S. Army Corps of Engineers – St. Louis District, St. Louis, Missouri, michael.t.rodgers@usace.army.mil

Abstract: In early 2012, low snowpack in the Rocky Mountains and the northern plains, followed by extreme heat, and prolonged drought in the plains and Midwest led to a long period of low water and record low stages on the Middle Mississippi River from June to February 2013. A drought of this magnitude had not occurred along the Mississippi River since 1988 and 1989. The U.S. Army Corps of Engineers (Corps) is responsible for maintaining a minimum 300 foot wide by nine-foot deep navigation channel. This task was especially challenging in 2012 as the drought carried on and conditions and forecasts worsened. However, due to strategic planning, engineering, and construction activities since the last major drought, the Corps was able to significantly lessen the impacts and provide a navigable channel throughout the drought and low water period through a combination of river engineering, dredging, forecasting, monitoring, and communication.

Although the Corps worked around the clock and seven days a week to dredge the channel, the amount of sediment that was dredged from the river channel was less than half of what needed to be dredged during the previous drought year. This is despite the fact that the number of low water days was more than in 1988/89 and the channel was dredged to greater depths in 2012. This paper will discuss what led to the significant improvement in the navigation channel, which included increased reliability and lower maintenance.

INTRODUCTION

The St. Louis District Corps of Engineers is responsible for maintaining a safe and dependable navigation channel on approximately 300 miles of the Mississippi River between Saverton, Missouri and Cairo, Illinois. The southernmost 195 mile section of the Upper Mississippi River, located between the confluences of the Missouri River and the Ohio River, is often referred to as the Middle Mississippi River. The Middle Mississippi River is a critical link in the inland navigation system and vital to the nation's economy. It is the middle link that connects the Lower Mississippi River and Ohio River systems with the Upper Mississippi River, Illinois River, and Missouri River systems. The Middle Mississippi River is unique because it is an open river system while the Upper Mississippi, Illinois Rivers, and Ohio Rivers use locks and dams to supplement navigation depths. The Lower Mississippi River is also open river system but has a much greater discharge that naturally supplements navigation. Therefore, maintaining navigation depths on the Middle Mississippi River has always been a significant challenge for river engineers. Engineers typically use a combination of river training structures, revetments, and maintenance dredging to keep the minimum nine-foot deep navigation depth year round.

While always a challenge, maintaining the navigation channel was made far more difficult in the fall and winter of 2012 due to extreme drought conditions in the Mississippi River watershed

(Figure 1). The drought was equal to or worse than any drought experienced in the past five decades. Water levels in the Middle Mississippi River reached near record lows, which posed a significant risk to commercial navigation traffic due to shallow channel crossings, reduced channel widths, and rock pinnacles located along the channel bottom (Figure 2).

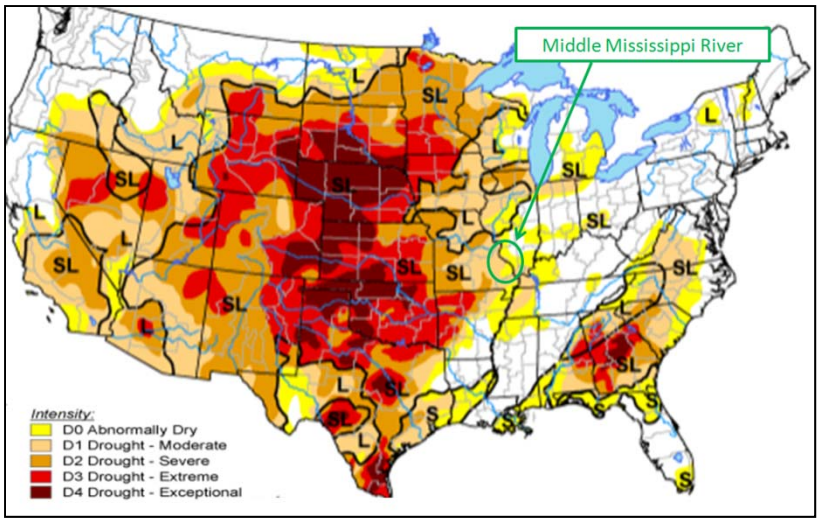

Figure 1. U.S. Drought Monitor map on January 1, 2013. (http://droughtmonitor.unl.edu/)

Figure 2. Drought and low water on the Middle Mississippi River meant exposed sandbars, hazards for navigation, and a narrow navigation channel.

EARLY SIGNS OF DROUGHT IN SPRING 2012

As early as April 2012 river engineers, water control managers, and the dredging team began preparing their staffs and upper management for the possibility of drought and probable low

water which would occur in the summer, fall, and winter of 2012. The weather in spring 2012 produced very little rainfall throughout the Midwest U.S. on top of a low snowpack in the Rockies and the plains, therefore the Mississippi River was much lower than normal for typical spring conditions. A flood level of 30 feet on the St. Louis gage is typically reached at least once during the spring rainy season, with a combination of inflows from the Upper Mississippi, Missouri, and Illinois basins. However, in 2012 the St. Louis gage only approached 20 feet briefly on just two occasions, in late March and again in early May. Otherwise, the stage remained well below normal throughout the spring and by early June was already ten feet below average. The river stages in 2012 were following a similar pattern to the stages early in the 1988/89 drought (Figure 3).

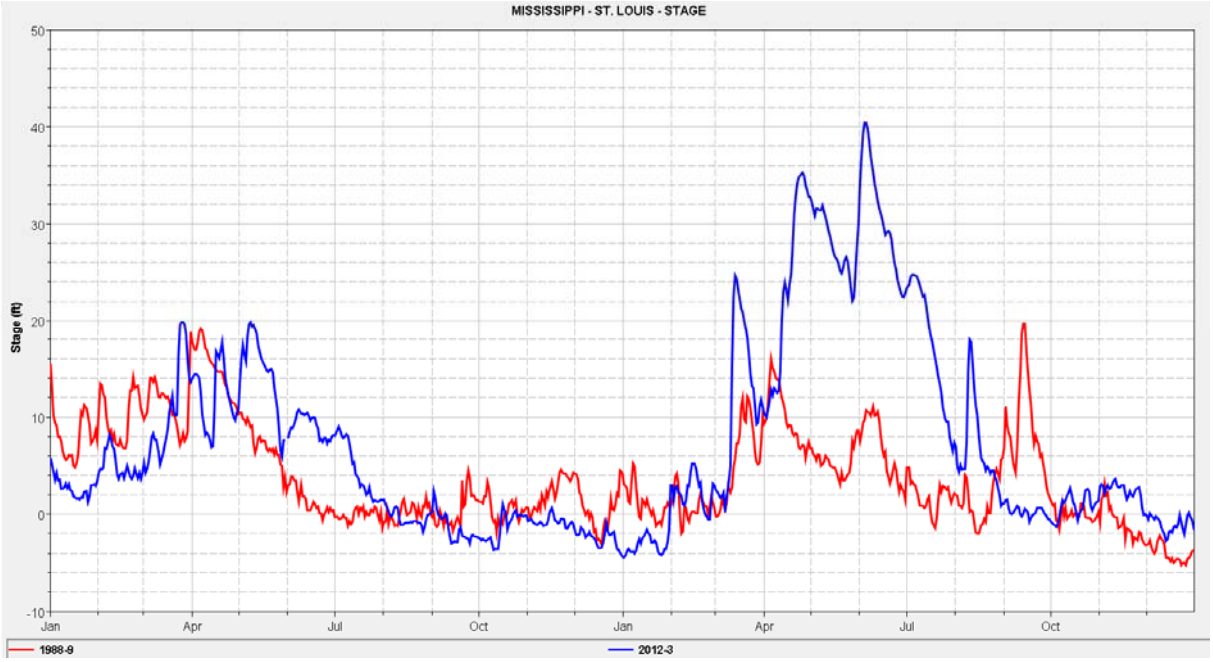

Figure 3. River stages at the St. Louis Gage over a 2-year period comparing 1988/89 with 2012/13.

The St. Louis District began communicating these conditions to the Corps Mississippi Valley Division (MVD) Office, River Industry Action Committee (RIAC), the River Industry Executive Task Force (RIETF), the United States Coast Guard (USCG), National Weather Service (NWS), and the United States Fish and Wildlife Service (USFWS). The teams discussed communication strategies, water management, forecasting, navigation channel monitoring, dredging capability, rock removal from the navigation channel, and various action levels/plans.

The team decided to start monitoring the navigation channel for trouble spots much earlier than a normal year. Channel reconnaissance surveys and pre-dredge surveys were collected early and often. The USCG Cutters and the Corps MV Pathfinder began patrolling the channel and resetting the channel marking buoys weekly. The St. Louis Harbor became narrow and congested as fleets encroached upon the navigation channel (Figure 4).

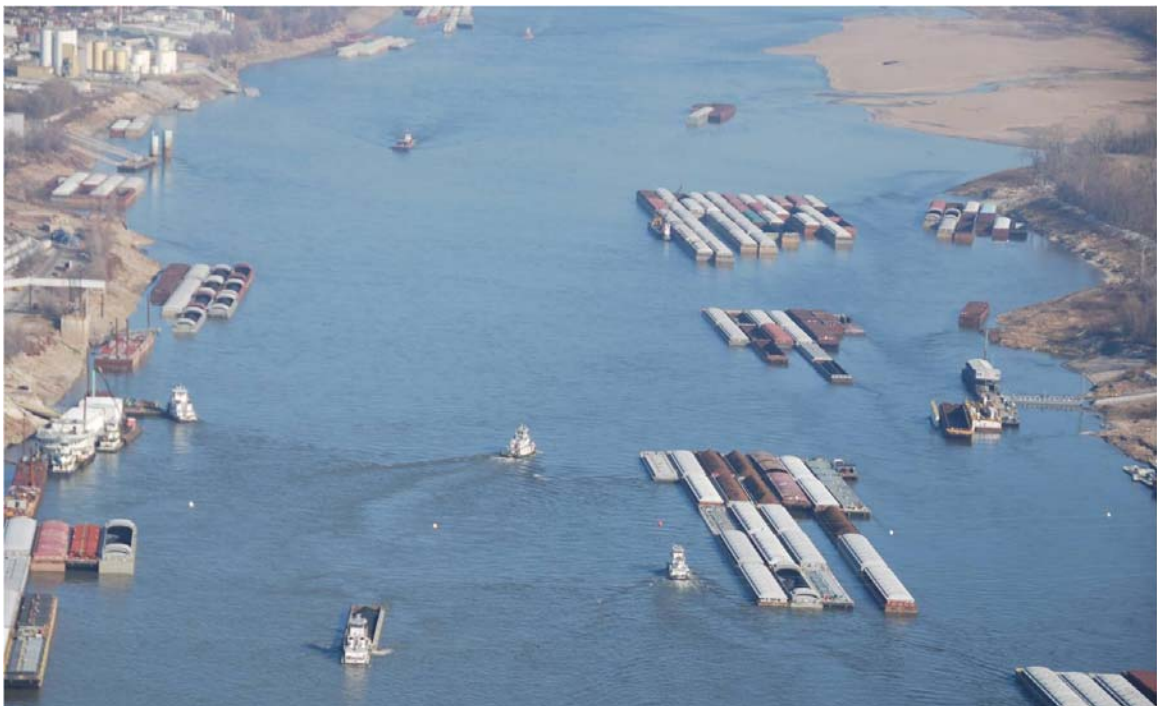

Figure 4. Low water conditions in the St. Louis Harbor meant that space for fleeting operations was limited.

DROUGHT RESULTS IN RECORD LOW WATER

Just as the Corps predicted in the spring of 2012, the drought took hold of the Midwest throughout an extremely hot summer. A sustained period of low water occurred on the Middle Mississippi River from June 2012 through the beginning of February 2013. The lowest stage at St. Louis during the low water period occurred in January 2013. A stage of -4.6 feet tied for the 7th lowest on record and was the lowest river had been since the drought of 1988/89 (Table 1). The length of the time the river remained at extreme low stages was also a concern. A stage of 0 feet on the St. Louis Gage is typically used by the Corps, the USCG, and the navigation industry to indicate low water and trigger additional action. The river stayed below 0 feet at St. Louis for 160 days during this period. By comparison, the river was below 0 feet for just 94 days in 1988 and 112 days in 1989. River engineers know that the longer the River stays below 0 feet, the more "lazy" it becomes as velocities and sediment carrying capacity declines. This results in more sediment accumulating in problematic reaches causing more problems for river industry.

Dredging during the low water event proved to be a significant challenge. Dredging operations began in early July 2012 and continued through February 2013 (Figure 5). The dredging team worked to prioritize dredging locations based on dredge efficiency and channel depths. Channel depths were continuously monitored through extensive channel patrol surveys. On typical years, the channel is dredged in order to maintain navigation depths 9 feet below a St. Louis stage of -3.5. Based upon forecasts for the fall and winter of 2012, the team decided to prepare the channel for a stage of -5.5 feet instead. Later in the year, when forecasts predicted that stages could be below -6.0 feet, the team decided to prepare the channel for a stage of -7.0 feet. This

new channel design was also predicated on the ongoing removal of rock pinnacles that were in the channel near Thebes and Grand Tower Illinois that would also allow depths to -7.0 when completely removed in January 2013 under an Urgent and Compelling Contract.

Rank	St. Louis Stage	Month/Year
1	-6.2	Jan 1940
2	-5.8	Jan 1963
3	-5.6	Jan 1964
4	-5.5	Dec 1937
5	-5.4	Dec 1989
6	-4.8	Jan 1957
7	-4.6	Jan 1956
	-4.6	Jan 2013
9	-4.5	Jan 2003
10	-4.3	Dec 1933

Table 1. A ranking of the lowest daily stages recorded at the St. Louis, Missouri river gage.

Figure 5. The Dredge Potter moves to the side to allow a tow to pass in September 2012.

The complexity and significance of the rock removal component of the mission cannot be overstated. This work required integrated and coordinated management along with the application of innovative technology and tools / removal methodologies. Risks associated with barge tow collisions with rock pinnacles were high, from both a fiscal and an environmental perspective. Current and future river construction contract needs were adjusted in order to fund the rock removal project. River engineering projects were reprioritized to allow for detailed plans and specifications to be produced to accommodate a tight project schedule. Removal of

the pinnacles involved advanced surveying techniques coupled with innovative removal methodologies. Work locations within the rock removal areas were prioritized to get the most dangerous (highest elevation) rock out first, with a secondary focus on providing optimal channel widths.

Water managers constantly collected water data, monitoring a number of hydrological and meteorological factors to forecast river conditions the rest of the low water team relied upon. Continuous monitoring of flows from the Middle Mississippi River tributaries and associated impacts played an important role in decision making. In close coordination with USCG and NWS, water managers operated Mel Price Locks and Dam, just upstream of St. Louis, under a deviation with a higher pool to alleviate impacts of water level fluctuations through the St. Louis Harbor. During the most critical water levels, the managers also utilized water in Carlyle Lake to augment flows for navigation purposes over the lower section of the Middle Mississippi River in order to temporarily increase stages.

Throughout the entire low water period, the District coordinated with project stakeholders including (but not limited to) RIAC, RIETF, the USCG, the NWS, and USFWS. The task of keeping the Middle Mississippi River open to commercial navigation is highly visible, politically sensitive, and extremely complex. Therefore, the district maintained close coordination of their activities with MVD, the Corps Headquarters Office in Washington D.C., the Assistant Secretary of the Army's (ASA) Office, the Department of Homeland Security and the White House. This required sending daily updates and information to all entities regarding: compliance with all relevant environmental regulations (National Environmental Policy Act (NEPA) and Fish and Wildlife Coordination Act (FWCA)); management of pool and reservoir elevations; forecasted river levels; status of the removal of the underwater rock pinnacles; dredging activities, including shoal locations; and providing a nearly continuous flow of channel and rock pinnacle surveys.
As a result of these activities during this low water event there were no accidents, groundings or unplanned closures of the Middle Mississippi River. This performance was unprecedented given that a similar drought in the late 1980's featured numerous groundings, accidents, channel closures, restrictions and a generally unreliable channel.

THE MIDDLE MISSISSIPPI RIVER NAVIGATION CHANNEL, NOW AND THEN

Accurate records of groundings during the 1988/89 drought are not readily available. However, according to newspaper articles, there were 22 groundings in just one weekend in December 1989 which caused the USCG to essentially close the entire Middle Mississippi River until conditions improved. By comparison, throughout the entire 2012/13 low water event there were no groundings or unplanned closures within the marked navigation channel. Some barges went aground on a few occasions, but in each situation it was determined that the tow had grounded outside of the marked channel.

What is the difference between the channel in 1988/89 and the one today? Following the drought of 1988/89 the St. Louis District embarked upon an aggressive river engineering project that resulted in the development, design and construction of innovative structures such as bendway weirs and chevrons that have significantly reduced channel maintenance dredging and resulted in a much more reliable channel during the 2012 drought. The Regulating Works

Project utilized innovative techniques to redesign the navigation channel which has led to the development of new types of river training structures.

Bendway Weirs were developed in the early 1990's as a means to improve navigation around the tight bends that are typical along the Middle Mississippi River. The development of these structures has been revolutionary for river engineers and the navigation industry. Over 175 bendway weirs have been constructed on this part of the River which has resulted in a significant reduction in the dredging of point bars and the elimination of accidents through these bends.

River engineers in the St. Louis District realized that for the project to be sustainable they had to adjust their design techniques and parameters in order incorporate environmental features into their navigation channel improvement projects. The engineers worked with closely with biologists in the Corps partnering agencies to develop different types of versatile structures in order to both protect the environment and to improve navigation. River training structures such as chevrons (Figure 6), off-set dikes, and W-dikes have successfully implemented by the river engineers in the St. Louis District. These types of structures have been shown to provide both navigation and environmental benefits.

Figure 6. Chevron river training structures near River Mile 32.

The St. Louis District also developed Hydraulic Sediment Response (HSR) models for use in the design of river training structures. After HSR models were fully developed, the District established the Applied River Engineering Center as a facility to conduct these physical models and other sediment studies of the Mississippi River and its tributaries. The use of the HSR models and AREC allowed the district to efficiently study and design multiple sets of river training structures that had both navigation and environmental benefits. The AREC facility has been used regularly to engage and collaborate with the environmental community during the entire design process. The technology has also allowed the engineers to be so efficient with the designs that the Project did not have enough capacity to implement the construction of these designs on a yearly basis. Therefore, many designs were put on the shelf to await funding.

When requests for projects eligible for the American Recovery and Reinvestment Act (ARRA) came about in 2009, the district was well positioned to act. Multiple river training projects qualified as "shovel-ready" and were funded by ARRA. The construction of these ARRA river training structures remedied many of the chronic dredging locations and led to a more reliable navigation channel.

Operational changes were also been undertaken to improve the district's responsiveness to low water events. A Project Delivery Team (PDT) consisting of elements from river engineering, water management, dredging, and surveying continue to meet weekly throughout the year to address river conditions in a timely manner. Outreach to both other government partners (USCG, NWS, etc.) and the river industry has led to a better understanding of, and response to, navigation concerns. A weekly channel status report is sent to the river industry and other invested partners. Internally, a river condition status report is generated weekly to anticipate dredging and surveying needs.

Surveying capabilities have also dramatically increased district responsiveness. Equipment improvements such as multi-beam sonar and increased surveying capacity utilizing two contract surveying companies have also led to an increased awareness of the state of the channel over the capabilities that were available in 1988/89. Survey data can now be sent directly from the boat to the office for post-processing and analysis leading to channel evaluations that can almost instantly be shared with the navigation industry.

Water management and forecasting have also greatly improved. Critical coordination occurred throughout the day and night with water managers upstream of St. Louis, including the Rock Island District for the Upper Mississippi and Illinois Rivers and the Northwest Division for the Missouri River. The St. Louis District constantly monitored inflows and adjusted the outflow at Mel Price Locks and Dam to alleviate impacts of water level fluctuations through the St. Louis Harbor. The District also utilized the available water in Carlyle Lake to augment flows for navigation purposes over lower portion of the Middle Mississippi River in order to temporarily increase stages by timing the releases as the water had to travel down the Kaskaskia River.

During low water, channel patrol efforts using the Corps M/V Pathfinder were increased to identify problem areas, replace or move buoys to better mark the narrowing channel. Assuring the channel is well marked prevents groundings which may further degrade the channel and defers dredging until a dredge can be assigned to that specific location. The USCG also increased their buoy tending runs. Schedules for the patrols between USACE and USCG are coordinated to maximize coverage on the system.

THE RESULTS OF THE RIVER ENGINEERING PROGRAM

In 1988 and 1989 alone, over 19 million cubic yards of material were dredged each year for a total of 38.1 million yards of material removed from the navigation channel. Compare that to the low water period of 2012/13 where only 9.3 million cubic yards of material were removed in just the one year. While the drought of 1988/89 encompassed two full dredging seasons and the drought of 2012/13 was only in one dredge season, the events can be compared considering that no two droughts are the same. Not only was significantly less material removed in 2012 by

comparing that year to either 1988 or 1989, but the channel was fully prepared for a stage of -7.0 at St. Louis, which was a full 3 feet lower than in 1988/89 (Table 2).

Dredge Season	Days below 0 ft at St. Louis	Dredge Volume (cubic yards)	9 ft Navigation Channel Prepared to a St. Louis Stage of:
1988	94	19,100,000	-4.0
1989	112	19,000,000	-4.0
2012/13	160	9,300,000	-7.0

Table 2. The period of low water and dredging volumes compared between the drought of 1988/89 and 2012/13.

The St. Louis District's river engineering program developed a ranking system of chronic dredging locations in order to prioritize the construction of river training structures. The system is based on a weighted average of the last 5 and 10 years of dredging in two mile river segments. The top ten dredging locations by volume in 1988/89 are shown in Table 3. The table shows the volume of material removed from these locations in 1988/89. The table also shows that the river engineering program has reduced the amount dredged from these locations by an average of 82%. The changes mentioned above highlight just a small portion of the changes that have occurred on the river in the last 25 years to reduce the number of lower water or confined channel dredging locations. Under multiple programs, over 175 bendway weirs were constructed since 1989 to widen the navigation channel and increase center channel depth. These same programs have funded multiple new dikes, chevrons, and other river training structures over the past 20 years to improve and maintain channel depth.

River Mile	1988-89 Rank	Dredged in 1988-89 (cy)	Current Rank	Dredged in 2012 (cy)	Percent Reduction
52 - 54	1	2,228,800	38	35,468	-98%
42 - 44	2	1,892,600	36	225,500	-88%
66 - 68	3	1,706,700	5	530,976	-69%
38 - 40	4	1,646,000	6	323,781	-80%
6 - 8	5	1,545,700	34	167,213	-89%
46 - 48	6	1,257,800	8	450,047	-64%
30 - 32	7	1,246,400	24	112,748	-91%
28 - 30	8	1,232,400	37	0	-100%
166 - 168	9	1,204,300	16	366,400	-70%
14 - 16	10	1,125,000	33	350,308	-69%

Table 3. The top ten ranked dredging locations in 1988/89 compared to 2012.

An analysis of the most troublesome dredging locations in 1988/89 compared to 2012 is even more dramatic. In 1988/89 the worst 20 miles of river accounted for over 15 million cubic yards of dredging over these two years. The worst dredging location for the 1988/89 time frame was the stretch of river from River Mile (RM) 54 to 52, near Cape Girardeau, Missouri. This stretch

was responsible for over 2.2 million cubic yards of dredging between 1988 and 1989. Since then, bendway weirs have been placed at the upstream extent of the stretch. In 2012, less than 36,000 yards were dredged in this reach for a 98% reduction.

The second-most dredged location in 1988/89 was between RM 44 and 42, near Thebes, Illinois. This reach of river required nearly 1.9 million cubic yards of dredging, with the dredging partially necessitated by the presence of submerged rock pinnacles that constrained the navigable channel. Since 1989, several additional dikes were constructed to better maintain flow alignment in the navigation channel. Efforts have also been made to remove the rock pinnacles to increase navigable channel width, both in 1989 and in 2012. In 2012, only 225,000 yards of material were dredged for a reduction of 88%.

The third-most dredged location was between RM 68 and 66, near Moccasin Springs, Missouri. In 1988/89, this area required over 1.7 million cubic yards of dredging. Dike extension was used in this reach to reduce dredging by 69% in 2012. Although this is a significant reduction, the reach still ranks currently as the 5th highest priority for work on the Middle Mississippi River based on dredging. To address the ranking, this stretch was recently studied with a HSR model with the principle goal of further alleviating the need for dredging. Construction of several innovative river training structures is scheduled for fiscal year 2016. The Project will not only reduce dredging in the main channel, but will add significant environmental enhancement in the form of a side channel or chute.

CONCLUSION

The nation's economy is heavily dependent upon the safe operation and reliability of the Middle Mississippi River corridor that transports 110 million tons per year or nearly $34 million worth of goods on a daily basis in and out of the St. Louis Harbor. Shut downs and delays to the river navigation industry can have profound effects on a regional and national level.

The entire 2012 low water effort resulted in a navigation channel that remained open for commerce throughout the drought, without any groundings or accidents within the channel, and generally led to a much more reliable channel for shippers. The implementation of a successful river engineering program led to the reduction in sediment and dredging volume as compared to a similar drought and low water period in 1988/89. Furthermore, improvements in hydraulic modeling, design of river training structures, water management techniques, bathymetric data collection, coordination with the towing industry and the Coast Guard, and the identification and removal of rock outcroppings from the riverbed can be also credited with the improvements.

This improvement in dredging was the result of an aggressive 20+ year long river engineering program that has reduced dredging costs and increased the safety and the reliability of the channel. The development and implementation of innovative river training structures, such as bendway weirs and chevrons, resulted in a much improved navigation channel while also creating diverse aquatic habitat.

In conclusion, the Middle Mississippi River Regulating Works Project since 1988/89 has resulted significant improvements to:

- Dredging – Significant reductions in the volume of dredge material resulting in a much lower Operations and Maintenance (O&M) cost.
- Depth – A river channel that can be maintained to deeper depths if needed, closer the authorized channel depth, for much less cost.
- Reliability – Shippers and carriers have much greater confidence in the ability of the River to carry goods when needed. This confidence means that more goods will be transported by the River every year that it can be demonstrated that the channel will be available full time and without delay.
- Safety – The 2012/13 low water period resulted in zero channel groundings and no incidents of hazardous chemicals spilled as a result of an accident.
- Habitat – The Middle Mississippi River contains more diverse aquatic habitat through the use of innovative river training structures such as chevrons, W-dikes, multiple round point structures, side channel enhancement dikes, and off-set dike extensions.

MISSOURI RIVER 2011 FLOOD – CHANNEL RESPONSE AND OBSERVATIONS

Chris Svendsen, Hydraulic Engineer, USACE Omaha District, Omaha, NE, christopher.j.svendsen@usace.army.mil; Dan Pridal, Hydraulic Engineer, USACE Omaha District, Omaha, NE, daniel.b.pridal@usace.army.mil;

ABSTRACT

The Missouri River 2011 flood event within Omaha District resulted in a sustained high peak flow with unprecedented duration. The Missouri River and entire floodplain experienced large areas of sediment erosion and deposition. Normal Corps activities include the monitoring of degradation and aggradation reaches on the Missouri River associated with Missouri River dam construction and also conditions within the navigation channel. Post-flood observations indicated sediment deposition, scour, and significant damage. Survey data was collected and hydraulic modeling performed in support of numerous programs for post-flood repairs. A review of the post flood status of several specific projects and observed channel response during and after the flood are presented.

INTRODUCTION

Introduction

The purpose of this report is to present gage stage trends on the Missouri River within the Omaha District from Ft Peck, MT, to Rulo, NE with a focus on 2011 flood impacts. Gages provide data with which to monitor changes in the river due to hydrologic events and construction of main stem dams and river structures. Record releases occurred from all Missouri River dams in 2011. This report addresses the stage to discharge relationship at each gage, the effects of the 2011 high flows, and how the stages have responded Additional response to or recovery from the 2011 event is expected to continue in many areas in the future.

The views expressed in this paper are those of the authors and do not necessarily reflect the official policy or position of the United States Army Corps of Engineers, the Department of the Army, Department of Defense, or the United States Government.

Description of Missouri River System

The Missouri River Mainstem system of dams is composed of six large earth embankments, which impound a series of lakes that extend for 1,257 miles from Gavins Point Dam near Yankton, SD to the head waters of Fort Peck Lake southeast of Glasgow, MT. These dams were constructed by the Corps of Engineers on the mainstem of the Missouri River for flood control, navigation, power production, irrigation, water supply, water quality, recreation and fish and wildlife enhancement. Fort Peck Dam, the oldest of the six, was closed in 1937. Fort Randall Dam was closed in 1952, followed by Garrison Dam in 1953, Gavins Point Dam in 1955, Oahe Dam in 1958 and Big Bend Dam in 1963. The dams provide nearly 988,000 acres of water surface area and extend a total length of 750 miles. There are 325 miles of open river between the lakes. The reservoirs contain an aggregate storage volume of approximately 73 million acre-feet, three times the average annual flow of the Missouri River at Sioux City, IA. There are 811 miles of open river downstream from Gavins Point Dam to the mouth of the Missouri River where it enters the Mississippi River at St. Louis, Missouri. The Omaha District Boundary ends at mile 498.

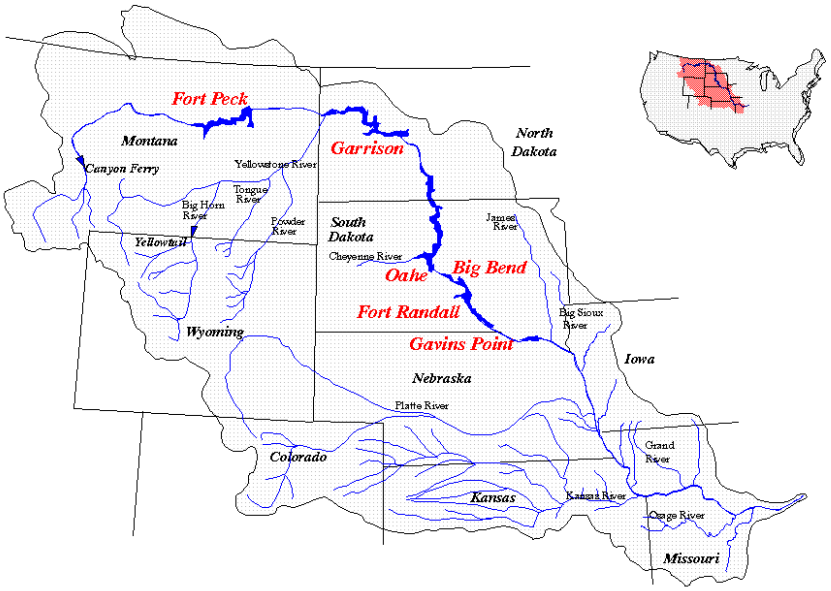

Figure 1 Missouri River Basin

Significance of 2011 Event

Flow Measurements and Observations

The 2011 runoff year was the highest runoff year of record in the upper Missouri River basin since records were initiated in 1898. Upstream of Sioux City, IA, annual runoff volume was estimated at 61 million acre-feet (MAF). In comparison, the previous greatest annual runoff volumes were 49 MAF in 1997 and a roughly estimated 50 MAF in 1881. For the period from March – July, the 1881 runoff volume was more than 40 MAF compared to 48.4 MAF for 2011 (USACE, 2013b).

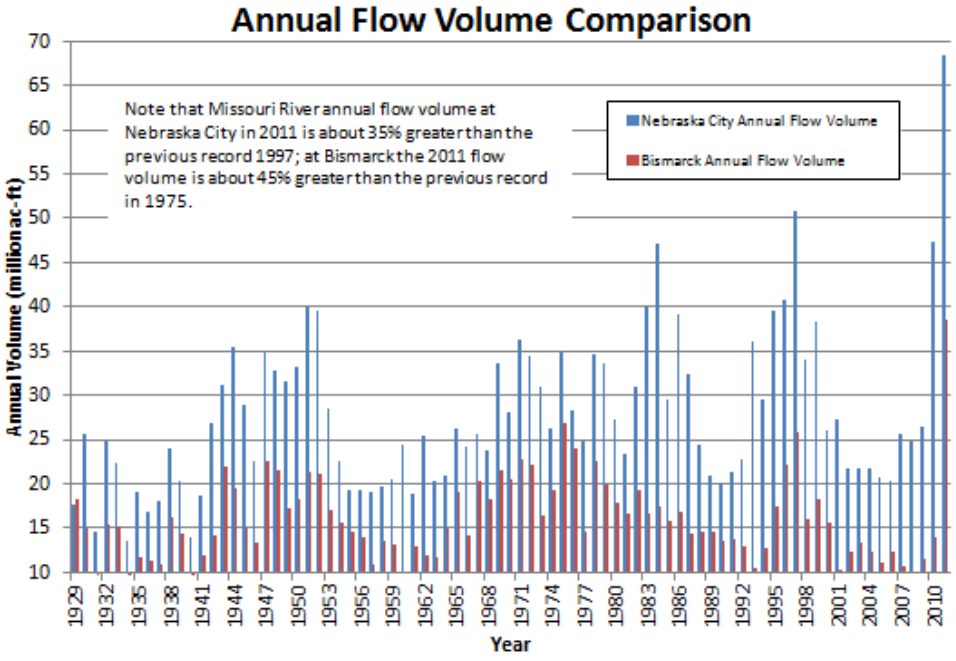

Figure 2 Nebraska City and Bismarck Annual Flow Volume Comparison

When compared to historic events, it should be recognized that historic river flows were affected by main stem dam construction and reservoir filling, primarily in the period 1953 to 1967. All flow frequency values reported in the comparison are post dam construction (USACE, 2003). As a result, compared to historic events is somewhat misleading since the reservoir system has significantly altered peak flows. Data from the USGS gage at Nebraska City is shown in Figure 3.

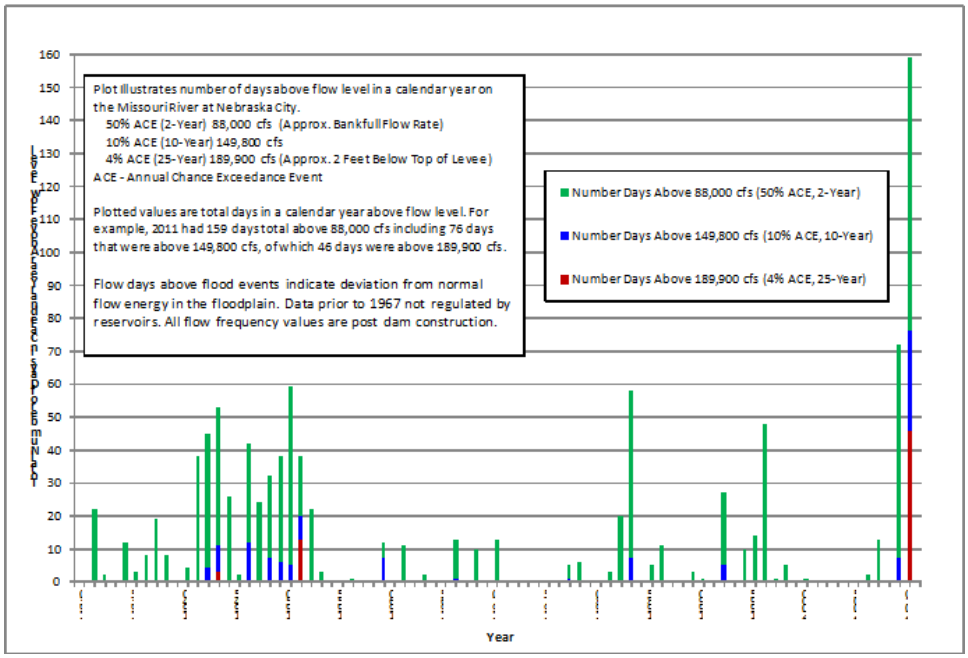

Figure 3 Nebraska City Days above Flow Value by Year

The above figure illustrates the severity of the 2011 event. Using the 189,900 cfs benchmark for comparison, the 2011 event dwarfs all other flood events on the Missouri River. This event was unique in the historic record with the floodplain inundated at a very high level for a prolonged duration. Table 1 presents additional information at both Nebraska City, NE, and Bismarck, ND.

Table 1 Nebraska City and Bismarck, Number of Days above Flow Value by Year

Nebraska City

Event	2011	1993	1984	1952	1944	Total (All Years)	2011 % of Total
189,900 cfs 4% ACE (25-Year)	46	0	0	13	3	62	74
149,800 cfs 10% ACE (10-Year)	76	5	7	20	11	169	45
88,000 cfs 50% ACE (2-Year)	159	27	58	38	53	1029	15

Bismarck

Event	2011	1997	1975	1952	1944	Total (All Years)	2011 % of Total
81,000 cfs 2% ACE (50-Year)	90	0	0	8	14	192	47
57,000 cfs 10% ACE (10-Year)	105	19	46	20	38	545	19

40,000 cfs 50% ACE (2-Year)	134	186	93	58	61	1716	8

Total refers to the number of days above given flow target since gage record began in 1929. Includes the period prior to dam construction. Historic large events tabulated to provide comparison to 2011.

Sediment Measurements and Observations

Sediment measurements were conducted at a number of locations by the USGS during the 2011 event. These sediment measurements during the 2011 event were compared to historic measurements from both the pre- and post-dam era. Measurements indicate a dramatic difference in the suspended sediment vs. flow relationship for the 2011 event. Suspended sediment plots from 2011 and other periods for comparison are illustrated for Nebraska City, NE in Figure 4 and for Bismarck, ND, in Figure 5 .

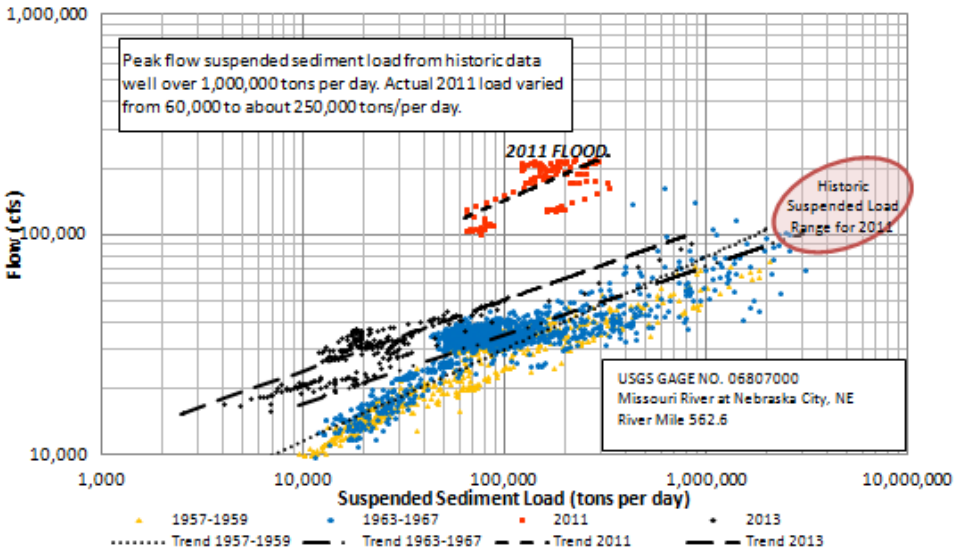

Figure 4 Nebraska City Suspended Sediment Load Comparison from Various Time Periods

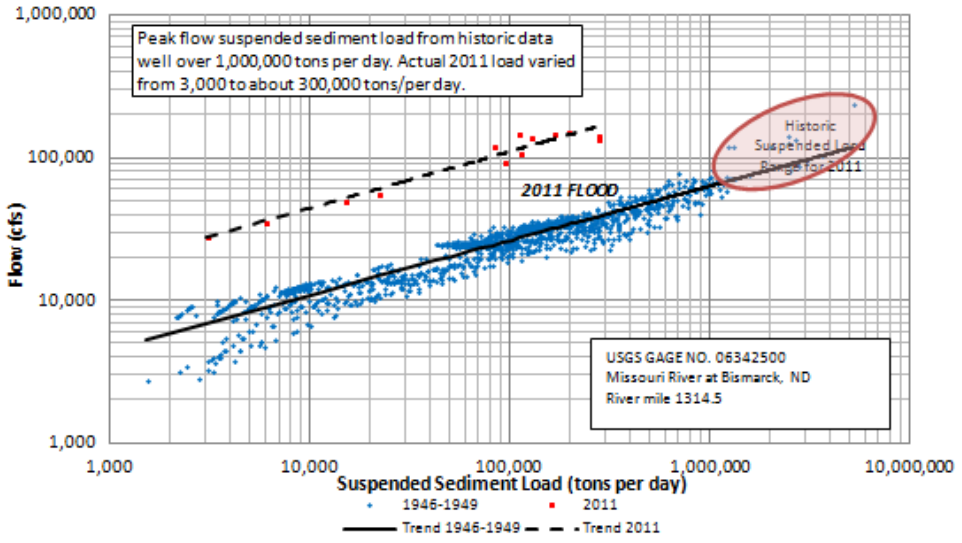

Figure 5 Bismarck Suspended Sediment Load from Various Time Periods

Gage Analyses and Methods

Stage trend plots presented in this report contain data points taken off rating curves or recorded historic data. Two methods are used to develop the rating curves. The first is to plot USGS field measurements (stage/discharge) for a certain water year and fit a rating curve through the points. The second method is to obtain average daily stage data from recorders at the gages and combine that information with average daily discharge measurements from dams and stage/discharge gages on tributaries or from a stage/discharge gage immediately upstream of the subject gage.

Major rivers such as the Missouri River often exhibit the characteristics of a looped rating curve as illustrated by individual gage data; one for the rising limb of the flood hydrograph when flows are increasing up to the occurrence of the flood peak and a second curve for the receding side of the flood hydrograph with decreasing flows from the peak.

Fort Peck Dam to Lake Sakakawea

Geographic Description

Fort Peck Dam is located on the Missouri River at RM 1771.5 in northeastern MT. The project was placed in operation for navigation and flood control in 1938. The Fort Peck degradation reach is considered to extend from the dam nearly 173 miles downstream to RM 1598. The Milk River is the major tributary in this reach entering the Missouri River about 10 miles downstream of the dam. The aggradation reach extends downstream from RM 1598 to the Williston, ND area. The Yellowstone River is the major tributary entering this reach near RM 1578.

Degradation Reach

This reach appears to be more stable than other reaches in the system. West Frazier Pumphouse and Wolf Point have behaved similarly. Trend plots show that the stages for a 10,000 cfs flow had dropped about three feet from 1950 to the mid-1980s, then changed little overall until 2011. Since 2011 the West Frazier gage showed slight degradation whereas the Wolf Point gage showed about 1.5 feet of degradation in 2012, followed by a slight rebound in 2013. Stages for the 20,000 and 30,000 cfs discharge have changed little since the mid-1980s at West Frazier, but dropped another 1 to 2 feet at Wolf Point by 2011, with a rebound occurring in 2013 at 20,000 cfs. At Culbertson, about 150 miles below the dam, the stages dropped about 1 to 3 feet depending on discharge from 1950 to 2011, and then slightly rebounded by 2013.

Table 2 Fort Peck Degradation Reach Elevation Changes at 10,000cfs

Gage	River Mile	1950	1984	2011	Total change
West Frazier	1751.3	2011.9	2008.8	2009.5	-2.4
Wolf Point	1701.2	1964.6	1961.5	1961.6	-3
Culbertson	1620.8	1888.5	1889.5	1887.4	-1.1

Aggradation Reach

Lake Sakakawea had high pool elevations through the mid-1990s that were followed by record low pools from 2005 through 2007 and then a high pool again in 2011. The extended time of high pool elevations in the mid 1990s probably caused an increase in deposited material from Williston, ND to the confluence with the Yellowstone River. However, much of this deposited sediment was probably re-suspended and then transported farther into the lake with low pool elevations during the first decade of the 21st century.

Table 3 Garrison Aggradation Reach elevation changes at 20,000 cfs

Gage	River Mile	1970	1985	2011	Total change
At Buford #5A	1577.5	1857.0	1859.3	1858.4	+1.4
Near Buford #6	1573.1	1854.0	1856.4	1857.3	+3.3
Williston	1552.7	1842.9	1845.6	1847.5	+4.6

Garrison Dam to Lake Oahe

Geographic Description

Garrison Dam is located in central ND on the Missouri River at RM 1390, about 75 river miles northwest of Bismarck and 11 river miles south of Garrison. Closure was made in April 1953. Since 1956, outflows from Garrison Dam have generally been through the power facilities, having a maximum capacity of about 38,000 cfs. Exceptions occurred in 1975, 1997, and 2011 when outflows of approximately 65,000, 50,000 and 150,000, respectively, were needed to pass high upstream runoffs.

The reach of the Missouri River between Garrison Dam and the headwaters of Lake Oahe covers a distance of about 80 miles of which the first 53 miles below the dam is considered the degradation reach. The Knife River enters the Missouri River approximately 14 miles downstream of the dam at RM 1376. The Heart River enters the aggradation reach just downstream of Mandan, ND at RM 1311.

Degradation Reach

The stage at the Garrison Dam tailwater gage has decreased slightly more than 11 feet at a discharge of 20,000 cfs in the period from 1953 and 2013. Most of this decrease occurred by 1980. The high flows from 1996 and 1997 caused another 1 foot of degradation. The 2011 event cause another 1 foot of degradation. All five gages located in this reach behave similarly.

Four gages in this reach show that the stage decreased in 2011. Records from the other two gages were inconclusive due to limited observations on the falling limbs of the hydrograph.

Table 4 Garrison Degradation Reach elevation changes at 20,000 cfs

Gage	River Mile	Original	1984	2011	Total change
Garrison Tailwater (1953)	1390.0	1680.3	1671.47	1669.5	-10.8
Stanton (1950)	1379.0	1676.5	1666.9	1665.2	-11.3
Fort Clark (1960)	1372.6	1668.5	1662.95	1659.5	-9
Hensler (1959)	1362.0	1660.7	1657.2	1655.8	-4.9
Washburn (1955)	1354.7	1656.1	1652.6	1650.2	-5.9
Price (1960)	1338.0	1642.4	1640.3	1638.2	-4.2

Aggradation Reach

Two gages are located in this reach. The 2011 event caused stages for both flows to lower significantly such that the stage for the 30,000 cfs flow in 2013 is about the same as in 1927. The stages for the 10,000 cfs flow fluctuated slightly until the 2011 event dropped the stage about 2 feet. The stages at Schmidt gage are affected by high Lake Oahe pool elevations. Current stages at the various discharges are lower than they were in the mid-1970s.

Table 5 Oahe Aggradation Reach elevation changes at 20,000 cfs

Gage	River Mile	Original	1985	2011	Total change
Bismarck (1927)	1314.5	1623.9	1624.3	1623.3	-0.6
Schmidt (1974)	1298.0	1611.2	1613.95	1616.2	+5

Fort Randall Dam to Lewis and Clark Lake

Geographic Description

Fort Randall Dam is located on the Missouri River at RM 880. The reservoir, Lake Francis Case, extends to the Big Bend Dam tailwater. Closure was made in July 1952. The Niobrara River is a major tributary located at RM 843.8.

Degradation Reach

The Fort Randall tailwater gage has decreased between 7 and 8 feet since 1952, most of which occurred by 1985. The 2011 event had little effect at this location. At the Greenwood gage the stages had decreased about one foot in 27 years (1960-1987). High flows in 2011 lowered the stages 1 to 1.5 feet. Some rebounding has occurred in 2012 and 2013.

Table 6 Fort Randall Degradation Reach elevation changes at 30,000 cfs

Gage	River Mile	Original	1984	2011	Total change
Fort Randall Tailwater (1952)	880.0	1239.8	1233.58	1232.7	-7.1
Greenwood (1960)	862.9	1228.8	1228.05	1225.9	-2.9

Aggradation Reach

The Verdel and Niobrara gages show the same pattern on the stage trend plots. Both show increasing trends from the mid 1970s until the high flows in 1995 when the stages decreased. By 1999 the stages were increasing again through 2008. Stages at both gages decreased between 3 and 4 feet in 2011. The stage at the Verdel gage was close to 3 feet higher for a 40,000 cfs flow on the increasing flow to peak curve than on the post flood curve and about 1 foot high at the Niobrara gage.

Table 7 Gavins Point Aggradation Reach elevation changes at 30,000 cfs

Gage	River Mile	Original	1985	2011	Total change
Verdel (1968)	846.5	1217.95	1220.2	1220	+2.05
Niobrara (1956)	842.9	1212.4	1218.3	1218.9	+6.5

Gavins Point Dam to Ponca, NE

Geographic Description

Gavins Point Dam is located at RM 811.1 on the Missouri River, 4 miles west of Yankton, SD and is the most downstream dam on the river. Therefore, there is no aggradation reach due to a reservoir is located downstream of this degradation reach. Closure was made July 1955.

Degradation Reach

The Gavins Point degradation reach extends from Gavins Point Dam downstream 58 miles to RM 753.18. The major tributaries in this reach include the James River at RM 797.5 and the Vermillion River at RM 772.0. The degradation trend is not limited to this reach and extends downstream to near Omaha, NE (approximately another 135 river miles).

Gavins Point tailwater gage over its period of record (1955 to 2013) shows a stage decrease of 13 feet for a flow of 20,000 cfs, most of which occurred by 1980. A decrease of about 1 foot occurred due to the 2011 flood event. Stages at the Yankton gage have decreased in a similar pattern to the tailwater gage.

The two most downstream gages in this reach (Maskell and Ponca) showed very little change in stages through the 1980's and early 1990's. Higher flows in 2010 and the record high flows of 2011 dropped stages between 2 and 4 feet. Since 2011, stages at the Maskell gage appear to be leveling off. Stages at Ponca have rebounded about 1 to 1.5 feet from the 2011 degradation level at the 20,000 cfs and above.

Table 8 Gavins Point Degradation Reach elevation changes at 30,000 cfs

Gage	River Mile	1955	1985	2011	Total change
Gavins Point Tailwater	811.0	1169.1	1159.8	1156.5	-12.6
Yankton	805.8	1163.4	1156.4	1153.8	-9.6
Maskell	775.4	1129.5	1124.8	1120.0	-9.5
Ponca	751.0	1096.5	1095.8	1089.0	-7.5

Missouri River Navigation Reach – Sioux City to Rulo, NE

Geographic Description

The Kensler Bend and the Bank Stabilization and Navigation Program (BSNP) Projects from Ponca (RM 753) to Rulo (RM 498), along with the construction of upstream dams, have drastically changed the characteristic of the Missouri River in this reach. Prior to construction, the river was a wide, sandy, sinuous channel containing numerous islands and sandbars and acting like any natural river system, by aggrading, degrading, or eroding its banks at any location dependent on the year. Today this reach is

narrower in cross-section, shorter in distance, with increased velocity, and is contained in rock-protected banks with constructed levees in many locations on the floodplain. A major influence in this reach is the Platte River at RM 594.

Generally, the stage (especially at the lower flows) has decreased in elevation to varying degrees upstream of Omaha. Downstream of the Platte River the stages have shown little change at the lower flows and an aggrading trend at the higher flows.

Navigation Reach

Overall, the stage at both Sioux City and Decatur shows a degradational trend. However, stages at both gages appeared to be leveling in the 1980s through the early 1990's. High flows in the mid 1990's caused a lowering of stages of about 4 feet at Sioux City and about 1 foot at Decatur. With the higher flow in 2010 and record high flows in 2011, both gages showed a decrease in stage elevations. The Sioux City gage, which decreased about 4 feet during the 2011 event, had rebounded about 1 to 2 feet depending on flows through 2013, while stages at the Decatur gage, which only decreased about 1 to 1.5 feet, also show some rebounding of stages. The Blair gage, which did not include any analysis of pre-2011 event stages, shows a slight increase in stages in 2012 and 2013.

Omaha's stage showed some degradation from 1930's through the early 1950's at all flows with a large decrease from the 1952 flood. A period of rebound and perhaps slight aggradation occurred through the mid-1970's. Since then, the stage at 40,000 cfs has shown very little overall change. Lower flows show a slight decreasing trend and higher flows a slight increasing trend. From 2010 to 2012 there had been between 0.5 to 3 feet of degradation at the various flows. All flows showed some rebounding in 2013 from 2011.

Nebraska City stages for flows below 70,000 cfs have been within the same range since 1990. Historic stages showed a mild decrease from years 1930 to 1950 followed by a period of mild increase. Stages for floodplain events above 100,000 cfs do indicate a slight rising trend since 1980. Nebraska City stages, as well as Plattsmouth and Brownille, show very little change since 2011.

At the Rulo gage, stages have fluctuated within about a one foot band for flows below 40,000 cfs since 1960. A slight aggradational trend is visible since the mid 1990's at higher flows. Since 2011, the stages have lowered between 0.5 and 1.5 feet at and below 40,000 cfs. The stage at a 70,000 cfs flow at Rulo increased about 0.5 feet between 2012 and 2013.

Table 9 Missouri River Sioux City to Rulo

Gage	River Mile	Original	1984	2011	Total change
Sioux City (1930)	732.2	1084.5	1077.4	1070.3	-14.2
Decatur (1957)	691.0	1040.3	1033.1	1030.7	-9.6
Omaha (1930)	615.9	967.7	966.9	965.6	-2.1
Nebraska City (1930)	562.6	913.7	914.9	915.5	+1.8
Rulo (1950)	498.0	845.7	847.0	846.5	+0.8

Water Surface Profile Evaluation Post 2011 Flood

Four water surface profiles are presented in this report within various reaches. Both the Garrison Dam to Lake Oahe and Fort Randall Dam to Springfield water surface profiles end in a reservoir. Most of the degradation in these reaches occurs in the region near the dam and the amount of degradation decreases as the distance from the dam increases. Within the reach below Garrison, the Oahe pool limits the degradation reach to between 70 and 90 river miles from the dam. In the river reach below Fort Randall the degradation limit is much shorter, primarily due to the location of the Niobrara River, and the degradation extent is only 35 to 40 miles downstream. Of course, the boundary between degradation and aggradation can move upstream or downstream due to pool levels, hydrologic cycles, and other factors.

The river stretch from Gavins Point Dam to Sioux City is interesting with two major processes at work. At the upstream end degradation is caused by the dam trapping all upstream sediment and releasing clear water into the river. In contrast to the other mainstem dam open river reaches, the river below Gavins Point Dam does not end at a reservoir. Near the downstream end of the reach, the construction of navigation channel structures to provide sufficient channel depth for navigation provide a strong influence.

Within the navigation channel reach from Sioux City to Rulo, the Platte River has a major impact on geomorphology. The change in water surface between different time periods is greatest at Sioux City and decreases as the profile approaches the Platte River. Downstream of the Platte River very little change is detected at the 40,000 cfs flow.

Stage Trend Summary

The 2011 flood event presented a challenge when evaluating trends. It was observed that the stages at many locations were different for the rising side of the event (increasing to peak flow) versus the declining side of the event (decreasing from peak flow). The differences in stage range from as little as a few tenths of a foot at some locations to about 6 feet at Ponca for a 40,000 cfs flow. At the degradation locations, the rising side event stages are higher while at aggradation locations the reverse is true. Compared to the degradation observed in 2011, the 2013 stages show varying amounts of rebound at many sites.

References

USACE, (2014a). 2013 Missouri River Mainstem Dams Tailwater Rating Curves and Trends, Omaha District Corps of Engineers, Jan 2014.

USACE, (2014b). Garrison Dam – Lake Sakakawea Headwaters Aggradation Evaluation of the Missouri River and Tributaries, Omaha District Corps of Engineers, January 2014.

USACE, (2013a). MRB Sediment Memorandum 28, Missouri River Fort Peck Project, Downstream Channel and Sediment Trends Study, Updated, Omaha District Corps of Engineers, April 2013.

Galloway, J.M., Rus, D.L., and Alexander, J.S., (2013b). Characteristics of sediment transport at selected sites along the Missouri River during the high-flow conditions of 2011: U.S. Geological Survey Scientific Investigations Report 2013–5006, 31 p.

USACE, (2012). Missouri River Stage Trends, Technical Report, Missouri River Basin Water Management Division, Omaha NE, August 2012.

Grigg, McCarthy, Lawrence, Ockerman, (2012). Review of the Regulation of the Missouri River Mainstem Reservoir System During the Flood of 2011, Independent Technical Review Panel, Missouri River Basin Water Management Division, Omaha, NE.

USACE, (2011). Missouri River Bank Stabilization and Navigation Project – Sioux City, IA to the Mouth, O&M Manual, Omaha District Corps of Engineers, November 2011.

USACE, (2006a). Missouri River Mainstem Reservoir System, Master Water Control Manual, Missouri River Basin. Northwestern Division, Reservoir Control Center, Omaha, NE.

USACE, (2006b). Analysis Outline, Revising Construction Reference Plane, Missouri River, Mil 811 to 498, Omaha District Corps of Engineers, Aug 2006.

USACE, (1994). Aggradation, Degradation, and Water Quality Conditions Missouri River Mainstem Reservoir System, Omaha District Corps of Engineers, January 1994.

USACE, (1990). Lake Sakakawea Headwaters Aggradation Study, 1962 – 1989, Omaha District Corps of Engineers, September 1990.

USACE, (1984). MRD Sediment Series #34, Aggradation and Degradation of the Missouri River Main Stem Dams, Omaha District Corps of Engineers, May 1984.

RAPID, QUANTITATIVE ANALYSIS OF THE COST EFFECTIVENESS OF STREAMBANK PROTECTION MEASURES USING THE BANK-STABILITY AND TOE EROSION MODEL (BSTEM)

Natasha Bankhead and Andrew Simon
Cardno Inc, P.O. Box 1236, Oxford, MS 38655; natasha.bankhead@cardno.com 662-380-1961; andrew.simon@cardno.com 662-832-1347

Abstract. Failure to undertake quantitative analysis of bank-protection schemes typically increases the risk and uncertainty in design and often results in greater cost due to either "over design" or by having designs or structures fail. The Bank Stability and Toe Erosion Model (BSTEM) is a fully deterministic simulation tool that has been used successfully across a wide spectrum of environments to predict streambank stability and to test the effectiveness of a broad range of mitigation schemes. The Dynamic version of the model using time-series flow data has been used in studies by Cardno, in the US, Australia and New Zealand to assist in selection of appropriate mitigation techniques and to compare their cost-effectiveness. Mitigation techniques are aimed at either reducing the driving forces acting on the bank and/or increasing the forces resisting hydraulic erosion and bank collapse. Resisting forces such as critical shear stress, effective cohesion and friction angle are measured *in situ*.

For a recent flood-recovery study conducted for the Burnett-Mary Regional Group (BMRG), Australia, simulations of different mitigation strategies included placing riprap at the bank toe, bank grading, re-vegetation, and construction of rock weirs or engineered log jams to deflect flows. Similar work in Auckland, New Zealand also included reduction of upstream channel gradient as a means of reducing hydraulic stresses. The effectiveness of a given mitigation strategy is based on comparison of predicted erosion volumes and lateral retreat with the no action alternative for an identical flow series. Where simulations with riprap are involved, traditional methods are used to calculate appropriate rock diameters using normal-depth calculations for hydraulic-parameter input. The cost of each mitigation scenario was based on local costs for rock or wood purchase, delivery and placement, heavy equipment, and the height and length of treated banks. The cost effectiveness of each treatment was then calculated by using: 1) total cost of the project, 2) the cost per meter of bank treated, 3) the cost per unit volume of streambank erosion prevented and 3) the cost per meter of streambank retreat prevented. As an extreme example, at one of the Burnett River sites, BSTEM predicted that protection of the bank toe and most of the bank face using rock would prevent bank erosion and retreat, but the unit cost would be about \$2,600/m of bank retreat or \$8,900/m^3 of soil-erosion prevented. Modeling of further mitigation strategies showed that, for example, that grading the bank to a 2:1 slope and planting riparian vegetation would prevent 97% of the erosion predicted under existing conditions, but would only cost \$150/m of bank retreat, and \$530/m^3 of soil-erosion prevented.

These data, in addition to typical BSTEM outputs such as erosion volumes and bank retreat distances, provides quantitative information about the performance of proposed streambank stabilization measures. In the case of BMRG, final decision making depends not only on the total cost of each project, but also the volume of fine sediment that can be prevented from entering the river system, and ultimately reaching the Great Barrier Reef.

INTRODUCTION

Failure to undertake quantitative analysis of bank-protection schemes typically increases the risk and uncertainty in design and often results in greater cost due to either "over design" or by having designs fail. The Bank Stability and Toe Erosion Model (BSTEM) is a fully deterministic simulation tool that has been used successfully across a wide spectrum of environments to predict streambank stability and to test the effectiveness of a broad range of mitigation schemes. The Dynamic version of the model with time-series flow data has been used in studies by Cardno Inc in the US, Australia and New Zealand, to assist in selection of appropriate mitigation techniques and to compare their cost-effectiveness. Mitigation techniques are aimed at either reducing the driving forces acting on the bank and/or increasing the forces resisting hydraulic erosion and bank collapse. Resisting forces such as critical shear stress, effective cohesion and friction angle are measured *in situ*. For a recent flood-recovery study on the Burnett River conducted for the Burnett-Mary Regional Group (BMRG), Australia, simulations of different mitigation strategies included placing riprap at the bank toe, bank grading, re-vegetation, and construction of rock weirs or engineered log jams to deflect flows.

The Burnett River is one of the Reef Catchments flowing through the city of Bundaberg in its downstream reaches before exiting to the Coral Sea. The Burnett River experienced severe flooding in early 2011 and 2013, with the latter flood breaking all historical records. As a result of these floods, damage to assets, infrastructure and the loss of agricultural land from bank erosion was considerable. In an effort to develop a strategy for prioritizing and determining resilient and cost-effective protection measures, it is essential to have an understanding of both site-specific and system-wide stability conditions. For site- and reach-specific solutions, this is accomplished by quantifying the driving (flow and gravitational) forces and resisting (shear strength) forces operating on the channel banks, and testing how alternative stabilization measures would perform over a range of flows. System-wide analysis then provides the spatial and temporal context of channel instability to determine the suitability of conducting various types of channel works (i.e. energy dissipation, bank stabilization, etc.) to protect assets and to aid in prioritization of those works.

METHODOLOGY

The geographic scope of this study extended from the mouth of the Burnett River east of Bundaberg, upstream to Eidsvold. In addition, the lower end of the Kolan River was included. These two reaches represent priority areas for investigation for the Burnett-Mary Regional Group (BMRG) to aid in their flood recovery efforts. BMRG selected eight sites along their study reach for a detailed investigation of current bank erosion rates, with which to develop potential mitigation measures that could be used to protect local assets. The investigation consisted of detailed field tests to quantify the geotechnical and hydraulic resistance of the bank and bank-toe materials were performed at each of the sites. Surveys of the banks were also carried out at each site to provide bank heights, angles, and stratigraphic layering for the tested bank. The data collected in the field were used to populate a Streambank Stability and Toe Erosion Model (BSTEM-Dynamic 2.0; Simon et al., 2000). These model results were used to calculate erosion rates for existing and mitigated conditions, which were then used in a cost-effectiveness analysis.

Simulations with BSTEM Dynamic were conducted for two non-mitigated cases to reduce uncertainty in model predictions and to provide a basis for simulating future erosion without mitigation (a no action alternative). The purpose of the first set of simulations was to calibrate BSTEM between two known surveys. Because detailed surveys for two points in time were not available, top-bank edges from GIS-based air photos were used to determine the amount of bank retreat that occurred between LiDAR data from 2009 and 2010 with the post-flood imagery shot in 2013. Mean-daily discharges from a nearby gauging station, adjusted for drainage area were used to establish the flow series encompassing the period bounded by the imagery. For the purposes of these simulations, the flow period used was 1 January 2009 to 31 July 2013. The amount of lateral retreat obtained from the imagery was then compared to the top-bank retreat predicted by BSTEM over the period. After successful calibration by iteration, the calibrated values were then applied to model potential future bank erosion under existing and mitigated conditions. For these model runs, BMRG and Cardno agreed to use a decade-long period to provide a meaningful comparison between erosion rates during wet and dry cycles. The period selected was slightly greater than ten years and spanned 1 January 2003 to 31 July 2013.

Estimating Cost-Effectiveness of Mitigation Measures Reducing land loss (bank retreat) and sediment loadings from bank erosion can be accomplished in a number of different ways depending on the objective of the program and the resources available. Quantifying reductions from application of different mitigation strategies can then be designed accordingly. For example, to protect agricultural assets it is perhaps the reduction in bank retreat that is of paramount concern. In contrast, a better metric for protection of storage area above dams, and sediment delivery to the estuary and the Coral Sea might be reduction in volume or mass of sediment. Thus, modeling results were expressed not only in absolute values (m^3/m and m) but as a percent reduction in those parameters as compared to the ten-year, "no action" simulations. Cost effectiveness of each of the modeled mitigation measures was accounted for at each site based on (1) estimates of unit costs for materials and labor, and (2) the specific requirements (length, height and area) for implementation of specific design elements at each site.

Bank Erosion Mitigation Scenarios Modeled Numerous combinations of bank treatments and protection schemes can be simulated within the BSTEM framework and all are related to how each scheme modifies the driving and/or resisting forces responsible for bank erosion. For example, placement of rock or large wood at the bank toe provides an increase in the resistance to hydraulic forces acting on the bank toe but does not address the hydraulic forces impinging on the toe or the shear strength of the overlying bank mass. Vegetative plantings, however, provide for not only an increase in the resistance to hydraulic forces but also additional root reinforcement to resist mass failures. Further, bank grading directly reduces the downslope, driving gravitational forces but does not alter resistance to hydraulic forces. Finally, bendway weirs or engineered log jams (ELJs) designed to keep the main flow thread away from the bank and re-direct it towards the center of the channel work to reduce the applied hydraulic forces acting on the bank toe and surface. These features do not modify either the gravitational, downslope forces or the shear strength of the *in-situ* bank material. In general, alternative strategies that were simulated include various combinations of rock facing (at the bank toe and along the bank surface), riparian planting, grading of banks, and the use of Bendway weirs/ELJs. Table 1 provides a list of the mitigation alternatives tested, and the input parameters modified in BSTEM to account for each alternative.

Table 1 Mitigation measures tested, and BSTEM input parameters modified to account for these measures.

Mitigation Measure	Modify critical shear stress of material	Modify soil shear strength to account for roots	Grade bank slope	Reduce applied shear stress acting on banks
Rock at toe, no grading	✓			
Rock at toe and up bank	✓			
Additional riparian planting	✓	✓		
Rock at toe with riparian planting above	✓	✓		
Rock at toe with riparian planting and bank grading	✓	✓	✓	
Bendway weirs/ ELJs				✓
Bendway weirs/ ELJs, with rock toe				✓
Bendway weirs/ ELJs, with riparian planting		✓		✓

Unit Costs and of Mitigation Alternatives Cost effectiveness can be defined as the cost of implementing a particular mitigation measure per unit of sediment or bank saved. The effectiveness of each of the simulated mitigation strategies is expressed herein, as a cost per unit volume of sediment-erosion reduction, and a cost per m of retreat reduced. To determine cost effectiveness, we must first be able to estimate the total cost of implementing a particular strategy. This is somewhat of a challenge without undertaking a detailed design with associated costs at each site. Reasonable estimates, however, may be obtained by applying the unit costs of materials and labor over the length, height and area covered by a particular alternative. Estimates of the required length of mitigation were estimated from inspection of the 2013 aerial photography for each main stem site. Consideration was given to the morphology of both the cross section and the reach. For example, if the site was located on an outside bend, it is prudent to protect not only the specific cross section but also the entrance and exit of the bend to prevent shifting the instability to another part of the bend.

Protection with Rock Rock is used in bank-protection schemes to resist hydraulic forces, typically at the toe of the bank to limit steepening and undercutting. The use of rock is generally combined with the placement of a filter fabric at the interface between the soil and the rock to limit winnowing of the finer materials. Rock is also used for the construction of weirs (flow deflectors) that extend into the flow field from the bank. In the case of a rock toe for example, one can estimate the purchase, delivery and placement of rock per tonne of rock and then calculate the amount of rock required for a given height and length of protection. BMRG provided Cardno with an estimate of $81.50/t for placed rock (I. Botha, written comm., 2013). The number of tonnes of rock required per meter of channel length varies according to whether it is placed against a vertical or sloping bank face (as in the case of toe protection) or on the channel bed (as in the case with a bendway weir). This is shown in Figure 1. By then applying the unit cost of $81.50/t we develop a relation between the unit cost (per m of channel or weir) and the height of the rock protection (Figure 2).

Costs for toe protection with rock, often referred to as longitudinal stone-toe protection (LSTP) were based on the unit costs of rock provided by BMRG ($81.50/t) and the red-colored equation

shown in Figure 2, where cost is a function of the height of the bank to be protected. Estimated costs for each site, therefore, are based on the projected height of LSTP specific to the conditions and geometry of the site. For estimating costs for bendway (rock) weirs which are typically placed as a series of equally-spaced structures extending slightly upstream into the flow, guidelines developed the U.S. Federal Highway Administration (based on research by the U.S. Army Corps of Engineers) are used. The amount of rock is determined by the height, length, spacing and number of structures, which are in turn a function of the width of the channel, the length of the reach to be protected and the depth of mean, annual high water. As a more conservative approach, and due to the apparent increase in the magnitude of peak-flow events in recent years in the study area, in this project the mean of the 11 highest daily flows (for each water year simulated) was used. Overall, as this is not an exercise in design but a means to estimate quantities of rock for approximate costing, the approach has been somewhat simplified. The following steps were used:

1. Determine the depth (d) of mean, annual high water;
2. Determine weir height (h) as 0.3d to 0.5d;
3. Calculate weir length (L) as ¼ of the channel width;
4. Calculate weir spacing (S) as 4 to 5 L;
5. Calculate the number of weirs using the length of the reach divided by S;
6. Calculate total cost by: determining the unit cost (per meter of weir length) for rock placement (of a given height) by the blue-colored equation in Figure 2 ($cost = 259.93 h 1.9528), then, multiplying the result by weir length (L) and by the number of weirs.

Protection with Vegetation Vegetation improves both the hydraulic and geotechnical resistance of banks as well as providing ecological benefits. Planting of the bank slope is generally combined with some kind of bank-toe protection with either rock or large wood. The cost of implementing a planting scheme is a combination of the cost of the plants and labor required for site preparation and planting. BMRG provided a unit cost of $2.50/plant (I. Botha, written comm., 2013). Because of some uncertainty in the number of plants required in different settings, we have instead estimated a unit cost of $5/$m^2$ based on previous experience.

Protection by Grading the Banks. Grading a bank slope reduces the gravitational, driving forces thereby increasing bank stability and is often combined with riparian plantings and bank-toe protection. This alternative requires the use of heavy equipment to perform cut and fill operations on the bank slope to batter it to an angle flatter then the friction angle of the material. The cost for mobilization and operation of the equipment can be variable due to location and accessibility, the height of the bank, access to the streambed, the amount of material to be moved per m of channel length, and disposal of the spoil. As such, the time required to perform the work can vary from several days to several months. We assume that four pieces of equipment would be required each day. They include a loader or bulldozer, an excavator or track hoe and two dump trucks. We further estimate an average, unit cost of $1,500 per day for each piece of equipment ($6,000/day total). We then estimate the number of days required to perform the work using an average of 2 days per 100 m of bank length. Given the estimated length of required mitigation at the sites, the time required for grading ranged from about 5 to 24 days for the eight sites investigated in this study.

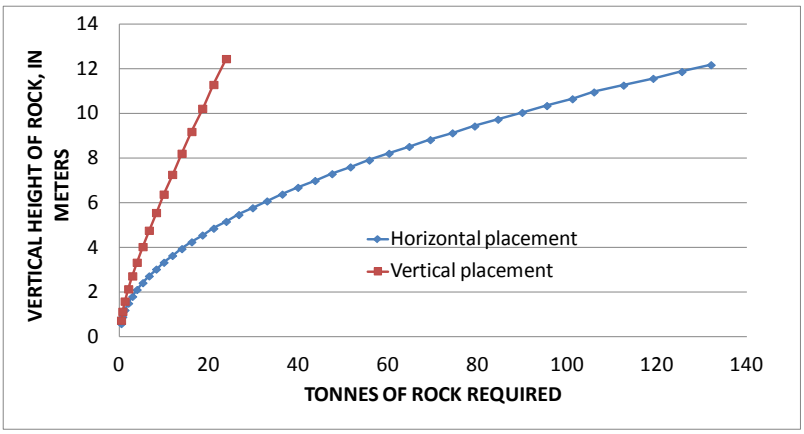

Figure 1 Tonnes of rock required relative to the height of the protected area for horizontal and vertical placement.

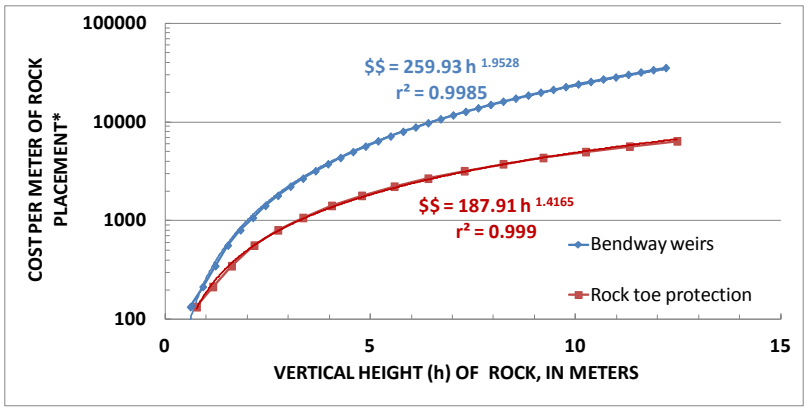

Figure 2 Estimate of the unit cost of rock placement (per meter of channel or weir length) as a function of the height of the protection. This does not include design costs and development of construction drawings.

Protection by Large-Wood Structures The use of large wood in bank-stabilization schemes is becoming more popular in many parts of the world, including Australia, because of the combined benefits to geomorphic and ecologic processes. The cost of wood structures such as engineered log jams (ELJs) can be quite variable and are often not reported in detail. Costs for construction of ELJs include the cost of the trees, delivery to the site and construction. Estimates of unit costs are done either per structure or per meter of bank protected. Estimates per structure are also quite variable because of differences in the number and sizes of logs required for different types of ELJs. For example, a recent ELJ bank-stabilization project on the O'Connell River, QLD, Australia, used about 90 logs in each of three log-jam structures at a cost of $55,000 (about $18,000 per structure or about $275 per meter). Other wood structures may contain as few as three or four logs depending on the objective of the structure (fish habitat, bank stabilization, flow deflection etc.). For the type of bank protection envisioned for the Burnett River, we assumed that each structure would require from 20 to 80 logs.

Based on an extensive review of available cost information and review by Cardno design engineers, we calculated two average-unit costs for ELJ construction: $194/m of channel length protected and $ 19,050 per structure. Because of the great variability in ELJ project costs we also provide the 75th percentile of unit costs as: $280/m of channel length and $29,600 per structure. Most of this information was obtained from North American sources but costs from two Australian projects (in Queensland and New South Wales) were also included. It should be stressed that the unit-cost estimates provided here and applied in the following sections of this report are just that, estimates. Additional uncertainty in cost estimates derived without full-scale design considerations may be related to:

- Difficult site conditions that may make placement more costly;
- Access to the streambed by heavy machinery;
- Vertical operational distance heavy machinery can operate from the bank top;
- Construction in wet (submerged) conditions;
- Differences in the cost of placing rock along a surface versus "keying" rock back into the bank at/or below bed level;
- Varying unit costs for rock of different sizes.

The unit costs described above are used to estimate the total cost of a modeled mitigation alternative, which in most cases involves combinations of treatments and their associated costs. To obtain actual costs for implementation at a given site, the costs for detailed design drawings, computation of the types and amount of materials, and access by heavy machinery would need to be undertaken. Still, with the unit-cost estimates developed here, reasonable estimates of total costs and cost effectiveness for each site can be provided.

RESULTS

Example from Shalom College Site (Figure 3). Results from the Shalom College site, which had the highest unit-erosion value, and largest bank retreat distance in the calibration runs, will be discussed here to provide an example of the way in which the BSTEM results were interpreted, and cost effectiveness analysis performed. The BSTEM results showed that without any remedial action at this site, an additional 52 m of retreat would occur over the next ten years, with all of that occurring during the wet period and associated large peak-flow events. About 98% of the total unit-volume eroded (about 780 m^3) also occurred during the wet period, indicating that only 2% of the hydraulic erosion occurred during the drier period.

The relatively high erosion rates seen at this site are the result of a high, bare bank composed of relatively weak materials that receives directed, accelerated flows due to a vegetated island in the reach. The result is that both moderate and high flows are deflected towards the bank toe, resulting in pervasive undercutting and representing an important process that would need to be addressed by mitigation. This interpretation is further supported by the results of the rock-toe and full-vegetation scenarios where, compared to the no action alternative of 783 m^3/m of erosion, 51.8 m^3/m and 353 m^3/m of erosion was predicted over the same period, respectively. In terms of effectiveness in reducing the amount of sediment delivered, the rock toe (keyed into the bank) reduces erosion 93 % while established vegetation would reduce erosion at the site by 55 %. The other metric for determining effectiveness of these two (and other) alternatives is the potential

reduction in lateral retreat. Although it is convenient to compare result in terms of percent reduction, it seems more meaningful in this case to compare absolute values. About 24 m of additional retreat is predicted for the full-bank vegetation case compared to about 4 m for the case with the rock toe. Two additional points about the comparison of these two alternatives need to be considered. First is the assumption that the planted vegetation will establish and will not die due to lack of water or being ripped from the bank by flood water. This point emphasizes the need for maintenance and protection of any vegetative plantings, particularly in their first year. The second point is the difference in the cost of these alternatives, with the installation of a rock toe that is keyed into the bank being considerably more expensive.

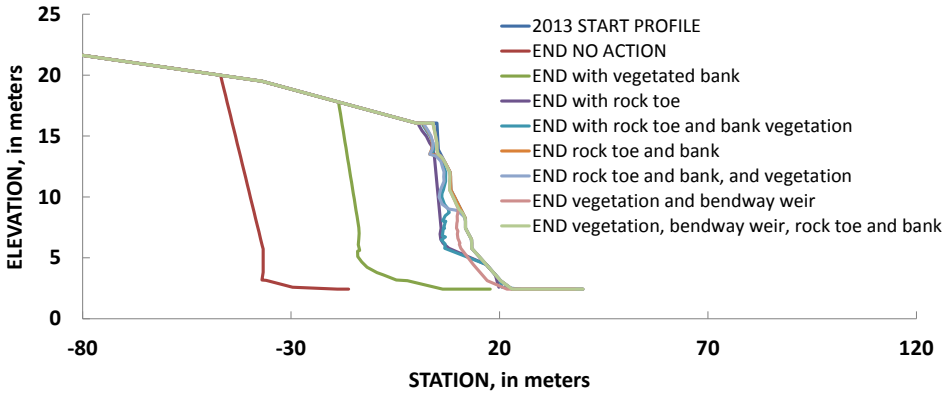

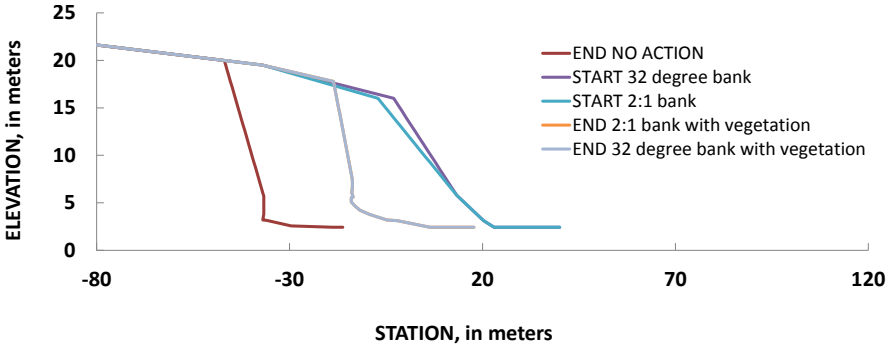

Figure 3 Top: photo of Shalom College site. Middle and bottom: Simulated, future bank retreat for the range of mitigation alternatives at the Shalom College site for the 10.6-year flow period used (2003-2013).

Predicted bank retreat and resulting geometries for a range of mitigation alternatives at this site at the end of the simulation period are displayed in Figure 3. Analysis of the BSTEM results showed that geotechnical failures were responsible for the bulk of the material delivered to the river, but reductions in hydraulic bank erosion and steepening through toe protection, resulted in significant reductions in the quantity of material delivered by mass failures. This provides evidence of the type of actions (ie. some kind of toe protection) that would be appropriate at this site. Indeed, the model runs including rock placement on the bank face and/or toe, resulted in considerably greater reductions in both total eroded volumes and bank retreat than those mitigation runs that involved only vegetation and/or grading. At this site, mitigation scenarios including bendway-weir structures, designed to deflect flow and reduce shear stresses applied to the banks, were also considerably more effective than vegetative plantings and/or grading. The height of rock required to successfully prevent bank toe erosion and subsequent bank oversteepening depends on the shear stresses acting on different parts of the bank, which are controlled by channel slope, flow depth and channel roughness. For example, where vegetated islands force flow into a narrower section of the channel, flow depths will be greater for a given discharge, and the height of the bank that requires rock reinforcement may, therefore, also be greater.

Cost Effectiveness of Mitigation Scenarios at the Shalom College Site (BMRG-03) As with any site, selecting a preferred alternative for the Shalom College site must be based on consideration of cost relative to an acceptable level of protection (magnitude of future land loss and likelihood of success). A summary of the estimated unit and total costs for the various mitigation alternatives at this site are shown in Table 2. The unit costs for mitigation scenarios involving vegetation and ELJs are considerably less ($66 to $260 per meter of bank length) than those requiring rock ($1,360 to $5,680 per meter of bank), whether it be for longitudinal stone toe protection, or for bendway weirs. Those mitigation runs that involve just vegetation and grading of the bank return relatively low costs per unit of sediment load or bank-top retreat saved, but they are also among the least effective measures in terms of total erosion reduction (Figure 4). Although the mitigation scenario that involves protecting the bank face and bank toe with rock (up to 11.1 m high) resulted in the highest percent reduction in terms of sediment volume at this site, the cost for this scenario is the highest estimated (about $3,00,000). This scenario is likely to be cost prohibitive and was included only to represent an end-member case. Considerably lower cost estimates were calculated for other mitigation st**r**ategies that reduced almost as much erosion and bank retreat (Figure 4). For example, if we compare the percent reduction in erosion and bank retreat for each mitigation in Figure 4 (red and blue bars) with the total cost for that mitigation (green bars), we can see that installation of ELJs with additional vegetative plantings on the bank face and toe regions, provides a much more cost-effective alternative ($138,000), while still providing a similar result as the rocked bank face and bank-toe scenario. It should be noted that although the alternative combining ELJs with vegetation is much more cost effective, it also has a higher risk associated with it than the hard engineering solution of protecting parts of the bank with rock. This is because it will take time for vegetation to establish, and the structure will thus be prone to large floods until any new vegetation can root firmly enough to anchor itself in place. There may, therefore, be some additional costs associated with management and protection of vegetation as it becomes established.

Table 2 Cost estimates for BMRG-03 for different mitigation scenarios, provided as total cost ($), costs by unit volume of sediment reduction ($/m^3), and per meter of bank retreat ($/m) prevented.

Scenario	**Protection**		**Unit Cost**	**Cost effectiveness**		
				Unit Cost		**Total Cost**
	Height	**Length**		**By volume**	**By retreat**	
	(m)	**(m)**	**($/m)**	**($/m^3)**	**($/m)**	**($)**
No Action	-	-	$0	$0	$0	$0
With vegetation	13.2	530	$66	$81	$1,230	$35,000
Rock at toe	4.1	530	$1,360	$988	$15,200	$722,000
Rock toe with vegetation	4.1	530	$1,430	$1,020	$15,600	$757,000
Rock toe and bank face	11.1	530	$ 5,680	$3,890	$61,600	$3,012,000
Rock toe and lower bank with vegetation	6.6	530	$ 2,790	$1,930	$30,200	$1,480,000
2:1 grading with vegetation	13.2	530	$186	$198	$2,440	$98,600
32 degree bank with vegetation	13.2	530	$186	$209	$2,710	$98,600
Vegetation with bendway weirs	13.2	530	$1,560	$1,080	$2,700	$824,000
Vegetation with ELJs	13.2	530	260	$181	$30,300	$138,000
Vegetation with bendway weir and rock toe	13.2	530	$2,920	$1,990	$30,300	$1,550,000
Vegetation with ELJs and rock toe	4.1	530	$1,620	$1,110	$16,800	$860,000

CONCLUSIONS

The primary objective of this study was to provide a means of determining strategies for cost-effective protection of local assets in the context of flood recovery and system wide channel-stability concerns. Site-specific stability issues at eight locations were studied to better understand system-wide trends, and investigate cost effectiveness of potential mitigation measures at these priority sites. At-a-site investigations of unit-erosion rates (expressed in m^3/m of channel) were carried out using BSTEM, populated using geotechnical and hydraulic-erodibility data collected *in situ* at each of the sites. The BSTEM results for various mitigation scenarios at each site showed that at some of the sites, protection of the bank toe was the essential component in managing and reducing streambank erosion, and therefore, banktop retreat. In these cases, the most successful mitigation measures were protection of the entire toe using rock, with the addition of vegetation to the banks often further reducing bank erosion by protecting the upper bank from both hydraulic and geotechnical erosion. At some sites, however, the before and after geometries output from BSTEM indicated that even where the toe was protected, some erosion could occur above the protected zone. In these cases, mitigation strategies that focused on reducing shear stresses in the entire near-bank zone, rather than just protection of the toe, were found to be more successful in terms of erosion reduction and prevention of bank top retreat.

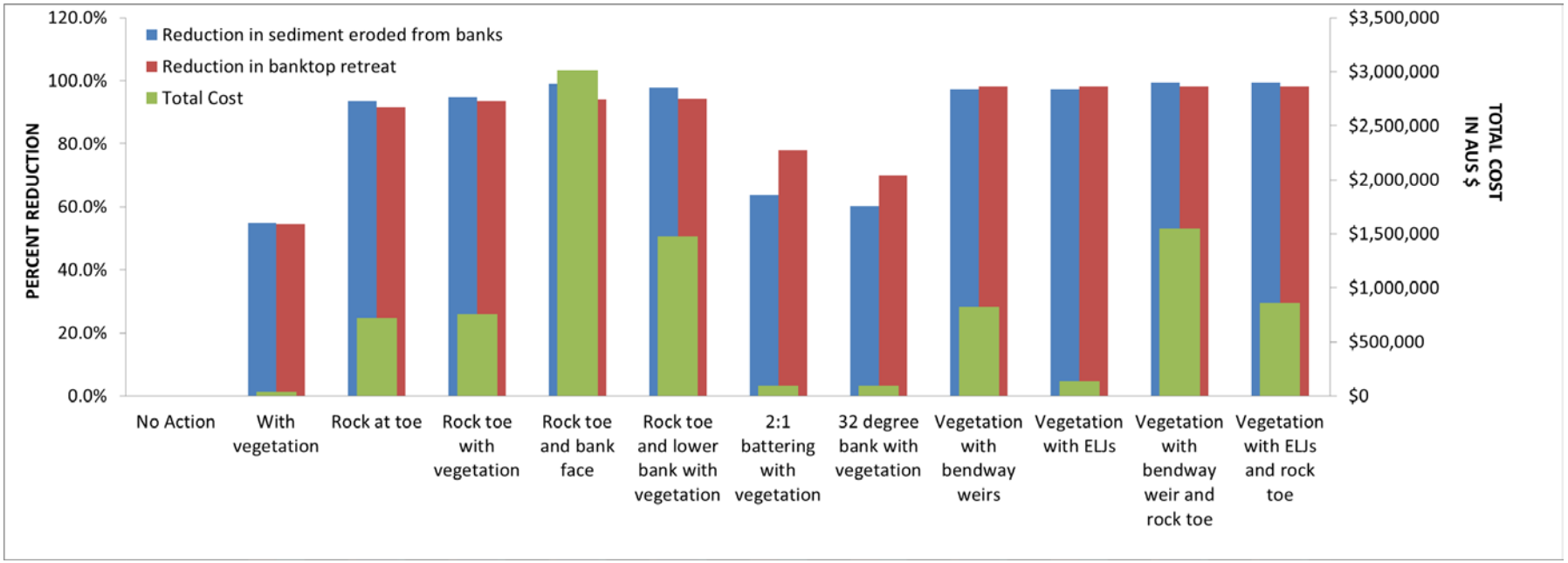

Figure 4 Plot showing percent reduction in sediment eroded at each site, and percent reduction in bank retreat, compared to the total cost for each mitigation scenario.

Cost estimates provided as part of this work served as an approximate guide for the mitigation scenarios presented. Overall, the scenarios involving rock in any form (rock toe or rock weirs) were the most expensive at any given site. The costs vary according to rock size, and height of bank protected, but were an order of magnitude higher than other measures at most sites, typically ranging from $1,000 to $3,000 per meter of bank. Planting of vegetation was the least expensive (approximately $5/m^2 of bank face or top) option. In general, mitigation runs including a rock component provided the greatest level of protection from bank erosion and sediment entering the channel, and those with vegetation alone, the least. It should also be noted, that the cost-effectiveness analysis showed that there are alternatives to the use of rock at some sites, with other combinations of mitigation strategies providing the same or only slightly less protection from future erosion. For example, the use of ELJs (with or without vegetation) often provided a good balance between bank protection and cost.

The results showed how the use of deterministic models, such as BSTEM can provide an effective way of quantifying the performance of proposed streambank stabilization measures. The balance between the cost-effectiveness of a given mitigation measure and the risk associated with the potential for ongoing erosion, and/or the failure of the implemented mitigation measure, must be considered on a site-by-site basis. In the case of BMRG, final decision making depends not only on the total cost of each project, but also the asset protection afforded, and the volume of fine sediment that can be prevented from entering the river system, and ultimately reaching the Great Barrier Reef.

REFERENCES

Brodie, J., McKergow, L.A., Prosser, I.P., Furnas, M., Hughes, A.O., and Hunter, H. 2003. Sources of Sediment and Nutrient Exports to the Great Barrier Reef World Heritage Area. Australian Centre for Freshwater Tropical Research Report Number 03/11, 192 p.

Simon, A., Curini, A., Darby, S.E., and Langendoen, E.J., 2000, Bank and near-bank processes in an incised channel. Geomorphology, 35: 193-217.

Simon, A., Pollen-Bankhead, N. and Thomas, R.E., 2011. Development and Application of a Deterministic Bank Stability and Toe Erosion Model for Stream Restoration. In: Simon, A., S.J. Bennett, J. Castro and C.R. Thorne (eds.), Stream Restoration in Dynamic Systems: Scientific Approaches, Analyses, and Tools. American Geophysical Union: Washington.

STREAMBANK EROSION: DEVELOPING RECESSION RATES BASED ON CONDITION CLASS AND FLOW STAGE CHARACTERISTICS

W. Barry Southerland, PhD, Fluvial Geomorphologist-Hydrologist, USDA-Natural Resources Conservation Service, West National Technology Support Center, 1201 NE Lloyd Blvd. Suite 1000, Portland, OR 97232, FAX: 503-273-2401; Lisa J. French, Project Coordinator, Cheney Lake Watershed, Inc., 18 E. 7th Avenue, South Hutchinson, Kansas 67505

ABSTRACT: In 2007 the Natural Resources Conservation Service National Water Quality and Quantity Technology Development Team began a collaborative six year streambank pin-based and bank profile recession rate study with Cheney Lake Watershed, Inc., Inc. The Cheney Lake Watershed is a designated Conservation Effects and Assessment Project (CEAP) Special Emphasis Watershed. The initial purpose was to determine the contribution of fine sediments from the 989 square mile watershed to the highly valued Cheney Lake Reservoir which provides water for the City of Wichita and to evaluate the downstream impacts of the current CRP, EQIP, WRP, and WHIP implementations. For the same time period, the USGS established suspended sediment load sampling (USGS depth integrated sampling procedures) at five gauge sites. Approximately one hundred erosion pins were strategically placed at ten streambank erosion sites to characterize five streambank erosion condition classes commonly represented within 782 square miles upstream from the USGS gauges. The five most probable erosion categories represent a significant presence or absence of characteristics such as roots, root mass, root depth relative to floodplain, bank angle, livestock impacts on streambanks, tension cracks, bank material, bankfull, bank height ratio, and other considerations to formulate BEHI (Bank Erodibility Hazard Index). The rate of lateral streambank recession was correlated to hydrologic runoff factors of flow duration above the inner-berm, assuming at least a bankfull event. This FISC paper is collaborative with, "The Dynamic Nature of Small Watersheds: Estimating the Inner Berm Geomorphic Channel Feature based on the Hydrologic Relationship of Channel Forming Events". In 2007 and 2008 the banks where comprehensively inventoried for condition, length of condition class, and bank height. Cheney Lake Watershed Inc. input and attributed over 186 miles of streambank conditions. The initial results show a significant pattern of recession rates relative to flow duration above inner berm flow. The findings will provide a reliable estimate of the portion of streambank suspended load contribution to the USGS sampler located on the North Fork of the Ninnescah Mainstem at the Whiteside Bridge. The data and analysis, along with the flow duration and intensity, will provide a considerably more robust result from the CEAP AnnAGNPS model because the streambank contributions to suspended sediment load will be proportionally accounted for as a reliable percentage of the total load. Just as significant is the utility of this information for ubiquitous, coarse, unconsolidated, high sand fraction soils, commonly found throughout the Midwestern U.S. Field staff in Midwest areas (Great Plains and Central Lowland physiographic provinces) with similar soil characteristics and predominantly thunderstorm-driven hydrology will have a field tool to reliably predict streambank erosion relative to their condition assessment and runoff conditions.

INTRODUCTION

There are many river models integrating sedimentology, hydrology, streambank conditions, soil stratigraphy and other physical input parameters to predict the streambank erosion associated with both average annual and high stage flow events (event-based). Streambank erosion rate by event-based flow stage is the more difficult proposition. It requires considerably more rigor in fieldwork and analysis to determine. It is often thought that more commonly used models are both validated and calibrated by a monitoring and assessment protocol. But the fact is, very few are both calibrated and validated by region or area to assure the erosion rates we receive are robust. Stakeholders, land operators, and planners ask the questions: How do I know the data you have gathered and the predictions you make are good or reasonable? What are the assumptions? Have you accounted for all of the physical and biological variables that affect streambank erosion in our watershed? These are good questions.

Paucity of field data is a major roadblock to river work. To approach any of these matters quantitatively one must have some data measured in the field. The value of river parameters can be estimated, but with no assurance of verity. Unfortunately, too many professionals approach such problems with the supposition that [the] computer can do all. In river work, computer modeling is an insidious procedure in which an air of surety hides questionable assumptions. A computer gives numerical answers, but the bases on which the computation rests are hidden (Leopold, 2001).

Leopold was not condemning models. His message was simple. Put field measured data into models based on real world morphometry and measures. Question the assumptions. Refine them when necessary and validate your model. Each time you consider re-calibration of a model or empirical-based tool, you must revalidate. This process will keep us out of the error margins which are often on order-of-magnitude away from real world data-based observations.

Exhibit A

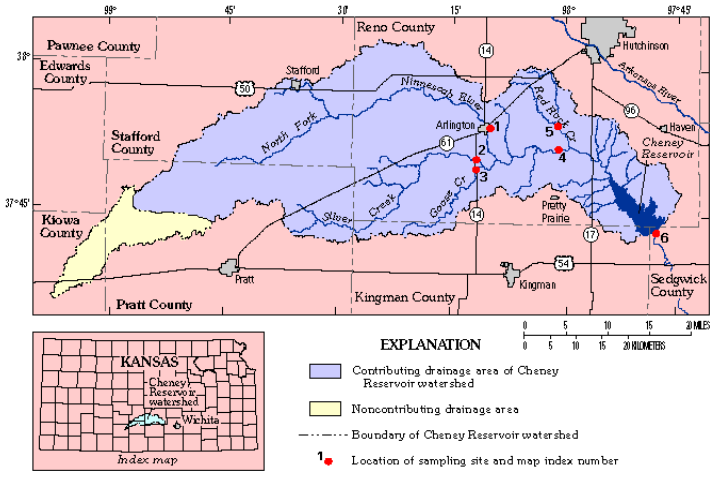

Figure 1. Location of Cheney Reservoir watershed in south-central Kansas and sampling sites used in this study.

The Cheney Lake Watershed is a designated Conservation Effects and Assessment Project (CEAP) Special Emphasis watershed (Exhibit A). This report provides an analysis of the

suspended load contribution from the banks of the contributing drainages within the 989 square miles of the Cheney Lake Watershed CEAP Project.

In 2007, an interdisciplinary team comprised of NRCS-Water Quality and Quantity Technology Development Team, Cheney Lake Watershed, Inc. with the Reno Conservation District, and the USGS completed an initial analysis report: Cheney Lake Watershed Streambank Erosion Analysis-CEAP Watershed (Southerland et al, 2007). Initial findings of streambank erosion contributions to suspended load were determined but it was based on a qualitative tool referred to as the Ventura Workshop Erosion and Sediment Yield Tool developed by Steffen, Lyle J., 1983. The estimated recession rate by condition class was developed in California. The recession rates were based on California studies over time and not calibrated nor validated for the Cheney Lake Watershed. This methodology was only used as an initial estimate of streambank erosion yield from the Cheney Lake Watershed. Three of four technical recommendations put forth in this report were adapted by the Cheney Lake Watershed, Inc. These findings led to the seven-year streambank erosion study resulting in both calibration and validation of streambank erosion rates by condition class.

The purpose of the special emphasis watershed study in the Cheney Lake Watershed is to evaluate the downstream impacts of conservation practices implemented through current USDA programs. The Annualized Agricultural Non-Pont Source Model (AnnAGNPS) will be calibrated and validated for a south central Kansas HUC eight watershed. Changes in offsite water quality will be described. Future watershed conservation practice implementations will also be evaluated to measure their offsite downstream impacts.

In order to appropriately calibrate the total loads in the AGNPS model it was essential to have a robust estimate of streambank erosion contributions to the suspended sediment load samplers. The streambank erosion study includes a surface runoff area of 782 square miles. Five USGS depth integrated sampling sites were established in 1996. Suspended load gauge data from several years were compiled to compute the average annual suspended load rate. This streambank and assessment field study will determine the annual rate and fraction of suspended load coming from streambanks contributed to the five United State Geological Survey (USGS) gauges.

The principle goal of this work was to provide measured data regarding the streambank erosion contributions of sediment for the AnnAGNPS model used in the CEAP project. A broader benefit of this work is the development of streambank recession rates for regions of the country that have similar hydrophysiographic and streambank conditions. The development of the Streambank Erodibility Visual Assessment Tool (SEVAT) calibrated to field measured bank is based on erosion pins and cross-sections by condition class. As a result of this assessment and analysis, these regions will have the opportunity to use real world recession rates on non-cohesive soils ubiquitous to the Midwestern United States.

METHODS AND ANALYSIS

In 2007 Cheney Lake Watershed, Inc., Reno County Conservation District and the USDA-NRCS-Water Quality and Quantity Technology Development Team (W2Q) became partners and

established 10 streambank erosion measurement sites with 30 annually measured bank profiles and 96 erosion pins. Bank erosion pin stations, concrete benchmarks with cross-sections, measured bank profiles, toe pins, bank erosion assessment worksheets, and photo references at ten sites were established. These ten sites varied in bank stability and erosion condition classes ranging from slight to severe (Photos 1 and 2).

Photos 1 and 2: Measuring Streambank Profile and Erosion Pins on Severe Erodibility Condition

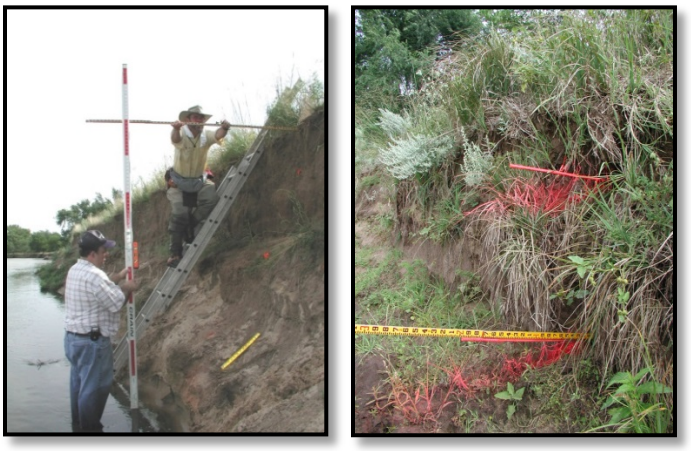

Concurrently, both the Bank Erodibility Hazard Index (BEHI) described in Dave Rosgen's Watershed Assessment of River Stability and Sediment Supply (WARSSS) (Rosgen, D.L. 2006) and a more simplified, "Streambank Erosion Visual Assessment Tool" (SEVAT) characterizing condition class, were implemented to provide a comparison between a tool well recognized and often implemented with the SEVAT scores. The objective is to develop SEVAT score sheets which is a combination of verbal description of erosion characteristics combined with extensive photo documentation at an erosion pin station site. The SEVAT tool will be a simpler tool for field offices to use on non-cohesive, coarse textured soil of the Midwest U.S. The SEVAT score sheet is still currently under development by the USDA-WNTSC and the Cheney Lake Watershed, Inc. and targeted for evaluation in 2015. SEVAT scores will be tied to erosion pin recession rates by condition class.

Within each major stream course, streambank conditions were delineated into five categories of streambank erosion rates: negligible (non-contributor), slight, moderate, high, or severe. Within all of the identified stream courses that were evaluated, the estimated height and length of eroded streambanks were assigned according to the height and length of eroded dimensions relative to the channel size and hydraulic geometry characteristics interpreted from ARCGIS. Areas rated negligible were culled from the contributing eroding banks. The five major stream courses are:

1. North Fork Ninnescah (Arlington) above USGS gauge #07144601
2. Silver Creek above USGS gauge #07144660
3. Goose Creek above USGS gauge #07144680
4. Ninnescah – Main-stem above USGS gauge #07144780
5. Red Rock Creek above USGS gauge #07144730

The data represent a combination of field morphometry, field reconnaissance, photo analysis, GIS measuring tools, wet and dry sieving of both bed and bank materials (Photo 3).

Photo 3: Wet and Dry Sieving at Multiple Locations

Bed and Streambank Particle Analysis

In the fall of 2007 and 2012, streambed and bank sieve analyses were completed in the North Fork of the Ninnescah, Photo 3. In 2007, sieve analyses were completed on two sites, one near the town of Arlington on the North Fork of the Ninnescah and one at Site NFN1 on the North Fork of the Ninnescah. The sieve analysis at Site NFN1 is located just upstream of the USGS Depth Integrated Sampling site at the Whiteside Bridge. The bed and bank wet sieve analyses were completed twice at Site NFN1 to compare, contrast and analyze particle size distribution and texture percentages over the six year study period. The two analyses yielded similar results (Figures 1 and 2).

Figures 1 and 2: Particle size distribution on streambanks located upstream of streambed

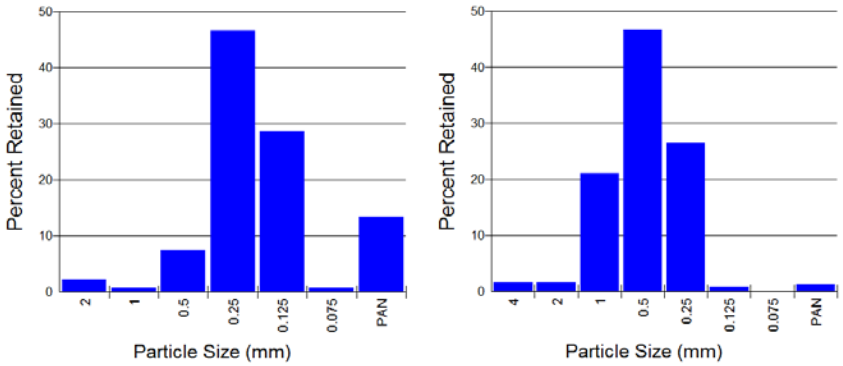

Streambank Streambed

The dominant soil association throughout all of the streambank study sites in the catchment is the Kanza-Ninnescah, a coarse, predominately sandy, non-cohesive soil that is highly prone to erosion. The data show that nearly all the 0.125mm to 0.25mm and finer materials in the streambanks were mobile once delivered to the water column and moving as suspended load along the streambed. A portion of the 0.25mm to 0.5 sized load is moving as suspended and some of this fraction settles out. The data indicates that the coarser 0.5mm to 1.0 mm sized particles are more present in the streambed post hydrograph recession limb and is not a suspended load component. When sieving of the coarse non-cohesive soils was complete the percent of streambank material parsed to be consistently mobile at a wide range of flows averages 43 to 50 percent. A conservative value of 45 percent was chosen based on the indication that 0.5mm to 1.0mm fraction remaining in the bed indicating that the larger-sized range of the material size .025 to .050mm typically remains as a bedload component. The results of the particle size analysis are consistent for both sampling periods. Particle sizes finer than 0.075mm, primarily silts and clays, are nearly one hundred percent transported to the Cheney Lake Reservoir.

RESULTS

The six year study involved the meticulous field measurements and data generation for ten streambank erosion sites in five streambank condition classes. Annual longitudinal profiles and annual cross sections were developed at each site. A total twenty-eight streambank profile and pin erosion sites along with 28 toe pins and 24 concreted benchmarks were established on ten sites.

Table 1: Streambank Erosion Study Site and Condition Class

Site Name	Condition Class: SEVAT	BEHI SCORE	Sub-watershed (Catchment)	Catchment Size
GC1	Slight	24	Goose Creek	27,935 ac (43.6m^2)
NFN3	Slight	30	NF Ninnescah	331,210 ac (517.5m^2)
SC1	Slight	27	Silver Creek	156,535 ac (244.6m^2)
NFN4	Moderate	32	NF Ninnescah	160,301 ac (250.5m^2)
GC2	Moderate	30	Goose Creek	27,935 ac (43.6m^2)
NFN6	High	36	NF Ninnescah	122,120 ac (190.8m^2)
SC2	High-Severe*	42	Silver Creek	67,758 ac (105.9m^2)
NFN1	Severe	40	NF Ninnescah	356,189 ac (556.5m^2)
NFN5	Severe	46	NF Ninnescah	150,835 ac (235.7m^2)
NFN2	Severe	49	NF Ninnescah	335,549 ac (524.3m^2)

*Condition Class Change during period of study.

The erosion on one severe site was so extreme between 2007 and 2010 that eight-foot pins set in the bank were washed out. However, the team established a cross-section tied to a concreted benchmark. The measure of toe pins and cross-sections and longitudinal profiles also provided data regarding validation of vertical bed stability (incision or aggradation). Table 1 describes Condition class of SEVAT compared to BEHI scores. The results of the SEVAT and BEHI scores show a consistent categorical pattern.

Table 2. Streambank Erosion Rates: Pin, Bank Profile, and Cross Sections

Site Name	Rating SEVAT	BEHI Rating*	Average Annual Recession Rate Ft 5 years	Period of collection Water Cycle Years	Above inner berm flow erosion rate Q_{ib} **	Stream
GC1	Slight	30	0.125	6		Goose
NFN3	Slight	24	0.223	6	.0011ft/hr cycle 3	NFN
SC1	Upper Slight	27	0.224	5		Silver
GC2	Moderate	30	0.50	6		Goose
NFN4	Moderate	32	0.91	6		NFN
SC2	High	42	1.1	6		Silver
NFN6	High	36	1.23	6		NFN
NFN5	Severe	46	2.1	5***		NFN
NFN1	Severe	40	3.02	5***	.045ft/hr cycle 2	NFN
NFN2	Severe	49	3.75	5***	.076ft/hr cycle 2	NFN

*not taking into account near bank stress ratings and two years of BEHI Ratings

**One runoff water cycle, year 2 based on 192 hours above Q_{ib}

*** Water Cycle 6 to be included.

Table 2 is a summary of the five to six year field data. The average annual recession rates of the Kanza-Ninnescah Soil Association ranged from 0.125ft/yr to 3.75ft/yr. These values are higher than the original estimates based on the Ventura Workshop Erosion and Sediment Yield Tool.

Discharges above inner berm flow at two sites located in the proximity of the principle USGS gage near the outlet of the study were analyzed by Thom Garday and W. Barry Southerland. The recession rates averaged between 0.0011ft/hr (for a condition class rating of slight) to 0.076 ft/hr (for a condition class rating of severe).

CONCLUSION

The Cheney Lake Watershed Conservation Effects and Assessment Project has come a long way since the first year of collecting field data and early model runs. Field-based streambank erosion data has been gathered, assessed, and used to provide input to the AnnAGNPS Model. Providing realistic and considerably more robust estimates of streambank erosion based on field-measured data will substantially improve the AGNPS CEAP model. In 2015 the final study will be concluded and report will be completed. Streambank contributions from suspended load estimates from the 2007 Cheney Lake Watershed Streambank Erosion Analysis-CEAP Watershed Technical Report range from 13 to 40 percent of the total suspended load, relative to the five originally gaged catchments. The overall percent of suspended load from the 2007 study was estimated at 13 percent. The preliminary estimates from measured data indicate that the suspended load contribution from banks is between 20 and 25 percent. A more in-depth analysis based on field data and the use of GIS will be used to determine amounts and percent contribution from streambanks will be completed in 2015.

Streambank erosion is highly variable throughout the USA due to integrative processes and variability of streambank material, geomorphic stream type, stratigraphy, change in runoff conditions, and past and present perturbations. This effort of CEAP modeling deserved realistic

input of streambank erosion based on field data, as its hydrophysiographic and streambank conditions are ubiquitous in the Great Plains of Central United States.

Streambank erosion pins and bank profiles were established to calibrate lateral recession rates on the several streambank types with typical conditions. The cost and personnel time committed to establish pins is minimal and the data are highly useful for future planning efforts and calibration of lateral recession rates. These data can be used to developed regional streambank erosion curves that would be characteristic of Midwestern areas and states similar to Kansas to assist NRCS planning efforts in the future. The Cheney Lake Watershed is large and diverse enough to establish an excellent database for streambank erosion and stability.

The appropriate parsing of suspended sediment load contribution from streambank contribution to total load was essential for a robust model. In 2014, after six years of field date collection, the annual recession rates based on condition class has been refined. Ten years would be more desirable and potentially within the prevue of the Cheney Lake Watershed, Inc.

There has been a tendency to use streambank erosion data throughout other regions of the country where the variability in recession rates are substantially different, given similar runoff conditions. Now is the time to begin this effort. There has never been a better time to commit to field collection of this valuable data as our reservoirs continue to fill at accelerated rates and suspended sediment loads from streambanks continue to be a significant source.

I would like to express my appreciation to the Cheney Lake Watershed, Inc. and the Reno Conservation District for supporting this critical data collection and analyses for the past seven years.

REFERENCES

Leopold, L.B. (2001) Let the Rivers Teach Us, Stream Notes July 2001, Stream Systems Technology Center, U.S. Forest Service, Rocky Mountain Research Station, Fort Collins, Colorado.

Rosgen, D.L. (2006). *Watershed Assessment of River Stability and Sediment Supply (WARSSS)*. Fort Collins, CO: Wildland Hydrology Books.

Southerland, W.B., French, Lisa, Garday, T. et al. (2007) Cheney Lake Watershed Streambank Erosion Analysis-CEAP Watershed Technical Report. USDA-NRCS and Cheney Lake Watershed, South Hutchinson, Kansas.

VEGETATION CALIBRATION IN A SEDIMENT TRANSPORT MODEL OF THE MIDDLE RIO GRANDE, NEW MEXICO

David Varyu, P.E., Hydraulic Engineer, Reclamation, Denver, Colorado, dvaryu@usbr.gov
Lisa Fotherby, Ph.D., P.E., Hydraulic Engineer, Reclamation, Denver, Colorado, lfotherby@usbr.gov

OVERVIEW

The purpose of this project is to develop a calibrated sediment transport and vegetation model for the Middle Rio Grande downstream of San Antonio (HWY 380 Bridge) to Elephant Butte Dam. Geomorphic conditions of flow, sediment transport, riparian vegetation and groundwater are linked in the SRH-1DV simulation. Hydraulics, sediment transport and groundwater conditions are defined by physical laws of nature, and the ecological factor, vegetation growth, is described by known plant response to the geomorphic factors. The establishment, growth and mortality of vegetation is tracked on a daily basis in response to dynamic physical conditions, and is tracked as individual plants located on every node at every cross section in the model (Fotherby 2012).

Model Description SRH-1DV is an adaption of SRH-1D, a one-dimensional mobile boundary hydraulic and sediment transport computer model for rivers and manmade canals. The base model simulates changes to rivers and canals caused by sediment transport. It can estimate sediment concentrations throughout a waterway given the sediment inflows, bed material, hydrology, and hydraulics of that waterway. Simulation capabilities include steady or unsteady flows, internal boundary conditions, looped river networks, cohesive and non-cohesive sediment transport, and lateral inflows. It uses cross section based river information (Huang and Greimann, 2011).

SRH-1DV simulates the processes of seedling growth and mortality as a function of species type, changing river stage and groundwater level, the rate of root growth, and the potential for scour velocity. SRH-1DV tracks the potential for species-specific plant mortality due to drowning, velocity scour, and desiccation. The model assumes that the river has an abundant seed source. During the seed dispersal and germination season, the model assumes that seeds will germinate and begin to grow at all points above the wetted channel. A seedling is initially very vulnerable to mortality, but as it continues to grow, the plant becomes more resistant to the plant stresses induced by desiccation, drowning or scour and it increases the local hydraulic roughness of the channel. If a cottonwood seedling survives to an age of three years, the cottonwood tree then becomes very resistant to removal by scouring erosion (http://www.usbr.gov/pmts/sediment/model/srh1d/1dv/ index.html accessed December 2012).

MODEL INPUT DATA

The model input for SRH-1DV is the same as input for SRH-1D – channel and floodplain geometry, bed material gradation, sediment transport function, and boundary conditions – with the addition of vegetation inputs. The vegetation inputs include spatially defined age and vegetation coverage percentages, along with germination, growth, and mortality parameters for every vegetation type modeled. In addition to these input files, a GIS-based shapefile from vegetation mapping is required to define vegetation conditions (type and location) at the start of the simulation. A table in the vegetation input file translates the vegetation mapping classifications into the vegetation types (plants) simulated in the model.

Geometry The model spatial extent is from just upstream of the US-380 Bridge in San Antonio, NM to Elephant Butte Dam (Figure 1). The input geometry combines a portion of the 2002 ag-deg data set (Holmquist-Johnson, 2004; ~RM89-RM60), a 2007 bathymetric survey of Elephant Butte reservoir (Ferrari, 2008; ~RM41-RM27), and from various local surveys associated with the development of the Delta Channel into the pool of Elephant Butte Reservoir (~RM60-RM41). Every measure was taken to ensure a consistent vertical datum, however some survey data did not report a vertical datum and professional judgment was employed where necessary to convert all geometric data into NAVD88 elevations.

The input geometry data was developed in a HEC-RAS file and a series of discharges were run. Cross sections were edited as necessary in terms of adding levees, blocked obstructions, and ineffective flow areas to the model geometry to produce hydraulic conditions representative of actual flow patterns. For example, in areas where the channel is not in the lowest elevation of a cross section, levees are implemented in the model geometry to keep the water in the perched channel. A total of 196 cross sections were used in the model, including 159 measured cross

sections and 37 interpolated cross sections. Maximum cross section spacing was limited to 2500 feet, except in the lower end of the reservoir pool where the cross section spacing is irrelevant because the cross section spacing is irrelevant because the cross sections remain inundated by the pool.

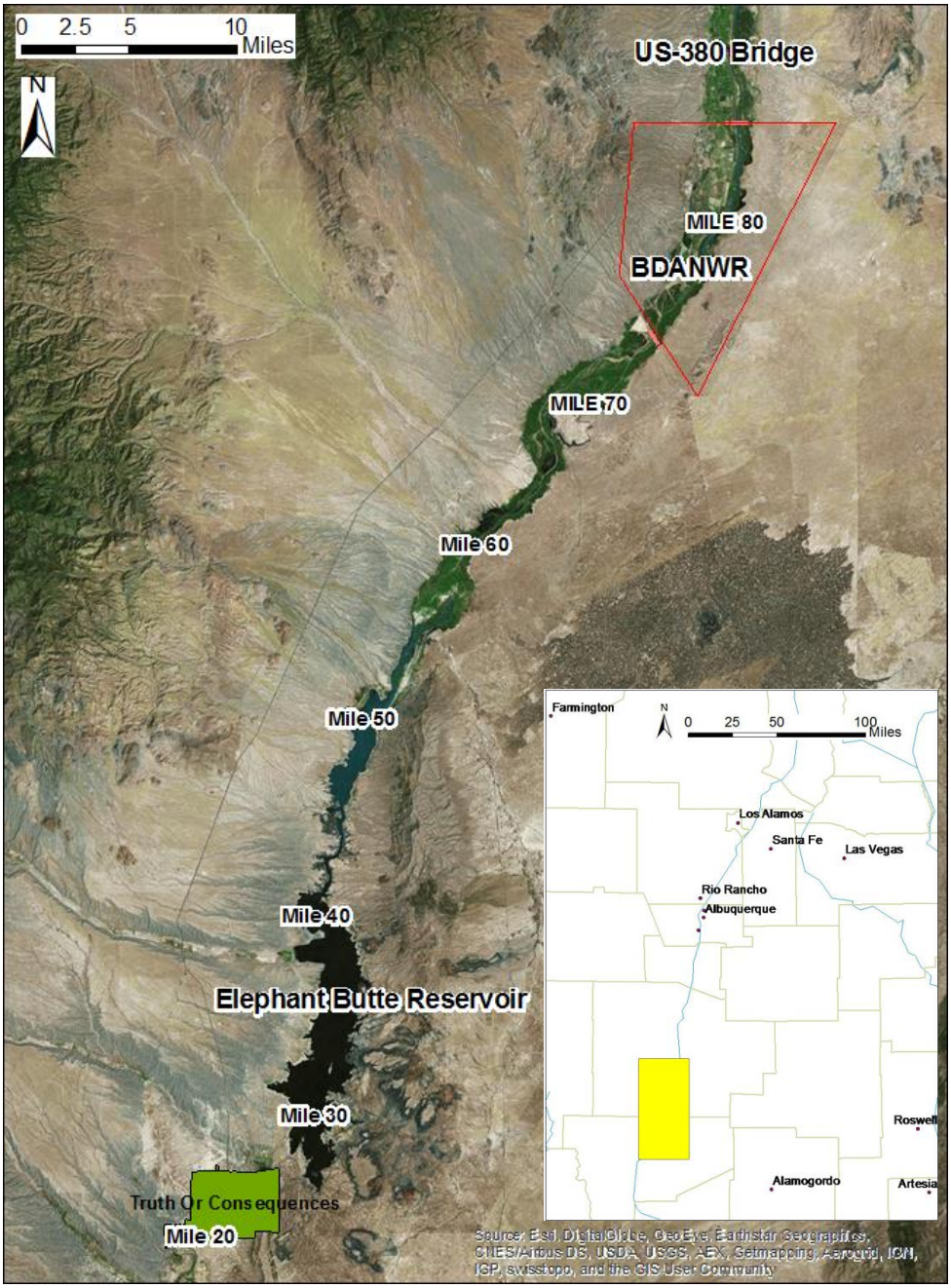

Figure 1 Overview map of model extent: US-380 Bridge to Elephant Butte Dam.

Bed Material and Sediment Transport Bed material data have been collected along the Rio Grande for various projects since the 1970s. Data appropriate for this model reach and time period were collected and prepared for model input. Twenty-eight sediment gradations are spatially assigned in the model, with the most downstream gradation located at EB-28 (~RM58). This gradation represents conditions for the model downstream of this point. The median grain size for the model domain is fairly uniform as compared to upstream reaches of the river, and a

range of 0.1 mm to 0.3 mm exists for all gradations employed in the model. The Engelund-Hansen transport formula is used in this model based on the size of the bed material in this spatial extent.

Boundary Conditions Boundary conditions need to be defined for the numerical model SRH-1DV. These include upstream conditions (flow rate and sediment discharge rate), downstream boundary condition (water surface elevation), and lateral flow and sediment contributions.

The temporal extent of this model begins in water year 2002 and ends with water year 2008. Daily discharge data from two USGS gages (08354800 Rio Grande Conveyance Channel at San Acacia, NM, 08354900 Rio Grande Floodway at San Acacia, NM) were combined to produce the upstream flow boundary condition for 10/01/2001 to 09/30/2008. The downstream boundary condition is defined as the water surface elevation of Elephant Butte Reservoir, and that daily data was transformed from local project datum to NAVD88 elevations. Figure 2 presents upstream boundary condition of incoming river discharge and the downstream boundary condition as the elevation of the Elephant Butte Reservoir pool.

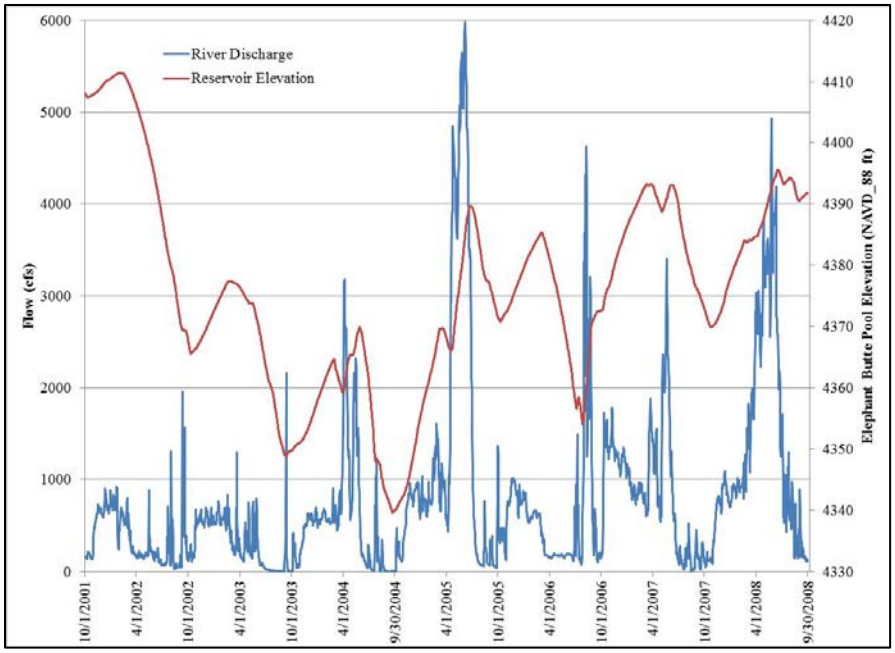

Figure 2 Downstream boundary condition; Elephant Butte Reservoir pool elevation.

The incoming sediment load at the upstream boundary of the model was developed by applying sediment rating curves based on dry, average, and wet flow regimes (Huang and Makar, 2012). Table 1 presents the classifications of the water year as Wet/Average/Dry, along with the coefficients a and b in for the power function rating curve sediment discharge to water discharge of the form $Q_s = aQ^b$.

Table 1 Water year type and sediment load coefficients used for upstream sediment supply.

Water Year	Flow Regime	coefficient a	coefficient b
2002	Dry	1.654	1.283
2003	Dry	1.654	1.283
2004	Average	2.895	1.229
2005	Wet	32.87	0.825
2006	Average	2.895	1.229
2007	Average	2.895	1.229
2008	Wet	32.87	0.825

Collins (2009) calibrated the gradation of the upstream sediment supply for the delta channel using published USGS data. Bureau of Reclamation Automated Modified Einstein Procedure (BORAMEP) was used to process USGS suspended sediment concentration data along with bed material gradation data to produce the gradation of the total sediment load at the upstream end of the reach. Sediment load gradations are assigned for five unique discharges ranging from 500 cfs to 6000 cfs (Figure 2).

Significant tributary contributions of water and sediment do not reach the mainstem of the Rio Grande in this reach due to levees. No lateral flow or sediment inputs are included in this model.

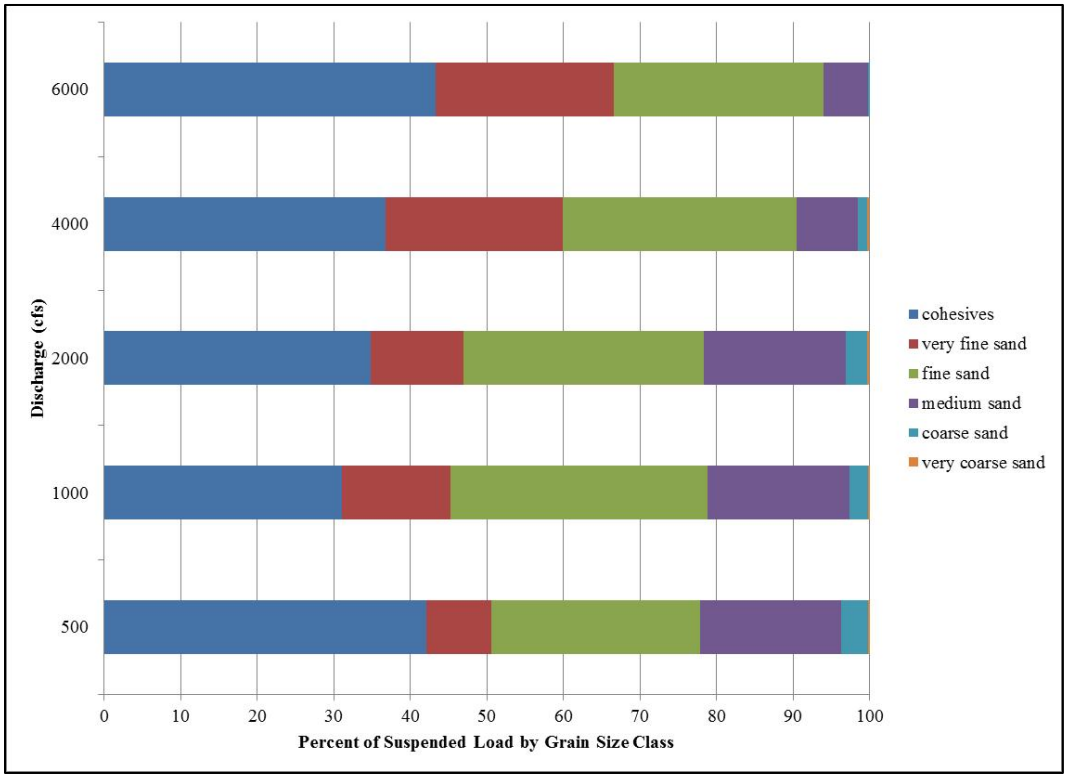

Figure 3 Changing gradation of upstream sediment supply as a function of discharge.

Vegetation data Vegetation was calibrated from initial to final conditions. The initial conditions were based primarily on the 2002 vegetation mapping (Callahan and White, 2004) which extends from upstream of this model domain to just downstream of river mile (RM) 62. Ancillary initial condition data from a 2004 vegetation map (Reclamation, 2005) was used as needed. The final conditions for the vegetation are derived from the 2008 vegetation mapping (Ahlers et al., 2010).

Discussion of Hink and Ohmart Classification and Interpretation The Hink and Ohmart (H&O) vegetation classification (Hink and Ohmart, 1984) was adapted and slightly modified by Reclamation biologists (Moore and Ahlers, 2003) while conducting habitat mapping for the southwestern willow flycatcher (SWFL), an endangered species. In general, the H&O system classifies vegetation based on species, height and whether there is a well-developed understory to supplement a canopy (overstory). Multiple vegetation species can be listed in the canopy/overstory and understory, where the first-listed species in the vegetation code is the most prevalent and the last listed is the least prevalent.

One of the modifications made by Moore and Ahlers (2003) was to try to better describe the vegetation density in 25% coverage increments. There were some methodological differences between the 2002 and the 2008 mapping, but in trying to maintain some consistency between the two datasets, they are interpreted and implemented as follows. The understanding during 2002 vegetation mapping was that nearly 75% vegetation coverage or more was needed for SWFL to find suitable nesting habitat. During the 2004 vegetation mapping, habitat occupations were

identified in areas where vegetation coverage was less than 75%, but still greater than 50%. The 2004 and 2008 vegetation mappings use a "d" indication (dense) at the tail end of the H&O classification to indicate vegetation coverage between 50-75%, where the 2002 data uses an "f" indication (full) for vegetation coverage greater than 75%. There was also an "s" indicator that was meant to indicate 'sparse' or 'scattered' (USACE et al., 2007), and the appropriate interpretation of this is unclear. For an area to be identified as 'covered' with vegetation there needs to be at least 25% coverage. It was assumed for this study that an identified area with an "s" qualifier was the same as if there was no qualifier.

A comparison of initial vegetation coverage (2002 and 2004 mapping) to final vegetation coverage (2008 mapping) includes 461 unique vegetation classifications, including a classification for no-grow areas (roads, railroad track) and open water areas (river and reservoir). Each unique vegetation classification can be one of 4 different density variations. For example, a lone stand of salt cedar, 5-15 feet high (H&O structural Type 5), can be sparse or scattered (s), dense (d), full (f) or have no density indicator.

Modified Hink and Ohmart Applied to SRH-1DV Input Transferring initial vegetation conditions defined by vegetation mapping classifications to the vegetation types and cross section locations simulated in SRH-1DV model requires some interpretation. In the modified H & O vegetation classification system, it is not uncommon to have the same vegetation type at two different ages in the same classification. A mature cottonwood can be present in the canopy and younger trees may form part of the understory. The SRH-1DV model does not simulate or track two of the same vegetation types on a single point. It was therefore necessary to have two vegetation types to represent the same species at different ages; one older and taller for the canopy, and one younger and shorter for the understory. This was not necessary for grasses or cattails as their maximum height does not exceed 15 ft. To ensure that twice as many germinations are not produced in SRH-1DV, only one age class for a given species is allowed to germinate. The younger category of a given species was arbitrarily assigned the ability to germinate, even though the older stands of some species, such as cottonwoods, would be more likely to supply seeds.

Vegetation mapping is normally classified by plant height (H&O vegetation structure) while vegetation modeling is based on plant age with plant height as a function of age. Fotherby (2012) provides growth rates for the vegetation types by age. These growth rates were used to translate vegetation height (H&O vegetation structure) into an age (SRH-1DV input).

Simulated Vegetation Types The model has to be able to distinctly represent a species' characteristics and responses to environmental conditions to justify simulation in this riparian vegetation model. Only riparian species that are frequently dependent on the water table for moisture can be well simulated; the species simulated in this Rio Grande model are Fremont cottonwood, Gooddings black willow (tree willow), sand bar willow (coyote willow), mulefat (seep willow), honey mesquite, cattail, Russian olive, tamarisk (salt cedar), and grasses (grass is a generic grouping of herbaceous and drought resistant upland grasses that provide ground cover) (Fotherby, 2012). Although there are many more species in the area, the number of simulated species is limited. There are a large number of parameters required for each species and all parameters cannot be calibrated or verified in each model. Fremont cottonwood is used here to represent cottonwoods, sand bar willow and mulefat are the representative riparian shrubs, honey mesquite is also assigned for screwbean and common mesquite, Russian olive is also assigned for New Mexico olive, only one tamarisk is simulated, and the only herbaceous representation is an upland grass that is resistant to desiccation. Roads and railroads are simply 'no-grow' zones.

Using two vegetation 'types' for different ages of the same species (older/taller and younger/shorter) as well as a no-grow designation (no plant establishment permitted) yields a total of 17 vegetation types: seven with two age/height classes, two with one age/height class, and the 'no-grow' vegetation type. A description of these vegetation types and references for SRH-1DV parameter selection are presented in Fotherby (2012).

Assigning Density to Initial Conditions Initial vegetation conditions in the model are also assigned from density reported in vegetation mapping. Vegetation densities in the modified H&O classification system are broken down in 25% vegetation cover increments. An 'open' polygon in the 2002, 2004, and 2008 vegetation mapping would indicate that there is less than 25% coverage, and the indicators "d" and "f" indicate 50-75% and 75-100%, respectively, where no indicator implies 25-50% vegetation cover. This is the total percentage of vegetation cover, regardless of how many species are present or listed in the category. Certain assumptions were made to implement the modified H&O information into a format suitable for SRH-1DV. First, vegetation densities for a given mapped

polygon are set at 37.5%, 62.5%, and 87.5%, depending on the presence/absence of an indicator ("d"/"f"). Second, the breakdown of relative percentages is based on their order as specified in the H&O classification method.

Table 2 presents the breakdown of implemented vegetation cover based on the number of species defined in each structure layer (canopy/overstory, or understory) of the vegetation code.

Table 2 Distribution of vegetation cover by code indicator and number of vegetation types.

	Number of vegetation types listed				
Total%	1	2	3	4	Total
25-50 (regular)	37.5				37.5
	20	17.5			37.5
	15	12.5	10		37.5
	12.5	10	7.5	7.5	37.5
50-75 (d=dense)	62.5				62.5
	33.3	29.2			62.5
	25	20.8	16.7		62.5
	20.8	16.7	12.5	12.5	62.5
75-100 (f=full)	87.5				87.5
	50	37.5			87.5
	35	30	22.5		87.5
	30	22.5	17.5	17.5	87.5

Vegetation Calibration Methodology The 2002, 2004, and 2008 vegetation maps used as model inputs and comparisons for model outputs are based on aerial percent coverage. The methodology used in this calibration process is based on percentages of model nodes (cross section points) located within a polygon. The assignment of vegetation species onto SRH-1DV model nodes is based on the polygon where the node is located and the percent vegetation cover specified in the input file. The number of nodes assigned a given vegetation type will be as close to, without exceeding, the assigned percent cover, or density.

The assessment of the model output worked in a similar manner. The model output reports a set of predicted vegetation types existing on every model node. Nodes are allowed to have more than one vegetation type, so the number of rows in the main model output text file equals the product of the number of model nodes multiplied by the number of vegetation types. The model nodes are located within the appropriate 2008 vegetation mapping polygon and the model outputs are compared to the observed data as recorded in the 2008 mapping polygons. The model comparison is not cross section based but rather polygon based since there are usually multiple segments of cross sections within a given polygon.

MODEL CALIBRATION

For this project, the ability to calibrate the sediment transport is important only in terms of being able to calibrate the vegetation data. For example, being able to exactly match the channel degradation due to the drop in Elephant Butte Reservoir elevation (base level lowering) is not necessary as long as the modeled degradation is sufficient to lower the water table elevation in the area and allow simulated vegetation mortality due to desiccation.

Almost half of the species for this Rio Grande study are being modeled for the first time in SRH-1DV. The parameters for each species are selected from a range of values identified in a literature review. Many parameter values required adjustment during calibration. Growth rates, germination seasons, dormant seasons and drought and inundation tolerance can all vary with regional climate differences and parameters from previous applications in different regions may not be suitable for the Rio Grande. The large number and detailed assignment of modified

H&O classifications for initialization of this model are another reason for a calibration investigation. The maximum spacing between cross section points was limited to 25 feet to ensure every vegetation polygon was represented by a model node. The number of model nodes is 66,198 for the model domain.

Through the course of the calibration process, adjustments were made to germination, growth, and mortality parameters for various plant species. A list of significant changes to the initial parameters (as defined by Fotherby 2012) is followed by a discussion of the final calibration results.

All Vegetation Types

- The model input competition tables are set up to define at what age a species will be out-competed by other species/age combinations. Therefore, each competition table was adjusted so that young tamarisk would out-compete other young vegetation types (further discussion of this adjustment below).
- Dormancy period extended from December 1 through January 1 to October 1 through March 31.

Mulefat

- Scour velocity needed to remove new and one year old plants reduced by one-third (to 0.67ft/s and 1 ft/s respectively).

Tamarisk

- Germination period extended from July 1 through September 30 to March 14 through November 15.

Upland Grass

- Scour velocity needed to remove new, one, and two year old plants reduced by one-half (to 1ft/s, 1.5ft/s, and 2ft/s respectively)

The list above does not encompass all of the iterations attempted in the calibration process, but only a summary of the changes between the initial set of vegetation parameters and the best-fit calibration parameters. The interpretation and implementation of the H&O classification system to SRH-1DV was at least as involved a process as calibration of the germination, growth, and mortality parameter for the vegetation species.

Vegetation Calibration Results There are 808 mapped polygons included in the calibration analysis. The final analysis methodology calculated the difference in percent coverage for all vegetation types within four different height categories (associated with the H&O structure classification): 0 to 15 feet, 15 to 20, 20 to 40, and over 40 feet. For the nine species being modeled (not counting the 'no-grow' vegetation type), there are 36 species/height categories being considered per polygon. The most common error is in the 0 to 15 feet range for all species except for Gooddings black willow (tree willow) and mesquite. This indicates that the germination process is a likely source of the most error in the simulation. Figure 4 shows the count of which age class represents the highest percent error per species per polygon.

If we consider the error of each vegetation type across the 808 vegetation polygons, we can discretize the error based on how many model nodes are within each polygon. Table 3 presents the grouping of polygons based on the number of model nodes within that polygon. The one polygon within the range "Q" is a polygon classified as "open water" and is the continuous riverine and reservoir polygon in the model, and the upper bound of this range was selected such that the midpoint of the range equaled the number of model nodes in this polygon.

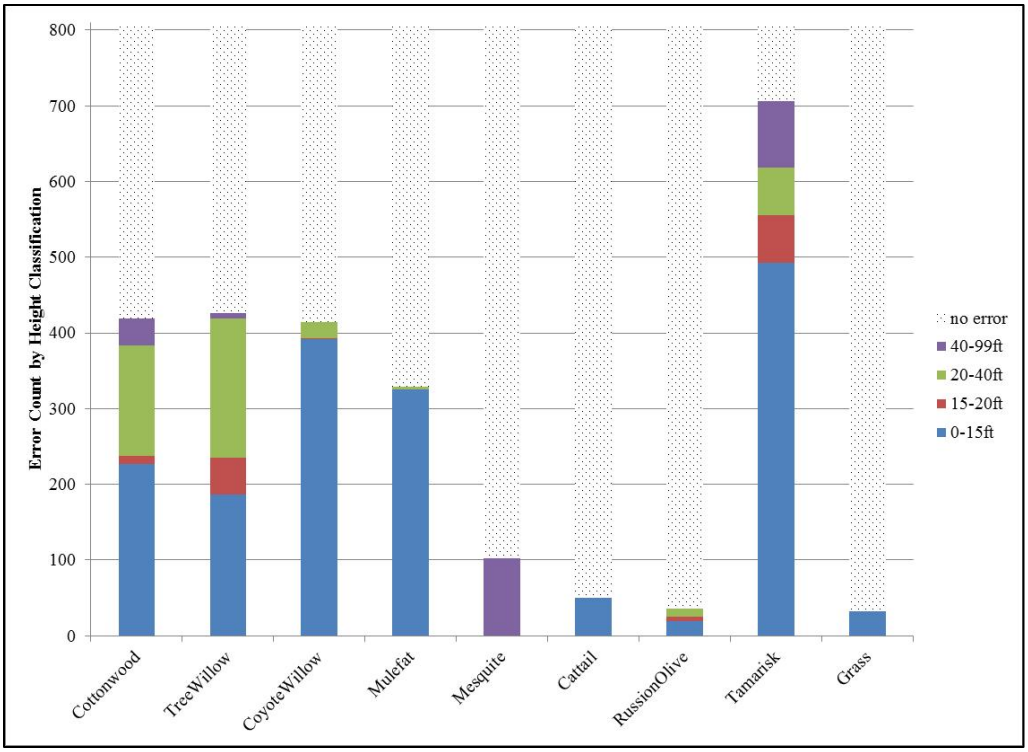

Figure 4 Count of age class representing the highest error per species polygon.

Table 3 Bin ranges used in analyzing error by number of model nodes in mapping classification polygons.

Range ID	Min Model Nodes	Max Model Nodes	Count Polygons in Range
A	1	5	116
B	6	10	132
C	11	20	168
D	21	30	125
E	31	40	63
F	41	50	44
G	51	60	31
H	61	70	25
I	71	80	11

Range ID	Min Model Nodes	Max Model Nodes	Count Polygons in Range
J	81	90	7
K	91	100	8
L	101	200	42
M	201	300	13
N	301	400	13
O	401	500	3
P	501	600	6
Q	601	29586	1

Figure 5 presents the average maximum absolute error (of the four height classifications) by vegetation type relative to the midpoint of the bin range. For example, consider the "O" bin range. There are three polygons that contain between 401 and 500 model nodes. If we consider just tamarisk, the maximum error for two polygons was in the 0 to 15 ft height range (-70% and 59%), and for one polygon was in the 40-99 ft height range (error of -25%). A negative error means SRH-1DV is predicting too much of a vegetation/height combination and a positive error indicates not enough of that vegetation/height combination is being predicted. The average of the maximum absolute error for tamarisk for the three polygons containing between 401 and 500 model nodes is 52%. This point is the peak error in Figure 5. The results in Figure 5 show good calibration (considering measured data specified in 25% bins), with tamarisk being the species that was least successfully calibrated. Another way to look at the calibration results is to consider the average (over the bin range) of the average error of the four height classifications for one

vegetation species. This is simply the average error of all 12 (four height classes by three polygons) error values associated with a bin range. Figure 6 presents the average error for each vegetation species by bin range.

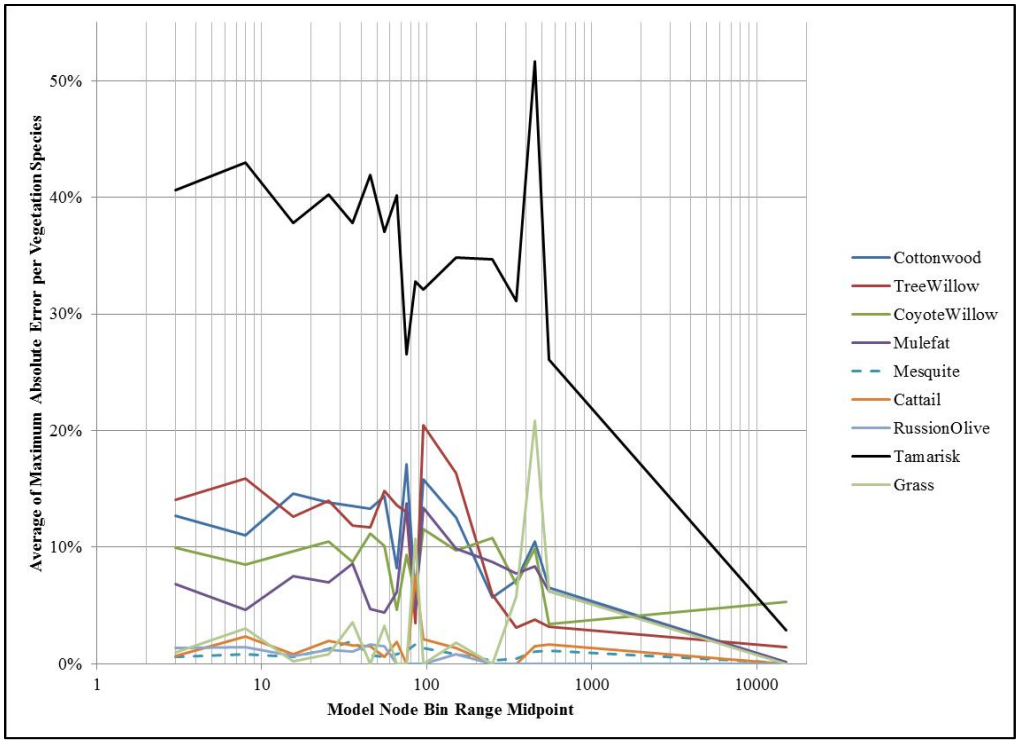

Figure 5 Plot of average of maximum error per vegetation species.

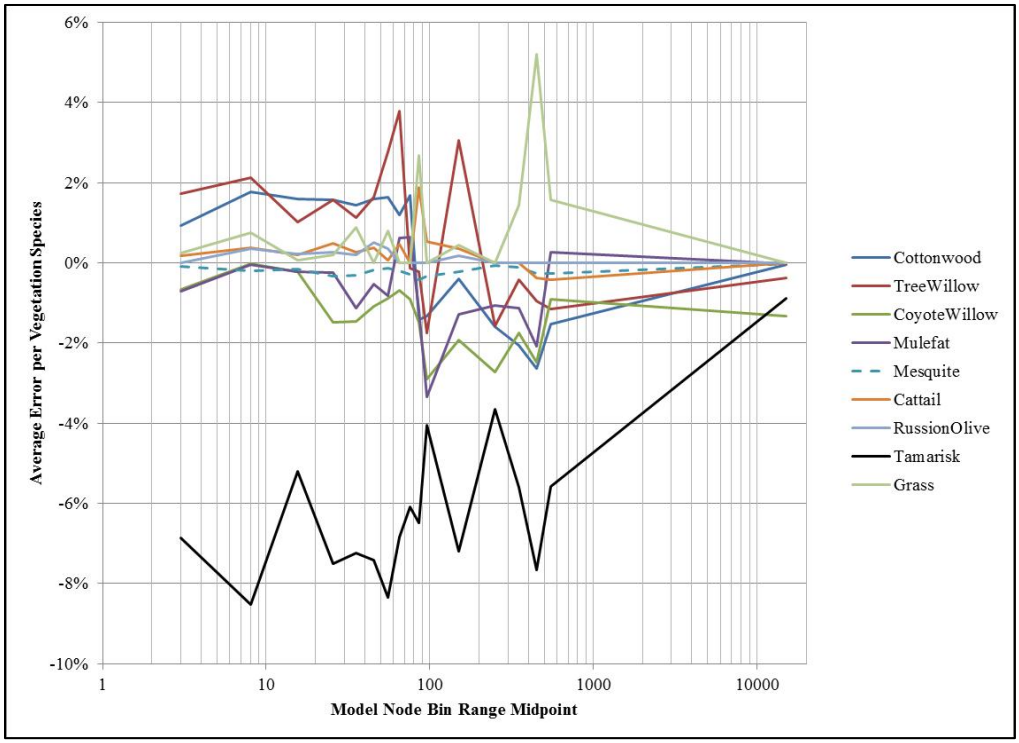

Figure 6 Average error per vegetation species.

These differences can be represented visually using ArcMap. Instead of trying to combine errors by bin ranges as was done above, the actual error for a given polygon can be presented for one vegetation species and height classification at a time. A python script was developed as a tool to translate SRH-1DV output text files into visually represented error polygons. Figure 7 presents an example plot that can be made for any combination of vegetation species and height classification, in this case Tamarisk for 0-15 ft (selected polygons outlined in cyan). The color coding is constructed in absolute terms and all errors that are negative are hatched horizontally while positive errors are hatched vertically.

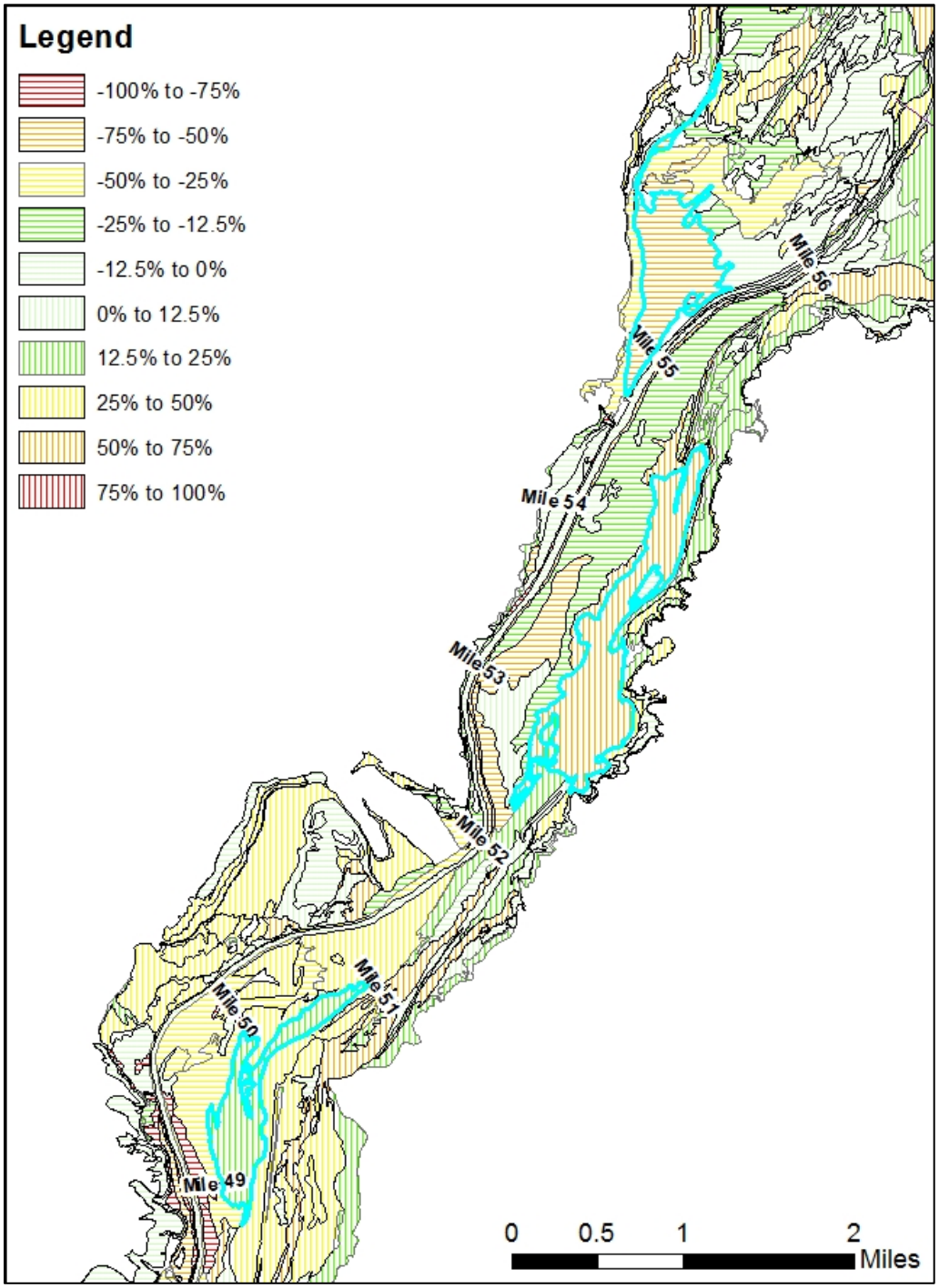

Figure 7 Vegetation polygons attributed by error in percent coverage for Tamarisk, 0-15 feet tall.

MODEL LIMITATIONS, ERROR SOURCES, AND AREAS OF IMPROVEMENT

This model, as with any, contains errors; some of which are due to data availability, some of which are due to limitations to the SRH-1DV model, and some are areas that could be improved (further calibrated) with more time and effort. A brief list describing some potential improvements follows:

- **Mapping inconsistencies**: In some instances the dominant canopy species for a 2008 polygon is not identified at all for the associated 2002 polygon.

- **Growth rates** are input into the model based on age and month of the year only. A wet year could allow for more tree growth (stalk diameter) than a dry year. The model could be adjusted to allow for this.

- **Lateral channel adjustment:** Some errors in the simulation are due to the fact that channel width change and lateral migration are processes not modeled in the 1D framework.

- **Anthropogenic influences:** channel excavation conducted by heavy machinery, channel clearing to increase morphodynamic response, and vegetation planting during habitat improvements are all actions taken on the river but are not simulated in the model.

- **Groundwater module:** the groundwater module is relatively coarse in the SRH-1DV. One soil type is incorporated in the Rio Grande model with one hydraulic conductivity value for the floodplain sediments, although two input types are allowed. This is a gross assumption, yet necessary as the data needed for accurately mapping hydraulic conductivity for this large area would be monumental.

- **Salinity:** Salt cedar (tamarisk) is considered a disturbance species, where it doesn't necessarily out-compete native species, but is able to take advantage of conditions where native species cannot survive (including high saline environments, hence the name). To overcome salinity not being simulated, tamarisk was modeled as a relatively competitive species, even though literature describes is as non-competitive. In this way, a native species that would not be able to germinate in the real world due to some level of salinity in the soil, is modeled as being outcompeted by salt cedar in SRH-1DV. The end result in the model is similar to reality, where the native species would not establish but salt cedar would. Incorporating salinity would make SRH-1DV more data intensive and it may not prove beneficial. Manipulating the competition table appears to be an appropriate surrogate for salinity modeling.

- **Interpretation of the modified H&O Vegetation data:** Implementing some bounded random number generator into SRH-1DV could allow for multiple vegetation age/heights to be assigned to model nodes according to the height range specified by the H&O classification system. Also, there are four density ranges from the modified H&O system at 25% increments. Similar to age, a random number generator could be implemented either within SRH-1DV or in the input file generation where the vegetation density could be any value as long as it was within the appropriate 25% range. It would be necessary to develop many simulations using the random number generators and statistically evaluate the outputs to determine if the central tendencies predict the observed end condition reasonably well.

CONCLUSIONS

The calibration of multiple species within SRH-1DV to the Middle Rio Grande was completed with good accuracy. The average error for all species/age combinations was well within the accuracy of the measured data. Further calibration may prove useful. In addition, a methodology for processing, presenting, and interpreting SRH-1DV results using ArcGIS has been developed and can be easily applied to future model runs.

Additional calibration, if conducted, would involve identifying the mode of mortality for all species within the model spatially and determining if that mechanism is being appropriately simulated. Germination would be looked at as well to see if plants are not only establishing in the right quantities but also identifying the mechanisms as to why establishment is or is not occurring in certain areas. Conducting multiple simulations using a bounded random

number generator to assign vegetation age and density appropriate to the H&O classification system would be another option in further calibration of SRH-1DV to the Middle Rio Grande.

A recent vegetation mapping using the H&O classification system was completed in 2012 and the final product will soon be available. Conducting a model validation for the period of 2008 to 2012 would provide insight as to the effectiveness of the model calibration and would help refine values assigned to various vegetation germination, growth, and mortality parameters. If the validation proves successful, then further calibration may not be necessary. The vegetation model, whether or not further calibration and validation are pursued, can be used for analyses of the effects of potential river maintenance actions and/or water operations. Absolute predictions of future conditions may not be a proper application of this model but rather a relative ranking of the effects in terms of sediment transport and vegetation conditions could be accomplished by employing this model.

Acknowledgements I would like to acknowledge the amount of research and literature review conducted by Lisa Fotherby in gathering the data necessary to apply appropriate values to the germination, growth, and mortality parameters for the SRH-1DV model, as well as providing additional review of this document. Dave Moore and Darrell Ahlers provide valuable information to interpreting and applying the Hink and Ohmart classification system. I would also like to acknowledge Victor Huang and Blair Greimann for developing both SRH-1D and the vegetation module for SRH-1DV.

REFERENCES

Ahlers, D., Johanson, V., Ryan, S., and Siegle, R. (2010). Southwestern Willow Flycatcher Habitat Suitability 2008: Highway 60 Downstream to Elephant Butte Reservoir, NM. Bureau of Reclamation. Technical Service Center. Fisheries and Wildlife Resources Group. Denver, Colorado.

Callahan, D., and White, L. (2004). Vegetation Mapping of the Rio Grande Floodplain 2002-2004. U. S. Department of the Interior, Bureau of Reclamation, Technical Services Center, Denver, Colorado.

Collins, K.L. (2009). 2007 Middle Rio Grande Maintenance Modeling: San Antonio to Elephant Butte Dam. Technical Report No. SRH-2009-29, U.S. Department of the Interior, Bureau of Reclamation, Technical Service Center, Sedimentation and River Hydraulics Group, Denver, Colorado.

Ferrari, R.L. (2008). Elephant Butte Reservoir 2007 Sedimentation Survey. Technical Report No. SRH-2008-04, U.S. Department of the Interior, Bureau of Reclamation, Technical Service Center, Sedimentation and River Hydraulics Group, Denver, Colorado.

Fotherby, L. (2012). Vegetation Modeling with SRH-1DV, Predicting the Interactions between Flow, Sediment, and Riparian Vegetation Research and Development. U.S. Department of the Interior, Bureau of Reclamation, Technical Service Center, Sedimentation and River Hydraulics Group, Denver, Colorado.

Hink, V.C., and Ohmart, R.D. (1984). Middle Rio Grande biological survey. U.S. Army Engineer District, Albuquerque, New Mexico. Contract No. DACW47-81-C-0015, Arizona State University. 193 pp.

Holmquist-Johnson, C.J. (2004). Sediment Model for the Middle Rio Grande – Phase 1. San Acacia Diversion Dam to Elephant Butte Reservoir. U.S. Department of the Interior, Bureau of Reclamation, Technical Service Center, Sedimentation and River Hydraulics Group, Denver, Colorado.

Huang, J. and Greimann, B. (2011). SRH-1D 2.8 User's Manual, Technical Report No. SRH-2012-03. U.S. Department of the Interior, Bureau of Reclamation, Technical Service Center, Sedimentation and River Hydraulics Group, Denver, Colorado.

Huang, J., and Makar, P. (2012), Investigation of Climate Change Impact on Reservoir Capacity and Water Supply Reliability, Technical Report No. SRH-2013-08, U.S. Department of the Interior, Bureau of Reclamation, Technical Service Center, Sedimentation and River Hydraulics Group, Denver, Colorado.

Moore, S. D. and Ahlers, D. (2003). 2002 Southwestern Willow Flycatcher study results, Appendix D, Southwestern Willow Flycatcher habitat suitability model. U.S. Department of the Interior, Bureau of Reclamation. Denver, Colorado.

USACE, U.S. Department of the Interior, Reclamation, New Mexico Interstate Stream Commission (2007). *The Upper Rio Grande Water Operations 2007 Environmental Impact Statement*, http://www.spa.usace.army.mil/Missions/CivilWorks/URGWOM/URGWOPS.aspx . Accessed December 2012

U.S. Bureau of Reclamation (2005). Habitat quantification of southwestern willow flycatcher nest sites, Rio Grande from La Joya to Elephant Butte Reservoir Delta, New Mexico – 2004. U.S. Department of the Interior, Bureau of Reclamation, Denver Colorado

REMOVING INVASIVE PLANTS FROM THE MOJAVE RIVER, AN EROSIVE INLAND DESERT RIVER SYSTEM IN SOUTHERN CALIFORNIA

Greg Norris, Assistant State Conservation Engineer, NRCS, Davis, CA, greg.norris@ca.usda.gov
Julia Grim, Geologist, NRCS, Davis, CA, julia.grim@ca.usda.gov

INTRODUCTION

In 2009, the Mojave Desert Resource Conservation District (MDRCD), in partnership with the Mojave Water Agency (MWA) and the USDA-Natural Resources Conservation Service (NRCS), began work to remove Arundo (*Arundo donex*) and saltcedar (*Tamarix ramosissima*) from areas within a 48-mile long riparian corridor within the Mojave River channel, referred to as Phases 3 and 4. Figure 1 provides a location map of the project area as it relates to the overall Mojave River watershed. As part of project planning, resource specialists from NRCS and MDRCD evaluated the potential impacts of the proposed project on stream function and riparian ecology.

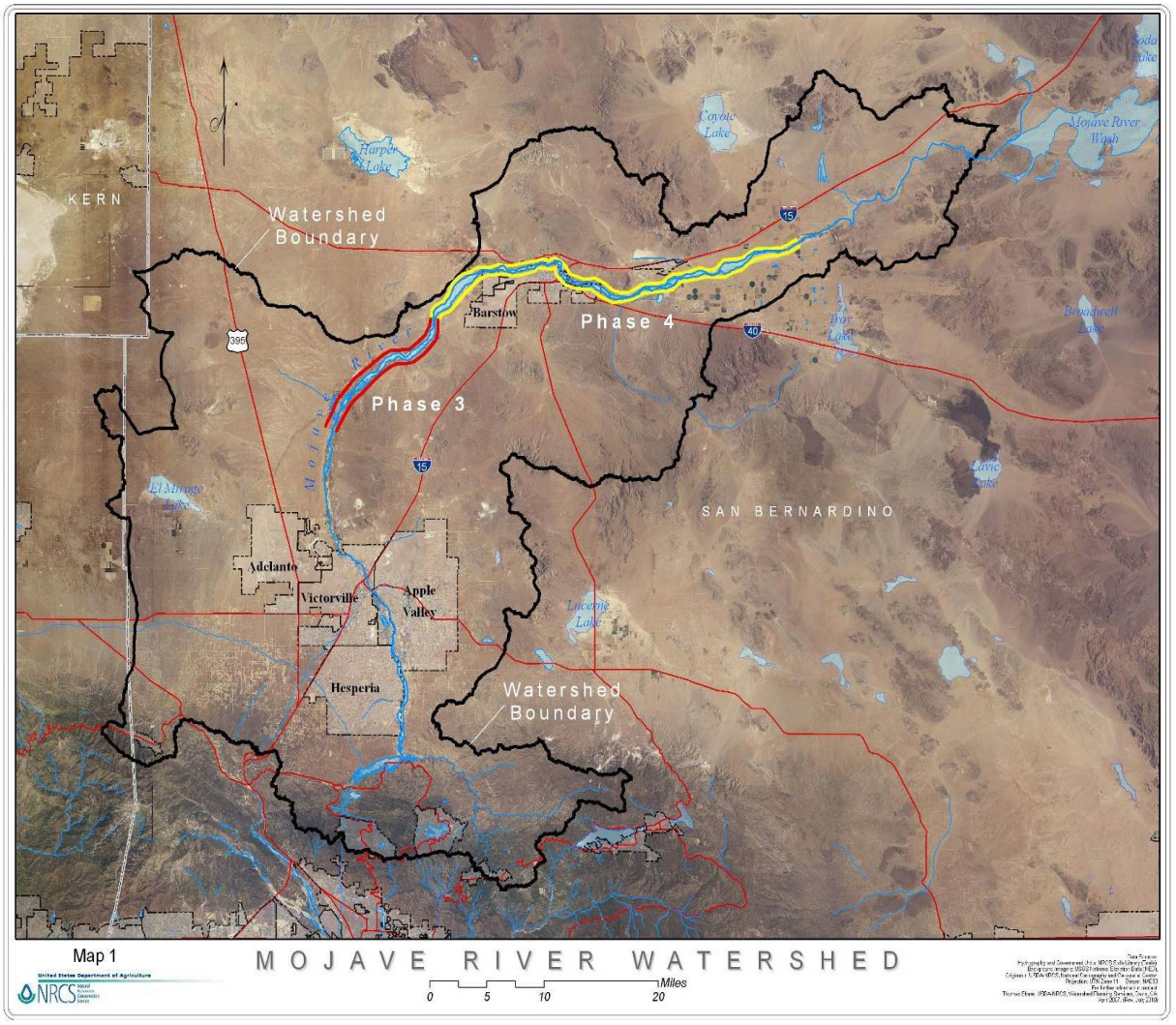

Figure 1 Map of Mojave River watershed showing the Phase 3 and 4 reaches.

The Mojave River is located in the high desert region of Southern California. It flows from the San Bernardino Mountains, inland through the Mojave Desert, to its terminus at Soda Lake. The flows in the alluvial reaches of the river are naturally ephemeral and flashy, but are greatly influenced by upstream water storage and imports, a flood control structure, levee confinement, locally high rates of groundwater withdrawal, and discharges from a municipal waste treatment facility. This altered hydrologic regime contributed to the establishment of non-native plants such as Arundo and saltcedar. Figure 2 depicts typical conditions found in these reaches and provides an example of how saltcedar plants invade the channel bed out-competing the native vegetation for moisture. The high density of these non-native species along some reaches further affect the geomorphology, hydrology, and ecology of the riparian community, by altering stream flow patterns and restricting channel capacity, consuming relatively large amounts of groundwater, and out-competing natives.

Figure 2 Typical condition of Mojave River within the Phase 3 and Phase 4 reaches.

METHODOLOGY

The evaluation team recognized a relationship between different areas of the river channel and critical resource concerns. Critical resource concerns were identified as streambank erosion, wind erosion, wildlife habitat, water conservation, and flooding. To help evaluate the effects of the critical resource concerns, the river channel was delineated into three distinct geomorphic categories based on function and the following characteristics: active channel, active floodplain, and terrace. Sub-reaches within the Phase 3 and Phase 4 reaches were further identified based on vegetation density and channel configuration. Then, each of the five resource concerns were evaluated for each geomorphic category within each sub-reach to determine whether there would

be a positive effect, negative effect, or no effect on the adjacent land uses if vegetation was removed. The team evaluated all potential combinations of land uses and resource concerns. If a negative effect was determined based on the criteria developed by the team, then a critical area was highlighted as needing special considerations with a recommended alternative for removal of invasive plants.

LAND USES

The evaluation team identified four typical land uses that occur adjacent to the Mojave River within the project Phase 3 and 4 reaches: private open land, public open land, homes and agriculture, and transportation infrastructure. For each sub-reach, the team evaluated how the resource concerns affect the adjacent land use if the invasive plants were removed. "Adjacent" for this project was defined as the distance extending from the river channel out to the point where the resource concern no longer has an effect.

CHANNEL FEATURES

Within the Phase 3 and Phase 4 project reaches, the team delineated the sub-reaches based on geomorphic and vegetative differences inferred from the 2007 MWA ortho-photography. The active channel, the low sand bars referred to as floodplain, and terraces were delineated using the MWA ortho-photography augmented by the team's field observations.

In several instances, some features were difficult to delineate because they were not apparent on the ortho-photos. For example, the low sand bars that form the floodplain were sometimes only a few inches higher than the active channel. Oftentimes these sand bars were only distinguishable from the active channel because there was some sparse vegetation, such as grasses, growing on them; or they had not been recently scoured or reshaped. Figure 3 shows an example of channel feature delineation for sub-reach 2 within the Phase 3 reach. The active channel, as mapped for this evaluation, appears in blue, the floodplain in green, and the terrace in orange. Vegetation maps were also used as an aid in delineating the channel features.

EVALUATION OF EFFECTS

The team evaluated the effects of invasive plant removal within each sub-reach and associated geomorphic feature relative to each land use (houses and agriculture, private open space, public open space, and roads/transportation) and each resource concern (wind erosion, flooding, habitat, water conservation, and stream bank erosion), for all sub-reaches in Phases 3 and 4. Table 1 provides an inventory of the results for one sub-reach (Phase 3, sub-reach 2) as an example. In Table 1, a plus (+) symbol indicates that invasive plant removal may reduce detrimental effects of specific resource concerns on particular land use categories. A zero (0) symbol indicates that invasive plant removal would most likely have no impacts, positive or negative, on effects of resource concerns on specified land use categories. A negative (-) symbol indicates that invasive plant removal may increase negative effects of specified resource concerns on particular land use categories.

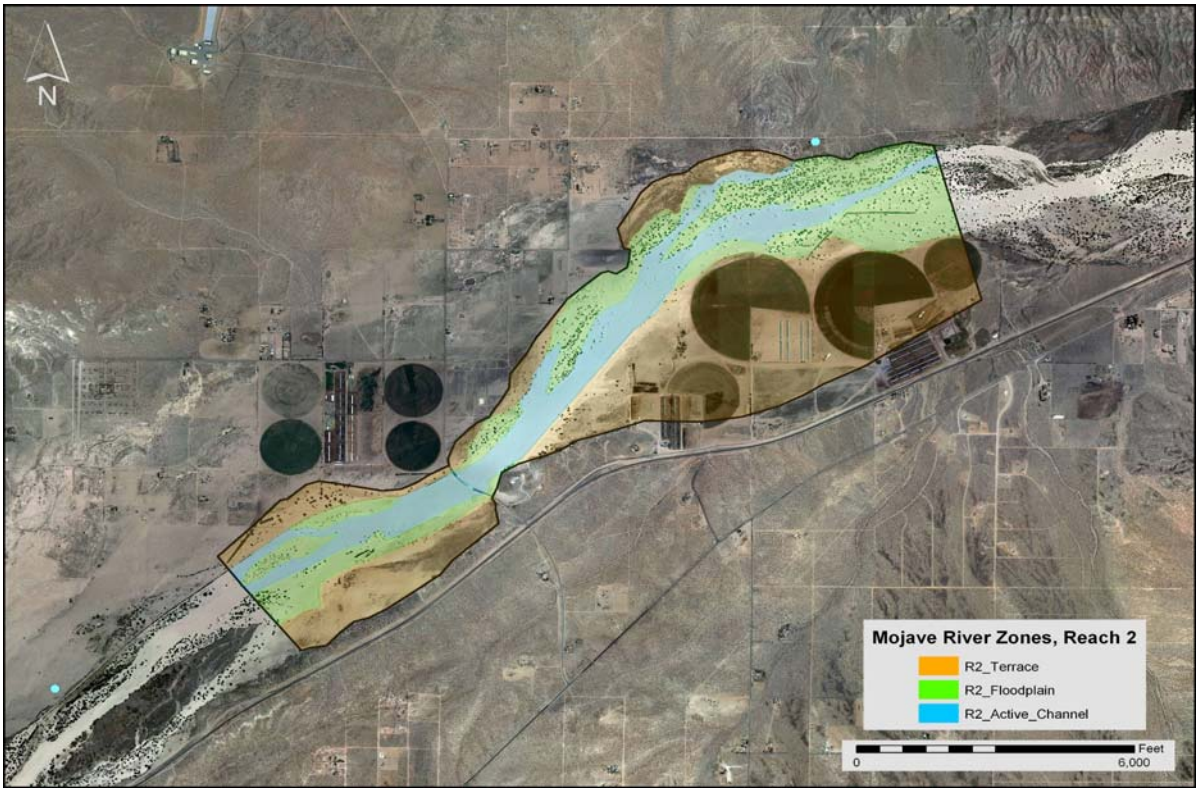

Figure 3 Channel features for Phase 3 sub-reach 2 (2007 MWA photo base).

Wind Erosion: Soil erosion due to wind was prevalent in the Phase 3 and Phase 4 reaches. Dune development and migration was easily identified in the 2005 and 2009 aerial images. In areas where invasive plants such as saltcedar existed, the soil tended to accumulate around the base of plants, functioning as soil traps. Because of this, the evaluation team recognized that invasive plants help prevent wind erosion. Modeling was performed to quantify the effects of vegetation on wind erosion.

Four typical existing conditions were modeled in and near the channel as follows:

- Dominate saltcedar with a nearly closed canopy
- Evenly mixed stand of saltcedar and native shrubs or trees with a nearly closed canopy
- Mixed stand of 25% saltcedar and 75% shrubs or trees with a nearly closed canopy
- Sparse vegetation of 25% saltcedar with 25% annual grasses

In conjunction with the four typical conditions above, four treatment options were modeled as follows:

- Dominate saltcedar killed using chemicals plus a 100 pounds per acre annual grass increase
- Evenly mixed stand of saltcedar and native shrubs or trees with saltcedar killed using chemicals, 100 pounds per acre annual grass increase
- Mixed stand of 25% saltcedar and 75% shrub or trees with saltcedar killed using chemicals, 50 pounds per acre annual grass increase
- Sparse vegetation with the 25% saltcedar canopy removed

Table 1 Example summary of effects for Phase 3, sub-reach 2

Reach Feature	**Houses & Agriculture**	**Private Open Space**	**Public Open Space**	**Roads & Transportation**
Active Channel	Wind –	Wind –	Wind –	Wind –
	Flood 0	Flood 0	Flood 0	Flood 0
	Habitat 0	Habitat 0	Habitat 0	Habitat 0
	Water Conservation +	Water Conservation +	Water Conservation +	Water Conservation +
	Streambank Erosion 0	Streambank Erosion 0	Streambank Erosion 0	Streambank Erosion 0
Active Flood Plain	Wind –	Wind –	Wind –	Wind –
	Flood -	Flood -	Flood -	Flood -
	Habitat -	Habitat -	Habitat -	Habitat -
	Water Conservation +	Water Conservation +	Water Conservation +	Water Conservation +
	Streambank Erosion -	Streambank Erosion -	Streambank Erosion -	Streambank Erosion -
Terrace	Wind -	Wind -	Wind -	Wind -
	Flood 0	Flood 0	Flood 0	Flood 0
	Habitat 0	Habitat 0	Habitat 0	Habitat 0
	Water Conservation +	Water Conservation +	Water Conservation +	Water Conservation +
	Streambank Erosion 0	Streambank Erosion 0	Streambank Erosion 0	Streambank Erosion 0

The eight options above were evaluated for two predominant soil types, Villa loamy sand and Cajon sand. Wind erosion rates for each condition and soil were estimated using the Wind Erosion Equation (Skidmore, 1968). The wind erosion modeling found that all treatment options had very high wind erosion rates compared to the soil loss tolerance of the individual example soils. Treatment for the dominant saltcedar condition resulted in an annual soil loss rate of 83 tons per acre, or 17 times the soil loss tolerance rate for Villa soil (USDA-NRCS, 2009). Treatment for the sparse vegetation area conditions resulted in an annual 395 tons per acre soil loss rate, which is 79 times the soil loss tolerance rate for Cajon soil (USDA-NRCS, 2009).

Removal of saltcedar in the Mojave River channel will increase wind erosion in varying degrees based on the method of treatment. Areas with a small, invasive plant canopy that is removed will have the lowest increase in wind erosion, approximately 1 ton per acre year, while the dominant saltcedar areas on Villa soil would have the greatest increase if removed, about 200 tons per acre year. Considerable dune activity would be expected if dense areas of invasive plants were sprayed, increasing the risk of damage due to sediment accumulation to sensitive areas such as the urban interface, rural farmsteads, roads, railroads, and producer field boundaries. Invasive plant areas not totally killed with chemicals and left clumpy with vegetation were predicted to accumulate soil around the base of the remaining plants. In areas that saltcedar was to be killed using chemicals, some annual grasses and forbs may grow due to increased sunlight and soil moisture post-spraying.

Streambank Erosion/Flooding: The evaluation team carefully assessed the risk of increased streambank erosion due to invasive plant removal because evidence has been documented in the literature that invasive plant removal, particularly saltcedar, can result in an unintended increase in streambank erosion. Helicopter herbicide applications in 2003 along a 12-km reach of the Rio Puerco, New Mexico, eliminated the saltcedar. Three years later a flood eroded about 680,000 cubic meters of sediment, increasing the mean channel width of the sprayed reach by 84 percent (Friedman, 2009). Erosion upstream and downstream from the sprayed reach during this flood was inconsequential (Friedman 2009). Streambanks for this analysis were considered a separate entity, generally being the transition between floodplain and terrace. At no location in the project area was saltcedar removal in the active channel or on the terrace considered a negative impact for streambank erosion or overbank flooding. Differences between the Rio Puerco and Mojave River are significant, but experience on the former helped guide recommendation for the Phase 3 and 4 reaches.

The impact of saltcedar removal in the active channel will generally increase flow area and reduce drag on the flow. In most river channels this would reduce flow depths, all other factors being equal. But, the Mojave channel width to depth ratio is high enough that a difference in depth would probably be minimal, except in reaches where there has been an extended interval from the last disturbance event. The thinning of vegetation in any given stream section would probably increase the capacity of the channel in that section. Saltcedar removal is expected to have little impact on the sparsely vegetated active channel areas.

The Corps of Engineers Mojave River channel maintenance plan describes the Corps' general goals and the estimated impacts of vegetation control in the active channel (U.S. Army Corps of Engineers (A), 1997). The Corps' document concludes that current channel conditions (1997) have a potential negative effect on streambanks due to excess vegetation. The vegetation in the channel tends to redirect flows toward the levees and streambanks causing erosion of unprotected slopes and overtopping. Any vegetation maintenance is to keep the centerline clear through urbanized areas, and maintain a buffer of adjacent wetlands and riparian vegetation to preserve their function of bank protection. In alignment with the Corps' goals, the team recommended that replacing vegetation where saltcedar removal occurred be made a priority in the near bank portions of the active channel.

Water Conservation: The team evaluated water conservation within the Phase 3 and 4 reaches of the Mojave River through removal of saltcedar. Groundwater pumping has steadily increased since the 1940s, reducing aquifer storage and creating an overdraft condition. This has caused changes in the quantity and distribution of recharge in the Mojave River (Stamos, 2001), leading to a loss of riparian habitat (Lines (A, B), 1996). This is evident in the decline of water levels in wells, which have dropped between 50 to 100 feet within the study area (Stamos, 2001).

The water table in healthy cottonwood-willow woodland is typically less than 10 feet below the surface. Willows and baccharis typically grow in narrow bands along the river edge in wetter areas than the cottonwood-willow woodland. Single-species cottonwood woodlands are common on terraces and slopes that are slightly elevated above the flood plain and the water table is typically 10-15 feet below the surface. Mesquite trees are typically widely spaced along the boundary of the riparian zone where water-table depths are 10-30 feet below the surface (Lines, (B) 1996).

Water savings due to saltcedar removal has been debated in the literature (Shafroth, 2005) as well as benefit/cost studies of water conservation gain, given the cost of mitigation measures (Barz, 2009). The ability of saltcedar to exclude native competition is contentious. Saltcedar roots generally reach deeper than roots of willow, mesquite, and cottonwood; and the invasive plant is able to capture moisture to the exclusion of the natives. In addition, saltcedar is more tolerant of low soil moisture conditions and can survive long drought periods more successfully than native species. Finally, saltcedar draws salt up through the soil column and deposits it on the surface through its leaf litter. The increased salinity further hinders native species (Swift, 2006).

Saltcedar may be able to tap into the water table at depths as great as 50 feet below the ground surface. Because of its rapid growth, saltcedar is commonly the dominant plant growing in the Mojave River channel (Lines (B), 1996).

It is estimated that saltcedar with a density of 71 to 100 percent uses 2.8 feet per acre of water per year. Healthy mesquite at a density of 71 to 100 percent is estimated to use 1.4 feet per acre of water per year (Lines (B), 1996). Reducing the density of saltcedar from 100 to 50 percent reduces water use by only about 10 percent (Hughes, 1972; and Van Hylckama, 1974).

Habitat: Invasive plants throughout the Phase 3 and 4 reaches have the ability to provide some level of habitat value in the form of protective cover and nesting structure (Brown and Johnson, 1998; Stromberg, 2009; and Van Riper, 2008). However, in the bigger picture, this habitat is not valuable if considering the overall negative habitat effects caused when the invasive plants outcompete and replace native plants (Anderson, 1977; Engel-Wilson and Ohmart, 1978; Kasprzyk and Bryant 1989; Howe and Knopf, 1991; Hunter, 1988; Lovich and de Gouvenain, 1998; and Zavaleta, 2000). The habitat value of native plants for native animal species is so high that even a little native plant habitat is much more desirable than a lot of invasive plant habitat. The only habitat condition that was considered where invasive plants would be left in place, was where the water table is too low to support native riparian vegetation. Even so, this consideration was rejected (from the habitat point of view) since leaving invasive species in place increases the potential to spread the plants, and their negative effects, to other locations. There may be some onsite short-term negative impacts to wildlife from the removal of the invasive plants, but the long-term onsite and offsite effect is overwhelmingly positive. The overall effect of invasive plant removal had been evaluated by the appropriate regulatory agencies prior to beginning of the project. Appropriate actions to avoid or minimize negative impacts associated with invasive plant removal were outlined through permitting and consultation with the applicable regulatory agencies.

DELINEATION OF NEGATIVELY EFFECTED AREAS

The team delineated the reach areas determined to be negatively affected due to invasive plant removal as depicted in Figures 4 and 5. These highlighted areas are deemed critical, as the proposed actions could increase the effects of resource concerns on adjacent land uses and should not have any plant removal or treatment, unless it is performed in such a way that the negative effects may be mitigated, using alternatives offered in the report. Figure 6 provides a close up view of areas delineated as “critical”. This type of map allows the user to control vegetation removal in an exact manner.

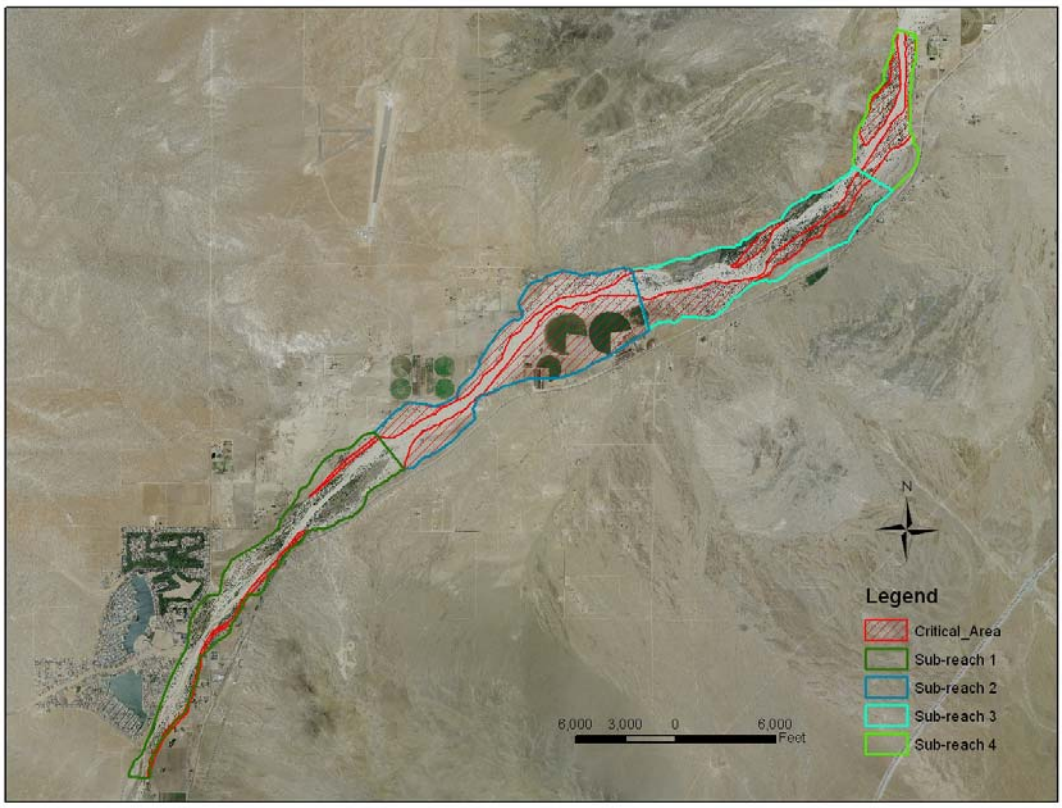

Figure 4 Negatively affected areas for Phase 3 reach.

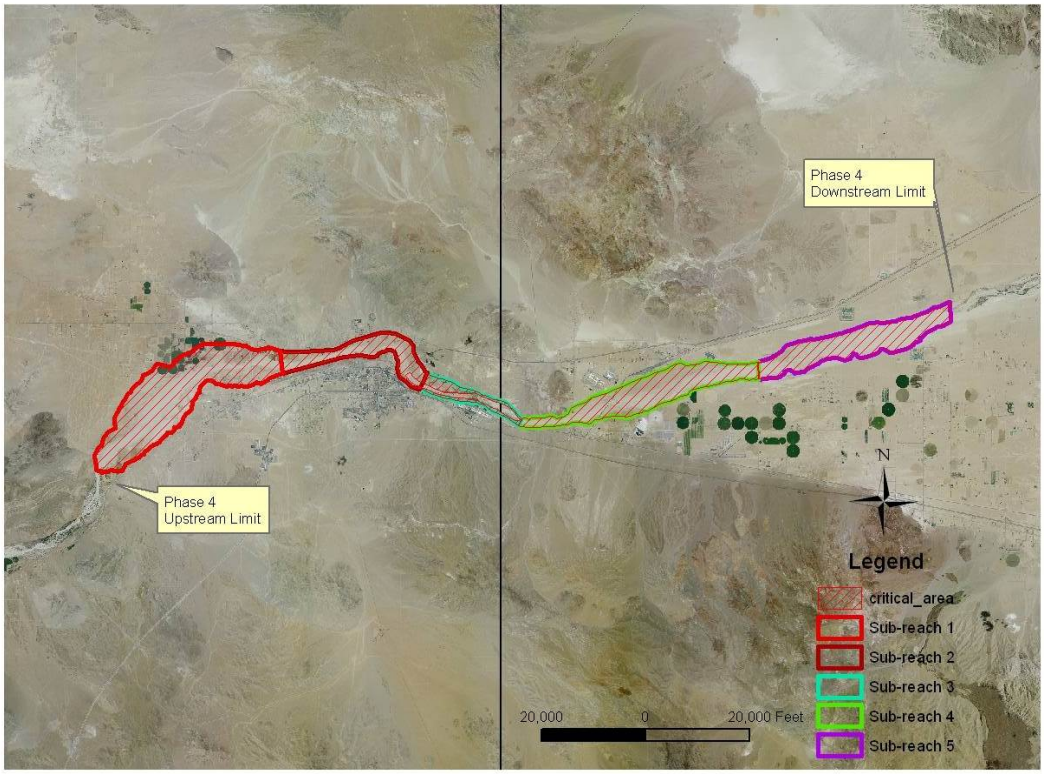

Figure 5 Negatively affected areas for Phase 4 reach.

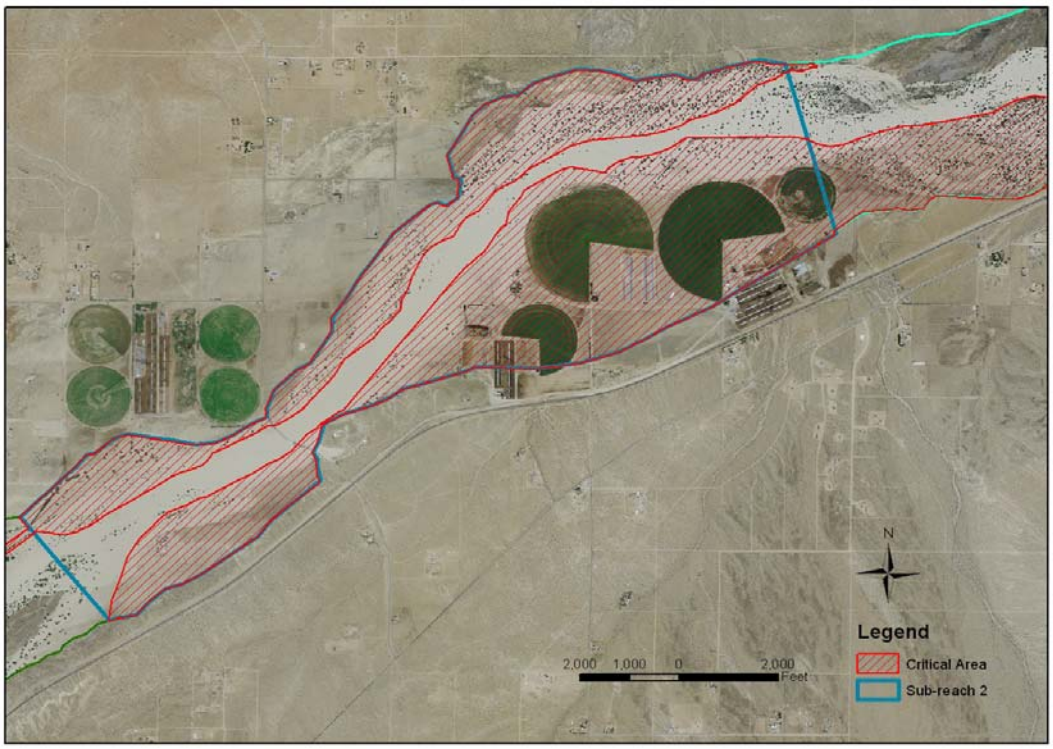

Figure 6 Zoomed in view of Phase 3, sub-reach 2 showing negatively affected areas.

TREATMENT ALTERNATIVES FOR CRITICAL AREAS

The team developed treatment alternatives for removing vegetation within the critical areas of the Phase 3 and 4 reaches. Alternatives included specific methods for vegetation removal, patterns of removal, amounts of vegetation removal, and re-vegetation directions. As an example, for active channel, floodplain, and terraces with mixed stands of saltcedar (25 to 50 percent canopy by area), the team developed the following directions:

1) Treat strips of saltcedar, where the strips are perpendicular to the prevailing wind direction, as evident by sand buildup behind existing saltcedar with a strip width no greater than 10 times the height of the average invasive plant, or (if not stripped) treat only 50 percent of all invasive plants in an every other plant pattern. The untreated strips should be at least 15 feet wide to stop saltation. Treated plants (dead) should remain standing, rather than being chipped on site or removed, to keep the standing plants in place (Skidmore, 1986); and

2) In conjunction with number 1, seed or plant native, soil-stabilizing, vegetation, such as desert panicgrass, (*Panicum urvilleanum)*; desert saltgrass, (*Distichis spicata)*; creeping wildrye, (*Leymus* (Elymus) *triticoides)*; scratchgrass, (*Muhlenbergia asperfolia);* and scale broom, *Lepidospartum squamatum*. Desert panicgrass appears to be adapted to deep sandy soils and dunes. The team observed this species in the active channel, as well as the active floodplain. Scratchgrass is adapted to floodplains with both saline or non-saline sandy soils. NOTE: the above species, except for wildrye, are warm season grasses and should be dormant during foliar herbicide applications and, if dormant, it is assumed that they would not be damaged during fall or early winter herbicide application. However, efforts should be made to direct spraying away from grasses and only onto target plants. The availability of seed or planting stock for creeping

wildrye and desert saltgrass can be intermittent. If desired, there is potential for conducting seeding trials using scratchgrass and, in the future, desert panicgrass with seed from Tucson PMC. Seeding or planting rates should be determined on the site-specific conditions and approved by an NRCS planting plan.

Other specific directions and alternatives were developed for floodplains and terraces with dominant saltcedar (stands with >50% canopy by area) and streambanks or levees with dominate invasive plants (stands with >50% canopy by area of invasive plants). Additional considerations were developed and outlined for establishment of native plants post removal of invasive plants.

SUMMARY

The team generally assessed the potential impacts of the proposed project on locally-identified resource concerns, including streambank erosion, wind erosion, wildlife habitat, water availability and use, and flooding. Recognizing that geomorphic units that together comprise the riparian corridor would respond differently to vegetation removal, the active channel, active floodplain and terraces within the 48-mile long study reach were mapped using GIS equipment and field reconnaissance. For each geomorphic unit, the team assessed whether vegetation removal would have a positive, negative, or insignificant effect on each of the resource concerns and adjacent land uses. Any areas having a negative effect due to vegetation removal were identified as critical and removal would either be avoided or mitigated. The planning report developed by the NRCS/MDRCD team included a map showing critical areas within the inventoried reach, technical guidelines for evaluating other reaches of the channel, and listed approved mitigation alternatives for critical areas.

Since 2009, the MDRCD has spent approximately $ 3,000,000 removing non-native vegetation either mechanically or through chemical treatment according to the plan. The work performed to date includes about 30 of the 48 miles evaluated within the plan. The remaining work will be completed as money becomes available.

REFERENCES

Anderson, B., Higgins, A., and Ohmart, R. (1977). “Avian use of saltcedar communities in the Lower Colorado River Valley,” USDA-Forest Service, General Technical Report RM-43, pp 128-136.

Barz, D., et al. (2009). “Cost/Benefit considerations for recent saltcedar control, middle Pecos River, New Mexico." Environmental Management 43, pp 282-298.

Brown, W.T., and Johnson, R.R. (1990). “Ecology and management of riparian breeding birds in saltcedar habitats along the Colorado River in Grand Canyon National Park,” Proceedings of Saltcedar Conference, University of Arizona, Tucson, AZ, pp 68-73.

Engel-Wilson, R.W., and Ohmart, R.D. (1978). “Floral and attendant faunal changes on the lower Rio Grande between Fort Quitman and Presidio, Texas,” Proceedings of the National Symposium for Protection and Management of Floodplain Wetlands, pp 139-147.

Friedman, J.M. (2009). "Erosional Consequences of Saltcedar Control," Environmental Management. (in review).

Howe, W.H., and Knopf, F.L. (1991). “On the imminent decline of Rio Grande cottonwoods in central New Mexico”, Southwestern Naturalist 36 , pp 218-224.

Hughes, W.C. (1972). "Simulation of saltcedar evapotranspiration," American Society of Civil Engineers Journal, v. 98, no.1R4, pp 533-542.

Hunter, W.C., Ohmart, R.C., and Anderson, B.W. (1998). "Use of exotic saltcedar (*Tamarix chinensis*) by birds in arid riparian systems," Condor 90 pp 11-23.

Kasprzyk, M.J., and Bryant, G.L. (1989). "Results of biological investigations from the lower Virgin River vegetation management study," Bureau of Reclamation, Boulder City, NV, p 75.

Laity, J. (2003). "Eolian Destabilization Along the Mojave River, Mojave Desert, California: Linkages Among Fluvial, Groundwater, and Aeolian Systems," Physical Geography, Vol. 24 (3): p. 196-221.

Lines, G.C. (1996). "Ground-water and surface-water relations along the Mojave River, southern California," U.S. Geological Survey Water-Resources Investigations Report 95-4189, p 43.

Lines, G.C., and Bilhorn, T.W. (1996). "Riparian vegetation and its water use during 1995 along the Mojave River, southern California," U.S. Geological Survey Water-Resources Investigations Report 96-4241, p 10.

Lovich, J.E., and de Gouvenain, R.G. (1998). "Saltcedar invasion in desert wetlands of the southwestern United States: ecological and political implications," Ecology of Wetlands and Associated Systems, Pennsylvania Academy of Science, pp 447-467.

Mojave Water Agency (1996). Investigation Report 96-4241, prepared in cooperation with the California Department of Fish and Game, p 10.

Righetti, M., and Armanini, A. (2002). "Flow resistance in open channel flows with sparsely distributed bushes," Journal of Hydrology 269, pp 55-64.

Shafroth, P. B., et al. (2005). "Control of Tamarix in the Western United States: Implications for Water Salvage, Wildlife Use, and Riparian Restoration," Environmental Management 35(3) pp 231-246.

Skidmore, E. L. (1968). "Wind Erosion Forces In the United States and Their Use in Predicting Soil Loss," Agriculture Handbook No. 346, ARS, USDA.

Stamos, C.L., Martin, P., Nishikawa, T., and Cox, B.F. (2001). "Simulation of ground-water flow in the Mojave River Basin, California," U.S. Geological Survey Water Resources Investigations Report 01-4002, p 129.

Stamos, C.L., Cox, B.F., Izbicki, J.A., and Mendez, G.O. (2003). "Geologic Setting, Geohydrology and Ground Water Quality near the Helendale Fault in the Mojave River Basin, San Bernardino County, California," U.S. Geological Survey.

Stromberg, J.,E., Glenn, M., Chew, and Nagler, P. (2009). "Changing perceptions of change: The role of scientists in Tamarix and river management," Restoration Ecology, 17(2) pp 177-186.

Van Riper, C., Paxton, K., and O'Brien, C. (2008). "Rethinking avian response to Tamarix on the lower Colorado River: A threshold hypothesis," Restoration Ecology, 16, pp 155-167.

Swift, C. E. (2006). "Saltcedar (Tamarix) Physiology, a Primer," (PowerPoint presentation). Colorado State University, Cooperative Extension.

USDA-NRCS (2009). Web Soil Survey.

US Army Corps of Engineers, L.A. District (1977). "Case Study Report #83, Mojave Forks Reservoir, Mojave River".

US Army Corps of Engineers, L.A. District (1997) (A). "Mojave River Floodplain Maintenance Plan".

US Army Corps of Engineers, L.A. District (1997) (B). "Mojave River Floodplain Maintenance Plan Appendix".

Van Hylckama, T.A. (1974). "Water use by saltcedar as measured by the water budget method: U.S. Geological Survey measured by the water budget method," U.S. Geological Survey Professional Paper 491-E, p 30.

Williams, R. (2006). "Erosion Control," University of Washington School of Environmental Science and Resource Management.

Zavaleta, E. (2002). "The economic value of controlling an invasive shrub," Ambio, 29 pp 462-467.

ESTIMATION OF DAILY SUSPENDED SEDIMENT AND MERCURY CONCENTRATIONS AND APPLICATION OF FLOW-NORMALIZED TREND ANALYSES TO ASSESS FLOODPLAIN RESTORATION, CARSON RIVER, NEVADA

Carl E. Thodal, Hydrologist, U.S. Geological Survey, Carson City, Nevada, cethodal@usgs.gov, Eric Morway, U.S. Geological Survey, Carson City, Nevada, emorway@usgs.gov, and Karen A. Thomas, U.S. Geological Survey (retired)

INTRODUCTION

The floodplain of the Carson River was severely destabilized and aggraded during the Comstock Lode mining boom of the late 19th century. The river flows about 180 miles from its headwaters on the eastern slopes of the Sierra Nevada in northeastern California to the Carson Sink in the high desert of western Nevada, draining nearly 4,000 square miles (Figure 1). The headwaters are in steep, volcanic and granitic terrain that is naturally susceptible to erosion. Hillslope erosion was exacerbated during the mining boom by extensive timber harvest from the upper watershed for mine-shaft structural supports and boomtown development. Moreover, sediment from an estimated ten million tons of waste rock and tailings from more than 200 stamp mills downstream of Carson City, Nevada is deposited along the floodplain and river channel (Figure 1). Carson River water quality is further compromised by the release of an estimated 7,500 tons of mercury used in the amalgamation process that was used to extract silver and gold from milled ores. In response to the mercury contamination, the U.S. Environmental Protection Agency (USEPA) listed more than 70 miles of the lower reach of the Carson River as a Superfund National Priorities Site in 1990 (USEPA, 2013).

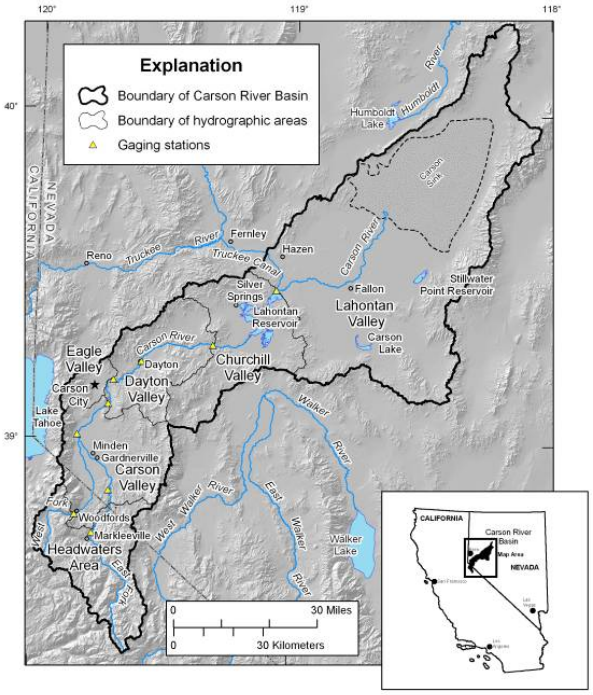

Figure 1 Location of Carson River Basin, California and Nevada

The Carson River has undergone significant geomorphological change that has destabilized its floodplain. As a result, agricultural and residential land has been lost to erosion and bank failure, and sedimentation has affected water quality, prompting efforts to stabilize the Carson River floodplain. Efforts in the mid-1960s to engineer flood control measures by channelizing the sinuous natural streambed, primarily along the East Fork Carson River are now acknowledged to have been a poor floodplain management practice. Renewed efforts beginning in the early 1990s by coalitions of private landowners, volunteers, non-profits, local school and conservation districts, and Tribal, County, State, and Federal agencies have included channel surveys, removal of sediment and constrictive debris, riparian vegetation plantings, flood protection, habitat enhancement, and bioengineered channel-stabilizing technologies (Azad, 2007). Conservation easements and public education about floodplains and recreational access are provided to promote awareness of floodplain value (http://water.epa.gov/type/oceb/upload/2006_11_02_showcase_showcasewatersheds.pdf).

River channel stabilization is apparent where rehabilitation projects, including riparian revegetation and placement of riprap, among others. have been completed (Azad, 2007), but reductions in sediment concentrations and loading have yet to be assessed. The U.S. Geological Survey (USGS) has monitored Carson River streamflow at the Fort Churchill gage (10312000) since 1911 (Figure 2). In October 1997, the USGS, in support of the USEPA Superfund Site Remedial Investigation program, began monitoring concentrations of suspended sediment, total mercury, and methyl mercury in water samples collected from the Carson River near Silver Springs (10312020) and below Lahontan Reservoir (10212150; Figure 2). Daily mean discharge recorded at USGS gaging stations ranged from 0 to 9,500 ft^3/s and averaged 330 ft^3/s as inflow and from 0 to 2,260 ft^3/s and averaged 400 ft^3/s as outflow. Instantaneous discharge measurements made above the reservoir during sampling events ranged from 0.2 to 4,200 ft^3/s and averaged 710 ft^3/s and below the reservoir ranged from 6 to 2,000 ft^3/s and averaged 620 ft^3/s. Sample summary statistics shown in table 1 indicate that Lahontan Reservoir is an effective sink for both suspended sediment and mercury. The statistical summary also indicates significant variability in concentrations. Results from a new statistical model to estimate trends and loading into Lahontan Reservoir are presented as metrics of the Carson River status and the possible effects of floodplain restoration efforts.

Table 1 Summary statistics for water sample concentrations, Carson River near Silver City, Nevada and below Lahontan Reservoir, 1997-2013; concentrations are nanograms per liter except suspended sediment concentrations are milligrams per liter

Constituent	Mean	Minimum	Median	Maximum	Count
10312020; Carson River near Silver Springs, Nevada					
Suspended sediment	220	1.0	61	3,600	309
Unfiltered mercury	2,500	34	1,000	36,000	281
Filtered mercury	29	9.0	25	100	281
Unfiltered methyl mercury	2.9	0.05	2.2	22	285
Filtered methyl mercury	1.2	0.02	1.0	6.8	285
10312150; Carson River below Lahontan Dam, near Fallon, Nevada					
Suspended sediment	28	6	32	100	134
Unfiltered mercury	250	0.04	250	740	134
Filtered mercury	11	2.4	8.4	52	135
Unfiltered methyl mercury	1.4	0.09	0.41	35	135
Filtered methyl mercury	0.6	0.04	0.2	13	133

Figure 2 Locations of selected USGS sampling sites, Carson River, Nevada

APPROACH

Statistical methods that attempt to estimate the mass of water-quality constituents conveyed with streamflow where concentrations are not continuously measured have been developed and evaluated for decades. These investigations aim to better understand temporal load behavior and reduce inherent biases and uncertainties associated with estimated loads (Hirsch, 2014, p. 2). While multiple regression models have demonstrated valid relations between continuous

streamflow and concentrations, analyses of long-term datasets (more than 20 years) have led to the development of models that can accommodate concentration-discharge relations that may change over time.

Exploration and Graphics for RivEr Trends (EGRET, Hirsch and De Cicco, 2014; http://pubs.usgs.gov/tm/04/a10/) is a USGS model written in R (R Core Team, 2014), an Open Source computer and statistical environment that adds flexible enhancements to earlier regression models. The EGRET package has exploratory graphics and statistical tools designed to identify long-term changes in streamflow by computing annual statistics for daily-mean streamflow. The period of analysis can be specified to explore monthly, seasonal, or annual trends in annual average, minimum, and maximum streamflow. Also included in the EGRET software package is the statistical modeling algorithm Weighted Regression on Time, Discharge, and Season (WRTDS; Hirsch et al., 2010) that estimates a continuous concentration time series where continuous streamflow data are available, but observations of constituent concentrations are intermittent. The WRTDS weighted regression equation (Equation 1) estimates daily concentrations by fitting the natural logarithmic function (*ln*) of concentration (*c*) to discharge (*Q*) and time (*t*); including seasonality as sine and cosine functions and ε is the unexplained variation. The regression coefficients (β_i) are estimated for every combination of *Q* and *t* in a weighting system defined by the proximity of each point in *Q* and *t* space (Hirsch and others, 2010).

$$ln(c) = \beta_0 + \beta_1 (ln(Q)) + \beta_2 (t) + \beta_3 sin(2\pi t) + \beta_4 cos(2\pi t) + \varepsilon \quad (1)$$

EGRET and WRTDS have been used to analyze data collected from the Carson River near Silver Springs (USGS site number: 10312020; Table 1 and Figure 2), along with daily streamflow data from the nearby USGS gaging station (USGS site number: 10312000; Figure 2; http://waterdata.usgs.gov/nv/nwis/dv/?site_no=10312000&agency_cd=USGS&referred_module=sw). Standard USGS protocols for measurement of streamflow discharge (Rantz and others, 1982) and isokinetic, depth-integrated water sampling using the equal-discharge-increment method (U.S. Geological Survey, variously dated) were followed for the data collection. Quality assurance and control (QA/QC), documentation, and data validation considerations are described in sampling and analysis plan documentation for mercury monitoring in the Carson River system (Praskins and Thomas, written commun., 2011).

RESULTS

Time series graphs of annual streamflow statistics for Carson River near Fort Churchill during the period of operation (water years 1911-2013) and during the sample collection period (water years 1998-2013) are shown in Figure 3. Both time periods indicate year-to-year variability with decreasing trends in average mean-daily streamflow. The short-term record also indicates decreasing trends in maximum and minimum streamflows. Potential causes of decreasing trends in streamflow cannot be determined with the available data, but changes in land- or water-use, drought, and climate change each may be contributing factors.

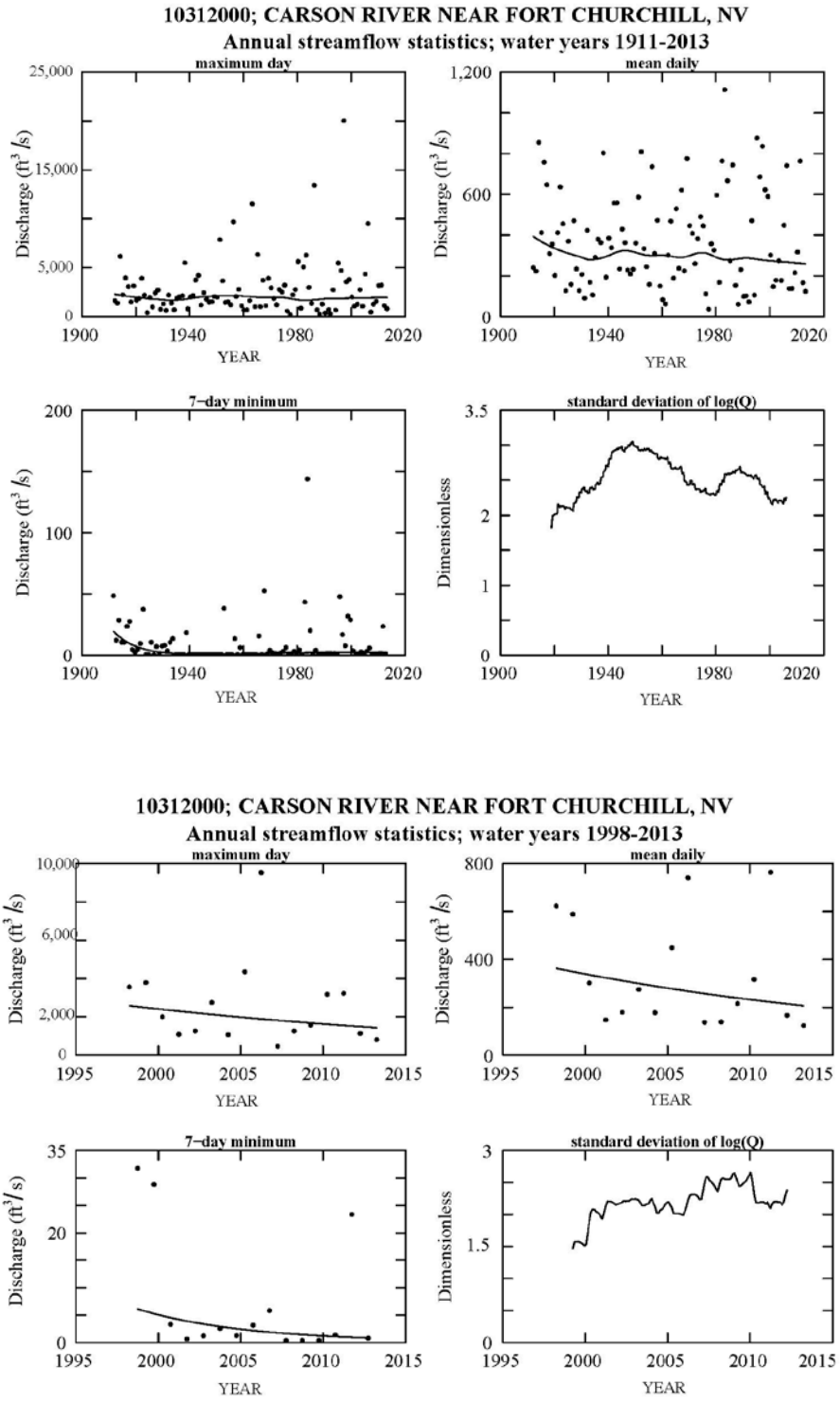

Figure 3 Selected time series of annual streamflow statistics computed for 1911-2013 and 1998-2013, Carson River near Fort Churchill, Nevada

Figure 4 compares mean daily discharge for the 7,457 days that span the suspended sediment sampling period (right box-and-whisker) to the mean daily discharge recorded on the 309 days on which sample collection took place (left box-and-whisker) and shows that sampling may have been biased toward higher streamflows, but is a fair representation of the streamflow distribution during the sampling period.

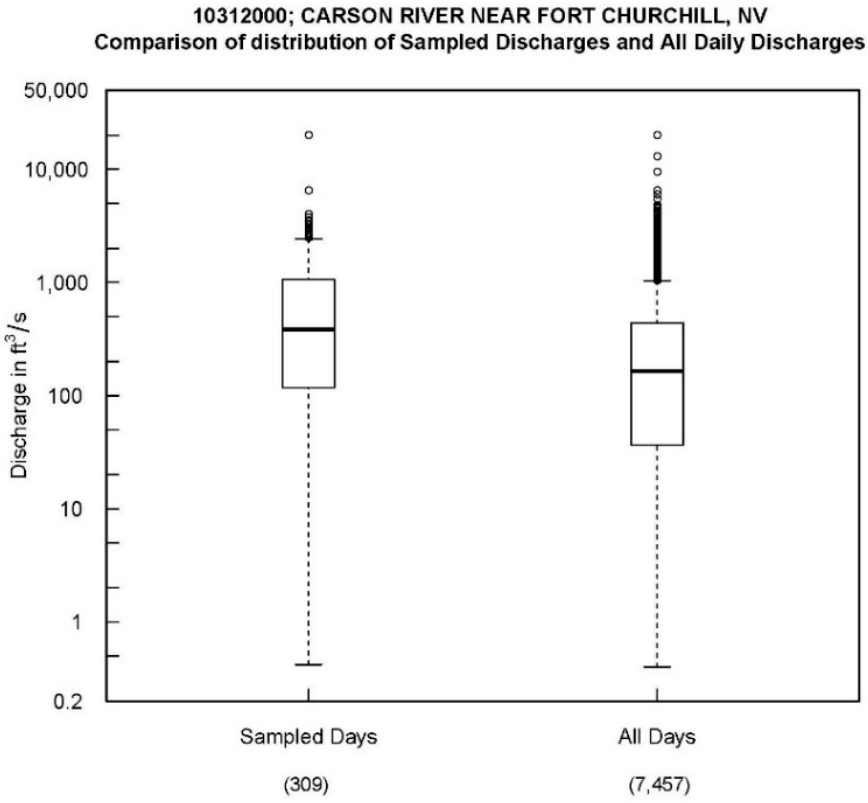

Figure 4 Box and whisker diagrams of mean daily streamflow during sample-collection days and all days during 1998-2013, Carson River near Fort Churchill, Nevada

Suspended sediment data and WRTDS-estimated daily concentrations as a continuous trace are shown in Figure 5a. Because the streambed of the Carson River near Silver Springs is deeply scalloped and has a mobile bedload, suspended sediment concentrations of particles less than 63 microns are computed using silt-sand percentage break determinations and are shown in Figure 5b. The WRTDS model fit is improved for the fine-grained particle size data because the sampling equipment is designed to sample suspended sediment that is at least 0.3 ft above the streambed. The mobile and uneven streambed of the Carson River results in coarser particles being intercepted by the sampler nozzle when it is downstream of submerged sand and gravel dunes.

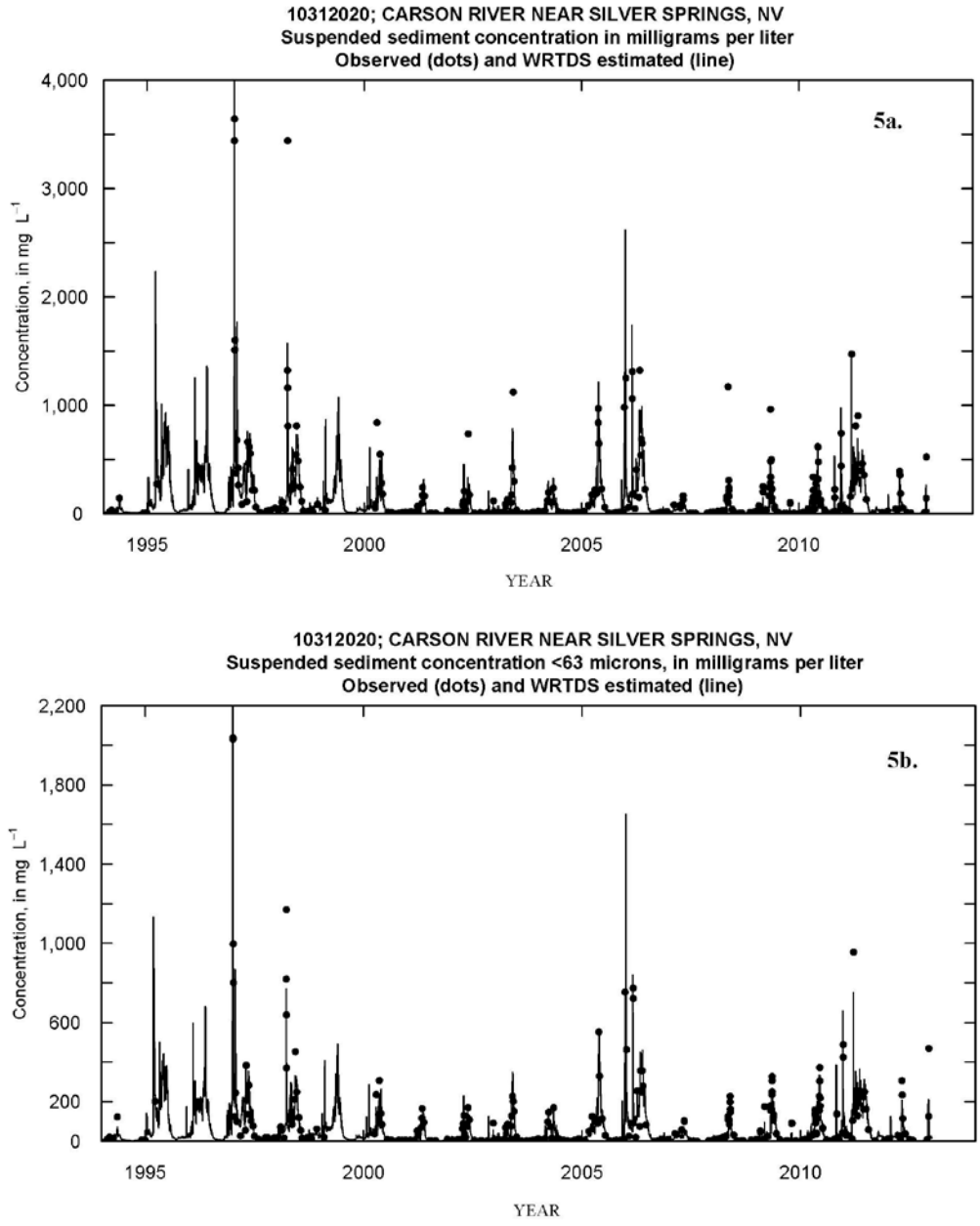

Figure 5 Observed (black dots) and estimated (black line) (5a) concentrations of suspended sediment and (5b) concentrations of suspended sediment less than 63 microns grain size, Carson River near Silver Springs, Nevada

Modeled changes in flow-normalized concentrations and fluxes (loads) for time periods that include all samples and for time periods that arbitrarily bracket the first and last halves of the sampling period are listed in Table 2. Estimated concentrations and fluxes of suspended sediment for the period 1994 through 2012 increased but at a lesser rate of annual change compared to estimates for the period 1994 through 2002. For the period 2002 through 2012 the trend had begun to decrease. Similarly, unfiltered concentrations of mercury and methyl mercury show a decreasing trends in concentrations of -9.5 and -6.9 percent, respectively, while the mass flux estimates decreased by 23 and 35 percent for the period 1998 through 2013. These trends may be

considered improvements, but there may be several contributing factors, including the decreasing trend in discharge, natural recovery of the historically destabilized channel, and floodplain rehabilitation efforts. However, in contrast to decreasing trends in unfiltered mercury and methyl mercury, increasing trends in concentration and flux of filtered mercury was estimated with the highest rate of increase (Table 2) and the flow-normalized concentrations and annual mean concentrations increase at nearly identical rates (Figure 6). The annual changes in average concentrations are relatively small: average suspended sediment concentrations decrease less than 2 milligrams per liter per year, while average filtered mercury concentrations increase by about 1 nanogram per liter (one part per trillion) per year.

Table 2 Estimated trends in concentrations and fluxes of suspended sediment, and mercury for selected time spans, Carson River near Silver Springs, Nevada

Constituent	Time period	Mean-annual percent change in:	
		Concentration	Flux
Suspended Sediment	1994 to 2012	0.1	0.24
	1994 to 2002	1.8	2
	2002 to 2012	-1.1	-0.98
Suspended Sediment, less than 63 microns	1994 to 2012	1.5	1.5
	1994 to 2002	2	2
	2002 to 2012	1	0.85
Unfiltered total mercury	1998 to 2013	-0.64	-1.5
	1998 to 2005	-0.65	-1.6
	2005 to 2013	-0.65	-1.6
Unfiltered methyl mercury	1998 to 2013	-0.46	-2.3
	1998 to 2005	-0.46	-1.9
	2005 to 2013	-0.57	-3.1
Filtered total mercury	1998 to 2013	3.6	4.2
	1998 to 2005	2.5	2.8
	2005 to 2013	3.8	4.6
Filtered methyl mercury	1998 to 2013	-0.35	0.52
	1998 to 2005	-0.18	1.2
	2005 to 2013	-0.51	-0.07

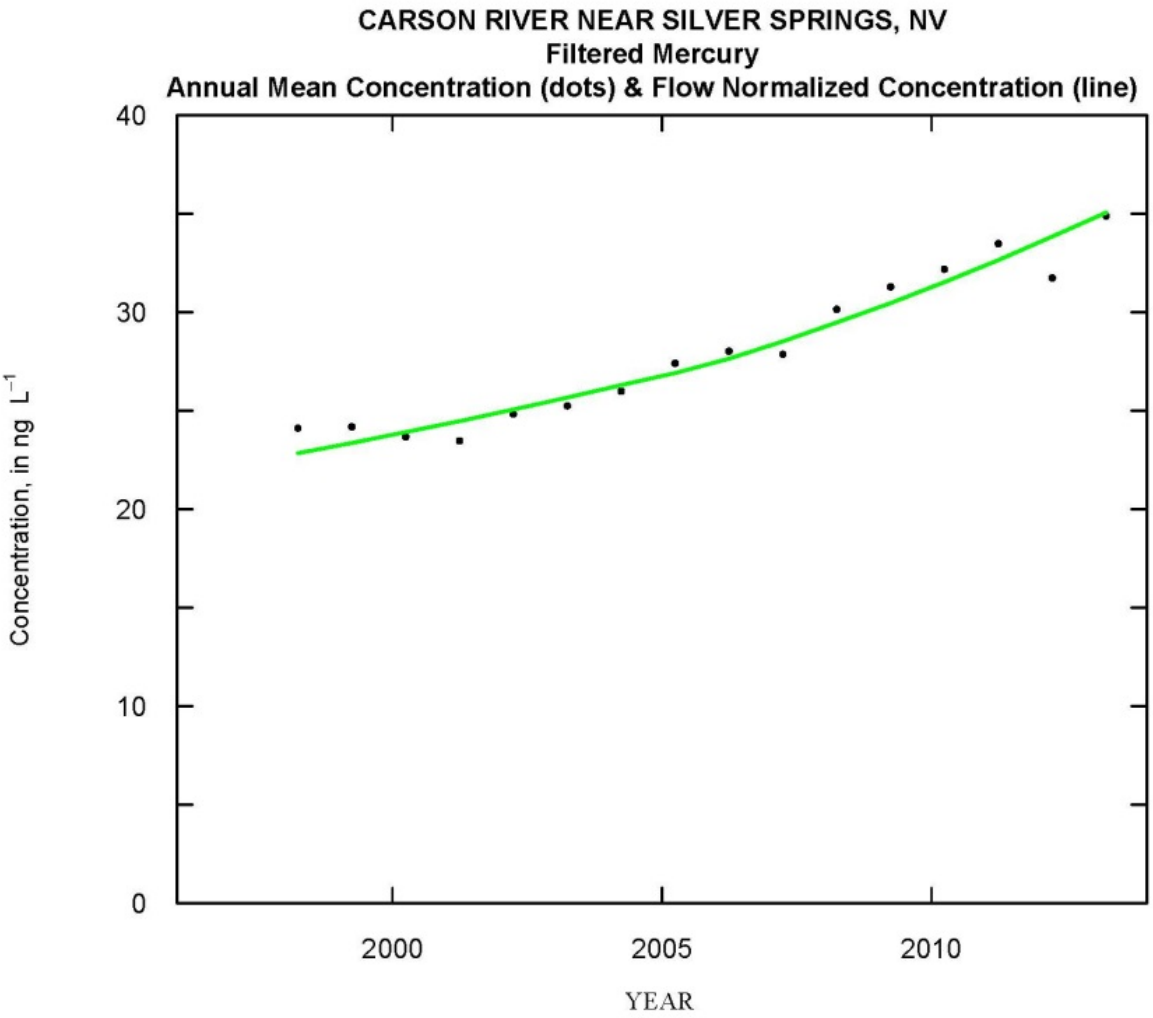

Figure 6 Annual mean filtered mercury concentrations (dots) and flow normalized concentration (line), Carson River near Silver Springs, Nevada

CONCLUSIONS

Statistical analyses, including trend estimation of the data collected in support of the USEPA Carson River Superfund Site Remedial Investigation, show decreasing concentrations and trends in suspended sediment and unfiltered total and methyl mercury. However, these subtle trends may be related to any of several factors, including decreasing streamflow, natural and engineered recovery of a destabilized watershed, or the gradual flushing and volatilization of mercury contamination from impacted sediment upstream of Lahontan Reservoir. The unanticipated increasing trend in filtered mercury concentrations may be related to a similar increasing trend in sample pH, or other unmeasured factors of which dissolved organic carbon and oxidation-reduction potential have been shown to be potential causative factors by other investigators (Aiken et al., 2011).

REFERENCES

Aiken, G.R., Gilmour, C.C., Krabbenhoft, D.P., and Orem, W., (2011). "Dissolved organic matter in the Florida Everglades: Implications for ecosystem restoration," Critical Reviews in Environmental Science and Technology, 41(6), pp 217-248.

Azad, Genie, (2007). Carson River watershed adaptive stewardship plan. Carson River Coalition and Carson Water Subconservancy District, http://www.cwsd.org/carson-river-watershed-adaptive-stewardship-plan/.

Hirsch, R.M. (2014). "Large biases in regression-based constituent flux estimates—causes and diagnostic tools," Journal of the American Water Resources Association, 50(6) pp 1401-1424.

Hirsch, R.M., and De Cicco, L.A. (2014). User guide to Exploration and Graphics for RivEr Trends (EGRET) and dataRetrieval; R packages for hydrologic data. U.S. Geological Survey Techniques and Methods book 4 (A10), *http://dx.doi.org/10.3133/tm4A10*.

Hirsch, R.M., Moyer, D.L., and Archfield, S.A. (2010) "Weighted Regressions on Time, Discharge, and Season (WRTDS), with an application to Chesapeake Bay River inputs," Journal of the American Water Resources Association, 46(5), pp 857–880, *http://onlinelibrary.wiley.com/doi/10.1111/j.1752-1688.2010.00482.x/full*.

R Core Team, 2014, R: A language and environment for statistical computing. R Foundation for Statistical Computing, Vienna, Austria. URL http://www.r-project.org/.

Rantz, S.E. and others (1982). Measurement And Computation Of Streamflow. Volume 1, Measurement Of Stage And Discharge; Volume 2, Computation Of Discharge. U.S. Geological Survey Water Supply Paper 2175, http://pubs.usgs.gov/wsp/wsp2175/.

U.S. Environmental Protection Agency, 2013, Explanation Of Significant Differences; Carson River Mercury Site, Washoe, Carson City, Lyon, And Churchill Counties, Nevada, NVD980813646.

U.S. Geological Survey (variously dated). National Field Manual For The Collection Of Water-Quality Data. U.S. Geological Survey Techniques of Water-Resources Investigations, book 9(A1-A9), http://pubs.water.usgs.gov/twri9A/.

MISSOURI RIVER HABITAT PROJECT DESIGN, PERFORMANCE, AND ASPECTS OF THE 2011 FLOOD

Daniel Pridal, Hydraulic Engineer, U.S. Army Corps of Engineers, Omaha, NE, daniel.b.pridal@usace.army.mil

Abstract: The Missouri River Recovery Program (MRRP) has constructed over thirty chute and backwater habitat areas on the Missouri River within the Omaha District that were consistent with shallow water habitat (SWH) creation requirements specified within the Biological Opinion (2000) and the Amended Biological Opinion (2003). Design and construction practices have evolved over the last 10 years due to project performance, objectives, and constraints. In addition, the 2011 Missouri River event within the Omaha District resulted in a sustained high peak flow with unprecedented duration. As a result, the Missouri River and entire floodplain experienced large areas of sediment erosion and deposition. Habitat project design process, construction aspects, and the observations related to 2011 flood impacts are presented. Conclusions regarding project performance with recommendations for future design improvements are provided.

INTRODUCTION

In 1989, The U.S. Army Corps of Engineers (Corps) initiated consultation with the U.S. Fish and Wildlife Service (Service) regarding operation of the Missouri River Main Stem Reservoir System. Consultation covered operation of the Missouri and Kansas Rivers as well as the Missouri River Bank stabilization and Navigation Project (BSNP). The 2000 Biological Opinion found that the actions proposed by the Corps would jeopardize the Interior least tern, pallid sturgeon, and piping plover. With the intent of precluding jeopardy to the species, the Service provided a Reasonable and Prudent Alternative (RPA). The Corps requested a re-initiation of the formal consultation and an amended Biological Opinion was provided in 2003. The Missouri River Biological Opinion and the Amended Biological Opinion (BiOp) set forth the requirements for the creation of shallow water habitat (USFWS, 2003). The RPA consisted of numerous elements pertaining to flow management, habitat diversity, and habitat area. The RPA performance standard for shallow water habitat acres established a goal of 20 to 30 acres per mile for the Missouri River from Ponca, Nebraska, located about 60 river miles downstream of Gavins Point Dam, to St. Louis, Missouri, a distance of 752 river miles. Since 2003, the Corps has completed construction of numerous projects intended to create shallow water habitat in this reach of the Missouri River. Following construction, monitoring activities have been conducted to evaluate the project performance. Activities have been conducted in both Omaha and Kansas City Corps of Engineers Districts (USACE, 2013). The Missouri River geometry and hydraulic characteristics change significantly between the two Corps Districts, which results in major differences in project formulation. The high floodplain energy associated with the flows and duration of the 2011 event resulted in significant changes within the floodplain including the constructed habitat projects. This paper focuses on observations related to habitat projects and

project performance within the Omaha District and the portion of the channelized Missouri River between Ponca, Nebraska, at river mile 752, and Rulo, Nebraska, at river mile 498.

Pallid Sturgeon Habitat: The pallid sturgeon is native to the Missouri and Mississippi Rivers and is adapted to the free flowing, warm water, and turbid habitats that are in a constant state of change. Floodplains, backwater, chutes, sloughs, islands, sandbars, and main channel waters formed the large river ecosystem that historically provided habitat for all life stages of pallid sturgeon in the river. Evidence of reproduction for wild origin pallid sturgeon is lacking. Destruction and alteration of big river ecological functions and habitat that was once provided by the Missouri River that followed Corps dam construction and channelization actions is believed to be the primary cause of declines in reproduction, growth, and survival of pallid sturgeon.

Shallow Water Habitat Definition: As set within the biological opinion, the parameters used to define shallow water habitat are Missouri River flow depths less than five feet (1.5m) and velocities less than two fps (0.6 m/s) (USFWS, 2003). For the purposes of assessing habitat creation, the effective discharge is defined as the 50% exceedance discharge from the August flow duration curve(s). Although the habitat accounting system is based on the effective discharge, data are also gathered and analyzed for a range of flows to provide an assessment of habitat diversity. Within the context of the RPA, shallow water habitat refers to:

- 50% exceedance August flow rate
- Flow depth less than 5 feet (1.5m)
- Flow velocity less than 2 ft/sec (0.6 m/s)

Channelized River Background:

Between 1912 and 1945, Congress, by funding and authorizing seven different acts, charged the U.S. Army Corps of Engineers with reservoir system construction, stabilizing the banks of the Missouri River, and providing a 9-feet deep by 300-feet wide navigation channel. Management activities resulting from these acts have included removing snags, protecting the river banks from erosion, and constructing and maintaining the navigation channel. This collection of projects is known as the Missouri River Bank Stabilization and Navigation Project (BSNP) (USACE, 2011). The Missouri River navigation project extends from its confluence with the Mississippi River at St Louis, Missouri, to Sioux City, Iowa, for a total distance of 734.2 river miles. For reference, Gavins Point Dam, the furthest downstream of the Missouri River reservoir system of six dams, is located at river mile 811. The reservoir system is operated to meet multiple authorized purposes, including navigation, as described in the Master Manual (USACE, 2006).

Stabilization and navigation objectives were accomplished through revetment of banks, construction of permeable dikes, cutoff of oxbows, closing minor channels, removal of snags and dredging. The BSNP is designed as a self-scouring channel that has not required maintenance dredging within Omaha District. In order to achieve the project objectives of bank stabilization and navigation, the river was shaped into a series of smoothly curved bends of the proper radii and channel width. Stabilization of the bank along the concave alignment of the design curve was accomplished with pile and rock-fill revetments. Dikes were constructed approximately perpendicular to the flow or slightly angled downstream along the convex bank, that were oriented to promote project objectives. BSNP structures are constantly attacked by river flows. Maintenance is conducted to ensure the structures provide river stability and channel dimensions

necessary for commercial navigation and other authorized purposes. Within the Omaha District portion of the navigation channel, the Missouri River has a top width generally between 600 and 700 feet. Dike spacing is also on the order of 600 to 700 feet. The typical BSNP components within the navigation channel are illustrated in Figure 1.

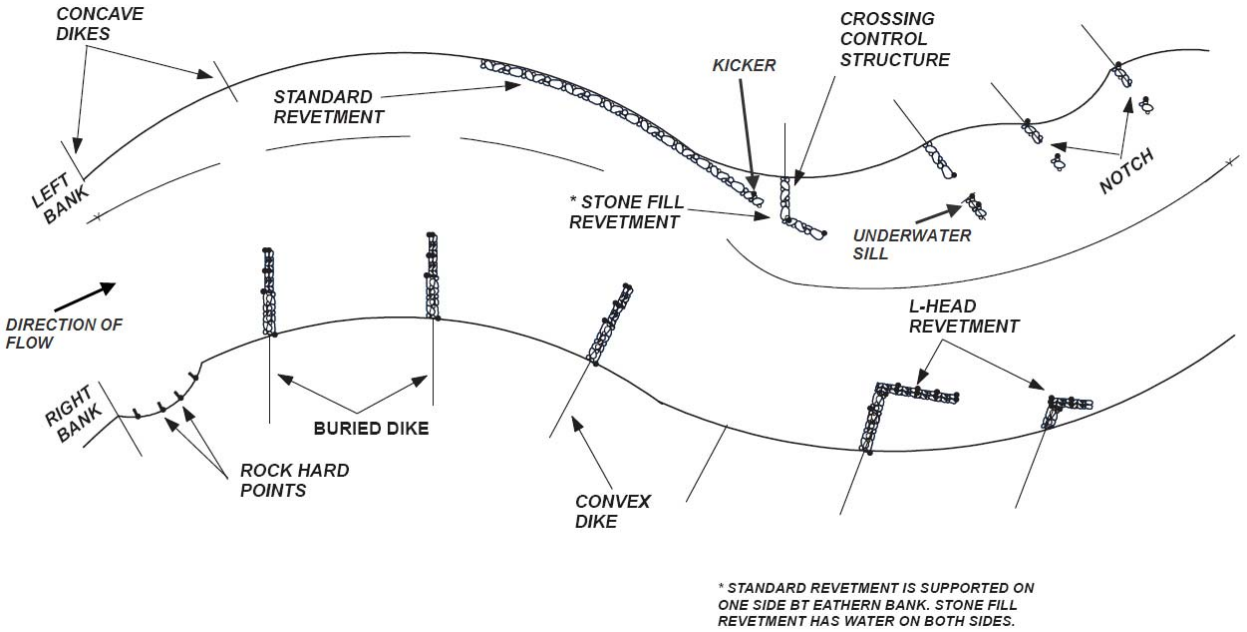

Figure 1 Typical Missouri River Navigation Channel Plan View

Habitat Project Types: Shallow water habitat is created using many different approaches that are generally classified according to the habitat type and location. Some projects are created within the main channel while other methods are within the adjacent floodplain. Habitat project types that have been used within the Omaha District include:

- Structure Modifications - Dike Notching (in-channel revetment and dikes)
- Backwater (off-channel)
- Pilot Channel (off-channel)
- Chute (off-channel)
- Major Dike Modification (in-channel dike lowering and chevron construction)

Employment of the various methods is often limited by physical parameters, available real estate, and other factors. For instance, bend curvature, site topography, adjacent infrastructure, and other factors may prevent sustainable construction of an off-channel chute. No actions are conducted without acquiring a real estate interest in all lands encompassing the project.

2011 EVENT

The duration and magnitude of the 2011 Missouri River flood event exceeds all other events in the recorded history of the river. Annual runoff volume frequency has been characterized as a 0.2 percent annual chance exceedance (500-year) event (Grigg et al., 2012). Historic events were

reviewed to provide context regarding 2011 event river flows. Sustained periods of prolonged floodplain flow indicate flow energy acting within the floodplain. In a simple method used to compare the 2011 event flow energy to historic events, the number of days when the Missouri River flowed within the floodplain were tabulated. When comparing contemporary to historic events, it should be recognized that historic river flows were affected by Missouri River main stem dam construction and reservoir filling, primarily from 1953 to 1967. All flow-frequency values reported in the comparison are post dam construction (USACE, 2003). As a result, comparing contemporary to historic events is somewhat misleading since the reservoir system has significantly altered its peak flows. For this simplified evaluation of floodplain energy, the 2-year event was assumed to roughly correspond with floodplain flow initiation. Data from the USGS gage at Nebraska City, Nebraska, which is located about 250 river miles downstream of Gavins Point Dam, is shown in
Figure **2**.

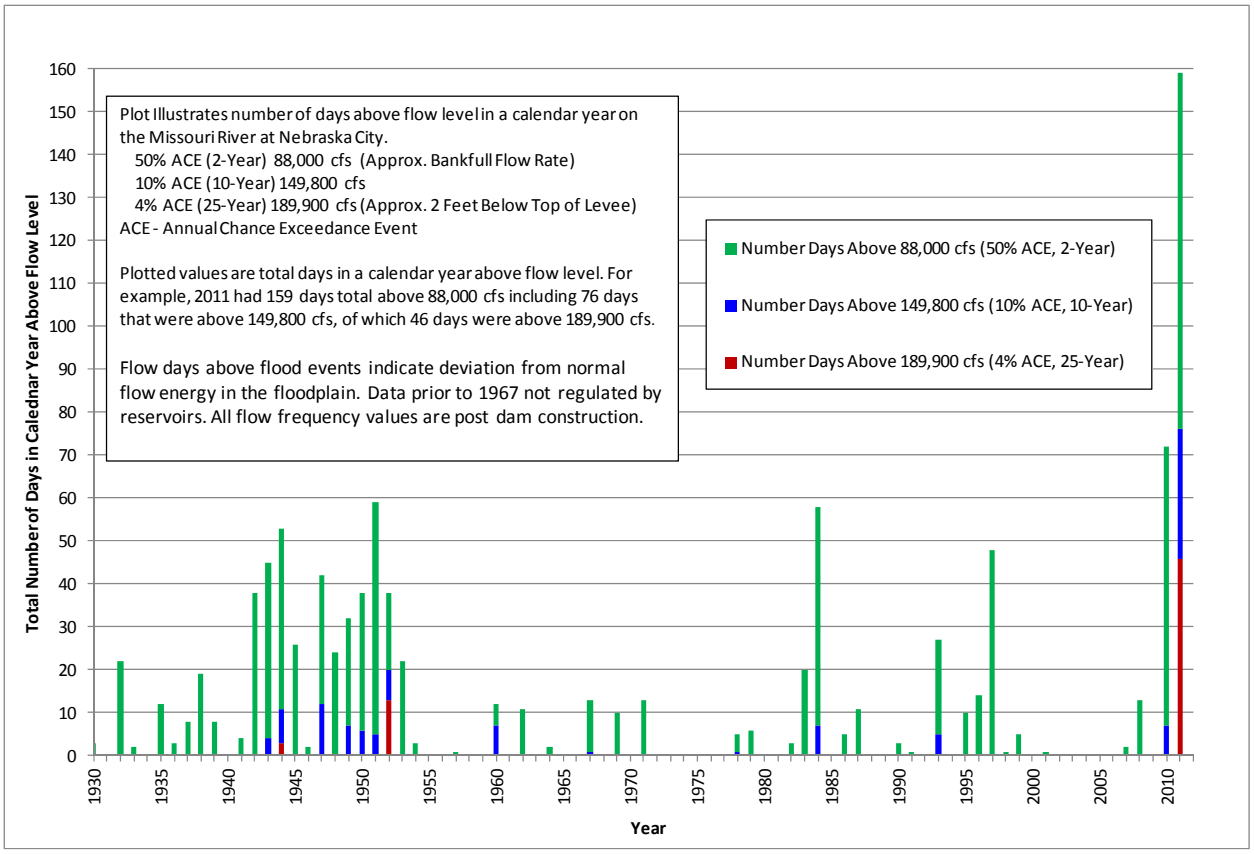

Figure 2 Nebraska City Days above Flow Value by Year

The above figure illustrates the severity of the 2011 event. The 2011 flow year at Nebraska City had 159 days with average daily flow above a 50% ACE (2-year) which roughly corresponds to the duration of floodplain flow or flow above the channel bank height. Furthermore, the 2011 event had 46 days with an average daily flow in excess of the post dam construction 4% (25-year) annual chance exceedance (ACE) event of 189,900 cfs. The prolonged duration of the 2011 event with flows above channel capacity dwarfs all other events which occurred on the historic

Missouri River. The 2011 event is the only event since mainstem dam construction was completed in the mid 1950s to have even a single day with the daily average flow greater than the 4% ACE (25-year). The average daily flow comparison illustrates that the 2011 event was unique with floodplain energy at a very high level for a prolonged duration that is unprecedented in the historic record.

HABITAT PROJECT PERFORMANCE EVALUATION

Habitat Projects Prior to the 2011 Event: Prior to the 2011 event, a total of 33 off-channel chute and backwater projects had been constructed in the Omaha District with varying size and location as shown in Table 1.

Table 1 Omaha District Off-Channel Projects Constructed Prior to 2011 Event

Site No.	Off Channel Projects	RM		Year	Length	State	SWH 2010 Acres[1]
		DS	US				
1	Ponca State Park Backwater	753		2004		NE	70
2	Glovers Pt Backwater	711.5		2005		Tribal	28.6
3	Glovers Point Chute	711.2	713.4	2005	11,100	Tribal	15
4	Hole In the Rock Backwater	706		2006		Tribal	5
5	Blackbird-Tieville-Decatur Flow Thru	688	698	2006		IA	7
6	Middle Decatur Chute	687.4	688.2	2009	4,640	NE	20
7	Lower Decatur Revet. Lower	685.7	687.3	2008	8,200	NE	7
8	Lower Decatur Chute	684.9	687.3	2008	2,400	NE	9
9	Louisville Bend Backwater	682	685	1995		IA	60
10	Fawn Island Chute	673.3	674.1	2010	2,979	IA	9
11	Three Rivers Revet. Lowering	669.4	670	2010	2,810	NE	12
12	Bullard Bend Backwater	663		2009		NE	25
13	Soldier Bend Backwater	660.4		2004		IA	26.8
14	Tyson Backwater	653.2		2009		IA	63.9
15	California Bend, IA, Chute	649.5	650.1	1999	4,000	IA	11.6
16	California Bend (IA) Backwater	649.5		2004		IA	16.3
17	California Bend, NE, Chute	648.5	650.1	2003	9,230	NE	36
18	Lower Calhoun Chute	637.1	637.6	2009	2,750	NE	9
19	Boyer Backwater	634.2		2010		NE	43
20	Boyer Chute	633.7	637.8	1994	16,760	IA	56
21	Council Bend Chute	616.8	617.8	2007	5,630	IA	18
22	Plattsmouth Lake Connect. Backwater	592.8	593.8	2005		NE	25
23	Plattsmouth Backwater Phase 2	592.3		2008		NE	25
24	Plattsmouth Chute	592.1	594.5	2005	12,070	NE	90
25	Tobacco Island Chute	586.3	588.4	2002	15,450	NE	23
26	Upper Hamburg Chute	552.2	555.9	1996	15,950	NE	97
27	Lower Hamburg Backwater	552		2005		MO	7
28	Lower Hamburg Chute	550.6	553.4	2005	13,200	MO	34
29	Kansas Bend Chute	544.5	546.4	2005	9,150	NE	23
30	Nishnabotna Chute	542.4	543.3	2005	5,780	NE	19
31	Langdon Bend Backwater	529		2000		NE	10
32	Deroin Bend Chute	516.4	520.5	2002	18,140	MO	85
33	Rush Bottoms Chute	499	502	2008	8,400	MO	12
	1 - Refers to the shallow water habitat acres as determined in a 2010 evaluation. This is pre-2011 high flow acres.						

The Corps utilized a monitoring and adaptive management program to verify that projects were within design objectives, that all Missouri River authorized purposes were functioning, and to inform future project design. In general, project performance prior to the 2011 event had been as expected. Critical points regarding constructed project performance through 2010 are:

- Projects were in different stages of development due to the time period since construction and other site specific factors such as historic flows, soil types, etc.
- Due to many factors, multiple habitat project types and sizes were constructed. Within the framework of the various project objectives and performance expectations, no significant performance differences were noted between habitat types.
- Several chute projects required minor maintenance on rock structures.

- No chutes experienced problematic erosion or widening and were within an acceptable range.
- Performance of habitat enhancement projects, such as features to promote depth diversity and add woody debris, had been reasonably successful.
- Sediment deposition had been noted in backwater areas as expected, with routine maintenance performed at some sites to maintain their function.

Habitat Project Assessment Following the 2011 Event: Following the 2011 event, the Omaha District performed numerous design and repair projects of critical infrastructure including dams and levees throughout the basin. Although a lower priority, habitat projects were also assessed and repairs performed as resources allowed. Inspection indicated that SWH habitat was lost in many constructed projects and gained in others. This also applied to the overall river corridor. However, much of the post-flood habitat does not appear to be sustainable and will likely experience future deposition. Flood damage varied significantly between constructed SWH projects. The high flood flows traveled downstream following the valley slope in the most energy-efficient manner crossing river bends. Erosion and deposition patterns typically associated with flow turbulence and velocity reduction due to primary flow direction exiting and entering the channel and floodplain were observed throughout the river corridor. Floodplain infrastructure and features, such as roads and levees, constricted the floodplain width and concentrated flows. Floodplain features as well as constructed habitat projects in the path of this flow zone were often severely impacted. Visible erosion and deposition areas were apparent throughout the floodplain corridor without an observed correlation to the presence or absence of SWH projects. Typical floodplain conditions post 2011 flood are shown in Figure **3**.

Figure 3 Typical Floodplain Conditions Post 2011 Flood.

Flood flows traveled across the river bends which resulted in degraded BSNP dikes and revetments at most bend entry and exit points, regardless of the presence of SWH projects. Floodplain material dynamics were noted throughout the Missouri River flow corridor with zones of both scour and deposition that occurred as the flood flows traveled linearly down the valley floodplain regardless of navigation channel alignment. Depending upon the location and river dynamics, constructed chute and backwater habitat projects in the floodplain were subject to the same floodplain dynamics and experienced both scour and deposition. Flood flow patterns in a typical area are illustrated in
Figure **4**.

Off Channel Chutes: Chute project response to the 2011 flow event varied significantly with location. A little less than half of the chutes required no or minor repairs. Constructed chute projects at about one-third of the sites experienced deposition that prevented flow-through chute connectivity at normal Missouri River flows and threatened sustainability. Minor sediment removal projects have been conducted at two sites, planning continues at a third site, and three sites likely will not be repaired due to excess sediment deposition. Many chutes experienced both erosion and deposition with varying levels. Chutes experienced rock structure damage, flanking of control structures, and both widening and deepening. These geometry changes resulted in chute flow above the amount desirable for both habitat and adjacent project purposes. Minor issues were addressed with repair of rock structures in many sites. At three other chutes which experienced significant erosion, new control structures were added to reduce the flow to an acceptable level and improve performance to meet design objectives.

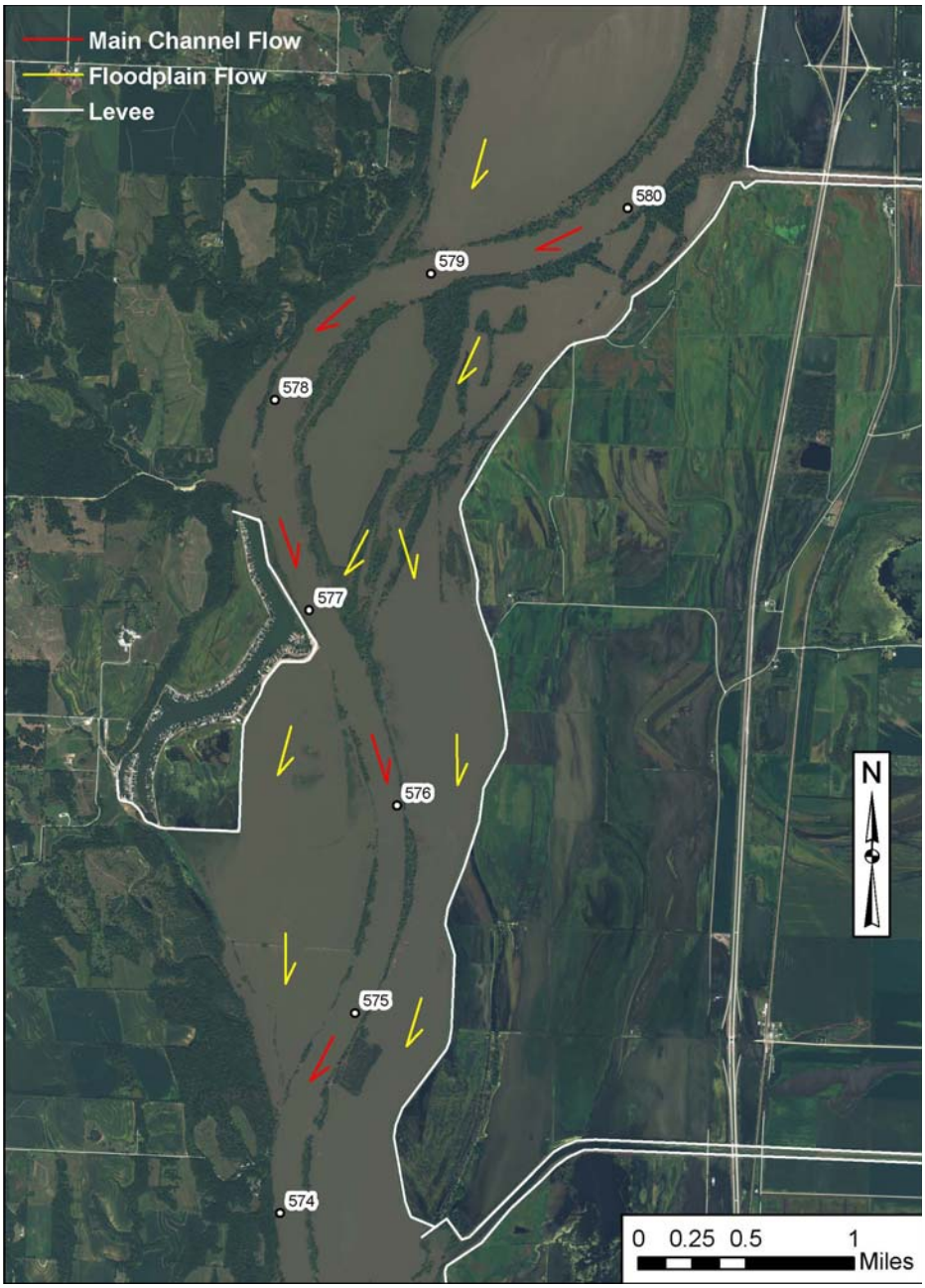

Figure 4 Typical Flood Flow Patterns

An inspection and subsequent evaluation of chute projects for factors which influenced the severity of damage noted a correlation to the previously discussed floodplain flow constrictions such as roads and levees, main channel curvature, and flow transfer across bends. For example, several chute projects that experienced erosion also were located in areas of floodplain constrictions which likely contributed to higher flow energy. Several chutes that experienced deposition were oriented against the path of prevailing floodplain flows. An example of a typical chute entrance that required repair is shown in
Figure 5.

Figure 5 Typical Post Flood Chute Entrance Requiring Repair

Backwater Area Evaluation: Backwater projects experienced variable levels of scour and deposition as a result of flood flows. It should be noted that backwater areas are known to be depositional during normal flow periods due to the Missouri River sediment load. However, post-flood surveys and observations indicated that the 2011 flood deposition generally raised bottom elevations within backwater areas. This deposition will likely reduce the interval before remedial sediment removal is necessary to maintain optimum function and provide shallow water depths during normal river flows.

A quantitative evaluation of backwater deposition volume directly attributed to the 2011 event has not been conducted. Qualitatively, observations indicated greater deposition tended to occur in backwater areas that had been constructed with variable depths and non-linear shorelines. Backwaters which were located in the lower portion of a bend with upstream features which reduced floodplain flow such as natural topography, road crossings, levees, and heavily forested areas generally experienced lesser amounts of deposition from the flood event. Conversely, backwaters that were located in the typical floodplain sediment deposition zone as floodplain topography created low velocity areas experienced greater deposition volumes. Most backwater areas experienced deposition at the entrance from the Missouri River that was in excess of the typical formation at normal flows. An example of a backwater area illustrating the entrance sediment deposition bar is included in
Figure **6**.

Figure 6 Typical Backwater at Low Winter Water Level Illustrating Entrance Sediment Bar

SUMMARY

The Omaha District Corps of Engineers has conducted significant SWH design, construction, and monitoring activities since 2004. The 2011 Missouri River event within the Omaha District resulted in a sustained high peak flow with unprecedented duration which significantly impacted the floodplain and constructed projects. Significant observations include:

- The 2011 event was unique with excess floodplain energy at a very high level for a prolonged duration that was unprecedented in the historic record.
- Prior to the 2011 event, no constructed chutes had experienced significant or problematic erosion and were operating within an acceptable range.
- The entire floodplain and features were severely altered by the 2011 flood event.
- Following the 2011 event, the Omaha District performed numerous design and repair projects on critical infrastructure including dams and levees throughout the basin. Although a lower priority, habitat projects were also assessed and repairs performed as resources allowed.
- Habitat and channel conditions are known to be dynamic. Future changes are expected as the river continues to recover during a more normal flow range following the 2011 event.
- The factors which correlated to constructed project response appeared to be surrounding floodplain features such as levee constriction and roads, bend layout with respect to transfer of flood flows, and floodplain topographic irregularities.
- Chute response varied significantly. About half of the chutes required no or minor maintenance. Several sites experienced deposition, several sites had significant scour.
- Chute changes usually consisted of degradation of the entrance control structure, flanking of internal control structures, and both chute widening and deepening.

- Measured chute:river flow ratios are useful to assess chute geometry changes as a result of the event.
- Backwaters had varying degrees of deposition that appeared to correlate with bend alignment, location within the floodplain, and upstream floodplain features.
- While backwaters are known to require periodic maintenance, the sediment deposited during the 2011 event generally reduced the interval before remedial sediment removal is necessary to maintain optimum function.

REFERENCES

Grigg, N., McCarthy, C., Lawrence, B., Ockerman, D. (2012). Review of the Regulation of the Missouri River Mainstem Reservoir System During the Flood of 2011, Independent Technical Review Panel, Missouri River Basin Water Management Division, Omaha, Nebraska.

USACE (2006). Missouri River Mainstem Reservoir System, Master Water Control Manual, Operation and Maintenance Manual, Missouri River Basin, Reservoir Control Center, U.S. Army Corps of Engineers, Northwestern Division, Omaha, Nebraska.

USACE (2011). Operation and Maintenance Manual, Missouri River Bank Stabilization and Navigation Project, Sioux City Iowa to the Mouth, U.S. Army Corps of Engineers, Omaha District.

USACE (2014). 2013 Annual Report for the Biological Opinion on the Operation of the Missouri River Main Stem System, Operation and Maintenance of the Missouri River Bank Stabilization and Navigation Project, and Operation of the Kansas River Reservoir System, U.S. Army Corps of Engineers, Omaha District and Kansas City District.

USFWS (2003). 2003 Amendment to the 2000 Biological Opinion on the Operation of the Missouri River Main Stem Reservoir System, Operation and Maintenance of the Missouri River Bank Stabilization and Navigation Project, and Operation of the Kansas River Reservoir System, U.S. Fish and Wildlife Service.

EVALUATION OF LEVEE SETBACKS AS A SUSTAINABLE SOLUTION ALONG THE MISSOURI RIVER

Tony D. Krause P.E. CFM, Chief, Flood Risk and Floodplain Management
USACE-Omaha, tony.d.krause@usace.army.mil;
Kelly Baxter, Economist, USACE-Omaha, kelly.d.baxter@usace.army.mil;
David J. Crane, Biologist, USACE-Omaha, david.j.crane@usace.army.mil;
Randall L. Behm P.E. CFM, Chair, National Nonstructural Flood Proofing Committee, USACE, randall.l.behm@usace.army.mil

The views expressed in this paper are those of the author and do not necessarily reflect the official policy or position of the United States Army Corps of Engineers, the Department of the Army, Department of Defense, or the United States Government.

ABSTRACT

The use of levee setbacks provides a sustainable strategy to reduce flood risk by enhancing protection of people and property, providing economic benefits, and improving established ecosystems. Following the 2011 Missouri River flood two efforts to evaluate levee setbacks were conducted; the Assessment of Conceptual Nonstructural Alternative Levee Setbacks along the Missouri River (ACNALS) (USACE, 2012), and the implementation of levee setbacks in two locations as part of the 2011 flood recovery. These efforts have shown levee setbacks as a viable alternative to in-place repairs of existing levee alignments.

The U.S. Army Corps of Engineers (USACE) portfolio of levees was constructed over a long time period stretching back to the early 1900s. As such, levee design and implementation is varied due to the multiple agencies engaged with levee programs, evolving societal goals with regard to the benefits and risk associated with levees, and evolving state of the practice both for levee design and environmental compliance. The 1994, the Galloway Report (IFMRC, 1994) similarly noted that:

> *The current flood damage reduction system in the upper Mississippi River Basin (including the Missouri River Basin) represents a loose aggregation of federal, local, and individual levees and reservoirs. This aggregation does not ensure the desired reduction in the vulnerability of floodplain activities to damages. Many levees are poorly sited and will fail again in the future. (Executive Summary)*

There are locations in levee systems where historic levee performance issues, hydraulic pinch points, and disconnected floodplain habitat intersect. These locations provide an ideal site for implementing levee setbacks.

The purpose of this paper is to discuss USACE Omaha District efforts to evaluate and construct levee setbacks along the Missouri River following the flood of 2011. This evaluation relies primarily upon the information in the ACNALS report as wells as the evaluations for the constructed levee setbacks.

INTRODUCTION

Since the passage of the Flood Control Acts in 1928 and 1936, the Federal Government has taken a lead role in the construction of flood-risk reduction projects. Levees have been one of the primary tools used to accomplish this task. The USACE inventory of levees is significant, with over 14,000 miles of levee segments identified in the National Levee Database (NLD). The majority of the inventory was constructed prior to modern water resource management requirements such as the National Flood Insurance Program (NFIP) floodway and National Environmental Policy Act. The Missouri River levee systems, located in between Omaha and Rulo, are representative of the inventory with levee alignments protecting large areas with recognized flood risk, life-cycle funding, and ecosystem concerns.

The Missouri River downstream of Omaha, Nebraska, and Council Bluffs, Iowa, consists of a navigation project with stabilized banks, an engineered channel, and a system of agricultural and urban levees protecting vast acres of farmland and residential areas. During the 1930s, protection of land was considered an incidental benefit of the navigation project. As discussed in the 1939 Missouri River Improvement Report (USACE, 1939):

> *While intended primarily for the improvement of navigation, works constructed on the Missouri River by the Federal Government have resulted in considerable benefits of other kinds. The most obvious of such incidental benefits is the protection afforded to bottom lands along the improved sections of the river. … The resulting security in the tenure of land has fostered a more stable agriculture in the valley, and increased the value of the lands and improvements.*

During the 1940s, protecting land with levees became a prominent part of the overall Missouri River plan with authorization for levee construction in the 1944 Flood Control Act (FCA).

Design for the Missouri River levees was authorized to provide minimum conveyance widths set by the FCA at 3,000 feet from Sioux City to the mouth of the Kansas River. Additionally, a buffer of 1,000 feet from the established bank line was identified. While much of the system does maintain these minimum conveyance widths, numerous locations exist with widths less than the 3,000-foot minimum. This issue exists most notably at bridge crossings where widths commonly vary from 1,200 to 1,600 feet. These alterations from the authorized buffer were primarily to include features in the protected area of the levee or reduce the cost of construction by building onto existing levees. The 1947 Definite Project Report (DPR) Supplemental on Levee Unit L-575 identifies locations where the levee was aligned without the minimum conveyance width in order to protect individual farmsteads and occupied residences, tie in with and increase the height of existing levees, or conform to existing bridge abutments.

Since the construction of the levee systems, a number of flood events have occurred causing levee breaches, significant damage, and routine wear and tear. Notably, the 1952, 1993, and 2011 floods resulted in levee breaches on the L-550 and L-575. In addition to the breach events, more frequent, less severe flood events such as the 1984 and 2010 events caused damage in the form of erosion and scouring to the levee systems, which was repaired through the PL 84-99 program. The Federal cost-shared Public Law 84-99 (PL 84-99) program provides assistance to repair damages caused by flood events. These repair costs are in-addition to routine non-cost-shared sponsor O&M costs.

Following the 1993 flood event, the Interagency Floodplain Management Review Committee was tasked to delineate the major causes and consequences of the 1993 Midwest flood. The committee evaluated the performance of existing floodplain management and related watershed management programs, which resulted in the publication of *Sharing the Challenge: Floodplain Management into the 21st Century*. Some of the conclusions from the this report include (IFMRC, 1994):

- *The need to consider both structural and nonstructural means to mitigate flood damages*
- *Levees can cause problems in some critical reaches by backing water up on other levees or lowlands*
- *Many levees are poorly sited and will fail again in the future*
- *Human activity throughout the basin has caused significant loss of habitat*

Adverse impacts to the ecosystem have been identified and linked to the disconnection between the Missouri River and its natural floodplain. Most notably, the US Fish and Wildlife Service (USFWS) 2000 (and 2003 amended) Biological Opinion on the Operation of the Missouri River Mainstem Reservoir System, Operation and Maintenance of the Missouri River Bank Stabilization and Navigation Project, and Operation of the Kansas River Reservoir System (BiOp) identifies the USACE as providing primary operational management of the Missouri River and is therefore responsible under the Endangered Species Act to take action within its authorities to conserve listed species impacted by the operation of the

Missouri River (USFWS, 2000 and 2003). The BiOp provided the USACE with a Reasonable and Prudent Alternative that, if accomplished, would likely avoid jeopardizing three listed species (pallid sturgeon, least tern, and piping plover).

EXISTING CONDITIONS

The current alignment of the Missouri River Levee System is based primarily on design concepts developed in the 1940s and early 1950s. Like most levee systems of that era, the overriding design goal included maximizing the size of the protected area behind the levee. Alignments for the levees were guided by available and affordable real-estate, minimizing levee lengths, and building onto existing locally-constructed levees to minimize project costs. The 1947 Missouri River Levees Detailed Project Report (DPR) notes (USACE, 1947):

> *Consistent with design criteria, prime consideration is given to protection of the maximum amount of land that is under cultivation or can be reclaimed after the levees are constructed. Attention is also given to alignment factors affecting the cost of construction and maintenance…*

By maximizing the amount of protected area and minimizing project costs, it was thought the levees would provide the highest benefit to the nation, both in terms economic development potential and flood risk reduction. At that time, the concept of maximizing the protected area was well received. This approach resulted in levee systems that are located in the active high-energy floodplain. Review of the levee alignments with historical imagery and mapping identifies numerous locations where alignments cut across abandoned meander channels, ridge and swale point bar morphology, chutes, and cutoff channels.

Flood Risk Conditions Multiple hydraulic constrictions exist along the Missouri River as a result of current levee and bridge alignments. A hydraulic constriction is a location with reduced conveyance in relation to upstream and downstream areas. To identify hydraulic constrictions, velocities for the 100-year flood event were modeled using the 2008 Missouri River Floodway model. Figure 1 shows modeled velocities in the Missouri River between Omaha and Rulo with annotation at various velocity peaks. Each of these velocity peaks is associated with a hydraulic constriction.

In general, the Missouri River levee systems are located near the river banks and their alignments are founded on a blanket of silts and clays, underlain by pervious sand and gravel. The geology corresponds to the historic braided channels typical to the Missouri River floodplain. The blanket of silts and clays provide an important layer of protection in the flood risk reduction function of the levee systems as a control of underseepage. The increased velocity associated with constrictions leads to increased flood risk through two primary methods, increased potential for erosion and scouring, and increased stages. Higher velocities are associated with higher potential for erosion and scour. Erosion and scour have the ability to alter stream and cross-section geometry, migrate riverine features, and/or damage the silt and clay blanket. At constriction points, the increased potential for erosion and scour makes the blanket layer more susceptible to damage.

The Galloway Report provided a review of the levee breaches in the 1993 flood event noting that 72% of the studied breaches were associated with areas occupied by one or more channels that had been active within the past 120 years. This report recommends the following (IFMRC, 1994):

> *Recommendation 8.1: The USACE in cooperation with the USGS and should conduct a detailed historical analysis of levee breaching to document specific levee locations and causes of high failure rates. This study should include geotechnical data and new field studies of hydraulic and geomorphologic factors that directly affect levee erosion and failure.*
>
> *Recommendation 8.2: On the basis of detailed floodplain mapping and historical levee evaluation, the USACE in cooperation with the USGS and SCS should identify alternative alignments for levees with high failure rates.*

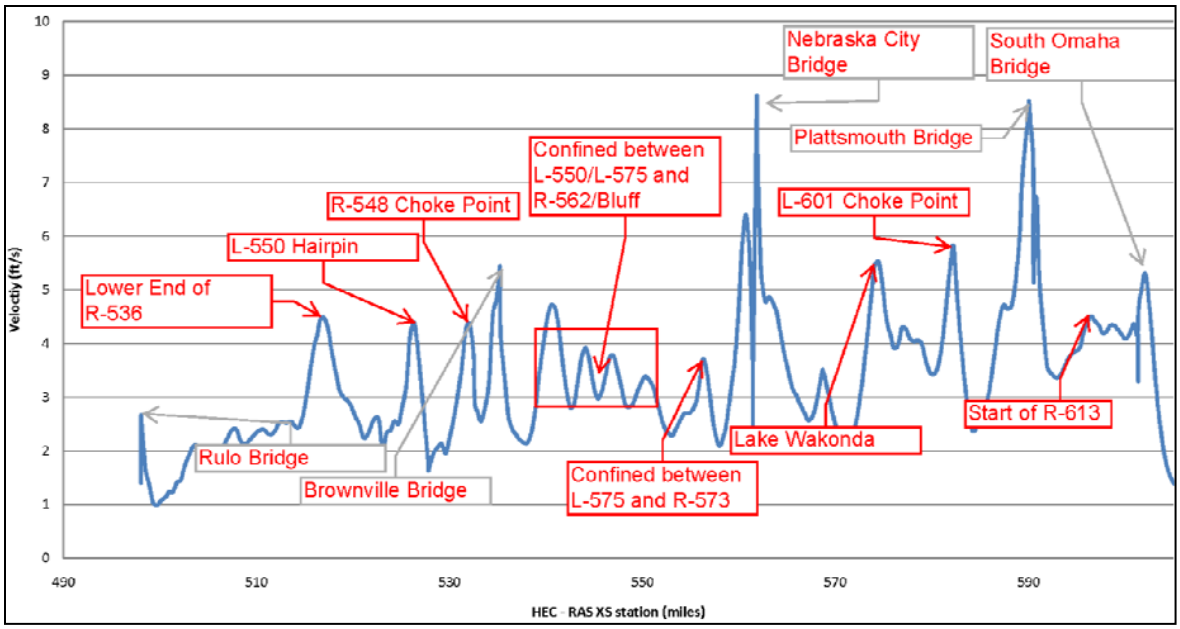

Figure 1 Missouri River 100-year velocities, Omaha to Rulo

Increased velocities at constriction points also result in increased water surface elevations, requiring larger amounts of energy to push water through the constricted conveyance locations. This was noted in the Galloway report (IFMRC, 1994):

> *Levees can cause problems in some critical reaches by backing water up on other levees or lowlands.*

Similarly, the Great Flood of 1993 Post-Flood Report (USACE, 1994) states:

> *By protecting the areas behind the levees, flood flows are partially constrained by the levees and forced to flow through a narrower cross section. This constriction causes flood levels to be higher for a specified distance upstream.*

Figure 2 presents stage trends of the Missouri River at Nebraska City, Nebraska from the 2012 Missouri River State Trends Report (USACE, 2012). This figure shows increasing stages for flows above 50,000 cfs. Following the 1984 Missouri River flood event, an evaluation of the adequacy of the Missouri River Levee System identified decreased levels of protection provided by the levee systems (USACE, 1986). The Upper Mississippi River System Flow Frequency Report (USACE, 2003) identified increasing stage trends at Omaha and Nebraska City, Nebraska. While it is certain that a rise in the stage-discharge relationship has occurred since the time of construction, this impact may come from many sources including the levee systems and floodplain aggradations. Estimates of the levee specific impacts was provided in multiple reports following the 1993 flood, including 0.5-2 feet with isolated areas having impacts as large as 4 feet (USACE, 1994) and 2-4 feet (USACE, 1995). These increased stages led to increased overtopping frequency for levee systems, as well as increased hydrostatic forces resulting in increased seepage potential.

Economic Conditions Figure 3 graphically presents the inter-relationship of levee site location, flood risk, habitat, and life cycle costs. On the Missouri River, these increased costs are incurred in a number of ways, including Federal costs through the Rehabilitation and Inspection Program (RIP), flood fight costs through the PL 84-99 expenditures, and habitat restoration costs through the Missouri River Recovery Program (MRRP). Local sponsor costs include ongoing O&M of levee systems. These costs are both

event-driven as well as ongoing. Due to the dispersed nature of the expenses amongst different entities, for different purposes, and in different time scales, they are difficult to fully quantify.

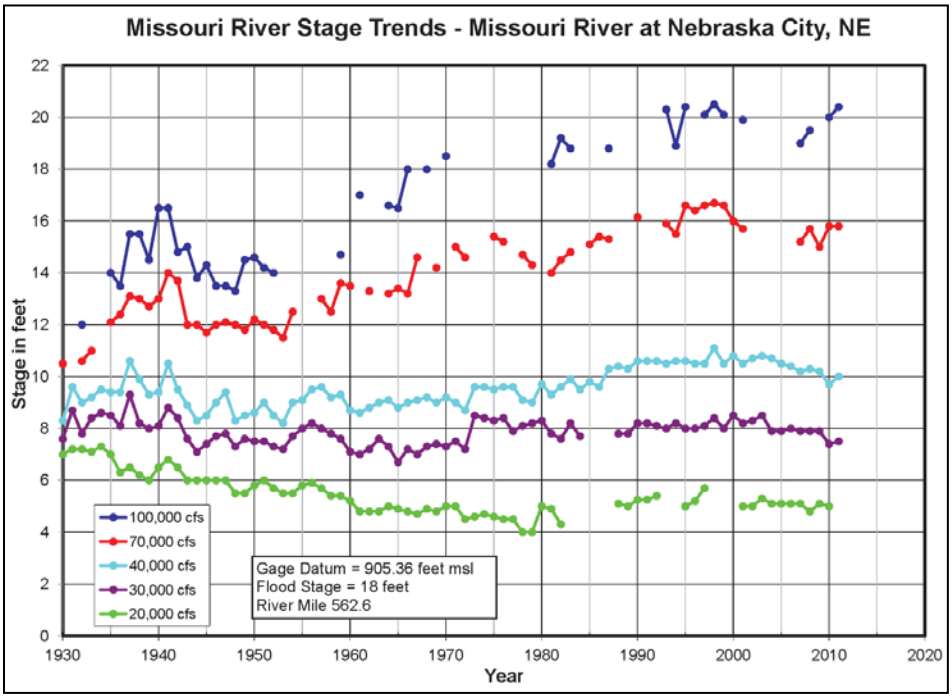

Figure 2 Missouri River at Nebraska City (USGS0680700) Stage Trends

Reviewing the costs of activities along the Missouri River does show that there are significant costs being incurred. Repair costs for levee systems L-575 and L-550 following the 2011 flood event were approximately $166.8 million. Total PL84-99 costs following the 1993 flood event for the Omaha District were approximately $7.6 million (~$12.1 million adjusted to 2014 dollars). Average annual costs for the MRRP, between 1992 and 2013, was approximately $30.8 million, this includes all activities involved in mitigating habitat lost due to construction of the BSNP along the entirety of the Missouri River.

Ecosystem Conditions Isolating the Missouri River from its floodplain has greatly impacted the river's ability to maintain its natural and beneficial ecological functions, and significantly changed the environmental conditions native species rely upon. Connectivity between a river and its floodplain are important to the flow, exchange, and pathways that move organisms, energy, and matter throughout watersheds (MNDNR, 2012). The high biodiversity typically found across natural floodplains cannot be maintained without the rejuvenating forces of floods and channel meandering (NRC, 2002).

Species-specific impacts due to today's degraded conditions can be observed across a suite of riparian and riverine flora and fauna. Disconnecting the land from the river has disrupted the periodic overbank flooding and erosion/deposition processes necessary for regenerating and maintaining cottonwood forests (Dixon, 2010). As a result of these alterations to the river-floodplain ecosystem, cottonwood forests that were once dominant along the river have ceased reproduction. Under the altered river conditions, 51 of 67 native mainstem fish species are now listed as uncommon or decreasing across all or part of their historic range. Benthic macroinvertebrate production has declined by 70% along the unchannelized river reaches (NRC, 2002). Over 80 species on the Missouri River have been listed under state statutes as rare, threatened, or endangered, including 24 fish, 22 birds, 14 plants, 6 reptiles, 6 mammals, 6 insects, and 2 mussels (Whitmore and Keenlyne, 1990).

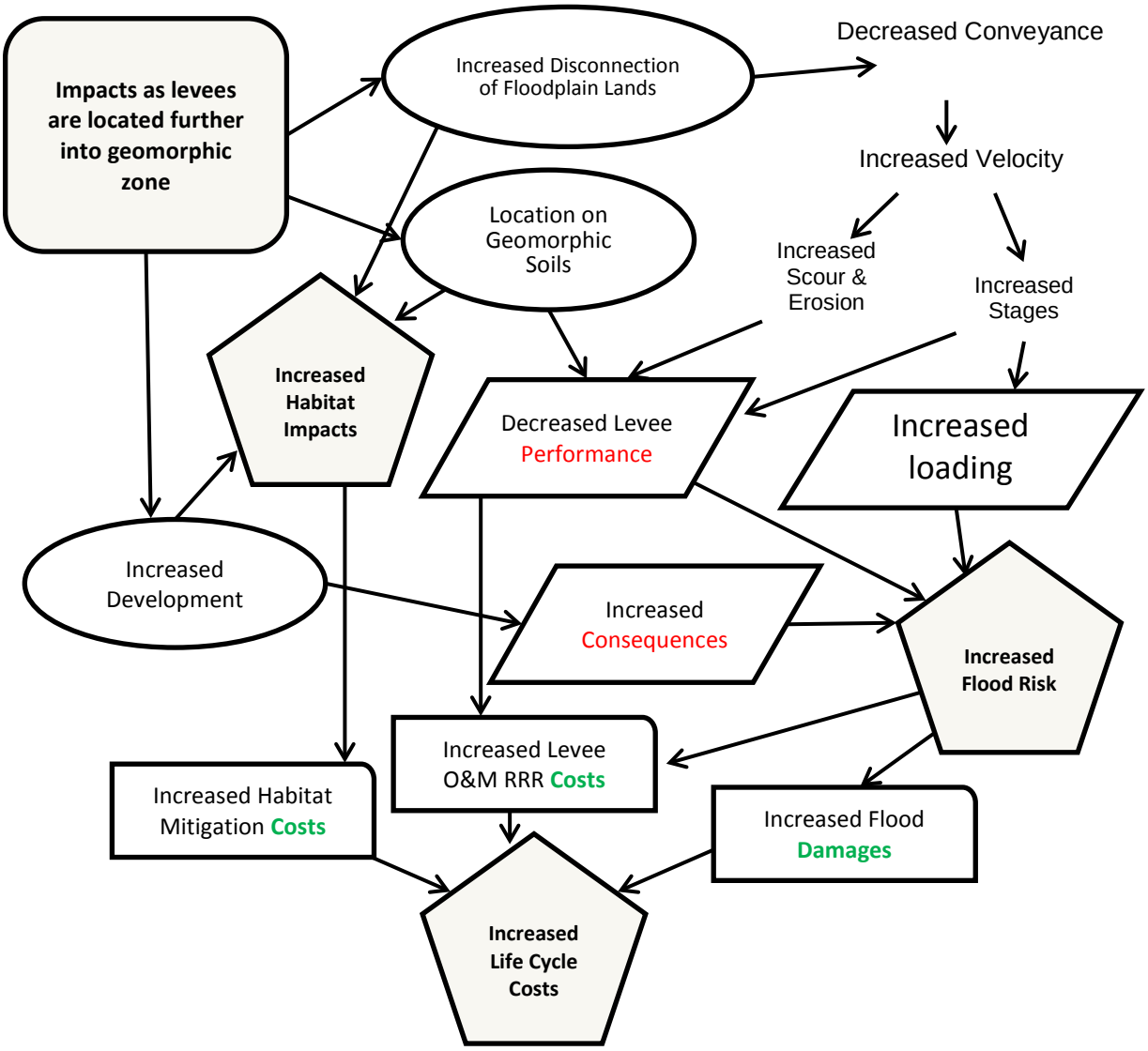

Figure 3 Interrelationships of Levee Locations in Geomorphic Zone and Lifecycle Costs

LEVEE SETBACK EVALUATION

Balancing flood risk reduction benefits with the impacts associated with levees in a financially beneficial manner is the goal of properly designed, constructed, operated, and maintained levee systems. The current understanding of riverine system management including flood-risk management, economic benefits, and habitat interactions has altered the way in which engineers approach levee system design. Implementing levee setbacks at select locations, such has hydraulic constrictions, provides a strategy to modify existing infrastructure with this modern understanding. Figure 4 provides a cross-sectional view of the levee setback concept.

The following sections discuss efforts to identify and quantify these benefits from the ACNALS, implementation of levee setbacks following the 2011 flood, and monitoring of those levee setbacks in subsequent years. The ACNALS evaluated three large-scale levee setbacks on L-575 and L-550 (each ~2.3 sq mi of floodplain connectivity). As a part of the post-2011 reconstruction, two hydraulic levee

setbacks were constructed on L-575 in Fremont County, Iowa. One setback is located at the Nebraska City constriction along Highway 2 within the Copeland Bend Wildlife Management Area (WMA), which reconnected approximately 760 acres of floodplain.

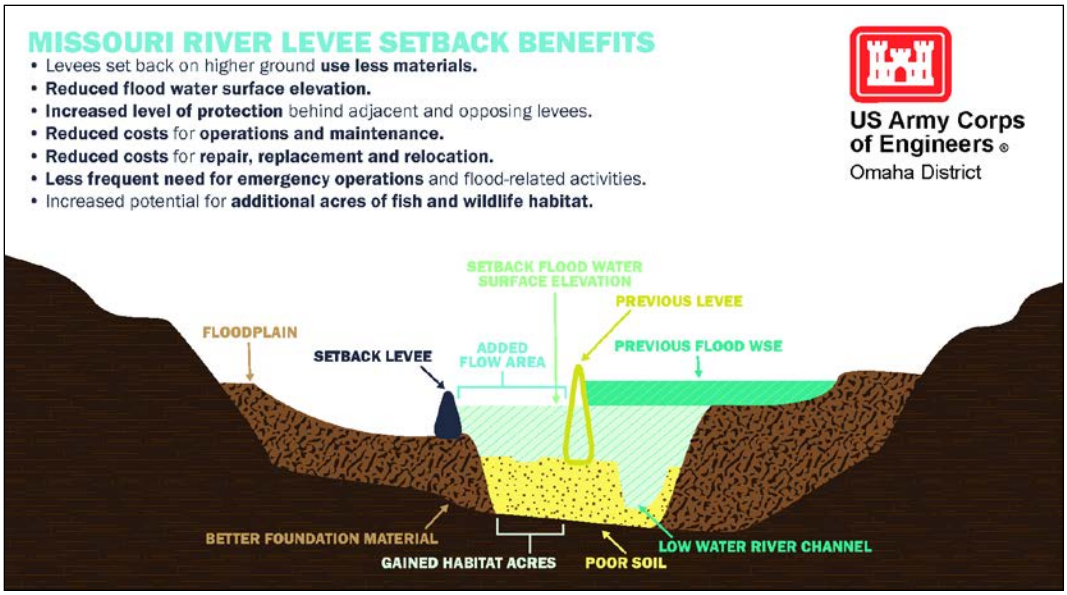

Figure 4 Levee Setback Concept Cross Section

The second setback is located at River Mile 557 within the Frazer Bend WMA, which reconnected approximately 980 acres of floodplain. Figure 5 provides an example of the levee setbacks assessed as part of the ACNALS. Figure 6 identifies the constructed levee setbacks on L-575. Overlaying the 1879 MRC mapping and historic performance of the levees shows similar themes as the Galloway report (IFMRC, 1994) which identified a correlation between breach locations and areas occupied by one or more active channels in the past. Figure 5 shows six historic breach locations, all of the four inlet breaches (as well as the two outlet breaches) are located in areas identifiable as active channels in the 1897 MRC maps.

Flood Risk Evaluation The ACNALS indentifies velocity reductions at identified pinch points; these reductions dropped pre-project velocities of 7.5 fps - 8.5 fps (feet per second) to 4.5 fps - 6.5 fps. Stage reductions resulting from this were four feet just upstream of the setbacks, and showed benefits of 0.10 feet 20 miles upstream. This level of benefit is in line with the estimated hydraulic impacts of levees in the post-1993 reports. These stage decreases have a significant effect on the calculated frequency of levee loading. For the L-575 and L-550 systems, the overtopping frequency could be decreased by 50% with similar decreases in loading frequency on the levee system prior to overtopping. Benefits to the adjacent systems (R-548, R-562, and R-573) are similar, with calculated loading frequencies cut in half.

The implemented levee setbacks show that at hydraulic constrictions, significant hydraulic benefits can be obtained with modest floodplain connectivity. The Nebraska City hydraulic constriction was one of the largest velocity peaks on the Missouri River from Omaha to Rulo (see Figure 1). The constructed levee setback altered the 100-yr velocity from 9.7 fps to 4.2 fps, dropping stages 1-2 feet through the project area. Frequency of overtopping the L-575 levee system (above Hwy 2) was altered from an 80-year to a 120-year frequency, and loading to 3 feet below the levee crest was altered from a 25-year to a 35-year frequency. This shows an overall reduction in loading of ~33%. At the River Mile 557 setback, 100-year velocities were reduced from 4.1 fps to 2.7 fps providing a stage reduction of 1.44 feet. This benefit is also experienced by the adjacent levee on the right bank of the river, R-573, which provides protection for the Omaha Public Power District Nebraska City Power Plant.

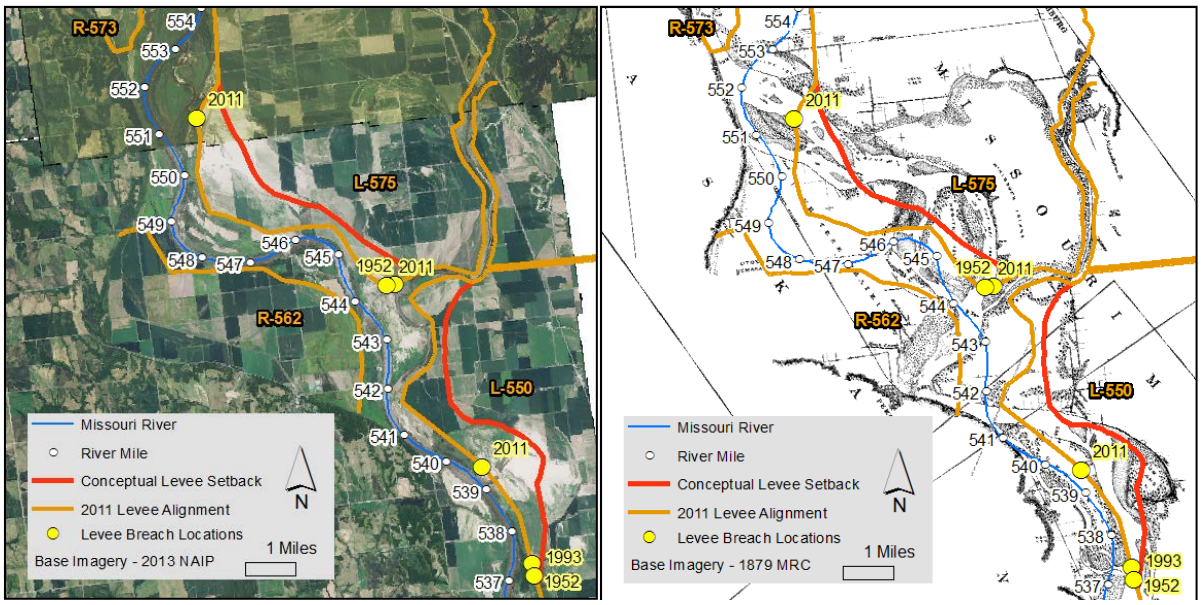

Figure 5 ACNALS Levee Setback (2013 Aerial Imagery and 1879 MRC)

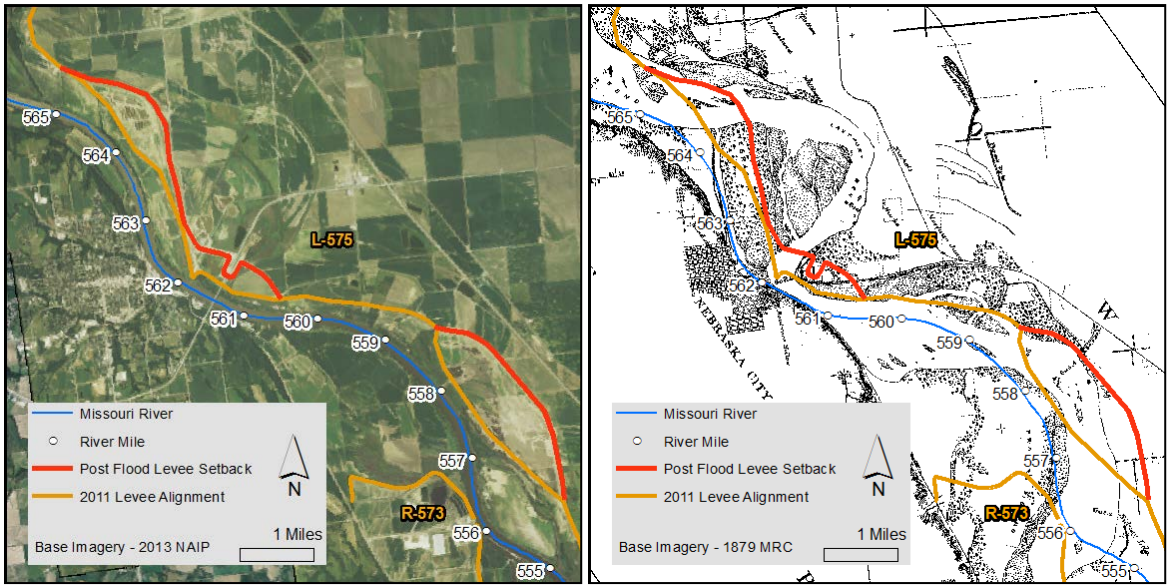

Figure 6 Constructed Levee Setbacks on L-575 (2013 Aerial Imagery and 1879 MRC)

While neither the ACNALS nor the constructed setbacks documentation included evaluation of levee performance, there were items of note. For the ACNALS evaluation, the distance of the levee setback was such that it was possible to identify higher elevations on which the levee could be founded. As a result, the frequency of loading the levee toe and maximum hydrostatic forces that the levee could be exposed to could be reduced. Similarly the River Mile 557, the setback alignment was based on a natural elevation change and benefits from reduced frequency of exposure. For both of the constructed setbacks, poor geotechnical characteristics of the site were a primary concern in deciding to realign the levee. This supports the assumption that movements away from the channel bank and toward the lower energy flood plain areas can obtain more resilient geotechnical conditions.

Economic Evaluation The objective of the ACNALS was to provide a comparison of levee setbacks in the framework of post-flood PIRs. Two alternatives were considered: the first looked at levee setbacks constructed with the same top of levee elevation as repair-in-place alternatives, the second looked at levee setbacks where the levee crest was lowered to provide the same frequency of overtopping protection provided by the repair in place alternatives. The ACNALS results showed that while levee setbacks were a more costly alternative, largely due to increased construction and real-estate costs, they still provided Benefit-Cost Ratios (2.3 to 2.52) comparable with the repair-in-place alternatives (3.11). The ACNALS also noted that many of the benefits of levee seatbacks were not quantified using this methodology. Unaccounted for benefits include reduced adjacent and/or upstream levee system exposure, less frequent emergency operations, reduced flood-related expenses, and ecosystem benefits. The Galloway report similarly noted (IFMRC, 1994):

> *The principal federal water resources planning document, Principles and Guidelines, is outdated and does not reflect a balance among the economic, social, and environmental goals of the nation. This lack of balance is exacerbated by a present inability to quantify, in monetary terms, some environmental and social impacts. As result, these impacts are frequently understated or omitted. Many critics of Principles and Guidelines see it as biased against nonstructural approaches.*

Table 1 provides a summary for the Benefit-Cost Ratio computations in the ACNALS.

With regard to the two implemented levee setbacks on L-575, these efforts were constructed as a least-cost alternative. As such, no benefit-cost analysis was conducted. Table 2 provides a cost comparison of the repair-in-place quantities and costs against the levee setback alternative. It shows a total cost savings of $5 million for the levee setback option, primarily due to increased quantities for the measures necessary for the repair-in-place option to protect against erosion and underseepage. Should a benefit-cost review be conducted it would show lower cost and increased benefits for the levee setback alternative.

Table 1 Benefit-Cost Summary for Conceptual Levee Setback Alternatives in the ACNALS Report

	Repair In Place Alternative	**Setback Alternative with Pre-Flood LOP**	**Setback Alternative with Pre-Flood Levee Top Elevation**
L-550 Level of Overtopping Protection	20 years	20 years	28 years
L-575 Level of Overtopping Protection	30 years	30 years	30 years upper L-575 56 years lower L-575
System Protected Area	72.9 sq mi	64.6 sq miles	64.6 sq mi miles
Traditional BCR computations:			
Total Cost ($M)	$166.00	$193.00	$212.00
Annual Cost ($M)	$10.70	$12.70	$14.00
Annual Benefit ($M)	$33.30	$32.10	$32.30
BCR	**3.11**	**2.52**	**2.30**
Other Benefits Associated with Levee Setback Alternatives Not Quantified:			
Reduced damage to critical infrastructure: • Two Public Power Stations, $6.8 million cost-savings based on 2011 event • Reduced damage to transportation and other infrastructure and decreased traffic disruption **Ecosystem restoration benefits** • Increased potential for 6,471 additional acres of fish and wildlife habitat		**System benefits:** • Increased level of protection behind adjacent and opposing levees • Reduced O&M and R,R&R costs for adjacent and opposing levees • Emergency, evacuation and cleanup cost-savings: • Less frequent need for emergency operations and flood-related activities	

Table 2 L-575 In-Place vs. Levee Setback quantities and Costs at Hwy 2

Item	Repair In-Place	Levee Setback
North of HWY 2		
Riprap	15,000 tons	5,400 tons
Temporary Stockpiling of Riprap	0	5,400 tons
Stripping	56,500 cu yd	95,500 cu yd
Sand Fill	350,000 cu yd	303,000 cu yd
Temporary Stockpiling of Sand	0	97,000 cu yd
Random Fill	23,400 cu yd	571,000 cu yd
Underwater Fill	50,000 cu yd	
Geotextile	11,000 sq yd	7,400 sq yd
Cohesive Fill	30,000 cu yd	295,000 cu yd
Topsoil	70,000 cu yd	115,400 cu yd
Levee Surfacing	5,000 tons	6,100 tons
Seeding	83 acres	117 acres
Rehabilitation of Existing Wells	40	0
Abandon Existing Wells	0	40
Sheet Pile	170,000 sq ft	0
Permanent erosion control mat (armor max)	200,000 sq ft	0
New Relief Wells	128	40
North of HWY 2 Cost	$14,220,644	$10,884,244
South of HWY 2		
Stripping	15,000 cu yd	31,900 cu yd
Sand Fill	85,185 cu yd	324,000 cu yd
Cohesive Fill	0	98,300 cu yd
Topsoil	14,056 cu yd	38,500 cu yd
Levee Surfacing (Restore Berm Road)	3,825 tons	1,370 tons
Seeding	18 acres	39 acres
Rehabilitation of Existing Wells	40	0
Abandon Existing Wells	0	0
New Relief Wells	102	0
South of HWY 2 Cost	$4,657,657	$2,910,382
Total Cost	**$18,878,301**	**$13,794,626**

Ecosystem Evaluation This ACNALS habitat assessment described conceptual biotic responses that would occur in relation to various flood frequencies and depths. The review identified that the reconnected lands have the capability of boosting primary and secondary productivity and provide increased fish access to floodplain habitat for rearing, foraging, and cover. Floodplain areas that have not been converted to cropland or other uses typically contain open water and some remnant areas of mature cottonwood and willow stands, shrub understory, green ash, American elm, and herbaceous wetland vegetation. These vegetative communities are indicative of the plant species and distribution that would most likely become established and successfully colonize the newly reconnected floodplain.

Construction of the two levee setbacks provided 1,740 acres (2.7 sq mi) of floodplain connectivity. Since establishing this connectivity, the general responses anticipated in the ACNALS report have started to occur in the reconnected floodplain. Over 320 acres of borrow pits used to obtain material for the setback construction were treated to encourage wetland establishment. Treatment of the pits involved shaping to incorporate depth diversity, irregular bank lines, gentle side slopes, and seeding.

In 2013, the USACE and the Iowa Department of Natural Resources (IDNR) engaged in monitoring the setbacks and borrow pit wetlands. The USACE evaluated vegetative composition of the wetlands while IDNR conducted a multi-taxon survey. While detailed quantitative data about wetland establishment and other biotic responses will require more years of surveying to obtain, the treated borrow pits are exhibiting wetland characteristics within one to two growing seasons. All borrow pits have some degree of hydrological connectivity with the Missouri River water table, allowing for development of hydric soils over time. Hydrophytic vegetation emerged from the soil's seed bank at all surveyed borrow pits. During certain times of the year, large open water areas contained upwards of tens of thousands of water fowl.

IMPLEMENTATION AND CHALLENGES

There are a number of programs which provide authority to support the implementation of a levee setback. Notably Section 205 and Section 1135 authorities address flood risk reduction and ecosystem benefits at constructed projects respectively. Additionally, post flood repairs can be an opportunity to implement a levee setback; as part of the PL 84-99 program, the levee sponsors have the option to implement a Nonstructural Alternative (NSA). ER 500-1-1 (5-17 c (6)) identifies acceptable costs for a NSA as "construction to promote, enhance, control, or modify water flows into, out of, through, or around the nonstructural project area". While this definition seems sufficiently broad as to incorporate a levee setback, there remain concerns if levee setbacks are an appropriate NSA.

Challenges preventing the implementation of levee setbacks include the requirement in ER 500-1-1 to use the least-cost alternative instead of the most beneficial alternative. ER 500-1-1 (5-11 e (3)) identifies that

> *If the public sponsor prefers an alternative method of repair that is not the least cost to the Federal government alternative, the public sponsor shall pay 100 percent of the additional costs above the least cost alternative.*

Most levee sponsors have established operating budgets consistent with the routine O&M costs and rely on the assistance and/or bonding activities for larger costs. Accordingly, large-scale costs such as levee setbacks are not likely economically feasible without assistance and/or sufficient lead time to establish financial capability.

In comparison with the in-place repair option, levee setbacks present unique challenges in locating real estate and borrow material sources. Typically, the non-federal levee sponsor would supply the real estate and borrow material for a new levee alignment to be constructed under the PL 84-99 program. The constructed levee setbacks are located primarily on land either owned by the USACE for MRRP habitat restoration purposes, or on land encumbered by Natural Resources Conservation Service (NRCS) easements for habitat purposes. This alleviated the need for the sponsors to provide the borrow material. While USACE real estate outgrant policies and procedures are being reviewed and clarified to avoid lapses in PL 84-99 role accountability, borrow sourced from federally owned land intended for habitat restoration for future levee rehab efforts remains a solution worth considering.

Post flood timing is a major challenge for implementation. The desire to rapidly reestablish protection requires careful attention to construction phasing. With regard to the implemented levee setbacks, material from the damaged original levee alignment could not be accessed or used for the setback construction until the setback was built to a 25-year level of protection. This requirement led to uncertainties that all old levee material could be incorporated into constructing the completed setbacks. In constructing future levee setbacks, timing of original levee degradation would be considered on a case by case basis with consideration for time of the year and other factors contributing to potential flood risk.

A systems approach to riverine management identifies the "triple bottom line" interconnectivity of flood risk, economics, and ecosystem impacts. Many of the authorities for implementation identified above have restrictions on the purposes of the efforts. For example, MRRP funds are primarily for projects benefiting habitat restoration, while PL 84-99 funds are for restoration of levee systems. Disconnects between the systems approach necessary for sustainable solutions and nonsystematic focused funding mechanisms is an impediment for implementation. Similarly interaction of various agency programs provides a challenge. During implementation of levee setbacks on L-575 concerns about programmatic conflicts of the NRCS was common.

CONCLUSIONS

In conclusion, the use of levee setbacks provides a sustainable strategy to modify existing levee systems to meet the triple bottom line benefits to flood risk, economics, and ecosystems. Conceptual analysis in the ACNALS report and the implementation and monitoring of levee setbacks in two locations as part of the 2011 Missouri River Flood recovery have shown levee setbacks to be an implementable and beneficial strategy. The ACNALS report identifies that significant flood risk reduction can be achieved by locating setbacks at hydraulic constrictions. The constructed levee setbacks on L-575 show that benefits can be achieved with modest-sized setbacks. The economic analysis in the ANCNALS and financial data from the constructed setbacks show economic viability of the concept as well economic benefits that may not be fully accounted for in traditional economic analysis. Ecosystem assessments and monitoring of the constructed levee setbacks have shown benefits in the reconnectivity of the floodplain including conditions encouraging hydric soil development and immediate biotic response. While there are a number of benefits of levee setbacks, challenges to implementation exist. These challenges include programmatic authorities as well as real estate and funding. In a post-flood situation, the desire to re-establish the protection in a short time may amplify these challenges

REFERENCES

Dixon M.D., Johnson W.C., Scott M.L., Bowen D. (2010). Status and Trend of Cottonwood Forests along the Missouri River. US Army Corps of Engineers, Omaha District. Report no. 78.

Interagency Floodplain Management Review Committee (IFMRC). 1994. (Brigadier General G.E. Galloway, Chair), Sharing the Challenge: Floodplain Management into the 21st Century. Washington, DC: U.S. Government Printing Office.

Minnesota Department of Natural Resources . 2012. Watershed Assessment Tool: Connectivity Concepts.

National Research Council (NRC). (2002). The Missouri River Ecosystem, Exploring the Prospects for Recovery. Committee on Missouri River Ecosystem Science, Water Science and Technology Board, Division of Earth Science and Life Studies. Washington, DC: National Academy Press.

U.S. Fish and Wildlife Service (USFWS). 2000. USFWS 2000 Biological Opinion on the Operation of the Missouri River Main Stem Reservoir System, Operation and Maintenance of the Missouri River Bank Stabilization and Navigation Project, and Operation of the Kansas River Reservoir System.

U.S. Fish and Wildlife Service (USFWS). 2003. USFWS 2003 Amendment to the 2000 Biological Opinion on the Operation of the Missouri River Main Stem Reservoir System, Operation and Maintenance of the Missouri River Bank Stabilization and Navigation Project, and Operation of the Kansas River Reservoir System.

U.S. Army Corps of Engineers, (March 1939). Improvement of the Missouri River. Omaha, Nebraska.

U.S. Army Corps of Engineers, Missouri River Division. (March 1947). Definite Project Report Missouri River Agricultural Levees Sioux City, Iowa to the Mouth. Omaha, Nebraska.

U.S. Army Corps of Engineers. (February 1947). Definite Project Report Supplemental Report on Levee Unite L-575. Omaha, Nebraska.

U.S. Army Corps of Engineers, Omaha District. (April 1986). Technical Summary Adequacy of Missouri River Levee System. Rulo, Nebraska to Omaha, Nebraska River Mile 498.0 to 624.8.

U.S. Army Corps of Engineers, Omaha District. (November 2003). Upper Mississippi River System Flow Frequency Study Hydrology and Hydraulics, Appendix F, Missouri River.

U.S. Army Corps of Engineers, North Central Division. (September 1994). The Great Flood of 1993, Post-Flood Report.

U.S. Army Corps of Engineers. (June 1995). Floodplain Management Assessment of the Upper Mississippi River and Lower Missouri River and Tributaries.

U.S. Army Corps of Engineers, Omaha District. April 2012. Assessment of Conceptual Nonstructural Alternative Levee Setbacks along the Missouri River (Lower L-575 / Upper L-550 and Lower L-550).

U.S. Army Corps of Engineers Missouri River Basin Water Management Division. (August 2012). Missouri River Stage Trends Technical Report. Omaha, Nebraska.

Whitmore, S.B., Keenlyne, K.D. (1990). Rare, threatened and endangered endemic species of the Missouri River floodplain. Missouri River Coordinator's Office, Report MRC-90-1, USFWS Pierre, South Dakota.

HYDRODYNAMIC MODELING TO EVALUATE THE INFLUENCE OF CONSTRUCTED SIDE-CHANNEL HABITAT ON LARVAL DRIFT OF PALLID STURGEON IN THE LOWER MISSOURI RIVER

Susannah O. Erwin, Research Geologist, Columbia Environmental Research Center, U.S. Geological Survey, Columbia, MO, 573-441-2978, serwin@usgs.gov; Robert B. Jacobson, Supervisory Research Hydrologist, Columbia Environmental Research Center, U.S. Geological Survey, Columbia, MO, 573-876-1844, rjacobson@usgs.gov

Abstract: Larval drift is a critical phase of ontogeny for many species of lotic fishes. Downstream advection and dispersion of drifting larvae or eggs is controlled by the complex interaction of flow regime, channel planform, local channel morphology, and the resulting hydraulic gradients. In many regulated rivers, channel engineering and perturbations to the flow regime may disrupt natural dispersal processes and prevent successful recruitment of native fishes. Here, we explore the influence of flow regime and channel morphology on the downstream transport, dispersion, and retention of free embryos of pallid sturgeon (*Scaphirhychus albus*), an endangered species endemic to the Mississippi River basin and the focus of significant conservation effort on the Missouri River. The transition from drifting free embryo to exogenously feeding larvae has been identified as a potential life stage bottleneck for the pallid sturgeon. We use a two-dimensional hydrodynamic model to evaluate the sensitivity of drift and dispersion to in-channel navigation structures, constructed shallow-water habitat, and flood hydrology. In the simulations, larvae were treated as passively drifting particles and calculated retention times were used as an index of potential for settling and retention within specific environments. During low flows, retention of larvae is promoted by shallow, low velocity conditions provided by constructed side-channel habitats. At higher flows, retention is driven by overbank flows that inundate the floodplain. Based on insights gained from the analysis of field data and modeling outputs, we consider the effects of flow regime modifications or channel re-engineering on the distribution and retention of free embryos within the Lower Missouri River.

INTRODUCTION AND BACKGROUND

The Missouri River has been profoundly transformed by over two centuries of river management and channel alterations (Jacobson and Galat, 2006). The river is the longest river in the United States and has a drainage area of more than 1,300,000 km^2, draining the eastern Rocky Mountains, Great Plains, and a small area of Canada (Figure 1A). Six large mainstem dams have substantially altered the natural flow regime, reducing the magnitude of annual floods and elevating base flows (Galat and Lipkin, 2000). The Lower Missouri River (LMOR) is defined as the 1,300 km of the Missouri River downstream from Gavins Point Dam near Yankton, South Dakota to the confluence with the Mississippi River, near Saint Louis, Missouri. Extensive channelization and construction of training structures (e.g. dikes and bank revetment) in the LMOR have converted the channel from one that was historically a broad, shallow, braided channel to a relatively deep and narrow navigation channel with less morphologic diversity (Jacobson and Galat, 2006).

Ongoing efforts to inform management of the Missouri River as part of Missouri River Recovery Program are focused on the recovery of three endangered or threatened species – the pallid

sturgeon (*Scaphirhynchus albus*), piping plover (*Charadrius melodus*), and interior least tern (*Sternula antillarum athalassos*) (U.S. Fish and Wildlife Service, 2000, 2003). Pallid sturgeon are endemic to the Mississippi River basin and are the focus of significant conservation efforts on the Missouri River. Subjected to years of heavy commercial fishing, declining water quality, a highly altered flow regime, and extensive habitat alternations, the pallid sturgeon was formally listed as a federally endangered species in 1990. Current recovery efforts focus on habitat restoration and hatchery augmentation, implemented through an adaptive management framework. However, it remains unclear what factor(s) are primarily responsible for decline of the species and what actions may be most effective in promoting successful recruitment.

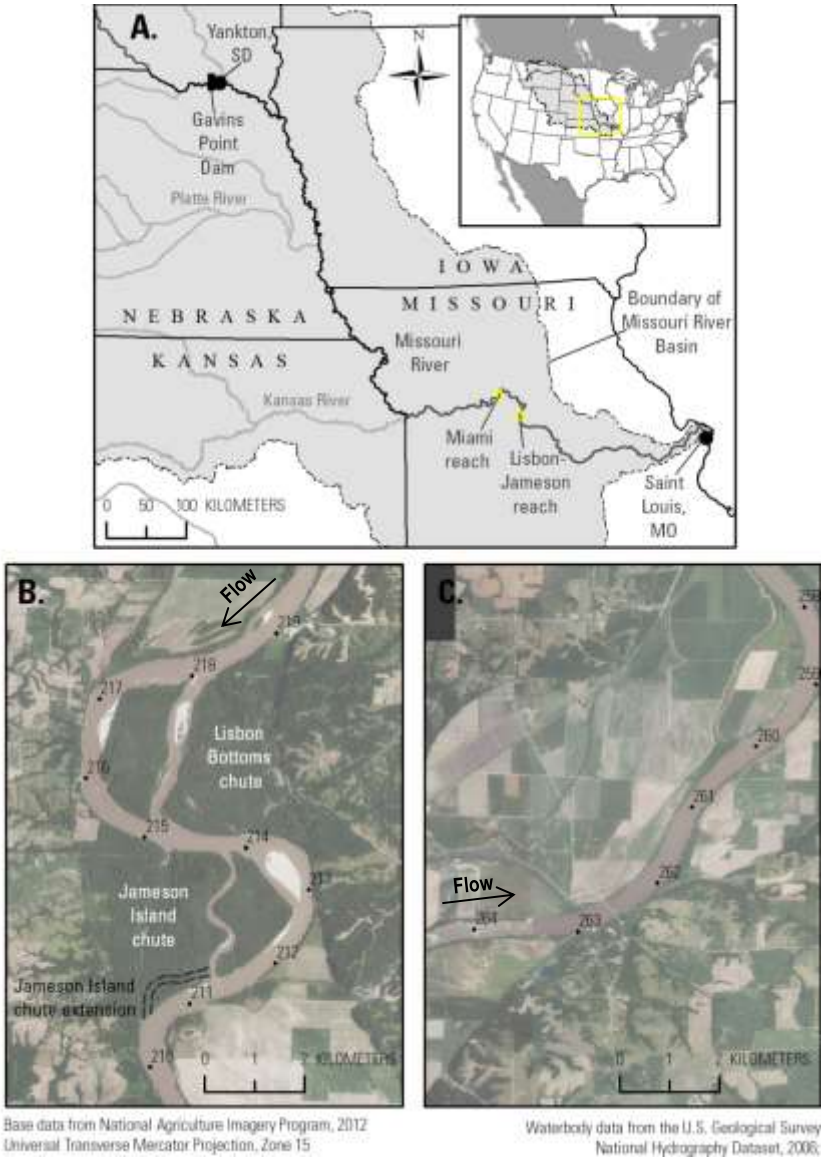

Figure 1 (A) The Lower Missouri River, (B) the Lisbon-Jameson reach (River Mile (RM) 210.0-219.1), and (C) the Miami reach (RM 259.6 – 263.5). River miles are the customary units of longitudinal measurement on the LMOR. They are measured upstream from St. Louis, MO and correspond to the channel position in 1960.

Recent research identifies the transition from drifting free embryo to exogenously feeding larvae as a life stage that may limit successful recruitment of pallid sturgeon in the Missouri River (Kynard and others, 2007; DeLonay and others, 2009a; Braaten and others, 2012). As is common for many lotic fishes (Muth and Schmulbach, 1984; Brown and Armstrong, 1985; Pavlov and others, 2008), pallid sturgeon undergo a period of drift and dispersal post-hatch. During this developmental phase, sturgeon free embryos may be transported several hundred kilometers downstream from the site at which spawning occurred (Kynard and others, 2007). On regulated rivers such as the Missouri River natural patterns of downstream transport and dispersal may be disrupted by extensive channel modifications and flow regulation (Erwin and Jacobson, 2014).

Construction of side-channel chutes has emerged as one of the primary restoration techniques used in the LMOR (Jacobson and others, 2004). The relatively shallow depths and slow velocities provided by such features are thought to increase the retention of drifting larvae within the LMOR, disrupting downstream advection in the channelized portion of the river and providing an environment suitable for foraging when the free embryos transition to exogenous feeding. Here, we present the preliminary results of a hydraulic modeling study designed to explore the influence of flow regime and channel morphology on the downstream transport, dispersion, and retention of larval pallid sturgeon.

STUDY AREA

We constructed two-dimensional hydrodynamic models for two reaches of the LMOR that represent end-member conditions. The Miami (Figure 1C) reach represents a typical channelized and leveed reach of the river, with relatively little in-channel complexity. The Lisbon-Jameson reach (Figure 1B) contains two constructed side-channel chutes and a greater degree of floodplain connectivity than occurs on most of the LMOR.

The 14.6-km Lisbon-Jameson reach is located approximately 22 km upstream from Boonville, MO and encompasses both the Lisbon Bottom and Jameson Island chutes (Figure 1B). The site is located within the U.S. Fish and Wildlife Service's Big Muddy National Fish and Wildlife Refuge and levee setbacks allow floodwater to inundate adjacent floodplains. The Lisbon Bottom chute (upstream chute) was formed as the result of levee breaks during the floods of 1993 and 1995 (Jacobson and others, 2004). The chute was allowed to evolve with minimal intervention until 1999, when a grade-control structure was installed at the downstream end of the chute and a notched hydraulic control structure was installed at the entrance to the chute. The Jameson Island chute (downstream chute) was intentionally constructed by the U.S. Army Corps of Engineers with the objective of creating habitat for pallid sturgeon (U.S. Army Corps of Engineers, 2012). Construction of the pilot channel occurred in 2006-2007 and the channel was subsequently widened during naturally occurring high flows. A chute extension was completed in summer 2014. These channel modifications, coupled with a high degree of floodplain connectivity and a relatively wide mainstem, produce a reach that represents one of the best-available sections of aquatic habitat within the LMOR.

The 8.4-km Miami reach is located at the town of Miami, MO (Figure 1C). Restoration activities in this reach have been limited to some dike notches, and levees restrict access to the floodplain. The reach is characterized by a navigation channel that is typical of the LMOR downstream from the border of Nebraska and Kansas. Both the Miami and Lisbon-Jameson reaches contain

extensive bank revetment and regularly spaced river-training structures, or dikes, designed to maintain a self-dredging navigation channel.

METHODS

The Lisbon-Jameson hydrodynamic model was developed following an extensive field campaign in spring and summer 2014. The Miami model was originally developed by USGS in 2006-2007 to evaluate the effects of modifications of releases from Gavins Point Dam on pallid sturgeon habitat dynamics. Methods used in the construction of the Lisbon-Jameson hydrodynamic model are described below, and methods used in the construction of the Miami model are described in detail by Jacobson et al. (2009).

Data Collection: Topographic data for the hydrodynamic models were generated by integrating data from hydroacoustic surveys, topographic ground surveys, and existing aerial LiDAR. Hydroacoustic surveys were performed using methods established by USGS (Reuter and others, 2008; Reuter and others, 2009). Surveys were conducted using a 200 kHz single-beam echo sounder with an 8 degree transducer coupled with real-time kinematic global positioning system (RTK-GPS) equipment to provide precise positioning. The echo sounder was calibrated for draft and sound velocity using a bar check. At Lisbon-Jameson, transects were surveyed at regularly-spaced 50-m increments in the main channel and 20-m increments in the chutes. Hydroacoustic data were supplemented by RTK-GPS ground surveys of sub-aerially exposed sand bars. Floodplain and bank topography was provided by aerial LiDAR collected in 2007 (National Elevation Dataset; http://ned.usgs.gov). Field data for the Miami reach were collected in 2006 and 2007, and transects were surveyed at 20-m intervals throughout the model domain (Jacobson and others, 2009).

Water surface profiles were surveyed over a range of discharges for model calibration. At Lisbon-Jameson, 6 main stem water surface profiles were surveyed at discharges ranging from 1,135 – 5,974 m^3s^{-1}. At Miami, seven water surface profiles were surveyed over discharges ranging from 588 – 3,136 m^3s^{-1}. Velocity data for model validation were acquired using 600 and 1200 kHz Teledyne RDI Rio Grande acoustic Doppler current profiler (ADCP) units, also integrated with RTK-GPS.

Hydrodynamic Modeling: We developed two-dimensional, depth-averaged hydrodynamic models to predict water-surface elevations, depths, and depth-averaged velocity throughout both study areas. Modeling was conducted using TUFLOW (BMT Group Ltd., Brisbane, Australia) and implemented within the Surface-water Modeling System (SMS, Aquaveo, Inc., Provo, Utah). TUFLOW solves the vertically-averaged, two-dimensional shallow water equations by means of finite difference method on a cartesian grid. The Miami model was originally developed and calibrated using an alternate hydrodynamic modeling program (see Jacobson and others, 2009), and was converted to TUFLOW as part of this analysis to facilitate comparison with the Lisbon-Jameson model. For the current application, the Miami model domain was extended to include overbank areas.

Topographic and bathymetric data were used to generate a computational grid for each modeling domain (4x4 m grid for Miami and 10x10 m grid for Lisbon-Jameson). We calibrated the models to measured water-surface elevations by iteratively adjusting channel roughness. Once

calibrated, we generated steady-state simulations for discharges ranging from base flow to overbank floods in 200-m^3s^{-1} increments (550 – 6,550 m^3s^{-1} at Miami and 600 – 7,000 m^3s^{-1} at Lisbon-Jameson).

We implemented a particle tracking algorithm within SMS to estimate residence times of passively drifting particles in each model domain (Aquaveo LLC, 2013). On a cell-by-cell basis, velocity vectors and magnitudes were used to generate flow paths through the model domains. Each simulation was seeded with 10,000 particles whose starting positions were uniformly distributed along a cross section perpendicular to flow near the upstream boundary of each reach. Simulations were run for 36 hours, at which point those particles not recirculating in eddies had long since exited the model domain.

RESULTS

Maps of inundation and velocity generated by flow simulations depict markedly different flow patterns in the two reaches. At Miami, simulated depth-averaged velocities during base flows display relatively little cross-stream variability due to the confined flow, relatively uniform channel width, and low sinuosity (Figure 2A). Similar patterns occur during bankfull flows; depth-averaged velocities are greater throughout the model domain, and eddies downstream from dikes become less prominent (Figure 2B). Overbank flows are contained within a relatively narrow corridor along the channel due to extensive levees along the reach (Figure 2C). For the entire range of flows simulated, the primary sources of hydraulic variability within the active channel are dikes used to maintain the navigation channel.

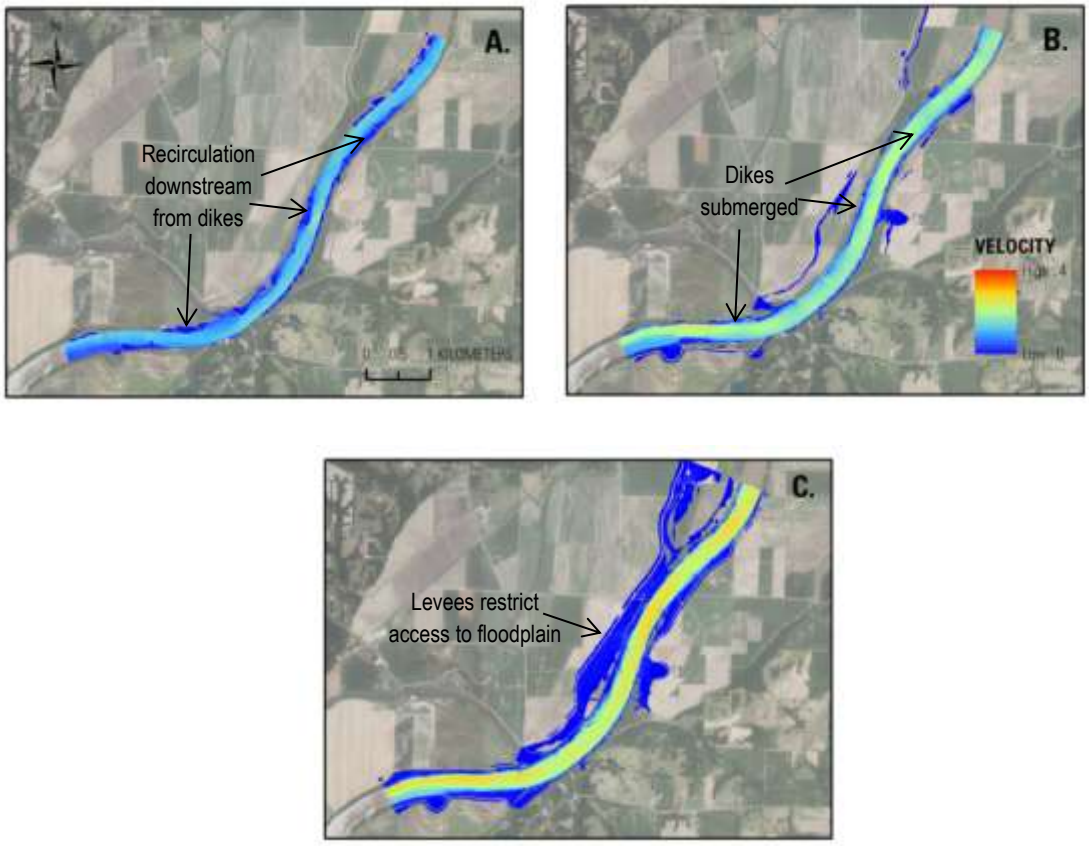

Figure 2 Simulated depth-averaged velocities for a subset of flows in the Miami modeling reach at (A) 950 m^3s^{-1}, (B) 3,750 m^3s^{-1}, and (C) 6,550 m^3s^{-1}.

The Lisbon-Jameson reach is morphologically and hydraulically complex. At base flows, bars, exposed dikes, and constructed side-channel chutes provide areas of low velocity and backwaters (Figure 3A). As discharge approaches bankfull conditions, bar and dikes become inundated but these features still provide substantial zones of hydraulic refugia (Figure 3B). Substantial areas of low velocity occur along the channel margins in the upstream and more developed chute, Lisbon; thus a wide distribution of velocities is maintained during moderate floods (Figure 4). As discharge overtops channel banks, mean velocities in both the main channel and chutes increase, but extensive areas of low velocity occur across the floodplain (Figure 3C).

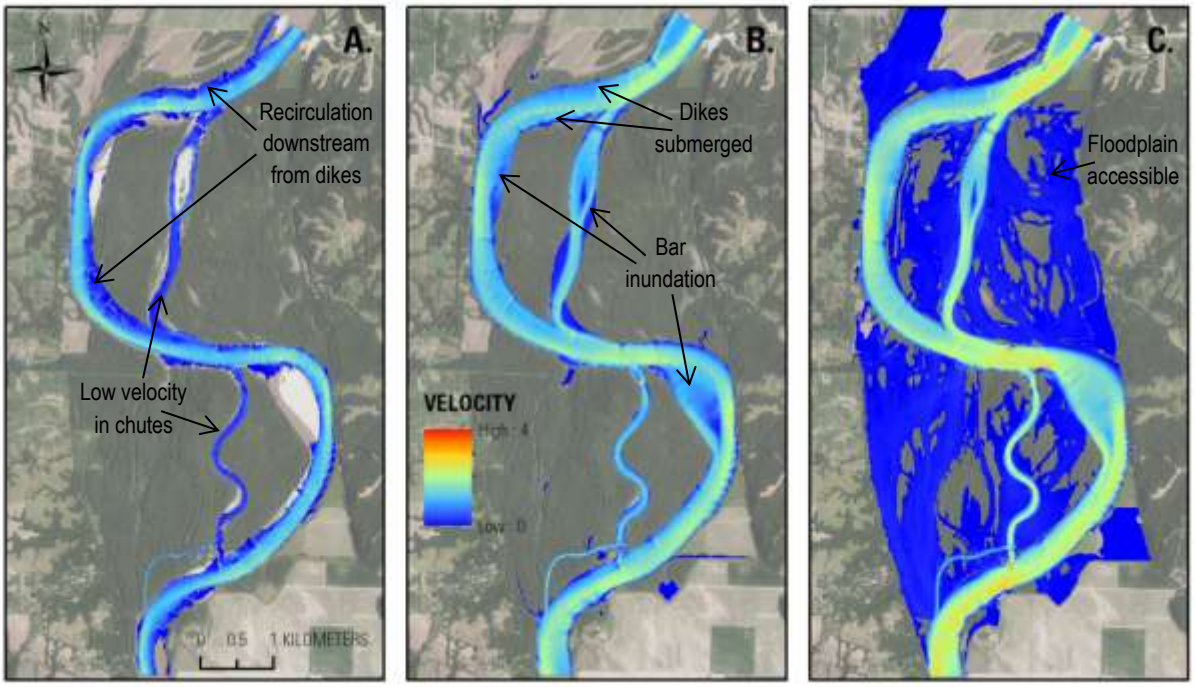

Figure 3 Simulated depth-averaged velocities throughout the Lisbon-Jameson modeling reach at (A) 1,000 m^3s^{-1}, (B) 4,000 m^3s^{-1}, and (C) 7,000 m^3s^{-1}.

The patterns in velocity depicted by the hydrodynamic simulations directly translate into differences in the routing of passively-drifting particles through the model domains. For the full range of discharges evaluated there is much greater variability in particle residence times calculated at Lisbon-Jameson as compared to those in Miami (Figure 5). Mean velocities do not differ substantially between the two reaches because currents in the navigation channel efficiently advect particles downstream. Thus, as flows increase, the median residence time steadily decreases in both reaches. In the Lisbon-Jameson reach, however, there is greater potential for retention within low-velocity environments, thus resulting in the long-tailed distribution of particle residence times observed for all flows (Figure 5A). Additionally, the

slight increase in the distribution of residence times at Lisbon-Jameson during large floods reflects the retention of particles on the floodplain that occurs during overbank flows. This effect is not observed at Miami because of the limited floodplain connectivity and the overwhelming ability of the navigation channel to convey water downstream.

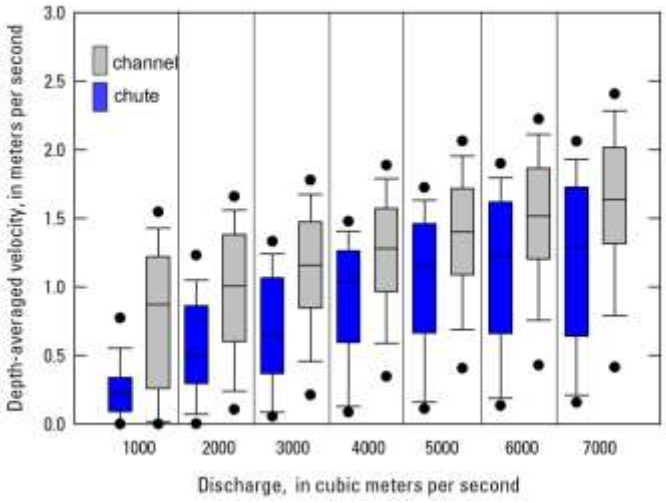

Figure 4 Box plot depicting the distribution of simulated velocities in the Lisbon-Jameson model, calculated for the two chutes and the main channel across a range of discharges.

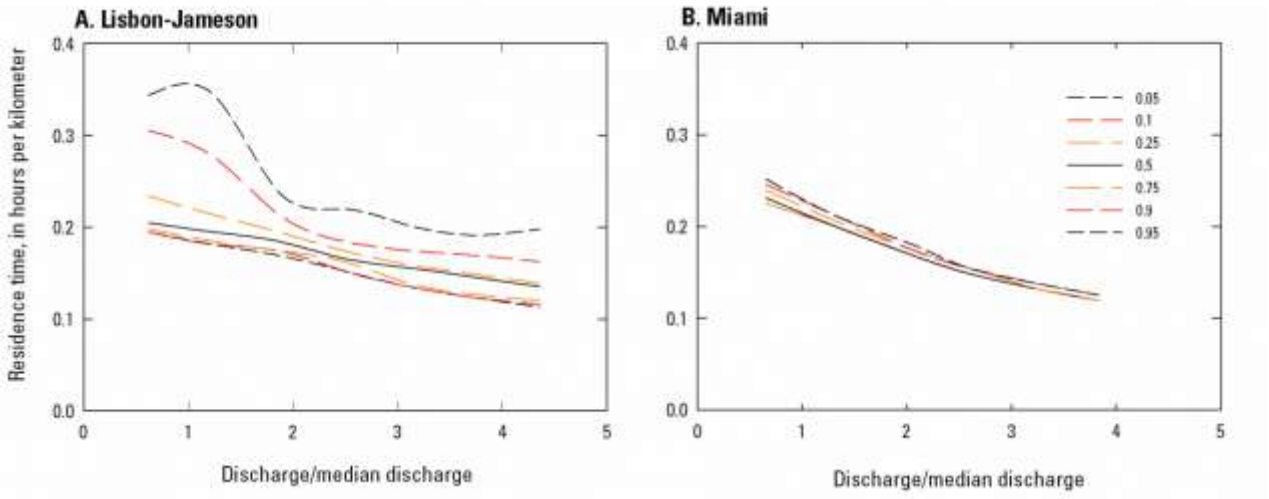

Figure 5 Distribution of particle residence times calculated for the Lisbon-Jameson (A) and Miami (B) modeling reaches. To allow comparison of calculated residence times between the two modeling reaches, values were normalized: (1) discharge was normalized by median discharge for each reach; and (2) residence time was normalized by mean reach length, as measured along the channel centerline throughout the model domain. Lines correspond to percentiles of particles (0.05 – 0.95), as indicated by legend in (B).

DISCUSSION AND SUMMARY

Once hatched, the transport and fate of pallid sturgeon larvae are largely unknown. Free embryos may drift for 9-17 days, depending on temperature-mediated development rate, before using up their yolk sac and transitioning to exogenous feeding (Kynard and others, 2002; Braaten and others, 2008; Braaten and others, 2012). During this time, swimming capabilities increase, and field experiments suggest that they tend to concentrate in the thalweg (Braaten and others, 2010) and drift at velocities slightly slower than mean water velocity (Braaten and others, 2008). Studies in the Upper Missouri River suggest that older larvae tend to drift slower as they settle, or orient to benthic habitats (Braaten and others, 2012), but the degree to which free embryo larvae engage in volitional swimming behaviors in the high velocities of the Lower Missouri River is unknown. Flume studies have begun to address these questions (Kynard and others, 2007; DeLonay and others, in press), but scaling up from experimental settings, where maximum flows have not exceeded 0.30 ms^{-1}, to the LMOR, where typical depth-averaged velocities are greater than 2 ms^{-1}, remains a fundamental challenge. Mean water velocities in the Lower Missouri River suggest larvae may drift hundreds of km per day (DeLonay and others, 2009b), but it is unknown how complex hydraulics along the river may interact with progressive larval development to determine actual drift distances, where larvae may be retained, and whether retention sites provide necessary food resources and protection from predation.

The analysis presented here highlights the geomorphic and channel engineering features that create channel complexity and promote retention of drifting particles within the LMOR. Typical sections of the LMOR, represented by the Miami modeling reach, are characterized by relatively uniform channel widths, low morphologic variability, and limited access to the floodplain. Thus, drifting particles or organisms are efficiently advected downstream and may not be able to exit the thalweg before the point at which they need to transition to the benthos and initiate exogenous feeding. The degree of exchange of free embryos between the thalweg and typical wing-dike structures is unknown. Restored reaches, such as Lisbon-Jameson, provide more complex hydraulic conditions that may transport the larvae into channel-margin habitats. It is hypothesized that such environments provide the food and cover required for survival of juvenile pallid sturgeon.

Several features of the Lisbon-Jameson reach contribute to hydraulic complexity captured by the model outputs and resulting particle tracking simulations. Heterogeneity in the simulated distribution of velocities results from not only the presence of constructed side-channel chutes, however, but also the relatively large channel width, variability in channel width, and sinuosity that lead to the secondary currents which drive the formation of bars. The reach also displays greater floodplain connectivity than much of the LMOR. Together, these characteristics of the Lisbon-Jameson reach increase channel complexity and hydraulic heterogeneity, thus increasing opportunities for drifting free embryos to exit the thalweg and access foraging habitats. Further research is needed to evaluate the relative contributions of these different geomorphic features to the retention of drifting free organisms within the LMOR in order to inform ongoing restoration efforts. Additionally, the presence of hydraulic conditions that are more conducive to retention and settling alone does not indicate that larvae will encounter conditions supportive of foraging or with adequate food resources. Identifying the habitat requirements of pallid sturgeon during these early life stages remains an area of active research.

ACKNOWLEDGEMENTS

This work received funding from the US Army Corps of Engineers, Missouri River Recovery Program, and the US Geological Survey Ecosystems Mission Area. Any use of trade, product, or firm names is for descriptive purposes only and does not imply endorsement by the US Government.

REFERENCES

Aquaveo LLC, 2013, Surface-water Modeling System User Manual v11.1: Provo, UT.

Braaten, P.J., Fuller, D.B., Holte, L.D., Viste, W., Brandt, T.F., and Legare, R.G., 2008, Drift dynamics of larval pallid sturgeon and shovelnose sturgeon in a natural side channel of the Missouri River, Montana: North American Journal of Fisheries Management, v. 28, p. 808-826.

Braaten, P.J., Fuller, D.B., Lott, R.D., Ruggles, M.P., Brandt, T.F., Legare, R.G., and Holm, R.J., 2012, An experimental test and models of drift and dispersal processes of pallid sturgeon (Scaphirhynchus albus) free embryos in the Missouri River: Environmental biology of fishes, v. 93, no. 3, p. 377-392.

Braaten, P.J., Fuller, D.B., Lott, R.D., Ruggles, M.P., and Holm, R.J., 2010, Spatial distribution of drifting pallid sturgeon larvae in the Missouri River inferred from two net designs and multiple sampling locations: North American Journal of Fisheries Management, v. 30, p. 1062-1074.

Brown, A.V., and Armstrong, M.L., 1985, Propensity to drift downstream among various species of fish: Journal of Freshwater Ecology, v. 3, no. 1, p. 3-17.

DeLonay, A.J., Jacobson, R.B., Chojnacki, K.A., Braaten, P.J., Bulliner, E.A., Elliott, C.M., Erwin, S.O., Fuller, D.B., Haas, J.D., Ladd, H.L.A., Mestl, G.E., Papoulias, D.M., and Wildhaber, M.L., in press, Ecological requirements for pallid sturgeon reproduction and recruitment in the Missouri River: a synthesis of science, 2005 to 2012: U.S. Geological Survey Scientific Investigations Report.

DeLonay, A.J., Jacobson, R.B., Papoulias, D.M., Simpkins, D.G., Wildhaber, M.L., Reuter, J.M., Bonnot, T.W., Chojnacki, K.A., Korschgen, C.E., and Mestl, G.E., 2009a, Ecological requirements for pallid sturgeon reproduction and recruitment in the Lower Missouri River: a research synthesis 2005 to 2008: U.S. Geological Survey Scientific Investigations Report 2009-5201.

DeLonay, A.J., Jacobson, R.B., Papoulias, D.M., Simpkins, D.G., Wildhaber, M.L., Reuter, J.M., Bonnot, T.W., Chojnacki, K.A., Korschgen, C.E., Mestl, G.E., and Mac, M.J., 2009b, Ecological requirements for pallid sturgeon reproduction and recruitment in the Lower Missouri River -- A research synthesis 2005-08 59 p. http://pubs.usgs.gov/sir/2009/5201/.

Erwin, S.O., and Jacobson, R.B., 2014, Influence of channel morphology and flow regime on larval drift of pallis strugeon in the Lower Missouri River: River Research and Applications. 10.1002/rra.2752.

Galat, D.L., and Lipkin, R., 2000, Restoring ecological integrity of great rivers: historical hydrographs aid in defining reference conditions for the Missouri River: Hydrobiologia, v. 422/423, p. 29-48.

Jacobson, R.B., and Galat, D.L., 2006, Flow and form in rehabilitation of large-river ecosystems: An example from the Lower Missouri River: Geomorphology, v. 77, no. 3-4, p. 249-269.

Jacobson, R.B., Johnson III, H.E., and Dietsch, B.J., 2009, Hydrodynamic simulations of physical aquatic habitat availability for pallid sturgeon in the Lower Missouri River, at Yankton, South Dakota, Kenslers Bend, Nebraska, Little Sioux, Iowa, and Miami, Missouri, 2006–07: U.S. Geological Survey.

Jacobson, R.B., Johnson III, H.E., Laustrup, M.S., D'Urso, G.J., and Reuter, J.M., 2004, Physical Habitat Dynamics in Four Side-channel Chutes, Lower Missouri River: U.S. Geological Survey Open-File Report 2004-1071.

Kynard, B., Henyey, E., and Horgan, M., 2002, Ontogenetic behavior, migration, and social behavior of pallid sturgeon, Scaphirhynchus albus, and shovelnose sturgeon, S. platorynchus, with notes on the adaptive significance of body color: Environmental Biology of Fishes, v. 62, p. 389-403.

Kynard, B., Parker, E., Pugh, D., and Parker, T., 2007, Use of laboratory studies to develop a dispersal model for Missouri River pallid sturgeon early life intervals: Journal of Applied Ichthyology, v. 23, no. 4, p. 365-374.

Muth, R.T., and Schmulbach, J.C., 1984, Downstream transport of fish larvae in a shallow prairie river: Transactions of the American Fisheries Society, v. 113, no. 2, p. 224-230.

Pavlov, D.S., Mikheev, V.N., Lupandin, A.I., and Skorobogatov, M.A., 2008, Ecological and behavioural influences on juvenile fish migrations in regulated rivers: a review of experimental and field studies: Hydrobiologia, v. 609, no. 1, p. 125-138.

Reuter, J.M., Jacobson, R.B., Elliott, C.M., and DeLonay, A.J., 2009, Assessment of Lower Missouri River physical aquatic habitat and its use by adult sturgeon (genus *Scaphirhynchus)* 2005-07: U.S. Geological Survey, U.S. Geological Survey Scientific Investigations Report 2009-5121, 81 p. http://pubs.er.usgs.gov/usgspubs/sir/sir20095121.

Reuter, J.M., Jacobson, R.B., Elliott, C.M., Johnson, H.E., III, and DeLonay, A.J., 2008, Hydraulic and substrate maps of reaches used by sturgeon (Genus *Scaphirhynchus*) in the Lower Missouri River, 2005–07: U.S. Geological Survey Data Series Report 386, 442 p. http://pubs.usgs.gov/ds/386/.

U.S. Army Corps of Engineers, 2012, Missouri River Recovery Program Project Implementation Report with Integrated Environmental Assessment and Section 404(b)(1) Evaluation: Jameson Island Unit Shallow Water Habitat Restoration Project: U.S. Army Corps of Engineers.

U.S. Fish and Wildlife Service, 2000, Biological opinion on the operation of the Missouri River main stem reservoir system, operation and maintenance of the Missouri River bank stabilization and navigation project, and operation of the Kansas River reservoir system: Bismark, ND, US Fish and Wildlife Service.

U.S. Fish and Wildlife Service, 2003, Amendment to the 2000 biological opinion on the operation of the Missouri River main stem reservoir system, operation and maintenance of the Missouri River bank stabilization and navigation project, and operation of the Kansas River reservoir system: Minneapolis, MN, US Fish and Wildlife Service.

IMPACT OF PRECIPITATION UNCERTAINTY ON SWAT MODEL PERFORMANCE

Milo Anderson, Environmental Engineer, USEPA-Region 5; Chicago, IL 60604; Phone: 312-886-6096 E-mail: Anderson.Milo@epa.gov
Yongping Yuan, Research Hydrologist, USEPA-Office of Research and Development; Las Vegas, NV 89119; phone: 702-798-2112; E-mail: yuan.yongping@epa.gov.
Ronald L. Bingner, Agricultural Engineer, USDA-Agriculture Research Services; Oxford, MS 38655; phone: 662-232-2966; E-mail: ron.bingner@ars.usda.gov

Abstract: The accuracy of a model output is, to a large degree, dependent upon the quality of the input data sets including their spatial and temporal resolution. Among those input data sets, precipitation is one of the most important because of its influence on the hydrological model's performance (defined as agreement between measured and simulated values) and its role in determining surface hydrologic processes. Rainfall data are often obtained from rain gage networks, which sometimes may not cover the study area. Usually, precipitation data from the nearest gage stations are used to represent the study area for model hydrological simulations. However, occasionally unusual meteorological conditions can make it necessary to consider precipitation data from gages as far away from the study watershed as the next county. The watershed south of the lake was within 10 miles of two National Oceanic and Atmospheric Administration National Climatic Data Center (NOAA NCDC) precipitation gauges on the north side of the lake, but for year 2010 the SWAT simulated flows using either of these gages as precipitation input data lacked correlation to flows observed at a United States Geology Survey (USGS) gauge on Chickasaw Creek. Due to 2010 being an unusually wet year, an assumption was that additional NOAA NCDC gauges were needed to capture the precipitation events occurred in the watershed; a particular storm occurred in the watershed may be affected by high variability of storm directional paths and variable amounts of rain/snow. By considering additional precipitation gauges within 35 miles of the watershed boundary, model performance as measured by R-squared correlation improved significantly. The nearby precipitation gauges essentially showed no correlation at a coefficient as low as 0.03 for year 2010, but using a combination of the additional gauges to capture the majority of precipitation events raised the coefficient to 0.60 for the same year.

Keywords: Precipitation; Grand Lake St. Marys Watershed; SWAT model; Runoff simulation

INTRODUCTION

The process of transformation of rainfall into runoff over a watershed is very complex, highly non-linear, and exhibits both temporal and spatial variability. Many models have been developed to simulate this process and Soil and Water Assessment Tool (SWAT) is one of these. No matter how complicated a model in simulating this process, the accurate representation of precipitation over the watershed is critical in obtaining the accurate runoff simulation and its transported pollutants.

Rainfall is commonly measured using a rain gauge, which is simply an instrument that is designed to measure the amount of rain that reaches the ground surface during a storm. Rain gauges are considered the most traditional method for measuring rainfall. They have been used historically to provide rainfall quantities and rates at a single point in space. As any measurements, errors can be induced during the measurement processes. One of the common and serious sources of errors in rain gauge measurements is wind-induced error. Another

common problem with rainfall gauge measurements is missing records. This is due to the high probability of gauge mechanical and electrical failures and is also caused by erroneous recording and publishing of rainfall measurements. As a result of measurement error and missing records, researchers and engineers often have to work with incomplete rainfall data from stations where rainfall records might be missing for a day or several days or rainfall data with measurement errors. This will limit most types of rainfall analyses such as calculation of water budgets, determining maximum rainfall intensities, and estimation of area-average rainfall intensities/rainfall amounts.

While rain gauges provide rainfall measurements at individual points, it is more of interest for hydrologic modelling to know rainfall amounts over an area, such as a small drainage basin or a watershed. Usually, the point measurements located in the watershed are assigned to the entire watershed if there is only one rainfall gauge available. The rainfall measurements from the closest rainfall gauge would be assigned to the watershed if there is no rain gauge available in the watershed. If there are more than one rain gauges available in the modelling area, techniques have been proposed to estimate area-average rainfall over an area from point measurements. The most commonly used approaches are based on weighted averaging of rainfall measurements from individual gauges that are located within or close to the area of interest. The Thiessen Polygon method is the most commonly-used method for estimating area-average from point measurements. The weight of a certain station is estimated based on its relative sub-area within the total area of interest. Are rainfall amounts over an area estimated from point measurements representative of the actual amount that happened over that area? How does one get an accurate rainfall estimate over an area based on point measurements (number of point measurements and distance of the point measurement to the interested area)? The overall objective of this study is to explore if common ways of area rainfall estimation provide representative rainfall values for a watershed through comparing SWAT model runoff simulations with field runoff observations.

METHODS AND PROCEDURES

Study Area and Its Background Information: Grand Lake St. Marys is located in Mercer and Auglaize County, northwestern Ohio (Figure 1) and is a very large size lake for its relatively small contributing watershed. The surface area of the lake comprises 17.5 percent of the overall watershed, and much of the remaining watershed is under agricultural production. There are multiple tributaries to the lake within the watershed, with the three largest tributaries making up 63% of lake's upstream drainage. Corn and soybeans are major crops. Other crops include alfalfa (8.5% of the watershed), and winter wheat/ Kentucky bluegrass (6.4% of the watershed) and hay (6.3% of the watershed). Due to the small acreage of farm land available in the watershed, many farmers own animal feeding operations to make a living and sustain local economy.

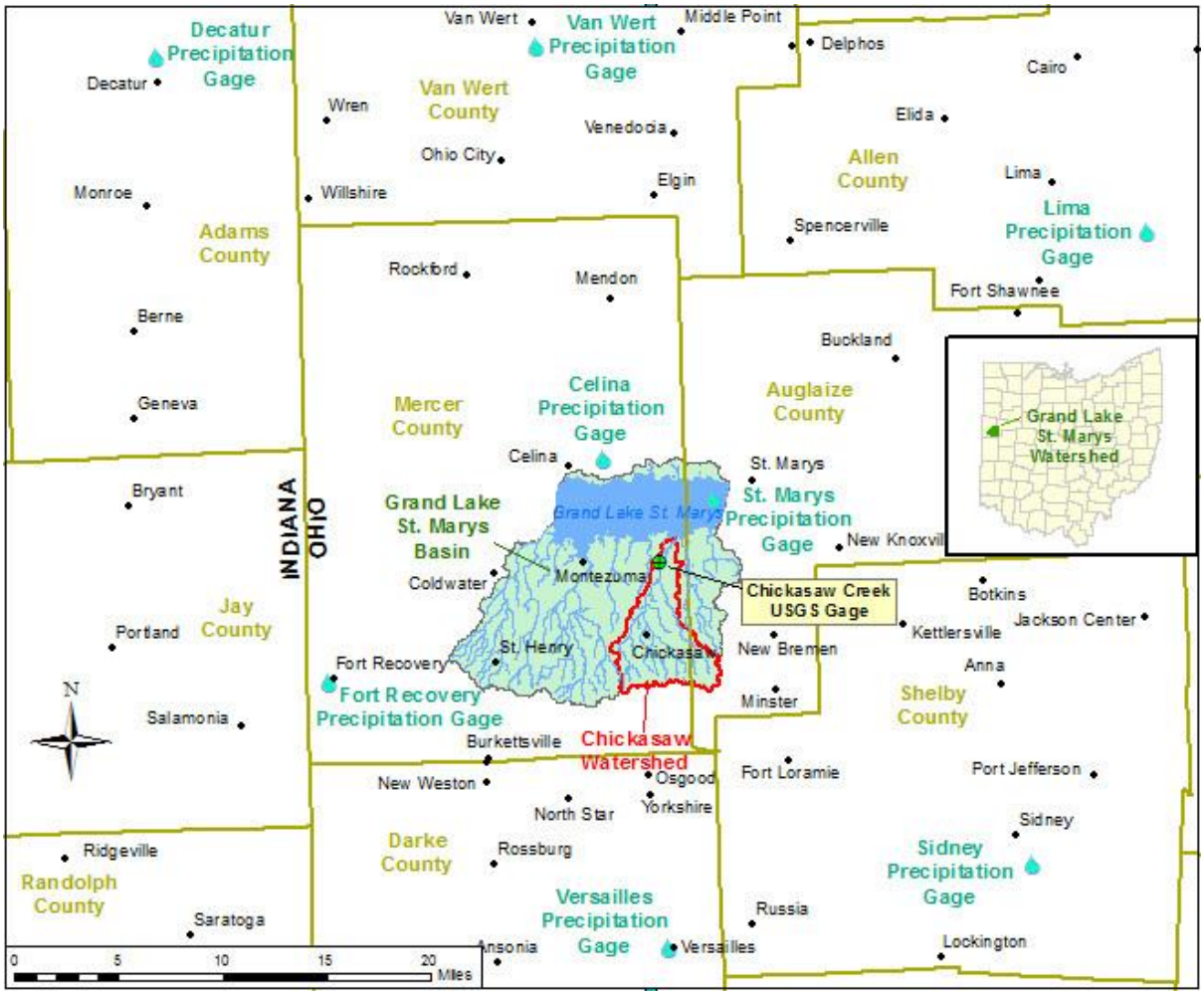

Figure 1 Locations of rural and municipal areas, USGS monitoring gages, and weather stations in the Grand Lake St. Marys Watershed, Mercer and Auglaize County, OH, USA

Grand Lake St. Marys (GLSM) is experiencing toxic levels of algal blooms resulting from phosphorus input from agricultural runoff. Since the outbreak of harmful algae bloom in the summer of 2010, the Ohio Environmental Protection Agency (OEPA) solicited potential short-term remedies from vendors and other interested parties. Thirty-four potential remedies were submitted in response to this solicitation. The submitted potential remedies were reviewed, evaluated and discussed by a technical committee comprised of six environmental scientists. In the absence of other information and from a strictly scientific basis, no single remedy (or proposed combination of remedies) was identified as leading to a probable effective solution. Notably, none of the proposed remedies has been tested on a scale as large as GLSM and therefore the effectiveness of those remedies when applied to GLSM cannot be predicted. The conclusion from this review is that none of the 34 remedies have a better chance for success than the application of alum alone. However, the committee did not believe that the use of alum alone, or any single management practice by itself, could improve the water quality of GLSM except perhaps only over the short term. The most important message from this committee is that the overriding need to improve the lake water quality is to improve the management of the GLSM watershed as a system. Any proposed remedies, however effective they might be in the short term, would be diminished or be completely negated by the continued input of phosphorus, other nutrients and sediment via tributaries. The goal of management of the GLSM watershed as system is implementing

management actions designed to improve the wellness and resiliency of the overall watershed. There is some urgency for the OEPA and EPA Region 5 to seek strategies on both short and long term solutions so as to improve the management of GLSM and its surrounding watershed with respect to sustainability and resilience. One of the questions concerning the longer term restoration of water quality for Grand Lake St Marys is if conservation practices can be adopted to limit nutrient loadings to the lake. The SWAT model is designed to simulate long-term impacts of land use and management on water, sediment and agricultural chemical yields at various temporal and spatial scales in a watershed (Arnold et al., 1998; Arnold and Fohrer, 2005; Gassman et al., 2007). It was chosen to evaluate the impact of conservation practices on nutrient loadings to the lake for this project. Before a model can reasonably simulate nutrient loadings, the runoff has to be reasonably simulated, which would be the first step before a model can be used to simulate nutrient loadings. The first step of the project is to evaluate SWAT runoff simulations.

Since daily flow was monitored at USGS 402913084285400 (Latitude 40°29'13" and Longitude 84°28'54") Chickasaw Creek at St. Marys Ohio (http://waterdata.usgs.gov/usa/nwis/uv?402913084285400). The Chickasaw Creek watershed with a drainage area of 16.4 square miles (42 square kilometers) was chosen as a pilot study.

SWAT Model Description: The Soil and Water Assessment Tool (SWAT) model is a continuous, long-term, physically based semi-distributed model developed to assess impacts of climate and land management on hydrological processes, sediment loading, and pollution transport in watersheds (Arnold et al. 1998). In the SWAT model, a watershed is divided into subwatersheds or subbasins, which are further partitioned into a series of hydrological response units (HRUs). HRUs are uniform units that share unique combinations of soil and land use. Hydrological components, sediment yield, and nutrient cycles are simulated for each HRU and then aggregated for the subbasins.

The hydrological cycle simulated in SWAT is based on the water balance equation:

$$SW_t = SW_0 + \sum_{i-1}^{t} (R_{day} - Q_{surf} - E_a - w_{seep} - Q_{gw})$$

where, SW_t and SW_0 are the final and initial soil water content on day i (mm H_2O), t the time steps on day i, R_{day} the rainfall that reaches the soil surface on day i (mm), Q_{surf} the surface runoff on day i (mm), E_a the evapotranspiration on day i (mm), w_{seep} the interflow on day i (mm), and Q_{gw} is the baseflow on day i (mm) (Neitsch et al. 2005).

The simulated hydrological components include evapotranspiration (ET), surface runoff, percolation, lateral flow, groundwater flow (return flow), transmission losses, ponds, and water yield (Arnold et al. 1998). Evaporation and transpiration are simulated separately in SWAT. Evaporation is computed using exponential functions of soil depth and water content and transpiration is estimated using a linear function of potential evapotranspiration (PET) and leaf area index. Three methods can be used to estimate PET: Hargreaves, Priestley-Taylor, and Penman-Monteith. The Pennman-Monteith method was used to calculate PET in this study. Surface runoff is simulated using a modification of the Soil Conservation Service (now the Natural Resources Conservation Service) Curve Number (SCS-CN) method (USDA, 2004) with daily rainfall. Curve number values used for runoff estimation are based on soil type, LULC, and land management conditions and are adjusted according to soil moisture conditions (Arnold et al. 1993). Percolation is estimated using the combination of a

storage routing technique and a crack-flow model (Arnold et al. 1998). The lateral flow is estimated simultaneously with percolation using a kinematic storage model. The groundwater flow (baseflow) into a channel is calculated based on hydraulic conductivity of shallow aquifer, distance from subbasin to main channel, and water table height. Transmission loss, amount of water removed from tributary channels by transmission, is calculated using procedures described in the SCS Hydrology Handbook. The canopy interception is estimated based on the canopy storage which is a function of vegetation type. Water yield, total amount of water leaving the HRU and entering main channel, is equal to surface runoff plus lateral flow and baseflow, and minus transmission loss and pond abstractions (Neitsch et al. 2005).

Model Input Preparation

The basic SWAT model inputs include a digital elevation model (DEM), Cropland Data Layer, and the Soil Survey Geographic Database (SSURGO) data. Other inputs include daily weather data and field management practices including planting, harvesting, fertilization and tillage information. In addition, streamflow data are also needed for model calibration and validation. The different datasets and their sources are given in Table 1.

The source of the Digital Elevation Model (DEM) data used for the SWAT modeling effort on GLSM was downloaded from USDA Data Gateway. The data is part of the National Elevation Dataset (NED), of which USGS is the original data source. The best horizontal resolution available was 3 meter grid cells, or one-ninth arc second, and this resolution of NED was used in SWAT modeling of GLSM tributary watersheds. Elevation data were converted to ArcGrid format, as required for input elevation data into SWAT. More information about NED can be obtained at http://ned.usgs.gov.

Table 1 Summary of Datasets and their sources used for building the model.

Datasets	Source
Elevation	United States Geological Survey (USGS)
Precipitation	National Climatic Data Center (NCDC)
Soil Classification	Soil Survey Geographic Database (SSURGO)
Landuse	Cropland Data Layer (USDA NASS)
Streamflow	United States Geological Survey (USGS)
Water quality	United States Geological Survey (USGS)

The Cropland Data Layer (CDL) originating from the USDA National Agricultural Statistics Service was used as the input land use/land cover dataset for SWAT modeling of GLSM tributary watersheds. Although SWAT can accommodate other land cover datasets such as the National Land Cover Dataset (NLCD), the CDL was used as it is ideally suited for watersheds that are largely agricultural in land use. The CDL includes information on what crops were planted in a given year on a field level, whereas the NLCD treats cropped fields collectively as a generalized single land use type, regardless of crop type. For modeling efforts in GLSM, the 2009 (56-meter pixel resolution), 2010 (30-meter pixel resolution), and 2011 (30-meter pixel resolution) versions of CDL were used. More information about CDL can be obtained at: http://www.nass.usda.gov/research/Cropland/metadata/meta.htm. As shown in Table 2, Chickasaw watershed is dominated by agricultural crop lands, where corn and soybeans are practiced over 50% of the entire watershed. The entire area of the

watershed is 11960 acres (4840 ha.) and the area draining to the USGS gauges is 10625 acres (4300 ha.).

Table 2 Summary of land use in the Chickasaw watershed

Land use	Area (Acres)	% of watershed area
Corn	4702	39.5
Soybean	2898	24.3
Alfalfa	1010	8.5
Winter wheat/ Kentucky bluegrass	758	6.4
Hay	748	6.3
Forest	384	3.2
Pasture	66	0.6
Urban	342	2.9
Water	11	0.1
Other crops*	1041	8.7
Total	11960	100

*other crops include various crop rotations.

The dominant soil associations in the Chickasaw watershed include Blount, covering 42% of the Chickasaw watershed with 4 soil layers; Pewamo, covering 32% of the watershed with 3 soil layers; and Glynwood, covering 20% of the watershed with 3 soil layers. These 3 soil types altogether comprise 93% of the watershed. The remaining 7% of the watershed is split among 13 soil types, and none of which exceed 3% of the watershed (most are below 1%). The major soil properties are listed in Table 3. Based on the Mercer County Soil Survey, the Blount is somewhat poorly drained, Pewamo is very poorly drained and Glynwood is moderately well drained (http://soils.usda.gov/survey/online_surveys/ohio/mercerOH1979/Mercer.pdf).

Table 3 Soil physical information from SSURGO used in SWAT modeling

Soil Type	Blount				Pewamo			Glynwood		
Layer	1	2	3	4	1	2	3	1	2	3
Depth from the soil surface (mm)	254	635	813	1524	330	940	1524	229	584	1524
Organic carbon content (% soil weight)	1.45	0.29	0.15	0.15	4.36	1.45	0.48	1.16	0.39	0.13
Moist bulk density (g/m^3)	1.45	1.55	1.6	1.73	1.45	1.55	1.6	1.38	1.58	1.75

Weather Data: Daily weather data hosted by the National Oceanic and Atmospheric Administration (NOAA) National Climate Data Center (NCDC) were used to serve as input into the SWAT model. Based on interviews and recommendations from local people, the lake itself appears to have an effect on approaching storms, resulting in different precipitation patterns on the south side of the lake where the Chickasaw watershed is located and on the north side of the lake where two weather stations which are the closest to the watershed are located (in Figure 1). In addition, meteorological observations indicate that the courses that storms travel can be highly variable, especially in relatively wet years. Thus, instead of the

usual modelling approach of just going with the closest gages, precipitation information from various directional precipitation gauges within 35-mile radius from the watershed boundary were collected in the hope of capturing precipitation coming from all directions of the watershed. This was done to explore the possibility of finding the representative precipitation pattern in the watershed.

SWAT Model Simulations and Performance Evaluation: Based on the DEM and selected outlets, the watershed was delineated into subbasins. Subsequently, the subbasins were partitioned into homogeneous units (HRUs), which shared the same land use, soil type, and slope range. In this study, a total of 30 subbasins were delineated, among which 27 subbasins drain to the USGS flow gauge station. HRUs were defined by applying a 10% threshold for land use, soil type, and slope range so any of these components that had a use/type/range less than 10% of a particular subbasin got eliminated from influencing the model result. The net effect of eliminating these minor influences was to significantly improve the efficiency of the model while not significantly affecting the result. Each HRU represents a unique combination of land use, soil type, and slope range, and collectively they provide much of the information needed by the SWAT model to characterize the watershed.

Model simulations were first performed using SWAT default values with precipitation data from the closest gauge (St. Marys). Next, model simulations were performed using SWAT default values with one precipitation gauge at a time for the remaining precipitation gauges from Figure 1. Finally, a hybrid precipitation file was developed to capture precipitation pattern of the watershed by using data from a single gauge to cover a range of consecutive dates based on which gauge best simulated actual precipitation events in term of timing and magnitude within that particular date range. To evaluate the model performance, four statistical measurements were used (Moriasi et al., 2007) including the coefficient of determination (R^2), Nash-Sutcliffe efficiency (NSE), RMSE-observations standard deviation ratio (RSR) and percent bias (PBIAS).

RESULTS AND DISCUSSION

Results from the Closest Precipitation Gauge: The first model simulation was performed using the SWAT default values and precipitation from the closest weather station, St. Marys precipitation gauge in which the missing records were substituted with the precipitation records from the Celina Precipitation gauge (Figure 1). For those two years of the model simulation for which observed flow data were available (2009 and 2010), the R^2 is 0.37 and 0.03 for 2009 and 2010, respectively (Figure 2). The R^2 of 0.37 for 2009 is within the acceptable range for an uncalibrated model simulation, but the R^2 of 0.03 for 2010 is unacceptable. Furthermore, the hydrographs in Figure 2 below show that the simulation did a fairly good job aligning with observed flow peaks for 2009, whereas the simulated peaks essentially aligned very poorly with observed peaks for 2010.

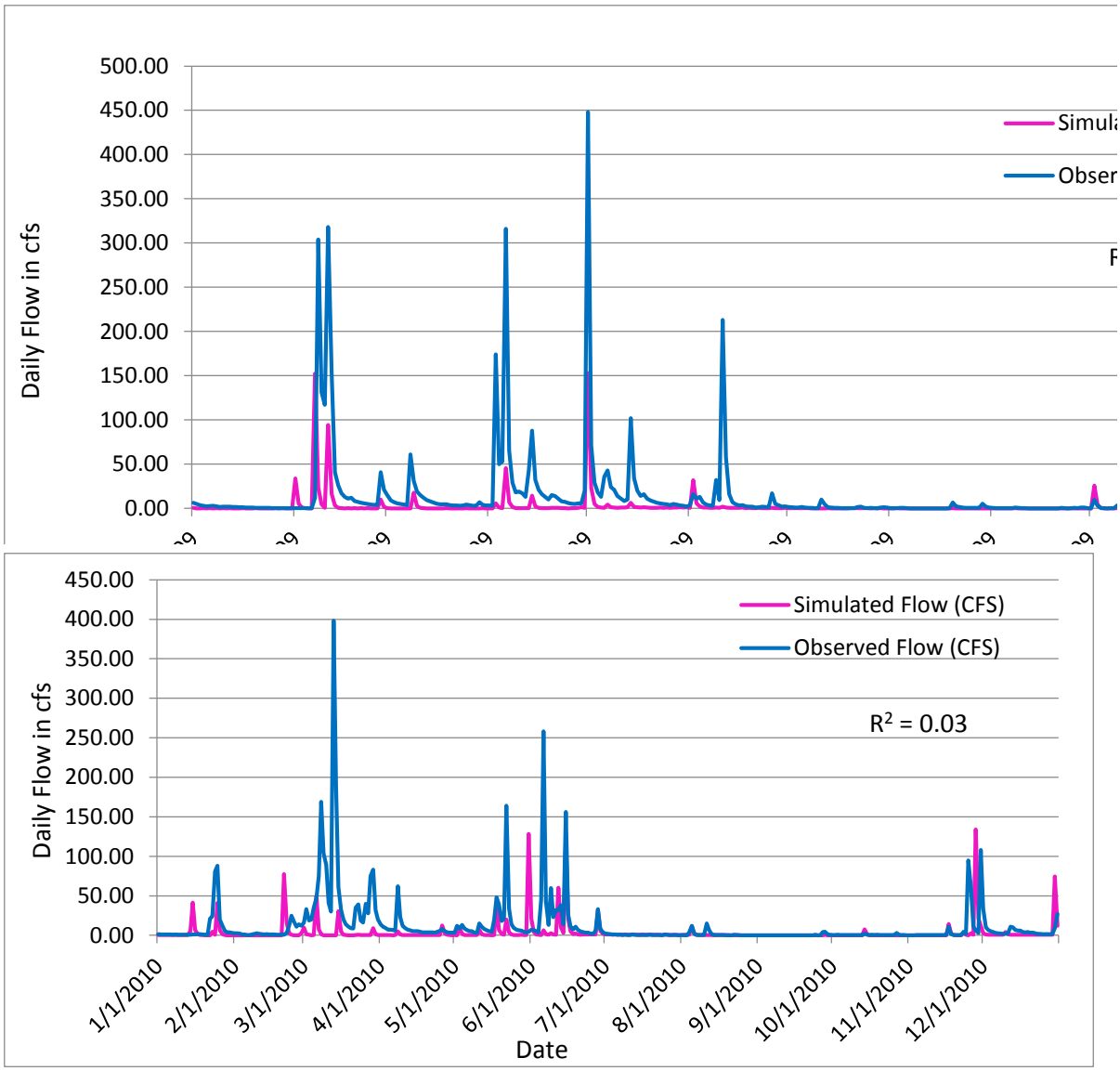

Figure 2 Flow hydrographs for initial uncalibrated model run with SWAT default values using precipitation data from St. Marys precipitation gauge.

The very poor correlation for Year 2010 of the model suggests that improvements to the model might be very difficult. After having tried model developers' recommendations for applying seasonal adjustments to the curve number for the Chickasaw watershed, it was found, unfortunately, very little improvement was achieved on model's performance. The poor correlation between simulated flow and observed flow led us to question the credibility of climate data. How well did the input precipitation dataset at the St. Marys weather station represent actual precipitation conditions in the watershed? The flow correlation coefficients were so low, especially for year 2010 (Figure 2), it seemed that the NOAA precipitation gage used did not match up with actual precipitation in the Chickasaw watershed based on the near-zero correlation of the simulated hydrograph comparing with the observed hydrograph for 2010 (Figure 2). Although the St. Marys precipitation gauge is only a few miles away from the Chickasaw watershed, the zero correlation of the hydrograph indicates that the precipitation gage is totally irrelevant to the flow generated in the watershed.

Results from other Precipitation Gauges: Additional SWAT simulations were performed using the SWAT default values and precipitation data from each of the weather gauges displayed in Figure 1. Table 4 shows the R^2 (correlation coefficients) for each gauge:

Table 4 SWAT model simulations with precipitation data from different precipitation gauges

R-squared	St. Marys	Celina	Decatur	Van Wert	Lima	Sidney	Versailles	Ft. Recov
Year 2009	0.37	0.50	0.17	0.37	0.17	0.14	0.02	0.06
Year 2010	0.03	0.07	0.03	0.07	0.02	0.23	0.04	0.06

As shown in Table 4, using precipitation data from the Sidney precipitation gauge to the southeast of the Grand Lake St. Marys watershed in neighboring Shelby County showed great improvements in correlating daily simulated and observed flows for the year of 2010. Further comparisons on a monthly basis gained more insights on weather patterns of the watershed; for example, in June of 2010, an R^2 of 0.59 was obtained using precipitation data from the Sidney precipitation gauge comparing an R^2 of 0.19 from the St. Marys precipitation gauge (Figure 3). It may be concluded that the first flow peak in this month was caused by a shared precipitation event occurring at both the watershed and the Sidney gauge.

The increased R^2 for June 2010 using precipitation data from the Sidney precipitation gauge is very encouraging, demonstrating that considering a more distant precipitation gauge from the modeled watershed can be promising in capturing the precipitation pattern of the watershed. The hydrograph above demonstrates that the more distant Sidney precipitation gauge might better represent precipitation of the watershed, at least for the first half of June in 2010. However, how well St. Marys precipitation gauge represents the second half of the month can't be overlooked, suggesting that weather experienced at the St. Marys precipitation gauge might better represent the precipitation pattern of the watershed for this time period.

This raised the question: what would be the best way to construct a precipitation file to represent the precipitation happened over the modeled watershed? A precipitation file covering the years 2009 and 2010 was constructed using observed precipitation from all 8 precipitation gauges (Figure 1). For the month of June 2010, it seemed that the Sidney precipitation gauge best represented most of the first half of June, and the St. Mary's precipitation gage represented the second half. Figure 4 illustrates the result of SWAT simulation with such a hybrid precipitation input file.

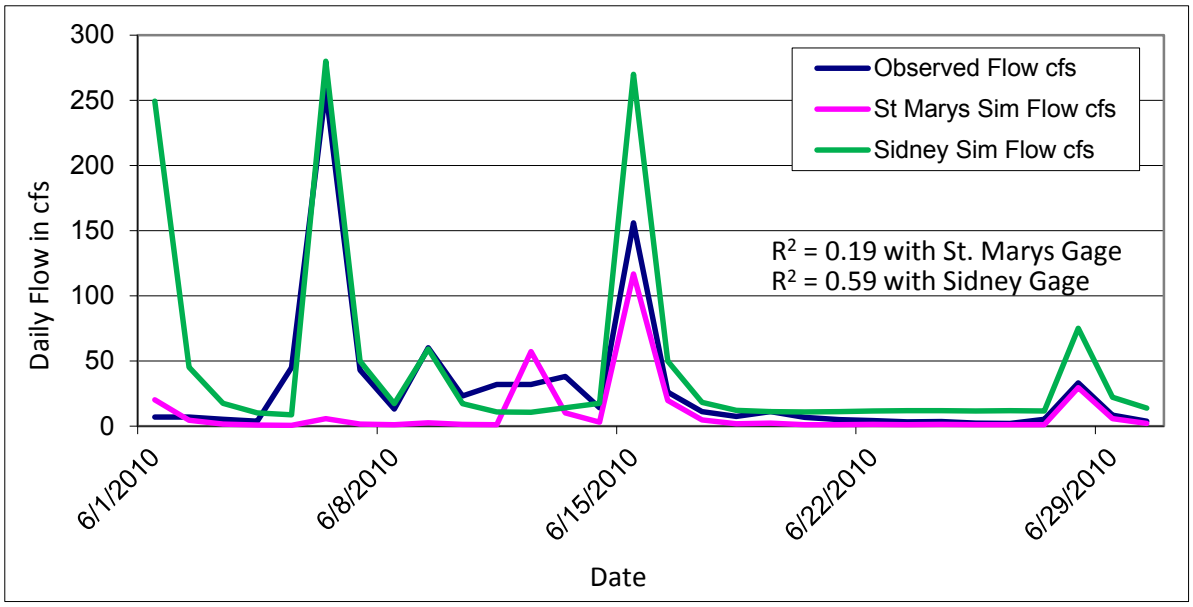

Figure 3 Simulated flow hydrographs using precipitation data from the Sidney precipitation and the St. Marys precipitation gauge vs observed flow hydrograph for June of 2010.

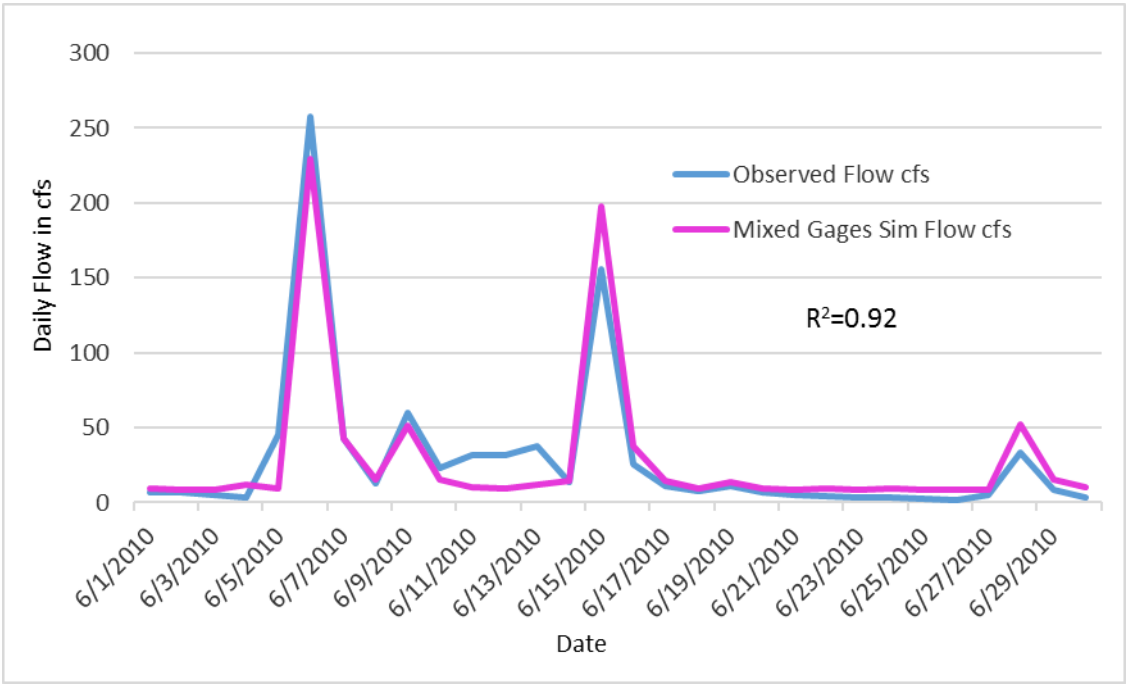

Figure 4 Simulated flow using a hybrid precipitation data from the Sidney precipitation and the St. Marys precipitation gauge vs observed flow for June of 2010.

The excellent result and correlation displayed in Figure 4 provided evidence that constructing a hybrid file from additional precipitation gauges nearby the watershed is necessary to represent the precipitation pattern of the watershed. St. Marys weather data would do a good job at picking up on weather systems coming out of the north, but adding other gages from all directions might pick up weather from all directions.

The result of using a hybrid precipitation input file constructed using a mix of observed daily precipitation data from all 8 precipitation gauges are shown in Table 5. The R^2 of 0.60 between model simulation and field observation displayed in Table 5 can be considered as excellent for an uncalibrated model simulation. The 2010 overall correlation using hybrid precipitation file increased to 0.60 from the dismal 0.03 using just the St. Mary precipitation data and 0.23 using just the Sidney precipitation data.

Table 5 Comparison of model performance using a hybrid precipitation data from all 8 precipitation gauges vs using only St. Marys Weather Station for water year of 2009 and 2010.

Simulated vs. Observed Flow R-squared Correlation	Using St. Marys Weather Station Precipitation Data	Using Hybrid Precipitation Data from All 8 Stations
2009	0.37	0.51
2010	0.03	0.60

Because the results speak so strongly for themselves, a meteorological perspective was sought out. The question of considering precipitation events from multiple gages as far away from the modeled watershed as the next county was posed to someone with a background in meteorology. The meteorologist considered it perhaps a trick question because from a meteorology perspective, it's absolutely appropriate to consider weather data from multiple gages when considering weather for a multi-county area commensurate in size to a major metropolitan area. It's what happens every evening in weather broadcasts in metro areas, or to quote the meteorologist above, "of course it's okay to consider precipitation gages in the next county!"

CONCLUSIONS

Accurate estimation of rainfall amount over a watershed is critical for getting accurate runoff simulation. The common practice of assigning the point measurements located in the watershed to the entire watershed may not represent the precipitation pattern over the watershed. This study shows that a watershed precipitation pattern could be influenced by precipitations from all directions. The closest precipitation gauge, the St. Marys on the north shore of Grand Lake St. Marys experienced a quite different weather pattern than the modeled Chickasaw Creek watershed, which is on the south side of the lake. Thus, it is important to construct a hybrid precipitation file from all 8 precipitation gauges within 35-mile radius from the boundary of the watershed.

ACKNOWLEDGEMENTS

The United States Environmental Protection Agency through its Office of Research and Development funded the research described here. It has been subjected to Agency review and approved for publication. The authors are grateful for the valuable comments and suggestions provided by reviewers.

Notice: Although this work was reviewed by the USEPA, and approved for publication, it may not necessarily reflect official Agency policy. Mention of trade names or commercial products does not constitute endorsement or recommendation for use.

REFERENCES

Arnold, J.G., Allen, P.M., and Bernhardt, G. (1993). "A comprehensive surface-groundwater flow model," Journal of Hydrology, 142(1-4), pp 47-69.

Arnold J.G., and Fohrer, N. (2005). "SWAT2000: current capabilities and research opportunities in applied watershed modelling," Hydrological Processes 19, pp 563-572.

Arnold, J.G., Srinivasan, R., Muttiah, R.S., and Williams, J.R. (1998). "Large area hydrologic modeling and assessment - Part 1: Model development," Journal of American Water Resour. Association, 34(1), pp 73-89.

Gassman P.W., Reyes M.R., Green C.H., and Arnold J.G. (2007). "The Soil and Water Assessment Tool: Historical Development, Applications, and Future Research Directions," Transactions of the ASABE, 50, 1211-1250.

Neitsch S.L., Arnold J.G., Kiniry J.R., Williams J.R. (2005). "Soil and Water Assessment Tool Theoretical Documentation," Temple, TX.

Moriasi D.N., Arnold J.G., Van Liew M.W., Bingner R.L., Harmel R.D., Veith T.L. (2007). "Model evaluation guidelines for systematic quantification of accuracy in watershed simulations," Transactions of the Asabe, 50(3), 885-900.

USDA, NRCS, (2004). National Engineering Handbook, Part 630, Hydrology. Chapter 8, Land Use and Treatment Classes.

USDA, NRCS, (2004). National Engineering Handbook, Part 630, Hydrology. Chapter 9, Hydrologic Soil-Cover Complexes.

USDA, NRCS, (2004). National Engineering Handbook, Part 630, Hydrology. Chapter 10, Estimation of Direct Runoff from Storm Rainfall.

MODELING INTERACTIONS OF FLOW AND VEGETATION FOR IMPROVED RIVERINE SYSTEM MANAGEMENT

Daniel Dombroski, Hydraulic Engineer, BOR, Denver TSC, CO, ddombroski@usbr.gov; Blair Greimann, Hydraulic Engineer, BOR, Denver TSC, CO; Yong Lai, Hydraulic Engineer, BOR, Denver TSC, CO; Victor Huang, Hydraulic Engineer, BOR, Denver TSC, CO; Lisa Fotherby, Hydraulic Engineer, BOR, Denver TSC, CO; Mark Stone, Assistant Professor, UNM Dept. Civil Eng., NM; Li Chen, Associate Research Professor, DRI Division of Hydrologic Sciences, NV

Abstract: The establishment, growth, and decline of riparian vegetation within impacted riverine systems is a growing challenge due to the increasing priority of maintaining ecosystem function while sustaining water supply and providing flood protection. A quantitative two-dimensional model is presented for predicting the interactions between flow and vegetation that is currently under development at BOR. The model is based upon the SRH-2D package, which contains a two-dimensional flow and mobile bed sediment transport model. The new SRH-2DV package incorporates a module that simulates the effect of vegetation on river and floodplain hydraulics through spatially distributed roughness. The coupled vegetation-hydraulic solver uses measured vegetation parameters to calculate a spatially-distributed, dynamic Manning's roughness coefficient while simulating the hydrodynamics of the system. Field and modeling work focused on a reach of the San Joaquin River near Fresno, California. Simulation results using the vegetation module are compared with measured water surface elevation and results from a manually-calibrated SRH-2D hydraulics model. We present initial simulation results from application to simple case studies and discuss the utility of expanding the predictive capabilities for application within more complex systems. Results from SRH-2DV will aid the science, economics, and policy of establishing environmental flows by addressing questions regarding the physical interaction of flow and vegetation in rivers and floodplains.

INTRODUCTION

The survival of riparian vegetation within managed river systems is a growing challenge due to the increasing priority of maintaining or restoring ecosystem function while balancing the need for water supply and flood protection. Riparian vegetation plays many important roles in the hydraulic, geomorphic, and ecologic processes of river systems (Naiman, 2010; Gurnell 2014). The ecological services provided by riparian vegetation are beneficial to both the river system and the human population surrounding the system (Groffman et al., 2003). Examples of these services include soil retention (Waters 1995), water quality improvement (Barling and Moore 1994), nutrient cycling (Dahm *et al*. 2002; Hill 1996), habitat provisioning (Keller *et al*. 1993; Stauffer and Best 1980), and flood damage mitigation (Brauman *et al*. 2007). The ecological services associated with riparian areas have been severely degraded in many river systems as the result of river engineering, floodplain development, and watershed development (Sweeney et al., 2004).

At the local scale, riparian vegetation increases flood risk by reducing effective flow areas and increasing hydraulic roughness (Rhee et al., 2008; Wilson et al, 2005; Green 2005). Reducing flow resistance in areas sensitive to flooding has historically been performed by vegetation removal (Darby, 1999; Masterman and Thorne 1992). At the watershed scale, however, vegetation-induced roughness has been

shown to enhance flood wave attenuation (Anderson 2006). Properly characterizing hydraulic roughness at the local scale is important for understanding hydrodynamic heterogeneity at the reach scale, including velocity and shear stress distributions and momentum exchange (Vermaas et al., 2011; Proust et al., 2013; Stone and Hotchkiss, 2007).

Vegetation resists flow due to drag forces on discrete elements and nonlinear interactions between multiple elements (Nepf, 2012). Flow resistance in natural systems is often characterized through the estimation of a dimensionless (e.g., Darcy friction factor *f*) or dimensional (e.g., Chezy coefficient *C* and Manning's *n*) roughness parameter that is used to model the hydraulics. Roughness parameters derive from a combination of empiricism and hydrodynamic theory and are generally interrelated deterministically. The roughness of a vegetated channel is generally a function of both the characteristics of the vegetation (e.g., size, density, flexibility, leaf area) and the flow (depth and velocity; due to streamlining effects). For computational convenience, however, roughness has historically been assumed independent of hydraulic conditions. Chow (1959) produced a list of bracketed roughness values corresponding to various vegetated flow types. Thompson & Roberson (1976) presented an analytical method for predicting roughness due to a flow through vegetation modeled as rigid or flexible cylinders. The method depends on estimation of a drag coefficient, stem spacing and diameter, and flexural rigidity. Kouwen & Li (1980) developed an iterative approach for calculating roughness as a function of vegetation rigidity, and estimated plant deflection in response to forcing exerted by the flow. The Kouwen & Li (1980) approach is generally applicable to grasses, and the authors provid a table with stiffness values for a large variety of grass types. Kouwen & Fathi-Moghadam (2000) describe methodology to estimate resistance due to coniferous trees in open-channel flow by modifying a previously existing model (Fathi-Moghadam & Kouwen, 1997) in order to account for variations in the flexibility between species. The authors obtained species-specific parameters for the equations by conducting intricate laboratory and field experiments to measure drag force on model trees. Darby (1999) presents a simplified cross-section based model for predicting roughness associated with sediment or vegetation. The approach applies one of six different empirically calibrated flow resistance equations at each computational node. An equation similar to the Kouwen & Li (1980) approach is used for flexible vegetation, while an equation similar to the Thompson & Roberson (1976) approach is used for nonflexible vegetation. A procedure for estimating roughness due to flow through stiff or flexible woody vegetation is described by Jarvela (2004). The method, limited to emergent vegetation, incorporates leaf area index (LAI) to account for the effect of leaf distribution on drag resistance. The author also presents (Jarvela, 2005) an analysis of flow structure over submerged flexible vegetation with a focus on velocity profiles and turbulence characteristics. Baptist et al. (2007) derive a Chezy-type formulation for calculating resistance due to submerged or emergent vegetation. The representative resistance coefficient includes contributions from the bed roughness, form drag from flow through the vegetation, and shear due to the velocity profile above the vegetation. Hession and Curran (2013) provide a literature review of trends and research in the topic of vegetation-induced roughness in fluvial systems; the authors discuss the spatio-temporal complexity of processes related to vegetation-flow-sediment interactions. Abu-Aly et al. (2014) present the results of two-dimensional hydraulic modeling using roughness derived from LiDAR. The authors demonstrate the effects of spatially-distributed roughness on hydraulics at the local and reach scale, and underscore the importance of systematically defining roughness at the resolution of the computational grid. The challenge of capturing the complexity of effects due to flow through a broad

range of vegetation types is reflected by the diversity of predictive methods developed during more than five decades of research.

Described herein is a deterministic computational tool for dynamically modeling spatially-distributed flow and vegetation interactions. An existing two-dimensional hydraulic and sediment transport model (SRH-2D) developed at the Bureau of Reclamation (BOR) Technical Service Center (TSC) is used as a basis for the new model development (SRH-2DV). The new SRH-2DV package iteratively computes hydraulic roughness due to vegetated flow as a function of the local hydraulics and vegetation characteristics. The algorithms and parameters applied are drawn from a combination of published literature and collaborative research. Results from SRH-2DV will aid the science, economics, and policy regarding riparian ecosystems by addressing uncertainties such as what impact riparian vegetation has on local flood conditions, how vegetation can be incorporated into restoration projects without increasing flood risks, and how management actions may impact habitat for endangered and threatened species.

METHODS

Model Development: The existing SRH-2D flow solver (Lai, 2010) is used as the computational base for the new SRH-2DV coupled flow and vegetation model. Hydraulic variables are computed by solving the depth-averaged dynamic wave equations using a finite volume numerical method. Solutions can be computed over an unstructured hybrid mesh (Lai, 1997; 2000), and the solver includes a seamless wetting-drying algorithm that is applied at each time step. With appropriate boundary conditions, constant or varying discharge flows may be simulated. The solver can compute subcritical and supercritical flow conditions without special treatment.

Bed shear stresses τ_{bx} and τ_{by} are calculated by the SRH-2D hydraulic solver using the Manning's roughness equation as follows:

$$\begin{pmatrix}\tau_{bx}\\ \tau_{by}\end{pmatrix} = \rho C_f \begin{pmatrix}U_x\\ U_y\end{pmatrix}\sqrt{U_x^2+U_y^2}; \quad C_f = \frac{gn^2}{h^{1/3}} \tag{1}$$

where ρ is water density, U_x and U_y are the x and y velocity components, g is gravity, h is flow depth, and n is the Manning's roughness coefficient. The user-specified Manning's n is generally spatially-distributed yet independent of the computed hydraulic variables, and is a primary "tuning" parameter used during model calibration.

In the SRH-2DV vegetation model, the solver was modified to calculate dynamic Manning's n values at each cell in the computational mesh due to vegetated flow. The approaches of Baptist et al. (2007) and Järvelä (2004) were implemented in the model; the required input parameters could readily be measured in the field and applied within the modeling framework. Additional methods can be built into the modeling framework based on availability of supporting field data and will be investigated in future research.

The Järvelä (2004) approach is valid for emergent, stiff and flexible woody vegetation. The authors proposed the following equation to calculate the friction factor f,

$$f = 4C_{dX}\mathrm{LAI}\left(\frac{U}{U_X}\right)^X \frac{h}{H} \tag{2}$$

where $C_{d\chi}$ is a species-specific drag coefficient, LAI is leaf area index (defined as one-sided leaf area to projected ground surface ratio), U is the flow velocity magnitude, U_χ is a reference velocity (set to 0.1 m/s for this study), and χ is a species-specific exponent (set to -0.57 for this study). The ratio of h (water depth) over H (plant height) is a scaling factor to account for partial submergence ($h<H$). The parameters LAI and H are measured in the field as described below. The variable flow velocity and water depth are obtained from the coupled hydraulic solver, where U is calculated as the resultant of the horizontal velocity components at each mesh cell. The value of the drag parameter $C_{d\chi}$ was based on prior work done by Fathi-Moghadam (1996) and then varied on a species-specific basis in order to calibrate the model response. Thus the friction factor is a function of spatial variation in the plant parameters and spatial and temporal variation in the hydraulic variables. In practice, the Manning's n is used by the hydraulic solver (Equation 1) and is computed from the friction factor as

$$n = h^{\frac{1}{6}}\sqrt{\frac{f}{8g}} \tag{3}$$

Roughness can alternatively be calculated using the Baptist (2007) approach according to

$$C_r = \sqrt{\frac{1}{(1/C_b^2) + (C_d mDH/2g)}} + \frac{\sqrt{g}}{\kappa}\ln\left(\frac{h}{H}\right) \tag{4}$$

where C_b is the Chezy bed coefficient, C_d is the drag coefficient, m is plant density, D is stem diameter, H is plant height, κ = 0.41 is the von Karman constant, and h is the flow depth. Thus the composite resistance coefficient C_r includes the effects of bed resistance, form drag of flow through the vegetation, and the boundary layer formed above the vegetation. For emergent vegetation, the logarithmic term in Equation 4 is dropped since the resistance is only a function of the bed roughness and vegetative form drag. For dense vegetation, the contribution of the bed roughness term may be considered insignificant compared to the contribution of the vegetative drag term (C_b =80 for this study). The water depth h is obtained from the coupled hydraulic solver and the parameters m, D, and H are measured in the field. The drag coefficient C_d was initially set to unity (Baptist, et al., 2007) and then varied on a species-specific basis in order to calibrate the model response. The resistance in Equation 4 is converted to Manning's n as

$$n = \frac{1}{C_r}h^{1/6} \tag{5}$$

Study Reach: The SRH-2DV vegetation model was tested by simulating the hydraulics in a reach of the San Joaquin River west of Fresno, California located between Friant Dam and the Chowchilla Bifurcation structure. This section was selected due to the presence of diverse riparian vegetation types and the availability of pre-existing field data.

Floodplain vegetation in the study reach was classified by Moise and Hendrickson (2002) to have 30 different dominant vegetation classes (Holland, 1986). To further classify woody types, Moise and Hendrickson added a numerical value from 1 to 6 indicating branch density (high to low) based on Hink and Omhart's work (1984). Moise and Hendrickson (2002) found eleven classes that covered 92% of the vegetated area within the study reach: (1) cottonwood riparian of branch density 3; (2) cottonwood riparian low density of branch density 4; (3) and (4) herbaceous, mixed riparian of branch densities 1 and 3; (5) mixed riparian low density of branch density 6; (6) riparian scrub; (7) and (8) willow riparian of branch densities 3 and 4; (9) and (10) willow scrub of branch densities 5 and 6; and (11) willow scrub low density of branch density 6. The vegetation classifications were compiled into a GIS shapefile comprised of polygons delineating the spatial extent of the dominant classes within the study reach.

A computational mesh with boundary conditions was available for the reach from previous hydraulic modeling in support of the San Joaquin River Restoration Project (Dombroski, Greimann, & Gordon, 2012). The existing model was calibrated by comparing simulated water surface elevation to measured water surface elevation at a similar discharge. The Manning's *n* was then manually adjusted in the channel and floodplain areas in order to bring the simulated water surface elevation in better agreement with the measurements. Manually adjusting the Manning's *n* in order to effect the water surface elevation is generally successful in reproducing the gross effect of bed and form roughness; however, the approach includes no explicit treatment of roughness due to vegetation, which limits the capability of the model in predicting vegetative effects.

Empirical Data and Field Work: Development and testing of the SRH-2DV vegetation model was dependent on data reconnaissance in support of the parameterized physical processes. A field study was conducted (Gillihan, 2013) at six 1000 ft^2 sites along the San Joaquin River, producing measurements of vegetation height, stem diameter, stem density, and leaf area index. Vegetation height and stem diameter was measured with a hypsometer (Nikon Forestry Pro Laser) and caliper, respectively. LAI was measured using a photosynthetically active radiation (PAR) sensor (Decagon AccuPAR model LP-80). The field measurement sites were selected as representative samples of the dominant vegetation classes identified by Moise and Hendrickson (2002); the measured vegetation parameters were then applied to all instances of the delineated vegetation classes within the shapefile. An attribute table was constructed to contain the input data required to parameterize the model for each vegetation classification. The shapefile in conjunction with the attribute table defines the spatial distribution of vegetation and corresponding parameters throughout the study reach. The shapefile and attribute table are read directly by the SRH-2DV model and the vegetation information is mapped to the computational mesh over which the hydraulic variables are solved.

Table 1 and Table 2 contain a summary of the parameter values and sources used in the Jarvela (2004) and Baptist (2007) approaches, respectively. Values listed as Variable generally may depend on vegetation class and location, and are used to tune the model response during calibration. Values listed as Measured were taken from the results of the field campaign, and Dynamic indicates quantities calculated by the hydraulic solver that may vary in space and time. The values of fixed parameters are given with reference to a source in the published literature.

For regions within the computational mesh where a vegetation-based roughness was not applicable (e.g., in-channel, no-grow, and anthropogenically disturbed areas) or not physically reasonable, a static value of n=0.035 was assigned by default.

Table 1 Identification of parameters used in the Jarvela (2004) approach for computing hydraulic roughness.

Parameter	Value	Source
C_{dX}	Variable	Model Calibration
X	-0.57	Aberle & Jarvela, 2013
U_x	0.1 m/s (0.328 ft/s)	Aberle & Jarvela, 2013
LAI	Measured	Gillihan, 2013
H	Measured	Gillihan, 2013
U	Dynamic	Hydraulic Solver
h	Dynamic	Hydraulic Solver

Table 2 Identification of parameters used in the Baptist (2007) approach for computing hydraulic roughness.

Parameter	Value	Source
C_D	Variable	Model Calibration
C_b	80	Gillihan, 2013
m	Measured	Gillihan, 2013
D	Measured	Gillihan, 2013
H	Measured	Gillihan, 2013
h	Dynamic	Hydraulic Solver

RESULTS

The SRH-2DV vegetated flow solver was tested by simulating the hydraulics within a reach of the San Joaquin River at flow rates Q = 1100 (31), 2500 (71), 4000 (113), and 7500 (212) cfs (cms). The capability of the hydraulic roughness module in estimating roughness due to vegetation was evaluated by comparing computed Manning's n to manually calibrated Manning's n and by comparing computed water surface elevation to measured water surface elevation at a similar discharge. Also available for comparison is simulated water surface elevation from the manually calibrated model (Dombroski, Greimann, & Gordon, 2012). Figures 1 and 2 show comparisons of water surface elevation results using the Baptist (2007) approach and Jarvela (2004) approach for calculating hydraulic roughness due to vegetation. Also shown is water surface elevation from a simulation using manually calibrated roughness and field measurements of water surface elevation for a similar discharge. The results indicate that the Jarvela (2004) approach, although resulting in under predicted water surface elevation, performs better than the Baptist (2007) approach, and compares favorably with the performance of the manually calibrated model for large extents of the model reach.

The simulated water surface elevation is in part determined by the distribution of Manning's n values computed by the model for each vegetation type. Compiled in Figure 3 and 4 are distributions of

Manning's *n* values for well-represented vegetation types in the modeled reach of the San Joaquin River. The distributions are compiled from the Manning's *n* value at each cell in the computational mesh as designated by the vegetation type polygons. The distributions shown in each figure include (A) the calculated values for wetted cells using the Jarvela (2004) approach, (B) the polygon values including those calculated in wet cells and the default value of n=0.035 in dry cells, and (C) the values taken from the manually calibrated model. Also shown in each plot are the mean (solid line) and standard deviation from the mean (dashed line) of the calculated Manning's *n* values for wetted cells. The distribution of calculated Manning's *n* values (blue) in each plot is representative of cells that are directly coupled to the hydraulics through Equation 2. For Mixed Riparian (Figure 3) and Willow Riparian (Figure 4) vegetation types, the compilation of Manning's *n* values are approximately normally distributed around the mean value. Manning's *n* values calculated for the Willow Scrub (not shown) vegetation type do not appear to be normally distributed, possibly due to species-specific parameters that are causing the calculated roughness values to be biased low. The cumulative count of a distribution of Manning's *n* values provides an indication of the relative influence a given vegetation type has in the hydraulic computations the model is performing. The gross effects of vegetative roughness in the hydraulic model will be driven by vegetation types that are largely inundated for the flow simulated. In the model reach of the San Joaquin River, many cells within the computational mesh are classified as Agricultural Field. The count of calculated Manning's values is far less, however, indicating that the portion of inundated agricultural field (and therefore the effect of agricultural vegetation on the hydraulics within the reach) is small.

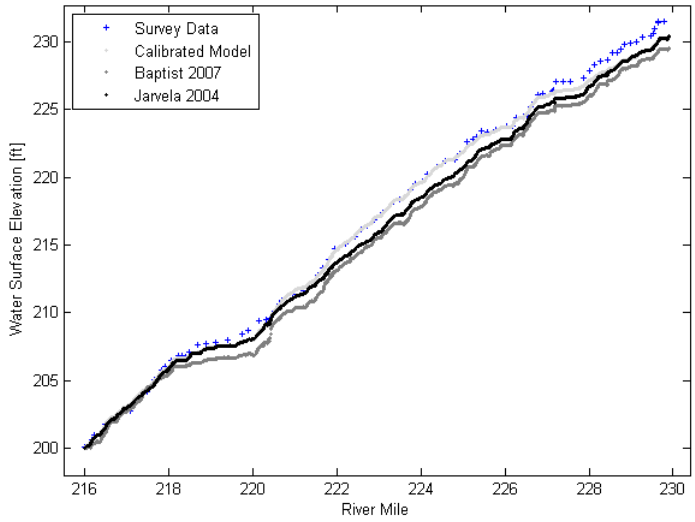

Figure 1 Simulated water surface elevation (ft) as a function of river mile (mi) for Q = 4000 cfs in a reach of the San Joaquin River. Shown for comparison are measured water surface elevation (blue), manually calibrated simulation results (light grey), simulation results using the Baptist (2007) approach (grey), and simulation results using the Jarvela (2004) approach (black). The figure demonstrates that the Jarvela (2004) approach performs better than the Baptist (2007) approach, although falls short of the performance of the manually calibrated model.

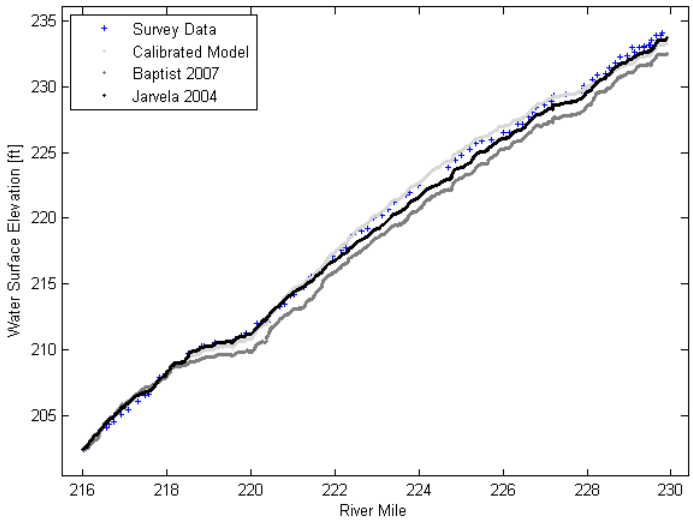

Figure 2 Simulated water surface elevation (ft) as a function of river mile (mi) for Q = 7500 cfs in a reach of the San Joaquin River. Shown for comparison are measured water surface elevation (blue), manually calibrated simulation results (light grey), simulation results using the Baptist (2007) approach (grey), and simulation results using the Jarvela (2004) approach (black). The figure demonstrates that the Jarvela (2004) approach performs better than the Baptist (2007) approach, although falls short of the performance of the manually calibrated model.

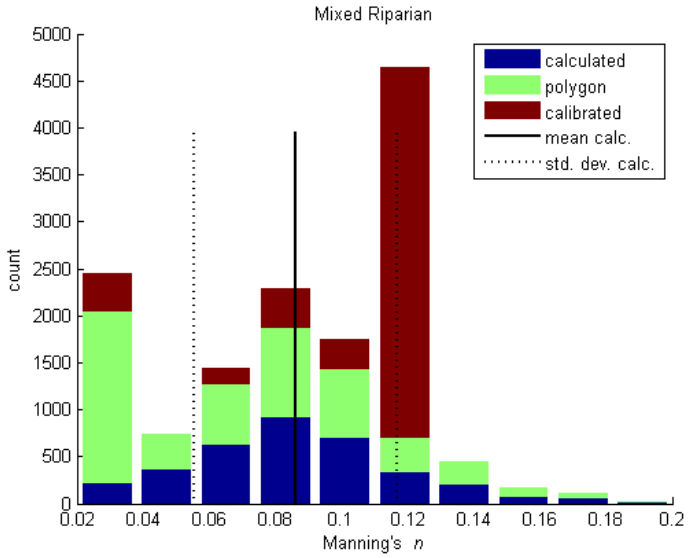

Figure 3 Distribution of Manning's *n* values for Mixed Riparian vegetation in the computational mesh of the modeled reach of the San Joaquin River. Shown in the figure are the calculated values for wetted cells using the Jarvela (2004) approach (blue), the polygon values including those calculated in wet cells and default values in dry cells (green), and the values taken from the manually calibrated model (red). Also shown are the mean (solid line) and standard deviation from the mean (dashed line) of the calculated Manning's *n* values for wetted cells.

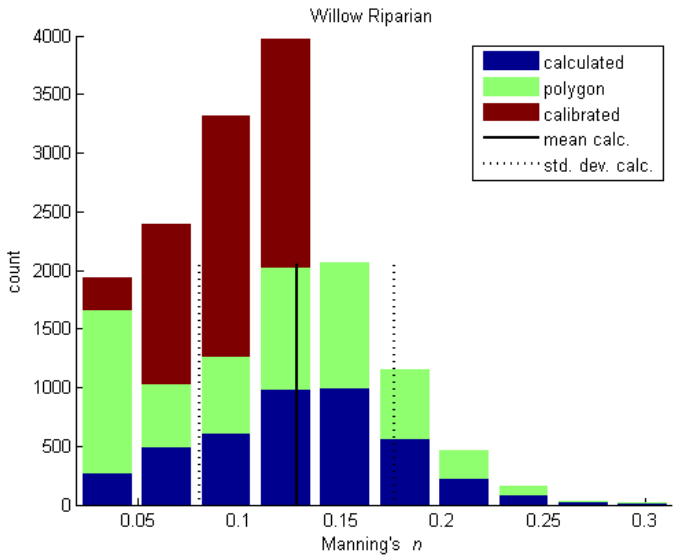

Figure 4 Distribution of Manning's *n* values for Willow Riparian vegetation in the computational mesh of the modeled reach of the San Joaquin River. Shown in the figure are the calculated values for wetted cells using the Jarvela (2004) approach (blue), the polygon values including those calculated in wet cells and default values in dry cells (green), and the values taken from the manually calibrated model (red). Also shown are the mean (solid line) and standard deviation from the mean (dashed line) of the calculated Manning's *n* values for wetted cells.

The comparisons in Figure 1 and 2 show that water surface elevation is underestimated in approximately the upper 2/3 of the model reach using the Jarvela (2004) approach for calculating roughness. This suggests that preferentially increasing the roughness in the upper portion of the model reach may produce simulated hydraulics that better match observed conditions. The mean calculated roughness values for the mixed riparian (Figure 3) and willow scrub (not shown) vegetation types tend lower than the bulk of calibrated roughness values for the same types, which suggests that the spatial distribution of mixed riparian and willow scrub vegetation types may be correlated to the underestimation of water surface elevation in the upper portion of the model reach. Upon inspection of the spatial distribution of mixed riparian and willow scrub vegetation types within the model reach, it is apparent that there is greater spatial coverage in the upper 2/3 of the reach. It was therefore hypothesized that tuning the parameters for the mixed riparian and willow scrub vegetation in order to increase calculated roughness for these types would result in simulated hydraulics that better match the observed conditions. The species-specific drag coefficient C_{dX} was increased from 0.43 to 0.75 for only the mixed riparian and willow scrub types and the model was run again using the Jarvela (2004) approach for calculating roughness. A comparison of water surface elevation for variation in the parameter C_{dX} for a simulated discharge of Q = 7500 cfs is shown in Figure 5. The comparison demonstrates that increasing the species-specific drag coefficient C_{dX} for the mixed riparian and willow scrub vegetation positively affected the simulated hydraulics by preferentially increasing water surface elevation through regions of the modeled reach that were underestimated using a constant value C_{dX}. The variation in parameter C_{dX} resulted in a shift in the distribution of calculated roughness towards larger values. Another test of parameter sensitivity was conducted by varying the exponent X in Equation 2 for the mixed riparian and willow scrub vegetation types. Increasing the fractional exponent X has the effect of increasing roughness, however, with a less than linear sensitivity. For the trial simulation, X was increased from -0.57 to -0.35 for the mixed riparian and willow scrub vegetation types, however the effect on the simulated water surface elevation was small

compared to the effect when varying the drag coefficient, C_{dX}. Comparison of water surface elevation at additional discharges and sensitivity analysis for varying input parameters is provided in Gillihan (2013).

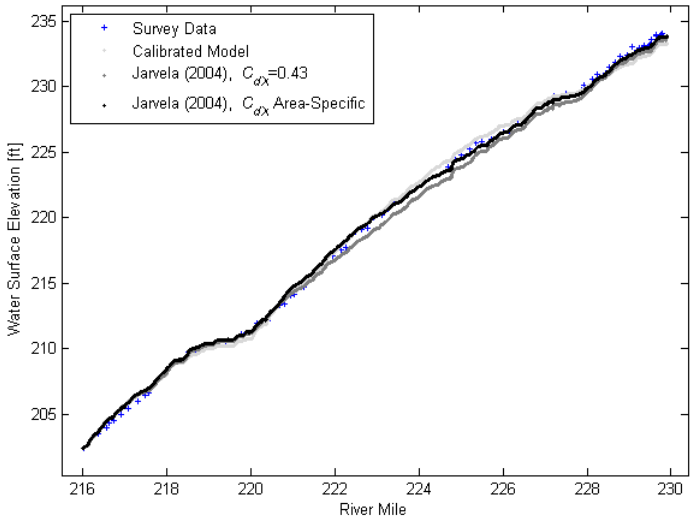

Figure 5 Simulated water surface elevation (ft) as a function of river mile for Q=7500 cfs in a reach of the San Joaquin River. Simulation results are shown for the Jarvela (2004) approach using constant C_{dX}=0.43 (grey) for all vegetation and C_{dX}=0.75 (black) for mixed riparian and willow scrub vegetation. Shown for comparison are measured water surface elevation (blue) and manually calibrated simulation results (light grey). The comparison demonstrates that increasing the species-specific drag coefficient C_{dX} for the mixed riparian and willow scrub vegetation positively affected the simulated hydraulics by preferentially increasing water surface elevation through regions of the modeled reach that were underestimated using a constant value C_{dX}.

DISCUSSION

The results demonstrate that the SRH-2DV model for simulating vegetated flow is generally successful in reproducing the effect of riparian vegetation on water surface elevation as compared to that of measurements and manually calibrated simulations. Distributions of calculated roughness values due to vegetation were generally consistent with values compiled in the literature (Hession & Curran, 2013). The Jarvela (2004) and Baptist (2007) approaches for computing roughness were both implemented in the model. The calibration procedure assumed variables computed by the hydraulic solver (U, h), vegetation characteristics measured in the field (LAI, H, m, D), and parameter values borrowed from published literature (X, U_X) to be known quantities; the parameters C_{dX} and C_d were assumed uncertain and subject to variation.

A likely source of significant error in the modeling is due to limitations imposed by applying locally measured vegetation parameters to spatially disparate zones within the computational mesh. Identical vegetation classes are likely only qualitatively equivalent and so it is predicted that accuracy improvements would be realized by comprehensive measurement of vegetation characteristics throughout the model domain.

The leaf area index is generally a convenient physically-based metric for quantifying vegetal density and area (Jalonen, Jarvela, & Aberle, 2013), and can be estimated by in situ observation or remote sensing. Further, the Jarvela (2004) approach incorporates water depth and velocity information, both of which are directly computed by the hydraulic solver. Given the spatially-detailed information that a two-dimensional hydraulic model can provide, it would be desirable to map measured vegetation parameters at similar scale and resolution (Abu-Aly, Pasternack, Wyrick, Barker, Massa, & Johnson, 2014), which would necessitate the use of remote sensing technologies.

The distributions of calculated roughness values produced by the model and the effect of varying the parameter C_{dX} in Equation 1 indicate that predicting the effects of vegetation on hydraulics is dependent on quantifying complicated species-specific coupling between the vegetation characteristics and local hydraulics. Further exploration of input parameter values and species dependency, a topic of active research (Aberle & Jarvela, 2013), will be useful in gauging applicability and evaluating performance of the algorithms.

Despite the uncertainties identified in the measured and parameterized vegetation characteristics applied in the SRH-2DV model, the simulation results demonstrate good qualitative performance as compared to observed conditions and calibrated results. It is anticipated that the model will serve as a useful tool for predicting the effects of projected vegetation changes and for use as a design tool in restoring riparian vegetation. As the challenges associated with measurement of vegetation characteristics over large spatial scales are overcome through developing remote-sensing techniques, the practicality and accuracy of vegetated-flow modeling will increase.

REFERENCES

Aberle, J., & Jarvela, J. (2013). Flow Resistance of Emergent Rigid and Flexible Floodplain Vegetation. *Journal of Hydraulic Research, 51*(1), 33-45.

Abu-Aly, T. R., Pasternack, G. B., Wyrick, J. R., Barker, R., Massa, D., & Johnson, T. (2014). Effects of LiDAR-derived, spatially distributed vegetation roughness on two-dimensional hydraulics in a gravel-cobble river at flows of 0.2 to 20 times bankfull. *Geomorph.*(206), 468-482.

Baptist, M., Babovic, V., Rodriguez Uthurburu, J., Keijzer, M., Uittenbogaard, R., Mynett, A., et al. (2007). On Inducing Equations for Vegetation Resistance. *Journal of Hydraulic Research, 45*(4), 435-450.

Chow, V. (1959). *Open-Channel Hydraulics.* New York: McGraw-Hill Co.

Darby, S. E. (1999). Effect of Riparian Vegetation on Flow Resistance and Flood Potential. *Journal of Hydraulic Engineering*, 443-454.

Dombroski, D., Greimann, B. P., & Gordon, E. (2012). *Hydraulic Studies for Fish Habitat Analysis.* Denver: Bureau of Reclamation.

Fathi-Moghadam, M., & Kouwen, N. (1997). Non-Rigid, Non-Submerged, Vegetation Roughness in Flood Plains. *Journal of Hydraulic Engineering*, 51-57.

Gillihan, T. (2013). *Dynamic Vegetation Roughness in the Riparian Zone.* Master Thesis, University of New Mexico, Department of Civil Engineering.

Hession, W. C., & Curran, J. C. (2013). The Impacts of Vegetation on Roughness in Fluvial Systems. In J. F. Schroder, D. R. Butler, & C. R. Hupp (Eds.), *Treatise on Geomorphology* (Vol. 12, pp. 75-93). San Diego, CA: Academic Press.

Jalonen, J., Jarvela, J., & Aberle, J. (2013). Leaf Area Index as Vegetation Density Measure for Hydraulic Analyses. *J. Hydr. Eng., 139*(5), 461-469.

Jarvela, J. (2004). Determination of Flow Resistance Caused by Non-Submerged Woody Vegetation. *International Journal of River Basin Management, 2*(1), 61-70.

Jarvela, J. (2005). Effect of Submerged Flexible Vegetation on Flow Structure and Resistance. *Journal of Hydrology*, 233-241.

Kouwen, N., & Fathi-Moghadam, M. (2000). Friction Factors for Coniferous Trees Along rivers. *Journal of Hydraulic Engineering*, 732-740.

Kouwen, N., & Li, R.-M. (1980, June). Biomechanics of Vegetative Channel Linings. *Journal of the Hydraulics Division, Proceedings of the ASCE, 106*(HY6), 1085-1103.

Lai, Y. G. (1997). An Unstructured Grid Method for a Pressure-Based Flow and Heat Transfer Solver. *Numerical Heat Transfer, Part B*, 267-281.

Lai, Y. G. (2000). Unstructured Grid Arbitrarily Shaped Element Method for Fluid Flow Simulation. *AIAA Journal, 38*(12), 2246-2252.

Lai, Y. G. (2010). Two-Dimensional Depth-Averaged Flow Modeling with an Unstructured Hybrid Mesh. *Journal of Hydraulic Engineering, 136*(1), 12-23.

Moise, G. H., & Hendrickson, B. (2002). *Riparian Vegetation of the San Joaquin River.* State of California Department of Water Resources.

Nepf, H. M. (2012). Hydrodynamics of Vegetated Channels. *Journal of Hydraulic Research*, 262-279.

Thompson, G. T., & Roberson, J. A. (1976). A Theory of Flow Resistance for Vegetated Channels. *Transactions of the ASAE*, 288-293.

SAND BAR VOLUME MODEL: IMPROVING MODELED SAND BAR RESPONSE IN MARBLE CANYON, ARIZONA

David Varyu, P.E., Hydraulic Engineer, Reclamation, Denver, CO, dvaryu@usbr.gov;
Blair Greimann, Ph.D., P.E., Hydraulic Engineer, Reclamation, Denver, CO, bgreimann@usbr.gov;
Nate Bradley, Ph.D., Physical Scientist, Reclamation, Denver, CO, dnbradley@usbr.gov:
Kendra Russell, P.E. International Affairs Specialist, Reclamation, Washington D.C., krussell@usbr.gov

Abstract: The empirical dataset of surveyed sand bar volumes in Marble Canyon on the Colorado River downstream of Glen Canyon Dam is analyzed. A subset of the empirical dataset is established based on bar and survey date consistency, resulting in the calibration dataset. The sand bar calibration dataset is represented by both the mean and median of the sand bar volume.

A conceptual model describing erosive and depositional processes for sand bars in Marble Canyon is described. A series of model formulations (termed Model V0 through V5) are developed and Model V3 is selected based on model performance calculated as the normalized sum of squared errors and adjusted R-squared. Confidence intervals are developed for the parameters and for the predicted bar volumes coinciding with calibration data survey dates.

Median and mean versions of Model V3 show similar percent improvement over the model V0 performance (86% for median, 89% for mean). The prediction confidence intervals contain 19 of the 28 observed bar volumes for both the mean and median V3 models. Deposition and erosion trends between survey dates are correctly predicted 25 out of 28 times for both the mean and median V3 models. The mean V3 model tended to perform better in the vicinity of high flow experiments (HFEs) as compared to the median V3 model.

INTRODUCTION

The Department of the Interior, through the Bureau of Reclamation (Reclamation) and the National Park Service (NPS) are preparing an environmental impact statement (EIS) for the adoption of a long-term experimental and management plan (LTEMP) for the operation of Glen Canyon Dam on the Colorado River. The EIS will fully evaluate dam operations and identify management actions and experimental options that will provide a framework for adaptively managing Glen Canyon Dam over the next 15 to 20 years.

The Sand Bar Volume Model (SBVM) was developed by Reclamation's Technical Service Center specifically for performing alternative analysis during the LTEMP EIS process. The sediment resource goal for the LTEMP EIS is "to increase and retain fine sediment volume, area, and distribution in the Glen, Marble and Grand Canyon reaches above the elevation of the average base flow for ecological, cultural, and recreational purposes." The Sand Budget Model (Wright et al., 2010) is useful for quantifying the overall sand budget within a reach, but does not consider the proportion of that sediment in the bed versus bars, and therefore does not explicitly reflect the sediment resource goal. The intent of SBVM is to represent a time series of all the bars in Marble Canyon by incorporating the empirical sand bar data, which is described in terms of sediment volumes relative to different reference elevations, into an analysis that more directly reflects the sediment resource goal. SBVM is only applicable to the Colorado River downstream of Glen Canyon Dam, and has currently been calibrated to the dataset consisting of sand bars in Marble Canyon (Figure 1).

REVIEW OF EMPIRICAL DATA

The U.S. Geological Survey's Grand Canyon Monitoring and Research Center (GCMRC) in collaboration with Northern Arizona University (NAU) have been performing repeat surveys of select bars throughout Marble and Grand Canyon for decades (Mueller et al., 2014). There are 25 bars in Marble Canyon, eight in Upper Marble Canyon (RM 0 to RM 30) and 17 in Lower Marble Canyon (RM 30 to RM 61) with 42 survey dates reported between 9/15/1990 and 9/21/2013. Data collected quantify the sediment area and volume relative to the water surface elevations (WSE) associated with a flow of 8,000 cubic feet per second (ft^3/s) and 25,000 ft^3/s (Grams, 2013). Data were binned as volume/area less than the 8,000 ft^3/s WSE, between the 8,000 and 25,000 ft^3/s WSE, and greater than the 25,000 ft^3/s WSE. To reflect the sediment resource goal of the LTEMP EIS, the sand bar data above the 8,000 ft^3/s WSE (8,000-25,000 ft^3/s and greater than 25,000 ft^3/s) is considered to represent the sediment above the elevation of the average base flow. The sediment below the 8,000 ft^3/s WSE is addressed with the Sand

Budget Model (Wright et al., 2010); the SBVM focuses on the portion of sediment referenced in the sediment resource goal of the LTEMP EIS.

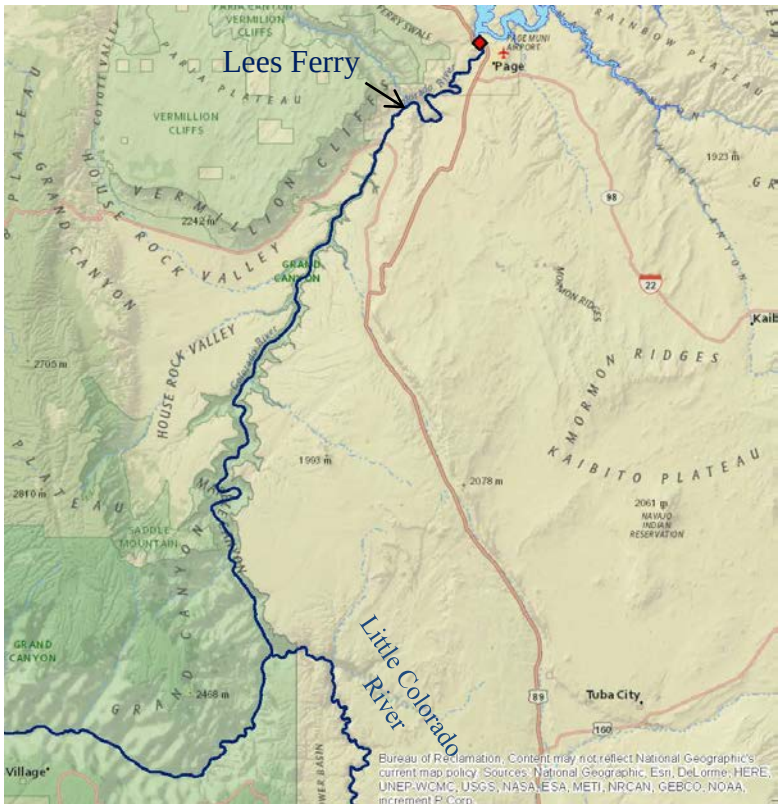

Figure 1 Location map: primary area of interest is Marble Canyon (Lees Ferry to Little Colorado River)

A consistent set of sand bars and survey dates was developed to be used as the calibration dataset. The development of the calibration dataset attempted to maximize the time span of observations but also maintain a consistent set of the highest number of sand bars possible. This approach yielded a calibration dataset of 29 dates (out of 42) and 14 sand bars (out of 25) from 7/26/1991 to 9/21/2013.

The SBVM represents a time series of all the bars in Marble Canyon, where the conglomeration of bars is represented by a single value; either the mean or median volume of those bars. Figure 2 is the distribution of bar volumes above the 8,000 ft^3/s WSE for a reported survey date. Note that the mean is always greater than the median, and that there is more variability in the median through time as compared to variability in the mean. The minimum and maximum bar volume is also shown in the graph; the maximum is always associated with 51-mile bar, the minimum is either 3-mile or 16-mile bar. An overarching assumption of the SBVM is that GCMRC selected bars to survey because those bars represent the variability in morphology and type found in the canyons, and that any inferences made via calibration to the surveyed bars would be representative of all of the sand bars, surveyed or not.

The surveys immediately after HFE events (1996, 2004, and 2008) all have mean volumes greater than 290,000 cubic feet (ft^3). Note that the HFE signal is not as pronounced in the median record; the surveys post-2004 and 2008 HFEs register a median value less than the survey that is approximately five months after the 1996 HFE. The time series of mean bar data likely represents the average conditions in the reach more accurately than the median, but both time series will be used as calibration datasets during model selection.

The trends in the mean and median data generally are the same except for the period from the late 1990s to the early 2000s. Figure 3 presents the correlation between the mean and median bar volume of the calibration dataset.

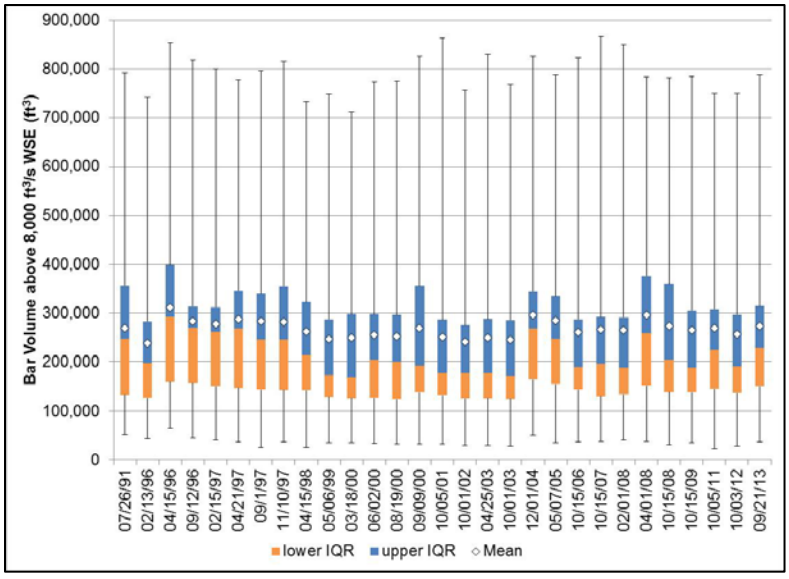

Figure 2 Calibration dataset statistics by date; bars identify minima and maxima and lower IQR refers to the 25th to 50th percentile and upper IQR refers to the 50th to 75th percentile.

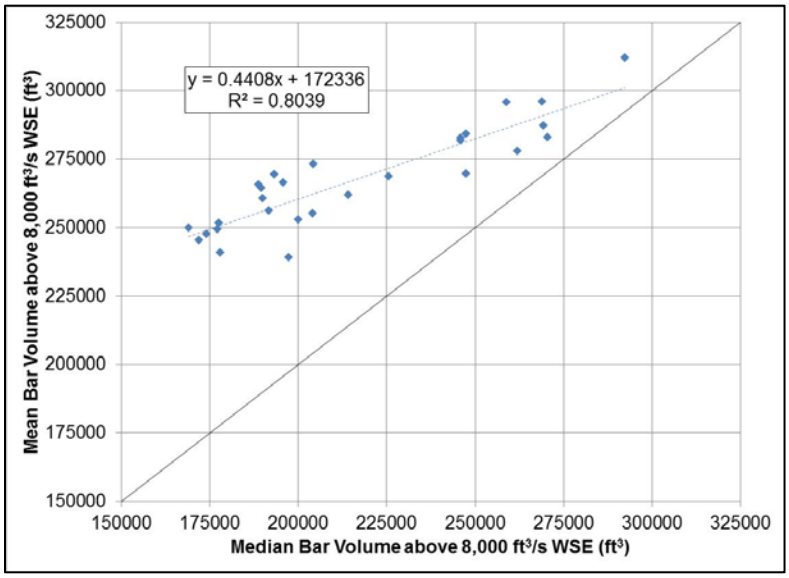

Figure 3 Correlation between mean and median bar volumes of the calibration dataset.

CONCEPTUAL MODEL AND MODELS TESTED FOR SELECTION

The impetus of model development was to find a way to predict bar responses to High Flow Experiments (HFE), sometimes referred to as controlled floods. The controlled high flow releases are meant to mimic natural flooding to an extent and benefit sediment-dependent resources such as sandbars. Building on the body of knowledge of sand bar behavior in Glen, Marble, and Grand Canyon – largely developed by GCMRC (Wiele et al., 2007; Wright and Kaplinski, 2011) – a general conceptual model was developed. The two fundamental processes which need to be captured are bar building (deposition) and bar erosion.

Sand bar deposition and bar building occur at high discharge and with high sediment concentration. The rate of bar building is largest during the early stages of an HFE, and tapers off as the bar becomes more 'full'; there is a physically reasonable maximum bar volume for each bar (Wiele and Torizzo, 2005). Also, the more 'empty' a bar

is, the higher the potential volume of deposition. An important aspect of deposition is the potential volume of sediment which a bar may contain.

The rate of sand bar erosion tends to be large during the first few to six months after a significant bar building event, then tapers off to a fairly constant rate. Early SBVM formulation experimented with combining depositional and erosional processes into a single term to capture bar volume change, but it soon became apparent that these two processes are governed by different processes under different conditions. The following discusses the model as consisting of two terms: one for depositional processes and one for erosional processes.

The general model formulation for a tool that can be used to predict bar volumes is presented in equation 1. There is a deposition rate and an erosion rate calculated at each time step in the model. The equation can be time-integrated get equation (2). A change in bar volume for a given time step is calculated by taking the difference between the erosion and deposition rates and converting to a volume by multiplying by time step and a porosity term. The bar volume for the next time step is the sum of the current time steps bar volume and the change in bar volume calculated at that time step (equation 3).

$$\frac{dS_b(1-\eta)}{dt} = Q_d - Q_e \tag{1}$$

where:

S_b = mean sand bar volume (ft^3) above a base flow rate water surface elevation
η = porosity of sediment (-)
Q_d = depositional flux of sediment into sand bar (ft^3/s)
Q_e = erosional flux of sediment from sand bars (ft^3/s)
t = time (s)

$$\Delta S_b(1-\eta) = \int_{t_1}^{t_2}(Q_d - Q_e)dt \tag{2}$$

$$S_{b(i+1)} = S_{b(i)} + \Delta S_{b(i)} \tag{3}$$

Five different sets of depositional and erosional terms are presented below. These five sets represent different models of depositional and erosional behavior; the erosion term Q_e in models V3 – V5 are identical and are paired with different depositional equations. Models V1-V5 can be compared to the average bar volume, identified as V0. That is, V0 assumes that the predicted bar volume for any time step is simply the average (mean or median as appropriate) bar volume. The model error associated with V0 will be a benchmark to which the model performance for V1-V5 can be compared.

Model V1: Flow only

$$Q_d = a_d {Q_x}^{b_d}$$
$$Q_e = a_e {Q_x}^{b_e}$$

Model V2: Storage only (*Q* is used indirectly to calculate S_{bv}, see below)

$$Q_d = a_d \left(\frac{S_{bv}}{S_b}\right)^m$$
$$Q_e = a_e \left(\frac{S_b}{S_{bv,max}}\right)^n$$

Model V3: Flow and Storage (no concentration term)

$$Q_d = a_d {Q_x}^{b_d} \left(\frac{S_{bv}}{S_b}\right)^m$$
$$Q_e = a_e {Q_x}^{b_e} \left(\frac{S_b}{S_{bv,max}}\right)^n$$

Model V4: Flow, Storage, Concentration (exponent on *Q*)

$$Q_d = a_d C {Q_x}^{b_d} \left(\frac{S_{bv}}{S_b}\right)^m$$

$$Q_e = a_e {Q_x}^{b_e} \left(\frac{S_b}{S_{bv,max}}\right)^n$$

Model V5: Flow, Storage, Concentration (exponent on product of *QC*)

$$Q_d = a_d (CQ_x)^{b_d} \left(\frac{S_{bv}}{S_b}\right)^m$$

$$Q_e = a_e {Q_x}^{b_e} \left(\frac{S_b}{S_{bv,max}}\right)^n$$

Where:

Q_d = deposition rate at time step i (ft^3/s)
Q_e = erosion rate at the time step i (ft^3/s)
Q_x = volumetric water discharge in Colorado River (ft^3/s) at River Mile 30 divided by 2,000 ft^3/s (-);
C = volumetric sand-sized sediment concentration within the Colorado River at River Mile 30 (-)
a_d, b_d, m = calibration parameters (ft^3/s), (-), (-), respectively
a_e, b_e, n = calibration parameters (ft^3/s), (-), (-), respectively.
S_{bv} = maximum available sand bar volume below the WSE at specific flow rate, Q (ft^3).
$S_{bv,max}$ = available sand bar volume at maximum flow rate of 45,000 ft^3/s (ft^3)

The calibration parameters are collectively called a calibration parameter set and include a_d, b_d, m, a_e, b_e, and n. The variable S_{bv} is derived from the empirical volume data for all available survey dates for the 14 bars used in the calibration dataset. S_{bv} is a variable describing the maximum potential sand bar volume at different flow rates. We currently have three data points to which to fit a curve and these points were developed as such:

- A zero sand bar volume was assigned to a discharge of 8,000 ft^3/s, as we are only concerned with the volume of sand above the 8,000 ft^3/s WSE.
- The maximum volume for each of the 14 bars associated as being between the 8,000-25,000 ft^3/s WSE were averaged (mean and median) and assigned to being the potential bar volume at 25,000 ft^3/s.
- The volume between the 8,000-25,000 ft^3/s WSE and the volume above the 25,000 ft^3/s WSE were summed for each survey date, and the maximum of those sums for each of the 14 bars were averaged (mean and median) and assigned to being the potential bar volume at 45,000 ft^3/s, which is the maximum planned release flow rate under the interim guidelines barring an excessively wet hydrologic year.

It is assumed for the sake of the S_{bv} equation that the available sand bar volume at a particular flow rate does not change in time. Further, a continuous function for the S_{bv} equation was desirable for optimization purposes. A logistic function was found to fit the data well and be continuous, once the discharge was scaled. Dividing the discharge by 2,000 ft^3/s provided the logistic functions for mean and median data (Figure 4).

As described in the presentation of the deposition and erosion models, the flow terms use the scaled discharge Q_x (Q/2000) and not the discharge Q, based on general early observations that a smaller base upon which an exponent is placed improves model performance. Also, dividing the flow by 2,000 ft^3/s is consistent with the flow terms in the model.

All models were implemented into the Mathworks® Matlab software. The modified Sand Budget Model (Wright et al., 2010; Russell and Huang, 2010) was developed as a sediment budget for Marble and Eastern Grand Canyon. Because we are focusing on the bars in Marble Canyon, the discharge and concentration time series at the middle of the canyon (RM30) is used as input to SBVM. The initial condition 7/26/1991 for the SBVM model is the average bar volume of 269,809 ft^3 for the mean and 247,433 ft^3 for the median of the calibration data. Because there are multiple parameters and the model is non-linear, optimization is dependent on the initial guess of parameter values. To increase the confidence in the results, a brute force grid search was employed for all models to locate the region of the global maximum, not just a local maximum. Parameter search domains for the mean and median model simulations were: 1E-20 to 1E20 for a_d and a_e; 0 to 30 for m and n; and at least -8 to 6 for b_d and b_e, although the search domain for b_d and b_e tended to be extended from -12 to 12 because the solution domain showed good performance near the bounds of the initial search domain.

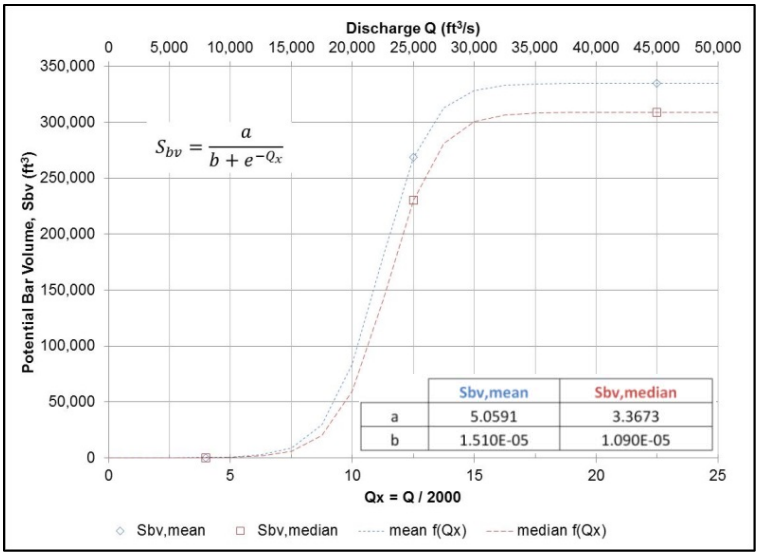

Figure 4 S_{bv} equation for the mean and median datasets

MODEL SEARCH DOMAINS

The bounded search optimization routine "Fminsearch" in Matlab was utilized once the best performing parameter sets were identified from the grid search. Multiple initial guess parameter sets were optimized for each model based on the results of the grid search.

OPTIMIZATION AND MODEL PERFORMANCE

Model V0; Average of calibration dataset This is the simplest model and is used as a benchmark to assess the results of models V1-V5. In this model, the predicted bar volumes are constant through time and are the mean for the mean bar volumes, and the median for the median bar volumes. Model performance is assessed as the sum of squared error (SSE) normalized to the appropriate average bar volume. The SSE for a mean bar volume of 267,754 ft^3 (normalized to this mean) is 0.125, and for a median bar volume of 204,013 ft^3 (normalized to this median) is 0.958. Figure 5 depicts the observed and the model V0 predicted bar volume above the 8,000 ft^3/s WSE.

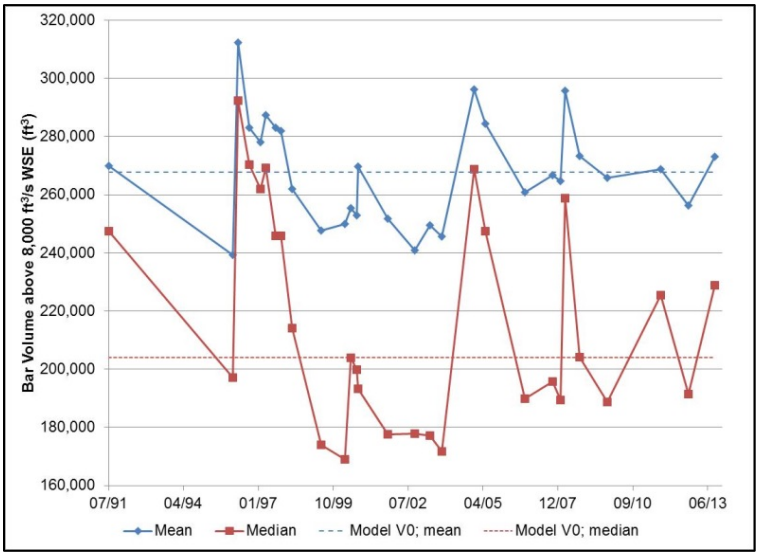

Figure 5 Model V0 depicted against the calibration datasets

Model V1; Flow Only This model uses only a flow term to predict erosion and deposition. There are no history effects accounted for in the erosion and deposition rates, meaning the bar volume existing at a given time step does not inform the rates of erosion and deposition. There is also no utilization of the S_{bv} curve relating the flow rate in the river to the presumed potential bar volume associated with that flow rate.

For both the mean and median cases, the top performing parameter sets (combinations of b_d, b_e, a_d, a_e) resulting from the grid search were used as initial guesses for the bounded Matlab optimization routine "Fminsearch", with the bounds coinciding with the step size specified during the grid search. For example, the grid search for this model had a step size of two for the exponents (b_d, b_e) and for the coefficients (a_d, a_e) the step size was two orders of magnitude. During the optimization for each parameter set, the search bounds were set to ±2 on the exponents and ±2 orders of magnitude on the coefficients.

The parameter sets resulting from the bounded optimization were plotted against their performance (Figure 6). The median optimization plot shows the behavior one would expect; the range for a given parameter decreases as the SSE decreases (performance increases). This behavior appeared for the V1 mean model as well, and gives greater confidence in the optimal parameter set than if the opposite were true (larger range for a given parameter as performance increased).

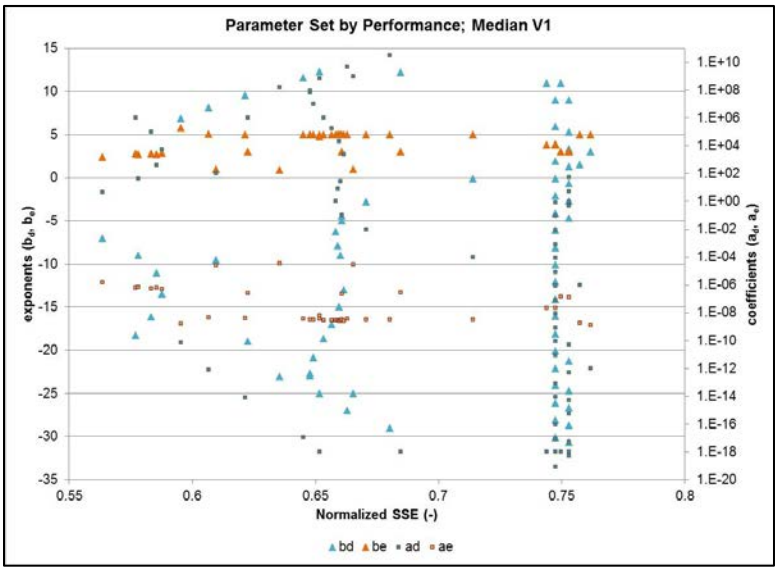

Figure 6 Parameter set performance after optimization for median V1 model

Model V2; Storage Only This model uses only a storage term to predict erosion and deposition. The flow rate at a given time step does not inform the rates of erosion and deposition, except for indirectly, where the flow rate selects the potential bar volume, S_{bv}, and thus the deposition is indirectly associated with flow rate. The erosion rate is simply calculated as a ratio of the current time step bar volume relative to the maximum bar volume; the smaller the bar gets, the slower the rate of erosion.

For the median case, the top performing parameter sets (combinations of m, n, a_d, and a_e) were used as initial guesses for the Matlab optimization routine "Fminsearch" with the bounds coinciding with the step size specified during the grid search as described for model V1. Due to the smooth nature of the mean performance surface, only one optimization was run.

The parameter sets resulting from the bounded optimization for the median data were plotted against their performance. The median optimization plot showed a different pattern than the median optimization plot for model V1; namely, there does not appear to be a convergent solution as the performance increases. Less confidence should be given to this model due to the non-convergent nature of the parameter sets relative to performance. The grid

search for Model V2 mean produced a smooth solution surface that leads to greater confidence in the optimized solution.

Model V3; Flow and Storage This model uses a flow term and a storage term to predict both erosion and deposition. This model is a combination of models V1 and V2. Flow rate and current bar volume inform the rates of erosion and deposition for that time step.

Only those parameter sets from the grid search for the mean model that resulted in an SSE less than or equal to one-half the SSE from model V0 were carried forward to optimization (n=429). If the same selection criteria was applied to the results of the grid search for the median model (using those that had an SSE equal to one-half the model V0 SSE), only about 1% of the parameter sets for the median model would have moved forward to optimization. To increase the sample set, the slope of a Weibull-distribution cumulative distribution function (CDF) was investigated. In the vicinity of an SSE = 0.577 the slope of the CDF transitions from variable to relatively constant. This location corresponds to 6% on the CDF, so the top 6% performing parameters sets from the median grid search (n=1226) moved forward to optimization.

The top performing parameter sets were used as initial guesses for the Matlab optimization routine "Fminsearch" with the bounds coinciding with the step size specified during the grid search as described for models V1. The parameter sets resulting from the bounded optimization were plotted against their performance (Figure 7). The optimization plot shows a pattern that would be expected in optimization; each parameter appears to converge as the performance increases (SSE decreases). This behavior suggests more confidence in the model and the optimized parameter set.

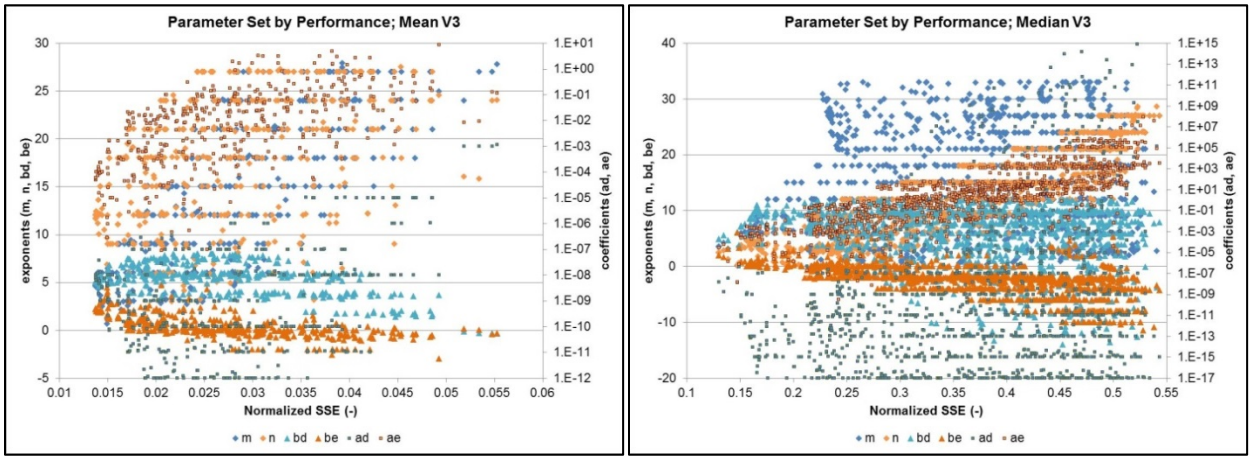

Figure 7 Parameter set performance for Model V3 mean (left) and median (right)

Model V4; Flow, Storage, and Concentration (linear) This model uses a flow term and a storage term to predict both erosion and deposition, much like Model V3, except that the addition of a concentration term is included to predict deposition rates. The exponent on the concentration term is fixed at 1.

Only those parameter sets from the grid search for the mean model that resulted in an SSE less than or equal to one-half the SSE from model V0 were carried forward to optimization (n=1410). If the same selection criteria was applied to the results of the grid search for the median model, (using those that had an SSE equal to one-half the model V0 SSE), only about 3% of the parameter sets for the median model would have moved forward to optimization. To increase the sample set, the slope of the CDF was investigated. In the vicinity of an SSE = 0.517 the slope of the CDF transitions from variable to relatively constant. This location corresponds to 5% on the CDF, so the top 5% performing parameters sets from the median grid search (n=1021) moved forward to optimization.

The top performing parameter sets were used as initial guesses for the Matlab optimization routine "Fminsearch" with the bounds coinciding with the step size specified during the grid search, as discussed in model V1. The parameter sets resulting from the bounded optimization for the median data are plotted against their performance

similar to Figure 6 and Figure 7. The median and mean optimization plot shows a similar convergence of the erosion parameters (n, b_e, and a_e) as for model V3. However, the deposition parameters (m, b_d, and a_d) do not appear to be converging with improved performance. In addition, the performance for model V4 does not achieve the same level as model V3, whether mean or median. This behavior not only reduces the confidence in the optimized parameter sets but also reduces the confidence in the model. The following model (V5) will allow the exponent on the concentration parameter to vary in an attempt to improve performance.

Model V5; Flow, Storage, and Concentration (power) This model uses a flow term and a storage term to predict both erosion and deposition, with the addition of a concentration term in the prediction of deposition rates. Unlike model V4, the concentration term has an exponent that is allowed to vary. The exponent is defined to equal the exponent on the flow term (b_d) so that the number of parameters does not increase.

Only those parameter sets from the grid search for the mean model that resulted in an SSE less than or equal to ½ the SSE from model V0 were carried forward to optimization (n=380). If the same selection criteria was applied to the results of the grid search for the median model, (using those that had an SSE equal to ½ the model V0 SSE), only about 1.3% of the parameter sets for the median model would have moved forward to optimization. To increase the sample set, the slope of the CDF was investigated. In the vicinity of an SSE = 0.617 the slope of the CDF has a noticeable break. This location corresponds to 6% on the CDF, so the top 6% performing parameters sets from the median grid search (n=1226) moved forward to optimization.

The top performing parameter sets were used as initial guesses for the Matlab optimization routine "Fminsearch" with the bounds coinciding with the step size specified during the grid search as described for models V1. The parameter sets resulting from the bounded optimization are plotted against their performance and the median and mean optimization plot showed convergence of the erosion and deposition parameters. The performance for model V5 does not achieve the same level as model V4, whether mean or median. This behavior reduces the confidence in the model.

Summary of Optimized Models Figure 8 presents a summary of the model performance for the mean and median dataset as a progression through models V0-V5. The percent improvement of the models compare models V1-V5 relative to the initial V0 model.

In both the mean and median cases, model performance improves from V0 through V3. Adding the concentration term reduces model performance. It is plausible that the explanation for this lies with the fact that the concentration used is a time series output from the modified Sand Budget Model rather than the actual measured data. Figure 6 from the Wright et al. (2010) paper showing that a significant amount of scatter exists in a concentration vs. discharge plot (not atypical) at River Mile 30. It is possible that using the measured (not model) concentration would improve model performance when including the concentration time series. However, the approach of using measured data means the model is no longer predictive under future flow and operational scenarios.

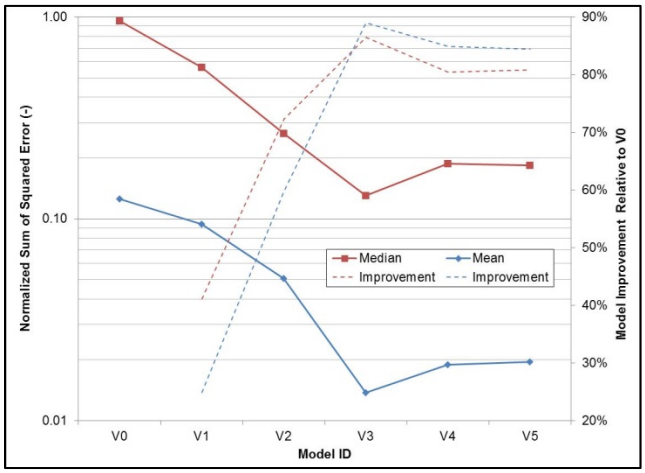

Figure 8 Summary of model performance (SSE) and percent improvement relative to model V0

It is apparent that model V3 is the best for both the mean and median datasets. It is the first model in the progression from V1-V5 that has six regressors, (models V1 and V2 had 4 each). Calculating an adjusted R^2 (or $\bar{R}^2$, r-bar squared) can help assess whether the added complexity is justifiable (http://www.mathworks.com/help/curvefit/evaluating-goodness-of-fit.html). Equation 4 presents the equation used to calculate the adjusted R^2 and Table 1 presents the results by model.

$$\bar{R}^2 = 1 - \frac{SSE(n-1)}{SST(v)} \quad (4)$$

Where:

SSE = sum of squared error (or sum of squared residuals)
SST = total sum of squares (= regression sum of squares + residual sum of squares)
n = number of response values
v = residual degrees of freedom = n-m
m = number of fitted coefficients

Table 1 Adjusted R-squared for models V1-V5; mean and median

	Model				
	V1	**V2**	**V3**	**V4**	**V5**
n	28	28	28	28	28
m	4	4	6	6	6
v = n-m	24	24	22	22	22
$\bar{R}^2$, median	0.27	0.66	0.82	0.74	0.74
$\bar{R}^2$, mean	0.16	0.55	0.87	0.81	0.81

The adjusted R-square values justify the additional complexity of transitioning from model V2 (with 4 regressors) to V3 (with 6 regressors), and suggest that models V4 or V5 do not offer improvement over V3.

CONFIDENCE INTERVALS

The Mathworks Matlab functions "nlparci" and "nlpredci" were used to develop the parameter confidence intervals and the prediction confidence intervals, respectively, both at the 95% confidence level. Table 2 presents the parameter confidence intervals for the median and mean datasets for model V3. Figure 9 presents the predicted sand bar volumes along with the predicted confidence intervals at the time steps corresponding to the observations.

Table 2 Parameter confidence intervals (CI) for model V3

	mean model			**median model**		
	Lower CI	**optimized**	**Upper CI**	**Lower CI**	**optimized**	**Upper CI**
a_d	-3.00E-08	9.86E-09	4.97E-08	-5.97E-08	1.49E-08	8.95E-08
a_e	-1.12E-04	4.83E-05	2.09E-04	-9.12E-05	2.78E-05	1.47E-04
b_d	3.593	5.015	6.437	3.283	4.917	6.550
b_e	0.924	2.272	3.620	0.140	1.965	3.789
m	0.993	4.697	8.400	1.074	3.569	6.063
n	7.105	11.664	16.224	-0.174	2.481	5.135

Both the mean and median prediction confidence intervals contain 19 of the 28 observed bar volumes (the first of the 29 observations – 7/26/1991 – was used as an initial condition for the model). The notable errors of the mean model are that it generally does not capture the cluster of measurements in summer/fall 1997, it under-predicts the erosion after the small depositional event in Fall 2000, and under-predicts the small depositional event in Fall 2007.

The notable errors of the median model are that it over-predicts the erosion before the 1996 HFE, under-predicts the deposition during the 2004 HFE, and under-predicts the erosion after the 2008 HFE.

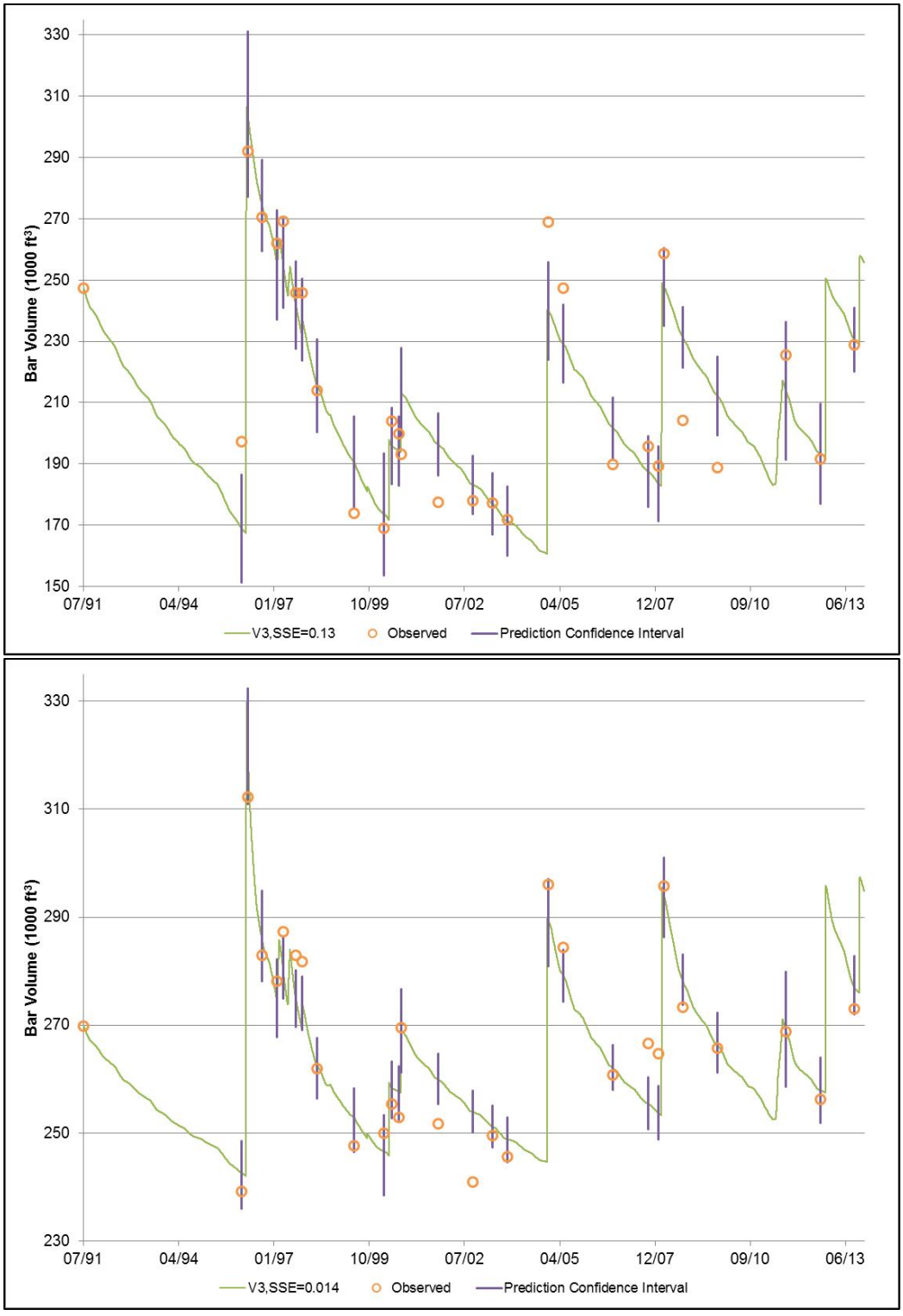

Figure 9 Model V3 predicted bar volume time series and prediction confidence intervals (median above, mean below)

Comparing observed vs. predicted trends of deposition or erosion between survey dates show that both models predict the trend correctly 25 out of 28 times. Both models miss the apparently mild depositional event between October 2006 and October 2007. The remaining trend errors for both the mean and median models occur in the 2000 to 2003 time frame.

Some parameter confidence intervals bound zero. The parameter confidence intervals developed by Matlab assume a normal parameter distribution, and this is likely not the case for the nonlinear model. Also, regression typically assumes that parameters are not correlated. An investigation of the optimized parameters shows that there is a correlation between the coefficients (a_d, a_e) and the flow exponents (b_e, b_e) respectively, as well as correlation between the coefficient a_e and the storage exponent n. No apparent correlation exists between the coefficient a_d and the storage exponent m. For physically practical purposes, a lower bound of zero should be imposed on all confidence intervals in Table 2.

SUMMARY

The empirical dataset of surveyed sand bar volumes in Marble Canyon on the Colorado River downstream of Glen Canyon Dam was analyzed. A subset of the empirical dataset was established based on bar and survey date consistency, resulting in the calibration dataset. The sand bar calibration dataset is represented by both the mean and median of the sand bar volume.

A conceptual model describing erosive and depositional processes for sand bars in Marble Canyon is described. A series of model formulations (termed Model V0 through V5) were developed and Model V3 is selected based on model performance calculated as the normalized sum of squared errors and adjusted R-squared. Confidence intervals were developed for the parameters and for the predicted bar volumes coinciding with calibration data survey dates.

Median and mean versions of Model V3 show similar percent improvement over the model V0 performance (86% for median, 89% for mean). The prediction confidence intervals contain 19 of the 28 observed bar volumes for both the mean and median V3 models. Deposition and erosion trends between survey dates are correctly predicted 25 out of 28 times for both the mean and median V3 models. The mean V3 model tended to perform better in the vicinity of HFEs as compared to the median V3 model.

REFERENCES

Grams, P.E. March 2013. Supervisory Hydrologist, Grand Canyon Monitoring and Research Center. Personal Communication.

Mueller, E.R., Grams, P.E., Schmidt, J.C., Hazel Jr., J.E., Alexander, J.S., Kaplinski, M (2014), "The Influence of Controlled Floods on Fine Sediment Storage in Debris Fan-affected Canyons of the Colorado River Basin", Geomorphology Vol 226, pp 65-75, doi:10.1016/j.geomorph.2014.07.029

Russell, K., and Huang, V. (2010). Sediment analysis for Glen Canyon Dam environmental assessment. Report to Upper Colorado Region, Bureau of Reclamation, Salt Lake City. Denver Technical Services Center, Bureau of Reclamation, Denver, Colorado.

Wiele, S., and Torizzo, M. (2005). Modeling of sand deposition in archaeologically significant reaches of the Colorado River in Grand Canyon,USA, in Computational Fluid Dynamics: Applications in Environmental Hydraulics, edited by P. D. Bates, S. N. Lane, and R. I. Ferguson, pp. 357-394, Wiley and Sons, Chichester, U. K., doi: I 0.1002/04700 15195.ch 14.

Wiele, S.M., Wilcock, P.R., and Grams, P.E. (2007), Reach-Averaged Sediment Routing Model of a Canyon River, Water Resour. Res., 43, W02425, doi:10.1029/2005WR004824.

Wright, S.A., and Kaplinski, M. (2011), "Flow Structures and Sandbar Dynamics in a Canyon River During a Controlled Flood, Colorado River, Arizona", J. Geophys. Res., 116, F01019, doi:10.1029/2009JF001442.

Wright, S. A., Topping, D. J., Rubin, D. M., and Melis, D. M. (2010). "An Approach for Modeling Sediment Budgets in Supply-Limited Rivers", Water Resour. Res., 46, W10538, doi:10.1029/2009WR008600.

PROCESSES LIMITING DEPTH OF ARROYO INCISION: EXAMPLES FROM THE RIO PUERCO, NEW MEXICO

Eleanor Griffin, Research Hydrologist, U.S. Geological Survey, Boulder, CO, egriffin@usgs.gov; and Jonathan Friedman, Research Hydrologist, U.S. Geological Survey, Fort Collins, CO, friedmanj@usgs.gov

Abstract: We examined channel flow and suspended sediment transport processes within the lower Rio Puerco arroyo, located in semi-arid north-central New Mexico, in an attempt to answer the question: Why did arroyo incision stop by about 1936? Channel flow model results show that in the narrow, incised channel of 1936, the boundary shear stress during a large flood was highest over the lower banks and bank toes, causing a higher potential for erosion of these surfaces than of the channel bed. This would have caused the channel (and arroyo) to widen, and the higher sediment fluxes from those surfaces would have inhibited the capacity of the flow to erode the bed. We found that volumes of sediment delivered to the channel from local erosion of the arroyo wall did not exceed the capacity of the flow to transport sediment, including sand, in suspension. However, sediment supplied from erosion upstream of our study reach may have reduced the capacity of the flow to erode the bed. Our results suggest that arroyo incision ended with the observed reduction in flood peak magnitude, frequency, and duration after 1941.

INTRODUCTION

Channel incision in the semi-arid southwestern United States in the mid- to late-1800s through early 1900s led to the development of arroyos, which are steep-sided, narrow gullies in which flood flows no longer overtop the walls (Hovey, 1902; Bryan and Post, 1927). Arroyos created hazards for travel and to livestock, and downcutting of the channel eliminated opportunities for flow diversion for irrigation (Bryan, 1928). Large volumes of sediment transported in the Rio Puerco downstream to the mouth between 1929 and the mid-1940s contributed to channel bed aggradation and increased flooding in the middle Rio Grande (Happ, 1948; Welsh, 1985). In addition, the high rate of sediment delivery to the Rio Grande decreased storage capacity of Elephant Butte Reservoir (Figure 1; Bryan and Post, 1927).

Between 1927 and 1936, the 55-km-long lower Rio Puerco arroyo (Figure 1) both widened and incised. Large floods in 1929, 1935 and 1936 contributed to an increase in arroyo volume by about 44.5 x 10^6 m^3 during this period (Friedman et al., 2014). Average arroyo width in this reach nearly doubled, increasing from 118 m in 1927 to 212 m by 1935 (Friedman et al., 2014). In the first 10 valley km (vk) downstream from Highway 6, arroyo depth increased from an average of about 12.1 m in 1927 (Bryan, 1928) to about 14.6 m by 1936 (Friedman et al., 2014). Arroyo volume can increase either by: 1) channel bed incision; 2) block failure of an arroyo wall undercut by channel or floodplain flow; or 3) erosion of inset terraces by meander migration. Eroded sediment can be redistributed within the arroyo, but some fraction of that sediment must be transported down-valley to the mouth in order to have a net increase in arroyo volume through time. In the lower 55 km of the Rio Puerco arroyo, we know that channel bed incision continued until shortly after the flood of record in 1929 and reached a maximum near Highway 6 by about 1936 (Elliott et al., 1999; Friedman et al., 2014). Much of the sediment eroded from the arroyo walls, channel bed, or inset terraces was transported down-valley and either deposited near the mouth, forming a delta, or transported into the Rio Grande (Bryan and Post, 1927; Tuan, 1966).

We examined the processes that caused incision of the channel bed and erosion of the arroyo walls in the first 10 km down-valley from the concrete sill near the Highway 6 crossing (Figure 1). A single arroyo cross section surveyed by K. Bryan in August 1936 (Elliott et al., 1999), located at vk 0.76, provides an example of the shape of the incising arroyo and inset active channel. At this location, the arroyo depth (height of the pre-arroyo valley floor above the channel bed) increased from 13.0 m in 1927 to 15.6 m in 1936, and subsequent aggradation on the bed reduced the depth to 14.9 m by August 1972 (Elliott et al., 1999). Dated sediment deposits in a trench excavated across the arroyo bottom at vk 0.84 km (the Highway 6 trench) indicate that the arroyo bottom has been aggrading since at least the early 1960s (Friedman et al., 2014). The question we address here is: Why did incision stop by about 1936?

Background: The Rio Puerco is an ephemeral tributary of the Rio Grande incised in fine valley-fill sediment, dominantly sand, silt and clay (Heath, 1983; Love, 1986). The watershed occupies 19,040 km^2 dominated by easily eroded sedimentary rocks (Heath, 1983). Elevation ranges from 3444 m at the summit of Mount Taylor, near the

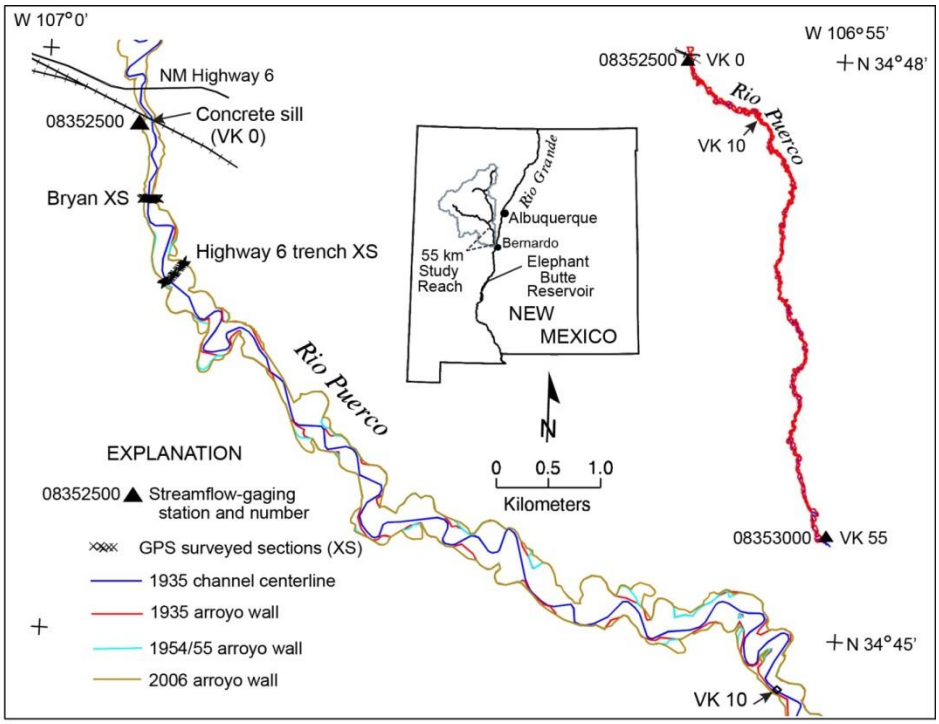

Figure 1 Map of the study reach. We focused this study on incision and arroyo wall erosion processes in the first 10 km downstream from the concrete sill on the downstream side of the railroad bridge near the Highway 6 crossing. Locations of two historical streamflow-gaging stations within the lower Rio Puerco arroyo are shown. Arroyo wall locations in 1935 (red line), the 1950s (light blue line), and 2006 (tan line) show the extent of arroyo widening since 1935. Where lines representing the 1935 and 1954/55 arroyo walls are visible, the arroyo has widened.

center of the watershed, to 1440 m at the mouth of the Rio Puerco near Bernardo (Figure 1). Floods usually are the result of sequences of summer to early fall monsoonal thunderstorms (Heath, 1983; Griffin et al., 2010). Mean annual precipitation varies from about 323 mm in the northeastern highlands to 212 mm at Bernardo, NM (1948 to 1997; Molnár and Ramírez, 2001).

Records available from the U.S. Geological Survey (USGS) streamflow-gaging stations Rio Puerco at Rio Puerco, NM (#08352500), located at vk 0 (Figure 1), and Rio Puerco near Bernardo, NM (#08353000), located at vk 55, indicate that annual peak flows have declined since the flood of record in September 1929 (Friedman et al., 2014). The magnitude of the peak flow on 23 September 1929 was 1,070 m^3/s at Rio Puerco (New Mexico State Engineer, 1930). This event was preceded by a flood with a peak discharge of 880 m^3/s in August 1929. The 1929 floods damaged the Atchison, Topeka, and Santa Fe (AT&SF) Railway Company railroad bridge at the Highway 6 crossing (Figure 1). During the bridge reconstruction in 1930, the concrete sill on the downstream side of the bridge was extended to the full width between abutments, and four concrete steps were added with a total drop from the sill to the downstream channel bed of 4.7 m (Powell, L.H., Chief Engineer, AT&SF Railway Company, written commun., 1953).

The Rio Puerco is known to carry high concentrations of sediment in suspension and to convey high suspended sediment loads (Nordin, 1963; Elliott et al., 1999; Bierman et al., 2005). More than 50% of 524 suspended sediment samples collected at the gage Rio Puerco near Bernardo between October 1947 and September 2002 had concentrations >100,000 mg/L (volume concentration (vol. conc.) > 0.0377; USGS Water-Quality data, 2014a). All samples with concentrations higher than 199,000 mg/L (vol. conc. 0.0751; n = 59) contained sand (Griffin et al., 2014).

The capacity of open channel flow to erode a surface is dependent in part on the sediment load already carried in the flow. Flow entering a reach that already is carrying the maximum sediment load cannot erode a surface unless there is an increase in the shear stress, which can be caused by a constriction in the channel or an increase in slope, for

example. In contrast, if the upstream sediment supply has been cut off by dam construction, then the magnitude of incision and widening can be extreme (Xia et al., 2014). Sand in suspension is transported at about the mean velocity of the fluid, whereas sand transported as bedload moves at the much lower velocity of the near-bed region of the flow. Suspended sediment samples collected by Nordin (1963) and annual suspended sediment loads (Elliott et al., 1999; Bierman et al., 2005) indicate that the dominant mode of sediment transport in this river is in suspension, and we assume that bedload transport is negligible.

Erosion of the Rio Puerco channel bed and arroyo walls is initiated by flow with locally increasing shear stress and increasing capacity to transport sediment, including the fine to very fine sand found in this system (Friedman et al., 2014). The process of wall erosion is dominated by undercutting of the cohesive wall by fluvial erosion along the exposed base of the wall (Figure 2). Layers of clay within the pre-arroyo valley-fill sediment provide cohesion that supports a steep wall face despite heights of more than 10 m. Field observations indicate that block mass failures occur when the wall has been undercut by 1.5 m or more. A single mass failure can deliver a large volume of sediment to the arroyo bottom. Sediment deposited on the arroyo bottom from wall mass failures temporarily protects the base of the wall from erosion. These failures also increase the local availability of sediment for transport, reducing the capacity of the flow to erode the bed.

Any geomorphic, hydrologic, or vegetative change that reduces the magnitude and duration of shear stress acting on the sediment surface can reduce the rate of incision. Possible changes include a reduction in runoff magnitude or duration through time, geomorphic changes that cause a reduction in bed gradient or an increase in flow width, or vegetative changes that add drag to the flow, reducing the shear stress on the sediment surface (see Simon et al., 2000). An increasing sediment load from erosion upstream also can reduce the capacity of flow to erode the bed.

We examined historical flow data (USGS, 2014a,b) and observed geomorphic changes in the arroyo (Friedman et al., 2014) to identify possible causes of the termination of incision in the lower Rio Puerco. We applied a physically based model for flow (Kean and Smith, 2004) to determine how observed widening of the arroyo bottom affected the boundary shear stress distribution during a large flood and the capacity of the flow to transport sediment in suspension. We compared the capacity of the flow to transport sediment with the available record of suspended sediment load transported past the gage near Bernardo (USGS, 2014a). Finally, we compared the extent of arroyo wall erosion determined from wall locations mapped from aerial imagery and LiDAR data covering the reach from vk 0 – 10 for four time intervals between 1935 and 2010.

Progression of incision and widening upstream from the study reach may have contributed to high sediment loads entering the reach, which could have limited the capacity of the flow to erode the bed in the study reach. Using available topographic data (Friedman et al., 2014), we can estimate the volumes of erosion and deposition within the

Figure 2 Example of a sharp bend in which channel flow has undercut the arroyo wall. The pre-arroyo valley-floor surface is about 10.5 m above the channel bed. The thickness of the undercut wall segment is about 7.6 m. Channel flow direction is from bottom of photo to middle left. (Photo taken April 3, 2010 by E. Griffin.)

study reach through time, but have no knowledge of volumes of sediment transported into the reach from upstream. Therefore, we can only infer the possible effects of increased incoming sediment loads on erosion of the arroyo bottom through time.

METHODS

Historical Flow and Suspended Sediment Transport: The streamflow-gaging station Rio Puerco at Rio Puerco, NM, located at the upstream end of our study reach (Figure 1), was operated from Water Year (WY) 1935 through 1976. Additional annual peak flows were determined from peak gage height and indirect discharge measurements at this station through WY 1991 (USGS, 2014b). Limited sediment data were collected at this site. The streamflow-gaging station Rio Puerco near Bernardo, NM, has been in continuous operation since WY 1941, and suspended sediment data are available beginning for WY 1956. We computed annual flow volumes at Rio Puerco for WY 1935 through 1976 and near Bernardo for WY 1941 through 2013 to examine changes through time. By the mid-1970s, the Rio Puerco channel had narrowed and woody vegetation canopy covered 47% of the arroyo bottom (Friedman et al., 2014), changing the flow distribution within the arroyo. Therefore, we applied linear regressions to determine the average relations between annual flow volume and suspended sediment load for the periods 1956 to 1975 and 1976 to 2013, and we estimated the sediment load for WY 1941 using the regression equation for the first period.

Topographic and Imagery Data Sources: Available topographic and imagery data include data from aerial Light Detection and Ranging (LiDAR) surveys conducted in April and July 2005 (Vincent et al., 2009) and March 2010 (Perignon et al., 2013). Arroyo features were mapped from imagery collected in 1935, 1954/55, 1975/79, and 2005 (Friedman et al., 2014). Bryan and Post (1927) and Bryan (1928) provided arroyo width and depth data collected in the late 1800s and early 1900s. All data have been referenced to the North American Datum of 1983 (NAD 83; horizontal datum) and to the North American Vertical Datum of 1988 (NAVD 88).

Channel Shape: Arroyo geomorphic data for the period of incision are almost entirely limited to measurements of arroyo width and depth. Channel width in 1935 determined from aerial imagery (Friedman et al., 2014) ranged from about 30 to 65 m, with an average of 41.1 m. The arroyo cross section surveyed by Bryan in August 1936 (Figure 3; Elliott et al., 1999) provides an example of the incised channel geometry near the end of the phase of incision. Top width of the inset channel in the 1936 Bryan cross section was 41.5 m, center depth was 4.6 m, cross-sectional area was 129 m^2, and the average bank angle was 20.3°.

Previous studies (Kean et al., 2009; Griffin et al., 2010) have shown that the sharp corners between the recently eroded channel bed and bank are areas of high shear stress, causing them to be short-duration, transient features. Therefore, we applied the Kean and Smith (2004) model using a channel shape similar to the 1936 Bryan cross section with a slightly rounded bank toe (**Case A**; Figure 3). We computed flow in the inset channel only, neglecting the terrace area to the right of the channel, artificially extending the banks upward in order to simulate flow in the early, narrow arroyo. For subsequent cases (B and C), we progressively widened the channel and reduced the bank angle as described below.

Nordin's (1963) cross sections surveyed in August and September 1961 near vk 55 provide examples of the channel that widened after initial incision. **Case B** is the channel shape from Case A, widened to match the width of the channel surveyed by Nordin (1963) on 19 August 1961, when measured discharge was 40.5 m^3/s. At a center depth of 1.89 m, top width was 35.9 m (36.5% wider than the channel shape in Case A at the same depth), cross-sectional area was 52.4 m^2, and the average bank angle was 15.3°. Again, for flow modeling purposes, the banks were extended upward at the same angle to accommodate the target flow.

Case C has the same bank geometry as Case B, but with the relatively flat segment in the center of the channel widened by 10 m. This channel shape simulates the wide, braided channel within the arroyo following the large floods of the 1930s and early 1940s (Friedman et al., 2014). Shrub canopy covered an average of only 9% of the arroyo bottom in 1935, and, in many cases, the shrubs present in 1935 were far from the channel (Friedman et al., 2014). In addition, frequent large floods between 1929 and 1936 prevented the establishment of vegetation on the channel bed (arroyo bottom). Therefore, we did not include drag on woody vegetation in these calculations.

Arroyo Wall Erosion: Erosion of the arroyo wall increases planimetric area of the arroyo, which can be used to estimate eroded sediment volumes. We mapped the 2010 arroyo wall locations from the 2010 LiDAR DTM

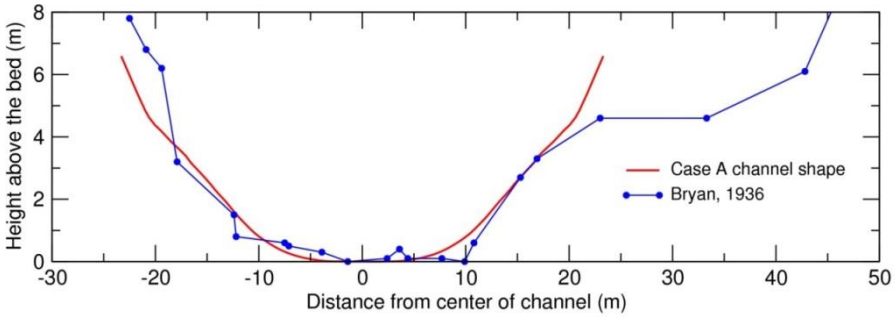

Figure 3 Initial modeled channel shape (Case A; red line), compared to the cross section surveyed by K. Bryan on 5 August 1936 (blue line; Elliott et al., 1999).

(Perignon et al., 2013) in the reach vk 0 – 10 for comparison with previously mapped wall locations in 1935, 1955, 1979, and 2005. We then mapped extents of wall erosion in each of four time intervals: from 1935 to 1955 (length = 20 yr); from 1955 to 1979 (length = 24 yr); from 1979 to 2005 (length = 26 yr); and from 2005 to 2010 (length = 5 yr). Although the last interval is considerably shorter than the others, there was a large flood within this interval (Vincent et al., 2009). For each of the four time intervals we identified: 1) average channel sinuosity; 2) the length of arroyo wall at the start of the interval exposed to channel flow at the base; 3) the length of arroyo wall at the start of the interval that was eroded by the end of the interval; 4) the total planimetric area eroded; and 5) the average wall erosion rate. The average arroyo wall erosion rate (m/yr) was computed by dividing the plan area eroded (m^2) by the length of wall eroded (m) and the number of years in the interval (yr). The computed erosion rates give the average movement of the arroyo wall through time at sites where the mapped change in wall location was >2 m (the minimum detectible movement; Friedman et al., 2014). The volume of sediment eroded from the arroyo wall between 1935 and 1955 was estimated by multiplying the eroded planimetric area by the estimated average height of the valley floor above the channel bed in 1955, about 14.4 m in this reach (Friedman et al., 2014).

Channel Flow Model Application: In a wide, unvegetated channel, the perimeter-averaged boundary shear stress, τ_b, is ρgRS, where ρ is the density of water in a clear-water flow (1,000 kg/m^3), or it is the bulk density of the fluid, ρ_f, in a sediment-laden flow, g is acceleration due to gravity (9.81 m/s^2), R is the hydraulic radius (m), and S is the water-surface slope, estimated here as the average bed slope. We assumed an average sediment density, ρ_s = 2,650 kg/m^3, and computed ρ_f using the equation

$$\rho_f = (1 - C_s)\rho_w + C_s \rho_s , \quad (1)$$

where C_s is the volume concentration of sediment in suspension and ρ_w is the density of water. We assumed that flow was quasi-steady and locally uniform in the down-valley direction and computed flow in the incised channel using the Kean and Smith (2004) model. This model includes the effects of friction on the lateral boundaries in the computation of the flow and boundary shear stress distributions. The model has been applied previously to compute flow in the narrow Rio Puerco channel of 2002 – 2007 in a reach with vegetated banks (Griffin et al., 2005) and in a reach in which bank vegetation had been killed by herbicide and removed by a flood (Griffin et al., 2010). This study is the first application of the model to compute flow in a narrow, deeply incised channel with large capacity. In all cases, the channel was assumed to be straight, with no secondary circulations in the flow.

We selected the magnitude of the annual peak discharge recorded on 23 September 1941, 480 m^3/s, as the target discharge (USGS, 2014b). This discharge is on the order of the mean annual peak flow for the record of the gage at Rio Puerco, 242 m^3/s, plus one standard deviation, 199 m^3/s (n = 51 yr). After 1941, annual peak flows exceeded 480 m^3/s only in 1972, 2006, and 2013. We applied the model to compute the depth of flow required to convey that discharge for each of the three cases for a narrow (Case A) to wide (Case C) channel.

Elevations of the channel bed determined from field survey data or estimated from trench stratigraphy near Highway 6 and Bernardo (Figure 1) combined with mapped channel centerline lengths through the 55 km-long arroyo segment indicate that an average channel bed slope of 0.0011 has been maintained through time since 1935 (Friedman et al., 2014). This slope is used for all of the calculations below. The average down-valley slope is 0.0016 (Griffin et al., 2014). Average sinuosity in 1935 was 1.33 (Friedman et al., 2014).

We assumed that channel bed roughness for flows with a meter or more depth was similar to that measured by Nordin (1963) in August and September 1961 (n = 0.014 to 0.016) and set the bed roughness, z_0, equal to 0.00016 m (Griffin et al., 2014). In a sand-bed stream, these flows are in the upper plane bed regime (Nordin, 1963; Guy et al., 1966). We estimated roughness of recently eroded banks starting 0.30 m above the bed as 0.005 m (Griffin et al., 2010). In the region of the lower bank and bank toe, we used a length-weighted average of the two values. We then calculated the depth required to convey the target discharge for each channel shape.

Computation of Suspended Sediment Transport: The capacity of the flow in the channel to transport sand and finer material in suspension was computed following the method of McLean (1992) and Smith and McLean (1977). We used the bed material distributions found by Griffin et al. (2014) to result in concentration profiles for each of 5 sediment sizes, ranging from medium silt to medium sand, that matched suspended sediment concentrations measured by Nordin (1963) on 20 September 1961 (Table 1). The transport of sand in suspension is dependent on the availability of sand for transport. Field observations (Nordin, 1963; Griffin et al., 2014) and suspended sediment measurements (USGS, 2014a) indicate that the availability of sand for transport has been highly variable through space and time. We assumed that channel bed porosity was 35%, giving a spatially averaged concentration of sediment in the bed, C_b, of 65%, and compensated for variability in availability of sand for transport by assuming sand covered only 25% of the bed in all cases (Topping et al., 2007; Griffin et al., 2014). Concentration profiles were computed for three segments of the channel flow in each case: 1) the middle of the channel over the nearly flat bed; 2) the lower bank and bank toe; and 3) the upper bank. We used the model-calculated τ_b distribution to determine the average τ_b in each segment, specified flow depth as the average depth in the segment, and computed the unit width sediment and sand fluxes (q_s and q_{sand}) in each segment. The total sediment and total sand fluxes in each case were computed by summing the fluxes in each segment.

In the absence of vegetative drag and form drag on topographic roughness elements, the skin friction shear stress, τ_{sf}, needed to compute the sediment transport, is equal to τ_b. Sediment is carried into suspension by turbulent diffusion, and the transport of sediment in suspension is determined by the ratio of the shear velocity, u_*, = $(\tau_b / \rho_f)^{1/2}$, to the sediment settling velocities (Yalin, 1972; Smith and McLean, 1977). Settling velocities for each particle size were determined using the method of Dietrich (1982). We estimated the near-bed reference concentration, C_a, using the equation

$$C_a = \frac{\gamma_0 C_b (T_* - 1)}{1 + \gamma_0 (T_* - 1)}, \tag{2}$$

(Smith and McLean, 1977) where T_* is the transport stage, equal to τ_b / τ_{cr} , τ_{cr} is the critical shear stress for erosion of sediment of a given size, and γ_0 = 0.004 (P.L. Wiberg, reported by McLean, 1992).

The computation of suspended sediment concentration profiles required iteration in each case, as the concentration of sediment in suspension affects the bulk fluid density (equation 1), which affects the sediment settling velocity (Dietrich, 1982). For each iteration, we modified the sediment settling velocities following the method of Dietrich (1982) and recomputed the suspended sediment concentration until the bulk fluid density from the previous iteration

Table 1 Bed material distribution assumed for suspended sediment calculations.

Sediment size (mm)	Fraction of bed material	Clear-water settling velocity (m/s)	Settling velocity with ρ_f = 1130 kg/m^3 (m/s)
0.016	0.40	0.00020	0.00015
0.050	0.14	0.0020	0.0015
0.065	0.20	0.0032	0.0025
0.13	0.19	0.0102	0.0081
0.26	0.07	0.0267	0.0231

was within 5% of the output bulk fluid density. Examples of the decrease in settling velocity for each grain size are shown in Table 1 for ρ_f = 1,130 kg/m^3 (vol. conc. 0.079).

Change in bed elevation (η) with time (t) is calculated from the 1-dimensional sediment continuity equation:

$$\frac{\partial \eta}{\partial t} = -\frac{1}{C_b}\left(\frac{\partial q_s}{\partial x}\right), \tag{3}$$

where x is distance downstream. Erosion of the bed can occur when there is an increase in the sediment flux through time, as during the rising limb of a flood, or with distance downstream. However, the capacity of a flow to erode the bed is strongly dependent on the sediment concentration already in suspension in the flow, which we cannot determine for the early 1900s floods in the study reach.

High concentrations of sand in suspension can cause a density gradient that dampens the turbulent mixing (Gelfenbaum and Smith, 1986; McLean, 1992). Data from Nordin (1963) and our field observations (Griffin et al., 2010) suggest that topographic irregularities in the Rio Puerco inhibit the development of a stable density-stratified flow, and we neglect that process here.

RESULTS

Annual Flow Volume and Suspended Sediment Load: Annual flow volumes from both gages (Figure 4) show a declining trend through time. Continuous flow data are not available for 1929, but the combined August and September flood magnitudes suggest that flow volume in that year was likely higher than in any year of the record. Floods in 1935 and 1936 produced high runoff volumes, but the largest flow volume in the period of record was in WY 1941, when high rainfall caused floods in May, September, and October (Heath, 1983). During the period of overlap in operation of the two gages from WY 1941 to 1976, the volume measured at Bernardo was an average of 94% of the volume measured at the upstream gage. Suspended sediment data from the gage near Bernardo also show a declining trend through time (Figure 5), with the relation between annual suspended sediment load and annual flow volume returning a higher load for a given flow volume in WY 1956 to 1975 than for the same flow volume in WY 1976 to 2013. Extrapolation of the regression for the early period to estimate flow volume in WY 1941 gives a total sediment load of 16.9 x10^6 metric tons (t), about the same as that in WY 1957.

Comparing the average annual sediment load for the period WY 1956 to 1975, 5.05 x 10^6 t/yr (sd = 2.80 x 10^6 t/yr; n = 19) to that for the period WY 1976 to 2013, 1.64 x 10^6 t/yr (sd = 1.01 x 10^6 t/yr; n = 37) shows a 66% decrease in the average annual load. Average annual flow volume also decreased, but only by 37%, from 40.0 x 10^6 m^3/yr (sd = 29.1 x 10^6 m^3/yr; n = 19) to 25.3 x 10^6 m^3/yr (sd = 19.3 x 10^6 m^3/yr; n = 37).

Channel Flow, Boundary Shear Stress, and Suspended Sediment Transport: Channel flow model results for **Case A** (Figure 6) show that as stage (center depth), h, increases from 1.10 to 5.10 m, the τ_b distribution changes from being relatively uniform across the bed and lower banks to showing areas of high stress over the bank toe and lower bank. Discharge increases from 33.0 m^3/s at h = 1.10 m to 480 m^3/s at h = 5.10 m, and the perimeter-averaged τ_b increases from 8.9 to 36.3 N/m^2. When h = 1.10 m, the model-calculated τ_b in the center of the channel is the same as ρghS. As flow depth increases, the difference between τ_b and ρghS in the middle of the channel increases, with a 30% difference between the two values when h = 5.10 m.

At h = 5.10 m, the average τ_b in the 7-m-wide zone of high stress over the bank toe is 51.5 N/m^2, 43% higher than the average in the middle of the channel, 35.9 N/m^2 (Figure 7A). The computed volume concentration of sediment in suspension, 0.0829, gives a total sediment flux of 39.8 m^3/s, and the computed sand flux is 13.4 m^3/s (Table 2). If the flow discharge were sustained at 480 m^3/s for one day and an unlimited supply of sediment, including sand, were readily available for transport, then the total sediment volume transported in a day could have been 3.44 x 10^6 m^3, and the sediment load could have been 9.11 x 10^6 t.

Flow depth in the wider channel of **Case B** required to convey 480 m^3/s is 4.16 m, 18% less than the depth in Case A. The maximum τ_b is reduced by 18%, and the difference between the average τ_b over the bank toe and τ_b in the

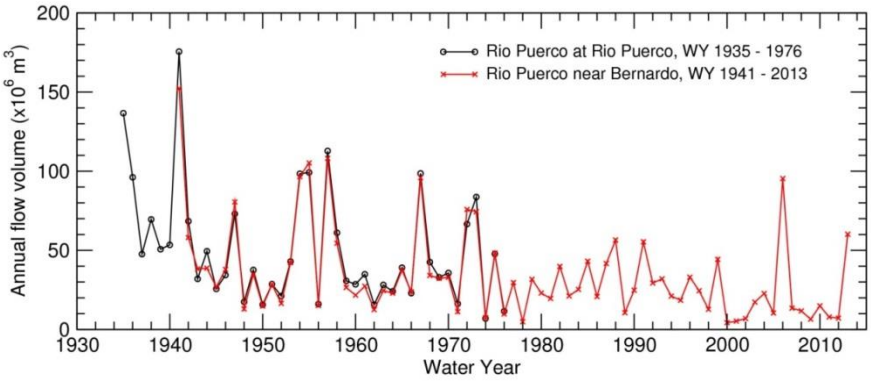

Figure 4 Annual flow volumes at the streamflow-gaging stations Rio Puerco at Rio Puerco (#08352500) and Rio Puerco near Bernardo, NM (#08353000). Declining trends in annual flow volumes are correlated with declining trends in annual peak flows.

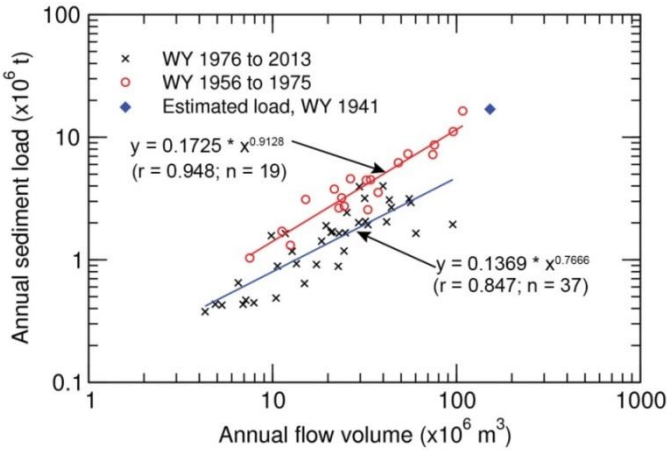

Figure 5 Annual sediment load as a function of annual flow volume from the record of the gaging station Rio Puerco near Bernardo, NM. Red circles are data for WY 1956 (the start of the sediment record) through 1975. Black xs are data for WY 1976 to 2013. The blue diamond is an estimate of the sediment load for WY 1941 based on the regression for WY 1956 through 1975 (red line).

middle of the channel is reduced by 17% (Figure 7). The computed τ_b in the middle of the channel is 11% less than the value of ρghS. The total sediment flux in this channel, 38.0 m^3/s, and sand flux, 12.7 m^3/s, are only 5% less than the computed fluxes in Case A (Table 2).

In the final example, **Case C**, the flow depth required to convey 480 m^3/s is reduced to 3.61 m, 29% less than depth in Case A, and the τ_b distribution approaches the more uniform pattern over the lower banks and bed, similar to the low-flow example of Case A. The maximum τ_b is 29% less than that in Case A, the average τ_b over the bank toe, 38.4 N/m^2, is only 11% greater than the average τ_b in the middle of the channel, and τ_b in the middle of the channel is only 4% less than ρghS. The total sediment flux is only 6.8% less than that in Case A, and the sand flux is 8.2% less (Table 2). The maximum τ_b in the middle of the channel is nearly the same in all 3 cases (Figure 7), ranging from 37.4 N/m^2 in Case C to 39.8 N/m^2 in case B despite the differences in flow depth.

The maximum q_s and q_{sand} (Table 2) are in the region of high τ_b over the lower bank and toe in each case. The maximum unit width fluxes are highest in the narrow channel and lowest in the wide channel, with q_s 24% lower and q_{sand} 27% lower in Case C than in Case A.

Wall Erosion: The extent of wall erosion from one point in time to another is related to the extent of unprotected arroyo wall exposed to channel flow at the start of the time interval (Table 3). In the reach from vk 0 to 10, the total

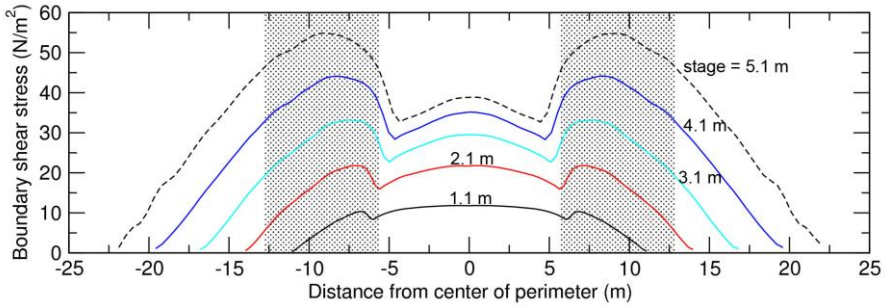

Figure 6 Change in boundary shear stress distribution with increasing flow stage from 1.1 to 5.1 m, Case A channel shape. The shading indicates areas of shear stress over the lower bank and toe.

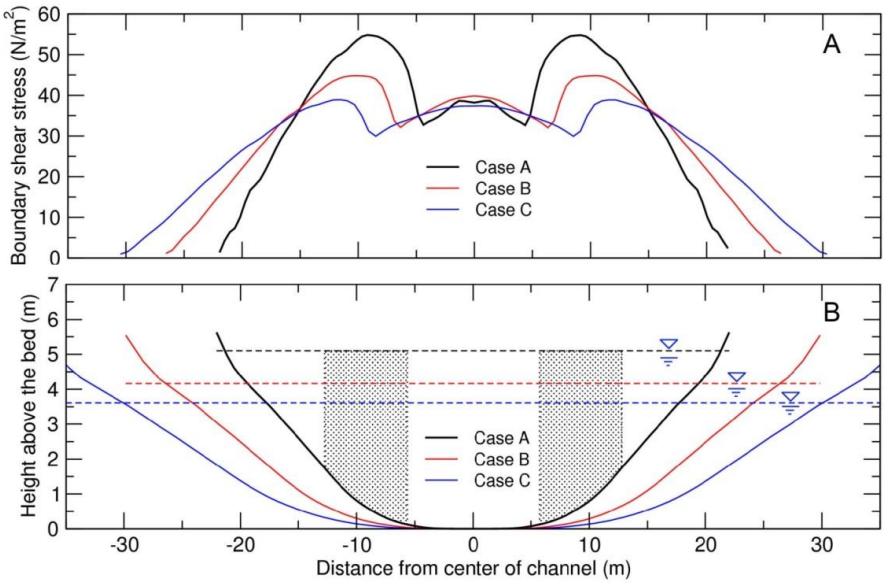

Figure 7 Model-calculated boundary shear stress (**A**) and channel shapes (**B**), with flow center depths that resulted in model-calculated discharge of 480 m^3/s. The shaded areas in B are the regions of high shear stress over the bank toe and lower bank in Case A.

length of wall segments exposed to channel flow at the base decreased from more than 6.3 km in 1935 to about 1 km by 1979. The total length of arroyo wall segments in 1935 that were eroded by 1955 was 7.9 km. Average arroyo width increased in this reach from 222 m in 1935 to 242 m by 1955. Multiplying the increase in arroyo area by the estimated height of the valley floor above the channel bed in 1955, 14.4 m, gives a volume of 2.85 x 10^6 m^3 eroded from the arroyo walls in this segment between 1935 and 1955. Assuming 35% porosity, the sediment volume eroded would have been about 1.85 x 10^6 m^3, with a total weight of 4.91 x 10^6 t, an average of 0.25 x 10^6 t/yr.

Despite the large decreases through time in annual flow volume and length of the arroyo wall exposed to channel flow at the base, the computed average wall erosion rates at sites that eroded all fall within a narrow range, from a minimum of 1.25 m/yr between 1935 and 1955 to a maximum of about 2.00 m/yr between 1979 and 2005.

DISCUSSION AND CONCLUSIONS

In all of the modeled flow cases, τ_b was above τ_{cr} for fine sand (D = 0.13 mm), 0.127 N/m^2. At the minimum modeled flow depth, h = 1.10 m, the perimeter-averaged τ_b, 8.9 N/m^2, was greater than that required to break up the clay armoring layer of the channel bed during Nordin's (1963) measurements (between 3.2 and 7.6 N/m^2). Therefore, all of the modeled flows potentially had the capacity to erode the arroyo bottom. Increasing the flow depth to 5.10 m in Case A resulted in an average shear stress over the lower bank and toe that was 43% higher than τ_b in the middle of the channel. Widening the channel reduced τ_b over the lower bank and toe so that by Case C,

with h = 3.61 m, τ_b over the lower bank and toe was only 11% greater than the average τ_b in the middle of the channel. The suspended sediment transport capacity of the 480 m^3/s channel flow was a maximum of 39.8 m^3/s in Case A. Despite a 26% reduction in mean τ_b from Case A to Case C, the capacity of the flow to transport sediment in suspension was reduced by only 7%.

The boundary shear stress distributions for Cases A, B, and C give an indication of the likely patterns of erosion during rising flow stage. The unit width sediment flux (q_s) varies with τ_b and h across the channel, and in all three cases, is maximum over the lower bank and toe (Table 2). However, the maximum q_s decreases by 24% as the channel widens from Case A to C, decreasing the potential for erosion (equation 3). During the rising limb of a flood, if the incoming sediment load is not at the capacity of the flow, increasing shear stress with stage would erode the wider channel (Case C) relatively uniformly across the bed. As stage rises in the incised, narrow channel (Case

Table 2 Channel flow and suspended sediment model results.

Parameter	Case		
	A	B	C
Center depth (m)	5.10	4.16	3.61
Average depth (m)	3.51	2.89	2.57
Top width (m)	42.7	52.4	60.1
XS area (m^2)	150.0	151.3	153.6
P (m)	44.6	53.7	60.8
R (m)	3.37	2.82	2.53
Mean τ_b (N/m^2)	36.3	30.5	27.0
Max τ_b (N/m^2)	54.8	44.8	38.9
Mean u (m/s)	3.20	3.17	3.12
Mean u_* (m/s)	0.191	0.175	0.164
Manning's n	0.0232	0.0210	0.0197
C_s	0.0829	0.0791	0.0773
C_{sand}	0.0279	0.0264	0.0257
$(q_s)_{max}$ (m^3/s)	1.19	0.99	0.90
$(q_{sand})_{max}$ (m^3/s)	0.41	0.34	0.30
Q_{total} (m^3/s)	480	480	480
Q_s (m^3/s)	39.8	38.0	37.1
Q_{sand} (m^3/s)	13.4	12.7	12.3

Table 3 Changes in arroyo wall erosion through time, vk 0 – 10.

Parameter	Time interval			
	1935 – 1955	1955 – 1979	1979 – 2005	2005 - 2010
Average sinuosity:	1.39	1.47	1.45	1.42
Length of wall exposed to channel flow at start of interval (m):	6,320	4,060	1,020	910
Length of wall at start of interval that eroded by end of interval (m):	7,900	3,210	1,410	450
Plan area eroded (m^2):	198,000	107,000	73,200	2,830
Average wall erosion rate at sites of erosion (m/yr):	1.25	1.39	2.00	1.26
Average arroyo width (m):	222	242	251	257

A), the much higher τ_b over the lower banks and toes would cause erosion of those surfaces at a higher rate than the bed. Higher concentrations of sediment over the lower banks and toe would give rise to a concentration gradient toward the center of the channel, causing mixing of the suspended sediment across the channel and inhibiting the capacity of the flow to erode the bed.

The estimated increase in volume of the lower Rio Puerco arroyo through both incision and widening between 1927 and 1935, 44.5 x 10^6 m^3 (Friedman et al., 2014), contained an estimated sediment volume of 28.9 x 10^6 m^3, or about 76.7 x 10^6 t. This total provides an average load of 9.6 x 10^6 t/yr, which is less than the estimated sediment load for WY 1941 (16.9 x 10^6 t/yr). The calculated potential sediment load for a single day of flow at 480 m^3/s in Case A, 9.11 x 10^6 t, is nearly the same as the average annual sediment load from 1927 to 1935. The sediment eroded from the arroyo walls between 1935 and 1955 in the reach from vk 0 – 10, an average of 0.25 x 10^6 t/yr, was only 5% of the average annual sediment load measured at the gage near Bernardo between 1956 and 1975 (5.05 x 10^6 t/yr). The results suggest that the suspended sediment load in the Rio Puerco often has been less than the capacity of the flow to transport sediment in suspension. Therefore, total sediment transport capacity in this system does not appear to have limited the capacity for incision.

The large reduction in length of wall segments exposed to channel flow (Table 3) was the result of increasing width of the arroyo bottom, increasing channel sinuosity, decreasing channel width after the 1940s, and increasing density of woody vegetation on the arroyo bottom through time (Friedman et al., 2014). The greater length of arroyo wall eroded from 1935 to 1955 than the length of wall exposed to channel flow in 1935 was in part the result of rapid channel migration down-valley, with average rates of up to 12 m/yr found by Friedman et al. (2014). The results indicate that arroyo wall erosion rates at sites of erosion averaged about 1.5 m/yr from 1935 to 2010. Although the trend in annual flow volume decreased through time, narrowing of the channel through time (Friedman et al., 2014) caused an increase in flow depth and τ_b as a function of discharge. In addition, sites of wall erosion between 2005 and 2010 were dominantly within sharp bends, where secondary circulations increased the shear stress along the outside of the bend, at the base of the arroyo wall (Engel and Rhoads, 2012). These changes appear to have compensated for the reduction in flow magnitude and volume through time.

The above results indicate that changes in the total suspended sediment transport capacity through time did not limit the capacity for incision. Instead, increased boundary shear stress over the lower bank and toe caused by friction on the lateral boundaries of the narrow, incised channel of 1936 would have contributed to a tendency to widen the channel (and arroyo) rather than further incise the bed. The decreasing flood peak magnitude, frequency and duration after 1941 also decreased the capacity for erosion in this system. A period of moderately low flows from WY 1948 through 1952 (Figure 4) may have provided an opportunity for widespread establishment of woody vegetation on the arroyo bottom, creating drag on future flows and a further reduction of τ_{sf} and potential to erode the bed.

Acknowledgments: The Pueblo of Isleta generously enabled the research to be conducted on their land and provided valuable historical information. Any use of trade, firm, or product names is for descriptive purposes only and does not imply endorsement by the U.S. Government.

REFERENCES

Bierman, P.R., Reuter, J.M., Pavich, M., Gellis, A.C., Caffee, M.W., and Larsen, J. (2005). "Using cosmogenic nuclides to contrast rates of erosion and sediment yield in a semi-arid, arroyo-dominated landscape, Rio Puerco Basin, New Mexico," Earth Surface Processes and Landforms, 30, pp 935-953.

Bryan, K. (1928). "Historic evidence on changes in the channel of Rio Puerco, a tributary of the Rio Grande in New Mexico," Journal of Geology, 36, pp 265-282.

Bryan, K., and Post, G.M. (1927). "Erosion and control of silt on the Rio Puerco, New Mexico," Report to the Chief Engineer, Middle Rio Grande Conservancy District, Albuquerque, New Mexico.

Dietrich, W.E. (1982). "Settling velocity of natural particles," Water Resources Research, 18(6), pp 1615-1626.

Elliott, J.G., Gellis, A.C., and Aby, S.B. (1999). "Evolution of arroyos: Incised channels of the southwestern United States," in Darby, S.E., and Simon, A., (eds.), Incised River Channels. Wiley, Chichester, UK, pp 153-185.

Engel, F.L., and Rhoads, B.L. (2012). "Interaction among mean flow, turbulence, bed morphology, bank failures, and channel planform in an evolving compound meander loop," Geomorphology, 163-164, pp 70-83.

Friedman, J.M., Vincent, K.R., Griffin, E.R., Scott, M.L., Shafroth, P.B., and Auble, G.T. (2014). "Processes of arroyo filling in northern New Mexico, USA," GSA Bulletin (in press).

Gelfenbaum, G. and Smith, J.D. (1986). "Experimental evaluation of a generalized suspended-sediment transport theory," in Knight, R.J. and McLean, J.R., (eds.), Shelf Sands and Sandstones, Canadian Society of Petroleum Geologists, Memoir II, pp 133-144.

Griffin, E.R., Kean, J.W., Vincent, K.R., Smith, J.D., and Friedman, J.M. (2005). "Modeling effects of bank friction and woody bank vegetation on channel flow and boundary shear stress in the Rio Puerco, New Mexico," Journal of Geophysical Research, 110, F04023.

Griffin, E.R., Smith, J.D., Friedman, J.M., and Vincent, K.R. (2010). "Progression of streambank erosion during a large flood, Rio Puerco arroyo, New Mexico," Proc. of the 2nd Joint Federal Interagency Conference, Las Vegas, NV, June 27 – July 1, 2010, 12 p.

Griffin, E.R., Perignon, M.C., Friedman, J.M., and Tucker, G.E. (2014). "Effects of woody vegetation on overbank sand transport during a large flood, Rio Puerco, New Mexico," Geomorphology, 207, pp 30-50.

Guy, H.P., Simons, D.B., and Richardson, E.V. (1966). "Summary of alluvial channel data from flume experiments, 1956-1961," U.S. Geological Survey Professional Paper 462-I, 96 p.

Happ, S.C. (1948). "Sedimentation in the Middle Rio Grande Valley, New Mexico," Bulletin of the Geological Society of America, 59, pp 1191-1216.

Heath, D.L. (1983). "Flood and recharge relationships of the lower Rio Puerco, New Mexico," New Mexico Geological Society Guidebook, 34th Field Conference, Socorro Region II, pp 329-336.

Hovey, E.O. (1902). "New York Academy of Sciences, Section of Geology and Mineralogy," Science, 15(384), pp 744-747.

Kean, J.W., and Smith, J.D. (2004). "Flow and boundary shear stress in channels with woody bank vegetation," in Bennett, S., and Simon, A., (eds.), Riparian Vegetation and Fluvial Geomorphology. American Geophysical Union Water Science and Application Monograph 8, pp 237-252.

Kean, J.W., Kuhnle, R.A., Smith, J.D., Alonso, C.V., and Langendoen, E.J. (2009). "Test of a method to calculate near-bank velocity and boundary shear stress," Journal of Hydraulic Engineering, 135(7), pp 588-601.

Love, D.W. (1986). "A geological perspective of sediment storage and delivery along the Rio Puerco, central New Mexico," in Hadley, R.F., (ed.), Drainage Basin Sediment Delivery. Institute of Hydrology, IAHS Publication 159, pp 305-322.

McLean, S.R. (1992). "On the calculation of suspended load for noncohesive sediments," Journal of Geophysical Research, 97(C4), pp 5759-5770.

Molnár, P. and Ramírez, J.A. (2001). "Recent trends in precipitation and streamflow in the Rio Puerco basin," Journal of Climate, 14(10), pp 2317-2328.

New Mexico State Engineer (1930). "The September flood," New Mexico State Engineer, Ninth Biennial Report, vol. 9, pp 257-264.

Nordin, C.F., Jr. (1963). "A preliminary study of sediment transport parameters, Rio Puerco near Bernardo, New Mexico," U.S. Geological Survey Professional Paper 462-C, 21 pp., U.S. Government Printing Office, Washington, D. C.

Perignon, M.C., Tucker, G.E., Griffin, E.R., and Friedman, J.M. (2013). "Effects of riparian vegetation on topographic change during a large flood event, Rio Puerco, New Mexico, USA," Journal of Geophysical Research: Earth Surface, 118, pp 1193-1209.

Simon, A., Curini, A., Darby, S.E., and Langendoen, E.J. (2000). "Bank and near-bank processes in an incised channel," Geomorphology, 35, pp 193-217.

Smith, J.D., and McLean, S.R. (1977). "Spatially averaged flow over a wavy surface," Journal of Geophysical Research, 82(12), pp 1735-1746.

Topping, D.J., Rubin, D.M., and Melis, T.S. (2007). "Coupled changes in sand grain size and sand transport driven by changes in the upstream supply of sand in the Colorado River: Relative importance of changes in bed-sand grain size and bed-sand area," Sedimentary Geology, 202, 538-561.

Tuan, Y.F. (1966). "New Mexican gullies: A critical review and some recent observations," Annals of the Association of American Geographers, 56, pp 573-597.

U.S. Geological Survey (2014a). National Water Information System, water-quality database, accessed 06/20/2014 at http://nwis.waterdata.usgs.gov/usa/nwis/qwdata.

U.S. Geological Survey (2014b). National Water Information System (NWISWeb): U.S. Geological Survey database accessed 9/16/2014 at http://waterdata.usgs.gov/nm/nwis/.

Vincent, K.R., Friedman, J.M., and Griffin, E.R. (2009). "Erosional consequence of saltcedar control," Environmental Management, 44, pp 218-227.

Welsh, M. (1985). "The United States Corps of Engineers in the Middle Rio Grande Valley, 1935-1955," New Mexico Historical Review, 60(3), pp 295-316.

Xia, J., Xiaojuan, L., Li, T., Zhang, X., and Zong, Q. (2014). "Response of reach-scale bankfull channel geometry to the altered flow and sediment regime in the lower Yellow River," Geomorphology, 213, pp 255-265.

Yalin, M.S. (1972). Mechanics of Sediment Transport, Pergamon Press, Oxford, UK.

ESTIMATING FLOW CONCENTRATION AND SEDIMENT REDISTRIBUTION ON SALINE RANGELAND COMMUNITIES

Sayjro K Nouwakpo, Research Professor, University of Nevada Reno, Department of Natural Resources and Environmental Science, snouwakpo@cabnr.unr.edu 775-784-6056; Mark Weltz, Rangeland Hydrologist and Research Leader, United States Department of Agriculture, Agriculture Research Service, mark.weltz@ars.usda.gov, 775-784-6057; Kenneth McGwire Associate Research Professor, Desert Research Institute, Division of Earth and Ecosystem Sciences, Ken.McGwire@dri.edu, 775-673-7324; Colleen G. Rossi, Water Quality Salinity Specialist, Bureau of Land Management, Salt Lake City, Utah, crossi@blm.gov, (801) 539-4028

ABSTRACT

In arid and semi-arid rangelands where vegetation is typically sparse, a synergistic relationship is assumed to exist between spatial distribution of plants and hydrologic and erosion processes. In these environments, an accurate understanding of sediment transport processes is key to developing informed management actions and addressing ecosystem response to global changes. In this study, data from rainfall simulation experiments in saline rangeland communities of the Upper Colorado River Basin were used to improve understanding on various sediment and solute transport processes in field conditions. During these experiments, hydrology, erosion and high-resolution surface microtopography changes were routinely measured, presenting a unique opportunity to answer many sediment transport questions relevant to these saline rangeland and other sparsely vegetated ecosystems. A series of variables were developed to quantify and characterize surface microtopographic changes as a function of hydrology, erodibility and hillslope configuration. Key findings from preliminary analyses include: (1) the dependence of deposition on plot slope and its independence on hydrologic and soil loss variables, (2) data supporting the process of increased downcutting as slope increased, (3) significance of accounting deposition processes in overall runoff energy quantification, (4) evidence of an equilibrium channel geometry with a given discharge that is marginally impacted by runoff duration.

INTRODUCTION

Hillslope runoff and soil erosion processes play a vital role in rangeland ecosystem sustainability due to their control on resource mobility but they also have significant implications in off-site resource transport. Nichols et al. (2013) found for example that hillslope processes contributed to 85% of sediment delivery from a 43.7 ha semi-arid shrub-dominated watershed. The influence of vegetation on hillslope runoff and sediment production forms the basis of current hydrology and erosion modeling technologies on rangelands (Nearing et al., 2011). Early attempts to apply empirical soil erosion models derived primarily from cropland data, such as the Universal Soil Loss Equation – USLE and the Revisited Universal Soil Loss Equation – RUSLE, on rangelands yielded unsatisfactory and contested results (Blackburn, 1980; Foster et al., 1981; Hart, 1984; Johnson et al., 1984; Mitchell and Roundtable, 2010; Spaeth et al., 2003; Trieste and Gifford, 1980). Weltz et al. (1998) point to the lumped nature and rigid structure of these empirical models as a key deficiency when applied to rangelands where biotic and abiotic interactions play a strong control on surficial processes.

The advent of physically-based soil erosion models such as the Water Erosion Prediction Project model-WEPP (Laflen et al., 1991) offered the opportunity to develop the scientific framework necessary to provide insight into the relationship between hydrologic processes and rangeland condition. These research efforts led to the Rangeland Hydrology and Erosion Model (RHEM) (Nearing et al., 2011), developed from experimental data specifically collected on rangeland sites across the Western U.S. As a process-based erosion model, RHEM models erosion and hydrology using the same fundamental principles as WEPP.

Runoff generation and erosion on the hillslope are modeled in response to hydrological inputs and hydraulic parameters that are adjusted based on soil intrinsic properties and land surface conditions.

In both WEPP and RHEM, the hillslope is divided into interrill areas where splash and sheet detachment and transport occur and rills where flow is concentrated and fluvial processes dominate. Accurate partitioning of hillslope erosion into interrill and concentrated-flow-dominated processes has a significant implication on rangeland erosion modelling especially following disturbances. Several studies (e.g, Al-Hamdan et al., 2012; Pierson et al., 2013) have demonstrated a significant increase in concentrated flow erosion when shrub-dominated rangeland are disturbed by fire or woody species encroachment compared to undisturbed conditions.

Concentrated flow erosion is a complex process because rill networks have a dual function of sediment and runoff production and storage as well as that of transport of these resources off-site and these intricately coupled functions are traditionally assumed to be controlled by rill flow hydraulics. The key to accurate concentrated flow erosion has therefore been that of adequate prediction of hydraulic parameters. A great deal of research efforts have been invested into relating rill detachment rate to flow hydraulic parameters such as average shear stress (e.g., Ghebreiyessus et al., 1994; Lyle and Smerdon, 1965; Nearing et al., 1997; Torri et al., 1987), stream power (e.g., Bagnold, 1977; Nearing et al., 1997; Zhang et al., 2003), effective stream power (e.g., Bagnold, 1980). Performance tests of these hydraulic parameters at predicting rill detachment rate in various experimental conditions (Al-Hamdan et al., 2012; Wirtz et al., 2013) resulted in no single parameter consistently best-fitting observed detachment rates, although (Al-Hamdan et al., 2012) found that the stream power performed well with rangeland erosion data. Wirtz et al. (2013) attributed discrepancies between observed and predicted erosions to the inherent emphasis of most hydraulic parameters on fluvial processes incising channel bottoms while diffusive processes such as headcut-retreat and bank-erosion make up a non-negligible portion of rill detachment.

Currently available hydraulic-driven-rill-detachment equations albeit incomplete, offer a widely accepted modeling framework but often rely on a good characterization of the channel network. One of the knowledge gap in process-based soil erosion modeling especially on rangelands is the lack of an adequate framework to characterize spatial extent of concentrated flow network. Another knowledge gap in these process-based modeling approaches concerns the mechanism of deposition.

As part of an effort to quantify salt transport from rangelands to the Upper Colorado River Basin (UCRB), experimental rainfall simulation studies were conducted in saline rangelands communities of this basin. Hydrology, erosion and high-resolution surface microtopography changes were routinely measured during these simulations, presenting a unique opportunity to answer many sediment transport questions relevant to these saline rangelands and other sparsely vegetated rangelands. The aim of this paper was to gain insight into the processes of concentrated flow erosion and deposition on saline rangelands by relating traditionally measured hydrologic and sediment yield data to observed expression of these processes in surface microtopography. This knowledge would provide a predictive framework for hydraulic parameter estimation on saline rangelands for use in physically-based erosion models such as RHEM.

MATERIAL AND METHODS

Study area: This study was part of a broader research effort aimed at quantifying salt transport from rangelands to the Upper Colorado River headwaters. Previous researchers (e.g., Hawkins et al., 1977; Riley et al., 1979; Tuttle and Grauch, 2009) have identified upland areas of the Upper Colorado River Basin in the Mancos Shale and Eagle Valley Evaporite geologic formations as major contributor to the river's salinity. For our study, two sites (Price and DryX hereafter) in the Mancos Shale geologic formation were then selected to conduct rainfall simulation experiments. These sites were selected for their contrasting slope ranges and differences in intrinsic properties of the soil.

The Price site was located near the city of Price, Utah at the geographic coordinates 39° 27' 47.22"N 110° 36' 26.16"W and average elevation of 1649 m. The soil on this site was mapped as a Persayo loam soil series and classified as loamy, mixed, active, calcareous, mesic, shallow, typic torriorthents. Measured slopes on the experimental site ranged from 0.6 to 10%. DryX was located near the city of Ferron, Utah at the geographic coordinates 38°58'38.50"N 111° 7'10.60"W and average elevation of 1893 m. The predominant soil type at DryX was mapped as a complex of Chipeta series soils with Badland areas. The taxonomic classification of the Chipeta series is clayey, mixed, active, calcareous, mesic, shallow, typic torriorthents. Measured slopes at the study area of the DryX site ranged from 11.4% to 24.5%.

Experimental setup

On each experimental site, a series of rainfall simulations were conducted on 6 m x 2 m erosion plots to quantify sediment and salt transport processes during rainfall-driven erosion processes. Erosion and hydrologic responses were assessed by measuring soil loss, runoff and solute transport under four rainfall intensities corresponding to return periods of 2 (50.8 mm/hr), 10 (88.9 mm/hr), 25 (114.3 mm/hr) and 50 (139.7 mm/hr) years. On each plot, a single rainfall event was applied to ensure the capture of the process of salt efflorescence (Bowles et al., 1982; Riley et al., 1982) whereby a salt crust is left at the soil surface by evaporation. Each rainfall intensity on each site was replicated three times leading to a total of twelve plots per site.

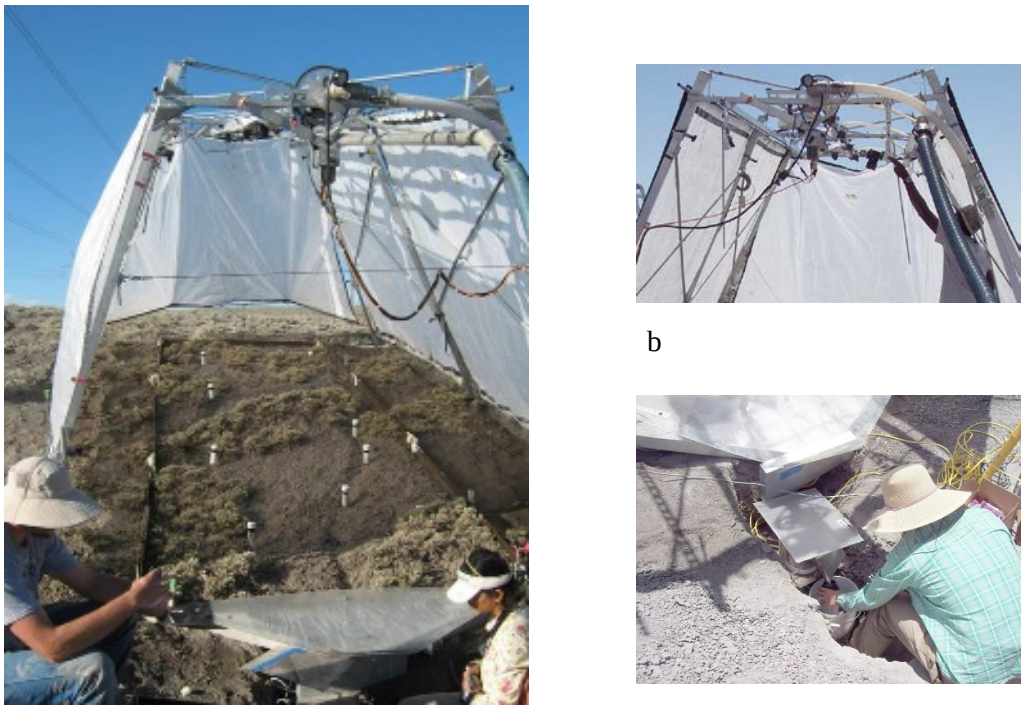

a b c

Figure 1 Experimental setup showing (a) rainfall simulator on 6 m x 2 m plot, (b) a close-up view of the camera mount and rail mechanism and (c) the supercritical flume used for runoff discharge measurement and runoff sampling.

A Walnut Gulch Rainfall Simulator (WGRS) (Paige et al., 2004) was used in this study (Figure 1a). A rail mechanism mounted lengthwise on the frame of the simulator supported a camera (Figure 1b) which was used to take overlapping pictures before and after each rainfall event to reconstruct soil surface microtopography at sub-millimeter resolution. A digital Single Lens Reflex (SLR) camera equipped with a

20 mm lens was used for acquiring the surface reconstruction pictures. The average camera-ground distance was 2.4 m and the overlap between adjacent pictures 0.15 m. Pictures were taken along two paths 0.76 m apart on either side of the central boom of the simulator. This image network configuration resulted in 80 to 90 pictures to cover each plot. Translucent side curtains on the simulator served the dual purpose of diffusing light, reducing excessive shadowing in the pictures and limited the effect of wind on rainfall distribution.

Soil surface analysis: Soil surface microtopography was reconstructed using the structure from motion software Agisoft PhotoScan 1.0 (Agisoft Llc, 2013). For each plot, PhotoScan produced pre- and post-rain point clouds which were manually edited to remove vegetation points in the software Cloud Compare (General Public Licence, 2014). Vegetation-free point clouds were then converted in Digital Elevation Models (DEMs) (Figure 2) and analyzed within the ArcGIS system (Esri, 2011).

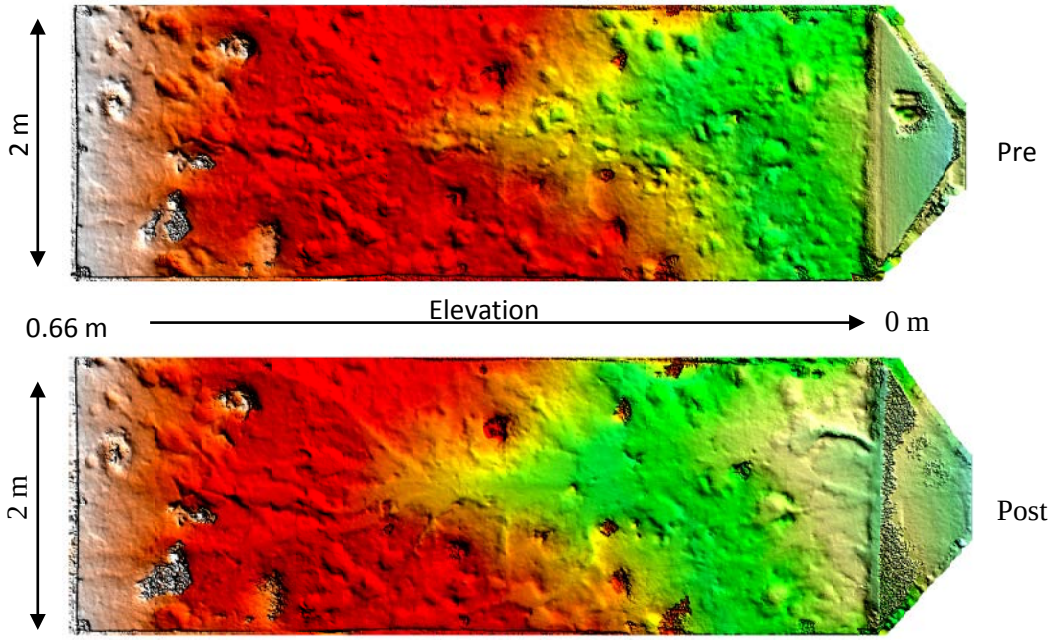

Figure 2 Example of 5-mm resolution DEMs representing soil microtopography reconstructed pre and post rainfall.

In this paper, changes in soil surface microtopography were related to sediment transport mechanisms. Changes to soil surface microtopography were quantified by subtracting post- from pre-rain DEMs, allowing the distinction between erosion areas (negative difference) and deposition areas (positive difference). To characterize soil surface response to erosive events, various areal and volumetric surface metrics were calculated from pre- and post-rain DEMs as well as the difference of DEMs.

Total erosion, deposition and net loss: The overall spatial extents of erosion processes TX_E and deposition TX_D were calculated as

$$TX_E = n \times A \quad (1)$$

$$TX_D = m \times A \quad (2)$$

where n and m are the number of grid cells with respectively negative and positive DEM differences and A is the grid size.

The volumes TV_E, TV_D and TV_N corresponding to erosion and deposition and net loss processes were also quantified as

$$TV_E = \sum_{i=0}^{i=n} \Delta Z_i \times A \tag{3}$$

$$TV_D = \sum_{j=0}^{j=m} \Delta Z_j \times A \tag{4}$$

$$TV_N = TV_E - TV_D \tag{5}$$

where *i* and *j* are respectively grid positions of erosion and deposition and ΔZ is the magnitude of elevation change.

Channel processes: Understanding mechanisms of erosion processes in concentrated flow pathways as they relate to other landscape attributes is crucial to accurate soil erosion modeling. In this study, flow concentration pathways were identified by applying the bottom-hat (also known as the black top-hat) mathematical morphology to the original DEMs. The bottom-hat operator detects local extrema in a two dimensional signals such as images and DEMs. This operator has been successfully applied to digital topographic data to delineate flow network and detect erosional incision (e.g., Rodriguez et al., 2002; Schwanghart et al., 2013). The detail presentation of the bottom-hat implementation is beyond the scope of this paper but in our study, the output of this operator was a spatial function whose minima were areas in the DEMs of local concavities. To minimize the effect of surface roughness in channel network detection, the original DEMs were smoothed using a 0.125 m^2 diamond-shaped structuring element similar to that used in Hyun-Chong et al. (2006). Concentrated flow pathways were considered as areas with bottom-hat responses lower than the plot average. Flow networks corresponding to the conditions pre- (Net_{pre}) and post- (Net_{post}) rain were merged to give a final flow network *Net*.

Spatial extent of erosion and deposition (CX_E and CX_D) that occurred within channels were obtained in a similar manner as TX_E and TX_D.

$$CX_E = n_c \times A \tag{6}$$

$$CX_D = m_c \times A \tag{7}$$

where n_c and m_c are the number of grid cells with respectively negative and positive DEM differences within *Net*. Likewise, CV_E, CV_D and CV_N were calculated by applying Eq. 3-5 to areas within *Net*.

Erosive forces can alter channel networks in both vertical and lateral dimensions depending on hillslope characteristics. These directional changes to the channel network were captured in $Net_{\Delta xy}$ and $Net_{\Delta z}$ for lateral and vertical changes respectively as:

$$Net_{\Delta xy} = Net_{post} \backslash Net_{pre} \tag{8}$$

$$Net_{\Delta z} = Net_{post} \cap Net_{pre} \tag{9}$$

where \ is the set difference operator and ∩ the intersection operator.

From the $Net_{\Delta xy}$ sub-network, spatial and volumetric metrics CX_{xyE}, CX_{xyD}, CV_{xyE}, CV_{xyD} and CV_{xyN} were calculated whereas $Net_{\Delta z}$ was used to obtain CX_{zE}, CX_{zD}, CV_{zE}, CV_{zD} and CV_{zN}.

Other secondary parameters were also calculated:

$$CXR = (CX_E + CX_D)/(TX_E + TX_D) \quad (10)$$

$$CVR_E = CV_E/TV_E \quad (11)$$

$$CVR_N = CV_N/TV_N \quad (12)$$

CXR, CVR_E and CVR_D express the space-based and volume-based ratio of concentrated flow processes that occurred on a plot.

The proportion of concentrated flow energy expenditure in lateral channel expansion versus vertical growth was quantified using two parameters α and α' calculated as:

$$\alpha = CV_{xyE}/CV_E \quad (13)$$

$$\alpha' = CV_{xyN}/CV_N \quad (14)$$

Deposition processes were also examined by calculating the proportion of eroded volume that was re-deposited at the plot level (*TDR*) and in the channels (*CDR*).

$$TDR = TV_D/TV_E \quad (15)$$

$$CDR = CV_D/CV_E \quad (16)$$

These surface changes metrics were related to hydrologic and erosion variables as well as plot slope (SLP). Hydrologic variables used were precipitation (*P*), runoff discharge (*R*), infiltration rate (*IR*), cumulative runoff (SR) and erosion information were sediment concentration (SC) and total sediment loss (S). Throughout this paper, the units are m^2 for spatial metrics (e.g., TX_E, CX_E), m^3 for volumetric surface metrics (e.g., TV_E, CV_E). *P*, *R* and *IR* are in mm, *SR* in 10^{-3} m^3, *SC* in g/L and *S* is in g.

PRELIMINARY RESULTS FROM THE PRICE SITE

Plot-wide erosion and deposition processes: Figure 3 shows the relationships between calculated plot-wide-surface-change metrics and hydrology, erosion and plot slope gradient. For erosion processes, volumetric metrics improved the correlation with hydrology and erosion variables (increased R^2) compared to the spatial metrics (e.g., TX_E vs TV_E), suggesting that incorporating the depth information is crucial to understanding erosion and deposition processes. This improvement in R^2 with the incorporation of depth information was observed throughout the analyses in this study therefore area-based metrics have been excluded as much as possible from other figures for conciseness.

TV_E had the highest correlation in all comparisons except with slope with which TX_E performed better, suggesting that in our experimental conditions at Price, overall eroded volumes were not a function of slope. Cumulative runoff *SR* and runoff rate *R* were better predictors of erosion volumes TV_E with R^2 of 0.60 and 0.74 compared to sediment concentration *SC* and cumulative sediment *S* (R^2 = 0.14 and 0.38 respectively). This finding suggests that a portion of observed sediment loss by weight (especially the colloidal soil fraction) has little contribution to overall surface microtopography. Also, runoff rate R better predicted erosion volumes than cumulative runoff. This finding is consistent with the existence of an equilibrium-channel-network-geometry for a specific runoff discharge with marginal influence of runoff duration. It is also important to note that rainfall events at the Price site did not vary significantly in length which may have masked the effect of runoff duration.

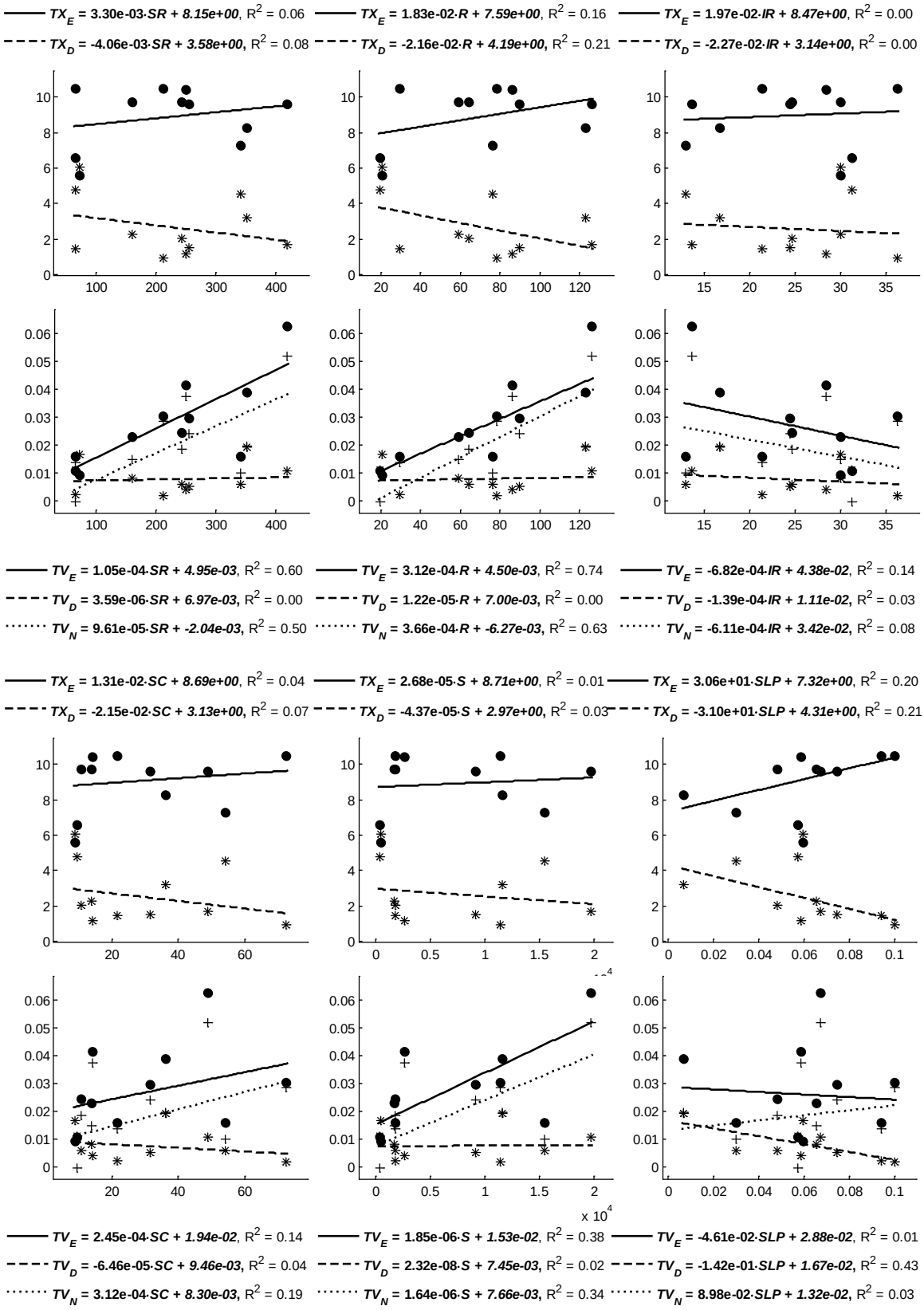

Figure 3 Plot-wide surface change metrics as a function of hydrology, erosion and slope variables.

Deposition processes (TX_D and TV_D) performed poorly against all hydrologic and erosion processes. For hydrologic processes, the largest correlation was found between TX_D and R with an R^2 of 0.21 but it is important to note that TX_D and TX_E are strongly correlated since they are complement of one another on a fixed plot area. This lack of dependence of deposition processes on hydrologic and erosion processes was likely the cause of the decrease in R^2 observed in most cases (except TV_E, TV_N vs. SC) when TV_E was replaced with TV_N. Nevertheless TV_D showed a systematic decreasing trend with slope (R^2 = 0.43), suggesting that sediment deposition volume was mainly controlled by plot slope on this site.

Channel processes: Figure 4 summarizes results of the microtopographic analysis in concentrated flow areas.

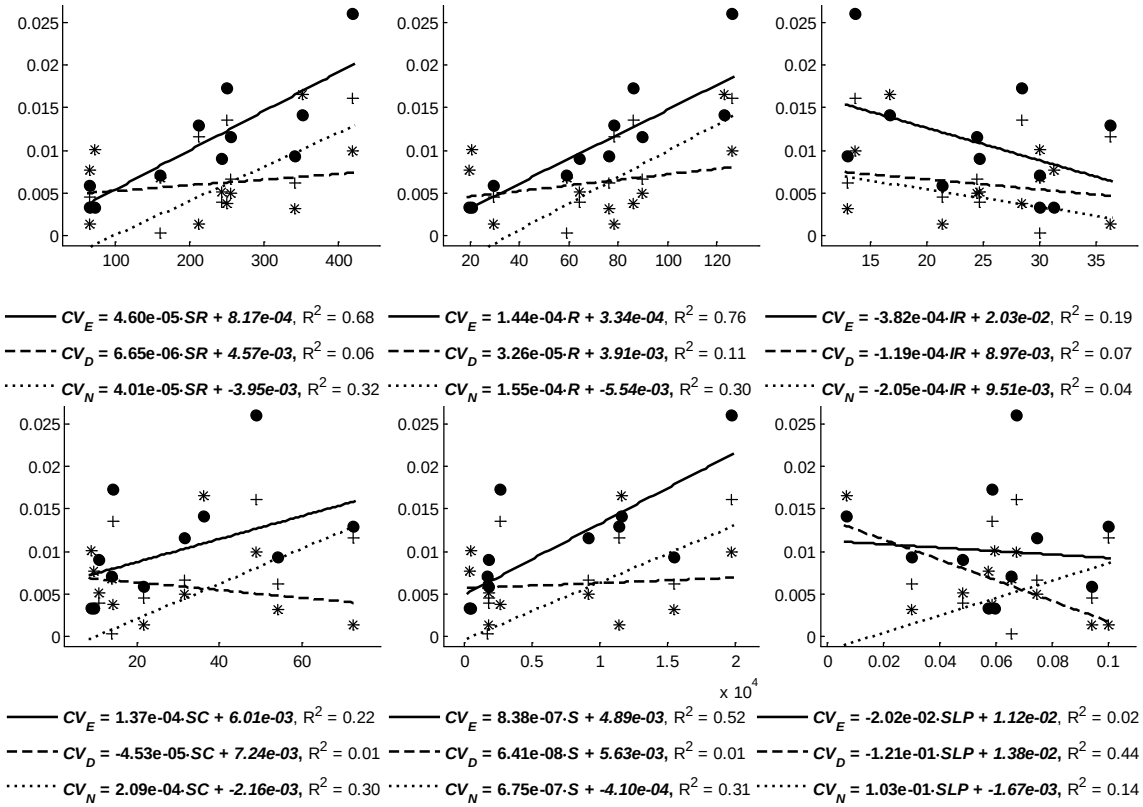

Figure 4 Concentrated flow processes as a function of hydrology, erosion and slope

Overall observations made for the plot-wide analysis are also valid here: (1) the incorporation of depth information in erosion volumes in channels improved correlation correlated with all variables (here again except for slope) with R^2 values for CV_E larger than those of CX_E (not shown in Figure 4), (2) runoff rate was a better predictor of eroded volume than cumulative runoff, (3) hydrology variables were better predictors of eroded volumes in channels than observed soil loss, (4) within channel deposition was primarily controlled by slope. Surface change metrics measured in channels were better correlated with hydrology, soil loss and slope variables than were plot-wide metrics indicated by an increase in R^2 in 21 of the 30 linear regressions on Figure 3 compared to Figure 4. However when TV_E and CV_E are plotted against precipitation P (Figure 5), one notices a slightly stronger correlation of P with TV_E. In other words, when relating surface change metrics to precipitation, R^2 increased with the inclusion of diffusive processes (sheet and splash erosion). This result is consistent with the current soil erosion theory which suggests a dependence of sheet and splash erosion processes on rainfall intensity. Likewise, when relating surface change metrics to runoff rate, R^2 was improved by excluding diffusive processes which is consistent with a dependence of concentrated flow processes (channel geometry) on runoff discharge.

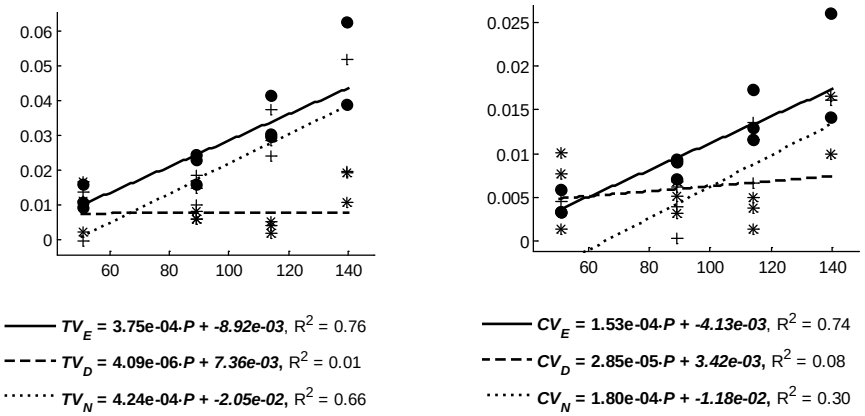

Figure 5 Plot-wide and channel erosion and deposition volumes as a function of precipitation

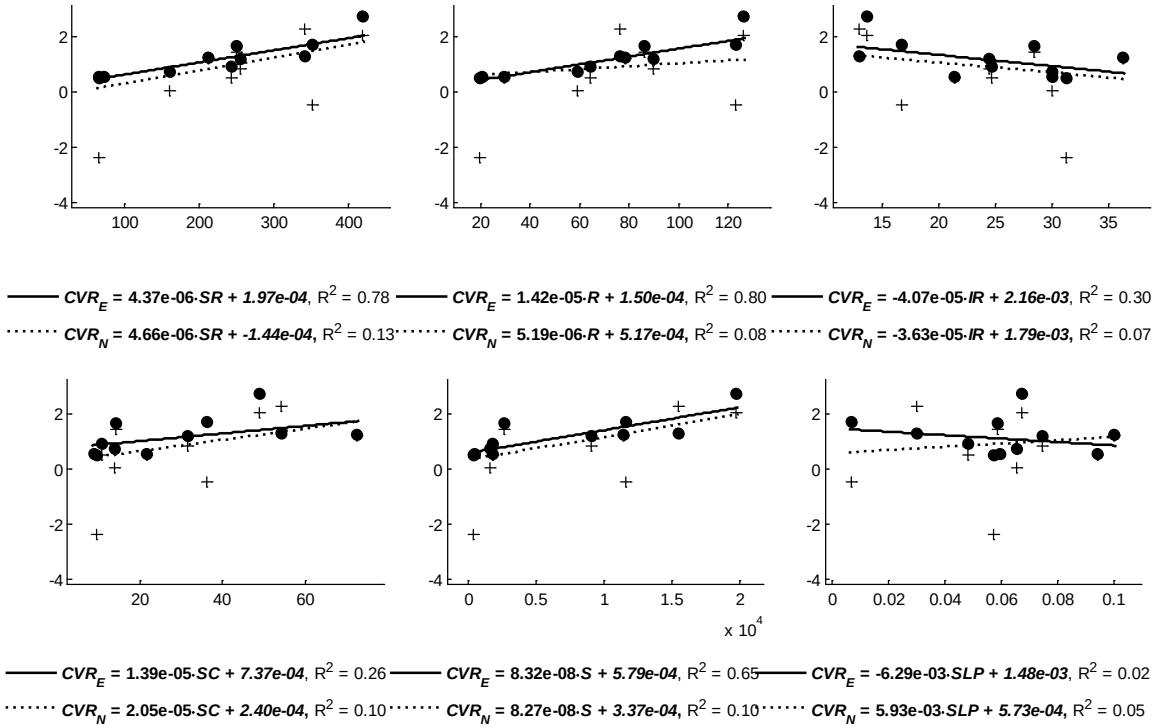

Figure 6 Area and volume-based ratios of flow concentration as a function hydrology, soil loss and slope

The ratios of flow concentration determined using volumes are shown in Figure 6. Overall the volume-based ratios showed again a stronger correlation with explanatory variables than the area-based ones. Also, an improvement in R^2 was observed with CVR_E compared to CV_E in Figure 4. This might be explained by the fact that CVR_E normalized channel erosion volumes to plot size and non-erodible contents (vegetation) which varied between plots due to practical field constraints. The R^2 values associated with CVR_N were, however, degraded compared to CV_N which is likely the result of confounding factors of deposition processes.

Figure 7 shows the relationship between α and α' (related to the energy spent on channel network expansion) as a function of hydrology and slope. A key finding that emerges from this analysis is that the hydrologic variable correlated better with α' than it did with α, suggesting that even though deposition volume might not be directly controlled by hydrologic parameters (Figure 3 and 4), its consideration is

essential in quantifying energy dissipated on channel widening. In other words, there might be a limit to sediment transport off-site for every incremental increase in runoff discharge (transport capacity concept).

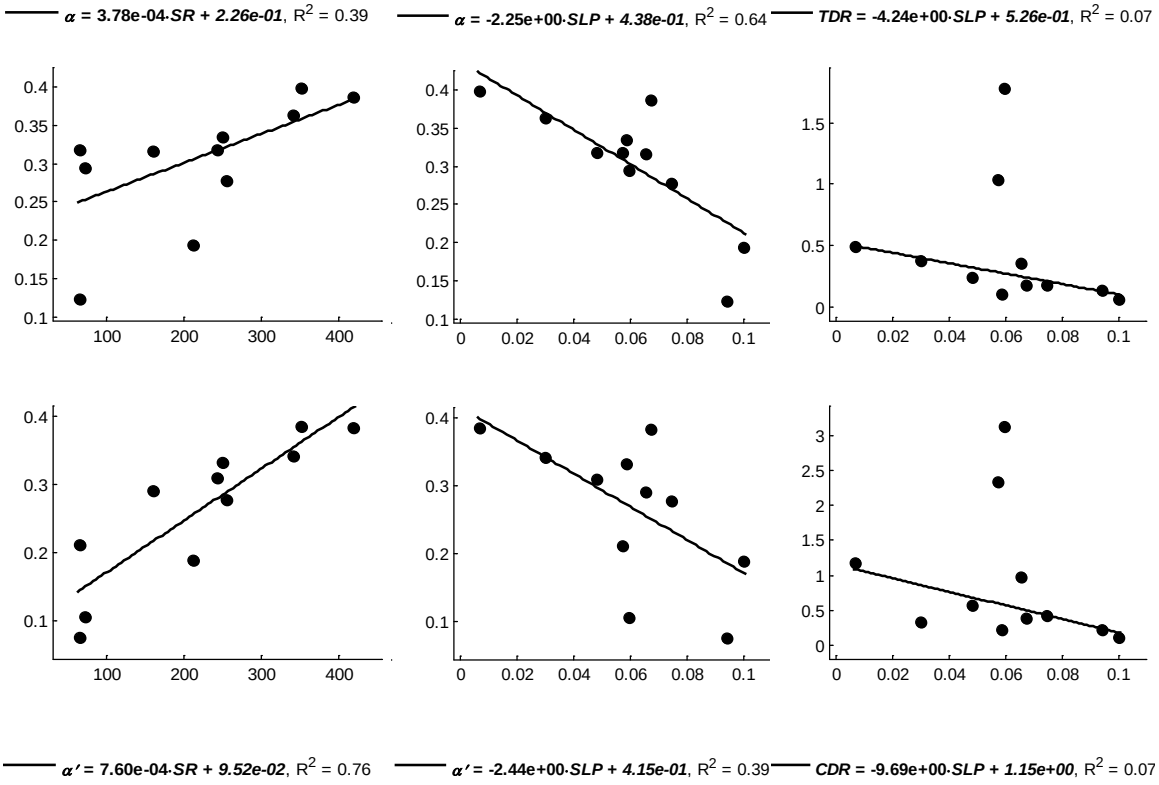

Figure 7 Volume-based channel expansion ratios (α = erosion volume based and α' = net volume based) as a function hydrology (*SR*) and slope. And plot-wide (*TDR*) and channel (*CDR*) deposition ratios as a function of slope

Another key finding in Figure 7 is the negative and relatively strong (R^2 = 0.64 for α and 0.39 for α') relationship between lateral energy expenditure and slope, consistent with the process of increase in downcutting relative to lateral expansion as slope increases. Also, Figure 7 shows that slope is negatively related to the proportion of re-deposited material (*TDR* and *CDR*), but the low number of observations adversely impacted the resulting R^2.

CONCLUSIONS

Rainfall simulations were conducted in saline rangeland communities of the Upper Colorado River Basin to quantify rainfall-driven salt transport from these environment to surface waters. Hydrology, erosion and high-resolution changes in surface microtopography measured during these simulations, were used in this study to answer many questions relevant to sediment transport processes in these saline rangelands and other sparsely vegetated rangelands.

Preliminary data show that analysis of the high resolution DEMs revealed that many interesting sediment transport processes that are traditionally difficult to quantify can now be examined with details and related to hydrologic inputs and landscape properties. Some of the key preliminary findings supported by our data include:

(1) the dependence of deposition on plot slope and its independence on hydrologic and soil loss variables,
(2) data supporting the process of increased downcutting as slope increased,
(3) significance of accounting deposition processes in overall runoff energy quantification,
(4) evidence of the existence of an equilibrium channel geometry with a given discharge that is marginally impacted by runoff duration.

This study will be valuable in developing semi-empirical equations for spatial extent and mass partitioning of soil loss between diffusive processes and concentrated flow erosion, as well as providing much needed insight into the processes of deposition and sediment storage.

REFERENCES

Agisoft LLC. (2013). Agisoft photoscan professional edition. Agisoft LLC, Russia.

Al-Hamdan O.Z., Pierson F.B., Nearing M.A., Williams C.J., Stone J.J., Kormos P.R., Boll J., Weltz M.A. (2012). Concentrated flow erodibility for physically based erosion models: Temporal variability in disturbed and undisturbed rangelands. Water Resources Research 48. doi:10.1029/2011wr011464.

Bagnold R.A. (1977). Bed load transport by natural rivers. Water Resources Research 13: 303-312. doi:10.1029/WR013i002p00303.

Bagnold R.A. (1980). An empirical correlation of bedload transport rates in flumes and natural rivers. Proceedings of the Royal Society of London Series a-Mathematical Physical and Engineering Sciences 372: 453-473. doi:10.1098/rspa.1980.0122.

ASCE. (1980). Universal soil loss equation and rangelands. Symposium on Watershed Management, Boise, ID. ASCE.

Bowles D.S., Nezafati H., Bhasker R.K., Riley J.P., Wagenet R.J. (1982). Salt loading from efflorescence and suspended sediments in the price river basin. Water Resources Planning Series. Utah Water Research Laboratory, Utah State University, Logan, Utah. p. 142.

ESRI. (2011). Arcgis desktop release 10. Evironmental Systems Research Institute, Redlands, CA.

Foster G.R., Simanton J.R., Renard K.G., Lane L.J., Osborn H.B. (1981). Application of the universal soil loss equation to rangelands on a per-storm basis - discussion. Journal of Range Management 34: 161-165. doi:10.2307/3898140.

General Public Licence. (2014). Cloudcompare v2.5. General Public Licence, USA.

Ghebreiyessus Y.T., Gantzer C.J., Alberts E.E. (1994). Soil erosion by concentrated flow: Shear stress and bulk density. Transactions of the ASAE 37: 1791-1797.

Hart G.E. (1984). Erosion from simulated rainfall on mountain rangeland in utah. Journal of Soil and Water Conservation 39: 330-334.

Hawkins R.H., Gifford G.F., Jurinak J.J. (1977). Effects of land processes on the salinity of the upper colorado river basin: Final project report. Utah State University, Logan, Utah. p. 196.

(2006). Extraction of stream channels in high-resolution digital terrain images using morphology. Geoscience and Remote Sensing Symposium, 2006. IGARSS 2006. IEEE International Conference on, July 31 2006-Aug. 4 2006.

Johnson C.W., Savabi M.R., Loomis S.A. (1984). Rangeland erosion measurements for the usle. Transactions of the ASAE 27: 1313-1320.

Laflen J.M., Lane L.J., Foster G.R. (1991). Wepp - a new generation of erosion prediction technology. Journal of Soil and Water Conservation 46: 34-38.

Lyle W., Smerdon E. (1965). Relation of compaction and other soil properties to erosion resistance of soils. Trans. ASAE 8: 419-422.

Mitchell J.E., Roundtable S.R. (2010). Criteria and indicators of sustainable rangeland management. University of Wyoming, Cooperative Extension Service.

Nearing M., Norton L., Bulgakov D., Larionov G., West L., Dontsova K. (1997). Hydraulics and erosion in eroding rills. Water Resources Research 33: 865-876.

Nearing M.A., Wei H., Stone J.J., Pierson F.B., Spaeth K.E., Weltz M.A., Flanagan D.C., Hernandez M. (2011). A rangeland hydrology and erosion model. Transactions of the Asabe 54: 901-908.

Nichols M.H., Nearing M.A., Polyakov V.O., Stone J.J. (2013). A sediment budget for a small semiarid watershed in southeastern arizona, USA. Geomorphology 180: 137-145. doi:10.1016/j.geomorph.2012.10.002.

Paige G.B., Stone J.J., Smith J.R., Kennedy J.R. (2004). The walnut gulch rainfall simulator: A computer-controlled variable intensity rainfall simulator. Applied Engineering in Agriculture 20: 25-31.

Pierson F.B., Williams C.J., Hardegree S.P., Clark P.E., Kormos P.R., Al-Hamdan O.Z. (2013). Hydrologic and erosion responses of sagebrush steppe following juniper encroachment, wildfire, and tree cutting. Rangeland Ecology & Management 66: 274-289. doi:10.2111/rem-d-12-00104.1.

Riley J.P., Bowles D.S., Chadwick D.G., Grenney W.J. (1979). Preliminary identification of price river basin salt pickup and transport processes. JAWRA Journal of the American Water Resources Association 15: 984-995. doi:10.1111/j.1752-1688.1979.tb01077.x.

Riley J.P., Chadwick D.G., Dixon L.S., James L.D., Grenney W.J. (1982). Salt uptake in natural channels traversing mancos shales in the price river basin , utah.

Rodriguez F., Maire E., Courjault-Radé P., Darrozes J. (2002). The black top hat function applied to a dem: A tool to estimate recent incision in a mountainous watershed (estibère watershed, central pyrenees). Geophysical Research Letters 29: 9-1-9-4. doi:10.1029/2001GL014412.

Schwanghart W., Groom G., Kuhn N.J., Heckrath G. (2013). Flow network derivation from a high resolution dem in a low relief, agrarian landscape. Earth Surface Processes and Landforms 38: 1576-1586. doi:10.1002/esp.3452.

Spaeth K.E., Pierson F.B., Weltz M.A., Blackburn W.H. (2003). Evaluation of usle and rusle estimated soil loss on rangeland. Journal of Range Management 56: 234-246. doi:10.2307/4003812.

Torri D., Sfalanga M., Chisci G. (1987). Threshold conditions for incipient rilling. Catena: 97-105.

Trieste D.J., Gifford G.F. (1980). Application of the universal soil loss equation to rangelands on a per-storm basis. Journal of Range Management 33: 66-70. doi:10.2307/3898231.

Tuttle M.L., Grauch R.I. (2009). Salinization of the upper colorado river—fingerprinting geologic salt sources. USGS Scientific Investigations Report. U.S. Geological Survey, Reston, Virginia. p. 62.

Weltz M.A., Kidwell M.R., Fox H.D. (1998). Invited synthesis paper: Influence of abiotic and biotic factors in measuring and modeling soil erosion on rangelands: State of knowledge. Journal of Range Management 51: 482-495. doi:10.2307/4003363.

Wirtz S., Seeger M., Zell A., Wagner C., Wagner J.F., Ries J.B. (2013). Applicability of different hydraulic parameters to describe soil detachment in eroding rills. Plos One 8. doi:10.1371/journal.pone.0064861.

Zhang G.H., Liu B.Y., Liu G.B., He X.W., Nearing M.A. (2003). Detachment of undisturbed soil by shallow flow. Soil Science Society of America Journal 67: 713-719.

TEMPERATURE SIMULATION OF A REACH OF THE METHOW RIVER NEAR WINTHROP, WASHINGTON

Jianchun Huang, Ph.D., P.E., Hydraulic Engineer, Bureau of Reclamation, Denver, CO, vhuang@usbr.gov; Jennifer Bountry, M.S., P.E., Hydraulic Engineer, Bureau of Reclamation, Denver, CO, jbountry@usbr.gov

Abstract: In this paper, a two-dimensional (2D) temperature model is tested within a reach of the Methow River near Winthrop, WA. The reach has a warm water tributary entering on river left and a cold water spring entering from river right. The 2D temperature model is spatially distributed in the lateral and longitudinal geographic extents, allowing for more accurate simulation of lateral changes in temperature across the channel than a 1D representation. The SRH-2D temperature model utilizes meteorological data as inputs (solar radiation, cloud cover, air temperature, dew point temperature, air pressure, and wind speed). Physical processes modeled include solar and atmospheric heating, effects of terrain and vegetation shading, heat exchange between water column and bed substrate, and losses due to evaporation, conduction, and back radiation. Two sets of data are used to test the model. Test one uses steady solution to simulate the lateral temperature mixing zone when warmer water from the Chewuch River enters from river left and colder water from Spring Creek enters from river right. Test two uses unsteady solution to simulate the continuous temperature change due to various water heat gains and losses.

INTRODUCTION

Lai and Mooney (2009) developed a two-dimensional (2D) temperature module for an existing 2D hydraulic and sediment transport model, SRH-2D. The 2D model incorporates data with both lateral and longitudinal geographic extents rather than lumping results into a point-to-point or uni-directional representation. The improved representation of spatial features allows more accurate simulation of lateral changes in temperature across the channel. The SRH-2D temperature model utilizes meteorological data as inputs (solar radiation, cloud cover, air temperature, dew point temperature, air pressure, and wind speed). Physical processes modeled include solar and atmospheric heating, effects of terrain and vegetation shading, heat exchange between water column and bed substrate, and losses due to evaporation, conduction, and back radiation.

In this research, the SRH-2D temperature model was verified in a reach of the Methow River near Winthrop, WA. The Methow River reach has a warmer water tributary entering on river left and a colder water spring entering from river right. Two sets of data were used to test the model. Test one involved using thermal infrared remote-sensing (TIR) imagery data that represents a grid of surface temperatures at a single river flow and a single point in time. This data was used to test how well the model can represent lateral changes in temperature across the channel. Surface water temperature can be different than depth-averaged temperature, which is computed by the 2D model. This difference may cause some variance in how well the 2D model results represent the TIR data, particularly in areas where the mixing rate of the river is slow or highly variable (due to stratification effects). However, the Methow is generally well mixed due to a steep slope and fairly shallow depths. Test two used three temperature loggers that provide continuous data over several months from spring to fall. The loggers provided a test of how well the model could represent temporal and longitudinal changes in temperature.

TEMPERATURE MODEL

Temperature Equation: The 2D depth-averaged flow equations are based on the assumptions that stream flows are shallow compared to width and the effect of vertical motion is negligible.
Conservation of thermal energy leads to the 2D depth-averaged temperature equation expressed as:

$$\frac{\partial hT}{\partial t}+\frac{\partial hUT}{\partial x}+\frac{\partial hVT}{\partial y}=\frac{\partial}{\partial x}\left[\frac{h\nu_t}{\sigma_t}\frac{\partial T}{\partial x}\right]+\frac{\partial}{\partial y}\left[\frac{h\nu_t}{\sigma_t}\frac{\partial T}{\partial y}\right]+\frac{\Phi_{net}}{c_w\rho_w}+\frac{q_{sp}}{A_{sp}}\left(T_{sp}-T\right) \quad (1)$$

In the above, T is depth averaged water temperature [C], x and y are horizontal Cartesian coordinates [m], t is time [s], h is water depth [m], U and V are depth-averaged velocity components [m/s] in x and y directions, respectively, ν_t is the turbulent viscosity and dispersion [m^2/s], σ_t is the turbulent Prandtl number, ρ_w is the water density [kg/m^3], $c_w$is the specific heat of water [J/kg/C], q_{sp} is the spring water flow rate [m^3/s] into the stream (zero if

spring flows out), A_{sp} is the area [m^2] of the spring water inflow, T_{sp} is the spring water temperature [C], and Φ_{net} is the net heat exchange [w/m^2] between water column and its surroundings (through water surface and streambed). The turbulent eddy viscosity (ν_t) is computed with a turbulence model (Rodi, 1993). The net heat flux, Φ_{net}, consists of six contributions as follows:

$$\Phi_{net} = \Phi_{ns} + \Phi_{na} + \Phi_{bed} - \Phi_{br} - \Phi_e - \Phi_c \tag{2}$$

where

Φ_{ns}= net solar radiation entering water surface;
Φ_{na}= net atmospheric radiation entering water surface;
Φ_{br}= heat loss by back radiation from stream (black body radiation);
Φ_e= evaporative heat loss at water surface;
Φ_c= conductive heat loss at water surface; and
Φ_{bed} = heat flux into stream at channel bed.

Solar Radiation: If measured solar radiation (Φ_{sm}) at water surface is available, the net solar radiation is computed as (Hauser and Schohl, 2003)

$$\Phi_{ns} = \Phi_{sm} R_s \tag{3}$$

where Φ_{sm} is measured solar radiation (shade free solar radiation at the water) and R_s is reflection and terrain and vegetation shading factor which is computed by the following equations (Hauser and Schohl, 2003):

$$R_s = \begin{cases} R_{sm} & \text{if } X_n \le B \text{ (shade free)} \\ 0.2 & \text{if } X_n > B+W \text{ (full shade)} \\ R_{sm}\frac{B+W-X_n}{W} + 0.2\frac{X_n-B}{W} & \text{if } B < X_n \le B+W \text{ (partial shade)} \end{cases} \tag{4}$$

In the above:

$R_{sm} = 1 - a(57.3\alpha)^{-b}$ = shade-free reflection factor (a and b see Table 1);
α = solar altitude in radians;
W = width of the stream cross section;
B = distance from trees to water edge;
$X_n = H_b \cos\beta / \tan\alpha$ = normal distance from trees to shadow edge;
H_b = tree and bank height from water surface;
$\beta = |\theta - 90/57.3|$ = angle between sun and stream axis normal in radian;
$\theta = \left|A_{zs} - \frac{A_{zr}}{57.3}\right|$ = angle between sun and stream axis in radian;
A_{zr}= river azimuth, clockwise from north to direction of flow in degree;
A_{zs} = sun azimuth in radian calculated by $\cos A_{zs} = -\frac{\sin\phi\sin\alpha - \sin\delta}{\cos\phi\cos\alpha}$.
ϕ = site latitude in radians; and
δ = is sun declination (between the sun and equator) in radians.

Table 1 Coefficients of solar radiation reflection.

Cloud Cover C	a	b
0-0.05	1.18	0.77
0.05 – 0.5	2.20	0.97
0.5 – 0.92	0.95	0.75
0.92 – 1.0	0.35	0.45

The solar altitude α is computed assuming spherical geometry, as follows (Huber and Harleman, 1968):

$$\sin\alpha = \sin\phi\sin\delta + \cos\phi\cos\delta\cos h \tag{5}$$

where ϕ is site latitude in radians, δ is sun declination in radians, and h is the sun hour angle in radians. If no measured solar radiation (Φ_{sm}) is available, the solar radiation that reaches the water surface can be estimated from (Martin and McCutcheon, 1999)

$$\Phi_{sm} = H_0 a_t C_a \tag{6}$$

where H_0 = the amount of radiation reaching the earth's outer atmosphere (Wm^{-2}); a_t= radiation scattering and absorption factor; C_a = the fraction of solar radiation not absorbed by clouds.
The fraction of solar radiation passing through the clouds is given by the cloud cover (C) as

$$C_a = 1 - 0.65C^2 \tag{7}$$

The flux of solar radiation that strikes the earth's outer atmosphere is estimated from

$$H_0 = \frac{H_{sc}}{r^2}[\sin\phi\sin\delta + \frac{12}{\pi}\cos\phi\cos\delta(\sin h_e - sinh_b)]\Gamma \tag{8}$$

H_{sc} = the solar constant (1390 Wm^{-2}); r = the relative distance (-) between the earth and sun; ϕ = the site latitude in radians; δ = sun declination (between the sun and equator) in radians; h_e and h_b = the solar hour angles at the end and the beginning of the time period over which H_0 is being calculated, respectively; and Γ = a correction factor for diurnal exposure to the radiation flux. The relative earth-sun distance can be estimated from

$$r = 1.0 + 0.017\cos\left[\frac{2\pi}{365}(186 - D_y\right] \tag{9}$$

where D_y = the Julian day of the year. The declination of the sun can be estimated from

$$\delta = \frac{23.45\pi}{180}\cos\left[\frac{2\pi}{365}(172 - D_y\right] \tag{10}$$

The hour angles (radians) at the beginning and ending of the period over which H_o is being calculated is computed from

$$h_b = \left\{\frac{\pi}{12}[(h_r - 1) - \Delta t_s + 12a_2]\right\} + b_2(2\pi) \tag{11}$$

$$h_e = \left\{\frac{\pi}{12}[h_r - \Delta t_s + 12a_2]\right\} + b_2(2\pi) \tag{12}$$

where h_r is the hour of the day from 1 to 24; the coefficient a_2 =1.0 for $h_r \leq 12$ and a_2 =-1.0 for $h_r > 12$. The coefficient b_2 varies with the magnitude of the quantity inside the curly brackets for both h_b and h_e in Eqs. (11) and (12). The coefficient b_2 = -1 for $\{\cdot\} > 2\pi$, b_2 = 1 for $\{\cdot\} < 0$, and b_2=0 otherwise.

The fraction of an hour between the standard meridian and the local meridian is Δt_s. In the United States, the standard meridians are at 75°, 90°, 105°, and 120° for eastern, central, mountain, and Pacific Time zones; respectively. The fraction can be calculated from

$$\Delta t_s = \frac{E_a}{15}(L_{sm} - L_{lm}) \tag{13}$$

where L_{sm} is the standard meridian, L_{lm} is the local meridian. $E_a = -1$ for west longitude and $E_a = 1$ for east longitude. For example, at Methow River at Winthrop, $L_{sm} = 120^o$ (Pacific Time zone), $L_{lm} = 120.167639^o$ (longitude of Winthrop), and $E_a = -1$ for west longitude.
The correction factor Γ in Eq.(8) is set to one at day time (between sunrise and sunset) and zero at night time. The standard time of sunset and sunrise can be estimated from

$$t_{ss} = \frac{12}{\pi}\cos^{-1}\left(-\frac{\sin\phi\sin\delta}{\cos\phi\cos\delta}\right) + \Delta t_s + 12 \tag{14}$$

$$t_{su} = -t_{ss} + 2\Delta t_s + 24 \tag{15}$$

The radiation scattering and absorption factor a_t in Eq.(6) can be estimated from

$$a_t = \frac{t + 0.5(1 - s - c_d)}{1 - 0.5R_g(1 - s - c_d)} \tag{16}$$

where c_d is a dust coefficient, which has a range of 0.0 to 0.13 and a typical value of 0.06; and R_g is the reflectivity of the water surface, which varies with the type of cloud cover as

$$R_g = a_3\left(\frac{180}{\pi}\alpha\right)^{b_3} \tag{17}$$

where α is the solar altitude in radians, calculated in Eq.(5) and a_3 and b_3 are coefficients (Table 2) depending on the cloud cover (C).

Table 2 Coefficients a_3 and b_3 describing the reflection of solar radiation at the water surface (source: Martin and McCutcheon, 1999; and Marciano and Harbeck, 1954).

Description	Fraction Cloud Cover (C)	a_3	b_3
Overcast	C> 0.9	0.33	-0.45
Broken	0.5 < C <0.9	0.95	-0.75
Scattered	0.1 <C <0.5	0.5	-0.97
Clear	C < 0.1	1.18	-0.77

The mean atmospheric transmission coefficient s and t in Eq. (16) is given by

$$s = \exp[-(0.465 + 0.134P_{wc})(0.129 + 0.171\exp(-0.88\theta_{am}))\theta_{am}] \tag{18}$$
$$t = \exp[-(0.465 + 0.134P_{wc})(0.179 + 0.421\exp(-0.721\theta_{am}))\theta_{am}] \tag{19}$$

where θ_{am} is the dimensionless optical mass, $P_{wc}$is the mean daily precipitable atmospheric water content, given by

$$P_{wc} = 0.85\exp(0.11 + 0.0614T_d) \tag{20}$$
$$\theta_{am} = \left(\frac{288 - 0.0065Z}{288}\right)^{5.256} / \left[\sin\alpha + 0.15\left(\frac{180\alpha}{\pi} + 3.855\right)^{-1.253}\right] \tag{21}$$

where T_d = the dew point temperature [C], Z = the site elevation (m) and α = the solar altitude in radians, calculated in Eq.(5).

Atmosphere Radiation: The net long-wave radiation (atmospheric radiation entering water surface) is computed as:

$$\Phi_{na} = 5.16432 \cdot 10^{-13}(1 + 0.17C^2)(T_a + 273.16)^6 \tag{22}$$

where C is cloud cover, fraction of the sky covered by clouds, and T_a is dry bulb air temperature [C].

Outgoing Black-Body Radiation: The outgoing black-body radiation emitted from the water surface is a function only of the water temperature, and it is given by (Huber and Harleman, 1968):

$$\Phi_{br} = \varepsilon_w\sigma(T_w + 273.16)^4 \tag{23}$$

where T_w is water-surface temperature [C], ε_w is emissivity (0.97 by Huber and Harleman (1968) and 0.98 by Tung et al. (2006), and σ is Stefan-Boltzman constant (5.672×10^{-8} w/m^2/K^4). In the current model, the depth averaged temperature T is used for T_w.

Evaporative Heat Loss: The evaporative heat loss is computed by:

$$\Phi_e = \rho_w L(a_1 + b_1 W_a)(e_s - e_a) \tag{24}$$

where:

$L = 4184(597 - 0.57T_w)$ =the latent heat [J/kg];
T_w = water surface temperature in Celsius;
W_a = wind speed (m/s);
a_1, b_1 = constants: a_1=0.0 to 4.0e-9; b_1=1.0e-9 to 3.0e-9;
$e_a = 2.171 \times 10^8 \exp\left[-\frac{4157}{T_d + 239.09}\right]$ = saturation vapor pressure [mb];
T_d = dew point temperature in Celsius; and
$e_s = \alpha_j + \beta_j T_w$ = saturation vapor pressure [mb] with coefficients in Table 3

Table 3 Coefficients to compute saturation vapor pressure.

T	j	αj	βj
0-5	1	6.05	0.522
5-10	2	5.10	0.710
10-15	3	2.65	0.954
15-20	4	-2.04	1.265
20-25	5	-9.94	1.659
25-30	6	-22.29	2.151
30-35	7	-40.63	2.761
35-40	8	-66.90	3.511

Conduction Heat Loss to Air: The conduction heat loss is:

$$\Phi_c = 0.61 \times 10^{-3} \rho_w L(a_1 + b_1 W_a) P(T_w - T_a) \tag{25}$$

where P is air barometric pressure [mb] and a_1 and b_1 are defined the same as in Eq.(24), T_w is water surface temperature [C], and T_a is dry bulb air temperature [C].

Heat Exchange with Stream Bed: Heat exchange between stream bed and stream water is significant for shallow streams and it consists of two contributions: conduction from bed to stream and net solar radiation entering bed. It is computed by the following expression:

$$\Phi_{bed} = \frac{k_b}{0.5\delta_b}(T_b - T_w) - (1 - A_b)(1 - \beta)\exp[-\eta(D - 0.6)]\,\Phi_{ns} \tag{26}$$

where k_b is the thermal conductivity of the streambed bed material, $\delta_b$is the effective bed thickness used for heat conduction computation, T_w is the water temperature, T_b is the effective stream bed temperature which is updated each time step by $T_b = T_b^{old} - \frac{\Phi_{\text{bed}}\Delta t}{\rho_b C_b \delta_b}$ with ρ_b and C_b the density and specific heat of the bed materials and Δt is the time step for simulation, A_b is albedo of bed material, β is fraction of solar radiation absorbed in the top 0.6m of surface water, η is extinction coefficient in water [1/m], and D is water depth [m].

RESULTS

Test Case with FLIR Data: Watershed Sciences (2009) provided TIR imagery for approximately 160 river miles in the Methow River Basin for the Yakama Tribe Fisheries. TIR images were collected with a temperature sensor mounted on the underside of a helicopter. Airborne TIR was used to map spatial temperature patterns in the Methow River. TIR images were recorded during a three-day flight from August 24 to August 26, 2009 over the

Methow, Twisp, and Chewuch Rivers. A four mile reach of the Methow River near Winthrop is used to simulate the two-dimensional temperature dynamics downstream of the Chewuch River Spring Creek confluences.

Simulated 2D water temperature is compared to measured surface temperature to test the ability of the model in predicting lateral thermal mixing. Surface water temperature (measured) may be different than depth-averaged temperature (computed) due to stratification. This difference may cause some variance in how well the 2D model results can represent the TIR data, particularly in areas where the mixing rate of the river is slow or highly variable. The Methow is, however, generally well-mixed due to a steep slope and fairly shallow depths. For this reason, the surface water temperature is used for the model upstream boundary condition.

Two river gage stations are located in the study reach: USGS 12448500 (Methow at Winthrop downstream of the confluence of the Methow and Chewuch) and USGS 12448000 (Chewuch at Winthrop upstream of the confluence). On August 26, 2009, the flow rate of Methow at Winthrop was 275 cfs and that of Chewuch at Winthrop was 89.1 cfs (Table 4). The combined flow in the Methow River and Spring Creek above the Chewuch is obtained from the difference between the two gages. Then, the incoming discharge for Spring Creek and the Methow River was solved by assuming the incoming temperature and discharge product for each tributary equals the temperature and discharge product in the downstream river at the gage. The flow rates at the Methow River above the Chewuch is set as 146.0 cfs and the combined flows from Spring Creek is set as 40.8 cfs., to reach a mixed temperature downstream of the Spring Creek 15.8 ^{o}C from the surveyed data. The calculation assumed that there is no heat sources and sinks within this short reach.

Table 4 Incoming flow rates and temperatures.

	Flow Rate (cfs)	Temperature (^{o}C)
Chewuch	89.1	17.3
Methow	146.0	15.4
Spring Creek	40.8	13.6

Figures 1 through 3 display measured water surface temperature and simulated water temperature results. Figure 1 shows measured water surface temperature in the vicinity of the Chewuch and Spring Creek confluences. The field data indicates the presence of temperature mixing zones downstream of the tributary confluences; the comparatively small inflow from Spring Creek produces a low temperature zone that is highly persistent in the streamwise direction, suggesting non-point source seepage along the bank. Figure 2 shows the SRH-2D simulated temperature using point-based model contributions from the Chewuch and Spring Creek. The simulation results qualitatively reproduce the zone of lateral temperature stratification downstream of the Chewuch River, however vastly under predict the extent to which the cold temperature zone persists along the bank downstream of Spring Creek.

Figure 3 shows the SRH-2D numerical temperature simulation with a non-point source of water seeping into the stream from Spring Creek. From the calibration process, it was determined that a combination of 20.7 cfs modeled as point source from Spring Creek and 20 cfs modeled as non-point source seeps produces qualitative agreement with the measurements (Figure 1), predicting mixing zones from both tributaries fairly well.

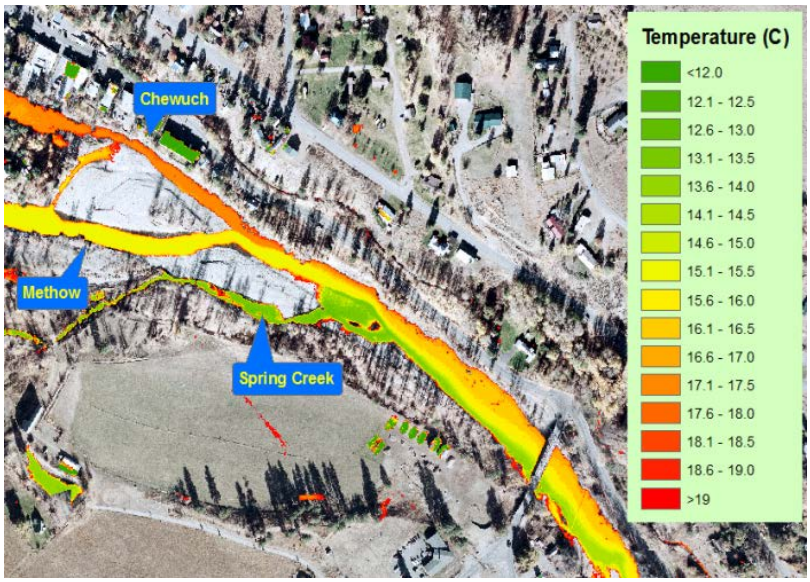

Figure 1 TIR imagery taken on August 26 2009 in the vicinity of the Chewuch River and Spring Creek. The color scale is mapped to measured water surface temperature. Warmer water from Chewuch River enters on the river left and colder water from the Spring Creek enters on the river right. Flow direction is from left to right.

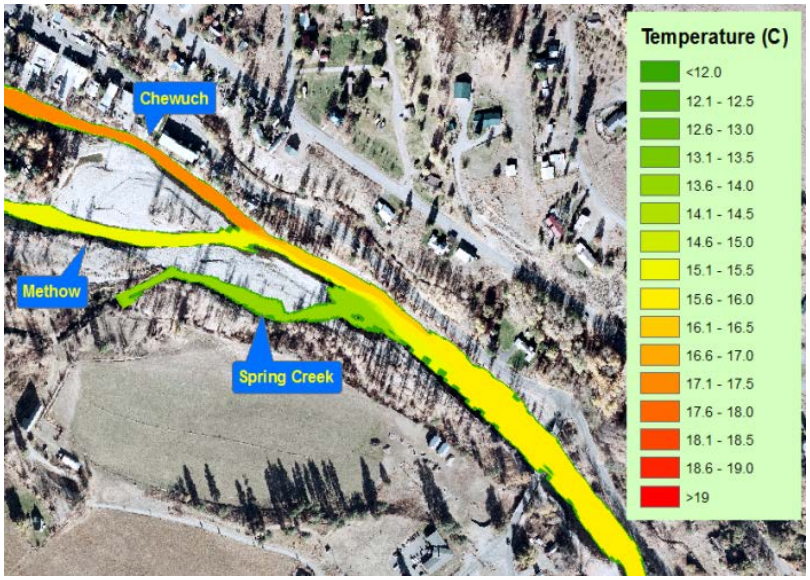

Figure 2 SRH-2D numerical simulation of water temperature at the confluences with the Chewuch River and the Spring Creek, with tributaries modeled as point sources. Color scale is mapped to predicted depth-averaged temperature. Flow direction is from left to right.

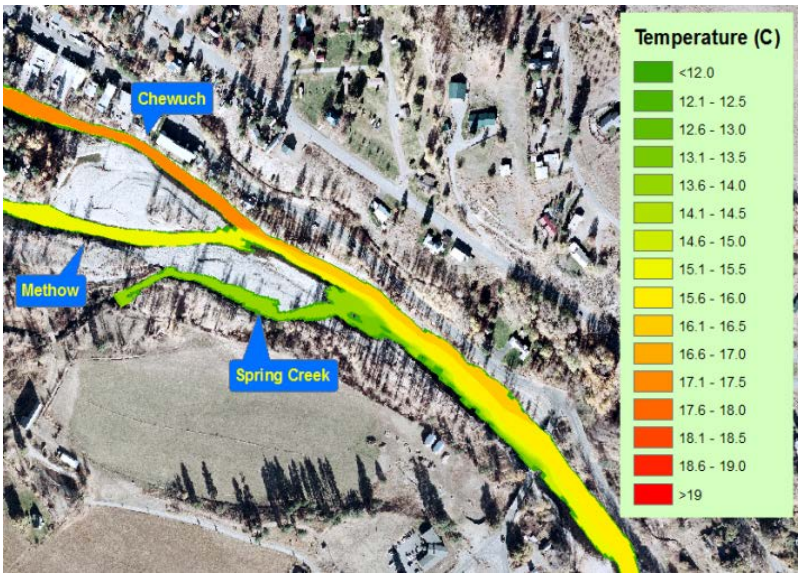

Figure 3 SRH-2D numerical simulation of water temperature at the confluences with the Chewuch River and the Spring Creek, with the Spring Creek contribution modeled as a combination of point-source and non-point source seeps from the right bank. Color scale is mapped to predicted depth-averaged temperature.

A sensitivity analysis was performed on the turbulent Prandtl number σ_t in Eq. (1). The turbulent Prandtl number is the ratio of momentum eddy diffusivity ν_t to thermal eddy diffusivity, and is typically on the order of one in natural turbulent flows. The results show that decreasing (increasing) the turbulent Prandtl number decreases (enlarges) the persistence of temperature gradients downstream of the tributary confluences.

Test Case with Log Data: In the second test case, SRH-2D is used to simulate unsteady flow and temperature over four months from June 1, 2012 to September 30, 2012. Several temperature loggers in the study reach provided continuous point temperature data that can be used to test model predictions of longitudinal changes in temperature. Three loggers provided continuous temperature measurements for upstream model boundary conditions at flow locations labeled Chewuch Mouth, Methow above Chewuch, and Spring Creek (Figure 4, Figure 5, and Table 5).

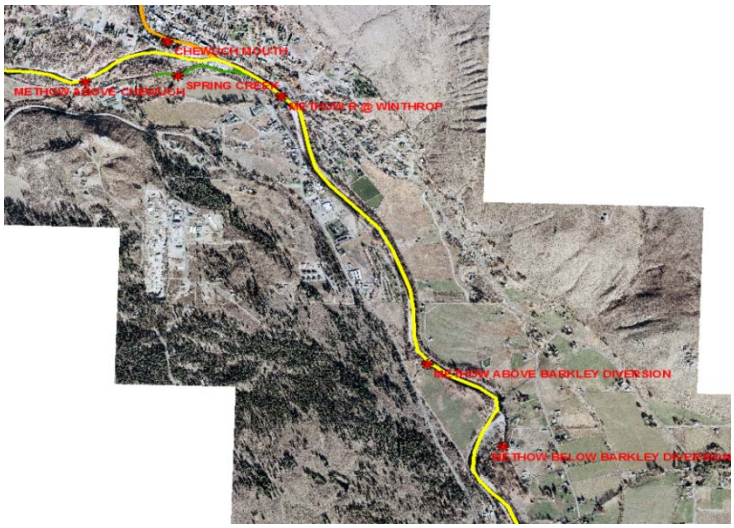

Figure 4 Temperature loggers located in the study reach.

Additional temperature logger data is needed to test model predictions along the channel. The logger location labeled Methow at Winthrop provided temperature downstream of the Chewuch and Spring Creek confluence at the US 20 bridge crossing in Winthrop. However, this location is in the temperature mixing zone; data was instead used from the logger located further downstream, labeled Methow above Barkley Diversion. Another logger, Methow below Barkley Diversion, located in the side channel which does not have a surface flow connection with the mainstem Methow River at the time of simulation and could not be used to test the model.

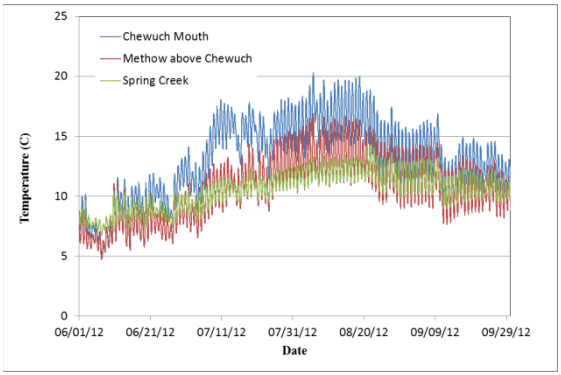

Figure 5 Methow, Chewuch, and Spring Creek inflow water temperatures used as upstream input boundary conditions for the model.

Table 5 Logger data available in the study reach.

Logger Location Label	Date Period
Chewuch Mouth	6/1/2005 to 9/18/2008, and 7/9/2010 to 10/11/2012
Methow Above Chewuch	6/30/2005 to 10/15/2009, and 7/16/2010 to 10/16/2012
Spring Creek	7/2/2005 to 10/15/2009, and 7/16/2010 to 10/16/2012
Methow at Winthrop	6/27/2005 to 10/13/2009
Methow above Barkley Diversion	11/26/2009 to 10/16/2012
Methow below Barkley Diversion	11/26/2009 to 10/16/2012

Two gage stations are located in the study reach (Figure 6): USGS 12448500 (Methow above Chewuch) and USGS 12448000 (Chewuch Mouth). There is no gage to measure flow in Spring Creek. The majority of the contribution from Spring Creek is due to ground seepage and the fish hatchery; further, there is no assumed correlation between the flow rates in the Methow and Spring Creek. For this reason, the same flow distribution used in the first test case was used in the second test case: 20.7 cfs from Spring Creek and 20 cfs from ground seepage on the right bank. Future field survey is recommended to measure the flow rate in the Spring Creek. The flow rate at the Methow above Chewuch is obtained by subtracting the flows at Chewuch and Spring Creek from the downstream gage at Methow at Winthrop.

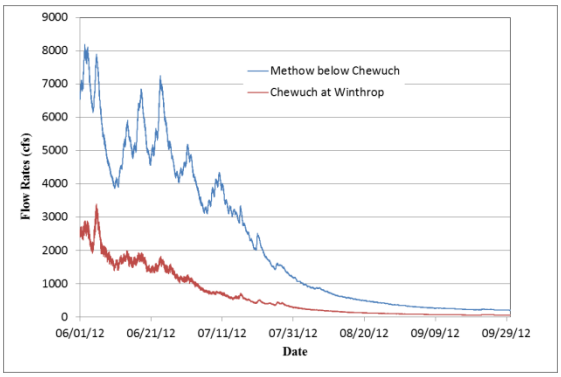

Figure 6 Methow and Chewuch River flow hydrographs used as upstream input boundary conditions.

The longitudinal temperature in the river is affected by the heat gain and loss at the water surface and channel bed. The dominant forms of heat gain are solar (short wave) radiation and atmospheric (long wave) radiation. The dominant forms of heat loss include back radiation from the stream, evaporative heat loss from the stream, and evaporative and conductive heat loss at the water surface. The heat flux to the channel bed is usually positive at day time and negative at night time. Solar radiation was not directly measured at the study reach, but was estimated from Eqs (6) to (21) given the cloud covering, elevation, and site latitude and longitude position.

Compared with logger data at the Methow above Barkley Diversion location, the model predicted the temperature fairly well Figure 7. The root mean square error is about 0.37°C. No temperature difference was observed in the channel transverse direction (well-mixed) at the Methow above Barkley Diversion location. The wind effect coefficients a_1 and b_1 as defined in Eq. (24) were set as 1.0×10^{-9} and 1.0×10^{-9}, respectively. The coefficients were set to their low ends in order to maintain a slightly increased temperature in the downstream direction. To better understand the effects of all source terms, a longer reach is recommended. In a small reach, the meteorological effects are small and the temperature is more driven by the upstream boundary conditions.

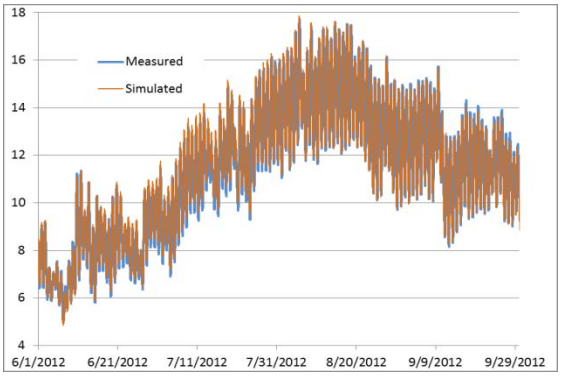

Figure 7 Measured and simulated water temperatures at the logger location labeled Methow above Barkley Diversion.

CONCLUSIONS

SRH-2D simulates the river temperature where water is well mixed in the vertical direction. First, the SRH-2D temperature module was tested using two sets of validation data from the Methow River near Winthrop, WA. Case one calculated a steady-state solution of the lateral temperature mixing zones downstream of the Chewuch (warmer water) and Spring Creek (colder water) confluences without any heat exchange with the air and channel bed. Case two calculated transient solutions of the temperature distribution driven by measured input hydrographs.
The model showed good accuracy in simulating the lateral temperature mixing zones downstream of tributary confluences when the model is well calibrated by adjusting the turbulent Prandtl number. In the Methow case, results show that the turbulent Prandtl number of one best reproduce the lateral temperature mixing. It was also shown that non-point source boundary conditions may be required to model spatially distributed contributions such as seepage of cold water from a spring.

The model was generally successful in reproducing the measured temporal variation in temperature measured at the Methow above Barkley Diversion location. In this four mile reach, the water temperature is mostly driven by incoming flow discharge and temperature, and not sensitive to weather/climate. For the Methow River, it is hypothesized from measured data that weather impacts to water temperature occur on the scale of multiple reaches, perhaps on the order of tens of river miles.

ACKNOWLEDGEMENTS

The authors would like to acknowledge the Research and Development Office, Science and Technology Program of the Bureau of Reclamation for providing funding to this research. The authors would like to thank Raymond "Jason" Caldwell, former employee of Bureau of Reclamation, who performed the research on modeling of daily and sub-daily stream temperatures which was used as input data in this study. The authors thank co-workers Yong

Lai, Blair Greimann, Dan Dombroski, and Subhrendu Gangopadhyay for discussions and insight. Dan Dombroski's peer review is appreciated.

REFERENCES

Hauser, G.E. and Schohl, G.A. (2003). "River Modeling System v4 – Vol. 2 Technical Reference," Report No. WR28-1-590-164, Tennessee Valley Authority, Norris, Tennessee.

Huber, W.C. and Harleman, D.R.F. (1968). "Laboratory and Analytical Studies of the Thermal Stratification in Reservoirs," Hydrodynamics Laboratory Technical Report No. 112, Department of Civil Engineering, Massachusetts Institute of Technology, Cambridge, Massachusetts, 277 pp.

Lai, Y., and Mooney, D. (2009). "On a Two-Dimensional Temperature Model: Development and Verification," World Environmental and Water Resources Congress, 1-14.

Marciano, J.J. and Harbeck, G.E. (1954). "Mass-transfer studies in Water-loss investigations—Lake Hefner studies". Technical Report: U.S. Geol. Survey Prof. Paper 269

Martin, J.L. and McCutcheon, S.C. (1999). "Hydrodynamics and Transport for Water Quality Modeling," CRC Press.

Rodi, W. (1993). "Turbulence models and their application in hydraulics," 3rd Ed., IAHR Monograph, Balkema, Rotterdam, The Netherlands.

Tung, C.P., Lee, T.Y., and Yang, Y.C. (2006). "Modeling climate-change impacts on stream temperature of Formosan landlocked salmon habitat," Hydrological Processes, Vol.20, 1629-1649.

PHYSICALLY BASED METHOD FOR MEASURING SUSPENDED-SEDIMENT CONCENTRATION AND GRAIN SIZE USING MULTI-FREQUENCY ARRAYS OF SINGLE-FREQUENCY ACOUSTIC-DOPPLER PROFILERS

David J. Topping, Research Hydrologist, U.S. Geological Survey, Flagstaff, Arizona, dtopping@usgs.gov;
Scott A. Wright, Research Hydrologist, U.S. Geological Survey, Sacramento, California, sawright@usgs.gov;
Ronald E. Griffiths, Hydrologist, U.S. Geological Survey, Flagstaff, Arizona, rgriffiths@usgs.gov; and
David J. Dean, Hydrologist, U.S. Geological Survey, Flagstaff, Arizona, djdean@usgs.gov

Abstract: As the result of a 12-year program of sediment-transport research and field testing on the Colorado River (6 stations in UT and AZ), Yampa River (2 stations in CO), Little Snake River (1 station in CO), Green River (1 station in CO and 2 stations in UT), and Rio Grande (2 stations in TX), we have developed a physically based method for measuring suspended-sediment concentration and grain size at 15-minute intervals using multi-frequency arrays of acoustic-Doppler profilers. This multi-frequency method is able to achieve much higher accuracies than single-frequency acoustic methods because it allows removal of the influence of changes in grain size on acoustic backscatter. The method proceeds as follows. (1) Acoustic attenuation at each frequency is related to the concentration of silt and clay with a known grain-size distribution in a river cross section using physical samples and theory. (2) The combination of acoustic backscatter and attenuation at each frequency is uniquely related to the concentration of sand (with a known reference grain-size distribution) and the concentration of silt and clay (with a known reference grain-size distribution) in a river cross section using physical samples and theory. (3) Comparison of the suspended-sand concentrations measured at each frequency using this approach then allows theory-based calculation of the median grain size of the suspended sand and final correction of the suspended-sand concentration to compensate for the influence of changing grain size on backscatter. Although this method of measuring suspended-sediment concentration is somewhat less accurate than using conventional samplers in either the EDI or EWI methods, it is much more accurate than estimating suspended-sediment concentrations using calibrated pump measurements or single-frequency acoustics. Though the EDI and EWI methods provide the most accurate measurements of suspended-sediment concentration, these measurements are labor-intensive, expensive, and may be impossible to collect at time intervals less than discharge-independent changes in suspended-sediment concentration can occur (< hours). Therefore, our physically based multi-frequency acoustic method shows promise as a cost-effective, valid approach for calculating suspended-sediment loads in river at a level of accuracy sufficient for many scientific and management purposes.

INTRODUCTION

Suspended-sediment concentration and discharge are poorly correlated in many rivers as a result of hysteresis in concentration and grain size produced by (1) changes in the upstream sediment supply and (2) hysteresis in bed roughness arising from lags between discharge and dune geometry during floods. Accurate sediment loads can be calculated in rivers exhibiting these types of hysteresis only if measurements of suspended-sediment concentration are made at time intervals more closely spaced than the timescales over which suspended-sediment concentration is observed to systematically vary independently of water discharge. Single-frequency acoustics have recently become popular for measuring suspended-sediment concentration at high temporal resolution. However, because acoustic attenuation and backscatter are both affected by changes in both the concentration and grain-size distribution of the suspended sediment, concentration biases exceeding a factor of two are common and concentration biases exceeding an order of magnitude are possible when only one acoustic frequency is used. Herein, we describe an unbiased physically based method for measuring suspended-silt-and-clay and suspended-sand concentration, and suspended-sand median grain size (D_{50}) using multi-frequency arrays of side-looking acoustic-Doppler profilers (ADPs), building on the work of Topping et al. (2004, 2006, 2007) and Wright et al. (2010). Data from and the locations of the study sites in this paper are available at: http://www.gcmrc.gov/discharge_qw_sediment/.

THEORETICAL FRAMEWORK

The initial theoretical development that ultimately led to the ability of using acoustics to measure suspended-sediment concentrations and grain-size distributions occurred during the early to mid 20th century, with much of this work occurring during World War II (Urick, 1975). Among the most important contributions of this early research

were the derivation and formalization of the sonar equations (National Defense Research Committee [NDRC], 1946; Urick, 1962). In our study, the following form of the active-sonar equation from Urick (1975) is used:

$$SL - 2TL + TS = RL + DT \tag{1}$$

where *SL* is the Source Level, 2*TL* is the 2-way Transmission Loss, *TS* is the Target Strength, *RL* is the Reverberation Level, and *DT* is the Detection Threshold. By standard convention, each of these terms is expressed as 10 times a base-10 logarithmic ratio of acoustic intensity, in units of decibels. Knowing the values of all of the terms in equation 1 is not required to approximately calibrate an ADP to measure suspended-sediment concentration. In many studies, only the values of 2*TL* and *RL* are used in combined, relative-backscatter form to develop such approximate calibrations (e.g., Thevenot et al., 1992; Gartner, 2004; Wall et al., 2006; Wright et al., 2010; Wood and Teasdale, 2013). These calibrations are referred to as approximate because they hold *TS* constant and therefore do not take into account how changes in the grain-size distribution of the suspended sediment affect *TS*. Depending on the instrument frequency and the grain-size distributions in suspension, neglecting the effects of changing grain size on *TS* can lead to substantial biases in ADP measurements of suspended-sediment concentration. Following the convention of Thevenot et al. [1992], the relative backscatter,

$$B = RL + 2TL \tag{2}$$

thus allowing equation 1 to be rewritten as:

$$SL - DT - B + TS = 0\ . \tag{3}$$

SL of the ADPs used in this study ranges from 191 to 196 dB; *DT* has been determined in this study to range from ~35 to 50 dB, and is the level associated with zero concentration of suspended sediment in the water. *B* is calculated for each cell along an acoustic beam where the amplitude of the acoustic signal strength, *A*, exceeds the effective noise floor. The effective noise floor is the sum of the ADP-measured noise floor and the noise-floor offset (determined by an iterative process that removes dependence of the measured acoustic attenuation and backscatter on cell number). In each cell,

$$RL = k_{SF}A \tag{4}$$

where *A* is the amplitude of the acoustic signal strength measured in counts, and k_{SF}=0.43 is a scale factor used to convert counts to decibels. By standard convention (Urick, 1975),

$$2TL = 20\log(r) + 2\alpha_W r + 2\alpha_S r \tag{5}$$

where *r* is the distance along the beam from the transducer to each cell in meters, 20log(*r*) is the spherical spreading loss term, α_W is the coefficient of absorption for acoustic energy in water in dB/m (depends only on temperature at the shallow-water and low-salinity conditions in rivers), and α_S is the sediment attenuation coefficient in dB/m. For convenience in solving for α_S, a new term is defined, the fluid-corrected backscatter (Wright et al., 2010),

$$B_F = RL + 20\log(r) + 2\alpha_W r \tag{6}$$

with α_S then being determined by **l**east-squares linear regression where the values of B_F are regressed on *r* (Topping et al., 2006, 2007b) while iteratively solving for the effective noise floor. In this regression, α_S is equal to -1/2 times the slope of the relation between *r* and B_F. Once α_S is known, *B* is then calculated in each cell where *A* exceeds the effective noise floor, finally allowing calculation of the beam-averaged backscatter, $\overline{B}$. $\overline{B}$ is *B* averaged first among all cells in a beam and them among all beams used on an ADP.

Attenuation: Acoustic attenuation caused by the presence of suspended sediment arises from two distinctly different physical processes that vary in importance largely as a function of instrument frequency, sediment grain size, and sediment density (Flammer, 1962). These processes are acoustic attenuation from: viscous losses arising from viscous drag between the water and sediment grains (Urick, 1948), and scattering losses arising from the

scattering of sound by the sediment grains in directions other than back toward the detector (Lamb, 1945; Urick, 1948; Morse, 1948). Viscous losses dominate when the suspended sediment is relatively fine whereas scattering losses dominate when the suspended sediment is relatively coarse. We use the conventions and methods of Urick (1948), Flammer (1962), Hay (1983), and Moore et al. (2013) to calculate a sediment attenuation coefficient (α_S) that includes the effects of both viscous- and scattering-losses as well as the effects of multiple grain sizes and wet densities of sediment. Following Urick (1948), α_S is the product of the unit sediment attenuation coefficient, α_{UNIT}, and the concentration of suspended sediment, C:

$$\alpha_S = \alpha_{UNIT} C \, . \tag{7}$$

In our study, the unit sediment attenuation coefficient is defined as the sediment attenuation coefficient at a suspended-sediment concentration of 1 mg/L, with α_S expressed in units of dB/m and C expressed in units of mg/L. α_{UNIT} is the combined ensemble-averaged viscous and scattering attenuation coefficients and is derived in this study using the equations of Moore et al. (2013), and making the appropriate conversions, such that it is expressed in units of decibel-liter per meter-milligram or dB-L/m-mg. Changes in the sorting and density of the suspended-sediment grain-size distribution and the frequency of the ADP all have a major influence on α_{UNIT} (Figure 1). From the example in Figure 1b, it is evident that there exists an optimal range of acoustic frequency, suspended-sand D_{50}, and suspended-silt-and-clay D_{50} where the sand contributes very little to α_{UNIT} and:

$$\alpha_S \approx \alpha_{UNIT} C_{SILT\text{-}CLAY} \tag{8}$$

where $C_{SILT\text{-}CLAY}$ is the suspended-silt-and-clay concentration. In many rivers the D_{50} of the suspended sand ranges from 0.0625 to ~0.25 mm (very fine to fine sand) and, in the absence of flocculation, the D_{50} of the suspended silt and clay ranges from ~0.0005 to ~0.01 mm (fine clay to fine silt). For the sorting of the grain-size distributions portrayed in Figure 1b, these median grain sizes result in a fair degree of separation between the value of α_{UNIT}

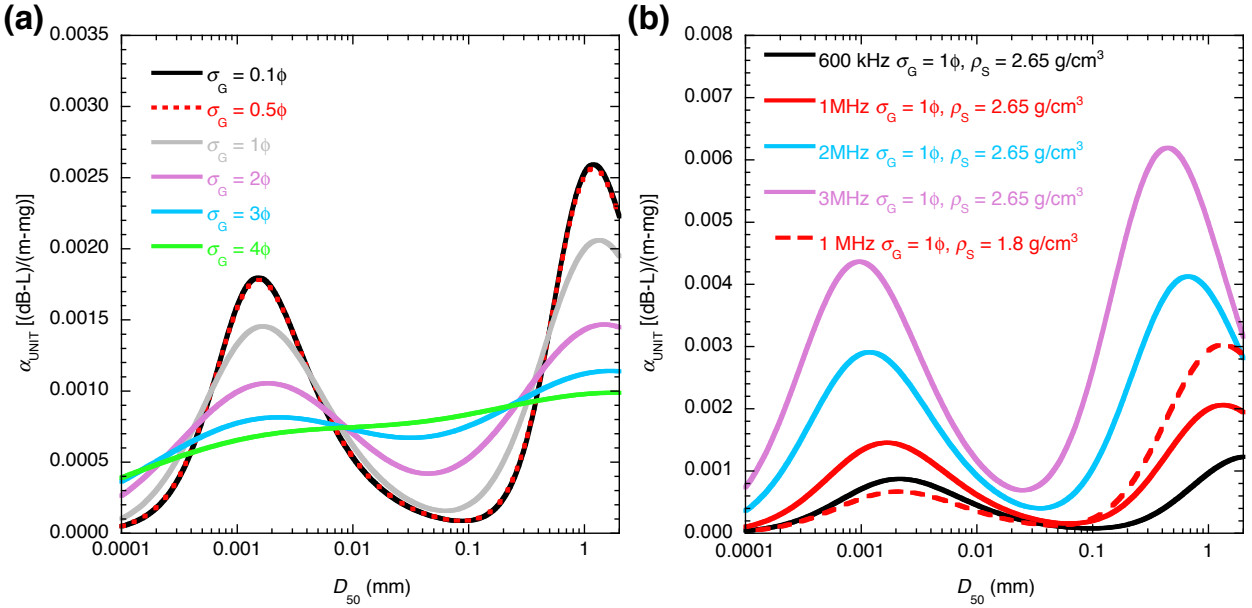

Figure 1 Effects of changes in (a) sediment sorting and (b) ADP frequency and sediment density (ρ_S) on α_{UNIT}. (a) Predicted values of α_{UNIT} at the 1-MHz frequency for the D_{50} of log-normal suspended-sediment grain-size distributions with geometric standard deviations (σ_G) of 0.1ϕ, 0.5ϕ, 1ϕ, 2ϕ, 3ϕ, and 4ϕ. ρ_S is held constant at 2.65 g/cm^3 (quartz density) in this example. (b) Predicted values of α_{UNIT} at acoustic frequencies of 600 kHz, 1 MHz, 2 MHz, and 3 MHz for the D_{50} of log-normal suspended-sediment grain size distributions with σ_G = 1ϕ and ρ_S = 2.65 g/cm^3, and α_{UNIT} at 1 MHz for the D_{50} of log-normal suspended-sediment grain size distributions with σ_G = 1ϕ and a montmorillonite wet ρ_S = 1.8 g/cm^3.

associated with the sand and the value of α_{UNIT} associated with the silt and clay, especially at lower acoustic frequencies. For these median grain sizes and acoustic frequencies, and so long as the suspended-sand concentration does not greatly exceed $C_{SILT\text{-}CLAY}$, $C_{SILT\text{-}CLAY}$ can therefore be reasonably accurately predicted by α_S. This result allowed Topping et al. (2006, 2007) and Wright et al. (2010) to develop their first-cut single-frequency approximate method of using acoustic attenuation to measure suspended-silt-and-clay concentration and acoustic backscatter to measure suspended-sand concentration.

Target strength and backscatter: Target strength, *TS*, is determined by the amount and nature of the sediment in suspension and by the dimensions of the ensonified volume (NDRC, 1946; Urick, 1975). Much research has been completed on the acoustic scattering effects of individual and, later, concentrations of particles in suspension (Rayleigh, 1896; NDRC, 1946; Urick, 1975; Sheng and Hay, 1988; Hay, 1991; Hay and Sheng, 1992; Thorne and Campbell, 1992; He and Hay, 1993; Thorne et al., 1993, 1995; Thorne and Hanes, 2002; Thorne and Buckingham, 2004; Thorne and Meral, 2008; Moore and Hay, 2009). Although the initial work in this field was conducted on regularly shaped particles, sufficient work using natural sand grains (in both single and mixtures of grain sizes) has allowed a sufficiently robust theory on how sound is backscattered by suspensions of sediment in water. The equation used to derive the relation for *TS* is the following version of the Thorne et al. (1993) equation:

$$P_{rms} = P_0 r_0 f \left[\frac{3Mtc}{8D\rho_S} \right]^{1/2} \frac{0.96}{ka_T \psi r} e^{(-2\alpha_N r)} \tag{9}$$

where P_{rms} is the reverberation-level pressure measured at the transducer (in Pascals), P_0 is the source-level pressure (in Pascals) at distance r_0 = 1 m from the transducer, r is the distance along the beam from the transducer (in meters), f is the nondimensional form function that describes the backscattering strength of sediment grains in water as a function of ka_S, $k = 2\pi/\lambda$ is the wave number (in 1/m), λ is the acoustic wavelength (in meters), a_S is the radius of the sediment grains (in meters), D is the diameter of the sediment grains (in meters), ρ_S is the density of sediment (in kg/m^3), M is the mass concentration of suspended sediment (in kg/m^3), t is the acoustic pulse duration (in seconds), c is the measured speed of sound (in m/s), a_T is the radius of the transducer (in meters), α_N is the attenuation coefficient (in nepers/m) resulting from the sum of α_W and α_S, and ψ is the non-dimensional near-field correction of Downing et al. (1995) that accounts for non-spherical spreading losses very near the transducer. We exclude this near-field correction because it is either negligible or, at higher frequencies, degrades the results by overcorrecting B_F in the first cell, thus resulting in negative biases in α_S that get larger with increasing $C_{SILT\text{-}CLAY}$.

The form function, f, used in this study is that of Thorne and Meral (2008), which takes into account both the effect of the non-spherical shape of natural sediment grains and the effect of multiple grain sizes. Relative to form functions evaluated for single-size spheres, these two effects combine to result in a substantial increase in f in the Rayleigh scattering regime ($ka_S < 1$), and a smaller decrease in the geometric scattering regime. Because this form function is used, M in equation 9 is the concentration of the grain-size distribution of suspended sediment with median grain size D_{50}. Hence, D in equation 9 is replaced with D_{50}. The fact that f and D_{50} are associated with a grain-size distribution and not just a single sediment grain size has major implications with respect to the derivation and physical interpretation of the target strength. The target strength derived below is therefore that for the entire grain-size distribution of sediment in suspension and not that for only sand. In cases where the amount of silt and clay greatly exceeds the amount of sand in suspension, the target strength will approach that for the suspended-silt-and-clay grain-size distribution and will be much different from the target strength for the suspended-sand grain-size distribution. One of the greatest source of error/bias in the methods used in previous studies that have related acoustic backscatter to the concentration of only suspended sand arises from these studies neglecting this important physical effect.

Because acoustic intensity is acoustic pressure squared and 1 neper = 8.686 dB, following the appropriate substitutions, simplifications, and rearrangement, equation 9 can be rewritten in the following decibel form:

$$RL = SL + \left[-20\log(r) - 2\log\alpha_W r - 2\log\alpha_S r \right] + 10\log\left[f^2 \frac{3Mtc}{8D_{50}\rho_S} \left(\frac{0.96}{ka_T} \right)^2 \right] \tag{10}$$

to be consistent with equation 1 and then further simplified to:

$$SL - B + 10\log\left[f^2 \frac{3Mtc}{8D_{50}\rho_S}\left(\frac{0.96}{ka_T}\right)^2 \right] = 0 . \quad (11)$$

Simple comparison of equation 3 and equation 11 suggests incorrectly that the right term of the three terms in equation 11 is essentially the target strength minus the detection threshold. Closer inspection of these two equations, however, indicates a problem arising from the conversion of equation 9 from pressure form to the logarithmic intensity form in equation 10 compatible with the sonar equations. When M goes to zero in equation 9, the reverberation-level pressure, P_{rms} also goes to zero. However, when M goes to zero in equation 11, RL goes to minus infinity, because the logarithm of zero is an infinitely large negative number. This problem can be corrected by limiting solution of equation 11 to only those cases where $M > 0$ and by adding a new term from equation 3, the detection threshold, DT. As used in this study, DT is slightly lower than the lowest measured RL in this study during conditions when the suspended-sand concentration was immeasurably small (<0.01 mg/L), conditions when RL is typically less than ~40 to 50 dB. Thus equation 11 can be written in final form as:

$$SL - DT - B = -TS = -10\log\left[f^2 \frac{3Mtc}{8D_{50}\rho_S}\left(\frac{0.96}{ka_T}\right)^2 \right] \quad (12)$$

and can be solved only when $M > 0$.

To finish the derivation of TS such that it is compatible with the backscatter – sediment-concentration relations derived from the sonar equations for constant grain size by Thevenot and others (1992), we: (1) convert M from SI units into the more conventional sediment-concentration units of mg/L and convert D_{50} from SI units into the more appropriate units of mm for sand and finer sediment (these two conversions cancel each other out), and (2) break TS in equation 12 into two parts, the Unit Target Strength, UTS, and, C, the concentration in mg/L of suspended sediment in a log-normal grain-size distribution with median grain size D_{50}. In this two-part form,

$$TS = UTS + 10\log C \quad (13)$$

where,

$$UTS = 10\log\left[f^2 \frac{3tc}{8D_{50}\rho_S}\left(\frac{0.96}{ka_T}\right)^2 \right] \quad (14)$$

and $UTS = TS$ when $C = 1$ mg/L. By virtue of equation 13 a tenfold change in C will result in a 10 dB change in TS when the grain-size distribution of the suspended sediment remains constant. Changes in the grain-size distribution affect both f and D_{50} in equation 13, resulting in a more complicated influence on TS than do changes in C.

The more complicated influence on TS of changes in the sand grain-size distribution under constant C is best illustrated through calculation of the Relative Unit Target Strength ($RUTS$), that is, the UTS relative to the UTS associated with a reference D_{50}, denoted as $D_{50\text{-REF}}$. $D_{50\text{-REF}}$ is the median grain size at a given location that best characterizes the D_{50} of the suspended sediment over the widest possible range in concentration. For convenience, the UTS associated with $D_{50\text{-REF}}$ is abbreviated as UTS_{REF}. $RUTS$ is calculated by simply subtracting UTS_{REF} from the UTS for all values of D_{50}. By virtue of the behavior of the $RUTS$, backscatter measurements made with higher-frequency ADPs are generally less sensitive to changes in suspended-sand D_{50} than are backscatter measurements made with lower-frequency ADPs. The $RUTS$ increases rapidly as a function of increasing D_{50} over most of the Rayleigh scattering regime, and only begins to plateau around ka_S ~0.5. The main implication of this result is that, when $ka_S < 0.5$, use of a single-frequency acoustic approach to measure suspended-sand concentration will be highly biased as a result of concentration-independent variation in D_{50}. Comparison between measured and theoretically determined values of the $RUTS$ are good (Figure 2). The behavior of the $RUTS$ as a function of frequency and D_{50} is

the physical process that allows accurate, that is, relatively unbiased, backscatter-based measurements of suspended-sand concentration and D_{50} to be possible when multiple acoustic frequencies are used.

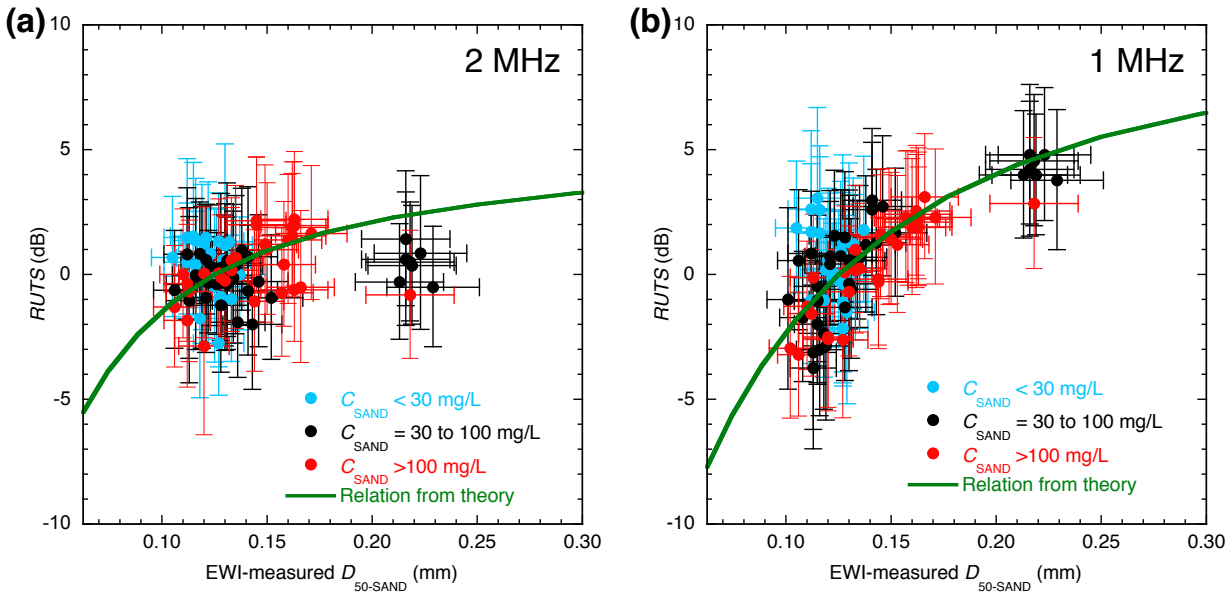

Figure 2 Comparisons of measured and theoretical values of *RUTS* at the Colorado River near river mile 30, 09383050, (CR30) study site, at (a) 2-MHz and (b) 1-MHz acoustic frequencies. Measured values of the *RUTS* are segregated into three different concentration ranges in these plots to allow evaluation of whether they depend on concentration; as indicated in these plots, there is no discernable dependence of the measured *RUTS* on concentration. $D_{50\text{-SAND}}$ error bars are 95%-confidence-level error bars that include both field and laboratory-processing errors in the EWI measurements of $D_{50\text{-SAND}}$; *RUTS* error bars are 95%-confidence-level error bars that include (1) both field and laboratory-processing errors in the EWI measurements of C_{SAND}, (2) a 2% estimated error in the ADP-calculated values of $\overline{B}$, and (3) the 95%-confidence-level error in the mean value of $\overline{B}$ time-averaged over the 1-hour interval centered on the temporal midpoint of the time of each EWI measurement.

Our derivation of the *UTS* and *RUTS* allows the Thevenot et al. (1992) simplification of the sonar equation to be re-derived in a convenient form for cases of varying grain size; a form that in this study uses backscatter measured at multiple frequencies to solve for both suspended-sediment concentration and D_{50}. In their simplification of the active sonar equation, Thevenot et al. (1992) showed that, when grain size is constant:

$$C = 10^{-0.1K+0.1B} \tag{15}$$

where C is sediment concentration in mg/L, B is relative backscatter (replaced in this study by $\overline{B}$ the beam-averaged backscatter), and K is a constant. Substituting equations 13 and 14 into equation 12 and rearranging equation 12 to be in the form of Thevenot et al. [1992] indicates that, when grain-size is allowed to vary, K is not truly constant, but is the sum of a constant part ($SL - DT$) and a varying part (*UTS*). The rearranged version of equation 12 after these substitutions is:

$$C = 10^{-0.1(SL-DT+UTS)+0.1\overline{B}}. \tag{16}$$

Thus, a generalized way to re-derive equation 15 such that grain size is free to vary is to define a new constant:

$$K_1 = SL - DT \tag{17}$$

and rewrite equation 16 as:

$$C = 10^{-0.1K_1 - 0.1UTS + 0.1\overline{B}} . \quad (18)$$

For the special case, where C is the concentration of suspended sediment with D_{50} equal to $D_{50\text{-REF}}$,

$$C = 10^{-0.1K_1 - 0.1UTS_{\text{REF}} + 0.1\overline{B}} . \quad (29)$$

Because

$$RUTS = UTS - UTS_{\text{REF}} \quad (20)$$

the general case where the median grain size of the sediment in suspension is allowed to vary can be written as:

$$C = 10^{-0.1K_1 - 0.1UTS_{\text{REF}} - 0.1RUTS + 0.1\overline{B}} . \quad (21)$$

Because UTS_{REF} is constant at a given study site, it is convenient to define another new constant:

$$K_2 = -\left(K_1 + UTS_{\text{REF}}\right) = -0.1\left(SL - DT + UTS_{\text{REF}}\right) \quad (22)$$

allowing the final more-general form of equation 15 for varying grain size:

$$C = 10^{K_2 + 0.1\left(\overline{B} - RUTS\right)} . \quad (23)$$

If only one frequency ADP is present, it is theoretically impossible to solve for both C and $RUTS$ for a given measured $\overline{B}$. However, if two or more frequencies are present, it is possible to iteratively solve for C and $RUTS$. This iterative approach is the basis for the method we use to calculate suspended-sand C and D_{50}.

As a grain-size distribution of suspended sediment broadens, the difference in the UTS between silt-and-clay- and sand-size sediment lessens as a result of the effect of decreased sorting on the form function. In cases where the geometric standard devation, σ_G, of a grain-size distribution is less than ~1.5ϕ, the UTS associated with silt grain-size distributions will be much less than the UTS associated with sand grain-size distributions. In these cases, the backscatter will be dominantly produced by sand-size sediment. Conversely, in cases where the σ_G of a grain-size distribution exceeds ~1.5ϕ, the UTS associated with silt grain-size distributions becomes a larger fraction of the UTS associated with sand grain-size distributions, and measurable backscatter will be produced by the silt-size sediment in addition to the backscatter produced by the sand-size sediment. Ultimately, in cases where the σ_G of a grain-size distribution exceeds ~3ϕ, the UTS associated with grain-size distributions of silt and clay will be nearly equal to the UTS associated with grain-size distributions of sand. Under these conditions, the backscatter produced by the suspended silt and clay is nearly as much as that produced by the suspended sand. Because the sorting of suspended silt and clay (σ_G = 2 to 3ϕ) is much broader than the sorting of suspended sand (σ_G = 0.63 to 0.65ϕ) at our study sites, a condition likely in most rivers, the backscatter produced by silt and clay must be accounted for under conditions when the concentration of the suspended silt and clay greatly exceeds that of the sand.

To allow accurate acoustic measurements of suspended-sand concentration to be made when even large concentrations of silt and clay are present (and most of $\overline{B}$ arises from the amount of silt and clay in suspension), a data-processing method was developed to allow separation of the part of $\overline{B}$ arising from sand-size sediment from the part of $\overline{B}$ arising from silt-and-clay-sized sediment. This method utilizes the differing theoretical behaviors of the UTS and α_S under different combinations of suspended silt and clay and suspended sand. An early empirical version of this method was described in Topping et al. (2007). The basis for the UTS part of this method is the development of a Base-Backscatter-Calibration (BBC) relation between $\overline{B}$ and the log-transformed EDI/EWI-measured suspended-sand concentration using equation 23 for conditions where the suspended sediment is

dominated by sand-size sediment with a median grain size within ¼ϕ of $D_{50\text{-REF}}$ and assumed constant sorting. Relations are then developed using both theory and empirical analysis to account and correct for the excess backscatter relative to this relation for conditions where the amount of silt and clay greatly exceeds the amount of sand in suspension. For accurate BBC relations to be developed, the average concentration of suspended sand along the beam must systematically relate to the EDI/EWI-measured velocity-weighted concentration of suspended sand in the cross section. Because of how the flow and suspended-sediment-concentration field interact with the local channel geometry at the locations of ADP deployments, there are typically differences between the average suspended-sand C and D_{50} in the part of the cross section ensonified by the ADP beams and the velocity-weighted suspended-sand C and D_{50} in entire EDI/EWI cross section. These differences lead to differences between the theoretically predicted (0.1 by equation 23) and empirically determined slopes and y-intercepts of the BBC relations. The BBC relation form of equation 23 allowing empirically determined slopes and y-intercepts is:

$$\log\left(C_{\text{SAND-REF}}\right) = K_2 + K_3\overline{B}_{\text{BASE}} \tag{24}$$

where $C_{\text{SAND-REF}}$ is the EDI/EWI-measured reference concentration in the river cross section of suspended sand with a median grain size equal to $D_{50\text{-REF}}$, and $\overline{B}_{\text{BASE}}$ is the base backscatter associated with $C_{\text{SAND-REF}}$.

The additional beam-averaged backscatter required to account for the amount of backscatter produced by the presence of suspended silt and clay at a given concentration of suspended sand is referred to as the excess backscatter, B'. Excess backscatter is calculated as:

$$B' = \overline{B} - \overline{B}_{\text{BASE}} . \tag{25}$$

Because

$$\overline{B} = TS + SL + DT \tag{26}$$

equation 25 can be rewritten as:

$$B' = \left(TS_{\text{SED}} + SL + DT\right) - \left(TS_{\text{SAND-REF}} + SL + DT\right) \tag{27}$$

and simplified to:

$$B' = TS_{\text{SED}} - TS_{\text{SAND-REF}} , \tag{28}$$

where TS_{SED} is the target strength of the suspended sand, silt, and clay mixture and $TS_{\text{SAND-REF}}$ is the target strength of $C_{\text{SAND-REF}}$. By definition, when all of the suspended sediment is composed of sand with $D_{50} = D_{50\text{-REF}}$, $B' = 0$. To derive the theoretically based value of B' at constant sand concentration and D_{50}, equation 13 can be rewritten as:

$$TS = 10\log\left[\frac{f^2}{D_{50}\rho_{\text{S}}}\right] + 10\log C + 10\log\left[\frac{3tc}{8}\left(\frac{0.96}{ka_{\text{T}}}\right)^2\right]. \tag{29}$$

After rearrangement and substitution of the quartz density of 2.65 g/cm^3 for the density of sand and replacement of the 0.1 theoretical slope of the BBC relation with the empirical slope K_3, equation 29 becomes:

$$B' = \left(\frac{1}{K_3}\right)\log\left[\left(\frac{f_{\text{SED}}}{f_{\text{REF}}}\right)^2\left(\frac{D_{50\text{-REF}}}{D_{50\text{-SED}}}\right)\left(\frac{2.65}{\rho_{\text{SED}}}\right)\left(1+\frac{C_{\text{SILT-CLAY}}}{C_{\text{SAND-REF}}}\right)\right] \tag{30}$$

where $C_{\text{SILT-CLAY}}$ is the concentration of silt and clay in mg/L, $D_{50\text{-SED}}$ is the median grain size of the sand, silt, and clay mixture in suspension, f_{SED} is the value of the Thorne and Meral (2008) form function calculated for the grain-size distribution of the sand, silt, and clay mixture, ρ_{SED} is the wet density of the sand, silt, and clay mixture, and f_{REF}

is the value of the Thorne and Meral (2008) form function associated with the $D_{50\text{-REF}}$ of the suspended sand. The theoretical behavior of B' predicted by equation 30 agrees well with the empirical behavior of B' (Figure 3).

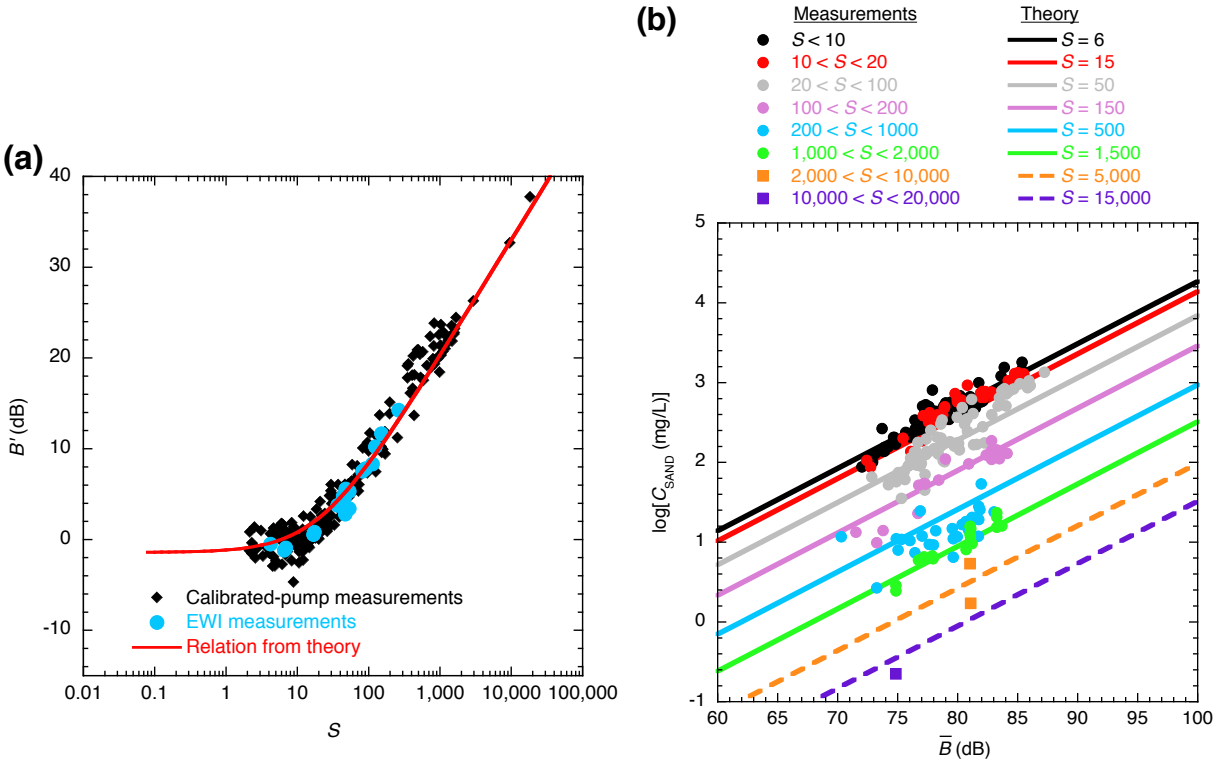

Figure 3 (a) B' plotted as a function of S for the 2-MHz ADP at the Rio Grande above Rio Grande Village, TX, 08375295, (RG-RGV) study site. The BBC relation used to calculate values of B' has a slope of 0.078. The theoretical relation for B' is derived using a sand grain-size distribution with $D_{50\text{-REF}}$ = 0.105 mm and σ_G = 0.65ϕ, and a silt and clay grain-size distribution with D_{50} = 0.002 mm, σ_G = 2.7ϕ, and a wet density of 2.65 g/cm^3. (b) Log(C_{SAND}) plotted as a function of $\overline{B}$ for 8 different ranges of S for the 2-MHz ADP at the RG-RGV study site. Measurements plotted are the same as in a. BBC relation fit to suspended-sediment measurements with $S \leq 10$ shown as solid black line; theoretical relations between $\overline{B}$ and log(C_{SAND}) at higher values of S calculated using the theoretical B' relation in a.

As a result of the theoretical behaviors of backscatter and attenuation under different suspended-sediment grain-size distributions, the backscatter produced by extremely high concentrations of suspended silt and clay can effectively mask the backscatter produced by sand when the ratio of suspended silt and clay to suspended sand, S, is high. As a result of backscatter masking by relatively high concentrations of suspended silt and clay, theoretically derived relations between $\overline{B}$ and log(C_{SAND}) at constant α_S become extremely steep (with almost no slope) at lower values of log(C_{SAND}), making it problematic to accurately solve for log(C_{SAND}). The steepness transition in these relations occurs at increasing values of S as the D_{50} of the silt and clay decreases. To calculate C_{SAND} using only the backscatter produced by the suspended sand, we subtract the silt-and-clay produced excess backscatter B' from measurements of $\overline{B}$ by using theoretically derived relations between $\overline{B}$, α_S, log(C_{SAND}), and S calculated on the basis of equations 8, 24, and 30 (Figure 4).

TWO-FREQUENCY *RUTS* METHOD

The two-frequency *RUTS* method for measuring C_{SAND} and D_{50} is an iterative process that uses as input (1) the single-frequency 1- and 2-MHz estimates of C_{SAND} calculated using the theory described in the previous section and (2) the theoretical relations between suspended-sand D_{50} and the *RUTS* at the 1- and 2-MHz frequencies. Because backscatter at higher frequencies is less affected by changes in the D_{50} of the suspended sand, the 2-MHz

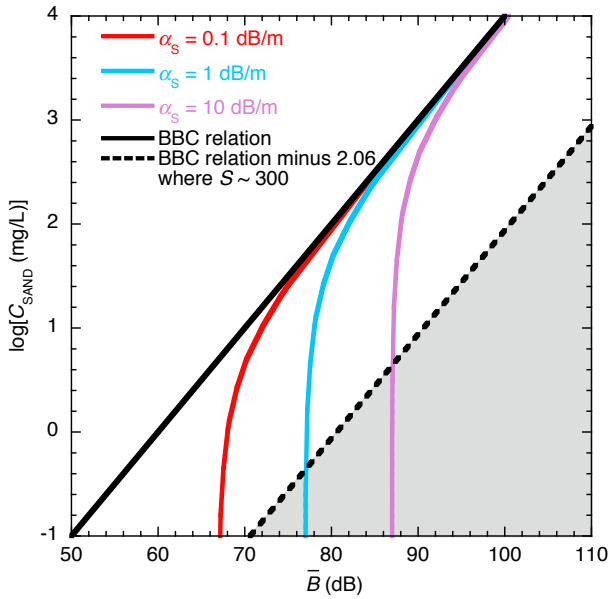

Figure 4 Behavior of theoretical relations between $\overline{B}$ and log(C_{SAND}) for different values of α_S at the 1-MHz frequency. The gray shaded regions indicate the regions of backscatter masking produced by relatively high concentrations of suspended silt and clay. Suspended-sand D_{50} = 0.125 mm, $\sigma_G = 0.63\phi$; suspended-silt-and-clay D_{50} = 0.001 mm, $\sigma_G = 3\phi$, ρ_S = 2.65 g/cm^3. BBC relation has a slope (K_3) of 0.1 and a y-intercept (K_2) of -6. Shown are the BBC relation and the relations between $\overline{B}$ and log(C_{SAND}) for the cases where α_S = 0.1, 1.0, and 10 dB/m. These relations between $\overline{B}$ and log(C_{SAND}) are near vertical when S exceeds ~300 in the gray shaded region.

estimate of C_{SAND} is chosen as the initial concentration estimate in this calculation. The difference in the values of $\overline{B}$ measured at the 1- and 2-MHz frequencies (corrected for B'), the theoretical *RUTS* relations, and the BBC relations for the 1- and 2-MHz ADPs are then used in an iterative fashion to calculate the D_{50} and concentration of the suspended sand that satisfies the constraint that the B'-corrected values of $\overline{B}$ measured at each frequency are associated with the same suspended-sand concentration. By this process, when the 1-MHz estimate of C_{SAND} exceeds the 2-MHz estimate, the suspended-sand D_{50} is calculated to be greater than $D_{50\text{-REF}}$ using the 1-MHz *RUTS* relation and the two-frequency value of C_{SAND} is calculated to be lower than the initial 2-MHz estimate of C_{SAND} using the 2-MHz *RUTS* relation and this new value of D_{50}. Conversely, when the 1-MHz estimate of C_{SAND} is lower than the 2-MHz estimate of C_{SAND}, the suspended-sand D_{50} is calculated to be less than $D_{50\text{-REF}}$ using the 1-MHz *RUTS* relation and the two-frequency value of C_{SAND} is calculated to be higher than the initial 2-MHz estimate of C_{SAND} using the 2-MHz *RUTS* relation and this new value of D_{50}. Compared to the initial single-frequency estimates of C_{SAND}, two-frequency measurements of C_{SAND} by this process are generally unbiased as a function of changing suspended-sand D_{50} (Figure 5). As expected on the basis of the theoretical behavior of the *RUTS* depicted in Figure 2, grain-size-driven biases in 1-MHz estimates of C_{SAND} are greater than in 2-MHz estimates of C_{SAND}.

RESULTS

Unless the range in suspended-sand D_{50} at a study site is smaller than about 1ϕ, two acoustic frequencies are required to produce measurements of suspended-sand concentration (C_{SAND}) that are unbiased by changes in the suspended-sand grain-size distribution. In cases where the range in suspended-sand D_{50} is smaller than about 0.75ϕ, reasonably unbiased results may be obtained by using only a single 2-MHz-frequency ADP, but only if the contribution of silt and clay to backscatter is accounted for. At our study sites, use of a single 1-MHz frequency ADP resulted in biased measurements of C_{SAND} regardless of the range in suspended-sand D_{50}. At almost all of our study sites, inclusion of B' resulted in a substantial reduction in the relative bias in the measurements of C_{SAND}. Furthermore, the inclusion of B' results in a much more substantial reduction in the maximum relative error. For

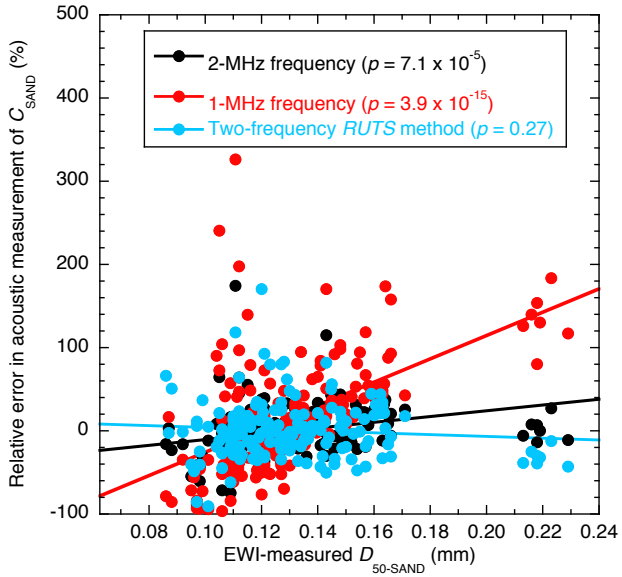

Figure 5 Relative errors in single-frequency and two-frequency acoustic measurements of C_{SAND} at the CR30 study site. F-tests conducted on the least-squares linear regressions fit to these relative errors indicate significant positive correlations (at the p = 0.05 critical level) between suspended-sand D_{50} and error for both the 1- and 2-MHz single-frequency measurements of C_{SAND}, but no significant correlation between suspended-sand D_{50} and error for the two-frequency measurements. The significant relation between suspended-sand D_{50} and error is much steeper at the 1-MHz frequency than at the 2-MHz frequency. These results indicate the presence of grain-size-driven bias in the single-frequency measurements of C_{SAND} that is larger at the lower frequency, as expected on the basis of the theoretical behavior of the *RUTS* depicted in Figure 2.

example, at the RG-RGV study site, the maximum relative error in the acoustic measurements of C_{SAND} when using the single-frequency method at 1 MHz neglecting B' is +95,900%; this enormous relative error decreases to +651% upon inclusion of the effects of B'. Furthermore, among the 173 paired acoustic and EWI measurements at the Colorado River near Grand Canyon, AZ, 09402500, study site, the maximum relative error in the acoustic measurements of C_{SAND} when using the single-frequency method at 2 MHz neglecting B' is +1,410%; this extremely large relative error decreases to +65.6% upon inclusion of the effects of B'.

The two-frequency acoustic measurements compare well with the physical measurements of the velocity-weighted suspended-silt-and-clay, suspended-sand concentrations, and suspended-sand median grain sizes in the river cross sections at the study sites on the Colorado River and Rio Grande (Figure 6). Wilcoxon-Mann-Whitney tests conducted on in- and out-of-sample data from the Colorado River study sites indicate that the in-sample and out-of-sample errors in the acoustic measurements of silt and clay concentration and sand concentration are not significantly different at the 0.05 critical level. In Figure 6a, the acoustic and physical measurements of suspended-silt-and-clay concentration are in good agreement over the range from ~100 mg/L to ~20,000 mg/L; in figure 6b, the acoustic and physical measurements of suspended-sand concentration are in good agreement over the range from ~2 mg/L to ~5,000 mg/L. Though not shown in figure 6a because the physical measurements are calibrated-pump measurements, acoustic and calibrated-pump measurements of suspended-silt-and-clay concentration have been found to agree well at concentrations as high as ~30,000 mg/L on both the Colorado River and Rio Grande. In Figure 6c, the acoustic and physical measurements of suspended-sand D_{50} are in reasonable agreement over the range from ~0.08 to 0.25 mm. Although the variance about the line of perfect agreement in Figure 6c appears larger than in Figures 6a-b, this is a visual artifact of the differences in scale between the figure panels; five orders of magnitude are plotted in Figures 6a-b, whereas less than one order of magnitude is plotted in Figure 6c. In reality, the variance about the line of perfect agreement in Figure 6c is smaller than in Figures 6a-b.

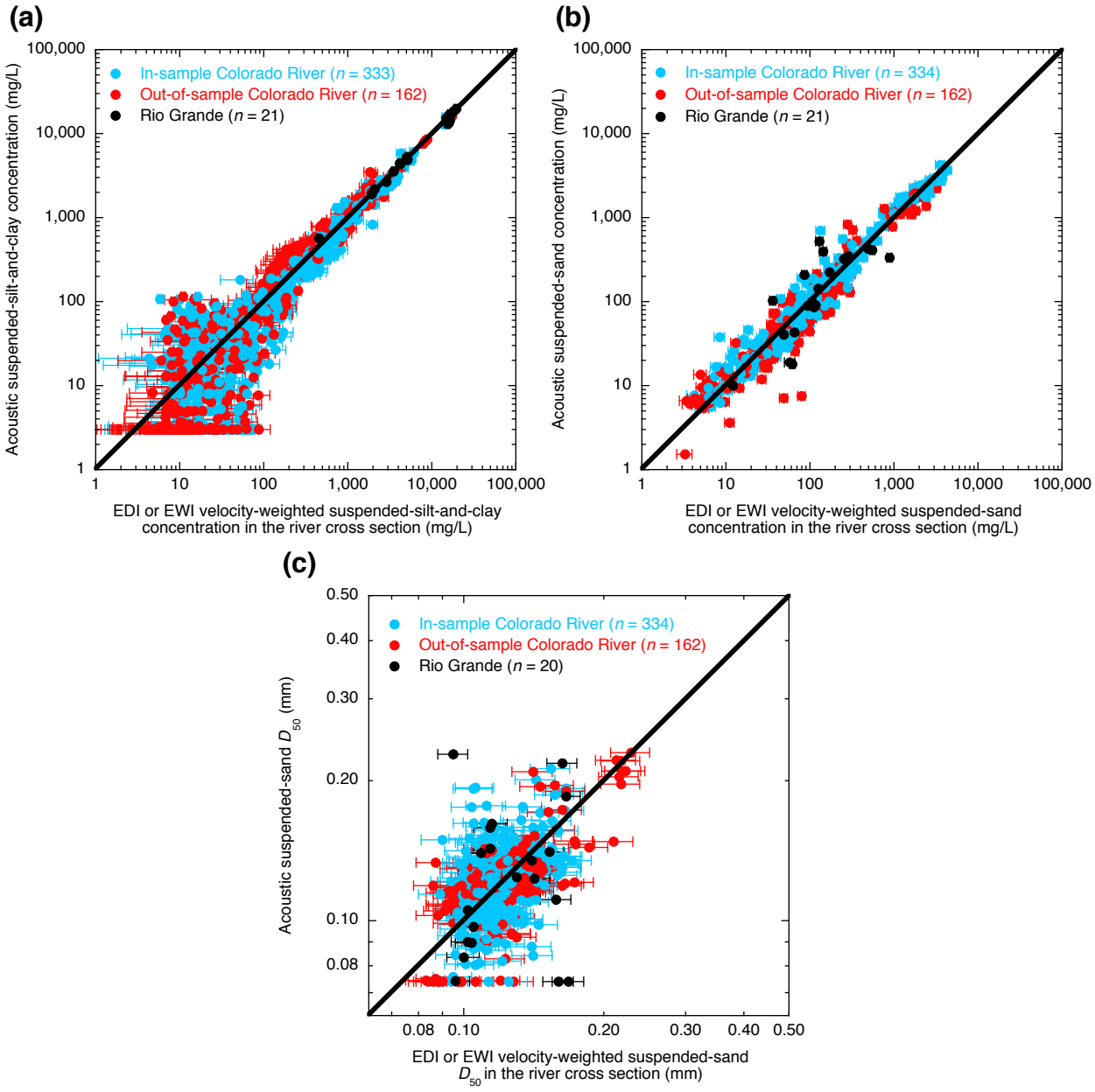

Figure 6 Two-frequency acoustic measurements of the velocity-weighted (a) suspended-silt-and-clay concentration, (b) suspended-sand concentration, and (c) suspended-sand D_{50} in the river cross section plotted as a function of the EDI or EWI-measured values of these parameters at the five Colorado River and Rio Grande study sites where the EDI/EWI measurement cross section is located within 200 m of the ADP arrays. Black solid lines are the lines of perfect agreement between the EDI/EWI measurements at the acoustic measurements. In-sample data are those used in the calibration of either of the two ADPs at a study site; out-of-sample data are not used in any calibration. Horizontal error bars indicate the 95%-confidence-level combined field and laboratory errors in the EDI/EWI measurements calculated using the methods in Topping et al. (2010, 2011).

For all three of the parameters plotted in Figure 6, the the log-transformed variance is approximately symmetric about the lines of perfect agreement, indicating the presence of little bias in the method; a result supported by F-tests conducted on the relative errors associated with each acoustic measurement. Only in the case of the acoustic

measurements of the suspended-sand D_{50} do the F-tests indicate the presence of bias; there is a tendency for a small positive bias in the acoustic measurements of suspended-sand D_{50} when $D_{50} < D_{50\text{-REF}}$ and for a small negative bias in these measurements when $D_{50} > D_{50\text{-REF}}$. Although the two-frequency acoustic measurements are generally unbiased, the presence of reasonably large variance about the lines of perfect agreement indicates that these measurements are subject to relatively large random error. For both suspended silt and clay and suspended sand, the log-transformed variance about the lines of perfect agreement decreases significantly with increasing concentration. In the case of sand, this decrease in variance is gradual, whereas in the case of silt and clay, this decrease in variance is rapid between concentrations of 1 and 100 mg/L and more gradual between concentrations of 100 and 20,000 mg/L. These negative correlations between concentration and the log-transformed variance about the lines of perfect agreement indicate that the relative errors in the acoustic measurements of suspended-silt-and-clay concentration and suspended-sand concentration both decrease with increasing concentration. For suspended-sand D_{50}, the log-transformed variance about the line of perfect agreement, and therefore the relative error in the acoustic measurements of suspended-sand D_{50}, is approximately constant across the measured 0.09 to 0.25-mm range.

REFERENCES

Downing, A., Thorne, P.D., and Vincent, C.E. (1995). "Backscattering from a suspension in the near field of a piston transducer," Journal of the Acoustical Society of America, 97(3), pp. 1614-1620, doi: 10.1121/1.412100.

Flammer, G.H. (1962). "Ultrasonic measurement of suspended sediment," U.S. Geological Survey Bulletin 1141-A, 48 pp.

Gartner, J.W. (2004). "Estimating suspended solids concentrations from backscatter intensity measured by acoustic Doppler current profiler in San Francisco Bay, California," Marine Geology, 211, pp. 169-187, doi: 10.1016/j.margeo.2004.07.001.

Hay, A.E. (1983). "On the remote acoustic detection of suspended sediment at long wavelengths," Journal of Geophysical Research, 88(C12), pp. 7525-7542, doi: 10.1029/JC088iC12p07525.

Hay, A.E. (1991). "Sound scattering from a particle-laden, turbulent jet," Journal of the Acoustical Society of America, 90(4), pp. 2055-2074, doi: 10.1121/1.401633.

Hay, A.E., and Sheng, J. (1992), "Vertical profiles of suspended sand concentration and size from multifrequency acoustic backscatter," Journal of Geophysical Research, 97(C10), pp. 15,661-15,677, doi: 10.1029/92JC01240.

He, C., and Hay, A.E. (1993). "Broadband measurements of the acoustic scattering cross section of sand particles in suspension," Journal of the Acoustical Society of America, 94(4), pp. 2247-2254, doi: 10.1121/1.407496.

Lamb, H. (1945), Hydrodynamics, Sixth edition, 738 pp., Dover Publications, New York.

Moore, S.A., and Hay, A.E. (2009). "Angular scattering of sound from solid particles in turbulent suspension," Journal of the Acoustical Society of America, 126(3), pp. 1046-1056, doi: 10.1121/1.3180696.

Moore, S.A., Le Coz, J., Hurther, D. and Paquier, A. (2013). "Using multi-frequency acoustic attenuation to monitor grain size and concentration of suspended sediment in rivers," Journal of the Acoustical Society of America, 133(4), pp. 1959-1970, doi: 10.1121/1.4792645.

Morse, P. M. (1948), Vibration and sound, Second edition, 468 pp., McGraw-Hill Book Co., New York.

National Defense Research Committee (1946), "Principles and applications of underwater sound," Summary Technical Report of Division 6, volume 7, 295 pp., Washington, D.C.

Rayleigh, Baron, Strutt, J.W. (1896). Theory of sound, vol. 2, 504 pp., Macmillan and Co., New York. [Google Books, http://books.google.com/books?id=Zm9LAAAAMAAJ&pg=PR5&source=gbs_selected_pages&cad=3#v=onepage&q&f=false, accessed on March, 13, 2014]

Sheng, J., and Hay, A.E. (1988), "An examination of the spherical scatterer approximation in aqueous suspensions of sand," Journal of the Acoustical Society of America, 83(2), pp. 598-610, doi: 10.1121/1.396153.

Thevenot, M.M., Prickett, T.L. and Kraus, N.C. (1992) "Tylers Beach, Virginia, Dredged material plume monitoring project 27 September to 4 October 1991," U.S. Army Corps of Engineers Dredging Research Program Technical Report DRP-92-7, 204 pp.

Thorne, P.D., and S.C. Campbell (1992), Backscattering by a suspension of spheres, *Journal of the Acoustical Society of America*, *92*(2), 978-986, doi: 10.1121/1.403967.

Thorne, P.D., and M.J. Buckingham (2004), Measurements of scattering by suspensions of irregularly shaped sand particles and comparison with a single parameter modified sphere model, *Journal of the Acoustical Society of America*, *116*(5), 2876-2889, doi: 10.1121/1.1808458.

Thorne, P.D., and Hanes, D.M. (2002). "A review of acoustic measurements of small-scale sediment processes," Continental Shelf Research, 22(4), pp. 603-632, doi: 10.1016/S0278-4343(01)00101-7.

Thorne, P.D., and Meral, R. (2008). "Formulations for the scattering properties of suspended sandy sediments for use in the application of acoustics to sediment transport processes," Continental Shelf Research, 28(2), pp. 309-317, doi: 10.1016/j.csr.2007.08.002.

Thorne, P.D., Hardcastle, P.J., and Soulsby, R.L. (1993). "Analysis of acoustic measurements of suspended sediments," Journal of Geophysical Research, 98(C1), pp. 899-910, doi: 10.1029/92JC01855.

Thorne, P.D., Waters, K.R., and Brudner, T.J. (1995). "Acoustic measurements of scattering by objects of irregular shape," Journal of the Acoustical Society of America, *97*(1), pp. 242-251, doi: 10.1121/1.413109.

Topping, D.J., Melis, T.S., Rubin, D.M., and Wright, S.A. (2004). "High-resolution monitoring of suspended-sediment concentration and grain size in the Colorado River in Grand Canyon using a laser-acoustic system," in Proc. of the 9th International Symposium on River Sedimentation, Yichang, People's Republic of China, 2004, edited by C. Hu and Y. Tan, pp. 2507–2514.

Topping, D.J., Wright, S.A., Melis, T.S., and Rubin, D.M. (2006). "High-resolution monitoring of suspended-sediment concentration and grain size in the Colorado River using laser-diffraction instruments and a three-frequency acoustic system," Proc. of the 8th Federal Interagency Sedimentation Conference, Reno, Nevada, April 2–6, 2006, CD-ROM, ISBN 0-9779007-1-1.

Topping, D.J., Wright, S.A., Melis, T.S., and Rubin, D.M. (2007). "High-resolution measurements of suspended-sediment concentration and grain size in the Colorado River in Grand Canyon using a multi-frequency acoustic system," Proc. of the Tenth International Symposium on River Sedimentation, Moscow, Russia, August 1–4, 2007, pp. 330–339, ISBN 978-5-89575-124-4, 978-5-89575-127-5.

Topping, D.J., Rubin, D.M., Grams, P.E., Griffiths, R.E., Sabol, T.A., Voichick, N., Tusso, R.B., Vanaman, K.M., and McDonald, R.R. (2010). "Sediment transport during three controlled-flood experiments on the Colorado River downstream from Glen Canyon Dam, with implications for eddy-sandbar deposition in Grand Canyon National Park," U.S. Geological Survey Open-File Report, 2010-1128, 111 pp.

Topping, D.J., Rubin, D.M., Wright, S.A., and Melis, T.S. (2011). "Field evaluation of the error arising from inadequate time averaging in the standard use of depth-integrating suspended-sediment samplers," U.S. Geological Survey Professional Paper, 1774, 95 pp.

Urick, R.J. (1948). "The absorption of sound in suspensions of irregular particles," Journal of the Acoustical Society of America, 20(3), pp. 283-289, doi: 10.1121/1.1906373.

Urick, R.J. (1962). "Generalized form of the sonar equations," Journal of the Acoustical Society of America, 34(5), pp. 547-550, doi: 10.1121/1.1918166.

Urick, R.J. (1975). Principles of Underwater Sound for Engineers, 384 pp., McGraw Hill, New York.

Wall, G.R., Nystrom, E. A., and Litten, S. (2006). "Use of an ADCP to compute suspended-sediment discharge in the tidal Hudson River, New York," U.S. Geological Survey Scientific Investigations Report 2006-5055, 26 pp.

Wood, M.S., and Teasdale, G. N. (2013). "Use of surrogate technologies to estimate suspended sediment in the Clearwater River, Idaho and Snake River, Washington, 2008-10," U.S. Geological Survey Scientific Investigations Report 2013-5052, 29 pp.

Wright, S.A., Topping, D.J., and Williams, C.A. (2010). "Discriminating silt-and-clay from suspended-sand in rivers using side-looking acoustic profilers," Proc. of the 2nd Joint Federal Interagency Conference, Las Vegas, Nevada, June 27-July 1, 2010.

SURROGATE ANALYSIS AND INDEX DEVELOPER (SAID) TOOL AND REAL-TIME DATA DISSEMINATION UTILITIES

Marian Domanski, Hydrologist, USGS, mdomanski@usgs.gov, 217-328-9758
Timothy Straub, Hydrologist, USGS, tdstraub@usgs.gov, 217-621-9587
Molly Wood, Hydrologist, USGS, mswood@usgs.gov, 208-387-1320
Mark Landers, Hydrologist, USGS, landers@usgs.gov, 678-924-6616
Gary Wall, Hydrologist, USGS, grwall@usgs.gov, 518-285-5621
Steven Brady, Computer Scientist, USGS, sbrady@usgs.gov, 785-832-3518

Abstract: The use of acoustic and other parameters as surrogates for suspended-sediment concentrations (SSC) in rivers has been successful in multiple applications across the Nation. Critical to advancing the operational use of surrogates are tools to process and evaluate the data along with the subsequent development of regression models from which real-time sediment concentrations can be made available to the public. Recent developments in both areas are having an immediate impact on surrogate research, and on surrogate monitoring sites currently in operation.

The Surrogate Analysis and Index Developer (SAID) standalone tool, under development by the U.S. Geological Survey (USGS), assists in the creation of regression models that relate response and explanatory variables by providing visual and quantitative diagnostics to the user. SAID also processes acoustic parameters to be used as explanatory variables for suspended-sediment concentrations. The sediment acoustic method utilizes acoustic parameters from fixed-mount stationary equipment. The background theory and method used by the tool have been described in recent publications, and the tool also serves to support sediment-acoustic-index methods being drafted by the multi-agency Sediment Acoustic Leadership Team (SALT), and other surrogate guidelines like USGS Techniques and Methods 3-C4 for turbidity and SSC.

The regression models in SAID can be used in utilities that have been developed to work with the USGS National Water Information System (NWIS) and for the USGS National Real-Time Water Quality (NRTWQ) Web site. The real-time dissemination of predicted SSC and prediction intervals for each time step has substantial potential to improve understanding of sediment-related water-quality and associated engineering and ecological management decisions.

INTRODUCTION

Streamflow, sediment, and water-quality data are needed to establish baseline information for water-resource managers to evaluate historical and current conditions and plan management alternatives. Real-time, continuous SSC data can be useful for monitoring river response downstream of areas affected by recent wildfires, construction or remediation activities, levee failures, or changing land uses. Additionally, real-time data can provide an early warning for operators of municipal water supply and hydroelectric facilities concerned with avoiding damage to infrastructure from sediment. Surrogates are becoming widely used to better understand physical and chemical processes in natural systems (Rasmussen and others, 2009). Acoustic technology is becoming increasingly used for velocity measurements and is also being used as a surrogate for sediment concentrations.

The Surrogate Analysis and Index Developer (SAID) tool is a standalone tool to assist in the development of ordinary least squares (OLS) regression models that relate response and predictor variables (Helsel and Hirsch, 2002) by providing visual and quantitative diagnostics to the user (figure 1). The tool is written in the Matlab® programming language. There is no limit on the number of explanatory variables to be used in the linear model and no requirement of which explanatory variables to use. SAID is under beta development and is not yet formally released as a USGS software product.

SAID has applications for relating surrogate-technology parameters such as turbidity, acoustics, and others. SAID can be used for processing acoustic parameters to be used as predictor variables for suspended-sediment concentrations (SSC).The sediment-acoustic method, which assumes a constant spatial suspended-sediment concentration and grain size distribution with respect to range along the acoustic axis of the beam, utilizes acoustic data from fixed-mount stationary acoustic Doppler velocity meters (ADVM). Some of the earliest USGS applications and research were done by Topping and others (2004, 2006, 2007), Wright and others (2010), Landers

(2012), and Wood and Teasdale (2013). The sediment-acoustic method, as described in these references, is used in SAID to compute the sediment attenuation coefficient and sediment corrected backscatter from ADVM acoustic parameters. SAID allows for quick adjustment of complex ADVM data-processing options, changes in the variables used in the regression, and evaluation of the created model. The tool also enables the user to transform loaded variables, build linear regression models, view linear model diagnostic statistics and plots, export the model information, and generate a predicted time series.

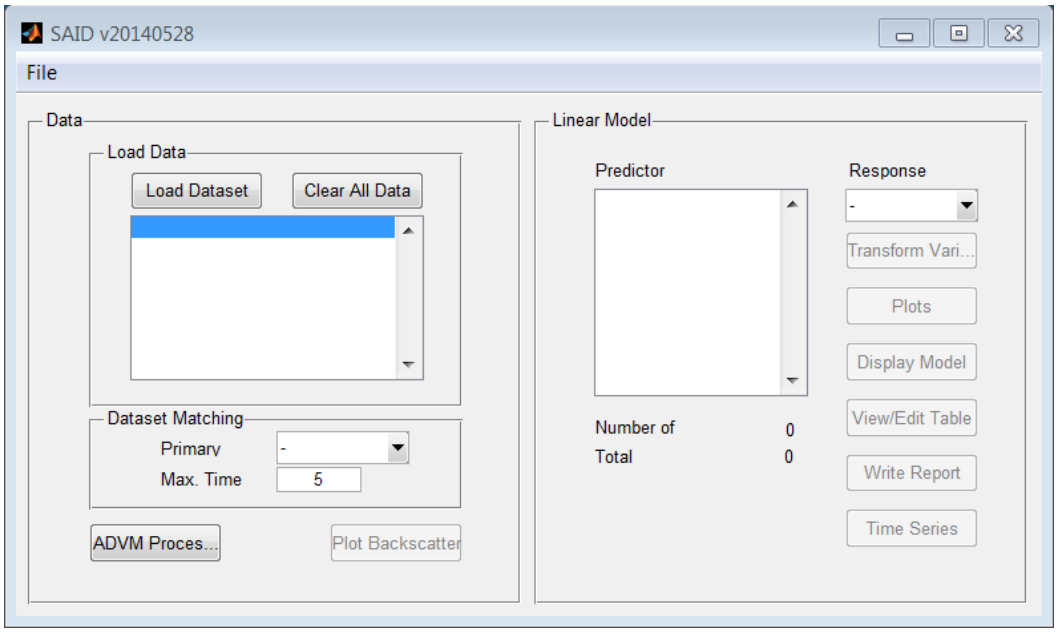

Figure 1 Main SAID window for beta version 20140528

This paper provides an overview on processing and loading data into SAID for developing regression models among surrogate data and measured constituents. In addition, this paper discusses the ADVM configuration parameters that are used in the calculation of acoustic surrogate parameters. Lastly, the paper gives an overview of how the regression models developed in SAID can be used in utilities that have been developed to disseminate predicted SSC in real-time.

SURROGATE ANALYSIS AND INDEX DEVELOPMENT

In the development of linear regression models, explanatory and response variables must be selected. These variables are contained in time series dataset files stored on disk. Because surrogate observations are continuous, and constituent observations occur at irregular time intervals, it is typical to store surrogate and constituent time series in separate dataset files. In order to choose observation sets of variables to develop a linear regression model, observations from the surrogate and constituent time series must be matched. Once a linear regression model is created from a set of matched observations, it must be evaluated for validity and appropriateness. SAID provides the ability to load and match datasets, select the response and predictor variables, and evaluate the created linear regression model. An overview of the dataset workflow is briefly described below and the following sections describe the process to develop regression models in more detail.

- ***Loading datasets***
  - Data that are stored on disk in ASCII files are loaded into memory by SAID.
- ***Choose primary datasets***
  - A dataset is selected that serves as the primary time series to synchronize observations. The selected dataset is known as the primary dataset and other loaded datasets become secondary datasets.
  - Adjusting the maximum time difference value (Max. Time) changes the upper limit of the time difference to which observations are synchronized.

- ***Choose linear model variables***
  - Available variables will be displayed in the Predictor Variables list box and the Response Variable drop-down list. SAID creates a linear model after a valid set of predictor and response variables are selected.
- ***Evaluate linear model***
  - SAID provides several diagnostic plots to determine if the created linear model created fits the assumptions of the OLS method.

Datasets: SAID is capable of loading two types of data. The term "loaded datasets" refers to datasets that have been loaded from disk. The data can be stored as tab delimited ASCII files or a collection of Argonaut ASCII files. Loaded datasets are not necessarily stored in separate files because of a constituent/surrogate relationship. Having dissimilar time steps is a typical reason for storing and loading datasets separately.

Variables with names that match the patterns CellXXAmpY and CellXXSNRY (where XX is the cell number, from 00 to 99, and Y the beam number, either 1 or 2) are dedicated variables for backscatter counts (Amp) and signal-to-noise ratio (SNR) and are used in the computation of the sediment attenuation coefficient and mean sediment corrected backscatter. These variables are not available for use in the creation of a linear model but are necessary in the computation of the ADVM acoustic surrogate metrics.

Variables named ADVMTemp and Vbeam also are dedicated variables used for the temperature and water depth. The temperature must be in units of degrees Celsius and is directly used in computing the ADVM parameters and is therefore necessary. The water depth is used to determine if the cell is out of water when the vertical orientation is selected in the ADVM Processing dialog box. A minimum Vbeam value also is set by the user in order to exclude samples taken when the water is below a certain depth.

During the time a dataset is being loaded, the program checks for variable names that are already loaded. If a variable that is in the dataset that is to be loaded exists in an already loaded dataset, then the selected dataset will not be loaded. Once the datasets are loaded, the data are then available for matching.

Matching Time-Series Observations: In order to build a linear model, it is necessary that a dataset with observations of predictor (surrogate) and response (water-quality) variables exist. Matching occurs in order to synchronize observations from the loaded datasets. The result of matching is the creation of a single dataset containing the matched data, which is then used to develop the linear model.

The primary dataset is the loaded dataset that contains the observations whose date and time of observation form the basis for matching in the secondary datasets. In a typical application for SAID, the primary dataset is the dataset that contains the constituent observations. The primary dataset is chosen by selecting it from the Primary Dataset drop-down list (figure 1). A linear model will not be created until a primary dataset is selected.

Secondary datasets are loaded datasets that contain observations that are matched to primary dataset observations. The term secondary dataset refers to all of the datasets that are not the primary dataset. Observations from the secondary datasets are only copied to the synchronized dataset if they have a date-time that matches a primary dataset observation within the user specified time interval allowance (Max. Time).

Selecting a primary dataset initiates the matching algorithm. For each observation in the primary dataset, SAID calculates the minimum absolute time difference between the observation date and time variables and the date and time variables of the secondary dataset being compared. If the minimum absolute time difference is less than or equal to the user specified value for the maximum time difference, the observations from the secondary dataset being compared are matched with the observations of the primary dataset and the values are copied to the matched dataset. If the minimum absolute time difference is greater than the user specified maximum time difference (Max. Time), then the corresponding variables in the observation in the matched dataset are set to an invalid value. In other words, the observation in the primary dataset will not be matched to an observation in the dataset being compared.

After a primary dataset is selected, the program will indicate that it is matching datasets and will remain unresponsive until the matching is complete. The time it takes for the program to create a matched dataset depends on the number of loaded datasets and the number of observations in each dataset. When the program has completed the matching algorithm, the variables available for use in the linear model are shown in the Predictor Variables and Response Variable lists.

Processing and Viewing Acoustic Backscatter Data (optional in SAID): The following ADVM-related parameters are required by SAID before the acoustic backscatter data are processed and acoustic surrogate parameters are computed:

- ADVM Configuration - Frequency, Effective Transducer Diameter, Slant Angle, Blanking Distance, Cell Size, Number of Cells
- ADVM Processing - Intensity Scale Factor (if Amp is selected for Backscatter Values), Minimum Mid-Point Cell Distance, Maximum Mid-Point Cell Distance, Minimum Vbeam

The configuration parameters are taken from a configuration record file that is saved by the ADVM with each ADVM data file. Once the required parameters in the ADVM Processing window have valid values, the ADVM parameters with at least one valid observation will be available in the Predictor Variables list. By clicking on the ADVM Processing button (figure 1), the ADVM configuration and processing options used in the calculation of the ADVM parameters can be changed (figure 2). ADVM configurations needed for input to SAID can be found in the setup parameters section of the ADVM software.

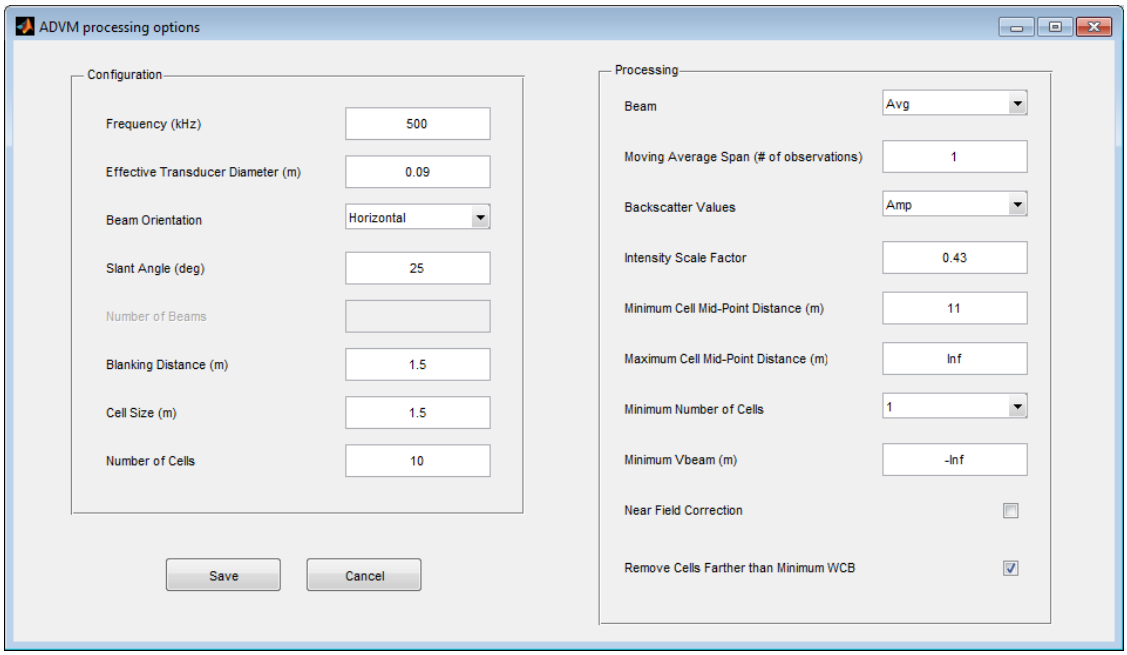

Figure 2 ADVM deployment configuration and acoustic parameter options window

Configuration Parameters: The following parameters indicate the ADVM type and setup and are necessary to compute the acoustic surrogate parameters (figure 2).

- ***Frequency*** – The frequency of the ADVM acoustic signal.
- ***Effective Transducer Diameter*** – The effective diameter in meters of the ADVM transducer. The effective transducer diameter is only used when the Near Field Correction option is selected in the Processing section.
- ***Beam Orientation*** – The orientation of the acoustic beams of the ADVM. If 'Vertical' is selected for this field, then the Vbeam for each observation is compared to the cell edges, and each cell that is out of water is marked as invalid.
- ***Slant Angle*** – The angle of the acoustic beam with respect to the vector that represents the cell distance from the instrument. This angle, along with the blanking distance, cell size, and number of cells, is used to find the mid-point distance of each cell along the acoustic beam.

- ***Number of Beams*** – The number of acoustic beams on the instrument. This value is not used. SAID assumes that the instrument has two beams.
- ***Blanking Distance*** – The distance in meters from the instrument to the beginning of the first cell. This value is used in the computation of the mid-point distance of each cell along the acoustic beam.
- ***Cell Size*** – The length of each cell in meters. This value is used in the computation of the mid-point distance along the acoustic beam of each cell.
- ***Number of Cells*** – The number of cells in the configuration of the ADVM under analysis. The number of cells directly affects the values displayed in the Minimum Number of Cells drop down list.

Processing Parameters: The following parameters control how ADVM backscatter data are screened and processed (figure 2).

- ***Beam*** – The beam number from which the backscatter values are taken. When 'Avg' is selected for this field, the average cell backscatter values are used.
- ***Moving Average Span*** – The span, in number of observations, used in a centered moving averaging of the backscatter time series. The span must be an odd positive integer.
- ***Backscatter Values*** – The backscatter values used in the computation of the ADVM parameters. When 'Amp' is selected, the backscatter values are multiplied by the value in the Intensity Scale Factor field. The Intensity Scale Factor field is made available only when 'Amp' is selected. (Caution: the model developed will be specifically for SNR or Amp units and cannot be switched without building a new model. All empirical testing for best model using SNR or Amp should be evaluated.)
- ***Intensity Scale Factor*** – The scaling factor to convert backscatter counts to decibels. This field is only available when 'Amp' is selected in the Backscatter Values drop-down list. The factor defaults to 0.43 (typical for SonTek® instruments); but should be taken from manufacturer literature for specific ADVMs.
- ***Minimum Cell Mid-Point Distance*** – The minimum distance in meters from the transducer that the mid-point of a cell has to be in order for it to be used in the computation of the ADVM parameters.
- ***Maximum Cell Mid-Point Distance*** – The maximum distance in meters from the transducer that the mid-point of a cell can be in order for it to be used in the computation of the ADVM parameters.
- ***Minimum Number of Cells*** – The required minimum number of valid cells that an ADVM sample has to have in order for its computed parameter to be included as an observation in the linear model.
- ***Minimum Vbeam*** – The minimum value for Vbeam that a sample must have in order for it to be used as an observation. Vbeam is the water height in meters that the ADVM reports.
- ***Near Field Correction*** – When the box is checked, a near field correction to the backscatter values is made (Downing and others, 1995). When the box is not checked, no near field correction is applied. In general, data from the near field should be avoided by setting the blanking distance and/or Minimum Cell Point distance greater than the near field for a given instrument.
- ***Water Corrected Backscatter (WCB) Profile Adjustment*** – When this box is checked, the range of cells that include and are beyond the cell with the minimum water corrected backscatter (minWCB) are not included in the calculation, unless the cell with the minWCB is the last or first cell in the range considered.
    - If the cell with the minWCB is the last cell, the value is retained and all cells are used to calculate the sediment corrected backscatter and attenuation coefficient.
    - If the cell with the minWCB is the first cell, all other cells are not considered, and the water corrected backscatter value in the first cell is used as the sediment corrected backscatter value for the observation, and no attenuation coefficient is calculated.

Viewing acoustic backscatter profiles: When a valid response variable is matched with valid predictor variables, the Plot Backscatter button will be made available. When this button is clicked, a window with three sets of axes is displayed. From the top, the axes show Sediment Corrected Backscatter (SCB), Water Corrected Backscatter (WCB), and Measured Backscatter (MB), all in decibels, versus the cell mid-point distance along the acoustic beam (figure 3). Also shown in the window is a list of observation numbers and times from the model. The observation times are taken from the primary dataset. Only the backscatter samples that correspond to observations in the linear model are shown. Selecting sample times in the list displays the plots of the backscatter values on the axes. Multiple observations can be selected and plotted.

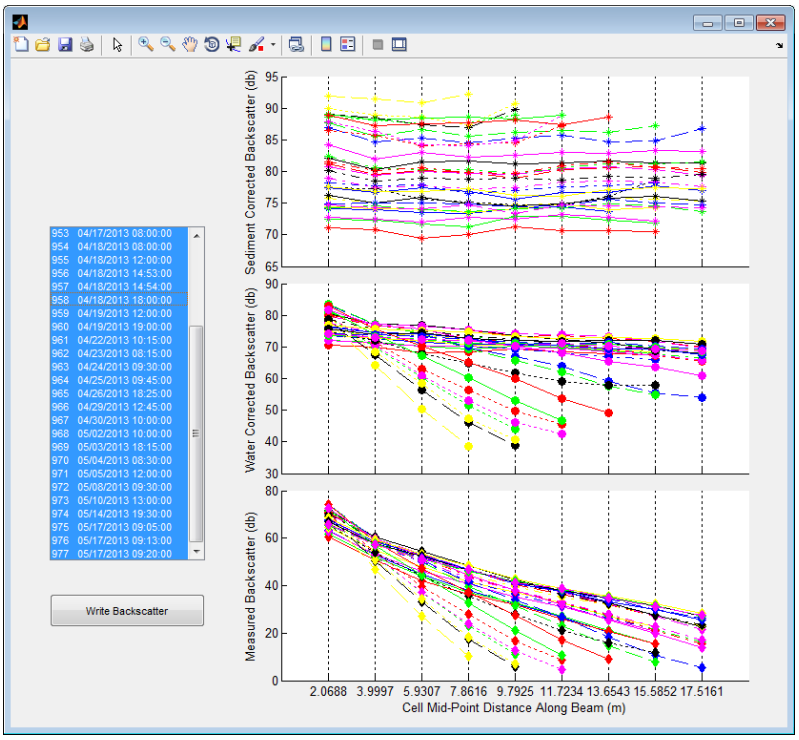

Figure 3 Backscatter profile plotting window

Development of Linear Regression Models: The available variables for use in the development of linear regression models in SAID appear in the Predictor Variable list and Response Variable in the Linear Model screen (Figure 4). There is no limit on the number of variables used in the creation of an Ordinary Least Squares (OLS) linear regression model, and there are no restrictions regarding which variables must be used. The Transform Variable button provides the option to transform a loaded variable using a transform function. When transformed, the variable will be available as a selection in the Predictor Variable list and the Response Variable drop down list.

As datasets are loaded, and if the Match Variable is a valid selection, the variables that are available for use in developing the linear model are shown in the Predictor Variables list and the Response Variable drop-down list. Selecting a variable in the Predictor Variables list, then one from the Response Variable drop-down list, will result in the generation of a model. Selecting the variable that is used for the Response Variable in the Predictor Variables list deselects the predictor variables and resets the response variable selection to the first in the list.

After a model is successfully created by selecting variables, a user can begin to evaluate the model results. This program includes tools to assist in model evaluation, available using the Plot Backscatter, View/Edit Table, Display Model, Write Report, Plots, and Time Series buttons. The number of observations used in the model is shown next to the Number of Observations label.

If a valid linear model exists within the program, the Number of Observations field will show the number of samples used in the development of the linear model. This corresponds to the number of valid observation values for the selected variables within the primary dataset. The Total Samples field shows the total number of samples in the loaded dataset. This number corresponds to the number of samples in the dataset that is selected in the Match Variable drop-down list.

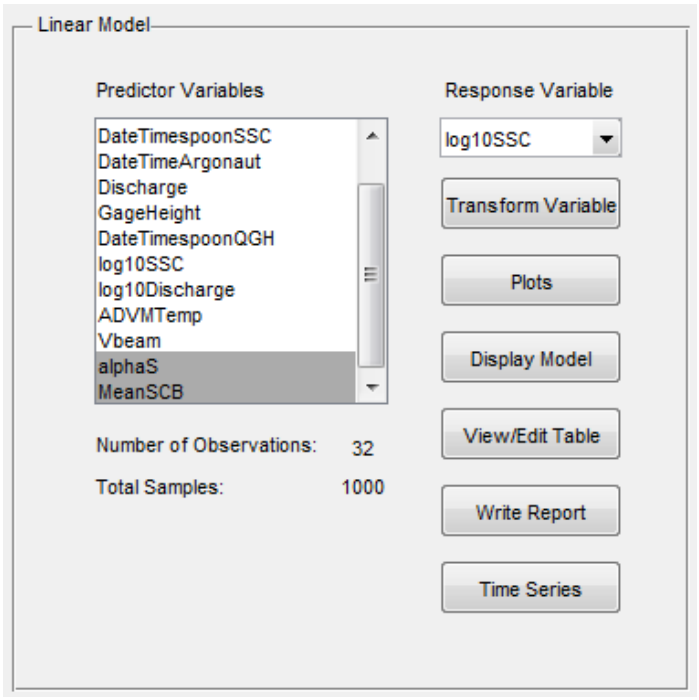

Figure 4 Linear Model options on the main SAID window

Evaluation of Regression Models: SAID provides several ways to graphically evaluate the linear model. Clicking on the Plots button within the main SAID window will display another window that provides several plotting options. In any plot figure, if Data Cursor Mode is enabled, any observation data point can be selected and the corresponding observation number will be shown along with the values plotted. The Model button will show different figures depending on if the linear model is a simple linear regression (SLR) or a multiple linear regression (MLR) or if the response variable is transformed. If the existing linear model is an SLR model, then a figure with the response observations plotted against the explanatory observed values will be shown (figure 5). When the existing model is an MLR, a partial residual plot for each variable in the model will be shown. If the response variable is transformed, then a linear-space plot will be shown with a smeared estimate fit line and confidence bounds.

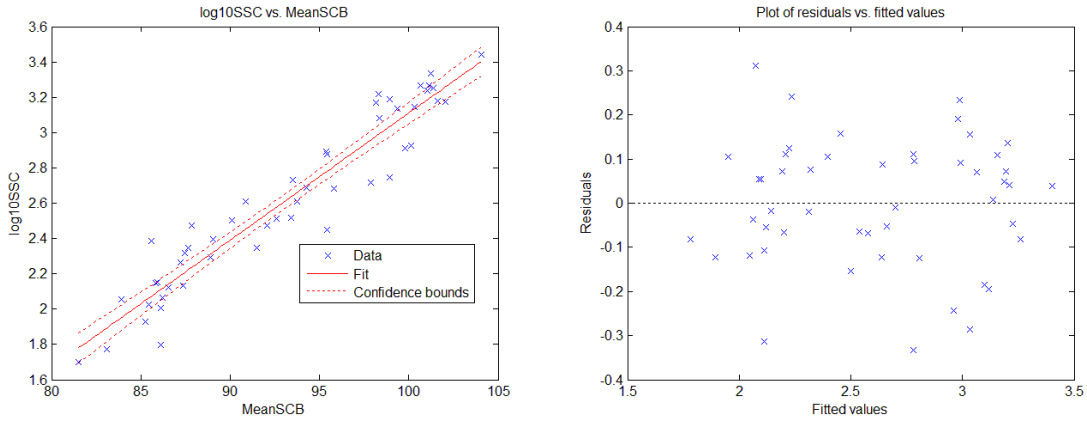

Figure 5 Linear model scatter plot and residual plot for a SLR model

Predicted versus observed plots can be selected to display the predicted response variable with the observed response variable. Also plotted is a one-to-one data line for comparison. If the response variable is transformed, then an additional figure will show the predicted versus observed values in linear space. Additionally the following residual plots can be selected:

- ***Raw Vs. Fitted***—Illustrates a plot of the raw residuals against the fitted response values.
- ***Probability***—Normal probability plot of raw residuals.
- ***Stan. Ser. Corr.***—Standard serial correlation plot of the residuals shown with a LOWESS fit line to detect autocorrelation. If the LOWESS fit line shows a trend that deviates far from 0, serial correlation may be present.
- ***Vs. Time***—Raw residuals plotted against time to see if a time dependent trend exists with the residuals.

The Display Model button will provide a window that displays the model results and statistics (figure 6). The information includes the linear equation, coefficient estimates, estimated confidence intervals, R^2 values for the model, and root mean squared error. This information also is written to a report with the Write Report button on the main SAID window.

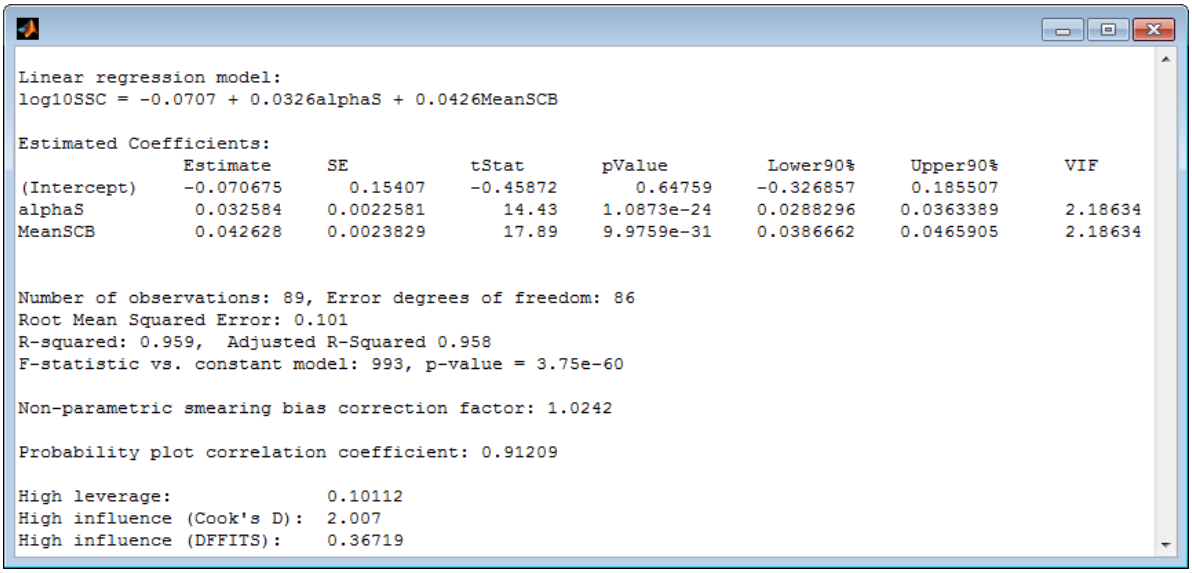

```
Linear regression model:
log10SSC = -0.0707 + 0.0326alphaS + 0.0426MeanSCB

Estimated Coefficients:
              Estimate      SE           tStat       pValue          Lower90%      Upper90%      VIF
(Intercept)    -0.070675      0.15407    -0.45872       0.64759     -0.326857     0.185507
alphaS          0.032584    0.0022581       14.43    1.0873e-24     0.0288296    0.0363389      2.18634
MeanSCB         0.042628    0.0023829       17.89    9.9759e-31     0.0386662    0.0465905      2.18634


Number of observations: 89, Error degrees of freedom: 86
Root Mean Squared Error: 0.101
R-squared: 0.959,  Adjusted R-Squared 0.958
F-statistic vs. constant model: 993, p-value = 3.75e-60

Non-parametric smearing bias correction factor: 1.0242

Probability plot correlation coefficient: 0.91209

High leverage:              0.10112
High influence (Cook's D):  2.007
High influence (DFFITS):    0.36719
```

Figure 6 Linear model regression model statistics window

Clicking on the View/Edit Table button will display a window that contains the observation information used in the model. The information shown is the observation number, the corresponding primary date and time variable, the response variable, and the predictor variables. Also shown are diagnostic statistics for each observation for outlier detection (Helsel and Hirsch, 2002). Calculated indicator values that exceed the corresponding critical values for the model are highlighted in red.

Observations can be removed by checking the boxes in the far left column and clicking the Remove Observation button. This action flags the date and time within the program and sets the variables that correspond to the date and time to an invalid value. Once a date and time is flagged as removed, any future variables that are used in the model will have the corresponding values set as invalid. This will continue until the Restore All Observations button is clicked, which clears the date and times flagged.

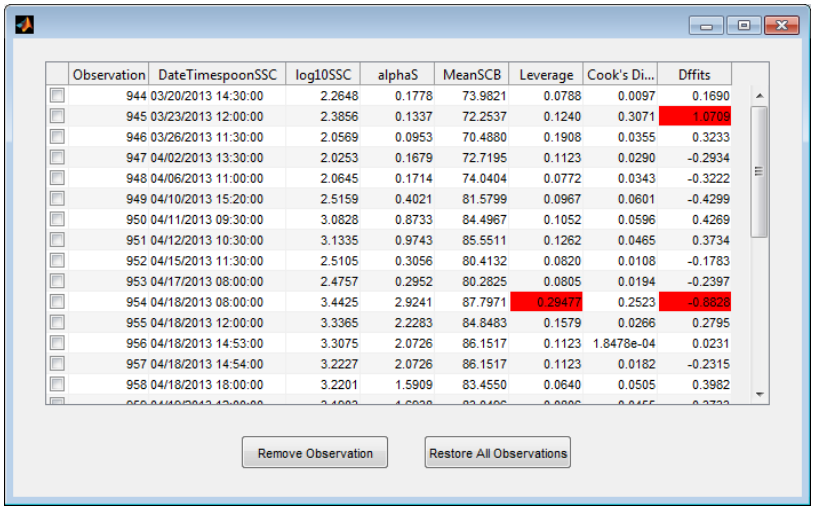

Figure 7 Observation table window used to view and remove observations from the model dataset

Generation of Report Output: To write a full summary report for the linear model, click on the Write Report button within the main SAID window. The user will be prompted for a location and name of a comma separated value file to write the report to. Selecting and entering a valid location and file name will write the report. The contents of the report include:

- ADVM configuration and processing options
- Dataset file names and locations
- Linear model summary and statistics
- Critical outlier indicator values
- The dataset observations that were used in the creation of the model along with Observation number, fitted response variable values, raw residuals, an estimate of the non-transformed variable with bias correction applied (if the response variable is transformed), and calculated outlier indicator values
- The observations that were removed from the model dataset

REAL-TIME DATA DISSEMINATION UTILITIES

After a surrogate regression model is developed and approved, the model can be used to generate continuous, real-time SSC estimates. The USGS has two utilities that make use of the computational algorithms in SAID to continuously estimate and display real-time sediment data:

- Real-time Acoustic Sediment Surrogate DAta Transfer (RASSDAT) program
- National Real-Time Water Quality (NRTWQ) program

RASSDAT is a Visual Basic Graphical User Interface (GUI) wrapped around a Python™ script that runs on a Windows® computer (figure 8), interfaces with the USGS National Water Information System (NWIS), and displays computed SSC on the NWIS Web Interface (http://waterdata.usgs.gov/nwis). NRTWQ is run from a centralized server and displays computed SSC on the NRTWQ Web site (http://nrtwq.usgs.gov/; figure 9). RASSDAT is under beta development and is not yet formally released as a USGS software product. Questions about RASSDAT development can be directed to the authors.

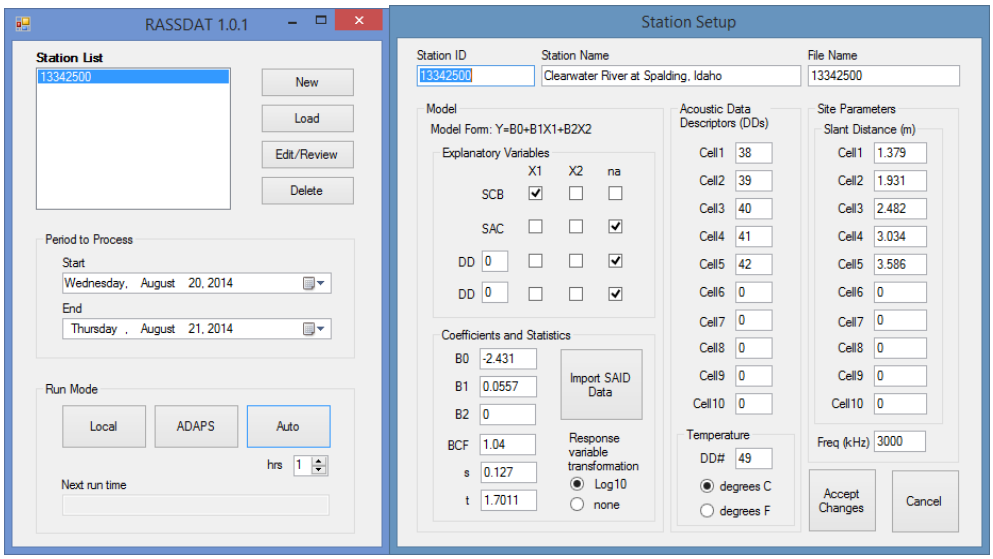

Figure 8 Screen captures of main processing (left) and station setup (right) windows from the USGS RASSDAT program, beta test version 1.0.1.

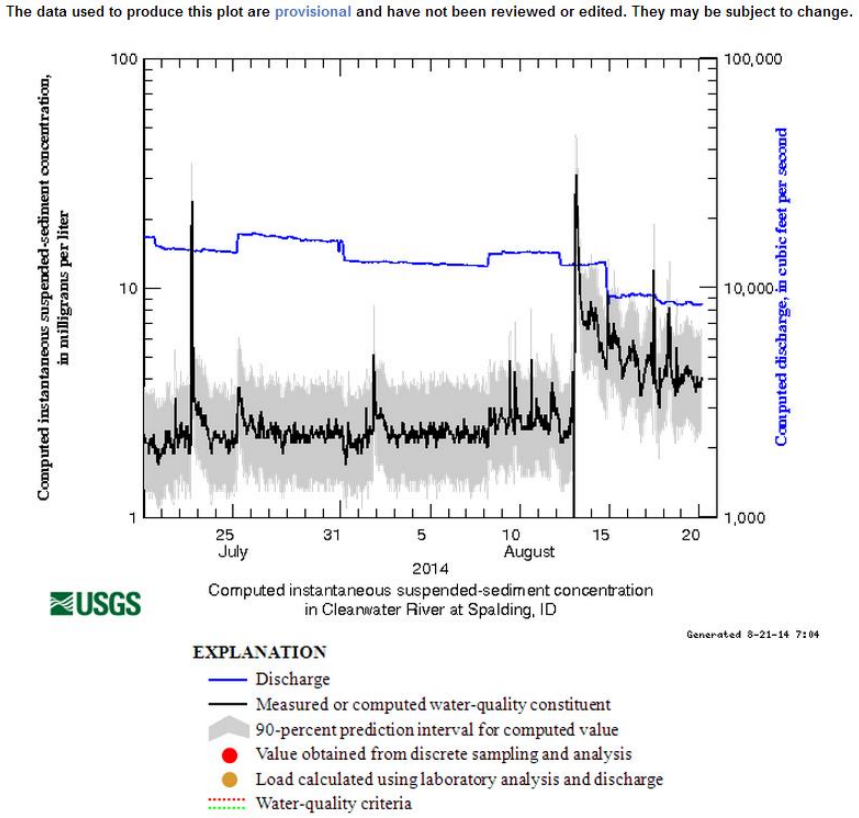

Figure 9 Screen capture from NRTWQ Web site showing example of SSC and SSC prediction intervals computed by using a sediment acoustic surrogate model developed for the Clearwater River at Spalding, Idaho (USGS Identification number 13342500).

SUMMARY

The use of continuous parameters as surrogates for water quality constituents has been successful in multiple applications across the Nation. Critical to advancing the operational use of surrogates are tools to process and evaluate the data along with the subsequent development of regression models from which real-time sediment concentrations can be made available to the public. Recent developments of these tools are having an immediate impact on surrogate research, and on surrogate technologies for monitoring, assessment, rapid decision making, and adaptive management. The Surrogate Analysis and Index Developer (SAID) standalone tool processes complex datasets and creates regression models that related surrogate to constituent data by providing visual and quantitative diagnostics to the user. SAID is currently under development and beta testing at the U.S. Geological Survey.

SAID can be used to create regression models between surrogate data and constituent measurements. Additionally, SAID is a standalone tool to assist in the development of ordinary least squares (OLS) regression models with any response and predictor variables by providing visual and quantitative diagnostics to the user. There is no limit on the number of variables that can be used in the linear model, and there are no restrictions regarding which variables must be used. The sediment acoustic method utilizes acoustic parameters from fixed-mount stationary equipment with the assumption that the sediment concentration along the acoustic beam path is constant for a given time period. Within SAID, the user can set ADVM configuration and processing options, transform a loaded variable, build linear regression models, view linear model diagnostic statistics and plots, export the model information, and generate a predicted time series.

After a surrogate regression model has been developed and approved, the model can be used to generate continuous, real-time SSC estimates. Results from SAID provide direct inputs to two USGS utilities: the Real-time Acoustic Sediment Surrogate DAta Transfer (RASSDAT) program and the National Real-Time Water Quality (NRTWQ) program. The output from these utilities are displayed on USGS Web sites as real-time continuously computed sediment data. RASSDAT, currently under development and in beta testing at USGS, is a Visual Basic Graphical User Interface (GUI) wrapped around a Python™ script that runs on a Windows® computer, interfaces with the USGS National Water Information System (NWIS), and displays computed SSC on the NWIS Web Interface (http://waterdata.usgs.gov/nwis). NRTWQ is run from a centralized server and displays computed SSC on the NRTWQ Web site. The real-time dissemination of predicted SSC and prediction intervals for each time step has substantial potential to improve understanding of sediment-related water-quality and associated engineering and ecological management decisions.

ACKNOWLEDGEMENTS

The USGS Midwest Region and the Federal Interagency Sediment Project supported the development of these utilities. The Midwest Region support was through the River Sediment and Nutrient Investigations Initiative. We thank the many beta testers for their thorough testing and comments. Any use of trade, firm, or product names is for descriptive purposes only and does not imply endorsement by the U.S. Geological Survey.

REFERENCES

Helsel, D.R., and Hirsch, R.M., 2002, Statistical methods in water resources—hydrologic analysis and interpretation: U.S. Geological Survey Techniques of Water-Resources Investigations, book 4, chap. A3, 510 p.

Landers, M.N., 2012, Fluvial suspended sediment characteristics by high-resolution, surrogate metrics of turbidity, laser-diffraction, acoustic backscatter, and acoustic attenuation. Ph.D. Dissertation, Georgia Institute of Technology. Available at http:hdl.handle.net/1853/43747 (accessed on 14 June 2012).

Rasmussen, P.P., Gray, J.R., Glysson, G.D., and Ziegler, A.C., 2009, Guidelines and procedures for computing time-series suspended-sediment concentrations and loads from in-stream turbidity-sensor and streamflow data: U.S. Geological Survey Techniques and Methods book 3, chap. C4, 53 p.

Topping, D. J., Melis, T. S., Rubin, D. M. and Wright, S. A. (2004), High-resolution monitoring of suspended-sediment concentration and grain size in the Colorado River in Grand Canyon using a laser acoustic system, in Proceedings of the 9th International Symposium on River Sedimentation, Yichang, China, 18-21 October, Tsinghua University Press, 2507-2514.

Topping, D. J., Wright, S. A., Melis, T. S., and Rubin, D. M. (2006), High-resolution monitoring of suspended-sediment concentration and grain size in the Colorado River using laser-diffraction instruments and a three-frequency acoustic system. Proceedings of the 8th Federal Inter-Agency Sedimentation Conference, Reno, NV, April 2–6, 2006, 555–559

Topping, D. J., Wright, S. A., Melis, T. S. and Rubin, D. M. (2007), High-resolution measurement of suspended-sediment concentrations and grain size in the Colorado River in Grand Canyon using a multi-frequency acoustic system, in Proceedings of the 10th International Symposium on River Sedimentation, Moscow, Russia, 1-4 August, 330-339

Wood, M.S., and Teasdale, G.N., 2013, Use of surrogate technologies to estimate suspended sediment in the Clearwater River, Idaho, and Snake River, Washington, 2008–10: U.S. Geological Survey Scientific Investigations Report 2013-5052, 30 p.

Wright, S. A., Topping, D. J., & Williams, C. A. (2010). Discriminating silt-and-clay from suspended-sand in rivers using side-looking acoustic profilers. 2nd Joint Federal Interagency Conference. Las Vegas, NV.

EFFECTIVE PARTICLE SIZES OF COHESIVE SEDIMENT IN NORTH MISSISSIPPI STREAMS

Roger Kuhnle, Research Hydraulic Engineer, National Sedimentation Laboratory, USDA-Agricultural Research Service, Oxford, MS, roger.kuhnle@ars.usda.gov;

Daniel Wren, Research Hydraulic Engineer, National Sedimentation Laboratory, USDA-Agricultural Research Service, Oxford, MS, daniel.wren@ars.usda.gov .

Abstract Knowledge of the size of cohesive sediment particles transported in streams is important information for predicting how the sediment and contaminants the sediment may be carrying will be transported by the flow. Cohesive sediments (less than 0.062 mm in diameter) generally are not transported in their primary dispersed particle sizes, but commonly assume larger sizes as aggregates and/or as flocs. Due to a lack of models for predicting effective particle sizes of fine sediments in streams, it is common for researchers and practitioners to assume that the sediment transported in a stream assumes the primary size of the sediment. Information on the effective sizes of fine sediment in streams is available for only a small number of streams. More data on the effective size of cohesive particles in streams is needed to allow more accurate modeling of their transport. In this investigation, measurements of the effective particle size were made using a portable laser particle size analyzer which was deployed in three streams during runoff events. The primary particle sizes were determined from samples of the suspended sediment which were collected in close proximity to and at the same time as the effective particle sizes were measured. The effective particle sizes were found to be coarser than the primary sizes and did not vary in a predictable manner with the stage of the streams during the runoff events. Ratios of the effective mean sediment size to the primary mean sediment size ranged from 6 to 21 for the three streams considered.

INTRODUCTION

Accurate determinations of the sizes of sediments are necessary for the study of sediment transport by flowing water. The grain size along with other physical properties of the sediment, including the composition, density, and shape are needed for determining how the sediment will be transported and how it will interact with materials in the water column such as chemicals and aquatic biota. The most widely accepted method for measuring particles greater than 62 microns in diameter is the use of sequentially sized sieves. For particles finer than 62 microns, pipettes and calculated fall velocities are typically used. Other techniques, based on automated fall-velocity determinations and laser-based measurements are also in use, but have not been standardized and tested and adopted by sedimentationists to the extent that sieve and pipette methods have been.

Measurements of the diameters of sand-sized sediments (62-2000 microns) and coarse silt-sized sediments (30-62 microns) that are transported in a channel have become routine and are repeatable if proper sediment collection and preparation methods are used (Rigby and Wren, 2013); however, the determination of the effective sizes of finer sediments in transport is problematic. As the size of the sediment decreases, properties such as cohesion and interactions with aquatic biota become important (Droppo, 2001) and measurement of size becomes more difficult. The effective particle size distribution (EPSD) of fine (< 62 microns in diameter) suspended sediment in fluvial transport is generally regarded to develop in balance with local conditions (Kranck, 1979), such that samples that are withdrawn from the channel, stored, and resuspended will have a particle size distribution that is not representative of the one present while the particles were in fluvial transport (Phillips and Walling, 1995). Measurements of fine sediment particles in fluvial transport must therefore be measured in situ.

Traditionally, studies of sediment transport by streams have made the assumption that the dispersed sizes of the inorganic material of the fine sediment fraction contain the information that is important for discerning how that sediment will be transported. However, because fine sediments in fluvial transport often consist of composite particles (Droppo, 2001; Walling and Woodward, 2000; Woodward and Walling, 2007) which may be composed of aggregates inherited from when the sediment was eroded (Meyer et al., 1980), or which formed by flocculation in the channel of the stream (Droppo, 2001), dispersed sediment size will not yield useful information on how fine sediment is transported or what it is carrying. Large differences in EPSD of fine sediments have been measured over separate sub-catchments of one basin (Woodward and Walling, 2007). Effective mean particle sizes have been found to be just slightly larger than the primary particle sizes (Williams et al., 2007) to more than two orders of magnitude larger than their constituent mineral grains (Woodward and Walling, 2007). Measurements from a wider variety of physical conditions and stream types are needed to determine the range of EPSD expected for different conditions. Measurements of EPSD and primary size distributions of fine sediments in fluvial transport from three streams northern Mississippi are presented and compared.

FIELD SITES

Samples of the fine suspended sediment in transport during runoff events were collected from three locations, Goodwin Creek, Yocona River, and Little Tallahatchie River, all located in the northern part of the state of Mississippi (Figure 1). The drainage areas upstream from the sample collection points were as follows: 18 km^2 for station 2 of Goodwin Creek, 679 km^2 for the bridge crossing of Mississippi State Highway 7 at the Yocona River, and approximately 3000 km^2 for the bridge crossing of Mississippi State Highway 7 at the Little Tallahatchie River. The samples from Goodwin Creek were collected 65 m upstream of the station 2 gauging station. The Yocona River samples were collected 10 m downstream of the bridge crossing of Mississippi State Highway 7 and south of Oxford. The samples from the Little Tallahatchie River were collected 300 m downstream of the bridge crossing of Mississippi State Highway 7 north of Oxford. Land use was 39 and 60 percent agriculture for the Yocona (Mississippi Department of Environmental Quality, 2003) and Little Tallahatchie Watersheds (Free Flow

Power, 2013), respectively. Recent surveys of land use at Goodwin Creek Watershed indicated that 8 percent of the land was cultivated (Kuhnle et al., 2008).

Figure 1. Map of the three sample locations: 1 – Little Tallahatchie River, 2 – Yocona River, 3 – Goodwin Creek.

Sample Collection

The collection of samples was undertaken as soon as practical after rainfall caused runoff events. Physical samples of sediment and water were collected while wading in water up to 1 m in depth. The samples were collected near the surface using 20 L buckets to ensure that sufficient quantities of sediment were collected to measure dispersed or primary sediment size distributions. After being transported to the laboratory and total weights had been measured, the samples were allowed to settle and the clear water was decanted. The sediment was collected and organic material was removed by treating with hydrogen peroxide. Samples were agitated overnight after the addition of sodium hexametaphosphate. Primary particle size distributions (PPSD) were determined in the laboratory following standard techniques using the pipette method (Brakensiek et al., 1979).

Measurement of Effective Particle Size Distributions

A self-contained portable laser particle size analyzer was used to collect measurements of EPSD of the fine sediments that were concomitant in time with the collection of physical samples. This instrument measures particle diameter using 32 logarithmically spaced size classes from 2.5 to 500 µm (LISST-100X, Type C from Sequoia Scientific). The size distribution of the particles is measured by volume with no assumptions made concerning density or mass. While the previous version of the instrument software only had the option of calculating the equivalent spheres size distribution, version 5.0 of the instrument software has the option to convert the diffraction data to particle diameters using algorithms which were developed using the light scattering properties of natural, random shaped particles (Agrawal et al., 2008). As fine sediment grains generally are not spherical, our experience with the new routines is that they yield more accurate size distributions than previous versions that used the spherical shape assumption. In some of the deployments the turbidity of the water was of a sufficient magnitude that the laser beam could not be pass through the measurement volume of the LISST. In these cases a 90 percent path reduction module was used to allow data to be collected.

The LISST was deployed in a vertical position with the measurement area perpendicular to the direction of the flow. The instrument was positioned near the bank in water depths of 0.6 to 0.9 m on the Yocona and Little Tallahatchie Rivers, and either near the bank or in the center of the channel mounted on a moored floating platform (Figure 2) on Goodwin Creek. The end of the instrument was mounted between 0.15 to 0.3 m below the surface of the flow.

Figure 2. Deployment of the LISST on tethered floating platform in Goodwin Creek during 06/10/2014 runoff event.

Effective size data was collected from five runoff events on Goodwin Creek, one runoff event on the Yocona River and one event on the Little Tallahatchie River (Table 1). Most of the samples were collected during relatively low stages in the channels after the peak flow had passed. Primary particle size data was measured for three of the events on Goodwin Creek and the events from the Yocona and Little Tallahatchie Rivers (Table 1).

Table 1. Dates and locations of sample collection.

date	location	Mean stage during sampling (m)	Relation to peak stage	Range in effective sizes (mm)	Range in primary sizes (mm)	Mean ratio effective to primary size
04/11/2013	Goodwin Creek, upstream of station 2	1.14	during	0.025 – 0.029	--	--
04/19/2013	Goodwin Creek, upstream of station 2	0.25	11 hours past	0.015 – 0.031	--	--
04/04/2014	Goodwin Creek, upstream of station 2	0.31	2.6 hours past	0.012 - 0.017	0.0029 - 0.0034	4.6
06/09/2014	Goodwin Creek, upstream of station 2	0.26	3.4 hours past	0.022 – 0.024	0.0029 - 0.0041	7.7
06/10/2014	Goodwin Creek, upstream of station 2	0.47	15.9 hours past	0.039 – 0.14	0.0062 - 0.0084	16.9
10/03/2014	Yocona River at MS Highway 7	1.01	6.5 hours past	0.039 – 0.045	0.0024 – 0.0027	15.2
10/15/2014	LittleTallahatchie River at MS Highway 7	3.26	7.8 hours past	0.017 – 0.065	0.0038 – 0.0041	10.5

RESULTS

Particle Sizes

The effective particle sizes with time for the sampled runoff events are presented in Figures 3 and 4. Changes in effective mean grain sizes over the periods measured (0.8 – 1.2 hr) on Goodwin Creek were nearly constant or changed gradually for three of the events, while the mean effective sizes during the 04/19/13 and 06/10/14 events increased by factors of 2.1 and 4.4, respectively. Changes in the trends of effective size were also small for the events sampled on the Yocona and Little Tallahatchie Rivers (Figure 4). Mean sizes of primary particles ranged from 0.0024 to 0.0084 mm with ratios of effective to primary sizes ranging from 4.6 to 16.9 (Table 1).

To investigate more fully the observed changes in effective sediment size during the 04/19/14 and the 06/10/14 runoff events on Goodwin Creek, the D_{16} and D_{84} particle sizes (sizes in which 16 and 84 percent of the distribution are finer) were plotted in Figure 3B and 3F. It is apparent for both of these runoff events that the D_{84} of the effective size distribution increased more rapidly than the D_{16} size. This was particularly true in the beginning part of the measured flows. Apparently the initial changes in mean size occurred mostly in the coarser part of the size distribution. This may be related to how flocs are created and destroyed during a runoff event.

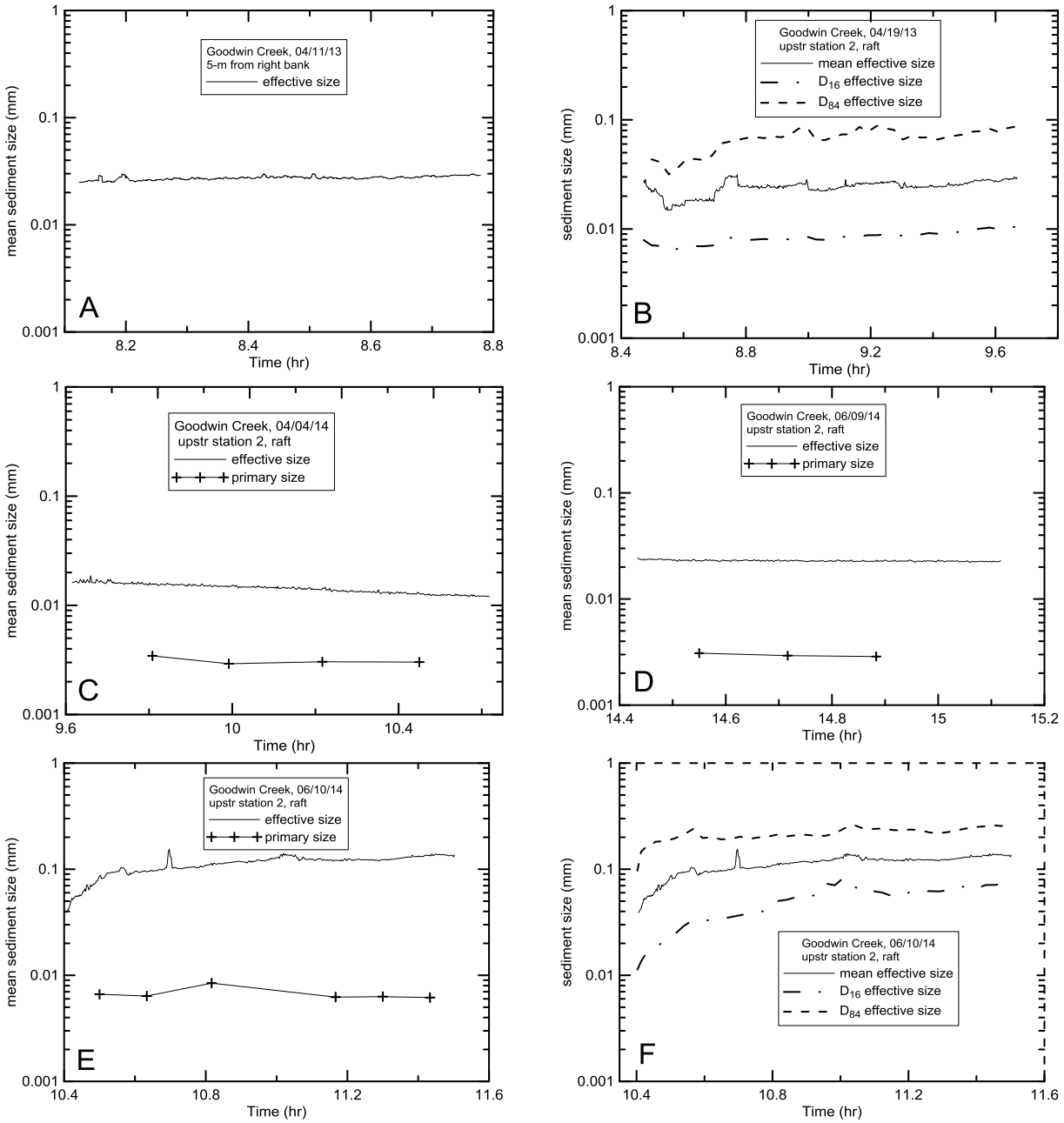

Figure 3. Effective and primary particle sizes measured in the main channel of Goodwin Creek 65 m upstream of gauging station 2.

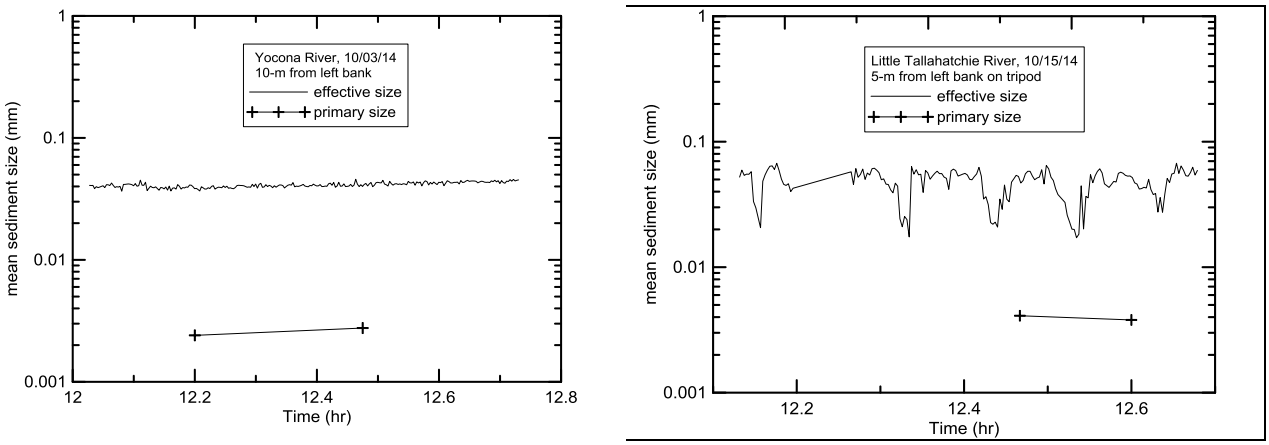

Figure 4. Effective and primary particle sizes measured at the Yocona River and Little Tallahatchie Rivers.

Discussion and Conclusions

The particle size data from this study indicates that the fine sediments of Goodwin Creek, Yocona River, and Little Tallahatchie River are transported as aggregated or flocculated collections of primary particles that range in size from about 5 to 20 times the mean diameter of the dispersed primary particles. Particle size data collected from multiple runoff events on Goodwin Creek have demonstrated that effective sizes may vary by more than an order of magnitude from different runoff events collected at the same site, while the mean sizes of primary particles varied only by about a factor of two. It has also been observed that effective sizes may vary by at least a factor for four over relatively short periods of time with nearly steady conditions of flow in the channel. The reasons for this range in effective sizes are possibly related to changes in the sources of sediment to the channel and how they were eroded and transported. It is clear that the effective particle sizes on the three watersheds were similar even though the drainage areas of the watersheds range over more than two orders of magnitude and channel lengths of the main channel upstream of the measurement sites were 10, 35, and 100 km for the Goodwin Creek, Yocona River, and Little Tallahatchie Rivers, respectively.

Past studies on the provenence of fine sediment conducted at Goodwin Creek have revealed that the dominant sources of sediment changed from surface to bank dominated during the course of a runoff event (Wilson et al., 2008, 2014) and may also vary with season and the characteristics of the rainfall and runoff. The different processes of erosion associated with different sediment source types would likely lead to different effective sediment size signatures in the channel of a stream. Aggregates of fine sediment, for example, may be more plentiful in sediment that was derived from bank erosion than from sediment that originated from upland sources. The intensity of the rainfall event and shape of the hydrograph also would likely affect the size of eroded particles and the evolution of particles as they are transported through the channels of a watershed. The season of the year may also be an important piece of information affecting effective sediment sizes particularly in watersheds with significant percentages of the land surface involved in agriculture activities such as tillage, planting, and cultivation. It has been shown from previous studies that the type and extent of agricultural practices have a direct effect

on the nature of runoff and the production of fine sediment from plots and watersheds (McGregor et al., 1969; Dendy et al., 1979; Kuhnle et al., 1996). This may also be true when biological activity affects particle flocculation (Droppo, 2001).

A related study conducted on the River Exe watershed in southern England (Williams et al., 2007), in which effective sizes were measured with a LISST-100, found that median of the EPSD ranged from about 70 to 200 microns over four runoff events. Two of the events were in the spring of the year and two were in the fall of the year and the durations of the measurements were 2.5 to 16 hours. These median values were about three to four times larger than the values measured in this study. It is not clear to what extent the differences in measured EPSD from the Exe watershed and the ones from this study were due to physical differences of the watersheds or to the effect of sampling differences. Measurements collected over larger portions of several runoff events from different seasons would yield a better picture of the variations present in EPSD on watersheds such as Goodwin Creek.

REFERENCES

Agrawal, Y. C., Whitmire, A., Mikkelsen, O. A., Pottsmith, H. C., (2008). "Light scattering by random shaped particles and consequences on measuring suspended sediments by laser diffraction", Journal of Geophysical Research, 113, C04023, doi:10.1029/2007JC004403, 11 pp.

Brakensiek, D. L., Osborn, H. B., Rawls, W. J., (1979). Field Manual for Research in Agricultural Hydrology. U. S. Department of Agriculture, Agricultural Handbook 224, 550 pp.

Dendy, F. E., Ursic, S. J., Bowie, A. J., (1979). "Sediment sources and yields from upland watersheds in north Mississippi". Proceedings Mississippi Water Resources Conference, Water Resource Research Institute, Mississippi. p. 49-54.

Droppo, I. G., (2001). "Rethinking what constitutes suspended sediment," Hydrological Processes 15, pp 1551-1564.

Free Flow Power Corporation, (2013). Sardis Lake Hydroelectric Project, Final License Application. FERC Project no. 13701, 276 pp.

Kranck, K., (1979). "Dynamics and distribution of suspended particulate matter in the St. Lawrence Estuary", Nat. Can. 106, pp 163-173.

Kuhnle, R. A., Bingner, R. L., Alonso, C. V., Wilson, C. G., and Simon, A., (2008). "Conservation practice effects on sediment load in the Goodwin Creek Experimental Watershed", Journal of Soil and Water Conservation. 63(6), pp 496-503.

Kuhnle, R. A., Bingner, R. L., Foster, G. R., Grissinger, E. H., (1996). "Effect of land use changes on sediment transport in Goodwin Creek". Water Resources Research, 32(10), pp 3189-3196.

McGregor, K. C., Greer, J. D., Gurley, G. E., Bolton, G. C., (1969). Runoff and sediment production from north Mississippi loessial soils. Bulletin 777, State College, MS Agricultural Experiment Station, Mississippi State University.

Meyer, L. D., Harmon, W. C., McDowell, L. L., (1980). "Sediment sizes eroded from crop row sideslopes", Transactions of the American Society of Agricultural Engineers, 23, pp 891-898.

Mississippi Department of Environmental Quality, (2003). Yocona River and Enid Reservoir Phase One Total Maximum Daily Load for Mercury. Mississippi Department of Water Quality, Jackson, MS, 47 pp.

Phillips, J. M., Walling, D. E., (1995). "An assessment of the effects of sample collection, storage and resuspension on the representativeness of measurements of the effective particle size distribution of fluvial suspended sediment", Water Research, 29(11), pp2498-2508.

Rigby, J. R., Wren, D. G., (2013). "A comparison and assessment of four sediment particle-size analysis methodologies", Proceedings of the Hydraulic Measurement and Experimental Methods Measurement Conference, ASCE, 2012.

Walling, D. E., Woodward, J. C., (2000). "Effective particle size characteristics of fluvial suspended sediment transported by lowland British rivers". In *The Role of Erosion and Sediment Transport in Nutrient and Contaminant Transfer*, IAHS Publication No. 263, International Association of Hydrological Sciences Press: Wallingford; pp 129-140.

Williams, N. D., Walling, D. E., Leeks, G. J. L., (2007). "High temporal resolution in situ measurement of the effective particle size characteristics of fluvial suspended sediment". Water Research, 41, pp 1081-1093.

Woodward, J. C., Walling, D. E., (1992). "A field sampling method to obtain representative samples of composite fluvial suspended sediment particles for SEM analysis," Journal of Sedimentary Petrology 64(4), pp 742-744.

Woodward, J. C., Walling, D. E., (2007). "Composite suspended sediment particles in river systems: their incidence, dynamics, and physical characteristics", Hydrological Processes, 21, pp 3601-3614.

Wilson, C. G., Kuhnle, R. A., Bosch, D. D., Steiner, J. L., Starks, P. J., Tomer, M. D., Wilson, G. V., (2008). "Quantifying relative contributions from sediment sources in Conservation Effects Assessment Project watersheds". Journal of Soil and Water Conservation. 63(6) pp 523-532.

Wilson, C. G., Kuhnle, R. A., Dabney, S. M., Lerch, R. N., Huang, C. H., King, K. W., Livingston, S. J., (2014). "Fine sediment sources on conservation evaluation assessment watersheds". Journal of Soil and Water Conservation, 69(5), pp 402-413.

SUSPENDED-SEDIMENT CONCENTRATIONS, YIELDS, TOTAL SUSPENDED SOLIDS, TURBIDITY, AND PARTICLE-SIZE FRACTIONS FOR SELECTED RIVERS IN MINNESOTA, 2007 THROUGH 2011

Christopher A. Ellison, Hydrologist, USGS, cellison@usgs.gov, 763.783.3121
Brett E. Savage, Hydrologic Technician, USGS, besavage@usgs.gov, 763.783.3133
Gregory D. Johnson, Senior Hydrologist, MPCA, gregory.johnson@state.mn.us, 651.757.2471

Abstract

Excessive sediment transport in rivers causes problems for flood control, soil conservation, irrigation, aquatic health, and navigation, as well as transporting harmful contaminants like organic chemicals and eutrophication-causing nutrients. In Minnesota, more than 5,800 miles of streams are identified as impaired by the Minnesota Pollution Control Agency (MPCA) due to elevated levels of suspended sediment.

The U.S. Geological Survey, in cooperation with the MPCA, established a sediment monitoring network in 2007 and began systematic sampling of suspended-sediment concentration (SSC), total suspended solids (TSS), and turbidity in rivers across Minnesota to improve the understanding of fluvial sediment transport relations. Suspended-sediment samples were collected from 14 sites from 2007 through 2011. Analyses of these data indicated that the Zumbro River at Kellogg in southeast Minnesota had the highest mean SSC of 226 milligrams per liter (mg/L) followed by the Minnesota River at Mankato with a mean SSC of 193 mg/L. The single highest SSC of 1,250 mg/L was measured at the Zumbro River during the 2011 spring runoff. The lowest mean SSC of 21 mg/L was measured at Rice Creek in the northern Minneapolis-St. Paul metropolitan area.

Total suspended solids (TSS) have been used as a measure of fluvial sediment by the MPCA since the early 1970s; however, TSS concentrations have been known to underrepresent the amount of suspended sediment. For this study, comparisons between concurrently sampled SSC and TSS indicated significant differences at every site, with SSC on average two times larger than TSS concentrations.

Regression analysis indicated that 7 out of 14 sites had poor or no relation between SSC and streamflow. Only two sites, the Knife River and the Wild Rice River at Twin Valley, had strong correlations between SSC and streamflow, with coefficient of determination (R^2) values of 0.82 and 0.80, respectively. In contrast, turbidity had moderate to strong relations with SSC at 10 of 14 sites and was superior to streamflow for estimating SSC at all sites. Suspended-sediment basin yields indicated that the Minnesota River had the largest mean annual sediment basin yield of 120 tons of sediment per year per square mile.

INTRODUCTION

Excessive sediment transported in rivers causes problems for flood control, soil conservation, irrigation, aquatic health, and navigation. Fluvial sediment becomes entrained in a stream by way of erosion from land surfaces, or from channel bed and bank erosion. Streams transport sediment by maintaining the finer particles in suspension with turbulent currents (suspended-sediment load) and by intermittent entrainment and movement of coarser particles along the streambed (bedload). Fine-grained sediment can serve to transport harmful contaminants such as organic chemicals, heavy metals, and eutrophication-causing nutrients (Baker, 1980).

The most recent U.S. Environmental Protection Agency compilation of States' water-quality reports under Section 305(b) of the Clean Water Act identifies sediment as one of the leading causes of impairment in the Nation's rivers and streams (U.S. Environmental Protection Agency, 2009, 2012). In Minnesota, more than 5,800 miles of streams are identified as impaired due to elevated levels of suspended sediments (Minnesota Pollution Control Agency, 2009a).

The Minnesota Pollution Control Agency (MPCA) incorporated a grab sampling procedure and laboratory analysis of total suspended solids (TSS) for measurement of fluvial sediment in the early 1970s. The grab sampling procedure and TSS measure were adopted by the MPCA for various reasons, including the assumption that the TSS method would provide an adequate representation of suspended sediment and the procedures for the collection and laboratory analysis of samples for suspended-sediment concentration were cost prohibitive. Marked differences between TSS and SSC field sampling procedures and subsequent laboratory analysis largely contribute to the significant differences between concentrations of TSS and SSC (Gray et. al, 2000). For field sampling, TSS samples

are collected at the center of the stream cross section (Minnesota Pollution Control Agency, 2011), whereas SSC samples are collected using federally approved (through the Federal Interagency Sedimentation Project) isokinetic samplers (Davis, 2005) and width- and depth-integrated procedures as described by Edwards and Glyssen (1999). The primary difference in laboratory procedures is that the TSS analytical method uses a pipette to extract a predetermined volume (subsample) from the original water sample to determine the amount of suspended material, whereas the SSC analytical method measures all of the sediment and the mass of the entire water-sediment mixture (American Public Health Association, American Water Works Association, and Water Pollution Control Federation, 1998). Gray et. al (2000) reported that the use of a pipette to obtain subsamples subjects the analyses to substantial biases compared to the SSC method.

The continued need to measure fluvial sediment and recent technological advances has led to the use of turbidity as a surrogate for suspended sediment, particularly in locations where streamflow alone is not a good estimator of SSC (Lewis, 1996; Rasmussen et. al, 2009). Optical turbidity sensors measure the amount of emitted light that is reflected by suspended particles in the water column, and have been used successfully to predict SSC, assuming the relation between the turbidity signal and SSC can be calibrated from physical samples (Lewis, 1996; Christensen et. al, 2000; Uhrich and Bragg, 2003; Rasmussen et. al, 2009). For this study, a portable desktop turbidity meter was used to measure turbidity concurrently with SSC sampling to investigate what relation may exist between turbidity and SSC for streams in Minnesota.

The purpose of the study presented here was to document findings based on sediment data collected by the U.S. Geological Survey (USGS), in cooperation with the MPCA, on selected rivers in Minnesota from 2007 through 2011. Specifically, the study examines suspended-sediment data to (1) describe suspended-sediment concentrations (SSC), total suspended solids (TSS), turbidity, and particle-size fractions for selected rivers across Minnesota's major watersheds; (2) quantify the difference between SSC and TSS; (3) develop relations among streamflow, SSC, TSS, turbidity, and suspended-sediment loads; and (4) estimate suspended-sediment loads and basin yields. This paper presents a condensation of the study by Ellison et. al (2014) and associated results.

DESCRIPTION OF THE STUDY AREA

A map of the State showing the locations of the sites in this study relative to the major watersheds and major streams in Minnesota is shown in Figure 1.

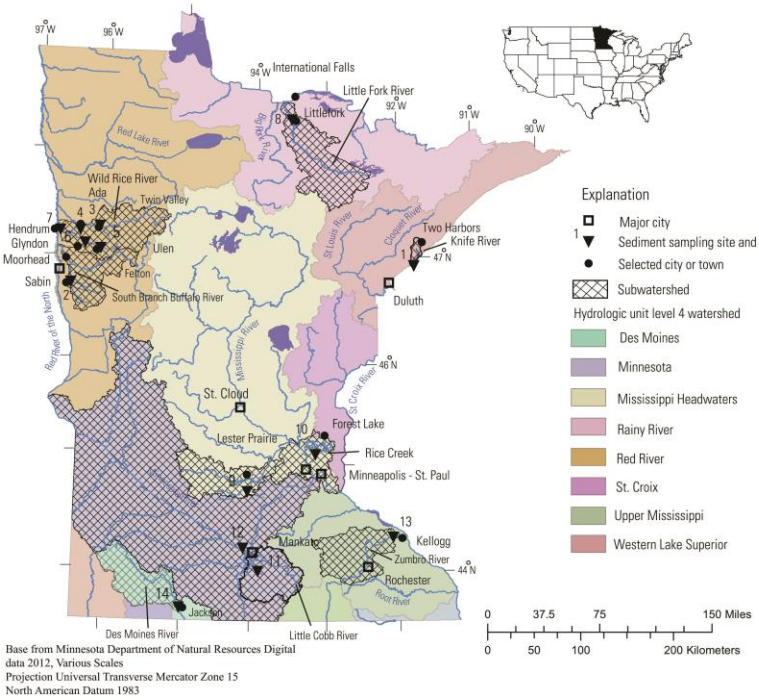

Figure 1 Major watersheds and locations of sediment sampling sites in Minnesota.

The 10 watersheds selected for this study represent a cross section of watershed characteristics present in Minnesota. Minnesota's geologic history of advancing and retreating glaciers affected most of the State and contributed to the development of the general soil types and topographic relief (Sims and Morey, 1972). Most of the northeastern part of the State is forested, but has some open pasture and sparse cultivated crops (Tornes, 1986). The far western and southern regions of Minnesota are intensively cultivated. Between these regions lies a transition area with a mixture of cultivated crops, pasture, and forests. Urban (developed) areas are scattered throughout the State, but the largest is the Minneapolis-St. Paul metropolitan area.

METHODS OF DATA COLLECTION AND ANALYSIS

Data were collected from February 2007 through November 2011. Fourteen sites were sampled 5–14 times per year during the open-water season (Table 1). Few samples were collected during the winter months because historically, less than 4 percent of annual loads were transported during the winter months (Tornes, 1986). Water samples were collected at all sites for analysis of SSC and particle-size fractions less than 0.0625 millimeters (mm) (fines). For this study, particles in suspension greater than 0.0625 mm are categorized as sands.

Table 1 Sediment sampling stations in selected watersheds in Minnesota, 2007 through 2011.
[USGS, U.S. Geological Survey; NAD 83, North American Datum of 1983; mi^2, square miles]

Site number (Figure 1)	USGS station number	Station name	Latitude (north) (NAD 83)	Longitude (west) (NAD 83)	Drainage area (mi^2)	Number of suspended-sediment samples
1	04015330	Knife River near Two Harbors, Minn.	46° 56' 49"	91° 47' 32"	84	27
2	05061500	South Branch Buffalo River at Sabin, Minn.	46° 46' 32"	96° 37' 40"	454	40
3	05062500	Wild Rice River at Twin Valley, Minn.	47° 16' 00"	96° 14' 40"	934	29
4	05063000	Wild Rice River near Ada, Minn.	47° 15' 50"	96° 30' 00"	1,100	29
5	05063340	South Branch Wild Rice River near Ulen, Minn.	47° 05' 17"	96° 15' 31"	141	25
6	05063400	South Branch Wild Rice River near Felton, Minn.	47° 07' 23"	96° 24' 25"	180	28
7	05064000	Wild Rice River at Hendrum, Minn.	47° 16' 05"	96° 47' 50"	1,560	27
8	05131500	Little Fork River at Littlefork, Minn.	48° 23' 45"	93° 32' 57"	1,680	34
9	05278930	Buffalo Creek near Glencoe, Minn.	44° 45' 50"	94° 05' 27"	373	44
10	05288580	Rice Creek below Old Hwy. 8 in Mounds View, Minn.	45° 05' 36"	93° 11' 42"	156	21
11	05320270	Little Cobb River near Beauford, Minn.	43° 59' 48"	93° 54' 30"	130	68
12	05325000	Minnesota River at Mankato, Minn.	44° 10' 08"	94° 00' 11"	14,900	32
13	05374900	Zumbro River at Kellogg, Minn.	44° 18' 43"	92° 00' 14"	1,400	34
14	05476000	Des Moines River at Jackson, Minn.	43° 37' 06"	94° 59' 05"	1,250	25

Streamflow data were obtained from existing USGS or MPCA/Minnesota Department of Natural Resources (MDNR) streamgages. Of the 14 sampling sites, 13 were colocated at the corresponding streamgage; the exception was the South Branch Wild Rice River near Ulen (site 5) where no streamgage was available. For the South Branch Wild Rice River near Ulen (site 5), streamflow was estimated by extending streamflow from a nearby USGS streamgage [South Branch Wild Rice River near Felton (site 6)] using the MOVE-1 (Maintenance of Variance Extension, Type 1) statistical program (Hirsch, 1982).

DATA COLLECTION

Suspended-sediment samples were collected at all 14 sites using isokinetic samplers and equal width and depth-integrating techniques following procedures by Edwards and Glysson (1999). Most samples were collected using a D–74 rigid bottle sampler suspended from a bridge during nonwadeable flows and a DH–48 hand-held sampler during wadeable flows. Following collection, samples were transported to the USGS sediment laboratory in Iowa City, Iowa, where they were composited into a single sample and analyzed for suspended-sediment concentration and fines particle-size fraction.

Grab samples for laboratory TSS analysis were collected in 1-liter (L) plastic containers near the centroid of the stream cross section following MPCA sampling protocols (Minnesota Pollution Control Agency, 2011). The TSS samples were collected at seven sites and were refrigerated and delivered to the Minnesota Department of Health laboratory in St. Paul, within seven days of the collection date.

Grab samples for field measurements of turbidity were collected at 13 of 14 sites (Minnesota River at Mankato were only collected periodically) from the centroid of the stream cross section in a 1-L plastic container. A subsample of the contents was transferred into a glass vial, which was then placed into the instrument cell compartment of a portable Hach model 2100P (Hach Company, Loveland, Colorado) turbidimeter to obtain the measurement.

Daily mean streamflow data were obtained from existing USGS or MPCA/MDNR streamgages to develop sediment transport relations and to calculate sediment loads. Streamflow data for 10 of the sites were from the USGS (*http://waterdata.usgs.gov/mn/nwis/sw/*), and streamflow data for 3 sites (sites 4, 9, and 13; Table 1) were from the MPCA (*http://www.dnr.state.mn.us/waters/csg/index.html*). The USGS and MPCA/MDNR determine streamflow at streamgages by use of the rating-curve method (the relation between streamgage height and streamflow) for each station following Rantz et. al (1982).

DATA ANALYSIS

Sediment concentration data and measures of daily mean streamflow were analyzed to obtain summary statistics and perform nonparametric match-pair tests, simple linear regression (SLR), and load estimation using S-Plus statistical analysis software (TIBCO Software Inc., 2010). The Wilcoxon signed-rank test (Helsel and Hirsch, 2002) was conducted to determine if significant differences could be detected between matched pairs of SSC and TSS.

For model development, SLR was used to calculate SSC based on daily mean streamflow, TSS, and turbidity. For SLR models, *p*-values were used to evaluate the model's null hypothesis for statistical significance [*p*-values less than (<) 0.05 indicated statistical significance], whereas the coefficient of determination (R^2) was used to assess the linear association between the response and explanatory variable and to assess how well the model was able to accurately predict outcomes of the response variable.

The SLR can be used to estimate unknown values of a response variable from a known quantity of an explanatory variable if a statistically significant correlation between the variables exists. For SLR to produce a useable model, assumptions are that the two variables are related linearly, that the variance of the residuals is constant (homoscedastic), and that the residuals are distributed normally (Helsel and Hirsch, 2002). These assumptions commonly are violated by measured water data, so the data are transformed to logarithmic values to satisfy these assumptions. Logarithmic base-10 (log10) transformation has been determined to be effective in normalizing residuals for many water-quality measures and streamflow (Helsel and Hirsch, 2002). There exists a consequence of transformation of the response variable, in this case SSC, which must be accounted for when computing SSC values. When the regression estimates are retransformed to the original units, bias is introduced (usually negative) in the

computed SSC values (Miller, 1951; Koch and Smillie, 1986). To correct for this retransformation bias, Duan (1983) introduced a nonparametric bias-correction factor (BCF) called the "smearing" estimator. The equation to compute the smearing BCF for base-10 logarithmic transformation follows (Duan, 1983):

$$BCF = (\sum_{i=1}^{n} 10^{e_i})/n \quad (1)$$

where

n is the number of samples, and

e_i is the difference between each measured and estimated concentration, in log units.

Regression-computed SSC values are corrected for bias by multiplying the retransformed SSC value by the BCF.

Sediment loads were estimated using S-LOADEST, which is an interface-driven, S-PLUS version of LOADEST, which is a FORTRAN program for estimating constituent loads in streams and rivers (Runkel et. al, 2004). The S-LOADEST program is based on a rating-curve method (Cohn et. al, 1989, 1992; Crawford, 1991) that uses regression to estimate constituent loads in relation to several explanatory variables, which most commonly are streamflow and time (seasonal component). The regression is developed using daily loads calculated from the sample concentration and daily flow for that sample.

SUSPENDED-SEDIMENT CONCENTRATIONS, TOTAL SUSPENDED SOLIDS, TURBIDITY, AND PARTICLE-SIZE FRACTIONS

Sediment samples were collected during a wide variety of streamflow conditions. The Zumbro River at Kellogg (site 13) had the highest mean SSC [226 milligrams per liter (mg/L)] among all sites. High SSC in the Zumbro River is attributed in part to the combined effects of climate, high topographic relief, and erodible soils. Steep terrain in the lower part of the watershed increases the erosion potential. The Minnesota River at Mankato (site 12) also had high mean SSC (193 mg/L). Although the Minnesota River Valley has low relief in the valley, the edges of the river valley are lined with steep bluffs and ravines (Minnesota Pollution Control Agency, 2009b). The Zumbro River at Kellogg produced the single highest SSC of 1,250 mg/L at a streamflow of 1,800 cubic feet per second (ft^3/s) during the 2011 spring snowmelt runoff. The Wild Rice River near Ada (site 4) had a mean SSC of 185 mg/L, similar in magnitude to the Minnesota River. Elevated SSC values on the main stem of the Wild Rice River have been linked to cultivated agriculture (Brigham et. al, 2001) and artificial channelization of the main stem from flood-control projects. One of the lowest mean SSC values of 37 mg/L occurred within the same watershed at the South Branch Wild Rice River near Ulen (site 5). The lowest mean SSC of 21 mg/L occurred at Rice Creek below Old Highway 8 in Mounds View (site 10) in the northern Minneapolis-St. Paul metropolitan area. The lowest SSC values of 2 mg/L were measured at the Little Cobb River near Beauford (site 11) on December 28, 2010, at a streamflow of 108 ft^3/s; at Rice Creek on September 15, 2010, at a streamflow of 31 ft^3/s; and at the Knife River near Two Harbors (site 1) on September 10, 2008, at a streamflow of 5 ft^3/s.

The TSS samples were collected concurrently with SSC samples at seven sites, and TSS concentrations followed similar spatial patterns as SSC. For example, similar to the SSC data, the largest mean TSS concentration of 182 mg/L was measured at the Zumbro River, whereas the smallest mean TSS of 25 mg/L was measured at the Little Fork River at Littlefork (site 8).

Variability in turbidity measurements was relatively smaller than SSC variability and followed spatial patterns similar to those of SSC and TSS. The Zumbro River and Wild Rice River near Ada had the largest mean turbidity values of 101 and 89 nephelometric turbidity ratio units (NTRUs), respectively. Rice Creek had the smallest single turbidity value along with a very narrow range of values (1 to 9 NTRUs). The narrow range of values observed at Rice Creek is attributed to the combined effect of low SSC and high percentage of sand-sized particles. Laboratory trials indicate that turbidity sensors are less sensitive to sand-sized particles than to fine-sized particles (Conner and De Visser, 1992; Hatcher et. al, 2000).

For particle sizes, suspended fines (sediment sizes less than 0.0625 mm) were documented in markedly higher percentages than suspended sands at all sites, with the exception of Rice Creek. The largest mean percentage of fines was at the Wild Rice River at Hendrum (site 7), where 92 percent of the material in suspension consisted of fines. Other large mean percentages of fines were at the South Branch Buffalo River at Sabin (site 2), Wild Rice River at

Twin Valley (site 3), and the Little Fork River with 88, 83, and 84 percent, respectively. Suspended fines were noticeably lower at Rice Creek when compared to other sites. Although fine-sized particles composed most of the total suspended sediment, the percentage of suspended sands was appreciable for many samples at many sites. The largest mean percentage of sand particles in suspension was observed at Rice Creek, where a mean of 45 percent of the material in suspension was sand-sized. Other substantial mean percentages of sands were measured at the Zumbro River, South Branch Wild Rice River near Felton (site 6), and the Minnesota River with 35, 33, and 28 percent, respectively.

COMPARISON BETWEEN SUSPENDED-SEDIMENT CONCENTRATIONS AND TOTAL SUSPENDED SOLIDS

For this analysis, the Wilcoxon signed-rank test (Helsel and Hirsch, 2002) was used to test if concurrently sampled pairs of SSC and TSS were different within sites. Box plots illustrate the variation in SSC and TSS at all sites (Figure 2) and are consistent with the Wilcoxon signed-rank test results, which indicated median values of SSC were larger than median values of TSS at each of the seven sites where TSS samples were collected concurrently with SSC. When comparing SSC to TSS median concentrations, the overall mean percent difference indicated that SSC was about 100 percent larger than TSS. The largest percent difference between median values of SSC and TSS was at the South Branch Buffalo River site and the smallest difference was at the Des Moines River.

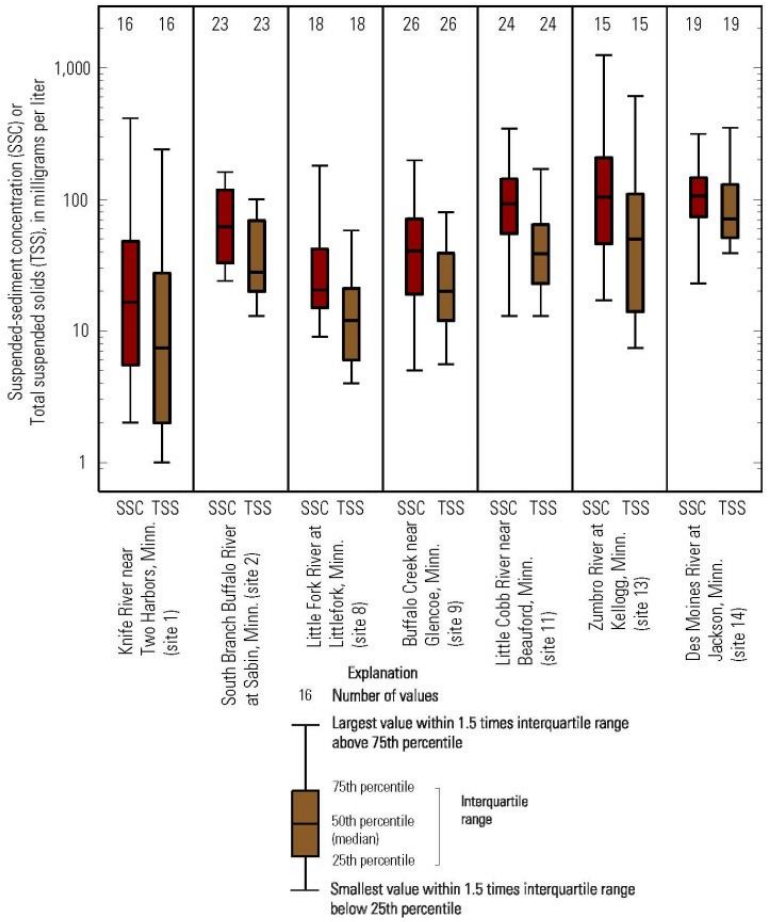

Figure 2 Boxplots of suspended-sediment concentrations (SSC) and total suspended solids (TSS) for selected sites in Minnesota, 2007 through 2011.

RELATIONS AMONG STREAMFLOW, SUSPENDED-SEDIMENT CONCENTRATIONS, TOTAL SUSPENDED SOLIDS, AND TURBIDITY

Variations in streamflow provide important information related to the timing and changes in sediment concentrations and has widely been used to develop SSC prediction models. The relation between SSC and streamflow for each site is presented in Table 2 and illustrated in Figure 3. Best-fit regression lines represent the relation between SSC and streamflow, and can be used to evaluate how SSC responds to changes in streamflow within and among sites. The gradient of the lines provides an indication of how quickly SSC changes with changes in streamflow. The strength of the relation can be seen in how closely the observed data fall along the regression line. Lines with steep positive gradients from left to right indicate SSC increases quickly as streamflow increases. In this study, the sites with the steepest gradients were the Knife River, Wild Rice River near Twin Valley, Wild Rice River near Ada, Little Fork River, Rice Creek, Minnesota River, and Zumbro River (Figure 3). Moderate gradients were observed at the South Branch Wild Rice River near Felton and the Des Moines River. Low or level gradients, which indicate that SSC changes little as streamflow increases, were observed at the South Branch Wild Rice River near Ulen, Buffalo Creek, and the Little Cobb River. The negative relation, indicated by a negative gradient, for the South Branch Buffalo River, is unusual. Negative gradients indicate that the amount of suspended sediment in streams may be diluted during periods of increased streamflow due to limited supply of sediment.

Table 2 Summary of simple linear regression models to evaluate suspended-sediment concentrations using streamflow as the explanatory variable for selected sites in Minnesota, 2007 through 2011.
[mg/L, milligrams per liter; R^2, coefficient of determination; BCF, Duan's bias correction factor; SSC, suspended-sediment concentration; Q, daily mean streamflow; <, less than]

Site number (Figure 1)	Station name	Number of samples used for regression	Regression model (mg/L)	R^2	Standard error residual (mg/L)	p-value	BCF
1	Knife River near Two Harbors, Minn.	27	$SSC = 0.9276 \times Q^{0.7175}$	0.82	12.7	<0.01	1.227
2	South Branch Buffalo River at Sabin, Minn.	40	$SSC = 280.7 \times Q^{-0.2213}$	0.22	10.7	<0.01	1.270
3	Wild Rice River at Twin Valley, Minn.	29	$SSC = 0.2691 \times Q^{0.9241}$	0.80	25.8	<0.01	1.212
4	Wild Rice River near Ada, Minn.	29	$SSC = 0.5526 \times Q^{0.8579}$	0.67	34.0	<0.01	1.417
5	South Branch Wild Rice River near Ulen, Minn.	25	$SSC = 26.1 \times Q^{0.0987}$	0.00	6.2	0.34	1.423
6	South Branch Wild Rice River near Felton, Minn.	27	$SSC = 20.93 \times Q^{0.3085}$	0.14	26.1	0.03	1.643
7	Wild Rice River at Hendrum, Minn.	27	$SSC = 24.84 \times Q^{0.2163}$	0.16	17.0	0.02	1.284
8	Little Fork River at Littlefork, Minn.	32	$SSC = 1.360 \times Q^{0.4563}$	0.65	3.8	<0.01	1.119
9	Buffalo Creek near Glencoe, Minn.	42	$SSC = 43.2 \times Q^{0.0897}$	0.02	10.2	0.19	1.581
10	Rice Creek below Old Hwy. 8 in Mounds View, Minn.	21	$SSC = 0.2842 \times Q^{0.9223}$	0.44	3.1	<0.01	1.263
11	Little Cobb River near Beauford, Minn.	68	$SSC = 102 \times Q^{0.0003}$	0.02	8.2	0.99	1.310
12	Minnesota River at Mankato, Minn.	32	$SSC = 9.738 \times Q^{0.3286}$	0.41	20.0	<0.01	1.173
13	Zumbro River at Kellogg, Minn.	18	$SSC = 0.0348 \times Q^{1.2314}$	0.54	61.5	<0.01	1.399
14	Des Moines River at Jackson, Minn.	25	$SSC = 23.07 \times Q^{0.2419}$	0.17	15.6	0.02	1.313

Results of the SLR analysis between SSC and streamflow presented in Table 2 provide a quantitative description of the plots shown in Figure 3. The relation between SSC and streamflow was significant statistically (p-value <0.05)

at 11 of the 14 sites (Table 2). The strongest correlations between SSC and streamflow were determined for the Knife River (R^2=0.82) and the Wild Rice River at Twin Valley (R^2=0.80). The Wild Rice River near Ada, Little Fork River, and Zumbro River had moderate R^2 values of 0.67, 0.65, and 0.54, respectively. Rice Creek and the Minnesota River had modest R^2 values of 0.44 and 0.41. The remainder of the sites (7 out of 14 sites) had poor relations between SSC and streamflow. The three sites that did not have a significant relation (p-values≥0.05) were the South Branch Wild Rice River near Ulen, Buffalo Creek, and Little Cobb River.

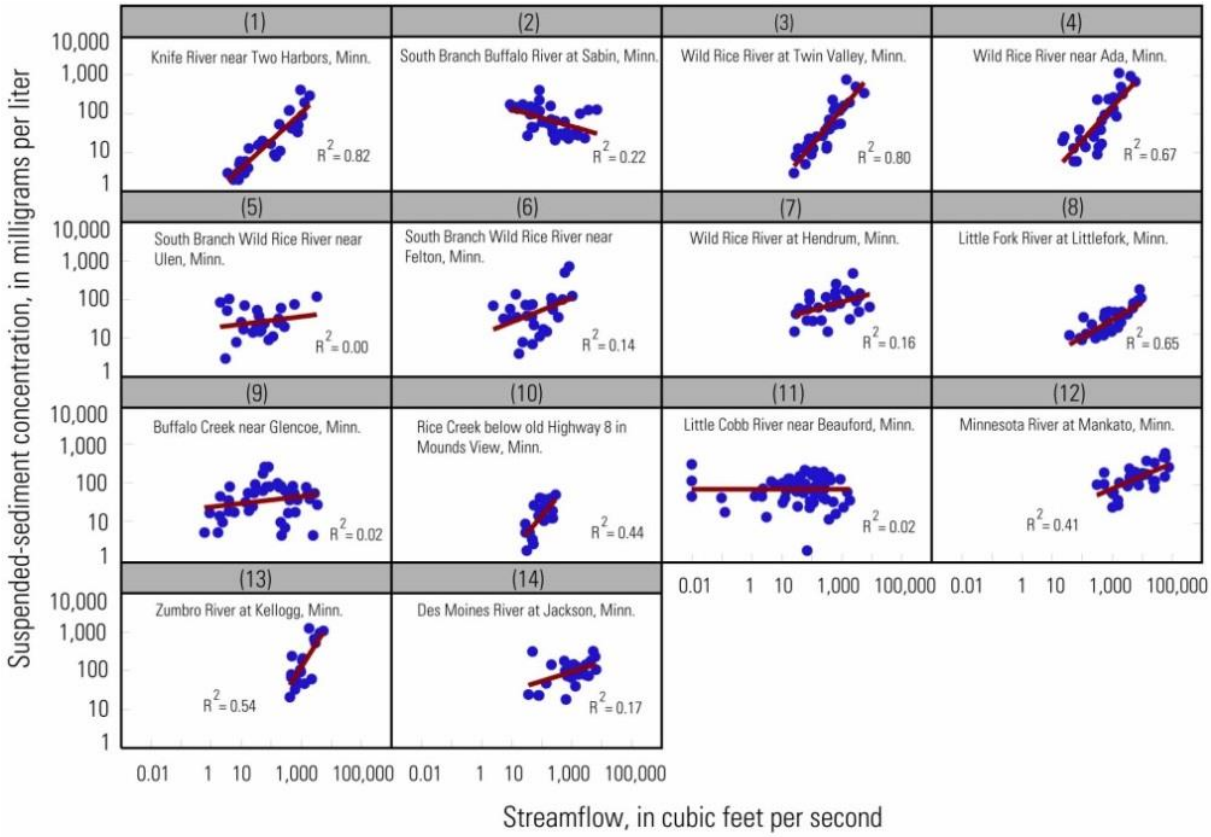

Figure 3 Relation between suspended-sediment concentrations and streamflow for selected sites in Minnesota, 2007 through 2011.

The overall relation between SSC and turbidity is shown in Figure 4, and regression models for the SSC-turbidity relation are presented in Table 3. The R^2 values for the SSC-streamflow models and SSC-turbidity models indicated that turbidity was correlated more strongly to SSC than was streamflow at all sampling sites (Tables 2 and 3). Among the largest increases in R^2 was at the Wild Rice River at Hendrum, which increased from 0.16 to 0.86 between the SSC-streamflow model and SSC-turbidity model. Two sites, the Knife River and the Wild Rice River at Twin Valley, had modest increases in R^2 values from 0.82 to 0.87 and from 0.80 to 0.82, respectively. The Wild Rice River near Ada, the Little Fork River, and the Zumbro River, had notable increases in R^2 values from 0.67 to 0.85, 0.65 to 0.82, and 0.54 to 0.63, respectively. For this study, there was not enough turbidity values available at the Minnesota River at Mankato (site 12) to develop the relation between SSC and turbidity.

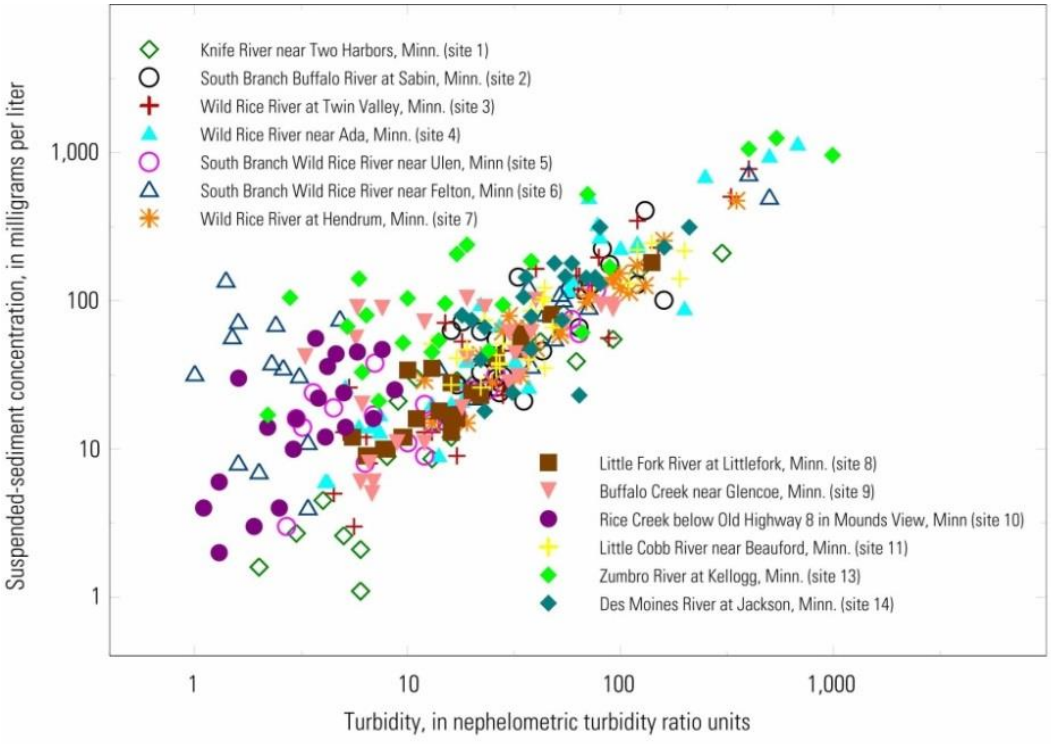

Figure 4 Relation between suspended-sediment concentration and turbidity for selected sites in Minnesota, 2007 through 2011.

Five sites with poor or no relation between SSC and streamflow had significant correlations and large increases in R^2 when using turbidity as the explanatory variable. For example, R^2 values for the Wild Rice River near Ulen and the Little Cobb River increased from 0.00 to 0.57 and from 0.02 to 0.70, respectively. For the South Branch Buffalo River, South Branch Wild Rice River near Felton, and Buffalo Creek, R^2 values increased from 0.22 to 0.54, from 0.14 to 0.50, and from 0.02 to 0.25, respectively. The smallest change was for Rice Creek, where only a 1-percent increase in R^2 was determined. These results indicate that turbidity was superior to streamflow in estimating SSC, and that turbidity may be beneficial as a surrogate for SSC in many of Minnesota's rivers.

Table 3. Summary of regression models to evaluate suspended-sediment concentrations using turbidity as the explanatory variable for selected sites in Minnesota, 2007 through 2011.
[mg/L, milligrams per liter; R^2, coefficient of determination; BCF, Duan's bias correction factor; SSC, suspended-sediment concentration; *Turb*, turbidity; <, less than]

Site number (Figure 1)	Station name	Number of samples used for regression	Regression model (mg/L)	R^2	Standard error residual (mg/L)	*p*-value	BCF
1	Knife River near Two Harbors, Minn.	20	$SSC = 3.452 \times Turb^{0.1686} \times (Turb^2)^{0.2821}$	0.87	7.5	<0.01	1.110
2	South Branch Buffalo River at Sabin, Minn.	27	$SSC = 2.520 \times Turb^{0.9061}$	0.54	11.6	<0.01	1.156
3	Wild Rice River at Twin Valley, Minn.	29	$SSC = 1.6789 \times Turb^{1.0442}$	0.82	11.1	<0.01	1.184
4	Wild Rice River near Ada, Minn.	29	$SSC = 2.2175 \times Turb^{1.0041}$	0.85	24.8	<0.01	1.177
5	South Branch Wild Rice River near Ulen, Minn.	19	$SSC = 16.74 \times Turb^{-0.4312} \times (Turb^2)^{0.4518}$	0.57	3.8	<0.01	1.125

6	South Branch Wild Rice River near Felton, Minn.	26	$SSC = 50.37 \times Turb^{-0.531} \times (Turb^2)^{0.3827}$	0.50	25.3	<0.01	1.319
7	Wild Rice River at Hendrum, Minn.	26	$SSC = 2.261 \times Turb^{0.8979}$	0.86	12.9	<0.01	1.043
8	Little Fork River at Littlefork, Minn.	23	$SSC = 1.784 \times Turb^{0.9428}$	0.82	1.7	<0.01	1.056
9	Buffalo Creek near Glencoe, Minn.	27	$SSC = 10.43 \times Turb^{0.5468}$	0.25	6.1	<0.01	1.383
10	Rice Creek below Old Hwy 8. in Mounds View, Minn.	20	$SSC = 3.487 Turb^{2.022}$	0.45	15.5	<0.01	1.266
11	Little Cobb River near Beauford, Minn.	23	$SSC = 4.765 \times Turb^{0.7351}$	0.70	7.0	<0.01	1.067
13	Zumbro River at Kellogg, Minn.	24	$SSC = 23.19 \times Turb^{0.6105}$	0.63	37.4	<0.01	1.261
14	Des Moines River at Jackson, Minn.	21	$SSC = 4.751 \times Turb^{0.8088}$	0.38	11.3	<0.01	1.164

SUSPENDED-SEDIMENT BASIN YIELDS

Suspended-sediment loads were calculated to estimate basin yields using the S-LOADEST program. The S-LOADEST program incorporates time-series data for streamflow, a dataset of constituent concentrations, and a time component to estimate annual and seasonal loads for the constituent of interest. The form of the regression equation used in the S-LOADEST model is described in Ellison et. al (2014). Mean annual basin yields for suspended sediment, suspended sands, and suspended fines are shown in Figure 5. Comparing annual sediment yields among sites across Hydrologic Unit Code Level 4 watersheds provides insight on erosion rates and describes the relative measure of degradation occurring on the landscape.

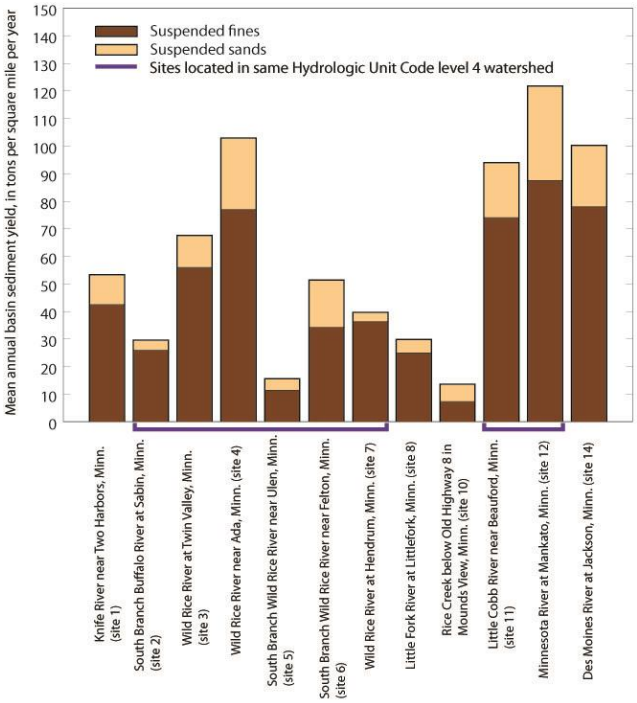

Figure 5 Mean annual basin yields of suspended sediment for selected sites in Minnesota, 2007 through 2011.

ACKNOWLEDGMENTS

This report presents a compilation of information supplied by many agencies and individuals. The authors would like to thank the Minnesota Pollution Control Agency, Wild Rice Watershed District, and the Rice Creek Watershed District for their assistance with this study. Dave Lorenz, Kristen Kieta, Joel Groten, Domenic Murino, Lance Ostiguy, Mark Brigham, and Christiana Czuba of the U.S. Geological Survey are acknowledged for assistance with office and field aspects of the study. Any use of trade, firm, or product names is for descriptive purposes only and does not imply endorsement by the U.S. Government.

REFERENCES

American Public Health Association, American Water Works Association, and Water Pollution Control Federation. (1998). Standard methods for the examination of water and wastewater (20th ed.): Washington, D.C., American Public Health Association, American Water Works Association, Water Environment Federation, [variously paged].

Baker, R.A. (1980). Contaminants and sediment—Volume 1, Fate and transport, case studies, modeling, toxicity: Ann Arbor, Mich., Ann Arbor Science, 558 p.

Brigham, M.E., McCullough, C.J., and Wilkinson, P. (2001). Analysis of suspended-sediment concentrations and radioisotope levels in the Wild Rice River Basin, northwestern Minnesota, 1973–98: U.S. Geological Survey Water-Resources Investigations Report 01–4192, 21 p.

Christensen, V.G., Jian, Xiaodong, and Ziegler, A.C. (2000). Regression analysis and real-time water-quality monitoring to estimate constituent concentrations, loads, and yields in the Little Arkansas River, south-central Kansas, 1995–99: U.S. Geological Survey Water-Resources Investigations Report 00–4126, 36 p. (Available at *http://pubs.er.usgs.gov/publication/wri004126*.)

Cohn, T.A., Delong, L.L., Gilroy, E.J., Hirsch, R.M., and Wells, D.K. (1989). Estimating constituent loads: Water Resources Research, v. 25, no. 5, p. 937–942. (Available at *http://dx.doi.org/10.1029/WR025i005p00937*.)

Cohn, T.A., Caulder, D.L., Gilroy, E.J., Zynjuk, L.D., and Summers, R.M.. (1992). The validity of a simple statistical model for estimating fluvial constituent loads—An empirical study involving nutrient loads entering Chesapeake Bay: Water Resources Research, v. 28, no. 9, p. 2,353–2,363. (Available at *http://dx.doi.org/10.1029/92WR01008*.)

Conner, C.S., and De Visser, A.M. (1992). A laboratory investigation of particle size effects on an optical backscatterance sensor: Marine Geology, v. 108, no. 2, p. 151–159. (Available at *http://dx.doi.org/10.1016/0025-3227(92)90169-I*.)

Crawford, C.G. (1991). Estimation of suspended-sediment rating curves and mean suspended-sediment loads: Journal of Hydrology, v. 129, p. 331–348. (Available at *http://dx.doi.org/10.1016/0022-1694(91)90057-O*.)

Davis, B.E. (2005). A guide to the proper selection and use of federally approved sediment and water-quality samplers: U.S. Geological Survey Open-File Report 2005–1087, 20 p. (Available at *http://pubs.usgs.gov/of/2005/1087/*.)

Duan, N. (1983). Smearing estimate—A nonparametric retransformation method: Journal of the American Statistical Association, v. 78, no. 383, p. 605–610. (Available at *http://dx.doi.org/10.1080/01621459.1983.10478017*.)

Edwards, T.K., and Glysson, G.D. (1999). Field methods for measurement of fluvial sediment: U.S. Geological Survey Techniques of Water-Resources Investigations, book 3, chap. C2, 89 p. (Available at *http://pubs.usgs.gov/twri/twri3-c2/*.)

Ellison, C.A., Savage, B.E., and Johnson, G.D. (2014). Suspended-sediment concentrations, loads, total suspended solids, turbidity, and particle-size fractions for selected rivers in Minnesota, 2007 through 2011: U.S. Geological Survey Scientific Investigations Report 2013–5205, 43 p., *http://dx.doi.org/10.3133/sir20135205*.

Gray, J.R., Glysson, G.D., Turcios, L.M., and Schwarz, G.E. (2000). Comparability of suspended-sediment concentration and total suspended solids data: U.S. Geological Survey Water-Resources Investigations Report 00–4191, 14 p. (Available at *http://pubs.usgs.gov/wri/wri004191/*.)

Hatcher, Annamarie, Hill, P.S., Grant, Jon, and Macpherson, P. (2000). Spectral optical backscatter of sand suspension—Effects of particle size, composition and color: Marine Geology, v. 168, p. 115–128 (Available at *http://dx.doi.org/10.1016/S0025-3227(00)00042-6*.)

Helsel, D.R., and Hirsch, R.M. (2002). Statistical methods in water resources—Hydrologic analysis and interpretation: U.S. Geological Survey Techniques of Water-Resources Investigations, book 4, chap. A3, 510 p., (Available at *http://pubs.usgs.gov/twri/twri4a3/*.)

Hirsch, R.M. (1982). A comparison of four streamflow record extension techniques: Water Resources Research, v. 18, no. 4, p. 1,081–1,088. (Available at *http://dx.doi.org/10.1029/WR018i004p01081*.)

Koch, R.W., and Smillie, G.M. (1986). Bias in hydrologic prediction using log-transformed regression models: Journal of the American Water Resources Association, v. 22, no. 5, p. 717–723. (Available at *http://dx.doi.org/10.1111/j.1752-1688.1986.tb00744.x*.)

Lewis, J. (1996). Turbidity controlled suspended sediment sampling for runoff event load estimation: Water Resources Research, v. 32, no. 7, p. 2,299–2,310. (Available at *http://dx.doi.org/10.1029/96WR00991*.)

Miller, C.R. (1951). Analysis of flow-duration sediment rating curve method of computing sediment yield: U.S. Department of Interior, Bureau of Reclamation, 55 p.

Minnesota Pollution Control Agency. (2009a). Minnesota's impaired waters and total maximum daily loads (TMDLs): accessed December 12, 2012, at *http://www.pca.state.mn.us/water/tmdl/index.html*.

Minnesota Pollution Control Agency. (2009b). Identifying sediment sources in the Minnesota River Basin: accessed January 9, 2013, at *http://www.pca.state.mn.us/index.php/view-document.html?gid=8099*.

Minnesota Pollution Control Agency. (2011). Standard operating procedures (SOP) intensive watershed monitoring—Stream water quality component: accessed August 2, 2012, at *http://www.pca.state.mn.us/index.php/view-document.html?gid=16141*.

Rantz, S.E., and others. (1982). Measurement and computation of streamflow—Volume 1, Measurement of stage and discharge, and volume 2, Computation of discharge: U.S. Geological Survey Water-Supply Paper 2175, 631 p. (Available at *http://pubs.usgs.gov/wsp/wsp2175/*.)

Rasmussen, P.P., Gray, J.R., Glysson, G.D., and Ziegler, A.C. (2009). Guidelines and procedures for computing time-series suspended-sediment concentration and loads from in-stream turbidity-sensor and streamflow data: U.S. Geological Survey Techniques and Methods, book 3, chap. C4, 54 p. (Available at *http://pubs.usgs.gov/tm/tm3c4/*.)

Runkel, R.L., Crawford, C.G., and Cohn, T.A. (2004). Load Estimator (LOADEST)—A FORTRAN program for estimating constituent loads in streams and rivers: U.S. Geological Survey Techniques and Methods, book 4, chap. A5, 69 p. (Available at *http://pubs.usgs.gov/tm/2005/tm4A5/*.)

Sims, P.K. and Morey, G.B. 1972. Geology of Minnesota–A centennial volume: St. Paul, University of Minnesota, Minnesota Geological Survey,. 632 p.

TIBCO Software Inc. (2010). TIBCO Spotfire S+: Somerville, Massachusetts, accessed November 9, 2012, at *http://spotfire.tibco.com/products/s-plus/statistical-analysis-software.aspx*.

Tornes, L.H. (1986). Suspended sediment in Minnesota streams: U.S. Geological Survey Water-Resources Investigations Report 85–4312, 33 p. (Available at *http://pubs.er.usgs.gov/publication/wri854312*.)

Uhrich, M.A., and Bragg, H.M. (2003). Monitoring in-stream turbidity to estimate continuous suspended-sediment loads and yields and clay-water volumes in the Upper North Santiam River Basin, Oregon, 1998–2000: U.S.
Geological Survey Water-Resources Investigations Report 03–4098, 43 p. (Available at *http://pubs.usgs.gov/wri/WRI03-4098/*.)

U.S. Environmental Protection Agency. (2009). National water quality inventory—Report to Congress, 2004 reporting cycle: U.S. Environmental Protection Agency Office of Water Report EPA–841–R–08–001, 37 p., accessed January 29, 2013, at *http://water.epa.gov/lawsregs/guidance/cwa/305b/upload/2009_01_22_305b_2004report_2004_305Breport.pdf*.

U.S. Environmental Protection Agency. (2012). Water quality assessment and total maximum daily loads information—Integrated report: accessed November 11, 2012, at *http://www.epa.gov/waters/ir/*.

COARSE PARTICULATE ORGANIC MATTER TRANSPORT IN TWO ROCKY MOUNTAIN STREAMS

Kristin Bunte, Research Scientist, Colorado State University, Engineering Research Center, 1320 Campus Delivery, Fort Collins, Colorado 80523, kbunte@engr.colostate.edu; Kurt W. Swingle, Environmental Scientist; 630 Iris Ave., Boulder, Colorado 80304, kskb@ix.netcom.com; Jens M. Turowski, Research Scientist, Helmholtz Centre Potsdam, GFZ German Research Centre for Geosciences, Telegrafenberg, D-14473 Potsdam, Germany, jens.turowski@gfz-potsdam.de and at Swiss Federal Research Institute WSL, Mountain Hydrology and Mass Movements, Zürcherstrasse 111, CH-8903 Birmensdorf, Switzerland; Steven R. Abt, Professor emer., Colorado State University, Engineering Research Center, 1320 Campus Delivery, Fort Collins, Colorado 80523, sabt@engr.colostate.edu; Daniel A. Cenderelli, Fluvial Geomorphologist/Hydrologist, USDA Forest Service, National Stream and Aquatic Ecology Center, 2150 Centre Ave., Fort Collins, CO 80526, dcenderelli@fs.fed.us.

Abstract Samples of coarse particulate organic matter (CPOM) were collected over one-month snowmelt highflow seasons in two high-elevation, subalpine, streams in the Rocky Mountains. Bedload traps developed for sampling gravel bedload were found to be suitable samplers for CPOM transport. When flow overtopped bedload traps, CPOM transport rates were adjusted to estimate and add the unsampled CPOM portion traveling higher in the water column; when nets overfilled, CPOM transport rate were adjusted for the reduction in captured transport. CPOM transport rates were well related to flow in consecutive samples but showed pronounced hysteresis over the diurnal fluctuations of flow, between consecutive days, and over the rising and falling limbs of the high-flow season. Hysteresis effects require intensive sampling and establishing separate rating curves for all rising and falling limbs in order to compute annual CPOM load. Annual CPOM export for the two streams was 2.7 and 4 kg/ha/year, but both streams exported 6.5 and 6.6 kg/ha/year in the forested portion of the watershed.

INTRODUCTION

Coarse particulate organic matter (CPOM) is comprised of particles 1-100 mm, and those particles play an important role as a food source for benthic organisms (e.g., Fisher and Likens, 1973). Furthermore, fluvial transport of CPOM is one of the forms in which carbon is exported from a basin. CPOM typically contributes about 2.5-10% of total carbon export (Wallace et al., 1995, 1997; Richardson et al., 2005), and knowledge of CPOM export is needed when establishing watershed carbon budgets that account for input, consumption, retention, and export. Dry CPOM supplied to a stream (e.g., as litter fall) tends to be transported on the surface over relatively short distances (up to several 100 m, Jones and Smock, 1991; Webster et al., 1994; Wallace et al., 1995) before becoming trapped around obstacles where particles become waterlogged, sink, and accumulate on the stream bottom. Submerged CPOM experiences carbon leaching, microbial colonization (conditioning), shredding by invertebrates, and physical abrasion (Foucreau et al., 2013). In snowmelt regimes, when CPOM deposits are re-entrained at the beginning of high-flow season, fully waterlogged CPOM from the channel bed, together with some dry CPOM that had been stranded along the banks, is transported through the watershed and exported. Studies of annual CPOM export are rare from high elevation Rocky Mountain streams where large tracts of forested land are located in the US (Webster and Meyer 1997; Turowski and Hilton, 2013). This study makes a start towards filling this gap.

Because CPOM is lightweight (compared to inorganic bedload) and easily entrainable by flow, one may postulate that transport rates of waterlogged CPOM are influenced by the interplay between (local) flow hydraulics and the dynamics of storage and release from local retention within the streambed and along the banks; hence transport is variable over time and with discharge. Several publications have suggested that CPOM transport rates respond very quickly to increased flow rates (Beschta, 1981; 1983a; Perry and Rose, 1984; Estep and Beschta, 1985; Wallace et al., 1995; Kiffney et al., 2000; Johnson et al., 2006; Beschta and Jackson, 2008; Turowski et al., 2013; Turowski and Hilton, 2013), whereas Angradi (1991) found no such relation. However, despite the relative importance of CPOM in the carbon budget and concerted efforts (Webster and Meyer, 1997; Richardson, 1992; Richardson et al., 2005, 2009), temporal dynamics of CPOM transport over the annual highflow season have not been adequately described.

Difficulties in measuring the downstream conveyance of CPOM have posed the biggest problem to advancing insights into its transport dynamics. CPOM export from a basin can be quantified by excavating and analyzing the annually accumulated material in debris basins (Bilby, 1981), but that practice reveals no insights into transport dynamics. The collection of all mobile CPOM in a screened sampling box under an overfall and emptying the box episodically, biweekly or daily during high flows (Wallace et al., 1995; Johnson et al., 2006), is a workable practice

reserved to small streams draining catchments of a few ha in size with discharges of a few liters/second. In larger streams, only portions of the CPOM transport can be sampled. Placing drift nets into the water column for minutes or hours at a time, episodically throughout the year (e.g., Newbern et al., 1981; Perry and Rose, 1984; Angradi, 1991; Jones and Smock, 1991; Kiffney et al., 2000) is limited to tranquil flows. Beschta (1981, 1983a) and Beschta and Jackson (2008) collected CPOM during stormflow events as by-catch in bedload samples in a 7.6 by 7.6 cm opening Hel-ley-Smith sampler with a 0.2 mm mesh-width net. However, those measurements are limited to the lower 7.6 cm of the water column and miss organic matter carried higher up. Turowski et al. (2013) collected CPOM transport in a high-energy mountain torrent, sampling the entire water column using bedload traps 0.2 m high (Bunte et al. 2007, 2008, 2010). They present the only transport relation known so far. In this study we: 1) demonstrate use of bedload traps for sampling CPOM transport in high-energy but wadeable streams during a high-flow season, 2) document CPOM transport and its variable relations to water flow (hysteresis) over a snowmelt high-flow season, and 3) provide estimates of annual CPOM export in two high elevation Rocky Mountain streams.

STUDY SITES

Study sites CPOM samples were collected in conjunction with gravel bedload sampling in two cobble-bed streams in the Rocky Mountains. The studies were conducted in 2001 and 2002 (Bunte, 2001; Bunte and Swingle, 2003), about 10 years before the widespread onset of pine beetle kill in the central Rocky Mountains. Both study streams have snowmelt runoff regimes and daily fluctuations of flow. See Table 1 for site and basin characteristics.

Table 1: Study site and basin characteristics for the two study streams.

	Little Granite Creek	East St. Louis Creek
Study site locations	Gros Ventre Range, 31 km SE of Jackson Hole, WY	Fraser Experimental Forest, 71 km NW of Denver, CO
Site coordinates	43º19'17.40"N; 110º 30"41.77"E	39º53'12.97"N; 105º52'38.42"W
Main flow direction: headwaters; main stem	SW; SE	NW; N
Min. and max. basin elevation (m)	2030 to 3220	2,889 to 3890
Drainage basin area (km^2)	13.09	8.03
[1)] % unforested	38 (above treeline)	38 (33 above tree line + 5 too dry)
[1, 2)] % partially forested, open canopy	41	-
[1)] % fully forested, (almost) closed canopy	21	62
Stream gradient (m/m) at site, over reach	0.012, 0.018	0.03, 0.093
Stream width at study site (m)	5.0	3.5
Stream length incl. tributaries (km)	14.5	6.0
Reach stream morphology	plane-bed; forced pool-riffle seq.	step-pool; occ. forced pool-riffle
Bed surface D_{16}, D_{50}, and D_{84} sizes (mm)	23, 67, 138	15, 108, 258
Bankfull flow (m^3/s)	2.83	0.764
Main lithology	sandstone, shale, limestn., granite	granite and schist

[1)] From Google Earth images; [2)] individual trees or tree groups discernible;

Little Granite Creek The Little Granite Creek study site (Figure 1a) in NW Wyoming is located 3.3 km above the confluence with Granite Creek. Downstream of Pleistocene glaciated headwater areas, the valley is typically confined by forested hillslopes (Lodgepole Pine (*Pinus contorta*), Engelmann Spruce (*Picea engelmannii*), Douglas Fir (*Pseudotsuga menziesii*)), but opens to a 45-50 m wide meadow 135 m upstream from the sampling site. The stream is incised about 1.1 m into the valley fill, keeping most high flows confined to the channel. The sampling site was located within a 25-m long straight run. Flow stage elevation was digitally recorded in 15-minute increments. Flow velocity was measured almost daily at about 20 verticals across the channel with an electromagnetic current meter at 0.6 of the flow depth to compute discharge and establish a hydrograph. Bankfull flow (Q_{bkf}) was estimated from field evidence and from the long-term flow record of a near-by stream adjusted by drainage area of the study stream.

East St. Louis Creek East St. Louis Creek is a steep, cobble-bed mountain stream (Figure 1b) in the Fraser Experimental Forest (http://www.fs.usda.gov/main/fraser/about/site-description) in central Colorado. The drainage basin is covered by glacial till, and near-stream valley slopes are typically gentle. Most of the basin is located in subalpine forest (Engleman spruce, Subalpine fir (*Abies lasiocarpa*), Lodgepole pine); there are a few quaking aspen (*Populus tremuloides*), alder (*Alnus incana*), and willows (*Salix* species). The streambed is typically incised by about 1 m

which prevents extensive overbank flooding. The sampling site was located in a short and locally wide plane-bed section a few meter upstream of a weir pond where discharge is recorded continuously at a crested weir. Bankfull flow was taken as the 1.5-year recurrence interval flow of a long-term flow record.

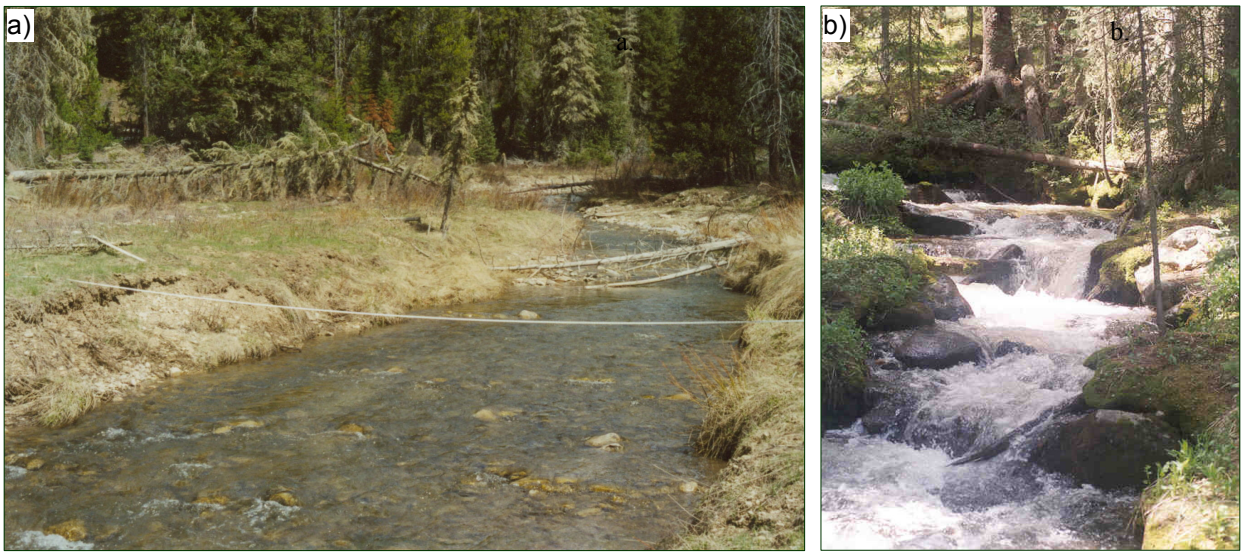

Figure 1: Upstream view of the Little Granite Creek (a) and East St. Louis Creek (b) study sites.

METHODS AND ANALYSES

Sampling with bedload traps and the sampling scheme Bedload traps (Bunte et al., 2004, 2007, 2008, 2010) that were used for sampling CPOM transport together with gravel bedload in this study (Bunte, 2001; Bunte and Swingle, 2003) have the shape of a shoebox without a bottom placed on its long side. The aluminum frame is 0.2 m high, 0.3 m wide, and 0.1 m deep; a net 1 to 1.6 m long with a 3.6 mm mesh width is attached to the frame (Figure 2a). The frame is placed onto a 0.41 by 0.35 m aluminum ground plate that is installed flush with the average height of the bed and anchored to the stream bottom with two metal stakes that are pounded into the bed. Adjustable straps attached to the frame are tied around the metal stakes and hold the sampler in place. This set-up allows bedload traps to be deployed for sampling times ranging from minutes to hours depending on transport rates and fill level of the net. For emptying, the string that closes the net at its downstream end is untied, the contents are shaken into a large bucket, and the string is re-tied for another round of sampling. Samples can thus be taken back-to-back during a field day, while the sampler frames remain fastened on the ground plates (Figure 2b). Four traps were installed about 1 m apart across the stream at the two study sites. Sampling covered an 8-10 hour period between the daily falling limbs of flow in the late morning and the daily rising limbs up to or just past daily peak flow in the evening. Bedload traps were removed from the stream bed overnight to avoid overfilling them.

Figure 2: Bedload traps installed at E. St. Louis Cr. (a); Retying the net after emptying the contents into buckets (b).

At Little Granite Cr., the 2002 snowmelt hydrograph had two distinct peaks, one on May 21 (85% Q_{bkf}) and one on June 1 (110% Q_{bkf}) (Figure 3a). CPOM sampling started at 21% Q_{bkf} on the first rising limb with 1-hour samples and continued daily until the end of the first discharge peak two weeks later. Over the second discharge peak, samples were collected alternately over intervals of 10 and 60 minutes. Sampling extended over another two-week period until flow had decreased to 40% Q_{bkf} on the second falling limb. Five to eight samples were collected each day, totaling 92 samples over the four-week high-flow season. At East St. Louis Cr., all CPOM samples were collected over 1-hour periods, starting at 44% of Q_{bkf} a week into the high-flow season, covering peak flow that was 70% of Q_{bkf}, and ending 17 days later at 36% of Q_{bkf} (Fig. 3b). Two to seven samples were collected per day on most days, totaling 73 samples.

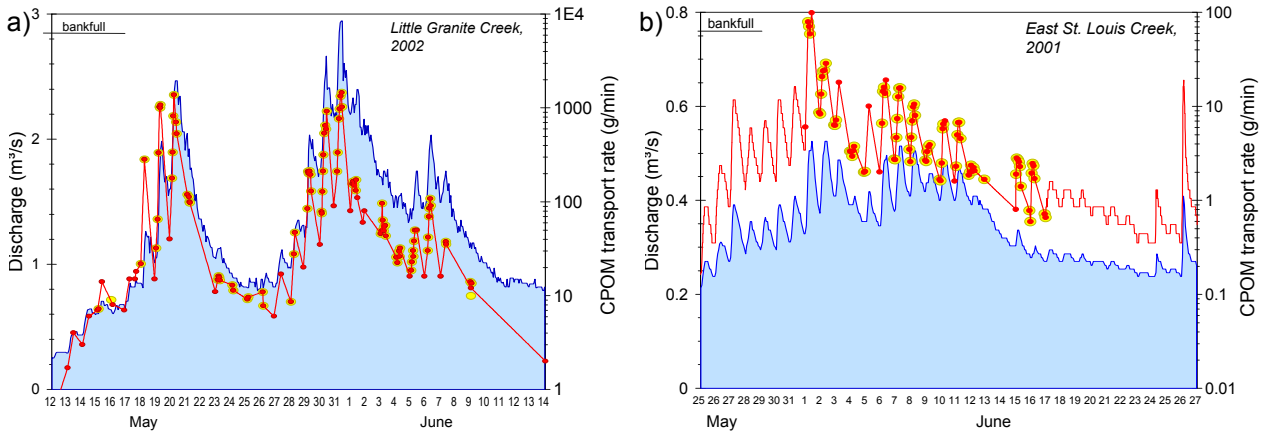

Figure 3: Peakflow portion of the annual hydrograph (blue line) with measured CPOM transport rates (yellow dots), those extrapolated for times of daily peak and low flow (red dots), and the interpolated continuous record of CPOM transport rates (red line) at Little Granite Creek (left) and East St. Louis Creek (right). Note different scales of plots.

CPOM composition Most of the CPOM collected in the bedload traps consisted of small cones from coniferous trees, cone scales, coniferous needles, small twigs and sticks (typically 1-3 cm in diameter, 10-30 cm long), leaves (mainly willow), small, spongy pieces of wood, and occasional hard pieces of bark. CPOM was dark brown in color and appeared as thoroughly soaked mulch from the forest floor. Dry needles were more frequent early in the high-flow season; at higher flows, sticks joined the CPOM mixture. Later in the high-flow season, rain, sleet, and hail washed, dislodged, and tore off dry needles and the green tips of coniferous trees that were included in the CPOM mix together with parts of fresh herbaceous plants. The CPOM composition in the study streams is similar to the CPOM the authors have collected during bedload measurements in several other Rocky Mountain streams.

The density of waterlogged CPOM is slightly higher than that of water. When water flow was still clear during moderate high flows, the authors observed CPOM to travel as bedload, rolling, sliding, and bouncing along the bed surface, especially the plump conifer cones and soaked wood pieces. At larger flows, CPOM moved in larger hops and in near-bed suspension; small organic particles moved as suspended load within the water column, while dry sticks floated. As flow approached bankfull flow conditions, the water was turbid, and the channel bed was not visible.

Field processing The combined sample volumes of wet CPOM and gravel bedload reached up to 20 liters. Early in the highflow season, sample volumes were comprised mostly of CPOM, but the CPOM portion decreased to less than half the volume later in the high-flow season. Samples collected near peak flow in the two study streams are shown in Figure 4. CPOM and gravel bedload were typically separated in the field to keep bagged sample volumes manageable and to minimize the number of bags with rotting CPOM to be dealt with later. Samples smaller than 1 liter were poured into a metal bowl and stirred with water to allow gravel bedload particles to sink; CPOM was then removed from the top by carefully decanting the wet organics into a bucket and helping the process along with a rubber spatula (Figure 5a). The action of stirring with water and decanting was repeated several times until all CPOM was removed. Large CPOM and gravel bedload samples were handled either in small batches as described above or pre-processed in a 20-liter bucket: after stirring with plenty of water and settling of the gravel particles, CPOM was removed from the top using a large wire-mesh spoon (Figure 5b). After repeating the process several

times, the remainder of the sample—bedload containing some CPOM—was separated in a bowl as described above. The volume of wet CPOM samples was determined in a clear 500 ml measuring cup or in a graded 10-liter bucket.

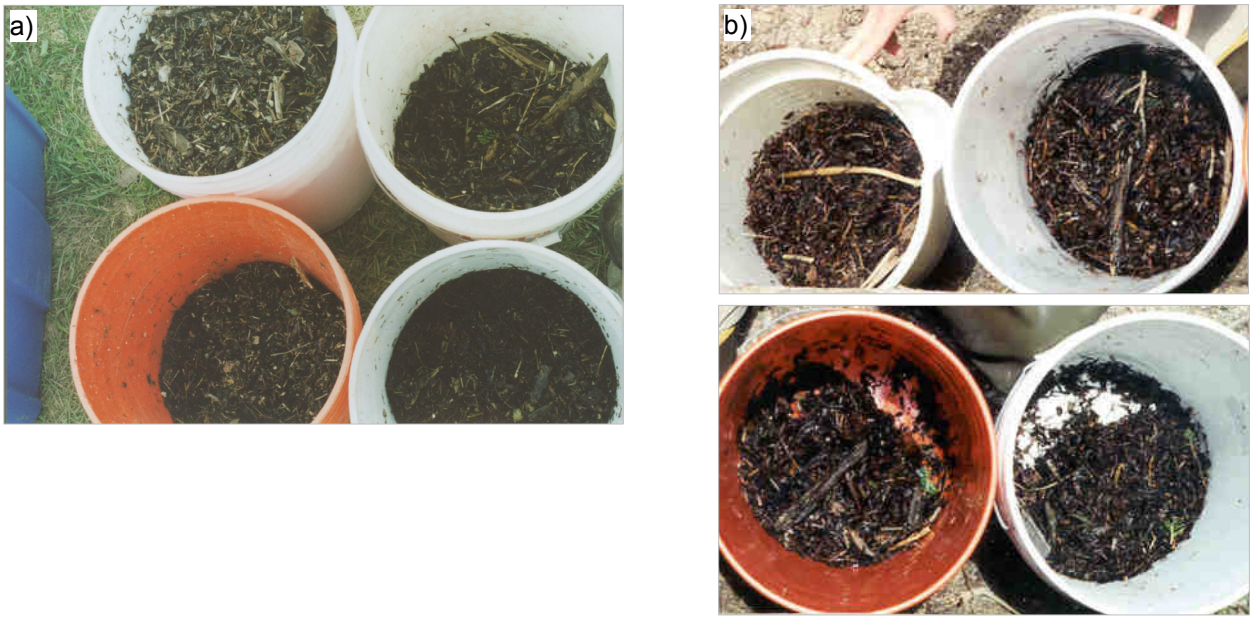

Figure 4: CPOM samples collected at high flow in the four traps at Little Granite (a) and East St. Louis Creek (b).

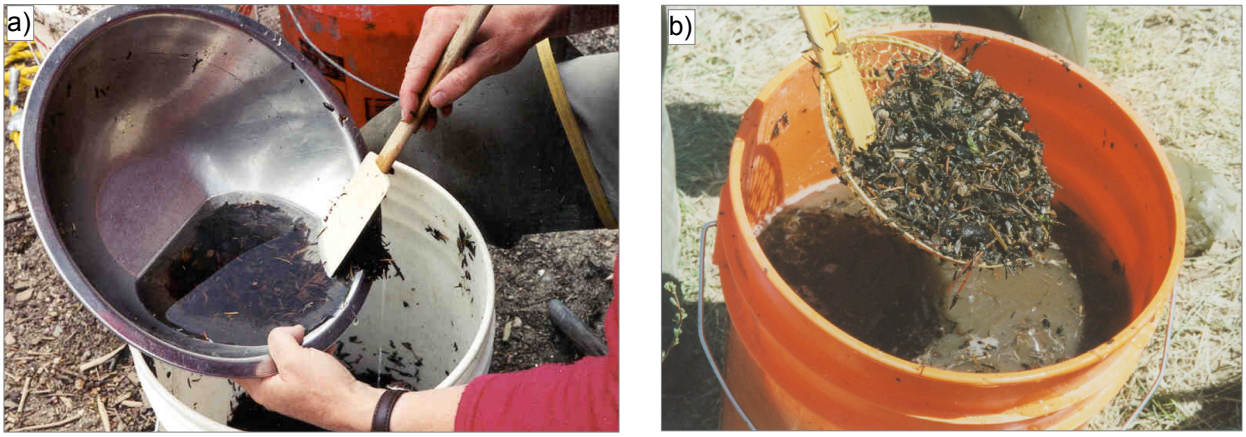

Figure 5: Field separation of CPOM from inorganic bedload in small (a) and large samples (b).

Computation of wet volumetric and dry mass CPOM transport rates Wet volumetric CPOM transport rates ($Q_{CPOM\ vol}$; l/hour) were computed individually for each stream width segment (w_1 *to* w_4) represented by one of the traps because trap spacing and sampling time differed slightly between traps. The cross-sectional wet volumetric CPOM transport rate is obtained from the sum over all width segments:

$$Q_{CPOM\ vol} = \frac{V_1 \cdot w_1}{w_s \cdot t_{s1}} + \frac{V_2 \cdot w_2}{w_s \cdot t_{s2}} + \frac{V_3 \cdot w_3}{w_s \cdot t_{s3}} + \frac{V_4 \cdot w_4}{w_s \cdot t_{s4}} \quad (1)$$

V is the CPOM volume per trap, w_s is the trap width, and t_s is the sampling duration. The summed stream sections equal the active stream width. A dozen CPOM samples from the two streams were dried to constant weight in a low temperature oven. The dry mass transport rate Q_{CPOM} (g/hr) is obtained from multiplying the wet volumetric transport rate by the mean dry weight of 112 g/l at E. St. Louis Cr. (std. dev. of 11.2 g) and 93.3 g/l at Little Granite Cr.

Adjustment for unsampled CPOM passing over the traps Flow sometimes overtopped the bedload traps—that extend 0.2 m above the bed—leaving near-surface CPOM transport unsampled. At Little Granite Cr., the two central

traps became overtopped at 20% Q_{bkf} and the two lateral ones at 30% Q_{bf}. The maximum overflow height reached 0.22 m during the brief periods of peak flow. To estimate the unsampled CPOM portion, a vertical concentration profile of CPOM needs to be assumed. If the concentration of waterlogged CPOM particles (C_{CPOM} [g/m^3]) is highest near the stream bottom, and given a near logarithmic velocity profile with the fastest flow (v [m/s]) near the water surface, CPOM transport rates per stream section (Q_{CPOM} [g/m^2·s] = $C_{CPOM} \cdot v$) are approximately even throughout the water column (Figure 6a). If, by contrast, C_{CPOM} is roughly even vertically through the water column, Q_{CPOM} is highest near the water surface (Figure 6b). If large amounts of CPOM (e.g., many dry sticks) float near the water surface, while waterlogged CPOM transport is concentrated near the bottom, a much larger portion of CPOM transport is missed by not sampling the top of the water column (Figure 6c).

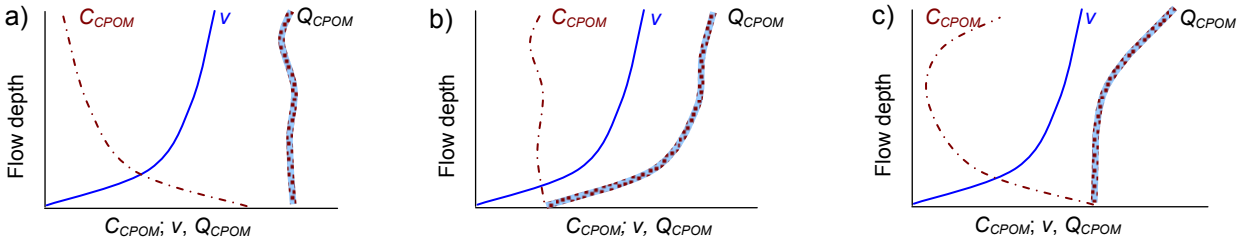

Figure 6: Interplay between C_{CPOM}, v, and Q_{CPOM}. Downward increasing trend of C_{CPOM} causes a vertically approx. even Q_{CPOM} profile (a). Vertically even C_{CPOM} causes highest Q_{CPOM} near the stream surface (b). Downward increasing C_{CPOM} together with high near-surface concentration also cause the highest Q_{CPOM} near the surface.

Based on visual field observation of where within the water column CPOM is transported, this study assumed a downward increasing trend for C_{CPOM} with a vertically even distribution Q_{CPOM} (Figure 6a) in which case the unsampled portion of CPOM transport is directly proportional to the height of flow overtopping the traps h_{top}. Overtopping heights were recorded at various flows Q for all traps, and h_{top} was described as a logarithmic function of Q where x and m are regression coefficients.

$$H_{top} = x\,(\log Q) + m \tag{2}$$

Once Q started overtopping one of the traps, overtop-adjusted transport rates $Q_{CPOM\ adj}$ were computed from measured transport rate $Q_{CPOM\ meas}$ as

$$Q_{CPOM\ adj} = \left(h_{trap} + \frac{h_{top}}{h_{trap}}\right) \cdot Q_{CPOM\ meas} \tag{3}$$

where the trap height h_{trap} which included the frame and the net thickness is 218 mm. During the brief peak flow periods, the overtop-adjusted cross-sectional $Q_{CPOM\ adj}$ rates at Little Granite Creek were up to twice the sampled values. At East St. Louis Creek, flows did not exceed 70% Q_{bkf}, and the sampling site was also considerably wider than the average stream width. Only one of the four traps became overtopped at 35% Q_{bkf}, and the maximal h_{top} was 6 cm at the highest measured flow. The overtopping adjustment increased cross-sectional CPOM transport rates by less than 6% for those flows.

Adjustment of 1-hour samples at Little Granite Creek During the first rising limb in 2002, almost all samples at Little Granite Cr. were collected over 1-hour sampling times, but 1-hour and 10-minute samples were collected alternately during the first falling limb and the second rising and falling limbs. CPOM transport rates computed from 10-minute samples ($Q_{CPOM\ 10}$) were generally larger than those computed from 1-hour samples ($Q_{CPOM\ 60}$) at similar flow (Figure 6a and b), indicating that 1-hour samples had a reduced sampling efficiency. This would occur when the nets overfilled or clogged which reduced through flow and capture rates. Differences in capture rates between sampling times were negligible early in the high-flow season, but $Q_{CPOM\ 10}$ exceeded $Q_{CPOM\ 60}$ by a factor of up to two at the highest transport rates near peak flow (Figure 6a). In order to use all samples collected over the highflow season in the analyses of annual CPOM export, the reduced sampling efficiency of the 1-hour samples was accounted for by adjusting 1-hour transport rates to those that might have been obtained by 10-minute sampling. The 1-hour and 10-minute CPOM samples were collected at alternate times, and because discharge changed quickly between samples, transport rates for the two sampling times cannot be directly related to each other. Instead, CPOM

transport rates for both sampling times were predicted for eight flow values evenly spaced between Q_{min} and Q_{max} from the second rising and falling limb CPOM rating curves (Figure 7a). To account for the inherent bias in predictions from a power function with data scatter, each predicted $Q_{CPOM\ 10}$ and $Q_{CPOM\ 60}$ was multiplied by a bias correction factor *CF*. From the several correction functions available (see discussion by Hirsch et al. 1993), the one proposed by Ferguson (1986, 1987) was selected for ease of computation ($CF = \exp(2.651\ SE_y^2)$ where SE_y is the standard error of the y-estimate.

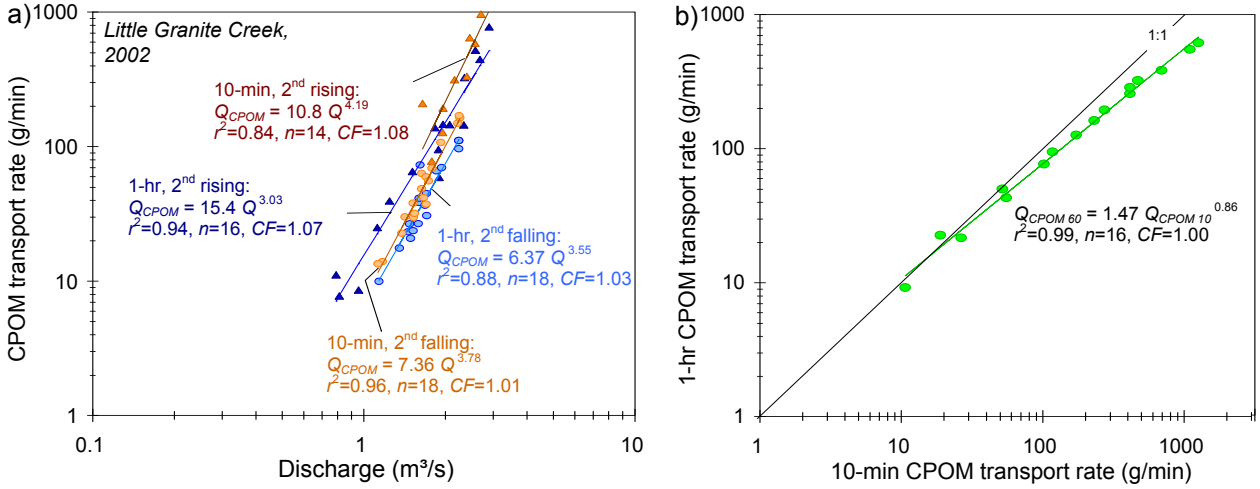

Figure 7: Relations of overtop-adjusted CPOM transport rates from 1-hour and 10-minute sampling with discharge during the second rising and falling limbs of flow at Little Granite Creek, 2002 (a). Relation between 1-hour and 10-minute Q_{CPOM} predicted from CPOM transport relations in panel (a) (b).

The relationship between predicted 1-hour and 10-minute Q_{CPOM} transport rates $Q_{CPOM\ 60}$ and $Q_{CPOM\ 10}$ was well defined with an r^2=0.99 (Figure 7b). Assuming that this relation established from data collected during the second discharge peak likewise applied to the first discharge peak, the inverse of the regression function in Figure 7b ($Q_{CPOM\ 60adj} = 0.666\ Q_{CPOM\ 10}^{1.155}$) was used to adjust all 1-hour CPOM transport rates >10 g/min for their reduced sampling efficiency; no adjustment was needed for small samples for which sampling time had no effect on sampling efficiency. After adjustments, there were 91 individual CPOM transport rates available over the high-flow season for computations of annual CPOM export at Little Granite Cr. Peak flow (70% Q_{bf}) and maximum Q_{CPOM} (81 g/min) were much lower at East St. Louis Cr., so a reduction in sampling efficiency of 1-hour samples was unlikely, and all 73 collected 1-hour samples were used without time adjustment to compute CPOM transport relations.

CPOM transport rates and relation to discharge The range of measured CPOM transport rates extended over more than two orders of magnitude in both study streams (Figure 8a and b). Due to pronounced hysteresis, Q_{CPOM} scattered over one order of magnitude in both streams for a given flow, and this resulted in a comparatively poor fit of the power function transport relationships $Q_{CPOM} = a \cdot Q^b$ fitted to all CPOM data (r^2 of 0.60 and 0.73) where *a* is the coefficient and *b* the exponent. By contrast, power function relations fitted to measured CPOM transport rates and flows for the individual rising and falling limbs were well defined in both study streams (r^2 between 0.85 and 0.96; see transport equations in Figure 8a and b), but differ notably among each other and from the relation for all data. The pronounced differences of transport relations between rising and falling limbs of flow makes clear that separate CPOM rating curves needed to be used to compute CPOM load over the high-flow season.

At East St. Louis Cr., the exponent *b* fitted to the relation $Q_{CPOM} = a \cdot Q^b$ for all data is 4.5, while exponents for individual rising and falling rating curves range between 6.6 and 7.1. At Little Granite Cr., Q_{CPOM} increases less strongly with flow, yielding an exponent of 3.5 for all samples, while exponents for individual limbs of flow are within 3.0 and 4.1. The Q_{CPOM} transport relations reported here are of similar steepness as the relation established by Turowski et al. (2013) for the Swiss Erlenbach torrent with an exponent $b = 4.42$, likewise sampled with bedload traps.

Computation of seasonal CPOM loads using a rating curve and a summation approach Both a rating curve and a summation approach were employed to compute seasonal and annual CPOM loads. For the rating curve

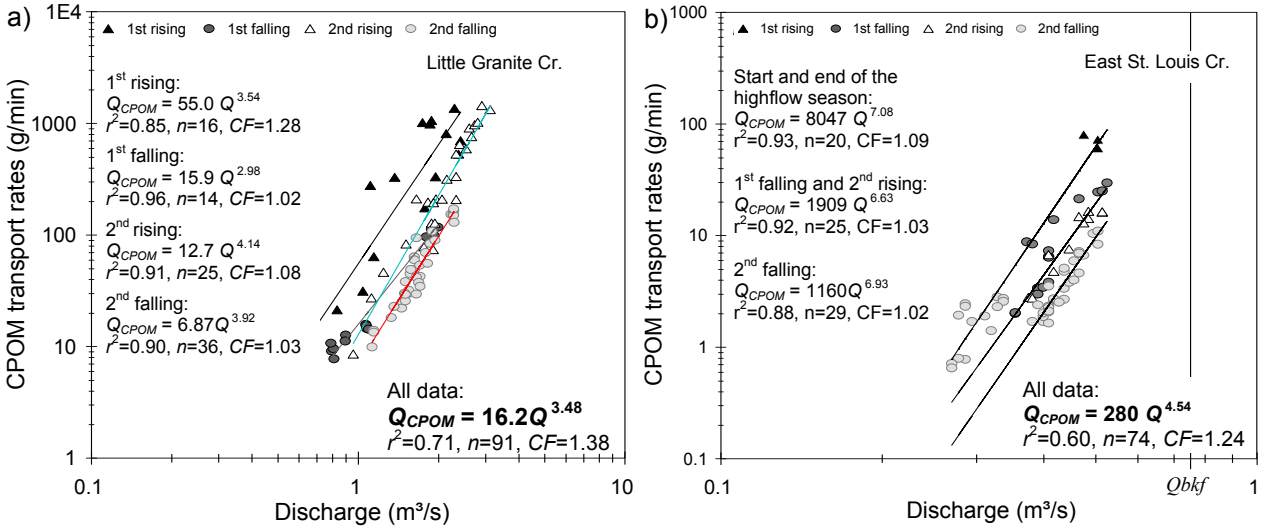

Figure 8: Relations of CPOM transport rates vs. discharge for seasonal rising and falling limbs of flow at Little Granite Creek (a) and East St, Louis Creek (b). All *p*-values are < 0.0001. Note different plot scales for a) and b).

approach, each flow value of the 15-minute hydrograph was multiplied by the CPOM transport rate (g/min) predicted for that flow from the respective power function $Q_{CPOM} = a \cdot Q^{b}$ rating curve (Figure 8a and b), multiplied by the Ferguson (1986, 1987) bias correction factor *CF*, multiplied by 15 to integrate over each 15-minute time increment, and summed over the rising and falling limbs of the high-flow season. Seasonal CPOM loads during the unmeasured flows prior to the high-flow season, the post high-flow falling limb, and late summer low flows were computed from a rating curve approach. Zero CPOM transport was assumed for both streams between fall and spring when flows are very low (5-10% of bankfull), and a snow cover shields most of the stream surface from CPOM input.

Summation approach The sequence of CPOM fluxes computed from samples collected over the daily rising limbs of flow (and adjusted for sampler overtopping and overfilling where needed) generally followed the diurnal fluctuations of flow. The lowest and highest daily transport rates fell onto the daily minima and maxima of flow at both streams. This correspondence can be used to extend the observed daily trends to peak- and low-flow times at which CPOM was not measured and to estimate daily maximum and minimum Q_{CPOM} when needed. CPOM transport rates were then interpolated geometrically (due to power-function relations of Q_{CPOM} with Q) between daily low-flows and peak flows to obtain a value for each 15-minute increment. This created a continuous 15-minute estimate of CPOM transport rates over the high-flow season (Figure 3a and b). Multiplication of Q_{CPOM} by the time of each 15-minute increment and summing over the sampled time period of the high-flow season yielded the CPOM load for the sampled portion of the highflow season. A rating curve approach was used to compute CPOM loads for the unsampled pre- and post high-flow seasons, extending trends from the CPOM rating curves for the first rising limb and the second falling limb, respectively, to lower flows. At Little Granite Cr., no hydrograph was available for the 80-day remainder of the seasonal falling limb between July 12 and Sept. 30, and a constant value of Q_{CPOM} = 0.05 g/min was assumed.

Simulating a hydrograph with bankfull flow at East St. Louis Creek Because CPOM transport rates increase with water discharge and hence with the highflow volume, a comparison of annual CPOM export between basins should be referenced to "normal" flow years, defined as years in which flows reach or slightly exceed the bankfull level for a few days. Flows at Little Granite Cr. peaked briefly at bankfull, approaching a normal year. For East St. Louis Cr. that had peaked at only 70% of bankfull flow, the study simulated a hydrograph that peaks at bankfull. To this end, measured peak flow was increased by 0.244 m^3/s to reach a bankfull flow of 0.764 m^3/s, and a smooth hydrograph was created by tapering off the mathematical flow addition towards the rising and falling limbs. CPOM transport rates were estimated by extrapolating the rating curves established for rising and falling limbs of flow in 2001 (Figure 8b). The predicted transport rates were then applied to each 15-minute time increment and summed over the new hydrograph. The stream's CPOM supply was considered sufficient to permit extension of the measured East St. Louis Cr. CPOM rating curves to bankfull flow because measured CPOM transport rates during a small flow peak on the falling limb of the hydrograph at the end of the high-flow season were higher than those

predicted from the falling limb rating curves that were based on measurements early on the falling limb. This suggested sufficient CPOM supply to allow CPOM transport rates to increase with increasing flow up to bankfull flow.

RESULTS

Annual CPOM export Annual CPOM export at Little Granite Cr. in 2002 computed from the summation approach was 3.6 metric tonnes (t) which represents a yield of 2.7 kg/ha/year. The vast majority (97%) of the annual export occurred during the 1-month high-flow season (Table 2), while only 0.4, 2.8, and 0.2% of the annual CPOM export occurred prior to high flow, after high flow, and later during summer low flows, respectively.

Table 2: CPOM transport rates and loads computed for hydrograph portions at Little Granite Cr. in 2002.

Time period	Hydrograph portion	Flow range (m^3/s)	No. of days	Range of transport rates (g/min)	Seasonal load (t)	% of annual export
April 18 - May 12	prior to high flow	0.08-0.34	24	0.001 – 1.5 *[1)]	0.013	0.4
May 12 - June 14	high flow	0.25-3.26	33	0.8 – 1458 [3)]	3.45	96.6
June 14 - July 11	falling limb	0.29-1.17	27	0.06 – 13 *[2)]	0.101	2.8
July 12 - Sept 30	late summer low *Q*	0.15-0.29 est.	80	0.05 *[2)]	0.006	0.2
Oct 1 – April 17	base flow	0.09-0.15 est.	201	0	0	0
2002 annual export (t)	entire year		365		3.57	100
Basin yield (kg/ha/yr)	entire year				2.73	

* estimated by extrapolation from rating curve for [1)] first rising limb; [2)] second falling limb; [3)] based on intensive sampling that facilitated using a summation approach.

Annual CPOM export at East St. Louis Cr. was 169 kg during the 2001 low-flow year, with a basin yield of 0.211 kg/ha/year—more than an order of magnitude less than exported from Little Granite Cr. Most of the CPOM export occurred within the high-flow period (82%), although notable amounts (11%) were still supplied during the falling limb (see 2001 in Table 3). Annual CPOM export at East St. Louis Cr. for a simulated bankfull hydrograph (see bf-year in Table 3) reached 3.2 metric tonnes, 19 times more than computed for the low-flow year. While this estimate might have some uncertainty because trends measured in the low-flow rating curves were extrapolated to higher flows (when perhaps supply exhaustion may set in), it shows the important role that runoff plays in annual CPOM export from a basin. Other studies have shown that differences in the CPOM export of more than an order of magnitude between years are not unusual (Bilby, 1981; Wallace et al., 1995).

Table 3: CPOM transport rates, loads, and yields for various hydrograph parts at East St. Louis Cr. in 2001 and for a year with a simulated a hydrograph reaching the bankfull level

Time period	Hydrograph part	Days	Flow range (m^3/s)		Range of transport rates (g/min)		Loads and yields		% of annual export	
			2001	bf-year	2001	bf-year	2001	bf-yr.	2001	bf-yr.
May 15 - June 1	rising limb	16	0.18-0.51	0.18-0.74	0.05-79 [1)]	0.05-1102 [1)]	0.0042	1.2	2.5	38
June 1 - June 17	highflow	12	0.34-0.53	0.53-0.76	1.6-99 [2)]	15.5-1363 [2)]	0.139	2.0	82	61
June 17 - July 15	falling limb	30	0.17-0.42	0.17-0.53	0.03-19 [1)]	0.01-15.5 [1)]	0.026	0.055	15	1.7
July 16 - Sept 30	late sumr. *Q*	77	0.044-0.19		~0-0.08 [3)]	~0-0.08 [3)]	0.00013		0.05	0.004
Oct 1 - May 14	base flow	230	0.028-0.044		0		0		0	
'01 ann. export (t)	entire year	365					0.169	3.24	100	
Yield (kg/ha/yr)	entire year						0.211	4.04		

[1)] Based on rating curve for 1st rising limb; [2)] based on summation approach and intensive sampling; [3)] based on rating curve for all data.

Comparison of CPOM export and yield CPOM export was slightly higher at Little Granite Cr. (3.6 t) compared that at East St. Louis Cr. (3.2 t) for the simulated bankfull hydrograph. Per basin area, though, East St. Louis Cr. yielded more CPOM (4.0 t) than Little Granite Cr. (2.7 t). For the forested portion of the basin area, both streams had similar CPOM exports of 6.6 and 6.5 kg/ha/year, a low estimate given that flows just briefly reached bankfull.

While little information exists for coniferous forests (Richardson et al. 2005), mean annual CPOM exports of about 0.4 to 10 kg/ha are reported for deciduous watersheds (Table 4). Per forested watershed area, CPOM export of 6.5 and 6.6 kg/ha/year from the two subalpine Rocky Mountain watersheds is comparable to export from deciduous forests such as in the Atlantic NE Hubbard Brook (e.g., Bilby 1981) and the Brazilian Mato Grosso (Johnson et al., 2006).

Table 4: Comparison of CPOM export reported for various streams with forested watersheds.

Location	Coweeta, NC watersheds C53, C54, C55	Hubbard Brook, NH watersheds W5, W6	Little Granite Cr., WY	East St. Louis [1], CO	Juruena, Mato Grosso, Brazil
Reference	Wallace et al. (1995)	Bilby & Likens (1980); Bilby (1981)	This study		Johnson et al. (2006)
Basin area (ha)	5.2 - 55	13 - 22	1309	803	1 - 2
Main forest type	deciduous	deciduous	coniferous		deciduous
CPOM export (kg/ha/yr)	0.14 - 1.2	7.1 - 15 [2]	2.7	4.0	3.7 [3]
CPOM export per forested watershed area (kg/ha/yr)	0.4 est.[4]	10 est. [4]	6.6 [5]	6.5 [5]	3.7 est. [4]

[1] est. for a year with bankfull flow; [2] based on 11 and 12 years prior to removal of debris dams; [3] based on a reported 3.5% portion of CPOC on total carbon export; [4] assuming basin areas are fully forested; [5] 21% basin area are fully forested; of the partially forested area (41%), half is counted to the fully forested area (=21% + 20.5% = 41.5% forested); 38% is above treeline or otherwise unforested; [5] 62% basin area are fully forested; 33% above treeline and 5% otherwise sparely forested.

DISCUSSION AND SUMMARY

Bedload traps with a 4-mm mesh were found suitable for sampling the CPOM-gravel bedload mix. Traps that extend through the entire water column over all flows would be desirable for a more complete capture of CPOM transport. However, during high flows, taller traps may not be able to withstand the greater force of flow near the top of the water column, possibly causing the traps to bend backwards and become dislocated from the ground plates. To estimate CPOM transport passing above the bedload traps, measuring profiles of the vertical CPOM concentration at increments through the water column at various flows might be useful. Care should be taken not to overfill the nets which may require a reduction in sampling times when loads are high. CPOM transport rates presented here may constitute a conservative estimate because the 4-mm mesh might not representatively sample the 1-4 mm portion of CPOM. However, based on the large amounts of captured conifer needles and needle fragments, elongated particles probably roll over the bed or tumble in the flow rather than go straight like an arrow that might pass straight through the mesh. Sampler nets with 1-mm mesh were also found to be less suitable for collecting CPOM because CPOM easily clogs those nets, causing a reduction in hydraulic and sampling efficiency (Bunte et al. 2015, *session 5C*). Since gravel bedload and CPOM are jointly transported and jointly captured in the sampler, it makes sense to combine field projects of bedload and CPOM sampling.

CPOM transport rates showed seasonal hysteresis that was more pronounced than what has been measured for gravel bedload transport at the study streams. The extremely supply driven (and limited) transport dynamics cause CPOM transport relations to differ drastically between individual rising and falling limbs of the high-flow hydrograph, as well as between the pre-and post runoff seasons (Bilby and Likens, 1980; Wallace et al., 1995). At Little Granite Cr., the season's first rising limb Q_{CPOM} was 4-5 times higher than Q_{CPOM} on the first falling limb, 3-4 times higher than on the second rising limb and about 6 times higher than on the second falling limb (Figure 8a). At East St. Louis Cr., Q_{CPOM} during the first rising limb was about 3 times higher than on the shared transport relation for the first falling and second rising limb (Figure 8b) and also about 6 times higher than on the second falling limb. During small rainfall peaks towards the end of the highflow season at East St. Louis Cr., Q_{CPOM} approached the relationship of the first rising limb, suggesting that CPOM was still available for transport on the falling limb in this in low-flow year.

The quick response of Q_{CPOM} to increasing flow in both streams indicates that CPOM is easily entrained and transported, i.e., transport is hydraulically controlled. However, the hysteresis relations, and transport rates that decrease over time, show that the response of CPOM flux to flow is also governed by the availability of CPOM supply which changes over the course of the high-flow season.

As Q_{CPOM} is strongly related to flow, 95% of the annual CPOM export was concentrated in the central one-month period of the snowmelt high-flow season in both study streams. Strong hysteresis effects during that period require that CPOM transport be intensively sampled and that separate CPOM rating curves are established for each portion of the typically multi-peaked snowmelt hydrograph. For example, had CPOM at Little Granite Cr. been sampled over only a few consecutive days (i.e., been limited to one of the rising or falling limbs of flow), and only one rating curve (together with bias correction factor CF) been used to compute the highflow CPOM load, computed loads might have varied between 1.7 tonnes (if field sampling was limited to the second falling limb) and 9.7 tonnes (if field sampling was limited to the 1st rising limb) depending on whether the field visit occurred early or late in the high-flow season. By contrast, using the appropriate rating curve for each limb resulted in a CPOM load of 3.5 tonnes which is very close to the annual load of 3.6 tonnes computed from the summation approach.

CPOM yields in the two high-elevation Rocky Mountain study streams with subalpine coniferous forests was 2.7 and 4.0 kg/ha/yr for bankfull flow events, but both streams yielded similar amounts (6.6 and 6.5 kg/ha/yr) per forested portion of the basin area. Those Rocky Mountain CPOM yields are similar to export reported for North Eastern deciduous forests (7-15 kg/ha/yr), and the Brazilian Mato Grosso. Due to high inter-annual variability, CPOM export is ideally based on the average of long-term observations. Failing that, it might be advisable to compute CPOM for normal flow years in which bankfull flow is reached or slightly exceeded for a few days.

Acknowledgement We thank Sandra Ryan and Mark Dixon for the 2002 flow data from Little Granite Creek and L. Porth, K. Elder, and B. Starr (all USDA Forest Service, Rocky Mountain Research Station, Fort Collins, CO) for the 2001 East St. Louis Creek flow data. Field work and part of the data analysis was funded by the USDA Forest Service Stream Systems Technology Center, Fort Collins, CO. Further analyses and part of the manuscript were prepared while K.B. received support from the Swiss Federal Research Institute (WSL) in Birmensdorf, CH. Sandra Ryan and Ellen Wohl (CSU) provided friendly reviews of the manuscript. We thank John Potyondy (USFS ret.) for vision, insight, and long-term support of our field studies.

REFERENCES

Angradi, T.R. (1991). "Transport of coarse particulate organic matter in an Idaho river, USA," Hydrobiologia, 211, pp 171-183.

Beschta, R.L., and Jackson, W.L. (2008). "Sedimentation studies following the Alsea Watershed study," In: Hydrological and Biological Responses to Forest Practices, J.D. Stednick (ed.). Ecological Studies, 199, pp 183-210. DOI: 10.1007/978-0-387-69036-0_12. Springer, New York, 316 pp.

Bilby, R.E. (1981). "Role of organic debris dams in regulating the export of dissolved and particulate matter from a forested watershed," Ecology, 62(5), pp 1234-1243.

Bilby, R.E, and Likens, G.E. (1980). "Importance of organic debris dams in the structure and function of stream ecosystems," Ecology, 61(5), pp 1107-1113.

Bunte, K. (2001). Field Testing the Sampling Efficiency of Bedload Traps at East St. Louis Creek, CO, Report submitted to the Stream Systems Technology Center, USDA Forest Service, Rocky Mtn. Res. Sta., Fort Collins, CO, 84 pp.

Bunte, K., and Swingle, K. (2003). Results from Testing the Bedload Traps at Little Granite Creek, 2002: Effect of Sampling Duration and Sampler Type on Bedload Transport Rates and Systematic Variability of Rating Curves with Basin Area and Stream Bed Parameters. Report submitted to the Stream Systems Technology Center, USDA Forest Service, Rocky Mtn. Res. Sta., Fort Collins, CO, 110 pp.

Bunte, K., Abt, S.R., Potyondy, J.P., and Ryan, S.E. (2004). "Measurement of coarse gravel and cobble transport using a portable bedload trap," J. Hydraul. Eng., 130(9), pp 879-893.

Bunte, K., and Swingle, K. (2009). Testing Bedload Traps with a 1.18 mm Mesh Width Netting. Report submitted to Stream Systems Technology Center, USDA Forest Service, Rocky Mtn. Res. Sta., Fort Collins, CO, 32 pp.

Bunte, K., Swingle, K., and Abt, S.R. (2007). Guidelines for Using Bedload Traps in Coarse-bedded Mountain Streams: Construction, Installation, Operation and Sample Processing. Gen. Tech. Rep. RMRS-GTR-191, Fort Collins, CO, U.S. Depart. of Agric., Forest Service, Rocky Mtn. Res. Sta., 91 pp. http://www.fs.fed.us/rm/pubs/rmrs_gtr191.pdf

Bunte, K., Abt, S.R., Potyondy, J.P., and Swingle, K.W. (2008). "A comparison of coarse bedload transport measured with bedload traps and Helley-Smith samplers," Geodinamica Acta, 21(1/2), pp 53-66.

Bunte, K., Swingle K.W., and Abt, S.R. (2010). "Necessity and difficulties of field calibration of signals from surrogate techniques in gravel-bed streams: possibilities for bedload trap samples," In: Bedload-surrogate

monitoring technologies, Gray, J.R., Laronne, J.B., and Marr, J.D.G (eds.), U.S. Geol. Surv. Sci. Invest. Rep. 2010-5091, 17 p. http://pubs/usgs.gov/sir/2010/5091.

Bunte, K., Swingle, K.W., Abt, S.R., and Cenderelli, D.A. (2015). "Effects of netting properties on flow hydraulics and transport rates sampled with bedload traps," In: SEDHYD 2015, 10th Fed. Interagency Sedimentation and 5th Fed. Interagency Hydrologic Modeling Conference, Session 5C, Physical measurement and monitoring.

Estep, M.A., and Beschta, R.L. (1985). Transport of Bedload Sediment and Channel Morphology of a Southeast Alaska Stream. Pacific Northwest Forest and Range Exp. Stat., Res. Note PNW-430, 15 pp.

Ferguson, R.I. (1986). "River loads underestimated by rating curves," Water Resourc. Res., 22(1), pp 74-76.

Ferguson, R.I. (1987). "Accuracy and precision of methods for estimating river loads," Earth Surface Process. Landforms, 12, pp 95-104.

Findlay, S., Likens, G. E., Hedin, L., Fisher, S. G., and McDowell, W. H. (1997). "Organic Matter Dynamics in Bear Brook, Hubbard Brook Experimental Forest, New Hampshire, USA," In: J.R. Webster and J.L. Meyer (eds.). Stream Organic Matter Budgets. J. North Am. Benth. Soc., 16(1), pp 43-46.

Fisher, S. G. and Likens, G. E. (1973). "Energy flow in Bear Brook, New Hampshire: An integrative approach to stream ecosystem metabolism," Ecol. Monogr., 43, pp 421–439.

Foucreau, N., Puijalon, S., Hervant F., and Piscart, C. (2013). "Effect of leaf litter characteristics on leaf conditioning and on consumption by Gammarus pulex," Freshwater Biol., 58, pp 1672-1681.

Hirsch, R.M., Helsel, D.R., Cohn, T.A., and Gilroy, E.J. (1993). Statistical Analysis of Hydrological Data. In: Handbook of Hydrology, Maidment, D.R. (ed.) McGraw-Hill, New York.

Johnson, M.S., Lehmann, J., Selva, E.C., Abdo, M., Riha S., and Couto, E.G. (2006). "Organic carbon fluxes within and streamwater exports from headwater catchments in the southern Amazon," Hydrol. Processes, 20, pp 2599-2614. DOI: 1.1002/hyp.6218

Jones, J.B., and Smock, L.A. (1991). "Transport and retention of particulate organic matter in two low-gradient headwater streams," J. North Am. Benth. Soc., 10(2), pp 115-126.

Kiffney, P.M., Richardson, J.S., and Feller, M.C. (2000). "Fluvial and epilithic organic matter dynamics in headwater streams of Southwestern British Columbia," Archiv für Hydrobiologie, 149, pp 109-129.

Newbern, L.A., Webster, J.R., Benfield, E.F., and Kennedy J.H. (1981)."Organic matter transport in an Appalachian Mountain river in Virginia, U.S.A," Hydrobiologia, 83, pp 73-83.

Perry, J.A., and Rose, F.L. (1984). "Organic carbon transport: Precision of measurement in stream systems," The American Midland Naturalist, 111(2), pp 400-404.

Richardson, J.S. (1992). "Coarse particulate detritus dynamics in small, montane streams of southwestern British Columbia," Can. J. Fisheries and Aquatic Sci., 49(2), pp 337-346.

Richardson, J.S., Bilby, R.E., and Bondar, C.A. (2005). "Organic matter dynamics in small streams of the Pacific Northwest," J. Am. Water Resourc. Assoc., 41(4), pp 921-934.

Richardson, J.S., Hoover, T.M., and Lecerf, A. (2009). "Coarse particulate organic matter dynamics in small streams: towards linking function to physical structure," Freshwater Biol., 54, pp 2116-2126.

Turowski, J.M., Badoux, A., Bunte, K., Rickli, C., Federspiel, N., and Jochner, M. (2013). "The mass distribution of coarse particulate organic matter exported from an alpine headwater stream," Earth Surf. Dynam. Discuss., 1, pp 1-29, doi:10.5194/esurfd-1-1-2013

Turowski, J.M., and Hilton, R. (2013). "A neglected riverine carbon transfer: The importance of coarse particulate organic matter for carbon export from a headwater catchment," Geophys. Res. Abstracts, 15, EGU2013-4168, 2013 EGU General Assembly 2013.

Wallace. J.B., Whiles, M.R., Eggert, S., Cuffney, T.F., Lugthart, G.J., and Chug, K. (1995). "Long-term dynamics of coarse particulate organic matter in three Appalachian mountain streams," In: Stream Organic Matter Budgets., J.R. Webster and J.L. Meyer (eds.). J. North Am. Benth. Soc., 14(2), pp 217-232.

Wallace, J.B., Cuffney, T.F., Eggert, S. L., and Whiles, M. R. (1997). "Stream organic matter inputs, storage, and export for Satellite Branch at Coweeta Hydrologic Laboratory, North Carolina, USA," In: Stream Organic Matter Budgets. J.R. Webster and J.L. Meyer (eds.). J. North Am. Benth. Soc., 16(1), pp 67-74.

Webster, J., Covich, A., Tank, J., and Crockett, T. (1994). "Retention of coarse organic particles in streams in the southern Appalachian Mountains," J. North Am. Benth. Soc., 13(2), pp 140-150.

Webster, J. R., and Meyer, J.L. (1997). "Organic Matter Budgets for Streams: A Synthesis," In: Stream Organic Matter Budgets, J.R. Webster and J.L. Meyer (eds.). J. North Am. Benth. Soc., 16(1), pp 141-161.

Webster, J.R., Benfield, E.F., Ehrman, T.P., Schaeffer, M.A., Tank, J.L., Hutchens, J.J., and Angelo, D.J.D. (1999). "What happens to allochthonous material that falls into streams?", Freshwater Biol., 41, pp 687-705.

SEDIMENT BUDGETS, TRANSPORT, AND DEPOSITIONAL TRENDS IN A LARGE TIDAL DELTA

Tara L. Morgan-King, hydrologist, U.S. Geological Survey Sacramento, California, tamorgan@usgs.gov; Scott A. Wright, research hydrologist, U.S. Geological Survey Sacramento, California, sawright@usgs.gov

INTRODUCTION

The Sacramento-San Joaquin Delta is the largest delta on the west coast of the United States. It is formed where the confluence of California's two largest rivers (the Sacramento and San Joaquin) meet the ocean tides and has a significant physical gradient from fluvial to tidal. It is a semi-diurnal system (two high and two low tides per day). Today, the Delta is one of the most manipulated in the United States. Once composed of many shallow, meandering and braided dendritic channels and dead-end sloughs and wetlands, it is now a network of leveed canals moving clear water around subsided islands. It historically has supported a biologically diverse tidal wetland complex, of which only 3% remains today (Whipple et al., 2012). It has also witnessed a collapse in the native fish populations. The Delta provides critical habitat for native species, however the hydrology and water quality are complicated by manipulations and diversions to satisfy multiple statewide objectives. Today water managers face co-equal goals of water supply to Californians and maintenance of ecosystem health and function. The Delta is a hub for both a multi-hundred-million dollar agricultural industry and a massive north-to-south water delivery system, supplying the primary source of freshwater to Central Valley farmers and drinking water for two-thirds of California's population. Large pump facilities support the water demand and draw water from the Delta, further altering circulation patterns and redirecting the net flow toward the export facilities (Monsen et al., 2007).

Fluvial sedimentation, along with organic accumulation, creates and sustains the Delta landscape. Hydraulic mining for gold in the watershed during the late 1800s delivered an especially large sediment pulse to the Delta. More recently, from 1955 to the present, a significant sediment decline has been observed that is thought to have been caused mostly by the construction of water storage reservoirs that trap the upstream sediment supply (Wright and Schoellhamer, 2004). Today, one concern is whether the volume of sediment supplied from the upper watershed is sufficient to support ecological function and sustain the Delta landscape and ecosystem in the face of climate change, sea level rise, and proposed restoration associated with the Bay Delta Conservation Plan (http://baydeltaconservationplan.com). Ecosystem health is a management focus and 150,000 acres of restoration is currently proposed, therefore it is of increasingly important to understand the quantity of sediment available for marsh and wetland restoration throughout the Bay Delta Estuary. It is also important to understand the pathways for sediment transport and the sediment budget into each of three Delta regions (figure 1) to guide restoration planning, modeling, and management.

In this paper, we present our preliminary findings while revisiting previous sediment flux research (Wright and Schoellhamer, 2005). Our current understanding of the hydrology of the Delta has been improved by a larger network of monitoring sites and new, higher quality

instrumentation to monitor turbidity, which we use as a surrogate for suspended sediment. The central Delta, specifically, is an extremely complicated and dynamic mixing zone hydrologically influenced by changes with river discharge, tides, seasons, diversions, and flow path modifications. Sacramento River flow into the central Delta is reduced by gates on the Delta Cross Channel (DCC figure 1) that are periodically closed, directing flows to the west Delta and San Francisco Bay. One critical issue is the migration of native fish through the Delta and the physical entrainment with the current into the south Delta. This often leads to mortality at the California and Federal pumping facilities and compromises population resilience (Kimmerer, 2008; Grimaldo et al., 2009). The annual spawning migration of delta smelt from Suisun Bay and the western Delta into the central and south Delta where they can potentially be entrained is believed to be triggered by the increase of Delta turbidity. The increased turbidity is caused by the influx of suspended sediment from the Sacramento River into the central Delta during the first major storm of the year (also known as the "first flush").

Our objectives for this paper are to 1) quantify annual sediment budgets for the Delta during water years 2011, 2012, and 2013, 2) to describe the primary pathways for sediment into each Delta region shown in figure 1, and 3) to explain the timing and magnitude of sources of sediment into the Delta. We evaluated the primary sediment peak of winter storms with a focus on the significance of the Georgiana Slough pathway (from GEO to MOK on figure 1) into the central Delta channels. One specific question we wanted to address is how much sediment moves into the central Delta during the peaks of the storm-related-sediment pulses during the initial prespawning migration of delta smelt compared to the total annual sediment load for a given water year (figure 2). The sediment information has been a missing link to migration and entrainment analysis. We know that the first significant rise in turbidity in winter, initiated by a big storm, is thought to initiate migration (Bennet et al., 2014; Grimaldo et al., 2009) and the majority of salvage (ie. captured and "saved" from entrainment) occurs during net negative flows (Kimmerer, 2009; Grimaldo et al., 2009). We hope, therefore, to help managers understand the effects of sediment and turbidity on fish migration in terms of the quantity and pathway of sediment that is transported to the pump facilities because salvage often leads to mortality.

METHODS

Turbidity, a surrogate measurement for calculating suspended-sediment concentrations (SSC) and load, is a water quality parameter that describes the cloudiness or opacity of the water due to suspended solids (Gray and Gartner, 2008). Turbidity as a surrogate has been successfully used for sediment analysis and demonstrated by Rasmussen and others (2005), Urich and Bragg (2003), Lietz and Debiak (2005), Wood and Teasdale (2013), Buchanan and Morgan (2010). Turbidity data from our network of sites described in figure 1 were corrected for calibration drift and fouling errors as described in Wagner et al. (2006).

Discharge data came from the California Department of Water Resources (DWR) and U.S. Geological Survey (USGS). Channel discharge was calculated from measurements using acoustic Doppler current profiler (ADCP) data and the index velocity method for tidal channels (Ruhl and Simpson, 2005). These data were accessed through the Water Information System (NWIS) http://waterdata.usgs.gov/ca/nwis, with exception to Mallard Island discharge data

which came from the DWR DAYFLOW website and was accessed from http://www.water.ca.gov/dayflow.

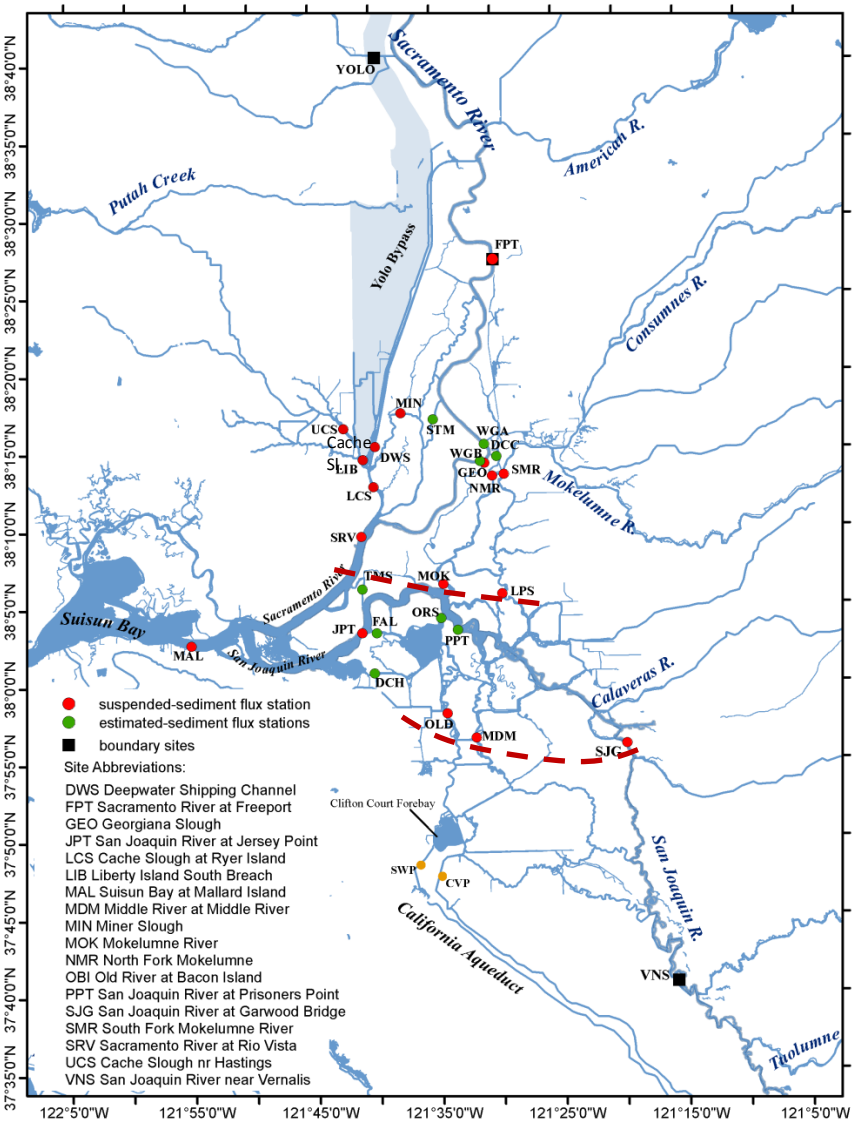

Figure 1. The north, central, and south regions of the Delta suspended-sediment-monitoring network are demarcated by the red dashed lines. We show 17 sediment-flux-monitoring stations, eight stations where sediment fluxes were estimated, and three boundary stations (FPT, YOLO, and VNS) which measure the primary sediment inputs from the Sacramento and San Joaquin Rivers. Measurements of tidal flow using acoustic Doppler current profilers were available at all stations so that fluxes could be estimated. The Georgiana Slough pathway is the channel between GEO and MOK.

The in-stream optical turbidity sensors and water samples were used to monitor suspended-sediment concentrations at seventeen sites (figure 1) strategically chosen from the larger network to allow for regional estimates of sediment loads and deposition. Suspended-sediment concentration data were collected across a number of Delta sites by the USGS during water years

2011-2013 (October 1, 2010–September 30, 2013). At all sites discussed herein, turbidity data was collected from optical sensors that are co-located with ADCPs to measure flow. Discharge weighted suspended-sediment concentrations (SSC_{xs}) were derived from depth-integrated water samples collected across the cross-section using the equal discharge increment technique and standard samplers (Edwards and Glysson, 1999). The output of the optical turbidity sensors were calibrated to the cross-sectional-average SSC so that a record of SSC, suspended-sediment flux (SSF), and loads could be computed. Yolo Bypass carries flow and sediment from the Sacramento River during floods and sediment loads were estimated using the methods in Wright and Schoellhamer (2005). Total sediment loads entering the Delta were determined by summing loads from the YOLO, FPT, UCS, NMR, SMR, and VNS stations (see figure 1). Sediment loads at Mallard Island were estimated using the approach discussed in McKee et al. (2013). The sediment entering the Delta, but not transported out at MAL, is considered to have been deposited in the Delta.

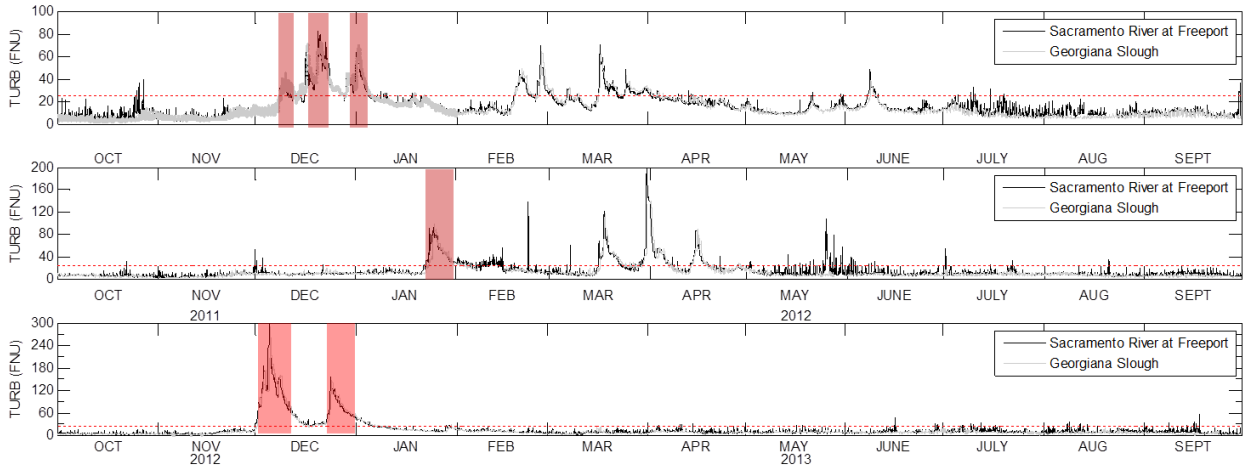

Figure 2. FTP and GEO turbidity time series, with the time periods isolated out for analysis in each of 2011 (top), 2012 (middle), and 2013 (bottom). These time periods isolated in red are thought to be the critical times associated with the initial migration of prespawning delta smelt. The red dashed line depicts the turbidity threshold of 25 FNU at FPT that was used to depict the storm pulse. Events identified as yielding the first flush span 22 days in 2011, 12 days in 2012, and 26 days in 2013. Note the differing y-axis for each graph.

RESULTS

DELTA SEDIMENT BUDGET AND DEPOSITION ZONES

The Sacramento River and San Joaquin Rivers are dominated by fluvial advection of sediment into the Delta, however the Sacramento River is the dominant source of flow and sediment (Wright and Schoellhamer, 2005). In general, the distributary channels throughout the Delta are also dominated by seaward advection, however, tidal dispersion and sediment settling also occurs. The average deposition/sediment budget for each of the three regions (north, central, and south) during the three-year time period discussed herein, is shown in figure 3 (left panel). The total sediment load into each Delta region for each year is shown in figure 3 (right panel). The largest sediment load to the Delta is from the north and decreases southward. On average,

roughly two-thirds of sediment supplied to the Delta is deposited, (Wright and Schoellhamer, 2005) however the proportion of sediment deposited varies from year to year as is to be expected. For 2011, around 69% of the total sediment load was deposited. In 2012, 45% of the total sediment was deposited, and in 2013, roughly 32% of the sediment was deposited.

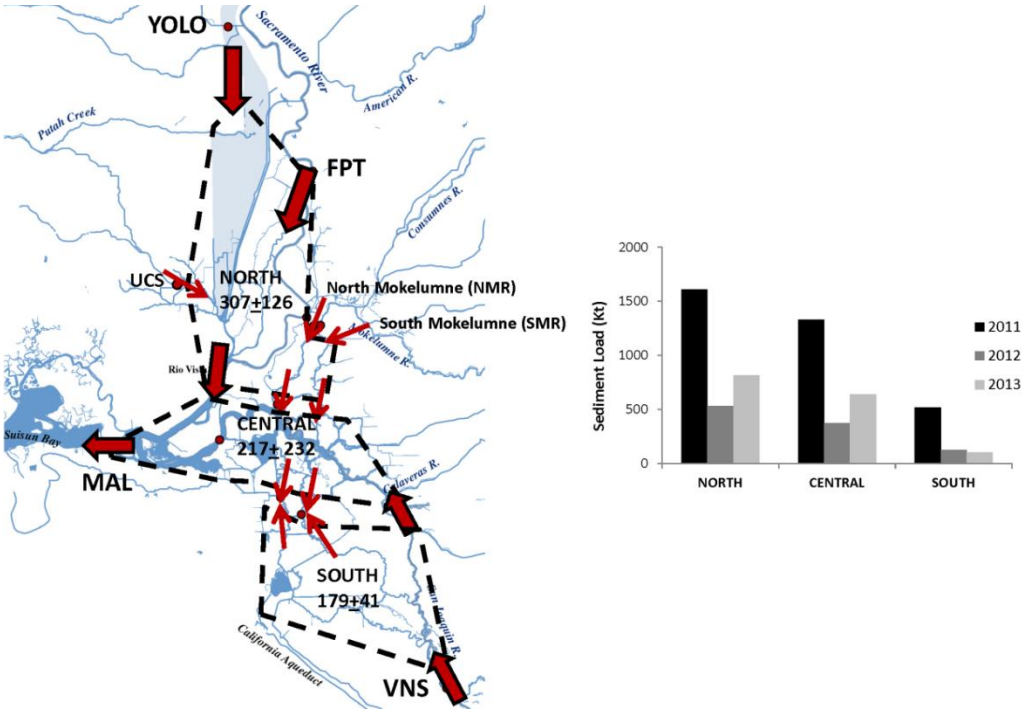

Figure 3. Map showing the Delta regions (left) defined by the black dashed line for north, central, and south Delta, and shows the average mass of deposition with the standard error. The bar graph (right) shows the annual sediment load in thousand metric tons to each region for each of 2011, 2012, and 2013. The sediment load from Rio Vista is considered part of the Central Delta. Bold arrows represent the primary paths for the Sacramento and San Joaquin Rivers. Additional pathways within the Delta are represented by red arrows. Note the opposing arrows for Old and Middle Rivers as sediment flux changes seasonally and with flow conditions.

PRIMARY PATHWAYS OF SEDIMENT

The primary pathways for fluvial sediment entering the Delta and it's regions, are shown in figure 3 (left panel) and figure 4 with bold arrows. The Sacramento and San Joaquin Rivers are the primary pathways of sediment from the watersheds to the north and south Delta respectively, however the maximum annual sediment flux was from the Sacramento River (1085 Kt at FPT in 2011) as shown in figure 4A, during an above average flow year. It carried three times as much sediment into the Delta than the San Joaquin River. In 2013 (a below average flow year), the volume of sediment supplied by the Sacramento River to the Delta was seven times that of the San Joaquin (roughly 80% of the total load into the Delta). Most of the sediment within the main-stem Sacramento River remains in suspension and is transported past Rio Vista and then seaward towards Suisun Bay. A portion of the sediment in the Sacramento River is also advected into various distributaries such as Miner Slough, Streamboat Slough, and Georgiana Slough (figure 4).

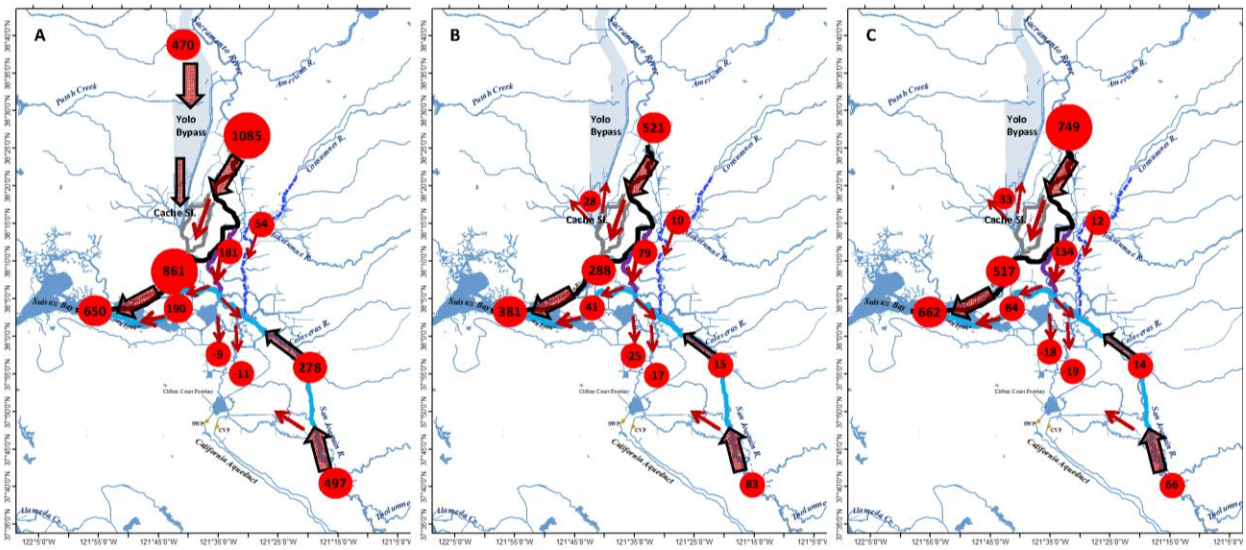

Figure 4. Primary pathways of sediment transport for 2011 (A), 2012 (B), and 2013 (C). The major riverine sediment pathways have red polygon arrows and the smaller distributary pathways are shown with red line arrows. The Sacramento River is represented by a black line and the San Joaquin River is represented by an aqua blue line. The east side Consumnes and Mokelumne River pathway to Little Potato Slough is represented by a blue-dashed line. Miner and Steamboat Slough distributaries are in gray, and Georgiana Slough is shown in purple. The sediment loads in thousand metric tons for various sites are shown with red circles proportionally sized.

The sediment from the Sacramento River is advected into distributaries and further transported either into the north Delta/Cache Slough region (north of LCS in figure 1 and figure 4) via 1) Sutter Slough (not shown) to Miner, or 2) Steamboat Slough, or 3) into the central Delta via Georgiana Slough (figures 1 and 4). Georgiana Slough and the Mokelumne River are influenced by the fluvial characteristics of the Sacramento River and sediment in these channels is advected to the central Delta. Most of the suspended sediment observed at site MOK (70% on average) comes from the Sacramento River via Georgiana Slough during the wet season and not directly from the tributaries of the Mokelumne. The Georgiana Slough pathway supplied a larger volume of sediment to the central Delta than the San Joaquin River during both 2012 and 2013 (figure 4B and 4C). In 2013, the annual sediment flux into the central Delta from the San Joaquin River at SJG, was 15% of the flux at MOK. Sediment originating from the Sacramento River can then make its way into the south Delta. In 2012, specifically, the sediment flux seaward from the central Delta was nearly equivalent to the sediment flux advected southward down Old and Middle Rivers (figure 4B).

DISCUSSION

DEPOSITIONAL PATTERNS

Proportional to sediment supply, on average, the north Delta had the least amount of deposition (30% on average) and the south Delta had the most (figures 3 and 4). This is because of the difference in the magnitude of flow in the Sacramento River compared to the San Joaquin River. Sacramento River sediment transport is dominated by advective processes; sediment remains in

suspension and is carried seaward past Rio Vista (SRV) to Suisun Bay (MAL). In contrast, a large portion of sediment advected down the San Joaquin River settles out of suspension and is deposited in the south Delta region especially during below average flows such as those occurring during 2012 and 2013. Based on a three year average, roughly 70% of the sediment advected down the San Joaquin River past Vernalis (VNS) is deposited in the south Delta Region.

The central Delta had approximately 50% deposition (and the most of any region) in 2011, but had little deposition in both 2012 and 2013. In these two years, the central Delta had the least sediment deposition of all three regions (23%). The Sacramento River alone supplied nearly 85% of sediment to the Delta proper and can account for roughly 70% of the sediment into the central Delta. Furthermore, our data suggest that for 2012 and 2013 (below average flows with little flow and sediment coming from the San Joaquin River watershed), a portion of the sediment entering the central Delta which is not advected seaward, moves further into the south Delta.

South Delta sediment is supplied from the north and the south direction and there is significant deposition. In 2011, when there was above average flow, sediment transport was predominantly seaward down the San Joaquin River. However, in 2012, 82% of the sediment load from the San Joaquin River observed at Vernalis (VNS) stayed in the south Delta. In addition, during 2012 and 2013, the quantity of deposition in the south Delta was greater than the mass of sediment advected down the San Joaquin River past VNS. Sediment is additionally advected into the south Delta from the central Delta because of the net negative flow that the large water pumps facilitate (figure 5). The sediment flux is in the landward direction into the south Delta via Old and Middle Rivers.

CENTRAL DELTA SEDIMENT

In this section, we address sediment transport pathways in the context of delta smelt migration. Specifically, we wanted to know the sediment transport pathways that lead to pumping curtailments either through increased turbidities in the south Delta or smelt salvage at the export facilities. To do this, we computed the sediment load from the first flush storm for each year of 2011, 2012, and 2013 to 1) determine the major contributions to the sediment load and thus increased turbidity in the central Delta and 2) to determine the sediment load of a first flush storm compared to the annual sediment load, to address the potential for making the Delta clearer in the summer if the first flush loads were reduced. Figure 2 shows the time periods which were isolated to compare the first flush sediment loads vs. the annual loads. Though these may not be the largest sediment loads of the year, the turbidity from a first flush event is correlated to fish migration (Sommer et al., 2011) and fish entrainment (Grimaldo et al., 2007) so we consider the first flush turbidity peaks to be the most critical time periods for delta smelt migration (Sommer et al., 2011, Bennett and Burau, 2014). We used a turbidity threshold of 25 FNU to define the first flush peaks at FPT (figure 2).

Sediment from Georgiana Slough is advected to the Mokelumne River and to the San Joaquin River. During low flow conditions, it is the main source of sediment to the central Delta. Compared to the total annual sediment load, the quantity of sediment which moves down Georgiana Slough during the first flush events shown in figures 2 and 6 varies from year to year and depends on flow conditions. In 2011, 21% of the annual sediment load down Georgiana

occurred within 22 days between December 8 and January 4, and 28% of the annual load occurred during the period of December 7 to January 9 (figure 6). Another 48% of the annual load was transported during mid-March to mid-April when approximately 50% of the total annual deposition into the central Delta occurred (figure 7 period 4). In 2012, only 12% of the

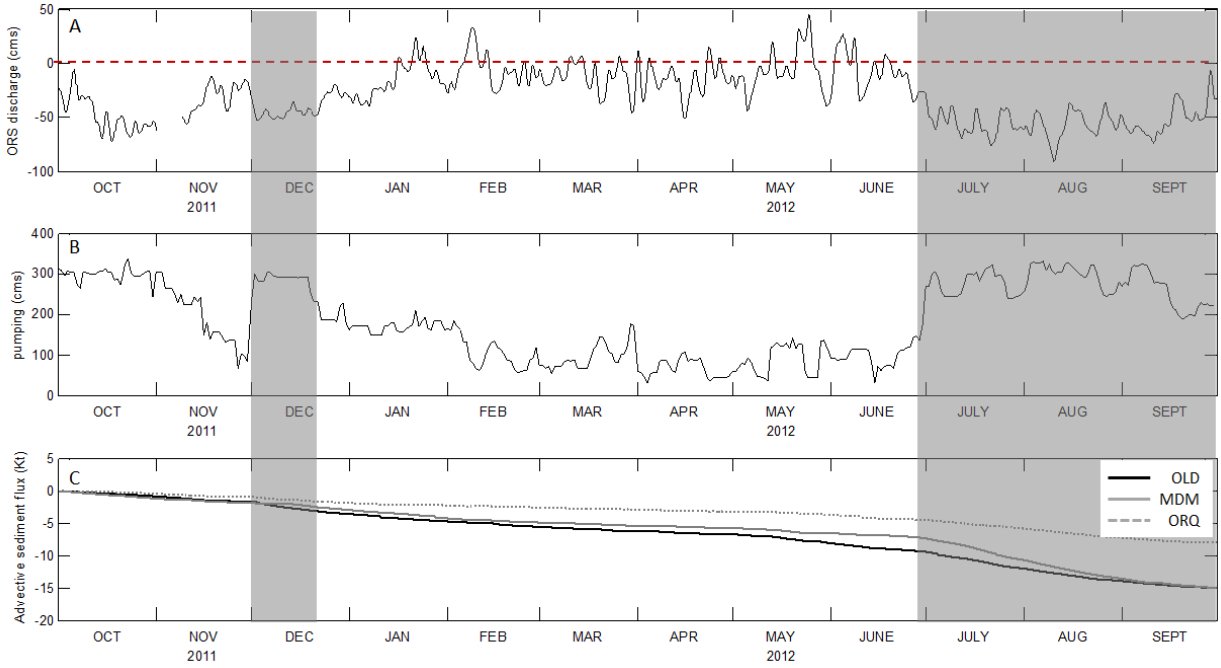

Figure 5. The highlighted gray areas in December and July-September represent more negative flow at ORS in 2012 (A) with increased pumping volumes (B), and a steeper negative advective sediment flux slope (C). Positive is ebb flow to the north and seaward; negative is towards the south Delta. Note that the daily pumping volume shown is for the combination of both State and Federal facilities.

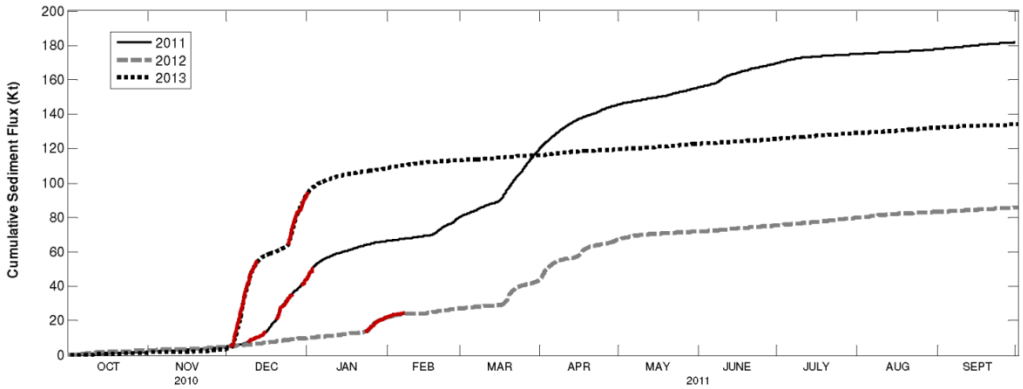

Figure 6. Georgiana Slough cumulative sediment load in thousand metric tons (Kt) for 2011, 2012, and 2013 showing the first flush sediment flux for the time periods outlined by the red lines here and coinciding with figure 2.

annual sediment load in Georgiana moved downstream towards MOK during the first flush compared to 2013, when 67% of the annual sediment load was advected downstream during the first flush time period. The largest first flush sediment load from the Sacramento River to the Delta occurred during 2013. Figure 8 shows the sediment supplied to the central Delta by each channel during the 2013 first flush. Eliminating this sediment supply to the Delta would significantly affect the quantity available for subsequent tidal and wind-wave resuspension. Sediment resuspension elevates turbidity and enhances habitat quality.

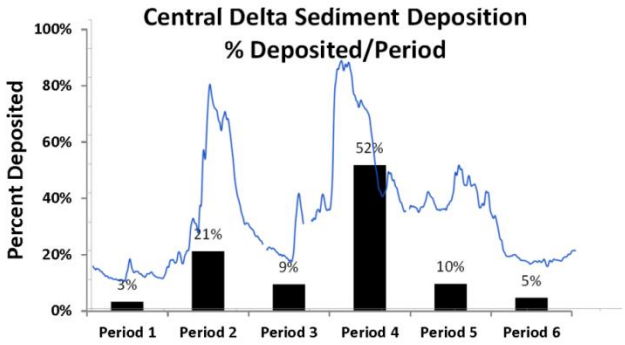

Figure 7. Approximate proportion of sediment deposition during 2011 within the central Delta from 6 different time periods. The blue line represents the tidally filtered FPT hydrograph image superimposed (unscaled) on the graph to show the flow patterns compared to the deposition patterns.

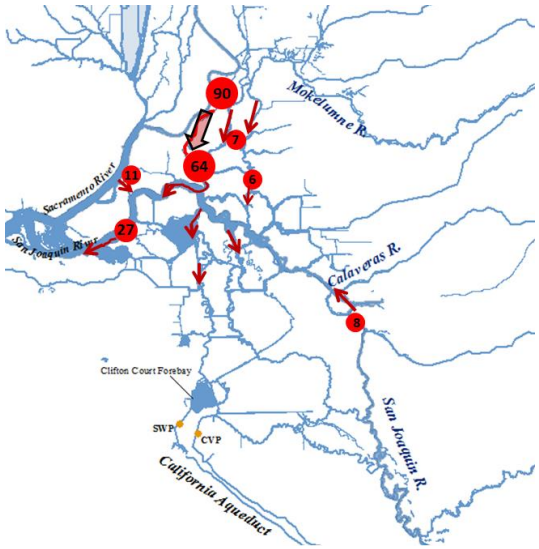

Figure 8. Total estimated sediment loads in thousand metric tons to the central Delta from each channel during 2013 for the time periods described in figure 2. Sizes of circles are intended to represent magnitude of sediment load and arrows represent direction of transport. The Georgiana Slough pathway to the Mokelumne is shown in red underneath the black arrow. The North and South Mokelumne tributaries are represented by one total (seven thousand metric tons).

CONCLUSIONS

The average sediment load during 2011-2013 to each of three Delta regions decreased from north to south. The north Delta has the largest sediment load, but proportionally, the smallest percentage of deposition because the Sacramento River is dominated by advective seaward sediment transport. Sediment supplied by the Sacramento River is additionally advected down various distributaries such as Sutter Slough, Miner Slough, Steamboat Slough, and Georgiana Slough.

Sediment from Georgiana Slough and the Delta Cross Channel is advected towards the Mokelumne River and into the central Delta; a major contribution to the total sediment supply into the central Delta is from the Georgiana Slough pathway. Sediment from Georgiana Slough is advected into the Mokelumne River and, during the 2013 first flush as described in figure 2, was nearly 70% of the load to the central Delta (south of the MOK and east of JPT). Less than 10% of the total sediment supply to this area was from the San Joaquin River during 2013. The 2013 annual sediment supply to the central Delta was dominated by one month of flow from the Sacramento River. If this supply was eliminated during the winter time period via upstream diversions along the Sacramento River, as proposed by the Bay Delta Conservation Plan, or some other means, the sediment supply to the central Delta in the 2013 example would be reduced by 70%.

Net flow (and advective sediment flux) is directed from the central Delta to the south Delta toward the export facilities and has been referred to by others as a hydrodynamic "pull" (Arthur et al. 1996, Monsen et al. 2007, Grimaldo et al. 2007). During low flow conditions both tidal dispersion and the effect of the pump facilities limit seaward transport where there is a predominantly net negative advective sediment flux from the south/central Delta into the south Delta.

REFERENCES

Anderson, C.W. (2004). Turbidity (version 2.0): U.S. Geological Survey Techniques of Water-Resources Investigations, book 9, Chap. A6, section 6.7.

Arthur, J.F., Ball, M.D., and Baughman, S.Y. (1996). Summary of federal and state water project environmental impacts in the San Francisco Bay-Delta Estuary, California. Pages 445-495 in J.T. Hollibaugh, editor. San Francisco Bay: the Ecosystem. American Association for the Advancement of Science, Pacifical Division, San Francisco.

Bennett, W.A. and Burau, J.R. (2014). Riders on the storm: selective tidal movements facilitate the spawning migration of threatened delta smelt in the San Francisco Estuary. Estuaries and Coasts. DOI 10.1007/s12237-014-9877-3

Buchanan, P.A., and Morgan, T.L. (2010). Summary of suspended-sediment concentration data, San Francisco Bay, California, water year 2007: U.S. Geological Survey Data Series 476, 30 p. (IP-006245).

Edwards, T.K., and Glysson, G.D. (1999). Field methods for measurement of fluvial sediment. U.S. Geological Survey Techniques of Water Resources Investigations 3:89. Chapter C2.

Grimaldo, L.F., Sommer, T., Van Ark, N., Jones, G., Holland, E., Moyle, P.B., Herbold, B., and Smith, P. (2009). Factors affecting fish entrainment into massive water diversions in a tidal

freshwater estuary: can fish losses be managed? North American Jounal of Fisheries Management 29:1253-1270. DOI: 10.1577/M08-062.1

Lietz, A.C., and Debiak, E.A. (2005), Development of rating curve estimators for suspended-sediment concentration and transport in the C-51 canal based on surrogate technology, Palm Beach County, Florida, 2004-05. U.S. Geological Survey Open-File Report 2005-1394, 25 p. http://pubs.usgs.gov/of/2005/1394.

McKee, L.J., Lewicki, M., Shcoellhamer, D.H. and Ganju, N.K. (2013). Comparison of sediment supply to San Francisco Bay from watershed draining the Bay Area and the Central Valley of California. Marine Geology. 345(1), 47-62.

Monsen, N.E., Cloern, J.E., and Burau, J.R. (2007). Effects of flow diversions on water and habitat quality: examples from California's highly manipulated Sacramento-San Joaquin Delta. San Francisco Estuary and Watershed Science. Vol 5(3), article 2. http://repositories.cdlib.org/jmie/sfews/vol5/iss3/art2.

Morgan, T.L. and D.H. Schoellhamer. (2013). Suspended-sediment flux and retention in a backwater tidal slough complex near the landward boundary of an estuary. Estuaries and Coasts, vol 36, 300-318.

Rasmussen, P.P., Gray, J.R., Glysson, G.D., and Ziegler, A.C. (2009). Guidelines and procedures for computing time-series suspended-sediment concentrations and load from in-stream turbidity sensor and streamflow data. U.S. Geological Survey Techniques and Methods Report 3 C4. http://pubs.usgs.gov/tm/tm3c4/.

Rasmussen, T.J., Ziegler, A.C., and Tasmussen, P.P. (2005). Estimation of constituent concentrations, densities, loads, and yields on lower Kansas River, northeast Kansas, using regression models and continuous water-quality modeling, January 2000 through December 2003: U.S. Geological Survey Scientific Investigations Report 2005-5165, 117 p. http://pubs.usgs.gov/sir/2005/5165/.

Ruhl, C.A., and Simpson, M.R. (2005). Computation of discharge using the index velocity method in tidally affected areas. U.S. Geological Survey Scientific Investigations Report No. 2005-5004, Sacramento.

Sommer T, Mejia F, Nobriga M, Feyrer F, Grimaldo L. (2011). The Spawning Migration of Delta Smelt in the Upper San Francisco Estuary. San Francisco Estuary and Watershed Science (2011) 9 (2), 16 p.

Uhrick, M.A. and Bragg, H.M.. (2003). Monitoring instream turbidity to estimate continuous suspended-sediment loads and yields and clay-water volumes in the Upper North Santiam River Basin, Oregon, 1998-2000. U.S. Geological Survey Water-Resources Investigation Report 03-4098, 44 p. http://pubs.er.usgs.gov/publication/wri034098.

Wagner, R.J., Boulger, R.W., Oblinger, D.J., and Smith, B.A. (2006). Guidelines and standard procedures for continuous water-quality monitors: station operation, record computation, and data reporting. U.S. Geological Survey Techniques and Methods 1-D3. 51. http://pubs.usgs.gov/tm/2006/tm1D3/.

Whipple, A.A., Grossinger, R.M., Rankin, D., STanfor, B., Askevold, R.A. (2012). Sacramento-San Joaquin delta historical ecology investigation: exploring pattern and process. Prepared for the California Department of Fish and Game and Ecosystem Restoration Program. A Report of SFEI-ASC's Historical Ecology Program, Publication #672, San Francisco Estuary Institute-Aquatic Science Center, Richmond, CA.

Wood, M.S., and Teasdale, G.N. (2013). Use of surrogate technologies to estimate suspended sediment in the Clearwater River, Idaho, and Snake River, Washington, 2008-10: U.S. Geological Survey Scientific Investigations Report 2013-5052, 30 p.

Wright, S.A. and Schoellhamer, D.H. (2005). Estimating sediment budgets at the interface between rivers and estuaries with application to the Sacramento-San Joaquin River Delta. Water Resources Research 41, 1-17.

Wright, S.A. and Schoellhamer, D.H. (2004). Trends in the Sediment Yield of the Sacramento River, California, 1957-2001. San Francisco Estuary and Watershed Science. 14 pages. https://escholarship.org/uc/item/891144f4.

THE STUDY OF MOST PROBABLE MEAN DAILY BANKFULL RUNOFF VOLUMES IN SMALL WATERSHEDS DOMINATED BY CONVECTIVE/FRONTAL CHANNEL FORMING EVENTS AND THE CO-INCIDENT INNER BERM CHANNELS – PART I.

Thomas J. Garday, Hydraulic/Civil/Mechanical Engineer
Little Rock AR 72202
meanderingriverman@gmail.com

Abstract

Small watersheds influenced pre-dominantly by rainfall of short-duration (<24 hours), exhibit an inner berm channel that resides below the floodplain. For modelling and calibration; the inner berm and floodplain are two distinct geomorphic stages of hydraulic and hydrologic significance. Bankfull discharge ($Q_{Bankfull}$) and stage represents the incipient floodplain level, the recurrence of $Q_{Bankfull}$ is derived from the annual flood-frequency distribution. Whereas the most probable one-day bankfull runoff volume ($Q_{Daily\ Bankfull}$) and stage coincides with the top of the inner berm sediment deposits (Q_{IB}) and calibrated to a flow duration. Both features can be surveyed and verified using hydraulic & hydrologic analyses and regional bankfull curves (discharge vs. drainage area). Part I presents an empirical procedure to develop ratios of most probable runoff volume to peak ($Q_{Daily\ Bankfull}$ to $Q_{Bankfull}$). Ratios are derived for 34 stream gages stratified by physiographic sections. Thirty three gages have 36 $Q_{Bankfull}$ published in 6 regional curve studies that span the Interior Plains Central Lowland Dissected Till Plains, Appalachian Highlands Piedmont province Piedmont Upland section, and the Atlantic Plain Coastal Plain (western) Embayed section. $Q_{Daily\ Bankfull}$ are derived from published $Q_{Bankfull}$ and calculated ratios, average annual durations are mapped on flow duration curves. Regional $Q_{Daily\ Bankfull}$ curves express Inner Berm growth by power relationships of drainage area. A handful of observations are noted in which published $Q_{Bankfull}$ plots on the $Q_{Daily\ Bankfull}$ regional curve, indicating co-incidence of $Q_{Daily\ Bankfull}$ to a geomorphic surface at Q_{IB}.

INTRODUCTION

A watersheds 'natural bankfull discharge' $Q_{Bankfull}$ is within a range of channel-forming discharges Q_{CF}, where Q_{Peak} is usually in the ~1 to 2-year return interval range ($Q_1 - Q_2$), Leopold, Wolman & Miller (1964). They recognize "*the channel is formed and re-formed during a range of flows lying between the lower limit of competence and an upper limit at which the flow is no longer confined within the channel.*" Wolman & Miller (1960) use 'geomorphic effectiveness' to describe a range of Q_{CF} exceeding threshold forces, that move the most material and perform the most work in modification of surface form. They all agree, $Q_{Effective}$ can often be approximated by $Q_{Bankfull}$, which in many rivers, is ~$Q_{1.5}$. They studied large watersheds whose hydrology was pre-dominantly snowmelt, groundwater or thunderstorm driven. They recognize maximum sediment flux is frequently transported by summer thunderstorms. Ideally, $Q_{Bankfull}$ fills the natural channel to the point of incipient flooding. Discharges above $Q_{Bankfull}$ would spill out onto the adjacent floodplains; suspended sediments and floating debris would transfer away from the channel to act upon the floodplain surfaces. The majority of $Q_{Daily\ Bankfull}$ is contained within the channel to act upon bed and banks dependent on material sizes and critical thresholds attained. $Q_{Daily\ Bankfull}$ is similar to Blench's (1951) dominant discharge *"a steady discharge that would produce the same result as the actual varying discharge."*

Klein (1976) stated one must understand the watershed's hydrologic regime before applying sediment transport equations. He used 'basin peakedness factors" to note hydrologic distinctions in basin characteristics. "Bankfull events" generated in small watersheds by thunderstorms are limited in energy, magnitude, runoff volume and duration; $Q_{Bankfull}$ is usually much larger than $Q_{Daily\ Bankfull}$, such that $Q_{1.5}$ does not produce 24 hours of Q_{CF}. Both Klein and Hewlett & Hibbert (1965) recognize that most of the transportation activity occurs within a short time of the hydrograph peak and recommended to separate 'quick flow' from total flow. Biedenharn & Copeland (2000) propose *for large watersheds* to use a steady mean daily discharge integrated from a flow duration curve with a proper bed-material-load rating curve to determine the flow class interval that moves the largest load fraction. They acknowledge "*mean daily values can under-represent the occurrence of short-duration, high magnitude flow events that occur within the averaging period. On large rivers such as the Mississippi River, the use of the mean daily values is acceptable because the difference between the mean and peak daily discharges is negligible. On smaller streams, flood events may last only a few hours, so that the peak discharge is much greater than the corresponding mean daily discharge."* The inner berm capacity, (Q_{IB}) is shaped over time by various runoff volumes. Melton (1936) recognized the geomorphic significance of the low-flow channel regime: "*those that nearly fill the channel but do not over-top its banks*". Q_{IB} often forms into a non-continuous bench of fine sediments, often vegetated and

alternating banks. Q_{IB} resides at the top of the sediment slope (e.g. point bars), where water slope tends to even out between pools and riffles.

PURPOSE AND SCOPE

In small watersheds where the majority of channel forming events are generated by convective/frontal precipitation (non-snowmelt); the Inner Berm capacity (Q_{IB}) is significant to the sediment regime. Q_{IB} typically convey 99 to 99.4% of all yearly Q_{Daily} at or below the sediment bench stage. In designing stream restoration, bank stabilization, fish passage, and road culvert/bridge crossings, it is important to recognize and match the inner-formation of Q_{IB} to drainage area. Part I outlines a mathematical procedure derived from continuous recording stream gages to estimate the most probable minimum one-day runoff volume ($Q_{Daily\ Bankfull}$), formed by $Q_{Bankfull}$. $Q_{Daily\ Bankfull}$ is the area under a 24-hour bankfull hydrograph; runoff volume and shape sets the duration (T_{CF}) of most effective Q_{CF}. $Q_{Daily\ Bankfull}$ also neatly approximates Q_{IB}. Part II: A study of $Q_{Daily\ Bankfull}$ in the Ninnescah River Watershed, Kansas, compares regionalized $Q_{Daily\ Bankfull}$ curves to surveyed Q_{IB} at fifteen watershed sites, 6 sites include USGS gage stations.

STUDY AREAS

The mathematical procedure is applied on 34 USGS stream gage stations across 4 hydro-physiographic provinces and 7 states. Eight principal authors identified and published 36 $Q_{Bankfull}$ at 33 gage stations: Emmert & Hase (2001) determined $Q_{Bankfull}$ for 8 gages on the Central Lowland Dissected Till Plains (Figure 1). Six gages on the main stem of Soldier Creek (Nemaha & Jackson Counties) allow study of typical growth of Q_{IB} in the downstream direction.

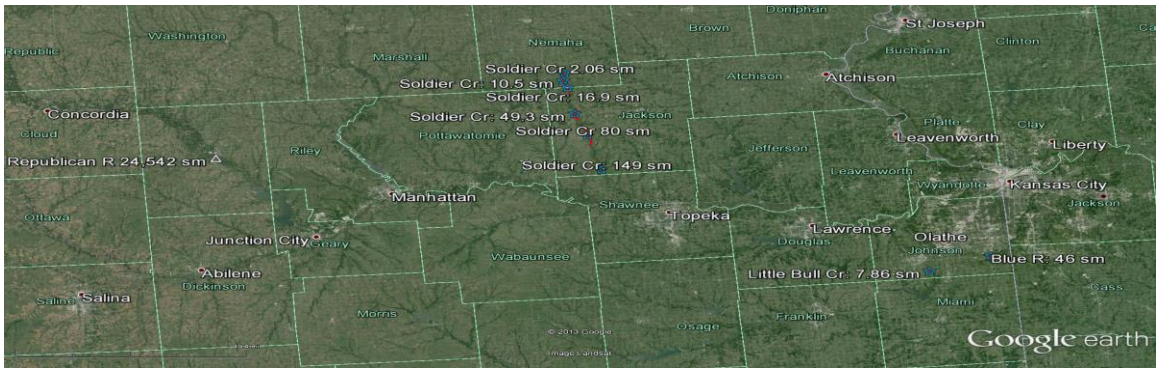

Figure 1 Eight gage locations on the Central Lowland Dissected Till Plains of Kansas

Leopold et al. (1964), White (2001), Cinotto (2003), McCandless et al. (2002), Harman et al. (1999) determined $Q_{Bankfull}$ for 20 gages on the Piedmont Upland section (Figure 2) across Pennsylvania, Maryland, and North Carolina.

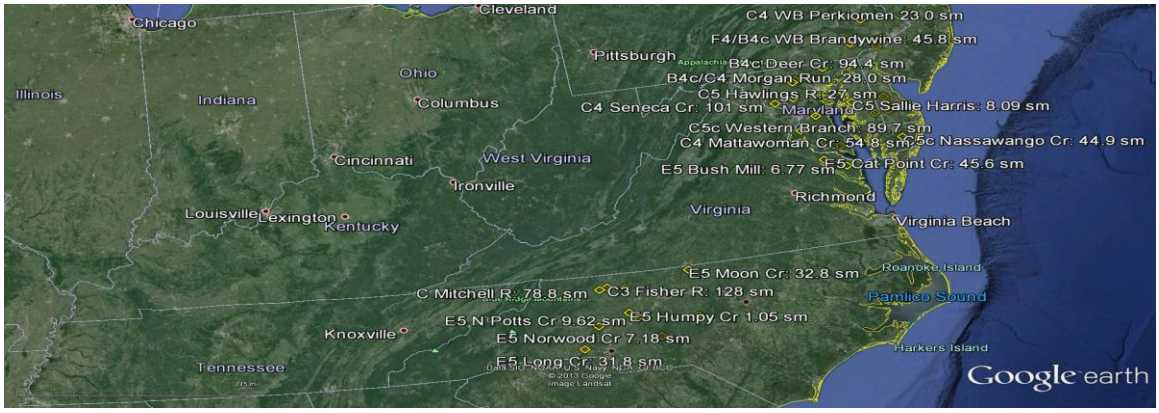

Figure 2 Twenty gage locations on the Piedmont Upland section (PA, MD & NC)

McCandless (2003) and Krstolic et al. (2007) determined $Q_{Bankfull}$ for 5 gages on the Atlantic Coastal Plain, western embayed section (Figure 3) spanning Delaware, Maryland and Virginia.

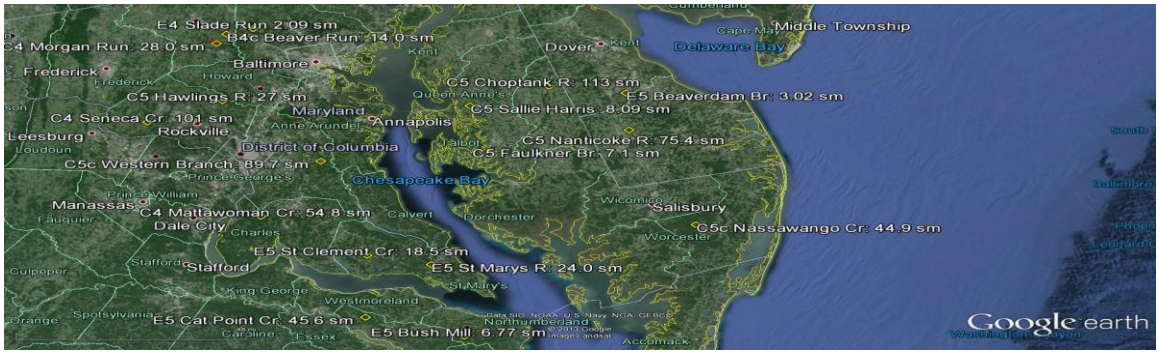

Figure 3 Gages located on the Atlantic Coastal Plain embayed section (DE, MD & VA)

METHODS

Determination of $Q_{Bankfull}$ Return Interval (RI)

The Log Pearson Type III distribution (LPIII) and the 1st order least squares curve-fit of the Weibull distribution are averaged to determine the recurrence intervals of $Q_{Bankfull}$. Outliers (annual Q_{Peak} too high or low) identified in the LPIII process were also removed from the Weibull plotting positions. Figure 4 shows the two flood frequency distributions for Seneca Creek at Dawsonville, Maryland USGS 01645000.

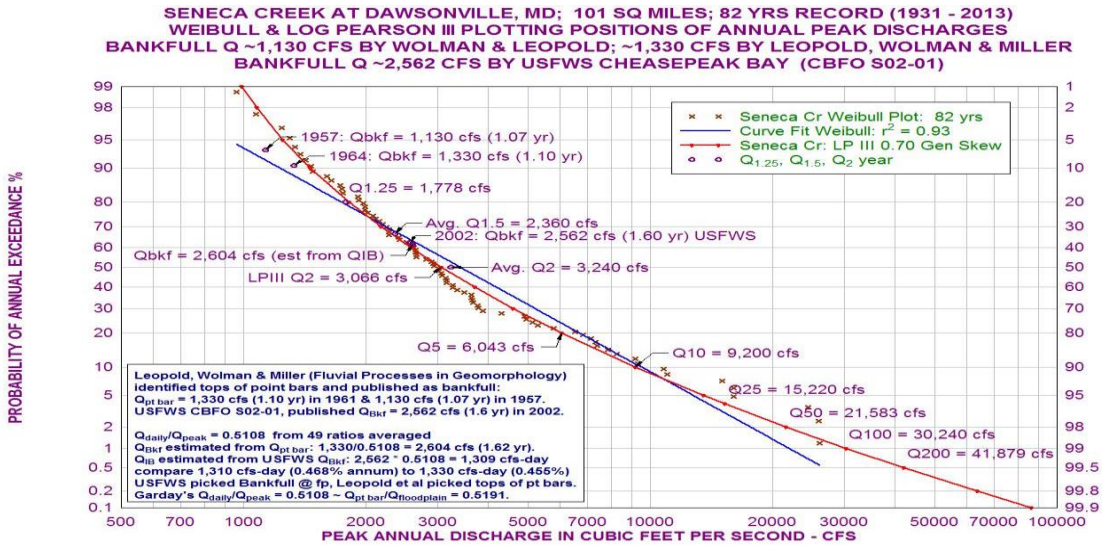

Figure 4 Log Pearson Type III and Weibull Distributions for Seneca Creek, Maryland

Approximation of Most Probable Duration (T_{CF}) for Q > $Q_{Daily\ Bankfull}$

For small watersheds, the bankfull event is modelled as a one-day hydrograph, the area under the hydrograph is $24*Q_{Daily\ Bankfull}$. Assumed hydrograph shape is trapezoidal below $Q_{Daily\ Bankfull}$, and triangular above with $Q_{Bankfull}$ at the apex. The trapezoidal base is 24-hour; it may start and end with or without base flow. The duration (T_{CF}) for which Q exceeds $Q_{Daily\ Bankfull}$ must equal the upper trapezoidal time base at $Q_{Daily\ Bankfull}$. Figure 5 shows the bankfull hydrograph based on these requirements for a gage on Soldier Creek in Kansas. Note the cross-shaded areas below $Q_{Daily\ Bankfull}$ must equal the cross-shaded area above $Q_{Daily\ Bankfull}$.

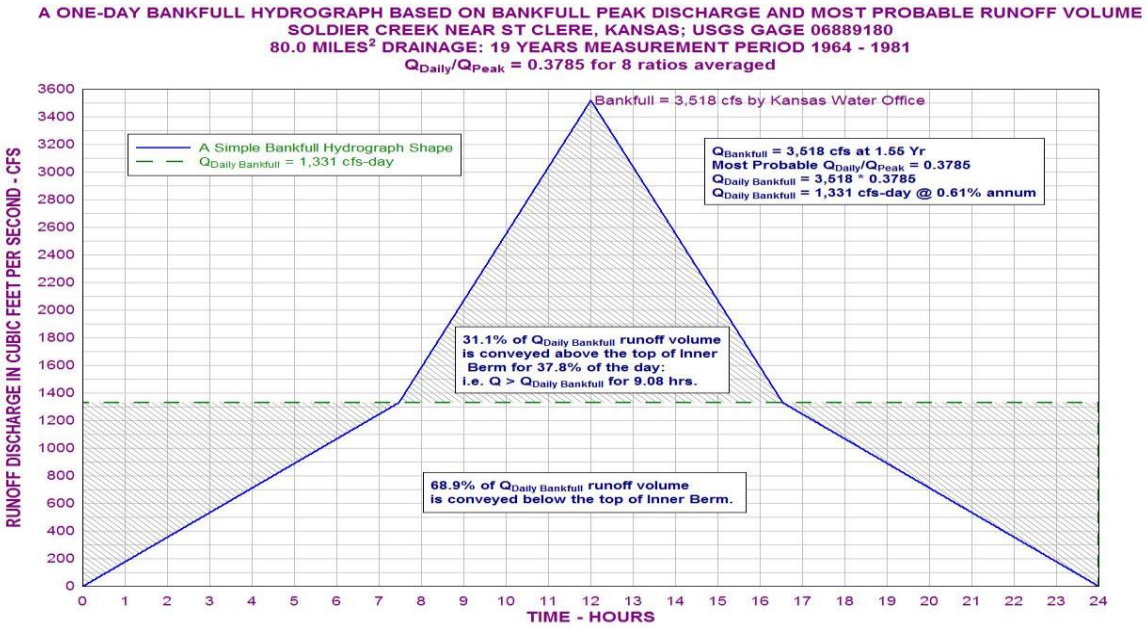

Figure 5 Assumed 1-day bankfull hydrograph shape based on peak and most probable runoff volume.

The duration (hours) of T_{CF}, represents strongest flow (Q exceeds $Q_{Daily\ Bankfull}$) in a minimal bankfull event, it can be solved by setting the sum of the trapezoidal and the triangular areas equal to the runoff volume in cfs-hours.

$$½ * (24 + T_{CF}) * Q_{Daily\ Bankfull} + ½ * T_{CF} * (Q_{Bankfull} - Q_{Daily\ Bankfull}) = 24 * Q_{Daily\ Bankfull} \quad (1)$$

$$T_{CF} = 24 * Q_{Daily\ Bankfull}/Q_{Bankfull}\ (\text{hours})\ \text{for which}\ Q > Q_{Daily\ Bankfull} \quad (2)$$

Computation of the Most Probable $Q_{Daily\ Bankfull}/Q_{Bankfull}$ Ratio

It is further assumed the long-term most probable $Q_{Daily\ Bankfull}/Q_{Bankfull}$ hydrologic ratio can be approximated using sufficient gage data: the average of Q_{Daily}/Q_{Peak} ratios for which Q_{Peak} is in the channel-forming range (Q_{CF}). Q_{CF} in all this work is generally between $Q_{1.25}$ and the mean annual flood (Q_{MA}). In calculating the return intervals of Q_{MA}, high outliers were removed from the flood averages. The return interval of Q_{MA} generally varies from 2.3 to 3.1 years it is somewhat sensitive to number of years of record relative to the magnitudes of floods in the period of record. Q_{MA} being a flood discharge is plotted on the LPIII curve and is not averaged with the Weibull distribution.

$Q_{Daily\ Bankfull}$ is computed as the product of $Q_{Bankfull}$ and the most probable Q_{Daily}/Q_{Peak} ratio.

$$Q_{Daily\ Bankfull} = Q_{Bankfull} * Q_{Daily}/Q_{Peak} \quad (3)$$

Computation is demonstrated using USGS gage 01645000 Seneca Creek at Dawsonville, MD. Seneca Creek $Q_{Bankfull}$ is documented by Leopold et al. (1964) and McCandless et al. (2002). For 82 years of annual maximums, 49 Q_{Peak} qualify as 1-day channel-forming events, 49 Q_{Daily}/Q_{Peak} ratios are averaged: 40 ratios involve Q_{Peak} between ~$Q_{1.25}$ and ~Q_2 and 9 ratios between ~Q_2 and ~Q_{MA}. Single event Q_{Daily}/Q_{Peak} ratios range from 0.12 to 0.75, but cumulatively, the running average or most probable Q_{Daily}/Q_{Peak} ratio converges to 0.51 and remains unchanged (to 2 decimal places) for the largest 15 Q_{Peak} at or below Q_{MA}.

Table 1 lists annual maximum discharges Q_{Peak} (column 3) in ascending order, the *largest* Q_{Daily} of the three days surrounding Q_{Peak} (1-day prior, on, or 1-day after) is chosen, (column 2) and single event Q_{Daily}/Q_{Peak} ratios (column 6). The most probable Q_{Daily}/Q_{Peak} ratio (0.5109) is the mean of all ratios (last value in column 7).

Table 1 Computations of Seneca Creek's most probable Q_{Daily}/Q_{Peak} Ratio

Date of annual peak	Q_{Daily} (cfs-day)	Q_{Peak} (cfs)	Probability Weibull Plot	Gage Ht. feet	Single Event Q_{Daily}/Q_{Peak} Ratio	Running Average: Q_{Daily}/Q_{Peak}
(1)	(2)	(3)	(4)	(5)	(6)	(7)
1/14/1968		1640	86.75	6.37		
7/1/1931	483	1730	85.54	6.08	0.2792	0.2792
4/20/1940	931	1740	84.34	6.41	0.5351	0.4071
3/27/1992	963	1750	83.13	6.55	0.5503	0.4548
3/22/2000	1330	1910	81.93	6.79	0.6963	0.5152
3/12/1962	1450	1920	80.72	6.83	0.7552	0.5632
8/8/1959	700	1970	79.52	6.9	0.3553	0.5286
8/20/1947	242	1990	78.31	6.75	0.1216	0.4704
6/30/1948	722	1990	77.11	6.78	0.3628	0.4570
1/3/1936	1370	2020	75.90	6.88	0.6782	0.4816
8/6/1995	936	2080	74.70	7.03	0.4500	0.4784
8/1/1945	1220	2110	73.49	6.9	0.5782	0.4875
1/30/1939	1400	2150	72.29	6.93	0.6512	0.5011
7/10/1970	980	2200	71.08	7.18	0.4455	0.4968
7/16/1949	729	2240	69.88	7.03	0.3254	0.4846
4/2/1990	1040	2270	68.67	7.24	0.4581	0.4828
10/23/1937	1630	2280	67.47	7.08	0.7149	0.4973
3/23/1950	1310	2280	66.27	7.12	0.5746	0.5019
9/17/1934	1080	2410	65.06	7.3	0.4481	0.4989
12/4/1950	1420	2420	63.86	7.26	0.5868	0.5035
1/9/1964	1290	2520	62.65	7.51	0.5119	0.5039
8/27/1937	1210	2610	61.45	7.45	0.4636	0.5020
8/13/1955	1950	2620	60.24	7.6	0.7443	0.5130
8/26/1965	717	2640	59.04	7.62	0.2716	0.5025
5/26/2009	1200	2650	57.83	7.65	0.4528	0.5005
11/9/1943	1360	2660	56.63	7.52	0.5113	0.5009
8/27/1967	1710	2660	55.42	7.64	0.6429	0.5064
9/1/1952	2080	2810	54.22	7.77	0.7402	0.5150
10/13/2011	908	2890	53.01	8.3	0.3142	0.5078
12/26/2009	2040	2930	51.81	7.98	0.6962	0.5143
6/2/1946	1880	2940	50.60	7.73	0.6395	0.5185
3/29/1984	2190	3010	49.40	7.92	0.7276	0.5253
9/14/1973	1280	3020	48.19	7.94	0.4238	0.5221
9/16/1999	1500	3060	46.99	7.95	0.4902	0.5211
6/10/1961	1060	3070	45.78	7.98	0.3453	0.5159
8/12/2001	887	3140	44.58	8.01	0.2825	0.5093
12/26/1973	1330	3160	43.37	7.95	0.4209	0.5068
6/13/1982	1460	3160	42.17	8.02	0.4620	0.5056
4/10/1983	2060	3260	40.96	8.09	0.6319	0.5089
9/14/1966	1580	3270	39.76	8.12	0.4832	0.5083
4/16/1993	1520	3350	38.55	8.15	0.4537	0.5069
9/4/1969	1840	3490	37.35	8.26	0.5272	0.5074
10/16/1942	1900	3620	36.14	8.31	0.5249	0.5078
2/12/1985	1980	3620	34.94	8.33	0.5470	0.5087
12/21/1957	1400	3640	33.73	8.35	0.3846	0.5059
5/12/2008	2560	3660	32.53	8.74	0.6995	0.5102
7/8/2005	1990	3750	31.33	8.83	0.5307	0.5107
10/9/1976	1780	3770	30.12	8.42	0.4721	0.5098
10/19/1996	2920	3880	28.92	8.49	0.7526	0.5149
5/27/2002	1360	4310	27.71	9.26	0.3155	0.5109

Durations of $Q_{Daily\ Bankfull}$ Annual Exceedance

Each gage is/was a continuous recording gage, (CRG) which produce Q_{Daily} for the respective period of record. Flow duration curves (FDC) were assembled using EXCEL spreadsheets that sorts and counts Q_{Daily} records by water year. Q_{Daily} from all water years are combined into 39 flow class intervals determined by the flow values closest to 100%, 99.99, 95, 90, 85, 80, 75, 70, 65, 60, 55, 50, 45, 40, 35, 30, 25, 20, 15, 10, 9, 8, 7, 6, 5, 4, 3, 2, 1, 0.9, 0.8, 0.7, 0.6, 0.5, 0.4, 0.3, 0.2, 0.1, and 0.05% annual exceedances. One percent annual exceedance (1% annum) is 3.6525 days/year or ~87.66 hours/year. The USGS rounds Q_{Daily} to the nearest integer above 10 cfs-day and to the nearest 10 cfs-day above 1,000 cfs-day. As percent annums are often developed from irrational fractions, it is not always possible to derive an integral flow on the specified exceedance class interval. For Seneca Creek, Q_{Daily} of 29 cfs-day is at 90.5% annum which is the closest integral flow to the desired 90.0% interval.

Leopold, Wolman & Miller (1964) identified bankfull durations of 0.40-0.60% annum common for the Maryland/Pennsylvania Piedmont Upland section (hydrologic records up to 1963). Nixon (1959), who studied rivers in the United Kingdom, concluded bankfull stage is co-incident with flows equaled or exceeded 0.6% annum on the FDC. Figure 6 shows three FDC's with similarities in shape but variations in annual duration of $Q_{Daily\ Bankfull}$. Seneca Creek at Dawsonville is plotted with Hawlings River near Sandy Spring, MD, both Upland section streams with similar $Q_{Daily\ Bankfull}$ durations. Whereas the $Q_{Daily\ Bankfull}$ duration of Beaverdam Branch at Houston, DE on the Coastal Plain (western) embayed section, downslope to the Piedmont Upland section, is ~twice as long.

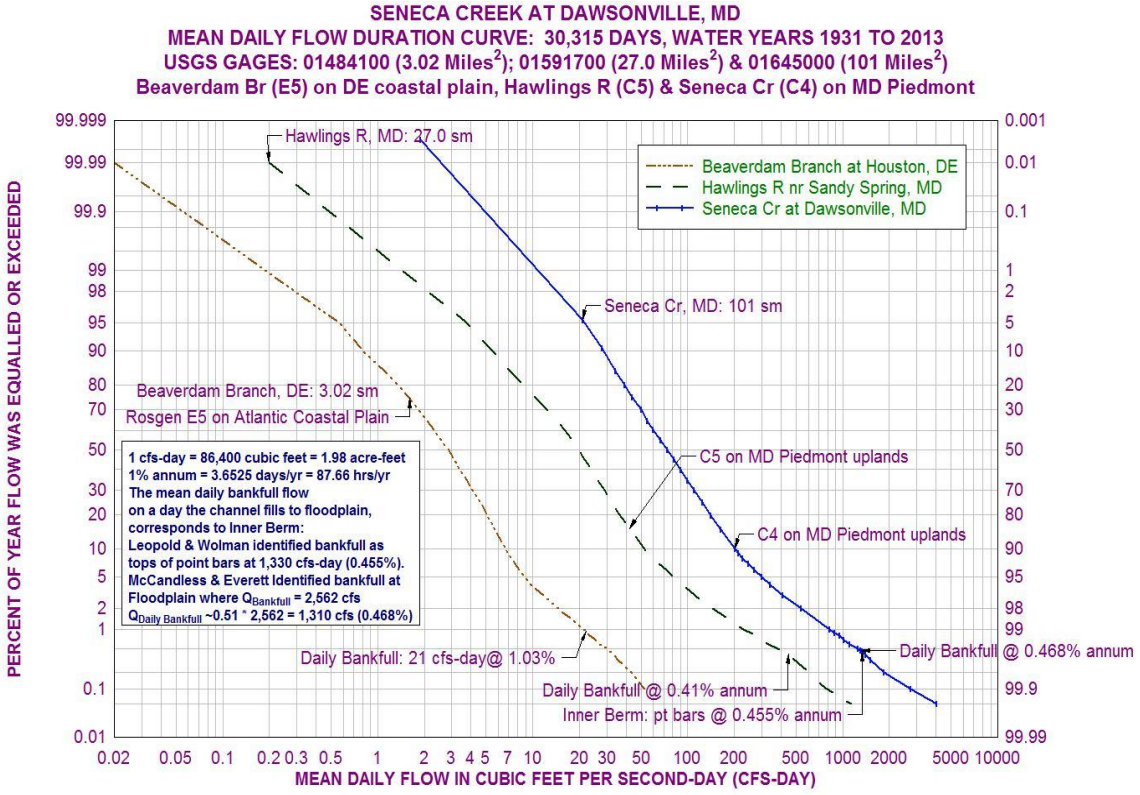

Figure 6 Flow Duration Curves of 3 Rosgen stream types in MD & DE across 2 physiographic regions

RESULTS

The gages (and results) are stratified by physiographic province according to Fenneman (1946). Results are presented in Tables (summarizing published $Q_{Bankfull}$, calculated Q_{Daily}/Q_{Peak} ratios, most probable $Q_{Daily\ Bankfull}$ and associated % annum durations), Figures (plots of Regional $Q_{Daily\ Bankfull}$ vs. DA & $Q_{Bankfull}$ vs. DA Curves), & Equations (first-order curve fits of Regional Curves using the DPLOT plotting program). The two derived power equations are substituted into equation 2 to express most probable duration T_{CF} that flow is above $Q_{Daily\ Bankfull}$.

Interior Plains Central Lowland Dissected Till Plains

Table 2 Summary of $Q_{Daily\ Bankfull}$ and percent annum for the Dissected Till Plains section

Gage #	Drainage Area (miles^2)	$Q_{Bankfull}$ (cfs)	Return interval of $Q_{Bankfull}$ (years)	Most probable Q_{Daily}/Q_{Peak} Ratio	$Q_{Daily\ Bankfull}$ (cfs-day) 1-day runoff volume	% annum: $Q_{Daily\ Bankfull}$ on FDC	Reference source for $Q_{Bankfull}$ (cfs) only
(1)	(2)	(3)	(4)	(5)	(6)	(7)	(8)
06889100	2.06	**191**	1.25	0.21	40.5	0.77	**KWO**
06914990	7.86	**659**	1.14	0.24	160	1.00	**KWO**
06889120	10.5	**688**	1.23	0.26	179	0.91	**KWO**
06889140	16.9	**823**	1.11	0.29	239	0.95	**KWO**
06893080	46.0	**1,736**	1.13	0.33	573	1.10	**KWO**
06889160	49.3	**2,600**	1.18	0.32	831	0.75	**KWO**
06889180	80	**3,518**	1.55	0.38	1,330	0.61	**KWO**
06889200	149	**3,279**	1.46	0.71	2,320	0.60	**KWO**
Kansas Regional Averages			**1.30**			**0.76**	

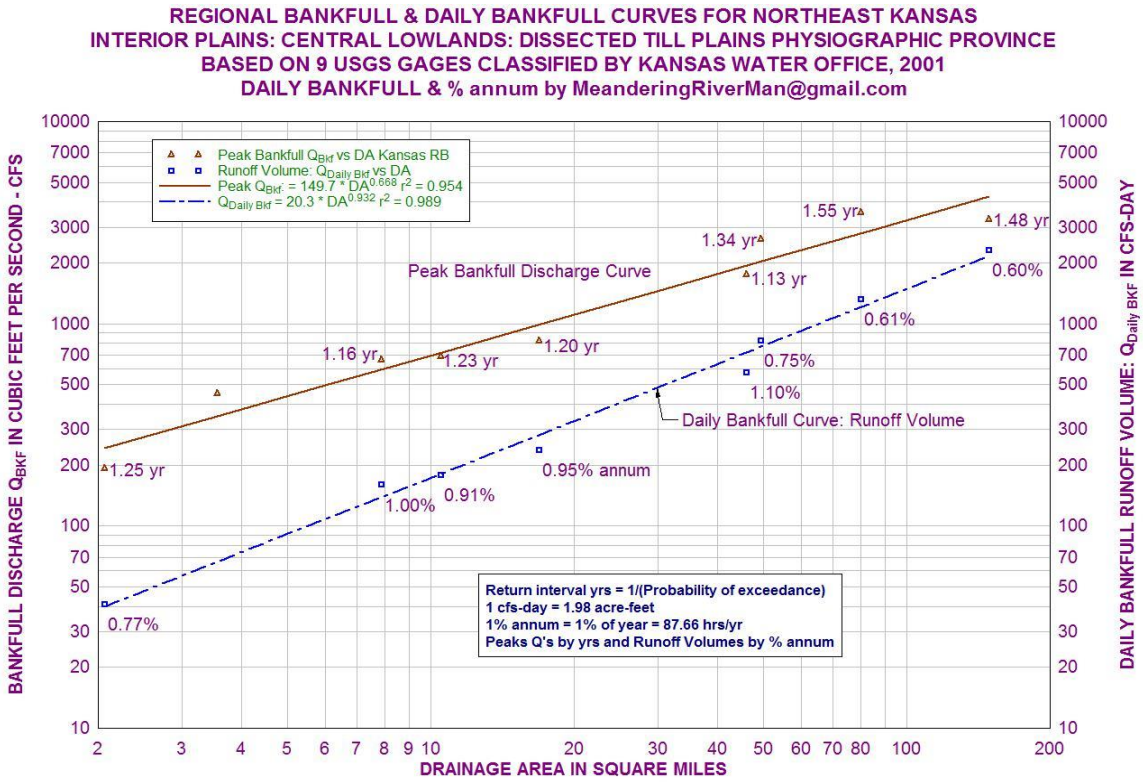

Figure 7 Regional $Q_{Bankfull}$ and $Q_{Daily\ Bankfull}$ Curves for Northeast Kansas

Equations 4, 5 & 6 apply to small watersheds in northeast KS for drainage areas 2.06 miles^2 to 149 miles^2.

$$Q_{Bankfull} = 149.7 * DA^{0.668} \quad \text{(cfs)} \quad r^2 = 0.954 \quad (4)$$

$$Q_{Daily\ Bankfull} = 20.31 * DA^{0.932} \quad \text{(cfs-day)} \quad r^2 = 0.989 \quad (5)$$

$$T_{CF} = 3.256 * DA^{0.264} \quad \text{(hours)} \quad (6)$$

Appalachian Highlands Piedmont province Piedmont Upland section

Generally, the North Carolina watersheds have ~25.3% less annual runoff, ~25% less channel-forming time, but ~22.5% more inner berm capacity than in similar watersheds of Maryland and Pennsylvania. The 20 gage set was stratified further by runoff criteria resulting in two sets of regional curves & power equations. Equations 7, 8 & 9 apply to small watersheds in NC Piedmont uplands for drainage areas 1.05 miles^2 to 128 miles^2.

Table 3 Summary of $Q_{Daily\ Bankfull}$ and percent annum for the Piedmont Upland section.

Gage #	Drainage Area (miles^2)	$Q_{Bankfull}$ (cfs)	Return interval of $Q_{Bankfull}$ (years)	Most probable Q_{Daily}/Q_{Peak} Ratio	$Q_{Daily\ Bankfull}$ (cfs-day) 1-day runoff volume	% annum: $Q_{Daily\ Bankfull}$ on FDC	Reference source for $Q_{Bankfull}$ (cfs) only
(1)	(2)	(3)	(4)	(5)	(6)	(7)	(8)
02117030	1.05	**83**	1.78	0.21	17.6	0.46	**NCSU**
02142538 30	7.18	**254**	1.23	0.35	88.7	0.77	**NCSU**
02121180	9.62	**507**	1.74	0.31	159	0.55	**NCSU**
02101800	15.5	**655**	1.37	0.44	291	0.61	**NCSU**
02144000	31.8	**1,041**	1.57	0.52	546	0.38	**NCSU**
02075160	32.8	**709**	1.68	0.62	441	0.26	**NCSU**
02114450	42.8	**2,236**	1.54	0.31	700	0.43	**NCSU**
02112360	78.8	**2,681**	1.58	0.40	1,080	0.31	**NCSU**
02113000	128	**3,687**	1.33	0.46	1,680	0.46	**NCSU**
NC Regional Averages			**1.54**	-		**0.47**	
01583000	2.09	**115**	1.45	0.16	18	0.60	**CBFO-S02-01**
01586210	14.0	**559**	1.44	0.24	137	0.50	**WRIR 03-4014**
01586210	14.0	**628**	1.60	0.24	154	0.42	**CBFO S02-01**
01475850	15.8	**601**	1.13	0.31	188	1.00	**WRIR 03-4014**
01480300	18.7	824	1.33	0.40	**333**	**0.60**	**WRIR 03-4014**
01472199	23.0	**1,000**	1.26	0.45	454	0.51	**WRIR 01-4146**
01586610	28.0	**970**	1.52	0.34	331	0.37	**WRIR 03-4014**
01586610	28.0	**1,024**	1.59	0.34	349	0.33	**CBFO S02-01**
01480500	45.8	**1,097**	1.24	0.55	602	0.65	**WRIR 03-4014**
01480617	55.0	**1,643**	1.33	0.42	686	0.78	**WRIR 03-4014**
01477000	61.1	**1,772**	1.22	0.41	733	0.82	**WRIR 03-4014**
01580000	94.4	**2,614**	1.31	0.35	905	0.60	**CBFO S02-01**
01645000	101	**2,562**	1.60	0.51	1,310	0.48	**CBFO S02-01**
01645000	101	**1,330**	1.08	0.51	679	1.37	**Leopold, Wolman & Miller**
MD/PA Regional Averages			**1.39**			**0.59**	
NC/MD/PA Regional Averages			**1.46**			**0.54**	
Maryland Piedmont upland gages							
North Carolina Piedmont upland gages							
Pennsylvania Piedmont upland gages							

$$Q_{Bankfull} = 68.87 * DA^{0.813} \quad \text{(cfs)} \quad r^2 = 0.948 \quad (7)$$

$$Q_{Daily\ Bankfull} = 16.98 * DA^{0.964} \quad \text{(cfs-day)} \quad r^2 = 0.990 \quad (8)$$

$$T_{CF} = 5.917 * DA^{0.151} \quad \text{(hours)} \quad (9)$$

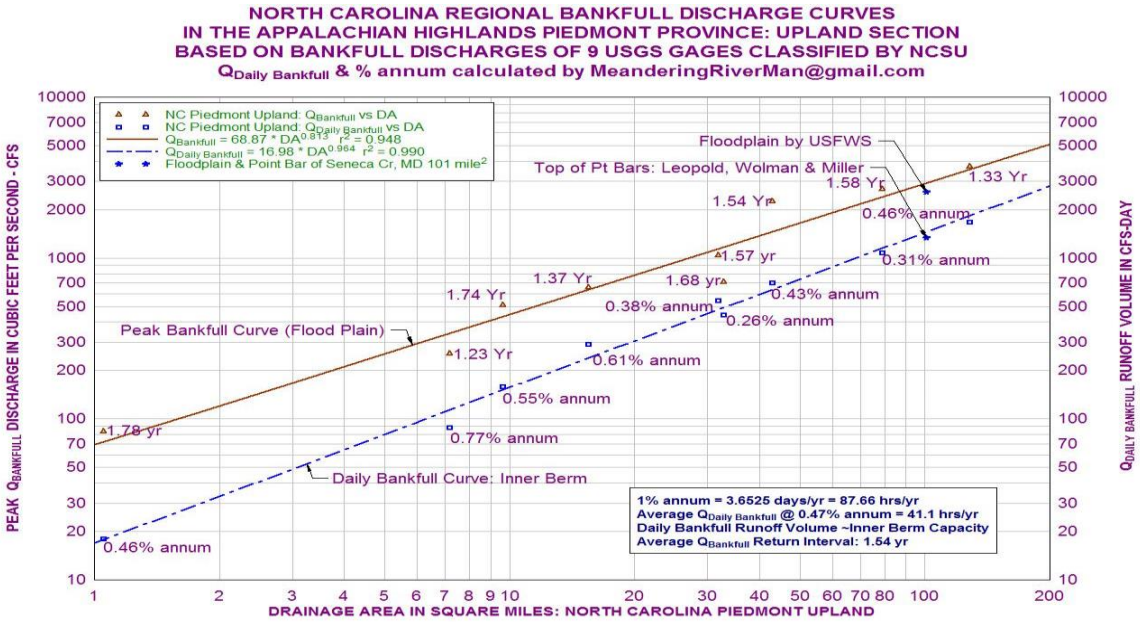

Figure 8: Regional $Q_{Bankfull}$ and $Q_{Daily\ Bankfull}$ Curves of Piedmont Upland section in North Carolina

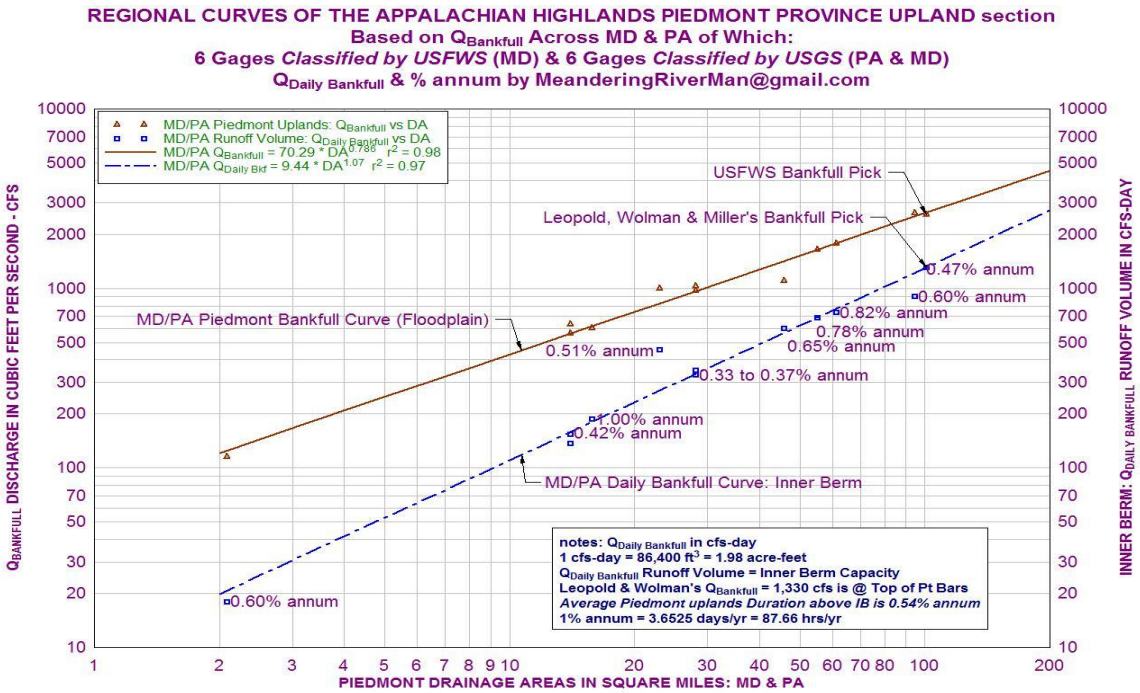

Figure 9 Regional $Q_{Bankfull}$ and $Q_{Daily\ Bankfull}$ Curves of Piedmont Upland section in MD & PA

Equations 10 - 12 apply for small watersheds in MD & PA Piedmont uplands for drainage areas 2.09 to 101 miles^2.

$$Q_{Bankfull} = 70.29 * DA^{0.786} \quad \text{(cfs)} \quad r^2 = 0.983 \quad (10)$$

$$Q_{Daily\ Bankfull} = 9.44 * DA^{1.07} \quad \text{(cfs-day)} \quad r^2 = 0.971 \quad (11)$$

$$T_{CF} = 3.223 * DA^{0.284} \quad \text{(hours)} \quad (12)$$

Atlantic Plain Coastal Plain (western) Embayed section

Table 4 Summary of $Q_{Daily\ Bankfull}$ and % annum for the Atlantic Coastal Plain (western) embayed section

Gage #	Drainage Area (miles^2)	$Q_{Bankfull}$ (cfs)	Return interval of $Q_{Bankfull}$ (years)	Most probable Q_{Daily}/Q_{Peak} Ratio	$Q_{Daily\ Bankfull}$ (cfs-day) 1-day runoff volume	% annum: $Q_{Daily\ Bankfull}$ on FDC	Reference source for $Q_{Bankfull}$ (cfs) only
(1)	(2)	(3)	(4)	(5)	(6)	(7)	(8)
01484100	3.02	**35**	**1.29**	0.59	21	1.03	**CBFO S03-02**
01661800	6.77	99	1.33	0.50	**50**	**1.01**	**SIR 2007-5162**
01661050	18.5	**273**	**1.23**	0.58	160	1.00	**CBFO S03-02**
01661500	24.0	**465**	**1.23**	0.54	252	0.91	**CBFO S03-02**
01658000	54.8	696	1.30	0.78	**540**	**1.05**	**CBFO S03-02**
Atlantic Coastal Plain Regional Averages			**1.28**	-		**1.00**	
FDC: Flow Duration Curve; 1 cfs-day = 1.98 acre-feet; 1% annum = 86.77 hrs./yr.							
Atlantic Coastal Plain Embayed section western gages							

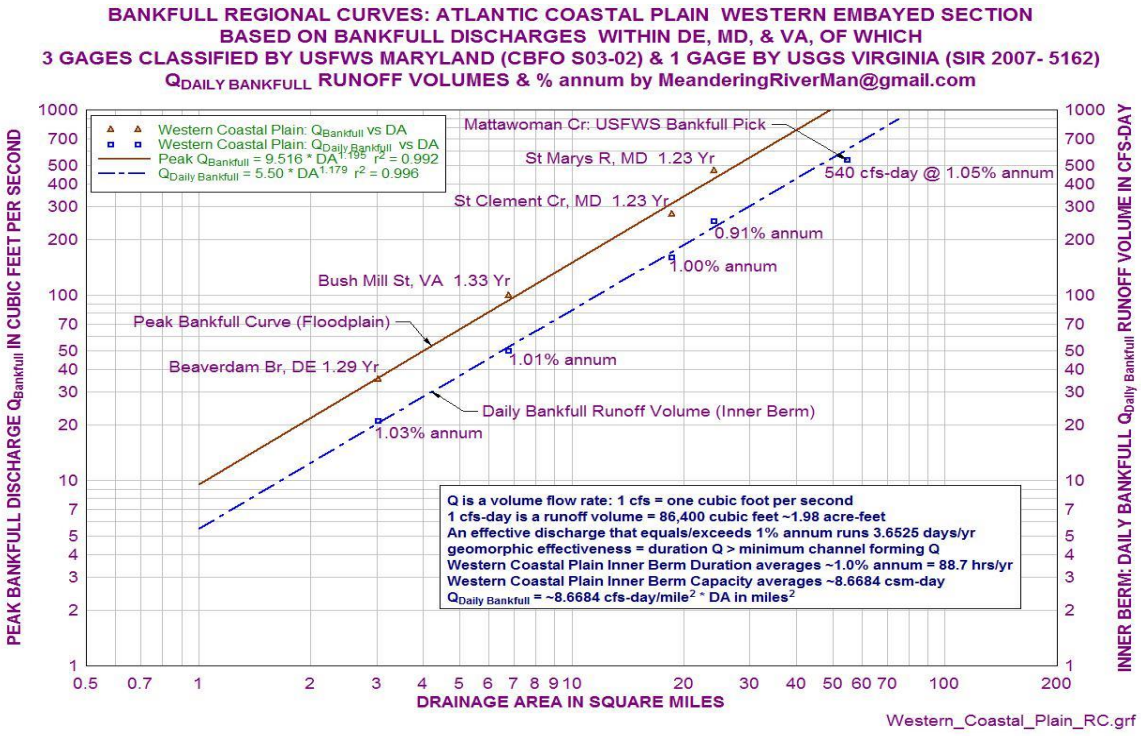

Figure 10 Regional $Q_{Bankfull}$ and $Q_{Daily\ Bankfull}$ Curves along the western Coastal Plain Embayed section

Equations 13 - 15 apply to small watersheds in DE, MD and VA coastal plain drainage areas 3.02 to 54.8 miles^2.

$$Q_{Bankfull} = 9.516 * DA^{1.195} \quad \text{(cfs)} \quad r^2 = 0.992 \quad (13)$$

$$Q_{Daily\ Bankfull} = 5.497 * DA^{1.179} \quad \text{(cfs-day)} \quad r^2 = 0.996 \quad (14)$$

$$T_{CF} = 13.864 * DA^{-0.016} \quad \text{(hours)} \quad (15)$$

DISCUSSION

The intention in developing $Q_{Bankfull}$ power equations and Regional Curves is not to supersede the work of the original authors, but to demonstrate the r^2 coefficients of the $Q_{Daily\ Bankfull}$ curves are generally better than for $Q_{Bankfull}$.

Co-Incidence of Regional $Q_{Daily\ Bankfull}$ Curves and Inner Berm (Q_{IB})

Seneca Creek: Leopold, Wolman & Miller (1964) published $Q_{Bankfull}$ at 1,330 cfs (1.1 year RI) at tops of point bars, 1,330 cfs-day corresponds to 0.46% annum flow duration. In 2002, McCandless and Everett, published $Q_{Bankfull}$ at 2,562 cfs (1.6 year RI). Using McCandless and Everett bankfull pick and Q_{Daily}/Q_{Peak} = 0.51, (derived from Table 1). Predicted $Q_{Daily\ Bankfull}$ = 2,562 cfs * 0.51 = 1,310 cfs-day at 0.47% annum on FDC, (Figure 6), a 1.6% difference.

$$Q_{Point\ Bar}/Q_{Floodplain} = 1{,}330/2{,}562 = 0.5191 \quad (16)$$

$$Q_{Daily\ Bankfull}/Q_{Bankfull} \sim Q_{Daily}/Q_{Peak} = 0.5109 \quad (17)$$

$$Q_{Daily}/Q_{Peak} \sim Q_{Daily\ Bankfull}/Q_{Bankfull} \sim Q_{Inner\ Berm}/Q_{Floodplain} \quad (18)$$

In Table 4 and Figure 10, $Q_{Bankfull}$ for Bush Mill Stream (01661800) and for Mattawoman Creek (01658000) are plotted to demonstrate that the USGS and USFWS identified geomorphic surfaces at 50 cfs (1.06 year) & 540 cfs (1.18 year) respectively, both plot close to the calculated Q_{IB} curve. On respective FDC's; 50 cfs-day plots at 1.01% annum, 540 cfs-day plots at 1.05% annum, both strongly agree with other $Q_{Daily\ Bankfull}$ durations of gages in the Atlantic Coastal Plain western embayed section.

Table 2, Figures 7 & 11 demonstrate changes in the Q_{Daily}/Q_{Peak} ratios (& $Q_{Daily\ Bankfull}$) of six gages on the main stem of Soldier Creek, (same valley type) are consistent in the *downstream direction.* As drainage area increases the inner berm stage (top of sediment bars) approaches bankfull (floodplain) stage. Simultaneously $Q_{Daily\ Bankfull}$ approaches $Q_{Bankfull}$ and the surrogate Q_{Daily}/Q_{Peak} ratio approaches unity. The two curves are asymptotic, but intersection of two linear curves would define "large watersheds", where Biedenharn & Copeland's (2000) assumptions hold true. Figure 11 is courtesy of Paul D. Miller, P.E. C.F.M., with GBA in Lenexa, KS. Mr. Miller surveyed & analyzed $Q_{Bankfull}$ for gages (red triangles) around the Kansas City area, then super-imposed his set with equations 4 (Central Kansas (Garday) and 5 (Q_{IB} (Garday)). His independent analyses, demonstrates *physical geomorphic features coincident with predicted* $Q_{Daily\ Bankfull}$.

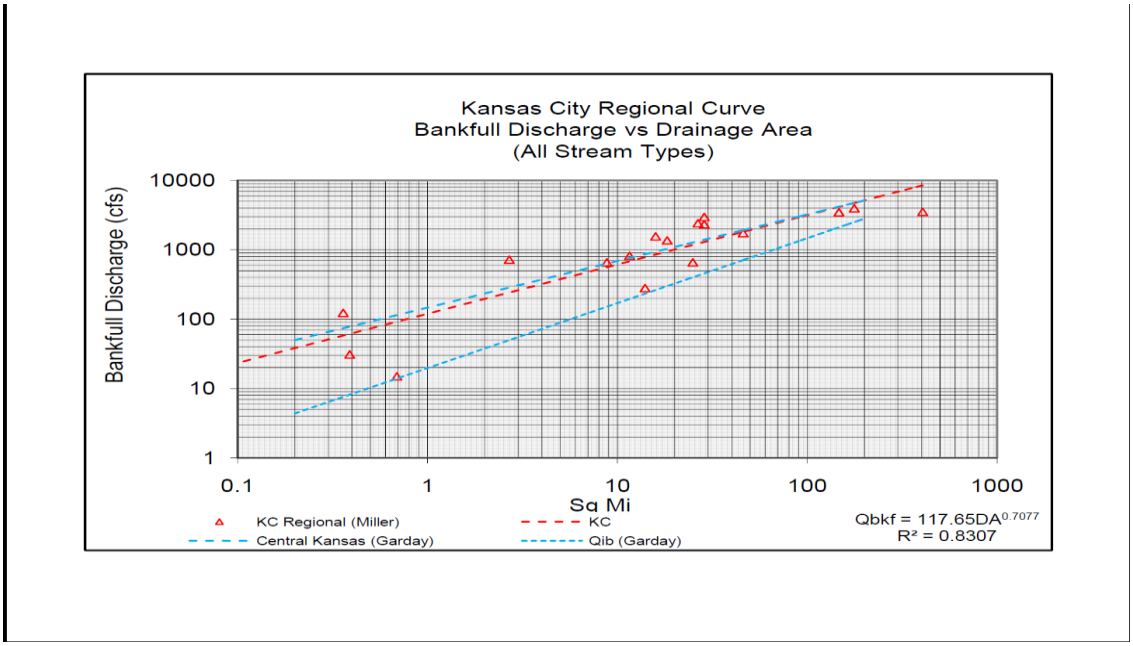

Figure 11 Kansas City Regional Bankfull Discharge Curves, Courtesy Paul D. Miller.

Most Probable Q_{Daily}/Q_{Peak} Ratios

Other methods to determine most probable Q_{Daily}/Q_{Peak} were evaluated: 15-minute instantaneous discharges were analyzed to use the largest 24-hour runoff volume under Q_{CF}. Surveys and analyses of 5 riffle cross-sections on the Sinsinawa River near Menominee; Illinois gage 05414820 at 39.6 miles^2 in the Wisconsin Driftless section: The Q_{Daily}/Q_{Peak} (**0.2243**) from averaging twenty (15-minute interval) storm hydrographs (1989-2004; $Q_{1.27} < Q_{Peak} < Q_{3.11}$) compared to Q_{Daily}/Q_{Peak} (**0.2338**) from averaging twenty three annual maximums (1967-2012; $Q_{1.25} < Q_{Peak} < Q_{2.99}$). Results of geomorphic surveys: $Q_{Bankfull}$ = 1,534 cfs and Q_{IB} = 364 cfs-day at 0.45% annum on FDC. Estimated $Q_{Daily\ Bankfull}$ = 359 cfs-day at 0.46% annum on FDC, actual $Q_{Inner\ Berm}/Q_{Bankfull}$ ~**0.2373**.

ACKNOWLEDGEMENTS

I must credit my survey team members who have shared their professional views and knowledge of riparian riverine systems over the years: Aaron Pugh, USGS geologist/hydrologist; Ron Redman, biologist/surveyor/WQ specialist, Arkansas Natural Resource Commission; Danny Goodwin, geographer/groundwater specialist, USDA NRCS; Christopher Haring, USACE geologist, Rock Island District. I would also like to thank Paul Miller, for sharing his Kansas City Regional Curves and all organizations - local, state, and federal, who have contributed funding to the USGS stream gage network, **Thank You**.

REFERENCES

Biedenharn, D. S. and Copeland, R. R. 2000, Effective discharge calculation, U.S. Army Corps of Engineers, ERDC/CHL CHETN-VIII-4, 10 p.

Blench, Thomas, 1951, Hydraulics of sediment-bearing canals and rivers: Vancouver, Evans Industries, Ltd.

Cinotto, P.J. 2003, Development of regional curves of bankfull-channel geometry and discharge for streams in the non-urban, piedmont physiographic province, Pennsylvania and Maryland, U.S. Geological Survey Water Resources Investigation Report 03-4014, 27 p.

Emmert, B.E. and Hase, K. 2001, Geomorphic assessment and classification of Kansas riparian systems, Kansas Water Office (KWO), USEPA No. CD997520-01.

Fenneman, N.M. 1946, Physical Divisions of the United States, U.S. Geological Survey Map, scale 1:7,000,000.

Harman, W.H. Jennings, G.D. Patterson, J.M. Clinton, D.R. Slate, L.O. Jessup, A.G. Everhart, J.R. and Smith, R.E. 1999. Bankfull hydraulic geometry relationships for North Carolina streams. AWRA Wildland Hydrology Symposium Proceedings. AWRA Summer Symposium. Bozeman, MT.

Hewlett, J.D. and Hibbert, A.R. 1965, Factors affecting the response of small watersheds to precipitation in humid area. International Symposium Forest Hydrology, pp 275-290.

Klein, M. 1976, Hydrograph peakedness and basin area. Earth Surface Processes and Landforms, Vol. 1, pp 27-30.

Krstolic, J.L. and Chaplin, J.J. 2007, Bankfull regional curves for streams in the non-urban, non-tidal coastal plain physiographic province, Virginia and Maryland, U.S. Geological Survey Scientific Investigations Report 2007-5162, 48 p.

Leopold, L.B. Wolman, M.G. and Miller, J.P. 1964, Fluvial processes in geomorphology, Dover Publications, Mineola, New York, 522 p.

McCandless, T.L. and Everett, R.A. 2002, Maryland stream survey: Bankfull discharge and channel characteristics of streams in the Piedmont hydrologic region, U.S. FWS Chesapeake Bay Field Office, CBFO S02-01, Annapolis, Maryland, 40 p.

McCandless, T.L. 2003, Maryland stream survey: Bankfull discharge and channel characteristics of streams in the Coastal Plain hydrologic region, U.S. FWS Chesapeake Bay Field Office, CBFO S03-02, Annapolis, Maryland, 29 p.

Melton, F.A., 1936, An empirical classification of flood-plain streams: Geog. Rev., v. 26, p. 593 – 610.

Miller, P.D., 2007, Kansas City Regional Curve, personal communication.

Nixon, M. 1959, A Study of the bankfull discharges of rivers in England and Wales: Institute Of Civil Engineering Proc., Paper No. 6322, pp 157-174.

Rosgen, D.L. 1996, Applied river morphology, Minneapolis, Minnesota, Printed Media Companies, 388 p.

Wolman, M.G. and Leopold, L.B. 1957, River flood plains: some observations on their formation, U.S. Geological Survey Professional Paper 282-C, pp 87-109.

Wolman, M.G. and Miller J.P. 1960, Magnitude and frequency of forces in geomorphic processes. Journal of Geology 68: pp 54-74.

A SIMPLIFIED MORPHODYNAMIC MODEL FOR GRAVEL-BED RIVERS

Alan Kasprak, Graduate Research Assistant, Department of Watershed Sciences, Utah State University, 5210 Old Main Hill NR 210, Logan, Utah, 84322-5210, 508.320.1186, alan.kasprak@gmail.com; Joseph M. Wheaton, Assistant Professor, Department of Watershed Sciences, Utah State University, 5210 Old Main Hill NR 210, Logan, Utah, 84322-5210, 435.554.1247, joe.wheaton@usu.edu; Konrad Hafen, Research Associate, Department of Watershed Sciences, Utah State University, 5210 Old Main Hill NR 210, Logan, Utah, 84322-5210, khafen74@gmail.com

Abstract: The evolution of gravel-bed rivers has major implications for the management and restoration of these streams and their associated aquatic habitat. This is particularly true in braided rivers, where abundant sediment supply and rapid fluctuations in streamflow lead to a high degree of dynamism. Because channel evolution frequently results from decadal to centennial scale forcings such as shifts in water or sediment supply, these timescales of change often preclude field-based measurement of channel morphodynamics. One potential alternative to field-based observation is numerical modeling. However, no morphodynamic model for gravel-bed rivers exists that can predict channel evolution at relevant spatiotemporal scales (e.g. decadal to centennial timescales at bar-scale resolution). Here we present a new event-based morphodynamic model that couples hydraulics driven by computational fluid dynamics with a simplified sediment routing algorithm based on sediment travel distances derived from field and laboratory data. This model efficiently quantifies morphodynamics at spatiotemporal scales coincident with those of channel change. Sediment travel distances, or path lengths, are estimated using morphologic unit spacing in modeled channels. We validate this model using high-resolution laboratory flume and field data collected annually on braided rivers. This morphodynamic model closes a longstanding knowledge gap in our ability to predict channel response at meaningful spatiotemporal scales. When used as a scenario-based exploration tool for predicting channel response to altered hydrologic or sediment regimes, it may provide valuable guidance for the management and restoration of gravel-bed rivers.

INTRODUCTION

Some of the most commonly studied processes in riverine environments occur over time and space scales that render traditional field-based observation impractical or impossible [Gurnell et al., 2009]. These fluvial dynamics include channel migration [Hooke, 1995; Black et al., 2010], shifts in channel form [Landon et al., 1998; Kondolf et al., 2002], and alterations in hydrology and/or sediment delivery [Kondolf, 1997; Montgomery and Buffington, 1998; Grams and Schmidt, 2005]. All of these dynamics occur frequently on timescales ranging from decades to centuries, and channel response to hydrologic and sediment regime shifts may manifest across a variety of spatial scales ranging from individual channel units (e.g. meters) to reaches spanning several kilometers. In such instances where the spatiotemporal scale of channel response renders field-based methods of observation intractable, representation of the fluvial environment using numerical models is invaluable both in terms of disentangling the relative efficacy of competing processes acting to shape channels and predicting future channel response to geomorphic forcings [Nicholas, 2005; Gurnell et al., 2012].

Despite the immense value of numerical models in the explanation and prediction of fluvial processes, the timescales at which channel evolution occurs render most available morphodynamic models (those which predict changes in channel form over time) impractical. Historically, one way of dealing with this problem has been to simplify the physics involved in modeling, giving rise to the so-called ‘reduced complexity’ or 'cellular automata' models [RC/CA; Murray and Paola, 1994; Coulthard et al., 2002; Thomas and Nicholas, 2002]. These models simplify the transport of water and sediment across a cellular network representing the riverscape using a rule set governing each process involved. Because these rule sets are simplified representations of the physics involved in hydrodynamics and sediment transport, RC

models achieve a great deal of computational efficiency, allowing calculations over large spatiotemporal extents (e.g. kilometer-scale, decadal-to-centennial timescales; Nicholas and Quine, 2007; Thomas et al., 2007). Yet this computational efficiency comes at the expense of field realism; because of the simplified nature of the physical processes, particularly the inability to conserve hydraulic momentum leading to inaccurate representation of pool dynamics and meander migration [Nicholas and Quine, 2007], reduced complexity models often fail to reproduce observed channel behavior at the spatial scales of change.

On the other hand, the subset of morphodynamic models driven by computational fluid dynamics (CFD; Bates et al., 2005) involve hydrodynamic components that approximate the solution of the Navier-Stokes Equations and subsequently drive sediment transport. To ensure computational stability, morphodynamics are typically computed by solving a form of the Exner equation (1) of sediment continuity (Paola and Voller, 2005) at fine time steps (seconds-minutes). The Exner equation predicts bed elevation change over time ($\partial z/\partial t$) as a function of sediment porosity (γ_p) and the spatio-temporal divergence of sediment flux (∇Qs). This reliance on rapid calculation of morphodynamic evolution comes at the cost of vastly increased computational overhead, making CFD-driven morphodynamic models suitable only over fine spatiotemporal scales for most users (e.g. hours-months at meter-scale resolution; Ferguson, 2007; Coulthard and Van de Wiel, 2012).

$$\frac{\partial z}{\partial t} = \frac{1}{1-\gamma_p}\left(\frac{\partial V_s}{\partial t} + \nabla \cdot Q_s\right) \quad (1)$$

We hypothesize that the fusion of CFD and RC-based morphodynamic modeling may present a novel way forward, in that the high spatial fidelity afforded by CFD-driven models may be coupled with a simplified, empirically-derived rule set for sediment transport and morphodynamic channel evolution (cf. Nicholas and Quine, 2007). As such, this paper presents a new, hybrid morphodynamic model termed the *Model of Riverine PHyiscal form and Ecohydromorphic Dynamics (MoRPHED.)*

THE MODEL

As with previously-developed morphodynamic models, MoRPHED contains routines for simulating hydrodynamics and uses these calculations to drive sediment transport. This section details the methods used in in each of these components, along with ancillary routines such as the parameterization of model boundaries, sediment grain size, and bank erosion. A flowchart of model operation along with required/optional inputs and outputs are shown in Figure 1, and these components are discussed throughout this section. The salient components of the model that directly impact our validation results are discussed here.

Hydraulic Model: The hydraulic component of MoRPHED is driven using the freely-available, open-source Delft3D software (Version 4.00.01, Deltares, Delft, Netherlands). Delft3D solves the shallow-water form of the Navier-Stokes equations, and herein we employed the model in two-dimensional (depth-averaged) form, as this provided an ideal compromise between computational efficiency and the ability to resolve hydraulics at the scale of our DEMs [Lane et al., 1999]. For all modeling, we employed Cartesian orthogonal grids generated using the RGFGRID module of the Delft3D suite and kept constant throughout a modeled event series, and adjusted the model time step to satisfy the Courant-Friedrichs-Levy condition. Models were run at a steady upstream discharge and were allowed to run to steady state (no observed change in depth, velocity, or inundation extent in QUICKPLOT model postprocessor).

For all simulations, discharge was specified at the upstream boundary and a corresponding water surface elevation was set at the downstream boundary. Delft3D requires an input DEM, along with simulated water discharge and boundary conditions. The downstream water surface elevation for each modeled

discharge was used to parameterize the hydraulic model boundary, and was calculated by determining reach-scale conveyance associated with reach-average slope and roughness [cf. USACE, 2010]. Although numerous hydraulic variables can be computed and exported from Delft3D, here we used (a) water depth, (b) flow velocity resolved into streamwise and lateral components, and (c) bed shear stress.

MoRPHED is an event-scale model, predicting channel evolution at the scale of individual floods. We do this for two reasons, (a) because the calculation of morphodynamics at coarser intervals allows for greatly reduced computational overhead associated with the model, and (b) because we argue that modeling at finer intervals, while allowing the ability to capture rapid transient events such as prograding bedload sheets and bank retreat during the course of a single flood, is difficult if not impossible to validate since the most common data geomorphologists have describe channel form only before and after a single event [Bertoldi et al., 2010; Williams et al., 2013; Mueller et al., 2014] along with sediment transport resulting from that event [Pyrce and Ashmore, 2003a, 2003b; Snyder et al., 2009; Kasprak et al., 2015].

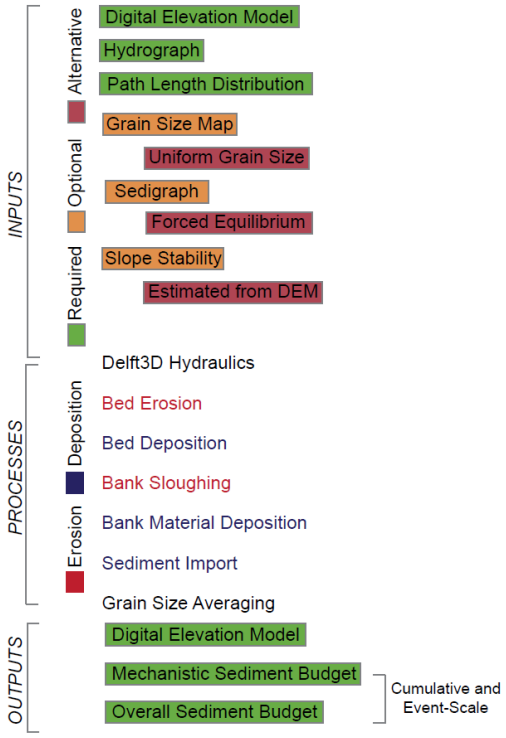

Figure 1 Flowchart of modules included in MoRPHED and their operation

Sediment Entrainment: MoRPHED employs a critical nondimensional value of the bed shear stress (Shields stress) to determine whether sediment can be entrained at a particular location. As our model is developed and used on gravel-bed rivers, the theory and threshold values of Shields stress for entrainment have been well studied in these settings. Incipient motion for gravel occurs when the Shields stress (τ^*) exceeds 0.03-0.07 [Buffington and Montgomery, 1997; Snyder et al., 2009]:

$$\tau^* = \frac{\tau_B}{(\rho_s - \rho)gD} \tag{2}$$

where ρ_s is sediment density (2650 kg/m^3), g is acceleration due to gravity, and D is the median particle size (see Section 2.4). The bed shear stress (τ_B) was computed using the output from Delft3D.

[Montgomery et al., 1996] proposed an event-scale model to predict sediment scour depth (D_s):

$$D_s = \frac{Q_b}{u_b \rho_s (1-\gamma)} \tag{3}$$

where Q_b is the average bedload transport rate during the event, u_b is the bedload velocity, and γ is the bed sediment porosity. Estimating Q_b, while straightforward, is often inaccurate as it is a strongly nonlinear process; however, most transport relations take a power-law form (e.g. Meyer-Peter Müeller equation):

$$Q_b = (\tau_b - \tau_{bC})^{1.5} \tag{4}$$

where the critical bed shear stress is given for a particular grain size by rearrangement of Equation 2. Bedload velocity is calculated via an equation of the form:

$$U_b = a(u_* - u_{*C}) \tag{5}$$

where u_*, the shear velocity, is computed as

$$u_* = \sqrt{\frac{\tau}{\rho}} \tag{6}$$

Which can be estimated directly from the bed shear stress obtained from Delft3D. The constant a in Equation 6 has been studied by many researchers [Garcia, 2008], and is generally around 9.

Sediment Transport and Deposition: Once entrained, sediment is mobilized downstream along flowlines which are delineated using velocity components from Delft3D to calculate velocity vectors.

At each cell along the flowpath, the volume of sediment to be deposited is given by a path length distribution (Figure 2). In the simplest sense, this distribution details the proportion of all eroded sediment which is deposited at a particular distance downstream. These distributions have been studied by numerous researchers and found to take several forms in braided rivers. Exponential decay, or heavy-tailed distributions (Figure 2A) are marked by a large number of particles that are mobilized short distances downstream, and may result from floods that do not generate sufficient shear stress for particle transport across the braidplain [Pyrce and Ashmore, 2003a, 2003b]. During floods which are competent across large areas of the braidplain, typical path length distributions exhibit peaks which correspond to the location of likely depositional sites downstream (Figures 2B, 2C). Kasprak et al. [2015] and Pyrce and Ashmore [2003a, 2003b] both noted that these depositional sites were most frequently the location of bar heads (e.g. flow diffluences; those places where one anabranch splits into multiple channels). As such particle path length distributions could be readily constructed using morphometric indices which described the characteristic diffluence spacing in braided channels. MoRPHED deposits sediment in cells along delineated flowpaths in a volume given by the path length distribution, which is specified by the user and can take a variety of forms in the model with chosen moment statistics (Gaussian, Exponential Decay, or any user-defined shape input using a text file).

Sediment Import and Export: For each simulated event, MoRPHED tracks the volume of sediment passing the downstream or lateral reach boundaries. In effect, export of sediment occurs when the user-specified path length distribution is longer than the flowpath delineated from a particular erosion cell. When this occurs, the remaining volume of sediment is recorded by MoRPHED as having been exported from the reach. Sediment import is user-specified and can be (a) set equal to the volume of sediment export during the preceding event (e.g. sediment equilibrium; Grams and Schmidt, 2005; Mueller et al.,

2014), (b) specified as a percent of sediment export during the preceding event, or (c) specified via a text file detailing volumetric sediment import during each event (e.g. sedigraph timeseries). Algorithmically, MoRPHED computes flowpaths from each wetted cell at the upstream reach boundary and distributes the total volume of imported sediment to each cell of each flowpath as specified in the user-input path length distribution.

MODELING SITE

The wandering gravel bedded River Feshie (Figure 3) is a tributary of the River Spey and drains 231 km^2 of mountainous, postglacial terrain. Underlain by metamorphic and igneous rocks, the basin ranges from around 230 m to 1260 m in elevation. The mean flow near the river's outlet was reported by Ferguson and Werritty [1983] as 8 m^3/s with Q_5 = 80 m3 sec^{-1}. Topographic data for the 1 km study reach of the Feshie consist of nine years of resurveys (2000, 2002-2008, 2013) comprising more than a decade of channel change using RTK-GPS (2000-2006) along with TLS and RTK-GPS fusion scans performed for three years (2007-8, 2013). Additionally, the Feshie dataset contains continuous hydrograph data (~55 years) and aerial photo records (~60 years), along with UK Ordnance Survey channel planform maps dating to 1869. The Feshie has been the site of a great deal of previous research ranging from bar morphodynamics [Ferguson and Werritty, 1983; Wheaton et al., 2013], development of riverine survey and DEM-differencing/change detection methodologies [Brasington et al., 2000; Hodge et al., 2009; Wheaton et al., 2009, 2013] and ongoing morphodynamic modeling efforts [Raj Baral et al., In Prep.]. The combination of annual resurveys capturing over a decade of channel change in combination with mapping and aerial photographs dating back over a century make the Feshie an ideal candidate with which to examine the performance of MoRPHED at annual and decadal scales.

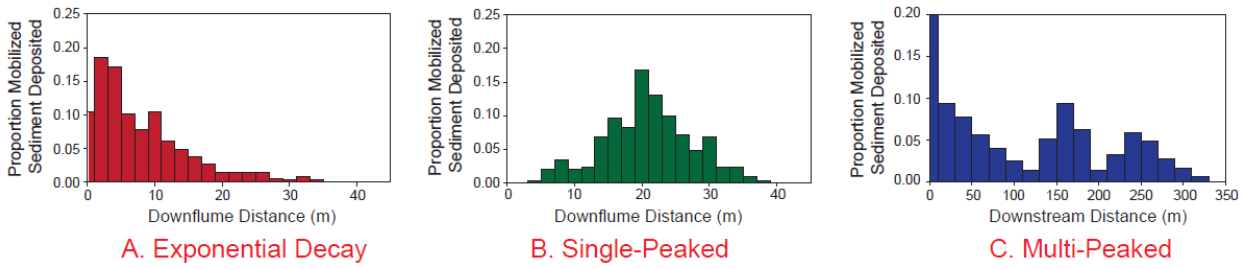

Figure 2 Example path length distributions

RESULTS AND ANALYSIS

Hydraulic Modeling and Validation: The use of Delft3D to model two-dimensional hydraulics in braided, gravel-bed rivers is discussed extensively by Williams et al., [2013], who specifically applied the model to the braided River Rees in new Zealand. As with Williams et al. [2013], the inundation extent outputs of Delft3D on the Feshie were compared with field-surveyed values and used to calibrate the model parameters (Colebrook-White roughness and horizontal eddy viscosity) until good agreement was reached.

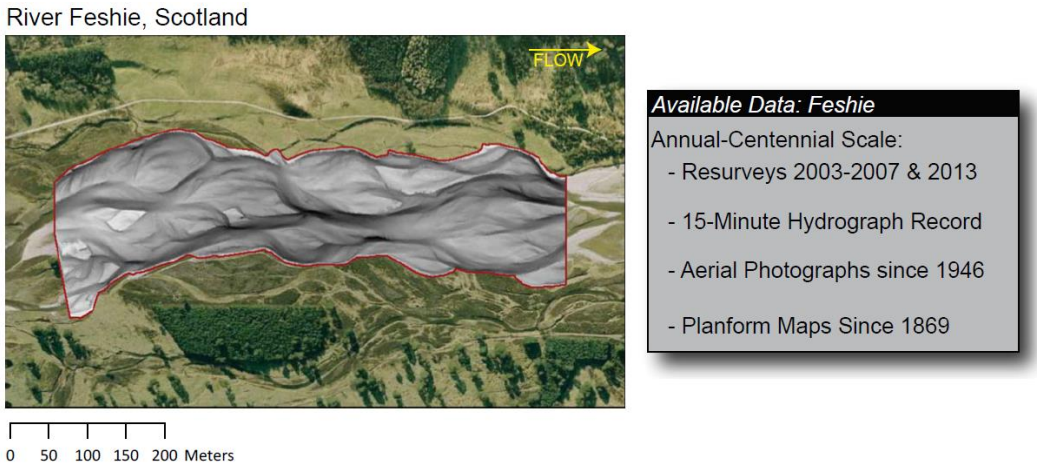

Figure 3 River Feshie modeling reach; base is a 2014 aerial photo with 1 m hillshade overlay

We leveraged existing surveys of wetted areas from 2003-2007 in concert with surveyed water depth in those years to examine the performance of Delft3D with regard to inundation extent and flow depth at randomly selected points across the braidplain. Because field surveys were conducted at low flows to facilitate rapid measurement of braidplain topography, here we are only able to validate the results of Delft3D at these low flows. However, Delft3D has been employed and validated on gravel-bed braided rivers at flood stage [Javernick, 2014], demonstrating that the model can accurately reproduce flood-stage hydraulic features and can be used to drive morphodynamic evolution at the event-scale. For modeling on the Feshie, we estimated discharge by downscaling the average observed flow for the relevant survey period at the nearest gauging station (SEPA # 8013, Feshie at Feshiebridge) located approximately 11 km downstream, using a coefficient of 0.71 [Wheaton et al., 2013]. We estimated the downstream water surface elevation using surveyed inundation extent in combination with the DEM for each year modeled. Downstream water surface elevations estimated from the spatial data were cross-checked using a reach-scale conveyance calculation [Williams et al., 2013].

Results of our validation of Delft3D on the Feshie at low flow are shown in Figure 4. Here we report (a) the mean of depth differences between modeled and observed values (D_{diff}), along with (b) the congruence of the modeled and measured inundation extents (F_c; cf. Bates and Roo, 2000) as described by the ratio of intersection and union areal extents. These two metrics are described by equations 12 and 13, respectively.

$$D_{diff} = \frac{\sum_i^n x_{mod} - x_{obs}}{n} \tag{7}$$

$$F_c = \frac{IA_{obs} \cap IA_{mod}}{IA_{obs} \cup IA_{mod}} * 100 \tag{8}$$

The validation metrics indicate that at low flow, Delft3D accurately predicted both depth and inundation extent across the Feshie study reach. Both D_{diff} and Fc are consistent with validation work performed by Williams et al., [2013], and are indicative of good agreement between hydraulic model and field-observed flow characteristics.

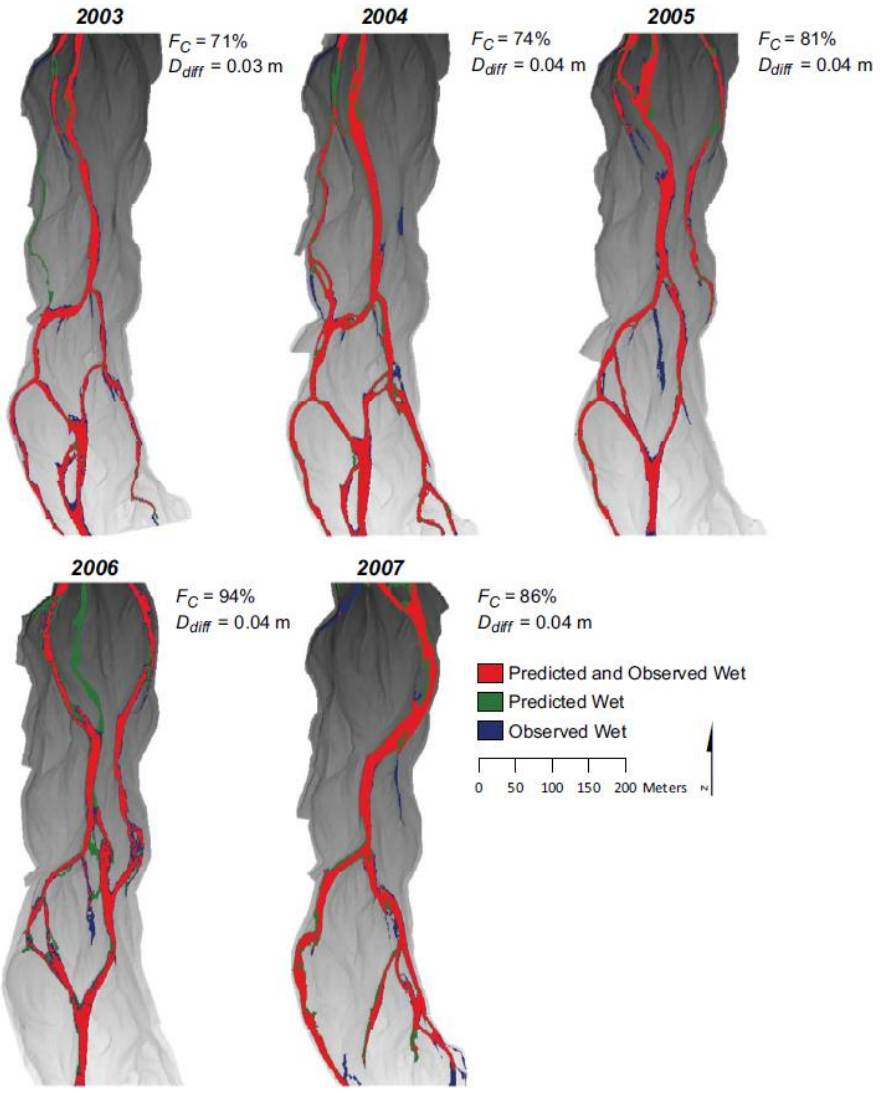

Figure 4 Hydraulic model validation on River Feshie. Mean depth of difference (D_{diff}; Equation 7) and congruence of fit (C_f; Equation 8) are shown for five years of survey data.

Morphodynamic Model Outputs: We modeled two one-year periods using MoRPHED, (a) the period between 2003 and 2004 and (b) the period between 2006 and 2007. We modeled the peak discharge of each flood over 42 m^3/s (high bankfull discharge; Wheaton et al., 2013), for a total of 5 floods in 2003-2004 and 16 floods in 2006-2007. For the hydrologic record and flood peaks over 42 m^3/s, see Wheaton et al., [2013]. We set sediment import equal to sediment export for each model run (reach-scale equilibrium; Figure 1). Though variable grain size is available in MoRPHED, a constant grain size of 0.1 m (representative D_{50} for the Feshie reach; Hodge et al., 2009) was used in these simulations. Bank erosion was not included, as refinement of process representations for lateral channel migration is ongoing. Modeled floods and resultant DEMs-of-Difference (DoDs) from the 2003-2004 and 2006-2007 model periods are shown in Figure 5 and compared with field-surveyed DoDs from the same period.

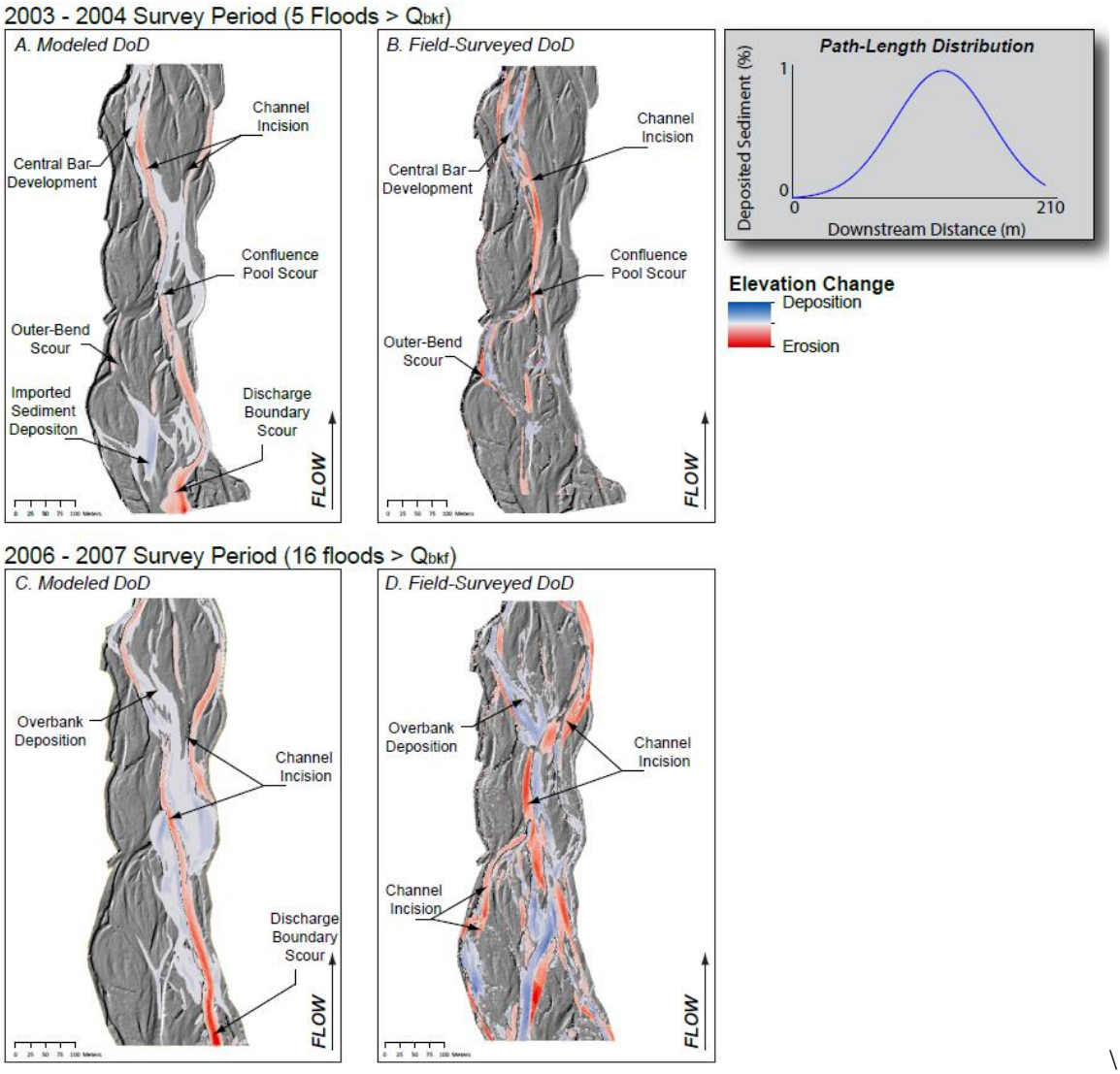

Figure 5 Modeled (A, C) and field-surveyed (B, D) geomorphic change on the River Feshie for 2003-2004 and 2005-2006 periods. DoDs are thresholded to only display geomorphic change greater than 0.1 m in magnitude.

For the 2003-2004 simulation, results of MoRPHED modeling agree reasonably well with geomorphic change observed in field surveys (Figure 6A, 6B). Continuous channel incision along the main anabranch is reproduced, along with bar edge trimming and associated deposition at the downstream end of the study reach. High-magnitude confluence pool scour is observed in both model and field surveys. However, while sediment scoured at the confluence is deposited immediately downstream in the MoRPHED simulation, this sediment appears to have been transferred further downstream (or out of the reach entirely) when examining the results of field surveys (Figure 5B).

In the 2006-2007 simulation, MoRPHED does not reproduce field-surveyed changes as well (Figure 6C, 6D). While certain areas of change are seen in both field and modeled data (e.g. channel incision and overbank deposition near the downstream end of the reach), the model does not appear to reproduce the dynamics of the numerous anabranches that underwent geomorphic change across the braidplain. We believe the simplified planform produced by MoRPHED is largely the result of not explicitly including

bank erosion in the model. As such, focused erosion leads to a largely single-thread channel planform, rather than lateral channel migration forcing avulsions and a dynamic braided channel planform [Ferguson, 2007]. Implementation of a bank erosion algorithm is an ongoing component of MoRPHED model development.

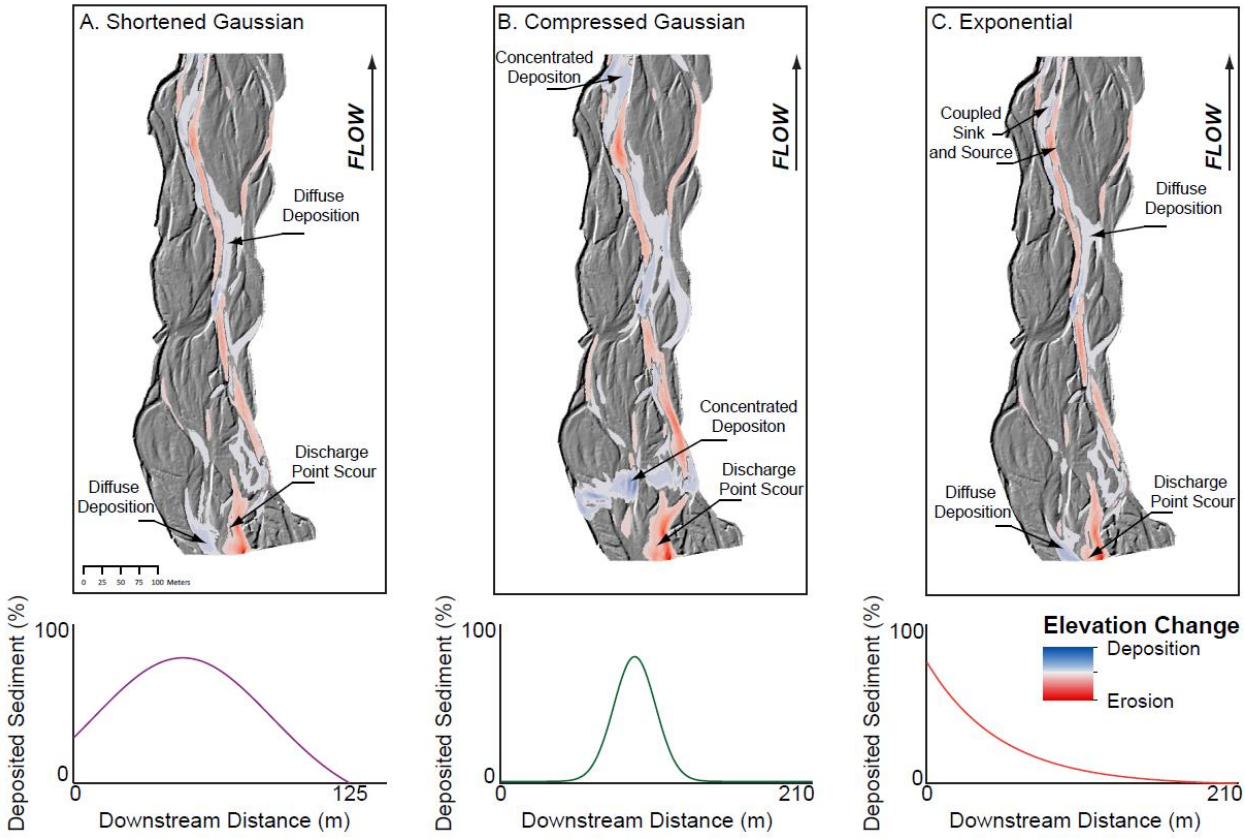

Figure 6 Results of modeling 2003-2004 period using three different path length distributions. DoDs are thresholded to only display geomorphic change greater than 0.1 m in magnitude.

In each model run, inaccuracies due to boundary effects can be observed, with high-magnitude scour at the upstream end of the reach due to channel bed erosion at water discharge points used in the Delft3D model. This scoured sediment (along with imported sediment) creates areas of deposition that were either (a) not observed in field surveys (Figure 6A, 6B), or were observed in a different anabranch than predicted by the model (Figure 6C, 6D).

Morphodynamic Process Representations: Whether or not certain processes are included in any morphodynamic model, along with the algorithms by which those processes are represented, has major implications for the computation efficiency and field-realism of the output solution. To this end, MoRPHED is not only a working morphodynamic model, but perhaps more importantly, provides an interchangeable framework by which users can explore the morphodynamic results of altering process representations. To illustrate this, we conducted three additional simulations using the 2003-2004 discharge record, each of which employs a modified path length distribution (Table 1). The results of these simulations are shown in Figure 6.

Table 1 Path length distribution parameters used in process representation modeling

Name	**Length (m)**	**Coefficient 1**	**Coefficient 2**
Default	210	$\sigma = 40$	$\mu = 125$
Shortened Gaussian	125	$\sigma = 40$	$\mu = 50$
Compressed Gaussian	210	$\sigma = 10$	$\mu = 125$
Exponential	210	$a = 0.1$	$b = 0.2$

While the shortened Gaussian and exponential distributions produced relatively similar model outputs, the compressed Gaussian distribution produced morphologies that reflected the high degree of coupling between erosion and deposition sites. This is particularly visible when observing the high-magnitude deposition resulting from sediment import or the concentrated deposition resulting from central bar trimming in Figure 6B. In Figures 6A and 6C, the deposition resulting from this bar scour is more longitudinally diverse, reflecting that deposition is spread over larger areas in the shortened Gaussian and exponential distributions. The focused nature of deposition in the compressed Gaussian distribution also has implications for erosion, with more high-magnitude erosional areas visible in Figure 6B; these erosional areas were likely not counter-balanced by the extensive depositional sheets seen in Figure 6A and 6C, and occur as more longitudinally-continuous, low-magnitude areas of scour.

CONCLUSIONS

This research seeks to develop a morphodynamic model that combines aspects of computational fluid dynamics with simplified morphologic-sediment transport relations to minimize computational overhead and allow increased simulation time at high spatial resolution. The MoRPHED model developed here has been run over two annual periods along a wandering, gravel bed river. During the 2003-2004 period, which was marked by a small number of peaks over the bankfull discharge (n = 5), the model reproduced field-surveyed geomorphic change reasonably well, although differences in the location of deposited sediment were observed, along with inaccuracies resulting from discharge point locations used in the hydraulic component of MoRPHED. In the 2006-2007 simulation, which was marked by a greater number of flows exceeding bankfull discharge (n = 16), the absence of a bank erosion algorithm in MoRPHED was notable, as the channel tended towards a single-thread planform in model simulations. Ongoing development of MoRPHED seeks to implement bank erosion dynamics and refine model boundary parameterization. MoRPHED is open-source software which is freely available at http://morphed.joewheaton.org, along with user manuals, tutorials, and example datasets.

ACKNOWLEDGEMENTS

Development of MoRPHED is supported by the National Science Foundation (Award #7086465). Extensive development assistance is provided by Philip Bailey (North Arrow Research), Matt Nahorniak (South Fork Research), James Brasington (Queen Mary University of London), and James Hensleigh, Sara Bangen, and Eric Wall (all of Utah State University and EcoLogical Research).

REFERENCES

Bates, P., and De Roo, A. (2000). "A simple raster-based model for flood inundation simulation," Journal of Hydrology, 236(1-2), 54–77, doi:10.1016/S0022-1694(00)00278-X.

Bates, P. D., S. N. Lane, S.N., and Ferguson, R.I. (2005). Computational fluid dynamics, Wiley Online Library.

Bertoldi, W., L. Zanoni, L., and Tubino, M. (2010). "Assessment of morphological changes induced by flow and flood pulses in a gravel bed braided river: The Tagliamento River (Italy)," Geomorphology, 114(3), 348–360, doi:10.1016/j.geomorph.2009.07.017.

Black, E., Renshaw, C. E., Magilligan, F.J., Kaste, J.M., Dade, W.B., and Landis, J.D. (2010). "Determining lateral migration rates of meandering rivers using fallout radionuclides," Geomorphology, 123(3-4), 364–369, doi:10.1016/j.geomorph.2010.08.004.

Buffington, J. M., and Montgomery, D.R. (1997). "A systematic analysis of eight decades of incipient motion studies, with special reference to gravel-bedded rivers," Water Resources Research, 33(8), 1993–2029, doi:10.1029/96WR03190.

Coulthard, T. J., and Van de Wiel, M.J. (2012). "Modelling river history and evolution," Philosophical transactions. Series A, Mathematical, physical, and engineering sciences, 370(1966), 2123–42, doi:10.1098/rsta.2011.0597.

Coulthard, T. J., Macklin, M.G., and Kirkby, M.J. (2002). "A cellular model of Holocene upland river basin and alluvial fan evolution," Earth Surface Processes and Landforms, 27(3), 269–288, doi:10.1002/esp.318.

Ferguson, R. (2007). "Gravel bed rivers at the reach scale, in Gravel-Bed Rivers VI: From Process Understanding to River Restoration," vol. 11, pp. 33–53, Elsevier.

Ferguson, R. I., and Werritty, A. (1983). "Bar Development and Channel Changes in the Gravelly River Feshie," Scotland, in Modern and Ancient Fluvial Systems.

Garcia, M. H. (2008). Sediment Transport and Morphodynamics, in Sedimentation Engineering, edited by M. H. Garcia.

Grams, P. E., and Schmidt, J.C. (2005). "Equilibrium or indeterminate? Where sediment budgets fail: Sediment mass balance and adjustment of channel form," Green River downstream from Flaming Gorge Dam, Utah and Colorado, Geomorphology, 71(1-2), 156–181, doi:10.1016/j.geomorph.2004.10.012.

Gurnell, A., Surian N., and Zanoni L. (2009). "Multi-thread river channels: A perspective on changing European alpine river systems," Aquatic Sciences, 71(3), 253–265, doi:10.1007/s00027-009-9186-2.

Gurnell, A. M., Bertoldi, W., and Corenblit D. (2012). "Changing river channels: The roles of hydrological processes, plants and pioneer fluvial landforms in humid temperate, mixed load, gravel bed rivers," Earth-Science Reviews, 111(1-2), 129–141, doi:10.1016/j.earscirev.2011.11.005.

Hodge, R., Brasington, J., and Richards, K. (2009). "Analysing laser-scanned digital terrain models of gravel bed surfaces: linking morphology to sediment transport processes and hydraulics," Sedimentology, 56(7), 2024–2043, doi:10.1111/j.1365-3091.2009.01068.x.

Hooke, J. M. (1995). "River channel adjustment to meander cutoffs on the River Bollin and River Dane, northwest England," Geomorphology, 14(3), 235–253, doi:10.1016/0169-555X(95)00110-Q.

Javernick, L. (2014). "Modeling Flood-induced Processes Causing Russell Lupin Mortality in the Braided Ahuriri River, New Zealand," University of Canterbury.

Kasprak, A., Ashmore, P., Hensleigh, J., Peirce, S., and Wheaton, J.M. (2015). "The Relationship Between Particle Travel Distance and Channel Morphology: Results from Physical Models of Braided Rivers, Journal of Geophysical Research: Earth Surface," doi:10.1002/2014JF003310.

Kondolf, G. (1997). "PROFILE: Hungry Water: Effects of Dams and Gravel Mining on River Channels, Environmental Management," 21(4), 533–51.

Kondolf, G. M., Piégay H., and Landon, N. (2002). "Channel response to increased and decreased bedload supply from land use change: contrasts between two catchments," Geomorphology, 45(1-2), 35–51, doi:10.1016/S0169-555X(01)00188-X.

Landon, N., Piégay, H., and Bravard, J. (1998). "The Drôme River incision (France): from assessment to management," Landscape and Urban Planning, 43.

Lane, S. N., Bradbrook, K.F., Richards, K.S., Biron, P.A., and Roy, A.G. (1999). "The application of computational fluid dynamics to natural river channels: three-dimensional versus two-dimensional approaches," Geomorphology, 29(1-2), 1–20, doi:10.1016/S0169-555X(99)00003-3.

Montgomery, D., and Buffington J. (1998). "Channel processes, classification, and response, in River Ecology and Management," edited by R. Naiman and R. Bilby, pp. 13–41, Springer-Verlag.

Montgomery, D. R., Buffington, J.M., Peterson, N.P., Schuett-Hames, D., and Quinn, T.P. (1996). "Stream-bed scour, egg burial depths, and the influence of salmonid spawning on bed surface mobility and embryo survival," Canadian Journal of Fisheries and Aquatic Sciences, 53(5), 1061–1070, doi:10.1139/f96-028.

Mueller, E. R., Grams, P.E., Schmidt, J.C., Hazel, J.E., Alexander J.S., and Kaplinski, M. (2014). "The influence of controlled floods on fine sediment storage in debris fan-affected canyons of the Colorado River Basin," Geomorphology, 226, 65–75, doi:10.1016/j.geomorph.2014.07.029.

Murray, A., and Paola, C. (1994). "A cellular model of braided rivers," Nature, (371), 54–57.

Nicholas, A. P. (2005). "Cellular modelling in fluvial geomorphology," Earth Surface Processes and Landforms, 30(5), 645–649, doi:10.1002/esp.1231.

Nicholas, A. P., and Quine, T.A. (2007). "Modeling alluvial landform change in the absence of external environmental forcing," Geology, 35(6), 527, doi:10.1130/G23377A.1.

Paola, C., and Voller, V.A. (2005). "A generalized Exner equation for sediment mass balance, Journal of Geophysical Research," 110(F4), F04014, doi:10.1029/2004JF000274.

Pyrce, R. S., and Ashmore, P.E. (2003a). "Particle path length distributions in meandering gravel-bed streams: results from physical models," Earth Surface Processes and Landforms, 28(9), 951–966, doi:10.1002/esp.498.

Pyrce, R. S., and Ashmore, P.E. (2003b). "The relation between particle path length distributions and channel morphology in gravel-bed streams: a synthesis," Geomorphology, 56(1-2), 167–187, doi:10.1016/S0169-555X(03)00077-1.

Snyder, N. P., Castele, M.R., and Wright, J.R. (2009). "Bedload entrainment in low-gradient paraglacial coastal rivers of Maine, U.S.A.: Implications for habitat restoration," Geomorphology, 103(3), 430–446, doi:10.1016/j.geomorph.2008.07.013.

Thomas, R., and Nicholas, A.P. (2002). "Simulation of braided river flow using a new cellular routing scheme," Geomorphology, 43(3-4), 179–195, doi:10.1016/S0169-555X(01)00128-3.

Thomas, R., Nicholas, A.P, and Quine, T.A. (2007). "Cellular modelling as a tool for interpreting historic braided river evolution," Geomorphology, 90(3-4), 302–317, doi:10.1016/j.geomorph.2006.10.025.

Wheaton, J. M. (2013). "Automated Derivation of Fish Habitat, Geomorphic Units & Transition Zones from Topography, in Eos, Transactions," American Geophysical Union, San Francisco, California.

Wheaton, J. M., Brasington, J.., Darby, S.E., and Sear, D.A. (2009). "Accounting for uncertainty in DEMs from repeat topographic surveys: improved sediment budgets," Earth Surface Processes and Landforms, 156(December 2009), n/a–n/a, doi:10.1002/esp.1886.

Wheaton, J. M., Brasington, J., Darby, S.E., Kasprak, A., Sear, D,, and Vericat, D. (2013). "Morphodynamic signatures of braiding mechanisms as expressed through change in sediment storage in a gravel-bed river," Journal of Geophysical Research: Earth Surface, 118(2), 759–779, doi:10.1002/jgrf.20060.

Williams, R. D., Brasington, J., Hicks, M., Measures, R., Rennie, C.D., and Vericat D. (2013). "Hydraulic validation of two-dimensional simulations of braided river flow with spatially continuous aDCP data," Water Resources Research, 49(9), 5183–5205, doi:10.1002/wrcr.20391.

SYNTHETIC BATHYMETRY METHOD DEVELOPMENT, VALIDATION AND APPLICATION TO FIVE PACIFIC NORTHWEST RIVERS

Zachary P. Corum, PE, Hydraulic Engineer, USACE Seattle District, Seattle, WA, zachary.p.corum@usace.army.mil; Travis D. Ball, Hydraulic Engineer, PE, CFM, USACE Seattle District, Seattle, WA travis.d.ball@usace.army.mil; Matthew J. Hubbard, Engineer 1, Brown and Caldwell, Tacoma, WA, mhubbard@brwncald.com

Abstract: This paper presents a simple, robust, and relatively efficient workflow to create and "burn in" high resolution synthetic river bathymetry data into existing LiDAR datasets. The Synthetic Bathymetry (SB) method uses widely available GIS and hydraulic modeling techniques to create physically-based synthetic bed elevation data without introducing significant error in computed water surface elevations and average channel velocities, under conditions where discharge at time of DEM data acquisition is known. The SB method was applied and validated on a small, steep, braided cobble bed river, large and small cobble bed wandering rivers with wide floodplains, and a small, entrenched, low gradient river with tidal influence all in Washington State – as well as a very large, flat gradient reservoir reach in Montana. As a test of the validity of the approach the results of models based on SB data were compared against models based on traditional survey methods, and against models based on LiDAR alone. For low (base) flows, bankfull (2-year) and 100-year flood flows the differences in computed water surface elevations, inundation area, and velocity were small (MAE in water surface elevation of less than 1 foot for all 5 study reaches under low flow, and less than 1 foot for all but the reservoir reach under 2 year and 100-year flood flows). At lesser flood flows to bankfull flows, the MAE in stage is modestly higher, as compared with the baseline models. For the reservoir reach, the model results were generally poor during 100-year flood flows as compared with the other rivers, however the error reduction in water surface elevation (from use of an unadjusted DEM alone) was nearly 30 feet. The good to excellent agreement of the SB models to the baseline in four of the five study reaches is attributed to the ability of the SB method to create the flow area needed to convey flood flows at comparable stages and velocities as survey based models. The SB method holds promise for speeding up and reducing the cost of 1-D and 2-D hydraulic modeling efforts where multiple decimal place accuracy is not required. The SB method can significantly reduce error in cases where only a DEM is available, and reduce the need for tedious, subjective terrain data manipulation commonly associated with interpolation between widely spaced cross sections. The SB method could improve the quality of models in cases where site conditions (unstable channel, remoteness, turbidity, safety) prevent bathymetric data collection but otherwise allow for above-water aerial survey techniques (photogrammetry, satellite, LiDAR, Structure from Motion). Other potential uses include estimation of bed elevations to track sediment movement under rapidly changing conditions, such as below a dam removal.

INTRODUCTION

This paper presents a relatively simple technique for creating physically based riverine bathymetric data from digital elevation models (DEMs) and discharge data using GIS and the US Army Corps of Engineers software HEC-RAS (USACE 2014). For the purposes of this paper DEM pertains to topographic datasets derived from photogrammetry or Light Detection And Ranging (LiDAR) techniques. The method described in this paper results in a “burned in” or “eroded” (synthetic) river bottom within a digital terrain model that otherwise lacks bathymetric data. In shallow rivers the method has shown promise at preserving riffle crest elevations, side channels, and large in-channel roughness elements. The technique can be used for any case where flow is nominally unidirectional, confined within banks, and is either known or can be estimated at time of topographic survey. Virtually any 1-D or 2-D modeling package that allows for computation of inundation maps can use this method.

The method, termed herein as the synthetic bathymetry (SB) method, has several potential applications in the fields of hydrology, hydraulics and fluvial geomorphology and is best suited for determining reasonably accurate water surface elevations in situations where data is scarce and/or where projects do not require stringent accuracy. The method also allows for filling in gaps between surveyed cross sections without interpolation, which helps preserve the near bank, and mid channel topography (large roughness elements) that may be important for 2-dimensional model studies. It also allows for a physically based estimate of riverbed elevations below the water surface which can be valuable for estimating long term geomorphic change over large areas.

This paper investigates the relative accuracy of one dimensional hydraulic models constructed from surveyed cross sections, from DEM data alone, and from DEM data blended with SB data. Published flood insurance study data or recently calibrated survey-grade hydraulic models are used as benchmarks to test the validity of the results using SB data.

BACKGROUND

LiDAR data sets are becoming widespread and have quickly become some of the most valuable data for hydrologic, hydraulic and geomorphic studies. The LiDAR data is usually extracted and processed for inclusion in a numerical model of hydrologic processes. Due to technical limitations many LiDAR datasets lack elevation information below the water surface (bathymetry), requiring collection of channel data with other methods. Alternately, models are used without this data due to cost constraints, reducing the quality of the results. As survey and post processing technologies improve, terrestrial floodplain topography can be acquired for large study areas in the time it takes to fly along the river in a helicopter or airplane. Despite their high resolution, most available LiDAR data sets used to create DEMs do not include bathymetric LiDAR data (now possible with certain sensors and shallow, clear water conditions – see River Bathymetry Tool Kit (McKean et al, 2009)). Other recent innovative methods to remotely survey the channel bottom, which also require clear water conditions, include correlation of aerial imagery based DEMs to physical measurements of depth (Javernick et al, 2014). Currently, several technologies are available to acquire high resolution topographic and bathymetric data to support floodplain studies (Bangen et al, 2014). Many of these technologies are complex and costly to use. Considerable effort and skill are necessary to check, verify, and blend available data to create a seamless riverine terrain model. Also, due to the high equipment costs associated with some technologies and large data sets created by modern equipment, considerable effort and expense are necessary to acquire, maintain, and post-process these data. But as two dimensional modeling moves to the forefront of hydraulic engineering practice, the demands for bathymetric data will continue to increase.

Thus, the current state of the practice is one where engineers and scientists have a plethora of terrestrial data sets to choose from, from which any number of cross sections can be created. Below-water bathymetric data, however, remain sparse and difficult to acquire in many settings. Use of interpolated or "best guess" bathymetry in hydraulic models introduces unknown errors that add uncertainty and risk to project findings and decisions resulting from the modeling. Fortunately, many of the issues resulting from missing bathymetry can be partly overcome by applying first principles and combining off-the-shelf GIS and hydraulic modeling software. This paper presents and validates one such method, termed the Synthetic Bathymetry (SB) method that allows for automatic manipulation of terrain data to "burn in" SB data under the LiDAR water surface to address circumstances where underwater survey data is lacking but improved model accuracy is desired.

SYNTHETIC BATHYMETRY METHODOLOGY

Commonly used open channel flow numerical models allow for computation of fluid depth based on first principles of open channel flow (conservation of energy, continuity of flow, conservation of momentum). If a numerical backwater model is used, such as HEC-RAS (USACE 2014), to perform a standard step backwater calculation, the energy losses due to cumulative expansion, contraction, and roughness losses can be accounted for in estimating the local variation in hydraulic conditions, such as velocity, depth, and stage. As with most open channel flow models, the quality of the hydraulic output depends on the quality of the input, namely survey data and how well the modeler captures the characteristics of the terrain.

For purposes of floodplain modeling and mapping, the goal is typically to first compute the losses in energy (expressed as fluid head) using standard step backwater computations, then to map the resulting water surface elevations across the terrain data used to construct the model. All major changes in cross section, planform, slope, and roughness need to be represented in the model to yield good estimates of local and cumulative energy losses. If a river model is constructed accounting for local changes in slope, width and roughness, then the depths and velocities can still be computed even if the bed elevations are not known with high accuracy. In this situation the accuracy of the results will be biased by the initial error in the bed elevations. Recognizing that LiDAR provides an extensive and detailed record of the water elevation at time of survey (calibration data), we can write the following equation for the LiDAR surveyed water surface elevation (WSE_{Survey}) resulting from a hydraulic simulation of the flow elevation at time of the LiDAR flight:

$$\mathbf{WSE}_{\mathbf{Survey}} = \mathbf{WSE}_{\mathbf{initial}} - \mathbf{E}_{\mathbf{initial}} \quad (1)$$

Where E represents error, the difference between the computed elevation ($WSE_{initial}$).and the "true" elevation and If the water level in the LiDAR is treated as terra firma in the model cross sections (as a false river bottom), all flow will then occur above the "correct" elevation. Thus the depth of flow above the initial "false bed" is the error in equation 1.

$$\mathbf{E}_{\mathbf{initial}} = \mathbf{WSE}_{\mathbf{initial}} - \mathbf{Z}_{\mathbf{false\ bed}} = \mathbf{Y}_{\mathbf{initial}} \quad (2)$$

Where:

$\mathbf{Z}_{\mathbf{false\ bed}}$ = **Bare earth LiDAR elev** = $\mathbf{WSE}_{\mathbf{Survey}}$

$\mathbf{Y}_{\mathbf{initial}}$ = **initially computed flow depth (above raw DEM)**

Expressed spatially, across a raster grid, at all locations within a raster cell,

$$\mathbf{E}_{\mathbf{initial\ (ij)}} = \mathbf{Y}_{\mathbf{initial\ (ij)}} \quad (3)$$

Where i and j denotes the spatial location of a given raster cell of a given dimension. It is then proposed that,

$$\mathbf{Z}_{\mathbf{SB\ (ij)}} = \mathbf{Z}_{\mathbf{false\ bed\ (ij)}} - \mathbf{Y}_{\mathbf{initial\ (ij)}} \quad (4)$$

Where $Z_{SB\ (ij)}$ represents a synthetic river bottom elevation at a given raster cell. By subtracting the initially computed flow depth ($Y_{initial\ (ij)}$) from the false bed ($Z_{false\ bed\ (ij)}$) at every raster cell, the synthetic river bottom is "burned" or "eroded" into the DEM, creating the SB data set ($Z_{SB\ (ij)}$). Note that the error is specific to each location in the modeled space, and that modern versions of both open channel flow and GIS software are needed to perform the above calculations. In this paper, Arc GIS version 10.1 and HEC-RAS version 5.0 were used. This version of HEC-RAS allows for simulation of 1- or 2-dimensional flows and rapid computation of inundation depth rasters (Geotiff format) at all points in the model domain. SB data creation requires low flow inundation depth rasters to be created at the same resolution as the underlying terrain raster (Figure 1).

Figure 1 below illustrates a short a portion of two Dungeness River low flow hydraulic models created to test the effects of the different bathymetric data sources on model accuracy (see low flow calibration and high flow calibration sections of this paper for more discussion). Figure 1 shows how the raw, LiDAR Only (LO) DEM compares with a SB based DEM, and how the approach uses GIS raster math to calculate the elevation of the SB raster data at the grid cell scale. Note the greater area of inundation present in the LO low flow model results – which is due to the effects of the artificially high false bed in the DEM. Also note the planar contours of the channel bed present in the LO DEM as compared with the SB DEM.

Once the "burned" or "eroded" DEM is created the quality of the resulting data needs to be checked by running the low flow hydraulic model extracted from the SB data. The low flow model should include reasonable flow resistance parameters and the best estimate for discharge available throughout the model domain. Using the water surface profile plot options and comparing the initial DEM-based plan to the SB-based plan in HEC-RAS allows for verification that the results are reasonable (Figure 2). Our experience is that minimal tuning of n-values is necessary to provide good fit between the computed and surveyed low flow water surface elevations. Figure 2 is representative of the quality of fit that results when low flow data is known with confidence and high quality LiDAR is used.

In application of the SB workflow (described during talk) we found that there are common difficulties when calibrating to low flow surveyed water elevations extracted from the DEM. These typically occur at the downstream end of the model (if the starting water surface is assumed to equal the surveyed water surface). Our initial experiences suggest that starting the model at normal depth will overcome most downstream boundary problems. Increasing n values locally can be used to force the river to deeper depths where pools are known to be present. If calibration difficulties are encountered throughout the model, this is most likely an indication of poor discharge estimates in the model. Even if available survey data is outdated, it should be used as a check of the SB DEM. If the SB data is suspect, it should be replaced with traditional survey data.

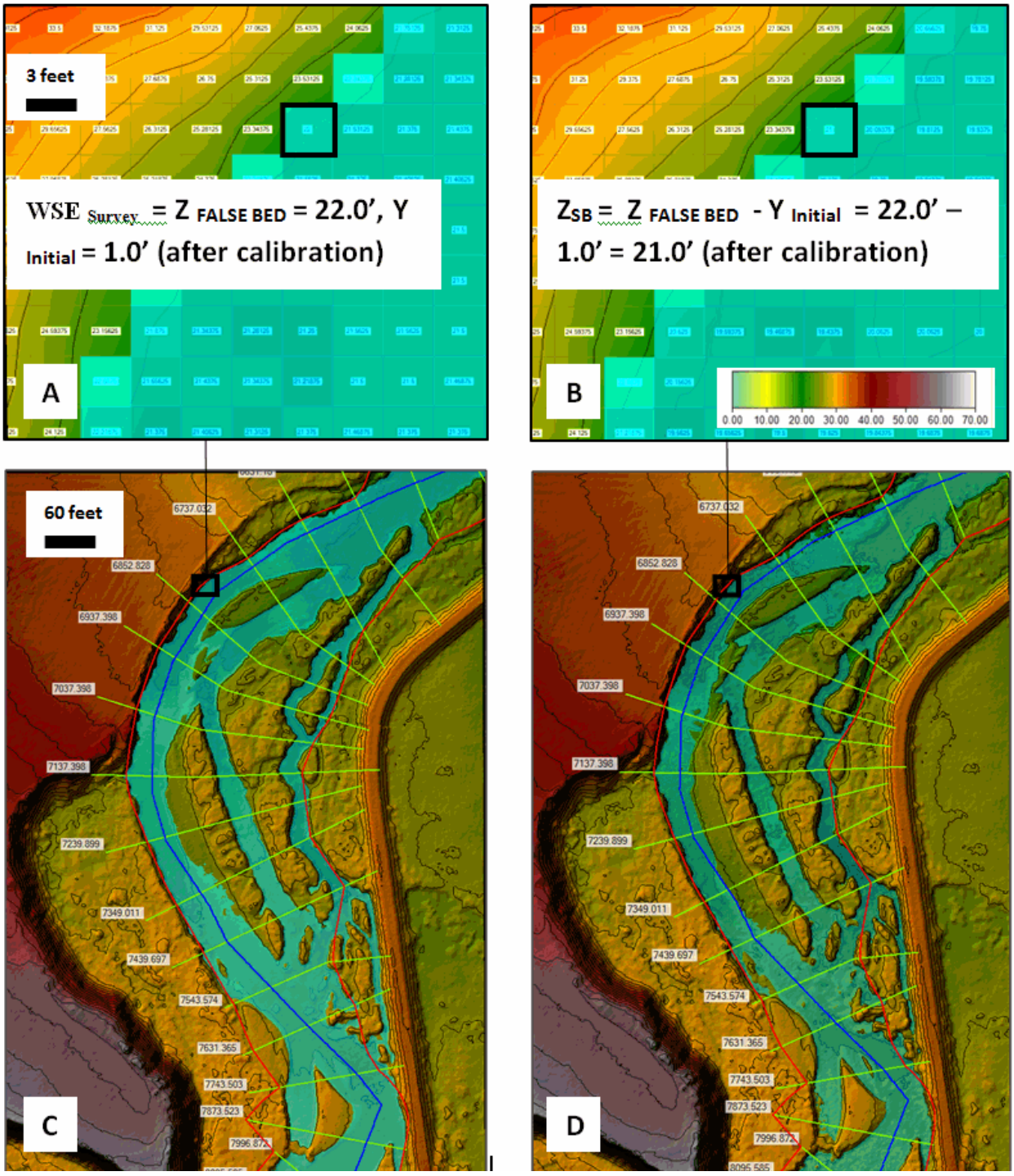

Figure 1: Dungeness River, WA (RM 1.3 to RM 1.6). (A) Close up showing initial LiDAR terrain grid cell center elevations ($Z_{FALSE\ BED}$). Each grid cell is 3 feet x 3 feet. Blue shaded numbers are cells that are wetted. Discharge at time of survey is 340 cfs. (B) Close up showing SB terrain computed grid cell center elevations (Z_{SB}), and how Z_{SB} is computed. (C) LiDAR terrain data overlaid with low flow hydraulic model cross sections, river centerline, banks, and resulting initial estimate of inundation area for flow at time of the LiDAR flight. Contour interval is 2 feet. Flow direction is south to north. (D) Synthetic bathymetry terrain data overlaid with low flow hydraulic model and computed inundation area. Note that all major geomorphic landforms with exception of deep pools are captured.

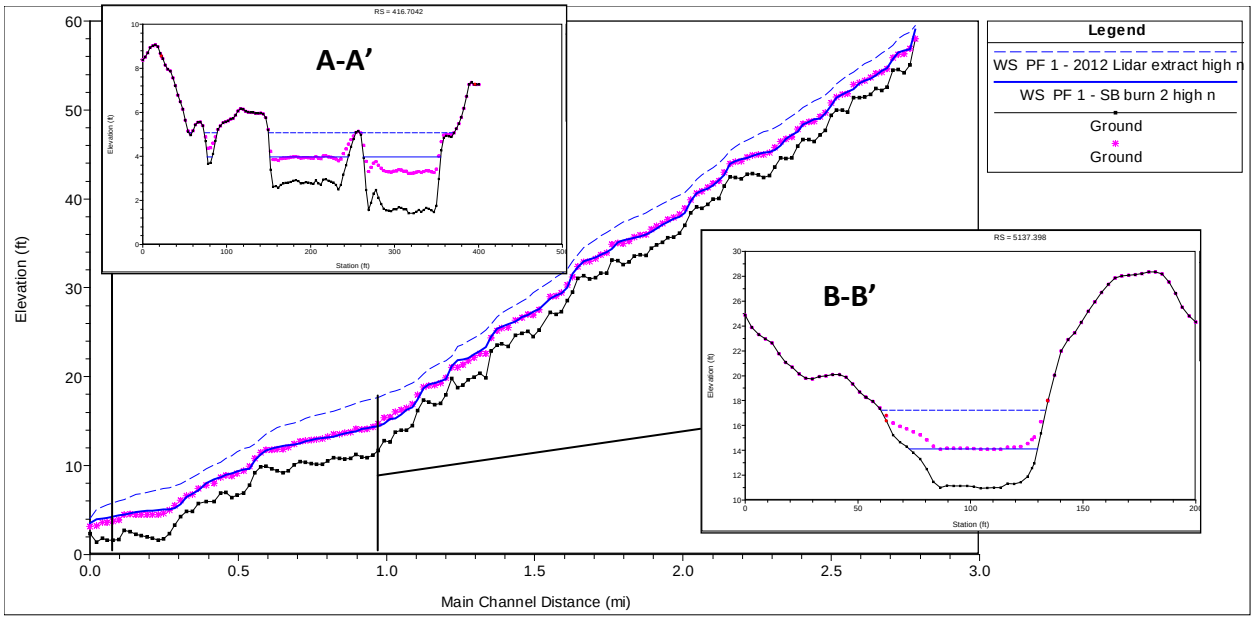

Figure 2 –Dungeness River, WA. Low flow hydraulic model verification against LiDAR surveyed water surface. In the water surface profile and cross sections the dashed blue line is initial estimate of water surface profile using LiDAR false bed elevation. Blue solid line is water surface computed after burning the initial depths into the LiDAR to create synthetic bathymetry (SB) data. Pink * is initial LiDAR surveyed water surface elevation (assumed to equal lowest point on cross section extracted from bare earth LiDAR) used to validate SB low flow model. Cross section A-A' shows how the method is able to burn side channels and main channels simultaneously while preserving large scale geomorphic features. The error in the depth is partly attributable to uncertainties about how much flow was in the main channel vs. the side channel. If the side channel was assumed dry, the main channel would have been stamped to a deeper elevation, which may have resulted in a better match. These errors are unavoidable without aerial photos to aid decisions on where to set limits of the channel in the model. Cross section B-B' is representative of how the method works in an ideal setting. The water surface matches the LiDAR survey, with minimal alteration of the cross section shape.

Note that the SB DEM is created after one or more calibration attempts to match low flow water elevations. This ensures that the low flow model and DEM have adequate conveyance to match low flow water surface elevations. In real rivers, as well as in numerical models, it is widely known that riffles are a primary control on flood elevations and that at high flows water surface elevations tend to follow a smoother longitudinal profile that drowns out bed elevation undulations more prominent at low flows. A fundamental assumption embedded in this approach is that as long as the SB DEM is the result of a well calibrated numerical model that captures riffle elevations (as shown in Figure 2 above), error in thalweg elevations between riffles will not significantly impact estimates of flood elevations. A primary goal of the high flow validation section of this paper is to test the validity of this assumption.

STUDY REACH DATA

Hydraulic models developed by others were acquired to establish baseline conditions for investigating the effects on the results of hydraulic models derived from ground survey based methods, from LiDAR alone, and from LiDAR blended with SB data. All baseline models used for validation purposes were developed by others. The Green River models were acquired from King County, prepared as part of a Preliminary Revised Flood Insurance Study (2007). The Skykomish River model was obtained from Snohomish County and was developed as part of a Revised Flood Insurance Study (2010). The Dungeness River model was developed by USACE Seattle District as part of a Feasibility Study (2014). The Clark Fork model was developed by USACE Northwest Division as part of the Columbia River Treaty Flood Risk Assessment (2012). All baseline models were used as-is, reflect real-world conditions and are based on modern modeling and mapping standards.

The Dungeness, Skykomish, and Green River in western Washington State, and the Clark Fork River, a tributary to the Columbia in Idaho and Montana were used for this study (Figure 3). For ease of comparison the Green River model was subdivided into the Middle and Lower Green Rivers based on a geologic reach break near river mile (RM) 32. All study reaches in Washington State are glacially modified alluvial floodplains, draining heavily forested mountains that have hydrology typical of the Puget Sound lowlands (high intensity fall and winter rains, spring snowmelt runoff). A flood control dam on the Green River caps flood flows at the pre-dam 2-year recurrence interval discharge, while the Skykomish and Dungeness are free flowing. In contrast, the Clark Fork River study reach is wholly contained by a bedrock gorge and is heavily influenced by hydroelectric dams located at both ends of the study reach, which causes the river to behave like a reservoir under all but the highest discharges.

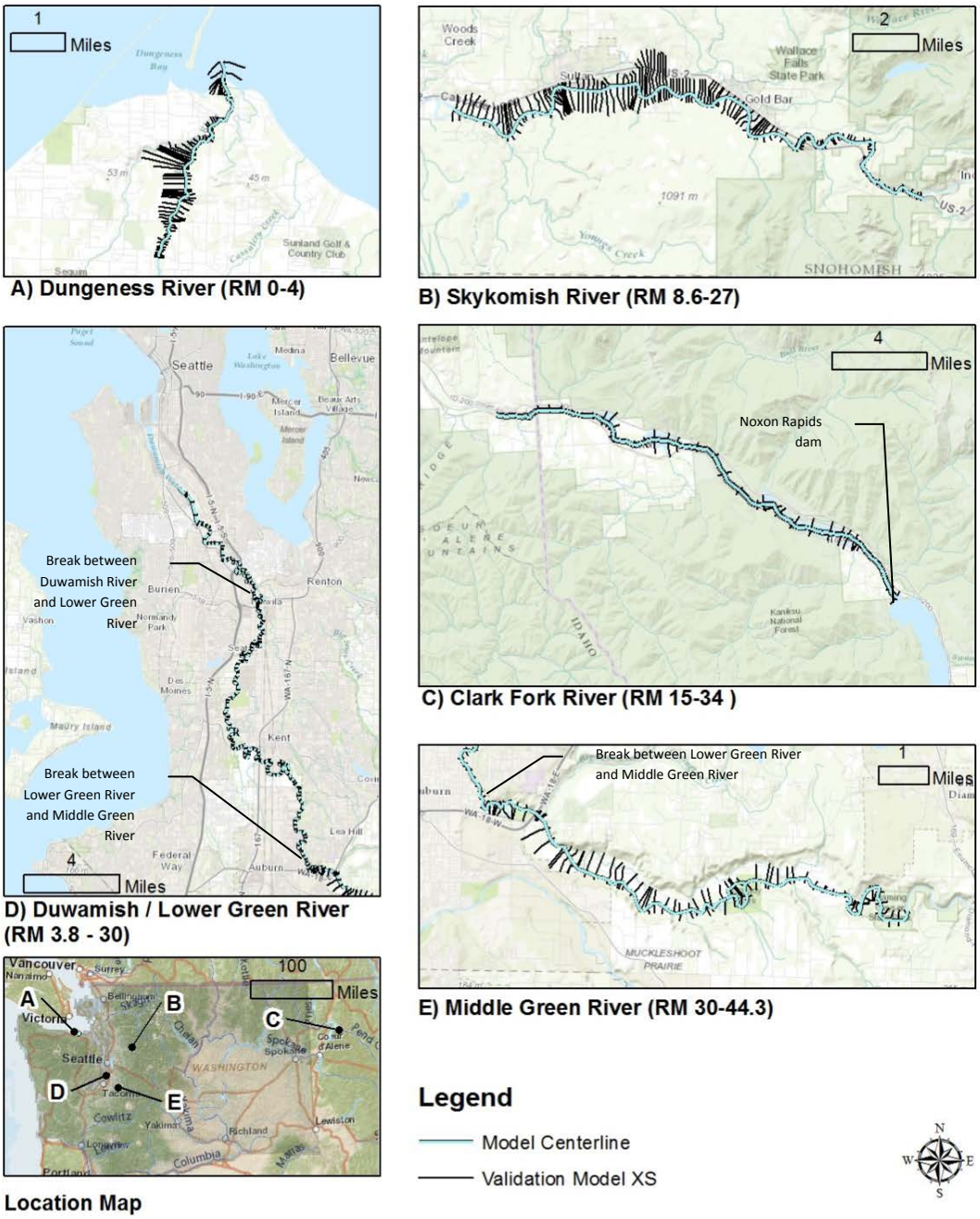

Figure 3: Location and vicinity maps of SB low flow and validation model reaches

The Dungeness River is the shortest and steepest of the study reaches, with the lowest 100-year discharge, while the Lower Green River is the longest and narrowest of the study reaches (Table 1). The flattest and most confined reach is the Clark Fork River – however the flat gradient is the result of a downstream dam. The natural valley gradient is much steeper given the canyon setting. The Dungeness, Skykomish, and Middle Green River are gravel/cobble bedded with boulders in places. The Skykomish River is the largest of the alluvial rivers studied, with large amplitude migrating meanders and wide floodplain All alluvial rivers studied are artificially confined by road embankments, revetments and levees near developed areas, the lower half of the Dungeness River and Lower Green River being the most confined. Hydrologic data available is of relatively high quality, with more than 80% of the study reaches gauged for all but the lower half of the Skykomish River. Flows at time of survey were about 10% of the 2 year discharge for the Dungeness and Green River, about 4% for the Skykomish, and about 22% for the Clark Fork, indicating that the discharge at time of survey was well below bankfull conditions.

Table 1: Study Reach Low Flow and Baseline Model Data

				Reach Average (Std Dev)		Discharge Estimates (cfs)		
Study Reach	**Length (miles)**	**Minimum % gaged in reach**	**Drainage Area (square miles)**	**EGL Slope & (EGL Stdev) (ft/ft) (1)**	**BFW/ BFD & (BFW/BFD Stdev) (ft/ft) (2)**	**@ time of survey**	**50% AEP (2-yr)**	**1% AEP (100-yr)**
A. Dungeness River, WA	2.8	95%	198	0.0044 (0.0024)	67 (95)	340	3,000	9,100
B. Skykomish River, WA	20.1	60%	563	0.0034 (0.0027)	42 (28)	1,040 to 2,400	37,800 to 51,700	118,000 to 156,900
C. Clark Fork River (ID, MT)	18.6	99%	22,067	0.000045 (0.0001)	23 (21)	17,000 to 19,400	78,000	140,000
D. Lower Green River, WA	26.1	91%	462	0.0004 (0.0002)	7 (4)	1,090 to 1,210	9,200	12,810 to 13,410
E. Middle Green River, WA	14.3	81%	390	0.0025 (0.0016)	18 (9)	660 to 1,090	9,200	12,250 to 12,810

(1) From 2-year discharge energy grade line computed from baseline (ground surveyed) model
(2) Bankfull Width (BFW) and Depth (BFD) computed from 2-yr discharge max depth and width (survey model)

SB LOW FLOW MODEL CALIBRATION

The key issues affecting the quality of the results of the SB method are determining the extent of low flow model cross sections, estimating the amount of flow present within the model at time of survey, and deciding how much to refine the model to achieve good match to the surveyed water surface elevations.

Table 2 below summarizes the error in the SB and LiDAR Only (LO) computed water surface elevations – in low flow conditions – for the five study reaches with respect to surveyed water surface elevations at each transect location in the model, after one or two calibration attempts. Calibration consisted of adjusting Manning's n values in the channel for the low flow model to better match the LiDAR surveyed water surface. In cases where significant amounts of flow was diverted at different elevations into side channels we either isolated all the flow into the dominant channel by limiting the cross section width, or constructed a connected side channel reach. The results were compared with the surveyed water elevations, which are extracted from the low point on each model cross section. Alternatively one could have used a 2-D model to estimate water elevations in the main and side channels at low flow.

The results for all five study reaches provide excellent-to-good matches of the surveyed water elevations during low flow conditions (average difference in computed low flow elevation is less than 0.1 to 0.5 feet from surveyed

elevation). In contrast the average error using only the LiDAR data ranges from 1.8 to 5.6 feet (and more than 25 feet in the Clark Fork reservoir reach). Note that in all cases additional refinements of the SB data to better match surveyed elevations were possible, however we viewed the low flow results as favorable enough to proceed to high flow validation.

Table 2: Low flow SB derived hydraulic model results after calibration vs. LO hydraulic model results as compared with low-flow surveyed water surface elevations

Study Reach	A. Dungeness, WA		B. Skykomish, WA		C. Clark Fork ID, MT		D. Lower Green, WA		E. Middle Green, WA	
Absolute Error in Computed WSE vs. Surveyed WSE	**SB** (ft)	**LO** (ft)	**SB** (ft)	**LO** (ft)	**SB** (ft)	**LO** (ft)	**SB** (ft)	**LO** (ft)	**SB** (ft)	**LO** (ft)
Median	0.03	1.81	0.46	3.12	0.66	25.84	0.07	5.61	0.22	2.12
Average	0.03	1.86	0.43	3.21	0.30	25.56	0.07	5.52	0.18	2.20
Stdev	0.29	0.48	0.47	0.91	0.62	1.63	0.41	2.05	0.36	0.79
Min	-0.7	0.9	-0.7	1.3	-0.9	17.2	-1.0	0.7	-1.5	0.6
Max	1.0	3.4	2.2	6.9	0.8	26.7	1.1	9.0	1.0	6.1
N=	145		222		42		292		185	
Reach length (mi)	2.8		20.1		18.9		26.1		14.3	

The excellent results on the 26-mile long Lower Green River reach were surprising given the tidal influence, however the survey at low tide and trapezoidal channel shape helped ensure that much of the channel conveyance area was captured in the initial terrain data. The higher-than-average errors in the Skykomish model are attributed to large uncertainties in flow at time of survey, effects of split flows around gravel bars, and errors and artifacts in the older vintage LiDAR data (trees, etc.). The excellent results for the Dungeness are partly attributed to the modern techniques used to acquire and post process the LiDAR data and the presence of a stream gage within the reach. The Clark Fork River reach – which is a backwatered canyon upstream of a dam – actually fairs better in the low flow than high flow model run (discussed in next section) because the known water surface at the downstream pool drives the water surface profile throughout the reach.

The good to excellent results over a wide range of channel sizes, slopes, and geomorphic types suggests that the SB method is capable of creating low flow hydraulic models that closely match surveyed water elevations, while preserving major geomorphic features of the channel (Figure 1D, Figure 2). Additionally, use of LiDAR data without adjustment may result in errors (under low flows) that exceed tolerances for most types of engineering studies. The effects of using unadjusted bare earth LiDAR data or SB terrain data without further parameter adjustment for flood conditions are presented in the next section.

SB HIGH FLOW MODEL VALIDATION

To validate the SB (and LO) DEMs, baseline hydraulic models developed by others to estimate floodplain depths and elevations were modified by re-cutting all cross sections from the original LO DEM and from the SB DEM. The steady flow step backwater models were then run with the new cross section data but without any further parameter or boundary condition adjustments to determine how the errors in the underlying terrain data affected the model results for the “bankfull” 2-year (50% annual exceedance probability) and “base” 100-year (1% annual exceedance probability) flood events.

Table 3 below summarizes the error in computed water surface elevation, flow area, average channel velocity, and average channel shear stress for the five study reaches from SB-based model and LO-based model with respect to results computed from the baseline models. The error statistics shown in Table 4 represent reach averages of the cross sectional difference between the results for the SB model or LO model and the baseline model. The percent change in error in Table 3 represents the reduction in error resulting from use of the SB model vs. the LiDAR only model.

Table 3: Study Reach Average Absolute Error Residuals in Computed WSE, flow area, velocity, and shear stress for SB and LiDAR Models with respect to Baseline Model

Study reach		A. Dungeness		B. Skykomish		C. Clark Fork		D. Lower Green		E. Middle Green		Study Average % Change	
		SB	**LO**	**SB**	**LO**	**SB**	**LO**	**SB**	**LO**	**SB**	**LO**	**Note 1**	**Note 2**
Δ 2-Yr WSE (ft)	Med	-0.2	1.2	0.4	1.1	0.7	25.8	-0.4	3.6	0.1	1.1	95%	96%
	Avg	-0.1	1.2	0.6	1.5	0.3	25.6	-0.2	3.5	0.1	1.3	92%	93%
	SD	0.3	0.5	1.0	1.2	0.6	1.6	0.6	0.8	0.5	0.9	29%	35%
	Min	-0.9	0.1	-1.4	-0.2	-0.9	17.2	-1.2	0.1	-0.9	0.1	1182%	967%
	Max	0.7	2.0	4.2	5.6	0.8	26.7	1.8	4.7	1.4	3.8	53%	62%
		SB	**LO**	**SB**	**LO**	**SB**	**LO**	**SB**	**LO**	**SB**	**LO**	**Note 1**	**Note 2**
Δ 100-Yr WSE (ft)	Med	0.0	0.9	0.3	0.7	4.9	30.2	-0.3	3.2	0.1	1.0	90%	89%
	Avg	0.0	0.9	0.5	1.2	4.7	29.9	-0.1	3.2	0.1	1.2	87%	87%
	SD	0.3	0.4	0.9	1.2	2.0	0.8	0.6	0.7	0.4	0.9	25%	-12%
	Min	-0.6	0.1	-1.2	-0.5	0.0	26.9	-1.0	0.1	-0.8	-0.6	332%	286%
	Max	1.3	1.8	5.8	7.0	7.3	30.6	1.7	4.3	1.3	3.4	42%	49%
		SB	**LO**	**SB**	**LO**	**SB**	**LO**	**SB**	**LO**	**SB**	**LO**	**Note 1**	**Note 2**
Δ 2-Yr Flow Area (ft^2)	Med	8	74	97	480	1617	-3465	13	64	46	551	85%	97%
	Avg	0	78	210	684	-333	-6521	-31	-15	75	863	39%	50%
	SD	77	121	879	1113	20411	19031	399	708	470	1183	40%	31%
		SB	**LO**	**SB**	**LO**	**SB**	**LO**	**SB**	**LO**	**SB**	**LO**	**Note 1**	**Note 2**
Δ 100-Yr Area (ft^2)	Med	21	122	92	535	6240	-2988	12	225	33	647	89%	133%
	Avg	8	421	145	762	8950	-3256	-36	334	134	1057	94%	150%
	SD	147	2124	1174	1205	25690	7542	411	960	543	1453	54%	-5%
		SB	**LO**	**SB**	**LO**	**SB**	**LO**	**SB**	**LO**	**SB**	**LO**	**Note 1**	**Note 2**
Δ 2-Yr Velocity (ft/s)	Med	-0.1	-0.3	-0.1	-0.3	-0.1	0.2	0.0	0.1	-0.1	-0.4	80%	90%
	Avg	0.0	-0.2	-0.2	-0.4	-0.1	0.6	0.0	0.2	0.0	-0.2	90%	95%
	SD	0.7	0.7	1.2	1.1	0.9	1.9	0.4	0.6	0.9	1.1	11%	19%
		SB	**LO**	**SB**	**LO**	**SB**	**LO**	**SB**	**LO**	**SB**	**LO**	**Note 1**	**Note 2**
Δ 100-Yr Velocity (ft/s)	Med	-0.1	-0.4	-0.1	-0.3	-0.7	0.3	-0.1	0.0	-0.2	-0.5	224%	243%
	Avg	-0.1	-0.3	-0.2	-0.4	-0.2	0.4	0.0	0.1	-0.1	-0.3	81%	95%
	SD	0.8	0.7	1.1	1.0	2.4	0.4	0.4	0.7	0.9	1.3	13%	-94%
		SB	**LO**	**SB**	**LO**	**SB**	**LO**	**SB**	**LO**	**SB**	**LO**	**Note 1**	**Note 2**
Δ 2-Yr Shear (lb/ft^2)	Med	0.0	0.0	0.0	0.0	0.0	0.0	0.0	0.0	0.0	0.0	50%	60%
	Avg	0.0	0.0	0.0	0.0	0.0	0.0	0.0	0.0	0.1	0.0	6%	35%
	SD	0.3	0.3	0.7	0.7	0.1	0.1	0.1	0.1	0.4	0.4	4%	9%
		SB	**LO**	**SB**	**LO**	**SB**	**LO**	**SB**	**LO**	**SB**	**LO**	**Note 1**	**Note 2**
Δ 100-Yr Shear (lb/ft^2)	Med	0.0	-0.1	0.0	-0.1	-0.1	0.0	0.0	0.0	0.0	-0.1	73%	121%
	Avg	0.0	0.0	0.0	0.0	0.0	0.1	0.0	0.0	0.1	0.0	8%	32%
	SD	0.4	0.4	0.8	0.6	0.4	0.1	0.1	0.1	0.4	0.5	2%	-73%

Note 1 – Study average % change is the difference in the LO reach average error statistic and SB reach average error statistic divided by the reach average LO error statistic, then averaged for all reaches (excluding Clark Fork).
Note 2 – Study average % change includes Clark Fork.

From Table 3 we can see that the study reach median error in SB model computed water surface elevation (WSE) ranged from -0.4 feet (Lower Green River) to 0.7 feet (Clark Fork) for the 2-year event, and ranged from -0.3 feet to 4.9 feet for the 100-year event (same reaches). The Dungeness and Middle Green models have the best overall match of the baseline WSEs, with 0.2 feet or less error on average for both the 2 year and 100-year events. Figure 5 provides a representative comparison of computed water surface profiles for all study reaches. The improvement in results from use of the SB method is most pronounced for the Lower Green, Clark Fork and Dungeness, which are all highly channelized or confined. The unconfined Middle Green and Skykomish have overbank floodplains that convey much of the flood flow, causing the results to be less sensitive to use of SB data.

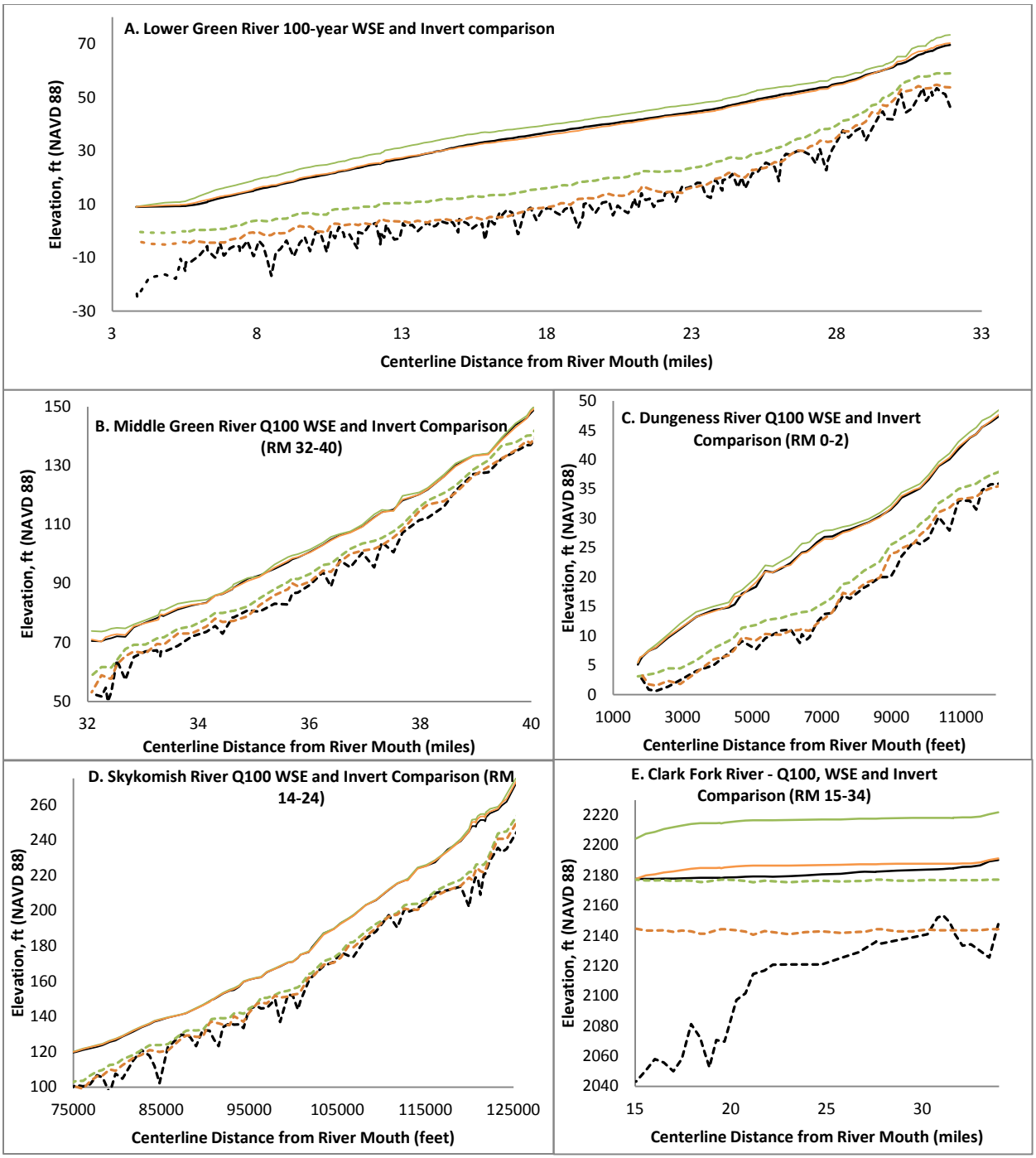

Figure 5. Computed 100-year flood water surface profiles and invert elevations for A) Lower Green (RM 3-32), B) Middle Green (RM 32-40), C) Dungeness (RM 0-2), D) Skykomish (RM 14-24), E) Clark Fork (RM 15-34). Green lines reflect initial bed elevation and computed WSE from original LO data, orange lines reflect SB bed elevation and computed WSE from SB data, black lines reflect surveyed bed elevation and computed WSE from baseline RAS model. Solid lines are computed WSEs, dashed lines are invert elevations.

The limitations and benefits of the SB method are seen from inspection of the Clark Fork results. Clearly the method cannot reproduce the river invert elevations submerged under the dam backwater, however the model still reduces average error in stage by more than 25 feet if one had used the LiDAR alone. For all but the Clark Fork the SB channel invert tracks the elevation of existing riffles quite closely, and results in hydraulic models that closely match

those of the baseline model in terms of WSE, flow area, velocity, and shear stress. Compared with models based on use of LiDAR alone, results are significantly improved for all study reaches.

The slight upward bias in flood stage resulting from the SB approach (under normal conditions) and more pronounced upward bias from use of LiDAR data without adjustment is when comparing total inundation area. Inundation area error is 0-5% in all reaches using the SB method, compared to 2-50% using the LO model. The error for the 2-year event is higher than that of the 100-year event for all but the channelized (trapezoidal) Lower Green. At higher stages the other reaches use more floodplain conveyance – which is not affected by the bathymetric data collection method.

SUMMARY

The SB method allows for creation of reasonable synthetic channel bathymetry data from LiDAR data, flow information, and widely available GIS and hydraulic software. The quality of the results can be easily demonstrated by comparing computed water elevations and velocities to the DEM water surface elevation at time of survey and to baseline model results or to high water marks. For this study the SB method results (comparison of computed flood stage to baseline) were excellent for a short steep sediment laden river with recent LiDAR and a gage within the reach, and poor for a reach upstream of a dam where true channel depths were many times that estimated using the SB approach. For a low gradient tidal river and medium gradient gravel bed river the results were very good. On a medium gradient wandering gravel bedded river with older LiDAR and higher uncertainty over low flow discharge the data were generally good to poor in isolated areas near bridges.

For all five study reaches the SB method significantly reduces the errors resulting from use of cross sectional data derived from LiDAR alone but does not eliminate the errors. This trend of reduced error is observed for all the flows analyzed and all the hydraulic parameters analyzed, other than depth. The median and average error when compared to baseline hydraulic models was typically less than 1 foot at bankfull stages, and under ideal conditions was less than 0.5 ft at 100-year flood stages. A river reach that is significantly affected by downstream backwater caused by a dam was used to check the quality of the method under non-ideal conditions. While the stage errors at low flow were less than 1 foot, the SB method was not able to create enough conveyance to pass 100-year flood flows with less than 4.7 feet of error (reach average). While this result at first glance is poor compared with the other reaches studied, the relative reduction in error compared with using a DEM without bathymetry is about six-fold. The location within a bedrock canyon suggests the error may not be significant with respect to adjacent development.

DISCUSSION

Under low and 2-year flood conditions we observed good to excellent matches of baseline and SB water surface elevations for all five study reaches, with the MAE of less than 1 foot for all but the Clark Fork reservoir reach. (Note that the results presented in this paper are not being compared to observed conditions at high flows which means that while the SB model results may provide a good match to the baseline model, the quality of the SB model with respect to real world conditions has only been evaluated for low flows and not under flood conditions). For nearly all flows and reaches, the results of the validation effort were surprisingly good (for the parameters that are typically meaningful for analysis and design, with the exception of maximum depth) considering that the SB based models lacked below-water survey data. This suggests that in similar conditions we would expect to have similar results, provided the quality of datasets and approach used to derive the SB data are similar.

To understand why the SB data results in a model that agrees well with the baseline, consider the significant error in maximum depth associated with models that still provided good to excellent estimates of flood stages (Figure 5) and inundation area. Concurrently, the good results of flow area, velocity, and stage shown in Table 3 (resulting from a 1-D step backwater model) suggest only reasonable estimates of cross sectional area, slope, and roughness are required. Because we are simulating physics of flow in one dimension, using open channel flow equations, all flow is assumed to be down valley, contained within banks, steady and uniform. During low flows, when LiDAR is typically acquired, these conditions are satisfied more often than not. We are simply using physical equations in the SB method (hydraulic model) to tell us how much space (area or volume) flow “takes up” at a given location. Then we are using GIS to create that space below the surface of a DEM for the river so it can pass the surveyed flow at the surveyed elevation. These results appear to confirm our primary assumption that as long as riffles are captured in the SB DEM that errors in flood stage will be small.

The quality of the results in this study are likely related to the setting and quality of the underlying data used to create the SB data. Reaches where the river was confined (Dungeness, Lower Green) with a trapezoidal cross section had the best agreement with the baseline models. The effort to create and apply SB data is significantly less than that needed to perform channel surveys. In less than one day we were able to use the technique to create a 40 mile long model that matched the baseline model computed 100-year flood elevations by less than 0.5 ft on average. While reach average hydraulic conditions computed from 1-D SB based models tracked closely with the baseline models, errors were higher at bankfull stages than at flood flows when the floodplain is active. Other difficulties were encountered where significant backwater was present, at hydraulic constrictions, and abrupt changes in grade or bed elevation. While no effort was made to calibrate the SB models to historical high water marks, we are confident that the close agreement with the baseline model results (with the exception of the Clark Fork) would allow for good calibration with reasonable parameters.

While the SB method will typically result in a DEM that includes a wider and shallower river than exists, it avoids the creation of artifacts common with using educated guesses or automated techniques to "burn" channels into DEMs from sparse survey data. For example all features above the water surface are preserved rather than "averaged out" as occurs when topography is created from widely spaced cross sections. This preserves side channels and bars that may be important for capturing flow paths or effects of macro roughness elements, however it will not capture deep pools or submerged features that may be important for habitat studies. This implies that a potential benefit of the SB approach is to improve the accuracy of a DEM (and model) between surveyed sections.

THE NEED FOR DUE DILLEGENCE AND REFINEMENT

This paper presents the promising results of a validation study of a method to create synthetic bathymetry for five rivers in the Pacific Northwest of varying size and geomorphic character. Until such time that the method has been validated for a wider range of channel types and rivers by other practitioners, we must recommend against applying it in cases where higher resolution survey grade data is warranted (i.e. life safety is of concern). In cases where flow data at time of DEM survey is lacking or uncertain, the SB approach will not provide reliable results, and could result in under-estimation of flood risk. Field data (discharge-elevation rating curves) may be needed to ensure the results are reasonable or to improve results. The potential cost savings of this method, while attractive, implore practitioners to collect detailed calibration and verification datasets to demonstrate the quality of the underlying SB data and model results. Models developed with this approach should be flagged as such, and a calibration and verification write-up should be included with model documentation. Before applying the SB method to a reach lacking a baseline model it is strongly recommended that one first independently validate the approach on a reach with a survey grade calibrated model to ensure that the approach is providing reasonable results. Further validation studies of the SB method with 1-D and 2-D unsteady state models are also recommended.

AKNOWLEDGMENTS

The authors appreciate the support of Seattle District staff and management and Clallam County, King County, and Snohomish County that provided baseline hydraulic models and data used to conduct the study. The authors wish to thank an anonymous reviewer that significantly improved the quality of the final manuscript.

REFERENCES

Bangen, S.J., Wheaton, J. M., Bouwes, N., Bouwes, B., Jordan, C. (2014) "A methodological intercomparison of topographic survey techniques for characterizing wadeable streams and rivers", Geomorphology, Volume 206, 1 February 2014, Pages 343-361

Javernick, L., Brasington, J., Caruso, B. (2014) "Modeling the topography of shallow braided rivers using Structure-from-Motion photogrammetry", Geomorphology, Volume 213, 15 May 2014, Pages 166-182

McKean, J. , Nagel, D., Tonina, D., Bailey, P., Wright, C.W., Bohn C., and Nayegandhi, A. (2009). "Remote Sensing of Channels and Riparian Zones with a Narrow-Beam Aquatic-Terrestrial LiDAR", Remote Sens. 2009, 1, November 2009, pages 1065-1096

USACE (2014). Combined 1D and 2D modeling with HEC-RAS. USACE Hydrologic Engineering Center.

FINLEY CREEK ALLUVIAL FAN GEOMORPHIC AND HYDRAULIC ANALYSES AND IMPLICATIONS FOR RESTORATION

Jeanne E. Godaire, Geomorphologist, Bureau of Reclamation, Denver, Colorado, jgodaire@usbr.gov; Sean Kimbrel, Hydraulic Engineer, Bureau of Reclamation, Denver, Colorado, skimbrel@usbr.gov

INTRODUCTION

Finley Creek, located on the Olympic Peninsula in western Washington, is a tributary of the Quinault River upstream of Lake Quinault. Previous observers have noted recent progressive lateral movement of the channel toward the eastern side of the Finley Creek alluvial fan, and aggradation and perching of the channel in the vicinity of the North Shore Road Bridge. The relationship between Finley Creek and the Quinault River is one of a long-term dynamic interaction between a large alluvial fan and mainstem river. The current sediment production from Finley Creek is of critical concern due to ongoing dredging at North Shore Road Bridge and the potential environmental effects of the dredging both upstream and downstream of the bridge (NPS, 2005) and sediment deposition and lateral Quinault River channel migration (GeoEngineers, 2011). Previous studies on Finley Creek have documented historical channel change using rectified aerial photography (Bountry et al. 2005) and the problems associated with aggradation and erosion on sections of Finley Creek (Kennard, 2009; Smillie, 2001; Jackson and Smillie, 1994).

The objectives of this study are to (1) provide a geomorphic analysis of conditions on Finley Creek in order to place current conditions into a long term context and to identify areas of potential avulsion and lateral erosion; and (2) conduct hydraulic modeling of various scenarios to guide the evaluation of alternatives for addressing aggradation near the North Shore Road Bridge and improvement of aquatic habitat on Finley Creek.

SETTING

Finley Creek flows from its headwaters in Olympic National Park to the south through a steep and narrow canyon with step-pool channel morphology. The stream emerges onto the Finley Creek alluvial fan, where channel morphology is braided at intermediate to high flows. Finley Creek joins the Quinault River just upstream of Quinault Lake near Quinault, Washington (Figure 1). Kestner Creek and Canoe Creek flow onto the Finley Creek alluvial fan on its western edge. The tributaries currently do not have a surface connection with Finley Creek but contain groundwater flow which is likely partially sourced from Finley Creek.

Flood frequency flows calculated indirectly by National Stream Statistics (Knowles and Sumioka, 2001) indicate a high-end 2-year event for Finley Creek is on the order of 2,500 ft^3/s while a 100-year flow is approximately 6,150 ft^3/s. A recently installed staff gage with time-lapse photography at the canyon mouth has continuously recorded stage. Flows of 1,557 and 1,240 ft^3/s through 2013 and 2014 have been measured at the Finley Creek Bridge—these flows are on the order of annual to 1.25-yr events and have been contained within the main channel of

Finley Creek. High flows mainly occur during the rainy season which on the Olympic Peninsula spans the months of October through March.

The Finley Creek alluvial fan is a moderate gradient, humid fan with a seasonally fluctuating discharge. Fluvial processes dominate on the fan and within its main channels; debris flow processes are dominant in the headwaters where steep tributaries join the main stem. The Finley Creek alluvial fan can be divided into an upper fan and lower fan based on changes in gradient and fan morphology (Figure 1). The upper fan is a higher gradient fan with one or two main channels that flow between interfluves stabilized by vegetation and soil development. These interfluves are young alluvial fan terraces, which have been abandoned by Finley Creek through avulsion and minor incision. The fan terraces consist of interbedded sand and gravel fluvial units. The upper fan is bounded by Pleistocene glaciofluvial deposits on the eastern edge and bedrock with steep gradient tributaries on the western edge. The lower fan is a lower gradient system with distributary channels that diverge from the main channel, some of which dissipate on the fan surface and others which deliver sediment to the Quinault River.

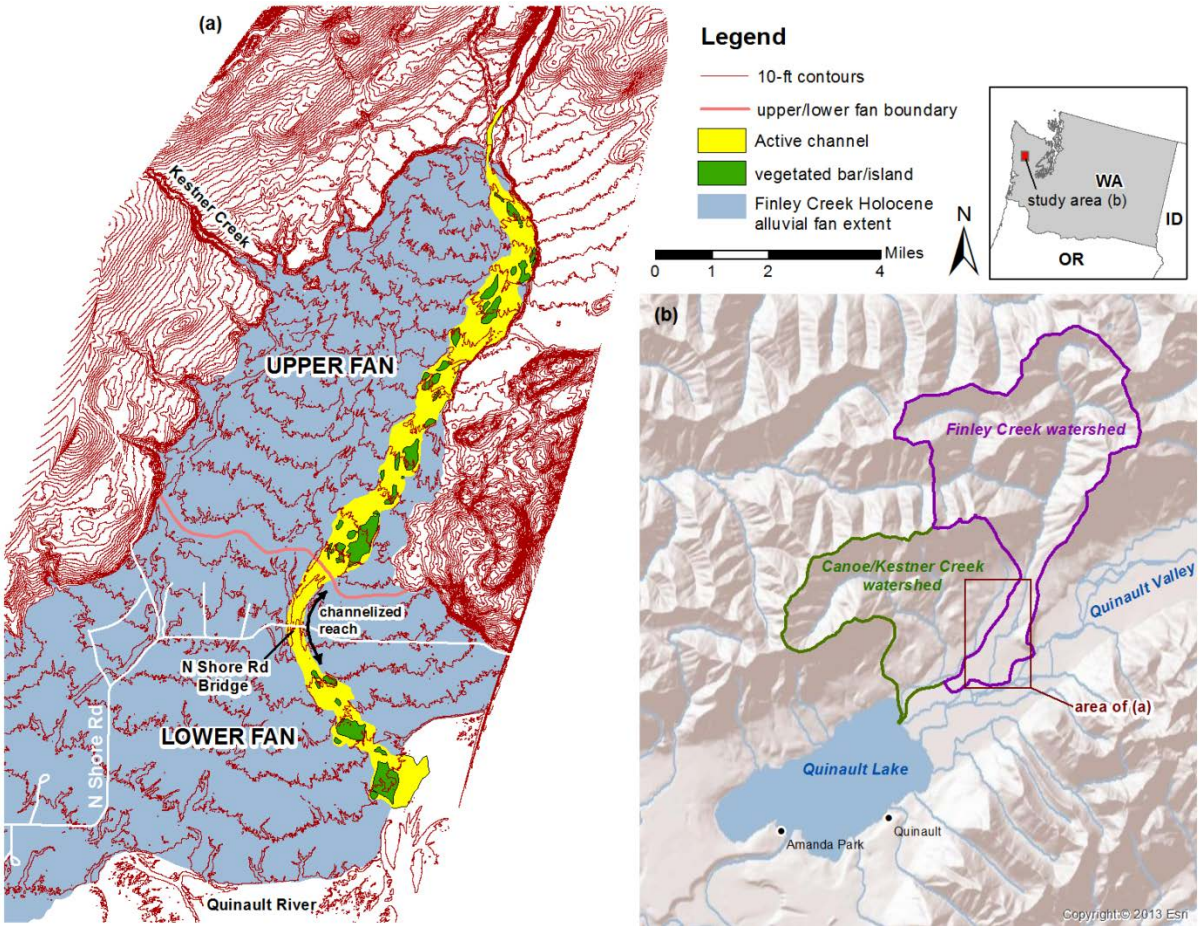

Figure 1 Location map showing (a) Finley Creek alluvial fan and (b) physiographic setting of study area.

Channel morphology of Finley Creek varies based on position within the alluvial fan and the amount of manipulation, and can be characterized in three segments: upper fan, lower fan and a channelized reach at the upstream part of the lower fan. On the upper fan, the main channel of Finley Creek is braided with high relief between the thalweg and top of unvegetated bars (Figure 2). Channel complexity is high with small pool and riffle areas during low flow. During high flow, the channel transitions to a braided morphology with abundant large woody debris and gravel bars. Mid-channel islands with immature vegetation such as alders and conifers occupy portions of the main channel and are transient features that are modified during high magnitude flows.

On the lower fan, the main channel is composed of a single braided channel that conveys the majority of flow to the Quinault River. Several large mid-channel islands exist with immature to mature vegetation (Figure 2). Many of these islands have been formed as the channel has scoured around older landscape features and isolated areas of the older alluvial surfaces as islands. Therefore the older character of the islands is in contrast to the immature islands in the active channel of the upper fan. In many locations, lacustrine sediment is exposed under the younger alluvium now contained on the islands in the lower fan. Prior to channel manipulation, the lower fan was largely a distributary system, where smaller channels branched from the main channel issuing from the upper fan. Blockage of many of the distributary channels by man-made berms or levees on the lower fan has prevented surface flow into many of the historical distributary channels, although several of these channels continue to convey baseflow from shallow groundwater. In the channelized reach in the vicinity of the North Shore Road Bridge, where the channel is constrained by levees, the channel is single thread with low relief and low complexity, and is a much narrower channel than the other reaches (Figure 2). Large woody debris is not abundant, partially due to clearing during gravel excavation.

Figure 2 Ground photos showing channel morphology in (a) upper fan; (b) channelized reach; (c) lower fan.

METHODS AND RESULTS

Various methods are employed to answer the study questions. Geomorphic and hydraulic analysis methods used in this study are:

- surficial mapping
- geomorphic change detection (Wheaton et al., 2010)
- mapping of potential sites of lateral erosion and channel avulsions
- numerical hydraulic modeling

Surficial mapping: The mapping for this project focuses on surficial deposits on the Finley Creek alluvial fan and highlights how recently surfaces have been activated by Finley Creek. Each map unit is a complex of ages; for instance, areas that have been active historically may include areas of older alluvium that have not been completely overprinted by historical lateral channel erosion or deposition. On the lower fan, deposits may also include underlying lacustrine sediment that is related to higher stages of Quinault Lake during the early to middle Holocene (~10-6ka). Mapping was performed remotely using historical channel mapping from Bountry et al. (2005), post-2005 channel mapping, 2011 LiDAR surface morphology and 2011 NAIP digital photography. Areas along the active channel were field checked; limited field checking was performed in areas away from the active channel. Where possible, exposures of the different alluvial deposits were described and photographed.

The youngest map units include the Finley Creek active channel and vegetated gravel bars and the Kestner Creek active channel and bars (Figure 3). The active channel map unit includes the area on Finley Creek alluvial fan that was actively being reworked by fluvial processes in 2011, the dates of the aerial photography and LiDAR. This includes the low flow and high flow channels, and unvegetated gravel bars. Vegetated bars or islands occur as mid-channel features with irregular surface morphology. The Kestner Creek active channel contains alluvium primarily derived from the Kestner Creek drainage, but may contain alluvium derived from Finley Creek as well, as it appears that the two drainages merged on the west side of the fan prior to the time covered by the historical channel mapping.

Historical alluvium includes areas on the Finley Creek alluvial fan that have been occupied historically since the late 1800s by either the main channel or distributary channels of Finley Creek (Bountry et al. 2005). The map units may include areas of older alluvium that have not been completely modified by historical channel activity. The historical alluvium is grouped into four main units based on the time period over which the area was actively being reworked by the main channel or distributary channels of Finley Creek (Figure 3): Historical alluvium III (post-1960), Historical alluvium II (1939-2002), and Historical alluvium IB (pre-1960) and IA (~1890s). Historical alluvium II contains overlapping time periods with III and IB because the time in which this area was occupied spans both units. The general pattern in historical alluviation has been a progressive shift of the active Finley Creek channel to the west on the fan, which was initiated by the log jams constructed by homesteaders in the late 1800s and into the 1930s at the canyon mouth on the upper fan to block flow from entering the western channels (Historical alluvium 1A and 1B). On the lower fan, levees were built near North Shore Road

Bridge in more recent decades to block flow from entering the western distributary channels (Historical alluvium II).

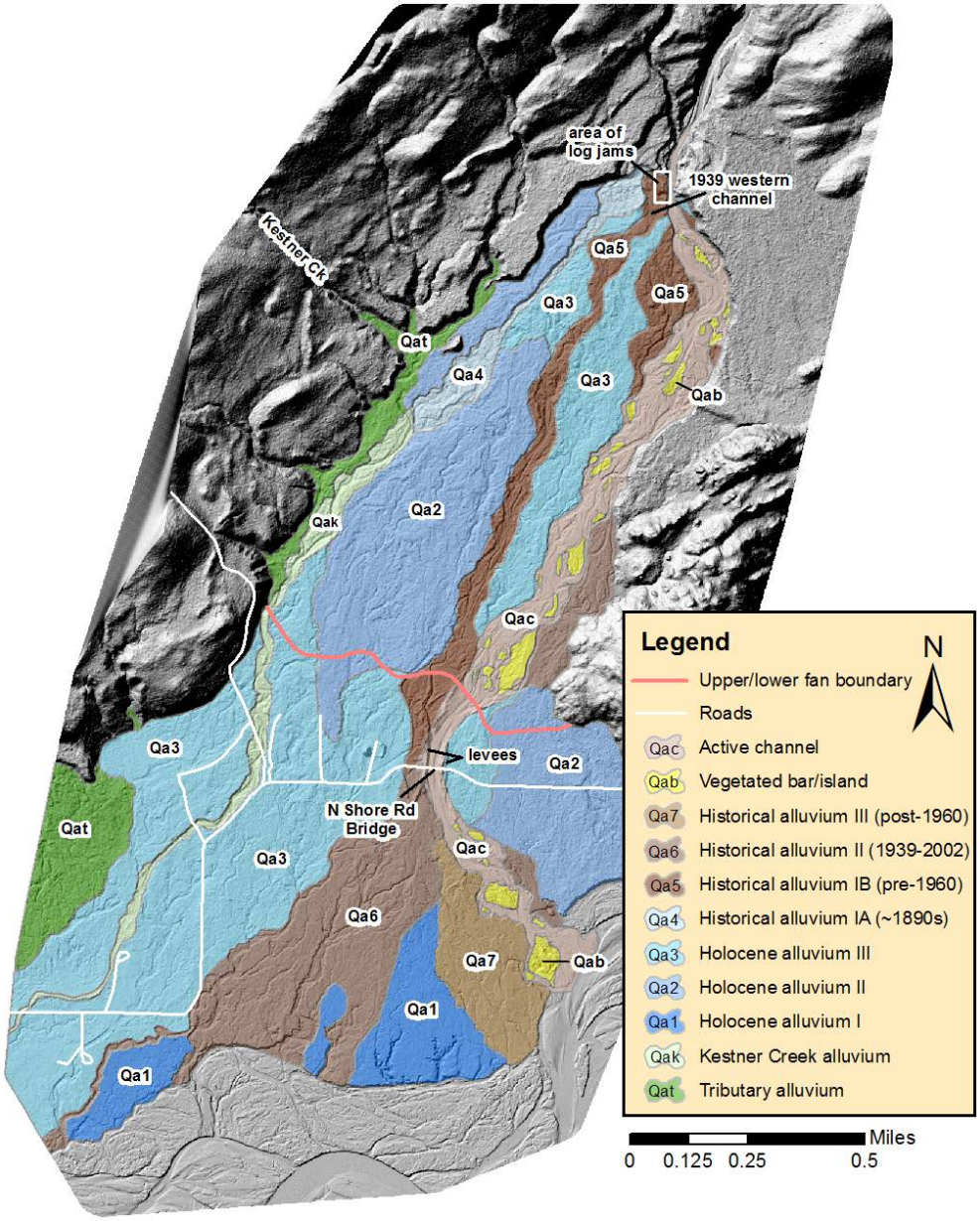

Figure 3 Surficial geologic map of Holocene units, Finley Creek alluvial fan. Basemap is a hillshade derived from 2011 LiDAR.

Holocene alluvium is mapped as three separate units based on surface morphology, soils and relative height above the active channel of Finley Creek. The units are numbered I, II and III in order of relative decreasing age. These units generally predate historical aerial photography and historical maps and therefore reflect areas of the fan that were active prior to the late 1800's. Based on limited radiocarbon data, these units appear to span the Late to Middle Holocene if underlying lacustrine units are included in the age estimate (<6ka) (Bountry et al., 2005).

Geomorphic Change Detection, patterns of erosion and deposition: Geomorphic Change Detection (GCD) software (V5.0, https://sites.google.com/a/joewheaton.org/gcd/home), which is based on the theory presented in Wheaton et al. (2010) was used to detect changes in erosion and deposition using changes in elevation between the 2002 and 2011, the dates of the LiDAR datasets (Figure 4). GCD was also used to develop a sediment budget along Finley Creek. Once the two datasets were converted into orthogonal and concurrent rasters, a threshold of 20 cm was applied to the DEM of difference, which was generated by taking the differences in the grid point elevations in 2002 and 2011. For the entire active channel area (active channel and vegetated islands map units), results show the alluvial fan had net deposition of more than 300,000 yd^3 in the 9 years between 2002 and 2011.

Areas of interest were further delineated in ArcGIS (Figure 4). Upstream of the North Shore Road Bridge (upper fan and upstream portion of lower fan), net deposition was 215,000 yd^3, in which 244,000 yd^3 of deposition and 29,700 yd^3 of erosion were calculated between the two datasets. There has been net erosion from the glacial terrace (labeled glacial terrace area, Figure 4) of -40,000 yd^3 based on 79,900 yd^3 of erosion and 39,900 yd^3 of deposition. The sediment budget calculations during this time period (2002-2011) show that the majority of sediment deposition is from headwater sources (e.g. landslides) since there is no sediment source within the fan (such as bank erosion) that shows net erosion similar to the net deposition in the active channel. The active channel in the channelized reach experienced net erosion (-7,000 yd^3) over the 9 year span, although this area was actively managed during this time period. In 2002 LiDAR (Oct 30th), the channel had just been excavated and in 2011 LiDAR (Nov-Dec), some deposition had already occurred following excavation. An increase in the volume of the berms or levees is also detected, with the river right levee gaining 14,000 yd^3, and the river left levee gaining 3,600 yd^3. Deposition in the western distributary area (labeled lower fan distributary area) is detected, with net erosion in the active channel downstream of North Shore Road Bridge to Quinault River (10,000 yd^3). In all areas downstream from North Shore Road Bridge (lower fan), net deposition (128,000 yd^3) is detected between 2002 and 2011.

Potential for future channel change, lateral erosion and channel avulsion: Finley Creek alluvial fan is a dynamic system, and has continued to evolve throughout the historical period. Channel change is a natural part of the Finley Creek system and will need to be considered in any recommendations for future management alternatives. The identification of areas most prone to lateral erosion and avulsion are important to identify and evaluate as part of identifying restoration alternatives. Areas of lateral erosion were identified on the basis of vertical stream banks observed and mapped during 2013 fieldwork (Figure 5). Vertical banks of unvegetated sediment are indicative of actively eroding areas and are typically located along outer bends in the channel where shear stress on banks is the highest. These areas are likely to continue to erode as long as the active channel is located in a similar position. Most areas of Finley Creek that are prone to lateral erosion are located along the western side of the active channel, where the channel is actively eroding. Areas prone to toppling are located along the eastern side of the upper fan active channel where fluvioglacial deposits crop out in the glacial terrace. This area has been eroding laterally since about 1952; however, undercutting at the channel level has caused toppling of the surface soil, depositing underlying sediment and large trees at the base of

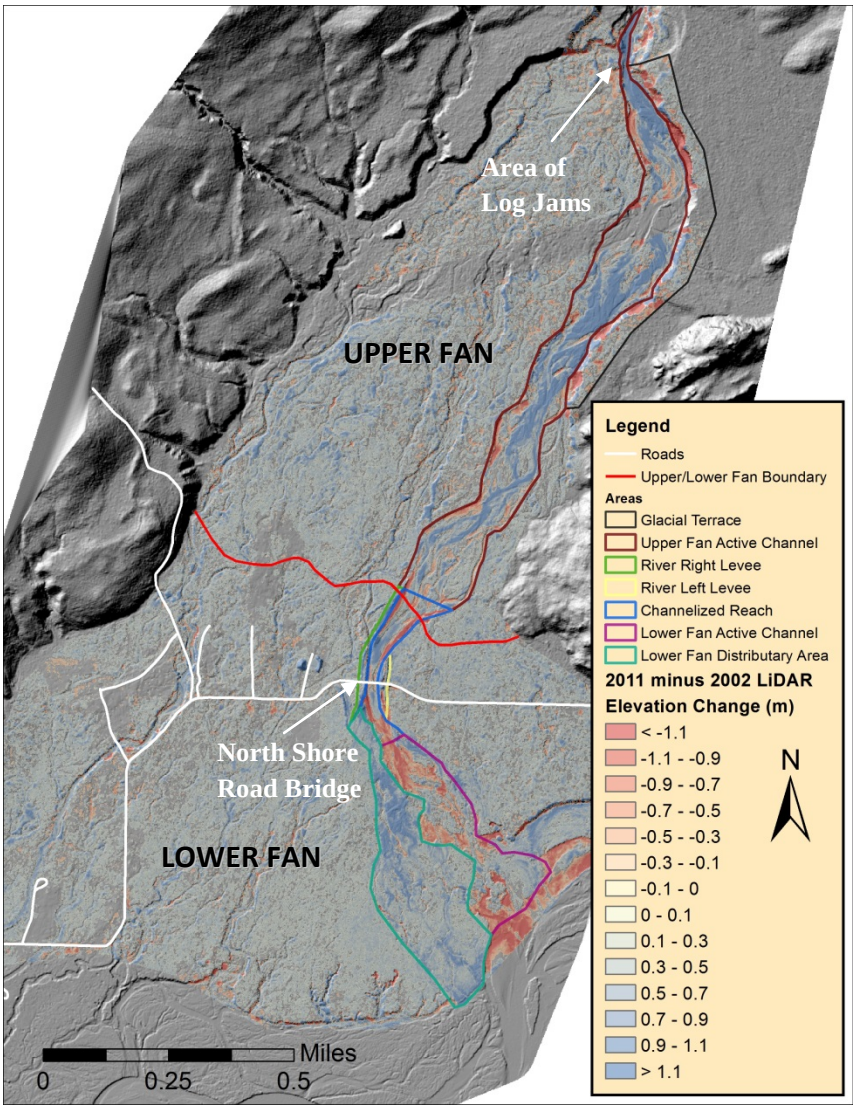

Figure 4 Erosion and deposition patterns of Finley Creek between 2002 and 2011 identified using Geomorphic Change Detection software.

the bluff. In addition, unraveling of the mostly unconsolidated glacial sediments has also generated a large amount of debris in the channel that provides some measure of bank protection along the eastern side of the channel on the upper fan. However, retreat of the bluff could continue through physical weathering and detachment of unconsolidated materials at the base of the bluff.

Channel avulsions could promote abandonment of some areas along the stream in which case the lateral erosion would shift to different areas than those shown in Figure 5. Areas of potential avulsion are located where the channel is most likely to shift position by abandoning its present channel for a new course (black circles in Figure 5). A channel avulsion could also occur where the distribution of flow and sediment shifts to a new location without completely abandoning, but leaving much less flow in, the old channel.

Potential avulsions areas were defined based on:

- Areas of low elevation adjacent to the active channel, especially those located along outer bends in the channel
- Presence of geologically recent or historical channels in overbank areas that have flow only in larger floods, but could be accessed by main channel flow
- Channels inundated in overbank areas as shown by the hydraulic model results
- Evidence for splays of the main channel, which indicate overbank inundation and preferred flow paths during high flows

Other areas of potential avulsion were identified that were not adjacent to the active channel in order to identify low elevation areas where the main channel could avulse if human constructs such as berms or levees were removed (white circles in Figure 5). These areas could also be avulsion areas even if human constructs are maintained, but the avulsion may take considerably longer to occur.

The area with the most potential for channel avulsion is located along the western side of the active channel upstream from the North Shore Road Bridge (area # 4, 5 and 10). This is an extensive area of low elevation where the current Finley Creek channel is perched above its surrounding floodplain, and held in place by man-made berms (area #10). When compared to surficial mapping (Figure 3), the avulsion areas are located mostly in areas that are mapped as historical alluvium.

Numerical hydraulic modeling: A fixed-bed two-dimensional (2D) numerical hydraulic model, SRH-2D (Lai, 2008), was employed to capture the inundation extent and hydraulic properties of flood flows experienced on the Finley Creek alluvial fan. Over the entire alluvial fan, only surface hydraulics are simulated, although observations indicate that there is significant surface water and groundwater interaction on the alluvial fan. Six different steady flows from the 1.5- to the 100-year discharge are simulated on the 2011 LiDAR surface, with the downstream stage-discharge boundary condition based on a modified HEC-RAS model of the Quinault River used in Bountry et al (2005). Manning roughness values were assigned to various areas including the channel (0.025-0.035), densely vegetated floodplain (0.1), sparsely vegetated floodplain (0.04), road prism (0.02), and structure footprints (0.08).

Lacking gaged discharge and measured water surface elevations for model calibration, a sensitivity test of the assumed water surface elevation was performed varying channel roughness and flood frequency. Modeling results of existing conditions for the 2- and 100-year events indicate that these flows are confined primarily to the active channel (Figure 6). Various restoration ideas developed with the consensus of the stakeholders can be simulated with the 2D numerical hydraulic model, such as the removal of various anthropogenic features (e.g. levees and log jams), which reduces the confinement of flows across the alluvial fan (Figure 6). Restoration ideas include removal of the historical log jams on the west side at the canyon mouth (Figure 3), removal of a portion of the western levee upstream of North Shore Road Bridge, construction of 7 to 8 road crossings through the road prism and raise of the road prism above the 100-year water surface elevation.

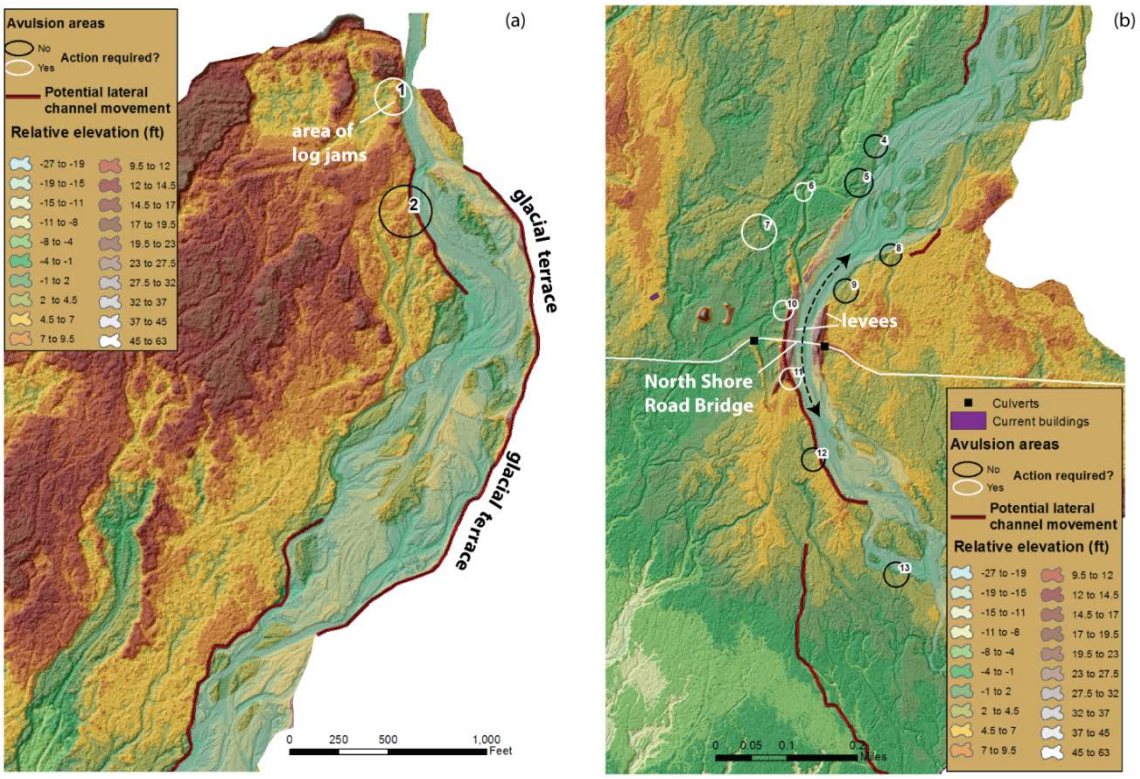

Figure 5 Finley Creek potential avulsion and lateral erosion areas. (a) upper fan; (b) lower fan. The avulsion areas are based on 2011 relative elevation map and field verification in 2014. The areas of potential lateral erosion were identified during field work in 2013. Avulsion areas are shown as circles; black circles show areas where man-made features do not block the channel from avulsing. White circles show areas where man-made features would either need to be removed or eroded before an avulsion could occur. Dashed line with arrows shows the channelized reach. The 2011 active channel is shown in light blue overlaid on the relative elevation map.

SUMMARY OF PRESENT CONDITIONS

Prior to human manipulation, Finley Creek existed as a multi-thread system that flowed through islands of alluvium with weakly developed soils and mature vegetation. With a natural decrease in gradient on the lower fan, flows became more distributary, depositing sediment on the fan surface and delivering sediment to the Quinault River. With the help of human constructs such as levees, repeated excavation of the channel, log structures and berms, the Finley Creek channel on both the upper and lower fan has been restricted to one main channel with intermittent mid-channel islands and immature vegetation and has shifted progressively to the east beginning in the late 1800s. In recent years (2002-2011), the main channel of Finley Creek on the upper fan has been dominated by deposition; the channel on the lower fan has been dominated by erosion. Landslides in the form of large debris avalanches appear to occur every few decades in the canyon upstream of the alluvial fan and are a periodic but persistent sediment source to the Finley Creek channel on the upper fan. Streambank erosion of the glacial terrace along the east

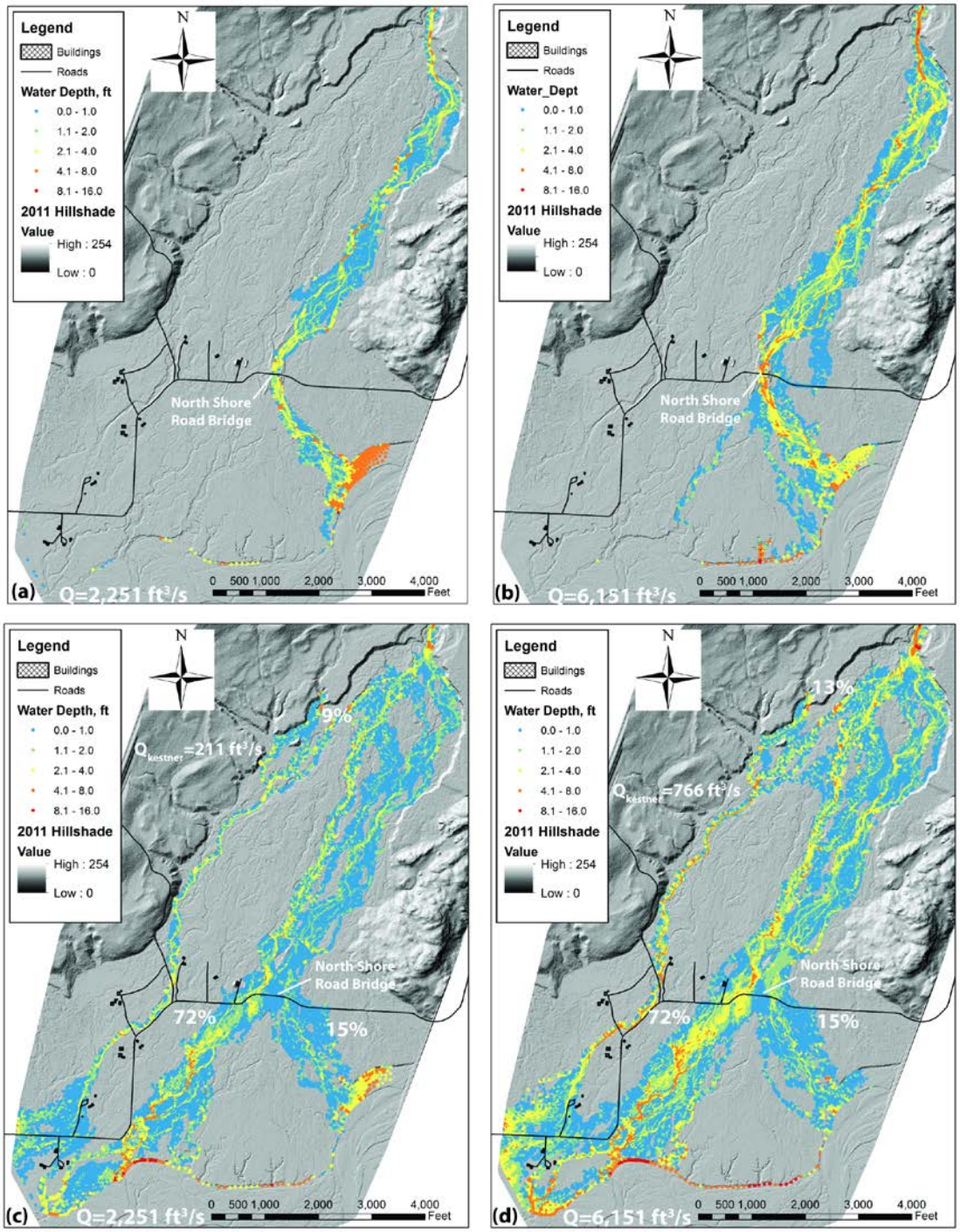

Figure 6 Hydraulic modeling results. (a) Existing condition (2011) 2-year discharge; (b) Existing condition (2011) 100-year discharge; (c) Example restoration condition, 2-year discharge and (d) Example restoration condition, 100-year discharge. Both restoration conditions (c) and (d) show modeling results with the removal of western levee at the North Shore Bridge and the log jam at canyon mouth and construction of channel crossings through North Shore road prism and raise of the road prism above the 100-year water surface elevation. Percentages show the distribution of flow among the various flow paths.

boundary of the upper fan and alluvial fan materials along the channel in the upper and lower fan area also provide sediment but total volume from these sources is not as large as the sediment contributions from the landslides. The area in the vicinity of the North Shore Road Bridge (the channelized section) has experienced net erosion likely because the channel has been excavated on an annual basis to increase channel conveyance under the bridge, however, sediment quickly refills the excavated area during the rainy season from November through February. Areas of potential avulsion are located mostly along the west side of the active channel on both the upper and lower fan at pre-existing historical channel paths. The 1939 western channel branch near the canyon mouth is not as likely to be an avulsion path even if the historical log jam is removed because the active channel appears to have incised in this location following the abandonment of the western channel. A major upstream landslide with large wood and a large sediment pulse would be necessary to cause an avulsion in this area.

IMPLICATIONS FOR RESTORATION

Hydraulic modeling of existing conditions shows that flows up to the 100-year magnitude are largely contained within the existing Finley Creek channel. Therefore, restoration alternatives will need to include active or passive removal of levees that block flow from entering former distributary areas on the lower fan. Restoration alternatives are currently being explored with coordination with local stakeholders. As an example, modeling of the 2-year and 100-year discharges show that if the western levee at the North Shore Bridge is removed and the channel aggrades 3 ft based on previous depths of channel filling following excavation, the following changes occur:

- Increased inundation in North Shore Road area primarily east of the current channel location and potential for flow on lower fan in west channel.
- Additional flow in western historical channels (Historical alluvium IA and IB) as a result of aggradation and west levee erosion/removal in which flow spreads across lower fan (50/50 split). Flow remains east of North Shore Road north-south trending section and there is no flooding of current structures.

Allowing flow onto the western part of the fan should reduce aggradation in the vicinity of the North Shore Road Bridge and also increase flow into historical channels and therefore habitat availability for various aquatic species. To accommodate flow and sediment across the North Shore Road in order to allow for year round road usage, the construction of seven to eight stream crossings in the road prism, with possibility of a road prism raise above the water surface elevation of the modeled 100-year discharge are included in the model (Figure 6c and 6d). Forded crossings, temporary bridges, and/or permanent bridge crossings are also potential alternatives that will be further investigated.

Active restoration by means of removing the log jam blocking the prehistorical channel at the canyon mouth would allow flows into 1890’s, 1939, and current channels, increasing flows into nearby Kestner Creek and reducing flow in Finley Creek at North Shore Road Bridge. Flow is mostly in western channel on the lower fan (70%+). With this scenario, some flow connectivity with Kestner Creek and the western part of alluvial fan causes possible overtopping of the North

Shore Road near known free-standing structures. Options for either protecting this area with structures or relocating structures would need to be considered for this restoration alternative.

Analyses that were key to the investigation of the alluvial fan are the surficial mapping and relative elevation mapping of the fan to define prehistoric and historic channels, and also to identify trends in lateral migration and potential avulsion areas. 2D numerical hydraulic modeling is key to identifying existing active flow paths during higher flows and for developing a snapshot of future active flow paths given various future actions on the alluvial fan. Challenges in developing a more sustainable road crossing across an alluvial fan requires the implementation of multiple crossings which allow for migration of the active channel across the fan with enough capacity to pass large flows that transport woody material and sediment. A better understanding of the surface water and groundwater interactions on the alluvial fan through coupled hydraulic modeling would be desirable for future analyses and would aid in the evaluation of aquatic habitat on Finley Creek and associated tributaries.

REFERENCES

Bountry, J., Randle, T., Piety, L., Lyon, E., Abbe, T., and Armstrong, B. (2005). Geomorphic Investigation of Quinault River, Washington, 18 km Reach of Quinault River upstream from Lake Quinault, Bureau of Reclamation, Technical Service Center, Denver, Colorado, 164 p.

GeoEngineers. (2011). Conceptual Design Report, Project Area 5 Restoration—Upper Quinault River, File No. 19117-002-00, GeoEngineers, Inc., 22 p.

Jackson, B. and Smillie, G.M. (1994). "Trip report for travel to Seattle, Washington and to the Quinault District of Olympic National Park, December 5-8, 1994," Water Operations Branch, Water Resources Division, Olympic National Park, 5 p.

Kennard, P. (2009). "Summary Memo, Finley Creek—OLYM, Trip Report for 6-4-09," MORA, 4 p.

Knowles, S.M. and Sumioka, S.S. (2001). The National Flood-Frequency Program—Methods for Estimating Flood Magnitude and Frequency in Washington, 2001: U.S. Geological Survey Fact Sheet FS-016-01, 4 p.

Lai, Y.G. (2008). SRH-2D version 2: Theory and User's Manual. Sedimentation and River Hydraulics – Two-Dimensional River Flow Modeling. U.S. Department of the Interior, Bureau of Reclamation, Technical Service Center, Denver, CO.

National Park Service (NPS). (2005). Olympic National Park Environmental Assessment for maintaining Finley Creek road access through continued removal of gravel. U.S. Department of the Interior, National Park Service, 112 p.

Smillie, G.M. (2001). "Trip report for travel to Olympic National Park, August 13 and August 17, 2001," Water Operations Branch, Water Resources Division, Olympic National Park, 5 p.

Wheaton, J.M.; Brasington, J.; Darby, S.E.; Sear, D. (2010). Accounting for Uncertainty in DEMs from Repeat Topographic Surveys: Improved Sediment Budgets. Earth Surface Processes and Landforms, 35 (2), 136-156. DOI: 10.1002/esp.1886.

WILDFIRE-INDUCED FLOODING AND EROSION-POTENTIAL MODELING: EXAMPLES FROM COLORADO, 2012 AND 2013

Steven E. Yochum, Hydrologist, US Forest Service, National Stream & Aquatic Ecology Center, Fort Collins, CO, steveneyochum@fs.fed.us; **John B. Norman, Soil Scientist**, NRCS, Soil Survey Division, Fort Collins, CO, john.norman@co.usda.gov.

prepared for the 5th Federal Interagency Hydraulic Modeling Conference
April 19-23, 2015, Peppermill Hotel, Reno, Nevada, USA

Abstract: Flooding and erosion potential for the High Park, Black Forest and West Fork Complex wildfires, in Colorado, were modeled using the Natural Resources Conservation Service (NRCS) curve number (CN) and Revised Universal Soil Loss Equation (RUSLE) methodologies. The CN technique, implemented within HEC-HMS, estimated direct runoff from rain events for both pre- and post-fire conditions, to develop estimates of increased flood hazard and potential threat to life and property. A spatial version of RUSLE was developed to predict pre- and post-fire sediment yields for each 10x10 meter area for hydrologic flow paths connected to the burn area. The pre- and post-fire CN runoff and RUSLE sediment erosion estimates were summarized at strategically-located pour points within and downstream of the wildfire burn areas. Results were computed at 96 pour points for the High Park Fire (87,000 acres), 52 pour points for the Black Forest wildfire (14,300 acres), and 70 pour points for the West Fork Complex wildfire (109,000 acres). Post-fire conditions were simulated to result in 100-year floods from 10-year rainfall events in the most severely-impacted watersheds and up to 70 to >200 times of sediment expected on an annual basis. The results are most appropriately used in a comparative manner, between catchments.

INTRODUCTION

The 2012 and 2013 Colorado wildfire seasons resulted in 20 substantial fires, including the West Fork Complex, Black Forest, and High Park (Figure 1) wildfires. Wildfires induce substantially increased flooding and erosion potential, with resulting impacts to life and safety, transportation and water supply infrastructure, property, and ecosystems. To address these issues, land managers, planners, and emergency response officials need prompt and spatially-explicit predictions of expected increases in flooding and sedimentation.

Figure 1 High Park Fire as viewed from Fort Collins, on day 1.

In response to requests from local, state, and federal agency partners, flooding and erosion potential for the High Park, Black Forest and West Fork Complex wildfires were modeled. The NRCS curve number (CN) and Revised Universal Soil Loss Equation (RUSLE) methodologies were implemented. The CN technique estimated direct runoff from rain events for both pre- and post-fire conditions, to develop estimates of increased flood hazard and potential threat to life and property. A spatial version of RUSLE was developed to predict pre- and post-fire sediment yields for each 10x10 meter area for hydrologic flow paths connected to the burn area. The pre- and post-fire CN runoff and RUSLE sediment erosion estimates were summarized to strategically-located pour points within and downstream of the wildfire burn areas. The magnitude of change in sediment yield and runoff were calculated for every pour point, to facilitate interpretation.

An overview of the implemented methods and results are provided, to assist other scientists and engineers with the task of providing officials with estimates of increased flooding and erosion potential after a wildfire. Similar approaches have been implemented by other workers (Livingston et al. 2005; Springer and Hawkins, 2005; Larsen and MacDonald, 2007; Rulli et al. 2013). Other tools are preferred by some practitioners (Canfield et al. 2005, Goodrich et al. 2005); Kinoshita et al. (2014) and Chen et al. (2013) provide comparisons between the results of differing methods. Due to limitations in modeling tools and data availability, and limits in scientific understanding of wildfire hydrology processes, these analysis results are most appropriately used in a relative manner for comparing runoff and sediment liberation potential between catchments. Despite this limitation, the provided methods do produce quantifiable results that are helpful for the informed development of response and restoration priorities, to protect life, property, and infrastructure in the hectic months that follow a wildfire.

METHODS

Wildfires cause hydrologic shifts for a number of years. Substantially increased runoff and sediment production result from the loss of vegetation and soil cover, as well as from hydrophobicity, where the fire-induced vaporization of hydrophobic compounds causes water to collect on the soil surface and run off, instead of infiltrate. The lack of vegetation interception and soil infiltration, from the loss of surface roughness from ground litter and hydrophobicity, can shift the rainfall response from infiltration-dominated processes to surface runoff-dominated processes. For example, watershed impacts due to recent wildfire caused a Swiss catchment to produce 100-year to 200-year runoff discharges from a 10-year rainfall event due to changes in infiltration capacity (Conedera et al. 2003), though scale effects with greater runoff enhancement in smaller catchments and tendencies towards overestimation in larger catchments have been noted (Stoof et al. 2011). Hydrophobicity, which tends to be more prevalent with increased sand content and lower soil water content, has been found to weaken within a few months of a fire but persist for at least 22 months in ponderosa and lodgepole pine forests of the Colorado Front Range (Huffman et al. 2001). Post-fire sediment yield is most dependent on ground cover, with percent ground cover explaining more than 80 percent of the variability in sediment yield (Benavides-Solorio and MacDonald 2001). Soil burn severity is hence fundamental for predicting sediment yield increases.

Predictions of post-fire sediment yield rely on mathematical models such as Revised Universal Soil Loss Equation RUSLE (Renard et al., 1997), Water Erosion Prediction Project WEPP (Elliot, 2004) and GeoWEPP (Renschler, 2003), as well as professional judgment (Robichaud et al., 2000). These methods have varying advantages and disadvantages for estimating the spatial distribution of post-fire soil loss, but all methods can require large amounts of time and energy to estimate soil loss and its associated risks over large spatial extents. With wildfires becoming more pronounced in the wildland-urban interface, rapid watershed management actions to protect sociological concerns, water quality, and ecosystem health are needed. This need for a rapid response to evaluate and manage post fire soil loss has increased the interest in using Geographic Information System (GIS) technology to spatially model post fire sediment yields. This has produced toolsets that use the above models as engines to estimate soil loss rates spatially.

Rainfall-runoff modeling was performed to simulate the expected flood response of the streams draining the wildfire areas. Additionally, predictions of post-fire sediment yield were developed using RUSLE. The implemented methods are presented below. Additional details are provided in the project reports (Yochum 2012; Yochum and Norman 2014).

Runoff Modeling

Runoff modeling was performed using the program HEC-HMS (version 3.5). The NRCS curve number (CN) technique for estimating direct runoff from rain events, combined with the NRCS dimensionless unit hydrograph method, was implemented. As documented in NRCS (2004b), the NRCS method for estimating direct runoff from individual storm rainfall events is of the following form:

$$Q = \frac{(P - I_a)^2}{(P - I_a) + S} \text{ if } P > I_a \quad (1)$$

$$Q = 0 \qquad \text{if } P \le I_a \quad (2)$$

where Q is the depth of runoff (inches), P is the depth of rainfall (inches), I_a is the initial abstraction (inches), and S is the maximum potential retention (inches). The equation derivation is not physically based but does respect conservation of mass (NRCS 2004b).

The Curve Number (CN) is defined as:

$$CN = \frac{1000}{10 + S} \quad (3)$$

The initial abstraction was initially described and has traditionally been used as:

$$I_a = 0.2S \quad (4)$$

To reflect the decreased storage of a fire impacted soil surface (due to a reduction of depression storage from the elimination of soil litter), the initial abstraction was assumed to be 0.1S for post-wildfire conditions in catchments that were substantially burned (>50% moderate + severe soil burn severity). Catchments that were not substantially burned were modeled with the standard I_a of 0.2S. The impact of the I_a adjustment on CNs was ignored; for the high CN (post-wildfire) conditions, smaller shifts in CN due to changes in I_a can be expected (Woodward et al. 2003).

The CN is a simple catchment-scale method that gives simplified results at a stream outlet, with more accurate results expected for larger, higher-intensity rain events. The method is

documented is in the NRCS National Engineering Handbook, Part 630, Hydrology, Chapters 9 and 10 (NRCS 2004a, NRCS 2004b), in Rallison (1980), as well as in numerous other publications. However, little quantitative information has been published of the database on which it was developed (Maidment 1992). In general, the method was developed for rural watersheds in various parts of the United States, within 24 states; was developed for single storms, not continuous or partial storm simulation; and was not intended to recreate a specific response from an actual storm (Rallison, 1980).

An overview of the general weaknesses of the CN method is provided in Hawkins (2014). Specifically in regard to rainfall-runoff modeling for wildfire areas, the reliability of the CN method for predicting peak flow from forested, mountainous watersheds is debatable. Forested watersheds in unburned conditions may be dominated by saturation-excess overland flow, where runoff is produced from relatively small and variable portions of a catchment when rainfall depths exceed the soil capacity to retain water. Newly burned catchments, on the other hand, may likely be dominated by infiltration-excess (Hortonian) overland flow, where surface runoff is generated when rainfall intensity is greater than soil infiltration capacity, and flow runs down the hillslope surface. Evidence of this surface runoff is provided by such features as surface rilling on freshly-burned hillslopes. Rainfall-runoff modeling performed in the San Dimas Experimental Forest (Chen et al. 2013) found that pre-fire runoff predictions were more accurate using the CN method, while KINEROS2 performed better for post-fire conditions. These results suggest fundamental shifts in runoff mechanisms between pre- and post-fire conditions, complicating modeling strategies. CN values are not well known for burned conditions, which is a primary source of potential error. Additionally, spatial rainfall variability due to orographic forcing can lead to additional modeling uncertainty, for the CN method as well as other rainfall-runoff modeling tools.

Despite the method's shortcomings, due to its relative simplicity, achievable data requirements on large scales, and the relatively-short timeframe needed to develop a model, as well as at least qualitatively-reasonable results when compared to actual post-fire runoff events, the CN method is a preferred tool for predicting the flow responses of wildfire areas. The best use of the modeling results is through comparison of different catchments flood response to identical rainfall events, for the prioritization of areas of concern. The use of peak flow ratios (i.e. post-fire peak flow/pre-fire peak flow) can be the most effective tool for comparisons.

CN

Curve numbers are values less than 100, with higher values corresponding to catchments with lower infiltration rates and higher runoff potential. In general, CN assignments are typically made using guidance provided in NRCS (2004a). CNs were assigned throughout the modeled catchments according to hydrologic soil group, vegetative type, and soil burn severity (Table 1). Soil burn severity is a dominant factor in CN assignments in burned areas. The average catchment CN was computed using an aerial averaging methodology. Catchment size was limited to areas that have similar runoff characteristics, and, where possible, to 2000 acres. As catchment size increased, CNs were computed for adjacent and serial catchments and flows were modeled, routed downstream, and combined with lower catchments to predict flow at downstream points of interest (Figure 2).

Table 1 CN assignments.

Cover Description	**A** HSG				**B** HSG				**C** HSG				**D** HSG			
	Unburned	Low	Moderate	High	Unburned	Low	Moderate	High	Unburned	Low	Moderate	High	Unburned	Low	Moderate	High
Herbaceous, Pasture, Alpine Meadow, Park	49	55	67	77	61	68	80	86	74	81	88	89	82	86	92	95
Oak-aspen—mountain brush mixture of oak brush, aspen, mountain mahogany, bitter brush, maple, and other brush	45	52	65	77	48	55	65	86	57	70	80	89	63	70	80	92
Ponderosa pine-juniper (grass understory)	49	57	65	77	58	65	75	86	73	78	83	89	80	85	90	92
Sagebrush (grass understory)	46	54	65	77	51	60	75	86	63	70	80	89	70	75	85	92
Lodgepole Pine Forest	49	57	65	77	60	65	70	86	73	78	83	89	79	83	87	92
Bare soil	77	77	77	77	86	86	86	86	91	91	91	91	94	94	94	94
Wetland	98	98	98	98	98	98	98	98	98	98	98	98	98	98	98	98

Hydrologic soil group (HSG) classifications were selected using soils data published in the NRCS SSURGO (Soil Survey Geographic) database. Using this method, soil are classified as being either A, B, C, or D type, where A allows the most infiltration and least runoff and D allows the least infiltration and greatest runoff. Vegetation type, from SWReGAP (Southwest Regional Gap Analysis Project) land cover mapping, was included in the CN assignments used for the modeling. Soil burn severity is the principle driver for increasing flow in runoff predictions. For these wildfires, soil burn severity was measured using the BARC process from satellite imagery.

A fair ground cover condition was generally assumed for the unburned values (Table 1) abstracted from NRCS (2004a), though a good ground condition was assumed for herbaceous/grassland. The CN values for burned conditions were primarily compiled from various grey literature and unpublished sources; they are approximate. Research is needed to better define these values.

Rainfall, Lag Time, Flow Routing, and Sediment Bulking

Rainfall depths used in the modeling were extracted from NOAA Atlas 14, Vol 8 (Perica et al. 2013), for the West Fork and Black Forest fire areas, and from NOAA Atlas 2, Volume 3 (Miller et al. 1973) for the High Park fire area. Six-hour rainfall durations and NRCS Type II rainfall distributions were assumed for the West Fork Complex Wildfire while 1-hour durations and TR-60 distributions were implemented for the Black Forest and High Park Wildfires. Areal reduction factors were applied as detailed in Miller et al. 1973. Where applied, these area reductions were implemented in all catchments; flow may be underpredicted in the smaller, upper catchments of such drainages.

Lag time (L), which is required to generate a hydrograph using the NRCS unit hydrograph methodology, was computed using the watershed lag method (NRCS 2010). The lag equation is:

$$L = \frac{l^{0.8}(S+1)^{0.7}}{1900Y^{0.5}} \tag{5}$$

, where l is the flow length (ft), Y is the average watershed land slope (%), and S is the maximum potential retention (in),

$$S = {}^{1000}\!\!\diagup\!\!_{cn'} - 10 \tag{6}$$

, where *cn'* is the retardance factor and is approximately equal to the CN. This method allows the rapid computation of differing lag times for pre- and post-fire conditions, reflecting the physical mechanism of more rapid flow response during post-fire conditions.

A Muskingum-Cunge procedure was used to route flow from upper catchments to the stream outlets. This 1-dimensional method allows for flow attenuation in the computations but does not provide a numerical solution of the full unsteady flow routing equations, as provided in such computational models as HEC-RAS. In each reach, flow routing was estimated using a single simplified cross section, channel slope, and Manning's *n* roughness estimates. Manning's *n* was selected using a visual estimation procedure, with a quality control step to assure that to maintain subcritical or approximately critical velocity was maintained, reflecting an assumption that existing or new channel bedform development prevents reach-average supercritical flow.

A simple multiplication factor was applied to the post-fire flood predictions to account for sediment bulking in the debris flows. For burned catchments, this multiplication factor was assumed to be 1.25 if the severe plus moderate soil burn severity aerial extent was greater than 50%, and 1.1 for catchments with between 15 and 50% soil burn severity.

Sediment Modeling

The RUSLE model was chosen to estimate pre- and post-fire sediment erosion rates. The RUSLE models (pre and post fire) are based on a spatial version of RUSLE outlined in Theobald et al. (2010) and Litschert et al. (2014). The ATREW methods entail calculating RUSLE (Equation 7) the standard way using widely available fine resolution spatial datasets to approximate the 6 RUSLE factors. The ATREW report provides guidance on parameterizing the RUSLE *C* and *P* factors based on commonly used landcover datasets (e.g., USGS National Landcover Dataset and USFS Existing Vegetation Dataset), as well as equations that scale GIS based terrain analysis for the *L* and *S* factors.

The advantages of this approach are (1) simple model parameterization using nationwide spatial datasets; (2) production of a sedimentation rate raster (each raster cell has a sedimentation rate); and (3), evaluate the resulting sediment yield rasters spatially to help prioritize soil treatment zones and emergency resource allocation. The RUSLE equation is:

$$A = R \cdot K \cdot L \cdot S \cdot C \cdot P \qquad (7)$$

where *A* is the average annual unit-area (tons per hectare per year), *R* is the rain erosivity factor (Mj mm/(ha h yr)), *K* is the soil erosivity factor, *L* is the slope length factor (m), *S* is the slope steepness factor, *C* is the cover management factor (>= 0), and *P* representing the management factor (>= 0). The sediment modeling entailed 4 general steps: (1) collection of geospatial dataset for the greater burn area (Table 2); (2) development of spatial RUSLE factors for pre and post fire conditions; (3) calculate RUSLE for pre- and post-fire scenarios (ArcGIS Raster Calculator); and (4) attribute computation points and values at risk with pre- and post-fire sedimentation rates. Pre- and post-fire sedimentation rate estimates were executed within a GIS using terrain analysis tools to calculate slope length (*L*) and steepness (*S*) factors with simple map algebra statements used to compute rainfall erosivity (*R*), soil erodibility (*K*) and cover management (*C*) factors from ancillary spatial datasets. The soil/cover management (*P*) factor was not incorporated in the analysis due to a lack of spatial information on management activity in the burn area. For each of the five RUSLE factors used, a 10-meter resolution raster dataset was

generated. The five RUSLE factor rasters where multiplied together to calculate the local (cell level) sedimentation rate. The local sedimentation rate values were accumulated downslope via a flow direction raster (Yochum and Norman 2014) and averaged by the contributing area above each raster cell. This results in the final sedimentation rate raster with values representing the average cumulative sedimentation rate in tons per year over 30 years for each scenario.

The rain erosivity (*R*) factor raster was generated by rasterizing the EPA EMAP HUC 8 polygon shapefile to a raster containing *R* factor values. The *R* factor raster was held constant between the pre- and post-fire scenarios due to a lack of information about change in rain erosivity values and the EPA EMAP values are based on 30 year averages. The HUC 8 *R* factor raster was masked out to match the cell size and processing extent.

Table 2 Spatial datasets sources used for the six RUSLE factors.

Factor	Source
R	U.S. Enviromental Protection Agency EMAP-West RUSLE Factors
K	USDA NRCS Web Soil Survey SSURGO spatial and tabular data
L & S	USGS National Elevation Dataset
C	USGS National Gap Analysis Program 30 meter landcover
P	Parameter not used in analysis due to lack of good spatial data

The development of soil erodibility (*K*) factor raster entailed summarizing KFFACT (SSURGO table attribute) to NRCS SSURGO map units and then rasterizing the map units in the same manner as the *R* factor. KFFACT (property of a soil horizon) was summarized to map unit delineations by calculating a depth/area weighted average based on horizon depths up to 15 centimeters and the component percent within a map unit. This was accomplished through queries developed in the SSURGO database downloaded from the USDA Geospatial Data Gateway website. The *K* factor raster was held constant for both scenarios even though burn severity alters soil erodibility. Altering soil erodibility based on burn severity between scenarios could be incorporated in future models but would require additional research.

The *L* and *S* factor were calculated jointly (*LS*) using basic terrain analysis methods outlined in Theobald et al. (2010) using a 10 meter elevation model. These methods include calculating a percent slope, aspect (radians), and accumulated upslope length. The accumulated upslope length process entailed accumulating number of contributing raster cells to a given cell based on the overland flow paths from the flow direction raster. The resulting slope, aspect and upslope length rasters were transformed using equations developed by Winchell et al. (2008, Equation 8) and Nearing (1997, Equation 10). These equations scale the values derived from the above terrain analysis to better fit within the frame work of the RUSLE equation and ensure that the units are correct. The slope length scaling equation is

$$LS_{i,j} = S_{i,j} * \frac{(A_{ij}+D^2)^{m+1} - A_{ij}{}^{m+1}}{X_{i,j}^{m+2} \cdot D^{m+2} \cdot 22.13^m} \quad (8)$$

, where LS_{ij} is the transformed slope length, D is the cell size of the analysis (10 meters), X aspect transformation (Equation 9), m slope transformation (Equation 10) and $S_{i,j}$ is the slope transformation function derived by equation 11. Aspect transformation were computed through:

$$X_{i,j} = \sin \alpha_{i,j} + \cos \alpha_{i,j} \quad (9)$$

, where $X_{i,j}$ is the transformed aspect values for raster cell *I* and *alpha* is aspect (radians clockwise from north) for raster cell *I*. Radians was used instead of degrees from north to prevent negative values from occurring when calculating COS of aspect in ESRI ArcGIS. The slope transformation is

$$\beta = \frac{\frac{\sin\theta_{i,j}}{0.0896}}{3(\sin\theta_{i,j}^{0.8}+0.56)} \quad (10)$$

, where *theta* is percent slope and the *m* coefficient is calculated by taking the ratio between *beta* and one plus *beta* ($\beta / 1 + \beta$).

The slope length ($LS_{i,j}$) factor raster was developed using the Nearing (1997) equation (Equation 8) in conjunction with equations 9, 10 and 11 to account for aspect and slope dynamics to better scale large flow path values (accumulated slope length). This is necessary because the accumulated flow path raster (A_{ij}) can have very large values which inflate sedimentation estimates. The *S* factor raster was developed by transforming percent slope using equation 11. Equation 11 scales slope values to reduce inflated soil loss values especially for slopes greater than 50%. As with the *R* and *K* factors the *L* and *S* factors were held constant between the pre and post fire models. The *S* factor transformation is computed as

$$S_{i,j} = 1.5 + \frac{17}{1+e^{(2.3-6.1*\sin\beta)}} \quad (11)$$

, where *beta* is the mean slope angle (Equation 10).

The *C* factor parameterization for the pre- and post- fire scenarios was developed using various source tables from different documents related to RUSLE. The pre-fire scenario parameterization involved developing a lookup table that assigns the existing landcover types (Southwest ReGAP) within the greater burn area their associated *C* factors (Yochum and Norman 2014). Table 3 in this project report was compiled by Theobald et al. (2010) for the ATERW report and provides a broad spectrum of landcovers found in most landcover datasets and can be modified based on local knowledge. The post-fire *C* factor parameterization entailed modifying the pre- burn *C* factor raster based on burn severity classes derived from the Burned Area Reflectance Classification (BARC) image. This process consisted of assigning the BARC burn severity classes *C* factor values (low burn = 1.03, moderate burn = 2.25 and high burn 3.75) (Larsen et al., 2007) that were then used to modify the pre-fire *C* factors by summing the two rasters together. Larsen et al. (2007) estimated that high burn severity area *C* factors changed by four hundred percent but didn't estimate moderate and low burn severity changes. *C* factors changes were selected using professional judgment.

The final sedimentation rate models for the pre- and post-fire scenarios were generated by first multiplying the 5 factors, accumulating the multiplied values downslope via the flow direction raster, and calculating an area weighted sedimentation rate. The area weighted sedimentation rate is calculated by dividing the accumulated sedimentation rate by the total accumulated drainage area (Yochum and Norman 2014). This aspect approximates the transportation of sediment from areas where sediment originates (steep slopes or burned areas) to areas that dampen sediment transport due to decreases in slope, unburned areas or flow distance. This assumes that sediment yields decreases from source areas downslope as slope decreases and distance increases.

RESULTS AND DISCUSSION

The results from the these three sets of models provided useful estimates of post-fire flooding and sedimentation rates that officials have used to prioritize management activities to reduce risk to life, property and infrastructure. Due to modeling limitations, the results are most appropriately used in a relative manner, comparing runoff and sediment liberation potential between catchments.

The 70 pour points for West Fork Complex wildfire (109,000 acres) indicate that severely burned catchments would experience a 50- or 100-year flood from a 10-year rainfall event and that 25-year rainfall events would produce more than 12 times the peak flow at some locations (Figure 2). Example maps produced for the project report are illustrated (Figures 3 and 4). The sediment modeling predicts that, on average, all catchments will experience 130 times more sediment, with one burn area (Papoose wildfire) accounting for 65% of the total sediment predicted to be delivered to the Upper Rio Grande river from the two fires.

Results at ninety six pour points were computed for the High Park wildfire (87,000 acres). Post-fire conditions were commonly predicted to induce 50- or 100-year floods from 10-year rainfall events across the High Park burn area, with the 25-year rainfall event expected to yield up to up to 10 times the pre-fire peak flow. Additionally, sediment yields were predicted to be 73 times

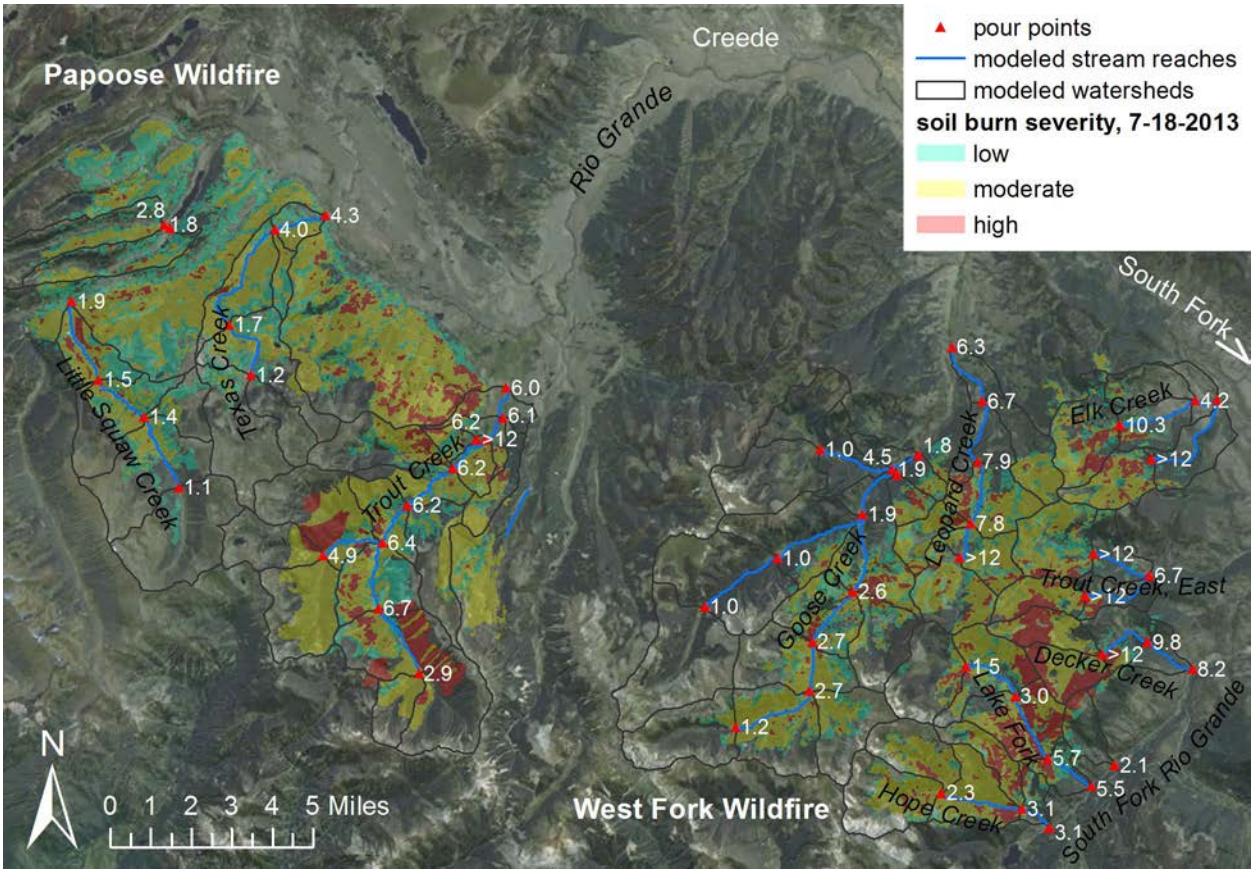

Figure 2 West Fork Complex wildfire peak flow magnification ratios (25-year rain event).

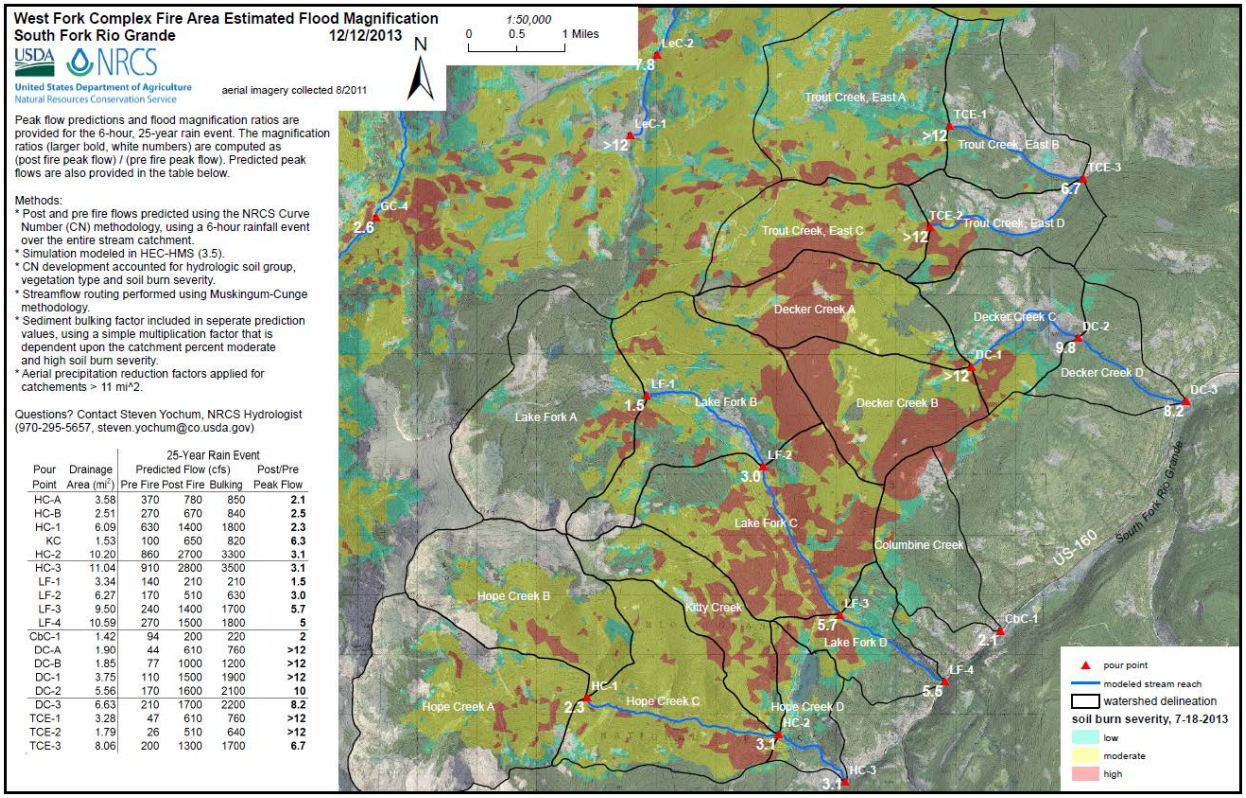

Figure 3 Example map providing pre- and post-fire flood predictions for the S. F. Rio Grande.

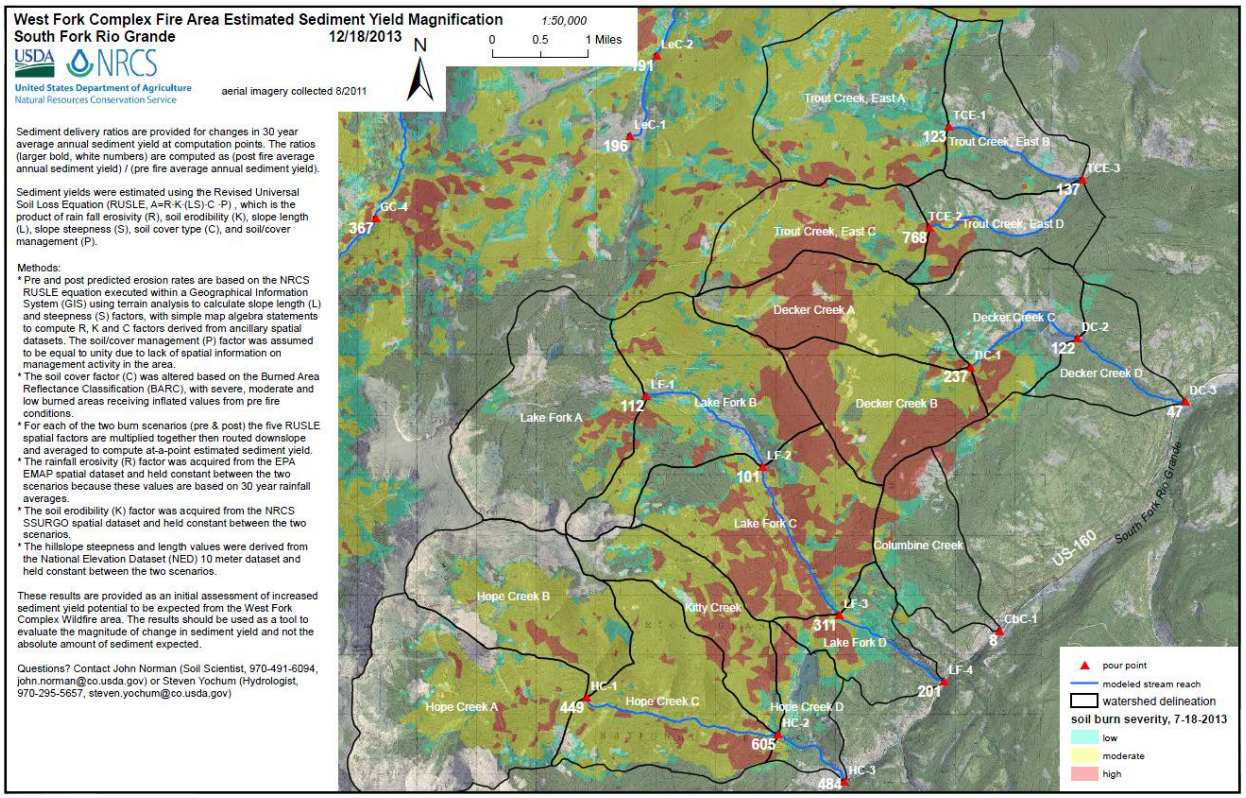

Figure 4 Example map providing pre- and post-fire erosion predictions for the S. F. Rio Grande.

greater than pre-fire conditions, with five catchments of the South Fork of the Cache La Poudre River having sediment magnification rates greater than 200.

Results at the 52 pour points for the Black Forest wildfire (14,300 acres) indicated that values at risk would experience a 100- or 200-year flood event from a 10-year rainfall event, with up to 15 times the pre-fire peak flow expected for the 25-year rainfall event. Sediment yield estimates predict sediment rates 75 times greater than pre-fire conditions with 15 values at risk having sediment magnification rates greater than 200.

CONCLUSIONS

Flow and sediment modeling was performed for the High Park (2012), Black Forest (2013) and West Fork Complex (2013) Wildfires. The results from the these three sets of models have provided useful comparative estimates of post-fire flooding and sedimentation rates (with respect to pre-fire conditions) that officials have used to prioritize management activities to reduce risk to life, property and infrastructure.

Substantial automation of the relatively-simple computational tools used to develop these estimates is possible; with support for the development or refinement of automation tools, results at the spatial scale presented in this report are likely feasible within the relatively-short Burn Area Emergency Response (BAER) process timeline.

ACKNOWLEDGEMENTS

Numerous individuals have contributed fieldwork, review, and other support for the modeling presented in this report. These individuals include David Levinson, Kari Sever, Sam Streeter, John Andrews, Claudia Hoeft, John Segars, Dustin Jager, Randy McKinley, Dan Moore, Jonas Feinstein, Rodney Clark, and Beau Temple. Their assistance has been highly appreciated.

REFERENCES

Benavides-Solorio, J., and MacDonald, L.H. (2001). “Post-Fire Runoff and Erosion from Simulated Rainfall on Small Plots, Colorado Front Range,” Hydrological Processes 15, 2931-2952.

Canfield, H.E., Goodrich, D.C., and Burns, I.S. (2005). “Selection of Parameters Values to Model Post-Fire Runoff and Sediment Transport at the Watershed Scale in Southwestern Forests,” Managing Watersheds for Human and Natural Impacts: pp. 1-12, doi:10.1061/40763(178)48.

Chen, L., Berli, M., and Karletta, C. (2013). “Examining modeling approaches for the rainfall-runoff process 18 in wildfire-affected watersheds: using San Dimas Experimental Forest.” Journal of the American Water Resources Association 1-16, doi:10.1111/jawr.12043.

Conedera, M., Peter, L., Marxer, P., Forster, F., and Rickenmann, D., R, L. (2003). “Consequences of Forest Fires on the Hydrogeological Response of Mountain Catchments: A Case Study of the Riale Buffaga, Ticino, Switzerland” Earth Surface Processes and Landforms 28, 117-129.

Elliot, W.J. (2004). “WEPP Internet interfaces for forest erosion prediction,” Journal of the American Water Resources Association, 40, 299-309.

Goodrich, D.C., Canfield, H.E., Burns, I.S., Semmens, D.J., Miller, S.N., Hernandez, M., Levick, L.R., Guertin, D.P., Kepner, W.G. (2005). “Rapid post-fire hydrologic assessment using the AGWA GIS-based hydrologic modeling tool,” Managing Watersheds for Human and Natural Impacts: pp. 1-12, doi:10.1061/40763(178)44.

Hawkins, R.H. (2014). “Curve Number Method: Time to Think Anew?” ASCE Journal of Hydrologic Engineering 19, 1059-1059, doi:10.1061/(ASCE)HE.1943-5584.0000954.

Huffman, E.L., MacDonald, and L.H., Stednick, J.D. (2001). "Strength and Persistence of Fire-Induced Soil Hydrophobicity Under Ponderosa and Lodgepole Pine, Colorado Front Range" Hydrological Processes 15, 2877-2892.

Kinoshita, A.M., Hogue, T.S., and Napper, C. (2014). "Evaluating pre- and post-fire peak discharge predictions across western U.S. watersheds," J. of the Am. Water Resources Association, 1-18, doi:10.1111/jawr.12226.

Larsen, I. J., and MacDonald, L.H. (2007). "Predicting postfire sediment yields at the hillslope scale: Testing RUSLE and Disturbed WEPP," Water Resources Research, 43 W11412, doi:10.1029/2006WR005560.

Litschert, S.E., Theobald, D.M., and Brown, T.C. (2014). "Effects of climate change and wildfire on soil loss in Southern Rockies Ecoregion." Catena 118, 206-219.

Livingston, R.K., Earles, T.A., and Wright, K.R. (2005). "Los Alamos Post-Fire Watershed Recovery: A Curve-Number-Based Evaluation," Managing Watersheds for Human and Natural Impacts: pp. 1-11. doi:10.1061/40763(178)41.

Maidment, D.R. (1992). Handbook of Hydrology. McGraw-Hill, Inc.

Miller, J.F., Frederick, R.H., and Tracey, R.J. (1973). *"Precipitation-Frequency Atlas of the Western United States."* U.S. Department of Commerce, National Oceanic and Atmospheric Administration, National Weather Service, NOAA Atlas 2, Vol 3, Silver Spring, Maryland.

Nearing, Ma., (1997). "A single continuous function for slope steepness influence on soil loss," Soil Science Society of America Journal, 61 (3), 917-919.

NRCS (2004a). "Hydrologic Soil Cover Complexes," USDA Natural Resources Conservation Service, National Engineering Manual, Chapter 9, 210-VI-NEH, July.

NRCS (2004b). "Estimation of Direct Runoff from Storm Rainfall," USDA Natural Resources Conservation Service, National Engineering Manual, Chapter 10, 210-VI-NEH.

Perica, S., Martin, D., Pavlovic, S., Roy, I., St. Laurent, M., Trypaluk, C., Unruh, D., Yekta, M., Bonnin, G. 2013 *NOAA Atlas 14 Volume 8 Version 2, Precipitation-Frequency Atlas of the United States, Midwestern States.* NOAA, National Weather Service, Silver Spring, MD.

Rallison, R.E. (1980). "Origin and Evolution of the SCS Runoff Equation," Proceedings of the Symposium on Watershed Management; American Society of Civil Engineers, Boise, ID.

Renard, K. G., G. R. Foster, G. A. Weesies, D. K. McCool, and D. C. Yoder. (1997). "Predicting soil erosion by water: A guide to conservation planning with the revised universal soil loss equation (RUSLE)," Agricultural Handbook 703, 404 pp., U.S. Department of Agriculture, Washington, D. C.

Renschler, C. S. (2003). "Designing geo-spatial interfaces to scale process models: The GeoWepp approach," Hydrological Processes, 17, 1005-1017.

Rodichaud, P.R. 2000. Fire effects on infiltration rates after prescribed fire in northern Rocky Mountain forests, USA, J. Hydrol., 231-232, 220-229.

Rulli, M.C., Offeddu, L., and Santini, M. (2013). "Modeling postfire water erosion mitigation strategies," Hydrology and Earth System Sciences, 17, 2323-2337.

Spinger, E.P., and Hawkins, R.H. (2005). "Curve Number and Peakflow Responses Following the Cerro Grande Fire on a Small Watershed." Managing Watersheds for Human and Natural Impacts: pp. 1-12, doi:10.1061/40763(178)40.

Stoof, C.R., Vervoort, R.W., Iwema, J., van den Elsen, J., Ferreira, A.J.D., and Ritsema, C.J. (2011). "Hydrological Response of a Small Catchment Burned by an Experimental Fire," Hydrology and Earth System Sciences Discussions 8, 4053-4098.

Theobald, D.M., D.M. Merritt, and J.B. Norman, III. (2010). "Assessment of Threats to Riparian Ecosystems in the Western U.S. A report presented to The Western Environmental Threats Assessment Center, Priveville, OR by the U.S.D.A.," Stream Systems Technology Center and Colorado State University, Fort Collins, 61p.

Winchell, M.F., S.H. Jackson, A.M. Wadley and R. Srinivasan. (2008). "Extension and validation of a geographic information system-based method for calculating the Revised Universal Soil Loss Equation length-slope factor for erosion risk assessments in large watersheds," Journal of Soil and Water Conservation 63(3): 105-111.

Woodward, D., Hawkins, R., Jiang, R., Hjelmfelt, Jr., A., Van Mullem, J., and Quan, Q. (2003). "Runoff Curve Number Method: Examination of the Initial Abstraction Ratio," World Water & Environmental Resources Congress 2003: pp. 1-10. doi: 10.1061/40685(2003)308.

Yochum, S.E. (2012) "High Park Fire: Increased Flood Potential Analysis," USDA NRCS, Colorado State Office, doi:10.13140/2.1.1282.3047

Yochum, S.E., Norman, J. (2014) "West Fork Complex Fire: Potential Increase in Flooding and Erosion" USDA NRCS, Colorado State Office, doi:10.13140/2.1.4165.8887.

NRCS POST-FIRE HYDROLOGIC MODELING IN NEW MEXICO 2012

Daniel S. Moore, P.E., Hydraulic Engineer, USDA-NRCS, Portland, Oregon, dan.moore@por.usda.gov

Abstract Wildfire can ravage enormous areas of the landscape and initiate extensive efforts among many agencies to combat the active event. Post-fire consequences also require attention, as the sudden watershed changes wrought by fire leave communities vulnerable to much larger floods, sedimentation, and debris flow. The Natural Resources Conservation Service (NRCS) in New Mexico played an important role both during and after large wildfires in the summer of 2012. Rapid application of the Emergency Watershed Protection (EWP) program funded several temporary USGS precipitation collection stations in the burned watersheds to help forewarn communities of possible flooding. Forest Service Burned Area Emergency Response (BAER) teams provided rapid assessment of the expected hydrologic consequences of the fire. NRCS followed up with detailed watershed modeling of Whitewater Creek, so that expected flood peaks and sedimentation could be quantified. Subsequent extreme storm events occurred in September 2013 in Whitewater Creek, New Mexico, and in Colorado's Front Range, the latter making national news. Development of the NRCS post-fire hydrologic analysis is detailed herein, with output including model performance of the 2013 observed event.

INTRODUCTION

Lightning sparked several outbreaks of wildfire in May 2012 that joined to became the largest in New Mexico recorded history. Lack of road access and the steep terrain of the Gila Wilderness Area hampered containment efforts, allowing the individual fires to grow rapidly. By the end of May, they had become one large wildfire known as the Whitewater-Baldy Complex.

The rugged landscape was not the only reason these fires escaped control. The watershed had already been under extreme drought conditions, with very little snowfall during the two previous winters. Air temperatures at the time of the outbreak were well above average, and high winds contributed to the merging of the fires. In early June, the Whitewater-Baldy Complex was only about 18 percent contained. By mid-June, containment increased to 56%. For about three months, the wildfire burned Ponderosa, Pinon/Juniper, and mixed conifer forests with relatively low burn temperatures. Rainfall in mid-July finally helped fire fighters gain momentum, with 95% containment attained in late July.

The wildfire burned about 465 square miles. The USDA Forest Service estimated final burn severity for the area within the fire perimeter to be 14 percent high, 12 percent moderate, 55 percent low or unburned, and 20 percent unknown (due to inadequate satellite imagery). Figure 1 shows the general location of the wildfire.

The NRCS Emergency Watershed Protection (EWP) program funded the installation of monitoring gages in the Whitewater-Baldy Complex burn area, to provide early warning to downstream communities of flood potential. The intensity of the wildfire and its large area prompted the Forest Service, in cooperation with the United States Geological Survey (USGS),

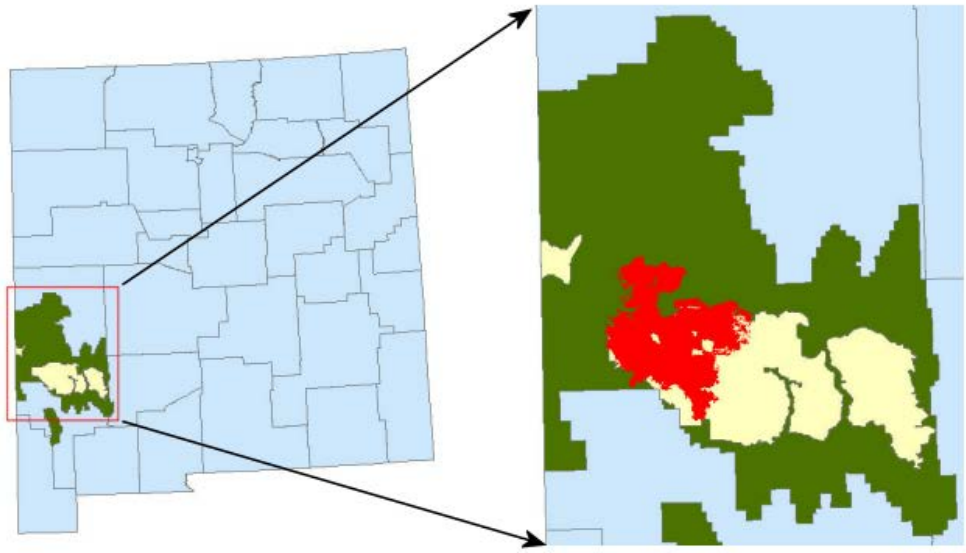

Figure 1 SW New Mexico, Gila National Forest (green), Gila Wilderness area (yellow), Whitewater-Baldy Complex wildfire (red).

to seek EWP funding from NRCS. The NRCS New Mexico State office worked with the New Mexico Department of Homeland Security and Emergency Management, which acted as the EWP local sponsor. USGS installed a streamflow gage on Whitewater Creek, near the Catwalk Recreational Area (figure 2). That station also received a precipitation gage. The location of the existing NRCS snow telemetry (SNOTEL) site is also shown in figure 2, along with additional precipitation gages installed by USGS using EWP.

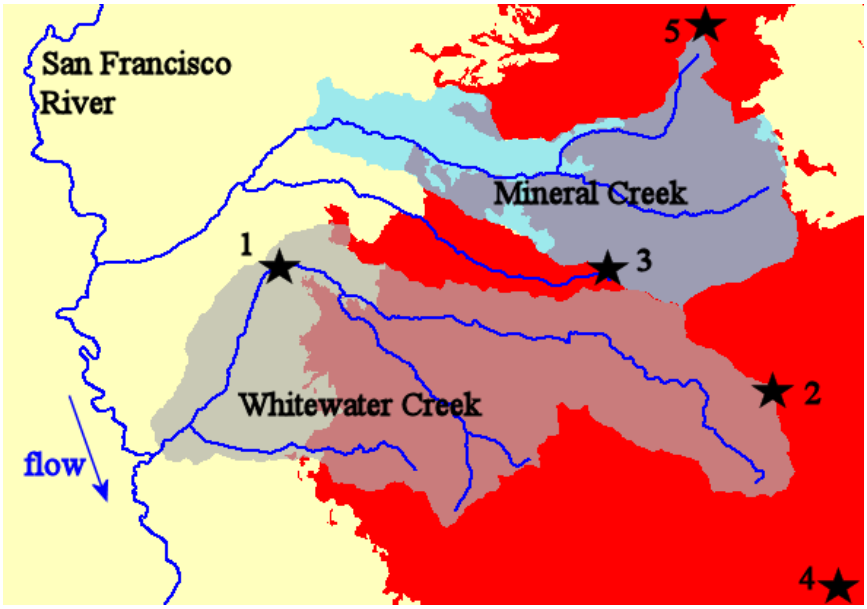

Figure 2 Gages in the burn area (red): Silver Creek Divide SNOTEL site (3), streamflow and precipitation at Catwalk (1), precipitation at Hummingbird Saddle (2), Mogollon Baldy Lookout (4), and Bear Wallow Lookout (5).

NRCS also performed a hydrologic analysis to assess flood potential for the community of Glenwood. In recent years New Mexico residents experienced flash flooding after wildfire. Hypothetical floods examined were pre-fire, post-fire immediately after the burn, and post-fire, one year later. Data from the newly installed precipitation and streamflow gages were used to verify that the hydrologic model produced reasonable results.

HYDROLOGIC MODELING DETAILS

After selecting a software application for watershed modeling, the hydrologist has key decisions to make about how to represent the landscape. These are an attempt to guide the model in partitioning precipitation between infiltration (and other losses) and runoff, and secondly, transforming remote runoff to an outlet hydrograph. The NRCS hydrologic model WinTR-20 employs the curve number runoff method, with curve numbers (generally between 30 and 99) that affect runoff volume (USDA-NRCS, 2004). Curve numbers are a subarea index, which includes losses to transpiration and ponding. Within the US Army Corps of Engineers model, HEC-HMS (USACE-HEC, 2013), these losses can be specified separately. The model provides several infiltration options, including curve numbers, and the Green-Ampt method. The latter is an attempt to model the physical infiltration process using soil characteristics such as hydraulic conductivity.

The draft NRCS National Technical Note Hydrologic Analysis of Post-Wildfire Conditions (USDA-NRCS, 2014), currently under review, provides a comprehensive guide to hydrologic modeling of post-wildfire conditions. The hydrologic model of Whitewater Creek, New Mexico, discussed in this paper is included in the technical note as a case study. The hydrologic modeling choices selected for Whitewater Creek were the HEC-HMS model, with Green-Ampt infiltration, and a user-specified unit hydrograph for runoff transformation.

Issues Particular to Post-Wildfire Modeling

The hydrologist has several challenges with burned watersheds. Adequate historical data records generally do not exist. The often remote and mountainous watersheds may never have been gaged or studied for rainfall-runoff behavior, which would establish indices such as curve numbers or peaking factors for synthetic unit hydrographs (UHs). Even if they were gaged, the gages would have to survive wildfire events to be available for monitoring the sudden watershed changes caused by the fire. New gages can be rapidly installed after an event, such as occurred for the Whitewater-Baldy Complex fire, but rarely is this action taken, and such data cannot provide insight into pre-fire runoff behavior.

Research literature to date does not provide post-wildfire modeling guidance that would remove much hydrologic judgement from the effort. The NRCS technical note (USDA-NRCS, 2014) gives several tables of post-wildfire runoff curve numbers (CNs) that have been compiled from previous hydrologic modeling efforts. Generally, these CNs have been selected using hydrologic judgement rather than being data-derived. One study of ten Appalachian forested watersheds, that did use data, found measured CNs varied significantly from published suggested values (Tedela, et al., 2012). The study also found very wide confidence limits for the measured values. One watershed, with a measured mean CN of 57, had 95 percent confidence interval of 32 to 83.

Other data-driven studies also found inability to achieve a stable CN value (Hawkins, 1993, and Springer and Hawkins, 2005).

Another source of uncertainty in hydrologic modeling of mountain watershed is in the use of synthetic unit hydrographs that include a user-specified peaking factor. The unit hydrograph transformation algorithm in WinTR-20 has a default peaking factor which applies to U.S. watersheds of average flow slopes and landscape storage effects. Mountain watersheds tend to have much steeper slopes and fewer storage effects than average. A hydrologist using WinTR-20 has the option to change this peaking factor, but the program does not make it obvious when it should be changed, and retaining the default is the likely practice, even for mountain watersheds. When using HEC-HMS the hydrologist cannot select an SCS peaking factor, but has only two hydrograph shape options: standard (the default peaking factor) and "Delmarva", a hydrograph shape developed by NRCS for the Delaware, Maryland, and Virginia peninsula, and often used for Eastern U.S. coastal watersheds. (A larger range of optional peak factors is planned for HEC-HMS version 4.1.)

To escape the need for a peak factor estimate, the hydrologist may consider other synthetic unit hydrograph options available in HEC-HMS. But similar user-entered factors are also required with those synthetic UH choices. For example, the Clark synthetic UH transform requires the user to specify a "storage coefficient" which, according to the user manual (USACE-HEC, 2013), may be determined from regional studies. The Snyder synthetic UH transform requires a "peaking coefficient" obtained, according to the user manual, "…using the best judgement of the user, or possibly from locally-derived relationships to watershed physical features."

The HEC-HMS model does offer a UH transform method that may get around the peaking factor issue: the user-derived UH. Of course, measuring the UH applicable to any given watershed requires data, but a synthetic UH may be derived if the user can determine an adequate time-area histogram of the watershed. Even without rainfall and runoff data, geographic information systems (GIS) may give the hydrologist the best handle on the shape of the mountain watershed hydrograph. Good resolution digital elevation models (DEMs) enable the land slope to be defined. More and more pertinent digital geographic data is becoming available, such as soil type, land cover, vegetation, and even burn extents and severities. The ArcGIS raster calculator (ESRI, 2010) enables the modeler to estimate flow velocities for overland flow slopes, collector channels, and major streams, and then travel times from any point in a watershed. This option was used for the Whitewater Creek study.

Soil hydrophobicity may be the most difficult effect of wildfire to model, and thereby the greatest source of uncertainty. The NRCS technical note discusses the phenomenon extensively, with numerous references, such as DeBano (2000) and Huffman, et al. (2001). Wildfire can result in soils becoming water repellent, but the pertinent landscape aspects vary widely and are not very quantifiable. Certain vegetation types, when burned, provide gaseous hydrocarbons that condense in cooler soil layers. Soil texture plays a role, in that coarse-grained soil is more susceptible than finer-grained soil.

Soil burn severity may have an important role in the strength of water repellency at a given location and the geographic extent. However, even as water repellency is created, the depth into

the soil of the top of the hydrophobic layer varies, and the thickness of that layer varies. Along with those unknowns comes variability in the time after a wildfire event that the hydrophobic characteristics persist.

The hydrologic modeler has a few reasonable options for estimating hydrophobic extent, but the uncertainty thrown into the runoff model is large and unquantifiable. For example, using GIS, a layer for soil burn severity could be combined with soil and vegetation layers to estimate where hydrophobic soil may exist, but the correlation may not be very good. Uncertainty also remains about whether hydrophobic soil restricts infiltration completely or only partially, and whether a sub-basin should be considered 100 percent hydrophobic or whether some lower fraction should be used. Relating to post-fire sedimentation, more erosion would tend to result from areas where loose soil exists above the hydrophobic layer, and rainfall on the unprotected soil can perch on the hydrophobic layer and run off similarly to a parking lot pavement. Again, the volume of such erosion would be highly uncertain.

As a result of all this uncertainty, the modeler must incorporate estimates about hydrologic conditions which cannot be verified. These estimates, along with the scarcity of gages, contribute to the fact that the hydrologic model cannot be calibrated. Model results will be reasonable, but the modeler should document areas of unknown variability. If post-wildfire data stations exist, such as in Whitewater Creek, the data can be used to adjust model input and examine the difference between modeled and measured runoff. However the geographic extent of the station network would generally remain too sparse for true model calibration.

Whitewater Creek Hydrologic Model

The total watershed area of Whitewater Creek upstream of the San Francisco River is 54.5 square miles. Upstream of the new Catwalk streamgage (figure 3) the drainage area is 36.2 square miles. Figure 3 shows how the basin was sub-divided for the hydrologic model. The inset of figure 3 is a single upstream sub-basin, shown in figure 4. Much of this discussion will focus on this sub-basin, as every other sub-basin is modeled similarly.

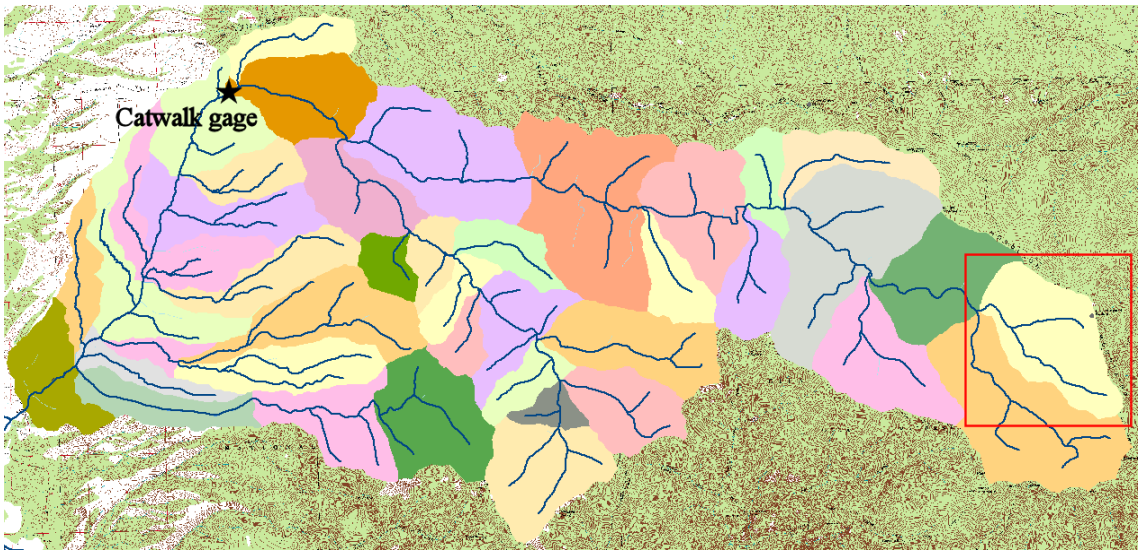

Figure 3 Whitewater Creek sub-areas, with inset of Baldy Fork (see figure 5).

For Green-Ampt infiltration, HEC-HMS requires soil data for initial moisture content, saturated content, matric suction, and hydraulic conductivity. Being within the Gila Wilderness, spatially distributed soil data are not available. However, a soil survey for part of Catron County outside the wilderness is available (USDA-SCS, 1985). The document shows that a typical soil of the area is the Tolman Series, for which the texture of the top two inches is described as cobbly loam, with permeability ranging between 0.6 to 2 inches per hour. For the entire watershed, the Green-Ampt parameters were estimated based on this soil type, with reference to the technical note table of hydraulic characteristics by soil texture. The assumed soil texture was loamy sand with porosity of 0.42 cubic inches of pore space per cubic inch of soil. Initial moisture content was assumed to be near field capacity, or 20 percent of the porosity. Wetting front suction was estimated at 4.33 inches and hydraulic conductivity 0.86 inches per hour.

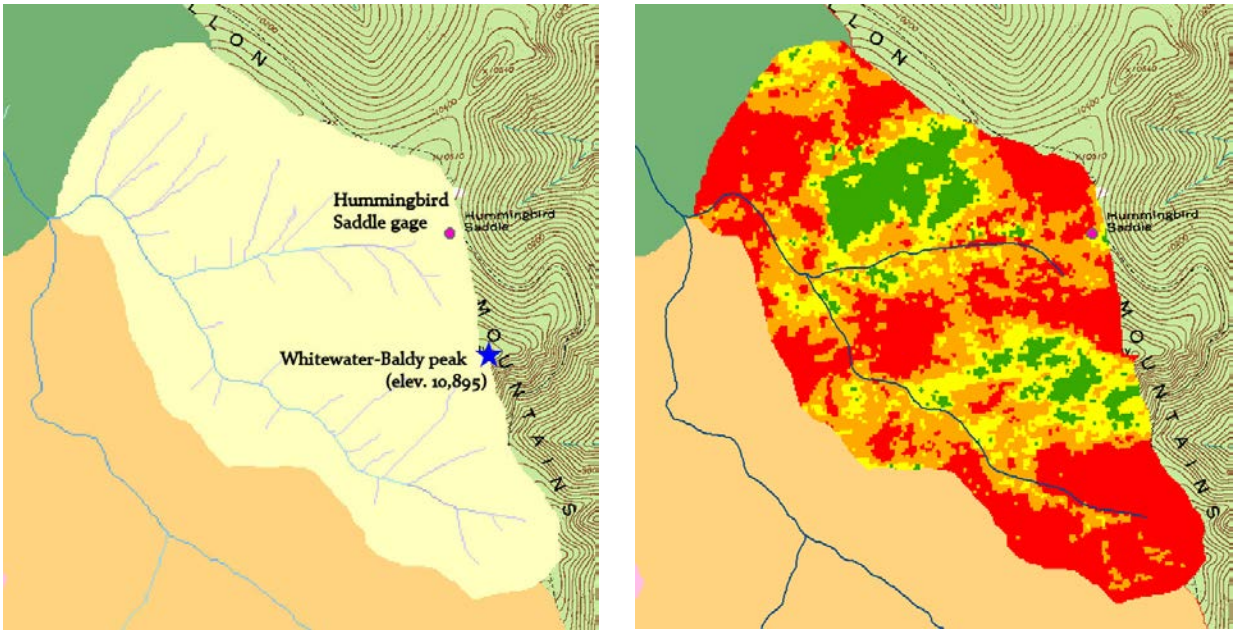

Figure 4 Baldy Fork sub-basin with burn severity raster on the right, (red = high, orange = medium, yellow = low, green= no burn).

Transformation of downstream runoff was accomplished using a unit hydrograph for each sub-basin derived from a GIS-estimated time-area histogram. Flow velocity for each ten-meter DEM cell was determined using Manning's equation, with a partitioning of cells into the catagories of overland flow, shallow-concentrated flow, or channel flow. The category was based on distance from the headwater ridge of each flowline. NRCS guidance (USDA-NRCS, 2010) suggests that overland flow will extend only up to 100 feet before transitioning to shallow-concentrated flow, which may extend another 1000 feet before becoming channelized. Separate Mannings roughness values are assumed for the different flow categories and for different types of vegetation or soil for each cell. In addition, burn severity was taken into account. (See figure 4).

Figure 5 shows the time band raster for Baldy Fork, derived using the ArcGIS raster calculator. Further details of the time-area histogram derivation is provided in USDA-NRCS (2014). The

time band table in figure 5 shows the number of cells that drain to the outlet in each 5-minute band. These data are copied to a spreadsheet and a time-area histogram created. Further spreadsheet manipulations result in the unit hydrograph shown in figure 6. Note that varying the conditions for travel time rasters results in separate unit hydrographs for pre-fire conditions, post-fire conditions immediately after the fire, and conditions after one year of healing.

The NOAA National Weather Service Precipitation Frequency Data Server (NOAA, 2013) was recently updated for New Mexico. Due to the flashy character of Southwest U.S. storms, a six-hour duration was selected for analysis, with rainfall amounts in table 1.

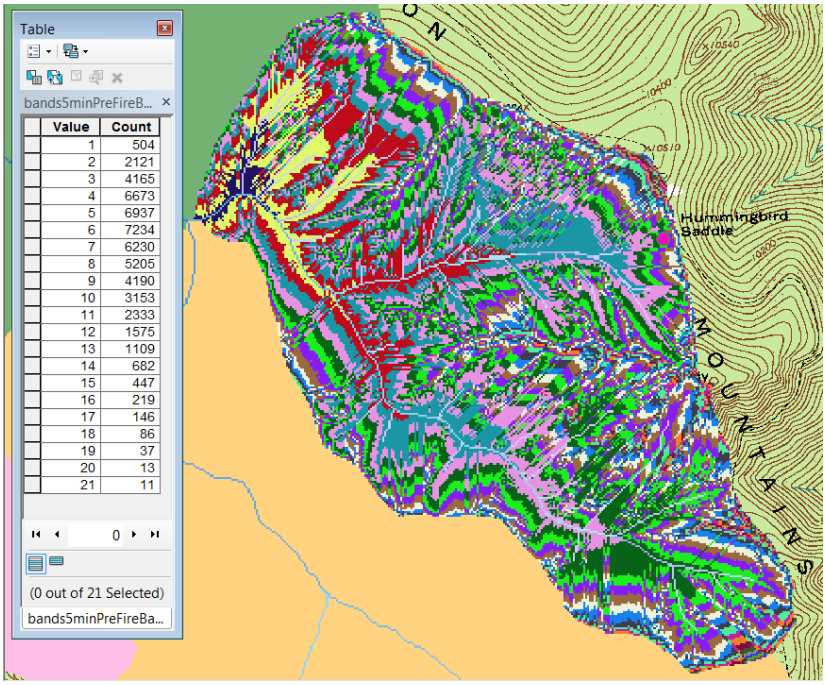

Figure 5 Twenty-one 5-minute travel time bands for Baldy Fork, with inset attribute table.

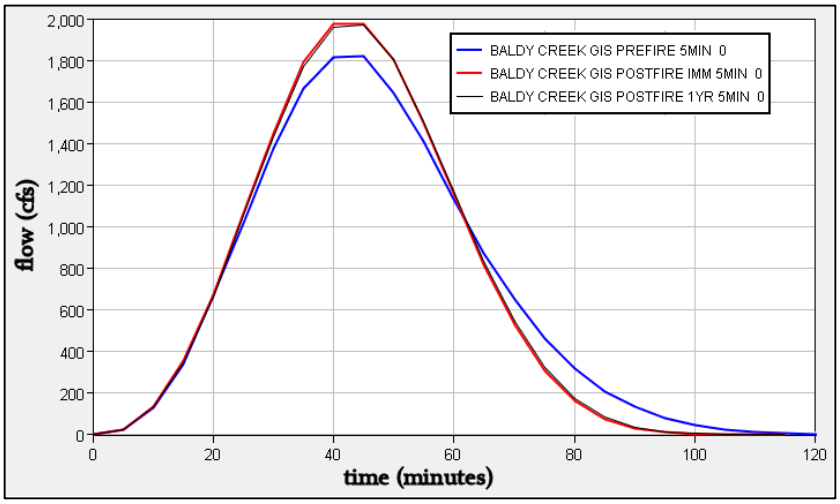

Figure 6 Synthetic GIS-derived unit hydrographs for Baldy Fork.

Table 1 Whitewater Creek watershed 6-hour duration storm totals

watershed area	precipitation		
	2-year (inches)	25-year (inches)	100-year (inches)
upper Whitewater	1.54	2.73	3.49
SF Whitewater	1.42	2.49	3.19
lower Whitewater	1.20	2.12	2.73

These rainfall amounts were distributed in time using a New Mexico variation of the standard NRCS Type II storm distribution. (The New Mexico variant results in a slightly higher peak than the NRCS Type II and causes the peak to occur earlier in the duration.) In addition, an areal reduction factor (ARF) was applied to the rainfall values of Table 1, based on the graph in figure 7, from Osborne, Lane, and Myers (1980). The Walnut Creek Experimental Watershed of figure 7 is near Tuscon Arizona, about 180 miles from Whitewater Creek, but in the same hydrographic region. Similar areal reduction is expected. The marked drop off of precipitation with distance, shown in figure 7, indicates that typical storms in the US Southwest are not large enough to cover the entire watershed of a size like Whitewater Creek. Typical storms may be 10 to 12 km in diameter, while Whitewater Creek is about 22 km wide, east to west. The storm centerings for the Whitewater Creek model are shown in figure 8, with locations selected which result in the largest runoff effect.

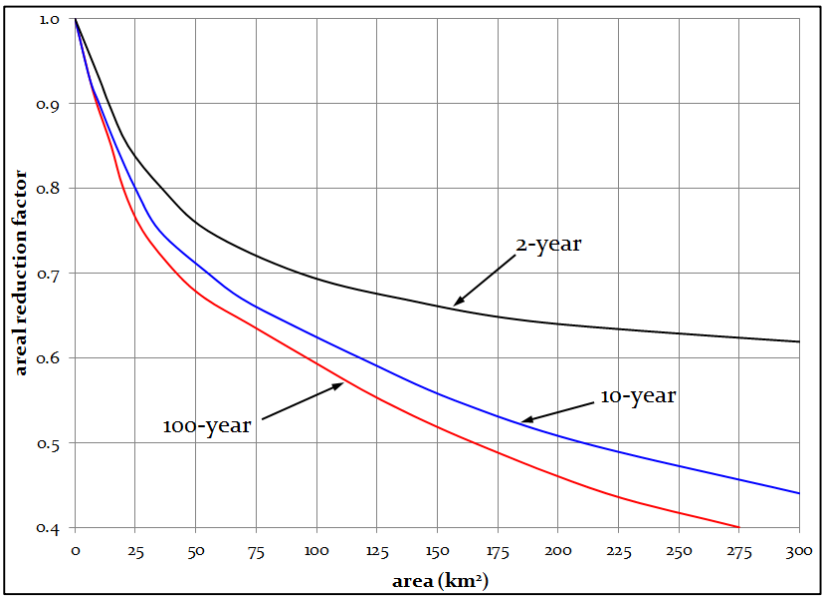

Figure 7 Areal reduction factors developed for 6-hour duration storms at Walnut Gulch AZ Experimental Watershed (modified from Osborn, Lane, and Myers 1980)

This analysis did not attempt to model sedimentation, but relied on a USGS report specifically concerning the Whitewater Baldy Complex wildfire (Tillery, Matherne, and Verdin, 2012) that estimated high probabilities in Whitewater Creek of debris flows from 30-minute duration

rainfall events for recurrence intervals of 2-year, 10-year, and 25-year. The report provides a map of Whitewater Creek sub-basins and their estimated propensity to generate sediment due to the wildfire. This information was used in this case study to bulk the modeled clear flow hydrographs, depending on their origin.

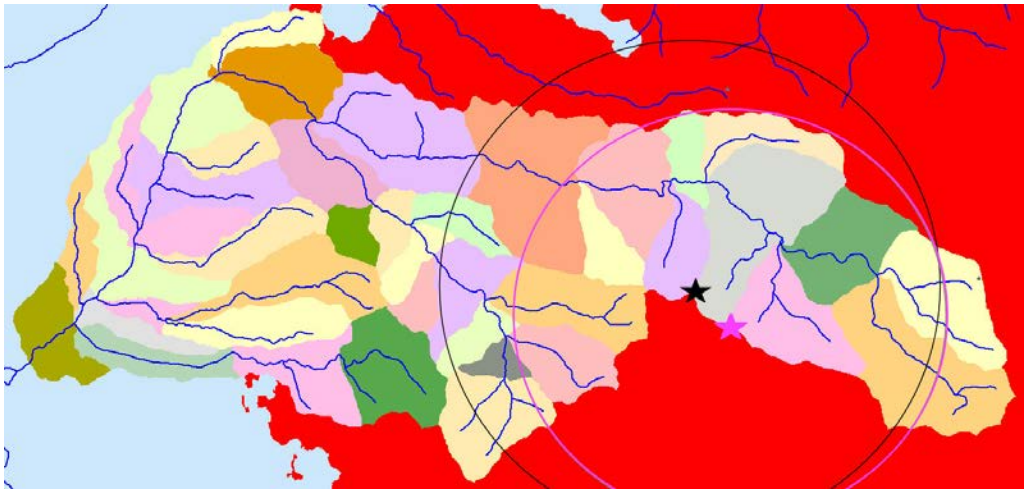

Figure 8 Storm centerings: UpperGrouse, 6 km radius (black), UpperLipsey, 5 km radius (pink)

MODEL RESULTS AND DISCUSSION

The HEC-HMS model can produce hydrographs for any of the sub-basin outlets of figure 3, but only the USGS gage at Catwalk (figure 2, gage 1) and the creek outlet to the San Francisco River (near Glenwood) are shown here. Three watershed scenarios were examined, pre-fire, immediately post-fire, and post-fire after one year of healing. Table 2 shows that varying storm center location and storm size (5- or 6-km radius) does not produce widely different results. Figure 9 shows the 100-year hydrograph at Glenwood for the 6-km radius storm.

Table 2 Model output: hydrograph peaks in cfs with areal reduction centerings from Figure 9.

storm	location	Grouse centering (6km radius)			Lipsey centering (5km radius)		
		pre-fire	post-fire (immed.)	post-fire (one year)	pre-fire	post-fire (immed.)	post-fire (one year)
100-yr	gage	10149	15734	14623	9246	15052	13500
100-yr	Glenwood	8776	14391	13245	7916	13899	12431
25-yr	gage	4384	9703	8696	4589	8654	7765
25-yr	Glenwood	3854	8713	7674	3934	7919	7060
2-yr	gage	31	4346	2878	56	3723	2405
2-yr	Glenwood	31	4121	2734	46	3555	2308

The observed event of 14-15 September, 2013, was modeled using the post-fire after one year scenario. The event magnitude was more rare than a 1,000-year recurrence, as shown in table 3. Some evidence of storm areal extent is provided by the fact that the Hummingbird Saddle gage during this event received minimal precipitation. The storm seems to have occurred closer to the

gage. Between 9 pm and midnight, while the Catwalk gage was recording 6.10 inches of rainfall, the Hummingbird Saddle gage received zero. For the three hours after midnight, rainfall at Catwalk dropped off considerably (0.75 inches, total) and Hummingbird Saddle recorded a similar total (0.93 inches). The Silver Creek Divide SNOTEL site (figure 2, gage 3) recorded precipitation of about two inches for that 24-hour period. (The SNOTEL precipitation gage is a cumulative collection cylinder, with historical records of daily observations.)

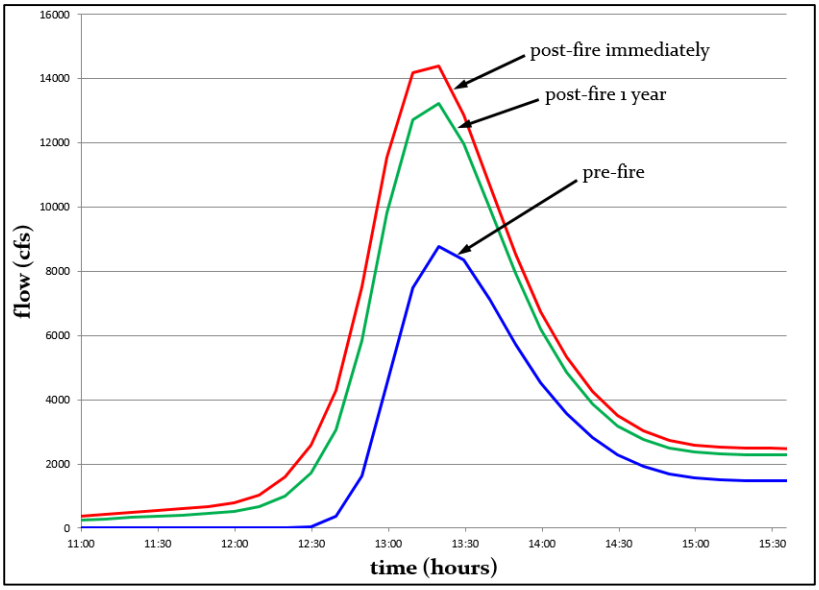

Figure 9 Model results, 100-year hydrographs at Glenwood for 6km radius storm.

Table 3 Observed storm event measured at Catwalk gage (blue) with NOAA precip-frequency.

storm centering at SF Whitewater confluence (rainfall in inches)							
	recurrence-->						
duration	50-year	100-year	200-year	500-year	1000-year	gage	14-15 Sep
1-hour	1.83	2.04	2.24	2.5	2.71	**3.01**	9-10 pm
2-hour	2.02	2.27	2.52	2.86	3.14	**4.09**	9-11 pm
3-hour	2.12	2.38	2.66	3.04	3.35	**6.10**	9-midnight
6-hour	2.48	2.8	3.14	3.61	3.99	**6.85**	9pm-3am

Areal reduction for the various storm frequencies (table 2) were of the "fixed" type, whereby the reduced rainfall value is applied to the entire storm area. These are not considered applicable to observed storms. In the absence of observed storm ARFs for the area, the reductions applied to the observed precipitation of September 2013 were taken from fixed ARF of figure 7; however the precipitation value applied to any given sub-basin was a reduction of the centered maximum value, proportional to the distance of the sub-basin from the storm center (assumed to be near the confluence of the upper Whitewater and SF Whitewater Creek, upstream of the Catwalk gage, figure 3).

The resulting model hydrograph at the USGS Catwalk gage, compared to the observed, is shown in figure 10. The two graphs are so remarkably close that the following points should be noted.

The model parameters were not adjusted in order to make the output match the observed. The same watershed scenario for postfire, after one year, was used here as for the modeling of recurrence flows. However, the model hydrographs of figure 10 is the result of only one possible scenario of storm size and centering. Other centerings could be justified using the same observed data. The assumed reduction of hydrophobic effect for the one year post-fire condition seems to have been in the ballpark, but the widespread nature of unknowns makes for difficulty judging which assumptions were better than others.

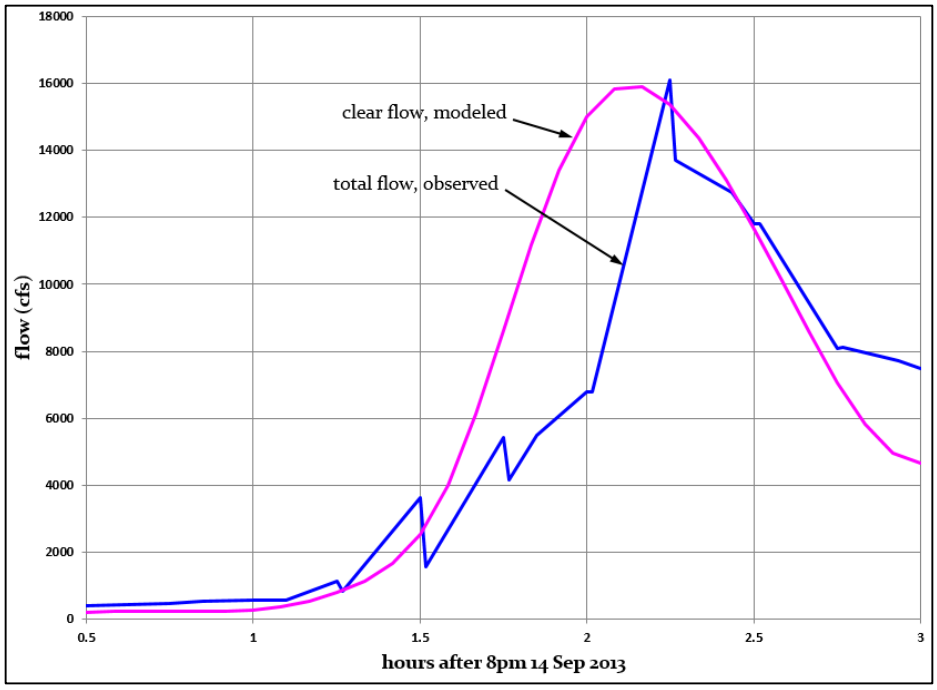

Figure 10 Catwalk gage modeled versus observed for the storm of 14-15 September 2013.

CONCLUSIONS

This case study has shown that reasonable model results can be obtained using the modeling options of HEC-HMS, Green-Ampt infiltration, and GIS-derived synthetic unit hydrographs. The extent of hydrophobicity and its effect on runoff remains a major source of uncertainty, but the assumptions made for Whitewater Creek, informed by detailed mapping of burn severity, appear to have resulted in a useful model.

REFERENCES

DeBano, L.F. (2000). The role of fire and soil heating on water repellency in wildland environments: a review, Journal of Hydrology, 231-232, 195-206.

ESRI (Environmental Systems Resource Institute). (2010). ArcMap 10.0 ESRI, Redlands, California.

Hawkins, R.H. (1993). Asymptotic determination of runoff curve numbers from data, Journal of Irrigation and Drainage Engineering, 119, 334-345.

Huffman, E.L., MacDonald, L.H., and Stednick, J.D. (2001). Strength and persistence of fire-induced soil hydrophobicity under ponderosa and lodgepole pine, Colorado Front Range, Hydrologic Processes, 15, 2877-2892.

NOAA National Weather Service Precipitation Frequency Data Server (2013). Available at http://dipper.nws.noaa.gov/hdsc/pfds/.

Osborn, H.B., Lane, L.J., and Myers, V.A. (1980). Rainfall/watershed relationships for Southwestern Thunderstorms. Transactions ASAE 23(1), 82-91.

Springer, E.P., Hawkins, R.H. (2005). Curve number and peakflow responses following the Cerro Grande Fire on a small watershed, In: Moglen, G.E., ed. Proceedings of Managing Watersheds for Human and Natural Impacts: Engineering, Ecological, and Economic Challenges, July 19-22, 2005, Williamsburg, VA, USA. Am. Soc. of Civil Engineers, Alexandria, VA.

Tedela, N.H., McCutcheon, S.C., Rasmussen, T.C., Hawkins, R.H., Swank, W.T., Campbell, J.L, Adams, M.B., Jackson, C.R., and Tollner, E.W. (2012). Runoff curve numbers for 10 small forested watersheds in the mountains of the Eastern United States, ASCE Journal of Hydrologic Engineering, 17, 1188-1198.

Tillery, A.C., Matherne, A.M., and Verdin, K.L. (2012). Estimated probability of postwildfire debris flows in the 2012 Whitewater-Baldy fire burn area, Southwestern New Mexico, USGS Open File Report 2012-1188, 11 pages.

USACE-HEC (U.S. Army Corps of Engineers, Hydrologic Engineering Center) (2013). HEC-HMS Technical Reference Manual. Davis CA, 138 pp.

USDA-NRCS (U.S. Department of Agriculture-Natural Resources Conservation Service) (2004). WinTR-20 User Guide. Washington DC. 145 pp.

USDA-NRCS (U.S. Department of Agriculture-Natural Resources Conservation Service) (2010). NRCS National Engineering Handbook, Part 630 Hydrology, Chapter 15, Time of Concentration.

USDA-NRCS (U.S. Department of Agriculture-Natural Resources Conservation Service) (2014). Hydrologic Analysis of Post-Wildfire Conditions, Draft National Technical Note, (under review).

USDA-SCS (U.S. Department of Agriculture-Soil Conservation Service) (1985). Soil Survey of Catron County, New Mexico, Northern Part, 199 pp.

HILLSLOPE EROSION AND SMALL WATERSHED SEDIMENT YIELD BEFORE AND AFTER FIRE IN SOUTHERN CALIFORNIA

Peter M. Wohlgemuth, Hydrologist, USDA Forest Service, Pacific Southwest Research Station, Riverside, California pwohlgemuth@fs.fed.us

Abstract: In 2002, a wildfire burned over an ongoing sediment flux study in the steep, chaparral-covered foothills of the San Gabriel Mountains of southern California. The study area had previously burned in 1960. Southern California experiences a Mediterranean climate with cool wet winters and hot dry summers. Average annual rainfall for the study area is 714 mm (80-year record) with an average two-year 30-minute peak intensity of 29 mm hr^{-1}. Hillslope erosion was measured in 30 cm collector traps. These traps were serviced multiple times per year to distinguish wet season from dry season erosion. Small watershed (1-3 ha) sediment yield was measured behind earthen debris dams. Three of the study watersheds were in mixed chaparral vegetation and one was in type-converted grass. One of the chaparral watersheds was burned in a prescribed fire in 2001 and did not re-burn in the wildfire. Hillslope erosion and small watershed sediment yield data were collected for 7 or 8 years prior to burning then for 5 or 6 years following fire, including the complete post-fire erosion record. Continuous rainfall was measured in a centrally-located weighing bucket recording raingage. Rainfall, both totals and intensities, was generally below average during the study period, especially immediately after the fires. Prior to fire, hillslope erosion was considerable, was an order of magnitude less under grass vegetation compared to chaparral, dry season erosion was equal to wet season erosion in all watersheds, but sediment yield was only minor and associated with high rainfall years at the watershed scale. In the first post-fire year, both hillslope erosion and small watershed sediment yield increased by 1-2 orders of magnitude over pre-fire levels and all parts of the landscape responded similarly. Hillslope erosion rates and small watershed sediment yields returned to pre-fire levels and patterns within two to three years post-fire. The magnitude and patterns of erosion following a prescribe burn in chaparral was very similar to those following a wildfire, although the recovery curve was somewhat flatter after the prescribed fire. Future studies will test a variety of predictive models against the current dataset as a benchmark to evaluate their performance as a tool for planning and risk assessment in southern California chaparral watersheds.

INTRODUCTION

Fire has been a part of the southern California landscape since before recorded history and is the disturbance event which drives much of the environmental response in southern California (Sugihara and Barbour 2006). Chaparral and coastal sage scrub vegetation communities have adapted to periodic burning and some species may require fire in order to reproduce (Keeley 2006). Furthermore, fire drives much of the surface erosion experienced across the landscape. With the removal of both the vegetation cover and the protective layer of organic litter post-fire hillside slopes are initially susceptible to dry ravel erosion and subsequently to raindrop splash (Rice 1974). Fire also alters the physical and chemical properties of the soil – bulk density and water repellency – promoting surface runoff at the expense of infiltration (DeBano 1981). This enhanced post-fire runoff removes more soil material from the denuded hillsides and can mobilize sediment deposits in the stream channels to produce debris flows with tremendous erosive power (Wells 1987). Post-fire accelerated erosion eventually abates as the re-growing

vegetation canopy and root system stabilize the hillslopes and provides protection against the agents of erosion (Barro and Conard 1991). However, in the interim, wildfires coupled with heavy winter rains can produce floods and debris flows that threaten human life, property, and infrastructure (roads, bridges, utility lines, communication sites) far downstream from the burn area itself. This places an extra burden on land managers and hazard protection agencies that must be able to predict post-fire watershed response and mitigate against any potentially negative consequences to these values at risk.

Although the patterns of post-fire erosion in southern California are generally understood, uncertainty about the magnitude of post-fire erosion events limits our ability to predict specific post-fire watershed responses. Prediction, usually in the form of numerical modeling, is only possible with a sufficient understanding of the quantitative effects of fire on erosion processes. Fortuitously, a wildfire on the San Dimas Experimental Forest burned over an ongoing sediment flux study and provided an opportunity to document and quantify the effects of fire on hillslope erosion and sediment yield in small watershed units in a semiarid, chaparral-covered, steepland environment. Results of this research could serve as a benchmark against which to test or evaluate existing models of post-fire erosion for the southern California area.

STUDY AREA

The San Dimas Experimental Forest (SDEF) is a nearly 7000 ha research preserve administered by the USDA Forest Service, Pacific Southwest Research Station, and has been the site of extensive hydrologic monitoring for over 80 years (Dunn et al. 1988). Established in 1933, with its headquarters at Tanbark Flat (34^{o} 12’ N latitude, 117^{o} 46’ W longitude) the SDEF is located in the San Gabriel Mountains, about 45 km northeast of Los Angeles, California (Figure 1).

Elevations in the study area range from 750 to 1050 meters and topography consists of a highly dissected mountain block with steep-walled canyons and steep channel gradients. Bedrock geology in the SDEF is dominated by Precambrian metamorphics and Mesozoic granitics that produce shallow, azonal, coarse-textured soils (Dunn et al. 1988). The SDEF experiences a Mediterranean-type climate, characterized by hot, dry summers and cool, moist winters. Temperatures range from -8^{o} C to 40^{o} C. Mean annual precipitation, falling almost exclusively as rain, is 714 mm (80-year record), but rain during individual years can range from 252 to 1848 mm. Over 90 percent of the annual precipitation falls between the months of November and April (Wohlgemuth 1996). The two-year 30-minute peak rainfall intensity (an index of rainfall erosivity) for the study area is 29 mm hr^{-1} (Bonnin et al. 2011).

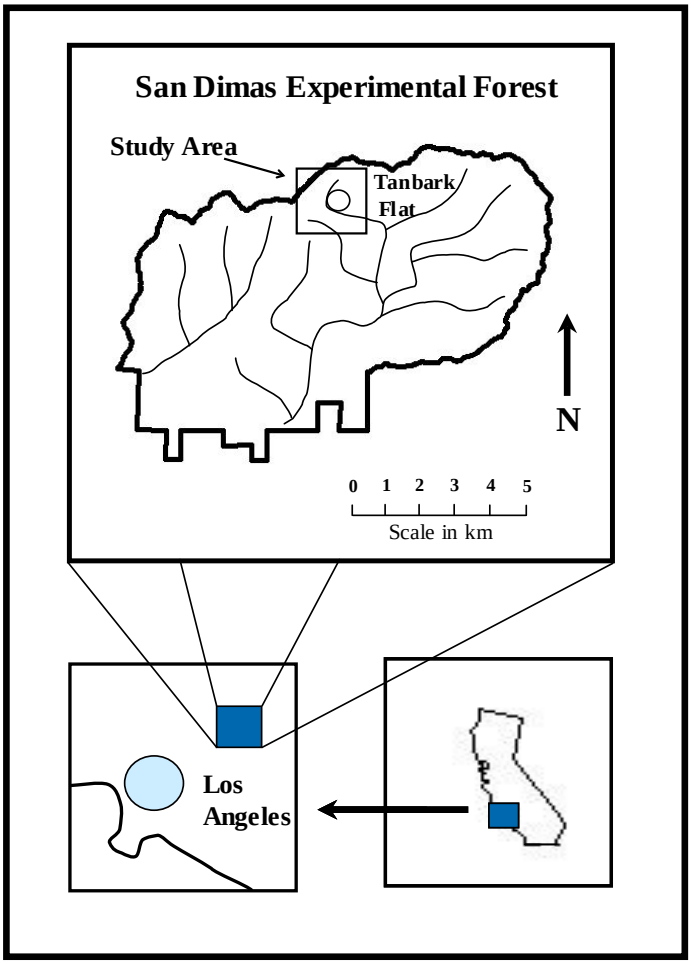

Figure 1 Location map of the San Dimas Experimental Forest.

Native vegetation in the SDEF consists primarily of mixed chaparral. Plant cover on south-facing slopes ranges from dense stands of chamise (*Adenostoma fasciculatum*) and ceanothus (*Ceanothus* spp.) to more open stands of chamise and black sage (*Salvia mellifera*). North-facing hillsides are dominated by scrub oak (*Quercus berberidifolia*) and ceanothus, with occasional hardwood trees – live oak (*Quercus agrifolia*) and California laurel (*Umbellularia californica*) – occurring on moister shaded slopes and along the riparian corridors (Wohlgemuth 2006). Fuel loadings of mature chaparral on the SDEF ranged from 110 to 135 Mg ha^{-1} (40-50 t ac^{-1}) (Ottmar et al. 2000). Management treatments following a wildfire in 1960 involved the vegetation type-conversion of some native chaparral watersheds to a mixture of perennial grasses. It was thought that type-conversion would aid in future fire control and would enhance water yield (Rice et al. 1965). To assist in the grass establishment, regenerating shrubs were sprayed with herbicides. These perennials included a variety of wheatgrass species (*Agropyron spp*.), Harding grass (*Phalaris tuberosa* var. *stenoptera*), big bluegrass (*Poa ampla*), smilo grass (*Piptatherum miliaceum*), veldt grass (*Ehrharta calycina*), and blando brome (*Bromus hordaceous*) (Corbett and Green 1965). By 2002, substantial amounts of buckwheat (*Eriogonum fasiculatum*) and

black sage had also established on the type-converted watersheds. Fuel loadings on the converted watersheds prior to the 2002 wildfire were 14-27 Mg ha^{-1} (5-10 t ac^{-1}) (Ottmar et al. 2000).

In 1994, a study was initiated to quantify sediment fluxes through several small (1-3 ha) headwater catchments in the SDEF that last burned in the 1960 wildfire (Wohlgemuth 1996). One of these chaparral watersheds was burned in a prescribed fire of moderate to high severity in 2001 (Wohlgemuth and Hubbert 2008). Following a winter drought and a hot, dry summer, almost all of the SDEF burned in a wildfire in late September 2002. A smoke plume that rose almost vertically indicated an absence of wind, which allowed the fire to burn relatively slowly, permitting longer fire residence times that resulted in substantial soil heating. In most parts of the SDEF, the fire burned at high severity, consuming all the aboveground biomass and leaving only the skeletons of the largest stems (Napper 2002). The areas that burned in the 2001 prescribed fire did not re-burn in the 2002 wildfire. Both fires burned over the aforementioned sediment flux study, providing a unique opportunity to quantify hillslope erosion and small watershed sediment yield following fire on the same sites for which there were extensive pre-fire measurements.

METHODS

In the sediment flux study, four small watersheds were selected to measure hillslope erosion: three in native chaparral vegetation and one in type-converted grass (Wohlgemuth 1996). Hillslope erosion was sampled using sheet metal collector traps (Figure 2) with a 30 cm aperture (Wells and Wohlgemuth 1987). Seventy-five traps sampled unbounded plots on both vertical hillslope transects and at the slope/channel interface in each watershed. The traps were installed in summer 1994. Sediment was collected for 7 years prior to the prescribed burn and 8 years prior to the wildfire. Sediment collection continued through the fifth (wildfire) or sixth (prescribed burn) post-fire winter. Hillslope erosion is expressed as a yield: the air-dried mass of collected debris per square meter of potential contributing area normalized to an annual rate based on the length of the collection period (kg m^{-2} yr^{-1}). The median value from these sediment collectors was used as a measure of central tendency for comparisons. These traps were serviced multiple times per year to distinguish wet season hillslope erosion lasting approximately four months from dry season hillslope erosion lasting about eight months.

Sediment was also trapped and measured behind earthen dams (Figure 3) constructed after the 1960 wildfire (Rice et al. 1965). These debris basins were re-activated in winter 1994. Sediment yields were calculated using an engineering end-area formula (Eakin 1939) based on repeated sag tape surveys of permanent cross sections (Ray and Megahan 1978). Sediment yield was measured for 7 or 8 years prior to and 5 or 6 years following the prescribed burn or wildfire as described above. Sediment yield was normalized by contributing area to account for catchments of different sizes and aggregated to annual totals (m^3 ha^{-1} yr^{-1}).

A centrally located weighing raingage recorded precipitation amounts and intensities throughout the study period.

Figure 2 Hillslope erosion sediment collector trap.

Figure 3 Debris basin for trapping small watershed sediment yield.

RESULTS AND DISCUSSION

Rainfall: Rainfall is the ultimate driver of all hydrologic erosion, both on the hillside slopes and in the channels of ephemeral streams. Annual rainfall totals and peak 30-minute intensities for the duration of the study period are arrayed in Table 1. During this period, both the highest (1848 mm) and the lowest (252 mm) rainfall totals of the entire 80-year record were experienced. Generally, high annual totals correlated positively with peak 30-minute intensities, but there were some notable exceptions (Table 1). Of the 13 years of study, only four exceeded the annual average rainfall and only four exceeded average peak intensity. The prescribed burn was followed by the record low annual total but with a peak intensity slightly above average, while the wildfire was followed by a sub-normal annual total and a peak intensity that was only half the long-term average (Table 1).

Hillslope Erosion: Surface erosion yields from the collector traps are arrayed by watershed and season in Table 1. Prior to fire, hillslope erosion was considerably less under the type-converted grass vegetation than the native chaparral, as previously reported (Wohlgemuth 1996, 2006). This difference may be explained by the density of plant stems providing barriers to surface erosion: chaparral typically has a density of about 1 stem per square meter while the grass has a density of thousands of stems per square meter, creating a variable resistance to the processes of

erosion between the two vegetation types. Furthermore, the amount of dry season erosion and wet season erosion was roughly equal in the unburned condition (as opposed to their yields over unequal time spans as displayed in Table 1). The protection afforded by the plant canopies and extensive litter layers prevented surface runoff on the unburned hillsides except during the most intense rainstorms. Thus wet season hillslope erosion was muted on the unburned landscape, being no greater than ravel, the pervasive erosion process during the dry season (Rice 1974).

Table 1 Median (n=75) hillslope erosion yields (kg m^{-2} yr^{-1}) by watershed and season. I_{30} is peak 30 minute rainfall intensity. Watershed Chaparral 3 was burned in a prescribed fire one year prior to the wildfire. Numbers in italics are post-fire values.

			Watershed							
	Rainfall		Grass		Chaparral 1		Chaparral 2		Chaparral 3	
Year	Total (mm)	I_{30} (mm hr^{-1})	Dry	Wet	Dry	Wet	Dry	Wet	Dry	Wet
1995	1227	20	0.02	0.05	0.28	0.64	0.32	0.67	0.20	0.45
1996	688	59	0.01	0.02	0.32	0.66	0.26	0.33	0.31	0.54
1997	738	18	0.01	0.01	0.30	0.47	0.26	0.35	0.28	0.36
1998	1367	53	0.04	0.02	0.34	0.48	0.36	0.43	0.44	0.42
1999	347	19	0.01	0.01	0.37	0.36	0.36	0.38	0.31	0.45
2000	526	16	0.01	0.01	0.26	0.49	0.33	0.40	0.28	0.40
2001	597	12	0.02	0.01	0.46	0.32	0.45	0.31	0.32	0.43
2002	252	33	0.02	0.01	0.33	0.16	0.29	0.22	*0.95*	*1.62*
2003	615	14	*0.18*	*4.68*	*1.41*	*8.70*	*0.74*	*5.12*	*0.34*	*0.95*
2004	408	17	*0.07*	*0.09*	*0.11*	*0.28*	*0.06*	*0.21*	*0.05*	*0.06*
2005	1848	49	*0.06*	*0.07*	*0.18*	*0.13*	*0.15*	*0.13*	*0.08*	*0.07*
2006	690	22	*0.05*	*0.02*	*0.20*	*0.14*	*0.15*	*0.08*	*0.16*	*0.06*
2007	277	17	*0.02*	*0.01*	*0.07*	*0.06*	*0.05*	*0.04*	*0.05*	*0.06*

In the first post-fire year, despite low rainfall totals (prescribed fire) or intensities (wildfire), yields of surface erosion increased by 1-2 orders of magnitude compared to pre-burn rates (Table 1), as the vegetative barriers were incinerated by fire and resistances to the forces of erosion were removed. Moreover, the pre-fire difference in yield between grass and chaparral vegetation disappeared, as fire eliminated any differential resistances among the vegetation types resulting in a very similar erosion response. However, in the immediate post-fire environment, wet season hillslope yield was substantially greater than dry season yield (Table 1), likely caused by the alterations in soil characteristics which affect post-fire hillslope hydrology and increased surface runoff (DeBano 1981).

In subsequent post-fire years the patterns of pre-fire surface erosion returned. Yield was once again greater under chaparral vegetation than under grass (Table 1), although the chaparral values were much smaller than in the pre-fire environment. Some of this reduction is likely due to the proliferation of re-growing near-surface vegetation (Barro and Conard 1991), but it could also reflect the loss of the easily mobilized sediment that exposed a less erodible material at the surface, effectively reducing the sediment supply (Wohlgemuth and Hubbert 2008). In addition, by the third post-fire year, dry season hillslope yields were greater than wet season yields (Table

1). This rapid return to pre-fire patterns suggests that recovery to hillslope erosion baseline levels can occur very quickly in this southern California locale.

Intuitively, wet season hillslope erosion should be related to rainfall. However, there is no discernable relationship between annual rainfall total or peak intensity and wet season hillslope erosion, either before or after fire (Table 1). This suggests that although rainfall is a necessary driver, hillslope sediment yield is governed more by the landscape sensitivity and differential resistances to the agents of erosion.

Small Watershed Sediment Yield: Sediment yield in the debris basins is arrayed by watershed in Table 2. Pre-fire watershed sediment yield was minor and associated with high rainfall years. More often than not, the annual sediment yield from these small watersheds was zero (Table 2). Prior to fire, watershed sediment yield was less in the grass vegetation than the chaparral (Table 2), presumably associated with the greater hillslope erosion, sediment delivery, and channel loading under the shrub vegetation. Immediately following fire, despite the low rainfall values, watershed sediment yields increased by 1-2 orders of magnitude over pre-fire levels (Table 2). Field observations confirmed both an extensive rill network, indicating the delivery of water and sediment from the burned hillsides, and channel scour of the existing in-channel deposits of stored sediment. Furthermore, first-year post-fire sediment yield from these small watersheds was roughly similar for both vegetation types, suggesting again the removal of differential resistances to promote a nearly equal erosion response. In subsequent post-fire years, watershed sediment yield was minor, associated with high rainfall, and greater in chaparral catchments compared to type-converted grass drainage basins. This very rapid return to pre-fire patterns of small watershed sediment yield again suggests that this environment can recovery very quickly to baseline conditions.

Table 2 Annual sediment yield (m^3 ha^{-1} yr^{-1}) by watershed. I_{30} is peak 30 minute rainfall intensity. Watershed Chaparral 3 was burned in a prescribed fire one year prior to the wildfire. Numbers in italics are post-fire values.

	Rainfall		Watershed			
Year	Total (mm)	I_{30} (mm hr^{-1})	Grass	Chaparral 1	Chaparral 2	Chaparral 3
1995	1227	20	0	0	0.63	0
1996	688	59	0	0	0	6.35
1997	738	18	0	0	0	0
1998	1367	53	0.71	1.66	5.45	3.72
1999	347	19	0	0	0	0
2000	526	16	0	0	0	0
2001	597	12	0	0	0	0
2002	252	33	0	0	0	*31.16*
2003	615	14	*32.19*	*11.26*	*24.87*	*2.11*
2004	408	17	*0.11*	*0*	*0.74*	*4.02*
2005	1848	49	*2.60*	*4.87*	*9.38*	*1.81*
2006	690	22	*0*	*0*	*0*	*0.58*
2007	277	17	*0*	*0*	*0*	*0*

Prescribed Fire Versus Wildfire: Prescribed burns are conducted under more moderate conditions of weather and fuel moisture to prevent an unplanned and costly fire escape. It is therefore generally assumed that the erosion response to a prescribed fire should be less than that from a wildfire (Loomis et al. 2003). However, for comparable chaparral-covered catchments in this study, the patterns of post-fire hillslope erosion and small watershed sediment yield are very similar: an immediate spike in sediment production followed by a quick return to baseline levels (Tables 1 and 2), perhaps suggesting that some threshold of landscape response is exceeded by all fire in these chaparral environments. The greater wet season hillslope erosion values following the wildfire compared to the prescribed fire (Table 1) can be explained by the total rainfall values but also by the time of burning. The prescribed fire burned in mid-May while the wildfire burned in late September. With initial heavy storms of the rainy season typically commencing in November or December, the areas of the prescribed fire had more time to heal, including some vegetation re-growth, than did the areas that burned in the wildfire. The prescribed-burn area was therefore better able to resist the hydrologic forces of winter storms than the freshly-burned hillsides after the wildfire. However, the prescribed fire has a slightly flatter recovery curve (2 years) than the wildfire (1 year), suggesting that the response to these two different types of fires is not identical (Table 1), perhaps reflecting the differences in rainfall totals and intensities.

A Benchmark for Post-fire Erosion Models: The value of this study is that it quantifies long-term hillslope erosion and small watershed sediment yield from the same plots and sites both before and after fire. As such, it provides a benchmark to evaluate the performance of predictive models of post-fire sediment yield from southern California chaparral environments. These models, which run the gamut from strictly empirical (Universal Soil Loss Equation; Wischmeier and Smith, 1978) to physically-based (Water Erosion Prediction Project; Laflen et al. 1991), are used by land management and hazard protection agencies to estimate the magnitudes of post-fire erosion events. Future work will involve the testing of a variety of predictive models against this dataset to evaluate their performance as a tool for planning and risk assessment in southern California chaparral watersheds.

SUMMARY

The timing and patterns of hillslope erosion and small watershed sediment yield were quantified when a prescribed fire and a subsequent wildfire burned over a sediment flux study, providing pre-fire and post-fire erosion values for the exact same sampling units, including the complete post-fire erosion record. The data suggest that, although there is not an exact correspondence, for this southern California chaparral locale erosion on the hillsides and the output from small catchments are remarkably similar: a 1-2 order of magnitude increase in immediate post-fire erosion over pre-fire yields followed by a relatively rapid recovery to baseline levels. Grass vegetation produced less erosion than comparable chaparral areas prior to fire, most likely because of differences in stem densities and channel loading, but these differences were erased immediately after fire and the landscape appeared to be eroding equally. Wet season hillslope erosion was especially enhanced following fire, most likely due to attendant changes in soil characteristics that promote overland flow. Although there appeared to be a relationship between rainfall and small watershed sediment yield, there seemed to be no association between wet

season hillslope erosion and either total rain or peak rainfall intensity. In chaparral vegetation the response to a prescribed fire was very similar to that of a wildfire, although there was a slightly flatter recovery curve following the prescribed burn, perhaps because of different rainfall patterns. This suggests that some threshold of landscape response is exceeded by all fire in these southern California chaparral environments.

REFERENCES

Barro, S.C., and Conard, S.G. (1991). "Fire effects on California chaparral systems: An overview," Environment International, 17 pp 135-149.

Bonnin, G.M., Martin, D., Lin, B., Parzybok, T., Yekta, M., and Riley, D. (2011). "Precipitation-Frequency Atlas of the United States." NOAA Atlas 14. US Department of Commerce.

Corbett, E.S., and Green, L.R. (1965). "Emergency revegetation to rehabilitate burned watersheds in southern California," Research Paper PSW-22, USDA Forest Service, Berkeley, CA.

DeBano, L.F. (1981). "Water repellent soils: A state-of-the-art," General Technical Report PSW-46, USDA Forest Service, Berkeley, CA.

Dunn, P.H., Barro, S.C., Wells, W.G., II, Poth, M.A., Wohlgemuth, P.M., and Colver, C.G. (1988). "The San Dimas Experimental Forest: 50 years of research," General Technical Report PSW-104, USDA Forest Service, Berkeley, CA.

Eakin, H.M. (1939). "Instructions for reservoir sedimentation surveys," Silting of Reservoirs. U.S. Department of Agriculture, Technical Bulletin 524, pp 153-164.

Keeley, J.E. (2006). "South coast bioregion," Fire in California Ecosystems, Suguhara, N.G. et al., eds. University of California Press, Berkeley, CA.

Laflen, J.M, Lane, L.J., and Foster, G.R. (1991). "WEPP – A next generation of erosion prediction technology," Journal of Soil and Water Conservation, 46(1), pp.34-38.

Loomis, J., Wohlgemuth, P.M., Gonzalez-Caban, A., and English, D. (2003). "Economic benefits of reducing fire-related sediment in southwestern fire-prone ecosystems," Water Resources Research, 39(9), pp. WES 3-1-WES 3-8.

Napper, C. (2002). "BAER Report, Williams Fire," USDA Forest Service, Angeles National Forest, FS-2500-8.

Ottmar, R.D., Vihnanek, R.E., and Regelbrugge, J.C. (2000). "Stereo photo series for quantifying natural fuels," Volume IV: Pinyon-juniper, chaparral, and sagebrush types in the Southwestern United States. PMS 883. National Wildfire Coordinating Group, Boise, ID.

Ray, G.A., and Megahan, W.F. (1978). "Measuring cross sections using a sag tape: A generalized procedure," General Technical Report INT-47. USDA Forest Service, Ogden, UT.

Rice, R.M. (1974). "The hydrology of chaparral watersheds," Proc. Symposium on Living with the Chaparral, Riverside, CA, Sierra Club, San Francisco, CA. pp 27-34.

Rice, R.M., Crouse, R.P., and Corbett, E.S. (1965). "Emergency measures to control erosion after a fire on the San Dimas Experimental Forest," U.S. Department of Agriculture, Miscellaneous Publication 970, pp 123-130.

Sugihara, N.G., and Barbour, M.G. (2006). "Fire and California vegetation," Fire in California Ecosystems, Suguhara, N.G. et al., eds. University of California Press, Berkeley, CA.

Wells, W.G., II. (1987). "The effects of fire on the generation of debris flows in southern California," Geological Society of America, Reviews in Engineering Geology, 7, pp 105-114.

Wells, W.G., II, and Wohlgemuth, P.M. (1987). "Sediment traps for measuring onslope surface sediment movement," Research Note PSW-393, USDA Forest Service, Berkeley, CA.

Wischmeier, W.H. and Smith, D.D. (1978). "Predicting rainfall erosion losses: A guide to conservation planning," Agriculture Handbook No. 537, U.S. Department of Agriculture, 58pp.

Wohlgemuth, P.M. (1996). "Hillslope erosion, channel routing, and sediment yield in small semiarid watersheds, southern California," Proc. 6th Federal Interagency Sedimentation Conference, Las Vegas, NV, Interagency Advisory Committee on Water Data, Subcommittee on Sedimentation, Washington, D.C., pp X54-X61.

Wohlgemuth, P.M. (2006). "Hillslope erosion and small watershed sediment yield following a wildfire on the San Dimas Experimental Forest, southern California," Proc. 8th Federal Interagency Sedimentation Conference, Reno, NV, Interagency Advisory Committee on Water Data, Subcommittee on Sedimentation, Washington, D.C.

Wohlgemuth, P.M., and Hubbert, K.R. (2008). "The effects of fire on soil hydrologic properties and sediment fluxes in chaparral steeplands, southern California," Proc. California Association for Fire Ecology Conference, San Diego, CA, General Technical Report PSW-189, USDA Forest Service, Albany, CA.

PREDICTING WATERSHED POST-FIRE SEDIMENT YIELD WITH THE InVEST SEDIMENT RETENTION MODEL: ACCURACY AND UNCERTAINTIES

Joel B. Sankey, Research Geologist, U.S. Geological Survey, Southwest Biological Science Center, Grand Canyon Monitoring and Research Center, Flagstaff, AZ, jsankey@usgs.gov; Jason McVay, Geospatial Research Specialist, Northern Arizona University, Remote Sensing and Geoinformatics Lab, Flagstaff, AZ, jlm683@nau.edu; Jason Kreitler, Research Geographer, U.S. Geological Survey, Western Geographic Science Center, Boise, ID, jkreitler@usgs.gov; Todd Hawbaker, Research Ecologist, U.S. Geological Survey, Geosciences and Environmental Change Science Center, Denver, CO, tjhawbaker@usgs.gov; Nicole Vaillant, Fire Ecologist, USDA Forest Service, Western Wildland Environmental Threat Assessment Center, Pacific Northwest Research Station, Prineville, OR, nvaillant@fs.fed.us; Scott Lowe, Assistant Professor, Boise State University, Department of Economics, Boise, ID, scottlowe@boisestate.edu

Abstract: Increased sedimentation following wildland fire can negatively impact water supply and water quality. Understanding how changing fire frequency, extent, and location will affect watersheds and the ecosystem services they supply to communities is of great societal importance in the western USA and throughout the world. In this work we assess the utility of the InVEST (Integrated Valuation of Ecosystem Services and Tradeoffs) Sediment Retention Model to accurately characterize erosion and sedimentation of burned watersheds. InVEST was developed by the Natural Capital Project at Stanford University (Tallis et al., 2014) and is a suite of GIS-based implementations of common process models, engineered for high-end computing to allow the faster simulation of larger landscapes and incorporation into decision-making. The InVEST Sediment Retention Model is based on common soil erosion models (e.g., USLE – Universal Soil Loss Equation) and determines which areas of the landscape contribute the greatest sediment loads to a hydrological network and conversely evaluate the ecosystem service of sediment retention on a watershed basis. In this study, we evaluate the accuracy and uncertainties for InVEST predictions of increased sedimentation after fire, using measured post-fire sediment yields available for many watersheds throughout the western USA from an existing, published large database. We show that the model can be parameterized in a relatively simple fashion to predict post-fire sediment yield with accuracy. Our ultimate goal is to use the model to accurately predict variability in post-fire sediment yield at a watershed scale as a function of future wildfire conditions.

INTRODUCTION

Fire suppression and the increased accumulation of fuels over the last century has led to a greater risk of high severity wildland fires for many watersheds of the western USA. Future climate change in the form of warmer temperatures and altered precipitation regimes may further increase wildfire potential (Flannigan et al., 2000, Westerling et al. 2006). Wildfire can impact watersheds through changes in the timing and amount of runoff, and increased erosion and sedimentation (Miller et al., 2011). These processes can negatively affect water quality, water supply, and other important ecosystem services such as sediment retention, which is a measure of the capacity for a watershed to withstand erosion and sedimentation.

When fire occurs on a landscape, burning immediately alters the existing distribution and structure of vegetation (Larsen et al., 2009). Vegetation can slow down overland flow of water and reduce the erosive force and sediment transport capacity of water. Vegetation can also trap and filter sediment transported by water. Collectively, these characteristics of vegetation contribute to the ability of a watershed to retain sediment, which results in the afore-mentioned ecosystem service. Combustion of vegetation thereby reduces watershed sediment retention.

Burning also directly alters soil characteristics (González-Pérez et al., 2004). Depending on the intensity of heat during a fire, soil organic content can be reduced and clay particles can become aggregated into fine silt-sized particles (Giovannini et al., 2001). The loss of organic material and a litter layer that otherwise provide a protective shield to the soil surface can increase soil erosion through increased exposure to rain splash, decreased infiltration, and increased sheet wash and rill erosion (DeBano, 2000). Intense heat also changes the carbon and nitrogen balance in soil, and can trigger a reduction in microbial activity (Choromanska and DeLuca, 2002). Collectively, these factors can increase erodibility of soil post-fire. In addition to post-fire changes in vegetation, increased erodibility further decreases watershed sediment retention.

The ability to efficiently and accurately model sediment retention at the scale of individual watersheds for a large number of watersheds is important (Miller et al., 2011). It provides a tool for resource managers to better understand and simulate how fire effects on vegetation and soil may affect the ecosystem service of sediment retention or conversely, post-fire sediment yield. The InVEST suite of ecosystem service models are an open source, stand-alone platform developed by Stanford University as part of the Natural Capital Project. The Sediment Retention model is designed to evaluate sediment retention at a watershed scale to enable the assessment of tradeoffs for natural resource management decisions (Tallis et al., 2014). The Sediment Retention model can be used to simulate how changes in vegetation and soil erodibility, which occur as a function of landscape processes such as fire, may affect watershed sediment retention or sediment yield. Moreover, the InVEST predictions under different scenarios of vegetation and soil condition can be evaluated as indicators of the potential relative change in the ecosystem service as a function of wildfire. The GIS-based Sediment Retention model implements the Universal Soil Loss Equation (USLE) (Wischmeier and Smith, 1978) to predict annual potential erosion at the pixel scale and annual sedimentation and retention at the watershed scale. The model takes into account landform, climate, soil, and vegetation properties. Users can also assess the influence of different vegetation types and soil properties.

For the western USA, Moody and Martin (2009) completed a comprehensive and exhaustive review and synthesis of measured post-fire sediment yields (Figures 1 and 2). Their study divided the western United States into four regions based on rainfall regimes: Pacific, Sub-Pacific, Arizona, and Plains, which vary by seasonal distribution of rainfall; and with sub-categories of Extreme, High, Medium, and Low rainfall intensity. Within these regions they identified all of the published measurements of post-fire sediment yield. The synthesis identified 135 measurements in 43 unique watersheds (defined at the Hydrologic Unit Code 8 “HUC-8” level) that spanned post-fire episodes from 1927 to 2007. They further identified whether the measurements were conducted on hillslope or channel landscape positions, whether they were conducted at point or plot scales, and whether they targeted a specific range of particle size

and/or transport mechanism. This resulted in a classification of each measurement into one of four types: Hillslope Points (H-Pt), Hillslope Plots (H-Plot), Channel Suspended Sediment (CSS), and Channel Volume (C-V) measurements (Moody and Martin, 2009). The Moody and Martin (2009) synthesis of post-fire sedimentation provides a baseline of field data to calibrate sediment yield predictions made with the InVEST Sediment Retention model in our study (Figures 1 and 2).

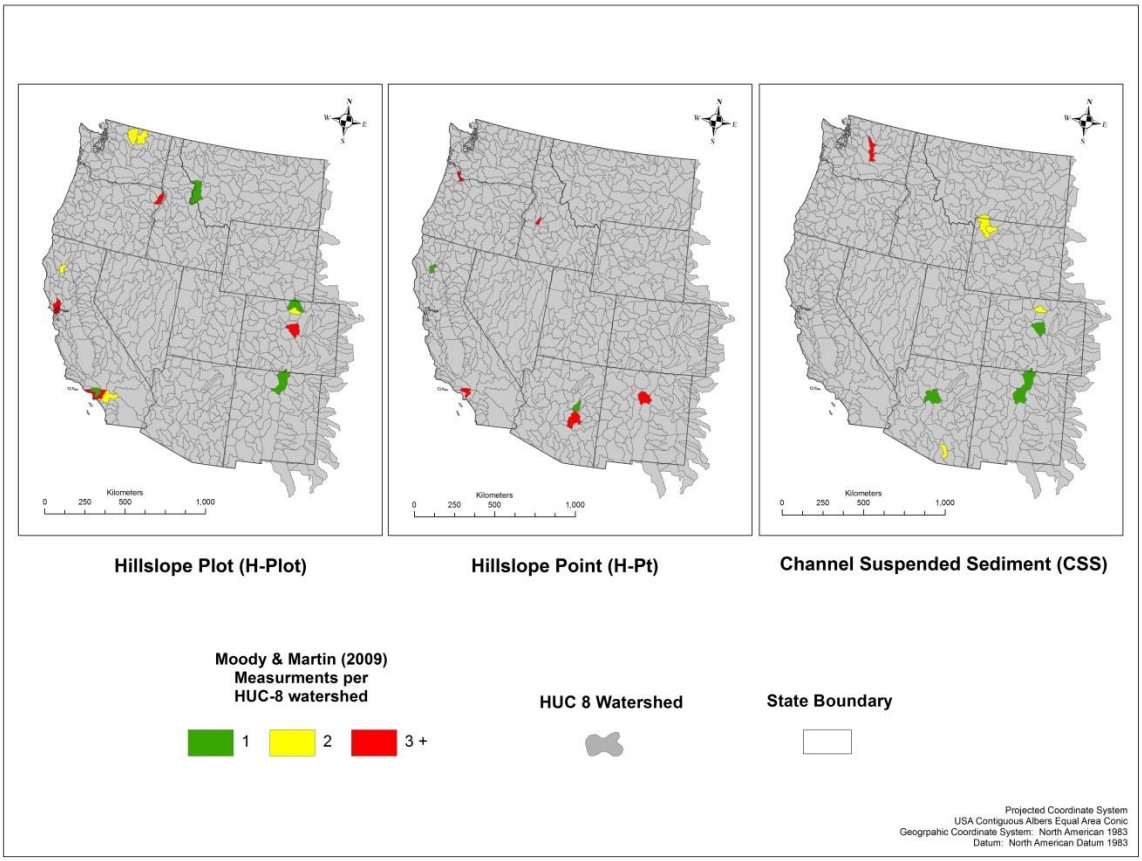

Figure 1 Number of hillslope plot (H-Plot), point (H-Pt), and channel suspended sediment (CSS) measurements synthesized by Moody and Martin (2009) per HUC-8 watershed in the western USA.

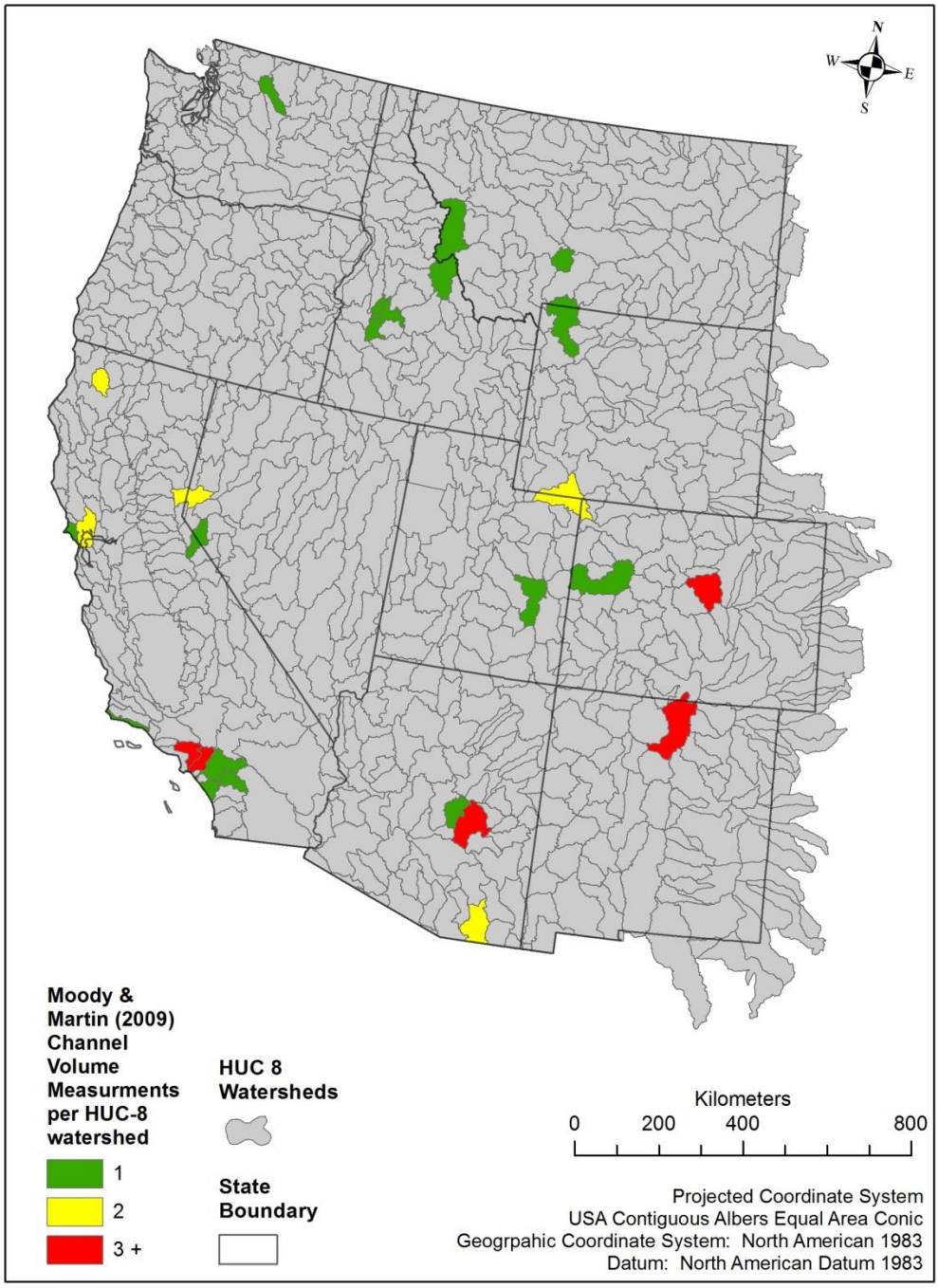

Figure 2 Number of channel volume (CV) measurements synthesized by Moody and Martin (2009) per HUC-8 watershed in the western USA.

OBJECTIVE

In this study, our primary objective was to parameterize and calibrate the InVEST Sediment Retention model to predict post-fire sediment yield at a watershed-scale as accurately as possible. We used measured post-fire sediment yields for watersheds reviewed in the Moody and Martin (2009) synthesis as the baseline calibration data set. We evaluated the relative ability of the model to accurately predict sediment yield for the 4 different types of measurements identified by Moody and Martin (2009). Because the Sediment Retention model is a watershed-scale model we hypothesized that it would most accurately predict measurements made within channel landscape positions (CSS or C-V), which presumably integrate over a greater upslope area of the watershed, than measurements made on hillslopes at plots (H-Plot) or points (H-Pt) within the watershed. Moreover, we hypothesized that the Sediment Retention model would most accurately predict channel volume (C-V) as opposed to channel suspended sediment (CSS) measurements because the model is not designed to target the more narrowly defined range of particle size fractions of sediment transported in suspension. Therefore, we first determined the best-fit parameter set for the particular measurement type that we identified as most appropriate through tests of the aforementioned hypotheses. Then we used the calibrated Sediment Retention model to predict sediment yield response to wildfire for all HUC-8 watersheds across the western United States.

METHODS

We predicted watershed sediment yield (tons/HA) with the InVEST Sediment Retention model for watersheds delineated at the HUC-8 level in the western USA (USGS, www.water.usgs.gov). In order to predict sediment yield, the Sediment Retention model requires Digital Elevation Model (DEM), land use/land cover (LULC), Soil Erosivity (R-Factor), and Soil Erodibility (K-Factor) raster datasets. The model requires a vector dataset that defines the watershed boundaries, and several user-defined tables that characterize important biophysical characteristics of the watersheds.

We used a 90 m resolution DEM (USGS, seamless.usgs.gov) with stream networks from the USGS National Hydrography Dataset (USGS, nhd.usgs.gov) “burned” in and small holes filled using the InVEST toolbox for ArcGIS. We used the National Land Cover Dataset (NLCD) 2006 (USGS, www.mrlc.gov) which has 16 land cover classes at 30 m resolution as the LULC raster.

The R-factor is a climatic indicator that estimates the kinetic energy of rainfall at the maximum 30 minute intensity. We converted an R-Factor vector layer produced by the Environmental Protection Agency (EPA) at the HUC-8 scale (EPA, www.epa.gov), to a 30-m R-Factor raster using a (multiplication) factor of 17.02 to convert from imperial to metric units (Tallis et al., 2014).

The K-Factor is an estimate of soil erodibility as a function of soil development and horizonation, texture, organic matter, and permeability. This was created from the State Soil Geographic Database (STATSGO) K-Factor vector data (USDA, Natural Resources Conservation Service; www.nrcs.usda.gov) and transformed into a 30-m raster dataset.

The Sediment Retention model requires a biophysical table characterizing response by land use/land cover type. Variables in the table include the sediment retention efficiency value which characterizes the relative ability of the vegetation type to slow down overland flow and trap and filter sediment transported by water. The sediment retention efficiency is a floating point index from 0 to 1, where 0.0 = minimum, and 1.0 = maximum, sediment retention. The biophysical table also includes the cover-management factor (C), and the support practice factor (P) values from the USLE. The C and P factors are important agricultural metrics that account for cover crop management and tilling practices, but were not integral to this study. As our study focused on pre- and post-fire conditions for a range of landcover types throughout the western USA, C and P factors were left at default values for all classes and all watersheds (Tallis et al., 2014).

A sediment threshold table containing information about expected reservoir lifetime, water volume, and annual sediment load is required for the intended assessment of the effect of sedimentation on hydropower, but not necessary to modify for our predictions of sediment yield. For the purpose of the table, we treated each watershed as the catchment area for a single reservoir and left default values in place (Tallis et al., 2014).

The Sediment Retention model takes into account a user-defined threshold flow accumulation number, which is the number of upstream pixel cells that must flow into a cell before it is counted as part of the stream network. The threshold flow accumulation number is therefore important for accurately characterizing the watershed drainage network. The Sediment Retention model also requires a slope threshold, which is included to account for agricultural landscapes on steep hillslopes. We heuristically experimented with different values for these variables but ultimately used the default of 1000 cells for threshold flow accumulation, and 75% slope threshold (Tallis et al., 2014).

We first predicted sediment yield for each HUC-8 watershed in the western USA using the aforementioned data and recommended default settings (Tallis et al., 2014). Next, we adjusted vegetation and soil characteristics in the input datasets in order to predict sediment yield for simulated post-fire characteristics of vegetation and soil. We specifically set the sediment retention efficiency value (i.e., of vegetation) to 0.0 for each watershed in the biophysical table, and we increased the soil erodibility (K) by one order of magnitude. These sediment retention and soil erodibility values were intended to simulate an extreme effect of fire in which the ability for vegetation to retain sediment is negated and soil erodibility is dramatically increased. These sediment retention efficiency and soil erodibility values were found heuristically to best predict measured sediment yield in the synthesis by Moody and Martin (2009). We compared sediment yield predicted with the InVEST model using the adjusted sediment retention and soil erodibility values to measured sediment yield reported in Moody and Martin (2009) for each HUC-8 watershed that contained at least one reported sediment yield measurement. We compared predictions to measurements aggregated by type (H-Pt, H-Plot, CSS, C-V) for each watershed. For watersheds with more than 1 measurement of a given type we calculated the mean of measured values of post-fire sediment yield by measurement type (which in some cases included unique measurements of the same type and within the same watershed but from multiple fires during the past century). To evaluate the accuracy of model predictions we focused on watersheds that had at least 3 post-fire measurements per type (Figures 1 and 2), and compared the mean measured post-fire watershed sediment yield to the yield predicted with the InVEST

Sediment Retention model using linear regression and by calculating an average prediction error (Root Mean Squared Error – RMSE).

RESULTS

InVEST model predictions of post-fire sediment yield were not significantly related to sediment yield measurements made with the C-SS, H-Plot, or H-Pt methods and reported in Moody and Martin (2009) (results otherwise not shown). The model accurately predicted mean post-fire sediment yield for those watersheds (n = 5) with at least 3 discrete channel volume (C-V) measurements reported in the Moody and Martin (2009) synthesis (Figure 3). The model accurately predicted approximately 50% of the variability in the mean C-V measurements. The RMSE average prediction error for these 5 watersheds (N ≥ 3 post-fire C-V measurements) was 149.29 tons/HA. The variance of reported channel volume measurements appeared to be large for some watersheds (e.g., standard error bars for measurement means in Figure 3) relative to the average prediction error of the model. Maps in Figures 4 and 5 show predicted sediment yield for all HUC-8 watersheds of the western USA based on: 1) the default parameters (Figure 4) for the InVEST Sediment Retention model (described in Methods section); and 2) the adjusted sediment retention efficiency and erodibility (K) values intended to simulate post-fire vegetation and soil conditions (Figure 5).

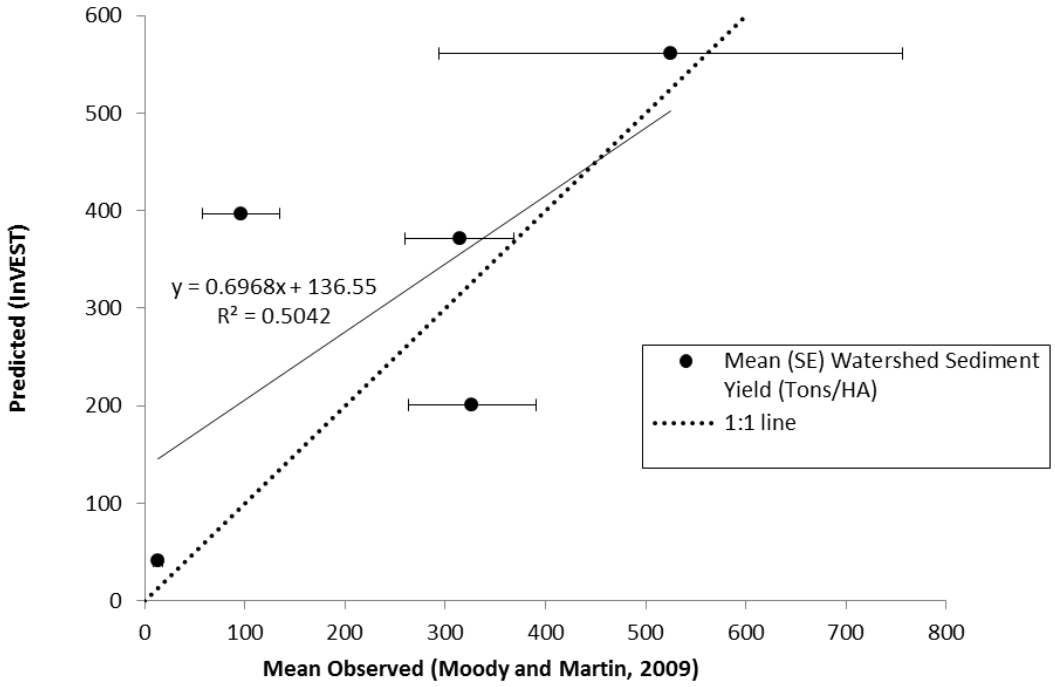

Figure 3 Post-fire sediment yield (tons/ha) predicted with InVEST plotted as a function of mean measured post-fire channel volume sediment yield for watersheds with at least 3 measurements reported in Moody and Martin (2009).

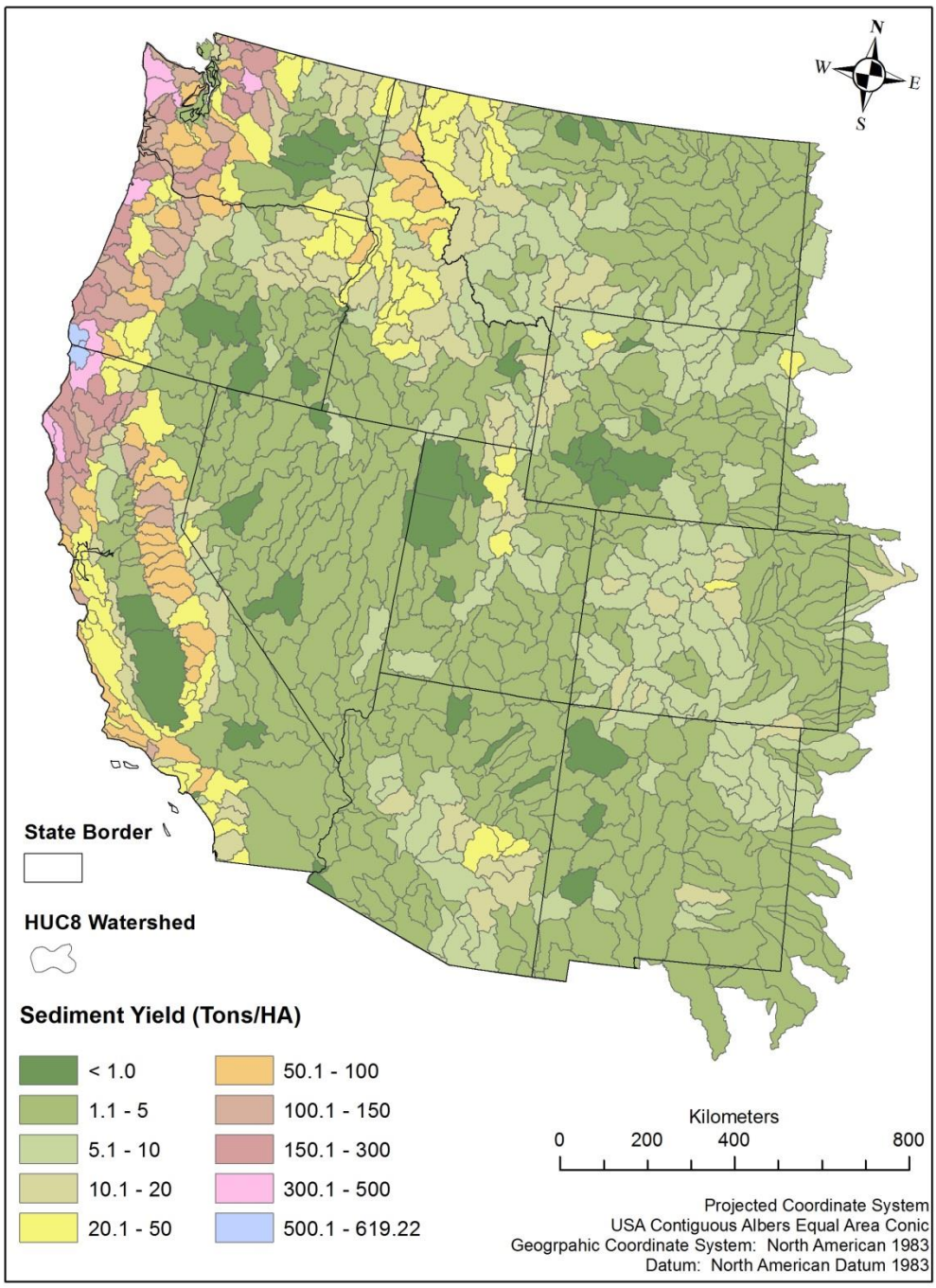

Figure 4 InVEST modeled sediment yield (tons/ha) for all HUC-8 watersheds using normal (default) input parameters.

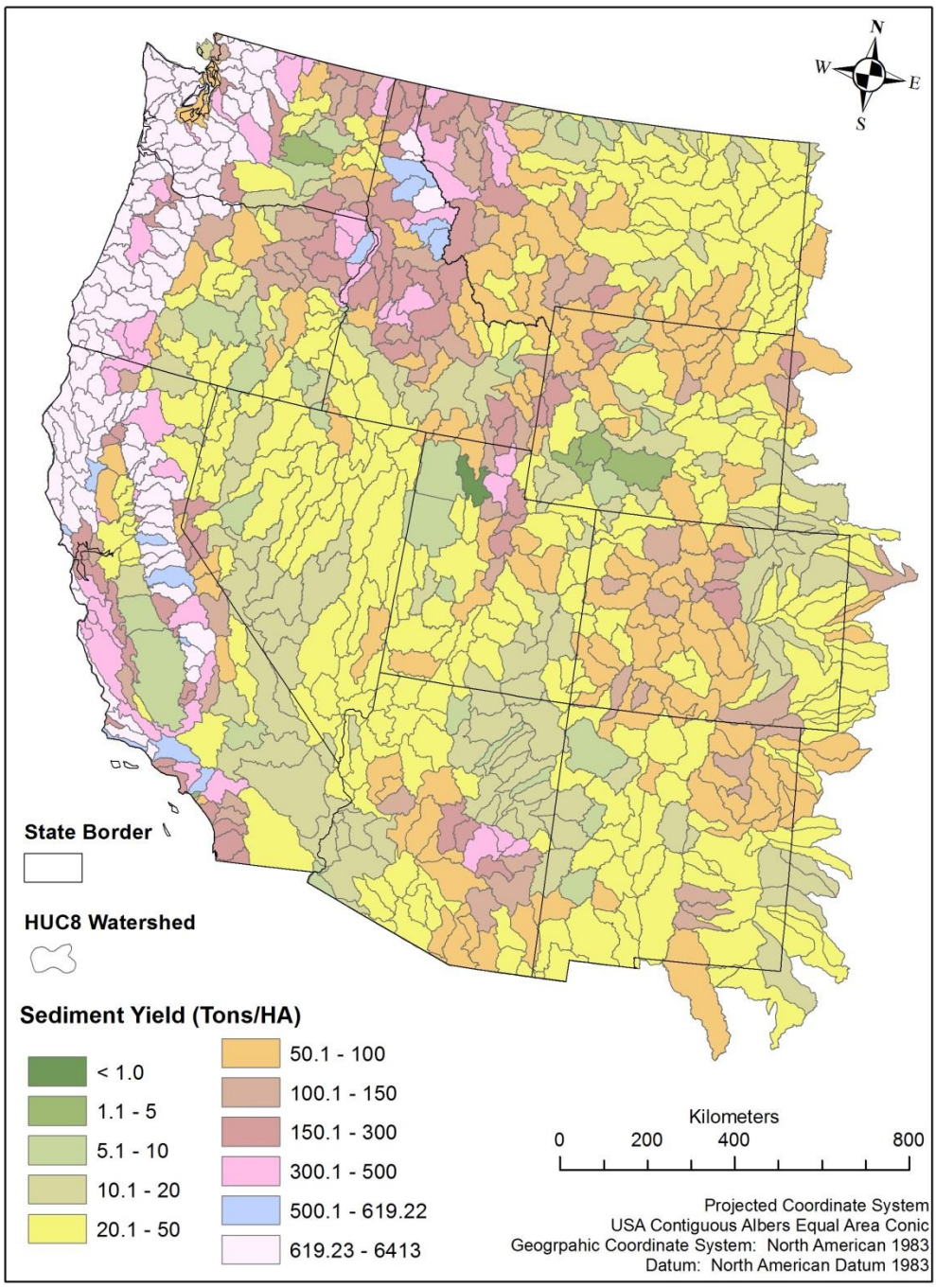

Figure 5 InVEST modeled sediment yield (tons/ha) for all HUC8 watersheds using input parameters modified to simulate post-fire conditions.

DISCUSSION

We evaluated the relative ability of the InVEST Sediment Retention model to accurately predict 4 different classes of post-fire sediment yield measurements synthesized for the western USA by Moody and Martin (2009). Channel volume measurements were the only measurement type for which we determined a significant relationship between model predictions and measured values of post-fire sediment yield. One explanation for why the InVEST Sediment Retention model might predict channel volume measurements with accuracy is because it is a watershed-scale model and measurements made within channel landscape positions are likely to integrate over a larger upstream area and are thus more comparable to the model domain; compared for example to measurements made on hillslopes (plots or point locations) within the watershed. The Sediment Retention model is not designed to predict specific ranges of particle sizes and therefore might also more accurately predict variability in channel volume measurements because they are not comprised of, or constrained to, a specific and narrow particle size range.

Relevant limitations of the model for predicting post-fire sediment yield are that it is based on the USLE and is designed to predict sedimentation as a function of sheet-wash erosion processes, but not from other erosion processes such as rilling, gullying, debris flows or other mass-wasting events (Tallis et al., 2014). The sediment retention efficiency index value that is parameterized by the model user for each LULC class has been identified as another potential limitation for prediction accuracy because few spatially explicit data at the relevant watershed scale are available to accurately characterize the biophysical interactions between vegetation, erosion, and sedimentation (Tallis et al., 2014). There are also few spatially explicit data that describe how the K factor varies as a function of fire within and among watersheds across such a large region; though soil erodibility is certainly known to increase with burning (DeBano, 2000; Giovannini et al., 2001).

Our parameterization of the model resulted in predictions that explained variability in post-fire sediment yield at a watershed-scale for the channel volume measurement type reviewed by Moody and Martin (2009). We anticipate that the methodology presented here for predicting post-fire sediment yield with the InVEST Sediment Retention model will have utility for evaluating the relative, potential vulnerability of watersheds to increased sedimentation as a function of future changes in wildfire frequency and occurrences throughout the western USA.

CONCLUSION

The InVEST Sediment Retention Model provides a GIS platform to efficiently model sediment yield and the ecosystem service of sediment retention at a watershed scale for a large number of watersheds. In this study, we showed that the model can be parameterized in a relatively simple fashion to predict post-fire sediment yield using site data where sediment yield measurements are characteristic of watershed-scale erosion and sediment delivery. Future work will focus on using the InVEST suite of models to assess tradeoffs for natural resource management decisions and to evaluate the potential vulnerability of watersheds throughout the western USA to post-fire sedimentation as a function of future changes in wildfire frequency and occurrence.

ACKNOWLEDGEMENTS

The project described in this publication was supported by a grant from the Department of the Interior Northwest Climate Science Center (NW CSC). This manuscript is submitted for publication with the understanding that the United States Government is authorized to reproduce and distribute reprints for Governmental purposes. Any use of trade, product, or firm names is for descriptive purposes only and does not imply endorsement by the U.S. government.

REFERENCES

Choromanska, U., & DeLuca, T. H. (2002). "Microbial activity and nitrogen mineralization in forest mineral soils following heating: evaluation of post-fire effects", Soil Biology and Biochemistry, 34, 263-271.

DeBano, L. F. (2000). "The role of fire and soil heating on water repellency in wildland environments: a review", Journal of Hydrology, 231, 195-206.

EPA, Landscape Ecology Branch. "Soil & Landform Metrics (Huc8)." Environmental Protection Agency, Washington D.C. [http://www.epa.gov/esd/land-sci/emap_west_browser/pages/wemap_download.htm, Accessed April, 2014].

Flannigan, M. D., Stocks, B. J., & Wotton, B. M. (2000). "Climate change and forest fires", Science of the Total Environment, 262, 221-229.

Giovannini, G., Vallejo, R., Lucchesi, S., Bautista, S., Ciompi, S., & Llovet, J. (2001). "Effects of land use and eventual fire on soil erodibility in dry Mediterranean conditions", Forest Ecology and Management, 147, 15-23.

González-Pérez, J. A., González-Vila, F. J., Almendros, G., & Knicker, H. (2004). "The effect of fire on soil organic matter—a review", Environment International, 30, 855-870.

Larsen, I. J., MacDonald, L. H., Brown, E., Rough, D., Welsh, M. J., Pietraszek, J. H. and Schaffrath, K. (2009). "Causes of post-fire runoff and erosion: water repellency, cover, or soil sealing?", Soil Science Society of America Journal, 73, 1393-1407.

Miller, M. E., MacDonald, L. H., Robichaud, P. R., & Elliot, W. J. (2011). "Predicting post-fire hillslope erosion in forest lands of the western United States", International Journal of Wildland Fire, 20, 982-999.

Moody, J. A., & Martin, D. A. (2009). "Synthesis of sediment yields after wildland fire in different rainfall regimes in the western United States" International Journal of Wildland Fire, 18, 96-115.

Tallis, H. T., Ricketts, T., Ennaanay, D., Nelson, E., Vigerstol, K., Mendoza, G., & Cameron, D. (2014). InVEST 2.5.6 beta User's Guide. The Natural Capital Project.

USDA, National Resource Conservation Service. "State Soil Geographic Database (STATSGO)". United States Department of Agriculture, Washington D.C. [http://water.usgs.gov/GIS/metadata/usgswrd/XML/ussoils.xml#stdorder, Accessed April, 2014].

USGS, Multi-Resolution Land Characteristics Consortium. "National Land Cover Dataset (NLCD) 2006." United States Geological Survey, Sioux Falls, SD. [http://www.mrlc.gov/nlcd06_data.php, Accessed April, 2014).

USGS, National Elevation Dataset. "3 Arc Second Digital Elevation model." United States Geological Survey, Sioux Falls, SD. [http://seamless.usgs.gov/, Accessed April, 2014.].

USGS, National Hydrography Dataset. "National Hydrography Dataset." United States Geological Survey, Sioux Falls, SD. [http://nhd.usgs.gov/, Accessed April, 2014.].

USGS, Water Resources. "Hydrologic Unit Maps" United States Geological Survey, Sioux Falls, SD. [http://water.usgs.gov/GIS/huc.html, Accessed April, 2014.].

Westerling, A.L., Hidalgo, H.G., Cayan, D.R., & Swetnam, T.W. (2006). "Warming and earlier spring increase western U.S. forest wildfire activity", Science 313, 940-943.

Wischmeier, W. H., & Smith, D. D. (1978). "Predicting rainfall erosion losses-A guide to conservation planning." Predicting rainfall erosion losses-A guide to conservation planning. Agriculture Handbook No. 537. Washington, DC: US Department of Agriculture.

UTILITIZATION OF ECOHYDROLOGIC MODELS IN FLOODPLAIN FISH PASSAGE AND HABITAT RESTORATION EVALUATION

Joshua A. Israel, Fish Biologist, U.S Bureau of Reclamation, Sacramento, CA. jaisrael@usbr.gov; Paul Bergman, Fisheries Biologist, Cramer Fish Sciences, Auburn, CA, pbergman@fishsciences.net; Chris Campbell, Ecohydrologist, CBEC Inc., West Sacramento, CA, c.campbell@cbecoeng.com; James Newcomb, Senior Environmental Scientist, Department of Water Resources, West Sacramento, CA, James.Newcomb@water.ca.gov; Maninder Bahia, Water Resource Engineer, Department of Water Resources, West Sacramento, CA, Maninder.Bahia@water.ca.gov

Abstract: Ecosystem restoration programs are playing an essential role in listed species management in California's Central Valley. Currently, the US Bureau of Reclamation and California Department of Water Resources are planning actions, evaluating alternatives, and assessing biological benefits of the Yolo Bypass Salmonid Habitat Restoration and Fish Passage Program as part of the Biological Opinion with NOAA-Fisheries required as part of operations of the Central Valley Project and State Water Project. Hydraulic modeling efforts for the evaluation of alternative fish passage structures and habitat restoration are critical elements of the assessment and optimization frameworks being undertaken. A two dimensional hydraulic model of the Yolo Bypass was constructed to undertake quantitative assessments of salmonid population response. This modeling indicates the importance of finer scale 3D modeling to inform juvenile population responses to potential project designs for structures increasing floodplain connectivity with the Sacramento River. Various biological metrics are being assessed using these hydraulic models to evaluate the benefits and limitations of floodplain restoration and fish passage alternatives for fishery resource recovery.

INTRODUCTION

Significant modifications have been made to the historic floodplain of California's Central Valley for flood damage reduction purposes and water supplies. The resulting losses of rearing habitat, migration corridors, and food web production for fish have significantly hindered native fish species that rely on floodplain habitat during part or all of their life history. The Yolo Bypass (Bypass), which currently experiences at least some flooding in approximately 80% of years, still retains many characteristics of the historic floodplain habitat that are favorable to various fish species. In approximately 70% of years, Fremont Weir overtops connecting the Bypass to the Sacramento River along its northern boundary, and Sacramento flows join flows from western tributaries. In approximately 10% of years, localized flooding is due to western tributary contributions only. The primary function of the Bypass is flood damage reduction, with most of it also managed as agricultural land. The Bypass has also been identified by several State and federal entities as a potential site for habitat restoration to ease pressure on and increase benefits to threatened and endangered fish species.

On June 4, 2009, the National Marine Fisheries Service (NMFS) issued its Biological Opinion and Conference Opinion on the Long-term Operation of the Central Valley Project (CVP) and State Water Project (SWP) (NMFS Operation BO). The NMFS Operation BO concluded that, if

left unchanged, CVP and SWP operations were likely to jeopardize the continued existence of four federally- listed anadromous fish species: Sacramento River winter-run Chinook salmon, Central Valley spring-run Chinook salmon, Central Valley steelhead, and Southern Distinct Population Segment (DPS) North American green sturgeon. The NMFS Operation BO sets forth Reasonable and Prudent Alternative (RPA) actions that would allow continuing SWP and CVP operations to remain in compliance with the federal Endangered Species Act (ESA). These include restoration of floodplain rearing habitat, through a "notched" channel that increases seasonal inundation within the lower Sacramento River basin. A second objective is to reduce migratory delays (i.e.: upstream adult fish passage, agricultural crossing modification, Lisbon Weir improvements) and stranding of fishes. A significant component of these risk reduction actions is lowering a section of the Fremont Weir (Figure 1) to allow juvenile fish to enter the bypass and adult fish to more easily ascend this hazard.

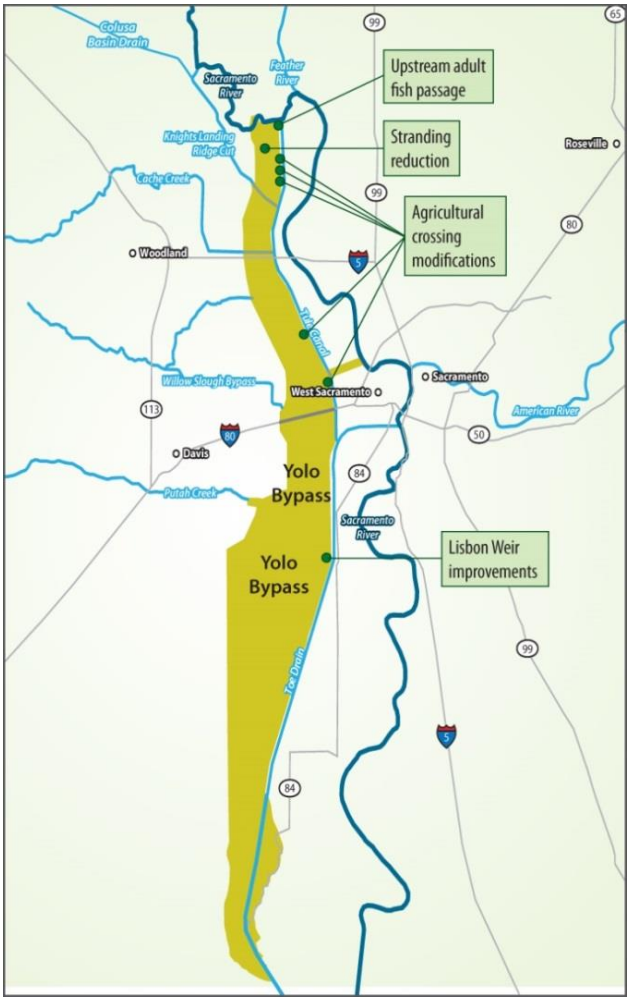

Figure 1 Yolo Bypass locality for projects increasing seasonal inundation and reducing adult straying and stranding.

Currently, the planning and environmental compliance process is considering a reasonable range of alternatives for implementing this RPA action. This includes a number of projects that are common elements, which will reduce stranding and migration delays, and other projects that represent potentially uniquely designed facilities with distinct benefits and risks for achieving

fisheries benefits. This presentation focuses on two modeling efforts underway to quantitatively assess the potential benefits of restoration actions for juveniles life stages of salmonids on ESA-listed fish populations. While other efforts are underway to use these models to benefits from alternative designs for adult passage, these results will not be discussed in this presentation. This presentation includes fishery benefit results from completed physical and biological modeling, discussion of a key uncertainty in our model, and description of our 2015's study to inform better modeling to reduce this uncertainty.

METHODS

MODELS: An interagency hydraulic modeling technical team evaluated a set of potential two-dimensional (2D) hydraulic models for use in evaluating different potential configurations of Fremont Weir gate and channel "notches" to allow larger and more frequent floodplain inundation events in the Bypass. The team ranked the models based on their model capabilities, other considerations, and optional model capabilities. Attributes characterized included performance, cost, public domain, breadth of user base, and model longevity. TUFLOW ranked high, and was selected based on its high performance, relative low cost, growing agency user base, Geographic Information System (GIS) interface, and quick run time. Technically favorable aspects with TUFLOW also included its ability to solve the full 2D shallow water equation, to provide numeric stability even with wetting and drying, to compute flows using weir equations automatically, and to allow support for hydraulic structure under potential operational control.

The model domain (see Figure 2) extends along the Sacramento River from River Mile (RM) 118 just south of the Tisdale Bypass near Wilkins Slough to RM 12 near Rio Vista and includes the entire Yolo Bypass. The domain extends 7 miles to the north along the Feather River and into the Sutter Bypass. The Feather-Sutter boundary was located far enough to the north of the flow split between the Yolo Bypass at Fremont Weir and the Sacramento River at Verona to minimize model boundary effects at the flow split (and the proposed gated channel at Fremont Weir). The domain includes the Sacramento Weir at RM 63 and extends 22 miles to the east along the American River to just below Nimbus Dam. The domain also includes various North Delta sloughs (i.e., Elk, Sutter, Miner, Steamboat, Haas, Cache, Lindsey, and Barker) and a boundary connection with the Delta Cross Channel and Georgiana Slough at RM 27.

The model domain is comprised of a combination of one-dimensional (1D) channels and 2D grids. The 1D channels describe the flow of water in the major sloughs, creeks, and rivers bordering or bisecting the flood control bypasses and are represented with a series of cross sections. The 2D grids describe the flow of water within the flood control bypasses when channel capacity is exceeded, flood control weirs are activated, and restricted height levees are overtopped. The TUFLOW model includes three separate 2D grids. The cell sizes for the grids are 400 feet-, 200 feet-, and 100 feet-square, which provide elevation values every 200 feet, 100 feet, and 50 feet, respectfully. The 200 foot grid covers the majority of the 2D domain. The 100

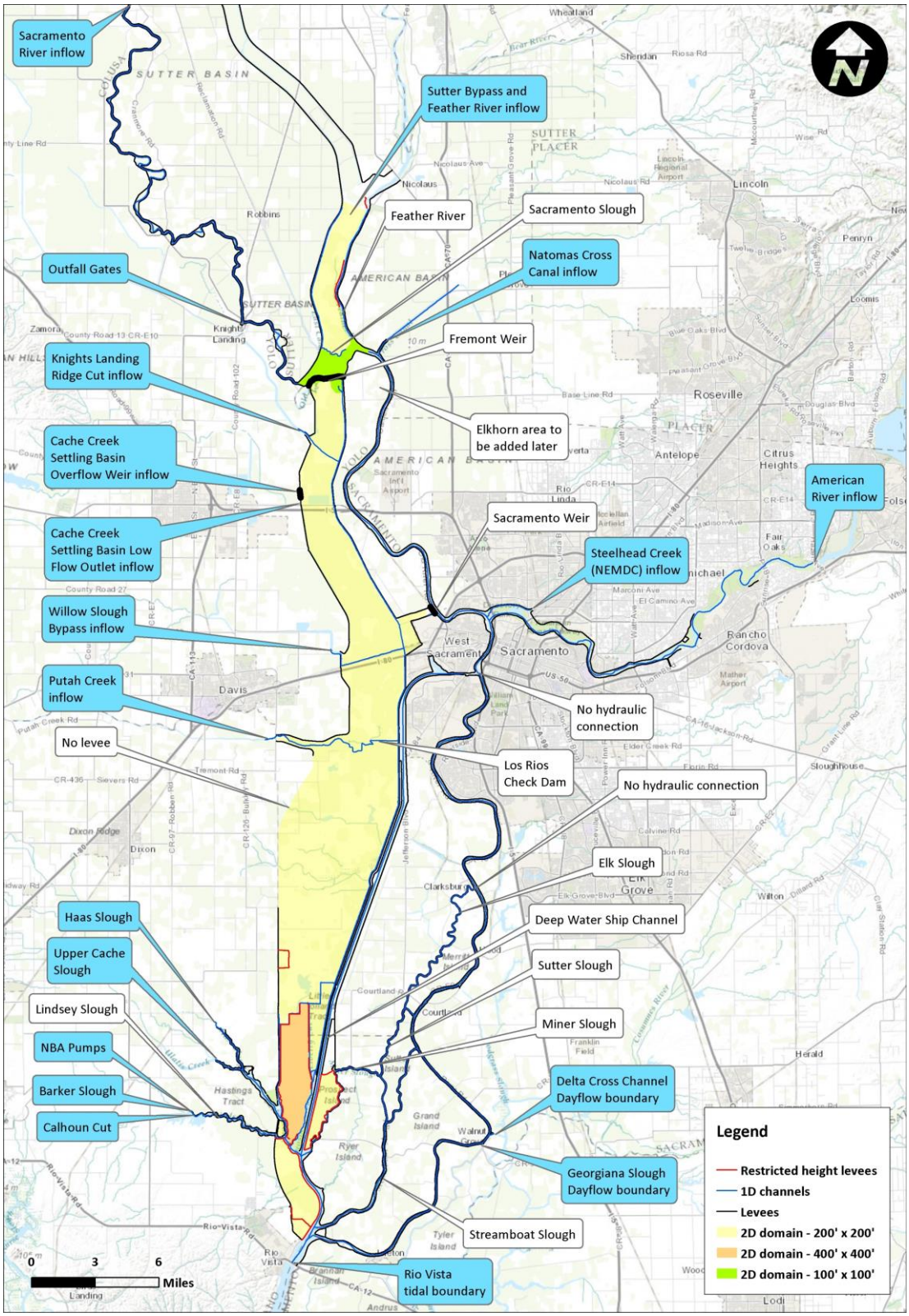

Figure 2 TUFLOW model domain and boundary locations. (Prepared for DWR by HDR and cbec).

foot grid represents the section of the Sacramento River between Knights Landing and Verona. The 400 foot grid represents Liberty Island. Each grid has elevations at each cell centroid, edge mid-point, and cell corner giving nine elevation values per cell. Multiple grids were used to vary the cell size spatially to balance required resolution and reduced runtimes. The grid elevations are assigned within the TUFLOW model based upon a Digital Elevation Model (DEM) with modifications to enforce localized features on the working agricultural landscape within the bypass. Exhaustive efforts were made to characterize boundary conditions, which were previously data limited, such as the west side tributaries, hydraulic structures in the Bypass, and Feather River and Sutter Bypass condition.

Long term daily hydrologic data was prepared for water years 1997 through 2012 to serve as existing conditions for the TUFLOW model. Inundation duration, frequency, and acreage were modeled for three potential alternative "notch" configurations relative to existing conditions (Table 1). These data were processed for the fisheries team to provide depth and velocity magnitude raster datasets covering the Bypass. Also, these results were processed into daily average discharge values for the Fremont Weir (including channel flows), the Sacramento at Verona, and the Sacramento River at Freeport.

Table 1 Small, medium, and large Fremont Weir notch configurations modeled.

Fremont Weir Notch	Small	Medium	Large	Existing
Bottom width (ft)	20	22.5	22.5	NA
Invert elevation (ft)	14	17.5	14	33

The Fisheries Benefit model keeps track of key life stage demographics resulting from potential restoration alternatives (Table 1). Its components include: (1) *model entry* – the abundance, size and timing of juvenile salmon entering the model; (2) *Yolo Bypass entrainment* – the entrainment of juvenile salmon onto the Bypass; (3) *rearing* – the life stage of juvenile salmon on the Bypass or in the mainstem Sacramento River ; (4) *emigration* – the downstream migration of juvenile salmon from Rio Vista, CA to San Francisco (Bay) entry; (5) *ocean residence* – the residence of salmon in the ocean; (6) *upstream migration*– the upstream migration of returning adults from the Bay upstream to Fremont Weir on the Sacramento River. Function and parameter values taken from appropriate literature and regional studies were used in the model. The assumption that juvenile fish are entrained from the Sacramento River onto the Yolo Bypass in proportion to the flow entering the Bypass was utilized, since no other information exists regarding this value.

METRICS: The utility of biological-physical coupled models to aid in this assessment is providing information on metrics useful for discerning benefits for ESA-listed species. Reclamation and DWR reviewed potential metrics prior to undertaking modeling, and thus were able to tailor models to emphasize results that are useful for comparing potential notches to existing conditions. Results from the hydraulic modeling are being used for independent consideration of attaining desirable inundated acreage targets and other landscape ecosystem metrics (Table 3). Results from the biological modeling, which are based upon the hydraulic model results, are being used for assessing population metrics useful for evaluating how the viability of salmon populations are impacted by these actions (Table 3).

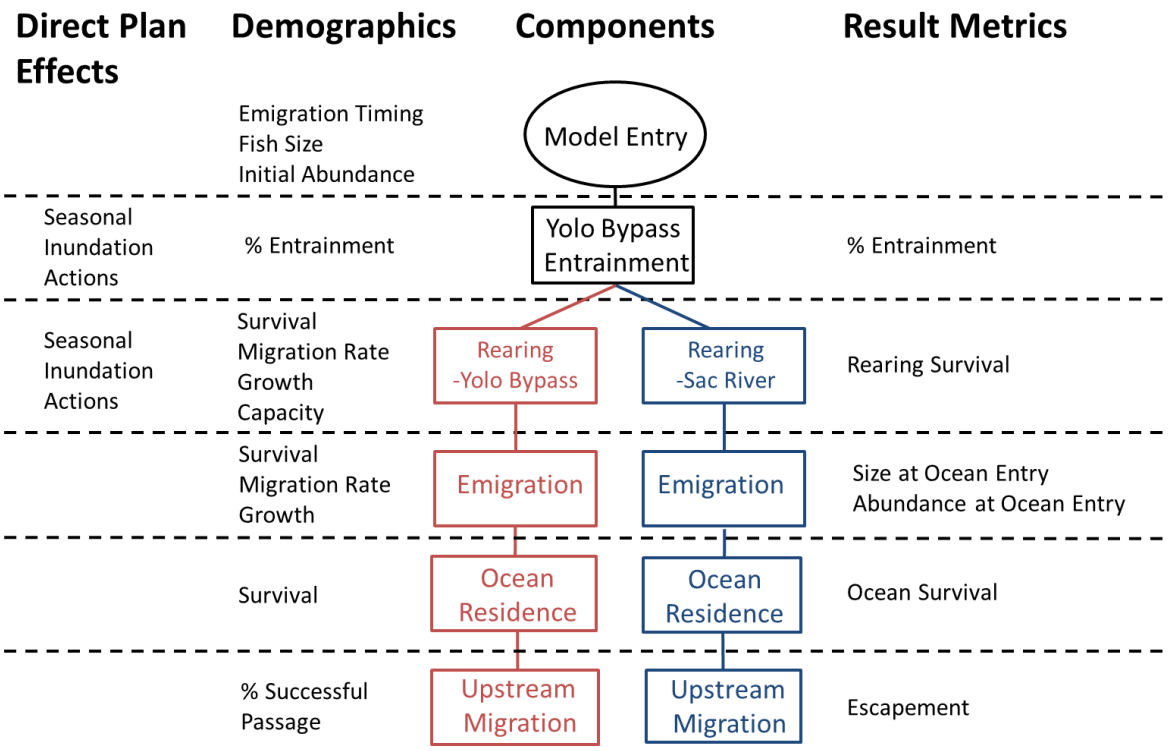

Figure 2 Conceptual diagram of the Yolo Bypass simulation model showing each of the model components, Chinook salmon demographics modeled for each component, and metrics that are used for comparison of fish benefits between management alternatives. (Prepared for Reclamation by CFS).

Table 3 Measures used for evaluation of potential alternatives from hydraulic and biological modeling.

Hydraulic Model Metrics	Biological Model Metrics
• Acreage Inundated • Duration Inundated • Frequency Inundated	• Entrainment onto floodplain • Amount of suitable habitat • Survival of juveniles • Juvenile to adult survival • Abundance of returning adults

MODELING OF A NON-PHYSICAL FISH BARRIER

Marcela Politano, Research Engineer, IIHR – Hydroscience & Engineering, The University of Iowa, Iowa City, IA, marcela-politano@uiowa.edu; Ezequiel Martin, Assist. Research Scientist, IIHR – Hydroscience & Engineering, The University of Iowa, Iowa City, IA, juan-martin@uiowa.edu; Yong Lai, Hydraulic Engineer, Technical Service Center, Bureau of Reclamation, Denver, CO, ylai@usbr.gov; Merlynn Bender, Hydraulic Engineer, Technical Service Center, Bureau of Reclamation, Denver, CO, mbender@usbr.gov; Dave Smith, Research Ecologist, US Army Corps of Engineers, Vicksburg, MS.

Abstract: Non-physical barriers (NPBs) are used to deter fish from entering an undesirable pathway without restricting flow. NPBs are commonly comprised of a bubble curtain, low-frequency sound, and hi-intensity light-emitting diode (LED) Modulated Intense Lights (MILs). In this study a 3D numerical model was developed to predict bubble, sound and light fields in the vicinity of an NPB. A Boussinesq approach was used to account for the reduction of density in the zones where bubbles are present. A simplified diffusive model for the sound intensity was developed. Two methods are proposed for light, one for high attenuation/scattering conditions based on P-N models and the other for low scattering conditions based on the superposition of analytical solutions for elementary one-dimensional cases. To validate the solvers, several experiments were simulated. A sample model application to a simplified NPB located in Georgiana Slough in the Sacramento River is presented and discussed.

INTRODUCTION

Non-physical barriers (NPBs) use behavioral stimuli such as bubbles, low-frequency sound, and high-intensity light-emitting diode (LED) Modulated Intense Lights (MILs) to deter fish from entering undesirable locations. The sound is concentrated within the bubble curtain due to the difference in the velocity of sound of water and air to prevent sound saturation. Lights projected onto the bubble curtain improve visibility for fish swimming in the direction of the curtain. This NPB arrangement is typically referred to as a Bioacoustic Fish Fence (BAFF).

The migration of juvenile salmonids in the San Joaquin and Sacramento Rivers is of great environmental interest due to decline of native species. Fish diversion into the Delta may result in delayed migration, elevated risk of predation, exposure to poor water quality conditions, and mortality in pumping facilities. The California Department of Water Resources (CDWR) and the U.S. Bureau of Reclamation (Reclamation) proposed to use a NPB to reduce the diversion of juvenile salmonids from the Sacramento River into the interior and south Delta. The effectiveness of NPBs in deterring fish is variable, depending on the location, barrier geometry, and river flows. NPB can also have unintended effects, such as increased predation upstream and downstream of the barrier. All the above increase the environmental risk requiring site specific study and evaluation. In this study a numerical model for a NPB was developed to better understand the effect of the barrier on the Sacramento River hydrodynamics and support the design and operation of a NPB to deter and direct fish movement.

NUMERICAL MODEL

In this study, we first developed the model equations to simulate the bubbles, sound and light fields. The model equations were then implemented into the open source code OpenFoam (Weller et al. 1998). OpenFoam is a collection of C++ libraries, based on object oriented programming, designed for continuum mechanics applications. A new solver, pisoFoamBLS, which includes simplified models for predicting bubbles, sound and light fields near a non-physical fish barrier, was developed based on the code pisoFoam using a modular approach. Several studies related to implementation of different solvers in OpenFoam may be found in the literature (Hussein 2009, Kassem et al. 2011, Flores et al. 2013, among others) and repeated herein.

MODELING OF BUBBLES

Mathematical Modeling

A bubbly flow, i.e., a discrete gas phase in a continuous fluid, is formed in bubble curtains. As illustrated in Figure 2, bubbles injected in an initially quiescent medium induce a motion in the liquid similar to that observed in buoyancy-induced flows. Three distinct zones can be observed in a bubble curtain:

1. The primary bubble zone: where bubbles accelerate as they detach from the nozzle

2. The plume zone: where bubble breakup and coalescence prevail to form the plume
3. The free bubble zone: where the dynamic process of breakup and coalescence have reached an equilibrium and bubbles rise without significant size change

Measurements of gas volume fraction, bubble frequency and chord length by Castillejos and Brimacombe (1987) indicate that bubble breakup in the plume zone predominantly occurs near the injection location. Close to the free surface, the bubble velocity decreases as liquid moves tangent to the free surface, which enhances coalescence and promotes larger bubble sizes.

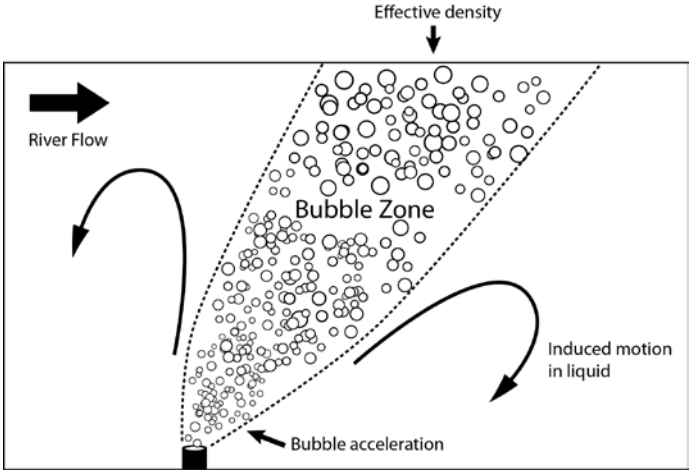

Figure 1. Induced liquid motion for a bubble curtain in a river

Most of bubble plume models found in the literature are intended for the free bubble zone region. The current modeling effort is based on the model presented by Buscaglia et al. (2002). The authors used a two-fluid approach assuming an incompressible mixture gas-liquid phase. In this approach, the Navier-Stokes equations are restored, significantly simplifying the formulation. The main advantage of this model is that an equation for the gas phase is included and therefore the shape of the bubble zone can be predicted. Future model improvements such as inclusion of a bubble size distribution, breakup and coalescence, bubble dissolution, bubble compression, bubble induced turbulence, etc., can easily be incorporated into the model using this formulation. Following Buscaglia et al. (2002), density differences are neglected except where they appear in the term multiplied by the acceleration due to gravity resulting in:

$$\nabla \cdot \vec{u}_m = 0 \tag{1}$$

$$\rho_l \frac{\partial}{\partial t}\vec{u}_m + \rho_l \nabla \cdot \left(\vec{u}_m \vec{u}_m\right) = -\nabla P + \nabla \cdot \left[\tau_m^{\mathrm{Re}} + \tau_m\right] + \rho_m \vec{g} \tag{2}$$

Eqs. (1) and (2) can be solved to compute pressure and velocity of the mixture phase with any single-phase CFD solver adding a source term in the momentum equation $\vec{S}_m = -(\rho_l - \rho_g)\alpha \vec{g}$. In this study an isotropic turbulence model $k-\varepsilon$ was used for turbulence closure. The gas velocity was obtained from the momentum equation for the gas phase. Inertia, gravity force and viscous shear stresses are significantly smaller than liquid-gas interfacial forces due to the small density and viscosity of the gas phase and are usually neglected. In this particular application, drag is the most important interfacial force and lift and virtual mass can be neglected resulting in:

$$-\nabla\left(P + \frac{2}{3}k\right) + \frac{3}{8}\frac{C_g^D}{R}\vec{u}_r\left|\vec{u}_r\right| = 0 \tag{3}$$

In a bubble curtain, bubble size can change due to breakup, coalescence, mass transfer and pressure variations. In this study, an equation for the bubble number density was used:

$$\frac{\partial N}{\partial t} + \nabla \cdot \left[\vec{u}_g \, N \right] = \frac{\nu^t}{Sc} \nabla^2 N_g \tag{4}$$

The bubble volume at a given position can be calculated from $v_b = \frac{P_c}{P} \frac{4}{3} \pi R_c^3$, where P_c and R_c are the pressure and radius at the injection point. The bubble zone can be determined using the gas volume fraction, which can be obtained from the mass conservation equation for the gas phase $\alpha = \frac{4}{3} \pi R^3 N$.

Model Comparison with Experiments

The model was used to simulate an experiment by Grevet et al. (1982) in which a water-filled cylindrical tank was agitated by a gas bubble stream, and compared against velocity data measured inside the tank. The modeled tank radius, *R*, was 0.3 m and the water height, *H*, 0.6 m. Bubbles were injected into the quiescent liquid through an orifice of 0.0127 m (0.5 inch) at a flowrate of 205 cm^3/s. Only one fourth of the tank was simulated to reduce grid size and computational time. Symmetry boundary conditions were used on the sides. Grid size was approximately 10^5 nodes. Since bubble velocities were not measured, it is assumed that bubbles enter the domain at their terminal velocity. Reasonable agreement was found between model predictions and experimental data for three axial positions (Figure 2). As rising bubbles leave the injector, they generate an inward flow at the left bottom side of the tank. The bubble stream then generates an upward flow in the center of the tank and a large clockwise vortical structure at the upper right side, with negligible radial velocities. The rising bubble velocity is terminated at the free surface and the liquid vertical moment is converted to horizontal flow. The horizontal flow is blocked by the tank wall and is redirected downward along the side wall. The model is considerably less accurate near the walls, but since wall interaction is not important in a bubble curtain, grid refinement was not performed to capture the velocity profile near the walls. The proposed model assumes one variable bubble size. Implementation of a bubble size distribution is expected to improve model accuracy. Figure 3 shows the gas volume fraction distribution in the tank. For the low gas volume fraction injected, bubbles concentrated in the core of the tank, rise almost uniformly in a nearly straight line. Near the injector, bubble velocity increases due to the upward liquid flow in the center of the tank. This local increase of the liquid velocity causes a reduction of the gas volume fraction. Conversely, bubble velocities are reduced near the free surface resulting in a local increase of the gas volume fraction.

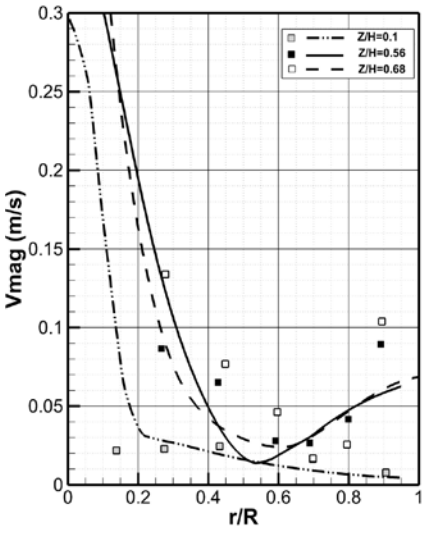

Figure 2. Comparison between predicted and measured velocity magnitude. Symbols: experiments by Grevet et al. (1982) and lines: model results

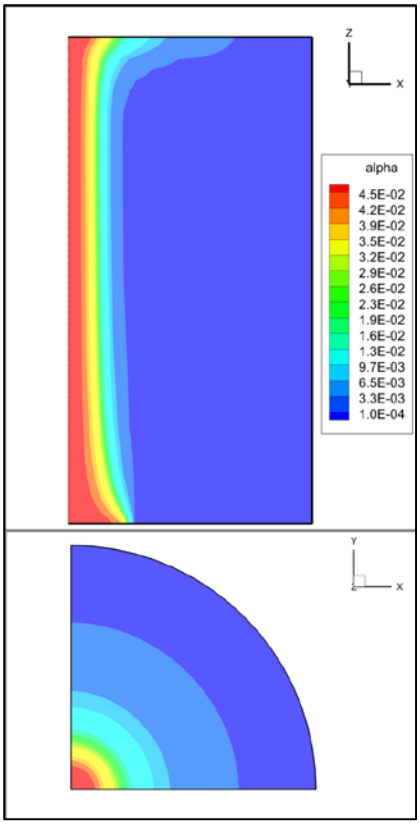

Figure 3. Gas volume fraction contours

MODELING OF SOUND

Mathematical Modeling

The acoustic field in a domain can be represented by an equation of acoustic energy conservation:

$$\frac{\partial W}{\partial t} = -\nabla \cdot \boldsymbol{I} - D \tag{5}$$

where W is the acoustic energy and $\boldsymbol{I}$ the acoustic energy flux. The last term in the RHS represents dissipation effects. In this study a method was developed to deal with the strong changes in fluid properties introduced by the presence of the bubble barrier as well as the multiple surfaces that partially absorb the sound signals at the boundaries. The diffusive equation used in architectural acoustics was identified as a viable candidate to fulfill these requirements. A Fick's law-type relation is postulated between the energy flux and the energy density, $\boldsymbol{I} = -\boldsymbol{D_W}\nabla W$, which adapted to give a dependence of the dissipation on W rather than $\boldsymbol{I}$, transforms the conservation equation for sound energy to:

$$\frac{\partial W}{\partial t} = -\nabla \cdot (\boldsymbol{D_W}\nabla W) - \alpha_W^2 |\boldsymbol{D_W}| W + S_W \tag{6}$$

where a general distributed source term S_W has also been included. A new parameter, an anisotropic diffusion coefficient $\boldsymbol{D_W}$, has been introduced, for which modeling is required. The expression for the dissipation term is such that the exponential decay of a plane wave in an isotropic media is recovered. Following Picaut (2002), absorption is modeled as a boundary condition. Picaut et al. (1999) proposed a diagonal tensor related to length-scale of domain for the diffusion coefficient:

$$\frac{D_{xx}}{\ell_x} = \frac{D_{yy}}{\ell_y} = \frac{D_{zz}}{\ell_z} = D_{3D} \tag{7}$$

with the diffusion proportional to sound speed ($D_{3D} \sim c$). Eq. (6) is a standard diffusion equation for which solution methods are well established and can be readily implemented in OpenFoam. Certain features of the sound field are lost by using this approach, such as the appearance of interference patterns and the rapid evolution of the sound field that can be found with the ray tracing method. However, it is questionable that those features are of significant importance for the current application, as it is expected that the cases of interest will be quasi-steady in both bubble-encapsulated and non-encapsulated sound fields as the fluid velocity is much smaller than the speed of sound, and the sound source are non-pulsating in time.
A set of linear attenuation coefficients and speed of sound data for bubbly flows presented by Silberman (1957) were used in this study.

Model Comparison with Experiments

The data presented by Würsig et al. (2000) represent one of the few reported field experiments with useful, albeit scarce, data for model validation. Sound levels produced by a pile-driving hammer in shallow waters were measured with and without a bubble curtain designed to mitigate the sound. Measurements of background noise are also available, but there is no measurement of sound levels near the source or inside the bubble curtain area. A slab geometry with an average depth of 8 meters was simulated. In Figure 4, the measured data on April 26, 1996 is shown along with the simulated results. The authors reported an overall sound level for frequencies spanning 100 Hz to 25.6 kHz, as well as results for the different one-octave bands. Notable differences in attenuation by the bubble curtain occur for the different frequencies, but it was found that the reported average trend for all frequencies is consistent with the results for low frequencies (as the sound intensity is largest for the 400 Hz octaves), and a representative frequency of 400Hz was chosen to perform the simulations. A uniform source for the background noise and an additional source near the coordinates' origin were obtained. The relationship between the wall attenuation coefficient and the diffusion parameter was established using the expression proposed by Silberman (1957). An extremely low value of $D_{yy}/D_{rr} = 1.6\text{x}10^{-4}$ was found from the experimental data, and as shown in Figure 4, the predicted decay matches well with the data. Finally, a mean gas volume fraction was estimated from the reported flow rate, assuming a terminal bubble velocity and a corresponding plume spreading angle. The resulting bubbly region is a ring, 25 m in diameter and 0.5 meter in thickness, with an estimated gas volume fraction of 0.02. It is reported that the resulting attenuation by the bubble barrier is about 3 to 5 dB, which agrees well with the estimated attenuation. The simulations required a smaller value of gas volume fraction to match the data of 0.003. When experimental data become available, further simulations and analyses should be performed to identify the reason for this discrepancy.

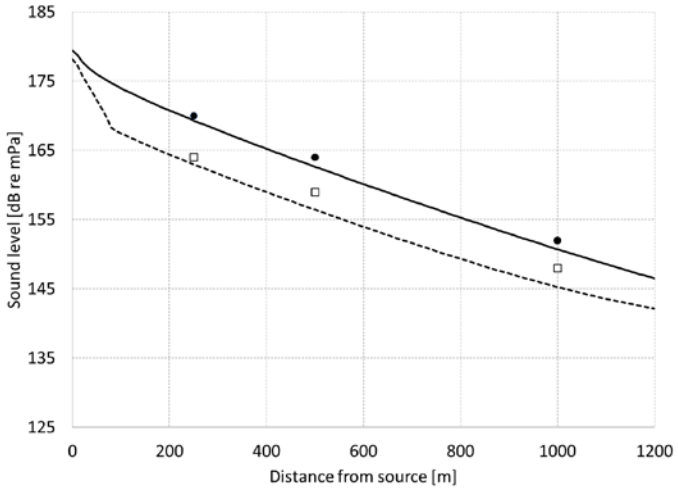

Figure 4. Sound levels in a slab. Symbols: Würsig et al. (2000) experimental data (black circles: bubble curtain off; white squares: bubble curtain on) and lines: simulation results

MODELING OF LIGHT

Mathematical Modeling

Calculations of light intensity can be extremely resource-intensive and are typically done using Monte Carlo simulations; or are based on semi-analytical approximations to an integro-differential equation. The latter approach was used in this study. The fundamental equation describing the light field in a continuous media is called the radiative transfer (RT) equation. The RT conservation equation balances the changes of spectral radiance (L) in a given direction with the processes that can modify it: *absorption*, *scattering* and *emission*. The attenuation of the beam is given by the *absorption*, defined by the absorption coefficient $a_{\mathrm{E}}(\boldsymbol{x},\lambda)$ times the radiance and all the scattering *out* of the beam direction that can be approximated as $-b_{\mathrm{E}}(\boldsymbol{x},\lambda)L$, with b_{E} the average of the volume scattering function. The elastic (i.e., without a change of wavelength) *scattering* for other directions *into* a given direction constitutes a source and is represented as an integral that accounts for all the contributions over all possible 4π solid angle directions to a given one. Finally, *emission* may correspond to an actual source or due to inelastic scattering from other wavelengths, and can be expressed as a general source s_{E}, per steradian. The complete RT equation can be written as (Mobley, 2001):

$$\Omega\nabla L(\boldsymbol{x},\theta,\varphi,\lambda) = -c_{\mathrm{E}}(\boldsymbol{x},\lambda)L(\boldsymbol{x},\theta,\varphi,\lambda) + \int_{4\pi} L(\boldsymbol{x},\theta',\varphi',\lambda)\beta_s(\boldsymbol{x},\theta',\varphi',\theta,\varphi,\lambda)d\Omega' + s_{\mathrm{E}}(\boldsymbol{x},\theta,\varphi,\lambda) \quad (8)$$

with β_s is the angle dependent volume scattering function and c_{E} the sum of a_{E} and b_{E}. Eq. (8) contains both an integral on the solid angle and spatial derivatives which can be very difficult to solve explicitly. In this study, the scalar irradiance, E, obtained by integration of L, was used. Extensive literature exists on different methods implemented to solve Eq. (8). In this study, two methods were implemented. A superposition of elementary solutions is proposed when scattering effects are not important and a P-1 model for high attenuation and/or scattering.

Certain apparent optical properties such as the diffuse attenuation coefficient can be approximated as a function of intrinsic properties for certain simple cases (Kirk, 2003; Kirk, 2006). Two simple solutions for the scalar irradiance can be found for planar and point sources by simple integration of Eq. (10):

$$E(z) = E_0\exp(-Kz) \quad (9)$$

$$E(r) = \frac{r_0^2}{r^2}E_0\exp(-Kr) \quad (10)$$

In the superposition of elementary solutions method, multiple elementary solutions are automatically combined to produce a light field that approximates the solution of RTE:

$$\nabla\cdot(\mathbf{u_E}E) = S_{\mathrm{E}} - KE \quad (11)$$

where $S_{\mathrm{E}} = 4\pi s_{\mathrm{E}}$, and K is the diffuse attenuation coefficient. To recover the solutions presented before (Eqs. 9 and 10), a dimensionless vector field is defined as $\mathbf{u_E}$ = (0,0,-1) for a plane source emitting in the z negative direction and $\mathbf{u_E} = \mathbf{e_r}$ the radial unit vector for the point source case. By presenting the solution as a result of a numerical integration it is possible to introduce more complex geometries and also variability of the attenuation factor, which can be calculated independently of the solution. With this simple scheme it is possible to reproduce background illumination due to natural daylight as a plane source, as well as including the stroboscopic lights of the barrier as point sources.

P-N models use a diffusive representation of the RTE, and as such its range of validity is for conditions with high attenuation and/or scattering (Sazhin et al., 1996). In general, P-N models are based on the expansion of the solution to RTE in orthogonal series of spherical harmonics. For the P-1 model only the first and third terms of the series are kept resulting in:

$$-\sum_{i=1}^{3}\frac{\partial}{\partial x_i}\frac{1}{3(a_{\mathrm{E}}+b_{\mathrm{E}})}\frac{\partial L^{(0)}}{\partial x_i} = 4\pi s_{\mathrm{E}} - a_{\mathrm{E}}L^{(0)} \quad (12)$$

Attenuation and absorption coefficients available in USEPA (2000) and Mobley (2001) as a function of water molecules, chlorophyll, inorganic matter and colored dissolved organic matter were used.

For a bubbly flow, the effect of the bubbles in the attenuation of light must also be considered. For most cases, it can be assumed than the bubble's radius R is much larger than the wavelength of the incident light. This condition is known as the geometric optic limit, for which both the geometric approximation and the Mie theory of scattering will predict the same far-field solution for the interaction of a plane wave and a single large sphere (Randrianalisoa and Baillis, 2014). It is a good assumption to neglect the absorption within the bubble and only consider the scattering contribution (Shamoun et al., 1999). For multiple scatters, the interaction between particles can be neglected if the characteristic spacing between particles is large compared to both the wavelength and the particle radius. In that case, the scattering characteristics can be obtained as a summation of the individual contributions. The resulting extinction coefficient due to bubbles is $c_{\mathrm{b}} = \frac{3}{4}\frac{\alpha}{R}$:

In this study reflections at the boundaries from the original sources were implemented using a cosine emission law.

Model validation

Some simple geometries were run to validate the implemented models and to highlight the differences between the two models. Unfortunately, no data for controlled bubbly flows were identified that could be simulated, other than some information on attenuation coefficients that was already included in the modelling process.

The dimensionless irradiance field for two point sources in a closed cavity were simulated. First reflections are possible in the bottom boundary only. The model predicts the irradiance reduction with the radial distance shown in Eq. (10) (Figure 5). Total irradiance shown on the left frames is the summation of incidente (middle frame) and reflected (right frame) irradiances. This case shows the feasibility of representing the modulated intense lights (MILs) for the fish barrier as the solution of superimposed single point sources.

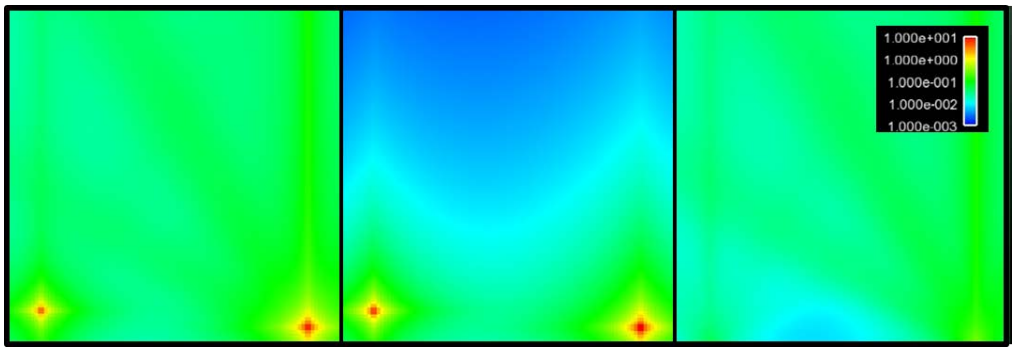

Figure 5: Total irradiance (left), incidente (middle) and reflected (right) from two point sources near the bottom of a cavity

The focus of the validation of the P-1 model was to demonstrate the effect of bubbles on the distribution of the irradiance. Figure 6 shows the basic profile for the case where no bubbles are present. As expected, the irradiance decays radially from the source with an equivalent diffuse attenuation coefficient $K = (3a_{\mathrm{E}}c_{\mathrm{E}})^{1/2}$. Two possible boundary conditions are shown in Figure 6 for the boundary closest to the source, the partial reflective condition (left frame) and full reflective conditions (right frame). As expected, the latter results in larger values for E, but given the rapid decay of the irradiance most differences between the two cases are localized to the region immediate to the source and very close to the boundary.

The deformation of the radial pattern due to the presence of a bubble curtain is shown in Figure 7. The extension of the curtain is shown with dashed lines. Several values of gas volume fraction with fully reflecting boundary were considered. The main effect of the bubbles is to concentrate the light field into a smaller region and with a larger maximum value for E. The distribution of the light field varies radically depending on whether the light source is contained in the bubble curtain, in which case very little illumination escapes the curtain, or whether the source is placed near the curtain, in which case bubbles act as a reflector.

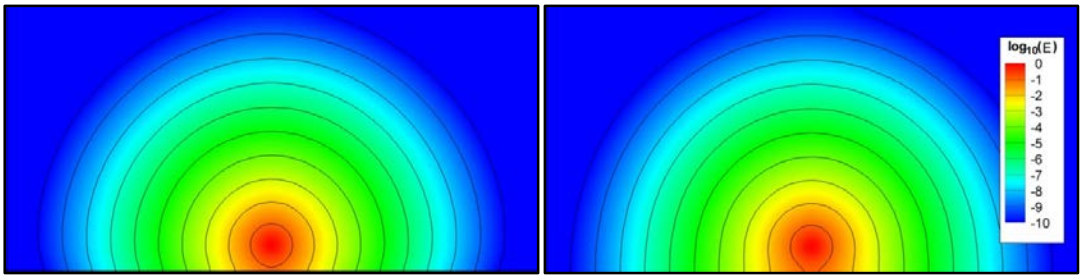

Figure 6. Unit irradiance source near a boundary. Left, lower boundary correspond to a water-air interface; right, fully reflecting boundary

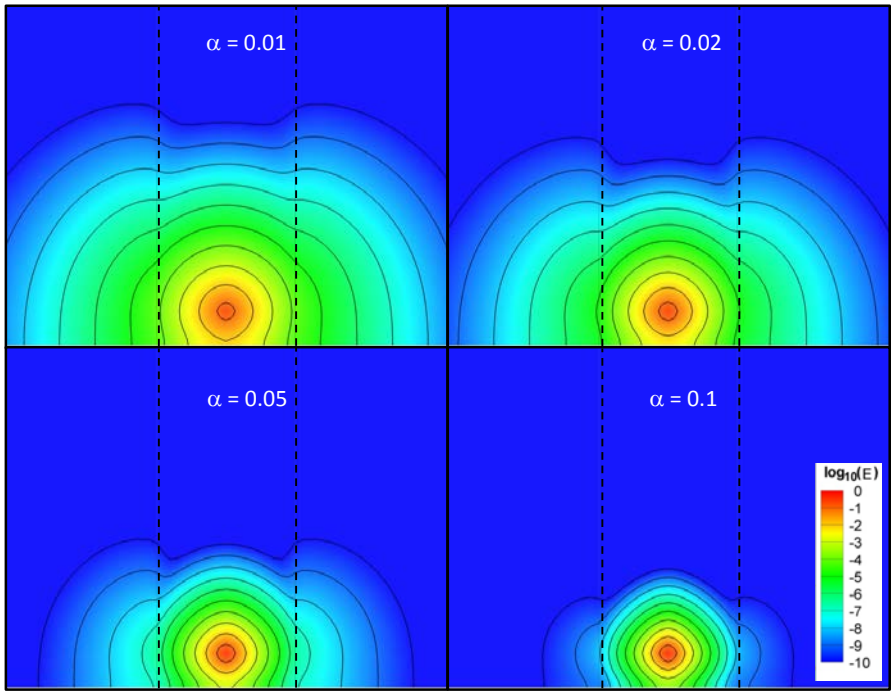

Figure 7: Unit irradiance source within a bubble curtain near a boundary

SIMULATION OF A NON-PHYSICAL FISH BARRIER

Simplified Georgiana Slough

A main channel with two bifurcations and a non-physical fish barrier upstream of the smallest stream was simulated to test the capability of the proposed model to predict the flow field and bubble, sound and light fields in the vicinity of a fish barrier (Figure 8). The geometry of the Georgiana Slough in the Sacramento River was used (McQuirk and Reeves, 2012). Since bathymetric information was not available a constant water depth of 9.1 m was used. This value was selected based on information of underwater sound measurements that were taken between 2.9 m to 14.6 m (McQuirk and Reeves 2012). In this paper a simulation using typical conditions in the Sacramento River upstream of the Georgiana Slough is presented. Flowrates upstream and downstream of the curtain were 334 m^3/s and 132 m^3/s, respectively. Small bubbles of 0.8 mm (0.03 inch) diameter were injected at the bottom of the river at a pressure of 1.91 10^5 Pa and at 25 ^{o}C. The diffusion coefficient was set using Eq. (12), with constant $D_{3D} = 0.1c_{water}$, l_z=10 m and l_x=l_y=200 m, a mixed boundary condition was imposed on the bottom and the side walls, and release conditions at the surface. Sound sources operating in the range 5-600 Hz with a mean sound level of 152 dB re 1μPa were installed in the field near Georgiana Slough (McQuirk and Reeves, 2012). A far field value (~200 m) of about 110 dB re 1μPa was reported. In this study, nineteen sound projectors were located immediately downstream of the bubble barrier and

each projector was modeled as a constant source of acoustic energy density of 0.01 W/m. Four lights sources of 10 W/m^3 were included upstream of the bubble barrier.

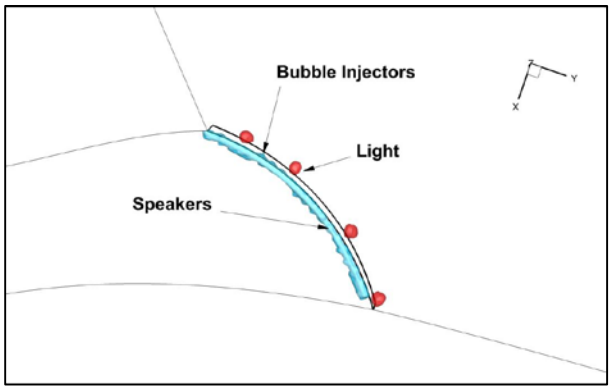

Figure 8. Simulated fish barrier

Figure 9 shows slices near the river bed (a), in the mid plane (b) and at the free surface (c). Vectors were interpolated in an equally-spaced structured mesh to enhance visualization. Bubbles significantly modify the flow pattern near the curtain. Two phenomena affect the gas volume fraction distribution; the most important is the buoyancy that drives bubbles toward the free surface and the other is the downstream convective transport by the river. The latter is significant at high river velocities and can be noted downstream of the curtain where the plume is directed towards the left bank. Upstream of the curtain and at small depths, the liquid velocity reverses direction due to the horizontal surface flow created when the plume reaches the free surface.

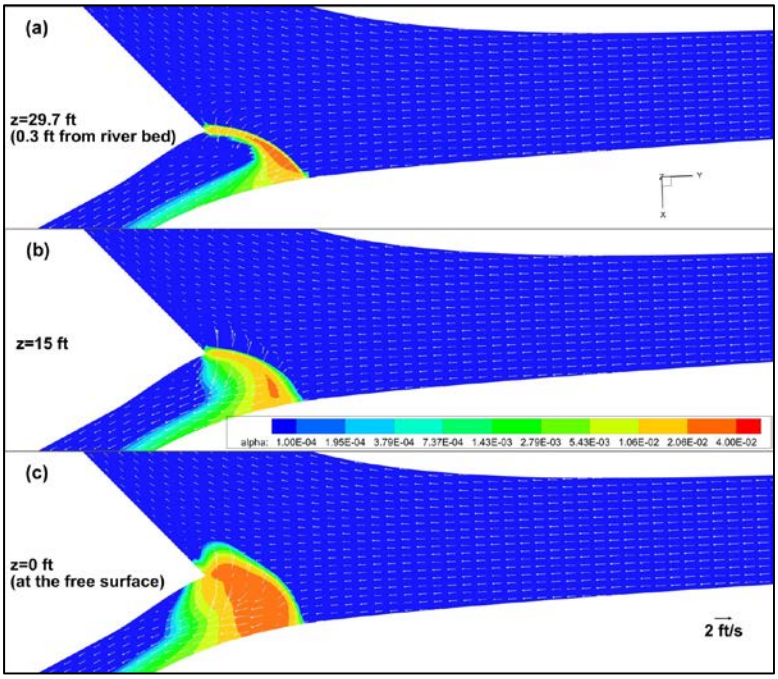

Figure 9. Gas volume fraction and velocity vectors at (a) 9 m (29.7 ft), (b) 4.5 m (15 ft) and (c) 0 m (0 ft)

Figure 10 shows flow characteristics near the bubble curtain. The frames in the top and middle show gas volume fraction isosurfaces and distribution of gas volume fraction at slices through the middle of the channels, respectively. Bubbles are transported away from the plume center by the strong surface current induced by the gas phase. The gas distribution and flow pattern are not symmetric relative to the bubble plume center due to the geometry and convective

transport by the river flow. Streamlines colored by velocity magnitude in the bottom frame show back flow near the inner wall of the larger branch towards the bubble curtain.

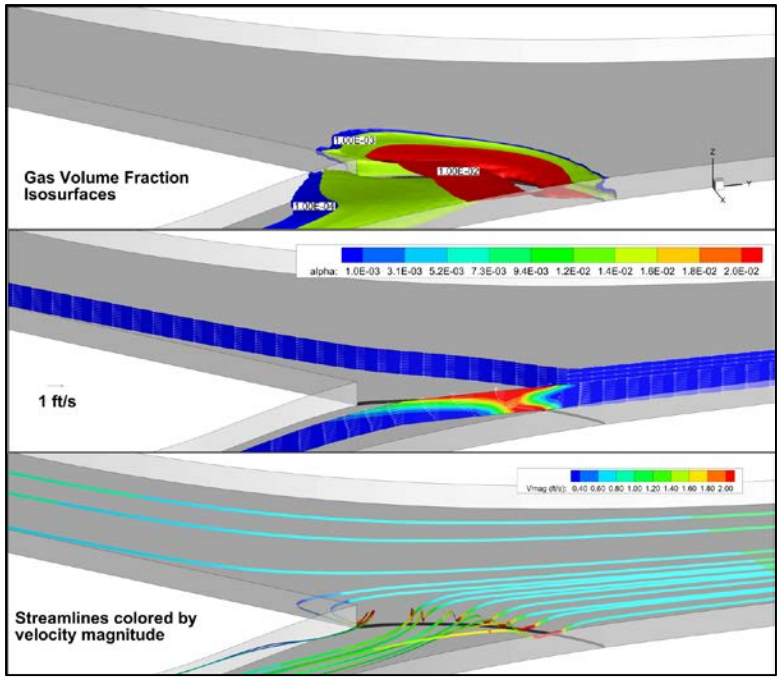

Figure 10. Gas volume fraction isosurfaces (top), gas volume fraction distribution in each river branch (middle), and streamlines colored by velocity magnitude (bottom)

Figure 11 shows the gas distribution and recirculation zones generated by the bubble curtain. As the bubble plume rises through the water column it entrains ambient water inducing two recirculating zones. Near the injector, the gas volume fraction is reduced as bubble velocity increases due to entrained liquid into the plume. On the other hand, near the free surface, the gas volume fraction increases for two phenomena, one is the increment in bubble volume due to decompression and the other is the reduction of liquid vertical velocity near the free surface. Note that since slip velocity increases with bubble size, a larger relative velocity is expected near the free surface. However, this effect is less important than the reduction of liquid velocity by the free surface.

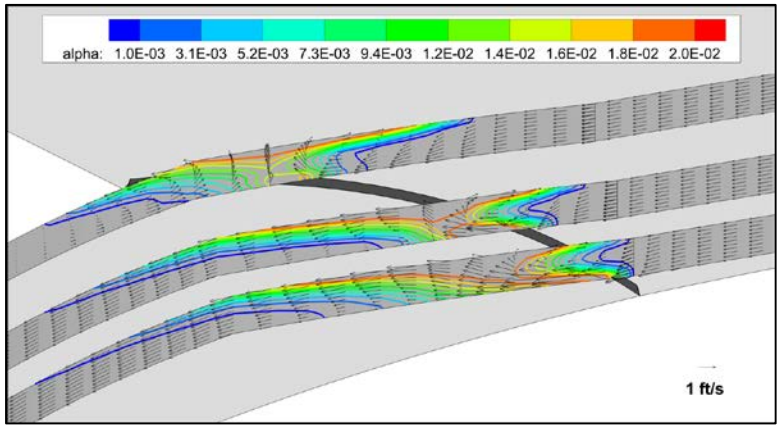

Figure 11. Gas volume fraction and velocity vectors near the bubble curtain

Figure 12 shows isosurfaces of sound energy. Bubbles encapsulate the sound within the fish barrier. However, some differences in the level of sound are observed due to increased sound attenuation by bubbles transported near the outer wall along the smaller channel.
Figure 13 shows the irradiance generated by the high-intensity LED MILs predicted with the superposition of elementary solution method (a) and P1 model (b). Light scattering and absorption by the bubbles results in an appreciable concentration of light within the fish barrier.

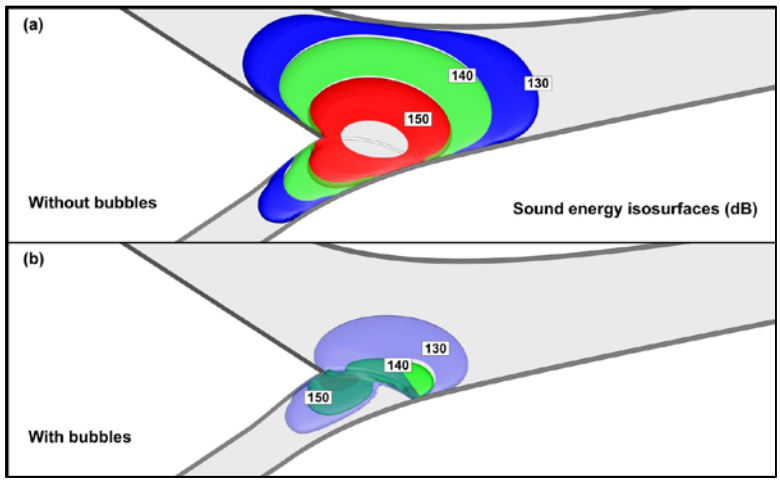

Figure 12. Isosurfaces of sound energy. Before bubble injection (a) and with bubble curtain (b)

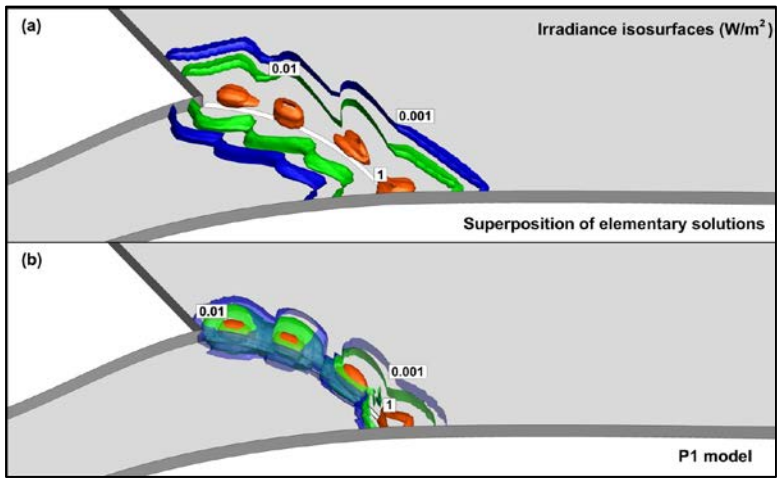

Figure 13. Isosurfaces of irradiance. Before bubble injection (a) and model P-1with bubble curtain (b)

CONCLUSIONS AND FUTURE DIRECTIONS

Numerical models for predicting the hydrodynamics, bubble, sound, and light distributions near a non-physical fish barrier were developed. The models were implemented using a modular approach in the open source code openFoam. A Boussinesq approach was used to account for the reduction of density in the zones where bubbles are present. The effect of the bubbles on the sound and light fields were considered through attenuation coefficient models found in the literature. Simple geometries were simulated to validate the implementation of the models. Model results for a non-physical fish barrier located in a bifurcation similar to Georgiana Slough indicate that the bubble plume has a strong effect on the flow pattern near the barrier. The resulting large-scale recirculations and increased accelerations near the barrier are expected to influence fish migration route. Sound and light are strongly coupled with the bubble plume. Bubbles effectively encapsulate both sound and light within the barrier region. According to the model, the effectiveness of bubbles to attenuate sound depends on the position of the speakers relative to the bubble plume. Since

the bubble plume location depends on the induced liquid movement as well as downstream transport by the river, optimal location of speakers is a function of the river flowrate and gas injection rate through the diffusers.
Additional research needs to include a full set of experimental data and monitoring near a fish barrier, at several river and barrier operational conditions, for better quantification of important variables. Examples include measurements of gas volume fraction, bubble size, river depth, liquid velocities, and sound and light fields. The complex three-dimensional nature of the problem will require measurement stations at several transects near the barrier. This is essential to fully validate and improve the developed numerical tool and identify areas where future modeling effort should focus.

REFERENCES

Buscaglia, G.C., Bombardelli F.A. and Garcia, M.H. (2002). "Numerical modeling of large-scale bubble plumes accounting for mass transfer effects". *Int. J. Multiphase Flow*, 28, pp 1763-1785.

Castillejos, A.H. and Brimacombe, J.K. (1987). "Measurement of physical characteristics of bubbles in gas-liquid plumes: Part II. local properties of turbulent air-water plumes in vertically injected jets". *Metallurgical Transactions B,* 18B, pp 659-671.

Flores, F., Garreaud, R. and Muñoz, R. (2013). "CFD simulations of turbulent buoyant atmospheric flows over complex geometry: solver development in OpenFoam". *Computers and Fluids,* 82, pp 1-13.

Grevet, J.H., Szekely, J. and El-Kaddah, N. (1982). "An experimental and theoretical study of gas bubble driven circulation systems". *Int. Journal of Heat Mass Transfer*, 25(4), pp 487-497.

Hussein, A.S. and El-Shishiny, H. (2009). "Influences of wind flow over heritage sites: a case study of the wind environment over the Giza Plateau in Egypt". *Environ Modell Software*, 24, 389–410.

Kassem, H., Saqr, K., Aly, H.S., Sies, M.M. and Wahid, M. (2011). "Implementation of the eddy dissipation model for turbulent non-premixed combustion in OpenFOAM". *Int. Communications in Heat and Mass Transfer*, 38, pp 363-367.

Kirk, J.T.O. (2003). "The vertical attenuation of irradiance as a function of the optical properties of the water". *Limnol. Oceanogr.*, 48, pp 9–17.

Kirk, J.T.O. (2006). "Light field around a point light source in the ocean". *Journal of Geophys. Res.*, 111, C07008.

McQuirk, J. and Reeves, R. (2012). "2011 Georgiana Slough Non-Physical Barrier performance evaluation project report". California Department of Water Resources, Sacramento, CA.

Mobley, C.D. (2001). "Radiative transfer in the ocean". in *Encyclopedia of Ocean Sciences*, edited by J. H. Steele, S. Thorpe, and K. Turekian, pp. 2321–2330, Elsevier, New York.

Picaut, J., Hardy, J. and Simon, L. (1999). "Sound propagation in urban areas: a periodic disposition of buildings". *Physical Review E*, 60, pp 4851-4859.

Picaut J. (2002). "Numerical modeling of urban sound fields by a diffusion process". *Applied Acoustics*, 63, pp 965-991.

Randrianalisoa, J. and Baillis, D. (2014). "Analytical model of radiative properties of packed beds and dispersed media". *Int. J. of Heat and Mass Transfer,* 70, pp 264-275.

Sazhin, S.S., Sazhina, E.M., Faltsi-Saravelou, O. and Wild P. (1996). "The P-1 model for thermal radiation transfer: advantages and limitations". *Fuel*, 75, pp 289-294.

Shamoun, B., Beshbeeshy, M.E.and Bonazza, R. (1999). "Light extinction technique for void fraction measurements in bubbly flow". *Exp. in Fluids*, 26, pp 16-26

Silberman E. (1957). "Sound velocity and attenuation in bubbly mixtures measured in standing wave tubes". *The Journal of the Acoustical Society of America*, 29, pp 925-933.

USEPA (2000). "Chesapeake Bay submerged aquatic vegetation water quality and habitat-based requirements and restoration targets: a second technical synthesis". http://archive.chesapeakebay.net/pubs/sav/savreport.pdf.

Weller, H., Tabor, G., Jasak, H. and Fureby, C. (1998). "A tensorial approach to computational continuum mechanics using object-oriented techniques". Comp. Phys. 12(6), pp 620–31.

Würsig, B., Greene, C.R. and Jefferson, T.A. (2000). "Development of an air bubble curtain to reduce underwater noise of percussive piling". *Marine Environmental Research*, 49, pp 79-93.

IMPACTS OF ROCK WEIRS ON FISH SWIM PATH SELECTION AND FATIGUE LEVLES

David L. Smith, Research Ecologist, US Army Corps of Engineers, Engineer Research and Development Center, Vicksburg, MS, david.l.smith@usace.army.mil; R. Andrew Goodwin, Research Environmental Engineer, US Army Corps of Engineers, Engineer Research and Development Center, Portland, OR, Vicksburg, MS, Andy.Goodwin@usace.army.mil; Yong Lai, Research Hydraulic Engineer, United States Bureau of Reclamation Technical Services Center, Denver, CO, ylai@usbr.gov; John M. Nestler, Senior Scientist, Badger Technical Services, Vicksburg, MS, John.m.Nestler@usace.army.mil

Abstract: The addition of rock weirs and other features is a common approach to stream restoration. We evaluate fish response to a pair of rock weirs installed in the Little Snake River, WY and explore the consequences of their presence in the stream in terms of fish movement and fish fatigue using a model. We model upstream fish movement of 5 size classes of salmonids, and use commonly accepted swim speeds and fatigue estimates to evaluate upstream movement. Fish can transition from a sustained to a prolonged or burst swim speed based on a local acceleration threshold. The flow field was computed using the model U2RANS and the resulting velocities averaged 1.4 m/s with a maximum of 3.8 m/s. We find that the largest fish are readily able to pass through the channel with low fatigue levels, while the smallest fish are unable to pass and have high fatigue levels. Moderate sized fish have two modes with some fish passing readily and with little fatigue while others don't pass and have high fatigue levels. The proportion of prolonged and burst swimming was highest for large fish. The results suggest that the rock weirs produce complex three-dimensional flow fields whose impacts depends on fish size and behaviour. Future work should focus on fish movement data collection near real stream restoration structures coupled with hydrodynamic modeling with U2RANS or other codes.

INTRODUCTION

Fragmentation and other effects of water resources development cause loss of populations and species of river fishes (Nilsson et al. 2005). Many species conservation and ecosystem restoration programs incorporate channel modifications such as rock weirs, intended to improve fish habitat, into their projects. Effective design criteria for incorporation of rock weirs into streams is based on stream stability and other engineering considerations and typically do not have a solid understanding of fish behavioral response to hydrodynamic consequences of rock weirs. Design criteria based solely on means of simple hydraulic variables may not capture the full behavioral repertoire of animals evolved to move in spatially and temporally complex aquatic environments. Rock weirs may be movement barriers to fish due to high velocities or excessive elevation change. If rock weirs are barriers to fish this may have fish population consequences because movement is disrupted or otherwise limited.

Fish employ at least three recognized swim behaviors during upstream migration: sustained, prolonged and burst swimming (Hoar and Randall 1978). Sustained swimming is generally employed over long time periods (hours, days) and is energetically efficient. Prolonged and burst swimming are short term (seconds, minutes) energy intensive behavior employed in high energy environments. Our goal is to mathematically represent upstream migration and quantify the

contribution of prolonged and burst swimming to passage by various sized fishes. We do this by: 1) using a computational fluid dynamics (CFD) CFD model of a restoration feature in a natural river; 2) simulating various sized fish implementing a mix of sustained and prolonger/burst swimming in complex hydraulic environments, and 3) analysis of resulting swim speeds, fatigue levels and passage success.

METHODS

A detailed CFD model is used to realistically simulate the hydrodynamic pattern in a selected section of river. The output of the CFD model is linked to a fish swim path selection model that creates virtual fish programmed to respond to hydrodynamic variables using Eulerian-Lagrangian-Agent Methods (ELAMs - Goodwin et al. 2006, 2013). The swim path selection model can be programmed with different behaviour rules that each represents a different assumption about the movement of observed fish. The outputs of competing movement rules can be evaluated for realism and explanatory power using techniques similar to those used for real fish. Virtual fish tracks can be analysed for swim distance, distance over ground, track complexity, track direction, passage rate past a fixed location (e.g. a fishway exit or an arbitrary finish line within the channel), and other useful descriptive measures. Species- and size-specific fatigue times based on swim speed and duration were derived from the literature.

Site Description and Computational Fluid Dynamics Model: We selected a 56-m long reach of the South Fork Little Snake River with a maximum width of about 5-m. This reach was characterized by steep slope, complex flow pattern (Figure 1A) with 3-D flow, two hydraulic jumps, and a wide range of depths and velocities created by a two u-shaped rock weirs (Figure 1B). To simulate this site, we used U^2RANS (Lai et al. 2003; Lai et al. 2004), a 3-D, unsteady, nonhydrostatic, model useful for simulating complex flow patterns in steep, geomorphically diverse river channels. The numerical mesh consists of about 160,000 cells with mixed hexahedrons and wedges. Maximum modeled pool depths are 1.6 m, maximum velocities at the weirs are greater than 3 m/s, and mean water velocities are 1.6 m/s (Figure 1).

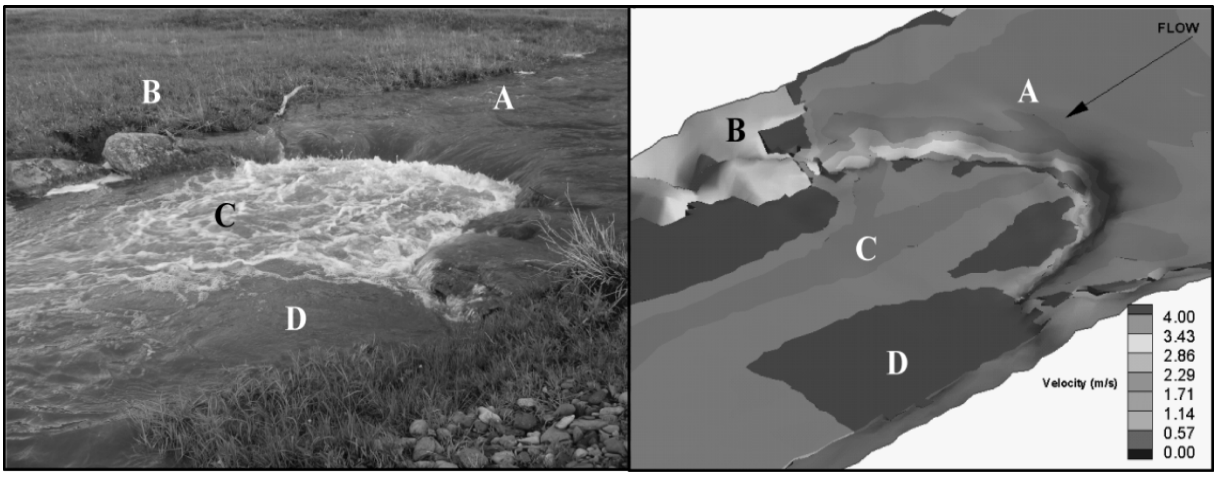

Figure 1 Photo and computational representation of the domain used to evaluate upstream fish movement. Point A shows approach to supercritical drop (height = 0.4 m) flow and velocities of 3 m/s. Point B shows complex rocks incorporated into the model. Point C is a high velocity jet of 2 m/s. Point D shows a low velocity zone (0.4 m/s).

Modeled Fish and Swimming Algorithm: We modelled fish with a default behavior of swimming upstream at a sustained speed of 2.0 body lengths per second (BL/s) using methods of Goodwin et al. (2006). Sustained upstream swimming is represented as a biased correlated random walk with turning angles drawn from a range of 0 to 5 degrees in the *xy* plane. We trigger a combined prolonged and burst swimming behavior (6 to 10 BL/s) using an acceleration threshold of 0.04 m/s^2. Both the sustained and prolonged/burst behaviors result in the fish swimming into the local flow vector. We manually calibrated the acceleration trigger by noting that a fish should implement swim strategies that minimize prolonged and burst swimming (to minimize fatigue) while still providing for upstream movement and ultimately passage through the domain.

One hundred fish per size class (0.38-, 0.52-, 0.63-, 0.73-, and 0.84-m) were parameterized with the size and swimming characteristics of upstream migrating steelhead (*Oncorhynchus mykiss*). A time step of 0.01 seconds was used because the domain is physically small and complex and larger time steps yield correspondingly less informative tracks. For example, given a time step of 0.1 seconds, a 0.84 m fish swimming at a maximum of speed of 10 BL/s can cover 0.84 m or roughly 20% of the channel width. The resulting swim path would miss much of the finer scale hydraulic complexity. Segments of virtual fish tracks exhibiting predicted swim velocities greater than 10 BL/s (occasionally occurs in small CFD domains for numerical reasons) were removed from the analysis during post processing. Simulation runs were terminated after 800 seconds because all fish had exited the model domain. Positions (*x*,*y*,*z*), swim speeds (BL/s and speed over ground (SOG), and the proportion of each behavior (sustained and prolonged/burst swimming) and fatigue (instantaneous and cumulative) were computed.

We estimated fatigue time using the well-known data on steelhead swimming and fatigue from Paulik et al (1957). Fatigue times are computed for modeled fish using estimates of swim speed (BL/s) as

$$lnT = -0.48 * swim\ speed\ \left(\frac{BL}{s}\right) + 6.466 \quad (1)$$

where *T* is fatigue time in seconds. The equation extends from approximately 1.5 to 7 BL/s. For speeds under 1.5 BL/s we specify *T* as 3600 seconds, or the upper time limit for sustained swimming. We extend the relationship beyond 7 BL/s to 10 BL/s. This does not imply that fish can only maintain sustained swimming for 3600 seconds. However, 3600 seconds yields a mathematically small estimate of fatigue for a given time interval suggesting long sustained swim times. Fatigue (%) for each time step was computed as

$$\left(\frac{t}{T}\right) \times 100 \quad (2)$$

where *t* is the model time interval in seconds. Cumulative fatigue time was simply the instantaneous fatigue time (%) summed over the intervals *t* by fish and stratified by fish size.

RESULTS

Mean cumulative fatigue varies by fish size with the larger fish accumulating the least fatigue and passing through the domain the fastest (Figure 2A). Larger fish, swimming at a sustained 2 BL/s, also have the highest mean SOG (Figure 2B). Larger fish have the highest passage rate

(~90%) while the smallest fish have the lowest (0%) (Table 1). Conversely, smaller fish implement the highest percentage of sustained swimming and the lowest percentage of prolonged/burst swimming (Table 1). This is due to the longer time smaller fish spend in the domain compared to larger fish (Figure 2C). To control for time and highlight the fatigue experienced by each size class of fish, we calculated the cumulative fatigue experienced by a fish per second and note that it is highest for the 0.38 size fish (Figure 2C).

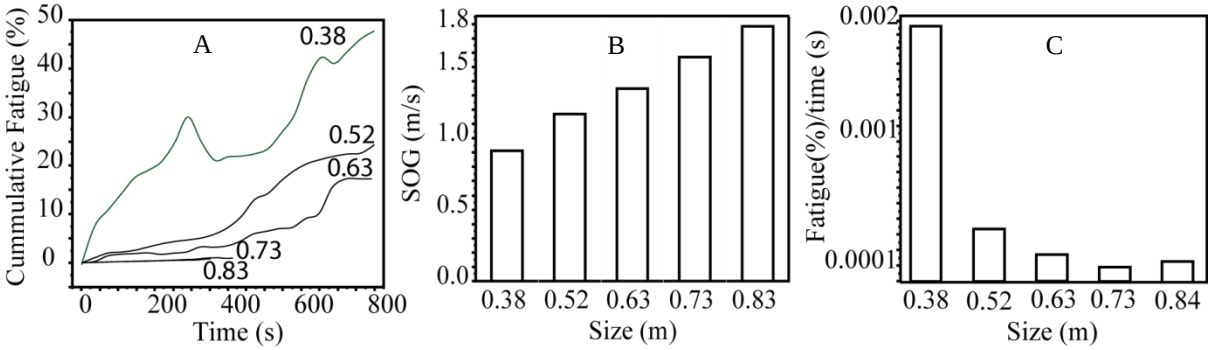

Figure 2 Mean cumulative fatigue (frame A), speed over ground (frame B), and accumulated fatigue per second (frame C) for each fish size class.

Table 1. The behavior and passage of the five size classes of fish

Size (m)	Sustained (%)	Prolonged/Burst (%)	Passage (%)
0.38	89	11	0
0.52	90	10	31
0.63	87	13	66
0.73	83	17	90
0.83	79	21	93

DISCUSSION

We show that it is possible to explore relationships among site specific geomorphology and hydraulic patterns with important biological attributes associated with fish behavior and fish passage. For example, larger fish pass at higher percentages and in shorter times than the smaller fish and the larger fish have higher SOG estimates than smaller fish. The inverse relationship between passage percentage and mean fatigue is also consistent with expectations as we would not expect fatigued fish to pass effectively. More subtlety, the simulation suggests that fatigue is not a simple correlate of swim speed. If it were, we would expect to observe that those fish that execute the most prolonged and burst swimming would also be the most fatigued. The smallest fish executed the least prolonged and burst swimming (Table 1) yet were the least successful at passage and were the most fatigued. We believe this reflects a complex dependency on fish size (and hence SOG) and the local hydraulic environment. We also note that there remains a basic question on how a fish decides, with incomplete knowledge of its environment, to transition from

sustained swimming to prolonged or burst swimming. Our premise was that prolonged and burst swimming should be not exceed the minimum needed to achieve passage. Embedded in this premise is the assumption that a fish knows the location and distance to the end point of the hydraulically challenging domain. This assumption may not be accurate, however. Improved methods of describing the decision process and behavior transitions and are needed.

Fatigue time analyses are common in the fish passage and fish swimming literature and are often used in conjunction with swimming speed information to estimate maximum distance a fish can swim in a given velocity field. Such analyses often assume uniform velocity such as might be found in a simple prismatic channel. With interest in complex natural fishways, stream restoration design and the burgeoning data available on fish movement via telemetry suggest that descriptions of fish behavior in complex, continuous velocity fields are needed. We have demonstrated one method that achieves the integration but acknowledge that much works remains to validate the approach.

Finally we note that the modelled river exhibited a range of hydraulic conditions with many point velocities exceeding the nominal swim speed criteria for adult steelhead of less than 0.6 m/s and vertical drops of 0.4 m (NMFS 2001). We demonstrated that passage was possible for some fish but not others in this environment. We conclude that simple velocity criteria may be difficult to apply in complex hydraulic environments with a wide range in velocities. Our results show that the combination of sustained and prolonged/burst swimming behaviour allows fish to pass through domains that simple criteria rule out. Further, it is possible to optimize the design using methods outlined in this study. This is a potentially important improvement over existing methods because rivers continue to be impacted by human activities and the need for effective mitigation has never been greater.

REFERENCES

Goodwin, R. A., M. Politano, J. W. Garvin, J. M. Nestler, D. Hay, J. J. Anderson, L. J. Weber, E. Dimperio, D. L. Smith, and M. Timko. 2014. Fish Navigation of Large Dams Emerges from Their Modulation of Flow Field Experience. Proceedings of the National Academy of Sciences (March 24): 1–6. doi:10.1073/pnas.1311874111.

Goodwin, R. A., Nestler, J. M., Anderson, J. J., Weber, L. J. & Loucks, D. P. 2006 Forecasting 3-D fish movement behavior using a Eulerian-Lagrangian-agent method (ELAM). Ecol. Model. 192, 197–223.

Hoar, W.S. and Randall, D.J. (editors). 1978. Fish physiology, volume VII: locomotion. Academic Press, New York.

Lai, Y.G., Weber, L.J., Patel, V.C., (2003). Non-Hydrostatic Three-Dimensional Method for Hydraulic Flow Simulation - Part I: Formulation and Verification. J. Hydraulic Engineering, ASCE, 129, 196-205.

Lai, Y. G., Weber, L. J., & Moedinger, J. (2004). A Three-Dimensional Unsteady Method for Simulating River Flows. In *World Water Congress 2001*, pp. 1–1).

National Marine Fisheries Service (NMFS). 2001. Guidelines for salmonid passage at stream crossings. Southwest Region.

Nilsson, C., Reidy, C.A., Dynesius, M., and Revenga, C. 2005. Fragmentation and flow regulation of the world's large river systems. Science. 308: 405-408.

Paulik, G.J., and DeLacy, A.C. 1957. Swimming abilities of upstream migrant silver salmon, sockeye salmon and steelhead at several water velocities. School of Fisheries, University of Washington, Technical Report 44.

FISH MOVEMENT NEAR INFRASTRUCTURE EMERGES FROM NATURAL RIVER ARCHITECTURE

R. Andrew Goodwin, Research Environmental Engineer,
U.S. Army Engineer R&D Center, Portland, OR, Andy.Goodwin@usace.army.mil

Abstract: Decades of empirical studies have identified many factors that affect the relationship between fish movement and water flow. How water flow pattern shapes the movement trajectories of fish near infrastructure remains unknown, however, and this knowledge gap impacts the success of existing and near-future engineered structures that are meant to improve the long-term health of fish populations. We present field evidence and an analysis of a hypothesis that describes fish movement near infrastructure in terms of naturally evolved behavior in free-flowing rivers for navigating heterogeneity arising from river architecture, where river architecture is defined as the geometric sum of contributions from the riverbed and embedded objects. The hypothesis assumes that fish modulate experienced changes in water acceleration (exchanges of force with the flow field) as the fish transits heterogeneity in the river. The acceleration-duration phenomenon that we identify as important in fish movement behavior has analogies to the acceleration-duration phenomena that have been implicated in sediment motion. Thus, it may be possible to interpret the hydraulic navigation of fish in rivers using phenomena involved also in the evolution of river architecture. We discuss numerical results from the application of the hypothesis to 47 flow fields at seven sites (dams) across 14 years when fish movement was monitored. Our hypothesis suggests that with a limited evolutionary history for navigating engineered structures, fish behavior reflects their naturally evolved response in free-flowing rivers. As such, we surmise that our hypothesis is applicable to fish outside the context of dams, in natural settings and near other forms of infrastructure such as fish diversion devices (booms and non-physical barriers), marine and hydrokinetic turbines, and also has implications for habitat design.

DOUBLE COUNTING, OVER CONSERVATIVE AND MISAPPLYING SAFETY FACTORS FOR STREAM SCOUR ANALYSES

David T. Williams, Ph.D., PE, PH, CFM, CPESC, F.ASCE
President, David T. Williams and Associates, Engineers, LLC, David@dtwassoc.com
1112 Oakridge Drive, #104, PMB 236, Fort Collins, Colorado 80525

EXTENDED ABSTRACT

Scour analyses are required for stream projects such as utility crossings, bridges, streambank protection, levees and floodwalls. In lieu of sophisticated numerical models, simplified approaches are often utilized. Neglecting local scour such as at bridges, the total scour using these simplified techniques is comprised of long term, general, bend, dune formation, and thalweg formation. There are no specific guidelines for application of safety factors for each of these components. Some techniques have safety factors inherently built into them but are not evident, often resulting in over conservative answers when additional safety factors are added. Some general scour methods include combinations of bend, dune and thalweg formation. These additional inclusions are often not evident or well documented, resulting in the unintended addition of these components and thus "double counting." In some cases, the computed scour depth is small (or zero) and the safety factor (often by adding an arbitrary scour depth) is applied to this small scour depth whereas the safety factor should have been applied to important variables that produced the total scour depth.

The safety factor is often applied only to the sum of the scour components thus giving equal "uncertainty" weighing to all the scour components. In most cases, with the use of engineering judgment, historic perspective, examination of how the scour techniques were developed, and the evaluation of the risks involved as a result of possible failure, one can estimate the appropriate safety factor for each scour component to come up with the total scour.

This presentation gives information on which techniques have safety factors inherently in them and what components are already included in the techniques. The presentation also gives guidelines on which variables should be used for application of safety factors and a suggested procedure to assure that scour components are appropriately combined.

THE UPPER BOUND OF PIER SCOUR DEFINED BY SELECTED LABORATORY AND FIELD DATA

Stephen T. Benedict, Hydrologist, U.S. Geological Survey, Clemson, South Carolina, benedict@usgs.gov
Andral W. Caldwell, Hydrologist, U.S. Geological Survey, Columbia, South Carolina, acaldwel@usgs.gov

Abstract The U.S. Geological Survey, in cooperation with the South Carolina Department of Transportation, conducted several field investigations of pier scour in South Carolina and used that data to develop envelope curves defining the upper bound of pier scour. To expand upon this previous work, an additional cooperative investigation was initiated to combine the South Carolina data with pier-scour data from other sources and evaluate the upper bound of pier scour with this larger data set. To facilitate this analysis, a literature review was conducted to identify potential sources of published data on pier scour, and selected data were compiled into a digital spreadsheet consisting of 569 laboratory and 1,858 field measurements. These data encompass a wide range of laboratory and field conditions and represent field data from 23 states within the United States and six other countries. This extensive database was used to define the upper bound of pier-scour depth, with respect to pier width, encompassing both laboratory and field data. The envelope curve provides a simple but useful tool for assessing the potential maximum pier-scour depth for pier widths of about 30 feet or less.

INTRODUCTION

The U.S. Geological Survey (USGS), in cooperation with the South Carolina Department of Transportation (SCDOT), collected 179 field measurements of clear-water pier scour and 141 measurements of live-bed pier scour in South Carolina (Benedict and Caldwell, 2006; 2009), with nominal pier widths ranging from 0.8 to 9 feet (ft). These data were used to develop field-derived envelope-curves that reflect the upper bound of clear-water and live-bed pier scour for bridges in South Carolina, using pier width as the primary explanatory variable. To expand upon this previous work, the USGS and SCDOT initiated an additional cooperative investigation to combine the South Carolina data with pier-scour data from other sources and evaluate upper-bound relations within this larger data set. A literature review was conducted to identify potential sources of pier-scour data, and selected data were compiled into a database consisting of 569 laboratory measurements and 1,858 field measurements from 23 states within the United States and six other countries (Benedict and Caldwell, 2014). These data substantially extended the nominal pier-width range (0.05 to 64 ft) and spatial extent associated with the South Carolina data. They provide a means to develop an improved upper-bound pier-scour envelope curve having broad application. Pier width has been noted by various investigators (Laursen and Toch, 1956; Melville and Coleman, 2000; Mueller and Wagner, 2005; Ettema and others 2011; and Arneson and others 2012) to be a primary variable that influences pier-scour depth, and therefore, pier width was the only explanatory variable used in the envelope curve. This paper presents preliminary findings providing a brief description of (1) the laboratory and field database, (2) the upper-bound envelope curve of pier-scour based on the compiled database, (3) the comparison of this upper-bound curve with the South Carolina pier-scour envelope curves, and (4) conclusions.

LABORATORY AND FIELD DATABASE

Benedict and Caldwell (2014) developed a digital pier-scour database, called the 2014 USGS Pier Scour Database (PSDb-2014), consisting of 569 laboratory and 1,858 field measurements compiled from selected authors. The laboratory data are measurements taken from 17 previous investigations and originally compiled by Sheppard and others (2011). Through a screening process that included data review and statistical analysis, Sheppard and others (2011) identified 441 of the laboratory measurements, with no skew to flow, that approximated equilibrium scour depths for the given flow, pier geometry, and sediment characteristics. These screened laboratory data provide a reliable source for evaluating the upper-bound relations of pier scour and were used in the current (2015) investigation to initially determine a pier-scour envelope curve. The field data were compiled from 32 previous publications and reflect measurements collected in 23 states within the United States and six other countries. A subset of 727 field measurements included in the PSDb-2014 was previously screened by Sheppard and others (2011), and identified as likely approximating equilibrium scour depths. From this subset of screened data, 410 field measurements with pier skews equaling zero degrees, or with adequate information to evaluate the influence of pier skew, were selected and used to corroborate and extend the pier-scour envelope curve defined by the laboratory data. An additional 558 pier-scour data, measured during high flows and having the previously noted selection criteria, were chosen from the remaining PSDb-2014 field measurements, and used as validation data to verify the pier-scour envelope curve defined with the screened laboratory and field data. [Note: Field measurements used in this investigation with piers skewed to flow were adjusted by dividing the scour depth by the pier-skew coefficient as determined from Arneson and others (2012).] Additional information regarding the PSDb-2014 and its associated report (Benedict and Caldwell, 2014) is available at the following web address: http://pubs.usgs.gov/ds/845.

THE UPPER BOUND OF PIER SCOUR IN LABORATORY AND FIELD DATA

Figure 1 displays the relation of pier-scour depth with respect to pier width using the 441 screened laboratory measurements identified by Sheppard and others (2011). A log-log scale is used to better display the upper bound of the data. With only two exceptions, the upper bound displays a well-defined relation as shown by the line in figure 1. The two data points that slightly exceed the line are associated with high Froude numbers (1.2 and 1.5). Jain and Fischer (1979) note that the flow conditions associated with these two measurements were very turbulent and unsteady, making the measurements questionable. Therefore, these two data points were excluded in defining the upper bound of the data. If the laboratory data in figure 1 are capturing the upper bound of pier-scour depth that is expected in the field, it would be reasonable to expect that the upper bound of the field data would conform to the extension of the line in figure 1.

Figure 2 shows the relation of scour depth and pier width for the 410 screened field data, previously described, using the same format as figure 1 with an extension of the envelope curve derived from the laboratory data. While there is more scatter in the upper bound of the screened field data than that of the laboratory data, it conforms well to the envelope curve of the laboratory data, indicating that the laboratory envelope curve provides a reasonable definition of the upper bound of pier scour in the field as well as the laboratory. There are two field measurements that exceed the envelope curve with exceedance values of 0.3 and 2.5 ft. The

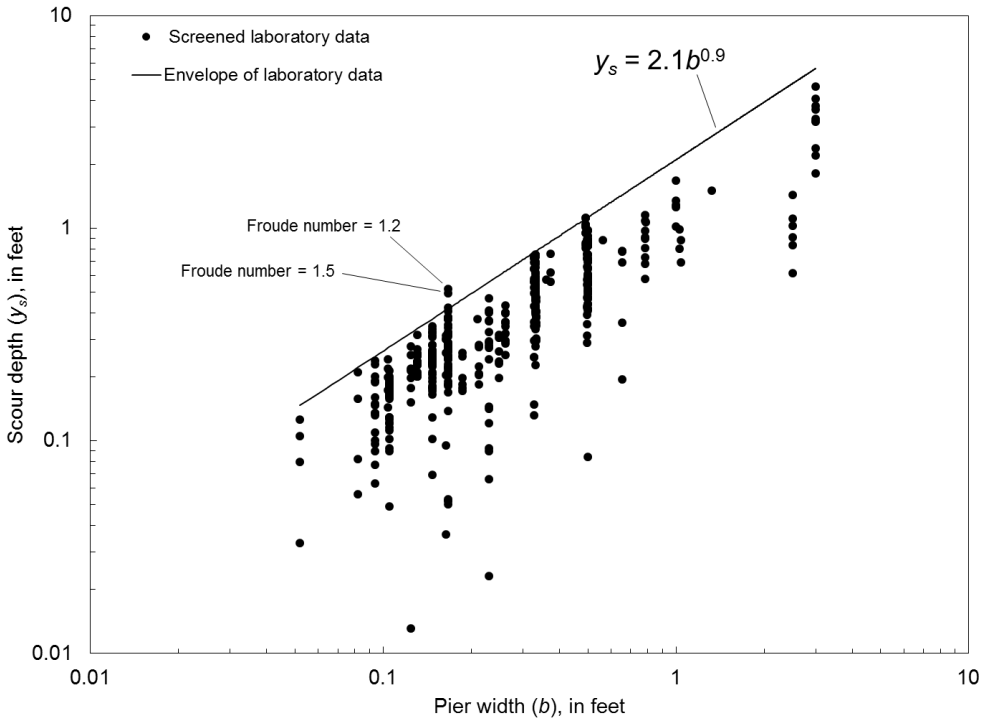

Figure 1 Relation of scour depth to pier width for the screened laboratory data.

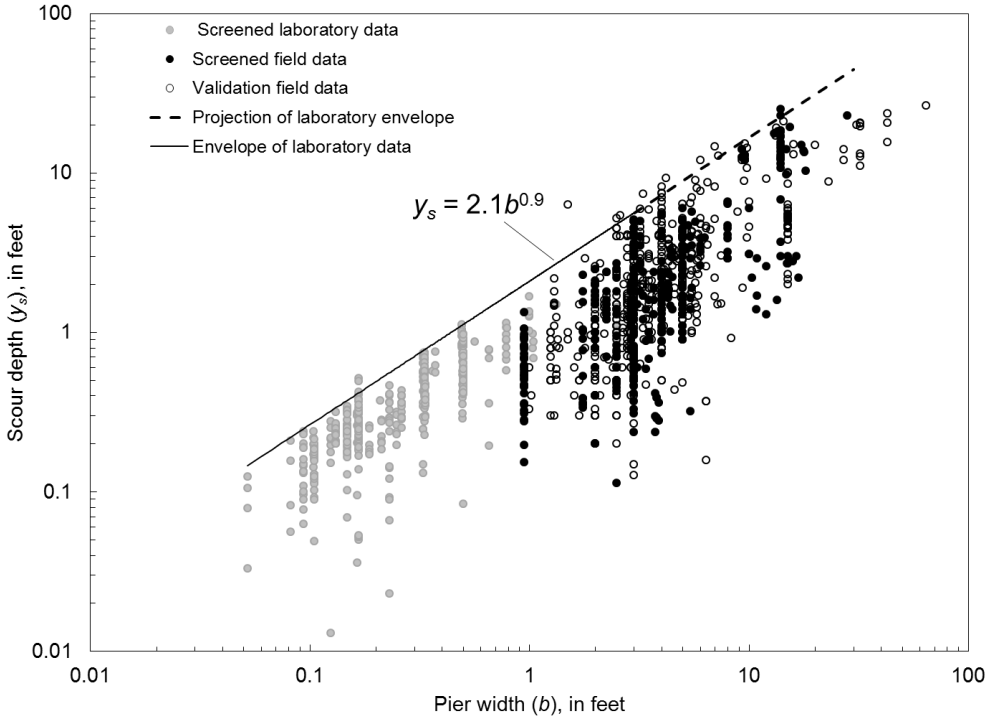

Figure 2 Relation of scour depth to pier width for the screened laboratory and field data, and validation field data.

complexities of the field, combined with the harsh measuring environment, make it difficult to measure pier scour to the same degree of accuracy as that of the laboratory, and therefore, it is expected that some field measurements may exceed the upper bound of the laboratory data. Because the exceedance values are small, no adjustment was made to the envelope curve to account for these two data points. The 558 validation field data measured during high flows as previously described, also are shown in figure 2. Only 11 of the validation data exceeded the envelope curve with small exceedance values ranging from 0.2 to 3.3 ft, with a median exceedance of 0.9 ft. The validation data provide further confirmation that the envelope curve shown in figure 2 is reasonable. The envelope curve in figure 2 represents preliminary findings for the current (2015) investigation and is subject to change.

COMPARISON WTIH THE SOUTH CAROLINA PIER-SCOUR ENVELOPE CURVES

Benedict and Caldwell (2006; 2009) developed clear-water and live-bed pier-scour envelope curves to be used as supplementary tools for evaluating the potential for pier scour at bridges in South Carolina. The format of the South Carolina pier-scour envelope curves are similar to those shown in figures 1 and 2 with pier width used as the primary explanatory variable. An objective of the current (2015) investigation is to evaluate the South Carolina envelope curves with the PSDb-2014 database to determine if they are reasonable or need modification. Figures 3 and 4 show the South Carolina pier-scour envelope curves for clear-water and live-bed scour conditions, respectively, along with the preliminary upper-bound envelope curve derived from the PSDb-2014 database. The South Carolina pier-scour envelope curves fall in close proximity to the PSDb-2014 envelope curve, indicating that the South Carolina pier-scour envelope curves

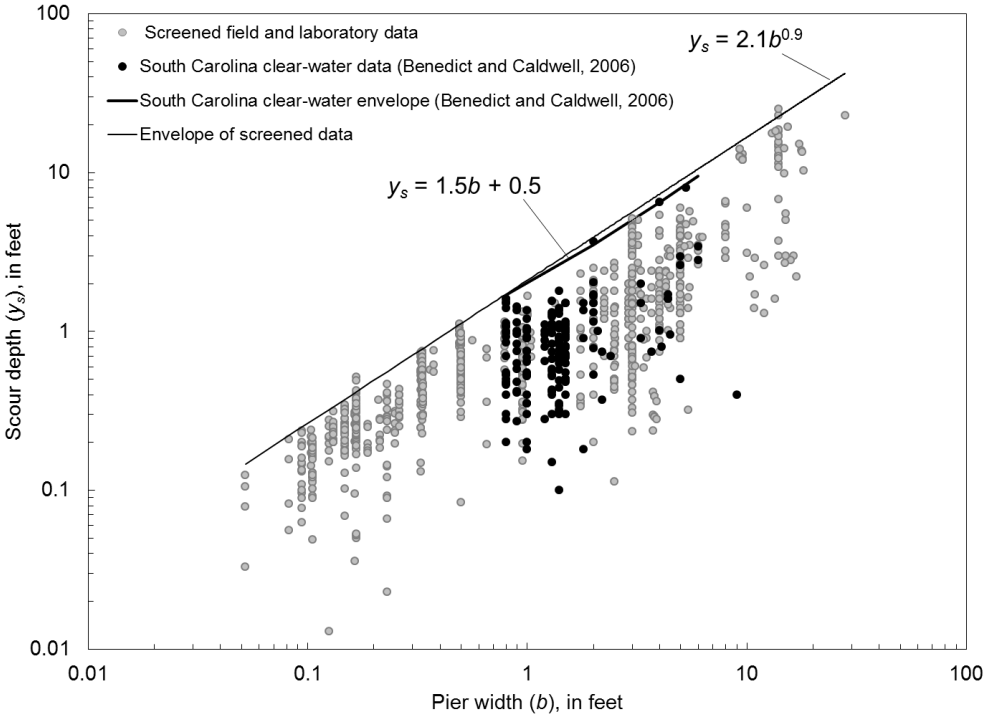

Figure 3 Comparison of the South Carolina clear-water pier-scour envelope curve to the upper-bound envelope curve derived from the screened laboratory and field data.

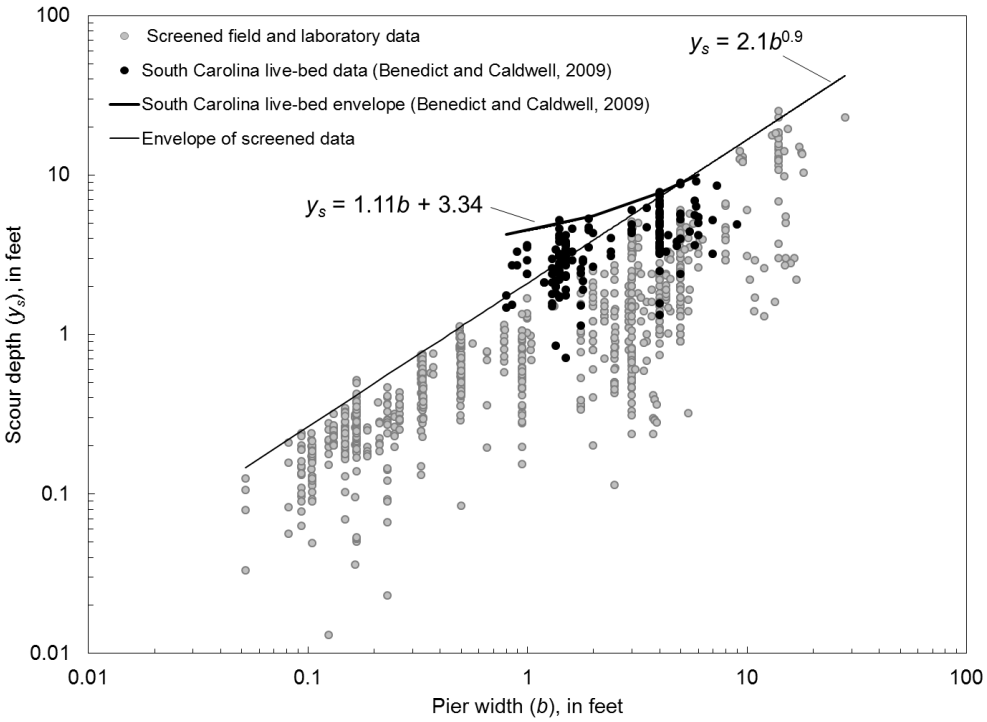

Figure 4 Comparison of the South Carolina live-bed pier-scour envelope curve to the upper-bound envelope curve derived from the screened laboratory and field data.

are reasonable. The small exceedance of the live-bed envelope curve (figure 4) can be attributed to the use of ground-penetrating radar that tends to have a larger measurement uncertainty (Benedict and Caldwell, 2009), which can lead to overestimates of scour. Current guidance and limitations for using the South Carolina pier-scour envelope curves can be found in Benedict and Caldwell (2006; 2009).

CONCLUSIONS

Current methods for predicting pier-scour depth have some uncertainty, and therefore, should be assessed for reasonableness. One way to make such assessments is by comparing predicted scour to historical field measurements. The recent investigations of pier scour in South Carolina demonstrate how a strategic sample of historic field data can be used to develop regional bridge-scour envelope curves for assessing scour potential. The preliminary pier-scour envelope curve based on the PSDb-2014 database indicates that the South Carolina bridge-scour envelope curves are reflecting a reasonable upper bound of pier scour under field conditions in South Carolina. The preliminary PSDb-2014 pier-scour envelope curve (figure 2) includes a larger range of pier widths and is therefore likely applicable to a broad range of pier widths. The South Carolina pier-scour envelope curves can be used as supplementary tools for assessing potential maximum pier-scour depth in South Carolina, and the preliminary PSDb-2014 pier-scour envelope curve likely will be applicable to a broader range of pier widths, inside as well as outside of South Carolina. Because of the complexity of scour, caution and judgment should be used in the application of the envelope curves presented in this paper, and they should not be relied upon as the only tool for assessing pier-scour potential. One can best assess anticipated scour by

compiling and studying the available information for a given site, bringing sound engineering principals to bear on the final estimate of anticipated pier-scour depth. Additional guidance and limitations for using the South Carolina pier-scour envelope curves can be found in Benedict and Caldwell (2006; 2009).

REFERENCES

Arneson, L. A., Zevenbergen, L. W., Lagasse, P. F., and Clopper, P. E. (2012). "Evaluating scour at bridges." Hydraulic Engineering Circular No. 18, 5th Ed., *Report FHWA-HIF-12-003*, Federal Highway Administration, Arlington, VA.

Benedict, S. T., and Caldwell, A. W. (2006). "Development and evaluation of clear-water pier and contraction scour envelope curves in the Coastal Plain and Piedmont Provinces of South Carolina." *U.S. Geological Survey Scientific Investigations Report 2005–5289*, Reston, VA.

Benedict, S. T., and Caldwell, A. W. (2009). "Development and evaluation of live-bed pier and contraction scour envelope curves in the Coastal Plain and Piedmont provinces of South Carolina." *U.S. Geological Survey Scientific Investigations Report 2009–5099*, Reston, VA.

Benedict, S. T., and Caldwell, A. W. (2014). "A pier-scour database: 2,427 field and laboratory measurements of pier scour." *U.S. Geological Survey Data Series 845*, Reston, VA.

Ettema, R., Constantinescu, G., and Melville, B. (2011). "Evaluation of bridge scour research: Pier scour processes and predictions." *NCHRP Report 175*, National Cooperative Highway Research Program, Transportation Research Board, Washington, D.C.

Jain, S. C., and Fischer, E. E. (1979). "Scour around circular bridge piers at high Froude numbers." *Report FHWA-RD-79-104*, Federal Highway Administration, Washington, D.C.

Laursen, E. M., and Toch, A. (1956). "Scour around bridge piers and abutments." *Bulletin no. 4*, Iowa Highway Research Board, Ames, IA.

Melville, B. W., and Coleman, S. E. (2000). *Bridge Scour*. Water Resources Publications, Highlands, CO.

Mueller, D. S., and Wagner, C. R. (2005). "Field observations and evaluations of streambed scour at bridges." *Report FHWA-RD-03-052*, Federal Highway Administration, McLean, VA.

Sheppard, M., Demir, H. and Melville, B. W. (2011). "Scour at wide piers and long skewed piers." *NCHRP Report 682*, National Cooperative Highway Research Program, Transportation Research Board, Washington, D.C.

THE UPPER BOUND OF ABUTMENT SCOUR DEFINED BY SELECTED LABORATORY AND FIELD DATA

Stephen T. Benedict, Hydrologist, U.S. Geological Survey, Clemson, South Carolina, benedict@usgs.gov

Abstract The U.S. Geological Survey, in cooperation with the South Carolina Department of Transportation, conducted a field investigation of abutment scour in South Carolina and used that data to develop envelope curves defining the upper bound of abutment scour. To expand upon this previous work, an additional cooperative investigation was initiated to combine the South Carolina data with abutment-scour data from other sources and evaluate the upper bound of abutment scour with the larger data set. To facilitate this analysis, a literature review was conducted to identify potential sources of published data on abutment-scour, and selected data, consisting of 446 laboratory and 331 field measurements, were compiled for the analysis. These data encompassed a wide range of laboratory and field conditions and represent field data from six states within the United States. The data set was used to evaluate the South Carolina abutment-scour envelope curves. Additionally, the data were used to evaluate a dimensionless abutment-scour envelope curve developed by Melville (1992), highlighting the distinct difference in the upper bound for laboratory and field data. The envelope curves evaluated in this investigation provide simple but useful tools for assessing the potential maximum abutment-scour depth in the field.

INTRODUCTION

> *Scant situations of hydraulic engineering are more complex than those associated with scour in the vicinity of a bridge abutment, especially one located in a compound channel. Accordingly, few situations of scour depth estimation are as difficult (Ettema and others, 2005).*

The complexity of abutment-scour processes has made it difficult to formulate prediction methods, and few would dispute the above assessment by Ettema and other (2005). Current scour-prediction equations largely consist of semi-empirical relations developed from simplified laboratory investigations (Sturm and others, 2011), and the performance of these equations can vary (Wagner and others, 2006; Benedict and others, 2007; Lombard and Hodgkins, 2008). While overprediction occurs frequently (and at times excessively), underprediction also is of concern. Because of the uncertainty in scour prediction, Hydraulic Engineering Circular No. 18 (HEC-18; Arneson and others, 2012) recommends that computed scour be evaluated for reasonableness by comparing with available historical data at or near the site of interest. Based on such an evaluation, the predicted scour can be modified if deemed appropriate. The wisdom and benefit of using historical flow and scour data to evaluate predicted scour is unquestionable. However, such data are frequently unavailable making the evaluation recommended in HEC-18 difficult, if not impossible. One way to address this issue of limited historical data is through the use of upper-bound envelope curves derived from laboratory and field measurements of abutment scour. While such envelope curves are not site (or near site) specific, they display the general trends for the upper bound of abutment scour over a wide range of conditions, providing a tool to help assess the maximum potential for scour. Envelope curves for abutment scour have been previously developed for laboratory and field data. With respect to laboratory data, Melville (1992) developed envelope curves using dimensionless variables associated with

selected laboratory data (96 measurements). With respect to field data, the U.S. Geological Survey (USGS), in cooperation with the South Carolina Department of Transportation (SCDOT), developed envelope curves for selected field data (209 measurements) in South Carolina (Benedict, 2003). These previous investigations demonstrate how envelope curves can be developed and used for assessing the maximum abutment-scour potential. To expand upon the previous work by Benedict (2003), the USGS and SCDOT initiated another cooperative investigation to compile additional laboratory and field data from other existing sources, and evaluate the upper-bound trends of abutment scour within this larger data set. A literature review was conducted to identify potential sources of abutment-scour data, and selected data were compiled into a digital database consisting of 329 field and 446 laboratory measurements. These data significantly extended the range of the data previously used by Benedict (2003) and Melville (1992), providing a means to evaluate the previously developed envelope curves. This paper presents preliminary findings providing a brief description of (1) the field and laboratory data used in the investigation, (2) the comparison of the field data with the Melville (1992) dimensionless envelope curve, (3) the evaluation of selected South Carolina abutment-scour envelope curves with additional field data, and (4) conclusions.

FIELD AND LABORATORY DATA

All of the field data, compiled from the previously noted literature review, were collected by the USGS and included 15 measurements from the USGS National Bridge Scour Database (NBSD; USGS, 2001), 92 measurements from the moderate-gradient streams of the South Carolina Piedmont with cohesive sediments (Benedict, 2003), 106 measurements from the low-gradient streams of the South Carolina Coastal Plain (none are tidally influenced) generally with sandy, non-cohesive sediments (Benedict, 2003), 93 measurements from the small, steep-gradient streams of Maine with coarse sediments (Lombard and Hodgkins, 2008), and 23 measurements from the low-gradient streams of the Alabama Black Prairie Belt with cohesive sediments (Lee and Hedgecock, 2008). Most of these data are historical scour measurements, similar to post-flood measurements, and are assumed to represent the maximum abutment-scour depth that has occurred at the bridge since construction. The field data are largely associated with clear-water scour conditions where sediments do not refill the scour holes as flood waters recede, providing justification for this assumption. Because the scour measurements were made during low-flow conditions, one-dimensional flow models were used to estimate the hydraulic properties. The post-flood nature of the scour measurements, in conjunction with the estimated hydraulics, makes these data less than ideal. These limitations should be kept in mind when using the USGS field data in any analysis. While the limitations of the USGS abutment-scour field data are acknowledged, this is currently (2015) the best available set of field data, and the large number of measurements (329) should be sufficient to gain insights into the general trends of abutment scour in the field. In addition to the USGS field data, two abutment-scour measurements at Interstate 70 crossing the Missouri River (Parola and others, 1998), associated with the 1993 flood also were included. The Missouri River data are perhaps the largest measured riverine abutment-scour depths in the United States (30 feet (ft) at the bridge and 56 ft upstream from the bridge) and were strongly influenced by a levee breach located approximately 350 ft upstream from the abutment. Additionally, the site has a drainage area of 500,000 square miles (mi^2). In contrast, the maximum drainage area for the South Carolina data is 8,830 mi^2 with a median value of approximately 100 mi^2. The adverse flow conditions and substantially larger drainage

area of the Missouri River site contribute to the larger scour depths than those of the South Carolina data. While the Missouri River data do not represent typical abutment scour, they were included in the analysis for perspective.

In addition to field data, 446 laboratory measurements of abutment scour reported by selected authors, including 96 measurements from Melville (1992), 191 measurements from Palaviccini (1993), 80 measurements from Sturm (2004), 17 measurements from Briaud and others (2009), and 62 measurements from Ettema and others (2010), were incorporated into the database. The data from Melville (1992) and Palaviccini (1993) were compiled from multiple authors of previous investigations, and are not listed here for brevity. The laboratory data are largely associated with non-cohesive sediments, with the exception of the Briaud and others (2009) investigation, which used cohesive sediments. Additionally, the data primarily represent clear-water scour conditions with the exception of 28 measurements from Ettema and others (2010) that represent live-bed scour conditions.

THE MELVILLE (1992) UPPER-BOUND ENVELOPE CURVE COMPARED WITH LABORATORY AND FIELD DATA

Melville (1992) used 96 laboratory measurements collected in rectangular flumes at threshold clear-water scour conditions to develop an envelope curve of abutment-scour depth (figure 1). The curve is based on the relation of relative scour depth (D_{sadj}/y) to relative abutment length (L/y), where D_{sadj} is the measured abutment-scour depth adjusted for the effect of abutment shape [see Melville (1992) for details on this adjustment], L is the abutment (also called embankment) length blocking flow, and y is the approach-flow depth. Melville (1992) noted that the upper bound of D_{sadj}/y generally increased with increasing L/y, and identified three abutment-length categories where the rate at which scour increased varied. These categories, identified in figure 1, included short abutments ($L/y \leq 1$) with the smallest scour potential, long abutments ($L/y \geq 25$) with the largest scour potential, and intermediate abutments between these values. The selected laboratory data from Palaviccini (1993), Sturm (2004), Briaud and others (2009), and Ettema and others (2010) also are shown in figure 1. All of the laboratory data falls within or close to the Melville (1992) envelope curve, indicating that the envelope curve is a reasonable representation of the approximate upper bound of abutment scour for laboratory data.

Figure 2 shows the previously described field data plotted with the Melville (1992) laboratory data and envelope curve. While the upper bound of the field data ($4.25y$) is significantly smaller than the laboratory data ($11y$), it is notable that this upper bound conforms well to the general shape and breakpoints associated with the Melville (1992) envelope curve. Based on this pattern, an envelope curve of the field data was drawn parallel to the laboratory envelope curve using the same breakpoint at the transition from intermediate to long abutments. The field data encompass the range of the three abutment-length categories; however, they are heavily weighted toward the long-abutment category where the potential for scour is greatest. The one Maine measurement that significantly exceeds the field-data envelope curve was collected using ground-penetrating radar (GPR), which is a useful tool for measuring scour. However, the interpretive nature of this method introduces uncertainty into the scour measurement which can lead to overestimates of scour (Benedict and Caldwell, 2009). The Missouri River data, the largest scour depths

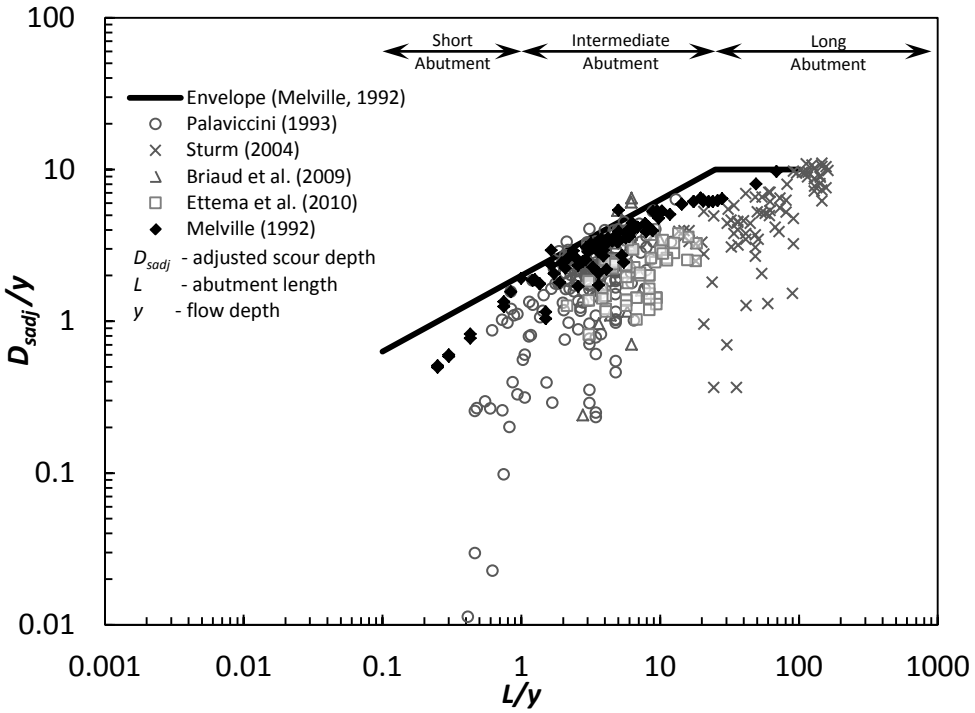

Figure 1 Relation of the relative scour depth (D_{sadj}/y) to relative abutment length (L/y), for selected laboratory data.

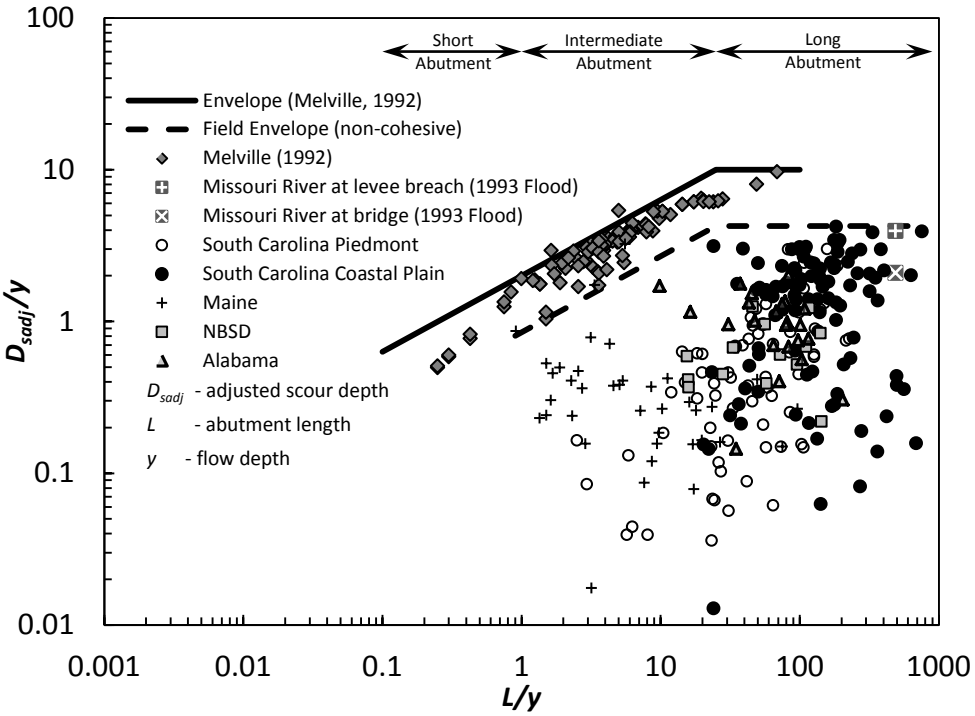

Figure 2 Relation of the relative scour depth (D_{sadj}/y) to relative abutment length (L/y), for selected laboratory and field data.

in this investigation, fall within the field envelope curve, providing a measure of confidence that the field envelope curve is reasonable. The significant difference in the upper bound of relative scour for the laboratory and field data, as shown in figure 2, is likely caused by multiple factors. The primary reasons for the discrepancy are thought to be short flow durations insufficient to produce equilibrium scour; approach-flow velocities significantly below threshold conditions for sediment motion that produce smaller scour depths than velocities at threshold conditions; and non-uniform sediments more resistant to scour.

VERIFICATION OF SELECTED SOUTH CAROLINA ABUTMENT-SCOUR ENVELOPE CURVES

Benedict (2003) used 209 field measurements of clear-water abutment scour to develop envelope curves for the Piedmont and Coastal Plain of South Carolina to be used as supplementary tools for evaluating the potential for abutment scour at bridges in South Carolina. Two envelope curves were developed for each region with one envelope curve using the geometric contraction ratio as the primary explanatory variable and the other curve using the abutment (or embankment) length blocking flow. Both variables are known to be strong explanatory variables for abutment-scour depth (Melville and Coleman, 2000; Benedict, 2003), thus providing justification for their use as explanatory variables. The geometric contraction ratio is a dimensionless variable that represents the severity of the contraction created by the bridge, with 0.0 being no contraction and 1.0 being 100-percent blockage. Larger geometric contraction ratios will tend to produce larger abutment-scour depths. The embankment length, measured from the edge of the floodplain to the abutment toe, is a relative measure of the blocked flow passing by the abutment with longer embankment lengths tending to block more flow, producing larger abutment-scour depths. As an example of these curves, figure 3 shows the South Carolina abutment-scour envelope curves with respect to the geometric contraction ratio for the Piedmont and Coastal Plain.

All of the previously noted field data are shown on this figure, with the exception of the largest Missouri River measurement, which was excluded for the purpose of the figure scale. With the exception of two data points, all of the field data falls within the Piedmont envelope curve with most of the data falling within the Coastal Plain envelope curve, providing a measure of validation for these curves. The one Maine data point that exceeds the envelope curve, as noted previously, was measured using GPR, giving some explanation for its exceedance. The exceedance of the Missouri River data can be attributed, in part, to the levee breach and the much larger drainage area, and highlights the importance of limiting the application of the South Carolina bridge-scour envelope curves to site characteristics similar to the South Carolina data used to develop them. Current guidance and limitations for using the South Carolina abutment-scour envelope curves can be found in Benedict (2003).

CONCLUSIONS

Current methods for predicting scour have some uncertainty, and therefore, should be assessed for reasonableness. One way to make such assessments is by comparing predicted scour to field measurements of historical scour. The recent investigations of scour in South Carolina

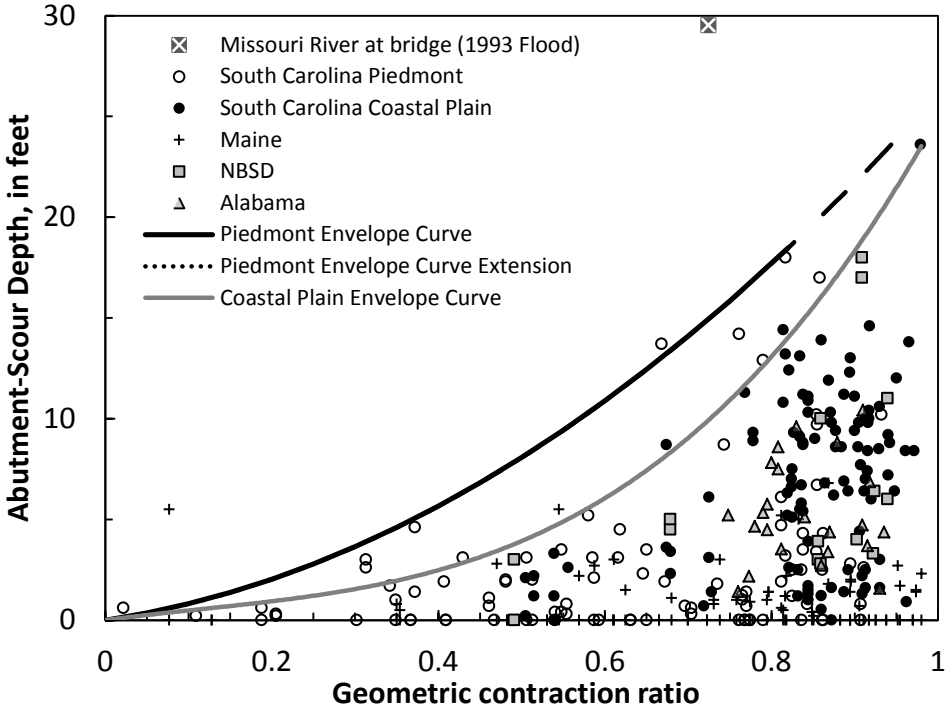

Figure 3 The South Carolina abutment-scour envelope curves with respect to the geometric contraction ratio compared with selected field data.

demonstrate how a strategic sample of historical field data can be used to develop regional bridge-scour envelope curves for assessing scour potential. The verification of these envelope curves with field data from other sources indicates that the South Carolina bridge-scour envelope curves are reflecting the upper bound of scour under field conditions in South Carolina. However, the exceedance of the Missouri River data highlights the importance of limiting the application of the South Carolina bridge-scour envelope curves to site characteristics similar to the South Carolina data used to develop the curves. A comparison of the field data with the laboratory data indicates that the upper bound of relative-scour depth in the field is significantly lower than the laboratory data, which likely is caused by the differing flow and sediment characteristics between these two environments. Because of the complexity of scour, caution and judgment are needed in the application of the envelope curves presented in this paper, and they should not be relied upon as the only tool for assessing abutment-scour potential. One can best assess anticipated scour by compiling and studying the available information for a given site, bringing sound engineering principals to bear on the final estimate of anticipated abutment-scour depth. Current guidance and limitations for using the South Carolina abutment-scour envelope curves can be found in Benedict (2003).

REFERENCES

Arneson, L. A., Zevenbergen, L. W., Lagasse, P. F., and Clopper, P. E. (2012). "Evaluating scour at bridges." Hydraulic Engineering Circular No. 18, 5th Ed., *Report FHWA-HIF-12-003*, Federal Highway Administration, Arlington, VA.

Benedict, S. T. (2003). "Clear-water abutment and contraction scour in the coastal plain and Piedmont provinces of South Carolina, 1996-99." *U.S. Geological Survey Water-Resources Investigations Report 03-4064*, Columbia, SC.

Benedict, S. T., and Caldwell, A. W. (2009). "Development and evaluation of live-bed pier and contraction scour envelope curves in the Coastal Plain and Piedmont provinces of South Carolina." *U.S. Geological Survey Scientific Investigations Report 2009–5099*, Reston, VA.

Benedict, S. T., Deshpande, N., and Aziz, N. M. (2007). "Evaluation of abutment scour prediction equations with field data." *Transportation Research Record*, 2025, 118-126.

Briaud, J.-L., Chen, H.-C., Chang, K.-A., Oh, S. J., and Chen, X. (2009). "Abutment scour in cohesive material." *NCHRP Report 24-15(2)*, National Cooperative Highway Research Program, Transportation Research Board, Washington, D.C.

Ettema, R., Yorozuya, A., Nakato, T., and Muste, M. (2005). "A practical approach to estimating realistic depths of abutment scour." *The 2005 Mid-Continent Transportation Research Symposium*, Iowa State University, Ames, IA.

Ettema, R., Nakato, T., and Muste, N. (2010). "Estimation of scour depth at bridge abutments." *NCHRP Report 24-20*, National Cooperative Highway Research Program, Transportation Research Board, Washington, D.C.

Lee, K. G., and Hedgecock, T. S. (2008). "Clear-water contraction scour at selected bridge sites in the Black Prairie Belt of the Coastal Plain in Alabama, 2006." *U. S. Geological Survey Scientific Investigations Report 2007–5260*, Reston, VA.

Lombard, P. J., and Hodgkins, G. A. (2008). "Comparison of observed and predicted abutment scour at selected bridges in Maine." *U. S. Geological Survey Scientific Investigations Report 2008–5099*, Reston, VA.

Melville, B. W. (1992). "Local scour at bridge abutments." *Journal of Hydraulic Engineering*, ASCE, 118(4), 615-631.

Melville, B. W., and Coleman, S. E. (2000). *Bridge Scour*. Water Resources Publications, Highlands, CO.

Palaviccini, M. (1993). "Predictor model for bridge abutments." thesis, presented to The Catholic University of America, Washington, D.C., in partial fulfillment of the requirements for the degree of Doctor of Philosophy.

Parola, A. C., Hagerty, D. J., and Kamojjala, S. (1998). "Highway infrastructure damage caused by the 1993 Upper Mississippi River basin flooding." *NCHRP Report 417*. National Cooperative Highway Research Program, Transportation Research Board, Washington, D.C.

Sturm, T. W. (2004). "Enhanced abutment scour studies for compound channels." *Report No. FHWA-RD-99-156*, Federal Highway Administration, McLean, VA.

Sturm, T. W., Ettema, R., and, Melville, B. W. (2011). "Evaluation of bridge-scour research: Abutment and contraction scour processes and prediction." *Web-Only Document 181*, National Cooperative Highway Research Program, Transportation Research Board, Washington, D.C.

U.S. Geological Survey. (2001). "National bridge scour database." accessed April 15, 2014, at http://water.usgs.gov/osw/techniques/bs/BSDMS/index.htm.

Wagner, C. R., Mueller, D. S., Parola, A. C., Hagerty, D. J., and Benedict, S. T. (2006). "Scour at contracted bridges." *Web-Only Document 83*, National Cooperative Highway Research Program, Transportation Research Board, Washington, D.C.

BAFFLE-POST STRUCTURES FOR FLOW AND BED-SEDIMENT CONTROL IN OPEN CHANNELS

Caroline Ubing[1], Robert Ettema[2], and Christopher Thornton[3]

[1]Graduate Student, Department of Civil and Environmental Engineering, Colorado State University; email: ubingc88@rams.colostate.edu

[2] Professor, Department of Civil and Architectural Engineering, University of Wyoming, 1000 E. University Ave., Laramie, WY 82071; (307)766-4658; email: rettema@uywo.edu

[3]Associate Professor and Lab Director, Department of Civil and and Environmental Engineering, Colorado State University; email: thornton@engr.colostate.edu

ABSTRACT

This paper presents theory and laboratory findings regarding the hydraulic performance of baffle-post structures used as a means for controlling flow in open channels. Such structures comprise one to two parallel rows of posts that extend slightly higher than the anticipated depth of flow, and offer a useful means for retarding flow in various channel situations where there is a need to reduce flow energy, possibly to reduce flow capacity to transport bed sediment and manage channel morphology. The laboratory findings were obtained using a tilting flume that produced data and observations on non-dimensional headloss and discharge coefficients and flow retardance (backwater flow profiles) associated with varying geometry of baffle-post structure. This information is of use in evaluating the extent to which a baffle-post structure, by retarding an approach flow, reduces the capacity of an approach flow to convey bed sediment and, thereby, promote channel bed aggradation.

INTRODUCTION

This study focuses on the hydraulic performance of baffle-post structures, illustrated in Figure 1. These structures act to slow or retard an approach flow, spread the flow across an approach channel, and sometimes disrupt large-scale turbulence structures in approach flows. They do so primarily by locally increasing flow resistance, reducing approach-flow velocities, and dissipating flow energy. The hydraulic performance of baffle-post structures, however, has received little attention. In particular, there appear to be no prior studies relating the geometric characteristics of baffle-post structures to hydraulic performance such as expressed using common indices, notably discharge and headloss coefficients associated with flow through baffle-post structures in open-channel flow.

By slowing or retarding an approach flow, and locally dissipating flow energy, baffle-post structures are used fairly often to help maintain the grade of a channel, and possible elevate and flatten the grade. This function is accomplished by the posts slowing and deepening the approach flow, letting flow and washload sediment pass, but causing a proportion of the approach bedload sediment transport to deposit on the channel bed upstream of the baffle-post structure.

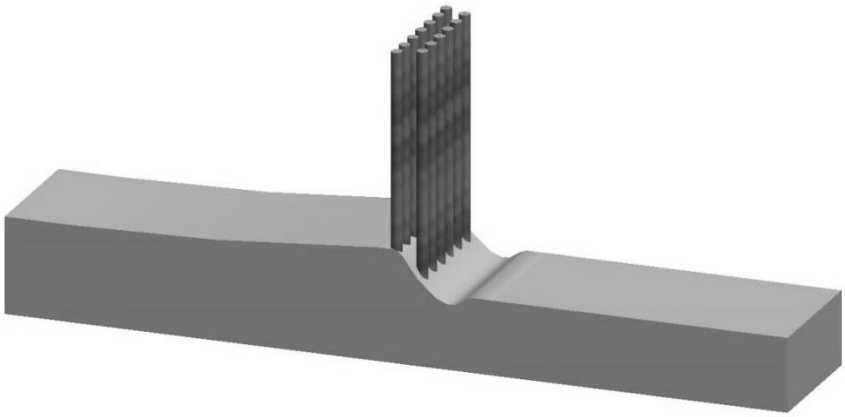

Figure 1: A Baffle post structure comprising a double row of posts spaced so as to suitably slow or retard an approach flow

The basic baffle-post structure consists of one to two rows of vertical posts. Depending on application, the post can be dowel timber, metal posts or rods, or tree trunks. When used in alluvial river channels, the posts typically are driven into the channel bed; in certain industrial uses, and laboratory flumes, the posts may be fixed to a base plate or cap block. The posts themselves usually are evenly spaced, with a second row staggered so that its posts align between those in the upstream row.

This paper briefly reviews the theory associated with the hydraulic performance of baffle-post structures, shows general trends for values of discharge coefficient and headloss related to them, and presents useful data for estimating the backwater extent (or M1 gradually varied flow profile) produced. This information is needed for evaluating the extent to which a baffle-post structure, by retarding an approach flow, reduces the capacity of an approach flow to convey bed sediment and, thereby, promote channel bed aggradation.

BACKGROUND THEORY

The essential function of a baffle-post structure is to retard an approach flow, slowing it, spreading it, and dissipating a portion of its energy. However, because flow at a baffle-post structure is non-uniform the analysis of structure hydraulic performance entails several simplifying approximations enabling baffle-post structure design to meet performance requirements within acceptable limits. The main requirement of interest for baffle-post structures in alluvial channels is the increase in water depth immediately upstream of the structure. A depth increase is associated with retarding of the approach flow so as to reduce the flow's capacity to transport bed sediment.

The hydraulic performance of a baffle-post structure can be evaluated in terms of the conservation of energy and continuity principles applied between the three flow cross sections indicated in Figure 2:

1. Between sections 0 and 1, where 0 indicates uniform approach flow well upstream of the structure, and 1 indicated a section immediately upstream of the structure; and,
2. Between sections 1 and 2, where 2 indicates the contracted section within the structure.

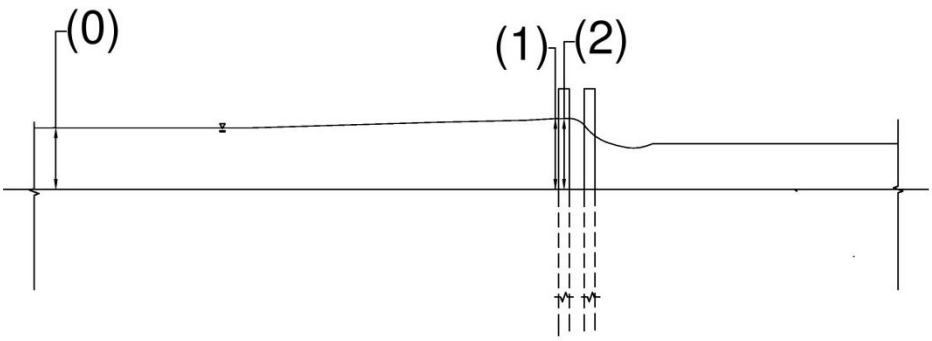

Figure 2: Three flow sections referenced for a double-row, baffle post structure

The specific energy diagram is a useful concept for explaining the hydraulic performance of a baffle-post structure. When the channel contracts, increasing the unit discharge, $q > q_0$, a set of curves exist, each with increasing value of critical depth, y_c, and E_{min}. Eventually, the contraction reaches critical width whereby E_{min} coincides with the initial specific energy, E_0. Associated with this critical flow depth is a critical width, b_c, defined as the maximum contraction the flow can pass through without becoming choked. In other words any constrictions narrower than b_c will produce an "overcritical" contraction so that there is not enough energy to maintain the given flow rate through the constriction. The critical width can be calculated as:

$$b_c = \left(\frac{3}{2}\right)^{3/2} \frac{Q}{\sqrt{gE_0^3}} \tag{1}$$

When the effective width of the flow constriction is less than b_c, the contraction acts as a "choke," as the available specific energy, E_0, is unable to pass the flow through the contraction. The flow backs up producing an M1 (backwater), gradually varied flow water surface profile, so as to elevate the magnitude of specific energy required to pass the flow through the contraction. The flow within the contraction stays critical, as the approach flow only backs up to the extent that generates the minimum energy needed to pass the given rate of flow through the contraction. The downstream flow may be supercritical or subcritical depending on the downstream conditions.

The additional energy becomes evident in the increased depth of flow at the contraction, and relatedly the energy increment, ΔE, needed to get the flow through the contraction. Figure 3 indicates the increase in specific energy and associated water depth upstream of the contraction. The increase in specific energy is dissipated as flow turbulence when the flow passes through the contraction and in a hydraulic jump formed immediately downstream of the contraction.

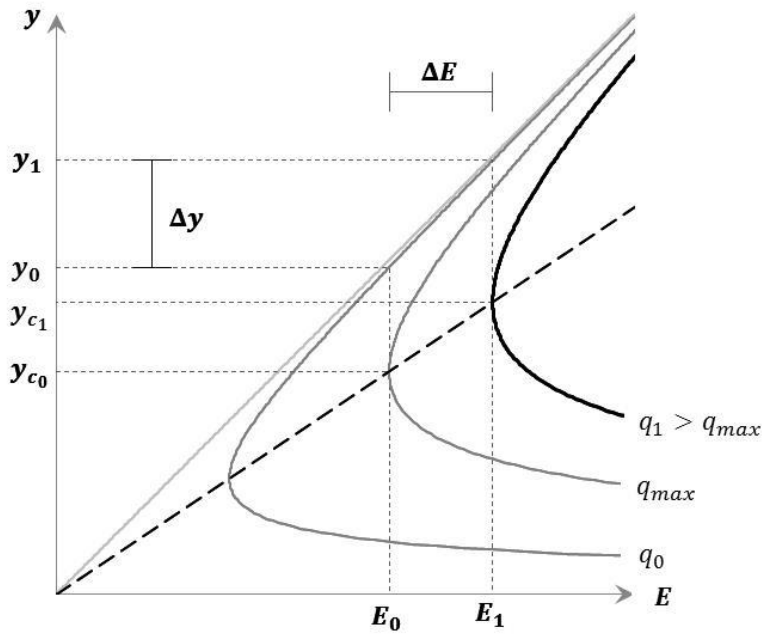

Figure 3: The increase in specific energy and upstream water level needed to pass the choked flow.

The additional energy, ΔE, needed to pass a give flow rate through a choked contraction can be evaluated in terms of the specific energy adjustments between sections 0 and 1: i.e.,

$$\Delta E = (y_1 - y_0) + \frac{q_0^2}{2gy_1^2} - \frac{q_0^2}{2gy_0^2} \tag{2}$$

Here, y_0 is the normal depth of flow for the uniform section well upstream of the structure, and y_1 is flow depth at section 1. Accounting for the headloss associated with flow resistance and the backwater curve, the headloss associated with the structure is:

$$\Delta E = h_{Lbaffle} = h_{L0} - h_{L0-1} = \left\{\left(\frac{fL}{8}\right)\left[\frac{(y_1/y_0)^3-1}{y_0(y_1/y_0)^3}\right]\right\}\left(\frac{u_0^2}{2g}\right) \tag{3}$$

It is common to express a local headloss, h_L, in terms of a headloss coefficient, C_L, and an average approach velocity, U_0, such as

$$h_L = C_L\left(\frac{u_0^2}{2g}\right) \tag{4}$$

Here

$$C_L = \frac{(y_1-y_0)+\frac{q_0^2}{2gy_1^2}-\frac{q_0^2}{2gy_0^2}}{\left\{\left(\frac{fL}{8}\right)\left[\frac{(y_1/y_0)^3-1}{y_0(y_1/y_0)^3}\right]\right\}\left(\frac{u_0^2}{2g}\right)} = \frac{1}{\left\{\left(\frac{fL}{8}\right)\left[\frac{(y_1/y_0)^3-1}{y_0(y_1/y_0)^3}\right]\right\}} C_L' \tag{5}$$

The term is a cumbersome expression relating to flow resistance in the approach to the structure, and shows that a unique value headloss coefficient, C_L, does not exist for a baffle-post structure.

DIMENSIONAL ANALYSIS

To work around the complications related to the non-uniform nature of the flow at a baffle-bar structure, it is useful to resort to dimensional analysis, which also offers a framework for assessing how approach-flow conditions and baffle-bar structure influence the hydraulic performance of baffle-bar structures. The dominant variables influencing flow and energy dissipation through a baffle-bar structure can be assembled and stated in the following functional manner:

$$f(N, D, s, l, Y_0, q_0, B, g, \nu) = 0 \tag{7}$$

Where N is the number of baffle bar rows, D is the baffle bar diameter, s is the lateral spacing, from center to center, of the baffle bars, l is the streamwise spacing, from center to center, of the baffle bars, y_0 is the flow depth at section 0, q_0 is the unit discharge at section 0, B is the width of the channel,g is the unit gravity constant, and ν is the kinematic viscosity of water.

Eq. (7) assumes fully turbulent flow with neglible surface tension effects. Applying the general principles of dimensional analysis, dimensionless relationships can be formed for C_L and C_D. Additionally, a dependent parameter of practical design interest is the depth increase parameter, y_1/y_0, as this parameter is usually required in order to select the geometric layout and dimensions of a baffle-bar structure. Therefore, an important functional relationship for design is,

$$\frac{y_1}{y_0} = f_D\left(N, \frac{s}{D}, \frac{l}{D}, \frac{y_0}{D}, Fr_0\right) \tag{8}$$

The laboratory experiments conducted for this study explore the relationship between the parameters in this equation.

LABORATORY EXPERIMENT

Experiments were conducted to determine the influences of baffle-post geometry (number of rows, post spacing and post diameters) on the hydraulic performance of baffle-post structures. The hydraulic parameters of interest are C_L' and y_1/y_0. They involved a re-circulating open channel flume that was 9.70m long, 0.20m wide and 0.36m deep at Colorado State University's (CSU) Hydraulic Laboratory.

The baffle-post models comprised cylindrical wooden dowels attached to a piece of wood secured to the top of the flume. The structure geometry was developed assuming 0.30m baffle post diameters for the prototype. Using a morphologic relationship, the posts were sized using a width ratio of 18 (prototype/model), which is based on a relaxed scaling approach used in the Mount Saint Helens GBS physical model. A 19.2 width ratio was adopted for practical purposes, as dowels are only available in standard sizes.

For single-row structures, post diameter and streamwise spacing were fixed. Only the relative lateral spacing $\frac{s}{D}$, was varied from 1.5 to 6.4. Experiments of single-row structures included two Froude numbers $(Fr_0 = 0.15, 0.45)$ and four relative depths. All three parameters (lateral spacing, streamwise spacing, and post diameter) were altered for the double row structure. Three

different relative depths were experimented at a range of Froude numbers ranging from 0.10 to 0.58.

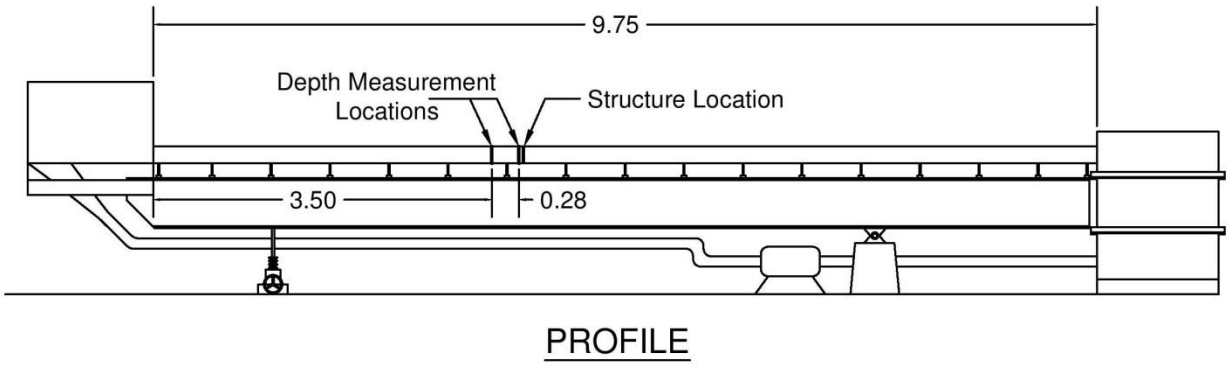

Figure 4: Profile view of the flume showing measurement locations for flow depths and velocities. Dimensions are in meters.

LABORATORY OBSERVATIONS AND DATA

The full set of observations and data are reported by Ubing (2015). This paper briefly describes the flow field at baffle-post structures, outlines the general trends obtained for the headloss coefficient, C_L', and a selection of data for the normalized flow depth increase y_1/y_0.

Flow Field at Baffle-Post Structures. When approaching the structure the flow transitions from uniform flow conditions into gradually varied flow conditions, where the depth is increasing gradually–until it reaches the maximum depth, directly upstream of the structure. Figure 5 illustrates the flow field. The depth increases to increase the specific energy upstream of the structure to pass the given flow discharge though the structure. At this point within the control volume, the velocity within the channel is the lowest. The flow accelerates through the structure, due to the width constriction. Directly downstream of the structure, the flow continues to accelerate, resulting in a rapid decrease in flow depth, eventually reaching the point of minimum flow depth, or maximum flow velocity. This location varies in its magnitude as well as its streamwise distance from the structure. Finally, the flow will gradually or rapidly increase, depending on initial flow conditions and the structure geometry. If choked flow conditions occurred, and the downstream depth become critical, it is likely that a hydraulic jump will occur within this section.

Figure 5: Side view of the flow field at a double-post baffle-post structure

Headloss Coefficient. The general impacts of structure geometry on the uniform flow headloss coefficient, C_L', are shown in Figure 7. Overall, C_L' decreased as the Froude number increased, because of the relationship between $C_L'$and Fr_0 indicated in Eq. (5). Lateral spacing, or *s/D*, has the greatest impact on C_L', causing the headloss coefficient to increases as lateral spacing decreases. As streamwise spacing increased, the headloss coefficient also decreased, but to a lesser extent. Finally, an increase in post diameter resulted in a slight increase in headloss coefficient. The discharge coefficient remained relatively constant over the experimented range of Froude numbers.

Closer spacing results in higher roughness through the baffles due to an increase in turbulence. When the flow openings are smaller, the flow vortices developed due to the baffle bars are closer together and more likely to interfere with each other, which results in a more turbulent flow and higher internal energy dissipation. The primary driver of an increase in energy dissipation is a direct result of higher blockage ratio, as shown in Figure 6. The additional baffle posts obstruct a larger flow area, producing higher resistance to flow, thus dissipating more flow energy.

At lower Froude numbers, the headloss coefficient also varied with relative depth, especially at smaller relative lateral spacing. Physically, the decrease in headloss coefficient with an increasing relative depth can be explained by the magnitude of the various vortices. At small relative depths, the downflow and horseshoe vortex will collide with the channel bottom, resulting in an increase in turbulence, which will further dissipate the energy within the flow. However, as the depth increases, the horseshoe vortex moves up the water column, no longer interacting with the channel bottom.

The relative depth appeared to have minimal impacts at the larger Froude number, due to the direct relationship between relative depth and energy dissipation. The relative change in water surface elevation produced by a structure increases as y_0/D increases. Therefore, both the velocity head, $\frac{u_0^2}{2g}$, and the energy dissipation, ΔE, increase, resulting in a less variable headloss coefficient. Furthermore, at a higher Froude number both the horseshoe and roller vortices are

much stronger and larger and possibly interacting at all three relative depths. Therefore, the additional energy dissipation as a result of the colliding flow paths is likely observed at all three relative depths, resulting in negligible differences in the headloss coefficient through the structure.

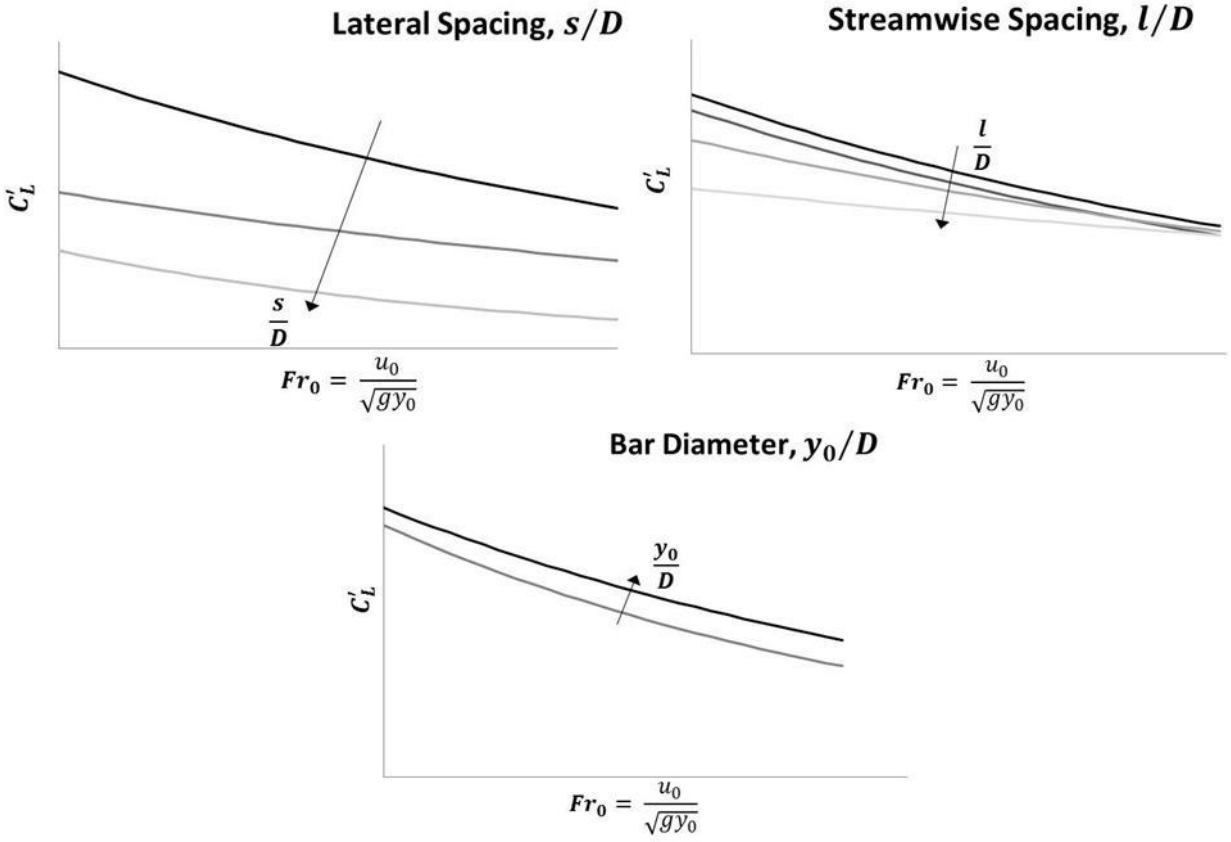

Figure 6: Schematic presentation of the general trends obtained for headloss coefficient C ′L *(Data in Ubing 2015)*

Backwater (Flow Retardance) Effect, y_1/y_0. The trends shown in Figure 7 illustrate how post spacing, *s/D*, and Froude number of approach flow, Fr_0, influence the values of the flow depth parameter y_1/y_0. Thus, the baffle-post structures created the backwater flow which acts to slow or retard an approach flow. The structures used to obtain the data for this figure entailed posts set at a streamwise spacing of *l/D* = 2. The value of y_0 for an approach flow (or flow prior to installation of a piffle-post structure) can be calculated, using say the Manning's equation, and then together with the value of Froude number, Fr_0, for the approach flow, the flow depth, y_1, at the baffle-post structure estimated using Figure 7. From the flow depth at the structure, y_1, the upstream dimensions of the backwater flow profile (M1 flow profile) can be calculated. In due course this backwater profile can be interpreted for its effect on the capacity of the approach flow to convey bed sediment.

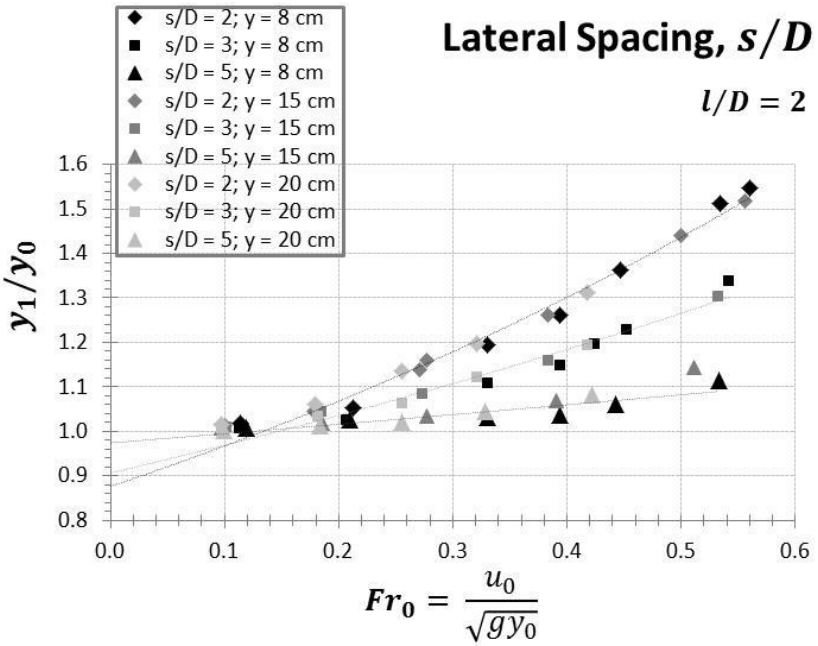

Figure 7: The variation of flow depth parameter y_1/y_0 for a double-row baffle-post structure with rows spaced at l/D = 2. The additional parameter in this figure is y_0/D, which exerts only a very small effect for the range of values investigated.

An important consideration in the use of baffle-post structures is the need for rock armoring to be placed around the base of the posts and the immediate downstream region where the flow passes through a hydraulic jump. The details related to tis consideration are presently under investigation at CSU.

CONCLUSIONS

This paper presents early observations regarding the impacts of geometric characteristics on the hydraulic performance of a baffle post structure. The observations, from laboratory experiments show that lateral spacing had the largest impact on the headloss and discharge coefficients; whereas, the post diameter and streamwise spacing appear to have near negligible impacts on the headloss and discharge coefficients. Relative flow depth impacted the headloss coefficient only at lower Froude numbers due to the magnitude of various flow vortices. At larger Froude numbers, the vortices are larger and stronger; therefore, colliding at three relative depths. In general, the headloss coefficient decreased as the Froude number increased. However, the discharge coefficient remained relatively constant within the range of tested Froude numbers.

Choked flow conditions only occurred at higher Froude numbers, with smaller relative lateral spacing. At smaller Froude numbers, the discharge through the channel was not large enough to induce choked flow conditions through the effective width of the structure. As the discharge increased and the critical width of the flow increased, the contraction became large enough to "choke" the flow.

Further work is needed to investigate other relevant aspects of the structure geometry such as baffle shapes, staggered rows, and random configurations. Also, further work is needed to determine the bed-protection needs to inhibit local scour at a baffle-post structure. Investigation

to the impact of the roughness of the baffle posts should be made to determine if the tree post will influence the energy dissipation through the structure. Additional experiments studying the impacts of variable diameter within a single structure is recommended as available materials may not provide uniform baffle posts. Finally, tests were conducted with initial Froude numbers varying between 0.10 and 0.58, all of which are within the region of subcritical flow. Supercritical flow does not occur often over large spatial extents in nature. However, the author recommends testing the structure in supercritical flow conditions to determine if the headloss coefficient curve deviates when $Fr > 1.0$.

The limitations inherent in determining general trends for discharge and headloss coefficients indicate that further investigation will benefit from an approach by means of dimensional analysis identifying the functional relationships between these parameters and approach-flow and structure geometry. Also of practical importance is the relationship between approach flow depth and flow depth at the structure, y_1/y_0; this parameter is significant in determining the backwater effects produced by a baffle-post structure.

ACKNOWLEDGEMENTS

This study was conducted as part of a background effort for a larger project aimed at designing and testing a series of grade-building structures for possible use in the Toutle River in Washington. The information presented here has yet to be further developed for potential use in this larger project, which is funded by the Portland District of the U.S. Army Corps of Engineers.

REFERENCES

Ubing, C. (2015). "The Hydraulics of Baffle-Post Structures." MS thesis, Colorado State University, Ft.Collins, CO

SUSPENDED-SEDIMENT TRANSPORT AND STORAGE: A DEMONSTRATION OF ACOUSTIC METHODS IN THE EVALUATION OF RESERVOIR MANAGEMENT STRATEGIES FOR A SMALL WATER-SUPPLY RESERVOIR IN WESTERN COLORADO

Cory A. Williams, Hydrologist, U.S. Geological Survey, Grand Junction, CO; Rodney J. Richards, Hydrologist, U.S. Geological Survey, Grand Junction, CO; Kent Collins, Hydraulic Engineer, Bureau of Reclamation, Lakewood, CO

Abstract: The U.S. Bureau of Reclamation (USBR) and local stakeholder groups are evaluating reservoir-management strategies within Paonia Reservoir. This small reservoir fills to capacity each spring and requires approximately half of the snowmelt-runoff volume from its sediment-laden source waters, Muddy Creek. The U.S. Geological Survey is currently conducting high-resolution (15-minute data-recording interval) sediment monitoring to characterize incoming and outgoing sediment flux during reservoir operations at two sites on Muddy Creek. The high-resolution monitoring is being used to establish current rates of reservoir sedimentation, support USBR sediment transport and storage models, and assess the viability of water-storage recovery in Paonia Reservoir. These sites are equipped with in situ, single-frequency, side-looking acoustic Doppler current meters in conjunction with turbidity sensors to monitor sediment flux. This project serves as a demonstration of the capability of using surrogate techniques to predict suspended-sediment concentrations in small streams (less than 20 meters in width and 2 meters in depth). These two sites provide the ability to report near real-time suspended-sediment concentrations through the U.S. Geological Survey National Water Information System (NWIS) web interface and National Real-Time Water Quality websites (NRTWQ) to aid in reservoir operations and assessments.

INTRODUCTION

The U.S. Bureau of Reclamation and local stakeholder groups are evaluating reservoir-management strategies within Paonia Reservoir. This small reservoir fills to capacity (live storage capacity is 15,553 acre-feet) each spring and requires approximately half of the snowmelt-runoff volume from its sediment-laden source waters, Muddy Creek (Bureau of Reclamation, 2014). Paonia Reservoir supports agriculture along the North Fork Valley. Reductions in water-storage capacity in the reservoir through time from sedimentation are affecting reservoir operation procedures (timing of reservoir fill and drawdown procedures to flush sediments interfering with gate operations) and may threaten continued operations of the reservoir. Storage losses also limit the availability of late-summer irrigation water for downstream diversions, especially during dry years when precipitation and natural sources of water become most scarce. Management strategies to mobilize sediments within the reservoir are in development. Active sediment removal techniques, such as dredging, are costly; therefore, an assessment of alternate management strategies, including passive removal techniques, is being evaluated. Sediment monitoring to characterize incoming and outgoing sediment flux during reservoir operations is needed to establish current rates of reservoir sedimentation, support USBR sediment transport and storage models, and assess the viability of water-storage recovery in Paonia Reservoir.

The U.S. Geological Survey (USGS), Bureau of Reclamation (USBR) and local stakeholder groups, including the North Fork Water Conservancy District and Fire Mountain Canal and Reservoir Company, are evaluating reservoir-management strategies with a goal of maintaining or increasing water-storage capacity within Paonia Reservoir. Two high-resolution (15-minute data recording interval) suspended-sediment monitoring sites were installed to monitor suspended-sediment flux into and out of Paonia Reservoir along Muddy Creek. The data collected supports the USBR hydrodynamic modeling of sediment transport and storage within, and downstream of, the reservoir.

The use of optical and acoustic surrogate techniques to characterize suspended-sediment flux can be highly effective in many river systems (Wood, 2014; Rasmussen *et al.*, 2009). Combinations of acoustic backscatter, acoustic attenuation, optical backscatter (turbidity), and seasonal effects are used to test the utility of these parameters as surrogates for suspended-sediment concentration on Muddy Creek. This project serves as a demonstration of the capability of these surrogate techniques to be used in small streams, less than 20 meters in width and 2 meters in depth, with suspended-sediment concentrations ranging from less than 10 to greater than 20,000 milligrams per liter (mg/L).

METHODS

Two USGS water-quality sites were established near Paonia Reservoir: Muddy Creek above Paonia Reservoir, CO – 385903107210800; and Muddy Creek below Paonia Reservoir, CO – 385626107212000) (fig. 1). Each site was instrumented with a 1.5 megahertz (MHz) side-looking Acoustic-Doppler Velocity Meter (ADVM) with voltage regulator, turbidity meter, automatic-pump sampler, and satellite telemetry. Suspended-sediment samples were collected from April 2013 to October 2013.

Suspended-sediment samples were collected using the equal-width-increment (EWI) method at 10 locations along the channel cross-section and were then composited for analysis (U.S. Geological Survey, 2006). Samples were collected using (1) a cable-suspended US D-74 depth integrated suspended-sediment sampler with quart glass bottle sampling container; or (2) a US DH-81 attached to US D-95 tetrafluoroethylene (TFE) cap and nozzles with a 3-foot wading rod and a 1-liter fluorinated ethylene propylene (FEP) bottle sampling container depending on flow conditions. Automatic-pump samples were collected in 1-liter polypropylene bottles. EWI and pump samples were sent to the USGS Iowa Water Science Center sediment lab for analysis (Guy, 1969). Approximately 15 EWI samples and 200 pump samples were collected at each site and were analyzed for concentration with additional grain-size analysis. Pump samples were analyzed for percent finer than 0.063 millimeters (mm), and suspended-sediment concentrations were adjusted using 'box coefficients' to correct these point-concentrations to represent cross-section average concentrations based on EWI/pump concentration pairs and streamflow (Edwards and Glysson, 1999). A full grain-size analysis was done on all EWI samples. Turbidity data were collected by using an optical turbidity meter using monochrome near infra-red LED light (780 – 900 nanometer wave length) with a detection angle of 90 degrees reported in formazin nephelometric units (FNU). The meter was operated and the data processed according to guidelines described in Wagner *et al.* (2006). Additional post-processing of the turbidity record was done to correct erroneous turbidity values, typically from fouling from filamental algae. A calibration check was completed in the lab after the instrument was removed for the season and a calibration drift correction was applied if necessary.

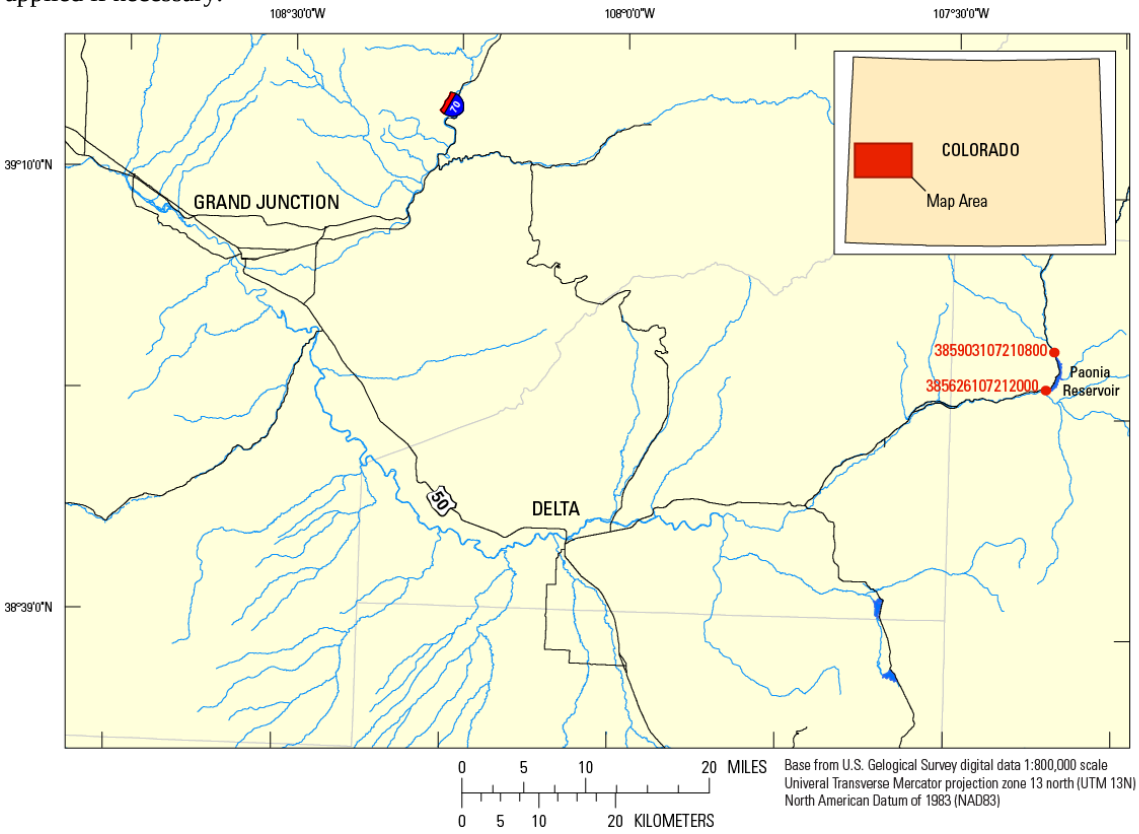

Figure 1 Map showing the location of Paonia Reservoir, and the location of USGS water-quality stations and station numbers in the North Fork Gunnison River Basin, in Western Colorado.

The multi-cell acoustic data collected by the ADVM (1,500 MHz side-looking instrument, 2.25–meter blanking distance along beam, 10 cells, 0.50-meter cell size along beam, 25° beam angle) are post-processed in a series of steps. During the deployment of the instrument, it became necessary to reconfigure the blanking distance to a length of 0.75-meters (along the beam) on August 29th in order to characterize the high-sediment concentrations associated with late-summer monsoon rain events. This was necessary because of excessive acoustic signal losses owing to the high sediment concentrations. Calculations for corrected acoustic backscatter and acoustic sediment attenuation followed the methodology outlined in Topping *et al.* (2004; 2006), Wright *et al.* (2010), and Wood and Teasdale (2013). Acoustic backscatter was corrected for losses including beam spreading (Downing *et al.*, 1995), fluid absorption (Urick, 1975), and near-field corrections (Downing *et al.*, 1995) resulting in a "fluid-corrected backscatter" profile across the 10-cell ensonified volume. The sediment attenuation was calculated from the slope of the fluid-corrected backscatter profile and represents transmission losses due to scattering, absorption, and attenuation due to sediment effects (Urick, 1975). Removing the losses from sediment attenuation from the "fluid-corrected backscatter" yields a "normalized-acoustic backscatter." Sediment attenuation and the average "normalized-acoustic backscatter" have been used in other studies to represent the suspended-silt-and-clay (fines) and suspended-sand portions of the suspended-sediment concentrations, respectively (Topping *et al.*, 2004; 2006, Wright *et al.*, 2010; Wood and Teasdale, 2013).

Suspended- sediment concentration predictions for the two sites were used to calculate the incoming and outgoing suspended-sediment load at Paonia Reservoir. A total suspended-sediment and suspended fines (<0.0625 mm) concentration and load were calculated at Muddy Creek above Paonia Reservoir, CO; and a total suspended-sediment concentration and load were calculated at Muddy Creek below Paonia Reservoir, CO. The suspended sand concentration and load (if present) was calculated as the difference between the total suspended-sediment concentration and load and the fine suspended-sediment concentration and load.

Above Paonia Reservoir: Muddy Creek above Paonia Reservoir, CO, is located approximately 1,000 m upstream of the reservoir (U.S. Geological Survey, 2014). The system is dynamic with large seasonal changes in streamflow and suspended-sediment concentration, especially during monsoonal-rain events. High suspended-sediment concentrations are common during the snowmelt-runoff period and late-summer monsoon season with suspended-sediment concentrations exceeding 20,000 mg/L.

A step-wise regression analysis was used to find the best-fit regression model based on normalized-acoustic backscatter, sediment attenuation (hereafter, *SedAtt*), turbidity (hereafter, *Turb*), and seasonality terms (Helsel and Hirsch, 2002). The final linear regression models for total suspended-sediment concentration and fine suspended-sediment concentration are:

$$\ln(totalSSC) = 4.7102 - 0.2261\ln(Q) + 0.7967\ln(SedAtt) + 0.6914\ln(Turb) + 3.3129(Sin) - 0.3699(Cos) \quad (1)$$

$$\ln(finesSSC) = 4.2950 + 0.7987\ln(SedAtt) + 0.7776\ln(Turb) + 3.7232(Sin) - 0.5886(Cos) \quad (2)$$

where *totalSSC* is the predicted total suspended-sediment concentration, in milligrams per liter (mg/L); *finesSSC* is the predicted suspended-sediment concentration for grain sizes less than 0.063 mm, in mg/L; *Q*, is streamflow, in cubic feet per second; *SedAtt* is the sediment attenuation, in decibels per meter; *Turb* is the turbidity 0–1,600, in formazine nephelometric units (FNU); *Sin*, is the sine wave component and *Cos*, is the cosine wave component of a Fourier Series seasonality term. A bias correction factor (smearing) was applied to each transformed prediction (Helsel and Hirsch, 2002). The linear regression diagnostics for the regression models are presented in table 1 and table 2.

Table 1 Regression diagnostics for sites bracketing Paonia Reservoir along Muddy Creek, April–October, 2013.
[R^2, coefficient of determination; RSE, residual standard error, in milligrams per liter; BCF, bias correction factor; mm, millimeters; --, no data]

Sediment size	Number of samples	R^2	RSE	BCF
Muddy Creek above Paonia Reservoir – 385903107210800				
Less than 2.0 mm	146	0.97	1.35	1.045
Less than 0.063 mm	146	0.98	1.28	1.031
Muddy Creek below Paonia Reservoir – 385626107212000				
Less than 2.0 mm	141	0.99	13.0	--

Table 2 Variance Inflation Factors for equations 1 and 2 at Muddy Creek above Paonia Reservoir, April–October, 2013.

[--, no data; *, VIF calculation excludes non-significant Cos term in Fourier Series seasonality term; ln(*Q*), natural logarithm of streamflow; ln(*SedAtt*), natural logarithm sediment attenuation; ln(*Turb*), natural logarithm turbidity; (*Sin*), sine component of Fourier Series; (*Cos*), cosine component of Fourier Series]

	Variance Inflation Factor (VIF)				
	ln(*Q*)	**ln(*SedAtt*)**	**ln(*Turb*)**	**(*Sin*)**	**(*Cos*)**
Equation 1*	1.2	2.3	2.6	2.8	--
Equation 2	--	2.2	2.6	3.2	1.5

Below Paonia Reservoir: Muddy Creek below Paonia Reservoir, CO, is located immediately downstream of Paonia Reservoir. The system is regulated and releases are governed by downstream water rights. The reservoir is filled in the spring during the snowmelt-runoff period and excess water spills over the spillway once the reservoir is at capacity. Releases during the summer and fall are from an elevated release structure (tower) within the reservoir. Due to the height and position of the tower in the reservoir dead pool, sand-sized sediments (0.063–2 mm) were not observed in waters leaving the reservoir in 2013.

A step-wise regression analysis was used to find the best-fit regression model based on backscatter, attenuation, turbidity, streamflow, and seasonality terms. The final linear regression model for total suspended-sediment concentration (very little sand was observed at this site, therefore no separate fine suspended-sediment model was needed) is:

$$totalSSC = 3.2215 + 0.5856(Turb) \quad (3)$$

where *totalSSC* is the predicted total suspended-sediment concentration, in mg/L, and *Turb* is the turbidity 0–1,600, in FNU. The linear regression model diagnostics are presented in table 1.

RESULTS

Above Paonia Reservoir: Predictions of total suspended-sediment are plotted against measured concentrations in figure 2. The regression analyses (eq. 1) indicates that for concentrations between 0 and 2,000 mg/L the predictions are very near the mean response; however, as the predicted concentration increases above 6,000 mg/L, greater error in the predictions are evident in the widening of the 95-percent confidence intervals (fig. 2B).

Overall, the predictions of total suspended-sediment concentration are near the mean response with a residual standard error of 1.35 mg/L (table 1), indicating that the loads calculated from the predictions are generally well defined (fig. 2). Additional sampling of conditions at higher concentrations in future years will provide improved characterization and opportunities for additional regression model refinement or continued validation of regression predictions.

The predicted fine suspended-sediment concentrations derived from equation 2 follow the same general trend as the total suspended-sediment concentrations. Predicted fine suspended-sediment concentrations below 2,000 mg/L are near the mean response with increases in error for predictions of greater concentrations. Similar to the predicted total suspended-sediment concentration, the relation of predicted and measured concentrations remains near the mean response with a residual standard error of 1.28 mg/L (table 1), indicating that the loads calculated from the predictions are generally well defined (fig. 3). Additional sampling of conditions at higher concentrations in future years will provide improved characterization and opportunities for additional regression model refinement or continued validation of regression predictions.

The total suspended-sediment concentrations vary throughout the year along with the grain size of the particles (fig. 4). Higher concentrations of total suspended sediment are observed in April and May during snowmelt runoff. During this period, larger portions of sand-sized particles are being suspended and mobilized. As the snowmelt period ends, in June, the total suspended-sediment concentration decreases rapidly and becomes much finer in grain size. Medium silt-sized to clay-sized particles dominate the system throughout much of the year. Large increases in total suspended-sediment concentration occur in the late-summer and early-fall months during monsoonal rains. These rain events produce the highest suspended-sediment concentrations of the year and are composed of silt-sized

and clay-sized particles (figs. 4 and 5). Muddy Creek becomes very turbid during these events and concentrations of suspended sediments are great enough to impede the effectiveness of the surrogate sensors. As a result, during some periods of the year, the total suspended-sediment load was estimated due to obscured turbidity and acoustic signals. Estimates of missing data were made such that the shape of the concentration peaks matched observed conditions of previous concentration peaks following techniques described in Porterfield (1972).

The temporal variations in the fine suspended-sediment concentrations are very similar to those of the total suspended-sediment predictions. During the snowmelt period, however, the fine suspended-sediments contribute less to total concentration than the sand-sized sediments, and from June through October, suspended-sediment concentration is almost entirely composed of silt-and clay-sized particles (fig. 5).

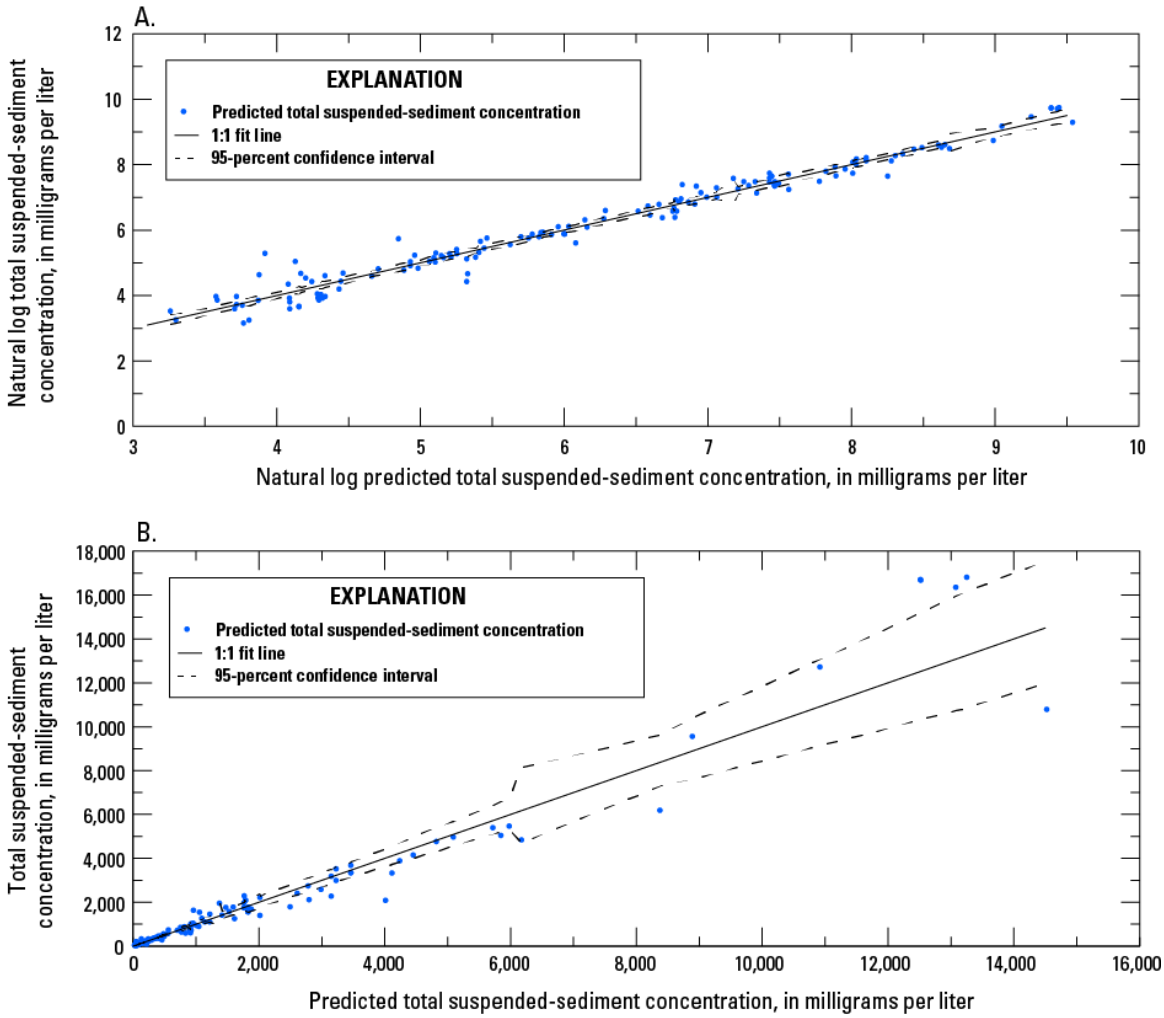

Figure 2 Relations between predicted and total suspended-sediment concentration with 95-percent confident interval for Muddy Creek above Paonia Reservoir in (A) logarithmic, (B) and normal space, April–October, 2013.

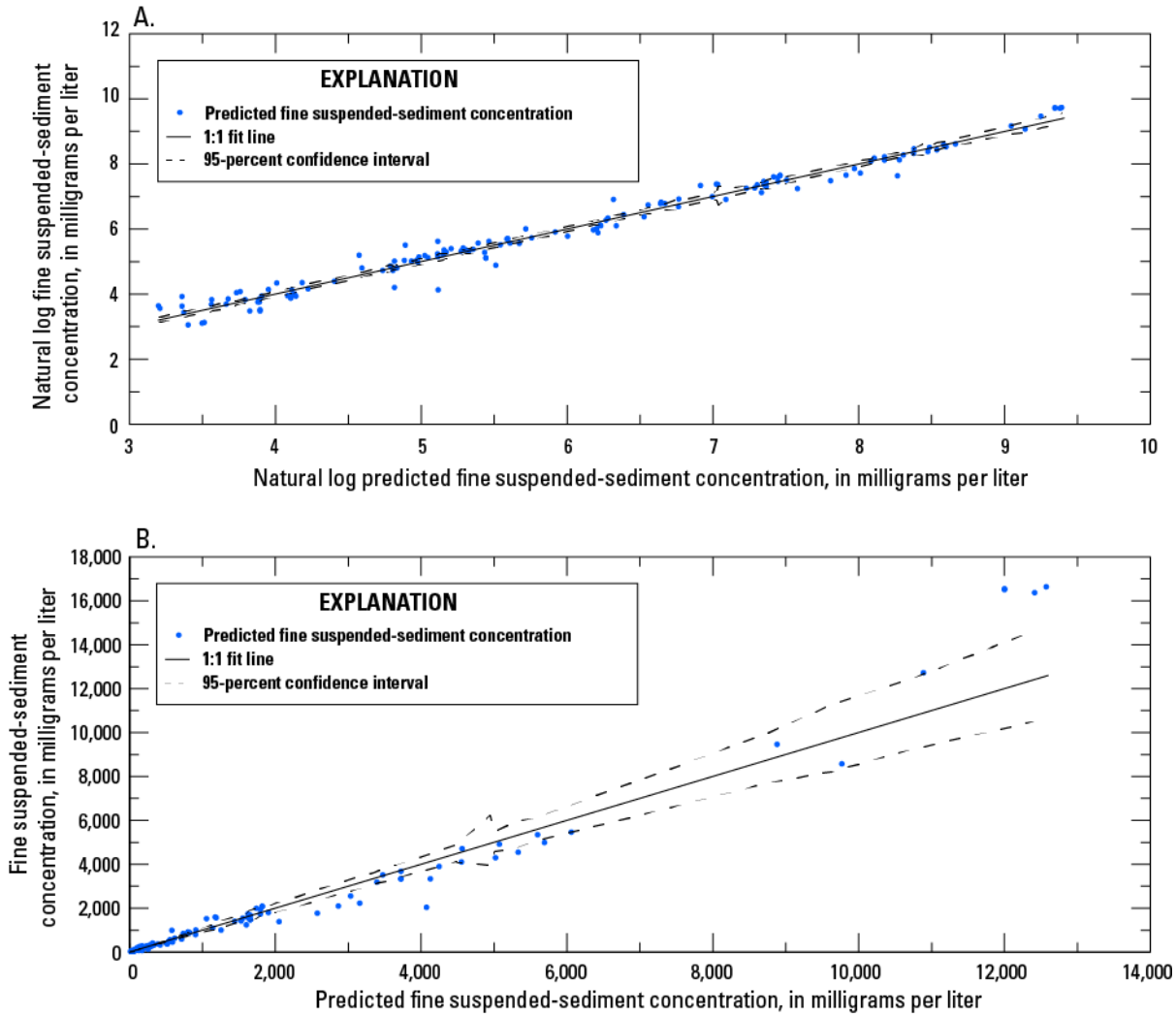

Figure 3 Relations between predicted and fine (grain size less than 0.063 millimeters) suspended-sediment concentration with 95-percent confident interval for Muddy Creek above Paonia Reservoir in (A) logarithmic, (B) and normal space, April–October, 2013.

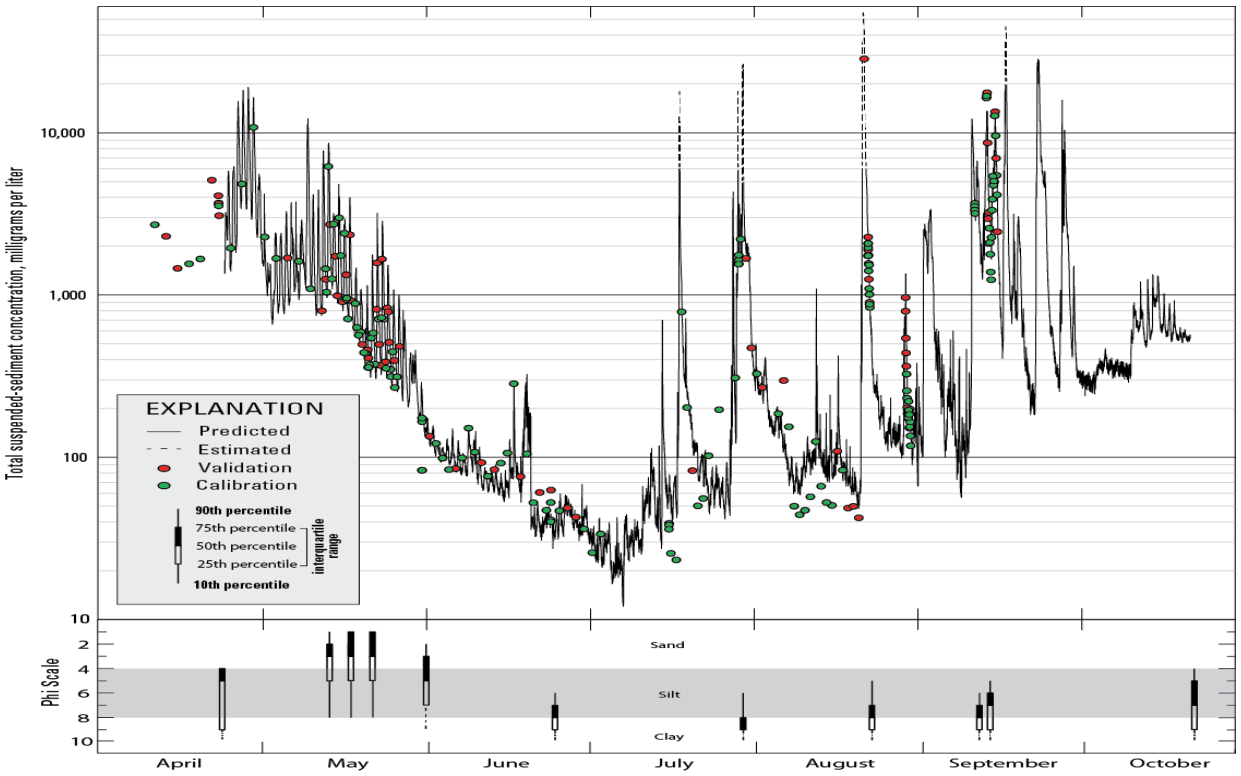

Figure 4 Predicted total suspended-sediment concentration with calibration data points, validation data points, and equal-width interval sample grain-size analyses for Muddy Creek above Paonia Reservoir, April–October, 2013.

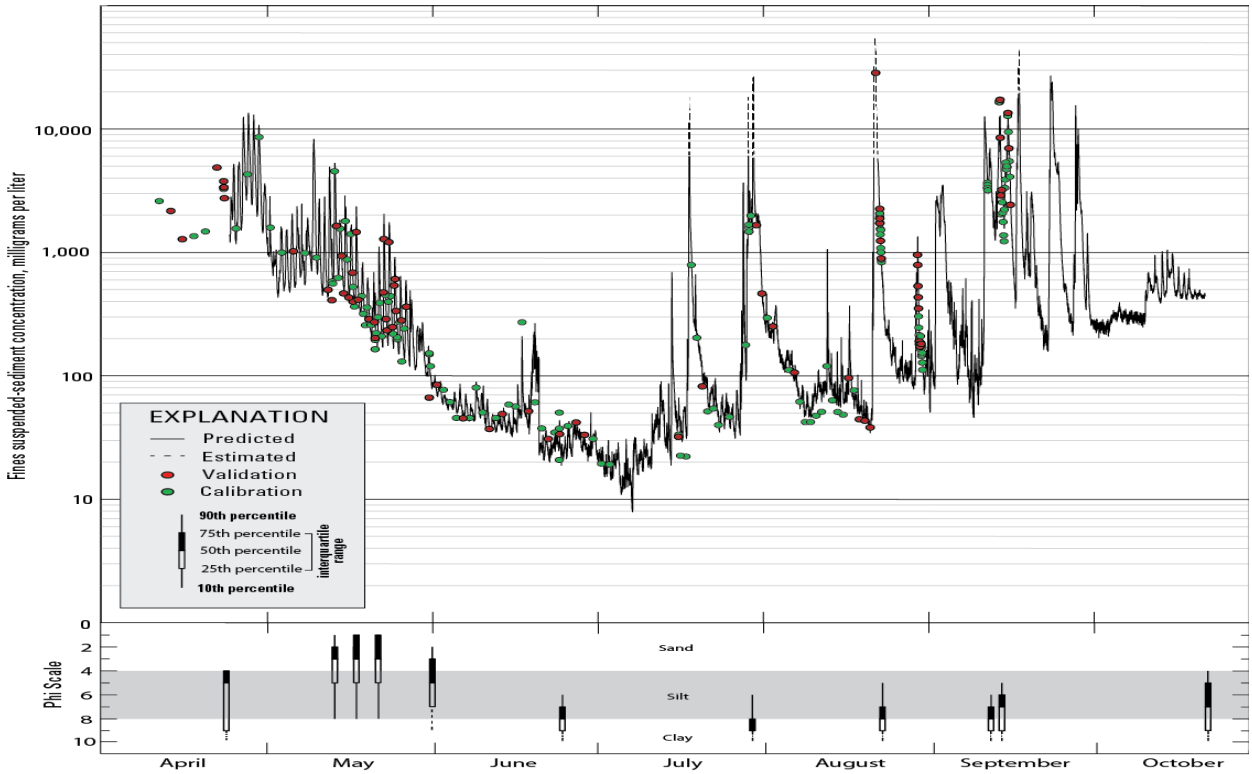

Figure 5 Predicted fine suspended-sediment concentration with calibration data points, validation data points, and equal-width interval sample grain-size analyses for Muddy Creek above Paonia Reservoir, April–October, 2013.

Below Paonia Reservoir: Predictions of total suspended-sediment concentrations are plotted against measured concentrations in figure 6. The predicted total suspended-sediment concentration from the regression analyses (eq. 3) indicates that the predictions scatter around the mean response with a residual standard error of 13.0 mg/L (table 1), indicating that the loads calculated from the predictions are well defined. The regulated nature of flows downstream of the reservoir result in less variability than suspended-sediment concentrations observed at the upstream site (fig. 7).

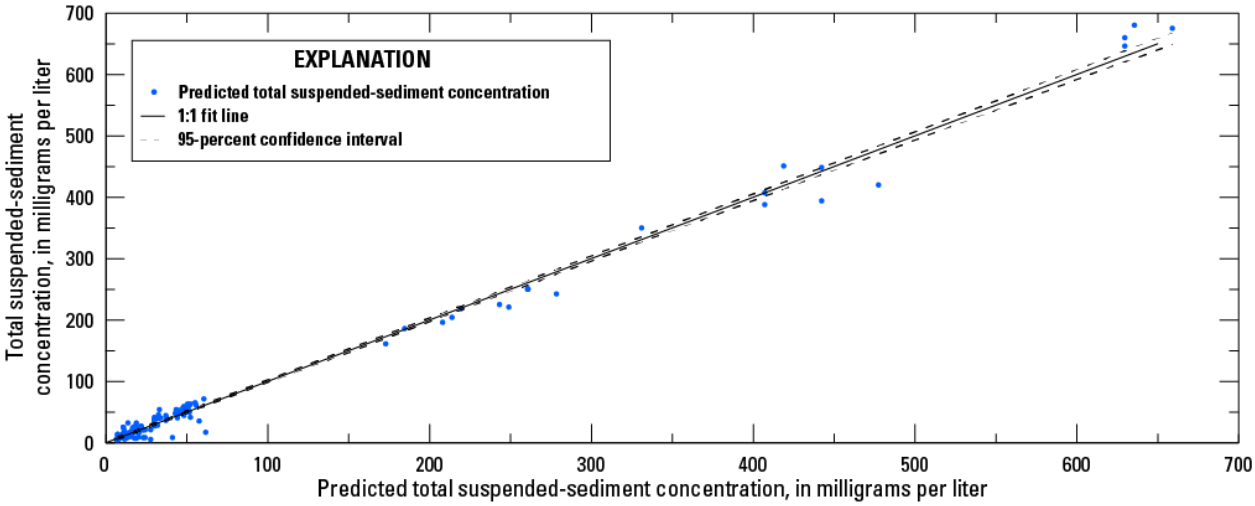

Figure 6 Relations between predicted and fine suspended-sediment concentration with 95-percent confident interval for Muddy Creek below Paonia Reservoir, April–October, 2013.

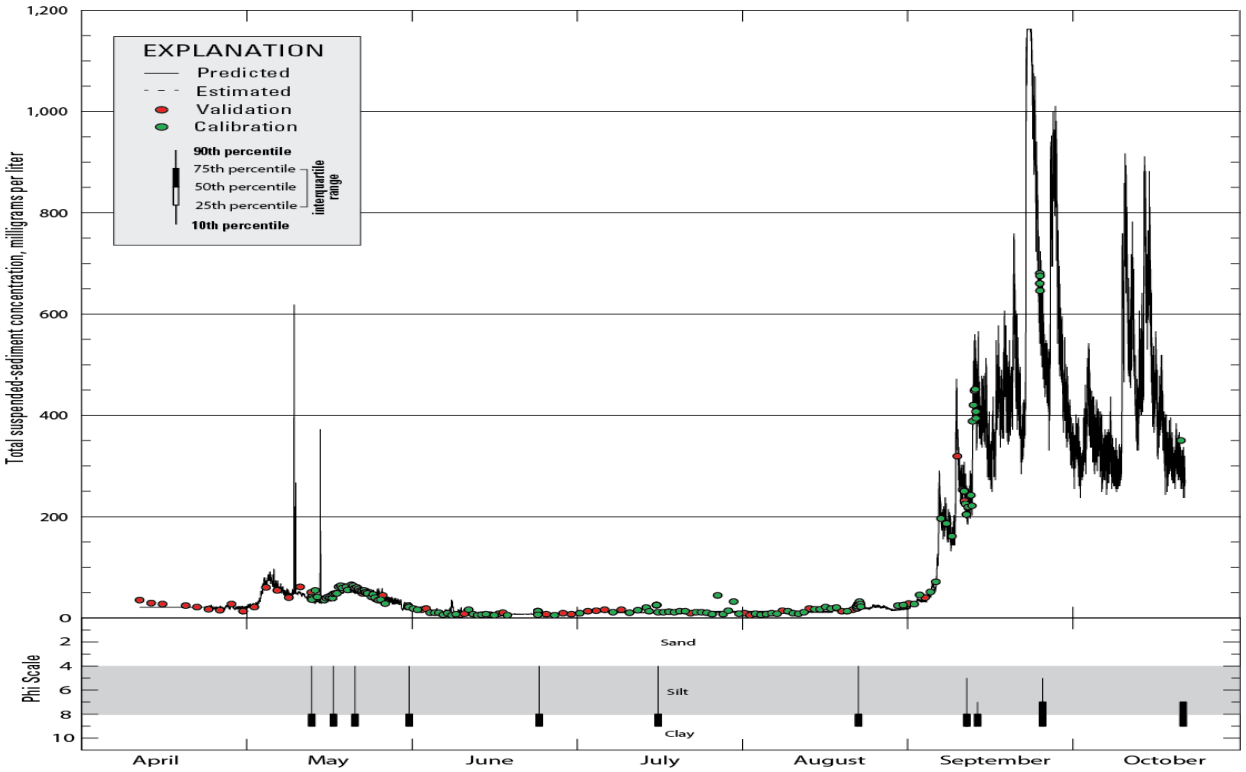

Figure 7 Predicted total suspended-sediment concentration with calibration data points, validation data points, and equal-width interval sample grain-size analyses for Muddy Creek below Paonia Reservoir, April–October, 2013.

Generally, total suspended-sediment concentrations below Paonia Reservoir remain minimal in comparison to the upstream site and are dominated by silt-sized and clay-sized sediments. Rapid, short-duration increases in total suspended-sediment concentration occur in May and are associated with the opening and closing of the gate on the outlet tower that controls water releases. In June, the reservoir is typically at full capacity and additional streamflow entering the reservoir exits through a combination of releases and spills. Reservoir geometry and sediment residence under these conditions trap much of the sediment entering the reservoir. When water levels in Paonia Reservoir are drawn down (typically by the end of the summer and early fall) greater suspended-sediment concentrations are observed as Muddy Creek meanders through newly exposed reservoir sediment deposits (fig. 7).

Sediment storage: A mass-balance analysis of incoming against outgoing total suspended-sediment load, calculated using the selected surrogate models, is shown in figure 8. Sediment monitoring in 2013 shows that approximately 75,000 tons of suspended sediment entered the reservoir (red line), and approximately 4,000 tons of suspended sediment was transported downstream (blue line). The majority of the total suspended sediment entering the reservoir occurred during snowmelt-runoff (~62,000 tons, in the light-yellow shaded region) with an additional increase occurring during the monsoon season (~12,000 tons, in the dark-yellow shaded region). The suspended-sand load (green line) also occurs during the snowmelt period with little sand being mobilized in suspension after the snowmelt period ends. The suspended-sediment load leaving the reservoir (4,000 tons) occurs later in the year and represents approximately 5 percent of the incoming load.

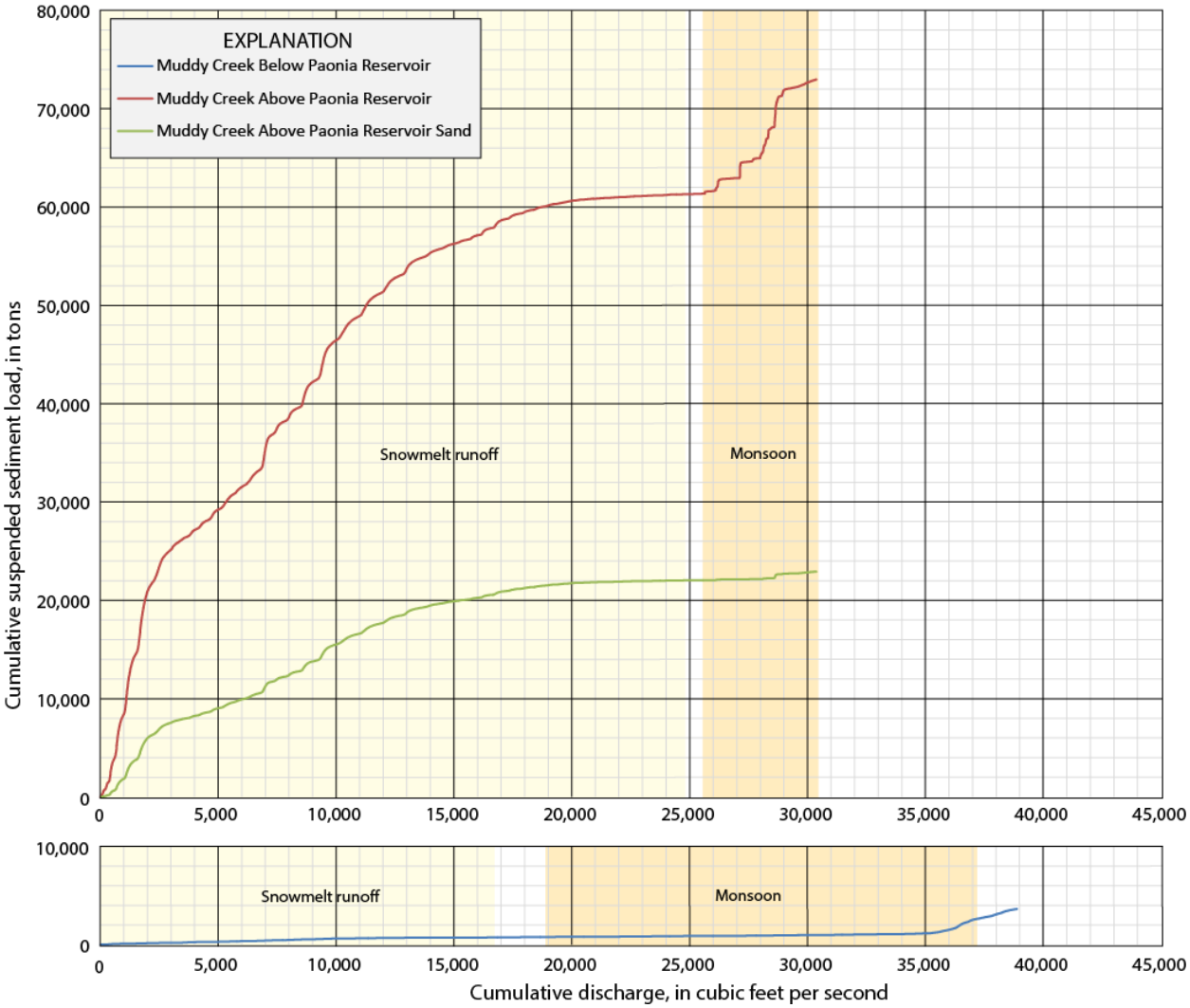

Figure 8 Mass curve of cumulative suspended-sediment load relative to cumulative discharge at Muddy Creek above Paonia Reservoir and Muddy Creek below Paonia Reservoir, April–October, 2013.

DISCUSSION

The development of regression models using suspended-sediment surrogates to characterize suspended-sediment concentration and flux is helpful in developing a management strategy to protect existing water storage and potentially increase lost storage due to sediment infilling. Based on the results from one year of observation and analyses, there is a substantial imbalance in the sediment transported into and out of Paonia Reservoir along Muddy Creek. The incoming suspended-sediment load consists of some finer sands, but silt-sized and clay-sized sediments dominate the suspended system. Most if not all of the sand portion of the incoming suspended load appears to be deposited in the reservoir. The outgoing suspended-sediment load appears to be dominated by clay-sized sediments with little to no fine-or-medium sand moving downstream of the reservoir. Differences in grain size of these sediments can be important to reservoir managers during calculation of storage-volume loss due to differences in the porosity (void spaces) associated between sediment deposits of differing grain-sizes. Additionally, the difference in grain size can be important when considering reservoir modifications to decrease retention of sediments (reservoir trap efficiency).

Using optical and acoustic high-resolution sediment monitoring to characterize suspended-sediment at Paonia Reservoir has shown to be an effective metric for evaluation of reservoir operational strategies. In 2013, substantial differences between incoming and outgoing total suspended-sediment loads indicate that mitigation efforts were largely unsuccessful. This is due, in part, to perceived limitations in the 2012 snowpack, and concerns that insufficient runoff may result in water shortages. This meant that reservoir operations during the early portion of the snowmelt runoff period were not used for sediment-flushing strategies. These flushing strategies include an approach where operations target delayed capture of later season flows for reservoir filling. The USBR hypothesizes that this operational strategy may help remove exposed reservoir sediments (while the reservoir storage level is near operational dead pool and much of the reservoir bed is exposed) because Muddy Creek is able to remobilize these deposited sediments and transport them towards the outlet tower. Reservoir filling began immediately in 2013, however, limiting options to flush sediments until late fall when reservoir levels were again exposing these sediments as water level in the reservoir fell. Additional modifications to the outlet tower may be necessary if mobilization of sand or coarser sediment is desired.

Successful monitoring of suspended sediment within this system using surrogates is useful in determining the type of management strategies that would be effective in increasing reservoir capacity or decreasing the present rate of capacity loss. Use of turbidity as a suspended-sediment surrogate within a simple-linear regression was appropriate for this study for conditions where sand-sized particles were absent. When present, sand-sized particles were not well characterized by changes in turbidity and incorporation of additional parameters (sediment attenuation, seasonality, and/or streamflow) was necessary. Exploring the relation between acoustic backscatter, sediment attenuation, turbidity, and seasonality effects has allowed for a more complex linear regression model to be developed that is effective in predicting suspended-sediment concentrations. It should be noted, however, that the regressions developed to date could change as subsequent data are incorporated into the regression under flow and reservoir management strategies of future years. Differences in seasonal streamflow patterns or reservoir management may change which combination of variables are statistically significant in predicting suspended-sediment concentrations in future monitoring efforts. Future plans for these two suspended-sediment monitoring stations include incorporation of near real-time reporting of suspended-sediment concentrations through the U.S. Geological Survey National Water Information System (NWIS) web interface (*http://watedata.usgs.gov.nwis*) and National Real-Time Water Quality websites (NRTWQ; *http://nrtwq.usgs.gov*) to aid real-time reservoir operations and assessments.

Any use of trade, firm, or product names is for descriptive purposes only and does not imply endorsement by the U.S. Government.

REFERENCES

Bureau of Reclamation (2014). Western Colorado area office – Water operations: Paonia Reservoir, accessed November 23, 2014 at http://www.usbr.gov/uc/wcao/water/rsvrs/ds/paonia.html.

Downing, A., Thorne, P.D., and Vincent, C.E. (1995). "Backscattering from a suspension in the near field of a piston transducer," Journal of Acoustical Society of America, 97(3), pp 605–610.

Edwards, T.K., and Glysson, G.D. (1999). "Field methods for measurement of fluvial sediment," U.S. Geological Survey Techniques of Water-Resources Investigations, 3(C2), 89 p.

Guy, H.P. (1969). "Laboratory theory and methods for sediment analysis," U.S. Geological Survey Techniques of Water-Resources Investigations, 5(C1), 58 p.

Helsel, D.R., and Hirsch, R.M. (2002). "Statistical methods in water resources," U.S. Geological Survey Techniques of Water-Resources Investigations, 4(A3), 522 p.

Porterfield, G. (1972). "Computation of fluvial-sediment discharge," U.S. Geological Survey Techniques of Water-Resources Investigations, 3(C3), 66 p.

Rasmussen, P.P., Gray, J.R., Glysson, G.D., and Ziegler, A.C. (2009). "Guidelines and procedures for computing time-series suspended-sediment concentrations and loads from in-stream turbidity-sensor and streamflow data," U.S. Geological Survey Techniques and Methods, 3(C4), 53 p.

Topping, D., Melis, T., Rubin, D., and Wright, S.A. (2004). "High-resolution monitoring of suspended-sediment concentration and grain size in the Colorado River using laser-diffraction instruments and a three-frequency acoustic system," Proc. 19th International Symposium on River Sedimentation, Yichang, China pp 2,507–2,514.

Topping, D., Wright, S.A., Melis, T.S., and Rubin, D.M. (2006). "High-resolution monitoring of suspended-sediment concentration and grain size in the Colorado River using laser-diffraction instruments and a three-frequency acoustic system," Proc. 8th Federal Interagency Sedimentation Conference, Reno, Nevada: pp 539–546.

Urick, R.J. (1975). Principles of underwater sound (2nd ed.). McGraw Hill, New York.

U.S. Geological Survey (2006). "Collection of water samples (ver. 2.0)," U.S. Geological Survey Techniques of Water-Resources Investigations, 9(A4).

U.S. Geological Survey (2014). National Water Information System: Mapper, accessed November 23, 2014 at http://maps.waterdata.usgs.gov/mapper/index.html.

Wagner. R.J., Boulger, R.W., Jr., Oblinger, C.J., and Smith, B.A. (2006). "Guidelines and procedures for continuous water-quality monitors--Station operation, record computation, and data reporting," U.S. Geological Survey Techniques and Methods 1-D3, 51 p. plus 8 attachments.

Wood, M.S. (2014). "Estimating suspended sediment in rivers using acoustic Doppler meters," U.S. Geological Survey Fact Sheet 2014-3038, 4 p.

Wood, M.S., and Teasdale, G.N. (2013). "Use of surrogate technologies to estimate suspended sediment in the Clearwater River, Idaho, and Snake River, Washington, 2008-10," U.S. Geological Survey Scientific Investigations Report 2013-5052, 30 p.

Wright, S.A., Topping, D, J., and Williams, C.A. (2010). "Discriminating silt-and-clay from suspended-sand in rivers using side-looking acoustic profilers," Proc. 2nd Joint Interagency Conference, Las Vegas, Nevada, 12 p.

ULTRASONIC MEASUREMENTS OF SUSPENDED SEDIMENT CONCENTRATIONS AT HARRIS BAYOU

Wayne Carpenter, Senior R&D Engineer, University of Mississippi, National Center for Physical Acoustics, University, MS, wocarpen@olemiss.edu;
Daniel Wren, Research Hydraulic Engineer, USDA, ARS-NSL, Oxford, MS, daniel.wren@ars.usda.gov;
Bradley Goodwiller, Research and Development Engineer, University of Mississippi, Dept. of Mechanical Engineering, University, MS, btgoodwi@olemiss.edu;
James Chambers, Associate Dean for Research and Graduate Programs and Associate Professor, University of Mississippi, Dept. of Mechanical Engineering, University, MS, chambers@olemiss.edu;
Thomas Kajdan, Graduate Research Assistant, University of Mississippi, Dept. of Civil Engineering, University, MS, alex.kajdan@gmail.com;
Cristiane Surbeck, Associate Professor, University of Mississippi, Dept. of Civil Engineering, University, MS, csurbeck@olemiss.edu;
Roger Kuhnle, Research Hydraulic Engineer, USDA, ARS-NSL, Oxford, MS, roger.kuhnle@ars.usda.gov

Abstract: The use of ultrasonic acoustic technology to measure the concentration of fine suspended sediments has the potential to greatly increase the temporal and spatial resolution of sediment measurements while reducing the need for personnel to be present at gauging stations during storm events. A laboratory investigation by Carpenter et. al (2009, 2014) was undertaken by the National Center for Physical Acoustics in cooperation with the USDA-ARS National Sedimentation Laboratory. In these experiments, two immersion transducers were used to measure attenuation from 20 MHz acoustic signals propagated through suspended clay (smectite and kaolinite) and silt particles (i.e. clays and silts ranging from 0.03–14 micrometer particle size diameter) for a wide range of concentrations (0.3–14 g/L). Attenuation curves for each particle classification were compared to the theoretical attenuation curves developed by Urick (1948) and Sheng and Hay (1988) for scattering as presented by Landers (2010), and a model for estimating concentration was created. Subsequently, a customized field deployable system was developed using the laboratory transducer design parameters and deployed as an acoustic surrogate monitoring fine sediment particles in suspension at Harris Bayou, in cooperation with personnel from the U. S. Geological Survey. Using the laboratory and field systems concurrently, the calibration measurements show good agreement between the laboratory grade equipment and the new prototype system. The results of laboratory calibration and testing of the prototype system at Harris Bayou will be presented.

INTRODUCTION

Growing populations and increased economic development, coupled with the effects of a warming climate, will place an increased strain on water resources. The accurate measurement of sediment transport in rivers and streams, typically associated with upland erosion, is an important and ongoing problem that affects water quality (Holeman, 1968). The use of ultrasonic acoustic technology as a surrogate method to monitor the concentration of fine suspended sediments has the potential to greatly increase the temporal and spatial resolution of sediment measurements.

METHODOLOGY

In order to improve the state of knowledge, laboratory investigations by Carpenter et. al (2009, 2014) were conducted at the National Center for Physical Acoustics with collaboration from the USDA-ARS National Sedimentation Laboratory. In the experimental setup, two immersion transducers were used to measure attenuation from 20 MHz acoustic signals propagated through suspended clay (smectite and kaolinite) and silt particles (i.e. clays and silts ranging from 0.03–14 micrometer particle size diameter) for a wide range of concentrations (0.3–14 g/L). Attenuation curves for each particle classification were compared to the theoretical attenuation curves developed by Urick (1948) and Sheng and Hay (1988) for scattering as presented by Landers (2010), and a model for estimating concentration was created assuming spherical-sized particles. The calibration curve is valid for silt-sized particles (D_{50} = 20 μm).

$$\alpha_s = SSC_v * k(\gamma - 1)^2 * \left(\frac{s}{s^2 + (\gamma + \tau)^2}\right) + \frac{k^4 * a_s^3}{5 * (1 + 1.3\,k^2 a_s^2 + 0.24\,k^4 a_s^4)} * \frac{8.686}{2} \quad (1)$$

where,

α_s is a coefficient of attenuation, measured in $\left(dB/_{cm}\right)$

SSC_v is the volumetric sediment concentration (*SSC* divided by the sediment density)

k is the wave number, $k = \frac{2\pi}{\lambda}$, where λ is the wavelength in cm

γ is the specific gravity of the sediment

a_s is the sediment radius in cm

$$s = \left[\frac{9}{4\beta a_s}\right] * \left[1 + \frac{1}{\beta a_s}\right]$$

$$\tau = \left[0.5 + \frac{9}{4\beta a_s}\right]$$

$\beta = \left[\frac{\omega}{2\nu}\right]^{0.5}$, $\omega = 2\pi f$ and ν is the kinematic viscosity of the water.

A customized field deployable system was developed using the laboratory transducer design parameters and a digital signal processor (DSP).

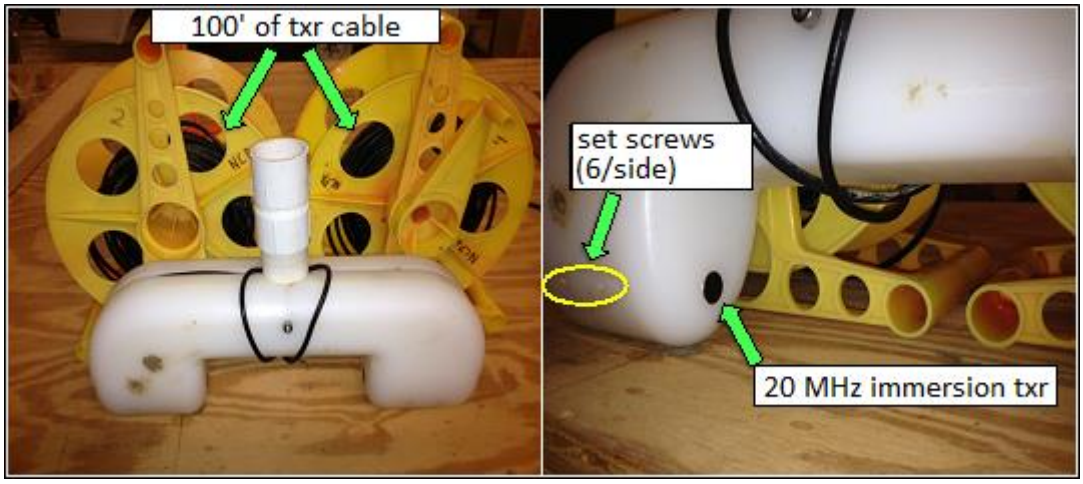

Figure 1 Field-Grade Transducer Casing

RESULTS

Using the laboratory and field systems concurrently, the calibration measurements show good agreement and a high level of reproducibility between the laboratory grade equipment and the new prototype system.

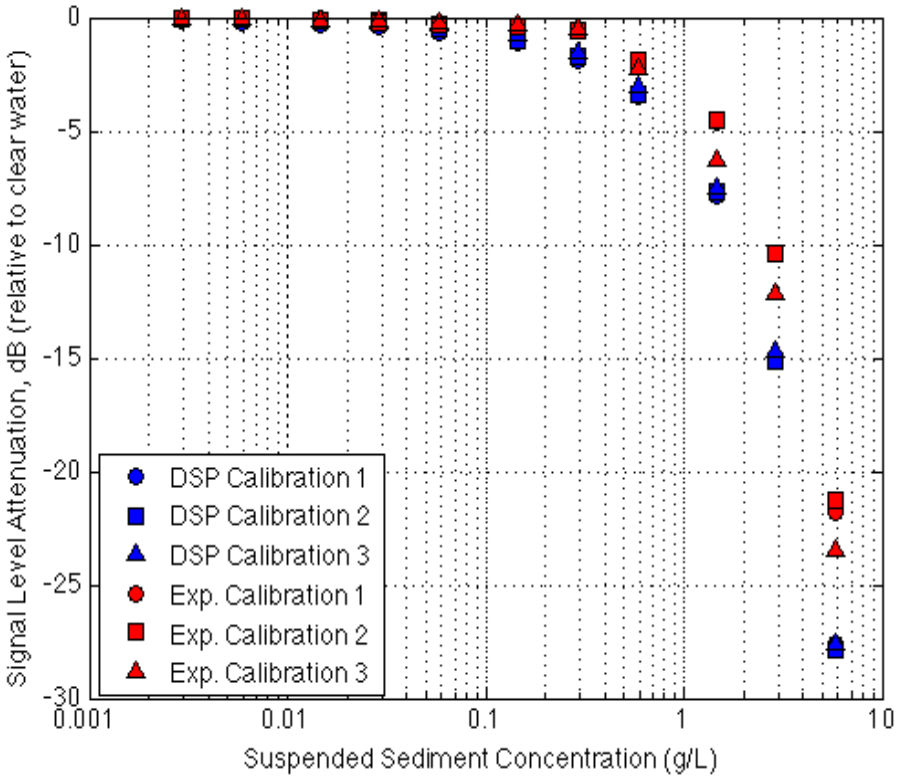

Figure 2 Comparison Plot DSP System vs. Experimental System

The red symbols represent the attenuation values computed by the verified experimental system during the three calibration experiments. The blue symbols represent the attenuation values that were found using the DSP system. Following the comparison, it was concluded the first well-defined signal drop was shown at 0.15 g/L. It is estimated that the upper detection threshold of the DSP system is ≈ 6.0 g/L.

Subsequently, the field system was deployed to monitor suspended fine sediment particles, less than 100 microns in diameter. In cooperation with personnel from the U. S. Geological Survey, the DSP system was deployed at Harris Bayou near Alligator, MS. The Harris Bayou watershed is a 71,592-acre watershed located in Bolivar and Coahoma Counties, Mississippi. The transducers were submerged in the bayou, and continuous in-situ measurements of fine suspended sediments were conducted. The acoustically measured suspended sediment concentration (SSC) data were compared with grab samples taken in predetermined intervals throughout the data collection period. Statistical methods were used to validate the accuracy of the acoustic prediction. However, field results were inconclusive, and the acoustic predictive model did not agree with the grab samples. Therefore, current studies are underway to examine the effect of water temperature on the acoustic prediction.

CONCLUSION

Multiple field trials were conducted at Harris Bayou to validate the prototype DSP system. A conversion scheme was successfully developed to convert the binary data from the field. The conversion routine can be used for future field trials. The acoustic SSC results were compared with the SSC found in the grab samples. It was shown that additional parameters, such as water temperature at near surface may be affecting the acoustic response of the system. Additional variation could result from the variation of pH, conductivity, and nutrient concentrations. This hypothesis should be evaluated in future work. It is recommended that an independent evaluation be conducted to determine if these factors have any effect on the acoustic response of the DSP system. Work is proceeding to calibrate the system with respect to temperature.

REFERENCES

Carpenter, W.O., Chambers, J.P., Wren, D.G., Kuhnle, R.A., Diers, J.A. (2009). "Acoustic Measurements of Clay-Size Particles," Journal of the Acoustical. Society of America Express Letters, 126(6).

Carpenter, W.O., Goodwiller, B.T., Wren, D.G., Kuhnle, R.A., Chambers J.P. (2014). "Acoustic measurement of suspensions of clay and silt particles using single frequency attenuation and backscatter," Applied Acoustics, Volume 85, pp 123-129.

Holeman, J.N. (1968). "The Sediment Yield of Major Rivers of the World," Water Resources Research, 4(4), pp 737-747.

Landers, M.N. (2010). "Review of methods to estimate fluvial suspended sediment characteristics from acoustic surrogate metrics," Joint Federal Interagency Conf. (2), pp 1-2.

Sheng, J., Hay, A.E. (1988). "An examination of the spherical scatterer approximation in aqueous suspensions of sand," Journal of the Acoustical Society of America, 83(2), pp 598610.

Urick, R.J. (1948). "The absorption of sound in suspensions of irregular particles," Journal of the Acoustical Society of America, 20(1), pp 283-289.

STUDYING SURROGATES TO ESTIMATE SUSPENDED SEDIMENT CONCENTRATIONS IN THE MISSOURI RIVER AT NEBRASKA CITY, NE

Extended Abstract

Jon F. Nania, Hydrologist, U.S. Geological Survey Iowa Water Science Center, Iowa City, IA, jfnania@usgs.gov

Fluvial sediments have various effects on river systems including adverse consequences for aquatic life, recreation, navigation, and reservoir storage capacity. Quantifying sediment transport is important in order to determine long-term trends in sediment transport, to understand the various effects from fluvial sediments, and to implement processes for minimizing adverse consequences. Traditionally, streamflow has been used as a surrogate to estimate instantaneous suspended sediment concentrations (SSC) and to compute sediment loads. However, streamflow alone may not be a reliable method for estimating SSC at locations that are effected by regulated flow, that have sediment inputs from a variety of sources, or have episodic sediment transport events which occur during a constant streamflow (Wood and Teasdale, 2013). Alternately, graphical methods for computing continuous concentration curves rely on interpretation supported by a subjective understanding of factors, often site-specific and undocumented, influencing sediment transport (Porterfield, 1972). To account for these factors, new techniques for using surrogates to estimate SSC are being developed and further study is needed refine these methodologies. The U.S. Geological Survey (USGS) has been studying three sediment surrogate methods at the Missouri River at Nebraska City, NE, streamgage.

The Missouri River at Nebraska City, NE, is a large river site, drainage area of 410,000 mi^2, and provides a unique study location with multiple and vastly different sediment sources. Sediment originates from the upper Missouri River with low SSC due to multiple dams, from the upper Platte River with Rocky Mountain snowmelt and lower Platte River alluvial sand, from runoff from the Loess Hills in Western Iowa with highly erodible aeolian silt soils, and from other local tributaries with agricultural runoff. This USGS streamgage, established in 1929 and operated in cooperation with the U.S. Army Corps of Engineers, is maintained by the USGS Iowa Water Science Center (IA WSC). Crews visit the site twice per week to collect measurements of streamflow and depth-integrated cross-sectional averaged SSC samples. Real-time streamflow data are computed from an established relation between stage, which is monitored real-time, and discharge which is updated routinely based on the streamflow measurements. Daily suspended sediment loads since 1957 have been computed by the USGS IA WSC using graphical methods for continuous concentration curves based on the sample results and daily streamflow, which is based on stage (Koltun and others, 2006). Averaged cross-section SSC samples since 1957 have ranged from approximately 100 milligrams per liter (mg/L) to 3,000 mg/L. Periodic analyses of the percent fine-grain material (less than 0.0625 mm) that is present in the SSC samples indicate material can vary spatially in the cross-section of the river and also vary temporally. The percent of fine-grain material ranges from less than 10 percent to over 90 percent (U.S. Geological Survey, 2014). Additional data collection for studying new surrogates at this location started in 2013 and is planned to continue through 2015 to include a variety of streamflow conditions. The additional data collection includes the installation of surrogate devices and more frequent analyses of the percent fine-grain material present in the SSC samples.

Three surrogate methods are being studied at the USGS streamgage on the Missouri River at Nebraska City, NE. These methods use turbidity, acoustic backscatter, and laser diffraction to develop a relation, by ordinary least-squares (OLS) regression, between SSC and the individual surrogate parameter. The dataset for each model is comprised of the cross-sectional averaged SSC samples and the corresponding recorded or computed surrogate values. The surrogate devices are mounted near the west bank in an area of uniform flow during a wide range of streamflow conditions. The Turbidity method uses turbidity data that are measured in formazine backscatter ratio units (FBRU) which has a broad operating range due to the data being calculated from infrared light at two backscatter angles. The turbidity data are recorded every 15 minutes by a data logger. The second method uses acoustic backscatter (ABS) measured by an acoustic Doppler velocity meter (ADVM) as a surrogate for SSC. Three ADVMs deployed at the site measure ABS recorded by a data logger every 15 minutes from each device. Two ADVMs have a frequency of 1500 kilohertz (kHz) and one ADVM has a frequency of 500 kHz. The 1500 kHz ADVMs are configured to determine if different measurement settings affect ABS during the same SSC conditions. The 500 kHz ADVM is installed to determine if model results at this site can be improved with a lower frequency. The third surrogate method uses laser diffraction technology to collect a volumetric measurement of SSC and of particle size distribution (PSD) divided into several size ranges. Water is pumped from the river for a short duration at one-hour intervals into a sample chamber where a laser is emitted through the sample volume. Logged every hour, volumetric SSC and PSD are measured depending on how the laser is diffracted through the sample volume. In addition to individual parameter models for SSC, combinations of some methods will also be used to assess models for SSC during varying particle size conditions. Combined models will determine if the different frequencies of ADVM data and the laser diffraction data for PSD together provide a better model for SSC at a site with such varying sediment sizes.

The use of surrogates at the Missouri River at Nebraska City, NE, streamgage, will provide significantly more data on sediment transport due to the frequency of the recording interval by each device. Rather than two cross-sectional averaged SSC samples per week, these surrogate methods can provide SSC information as often as data are recorded. The varying presence of fine-grain material at this site will also help refine methodologies to adjust for this condition. The results from this study will be used to identify the method that provides the best estimates for SSC in the Missouri River at Nebraska City, NE, and the applicability for use at similar locations.

REFERENCES

Koltun, G.F., Eberle, M, Gray, J.R., and Glysson, G.D., User's Manual for the Graphical Constituent Loading Analysis System (GCLAS), U.S. Geological Survey Techniques and Methods 4-C1, 51 p.

Porterfield, George, 1972, Computations of fluvial-sediment discharge. U.S. Geological Survey Techniques of Water Resources Investigations, book 3, chap. C3, 66 p.

U.S. Geological Survey, 2014, U.S. Geological Survey National Water Information System, accessed October 31, 2014, at *http:waterdata.usgs.gov/nwis*.

Wood, M.S., and Teasdale, G.N., 2013, Use of surrogate technologies to estimate suspended sediment in the Clearwater River, Idaho, and Snake River, Washington, 2008-10: U.S. Geological Survey Scientific Investigations Report 2013-5052, 30 p.

HYDROACOUSTIC SIGNATURES OF COLORADO RIVERBED SEDIMENTS IN MARBLE AND GRAND CANYONS USING MULTIBEAM SONAR

Daniel Buscombe, Research Geologist, US Geological Survey, Southwest Biological Science Center, Grand Canyon Monitoring and Research Center, Flagstaff, AZ, dbuscombe@usgs.gov;
Paul E. Grams, Research Hydrologist, US Geological Survey, Southwest Biological Science Center, Grand Canyon Monitoring and Research Center, Flagstaff, AZ, pgrams@usgs.gov;
Matt A. Kaplinski, Research Associate, School of Earth and Environmental Sustainability, Northern Arizona University, Flagstaff, AZ, matt.kaplinski@nau.edu;
Robert Tusso, Hydrologist, US Geological Survey, Southwest Biological Science Center, Grand Canyon Monitoring and Research Center, Flagstaff, AZ, rtusso@usgs.gov;
David M. Rubin, Research Professor, Department of Earth and Planetary Sciences, University of California Santa Cruz, Santa Cruz, CA, drubin@ucsc.edu

INTRODUCTION

Characterizing the large-scale sedimentary make-up of heterogeneous riverbeds (Nelson et al., 2014), which consist of a patchwork of sediment types over small scales (less than one to several tens of meters) (Dietrich and Smith, 1984) requires high resolution measurements of sediment grain size. Capturing such variability with conventional physical (e.g. grabs, cores, and dredges) or underwater photographic sampling (Rubin et al., 2007; Buscombe et al., 2014a) would be prohibitively costly and time-consuming. However, characterizing bed sediments using high-frequency (several hundred kilohertz) acoustic backscatter from swath-mapping systems has the potential to provide near complete coverage of the bed (Brown and Blondel, 2009; Brown et al., 2011; Snellen et al., 2013), at resolutions down to a few centimeters, which photographic sampling could not practically achieve within the same time and with the same positional accuracy.

In shallow water, the physics of high frequency scattering of sound are relatively poorly understood, therefore acoustic sediment classification are almost always statistical (Snellen et al., 2013). Many such methods proposed to date are designed for characterizing large areas of seabed (Brown and Blondel, 2009; Brown et al., 2011) at relatively poor resolution (tens of meters to several hundred meters) and therefore rely on aggregation of data over scales much larger than the typical scales of sediment patchiness on heterogeneous riverbeds. In response to this need, Buscombe et al. (2014b, 2014c) developed a new statistical method for acoustic sediment classification based on spectral analysis of backscatter. This method is both continuous in coverage and of sufficient resolution (order meter or less) to characterize sediment variability on patchy riverbeds. Here, we apply these methods to multibeam echosounder (MBES) data collected from the bed of the Colorado River in Marble and Grand Canyons.

Sediment dynamics on the Colorado River in Grand Canyon National Park have been studied for several decades (e.g. Howard and Dolan, 1981; Rubin et al., 2002). Particular focus has been given to sandbars in large eddies downstream of tributary debris fans (Schmidt, 1990) because they are considered valuable resources by stakeholders and managers. Due to the severe limitations in sand supply imposed by Glen Canyon Dam (Howard and Dolan, 1981; Topping et

al., 2000; Hazel et al., 2006), understanding the effectiveness of sandbar management practices, such as controlled floods (Rubin et al. 2002; Topping et al., 2006; Hazel et al., 2010), and the long-term fate of sand in Grand Canyon over decadal timescales, requires construction of accurate sand budgets, which involves detailed monitoring of influx, efflux and changes in sand storage (Topping et al., 2000; Topping et al., 2010; Grams et al., 2013) and assessments of uncertainties in sand-budget calculations (Grams et al., 2013).

In order to estimate the sand budget, it is necessary to estimate what component of observed morphological changes is sand and what component is coarser. Grams et al. (2013) classified sand and coarse substrates using topographic roughness derived from digital elevation models, but the classification skill was estimated to be only 60-70%. In addition, sand bedforms had to be delineated manually, and validation was based on grain-size observations with positional uncertainties up to tens of meters. Because the morphology of the Colorado riverbed in Grand Canyon is mapped - to a large extent - using MBES (Kaplinski et al., 2009), the primary motivation for the present study is to examine how uncertainties in sand budgets can be constrained by producing maps of surface sediment types using the completely automated methods of Buscombe et al (2014b, 2014c) based on statistical analysis of MBES acoustic backscatter.

SITES AND DATA

MBES soundings, backscatter and underwater video camera images were collected in August 2013 from three short (approx. 500-1000m) reaches around sediment and flow gaging stations (Figure 1). Site 1 (hereafter, RM30), in Upper Marble Canyon at river-mile 30, is a relatively straight section of channel within the Redwall Limestone above Shinumo Wash. Site 2 (hereafter, RM61), in Lower Marble Canyon at river-mile 60, is within the Tapeats Sandstone just above the confluence with the Little Colorado River. Site 3 (hereafter, RM87), in Eastern Grand Canyon at river-mile 87, near Phantom Ranch within the Upper Granite Gorge, comprises two sections separated by a riffle and debris fan on river left. These sites were chosen to test scattering signatures of bed sediment because they collectively include a majority of the range of sediment, flow, geomorphic and geological settings found in this canyon river.

MBES data were collected using a Reson® 7125 multibeam sonar, operating at 400 kHz with a configuration that produces a 512 beam swath across a total subtended angle of 135°. This geometry permits swath widths of up to seven times the water depth. Each beam has a 0.5° across-track by 1.0° along-track angular width. Each echo is registered simultaneously by all 512 beams, which constitutes one ping. Pings are recorded up to 50 times per second. More details of sonar data collection are described in Kaplinski et al. (2009, 2014).

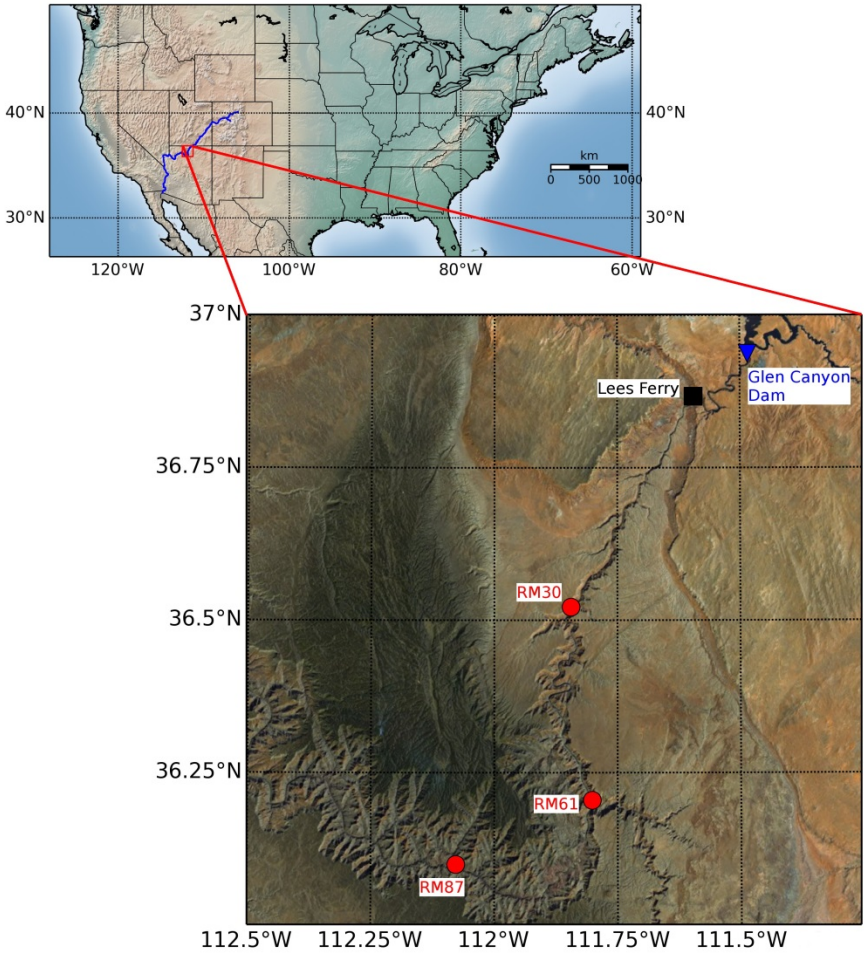

Figure 1 Map of survey locations on the Colorado River in Marble (RM30 and RM61) and Grand (RM87) Canyons.

A cabled video-microscope system was used to collected high-resolution (0.02mm/pixel) images of the bed. The system consists of a video camera fitted with macro lens, inside a protective metal housing. The transparent faceplate of the camera housing, fitted with LED lights for illumination, makes contact with the bed. Data collection involves navigating to each location, turning the boat to face the current, and lowering the video to the bed using an electric winch. The video is relayed instantly to the winch operator. For more details about the system, see Rubin et al. (2007, 2010). Coordinates of sample locations were measured by tracking the boat using a shore-based robotic laser-tracking system from established survey control points (Kaplinski et al., 2009). This method allows bed-sediment sampling at moderately high spatial density (up to tens of samples over tens of square meters) (Rubin et al., 2010) and hundreds of images can be obtained in a few hours. Another advantage of this approach over conventional physical sampling is that it samples only those sediments that are exposed on the bed surface. This is important because, given the high frequency of the MBES sound source, acoustic penetration into the bed is negligible, therefore the measured backscatter amplitude reflects the

composition of bed surface sediment (and possibly form roughness within the beam footprint) only.

The underwater video camera images were used to characterize bed-sediment, at a point, into three categories: 1) 'sand': homogeneous sandy surfaces (where no distinction was made between plane bed, ripples and dunes); 2) 'gravel': coarse substrates encompassing homogeneous gravels and sand-gravel mixtures (sand in the interstitial spaces of gravel clasts), in the size range deemed to be movable by typical flows; and 3) 'rock', a category which includes boulders, bedrock ledges, and cobbles large enough to be considered immovable by typical flows. These qualitative assessments were made by an experienced field technician operating the winch, based on both the image and the feel of the winch as the video housing hit the bed surface.

Figure 2 Underwater video images along a ~50m (river left to river right) transect at RM 30, showing typical sediment heterogeneity.

Another underwater video camera system - a towed video sled with a wider field of view, equipped with powerful lights and lasers for scale - was also used to observe the bed. These data were collected at a different time (May 2012) in the RM30 and RM61 pools, along with MBES data, and were used to assess the plausibility of sediment classifications applied to an earlier data set (outside the calibration).

DATA PRE-PROCESSING

Several quality control and quality assurance procedures are performed to ensure only high-quality amplitude data are used for bed sediment characterization. These checks, detailed in Kaplinski et al. (2009, 2014) and Buscombe et al. (2014b), include:

1. Patch tests to determine the offset angles and timing between the various system components.
2. Beam-angle tests are used to determine the uncertainty of soundings for all beam angles.
3. Quality assurance assessments performed in real time during the surveys by continuously monitoring across-track swaths and comparison between adjacent overlapping sweeps.
4. Manual sweep editing and systematically stepping through overlapping sweeps.
5. Automated spatial filtering procedures, designed to identify artifacts based on excessive bathymetric slopes; and incorrect beam locations.

The raw high-frequency echoes recorded by the receive beams MBES are corrected for beam geometry effects (angle of sound incidence and area of beam of the sloping bed) and radiometric effects (source and transmission losses) using the methods detailed in Buscombe et al. (2014b). Backscatter was corrected for water and suspended sediment attenuation using the median size and concentration of sand, and concentration of silt and clay. These were available every 15 minutes from gages in the same survey reach (Griffiths et al., 2012). It was assumed that the median silt grain size is 2 μm (Voichick and Topping, 2014). It was further assumed that sand and silt are homogeneously mixed through the water column. This assumption is physically unreasonable for sand. However, sand suspensions were so dilute so as to make negligible difference to the sediment attenuation calculation, so the assumption of homogeneous mixing was made for numerical convenience. For water attenuation corrections, measurements of temperature and salinity were also available every 15 minutes from sondes at each gaging station.

SPECTRAL ANALYSIS

Backscatter data from the three survey reaches were processed using the spectral analysis methods presented in Buscombe et al. (2014b) which use the (per beam, per ping) amplitudes of backscattered sound associated with time-of flight bathymetric soundings (range to the bed). This recorded amplitude is either the peak amplitude, or the amplitude associated with the highest phase-coherence between the source sound wave envelope and the echo wave envelope. Either way, it is considered the integral of the portion of reflected sound at incidence angle from all scatterers in the insonified area of the bed (the beam footprint).

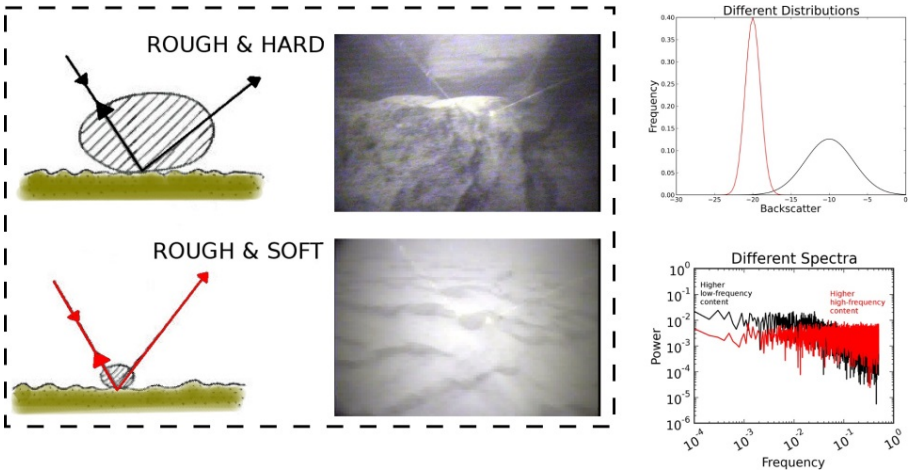

Figure 3 Schematic showing hypothesized backscatter distributions and spectra for rough/hard substrate (rock) and rough/soft substrate (rippled sand).

The method quantifies the variation in length- and amplitude-scales of backscatter over small areas of gridded surfaces, using windowed spectral (frequency domain) analysis (Figure 3). Because backscatter is a measure of the hardness (impedance) of a substrate, this approach is somewhat independent of the roughness of the topography, which may not be uniquely related to

a given substrate type (for example, the occurrence of gravel dunes). The method works by carrying out spectral analysis of gridded backscatter (the median value per grid cell) that has been detrended and tapered (Figure 4). Backscatter power spectra are computed to produce scale and amplitude metrics that collectively characterize the length scales of stochastic measures of riverbed scattering, termed `stochastic geometries' by Buscombe et al. (2014b). Backscatter aggregated over small spatial scales has spectra that obey a power-law in 1D (Figure 4). Relationships exist between stochastic geometries of backscatter and areas of rough and smooth sediments (Buscombe et al., 2014c).

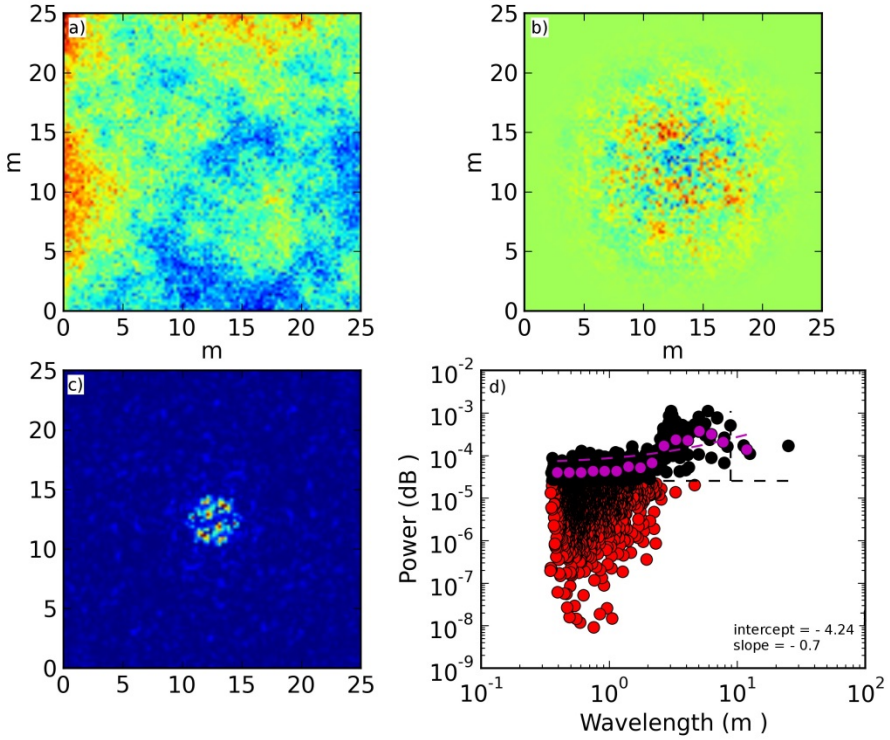

Figure 4 A window of backscatter (a) is detrended and Hann tapered (b). The 2D power spectral density of this surface (c) is collapsed to a 1D form (d) from which statistics are calculated (from the data that are statistically significant at the 95% level, shown as black dots) such as the slope and the intercept. These statistics have been shown to be sensitive to changing substrate type by Buscombe et al. (2014b, 2014c).

A grid size of 0.25 x 0.25 m was chosen for construction of surfaces because this was the smallest scale at which there were, consistently across sites, multiple usable soundings. A window size of 25 x 25 m was chosen based on examination of individual spectra and the criteria suggested by Buscombe et al (2014c). Windows are moved around the surface such that the outputs from one window are ascribed to the central cell of the window. The window is then shifted by a specified amount in space in 2 directions, and the calculations are repeated. This process is repeated until the entire surface has been analyzed by systematic windowing. A shift length of 0.25 m (1 grid cell) was chosen so the output surfaces were the same spatial resolution

as the input surfaces. In this configuration, the value in each output grid cell is the ensemble average of 1000 individual spectra for a window passing over that point.

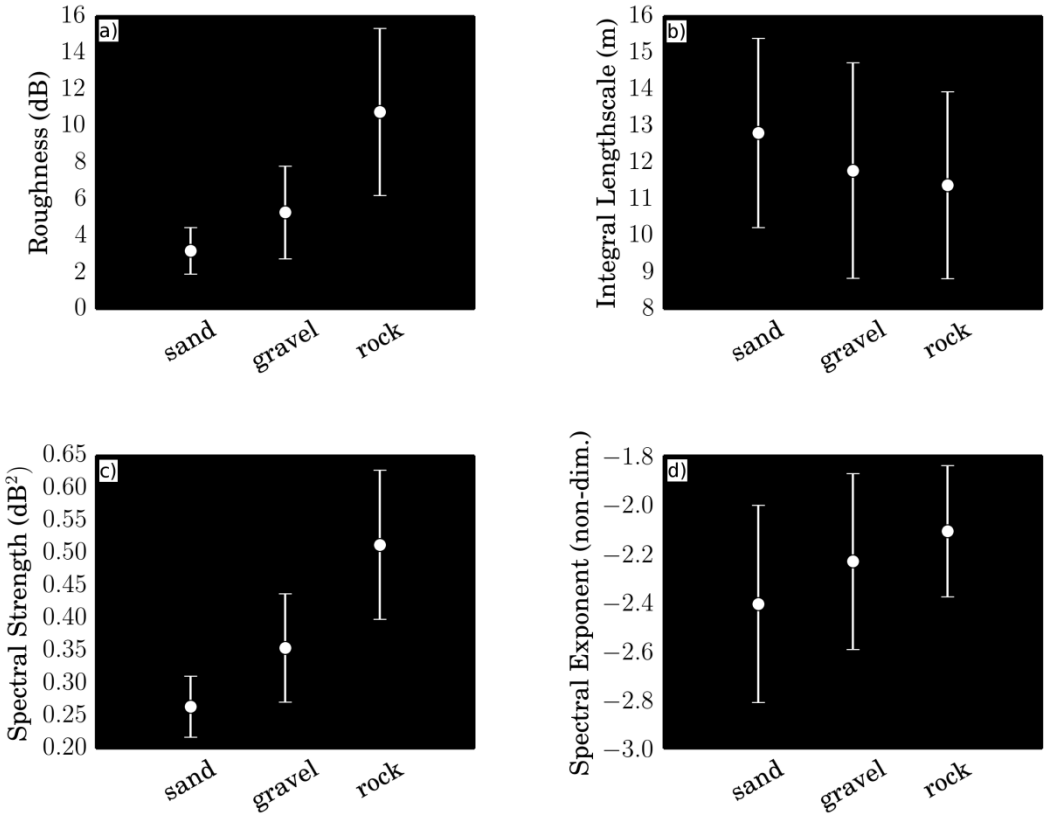

Figure 5 Example of spectral signatures of 3 different sediment substrates at RM 87. Roughness (a) is the root mean square variance in amplitude; integral lengthscale (b) is a measure of persistence; spectral strength (c) is a measure of power at low frequencies; and spectral exponent (d) is a measure of the rate of decay of power with increasing frequency. In each subplot, the dot represents the mean quantity per co-located substrate and the bars are the range of values.

SEDIMENT SPECTRAL SIGNATURES

Four parameters are calculated from each computed log-transformed spectrum, according to the methods detailed in Buscombe et al (2014b): 1) the spectral strength, ω, which is the intercept of the regression through the statistically significant portion of the spectrum, and a measure of the variance in the data at low frequencies (large wavelengths); 2) the spectral exponent, γ, which is the slope of the regression through the statistically significant portion of the spectrum, and a measure of the decay in power as a function of frequency, or the number of frequencies required to describe the data (spectral width) and therefore a measure of how complicated the data is; 3) the acoustic 'roughness', σ, which is the overall power in the spectrum over all frequencies; and 4) the integral lengthscale, which describes the lengthscale over which the surface is typically statistically significant. These 4 parameters were found by Buscombe et al (2014c) to have the

strongest correlations with co-located substrate types (Figure 5) identified in the underwater video streams. Of these, the spectral strength, exponent and roughness were used to develop an acoustic sediment classification because they have high between-substrate variability, low between-site variability, low within-substrate variability, and the magnitude of values scale with substrate size.

SEDIMENT CLASSIFICATION

Towards an aim of classifying each 0.25 × 0.25 m grid cell into three sediment types, Buscombe et al. (2014c) developed an approach based on decision tree learning. A decision tree (Breiman et al., 1984) recursively partitions the space into smaller homogeneous subsets using a set of binary condition rules such that the samples with the same labels are grouped together. The basic process is as follows: 1) for each attribute (spectral slope, strength, and roughness), find the feature that best divides the training data (attribute value at each substrate location) such as information gain from splitting on the attribute; 2) create a decision node that splits on the attribute with the highest information gain; and 3) recurse over the sub-lists obtained (at descendant nodes) by splitting on the previous decision node until no more splits are possible. More details are provided in Buscombe et al. (2014c).

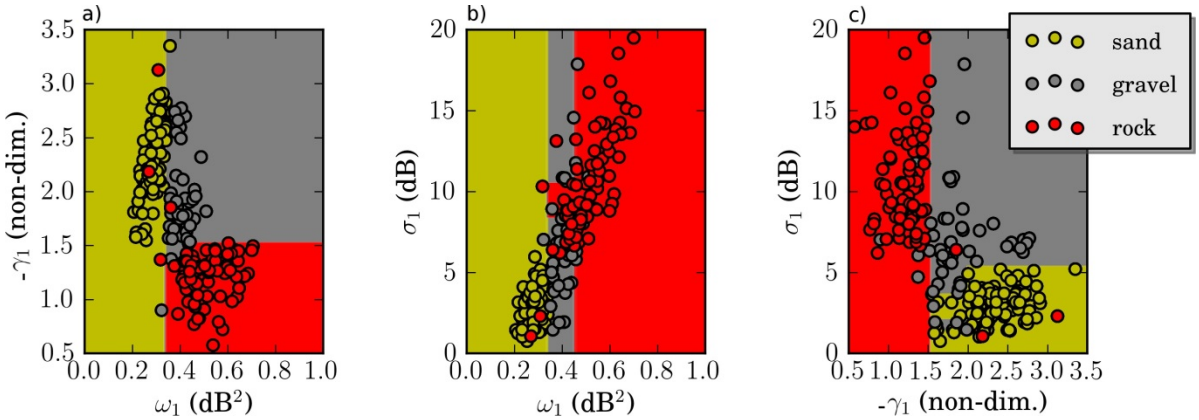

Figure 6 Decision surfaces of paired parameters based on aggregation of observations from RM30, RM60 and RM87 pools (circles), with a constraint that each decision node must have at least 50 samples: (a) ω and -γ ; (b) ω and σ; and (c) -γ and σ. The yellow, grey and red portions of the parameter space show where the decision tree would classify as sand, gravel and rock, respectively.

Classifications were carried out using a calibration based on data aggregated from all three sites (RM 30, RM 61, and RM 87). Trees were constructed with a single constraint that a minimum of 50 samples were required to be at a terminal node. The decision surface (Figure 6) shows the observations as colored markers, and a relatively straightforward partitioning of space between pairs of the 3 spectral parameters input into the decision tree algorithm. An example work flow from map of gridded corrected backscatter, to maps of spectral quantities with the same resolution, to final classification, has been provided for the RM 30 site (Figure 7). The classification skill for sand, gravel and rock is 97, 81, and 95 % respectively. Finally, another

sediment classification map is provided for RM 61 (Figure 8) overlying an aerial photo for geomorphic context.

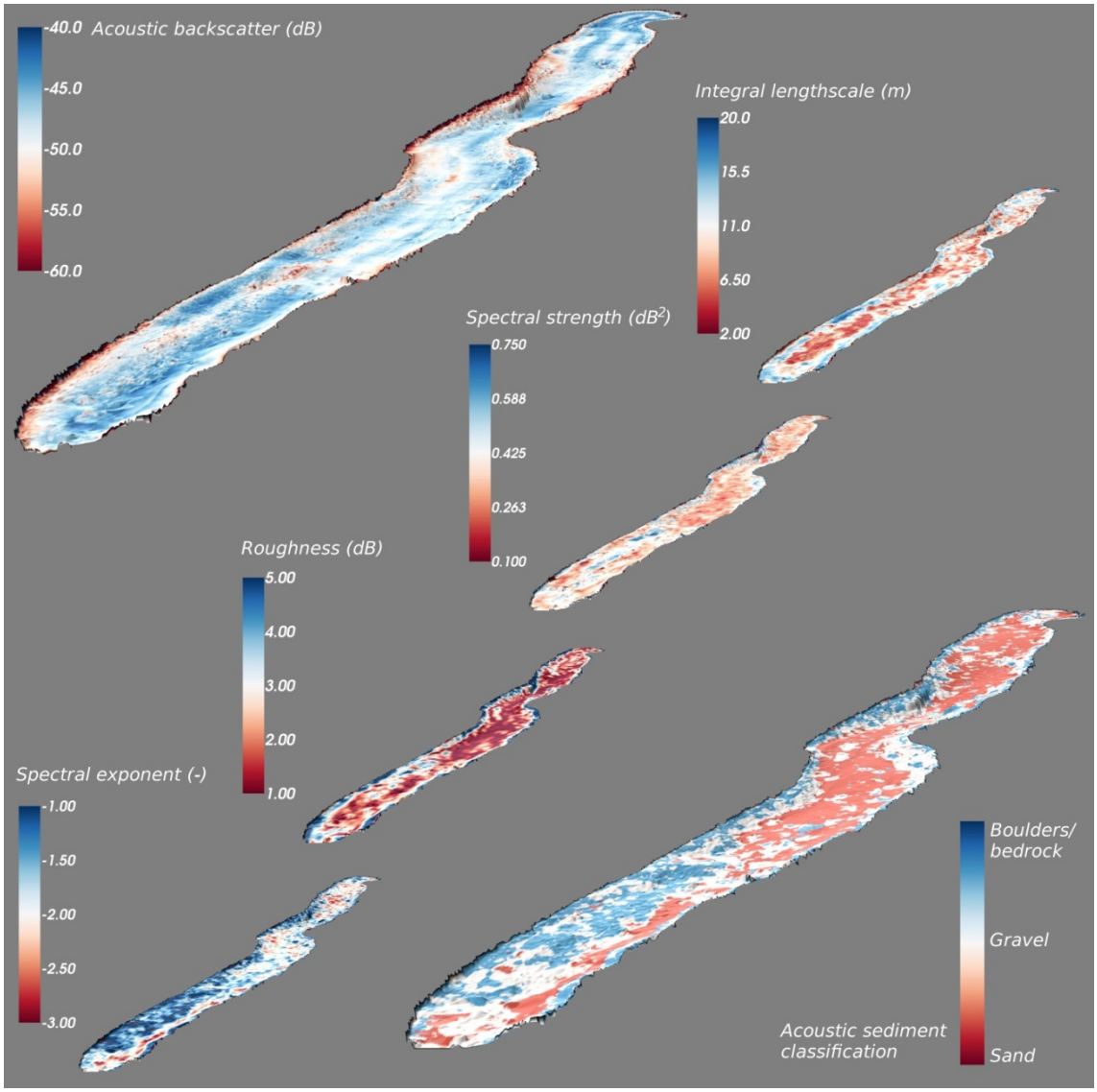

Figure 7 Example of processing stages from data collected at RM 30. Upstream to downstream is bottom left to upper right. Each map is a 3D DEM of the survey pool draped with a different quantity. From gridded acoustic backscatter (top), various maps of spatially explicit stochastic geometries (middle), derived from the windowed spectral analysis procedure, are merged in a decision tree classification to produce a map of sediment types (bottom).

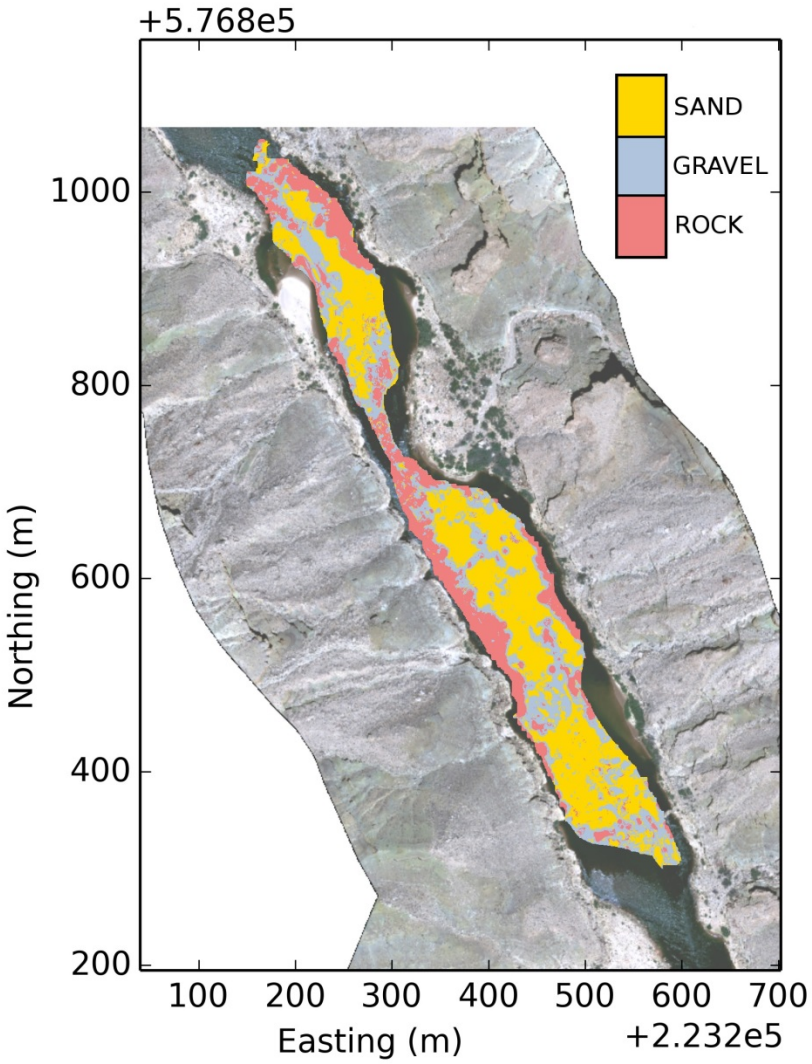

Figure 8 Example of sediment classification map at RM 61.

SUMMARY

Capturing the spatial variability in classifications of riverbed sediments is challenging using high-frequency hydro-acoustic instruments. However, the method proposed by Buscombe et al (2014b, 2014c) has been shown to be potentially useful to classify grain-scale roughness and hardness on the Colorado riverbed in Marble and Grand Canyons. The method uses high-frequency acoustic backscatter from multibeam sonar to classify heterogeneous riverbed sediments by type (sand, gravel, rock) continuously in space and at small spatial resolution.

Spatially explicit maps of the stochastic geometries (length- and amplitude-scales) of backscatter are related to patches of riverbed surfaces composed of known sediment types, as determined by geo-referenced underwater video observations. Statistics of backscatter magnitudes alone are found to be poor discriminators between sediment types. However, the variance of the power spectrum, and the intercept and slope from a power-law spectral form (termed the spectral

strength and exponent, respectively) successfully discriminate between sediment types. A decision tree approach to classifications was able to classify spatially heterogeneous patches of homogeneous sands, gravels (and sand-gravel mixtures), and cobbles/boulders with 95, 88, and 91% accuracy, respectively. This data-driven approach allows bed sediment classifications at unprecedented resolution.

REFERENCES

Brown, C.J., and Blondel, P. (2009). "Developments in the application of multibeam sonar backscatter for seafloor habitat mapping," Applied Acoustics (70), pp. 1242-1247.

Brown, C.J., Smith, S.J., Lawton, P., and Anderson, J.T. (2011). "Benthic habitat mapping: A review of progress towards improved understanding of the spatial ecology of the seafloor using acoustic techniques," Estuarine, Coastal and Shelf Science (92), pp. 502-520.

Breiman, L., Friedman, J.H., Olshen, R.A., Stone, C.J. (1984). Classification and regression trees. Wadsworth and Brooks/Cole Advanced Books and Software, Monterey, California.

Buscombe, D., Rubin, D.M., Lacy, J.R., Storlazzi, C.D., Hatcher, G., Chezar, H., Wyland, R., and Sherwood, C.R. (2014a). "Autonomous bed-sediment imaging-systems for revealing temporal variability of grain size," Limnology and Oceanography: Methods (12), pp. 390-406.

Buscombe, D., Grams, P.E., and Kaplinski, M.A. (2014b). "Characterizing riverbed sediments using high-frequency acoustics 1: Spectral properties of scattering," Journal of Geophysical Research - Earth Surface (119), F003189, doi:10.1002/2014JF003189.

Buscombe, D., Grams, P.E., and Kaplinski, M.A. (2014c). "Characterizing riverbed sediments using high-frequency acoustics 2: Scattering signatures of Colorado River bed sediments in Marble and Grand Canyons," Journal of Geophysical Research - Earth Surface (119), JF003191, doi:10.1002/2014JF003191.

Dietrich, W.E., and Smith, J.D. (1984). "Bed load transport in a river meander," Water Resources Research (20), pp. 1355-1380.

Grams, P.E., Topping, D.J., Schmidt, J.C., Hazel, J.E., and Kaplinski, M.A. (2013). "Linking morphodynamic response with sediment mass balance on the Colorado River in Marble Canyon: Issues of scale, geomorphic setting, and sampling design," Journal of Geophysical Research - Earth Surface (118), pp. 361-381.

Griffiths, R.E., Topping, D.J., Andrews, T., Bennett, G.E., Sabol, T.A., and Melis, T.S. (2012). "Design and maintenance of a network for collecting high-resolution suspended-sediment data at remote locations on rivers, with examples from the Colorado River." U.S. Geological Survey Techniques and Methods, book 8, chapter C2, 44 p.

Hazel, J.E., Grams, P.E., Schmidt, J.C., Kaplinski, M. (2010). "Sandbar response following the 2008 high-flow experiment on the Colorado River in Marble and Grand Canyons," U.S. Geological Survey Scientific Investigations Report 2010-5015, 52 pp.

Hazel, J.E., Topping, D.J., Schmidt, J.C., and Kaplinski, M.A. (2006). "Influence of a dam on fine-sediment storage in a canyon river," Journal of Geophysical Research - Earth Surface (111), pp. F01025.

Howard, A., and Dolan, R. (1981). "Geomorphology of the Colorado River in the Grand Canyon," The Journal of Geology (89), pp. 269-298.

Kaplinski, M.A., Hazel, J.E., Grams, P.E., and Davis, P.A. (2014). "Monitoring fine-sediment volume in the Colorado River ecosystem, Arizona: Construction and analysis of digital elevation models," U.S. Geological Survey Open-File Report 2014-1052, 29 pp.

Kaplinski, M.A., Hazel, J.E., Parnell, R., Breedlove, M., Kohl, K., and Gonzales, M. (2009). "Monitoring fine-sediment volume in the Colorado River Ecosystem, Arizona: Bathymetric survey techniques," U.S. Geological Survey Open-File Report 2009-1207, 41 pp.

Nelson, P.A., Bellugi, D., and Dietrich, W.E. (2014). "Delineation of river bed-surface patches by clustering high-resolution spatial grain size data," Geomorphology (205), pp. 102-119.

Rubin, D.M., Chezar, H., Harney, J.N., Topping, D.J., Melis, T.S., and Sherwood, C.R. (2007). "Underwater microscope for measuring spatial and temporal changes in bed-sediment grain size," Sedimentary Geology (202), pp. 402-408.

Rubin, D.M., Topping, D.J., Chezar, H., Hazel, J.E., Schmidt, J.C., Breedlove, M., Melis, T.S., Grams., P.E. (2010). "20,000 grain-size observations from the bed of the Colorado River, and implications for sediment transport through Grand Canyon," 9th Federal Interagency Sedimentation Conference.

Rubin, D.M., Topping, D.J., Schmidt, J.C., Hazel, J.E., Kaplinski, M., and Melis, T.S. (2002). "Recent sediment studies refute Glen Canyon Dam hypothesis," Eos (Transactions, American Geophysical Union) (83), pp. 277-278.

Schmidt, J.C. (1990). "Recirculating flow and sedimentation in the Colorado River in Grand Canyon, Arizona," The Journal of Geology (98), pp. 709-724.

Snellen, M., Eleftherakis, D., Amiri-Simkooei, A., Koomans, R.L., and Simons, D.G. (2013). "An inter-comparison of sediment classification methods based on multi-beam echo-sounder backscatter and sediment natural radioactivity data," Journal of the Acoustical Society of America (134), 959-970.

Topping, D.J., Rubin, D.M., Grams, P.E., Grifths, R.E., Sabol, T.A., Voichick, N., Tusso, R.B., Vanaman, K.M., and McDonald, R.R. (2010). "Sediment transport during three controlled-flood experiments on the Colorado River downstream from Glen Canyon Dam, with implications for eddy-sandbar deposition in Grand Canyon National Park," U.S. Geological Survey Open-File Report 2010-1128, 111 pp.

Topping, D.J., Rubin, D.M., Schmidt, J.C., Hazel, J.E., Melis, T.S., Wright, S.A., Kaplinski, M., Draut, A.E., and Breedlove, M.J. (2006). "Comparison of sediment-transport and bar-response results from the 1996 and 2004 controlled-flood experiments on the Colorado River in Grand Canyon," 9th Federal Interagency Sedimentation Conference.

Topping, D.J., Rubin, D.M., and Vierra, L.E.J. (2000). "Colorado River sediment transport 1. Natural sediment supply limitation and the influence of Glen Canyon Dam," Water Resources Research (36), pp. 515-542.

Voichick, N., and Topping, D.J. (2014). "Extending the turbidity record – making additional use of continuous data from turbidity, acoustic-Doppler, and laser diffraction instruments and suspended-sediment samples in the Colorado River in Grand Canyon," U.S. Geological Survey Scientific Investigations Report 2014-5097, 31 p.

®, Any use of trade, product, or names is for descriptive purposes only and does not imply endorsement by the U.S. government.

APPLICATION OF CROSS-PLOT ANALYSIS ON A LEVEE USING TIME LAPSE SIESMIC REFRACTION TOMOGRAPHY AND ELECTRICAL RESISTIVITY TOMOGRAPGY.

Leti Wodajo, Graduate student, ltwodajo@go.olemiss.edu, University of Mississippi, University, MS; Dr. Craig Hickey, Associate Director for Applied Research National Center for Physical Acoustics & The University of Mississippi Research Associate Professor of Geological Engineering, University, Mississippi, chickey@olemiss.edu; Dr. Chung Song, The University of Mississippi Associate Professor of Civil Engineering, csong@olemiss.edu, University of Mississippi, University, MS.

Abstract

Out of the estimated 100,000 miles of levees in the United States a staggering 91% of these levees are not in an acceptable condition. Levee failures due to flood from hurricanes or heavy rainfalls occur without early warning and cause catastrophic damage. Therefore, the development of rapid assessment system of levees is greatly required to delineate weak locations and prioritize compromised locations. This study implements the use of surface based time-lapse geophysical methods known as seismic refraction tomography (SRT) and electrical resistivity tomography (ERT) on the Francis Levee Site. The Francis Levee site is located in Bolivar County, 0.5 miles west of Francis, Mississippi. The Francis Levee site was affected by the 2011 Mississippi river flood with multiple sand boil formations at the toe of the clay apron on the landside. Multiple geophysical surveys were conducted during spring 2014. It should be noted that similar methods of investigation are also applicable on earthen dams. The large number of dams in the Unites States and their risk of failure is alarming considering their old age and engineering design. Out of the 75,000 earthen dams in the US reported by the National Dam Inventory (2009), 56,000 are privately owned and do not undergo through investigation. This statistics necessitates the development of rapid and economical method of integrity assessment.

INTRODUCTION

The 2011 flood report by the Mississippi Levee Board, identified as many as twelve areas associated with seepage. The Francis levee site is one of the locations affected by the flood. Francis levee site (Station 150, 34° 5'9.48"N, 90°51'52.56"W) is located 0.8 kilometers west of Francis, Mississippi. During the 2011 flood event, three main sand boils were observed and mitigated by the construction of sand bag berms. After the initial mitigation, the US Army Corps of Engineers (USACE) extended the berm of the levee and constructed 16 relief wells. Figure 1 shows the location of the Francis Levee site on a Google map and an aerial photograph taken during the mitigation of the levee. This site was chosen for the geophysical study due to its close proximity to the University of Mississippi and the availability of borehole information.

Figure 1 Location of Francis Levee Site (left) and aerial photograph during mitigation (right)

Nimrod (2011) noted during the 2011 flooding the first sand boil surfaced at toe of the (berm) apron on the landside of the levee inside a drainage trench. The sand boil was mitigated with sand bags and by impounding water above the seepage area. After the first sand boil was mitigated, two additional sand boils surfaced 90 m to the northeast of the first one. Sand bags were used to mitigate these new sand boils. Figure 2 shows the locations of the three sand boils with red dots and a photograph of one of the later sand boils.

Figure 2 Location of sand boils (left) and mitigation of sand boil with sand bags (right)

The rapid assessment of the potential hazards associated with earthen dam and levee failures requires advanced screening tools to delineate, classify, and prioritize compromised locations. Screening such a large number of dams and levees requires the use of some type of remote sensing and/or geophysical technique. Geophysical methods provide a means of evaluating large areas of the subsurface rapidly. The results are can be used to optimize drilling requirements. Geophysical methods are also non-destructive and non-invasive with a simple and portable setup.

The overall objective of this study is to advance the use of remote sensing and multiple geophysical techniques for the early identification of compromised zones in levees. Geophysical monitoring and condition assessment of the Francis Levee was conducted with the use of different methods including seismic refraction tomography (SRT), electrical resistivity tomography (ERT), multichannel analysis of surface waves (MASW), electromagnetic (EM34) survey, and remote sensing surveys. The first phase of this study was conducted in the Spring 2014. Addition sets of measurement were planned for Fall 2014 during low water level but were not conducted due to weather and logistical problems.

In this paper, preliminary results from seismic refraction tomography (SRT) and electrical resistivity tomography (ERT) from the first set of surveys (Spring, 2014) at the Francis Levee site is presented. Focus will be on identifying seepage paths that start on the waterside of the levee and are responsible for the sand boil formations on the landside.

Uyank (2011) divided factors that can affect seismic velocities through soils and rocks into three main groups. Lithological properties of soils (grain sizes, grain shape, grain type, grain size distribution, amount of compaction, amount of consolidation and cementation), physical properties of soils (porosity, permeability, density, degree of saturation, pressure, and temperature), and elastic properties of soils (shear modulus (G), bulk modulus (K), Young modulus (E), Poisson's ratio (ν) and Lamé constant (λ)). All these factors are interrelated and affect the seismic velocity of soils. Therefore, analyzing 2D velocity distribution tomograms obtained from seismic refraction surveys provides valuable information on the integrity of the subsurface of dams and levees (Kim et. al., 2011, Bedrosian et. al., 2012, Moustafa et. al., 2012). In Particular, we expect that subsurface zones with higher permeability will have lower p-wave velocity. An area of seepage with fines washed out will have a high resistivity area if it is not fully saturated.

Electrical resistivity is a physical material property that represents the material's ability to oppose the flow of electrical current. The resistivity of a given soil (sand/clay) can have a wide range values due to differing porosity (ϕ), saturation (S_w), pore fluid resistivity (ρ_w), and the presence of clay content. This makes electrical resistivity an ideal method in the early detection of subsurface seepage through dams and levees (Cho et. al., 2007, Sjödahl et. al, 2008, Chinedu et al., 2013 Lin et. al., 2014, Al-Fares, 2014). Case (2012) applied the electrical resistivity method to a model embankment dam where resistivity tomograms are used to infer the subsurface conditions and assist in the resolution of zones susceptible to preferential flow.

SURVEY SETUPS AND PROCESSING

The data acquisition for seismic refraction surveying requires placing a line of multiple geophones on the ground surface and creating seismic waves using an impact source at a shot point location. The geophones record direct and refracted energies which are stored as waveform using a seismograph. The first arrival time is the relevant information required from the data. The first arrival time is the time it takes for the first seismic energy to travel from the source to a geophone. These first arrival times are determined for all geophones of the spread and are used to determine the velocity of seismic waves in the subsurface.

For the P-wave seismic refraction surveys, 48 vertical component 10 Hz geophones with 2 m spacing were used. The whole length of each survey line is covered using a 24-geophone roll-along. Data were collected with a sample interval of 0.125 msec and a record length of 2 sec. Shot records were collected 1 m offset from the first and last geophones and in between all geophones.

Depending on the quality of the data, multiple shot records might be obtained at one location and added together to increase the signal to noise ratio. An 8 lbs sledgehammer was used as a seismic source. Rayfract^{TM}, commercially available software, was used for the inversion of all seismic refraction data. Surfer^{TM}, commercially available imaging software, was used to build the tomograms after processing with Rayfract^{TM}. After first arrival times are picked, an inversion technique is implemented and a 2-D velocity tomogram is obtained which is a station location (distance) versus depth image showing the velocity distribution in the subsurface. The velocity tomogram is plotted using color scales depending on the value of the velocity obtained for each grid after processing the first arrival times. In addition to the velocity tomogram, a ray coverage tomogram, a plot showing the number of rays passing through the grids used to obtain the velocity tomogram is obtained. A high number of ray coverage is an indication that more rays traveled through that area of the subsurface. Low ray coverage on the other hand is an indication that the rays avoided to travel through that location and took a preferred high velocity path in the surrounding subsurface.

In this study, the electrical resistivity method is used to study the distribution of electrical properties in the subsurface by injecting electrical current and measuring the induced potential at various locations along the ground surface. The final product is a 2D distance versus depth electrical resistivity distribution tomogram. Electrical resistivity surveys were conducted using 112 electrodes with 1 m spacing. Dipole-dipole electrode configuration was chosen. Case (2012) showed that the dipole-dipole electrode configuration has a higher sensitivity to horizontal changes, depth of investigation, and horizontal data coverage. The whole length of each survey line is covered using a 56-electrodes roll-along. EarthImager 2D, a commercially available inversion software, was used for the inversion and imaging of all the electrical resistivity data.

RESULTS

Both the P-wave seismic refraction and electrical resistivity surveys were conducted along three 478 m long lines. Figure 3(a) shows the location of the three survey lines and the sand boils. Survey line 1 is on the water side of the levee, survey line 2 is on the berm of the levee and between the levee and the first sand boil, survey line 3 is on the landside of the levee and between the first sand boil and the two sets of sand boils. Each survey line starts at the northern end and progresses southward parallel to the levee.

To cover the entire 478 m length of each survey line, eight roll-along spreads for the seismic refraction and six roll-along spreads of electrical resistivity surveys were conducted. In this paper, results from three locations (rolls) along each line will be presented. The three selected locations are shown in Figure 3(b). These locations are chosen because they show anomalies that might be associated with a pathway for seepage responsible for the formation of the three sand boils on the land side of the levee.

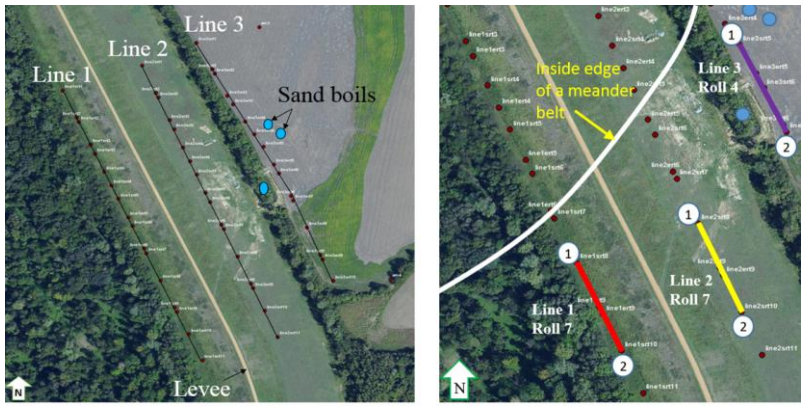

Figure 3 (a) Location of P-wave seismic refraction and electrical resistivity survey lines, (b) Seismic refraction and electrical resistivity survey lines

The white line in Figure 3(b) represents the inside edge of a meander belt from an old river channel composed of complex deposits and sedimentary structures. Figure 4(a) represents a typical cross-section of a meander belt (Saucier, 1994). The cross section shows that the old river channel is filled with vertical structures of medium-course sand and gravel at the bottom, fine-medium grained sand in the middle, and a very fine grained silt and sand at the top. There is a ridge and swale formation in the top silt and sand layer with swale fill clays. There are also clay drapes in between each vertical structure. Measuring from the edge of the natural levee the ridge and swale formation ranges from 6m to 9m of depth. The depth from the bottom of the ridge and swale formation to the bottom of the old river channel is site specific and ranges from 18m to 24m.

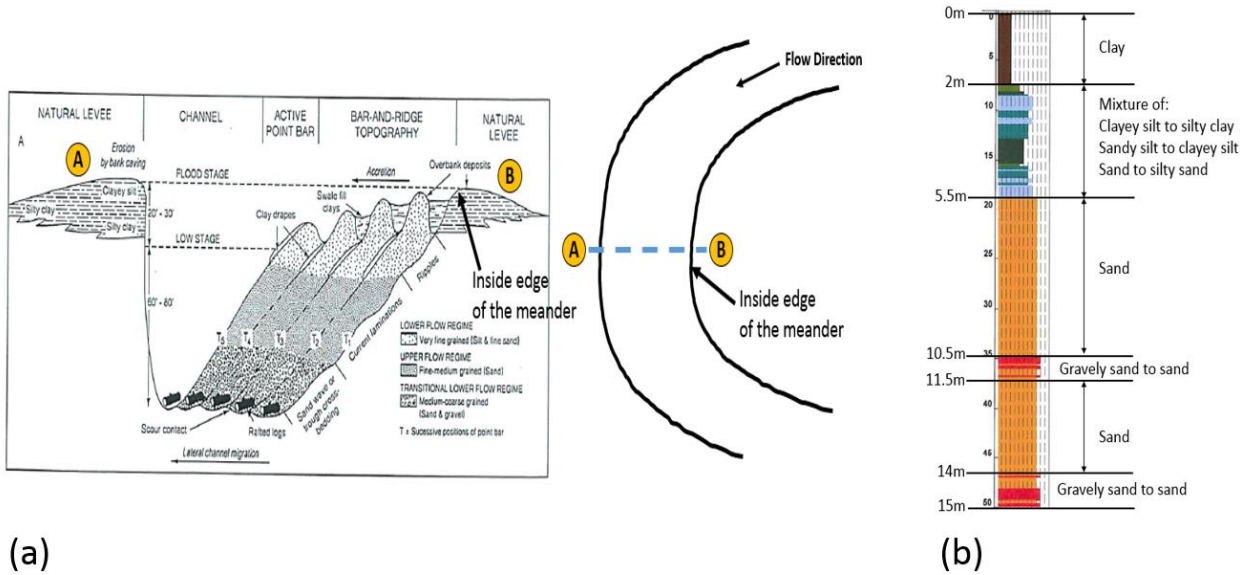

Figure 4 (a) Cross-section of a typical meander belt (Saucier, 1994), (b) An example of borehole information, modified from Brackett (2012)

An example of borehole information close to the three survey lines and inside the meander belt is shown in Figure 4(b). The borehole goes to a depth of 15m (50ft). Considering the 2m clay layer on the top is natural soil deposit after the ridge and swale formation, the bottom of the borehole lies just below the ridge and swale formation and inside the fine-medium grained sand layer in the middle.

After the 2011 flood event, the U.S. Army Corps of Engineers (USACE) mitigated the problem with an installation of water relief wells on the landside of the levee at the end of the apron (berm). Ground water elevation readings from all the relief wells were measured alongside geophysical measurements. Figure 5 shows the average ground water elevation based on the well readings and the above sea level (ASL) elevations of the three survey lines. Based on the ground water elevation shown in Figure 5 and the borehole information in Figure 4(b), the sand layer is fully saturated.

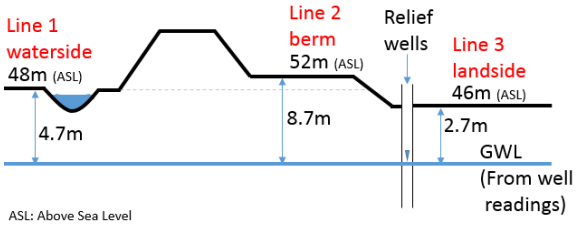

Figure 5 Ground water elevations from well readings

P-wave seismic refraction data was processed using a travel (arrival) time plot analysis for the survey on the water side. Water saturated soils commonly have p-wave seismic velocity of 1500m/s or higher. Based on the travel time plot analysis shown in Figure 6, the subsurface is interpreted to be a two-layer structure. The depth of the water saturated soil with a P-wave velocity of 1667m/s is at a depth of about 8m. The saturated zone predicted from the seismic data is much deeper than one on predicated based on the ground water elevation from the well readings.

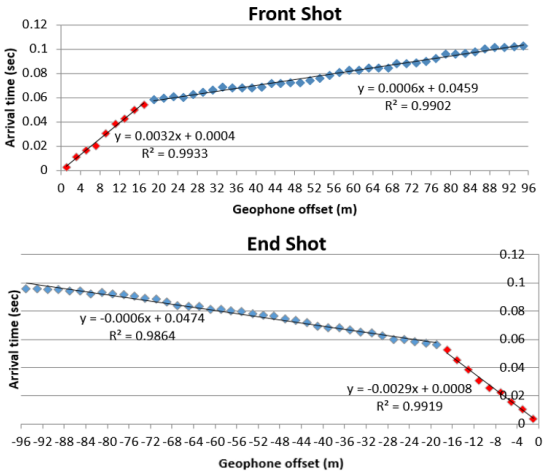

	front shot	end shot	average
Vp1 (m/s)	312.5	344.83	328.665
Vp2 (m/s)	1666.67	1666.67	1666.67
Z1 (m)	7.69	7.94	7.815

Figure 6 Travel time plot analysis for survey line 1 (336m to 430m)

Based on the depth of the 2nd layer obtained from the travel time analysis, an initial model for tomography processing is produced with the 1666m/s is close to 8m (Figure 7). The resulting P-wave velocity tomogram in meters/second is shown on the right of Figure 7. There are two velocity anomalies with lower velocity between 15m and 25m of depth annotated with the box.

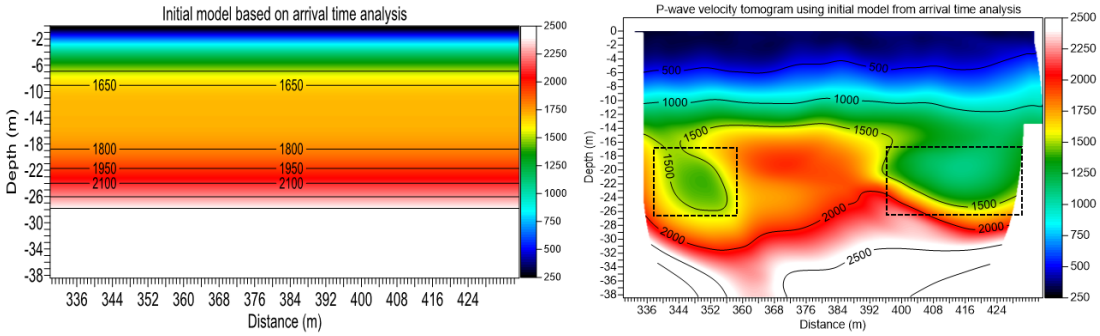

Figure 7 Initial model based on arrival time plot and associated velocity tomogram.

The same survey location in Figure 7 (336m – 430m) is processed again using the 1D-gradient smooth initial model obtained from Rayfract™. Figure 8 shows the Rayfract™ initial model on the top and the associated velocity tomogram on the bottom left and the ray coverage on the bottom right. The velocity tomogram shows similar features to the velocity tomogram in Figure 7 except for the less pronounced anomaly on the left. This indicates that the tomography results are not controlled by the initial model. RayfractTM generated initial models are therefore used for all refraction processing.

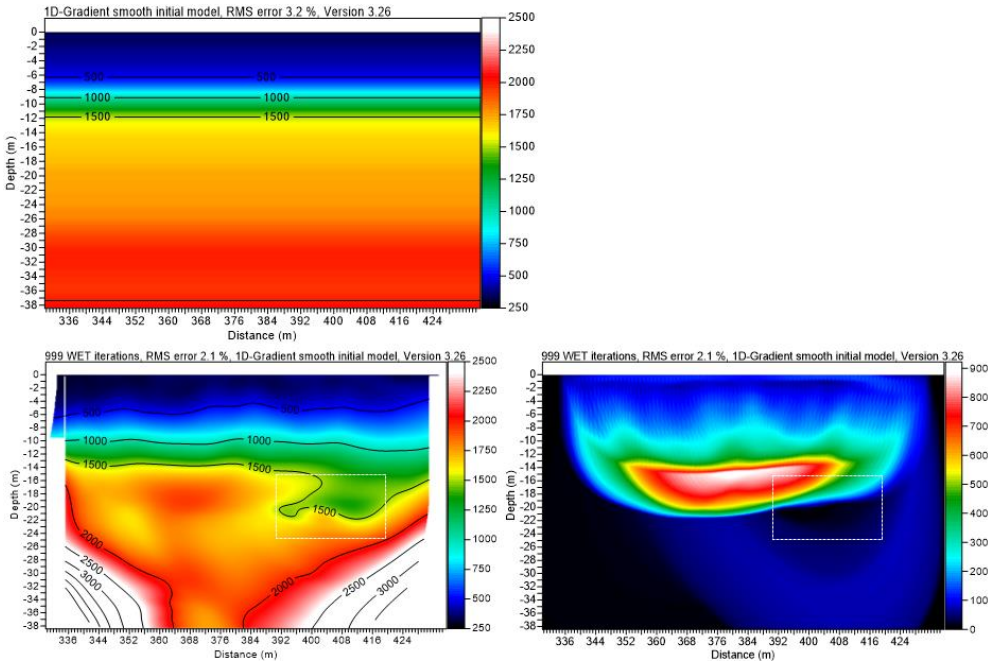

Figure 8 Rayfract™ initial model and inversion results

The velocity tomogram in Figure 8, indicates a P-wave velocity ranging from 350 m/s near the surface to 3000 m/s at 34 m below the surface. Comparing to the borehole information, suggest that the soil between the surface and the 500 m/s contour is clay at the top overlying a mixture of clayey silt to silty sand. Below the 500m/s contour line it is mostly sand. The 1500-1800 m/s P-wave velocity is usually used as indicator of ground water level, because the speed of sound in water is close to 1500 m/s. Seismic interpretation based on the velocity tomogram indicates that the saturated zone is at a depth of around 14m for the first half of the survey line. This depth is in much deeper to what would be predicted from the well readings.

With increasing depth, elastic properties such as bulk modulus will increase due to the added compaction of the overburden pressure (effective stress). An increase in bulk modulus with depth will cause an increase in P-wave velocity with depth. However, lithology can have an effect. Unsaturated sand is expected to have a lower P-wave velocity compared to clay due to high porosity and low bulk modulus. There is a pull down in the 1500 m/s velocity contour annotated with the white box in Figure 8. This location has a lower velocity compared to adjacent material at the same depth. The same location is indicated on the ray coverage tomogram (shown on the bottom right of Figure 8) with an area of low ray coverage. A combination of low P-wave velocity and low ray coverage is an indication of weak compaction or possible void formation due to an internal erosion (washing out of fines) caused by seepage. Seismic waves travel through a preferred path of high P-wave velocity, which can be associated with good compaction (high bulk modulus). When seismic waves encounter low velocity zones, they travel through surrounding areas with higher velocity zones and do not go through the low velocity zones which leads to the formation of localized low ray coverage areas as shown in Figure 8. Another possible reason for the low velocity area could be a zone of high pore pressure causing a decrease in the effective stress of the area and therefore dropping the velocity.

The results for the seismic surveying on the berm of the levee are shown in Figure 9. The P-wave velocity tomogram is on the left and the ray coverage tomogram on the right for. The above sea level elevation of the berm (line 2) is 4 m higher than the elevation on the waterside (line 1). This is due to the 4 m sand layer used for the construction of the berm. The water table indicated by the 1500 m/s contour line is at a deeper depth of 20m which is located 2m shallower on survey line 1. There is an anomaly of low velocity and low ray coverage indicated within the white box. The depth of the anomaly is too shallow to be seepage path associated with the sand boil formation.

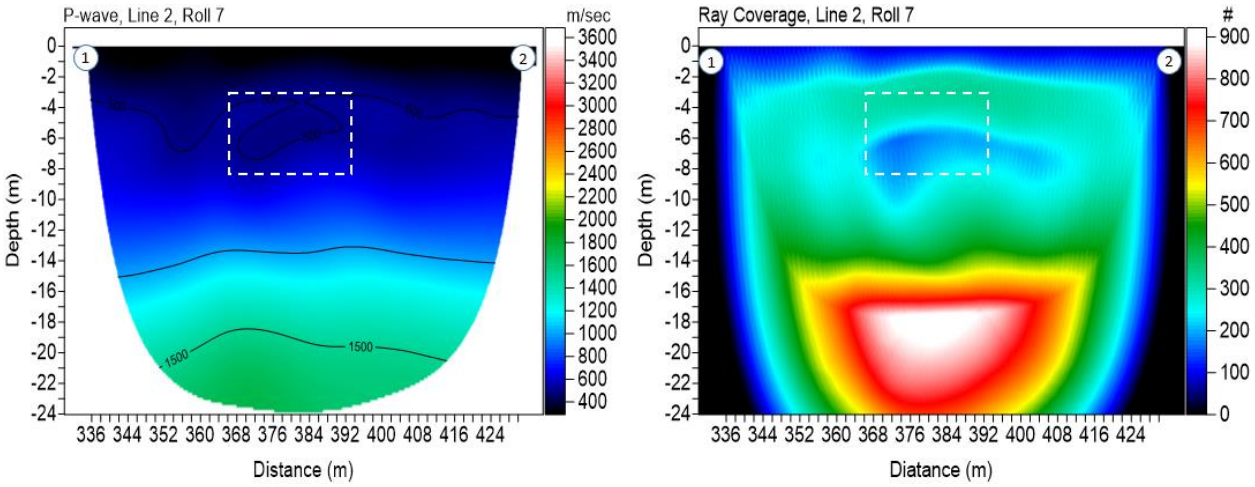

Figure 9 P-wave velocity (left) and ray coverage tomogram (right) for Line 2 (336m – 430m)

The results of the p-wave seismic refraction survey on the landside of the levee, line 3 (192m – 286m), is shown in Figure 10. The p-wave velocity tomogram is on the left and the ray coverage tomogram on the right. Surface elevation of survey line 3 is 2m below survey line 1 and 6m below survey line 2. The ground water table (1500 m/s contour line) is located at a depth of 13 m which is consistent with the observation on the other seismic surveys. The white box indicates an anomaly with a low P-wave velocity and low ray coverage which we interpret as an indication of a weak zone in the subsurface.

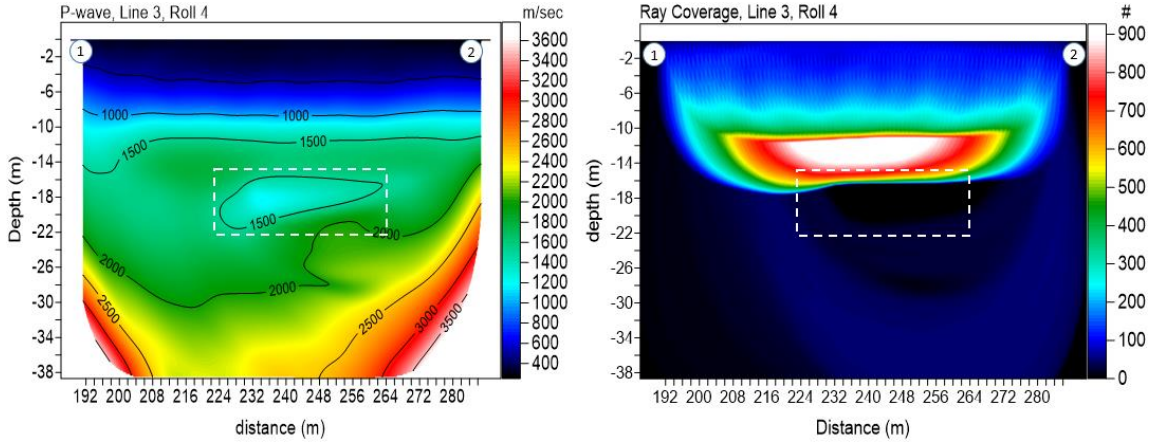

Figure 10 P-wave velocity (left) and ray coverage tomogram (right) for Line 3 (192m - 286m)

The electrical resistivity tomogram for Line 1 (336m - 430m) is shown in Figure 11. The electrical resistivity values are given in Ohm-m. Borehole information is added on the left of Figure 11 to aid with the interpretation of the result. The broken lines on the figure indicate different layers that are observed based on resistivity values.

In Figure 11, the low resistivity region between the top surface and the first broken line is an indication of the clay and silty sand layer. The same location is indicated in Figure 8 between the surface and the 500m/s contour line. Mavok, Mukerji, and Dvorkin (1998) showed that clays have lower resistivity (higher conductivity) than sands due to their high cation exchange capacity. In sands, electrical conductivity is solely based on the conductivity of the pore fluid; whereas in clays, in addition to the pore fluid electrical conductivity takes place through the charged and interconnected surface of the clays.

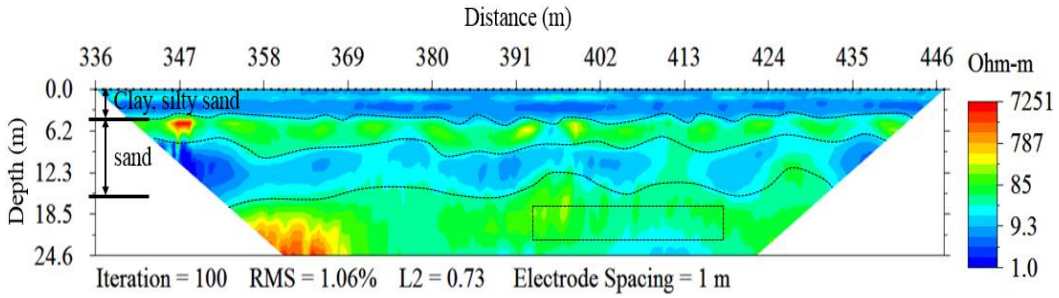

Figure 11 Electrical resistivity tomogram for Line 1 (336 m - 448 m)

The borehole indicates sand at depths greater than 5m. The resistivity data shows a layer between 4m and 8m consistent with sand. However, there is a drop in resistivity to 5-10 Ohm-m within the sand zone at a depth of 8m. Calculation using Archie's first law was made to check if such a low velocity in the sand layer can be achieved by a fully saturated clean sand. Using an electrical resistivity of 15 Ohm-m for the pore fluid and cementation factor for sand between 1.8 and 2, it requires unrealistic porosity to achieve a resistivity lower than 10 Ohm-m for clean sand only due to saturated water. This suggests that there must be a mixture of clay in the sand layer not indicated in the borehole information. The low resistivity structure may be due to the swale fill clays in the vertical structure of the meander geomorphology. The black broken box in the resistivity tomogram indicates the location of the seismic anomaly shown in Figure 8. There is no anomaly at that location indicating a possible location of seepage.

The electrical resistivity survey on the berm of the levee did not yield usable information due to high noise in the data. This problem is due to the high contact resistance of the top dry sand layer. Electrical resistivity survey works when there is good contact between the electrodes and the ground. Attempts were made to reduce the contact resistance by pouring salt water around the electrodes but only slight reduction around the electrodes was observed which did not improve the overall quality of the data.

SUMMARY

Multiple geophysical methods were conducted at the Francis Levee site. In this paper, part of seismic refraction tomography and electrical resistivity tomography results that focus on identifying seepage paths responsible for sand boil formations were presented.

Although electrical resistivity surveys are not completed as planned, results from seismic refraction tomography show an indication of a possible seepage path that can be associated with the three sand boil formations. The location of low P-wave velocity and low ray coverage anomalies observed in the seismic refraction results are shown with the green circles in Figure 12. A possible seepage path is drawn by connecting these anomalies. The three sand boils indicated with the blue circles are in close proximity to the estimates seepage path. It should be noted that the seepage path is perpendicular to the levee and follows the trend of the meander belt. Flow path parallel to the meander is expected because the soil deposit inside the meander has low compaction and high permeability compared to the native ground. Water can flow through the highly permeable sand and gravely sand and cause sand boil formations at locations where the overburden clay layer is thin.

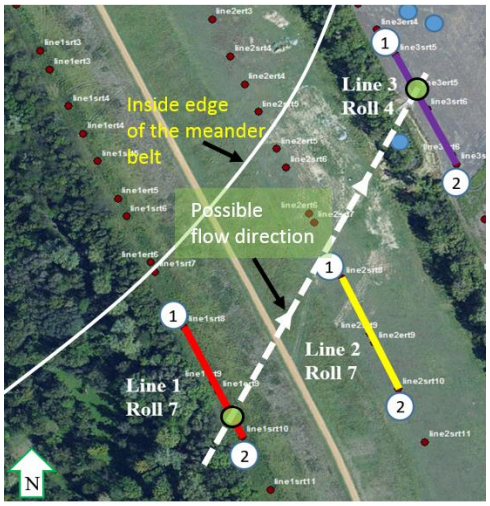

Figure 12 Possible seepage path

It is possible that water flows from the waterside to the landside through the path shown in Figure 12. At places where the overburden clay layer is thin above the seepage path, water can flow to the surface causing sand boil formations.

REFERENCES

Al-Fares, W., (2014) "Application of Electrical Resistivity Tomography Technique for Characterizing Leakage Problem in Abu Baara Earth Dam, Syria," International Journal of Geophysics, 2014, Article ID 368128.

Bedrosian, P. A., Burton, B. L., Powers, M. H., Minsley, B. J., Philips, J. D., and Hunter, L. E., (2012), "Geophysical investigations of geology and structure at the Martis Creek Dam, Truckee, California," *Journal of Applied Geophysics*, 77, pp. 7-20.

Case, J., (2012). "Inspection of Earthen Embankment Dams Using Time Lapse Electrical Resistivity Tomography," ProQuest Dissertations and Theses, 51-01, 124p.

Chinedu, A. D., and Ogah, A. J., (2014), "Electrical resistivity imaging of suspected seepage channels in an earthen dam in Zaria, North-Western Nigeria," *Open Journal of Applied Sciences*, 3, pp. 145-154.

Cho, I., and Yeom, J., (2007), "Crossline resistivity tomography for the delineation of anomalous seepage pathways in an embankment dam," *Geophysics*, 72, pp. G31–G38.

EarthImager™ 2D Resistivity Inversion Software Instruction Manual, Version 2.4.0, 2007.

Kearey, P., Brooks, M., (1984). An Introduction to Geophysical Exploration, Blackwell Science, Oxford.

Kim, K. Y., Jeon, K. M., Hong, M. H., and Park, Y., (2011), "Detection of anomalous features in an earthen dam using inversions of P-wave first-arrival times and surface-wave dispersion curves," *Exploration Geophysics*, 42, pp. 42-49.

Lin, C. P., Hung, Y. C., Wu, P. L., and Yu, Z. H., (2014), "Performance of 2-D ERT in investigation of abnormal seepage: a case study at the Hsin-Shan earth dam in Taiwan," Journal of Environmental and Engineering Geophysics, 19, pp. 101-112.

Mavko, G., Mukerji, T., Dvorkin, J., (1998). The Rock Physics Handbook, The Rock Physics Handbook. Cambridge Univ. Press, Cambridge.

Moustafa, S. S., Ibrahim E. H., Elawadi, E., Metwaly, M., and Agami, N., (2012), "Seismic refraction and resistivity imaging for assessment of groundwater seepage under a dam site, southwest of Saudi Arabia," *International Journal of the Physical Sciences*, 7, pp. 6230-6239.

Nimrod, P., (2011). 2011 Flood Report, A Success Story, Mississippi Levee Board.

Rayfract™ Standard License Version 3.26, Instruction Manual, Intelligent Resources Inc., 1996-2006.

Sjödahl, P., Dahlin, T., Johansson, S., and Loke, M. H., (2008), "Resistivity monitoring for leakage and internal erosion detection at Hällby embankment dam," *Journal of Applied Geophysics*, 65, pp. 155–164.

Saucier, R. T., (1994), Geomorphology and quaternary geologic history of the lower Mississippi valley, U.S. Army Engineer Waterways Experiment Station, Volume 1.

Uyank, O., (2011). "The Porosity of Saturated Shallow Sediments from Seismic Compressional and Shear Wave Velocities," Journal of Geophysics, 73, pp. 16-24.

A SIMPLIFIED BATHYMETRIC SURVEY SYSTEM USING A MODIFIED SOUNDER GPS

Theodore L. Huscher, P.G., Geologist and David Griffith, Water Quality Specialist, USDA-Natural Resources Conservation Service, Lincoln, NE

Abstract

Nebraska NRCS improved the accuracy of bathymetric reservoir surveys and simplified field data collection and data analysis used to calculate sedimentation rates and stage storage determinations for dam rehabilitation work, using a sonar-based depth finder GPS unit with 3-D recording/mapping capability. Portability of the unit and set-up time was improved by mounting the unit's monitor and external antennae onto the lid of a standard 5-gallon bucket. The bucket provides cable storage and protection until used. The unit and battery were modified to use vehicle power adapters, resulting in a readily chargeable and transportable system that is easily set up for field use by a two-person field crew, rather than previous method requiring three or four persons, adding efficiency of operation. With proper software, data are translated into an up-to-date survey of reservoir bathymetry. Data must be corrected for the depth of transducer below water level, the measured reservoir water level, and errant shallows readings caused by minimal depths or false shallow readings due to signal reflection off vegetation. Shallows, vegetation, and other non-germane features are visually confirmed in the field before data synthesis in the office. Technical aspects of system set up, and advantageous features, use of the equipment, helpful suggestions and cautions are highlighted, presenting optimal utilization of this system.

PRACTICE AND PROCEDURES

The Nebraska USDA-Natural Resources Conservation Service (NRCS) adapted a Garmin GPSmap 536s[1] sounder/depth finder system to a standard 5-gallon bucket lid-mount for quicker, more efficient bathymetric survey data collection (Figure 1). This system provides for ease of transport, set up and storage (Figure 2), and needs only a boat and two people to operate (Figure 3). Utilizing a high sensitivity global positioning system (GPS) receiver and dual-beam transducer (sonar transponder) (Figure 4) to plot location and water depth, the system transfers stored data using a Secure Digital (SD) card for rapid download to a computer. Data processing involves opening the *.adm file extension, and loading it into the MapSource® software program, transferring it and saving the data as a text file.

[1] The use of trade names of all commercial products mentioned in this paper shall not be construed as endorsements by the USDA-NRCS of these products. They are presented for informational purposes only.

Figure 1 5-gallon bucket lid-mounted Garmin GSPmap 536s sounder/depth finder system. Transom mount (at right) resting on bucket lid.

Figure 2 Depth finder system components: Garmin GSPmap 536s sounder/depth finder, dome antennae (both mounted on bucket lid), battery charger with vehicle adapter plug, 12V battery with vehicle adapter socket, and transducer clipped to bucket rim. Top of transom mount visible at lower right. The Garmin monitor cover shown removed at lower middle.

Figure 3 Manual depth readings are used to verify depth finder readings. This is done to confirm depth finder accuracy and/or determine the need for a correction factor.

Figure 4 Transducer (lower left) shown where it is to be bolted to the bottom of the transom mount and depth adjusted on site. External GPS antennae shown mounted to bucket lid.

The text file is cut and pasted into an Excel spreadsheet, processed and saved as a *.csv file extension format for import into the ESRI ArcMap GIS program. ESRI ArcMap is used to analyze the data and display the map. The shoreline is digitized from the National Agricultural Imagery Program (NAIP) imagery. The *.csv file can be imported and overlaid onto the imagery. The 3D Analyst routine in ArcMap is used to create a Triangular Irregular Network (TIN) of the data points and the shoreline (Figure 5). The TIN creates bathymetric contours and enables calculation of reservoir volume. Surveyed benchmarks and the inlet riser structure elevation serve as points of known reference. Shoreline points serve as the zero contour to tie bathymetric data to the surrounding ground topography (Figure 6). The distance of the transducer below the water surface is measured (Figure 3) to provide a plotting correction factor for the data processing phase of the survey.

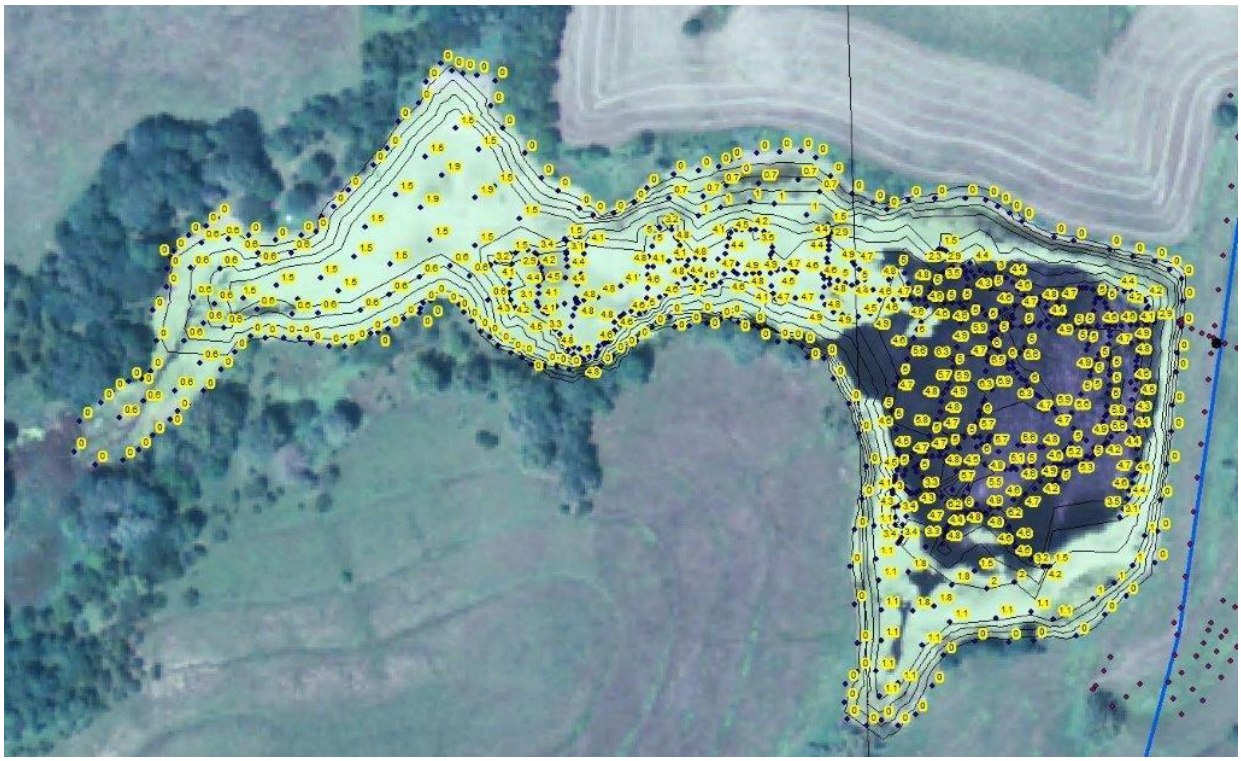

Figure 5 Map of plotted waypoints with extrapolated bathymetric depths, contours and surveyed zero elevation shoreline overlain on current aerial image.

Optionally, a measured keel depth, or a tape measurement of the (negative) distance from the transducer to the water line, can be entered allowing the unit to correct the transducer depth directly for that survey. Errant shallow depths, below the instrumentation sensitivity threshold, and the occurrence of vegetation that may obscure or influence bottom depth readings are corrected during the data rendering (smoothing) phase of the survey plotting. These corrective measurements should be confirmed during the survey by measuring the water depth to reservoir bottom, and top of vegetation, from water level using a range pole, survey rod or survey grade GPS, recorded, and compared to the depth measurement displayed on the unit (Figures 3 and 7).

Figure 6 Shoreline survey using survey grade GPS system provides a zero depth for bathymetric survey.

Figure 7 Wadable lake bottom surveyed with GPS, extending to depth/shoreline. This is the preferred way to confirm location and depth to adjust and correct depth finder readings if necessary.

The system allows for use of two people in the field; a boat driver and bathymetric survey equipment operator. Using two people provides for safety, increased speed, accuracy, and efficiency in conducting a bathymetric survey, as opposed to using a smaller or larger team. The team coordinates to prepare the boat for launch, system set up, adjusting the transducer to a transom mount assuring a proper and equipment safe reading depth, and connecting the transducer cable to power (Figures 8 through 13). Once powered up the unit requires a short time to acquire a satellite signal. A calm weather day on the water is preferred for more accurate data collection as well as general boating safety.

Figure 8 On-shore preparations. Transducer connected to transom mount (lying on its side on back seat of boat) with cable electrical running to depth finder mounted to bucket lid. Survey rod, used to confirm depth against finder reading, is shown at boat's starboard side.

After the transducer is in place, the desired chart/sonar split-screen readout is selected to simultaneously show geographic location and depth to bottom (Figure 14). A pre-loaded (or integrated) U.S. inland lakes map can be used to indicate nearby features and landmarks. However, shoreline accuracy is questionable and should be monitored visually. Signal reception is greatly enhanced with the use of the external GPS antennae, with the bucket lid serving as a convenient location for mounting (Figures 2, 4, 8 and 12). Heading and north arrow are also displayed and, once moving, boat speed by GPS as well. A minimum depth warning signal can also be programmed into the system.

Figure 9 Transom mounted transducer about to be lowered into water.

Figure 10 Close-up of transducer mounted to transom mount, about to be lowered into water and then depth adjusted.

Figure 11 Transom mount screw clamp being tightened and transducer adjusted to proper reading depth. The transducer depth is then measured from the water surface (and recorded as a correction factor).

Figure 12 Cable connection from depth finder (right) to transducer cable (left).

Figure 13 Power cable connection from depth finder plug (right) to 12V battery socket (middle).

When operating the system on the water, the forward facing boat driver watches for hazards, steering the boat for complete coverage of the reservoir pool using landmarks where possible. The backward facing unit operator collects depth data by marking waypoints with the unit, checks for measurements coverage and data gap filling via the unit's map display, calls out displayed depths to let the driver know when shallows approach and monitors areas behind the boat. This arrangement allows for ready communication between boat driver and unit operator to coordinate efforts and concerns.

There are many advantages to this system. The chart/sonar split-screen display allows for real-time situational monitoring in three dimensions and improves overall reservoir bathymetry coverage (Figure 14). The recording of depth measurement points or waypoints is simplified by toggling back to split-screen depth and map view to observe the locations of recorded waypoints. This process simultaneously facilitates selection of the next waypoint while monitoring depth to avoid shallows. The real time read out also allows the unit operator to readily see where the boat is located and to notify the boat driver which direction to drive the boat to complete coverage of the area while the boat driver watches for visible hazards such as potential emergent structures, vegetation, trees, stumps or known or suspected shallows. Waypoints can be collected as frequently as desired without requiring the boat to stop. Map scale can be adjusted for fine-tuned gap filling by zooming in and out. A scale bar and distance display show the current map scale setting.

Figure 14 Dual display depth finder monitor readings of location, heading (top) and depth (bottom).

Shallow depths of approximately one foot or less should be avoided because they are insufficient for signal rebound and accurate reading by the transducer. Shallow water causes the unit to repeat the most recent shallowest depth, alerting the unit operator by blinking a continuous single depth reading, e.g., 0.9 foot, and the unit's depth recording capability is thus frozen. Waypoint recording should be halted and the depth noted so the erroneous data can be adjusted later. To return the unit to normal operation, the system is then taken to water deep enough to provide signal reception to clear the sonar. Generally water depths approaching four feet will suffice to auto reset the unit. Waypoint recording may then resume. Mud-churned waters may also cause the signal to be interrupted or to erroneously read as too shallow. These errant depth readings and time it takes to reset the unit can greatly increase the time needed to conduct a bathymetric survey in the field and data correction back at the office.

If a shallow water alarm depth is not programmed into the unit prior to commencement of the field work, attention must be paid when the depth reading begins to blink on the display. Calculating a reasonable warning depth alarm-level may take some trial and error through exploring shallower areas to determine the minimum depth resulting in the sonar fouling. By adding an additional "cushion value" to the established minimum depth for an accurate measurement, more time is available to maneuver away from the shallows when the shallow

water alarm is activated as the system alerts the crew to the hazard. This results in minimizing unnecessary delays and maximizing field time productivity.

Monitoring current depth read outs is critical to look for drop offs, channels, and to avoid shallows, the latter of which can cause problems for the boat motor propeller and sonar system. The display scrolls the "bottom" surface across the screen while reading depths and adjusting the scale when greater depths are encountered. An alert team is one that monitors shallows both visually from the boat and by watching the unit's depth display. Hazards are thus avoided and the survey will proceed in an overall safer and more time-efficient manner.

If sonar reflects off benthic aquatic vegetation rather than the bottom, an erroneous (too shallow) depth reading may result. Conducting periodic soundings with a measured weighted line or survey rod can help validate bottom depths while measurements from the water surface to the top of the plants can help determine an average height of subaqueous vegetation (Figures 3 and 7). A correction factor can be calculated accordingly where depth measurements appear to be too shallow due to vegetation reflection readings. This correction factor must be added later into the bathymetric survey plot with special attention to areas with vegetation that are visually confirmed and noted, as previously discussed.

The internal storage capacity of the lidded 5-gallon bucket allows for a convenient, mostly buoyant place to store cables, the 12 volt dry cell battery, operator's manual, tape measure and charger (removed before taking into boat) (Figure 2). The lid-mounting of the system monitor and external GPS antennae (Figures 1 and 2) provides a ready-made recording station for the seated unit operator. The 12-volt dry cell battery can be wired to a vehicle power outlet (socket or "female") adapter (Photo 13). Some commercially available 12-volt battery chargers come with a versatile quick connect harness adapter for use with a vehicle power adapter "male" plug. The depth finder unit's power wiring harness can be wired to terminate as a vehicle power adapter plug. This battery adapter system provides for greater versatility for charging the battery in the office, on the road or in the field from a vehicle's power outlet. It also enables quick connection to the depth finder unit.

RESULTS

Nebraska NRCS bathymetric surveys were previously conducted by a three person boat crew consisting of; a boat driver, a technician to type depth measurements into a survey grade GPS rover unit as soundings were called out by a third person using a survey rod to sound the bottom. Often a fourth person was needed onshore to set up and guard a GPS base station reception unit to prevent tampering or theft. The previous system also required a near or complete stop of the drifting boat to obtain an accurate depth sounding measurement and GPS fix to establish location, all of which added time to complete the field survey data acquisition.

The changes implemented simplify how Nebraska NRCS conducts its bathymetric reservoir surveys. The time required conducting surveys, and the number of necessary personnel is dramatically reduced. The streamlining of data collection, and utilization of state-of-the-practice sonar equipment result in a significant increase in time efficiency, improve personnel safety in the field, and more precise bathymetric mapping.

SUBSURFACE HYDROLOGIC EFFECTS ON SEDIMENT DEPOSITION

Zhaoxia Li, Huazhong Agricultural University, Wuhan, CHINA, zxli@mail.hzau.edu.cn
Sayjro Nouwakpo, University of Nevada, Reno, Nevada, snouwakpo@cabnr.unr.edu
Chi-hua Huang, USDA-ARS, W. Lafayette, Indiana, chi-hua.huang@ars.usda.gov

EXTENDED ABSTRACT

Quantification of soil erosion processes has been traditionally focused on soil detachment and sediment transport while efforts in quantifying sediment deposition process are relatively minor. Although soil erosion has been considered as a surface hydrologic process governed by the mechanics and hydraulics of the rainfall and surface flow, there are increasing numbers of literature evidences showing effects of subsurface hydrology on soil erosion processes, some recent examples: Fox et al., 2007; Chu-Agor et al., 2008; Nouwakpo et al., 2010. There are many components of the sub-surface hydrology that may or may not have any impacts on soil erosion. The specific component we are interested in is the near-surface hydraulic gradient which controls whether surface water flows into, i.e., downward drainage, or out of the soil surface (upward seepage). These findings show that as the near-surface hydraulic gradient is shifted from a natural gravity drainage condition to an upward seepage (artesian) condition, soil erosion is greatly enhanced. The question is whether the change in the near-surface hydraulic gradient affects the sediment deposition process.

In a recently published paper from a rainfall simulation study conducted in a laboratory 3.7-m (w) by 9.7-m (l) soil box, we observed the further advancement of the deposition zone when the soil box was free drained as compared to when the box was set to seepage (Nouwakpo and Huang, 2012). This is illustrated here where the deposition areas, shown in green, appeared further into the upper edge of the soil box under drainage (lower graphs) vs. under seepage (upper graphs) (reference here). This graph also shows deeper and more pronounced rills (darker red color) under the seepage condition. The net sediment delivery measured at box outlet supported prior findings of a higher sediment delivery under the seepage condition. Although we have visual evidences of soil profile drainage may have enhanced the development of sediment deposition areas, we need quantitative results to support this observation.

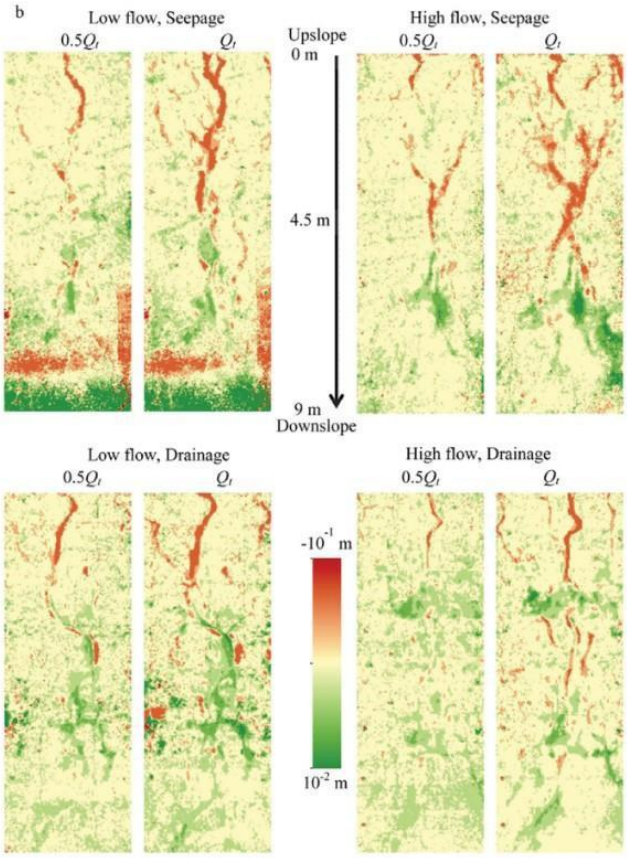

We designed another soil box system specifically to quantify sediment deposition. The box system contains a sediment source box that feeds runoff into a 5-m long rill channel which has water table control to set the rill channel to free drainage, saturation or seepage. The sediment source box and the rill channel have their own programmable rainfall simulator such that the amount of runoff from source box and the study channel can be separately controlled. By regulating the amount of sediment from the source box, the rill channel can have net erosion when the feed sediment at the top of the rill channel is less than the discharged sediment at the outflow end of the channel. Net deposition in the rill channel occurs when the inflow feed sediment is greater than the outflow sediment. For the results shown in this presentation, the rainfall intensities for the feeder box and rill channel were kept constant while the subsurface hydrology of the rill channel was set to one of the following: free drainage, saturation, low seepage (240 ml/m2/min) and high seepage (480 ml/m2/min). For each hydrologic treatment, the amount of feed sediment was varied, by varying the fraction of the feeder box surface covered by a furnace filter, from zero to a maximum rate that the feeder box could generate. Hence, the rill channel went through a transition from net erosion with low sediment feed to net deposition with high sediment feed.

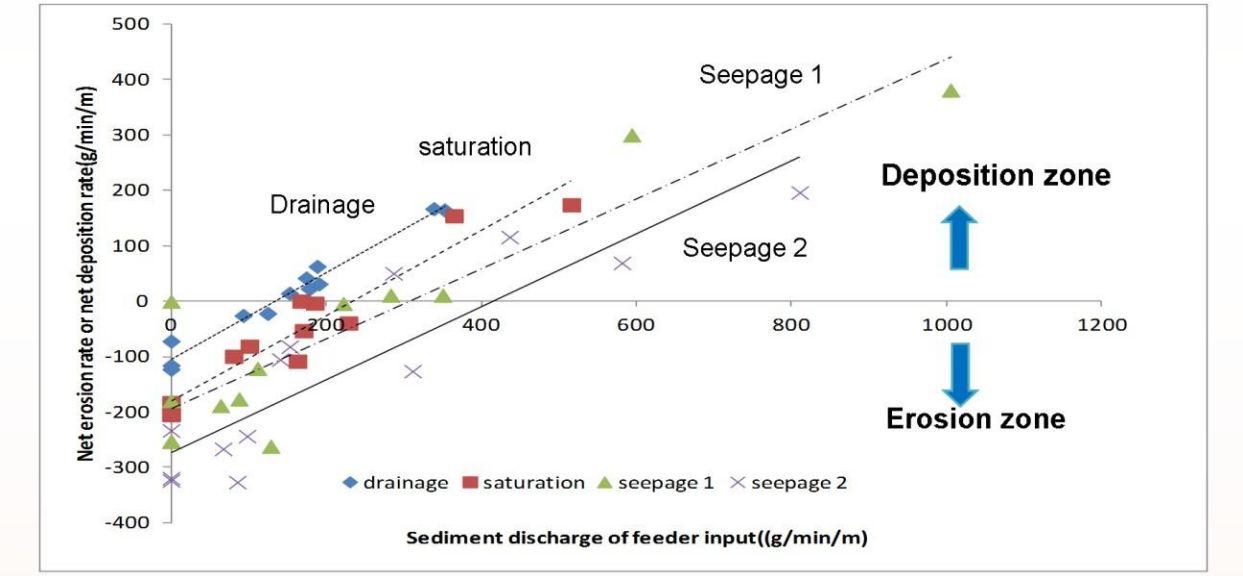

The graph shows the sediment feed rate (x-axis) and net erosion or deposition (y-axis), which is the difference between the feeder input to the rill channel and the rill channel output. As the subsurface hydrology of the rill channel is shifted from drainage, to saturation and seepage, the results show increased erosion and decreased deposition. In other words, soil drainage not only reduces soil erosion, it also enhances sediment deposition. Conversely, saturation and seepage conditions will enhance soil erosion and hinder sediment deposition.

Our results present some challenges in the current thinking of soil erosion processes. If we define the equilibrium sediment discharge as the crossing point from net erosion to net deposition, then this amount increases as the rill channel is shifted from drainage to seepage regime. In our case, the erosion-deposition crossing varies from ~130 to 410 g/m^2/min when the subsurface hydrology changes from drainage to seepage.

In the current erosion model concept, the equilibrium sediment discharge, when neither erosion nor deposition occurs, can be considered the sediment transport capacity, or Tc. However, current concept of Tc is solely based on surface hydraulics and sediment characteristics. In this study, the same soil was used in the feeder box and rill channel, and the same rainfall rate was maintained, hence surface hydraulics and sediment properties were invariant. The challenging question is what is Tc?

The second challenge in current erosion modeling concept is the calculation of sediment deposition. Currently, sediment deposition is based on surface flow hydraulics, sediment characteristics (mainly, size distribution) and sediment concentration. Again, in our research, the sediment property and surface flow hydraulics are somewhat constant. But we show the seepage condition has much greater sediment concentration but much less sediment deposition. Again, this is a deficiency in current sediment deposition equation.

In summary, we have quantified sediment deposition in a rill channel and found the amount of deposition is highly dependent on the subsurface hydrology. Our results show that current process-based erosion modeling concept where erosion and deposition equations based solely on surface flow hydraulics and sediment properties is deficient. It requires a major rethinking on how to incorporate the surface hydrology to properly quantify erosion, deposition, and sediment transport processes on the landscape.

REFERENCES

Chu-Agor, M., Fox, G., Cancienne, R., and Wilson, G. (2008). Seepage caused tension failures and erosion undercutting of hillslopes. J. Hydrol. 359:247–259.

Fox, G., Chu-agor, M., and Wilson, G. (2007). Erosion of noncohesive sediment by ground water seepage: Lysimeter experiments and stability modeling. Soil Sci. Soc. Am. J. 71:1822–1830.

Nouwakpo, S.K., Huang, C., Bowling, L., and Owens, P. (2010). Impact of vertical hydraulic gradient on rill erodibility and critical shear stress. Soil Sci. Soc. Am. J. 74:1914–1921.

Nouwakpo, S.K., and Huang, C. (2012). The role of subsurface hydrology in soil erosion and channel network development on a laboratory hillslope. Soil Sci. Soc. Am. J. 76:1197-1211.

REPRESENTATIVENESS OF SOIL SAMPLES COLLECTED TO ASSESS MINING-RELATED CONTAMINATION OF FLOOD PLAINS IN SOUTHEAST KANSAS

Kyle Juracek, Research Hydrologist, U.S. Geological Survey, Lawrence, Kansas, kjuracek@usgs.gov

INTRODUCTION

Historical lead and zinc mining in the Tri-State Mining District (TSMD), located in parts of southeast Kansas, southwest Missouri, and northeast Oklahoma, has resulted in a substantial ongoing input of lead and zinc to the environment (Juracek, 2006; Juracek and Becker, 2009). In response to concern about the mining-related contamination, southeast Cherokee County, Kansas, was listed on the U.S. Environmental Protection Agency's (USEPA) National Priority List as a Superfund hazardous waste site (fig. 1). To provide some of the information needed to support remediation efforts in the Cherokee County Superfund site, a study was begun in 2009 by the U.S. Geological Survey (USGS) that was requested and funded by USEPA. As part of the study, surficial-soil sampling was used to investigate the extent and magnitude of mining-related lead and zinc contamination in the flood plains of the Spring River and several tributaries within the Superfund site. In mining-affected areas, flood-plain soils had lead and zinc concentrations that far exceeded background levels as well as probable-effects guidelines for toxic aquatic biological effects (Juracek, 2013). Lead- and zinc-contaminated flood plains are a concern, in part, because they represent a long-term source of contamination to the fluvial environment.

An important issue is the within-site representativeness of the surficial-soil samples collected. Specifically, the question is whether or not the samples collected provide an acceptable representation of the lead and zinc concentrations at each site for the purpose of characterizing and comparing sites. The distribution of mining-contaminated sediment on flood plains is determined by several factors including the size and density of the contaminated particles, flood-plain width and topography, flood characteristics (frequency, magnitude, duration), and fluvial geomorphic processes. To evaluate within-site representativeness, additional samples were simultaneously collected to assess within-site variability. In this paper, the specific objectives were to:

(1) Describe the collection and analysis of surficial-soil samples using a 5-point sampling technique;
(2) Describe the collection and analysis of additional surficial-soil samples to assess within-site variability; and
(3) Evaluate the within-site representativeness of the original 5-point samples for assessing mining-related contamination.

DESCRIPTION OF STUDY AREA

The Cherokee County Superfund site is a 115 square mile area located within the TSMD (fig. 1). For about 100 years (1850-1950), the TSMD was one of the primary sources of lead and zinc ore in the world (Brosius and Sawin, 2001). Mining activity in the TSMD ended in the 1970s. Background sediment concentrations of lead and zinc in the Superfund site were estimated by Pope (2005) to be 20 and 100 milligrams per kilogram, respectively.

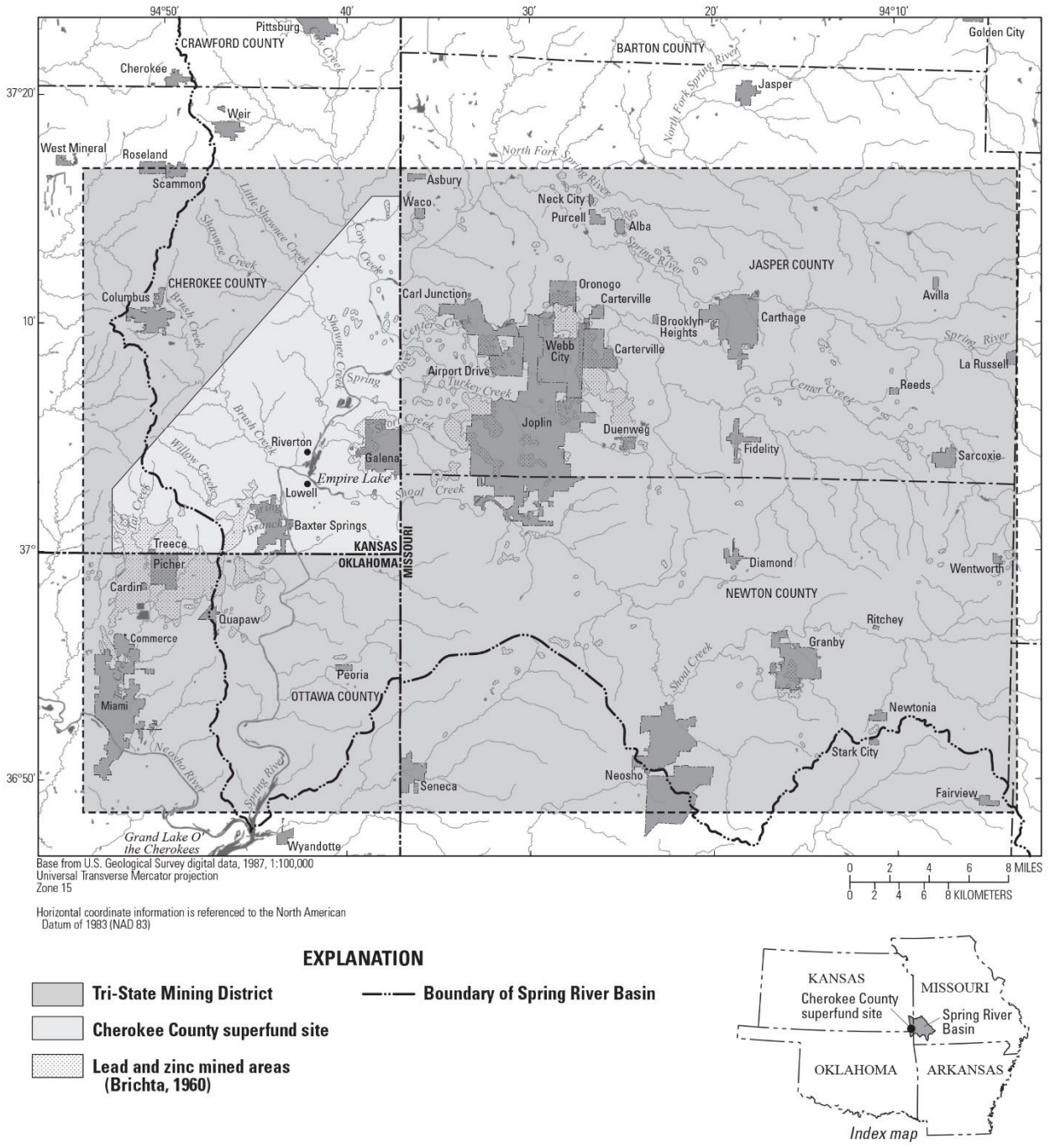

Figure 1. Location of the Spring River and its tributaries, the Cherokee County Superfund site, and lead- and zinc-mined areas in the Tri-State Mining District, Kansas, Missouri, and Oklahoma.

The Superfund site is drained by the Spring River, its tributaries, and Tar Creek. Principal tributaries to the Spring River in Cherokee County include Brush Creek, Cow Creek, Center Creek, Shawnee Creek, Shoal Creek, Short Creek, Turkey Creek, and Willow Creek. Several of the tributaries, as well as Tar Creek, drain areas that were substantially affected by historical lead and

zinc mining (fig. 1). On average, the width of the Spring River flood plain in the Superfund site is about 1 to 1.5 miles. The width of the tributary and Tar Creek flood plains generally is about 0.5 mile or less.

METHODS

As part of a study to assess the extent and magnitude of mining-related lead and zinc contamination (Juracek, 2013), information was obtained through an analysis of surficial-soil samples collected from the Spring River flood plain, tributary flood plains, and the Tar Creek flood plain in the Superfund site. Sampling sites for the Spring River flood plain, as compared to the other flood plains, were selected using different schemes as described below.

Sampling site selection: The selection of surficial-soil sampling sites for the Spring River flood plain involved several steps. First, all one-square-mile sections that were located mostly (that is, at least 50 percent) or completely in the Spring River flood plain were identified using USGS 1:24,000-scale topographic quadrangle maps. Second, the selected sections were divided into quadrants. Third, for each section, a quadrant was randomly selected for sampling. The random-selection process involved the use of coin flips to determine if the quadrant was north or south and east or west. Using this process, either the northwest, northeast, southwest, or southeast quadrant was selected for each section. If the randomly selected quadrant for a section was unusable, either because it was located mostly out of the flood plain or because access permission from the land owner was not granted, the next quadrant was selected using a clockwise rotation. A total of 30 Spring River flood-plain surficial-soil sampling sites were selected. Typically, the flood-plain soil was sampled at the center of each randomly selected quadrant.

Tributary streams for which flood-plain surficial soils were sampled included Brush Creek, Cow Creek, Shawnee Creek, Shoal Creek, Short Creek, Spring Branch, Tar Creek, Turkey Creek, and Willow Creek (fig. 1). Tar Creek is not a direct tributary of the Spring River. It flows into the Neosho River, which subsequently joins the Spring River at Grand Lake O' the Cherokees in Oklahoma. Tar Creek was included because it drains a part of Cherokee County that was substantially affected by historical lead and zinc mining activity (fig. 1). Along each stream, one to three transects were established for the purpose of sampling. Each transect extended perpendicularly away from the channel on one or both sides as dictated by the location of the flood plain and site accessibility. Twenty transects were established. Along each transect, two to four flood-plain sampling sites were selected. The distance between successive sampling sites (when two or more sites were sampled on the same side of the channel) ranged from about 10 to about 300 feet depending on flood-plain width, number of sites, and site conditions. A total of 59 tributary flood-plain surficial-soil sampling sites were selected.

Sample Collection and Preparation: The Spring River flood-plain surficial-soil samples were collected in the fall of 2009. The tributary flood-plain surficial-soil samples (including Tar Creek) were collected in the spring of 2011. All flood-plain surficial-soil samples were collected to a depth of about 1 inch. At each Spring River flood-plain site, the soil was sampled at the selected center location and typically at a distance (hereafter referred to as the sampling radius) of 100 feet north, south, east, and west of the center. This sampling method is referred to as the 5-point sampling technique (fig. 2). For the tributary flood-plain sites, the 5-point technique was used with

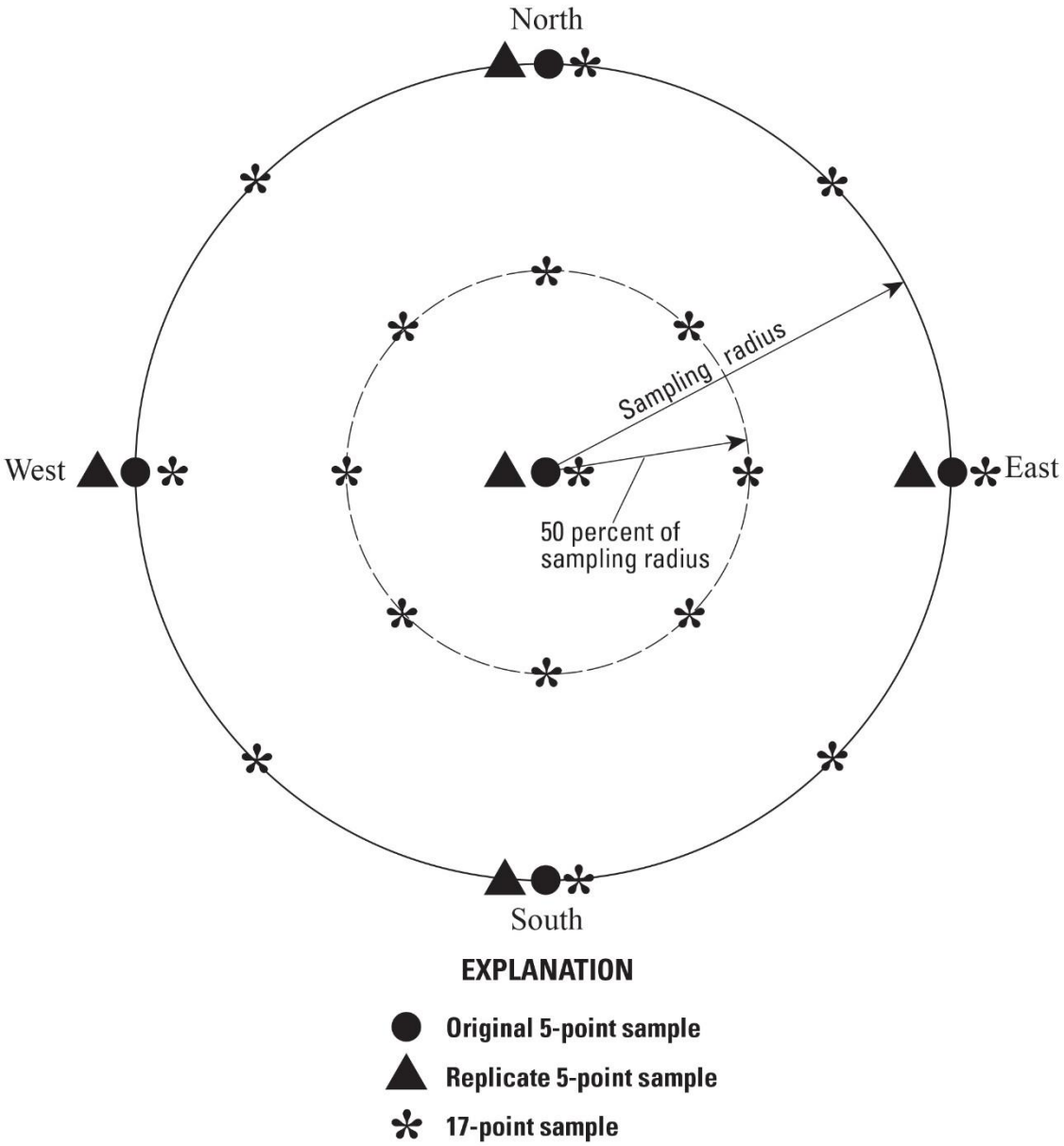

Figure 2. Diagram showing the 5- and 17-point sampling techniques.

a sampling radius that ranged from 5 to 50 feet depending on the width of flood plain available for sampling and the number of sampling sites per transect. Along each transect, samples collected using the 5-point technique were non-overlapping.

At each sampling site, an equal volume of soil was collected at the five locations using a 5-inch long section of cellulose acetate butyrate transparent tubing (2.6-inch inside diameter) that was pushed by hand into the soil. The tubing was thoroughly cleaned with a clean paper towel prior to each reuse. For each site, the soil from the five locations was combined in a plastic bag and transported back to the USGS laboratory in Lawrence, Kansas, for subsequent sample preparation.

Following air drying, each bulk sample was spread out on a clean plastic sheet and all visible organics (for example, plant fragments, seed pods, and roots) were removed using stainless steel tweezers. Each sample was disaggregated using a rubber-tipped pestle until the entire sample passed through a 4-millimeter stainless steel sieve. Then, each disaggregated sample was placed in a glass bowl and homogenized using a plastic spoon to provide a composite sample for each site. All utensils used in sample preparation were thoroughly cleaned with deionized water and wiped dry with a clean paper towel before each reuse.

Sample Collection to Assess Representativeness: To evaluate the within-site representativeness of the 5-point samples collected, two additional sets of samples (each set representing about 10 percent of the total samples collected) were simultaneously collected to assess within-site variability. First, replicate 5-point samples were collected in juxtaposition with the original 5-point samples (fig. 2) at three Spring River and six tributary flood-plain sampling sites. Second, 17-point samples were collected at three Spring River and five tributary flood-plain sampling sites. In the 17-point technique, the soil was sampled at the center and at 100 and 50 percent of the selected sampling radius north, northeast, east, southeast, south, southwest, west, and northwest from the center (fig. 2). Following collection, these additional samples were prepared for analysis in the same manner as the original samples.

Chemical Analyses: The flood-plain surficial-soil samples were analyzed for lead and zinc concentration at USEPA facilities using x-ray fluorescence (XRF) (U.S. Environmental Protection Agency, 2007). All samples were analyzed as bulk samples. The samples collected from the Spring River flood plain were analyzed using a handheld XRF instrument. The samples collected from the tributary flood plains were analyzed using a stationary XRF instrument.

XRF analytical variability was assessed by the triplicate analysis of multiple samples to determine the deviation from the mean concentration. For the Spring River flood-plain samples, the analytical variability for lead ranged from $\pm$2 to $\pm$38 percent with a mean variability of $\pm$17 percent (9 samples). For zinc, the analytical variability ranged from $\pm$2 to $\pm$33 percent with a mean variability of $\pm$11 percent (10 samples). For the tributary flood-plain samples, the analytical variability for lead ranged from $\pm$1 to $\pm$12 percent with a mean variability of $\pm$4 percent (70 samples). The analytical variability for zinc ranged from 0 to $\pm$12 percent with a mean variability of $\pm$3 percent (70 samples). The larger variability for the Spring River flood-plain samples likely was caused, in part, by the use of a handheld XRF instrument.

To assess the comparability of the XRF analyses with another method, split-replicate samples from three Spring River and six tributary flood-plain surficial-soil sampling sites were analyzed at a USGS laboratory for lead and zinc concentration using spectroscopic methods (Fishman and Friedman, 1989; Arbogast, 1996; Briggs and Meier, 1999). For each site, the composite sample was split to provide the original and split-replicate samples. The spectroscopic methods used provided total (at least 95 percent of the element present) rather than total-recoverable concentrations. Analytical variability for the spectroscopic methods was about 10 percent or less (Juracek, 2013).

Overall, including the results for both the Spring River and tributary flood plains, lead and zinc concentrations determined by spectroscopic methods typically were larger. Lead and zinc concentrations for the three Spring River split-replicate samples averaged 55 and 28 percent larger, respectively. Lead concentrations for the six tributary split-replicate samples ranged from 56 percent smaller to 94 percent larger. Zinc concentrations for the six tributary split-replicate samples ranged from 3 to 70 percent larger.

RESULTS AND DISCUSSION

Within-site representativeness of the original 5-point surficial-soil samples was evaluated using two additional sets of samples that were simultaneously collected. On average, lead and zinc concentrations in the replicate 5-point samples collected from the Spring River flood plain were within about $\pm$11 and $\pm$15 percent of the concentrations in the original 5-point samples, respectively (table 1). For lead, the average variability for the replicate samples was computed using only two of the three sampling sites because the lead concentration was less than the XRF limit of detection for one of the original samples. On average, lead and zinc concentrations in the replicate 5-point samples collected from the tributary flood plains were within about $\pm$8 and $\pm$4 percent, respectively (table 1). The larger variability measured for the Spring River samples possibly was caused, in part, by the use of a handheld (as opposed to stationary) XRF instrument for the chemical analyses.

Lead and zinc concentrations in the 17-point samples collected from the Spring River flood plain were, on average, within about $\pm$27 and $\pm$23 percent of the concentrations in the original 5-point samples, respectively (table 1). Lead and zinc concentrations in the 17-point samples collected from the tributary flood plains were, on average, within about $\pm$11 and $\pm$14 percent, respectively (table 1). The larger variability documented for the Spring River 17-point samples may be indicative of greater spatial variability associated with the use of a larger sampling radius. Also, the larger variability for the Spring River samples possibly was caused, in part, by the use of a handheld XRF instrument for the chemical analyses. Finally, the larger variability measured for the 17-point samples, compared to the replicate 5-point samples, may be indicative of the fact that more spatial complexity in flood-plain lead and zinc concentrations is being captured by the 17-point samples.

SUMMARY AND CONCLUSIONS

To assess the within-site representativeness of flood-plain surficial-soil samples collected using a 5-point sampling technique to characterize the extent and magnitude of mining-related lead and zinc contamination in the Cherokee County (Kansas) Superfund site, additional 5- and 17-point samples were simultaneously collected and analyzed. On the basis of the similarity of the chemical results obtained, it was concluded that, for the flood-plain sampling sites selected, the 5-point samples provided representative data for the purpose of assessing lead and zinc contamination.

REFERENCES

Arbogast, B.F. (1996). Analytical methods manual for the Mineral Resource Surveys Program: U.S. Geological Survey Open-File Report 96–525, 248 p.

Brichta, L.C. (1960). Catalog of recorded exploration drilling and mine workings, Tri-State Zinc-Lead District—Missouri, Kansas, and Oklahoma: U.S. Bureau of Mines Information Circular 7993, 13 p.

Briggs, P.H., and Meier, A.L. (1999). The determination of forty two elements in geological materials by inductively coupled plasma-mass spectrometry: U.S. Geological Survey Open- File Report 99–166, 15 p.

Brosius, Liz, and Sawin, R.S. (2001). Lead and zinc mining in Kansas: Kansas Geological Survey Public Information Circular 17, 6 p.

Fishman, M.J., and Friedman, L.C., eds. (1989). Methods for determination of inorganic substances in water and fluvial sediments: U.S. Geological Survey Techniques of Water-Resources Investigations, book 5, chap. A1, 545 p.

Juracek, K.E. (2006). Sedimentation and occurrence and trends of selected chemical constituents in bottom sediment, Empire Lake, Cherokee County, Kansas, 1905-2005: U.S. Geological Survey Scientific Investigations Report 2006—5307, 79 p.

Juracek, K.E., and Becker, M.F. (2009). Occurrence and trends of selected chemical constituents in bottom sediment, Grand Lake O' the Cherokees, northeast Oklahoma, 1940-2008: U.S. Geological Survey Scientific Investigations Report 2009—5258, 28 p.

Juracek, K.E. (2013). Occurrence and variability of mining-related lead and zinc in the Spring River flood plain and tributary flood plains, Cherokee County, Kansas, 2009-11: U.S. Geological Survey Scientific Investigations Report 2013—5028, 70 p.

Pope, L.M. (2005). Assessment of contaminated streambed sediment in the Kansas part of the historic Tri-State Lead and Zinc Mining District, Cherokee County, 2004: U.S. Geological Survey Scientific Investigations Report 2005—5251, 61 p.

U.S. Environmental Protection Agency. (2007). Field portable x-ray fluorescence spectrometry for the determination of elemental concentrations in soil and sediment, method 6200: accessed January 2010, at *http://epa.gov/epawaste/hazard/testmethods/sw846/pdfs/6200.pdf*

Table 1. Lead and zinc concentrations for original 5-point samples, replicate 5-point samples, and 17-point samples collected from the Spring River and tributary flood plains, Cherokee County, Kansas. [mg/kg, milligrams per kilogram; %, percent; <, less than; --, not available. Each parenthetical percentage indicates the difference from the original sample concentration.]

Surficial-soil sample	Lead, in mg/kg	Zinc, in mg/kg
Spring River flood plain		
SRF-1, original 5-point	24	56
SRF-1, replicate 5-point	22 (-8%)	48 (-14%)
SRF-3, original 5-point	<19	78
SRF-3, replicate 5-point	19 (--)	67 (-14%)
SRF-7, original 5-point	21	186
SRF-7, replicate 5-point	18 (-14%)	155 (-17%)
SRF-4, original 5-point	16	53
SRF-4, 17-point	19 (+19%)	45 (-15%)
SRF-9, original 5-point	29	75
SRF-9, 17-point	13 (-55%)	41 (-45%)
SRF-29, original 5-point	47	200
SRF-29, 17-point	50 (+6%)	216 (+8%)
Tributary flood plains		
BC2-2, original 5-point	66	200
BC2-2, replicate 5-point	63 (-5%)	173 (-14%)
CC1-3, original 5-point	55	158
CC1-3, replicate 5-point	45 (-18%)	159 (+1%)
SB2-1, original 5-point	697	3,515
SB2-1, replicate 5-point	638 (-8%)	3,456 (-2%)
TrC1-2, original 5-point	5,363	25,500
TrC1-2, replicate 5-point	4,943 (-8%)	24,900 (-2%)
TkC1-3, original 5-point	475	2,839
TkC1-3, replicate 5-point	483 (+2%)	2,725 (-4%)
WC1-1, original 5-point	210	927
WC1-1, replicate 5-point	218 (+4%)	954 (+3%)
BC1-2, original 5-point	50	90
BC1-2, 17-point	52 (+4%)	118 (+31%)
CC1-2, original 5-point	63	165
CC1-2, 17-point	50 (-21%)	148 (-10%)
ShC2-1, original 5-point	281	2,007
ShC2-1, 17-point	291 (+4%)	1,887 (-6%)
SB2-3, original 5-point	233	973
SB2-3, 17-point	272 (+17%)	1,161 (+19%)
TrC3-1, original 5-point	62	290
TrC3-1, 17-point	69 (+11%)	302 (+4%)

MORPHOLOGICAL EVOLUTION OF FLUVIAL AND ESTUARINE SEGMENT FLOWS

Geraldo Wilson Júnior, Docteur d'Etat, COPPE/Federal University of Rio de Janeiro-UFRJ, Rio de Janeiro, Brazil, jrwilsong@gmail.com;
Mario Grüne de Souza e Silva, M.Sc., COPPE/UFRJ, Rio de Janeiro, Brazil, mariosilva@poli.ufrj.br

Abstract: Fluvial sedimentological equilibrium is reached when the sediment load discharging into a longitudinal segment equals the solid phase leaving that stretch. In such segments, natural and anthropogenic phenomena may occur as, for example, the formation of sand banks and beaches, erosion, mud slumps, silting, formation of meanders, oxbows and riverbed configurations, with expressive ecosystem interferences. In this paper, the following are shown: (i) qualitative and quantitative descriptions of the hydrodynamic, sedimentological, morphological and phytosociologic processes within fluvial and estuarine systems; (ii) validation and modernization of the methodology for hydrosedimentologic studies developed in Brazil; (iii) the importance of land, bathymetric, remote sensing surveying and (iv) application and validation of this methodology in Brazilian open channels systems. Qualitative and quantitative cases are outlined: (1) Sedimentological and morphological aspects of the *Paraguay* River in the *Pantanal of Mato Grosso* State. (2) *Morro Grande* bathymetry estimate of the *Preto* River Reservoir, in the state of *Rio de Janeiro*, using Remote Sensing analysis. (3) Hydrodynamic, sedimentological and morphological aspects of a *São Francisco* River stretch, and (4) the phytosociologic problems carried out by the diversion of the *Macacu* River into the *Guapimirim* River, which cross one of the few remnant mangrove areas in the *Rio de Janeiro* State. Results showed that the periodic land, bathymetric and Remote Sensing surveys are indispensable tools for the qualitative and quantitative descriptions of the sediment movements in open channel flows methodology.

INTRODUCTION

In open channel flows two phases move: a liquid, governed by the laws of Fluid Mechanics and a solid, composed of sediment particles, which moves in contact with the river bed, or in suspension in the middle of the turbulent flow (Wilson-Jr., 2009). When the mass of sediment that penetrates some stretch is equal to the mass that flows out of it in a period of time, it is said that the sedimentological equilibrium was achieved. The size of the stretch and the period of time that characterize this equilibrium define the scales - spatial and temporal - of the morphological process in the stream. In fluvial flows, the equilibrium time scale is a multiple of a hydrological year. The mean longitudinal profile of a river stretch, for example, remains stable during this period of time. However, in the equilibrium segments, natural morphological phenomena of disequilibrium may occur during a hydrological year, as: meandering, sand banks, erosion, mud slumps, cut-off, silting, and others. Sub-stretches of sedimentological disequilibrium appear and advance along the stretch their analysis depending on the spatial scale of observation.

Anthropogenic interferences in the river's bed and on the watershed add up to these phenomena, and must be detached and controlled, because they are capable of modifying the equilibrium conditions of the stretch, with severe consequences to the environment, engineering projects, and specifically to the phytosociological processes.

OBJECTIVES AND STUDIED CASES

The main objectives of this paper are: (i) To consider the concatenation of hydrodynamic, sedimentologic, morphologic and phytosociological processes within fluvial and estuarine systems; (ii) To present a Brazilian methodology for hydrosedimentologic studies in watersheds, (iii) To emphasize the importance of land, bathymetric and Remote Sensing surveys as special measurements to calibrate these studies, and (iv) To apply this methodology in fluvial systems.

Four Brazilian cases were outlined: (1) Sedimentologic and morphological aspects of the *Paraguay* River in the *Pantanal Matogrossense*, MS; (2) *Morro Grande* Reservoir bathymetric estimate using Remote Sensing, RJ; (3) Morphological aspects of a *São Francisco* River stretch, BA, and (4) Phytosociological problems carried out by the diversion of a river into a remnant mangrove area in the *Rio de Janeiro* State.

METHODOLOGY OF SEDIMENTOLOGICAL AND MORPHOLOGICAL PROCESSES

Sediments are placed in motion or have their movement changed by the natural elements' action, e.g. rain, currents, winds, waves, tides; and by human interventions in the river bed and the watershed basin, that sum out with the natural ones, as: dams, navigation, dredging, mining, waste, deforestation, irrigation, sport, leisure and touristic activities (Figure 1). In other words, the sediments are placed in motion or have their movement changed, every time the river bed and watershed suffer an alteration. Then, two types of solid movement can occur in fluvial streams: (i) Movement of sediments from the river bed that either move in contact with the bed most of the time, or in suspension; (ii) Movement of sediments from the watershed basin, mostly carried out by the rain, generating the wash-load. These sediments are finer than the bed load material and are transported in suspension, by the river, through long distances.

Depending on the case, a non-linear relationship between the liquid flow and the bed sediment discharge is possible:

$$q_b = a\, q^{n_s} \tag{1}$$

where q_b = the solid discharge per unit width, in mass, force or volume per time; q = liquid flow, that can be expressed in the same units. a and $n_s > 1$, are positive constants, that depend on the hydrosedimentological characteristics of the river stretch.

However, the wash load movement, which corresponds to the quickest response of the river to the fluvial basin modification, relates directly to the soil loss in the watershed. Thereby, to estimate the solid discharge of river stretches, it is essential to distinguish and to know the sources of sediments that are being transported and spread over the studied reach.

For some decades, Wilson-Jr. (2009) has dedicated himself, through tests in laboratory channels, creeks, brooks, rivers and estuaries, to developing a methodology to characterize sediment motion in open channel flows. This methodology allows the simultaneous application of bathymetric, hydrometric and sedimentometric measurements, the use of tracers (radioactive, chemicals and fluorescent), Remote Sensing and GIS.

According to this methodology, for the sediment motion description in water streams, three steps are necessary (Figure 2) (Wilson-Jr., 1999, 2009): (i) Knowledge of the watershed; (ii) *In-situ* measurements of the solid motion, in a representative reach of the flow, and during these measurements' period; (iii) Determination of the hydrodynamic, sedimentologic and hydrometeorological characteristics of the representative watershed segment.

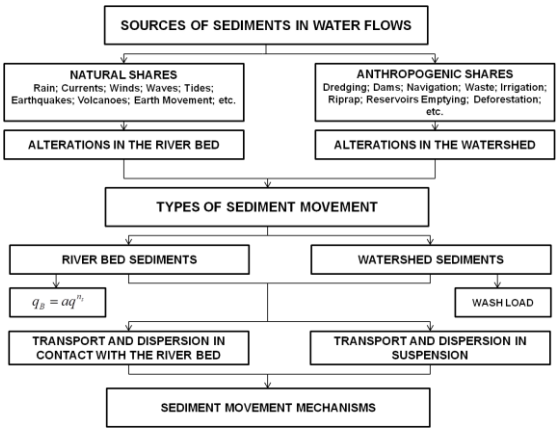

Figure 1. Sources and types of sediment movements (Wilson-Jr., 2009)

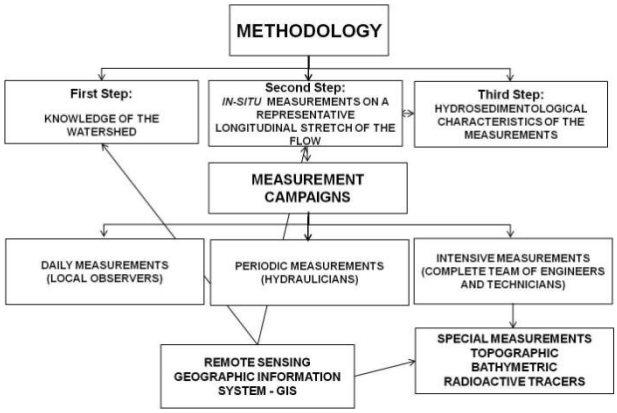

Figure 2. Methodology for sedimentological and morphological studies in open channel flows (Wilson-Jr., 1999, 2009)

First step: Knowledge of the watershed basin

The knowledge of the watershed delimited by the project involves the understanding of their geographic, geologic, hydro-meteorological, sedimentologic, socio-economic and historical characteristics, among others. Knowledge of these characteristics comes from office and field works, and involves the interaction of specialists in these specific fields. In this step, the aerial photography, satellite images and GIS techniques are very useful. They allow identifying fixed (topographic, pedology) and varying (forest cover and soil type) characteristics of the basin, which condition the water and sediment contributions.

Second step: *In-situ* measurements campaigns

It is recommended that the hydrosedimentological measurements in the river be conducted in a stretch of uniform flow and that its hydrodynamic and morphological characteristics be representative of a great extension of the flow. However, in many cases, the studied river stretch is determined by the project: the erosion downstream of a dam, the aggradation of a hydroelectric power plant reservoir and a complex navigational stream due to its sediment banks are some examples. For the quantification of the sediment movement in this representative river stretch, three superposed measurements campaigns are necessary: daily, periodic and intensive.

Daily measurements campaign

This consists of the water level record and the water sample collection to determine the concentration and granulometry of the suspended sediment. These daily values, along with the pluviometric and evaporation data, characterize the hydrologic cycle considered.

Periodic measurements campaign

They must be performed as a function of the hydrometeorological conditions, as a complement to the daily observations. They consist of, e.g. velocity measurements and liquid discharge calculations; watershed erosion and aggradation monitoring; detailed sample of the bed sediments; bathymetric survey, including the measurement of the waterline and bed slopes, flood levels, bed forms records, water flow and watershed basin morphological characteristics.

Intensive measurements campaign

Performed in well defined hydrological conditions, generally during the rainy seasons, when there is a larger sediment production, or during the average discharge period, when there is a sediment

motion representative of the bed forming discharges. Intensive measurements are performed at the same time as the ones of the previous campaigns and include: longitudinal bathymetry of the stretch, bed forms records and special measurements of the bed sediment discharges.

Third step: Hydrometeorologic characteristics during the *in-situ* measurements

The information obtained during the measurements campaign, especially those obtained during the Intensive Measurements Campaign, are limited in time and to defined hydrometeorological conditions, which need to be well known, so the data can be extrapolated.

Special measurements of the sediment movement

The periodic observations campaign results enable the definition of analytical relations between hydrodynamic and sedimentological quantities for the representative river stretch. The daily campaign allows those relations to be extended to hydrological cycle(s). However, the special measurements results are the ones that enable the **calibration** and **validation** of the analytical expression and models obtained. This methodology was developed in Brazil with the use of radioactive tracers and bathymetric surveys as special measurements. It was successfully applied in the *Ivai* River's watershed, in *Paraná* State (Wilson-Jr. *et al.*, 1980). The radioisotopes technique has been very efficient as a selective criterion of bed load formulas. In the *Ivai* River, the methodology enabled the selection of classic sediment motion formulas and their validation through comparison with data obtained by labeled sediments with radioisotopes. The use of tracer techniques enables the determination of kinematic and dynamic characteristics of the flow and sediment. They provide accurate data of the amount transported; sediment trajectories and velocities; residence time in the water flow; liquids and solid circulation; dispersion of liquid pollutants and of those fixed on sediments.

However, as the usage of radioisotopes in open channel flow is restricted to the Nuclear Energy Institutes, other methods are being considered for the direct measurement of sediment motion. In this paper, the usage of Remote Sensing technique and GIS as special measurements is considered, along with bathymetric surveys, for models calibration and validation. This technique is also being used for the knowledge of the watershed basin, as schematized in Figure 2. Following, four Brazilian cases were selected to illustrate the use of special measurements to calibrate and validate the descriptive models of sediment in open channel flows. The regions were the studies took place were outlined in the Figure 3.

Figure 3. Regions where studies were realized

SEDIMENTOLOGICAL BALANCE OF THE FERRADURA ISLAND STRETCH OF THE *PARAGUAY* RIVER (CASE I)

The morphological evolution with time, of a bed stretch of the *Paraguay* River was performed through comparisons between the topobathymetric measures taken in different occasions by the Brazilian Navy and published in 1:10,000 scales. The considered stretch, in which it was possible

to count on two measurements, was that of *Ferradura* Island, in Km 1255 of the *Pantanal* International Waterway. The bathymetries of the Figures 4 and 5 were made in 1974 and 1994, respectively, allowing for the stretch's morphological comparison in this 20-years period. Erosion and sedimentation rates were determined through the calculation of liquid and solid volume variations between the limits established for the stretch. Three methods were used: Contour Lines, Cross Sections Methods and Software Surfer® 7.0's use (Wilson-Jr. and Andrade, 2000).

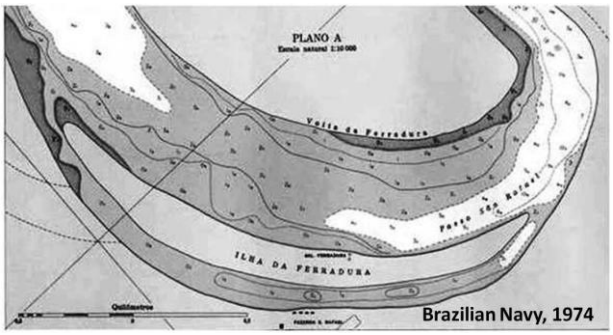

Figure 4. Topobathymetric measures on the *Ferradura* Island Region of the *Paraguay* River at 1974

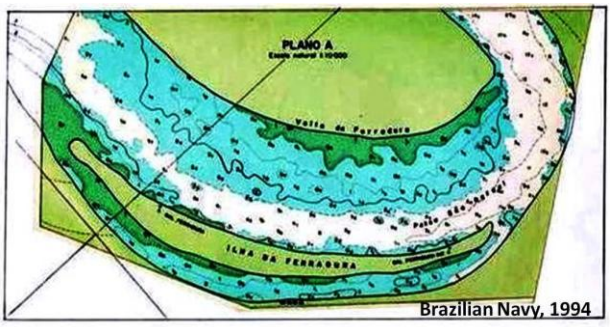

Figure 5. Topobathymetric measures on the *Ferradura* Island Region of the *Paraguay* River at 1994

The **Contour Lines Method** is based on the determination of the areas corresponding to each water level. For a better visualization of the area to be determined, a plane cutting the river segment in the desirable level is considered. The superior flooded areas also contain the interior levels' areas. Thus, obtaining the values of the areas corresponding to each level, a graph of flooded areas as a function of the water level can be constructed, and through the resulting curve, the final reach volume calculated. The increase in flooded areas can be seen for all levels in Figure 6. The volumes were: $V_{1974} = 4.04 \times 10^{-3}$ km^3 and $V_{1994} = 4.61 \times 10^{-3}$ km^3, with a volumetric increase of 0.57×10^{-3} km^3, i.e. an erosion rate 28,500 m^3/year.

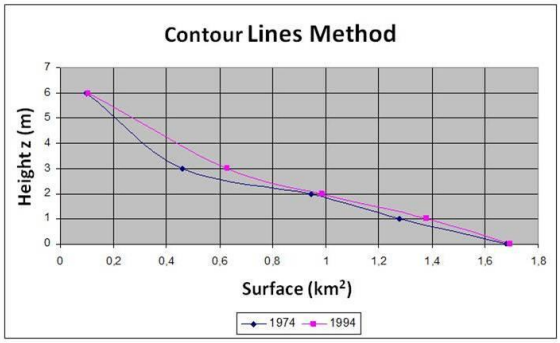

Figure 6. Flooded areas as function of water level

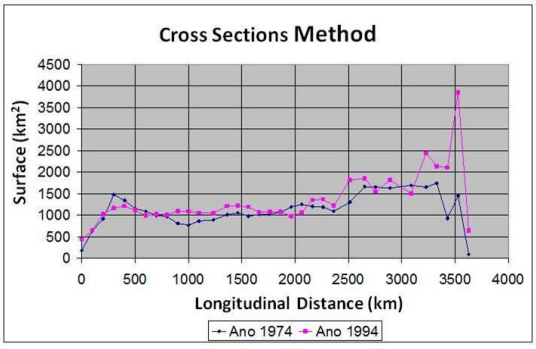

Figure 7. Longitudinal profile in the *Ferradura* Island reach

The **Cross Sections Method** consists in dividing the river stretch in sections whose areas can be determined. Afterward, the studied stretch's volume is calculated. Since it is a curved stretch, it was decided to consider four rectilinear sections of the longitudinal axis, from which were traced perpendicular lines spaced 100.0 m of terrain, considered such as not to intercept within the river channel. Results of this application are presented in Figure 7, where the segments of erosion and sediment deposition can be distinguished along the twenty years. The water volumes were: $V_{1974} = 4.15 \times 10^{-3}$ km^3 and $V_{1994} = 4.99 \times 10^{-3}$ km^3, presenting a volumetric increase of 0.84×10^{-3} km^3, that is, an erosion rate 42,000 m^3/year.

The **Surfer Software** makes the volume determination very fast, besides generating several graphical outputs, among which 3D drawings, as shown in Figures 8 and 9. Results obtained with Surfer® were: $V_{1974} = 4.38 \times 10^{-3}$ km^3 and $V_{1994} = 4.96 \times 10^{-3}$ km^3, presenting a volumetric increase of 0.58×10^{-3} km^3, that is, an erosion rate 29,000 m^3/year.

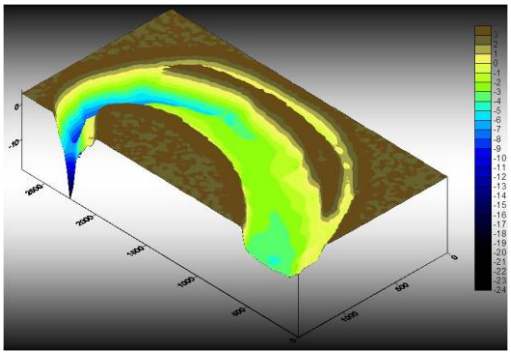

Figure 8. 3D representation of the *Ferradura* Island stretch of the *Paraguay* River in 1974

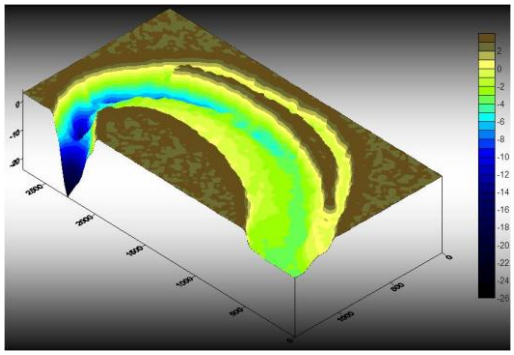

Figure 9. 3D representation of the *Ferradura* Island stretch of the *Paraguay* River in 1994

For the final erosion rates determination, the mean of the values obtained by the Contour Lines Method and the Surfer® application was calculated, obtaining an erosion rate 28,750 m^3/year. Results obtained with the Cross Sections Method presented an erosion rate larger than those obtained by the other ones. This may be due to the distance between cross sections. The larger is the distance between sections, the larger is the interpolation error between the sections' areas. This method is not recommended for very sinuous and irregular reaches.

From the analysis of the Figures 4 to 9, it is observed that along with the deepening of the riverbed that occurs, mainly in the downstream stretch, there is a sandbanks' increase at the upstream entrance of the river's right arm that goes around the *Ferradura* Island. This makes navigation harder through this arm, and also, in the convex part of the left margin, in the center of the segment. The sandbanks' volumes calculated in the years 1974 and 1994, are the following: $V_{Sb1974} = 1.06 \times 10^5$ m^3 and $V_{Sb1994} = 2.52 \times 10^5$ m^3, with a volumetric sandbanks' increase of 1.46×10^5 m^3, i.e., an aggradation rate equal 7.300 m^3/year during these 20 years.

Comparing all these values, it can be concluded that in the study period, the segment presented a sedimentological disequilibrium with predominantly erosive process. However, it has to be mentioned that the aggradation consequences at the entrance of the right arm of the *Ferradura* Island were serious, making navigation and access to the farms located in these margins difficult.

MORRO GRANDE RESERVOIR BATHYMETRIC ESTIMATE USING REMOTE SENSING ANALYSIS (CASE II)

Borges (2004) and Borges *et al*. (2007) used Remote Sensing to study the aggradation in the *Morro Grande*'s reservoir, *Rio de Janeiro* State, Brazil, using a high IKONOS resolution image and some bathymetric survey data, related by Bayesian Kriging method. They investigated the spatial variability in the ground-truth bathymetric dataset and the spatial variability in the image.

The geostatistical analysis showed that a similar behavior and correlation structure is present in both data sets (ground-truth and image) as well as a relationship does exist between the ground and the image. Indeed, the results showed a good correlation between the IKONOS image and the bathymetric measurements, where the Kriging method improved the estimates obtained by the common methods of statistical regression.

The data analysis was recommend for : (i) the estimation and monitoring of reservoirs and rivers aggradation, and (ii) for dredging management and maintenance of navigation channels, once the best correlation between imagery and bathymetric data are obtained for stretches with low depth, i.e., the most aggradated or shallow stretches.

Figure 10 (Borges *et al.*, 2007) shows the IKONOS image and, superposed, the estimated bathymetric through the image, which was adjusted with field data. Continuing this work, Wilson-Jr. (2009) proposed the study of the temporal evolution of sediment banks and river reaches morphology, assisted by Remote Sensing and GIS, for the calibration and validation of sediment transport models.

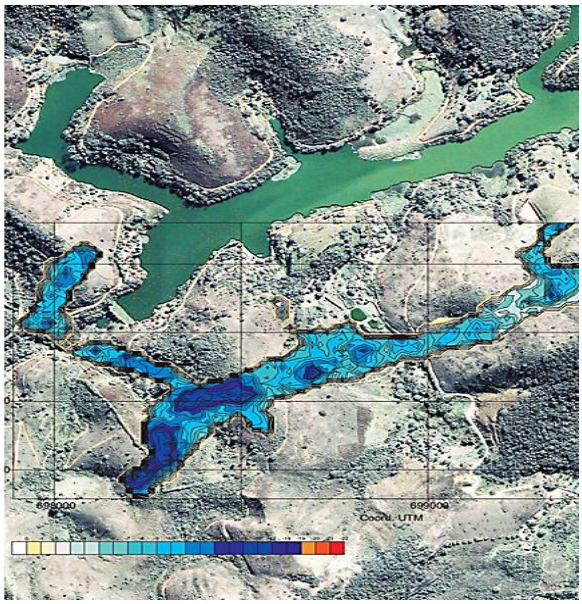

Figure 10. IKONOS image and estimated bathymetry of the Morro Grande Reservoir (Borges et al., 2007)

MORPHOLOGICAL CHARACTERIZATION OF A STRETCH OF THE *SÃO FRANCISCO* RIVER (CASE III)

São Francisco headwater is located in *Minas Gerais* State – Brazil, in *Serra da Canastra*. Until its mouth, in the Atlantic Ocean, on the border of *Sergipe* and *Alagoas* States, it travels 2,830 km, draining areas of seven states. Approximately 2,000 km are (or were!) navigable, so this river is also responsible for the flux of Brazil's Southeast, Midwest and Northeast regions' productions.

***Iuiú* Irrigation Project**

The *Iuiú* Basic Irrigation Project was elaborated in the year 2000 and intended for the agricultural development of an area of 500 km^2, located Southwest of *Bahia* State (Figures 11 and 12), on the border of *Minas Gerais* State, near the *Verde Grande* River mouth. The expected liquid flow for the *Iuiú* Project was 29.7 m^3/s of water captured from the *São Francisco* River. The river stretch of the project is located between two hydrosedimentological stations: *Manga* 30.0 km upstream, in *Minas Gerais* State, and *Carinhanha* 20.0 km downstream, in *Bahia* State.

Figure 12 highlights the river stretch that is being studied for the *Iuiú* Irrigation Project, the location of the hydrosedimentological stations, the alternatives for water intake and the sediment banks that were analyzed during the period of 1985 to 2011. In the drought period, when the hydrosedimentological survey was made by Wilson-Jr. (2000), the measured liquid flow was 1,045 m^3/s. It corresponds to 3.0 % of the minimum flow rate of the *São Francisco* River.

Hydrosedimentological and morphological aspects of the *Iuiú* Irrigation Project stretch

The Water Intake Project in the *São Francisco* River represents an anthropogenic interference in a river stretch whose sediment dynamics have special qualitative and quantitative characteristics. As this stretch is 10.0 km long, the sedimentological and morphological processes assume local importance, and must be addressed on a medium (≤ 30.0 m) and high resolution scale (≤ 2.0 m).

For the water intake alternative selection and for future hydrosedimentological studies, Wilson-Jr. (2000) proposed the methodology presented on Figure 2, in which parts of the first and second steps were completed. Concerning the first step, called Watershed Basin Knowledge, beyond the studies of reports, a field visit was made to the *São Francisco* River Watershed, on the segment between *Manga* (MG) and *Carinhanha* (BA), on the downstream stretches of the *Verde Grande* and *Carinhanha* Rivers and on the port regions of *Malhada*, *Carinhanha* and *Manga*. As the representative stretch of the *São Francisco* River was imposed by the project and it is delimited by *Manga*'s and *Carinhanha*'s stations, a special measurement campaign involving hydro-sedimentological, morphological and bathymetric surveys was conducted on the alternative stretch and was described in Wilson-Jr. (2000).

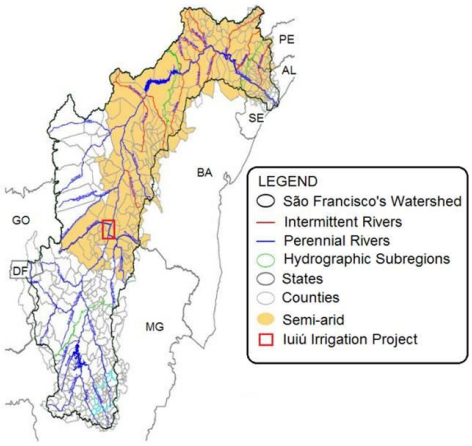

Figure 11. Semi-arid region of the *São Francisco* River watershed (Souza e Silva, 2013)

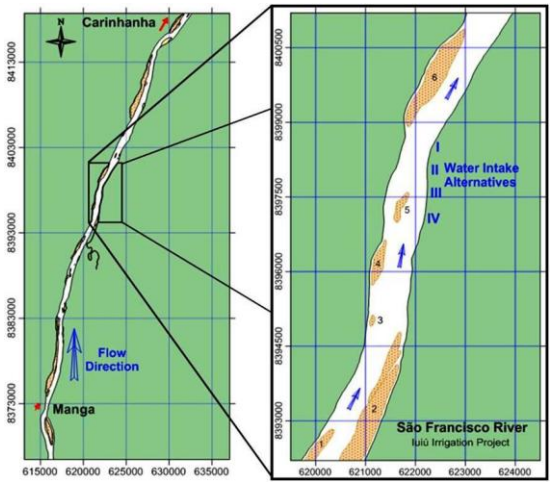

Figure 12. *Iuiú*'s irrigation project stretch water intakes alternatives and sediment banks localization

Movable sediment banks

The *São Francisco* River stretch on the site of the water intakes alternatives is not rectilinear (Figure 12). Its cross sections are asymmetric and because of the liquid flow variations during the hydrological cycle ($Q_{min} \cong 1{,}000$; $Q_{max} \cong 12{,}000\ m^3/s$), varied bed forms, islands and sediment deposits can be observed *in-situ* and on the satellite images. During the drought periods, the sediment deposits emerge, enabling the development of subsistence farming by the riverside population. With the arrival of the rainy season, the water level of the river rises, floods and washes most of the plantations, modifies the banks and islands, removes and deposits sediments, fertilizes the soil, sculpts the margins, the river bed, the movable banks, alters old bed forms and create new ones. During the field visit of July 2000, three sediment banks were observed: Banks 2, 4 and 6 (Figure 12). In this paper, assisted by Remote Sensing techniques during the period of 1985 to 2011, three other sediment banks were noted: Banks 1, 3 and 5. The temporal evolution analysis of these six banks is one of the main objectives of this work.

Remote Sensing Techniques Usage

The morphological evolution study of the *São Francisco* River stretch started with the use of LANDSAT-5 TM satellite images that were immediately provided by INPE (National Institute of Spatial Research) at no cost and extended for a period of 27 years. The first objective of this step was to verify that the LANDSAT-5 image has sufficient resolution to reproduce the borders of the river and sediment banks in the *São Francisco* River stretch, on the *Iuiú* Project area.

This step was called LANDSAT-5 TM Image Validation, and it is shown in Figure 13. Three softwares were used to manipulate the satellite images: ENVI®, Surfer® and AutoCAD®. The first one to manipulate the images and digitize the river stretch and sediment banks' borders; Surfer® to draw the maps, calculate the geometries and evaluate the morphological characteristics of the stretch, and AutoCAD® to adjust the map dimensions obtained in the field and satellite images. The forms and borders of the margins and banks determined by the LANDSAT-5 images and the field topographic and bathymetric survey were compared, as shown in the Figure 13. The image used was from 07/11/2000, because it was the closest to the period when the field survey was made: 07/06 to 07/09/2000 (Wilson-Jr., 2000). The field's survey calibration was made through the determination, with a GPS (Global Positioning System), of known polygons areas on the ground.

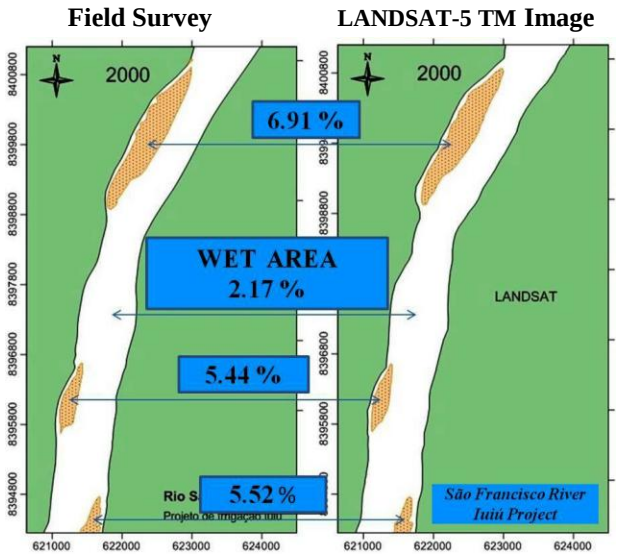

Figure 13. LANDSAT-5 TM image validation

The points' coordinates precision obtained in the field varied from 1.0 to a maximum of 3.0 m, which is inferior to the LANDSAT-5 image resolution. The Image Validation was made by comparing the dry and wet areas seen by satellite on the *São Francisco* River stretch, to the field data, as shown in Figure 13. The maximum discrepancy between the field survey areas and the ones determined with the satellite image was approximately 7.0 %. This value was considered acceptable, and it was concluded that the LANDSAT-5 TM images can be used for the temporal evolution study of the morphological variations of the *São Francisco* River stretch.

Morphological evolution of sediment banks

To evaluate the morphological evolution of the *Iuiú* Project region, 26 satellite images that represented the dry season ($Q \cong 1{,}000\ m^3/s$) and the years of 1985 to 2011, were used. Only the year 2002 was not considered, because an adequate LANDSAT-5 image was not available for the dry season. Afterward the initial images treatments phases, i.e. the georeferencing, resizing and borders' digitations, the banks and islands forms were analyzed, covering these 27 years.

The sum of the emerged areas of the six sediment banks on each image, named Dry Area; and the complement of this sum in relation to the delimited domain of the *São Francisco* River stretch, named Wet Area, were used to estimate the sedimentological behavior of the stretch. The results are shown in Figure 14, hereafter. One realizes that there was an increase of the Dry Area, and consequently, a decrease of the Wet Area, throughout the first 17 years (1985-2001). This finding indicates that the *Iuiú*'s Irrigation Project stretch was not in sedimentological equilibrium and showed a tendency to aggradation. The estimated aggradation value was around 7.70 % in relation to the recorded area values of 1985. Nevertheless, from 2003 to 2011, the dry and wet areas oscillate around constant values, indicating that the *São Francisco* River stretch reached a sedimentological equilibrium during this more recent period.

The aggradation of the *São Francisco* River stretch becomes even more evident when the temporal variations of the dry area of each sediment bank are analyzed. Figure 15 shows the annual variations of dry area of the six banks. The presentation of the banks was made in

ascending order of dry area values in relation to the total area of the studied stretch, so the highest values would stay on the back of the figure and would not hide the value of the smaller banks.

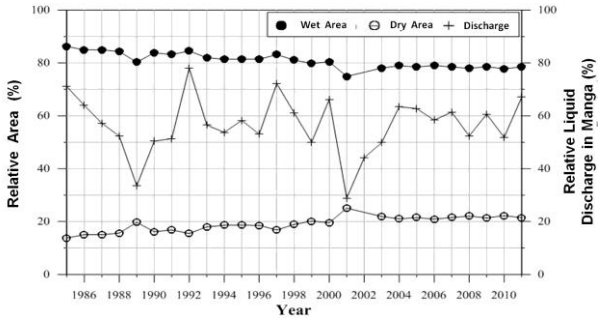

Figure 14. Annual evolutions of the relative dry and wet areas of the *Iuiú* Project in the *São Francisco* River

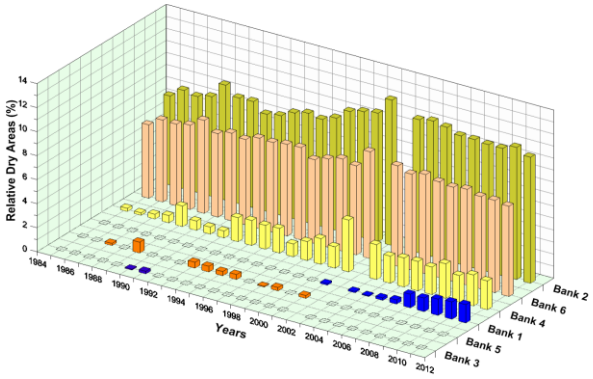

Figure 15. Morphological evolution of the *São Francisco's* sediment banks, from 1985 to 2011

The analysis of the annual images showed that some of the sediment banks are intermittent, while others are permanent. It also showed that some banks migrate downstream, while others remained stationary but had annual morphological modifications. Banks 2, 4 and 6 of Figures 12 and 15 are permanent and present in all of the 26 analyzed images. Bank 1 can also be considered permanent, although it has only reached the *Iuiú*' area in 2001. Before then, the bank fell outside the map's limits, but as Bank 2 it later extended itself downstream.

Banks 3 and 5 represent intermittent movable deposits, common on some Brazilian rivers of the *Amazonas* and *Prata* Basins, which arise during some years, generally after flood seasons, but are gradually eroded on the subsequent periods, with lower water levels. Bank 3 was only present in 1990 and 1991, while Bank 5 emerged in 1987, 1989, of 1993 to 1996, and again in 1998, 1999 and 2001. A great challenge, and, consequently a great motivation to continue the morphodynamic studies on the *São Francisco* River, consists in explaining analytically the formation and disappearances of these movable banks. Certainly, the application of the methodology sketched in Figure 2 will allow the progress in this direction.

PHYTOSOCIOLOGIC PROBLEMS CARRIED OUT IN THE *GUAPI* ESTUARY, *RIO DE JANEIRO* STATE (CASE IV)

The *Guapi* River crosses one of the few remnant mangrove areas in the *Rio de Janeiro* State. This estuarine flow was formed by the *Guapimirim* River, after receiving the *Macacu* River. It crosses the *Atlântica* Forest (an ecosystem of altitude fields, riparian forest, marshes and mangroves).

The *Macacu* River has its sources in the *Órgãos* Mountains, *Rio de Janeiro* State. It covers 74.0 km until joining *Guapi* River and more 20.0 km from this point to *Guanabara* Bay. The *Macacu* and *Guapi* Rivers watershed drainage surface is 1,640 km^2 (Figures 16 and 17).

Originally, *Guapimirim* and *Macacu* Rivers did not have any connection each other, and flowed independently into the *Guanabara* Bay. At the end of 40 decade, the National Works and Sanitation Department – DNOS, carried out several works in this region including the rectification of meanders; the opening of drainage channels; the buildings of dykes and floodwalls (Pires, 2010). A particular work was the *Imunana* Channel construction, which connected the *Macacu* with the *Guapimirim* River, an estuarine region that until this work remained flooded. Subsequently, a water intake system was installed into this channel to supply neighboring cities

and a submerged dam was built to elevate the water level and restrain the salt-water intrusion. The downstream flow was called *Guapi* River.

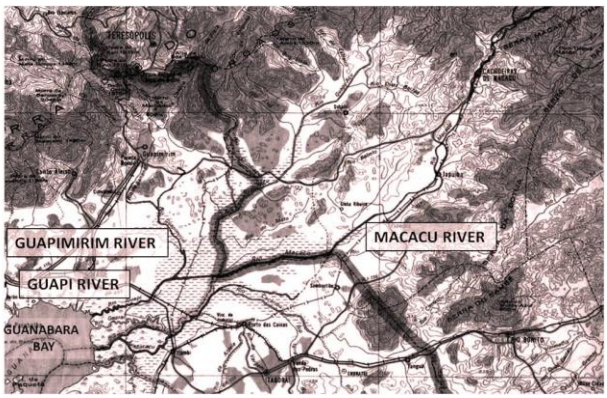

Figure 16. Macacu, Guapimirim and Guapi Rivers

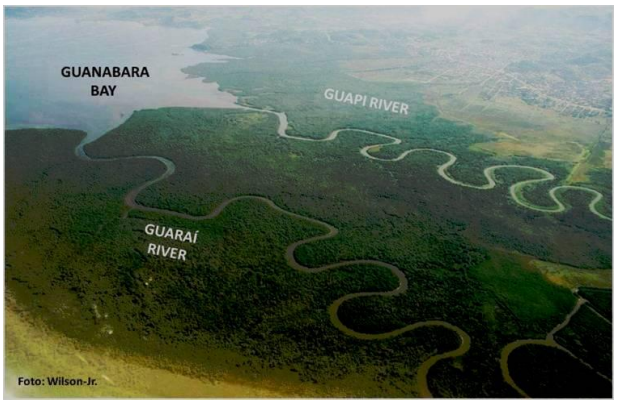

Figure 17. Guaraí and Guapi estuaries

Nowadays, the soil predominant usage is rural: agriculture and castle-raising. The vegetation presents some fragments from the *Atlântica* Forest and a considerable industrial development due to the *Rio de Janeiro* Petrochemical Complex – COMPERJ installation is predictable.

In spite of its environmental conservation organizations: (i) fluvial – *Órgãos* Mountain National Park; Environmental Protection Areas (*APA*) of *Petropólis* Municipality and of *Macacu* River watershed; and (ii) estuarine – *Guapimirim APA* and *Guanabara* Ecological Station; this region has been still submissive to the same former anthropogenic interventions. The vegetation suppression has been intensively practiced, for obtaining new sugar-cane and coffee cultivation areas; and the mangrove wood has been used to feed the brick-works industry. With the fluvial water discharge increase from the *Macacu* River, the *Guapimirim* River bordering forest, which was mainly composed of *Rhizophora* mangle *Linnaeus* (red mangrove), of *Laguncularia racemosa* (*L.) Gaertn f.* (white mangrove) and of *Avicennia schaueriana Stapf & Leechman* (black mangrove), was partially extinguished.

At 1984, when the *Guapimirim APA* was conceived, the mangrove vegetation cutting was forbidden. Nevertheless, in spite of the high resilience power of this ecosystem, the mangrove area that had already been cut did not return to its original conditions, on account of the salt-wedge regression that occurred after the *DNOS* interferences. With the salinity decrease and the hydro corium dispersion of riparian vegetation fragments from upstream, the degraded mangrove areas were gradually replaced by the *Tabebuia cassinoides ecosystem* or *caxetal* ecosystem in Portuguese. As well as the sand banks, shoals and mangrove systems, the *caxetal* system is a littoral marshland ecosystem, which is subject to a fluvial influence (Ziller, 1992). Its species, mainly the *Tabebuia cassinoides* (*Lam.*) *DC* is very resistant to an almost continuous flooding.

So, with the hydrodynamic process changes in the *Guapimirim* fluvial-estuarine system, the phytosociological process also changes, and, it is now affecting local sedimentological and morphological processes, modifying, in particular, the riparian vegetation and the sedimentological equilibrium of the flow segments.

CONCLUSIONS AND RECOMMENDATIONS

The use of topobathymetric measurements and of Remote Sensing and GIS are essential for calibration and validation studies on Sedimentological and Morphological Processes.

The morphological variations of the *Paraguay* River, in the *Ferradura* Island segment, were determined by comparing the topobathymetric curves taken in a 20-years period. Results showed that the segment presented a sedimentological disequilibrium with predominantly erosive process, estimated equal 28,750 m^3/year. However, the aggradation rate equal 7,300 m^3/year was at the entrance of a riparian farm, making the navigation and the farm's access impracticable.

Borges (2004) used high resolution IKONOS images to reproduce the bathymetric of the *Morro Grande* Reservoir in *Rio de Janeiro* State. The adopted treatment showed a great potential to be applied: (i) in the estimate and monitoring of sediments deposits in reservoirs and water streams with depths less than 10.0 m and (ii) on the management of dredging operations and maintenance of navigation channels, once the best results were obtained for aggradated shallow stretches.

It was also showed that LANDSAT-5 TM Satellite Images can be used for the morphological study of a river stretch. These images were used to describe the temporal evolution, during 27 years, of sediment banks and margins of a 10.0 km stretch in the *São Francisco* River. It is recommended that these Remote Sensing, GIS techniques and the topobathymetric measurements be introduced on the Sediment Movement Study Methodology steps, as suggested in Figure 1 of this paper, that is: (i) on the Watershed Basin Knowledge, and (ii) as special measurement of the Sedimentological and Morphological Processes. They enable the calibration and validation of qualitative and quantitative sediment transport models and the understanding of correlated phenomena, as the Phytosociological Process, e.g. the mangrove changes which are taking place on the *Guapi* Estuary borders, in *Rio de Janeiro* State.

Instead of an instantaneous vision of the measurements stations, these tools provide the observer with a wide and detailed vision of the watershed basin, the river stretch and even the bed changes.

ACKNOWLEDGEMENTS

The authors express their sincere gratitude to PENO/COPPE/UFRJ, CAPES, FAPERJ and CNPq for the institutional support received, without which, the realization of this work would not have been possible.

REFERENCES

Borges, F.S.P. 2004. *Estimativa de batimetria utilizando Sensoriamento Remoto e Krigagem Bayesiana. Estudo de Caso: Reservatório Morro Grande, Rio de Janeiro* (in Portuguese). M. Sc. Dissertation. COPPE/UFRJ. RJ.

Borges, F.S.P., Rotunno Filho, O.C., Wilson-Jr., G. 2007. Estimate of open channel flow bathymetry using Remote Sensing and the Bayesian Kriging method. ICGRHWE'07/EM25'07. Guangzou, Three Gorges. China.

Pires, I.O. 2010. *Manguezais da Região do Recôncavo da Baía de Guanabara: Revista através dos Mapas* (in Portuguese) Journal of Integrated. Coastal Zone Management, pp. 1-9.

Souza e Silva, M.G. 2013. *Análise de Processos Hidrossedimentológicos em Escoamentos com Superfície Livre: Trecho do Projeto de Irrigação Iuiú no Rio São Francisco.* M. Sc. Dissertation. COPPE/UFRJ. RJ.

Wilson-Jr., G. 1999. *Estudo do Movimento Sedimentar em Escoamentos com Superfície Livre* (in Portuguese). XIII Brazilian Symposium of Hydric Resources. Belo Horizonte, MG.

Wilson-Jr., G. 2000. *Estudos Hidráulicos e Sedimentológicos Referentes às Alternativas de Tomada d'Água do Rio São Francisco para o Projeto de Irrigação Iuiú* (in Portuguese). COPPETEC/PENO-1825/UFRJ, 198 *p. il*. RJ.

Wilson-Jr., G. 2009. *Evolução Morfológica de Trechos Hidroviários* (in Portuguese). 6th Meeting of Inland Hydroways Transport and Development. SOBENA, Rio de Janeiro.

Wilson-Jr., G., Rodriguez, H.T., Santos, J.S. 1980. *Estudos Hidráulicos e Sedimentológicos Realizados no Trecho Inferior do Rio Ivai, Noroeste do Estado do Paraná.* (in Portuguese). AEO: Hydrology Project. 1974-1980. PR.

Wilson-Jr., G., Andrade, R. 2000. *Variações Morfológicas e Sedimentológicas do Trecho da Ilha da Ferradura, no Rio Paragua*i (in Portuguese). 4th National Meeting of Sediment Engineering. IV ENES. Santa Maria, RS.

Ziller, S.R. 1992. *Análise Fitossociológica de Caxetais* (in Portuguese). M.Sc. Dissertation. Forest Science Program. UFPR, PR.

FLOW ENERGY AND BEDLOAD-TRANSPORT EFFICIENCY: THE FROUDE NUMBER AS A METRIC FOR BEDLOAD TRANSPORT RATES

Andrew Simon, Cardno, Senior Consultant, P.O. Box 1236, Oxford, Mississippi 38655 USA; andrew.simon@cardno.com; and Michael Singer, Department of Earth and Environmental Sciences, University of St. Andrews, St Andrews, KY16 9AL, UK; and Earth Research Institute, University of California Santa Barbara, Santa Barbara, California 91306, USA; bliss@eri.ucsb.edu

INTRODUCTION

The study reported in this short paper is preliminary in nature. The ideas and impetus behind this work stem from decades of research on unstable channels and was initiated in the 1990's as part of studies on channel evolution of the Toutle River System in the aftermath of the 1980 eruptions of Mount St Helens (Simon, 1992; 1999). This earlier work included a strong focus on trends of non-linear decay in flow energy and the processes (Graf, 1977) responsible for minimizing energy in an adjusting alluvial stream (Simon and Thorne, 1996). Applied to the suite of extremal hypotheses published in the 1970's and 1980's and placed within the framework of open systems theory with its references to minimizing entropy in landscapes, the associated theory that conditions at critical flow represent the most efficient means for channels to transmit water (Blench, 1966) and sediment (Kirkby, 1977) is considered. If this is to be realized, then maximum sediment transport should occur at hydraulic conditions representing minimum energy for that discharge (ie. critical flow; Froude number equals 1.0). To test this hypothesis, unit bedload transport data and associated hydraulic data were required, which span subcritical and super-critical flow regimes.

Geomorphically we can describe these adjustments in terms of measureable changes in geometry, its effects on boundary roughness and associated hydraulic conditions. Channel widening, particularly when associated with degradation, was found to be the most effective process in reducing flow energy, as all three components of total mechanical energy are reduced (ie. datum [elevation], hydraulic depth, and velocity) (Simon, 1992; Simon and Thorne, 1996). Further, energy slope represents the dissipation of energy over the reach. At Mount St. Helens with its braided channels, plentiful sediment supply, and cohesionless banks and terrace slopes, channel widening is and will remain (assuming no additional disturbances), the dominant process on the North Fork Toutle River for the next century (Simon and Klimetz, 2012). Channel widening of hundreds of meters has resulted in extremely shallow flow depths and frequent observations of critical-flow conditions (standing waves). Similar observations are common on braided streams. Over the course of adjustment, wide, shallow channels form where some peak flows oscillate between sub-critical and super-critical flow regimes (Simon, 1992) trending towards critical. The results further allow for an energy-based explanation for the hierarchy of channel-adjustment processes, their role in minimizing flow energy, and the importance of both bed and bank erosion in channel evolution (Simon and Thorne, 1996).

Sediment transport in rivers and streams is typically predicted as a function of shear-stress based theory, which when applied to bulk properties of channelized streamflow, places a large importance on the depth of flow and water surface (or energy) slope. This theory is based on the Law of the Wall, a logarithmic velocity gradient with increasing velocity with distance above the bed, with a corresponding decrease in boundary shear stress. It is these conditions that are responsible for rotating sediment grains out of pockets on the bed surface. Accordingly, a larger flow depth for a given slope produces a higher integral of shear stress applied to a bed particle and, therefore, a higher sediment flux rate. Such theory and its inclusion in sediment transport equations may not accurately represent observed sediment transport rates in a range of natural environments including sandy beach shorelines, alluvial fans, river bars, and floodplains, where flow is characteristically shallow, bed slopes are steep (≥1%), and beds are generally smooth with larger particles sparsely accumulated over a finer substrate. In such environments, vertical velocity and shear stress gradients may not be relevant at the scale of particles on the bed surface and sediment may be entrained in flows that are near the length scale of particles on the bed.

NEED FOR NEW SEDIMENT-TRANSPORT THEORY

Shear stress based theory tends to predict zero transport under such conditions because the critical flow depth has not been reached, yet particles in these environments typically move at high rates over smooth beds (Laronne and Reid, 1993) in rapid, shallow flows approaching or exceeding the critical value (Froude number ≥ 1):

$$F_r = \frac{u}{\sqrt{gh}} \tag{1}$$

Where u = downstream flow velocity, in m/s; g = acceleration of gravity, in m/s^2; and h = flow depth in m.

We hypothesize that in such rapid, shallow flows the processes by which sediment moves are not well characterized by theory designed for particle rotation out of pockets. Rather, they are more reasonably responsive to a square wave of flow pushing along the stoss particle boundary. In these shallow, rapid flow regimes, sediment particles on the bed are typically not encumbered by clast support, so transport only requires a flow force large enough to push particles with median diameters far greater than the bed roughness scale (e.g., mean friction angle (Buffington et al., 1992; Kirchner et al., 1990)), and do not rotate out of pockets. Once entrained, these relatively coarse particles may continue to move as long as this flow force is maintained and the bed surface remains smooth (preventing grain to grain interactions that would slow them to a halt).

Shear stress approaches are typically very sensitive to empirically defined values of critical shear stress for entrainment, which are known to vary dramatically for non-uniform sediment mixtures (Wiberg and Smith, 1987; Buffington and Montgomery, 1997). Based on the understanding that entrainment is sensitive to bed material grain-size distribution, critical shear stress is typically

computed as a power law of the ratio of particle sizes subject to movement to median bed-grain sizes (Andrews, 1983; Egiazaroff, 1965) or more recently, by sand fraction in the bed (Wilcock and Crowe, 2003), both of which are assumed to account for the effects of relative grain protrusion/hiding and pocket angle rotation on entrainment.

In cases of rapid shallow flow over smooth beds, these calculations of critical (or reference) shear stress yield values near zero, suggesting that any positive value of flow will move sediment particles on the bed surface (i.e., there are no frictional forces to overcome associated with clast support). Even assuming near zero critical shear stress, surface based equations that were designed for gravel-bed rivers (e.g., (Parker, 1990; Wilcock and Crowe, 2003)) still may not perform well under shallow rapid flow regimes over smooth, unarmored beds lacking developed bar morphology (Hassan, 2005; Laronne et al., 1994; Singer and Michaelides, 2014). Consequently, re-calibration of these equations has been undertaken to overcome the limitations in these approaches and to more accurately hindcast high observed flux rates (e.g., ephemeral dryland sediment flux in Nahal Eshtemoa, Israel (Powell et al., 2003)). However, these empirical tweaks to existing equations do not yield new insight into transport processes within shallow, rapid flow regimes. Thus, we in the sediment transport community continue to grapple with the process controls on flux rates and morphologic development in many such fluvial environments. Here, we re-investigate published sediment flux rates for controlled conditions within a range of field and flume datasets and the corresponding hydraulics to develop new insight into sediment transport under rapid, shallow flow regimes.

FLOW-ENERGY BASED HYPOTHESIS

Controversial theories of minimum stream power and rate of energy dissipation were developed in the late 1970's and early 1980's as a means of describing the equilibrium shape of alluvial channels (Yang, 1976; Chang, 1979; Yang and Song, 1979; Chang, 1980; Yang et al., 1981). These theories were the subject of extensive debate in the geomorphic and engineering literature. Chorley (1962) describes channel adjustment in terms of open systems theory "*...wherein the import and export of energy and material are equated by means of an adjustment of the form, or geometry, of the system itself*." (Chorley, 1962, p. B3). Simon (1992) reported that the theories were applicable to the adjustment of alluvial streams, noting that channel widening and reduction in flow depths was a critically important process in minimizing flow energy. This work further showed that equilibrium geometries for the North Fork Toutle River tended towards a minimum specific energy, representing a maximum unit discharge, critical flow and a Froude number of 1.0 (Simon and Thorne, 1996). Blench (1966) and Ergenzinger (1987) also indicate that gravel-bounded streams with no lateral constraints such as cohesive materials or root reinforcement and are controlled only by hydraulic, excess shear stress conditions adjust to a Froude number near 1.0.

An associated theory of maximum sediment-transport efficiency (Kirkby, 1977) was also developed at this time using the corollary that the dissipation of minimum energy by the flow

signified maximum efficiency of bedload transport. If these parallel theories are to be substantiated with bedload-transport data, it holds that maximum, unit bedload transport should occur at a minimum specific energy, which equates to a Froude number of 1.0 (critical flow). The Froude number, representing the ratio between inertial to gravitational forces is an easily measurable metric obtained from discharge measurements.

Based on the parallel theories of minimization of energy and maximization of sediment-transport efficiency, the following hypothesis, can be stated and tested using bedload-transport and associated hydraulic data. That is "unit bedload-transport rates should peak at a Froude number close to 1.0, representing the maximum amount of bedload transport (per unit wdith) that can occur per unit of energy expended."

SUMMARY OF FINDINGS

The hydraulic and sediment transport data used in this study come from about two decades of collecting and collating reports from the US Geological Survey and other agencies. Laboratory bedload-transport and hydraulic data were obtained from unpublished sources at the USDA-ARS, National Sedimentation Laboratory, and Colorado State University, as well as from the literature (ie. Gilbert, 1914; Stein, 1965; Foley, 1975; Nordin, 1976; and others). Field data were obtained from unpublished sources at the USGS Cascades Volcano Observatory, and from the literature. Sampling locations include the North Fork Toutle and Toutle Rivers, Washington (Dinehart, 1998); the Tanana River, Alaska (Burrows et al., 1979; Harrold and Burrows, 1983); the Jordan River, Israel (Inbar and Schick, 1979); and the East Fork River, Wyoming (Emmett, et al., 1982). The transport data cover sand- and gravel-sized bed material with median diameters ranging from 0.19 to 300 mm over Froude numbers ranging from 0.2 to greater than 3.0. All data were normalized by unit width to obtain unit-bedload transport rates (q_s) in kg/m/s and, by particle size (where d_{50} of the material was available) to test the utility of predicting dimensionless unit bedload transport (q^*) across the range of sizes:

$$q^* = q_s \sqrt{\left(\frac{\rho_s - \rho}{\rho}\right) g d_{50}{}^3} \qquad (2)$$

where q^* = dimensionless bedload transport rate; q_s = unit bedload transport rate, in kg/m/s; ρ_s = sediment density, assuming 2.65 kg/m^3; ρ= density of water, assuming 1.0 kg/m^3; d_{50} = median size of sediment, in m.

The various datasets indicate a reasonably tight relation (in semi-log space) between unit bedload transport rate and Froude number, with a peak transport rate occurring in the region of a Froude number of 1.0 (Figure 1). Transport rates increase sharply through the sub-critical regime, reach a flat peak at about 1.0 and then decrease slightly through the supercritical regime. This relation and its general form holds for the combined flume and field data over sand- and gravel-size ranges, and indicates that unit bedload-transport rates can be predicted with only measurements

of flow velocity and depth. Further study is required to determine the nature of the increased scatter in the vicinity of F_r = 1.0 and whether this is due to experimental and/or sampling issues.

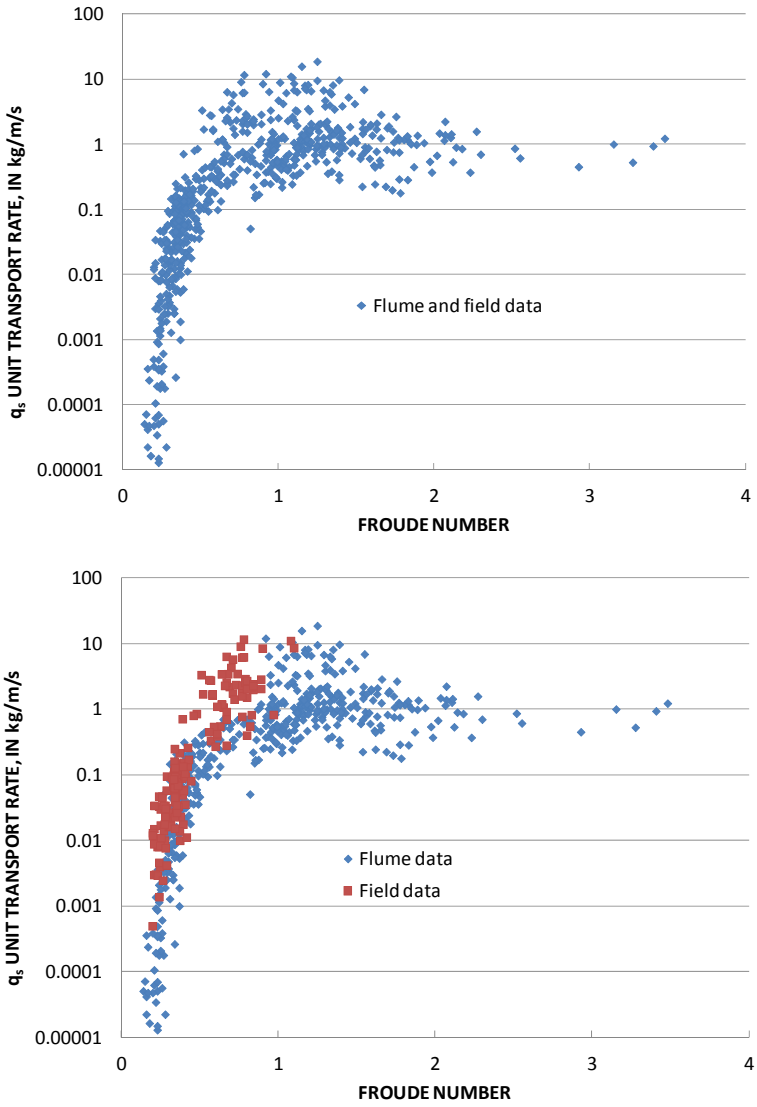

Figure 1 Unit bedload-transport rate (per unit width) and Froude number

To check the consistency of the relation over the range of particle sizes represented by the data, the transport data are converted to the non-dimensional form by dividing by particle size. The resulting relation between q^* (equation 2) and the Froude number is shown in Figure 2. Again we see a sharp increase in transport rates with increasing Froude number through the sub-critical flow regime, reaching a peak value in the region near F_r = 1.0. This plot predominantly includes the flume data. Particle size was missing from some of the extensive field datasets and will be incorporated in future analyses and publications.

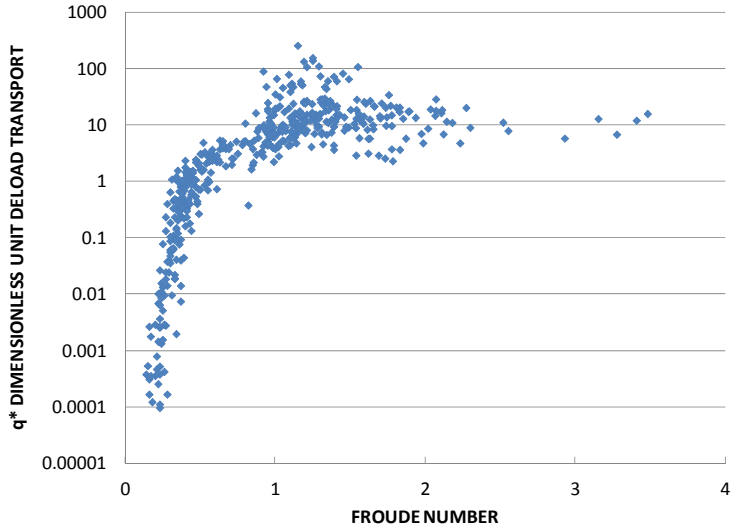

Figure 2 Variation in dimensionless unit bedload transport (q^*) with Froude number

The preliminary results from our analysis presented here support the hypothesis that the Froude number, i.e., a dimensionless relation between inertial and gravitational forces, has marked influence over unit bedload-transport rates, and that maximum rates occur at or near critical flow. This is an interesting development that could have great implications for sediment-transport theory and provide for a more simplified approach to estimating bedload-transport rates. Extension of this result from mechanistic sediment-transport theory to geomorphic-systems theory is also compelling. This work is still in progress. We are currently investigating the consistency of this relation across these and additional datasets after correcting for the effects of flume side walls and using dimensionless particle sizes rather than absolute values of grain size. We believe these steps will improve the resolution of this relation and that we can create a new, simplified sediment transport equation based on Froude number.

REFERENCES

Andrews, E.D., (1983). Entrainment of gravel from naturally sorted riverbed material: Geological Society of America Bulletin, 94, p. 1225-1231.

Blench, T., (1966). Mobile-Bed Fluviology. T. Blench and Associates Ltd., Edmonton, 300 pp.

Buffington, J.M., Dietrich, W.E., and Kirchner, J.W., 1992, Friction angle measurements on a naturally formed gravel streambed - implications for critical boundary shear-stress: Water Resources Research, 28(2): 411-425.

Buffington, J.M., and Montgomery, D.R., (1997). A systematic analysis of eight decades of incipient motion studies with special reference to gravel-bedded rivers: Water Resources Research. 33(8): 1993-2029.

Burrows, R.L., Parks, B., and Emmett, W.W., (1979). Sediment transport in the Tanana River in the vicinity of Fairbanks, Alaska, 1977-78. US Geological Survey Open-File Report 79-1539, Anchorage, Alaska, 37 p.

Chang, H.H., (1979). Geometry of rivers in regime. J. Hydraulics. Div. ASCE, 105: 691-706.

Chang, H.H., (1980). Geometry of gravel streams. J. Hydraulics. Div. ASCE, 106: 1443-1456.

Chorley, R.J., (1962). Geomorphology and general systems theory. U.S. Geological Survey Professional Paper, 500-B: 10 pp.

Dinehart,R.L., (1998). Sediment transport at gaging stations near Mount St. Helens, Washington, 1980-90: Data collection and analysis. US Geological Survey Professional Paper 1573, 105 p.

Egiazaroff, I.V., (1965). Calculation of non-uniform sediment concentrations: J. Hydraulic Eng., 91(4): 225-248.

Emmett, W.W., Myrick, R.M., and Meade, R.H., (1982). Field data describing the movement and storage of sediment in the East Fork River, Wyoming. Part III. River Hydraulics and Sediment Transport, 1980. USGS Open-File Report 82-359, Denver, Colorado, 289 p.

Ergenzinger, P., (1987). Chaos and order the channel geometry of gravel bed braided rivers. In: F. Ahnert (Editor), Geomorphological Models. Catena Suppl., 10: 85-98.

Foley, M.G., (1975). Scour and fill in ephemeral streams. California Institute of Technology, Pasadena, CA.

Gilbert, G.K., (1914). The transportation of debris by running water: U.S. Geological Survey Professional Paper 86, 263 p.

Graf, W.L., (1977). The rate law in fluvial geomorphology: American Journal of Science, 277: 178-191.

Hassan, M.A., (2005), Characteristics of gravel bars in ephemeral streams: Journal of Sedimentary Research, 75(1): 29-42.

Harrold, P.E. and Burrows, R.L., (1983). Sediment transport in the Tanana River near Fairbanks, Alaska, 1982. USGS Water-Resources Investigations Report 83-4213, Anchorage, Alaska, 53 p.

Inbar, M., and Schick, A.P., (1979). Bedoload transport associated with high stream power, Jordan River, Israel. Proc. National Academy of Sciences, 76(6), 2515-2517.

Kirchner, J.W., Dietrich, W.E., Iseya, F., and Ikeda, H., (1990), The variability of critical shear stress, friction angle, and grain protrusion in water-worked sediments: Sedimentology, 37: 647-672.

Kirkby, M.J., (1977). Maximum sediment efficiency as a criterion for alluvial channels. In: K.J. Gregory (Editor), River Channel Changes. Wiley, New York, pp. 429-442.

Laronne, J.B., and Reid, I., (1993). Very high-rates of bedload sediment transport by ephemeral desert rivers: Nature, 366(6451): 148-150.

Laronne, J.B., Reid, I., Yitshak, Y., and Frostick, L.E., (1994). The non-layering of gravel streambeds under ephemeral flood regimes: Journal of Hydrology, 159(1-4): 353-363.

Nordin, C.F. , Jr . , (1976). Flume Studies with Fine and Coarse Sands, Open File Report 76-762, U.S. Geological Survey, Washington, D.C., 1976, 18 p.

Parker, G., (1990)., Surface-based bedload transport relation for gravel rivers: Journal of Hydraulic Research, 28, (4): 417-436.

Powell, D.M., Laronne, J.B., and Reid, I., (2003). The dynamics of bedload sediment transport in low-order, upland, ephemeral gravel-bed rivers: Advances in Environmental Monitoring and Modelling, 1(2): 1-27.

Simon, A., (1992). Energy, time, and channel evolution in catastrophically disturbed fluvial systems. Geomorphology 5: 345-372.

Simon, A., (1999). Channel and drainage-basin response of the Toutle River System in the aftermath of the 1980 eruption of Mount St. Helens, Washington. USGS Open-File Report 96-633, Vancouver, Washington, 130 p.

Simon, A., and Klimetz, P.D., (2012). Analysis of Long-Term Sediment Loadings from the Upper North Fork Toutle River System, Mount St. Helens, Washington., USDA-ARS National Sedimentation Laboratory Technical Report Number 77, Oxford, MS. 109 p.

Simon, A., and Thorne, C.R., (1996). Channel adjustment of an unstable coarse-bedded stream: Opposing trends of boundary and critical shear stress and the applicability of extremal hypotheses. Earth Surface Processes and Landforms, 21, 155-180.

Singer, M.B., and Michaelides, K., (2014). How is topographic simplicity maintained in ephemeral dryland channels?: Geology, 42(12):1091-1094, doi:10.1130/G36267.1.

Stein, R.A., (1965). Laboratory studies of total load and apparent bed load. Journal of Geophysical Research, 70(8): 1831-1842.

Wiberg, P., and Smith, J.D., (1987). Calculations of the critical shear stress for motion of uniformand heterogeneous sediments. Water Resources Research, 23(8), 1471-1480.

Wilcock, P.R., and Crowe, J.C., (2003). Surface-based transport model for mixed-size sediment: Journal of Hydraulic Engineering, 129: 120-128.

Yang, C.T., (1976). Minimum unit stream power and fluvial hydraulics. J. Hydraul. Div. ASCE, 102(HY7): 919-934.

Yang, C.T. and Song, C.C.S., (1979). Theory of minimum rate of energy dissipation. J. Hydraul. Div. ASCE, 105(HY7): 769-784.

Yang, C.T., Song, C.C.S. and Woldenberg, M.J., (1981). Hydraulic geometry and minimum rate of energy dissipation. Water Resources. Research, 17 (4): 1014-1018.

EFFECT OF UPSTREAM SEDIMENT SUPPLY AND FLOW RATE ON THE INITIATION AND TOPOGRAPHIC EVOLUTION OF SANDBARS IN LABORATORY AND NUMERICAL CHANNELS

Paul J. Kinzel, Hydrologist, U.S. Geological Survey, Geomorphology and Sediment Transport Laboratory, Golden, Colorado
pjkinzel@usgs.gov
Brandy L. Logan, Water Resources Specialist, Stream and Lake Protection Section, Colorado Water Conservation Board, Department of Natural Resources, Denver, Colorado
brandy.logan@state.co.us
Jonathan M. Nelson, Research Hydrologist, U.S. Geological Survey, Geomorphology and Sediment Transport Laboratory, Golden, Colorado
jmn@usgs.gov

Abstract The evolution of barforms from a bed of uniform sediment and changes in sediment storage were measured in a laboratory flume and simulated numerically. Flume experiments were conducted with several upstream sediment supplies and flow conditions. For the sediment supply rates (no upstream supply, equilibrium supply, and 133, 166, and 200 percent of the equilibrium supply) and flow rates examined, the plane bed tended to evolve into mid-channel bars early in the runs ~15 minutes. As the flume experiments progressed, the bed transitioned to a lower mode configuration of alternate bars or a single-thread meandering thalweg. Increasing the upstream sediment supply to 133 percent or more of the equilibrium rate, increased the height and volume of deposited sediment relative to experiments conducted at the equilibrium rate and those experiments without sediment supply. Experiments conducted at flow rates of 0.5 and 1.0 L/s without sediment supply demonstrated that an increase in flow corresponded to a greater volume of erosion. A coupled two-dimensional flow and sediment transport model, Nays2DH, was used to simulate the evolution of bed topography for three sediment supply rates. We compared the morphodynamics and sediment storage predicted by Nays2DH for two initial bed conditions: one set of calculations used a plane bed with a small upstream perturbation as the initial bed condition, and the other set used the bed topography measured 15 minutes after the start of the flume run. Whereas initializing the model with measured flume topography provided a somewhat better analog to the final evolved morphology, predictions of sedimentation were not substantially improved over simulations using the plane bed as the initial condition.

INTRODUCTION

Flow and sediment management have been identified as tools to rehabilitate river corridors impaired by upstream regulation (National Research Council, 1999; U.S Department of Interior, 2006). Management strategies may be directed toward increasing the height of fine-grained deposits along channel margins or increasing barform heights for the preservation or enhancement of in-channel habitat. A number of adaptive management programs are in place in the United States that have objectives related to geomorphic change. A few examples of these programs are the Colorado River in Grand Canyon, the Trinity River in California, and the Platte River in Nebraska. In the case of the Platte River, the Bureau of Reclamation and U.S. Fish and Wildlife Service have identified short duration near-bankfull flows from 1 to 3 days in duration to test the ability of these flows to scour vegetation and build ephemeral sandbars to benefit

nesting species of concern (the least tern and the piping plover, U.S. Department of the Interior, 2006). Sediment augmentation has been recently used in the Platte River to offset reduction in sediment supply created by a clear water return from an upstream hydropower canal. The Platte River Recovery Implementation Program (PRRIP) initiated a pilot study aimed at adding 100,000 tons of sediment to the Platte River (PRRIP, 2014). Due to the magnitude and cost of adaptive management programs, predicting the outcome of management actions becomes an important means to design strategies to achieve the desired goals economically and effectively.

Predicting river response to different physical stimuli can be a difficult task. One of the tools available to river scientists is numerical models that can simulate morphologic change in rivers resulting from various management scenarios, including hydrograph change and sediment input. However, the detailed field information required to run, calibrate, and verify these models may be unavailable, potentially incomplete, or difficult to collect. Specifically, river bed topography before, during, and after flow manipulation may be lacking, as might information regarding the sediment supply rate during the management activities. Additionally, it is not always clear if a model has a range of applicability that encompasses the physical settings of the problem at hand.

Flume experiments have been used by researchers as a means to understand and observe channel evolution processes (Fujita and Muramoto, 1985; Fujita, 1989; Germanoski and Schumm, 1993; Marti and Bezzola, 2006; Madej et al., 2009). Flume experiments can also provide the data necessary for input, calibration, and verification of morphodynamic models (Jang and Shimizu, 2005; Takebayashi and Okabe, 2009). Combining numerical and physical modeling, therefore, offers a more comprehensive approach to predicting the outcomes of river management actions for at least two reasons. It can identify and provide a means to assess conditions that drive model predictions and provide a better understanding of the physical processes involved.

The intent of this paper is twofold. First, we discuss a series of flume experiments designed to explore the effect of upstream sediment supply and discharge alterations on erosion and deposition patterns in a straight channel with an initial plane bed. Second, we applied a coupled flow and sediment transport model to simulate and predict the morphologic changes observed in the flume. The flume experiments were conducted to address how the magnitude of upstream sediment supplied influenced the spatial and temporal patterns of erosion and deposition in a straight channel. In addition, we wanted to understand the effect of flow rate on the deposition and erosion patterns in a coarse, bedload dominated system. These effects are related to many types of management actions and, in particular, are directly relevant to those actions that involve manipulating flow and sediment supply to achieve bar formation. The numerical experiments were conducted for model testing and validation, and to gain an understanding of the influence of boundary conditions (input sediment load and initial topography) on predictions of channel evolution.

METHODS

Flume Experiments Over 30 flume experiments were conducted at the U.S. Geological Survey's Geomorphology and Sediment Transport Laboratory in Golden, CO using a 7-m long and 1.2-m wide tilting and recirculating flume. The flume slope was set to 1.25 percent. Vertical plywood walls were attached to the flume bed to restrict the width of the test channel to 0.50 m and the flow in the flume was adjusted with a computer controlled valve. The sediment used in the experiments was a well-sorted sand d_{50} = 0.6 mm, $\sigma = \sqrt{D_{84}/D_{16}}$ = 1.2. Sediment was introduced at the upstream end of the flume using a motorized sediment feeder. Higher sediment supply rates were achieved by augmenting the feeder supply by manually distributing sand evenly across the upstream end of the flume. We determined the sediment transport rate for a given flow by trapping sediment at the downstream end of the flume at that flow over a set time interval and weighing the dried material. The mean equilibrium transport rate measured for a 1L/s flow was approximately 3.3 $x10^{-3}$ kg/s. The bed of the test channel was screeded at the beginning of each experiment and the initial plane bed topography of the test channel was surveyed. Topographic surveys were repeated at 15-minute intervals over the duration of each experiment. We used a topographic measurement system that included a motorized traverse that spanned the width and length of the flume, a laser mounted to the traverse with its long axis pointing perpendicular to the flume bed, and a video camera oriented to capture an oblique image of the laser spot on the sand. Details of the mapping system are presented in Kinzel and others (2010). During the experiments it was necessary to drain the flume before the bed was surveyed. This was because the refraction of the laser through a small depth of water (< 0.01 m) could not be compensated for accurately, due to the inability to resolve distinct water surface and bed reflections in the images. An ultrasonic sensor was integrated to detect the water surface. The water-surface elevation was measured with the ultrasonic sensor at the end of each flume run.

A series of flume runs was conducted to evaluate channel response to varying sediment loads at a similar discharge. A discharge of 1.0 L/s was used for each of these experiments and with sediment supply rates equal to 0, 100, 133, 166 and 200 percent of the equilibrium transport rate. Each experiment lasted 2 hours to allow sufficient time for the sediment to move through the test section located between 2 and 4 m downstream of the most upstream transect measured. A series of flume runs was also conducted at 0.5 and 1.0 L/s without sediment supply to examine the change in morphology and sedimentation from clear-water flow alteration.

Plots of volumetric change as a function of the vertical deviation from the initial plane bed were made by determining the volume in 1-mm elevation bins within the test section of the flume. The test section was positioned to minimize the effect of the flume boundaries (upstream entrance and downstream tailgate) on the erosion and deposition patterns in the flume.

Numerical Modeling We used a two-dimensional, depth averaged, unsteady, coupled flow and sediment transport model, Nays2DH Version 1.0, to try to reproduce the spatial and temporal evolution of barforms observed in the flume experiments and the concomitant changes in sediment storage. Nays2DH is based on the numerical solution of the shallow water equations in a curvilinear orthogonal, structured grid and is a combination of two models: Nays2D and Morpho2D (iRIC Project, 2014). Nays2D is described in Shimizu (2002) and Morpho2D in Takebayashi (2005) and Takebayashi and Okabe (2009). Nays2DH is one of the models in the

international River Interface Cooperative (iRIC) software, described by Nelson and others (2010). The software is available at no cost and can be downloaded from http://i-ric.org/en/introduction. A general curvilinear coordinate system is used in Nays2DH. For our straight channel simulations we used a numerical grid with 0.02 m x 0.05 m grid cells in the stream-normal and stream-wise directions. Model inputs included the initial bed topography of the flume, downstream water-surface elevation, flow rate, and hydraulic roughness in the form of Manning's n. Nays2DH assumes a non-slip condition along the side-wall boundary.

Nays2DH supports both bedload and suspended sediment transport, and can perform calculations on uniform and mixed-grain sediment beds. The sediment bed in the flume was modeled with a uniform grain diameter of 0.6 mm. Nays2DH uses either the Meyer-Peter Müller (1948) or Ashida and Michiue (1972) equation to compute bed load transport. In our simulations, the Ashida and Michiue equation was used. The bedload transport vector was calculated using the Watanabe formula (Watanabe et al., 2001).

Two sets of model simulations were carried out. In the first set, a common technique to perturb the numerical calculation and stimulate the development of bar morphology from the initially plane bed was used. This technique uses a plane bed topography for the initial condition, and places a rectangular region with a slightly higher bed elevation (bump) at the upstream end of the model domain (Jang and Shimizu, 2005). In the second set of simulations, the flume topography measured after 15 minutes into the run was used directly as the initial condition for the bed topography.

Other modeling experiments were performed to examine the influence of secondary flows on the morphodynamics. Secondary (helical) flows can be treated in Nays2DH by using one of two approaches. One option involves solving an equation for depth-averaged vorticity in the streamwise direction. The other option allows the user to directly specify the strength of secondary flows. This parameter controls the near bed velocity and the direction of bedload transport:

$$\tilde{u}_b^n = \tilde{u}_b^s N^* \frac{h}{r_s} \quad (1)$$

Where: $\tilde{u}_b^n$ = the near-bed velocity in the transverse direction

$\tilde{u}_b^s$ = the near-bed velocity in the stream-wise direction

N^* = the strength of secondary flows, =7 per Engelund (1974))

$\frac{h}{r_s}$ = the ratio of the depth to the radius of streamline curvature

RESULTS

Sediment Experiments Our first experiments demonstrated, albeit somewhat intuitively, that if we supplied sediment at the equilibrium transport rate, the flume channel would degrade less and build bars to higher elevations than without sediment supply. Subsequent experiments demonstrated it was necessary to increase sediment supply 133 percent or more of the equilibrium transport rate for bars to be built to higher elevations than those built with the equilibrium rate. The change in elevation from the initially plane bed for three sediment supply rates and sedimentation after 2 hours with a flow of 1 L/s are shown in figure 1.

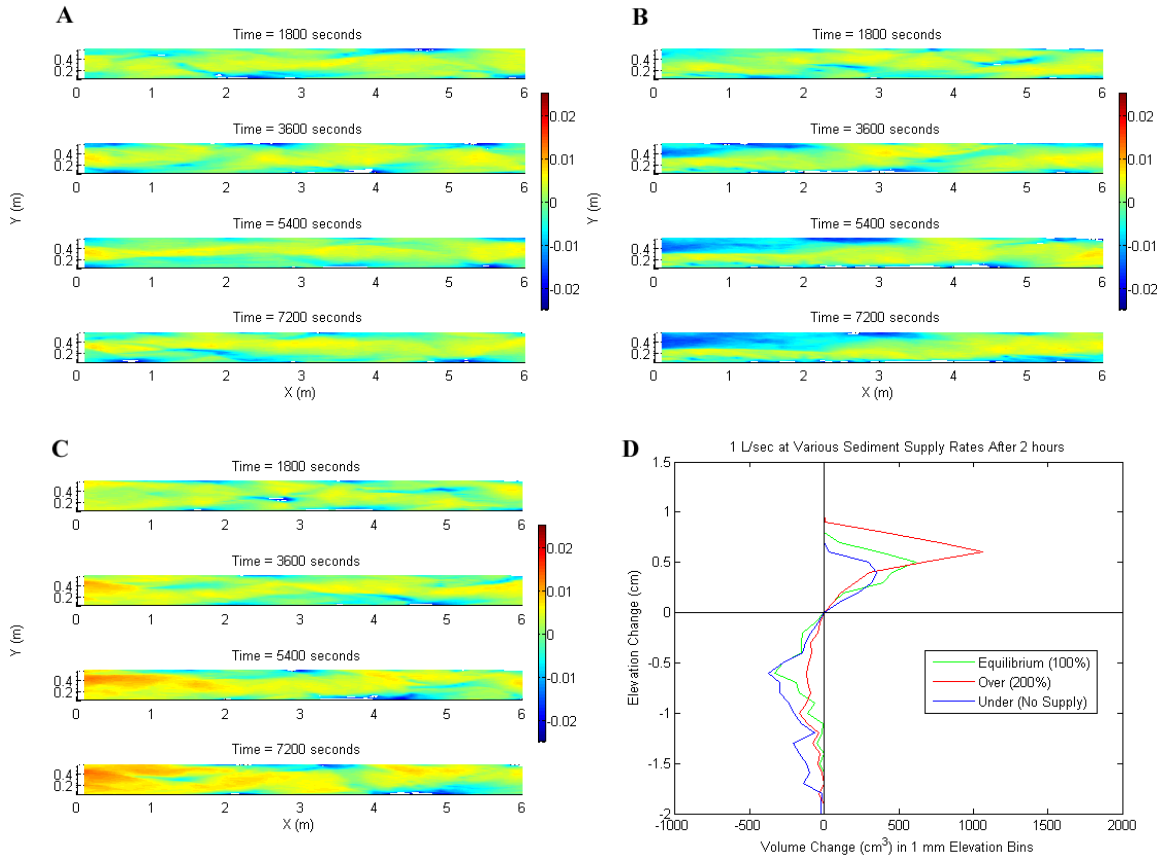

Figure 1 Changes in the bed elevation of the flume, in meters, measured over 2 hours with a flow of 1.0 L/s and sediment supplied at (A) the equilibrium transport rate (B) no upstream supply and (C) double the equilibrium transport rate. Plot showing erosion and deposition volumes measured in the test section as a function of elevation for the various supply rates after 120 minutes (D).

The differences between the supply rates are most discernable in the upper portion of the flume. For the flume run conducted with the equilibrium transport rate (Fig. 1A), the net change in the volume of the test section was a relatively small gain of 358 cm^3. The undersupply run (Fig. 1B) was dominated by erosion in this section and the net change in sediment volume in the test section was a loss of 1768 cm^3. The run with twice the equilibrium transport rate (Fig. 1C) resulted in a delta at the upstream end of the flume that continued to propagate downstream as

the experiment progressed, resulting in a net increase in sediment volume of 2273 cm^3 in the test section.

The morphology of the runs shown in figure 1 could be classified as alternate bars with deeper regions periodically forming along opposing channel walls. A volumetric change plot, which is computed over the inner third of the flume (test section) also highlights differences between the 3 sediment supply rates (Fig. 1D). The volume and height of deposition is highest for double the equilibrium supply rate, whereas the volume of erosion is highest when sediment is not supplied. Not surprisingly, supplying sediment at the equilibrium transport rate shows more equivalent volumes of erosion and deposition.

Flow Experiments A series of experiments was conducted to simulate the effect of flow regulation on channel morphology. These experiments are analogous to river reaches that have experienced alterations in flow due to dams or diversions. Two discharges were examined in detail, 0.5 and 1 L/s. Multiple runs were conducted for each discharge without upstream sediment supply and each lasting a duration of 1 hour.

Figures 2A and 2B illustrate the topographic changes that were measured for Run 3 (1 L/s) and Run 9 (0.5 L/s). The experiments conducted at 1.0 L/s displayed a similar pattern of channel evolution. Typically the channel formed higher mode bars during the initial 15 minutes of the experiment (Fig 2A). Following the 15-minute survey, when flow in the flume resumed, the channel evolved to have a more meandering pattern in which the main thalweg was found along alternating sides of the flume. The experiments conducted at 0.5 L/s (Fig. 2B) initiated bed forms in the first 15 minutes that, based on visual inspection, were less symmetric and of lower relief than the higher mode bars that developed early in the 1.0 L/s experiments. The initiation and progression of upstream erosion during the 1-hour flume run was also less clearly defined for the lower 0.5 L/s flow. Volumetric plots of the elevation changes after 1 hour for each run at 0.5 and 1.0 L/s show variability among each flow rate (Fig. 2C).

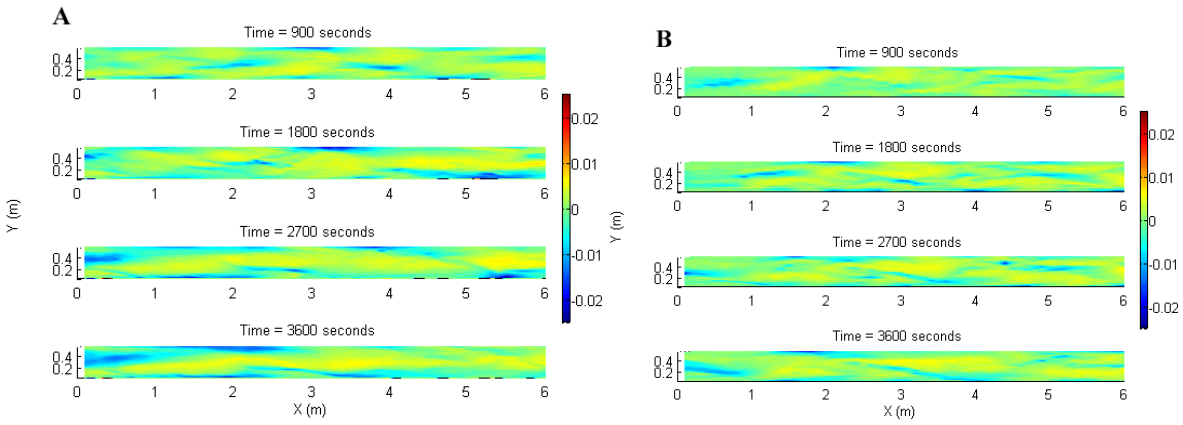

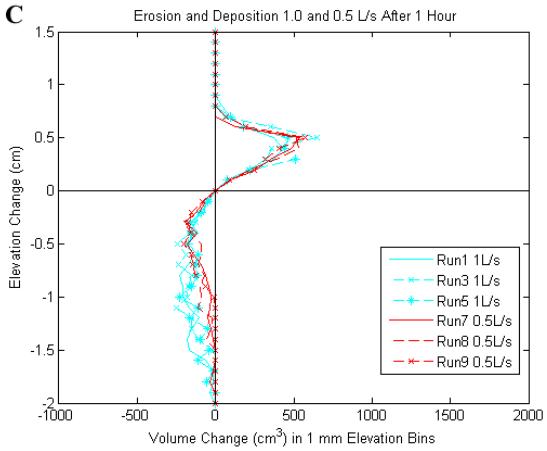

Figure 2 Changes in the bed elevation of the flume, in meters, measured over 1 hour for two flow rates (A) Run 3 at 1 L/s and (B) Run 9 at 0.5 L/s. Plot showing the erosion and deposition measured in the test section for various flow rates after 1 hour (C).

The greatest disparity in sedimentation between the flow rates was observed in the amount of erosion; the height of bar forms were rather consistent. The higher discharge caused more total erosion and erosion to lower elevations. This morphologic response is akin to that of a flushing event wherein water devoid of sediment is released into a channel from a dam or hydropower return canal.

Nays2DH Simulations The roughness value used in Nays2DH was determined by calibrating the water-surface elevation measured at 2 hours into the flume run with the model predicted water surface. This water-surface elevation was influenced by drag from bedforms created during the flume run, but acknowledging that drag changed because of bed evolution we reasoned this profile was most appropriate for calibration. The best calibration (root mean square error of 0.001 meter between measured and modeled water-surface elevations) was found using a Manning's n of 0.03. While Nays2DH can accept varying sediment supplies at the upstream end by specifying the ratio of supplied sediment transport to the equilibrium rate, there is presently no ability to input a transport rate to exactly match observations. We found better agreement in transport rate with our observations using the Ashida Michiue equation (~2.0 $x10^{-3}$ kg/s, i.e., 60.6 percent of the measured transport rate of the flume experiments) rather than the Meyer-Peter Müller equation (~2.0 $x10^{-2}$ kg/s, an order of magnitude greater than Ashida Michiue), which is expected as the latter was developed for fine gravel. Modeling experiments were conducted to compare two approaches for inducing bed instability and initiating bar development in a straight channel. Model results using an initial plane bed with a small bump placed immediately upstream as input are shown in figure 3. Figure 4 shows the outcome from using the flume topography measured at 15 minutes as the initial bed condition.

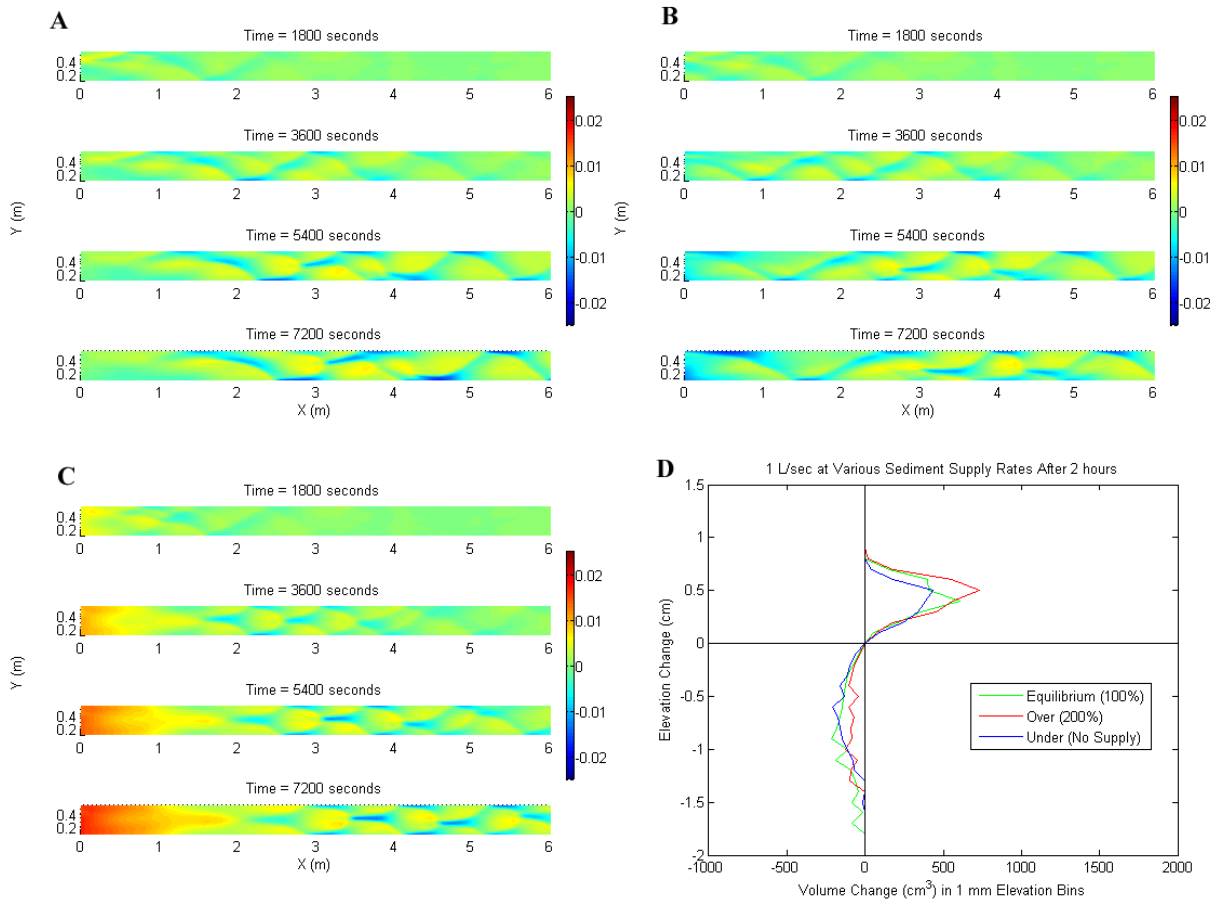

Figure 3 Changes in bed elevation predicted by Nays2DH using a plane bed with upstream perturbation as input and sediment supplied at (A) the equilibrium rate, (B) 0 percent of the equilibrium rate, and (C) 200 percent of the equilibrium rate. Plot showing erosion and deposition volumes predicted by Nays2DH in the test section as a function of elevation for the various supply rates after 2 hours (D).

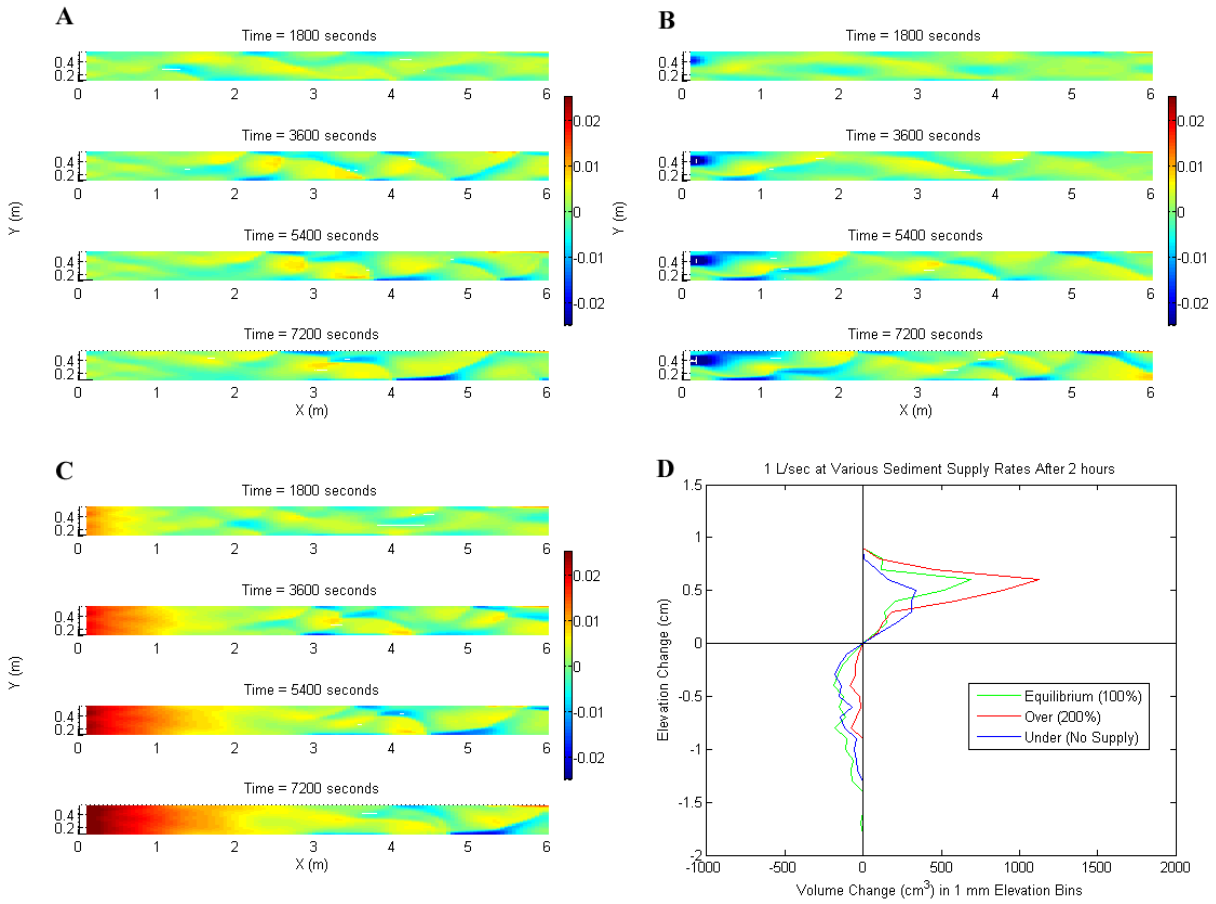

Figure 4 Changes in bed elevation predicted by Nays2DH using the antecedent bed topography in the flume measured at 15 minutes as input and sediment supplied at (A) the equilibrium rate, (B) 0 percent of the equilibrium rate and (C) 200 percent of the equilibrium rate. Plot showing erosion and deposition volumes predicted by Nays2DH in the test section as a function of elevation for the various supply rates after 2 hours (D).

Including secondary flows by computing the depth-averaged vorticity in the streamwise direction resulted in excessively weak alternate bar formation that did not match experimental results. Using the second option and increasing the strength of the secondary flow parameter N^*, from the default value of zero, was shown to induce more substantial variations in bed morphology and sediment storage. However, because we were simulating flow in a straight flume channel, we reasoned that adjusting this parameter was somewhat subjective and more justifiable for stronger meander bends, therefore the results are not discussed here. Nays2DH also is able to simulate periodic boundary conditions. If periodic boundary conditions are used, the sediment and hydraulic conditions calculated at the downstream end of the model domain are applied to the upstream end. However, in the present version of Nays2DH if periodic boundary conditions are enabled the supply of sediment at the upstream boundary cannot be changed from the equilibrium condition. Therefore, to ensure consistency among all supply rates modeled, we disabled this boundary condition for all runs.

DISCUSSION AND CONCLUSIONS

Two sets of flume experiments were carried out: one set with increasing sediment supply, the other with clear-water inflow at different flow rates. In conjunction these two sets of runs show the separate effects of flow rate and sediment supply changes on the morphologic evolution of a plane-bed channel. These experiments were conducted to illustrate and explore basic morphologic responses and serve as simple analogs to river management activities. The sediment supply experiments (Fig. 1) indicated that it was necessary to increase the supply at or above 133 percent of the equilibrium rate to appreciably increase bar heights. Although all runs showed both degradation and bar formation, the height of the bedforms was greater and degradation was smaller for the higher sediment supply rate (Fig. 1D), highlighting the role of sediment transport in bar formation and maintenance. In the clear-water flow experiments without upstream sediment supply, greater flow rates induced increased bed degradation, but did not contribute to the creation of bed forms with higher elevation (Fig. 2). This observation corroborates the idea that increased transport capacity (i.e., higher flow rates) must be accompanied by increased sediment availability in order to create and maintain higher bars and topographic relief.

The Nays2DH numerical model was used to simulate the conditions employed in the laboratory flume. The principal difficulties in the modeling effort were to accurately compute the sediment transport rates and to determine the ideal starting bed conditions for the onset of plane bed instability. Therefore, the primary causes for the differences between the physical flume experiments (Fig. 1) and the numerical simulations (Figs. 3 and 4) may be attributed to the boundary conditions supplied to the model. The initiation of morphologic evolution using an initially plane bed with an artificial perturbation produced higher mode bars at the end of the simulations than did predictions using the natural perturbations present in an antecedent flume topography, which more closely resembled the alternate bar or single-thread meandering morphology observed in the flume.

The initiation and progression of the scour under the no supply case was more pronounced using the antecedent bed condition over the plane bed topography but did not advance downstream to the extent of the flume observations. In addition, the delta predicted at the upstream end of the flume for each modeled over supply case was higher than observed in the flume. These observations indicate the transport rate calculated by the model was not sufficient in either input condition to advance these features, and it may be a direct consequence of the use of the Ashida and Michiue transport equation, which was shown to underestimate the equilibrium transport rate of the experimental conditions by over 39 percent.

The erosion and deposition volumes predicted by either input bed condition were about the same for the equilibrium supply case. For the under supply case, both models over predicted aggradation and under predicted degradation. Turning to the over supplied case, the plane bed input condition under predicted aggradation, whereas using the antecedent topography as input under predicted the degradation. Thus, it can be concluded that although using a natural perturbation produced a morphology that was more analogous to the final evolved flume topography, the transport rates predicted by the model were not sufficient to match the sedimentation observed in the test section. As above, the likely explanation is that the transport

rate computed by the model was less than that of the experiments. Unfortunately, Nays2DH does not at present offer a means to scale existing transport equations to match the observed conditions.

Future work will include comparing the flume experiments and, ultimately, morphologies from river management experiments with predictions from other models in iRIC. These models offer different approaches to sediment transport modeling, such as other transport equations, and can account for three-dimensional flow effects. While resulting in somewhat more computationally expensive models, inclusion of additional boundary conditions (e.g. side wall friction) and three-dimensional simulation of the flow structure and its influence on sediment transport can provide more accurate representation of the dynamics of channel evolution.

REFERENCES

Ashida, K., and Michiue, M. (1972). "Study on hydraulic resistance and bedload transport rate in alluvial streams," *in* Transcripts of the Japan Society for Civil Engineers, pp. 59–69.

Engelund, F. (1974). "Flow and bed topography in channel bends," Journal of the Hydraulics. Division, ASCE, 100(11), pp. 1631-1648.

Fujita, Y. and Muramoto, Y. (1985). "Studies on the process and development of alternate bars", Reprinted from Bulletin of the Disaster Prevention Research Institute Kyoto University, Volume 35, pp. 55-86.

Fujita, Y. (1989). "Bar and channel development in braided streams," *in* S. Ikeda and G. Parker eds., River Meandering, Water Resources Monograph 12, American Geophysical Union, pp. 417-462.

iRIC Project (2014). Nays2DH Solvers Manual. 60 p., accessed October 1, 2014, at http://i-ric.org/en/downloads.

Germanoski D, Schumm S.A. (1993). "Changes in braided river morphology resulting from aggradation and degradation." Journal of Geology, 101, pp. 451–466.

Jang, C. and Shimizu, Y. (2005). "Numerical simulation of relatively wide, shallow channels with erodible banks," Journal of Hydraulic Engineering, 131(7), pp. 565-575.

Kinzel, P.J., Nelson, J.M., McDonald, R.R. and Logan, B.L. (2010). "Topographic evolution of sandbars: laboratory experiment and computational modeling," Proc. of the Joint 9th Federal Interagency Sedimentation Conference and 4th Federal Interagency Hydrologic Modeling Conference, June 27 – July 1, 2010, Las Vegas, Nevada, 8p.

Madej, M.A., Sutherland, D.G., Lisle, T.E. and Pryor, B. (2009). "Channel responses to varying sediment input: A flume experiment modeled after Redwood Creek, California," Geomorphology, 103, pp. 507–519.

Marti, C. and Bezzola, G.R. (2006). "Bed load transport in braided gravel-bed rivers," *in* G.H. Sambrook Smith, J.L. Best, C.S. Bristow, and G.E. Petts, eds., Braided Rivers: Process, Deposits, Ecology and Management, Blackwell Publishing, pp. 199-215.

Meyer-Peter, E. and Müller, R. (1948). "Formulas for bed-load transport." Proc., 2nd Congress, IAHR, Stockholm, Sweden, 2(2), pp. 39-64.

National Research Council. (1999). Downstream: Adaptive Management of Glen Canyon Dam and the Colorado River Ecosystem. Washington, D.C.: National Academy Press.

Nelson, J.M., Shimizu, Y., Takebayashi, H. and McDonald, R.R. (2010). "The international river interface cooperative: public domain software for river modeling," in *Proceedings of the Joint 9th Federal Interagency Sedimentation Conference and 4th Federal Interagency Hydrologic Modeling Conference*, June 27 – July 1, 2010, Las Vegas, Nevada, 8p.

Platte River Recovery Implementation Program (PRRIP) (2014). Sediment augmentation—Final pilot study report: 87 p., appendices, accessed July 2014 at https://www.platteriverprogram.org/PubsAndData/ProgramLibrary/PRRIP%20Final%20Sediment%20Augmentation%20Pilot%20Study%20Report.pdf.

Shimizu, Y. (2002). "A method for simultaneous computation of bed and bank deformation of a river," *in* Proc. of the International Conference on Fluvial Hydraulics, River Flow 2002, Louvain-la-Neuve, Belgium, vol. 2, pp.793-802.

Takebayashi, H. and Okabe, T. (2009). "Numerical modeling of braided streams in unsteady flow," Water Management, Institution of Civil Engineers, Thomas Telford Publishing, Volume 162, Issue 3, pp.189-198.

Takebayashi, H. (2005). "River configuration in middle-lower reach of river basin," Journal of Japan Society of Fluid Mechanics, 24(1), pp. 27-36.

U.S. Department of the Interior (2006). Platte River Recovery Implementation Program Final Environmental Impact Statement. Volume 1.

Watanabe, A., Fukuoka, S., Yasutake, Y. and Kawaguchi, H. (2001). "Method for Arranging Vegetation Groins at Bends for Control of Bed Variation," Advances on River Engineering, 7, pp. 285-290. (in Japanese).

USE OF FLUX AND MORPHOLOGIC SEDIMENT BUDGETS FOR SANDBAR MONITORING ON THE COLORADO RIVER IN MARBLE CANYON, ARIZONA

Paul E. Grams, Research Hydrologist, U.S. Geological Survey, Flagstaff, Arizona, pgrams@usgs.gov; Daniel Buscombe, Research Geologist, U.S. Geological Survey, Flagstaff, Arizona, dbuscombe@usgs.gov; David J. Topping, Research Hydrologist, U.S. Geological Survey, Flagstaff, Arizona, dtopping@usgs.gov; Joseph E. Hazel Jr., Research Associate, Northern Arizona University, Flagstaff, Arizona, Joseph.Hazel@nau.edu; Matt Kaplinski, Research Associate, Northern Arizona University, Flagstaff, Arizona, matt.kaplinski@nau.edu

INTRODUCTION

The magnitude and pfattern of streamflow and sediment supply of the Colorado River in Grand Canyon (Figure 1) has been affected by the existence and operations of Glen Canyon Dam since filling of Lake Powell Reservoir began in March 1963. In the subsequent 30 years, fine sediment was scoured from the downstream channel (Topping et al., 2000; Grams et al., 2007), resulting in a decline in the number and size of sandbars in the eastern half of Grand Canyon National Park (Wright et al., 2005; Schmidt et al., 2004). The Glen Canyon Dam Adaptive Management Program (GCDAMP) administered by the U.S. Department of Interior oversees efforts to manage the Colorado River ecosystem downstream from Glen Canyon Dam. One of the goals of the GCDAMP is to maintain and increase the number and size of sandbars in this context of a limited sand supply. Management actions to benefit sandbars have included curtailment of daily streamflow fluctuations, which occur for hydropower generation, and implementation of controlled floods, also called high-flow experiments.

Studies of controlled floods, defined as intentional releases that exceed the maximum discharge capacity of the Glen Canyon Dam powerplant, implemented between 1996 and 2008, have demonstrated that these events cause increases in sandbar size throughout Marble and Grand Canyons (Hazel et al., 2010; Schmidt and Grams, 2011; Mueller et al., 2014), although the magnitude of response is spatially variable (Hazel et al., 1999; 2010). Controlled floods may build some sandbars at the expense of erosion of sand from other, upstream, sandbars (Schmidt, 1999). To increase the frequency and effectiveness of sandbar building, the U.S. Department of Interior adopted a "high-flow experimental protocol" to implement controlled floods regularly under conditions of enriched sand supply (U.S. Department of Interior, 2012). Because the supply of sand available to build sandbars has been substantially reduced by Glen Canyon Dam (Topping et al., 2000) and depends entirely on infrequent tributary floods, monitoring of both sandbars and gross sand storage (the sand budget) is required to evaluate whether the high-flow protocol is having the intended effect of increasing sandbar size without progressively depleting sand from the system.

There are many challenges associated with monitoring sand storage and active sand deposits in a river system as large and complex as the 450-km segment of the Colorado River between Glen Canyon Dam and Lake Mead. Previous studies have demonstrated the temporal variation in sand storage associated with sand-supply limitation (Topping et al., 2000) and the spatial variability in the amount of sand stored in eddies and the channel associated with channel hydraulics (Grams et al., 2013). In this study, we report on companion measurements of sand flux and morphologic change to quantify, for the first time, the relation between changes in sand mass balance, changes

in within-channel sand storage, and changes in sandbars comprehensively for a 50-km river segment of the Colorado River in lower Marble Canyon within Grand Canyon National Park.

We show that, when measured over the scale of a 50-km river segment, these complementary measurements of the sand budget agree within measurement uncertainty and provide a rare opportunity to integrate the temporally rich sand-flux record with the spatially rich morphologic measurements. Both methods show that sediment was evacuated from lower Marble Canyon over the 3-year study period. The flux-based budget shows the timing of changes in storage relative to dam-release patterns, while the morphologic measurements depict the spatial distribution of erosion and deposition among different depositional settings.

Figure 1 Map of Colorado River between Lake Powell and Lake Mead. Marble Canyon is the river segment between Lees Ferry and the Little Colorado River confluence. The focus of this study is lower Marble Canyon, which is the 50-km segment of Marble Canyon that begins 50 km downstream from the mouth of the Paria River. Grand Canyon is the segment of the Colorado River from the Little Colorado River confluence to Lake Mead.

METHODS

Flux-based Sand Budget: Streamflow and suspended sediment transport are monitored continuously (15-minute intervals) at the upstream and downstream ends of lower Marble Canyon (Figure 1). Streamflow is gaged by standard gaging methods (Rantz et al., 1982) and sediment concentration is monitored with acoustic instruments that are calibrated to conventional suspended-sediment samples (Griffiths et al., 2012; Topping et al., 2015). These data are used to compute 15-minute sediment loads separately for mud (silt and clay) and sand. The instantaneous values for discharge and concentration from each gage and sand budgets computed

for any time interval between 2002 and present are available at www.gcmrc.gov/discharge_qw_sediment/.

Morphologic-based Sand Budget: Riverbed and sandbar topography were measured by surveys with total stations, singlebeam sonar, and multibeam sonar during separate two-week field campaigns in May 2009 and May 2012. Multibeam sonar was used to map the river channel in all locations with sufficient depth, generally 2 m or deeper. Singlebeam sonar was primarily used to map shallower depths along the channel margins. Some reaches were mapped entirely with singlebeam sonar. Total stations were used to survey sand deposits along and above the water's edge. Gravel bars, talus slopes, and debris fans were not typically surveyed. Areas of the channel where upstream navigation was not possible and areas of the banks dominated by established woody riparian vegetation also were not surveyed. Thus, most of the area of the channel not surveyed consists of immobile or rarely mobile gravel and boulders; most of the area on the channel margins not surveyed has been stabilized by vegetation. Details on the methods of data collection, processing, construction of digital elevation models (DEMs), and analysis of uncertainty are described in Hazel et al. (2008) and Kaplinski et al. (2009; 2014).

The difference between the 2009 and 2012 DEMs was computed for each 1-m grid cell and uncertainty was assigned based on the method of data collection (Kaplinski et al., 2014). Volumes of erosion, deposition, and net change were tabulated by geomorphic unit. The primary geomorphic units are eddy, channel adjacent to eddy, other channel, onshore sandbar, and sandbar above reference stage (Figure 2). Eddies were defined as regions of recirculating flow based on water-surface streamflow paterns at 8,000 ft^3/s. The channel adjacent to the eddy is the entire width of downstream-directed current in the channel adjacent to the length of an eddy. The onshore sandbar category is comprised of all the morphologic types of sandbars described by Schmidt (1990) that occur in eddies. The geomorphic units were mapped in a geographic information system (GIS) with May 2009 digital ortho-rectified imagery as a base and subsequently checked in the field for accuracy. For the purposes of volumetric calculations, onshore sandbars are the portions of the sand deposits in eddies that are above the subhorizontal plane (defined by water surface) associated with a discharge of 8,000 ft^3/s. Thus, changes in the onshore sandbars represent changes in sand volume above the 8,000 ft^3/s stage. The "other channel" category includes all portions of the channel not included in the categories described above.

Uncertainty in the estimate of morphologic change is based on the method of data collection, potential changes in storage for the 30% of the reach that was not mapped, and the potential that some topographic change comprised sediment other than sand. For areas mapped by multibeam sonar and singlebeam sonar, we estimate the uncertainty to be ±0.06 m and ±0.12 m, respectively, based on analysis of repeat maps over stable areas reported by Kaplinski et al. (2014). We estimate uncertainty for areas mapped by total station to be ±0.04 m. These values were multiplied by the area mapped by each method, using the method with greatest uncertainty for areas mapped by different methods in each year. The potential change for the portion of the reach not mapped was estimated based on the mean change in each map unit for the portion of the reach that was mapped. Determining the proportion of morphologic change that involved sand is challenging, because bed texture measured before or after the topographic change is not necessarily indicative of the texture of the material that was eroded or deposited. A comprehensive analysis considering both the direction and magnitude of topographic change and

textural changes is ongoing. In this analysis, we make the conservative estimate that as much as 30% of the morphologic change involved sediment other than sand. We assume each of the sources of uncertainty to be independent and, therefore, the uncertainties are summed in quadrature to arrive at an estimate of gross uncertainty for lower Marble Canyon.

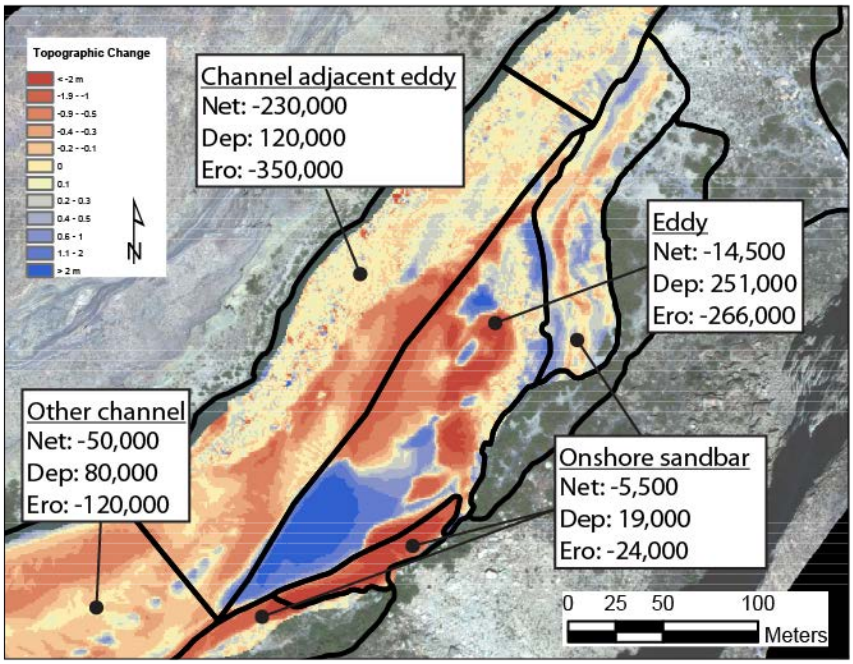

Figure 2 Illustration of sediment storage environments in lower Marble Canyon. Values indicate the volumes, in cubic meters, of net sand storage change, deposition, and erosion summed by indicated map unit for all areas mapped in lower Marble Canyon. Line separating onshore sandbars from eddy is water edge at 8,000 ft^3/s in May 2009. This example location is 71 km downstream from Lees Ferry. Streamflow is from upper right to lower left. All values are in cubic meters.

RESULTS

Comparison of Flux-based and Morphologic-based Sand Budgets: The sand budget computed by measurements of sand flux, and the sand budget computed as the difference between the two topographic surveys, agree within measurement uncertainty. Between May 1, 2009, and May 1, 2012, approximately 2.49 x 10^6 metric tons (Mg) of sand entered lower Marble Canyon at gage 9383050 (Figure 1) and approximately 3.06 x 10^6 Mg of sand was exported past gage 9383100. Ungaged tributaries added an estimated 20,000 Mg of additional sand to the reach. With uncertainty, this results in a flux-based sand budget of -550,000 ± 300,000 Mg (Figure 3). Based on a particle density of 2650 kg/m^3 and 35% porosity, that is equivalent to 320,000 ± 70,000 m^3 of net sand loss in the reach. Over the same time period, the repeat topographic measurements indicate approximately 770,000 m^3 of erosion and 470,000 m^3 of deposition resulting in a net change of -300,000 ± 250,000 m^3.

Most of the net changes in sand storage occurred in the areas of channel adjacent to eddies (Figure 2). However, net change in storage may not be the best metric to evaluate the relative

capacity of each storage environment. Although the net change in storage in eddies was relatively small, eddies were actually the most active storage environments in terms of gross storage change. Gross storage change is defined as the sum of the absolute values of erosion and deposition. For this period of net sand loss from lower Marble Canyon, there was widespread erosion in both the eddy and channel storage environments. However, erosion in eddies was compensated by an almost equally large volume of deposition. Relatively little deposition occurred in the channel. Thus, despite the relatively small net change, eddies were the most active storage environment. This new observation regarding the relative role of the eddy and channel storage environments likely has implications for the processes by which sand accumulates and evacuates from the river.

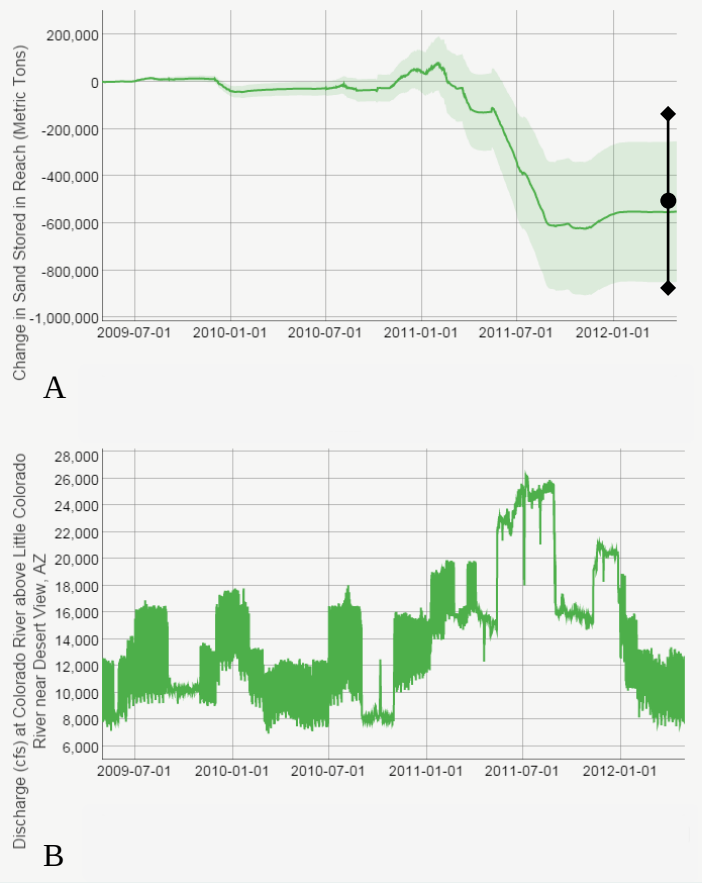

Figure 3 (A) Cumulative change in sand storage for lower Marble Canyon from May 1, 2009 to May 1, 2012. The solid line shows the zero-bias estimate; the shaded region shows the uncertainty band, which increases with time. The point with error bars shows the morphologic-based sand budget for the same period converted to units of mass, with uncertainty. (B) Discharge of the Colorado River at the upstream end of lower Marble Canyon (U.S. Geological Survey gage 9383050). Plot generated Nov. 6, 2014 at www.gcmrc.gov/discharge_qw_sediment/.

Spatial Variability in Sandbar Erosion and Deposition: The parts of sandbars that are exposed above the water surface and available for use by river runners as campsites are of the greatest management interest. Those areas, however, comprise a small proportion of the total

sediment budget. Both the net and gross changes in onshore sandbars were small fractions of the gross changes in other storage environments (Figure 2). Only 2% of the 300,000 m^3 of net storage change in lower Marble Canyon occurred in onshore sandbars above the elevation associated with a discharge of 8,000 ft^3/s, despite the fact that flows exceeded 8,000 ft^3/s over 95% of the time.

While changes in the channel, eddy, and sandbar storage environments are related on some relatively large spatial scale, changes in onshore sandbars and the adjacent eddy and channel appear to be poorly correlated. Over some spatial scale, when sand is depleted from the channel and eddies, more sandbars decrease in size than increase in size. This is shown in a plot of the cumulative changes in each geomorphic unit (Figure 4). Although the cumulative changes do not track precisely, there is consistency between loss of sand from the channel and eddies and decreases in the volume of sand in sandbars. Although this correspondence in the general direction of change exists, the changes are not well correlated at the scale of individual eddies (Figure 5). It is therefore not possible to predict the response of individual sandbars based on the response of the adjacent channel. Correspondingly, responses for individual sandbars cannot be inferred to be representative of the status of sand storage in the adjacent eddy and channel. Based on the data shown in Figures 4 and 5, it appears that there is correlation between onshore sandbar response and eddy/channel response at scales of a few km. However, the spatial scale of this coupling is likely to depend on many factors, including the length of the time interval analyzed, streamflow during the interval, the amount of sand-storage change, and the sand grain size. Thus, further investigation considering these and other factors is required.

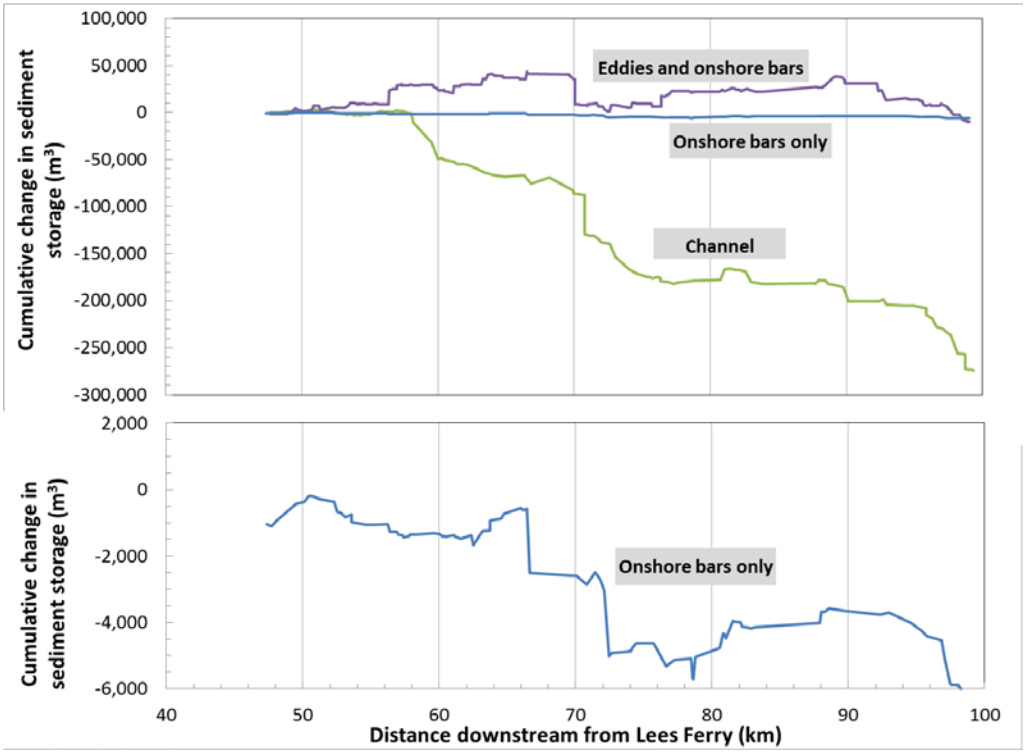

Figure 4 Cumulative downstream change in net sediment storage in lower Marble Canyon by depositional setting. Top panel shows all depositional settings, bottom panel shows the same data for onshore bars only at increased vertical scale.

Evaluation of Sandbar Sampling Design: Comprehensive measurements of onshore sandbar change made throughout lower Marble Canyon between 2009 and 2012 provide the opportunity to evaluate the sampling design for site-based sandbar monitoring that has been in place since 1990. Changes in sandbar topography have been monitored annually since 1990 at study sites throughout Marble and Grand Canyons (Hazel et al., 2010). In lower Marble Canyon, topographic changes of 18 sandbars in 14 different eddies are monitored above the 8,000 ft^3/s reference stage (Hazel et al., 2010). The success or failure of management actions, such as controlled floods, to cause net increases in sandbar size is based largely on the changes in sandbar volume measured at these sites. The maps of geomorphic units described above show that lower Marble Canyon contains 176 eddies larger than 1000 m^2 (combined area of eddy and onshore sand deposits), 84 of which had onshore sandbars larger than 100 m^2 and were mapped in both 2009 and 2012. Thus, the 18 sandbars that are monitored annually comprise a relatively small sample of the total number of large sandbars. Below, we compare topographic changes at the 18 sandbars that are monitored annually with changes that occurred at all 84 sandbars mapped in 2009 and 2012.

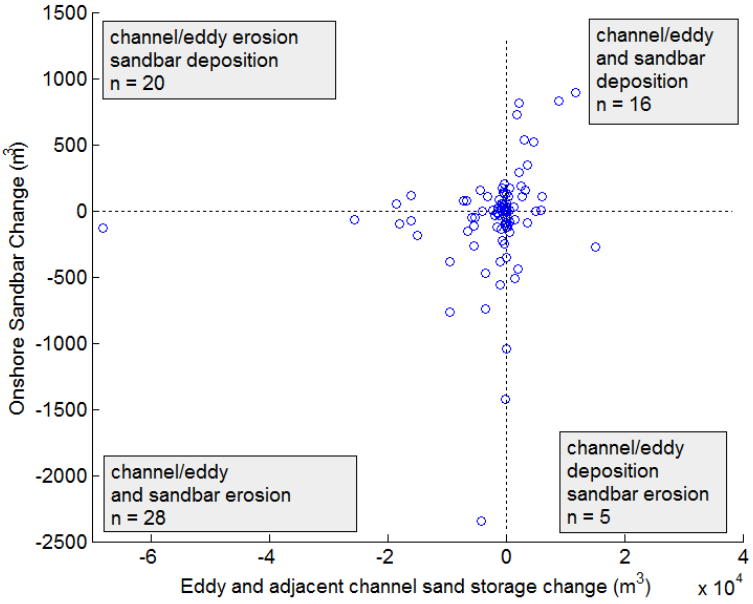

Figure 5 Change in onshore sandbar volume as function of change in channel and eddy storage for the corresponding eddy. This shows that changes in onshore sandbars are not well-correlated with sediment storage change in the same eddy and adjacent channel.

The mean change in sandbar thickness (volume normalized by area) between 2009 and 2012 for these sites (-0.06 m ± 0.06 m standard error), is consistent with the mean change among the much larger sample of 84 sandbars mapped throughout lower Marble Canyon (-0.10 m ± 0.06 m standard error) (Figure 6A). While the mean responses among the two sample sizes are similar for this period, they do not necessarily reflect the full range of sandbar responses, in particular those sites with large gains or large losses. The variance of sand thickness change between 2009 and 2012 among all sandbars in lower Marble Canyon (σ^2=0.12) is double the variance among the 18 monitoring sites (σ^2=0.06), showing that for this period, the monitoring sites had smaller-

magnitude changes than was observed among all sandbars. This suggests that while the set of long-term monitoring sites may adequately represent mean sandbar condition, it fails to capture the full extent of variability in sandbar condition. A bootstrap analysis using all 84 sites surveyed in 2009 and 2012 in lower Marble Canyon indicates that a random sampling of fewer than the current number of monitoring sites would be unlikely to capture mean bar condition better than the current configuration of monitoring sites. The standard error on the mean sandbar thickness as a function of sample size (Figure 6B) suggests that the 18 sites regularly surveyed would capture the trend in the mean sandbar thickness to within approximately 10 cm. While this is a marginally acceptable uncertainty, Figure 6B suggests that one would expect an exponential increase in this uncertainty with decreasing sample size, which is an important consideration for sampling design elsewhere in the canyon.

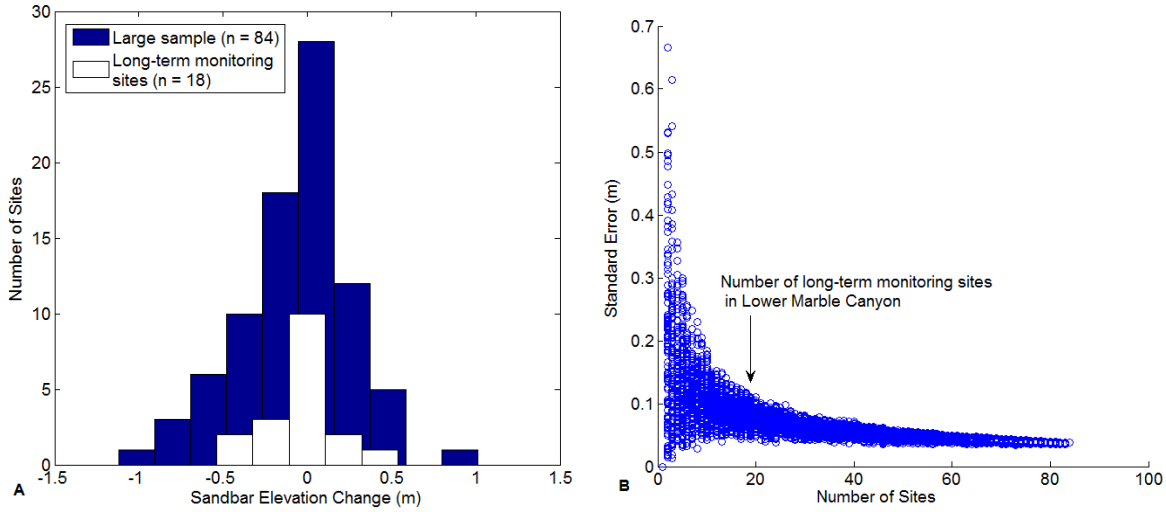

Figure 6 (A) Histograms showing frequency distribution of changes in sandbar elevation for the 84 onshore sandbars measured in lower Marble Canyon (blue) and the 18 of those that are also long-term monitoring sites (white). (B) Bootstrap simulation of expected standard error for estimates of sandbar thickness change as a function of sample size. Measurements of thickness change for 84 sandbars in lower Marble Canyon were sampled randomly using increasing sample size (1 to 84). For each sample size, 100 random selections of (1 – 84) sites were made from among the 84 sites, and the standard error calculated and plotted.

DISCUSSION AND CONCLUSIONS

The goals of resource managers on the Colorado River in Grand Canyon National Park include maintaining and improving the condition of alluvial sandbars in a system that has been perturbed into severe fine-sediment deficit by an upstream dam (Schmidt and Wilcock, 2008). While controlled floods are the most cost-effective management tool that is currently available to achieve that goal, it is uncertain whether sand supply is sufficient to support repeated sandbar building in the context of other dam operations, which also export fine sediment (Wright and others, 2008; Wright and Grams, 2010). The data reported here span a 3-year period that did not include controlled floods but did include over 3 months of steady dam releases that greatly exceeded the range of normal dam operations (Figure 3). The measurements of sand flux and the

measurements of sediment storage change both indicate that these releases evacuated on the order of 300,000 m^3 (500,000 Mg) of sediment from lower Marble Canyon.

Previous attempts to construct a closed sand budget for lower Marble Canyon based on measurements of morphologic change for short monitoring reaches were unsuccessful, because large spatial variability in erosion and deposition resulted in the inability to extrapolate measurements from short reaches to the entire 50-km segment (Grams et al., 2013). In this case, mapping morphologic change in approximately 70% of the same segment resulted in good agreement between the flux-based and morphologic-based budgets. This greatly increases confidence in both the measurements of flux and morphologic change. The results further demonstrate the challenge associated with using morphologic measurements to infer a sediment budget at a scale larger than the reach measured. Although a 10-km study reach might often be considered to be of sufficient length to be representative of a longer river segment, it is clear that in lower Marble Canyon, there are significant differences in the magnitude of sand-storage change between adjacent 10-km reaches (Figure 4). Therefore, without detailed knowledge about the behavior of all major sand-storage locations, it would not be possible to construct an accurate morphologic-based sediment budget for a long river segment like lower Marble Canyon based on a sub-sample of the segment.

The measurements of flux show that nearly all of the sand evacuation occurred during the high releases of summer 2011 (Figure 3). The maps of channel topographic change reveal the locations of that sediment evacuation. Previous studies concluded that most sand-storage changes in Marble and Grand Canyons occurred within zones of recirculating flow – eddies (Hazel et al., 2006). Our findings support that conclusion with some qualification. Between 2009 and 2012 in lower Marble Canyon, eddies were the most active sediment storage environment, but exhibited very little net change in sediment storage. Most net change in sediment storage occurred in the main channel adjacent to eddies. The Hazel et al. (2006) study was conducted over a period that that followed relatively high dam-release volumes and focused on changes that occurred over a short period during a controlled flood. In contrast, we studied changes over a three-year period following relatively low dam-release volumes. This illustrates that the behavior of different storage environments can vary widely depending on the period examined. Because both eddy and channel storage environments are very large and either may dominate the signal of net change in sand storage, both must be measured to compute an accurate sediment budget.

The observations also demonstrate that the entire debris-fan eddy complex (Schmidt and Rubin, 1995) is the dominant storage environment, not just the recirculation zone. The channel adjacent to the eddy includes a scour hole and pool exit slope, both of which accumulate and evacuate sediment. While the channel adjacent to eddies was the dominant location of net change in this period of scour, it is possible that the relative proportions of change between the eddies and channel could reverse in other periods.

This period of sand evacuation followed a period of large tributary inputs and sand accumulation from 2004 through 2010 (Topping et al., 2010). Repeat topographic maps of short reaches within lower Marble Canyon from 2002, 2004, and 2009 also indicate that 2009 was a period of enriched sand storage. We speculate that both channel and eddy sand-storage locations were relatively full at the beginning of the high dam releases in 2011. During the elevated sand concentrations that occurred as sand was exported from the reach, it is likely that eddies were

locations of substantial mixing between the bed and suspension, while sand was simply scoured from other storage locations. In this way, the eddies behave as a buffer for sand evacuation. If all of the sand mobilized in the 2009-2011 interval had been eroded (i.e. the sand deposited in eddies was instead exported), the net loss of sand could have been nearly twice as large as actually occurred. At least 250,000 m^3 of easily mobilized sand remained in storage within the eddies. Thus, if the 2011 high releases continued for a longer period of time, we would expect that sand evacuation would have continued at a high rate for much longer. This is consistent with the measurements of sand flux, which do not indicate a decline in the rate of evacuation during 2011 (Figure 3).

On the scale of the entire 50-km segment of lower Marble Canyon, the changes in onshore sandbars tracked with the overall decline in sand storage. There was net loss of sand from the river channel and net decrease in the volume of sand in onshore sandbars. Previous studies have shown that for short time periods (e.g. the several day span of a controlled flood), there can be widespread deposition on the onshore sandbars while there is net sand loss from the deeper parts of eddies and the main channel (Schmidt, 1999; Hazel et al., 2010; Wright and Kaplinski, 2011). The findings from this comprehensive sand budget for lower Marble Canyon suggest that over the time scale of a few years (e.g. the 3-year period of this study) or longer, onshore sandbars generally increase in size when the sand budget is positive and decrease in size when the sand budget is negative.

There is not, however, a direct correlation in the response between the combined channel/eddy storage environment and the adjacent onshore sandbar. The change in onshore sandbars can be muted or amplified relative to the change in the adjacent eddy and channel. In some cases, the change in the onshore sandbar is the opposite sign of the change in the channel and eddy. This means that in order to monitor both the status of the sand budget and the status of onshore sandbars, it is necessary to monitor both, even though the net changes in the onshore sandbars are small relative to the overall sand budget. Further investigation is required to better describe the spatial scale at which channel, eddy, and onshore sandbar response are coupled. Sandbar sampling design is further informed by an examination of the change in sandbar elevation for the onshore sandbars mapped in lower Marble Canyon. This analysis indicates that the 18 sites currently monitored in the 50-km reach is likely a minimum sample size to reasonably represent the mean response exhibited in the larger set of 84 sandbars.

REFERENCES

Grams, P. E., Schmidt, J. C., and Topping, D. J. (2007). "The rate and pattern of bed incision and bank adjustment on the Colorado River in Glen Canyon downstream from Glen Canyon Dam, 1956-2000," *Geological Society of America Bulletin, 119*(5/6), 556-575.

Grams, P. E., Topping, D. J., Schmidt, J. C., Hazel, J. E., and Kaplinski, M. (2013). "Linking morphodynamic response with sediment mass balance on the Colorado River in Marble Canyon: Issues of scale, geomorphic setting, and sampling design," *Journal of Geophysical Research, 118*, 21.

Griffiths, R. E., Topping, D. J., Andrews, T., Bennet, G. E., Sabol, T. A., and Melis, T. S. (2012). "Design and maintenance of a network for collecting high-resolution suspended-sediment data at remote locations on rivers, with examples from the Colorado River," *U.S. Geological Survey Techniques and Methods, book 8, chapter C2*, 44.

Hazel, J. E., Topping, D. J., Schmidt, J. C., and Kaplinski, M. (2006). "Influence of a dam on fine-sediment storage in a canyon river," *Journal of Geophysical Research, 111*(F01025).

Hazel, J. E., Kaplinski, M., Parnell, R., Manone, M., and Dale, A. (1999). Topographic and bathymetric changes at thirty-three long-term study sites, in *The Controlled Flood in Grand Canyon*, edited by R. H. Webb, J. C. Schmidt, R. A. Valdez and G. R. Marzolf, American Geophysical Union.

Hazel, J. E., Jr., Grams, P. E., Schmidt, J. C., and Kaplinski, M. (2010). "Sandbar response following the 2008 high-flow experiment on the Colorado River in Marble and Grand Canyons," *U.S. Geological Survey Scientific Investigations Report 2010-5015*, 52.

Hazel, J. E., Jr., Kaplinski, M., Parnell, R. A., Kohl, K., and Schmidt, J. C. (2008). "Monitoring fine-grained sediment in the Colorado River Ecosystem, Arizona-Control network and conventional survey techniques," *U.S. Geological Survey Open-File Report 2008-1276*, 15.

Kaplinski, M., Hazel, J. E., Jr., Grams, P. E., and Davis, P. A. (2014). "Monitoring Fine-Sediment Volume in the Colorado River Ecosystem, Arizona: Construction and Analysis of Digital Elevation Models," *U.S. Geological Survey Open-file Report 2014-1052*, 36.

Kaplinski, M., Hazel, J. E., Parnell, R., Breedlove, M., Kohl, K., and Gonzales, M. (2009). "Monitoring Fine-Sediment Volume in the Colorado River Ecosystem, Arizona: Bathymetric Survey Techniques," *U.S. Geological Survey Open-File Report 2009-1207*, 41.

Mueller, E. R., Grams, P. E., Schmidt, J. C., Hazel, J. E., Jr., Alexander, J. S., and Kaplinski, M. (2014). “The influence of controlled floods on fine sediment storage in debris fan-affected canyons of the Colorado River basin,” Geomorphology, 226, 65-75.

Rantz, S. E. (1982). "Measurement and computation of streamflow: Volume 1. Measurement of Stage and Discharge," *U.S. Geological Survey Water Supply Paper 2175*, 313.

Schmidt, J. C. (1990). "Recirculating flow and sedimentation in the Colorado River in Grand Canyon, Arizona," *Journal of Geology, 98*, 709-724.

Schmidt, J. C. (1999). Summary and synthesis of geomorphic studies conducted during the 1996 controlled flood in Grand Canyon, in *The 1996 Controlled Flood in Grand Canyon scientific experiment and management demonstration*, edited by R. H. Webb, J. C. Schmidt, R. A. Valdez and G. R. Marzolf, AGU, Washington, D.C.

Schmidt, J. C., and Rubin, D. M. (1995). Regulated streamflow, fine-grained deposits, and effective discharge in canyons with abundant debris fans, in *Natural and anthropogenic influences in fluvial geomorphology*, edited by J. E. Costa, A. J. Miller, K. W. Potter and P. R. Wilcock, pp. 177-195, American Geophysical Union.

Schmidt, J. C., and Wilcock, P. R. (2008). "Metrics for assessing the downstream effects of dams," *Water Resources Research, 44*(W04404).

Schmidt, J. C., and Grams, P. E. (2011). The high flows--physical science results, in *Effects of three high-flow experiments on the Colorado River ecosystem downstream from Glen Canyon Dam, Arizona, U.S. Geological Survey Circular 1366*, edited by T. S. Melis, pp. 53-91.

Schmidt, J. C., Topping, D. J., Grams, P. E., and Hazel Jr., J. E. (2004). System-wide changes in the distribution of fine sediment in the Colorado River corridor between Glen Canyon Dam and Bright Angel Creek, Arizona: U.S. Geological Survey, Grand Canyon Monitoring and Research Center, Flagstaff, Ariz., 107 p. http://www.gcmrc.gov/library/reports/Physical/Fine_Sed/Schmidt2004.pdf

Topping, D. J., Rubin, D. M., Grams, P. E., Griffiths, R. E., Sabol, T. A., Voichick, N., Vanaman, K. M. (2010). Sediment transport during three controlled-flood experiments on

the Colorado River downstream from Glen Canyon Dam, with implications for eddy-sandbar deposition in Grand Canyon National Park : U.S. Geological Survey Open-file Report 2010-1128, 111 p.

Topping, D. J., Rubin, D. M., and Vierra, L. E. J. (2000). "Colorado River sediment transport 1. Natural sediment supply limitation and the influence of Glen Canyon Dam," *Water Resources Research*, *36*(2), 515-542.

Topping, D.J., Wright, S.A., Griffiths, R.E., Dean, D.J. (2015). "Physically based method for measuring suspended-sediment concentration and grain size using multi-frequency arrays of acoustic-Doppler profilers," in Proc. of the 3rd Joint Federal Interagency Conference, Reno, Nevada, April 19-23, 2015.

U.S. Department of the Interior (2012). Environmental Assessment: Development and Implementation of a Protocol for High-Flow Experimental Releases from Glen Canyon Dam, Arizona, 2011 through 2020, Bureau of Reclamation, Salt Lake City, Utah, 546 p, http://www.usbr.gov/uc/envdocs/ea/gc/HFEProtocol/index.html.

Wright, S. A., and Grams, P. E. (2010). Evaluation of water year 2011 Glen Canyon Dam flow release scenarios on downstream sand storage along the Colorado River in Arizona, U.S. Geological Survey Open-file Report 2010-1133, 19 p.

Wright, S. A., & Kaplinski, M. (2011). “Flow structures and sandbar dynamics in a canyon river during a controlled flood, Colorado River, Arizona,” *Water Resources Research*, 116(F01019). doi:10.1029/2009JF001442, 2011

Wright, S. A., Melis, T. S., Topping, D. J., and Rubin, D. M. (2005). Influence of Glen Canyon Dam operations on downstream sand resources of the Colorado River in Grand Canyon, in *The state of the Colorado River ecosystem in Grand Canyon*, edited by S. P. Gloss, J. E. Lovich and T. S. Melis, pp. 17-31, U.S. Geological Survey Circular 1282.

Wright, S. A., Schmidt, J. C., Melis, T. S., Topping, D. J., and Rubin, D. M. (2008). "Is there enough sand? Evaluating the fate of Grand Canyon sandbars," *GSA Today*, *18*(8).

PREDICTING AND COMPARING MEASURED BULKING AND PEAK DISCHARGE USING MULTIPLE METHODS FOR POST FIRE HYDROLOGIC AND SEDIMENTATION ANALYSIS ON THE DUMP FIRE IN SARATOGA SPRINGS

Nathaniel Todea, USDA Natural Resources Conservation Service Hydraulic Engineer, 125 South State Street Room 4010, Salt Lake City, Utah 84106, 801.524.4573, Nathaniel.Todea@ut.usda.gov

Abstract: As part of the 2012 Utah fire season, analysis of the Dump Fire was conducted to design sediment basins. The event was estimated to be a 1.25-inch storm that lasted 25 minutes and dropped an estimated bedload of 70,000 tons of material, which damaged houses, inundated basements, and overtopped a small basin. The event is comparable to two times the 100-year (1% chance event) flow. The Dump Fire was analyzed as a part of the United States Department of Agriculture Natural Resources Conservation Service Emergency Watershed Protection Program.

The Dump Fire watershed is located near Saratoga Springs, Utah, which is on the eastern edge of the Basin and Range physiographic region. It was analyzed using the United State Department of Agriculture Agricultural Research Service Automated Geospatial Watershed Assessment Tool (USDA-ARS AGWA). The runoff curve number (CN) and derived hydrologic characteristics were calibrated using local stream gage networks, regression equations (USGS StreamStats), National Oceanic and Atmospheric Administration (NOAA), National Weather Service NOAA Atlas 14 rainfall distribution, and modified cumulative Kirpich time of concentration methods for the pre-fire condition.

Furthermore, specific papers and their methods were analyzed and compared for modifications to CN based on burn severity and reduction of cover, changes to lag time, and other basin characteristics. Peak discharge and area of basin burned based on lithology and peak discharge was considered. Lag times were changed due to relative increases in CN. Fire related debris flow volumes from the Western U.S. regression model were used to compare final results.

Of the 70,000 tons of bedload material, about 15% made it to a housing development downstream. Typically, the ratio of sands and colloidal to bedload was estimated at 10:1 or 3:1 ratios. Since the AGWA value was within reason for the total sediment and sands as a percentage (i.e. 10%), it was assumed to be comparable to total bedload in this case. Overall, AGWA was found to be a reliable to tool for sedimentation / bulking values in this situation.

BACKGROUND

In late June 2012 wildfire burned the watershed above the Utah communities of Saratoga Springs and Eagle Mountain, about 40 miles south of Salt Lake City. Reported to have been sparked by target shooters, the fire burned approximately 6,000 acres and required the evacuation of an estimated 9,000 residents. No serious injuries or damages were reported as a result of the event, which became known at the Dump Fire. Local residents protested the name, which came about because the fire was started near an old dump. This case study will refer to the event as the Saratoga Springs Fire. See Figure 1 for location.

The wildfire prompted the City of Saratoga Springs to request assistance from the NRCS through the Emergency Watershed Protection Program (EWP). Storm damages following an early September rainfall event (only about a month after the fire) occurred before counter-measures could be installed. NRCS performed a post-fire hydrologic analysis in support of the design of a sediment basin to protect residents from the accelerated erosion and sedimentation caused by the fire. Figures 2 and 3 illustrate the burning watershed from the point of view of the community of Eagle Mountain.

The storm of 1 September 2012 was centered over an unnamed tributary and Israel Canyon, which drain into Saratoga Springs. Local officials reported that the rainfall was 1.25 inches over a 25-minute duration. NRCS engineers estimated that the subsequent runoff deposited a bedload estimated at 70,000 tons. The mud slurry damaged houses, inundated basements, and filled and overtopped a small debris basin. The event was comparable to two times the 100-year (1% chance event) flow. The flow direction into the residential areas of Saratoga Springs is shown in Figure 4. The drainages discharge onto an alluvial fan that slopes into residential development where mud slurry, small boulders, cobbles, and gravel were deposited during the storm (Figures 5 and 6). This debris

damage was caused by the vulnerability of the watershed immediately following the fire, which increased erosion and mudflows in the steep gradient alluvial fan.

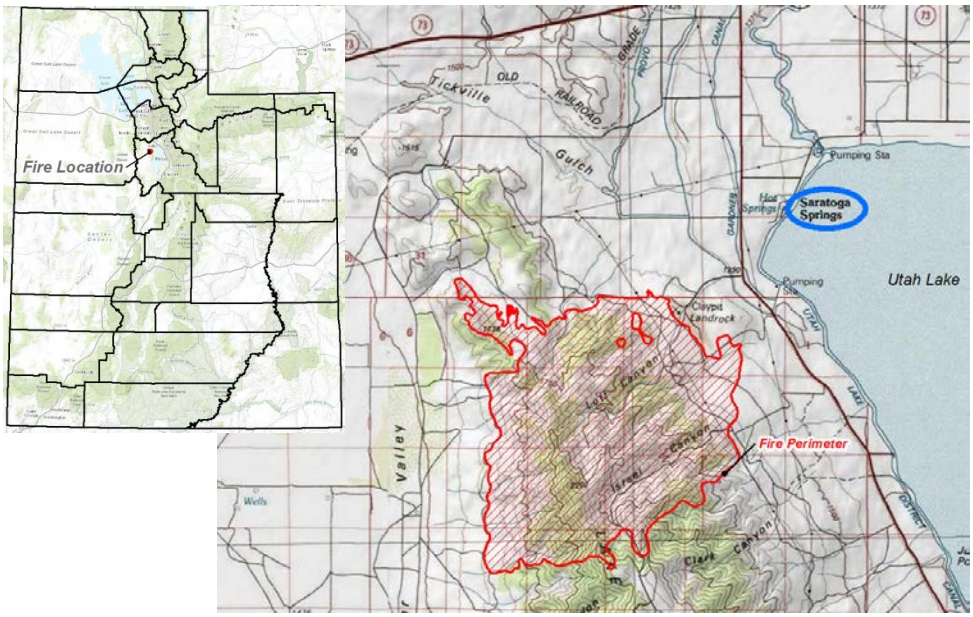

Figure 1. State of Utah and fire location, about 40 miles south of Salt Lake City.

Figure 2. Burning watershed from Eagle Mountain UT, 21 June 2012. photo by Cindi Braby, Eagle Mountain UT.

Figure 3. Burning watershed from Eagle Mountain UT, 22 June 2012.photo by Cindi Braby, Eagle Mountain UT.

Figure 4. Burned watershed flow direction into Saratoga Springs UT from 1 Sep 2012 event.

Figure 5. Sediment laden flow through residential neighborhood (credit Utah County)

Figure 6. Typical sediment composition in residential area. (credit City of Saratoga Springs)

METHODS

As part of the post-fire hydrologic analysis for the Saratoga Springs fire, a number of computer programs were used. Runoff hydrographs were determined using the NRCS hydrology program WinTR-20 (USDA-NRCS(a) 2004). The model Automated Geospatial Watershed Assessment Tool, or AGWA, (Goodrich et al. 2006 and USDA-ARS 2014) was used to determine sedimentation rates. AGWA was created by the USDA Agricultural Research Service, Southwest Watershed Research Center in Tuscon AZ. It combines previously existing models KINEROS2 (Smith et al. 1995, Woolhiser et al. 1990) and SWAT (Arnold et al. 2012).

The runoff curve number (CN) and derived hydrologic characteristics from local stream gage networks and regression equations (USGS StreamStats) were used to determine the logical pre-fire inputs. NOAA Atlas 14 rainfall distribution and modified cumulative Kirpich time of concentration methods were also used.

Changes to the time of concentration, T_c, and CN inputs into WinTR-20 and AGWA were based on past studies for post-fire analysis. Goodrich et al., (2005) provides support for modification of CN values, given reduction of cover and burn severity. McLin et al. (2001) provides a method to estimate change in lag time associated to relative increases in CN.

Two methods were used to analyze the viability of derived post-fire peaks and debris flow volumes. These include the Cannon and Gartner (2005) regression equations for estimating peak debris flow, given burn area and lithology of burn area, basin gradient, and storm rainfall; and the Gartner et al. (2008) regression equations for estimation of debris flow volumes.

Typically, the ratio of sands and colloidal grain sizes to bedload is estimated at 10:1 or 3:1 ratios. Since the AGWA value was within reason for the total sediment and sands as a percentage (i.e. 10%), it was assumed to be comparable to total bedload in this case.

For the hydrologic analysis of the burned watershed above Saratoga Springs, the entire watershed was assumed to have experienced moderate burn severity.

An initial estimate of pre-fire sedimentation conditions was made using the map of Bridges (1973) which shows estimated yearly sediment yield and a breakdown between sheet and rill erosion versus channel and gully erosion. For the Saratoga watershed, pre-fire sediment yield is estimated to range between 0.1-0.2 acre-feet per square mile per year. with sources being 60% sheet and rill and 40% channel and gully.

Pre-fire Flow Ranges The first step in estimating the pre-fire watershed condition was to review existing gages in the area to determine reasonable pre-fire flows for the 25-, 50-, and 100-year (4%-, 2%- and 1%-chance) events.

After this was completed, WinTR-20 was used with NOAA Atlas distributions and a modified cumulative Kirpich equation. Runoff curve numbers were modified between ground cover conditions and used USDA – NRCS National Engineering Handbook, Part 630, Hydrology, Chapter 9, Hydrologic Soil-Cover Complexes (USDA NRCS(b), 2004), the United States Geologic Survey (USGS) National Land Cover Database (NLCD) (Fry et al, 2011), and the NRCS SSURGO database (USDA-NRCS(c), 2012).

Stream Gages Six nearby stream gages were analyzed to help estimate peak flows for the pre-fire watershed above Saratoga Springs. The stream gages are listed in Table 1 and are shown on the Figure 7 map. Their statistics were taken from the StreamStats report appendix (Kenney et al. 2007). Discharge per unit area (cubic feet per second / square mile, CSM) was computed for each probability and graphed (Figure 8).

Table 1. Six stream gages near Saratoga Springs, UT

# on fig. CS5-8	USGS #	Drainage (sq. mi.)	gage name
1	10172790	5.77	Settlement Canyon nr Tooele UT
2	10172805	5.38	N. Willow Creek nr Grantsville UT
3	10172800	4.19	S. Willow Creek nr Grantsville UT
4	10166430	26.5	W. Canyon Creek nr Cedar Fort UT
5	10172765	6.7	Clover Creek abv Big Hollow nr Clover UT
6	10172910	16.8	Settlement Creek abv Resvr nr Tooele UT

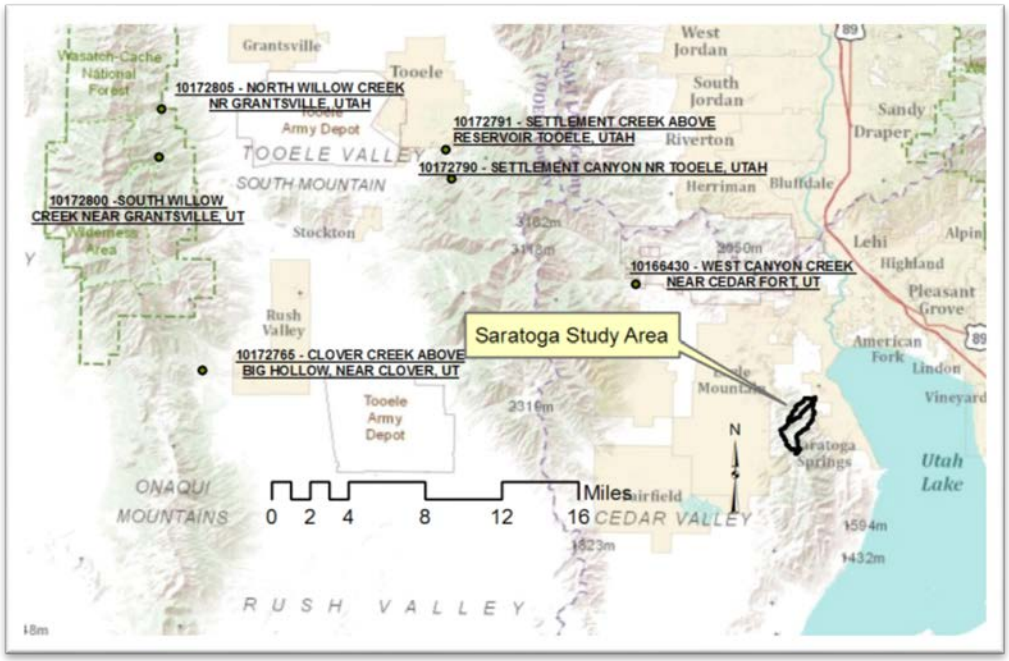

Figure 7. Location of stream gages and study area

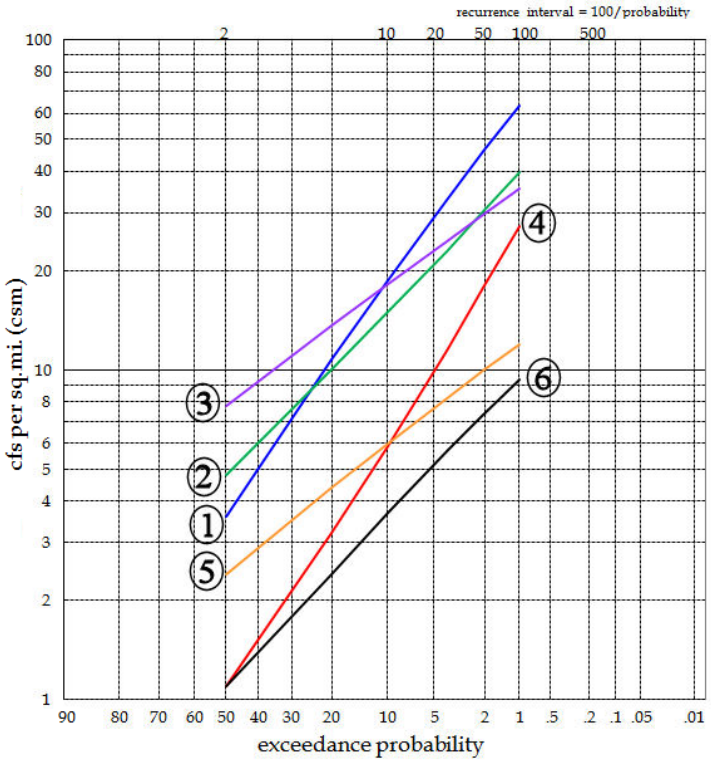

Figure 8. Stream gage regression output converted to discharge per unit area

Of the six nearby gaged watersheds, numbers 1 through 3 (Table 1) are most similar in drainage area, although the modeled watershed area above Saratoga Springs is 2.5 square miles, which is about half the size of three nearby gages. In Figure 8, the graphs of those three gages are the higher ones: blue, green, and violet.

T_c Pre-fire The upper range CSM exceedance probability was used to determine the pre-fire inputs into WinTR-20. The T_c was estimated to be 1 hour, or an average velocity of 6.0 feet per second. The upper elevation of the watershed is 7,500 feet above mean sea level, the watershed outlet is at 4,875 feet above mean sea level, and the longest flow path is 3.8 miles in length.

CN Pre-fire The CN look-up values were adjusted pending NEH, part 630, Chapter 9 ground cover conditions (USDA-NRCS(b), 2004) based on NLCD and SSURGO data. The generated T_c, adjusted CN, and NOAA Atlas 14 rainfall distribution were entered into WinTR-20. The CN was adjusted until the WinTR-20 output and calculated CSM matched the range of CSM of nearby stream gages.

Post Fire Peaks and volumes of sediment The burned watershed above Saratoga Springs has a total drainage area of 4.91 square miles. For WinTR-20 analysis, the burned area was divided into three subareas, as shown in Figure 9. Subareas 1 and 2 converge and provide outlet to the Saratoga Springs residential areas shown in Figures 4 through 6. Subarea 1 is known as Israel Canyon. See Tables 2 and 3 for WinTR-20 basic input related to these subareas, including selected pre-fire and post-fire CN.

Table 2. Burned watershed subarea input to WinTR-20.

subarea	drainage (sq.mi.)	CN (pre-fire)	CN (post-fire)	T_c (hrs, pre-fire)	T_c (hrs, post-fire)
1	1.81	62	74	0.92	0.85
2	0.60	74	80	0.40	0.37
1 + 2	2.50	65	75	1.00	0.92

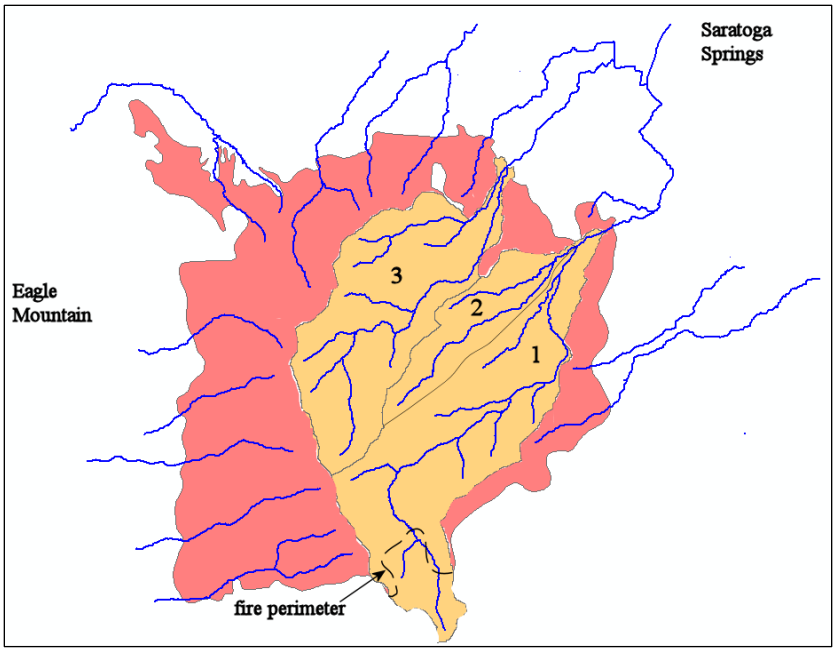

Figure 9. Burned zone (red) and sub-areas upstream of Saratoga Springs.

CN Post-fire Modification Post-fire CN were selected based on Goodrich (et al. 2005), which stated that, "there [is] a 15% reduction in cover for low-severity burns, a 32% reduction for moderate-severity burns, and a 50% reduction for high-severity burns" (Figure 10).

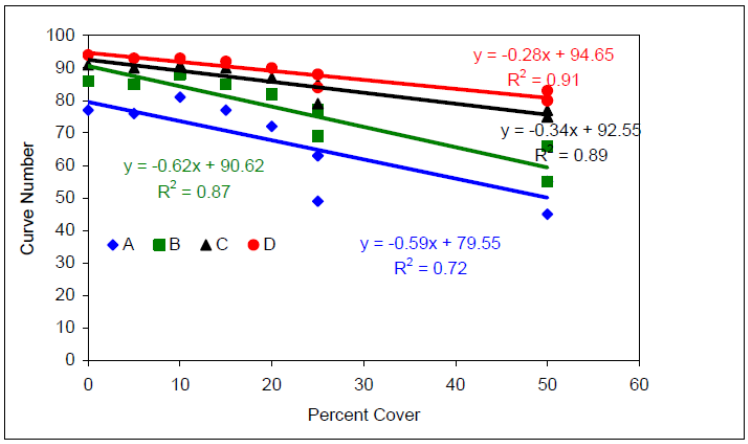

Figure 10. Curve number from cover, for hydrologic soil groups (Goodrich et al. 2005).

Table 3 shows the CN increase from pre-fire to post-fire CN used in this study. The table associates these with the standard National Land Cover Dataset (NLCD) and hydrologic soil groupings (hsg).

Table 3. Increase in runoff curve number from pre-fire to post-fire conditions.

burn severity	NLCD	cover name	hsg A	hsg B	hsg C	hsg D
Low	41	Deciduous Forest	4	5	3	2
	42	Evergreen Forest	4	16	10	8
	43	Mixed Forest	4	5	3	2
	51	Shrubland	2	2	1	1
Moderate	41	Deciduous Forest	10	10	5	5

	42	Evergreen Forest	10	21	12	11
	43	Mixed Forest	10	10	5	5
	51	Shrubland	5	5	3	2
High	41	Deciduous Forest	15	16	8	7
	42	Evergreen Forest	15	27	15	13
	43	Mixed Forest	15	16	8	7
	51	Shrubland	10	11	6	3

Time of Concentration Post-fire Modification T_c was adjusted using McLin et al. (2001), which suggest that lag time decreases from the pre-burn to post-burn condition as a result of increase in CN (Figure 11). Note that this depends on channel blockages caused by the fire, and frequency that the watershed experiences wildfire. Channel blockages can possibly increase lag times. In this case, however, the watershed cover is generally mixed with deciduous forest and low-lying shrubs and no channel blockages were assumed. Furthermore, the roughness of the watershed was assumed to decrease as a result of fire. For this case study, the following rule of thumb was adopted for changes in runoff velocity and associated change in time of concentration: velocity increases 0.5 feet per second for low severity burns, 1.0 feet per second for moderate severity burns, and 1.5 feet per second for high severity burns.

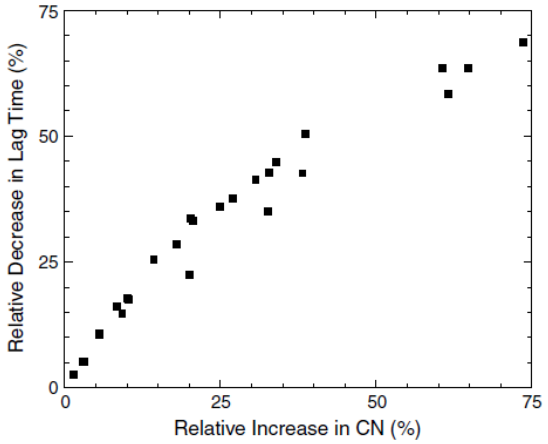

Figure 11. Interdependency of CN and lag time, Cerro Grande Wildfire McLin (et al. 2001)* *Relative change is defined as the sum of pre-fire and post-fire values divided by pre-fire values.

AGWA The AGWA model was used to model sediment rates. AGWA has a GIS interface and uses one of two routines to route runoff using the kinematic wave equation in the sub-model KINEROS2. In AGWA the landscape, including land uses and management practices, are handled by the sub-model SWAT. Table 4 shows output parameters for KINEROS and SWAT. Although AGWA produces both flow hydrographs and sedimentation rates, only the latter was used for the current study.

Table 4. Output Variables Available in AGWA.

KINEROS - ■ Infiltration (mm; m^3/km), ■ Infiltration (in; ac-ft/mi), ■ Runoff (mm), Runoff (m3), ■ Sediment yield (kg/ha), ■ Peak flow (m^3/s), Peak flow (mm/hr), ■ Sediment discharge (kg/s)	SWAT-■ Channel Discharge (m^3/day), ■ ET (mm), ■ Percolation (mm), Surface runoff (mm), ■ Transmission loss (mm), ■ Water yield (mm), ■ Sediment yield (t/ha), ■ Precipitation (mm)

Bulking Another way to estimate sedimentation is to consider typical runoff bulking factors for recently burned watersheds. This was done to further support concentration volumes that were deposited on the alluvial fan. Considering a 20% bulking factor, an event sedimentation volume can be estimated and applied to WinTR-20 post fire results.

Western Regional Equation The empirical Western U.S. regression model to estimate fire-related debris-flow volumes Gartner et al. (2008) was used to estimate post fire sediment. The equation used is presented below (Equation 1). The Western U.S. regression model to estimate fire-related debris-flow volumes Gartner et al. (2008) was taken from the Giraud and Castleton (2009) investigation.

$$lnV = 0.59(lnS) + 0.65B^{1/2} + 0.18R^{1/2} + 7.21 \qquad \text{(eq 1)}$$

V = volume (cubic meters)
S = basin area with slopes greater than or equal to 30% (square kilometers)
B = basin area burned at moderate and high severity (square kilometers), and
R = total storm rainfall (millimeters)

Comparative Analysis to Existing Studies: Figure 12 from McLin et al. (2001) illustrates that the change in peak discharge per unit area caused by wildfire can be quite large, therefore the pre and post fire ranges from Figure 12 were considered.

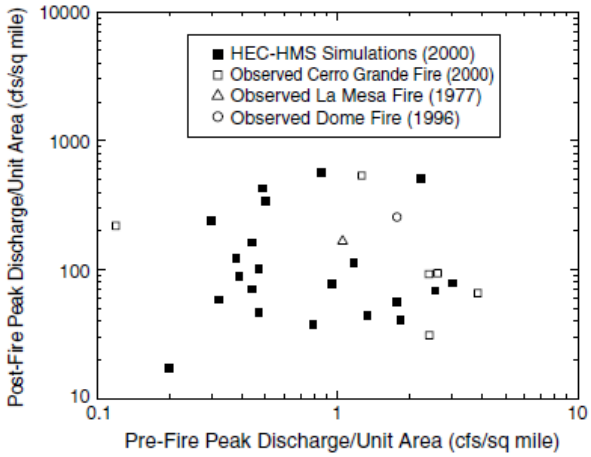

Figure 12. Comparison of observed and simulated pre-and post-fire peak discharges per unit drainage basin area in New Mexico. (McLin et al, 2001)

Regional Equations The regression equations of Cannon and Gartner (2005) were also used to estimate post-fire flow. Since the Saratoga Springs watershed is sedimentary, the regression equation (eq. 2) from Cannon and Gartner (2005) was used to compute an estimated peak discharge. Since the equation units are SI, conversions are required. For the Saratoga Springs watershed, 2.5 square miles converts to 6.47 square kilometers.

$$Q_p = 17A_b^{0.4} \qquad R^2 = 0.42 \qquad \text{(eq. 2)}$$

Bridges Map The Bridges (1973) map entitled "Estimated Sediment Yield Rates for the State of Utah" references many data sources as part of the map, including: 1) Great Basin Upper Colorado and Lower Colorado Regions, Comprehensive Framework Study, Appendices VIII, Water Management, June 1971, Pacific Southwest Inter-Agency Committee/Water Resources Council, 2) Utah State soils map and soil descriptions, 3) Reservoir Surveys by SCS and USBR, 4) suspended load measurements by USGS, USGR and SCS, 5) Watershed studies by SCS, and 6) General knowledge of the state from regular SCS program work. The author notes, "Do not use these rates to determine sediment yields at specific sites. Large variations in sediment rates may occur within the delineated areas".

According to the United States Department of Agriculture, Soil Conservation Service map (Bridges, 1973) the sediment yield for the Saratoga watershed ranges between 0.1-0.2 acre-feet/square mile/year with a 60% sheet and rill erosion and 40% channel and gully erosion.

The range of erosion rates for the Saratoga Springs watershed from the 1973 map are plotted (Figure 13). On the graph, the red squares represent the acre-feet/square mile/year rate that correlates to the tons for 2.5 square miles, pre-burn condition. The blue diamonds on the graph show values assuming a 0.45 acre-feet/square mile/year rate plotted in total tons, a conservative pre-fire condition. Finally, the green triangles represent the breakdown of erosion types (60% sheet / rill erosion, 60% other colloidal material, 40% channel and gully erosion), a post-fire condition.

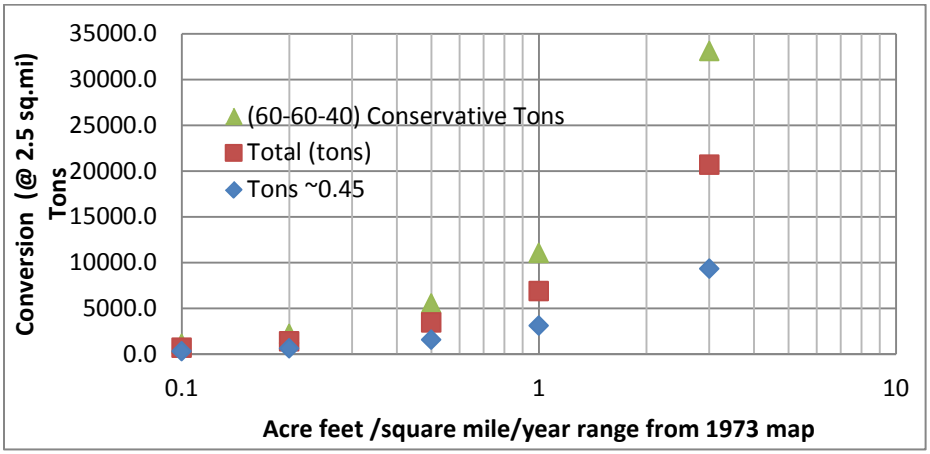

Figure 13. Range of annual erosion rates from Bridges (1973).

RESULTS

WinTR-20 Pre and Post Fire: The WinTR-20 provides pre-fire flow calculations that correlated well to the USGS stream gages CSM provided in Figure 8. Table 5 below illustrates these results. The lower return intervals from WinTR-20 pre-fire results are higher and the higher return intervals are lower than USGS calculated CSM. For estimation purposes, the upper results for the 25 year (4% chance), 50 year (2% chance) and 100 year (1% chance) will be focused on during the rest of the paper. Table 6 reflects the pre and post fire peak discharges.

Table 5. Cubic feet per second per square mile (CSM) from WinTR20 pre-fire results and selected stream gages

	2-year (50% chance) (CSM)	5 year (20% chance) (CSM)	10 year (10% chance) (CSM)	25 year (4% chance) (CSM)	50 year (2% chance) (CSM)	100 year (1% chance) (CSM)
WinTR-20 Pre-fire	0	2.5	6.8	28.4	58	100.8
Observed CSM from Figure 8	~5	12	<20	30	45	60

Table 6. Burned watershed pre-fire and post-fire peak flow output from WinTR-20.

Subarea	2-year (cfs)	5-year (cfs)	10-year (cfs)	25-year (cfs)	50-year (cfs)	100-year (cfs)
1 (pre-fire)	0	0	0	25	65	127
1 (post-fire)	14	57	118	234	359	514
2 (pre-fire)	6	29	62	126	195	280
2 (post-fire)	39	92	149	248	347	466
1+2 (pre-fire)	0	6	17	71	145	252
1+2 (post-fire)	26	92	179	342	516	728

The WinTR-20 output in Figure 14 shows the considerable increase in runoff peaks and volumes due to the fire. The peaks are predicted to more than double, with the 25-year (4% chance) event (red dashed for post-fire versus black dashed for pre-fire) rising from 71 cfs to 342 cfs. The runoff volume (represented by the area under each

curve and in Table 6) is predicted to increase runoff from the pre-fire to post-fire event, 192% to 122% for the 25-year to 100-year events.

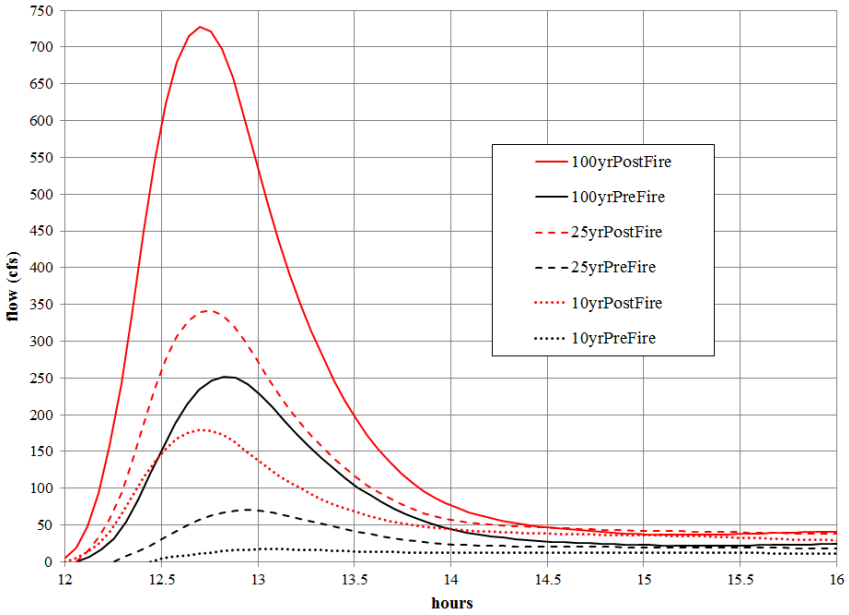

Figure 14. Burned watershed pre-fire and post-fire hydrographs from WinTR-20.

Table 6. Storm totals runoff for various recurrence intervals, input to WinTR-20 and post fire runoff values for Subarea 1+2.

Percent Chance	2-year (50% chance)	5-yr (25% chance	10-yr (10% chance)	25-yr (4% chance)	50-yr (2% chance)	100-yr (1% chance	200-yr (0.5% chance	500-yr (0.2 chance
Pre-Fire runoff (inches) Subarea 1+2	0.01	0.03	0.07	0.13	0.19	0.27	0.35	0.48
Post Fire runoff (inches) Subarea 1+2	0.09	0.17	0.25	0.38	0.48	0.60	0.73	0.92
Pre Fire - Runoff in acre feet over 2.5 sq.mi	1	4	9	17	25	36	47	64
Post Fire - Runoff in acre feet over 2.5 sq.mi	12	23	33	51	64	80	97	123

AGWA The sediment for the 25-year (4% chance) storm was estimated to be 10,303 tons and the 100-year (1% chance event) storm was estimated to be 27,897 tons.

Bulking An event sedimentation volume was estimated considering a 20% bulking factor on the WinTR-20 post fire results. The information in Table 7 was derived by taking the post-fire clear flow hydrographs of Figure 14, from WinTR-20, and considering the event sedimentation rate to be 20% at each time-step. The area under the sedimentation hydrograph provided a volume, which was converted to tons by assuming a sediment unit weight of 108 pounds per cubic foot in Table 7.

Table 7. Burned watershed post-fire event total sediment runoff in tons.

event totals	25-yr (4% chnance) (tons)	50-yr (2% chance) (tons)	100-yr (1% chance) (tons)
sediment	23,705	29,943	37,429

Western U.S. Regression Model The empirical Western U.S. regression model to estimate fire-related debris-flow volumes Gartner et al. (2008) was estimated to be between 34,550 – 51,182 tons for the 2- to 100-year (50% to 1% chance) rainfall events. These numbers are high since the model assumes that watersheds typically have moderate to high severity burns.

Table 8 shows the WinTR-20 pre-fire and post-fire peaks (in cfs per square mile) for comparison with Figure 12. The current case study results would plot generally lower on the figure than the New Mexico watersheds, the WinTR-20 results are considered reasonable.

Table 8. Saratoga Springs burned watershed pre-fire and post-fire peaks (csm) from WinTR-20.

flood	25-year (4% chance)	50-year (2% chance)	100-year (1% chance)
Pre-fire (CSM)	28.4	58	100.8
Post-fire (CSM	136.8	206.4	291.2

Regional Equations The regression equations of Cannon and Gartner (2005) after inserting 6.47 as A_b into the equation results in a Q_p of 35.88 cubic meters per second, or a Q_p of 1267 cfs after converting to English units . This results in 506 CSM; and the WinTR20 post-fire result is 728 cfs or 291 CSM.

CONCLUSIONS

The review of USGS stream gages and making modification to the CN to have both values correlate was an attempt to familiarize one on potential results, pre-fire. Once this was done a post-fire CN was applied and T_c was lowered. This resulted in both higher peaks and bigger volumes of runoff. AGWA, a 20% bulking to WinTR-20 post fire results, and the Western Regional Equation overall correlated well. These results were compared to McLin et al (2001) pre- and post- fire peak discharges per unit drainage basin area and to a range or potential erosion values, Bridges sedimentation map (1973).

Typically, one would think of using the peak discharge of post-fire analysis using WinTR-20, while increasing the CN and decreasing the $_{Tc}$. The peak discharge during the flood event and high water marks were observed as being in range for the post-fire WinTR-20 results. The Cannon and Gartner (2005) estimate of over 1,200 cfs may be reasonable and could be used for preliminary or lower and upper bound limits; the lower limit at 75% of the total, and the upper at 100% of the total.

The range of sediment, bulking and mud slurries were in a range of 10,000 tons to over 50,000 tons for the post-fire 25- to 100-year (4% to 1% chance) events. The AGWA range is between 10,000 and 50,000 tons for the 25- to 100-year (50% to 1% chance) post-fire event. The bulking at 20% is 23,000 to 37,000 tons for the post-fire event. The western regional equation produced a number of 34,600 – 51,200 tons. Between the sand, colloidal, and bedload the percentages can vary. For the sediment, sand and colloidal the numbers above could still be a low estimate. Bedload at either 1:3 or 1:10 ratio could be still be small. However, due to the system being flushed by previous storm events, these ratios may be accurate. A range of 5,000 to 17,000 tons could be accounted for bedload.

ACKNOWLEDGEMENTS

The author appreciates the assistance, review, and support of Claudia Hoeft, Dan Moore, Steve Yochum, Kent Sutcliffe, Norm Evenstad, Bronson Smart, the AGWA ARS staff, and Utah USDA NRCS.

REFERENCES

Arnold, J. G., D. N. Moriasi, P. W. Gassman, K. C. Abbaspour, M. J. White, R. Srinivasan, C. Santhi, R. D. Harmel, A. van Griensven, M. W. Van Liew, N. Kannan, M. K. Jha, SWAT: Model Use, Calibration and Validation. Transactions of the ASABE. 55(4): 1491-1508.

Bridges, B.L. 1973. Map: Estimated sediment yield for the State of Utah. Erosion and Sedimentation, Western US Water Plan, prepared by SCS August 1973.

Cannon, S.H. and Gartner, J.E. 2005. Wildfire-related debris flow from a hazards perspective, in Jakob, M. and Hungr, O., Debris-flows hazards and related phenomena: Chichester, United Kingdom, Springer-Praxis Books, p. 362–385.

Fry, J., Xian, G., Jin, S., Dewitz, J., Homer, C., Yang, L., Barnes, C., Herold, N., and Wickham, J., 2011. Completion of the 2006 National Land Cover Database for the Conterminous United States, *PE&RS*, Vol. 77(9):858-864.

Gartner, J.E., Cannon, S.H., Santi, P.M., and deWolfe, V.G. 2008. Empirical models to predict the volumes of debris flows generated by recently burned basins in the western U.S. Geomorphology, 96, 339-354.

Giraud, R.E., and Castleton, J.J. 2009. Estimation of Potential Debris-Flow volumes for Centerville Canyon, Davis County, Utah. Report of Investigation 267 Utah Geological Survey, Utah Department of Natural Resources, Salt Lake City, Utah.

Goodrich, D.C., H. E. Canfield, I.S. Burns, D.J. Semmens, S.N. Miller, M. Hernandez, L.R. Levick, D.P. Guertin, and W.G. Kepner. 2005. Rapid Post-Fire Hydrologic Watershed Assessment using the AGWA GIS based Hydrologic Modeling Tool. Proc. ASCE Watershed Manage. Conf., July 19-22, Williamsburg, VA.

Kenney, T.A., Wilkowske, C.D., and Wright, S.J. 2007. Methods for estimating magnitude and frequency of peak flows for natural streams in Utah: U.S. Geological Survey Scientific Investigations Report 2007-5158, 28 p.

McLin, S. G., Springer, E. P., and Lane, L. J. 2001. Predicting floodplain boundary changes following the Cerro Grande wildfire. Hydrological Proc., 15(15): 2967-2980.

Smith, R.E., Goodrich, D.C., and Quinton, J.N. 1995. Dynamic, distributed simulation of watershed erosion: The KINEROS2 and EUROSEM models, Journal of Soil and Water Conservation, 50(5):517-520.

USDA-ARS (U.S. Department of Agriculture-Agricultural Research Service). 2014. AGWA (Automated Geospatial Watershed Assessment Tool) website, through the ARS Southwest Watershed Research Center, Tuscon AZ, http://www.tucson.ars.ag.gov/agwa/.

USDA-NRCS(a) (U.S. Department of Agriculture-Natural Resources Conservation Service), 2004. WinTR-20 User Guide. Available at http://go.usa.gov/KoZ/. Accessed in April 2013.

USDA-NRCS(b), 2004. National Engineering Handbook, Part 630 Hydrology, Chapter 9, Hydrologic Soil-Cover Complexes.

USDA-NRCS(c), 2012. Soil Survey Geographic (SSURGO) Database. Available online at http://sdmdataaccess.nrcs.usda.gov/. Accessed [2012].

Woolhiser, D.A., Smith, R.E., and Goodrich, D.C. 1990. KINEROS, A kinematic runoff and erosion model: Documentation and User Manual. U.S. Department of Agriculture, Agricultural Research Service, ARS-77, 130 pp.

STREAM RESTORATION WITHIN A CONFINED SPACE: A CASE STUDY ON THE MIDDLE RIO GRANDE

Jonathan AuBuchon, Hydraulic Engineer, Albuquerque, NM, jaubuchon@usbr.gov; Chi Bui, Hydraulic Engineer, Albuquerque, NM, cbui@usbr.gov

BACKGROUND

The Rio Grande downstream of Cochiti Dam, as described by Happ (1948), Dewey et al. (1979), Lagasse (1980), Salazar (1998), Makar et al. (2006), and Makar and AuBuchon (2012), has seen the frequency of large magnitude floods and the sediment supply decrease over the last few decades. This has decreased the mobility of the medial and point bars and allowed the vegetation to become established, further amplifying the stability of the banks and the channel planform. Since the closure of Cochiti Dam in 1973, the downstream channel has continued to narrow through incision and vegetation encroachment, isolating the main channel from its floodplain. Richard (2001) and Shah et al. (2006) found that Cochiti Dam has had a high trapping efficiency, close to 98%, which as Lagasse (1980), Scurlock (1998), Massong et al. (2008), and Bauer (2009) described has led to the exposure of a dominant gravel fraction in the bed material in the first 30+ miles downstream of Cochiti Dam. Recent analyses by AuBuchon and Bui (2014) showed that within the first 5 miles of the Rio Grande below Cochiti Dam the active channel width has fluctuated around 200 feet and the slope has flattened to about 0.0012 over the last 2-3 decades. In addition, the channel planform has abandoned some of its variability with a decrease in the average number of channels from 2-3 prior to 1962 to about 1-2 since 1972. The sinuosity still fluctuates slightly, although not to the extent that it did prior to 1962, suggesting that there are local areas of instability, amidst the observed stability.

In 2011, the watershed of the Peralta Arroyo was burned by the Las Conchas fire, which has affected the stability of the slopes on the upper watershed. This has resulted in rainfall runoff events moving a significant volume of water and sediment into the lower portions of the Peralta Arroyo watershed. On September 13, 2013, a rainfall runoff event occurred over this watershed and brought enough sediment downstream to the confluence with the Rio Grande that the river was completely blocked (see Figure 1). Collected survey data revealed that about 2–5 feet of sediment was deposited in the Rio Grande from this event, in essence creating a miniature dam on the river. This sediment block created an opportunity for overbanking flows on a terrace that had been isolated from the main channel for decades. The backed up water also created engineering and reservoir operation concerns.

The engineering and reservoir operation concerns included being able to safely release floodwaters stored in Cochiti and minimizing the risk of unconsolidated spoil levee failure, property flooding, and ineffective farm field drainage. For the short term these were addressed by excavating a pilot channel through the sediment block on the main channel. A longer term design was required though to avoid future intervention and allow the natural fluvial and riverine processes to occur with as much freedom as possible while still addressing engineering and reservoir operation concerns.

Figure 1 Sediment deposit at Peralta Arroyo confluence. Photograph taken on 9/17/13.

DESIGN

Key aspects that were used to develop the long term design were 1) observations of the river's response when the channel was blocked, 2) analysis of sediment (channel competency and capacity), 3) addressing the engineering and reservoir operation concerns, and 4) encouraging overbank flows on the eastern terrace.

The first aspect concerns two observations made of the river's response to the sediment block in the river. The first was the observation of incision due to head cutting (see Figure 2) on the southern end of the eastern terrace. As the overbanking flow paths merged together and dropped into an abandoned river channel, enough energy was developed to start carving new channel locations. While the overbank flows only lasted for about 1.5 months, some of the carved new channels extended back a hundred feet or more, incising 1-3 feet. Massong et al. (2010) found that the general governing process for locational changes through this reach of the Rio Grande is lateral migration. Over the years the lateral migration of the banks has decreased through this reach of the Rio Grande, as the coarse fraction in the bed and the dense vegetation growth on the banks helped to minimize further bed and bank erosion. The observation of incision on the eastern terrace reveals that under the right circumstances, and given enough time, a slightly different planform change process may occur in this reach. Since the eastern terrace has significantly less vegetation and more sand than the existing channel banks and bed, respectively, there is less resistance to erosion. As erosion proceeds with time, conditions may set up that cause the Rio Grande to "avulse" from its existing path to a new main channel location on the eastern terrace.

Figure 2 Incision on southern end of eastern terrace. Left: Vertical drop at one of the incision fingers during the overbanking flow. Right: One of the longer incision fingers. Photographs were taken on 9/17/2013 and 10/17/2013 respectively.

The second observation was where and how overbanking occurred on the eastern terrace. Once a pilot channel had been cut through the sediment block on the Rio Grande, flows were increased from Cochiti Dam until a flow of about 2,200 cfs was reached. The observed flow paths at the 2,200 cfs flow rate (orange flow arrows) are shown in Figure 3. While overbank flows were occurring, standing water at the toe of the east side, unconsolidated spoil levee was not observed. On October 21, 2013 releases were made at Cochiti Dam to temporarily increase the flow to 3,500 cfs and then about 5,300 cfs in an effort to assess the current capacity of the system. Figure 3 shows the measurement and observations made that day by AuBuchon and Bui (2013). These observations helped identify some of the features that would be needed in the long term design to address engineering and reservoir operation concerns (discussed later).

The second key aspect considered two basic questions addressing sediment. The first question is whether the flow of a design channel would be competent to move the material found in the eastern terrace. The second question is whether a design channel would have the capacity to transport sediment (both incoming and self-generated through morphological adjustments) at flows between 5,000 and 6,000 cfs. This flow range has been the observed maximum flow releases during the spring snow-melt runoff on the Rio Grande from Cochiti Dam over the last decade.

To address the first question, soil samples were collected at five locations in the eastern terrace. Samples were collected with a hand auger to a depth of about 2.5 feet below the eastern terrace surface. The results of the gradation analysis on the soil samples are summarized in Table 1. The results in Table 1 were used to calculate the critical shear stress for particle mobility using the Shield's approach for incipient motion as described by Yang (1996). A one-dimensional hydraulic model provided the necessary inputs to calculate the normal shear stress according to Brown (1996). The critical and normal shear stress results were then compared to provide an estimate of the initial bed stability (Table 2). From these results it is seen that a design channel would be competent to move the majority of the material in the eastern terrace with sustained

high flows of 5,000 cfs or higher. However, there are larger particles present in the eastern terrace that the channel may not be competent to move, suggesting an armor layer could develop.

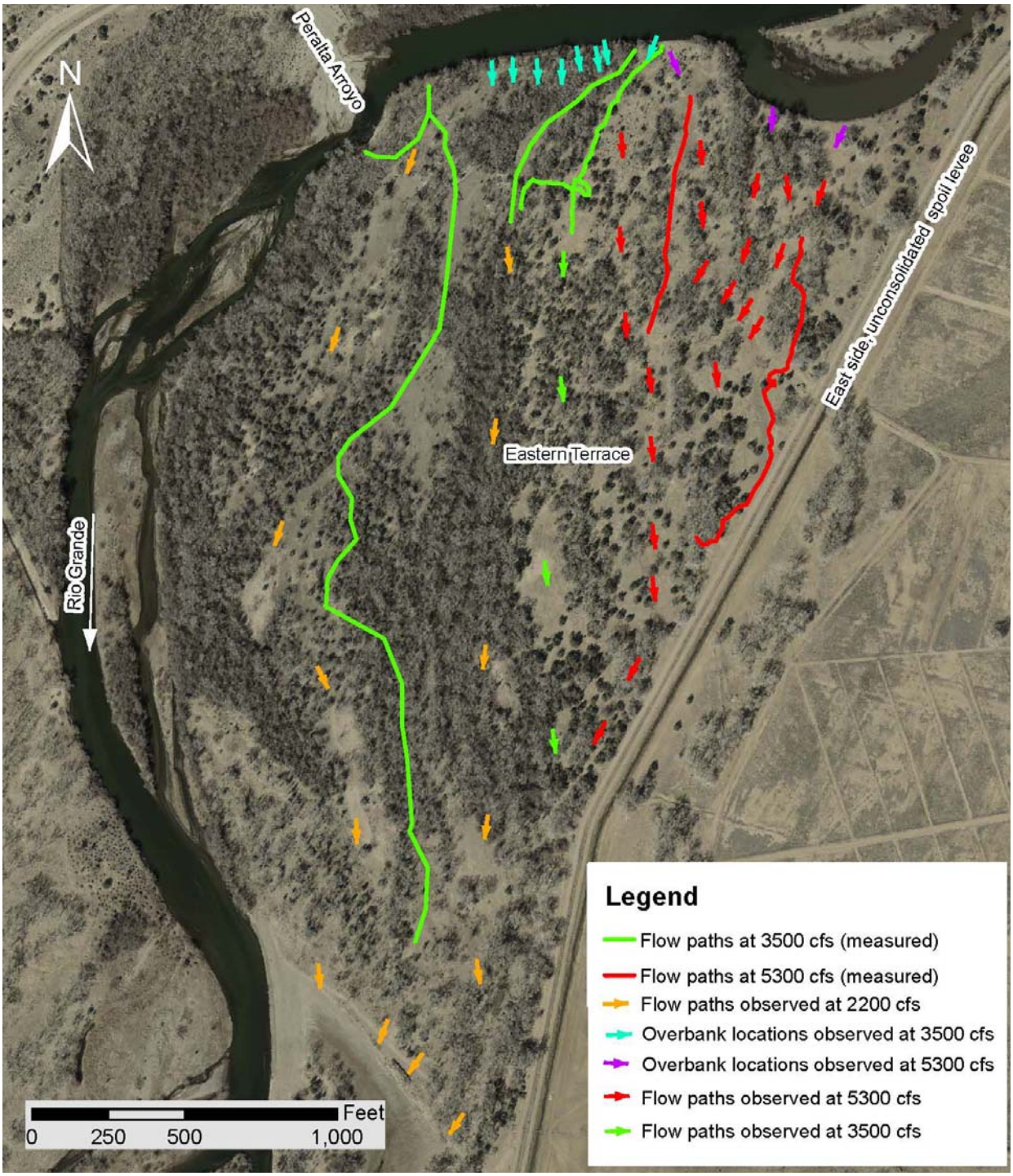

Figure 3 Observed flow paths on the eastern terrace during a short term high flow release in 2013. The background map is from Reclamation's 2012 aerial photography of the Rio Grande.

Table 1 Gradation results (median size – d_{50} and one standard deviation coarser than the median size – d_{84}) of eastern terrace bed material samples. Sample numbers are listed geographically by sample location from upstream to downstream.

Sample #	D_{50} (mm)	Description (D_{50})	D_{84} (mm)	Description (D_{84})
5	0.07	Very fine sand	20	Coarse gravel
1	0.062	Very fine sand	0.31	Medium sand
4	0.084	Very fine sand	10.5	Medium gravel
2	0.0083	Fine silt	14	Coarse gravel
3	14	Medium gravel	100	Small cobbles

Table 2 Critical and normal shear stress results (median size – d_{50} and one standard deviation coarser than the median size – d_{84}) of eastern terrace bed material samples. Sample numbers are listed geographically by sample location from upstream to downstream.

Sample #	D_{50} Critical shear stress (lb/ft^2)	D_{84} Critical shear stress (lb/ft^2)	Normal shear stress at 5,000 cfs (lb/ft^2)	Normal shear stress at 6,000 cfs (lb/ft^2)
5	<0.1	0.3	0.5	0.6
1	<0.1	<0.1	0.5	0.6
4	<0.1	0.2	0.4	0.5
2	<0.1	0.2	0.4	0.5
3	0.2	1.5	0.2	0.3

An additional assessment was also made to look at the competence of a design channel to erode its banks given the information available about the material in the eastern terrace. This assessment was made using the Bank Stability and Toe Erosion Model (BSTEM) described by Simon et al (2000), Simon and Collison (2002), Pollen-Bankhead and Simon (2009), and Simon et al. (2010). The initial channel condition runs with the BSTEM model (no vegetation establishment) projected unstable bank conditions for the design channels, except in the areas where there was a coarser bed material fraction. The presence of coarse particles and the possibility of future vegetation growth (Figure 4) indicate that the banks of a design channel through the eastern terrace may become more stable over time.

To address the second sediment question we first need to understand the available incoming sediment supply. Richard (2001) noted that although the sediment supply on the Rio Grande has been decreasing since the late 1950s, there was a pronounced decrease in the sediment supply immediately below Cochiti Dam after its closure. In the years leading up to the Cochiti Dam closure, the Rio Grande had an annualized average suspended sediment concentration around 2,000 mg/L. This dropped to an annualized average suspended sediment concentration of about 40 mg/L after the closure of Cochiti Dam. An estimate of the incoming sediment supply may be obtained by assuming the annualized average suspended sediment concentration is reflective of the sediment input immediately below the dam and assuming a representative flow rate. The median flow rate (590 cfs) at the USGS gaging station on the Rio Grande below Cochiti Dam, NM (08317400) was used to provide a representation of the flow rate since the closure of Cochiti Dam. The daily incoming sediment supply then for the reach immediately below the dam is roughly 60 tons per day.

Figure 4 First season vegetation growth on bed of design channel near outlet of flow path 2, looking upstream. Photograph was taken on 10/1/2014.

The transport capacity of any channel is very dependent upon slope. The localized slope of the Rio Grande around the Peralta Arroyo confluence is shown in Figure 5 before and after the September 2013 rainfall-runoff event on the Peralta Arroyo. The January 2009 survey data reflects relatively unchanging slope conditions (0.0012) since the early 2000s. The slope increase seen in the 9/20/13 data set (estimated slope of around 0.0038) reflects the large sediment input after the September 2013 event. The third data set reflects conditions on the Rio Grande 2 months after the September 2013 event, and about 1 month after a pilot channel was constructed through the sediment block on the main channel. The slope of the river bed from this data collection effort was found to be around 0.0011. Comparing the localized slope values of the Rio Grande for all three surveys reveals the impact a temporary higher sediment load has on the local river morphology and also the tendency of the river to adjust towards a certain slope value based on average sediment loads.

Based on the previously discussed observations of head cutting on the eastern terrace and the measured slope adjustments around the Peralta Arroyo, an initial slope value of 0.0028 was used for the design channels on the eastern terrace. This steepened slope is not expected to be stable, but was chosen to help induce morphological change. It is expected that the slope of any design channel on the eastern terrace will eventually adjust to around the observed reach tendency, unless the eastern terrace is abandoned as a flow path entirely or the sediment load changes significantly.

Using this initial design slope and the channel hydraulics (derived from a 1-dimensional hydraulic mode) a rough idea of the sediment transport capacity of the design channel at 5,000 cfs was estimated. The estimation approach used a Monte Carlo error analysis assuming hydraulic relations for wide, steady, uniform flow as described by Wilcox et al. (2009). Using this approach, the transport capacity of the initial design channel at 5,000 cfs is calculated to be almost a 100x greater than the estimate of incoming sediment supply discussed previously. The transport capacity of the design channel with an adjusted slope near the reach tendency is estimated to drop to almost a third of this value. This would indicate that the initial channel design has the capacity to transport the incoming sediment load and sediment eroded from the bed and banks as morphological adjustments occur. It also indicates that as adjustments occur, especially along the longitudinal profile, the transport capacity would also decrease with time.

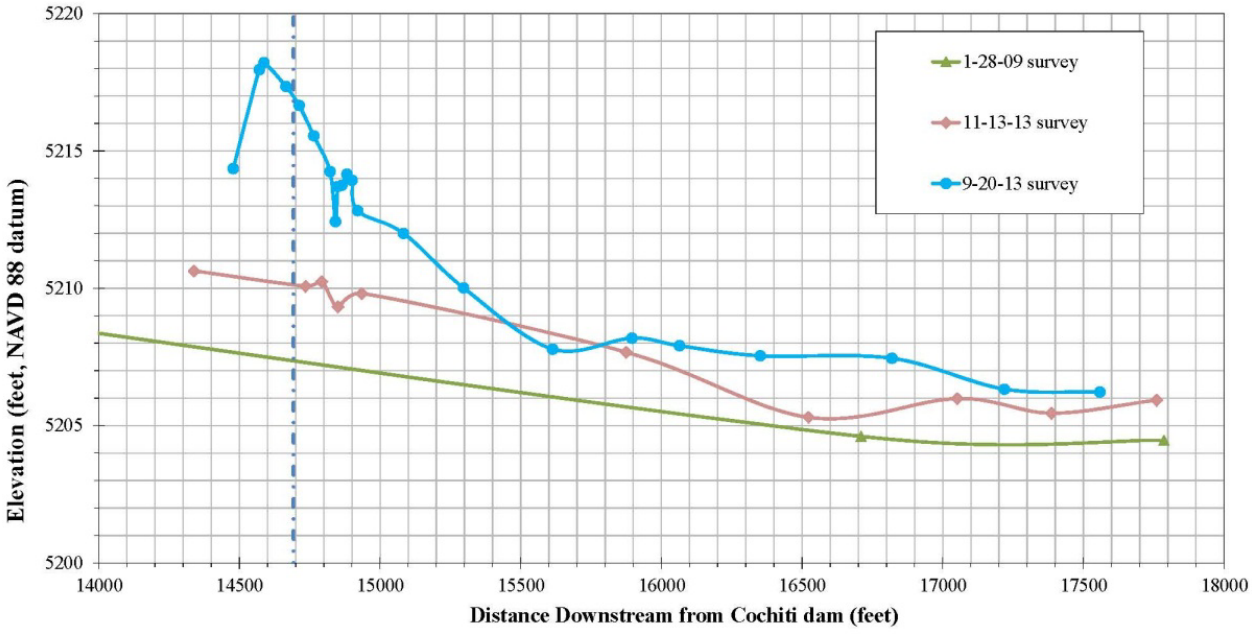

Figure 5 Rio Grande Profile between ~ 200 feet upstream and ~0.5 miles downstream of Peralta Arroyo.

The third key aspect of the long term design was addressing the engineering and reservoir operation concerns. From a reservoir operation perspective the primary concern with a potential sediment block is being able to safely evacuate stored floodwater in Cochiti Dam in a timely manner. Within a week of the September 13, 2014 event, upstream rainfall events had brought in almost 30,000 acre-feet of water to Cochiti Dam. Because of the sediment block at Peralta Arroyo, this water could not be safely released. While the construction of a pilot channel through the sediment block resolved this concern, it was desirable to solve this concern in the future without requiring the intrusion of construction equipment into the river. To mitigate this future risk for the long term design, multiple design channels with different inlets were designed in the eastern terrace. This provided redundancy to bypass the Peralta Arroyo confluence in case a similar event occurred in the future.

Engineering concerns also arose due to the flooding that occurred as a result of the sediment block. The three primary engineering concerns were unconsolidated spoil levee failure due to seepage, property flooding, and ineffective farm field drainage. The concern with the unconsolidated spoil levee failure is associated with pooling of this water at the toe which created seepage on the landward side, as shown in Figure 6. This issue was addressed by placing design features on the eastern terrace to intercept and redirect overbanking flows. Observations of the overbank flow paths, as shown in Figure 3, were directly used to strategically place design features to intercept and redirect flow heading to the unconsolidated spoil levee. The property flooding risk is directly related to the failure of the unconsolidated spoil levee, since the soil levee separates the river from the nearby agricultural land and nearby communities. Because of this relationship any reduction in the risk of levee failure also reduces the property flooding risk. The elevated water levels associated with the sediment block were the primary concern behind the farm drains not operating as designed. By incorporating multiple pathways in the design for the water to be conveyed downstream, the risk of future sediment blocks creating elevated river water levels is minimized.

Figure 6 Seepage and pooling at the unconsolidated spoil levee. Left: Observed seepage on the landward side of the spoil levee. Right: Water pooled on the river side of the spoil levee. Photographs were taken on 9/26/2013 and 10/21/2013 respectively.

The fourth and final aspect of the long term design involved encouraging opportunities for overbank flows to help increase the morphological diversity of the channel. The observations of the overbank flow paths shown in Figure 3 were used to help identify locations where overbanking flows occurred and did not pose a risk to the unconsolidated spoil levee. A temporary spoil levee was then constructed to help contain higher flows within this area. This allowed overbanking flows, such as seen in Figure 7, access to slightly over half of the area observed to be flooding at a flow of 3,500 cfs, and about a third of the flow at 5,000 cfs.

Figure 7 Overbanking flows on the eastern terrace at 3,500 cfs. Photograph was taken on 10/21/2013.

The consideration of all 4 key aspects of the long term design led to the final design, as shown in Figure 8. This design included construction of three channels on the terrace (yellow lines) following locations where the main overbanking flow paths were observed. It also included strategically excavating and placing material (red line) to intercept and redirect overbanking flows away from the unconsolidated spoil levee into the constructed channels. A final component of the design was to place excavated material, as a spoil berm (green line), on the east side of the excavated channels. This provides an immediate channel capacity between 5,000 and 6,000 cfs, while still allowing overbank flooding to occur. The inclusion of multiple channels, a redirection berm and ditch, and a spoil berm also provided a level of redundancy that allows for complex system responses without the need for substantial intervention.

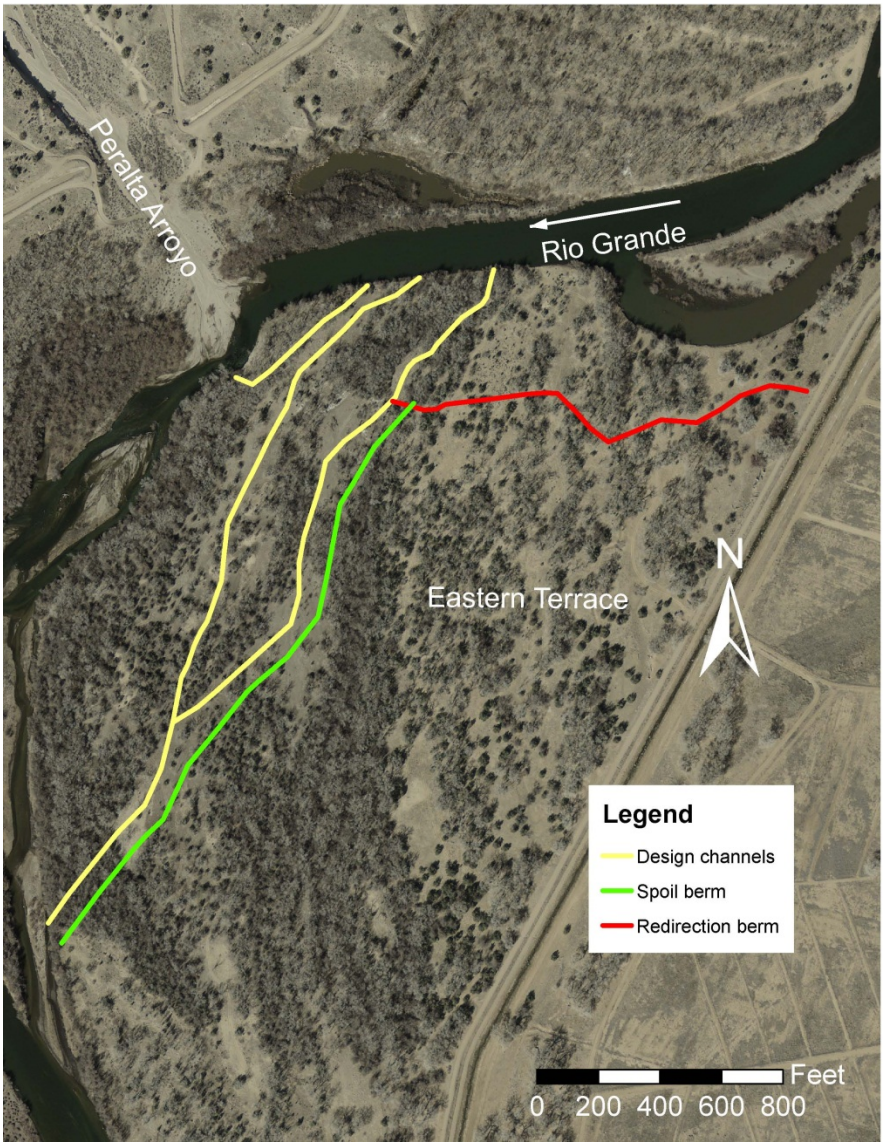

Figure 8 Long term design components for the eastern terrace flow augmentation. The background map is from Reclamation's 2012 aerial photography of the Rio Grande.

EXPECTED RESPONSE

The long term design was constructed in the spring of 2014. In late spring/early summer a small spring snow-melt runoff of slightly less than 2,000 cfs caused a few of the design channels to flow, see Figure 9. While very little morphological change occurred, the channel was visually winnowing finer material, like the sands, and transporting them downstream, as shown in Figure 9. Since the channel banks and bed are expected to adjust, the presence of large trees left at the edges of the construction footprint will hopefully also provide local conditions, as the trees fall into the river, where complex flow patterns will develop. These flow patterns may aid in the formation of channel complexity and create greater diversity in the morphology of the channels.

Figure 9 Looking downstream on one of the constructed channels. Left: Channel during spring runoff flows. Right: Channel after the spring runoff flows. Note the presence of sand deposits from upstream winnowing in the channel. Photographs were taken on 5/9/14 and 10/1/14, respectively.

A long term design that allows for dynamic change within a restrained system was facilitated by considering 4 key aspects. These aspects included observing the river's response to a disturbance event, analyzing the sediment (channel competency and capacity), addressing the engineering and reservoir operation concerns, and encouraging the continuation of overbank flows. This design process allowed the Rio Grande within this confined river reach more freedom to self-adjust, creating opportunities for diverse morphological features to develop on a previously abandoned floodplain terrace.

ACKNOWLEDGEMENTS

Kai-t Blue-sky, Jacob Pecos and other staff/consultants of the Pueblo de Cochiti have assisted with the coordination, selection, and design of this work. Vincent Benoit, Suzanne Devergie, and Nathan Holste have participated in data collection and field reconnaissance trips at this site. Jason Casuga, Victor Chavez, Carolyn Donnelly, and Robert Padilla have also provided valuable insight and ideas throughout the project development process.

REFERENCES

AuBuchon, J. and Bui C. (2013). Peralta Arroyo: October 21, 2013 Trip Report. U.S. Bureau of Reclamation, Albuquerque, NM.

AuBuchon, J. and Bui, C. (2014). Peralta Arroyo Eastern Terrace Flow Augmentation Design Report. U.S. Bureau of Reclamation, Albuquerque, NM.

Bauer, T. R. (2009). Evolution of Sedument on the Middle Rio Grande, New Mexico. U.S. Bureau of Reclamation, Denver, CO.

Brown, S.A. (1986). Use of Riprap for Bank Protection: Literature Review Report. U.S. Department of Transportation, Federal Highways Administration, McLean, VA.

Dewey, J. D., Roybal, F. E., and Funderburg, D. E. (1979). Hydrologic Data on Channel Adjustments 1970 to 1975, on the Rio Grande Downstream from Cochiti Dam New Mexico: Before and After Closure. U.S. Geological Survey, Water Resources Investigations 79-70.

Happ, S. C. (1948). "Sedimentation in the Middle Rio Grande Valley, NM." Geological Society of America Bulletin, 59(12), pp 1191–1216.

Lagasse, P. F. (1980). An Assessment of the Response of the Rio Grande to Dam Construction – Cochiti to Isleta Reach. U.S. Army Corps of Engineers, Albuquerque, NM.

Makar, P., and AuBuchon, J. (2012). Channel Conditions and Dynamics of the Middle Rio Grande. U.S. Bureau of Reclamation, Albuquerque, NM.

Makar, P. W., Massong, T. M., and Bauer, T. R. (2006). "Channel Widths Changes Along the Middle Rio Grande, NM." Proc. Joint 8th Federal Interagency Sedimentation Conference and 3rd Federal Interagency Hydrologic Modeling Conference, Reno, NV, pp 942–949

Massong, T. M., Makar, P. W., and Bauer, T. R. (2008). Rio Grande Geomorphic Summary Final. U.S. Bureau of Reclamation, Albuquerque, NM.

Massong, T. M., Makar, P. W., and Bauer, T. R. (2010). Planform Evolution Model for the Middle Rio Grande, NM. Albuquerque, NM.

Pollen-Bankhead, N. and Simon, A. (2009). "Enhanced application of root-reinforcement algorithms for bank-stability modeling." Earth Surface Processes amd Landforms, 34 (4), pp. 471-480.

Richard, G. A. (2001). Quantification and Prediction of Lateral Channel Adjustments Downstream from Cochiti Dam, Rio Grande, NM. Colorado State University, Fort Collins, CO.

Salazar, C. L. (1998). Morphology of the Middle Rio Grande From Cochiti Dam to Bernalillo Bridge, NM. Colorado State University, Ft. Collins, CO.

Scurlock, D. (1998). From the Rio to the Sierra: An Environmental History of the Middle Rio Grande Basin. U.S. Department of Agriculture, General Technical Report RMRS-GTR-5. Ft. Collins, CO.

Shah, S., Novak, S., and Julien, P. (2006). Cochiti Dam Reach: Cochiti Dam to Galisteo Creek Hydraulic Modeling Analysis 1962 - 2004. Colorado State University, Fort Collins, CO.

Simon, A., Curini, A., Darby, S.E., and Langendoen, E.J. (2000). "Bank and near-bank processes in an incised channel."Geomorphology, 35 (3-4), pp. 193-217.

Simon, A. and Collison, A.J. (2002). "Quantifying the Mechanical and Hydrologic Effects of Riparian vegetation on Streambank Stability." Earth Surface Processes amd Landforms, 27 (5), pp. 527-546.

Simon, A., Bankhead, N., and Thomas, R. (2010). "Iterative Bank-Stability and Toe-Erosion Modeling for Predicting Streambank Loading Rates and Potential Load Reductions." Proc. Joint 9th Federal Interagency Sedimentation Conference and 4th Federal Interagency Hydrologic Modeling Conference, Las Vegas, NV, 11 pp.

Wilcox, P., Pitlick, J., and Cui, Y. (2009). Sediment Transport Primer Estimating Bed-Material Transport in Gravel-bed Rivers. U.S. Department of Agriculture, Forest Service, General Technical Report (RMRS-GTR-226), Albuquerque, NM.

Yang, C.T. (1996). Sediment Transport:Theory and Practice. McGraw-Hill Companies, Inc. New York, NY.

THE APPLICATION OF *WARSSS* FOR A WATERSHED-BASED SEDIMENT BUDGET AND POST-FIRE STREAM RESTORATION: THE HAYMAN FIRE, TRAIL CREEK WATERSHED, COLORADO

Dave Rosgen, Ph.D., Professional Hydrologist, Wildland Hydrology, Fort Collins, CO, Dave@wildlandhydrology.com; Darcie Frantila Geenen, Wildland Hydrology, Fort Collins, CO, Darcie@wildlandhydrology.com; Brandon Rosgen, Hydrologist, Wildland Hydrology, Fort Collins, CO, Brandon@wildlandhydrology.com

INTRODUCTION

The Hayman Fire started on June 8th, 2002, and burned over 138,000 acres and 133 homes. The burn area involved a large portion of the 186 mi^2 Horse Creek Watershed on the Pike National Forest, Colorado. Eight years following the fire, disproportionate sediment yields and river impairment were still prominent in the burn area. Thus a watershed assessment was conducted in 2010 and 2011 to ascertain erosional and depositional processes to identify the causes of impairment by specific location. The results of the watershed assessment were used to develop a master restoration plan to reduce the accelerated sediment yields in the areas affected by the burn.

The watershed assessment utilized the *Watershed Assessment of River Stability and Sediment Supply (WARSSS)* methodology (Rosgen, 2006b). *WARSSS* is a three-phase approach that assesses large watersheds with a practical, rapid screening component that integrates hillslope, hydrologic, and channel processes. It is designed to identify the location, nature, extent, and consequences of various past, existing, and proposed, land use impacts.

The initial two phases of *WARSSS* involving the *Reconnaissance Level Assessment (RLA)* and the *Rapid Resource Inventory for Sediment and Stability Consequence (RRISSC)* levels were conducted on the 186 mi^2 Horse Creek Watershed (Rosgen and Rosgen, 2010). The *RLA* and the *RRISSC* assessments identified the Trail Creek Watershed within the Horse Creek Watershed as *High Risk* for disproportionate sediment supply and river impairment. Based on the results of *RLA* and *RRISSC*, the Trail Creek Watershed advanced to the third and most detailed phase of *WARSSS*, the *Prediction Level Assessment (PLA)*. The *PLA* phase was directed to:

1. Identify the erosional and depositional processes that are disproportionately contributing sediment to Trail Creek
2. Quantify sediment loading by location, process, and land use
3. Develop a master plan for watershed restoration

The *PLA* methodology and results are summarized in this paper. These results were used to prioritize the locations within the Trail Creek Watershed for mitigation and restoration based on the magnitude of sediment sources for a variety of land uses. This paper also discusses design solutions for the identified areas with disproportionately high sediment yields throughout the watershed. The designs address typical sediment yield processes for hillslope and channel processes at representative or typical impaired stream type and landscape type locations.

THE *WARSSS* METHODOOGY: THE *PLA* RESULTS

The majority of the Trail Creek Watershed was burned during the Hayman Fire. The watershed involves nearly *16 mi^2* of drainage area within the South Platte River drainage in Colorado. The watershed is located in the Granitic geology associated with the Pikes Peak Batholith composed of erosive grussic granite soils. The confluence of Trail Creek is at West Creek near the community of West Creek. Ownership within the watershed is predominantly USDA Forest Service, Pike National Forest, with some private land inholdings in the upper watershed. The Trail Creek Watershed was delineated into 58 sub-watersheds, each given a unique number ID.

The *PLA* analysis identified and quantified annual sediment yields from hillslope, hydrology, and channel processes (Figure 1). Hillslope processes included assessments of the introduced sediment from surface erosion and roads and trails. Flow-related sediment was analyzed from a change in hydrology due to the fire. The assessment of channel processes included streambank erosion, degradation (bed erosion) due to headcuts and incising channels, and the combined sediment yield of the 58 sub-watersheds and the mainstem Trail Creek.

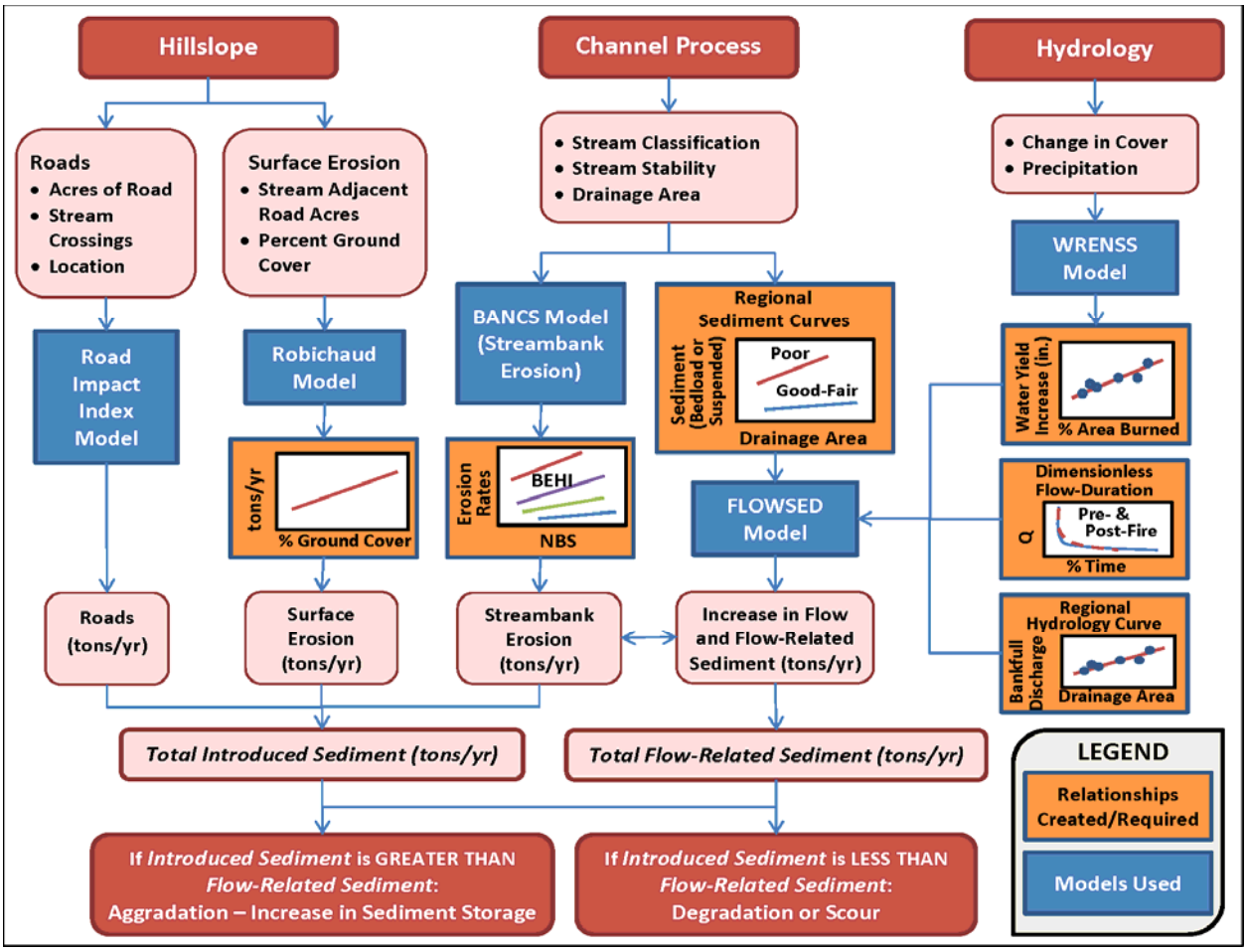

Figure 1 The procedure to quantify the sediment sources by major process (Rosgen, 2011a).

Hydrology

Increases in annual water yield following wildfires, although highly variable, can be expected (DeBano *et al*., 1998; Robichaud *et al*., 2000, 2002, 2003). Intense short duration storms characterized by high rainfall intensity and low volume have been associated with high stream peak flows and significant erosion events after fires (DeBano *et al*., 1998; Neary *et al*., 1999; Moody and Martin, 2001; Robichaud *et al*., 2002). Continued frequent and high magnitude storms will generate excess sediment yields based on flow-related channel response for the Trail Creek Watershed and other tributaries involved in the Hayman fire. According to MacDonald (2009), the Hayman fire will continue to produce sediment from the more extreme storm events because of the limited recovery potential for revegetation to offset evapotranspiration and interception losses. The growing conditions on most of the Hayman fire are very poor due to the coarse-textured soils and low precipitation relative to potential evapotranspiration. Vegetative cover is not expected to increase much beyond the current levels in areas without coniferous trees. If the amount of ground cover is not able to return to pre-fire levels, there will be a continuing susceptibility for a higher than normal streamflow "peak" response to high-intensity summer thunderstorms (MacDonald, 2009).

The hydrologic assessment for Trail Creek and its tributaries involved an application of the WRENSS water yield model (USEPA, 1980), completed by J. Nankervis, 2010, Blue Mountain Consultants. The water yield model simulates the increase in yield based on the percent of the stand that was burned for each sub-watershed to determine the inches of increased annual water yield due to the fire. The increase in flow is reflected in changes in a flow-duration curve, normalized for the flows of each sub-watershed and the mainstem Trail Creek. Changes in pre- and post-fire flow-duration curves were simulated as part of the flow-related sediment yield increase due to the wildfire for each sub-watershed and the entire Trail Creek Watershed.

The pre-fire water yield for the Trail Creek Watershed was predicted at *3,689 acre-ft* and the post-fire water yield at *6,560 acre-ft*. The total water yield increase from pre-fire to post-fire conditions was predicted to be *2,871 acre-ft*, representing a *44%* increase.

Bankfull Discharge

Bankfull discharge is the frequent peak flow that fills the channel to the incipient level of flooding. It often is associated with a return interval of 1 to 2 years and is coincident with the effective discharge or channel forming flows. Bankfull discharge was determined using the continuity equation ($Q = A * \bar{u}$) by estimating velocity ($\bar{u}$) and calculating the bankfull cross-sectional area (A). The calculated bankfull discharge was then compared to a regional curve developed for this project representing bankfull discharge *vs*. drainage area (see Rosgen, 2011b). This regional curve is based on calibrated, field-determined bankfull values at streamgage sites in the same hydro-physiographic province as Trail Creek. Velocity was estimated using a variety of methods, such as flow resistance to relative roughness and Manning's '*n*' by stream type (Rosgen, 1996, 2006b). The bankfull discharge at the mouth of each sub-watershed was determined from the regional curve relation of bankfull discharge *vs*. drainage area.

Flow-Related Sediment Yields

The flow-related sediment yield represents an integration of all introduced sources (including sediment supply from channel and hillslope processes) and the increased flow from flow-duration curves. The FLOWSED model (Rosgen, 2006a, 2006b) was applied to determine flow-related sediment yield increases due to the fire. The model uses dimensionless relations of the flow-duration curves from the WRENSS water yield analysis, along with dimensionless sediment rating curves. The normalization parameter to convert the dimensionless flow-duration curves to dimensional is the bankfull discharge determined from a regional curve of bankfull discharge *vs*. drainage area. Bankfull sediment values are used to convert the dimensionless sediment rating curves to dimensional curves. Flow-related sediment yield is then calculated based on routing the flow increase through sediment rating curves established by stream type and stability categories. This prediction assists in determining individual sub-watersheds that may be disproportionately contributing sediment based on their sediment supply, channel condition, and stream type related to the increases in post-wildfire peak flows and corresponding flow-related sediment.

In the absence of measured bankfull sediment data, similar to the approach used to estimate bankfull discharge, bankfull bedload and suspended sediment data by drainage area can be developed for a given geological region by stability. Regional sediment curves by channel stability were developed for the batholith geology (Pikes Peak, grussic granite geology) for this assessment (see Rosgen, 2011b).

The FLOWSED model was run for each of the 58 sub-watersheds and for the entire Trail Creek Watershed. The flow-related sediment yield from the post-fire, existing condition is compared to the introduced sediment supply from roads, surface erosion, and streambanks. If the combined introduced sediment values exceed the existing annual sediment yield, then excess deposition (increased channel sediment storage) is indicated. If annual flow-related sediment yield values are greater than the combined introduced sediment supply, then channel scour (bed erosion) is indicated.

The flow-related increase in sediment for the Trail Creek Watershed due to changes in the flow-duration curves and the sediment rating curves from the FLOWSED model resulted in an increase from the pre-fire to post-fire total sediment yield of *1,250 tons/yr* to *20,838 tons/yr*, which represents an increase of *19,588 tons/yr*. The total yield is comprised of approximately 26% bedload sediment and 74% suspended sediment. Overall, for a 44% increase in water yield, there is a corresponding 94% increase in total sediment (based on flow-related increases) for the Trail Creek Watershed. The significance of the increased streamflow peaks cannot be overlooked based on the magnitude of the total sediment yield consequence. Annual sediment yields from the introduced supply of roads, trails, surface erosion, and streambank erosion compared to the flow-related sediment yields are helpful in identifying sediment sources to set priorities in restoration and stabilization proposals to reduce sediment.

Hillslope Processes

Surface Erosion

Sediment yields due to surface erosion following fires can decrease by an order of magnitude following the first year, and by seven years, negligible erosion can result (Robichaud and Brown, 1999; Robichaud *et al*., 2002). MacDonald (2009) emphasizes that surface erosion rates are highly dependent on the amount of surface cover. According to the research reported by Robichaud and Wagenbrenner (2009), due to increasing ground cover in the Hayman fire burn area, a major reduction in sediment yield resulted between 2002 to 2008. For slopes in the 15–40% range and for ground cover greater than 50%, limited sediment yields from surface erosion is anticipated based on data six years following the fire. By 2008, although in the presence of high intense rainstorms, sediment yields are greatly reduced from the initial erosion and sedimentation rates. Based on the conducted research, it may be inferred that the highest potential for sediment yields from surface erosion are more likely to occur adjacent to stream systems on very steep slopes with less than 20% ground coverage.

As a result of Robichaud and Wagenbrenner (2009) research, a negative exponential relationship of erosion rate (tons/acre) as a function of ground cover density (%) was developed for this analysis (see Rosgen, 2011b). The sediment delivery data was derived from surface erosion processes for relatively short slope lengths adjacent to ephemeral channels, and for 20–40% slopes based on ground cover density. The erosion rates represent delivered sediment within approximately 100 ft from the surface erosion source. Ground cover densities were determined for each 100 foot zone on both sides of each drainage to obtain the sediment yield from surface erosion in tons/acre/yr. Aerial photo interpretations from ground truth signatures contrasting roads as zero percent ground cover up to 90% were used to obtain ground cover percentage in these 100 foot, stream-adjacent slope zones. These variables were then used to determine the increase in sediment supply from surface erosion processes based on the surface erosion rate multiplied by the total acres for that condition. Although there is evident surface erosion on mid-to-upper slopes, the potential to provide for increased sediment supply is diminished as these locations are far removed from the stream-adjacent slopes. In cases where field observations (ground truthing) indicated lower ground cover than the aerial photo-interpretation, the following procedure was followed to obtain surface erosion contributions for each sub-watershed:

1. Determine the acres of burn intensity within the near-bank zone (100 feet each side of channel) using categories as previously mapped of *High*, *Moderate*, *Low*, and *Unburned* conditions
2. Calculate the percentage of area for each burn intensity condition
3. Determine the percent ground cover for each burn intensity condition using 30% ground cover for *High* intensity, 55% for *Moderate*, 75% for *Low*, and 85% for *Unburned*
4. Calculate the weighted percent ground cover for each burn intensity condition
5. Calculate the ground cover distribution for the sub-watershed
6. Calculate the corresponding erosion rate based on the relationship to the percentage of ground cover

The predictions of sediment yields related to surface erosion resulted in a total of *2,542 tons/yr* from the Trail Creek Watershed. The total surface erosion from individual sub-watersheds is estimated at *1,908 tons/yr*, and the surface erosion adjacent to the mainstem Trail Creek is estimated at *634 tons/yr*. Overall, surface erosion contributes approximately 12% of the total introduced sediment in the sub-watersheds, mainstem Trail Creek, and the Trail Creek Watershed.

Roads and ORV Trails

Over the long-term, studies by Colorado State University indicate that roads and ORV trails generate and deliver as much sediment to the stream channel network as high-severity wildfires (MacDonald, 2009). Sediment from stream encroachment, crossings, cut bank erosion, fill erosion, and poor drainage on the main Trail Creek road results in disproportionate sediment yields. Another source of sediment is from the encroachment of the road system on alluvial fans, which has over-steepened the channels causing headcuts and the routing of sediment from the fans directly into Trail Creek. The Trail Creek road parallels and crosses the stream channel multiple times throughout its length. The majority of the ORV road and trail systems follow in close proximity to the drainageways.

The Road Impact Index (RII) model (Rosgen, 2006b) was used to predict the delivered road erosion sediment from road cuts, surfaces, and fill slopes (RII = road density multiplied by the number of stream crossings). Reasonable

validation agreement of the measured road erosion rates from the Hayman fire research (Libohova, 2004) and the sediment yield prediction from roads using the RII suggests the RII is an appropriate model utilized for this assessment. The acres of road surfaces exposed were broken into three classes based on the type of road or trail, and the typical side-slope gradient. The acres of road divided by the sub-watershed acres multiplied by the number of stream crossings by slope position were used to determine the sediment yield (tons/acre/yr).

The total sediment yield of the Trail Creek Watershed from roads and trails (erosion delivered to stream channels) is *848 tons/yr* based on 8.9 miles of roads and trails. The total sediment from the sub-watersheds, separate from the main Trail Creek road, is *258.1 tons/yr* based on 4x4 and ORV trail systems involving less acres/road length. The main Trail Creek road contributes *589.9 tons/yr* due to its close proximity to the mainstem Trail Creek. Overall, the roads and trails contribute *approximately 11%* of the introduced sediment for the mainstem Trail Creek, *approximately 2%* of the introduced sediment for the sub-watersheds, and *approximately 4%* of the introduced sediment for the Trail Creek Watershed.

Channel Processes

According to MacDonald (2009), most of the sediment due to the fire is coming from rill, gully, and channel erosion rather than hillslopes. Large amounts of sediment are still generated seven years after the fire (MacDonald, 2009). This increase in sediment can be attributed to extreme storms where there is still sufficient surface runoff to cause further channel incision and streambank erosion. Increases in the headward expansion of the drainage network are evident and widespread due to the increased peak flows and decreased flow resistance from destroyed riparian vegetation following the fire. Headcuts result in an over-steepening of the energy slope and corresponding channel bed degradation. Consequently, slope rejuvenation occurs leading to a corresponding accelerated increase in bed and bank erosion rates with increased sediment supply.

River Stability Analysis using Reference & Representative Reaches

Because there are 178 miles of stream channels within the Trail Creek Watershed, it was not practical to traverse each channel length, providing a detailed assessment of each channel. To characterize the major reaches in the watershed, the following procedure was utilized that allows for extrapolation of detailed stream channel process relations to other reaches of similar stream type and condition. Stream impairment and sediment supply are based on:

1. Development of typical, *representative reaches* that represent a range of stability and sediment supply conditions for the various stream types that occur within the Trail Creek Watershed
2. Departure of the representative reaches from the stable, *reference reach* condition for various stream types and landscape types with defined boundary conditions and controlling variables

River stability is evaluated for each reference and representative reach following the procedures in Rosgen (2006b). The evaluation is conducted on the reference reaches to validate a "Good" overall stability, and the data is used in the departure analysis of the representative reaches compared to reference conditions. Estimates of vertical stability, lateral stability, channel enlargement, and sediment supply are assessed, including streambank erosion, channel competence, and transport capacity evaluations. Streambank erosion is assessed using the *Bank Assessment for Non-point source Consequences of Sediment (BANCS)* model (Rosgen, 2001, 2006b). Competence is determined using the revised Shields relation for initiation of motion (Rosgen, 2006b); sediment transport capacity is evaluated using the POWERSED model (Rosgen, 2006a) as programmed in RIVERMorph™. The POWERSED model is also used to determine channel response (aggradation, degradation, or stable) for each representative reach as a departure from the reference condition. The river stability evaluation provides a quantitative expression of the stable form of stream types that may be potentially implemented as part of mitigation or restoration.

Overall, sixteen *representative reaches* and five *reference reaches* were obtained to document a range of stream types and conditions that occur within the Trail Creek Watershed. Data for each stream type and landscape type include the morphological characterization (dimensions, pattern, profile, and channel materials) to determine the departure of each representative reach from the potential, stable stream type (reference reach). If restoration designs are required, the reference reach data is also used to scale the morphological characteristics of the stable form to apply to the restoration reaches that have similar landscape types, boundary conditions, and controlling variables.

The data from the representative reaches were extrapolated to reaches with similar stream types and conditions within the watershed. For example, for the typical "Poor" stability, F4 stream types (entrenched channels with high width/depth ratios and high banks on both sides; see Rosgen, 1994, 1996 for stream type and valley type descriptions), unit erosion rates in tons/yr/ft of streambank erosion were obtained; these rates were extrapolated to other similar "Poor" stability, F4 reaches. The reaches that indicated *moderate* to *very high* sediment supply or channel instability were mapped in detail. Approximately 55 miles (31%) of the streams in the Trail Creek Watershed were traversed obtaining direct observations of stream types and associated stability. The remaining two-thirds of the reaches utilized extrapolated relations due to similar boundary conditions and controlling variables. Based on stable, low sediment supply indicators at the mouth of several small watersheds, values of "Good" were used to predict the potential, flow-related sediment increases. Because of the distinctly evident stable conditions, more detailed site investigations were not warranted; thus these small watersheds were not mapped in the same detail (streambank erosion rates, stream type, and condition) as the "Fair" and "Poor" condition sub-watersheds.

Streambank Erosion

Streambank erosion is accelerated in the presence of aggradation, central bars, channel incision, increased peak flow magnitude and frequency, debris jams, and change in riparian vegetation that decreases frictional resistance. The BANCS model (Rosgen, 2001, 2006b) was used to predict streambank erosion rates on the reference reaches, representative reaches, sub-watersheds, and mainstem Trail Creek. The BANCS model utilizes two tools to predict streambank erosion: 1) The Bank Erosion Hazard Index (BEHI), and 2) Near-Bank Stress (NBS). The BANCS model evaluates the bank characteristics and flow distribution along river reaches and maps BEHI and NBS risk ratings commensurate with streambank and channel changes. Annual erosion rates are estimated using the BEHI and NBS ratings, and then are multiplied by the bank height and corresponding bank length of a similar condition to estimate the tons of sediment per year.

The erosion rates for the reference reaches indicate baseline or geologic rates; whereas the erosion rates from the representative reaches indicate a potential departure from the reference condition, or an acceleration of this process. Stream reaches were mapped in each major sub-watershed and along the mainstem Trail Creek to spatially locate disproportionate accelerated sediment supply from streambank erosion. The total tons of sediment from streambank erosion are weighted by the length and condition for each sub-watershed and the mainstem Trail Creek. This allows the locations with very high sediment contributions to be identified within the sub-watersheds and their relative contribution to total sediment yield. Not all of the sediment, however, that is dislodged or entrained from the banks is routed out of the watershed. Much of the sediment from the streambank erosion process is stored temporarily in the channel. Sediment budgets for each sub-watershed, reference reach, and representative reach include the specific contributions from streambank erosion. Because streambank erosion can be mitigated or reduced through various streambank stabilization methods, this data is used to set priorities for restoration and stabilization recommendations.

Overall, streambank erosion contributes *14,087 tons/yr* of introduced sediment for the sub-watersheds, which represents *87%* of the total introduced sediment. The streambanks along the mainstem Trail Creek contribute *4,031 tons/yr* of introduced sediment, which represents *77%* of the total introduced sediment along the river corridor. Overall, for the entire Trail Creek Watershed, streambank erosion makes up *84%* of the introduced sediment and contributes *18,118 tons/yr* to the post-fire total sediment yield of *20,838 tons/yr*. These values indicate the significant contribution of streambank erosion to the introduced or accelerated sediment supply.

Stream Type Succession

Wildfire-induced changes in the boundary conditions (riparian vegetation and flow resistance) and the flow and sediment regimes promote changes in river morphology and stream type. Typical channel responses to the fire effects are generally increased streambank erosion, channel enlargement, aggradation, degradation, lateral migration, and channel avulsion. The extent, nature, and direction of change is dictated by the landscape type and stream type associated with a given stream reach and its condition prior to the fire. Recognizing disequilibrium or unstable reaches and understanding what the stable form should be is instrumental to this effort on Trail Creek and its tributaries.

Stream type succession is used to interpret and predict the potential stable morphological state. Twelve stream succession scenarios and stream type shifts toward stable end points for each scenario are presented in Rosgen (2006b). These scenarios represent various sequences from actual rivers and are used to assist in predicting a river's

behavior based on documentation of similar response from similar types for imposed conditions. It is important to select the appropriate scenario and current stage of stream succession to assist in selecting the stable, end point stream type for restoration. The use of stream succession in design is dependent on the existing stream type and the stable, potential type based on a landscape type that matches the boundary conditions and the controlling variables. Based on the stream succession scenarios, Table 1 shows the typical, impaired stream types and their respective stable, potential stream types within specific landscape types.

Table 1 Existing, impaired stream types compared to the stable, potential stream types stratified by landscape types for the Trail Creek Watershed.

Existing, Impaired Stream Type	Existing Landscape Type	Stable, Potential Stream Type
A4	Short Alluvial Fan	B4a
A4	Long Alluvial Fan	D4
D4	Terraced Alluvial	C4
F4b	Colluvial	B4
F4b	Terraced Alluvial	B4
F4b	Short Alluvial Fan	B4
F4b	Long Alluvial Fan	D4
F4	Terraced Alluvial	C4
F4	Terraced Alluvial (confined)	B4c
G4	Terraced Alluvial	B4
G4	Short Alluvial Fan	B4
G4	Long Alluvial Fan	D4
B4 “Fair” or “Poor”	Terraced Alluvial	Stable B4
C4 “Fair” or “Poor”	Terraced Alluvial	Stable C4

Summary of Sediment Supply and Sub-Watershed Priorities

The contributions of the total introduced sediment supply to the total post-fire annual sediment yield for the Trail Creek Watershed are shown in Table 2. The total introduced sediment yield is higher than the flow-related annual sediment yield because not all of the sediment is routed out of the basin. Approximately *661 tons/yr* can potentially be related to excess sediment (channel storage) of the total flow-related increased sediment. The stored sediment in the channel is made available during subsequent stormflow runoff events and is reflected as an increase in flow-related channel source sediment.

The contributions of each erosional process for the 58 sub-watersheds are summarized in Rosgen (2011b). Priorities to address the sediment supply for the 58 sub-watershed were established based on a weighted sediment supply by area (see Rosgen, 2011b). The watershed master plan for restoration focuses on the high priority sub-watersheds to reduce the annual sediment supply based on the sediment sources.

Table 2 Relative contributions of erosional or depositional processes to total annual sediment yield for the Trail Creek Watershed.

Erosional or Depositional Processes	Total Annual Sediment Yield (tons/yr)	Percent of Total Introduced Sediment
Surface Erosion	2,542	12%
Roads & Trails	848	4%
Streambanks	18,109	84%
Total Introduced Sediment	21,499	100%
Erosional or Depositional Processes	**Total Annual Sediment Yield (tons/yr)**	**Sediment Deposition/ Increased Channel Storage (tons/yr)**
Post-Fire Flow-related Total Sediment Yield (FLOWSED)	20,838	661

THE WATERSHED MASTER PLAN FOR RESTORATION

The watershed and river restoration plan is based on the Natural Channel Design (NCD) methodology (Rosgen, 2007, 2011a). The watershed restoration master plan and design considers the stated objectives and offers a variety of solutions for a wide range of conditions. The following objectives help define the proposed watershed and river system restoration and sediment reduction plan:

1. Reduce sediment supply from disproportionate sources identified by erosional process, land use, and specific locations within the watershed
2. Quantify the sediment supply reduction by proposed restoration
3. Develop restoration scenarios that address the cause of impairment
4. Improve fish habitat diversity and function
5. Stabilize streambanks and streambeds
6. Utilize a natural channel design methodology that results in a natural appearance
7. Accelerate the recovery processes from the Hayman Fire
8. Re-establish a functional riparian corridor
9. Reduce road and trail maintenance
10. Provide for improved recreational opportunities
11. Provide ecological restoration (including habitats for birds, fish, mammals, and amphibians)
12. Reduce flood stage
13. Accommodate floods and reduce flooding impacts on adjacent road
14. Create cost-effective and low-risk restoration solutions
15. Be complimentary to the central tendency of natural systems
16. Provide a demonstration reach for extrapolation of similar applications
17. Provide an opportunity for research and restoration monitoring

Hydrologic Processes

The increase in peak flows due a reduction in evapo-transpiration will continue until a forested stand is re-established. Decades will be required to reach a full hydrologic utilization. Planting coniferous trees on the burned landscape will help accelerate the re-establishment of a forested stand for the potential long-term condition.

Restoration Plan for Hillslope Processes

Surface Erosion

Surface erosion reduction is planned within the *100 foot buffer* to existing streams because this zone has the highest probability of delivered sediment. The highest priorities are also set adjacent to perennial channels. The annual sediment contribution of approximately *2,542 tons/yr* makes this effort worthwhile. The following recommendations are designed to reduce this sediment source.

Because ground cover density is directly related to erosion rates and sediment supply, any sites with a ground cover density less than *40%* will need treatment. Treatment includes reseeding with a grass hay or straw mulch surface. Adding debris such as small logs, tops, and branches will also help reduce soil loss transport. The highest priorities for treatment are on slopes adjacent to perennial streams. The locations of the lowest ground cover density based on burn intensity for each sub-watershed are also zones of highest priority for surface erosion contributions.

Where sufficient space allows, constructing a bankfull bench against the toe of the slope is also recommended rather than allowing the sediment to be routed directly into the stream channel. The bench is most appropriate adjacent to B and C stream types. The materials for the entire bench width and length are generated from borrow sites. The borrow sites can also be used as a sediment detention basin. It is also necessary to establish vegetation on the bench to add as a potential sediment filter and sediment catch. Native bunchgrasses, such as big mountain brome, are appropriate species for the bench as these sites are not typically in wetland areas. The design requires approximately *89 yds*^{3} of fill per *100 ft* of constructed bench based on a bench width of *12 ft* and a mean depth of *2.0 ft*. Thus the borrow depression would be sufficiently deep and spaced to provide the needed fill. There is a net balance of cut and fill by design.

Overall, it is anticipated that at least *50%*, or *1,270 tons/yr*, can be reduced by increasing ground cover to above *65%* and by installing benches and establishing riparian vegetation on stream-adjacent slopes that are contributing to sediment delivery from surface erosion.

Roads & Trails

The *WARSSS* assessment indicated that the mainstem Trail Creek road contributes approximately *589.9 tons/yr* of delivered sediment compared to the total of *848 tons/yr* from the trails, off-road 4x4 roads systems, and the mainstem Trail Creek road. To reduce the delivered sediment and erosional debris from the Trail Creek road directly into Trail Creek, decreasing the *number* of stream crossings is recommended. Relocating the main Trail Creek road in two major locations will potentially reduce six crossings.

It is also recommended to reduce the fill erosion along many actively eroding road fill sites that are responsible for direct sediment contributions to Trail Creek; the following practices are recommended:

1. Relocate the channel away from the road fill slope to reduce the toe erosion from lateral channel migration
2. Place grass seed and native grass hay mulch or straw mulch over the seed on the fill slopes; native grass hay mulch is preferred as it is not as susceptible to wind transport as straw mulch and provides additional seed source
3. Move the localized road prism farther away from the channel without total relocation at locations where feasible
4. Stabilize channels cut through fills with step–pool grade control structures, side-slope reduction, and seeding and mulching
5. Place woody debris on fill slopes, including limbs, tops, branches and small logs, perpendicular to the slope; seed and mulch the slopes
6. Construct small terraces perpendicular to the slope to reduce rill erosion; seed and mulch the terraces
7. Construct a bankfull bench between the toe of fill slope and the channel where the channel impinges on fill
8. Install the toe wood structure with sod mats and willow transplants (or soil lifts with cuttings) on the bankfull bench to prevent Trail Creek from eroding the fill material

Also, reseeding and grading the road surface to reduce surface rills and maintain drainage features are recommended. Improving the road surface drainage is also advised as follows:

1. Out-slope the road to reduce concentration of water and sediment on the inside ditch line; this avoids the concentration of water from sub-surface interception and disperses the flow instead of concentrating such flows on the road and ditch-line surface
2. Place rolling “Kelly dips” on slope gradients greater than three percent
3. Construct sediment detention depressions at drainage outfalls or at drainage turnouts to encourage infiltration and sediment deposition

Headcut channels intercepted by the road should also be stabilized with step–pool grade control. This will help reduce the current high maintenance of sediment deposition on the road surface and will prevent over-steepening of the channel at the toe of the road.

It is anticipated that the aforementioned recommendations can effectively reduce the existing sediment yield from the Trail Creek road by approximately *413 tons/yr*, representing a *70%* sediment reduction.

In addition to the Trail Creek Road, numerous ORV roads and trails parallel and cross the channels in the Trail Creek Watershed; it is recommended to relocate the majority of these systems that are frequently introducing direct sediment away from the drainage proximities. Based on the immediate proximity of the ORV roads and trails to the adjacent channels and their steepness, it would be extremely difficult with a poor likelihood of success to institute sediment mitigation on these systems. The proposed ridge routes are available and feasible for these trails without changing their origin or destination sites (see Rosgen, 2011c). This recommendation can reduce nearly *200 tons/yr* of delivered sediment to Trail Creek.

Restoration Plan for Channel Processes

Due to high sediment yield results from flow-related increases, stream channel restoration and stabilization can be effective to reduce this accelerated sediment supply. The restoration work includes protecting streambeds and streambanks from the increased flows and re-establishing floodplain connectivity where possible. Creating a functioning riparian corridor is also recommended for the long-term stability of stream channels. Aquatic habitat will also be improved with such river restoration and stabilization work. The proposed restoration of the stream channels to reduce the accelerated sediment supply focuses on converting unstable stream types to stable stream types and reducing the streambank erosion.

Typical Design Scenarios

The *representative reaches* were established, measured, quantified, and evaluated in great detail to develop typical design scenarios that can be extrapolated to other locations in the Trail Creek Watershed where this level of detail was not obtained but is assumed to be similar. The reference reaches were established to provide the stable design criteria to develop the proposed design for the representative reaches. The nine design scenarios shown in Table 3 were developed to represent the range of stream types and stability conditions that require restoration within the Trail Creek Watershed. Each of the design scenarios is related to a specific location within the watershed for demonstration purposes. The appropriate scenario can then be extrapolated to other reaches of the same stream type, landscape type, and stability condition as the representative reach.

Table 3 The nine typical design scenarios developed to extrapolate to other locations in the Trail Creek Watershed for restoration.

Stream Type Conversions		
Existing, Impaired Stream Type	**Proposed Stream Type**	**Landscape Type**
1. D4 Poor	C4 Good	Terraced Alluvial
2. F4 Poor	B4 Good	Terraced Alluvial (confined)
3. G4 Poor	B4 Good	Terraced Alluvial
4. C4 Poor	C4 Good	Terraced Alluvial
5. F4b Poor Tributary	D4	Alluvial Fan
6. F4b Tributary	B4 Good	Alluvial Fan
7. A4a+ Poor	A4a+ Good	Colluvial
8. A4a+ Poor	D4	Alluvial Fan
9. A4a+ Poor	B4a Good	Alluvial Fan (short fan)

Each typical design scenario includes detailed descriptions of 1) General Description and Morphological Data; 2) Bankfull Discharge, Cross-Sectional Area, and Mean Velocity; 3) Plan View Alignment; 4) Cross-Section Dimensions; 5) Longitudinal Profile; 6) Structures; 7) Riparian Vegetation; 8) Cut and Fill Computations; 9) Streambank Erosion; 10) Flow-Related Sediment; and 11) Sediment Competence (see Rosgen, 2011c, for the detailed design scenarios).

The flow-related sediment and potential sediment reductions, including streambank erosion contributions, for the existing and proposed design reaches are documented in Rosgen (2011b). The majority of the design scenarios convert "Poor" condition stream types to "Good" stream types and unit sediment transport reductions are computed. However, the typical design scenarios 5 and 8 in Table 3 convert A4a+ and F4b stream types to the braided, D4 stream type with sediment detention basins and surface storage on alluvial fans. The typical designs for these scenarios store 100% of the sediment yield and are associated with a zero sediment transport to the mainstem Trail Creek.

The sediment reduction potential by implementing the proposed stream restoration design scenarios involving 3,025 ft of stream channels is approximately *1,600 tons/yr* for 7 of the 9 scenario locations. The remaining 2 scenarios associated with creating D4 stream types with sediment detention basins on alluvial fans result in reductions of

approximately *5,468 tons/yr* of sediment. In total, over *7,000 tons/yr* of sediment could be kept out of Trail Creek per year based on the implementation of the nine scenarios presented. This represents approximately *29%* of the total annual sediment yield in the Trail Creek Watershed. Extrapolating and implementing the design scenarios to appropriate locations will result in even greater sediment yield reductions.

Total Potential Sediment Reductions

The potential sediment reductions associated with implementing the nine typical design scenarios and the recommendations for hillslope processes are presented in Table 4. The total potential reduction is approximately *8,853 tons/yr*, representing approximately *37%* of the total annual sediment yield.

Table 4 The potential sediment reductions by implementing the recommendations for hillslope and channel processes.

Total Sediment Contribution Reductions	
Hillslope Processes	
Surface Erosion	*1,270 tons/yr*
Trail Creek Road	*413 tons/yr*
ORV Roads and Trails	*200 tons/yr*
Channel Processes	
The Nine Typical Design Scenarios	*7,000 tons/yr*
Total Potential Reduction	***8,853 tons/yr***

SUMMARY

The Trail Creek Watershed master plan for stream restoration and sediment reduction is the result of a detailed watershed assessment that has directed the proposed restoration to impaired streams. The assessment also identified the source of impairment including hillslope, hydrology, and channel processes. The master plan identified priorities of restoration based on disproportionate sediment supply contributions and the various sources, including streambed and streambank erosion from post-fire related streamflow increases, and direct introduction by surface erosion and roads and trails. These various erosional processes were identified and specific restoration scenarios were proposed to reduce the sediment supply and restore the physical and ecological function.

Each of the 17 specific, multiple objectives for the master restoration design for the Trail Creek Watershed are potentially met with the implementation of the various scenarios and locations proposed. Overall, the various restoration scenarios within the Trail Creek Watershed were developed to extrapolate general hydrology, sedimentological, and morphological relations and to create the dimensions, pattern, and profile of stable stream types scaled for individual reaches.

These subsequent designs are intended to accelerate the recovery of the Trail Creek Watershed from the adverse impacts of the Hayman fire. The proposed design scenarios and subsequent implementation will potentially direct the future of watershed restoration following large wildfires. The procedures can also be used for other watersheds that are currently impaired due to the Hayman fire in the South Platte Basin in a timely manner. Overall, the field assessment for the entire Horse Creek Watershed was completed in eight months and the assessment report and master restoration plan was completed in six months.

An individual 404 permit was issued for the master restoration plan for the entire Trail Creek Watershed to be implemented over 20 years, and project implementation began in 2011. The Forest Service (Pike and San Isabel National Forest) is monitoring the physical and biological response of the WARSSS-based restoration. The research and monitoring will document the benefits of restoration and watershed recovery.

REFERENCES

DeBano, L.F., Neary, D.G., and Ffolliott, P.F. (1998). Fire's Effects on Ecosystems. New York, NY: John Wiley & Sons, 333 pp.

Libohova, Z. (2004). Effects of Thinning and a Wildfire on Sediment Production Rates, Channel Morphology and Water Quality in the Upper South Platt e River Watershed. Thesis, Colorado State University, Fort Collins, Colorado.

MacDonald, L. (2009, Personal Communication). Hayman Fire: Current Status and Management Options. Memorandum dated September 12, 2009.

Moody, J.A., and Martin, D.A. (2001). Hydrologic and Sedimentologic Response of Two Burned Watersheds in Colorado. Water Resources Investigation Report 01-4122. Denver, CO: U.S. Geological Survey.

Neary, D.G., Klopatek, C.C., DeBano, F.F., and Ffolliott , P.F. (1999). Fire Effects on Belowground Sustainability: A Review and Synthesis. *Forest Ecology and Management, 122*, 51–71.

Robichaud, P.R., and Brown, R.E. (1999). What Happened after the Smoke Cleared: Onsite Erosion Rates after a Wildfire in Eastern Oregon. In: D.S. Olsen, & J.P. Potyondy (Eds.), *Proceedings, Wildland Hydrology Conference*, June, 1999, Bozeman, MT. Hernon, VA: American Water Resource Association, 419–426.

Robichaud, P.R., Beyers, J.L., and Neary, D.G. (2000). Evaluating the Effectiveness of Postfire Rehabilitation Treatments. General Technical Report RMRS-GTR-63. Fort Collins, CO: USDA Forest Service, Rocky Mountain Research Station, 85 pp.

Robichaud, P., MacDonald, L., Freeouf, J., Neary, D., and Martin, D. (2002). Hayman Fire Case Study Analysis: Postfire Rehabilitation, pp. 241–262. *Interim Report*, R.T. Graham (Ed), Hayman Fire Case Study, General Technical Report RMRS-GTR-114. Ogden, UT: USDA, Forest Service, Rocky Mountain Research Station.

Robichaud, P.R., MacDonald, L., Freeouf, J., Neary, D., Martin, D., & Ashmun, L. (2003). Postfi re Rehabilitation of the Hayman Fire, pp. 293–313. In: R.T. Graham (Ed), *Hayman Fire Case Study*, General Technical Report RMRS-GTR-114. Ogden, UT: USDA, Forest Service, Rocky Mountain Research Station, 396 pp.

Robichaud, P., and Wagenbrenner, J. (2009). Hayman Fire Rehabilitation Treatment Monitoring Progress Report Addendum, 2002–2008: Sediment yields, runoff , and ground cover in the first five years after the Hayman Fire. Moscow, ID: USDA Forest Service, Rocky Mountain Research Station.

Rosgen, D.L. (1994). A Classification of Natural Rivers. *Catena, 22*, 169–199.

Rosgen, D.L. (1996). *Applied River Morphology*. Pagosa Springs, CO: Wildland Hydrology.

Rosgen, D.L. (2001). A Practical Method of Computing Streambank Erosion Rate. In: *Proceedings of the Seventh Federal Interagency Sedimentation Conference, Vol. 1*, II-9–II-15. Reno, NV: Subcommittee on Sedimentation.

Rosgen, D.L. (2006). FLOWSED/POWERSED: Prediction Models for Suspended and Bedload Transport. In: *Proceedings of the Eighth Federal Interagency Sediment Conference*. Reno, NV: Subcommittee on Sedimentation.

Rosgen, D.L. (2006b). *Watershed Assessment of River Stability and Sediment Supply (WARSSS)* (2nd edition 2009). Fort Collins, CO: Wildland Hydrology.

Rosgen, D.L. (2007). Rosgen Geomorphic Channel Design. In: J. Bernard, J.F. Fripp, & K.R. Robinson (Eds.), *Part 654 Stream Restoration Design National Engineering Handbook (210-VINEH)*. Washington, DC: USDA, Natural Resources Conservation Service.

Rosgen, D.L., and Rosgen, B.L. (2010). Horse Creek Watershed *RLA* and *RRISSC* Assessments (Report submitted June 17th, 2010, to the Coalition for the Upper South Platte). Fort Collins, CO: Wildland Hydrology, 93 pp.

Rosgen, D.L. (2011a). Natural Channel Design: Fundamental Concepts, Assumptions, and Methods. In: A. Simon, S.J. Bennett, & J.M. Castro (Eds.), *Stream Restoration in Dynamic Fluvial Systems: Scientific Approaches, Analyses, and Tools*, Geophysical Monograph Series 194, pp. 69-93. Washington, D.C.: American Geophysical Union.

Rosgen, D.L. (2011b). Trail Creek Watershed Assessment & Conceptual Restoration Plan: The *WARSSS* Results of the Hayman Fire (Report submitted February 18, 2011, to the Coalition for the Upper South Platte). Fort Collins, CO: Wildland Hydrology, 146 pp., 5 Appendices.

Rosgen, D.L. (2011c). The Trail Creek Watershed Master Plan for Stream Restoration and Sediment Reduction (Report submitted April 22, 2011, to the Coalition for the Upper South Platte). Fort Collins, CO: Wildland Hydrology, 322 pp., 1 Appendix.

U.S. Environmental Protection Agency (1980). (WRENSS) An Approach to Water Resource Evaluation of Non-point Silvicultural Sources (A Procedural Handbook). EPA-600/8-80-012. Athens, GA: Environmental Research Laboratory.

HYBRID HYDRAULIC MODELING OF RIVER-TRAINING STRUCTURES IN SINUOUS CHANNELS

S. Michael Scurlock, Ph.D, Post-Doctoral Fellow, Colorado State University, scurlock@engr.colostate.edu; Amanda L. Cox, Ph.D, Assistant Professor, Saint Louis University, coxal@slu.edu; Drew C. Baird, Ph.D, Hydraulic Engineer, United States Bureau of Reclamation, dbaird@usbr.gov; Christopher I. Thornton, Ph.D; Associate Professor, Director Engineering Research Center, Colorado State University, thornton@engr.colostate.edu; Steven R. Abt, Ph.D; Senior Research Scientist/Scholar, Colorado State University, sabt@engr.colostate.edu

Abstract: Hybrid hydraulic modeling research, which integrates physical and numerical modeling, is currently being conducted to develop empirical design procedures for river-training structures. Transverse features are rock structures, usually installed in series around a river bend, which can control near-bank flow velocities, increase bank stability, decrease the effect of secondary currents, and promote habitat. An extensive database was developed from physical modeling of transverse features in a native-topography channel. The laboratory database is being used to calibrate and validate computational fluid dynamic (CFD) models, which will be used to approximate flow fields for varying structure designs. Empirical design procedures will then be developed from the resulting numerical-modeling database. The hybrid hydraulic modeling approach is detailed and results are presented from the CFD model calibration and validation to laboratory data.

INTRODUCTION

Hydraulic modeling has historically been grouped into the paradigms of either theoretical or empirical derivation. In essence, theoretical models are derived from conservation fundamentals while purely empirical methods rely on statistical methods to fit observed data. Due to the complex nature of fluid flow, the majority of theoretical models have a degree of associated empiricism; e.g. Manning *n*, viscosity, energy loss coefficients, which must be calibrated using observed hydraulic data. However, the core of the theoretical models is grounded in the Navier-Stokes equations. Empirical models used for hydraulics, such as stage-discharge relationships, scour-depth studies, rip-rap sizing, or stilling basin design, typically implement pertinent design parameters grouped into physically meaningful groups with numerical weights tailored to a collected dataset.

With increasing computational power and efficiency, theoretical models have evolved into robust, three-dimensional computational fluid dynamics (CFD) simulations. Such simulations have been shown effective in the evaluation of complex hydraulic conditions. While validated, the widespread use of CFD has not been realized in the current applied engineering and scientific realms. Theoretical models incorporating assumptions of the behavior of flow are widespread for practitioners, including HEC-RAS one-dimensional and two-dimensional code; however, the assumptions of such models significantly limit accuracy of results in complex flow environments where they are violated. In one-dimensional and two-dimensional theoretical flow simulations, assumptions break down when there are spatially rapidly-varied flow conditions containing a significant vertical flow component. Codified and widely implemented theoretical modeling codes such as HEC-RAS utilize empirical equations to account for the instances where assumptions break down, such as in the instance of a hydraulic jump or encountering an instream structure. The research presented in this proceeding illustrates a novel approach for hydraulic modeling methods by examining the feasibility of the combination of both theoretical and empirical models to develop design procedures for riverine structures. Proposed methods for the development of empirical design guidelines for transverse instream structures using data gathered from three-dimensional CFD simulations are expounded and detailed.

The Middle Rio Grande River between Cochiti Dam and Elephant Butte Reservoir in New Mexico has been the focus of extensive river restoration work since the upstream Cochiti Dam installation in 1975. The dam effectively disconnected the sediment continuity to the downstream reach, resulting in a geomorphic shift from a historically braiding channel to a slightly sinuous, incising system. The United States Bureau of Reclamation (Reclamation), as the responsible party for management of the river, launched an investigative study on the performance of transverse

in-stream structures jointly with Colorado State University (CSU). Research performed by CSU and Reclamation has provided a wealth of physical model hydraulic data surrounding transverse in-stream structures and quantitative design guidelines for structure installation.

Transverse in-stream structures are a type of river-training structure that has the primary goal of halting bank migration in a meandering system. Structures extend from the outer-bank of the channel into the center, diverting flow from the outer-bank to the relocated channel thalweg at the structure tips. Nomenclature for transverse in-stream structures varies dependent upon the crest height and intended flow pattern. Bendway-weirs, spur-dikes, and bank-attached vanes are types of in-stream structures, planimetrically identical, yet different in their cross-sectional geometries and intended hydraulic effects. Planimetric and cross-section schematics of the three identified in-stream structures are provided in Figure 1, which expounds differences between structure classifications in the cross-sectional view. In a general hydraulic sense, bendway weirs redirect conveyance perpendicularly and over the top of the structure crests, spur-dikes shift flows around the structure tip, and bank-attached vanes combine both crest overtopping and shifted flow to redirect conveyance to the channel center.

Design recommendations for transverse in-stream structures are typically anecdotal and do not provide specifics of hydraulic performance based upon alteration of design parameters within recommended ranges. Examples of guidelines include NRCS (2005) for bank-attached vanes, Lagasse et al. (2009) for spur-dikes, and McCullah and Gray (2005) for bendway weirs. Scurlock et al. (2014) presented a quantitative model for estimation of normalized maximum and average velocities at various locations within a channel resulting from structure installations. The general mathematical model presented by Scurlock et al. (2014) is given as Equation 1.

$$MVR, AVR = a_1 + a_2\left(A^*\right)^{a_3}\left(\frac{L_{ARC}}{T_W}\right)^{a_4}\left(\frac{R_C}{T_W}\right)^{a_5}\left(\frac{L_{W-PROJ}}{T_W}\right)^{a_6}\left(\frac{D_B}{D_B-\Delta z}\right)^{a_7}\left(\frac{2\theta}{\pi}\right)^{a_8} \quad (1)$$

where:

MVR = maximum velocity ratio;

AVR = average velocity ratio;

A^* = percentage of baseline cross-sectional area blocked by structure;

$L_{W\text{-}PROJ}$ = projected length of structure into channel [L];

L_{ARC} = arc length between centerline of structures [L];

R_C = radius of curvature of channel bend centerline [L];

T_W = averaged top width of channel measured at baseline in bend [L];

D_B = averaged maximum cross-section baseline flow depth in bend [L];

Δz = elevation difference between water surface and structure crest at the tip [L];

θ = structure plan angle [radians];and

$a_1, \ldots, a_6$ = regression coefficients.

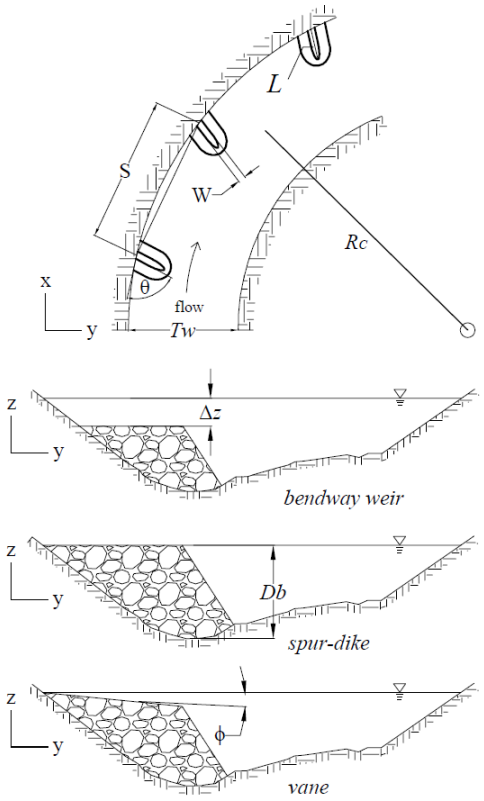

Figure 1 In-stream structure geometric parameter definitions

Heintz (2002), Darrow (2004), and Schmidt (2005) evaluated hydraulic performance of transverse in-stream structures in a physical model at CSU. Using physical model data collected from these studies from a 1:12 Froude scale model of two trapezoidal representations of the prototype Middle Rio Grande River, Equation 1 was optimized to predict normalized velocities at the outer-bank, centerline, and inner-bank of the channel for spur-dike and bank-attached vane installations. A total of 130 independent data points were used for regression analysis, representing a statistically large database for equation development.

Further research was conducted at CSU by Thornton et al. (2011), Scurlock et al. (2014a), and Scurlock et al. (2014b) on spur-dikes, bendway-weirs, and bank-attached vanes installed in a physical model representation of natural channel geometry. Survey data were obtained from two channel bends in the Middle Rio Grande and were constructed within the spatial constraints of the trapezoidal physical model. A total of four bendway-weir configurations, one spur-dike, and one bank-attached vane configuration were evaluated in the natural channel with comprehensive velocity fields realized through data collection with an acoustic Doppler velocimeter (ADV). Data collected in the natural topography physical model elucidated important hydraulic characteristics regarding transverse in-stream structures; however, evaluated configurations do not substantiate regression analysis using the model of Equation 1.

The primary goal of the current research is to investigate methods of compiling a large dataset for the bendway-weir structure type in attempt to develop quantitative design guidelines similar to the model of Equation 1. To facilitate this development, a dataset of significant size would be required, at least one order of magnitude higher than the four physically modeled natural-topography bendway-weir configurations. Physical modeling can be time consuming and resource intensive; factors which can inhibit the compilation of the requisite dataset for design guideline development. Utilizing CFD, it may be possible to take numerically simulated results from modeled bendway-weir configurations and compile a dataset large enough for empirical development. The feasibility of developing bendway-weir design guidelines using CFD is examined using calibration and validation procedures with the physical model data of Scurlock et al. (2014a) and Scurlock et al. (2014b). It is shown that CFD methodologies

present a viable alternative to physical modeling or field data collection for the development of empirical equations, representing a hybrid approach to hydraulic modeling.

NUMERICAL MODEL SELECTION

A proven, reliable, and reproducible model was desired for the completion of numerical evaluation of laboratory data. A balance between desired accuracy and required computational resources must be achieved during numerical modeling. While large-eddy simulations and direct-numerical solutions outperform Reynolds-averaged Navier-Stokes (RANS) models in resolving turbulent and separating flows (Kang and Sotiropoulos, 2012; Constantinescu et al., 2011), the required computational times are substantially greater and unfeasible for the proposed research objectives. A numerical code using a RANS approach with an appropriate turbulence model was investigated. FLOW-3D is a commercial numerical package created by Flow Science which has been proven in open-channel flow applications and in-stream structures (Rodriguez, 2004; Abad et al., 2008; Plymesser, 2014; Kolden, 2013). The model incorporates a Fractional-area-volume-obstacle-representation (FAVOR) method for solid object interfaces and volume-of-fluid (VOF) method for free-surface fluid interfaces. FLOW-3D uses a rectilinear, orthogonal grid system in conjunction with FAVOR and VOF to rapidly develop discretized meshes around complex objects, which is preferable when investigating multiple geometries.

The RNG k-ε turbulence mode, an option incorporated into FLOW-3D model, was found to be an appropriate numerical method of representing overall hydraulic trends while accounting for smaller scales of turbulence than other RANS turbulence closure models. The RNG k-ε model presented by Yakhot et al. (1992) accounts for different scales of turbulent motion influencing the transport of k and ε and may improve RANS model resolution of rotating flows. All simulations were conducted using the RNG k-ε RANS model with the standard turbulent mixing length coefficient of 0.09. Pressure was solved for implicitly and momentum advection was set as a second-order monotonicity preserving explicit scheme akin to the PRIME method of Maliska and Raithby (1983).

Meshing proficiency, graphical display capabilities, ease of user interaction, numerical method flexibility, and application track record led to the selection of FLOW-3D as the model of choice to meet project objectives. With the numerical package selected and specific code aspects of the model determined, the spatial domain of the simulation was then defined in order for the mesh to be generated and the numerical code executed. Representations of the physical model channel and in-stream structures were created to serve as the boundaries for the numerical simulations.

GEOMETRY REPRESENTATION AND MODEL SETUP

Representation of a physical surface as a boundary in a numerical mesh requires surveyed data and a method for interpolation between known data points. The nature of the FAVOR model in FLOW-3D allows for rapid integration of new components to surfaces. This concept works well in the context of the current research. A baseline model was created as an individual surface and in-stream structure configurations were represented as independent surfaces and brought into the model separately.

The creation of the numerical domains utilized high-resolution LiDAR data of approximately 15 million individual points parsed to approximately 6 thousand points for surface generation. Parsed data were imported to AutoCAD Civil 3D and developed into a surface using a triangular-irregular network (TIN) which was then exported to FLOW-3D. The same process was followed with bendway-weir configurations. Figure 2 illustrates a schematic of the bendway-weir configurations installed with a topographic representation interpolated from LiDAR data. FLOW-3D requires that the flume outlet be oriented on an orthogonal axis. The model was rotated and linearly translated to ensure that the outlet was oriented parallel to x = 0 ft. Initial and boundary conditions within FLOW-3D are specified once the surface has been imported to the program. The developed baseline surface was added, the mass-flow outlet was designated, and the domain inlet was defined as a constant mass input. Constant mass input boundary conditions designate the full cross section with a uniform deliverance of volumetric flow and do not initially contain information regarding developed velocity profiles expected in a physical laboratory or field. This entrance effect was mitigated by extending the model input section approximately 10 channel widths upstream allowing uniform cross-section inflow to develop along the channel before it encountered the test area. Downstream boundary conditions were specified at water-surface elevations observed during laboratory testing. Figure 3 provides

an example of the numerical model topography depicting the baseline model (in grey) along with a bendway-weir structure installation (in red).

MODEL CALIBRATION

Numerical models may be calibrated to specific applications through adjustment of spatial grid resolution, maximum permitted time step, surface roughness, turbulence parameters, mass inflow, fluid properties, initial conditions, and boundary conditions. In the case of modeling bendway-weirs using FLOW-3D, grid independence, time step, surface roughness, and mass inflow was adjusted during the calibration process. Initial grid, time step, and mass inflow calibrations were performed on the baseline model and then applied to the bendway-weir configurations. Approximately 3,000 ADV data were used for the baseline calibrations as reported in Scurlock et al. (2012). Total velocity measurement variability from instrumentation thresholds as reported from Scurlock et al. (2012) amounted to ± 4.5% of the measured value. Surface roughness was calibrated to baseline and structure installation configurations.

Numerical grid independence is an evaluation of the level of mesh resolution required for efficient and accurate representation of fluid dynamics throughout the solution domain. Both spatial precision and solution accuracy increase with finer grid resolution up to a threshold at which further reduction of grid size does not warrant computational expense. To prove grid independence, an original Cartesian mesh of size {x,y,z} = {1.5 ft, 1.5 ft, 0.5 ft} was evaluated then split by a factor of two for reevaluation. Global mean absolute difference was computed between the flow velocities for each mesh and a mean absolute percent difference (MAPD) tolerance was established at 5%. *MAPD* was calculated using the grid points from the coarser mesh as comparison locations and used the finer mesh for deviation normalization. Five grid sizes were evaluated and grid independence for the baseline model was established at a spacing {0.1875 ft, 0.1875 ft, 0.0625 ft}. The *MAPD* between the last grid iteration was 2.6% for depth-averaged velocity points and 3.7% for all velocity data, largely centered in small, localized areas at the flow boundaries.

Time-step discretization is another dimensional grid in addition to the spatial mesh which must be specified for numerical model execution. Time-step sizing is not as important as spatial grid resolution for data precision; a smaller time step will generally not provide more information than a larger one. However, the explicit nature of the momentum advection numerical scheme and Courant-Friedrichs-Lewy (CFL) limitations makes the time-step size fundamental for local numerical stability as well as for attenuation of global numerical oscillation perturbations (Courant et al., 1928). Time-step independence was proven by iterating maximum time step size. CFL limitations dictate that the time step must be small enough to reconcile all advective motion within a given grid cell, or that the speed at which the mass travels through a certain distance cannot exceed the numerical computation speed. As such, the time step was automatically reduced if CFL requirements were violated.

Surface roughness affects the frictional resistance on the flow and all hydraulic properties within the channel. Five roughness iterations were carried out to bracket the minimum deviation between numerical and physical results. Flow depths, 60% depth laboratory velocity locations, and the full set of laboratory velocity data collection locations were used for comparison between numerical and physical models. A surface roughness value of 0.07 ft produced the most accurate results at a precision level of ± 0.01 ft.

Using the calibrated mesh size, time step, and roughness value, a full-domain simulation was performed on the baseline model. It was observed that flow depths as well as velocities were greater than those recorded in the physical model, indicating that the volumetric flow rate in the numerical model was in excess of that in the physical model. The physical model surface was not impermeable and an amount of seepage was present during operation. A calibration adjustment of the numerical flow rate to 11.5 ft^3/s produced more accurate results and the discharge reduction of 0.5 ft^3/s, representing 4.7% of the bankfull flow rate, was applied to all subsequent numerical simulations.

The calibrated numerical baseline model was run at 11.5 ft^3/s until a steady-state condition was achieved. Numerical model data were extracted at the physical data-collection locations for comparison. Flow depths throughout the solution domain matched physical values well with mean-absolute deviation of 0.026 ft and *MAPD* of 3.78%. Velocity magnitudes at 60% flow depth were represented well with important regions of flow for the project

objectives resolved. Regions of high and low flow at the respective outer-bank and inner-bank were nearly identical in both models and velocity magnitudes were of approximately the same. The *MAPD* was calculated at 11.67%, the median was 9.00%, and the standard deviation was 12.33%, indicating a strong right-skew. Approximately 55% of the data were represented with less than 10% difference and 84% of data were predicted with 20% difference or less.

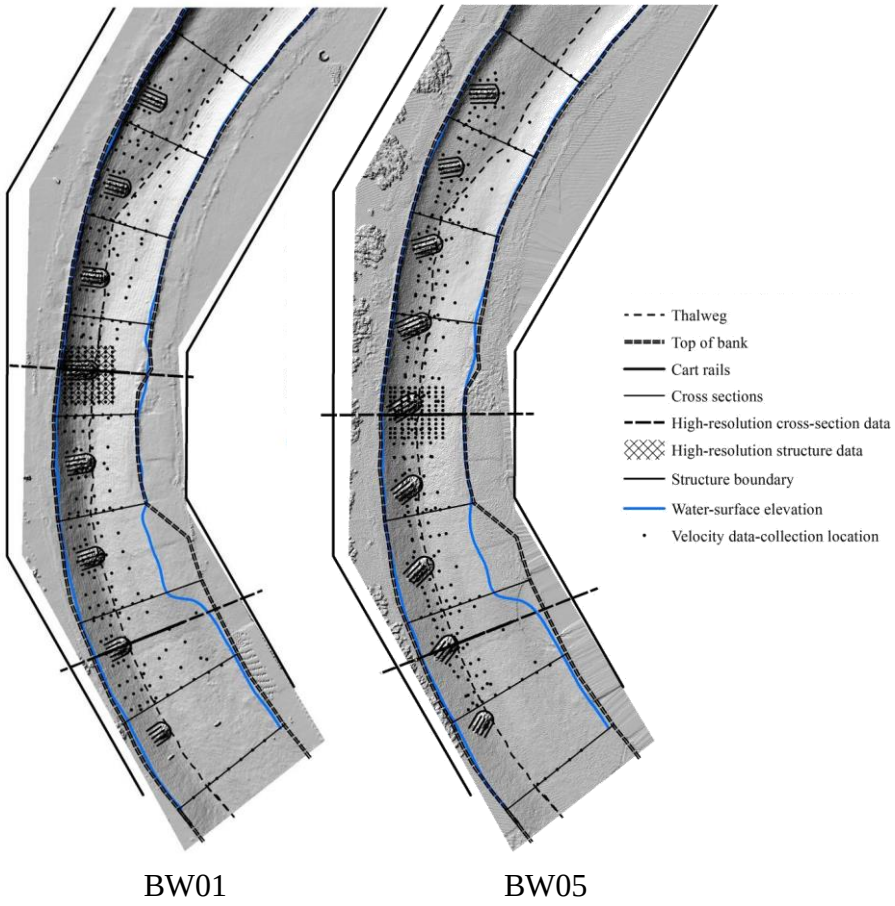

Figure 2 Bendway-weir configurations, flume schematic, and data-collection locations

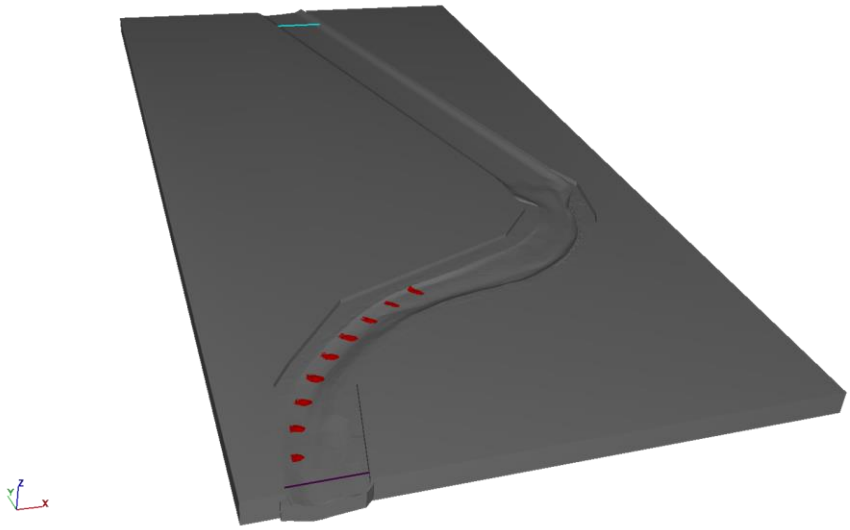

Figure 3 Geometric representation of baseline model (grey) and installed structures (red)

A calibration simulation at 11.5 ft^3/s was performed on the BW05 bendway-weir configuration from Scurlock et al. (2014b) with uniform surface roughness set at R = 0.07 ft and compared to the physical model dataset. Figure 3 illustrates the BW05 structure configuration and velocity data-collection locations. Roughness values for the structures were iterated and deviations between numerical and physical results increased with roughness greater than the bed surface. The structures were then set uniformly at 0.07 ft of surface roughness. Mean-average difference for flow depth was calculated as 0.04 ft and the *MAPD* was found to be 4.61%. Distributions of velocity in the physical and numerical model of the BW05 configuration are presented in Figure 4. The numerical model velocity distribution adheres closely to magnitudes at 60% flow depth in the physical model with shifted conveyance to the channel center, acceleration over structure crests, acceleration around structure tips, and outer-bank velocity increases captured. A notable area of accuracy of the numerical and physical model occurs at the shear layer between the reduced outer-bank velocity zone and increased channel-center velocity zone. The gradient zone was well resolved by the numerical model especially in the downstream regions of the channel. Discrepancies in the velocity distributions were mainly concentrated in the leeward areas of the bendway weirs and at the downstream extent of the model where a planimetric expansion occurred. The RNG κ-ε turbulence model used in the numerical model has limitations in application to highly turbulent flows with strong vorticity components and flow separation (Menter, 1994), such as observed in the areas of higher difference. Overall, 60% velocity magnitudes were predicted with a right-skewed difference distribution with a *MAPD* of 14.30%, median of 9.21%, and standard deviation of 16.53%. Seventy-nine percent of the data were predicted at better than 20% relative difference and 52% were predicted at 10% difference or less.

A high-density data collection cross section for BW05 transected behind the structure crest and passed through the zone of reduced outer-bank velocity. Approximately 300 ADV data collection points were spaced across this cross section. The distributions of velocity magnitudes between the physical and numerical models were similar as illustrated in Figure 5. A high velocity core was centered in the channel due to bendway-weir flow redirection, high velocity was noted above the structure crest, and low velocity zones were located behind the structure and at the inner-bank boundary. The gradient between the high velocity in the channel center and low velocity in the leeward shadow of the structure was represented well by the numerical model. The zone of high velocity in the channel center was slightly larger in size and of higher magnitude for the physical model. The majority of the channel cross-section was predicted with relatively low differences; 54% of the data were below 10% difference and 81% were below 20% difference. The calculated cross-sectional *MAPD* was 12.80%, median difference was 8.99%, and standard deviation was 13.67%

MODELVALIDATION

Numerical model validation consists of application of a calibrated numerical algorithm to an independent, yet similar simulation to which the numerical model was tailored to apply. If a numerical model performs well in describing a validation situation when no parameters are adjusted, then confidence is warranted for interpretation of further simulation extrapolations. The downstream minimum, BW01 configuration from Scurlock et al. (2014a) was used for the validation dataset for the bendway weir structure type. Figure 3 details the structure schematic and data-collection locations overlaid on a LiDAR topographic survey.

Numerical simulations for BW01 were performed at a steady 11.5 ft^3/s flow rate with calibrated parameters and boundary condition water-surface elevations observed in the physical model. Numerical data were extracted at the physical data-collection locations for comparable analysis. Flow depths for BW01 were predicted with an average difference of 0.034 ft and *MAPD* of 4.34%. Planimetric velocity magnitude distributions at 60% flow depth for the physical and numerical model are displayed in Figure 6. The distribution of velocity within the BW01 structure field was complex and varied rapidly between high and low velocity magnitudes. Velocity contours between models matched closely, with high velocities centered off the structure tips, structure-crest acceleration, outer-bank acceleration over the structure crests, and reduced velocity zones in the leeward zone of the structures. Transition gradient zones between regions of high and low velocity were similar between the two datasets and the numerical model represented the overall flow conditions of the physical model with high accuracy. The most flagrant discrepancies in the velocity magnitude distributions occurred at the leeward side of the fifth and sixth structures moving downstream in the structure configuration series. In this leeward zone, the numerical model simulated high velocities on the order of the outer-bank increased zone while the physical model contained data which indicated a region of reduced velocity. The distribution of difference percentage was strongly right-skewed with a *MAPD* of

44.62%, a median of 14.83%, and a standard deviation of 111.47%. The majority of data in the solution domain contained differences much lower than the regions near the fifth and sixth structure. Sixty-two percent of the data had relative difference of less than 20% and 35% of the data were below 10% relative difference. Median difference of 14.83% exceeded the BW05 calibration median difference of 9.21%.

An upstream high-resolution data cross-section transected the majority of the fourth structure crest in the BW01 configuration series. The cross-sectional topography and numerical and physical velocity magnitude distributions are presented in Figure 7. Velocity magnitude distributions between the two models share similar overall patterns. The largest velocities were centered over the tip of the structure crest, a low velocity region existed at the inner-bank, and acceleration over the structure crest was noted. Numerical results also produced higher velocities and less boundary interference near the channel thalweg than observed in the physical model. However, on a cross-sectional scale, results of the two models are visually equivalent. The majority of the cross section was well predicted, with a *MAPD* of 8.92%, median difference of 7.85%, and standard deviation of 6.02%. The median difference for the validation configuration was less than that of the cross-sectional calibration median difference of 8.99%.

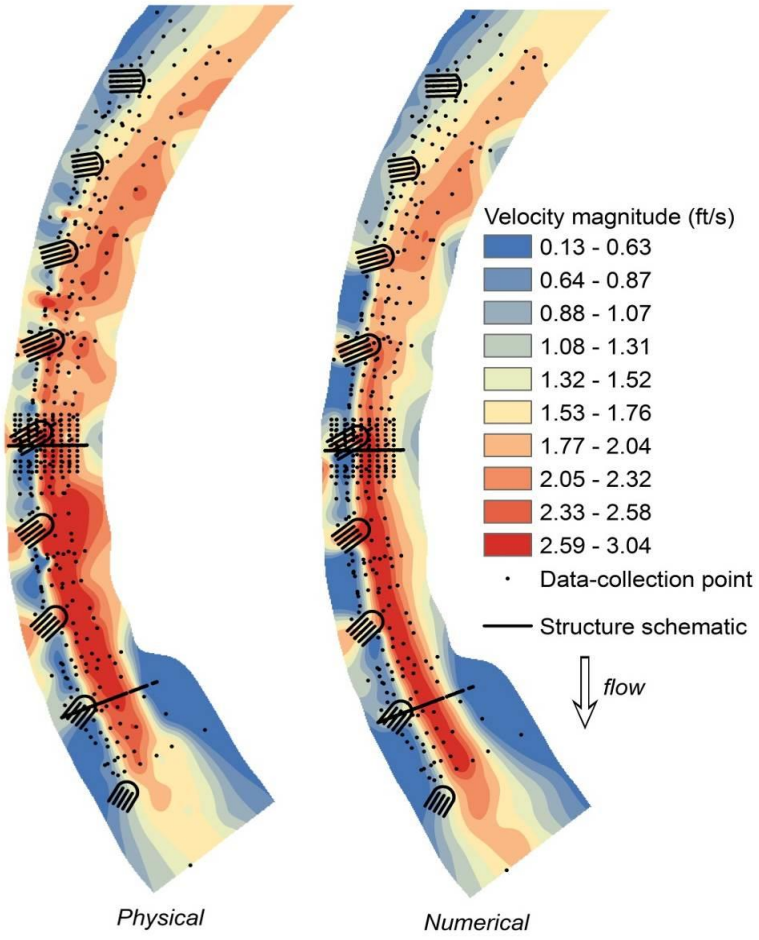

Figure 4 Physical and numerical velocity magnitudes, calibrated BW05

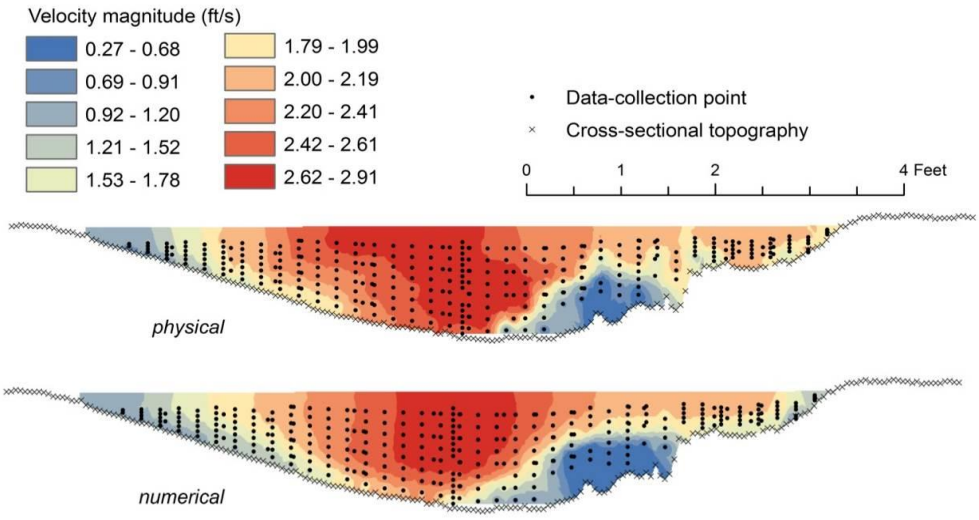

Figure 5 Velocity magnitude distributions, BW05XSA; downstream perspective

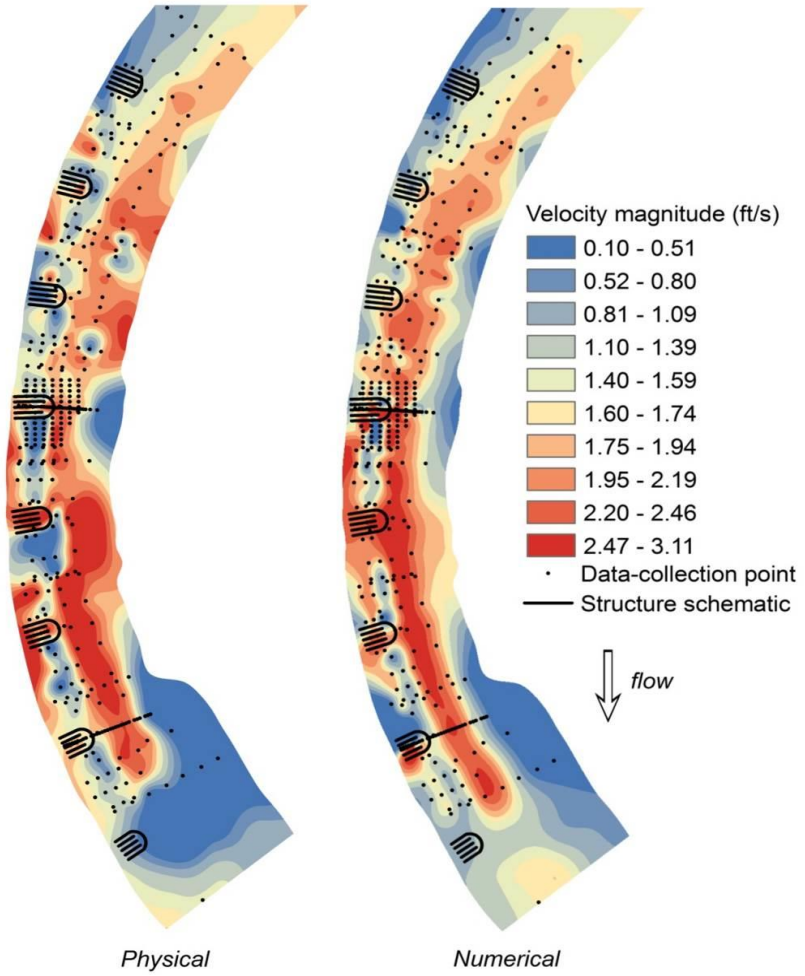

Figure 6 Velocity-magnitude distribution, BW01 bendway-weir validation simulation

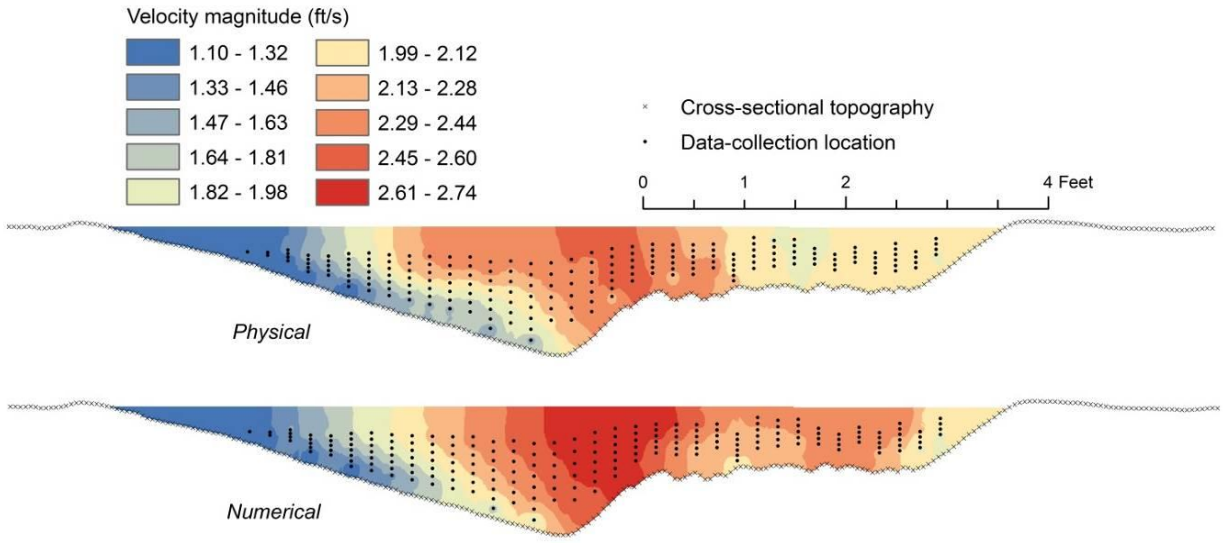

Figure 7 BW01XSA velocity magnitude distribution, bendway-weir validation simulation

SUMMARY AND CONCLUSIONS

Approximation of open-channel hydraulics may be achieved through the theoretical or empirical solutions. Prediction of flow conditions using theoretically grounded CFD methods has been proven to be accurate for in-stream structure hydraulics; however, widespread implementation of three-dimensional numerical modeling has yet to be fully integrated into typical engineering design. Designers typically employ empirical equations to account for scenarios in which typical one-dimensional and two-dimensional models are inaccurate. This study investigated the feasibility of using CFD to compile a large enough database for the development of an empirical model from numerical results, representing a hybrid modeling approach.

A CFD model was chosen and physical models of bendway weirs in a meandering river channel were represented numerically. Grid independence, maximum time-step independence, surface roughness, and seepage losses were calibrated using baseline flow data and one bendway-weir configuration and then validated using a separate bendway-weir configuration. Pursuant to the goals of empirical model development, the velocity magnitudes between the observed physical model data and predicted numerical results were compared. It was found that the numerical model represented observed velocity trends well and the general flow patterns were captured. Median percent differences in velocity magnitudes of comparable datasets were on the order of 10% and right-skewed, indicating a global representation of flow patterns with localized regions where results did not match.

Calibration and validation results accentuate the potential of CFD as a method of compiling a large enough dataset for empirical model development. A series of structure configurations at various geometry parameters will be created and placed within the baseline numerical model and simulations will be performed. Results of this process will provide substantial information about the effects of bendway-weir geometries on resulting flow fields and aid in the development of structure design procedures.

REFERENCES

Abad, J.D., Rhoads, B.L., Guneralp, I., and Garcia, M.H. (2008). "Flow structure at different stages in a meander-bend with bendway weirs." *Journal of Hydraulic Engineering.* 134:8. 1052-1063.

Constantinescu, G., Koken, M., and Zeng, J. (2011). "The structure of turbulent flow in an open channel bend of strong curvature with deformed bed: Insight provided by detached eddy simulation." *Water Resources Research.* 47, 1-17.

Courant, R.; Friedrichs, K.; Lewy, H. (1928), "Über die partiellen Differenzengleichungen der mathematischen Physik", Mathematische Annalen (in German) 100 (1): 32–74, Bibcode:1928MatAn.100..32C, doi:10.1007/BF01448839, JFM 54.0486.01, MR 1512478

Darrow, J.D. (2004). "Effects of bendway weir characteristics on resulting flow conditions." M. S. Thesis. Colorado State University, Department of Civil Engineering. Fort Collins, Colorado.

Heintz, M.L. (2002). "Investigation of bendway-weir spacing." M. S. Thesis. Colorado State University, Department of Civil Engineering. Fort Collins, Colorado.

Kang, S. and Sotiropoulos, F. (2012). "Numerical modeling of 3D turbulent free surface flow in natural waterways." *Adv. in Water Resources*, 40 (2012) 23-36.

Kolden, E. (2013). "Modeling in a three-dimensional world: Whitewater park hydraulics and their impact on aquatic habitat in Colorado." M. S. Thesis. Colorado State University, Department of Civil Engineering. Fort Collins, Colorado.

Lagasse, P.F., Clopper, P.E., Pagan-Ortiz, J.E., Zevenbergen, L.W., Arneson, L.A., Schall, J.D., and Girard, L.G. (2009). "Bridge scour and stream instability countermeasures: experience, selection, and design guidance." 3rd ed. HEC-23. Federal Highway Administration. FHWA-NHI-09-111.

Maliska, C.R. and Raithby, G.D. (1983). "Calculating 3-D fluid flows using non-orthogonal grid." *Proc. Third Intl. Conf. on Numerical Methods in Laminar and Turbulent Flows*, 656-666.

McCullah, J.A. and Gray, D., 2005, "Environmentally Sensitive Channel- and Bank-Protection Measures," NCHRP Report 544, Transportation Research Board, National Academies of Science, Washington, D.C.

Menter, F.R. (1994). "Two-equation eddy viscosity turbulence models for engineering applications." *AIAA Journal* 32(8). 1598-1605

Natural Resources Conservation Service (2005). "Design of stream barbs." *Tech. note 23.* Department of Agriculture. Portland, OR.

Plymesser, K.E. (2014). "Modeling fish passage and energy expenditure for American Shad in a steppass fishway using a computation fluid dynamics model." Ph.D Dissertation.Montana State University, Dept. of Civil Engineering.

Rodriguez, J.F., Bombardelli, F.A., Garcia, M.H., Frothingham, K.M., Rhoads, B.L., Abad, J.D. (2004). "High-resolution numerical simulation of flow through a highly sinuous river reach." *Water Resources Management*, 18: 177-199.

Schmidt, P.G. (2005). "Effects of bendway weir field geometry characteristics on channel flow conditions." M. S. Thesis. Colorado State University, Department of Civil Engineering. Fort Collins, Colorado.

Scurlock, S.M., Cox, A.L., Baird, D.C., Thornton, C.I., Parker, T.R., and Abt, S.R. (2012) "Middle Rio Grande Physical Modeling - Native topography: Construction and evaluation of baseline hydraulic conditions." Colorado State University, Department of Civil Engineering, Fort Collins, CO.

Scurlock, S.M., Thornton, C., Baird, D., and Abt, S. (2014). "Quantification of transverse in-stream structure hydraulics." *Journal of Hydraulic Engineering*. DOI: 10.1061/(ASCE)HY.1943-7900.0000952.

Scurlock, S.M., Thornton, C.I., and Abt, S.R. (2014a). "Middle Rio Grande physical modeling – Evaluation of bendway-weir structures with the native-topography channel." Technical report prepared for the United States Bureau of Reclamation, Albuquerque Area Office. October, 2014.

Scurlock, S.M., Thornton, C.I., and Abt, S.R. (2014b). "Middle Rio Grande physical modeling – Reevaluations and comparison of instream structures within the native-topography channel." Technical report prepared for the United States Bureau of Reclamation, Albuquerque Area Office. In Peer Review.

Thornton, C.I., Cox, A.L, Ursic, M.E., and Youngblood, N.A. (2011). "Data report for completed bendway-weir configurations within the native topography model." Colorado State University, Department of Civil and Enviromental Engineering. Fort Collins, CO.

Yakhot, V., Orszag, S.A., Thangam, S., Gatski, T.B. & Speziale, C.G. (1992), "Development of turbulence models for shear flows by a double expansion technique." *Physics of Fluids A*, 4(7): 1510-1520.

A CYCLIC STREAM EVOLUTION MODEL INTEGRATING HABITAT AND ECOSYSTEM BENEFITS, INCORPORATING SPACE-TIME SUBSTITUTION

Brian Cluer, Regional Geomorphologist, NOAA Fisheries, Santa Rosa, CA 95472 (brian.cluer@noaa.gov); Colin Thorne, ESA Vigil-Agrimis, Portland OR 97214 (cthorne@esassoc.com)

Abstract While channel evolution models (CEM) provide an organizational structure for considering river channels and their complex response to disturbances (for example; changes in base level, channelization, levees, or alterations to the flow and sediment regimes), physically and ecologically streams comprise more than their channel. We present a revised model, updated in light of several decades of research and practical experience, including realization that the single thread, meandering channel form may not represent the natural or pre-disturbed state, or the potential evolutionary end-state, an assumption implicit to CEMs. The new Stream Evolution Model (SEM) includes precursor and successor stages featuring floodplain interactions and multi-threaded channels, and stream evolution as a cyclical phenomenon within which natural channels evolve (Figure 1).

The SEM links habitat and ecosystem benefits to the hydrologic, hydraulic, morphological and vegetative attributes of each evolutionary Stage, highlighting the interactions between physical and biological processes (Figure 2).

Consideration of the links between stream evolution and ecological services leads to improved understanding of the ecological status of modern, managed rivers compared to their unmanaged, natural counterparts. The potential utility of the SEM, with its interpretation of habitat and ecosystem benefits, includes improved river management decision making with respect to future capital investments in river conservation, restoration, and species recovery (Figure 3).

This presentation adds original, new capabilities to the version of the Stream Evolution Model published in 2013 in the Journal *River Research and Applications*. The new version considers space-time substitution to account for the effects of upstream propagation of nickpoints and downstream delivery of excessive sediment loads, together with implications for habitats and ecosystems (and their conservation or restoration).

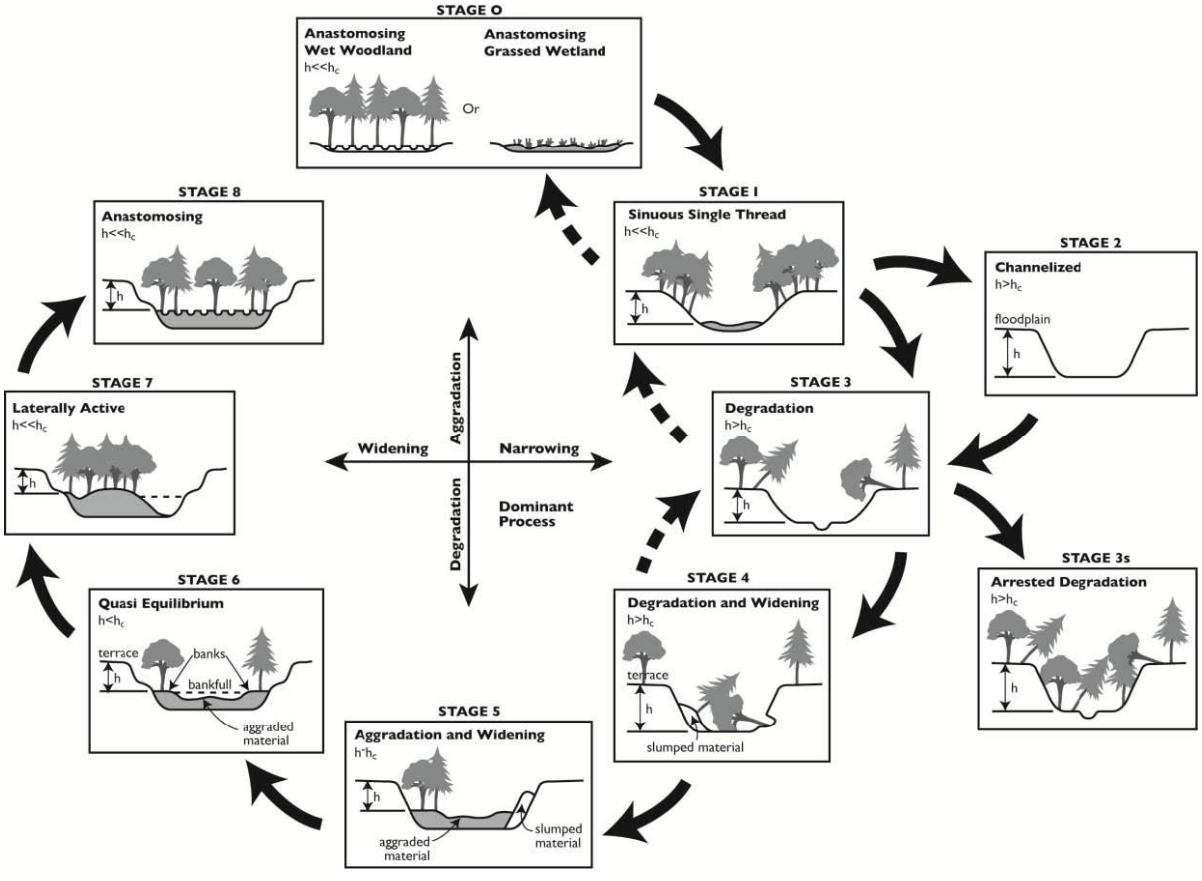

Figure 1 Stream Evolution Model based on: combining the former CEMs (Schumm et al. 1984; Simon and Hupp 1986); inserting a precursor stage (Stage 0) to better represent pre-disturbance conditions; adding two successor stages (Stages 7 and 8) to cover late-stage evolution; and, representing incised channel evolution as a cyclical rather than a linear phenomenon. Dashed arrows indicate 'short-circuits' in the normal progression indicating, for example, that a Stage 0 stream can evolve to Stage 1 but then recover to Stage 0, a Stage 4-3-4 short-circuit which occurs when multiple head cuts migrate through a reach and which may be particularly destructive. Stage 2 is a constructed stage in which the stream is channelised, while Stage 3s is outside the cycle and represents an evolutionary "dead end" where an erosion resistant layer in the local lithology stabilizes the bed and banks on an incised channel.

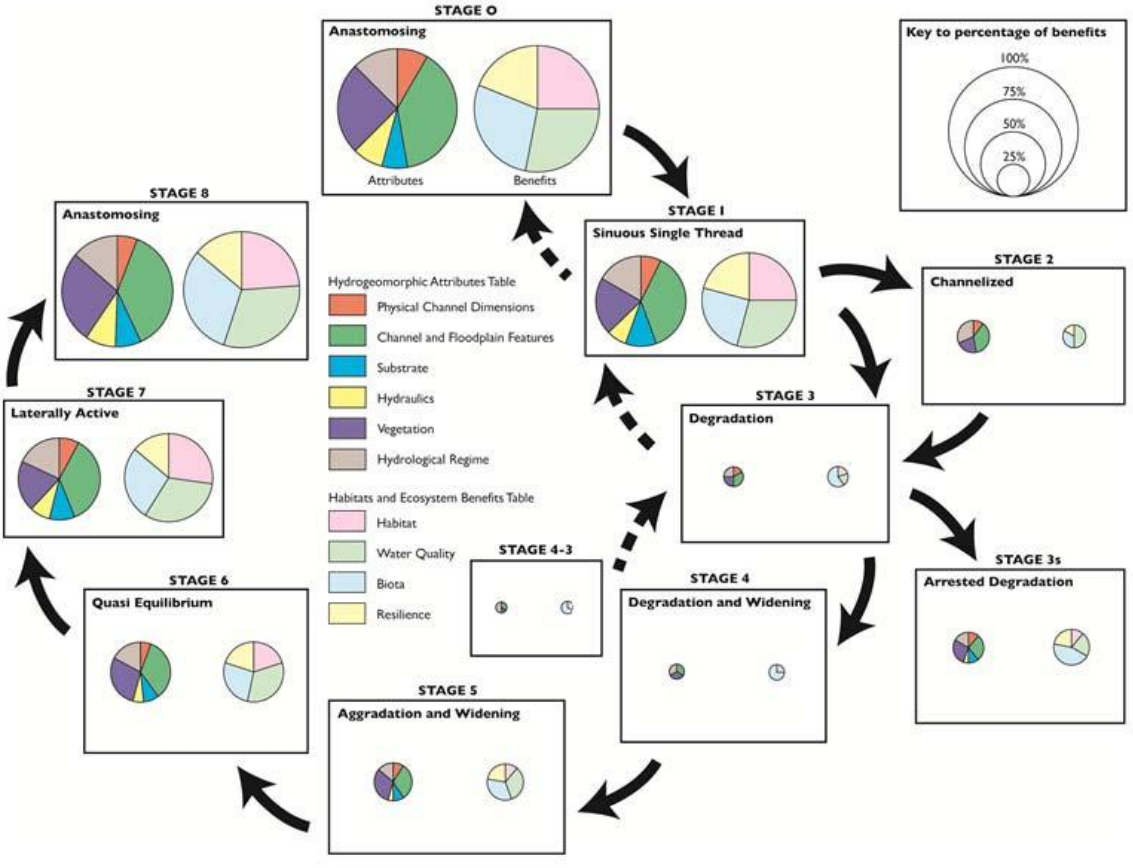

Figure 2 Habitat and ecosystem benefits associated with each SEM stage, set out using the same spatial pattern as Figure 1. Each stage is represented by two pie charts whose diameters indicate the relative percentage of maximum benefits provided by a pristine stream in Stage 0. For each stage, the pie chart on the left summarizes the richness and diversity of the hydromorphic attributes, while the pie chart on the right summarizes the associated habitat and ecosystem benefits.

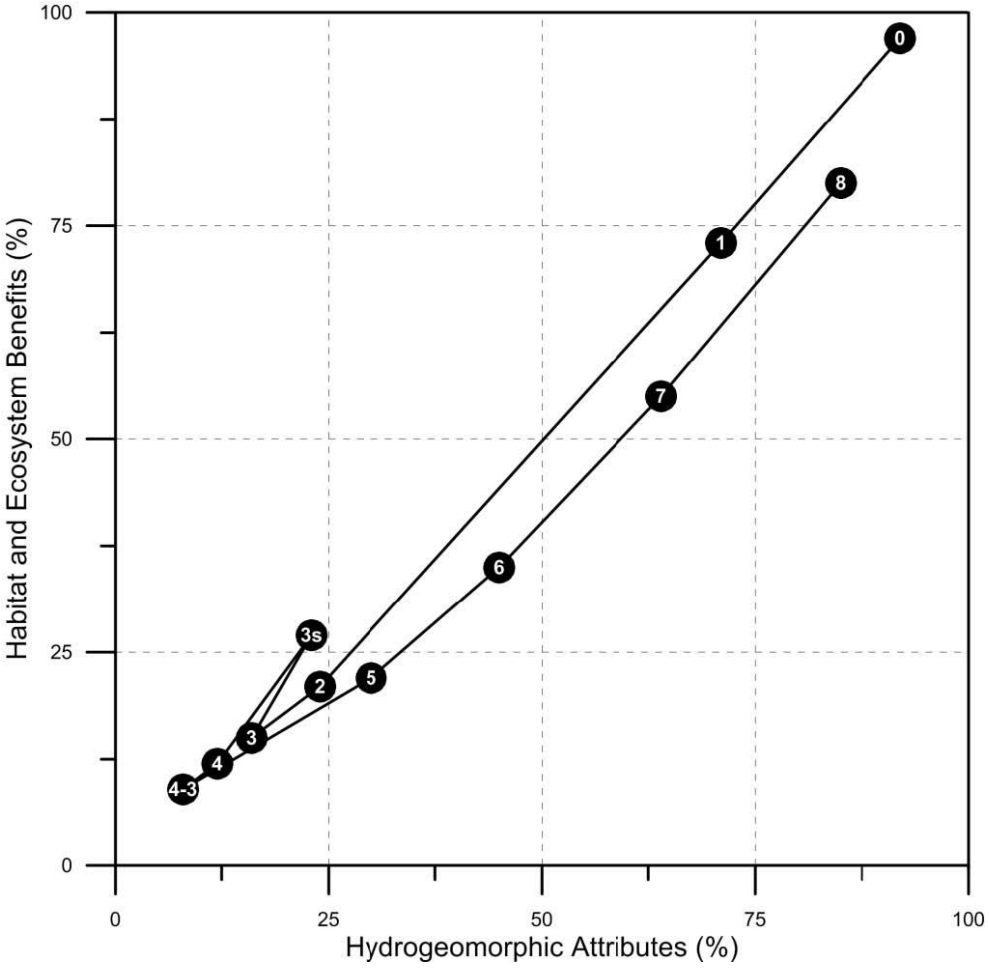

Figure 3 Relationship between hydrogeomorphic attributes and habitat and ecosystem benefits, in proportion to fully functional stream in a Stage 0 condition. There are two main clusters: streams that have greater than 50% of their pristine hydrogeomorphic attributes habitat and ecosystem benefits; and, streams with less than 30%. Stage 6 (Quasi-equilibrium) streams are intermediate. The most abrupt difference between adjacent stages is that from Stage 1 to Stage 2, where scores drop from nearly 75% in a single-thread channel to less than 25% in a channelised stream, due primarily to floodplain disconnection. The existence of a hysteresis loop reveals that habitat and ecosystem benefits recover less quickly and less completely than do the corresponding hydrogeomorphic attributes over long time scales. It is likely that the loop is broader over short times scales.

REFERENCES

Cluer, B. and Thorne, C. R. 2013 (online), 2014 (in print). A stream evolution model integrating habitat and ecosystem benefits, *River Research and Applications*,30, 135-154.

Schumm, S. A., Harvey, M. D. and Watson, C. C. 1984. Incised channels: morphology, dynamics, and control, *Water Resources Publications*, Littleton, CO.

Simon, A. and Hupp, C. R. 1986. Geomorphic and vegetative recovery processes along modified Tennessee streams: an interdisciplinary approach to disturbed fluvial systems, *Forest Hydrology and Watershed Management*, IAHS-AISH Publ.167.

COMPOSITE MODELING OF THE HALFWAY WASH FISH BARRIER

Mike Sixta, M.S., P.E., Hydraulic Engineer, U.S. Bureau of Reclamation, Denver, CO, msixta@usbr.gov; Kendra Russell, M.S., P.E., Hydraulic Engineer, U.S. Bureau of Reclamation, Washington DC, krussell@usbr.gov; Leslie Hanna, Hydraulic Engineer, U.S. Bureau of Reclamation, Denver, CO, lhanna@usbr.gov

BACKGROUND

The lower Virgin River in Southeast Nevada is home to two native fish species currently listed as endangered. These fish populations are under threat due to the upstream invasion of non-native fish from Lake Mead. The Virgin River Fishes Recovery Plan outlines the steps necessary to recover the endangered fishes, calling for the construction of fish barriers on the river. Fish barriers play a central role in the re-establishment of native fish populations by preventing the current and future upstream migration of invasive, non-native fishes. Once a barrier is constructed, the non-native fish can be eradicated from the river upstream of the barrier and the native populations re-introduced. The barrier then prevents future invasion of non-native species, allowing the native fish populations to rebound.

INTRODUCTION

The Bureau of Reclamation was tasked with designing an effective fish barrier on the lower Virgin River in an area referred to as Halfway Wash; approximately 16 miles upstream of Lake Mead in the northwest corner of Arizona. A project location map is shown in Figure 1. This structure will be the most downstream structure on the lower Virgin River. The barrier is to be located where the river valley consists of a wide, relatively flat floor bounded by steep canyon walls. The valley floor is about 1,600 feet wide with a maximum elevation change of about 10 feet across its width. Only during very large flood events does the river occupy the entire width of the river valley.

A composite set of models, each at varying spatial scales, was utilized to propose a fish barrier design concept that would optimize its use as a deterrent to non-native fish passage while minimizing erosion immediately downstream of the structure. Composite modeling is when numerical models are used in conjunction with physical modeling to obtain more detailed information (Rahmeyer et al., 2011). Each modeling technique has its own sets of uses and limitations. Therefore, the collaborative results from the concurrent use of multiple models allowed for a more accurate and thorough analysis of the proposed barrier.

A geometrically scaled physical model along with two-dimensional (2D) numerical modeling of the local hydraulics and sediment were employed to achieve project goals. The project goals, besides limiting the passage of non-native fish species, were to assess the barrier effectiveness through evaluating local hydraulics at various discharges of interest and structure stability through determining the scour and aggradation effects of the barrier. The physical model was used to optimize the fish barrier design while verifying that design criteria were met and evaluating potential scour immediately downstream of the structure. The Sedimentation and River Hydraulics Two-Dimensional (SRH-2D) numerical model was used to evaluate the overall

effect the structure would have on the surrounding area hydraulics as well as predict the erosion patterns downstream of the structure, which was accomplished through the use of two separate modules; the first being fixed bed hydraulics and the second being mobile bed sediment transport. Together, this suite of modeling techniques allowed for the development and comprehensive evaluation of an effective fish barrier.

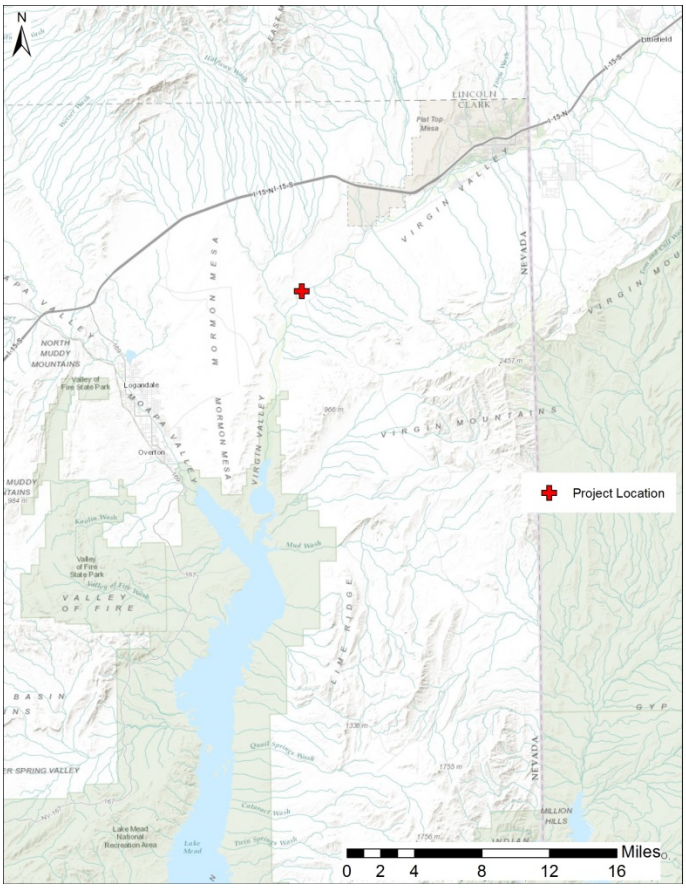

Figure 1 Project location map.

PREFERRED DESIGN ALTERNATIVE

The primary purpose of the fish barrier was to create enough of a vertical discontinuity and increases to in-stream velocities to prevent the upstream passage of invasive, non-native fishes. At low flows, the barrier will create a vertical discontinuity in the stream surface that the fish will not be able to jump over. At high flows, the barrier will be partially submerged and the vertical discontinuity will not develop, but the stream velocity will be above the highest dash speed of the fish. At intermediate flows, the barrier will produce a combination of vertical discontinuity and high stream velocities that will prevent fish passage. The Bureau of Land Management (BLM) provided Reclamation with design requirements that the barrier create a minimum 5 foot tall vertical discontinuity and increase the stream velocities to at least 11.5 ft/s whenever the vertical discontinuity criterion was not met.

The design flow for the structure was given as 45,000 ft^3/s. However, flows in the river are more often in the range of 100-to-5,000 ft^3/s. Therefore, the barrier had to be designed to perform well throughout this full range of flow conditions. An ogee shaped crest is generally considered the most efficient design for passing large flood events and was chosen for the design.

The next question that had to be addressed was how to maximize energy dissipation while also providing an upstream fish deterrent for this range of flow conditions. Past field observations have indicated that a roller bucket design for the barrier energy dissipater may also serve as a good deterrent to upstream fish passage; the roller bucket produces extreme turbulence in the localized area at the toe of the structure where the fish would normally stage to jump over the barrier. The turbulence within the bucket is much more disorganized than would occur in a typical hydraulic jump basin, making it more difficult for fish to stage for a jump at that location.

Utilizing the ogee crest and roller bucket concepts, a physical model study was completed by Reclamation's Hydraulic Investigations & Laboratory Services Group, evaluating several design iterations in ultimately determining the preferred barrier design that was deemed the most effective for meeting all design criteria (Hanna and Lentz, 2012). The outline of the preferred design alternative is shown in Figure 2.

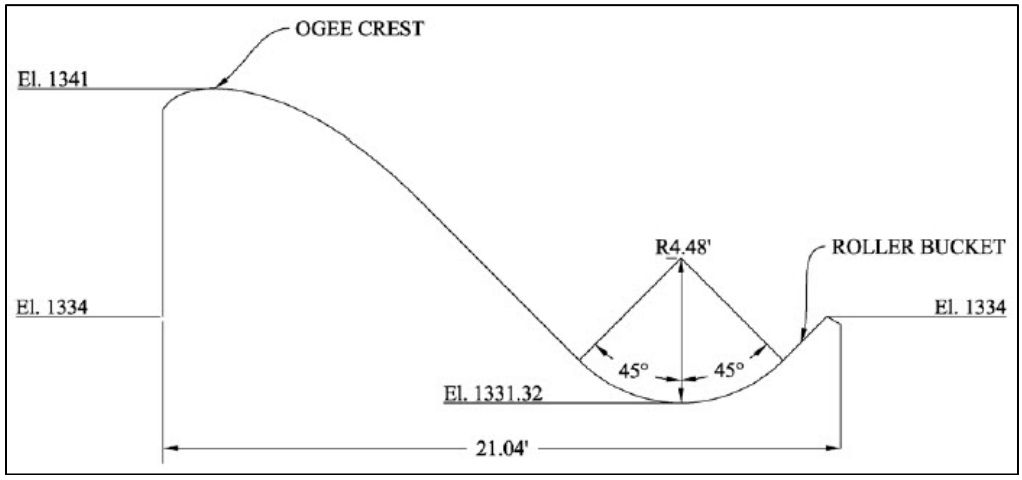

Figure 2 Preferred design alternative of the Virgin River fish barrier (prototype dimensions and elevations).

MODELING METHODOLOGY

All models require simplifying assumptions and thus have limitations. The choice of model is often governed by time and budget constraints, access to and knowledge of existing models, and the ability to develop the model (data availability). It is important to understand the formulation of the selected model, recognize the model limitations, and apply the model in a manner that takes advantage of its strengths. Model predictions will always include some uncertainty because the physical processes being modeled are not completely represented.

A composite suite of models was utilized to evaluate both the stability and predicted effects the proposed fish barrier will have on the river system. A physical model was used to optimize the

fish barrier design while verifying that design criteria were met and evaluating potential scour immediately downstream of the structure (Hanna and Lentz, 2012). A two-Dimensional (2D) numerical hydraulics and sediment transport model was used to evaluate the overall effect the structure would have on the surrounding area hydraulics as well as predict the erosion patterns surrounding the structure and scour downstream of the structure (Russell and Sixta, 2012).

Physical Model: Due to such a large width of the river channel and the wide range of flow conditions to be tested, a 1:5 geometric scale sectional physical model was used to represent the structure (Hanna and Lentz, 2012). The width of the barrier inside a 4-foot wide testing flume represented a 19.75 foot slice of the prototype barrier. Froude similitude was used to establish a kinematic relationship between the model and the prototype. Sand was placed downstream of the barrier to evaluate local scour depths and erosion patterns. This was a qualitative evaluation relative to each subsequent design given that the river channel is made up of silts and sand and not possible to be accurately represented geometrically in the model using Froude similitude. The layout of the physical model is shown in Figure 3.

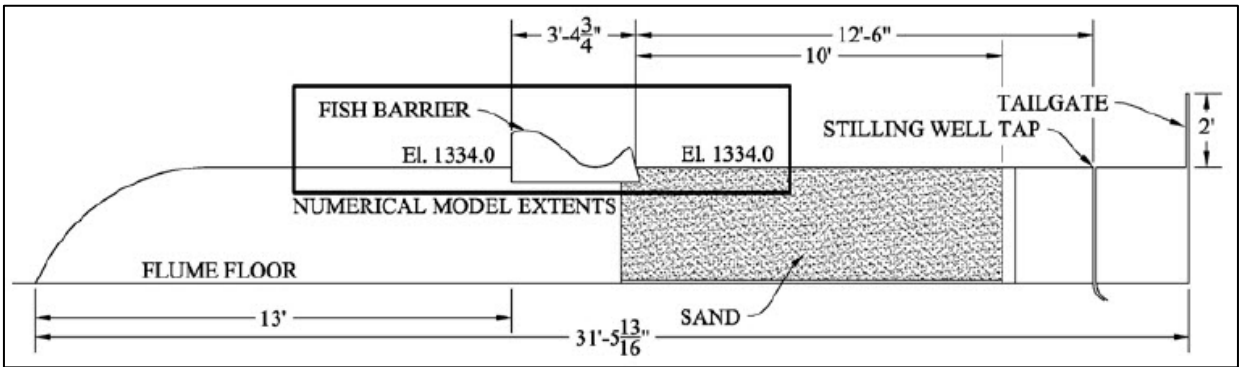

Figure 3 Physical model layout (dimensions in model scale, elevations in prototype scale).

Tailwater depths in the model were set to match depths determined from a one-dimensional HEC-RAS model of the Virgin River. Upstream depths were measured 4 model-feet upstream from the barrier crest. Downstream depths were measured 12.5 model-feet downstream from the roller bucket. Other water surface measurements and velocities were taken along the length of the structure to determine if design criteria were properly met. Model flow rates were measured using calibrated venturi meters.

Two-Dimensional (2D) Numerical Model: SRH-2D is a two-dimensional (2D) hydraulics and sediment transport (mobile-bed) model for river systems developed by Reclamation at the Technical Service Center (Lai, 2008). SRH-2D solves the depth-averaged dynamic wave equations with a depth-averaged parabolic turbulence model using a finite-volume numerical scheme. The model adopts a zonal approach for coupled modeling of channels and floodplains; a river system is broken down into modeling zones (delineated based on natural features such as topography, vegetation, and bed roughness), each with unique parameters such as flow resistance. One of the major features of SRH-2D is the adoption of an unstructured hybrid mixed element mesh, which is based on the arbitrarily shaped element method of Lai (2000) for geometric representation. This meshing strategy is flexible enough to facilitate the implementation of the zonal modeling concept, allowing for greater modeling detail in areas of

interest that ultimately leads to increased modeling efficiency through a compromise between solution accuracy and computing demand.

The SRH-2D modeling was broken up into two distinct efforts (Russell and Sixta, 2012). Fixed bed, hydraulic conditions were first modeled; to determine an appropriate model extent (primarily width), to perform a flow roughness calibration, and to obtain hydraulic model results to address some of the study questions. Modeling of the mobile channel dynamics and sediment transport commenced after a satisfactory hydraulics model was constructed and calibrated.

Due to the increased computational demand for the mobile-bed modeling, separate meshes/model domains were generated using Surface-water Modeling System (SMS) software for the hydraulics and sediment transport modeling. The model domain spanned laterally valley wall-to-valley wall and longitudinally 0.9 river miles upstream and 2.0 (hydraulics) and 0.9 (mobile-bed) river miles downstream of the fish barrier. A total of 56,500 and 21,000 mixed quadrilateral/triangular elements were used to represent the model domain for the hydraulics and sediment transport modeling, respectively. In each mesh, the resolution was denser (~5X; longitudinal spacing) at the fish barrier in order to better capture its geometry as it was a feature of focus.

A combination of several data sets was used to construct the topography of the study area. Ground survey data were collected upstream and downstream of the proposed fish barrier before December, 2010 (exact date is unknown) and on June 20, 2011 and July 5, 2011. These data were mainly used to represent the wetted portion of the channel (bathymetry). To supplement the survey data in the floodplain areas, a Digital Terrain Model (DTM) containing elevations of natural terrain features was obtained. The data making up the DTM was collected using airborne Interferometric Synthetic Aperture Radar (IfSAR) technology. The IfSAR data had a 5-meter posting with a published vertical accuracy of +/- 1 meter. The ground survey and IfSAR data were combined to create a representative topographic surface in ArcGIS using a Triangulated Irregular Network (TIN) methodology that each mesh was solved against.

Four distinct roughness zones were used in the model domain; 1) main channel, 2) vegetated floodplain, 3) cleared floodplain, and 4) fish barrier. Delineation of these zones utilized aerial photography in combination with information from the ground survey data. The corresponding material type roughness values used in the modeling were set through an iterative model calibration process. The resultant roughness values were 0.020 for the main channel, 0.045 for vegetated floodplain, 0.025 for cleared floodplain, and 0.013 for the fish barrier. The same roughness coefficients were used for both the hydraulics and sediment transport modeling and all were held constant for the entire range of discharges modeled.

Bed sediment gradations and sediment supply are needed for sediment transport modeling. For this study, uniform surface and subsurface gradations were applied to the entire model domain. Ten (10) geologic test pits and three (3) drill holes were excavated near the proposed fish barrier site. Sediment data was measured at each location for multiple depths. Based on that information, a change in bed material was detected at 5 feet of depth. Therefore, sediment gradations were averaged for the top surface layer (less than 5 feet) and subsurface layer (greater than 5 feet). A uniform two layer gradation with 5 sediment size classes was used over the entire

model domain due to the small number of samples surveyed. Vertical erosion limits were not set for the subsurface layer. Sediment supply was determined using the Engelund and Hansen (1972) sediment transport formula to calculate capacity, which is the amount of sediment that can be transported while maintaining a stable bed locally.

Seven (7) steady state discharges were simulated in the 2D hydraulics and sediment transport models: 200 ft^3/sec, 600 ft^3/sec, 1,000 ft^3/sec, 5,000 ft^3/sec, 10,000 ft^3/sec, 30,000 ft^3/sec, and 45,000 ft^3/sec. These discharges range from a regularly occurring high flow to a conservative design flow. In addition, three (3) unsteady hydrographs were simulated for the sediment transport modeling. All three hydrographs represented flood flows happening on a less than annual basis. The hydrographs represented the 1995 flood, a high flow flood, and a scaled synthetic design flow flood to peak at 45,000 ft^3/sec. The hydrographs have duration of less than 12 days. For the unsteady flow simulations, the annual peak stream flow and average daily stream flow at the nearest USGS gage (Virgin River at Littlefield, AZ 09415000) were used to determine the magnitude and shape of storm hydrographs for the Virgin River in the project area. The only time flow was above the largest design flow under consideration (45,000 ft^3/sec) was in 1989 when there was a dam break upstream.

MODEL RESULTS DISCUSSION

Physical Model: Three (3) designs were evaluated with the physical model before settling on one that met either the surface drop and/or velocity criteria for all flow conditions tested. For each test condition, depth measurements along the barrier were taken through the flume glass sidewall, perpendicular to the urethane surface at 0.5-to-1.0 foot incremental drops in elevation until the determined tailwater surface was reached. Measured depths were used to calculate average velocities flowing over the barrier at each location. Velocities were also measured using a Swoffer propeller meter at the model centerline when flow depth was adequate. These velocities were not averaged over the full flow depth, so in most cases the readings are higher than the average velocity calculated using the depth measured near the same location.

Surface drop criteria for the preferred alternative design was met for flows up to 1,000 ft^3/sec and velocity criteria was met for flows of 1,000 ft^3/sec and above (Table 1). This overlap in meeting both criteria brings an added level of confidence in achieving acceptable performance throughout the range of flow conditions expected at the barrier.

Table 1 Measured stream surface drop and velocity for preferred alternative design.

Prototype Discharge (ft^3/s)	Stream Surface Drop (ft)	Maximum Calculated Prototype Velocity (ft/s)	Maximum Measured Prototype Velocity (ft/s)
200	6.1	8.0	N/A
600	5.7	11.5	N/A
1,000	5.5	15.4	N/A
5,000	4.5	16.0	N/A
10,000	3.9	15.4	16.3
20,000	3.5	16.0	19.4
30,000	2.9	16.7	19.2
45,000	1.7	18.2	19.2

Although actual scour depths could not be simulated due to scaling issues, the patterns of erosion that would occur could be reasonably represented in the physical model using fine sand. Therefore, erosion measurements were conducted to get qualitative data on resulting erosion patterns relative to each test. The maximum scour depth was measured and documented along with the distance from the barrier (referenced to downstream edge of the roller bucket) where it occurred. Table 2 shows the scour depths and corresponding distance for each flow rate tested for the preferred alternative design. Results show that as flow increases, maximum scour depths increase and move further downstream. For flows up to 1,000 ft^3/sec erosion occurs close to the downstream edge of the barrier. Erosion occurs next to the structure with low discharges because velocities are low, and therefore flow at the end of the roller bucket tends to drop vertically downward over the downstream edge resulting in erosion in close proximity to the barrier, but also not very deep. At flows of 5,000 ft^3/sec and above, the flow pattern appeared to go through a transition. The patterns of erosion indicated that scour produced downstream from the barrier should not endanger that stability of the structure. However, it's important to note that the structural design for the barrier was not determined from this study.

Table 2 Scour depths and corresponding distance for preferred alternative design.

Prototype Discharge (ft^3/s)	Barrier Design #3	
	Sand Depth (ft)	Downstream Distance from Barrier (ft)
200	0.5	0.10
600	0.58	0.31
1,000	0.58	1.46
5,000	1.54	8.21
10,000	2.25	12.10
20,000	3.71	21.50
30,000	5.29	27.0
45,000	7.50	28.0

Two-Dimensional (2D) Numerical Model: As mentioned previously, the 2D numerical modeling was broken into two separate efforts; fixed-bed hydraulics modeling and mobile-bed sediment transport modeling. The main objective of the hydraulics modeling was to quantify differences among the currently existing and proposed conditions over a range of flow conditions. The predicted hydraulic parameters of interest included flow depth, water surface elevation, and velocity magnitude and direction. The spatial distributions of these parameters were examined to determine the location and magnitude of the differences between the existing and proposed conditions, which were used to forecast project impacts. This was accomplished by differencing raster grids representing the specific model hydraulic parameters in ArcGIS.

The spatial distribution of the differences in water depths near/around the fish barrier for the 45,000 ft^3/sec event is shown in Figure 4. Results show an overall increase in depth upstream of the fish barrier and decrease in depth downstream of the barrier. The relative magnitudes of depth decreases downstream of the barrier are small as compared to the depth increases upstream of the barrier; the biggest differences occur within close proximity of the barrier. The results also show the barrier to back water upstream approximately 0.4 miles.

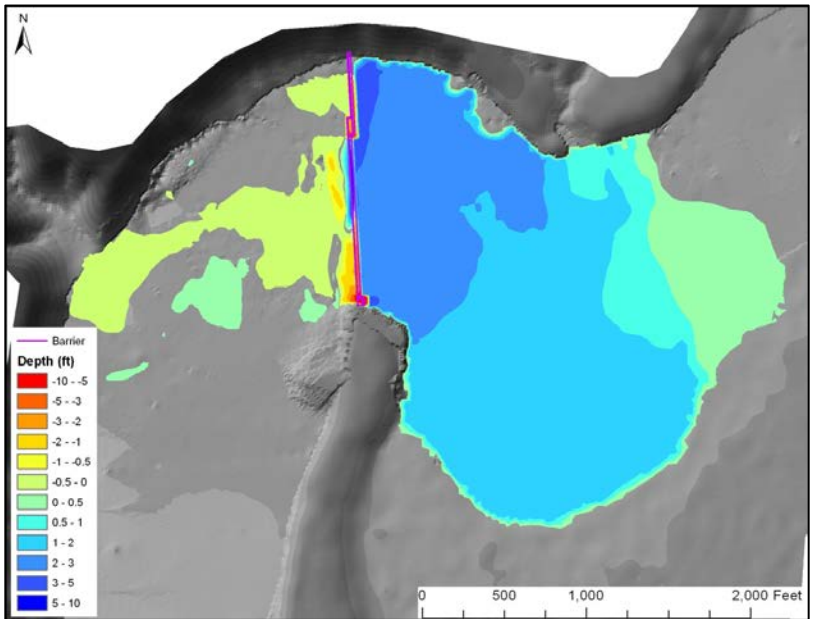

Figure 4 Depth difference (proposed – existing) for the 45,000 ft^3/sec event. (Flow is from right-to-left).

Resultant velocity magnitude and vectors for the 45,000 ft^3/sec event with the proposed barrier showed flow to be distributed along the entire barrier, but not with a consistent magnitude. Velocities were seen to be larger along the southern portion of the barrier. The average velocities for the 45,000 ft^3/sec event just upstream of the barrier ranged from 6-8 ft/sec, while the average velocities just downstream of the barrier ranged from 7-9 ft/sec on the northern half, and 12-18 ft/sec on the southern half. (These velocities can be compared against the design criteria of 11.5 ft/s. However, it's important to keep in mind that they refer to the velocities in the main channel and not on the barrier itself). Furthermore, the velocity vectors showed slower recirculation zones on the northern end of the barrier on both the upstream and downstream sides.

Sediment transport modeling was used to predict the erosion/deposition patterns near/around the structure. The first set of mobile-bed simulations used a constant, steady flow that was carried out for 10 days for both the existing and proposed barrier conditions. The net change in bed elevation, relative to the initial bed at time zero is shown in Figure 5 for the design event (45,000 ft^3/sec). Based on results from all of the steady flow runs, the following conclusions were made:

- At 200 ft^3/sec there is little change to the bed elevation for both the baseline and barrier conditions; flow must be greater than 200 ft^3/sec to move appreciable amounts of sediment within the system.

- For the baseline condition, erosion occurs along the south valley wall. There is potential for the river planform to shift toward the south and straighten under this condition.

- For the proposed condition, erosion will occur downstream of the barrier and it appears likely that the river planform will shift to the south and straighten (similar to the baseline condition). The model does not include the differences in potential erodibility of cleared versus vegetated areas on the banks and floodplain. Although all of the simulations above 10,000 ft^3/sec show this planform change, it may be a slow developing process.

- For the proposed condition, the backwater upstream of the barrier creates a net depositional area. However, there is some local scour in certain places. Most notably a bar develops on the south side of the channel which concentrates the flow in the north portion. Local scour occurs where the flow is concentrated.

- For the proposed condition, it is likely that alternating bars will form upstream until the river is out of the barrier backwater influence. This process will likely develop slowly and will depend on the amount of time and frequency that the river discharge is greater than 200 ft^3/sec.

- In the proposed condition, bank erosion may be an issue where the flow is concentrated upstream of the barrier. The sediment transport model does not include bank erosion, but it is likely that the right bank upstream of the barrier will experience some bank erosion.

- Immediately downstream of the barrier, erosion occurs. However, this erosion does not include plunging scour off of the barrier roller bucket and is potentially under predicted. Further downstream the erosion represents the reach average scour.

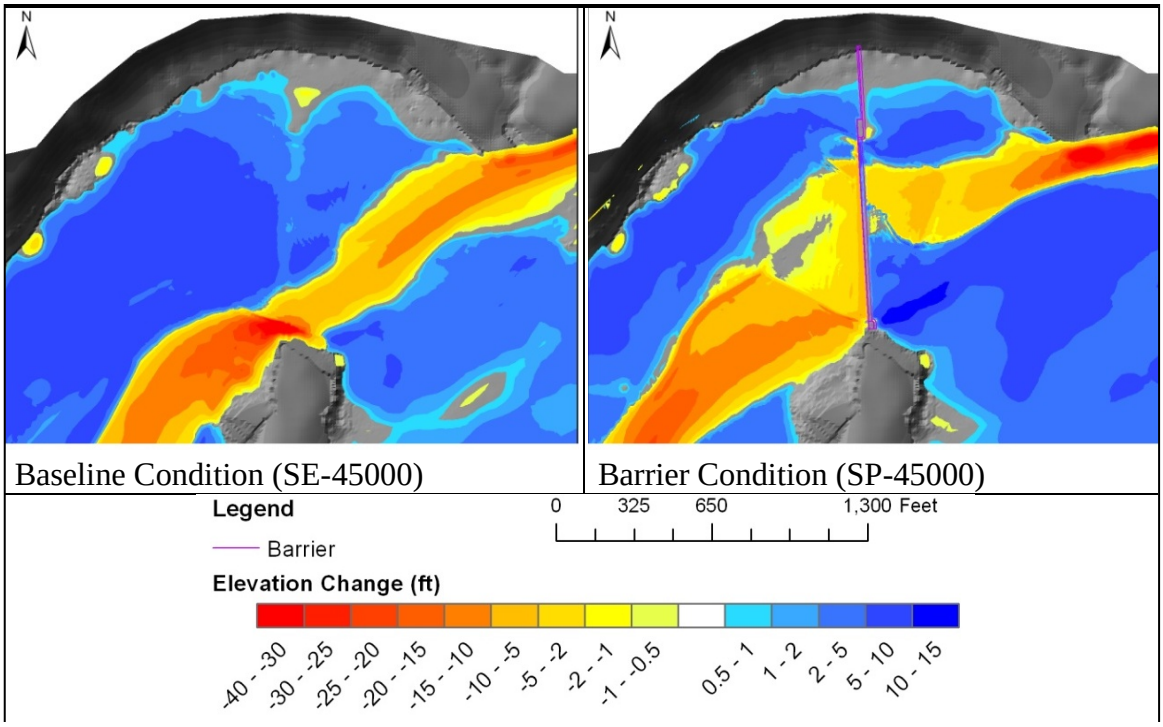

Figure 5 Change in bed elevation for existing and proposed conditions at 45,000 ft^3/sec. (Flow is from right-to-left).

Based on the flow record, high steady flows are unlikely to occur at this location. As a result, the prolonged steady flow simulations were viewed as a conservative estimate of the erosion that will occur in the study reach. Three unsteady hydrographs were simulated to provide a more realistic prediction of the erosion and deposition patterns. The evolution of the bed elevation throughout the simulations were evaluated and seen to produce similar erosion and deposition patterns although the magnitude of bed change varies. Deposition occurs upstream of the barrier in all three scenarios. For the 45,000 ft^3/sec peak hydrograph, a deeper main channel is eroded. This is similar to the steady flow results where the flow was concentrated upstream of the barrier due to bar development.

Downstream of the barrier, there is a pocket of increased erosion that occurs on the north abutment in all three hydrographs. Erosion did occur in this location during the steady flows but the magnitude was less. As expected, further erosion occurs downstream of the barrier. One of the most noticeable differences between the 45,000 ft^3/sec steady flow and the 45,000 ft^3/sec hydrograph is that during the steady flow simulation, deposition occurs downstream of the barrier on the left and right banks; a single thread main channel is clearly defined. However, for the hydrograph simulation, the majority of the downstream valley bottom is degraded. It appears that the channel has started to straighten and shift towards the south. Figure 6 shows the net eroded/deposited depth, relative to the initial bed at time zero for the last time step (t = 11 days) of the 45,000 ft^3/sec simulation. The river channel has started moving towards the planform shown in the steady flow runs, but was unable to completely develop and shift its alignment.

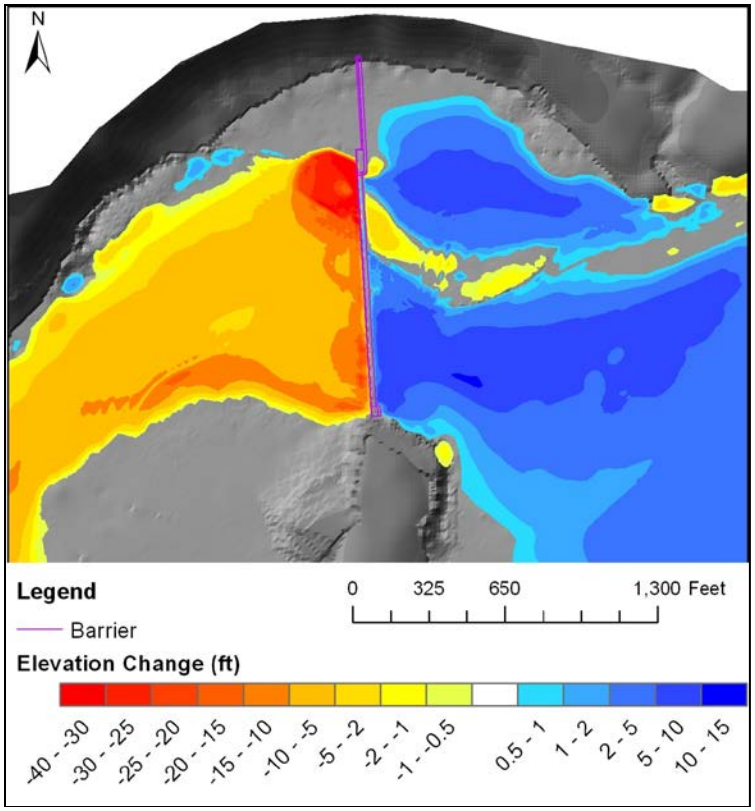

Figure 6 Change in bed elevation for the final time step (t= 11 days) for the synthetic 45,000 ft^3/sec peak hydrograph.

The 2D sediment transport numerical model cannot predict local scour due to the inability of quantifying plunging flow, but it can predict the decrease in river bed elevations due to the reduction in sediment load caused by the structure and larger discharges. Therefore, the 2D model was used to estimate the "reach average" erosion. The reach average erosion is that erosion that occurs over a large spatial scale and is relatively uniform in the streamwise direction. The reach average erosion was approximately 20.5 feet, which was considered the maximum total bed scour that the fish barrier's foundation should be designed around. However, it's also worth keeping in mind the scour findings from the physical modeling showing that as flow increases, maximum scour depths increase, but also move further downstream.

SUMMARY AND CONCLUSIONS

The Bureau of Reclamation was tasked with designing an effective fish barrier on the lower Virgin River in an area that is referred to as Halfway Wash. The barrier is designed to prevent upstream non-native fish passage by creating a vertical discontinuity in the river that fish are unable to jump over as well as increasing the stream velocities above the maximum dash speed of the fish. A composite of models, each at varying spatial scales, was utilized to propose a fish barrier design concept that would optimize its use as a deterrent to fish passage while minimizing erosion immediately downstream of the structure. Each modeling technique has its own sets of uses and limitations. Therefore, the collaborative results from the concurrent use of multiple models allowed for a more accurate and thorough analysis.

Scaled physical modeling along with 2D numerical modeling of local hydraulics and sediment were employed to achieve project goals of preventing fish passage while maintaining structural stability of the feature preventing fish passage. An ogee crest with roller bucket concept was used in the design of the fish barrier. The physical model showed a design that met both drop height and velocity design criteria with an overlap of discharges. Patterns of erosion showed that as flow increases, maximum scour depths increase and move further downstream of the barrier. The 2D hydraulics modeling showed non-uniform velocities upstream and downstream of the barrier, and that the barrier will back water upstream approximately 0.4 miles during the 45,000 ft^3/sec design flow. The 2D sediment modeling showed that flow must be greater than 200 ft^3/sec to move appreciable amounts of sediment within the system. The backwater upstream of the barrier was seen to create a net depositional area with some local scour in areas where the flow is concentrated. Erosion occurs immediately downstream of the barrier. Further downstream the erosion represents the reach average scour, which was approximated to be 20.5 feet. Together, this suite of modeling techniques allowed for the development and comprehensive evaluation of an effective fish barrier.

REFERENCES

Engelund, F., and Hansen, E. 1972. *A monograph on sediment transport in alluvial streams.* Teknish Forlag, Technical Press, Copenhagen, Denmark.

Hanna, L.J., and Lentz, D. 2012. "Halfway Wash Fish Barrier Physical Hydraulic Model Study." *Hydraulic Laboratory Report HL-2012-01*. U.S. Department of the Interior, Bureau of Reclamation, Technical Service Center, Hydraulic Investigations and Laboratory Services Group, Denver, CO.

Lai, Y.G. 2000. "Unstructured grid arbitrarily shaped element method for fluid flow simulation." *AIAA Journal*. 38(12), 2246-2252.

Lai, Y.G. 2008. "SRH-2D version 2: Theory and User's Manual." Sedimentation and River Hydraulics – Two-Dimensional River Flow Modeling. U.S. Department of the Interior, Bureau of Reclamation, Technical Service Center, Denver, CO.

Rahymeyer, W., Barfuss, S., and B. Savage. 2011. "Composite Modeling of Hydraulic Structures." *The Association of State dam Safety Officials, Dam Safety 2011 Conference Proceedings*.

Russell, K., and Sixta, M. 2012. "Evaluation of Hydraulics and Sediment Transport for Proposed Fish Barrier at Halfway Wash." Virgin River, AZ. Upper Colorado Region. U.S. Department of the Interior, Bureau of Reclamation.

COUPLED SEDIMENT YIELD AND SEDIMENT TRANSPORT MODELING TO SUPPORT WATERWAY NAVIGATION PLANNING IN NORTHEAST BRAZIL

Calvin T. Creech, PhD, PE, Lead Hydraulic Engineer, US Army Corps of Engineers, Brasília, DF, Brazil, Calvin.T.Creech@usace.army.mil
Rafael Brito Siqueira, Development Analyst, CODEVASF, Brasília, DF, Brazil, rafael.siqueira@codevasf.gov.br
James P. Selegean, PhD, PE, Lead Hydraulic Engineer, US Army Corps of Engineers, Detroit, MI James.P.Selegean@usace.army.mil
Carol Miller, PhD, PE, Professor, Wayne State University, Detroit, MI, ab1421@wayne.edu
Pedro Cunha, Agência Nacional de Águas, Brasília, DF, Brazil, Pedro.cunha@ana.gov.br

Abstract

The São Francisco River Basin - located in northeast Brazil - has undergone a significant amount of anthropogenic changes in the last several decades, including agricultural expansion, irrigation activities, mining, and the construction of large dams. Together, these changes have altered the historic sediment budget and have led to an aggradation of sediments in the navigation channel, impacting the ability to efficiently ship commodities to regional ports. In an effort to aid decision makers in future waterway navigation planning, a SWAT model of the 630,000 km^2 São Francisco River basin was developed and used to calculate a basin-wide sediment budget.

The SWAT model of the São Francisco River Basin was calibrated for hydrology and sediment loads. Monthly discharges were calibrated at ten Agência Nacional de Águas (ANA) gages, with NSE values ranging from 0.52 to 0.72 for a six-year simulation. An additional seven ANA gages were used to validate the model, resulting in NSE values between 0.51 and 0.88 for these additional gages. Sediment loads were calibrated to an ANA sediment gage located in the Middle São Francisco River Navigation Channel, with a PBIAS of -12.6. A sediment budget was calculated and approximately 94% of the sediment that is shoaling in the navigation channels originates from overland sources. A total of approximately 23 million tonnes of net sediment is deposited in the bed of the São Francisco River and major tributaries annually. This net deposition has contributed to an impaired navigation channel due to shoaling of sandy sediments in the navigation channel.

Combining a geomorphology study with the SWAT model, conceptual designs for navigation improvements were developed for the São Francisco River navigation channel. A HEC-RAS sediment transport model was built for the navigation channel to predict long-term navigation sustainability using spur dikes and cut-off dikes at the critical shoals. This conceptual design was shown to be a viable long-term alternative to maintaining a sustainable, economically feasible navigation channel when compared to the current practices of maintenance dredging alone.

Keywords: Sediment Budget, Waterway Navigation, Sediment Transport, Sediment Yield

INTRODUCTION

The Companhia de Desenvolvimento dos Vales do São Francisco e do Parnaíba (CODEVASF) and the US Army Corps of Engineers (USACE) engaged in an intergovernmental partnership agreement to support river engineering, navigation improvements, and bank stabilization projects along the São Francisco River in northeast Brazil. The São Francisco River is an important north-south corridor of navigation in Brazil, which links the important agricultural and mining activities that occur in the southern states of Minas Gerais and Bahia to the northeast part of the country. The São Francisco River Basin has undergone significant landuse changes over the previous few decades. Large percentages of the watershed have been converted from native vegetation to either grazing or intense row crop agriculture. In addition, hydropower dams and large-scale irrigation projects have been constructed and the expansion of row crop farming as well as dam and pumping plant construction is expected to continue in the basin. The impacts associated with these watershed changes are currently not well understood, and a numerical watershed yield model and navigation sediment transport model were developed to improve the overall understanding of the sediment dynamics (yield and transport) in the São Francisco River Basin and navigation channel.

The São Francisco River is approximately 2,900 kilometers in length with a watershed area of 630,000 km^2 (see Figure 1). It is the longest river that is entirely contained within Brazil and includes portions of the states of

Alagoas, Bahia, Goiás, Minas Gerais, Pernambuco, Sergipe, and the Federal District. The upstream boundary of the navigation channel begins at a small port city – Pirapora, Minas Gerais. The navigation channel then continues through a low sinuosity alluvial river valley for 1,015 km until it reaches the upstream end of a large reservoir, the Sobradinho reservoir. Navigation continues approximately 200 kilometers through the Sobradinho reservoir (which includes a navigation lock), and then another 42 kilometers downstream of the reservoir through a rock controlled section of river. The navigation channel terminates at the twin port cities of Juazeiro, Bahia, and Petrolina, Pernambuco. The São Francisco River continues downstream of Petrolina/Juazeiro for an additional 675 river kilometers through three large hydropower dam systems (which do not include any navigation locks) to its outlet in the Atlantic Ocean. There is no commercial navigation downstream of Petrolina/Juazeiro.

Figure 1 Location Map and Boundary of the São Francisco River Basin

Approximately 13 million people live in the São Francisco River Basin, with the highest density living in the south (headwaters), especially near the Belo Horizonte metropolitan area. The climate ranges from humid in the headwaters (south) to semi-arid in the Lower São Francisco River (north). Vegetation associated with a cerrado ecosystem is present in the headwaters with a high diversity of mixed forest, and a caatinga ecosystem (sparse and stunted vegetation) is associated with the semi-arid region of the watershed to the north. More information regarding physical characteristics of the São Francisco Basin is found in CODEVASF & ANA (2002) and Biswas et al. (1999), which presents an overview of the site location, weather, vegetation, hydrology, navigation, dams, development, geomorphology, geology, and other watershed feature information.

METHODS

Modeling Framework

A decision support system is necessary for planning the waterway development within the São Francisco River Basin. The primary navigation impedance in the São Francisco River waterway is shoaled alluvial sediment (primarily medium sand), which reduces the navigation draft and prohibits year-round commercial transport of agricultural goods and mining commodities. To address these concerns, a numerical modeling framework to support navigation planning was developed and then applied to the São Francisco River in Northeast Brazil. This modeling framework includes the development of a hydrology and sediment yield model of the São Francisco River Watershed, coupled with a sediment transport model of the navigable waterway. The results of this watershed model were used for determining sub-watersheds that are primary sources of sediment and also used as input values for the sediment transport model. The sediment transport model was developed for the Middle São Francisco River, where the current alluvial navigation channel is defined.

The modeling approach consists of nine steps (graphically presented in Figure 2). First, an understanding of the existing sediment dynamics of the basin is developed using the Soil and Water Assessment Tool (SWAT) as the sediment yield model. Next, this information is used to develop a sediment budget for the watershed, which indicates the primary sediment sources and sinks. The sediment budget allows for decision makers to prioritize sediment mitigation measures (either focusing on upland sediment management, bank stabilization, or other mitigation areas). The sediment mitigation measures then can be applied into a watershed development plan. The future conditions of the watershed plan are then modeled in a future sediment yield model (using SWAT) to understand the future sediment dynamics of the system.

In parallel to the sediment management planning and modeling, an understanding of the fluvial system is necessary for navigation planning purposes. A geomorphology study of the waterway allows for a determination of what types of measures may be suitable for improvement of the shoaling issues. The geomorphology study feeds into a conceptual design of a navigation plan that can consist of dredging, and riverine training structures, such as spur dikes, cutoff dikes, and other navigation structures. The sediment dynamics of the future watershed plan and the conceptual design of the waterway can then be modeled in a sediment transport model to predict the effectiveness of the proposed conceptual designs and to make iterative revisions in order to finalize a proposed navigation plan.

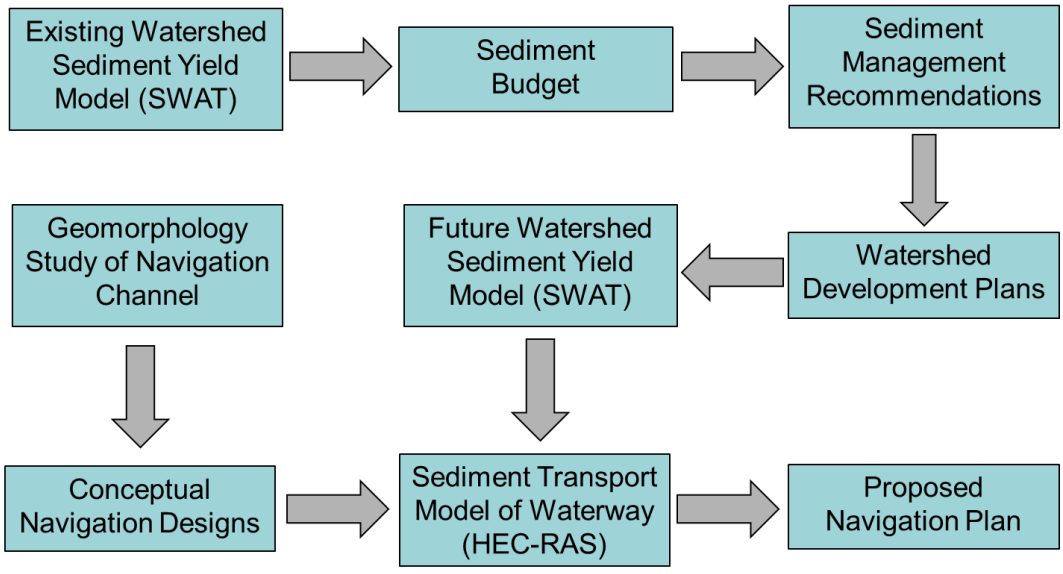

Figure 2 Waterway Modeling and Planning Framework

Hydrology and Sediment Yield Model

The Soil and Water Assessment Tool (SWAT) was the model selected to evaluate the sediment dynamics of the São Francisco River Basin. The primary data that was used to build a hydrology and sediment yield model in SWAT include the following: topography, soils, landuse, reservoirs, irrigation withdrawals, weather (precipitation, temperature, relative humidity, solar radiation, and wind), and river gages (streamflow and sediment gages). The topography, soils, and landuse layers were overlaid in ArcSWAT and were used to create Hydrologic Response Units (HRUs). Areas that have similar slopes, soil classification, and landuse were grouped into a single HRU, with each subwatershed consisting of numerous HRUs.

The topography data were obtained from the Advanced Spaceborne Thermal Emission and Reflection Radiometer (ASTER) by NASA (NASA, 2013). This data consists of a 30m Digital Elevation Model (DEM) for the entire basin. The DEM data was divided into three slope classes 1) 0-1%; 2) 1-2%; and 3) Over 2% (see Figure 3a for derived slope classes).

Soils data were obtained from the Empresa Brasileira de Pesquisa Agropecuária (Emprapa, 1981), which had previously been converted to a digital format by the U.S. Geological Survey's EROS Data Center. There are seventy soil groups defined in the overall Brazil Soil Dataset within the São Francisco River watershed. See Figure 3b for a map of the soils in the watershed. Soil physical and chemical property data were not directly available in the Embrapa dataset; therefore, a second soil dataset was used to extract soil property information and was applied directly to the Embrapa soil boundaries. The International Soil Reference and Information Centre (ISRIC) provides a soil data set at a 5 arc-minute resolution for the world, including soil physical and chemical properties (Batjes, 2012).

The GlobCover 2005 (European Space Agency, 2006) was used to assign the landuse to the São Francisco River SWAT model. GlobCover 2005 is a global dataset with 300m x 300m resolution of landcover from the year 2005. Figure 3c includes the landuse data used in the SWAT model.

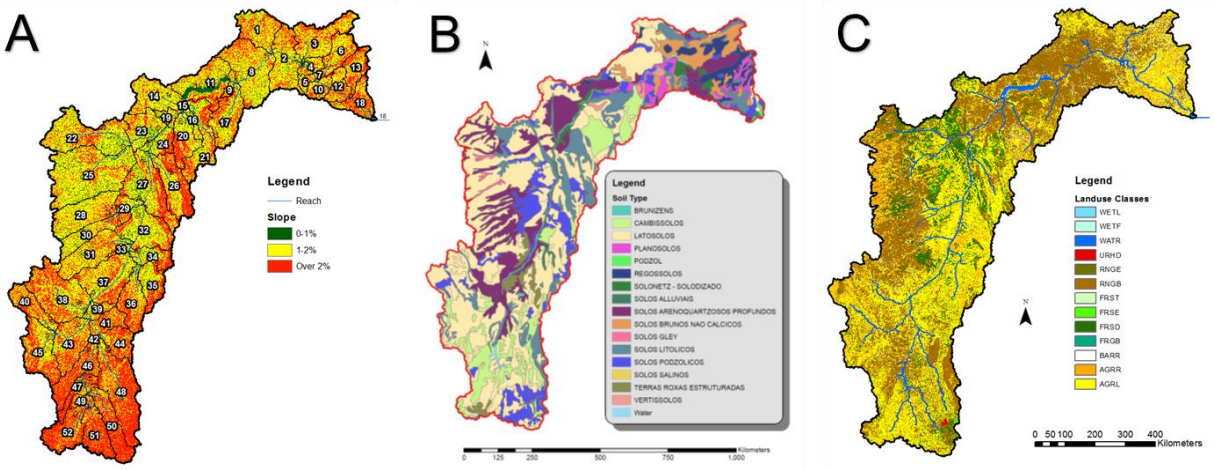

Figure 3 HRUs Built from A – Slope (ASTER, 2013); B – Soils (Embrapa, 1981); and C – Landuse (European Space Agency, 2006)

Five of the largest reservoirs in the São Francisco Basin were added to the model. These reservoirs include the Três Marias, Sobradinho, Luiz Gonzaga, Paulo Afonso and Xingó reservoirs. Irrigation practices were also added to the SWAT model. Irrigation within the basin is permitted throughout the São Francisco River watershed, with most projects owned and constructed by CODEVASF. There are a total of 26 major irrigation sources identified by CODEVASF (2013) and these were input into the SWAT model.

Weather data for the São Francisco River Basin were obtained from the Global Weather Data website http://globalweather.tamu.edu/. These data includes temperature, precipitation, wind, relative humidity, and solar radiation weather. Weather data were collected from 1995 through 2006 at 1,254 locations throughout the basin.

Although the modeling was designed to include daily output from 2001-2006, all data from 1995 through 2006 were collected in order for the model to have a sufficient "hotstart" period (from January 1, 1995 through December 31, 2000). Existing conditions, historic conditions (using pre-European settlement landuse data and the removal of anthropogenic activities such as hydropower and irrigation), as well as future conditions of the hydrology and sediment were modeled using the developed SWAT model.

The Nash Sutcliffe Efficiency (NSE), developed by Nash and Sutcliffe (1970) was the primary hydrological statistical measure to determine if calibration was achieved. The NSE is a measure of how much better a model predicts hydrologic behaviors compared to the mean of the observed data. The calibration of sediment yield for typical SWAT modeling studies is based on a Percent Bias (PBIAS) statistical technique, which was applied to this study. The São Francisco Basin SWAT model was first calibrated to the hydrology of a gage in the Middle São Francisco basin at Morpará (ANA gage 46360000). Monthly flow simulations yielded a NSE = 0.66 and daily flow simulations yielded a NSE = 0.56 for a simulation from 2001-2006 (Figure 4).

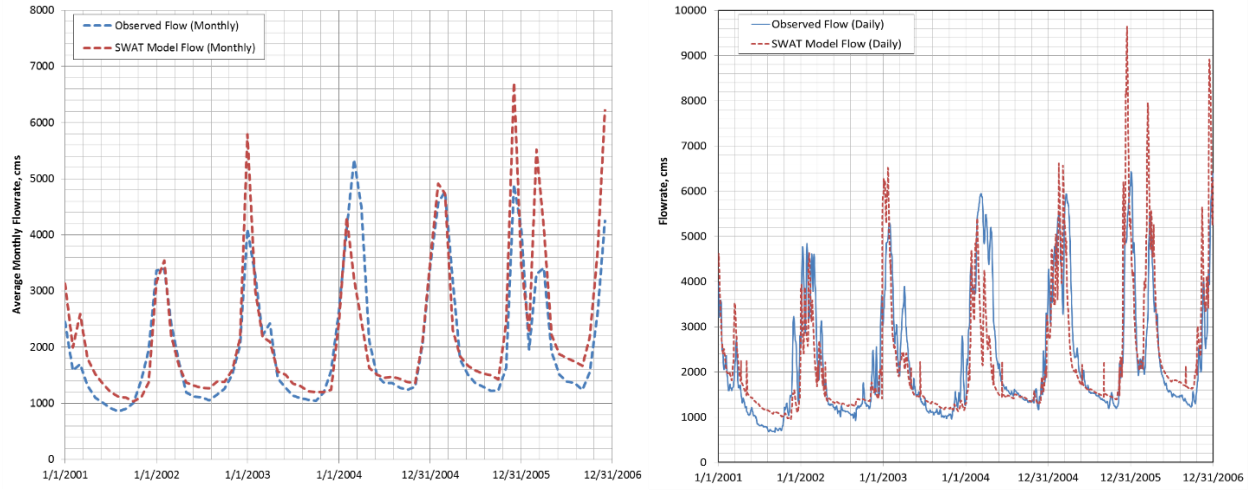

Figure 4 Monthly (left) and Daily (right) Hydrology Calibration at Morpará Gage

The hydrology was calibrated at ten locations throughout the basin and validated at seven additional gages along the São Francisco River's main channel. All calibration and validation yielded a minimum of satisfactory results based on recommended procedures from Moriasi et al (2007), and is presented in Table 1.

The Morpará Gage (ANA Gage 46360000) was selected for the initial basin-wide calibration of the SWAT model for sediment. This gage was selected for the following reasons: 1) the gage includes a long daily flow record (since 1954) and is still an active gage; 2) the gage includes both flow and sediment records; 3) the gage is in the middle São Francisco River (the focus area of navigation impacts); and 4) the gage is not heavily influenced by dams/reservoirs. Suspended sediment data are collected at the Morpará gage four times per year using a USDH-59 sampler, which collects suspended sediment loads. Previous studies have found that the bedload in this reach is approximately 25% of the suspended load (Creech, 2014). These data were compiled into a flow-sediment load rating curve and monthly sediment loads were calculated for the duration of the SWAT simulation (2001-2006). The SWAT output was compared to the observed sediment loads, and a PBIAS of -12.6 was calculated for the length of the simulation (Figure 5). According to Moriasi et al. (2007) this is considered a "Very Good" calibration of monthly sediment loads.

Calibration of the hydrology and sediment for the São Francisco River baseline conditions was achieved by adjusting 15 variables for the hydrology, and 14 additional variables for sediment loads. These variables and the final values of each are listed in Table 2 and 3. Calibration was achieved combining manual methods and utilizing the automated calibration programs SWAT-CUP. All other variables not listed in Table 2 and 3 applied default SWAT values.

Table 1 Hydrology Calibration and Validation within the São Francisco and Major Tributaries

ANA Name	Gage	SWAT Basin	Type	NSE	Description
Rio Pará	40330000	74	Calibration	0.66	Good
Rio Paraopeba	40850000	75	Calibration	0.72	Good
Rio das Velhas	41818000	73	Calibration	0.63	Satisfactory
Rio Jequitaí	42145498	66	Calibration	0.67	Good
Rio Paracatu	42980000	62	Calibration	0.61	Satisfactory
Rio Urucuia	43980002	58	Calibration	0.57	Satisfactory
Rio Verde Grande	44670000	57	Calibration	0.6	Satisfactory
Rio Carinhanha	45260000	49	Calibration	0.58	Satisfactory
Rio Corrente	45960001	42	Calibration	0.67	Good
Rio Grande	45965000	26	Calibration	0.52	Satisfactory
Rio São Francisco upstream of Pará	40100000	76	Validation	0.51	Satisfactory
Rio São Francisco at Manteiga	42210000	60	Validation	0.73	Good
Rio São Francisco at Manga	44500000	56	Validation	0.75	Very Good
Rio São Francisco at Bom Jesus de Lapa	45480000	44	Validation	0.76	Very Good
Rio São Francisco at Morpara	46360000	27	Validation	0.66	Good
Rio São Francisco at Juazeiro	48015000	12	Validation	0.88	Very Good
Rio São Francisco at Ibó	48590000	4	Validation	0.57	Satisfactory

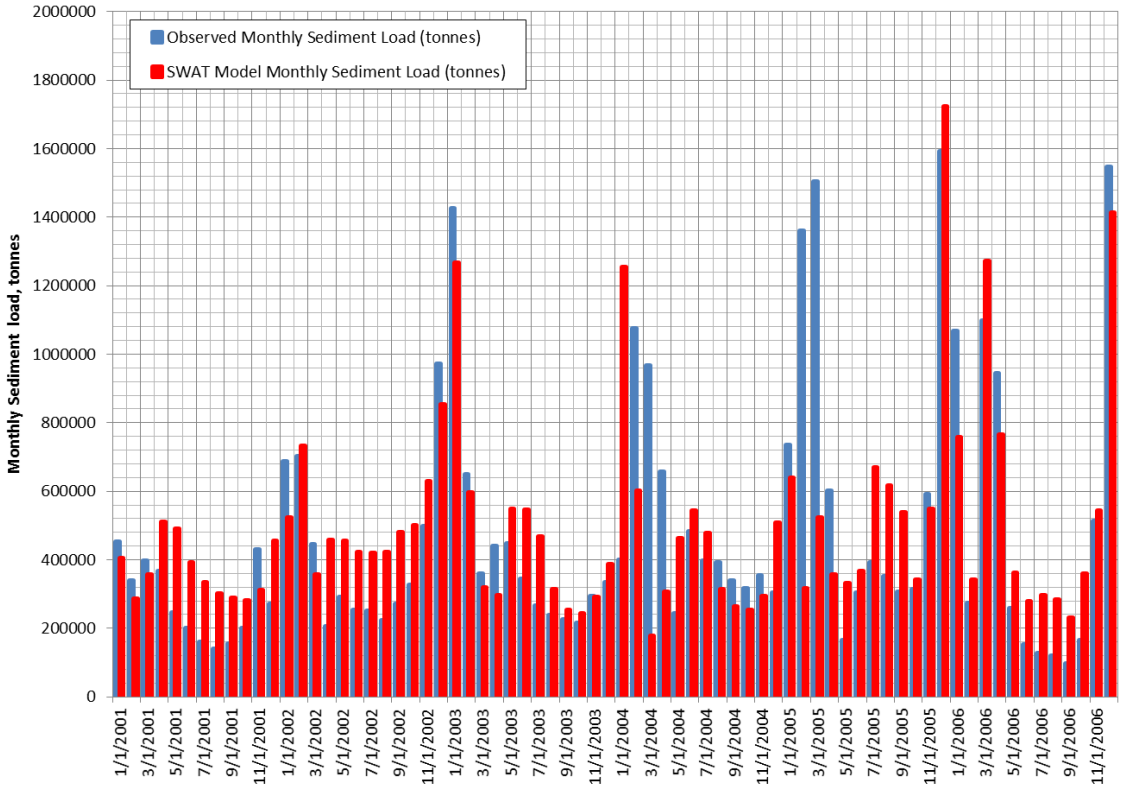

Figure 5 Monthly Suspended Sediment Load Calibration at Morpará Gage

Table 2 Calibration Parameters for Baseline SWAT Model (Hydrology)

Parameter	Table	Description	Sensitivity (P-Value)	Initial Estimated Value	Value Used
ALPHA_BF (days^{-1})	.gw	Baseflow alpha days	0.0173	0.0095	0.0095
OV_N	.hru	Manning's "n" value of overland flow	0.120	0.08	0.096
SOL_K (mm/hr)	.sol	Saturated hydraulic conductivity	0.125	Varies	R: -0.15
RCHRG_DP	.gw	Deep aquifer percolation fraction	0.207	0.10	0.02
ESCO	.hru	Soil evaporation compensation factor	0.366	0.95	0.88
CH_K1 (mm/hr)	.sub	Hydraulic conductivity in tributaries	0.378	5	5
SLSUBBSN (m)	.hru	Average slope length	0.453	90	113
CH_K2 (mm/hr)	.rte	Hydraulic conductivity in main channel	0.498	5	3
REVAPMN (mm)	.gw	Depth of water in shallow aquifer for revap	0.503	100	58
CN2	.mgt	Runoff curve number	0.508	Varies	R: -0.09
CH_N2	.rte	Manning's "n" value for main channels	0.601	0.03	0.022
GW_DELAY (days)	.gw	Groundwater Delay	0.618	30	32
SOL_AWC	.sol	Available Water Capacity of the Soil Layer	0.627	Varies	R: -0.14
CH_N1	.sub	Manning's "n" value for tributary channels	0.771	0.03	0.05
GW_REVAP	.gw	Groundwater revap coefficient	0.880	0.02	0.038

R: Relative Change from Default Values (multiply default value by 1 + R)

Table 3 Calibration Parameters for Baseline SWAT Model (Sediment)

Parameter	Table	Description	Value Used
CH_WDR (m/m)	.rte	Channel width/depth ratio	10
CH_COV1	.rte	Channel erodability factor	0.6
USLE_P	.mgt	Universal Soil Loss Equation Support Practice Factor	0.15
LAT_SED (mg/l)	.hru	Sediment concentration in lateral flow	0
CH_BNK_KD (cm^3/N-s)	.rte	Erodability of Channel Bank Material	0.1
CH_BED_KD (cm^3/N-s)	.rte	Erodability of Channel Bed Material	1
CH_BNK_D50 (μm)	.rte	Median particle size of bank material	500
CH_BED_D50 (μm)	.rte	Median particle size of bed material	500
CH_BNK_TC (N/m^2)	.rte	Critical Shear Stress of Channel Bank	0.2
CH_BED_TC (N/m^2)	.rte	Critical Shear Stress of Channel Bed	0.08
CH_ERODMO1-12	.rte	Erodability Factor by Month	1
CH_EQN	.rte	Sediment Transport Equation	1
RES_SED (mg/l)	.res	Initial Sediment Concentration in Reservoir	1
RES_NSED (mg/l)	.res	Normal Sediment Concentration in Reservoir	1

Geomorphology Study and Sediment Transport Model

The São Francisco River has a very mild slope (ranging from approximately 0.00006 m/m at the downstream reaches to 0.00013 m/m at the upstream reaches). The width of the river ranges from approximately 200 meters in the upper reaches of the navigation channel to approximately 1 km in the lower reaches (upstream of the Sobradinho Reservoir). Widths can be much larger and in some locations the bank to bank width is over 2 km where islands are present. Depths are on average 2-3 meters deep; however, the navigation channel ranges from 0.3 meters to over 18 meters according to a survey of the navigation channel conducted in 2012 by the Administração da Hidrovia do Rio

Sao Francisco (AHSFRA, 2012). AHSFRA is responsible for the operation and maintenance of the navigable portion of the waterway.

Upon evaluation of the current morphological conditions of the navigation channel a pattern of the plan-form was observed. The São Francisco River within the boundaries of the navigation channel generally consists of a narrow and deep section of the river which is horizontally controlled by a rocky bank, with extremely low bank erosion rates. Downstream of the horizontally controlled section, the river begins to widen and in many cases an island may be present in the wide portions of the river. Navigation is typically impeded most significantly either downstream or upstream of the islands in the wider portions, and where the transport capacity of the river is low. Due to the rocky knick points that control many sections of the river, the river evolutionary rates are extremely low. The slow evolutionary patterns are evidenced by comparing historic 19th century surveys of the river to the present day morphology. In the early 1850s, Henrique Guilherme Fernando Halfeld was commissioned by Dom Pedro II, the Emperor of Brazil, to survey the São Francisco River from Pirapora, Minas Gerais to the Atlantic Ocean (Halfeld, 1860). These detailed Halfeld maps provide significant insight into the conditions of the São Francisco River prior to major development in the basin. After reviewing these maps it was shown that there is very little difference between current widths of the river and the river widths in 1852-1854 when the originally surveys were conducted. See Figure 6 for a comparison of the river morphology near Paratinga, Bahia in 1852 and 1999, which demonstrates that the river has a similar morphology, width, and location of islands between these time periods (although there are some changes to the shape and size of some of the islands). This is a typical result when comparing the majority of the locations of the navigation channel that have not been influenced by reservoirs associated with dams.

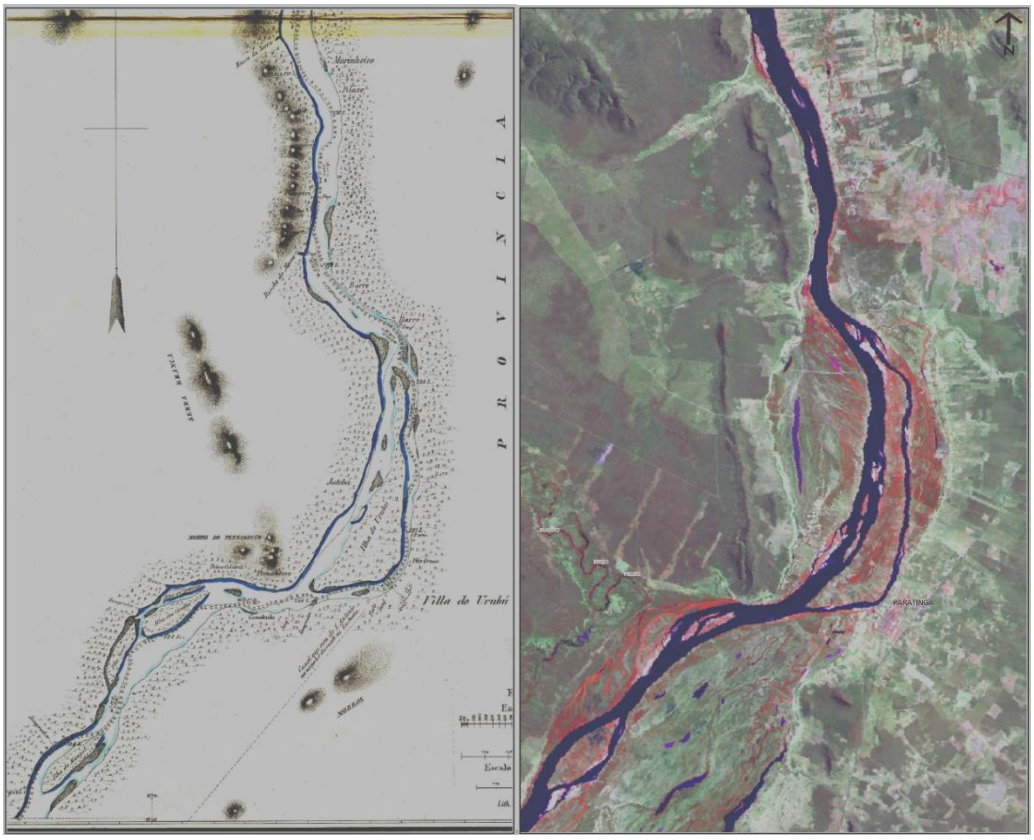

Figure 6 São Francisco River Morphology Surveyed in 1852 (left) and from aerial survey in 1999 (right) at Paratinga, Bahia, Brazil

Prior to the sediment transport modeling, an analysis of the fluvial geomorphology of the river was conducted. The Middle São Francisco River was first divided into sub-reaches based on hydrologic and geomorphic characteristics. The upper and lower limits of each reach are defined at confluences of major tributaries (i.e., where significant increases in flow and sediment exist). Major tributaries contribute a significant load of sediment and flow to the São

Francisco River, leading to potentially differing geomorphic conditions. Between the major tributaries, it was assumed that there is limited hydrologic or geomorphic changes to the slopes, width/depth ratios, sinuosity, etc. The assumption of similar geomorphic characteristics between major tributaries was qualitatively validated by investigating maps of each defined segment. The widths, depths, sinuosity and other dimensionless characteristics were verified to be similar for each defined reach. No major geologic conditions were noted to contribute to a major geomorphic changes in any of the defined reaches. Therefore, the geomorphic reaches are defined based only on the confluences of major tributaries. For each geomorphic reach a specific width of the river is necessary in order to maintain a sustainable self-scouring channel. In locations where the identified width is exceeded navigation shoals may persist. Therefore, a reduction in the effective width (using river training structures) was identified and applied for a conceptual design to be tested and modeled in the HEC-RAS sediment transport model.

RESULTS

SWAT is able to calculate the bank erosion, bed erosion, overland sediment sources, reservoir sedimentation, and net annual sediment loads to the Atlantic Ocean at the watershed scale. Together, these variables make up the São Francisco Basin's sediment budget. The sediment output was evaluated at the average annual scale to determine the sediment sources and sinks for the overall watershed. Each of the net average annual sediment source and sink data are summarized in Figure 7 based on the six-year SWAT simulation. This figure shows that a small percentage of the gross sediment erosion comes from the banks of the São Francisco River and the major tributaries (approximately 6%). The much larger contribution of the net sediment to the shoaling navigation channel is from the upland overland sources and small tributaries (approximately 94% of the net erosion). Most of the sediment that is delivered to the São Francisco River is deposited in the five major reservoirs modeled in the basin (approximately 72%). Only a small percentage is deposited in the São Francisco River floodplain (less than 1%). This may be due to the limited over-bank flooding that occurs due to regulation of the major reservoirs. Overall, the model predicts approximately 23 million tonnes of sediment per year (approximately 25% of the sinks) is deposited within the São Francisco River navigation channel and major tributaries, leading to a net aggradation in the system.

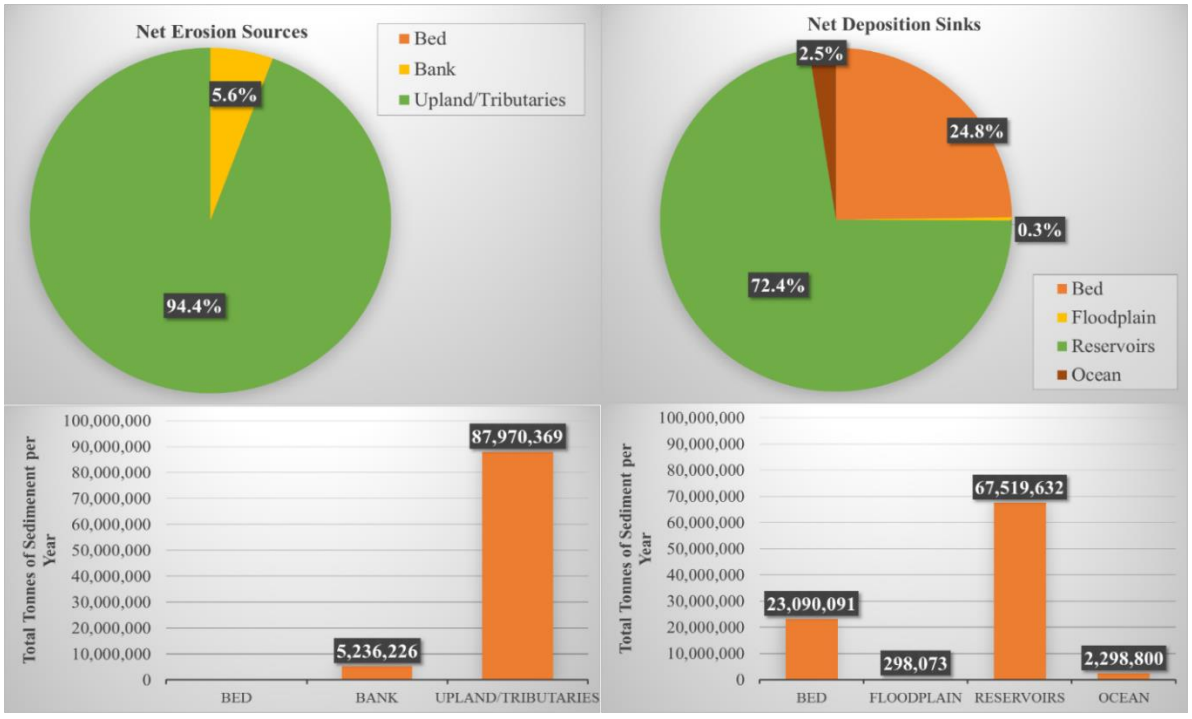

Figure 7 Sediment Budget: Net Sources (Left) and Sinks (Right) of Sediment in the São Francisco River Basin

Approximately 2.5% of the sediment sinks is associated with the delivery of sediment to the Atlantic Ocean at the São Francisco River mouth. Syvitsky and Milliman (2007) developed a predictive model for suspended sediment delivery of major rivers to the oceans using dimensional analysis of the sediment load, area, topographic relief, fluid

density, and gravity. Using this model, Syvitsky and Milliman (2007) calculated that the São Francisco River should deliver approximately 6.4 million tonnes of sediment per year to the Atlantic Ocean (compared to the 2.3 million tonnes that the SWAT model calculated). A suspended sediment gage at Propriá, Sergipe (ANA gage 49705000, located approximately 69 km upstream from the São Francisco River mouth) shows the long-term suspended sediment load (from 1977-1999) is approximately 2.7 million tonnes per year. The Propriá gage is located in the São Francisco River estuary without any major tributaries between Propriá and the São Francisco River mouth, and may be used to represent the sediment load to the Atlantic Ocean. The SWAT model annual average sediment load results are similar to the long-term sediment load at the Propriá gage. The overestimation by Syvitsky and Milliman (2007) may be due to the selected reservoir trapping factor of 0.30 (representing a 70% reservoir trapping efficiency). Due to the three major dams just upstream of the mouth, a trapping efficiency of 85% may be more appropriate, which would bring the Syvitsky and Milliman reservoir trapping factor to 0.15. This would change their prediction of sediment delivery to the Atlantic Ocean from the São Francisco River to 3.2 million tonnes per year; a value closely resembling the observed long-term average at the Propriá gage.

Based on the required reductions in width of the São Francisco River navigation channel for each geomorphic reach, conceptual river training structure designs were developed and analyzed in a sediment transport model. An example of a conceptual design is shown in Figure 8. After the structures were input into the sediment transport model, the results of a six-year simulation were analyzed. The primary analysis consisted of investigating the depths of the thalweg along the navigation channel. This provided confirmation that the proposed design (based on geomorphic characteristics of each reach) would provide a sufficient amount of self-scour along the navigation channel. In several instances the self-scouring goal of 2.0 meters at the low water datum (an economically viable navigation draft) was not achieved, and the structures were revised. After the revised structures were added to the model, the channel was able to maintain a self-scour depth of at least 2.0 meters along the channel for each geomorphic reach. The results of the final navigation depths are shown in Figure 9.

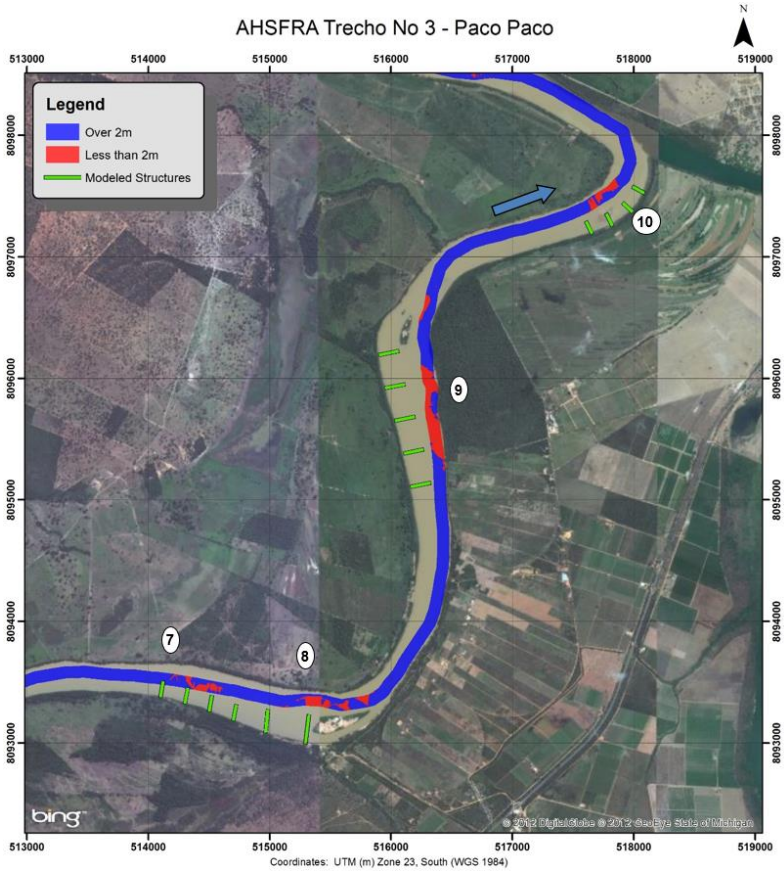

Figure 8 Typical Structure Design for Improved Navigation in the São Francisco River

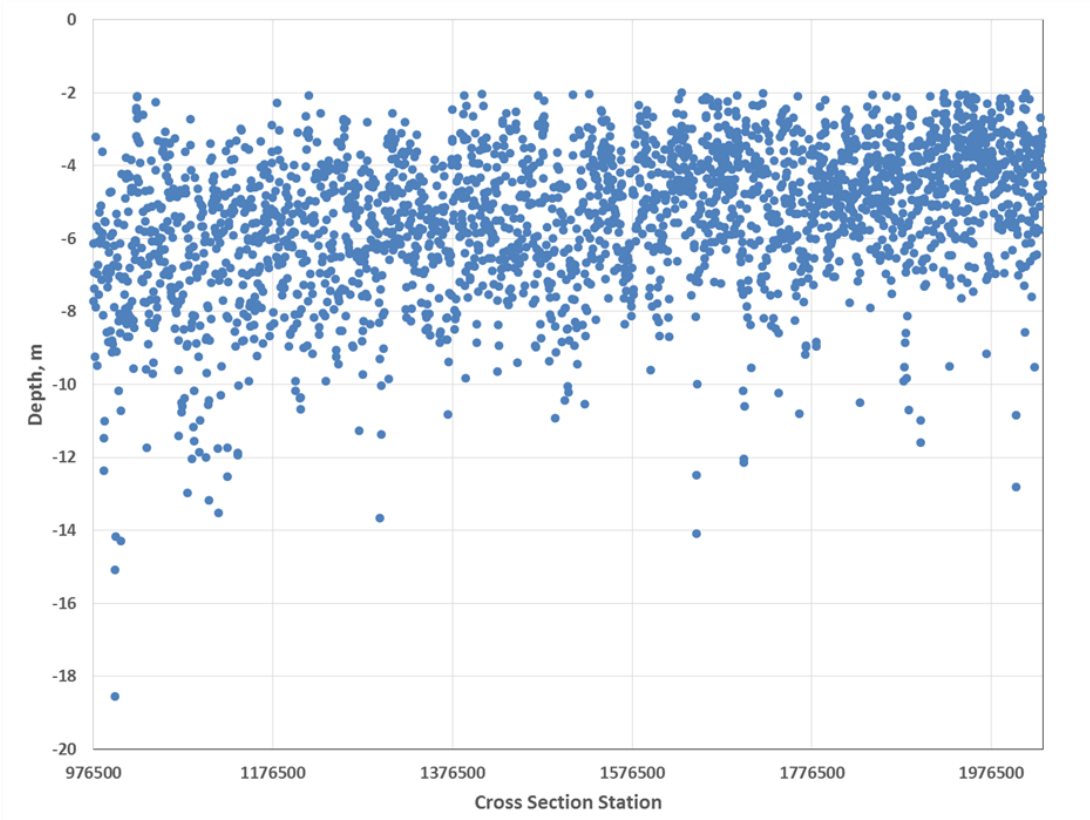

Figure 9 Predicted Navigation Channel Depths following a Six-Year Sediment Transport Simulation

CONCLUSIONS

A SWAT model of the São Francisco Basin was developed to calculate a modern sediment budget for the watershed and to analyze the changes to the sediment budget since Pre-European settlement. Based on the SWAT model results, currently only a small component of the existing sediment budget is due to bank erosion of the São Francisco River. Approximately 5.6% of the sediment that is causing shoals in the São Francisco River may have originated in the banks of the São Francisco River or the banks of the major tributaries. The remaining 94.4% of the sediments that are causing shoals originated from overland sediment sources or sediment erosion occurring in minor tributaries. Due to the high percentage of sediments that originated in the uplands and minor tributaries, bank erosion measures alone will have a negligible effect on the existing shoals in the São Francisco River navigation channel, and an improved navigation channel will only result from minimizing sediment yields at upland sources and by projects designed to improve navigation at the shoal locations.

The sediment transport model confirms the effectiveness of the conceptual layout of self-scouring structures, and the proposed alignments of structures can be used as a guide for planning long-term structural solutions for improving navigation of the Sao Francisco River. The linked sediment yield and sediment transport modeling is a system wide model, which characterizes likely future conditions throughout the entire system, and the modeling demonstrates that the layouts and approaches used will likely not create new navigation hazards. The modeling conducted in this alternative analysis should only be used as a guide for general structure layouts and planning purposes. Any specific project will need to develop a site-specific model or analysis in order to verify the effectiveness of the proposed self-scouring structures. In addition, other concerns such as bank erosion associated with the proposed designs (particularly on the opposite bank) will need to be investigated for any site-specific project that will be developed into a basic or executive design. Therefore, although the model will not support detailed analysis at the site-specific level, the modeling results can be used for general planning purposes such as calculating costs to efficiently develop the Sao Francisco River navigation channel.

REFERENCES

AHSFRA (2012). Bathymetry Data of the São Francisco River Navigation Channel, 2012. Unpublished raw data.

Batjes, N.H. (2012). ISRIC-WISE derived soil properties on a 5 by 5 arc-minutes global grid (ver. 1.2). Report 2012/01, ISRIC – World Soil Information, Wageningen (with data set, available at www.isric.org) Report 2012/01. 52 pp.

Biswas, A.K., Cordeiro, N.V., Braga, B.P.F., and Tortajada, C. (1999). *Management of Latin American River Basins: Amazon, Plata, and São Francisco*. United Nations University Press, Tokyo, Japan.

CODEVASF (2013). Irrigation permitted data. Unpublished raw data.

CODEVASF & ANA, (2002). Multitemporal Analysis of the Dynamic of Alteration of the Conformation of the Sao Francisco Riverbed – Middle Course. Brasilia.

Creech, C.T. (2014). *Coupled Sediment Yield and Sediment Transport Model to Support Navigation Planning in Northeast Brazil.* Dissertation, Wayne State University. Ann Arbor: Proquest/UMI, 2014. (Publication No. 3646957)

Emprapa (1981). Mapa de solos do Brasil. Excala 1:5,000,000. Rio de Janeiro, 1981. 9 p. Communicado expositivo do mapa de solos do Brasil.

European Space Agency (2006). GlobCover Dataset. http://due.esrin.esa.int/globcover/. Accessed on 17 June, 2013.

Halfeld, H.G.F. (1860). Atlas e relatorio concernente a exploração do Rio de S. Francisco desde a Cachoeira da Pirapora até ao Oceano Atlantico : levantado por Ordem do Governo de S. M. I. O Senhor Dom Pedro II, Rio de Janeiro, Brazil.

Moriasi, D.N., Arnold, J.G., Van Liew, M.W., Binger, R.L., Harmel, R.D., and Veith, T.L. (2007). Model Evaluation Guidelines for Systematic Quantification of Accuracy in Watershed Simulations. *Transactions of the ASABE,* 50 (3), 885-900.

NASA (2013). Advanced Spaceborne Thermal Emission and Reflection Radiometer Website. Accessed on 17 June 2013. http://asterweb.jpl.nasa.gov/

Nash, J.E. and Sutcliffe, J.V. (1970). River flow forecasting through conceptual models. Part I – A discussion of Principles. Journal of Hydrology, 10 (3), 282-290.

Syvitski, J.P.M., and Milliman, J.D. (2007). Geology, Geography, and Humans Battle for Dominance over the Delivery of Fluvial Sediment to the Coast Ocean. Journal of Geology, Vol. 115, No. 1, pp. 1-19.

SEDIMENT DYNAMICS ON RIVER NETWORKS: INCORPORATING SOURCES, STORES, AND SINKS FROM A SEDIMENT BUDGET INTO A NETWORK-MODELING FRAMEWORK

EXTENDED ABSTRACT

Jonathan A. Czuba, Department of Civil, Environmental, and Geo- Engineering and St. Anthony Falls Laboratory, University of Minnesota, Minneapolis, Minnesota, czuba004@umn.edu;
Efi Foufoula-Georgiou, Department of Civil, Environmental, and Geo- Engineering and St. Anthony Falls Laboratory, University of Minnesota, Minneapolis, Minnesota, efi@umn.edu;
Karen B. Gran, Department of Geological Sciences, University of Minnesota, Duluth, Minnesota;
Patrick Belmont, Department of Watershed Sciences, Utah State University, Logan, Utah;
Peter R. Wilcock, Department of Watershed Sciences, Utah State University, Logan, Utah

Many streams and rivers throughout the U.S. have experienced degraded water quality and declines in both number and diversity of aquatic species. These changes are undesirable consequences of an intensification and expansion of human actions on the landscape combined with climatic trends occurring in the last few decades. The Minnesota River Basin (MRB) is no exception. Changes in agricultural management in the MRB, including installation of tile drainage, have reduced surface runoff and erosion from agricultural fields in recent decades. However, increased drainage has also increased streamflow and therefore amplified erosion of streambanks and bluffs. As a result, no net change in suspended sediment loading has been observed, but rather a drastic shift in sediment sources from upland agricultural fields to near-channel river banks and bluffs (Belmont et al., 2011; Schottler et al., 2014). Targeting management actions to ultimately improve ecosystem health and function requires navigating the cascade of changes from streamflow to sediment to river biology.

In the MRB, the locations and rates of erosion and deposition of major sediment sources and sinks (i.e., bluffs, streambanks/floodplains, agricultural fields, and ravines) have been well documented over millennial and decadal timescales (Belmont et al., 2011; Gran et al., 2011a, 2011b, 2013). But robust modeling of watershed sediment dynamics (i.e., generation, transport, and storage of sediment through the entire river network) requires understanding how these features are arranged within the river network, the "skeleton" of the landscape, and how process-based time delays of input, storage, and transport set the system in motion. We investigate the sediment dynamics of the Le Sueur River Basin, the major sediment-generating subbasin of the MRB, using a sediment budget to inform a modeling framework that incorporates simple reach-scale process dynamics into a river network context (Czuba and Foufoula-Georgiou, 2014, 2015). We seek to better understand how fine and coarse sediment moves through an entire river network over decadal to century time scales, given a heterogeneous distribution of sources, transport pathways set by the river network, and underlying process dynamics. We also extend this understanding to discuss implications for watershed scale sediment management and policy.

The network-based modeling framework of Czuba and Foufoula-Georgiou (2014, 2015) focuses on understanding large-scale system functioning and predicting the emergence of vulnerabilities, "hotspots" of change, and system resilience for guiding effective landscape management decisions. Landscapes are too complex to be modeled with fully distributed deterministic models that consider all the small-scale physics and interactions, due to large and unavoidable uncertainties associated with the myriad of relevant processes. Besides, changes in climate, land use, and water management impose non-stationary conditions and also nonlinearities in the system make it sensitive to small perturbations. Instead, the aim of this framework is to capture the most important interactions and amplifications by exploring the system connectivity and its transport pathways including residence times, threshold behavior, and physical transformations. The framework focuses on understanding network transport by: (1) decomposing the landscape into a connected network of elements including river channels, wetlands, agricultural fields, etc., (2) spatially and temporally distributing inputs of water and sediment, and (3) tracking these inputs through individual landscape elements through process-based time delays.

The application of this framework so far has focused on the dynamics of water and sediment on the landscape. The transport of sediment has been reduced to simple time delays as functions of upstream drainage area and channel slope by combining and reducing equations for uniform flow hydraulics, (at capacity) sediment transport, hydraulic geometry scaling, and intermittent sediment-transporting flows (see Czuba and Foufoula-Georgiou, 2014 for the derivation and limitations of mud, sand, and gravel transport time-delay equations). This framework has successfully answered questions as to likely hotspots of fluvial geomorphic change that have been validated with field observations. Specifically, the framework has been used to identify vulnerable reaches of a river network prone to high rates of channel migration by highlighting where bed-material sediment has a tendency to persist and thereby force channel migration through the bar-push mechanism, i.e, more rapid accretion of the point bar along the inner bank forcing erosion of the outer bank (Czuba and Foufoula-Georgiou, 2015).

We apply and advance this framework to capture the dynamics of sediment-size classes of mud, sand, and gravel in the Le Sueur River Basin. Sediment input to the network is informed based on the locations and erosion or deposition rates of bluffs, streambanks/floodplains, agricultural fields, and ravines as well as physically-based process dynamics of sediment generation. Sediment transport closely follows the approach developed by Czuba and Foufoula-Georgiou (2014). The advancement of the framework is in allowing for feedback between the accumulation of mass, geomorphic properties, and sediment transport (via travel time) within a reach. Thus, we now couple geomorphic properties with density-dependent transport, all within a network context. Furthermore, we explore how floodplain storage (via additional storage delays) affects the system dynamics.

As part of this ongoing research, we are exploring: (1) how the heterogeneity of landscape features affects the spatial distribution of sediment impacts, e.g., confined to select reaches near the sources, (2) timescales of movement of sediment through the system, including floodplain storage, that can better inform legacy effects and hysteresis, and (3) the implications of system dynamics for targeting management actions that will most effectively reduce the detrimental impacts of sediment.

REFERENCES

Belmont, P., et al. (2011). "Large shift in source of fine sediment in the Upper Mississippi River," Environmental Science & Technology, 45, pp 8804–8810, doi:10.1021/es2019109.

Czuba, J.A., and Foufoula-Georgiou, E. (2014). "A network-based framework for identifying potential synchronizations and amplifications of sediment delivery in river basins," Water Resources Research, 50(5), pp 3826–3851, doi:10.1002/2013WR014227.

Czuba, J.A., and Foufoula-Georgiou, E. (2015). "Dynamic connectivity in a fluvial network for identifying hotspots of geomorphic change," Water Resources Research, doi:10.1002/2014WR016139.

Gran, K.B., Belmont, P., Day, S.S., Finnegan, N., Jennings, C., Lauer, J.W., and Wilcock, P.R. (2011a). "Landscape evolution in south-central Minnesota and the role of geomorphic history on modern erosional processes," GSA Today, 21(9), pp 7–9, doi:10.1130/G121A.1.

Gran, K., Belmont, P., Day, S., Jennings, C., Lauer, J.W., Viparelli, E., Wilcock, P., and Parker, G. (2011b). "An integrated sediment budget for the Le Sueur River Basin," Minnesota Pollution Control Agency, report number wq-iw7-29o, Mankato, MN. 128 p. (http://www.pca.state.mn.us/index.php/view-document.html?gid=16202) last accessed 20 Jan. 2015.

Gran, K.B., Finnegan, N., Johnson, A.L., Belmont, P., Wittkop, C., and Rittenour, T. (2013). "Landscape evolution, valley excavation, and terrace development following abrupt postglacial base-level fall," GSA Bulletin, 125(11-12), pp 1851–1864, doi:10.1130/B30772.1.

Schottler, S.P., Ulrich, J., Belmont, P., Moore, R., Lauer, J.W., Engstrom, D.R., and Almendinger, J.E. (2014). "Twentieth century agricultural drainage creates more erosive rivers," Hydrological Processes, 28(4), pp 1951–1961, doi:10.1002/hyp.9738.

USING 15-MINUTE ACOUSTIC DATA TO ANALYZE SUSPENDED-SEDIMENT DYNAMICS IN THE RIO GRANDE IN THE BIG BEND REGION

David J. Dean, Hydrologist, U.S. Geological Survey, Grand Canyon Monitoring and Research Center, Flagstaff, Arizona, djdean@usgs.gov; David J. Topping, Research Hydrologist, U.S. Geological Survey, Grand Canyon Monitoring and Research Center, Flagstaff, Arizona, dtopping@usgs.gov; Ronald Griffiths, Hydrologist, U.S. Geological Survey, Grand Canyon Monitoring and Research Center, Flagstaff, Arizona, rgriffiths@usgs.gov; Thomas A Sabol, Hydrologist, U.S. Geological Survey, Grand Canyon Monitoring and Research Center, Flagstaff, Arizona, tsabol@usgs.gov; John C. Schmidt, Professor, Utah State University, Logan, Utah, jack.schmidt@usu.edu; Jeffery Bennett, Physical Scientist/Hydrologist, National Park Service, Big Bend National Park, Texas, jeffery_bennett@nps.gov

INTRODUCTION

The Rio Grande in the Big Bend region is subject to rapid geomorphic change consisting of channel narrowing during years of low flow, and channel widening during rare, large, long duration floods. Since the 1940s, there have been large declines in mean and peak stream flow, and the channel has progressively narrowed. Large, channel widening floods are infrequent and have failed to widen the channel to widths measured prior to the onset of channel narrowing in the 1940s. Before the most recent channel-widening flood in September 2008, the Rio Grande in the Big Bend was more than 50 percent narrower than measured in the 1940s.

Channel narrowing results in increased flood frequency and flood magnitude due to the loss of channel capacity and flood conveyance (Dean and Schmidt, 2011). Channel narrowing also results in the loss of important aquatic habitats such as backwaters and side-channels, because these habitats accumulate sediment and are converted to floodplains. Environmental managers are attempting to construct an environmental flow program for the purposes of minimizing channel narrowing during low flow years such that channel capacity, flood conveyance, and important aquatic habitats are maintained. Effective mitigation of channel narrowing processes requires an in-depth understanding of the predominant sediment source areas, the quantity of sediment input from those source areas, the parts of the flow regime responsible for the greatest sediment deposition, and the effect of managed flows in ameliorating the sediment loading that occurs within the channel.

Here, we analyze data collected with acoustic instrumentation at high temporal resolution to quantify suspended-sediment transport during a variety of flood types. We also investigate the effect of long duration managed flows in promoting sediment export and minimizing channel narrowing.

STUDY AREA AND BACKGROUND

The Rio Grande in the Big Bend region of the Chihuahuan Desert extends from the confluence with the Rio Conchos 490 km downstream to Amistad Reservoir (Figure 1), and is the international boundary between the United States and Mexico. Prior to the 1940s, the hydrology

of the Rio Grande in the Big Bend region was comprised of a snowmelt flood pulse in late spring and early summer from the upper Rio Grande, followed by a much larger summer flood pulse from the Rio Conchos basin driven by rains of the North American Monsoon and dissipating tropical storms in northern Mexico (Dean and Schmidt, 2011; Dean et al., 2011, Dean and Schmidt, 2013). Dam construction and agricultural diversions on the upper Rio Grande completely eliminated the spring snowmelt pulse from the Rio Grande in the Big Bend by the 1940s (Dean and Schmidt, 2011). Dam construction and water development on the Rio Conchos also contributed to reductions in mean and peak flow on the Rio Grande in the Big Bend region, however, large floods driven by dissipating tropical storms in northern Mexico occasionally still occur on the Rio Conchos when reservoir capacity is exceeded (Dean and Schmidt, 2013).

The current flood hydrology of the Rio Grande is highly variable. The lowest flows occur during the winter and spring, and base flows are commonly less than 1.5 m^3/s. High flows usually begin in May and June and can be generated by localized, convective thunderstorms lasting a few hours or days, or can be caused by longer duration dam releases from Luis L. Leon Dam on the Rio Conchos. Flash floods associated with convective thunderstorms contribute large amounts of sediment to the Rio Grande. Dam release floods from Luis L. Leon Dam are generally of moderate magnitude (40 to 200 m^3/s) and usually last longer than 5 days. Channel reset floods have peak discharges greater than 1,000 m^3/s, and have durations of weeks to months. Floods of this magnitude were common in the early 1900s, but are now rare.

Geomorphic investigations show that the modern Rio Grande in the Big Bend region is a river in geomorphic disequilibrium (Dean and Schmidt, 2011; Dean et al., 2011, Dean and Schmidt, 2013). This disequilibrium is characterized by channel narrowing over decadal timescales, and episodic channel widening during large floods (i.e., channel reset events, >1,000 m^3/s) originating in the Rio Conchos basin. Between channel reset events, the Rio Grande rapidly narrows by oblique and vertical accretion of fine sediment on floodplains and formerly active channel bars. Between 1991 and 2008, the river narrowed between 36 and 52 percent through the accretion of sediment that exceeded three meters in thickness (Dean and Schmidt, 2011; Dean et al., 2011). The most recent channel resetting flood occurred in 2008 and the channel is in a new phase of narrowing (Dean and Schmidt, 2013). The rapid rates of channel narrowing and sediment accumulation in the Rio Grande indicate that the river presently resides in a state of sediment surplus. Although general patterns of sediment surplus have been described, sediment inputs, and sediment-transport processes associated with this surplus condition remain unquantified.

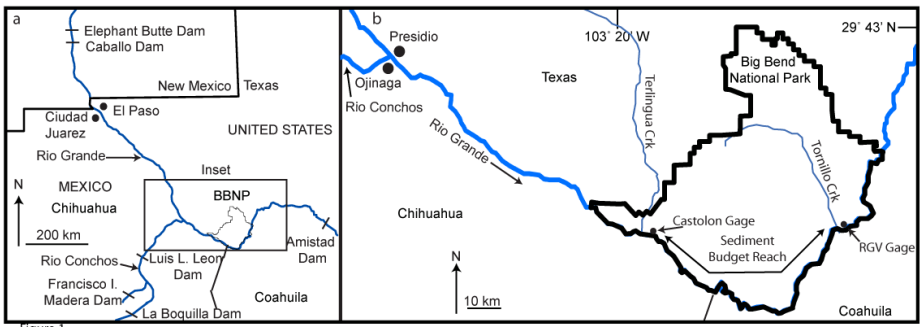

Figure 1 (a) Map of the Big Bend region. (b) Study Area

Little is known of the relative contributions of sediment from various source areas, the ranges in suspended-sediment concentrations and loads associated with different types of floods, the longitudinal trends and continuity of sediment transport along the river corridor, and whether all flood events or only a subset of floods contribute to the sediment surplus condition. We use 15-minute stream-flow and suspended-sediment transport data collected using acoustic instrumentation at discrete locations along the Rio Grande to begin to address these knowledge gaps. Using these data, we analyze suspended-sediment dynamics during two parts of the flood regime, (1) short-duration tributary-derived flash floods, and (2) longer-duration dam release floods from Luis L. Leon Dam on the Rio Conchos. We analyze the degree to which flash floods contribute to sediment accumulation within the channel, and examine the hypothesis that dam releases help to ameliorate sediment surplus conditions.

METHODS

Continuous Acoustic Suspended-Sediment Monitoring: In rivers, the concentrations of some grain-size fractions of suspended sediment are typically controlled or regulated by changes in the upstream supply of those fractions. These supply-driven changes in suspended-sediment concentration can vary somewhat independently of the water discharge (Colby, 1963; Guy, 1970; Dinehart, 1982; Topping et al., 2000a, 2000b). The development of a progressive lag between suspended-sediment concentration and the kinematic discharge wave during a flood may result in poor correlation between water discharge and suspended-sediment concentration (Heidel, 1956; Dinehart, 1982). Increased form drag caused by bedform development during floods may also result in reduced suspended-sediment concentrations for the same discharges (Kleinhans et al., 2007). In the case of the Rio Grande in the Big Bend region, the upstream supplies of water and sediment are at times completely decoupled. Water during low flows is primarily supplied from the dam-regulated Rio Conchos and shallow aquifers, whereas water during high flows may be supplied from the Rio Conchos, any number of ephemeral tributaries within the region, and occasionally from the Rio Grande upstream from the Rio Conchos. Sediment is generally supplied by the Rio Conchos, local tributaries, and during higher discharge, may also be supplied by erosion of the floodplains that have developed in the formerly braided channels of the Rio Grande. Thus, at no time can stable relations between the discharge of water and suspended-sediment concentration be assumed.

Computation of accurate sediment loads in rivers where the transport of suspended sediment is, at least partially, regulated by changes in the upstream sediment supply requires high-resolution measurements of suspended-sediment concentration that are discharge-independent. To make these discharge-independent measurements of suspended-sediment concentration and grain size at high temporal resolution, we use a multi-frequency acoustic method that was developed and tested on the Colorado River in Grand Canyon National Park (Topping et al., 2004; Topping et al., 2007). This method utilizes 15-minute measurements of acoustic attenuation and backscatter using an array of 1 and 2 MHz side-looking acoustic-Doppler profilers (Topping et al., 2015). The basics of this method are as follows: (a) acoustic attenuation is used to calculate the velocity-weighted suspended-silt-and-clay concentration in the river cross section, (b) acoustic backscatter is used to calculate the apparent suspended-sand concentration at each frequency corrected for the backscatter produced by the silt and clay, (c) the apparent suspended-sand concentrations calculated at each acoustic frequency are then used in combination with theory to

calculate an unbiased two-frequency measure of the velocity-weighted suspended-sand concentration and median grain size in the river cross section.

In November 2010, the USGS Grand Canyon Monitoring and Research Center (GCMRC), Utah State University (USU), and the National Park Service (NPS) installed two continuously operating suspended-sediment gaging stations on the Rio Grande near Castolon, Texas, and Rio Grande Village, Texas (Figure 1b). The Castolon sediment gage (Rio Grande above Castolon, Texas, 08374535) was established approximately 1.8 km upstream of the Castolon stream gage (Rio Grande near Castolon, Texas, 08374550), and the RGV sediment gage (Rio Grande above Rio Grande Village, Texas, 08375295) was established approximately 400 m upstream from RGV stream gage (Rio Grande at Rio Grande Village, Big Bend National Park, Texas, 08375300). Each sediment gage consists of a 1 MHz and 2 MHz side-looking acoustic-Doppler profiler, and an ISCO 6712 automatic pump sampler[1]. For ease of communication, the Castolon and RGV sediment and stream gages are referred to as the Castolon and RGV gages.

Acoustic attenuation and backscatter data were calibrated using physical suspended-sediment samples. At high flows, standard depth-integrated samples were collected using a US D-74 sampler (Edwards and Glysson, 1999) using the Equal-Width-Increment (EWI) method (Edwards and Glysson, 1999) at 10 equally spaced verticals across the channel using the additional transits recommended by Topping et al. (2011). At low flows, EWI measurements were made using a US DH-48 sampler and the same numbers of verticals and transits (Edwards and Glysson, 1999). During night-time hours, and when field crews were not available, suspended-sediment samples were collected automatically by the pump sampler. Samples collected by the pump sampler were calibrated to the cross section using paired EWI-pump measurements. These calibrations were developed for silt and clay and for multiple individual size classes of sand, as recommended by Edwards and Glysson (1999). The outcomes of the pump-sampler calibration are calibrated-pump measurements of the velocity weighted suspended-silt-and-clay concentration, suspended-sand concentration, and suspended-sand median grain size (albeit with larger error than the EWI measurements).

Sediment loads were calculated using the calibrated acoustic data, the EWI measurements, and the calibrated-pump measurements using the standard methods described by Porterfield (1972). Calibrated acoustic data at the two sediment gages were combined with discharges measured at the nearby Castolon and RGV stream gages to calculate instantaneous loads of suspended silt and clay and suspended sand. These instantaneous loads were then integrated over the hydrograph to calculate cumulative loads. Calibrated acoustic data include instantaneous concentrations of silt and clay, and sand, and the instantaneous median grain size of the suspended sand. All EWI and calibrated-pump and acoustic data are available on the USGS-GCMRC website, http://www.gcmrc.gov/discharge_qw_sediment/. This website also includes a sediment budget tool that calculates the change in sediment storage between the Castolon and RGV gages (i.e. the sediment budget reach) for any time period of interest. Uncertainty bands calculated using the sediment budget tool include biases in discharge calculations, uncertainty in the quantity of sand bedload (assumed to be 5% of total sand load), small biases in the

[1] Any use of trade, product, or firm names is for descriptive purposes only and does not imply endorsement by the U.S. Government.

suspended-sediment measurements, and uncertainty in the contribution of suspended sediment from ungaged tributaries.

RESULTS

Here, we examine suspended-sediment transport dynamics during two parts of the Rio Grande flow regime. First, we analyze suspended-sediment transport during two periods when flash floods occurred in 2011 and 2013. The periods of flash floods are just two of many that have occurred since installation of the sediment gages, and are discussed here because they are representative of these types of events. Second, we analyze suspended-sediment transport during longer duration dam release floods that occurred in 2011, 2012, and 2013.

Sediment Dynamics During Flash Floods: Flash floods generally cause sediment deposition within the channel. Large suspended-sediment concentrations occur during flash floods, however, discharge and suspended-sediment concentration can attenuate rapidly downstream. This is clearly illustrated during the flash flood that occurred on 6/2/2011 as depicted in Figure 2a-d. This flood was sourced in the Rio Conchos basin and was nearly 200 m^3/s at the confluence of the Rio Conchos and the Rio Grande. At the Castolon gage, over 125 km downstream, discharge attenuated to 80 m^3/s, and was only approximately 20 m^3/s at the RGV gage (see Figure 1 for locations).

Sediment concentrations also significantly attenuated downstream. At the Castolon gage, the peak silt and clay concentration was 14,200 mg/L, and downstream, at the RGV gage, the peak silt and clay concentration was an order of magnitude less at 1,470 mg/L (Figure 2a). The peak sand concentration at the Castolon sediment gage was 260 mg/L, and was less than one mg/L at the RGV sediment gage (Figure 2b). The nearly complete attenuation of flow and sediment resulted in the deposition of more than 96 percent of the silt and clay load, and 100 percent of the sand load between the Castolon and RGV sediment gages during this flood.

For the same supply of sand on the bed, increases in flow will result in increases in the concentration and grain size of suspended sediment (Rubin and Topping, 2001). Thus, if increases in flow cause increases in suspended-sediment concentration and decreases in suspended-sediment grain size, changes in the sediment supply occurred (either from upstream or the floodplains). During the flash flood depicted in Figure 2a-d, silt and clay concentrations were higher on the falling limb of the flood (Figure 2a, c), resulting in a strong counterclockwise hysteresis loop for discharge and silt and clay concentration (Figure 2c). This indicates that a progressive lag developed between the kinematic discharge wave and the suspended silt and clay; the water and sediment both had the same tributary source, but the kinematic discharge wave "outran" the suspended sediment traveling at or below the velocity of the water. Sand concentrations however, was greatest during the largest discharges (Figure 2b), but the largest concentrations had the finest grain sizes (Figure 2d). Thus, silt and clay transport at both gages was primarily controlled by the upstream supply of sediment and the downstream rate of sediment transport relative to the flood wave, and not flow magnitude at the sediment gages. The negative relationship between suspended sand concentration and the grain size of suspended sand whereby the grain sizes of the suspended sand were finer for increasing concentration (Figure 2d) also indicate that sand transport at Castolon was controlled by the upstream supply.

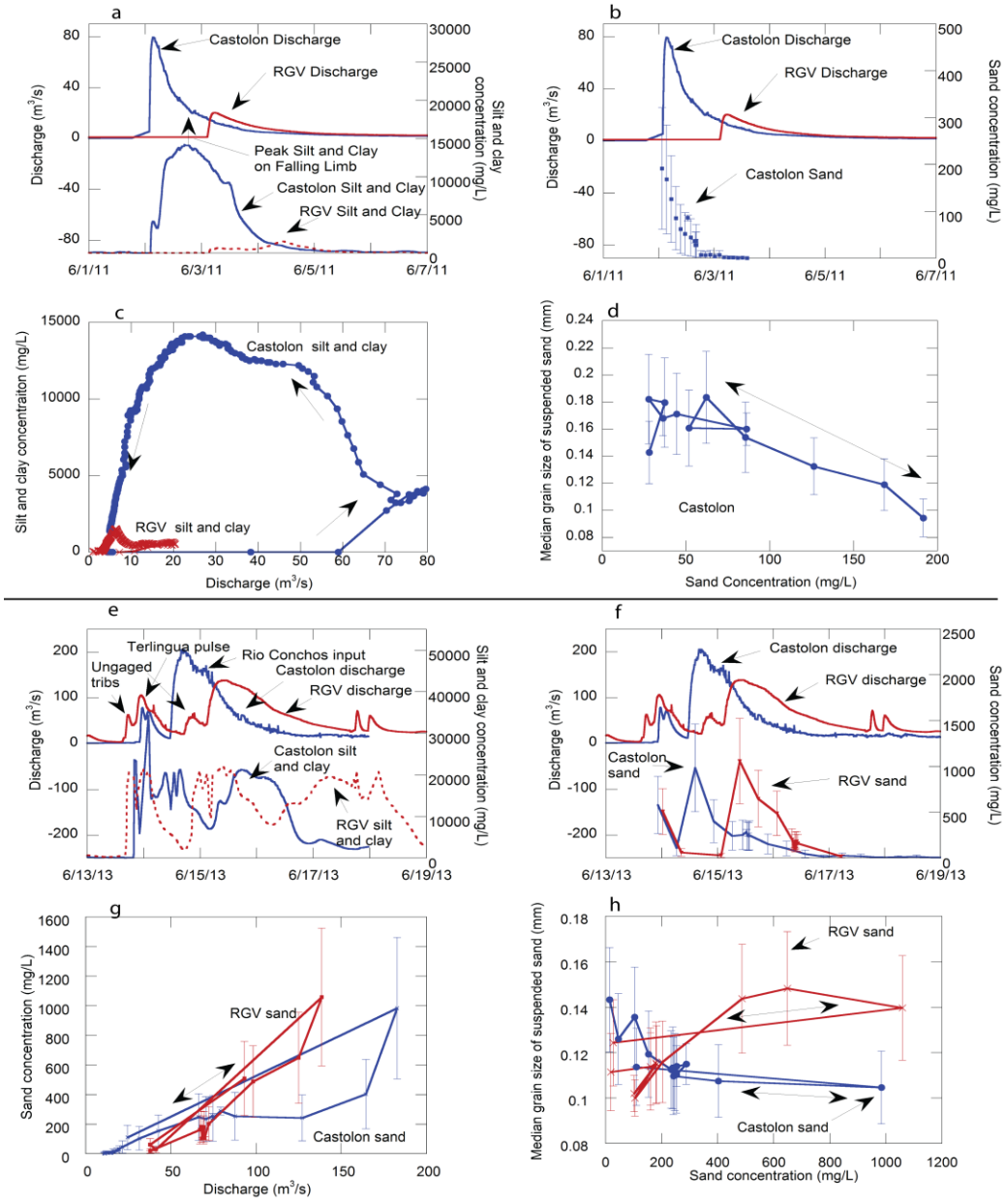

Figure 2 Suspended-sediment dynamics for flash flood between 6/2/2011 and 6/6/2011 (days 244-248)(a-d). Time series of discharge and sediment concentration are shown in (a) and (b). Counterclockwise hysteresis loop between discharge and silt and clay concentration shown in (c), and declines in sand grain size with increasing concentration show in (d). Suspended-sediment dynamics for flash flood event between 6/13/2013 and 6/19/2013 (days 986-992)(e-h). Time series of discharge and sediment concentration are shown in (e) and (f). Relations between discharge and sand concentration shown in (g), and relations between sand concentration and grain size shown in (h). Double-headed arrows show relations that are roughly linear in nature. Time-series are in days since 10/1/2010 because the start of the 2011 water year roughly corresponds to the installation date of the sediment gages. Data in b,d, and f-h show physical measurements only because some short-term biases existed in the acoustic data.

The second period of flash flooding shown here occurred between 6/13/2013 and 6/19/2013 (days 986-992, Figure 2e-h), and consisted of many flash floods from multiple source areas, including: ungaged tributaries both upstream and within the sediment budget reach, Terlingua Creek which is a large tributary approximately 9 km upstream from the Castolon gage, and a much larger pulse of water from the Rio Conchos. Peak flow magnitudes were more than twice as large as the previous flash-flood example.

Suspended-sediment dynamics were much more complex during the 2013 floods compared to in the 2011 flash flood example. The largest spikes in sediment concentration occurred at Castolon and were driven by the flash flood from Terlingua Creek. Silt and clay concentrations were over 34,000 mg/L, and sand concentrations were 877 mg/L at the Castolon sediment gage during this initial spike (Figures 2e-f).

With the exception of the initial flash from Terlingua Creek, concentrations of both silt and clay and sand during the remaining high flows were roughly equal at the two gages (Figure 2e-f). However, there was significant discharge attenuation between the Castolon and RGV gages, and thus, elevated sand concentrations occurred for a shorter period of time at the downstream RGV gage (Figure 2e-f). The attenuation of flow, and the shorter duration of elevated sediment concentrations at the downstream gage, resulted in the deposition of approximately 18,000 metric tons of sand, and over 110,000 metric tons of silt and clay.

Sand concentration at both sites increased relatively linearly with increasing discharge (Figure 2f-g). However, the suspended sand was finest at higher discharges at Castolon (Figure 2h), and the suspended sand was the coarsest at higher discharges at RGV. Thus, suspended-sand transport at Castolon was partially regulated by the upstream supply as evidenced by the fining of the suspended sand at the highest discharges, whereas sand transport was mostly regulated by flow at RGV, because larger discharges always transported more sand, and the median grain sizes of sand coarsened with increasing discharge. Higher sand concentrations, and coarser grain sizes with increasing discharge suggest that transport at RGV was primarily controlled by flow. Thus, sand transport at the two gages was controlled by different mechanisms (i.e. supply vs flow), and this is depicted in the different trends between sand concentration and the median grain size of sand in transport.

Sediment Dynamics During Dam Release Floods: Floods have been released annually from Luis L. Leon Dam since 2011. Here, we discuss some of the basic sediment-transport data from these releases. The first two dam release floods (2011 and 2012) were both of similar magnitude and duration; they were both between 50 and 70 m^3/s, and each lasted approximately 8-10 days (Figure 3a-b). The 2013 dam release flood (Figure 3c) consisted of three distinct pulses over the duration of approximately two and half months. The initial pulse was steady at approximately 180 m^3/s for approximately 15 days. The second pulse lasted approximately 10 days and peaked at 80 m^3/s, and the third pulse was steady at approximately 110 m^3/s for about 10 days. During each of the dam release floods, there were concurrent flash floods, indicated by the abrupt discharge spikes shown in Figure 3. These are not the same flash floods described in the previous section of this paper.

Trends in Suspended-Sediment Concentration and Grain Size During Dam Release Floods: Trends in sediment concentration and grain size for the three dam release floods provide insight into the relative supply of sediment near the sediment gages, and the evolution of the sediment supply over time. During the steady-state parts of each dam release, mean silt and clay concentrations were larger downstream at RGV compared to concentrations at Castolon (Figure 4a). The largest mean silt and clay concentrations occurred in 2012, and this was likely a result of the frequent 2012 flash flood activity that occurred before and during the dam release, thereby increasing the supply of silt and clay within the channel. The lowest mean silt and clay concentrations occurred during the largest and longest duration dam releases in 2013. The smaller silt and clay concentrations in 2013 indicate that the supply of readily-transportable silt and clay within the channel had been depleted over the longer duration of these dam releases.

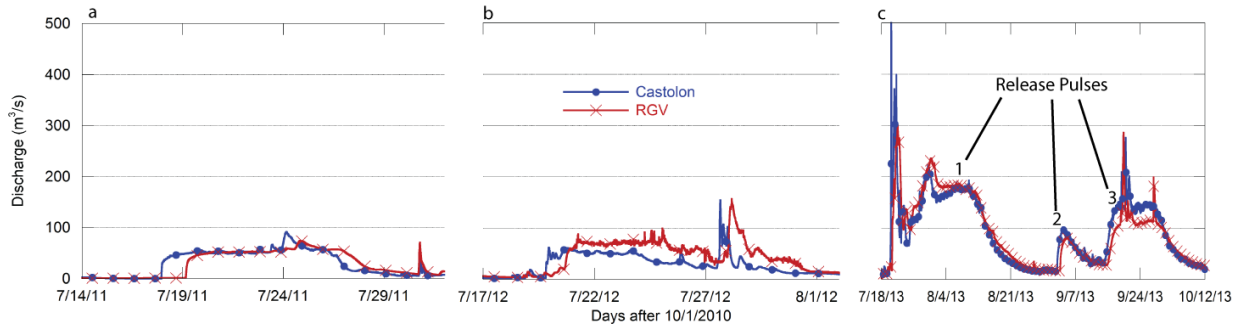

Figure 3 Luis L. Leon Dam releases in 2011 (a), 2012 (b), and 2013 (c).

The trends of sand transport during the dam releases were different than the trends in silt and clay transport. In 2011 and 2012, sand concentrations during the steady-state parts of the releases at the Castolon sediment gage were roughly twice as large as concentrations measured at the RGV sediment gage (Figure 4a). In 2011, the mean sand concentrations were approximately 60 mg/L at the Castolon gage, and 34 mg/L at the RGV gage. In 2012, mean sand concentrations were approximately 230 mg/L at the Castolon sediment gage and 125 mg/L at the RGV sediment gage.

Unlike during the 2011 and 2012 releases, mean sand concentrations during the 2013 release were higher at the RGV gage than at the Castolon gage (Figure 4a). During the steady-state part of pulse 1, mean sand concentrations at the Castolon sediment gage were approximately 550 mg/L, and mean sand concentrations were 650 mg/L at the RGV sediment gage. During pulse 2, mean sand concentrations were 160 mg/L at the Castolon sediment gage, and 175 mg/L at the RGV sediment gage (Figure 4a), and during pulse 3, mean sand concentrations were 257 mg/L at the Castolon sediment gage, and 475 at the RGV sediment gage. Although the error bars overlap in 2011, 2012, and pulses 1 and 2 of 2013, the general shift from higher upstream sand concentrations in 2011 and 2012 to higher downstream sand concentrations in 2013 is important because it provides insight into the evolution of the sand supply near each gage.

The average median grain sizes of suspended sand were generally much coarser at Castolon than at RGV (Figure 4b). Median grain sizes at the two sites were only similar during the 2012 dam release, and during pulse 3 of the 2013 dam release (Figure 4b). The finer median grain sizes at

Castolon in 2012, and during pulse 3 of 2013 may have been influenced by the flash flood activity that occurred coincidently with the releases. Thus, the channel was likely enriched with respect to the finer fractions of sand antecedent to these releases.

In 2011 and 2012, the larger concentrations of sand at Castolon indicate that there was a greater sand supply upstream of the sediment budget reach, and that sand supply was also generally coarser than the sand at the RGV gage (Figure 4). The increase in concentration over time at the RGV sediment gage indicates that the sand supply in the downstream portion of the budget reach became enriched with respect to the sand supply that existed in 2011 and 2012. The increase in downstream sand supply was likely caused by the frequent flash flood activity that occurred between the 2012 and 2013 releases, which would have loaded the channel with sediment prior to the 2013 release.

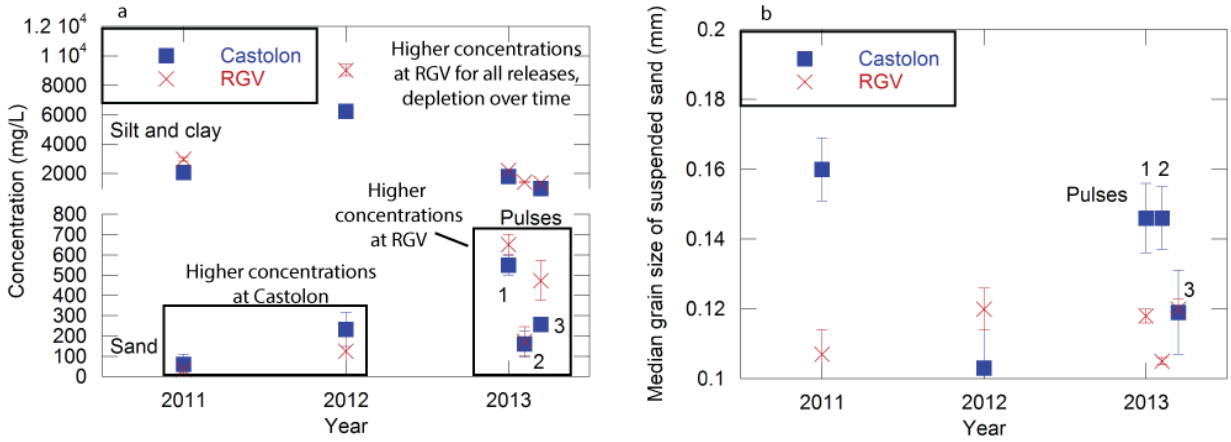

Figure 4 Mean sand concentrations (a) and median sand grain sizes (b) during the steady-state parts of the three dam release floods. Error bars represent 95 percent confidence intervals around the mean. For clarity, mean concentrations and median grain sizes were calculated without including the spikes in concentration during concurrent short-duration flash floods.

The long duration of the 2013 dam releases appears to have resulted in the partial depletion of transportable sand above the Castolon sediment gage. During the second and third pulses of the 2013 release, sand concentrations at the Castolon gage were much lower than concentrations during pulse one, which indicates that the sand supply was becoming depleted above/at the Castolon sediment gage, and erosion was occurring throughout the duration of the release. Sand concentrations during pulse 3 at RGV, however, were nearly as high as pulse 1 which indicates that erosion from upstream reaches was resulting in the enrichment of sand in the downstream parts of the budget reach.

Analyses of the Change in Sediment Storage During Managed Flows: Dam release floods have the potential to export sediment from the budget reach. The amount of export is controlled by the magnitude and duration of the releases, and the amount of sediment supplied from ephemeral tributaries. Analyses of the change in storage during the dam release floods show differing results over the three years; the central estimate of the silt and clay budget in 2011 was negative, while the central estimates of the silt and clay budgets in 2012 and 2013 were positive.

The central estimate of the change in storage for the silt and clay budget in 2011 indicates that 11,000 ± 25,000 metric tons of silt and clay were eroded from the budget reach (Figure 5a). A series of flash floods during the second half of the flood offset some of the export that occurred during the first half, and the uncertainty bands indicate that the silt and clay budget in 2011 was indeterminate (Figure 5a). During the steady-state part of the dam release flood, however, the silt and clay budget was clearly negative, which indicates that erosion was occurring throughout the duration of the release (Figure 5a). The central estimates of the change in the storage of silt and clay for the 2012 and 2013 dam release floods were both positive, yet the uncertainty bands indicate that the silt and clay budgets in these years were also indeterminate. Approximately 56,000 ± 244,000 metric tons of silt and clay accumulated during the 2012 release, and 250,000 ± 850,000 metric tons of silt and clay accumulated during the 2013 releases. Similar to the 2011 release, the estimate of the change in storage during the 'steady-state' parts of these releases do show that silt and clay was being eroded (Figures 5c, e). Flash flood activity during these floods, however, offset these negative changes in the budgets.

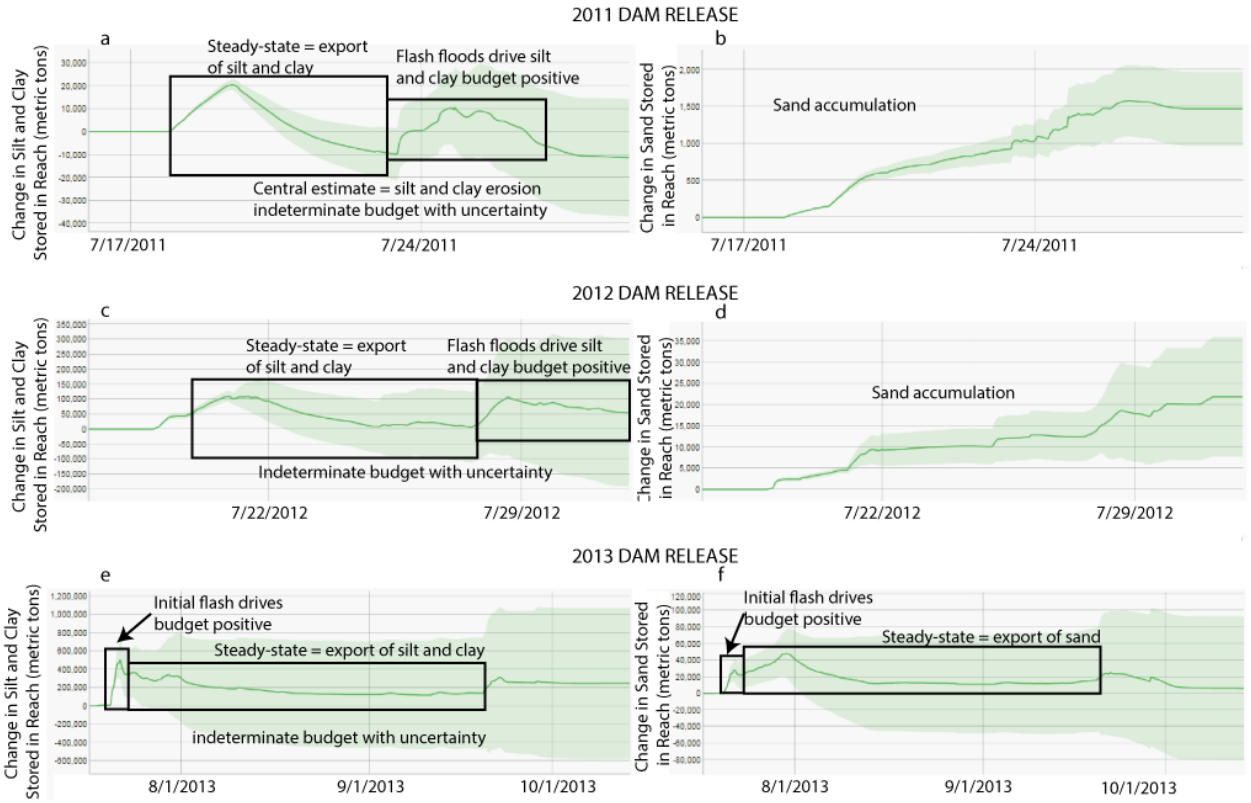

Figure 5 Changes in sediment storage for the 2011(a-b), 2012 (c-d), and 2013 (e-f) dam release floods.

Positive changes in the storage of sand occurred during the 2011 and 2012 dam release floods. In 2011, the budget reach accumulated 1,500 ± 500 metric tons of sand, and in 2012, the budget reach accumulated 21,000 ± 14,000 metric tons of sand. These changes were primarily driven by the much larger suspended-sand concentrations upstream at the Castolon sediment gage, thereby resulting in more sediment being transported into the budget reach than was exported. In 2013, the larger downstream sand supply, and the larger suspended-sand concentrations at RGV

relative to Castolon resulted in a sediment budget that was much less positive compared to 2011 and 2012 (6,400 ± 86,600 metric tons), and the 2013 sand budget was indeterminate. Although many of the sediment-budget predictions were indeterminate during the dam release floods, general trends in the central estimate of the change in storage offer important insights into the erosion and deposition patterns during these releases. Additionally, specific trends in concentration and median grain size obtained from the acoustic data help corroborate these trends.

CONCLUSIONS

The Rio Grande in the Big Bend region is in a stage of channel contraction following the 2008 channel resetting flood. Channel contraction occurs through the accumulation of sediment within the channel, and on bars and floodplains. The sediment responsible for this contraction is largely supplied by tributary-derived flash floods during the summer thunderstorm season. Continuous suspended-sediment monitoring at two sites on the Rio Grande has provided the ability to constrain the sediment contributions during tributary floods, and evaluate the impacts of long-duration dam release floods in alleviating the degree of tributary-sourced sediment loading that occurs.

Although the general sediment conditions on the Rio Grande consist of sediment surplus, periods of sand supply limitation can persist in downstream reaches after channel reset floods until the tributary sediment supply overwhelms the enlarged channel. Sand supply limitation was observed during the dam release floods in 2011 and 2012 whereby sand concentrations were much higher upstream at the Castolon sediment gage compared to the RGV gage downstream. Frequent summer storm activity, and associated flash floods, resulted in increases in the downstream sand supply by 2013. This increase in the downstream sand supply was apparent during the 2013 dam release because suspended-sand concentrations were larger in downstream reaches compared to upstream reaches for the same discharges. Continuous 15-minute sediment transport measurements provided the means for identifying these temporal changes in supply.

Analyses of suspended-sediment transport during long-duration dam releases shows that during the steady-state parts of these releases, sediment is evacuated from the sediment budget reach. This is corroborated by the decrease in sand concentration at the upstream gage for the same discharges during the 2013 dam release, the negative changes in the storage of silt and clay during the steady-state parts of the dam releases, and the decline in suspended sediment concentrations throughout the duration of the 2013 dam release. However, the amount of sediment evacuated during steady-state dam releases may be completely offset by sediment contributions from just a few flash floods. Therefore, larger or longer duration dam releases than those observed during the 2010-2013 period of this study are likely required to result in net sediment evacuation, channel enlargement, and habitat maintenance.

ACKNOWLEDGEMENTS

This study was funded by the NPS, USGS, and the Commission of Environmental Cooperation. Thanks to Joe Sirotnak, Phil Wilson, Billie Brauch, David Larson, Keith Sauter and the NPS

River Rangers at Big Bend National Park. Special thanks to Hunter Edwards, Jeff Kelsch, Jeff Renfrow, Kelon Crawford, Dana Milani, and Trevor Bryan for their endless days in the field.

REFERENCES

Colby, B. R. (1963). "Fluvial sediments--a summary of source, transportation, deposition, and measurement of sediment discharge," U.S. Geological Survey Bulletin, 1181-A, 47.

Dean, D. J., and Schmidt, J. C. (2011). "The role of feedback mechanisms in historic channel changes of the lower Rio Grande in the Big Bend region," Geomorphology, 126(3), pp 333-349.

Dean, D. J., Scott, M. L., Shafroth, P. B., and Schmidt, J. C. (2011). "Stratigraphic, sedimentologic, and dendrogeomorphic analyses of rapid floodplain formation along the Rio Grande in Big Bend National Park, Texas," Geological Society of America Bulletin, 123(9-10), pp 1908-1925.

Dean, D. J., and Schmidt, J. C. (2013). "The geomorphic effectiveness of a large flood on the Rio Grande in the Big Bend region: Insights on geomorphic controls and post-flood geomorphic response," Geomorphology, 201, pp 183-198.

Dinehart, R.L. (1998). "Sediment transport at gaging stations near Mount St. Helens, Washington, 1980-90. Data collection and analysis," U.S. Geological Survey Professional Paper, 1573, 105 p.

Edwards, T. K., and Glysson, G. D. (1999), "Field methods for measurement of fluvial sediment," Techniques of Water-Resources Investigations of the U.S. Geological Survey, Book 3, Chapter C2, edited, 89 p.

Guy, H. P. (1970). "Fluvial sediment concepts," Techniques of Water-Resources Investigations of the U.S. Geological Survey, Book 3, Chapter C1, 55p.

Heidel, S. G. (1956). "The progressive lag of sediment concentration with flood waves," American Geophysical Union Transactions, 37(1), pp 56-66.

Kleinhans, M.G., Wilbers, A.W.E., and ten Brinke, W.B.M. (2007). "Opposite hysteresis of sand and gravel transport upstream and downstream of a bifurcation during a flood in the Rhine River, the Netherlands," Netherlands Journal of Geosciences, 86(3), pp. 273-285.

Porterfield, G. (1972). "Computation of fluvial sediment discharge," U.S. Geological Survey Techniques of Water-Resource Investigations, Book 3, Chapter C3, 66p.

Rubin, D. M., and D. J. Topping (2001). "Quantifying the relative importance of flow regulation and grain size regulation of suspended sediment transport α and tracking changes in grain size of bed sediment β," Water Resources Research, 37(1), 133-146.

Topping, D. J., Rubin, D. M., and Vierra, L. E. (2000a). "Colorado River sediment transport: 1. Natural sediment supply limitation and the influence of Glen Canyon Dam," Water Resources Research, 36(2), pp 515-542.

Topping, D. J., Rubin, D. M., Nelson, J. M., Kinzel, P. J. and Corson, I. C. (2000b). "Colorado River sediment transport: 2. Systematic Bed-elevation and grain-size effects of sand supply limitation," Water Resources Research, 36(2), pp 543-570.

Topping, D. J., Melis, T. S., Rubin, D. M., and Wright, S. A. (2004). "High-resolution monitoring of suspended-sediment concentration and grain size in the Colorado River in Grand Canyon using a laser acoustic system," in Proc. of the 9th International Symposium on River Sedimentation, Yichang, People's Republic of China, 2004, edited by C. Hu and Y.Tan, pp 2507-2514.

Topping, D. J., Wright, S. A., Melis, T. S., and Rubin, D. M. (2007). "High-resolution measurements of suspended-sediment concentration and grain size in the Colorado River in Grand Canyon using a multi-frequency acoustic system," in Proc. of the 10th International Symposium on River Sedimentation, Moscow, Russia, 2007, August 1-4, 2007, pp 330-339.

Topping, D.J., Rubin, D.M., Wright, S.A., and Melis, T.S. (2011). "Field evaluation of the error arising from inadequate time averaging in the standard use of depth-integrating suspended-sediment samplers," U.S. Geological Survey Professional Paper, 1774, 95 pp.

Topping, D.J., Wright, S.A., Griffiths, R.E., Dean, D.J. (2015). "Physically based method for measuring suspended-sediment concentration and grain size using multi-frequency arrays of acoustic-Doppler profilers," in Proc. of the 3rd Joint Federal Interagency Conference, Reno, Nevada, April19-23, 2015.

PRELIMINARY ANALYSIS OF SUSPENDED SEDIMENT RATING CURVES FOR THE KALAMAZOO RIVER AND ITS TRIBUTARIES FROM MARSHALL TO KALAMAZOO, MICHIGAN

David T. Soong, USGS, 405 N. Goodwin Ave., Urbana, Illinois, dsoong@usgs.gov; Christopher J. Hoard, USGS, 6520 Mercantile Way, Lansing, Michigan, cjhoard@usgs.gov; Faith A. Fitzpatrick, USGS, 8505 Research Way, Middleton, Wisconsin, fafitzpa@usgs.gov; Ronald B. Zelt, USGS, 5231 S. 19th Street, Lincoln, Nebraska, rbzelt@usgs.gov

ABSTRACT: Suspended sediment concentration (SSC) rating curves for the Kalamazoo River and its tributaries from Marshall to Kalamazoo, Michigan, U.S.A., were developed based on measured data. The slopes of the at-site SSC rating curves were of two general types: either increasing or decreasing with increasing discharges. By examining the basin characteristics and flow patterns, streams with negative SSC rating curve slopes were associated with groundwater-dominated streams and those with positive slope terms were associated with surface-water dominated streams. A panel regression with fixed-effects analysis was applied to the pooled at-site data according to various grouping criteria. The results from the subgroups which considered groundwater and surface-water dominance, seasonality, and dam effects showed better fit than the at-site SSC rating curves did. It was assumed that the rating curve slopes for sites in each subgroup were the same but their intercepts varied from site to site. The groundwater and surface-water dominance division was used as the basis for estimating SSC at ungaged sites. The study was conducted as a component of hydrodynamic modeling under the Enbridge Line 6B pipeline oil-spill recovery activities.

INTRODUCTION

Background: The July 25, 2010 oil spill that occurred near Kalamazoo, Michigan, was one of the largest oil spills into freshwater in North American history. The Enbridge Line 6B pipeline released approximately 843,000 US gallons of dilbit (http://www.epa.gov/enbridgespill/, accessed February, 2013), which is bitumen diluted with natural gas condensate, into a wetland draining to Talmadge Creek and then to the Kalamazoo River downstream from Marshall, Michigan. The spill impacted 38 miles of the waterway. Less than a month after the spill, the dilbit submerged, likely because of mixing and forming aggregates with fine-grained particles of mineral sediment and organic matter (Dollhopf et al., 2014). The large quantity of oil released required the development and implementation of new approaches for detection and recovery of submerged oil and oil-particle aggregates (OPAs) (Dollhopf et al., 2014). Fitzpatrick et al. (this volume) provided a detailed overview of the hydrodynamic modeling work that was done for the spill response. The modeling, which started in 2011 and continued into 2014, helped to answer questions about the fate and transport of the remaining submerged oil in the Kalamazoo River, and whether the oil would be transported out of the Morrow Lake delta and past Morrow Dam. To establish hydrodynamic model boundary conditions suspended sediment samples were collected from the oil-affected reach for analysis of suspended sediment concentrations and loads. This paper describes the challenges encountered in the development of rating curves for estimating the suspended sediment concentrations (SSC) for the hydrodynamic models used to predict the movement of sediment and OPA.

Study Reach: The study reach extended 38 miles from the site of the pipeline spill at Talmadge Creek downstream to the confluence with the Kalamazoo River, and downstream on the Kalamazoo River to Morrow Dam (Fig. 1). Some of the tributaries included in the study are too small to identify in figure 1 but are listed in table 1. Table 1 is a list of study reaches from the upstream to downstream direction together with their drainage areas and streamflow gage status.

Suspended Sediment Rating Curve: A water discharge (Q_w) to suspended sediment concentration (SSC) rating equation is referred to as an SSC rating curve in this paper. An SSC rating curve commonly takes the simple log-linear form as:

$$\log_{10}(SSC) = a + b \times \log_{10}(Q_w) + \varepsilon \quad (1)$$

where:

$\log_{10}(SSC)$ = the $\log_{10}$ transformed SSC, in milligrams per liter (mg/l),
$\log_{10}(Q_w)$ = the $\log_{10}$ transformed Q_w at the time of SSC measurement or estimation, in cubic feet per second (cfs),
a is the intercept and b is the slope of the linear regression, and
ε is an error term.

The SSC rating curve has been widely used for estimating SSCs in rivers at similar flow conditions (Colby, 1956; Porterfield, 1972). However, when applying the ordinary least-squares (OLS) method to estimate the regression equation parameters based on the logarithms of measured SSC and Q_w, the resulting equation may underestimate SSC at high flows (Ferguson, 1986; Singh and Durgunoglu, 1989). Some authors (for example, Asselman, 2000) have proposed using nonlinear least-squares regression to mitigate this potential underestimation. Transforming $\log_{10}$(SSC) back to SSC can introduce a bias and Helsel and Hirsch (1992) recommend addressing the bias by using the Smearing estimator.

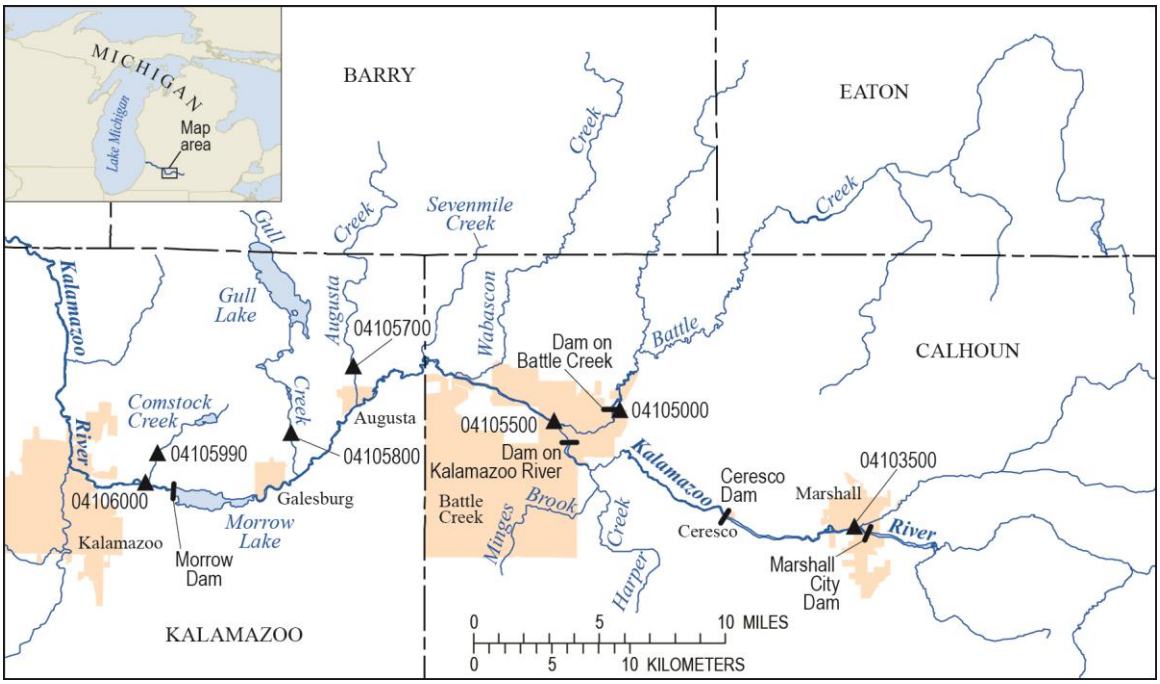

Figure 1 Diagram showing the study reach in the Kalamazoo River Basin.

Developing an SSC rating curve is challenging because SSC samples are typically limited in number and scattered around the rating curve. Scatter contributes to uncertainty of derived rating curves (Porterfield, 1972). Glysson (1987) illustrated many possible causes that could lead to variability in rating curves, such as seasonality and asynchrony of sediment peaks in relation to discharge peaks. Colby (1956) discretized the rating curve with partial-year records when seasonal variations were obvious. Different SSC values could be expected at equivalent Q_w in the rising and falling limbs of a storm hydrograph (hysteresis effect) (Ahanger et al. 2013; Baca, 2008). Considerations for deriving a meaningful at-site SSC rating curve may include (1) the coverage of the ranges of discharge and SSC to be estimated (that is, avoid extrapolation beyond the range of measured data), (2) the amount of measured data at specific flow ranges of interest for an application, and (3) exclusion of extreme sediment-transport rates from mixed populations of sediment-production processes (such extremes might occur after a dredging or dam removal).

Physiography and human activity (such as roads and structures) are common factors in the sediment concentration regimes. With the sediment availability and delivery governed by watershed and channel (hydraulic) characteristics, the parameters a and b (equation 1) are unique at individual sites. There have been

attempts to attribute physical meaning to the parameters *a* and *b*. For example, Morgan (1995) considered that the intercept, *a*, represents an index of erosion severity, and slope parameter *b* indicates the extent to which new sediment sources become available as discharge increases. Based on sediment characteristics in the Lower Yellow River, Mai et al. (1990) interpreted *a* to characterize the boundary conditions, such as the incoming sediment composition, and *b* to characterize the sediment carrying capacity. Asselman (2000) did not find these parameters to have any physical meaning.

Table 1 Rivers included in the study and their drainage areas and streamflow gage status in upstream to downstream order. Drainage areas for ungaged locations are calculated at the confluence with the Kalamazoo River.

Station Number or Ungaged	***Site Name***	***Drainage Area, mi^2***
04103500	Kalamazoo River at Marshall, MI	449
Ungaged	Talmadge Creek, MI	3.3
Ungaged	Bear Creek, MI	14.8
Ungaged	Minges andHarper Creek, MI	54.9
04105000	Battle Creek at Battle Creek, MI	241
04105500	Kalamazoo River near Battle Creek, MI	824
Ungaged	Wabascon Creek, MI	43.1
Ungaged	Sevenmile Creek, MI	16.4
04105700	Augusta Creek near Augusta, MI	38.9
04105800	Gull Creek at 37th Street near Galesburg[1], MI	38.1
04105990	Comstock Creek at E. Main Street near Kalamazoo[2], MI	18.3
04106000	Kalamazoo River at Comstock, MI	1,100

1. Gull Creek at 37th Street near Galesburg (04105800) has daily streamflow records between 10/01/1964 and 02/02/1973.
2. Comstock Creek at E. Main Street near Kalamazoo (04105990) has 28 field discharge measurements between 02/06/1964 and 09/03/2002.

MEASURED DATA AND ASSESSMENT

Data collected during the project: The USGS collected SSC data in August 2012, January through April 2013, and in March 2014. For each round of water samples, SSC samples were collected at five gaged sites (table 2) in the study reach. Samples were not collected at the two historical gage sites on Gull and Comstock Creeks.

Table 2 Description of data collection stations and suspended-sediment data availability

Station Number	***Site Name***	***Number of Project samples***	***Number of Historical samples***
04103500	Kalamazoo River at Marshall, MI	6	0
04105000	Battle Creek near Battle Creek, MI	6	0
04105500	Kalamazoo River near Battle Creek, MI	6	0
04105700	Augusta Creek near Augusta, MI	6	4
04105800	Gull Creek at 37th Street near Galesburg, MI	0	4
04105990	Comstock Creek at E. Main Street near Kalamazoo, MI	0	4
04106000	Kalamazoo River at Comstock, MI	6	4

Historical data: SSC data collected in the mid-1980s from 29 sites covering the main stem and tributaries of the Kalamazoo River were retrieved (C. Hoard, USGS, written communication, February, 2013). Four of the 29 sites are in the study reach and each of the four sites has four samples. Table 2 summarizes the sites and SSC data points available for the study and table 3 lists the data. Hereafter, the gaged sites will be referred to by their station numbers.

Table 3 List of available suspended sedimentation concentrations (milligrams per liter, mg/l) according to the location, date, discharge (in cubic feet per second, cfs), and water temperature (in Celsius). [SSC: suspended sediment concentration]

Station Number	Sample Date	Instantaneous discharge, in cfs	SSC, in mg/l	Water Temperature, in ℃
04103500	8/16/2012	243	20	21.72
04103500	1/15/2013	422	23	1.3
04103500	2/1/2013	575	18	0.11
04103500	3/18/2013	259	51	3.15
04103500	4/22/2013	1150	25	11.18
04103500	3/31/2014	826	27	7.0
04105000	8/16/2012	57	9	20.34
04105000	1/15/2013	273	8	0.67
04105000	2/1/2013	398	17	0.06
04105000	3/18/2013	422	45	1.48
04105000	4/22/2013	1410	48	9.07
04105000	3/31/2014	937	23	3.2
04105500	8/16/2012	436	23	21.02
04105500	1/15/2013	813	22	0.87
04105500	2/1/2013	1500	29	0.03
04105500	3/18/2013	1040	48	2.42
04105500	4/22/2013	3000	91	9.1
04105500	3/31/2014	2060	14	5.1
04105700	8/1/1986	39	35	20.5
04105700	10/7/1986	104	7	10.5
04105700	6/15/1987	27.3	44	21.2
04105700	9/91987	28	45	18
04105700	8/16/2012	24	20	18.1
04105700	1/15/2013	46	18	0.22
04105700	2/1/2013	111	14	0.1
04105700	3/18/2013	37	24	2.85
04105700	4/22/2013	89	22	8.7
04105700	3/31/2014	75	6	4.7
04105800	7/31/1986	47	6	27
04105800	10/7/1986	102	3	15.5
04105800	6/15/1987	15.4	8	27
04105800	9/9/1987	30.7	5	24
04105990	7/31/1986	7.6	3	25.5
04105990	10/71986	19.5	3	17
04105990	6/15/1987	4.54	5	30
04105990	9/9/1987	6.24	1	25
04106000	7/31/1986	778	8	26
04106000	10/9/1986	3100	7	13.5
04106000	6/17/1987	580	11	27
04106000	9/11/1987	762	39	22
04106000	8/16/2012	445	18	22.5
04106000	1/15/2013	1210	22	2.2
04106000	2/1/2013	2090	9	0.1
04106000	3/18/2013	1440	31	2.6
04106000	4/22/2013	3750	74	8.2
04106000	3/31/2014	2290	5	5.0

Timing of collected data: The SSC data were collected near the storm peaks or slightly afterward during the falling limbs of the hydrograph (Fig. 2). The magnitudes of SSC collected on March 31, 2014 were much lower than those for samples collected previously. As part of the oil-mitigation work, sediment from the channel upstream of the Ceresco Dam, located approximately 3.75 miles downstream from the confluence of Talmadge Creek and the Kalamazoo River, was dredged and removed. Additionally, the channel was shaped to a wide floodplain channel and the Ceresco Dam (near Ceresco in Fig. 1) was notched in October 2013. Because of this dredging and channel alteration, the March 31, 2014 SSC data at sites 04105500 and 04106000 were not included in this analysis.

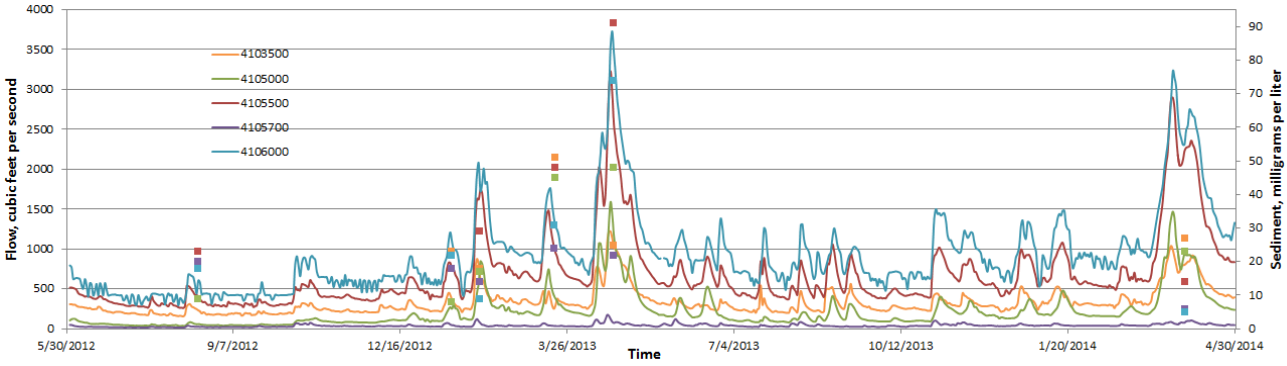

Figure 2 Timing of suspended sediment concentration data collection in relation to flow from June 1, 2012, to April 30, 2014. (Solid lines represent the hydrographs and dots show suspended sediment concentrations.)

Flow regimes of collected data: Both project and historical SSC data are plotted in relation to the flow duration curves (FDCs) to determine how well they represented the full streamflow regime. The FDCs were developed using mean-daily streamflow records from water years (WY) 2001 to 2014. The flow exceedance probability used for plotting the SSC data was computed based on the instantaneous discharge reported with each sample, assuming the differences between mean daily discharge and instantaneous discharge are not appreciable. The SSC data spanned a wide range of flow duration at each site (Fig. 3).

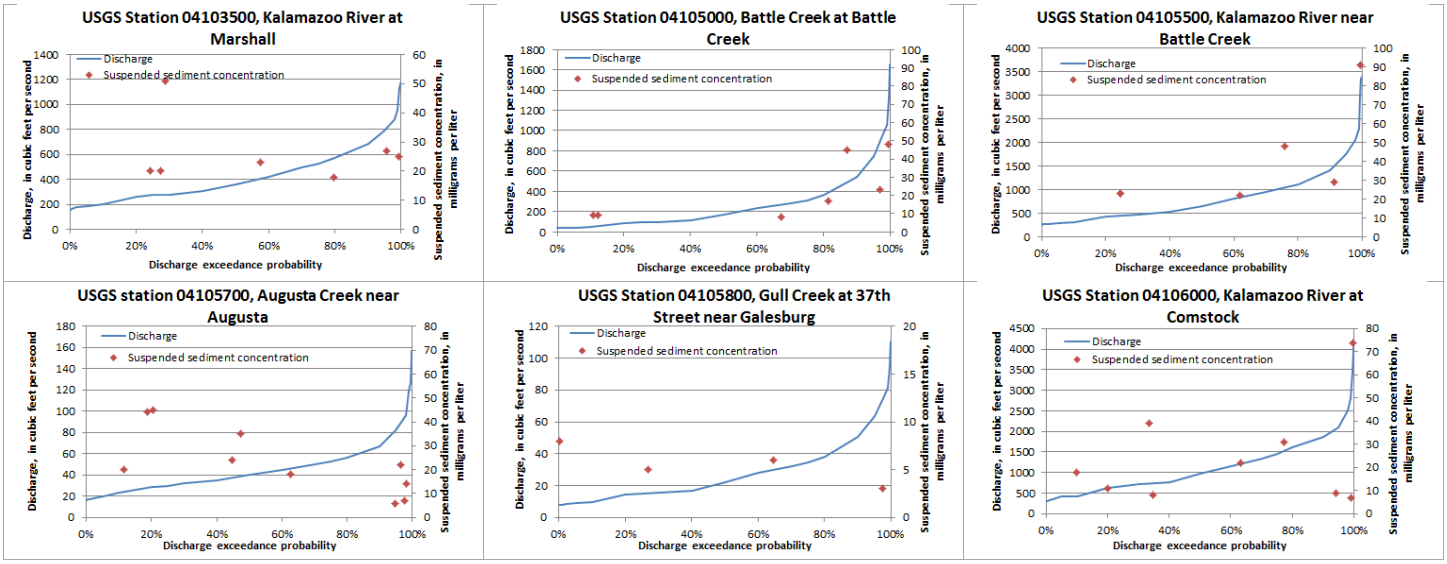

Figure 3 Coverage of suspended sediment concentration data in relation to discharge exceedance probability (flow-duration curve). Note as discussed in the "Timing of Collected Data" section, the March 31, 2014 SSC data at Kalamazoo River near Battle Creek (04105500) and Kalamazoo River at Comstock (04106000) were not included in this analysis.

The FDC for site 04105990 was not developed because the site has only 28 historical miscellaneous streamflow measurements. However, based on the 28 streamflow measurements, the range of flows for Comstock Creek is from 1.76 to 19.5 cfs, and the SSC measurements are considered to have covered the range of flows reasonably well.

AT-SITE SSC RATING CURVES AND SITE CHARACTERISTICS

At-site SSC rating curves: Figure 4 shows log-log plots of Q_w and SSC data for each site, along with the rating curve obtained from OLS regression. All data except for the two samples collected on March 31, 2014 at sites 04105500 and 04106000, were used in developing the at-site rating curves. Each at-site SSC rating curve was obtained from OLS regression between all remaining $\log_{10}(Q_w)$ and $\log_{10}(SSC)$ data pairs. Although the dataset sizes were limited, the trend of the resulting rating curves was considered representative because the sampled SSC data spanned much of the respective FDCs.

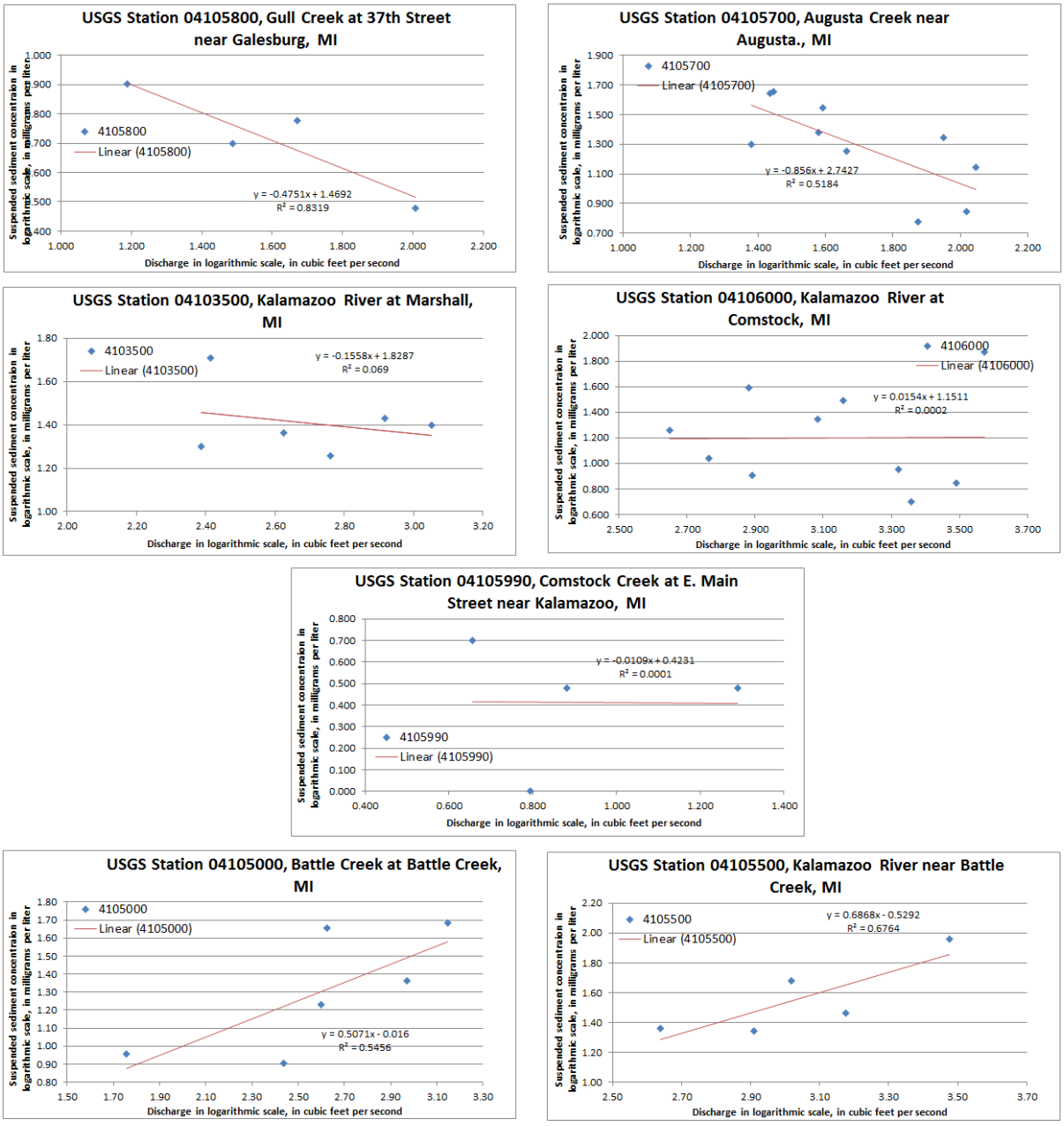

Figure 4 Relations of suspended sediment concentration (SSC) to discharge (Q_w) in logarithmic plots and SSC rating curves developed for seven study sites. [y stands for $\log_{10}$SSC, x stands for $\log_{10}Q_w$, and R^2 is the coefficient of determination]

The regression analysis resulted in negative SSC-rating slope estimates at sites 04105700 and 04105800; and weakly negative slopes at sites 04103500 and 04106000. In contrast, the positive slope estimates at sites 04105000 and 04105500 are more typical, in that SSC increases as Q_w increases (Porterfield, 1972). The SSC-rating slope at site 04105990 is difficult to assess with the scatter in the limited data points. Physically, decreasing SSC at increasing Q_w indicates that either the amount of sediment supply is similar at all flow rates, exhausted after early season flushing, or became supply-limited after the early part of each hydrograph pulse; or the transport of sediment is limited because of hydraulic carrying capacities. To understand whether the sediment transport is supply-limited or transport-limited, additional information on the amount and particle sizes of sediment is needed for analysis. The challenges to resolve for the present study are to: (1) use the available samples to improve the at-site analysis, and (2) use the at-site results to estimate SSC at ungaged locations.

Temperature effect on SSC: Some of the SSC data were collected between January and March at water temperatures between 5°C and 0°C and their values were higher than other samples collected at those sites in warmer weather (table 3). Barton and Albertson (1953) experimentally demonstrated that the depth-averaged SSC increases with a decrease in water temperature, and Colby (1956) documented that for finer sediment in the size range from 0.016 to 0.062 millimeter, there was a 57 percent increase in SSC as temperature dropped from 80 °F (26.7°C) to 40 °F (4.4°C). Plots made of the two subsets of the at-site data--those with water temperature above 5°C, and those with water temperature below 5°C--suggested a seasonal effect may exist in the study area as indicated by the different rating slopes in the two subsets at sites with adequate data.

Dam effects versus free-flowing reaches: There are several transverse (across the river) structures in the study reach including decommissioned dams (upper structure removed), a low-head dam, and hydropower dams. These transverse structures slow current velocity and cause coarse-grained sediment to settle. Depending on the incoming flow and incoming sediment magnitudes and particle sizes, in general the run-of-river conditions in these impoundments will not prevent fine sediment from being transported downstream. Therefore, SSC measured downstream from some of these dams could rise rapidly when streamflow increases from low to high discharges (i.e., a steeper rating-curve slope). In free-flowing channels, sediment deposits along the low-gradient reaches can produce similar effects. At regulated sites, the incoming flows and dam operations at the time of measurements can alter the relation between measured SSC and flow.

Among the gaged sites, the Kalamazoo River at Marshall and the Kalamazoo River at Comstock are located downstream from hydropower dams. Marshall has a small hydropower station by its dam that receives water from the Marshall pool through a side-channel. About 8 miles downstream from Marshall is a decommissioned dam at Ceresco. The operational rules at Morrow Dam are designed to release the amount of discharge flowing into its pool, as estimated from flows reported at the Kalamazoo River near Battle Creek gage, when discharges are above 1,000 cfs. Battle Creek is one of the largest tributaries of the Kalamazoo River, and the gage at Battle Creek at Battle Creek is located about 2.9 miles upstream from a low-head dam. Also, the gage on the Kalamazoo River near Battle Creek is located about 0.35 miles downstream from the low-head dam on Battle Creek.

Monthly hydrographs: Mean monthly streamflow hydrographs for six of the gaged sites are presented in figure 5 using data from water years (WYs) 1987 to 2011 except for the Gull Creek site, which used data from WYs 1964 to 1972. In general, streamflow rises from base flow in October to annual peaks in March or April, and then declines through August and remains low through September. Hydrograph bars in figure 5 are coded with two colors; the orange bars are those whose hydrograph patterns are clear and with low base flows in August to October; the blue ones are those with comparatively higher base-flow magnitudes and with monthly volumes fluctuating in the higher discharge period (signifying greater groundwater and surface water exchange). The hydrographs with blue bars are also associated with sampling sites that have negative SSC-rating-curve slopes. The monthly discharges were graphed using per unit area values, and it was observed that peak magnitudes for those coded with blue generally have lower values than those that are coded with orange.

Watershed and stream characteristics: Watershed characteristics such as the basin relief and geology (soil erodibility and permeability, and sediment delivery and storage), geomorphology of the channel (channel

sinuosity, narrow or floodplain channels, bank and bed erodibility), and land-cover changes are factors affecting sediment yield from a watershed. On a large scale, most of these factors are also affecting streamflow from the watershed. Therefore, the streamflow patterns can serve as a surrogate for analyzing the sediment yields. On this basis, the watershed and stream characteristics that could serve as indictors for explaining SSC rating curves at the gaged sites and help extending the results of gaged sites to ungaged sites were sought.

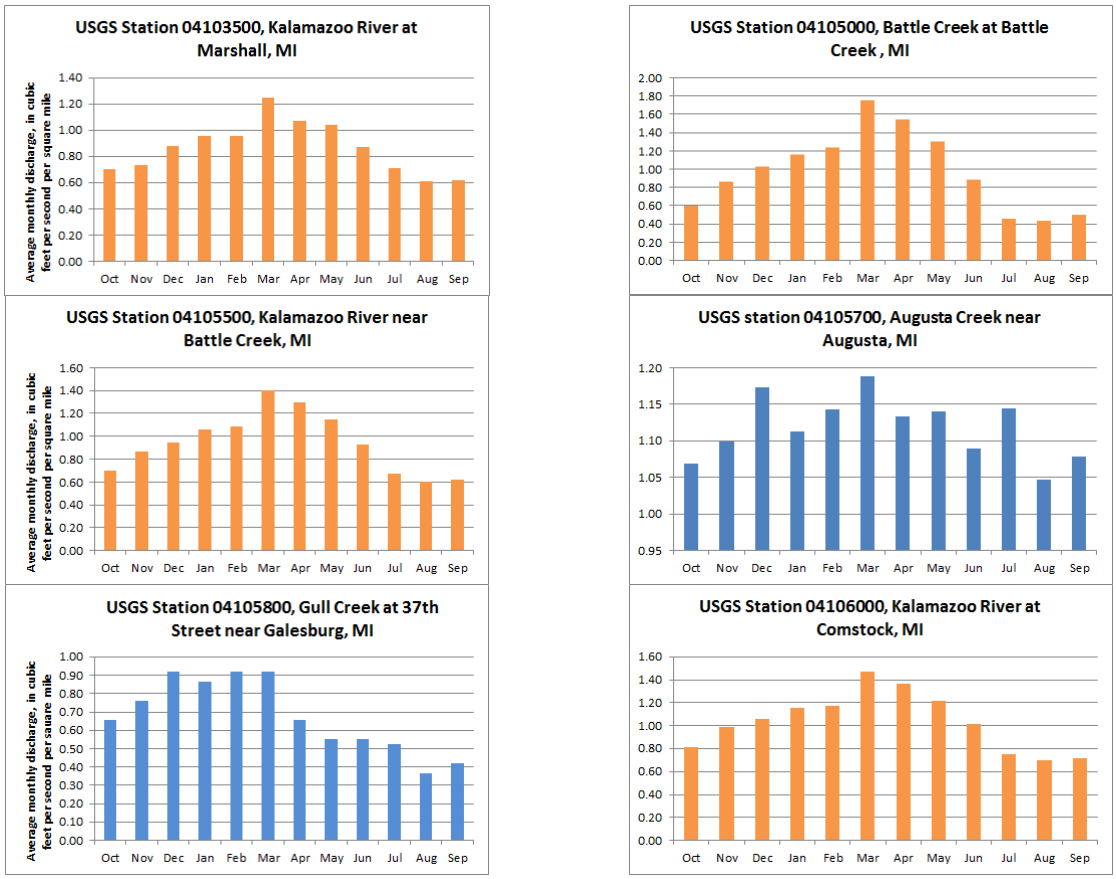

Figure 5 Mean monthly streamflow hydrograph patterns for sites in the study reach that have suspended sediment samples. Hydrographs coded in orange are considered to have clear yearly seasonal rising and falling patterns and with low base flows in August to October; those coded in blue have comparatively higher base-flow magnitudes and large monthly volumes fluctuations in the remaining months. Statistics were computed for water years (WYs) 1987 to 2011 except for the Gull Creek site, which used data from WYs 1964 to 1972.

Wesley (2005) used a "flow stability" index to classify the streamflow patterns of a watershed. A stream with more stable flows is characterized by lower peak flows and higher base flows than a stream with less stable flows. One component of the flow stability index (Wesley 2005) was the ratio of mean high flow to mean low flow. The dominance of stable streams (streams with low flow stability ratios) is mainly due to abundance of permeable surficial soils and geology, which promote groundwater inflow and outflow (Wesley, 2005). Groundwater dominated streams generally have cooler water temperatures than surface-water dominated streams. Surface-water dominated streams generally have relatively warmer water temperatures and higher flow-stability ratios because of faster responses to rainfall or snowmelt than groundwater dominated streams (Wesley, 2005). Less permeable soils, land-use changes (agriculture or development of less pervious surfaces), and channelization contribute to higher stream flow stability ratios. However, wetlands and lakes, wide floodplains that create channel storage also contribute to low flow-stability ratios. Wesley (2005) suggested that a ratio between 1.0-2.0 indicates a typical self-sustaining cold-water trout stream, between 2.1-5.0 indicates warm-

water streams, between 5.1-10.0 indicates somewhat flashy warm-water rivers, and >10.0 represents very flashy warm-water rivers.

Relevant characteristics found in Wesley (2005) for describing the watershed and stream and the flow-stability index of the gaged and ungaged sites in the study reach are presented in table 4. The high urban land cover in the Comstock Creek watershed might have caused the inconsistency in SSC data collected at the Comstock Creek site. For sites where such information is unavailable, the stream temperature class, defined as cold- or warm-water as described in Wesley (2005), is used as the indicator. A cold-water stream (groundwater dominated) has a low flow-stability index and the annual hydrographs are typical of those coded in blue in figure 5; the warm-water streams (surface-water dominated) have more diverse flow-stability indexes and annual flow patterns, most likely due to channel patterns.

Table 4 Watershed and stream characteristics and flow stability index for study sites along the main stem and tributaries used in hydrodynamic modeling work. [GW: groundwater; SW: surface water]

River Reach	***Stability Index***	***Watershed and stream characteristics (Wesley, 2005)***	***Classification***
Marshall pool above the Marshall Dam on the Kalamazoo River at Marshall, MI	4.4	Heavily influenced by inflows from Rice Creek, which is groundwater dominated and comes in from upstream of the Marshall Dam. The measurement site is downstream of Marshall Dam.	Mixed
Talmadge Creek, MI	N/A	A cold-water stream; with gravel and coarse sand substrate.	GW dominated
Bear Creek, MI	N/A	A cold-water stream, having gravel and cobble substrate.	GW dominated
Minges and Harper Creek, MI	N/A	A cold-water stream.	GW dominated
Battle Creek, MI	7.0	A surface-water dominated stream, has channelization near the mouth, drainage includes urban area; located at upstream of Battle Creek Dam.	SW dominated
Kalamazoo River above the junction with Battle Creek, MI	3.4	Located downstream of Battle Creek Dam which is an urban area.	SW dominated
Wabascon Creek, MI	N/A	A warm-water stream. Drains a mixture of moderate-relief plains. Flows through several lakes and swamps.	Mixed
Sevenmile Creek, MI	1.6	A cold-water stream; substrate features gravels overlain by sand.	GW dominated
Augusta Creek, MI	2.2	A cold-water stream; features a series of wetlands and reservoirs. The substrate dominated with gravel and cobbles.	GW dominated
Gull Creek, MI	N/A	A warm-water stream. Gull Lake is located at headwater and Gull Creek flows through several lakes and swamps. Substrate: gravel and cobble.	Mixed
Comstock Creek, MI	N/A	A warm-water stream, drains through a few small lakes. 85 percent is in an urban area.	Mixed
Kalamazoo River near Comstock, MI	2.9	Located downstream of Morrow dam, whose release has been controlled by gates and turbine operations.	Regulated

DEVELOPING SSC RATING CURVES FOR GAGED AND UNGAGED SITES

Supplemental measures to improve the accuracy of at-site SSC rating curves are needed because of the small number of samples collected at each site. Furthermore, the distinctive SSC rating slopes could be caused by effects of water temperature, dam, and watershed and stream characteristics individually or in combination. The modeling challenges include determining the at-site SSC rating curves by incorporating these factors and then estimating SSCs for the ungaged sites.

Panel regression with fixed-effect analysis for gaged sites: The SSC data presented in table 3 were pooled as panel data for regression analysis, and the fixed-effects model was applied to analyze the panel data. Data were grouped in the analysis according to the causative factors: dammed or free-flowing reaches, winter or non-winter seasons, and surface-water or groundwater dominated watersheds. An assumption made was that the slope parameter *b*-the sediment source term-was similar for sites in each of the five subgroups, but the intercept, parameter *a*, varied from site to site. The assumption was based on reasoning that the magnitude of SSC is a function of channel erosive power and conveyance capacity. The following five subgroupings were tested and the goodness of fit between measured and estimated SSC was evaluated using the quantitative statistics presented in table 5.

- Group 1: Results from at-site linear regression analysis; i.e., no groups, no panel regression. This is the baseline condition.
- Group 2: The free-flowing and dammed reaches partition. Sites 04105700, 04105800, and 04105990 belong to the free-flowing reaches, and sites 04103500, 04105000, 04105500, 04106000 belong to the dammed reaches.
- Group 3: The groundwater and surface-water dominated reaches partition. Sites 04105000 and 04105500 belong to the surface-water dominated group, the remaining 5 sites belong to the groundwater-dominated group.
- Group 4: A further partition of Group 3 into winter (January through March) and non-winter months (the rest of the year).
- Group 5: Similar to Group 4, but the at-site SSC rating curve is used for site 04103500 and this site is not used in the panel analysis. An additional constraint is imposed at site 04106000: when Qw <= 1000 cfs (up to four turbines opened) the data are classified under groundwater-dominated stream (the dam effectively traps sediment), and when Qw is larger than 1000 cfs, the data are classified under surface-water dominated streams.

Table 5 Quantitative statistics of estimated suspended sediment concentrations for the five groupings studied. [R^2, coefficient of determination; PBIAS: ratio of deviation of simulated from measured data; NSE: Nash-Sutcliffe efficiency; and RSR: ratio of the root-mean-square error to the standard deviation of measured SSC data. Moriasi et al. (2007) recommended the use of the latter three statistics.]

Parameter	*Group 1*	*Group 2*	*Group 3*	*Group 4*	*Group 5*
R^2	0.77	0.72	0.72	0.76	0.78
PBIAS	-0.11	-0.13	-0.13	-0.11	-0.11
NSE	0.57	0.47	0.49	0.55	0.60
RSR	0.65	0.73	0.71	0.67	0.64

Group 5 results had a better fit and the least variance among the groups; therefore, parameters *a* and *b* (table 6) for that group were used to construct the SSC rating curves at specified gaged locations.

Estimation of parameters *a* and *b* for ungaged sites: For ungaged tributary sites, it was assumed that parameter *a* is a function of basin characteristics and that parameter *b* can be transferred from gaged sites that have similar watershed and channel characteristics.

Parameter *a* for ungaged sites was obtained using the assumption that they can be transferred from gaged sites to ungaged sites based on the criterion of whether the stream is groundwater or surface-water dominated. Table 7 lists the two parameters used for the ungaged study sites.

CONCLUSIONS

Suspended sediment concentration (SSC) rating curves for gaged and ungaged sites in the Kalamazoo River and its tributaries from Marshall to Morrow Dam were developed. Despite the paucity of measured SSC data, the developed rating curves adequately covered the range of flows at each study site. Several sites had negative SSC rating curve slopes, in contrast to the typical SSC rating curve pattern in which SSC increases as streamflow

increases. This variability added an additional challenge to the SSC rating curve analysis for this study. By pooling at-site data as panel data and grouping them according to possible causative factors, a fixed-effects model analysis found classifying study sites according to their groundwater or surface-water dominance yielded better quantitative statistics than other groupings tested. For ungaged sites in the study area, it was assumed the parameters of SSC rating curves could be transferred from gaged sites reasonably well, based on the similarity in watershed and channel characteristics.

Table 6 Parameters *a* and *b* for estimating suspended sediment rating curves at sites with measured data. Winter was designated as January 1 through March 31, and non-winter period was designated as April 1 through December 31.

River Reach	***Season***	***a***	***b***
Marshall pool above the Marshall Dam on the Kalamazoo River at Marshall, MI	Winter	1.943	-0.203
Marshall pool above the Marshall Dam on the Kalamazoo River at Marshall, MI	Non-winter	1.943	-0.203
Battle Creek, MI (tributary)	Winter	0.554	0.277
Battle Creek, MI (tributary)	Non-winter	-0.161	0.603
Kalamazoo River above the junction with Battle Creek, MI	Winter	0.654	0.277
Kalamazoo River above the junction with Battle Creek, MI	Non-winter	-0.184	0.603
Augusta Creek, MI (tributary)	Winter	2.02	-0.432
Augusta Creek, MI (tributary)	Non-winter	2.279	-0.544
Gull Creek, MI (tributary)	Winter	0.554	0.277
Gull Creek, MI (tributary)	Non-winter	1.579	-0.544
Comstock Creek, MI (tributary)	Winter	0.554	0.277
Comstock Creek, MI (tributary)	Non-winter	1.064	-0.544
Kalamazoo River near Comstock, MI when Q>1000	Winter	0.379	0.277
Kalamazoo River near Comstock, MI when Q>1000	Non-winter	-0.773	0.603
Kalamazoo River near Comstock, MI when Q<=1000	Winter	0.379	0.277
Kalamazoo River near Comstock, MI when Q<=1000	Non-winter	2.719	-0.544

Table 7 Parameters *a* and *b* for estimating suspended sediment rating curves at ungaged sites used in hydrodynamic modeling. Winter was designated as January 1 through March 31, and the non-winter period was designated as April 1 through December 31.

River Reach	***Time period***	***a***	***b***
Talmadge Creek, MI (tributary)	Winter	0.554	0.277
Talmadge Creek, MI (tributary)	Non winter	-0.161	0.603
Bear Creek, MI (tributary)	Winter	0.554	0.277
Bear Creek, MI (tributary)	Non-winter	-0.161	0.603
Minges and Harper Creek, MI (tributaries)	Winter	0.554	0.277
Minges and Harper Creek, MI (tributaries)	Non-winter	-0.161	0.603
Wabascon Creek, MI (tributary)	Winter	2.02	-0.432
Wabascon Creek, MI (tributary)	Non-winter	2.279	-0.544
Sevenmile Creek, MI (tributary)	Winter	0.554	0.277
Sevenmile Creek, MI (tributary)	Non-winter	-0.161	0.603

Tributaries with negative SSC-rating slopes were found to come from watersheds that are characterized by lower stream temperatures and permeable surficial soils and geology indicative of groundwater-flow dominated systems. Such streams generally have low flow stability indices. However, surface-water dominated watersheds can also have a lower flow stability index if the channels have abundant storage. Classification of the watershed and channel characteristics as described in this paper improves the estimation of the SSC-rating curve at both gaged sites and ungaged sites. This identification can be an important consideration for the analysis and modeling of watershed streamflow and sediment.

REFERENCES CITED

Ahanger, M.A., Asawa, G.L., and Lone, M.A. (2013). Hysteresis effect on sediment rating curves, J. Acad, Indus. Res. V1(8), pp: 481-484.

Asselman, N.E.M. (2000). Fitting and interpretation of sediment rating curves. Journal of Hydrology V.234 (2000), pp: 228-248.

Baca, P. (2008). Hysteresis effect in suspended sediment concentration in the Rybarik basin, Slovakia; Hydrological Science-Journal-des Sciences Hydrologiques, 53(1) February 2008; p 224-235.

Barton J.R., and Albertson, M.L. (1953). Temperature, seepage, and turbulence as factors affecting suspended sediment concentration: Colorado State University, Agricultural and Mechanical College, Department of Civil Engineering, AgrReport No. CE 53JBR12, 83 p.

Colby, B.R. (1956). Relationship of sediment discharge to streamflow: USGS Open File Report, prepared by Quality of Water Branch – April 1956, 184 p.

Dollhopf, R.H., Fitzpatrick, F.A., Kimble, J.W., Capone, D.M., Graan, T.P., Zelt, R.B., Johnson, R. (2014). "Response to heavy, non-floating oil spilled in a Great Lakes river environment: a multiple-lines-of-evidence approach for submerged oil assessment and recovery," Proceedings, 2014 International Oil Spill Conference, Savannah, GA, pp 434-448.

Ferguson, R.I. (1986). River loads underestimated by rating curves, Water Resources Research, 22(1), pp 74-76.

Fitzpatrick, F.A., Johnson, R., Zhu, Z.D., Waterman, D., McCulloch, R.D., Hayter, E.J., Garcia, M.H., Boufadel, M., Dekker, T., Hassan, J.S., Soong, D.T., Hoard, C., and Lee, K. (this volume). Integrated modeling approach for fate and transport of submerged oil an oil-particle aggregates in a freshwater riverine environment: (manuscript published in this proceedings).

Glysson, G.D. (1987). Sediment transport curves; U.S. Geological Survey, Open-File Report 87-218, Reston, Virginia, 47 p.

Helsel, D.R., and Hirsch, R.M. (1992). Statistical methods in water resources: U.S. Geological Survey, Water Resources Division, Reston, Virginia, 22092. 522 p.

Holtschlag, D.J., and Croskey, R.M. (1984). Statistical models for estimating flow characteristics of Michigan streams; U.S. Geological Survey Water-Resources Investigations Report 84-4207, 81 p.

Mai, Q.W., Zhao, Y.A., Pan, X.D., and Fan, Z.I. (1990). Feature of flow-sediment regime and regularities of siltation – scour on the lower Yellow River, *in* Sedimentation and Soil Conservation, Collected Research Papers, Vol. 2. Yellow River Conservancy Commission. Zhengzhou, China. p. 100-146.

Morgan, R. P.C. (1995). Soil Erosion and Conservation (2nd edition), Longman, London, 320 P.

Moriasi, D.N., Arnold, J.G., Van Liew, M.W., Bingner, R.L., Harmel, R.D., and Veith, T.L. (2007). Model evaluation guidelines for systematic quantification of accuracy in watershed simulation: Transaction of American Society of Agricultural and Biological Engineers, v. 50, no. 3, p. 885– 900.

Porterfield, G. (1972). Techniques of water-resources investigations of the United States Geological Survey; Chapter 3, Computation of fluvial-sediment discharge, U.S. Geological Survey, Book 3, Applications of Hydraulics, 66 P.

Singh, K.P., and Durgunoglu, A. (1989). Developing accurate and reliable stream sediment yields: Sediment and the environment, IAHS publication, Wallingford, 184. Proceedings of the Baltimore symposium, May 1989: pp. 193-199.

Wesley, J.K. (2005). Kalamazoo River assessment, State of Michigan, Department of Natural Resources, Number 35, 377 P.

FROM MOBILE ADCP TO HIGH-RESOLUTION SSC: A CROSS-SECTION CALIBRATION TOOL

Justin A. Boldt, Hydrologist, U.S. Geological Survey,
Kentucky Water Science Center, Louisville, KY, jboldt@usgs.gov

INTRODUCTION

Sediment is a major cause of stream impairment, and improved sediment monitoring is a crucial need. Point samples of suspended-sediment concentration (SSC) are often not enough to provide an understanding to answer critical questions in a changing environment. As technology has improved, there now exists the opportunity to obtain discrete measurements of SSC and flux while providing a spatial scale unmatched by any other device.

Acoustic instruments are ubiquitous in the U.S. Geological Survey (USGS) for making streamflow measurements but when calibrated with physical sediment samples, they may be used for sediment measurements as well. The acoustic backscatter measured by an acoustic Doppler current profiler (ADCP) has long been known to correlate well with suspended sediment, but until recently, it has mainly been qualitative in nature. This new method using acoustic surrogates has great potential to leverage the routine data collection to provide calibrated, quantitative measures of SSC which hold promise to be more accurate, complete, and cost efficient than other methods.

This extended abstract presents a method for the measurement of high spatial and temporal resolution SSC using a down-looking, mobile ADCP from discrete cross-sections. The high-resolution scales of sediment data are a primary advantage and a vast improvement over other discrete methods for measuring SSC. Although acoustic surrogate technology using continuous, fixed-deployment ADCPs (side-looking) is proven, the same methods cannot be used with down-looking ADCPs due to the fact that the SSC and particle-size distribution variation in the vertical profile violates theory and complicates assumptions.

A software tool was developed to assist in using acoustic backscatter from a down-looking, mobile ADCP as a surrogate for SSC. This tool has a simple graphical user interface that loads the data, assists in the calibration procedure, and provides data visualization and output options. This tool is designed to improve ongoing efforts to monitor and predict resource responses to a changing environment. Because ADCPs are used routinely for streamflow measurements, using acoustic backscatter from ADCPs as a surrogate for SSC has the potential to revolutionize sediment measurements by providing rapid measurements of sediment flux and distribution at spatial and temporal scales that are far beyond the capabilities of traditional physical samplers.

CALIBRATION METHOD

The conversion from echo intensity, also known as raw backscatter (RB, in counts), to sediment-corrected backscatter (SCB, in dB) uses the following equation (Gartner, 2004):

$$SCB = K_c * RB + 20 * \log_{10}(\psi R) + 2\alpha_w R + 2\alpha_s R \quad (1)$$

where K_c is the instrument- and beam-specific echo intensity scale factor (dB/count), ψ is the non-dimensional function describing the non-spherical spreading of the backscattered signal in the near field (Downing et al., 1995), R is the range or distance along the beam (m), α_w is the sound absorption coefficient (dB/m) (Schulkin and Marsh, 1962), and α_s is the sediment attenuation coefficient (dB/m) (Wright et al., 2010; Landers, 2010). In Eq. (1), the first term converts the raw backscatter from counts to decibels, the second term corrects for beam spreading, the third term corrects for water absorption, and the fourth term corrects for sediment attenuation.

The sediment attenuation coefficient can either be measured using the slope of the water-corrected backscatter (WCB) profile (Wright et al., 2010) or computed using knowledge of the suspended-sediment characteristics. The first method assumes uniform SSC over the range from which the slope is obtained. Vertical SSC profiles usually are not uniform with depth, but the upper portion of the SSC profile may be nearly uniform, and this assumption may be acceptable in certain environments. The second method requires analysis of the density and particle-size distribution of the sediment, but its application to a real-world environment is complex to say the least. Both of these sediment attenuation estimation methods are the subject of ongoing research.

The SCB to SSC calibration method relies on concurrent measurements of ADCP acoustic backscatter and suspended-sediment concentration at points throughout the water column at one or more stationary, vertical locations [Figure 1(A–B)]. The acoustic backscatter data from a stationary ADCP profile are time-averaged over the period during which the suspended-sediment point samples were collected. The calibration procedure requires that each physical sediment sample is temporally and spatially matched to a SCB value [Equation (1)]. A linear regression between the matched values is determined such that

$$\log_{10} \mathrm{SSC} = \mathrm{a} * \mathrm{SCB} + \mathrm{b} \tag{2}$$

where a is the slope and b is the y-intercept [Figure 1(C)]. Once the slope and intercept values have been determined for the calibration data (stationary verticals), any sequential ADCP data (e.g., transects or cross-sections) can be converted to SSC using the following equation:

$$\mathrm{SSC} = 10^{(\mathrm{a}*\mathrm{SCB}+\mathrm{b})} \tag{3}$$

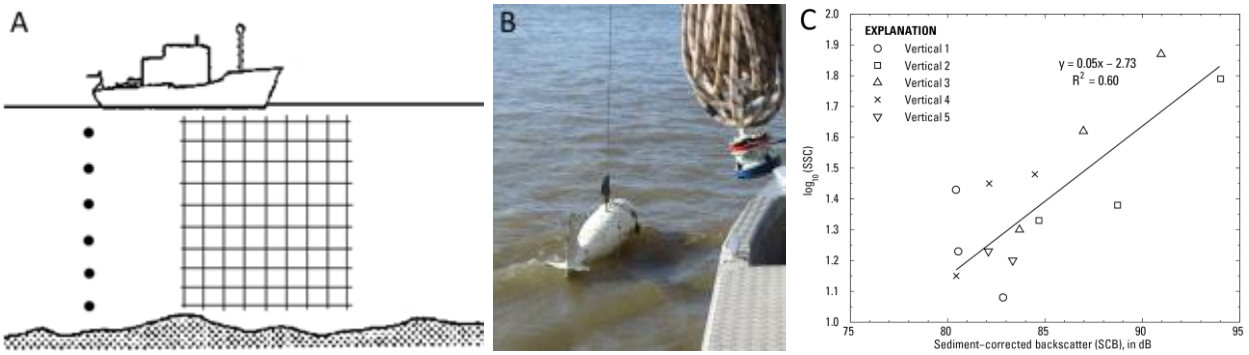

Figure 1 (A) Schematic showing physical sediment samples (points) and stationary ADCP profile time-series (grid). (B) Photo of suspended-sediment sampler and ADCP. (C) Example of linear regression between suspended-sediment concentration (SSC) and sediment-corrected backscatter (SCB).

RESULTS

Although a single vertical can be used to develop a calibration, research to date indicates that a more robust calibration results from using multiple verticals. A convenient method is to use the verticals associated with an equal-discharge-increment (EDI) suspended-sediment sample. This method consists of taking several point samples of suspended sediment throughout the water column in addition to the standard depth-integrated sample at each EDI vertical. The point samples are used to develop the calibration, and the EDI-computed SSC provides a standard measurement of suspended-sediment concentration with which to validate the composite value output by the software tool. An example of a calibrated cross-section is shown in Figure 2. The color contours represent the suspended-sediment concentration. A composite SSC value is reported for the cross-section which may be validated with an EDI composite or other reference measurement of suspended-sediment. When combined with ADCP velocity data, the sediment flux throughout the cross-section can be computed. The software tool provides all of these data visualization options, and additional information about the tool can be found at the USGS Sediment Acoustics webpage (http://water.usgs.gov/osw/SALT/).

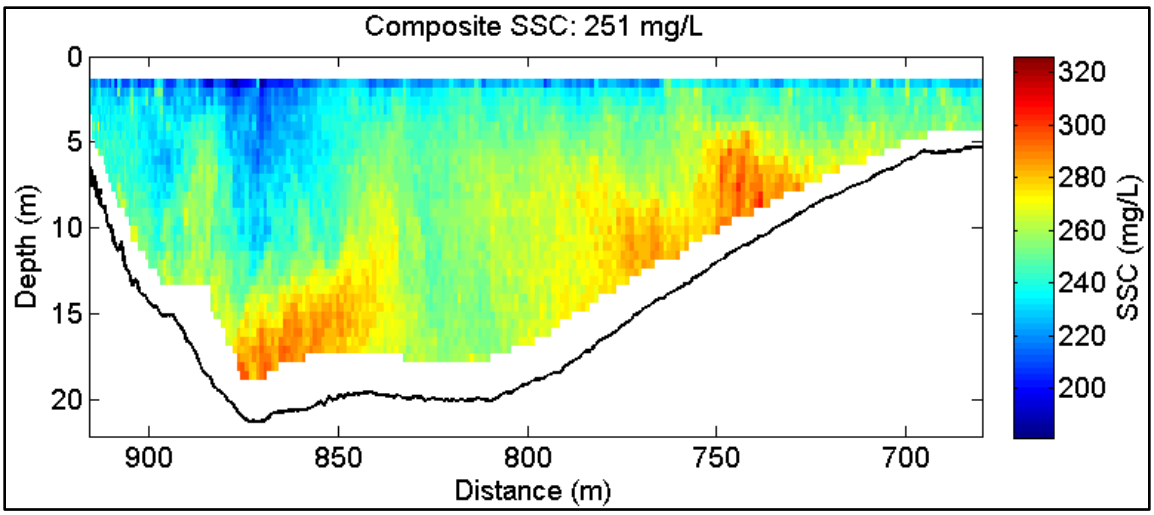

Figure 2 Calibrated cross-section showing color contours of suspended-sediment concentration.

The primary benefit of this method is the vast improvement in spatial scale. Side-looking ADCP deployments are best for continuous monitoring of suspended-sediment, but repeat cross-sections with a down-looking ADCP provide spatial and temporal scales unmatched by any other device. The main limitation of this calibration procedure is that each calibration is specific to the instrument (frequency and beam scale factors) and the particle-size distribution at each site. Changing sediment conditions cause a previous calibration to be invalid due to the complex relationship between sediment characteristics and acoustic backscatter. There is ongoing work to determine how transferable a calibration is over small changes in particle-size distribution for a single site. Another limitation is that this method only applies to measurements of suspended sediment, not bedload measurements. Because the data come from an ADCP, there exist the unmeasured areas on the top and bottom due to the blanking distance and side-lobe interference, respectively; although, estimation algorithms are under development.

SUMMARY

A calibration procedure is presented for converting ADCP acoustic backscatter data to suspended-sediment concentration, which is especially powerful when applied to a full channel cross-section. The calibration method relies on concurrent measurements of ADCP acoustic backscatter and suspended-sediment concentration at points throughout the water column at one or more stationary, vertical locations, and a software tool was developed to standardize and expedite the calibration process. As a result, it is possible to provide rapid measurements of sediment flux and distribution at spatial and temporal scales that are far beyond the capabilities of traditional physical samplers.

REFERENCES

Downing, A., Thorne, P.D., and Vincent, C.E. (1995). “Backscattering from a suspension in the near field of a piston transducer.” J Acoust Soc Am, 97, 1614–1620.

Gartner, J.W. (2004). “Estimating suspended solids concentrations from backscatter intensity measured by acoustic Doppler current profiler in San Francisco Bay, California.” Marine Geol., 211, 169–187.

Landers, M.N. (2010). “Review of methods to estimate fluvial suspended sediment characteristics from acoustic surrogate metrics.” 2nd Joint Federal Interagency Conference, Las Vegas, NV.

Schulkin, M. and Marsh, H.W. (1962). “Sound absorption in sea water.” J Acoust Soc Am, 34, 864–865.

Wright, S.A., Topping, D.J., and Williams, C.A. (2010). “Discriminating silt-and-clay from suspended-sand in rivers using side-looking acoustic profilers.” 2nd Joint Federal Interagency Conference, Las Vegas, NV.

IN SITU DENSIMETRIC MEASUREMENTS AS A SURROGATE FOR SUSPENDED-SEDIMENT CONCENTRATIONS IN THE RIO PUERCO, NEW MEXICO

Jeb E. Brown, Hydrologic Technician, U.S. Geological Survey, Albuquerque, NM,
jebbrown@usgs.gov
John R. Gray, Scientist Emeritus, U.S. Geological Survey, Reston, VA,
graysedimentology@gmail.com
Nancy J. Hornewer, Hydrologist, U.S. Geological Survey, Flagstaff, AZ,
njhornew@usgs.gov

Abstract: Surrogate measurements of suspended-sediment concentration (SSC) are increasingly used to provide continuous, high-resolution, and demonstrably accurate data at a reasonable cost. Densimetric data, calculated from the difference between two in situ pressure measurements, exploit variations in real-time streamflow densities to infer SSCs. Unlike other suspended-sediment surrogate technologies based on bulk or digital optics, laser, or hydroacoustics, the accuracy of SSC data estimated using the pressure-difference (also referred to as densimetric) surrogate technology theoretically improves with increasing SCCs. Coupled with streamflow data, continuous suspended-sediment discharges can be calculated using SSC data estimated in real-time using the densimetric technology.

The densimetric technology was evaluated at the Rio Puerco in New Mexico, a stream where SSC values regularly range from 10,000-200,000 milligrams per liter (mg/L) and have exceeded 500,000 mg/L. The constant-flow dual-orifice bubbler measures pressure using two precision pressure-transducer sensors at vertically aligned fixed locations in a water column. Water density is calculated from the temperature-compensated differential pressure and SSCs are inferred from the density data.

A linear regression model comparing density values to field-measured SSC values yielded an R^2 of 0.74. Although the application of the densimetric surrogate is likely limited to fluvial systems with SSCs larger than about 10,000 mg/L, based on this and previous studies, the densimetric technology fills a void for monitoring streams with high SSCs.

INTRODUCTION

Surrogate measurements of suspended-sediment concentrations (SSCs) can produce continuous, real-time measurements at reasonable costs compared to the traditional collection and analysis of physical samples (Porterfield, 1972; Edwards and Glysson, 1999; Nolan et al., 2005; Koltun et al., 2006; Gray et al., 2008; Gray and Simões, 2008; and Gray and Landers, 2014). The state-of-the-art surrogate technologies as described by Gray and Gartner (2010) include optical backscatter (turbidity), laser diffraction, and hydroacoustics. Although these technologies are proving to be useful for continuously monitoring SSCs in operational programs, most tend to saturate – that is, reach an upper measurement limit – when SSC values exceed 4,000-8,000 milligrams per liter (mg/L) depending on the technology and the characteristics of the sensor selected. SSCs in flows in many rivers around the world, including many unregulated channels in the southwestern United States, episodically exceed 10,000 mg/L, sometimes by more than an order of magnitude (Beverage and Culbertson, 1964), thus rendering the aforementioned SSC

surrogate technologies ineffectual when most sediment transport occurs during higher flows. The densimetric SSC surrogate method effectively enables measurements of SSCs – theoretically with improving accuracy – as SSCs rise above about 10,000 mg/L. Although evaluations of the densimetric technology as a surrogate for moderate-to-high SSCs previously have been administered with mixed results (Larsen et al., 2001; Gray et al., 2010), new interest expressed by the Federal Interagency Sedimentation Project, in a surrogate technology capable of operating under high SSCs, has led to revisiting the densimetric technology.

Previous Research: Lewis and Rasmussen (1999) used precision-pressure transducers to calculate fluid density in a laboratory using glass-microspheres at an SSC of 542 mg/L to within ± 14 mg/L. Calhoun and Rasmussen (2001) also analyzed differential-pressure readings to estimate SSCs and reported good results in the laboratory. The results of field applications by Calhoun and Rasmussen in two creeks in northern Georgia were less convincing largely due to complications from variations in flow velocity, water temperature, and dissolved solids.

Sumi et al. (2002) successfully used two different pressure devices in Japan: (1) a floating, submersible device designed for use in reservoirs, and (2) a differential-pressure device mounted on the banks of a river requiring a submersible pump to deliver water to the sensors. However, the first device was limited to use in reservoirs and the second lacked in situ measurement capability. Hsu and Cai (2010) used two submersible pressure transducers and reported good results in the laboratory. Field results were limited to a single period runoff period, yet the preliminary findings were promising.

Larsen et al. (2001) used a prototype dual-orifice bubbler manufactured by Design Analysis Associates, Inc. (use of firm names in this report is for identification purposes only and does not constitute endorsement by the U.S. Geological Survey) for monitoring SSCs in a Puerto Rico stream. The in situ densimetrically derived SSC values generally were synchronous with the runoff hydrograph. However, the authors considered the maximum observed SSC values of about 17,000 mg/L to be marginal with respect to the low-end SSC measurement capability of the non-temperature-corrected device. The technology was considered worthy of additional research in rivers with high SSCs, in part because no other surrogate technology has been identified for monitoring highly concentrated streamflows.

The same densimetric dual-orifice bubbler used in Puerto Rico subsequently deployed at the Paria River at Lees Ferry, Arizona (Gray et al., 2010), also yielded mixed results in spite of SSC values that exceeded 100,000 mg/L, or about five times the maximum SSC value measured in the Puerto Rico study. It was surmised that bedforms might have intermittently buried the bottom orifice line, thus rendering as spurious any inferred SSC values.

Regarding the Puerto Rico and northern Arizona densimetric tests, Gray et al. (2010) concluded, “In spite of its sound theoretical underpinnings, the field performance of the Double Bubbler in Puerto Rico and northern Arizona, has yet to be fully resolved. Research is continuing into whether development and use of empirical relations from calibration data in lieu of the theoretical considerations are warranted. The required computational scheme presupposes that the SSC in the vertical profile between the sensors is more or less equal to that above the higher sensor. This assumption is difficult to verify and may not be valid. The technology is unreliable

for measuring SSC at less than about 10 g/L [10,000 mg/L], and the actual lower measurement threshold may be at a somewhat larger SSC. The technology is incapable of measuring SSC when the top orifice is out of water. Spurious data are numerous and are believed to be associated with flow turbulence or orifice blockage by bedforms. Continuous pressure-difference measurements may be useful in developing a continuous SSC trace under some circumstances but are not yet considered sufficiently reliable to replace traditional suspended-sediment-monitoring techniques."

In summary, previous studies support the theoretical truism that a positive correlation between SSC and values of fluid density exists in streamflow. However, no previous study has yet conclusively reported reliable, robust field results for inferring SSC values from continuous densimetric measurements. Results of the study described herein add to the knowledge gained from the aforementioned studies by determining the viability of a commercially available instrument for measuring in situ stream water density as a surrogate for SSC.

STUDY SITE AND METHODS

Rio Puerco Study Site: The study site (figure 1) is located at the Rio Puerco near Bernardo, New Mexico, U.S. Geological Survey (USGS) streamflow- and suspended-sediment gaging station (08353000) approximately 0.5-mile upstream from the confluence with the Rio Grande. The Rio Puerco is an ephemeral, incised arroyo in northwest New Mexico with a drainage area of 6,080 square miles. Streamflow is generally produced by summer monsoonal storms or dissipating fall tropical storms (Western Regional Climate Center, 2015). The daily discharge record since 1939 reports a maximum of 7,000 cubic feet per second (ft^3/s), a median of 39.0 ft^3/s and a mean of 126 ft^3/s, excluding flows less than 1 ft^3/s (USGS, 2015). Except for the headwaters, the stream flows through alluvium and valley fill dominated by fine sand-, silt-, and clay-size sediments in unlimited supply for fluvial transport (Nordin, 1963).

The Rio Puerco is renowned for conveying some of the world's largest SSCs. SSCs regularly range from 10,000 mg/L to 200,000 mg/L; Beverage and Culbertson (1964) reported a value of 564,000 mg/L measured on July 24, 1949.

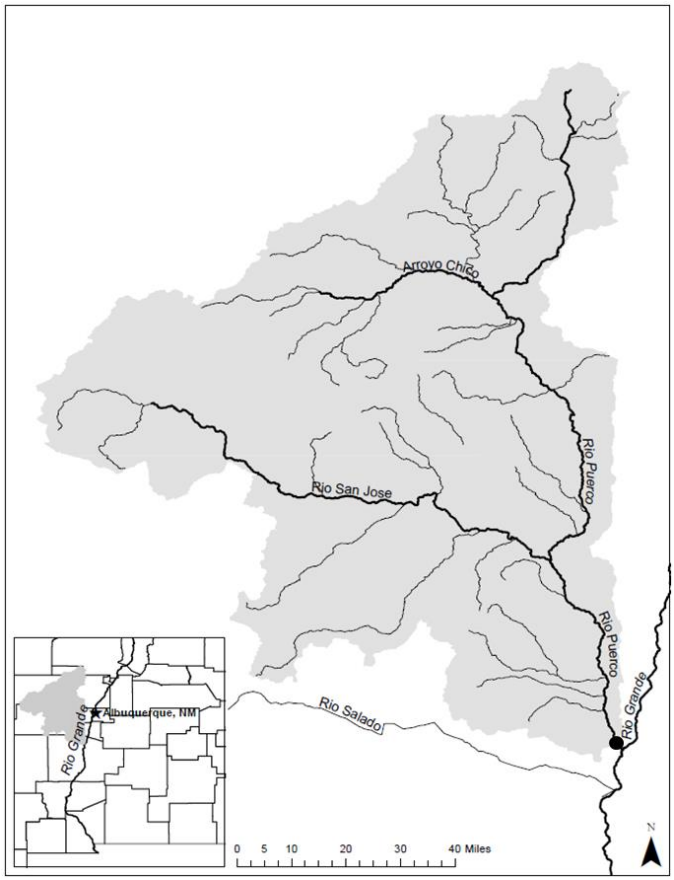

Figure 1 Map of the Rio Puerco watershed in New Mexico. The USGS Rio Puerco near Bernardo, NM, streamflow- and suspended-sediment gaging station (08353000) is located upstream from the confluence with the Rio Grande (black circle).

Methods: Simultaneous pressure readings are obtained using a constant-flow dual-orifice bubbler and recorder manufactured by Sutron Corporation. The two orifices are separated by a fixed distance and vertically aligned in the water column. Differential pressure, computed from the two simultaneous precision-sensor pressure readings, is used to determine the temperature-compensated density of the stream water. The simplified density equation, as given in the Sutron manual (Sutron, 2014), is:

$$\rho_{sw} = \frac{P_2 - P_1}{z} * 2.3066587 \quad (1)$$

where ρ_{sw} is the density of the stream water in grams per milliliter (g/mL), P_1 and P_2 are the pressures in lbs/in² of the upper and lower orifices, respectively, and z is the distance between the orifices, in feet. Figure 2 shows a schematic of the channel at the study site and the orientation of the orifices in the stream. As increases in SSCs correspond to concomitant increases in the density of stream water, the increased density is attributable to an increase in SSC, with some assumptions. Subtraction of the density of pure water, at the temperature of the stream water, results in a value that may be assumed to represent SSC, as shown in equation 2:

$$SSC_{est} = (\rho_{sw} - \rho_{pw}) * 1{,}000{,}000 \quad (2)$$

where SSC_{est} is estimated SSC in mg/L, ρ_{pw} is the density of pure water in g/mL at the temperature of stream water, and 1,000,000 is a conversion factor. Of necessity, equation 2 is based on the following assumptions:

1. both orifices reference the same water surface,
2. the SSC is large enough to exceed a minimum signal-to-noise ratio,
3. the density of suspended sediment and dissolved solids remain constant, and
4. no SSC gradient is present between the lower orifice and the water surface in the vertical water column.

A failure for the orifices to reference the same water surface, and (or) unacceptably low SSC values (assumptions 1 and 2) lead to a lower signal-to-noise ratio, which results in increased uncertainty in the estimation of SSCs, whereas a breakdown in the remaining assumptions (3 and 4) may result in biased data. Water density varies with temperature and as such the density data must be adjusted for ambient water temperature. Water temperatures were measured with a Forest Technology Systems (FTS) digital temperature probe located at the midpoint between the two bubbler orifices and was used to correct the density data. Although the density of water is temperature dependent, Skinner (1982) found that a 1 degree Celsius (ºC) change in temperature was equivalent to a SSC of 160 mg/L, which would be negligible in streams with exceptionally large SSCs.

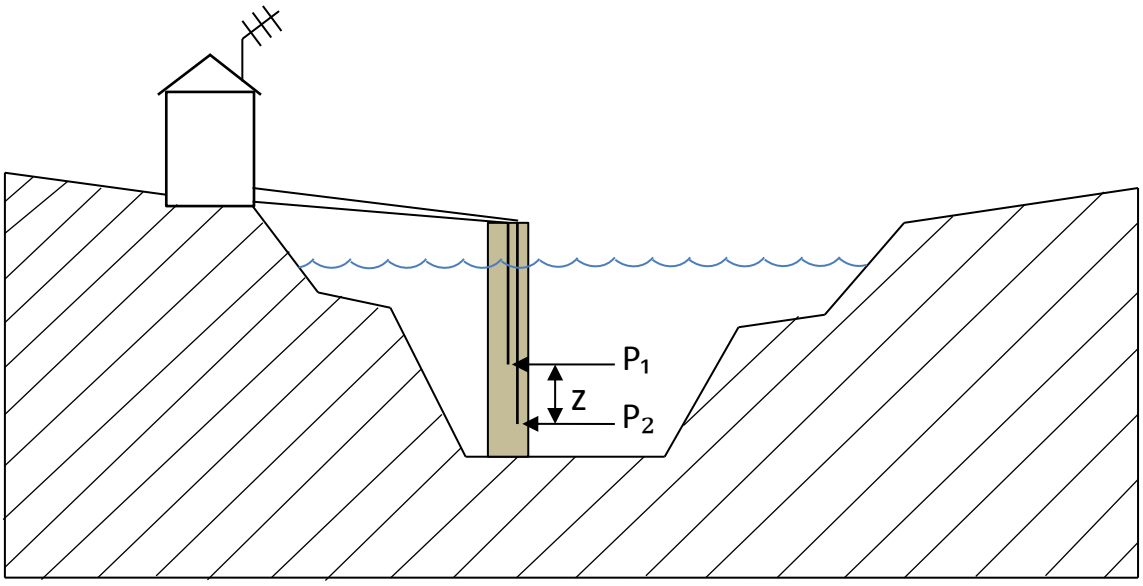

Figure 2 Schematic of the installation of the constant-flow dual-orifice bubbler at the USGS Rio Puerco near Bernado, NM, streamflow- and suspended-sediment gaging station (08353000). P_1 and P_2 represent the bubbler orifices at which depths their respective pressure readings are made. The distance, z, is the vertical separation between orifices. The data-collection platform and two automatic-pumping samplers are located in the gage house.

The two orifices at which pressure measurements were made were mounted in the channel with a vertical separation of 2 feet. Subsequent differential-pressure measurements require that the upper orifice be submerged by at least 0.2 foot. In general, the larger the separation between orifices and the greater the depth over the upper orifice, the stronger the derived signal-to-noise ratio, ergo, the greater accuracy of the computed SSCs.

Water samples for subsequent SSC analyses were collected using two automatic-pumping samplers (Teledyne ISCO 6712) with intake lines mounted in close proximity to the lower bubbler orifice. The samplers were triggered using a 1640 liquid-level actuator manufactured by Teledyne ISCO and samples were collected every 30 minutes during liquid-level actuator submergence. These point samples were compared with suspended-sediment samples collected manually with a depth-integrating isokinetic sampler using the equal-width-increment methods following USGS sampling protocols (Edwards and Glysson, 1999; Nolan et al., 2005; Gray et al., 2008; Gray and Landers, 2014). Samples were analyzed at the USGS New Mexico Water Science Center's sediment laboratory by methods described by Guy (1969). The comparison showed that suspended sediment in the stream is well mixed at this site.

RESULTS AND DISCUSSION

During the study period from July 2013 to September 2013, measured SSCs in the Rio Puerco ranged from 6,730-195,000 mg/L with a median value of 29,500 mg/L. During this period, runoff from monsoonal storms produced 14 discrete high flows (peak flows exceeding 30 ft^3/s). A total of 949 automatically pumped samples were collected and analyzed. Density values, calculated from differential-pressure measurements made every 15 minutes, ranged from 0.70-1.15 g/mL with a median of 1.04 g/mL. Water-temperature data were collected concomitant with the differential-pressure data every 15 minutes and ranged from 14.2ºC to 26.8ºC with a median temperature of 21.7ºC.

Figures 3-6 depict four of the larger flows during the study period (defined here as at least 24 consecutive hours of flow exceeding 30 ft^3/s) and show streamflow and observed and estimated SSCs (estimated SSCs were derived from equation 2). Estimated SSCs follow the general trend of observed SSCs, but estimated SSC values generally display a wide scatter due to noise in the differential-pressure readings, possibly induced from turbulence at or below the water surface. Although not included in this analysis, a moving average applied to the estimated SSC would smooth the curve, but differences between the observed and estimated SSCs would still be present.

In general, the estimated SSC values follow the same pattern as the observed SSC values. The densimetric surrogate estimated the peak SSC reasonably well for the flows shown in figures 3 and 4, but underestimated the peak for the flow shown in figure 5 and the beginning of the flow shown in figure 6. The densimetric surrogate tended to overestimate SSCs as the observed SSCs decreased. This is best shown in figure 5, but also is evident in figures 3 and 4. It is likely that SSC needs to be somewhat larger than 10,000 mg/L at this site for the densimetric surrogate to provide acceptably reliable data. Further investigation is required to better understand the operational constraints of this densimetric instrument at this site.

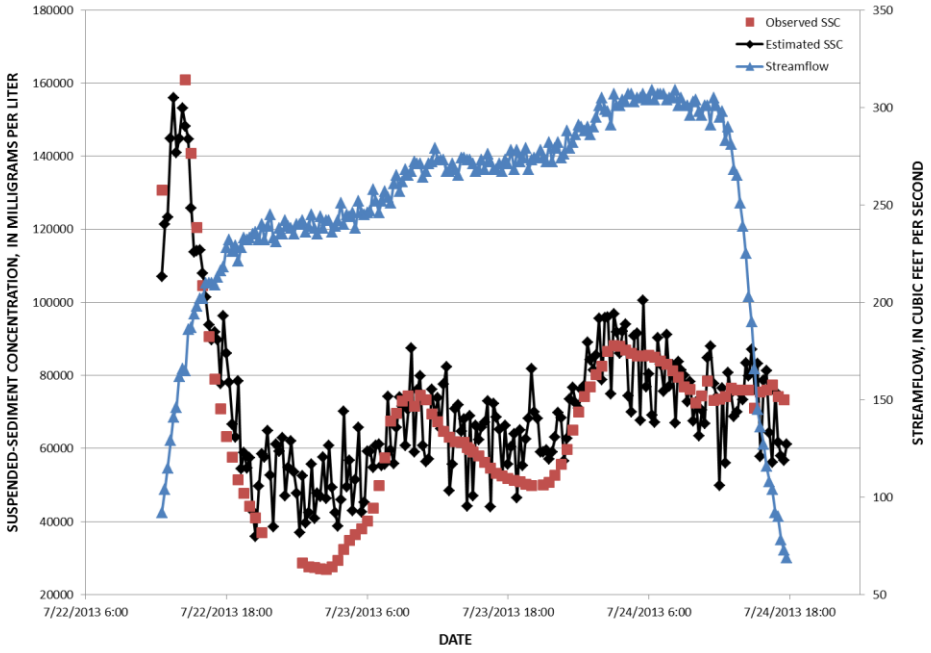

Figure 3 Estimated and observed suspended-sediment concentration and streamflow for July 22 – 24, 2013, at the Rio Puerco near Bernardo, NM, study site.

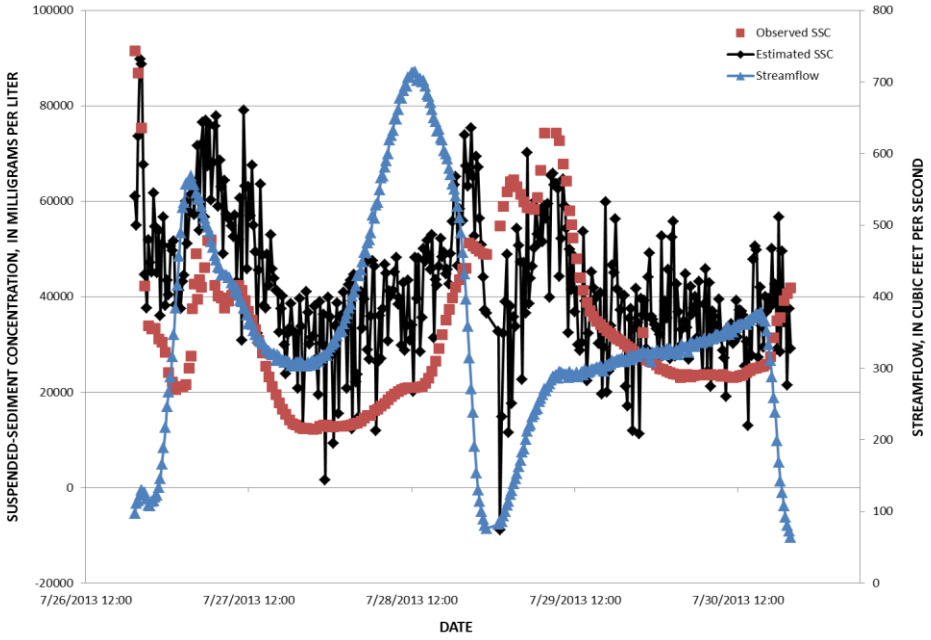

Figure 4 Estimated and observed suspended-sediment concentration and streamflow for July 26 – 30, 2013, at the Rio Puerco near Bernardo, NM, study site.

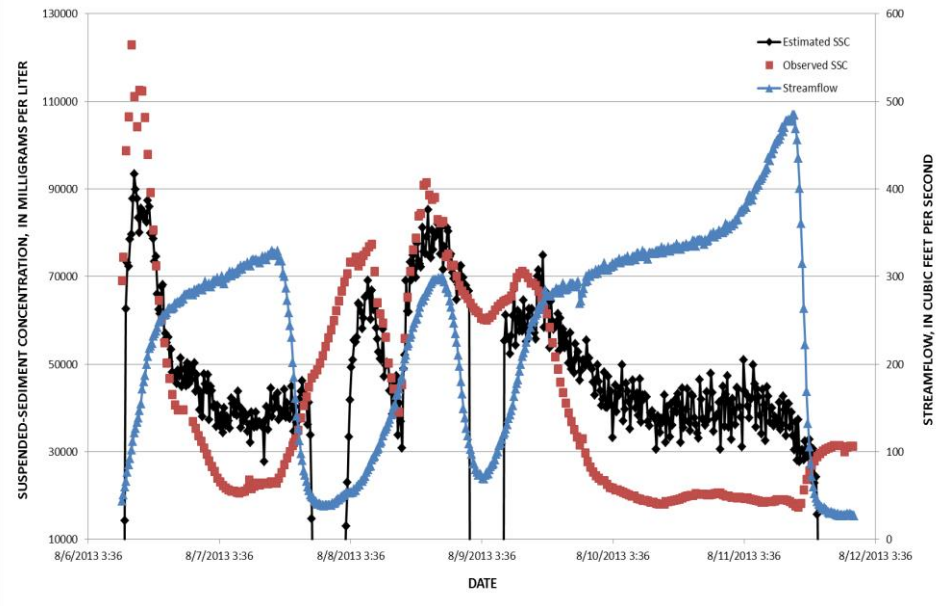

Figure 5 Estimated and observed suspended-sediment concentration and streamflow for August 6 – 12, 2013, at the Rio Puerco near Bernardo, NM, study site. The two periods near August 8 – 9 where estimated SSC drops below the x-axis were due to the water surface receding below the upper orifice during those periods.

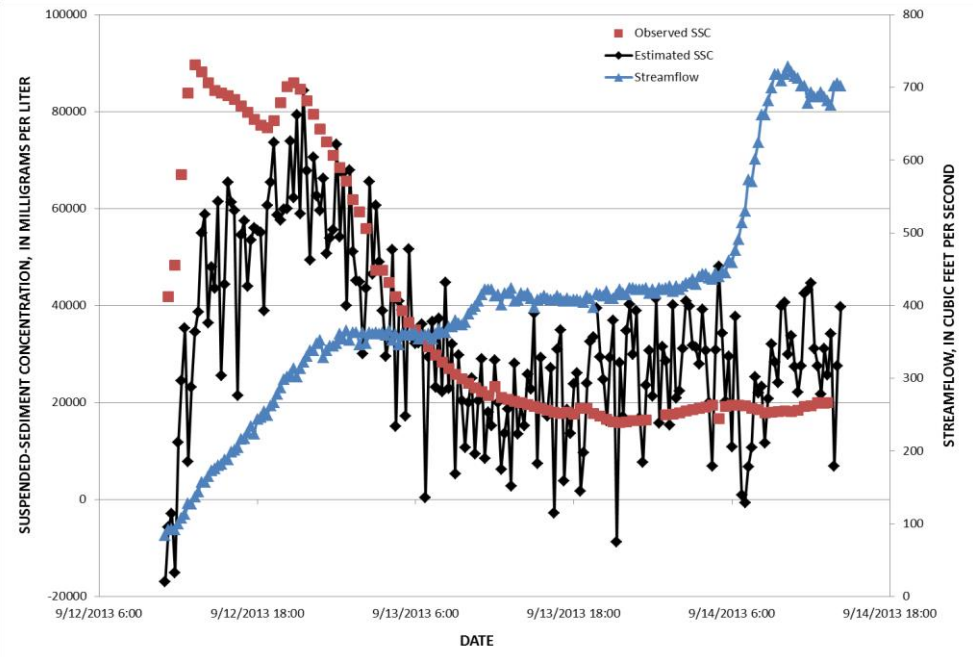

Figure 6 Estimated and observed suspended-sediment concentration and streamflow for September 12 – 14, 2013, at the Rio Puerco near Bernardo, NM, study site.

The data collected from the 14 periods of runoff were analyzed to identify and eliminate probable outliers. The resulting paired data—observed SSCs with estimated SSCs—were used to create a simple linear regression model (Helsel and Hirsch, 2002). Figure 7 shows the scatterplot; resulting ordinary least squares regression line; R^2; and the number of paired samples used in the regression. The coefficient of determination of 0.74 suggests that a reasonable correlation between estimated and observed SSC exists.

These data indicate that the densimetric suspended-sediment surrogate technology provides unequivocally superior estimates of SSC compared to estimates derived from a suspended-sediment-transport curve developed from streamflow and concentration data for the site (Porterfield, 1972; Gray and Simões, 2008). Because there is little correlation between streamflow and SSC at this site, it is difficult to accurately estimate SSC using the transport curve (figure 8).

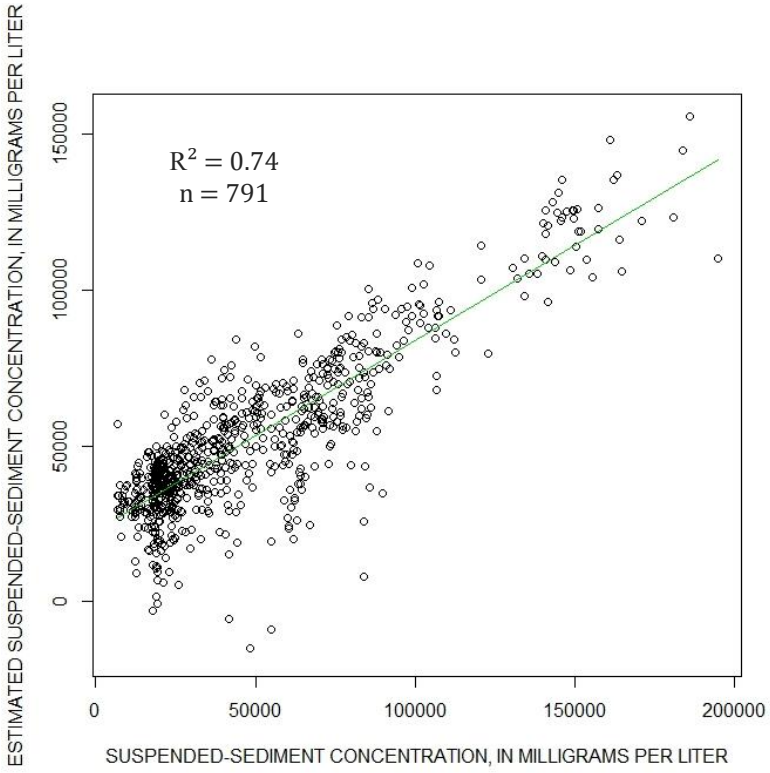

Figure 7 Scatterplot comparing differential pressure derived suspended-sediment concentration estimates with observed SSCs from paired data at the Rio Puerco near Bernardo, NM, study site during July to September, 2013. The ordinary least squares line is shown in green.

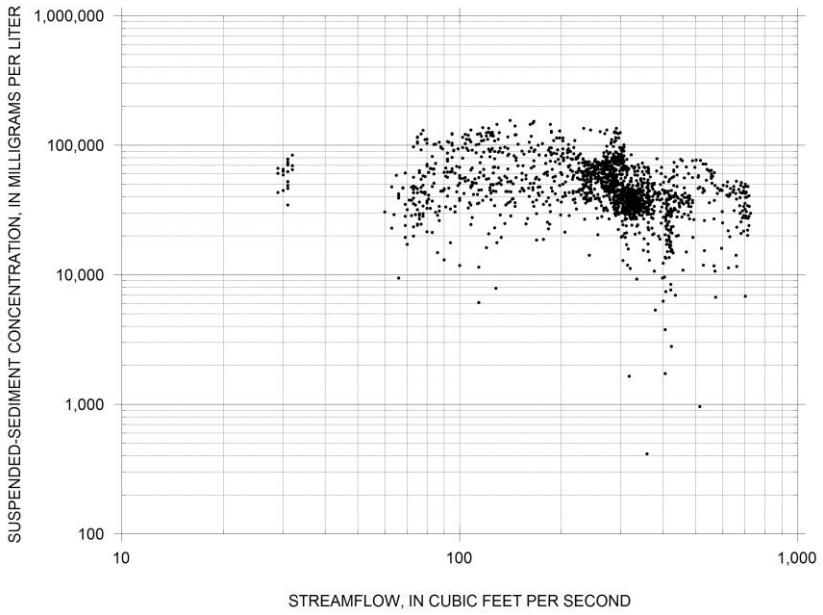

Figure 8 Scatterplot comparing observed suspended-sediment concentration to streamflow from paired data at the Rio Puerco near Bernardo, NM, study site during July to September, 2013.

CONCLUSION

The densimetric surrogate technology for continuously monitoring SSCs was developed to address a monitoring niche unfulfilled by any other surrogate technology: to provide reliable SSC data in fluvial systems that convey high-to-hyperconcentrated SSCs. Tests of the relation between densimetric and observed SSC values in New Mexico's Rio Puerco—renowned for conveying some of the largest SSCs in the world—in July-September 2013 during runoff from monsoonal storms yielded an R^2 of 0.74.

Much of the uncertainty in densimetric measurements is likely attributed to site-specific issues including turbulence at and below the water surface, the presence of low SSCs, and sufficient depth to achieve a computationally useful ratio of depth over the top orifice to depth over the lower orifice. In spite of the moderate accuracy of the technology as indicated by the R^2 of 0.74, two key characteristics – the temporal continuity of the technology and saturation-free performance – make this a valuable technology for monitoring sediment-laden streamflows.

The study results indicate that the densimetric technology is capable of providing an empirically derived SSC time series that is, or at least can be superior to those derived from a transport curve when SSC values exceed about 10,000 mg/L. The other sediment-surrogate technologies described by Gray and Gartner (2009) saturate at SSCs lower than or within the same approximate range at which the densimetric technique becomes effective. Hence, the densimetric technique is a demonstrably reliable method for monitoring highly concentrated and hyperconcentrated streamflows at the Rio Puerco site. Additional deployments of the densimetric technology are recommended at other rivers that episodically convey SSCs exceeding 10,000 mg/L to further test this technology and to produce continuous records of suspended-sediment transport where no reasonable alternative is available.

REFERENCES

Beverage, J.P., and Culbertson, J.K. (1964). "Hyperconcentrations of suspended sediment," Journal of Hydraulics Division, ASCE 90, pp 117-128.

Calhoun, D.L., and Rasmussen, T.C. (2001). "Densimetric monitoring of suspended-sediment concentrations," Northeastern Georgia, In: Proceedings of the 7th Federal Interagency Sedimentation Conference, Reno, Nevada, March 25-29, 2001. http://pubs.usgs.gov/misc/FISC_1947-2006/pdf/1st-7thFISCs-CD/7thFISC/7Fisc-V1/7preface.pdf.

Edwards, T.E., and Glysson, G.D. (1999). "Field methods for collection of fluvial sediment," U.S. Geological Survey Techniques of Water-Resources Investigations, book 3, chap. C2. pp 89. http://water.usgs.gov/osw/techniques/Edwards-TWRI.pdf.

Gray, J.R., and Gartner, J.W. (2009). "Technological advances in suspended-sediment surrogate monitoring," Invited paper, Water Resources Research, vol. 45, W00D29, doi:10.1029/2008WR007063, pp 20. http://water.usgs.gov/osw/techniques/2008WR007063.pdf.

Gray, J.R., and Gartner, J.W. (2010). "Surrogate technologies for monitoring suspended-sediment transport in rivers," Sedimentology of Aqueous Systems, London, Wiley-Blackwell, Chapter 1. http://water.usgs.gov/osw/techniques/sed_aq_sys_chap_1_pdf_from_wb_3_16_2010.pdf.

Gray, J.R., Glysson, G.D., and Edwards, T.E. (2008). "Suspended-sediment samplers and sampling methods," In: Sediment Transport Measurements, M. Garcia (ed.), Sedimentation Engineering - Processes, Measurements, Modeling, and Practice, American Society of Civil Engineeers, Manual 110, chap. 5.3, pp 320-39. http://water.usgs.gov/osw/techniques/Diplas_Kuhnle_others.pdf.

Gray, J.R., and Landers, M.N. (2014). "Measuring suspended sediment," In: Ahuja S. (ed.) Comprehensive Water Quality and Purification, vol. 1, United States of America: Elsevier, pp 157-204. http://water.usgs.gov/osw/techniques/sediment/gray_landers_elsevier_chapter_12_10_17_2013.pdf.

Gray, J.R., and Simões, F.J.M. (2008). "Estimating sediment discharge," In: Sedimentation Engineering – Processes, Measurements, Modeling, and Practice, Manual 110, edited by M. Garcia, American Society of Civil Engineers, pp 1067-1088. http://water.usgs.gov/osw/techniques/Gray_Simoes.pdf.

Gray, J.R., Hornewer, N.J., Larsen, M.C., Fisk G.G., and Macy, J.P. (2010). "Pressure difference," In: Gray, J.R., and Gartner, J.W., eds., Section 1.2.4, Chapter 1, Surrogate technologies for monitoring suspended-sediment transport in rivers: Poleto, Cristiano, and Charlesworth, Susanne, eds., Sedimentology of Aqueous Systems, London: Wiley-Blackwell, pp 23-28. http://water.usgs.gov/osw/techniques/sed_aq_sys_chap_1_pdf_from_wb_3_16_2010.pdf.

Guy, H.P. (1969). "Laboratory theory and methods for sediment analysis," U.S. Geological Survey Techniques of Water-Resources Investigations, book 5, chap. C1, pp 59. http://pubs.usgs.gov/twri/twri5c1/.

Helsel, D.R. and Hirsch, R.M. (2002). "Statistical methods in water resources," U.S. Geological Survey Techniques of Water-Resources Investigations, book 4, chap. A3, pp 522.

Hsu, Y., and Cai, J. (2010). "Densimetric monitoring technique for suspended-sediment concentrations," Journal of Hydraulic Engineering, ASCE, 2010.136, pp 67-73.

Koltun, G.F., Eberle, M., Gray, J.R., and Glysson, G.D. (2006). "User's manual for the Graphical Constituent Loading Analysis System (GCLAS)," U.S. Geological Survey Techniques and Methods, book 4, chap. C1, pp 50. http://pubs.er.usgs.gov/usgspubs/tm/tm4C1.

Larsen, M.C., Figueroa-Alamo, C., Gray, J.R., and Fletcher, William (2001). "Continuous automated sensing of streamflow density as a surrogate for suspended-sediment concentration sampling," In: Proceedings of the 7th Federal Interagency Sedimentation Conference, Reno, Nevada, March 25-29, 2001. http://pubs.usgs.gov/misc/FISC_1947-2006/pdf/1st-7thFISCs-CD/7thFISC/7Fisc-V1/7preface.pdf.

Lewis, A.J., and Rasmussen, T.C. (1999). "Determination of suspended sediment concentrations and particle size distributions using pressure measurements," Journal of Environmental Quality, 28, pp 1490-96.

Nolan, K.M., Gray, J.R., and Glysson, G.D. (2005). "Introduction to suspended-sediment sampling," U.S. Geological Survey Scientific Investigations Report 2005-5077. http://pubs.er.usgs.gov/pubs/sir/sir20055077.

Nordin, C.F., Jr. (1963). "A preliminary study of sediment transport parameters, Rio Puerco near Bernardo, New Mexico," U.S. Geological Survey Professional Paper 462-C, pp 21. http://pubs.er.usgs.gov/publication/pp462C.

Porterfield, G. (1972). "Computation of fluvial-sediment discharge," U.S. Geological Survey, Techniques of Water-Resources Investigations, book 3, chap. C3, pp 66. http://water.usgs.gov/pubs/twri/twri3-c3/.

Skinner, J.V. (1982). "A fluid-density gage for measuring suspended-sediment concentration," Part A, in Measurement and Analysis of Sediment Loads in Streams, Federal Interagency Sedimentation Project, 125 P.; http://water.usgs.gov/fisp/docs/Report_X.pdf.

Sumi, T., Morita, S., Ochi, T., and Komiya, H. (2002). "Development of the suspended-sediment concentration measuring system with differential pressure transmitter in rivers and reservoirs," In: Proceedings of the Hydraulic Measurements and Experimental Methods Conference, ASCE.

Sutron (2014). "Accubar constant flow bubble gauge/recorder 56-0133 and dual orifice bubble gauge/recorder 56-0134 operations & maintenance manual," revision – 1.73, February 14th, 2014. http://www.sutron.com/documents/constant-flow-bubblers-manual-5.pdf.

U.S. Geological Survey (2015). "USGS 08353000 Rio Puerco near Bernardo, New Mexico," U.S. Geological Survey National Water Information System. http://waterdata.usgs.gov/usa/nwis/uv?site_no=08353000.

Western Regional Climate Center, 2015. "Climate of New Mexico," http://www.wrcc.dri.edu/narratives/newmexico/.

LARGE RIVER BED SEDIMENT CHARACTERIZATION WITH LOW-COST SIDESCAN SONAR: CASE STUDIES FROM TWO SETTINGS IN THE COLORADO (ARIZONA) AND PENOBSCOT (MAINE) RIVERS

Daniel Buscombe, Research Geologist, Grand Canyon Monitoring and Research Center, Southwest Biological Science Center, USGS Flagstaff, AZ, dbuscombe@usgs.gov;
Paul E. Grams, Research Hydrologist, Grand Canyon Monitoring and Research Center, Southwest Biological Science Center, USGS Flagstaff, AZ, pgrams@usgs.gov;
Theodore S. Melis, Physical Scientist, Grand Canyon Monitoring and Research Center, Southwest Biological Science Center, USGS Flagstaff, AZ, tmelis@usgs.gov;
Sean M.C. Smith, Assistant Professor, School of Earth and Climate Sciences, University of Maine, Orono, ME, sean.m.smith@maine.edu

Mapping subaqueous riverbed sediment grain size across channels and in nearshore areas typically used by fish and benthic invertebrates is difficult where and when the water flow is too swift or deep to wade yet impractical to access with large boats and instruments. Fluvial characteristics can further constrain sampling options, particularly where flow depth, water column turbidity or channel bottom structure prohibit use of aerial or bottom deployed imaging platforms.

Sidescan sonar returns that image swaths of the bed from a vessel have the potential to meet the technical shortfall confronting bed sediment change detection in large rivers. Inexpensive, easy to use sonar devices designed to be mounted to small durable vessels are commercially available. They are lightweight and have low power demands, providing opportunities for use in a large range of rivers by one or two personnel. The modern sidescan transducers are low profile and require minimal draft, making them suitable for imaging in very shallow water. Swath mapping using these devices has the potential to rapidly map bed sediments, structural features and large woody debris, with minimal logistics and cost. Coupled with a GPS or other type of vessel tracking, they can produce geo-referenced images of the acoustic returns and relate spatial variations in the signal ('bed texture') to the grain size of the bed surface sediments and structural changes (Figure 1).

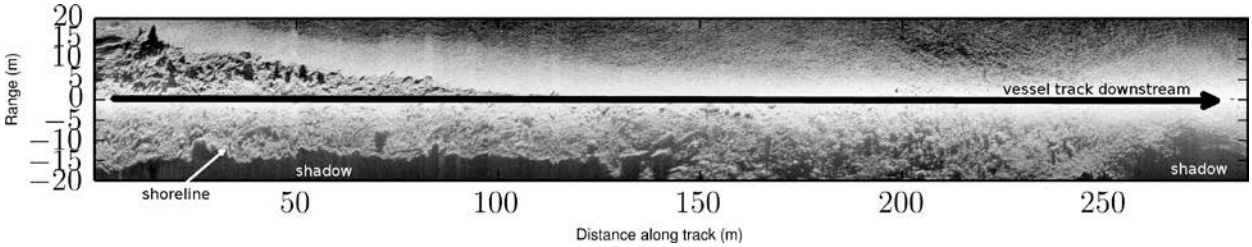

Figure 1 An example merged (port and starboard) sidescan sonar echogram. The transducer sends out a high-frequency (typically several hundreds of kHz) acoustic beam perpendicular to the vessel heading on either side (positive ranges are port and negative ranges are starboard) and records the amplitude of the returning echoes from a wide swath. One ping constitutes the simultaneous acquisition of data from the two sidescan beams at an instant, returning a swath composed of pixels whose intensity relates to the echo strength, determined by the acoustic impedance and reflection at those locations. A small strip of the bed is imaged with each ping,

building an echogram that provides near continuous coverage as the vessel moves slowly along-track (up or downstream).

The typical spatial resolution (pixel size) of a sonar signal return varies from decimeters to meters depending on range and acoustic parameters. The acoustic texture relates to morphological form roughness rather than the grain-scale roughness. The strength of the returned echo is a function of the bed sediment composition. A harder surface with greater acoustic impedance, such as bedrock and cobbles, will return more acoustic energy than a softer bed such as sand. The predictable relation between the sonar signal, acoustic texture and substrate properties provides a basis to distinguish dominant grain sizes and structures of a sedimentary environment (Figure 2).

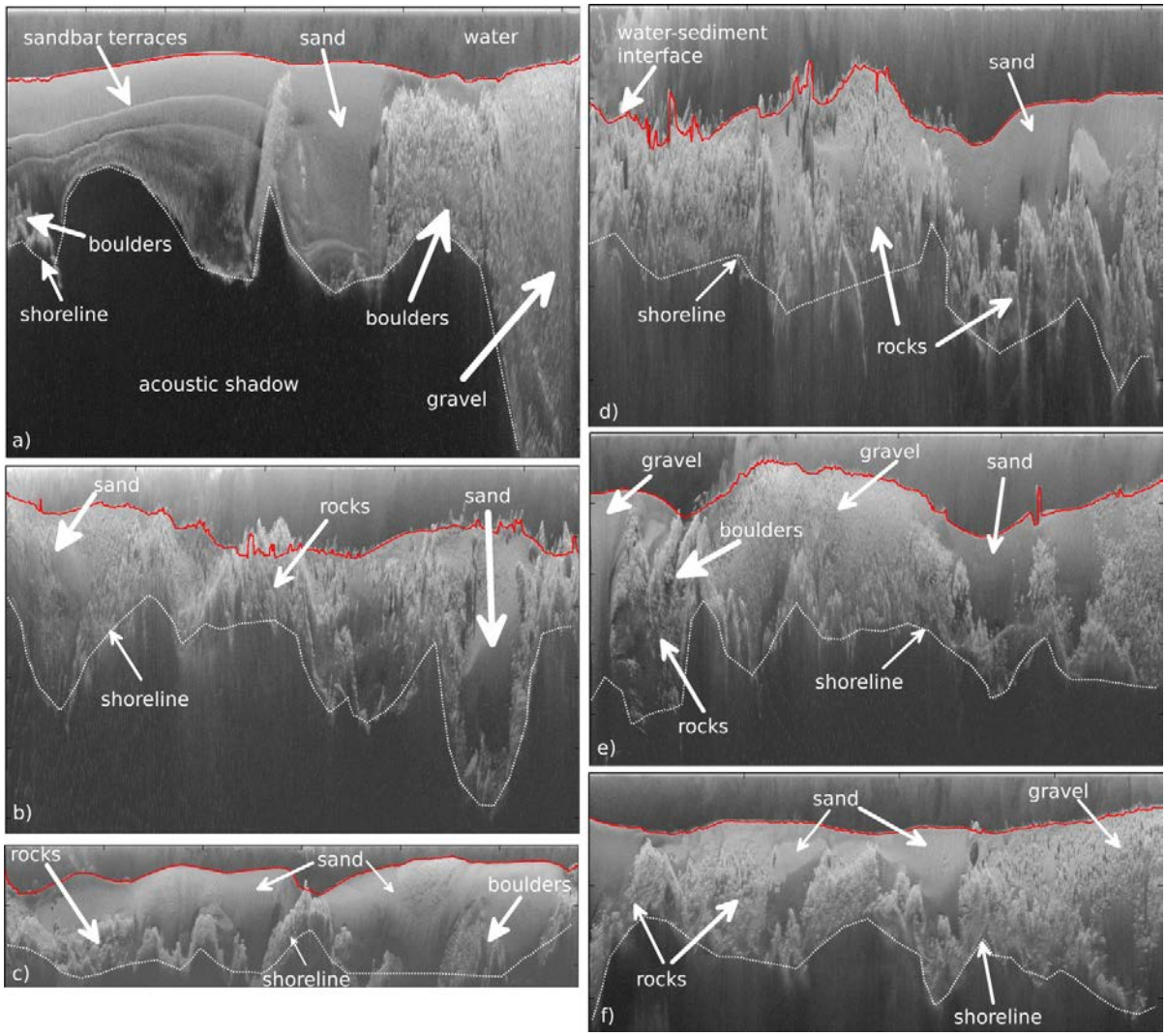

Figure 2 Examples of raw starboard sidescan sonar echograms (left to right, upstream to downstrean) collected with a Humminbird® instrument. The top of each image is the water column, and the bottom the acoustic shadow caused by the shoreline. Some sediment types have been identified. The label ‘rocks’ refers to bedrock outcrops. The line delimiting the water and the bed has been detected automatically. The challenge is to develop an automated means to

classify, in a robust manner, sediments that can be recognized by a trained eye. ®, Any use of trade, product, or names is for descriptive purposes only and does not imply endorsement by the U.S. government.

Here we discuss considerations in the use of sidescan sonar for riverbed sediment classification using examples from two large rivers, the Colorado River below Glen Canyon Dam in Arizona and the Upper Penobscot River in northern Maine (Figure 3). These case studies represent two fluvial systems that differ in recent history, physiography, sediment transport, and fluvial morphologies. The bed of the Colorado River in Glen Canyon National Recreation Area is predominantly graveled with extensive mats of submerged vegetation, and ephemeral surficial sand deposits exist below major tributaries. The bed is imaged periodically to assess the importance of substrate type and variability on rainbow trout spawning and juvenile rearing habitats and controls on aquatic invertebrate population dynamics. The Colorado River bed further below the dam in Grand Canyon National Park is highly dynamic. Tributary inputs of sand, gravel and boulders are spatially variable, and hydraulics of individual pools and eddies vary considerably in space and in response to varying dam operations, including experimental controlled flood releases to rebuild eroding sandbars. The bed encompasses the full range of non-cohesive sediments, deposited in complicated spatial patterns. The mobile portion of the Penobscot River is generally more uniform, and consists predominantly of embedded gravels interspersed between bedrock outcrops with small isolated sand patches in sections with modest or low gradients. Patches of large cobbles, boulders and bedrock outcrops are present in the lower reaches of the river near locations of two recent dam removal projects but are of limited extent below the "head of tide" on the river. Aggregations of coarse materials often correspond to locations with abrupt bed elevation drops in the Upper Penobscot River.

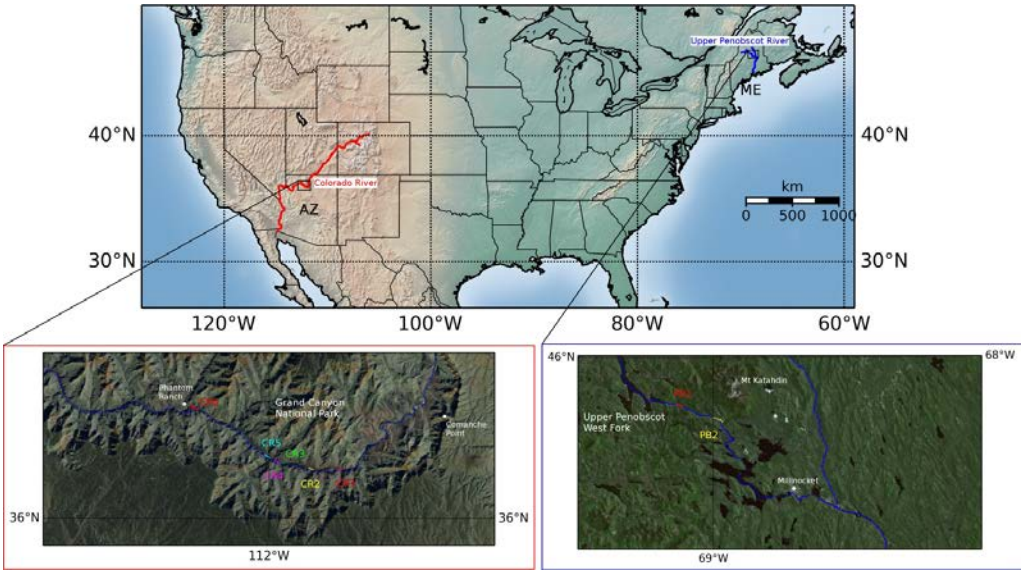

Figure 3 Location of the Colorado and Penobscot Rivers an d some sampling reaches (inset). The sites that will be discussed in this presentation are PB1 and PB2 on the Penobscot and CB1 through 6 on the Colorado.

First, we discuss data collection 'best practices' based on experience in varied environments. Second, we relate uncertainties in instrument positioning and boat attitude (heading and pitch) to sidescan bed-sediment texture measurements. Third, we present methods to relate raw echoes to backscatter amplitudes (in dB Watts) and acoustic impedances by correcting for transmission, spreading and absorption losses, the sonar footprint and instrumental factors such as time-varying transducer power. Fourth, we discuss the merits (and some pitfalls) of likely approaches to automated bed-sediment classification from sidescan imagery, such as textural classification based on machine learning and spectral signal decomposition. Finally, we present a promising spectral technique for automated sediment classification from sidescan echograms (Figure 4). The recursive application of the wavelet transform over small overlapping windows of the echogram provides a robust measure of variation in wavelengths of alternating patterns of strong and weak echoes. The greater this variation, the more textured the echogram and the coarser the substrate. The method provides an objective quantification of textures in physical units (length), for the purpose of riverbed sediment classification. We will evaluate this method using data from all contrasting case study sites.

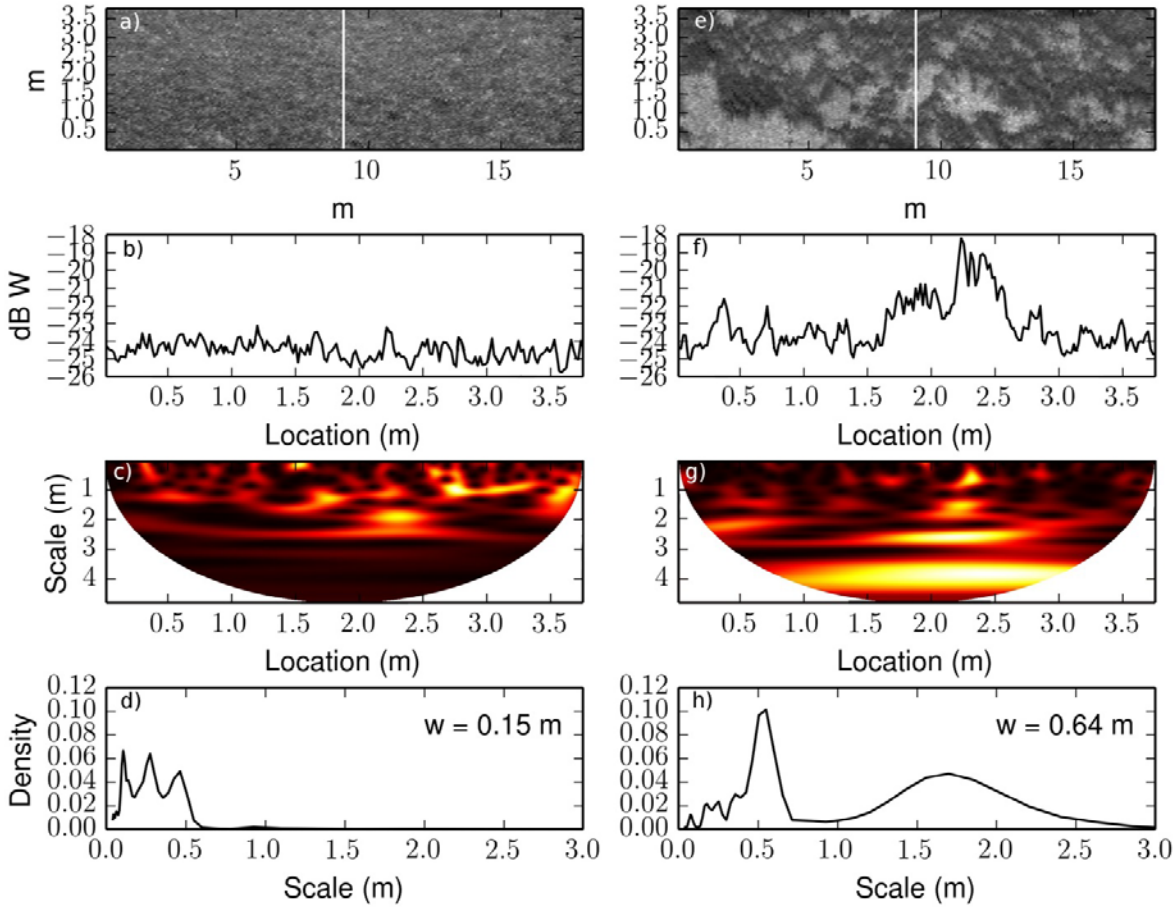

Figure 4 Example analysis of a small patch of homogeneous echogram texture: (a) a 200 x 200 pixel (~4 x 17m) window showing the textural signature from small well-sorted gravel at site in PB1 (Figure 3); (b) the trace through the white line in (a); (c) the continuous wavelet transform

of the data in (b) showing areas of high spectral power in lighter shades and low spectral power in darker shades; and (d) the normalized autospectral variance derived from (c) which shows spectral energy in a narrow band of scales. Panels e) through h) are the same for a 200 x 200 pixel (~4 x 17m) window showing the textural signature from small boulders at the same site. These different signatures for different substrate types are used to classify sediments in an objective and fully automated fashion.

RESERVOIR SUSTAINABILITY WORKSHOP AND NATIONAL RESERVOIR SEDIMENTATION TEAM

Timothy J. Randle, Supervisory Hydraulic Engineer, trandle@usbr.gov; Sean Kimbrel, Hydraulic Engineer, skimbrel@usbr.gov; and Kent L. Collins, Hydraulic Engineer, kcollins@usbr.gov; Bureau of Reclamation, Sedimentation and River Hydraulics Group, Denver, Colorado

ABSTRACT

A Reservoir Sustainability Workshop with national and international specialists was convened in Lakewood, Colorado, July 10-12, 2012 to develop and describe practical solutions for managing sediment for long-term reservoir sustainability. The workshop was sponsored by the Federal Advisory Committee on Water Information, Subcommittee on Sedimentation and the U.S. Society on Dams.

One of the recommendations made during the workshop was to form the National Reservoir Sedimentation Team. The Subcommittee on Sedimentation adopted this recommendation and formed this new team to provide short-course training on reservoir sedimentation and sustainability, provide web-based resources for agencies and the public, recommend interagency protocols for web-based storage and retrieval of reservoir survey datasets, encourage storage of reservoir capacity and sedimentation data in the national reservoir database RESSED, and formulate a white paper on reservoir sedimentation and sustainability.

INTRODUCTION

All rivers transport sediment of various sizes (e.g., clay, silt, sand, gravel, cobbles) and rates. Therefore, reservoirs located on a stream channel accumulate sediment over time unless sediments are trapped by an upstream reservoir. Coarser sediments (sand, gravel, and cobble) entering the reservoir deposit first and often form a delta at the upstream end of the reservoir (Figure 1). The formation of a reservoir delta depends on a significant supply of coarse sediment and the reservoir operating level (Morris and Fan, 1998). Finer sediments (clay and silt) deposit farther downstream along the reservoir bottom. Sediment often accumulates at all elevations of the reservoir. Outlets at most federal dams were typically designed to remain above the sediment accumulation during the first 50 or 100 years of operation (sediment design life). The rate of sediment accumulation depends on the upstream sediment supply and the trap efficiency of the reservoir.

RESERVOIR SEDIMENTATION IMPACTS

One of the most obvious impacts from reservoir sedimentation is the loss of water storage capacity (Figure 2), which will eventually lead to the reduced reliability of water supply and power. Reduced reliability will have the largest impact in regions exposed to multiple-year droughts, which may be exacerbated by the effects of climate change. Other serious impacts often occur long before the reservoir completely fills with sediment:

- Burial of dam outlets, water intakes, boat marinas, and boat ramps (Figure 3).
- Reduction in surface area for recreation (Figure 4).
- Increased dam safety risks from sediment loads against the dam, abrasion of outlets and spillways, and loss of functioning outlets (Figure 5).
- Degradation of the downstream channel bed and stream-bank erosion (Figure 6).
- Alteration of downstream channel and riparian habitat (Figure 7).
- Aggradation of upstream channels, which can lead to reduced conveyance capacity, increased flooding stage, and increased ground water table (which can cause waterlogging and soil salinization).

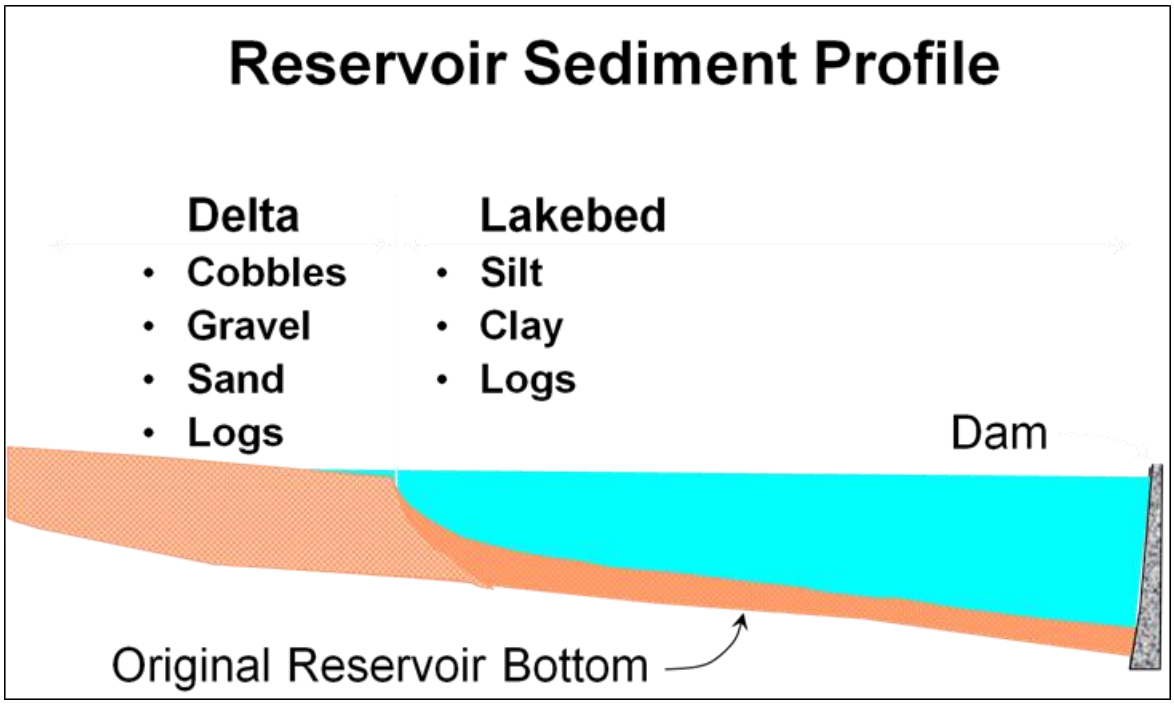

Figure 1 Typical longitudinal profile of a reservoir with a delta and lake bottom sediment deposits.

RESERVOIR SUSTAINABILITY WORKSHOP

The future project benefits of the nation's reservoirs are threatened by continued sedimentation. Therefore, a workshop of national and some international specialists was convened in Lakewood, Colorado, July 10-12, 2012 to discuss potential solutions to reservoir sedimentation (Randle and Collins, 2013). The workshop objective was to develop and describe practical options for managing sediment for long-term reservoir sustainability in the United States. The workshop was organized and sponsored by the Federal Advisory Committee on Water Information, Subcommittee on Sedimentation (SOS) and the U.S. Society on Dams, Hydraulics of Dams Committee. The Subcommittee on Sedimentation provided some financial support for the workshop.

The three-day workshop consisted of a series of sessions. Each session began with an invited lecturer (Figure 8) followed by four separate and concurrent small-group discussions that focused on specific questions. The small groups gave everyone an opportunity to provide input and allowed different groups to concurrently address different questions (Figure 9). Afterward, all participants reconvened for a summary of the four small group discussions. The questions that the small groups focused on are listed below:

- What are impacts associated with reservoir sedimentation?
- What are useful categories of reservoir sedimentation?
- What are the reservoir sediment monitoring recommendations?
- What are the effective reservoir sustainability methods?
- When are specific sustainability methods most applicable?
- What are the environmental effects of reservoir sediment management?
- What further research is needed and what are the priorities?

Figure 2 Sedimentation has almost completely filled the reservoir behind Matilija Dam near Ventura, California.

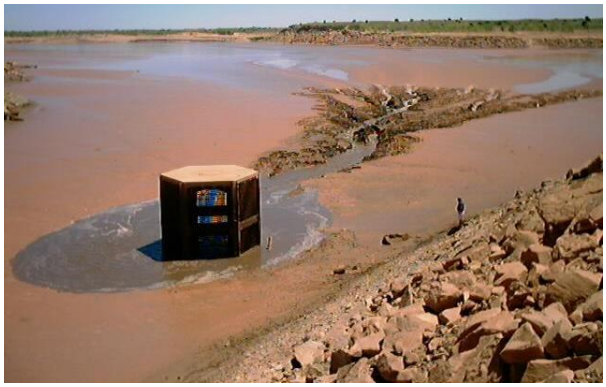

Figure 3 Reservoir sedimentation has impaired the outlet at Sumner Dam near Fort Sumner, New Mexico.

Figure 4 The reservoir delta has reduced the surface area available for recreation at Lake Powell near Hite, Utah.

Figure 5 Sand has abraded the spillway at the Milburn Diversion Dam near Sargent, Nebraska.

Figure 6 Channel degradation downstream from Sumner Dam near Fort Sumner, New Mexico.

Figure 7 Channel Degradation and narrowing of the Platte River near North Platte, Nebraska.

Figure 8 Invited lecturers help to introduce each workshop topic.

Figure 9 Small group breakout sessions were used to concurrently discuss different aspects of each workshop topic.

The workshop was kept to a manageable size by inviting the following organizations with expertise in managing reservoirs and sedimentation:

- Subcommittee on Sedimentation Member Organizations
  - U.S. Army Corps of Engineers (Meg Jonas, Dan Pridal, John Remus, Jerry Webb)
  - U.S. Department of Agriculture
    - Agricultural Research Service (Matt Römkens)
    - Natural Resources Conservation Service (Kerry Robinson)
  - U.S. Department of the Interior
    - Bureau of Land Management (Robert Boyd, Andrew Moss, Dan Staton)
    - Bureau of Reclamation (Michael Beus, Kurt Brown, Kent Collins, Ron Ferrari, Blair Greimann, David Harpman, Victor Huang, Sean Kimbrel, Cassie Klumpp, Yon Lai, Jan Oliver, Tim Randle)
    - Geological Survey (John Gray, Kyle Juracek)
    - National Park Service (Patrick Mangan)
  - Environmental Protection Agency (Gina Christiano)
  - American Society of Civil Engineers (Tim Randle)
  - Colorado Water Resources Institute (Amanda Cox)
- U.S. Society on Dams, Hydraulics on Dams Committee (Marty Teal)
- North Fork Water Conservancy District (Tom Alvey, Trey Denison, Bruce Marvin)
- Los Angeles County Flood Control District (Chris Stone)
- Universities
  - Brigham Young University (Rollin Hotchkiss)
  - Colorado State University (Amanda Cox)
  - Kyoto University (Tetsuya Sumi)
  - Oregon State University (Desirée Tullos)
  - Stanford University (Tom Zigterman)
  - University of South Carolina (Enrica Viparelli)
- Consultants
  - Golder Associates Inc. (George Annandale)
  - Gregory L. Morris Engineering (Greg Morris)
  - WEST Consultants, Inc. (Marty Teal)

The following lectures were provided to introduce each workshop session and stimulate subsequent discussions among the small breakout groups:

- Reservoir Sedimentation Keynote Lecture (Gregory Morris, GLM Engineering)
- Sustainable Water Supply: Policy Implications (George Annandale, Golder Associates)
- Reservoir Sedimentation Categories (Kent Collins, Reclamation)
- Frequency and Extent of Reservoir Sediment Monitoring and the REServoir SEDimentation (RESSED) database (John Gray, USGS)
- Data Collection Technologies (Ron Ferrari, Reclamation)
- Reservoir Sustainability Options (Tetsuya Sumi, Kyoto University)
- Applicability and Cost of Reservoir Sediment Management Options (Rollin Hotchkiss, Brigham Young University)
- Elwha River Restoration Sediment Management (Tim Randle, Reclamation)
- Environmental Effects of Reservoir Sediment Management Options (Kyle Juracek, USGS)
- Modeling Turbidity Currents (Yong Lai, Reclamation)

RESERVOIR SUSTAINABILITY SOLUTIONS

Several categories of reservoir sustainability solutions exist. Combinations of reservoir sediment management methods may be needed to achieve sustainability:

- Watershed land-use practices can reduce the sediment yield entering a reservoir. A wide range of methods can be employed that reduce landslides (Figure 10), soil erosion, and stream-bank erosion.

- Sediment bypass around the reservoir would keep sediments from entering the reservoir. For example, an upstream diversion weir could be constructed to divert river flows with high sediment concentrations into a tunnel or pipe that conveys the sediment around the reservoir and past the dam (Figure 11).
- Passing inflowing sediments through the reservoir also would limit sediment deposition. The venting of turbidity currents through a low-level outlet in the dam (Figure 12) or drawing the reservoir down during periods of high sediment inflow would pass sediment through the reservoir.
- Sluicing of sediment during partial reservoir drawdown would help evacuate sediments near the sluice gates.
- Flushing of sediments previously deposited in the reservoir would help recover storage capacity. Emptying the reservoir is necessary to increase the flow velocity and sediment transport capacity through the reservoir (Figure 13). Downstream sediment concentrations can be very high during flushing.

Figure 10 Landslide stabilization in Japan reduces the watershed sediment yield.

Figure 11 A tunnel was constructed along the Miwa Reservoir in Japan to bypass river flows with high sediment concentration.

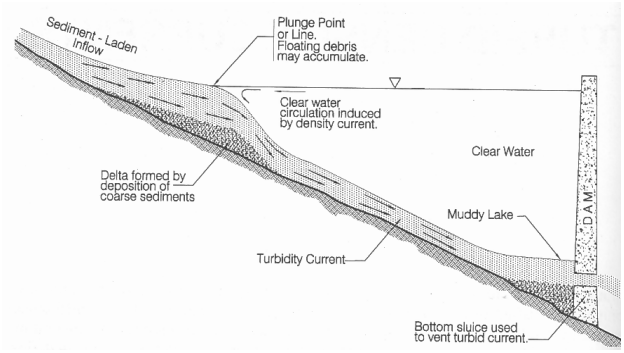

Figure 12 Sediment laden inflows can form a turbidity current along the reservoir bottom and it may be possible to vent this high sediment concentration through a low-level outlet in the dam (Morris and Fan, 1998)

Figure 13 Lowering the reservoir can result in the erosion and downstream flushing of sediments (Lake Aldwell behind Elwha Dam, Washington).

- Sediment removal also would help recover storage capacity. Sediment can be removed by hydraulic dredging (Figure 14), mechanical dredging (Figure 15), and dry excavation. Sediments can be conveyed from the reservoir by sediment slurry pipeline, truck transport, or conveyor belt. Removed sediments can be discharged into the downstream river channel or delivered to a disposal site.

Some sediment management methods would affect reservoir storage operations:

- Flushing that is implemented during the non-flood season by complete reservoir drawdown.
- Sluicing that is implemented during the flood season with partial or full reservoir drawdown.
- Dry excavation, which requires emptying reservoir and using conventional excavation equipment to remove sediment.

Figure 14 Hydraulic dredging of reservoir sediments for transport through a sediment slurry pipeline (Strontia Springs Reservoir, Colorado).

Figure 15. Mechanical dredging of reservoir sediments and transport by truck (Japan).

Other sediment management methods would have much less effect on reservoir storage operations:

- Upstream check dams.
- Bypassing sediment through or around the reservoir.
- Density current venting.
- Hydraulic dredging.
- Barge-based mechanical dredging.
- Hydrosuction sediment removal systems.
- Pressure sluicing under a full reservoir to remove sediment near the outlet.

WORKSHOP FINDINGS

Overview Findings:

- Continued reservoir sedimentation will eventually eliminate or substantially reduce the benefits for which the reservoirs were authorized, designed, and constructed. Sediment management alternatives exist to achieve sustainable reservoir management. The cost of these alternatives is not well known, but failure to manage reservoir sediment will eventually result in substantial dam decommissioning costs and either the loss of project benefits or increased costs of future water storage.
- Federal reservoirs are functioning as originally authorized and designed, which also means they trap sediment that is naturally transported by all rivers and streams. Policy makers likely are not aware that the numerous benefits provided by the nation's reservoirs are not sustainable over the long term without sediment management.
- Population increases over time will result in increased demand for water supply while reservoir storage capacity is being reduced due to sedimentation.
- In some regions, climate change may lead to increased hydrologic variability. Increased variability will reduce water supply reliability during droughts and increase rates of reservoir sedimentation during floods, which also reduces reservoir reliability.
- The present course of reservoir sedimentation will result in lost opportunities for future generations, force them to pay for dam decommissioning, and force them to choose more expensive water storage alternatives than those that were available to previous generations.

- Economic analysis of reservoir sediment management needs to account for inter-generational equity, the future value of reservoir storage, and the eventual dam decommissioning cost if no action is taken. A life-cycle design approach for reservoirs would promote sustainability over the traditional design-life approach.
- A great deal is known about reservoir sedimentation processes. More research is still needed, but enough is known to start addressing the problem.

Reservoir Sediment Monitoring:

- Reservoir sediment monitoring and reporting is needed to track and forecast sedimentation. A publicly available and updatable reservoir sedimentation database is also needed Reservoirs should be surveyed at minimum intervals based on the rates of sedimentation. Reservoirs should also be surveyed after significant inflow floods (e.g., after 10-year flood peak or greater).
- Reservoir sediment survey costs have substantially decreased over the past few decades while the quantity and precision of the data have greatly improved.
- Capabilities to continuously measure sediment transport through surrogate technologies (e.g., hydro-acoustics, turbidity) have also improved over time.

Reservoir Sustainability Solutions:

- Each reservoir sediment management method has a range of applicability. Guidelines are needed to help determine the most applicable sediment management method (or combination of methods) for a given reservoir.
- For each reservoir, eventually develop a plan for either long-term sustainability or decommissioning. Watershed and reservoir demonstration sites are needed to collect data, and test methods and models.
- Reservoir sediment monitoring data are needed to measure sedimentation rates and determine management priorities. Sediment monitoring data should include the volume and spatial distribution within the reservoir, grain size, bulk density, chemical composition, and cohesive properties.
- Environmental problems associated with reservoir sediment can be managed or mitigated with sufficient investigation and understanding of physical, chemical, and biological processes. Lack of understanding will result in unintended consequences.

Sediment Management Research Needs:

- Develop techniques or methods to reduce sediment measurement costs and improve the efficiency of measurements for sediment inflow and thickness within the reservoir, grain size, bulk density, and chemical characteristics.
- Develop methods or models to assess the effectiveness of watershed land-use practices.
- Develop reservoir sediment models to simulate turbulence and sediment entrainment, turbidity currents, and downstream effects.
- Develop improved design methods for dam outlets and bypass tunnels or pipes. Important topics would include the entrainment of sediment into outlets, controlling abrasion, and allowing for maximum reservoir drawdown.
- Develop improved methods for the treatment of contaminated sediment both in situ and at off-site locations.
- Develop improved understanding of how various species of fish or other aquatic organisms respond to periods of high sediment concentration.
- Develop economic analysis methods that account for intergenerational equity and the future value of water storage.
- Explore financial opportunities to pay for reservoir sediment monitoring and management.

NATIONAL RESERVOIR SEDIMENTATION TEAM

Based on the recommendations from the Reservoir Sustainability Workshop, the Subcommittee on Sedimentation has formed the National Reservoir Sedimentation Team (NRST), which is comprised of representatives from the Bureau of Reclamation, U.S. Army Corps of Engineers, other SOS-member organizations, universities, and consultants (Table 1 and Figure 16).

The Objectives and Mission of the NRST are listed below:

- Provide training on reservoir sedimentation and sustainability.
- Provide publically available web-based resources.
- Develop interagency protocols for web-based storage and retrieval of reservoir survey datasets.
- Encourage storage of sediment survey data in the national reservoir database RESSED.
- Formulate a white paper on reservoir sedimentation and sustainability.

Table 1 Founding members of the National Reservoir Sedimentation Team.

Name	Title	Organization
Mustafa Altinakar	Director and Research Professor, National Center for Computational Hydroscience and Engineering	University of Mississippi
Paul Boyd	Hydraulic Engineer, River and Reservoir Engineering Section	U.S. Army Corps of Engineers
Kent Collins	Civil Engineer (Hydraulics), Sedimentation and River Hydraulics Group	Bureau of Reclamation
Deborah Cooper	Research Hydraulic Engineer, River Engineering Branch	U.S. Army Corps of Engineers
Darrell Eidson	Hydraulic Engineer, Hydrology and Hydraulics Branch	U.S. Army Corps of Engineers
Ron Ferrari	Civil Engineer (Hydraulics), Sedimentation and River Hydraulics Group	Bureau of Reclamation
Rollin Hotchkiss	Professor and Chair, Department of Civil and Environmental Engineering	Brigham Young University
Meg Jonas	USACE	U.S. Army Corps of Engineers
Kyle Juracek	Research Hydrologist, Kansas Water Science Center	U.S. Geological Survey
Sean Kimbrel	Civil Engineer (Hydraulics), Sedimentation and River Hydraulics Group	Bureau of Reclamation
Matt Kondolf	Dept Landscape Architecture and Environmental Planning	University of California, Berkeley
Greg Morris	President	Gregory Morris Consultants
Peter Nelson	Colorado Water Resources Research Institute (CWRRI)	Colorado State University
Tim Randle	Reclamation Manager, Sedimentation and River Hydraulics Group	Bureau of Reclamation
Rene Vermeeren	Chief, Hydrology and Hydraulics Branch	U.S. Army Corps of Engineers
Frank Weirich	Iowa Institute of Hydraulic Research, Hydroscience and Engineering	University of Iowa

The NRST is currently focused on the first objective, which is training of reservoir sedimentation and sustainability provided through short courses or workshops, such as the Federal Interagency Sedimentation Conference and other times when possible. These short courses and workshops would be open to the public.

The next objective of the NRST is the development of web-based resources to be posted on the SOS website. These web-based resources would include the following types of information:

- Answers to frequently asked questions

- Protocols for answering new questions posed by the public
- Photo gallery
- Bibliography and publications

Figure 16 Photograph of National Reservoir Sedimentation Team members. Standing left to right are Rollin Hotchkiss, Deborah Cooper, Frank Weirich, Peter Nelson, Sean Kimbrel, Ron Ferrari, Meg Jonas, Tim Randle, Darrell Eidson, Paul Boyd, Kyle Juracek, Mustafa Altinakar, and Rene Vermeeren. Seated left to right are Greg Morris and Matt Kondolf.

The third objective of the NRST is to develop interagency requirements for web-based storage and retrieval of reservoir survey datasets. NRST members will brainstorm ideas to encourage the storage of sediment survey data in the national reservoir database RESSED.

As part of the fourth objective, the SOS website (http://ida.water.usgs.gov/ressed/) and RESSED database are excellent tools for acquiring, summarizing, and sharing information on reservoir sedimentation. Agencies and other organizations are also encouraged to make reservoir sedimentation data available to the public through RESSED. The NRST will be tasked with developing protocols for web-based storage and retrieval of reservoir survey datasets that would be hosted on individual agency web sites.

The last objective is to develop a white paper on reservoir sedimentation and sustainability to inform policy makers about the life-cycle approach to managing sediment in reservoirs.

SUMMARY AND CONCLUSION

The convening of the Reservoir Sustainability Workshop and the formation of the National Reservoir Sedimentation Team are key steps forward in the development of information and awareness about reservoir sedimentation and sustainability. The technical information and policy implications will be important for mangers of dams and reservoirs throughout the nation as they may seek to implement sustainable sediment management practices for the benefit of future generations.

REFERENCES

Morris, Gregory L. and Fan, Jiahua. (1998). *Reservoir Sedimentation Handbook, Design and Management of Dams, Reservoirs, and Watersheds for Sustainable Use*, McGraw-Hill Book Company, New York, NY, 25 Chapters.

Randle, T. J., Collins, K. L., and Gray, J. R. (2013). Avoiding the Inevitable? Capacity Loss from Reservoir Sedimentation. *EOS Transactions American Geophysical Union*, 94(1), 4-4.

Randle, T. J. and Collins, K. L. (2013). Reservoir Sustainability Workshop, Lakewood, Colorado, July 10-12, 2012 in *proceedings of the 33rd USSD Annual Meeting and Conference*, Challenges and Risks of Managing Aging Infrastructure under a New Financial Reality, February 11-15 in Phoenix, Arizona.

PROGRESS TOWARD DEVELOPING A NATIONAL, DYNAMIC RESERVOIR-SEDIMENTATION DATABASE

John Gray, Scientist Emeritus, USGS, Office of Surface Water, Headquarters, Reston, VA
jrgray@usgs.gov

Progress toward efforts to develop publically accessible and updatable REServoir-SEDimentation survey information (RESSED) database – last described in the Proceedings of the 9th Federal Interagency Sedimentation Conference – is encouraging. Since 2009, RESSED has:

- Been successfully ported from Microsoft Access to the user- and web-friendly FilemakerPro database management system.
- A completely revised, logical, and modern schema.
- A beta-tested data-entry module.
- A quality-control function to ensure security for data-entry.
- A reports-production module.
- Data describing changes in capacities for hundreds of additional reservoirs as part of thousands of capacity surveys.
- Most reservoir capacity data available from the U.S. Army Corps of Engineers and the Bureau of Reclamation.
- Acquired permanent maintenance-level support of the U.S. Geological Survey.
- Interest and vocal support from Senior Staff, U.S. House of Representatives.

A number of challenges in the RESSED database-development effort remain. These include:

- A vexing number of ingrained, mostly historical errors in the stored data, although many errors have been identified and culled out.
- A desire expressed among some collaborators to enable porting of spreadsheet-based reservoir sedimentation data directly to RESSED, which raises a number data-transfer and data-quality issues.
- Insufficient resources to expand the development effort to include public-data entry, or to continue development of the version of RESSED envisioned to be most useful in the 21st century.

The eventual goal for the RESSED database is to provide an access for any valid user to enter and retrieve reservoir capacity-change and related data, and to interface it where advantageous with other applications, including the National Inventory of Dams, National Hydrography Dataset, and StreamStats. The time for enhancement of RESSED is now, given the need for early warning on reservoir-storage losses resulting from the inevitable and inexorable accumulation of sediment.

USACE RESERVOIR SEDIMENTATION SURVEY DATABASE (RESSED) ORACLE CONVERSION

Deborah Cooper, Research Hydraulic Engineer, US Army Engineer Research and Development Center, Vicksburg, MS, Deborah.R.Cooper@usace.army.mil

Abstract

Reservoirs are vital for providing flood risk reduction, water supply, energy generation, navigation, irrigation, recreation, and other services. Sediment deposition reduces the useful life of reservoirs, affecting their authorized function. Reservoir Sedimentation Survey Database (RESSED), a database in FileMaker Pro© (FMP) maintained by the U.S. Geological Survey (USGS), contains reservoir information from U.S. Army Corps of Engineers (USACE) districts and other federal agencies for updating and verifying data and creating reports concerning reservoir sedimentation. The data in RESSED can be used to calculate and track changes in reservoir storage characteristics, track and report current and future impacts of sedimentation, quantify sediment budgets, estimate erosion rates in a reservoir's watershed, and export data into other databases. Data captured from FMP to Oracle© provides a basic interface to view RESSED data in the CorpsMap©, an enterprise geospatial platform for USACE that is capable of communication with other data platforms. This paper will discuss the USACE-RESSED data conversion application.

INTRODUCTION

USACE manages more than 700 locks and dams that provide flood risk reduction, water supply, energy generation, navigation, irrigation, recreation, and other services. Sediment deposition (Figure 1) reduces the useful life of the reservoirs these dams produce, affecting their authorized function. More than 50% of USACE reservoirs report moderate to severe impacts of performance within their authorized function before 25% of storage capacity is lost due to reservoir sedimentation. Increasing deposition of sediment in reservoirs is recognized as a growing problem in the United States, with implications for impacts on water supply, water quality, and navigation. The 1996 National Water Quality Inventory (Section 305(b) Report to Congress) indicates that sediments are ranked as a leading cause of water quality impairment in assessed rivers and lakes (Kuhnle and Simon 2000). Quantifying the rate that sediment moves through or is deposited in a reservoir is vital to managing the nation's water resources. Reservoir sedimentation data is essential to assessing changes in reservoir capacity and future reservoir sustainability.

Locating and comparing datasets is challenging because reservoir sedimentation records are scarce, various methods of measuring can be incompatible, and the procedures may have high rates of measurement uncertainty. A *High Country News (HCN)* analysis of US Bureau of Reclamation (USBR) data provides a good example of why locating and comparing datasets is challenging. This analysis, which offers the most recent publicly accessible surveys for eight of

11 Western states, reveals that 35 USBR reservoirs have lost approximately 4.6 million acre-ft of storage capacity to sedimentation.

Figure 1 Sediment Deposition in Matilija Reservoir, CA (USBR 2010)

That's about 8% of total storage in USBR reservoirs, or enough water to serve at least nine million households. The surveys examined by *HCN* cover less than 10% of the dams managed by USBR. Other challenges are that many of USBR's surveys are two decades old and Utah was only able to locate data for 18 of its 133 reservoirs larger than 1,000 acre-ft (Weiser 2011). The lack of reservoir sedimentation data is not a state or regional issue rather it is a national issue. A standardized, web accessible database may provide more accurate data sets for analysis of the effects of sedimentation on reservoir sustainability.

The USGS manages the nation's largest reservoir sedimentation database, RESSED. RESSED, a database in FileMaker Pro© (FMP), is a comprehensive reservoir sedimentation database for U.S. reservoirs (http://water.usgs.gov/osw/ressed) containing data compiled by the Soil Conservation Service, now the Natural Resources Conservation Service (NRCS). Version 1.0 of this interactive and enhanced reservoir sedimentation survey database consists of a comprehensive compilation of reservoir information related to wet and dry surveys, storage, elevation, area capacity, reservoir operations, and other reservoir information for 1,824 large and small USACE, USBR, Tennessee Valley Authority (TVA), NRCS, and other federal, municipal, and utility agency reservoirs and lakes. The data in RESSED can be used to calculate and track changes in reservoir storage characteristics, track and report current and future impacts of sedimentation, quantify sediment budgets, estimate erosion rates in a reservoir's watershed, and can be exported into other databases.

To date, USACE districts have performed quality assurance and quality control on RESSED data. The Institute for Water Resources (IWR) is conducting ongoing research of reservoir sedimentation and the impacts of climate change on reservoir sedimentation through the Reservoir Sediment Information (RSI) research work unit and the USACE Response to Climate

Change Program. Data capture of reservoir survey and area capacity data from the USGS RESSED FMP platform became necessary to store and display reservoir information consistent with established USACE enterprise databases, such as the Corps Water Management System (CWMS) and the National Inventory of Dams (NID). Once the RESSED data was captured in CorpsMap©, USACE developed the Reservoir Sedimentation Information system production site for entering basic reservoir survey and capacity data for uploading data to RESSED. While the production site was developed with references to NID and CWMS databases, the data capture from RESSED established a platform for uploading data to RESSED. This paper will discuss the USACE-RESSED data conversion application.

RESERVOIR SEDIMENTATION INFORMATION SYSTEM PRODUCTION SITE

The Reservoir Sedimentation Information (RSI) system production site was developed by USACE to provide a comprehensive summary of USACE reservoir conditions. The overarching intent of this system is to store and display reservoir information to assist with evaluation of sedimentation trends and reservoir life expectancy with respect to a changing climate. The initial iteration of this dynamic system focuses on input and display of reservoir metadata. Reservoir information is available for viewing by all users. To edit or upload data requires the acquisition of permissions provided by an administrator.

To access the RSI production site users must:

1. Log on to https://maps.crrel.usace.army.mil/apex/f?p=303
2. Click the CAC Login button
3. Enter the 4-digit PIN

Upon logging into the system, the user will be able to view everything in the application as the read-only role of Data Reviewer. To obtain additional privileges of editing or uploading data, the user should email one of the points of contact (POC) listed on the Help tab. After emailing a RSI POC, if the user is eligible for additional privileges, the RSI Production Site team will grant the user District Data Manager (DDM) privileges based on the corresponding district. After the Production Site team grants privileges, the user will receive an email notifying him or her of a role change in RSI. The District Data Manager privilege will allow users to edit data for their specific district only, while still allowing them to view data from other districts as they did with the Data Reviewer role, i.e., the District Data Manager for the Vicksburg District can view any district's data but can only edit data for the Vicksburg District.

The RSI system production site consists of four main tabs: Home, Reservoirs, Map, and Help. Descriptions and graphic illustrations of each tab are provided below.

Home Tab

The Home tab provides introductory information on the RSI Production Site and describes each of the successive tabs (see Figure 2 below).

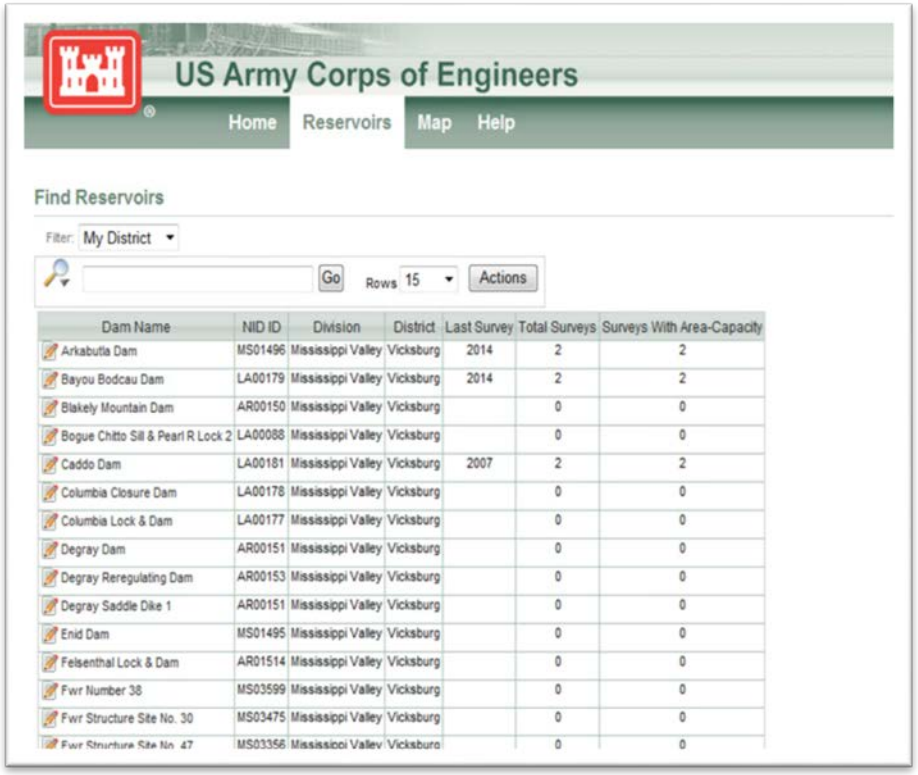

Figure 2 Reservoirs Tab

Reservoirs Tab

The Reservoirs tab allows a user to view detailed information about all USACE reservoirs listed in the NID database. The dam name, NID ID, division, and district are directly linked to the NID database and cannot be modified or edited within the RSI production site. Data associated with a particular reservoir, found in the last survey, total surveys, and surveys with area-capacity fields on the production site, can be viewed and, with special permissions, edited by the District Data Manager aligned to that particular reservoir. The dams can be filtered by an individual district or all districts. A reservoir can be located by typing the name of the reservoir in the search window and clicking "Go." The user can then click the pencil icon to view detailed information and/or enter data for the specific dam that was searched for. Five sub-tabs will appear under the Reservoirs tab: Detail, Surveys, Storage Allocation, Documents, and Graphs.

Detail Sub-Tab

The Detail sub-tab allows a user to view detailed information about a particular USACE reservoir. Information on this sub-tab is still directly linked to the NID database. A map showing the reservoir location and NID information is also displayed (shown in Figure 3 below).

Figure 3 Reservoirs Detail Sub-tab

Surveys Sub-Tab

Survey data is entered by clicking the "Add New Survey" button on the Surveys sub-tab and entering data under the Survey Detail tab (see Figure 4a below). Values with asterisks indicate mandatory fields. Clicking the "Add" button after entering all the required information displays the survey data in a table at the top of the page. Clicking the pencil icon next to an added survey and clicking a red "Upload Area-Capacity" arrow (Figure 4b) allows the user to upload Area-Capacity data for the corresponding survey. After uploading the Area-Capacity data, data can be edited in this window by clicking the pencil icon next to the row to be edited. Note that the Area-Capacity data can also be downloaded by clicking on a green "Download Area-Capacity" arrow.

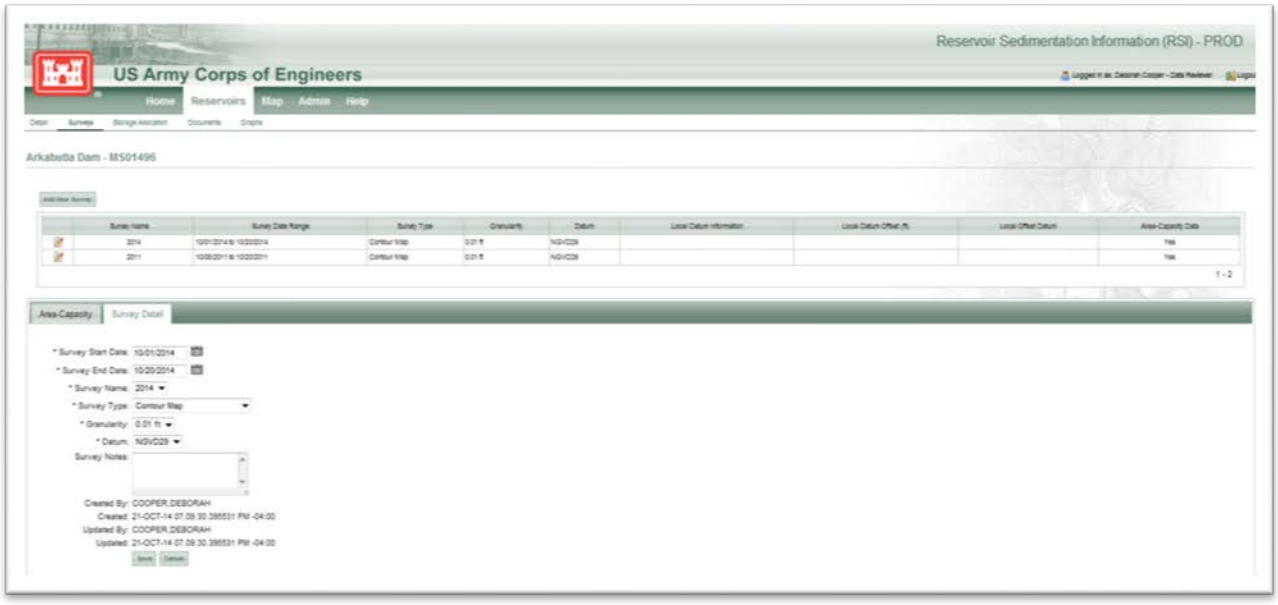

Figure 4a Reservoirs Surveys sub-tab and Survey Detail tab

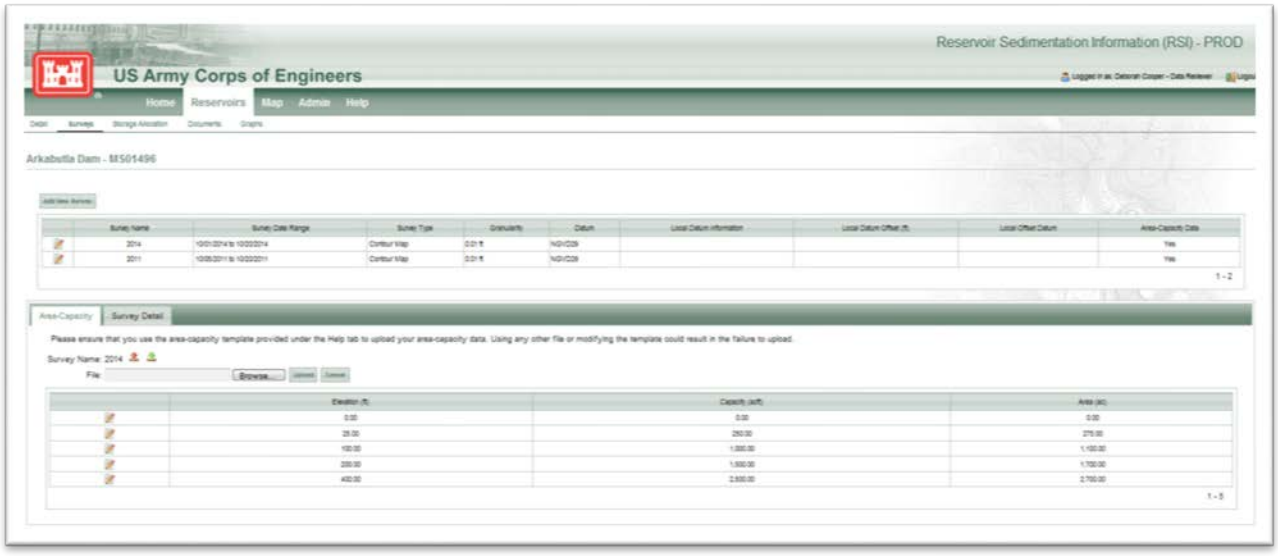

Figure 4b Reservoirs Surveys sub-tab and Area-Capacity tab

Storage Allocation Sub-Tab

Data from the Corps Water Management System (CWMS) is displayed under the Storage Allocation Tab. If reservoir data is not found in CWMS, no data will be displayed.

Documents Sub-Tab

The user can upload documents for storage under the Documents sub-tab. Area-Capacity spreadsheets, documents, images, maps, presentations, reports, videos, and other files can all be stored for retrieval on this site (shown in Figure 5 below).

Figure 5 Reservoirs Documents Sub-tab

Graphs Sub-Tab

Capacity data is plotted under the Graphs tab (shown in Figure 6 below). If the reservoir elevation data is entered in CWMS, data from the CWMS site can be plotted here as well.

Map Tab

The Map tab displays active reservoir survey data sites.

Help Tab

Technical assistance information, a RSI Quick Guide, and an Area-Capacity spreadsheet template (that must be used for uploading area-capacity data to the RSI System Production Site) are all found under the Help tab. Users must use the provided Area-Capacity template to ensure that data is properly uploaded and displayed in the Reservoirs Surveys window. To enter data for additional reservoirs, the user must begin the process again by navigating to the Reservoirs tab. On the Reservoirs tab, the user can then search for and locate another reservoir to initiate survey data input.

Figure 6 Reservoirs Graphs Sub-tab

CONCLUSION

Testing of the RSI system production site will be initiated by district input of survey and area-capacity data in FY15. The plan is to expand the site to include additional reservoir data as it becomes available, enhance the input tools, and standardize the reservoir data analysis across USACE. The RSI production site will ensure that districts can maintain the most currently available and consistent data from databases such as RESSED, CWMS, and NID. It does this by using the provided Oracle© interface to view RESSED data in CorpsMap© and as a mechanism for the USACE data platform to communicate with RESSED as well as other data platforms.

REFERENCES

Kuhnle, R.A. and Simon, A. (2000) "Evaluation of Sediment Transport Data for Clean Sediment TMDLs" National Sedimentation Laboratory, USDA Agricultural Research Service, p 3.

Morris, G. L. and Fan, J. (2010). ***Reservoir Sedimentation Handbook,*** p 10.1.

Strand, R.I., and E.L. Pemberton (1982). **Reservoir Sedimentation**, U.S. Bureau of Reclamation, Sedimentation and River Hydraulics Group, p 48

Weiser, M., (2011). "Sedimentation is a Building Problem in the West's Reservoirs", *High Country News*, April 20, 2011, http://www.hcn.org/issues/43.6/muddy-waters-silt-and-the-slow-demise-of-glen-canyon-dam/sedimentation-a-building-problem-in-the-wests-reservoirs

RESERVOIR SEDIMENTATION AND SUSTAINABILITY IN USACE: STATUS REPORT

Meg Jonas, Senior Hydraulic Engineer, USACE Headquarters, Engineering & Construction, Washington, DC, meg.m.jonas@usace.army.mil;

Abstract Sediment deposition in Corps reservoirs reduces the useful life and can severely impact authorized project purposes including flood risk management, hydropower, recreation, water supply, and environmental quality. Within the United States, the US Army Corps of Engineers (USACE) maintains and operates almost 400 dams and reservoirs for flood damage reduction. Sedimentation affects (or will affect) all these projects to some degree, and may be one of the most significant impediments to long-term sustainable operation. Reservoir sedimentation and sustainability are closely linked. Anticipated future conditions (decreased firm yield due to climate change, along with increased demand for water) will work in conjunction with the diminished reservoir storage due to sedimentation to reduce our reliable water supply. This paper will discuss the current status of data on Corps projects and types of impacts that have been observed. It will also cover ongoing Corps activities related to reservoir sedimentation and sustainability, including efforts that are proposed or underway at various Corps projects to mitigate the impacts of reservoir sedimentation. Activities related to reservoir sedimentation fall under multiple components of USACE. This paper will review and summarize those activities across the organization. USACE is involved in the Reservoir Sustainability Task Committee and the National Reservoir Sedimentation Team (under the ACWI Subcommittee on Sedimentation). This paper will provide an update on USACE activities related to reservoir sustainability.

INTRODUCTION

Reservoir sedimentation problems affect multiple business lines within the Corps, and related activities are funded by multiple programs. This paper will identify current ongoing efforts and stakeholders within the Corps.

RESERVOIR SEDIMENTATION SURVEYS

Reservoir sedimentation surveys are performed by each individual Corps district. Funding normally comes out of reservoir project funding. Surveys are often deferred in order to fund higher priority items. However, other funding sources may become available: funds that cannot be expended on other projects, or unusual funding sources such as ARRA. These other funding sources often have a very short window of opportunity, and the key to obtaining them is the district's ability to move quickly, that is, their readiness to take advantage of funding that comes up suddenly. Sponsors also fund surveys.

All the aspects of a reservoir sedimentation survey are determined by the district, including:

- Type of survey (range line or bathymetric)
- Extent of survey (entire flood control pool or a portion thereof)

- Use of aerial survey data to augment hydrographic survey data
- Who performs the survey (contractor or in-house staff)
- Method of data reduction, and who performs it (contractor or in-house staff)

There is significant variability among Corps districts in all aspects of reservoir sedimentation surveys.

RESERVOIR SEDIMENTATION DATABASE

USACE has been working with USGS on a reservoir sedimentation database, RESSED, to facilitate national reporting of reservoir sedimentation survey results, survey status, and other items (sediment management measures, sedimentation problems, etc.) One key element is obtaining data from each individual Corps district to populate the database.

Under the Responses to Climate Change program, the Corps is evaluating the potential impact of climate change on reservoir sedimentation. Multiple activities are being performed under this program. One activity includes reviewing available sediment information to identify data gaps and estimate the costs required to bring reservoir sedimentation information up-to-date.

CORPS PROGRAMS AND ENTITIES WITH INTEREST IN RESERVOIR SEDIMENTATION

Multiple Corps programs and entities have aspects related to reservoir sedimentation. The most significant are listed below.

Operations. The operation of each reservoir project is affected by reservoir sedimentation and related problems, which may include lack of access to boat ramps, inability to operate outlet works, blockage of water supply intakes, and other impacts.

Water Supply. Sedimentation normally has the most significant impacts on water supply storage.

Responses to Climate Change (RCC). Climate change may impact sediment yields. The RCC program has funded work on reservoir sediment information (discussed above), as well as other studies such as paired reservoir studies. A study of Coralville Reservoir by Rock Island District evaluated the impacts of storage loss due to sedimentation (under current conditions) on spillway flows for simulations of historic flood events.

Committee on Channel Stabilization. This Headquarters-level committee is composed of experts in alluvial channel processes and river engineering from throughout the Corps. Reservoir sedimentation falls under this committee's area of expertise, and the committee (or individual committee members) have been involved in many ongoing efforts.

RESEARCH AND DEMONSTRATION PROGRAMS RELATED TO RESERVOIR SEDIMENTATION

There is no program dedicated solely to reservoir sedimentation and sustainability research. The research and demonstration programs listed below cover multiple items, some of which are related to reservoir sedimentation:

- Flood Risk Management Research Area
- Regional Sediment Management
- Engineering with Nature
- Great Lakes Tributary Modeling Program

GUIDANCE RELATED TO RESERVOIR SEDIMENTATION

The following Corps guidance addresses reservoir sedimentation:

Engineer Manual (EM) 1110-2-4000, Sedimentation Investigations of Rivers and Reservoirs. Provides guidance on procedures for river and reservoir sedimentation investigations (1995, currently being updated).

Engineer Regulation (ER) 1110-2-4001, Notes on Sedimentation Activities. This regulation prescribes general requirements for submittal of annual reports on Corps of Engineers activities in the field of sedimentation (1981).

Engineer Regulation (ER) 1110-2-8153, Sedimentation Investigations. This regulation prescribes the procedure and rationale for conducting sedimentation investigations in support of the hydrologic analysis and hydraulic design of civil works projects, and environmental impact analyses (1995).

TRAINING RELATED TO RESERVOIR SEDIMENTATION

There is currently no Corps training offered related to reservoir sedimentation. Corps personnel are assisting in the short course on reservoir sedimentation and sustainability at the 2015 SedHyd conference.

EXAMPLES OF DISTRICT PROJECTS RELATED TO RESERVOIR SEDIMENTATION

The list below gives some examples of district activities.

Baltimore District, Susquehanna River Basin. Watershed assessments and sediment transport modeling have been performed to evaluate alternatives at Conowingo Dam, with the goal of protecting water quality, habitat and aquatic life in the lower Susquehanna River and the Chesapeake Bay.

Tulsa District, Neosha River. The Kansas Water Office has requested approval to dredge sediment from the conservation pool of John Redmond Reservoir in order to restore water supply storage capacity that has been lost to sedimentation.

Kansas City District, Kansas River Basin. Reservoir sustainability efforts have been initiated to evaluate alternatives for sediment management alternatives at Perry Lake and Tuttle Creek Lake.

Omaha District, Missouri River. The district is evaluating sediment flushing at Gavins Point Dam in Phase II of its Lewis and Clark Lake Sediment Management Study as part of the Missouri River Recovery Program.

Los Angeles District, Santa Ana River. Orange County Water District (OCWD) is proposing a demonstration project in which sediment would be removed from behind Prado Dam, and conveyed to the Lower Santa Ana River below the dam for re-entrainment.

INTERAGENCY ACTIVITIES RELATED TO RESERVOIR SEDIMENTATION

The Corps is represented on the ACWI Subcommittee on Sedimentation (SOS). The Corps also has representatives on the SOS working group on reservoir sedimentation and sustainability (the National Reservoir Sediment Team). The SOS passed a resolution on reservoir sustainability, which was recently approved by ACWI.

OTHER ACTIVITIES

Personnel from Omaha District are working on projects in the Mekong River Delta, along with personnel from the US Bureau of Reclamation.

SUMMARY AND CONCLUSIONS

There are many Corps activities related to reservoir sedimentation and sustainability. This is a “first cut” at listing all pertinent Corps activities, and is no doubt incomplete. Next steps include making the list of activities more complete, and improving coordination between these activities.

ANALYSIS OF EXTREME FLOOD SIGNATURE: CAN 2-D HYDRAULIC MODELING MATCH OBSERVATIONS?

Rebecca Kallio, Hydraulic Engineer, Bureau of Reclamation Technical Service Center, rkallio@usbr.gov;
Jeanne Godaire, Geomorphologist, Bureau of Reclamation Technical Service Center, jgodaire@usbr.gov

INTRODUCTION

Paleoflood hydrology is critical to the understanding of flood magnitude-frequency responses because it extends the timescale of the gaged record to include extreme floods that occurred prior to human observation. Paleoflood studies usually produce flood chronologies that can be used to improve flood-frequency analysis and flood hazard evaluations. Paleoflood studies rely on assumptions of shear stress values necessary to erode stream terraces with stable soils and the predictive capability of the hydraulic model to generate accurate peak discharge estimates to produce a paleoflood signature, deposition on or erosion of a stream terrace surface. While a range of values is reported that includes uncertainty in the peak discharge estimates, only limited comparisons between physical observations of large historical floods and the model simulations of the same events have been performed. These comparisons typically have involved historical floods that are decades old and therefore many of the flood indicators have been removed or obscured from field observation. A post-flood investigation of a recent extreme flood can provide a more robust estimate of the uncertainty in model predictions of surface erosion and deposition and can also provide greater overall understanding of flow dynamics during extreme floods and the shear stress values necessary to leave a signature, erosion or deposition of surface sediment.

This study poses the following questions: (1) how well does the hydraulic model simulate a recent, extreme flood; (2) do field observations and model predictions indicate surface erosion in the same areas during an extreme event; (3) do field observations and model predictions infer sediment deposition in the same areas during an extreme event; and (3) what are the limitations of the model and paleoflood studies in general to predict the modification of stream terraces or areas of sediment deposition during extreme floods?

To answer these questions this study will: (1) survey high water marks and make field observations and interpretations of erosion and deposition during a recent large flood; (2) construct 2D hydraulic models to simulate the extreme flood; and (3) compare model predictions with the surveyed flood stage and real world observations of erosion, deposition and other modifications to the stream channel.

PALEOFLOOD HYDROLOGY

Paleoflood hydrology has been used for the past century in a wide variety of settings throughout the world (Costa, 1986; Patton, 1987; Baker et al., 1988). Early studies by Mansfield (1938) on the Ohio River and Jahns (1947) on the Connecticut River recognized that historical floods on those rivers overtopped stream terraces that had not been inundated for thousands of years. The stratigraphic record present along streams in the form of terrace and flood plain deposits can be direct indicators of the magnitude of large floods on a river and may be 10 to 100 times longer than conventional stream gaging records of large floods (e.g., Patton, 1987; Baker, 1989; Jarrett, 1991).

One widely-used technique in paleoflood studies uses the fine-grained sedimentological record that accumulates in backwater areas (slackwater) to construct a detailed history of past floods (e.g., Patton et al., 1979; Kochel and Baker, 1988). This technique can be extremely useful in characterizing the frequency of large floods, but can fall victim to the inherent assumption that a sequence of slackwater sediments represents a complete and continuous record of floods at a particular site. In addition, the physical setting of a backwater site may not be ideally suited for reconstructing or accurately estimating the peak discharge for the flood associated with a particular sequence of slackwater deposits in one-dimensional hydraulic models. Two-dimensional hydraulic modeling (e.g., Denlinger et al., 2002) can aid in estimating peak discharges in these complex geometries.

Another methodology uses the age of a terrace surface that lacks clear evidence of recent inundation, erosion and deposition, or alternatively displays evidence for long-term stability, to establish an upper limit to flooding. This non-inundation approach can be very useful in flood hazard assessment because geomorphic and stratigraphic information derived from the terrace surface can provide an upper limit or bound on the age and magnitude of extreme floods (Levish, 2002). Rather than constructing a detailed record of past floods, the non-inundation approach focuses on identifying a non-exceedance bound. Establishing a non-exceedance bound is accomplished by identifying terrace surfaces that serve as limits for the paleostage of large floods and estimating ages for those terraces (Figure 4). These bounds do not represent actual floods, but instead limits the peak flood stage over some measured time interval. Simply stated, a non-exceedance bound is a maximum stage that has not been exceeded in the time period since the terrace surface stabilized. The maximum stage can be used to estimate peak discharge given some knowledge of the channel characteristics.

SETTING

The study reach is located along Cottonwood Creek in El Paso County near Colorado Springs, Colorado approximately 60 miles south of Denver (Figure 1). The Cottonwood creek watershed is about 18.9 mi^2, heading in the southern portion of the Black Forest region and draining to the southwest into Fountain Creek. A flood of record during June 2012 on Cottonwood Creek provided an ideal dataset to study recent flood signatures and physical/hydraulic properties associated with a large-magnitude flood in a small watershed. The study reach is located within the city of Colorado Springs open space and begins 150 feet downstream of the East Woodman Bridge, extending downstream 5,800 feet to just upstream of Rangewood Drive Bridge. Cottonwood Creek is incised into Cretaceous bedrock and about 10-20 ft. below housing developments. Limited grade control features and other human structures within the reach provide a mostly natural setting in which to study the geomorphic characteristics of the flood. Drainage area associated with the study reach is approximately 10.2 mi^2 as documented at the USGS stream gage no. 07103980.

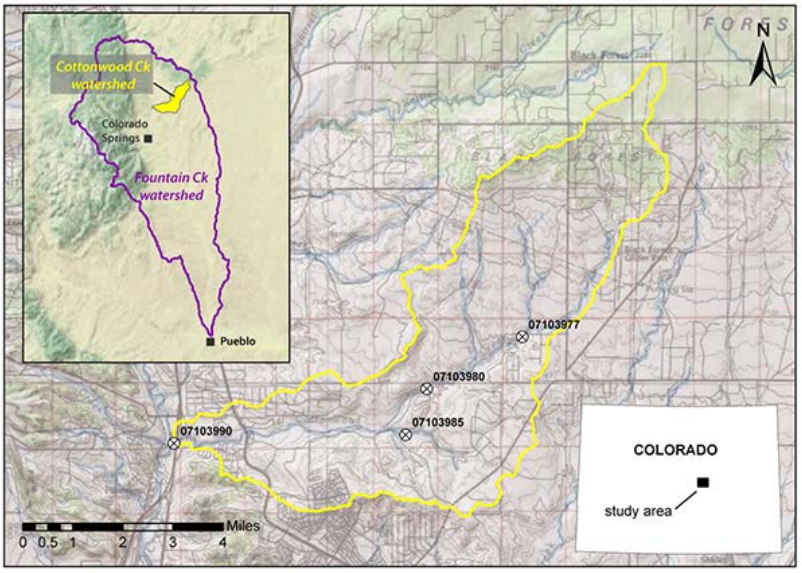

Figure 1 Cottonwood Creek study reach located downstream of East Woodman Road near Colorado Springs, CO. USGS stream flow gage stations are denoted on the map with cross hatched circles.

THE JUNE 6, 2012 FLOOD, COTTONWOOD CREEK, COLORADO SPRINGS, CO

Peak flows on Cottonwood Creek typically occur during the summer months of June through September and are commonly caused by convective storm systems which deliver moisture in the form of intense thunderstorms in the late afternoon and early evening hours. The flood of June 6, 2012 peaked between 8:15 and 8:30 pm and had a peak discharge of 1,610 ft^3/s at USGS stream gage no. 07103980 (Cottonwood Creek at Woodmen Road near Colorado Springs, CO), which was the peak of record for the 20-year history of the stream gage (Figure 2). The flood lasted approximately 2 hours with a slightly more gradual rising limb and a steep falling limb. Within about 81/2 hours, flows had returned to less than 10 ft^3/s at the stream gage. During August 2013 a larger-magnitude peak discharge of 3,500 ft^3/s was recorded after the field survey of high water marks.

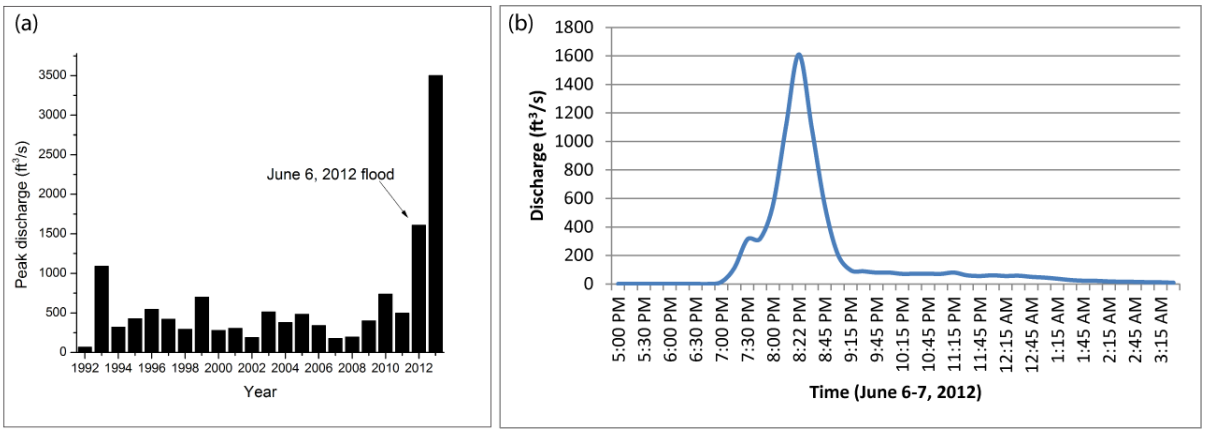

Figure 2 Hydrologic data, Cottonwood Creek at Woodmen Road near Colorado Springs, CO (USGS gage no. 07103980). (a) Peak discharge data; (b) runoff hydrograph, 15-minute discharge data, June 6-7, 2012.

MODEL SELECTION

Reclamation Technical Service Center (TSC) utilizes hydraulic modeling as part of paleoflood studies to estimate peak discharge magnitude associated with the stage of slackwater deposits and stream terraces. The majority of detailed paleoflood studies have used Sedimentation and River Hydraulics 2D (SRH-2D) (Lai, 2008) for 2D hydraulic modeling. This study used SRH-2D to test the current methodology that is incorporated into the paleoflood studies. SRH-2D can analyze flow complexities of the interaction between the main channel, banks, and floodplain that are best represented with an unstructured arbitrarily-shaped mesh.

SRH-2D was used to model flow under steady and unsteady-state conditions. Steady state analysis was used to determine whether modeled depth averaged maximum water surface elevations matched field observations and to compare the modeled depth average maximum shear stress values with erosional and depositional areas. Unsteady-state flow modeling was performed to examine the variation in shear stress values at different points in the flood hydrograph for selected observation areas. To define the SRH2D downstream boundary condition, an Army Corps of Engineers Hydrologic Engineering Center River Analysis System (HEC-RAS) (U.S. Army Corps of Engineers Hydrologic Engineering Center, 2010) model was constructed for the study reach. The HEC-RAS model was extended 650 feet downstream of the study reach to ensure the boundary condition would not impact SRH2D model results.

DATA COLLECTION

This section describes the field survey, topographic, and geomorphic data that were collected for this study. The collection methods, locations, and data uncertainty are described.

Survey Data and Terrain Development

The terrain developed for the study reach used a combination of in-channel surveyed points and contour data. Site specific survey points were collected by the authors on June 5, 2013 to identify the stage and lateral extent of the June 6, 2006 flood and to further define the channel topography. The June 6, 2012 flood was the event of record and it was assumed that the highest high water marks were a result of this event. To define the flood stage and lateral extent, we surveyed trim lines, flotsam and tops of sandy flood deposits. An effort was made to find the highest flood indicators to identify the peak stage of the flood. In order to define channel topography, survey points were collected to capture the channel thalweg, sand bars and banks. All survey points were collected using Real Time Kinematic (RTK) Global Positioning System (GPS) equipment. An NGS Online Positioning User Service (OPUS) solution was obtained for control at the base station. Positional accuracies for RTK and this survey are +/- 0.05 feet horizontally and +/- 0.10 feet vertically. The survey used NAD 1983 (2011) Epoch 2010.00, State plane coordinates,

Colorado Central zone in U.S. Survey Feet (USFT), based on station Marshall Field Cors Arp with coordinates 1298154.39 N and 3448788.1 W.

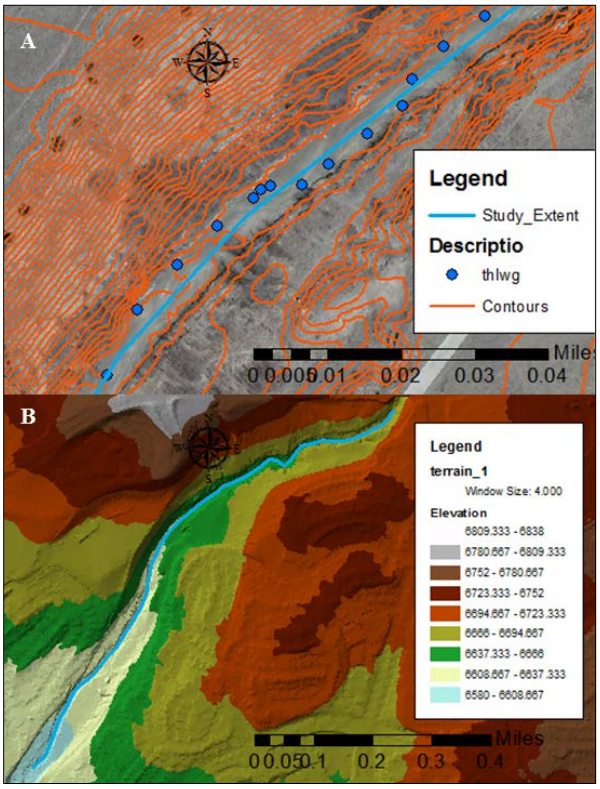

Figure 3 A) Example of survey data and contour lines along Cottonwood Creek, B) Terrain developed for the study reach.

The City of Colorado Springs contracted with Sanborn to provide a digital orthoimagery dataset. The imagery was acquired over approximately 240 square miles of the City of Colorado Springs, Colorado. Sanborn acquired new 0.5-foot pixel imagery of the Colorado Springs area in the spring of 2010 during leaf-off conditions. The acquisition was performed using Sanborn's UltraCam-D digital camera system and aircraft equipped with AGPS/IMU. Digital orthoimagery was produced using existing DEM, updated as needed to support production of the orthoimagery. The City of Colorado Springs used the imagery to develop 2-foot contour lines for the Cottonwood Creek basin.

The digital imagery of the study reach was collected while water was in the stream; therefore, the channel survey points collected in 2013 were used to define the channel bed and then combined with the 2-foot contours to develop a t errain for the study reach (Figure 3). GPS surveyed points were taken along the stream bank and compared to Sanborn contour data. The points were within the ±1 foot tolerance and provide confidence in the topographic data.

Geomorphology

Surficial geologic mapping involves the delineation of surficial geologic features on the landscape. When mapping along river corridors, these features typically include stream terraces, bedrock outcrops, axial and tributary stream channels, eolian landforms, and other deposits along valley margins, such as landslide deposits and glacial deposits. Surficial map units are landforms that can be grouped together based on similar physical or geomorphic characteristics such as position in the landscape, surface morphology, sedimentology, soil development and process of formation. Deposits in this study are mapped along the Cottonwood Creek stream corridor and therefore are typically composed of fluvially-derived sediments and are landforms that were created and modified by fluvial processes. The extent and character of these features provide information concerning controls on lateral and vertical channel movement over longer time frames than the historical period and many times are important factors in explaining variation in channel morphology along the length of the study reach. Surficial geologic units defined in this study are described on the basis of surface morphology, character of deposits, vertical and lateral relation to other mapped units, relative or absolute age, and geographic location. Stratigraphic descriptions were performed on a limited number of exposures along the channel banks using sedimentological terminology from Boggs (1995) and soil nomenclature from Birkeland (1999) in order to understand the depositional processes associated with the stream deposits. Five Sediment samples were collected from the surface of alluvial deposits near model observation points along Cottonwood Creek and submitted for particle size analysis and bulk density determinations at Colorado State University Soil, Water and Plant Testing Laboratory. Bulk density samples were collected using a soil core sampler.

Flood observations were made during field work in July and August 2013. Types of features that were noted included depositional features such as sand bars, flotsam and debris lines. Scour features included trim lines, scoured bedrock and vertical bank exposures. When combined the observations reveal the stage of flood waters and areas where the channel was scoured both vertically and laterally during the flood.

GEOMORPHIC OBSERVATIONS AND MAPPING

In order to compare the geomorphic effects of the June 6, 2012 flood with model predictions, high water marks and other features created during the flood were documented during field observations. T he main goal of the geomorphic mapping of flood features was to determine areas of deposition and erosion along the channel during the 2012 flood. Areas that were above the level of low bars were mapped based on whether they appeared to be primarily depositional or erosional areas. Depositional areas consisted of abundant flotsam and sand deposits which were deposited on younger terraces or in areas of recirculation, such as upstream of sharp meander bends, or in small tributary or sideslope gullies along the margins of the channel (Figure 4). Erosional areas consisted of scoured bedrock benches, and areas with distinct trim lines or vertical bank exposures of fluvial sediment or bedrock. Low bars were not mapped as areas of deposition because these areas are also modified by lower stage flows than the 2012 flood.

A surficial geologic map was also produced to show the extent of the channel, channel bars, terraces (labeled younger and older on a relative scale), bedrock benches and bedrock outcrops in the channel. Mapped flood features generally correspond to specific landforms that were mapped in the reach; for example, many depositional areas were located on younger stream terraces and erosional areas were located on bedrock benches. Mixed depositional and erosional areas occur within the channel itself but cannot be related to the 2012 flood because they have been modified by more recent, lower flows.

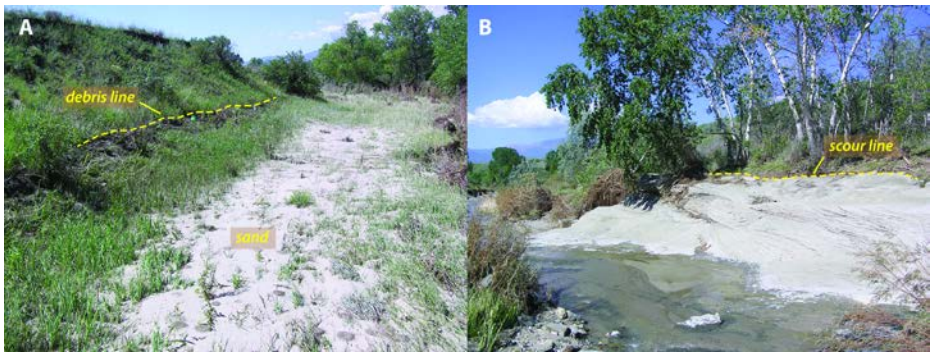

Figure 4 Example of erosional and depositional areas; A. depositional area showing sand and debris line from recent flood; B. erosional area showing scour line on bedrock outcrop.

HYDRAULIC MODELING

Boundary Condition

Hydraulic models require an exit boundary condition to converge on solutions for various hydraulic parameters. SRH-2D requires either a r ating curve or a known downstream water surface elevation to satisfy a b oundary condition. There was no flow or stage data at the downstream end of the model. As such, a HEC-RAS model was developed for the Cottonwood Creek Study using HEC-geoRAS (U.S. Army Corps of Engineers, 2010) to develop the geometry. The HEC-RAS model was extended far enough beyond the downstream boundary of the 2D model that the computed water surface elevation in the HEC-RAS model at the station of the outlet of the 2D model was not influenced by the boundary.

The flow data was obtained from USGS gaging station located at cottonwood creek for the June 6, 2012 flooding event. A manning's n of 0.03 and 0.06 was selected for the main channel and the left and right bank, respectively for the channel roughness (Chow, 1959). The HEC-RAS boundary condition used for both steady-state and unsteady-state was the normal depth. The normal depth can be determined by the slope of the channel and Cottonwood Creek has a slope of 0.025 ft/ft that was derived from the contour data. This HEC-RAS boundary condition will be referred to the regular boundary condition. We performed a boundary conditions sensitivity analysis and altered the slope to 0.03 ft/ft and 0.02 ft/ft.

Mesh Generation

Table 1 Manning's n values selected for study reach areas.

Material Type	High n	Mid n	Low n
Channel	0.035	0.03	0.025
Overbank grass	0.055	0.05	0.045
Overbank shrub	0.08	0.07	0.075
Overbank tree	0.1	0.095	0.09

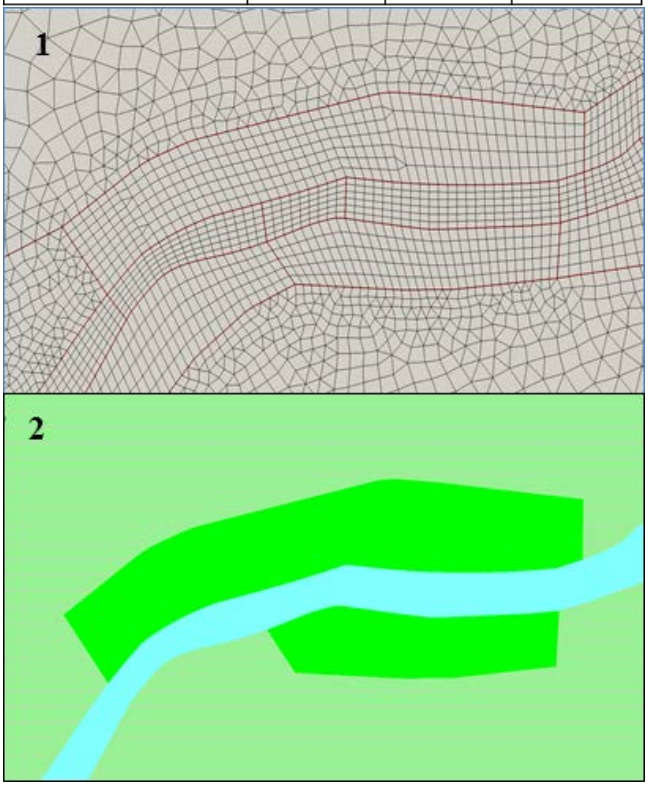

Figure 5 (1) Quadrilateral elements in the main channel and triangular elements on the over bank areas. (2) Material properties for the main channel, the dense vegetated area, and grassed and small shrub vegetated area.

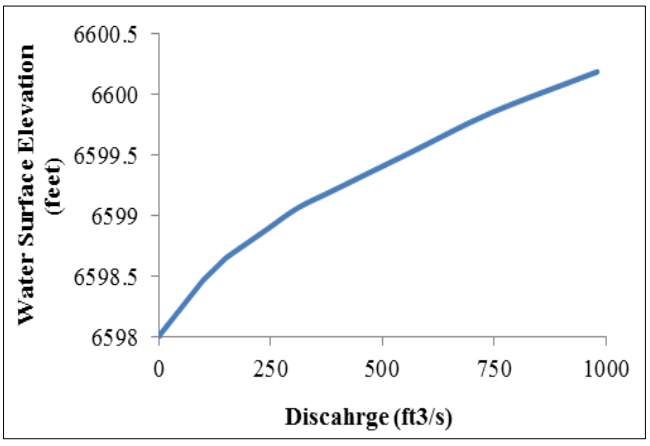

Figure 6 The rating curve developed at River station 812.67 feet for SRH-2D unsteady-state model downstream boundary condition.

Two main components of the 2D model are the mesh and the topography. The mesh was constructed in Surface water Modeling System (SMS) version 10.1 and contains all spatial data such as ground/bed elevations, channel roughness, and overbank roughness. Elevation values are stored at each node while roughness values are stored in each element (Figure 5). The average cell size within the main channel was 10 feet longitudinally and 8 feet laterally. Mesh cell sizes increased with increasing distance from the main channel. The entire mesh contained 17,320 cells. The mesh elevation is imported from ArcGIS and is interpolated to each mesh node. Roughness is assigned to polygons created to construct the mesh. Based on site visit observations and aerial photography the study reach was broken up into four roughness areas: the main channel, overbank grass, overbank shrub and overbank tree (Table 1) and were estimated from (Chow, 1959).

Model parameters

The 2D model was run under both steady state and unsteady state conditions with slightly different input parameters. For steady-state flow the inlet discharge was 1610 ft^3/s. The model had a simulation time of 74 hours with a time step of 2 seconds. Three boundary conditions of 6599.71 feet, 6600.21 feet, and 6600.71 feet developed from the HEC-RAS model were modeled to observe where water surface elevations converged to a common elevation. Convergence indicates the boundary condition no longer impacts the water surface elevation. Model results downstream of this location would be considered void since they are driven by the boundary conditions and not flow dynamics of the river system.

For the unsteady flow model the total time simulated was 80 hours and a time step (model time integration) of 1 second. A rating curve was used for the downstream boundary condition. The rating curve was taken from the HEC-RAS model at river station 812.67 feet (Figure 6).

Soil Samples and Shear Stress

Julien (1998) defined the critical shear stress as the beginning of motion when the ratio of hydrodynamic focus exceeds the submerged weight of a particle.
Julien developed a graphical relationship between critical shear stress and median grain size d_{50} on a flat horizontal surface (Table 2). This method also assumes that fractions of sediment enter motion at the same values of applied shear stress.

Table 2 Threshold shear stress conditions for granular material at 20˚ C (Julien, 1988).

Size Class	Shear Stress Range (Pa)
Medium Silt	0.010-0.083
Coarse Silt	0.084-0.110
Very Fine Sand	0.111-0.145
Fine Sand	0.146-0.194
Medium Sand	0.195-0.270
Coarse Sand	0.271-0.470
Very Coarse Sand	0.471-1.260

In previous paleoflood studies, these values have been used to infer surface erosion of stream terraces when the critical shear stress is exceeded during a modeled flood. Discharges necessary to produce the critical shear stress and inundate a particular stream terrace are given a range based on uncertainty in the model, topography, and flood stage associated with the range of critical shear stress values.

Field evidence of surface erosion or stability is used as an indicator of whether floods have recently overtopped terrace surfaces, providing lasting visible evidence of surface modification. These modifications take the form of secondary or overflow channels, bar and swale topography, channel splay deposits, or reentrant channels near the downstream ends of terrace surfaces. Soil/stratigraphic evidence in the form of truncated or buried soils would also indicate overtopping of the terrace surface. On the contrary, soils that show long term stability indicate the lack of flooding on the terrace over the timeframe of the developing soil. Discharge estimates for overtopping terraces with stable soils rely on these critical shear stress values in order to define a range of discharges that would erode the soil if the discharge had occurred over the timeframe of the developing soil (Levish, 2002).

The hypothesis for this study was that critical shear stress values should exceed the threshold critical shear stress on erosional surfaces and be below the threshold critical shear stress on depositional surfaces, thus reflecting higher stream power in the areas that were eroded. To test whether critical shear stress can be used to differentiate erosional versus depositional areas, we collected sediment samples from the upper 10cm of surface sediments on stream terraces at three different sites, COTT2, COTT3, and COTT4.The locations of the sediment samples correspond to the locations of stratigraphic descriptions of terrace deposits. Particle size analysis was completed for all three sites, whereas bulk density was completed only for COTT2 and COTT3 (Table 3). Bulk density was not completed for COTT4 because the sample lacked cohesion and crumbled apart during sampling. Soils were analyzed and characterized at the Soil, Water and Plant testing Laboratory at Colorado State University in Fort Collins, CO. Based on the soil samples data we concluded that the critical shear stress for our study reach was a very coarse sand corresponding to a threshold shear stress of 0.55 Pa.

Table 3 Soil sample results for Cottonwood creek.

Sample ID	Bulk Density (g/cm^3)	% Retained By Sieve Size (mm)						% Composition			Texture
		2	1	0.5	0.25	0.106	0.053	Sand	Silt	Clay	
COTT2	1.50	2.92	4.37	8.89	15.38	18.54	8.82	56	18	26	Sandy Clay Loam
COTT3	1.59	1.61	1.89	8.23	51.95	9.08	3.85	75	8	17	Sandy Loam
COTT4	N/A	1.91	3.75	6.49	28.45	32.28	2.83	74	6	20	Sandy Clay Loam

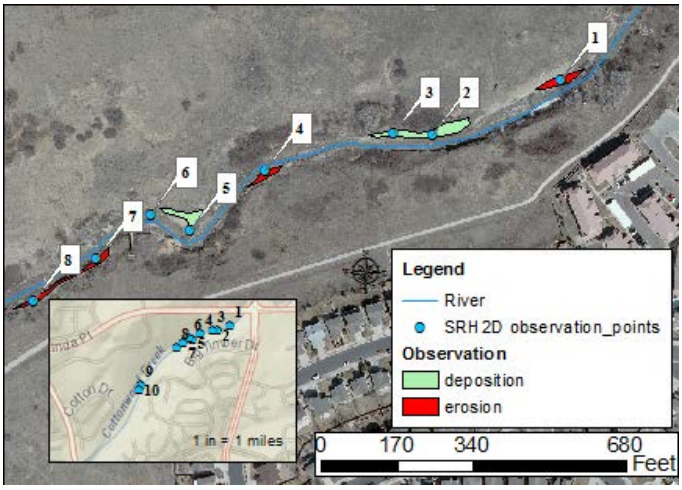

Figure 7 Location of observed erosion and deposition and the monitoring shear stress points in the SRH-2D model.

We wanted to determine if the threshold critical shear stress identified in the soil samples was exceed in the study reach, how much it was exceeded by, and for what duration. SRH-2D allows users to identify monitoring points, locations where simulated results are recorded at each time step. Ten monitoring points were placed within field observation polygons identified as areas of deposition and scour that were associated with the 2012 flood (Figure 7) Monitoring points 1, 4, 7, and 8 were located in polygons with observed erosion and monitoring points 2, 3, 5, 6, 9, and 10 were located within polygons where deposition was observed.

RESULTS

Model Extent

The results of the HEC-RAS model for the three boundary conditions provided three water surface elevations for SRH-2D steady-state downstream boundary conditions of 6600.71 feet, 6600.21 feet, and 6599.71 feet. The SRH-2D steady-state model water surface elevations for the high, regular, and low modeling scenarios were plotted (Figure 8) and show that the boundary condition had no impact for model results upstream of 4933.69 (HEC-RAS station 812.67 feet). The model extent in this study refers to all results upstream of station 812.67 feet.

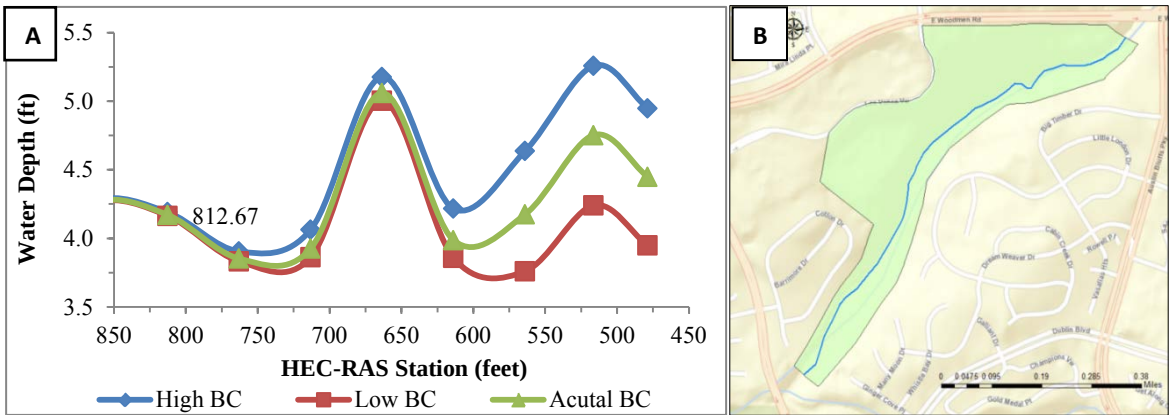

Figure 8 A) The 2D water surface profiles results for high downstream boundary condition, "Reg" or Regular downstream boundary condition and Low boundary conditions. B) The SRH-2D modeling extends to project station 4933.69 feet.

Model Uncertainty – Water Surface Elevation

Model uncertainty for water surface elevation was estimated to be ±1.02 ft. for the modeled reach. The modeled water surface elevation uncertainty was computed using the sum in quadrature equation (Taylor, 1997):

$$\sigma_\tau = \sqrt{\sigma_s^2 + \sigma_r^2 + \sigma_d^2}$$

Where σ_τ = absolute error, σ_s = topography error, σ_r = the roughness error, and σ_d = the error in the discharge measurement.

The terrain data for the study reach was developed from contours and surveyed points. Because there are two sources of data to develop the terrain the sum in quadrature equation was used to define the topographic uncertainty. The contour data is at 2 feet intervals which has an uncertainty of ± 1 foot. The vertical error associated with the surveyed point is ±0.1 feet. The total error for topography (σ_s) is 1.01 feet.

Roughness uncertainty (σ_r) was set at 0.03 ft. by comparing the difference in water surface elevation between selected roughness values and a 25% increase in roughness at a flow of 1610 ft^3/s. Differences in modeled water surface elevations ranged from 0.43 to 0 feet. An average value of 0.03 feet was used as a general indicator.

For a flow measurement to qualify as "good" under USGS standards it should be within ± 5 percent of the true value and a "poor" measurement is considered to have greater than 8 percent error (Sauer & Meyer, 1992). The daily discharge measurements at Cottonwood Creek generally receive a fair or poor rating. The 2012 water year report indicates that records are fair to poor because flow is affected by erosion-control and livestock-watering reservoirs and groundwater withdraws. For purposes of uncertainty estimation, the error in a given flow value was assumed to be ± 8 percent (e.g. 128.8 ft^3/s for 1610 ft^3/s). This translates to an estimated water surface elevation uncertainty (σ_d) of ± 0.17 feet at 1610 ft^3/s.

Water surface elevation fit

A comparison between the measured water surface elevations and the modeled steady state water surface elevations determine how well the model replicated flow depth. The survey points identified as flotsam were used as the

measured water surface elevation and were compared to the water surface elevations for the SRH-2D unsteady model (Figure 9). A comparison of 49 locations along the study reach found that the modeled water surface elevation was on average 0.81 feet above the measured water surface elevations. This indicates an over prediction of water surface elevation, on average, by 1.2 feet in the upper reach (River Stations 5746.36-4160.24), slightly over predicted water surface elevation by 0.3 feet in the middle reach (River Stations 4532.63-2736.01), and over predicted water surface elevations on average 1.1 feet in the lower reach (<2736.01 River Station) of the model.

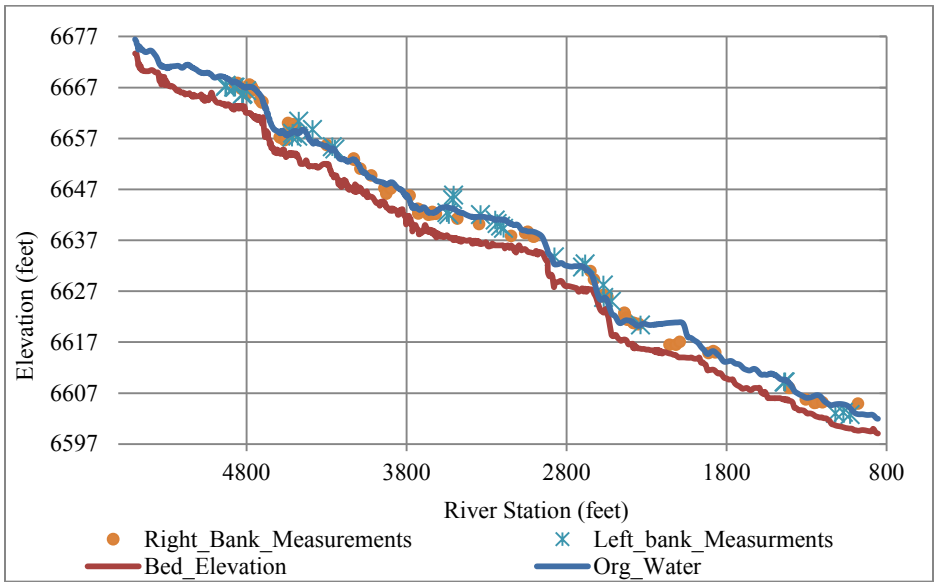

Figure 9 A comparison between the field measured and computer modeled water surface elevations for Cottonwood Creek study reach.

Critical Shear Stress Analysis

The ten SRH-2D monitoring points provided time series data for flow depth and critical shear stress. These values were plotted together against time (Figure 10). There was no flow at monitoring points 5, 6, 7, 8 and 10. For the monitoring points that did receive flow, they all exceed the critical shear stress values of 0.55 Pa. Although all surfaces showed modification in the form of either deposition or erosion, the methodology used in the paleoflood studies would have only assumed surface erosion above the critical shear stress value. Observation points 1 and 4 showed signs of erosion; however, observations sites 2, 3, and 9 were all mapped as locations where deposition had occurred. Observation points 1 and 4 had modeled peak critical shear stress values that were between 300 and 700 times larger than the threshold critical shear stress. They also experienced shear stresses that exceeded the threshold critical shear stress for over ten hours. Observations points 2, 3, and 9 had modeled peak critical shear stresses that were between 80-300 times larger than the threshold critical shear stress for durations around one hour.

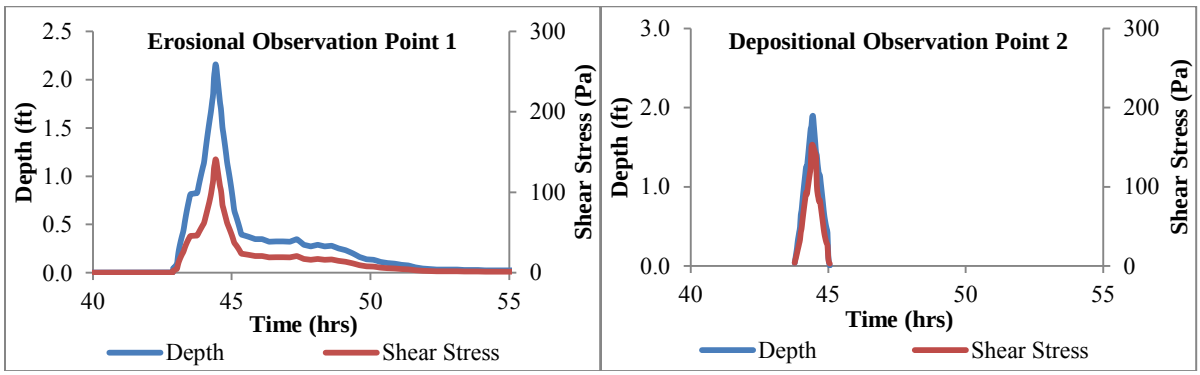

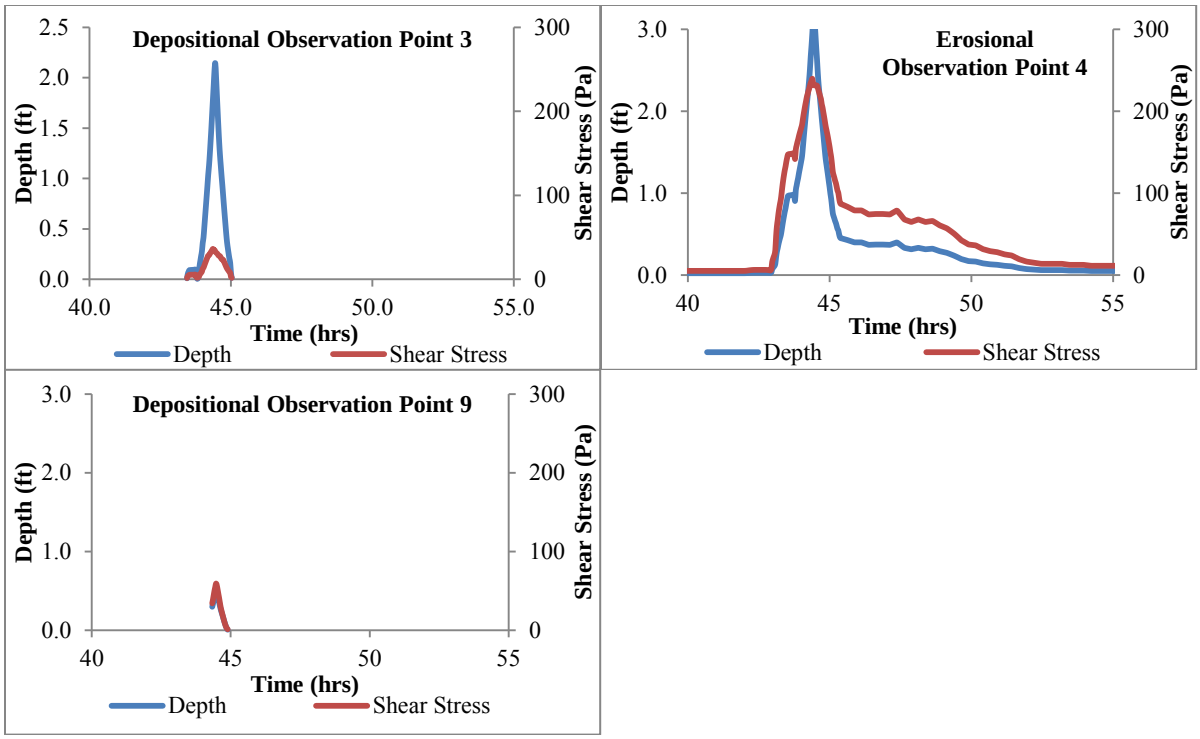

Figure 10 The charts plot the change in shear stress and depth over time for the describe monitoring points. Note the proposed threshold critical shear stress of (0.55 Pa).

DISCUSSION

Comparison of modeled water surface elevations and stage of high water marks

Modeled water surface elevations were within approximately 1ft of the field surveyed high water marks. Because the hydraulic model had a water surface elevation uncertainty of 1.02 feet this fit is within the range of uncertainty and is considered satisfactory. Higher resolution topographic data inside the channel would have the greatest impact on reducing the hydraulic model uncertainty. Finally, the uncertainty in collecting water marks is very difficult to quantify. Flow around objects in the channel is dynamic and complex where debris can be deposited throughout the hydrograph, making it difficult to discern the correct flood stage from the high water marks. Debris can be super elevated from in channel vegetation or obstructions, can be entrained during the hydrograph rising limb, or be suspended during the peak and then deposited during the falling limb at a lower channel elevation. To ensure high quality measurements of high water marks, a large number of measurements should be taken to rule out the mentioned outliers. This study measured over 233 high water marks over a one mile study reach and was considered satisfactory.

Comparison of steady state model output and field observations

For depth-averaged values in the steady state model, the SRH-2D model shows good correspondence with field observations. In other words, higher shear stress is computed in areas that were mapped as erosional and lower shear stress values are computed for areas that were mapped as depositional. Deviations from this pattern occur along the margins of the surfaces at their boundary and in transitional areas between erosional and depositional areas, where high shear stress values are computed at the upstream portions of the depositional areas.

Comparison of unsteady state model output and field observations

Results from the unsteady flow modeling at observations points along the study reach show that threshold critical shear stress is exceeded at every observation point regardless of whether the observation point was within an erosional or depositional area. We concluded that the Julien defined critical shear stress for our study site was not a

good predictor of erosion or deposition. The three assumptions of the Julien method (flow occurs over a plane bed, the particles shape are uniform, and the particles are non –cohesive) may have contributed to the low correlation. Our study site had steep bed slopes, segments of bedrock, and bank vegetation all of which affect the flow of sediment. Our soil samples had as high as 26% clay content indicating particle cohesion. Finally, natural stream systems have imbrication or armoring of the bed. It is likely that our site could have had imbrication or interlocking sediment particles of varying shape impacting sediment transport. These three conditions may have contributed to the poor correlation between the Julien comparison of grain size and critical shear stress and our site.

Maximum shear stress values also varied and appeared to have no distinct difference in values between erosional and depositional surfaces. The results also show that the duration and depth of inundation on erosional surfaces was much greater than on depositional surfaces, which may be the reason why these areas experienced greater removal of sediment.

CONCLUSIONS

Geomorphic observations of an extreme event can provide insight into flood dynamics. One dimensional and two dimensional modeling provided quantitative data on flow velocities, depths and shear stress for the June 6, 2012 flood. There was a strong agreement between field observations and modeled results of flood stage. Anomalies occurred in locations where three dimensional flow effects were likely during the flood. Critical shear stress as an indicator of surficial erosion is currently used to develop non-exceedance bound discharges for paleoflood studies; this research shows that the critical shear stress value can only be used to develop a minimum stage and discharge required to modify a fluvial surface; other parameters should be explored to better define the range of peak discharges for paleoflood studies.

REFERENCES

Baker, V.R., 1989, Magnitude and frequency of palaeofloods, *in* Beven, K., and Carling, P., (eds.), Floods: Hydrological, sedimentological, and geomorphological implications: New York, John Wiley and Sons, p. 171-183.

Baker, V.R., Kochel, R.C., and Patton, P.C., (eds.), 1988, Flood geomorphology: New York, John Wiley and Sons, 503 p.

Birkeland, P.W. (1999). Soils and Geomorphology. Oxford University Press, New York, 430 p.

Boggs, S., Jr. (1995). Principles of Sedimentology and Stratigraphy. Prentice Hall, Englewood Cliffs, New Jersey, 774 p Chow, V. T. (1959). Open-Channel Hydraulics. New York: McGraw - Hill Book Co.

Costa, J.E., 1986, A history of paleoflood hydrology in the United States: Eos, Transactions of the American Geophysical Union, v. 67, no. 17, p. 425, 428-430.

Denlinger, R.P., O'Connell, D.R.H., and House, P.K., 2002,Robust determination of stage and discharge: An example from an extreme flood on the Verde River, Arizona: in House, P.K., Webb, R.H., Baker, V.R., and Levish, D.R., (eds), Ancient Floods, Modern Hazards: Principles and Applications of Paleoflood Hydrology, Water Sciences and Application Volume 5, American Geophysical Union, Washington D.C., p. 127-146**.**

Environmental Systems Research Insitute (ESRI). (2011). ArcGIS Desktop: Release 10. Redlands, CA: Environmental Systems Research Institute.

Jahns, R.E., 1947, Geologic features of the Connecticut Valley, Massachusetts, as related to recent floods: U.S. Geological Survey Water-Supply Paper 996, 158 p.

Julien, P. Y. (1988). Erosion and Sedimentation. Cambridge: Cambridge University Press.

Jarrett, R.D., 1990, Paleohydrologic techniques used to define the spatial occurrence of floods: Geomorphology, v. 3, no. 2, p. 181-195.

Kochel, R.C., and Baker, V.R., 1988, Paleoflood analysis using slackwater deposits, *in* Baker, V.R., Kochel, R.C., and Patton, P.C., (eds.), Flood Geomorphology: New York, John Wiley and Sons, p. 357-376.

Lai, Y. (2008). "SRH-2D version 2: Therory and User's Manual", Sedimentaion and River Hydraulics- Two Dimensional River Flow Modeling. Denver, CO: US Bureau of Reclamation, Technical Service Center.

Levish, D.R., 2002, Paleohydrologic Bounds--Non-Exceedance Information for Flood Hazard Assessment, *in* House, P.K., Webb, R.H., Baker, V.R., and Levish, D.R., (eds.), Ancient Floods, Modern Hazards, Principles

and Applications of Paleoflood Hydrology: Washington, D.C., American Geophysical Union, Water and Science Application 5, p. 175-190.

Madole, R.F. (2003). Geologic Map of the Falcon NW Quadrangle, El Paso County, Colorado. U.S. Geological Survey Open File Report 03-8, 16 p., 1 sheet, scale 1:24,000.

Mansfield, G.R., 1938, Flood deposits of the Ohio River, January-February, 1937, a study of sedimentation, in Grover, N.C., (ed.), Floods of Ohio and Mississippi Rivers, January-February, 1937: U.S. Geological Survey Water Supply Paper 838, p. 693-736.

Patton, P.C., 1987, Measuring rivers of the past: A history of fluvial paleohydrology, in Landa, E.R., and Ince, S., (eds.), The History of Hydrology: History of Geophysics: Volume 3, American Geophysical Union, Washington, D.C., p. 55-67.

Patton, P.C., Baker, V.R., and Kochel, R.C., 1979, Slack water deposits-- A geomorphic technique for the interpretation of fluvial paleohydrology, in Rhodes, D.D., and Williams, G.P., (eds.), Adjustments of the fluvial system: Dubuque, Iowa, Kendall/Hunt Publishing Company, p. 225-253.

Sauer, V. B., & Meyer, R. W. (1992). Determination of error in individual discharge measurements. US Geological Survey. Taylor, J. R. (1997). An Introduction to Error Analysis: the Study of Uncertainties in Physical Measurements (2 ed.). Sausalito, California: University Science Books.

Thorson, J.P., Carroll, C.J. and Morgan, M.L. (2001). Geologic Map of the Pikeview Quadrangle, El Paso County, Colorado. U.S. Geological Survey Open File Report 01-3, 30 p., 1 sheet, scale 1:24,000.

U.S. Army Corps of Engineers. (2010). Hydrologic Engineering Center HEC-geoRAS, an application for support of HEC-RAS using ARC/INFO: User Manual Version 4.0. Davis, California.

U.S. Army Corps of Engineers Hydrologic Engineering Center. (2010, January). HEC-RAS. River Analysis System Version 4.1.0. Davis, California, United States of America: U.S. Army Corps of Engineers.

SETTING THE STAGE FOR CHANGE: GEOMORPHIC RESPONSE OF A SECONDARY CHANNEL ON THE RIO GRANDE

Jonathan AuBuchon, Hydraulic Engineer, Bureau of Reclamation, Albuquerque, NM, jaubuchon@usbr.gov; Mark S. Nemeth, Supervisory Civil Engineer, Bureau of Reclamation, Albuquerque, NM, mnemeth@usbr.gov.

INTRODUCTION

Anthropogenic and natural changes have influenced the morphology of the Rio Grande over the last century, especially in the reach below Cochiti Dam. The channel degradation that followed the closure of Cochiti Dam (1973) resulted in a floodplain that is rarely inundated and a river that is narrower and deeper, creating bank erosion and habitat diversity concerns as documented by Happ (1948), Dewey et al. (1979), Lagasse (1980), Salazar (1998), Scurlock (1998), Richard (2001), Makar et al. (2006), Massong et al. (2008), and Makar and AuBuchon (2012).

Makar and AuBuchon (2012), Richard (2001), and Shah et al. (2006) document the decrease in the frequency of the large magnitude floods, the sediment supply, and the mobility of the medial and point bars. The increased bar stability has simultaneously allowed an increase in vegetation establishment, which has increased the stability of the banks and the channel planform. Over the last few decades the channel has continued to narrow through incision and vegetation encroachment, both of which have served to further isolate the main channel from its floodplain. At the same time the exposure of a dominant gravel fraction in the bed material as shown by Salazar (1998) and Bauer (2009), and vegetation encroachment on the banks and bars has reduced the degrees of freedom for the river to adjust, increasing the channel stability and uniformity.

In the river reach below Cochiti Dam (~ first 5 miles downstream) recent analyses by AuBuchon and Bui (2014) have shown that the active channel width has fluctuated around 200 feet and the slope has flattened to about 0.0012 over the last 2–3 decades. The channel planform has also abandoned some of its variability with a decrease in the average number of channels from 2–3 prior to 1962 to about 1–2 since 1972. The sinuosity still fluctuates slightly, although not to the extent that it did prior to 1962, suggesting that there are local areas of instability amidst the observed stability.

PROJECT DESCRIPTION

In 2008, the U.S. Bureau of Reclamation constructed a project about four miles south of Cochiti Dam that combined erosion control and habitat restoration goals. The design at this location blocked off an existing side channel where there was a bank erosion concern and constructed a new secondary channel slightly downstream. This new side channel was constructed through a relatively stable island feature deposited in the 1950s; this date was based on tree-ring aging performed by Bio-West (2005). The composition of the island deposits are primarily gravels among a matrix of sand, as shown in the red circle on Figure 1.

The side channel was designed by Bio-West (2006; 2007) to mimic other naturally occurring side channels in the area. The design bottom width was about 10 to 25 feet, with a 5.5-foot to 7-foot design depth range from the island surface. While initial draft concepts explored the possibility of planting vegetation on the channel sides to provide stability, this was quickly abandoned in favor of allowing the river freedom to adjust. The high banks of the island surface were estimated by Bio-West (2005) to be about 8 to 10 feet above the river bed. This information, coupled with observations of bank erosion at similar locations, suggested that the river would be able to move the sediment at this site, creating an opportunity for the river to adjust the channel dimensions.

During construction the side channel outlet was moved downstream to avoid removing a mature stand of cottonwoods. This resulted in a channel length increase of about 100 feet. The relocation effort also took advantage of existing sparsely vegetated areas through which the new channel could be constructed, one of which is shown staked out with pink flagging in Figure 1. The actual constructed bottom width of the channel was about the width of two wheel tractor-scrapers (CAT 621G), or about 20 feet as shown in Figure 2. The actual excavated depth was estimated to be about 5 feet.

Figure 1 Proposed side channel location at RM 228.9 river maintenance priority site looking at upstream bend. Photo taken on November 29, 2007.

Figure 2 Constructing the side channel at RM 228.9 river maintenance priority site. Each path is the width of one tractor-scraper. Photo taken on January 30, 2008.

OBSERVATIONS

In the years since the construction of the new side channel, the river's morphological response has created a rich variety and complexity of stream features. High spring snow melt flows during the initial years of the project (see Figure 3 where flows are above 3500 cfs for an extended period of time in 2008 [55 days], 2009 [28 days], and 2010 [7 days]) provided the energy for change, creating width, depth, and sinuosity changes. The erosion of bed and bank material during the initial years (2008 to 2010) created a sediment source (sands and coarser materials) for the river. This is a significant change since the closure of Cochiti Dam in 1973, as Shah et al. (2006) and Richard (2001) found that Cochiti Dam, just 4.5 miles upstream, has had a high trapping efficiency, close to 98%. The initial years of high flow not only created a sediment source, but they also winnowed the finer material out of the channel bed (see Figure 4) and deposited bars that have a nominal size in the very coarse gravel range (see Figure 5, 2009 survey).

The high spring runoff years were followed by lower spring snow melt flows that allowed the establishment of plant species. Summer monsoon flows between 2011 and 2014 have also brought additional sediment into the reach. Of particular note are the higher turbidity measurements in 2013 shown in Figure 3. In 2013, an unusually high discharge from a tributary of the Rio Grande upstream of the project site blocked the river and created conditions that significantly increased the local turbidity throughout the reach. This event, as well as other smaller sediment spikes, shown in Figure 3, during the monsoon seasons of 2011, 2012, and 2014, likely contributed additional finer material, as was noted in a 2014 re-survey of the bed material present on the 2009 surveyed bar (see Figure 5). It should be noted that the gravel predominant in the 2009 measurement was still present in the 2014 measurement, just overlain by finer material. These observations indicate that both water and sediment have helped shape the river's morphological response on the constructed side channel.

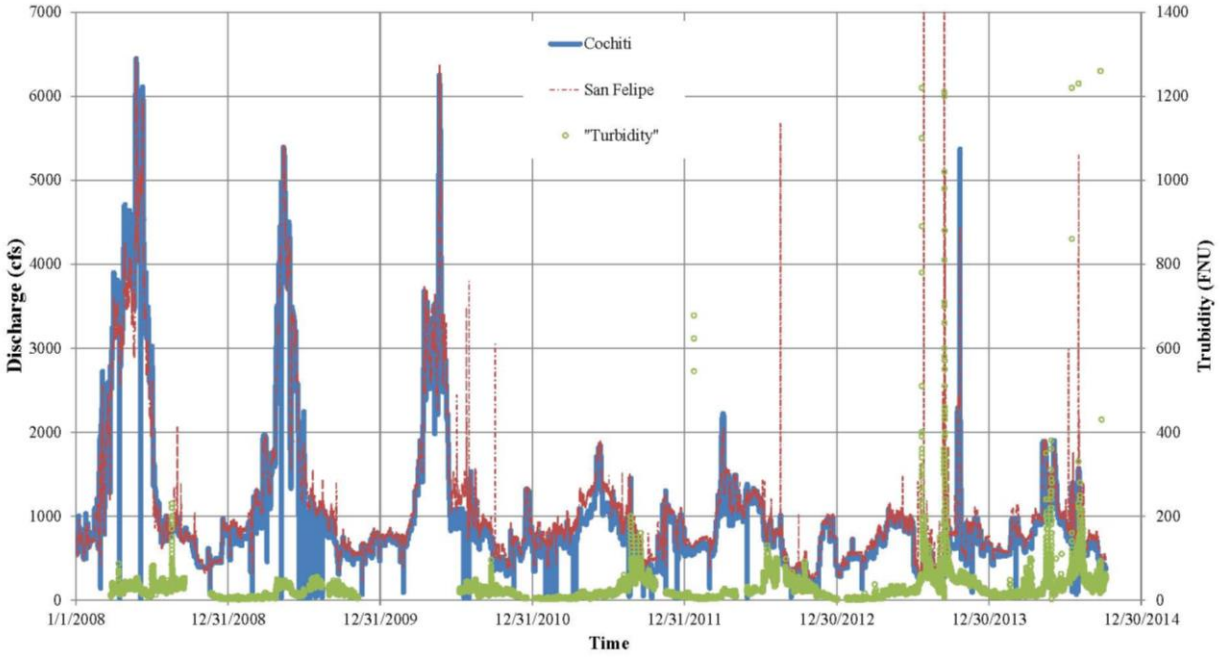

Figure 3 Discharge and turbidity (formazin nephelometric units–FNU) measurements at the USGS gage 08317400 Rio Grande Below Cochiti Dam, NM and discharge measurements at the USGS gage 08319000 Rio Grande at San Felipe, NM between January 2008 and October 2014.

Figure 4 Constructed side channel looking upstream. Note gravel bar on river right and gravel on the river left bank. Photo taken by L. Malone on August 4, 2009.

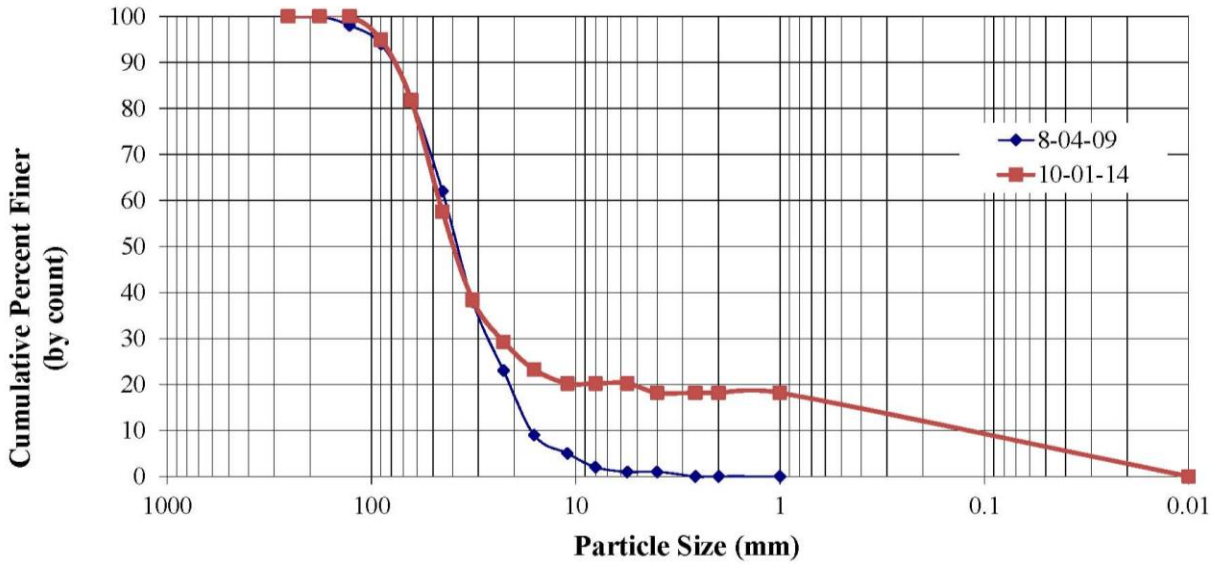

Figure 5 Grain size distribution plots (by count) of a bar forming on river left between CI-52.3B and CI-53.5B. Results are from measurements conducted using Wolman's (1954) methodology.

The specific morphological response of the constructed side channel is shown in planimetric view in Figure 6. A study of Figure 6 reveals not only a change in width and sinuosity, but also that the development of the meander bends is reflective of the locations where a major curvature was introduced during construction. Over the sequence of the provided aerial photography, this curvature has become more pronounced with downstream migration of the meander bends. Also of note in Figure 6 is the appearance of small channels on the backside of some of the meander bars which may indicate potential channel cutoffs and additional channel changes in the future.

Changes in the profile view over roughly the same time period are shown in Figure 7. The water surface elevation plot in Figure 7 reveals that the slope is adjusting with time (from ~0.0024 in 2009 to ~0.008 in 2012). The bed elevation plot in the same figure reveals a similar slope reduction (from ~0.0031 at the time of construction to ~0.0023 in 2009). The bed elevation plots also show the increase in depths along the thalweg with time. The August 2009 bed survey used an Acoustic Doppler Current Profiler (ADCP), so a higher resolution of the bed topography was possible. The January 2009 survey measured the depths at four cross section line across the constructed side channel; the profile plot only shows the deepest depth recorded at these four locations. Cross-sectional areal changes on the constructed side channel are shown in Figure 8. This figure provides a graphic illustration of the increase in cross section area (changes in width and depth) from construction to after the first two major spring runoff events in 2008 and 2009.

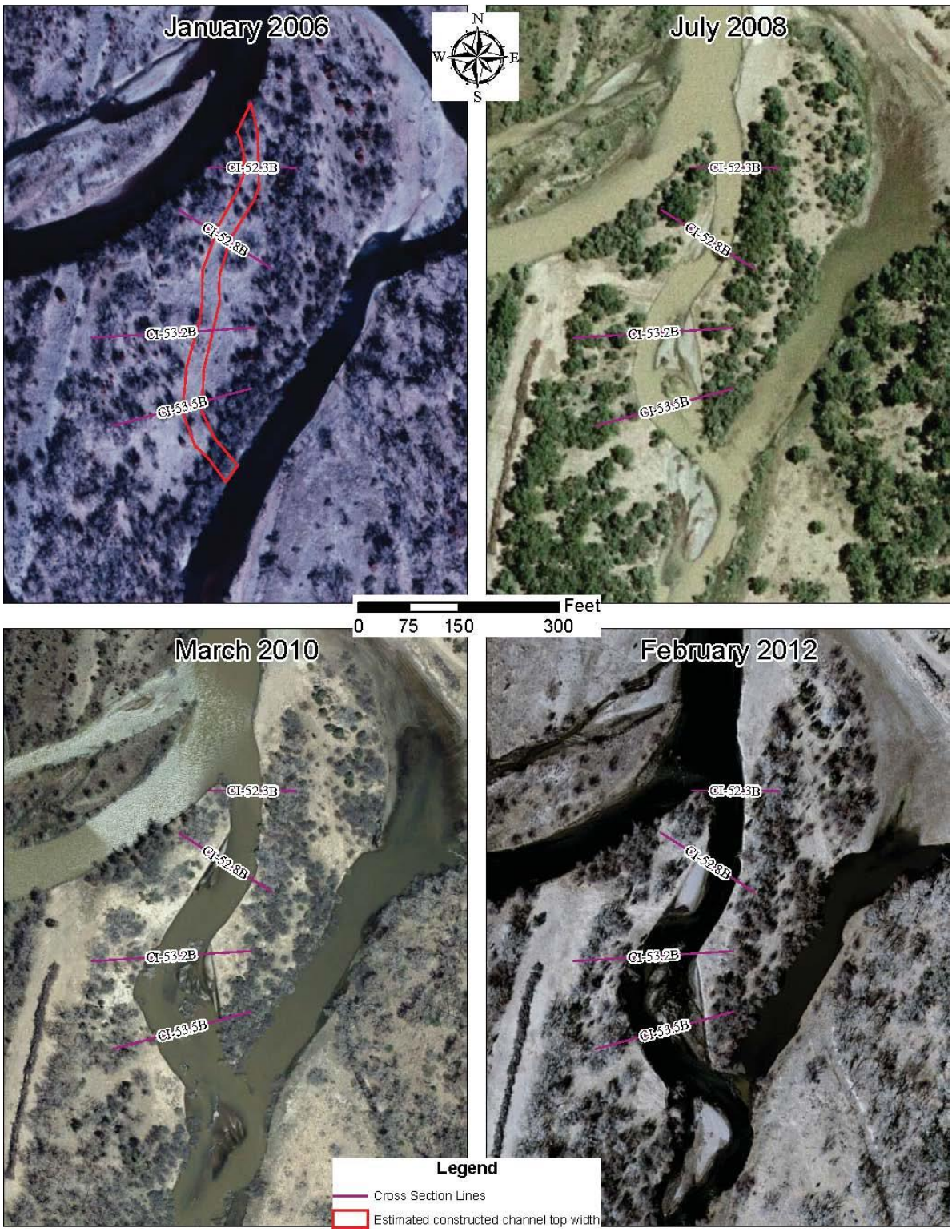

Figure 6 Planform changes observed on constructed side channel, from top left to bottom right: 2006 Reclamation aerial photography with estimated constructed channel top width, 2008 Reclamation post runoff aerial photography, 2010 Middle Rio Grande Council of Government (MRCOG) spring runoff aerial photography, 2012 Reclamation aerial photography.

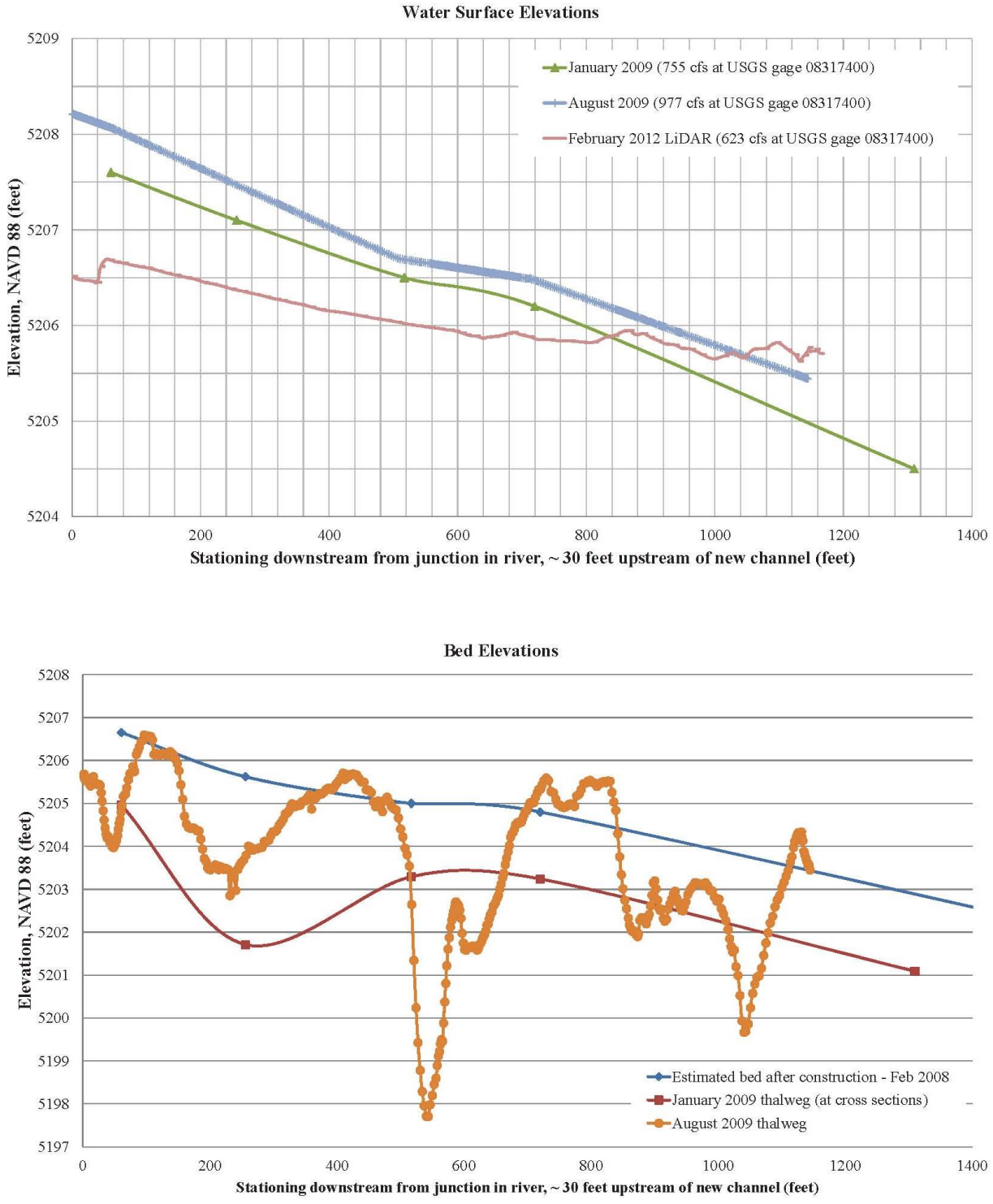

Figure 7 Slope changes on constructed side channel through time.

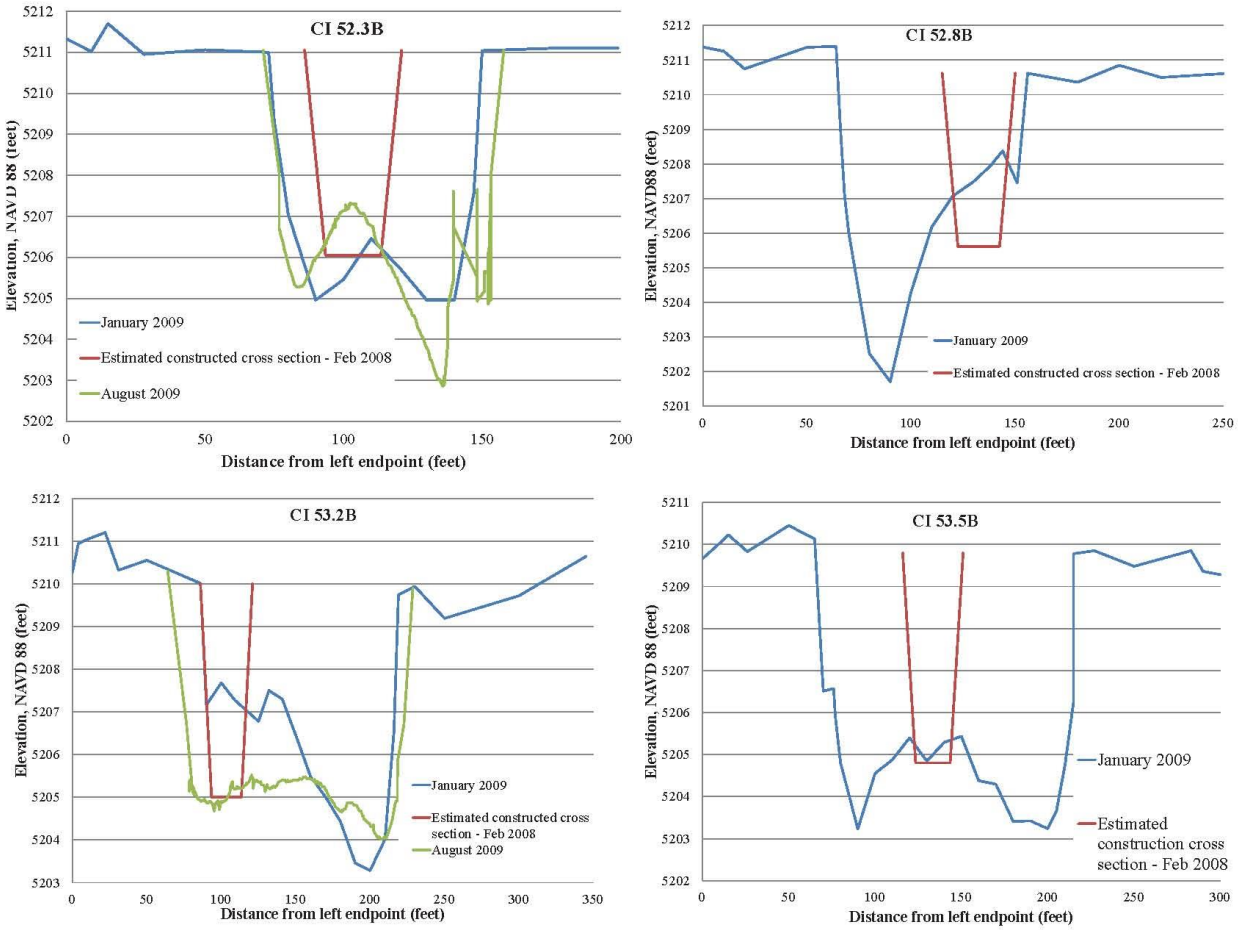

Figure 8 Cross-sectional changes on constructed side channel through time. Top two cross-section graphs are in the upper half of the constructed side channel. The bottom two cross-section graphs are in the lower half of the constructed side channel.

A summary of the planimetric changes that occurred on the constructed side channel is provided in Table 1. These changes were measured from the aerial photography shown in Figure 6. A similar planimetric analysis (Table 2) was performed using the same aerial photography sets on an upstream existing side channel. The constructed side channel showed a significantly more diverse morphological response than the existing side channel, with a larger range in the variability of number of bars, size of bars, and number of dead vegetation clusters in the channel. The side channel that was abandoned during construction was also assessed using this planimetric analysis (see Table 3), but for the time period prior to construction, this included three sets of aerial photography prior to the closure of Cochiti Dam. The width and sinuosity increases in the constructed side channel were seen to be similar to the abandoned side channel responses prior to construction of Cochiti Dam. Similarly, the quantity of bars observed in the constructed side channel was on par with the abandoned side channel up to about 1992; the volume of sediment available before Cochiti Dam though was far in excess (see maximum bar size) of what the constructed side channel could generate. The constructed side channel, though, had a significantly higher number of dead vegetation clusters than the abandoned channel, even before the closure of Cochiti Dam.

Table 1 Planimetric measurements of constructed side channel from aerial photography.

	February 2008	**July 2008**	**March 2010**	**February 2012**
Average width (feet)	64	83	110	107
Sinuosity	1.00	1.14	1.17	1.19
Number of bars	2	6	5	14
Minimum bar size (square feet)	1,883	1,147	161	67
Maximum bar size (square feet)	2,525	4,573	7,639	16,172
Number of dead vegetation clusters in channel: trees, wood piles, clumps of vegetation matted together, etc.	0	16	29	24

Table 2 Planimetric measurements of nearby side channel (unaffected by construction activities) from aerial photography.

	January 2006	**July 2008**	**March 2010**	**February 2012**
Average width (feet)	212	210	220	209
Sinuosity	1.17	1.16	1.20	1.22
Number of bars	6	6	5	9
Minimum bar size (square feet)	133	1,109	489	444
Maximum bar size (square feet)	8,201	5,407	2,513	10,281
Number of dead vegetation clusters in channel: trees, wood piles, clumps of vegetation matted together, etc.	1	1	1	1

Table 3 Planimetric measurements of abandoned side channel from aerial photography.

	1949	**1962**	**1972**	**1992**	**2001**	**2006**
Average width (feet)	407	264	137	126	123	119
Sinuosity	1.04	1.11	1.13	1.38	1.41	1.30
Number of bars	9	4	5	4	2	2
Minimum bar size (square feet)	1,052	8,745	537	460	27,249	1,329
Maximum bar size (square feet)	177,638	222,716	50,210	74,713	52,283	4,385
Number of dead vegetation clusters in channel: trees, wood piles, clumps of vegetation matted together, etc.	1	1	1	3	3	5

While there was likely some dead vegetation that made its way to the side channel from upstream, the larger wood piles were a result of trees that were left near the constructed side channel and which fell into the river as the side channel widened and deepened (Figure 9). In effect, the toppled trees created irregularities in the flow that increased the local channel sinuosity and width, in addition to providing traps for sediment, seeds, and other debris carried by the river (Figure 9). It is likely the presence of these trees that have helped create the rich

variety and complexity of morphological features that have developed over time, as can be seen in the time sequence of photographs in Figure 10 and Figure 11.

Figure 9 Left: Cottonwood tree that fell near CI-53.2B. Photo taken on April 16, 2008. Right: Same cottonwood tree that fell near CI-53.2B. Photo taken on October 1, 2014.

Figure 10 Temporal sequence of photographs looking downstream at the bend around CI 52.3B: 1–11/14/07, 2–1/30/08, 3–4/16/08, 4–5/27/08, 5–8/7/09, 6–6/16/10, 7–10/17/13, and 8–10/1/14.

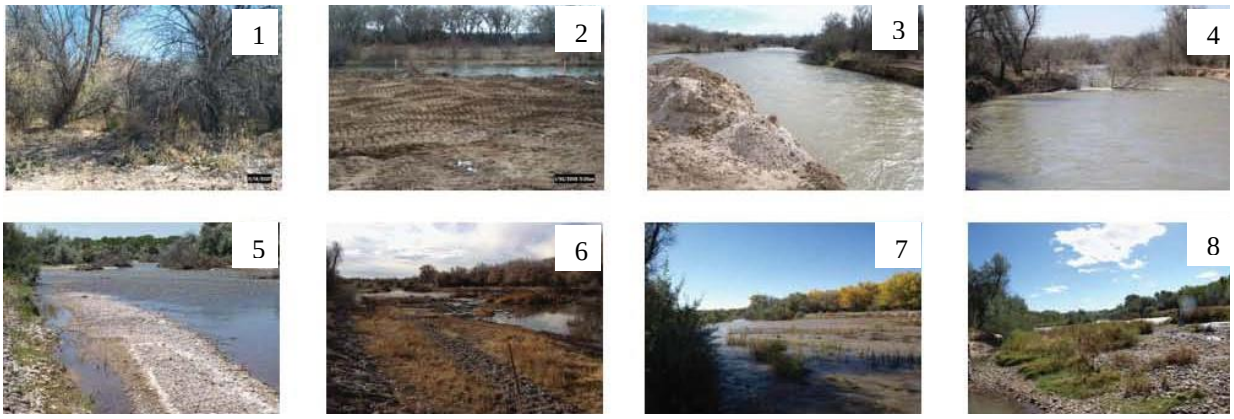

Figure 11 Temporal sequence of photographs looking downstream from around CI 53.5B: 1–11/14/07, 2–1/30/08, 3–3/6/08, 4–4/16/08, 5–6/16/10, 6–11/21/12, 7–10/17/13, and 8–10/1/14.

RECOMMENDATIONS

Experience with the fluvial geomorphic response of this secondary channel on the Rio Grande can provide a basis for recommendations for future stream restoration projects. These are shown below.

- Know your river's history. Understanding the historical morphological response and the changes in the system drivers, like water and sediment, is key in developing design concepts that work with the river processes to meet a variety of design goals.

- Know your river now. Spend time in the field, with repeat visits during different seasons to assess changes in the vegetation, bed and bank materials, and general river responses over time. Understand whether your system can benefit from an increase in the sediment supply and what size sediment would be beneficial. In addition, assess if there are potential sources and sinks for this sediment within your design area.

- Provide freedom for the river, where possible, to be a river. Let the river adjust the channel dimensions, especially in areas where the additional sediment supply is needed. Keep large trees near the constructed edges of the channel that may fall into the channel and cause complex flows that create rich and diverse morphological forms that cannot be replicated with construction equipment.

- Plan for an adaptive management process to best take advantage and document morphological changes that occur after construction.

ACKNOWLEDGMENTS

Kai-t L.V. Blue-Sky, Jacob Pecos and other staff and consultants of the Pueblo de Cochiti have assisted with the coordination, selection, and design of this project, along with facilitating permission from the Pueblo de Cochiti for writing this paper. Vincent Benoit and Laeldre Malone have participated in data collection and field reconnaissance trips at this site.

REFERENCES

AuBuchon, J. and Bui, C. (2014). Peralta Arroyo Eastern Terrace Flow Augmentation Design Report. U.S. Bureau of Reclamation, Albuquerque, NM.

Bauer, T. R. (2009). Evolution of Sedument on the Middle Rio Grande, New Mexico. U.S. Bureau of Reclamation, Denver, CO.

Bio-West. (2005). Cochiti Priority Site #3: geomorphic Assessment Report. Bio-West, Inc., Logan, UT.

Bio-West. (2006). Cochiti River Mile 228.9 Final Design Drawing Set. Bio-West, Inc., Logan, UT.

Bio-West. (2007). Middle Rio Grande Project Cochiti Priority Site: Final Design Report. Bio-West, Inc., Logan, UT.

Dewey, J. D., Roybal, F. E., and Funderburg, D. E. (1979). Hydrologic Data on Channel Adjustments 1970 to 1975, on the Rio Grande Downstream from Cochiti Dam New Mexico: Before and After Closure. U.S. Geological Survey, Water Resources Investigations 79-70.

Happ, S. C. (1948). "Sedimentation in the Middle Rio Grande Valley, NM." Geological Society of America Bulletin, 59(12), pp 1191–1216.

Lagasse, P. F. (1980). An Assessment of the Response of the Rio Grande to Dam Construction – Cochiti to Isleta Reach. U.S. Army Corps of Engineers, Albuquerque, NM.

Makar, P., and AuBuchon, J. (2012). Channel Conditions and Dynamics of the Middle Rio Grande. U.S. Bureau of Reclamation, Albuquerque, NM.

Makar, P. W., Massong, T. M., and Bauer, T. R. (2006). "Channel Widths Changes Along the Middle Rio Grande, NM." Proc. Joint 8th Federal Interagency Sedimentation Conference and 3rd Federal Interagency Hydrologic Modeling Conference, Reno, NV, pp 942–949

Massong, T. M., Makar, P. W., and Bauer, T. R. (2008). Rio Grande Geomorphic Summary Final. U.S. Bureau of Reclamation, Albuquerque, NM.

Richard, G. A. (2001). Quantification and Prediction of Lateral Channel Adjustments Downstream from Cochiti Dam, Rio Grande, NM. Colorado State University, Fort Collins, CO.

Salazar, C. L. (1998). Morphology of the Middle Rio Grande From Cochiti Dam to Bernalillo Bridge, NM. Colorado State University, Ft. Collins, CO.

Scurlock, D. (1998). From the Rio to the Sierra: An Environmental History of the Middle Rio Grande Basin. U.S. Department of Agriculture, General Technical Report RMRS-GTR-5. Ft. Collins, CO.

Shah, S., Novak, S., and Julien, P. (2006). Cochiti Dam Reach: Cochiti Dam to Galisteo Creek Hydraulic Modeling Analysis 1962 - 2004. Colorado State University, Fort Collins, CO.

Wolman, M.G. (1954). "A Method of Sampling Coarse River Bed Material." Transactions of the American Geophysical Union, 35 (6), pp 951-956.

BANK EORISON MODELING WITH SRH-2D ON THE RIO GRANDE, NEW MEXICO

Yong G. Lai, Ph.D., Hydraulic Engineer, Technical Service Center,
U.S. Bureau of Reclamation, Denver, CO, ylai@urbr.gov

Abstract A number of sites along the Rio Grande in New Mexico have been experiencing significant bank erosion. A good understanding of bank erosion along the river is necessary for habitat restoration projects and river maintenance planning. This includes the ability to estimate future bank erosion location and its rate. The new geofluvial model SRH-2D, which couples lateral bank erosion modules with the original vertical mobile-bed erosion model, has been developed recently. The model has been verified elsewhere as a useful numerical model that simulates simultaneously the vertical stream bed erosion and lateral bank erosion. In this study, the new SRH-2D is used to evaluate whether the new model is applicable to Rio Grande bank erosion modeling, and the study also establishes the modeling procedure. A specific site at RM 111 on the Rio Grande, New Mexico, is selected for the purpose.

INTRODUCTION

Stream bank erosion is a natural geomorphic process occurring in all alluvial channels; it can be an important form of channel adjustment in unstable alluvial environments. Hence bank erosion should be accounted for in geomorphic analyses, river restoration, dam removal, and channel maintenance projects. Along the Rio Grande in New Mexico, for example, many sites have been experiencing bank erosion. These sites need frequent river maintenance work and the cost can be prohibitive if unmanaged. A good understanding of the bank erosion locations and retreat rates is necessary for river maintenance prioritization, planning and project design. Numerical modeling assessment is a viable alternative for these purposes.

In recent years, one-dimensional (1D) and two-dimensional (2D) numerical models have become important tools for predicting channel responses. For example, a number of stream-specific mobile-bed sediment transport models are becoming available for project applications such as HEC-RAS, SRH-1D, CONCEPTS, CCHE2D and SRH-2D. They are versatile and offer extensive capabilities and choices in modeling the vertical stream bed changes (a few also have the lateral erosion modeling capability). Recently, SRH-2D has been extended to include the bank erosion modules; this new geofluvial capability has been tested, validated and applied to a number of rivers (Lai and Wu 2013; 2014; Lai 2014; Lai et al. 2015a; 2015b). This new development motivated the present study; and it intends to answer the question of whether the current state-of-the-art multi-dimensional geofluvial model SRH-2D can be useful in predicting bank erosion on the Rio Grande. In the past, a few bank erosion sites on the Rio Grande were assessed through field study and using a point-based bank erosion model (Bankhead et al. 2012). However, the point-based models have limited use for predicting future changes. More advanced geofluvial modeling was sought by the Bureau of Reclamation Albuquerque Area Office. In this study, I report the application of SRH-2D to a particular bank erosion site on the Rio Grande, New Mexico (River Mile 111). The study has the following objectives: (a) establish the application and calibration procedure of SRH-2D to the field case, and (b) assess the model performance by comparing the model results with the field data. The study paves the way for future potential applications of SRH-2D to the Rio Grande for bank erosion assessment; it also

adds to the list of successful applications of SRH-2D for combined vertical and lateral erosion modeling.

ABOUT THE STUDY SITE

The bank erosion site selected for the present study is located at River Mile (RM) 111, downstream of the San Acacia Diversion Dam, on the Rio Grande, New Mexico. A series of historical aerial photographs are available between 2002 and 2012 and they are used to help delineate the bank erosion processes at the study site. In particular, the bank retreat distance is obtained and is used to calibrate the numerical model in this study.

The modeling starts from October 2005 and ends in September 2010, about a 5-year modeling period. The aerial photographs from January 2006 and in the summer of 2010 are shown in Figure 1. In the plot, the 5-year bankline retreat is also displayed. The October 2005 terrain used by the model is reconstructed from the July-August 2005 cross sectional data surveyed by Tetra Tech., Inc., and the 2003 DTM data and 2012 LiDAR in dry areas such as bank tops and floodplains. Photos taken at the RM 111 site during a field trip by the author on February 6, 2013 are shown in Figure 2.

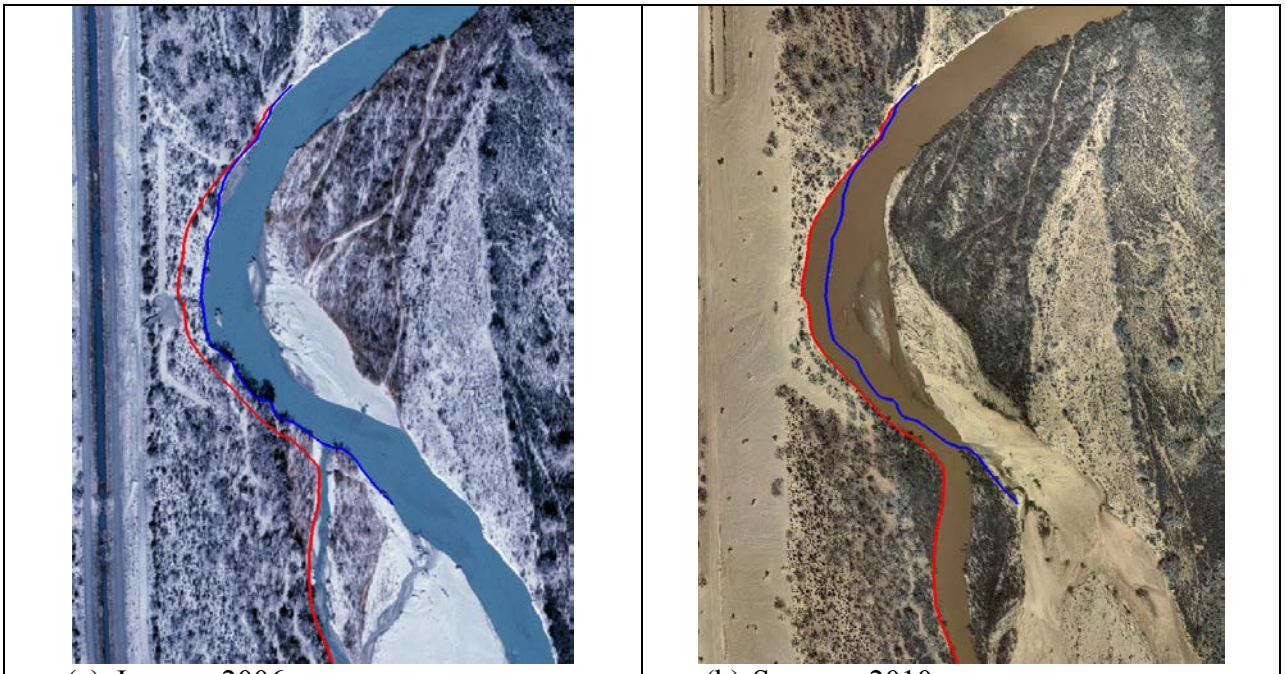

(a) January 2006 (b) Summer 2010

Figure 1. Aerial photographs between January 2006 and summer 2010 at RM 111; also shown are the banklines: Blue=2006; Red=2010

(a) Looking Upstream (b) Looking Downstream

Figure 2. Photos taken at RM 111 during the February 6, 2013 field trip

NUMERICAL MODEL AND MODELING DETAILS

SRH-2D Model Description SRH-2D is a teo-dimensional, depth-averaged, hydraulic and sediment transport model for river systems under development at the Bureau of Reclamation. The hydraulic flow model, documented by Lai (2008; 2010), has been widely used by internal and external users. The sediment transport mobile-bed module is used to predict stream-bed vertical changes and has been described by Lai and Greimann (2008; 2010) and Lai et al. (2011). The sediment module tracks multi-size, non-equilibrium sediment transport for suspended, mixed, or bed load for both cohesive and non-cohesive materials. In recent years, SRH-2D has been developed to include bank erosion modules. Two bank modules are developed: the uniform retreat module and the mechanistic failure module. The two adopt the same basal erosion (lateral erosion) algorithm given a shear stress distribution on a wetted bank. The main difference lies in the mass failure algorithm. The uniform retreat module assumes that the bank is retreating uniformly as a whole. The mass failure process is computed by assuming that a constant bank angle (e.g., the angle of repose) is maintained, and the loss of the bank material equals to the basal erosion. The uniform retreat module is developed primarily for uniform non-cohesive banks undergoing the dry granular and shallow slide processes. It may also be applied to cohesive banks or banks with other mass failure processes if only gross bank retreat amount is of the interest, when actual physical processes are too complex to model, or if there is a lack of measured bank data. The mechanistic failure module is developed primarily for multi-layer cohesive banks; the development is based on t he Bank Stability and Toe Erosion Model (BSTEM) as reported by Simon et al. (2000; 2011) and Langendoen and Simon (2008). The integration of key BSTEM algorithms into SRH-2D was documented by Lai et al. (2013; 2015a).

The technical details of the geofluvial modeling capability of SRH-2D are not reported herein; interested readers are referred to the review by Lai (2014), along with other works by Lai and Wu (2013; 2014) and Lai et al. 2015a. With the latest SRH-2D, main channel fluvial processes may be solved with the regular 2D depth-averaged mobile-bed module, while the lateral bank erosion processes are solved with bank modules. In this study, the latest geofluival SRH-2D model is used and the uniform retreat bank module is used.

Modeling Procedure Modeling is carried out in two stages: hydraulic analysis and bank erosion mobile-bed analysis. Hydraulic analysis is a necessary step to check and verify the model development and setup; the results are needed as the initial condition for bank erosion modeling. Often it also helps guide a proper selection of the solution domain (model boundaries) and the development of the mesh. Bank erosion modeling is carried out after the hydraulic analysis is completed. SRH-2D modeling, in general, is carried out in the following steps: (1) Selection of the solution domain; (2) Mesh generation for the solution domain; (3) Topography and flow roughness and bed gradation representations on the mesh; (4) Model calibration; and (5) Model application. Steps 1-3 are discussed first; followed by hydraulic analysis and bank erosion modeling for model calibration. In this study, model application is not carried out due to limited scope of the study.

Solution Domain, Mesh and Initial Terrain The solution domain may be limited by the availability of terrain data and the area of interest. For this study the solution domain is shown in Figure 3a. It runs from cross sections SA-1243 to SA-1262 and has a longitudinal extent of about 1.8 miles. The upstream boundary is located upstream of SA-1246 and the downstream boundary is located near SA-1262. A 2D mesh is generated with the Surface Water Modeling System software (SMS). It consists of a total of 11,722 mixed quadrilateral and triangular cells and 11,584 nodes (Figure 3b). Once the 2D mesh is generated, the October 2005 terrain and bathymetric survey data are interpolated onto the 2D mesh. The terrain represented by the 2D mesh is shown in Figure 3c.

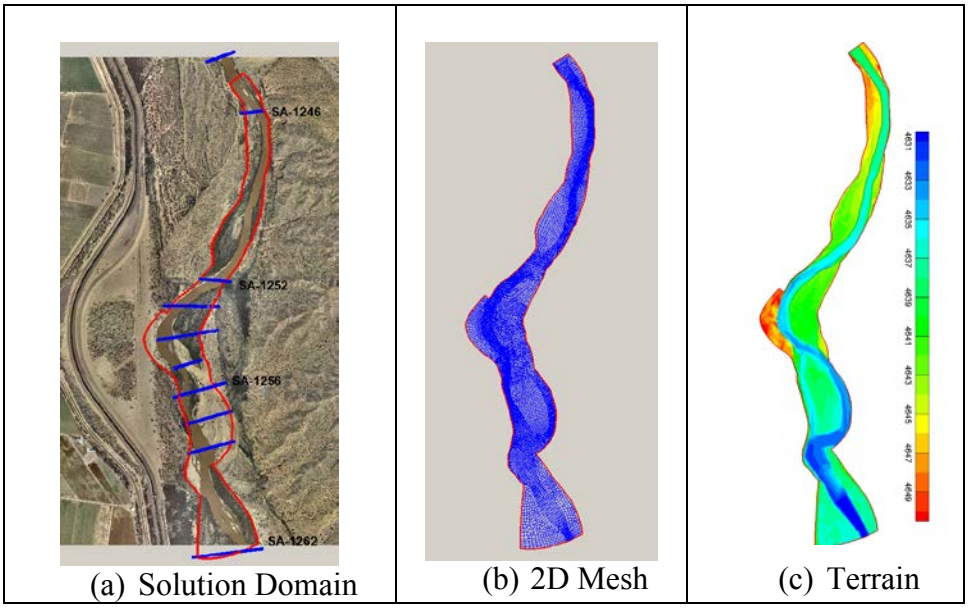

(a) Solution Domain (b) 2D Mesh (c) Terrain

Figure 3. Solution domain (Left), 2D mesh (Middle) and terrain (Right) at RM 111 study site

Flow Resistance and Bed Gradation The flow resistance and initial bed/subsurface sediment gradations are two major model inputs. The flow resistance is computed with the Manning's roughness equation. In this study, the Manning's coefficient of 0.026 is used in the main channel and bare bars based on the study carried out in the reach upstream of San Acacia Diversion Dam (Lai, 2007). No separate calibration for the roughness coefficient is carried out due to lack of data.

Initial bed and subsurface sediment gradations are represented by four bed zones as shown in Figure 4a. Each zone is assigned with thickness of the surface and sub-surface layers along with the sediment gradation (cumulative sediment size distribution). Sediment gradation surveys were carried out by Bauer (2006) between June 15-20, 2006 and again between July 17-19, 2006. These survey data are used for the present modeling. The survey points within the study area are displayed in Figure 4b while the gradations of these survey points are plotted in Figure 4c and d.

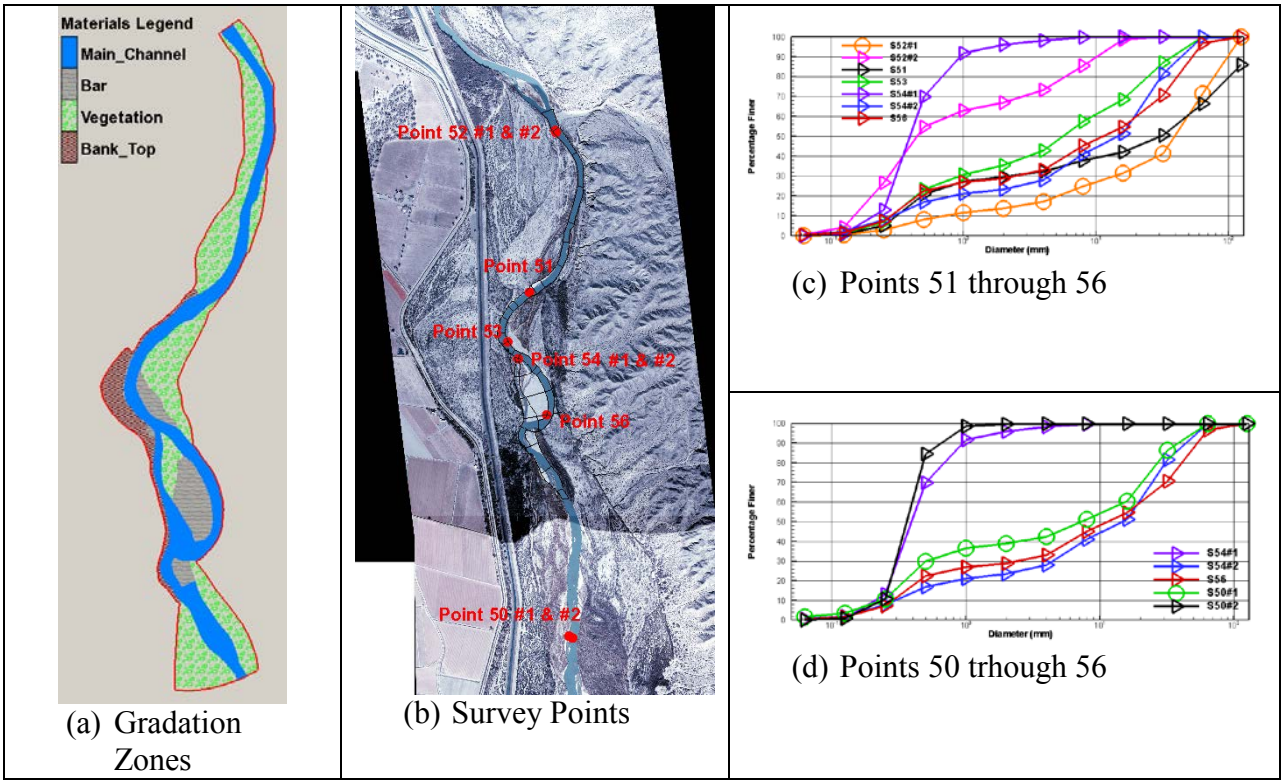

(a) Gradation Zones

(b) Survey Points

(c) Points 51 through 56

(d) Points 50 trhough 56

Figure 4. Zonal partition of the solution domain for bed gradation, survey points and the measured cumulative distribution at survey points

Boundary Conditions and Other Model Inputs A time-series flow hydrograph from July 2005 to the end of 2010 is used for the simulation; the data are based on the runoff data recorded at the USGS San Acacia Floodway station (#08354900) (Figure 5a). The time series discharges are used as the upstream boundary condition. The upstream sediment supply is based on the capacity equation of Parker (1990) since the measured sediment flux data are unavailable. Discharges less than 1,000 cfs are excluded from sediment modeling as done by Lai (2009) and Lai (2011) for the Rio Grande since low flows do not change the channel morphology appreciably and the exclusion reduces the computing time. At the downstream boundary, the normal depth boundary condition is applied. The normal depth assumption is adequate for the present study since the selected downstream boundary is located quite far away from the RM 111 bend which is the zone of interest of the study; the outlet is also located in a relatively straight channel.

A total of seven sediment size classes are used, from 0.002 to 125 mm, to represent the bed material load. The partition of the seven classes is shown in Table 1. The sediment erosional rate

potential uses the Parker (1990) sediment transport equation. The bedload adaptation length is chosen to be 170 ft (about the average channel width of the study reach), and the active layer thickness is 30 mm which is about twice the mean particle diameter in the main channel.

Table 1. Size ranges of each sediment size class

Sediment Size Class	Size Range (mm)
1	.002 to .0625
2	.0625 to .25
3	.25 to .5
4	.5 to 2.0
5	2.0 to 8.0
6	8.0 to 32
7	32 to 125

Bank Module Inputs Additional input parameters are related to the bank properties for a coupled geofluvial modeling; the right bank within the bend is simulated as shown in Figure 5b. In the figure, both bank toe and top lines are displayed. The mesh within the bank zone consists of quadrilateral cells and has a total of five lateral nodes. Longitudinally, fifteen (15) bank profiles are simulated; the toe and top nodes of each bank profile are displayed in Figure 5b as black dots.

A separate input file is used for the bank erosion module and it contains bank erosion input parameters for each of the 15 banks. The input parameters are summarized below:

- A constant time step of 1 hour is used for the bank erosion module (as compared with 5 seconds time step for the flow and sediment transport modeling);
- Each bank is simulated using the uniform retreat module with the following input parameters;
    - All banks have the same bank porosity of 0.4 and critical shear stress of 0.0 Pa, with the initial angle of the bank profile unchanged;
    - The volumetric composition of the bank sediment in terms of the seven size classes in Table 1 is specified as: 13%, 29%, 29%, 29%, 0%, 0%, and 0%; and
    - The erodibility coefficient is calibrated and the final values were: 2.0e-5 for banks 2 to 10; 5.0e-6 for banks 11 to 12; 2.0e-6 from banks 13 to 15.

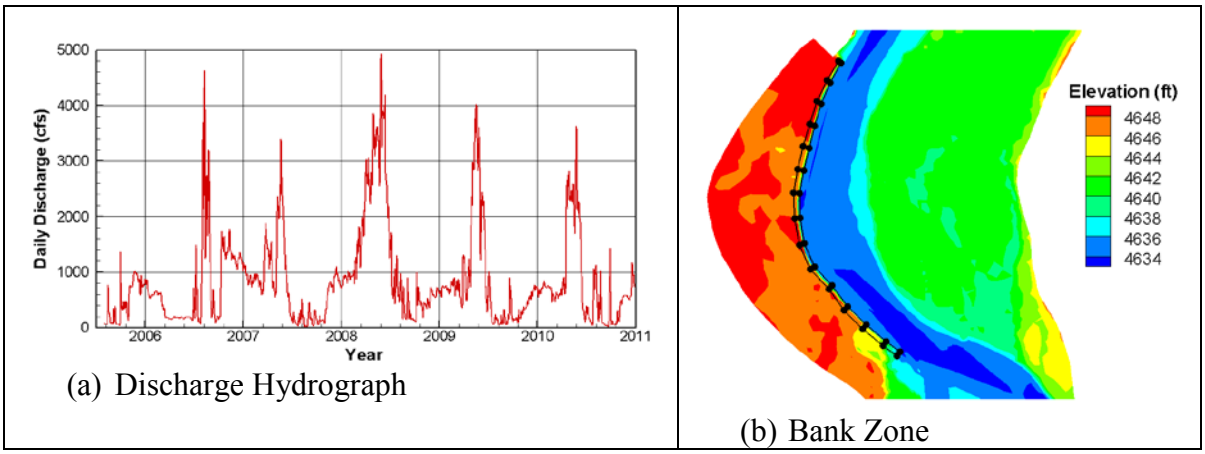

(a) Discharge Hydrograph

(b) Bank Zone

Figure 5. Daily flow discharge data (Left) and bank zone (black polygon on the Right) along the outer bank of the bend (right black circles represent bank toes of all bank profiles and left ones are top nodes)

RESULTS AND DISCUSSION

Simulation is carried out from October, 2005 to September, 2010. First a constant discharge of 1,000 cfs is simulated without the bank erosion module. The flow results are discussed first since it is used as the initial condition. It is also used as the cutoff discharge for the bank erosion mobile-bed modeling. The bank erosion modeling results are presented and discussed afterwards.

Flow Results The predicted flow velocity and shear stress for the 1,000 cfs discharge are shown in Figure 6 (shear stress unit conversion: lb/ft^2 = 47.838 Pa). The results show that flow in the upstream section above the bend has higher velocity and shear stress than the downstream section, due possibly to narrower upstream cross sections. The RM 111 bend is only subject to moderate fluvial loading with shear stress around 1.0 Pa at the 1,000 cfs flow. This is a bit surprising considering that this bend has been subject to bank erosion over the study period. Without bank erosion modeling, the hydraulic flow results alone may be used infer the bank erosion mechanisms. First, the bank at the bend might consist of weaker materials than those upstream, owing to geological reasons or vegetation roots, as the shear stress is not very high. The field observation by the author in February, 2013 seemed to confirm the above conjecture. It was found that the banks at RM 111 composed of very fine, unconsolidated, easily erodible materials. Also, the banks were mostly bare without much vegetation presence except near the downstream section. Second, non-fluvial processes such as seepage and/or piping may contribute to bank erosion. If this is the case, rainfall events would also influence the erosion process and a fluvial based method alone might be insufficient to capture all processes. At the best, the erodibility coefficient used by SRH-2D model needs to take the non-fluvial processes into consideration. Without detailed field study and monitoring data, I could not identify the processes for sure.

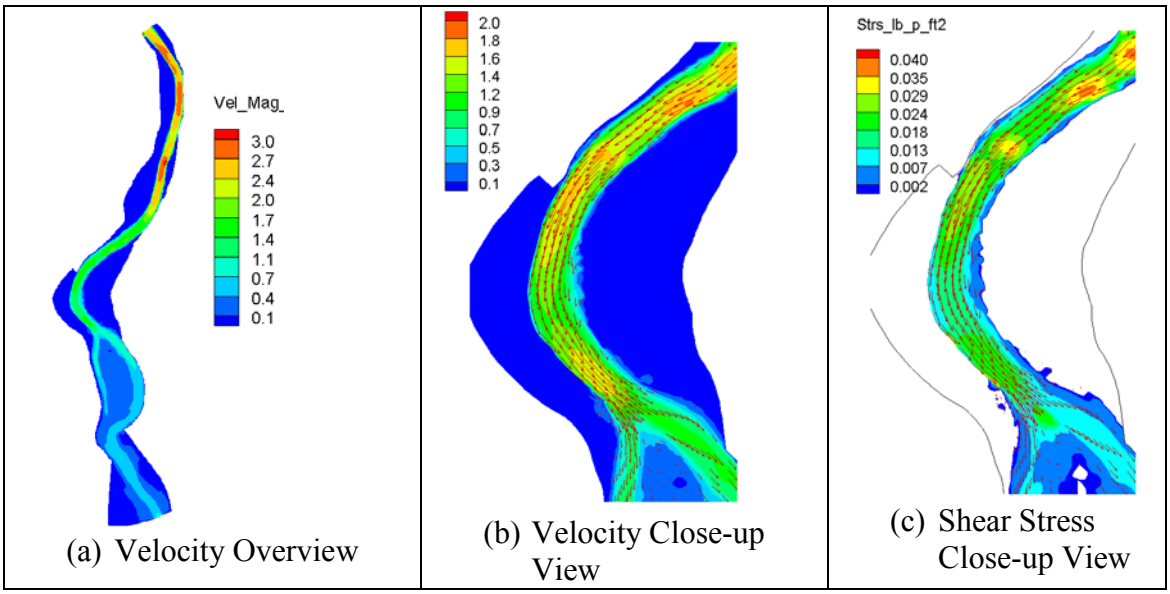

(a) Velocity Overview

(b) Velocity Close-up View

(c) Shear Stress Close-up View

Figure 6. Simulated velocity and shear stress at 1,000 cfs discharge with the 2005 terrain

Bank Erosion Modeling Results Bank erosion mobile-bed modeling is carried out in an attempt to calibrate the model using the bank retreat data computed from the historical aerial photographs. The modeling study assumes that fluvial processes are responsible for the bank erosion at the RM 111 site. For the modeling, the erodibility coefficient is chosen as the main calibration parameter.

All model input parameters and initial and boundary conditions have been discussed above. The calibration model run starts the simulation in October 2005 and ends in September 2010. The final 2010 bankline predicted by the model is plotted in Figure 7 and it is represented by the red dots of both bank toe and top points. In the figure, the January 2006 and summer 2010 historical aerial photographs are also shown for comparison. It is seen that the calibrated model did a reasonably good job in capturing the bank retreat over the 5-year period; up to about 78 feet of bank retreat distance is predicted at a few cross sections which is in agreement with the historical data.

With the calibration model, erodibility coefficient is chosen as the primary calibration parameter. However, its value has to be changed along the outer bank with a large reduction of erodibility at the downstream section of the bank. The calibrated model uses the following erodibility values: 2.0e-5 for banks 2 to 10; 5.0e-6 for banks 11 to 12; and 2.0e-6 from banks 13 to 15. A reduction of erodibility for banks 11-15 is justified as the banks in this area were reinforced by the presence of the vegetation as shown in Figure 7a as well as the photos shown in Figure 2.

During calibration it is found that a very small critical shear was required in order to simulate the bank erosion reasonably. This may or may not be physically correct. I attribute the cause to the poor representation of the terrain in the bend area.

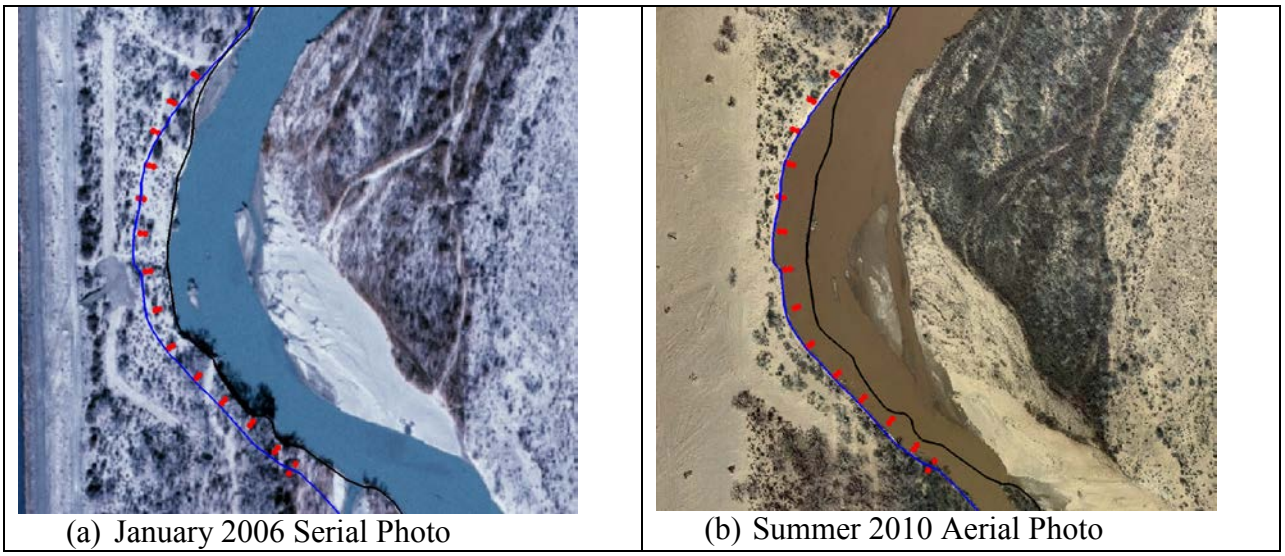

(a) January 2006 Serial Photo (b) Summer 2010 Aerial Photo

Figure 7. Comparison of bankline location and the historical bankline changes. Black line: January 2006 bankline; Blue line: summer 2010 bankline; Red dots: Predicted 2010 bankline

CONCLUDING REMARKS

The new geofluvial SRH-2D model, which coupled bank erosion modules with the mobile-bed model, is applied to predict the bank erosion at RM 111 on the Rio Grande, New Mexico. The simulation starts with the reconstructed river terrain representing the October 2005 river condition, and ends in September 2010. The 5-year simulation is carried out by using the actual, recorded daily discharge at the USGS gaging station 08354900, the Rio Grande Floodway at San Acacia, NM. The study finds that SRH-2D model is robust and ready to use with its uniform retreat bank erosion module for engineering applications. The main bank erosion calibration parameter is the erodibility coefficient that quantifies the rate of retreat at each simulated bank. The erodibility coefficient is used to represent primarily the fluvial processes. The effect of vegetation protection may also be included. However, the erodibility coefficient may also be used to represent non-fluvial processes if they are identified and quantified in the field. Once calibrated, the numerical model can perform a reasonable job in predicting the right amount of bank retreatment.

Despite the success, there are areas that need further attention and improvements in the future. They include the following:

- Field study is recommended at bank erosion sites focusing on identifying the dominant bank erosion mechanisms. SRH-2D is developed primarily for fluvial processes. If non-fluvial processes are also important, the model would be less accurate, although the erodibility coefficient can be adjusted to take non-fluvial processes into account to a certain extent.
- The terrain data, mainly in the main channel of the retreating banks, are too scarce in the present study. We believe the October 2005 terrain reconstructed from the available data is not accurate enough for this study. High uncertainty in the terrain may cause doubts on

the reasonableness of the calibrated erodibility coefficient. Erodibility should be a physical parameter; however, it is possible that the calibrated value of this study may also contain a non-physical portion that is necessary to compensate the high uncertainty of the terrain data. In the future, a bathymetric survey near the banks is recommended for SRH-2D bank erosion modeling in order to predict potential future bank changes more reliably if such data are not already available or too sparse.

ACKNOWLEDGEMENT

The author acknowledges the technical assistance and peer review provided by Paula Makar at the Bureau of Reclamation.

REFERENCES

Bankhead, N., Simon, A., Klimetz, L., and Klimetz, D. (2012). Application of the Bank-Stability and Toe-Erosion model (BSTEM) at Sites along the Rio Grande, New Mexico. U.S. Department of Agriculture – Agricultural Research Service. National Sedimentation Laboratory.

Bauer, T.R., (2006). 2006 Bed Material Sampling on the Middle Rio Grande, NM, U.S. Bureau of Reclamation, Technical Service Center, Sedimentation and River Hydraulics Group, Denver, CO.

Lai, Y.G. (2007). Erosion Analysis Upstream of the San Acacia Diversion Dam on the Rio Grande River. Technical Report. Technical Service Center, U.S. Bureau of Reclamation.

Lai, Y.G. (2008). SRH-2D Theory and User's Manual version 2.0, Technical Service Center, Bureau of Reclamation, Denver, CO.

Lai, Y.G. and Greimann, B.P. (2008). "Modeling of erosion and deposition at meandering channels," World Environmental & Water Resources Congress, ASCE, May 12-16, 2008, Honolulu, Hawaii.

Lai, Y.G. (2009). Sediment Plug Prediction on the Rio Grande with SRH-2D Model. Technical Report No. SRH-2009-41. Technical Service Center, Bureau of Reclamation.

Lai, Y.G. (2010). "Two-Dimensional Depth-Averaged Flow Modeling with an Unstructured Hybrid Mesh." J. Hydraul. Eng., ASCE, 136(1): 12-23.

Lai, Y.G. and Greimann, B.P. (2010). "Predicting contraction scour with a two-dimensional depth-averaged model." J. Hydraulic Research, IAHR, 48(3), 383-387.

Lai, Y.G. (2011). Prediction of Channel Morphology Upstream of Elephant Butte Reservoir on the Middle Rio Grande. Technical Report No. SRH-2011-04, Technical Service Center, Bureau of Reclamation.

Lai, Y.G., Greimann, B.P., and Wu, K. (2011). "Soft bedrock erosion modeling with a two-dimensional depth-averaged model," J. Hydraul. Eng., ASCE, 137(8): 804-814.

Lai, Y.G. 2013. A Coupled Stream Bank Erosion and Two-Dimensional Mobile-Bed Model. Technical Report No. SRH-2013-07, Technical Service Center, Bureau of Reclamation, Denver, CO.

Lai, Y.G. and Wu, K. (2013). "Modeling of Vertical and Lateral Erosion on the Chosui River, Taiwan," ASCE World Environmental and Water Resources Congress, Cincinnati, Ohio, May 19-23.

Lai, Y.G. (2014) "Advances in Geofluvial Modeling: Methodologies and Applications." Advances in Water Resources Engineering, Handbook of Environmental Engineering, Volume 14, C.T. Yang and L. K. Wang (eds), Humana Press, Springer Science and Business Media.

Lai, Y.G., and Wu, K. (2014). "Combined Vertical and Lateral Channel Evolution Modeling." Proc. 11th International Conference on Hydroinformatics, New York City, USA.

Lai, Y.G., Thomas, R., Ozeren, Y., Simon, A., Greimann, B.P., Wu, K. (2015a). "Modeling of multi-layer cohesive bank erosion with a coupled bank stability and mobile-bed model." To appear in Geomorphology.

Lai, Y.G., Gaeuman, D, Bandrowski, D.J. (2015b). "Morphological impact of a rehabilitation project: SRH-2D modeling assessment." Joint 10th Federal Interagency Sedimentation Conference and 5th Federal Interagency Hydrologic Modeling Conference, Reno, Nevada, April 19 –23, 2015.

Langendoen, E.J. and Simon, A. (2008). "Modeling the evolution of incised streams. II: Streambank erosion." J. Hydraul. Eng., ASCE, 134(7): 905-915.

Parker, G., (1990). "Surface-Based Bedload Transport Relation for Gravel Rivers." J. Hydraulic Research, 28(4):417-436.

Simon, A., Curini, A., Darby, S.E., and Langendoen, E.J. (2000). "Bank and near-bank processes in an incised channel." Geomorphology, 35(3-4): 193–217.

Simon, A., Pollen-Bankhead, N., and Thomas, R.E. (2011). "Development and application of a deterministic bank stability and toe erosion model for stream restoration." In: Stream Restoration in Dynamic Fluvial Systems: Scientific Approaches, Analyses, and Tools, American Geophysical Union, Geophysical Monograph Series 194. pp. 453-474.

COMPLEX GEOMORPHIC RESPONSES TO BASE LEVEL FLUCTUATIONS: A CASE STUDY ON THE RIO GRANDE UPSTREAM OF ELEPHANT BUTTE RESERVOIR

Nathan Holste, Hydraulic Engineer, Bureau of Reclamation, Denver, CO, nholste@usbr.gov

INTRODUCTION

The Rio Grande has episodically become disconnected from the Elephant Butte Reservoir pool in southern New Mexico after drought-induced periods of drastic reservoir recession, most recently from 1998 to 2004. Relatively high sediment loads coupled with low water discharge and a flat valley slope caused the river channel to lose form within the reservoir delta. Water and sediment could not be effectively delivered to the reservoir pool due to the lack of an established channel, which led to high evapotranspiration water loss within the delta area. Therefore, a channel was constructed between 2000 and 2004 to reconnect the river to the reservoir pool. Annually recurring adaptive maintenance of the excavated channel has been required to remove accumulated sediment, clear vegetation, and repair spoil berms. Upstream of the delta area, concerns have included sediment plugs that blocked the main channel and headcuts that caused bank instability and habitat loss. These issues motivated an assessment of channel conditions and dynamics within a geomorphic framework that considers the primary physical processes that govern alluvial river morphology. A reach length of 60 miles was evaluated from Elephant Butte Dam to the Highway 380 Bridge, with emphasis on the subreaches closest to the reservoir pool.

This reach of the Rio Grande is highly dynamic and behaves with a great deal of complexity. The geomorphic drivers of water discharge and sediment load, coupled with the primary control of downstream base level (reservoir pool) elevation, have varied significantly from the early 1900s to the present. After a period of initial reservoir filling that followed dam construction in 1915, the reservoir water surface has fluctuated over a vertical range of 150 feet (a shift in the horizontal water surface of around 32 river miles) corresponding to wet and dry climatic periods. Given that the Rio Grande's water and sediment inputs are varying while the downstream control is changing, it is clear that a complex series of responses should be expected. The river's planform, cross-sectional shape, slope, bed elevation, and other morphological characteristics are continuously changing in response to alterations in water discharge, sediment load, base level, and anthropogenic actions (Schumm, 1977; Watson et al., 2007).

The relationship between upstream geomorphic drivers and the downstream control often results in a sediment imbalance upstream of the reservoir pool. An imbalance between sediment supply and sediment transport capacity is the prevailing condition within this reach of the Rio Grande, which causes frequent channel adjustments over both space and time. Analysis demonstrates that the slope and bed elevation of the Rio Grande through this reach respond to a rising or falling reservoir pool. Locations near the reservoir pool tend to adjust quickly, while channel response further upstream occurs later in time and at a lesser rate. Backwater effects from the reservoir may amplify or dampen channel adjustment to upstream water and sediment discharge. Although periods of degradation have been initiated when a high flow event occurs while the reservoir pool is low, aggradation is the most dominant characteristic of this reach.

Sediment balance implies a relative equality between the material made available to a stream from a watershed (sediment supply) and the capacity of a stream to convey the available material (sediment transport capacity). Sediment supply to a river is primarily a function of water discharge and the quantity and characteristics of available sediment. Sediment transport capacity is determined by the channel morphology and its interaction with flowing water. The fundamental cause of most channel and floodplain adjustments is an imbalance between sediment supply and transport capacity (Lane, 1955; Schumm, 1977). Figure 1 shows that the rate of sediment transport in a river, or section of river, is governed by a limited sediment supply (supply limited) or a limited transport capacity (capacity limited) (Julien, 1998). The relative magnitude of these two variables determines the response of the river. Where an alluvial river system has excess transport capacity, typical adjustments include channel incision, bank erosion, and potential planform change from a braided sand bed channel to a single thread, mildly sinuous channel with a coarser bed. Additionally, a reduction in sediment supply generally results in a narrower, deeper channel with a flatter local slope and increased sinuosity. Where a river has excess sediment supply and limited transport capacity, channel aggradation will occur. Aggradation usually causes a wider, shallower channel with a steeper slope, decreased sinuosity, and reduced flow capacity (Reclamation, 2012).

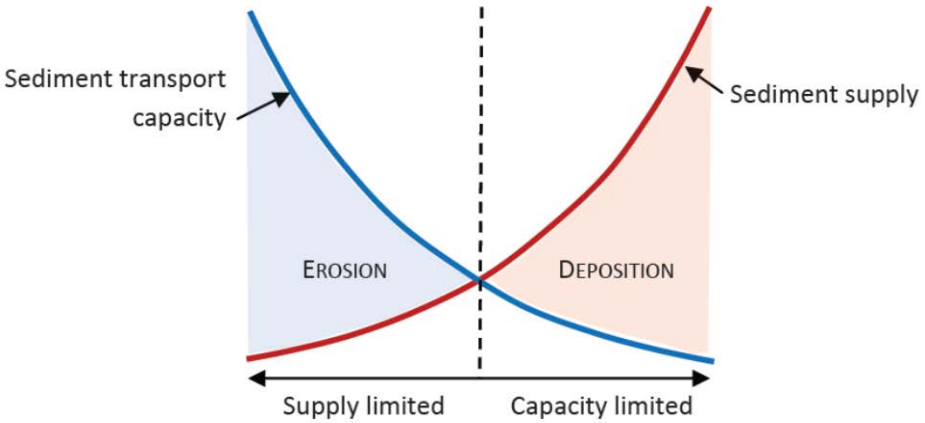

Figure 1 Sediment transport and supply curves (after Julien, 1998).

Lane (1955) proposed a qualitative relationship for adjustment in alluvial streams as a function of sediment supply and transport capacity. This relationship, known as Lane's balance ($Q_s d_{50} \sim QS$), states that the river's sediment load (Q_s) and median sediment size (d_{50}) are proportional to the river's water discharge (Q) and slope (S). Although the relationship is indeterminate, it provides a conceptual framework for evaluating the direction of change that would restore balance to a river system where one or more of the parameters have been altered. The concept of Lane's balance and sediment balance was first discussed by Davis (1895), who explained how the gradient of a stream adjusts so that the capacity to do work (related to sediment transport capacity) is equal to the work that must be done (related to sediment supply). Davis's description of work is essentially the river's ability to effectively transport the available water and sediment. The river morphology adjusts in an attempt to balance the energy of the flow with the sediment regime.

GEOMORPHIC DRIVERS

Sediment balance, or imbalance, is affected by two types of factors: drivers of channel adjustment and controls on channel adjustment (Makar and AuBuchon, 2012). During a period of years, decades, or centuries, the primary drivers that determine alluvial channel morphology are the flow regime and sediment load (Schumm, 1977; Watson et al., 2007).

Flow Magnitude, Frequency, and Duration: On the Middle Rio Grande, flood and sediment control dams have altered the hydrologic regime by reducing flood peaks. Natural climate cycles have also affected streamflow characteristics. During dry periods from 1943–1978 and 1996–present, most of the recorded peak flows are substantially less than 5,000 cfs and the annual flow volume is typically less than one million acre-feet. Wetter cycles from 1903–1942 and 1979–1995 resulted in peaks significantly greater than 5,000 cfs and annual flow volumes greater than one million acre-feet. The sequencing, or relationship, between monsoon and spring runoff events contributes to the sediment balance complexity because much of the sediment is supplied to the river during monsoons and transported during spring runoff flows.

Figure 2 illustrates the total annual valley flow volume, as calculated by combining values from the Rio Grande at San Marcial (USGS Gage 08358500), Rio Grande Floodway at San Marcial (USGS Gage 08358400), and the Rio Grande Conveyance Channel at San Marcial (USGS Gage 08358300). The gage locations are combined in order to maintain consistency across the period of record while accounting for operation of the Low Flow Conveyance Channel (LFCC) from 1952 to 1975 and 1983 to 1985. The annual flow volume incorporates both the magnitude and duration of flow events so it is a good indication of the energy provided to the river. The channel planform has narrowed and become more uniform as decreased peak flows have not reworked the channel to the degree it had been in the past (Makar and AuBuchon, 2012). It is evident that flows upstream of Elephant Butte are quite dynamic; the variability exists within wet-dry cycles and across the entire period of record.

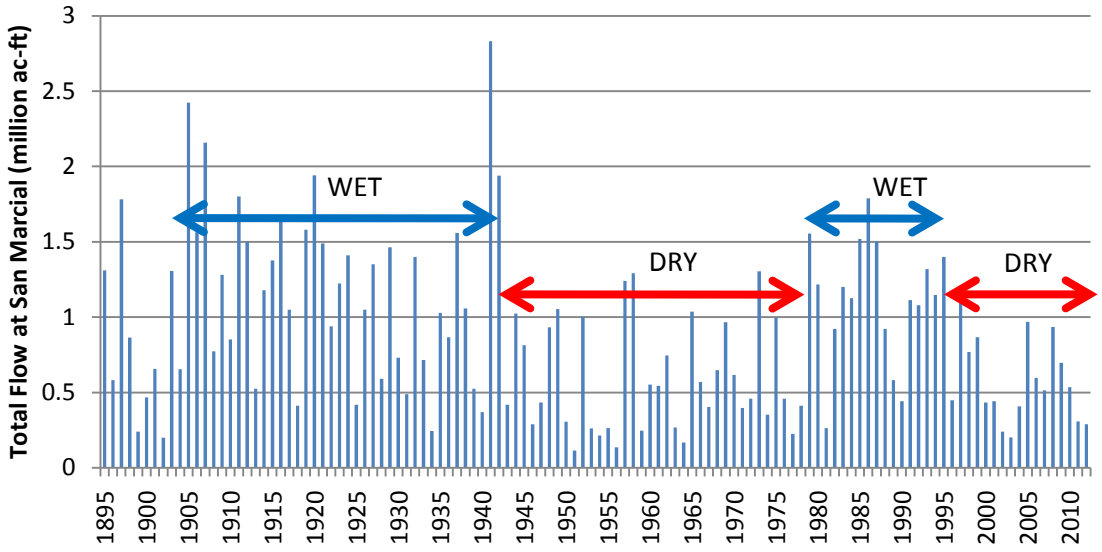

Figure 2 Annual valley flow volume at San Marcial (1895–2012).

Sediment Supply: Sediment supply is coupled with water discharge as the primary drivers of channel morphology and is also half of the sediment balance relationship. For an alluvial channel, sediment particles at a given location must have been eroded from within the watershed above the cross section and transported by flow from the place of erosion to the cross section (Julien, 1998). The Rio Grande is a sediment-laden river with many sources contributing to the total load including upland erosion (overland flow), tributaries (arroyo flow), and bed/bank erosion (main channel flow). Sediment supply is difficult to quantify due to the highly spatially and temporally variable physical processes that are not easily measured.

Sediment loads have been reduced on the Middle Rio Grande as a result of reduction of peak flows, deposition in reservoirs, and other sediment control measures (Makar and AuBuchon, 2012). Figure 3 is a double mass curve of cumulative suspended sediment load versus water discharge at San Marcial. It should be noted that suspended load is only a portion of the total load and does not include coarser particles that are transported near the bed. A steeper slope on the graph indicates that a greater volume of sediment is being carried for an equal discharge, as compared to a flatter slope that represents a smaller volume of suspended sediment for the same discharge. The figure shows a high concentration of sediment from 1955 to 1977, a slightly lower concentration from 1978 to 1982, and an even lower concentration from 1983 to 1992. Beginning in 1993, the concentration increased for a period through 2006, after which it decreased again between 2007 and 2012. Data from future years may show if a true shift occurred in 2007, or if the current period is statistically similar to 1993–2006.

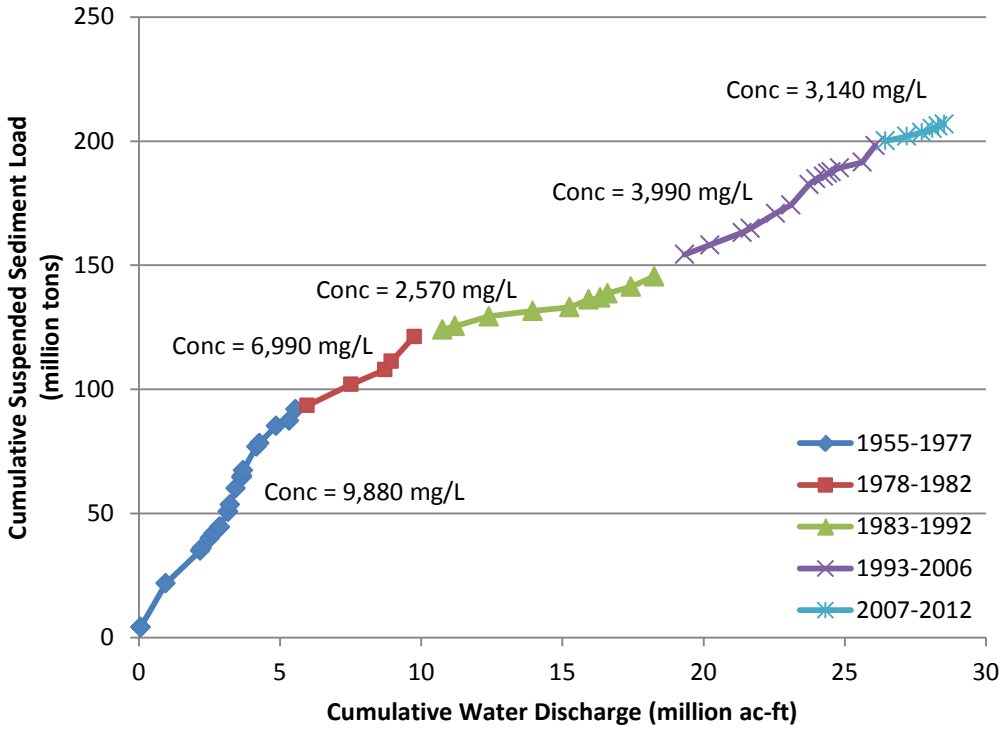

Figure 3 Cumulative suspended sediment load versus discharge at San Marcial Floodway Gage.

GEOMORPHIC CONTROLS

Controls can be defined as factors that limit or influence the effect that drivers have on channel adjustment (Makar and AuBuchon, 2012). These factors are further characterized as channel and floodplain controls or base level control.

Channel and Floodplain: The channel boundary consists of the stream bed and stream banks; the material composition of these features significantly affects channel planform and cross-sectional geometry. Bed and banks that are erodible allow the river to freely shift shape, position or pattern. The relative stability and roughness of the bed and banks often determines whether the channel will adjust laterally or vertically. When sediment transport capacity exceeds supply, a channel with an erodible bed and resistant banks will tend to incise. Over time, the bed material may coarsen and incision may continue below the vegetative root mass elevation, thus stabilizing the bed and destabilizing the banks. At this time, lateral erosion of the banks will occur as described in the Channel Evolution Model (Schumm et al, 1984; Watson et al., 2007). Coarser bed and bank material typically provide enhanced stability, but fine-grained cohesive sediments may also be relatively erosion resistant. The presence of clay layers has been well documented within the study area (Hilldale, 2003; Bauer, 2007). Cohesive silt and clay are usually most prominent on bars and floodplain surfaces, although there have been observations of clay spanning the entire width of the riverbed. Existing clay layers may have been deposited long ago in former overbank or reservoir pool areas, but there is also a significant amount of cohesive material deposited annually by arroyo flows. Bed material grain size is classified as fine sand (0.125–0.25 mm) for the majority of the study reach and medium sand (0.25–0.5 mm) for the most upstream 10–20 miles. Coarsening has occurred during the previous 40 years, a trend that is consistent with other reaches throughout the Middle Rio Grande (Makar and AuBuchon, 2012).

Floodplain characteristics also act as a control on channel adjustment. A well-connected floodplain where overbanking flows frequently occur provides a negative feedback mechanism that dissipates energy during large floods. A positive feedback loop occurs in channels with a disconnected floodplain as the energy is confined to the channel and increasing velocity and shear stress are amplified. Floodplain confinement is a control that limits lateral migration and the width of overbanking flow due to natural geologic outcrops or artificial levees. Lateral constraints confine sediment-carrying flood waters and may increase the depth of deposition because the available area is reduced. Deposition across a river and floodplain cross section is not uniform, owing to the vertical sediment concentration profile and local site conditions. Many cross sections within this reach show a channel perched above the floodplain, and a floodplain perched above the valley. Overbanking flows within these areas are often separated from main channel flows, thereby reducing channel sediment transport capacity and contributing to sediment imbalance. A perched system is indicative of disequilibrium and increases the probability of channel avulsions or levee breaches.

Base Level: Base level, the downstream limit of the stream network and origin of the thalweg profile, controls the longitudinal water surface profile for typical alluvial rivers. Changes in base level have the potential to initiate instability within the river system (Watson et al., 2007). Table 1 distinguishes the primary causes of bed elevation change that progresses downstream from that

of an upstream progression. Base level lowering, such as a drop in reservoir pool elevation, locally increases slope at the channel outlet (e.g., reservoir delta) thus increasing sediment transport capacity. If the increased capacity exceeds sediment supply, the abrupt break of slope (headcut or knickpoint) migrates upstream through the system. The peak rate of degradation is dependent on discharge and usually occurs fairly quickly and then slows over time, while also declining at further distances upstream. Incision may trigger bank instability that generates lateral erosion and channel widening. Bank erosion provides additional sediment input to the stream and the system oscillates through a series of adjustments to the new base level until relative stability is restored. (Stability may never be restored if the base level continues to fluctuate and there is not a balance between sediment supply and transport capacity.) In the absence of a geologic control, the final gradient resembles the same form as the original slope, but at a lower bed elevation throughout the affected reach (Knighton, 1998; Watson et al., 2007).

Table 1 Main Causes of Streambed Elevation Change (adapted from Knighton, 1998).

Type of Bed Elevation Change	**Upstream Driver: Cause of Downstream Progression**	**Downstream Control: Cause of Upstream Progression**
Degradation	water discharge increase; sediment supply decrease	base level fall
Aggradation	water discharge decrease; sediment supply increase	base level rise

Conversely, a rise in base level reduces local transport capacity at the river/pool interface and initiates or increases deposition. Lai and Capart (2008) conducted physical and numerical modeling to examine longitudinal delta profile evolutions over time for a constant base level and a steadily rising base level. For both cases, the greatest amount of aggradation occurred at the intersection of the pool water surface and the riverbed, while the rate of aggradation decreased further upstream. The rising base level models showed that the zone of greatest aggradation moved upstream in response to the advancing reservoir pool shoreline. At a constant location significantly upstream of the reservoir pool, there was more aggradation during the rising base level experiment than the steady base level experiment.

Reservoir and Riverbed Elevation Analysis: Construction of Elephant Butte Dam began in 1908 and was completed in 1916, with water storage operations beginning in 1915. The dam's spillway is an uncontrolled ogee crest weir and has a crest elevation of 4452.5 feet in the NAVD88 datum (Ferrari, 2008). The reservoir pool filled fairly rapidly between 1915 and 1920, and then declined slightly until large floods in 1941 and 1942 completely filled the reservoir. Between 1942 and 1951, the average annual pool elevation dropped 114 feet. The reservoir pool stayed fairly low through the end of the dry period in 1978 and then increased 101 feet to full pool elevation in 1986 due to large flows in the 1980s. The reservoir was essentially full between 1985 and 1995 before declining slightly through 1998. Between 1998 and 2004, the average pool elevation dropped 90 feet. A moderate increase of 35–40 feet occurred between 2004 and 2009 prior to a similar decrease of 30–40 feet through 2012.

Figure 4 shows a time series plot of the pool water surface elevation compared to the riverbed elevation at San Marcial. San Marcial is about 42 miles upstream of Elephant Butte Dam, 31 miles upstream of the average 2012 pool elevation, and 5 miles upstream of the full pool

elevation. The largest rates of aggradation (1920–1948 and 1978–1995) have occurred during periods of increasing or full reservoir pool elevations. Periods of riverbed degradation (1949–1972 and 2005–2011) correspond to low or decreasing reservoir pool elevations. The periods of degradation began during large spring runoff events of 1949 and 2005, both about 7 years after the reservoir pool started to lower. Bed elevation stabilized briefly from 1950 to 1956, before large flows in 1957 and 1958 initiated a more constant degradational trend through about 1972. The 1949–1972 degradation rate was only about one half to one third that of the recent rate, most likely due to the substantially higher historical sediment load (Figure 3). Short-term degradation during 1937 (Happ, 1948), 1991, and 1995 was caused by avulsions or sediment plugs that reduced upstream sediment supply. A sediment plug also occurred in 2005, but the degradational effect persisted over a longer period of time because of the lowered reservoir pool. All three of the primary degradation causes (Table 1) were present during the 2005 spring runoff: water supply increase, sediment supply decrease, and a lowered base level. Although degradation has occurred during the identified periods, the overall dominant historic trend is aggradational. The average riverbed elevation at San Marcial has increased by about 21 feet since 1895 and by about 18 feet since Elephant Butte water storage began in 1915.

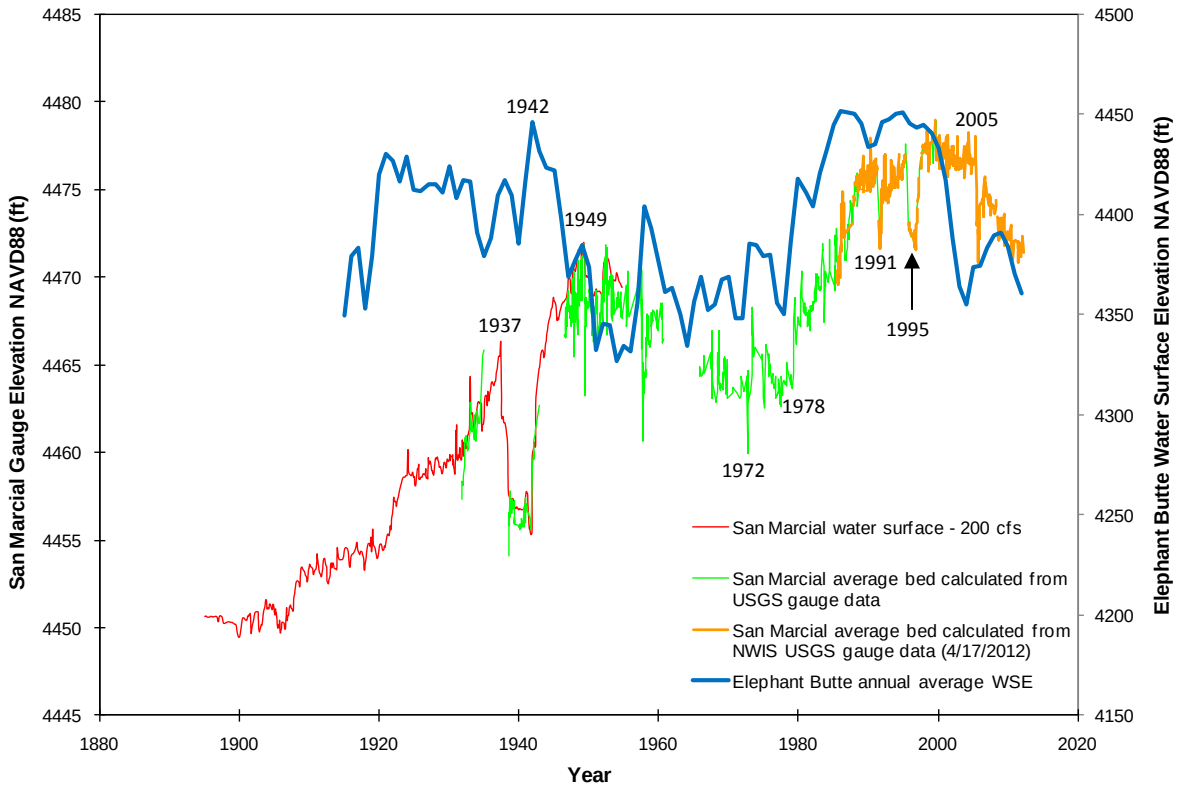

Figure 4 Elevation changes of the USGS San Marcial gage and Elephant Butte Reservoir pool over time (modified from Makar 2013, pers. comm.).

It is instructive to consider the various geographic locations of the reservoir pool shoreline in the context of the river and reservoir longitudinal profiles. Figure 5 overlays six different pool

elevations on surveyed profiles from 1915, 1988, 1999, and 2007. The two most apparent observations from the graph are the sediment deposition along the length of the profile and the tremendous range in horizontal and vertical reservoir pool locations. It is evident that the original 1915 slope was fairly uniform from the dam upstream to EB-10 (near San Marcial). The more recent profiles show a break in slope (pivot point or knickpoint) at the Narrows where the greatest amount of historical aggradation has occurred. This is also the historical average pool elevation, corroborating the model results of Lai and Capart (2008). Degradation at the Narrows and locations further upstream can be observed in the profiles between 1999 and 2007, corresponding to a decline in reservoir pool elevation. Strand and Pemberton (1982) describe the development of a topset slope and foreset slope during the delta formation process. They found that, on average, the topset slope is half of the original channel slope and the foreset slope is 6.5 times steeper than the topset slope. The grade break between the two slopes is known as the pivot point, which becomes a knickpoint or headcut within the river channel after the pool water surface lowers. This process sets up conditions that promote upstream migration of riverbed degradation after a period of reservoir lowering.

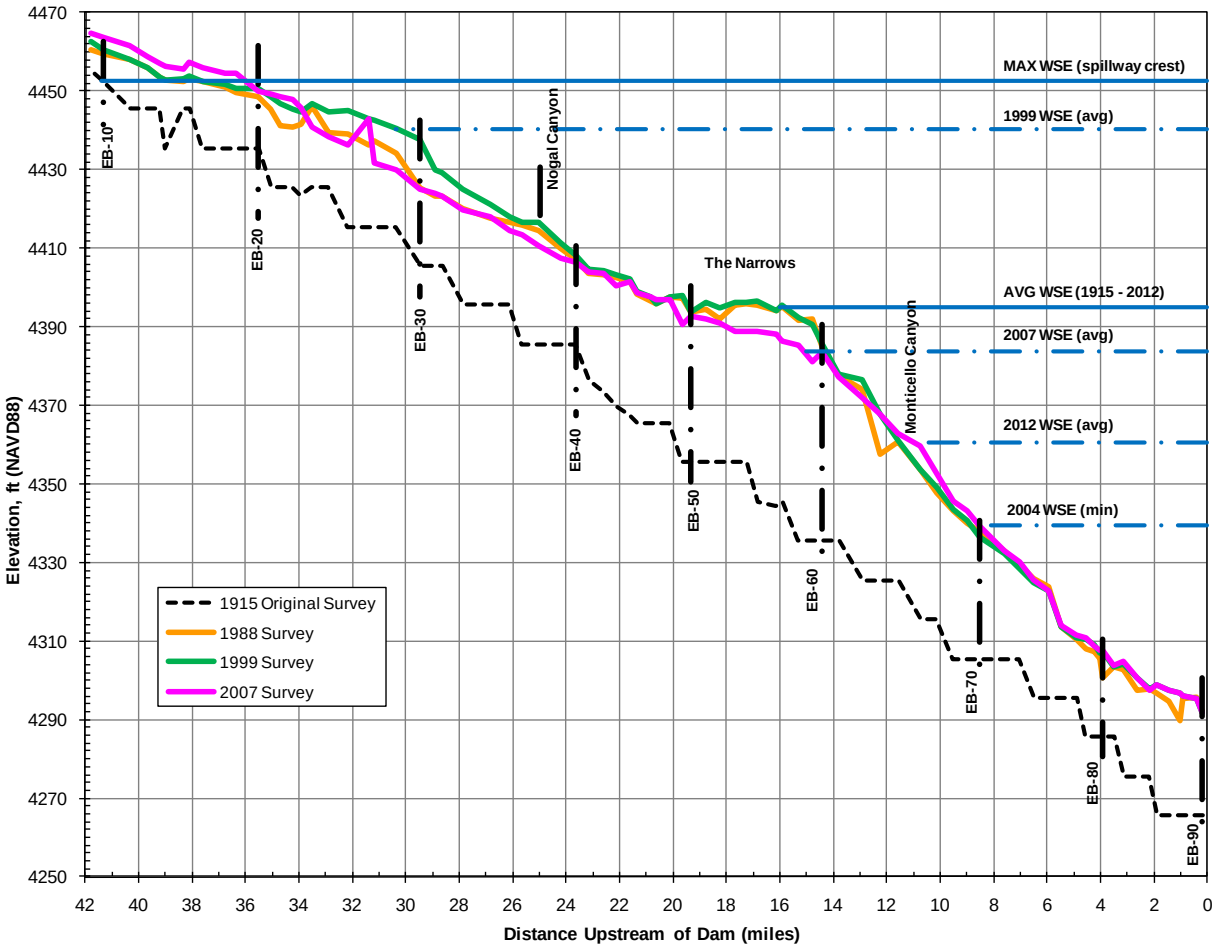

Figure 5 Elephant Butte Reservoir longitudinal profiles and pool elevations (modified from Ferrari, 2008).

Comparing the 1999 and 2004 reservoir water surfaces within the context of the longitudinal profiles also shows why channel excavation was needed to maintain a connection from the river to the reservoir pool. The flat slope in many areas combined with low flows and relatively high sediment loads did not provide enough energy for the river to carve its own channel through several miles of delta. After initial construction was completed in 2004, the channel has required annual maintenance to adapt to the dynamic nature of the delta area. Concerns were expressed that the recurring maintenance may cause reach-wide riverbed degradation, which led to a more detailed analysis of the constructed channel during the maintenance period. Figure 6 demonstrates that during recurring maintenance, the average thalweg elevation responded directly to the reservoir pool: aggradation occurred between 2004 and 2010 as the pool elevation increased and degradation occurred between 2010 and 2012 while the pool receded. In this dynamic and complex system, geomorphic effects that may have been caused by maintenance actions are not discernable compared to the significant effects from the geomorphic drivers and the primary control of base level elevation.

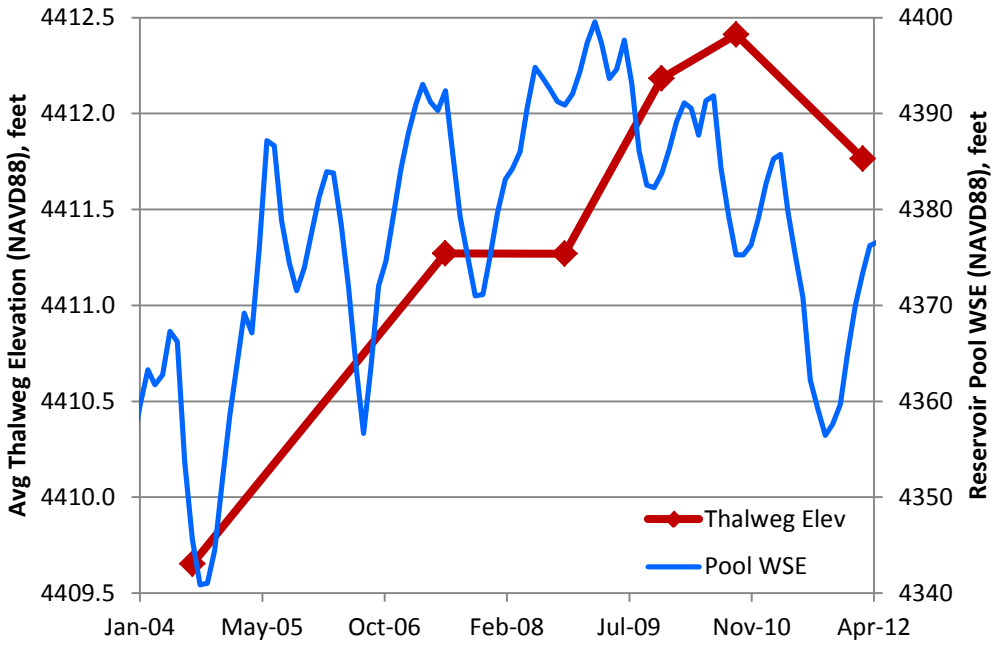

Figure 6 Distance-weighted average thalweg elevation over time for the constructed channel (between EB-28 and EB-50) during recurring channel maintenance.

Reservoir and Riverbed Slope Analysis: River slope is one of the best indicators of the river's ability to do morphological work (Watson et al., 2007) and, as discussed earlier, slope directly affects the transport capacity and sediment balance of a river system. An increase or decrease in the river slope over time provides insight regarding the river's response to changes in upstream drivers (water and sediment discharge) and downstream control (base level). Changes in slope are a measure of the relative bed adjustment between the upper and lower sections of a reach; if all cross sections aggraded or degraded equally the slope would not change. A steeper slope that provides increased transport capacity would result from aggradation at the upper portion of a reach and/or degradation at the lower end. A flatter slope that provides reduced transport

capacity could be created by degradation at the upstream section of a reach and/or aggradation downstream. Figure 7 presents thalweg profiles of the Rio Grande from the Highway 380 Bridge to the Narrows between 1999 and 2012. The pivot point corresponding to the reservoir pool elevation and the upstream depositional wedge are clearly evident in the 1999 profile. Little change occurred during the 1999–2004 low flow years before upstream headcut migration occurred during the 2005 spring runoff. The 2005 profile also shows the sediment plug near RM 72 and the deposition between RM 46–50 of material eroded from upstream. Finally, there is a zone of convergence between RM 74–78 where the profiles are relatively constant for all years.

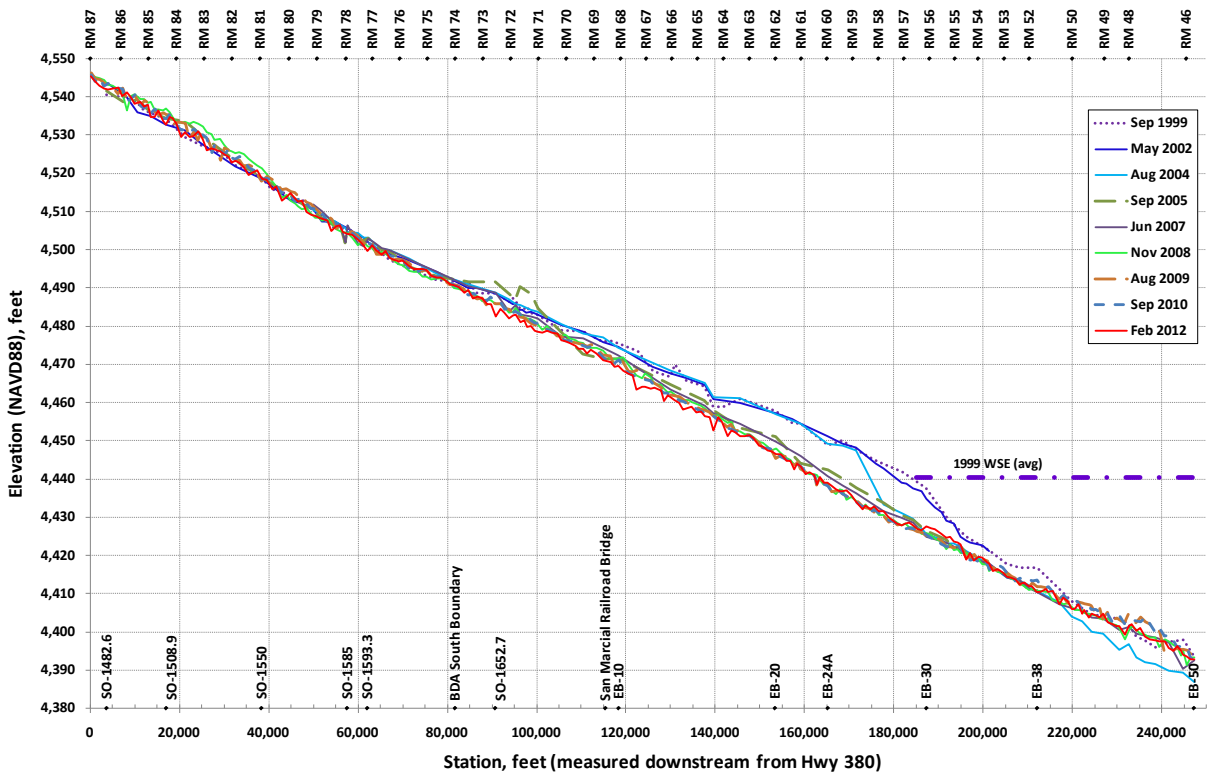

Figure 7 Thalweg profiles from Highway 380 Bridge to the Narrows.

Figure 8 shows the relationship between channel slope and reservoir pool elevation, and also channel slope over time for different Rio Grande subreaches upstream of the reservoir pool. The upper subreach contains 9 miles, measured along the thalweg, from near RM 68 to near RM 60 (EB-10 to EB-24A) and the lower subreach contains 9 miles, from near RM 60 to near RM 52 (EB-24A to EB-38). Results for the entire 18-mile reach are also shown for comparison. Subreach and reach lengths, in addition to longitudinal profile stationing, were measured along the 2010 thalweg. The lower subreach was partially inundated by the reservoir pool in 1999 and includes the transition into the channel construction work area that began in 2000. The lower subreach also includes the 1999 pivot point at EB-30 and is assumed to be the critical subreach in which transport capacity must exceed sediment supply for a headcut to migrate upstream of RM 60. Downstream of the lower subreach, the section between EB-38 and EB-50 was not included because data were not always available, and it should also be noted that this area is flatter as the Rio Grande enters the Narrows. The figure illustrates the highly variable slope over

time as the river attempts to adjust to changes in downstream base level or upstream drivers. The lower subreach is particularly sensitive to the reservoir pool and the river slope trend closely follows the pool elevation. Although the response is not as dramatic, the slope adjustment of the overall reach is also in sequence with the reservoir pool elevation, steepening when the pool elevation drops and flattening when the pool elevation rises. For the upper subreach, the change in slope is out of phase with changes to the pool elevation. This indicates a delayed response in which the upper subreach adjusts to changes in the lower subreach. Note that lines connecting discrete slope values in the graphic illustrate trends over time (direction of slope change), and actual channel slope values are labeled on the reversed y-axes (steeper slopes are near bottom of graph).

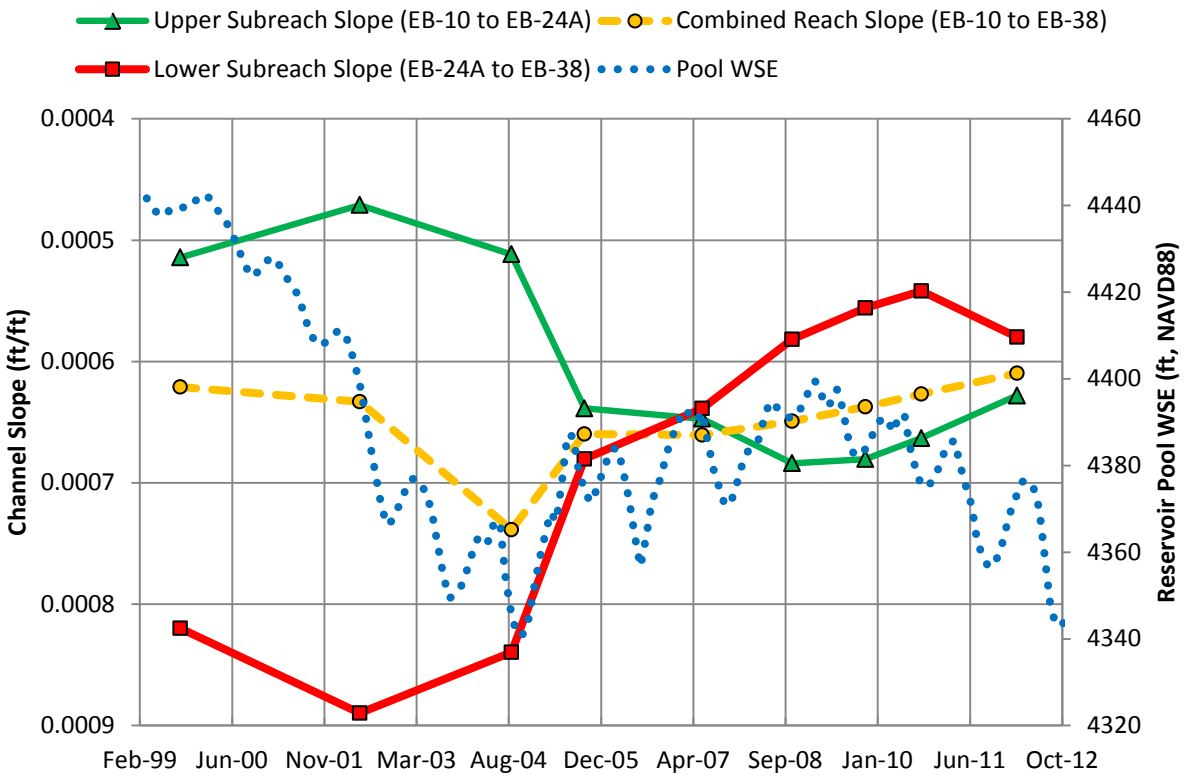

Figure 8 Changes to channel slope and reservoir pool elevation over time (1999–2012).

Using a constant water surface elevation in the reservoir at the average 2008 level, mobile bed modeling results predict that the stable slope between RM 78 and RM 46 is flatter than the existing slope. This means that a combination of aggradation in the lower portion of the modeled reach (~RM 62–46) and degradation in the upper portion of the modeled reach (~RM 62–78) is expected for the given hydrology, sediment, and base level conditions (Reclamation, 2012). As part of a sensitivity analysis, Reclamation (2012) also found that for some discharge scenarios this reach did not achieve equilibrium even after 120 years of simulation. The model results support the empirical conclusion that the Rio Grande upstream of Elephant Butte Reservoir is inherently unstable and terms such as equilibrium or stable slope do not apply for timescales less than about 100 years.

REFERENCES

Bauer, T. (2007). 2006 Bed Material Sampling on the Middle Rio Grande, New Mexico. Bureau of Reclamation, Technical Service Center, Sedimentation and River Hydraulics Group, Denver, Colorado, 44 pp.

Davis, W.M. (1895). "The Development of Certain English Rivers," Journal of Geography, v. 5, pp. 127–146.

Ferrari, R.L. (2008). Elephant Butte Reservoir 2007 Sedimentation Survey. Technical Report SRH-2008-4. Bureau of Reclamation, Technical Service Center, Sedimentation and River Hydraulics Group, Denver, Colorado, 153 pp.

Happ, S.C. (1948). "Sedimentation in the Middle Rio Grande Valley, NM," Geological Society of America Bulletin, 59(12), pp. 1191–1216.

Hilldale, R. (2003). Middle Rio Grande Substrate Exploration. Bureau of Reclamation, Technical Service Center, Sedimentation and River Hydraulics Group, Denver, Colorado.

Julien, P.Y. (1998). Erosion and Sedimentation. Cambridge University Press, Cambridge, United Kingdom.

Knighton, D. (1998). Fluvial Forms and Processes: A New Perspective. Arnold, London England and Oxford University Press, New York, New York.

Lai, S.Y.J., and Capart, H. (2008). "Response of Hyperpycnal Deltas to a Steady Rise in Base Level," Proceedings of the 5th IAHR Symposium on River, Coastal, and Estuarine Morphodynamics, edited by C.M. Dohmen-Janssen and S.J.M.H. Hulscher, Taylor and Francis, London, pp. 57–62.

Lane, E.W. (1955). "Design of Stable Channels," Transactions of the ASCE, Vol. 120, pp. 1234–1279.

Makar, P., and AuBuchon, J. (2012). Channel Conditions and Dynamics of the Middle Rio Grande River. Bureau of Reclamation, Technical Service Center, Denver, Colorado, and Upper Colorado Region, Albuquerque Area Office, Albuquerque, New Mexico, 94 pp.

Reclamation. (2012). Middle Rio Grande River Maintenance Program Comprehensive Plan and Guide. Bureau of Reclamation, Upper Colorado Region, Albuquerque Area Office, Middle Rio Grande Project, Albuquerque, New Mexico, 202 pp.

Schumm, S.A. (1977). The Fluvial System. John Wiley and Sons, New York.

Schumm, S.A., Harvey, M.D., and Watson, C.C. (1984). Incised Channels: Morphology, Dynamics and Control. Water Resources Publications. Littleton, Colorado.

Strand, R.I., and Pemberton, E.L. (1982). Reservoir Sedimentation Technical Guideline for Bureau of Reclamation. U.S. Bureau of Reclamation, Denver, Colorado. 48 pp.

Watson, C.C., Biedenharn, D.S., and Thorne, C.R. (2007). Stream Rehabilitation. Cottonwood Research, LLC. Fort Collins, Colorado.

RESTORING ALLUVIAL FAN CONNECTIVITY FOR POST-FIRE FLOOD ALLEVIATION AND SEDIMENT REDUCTION

Dave Rosgen, Ph.D., Professional Hydrologist, Wildland Hydrology, Fort Collins, CO, Dave@wildlandhydrology.com; Brandon Rosgen, Hydrologist, Wildland Hydrology, Fort Collins, CO, Brandon@wildlandhydrology.com

INTRODUCTION

The Waldo Canyon Fire burned 18,247 acres within the foothills and mountains of the Rampart Range immediately northwest of Colorado Springs, Colorado, in El Paso County. The fire started Saturday, June 23rd, 2012, and was fully contained Tuesday, July 10th, 2012, after destroying 346 homes. The four major watersheds affected by the Waldo Canyon Fire were Camp Creek, Douglas Creek, Fountain Creek, and West Monument Creek. Using GIS, these four watersheds were delineated into 89 sub-watersheds.

A post-fire *Watershed Assessment for River Stability and Sediment Supply (WARSSS)* study was conducted within the four watersheds impacted by the Waldo Canyon Fire in the fall of 2012 and completed in April, 2013 (Rosgen, 2006; Rosgen *et al*., 2013a). The *WARSSS* study is a cumulative watershed effects analysis that quantifies changes in water yield, hillslope erosional processes, and stream channel impacts, including streambank erosion due to disturbance. The assessment found that the prevailing consequences of the Waldo Canyon Fire included: 1) an increased magnitude and frequency of peak flows; 2) accelerated sediment yield from hillslope erosional processes, including rill, gully, and debris flow/debris torrents; 3) streambank erosion and channel enlargement due to destruction of riparian vegetation and increased flows; and 4) channel incision and subsequent abandonment of fluvial features, including alluvial fans.

The results of the *WARSSS* study form the foundation for a multi-watershed master plan to direct restoration efforts to reduce delivered sediment, restore the stability and function of the stream and riparian systems, and accelerate the watershed recovery processes (Rosgen *et al*., 2013b). The results were used to develop design scenarios for post-fire restoration priorities directly related to individual erosional processes by specific sub-watershed location.

This paper focuses on one of the restoration design scenarios related to restoring alluvial fan functions to meet the primary restoration objectives. Ephemeral, fan-head trenches (gullies) within alluvial fans were raised to reconnect to the original fan surface to reduce the flood and debris flows that were directly routed into the trunk stream. Once connectivity of the fan was restored, flood flows were dispersed and sediment was stored. Fill material for the gully was obtained from excavating sediment detention basins at the start, middle, and lower sections of the fan, and braided channels were constructed on the fan surface to match the natural channel form. Log crib walls were constructed for grade control on the upslope end of the sediment detention basins with log sills buried flush on the fan surface to prevent channel incision. An example is presented on the flow and sediment response of restoring alluvial fan function.

IMPACTS OF THE WALDO CANYON FIRE

Rill and gully erosion is common within the fire-scarred landscape associated with soils comprised of highly-weathered grussic granite from Pikes Peak Batholith (Figure 1). Such rills and gullies increase the time of concentration of flows that lead to increased peak flows and associated debris flows.

The post-fire floods and debris flows resulted in major destruction to property and loss of lives. Damage to water transmission lines caused millions of dollars of damage to infrastructure to the Colorado Springs Utilities (Figure 2). A fatality occurred due to debris flows similar to the one shown in Figure 3 that occurred on Highway 24 following a post-fire storm in August, 2013. Furthermore, a 1.0-inch in 30 minute precipitation event created a 1,100 cfs debris flow in Williams Canyon (2.69 mi^2 drainage area with a bankfull discharge of 9.0 cfs) (Figure 4). The sediment supply from debris flows overwhelmed multiple receiving streams and induced stream aggradation (Figure 5). The erosional debris accumulated in downstream channels (Figure 6) and reservoirs (Figure 7).

High rates of sediment are also delivered downstream with subsequent flows when streams become incised in the erosional debris. The incised gullies increase sediment transport capacity due to the increased slope and decreased

width/depth ratio (Figure 8). Further channel aggradation was evident in the receiving streams due to the very high sediment supply delivered from upstream.

Figure 1 Rill and gully development from a recent storm on a fire-scarred landscape of the Waldo Canyon Fire.

Figure 2 Damage to water transmission lines, North Monument Creek.

Figure 3 An alluvial fan being formed on Highway 24 following a post-fire flood. The flooding resulted in a fatality due to debris flows onto the highway.

Figure 4 Destruction of homes following a post-fire flood and debris flow in Williams Gulch associated with the Waldo Canyon Fire.

Figure 5 Stream aggradation due to excess sediment deposition, North Monument Creek.

Figure 6 Erosional debris following a post-fire flood in Waldo Canyon.

Figure 7 Loss of reservoir storage due to excess sediment deposition following the Waldo Canyon fire in the Monument Creek drainage.

Figure 8 Erosional debris in a 3rd order stream following post-fire flooding in Chuckwagon Creek; note the new deposition and subsequent channel incision and headward advancement of the gully.

Hydrology Impacts: The effects of wildfire on increased peak flows and associated channel source sediment are well-documented (Moody, 2001; Kunze and Stednick, 2006; Moody and Martin, 2009). Relatively frequent precipitation events associated with high intensity, short duration storms are related to unusually large flood peaks (Neary *et al*., 2005; Moody and Martin, 2001a). Jarrett (2013) demonstrated that relatively frequent precipitation events following wildfires result in extremely rare, infrequent flood magnitudes; the predicted peak flows for a given precipitation by drainage area are shown in Figure 9 (Jarrett, 2013). A post-flood, 1.0-inch in 30 minute storm (frequent return period) generated 1,100 cfs (a rare flood) in Waldo Canyon associated with a 1.7 mi^2 drainage area and a bankfull peak flow discharge of 10 cfs. In Northfield Gulch (associated with a drainage area of 0.5 mi^2 and a bankfull discharge of 3.0 cfs), a 1.0-inch per hour storm predicted a flood peak of 210 cfs, where the observed value was 180 cfs (Figure 10).

Stednick and Webb (2014) indicated that post-fire floods can be up to three orders of magnitude greater than pre-flood conditions. Post-fire peak flows have been reported on the Hayman fire in Colorado on small drainage basins that can vary from 600 csm ($ft^3/sec/mi^2$) to over 1,064 csm from a 4.3-inch storm (Robichaud and Wagenbrenner, 2009). Post-fire peak flows have increased from 3.7 csm to over 600 csm on North Douglas Creek on the northern end of the Waldo Canyon Fire.

Moody and Martin (2001b) state that high sediment yields may persist for four to seven years following wildfires. However, hydrologic recovery in certain landscapes is much longer than anticipated; for example, the Hayman fire that burned 12 years ago is still producing high peak flows and disproportionately high sediment yields compared to pre-fire conditions (Rosgen *et al*., 2013a; Stednick and Webb, 2014). Sediment supply recovery from debris flows and associated channel source sediment related to peak flows is not rapid.

The influence of the loss of vegetative cover on streamflow response following wildfires is critical in addressing restoration strategies for recovery (Beanvides-Solorio *et al*., 2005). Hydrologic recovery and decreasing flow-related, channel source sediment is a long-term proposition related to re-establishing the riparian community following wildfires in Colorado. However, decades will be required to reach a full hydrologic utilization due to the cold climate, relatively low precipitation, steep slopes, shallow soils, high elevations, and short growing seasons.

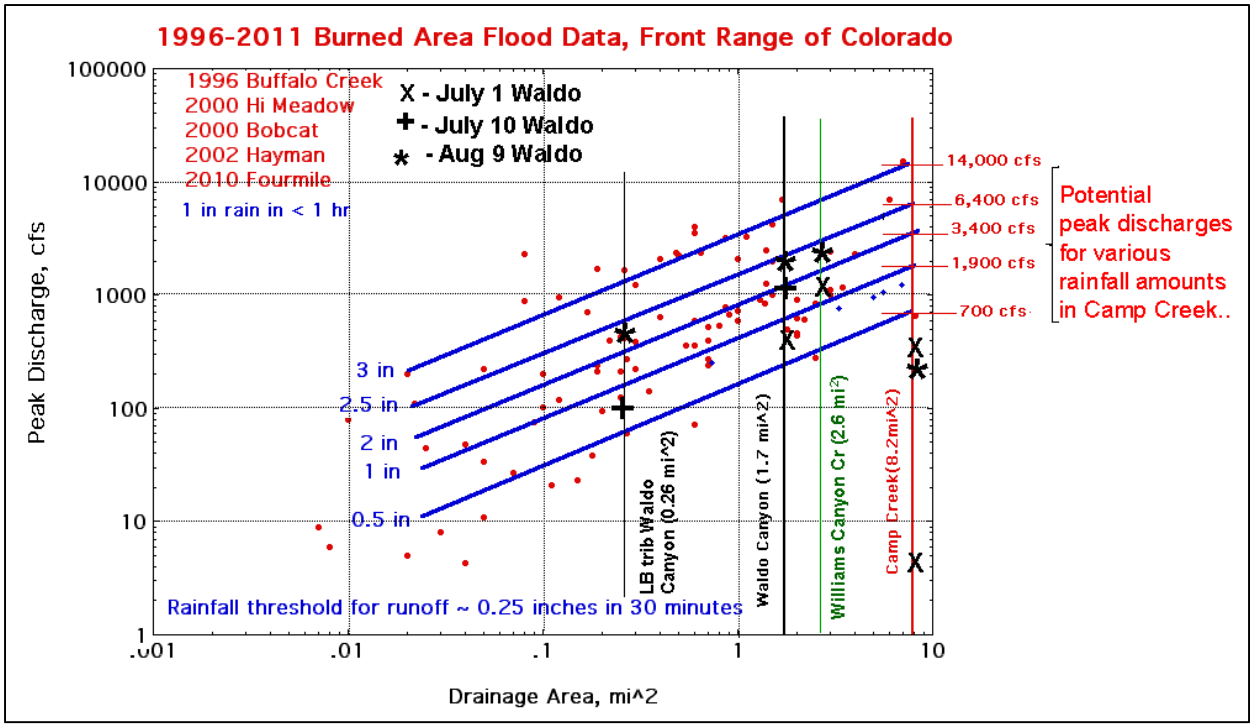

Figure 9 Peak flow data for various precipitation rates by drainage area for various burned watersheds on the Front Range of Colorado (Jarrett, 2013).

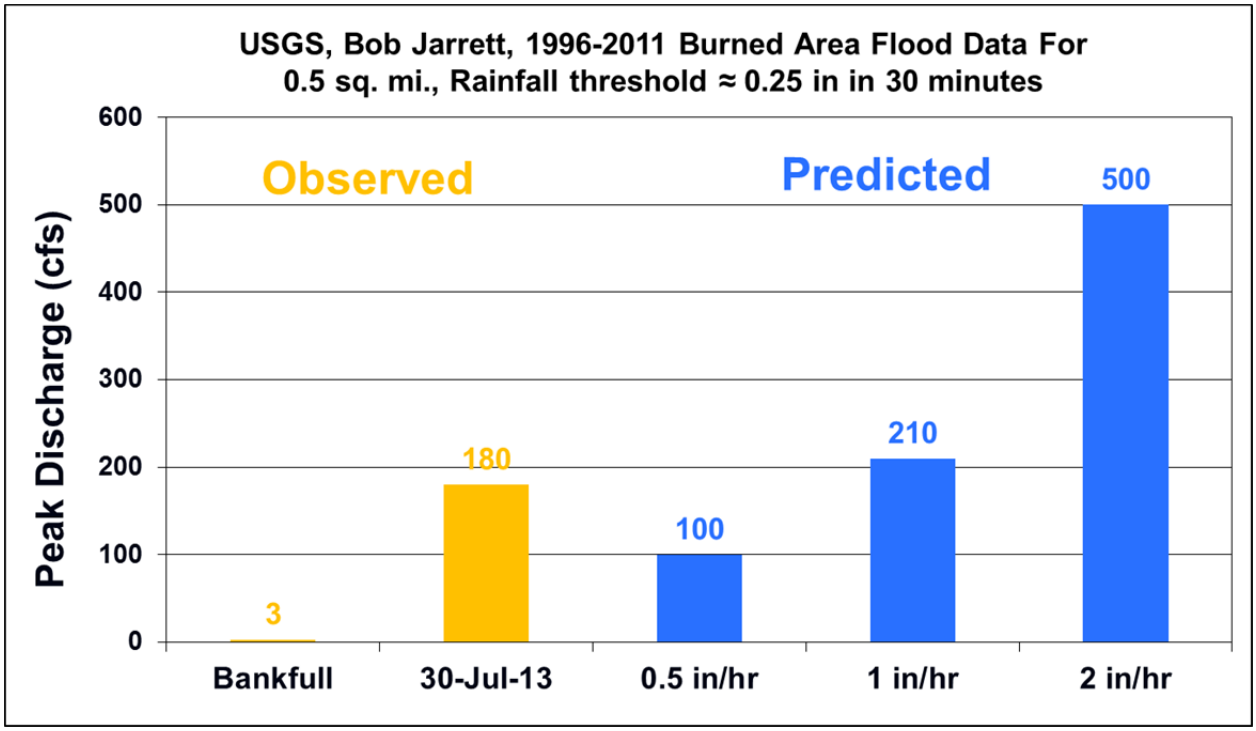

Figure 10 Predicted versus observed post-fire peak discharge for Northfield Gulch by storm intensity rates (Jarrett, 2013).

POST-FIRE ASSESSMENT AND MASTER RESTORATION PLAN

In total, 89 sub-watersheds and 237 miles of stream channel were evaluated within the four major watersheds impacted by the Waldo Canyon Fire to quantify the sediment supply from hillslope, hydrology, and channel processes (Rosgen *et al*., 2013a). The sediment supply was evaluated for each sub-watershed and was totaled for the entire fire area. The total introduced sediment from the Waldo Canyon Fire is estimated to be *51,479 tons/yr*.

The surface erosion from hillslope processes accounted for approximately *18,085 tons/yr*, or 35% of the total introduced sediment. Contributions from roads and trails accounted for approximately *2,035 tons/yr*, or 4% of the total introduced sediment.

Channel processes were evaluated for each stream reach by sub-watershed using the stability methods in *WARSSS* (Rosgen, 2006). The FLOWSED/POWERSED model was used to evaluate sediment transport capacity, and streambank erosion rates were estimated using the BANCS model. Overall, the sediment yield from streambank erosion accounted for *31,480 tons/yr*, or 61% of the total sediment yield (Rosgen *et al*., 2013a). Moody and Martin (2001b) predicted that 80% of introduced sediment from wildfires was from channel sources and 20% was from hillslopes based on the assessment of other fires on the Colorado Front Range.

Changes in hydrology were evaluated using the WRENNS model (USEPA, 1980); post-fire changes in water yield and peak flows were estimated based on the severity of the burn, the percentage of the watershed burned, pre-existing stand composition, and precipitation by elevation/aspect zone. The results from WRENNS were used to determine the flow-related increases in sediment yield using the FLOWSED model.

The results of the *WARSSS* study were used to direct a multi-watershed mater restoration plan (Rosgen *et al*., 2013b). Priority areas for restoration were established for each sub-watershed based on the highest risk and highest sediment producers from the *WARSSS* analysis. Design scenarios were developed to represent the range of stream types and stability conditions that require restoration within the watersheds using representative and reference reaches. The appropriate scenario can then be extrapolated to other reaches of the same stream type, landscape type, and stability condition.

Post-fire rehabilitation often focuses on hillslope processes because of the fast recovery rates; remediation to reduce surface erosion often includes aerial seeding, mulching, planting trees, placing contour logs on burned slopes, and contour trenching. The majority of the work completed by the USDA Forest Service BAER (Burned Area Emergency Rehabilitation) teams focused on surface erosion processes. Although it is important to maintain surface soils and revegetate as soon as possible, the restoration designs must also account for channel source sediment, which contributed 61% of the total sediment yield. The recovery of channel processes is often slow due to the long-term, peak flow increases and associated debris flows, especially in incised and entrenched stream systems. The remainder of this paper focuses on one of the restoration scenarios that accounts for excess channel source sediment related to incised and entrenched stream systems within alluvial fan landscapes.

RESTORING ALLUVIAL FAN CONNECTIVITY

Active alluvial fans and associated braided channels are the natural solution to sediment detention of the erosional material delivered from upper slopes to prevent direct sediment introduction into main trunk streams. The braided, D stream types are the natural, functioning channels on active alluvial fan surfaces that deposit sediment, decrease velocity, increase infiltration, and attenuate flood peaks (see Rosgen, 1994, 1996, for stream type descriptions).

A functioning alluvial fan as displayed in Figure 11 was enlarged following the major 1982 Lawn Lake Flood in Rocky Mountain National Park, Colorado. The Lawn Lake Flood was estimated to be the largest flood since the end of the last glacial retreat at the start of the Holocene period, 10,000 years ago (Jarrett and Costa, 1986). Extensive debris flows were deposited on the fan surface from the upstream lake breach and the associated high energy/high sediment supply from A3a+ stream types that cut into unconsolidated, glacial till with lateral moraine deposits of boulders, cobble, gravel, and sand. The natural grading of the fan deposited the coarser, boulder material at the apex and decreased the surface grain size to sand at the lower lobe. The fan prevented the bulk of the coarse, erosional debris from reaching Fall River, located immediately below the fan, as shown three days following the flood in

Figure 12. Regardless of the magnitude of the flood, the Fall River retained its naturally stable morphology due to its stable riparian corridor and floodplain connectivity.

Figure 11 Alluvial fan and braided, D stream type on the Roaring River in Rocky Mountain Park following the 1982 Lawn Lake flood.

Figure 12 Fall River in Rocky Mountain National Park, one-quarter mile below the alluvial fan of the Lawn Lake Flood. This photo was taken three days following the flood that was estimated at approximately 14,000 cfs.

Fan head trenches, or incised channels associated with A, F, and G stream types, often form due to the increased post-fire stormflow peaks (Figure 13). When stream channels abandon the fan surface and become incised in alluvial fans, they become high supply and high transport systems; thus the sediment yield is not only routed from farther upstream but is cut through portions of the fan deposit as well. The incised streams have increased velocity, stream power, and sediment transport capacity, thereby delivering excess sediment to the receiving streams. Under this scenario, the alluvial fan ceases to properly function.

Figure 13 A fan-head trench, an F4 stream type, incised in grussic granite soils within an alluvial fan on a tributary to Trail Creek following the Hayman Fire of 2002 in the South Platte River basin, Colorado.

An example of the fan head trench scenario occurred on North Douglas Creek within the Waldo Canyon Fire area. Deposition from debris flows on a fan surface is shown in Figure 14 following a storm; within one month following the deposit, an 8.0 ft headcut gully developed at the same location (Figure 15).

Figure 14 Erosional debris deposited on North Douglas (note the curved tree).

Figure 15 Channel incision (G4 to F4 stream type) at the same location as shown in Figure 14 (note the arrow directed to the same curved tree).

Restoration Design: To reduce the sediment delivered to mainstem stream systems from anticipated debris flows, the fan head trenches associated with incised A, G, and F stream types were reconnected to the alluvial fan surface with fill material to naturally create a braided, D4 stream type. Sediment debris basins were excavated to obtain the material to reconnect the incised channels with the original fan surface and to provide for sediment storage and help attenuate flood peaks. Once the basins are filled, the flood debris is designed to spread onto the fan surface with a braided channel system that will persist as long as there is a high sediment supply.

The restoration design is shown in Figure 16, featuring an interlocked crib wall to prevent headcutting during runoff events. Additional log or rock sills are located within the gully fill on the fan surface to prevent future channel incision and maintain fan function (Figure 16).

If the basins are cleaned out on a frequent basis and clear water discharge results, then a single-thread, B stream type can be constructed at the lowest basin on the fan lobe to direct streamflows to a receiving stream that overtop the basin. The B stream types are stable stream types found on inactive alluvial fans or when the incised channels become stabilized through stream succession processes in confined fluvial landscapes (Rosgen, 1996).

Where possible, restoring active fan function is the top priority for all ephemeral, 2nd and 3rd order streams affected by the Waldo Canyon Fire. The following is a summary of the specific objectives of this design scenario:

- Store sediment before it is delivered to downstream channels
- Reduce the accelerated streambank erosion rates
- Eliminate any advancing or future headcuts
- Develop sediment detention storage basins
- Attenuate flood peaks

Case Example: North Douglas Creek: Based on the *WARSSS* assessment, North Douglas was identified as a high priority sub-watershed due to the high probability of debris flows and flow-related sediment increases located immediately above thousands of homes in Colorado Springs. An incised, F4 gully over 6.0 ft deep was cut into a large alluvial fan in the sub-watershed. Although the drainage area is only 1.7 mi^2 with approximately 12.0 cfs bankfull discharge, the *WARSSS* assessment predicted approximately *10,000 tons/yr* of sediment from post-fire storms (Rosgen *et al*., 2013a).

Five sediment basins were constructed along the large alluvial fan to obtain sufficient material to fill the incised channel and to accommodate the predicted sediment yield (Figure 16 and Figure 17). The Water Resources Department at Colorado State University monitored the flows and sediment in North Douglas Creek to obtain detailed data on reactivating alluvial fans and creating sediment basins (Stednick and Webb, 2014). Streamflow measurements were obtained above the first basin, and each basin was monitored following storm events.

Following a July 1, 2013 storm, *2,751 tons* were stored in the first basin with a flow of 120 cfs (an order of magnitude higher than bankfull discharge). The constructed basin (Figure 18) is compared to the post-fire storm results depicting a completely filled basin (Figure 19). By the end of the storm season following eight, individual storms, all five basins were filled with an estimated *10,000 tons* of sediment (Stednick and Webb, 2014); additionally, one foot of sediment deposited on the fan surface, and a braided, D4 stream type was created naturally (Figure 19). In all but the last storm, no flows or sediment were delivered downstream of the last basin on the fan; the last storm on September 23, 2013, associated with over 773 cfs from a 7.0-inch rainstorm, filled the sediment basins and resulted in minor flows and sediment delivered downstream without incident or reported damage.

The relationship between the sediment captured in cubic yards versus peak flow discharge is shown in Figure 20 as developed by Stednick and Webb (2014). This relationship does not include the last storm that produced 773 cfs and the sediment that overfilled the basins and deposited on the fan surface.

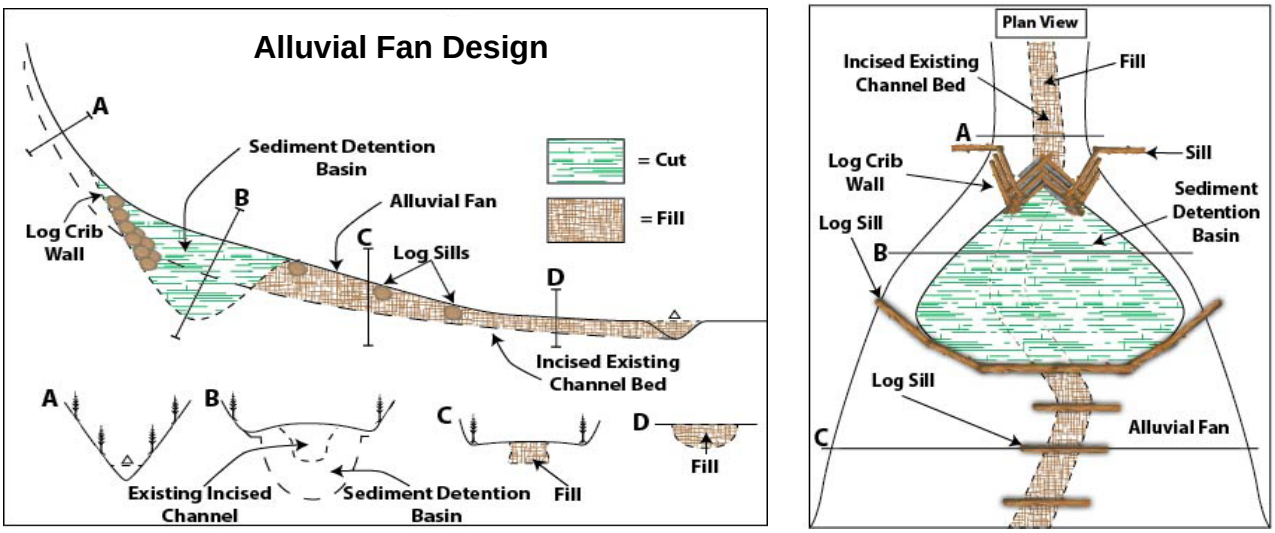

Figure 16 The design to reactivate alluvial fans and create braided, D stream types featuring a proposed debris basin with a crib wall and log sills (Rosgen, 2013b).

Figure 17 Post-construction of the five debris basins installed on North Douglas Creek on an alluvial fan.

Figure 18 Newly constructed debris basin and crib wall on North Douglas Creek where the excavated material was used to fill the deep and wide gullies (note the arrow indicating the location of the rock and exposed root wad).

Figure 19 The debris basin completely filled with sediment and ash deposits, looking downstream on fan surface, North Douglas Creek (note the same exposed root wad and rock as shown in Figure 18).

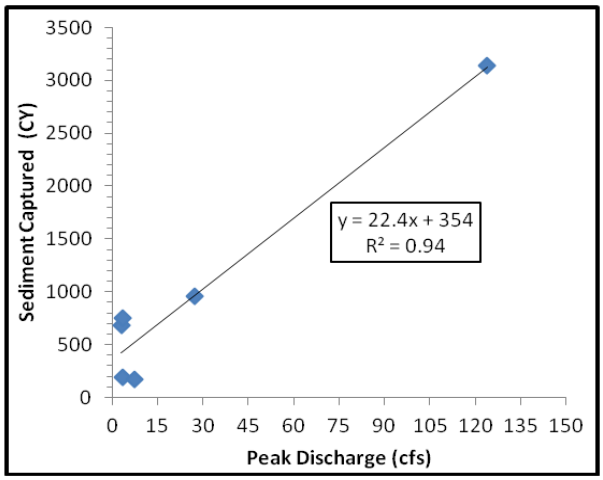

Figure 20 Relation of sediment storage by flow discharge; this does not include the 773 cfs streamflow that filled the basins and deposited one foot of sediment on the fan surface (from Stednick and Webb, 2014).

Discussion: The estimated design, oversight, and implementation costs of the debris basins vary between $4.00−$10.00 per ton of sediment saved. The costs per ton to dredge sediment from downstream reservoirs for water storage varies between $90.00−$120.00 per ton; thus it is much more cost effective to retain the sediment within the watershed. The reduced risk to downstream homeowners and the mitigation of potential adverse ecological impacts associated with sediment deposition in stream channels also provide strong motivation for implementing this approach.

Overall, restoring the alluvial fan connectivity with detention basins has saved thousands of tons of sediment from being directly delivered to the urban development immediately below the Waldo Canyon Fire perimeter. Over 40 sediment basins were constructed in 2013 on many of the high risk tributaries and all were successful at reducing delivered sediment. Due to the efficiency of the sediment detention basins, the City of Colorado Springs has since established a permanent basin at the end of the chain of basins on North Douglas Creek to reduce future flooding and sediment problems above adjacent subdivisions; the basin will be cleaned out when filled with sediment from future storms. Furthermore, the Forest Service BAER team recently approved the debris basin approach to be considered in their arsenal of recommended treatments nationwide.

Restoring alluvial fan connectivity with sediment detention basins was also successfully implemented in 2012 on numerous tributaries within the Trail Creek Watershed affected by the Hayman Fire of 2002 (Rosgen, 2011). The performance of these basins following post-fire storms promoted the application on the Waldo Canyon Fire and elsewhere. The approach was subsequently implemented within the Shultz Fire Burn Area in Flagstaff, Arizona (Natural Channel Design, Inc., 2012), saving thousands of tons of sediment from damaging downstream subdivisions.

SUMMARY

The erosional and depositional processes must be understood following wildfires to appropriately prescribe treatments that address the impairment. Restoration priorities by process and locations are always challenging when faced with limited budgets and time constraints. The challenge presented to managers is to have the most effective measures available that properly address the erosional processes when faced with post-fire rehabilitation prescriptions, which must be cost-effective, low risk, and meet specific objectives. The recent application and positive performance of reactivating alluvial fans for extensive sediment reduction and flood attenuation due to post-fire impacts shows excellent promise to assist in future flood restoration/rehabilitation efforts.

REFERENCES

Blair, T., and McPherson, J. (1994). Alluvial Fans and their Natural Distinction from Rivers based on Morphology, Hydraulic Processes, Sedimentary Processes and Facies Assemblages. *Journal of Sediment Research, 64*, 450−489.

Benavides-Solorio, J.D., and MacDonald, L.H. (2005). Measurement and Prediction of Post-Fire Erosion at the Hillslope Scale, Colorado Front Range. *International Journal of Wildland Fire, 14*, 457–474.

Kunze, M.D., and Stednick, J.D. (2006). Streamflow and Suspended Sediment Yield following the 2000 Bobcat Fire, Colorado. *Hydrological Processes, 20*, 1661–1681.

Jarrett, R.D., and Costa, J.E. (1986). *Hydrology, Geomorphology, and Dam-break Modeling of the July 15, 1982 Lawn Lake Dam and Cascade Lake Dam Failures, Larimer County, Colorado* (USGS Professional Paper 1369). Washington, DC: U.S. Government Printing Office.

Jarrett, R. (2013). Documentation of the July 1st and 10th, and August 9, 2013 Peak Discharges in the 2012 Waldo Burn Area Streams. Report created August 22, 2013, Lakewood, CO.

Moody, J.A. (2001) Sediment Transport Regimes after a Wildfire in Steep Mountainous Terrain. In: *Proceedings of the Seventh Federal Interagency Sedimentation Conference*, March 25–29, 2001, Reno, NV.

Moody, J.A., and Martin, D.A. (2001a). Initial Hydrologic and Geomorphic Response following a Wildfire in the Colorado Front Range. *Earth Surface Processes and Landforms, 26*, 1049–1070.

Moody, J.A., and Martin, D.A. (2001b). Post-Fire, Rainfall Intensity–Peak Discharge Relations for Three Mountainous Watersheds in the Western USA. *Hydrological Processes, 15*, 2981–2993.

Moody, J.A., and Martin, D.A. (2009). Forest Fire Effects on Geomorphic Processes. In: A. Cerdá, & P.R. Robichaud (Eds.), *Restoration Strategies after Forest Fire.* Enfield, NH: Science Publishers, Inc.

Moody, J.A., Martin, D.A., and Cannon, S.H. (2008). Post-Wildfire Erosion Response in Two Geologic Terrains in the Western USA. *Geomorphology, 95*, 103–118.

Natural Channel Design, Inc. (2012). Schultz Fire and Flood Assistance Area: Sediment Analysis Refinement & Reduction Option Final Report. Report submitted to Coconino County Public Works. Flagstaff, AZ: Natural Channel Design, Inc, 103 pp.

Neary, D.G., Ryan, K.C., DeBano, L.F., Landsberg, J.D., and Brown, J.K. [Eds.] (2005). Wildland Fire in Ecosystems: Effects of Fire on Soil and Water (RMRS-GTR-42-vol 4). Ogden, UT: USDA Forest Service, Rocky Mountain Research Station, 250 pp.

Robichaud, P., and Wagenbrenner, J. (2009). Hayman Fire Rehabilitation Treatment Monitoring Progress Report Addendum, 2002–2008: Sediment yields, runoff, and ground cover in the first five years after the Hayman Fire. Moscow, ID: USDA Forest Service, Rocky Mountain Research Station.

Rosgen, D.L. (1994). A Classification of Natural Rivers. *Catena*, *22*, 169–199.

Rosgen, D.L. (1996). *Applied River Morphology* (2nd ed. 2001). Pagosa Springs, CO: Wildland Hydrology Books.

Rosgen, D.L. (2006). *Watershed Assessment and River Stability for Sediment Supply (WARSSS)* (2nd ed. 2009). Fort Collins, CO: Wildland Hydrology Books.

Rosgen, D.L. (2011). The Trail Creek Watershed Master Plan for stream Restoration & Sediment Reduction. Report submitted to the Coalition for the Upper South Platte. Fort Collins, CO: Wildland Hydrology, 322 pp.

Rosgen, D.L., Rosgen, B., Collins, S., Nankervis, J., & Wright, K. (2013a). Waldo Canyon Fire Watershed Assessment: The *WARSSS* Results. Report submitted to the Coalition for the Upper South Platte. Fort Collins, CO: Wildland Hydrology, 80 pp., 4 Appendices.

Rosgen, D.L., Rosgen, B., Collins, S., & Nankervis, J. (2013b). The Waldo Canyon Fire Master Plan for Watershed Restoration & Sediment Reduction. Report submitted to the Coalition for the Upper South Platte. Fort Collins, CO: Wildland Hydrology, 146 pp., 3 Appendices.

Stednick, J.D., and Webb, R. (2014). Post-Fire Streamflow, Soil Erosion, and Sediment Detention Structure Performance on North Fork Douglas Creek, Waldo Canyon Fire (Report submitted June 13, 2014, to Colorado Water Conservation Board, Department of Natural Resources). Fort Collins, CO: Colorado State University, Watershed Science Program, 36 pp.

U.S. Environmental Protection Agency (1980). *(WRENSS) An Approach to Water Resource Evaluation of Non-point Silvicultural Sources (A Procedural Handbook)* (EPA-600/8-80-012). Athens, GA: Environmental Research Laboratory.

THE AUTOMATED GEOSPATIAL WATERSHED ASSSESMENT TOOL (AGWA): USING RAINGAGE, RADAR AND STREAMFLOW RECORDS FROM BURNED WATERSHEDS TO EVALUATE AND IMPROVE PARAMETER ESTIMATIONS

B. Scott Sheppard, M.S. candidate, Hydrology, University of Arizona, bss1@email.arizona.edu; I. Shea Burns, Support Scientist, USDA-ARS-SWRC, Tucson AZ, USA, shea.burns@ars.usda.gov; Gabriel Sidman, GIS Analyst, Winrock International, Washington D.C., USA, gabriel.sidman@winrock.org; D. Phillip Guertin, Professor, School of Natural Resources, University of Arizona, Tucson AZ, USA, dpg@email.arizona.edu; David C. Goodrich, Research Hydraulic Engineer, USDA-ARS-SWRC, Tucson AZ, USA, dave.goodrich@ars.usda.gov

Abstract: Precipitation and runoff records from several burned watersheds have been used to evaluate the performance of the AGWA/KINEROS2 modeling scheme that Department of Interior Burned Area Emergency Response (DOI BAER) teams use to assess risk immediately following a wildfire. Although DOI BAER teams use this parameterization/modeling framework to assess the relative change in watershed behavior following a wildfire by driving the model with National Oceanic and Atmospheric Administration (NOAA) design storms, calibrations performed on actual events using rainfall estimations provided by rain gages and radar provide insight into the model's performance, and potentially inform changes and developments to the AGWA parameter estimation scheme. Results indicate that current parameter modifications made by AGWA to represent fire provide reasonable results for DOI BAER risk assessments, though additional modifications to saturated hydraulic conductivity may be necessary to represent a broader range of storm sizes and intensities.

INTRODUCTION

Runoff response to rainfall changes following a wildfire (DeBano et al., 1998). This is a result of the removal of canopy cover and organic litter (duff), which decreases interception and surface roughness respectively. Hydrophobic soils can also form as a result of wildfire, which can reduce infiltration rates. The loss of interception, decrease in surface roughness and decrease in infiltration rates all contribute to an increase in surface runoff. This increase in surface runoff presents a risk of flooding and erosion. Hydrologic modeling is often used in order to anticipate this risk, and target areas for mitigating efforts.

AGWA Background: AGWA (see: www.tucson.ars.ag.gov/agwa or http://www.epa.gov/esd/land-sci/agwa/) is a GIS interface jointly developed by the USDA-Agricultural Research Service, the U.S. Environmental Protection Agency, the University of Arizona, and the University of Wyoming to automate the parameterization and execution of a suite of hydrologic and erosion models (SWAT and KINEROS2 – the latter with the Rangeland Hydrology and Erosion Model (RHEM) and the Water Erosion Prediction Project (WEPP) for hillslope erosion options). Through an intuitive interface the user selects an outlet from which AGWA delineates and discretizes the watershed using a digital elevation model (DEM). The watershed model elements are then intersected with nationally available data sets for soils and land cover to derive the requisite model input parameters. The soils layer provides a texture-based estimation of saturated hydraulic conductivity (Ks), and the land cover layer provides information associated with land cover types, such as percent cover, interception, and hydraulic

roughness (Manning's *n*). With the addition of a burn severity map, AGWA can be used to change the existing land cover to reflect burned conditions.

The key challenge to using AGWA in a post-fire context is developing rules to change important model parameters (canopy cover, interception, saturated hydraulic conductivity and hydraulic roughness) as a function of the original cover type and the degree of disturbance based on the burn severity map. To account for burn effects, AGWA reduces the percent canopy cover (CC) parameter using a land cover look up table. Currently for severe, moderate, and low burn severity the CC for a given land cover vegetation class is reduced by 50%, 32%, and 15%, respectively (Burns et al., 2013). AGWA increases the soil texture based Ks using equation (1) based on percent canopy cover (CC) for all land cover types; therefore reductions in CC due to fire will decrease Ks from pre-fire conditions which result in an increase in post-fire runoff.

$$Ks = Ks_{soil} * e^{0.0105*CC} \quad (1)$$

However, preliminary calibration efforts have shown that changes to land cover look-up tables for burn severity alone were insufficient to calibrate Ks for several of the events examined in this study. This could imply that the model input for soils is not sufficiently representative of reality, that the CC reduction percentages are not large enough, that hydrophobic conditions have developed, or that Ks is also a function of rainfall intensity or amount.

METHODS

Changes in soil infiltration and hydraulic roughness are often a result of fire (Canfield et al., 2005). They are also sensitive parameters in the KINEROS2 model (Yatheendradas et al., 2008) and were therefore altered during calibration to match observed runoff in an attempt to determine how they might be altered in AGWA post-fire lookup tables. Gridded searches of the saturated hydraulic conductivity (Ks) and hydraulic roughness (n) parameter space were conducted using the Nash-Sutcliffe (NSE) and the Kling-Gupta Efficiencies (KGE) in order to determine their optimal calibrating multipliers. Multipliers were used to alter parameter values in order to maintain the spatial variability of the parameters given by the spatial data layers, while keeping the number of calibrating parameters small. For this initial investigation the CC parameter was set to zero, and calibrating multipliers were applied to all hillslope model elements in the watershed.

Storms of various sizes at three different small watersheds, Marshall Gulch (8 km^2) in the Santa Catalina Mountains outside of Tucson Arizona, Starmer Gulch (3 km^2) on the Las Alamos National Lab, New Mexico, and Eagle Creek (21 km^2) near Ruidoso, New Mexico, were used in this effort. These storms ranged in total accumulated rainfall depth of 6 to 41 millimeters, observed total outflow volumes ranged from 0.25-4.6 millimeters yielding runoff to rainfall ratios of 0.02-0.25. Peak flows ranged from 0.2-5.9 millimeters/hour. All storms used for analysis were reasonably well modeled with the lowest NSE value being 0.64.

RESULTS

Initial calibrations indicated that there is a correlation between the calibrated Ks values (figure 1), calibrating Ks multipliers (figure 2) and the total depth of the rainfall in an event. This will be explored further with the intention of determining rainfall intensity based thresholds for calibrating Ks multipliers.

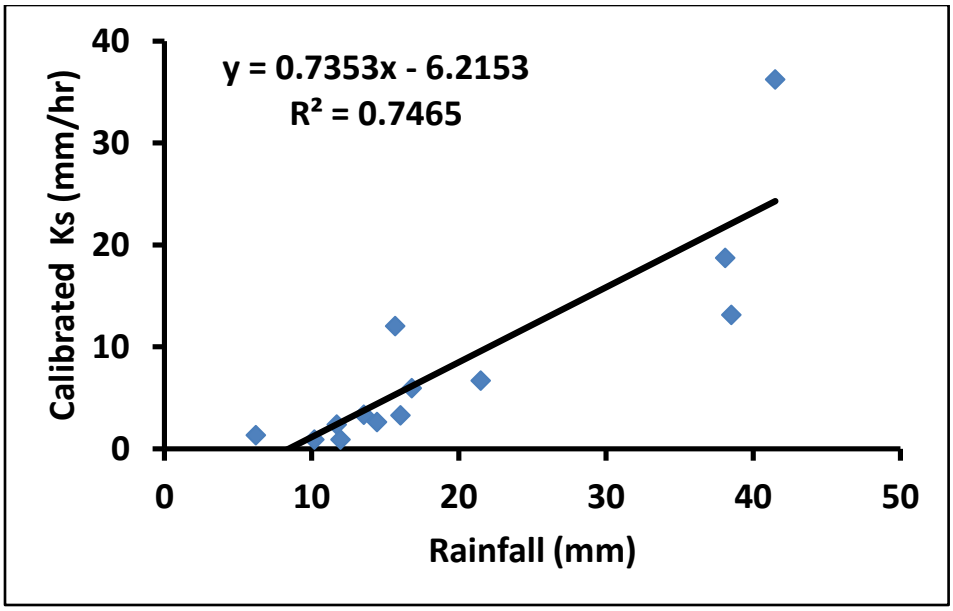

Figure 1 Correlation of rainfall amounts and calibrated Ks values (mm/hr).

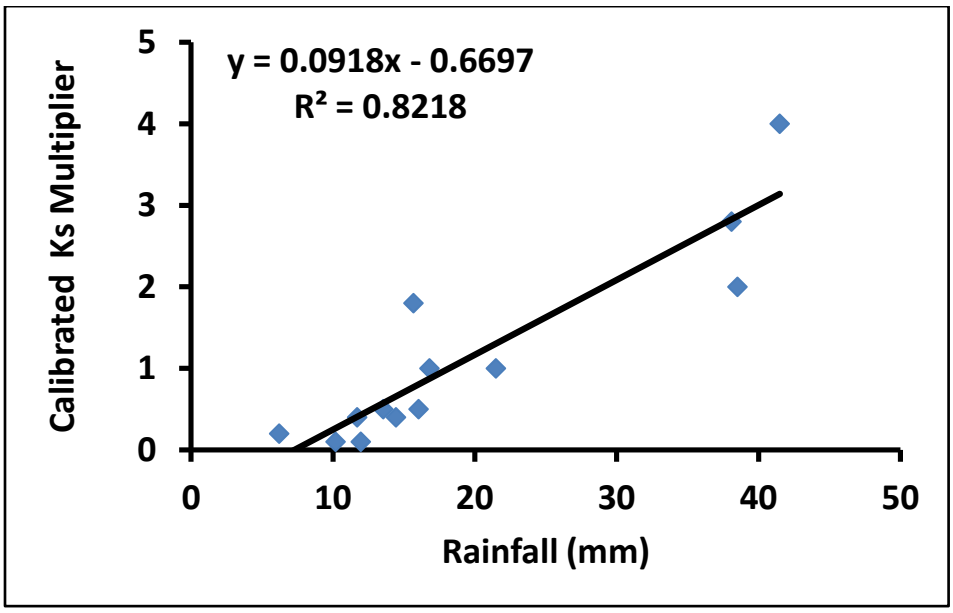

Figure 2 Correlation of rainfall amounts and calibrated Ks multiplier values.

Although many burned watersheds had stream flow and rain gages installed following a wildfire, pre-fire data is rarely available, and storm events appropriate for model calibration are infrequent. The record of data at Marshall Gulch following the 2003 Aspen Fire is the longest record of stream flow and rainfall data used in this study. Dating from 2003-2013, this record gives the opportunity to use data from ten years following a wildfire as a proxy for pre-fire conditions. The storms of 7/29/2003 and 7/15/2013 show that it takes much less rainfall on a burned landscape (figure 3, table 1) to generate similar peak flow on a forested landscape (figure 4, table 1). This is the difference between a storm that is likely to occur every year and a NOAA twenty-five year return period, one-hour design storm.

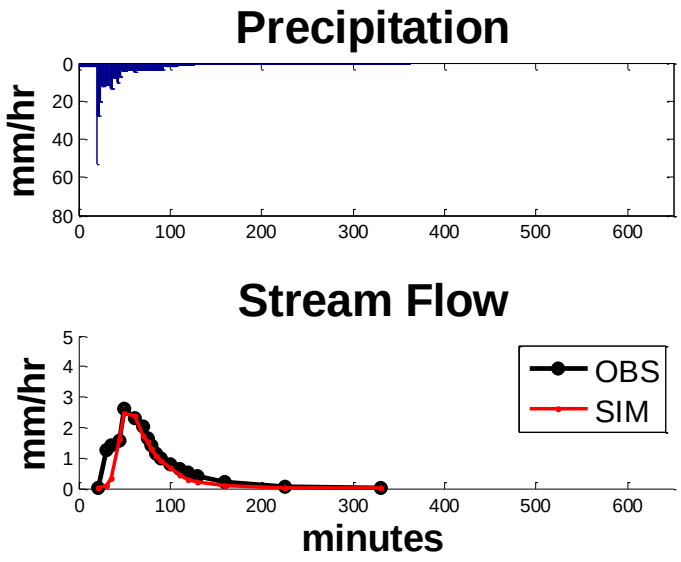

Figure 3 Hyetograph from storm of 7/29/2003 (upper) and simulated and observed streamflow (lower) at the Marshall Gulch Pima County Flood Control gage using Ks and roughness parameters listed in table 1.

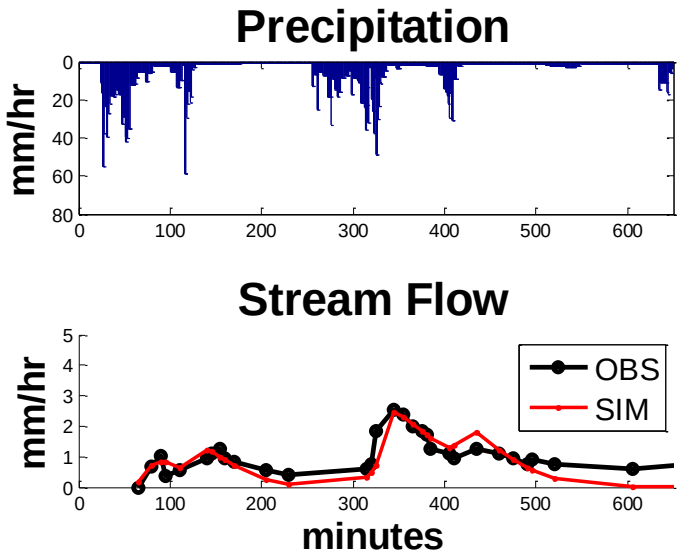

Figure 4 Hyetograph from storm of 7/15/2013 (upper) and simulated and observed streamflow (lower) at the Marshall Gulch Pima County Flood Control gage using Ks and roughness parameters listed in table 1.

Table 1 Rainfall, runoff to rainfall ratio (RO Ratio), observed (OBS) and simulated (SIM) stream flow, Nash-Sutcliffe Efficiency (NSE), and calibrated values of Ks and Manning's *n* (n) for storm events 7/29/2003 and 7/15/2013.

			Peak (mm/hr)		Volume (mm)				
Storm	Rain(mm)	RO Ratio	OBS	SIM	OBS	SIM	NSE	Ks	n
7/29/2003	10.19	0.25	2.62	2.46	2.57	1.96	0.75	1.35	0.03
7/15/2013	58.73	0.21	2.52	2.47	12.43	6.92	0.64	4.50	1.28

The Marshall Gulch responses to storms similar to a NOAA five year return period, one-hour design storm also show quite different behavior for burned (figure 5, table 2) and unburned conditions (figure 6, table 2). Peak flows for burned conditions were nearly five times greater than forested conditions.

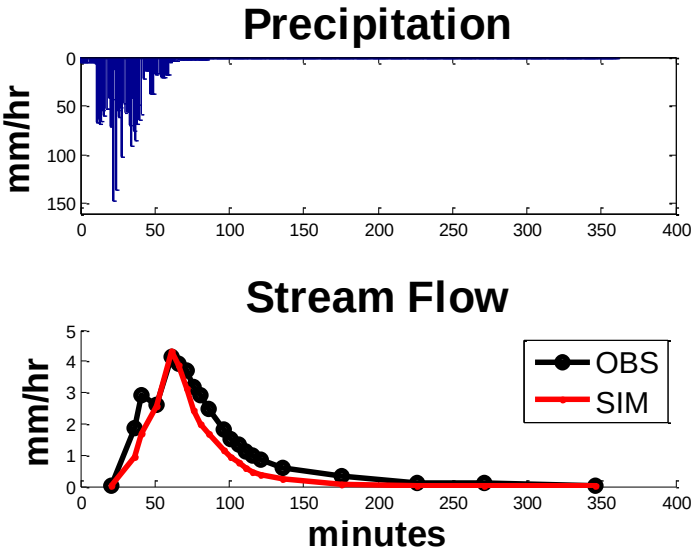

Figure 5 Hyetograph from storm of 7/24/2003 (upper) and simulated and observed streamflow (lower) at the Marshall Gulch Pima County Flood Control gage using Ks and roughness parameters listed in Table 2.

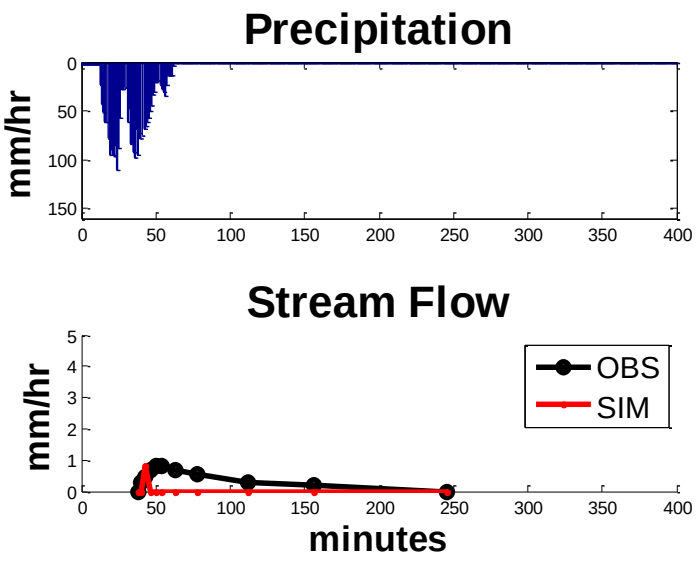

Figure 6 Hyetograph from storm of 7/27/2013 (upper) and simulated and observed streamflow (lower) at the Marshall Gulch Pima County Flood Control gage using Ks and roughness parameter listed in Table 2.

Table 2 Rainfall, runoff to rainfall ratio (RO Ratio), observed (OBS) and simulated (SIM) stream flow, Nash-Sutcliffe Efficiency (NSE), and calibrated values of Ks and Manning's *n* (n) for storm events 7/24/2003 and 7/27/2013. Rainfall amount is equivalent to NOAA five year return period, one-hour design storm.

			Peak (mm/hr)		Volume (mm)				
Storm	Rain(mm)	RO Ratio	OBS	SIM	OBS	SIM	NSE	Ks	n
7/24/2003	41.49	0.11	4.14	4.34	4.58	3.23	0.85	36.00	0.06
7/27/2013	44.60	0.02	0.83	1.17	0.72	0.06	-0.54	15.00	1.44

DISCUSSION

Figures 3 through 6 and tables 1 and 2 demonstrate that the calibrated model better reproduces the 2003 event (burned conditions) hydrographs than the 2013 event (proxy for unburned conditions) hydrographs. This is likely because the KINEROS2 model only represents overland flow generation as infiltration excess, the expected dominant runoff process in burned conditions/areas, and in unburned, forested conditions shallow subsurface flow is an important runoff process which KINEROS2 does not represent. In addition events with low runoff ratios are difficult to model as the uncertainties associated with observed rainfall can be a very large part of the overall runoff signal (high noise to signal ratio – Goodrich et al., 2012).

The difference in the observed responses to the storms of 7/24/2003 and 7/27/2013 provided an opportunity to see how well the AGWA relative difference approach used by DOI BAER teams anticipates change in response to a NOAA five year, one-hour design storm. Hydrographs of the uncalibrated simulated flows at the outlet of Marshall Gulch are shown below (figure 7). The percent change in peak flow for the modeled flows was 456% (table 3), i.e. peak flows in burned conditions are expected to be roughly 5.6 times greater than unburned conditions. For observed

flows a 399% (table 3) increase was calculated, i.e. peak flows in burned conditions are expected to be roughly 5 times greater than unburned conditions. This comparison of storms shows that the method used by DOI BAER would have been a very reasonable estimate of peak flow for use in risk assessment.

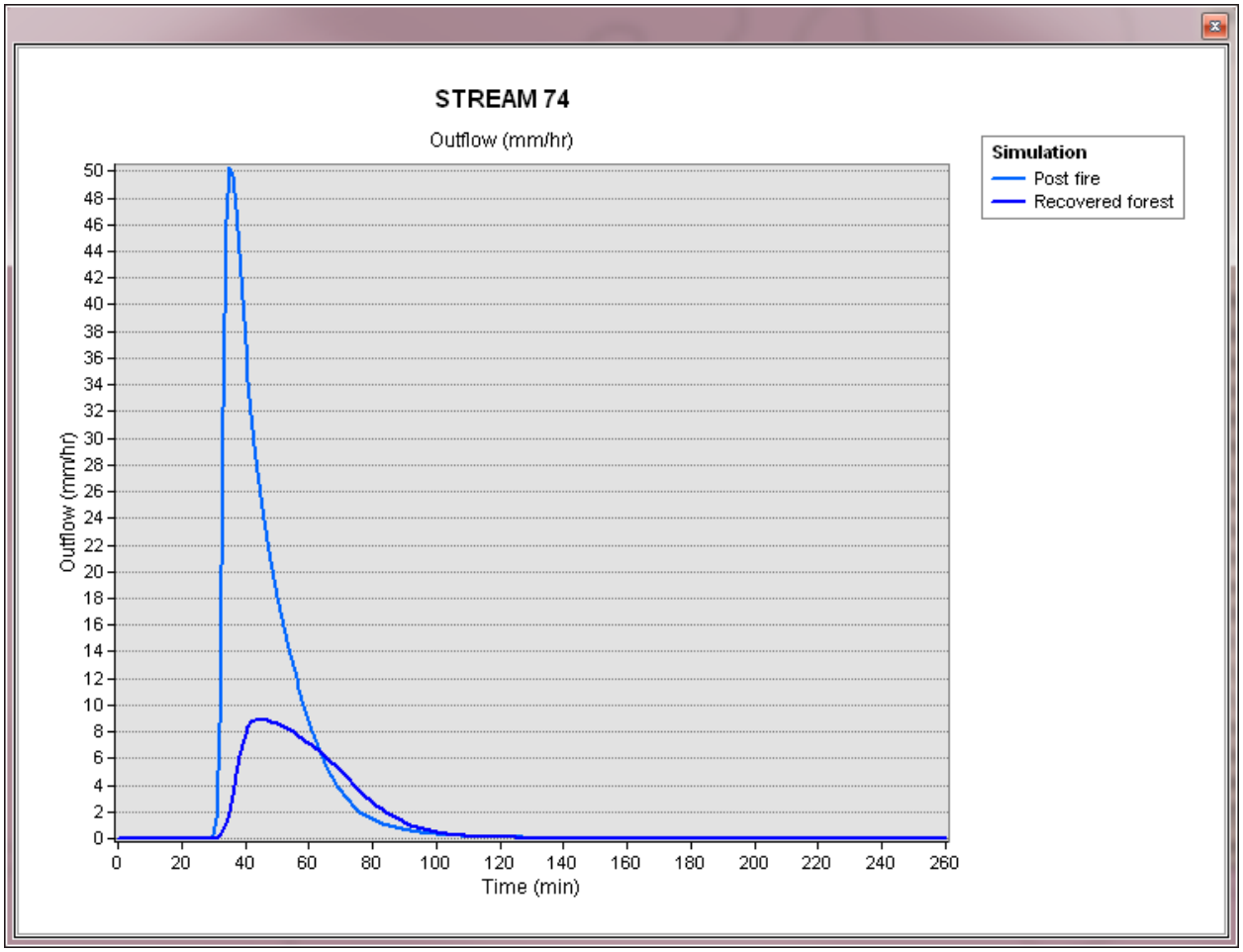

Figure 7 AGWA hydrograph output for uncalibrated KINEROS2 simulations of unburned and burned conditions responding to a NOAA five year, one-hour design storm.

Table 3 Percent change determined by modeling results and by observed data for NOAA five year, one-hour return storm.

	AGWA/K2	OBS
Unburned Conditions Peak Flow (mm/hr)	9	0.83
Burned Conditions Peak Flow (mm/hr)	50	4.14
Percent Difference	456	399

FUTURE WORK

Further investigations will be made using both rain gage records and bias corrected radar precipitation estimates to determine if thresholds can be established for calibrating Ks multipliers

for differing intensities of rainfall. Additional storms from Marshall Gulch, Starmer Gulch, Eagle Creek, and other watersheds will be calibrated to determine how similar or different the calibrating multipliers for Ks and surface roughness are at different locations. Once the correlation between rainfall intensity and Ks is better understood, refinement of this parameter for post-fire modeling use will be performed by including canopy cover values and applying calibrating multipliers only to burned hillslope elements in order to improve post-fire modeling use. Watershed recovery as a function of time since fire will also be investigated using post-fire events over long periods of time where they are available. In addition, remotely sensed estimates of cover condition over time will be assessed to see if they provide a reasonable surrogate measure for recovery.

REFERENCES

Burns, I.S., Korgaonkar Y., Guertin, D.P., Goodrich, D.C., Kepner, W.A., Miller, and S.N., Semmens, D.J. (2013) Automated Geospatial Watershed Assessment (AGWA) 3.0 Software Tool. USDA Agricultural Research Service and U.S. EPA, Washington, DC (http://www.tucson.ars.ag.gov/agwa/).

Canfield, H.E., Goodrich, D.C., and Burns, I.S. (2005). Application of models to predict post-fire runoff and sediment transport at the watershed scale in southwestern forests. Proc. Amer. Soc. Civil Engr. 2005 Watershed Management Conference, Williamsburg, VA, July 22-25, 12p., CD-ROM.

DeBano, L. F., Neary, D.G. and Ffolliott, P.F. (1998) Fire's Effects on Ecosystems. John Wiley and Sons, New York. 338p.

Goodrich, D.C., Burns, I.S., Unkrich, C.L., Semmens, D.J., Guertin D.P., Hernandez, M., Yatheendradas, S. Kennedy, J.R., and Levick, L.R. (2012). KINEROS2/AGWA: Model use, calibration, and validation, Trans. of the ASABE. 55(4): 1561-1574.

Yatheendradas, S., Wagener, T., Gupta, H., Unkrich, C.L., Goodrich, D.C., Schaffner, M., Stewart, A. (2008). Understanding uncertainty in distributed flash flood forecasting for semiarid regions. Water Resources Research, Vol. 44, W05S19, doi:10.1029/2007WR005940.

COMBINING FIRE AND EROSION MODELING TO TARGET FOREST MANAGEMENT ACTIVITIES

William J. Elliot, U.S. Department of Agriculture, Forest Service, Rocky Mountain Research Station, 1221 South Main Street, Moscow ID 83843 welliot@fs.fed.us
Mary Ellen Miller, Michigan Technology Research Institute, Michigan Technological University, 3600 Green Court, Suite 100, Ann Arbor, MI 48105 marymill@mtu.edu
Nic Enstice, Sierra Nevada Conservancy, 11521 Blocker Dr., Suite 205, Auburn, CA 95693 Nic.Enstice@sierranevada.ca.gov

Abstract Forests deliver a number of important ecosystem services including clean water. When forests are disturbed by wildfire, the timing, quantity and quality of runoff are altered. A modeling study was carried out in a forested watershed in California to determine the risk of wildfire, and the potential post-fire sediment delivery from approximately 6-ha hillslope polygons within a 1500-km^2 basin following a wildfire event. Wildfire intensity was estimated with the FlamMap prediction tool and fire risk with the FSim tool, based mainly on topography, current vegetation conditions, and wind speed and direction. The estimation of soil burn severity was based on predicted flame length for each modeled 30-m pixel and the prefire vegetation for each hillslope polygon. Sediment delivery was estimated from each hillslope polygon using the Water Erosion Prediction Project (WEPP) Model in a GIS framework. Polygons that generated the greatest amount of sediment, impacted other values at risk in the basin, or were critical for reducing fire spread were "treated" by reducing the amount and type of fuel available for a wildfire. The fire and erosion models were run a second time for treated conditions to see if the treatment resulted in a reduced fire intensity and probability, and hence a reduced erosion rate. The estimated erosion rates the first year after the fire dropped from 46 Mg ha^{-1} before treatment to 26 Mg ha^{-1} for polygons that had received fuel treatments. If the reduction in the probability of wildfire occurrence and the effects of a quarter century of fuel treatments are considered together, then the treatments are predicted to significantly impact long-term (century scale) erosion rates by lowering "average annual" erosion rates by 19%.

INTRODUCTION

Managers in fire-prone watersheds are looking for ways to protect communities, forest resources, municipal water supplies, and other societal values from the detrimental and expensive effects of wildfire. Increased fuel loads from past decades of fire suppression (Agee 1993; Keane et al. 2002) and climate change (Flannigan et al. 2000; Westerling et al. 2006) are increasing the risks of large, high severity wildfires in Western forests and shrublands. These high-severity fires in turn increase the risk of flash floods and surface erosion (Forrest and Harding 1994; Robichaud et al. 2013). Increased post-fire erosion rates can severely degrade water quality and reduce reservoir storage capacity (Tiedemann et al. 1979; Moody and Martin 2001; Neary et al. 2005). In response to these risks, land managers responsible for protecting forestlands and watersheds, especially those that provide municipal water supplies, are considering ways to mitigate the effects of wildfire on water resources through the use of fuel reduction treatments (Sidman et al. 2015). Fuel reduction treatments, such as thinning and prescribed burning, have been shown to be effective in modifying fire behavior and fire severity (Cochrane et al. 2012; Reinhardt et al. 2008). A reduction in fire severity can then reduce threats to important ecosystem services including the availability of clean water, recreation opportunities, and timber, as well as fish and wildlife habitat. However, the costs associated with fuel reduction treatments can limit their application (GAO 1999 and 2007; Sampson et al. 2000).

A study was carried out on 1500-km^2 of the Upper Mokelumne Basin to see if the costs for fuel reduction treatments can be justified. The basin is located on the western slope of northern California's Sierra Nevada Mountains. The North Fork of the Mokelumne River cuts through granite to form deep canyons

and flows through a rugged landscape with granite domes, much like its neighbor to the south – Yosemite National Park. The vegetation ranges from mixed oak woodlands below 900 m, to mixed conifer forests between 900 and 2000 m. Between 2000 and 2750 m the forests are dominated by California Red Fir (*Abies magnifica*), and above 2750 m barren rock outcrops predominate. The Mokelumne Wilderness area encompasses much of the Northern portion of the watershed. Recreational activities include fishing and camping, but the river is particularly famous for white water rafting and kayaking. The basin is an important water source for agriculture and provides drinking water to 1.3 million residents of in the San Francisco Bay area. The Mokelumne River also provides hydropower with a generating capacity of 215 MW. The extensive forest stands within the basin are under both public and private ownership. Much of the forested land is at risk to wildfire as evidenced by the 2004 Power Fire (70 km^2) within the basin (Figure 1), and the nearby Rim (2013; 1,040 km^2) and King (2014; 390 km^2) fires. Major landowners include the U.S. Forest Service, Bureau of Land Management, and Sierra Pacific Industries (Buckley et al. 2014).

In order to spatially prioritize fuel treatments and to determine the economic value of increasing treatments compared with a "do-nothing" scenario during this time of increasing fire threat, the U.S. Forest Service, The Sierra Nevada Conservancy, and The Nature Conservancy brought together a diverse set of stakeholders to form the Mokelumne Avoided Cost Analysis (MACA) committee (Buckley et al. 2014). Stakeholders included land, water and utilities managers, federal, state and local agencies, local stakeholders, and environmental organizations. The MACA committee developed a methodology to forecast the impacts of fuel treatments on wildfire risks and erosion rates in watersheds both before and after wildfire in order to link the benefits associated with fuel treatments with their costs.

MODELING APPROACH

To forecast the benefits of fuel treatments on the Mokelumne Basin we modeled erosion under four distinct conditions:

1) current vegetation conditions in the absence of fire;
2) after a fire assuming current fuel conditions;
3) after proposed fuel treatments; and
4) after a fire following the application of proposed fuel treatments.

The mapped erosion predictions following wildfire (condition 2, Figure 1) in conjunction with the burn severity predictions, asset locations within the basin and other considerations were used by the MACA Advisory committee to plan and prioritize fuel reduction treatments within the basin. The application of these treatments which included prescribed fire and mechanical and hand thinning could impact erosion rates within the watershed, so the effects of these treatments were modeled for the third condition. Fuel treatments were planned for elevations between 300 and 2,000 meters in the watershed covering most of the mixed conifer forests. Fuel loading and canopy cover were assumed to be changed as a result of these treatments. The effect of treatments on burn severity was then modeled and new predictions of burn severity were used to model post-fire erosion after treatments for the fourth condition. Our modeling results were used in two ways. The first application was to prioritize treatments based on post-fire erosion risk (Figure 1). The second application was to synthesize our modeling results from the four runs to quantify the watershed benefits and compare them to the cost of treatments to determine whether the costs of proactively treating forests prefire are justified by the savings from either not having a wildfire occur or from a reduction in wildfire severity.

We used three different models sequentially to quantify the reduction in sediment due to fuel treatments within the Mokelumne basin. The first model, FlamMap (Finney 2006), was used to predict burn severity both before and after proposed fuel reduction treatments. Probability of fire occurrence was modeled using the Fire SIMulation system (Fsim, Finney et al. 2011). The Water Erosion Prediction Project (WEPP)

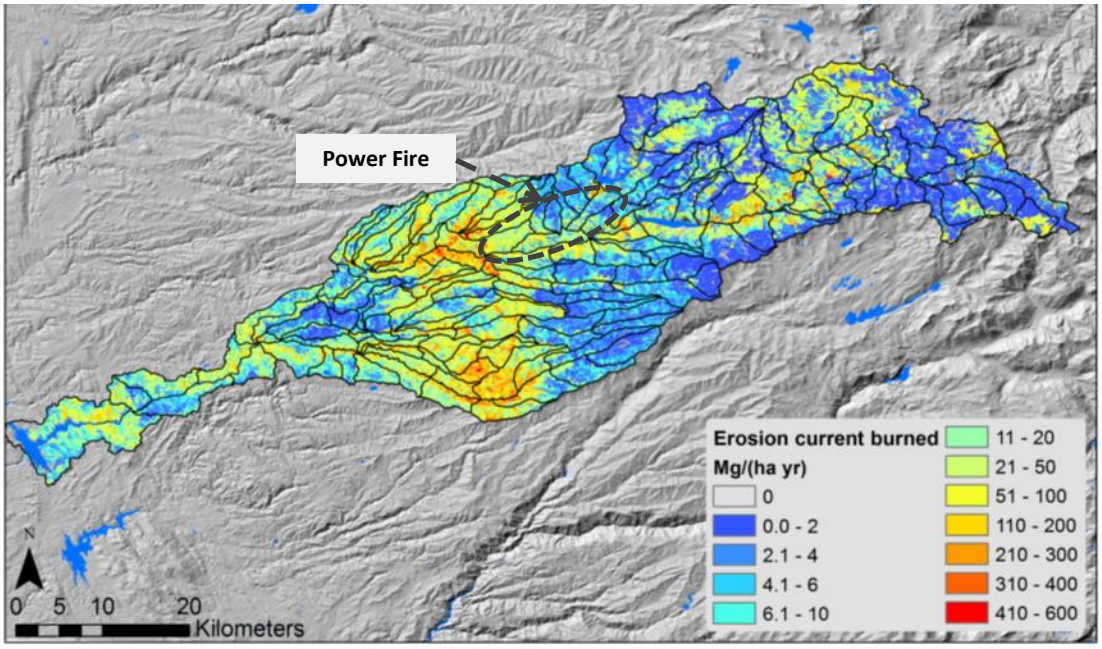

Figure 1 Map of predicted post-fire erosion for the first year after the fire for the Mokelumne Basin for current (untreated) vegetation conditions. The area burned by the 2004 Power Fire is outlined

model (Laflen et al. 1997) used burn severity predictions from FlamMap to predict hillslope erosion following wildfire both before and after treatments.

FlamMap FlamMap is a spatial fire behavior model that uses land cover, topography, and fuel characteristics data from the Landfire database (Rollins 2009), along with fuel moisture and weather data (Finney 2006). Resulting fire behavior predictions are pixel-based (30-m resolution) and include fire line intensity (kW m^{-1}), heat per unit area (kJ m^{-2}), and flame length (m). The soil and vegetation burn severity category and ground cover for erosion modeling were determined from the predicted flame length for each pixel (Table 1). Determining where to make the cutoffs in flame length for severity categories was based on the distribution of severity observed on post wildfire field studies and the distribution of fire severity following a recent fire in the basin (Power Fire, 2004; Figure 1).

FSim The Fire SIMulation system (FSim) uses historical weather data, topography, past wildfire ignitions, fuel and vegetation data to simulate wildfire ignition, fire growth, and suppression (Finney et al. 2011). The model estimates burn probability by simulating 10,000 to 50,000 years of fire seasons under the same vegetation and fuel conditions. Burn probability is the number of simulations in which a pixel burns divided by the total number of simulations (Finney et al. 2011). For the Mokelumne basin, FSim was run using vegetation data from the same Landfire database as the other modeling activities, but at a 90-m resolution. Modeling was carried out for three elevation zones in order to account for differences in ignition patterns. Calibration runs were undertaken to adjust parameters in order to match predictions with historical fire occurrences for each zone. Once calibrated, the model was run for 40,000 fire seasons. Additional details can be found in Buckley et al. (2014).

WEPP WEPP is a process-based model that predicts runoff and sediment yields from planar hillslopes and small, unchannelized watersheds (Flanagan and Nearing 1995). The surface hydrology component of the WEPP model uses climate, soils, topography, and vegetation input files to predict infiltration, runoff volume, and peak discharge for each simulated storm or snowmelt runoff event. WEPP then uses the

Table 1 WEPP soil and vegetation severity categories as determined by flame lengths predicted by FlamMap

	FlamMap Flame Length (m)			
	0	0 – 1.2	1.2-2.5	2.5≤
WEPP Burn Severity Category	Unburned	Low	Moderate	High
WEPP Soil Category and ground cover (%) if pre fire vegetation was grass	Unburned 60-80	Low 60	Low 45	Low 15
WEPP Soil Category and ground cover (%) if pre fire vegetation was forest	Unburned 99	Low 60	Low 45	High 15

same inputs and runoff predictions to calculate rill and interrill erosion, as well as sediment yield from the hillslope (Flanagan and Nearing 1995). The need to predict post-fire erosion rates across the entire 1500-km^2 Upper Mokelumne Basin necessitated the use of the Geo-spatial interface for the Water Erosion Prediction Project (GeoWEPP) (Renschler 2003). GeoWEPP facilitates the use of WEPP across large areas by converting GIS data into WEPP input files, running WEPP, and then compiling the results into a spatial maps and text summaries.

DEVELOPMENT AND COMPILATION OF INPUT DATA

Prior to preparing model inputs, land cover, soil and topography data were collected in the watershed at various elevations and forest conditions from multiple sources to ensure accuracy. The Landfire vegetation files used as input to the fire spread models were modified to incorporate detailed local knowledge of site conditions. These same files were used to support prefire WEPP runs, and to aid in developing post fire soil and vegetation files. For the spatial WEPP modeling, the Upper Mokelumne Basin was divided into 244 sub-watersheds averaging about 6 km^2 in area, using a Digital Elevation Model (DEM) and ESRI watershed tools, in order to address climate variability and for computational efficiency. Sub-watersheds were used to create smaller raster inputs (DEM, soil, land cover) for batch files. These batch files were then modeled in a batched version of GeoWEPP (Miller et al. 2011). In the cases where the sub-watersheds contained more than one drainage outlet or the model failed to run, the sub-watersheds were rerun using GeoWEPP for ArcGis 9.3. The resulting erosion prediction maps from the batch runs were then merged into a final erosion map for each of the four conditions (Figure 1).

Climate Data WEPP uses a stochastic weather generator called Cligen (Nicks et al. 1995) to generate a daily weather sequence, including the precipitation amount and duration, minimum and maximum temperatures, dew point, mean solar radiation, and wind speed and direction. The input to Cligen is from a database of more than 2,600 long term climate stations within the United States. The U.S. Forest Service has complemented this database with Rock:Clime, an interface to Cligen that estimates mean monthly rainfall amounts between stations (Elliot et al. 1999; Scheele et al. 2001). The interface also allows users to change the number of wet days within a month, and to alter the average maximum and minimum temperatures either manually, or based on an adiabatic lapse rate for maximum temperature of -6°C km^{-1} and a lapse rate for minimum temperatures of -5°C km^{-1} between the nearest weather station and the site of interest (Scheele et al., 2001). The interpolation is particularly important in mountainous areas such as the Mokelumne Basin because of the large changes in climate conditions that occur with changes in elevation over relatively short distances (Table 2), as well as the paucity of climate stations in remote mountainous areas. The interpolation procedure in Rock:Clime modifies the monthly precipitation for a selected climate station based on elevation and PRISM data (Parameter-elevation Regressions on

Table 2 Stochastically generated climate zones for the Mokelumne Basin

Physical Elevation Range (m)	Climate Zones	Modeled Elevation (m)	Avg Annual Precip (mm)
100 – 300	Tiger Low Rock:Clime/PRISM	259	799
300 – 600	Tiger Low2 Rock:Clime/PRISM	535	951
600 – 900	Tiger Creek Station	719	1176
900 – 1200	Calaveras Low Rock:Clime/PRISM	1093	1138
1200 – 1500	Calaveras Big Trees Station	1432	1383
1500 – 2000	Calaveras Big Trees High Rock:Clime/PRISM	1868	1336
2000 – 2400	Twin Lakes Station	2386	1249
≥2400	Twin Lakes High Rock:Clime/PRISM	2646	1438

Independent Slopes Model, Daly et al. 2004). The PRISM database with a spatial resolution of 4 km^2 is used by Rock:Clime.

Three NOAA weather stations in the Cligen database are located within or near the Mokelumne Basin. These stations (Twin Lakes, Calaveras Big Tree, and Tiger Creek; Figure 2) were used to develop an additional five climate files with the Rock:Clime interface. The additional climates were needed to account for the impacts of elevation changes in the watershed (Table 2). Each climate input file contained 50 years of daily stochastically-generated weather data. The average elevations of the initial WEPP sub-watersheds were then used to select the appropriate climate zone (Figure 2) for each sub-watershed.

Land cover and plant/management input files for WEPP Land cover data were obtained from the Landfire Project (Rollins, 2009). For this analysis, we used the Landfire land cover data that were modified with field observations for the fire modeling runs (Buckley et al. 2014). In addition to making the process more efficient by using the same data set, this ensured consistency across the modeling efforts. We then reclassified the land cover data layer into WEPP database cover types (e.g. Forest, Young Forest, Shrubs, Bunch or "Good" Grass, Sod or "Poor" Grass) in order to model background erosion rates from the Mokelumne Basin without fire. In the WEPP database, the land cover type is linked to both vegetation and soil properties (Elliot 2004).

For modeling post-fire conditions, the FlamMap burn severity maps from before and after fuel reduction treatments were used to reclassify land cover into unburned, low, moderate, and high burn severity classes (based on Table 1). In order to model the potential erodibility effects of the fuel reduction treatments, we used the map of proposed treatments developed for this analysis (Buckley et al., 2014). We assumed that the prescribed fire treatments would have a low severity soil condition for the year following the treatment with 85 percent ground cover, and the thinning-only treatments would have unburned soil properties and 90 percent cover (Elliot and Miller 2004).

Soils Data For the WEPP modeling, we used Landfire soil layers that were derived from STATSGO (STATe Soil GeOgraphic) data (USDA 1991). This dataset included: maximum soil depth; percent rock fragments (> 2.0 mm), sand, silt, and clay. The percent-sand, -silt and -clay layers were used to classify each soil pixel into one of the four soil texture classes represented in the WEPP forest soil database (sandy loam, loam, silt loam, and clay loam). WEPP input parameters (e.g., effective hydraulic conductivity, soil albedo, and interrill and rill erodibility) specific to each soil texture class were then used in the modeling (Elliot et al. 2000). Soil properties were based on the predicted burn severity and the type of vegetation that burned (forests, shrubs or grasses).

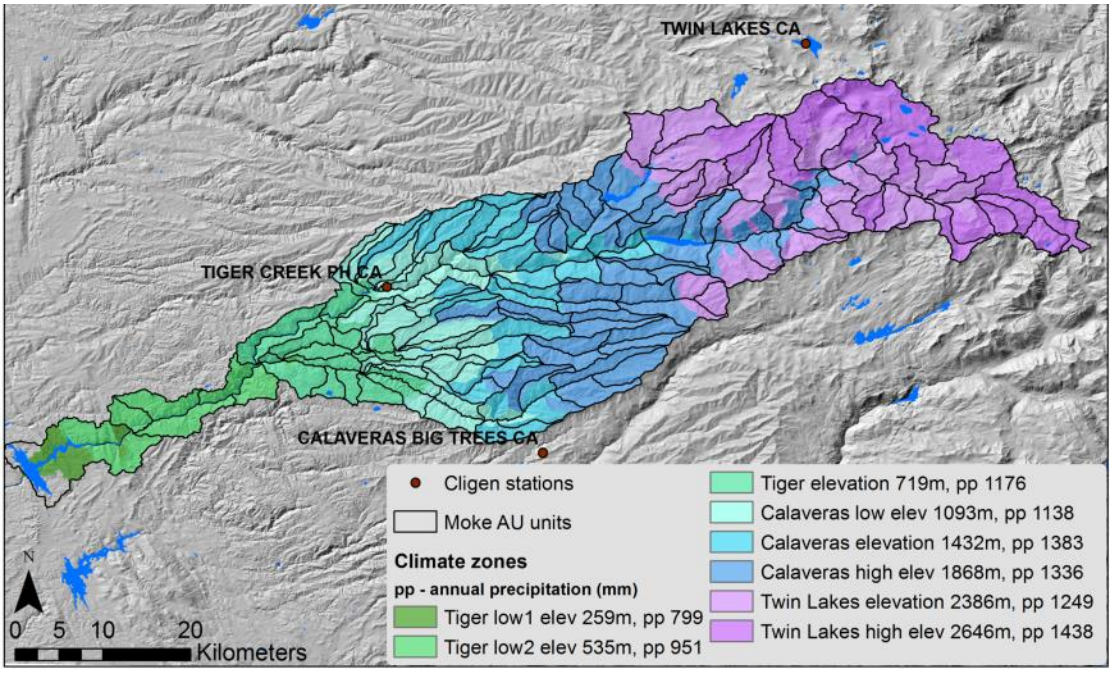

Figure 2 Map displaying the distribution of climate zones within the Mokelumne Basin and showing the boundaries of the Analysis Units (AUs)

RESULTS

Sediment delivery from hillslopes in the Mokelumne Basin was estimated and mapped for four conditions. The first condition determined background erosion rates without fire under the current vegetation conditions. Average erosion in the unburned basin was 0.67 Mg yr^{-1} ha^{-1} for the entire basin and 0.4 Mg yr^{-1} ha^{-1} in the lower elevation portion of the watershed where treatments were planned. Forested hillslopes typically did not generate significant erosion, but the steep, barren rocky slopes in the upper portions of the basin were highly erosive as is typical of high elevation areas in the Sierra Nevada Mountains (Brooks et al. 2010). The next run used the FlamMap predictions of burn severity under the current vegetation conditions to predict post-fire erosion (Figure 1). Average first year post-fire hillslope erosion in the Mokelumne Basin was 32 Mg yr^{-1} ha^{-1}, 50 times higher than the unburned conditions.

The mapped post-fire erosion predictions for current conditions along with the fire modeling results and other considerations were used by the MACA committees and stakeholders to help plan and prioritize a fuel reduction treatment strategy within the basin. The treatment selection process focused on reducing risks from fire and post-fire sediment to water utility and other infrastructure (Buckley et al. 2014). Wilderness and roadless areas were for the most part excluded from the analysis as treatments could not be carried out in these areas and they do not possess infrastructure that would be threatened by wildfire. An online GIS platform was created to allow stakeholders to review the data and then easily select treatment analysis units and provide a rational for their decisions. The watershed was divided into 148 potential treatment Analysis Units (AUs) with an average area of 10 km^2 (Figure 2). The post-fire erosion and burn probability maps were averaged by AUs and then classified into five risk quantiles. To further help stakeholders choose AUs for treatments, additional map layers containing towns, roads, building densities, land ownership, topography, transmission lines, hydropower facilities, wilderness areas, and water conveyances were provided. Stakeholder and MACA committee selections were then combined and through an iterative process, 46 AUs were selected for treatment. Recent studies indicate the minimum

Table 3 Summary of the results from the four hillslope erosion model runs for the entire Mokelumne Basin

	Current Condition	Fire Following Current Condition	Treatment Effects	Fire Following Treatment
Average Erosion in Basin	0.67 Mg ha^{-1}	32 Mg ha^{-1} in year 1	0.69 Mg ha^{-1}	26 Mg ha^{-1} in year 1
Range	0 – 84 Mg ha^{-1}	0 – 566 Mg ha^{-1}	0 – 84 Mg ha^{-1}	0 – 535 Mg ha^{-1}
Standard Deviation	3.0 Mg ha^{-1}	55 Mg ha^{-1}	2.5 Mg ha^{-1}	44 Mg ha^{-1}

Table 4 Summary of results from the four hillslope erosion model runs for only the treated portions of the Mokelumne Basin

	Current Condition	Fire Following Current Condition	Treatment Effects	Fire Following Treatment
Average Erosion in Basin	0.40 Mg ha^{-1}	46 Mg ha^{-1} in year 1	0.69 Mg ha^{-1}	26 Mg ha^{-1} in year 1
Range	0 – Mg ha^{-1}	0 – 566 Mg ha^{-1}	0 – Mg ha^{-1}	0 – 535 Mg ha^{-1}
Standard Deviation	2.5 Mg ha^{-1}	69 Mg ha^{-1}	2.5 Mg ha^{-1}	36 Mg ha^{-1}

area needed to be treated in a watershed to lower burn probability is 10-20% (Finney et al. 2007) and that strategically treating 35% would be ideal for reducing risks (Ager et al. 2013). The proposed treatment AUs covered about 29% of the Upper Mokelumne watershed (Buckley et al. 2014), which is more than enough to reduce fire probability within the entire watershed.

The application of these treatment prescriptions, which included prescribed fire, biomass removal, and thinning, would not only impact fire behavior, but also could result in soil erosion, so the effects of these treatments on soil erosion were modeled for the third condition. Fuel treatments were planned only in the lower portions of the watershed and the average predicted erosion rate from these treatments was 0.69 Mg yr^{-1} ha^{-1}, an average increase of 0.02 Mg yr^{-1} ha^{-1}over the current condition run without treatments. Canopy cover and fuel loads decreased as a result of these treatments and the treated landscape was modeled in FlamMap. The treated FlamMap burn severity predictions were used to model the first year post-fire erosion for the treated watersheds. The average first year post-fire erosion rate (after fuel treatments) for the whole watershed was 26 Mg yr^{-1} ha^{-1}, or 6 Mg yr^{-1} ha^{-1} less than the average post-fire erosion rates without treatments (Table 3). In the second year post-fire, erosion rates for both the current conditions and treated conditions would likely drop to only 10% of their first year post-fire values, and return to pre-fire levels in year three post-fire (Robichaud et al., 2008). If only the treated portions of the basin are considered; the reduction in post-fire erosion between the current conditions and treated runs is even greater: 20 Mg yr^{-1} ha^{-1} (Table 4).

Predictions of both burn severity and post-fire erosion rates are comparable to field and satellite derived measurements collected in or near the basin. Model validation of post-fire erosion is very difficult given the high variability in post-fire erosion rates and uncertainties involved when predicting future fire effects and climate scenarios. However, the ratio of high, moderate, and low burn severity from the FlamMap derived predictions for post-fire burn severity were consistent with a satellite-derived map of burn severity for the burned areas of the Power Fire that burned within the Mokelumne Basin in 2004. Field measurements of post-fire erosion rates from the nearby Cannon Fire ranged from 2.5-15 Mg yr^{-1} ha^{-1}

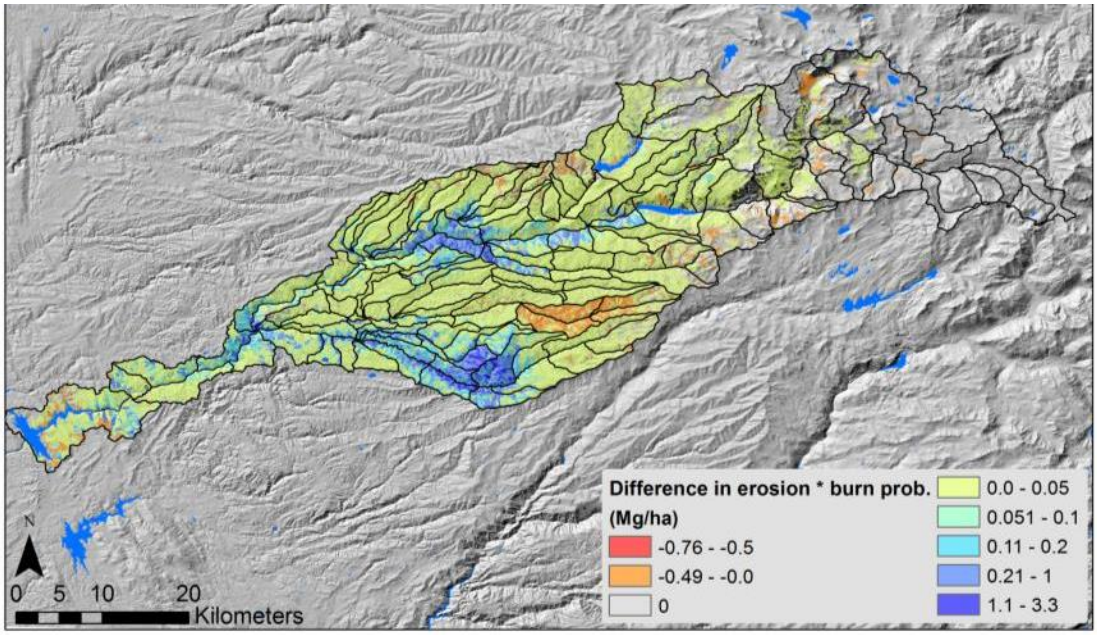

Figure 3 Map of the differences between post-fire erosion predictions for current conditions x burn probability for current conditions and post treatment x burn probability post treatment.

(Robichaud et al. 2008) and the Cannon Fire site is drier than the Mokelumne Basin, with a mean annual precipitation of only 658 mm compared to the range of 799-1438 mm expected in the Mokelumne Basin. Erosion rates measured following other wildfires further south in the Sierra Nevada Mountains were 25 Mg ha^{-1} (mulched) to 46 Mg ha^{-1} (untreated) for a high severity site in the Cedar Fire (Robichaud et al. 2013), where the annual precipitation was 398 mm yr^{-1}. While these comparisons do not validate our modeling, they do demonstrate our results are reasonable.

Frequency of Burning The fire behavior modelers (Buckley et al. 2014) also provided spatial predictions of fire probability derived from the FSim model (Finney et al. 2007) for both current conditions and after the application of fuel reduction treatments. One of the benefits of fuel reduction treatments is a decrease in fire probability due to changes in fuel load properties and canopy, a benefit that can extend into untreated areas. The probability of fire in a given year is fairly low for most of this relatively moist basin, with a fire return interval about 300 years for the forested areas. In order to incorporate fire probability into erosion modeling, it is necessary to multiply the sediment predicted following a wildfire event by the probability of that fire occurring (Elliot, 2013). We can do this for both the untreated and treated post fire erosion estimates. Figure 3 is a map of the difference between the first year post-fire erosion under current conditions multiplied by current burn probability and first year post-fire erosion following treatments multiplied by burn probability after treatments. Overall the modeled treatments are predicted to decrease burn severity, fire probability and post-fire erosion rates. The average reduction in post-fire erosion for the entire basin due to fire between the current conditions and post treatment was 0.05 Mg yr^{-1} ha^{-1}. This metric, however, does not allow us to examine the effects of the treatments on erosion rates in the absence of fire. In order to estimate long term (century scale) "average annual" erosion rates we needed to consider all four conditions (Elliot, 2013).

To estimate "average annual" erosion rates we needed to account for erosion in both fire and non-fire years, as well as the effects of treatments on erosion rates and burn probabilities (Elliot 2013; Miller et al. 2011). Under current conditions, long term hilllslope erosion rate *Average Erosion*$_{cc}$ can be represented

by Equation 1. If we assume the effects of fuel reduction treatments last 25 years, then Equation 2 represents long term erosion rates *Average Erosion*$_{tr}$ with regular fuel reduction treatments.

$$Average\ Erosion_{cc} = E_{cc\_fire} * bp_{cc\_fire} + (1 - bp_{cc\_fire}) * E_{nf} \quad \text{(Eq 1)}$$

$$Average\ Erosion_{tr} = E_{tr\_fire} * bp_{tr\_fire} + (1 - bp_{tr\_fire}) * (24 * E_{nf} + E_{tr})/25 \quad \text{(Eq 2)}$$

where:

E_{cc_fire} is the mapped post-fire erosion rates for current conditions.
E_{tr_fire} is the mapped post-fire erosion rates following fuel treatments.
E_{tr} is the mapped erosion rates due to the effects of the fuel treatments.
E_{nf} is mapped erosion rates for current conditions in the absence of fire.
bp_{cc_fire} is the mapped probability of fire under current conditions.
bp_{tr_fire} is the mapped probability of fire following fuel treatments.

These equations were used in conjunction with our four model runs to develop long term "average annual" erosion rates for the treated portions of the basin with and without fuel reduction treatments every twenty five years. Model results for long term average erosion rates for current conditions were 0.64 Mg yr^{-1} ha^{-1} (Equation 1 averaged for hillslopes selected for treatment, if they were not treated), compared to 0.52 Mg yr^{-1} ha^{-1} if the designated treatment area is in fact treated as modeled (Equation 2 averaged for all treated hillslopes if they were treated). Our predictions indicate that regular treatments will significantly reduce long term overall erosion rates by lowering the "average annual" erosion rate by 19%.

DISCUSSION

The goal of the MACA committee was to determine whether an economic case could be made for increased investment in fuel reduction treatments in the Upper Mokelumne Basin in the face of increasing wildfire threats. This is a challenging task as it is difficult to assign economic value to resources such as fish and wildlife habitat, tourism and recreational opportunities, and cultural sites, which ultimately were left unquantified in the final analysis. To simplify the analysis the committee focused on resources that could be readily assigned a dollar value. These included the avoided sediment costs as well as the cost of homes, infrastructure, treatment implementation costs, timber, carbon sequestration, and fire suppression and cleanup costs. Based on the fire model results and expert review, five fires from the modeling became the focus of the economic analysis, such that those five fires (or similar ones) are likely to occur within the watershed over a 30-year period. The fire behavior models predicted a significant decline in both fire size and intensity due to fuel treatments. Low and high estimates of the dollar value of the resources that would be lost if one of the five fires occurred were tabulated with and without the fuels treatments. The analysis predicted that the economic benefits of the fuels treatments were two to three times more than the costs of treatments. Total treatment cost for the 46 Analysis Units (AUs) was estimated to be $68 million (including maintenance costs over 30 years) compared to the lower estimated avoided cost of $126 million and the higher estimate of $224 million if those fires burned on an untreated landscape. The assumptions of the potential fire size and potential costs of future fires were intentionally conservative. Over the 30-year time frame, the five fires are predicted to burn a total of 21,000 ha with high severity, accounting for 27 percent of the burned area (Buckley et al. 2014). Contrasting this with two major recent wildfires that occurred on either side of the Mokelumne Basin, the Rim Fire (2013) burned 104,000 ha and the King Fire (2014) burned 39,000 ha, with 38 and 47 percent respectively, of their area burning at high severity (http://www.fs.fed.us/postfirevegcondition/index.shtml). These individual fires were much larger and burned at a higher severity than the modeled fires that were used to create cost estimates, therefore the potential costs associated with our modeled future fires are likely underestimated.

Avoided cost due to sediment may have been undervalued by this process due to an inability to sufficiently quantify the potential impacts to aquatic and recreational resources, hydropower and treatment

costs from potential post-fire sediment depositions in key reservoirs. The estimated value of avoided sediment costs was approximately $1 million, attributed to lost water storage potential. This is a relatively small amount compared to the costs associated with saving structures ($32-$45.6 million) or avoiding cleanup costs ($22.5 million) (Buckley et al. 2014). The hydroelectric utility operating in the Mokelumne Basin was not concerned about sediment as the watershed is equipped with multiple water conveyances that allow the utility select different water sources (Buckley et al. 2014). The water utility relies on upstream hydroelectric dams to trap sediments before they reach the Pardee Reservoir at the lower end of the basin where most of the drinking water intakes are located. Loss of reservoir storage capacity was not a concern to either utility company, but this attitude could change due to persistent drought conditions in Western states, with reduced snowpack due to climate change (Mote, 2006) or if one of the water storage reservoirs were lost due to a reduction in useful storage capacity. The Tiger Creek Afterbay reservoir with a storage capacity of 4.8 million m^3 was constructed in 1931 for a hydroelectric plant. A rudimentary bathymetric survey carried out in 2013 estimated storage has dropped to just 1.2 million m^3, a loss of about 75% of its original capacity (Buckley et al. 2014). Elsewhere in the U.S., loss of water reservoir storage capacity in watersheds recently impacted by wildfire has cost water utilities millions of dollars in additional water treatments and dredging expenses. Denver Water has spent $26 million treating drinking water and dredging Strontia Springs Reservoir following the Buffalo Creek (1996) and Hayman (2002) wildfires and the Los Angeles County Public Works plans to spend $190 million dredging four reservoirs impacted by sediment from the 2009 Station Fire (US Department of Interior, 2013). In California, state legislators are considering increasing reservoir storage capacity, the cost of storage for new usable water averages $20/$m^3$ for the proposed reservoirs (http://www.fresnobee.com/2014/06/01/3956458/should-calif-add-new-dams.html). The loss of reservoir storage due to sediment from a single 28,000 ha fire delivering only a tenth of its sediment to the reservoir (about 100,000 m^3) would be $2 million.

CONCLUSIONS

By linking fire behavior and post-fire hydrology models we were able to create a risk assessment map that allowed land and water managers in the Mokelumne Basin to prioritize fuel reduction treatments to protect both land and water resources. These managers are seeking ways to mitigate post-fire erosion and flooding before a wildfire occurs. The potential for dramatic increases in post-fire runoff, erosion and sedimentation is well documented. The importance of targeting limited fuel treatment resources to areas where the greatest benefits are achieved is gaining recognition as society increasingly understands the importance of improved watershed management. Work is ongoing to improve the application of these models and their linkages in order to provide land managers with increasingly refined and spatially-explicit data that will help them to better protect valuable water resources in fire prone regions.

REFERENCES

Agee, J.K. (1993). 'Fire ecology of Pacific Northwest forests.' 493 pp. Island Press, Washington, DC.

Ager, A.A., Finney, M.A., Kerns, B.K., and Maffei. H. (2007). "Modeling wildfire risk to northern spotted owl (Strix occidentalis caurina) habitat in Central Oregon, USA," Forest Ecology and Mngt. 246(1), pp 45-56.

Ager, A.A., Vaillant, N.M., and McMahan, A. (2013). "Restoration of fire in managed forests: a model to prioritize landscapes and analyze tradeoffs," Ecosphere, 4(2), art 29.

Brooks, E.S., Elliot, W., Boll, J., and Wu, J. (2010). Final Report: Assessing the sources and transport of fine sediment in response to management practices in the Tahoe Basin using the WEPP model. Online at < http://www.fs.fed.us/psw/partnerships/tahoescience/sediment_sources.shtml>. (Accessed January, 2015). 74 p.

Buckley, M., Beck, N., Bowden, P., Miller, M.E., Hill, B., Luce, C., Elliot, W.J., Enstice, N., Podolak, K., Winford, E., Smith, S.L., Bokach, M., Reichert, M., Edelson, D., and Gaither, J. (2014). Mokelumne watershed avoided cost analysis: Why Sierra fuel treatments make economic sense. Report prepared for the Sierra Nevada Conservancy, The Nature Conservancy, and USDA, Forest Service. (Sierra Nevada Conservancy, Auburn, CA) Online at < http://www.sierranevadaconservancy.ca.gov/mokelumne > [Accessed January, 2015).

Cochrane, M.A., Moran, C.J., Wimberly, M.C., Baer, A.D., Finney, M.A., Beckendorf, K.L., Eidenshink, J., and Zhu, Z. (2012). "Estimation of wildfire size and risk changes due to fuels treatments," Int. Jour. of Wildland Fire. 21, pp 357–367.

Daly, C., Gibson, W.P., Doggett, M., Smith, J., and Taylor, G. (2004). "Up-to-date monthly climate maps for the conterminous Unites States," Proc., 14th AMS Conf. on Applied Climatology, 84th AMS Annual Meeting Combined Preprints, Amer. Meteorological Soc., Seattle, WA, January 13-16, 2004, Paper P5.1, CD ROM.

Elliot, W.J. (2004). "WEPP internet interfaces for forest erosion prediction," Jour. of the American Water Resources Association 40, pp 299-309.

Elliot, W.J. (2013). "Erosion processes and prediction with WEPP technology in forests in the Northwestern U.S." Trans ASABE. 56(2), pp 563-579.

Elliot, W.J., Hall, D.E., and Scheele, D.L. (1999). Rock:Clime Rocky Mountain Research Station Stochastic Weather Generator Technical Documentation. USDA Forest Service Rock Mountain Research Station (Moscow, Idaho) Available at http://forest.moscowfsl.wsu.edu/fswepp/docs/rockclimdoc.html [Verified January, 2015].

Elliot, W.J., Hall, D.E., and Scheele, D.L. (2000). Disturbed WEPP (Draft 02/2000) WEPP interface for disturbed forest and range runoff, erosion and sediment delivery. USDA Forest Service Rock Mountain Research Station (Moscow, Idaho) Available at http://forest.moscowfsl.wsu.edu/fswepp/docs/distweppdoc.html. [Verified January, 2015].

Elliot, W.J., and Miller, I.S. (2004). "Measuring Low Rates of Erosion from Forest Fuel Reduction Operations," Presented at the Annual International Meeting of the ASAE and CSAE. Paper Number: 045018. 1-4 August, Ottawa, Canada. St. Joseph, MI: ASAE, 10 p.

Finney, M.A. (2006). "An overview of FlamMap modeling capabilities," In: Andrews, P.L., and Butler, B.W. (comps.). Fuels Management – How to measure success: Conference Proceedings. RMRS-P-41. pp 213-219.

Finney, M.A., McHugh, C.W., Grenfell, I.C., Riley, K.L., and Short, K.C. (2011). "A simulation of probabilistic wildfire risk components for the continental United States," Stochastic Environmental Research and Risk Assessment, 25(7), pp 973-1000.

Finney, M.A., Seli, R.C., McHugh, C.W., Ager, A.A., Bahro, B., and Agee, J.K. (2007). "Simulation of Long-Term Landscape-Level Fuel Treatment Effects on Large Wildfires," Int. Jour. of Wildland Fire, 16, pp 712-727.

Flanagan, D.C., and Nearing, M.A. (1995). USDA – Water Erosion Prediction Project: hillslope profile and watershed model documentation, USDA-ARS National Soil Erosion Research Laboratory, NSERL Report No. 10. (West Lafayette, Indiana).

Flannigan, M.D., Stocks, B.J., and Wotton, B.M. (2000). "Climate change and forest fires," Science of the Total Environment, 262, pp 221-229.

Forrest, C.L., and Harding, M.V. (1994). "Erosion and sediment control: preventing additional disasters after the Southern California fires," Jour. of Soil and Water Conservation 49(6), pp 535-541.

GAO (1999). Western national forests: a cohesive strategy is needed to address catastrophic wildland fire threats, Government Accounting Office Report GAO/RCED–99–65. (Washington, DC).

GAO (2007). Wildland fire management: better information and a systematic process could improve agencies' approach to allocating fuel reduction funds and selecting projects, US General Accounting Office (Washington, DC).

Garbrecht, J., and Martz, L.W. (1999). TOPAZ: an automated digital landscape analysis tool for topographic evaluation, drainage identification, watershed segmentation and subcatchment parameterization. USDA Agricultural Research Service Publication No. GRL 99-1. (El Reno, Oklahoma).

Gesch, D.B. (2007). "The National Elevation Dataset," in Maune, D., ed., Digital Elevation Model Technologies and Applications: The DEM Users Manual, 2nd Edition: Bethesda, Maryland, American Society for Photogrammetry and Remote Sensing, pp 99-118.

Gesch, D., Oimoen, M., Greenlee, S., Nelson, C., Steuck, M., and Tyler, D. (2002). "The National Elevation Dataset," Photogrammetric Engineering and Remote Sensing, v. 68, no. 1, pp 5-11.

Keane, R.E., Ryan, K.C., Veblen, T.T., Allen, C.D., Logan, J., and Hawkes, B. (2002). Cascading effects of fire exclusion in Rocky Mountain ecosystems: A literature review, USDA Forest Service Rocky Mountain Research Station General Technical Report RMRS-GTR-91. (Fort Collins, Colorado).

Laflen, J.M., Elliot, W.J., Flanagan, D.C., Meyer, C.R., and Nearing, M.A. (1997). "WEPP-predicting water erosion using a process-based model," Jour. of Soil and Water Conservation 52(2), pp 96-102.

Miller M.E., MacDonald, L.H., Robichaud, P.R., and Elliot, W.J. (2011). "Predicting post-fire hillslope erosion in forest lands of the western United States," Int. Jour. of Wildland Fire 20, 982-999.

Moody, J.A., and Martin, D.A. (2001). Hydrologic and sedimentation response of two burned watersheds in Colorado. U.S. Geological Survey Water Resources Investigative Report 01-4122. (Denver, Colorado).

Mote, P.W. (2006). "Climate-driven variability and trends in mountain snowpack in Western North America," Jour. of Climate, 19, pp 6209-6220.

Neary, D.G., Ryan, K.C., and DeBano, L.F. (2005). Wildland fire in ecosystems: effects of fire on soils and water. USDA Forest Service, Rocky Mountain Research Station General Technical Report 42, vol. 4. (Ogden, Utah).

Nicks, A.D., Lane, L.J., and Gander, G.A. (1995). "Weather generator," In Flanagan, D.C., and Nearing, M.A. (Eds.) USDA-Water Erosion Prediction Project Hillslope Profile and Watershed Model Documentation pp. 2.1-2.22. (USDA Agricultural Research Service: West Lafayette, Indiana).

Reinhardt, E.D., Keane, R.E., Calkin, D.E., and Cohen, J.D. (2008). "Objectives and considerations for wildland fuel treatment in forested ecosystems of the interior western United States," Forest Ecology and Mgt 256, pp 1997-2006.

Renschler, C.S. (2003). "Designing geo-spatial interfaces to scale process models: the GeoWEPP approach," Hydrological Processes 17, pp 1005-1017.

Robichaud, P.R., Wagenbrenner. J.W., Brown. R.E., Wohlgemuth, P.M., and Beyers, J.L. (2008). "Evaluating the effectiveness of contour-felled log erosion barriers as a post-fire runoff and erosion mitigation treatment in the western United States," Int. Jour. of Wildland Fire, 17(2) pp 255-273.

Robichaud, P.R., Wagenbrenner, J.W., Lewis, S.A., and Ashmun, L.E. (2013). "Post-fire mulching for runoff and erosion mitigation Part II: Effectiveness in reducing runoff and sediment yields from small catchments," Catena 105, pp 93-111.

Rollins, M.G. (2009). "Landfire: a nationally consistent vegetation, wildland fire, and fuel assessment," Int. Jour. of Wildland Fire, 18, pp 235-249.

Sampson, R.N., Atkinson, R.D., and Lewis, J.W. (2000). "Indexing resource data for forest health decision making," Jour. of Sustainable Forestry 11, pp 1-2 – 1-14.

Scheele, D.L., Elliot, W.J., and Hall, D.E. (2001). "Enhancements to the Cligen weather generator for mountainous or custom applications," Procs. from Soil erosion research for the 21st century. (Eds. J.C. Ascough, II, and D.C. Flanagan), American Society of Agricultural Engineers: St. Joseph, Michigan, pp 392-395.

Sidman, G., Guertin, D.P., Goodrich, D.C., Thoma, D., Falk, D., and Burns, I.S. (2015). A coupled modeling approach to assess the impact of fuel treatments on post-wildfire runoff and erosion, Int. Jour. of Wildland Fire, (in press).

Tiedemann, A.R., Conrad, C.E., Dieterich, J.H., Hornbeck, J.W., and Megahan, W.F. (1979). Effects of fire on water. A state-of-knowledge review. USDA Forest Service, General Technical Report WO-10 (Washington, D.C.).

U.S. Department of Agriculture (USDA). (1991). State soil geographic (STATSGO) data base data use information, U.S. Department of Agriculture Miscellaneous Publication 1492. (Washington, D.C.)

U.S. Department of the Interior. (2013). USDA and Interior Announce Partnership to Protect America's Water Supply from Increased Wildfire Risk [Press release]. Available at: http://www.doi.gov/news/pressreleases/usda-and-interior-announce-partnership-to-protect-americas-water-supply-from-increased-wildfire-risk.cfm.

Westerling, A.L., Hidalgo, H.G., Cayan, D.R., and Swetnam, T.W. (2006). "Warming and earlier spring increase western U.S. forest wildfire activity," Science 313, pp 940-943.

CLIMATE CHANGE IMPACTS AND MITIGATION/ADAPTATION: COPING WITH WEATHER EXTREMES FROM AN ENGINEERING STUDENT'S PERPECTIVE

Brittany R. Bennett, M.S.E. Candidate, The Catholic University of America, Washington, D.C., 19bennettb@cardinalmail.cua.edu

Abstract: Nowadays civil engineering students of engineering should be knowledgeable about global climate change, due to the fact that it is one of today's greatest challenges our society faces to existing and future infrastructure. For example, in the case of all water-related infrastructure and planning, design, construction, maintenance and operation, there are increasing impacts from extreme weather events. Future engineers need to be prepared for meeting those challenges for mitigation and/or adaption with a result of climate resilience. Federally developed resources and regional case studies will be drawn upon in order to provide useful guidance to water engineering students, or current engineers embracing a climate change approach. The unique perspective of a current student will also provide useful feedback in the development of higher education.

INTRODUCTION

Due to a changing climate, the USACE has identified that "all infrastructure is potentially affected and needs adaptation". Following the 2009 request of President Obama, an interagency Climate Change Adaptation Task Force has crafted numerous recommendations for policy. These include useful guiding principles and strategies for many agencies. At an operational level, regional water resources and related structures (e.g. hydropower dams, water treatment plants) have been studied and some adjustments made.

OBJECTIVES

1. Clarifying relevant climate impacts to water infrastructure, based on the current state of climate science.
2. Determining the actionable goals for intersecting climate and water sectors.
3. Identifying the key strategies for determining risk and associated, imperative, action, and measure which are applicable to various projects.
4. Compiling a useful directory of decision-making and planning tools, which are existing or in-development .
5. Analyzing examples of responsive adjustments made or identified as needed by U.S. water entities.
6. Providing suggestions for relevant preparation in higher education.

CLIMATE IMPACTS TO U.S. WATER INFRASTRUCTURE

Climate is average weather over a time, and a prime environmental factor that determines the life of an area. The climate is warming, not for the first time, but this time it is largely due to the activities of humans and there is now a scientific consensus. Changes to natural cycles in response to man-made activities, especially the hydrologic cycle, must be understood for managers within reliant sectors and for climate users, in order to make sustainable decisions.

Significant changes in temperatures and precipitation patterns affect local water budgets, streamflows, runoff patterns, and extreme weather events. The US has seen the greatest temperature increase and increase in weather extremes, while in the UK there have been more studies on watershed change. The challenges are most significant in urban areas where infrastructure was built to handle a particular environment that is no longer what it was today, and in rural areas where human practices cannot be improved to mitigate global change, and resources for adapting are limited.

Water budgets quantify the hydrologic cycle in the open system including parts in land, air, and in between. A water budge can be considered at the global and regional scales. It accounts for rates of water movement and changes in water storage in a specific unit. Calculations can be done to predict changes and availability. While the concept is simple, accurate determinations are difficult to obtain due to the number of uncertainties present at every scale. There are two sources of uncertainty in water-budget calculations: natural variability and error in measurements. Natural variability occurs in all aspects of the hydrologic cycle, and is becoming more difficult to predict.

The change of temperature is a controlling factor. Higher temperatures allow for larger amounts of water vapor to be to be stored in the atmosphere and cause rates of evapotranspiration to increase. These shifts affect the dynamics of water storage and movement. This is source of complication because the budget is no longer held in steady amounts in the various categories and locations. Quantities and properties for specific watersheds are shifting significantly.

In the past century, changing streamflow and runoff rates have been observed for most rivers and steams. In the US, increasing streamflows have been observed in the East. In the Central US major river basins streamflow and runoff are decreasing. Annual precipitation has been increasing in most of the US, except for in the Midwest, where it has been decreasing. Annual flows of the Colorado, Rio Grande and San Joaquin river basins have decreased 8-20%. Frequency of heavy precipitation events has been increasing throughout most of the US as well. In the Western US and Alaska, storage re-charge is impacted by decrease in the contribution of ice melt.

While the measured extremes now occurring may be greater in the US, it is in the UK that more studies are being done to model climate impacts on strategic river flows. Model projections for the River Medway, in England found a persistent lowering of mean daily river flows for all months and for all projection time slices. This signal was evident, even after considering for uncertainties in the exercises. (Cloke, 2010)

The effect of temperature on soil moisture may account for the lower runoff amounts for some watersheds. Dry soil will absorb more of the rainfall, contributing to more interflow and groundwater flow. However, the driest soils, which can become caked, may not readily absorb rainfall, leading to higher rates of runoff at the beginning of a rainfall event. Droughts are a significant concern. In the US, they have not been found to be increasing in frequency, because they already occur with annual frequency in the Midwest. However, the length of the droughts, and decrease in rainfall may be steadily increasing. The distance in these regions from large water sources, make the situation more fragile.

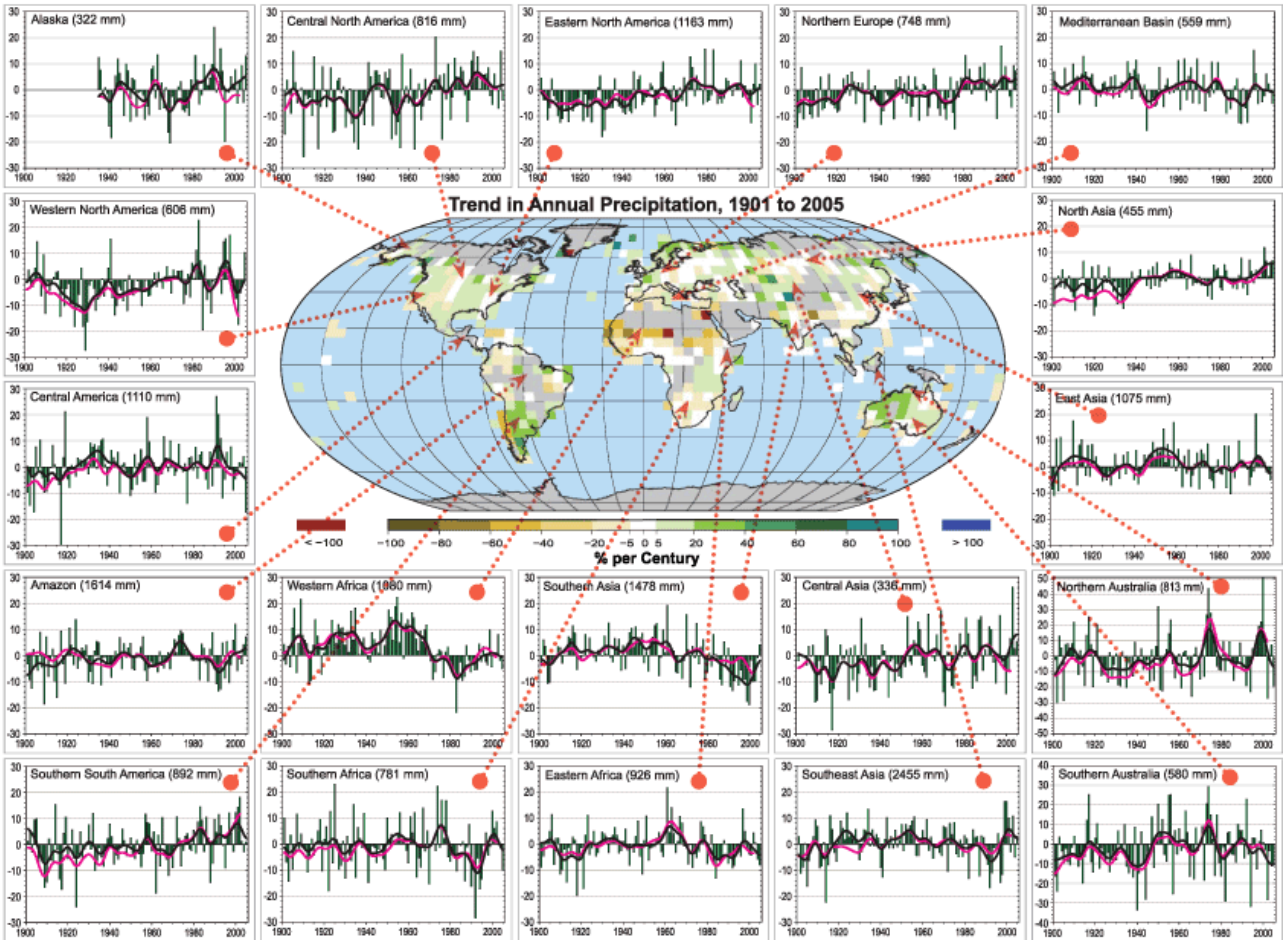

Figure 1. The diagram shows annual precipitation trends (1901-2005) at various regions (Source: IPCC Fourth Assessment Report, 2007, Chapter 3, Figure 3.14).

Temperature increase can cause higher rates of evapotranspiration. Surface waters exposed to higher temperatures see a greater loss in evaporation, and decrease in stored quantity. The additional water vapor passing into the atmosphere may be steadily retained, reducing storage in lakes and rivers. Some of the additional water vapor may also be transported across watersheds in shifting patterns, and contribute to the more extreme rainfall events.

The properties of the local watershed are the significant determinations of hydraulic characteristics in an area. These include total area, slope, elevation, soil and rock types and permeability, storage, density, roughness, and antecedent moisture content. Some of these features are influence by the hydro-meteorological changes discussed above, and others are undergoing change with land use patterns. Land use shifts together with climate shifts, contribute to total watershed change. It's important that future development planning take both of these into account.

Storage, run-off, and antecedent moisture content in particular, are hydraulic characteristics within watersheds which are affected by climate. Both of these measures change continuously but notable shifts may occur with climate change as well as notable extremes.

Antecedent moisture content (AMC) is the relative wetness or dryness of soil prior to a rainfall event. Run-off, infiltration, and interflow are highly affected by AMC. Factors which influence AMC include air temperature, humidity and wind levels, as well as evaporation and transpiration rates. Climatic changes in air temperature, humidity (water vapor), and evapotranspiration rates can alter AMC content.

In regions which experience higher temperatures for longer periods of time, soils may be drier prior to more rainfall events, leading to higher initial infiltration, greater interflow, and lower run-off. Yet, in the cases where temperatures remain high and rainfall events are less frequent, it is possible for caking and cracking to occur in the soil. This can cause initial flooding, because the rainfall is not as ready absorbed. The cracking phenomenon has been observed temporally in clay soils, in particular (Kishné, 2010). While climate changes can influence this dynamic, it will vary with the local soil type.

Periods of freezing and frost also influence soil moisture content. The storage capacity and moisture content of limestone soils increase with freezing and frost events. In the case of increased temperatures, regions with these types of soils may see a reduction in total storage capacity. This could cause more runoff and less moisture availability. (White, 2001)

Climate change slightly increases transpiration rates, yet a large factor in climate change CO2 slightly decreases transpiration rates. The increase in temperature causes plants to transpire more, while greater concentrations in CO2 close the stomata and lead to less transpiration. This dynamic underscores the complications in distinguishing local impacts from global. In general, the increase in temperature has the greatest effect. (State of California)

Land uses also highly influence evapotranspiration and runoff. Shifts in regional land use from undeveloped land, cropland, or woodland to urban and industrial uses decrease the % of evapo-transpiring land which has plant, soil, or water surface. Landscape changes such as these, lead to increased rates of run-off and decreased rate of evapotranspiration. Surface cover is an important input along with precipitation, soil type and moisture conditions. Some models are being developed which can run various surface cover (or development) scenarios. These models are useful, in that they can help determine the impact of greening in urban areas for the purpose of adapting to climate change. (Gill, 2012)

The hydrologic changes mentioned above, all impact the availability of water as resource. It is becoming increasingly important to understand the implications of climate change at the regional and local levels where demands occur. Changes in the global climate have impacts which cross many kinds of borders, whether they are natural or political boundaries. Climatic shifts are influences the extremity of weather events and in some cases the area storm events may cover can include multiple watersheds, states, or countries. The land uses in one region can influence the climate of another region, which in turn influence the hydrology.

Land use is a factor which can be controlled, although the effects of past use can be difficult to eliminate or restore. Models which can run various development scenarios with changing inputs may become increasingly necessary. Management changes occurring are due to the frequencies

in extreme weather events. Management areas include maintaining water availability, controlling floods, operating exposed infrastructure, and managing particular ecosystems and species populations.

Structural difficulties arising from climate change on land are dealing with increasing salinity and soil saturation, and to a lesser extent (depending on the region) sea level rise. Increasing salinity affects drinking water and necessary treatment. Salinity also impacts various ecosystems which may provide other services such as food, medicine, wood products, or storm protection. Preparation for increasing salinity should include planning and mapping for protection, changes in practice, or exclusion from expensive engineering. Increasing soil saturation may contribute to landslides, structural instability or collapse, and changes in agricultural production. Preparation for increasing soil saturation could follow a similar strategy.

ACTIONABLE GOALS FOR CLIMATE AND WATER SECTOR

The actionable goals for the water sector and associated fields of engineering in dealing with climate change, are simply to continue to meet long-established goals, in face of modern changes to the environment. According to the USACE's webpage on adapting to climate change:

> *"The US Army Corps of Engineers (USACE) must be able to perform our missions and operations despite dynamic conditions, whether these result from climate change alone or in combination with other global changes such as demographic shifts, land use/land cover changes, world population growth, aging infrastructure, persistent conflict, declining biodiversity, globalization, climate variability and change, and changing social values and economic conditions."*

From the perspective of an engineering student, this implies a need for gaining knowledge and familiarity with certain challenges, such that whatever the engineer designs or operates has a longevity and can withstand predicted shifts from a current condition (e.g. rainfall, moisture, wind speeds, etc.), wherever it is located. It is implied that these challenges are to be met with diligence, and not ignorance to the current state of knowledge. The engineer, should in fact draw from the available science and from the predictions which are being made by climate scientists. This may seem challenging. How does the engineer know where to find this information, and how do they communicate with other specialists?

KEY STRATEGIES

Strategies related to climate change, may deal with either mitigation or adaption. Mitigation strategies can occur at individual or micro-level. Numerous actions taken at that level can which all have the same impact of reducing emissions. However, adaptation requires more coordination and occurs at the socio- or macro-level. Adaptation involves different groups or sectors finding the best way to respond to the same phenomena.

The current state of the science is sufficient enough, at this point, that application can begin. An important feedback loop is beginning in climate science, as scientific investigation informs the experience and experience will inform future investigation.

A lot of key organizational changes have occurred recently within key scientific and administrative bodies. Publications from a number of reports from various industries and agencies have also been made public. Action at some level has begun in nearly all states and agencies. At this point, it seems that most of the changes have occurred at the scientific and political level. This information and policy are great directives to further more useful advances in mitigation and adaptation.

It is important to move from scattered action to strategic action which occurs to some degree at every level, because the impacts are broad. Emissions cannot be simply reduced in a single region or industry, with the expectation that the temperature and precipitation increases or decreases will return back to normal. There needs to be a high level of coordination across sectors and political boundaries.

Key Bodies, Legislation, and Reports:

- IPCC
- USGCRP - United States Global Change Research Program
- White House CEQ Federal Instructions for Adapting
- Regional GHG initiative (NEUS)
- CA AB32 Act (California "Global Warming Solutions Act")
- NRC report (adaptation)
- Insurance companies report
- Security Exchange Commission disclosure
- EIA's – incorporating climate change impacts
- USACE – "all infrastructures potentially affected and need adaptation"

In particular, the White House CEQ's Federal Instructions, given to all federal agencies a couple years ago, contains principles useful to various fields. They are summarized below.

- *Adopt Integrated Approaches:* Adaptation should be incorporated into core policies, planning, practices, and programs whenever possible.
- *Prioritize the Most Vulnerable*: Adaptation strategies should help people, places, and infrastructure that are most vulnerable to climate impacts and be designed and implemented with meaningful involvement from all parts of society.
- *Use Best-Available Science*: Adaptation should be grounded in the best-available scientific understanding of climate change risks, impacts, and vulnerabilities.
- *Apply Risk-Management Methods and Tools:* Adaptation planning should incorporate risk-management methods and tools to help identify, assess, and prioritize options to reduce vulnerability to potential environmental, social, and economic implications of climate change.
- *Apply Ecosystem-based Approaches:* Adaptation should, where appropriate, take into account strategies to increase ecosystem resilience and protect critical ecosystem services on which humans depend, to reduce vulnerability of human and natural systems to climate change.

(http://www.whitehouse.gov/administration/eop/ceq/initiatives/adaptation)

The best available science is being done in many places, but much of it related to climate change

has been reviewed and summarized by IPCC. The next assessment will be done next year. Four reports are currently available. (http://www.ipcc.ch/publications_and_data/publications_and_data_reports.shtml#.UKf1MYdZWv0)

The best technologies and applications for climate change adaptation leverage the internet, and compile data from multiple sources. These data inputs can be used to inform management of GHG emissions, by flagging the greatest uses and indicating where the easiest or greatest reductions can be made. Utilizing various performance technologies can generate savings which may be found in many areas including labor, time, travel, physical infrastructure, energy, and consumption. Due to the large volume of data can and is being generated from connecting so many 'things', some new references are being made to 'big data' and the 'internet of things'.

The key will be learning to efficiently interpret this data and digest it. This is still a largely intuitive process, which requires more training of managers in what to look for, how to look, and how to use the information available. While 'things' are becoming more and more connected and better understood it's important that 'people' (e.g. managers of various sectors or resources or organizations) remain just as connected, so that advances are shared in a timely way. An example where that dynamic plays out is in the case of environmental requirements for data server storage (Jonassen, 2012). While it is now known that they still function properly under moderate ambient temperatures, many centers are still cooled. These situations could be adapted for easy savings in energy use and emissions.

DIRECTORY OF TOOLS, EXISTING AND IN-DEVELOPMENT

An up-to-date list will be included as part of the presentation / poster

CASE STUDIES OF ADAPTATION TO CLIMATE CHANGE IN THE U.S. WATER SECTOR

The majority of case studies on this topic are in the assessment and planning stage. A few examples:

1. The NDWAC report identifies current water sector needs and challenges utilities face when attempting to mitigate and adapt to the impacts of climate change ("Overview of Climate Ready Water Utilities Working Group Report.").
2. Metropolitan Washington Council of Governments inter-agency initiative ("Climate Change - Building Resilience") focuses on mitigation, in compliance with federal direction, and resiliency.
3. The District Department of Transportation (DDOT)'s Adaptation Plan includes water infrastructure ("Climate Change Adaptation Plan")

RECOMMENDATIONS FOR HIGHER EDUCATION

A number of important inputs in hydrology are changing temporally leading to changes in water availability. While the many changes are being studied by experts in different areas, barriers

remain for effective management of water resources and adaptation of urban areas. Some recommendations can be made to reduce these barriers and better sync management change with climate change so that adverse impacts are decreased, and so that students are properly trained and prepared to enter these fields.

The first two suggestions are related to engineering as a whole, wherein clarification would improve education, and wherein students themselves may make contributions. The rest are primarily focused on the realm of improving higher education through specific course integrations.

Terms: Within this paper many terms were used, some interchangeably and some not well-explained. Not all managers will be familiar with the list of terms related to climate. Various fields have preferred terms, or unique terms. More uniform terminology and metrics could make current scientific understanding more accessible and communication across disciplines/sectors more efficient. Uniform metrics would allow for the more efficient education and training of managers, as well as give them tools to more quickly assess key local changes and adaptation options. Improvements could also be more clearly made and shared. Students in multiple disciplines would be able to collaborate more effectively, enabling conversations which lead to deeper understanding and more creative solutions to problems in their communities.

Economics and community-based approaches: No models were found in the research of this paper which related climate change to specific economic valuations of various ecosystem services. This is an important factor in decision making. Many engineering students are educated in economics for the purpose of managing projects. However, because the impacts of climate change are so broad, and because the economic implications are not well understood, these students are at a disadvantage in today's workplace. In real-world projects, the involvement of local community may be a key concern in adapting regional areas. Therefore it is suggested that students become familiar with community interaction. Motivated citizens (a.k.a. the end-users of services and products such as roads or drinking water) may find the time and interest in monitoring local watershed changes, and reporting these inputs to experts in modeling. They may also communicate with managers to inform them of practicality of land use changes in response to these changes. Students should be introduced to a community-based approach to managing and developing water-related projects. Practically speaking, this could be addressed by including modules in existing and sometimes required management courses, by new courses on climate management, or by recommending courses on economic development or introductory courses on environmental/climate science.

Integration of sustainability criteria to engineering degree program accreditations: Example:

- The National Architectural Accrediting Board (NAAB) is updating the criteria it uses to accredit degree-granting architecture schools in the U.S. to include full integration of sustainability criteria (instead of requiring unique courses on sustainability). This could likewise, be instituted by the Accreditation Board for Engineering and Technology (ABET).

Science and sustainability courses: Examples:

- Sustainability course (http://architecture.cua.edu/res/docs/Curriculum/SustainMinorCourses-2014-082014.pdf)

- LEED lab (http://www.leedlab.com)
- Technologies for Sustainable Societies (http://osoc.berkeley.edu/catalog/gcc_search_sends_request?p_dept_cd=CIV+ENG&p_title=&p_number=292A)
- Introduction to environmental science (a standardized course)

Other courses: Examples:

- Climate Change Mitigation (http://osoc.berkeley.edu/catalog/gcc_search_sends_request?p_dept_cd=CIV+ENG&p_title=&p_number=107)
- Adapting roads (http://www.idrrim.com/ressources/documents/5/2710,ROADAPT-course-October-20-21.pdf)
- Alternative energy (http://eecs.cua.edu/renewable-energy/index.cfm)
- Introduction to environmental engineering (a standardized course)

REFERENCES

"Arctic Sea Ice Shatters Previous Low Records; Antarctic Sea Ice Edges to Record High." The National Snow and Ice Data Center, n.d. Web. 28 Oct. 2012. <http://nsidc.org/news/press/20121002_MinimumPR.html>.

Bindoff, N., Willebrand J., Artale V. , Cazenave A., Gregory J. , Gulev S., Hanawa K., Le Quéré C., Levitus S., Nojiri Y., Shum C.K., Talley L., Unnikrishnan A., Observations: oceanic climate and sea level. In: Climate change 2007: The physical Science Basis. Contribution of Working Group I to the Fourth Assessment report of the Intergovernmental Panel on Climate Change [Solomon S., D. Qin, M. Manning, Z. Chen, M. Marquis, K.B. A]

"Business Risk Assessment and the Management of Climate Change Impacts - 12 Cities." (n.d.): n. pag. Wwf.org. World Wildlife Foundation. Web. <http://wwf.org.ph/wwf3/downloads/publications/Business%20Risk%20Assessment%20and%20the%20Management%20of%20Climate%20Change%20Impacts%20-%2012%20Cities.pdf>.

"Climate Change." Weather Forecast & Reports. Weather Underground, n.d. Web. 28 Oct. 2012. <http://www.wunderground.com/climate/?MR=1>.

"Climate Change - Building Resilience." MWCOG.org. Metropolitan Washington Council of Governments, n.d. Web. 20 Jan. 2015. <http://www.mwcog.org/environment/climate/resilience.asp>.

Cloke, H. L., C. Jeffers, T. Byrne, J. Lowe, and F. Pappenberger. "Climate Impacts on River Flow: Projections for the Medway Catchment, UK, with UKCP09 and CATCHMOD." Http://www.ecmwf.int. European Centre for Medium-Range Weather Forecasts, 19 July 2010. Web. 8 Nov. 2012. <http://www.ecmwf.int/staff/florian_pappenberger/publications/pdf/clokeHP2010-climateimpacts-published.pdf>.

Cook, B., et al. (2014). "Global warming and 21st century drying." Climate Dynamics 43(9-10): 2607-2627.

District Department of Transportation. "Climate Change Adaptation Plan." (n.d.): n. pag.

"Global Warming Frequently Asked Questions." . National Oceanic and Atmospheric Administration -National Climatic Data Center, n.d. Web. 28 Oct. 2012.

<http://www.ncdc.noaa.gov/cmb-faq/globalwarming.html>.
Hammill, Anne, and Tom Tanner. "Climate Risk Screening & Assessment Tools." Climate Risk Screening & Assessment Tools (2010): n. pag. Http://www.ddrn.dk. Danish Development Research Network. Web. <http://www.ddrn.dk/filer/forum/File/Anne_Hammill.pdf>.
Hunt, A. and Watkiss, P. (2011) Climate change impacts and adaptation in cities: a review of the literature. Climatic Change, 104 (1). pp. 13-49. ISSN 0165-0009
"IV. Climate Change Risk Management." Whitehall Papers 69.1 (2007): 28-37. Http://www.undp.org. United Nations Development Programme. Web. 1 Jan. 2015.
Jonassen, Rachael G. Climate Change: What You Can Do Now. McLean, VA: LMI, 2012. Print.
Jones, R. 2010. A risk management approach to climate change adaptation. In: Climate change adaptation in New Zealand: Future scenarios and some sectoral perspectives. Nottage, R.A.C., Wratt, D.S., Bornman, J.F., Jones, K. (eds). New Zealand Climate Change Centre, Wellington, pp 10 - 25.
Kishné, Andrea Sz., Cristine L.S. Morgan, Yufeng Ge, and Wesley L. Miller. "Antecedent Soil Moisture Affecting Surface Cracking of a Vertisol in Field Conditions." Geoderma 157 (2010): 109-17. Http://www.sciencedirect.com. Science Direct. Web. 9 Nov. 2012. <http://www.sciencedirect.com/science/article/pii/S0016706110001084>.
Lin, Samuel (2011). CE 593 Class Slides, CE Department, CUA, Washington, D.C.
National Drinking Water Advisory Council (NDWAC). "Overview of Climate Ready Water Utilities Working Group Report." (2011): n. pag. Http://water.epa.gov. U.S. Environmental Protection Agency. Web. <http://water.epa.gov/infrastructure/watersecurity/climate/upload/NDWAC-overview-of-CRWU-10.pdf>.
"NASA, NOAA Find 2014 Warmest Year in Modern Record." ScienceDaily. ScienceDaily, 16 Jan. 2015. Web. 16 Jan. 2015. <http://www.sciencedaily.com/releases/2015/01/150116153905.htm>
"Mean Sea Level Rise." Aviso, n.d. Web. 28 Oct. 2012. <http://www.aviso.oceanobs.com/en/news/ocean-indicators/mean-sea-level/>.
McLaughlin, B. J., etc. (2011). “Anticipating Climate Change”, Civil Engineering, ASCE, April, 2011.
Shaw, E. M., etc. (2011). Chapter 19, Hydrology in Practice, 4th Edition, Spon Press, London and New York
State of California. Department of Water Resources. Bay-Delta Office. Http://baydeltaoffice.water.ca.gov. By Roy Peterson, Richard Snyder, and Morteza Orang. N.p., n.d. Web. 09 Nov. 2012. <http://baydeltaoffice.water.ca.gov/climatechange/200610_ClimateChangeET_CALFEDScience_rpeterso.pdf>.
"State of the Climate Global Analysis September 2012." National Oceanic and Atmospheric Administration -National Climatic Data Center, n.d. Web. 28 Oct. 2012. <http://www.ncdc.noaa.gov/sotc/global/>.
United States. United States Global Change Research Program. Globalchange.gov. United States Global Change Research Program, n.d. Web. 28 Oct. 2012. <http://www.globalchange.gov/publications/reports/scientific-assessments/us-impacts/full-report>.
White, Kasey S. IPCC Third Assessment Report :Working Group II: Impacts, Adaptation and Vulnerability. Rep. Ed. James J. McCarthy, Osvaldo F. Canziani, Neil A. Leary, and David

J. Dokken. Intergovenmental Panel on Climate Change, 2001. Web. 09 Nov. 2012. <http://www.grida.no/publications/other/ipcc_tar/?src=/climate/ipcc_tar/wg2/>.

DOWNSTREAM SEDIMENT IMPACTS ON FISH RESTORATION, RIVER DYNAMICS, FLOODPLAIN DEVELOPMENT, AND WATER QUALITY FROM BREACHING THE ELWHA AND GLINES CANYON DAMS, NEAR PORT ANGELES, WASHINGTON

Dr. Frank Reckendorf, Fluvial Geomorphologist, Reckendorf and Associates, Salem, Oregon, frecken@mac.com
Dr. Barry Southerland, Fluvial Geomorphologist, NRCS, WNTSC, Water Quality and Quantity Technology Development Team, Portland, Oregon, barry.southerland@por.usda.gov

INTRODUCTION

The Natural Resources Conservation Service (NRCS) in Washington generated a request for post-project appraisals of Engineered Log Jams (ELJs) in December of 2005. In February of 2006 the Washington NRCS in Spokane, and the West National Technical Support Center of NRCS in Portland, Oregon, assembled an interdisciplinary team including two fluvial geomorphologists, a fisheries biologist, and a stream-mechanics engineer. They were to study the results of the ELJs Implementation since the mid1990s in the State of Washington. One major study site was the ELJs on the Lower Elwha River. During the 2010 evaluation of the Lower Elwha it was decided to extend the study to look at the effects of sedimentation on the Elwha River and the ELJs once a large dam removal project started in 2011. We monitored 49 ELJs on the Lower Elwha River between 2006 and 2013.

Two hydroelectric dams were constructed on the Elwha River by a private company in the early part of the last century. Elwha Dam was constructed in 1910, and the Glines Canyon Dam in 1925. They were constructed without regard to fish passage facilities, although regulations were in effect in Washington at the time. The dam's lack of fish passage decimated native populations of salmon including spring Chinook known to exceed 100 pounds. The dams altered the natural hydrologic regime, caused downstream scour to occur below both dams, and an increased transported particle size passing through the spillway, because the coarser material is trapped. The downstream scour after the dams are built causes there to be an increase insize because the flow contains less load. This condition is called hungry water. In addition, the altered hydrology caused an increase in downstream temperatures, and decreased transport of large woody debris (McHenry et al., 2007).

STUDY AREA

The Elwha River watershed is in the Olympic Peninsula, with its headwaters on the slopes of Mt. Olympus in Olympic National Park. About 80 percent of the Elwha River watershed lies within the Park boundaries. Limited development occurs within Olympic National Park, so the Elwha has largely remained in its natural condition above the dams.

Construction began on the Elwha Dam, located at RM 6, in 1913. The dam was 108 feet high. Construction began on the Glines Canyon Dam, located at RM 13, in 1926. This dam was 220 feet high. The portion of the Elwha River impacted by sediment that is discussed in this study

extends from RM 2.5 to the mouth at the Puget Sound near Port Angeles. The ELJ study site is located between RM 2.25 and RM 1.33, downstream of both dam sites.

SETTING

The watershed has a drainage area of 325 square miles. The period of record, including pre-dam construction and pre-breaching, had a bankfull discharge in the range between 6,500 to 8,250 cfs with a drainage area of 270 square miles to the ELJs. Table 1 shows the recent high flows of significance since ELJ implementation.

Year	Discharge (cfs)	Log Pearson III
2002	25,700	9Q
2003	29,700	17Q
2006	20,900	5Q
2007	35,900	37Q
2010	22,300	6Q
2013	11,100	1.6Q

Table 1 USGS Gage 12045500

The tortuosity, defined as R_c/W_{bkf}, (Rc is Radius of Curvature and W_{bkf} is Width at bankfull Q), in the ELJ evaluation reach varied from 2.5 ft/ft to 2.6 ft/ft. Prior to dam removal the Elwha was migrating laterally towards the left streambank at the study site. Local scallop patterns were present on the left streambank, and excessive streambank loss is still a major concern.

The Elwha River is typical of many Northwestern rivers that have undergone channel modification by straightening, gravel removal, and destruction of the riparian vegetation. Historically, under natural conditions the Elwha River was a pool/riffle, gravel-bed system. The riparian area functioned hydraulically with the river adding a large woody debris component that was functionally important for salmonid habitat. After the dams were constructed, the Elwha River lost legendary fish runs of ten species, destroying the habitat complexity. Before the dams were removed, it provided limited spawning and rearing habitat for remnant populations of native Pacific Salmon (McHenry et al., 2007). Two species, Chinook salmon and bull trout, are listed as threatened under the Endangered Species Act and steelhead is proposed for listing (McHenry et. al, 2007).

The construction of the two dams changed the hydraulics, sedimentation, and meander geometry downstream. The absence of sediment loads below the dams caused scour to occur downstream all the way to the mouth of the Elwha River. The bed load component played a much greater role in determining the medium load size in the river with the dams in place, causing an increase in the bed material load.

The post-dam hydraulics caused roughly three feet of downcutting to a coarse cobble material with a d_{50} of roughly 190 mm.

Figure 1 Downcutting shown in the left portion exposed an old channel, which is, now, a floodplain. The right portion of the image shows this old channels remnant floodplain as it was 50 years ago.

Figure 2 Close up of the streambank of the remnant floodplain shown in the right part of Figure 1. This figure shows a cantilever overhang that is sloughing as described by Reckendorf (2009 and 2010).

There was still sediment contributed to the Elwha River from the uncontrolled drainage area below the dams, including streambank erosion such as shown in Figures 1 and 2, and from sediment that was passed through the spillways of both dams. Prior to dam removal, the Lower Elwha study area had a bimodal sediment distribution, with some of the gravel bed with a d_{50} of roughly 50 mm associated with the current flow regime. In addition, part of the bed and bar had a d_{50} of roughly 130 mm, associated with coarse (cobble) bed material exposed through the downcutting process. The maximum d_{50} was roughly 200 to 225 mm (coarse cobbles). The velocity that could transport a 225 mm particle with a flow depth of 10 feet is estimated to be 15 ft/second (Simon and Senturk, 1977).

The post-dam downcutting resulted in the exposure of coarse streambanks (Figure 3) and in cobble beds and bars throughout the Lower Elwha, as shown in Figure 4.

Figure 3 The coarse cobble bed materials on a bar and in the lower bank prior to breaching the dams.

Figure 4 Coarse bed material next to an ELJ prior to dam breach.

There was an estimated 18 million cubic yards of gravel, sand, and silt accumulated in the two reservoirs (NPS, 2015). There was a projected potential release of 13 million cubic yards after the dams were breached (Glines, 2014). Sediment from the dams was expected to move downstream in pulses associated high flows. The largest sediment pulse, or flux, would be expected to occur after the major draw-down of the Elwha Dam and partial draw-down of Glines Canyon Dam in 2011. For the 2011-2012 winter runoff, the maximum post-breach Q was 10,300 cfs.

Observations at the upper end of Glines Canyon Dam in October of 2013 indicated new deposition of coarse gravel with an average size of 25 mm. There were also some small gravel bars with an estimated d_{50} of 10 mm. However, most of the post reservoir deposition was sand.

Extensive sedimentation after the two dam breaches likely caused sediment intrusion into spawning gravels of the type pointed out by Reckendorf and Van Liew (1988), and Everett, Lotspeich, and Meeham (1982). These studies showed that even a small sediment supply in winter runoff of sand and silt particles caused sufficient packing of sediment intruded into the gravel above spawned eggs to reduce dissolved oxygen to lethal levels for salmonid egg survival. Streamflow under normal circumstances would have kept new redds saturated with dissolved oxygen as water is pushed through the open gravel.

DAM REMOVAL EFFECTS

The Elwha Ecosystem and Fisheries Restoration Act of 1992 authorized the Department of Interior to remove the dams beginning in 2009. Dam removal started in September of 2011. The Elwha Dam was fully removed by March of 2012. The Glines Canyon Dam was partially cut down from 220 to 60 feet by then, and was fully removed by the spring of 2014.

According to the Peninsula Daily News (Rice, 2011) the storm events on December 9 through 11, 2011, caused the flushing of 1.5 to 2.0 million cubic yards of sediment from Lake Mills above Glines Canyon Dam and Lake Aldwell above Elwha Dam. The newspaper reported that a three-storm event raised the peak flow on the Elwha River to 17,000 cfs. This caused extensive streambank erosion resulting in the loss of riparian trees along the river.

Sedimentation started large, new lateral and center bars, which appeared when the flow receded after the 2011-2012 runoff. During the 2012 event, a new first flat depositional surface developed at RM 2.5, at the upstream end of the evaluation reach. The top of the first flat depositional surface formed about 2.5 feet above the adjacent new lateral bars, which is shown in Figure 5, as observed in 2013. This new first flat depositional surface has been observed upstream as far as RM 12.8, at the Elwha River Bridge near Glines Canyon Dam. Figure 6 is an example of the consistent first flat depositional feature in the study area, and it occurs all the way downstream to the mouth of the river.

Figure 5 The top of the first flat depositional surface formed about 2.5 feet above the adjacent new lateral bars, as observed in 2013.

Figure 6 An example of the consistent first flat depositional feature in the study area. It occurs all the way to the mouth of the river at the Puget Sound.

A new flat depositional surface is apparent around ELJs such as shown in Figures 7. This new first flat depositional surface varies in height from 2.5 feet to 3.0 feet above the adjacent lateral bars. The first flat depositional surface is still growing from deposition that occurred during recent winter runoff.

The first flat sedimentation after the first dam flush (pulse) and the new bar deposition have essentially covered most of the coarse cobble channel and bars. The new first flat depositional surface extends right into ELJs such as shown in Figures 7 and 8, and has filled pools created by the ELJs.

Figure 7 A new flat depositional surface is apparent around an ELJ.

Figure 8 Another new flat depositional surface apparent around an ELJ.

The gravel that had previously been deposited above Glines Canyon Dam now has the opportunity to pass through the sites where the Glines Canyon and Elwha Dams once stood, and can now again provide gravel substrate to the lower reach of the ELJ study site. The size of the gravel that now reaches the channel area developed through the old Lake Mills has a d_{50} with a typical range between 10 to 25 mm.

Side channels along the Elwha River received extensive sedimentation essentially filling side channels. The falling stage of the post-breach hydrograph, with subsequent flood events, partially opened up new side channels. The side channels evaluated in 2013 had extensive new first flat depositional surfaces.

Deposition on the ELJs was observed to be as high as three feet above the first flat depositional surface on ELJ logs. This depositional surface is not continuous and reflects scour during subsequent breach flood flows. This likely occurred during the falling stage of post-breach events but could also have occurred in subsequent events. However, the post-scour effects have not transported the sediment out of the pools under the ELJs.

On the Lower Elwha, most of the pools, including pools under ELJs constructed between 1999 - 2011, filled with sediment during the 2011–2012 winter runoff. This occurred again during the 2012 – 2013 winter runoff, which filled the pools constructed in 2012. There are 49ELJs in the 2013 evaluation; whereas, there were 37 in the original study. From the thirty seven observed in 2007, three ELJs had washed out. Six ELJs were added in 2013 after the winter runoff of 2012 - 2013. Therefore, 37 ELJs could have been impacted by the sediment releases in 2011, 2012, and 2013.

Observations in October 2013 found that 35 of the 37 observed in 2007 were very shallow or non-existent such as those shown in Figure 7. There was essentially no summer refuge or adult holding pools for salmon under the 35 ELJs as the pools filled with sediment. Where the Elwha has been narrowed by opposing ELJs, identified as 10-1 and 10-2, scour has kept the pools under the two ELJs open for summer refugia.

As reported by the Peninsula Daily News (Rice, 2011) the large December 2011 runoff greatly impacted the water supply for the water intake for the Elwha Tribe Hatchery. The water intake for the City of Port Angeles was also significantly impacted by the sediment flux from the two dams.

CONCLUSIONS

After the two dams on the Elwha River had been constructed, there was extensive downcutting in the downstream reaches of the Lower Elwha River. Roughly three feet of river bed downcut to a coarse cobble surface with a rough d_{50} of 190 mm. There is post-dam sedimentation of small gravel with a rough d_{50} of 10 to 25 mm. Before the dam breaches, most locations on the Lower Elwha had a bi-modal distribution of average particle sizes. There was gravel with an average d_{50} of 50 mm associated with coarse cobbles with a d_{50} of 190 mm, and a maximum d_{50} of 225 mm.

The average flow velocity that could transport an average size of 225 mm is 15 feet per second (fps).

Such a flow velocity of 15 fps has probably not occurred in post-dam time, so the coarse cobbles likely represent a paleo-channel formed in Holocene or Late Pleistocene time. By comparison the average flow that would transport a d_{50} with an average size of 50 mm (pre-breach flow regime) would have a velocity of 8 fps. The post-dam flow sized particles could easily be transported by flood runoff in historic time.

The Elwha Rivers hydrologic regime has substantially changed because of the removal of the two dams. Extensive sedimentation created a new first flat depositional surface along many of the lateral bars that covered the coarse-cobble substrate. The sediment flux also created new lateral bars and greatly expanded center bars. The sediment pulses in the 2011-2012 and 2012-2013 events extensively filled the side channels, and they are gradually opening again.

ELJs that were installed along the Elwha starting in 1999 had their foundations in coarse cobbles, for the most part. This coarse-grained foundation adds to their stability. The post-dam sedimentation filled most of the pools under the ELJs constructed between 1999 – 2011, such that there is little summer refugia for salmon, especially adults. Two of the ELJs still have good pools that can be used for summer refugia. These two are opposite one another and have constricted the channel width such that there is increased shear stress on the channel bed and bank (which is the ELJ) so scour keeps the pools open. This would appear to be one solution to maintain pools under the ELJs in the future. The difficulty will be to keep the Elwha channel, which is presently wide, confined between ELJs.

Sedimentation is still occurring in the Lower Elwha, and sediment is being added to the first flat depositional surface, and to existing ELJS> Sedimentation is likely intruding into spawning gravel. It will likely constrain new spawning as long as large sediment loads get reworked down the channel with winter pulses of sediment.

The reworking of sand and fines sediment from the reservoir as well as that now deposioted on bars, will likely constrain being able to have clean flushing flows that sour out the polls under ELJs in the foreseeable future. This along with the sediment intrusion into spawning gravels ,from the excess sediment supply, will also constrain recovery of salmon populations for some time.

REFERENCES

Everett, F., Lotspeich, F., and Meehan, W. (1982). New perspectives on sampling, analysis, and interpretation of spawning gravel quality. In Armantrout, N. B. (ed.) Acquisition and Utilization of Aquatic Habitat Inventory Information, p 325-333. Western Division, American Fisheries Society, Portland, Oregon.

Glines, J. (2014) Environmental Monitor Newsletter, January 14, 2014.

McHenry, M., Pess, G., Abbe, T., Coe, H., Goldsmith, J., Liermann, M., McCoy, R., Morley, S., and Peters, R. (2007). “The physical and biological effects of engineered logjams (ELJs) in the Elwha River, Washington.”

Elwha River Engineering Logjam Monitoring Report for (1999 – 2006). Lower Elwha Klallam Tribe, Fisheries Department, Port Angeles, Washington, 82p.

National Park Service (2015). www.doi.gov. Last updated 1/04/15.

Reckendorf, F. (2010). Streambank erosion causes and large woody material solutions for streambank erosion and sediment reduction. 2nd Joint Federal Interagency Sedimentation Conference, Las Vegas, Nevada, June 27 – July 1, 2010. 12p.

Reckendorf, F. (2009). Causes of streambank erosion. Geological Society of America, Annual Meeting Abstracts. October 18 – 21, 2009, Portland, Oregon. Abstract no 22, p. 575.

Reckendorf, F. and Van Liew, M. (1988). Sampling of sediment intrusion into artificial redds in the Tucannon Watershed, Washington. Proceedings of the sixth Symposium on Coastal and Ocean Management Charleston, South Carolina, pages 964-978.

Rice, A. (2011). Storms bring massive amounts of Elwha river sediment downstream. www.Peninsuladailynews.com, Port Angeles, Washington.

Simon, D. and Senturk, F. (1977). Sediment Transport Technology. Water Resources Publications. Figure 9.8m

SANDBAR GROWTH AND DECAY ON THE MISSOURI RIVER DURING THE HIGH FLOWS OF 2010 AND THE HISTORIC 2011 FLOOD

Jake Gusman, P.E., Project Manager, WEST Consultants, San Diego, CA, jgusman@westconsultants.com; Vicki Tripolitis, EIT, Hydraulic Engineer, WEST Consultants, San Diego, CA, vtripolitis@westconsultants.com; Cameron Jenkins, P.E., Hydraulic Engineer, WEST Consultants, San Diego, CA, cameronj@westconsultants.com; Christopher Svendsen, P.E., Hydraulic Engineer, U.S. Army Corps of Engineers, Omaha District, Omaha, NE, christopher.j.svendsen@usace.army.mil; Daniel Pridal, P.E., Chief, Sedimentation and Channel Stabilization Section, U.S. Army Corps of Engineers, Omaha District, Omaha, NE, daniel.b.pridal@usace.army.mil

Abstract: The U.S. Army Corps of Engineers, Omaha District implements an Emergent Sandbar Habitat (ESH) construction program on the Missouri River to create nesting habitat for the interior least tern and piping plover bird populations. Beginning in August 2010, high flows prompted the Corps to initiate physical monitoring of six sites to document whether the flow level and duration were sufficient to create sandbars suitable for nesting. In 2011, a historic flood resulted in dam releases reaching 160,000 cfs, approximately a 0.2% annual chance exceedance (500-year) event. The monitoring period was extended to capture sandbar formation during this event and to document the subsequent degradation once the high water had receded.

Analysis of the data for the high flows of 2010 and 2011 yielded important insights regarding the sediment volume change at each site, total sandbar area, individual sandbar characteristics (wetted perimeter to area ratio, average side slope, average sandbar height, etc.), and the mechanisms for sandbar growth and decay. A two-dimensional, fixed-bed hydrodynamic model was constructed for one of the survey sites using the ADH (ADaptive Hydraulics Modeling System) program. Computed flow depth, velocity, and shear stress were analyzed during periods of sandbar growth and decay. For the highest flows, there was a zone with highly transient sandbars—a zone in which bed material was continuously moving, depositing, and eroding. These highly transient sandbars did not persist after the floodwaters receded. As expected, sandbars were more likely to persist in areas of reduced shear stress, velocity, and depth.

The location of the thalweg versus the location of major sandbars has a strong correlation to the sandbar decay rate. In periods when the thalweg was close to the major sandbars, the decay rate was significantly higher. As the thalweg moved away from the sandbars (e.g., toward one of the banklines), the decay rate was lower. Based on the survey data, wind erosion was not a significant factor in sandbar decay following the 2011 flood. The rate of sandbar erosion was directly related to sandbar area. Sites with the largest sandbars generally eroded at the highest rate. Finally, the sandbar area at each site was projected 10 years into the future based on observed sandbar growth/decay, thalweg location, and site characteristics.

INTRODUCTION

Emergent Sandbar Program: The U.S. Army Corps of Engineers, Omaha District implements an Emergent Sandbar Habitat (ESH) construction program to create nesting habitat (see Figure 1) for the interior least tern (*Sternula antillarum)* and piping plover (*Charadius melodus*) bird populations. In contrast to islands, sandbars are temporary formations and comparatively dynamic in nature that change dramatically in form and extent both within and among seasons. The ESH program was implemented based on the Amended Missouri River Biological Opinion (BiOp) issued in 2003 by the U.S. Fish and Wildlife Service. The BiOp provides the Corps with reasonable and prudent alternatives with respect to providing sufficient ESH acreage in order to support least tern and piping plover populations on the Missouri River. The BiOp also suggests that the flows from Gavins Point be used to create ESH. The Corps has not attempted to utilize flows for the creation of ESH. Instead, the Corps has relied on mechanical construction to augment ESH acres, but high water events occurring in 2010 and 2011 resulted in the natural formation of ESH.

Figure 1 Missouri River Sandbar Habitat

Recent High Flows and Sandbar Monitoring: Discharge from Gavins Point Dam exceeded 45,000 cubic feet per second (cfs) from late August through mid-December 2010 (see Figure 2)—the first instance of extended flows of this size since the ESH program began. Flow contributed by the James River (1960 RM 800) and Vermillion River (RM 772) increased this flow to greater than 50,000 cfs during this period, peaking at over 63,000 cfs on 4 August 2010. The Corps initiated physical monitoring of six sites to capture sandbar response to the large flows. The goal was to document whether the flow level and duration were sufficient to create sandbars suitable for nesting. In 2011, the historic flood resulted in dam releases reaching 160,000 cfs, approximately a 0.2% annual chance exceedance (500-year) event. The ESH

monitoring period was extended to capture the formation of sandbars during this event and to document the subsequent degradation once the high water had receded.

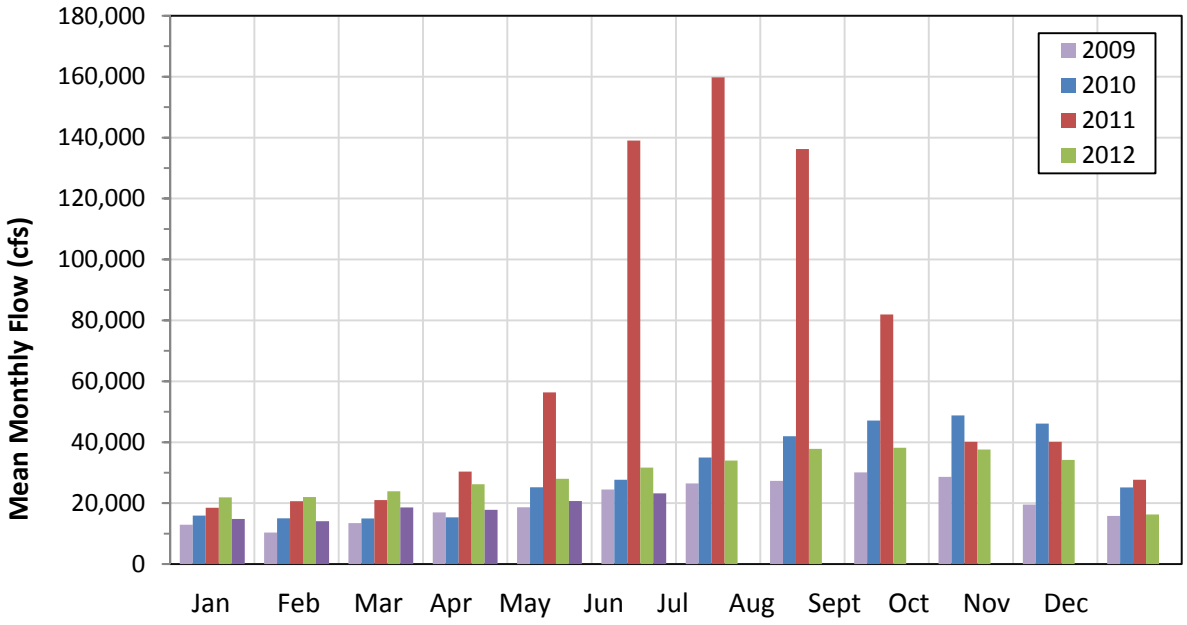

Figure 2 Gavins Point Dam Mean Monthly Flows

SEDIMENT VOLUME CHANGE

High-density hydrographic surveys, with an average of 10 cross sections per mile, were completed in 1995 and 2013. The high-density data sets were merged with LiDAR survey data of islands and overbanks to create elevation surfaces (see Figure 3 for an example). The difference between the two surfaces was then used to identify major changes in sediment volume. An elevation change over 15 feet was considered a major change. There are 45 locations with elevation differences over 15 feet with 33 of them based on erosion and 12 based on deposition (see Figure 4 for example). Most of the major erosive areas are locations where the river has encroached on its banks. However, some of these erosion areas are located further away from the banks.

Between 1995 and 2013, net erosion exceeded 55 million cubic yards within the study reach (approximate 1960 River Mile 753 to 810). The study reach was divided into six segments and only one (RM 790.3 to 800) showed net deposition (3.4 million cubic yards). The highest net erosion occurred in the most downstream segment (RM 753 to 763), totaling over 22.3 million cubic yards. Table 1 shows the volume change for all six segments.

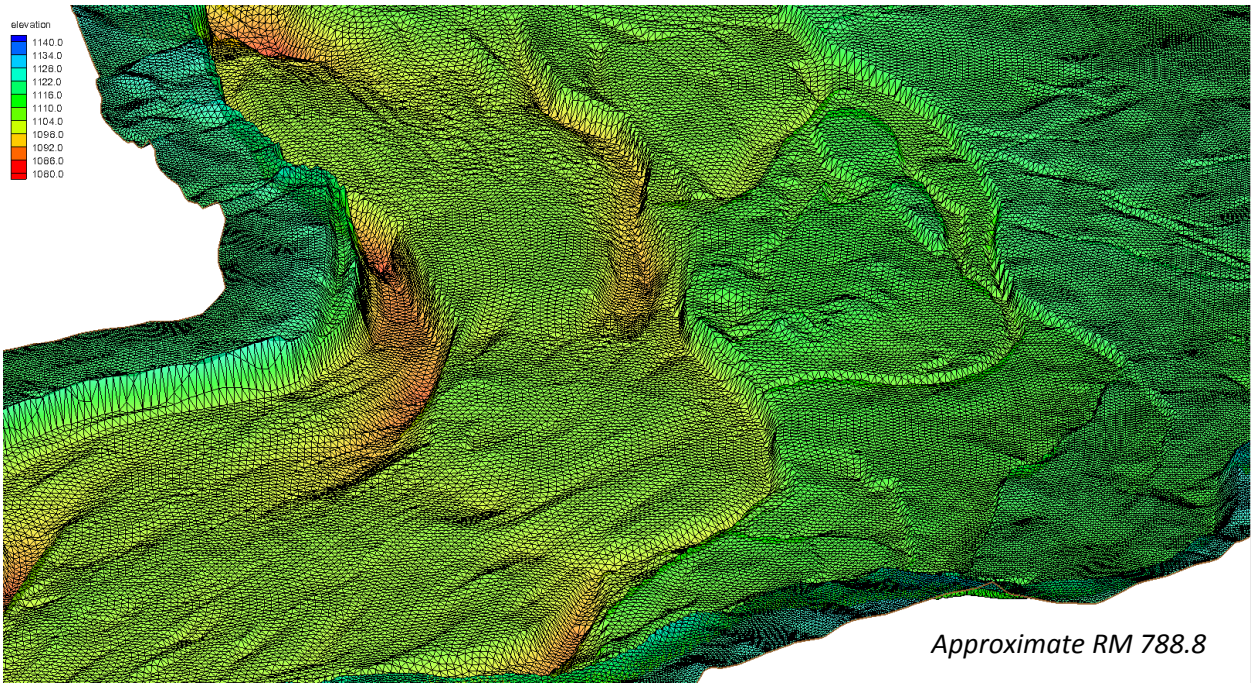

Figure 3 Example of a Finished Surface

Table 1 Volume Change (1995 to 2013) based on High-density Survey and LiDAR Data

Segment	Segment Boundary		Change in Volume (cubic yards)		
	Sediment Range	1960 RM[1]	Erosion[2]	Deposition	Total
1	783.6 – 793.9	753 – 763	(28,766,000)	6,397,000	(22,369,000)
2	793.9 – 804.2	763 – 771	(17,394,000)	10,206,000	(7,188,000)
3	804.2 – 814.7	771 – 780.5	(25,823,000)	11,867,000	(13,956,000)
4	814.7 – 824.1	780.5 – 790.3	(17,449,000)	7,661,000	(9,788,000)
5	824.1 – 834.5	790.3 – 800	(10,167,000)	13,539,000	3,372,000
6	834.5 – 845.1	800 – 810	(11,175,000)	5,950,000	(5,225,000)
Total	783.6 – 845.1	753 – 810	(110,774,000)	55,621,000	(55,153,000)

1. Approximate 1960 river mile location.
2. Values in parentheses represent negative numbers, i.e., areas of erosion; positive values are shown without parentheses and represent deposition.

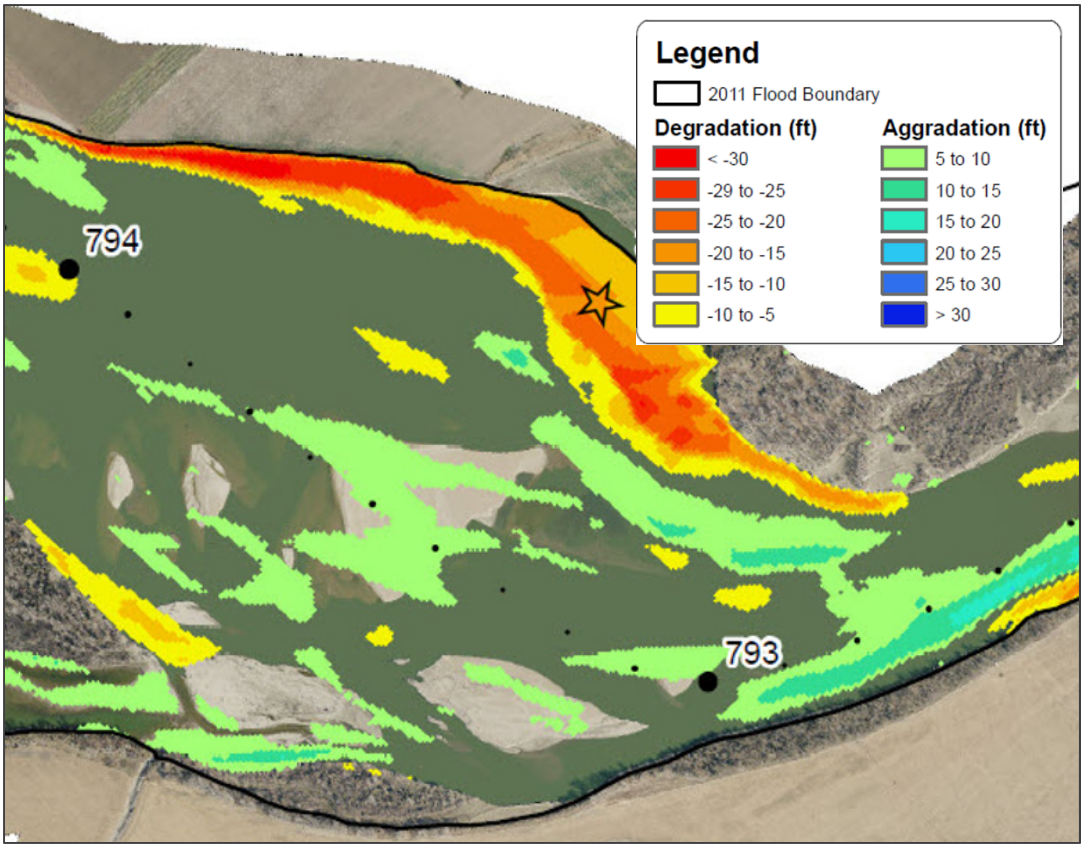

Figure 4 Example of Major Elevation Change (River Mile 793 to 794)

ESH SURVEY SANDBAR AREA ANALYSIS

Sandbar Survey Sites: The ESH surveys were conducted at approximate 1960 river miles 761, 770, 776, 782, 793, and 795, for sites ranging from a half mile to a mile in length (see Figure 5). The average width of the sandbar sites ranged from 2,759 feet (Site 761) to 4,100 feet (Site 770). The average site width was approximately 30 percent larger than the average width of the corresponding river segment. Most sites lie within fairly straight stretches or with slight bends in the channel. However, Site 776 is located near the apex of a sharp bend. Although Site 782 is located within a fairly straight section of the river, it differs from the other straight section sites because it is located just downstream of a large vegetated island that splits the channel flow. Sites 795 and 793 are within the same segment, and located only two miles apart.

In general, two surveys were performed per year in 2010, 2011, and 2012, with one survey in 2013. To evaluate the survey results, sandbar elevations and areas were analyzed at the 10-, 50-, and 90-percent exceedance flow levels (i.e., the flow level exceeded 90 percent of the time). To be considered a sandbar, a minimum area of one acre was required at the 90-percent flow level.

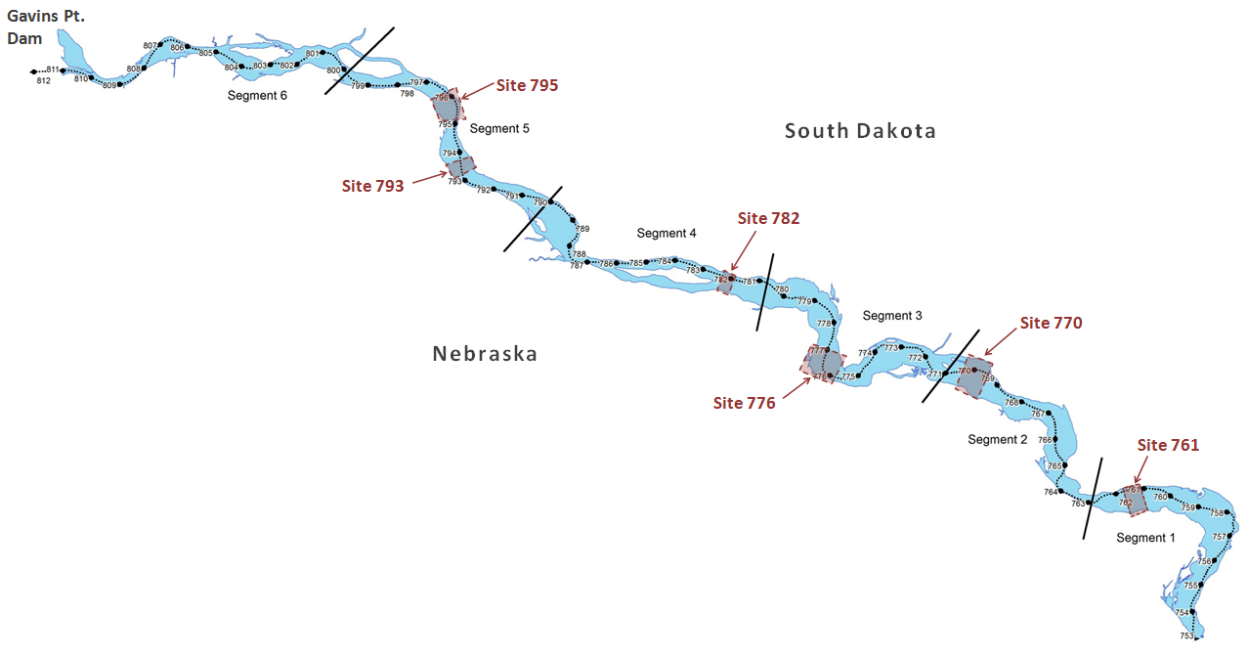

Figure 5 Missouri River ESH Sites and Study Extents

Total Sandbar Area: The total sandbar area was estimated at each study site for each season surveyed. These areas were then used to estimate the rates of growth and decay of the sandbars during the study period, and for use in projecting the rates of decay 10 years into the future.

Emergent sandbar habitat acreage is defined by USACE (2011) as all bare or sparsely vegetated sandbars available to terns and plovers. By definition, this encompasses new ESH (non-vegetated sandbars) as well as old ESH (sandbars that have aged and been subject to limited vegetation encroachment and erosion). Aged sandbars, however, should not be confused with islands that have woody riparian vegetation. Sandbars have only sparse plant cover and little or no woody vegetation. In the current study, islands were not considered ESH, and were not included in total sandbar area computations. In addition, point bars (formed on the inside of river bends) and shoreline deposition were not included in the total area. Figure 6 shows an example of what was included when determining total sandbar area.

All but two of the sites had the largest ESH area occur during summer 2011—Sites 761 and 776 had the largest ESH during fall 2011. Overall, the results show significant increases in ESH area (90-percent flow level) during the historic 2011 flood—from an average of 60.6 acres per mile in winter 2010 to 136.5 acres per mile in summer 2011 (see Table 2). ESH area ranged from 55.8 acres per mile (Site 776) to 223.5 acres per mile (Site 770) in summer 2011. At the 10- and 50-percent flow levels, average ESH went from 0.5 and 25.5 acres per mile in winter 2010 to 52.2 and 94.0 acres per mile, respectively, in summer 2011. After the historic flood, the average total sandbar area (90-percent flow level) decreased to 51.4 acres per mile by fall 2013 (20.0 and 44.4 acres per mile for the 10- and 50-percent flow levels).

Table 2 Average Total Sandbar Area per Mile

Season/ESH Level	Site Average (acres/mile)		
	10%	50%	90%
Fall 2010	0.5	15.6	63.5
Winter 2010	0.5	25.5	60.6
Summer 2011	52.2	94.0	136.5
Fall 2011	48.3	86.8	117.2
Spring 2012	35.5	66.6	85.7
Fall 2012	23.1	48.7	58.1
Fall 2013	20.0	44.4	51.4

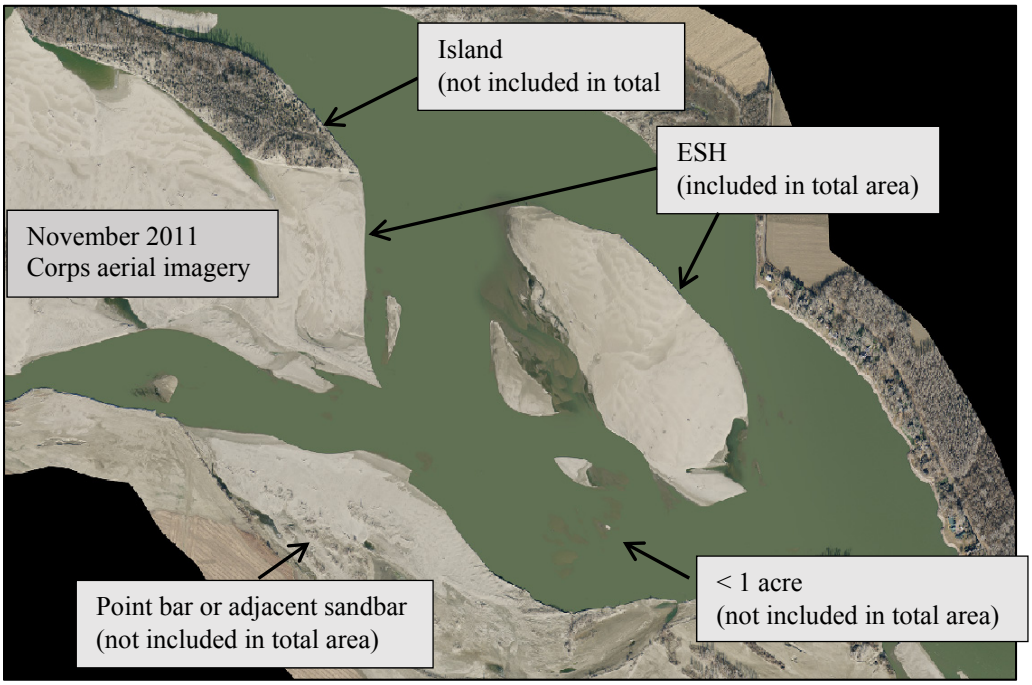

Figure 6 Example of Areas Included and Not Included in Total ESH Area

Sandbar Characteristics: In winter 2010, the average size of an individual sandbar (90% flow level) ranged from 2.2 acres at Site 782 to 31.9 acres at Site 795. The average sandbar size was 14.1 acres across all sites. In fall 2011, the average size of an individual sandbar (90% flow level) ranged from 14.6 acres at Site 782 to 78.6 acres at Site 776. The average sandbar size was 37.2 acres across all sites. Overall, the habitat formed during the 2011 flood was much larger in total area compared to the ESH formed in winter 2010. Although the total area at each site was greater in fall 2011, there were more sandbars in winter 2010 (25 versus 17 across all sites).

Wetted perimeter to area ratios (90% flow level) ranged from 369 feet per acre (Site 793) to 1,119 feet per acre (Site 782) in winter 2010. In fall 2011, sandbars were much larger. As a result, the wetted perimeter-to-area ratios were much lower overall, ranging from 146 feet per acre (Site 776) to 298 feet per acre (Site 793). The average sandbar height above the 90% flow

level was 1.1 feet in winter 2010 (ranging from 0.7 to 1.4 feet). The average height increased to 3.3 feet by fall 2011 (ranging from 2.1 to 4.3 feet). In winter 2010, the average sandbar slope was 1.4 percent. By fall 2011, it had increased to 2.0 percent.

Geomorphic and Bed Material Impacts: Thalweg depths and movement were analyzed at the 50-percent flow level (see Figure 7 for an example). The average thalweg generally deepened due to the high flows of 2010, as well as between summer and fall 2011. Thalweg movement varied between sites. For some sites, there was only minor change between seasons, while other sites experienced significant movement from season to season. The average bed material size (D_{50}) did not change significantly during the 2011 flood, indicating that the riverbed is largely homogeneous and the sandbar sites are not bed material limited.

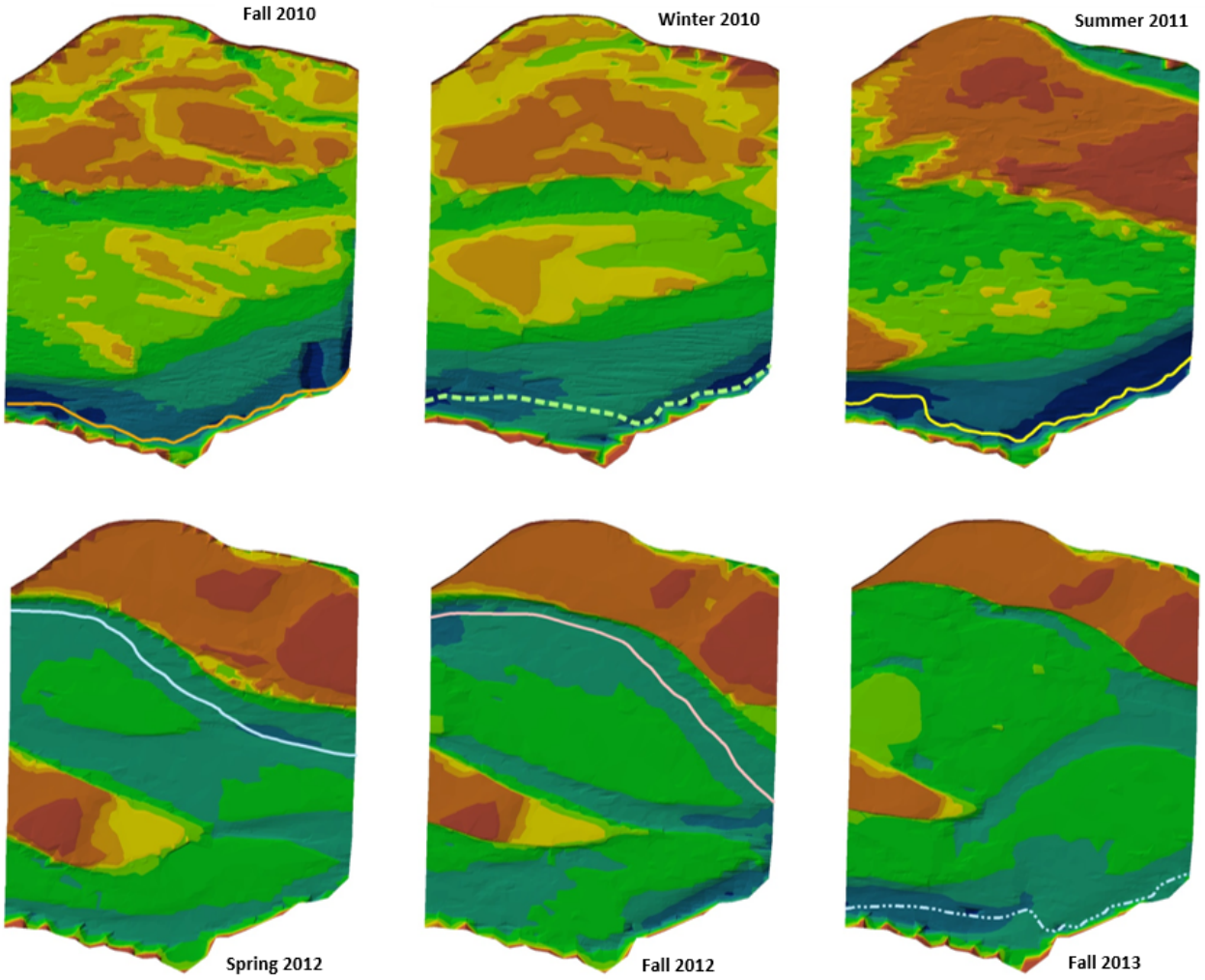

Figure 7 Thalweg Locations for Each Season Surveyed – Site 761

Sandbar Growth and Decay: A major question in the 2003 BiOp Amendment is whether a flow of 60,000 cfs for 60 days will produce sandbars within the study reach. Although the study data do not provide a definitive answer to this question, some observations can be made. The high releases from Gavins Point Dam in 2010 were on the order of 45,000 cfs. Tributary flows, particularly from the James River (RM 800), helped to increase the total flow through the project reach during the fall 2010 survey period. Flows peaked above 63,000 cfs on 4 August 2010, exceeding 50,000 cfs through mid-August and from the beginning of September through mid-November. Although these flows were much higher than normal flows, they were too small to create significant ESH area. In contrast, the 2011 flows were much higher than 60,000 cfs, and greatly increased ESH area.

Every significant sandbar-building flood event affects future building events. If the 60,000 cfs flow would have occurred in 2010 for a longer duration, it may have created more significant sandbar habitat. The current remaining sandbars were formed by large flows and many remain above the 10-percent flow level. If the 60,000 cfs flow occurred today, it may not act as a building event because it could erode the existing high-elevation sandbars rather than form new sandbars.

Relative shear stress over a sandbar and/or adjacent to a sandbar is a good indicator of whether the sandbar would be eroded away by the time of the next survey. Typically, initiation of particle movement is modeled with the Shields method. Inversely, low shear stresses indicate depositional areas. Using this approach and assuming a 0.4 mm median particle size, deposition is assumed to occur for shear stresses of approximately 0.005 lb/ft^2 or lower, under normal flow conditions. This appears to be appropriate for determining sandbar persistence for the lower flow periods, but not necessarily for the higher flows.

The location of the thalweg versus the location of major sandbars has a strong correlation to the sandbar decay rate. In periods when the thalweg was close to the major sandbar(s), the decay rate was significantly higher. As the thalweg moved away from the sandbars (e.g., toward one of the banklines), the decay rate was lower. Based on the survey data, wind erosion was not a significant factor in sandbar decay following the 2011 flood.

The study also examined correlations between sandbar growth and two-dimensional hydraulic model results at Site 795 (see Figure 8 for an example of the results). For the highest flows, there was a zone with highly transient sandbars. Surveyed sandbars within this zone represent snapshots in time, with bed material that is continuously moving, depositing, and eroding. The highly transient sandbars did not persist after the floodwaters receded. As expected, sandbars were more likely to persist in areas of reduced shear stress, velocity, and depth.

There was an average flow depth of 3.0 feet above the sandbars created between fall and winter 2010. This depth increased to 12.5 feet for sandbar area formed between summer and fall 2011. The rate of sandbar erosion following the 2011 flood was directly related to sandbar area. Sites with the largest sandbars generally eroded the quickest (based on the percent decrease in area between fall 2011 and spring 2012).

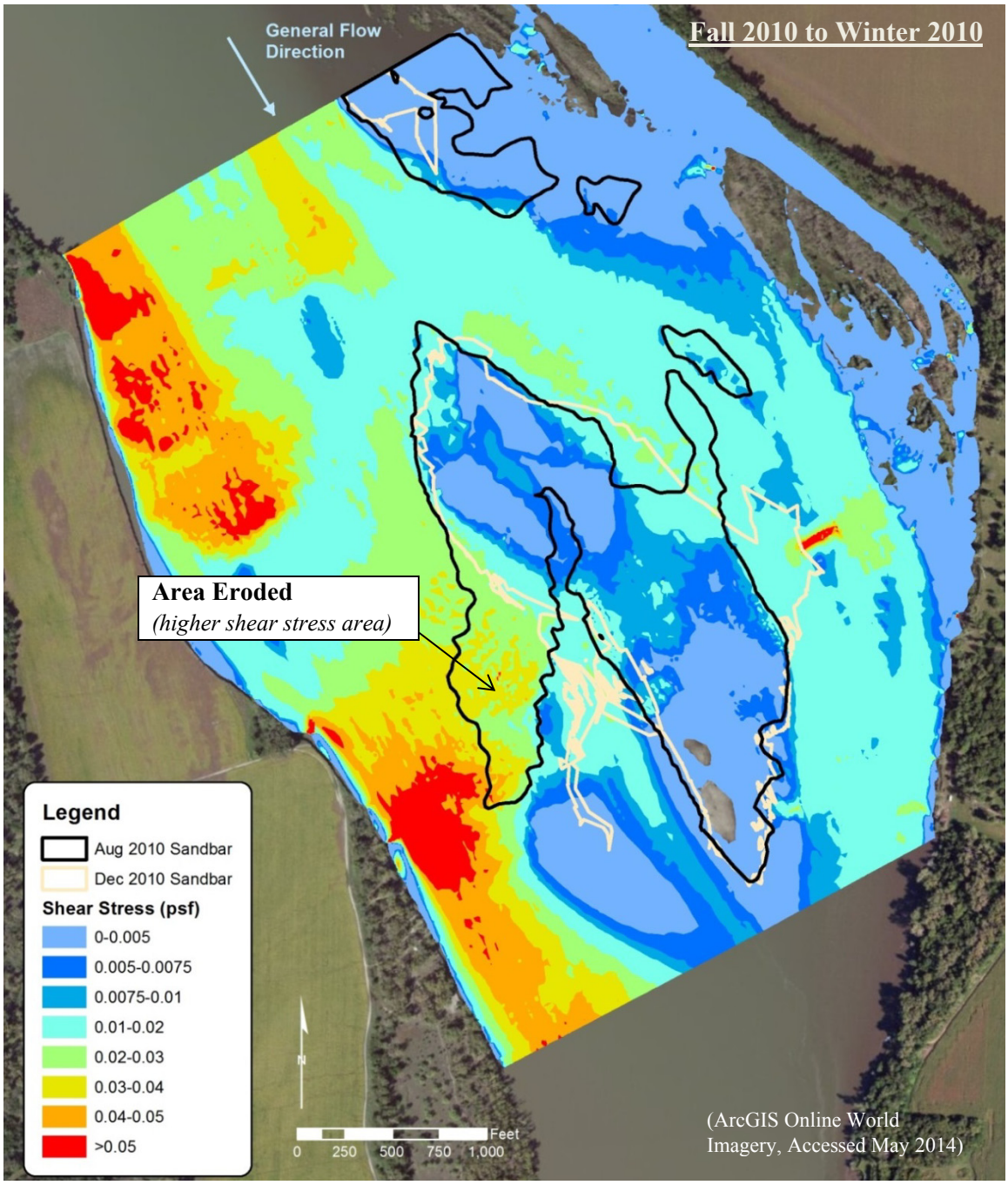

Figure 8 Computed Shear Stress (Fall 2010 at 52,000 cfs) – Sandbar Decay

Sandbar formation is a dynamic sediment transport process. Figure 9 compares the 90-percent sandbars at Site 795 for all survey periods. This figure shows where the sandbars are highly transient versus areas where the sandbars are relatively persistent. The surveyed sandbars, especially within the highly transient zone, represent snapshots in time of bed material that is continuously moving, depositing, and eroding. Moreover, these highly transient sandbars did not persist after the floodwaters receded. As expected, sandbars are more likely to persist in areas of reduced shear stress, velocity, and depth.

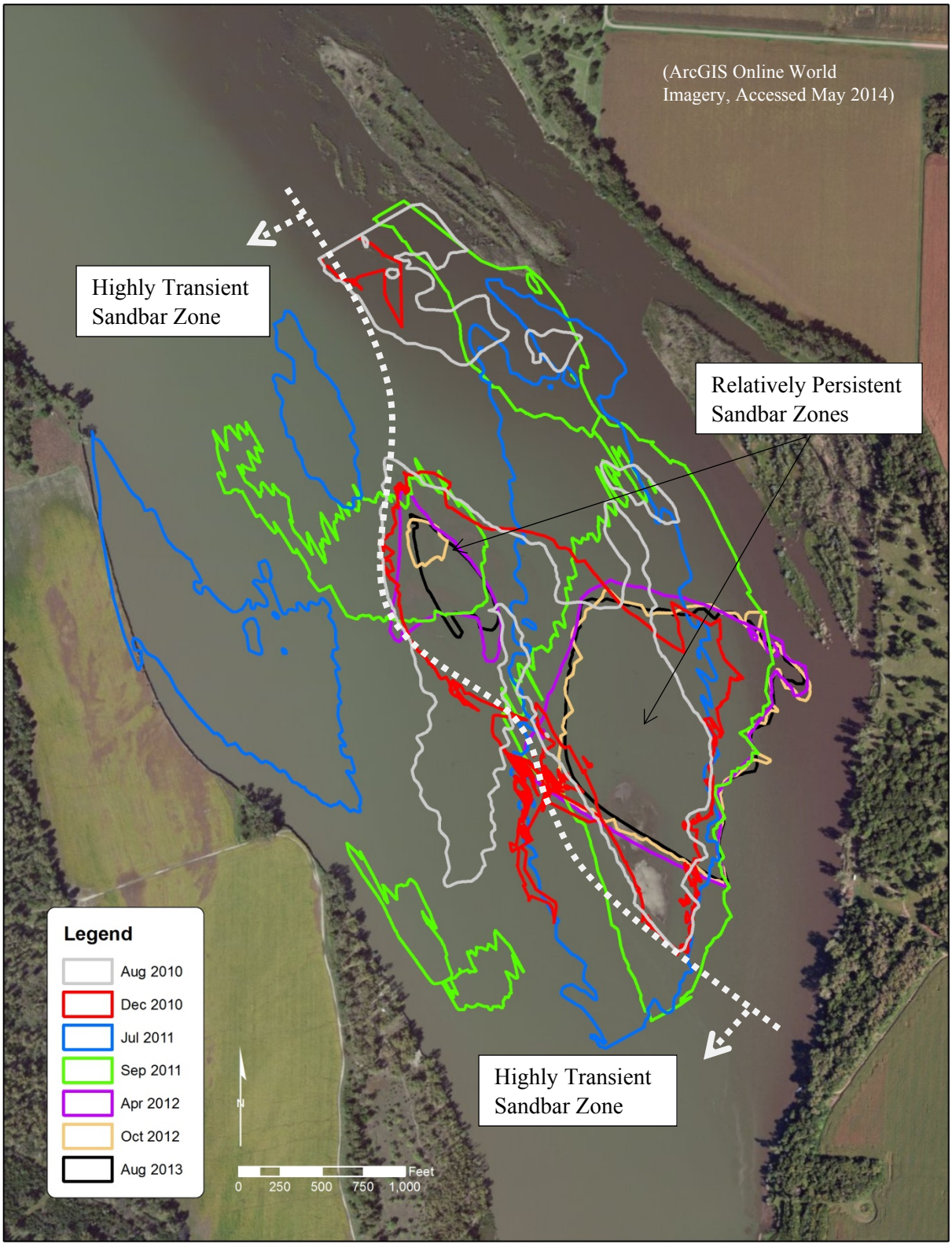

Figure 9 Sandbars (90% flow level) at Site 795 – All Survey Periods

Sandbar Area Projections: The total sandbar area at each site was projected 10 years into the future (see Figure 10 for an example) based on the observed sandbar growth/decay, thalweg location, site characteristics, and engineering judgment. In particular, the variability of the thalweg and its most recent surveyed location were strongly correlated to the sandbar projections. Projected decay of the 90-percent flow level sandbar area was the greatest at Site 770 and the least at sites 793 and 795. The location of the thalweg during the study period, as well as the overall site width, had a direct impact on the sandbar projections. For comparison, USACE (2011) indicates that the projected life expectancy of a constructed sandbar is 5 to 10 years. This is dependent on rates of erosion and vegetation encroachment, as well as flows and potential ice jams or thalweg shifts. The lifespan of a sandbar may be extended through maintenance activities such as vegetation removal and reshaping.

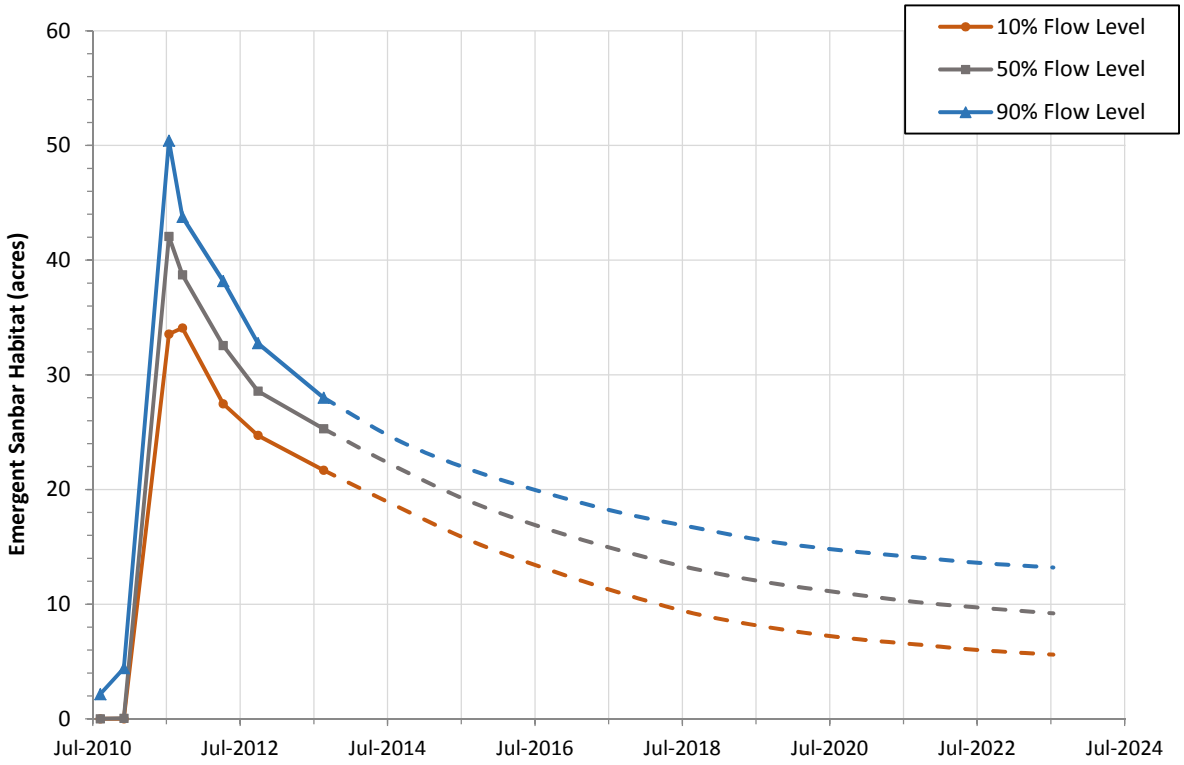

Figure 10 Projected Rates of ESH Growth/Decay – Site 782

REFERENCES

USACE (2011). *Final Programmatic Environmental Impact Statement for the Mechanical and Artificial Creation and Maintenance of Emergent Sandbar Habitat in the Riverine Segments of the Upper Missouri River*. Volume 1: Final Programmatic Environmental Impact Statement.

WEST Consultants (2014). *Geomorphic Change Evaluation in Support of ESH, Final Report*, prepared for the U.S. Army Corps of Engineers, Omaha District, July 2014.

SAN JOAQUIN RIVER SPAWNING HABITAT SUITABILITY STUDY

Elaina Gordon, Hydraulic Engineer, US Bureau of Reclamation, Denver, CO,
egordon@usbr.gov, (303)445-2550
Blair Greimann, Hydraulic Engineer, US Bureau of Reclamation, Denver, CO,
bgreimann@usbr.gov, (303)445-2563

Abstract: The availability of quality spawning habitat within the San Joaquin River downstream of Friant Dam (Reach 1A) is crucial for successful reintroduction and sustained population of Chinook salmon. Several uncertainties exist as to the suitability of existing spawning habitat within Reach 1A and how sediment transport may affect efforts aimed at improving spawning and incubation habitat. Multiple studies are currently underway or have been completed to help identify the quality of the hyporheic environment as it relates to successful spawning and fry emergence, including evaluations of water quality within the hyporheic zone (DO, water temperature, fine sediment accumulation), egg survival, mesohabitat, bed material size and mobility, scour and deposition, and channel morphology changes associated with alteration to the flow regime. In addition, bedload and suspended load monitoring have been conducted within the reach since 2010.

Critical to identification of potential spawning areas are the bed material and hydraulic conditions within the reach during probable spawning periods of spring-run and fall-run Chinook salmon. This current study combines bed material characterization efforts with two-dimensional hydraulic modeling results to identify areas considered potentially suitable spawning habitat based upon depth and velocity requirements. The suitability of the potential spawning habitat is evaluated with GIS parameterization of substrate and hydraulic conditions, and correlation of surveyed redds, substrate, and hydraulic conditions are examined and quantified.

INTRODUCTION

The San Joaquin River Restoration Program (SJRRP) aims to "restore and maintain fish populations in good condition in the main stem of the San Joaquin River below Friant Dam to the confluence of the Merced River, including naturally-reproducing and self-sustaining populations of salmon and other fish." The SJRRP Fisheries Management Plan identifies spawning and incubation as a life stage to be supported for successful completion of the salmon life cycle.

SJRRP's current understanding of the system is that sufficient availability and quality of spawning habitat within Reach 1A of the San Joaquin River is imperative to sustaining a population of Chinook salmon (*Oncorhynchus tshawytscha*). Multiple studies are currently underway or have been completed to help identify the quality of the surface water and hyporheic environments as they relate to successful spawning and fry emergence (current efforts summarized in Section 3.2 of 2014 Monitoring and Analysis Plan; SJRRP, 2013a). These include efforts to evaluate water quality within the hyporheic zone (DO [Reclamation, 2012a], water temperature effects [Reclamation, 2012a], fine sediment accumulation [SJRRP, 2010a; SJRRP, 2013b]), egg survival (SJRRP, 2012), mesohabitat characterization (SJRRP, 2010b), spawning habitat use by transported fall-run Chinook (SJRRP, 2011; SJRRP, 2013c), bed material size and mobility (Tetra Tech, 2012a,b; SJRRP, 2012; SJRRP, 2013d), scour and deposition (SJRRP, 2011), and channel morphology changes associated with alteration to the flow regime (SJRRP, 2011; SJRRP, 2012; SJRRP, 2013e). In addition, bedload and suspended load monitoring have been conducted within the reach since 2010 (Graham, Mathews & Associates, 2012; Reclamation, 2014a). Most recently, spatial characterization of hydraulic conditions within Reach 1A was completed through two-dimensional hydraulic modeling across a wide range of flows (Reclamation, 2014b), and continuous facies mapping of the bed material was completed within the low-flow channel (SJRRP, 2014b).

The purpose of this current study is to initially characterize potential spawning locations within Reach1A of the San Joaquin River from Friant Dam to Highway 99 (HW99) based upon suitable hydraulics, bed material, and surface water temperature (figure 1). These potential areas will then analyzed for patterns of correlation and compared with mapped spawning redds within the reach over the past 2 years. This effort is part of a larger study to characterize suitability of spawning and incubation habitat based on physical, biological, and chemical criteria.

POTENTIAL SPAWNING HABITAT QUANTITY

Requirements for spawning Chinook salmon evaluated in this initial assessment of potential spawning habitat area include hydraulic conditions, substrate, and surface water temperature. Multiple other aspects of spawning habitat quality may impact where a fish chooses to spawn and are only briefly discussed within this paper. However, we recognize the importance of many additional variables influencing spawning habitat quality and ultimately on the incubation habitat provided for successful emergence. These are anticipated to be incorporated into future analyses.

With respect to hydraulic conditions for spawning Chinook, water depth must be sufficient to cover the fish during spawning, and velocity must be adequate to flush finer particles downstream during the process of red construction, but not so great that eggs do not remain in the egg pocket or adults have to expend too much energy holding position in the water column (SJRRP, 2014a). The SJJRP Spawning and Incubation Subgroup reviewed habitat suitability indices (HSI) from studies on the Tuolumne, Stanislaus (Aceituno, 1990, 1993), and Merced (Gard, 1997) Rivers (all tributaries to the San Joaquin River) and suggested the criteria for suitable spawning depths for the San Joaquin River to be between 0.7 and 3.7 feet (ft) and velocities between 0.8 and 3.4 ft/s. These values correspond to the criteria from the Stanislaus River and encompass the ranges for all three rivers, thereby providing the greatest flexibility for evaluation on the San Joaquin River.

Chinook salmon generally select larger substrate to spawn in than other Pacific salmon species. Suitable spawning gravel consists of a mixture of particle sizes from sands to cobbles, with a median diameter (D50) of 2.5 to 5 cm (SJRRP, 2010c). A review of reported spawning substrate in Central Valley System suggests that the preferred substrate size ranges between 2.5 and 10 cm in diameter, and some studies indicate spawning in substrate up to 30 cm in diameter (SJRRP, 2010c). Substrate requirements for spawning are highly correlated to fish size with large fish capable of using larger substrate materials than small fish (SJRRP, 2014a) to build a redd. Moir and Pasternack (2010) found that Chinook often utilize coarser substrate when higher velocities are present. Fine sediment within the system has a large influence on the incubation habitat once the eggs are laid (Tappel and Bjornn, 1983). However, the presence and influence of fine sediment on egg survival is a topic currently under investigation, the results of which will be incorporated into future designation of suitable incubation habitat.

Chinook salmon have specific water temperature requirements before and during spawning in order to survive and deposit their eggs (SJRRP, 2014a). Surface water temperatures for successful spawning and incubation are illustrated in table 1. The critical temperature range defines the range over which a fish shows definite signs of thermal stress (Elliot, 1981).

Table 1 Temperature Requirements for Spawning and Incubation (from SJRRP, 2010).

	Spawning	**Incubation and Emergence**
Optimal	≤ 57 °F (13.9 °C)	≤ 55 °F (13 °C)
Critical	60-62.9 °F (15.6-17°C)	58-60 °F (14.4-15.6°C)
Lethal	≥62.6 °F (17 °C)	≥62.6 °F (17 °C)

Two-dimensional Hydraulic Modeling: Two-dimensional hydraulic models of Reach 1A of the San Joaquin River were developed and calibrated using SRH-2D (Reclamation, 2008) to spatially characterize hydraulic conditions throughout the reach as a tool for predicting the availability of spawning habitat (Reclamation, 2014b). For computational efficiency, the reach was modeled in two sections: the first is from Friant Dam (Mile Post (MP) 267) downstream to Highway 41 (HW41) Bridge (MP 255) and is referred to as Reach1A_01, and the second extends from HW41 downstream to Highway 99 (HW99) Bridge (MP 243) and is referred to as Reach1A_02.

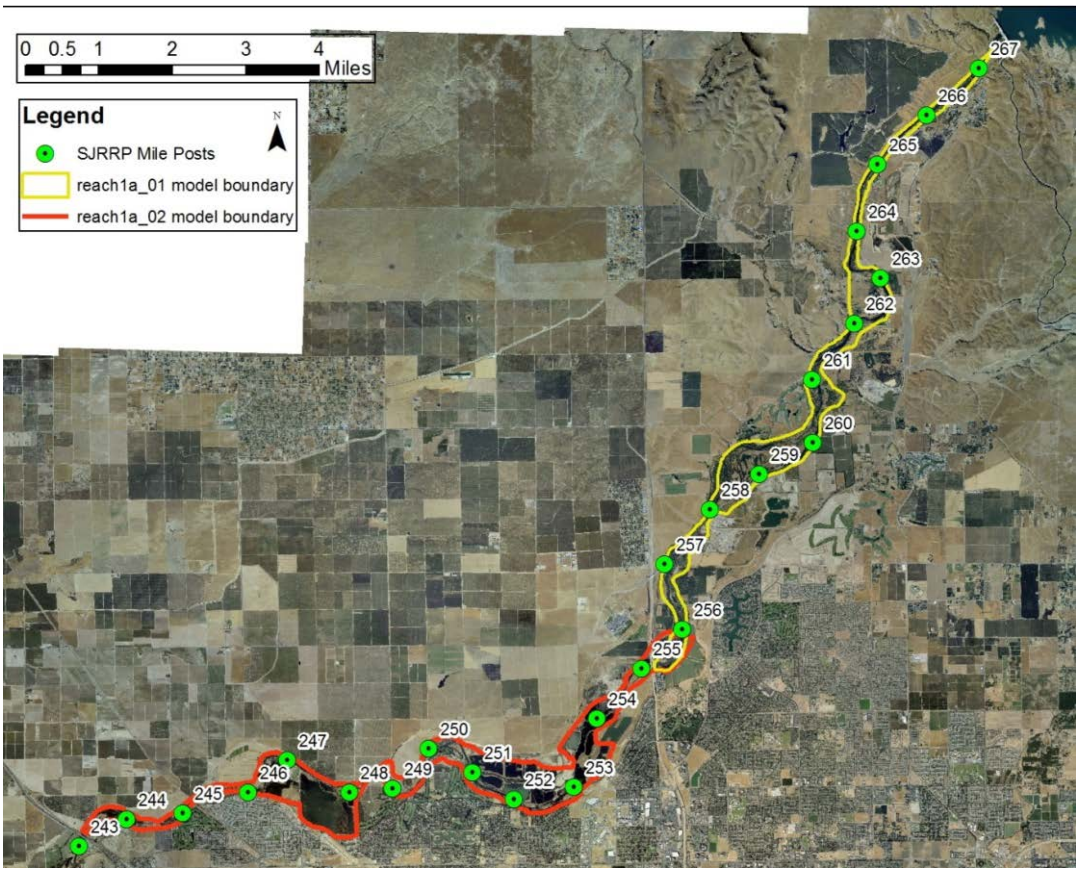

Figure 1 Map of modeled reaches. Reach 1A_01 extends from Friant Dam (MP 267.5 to HW41 (MP 255) and Reach 1A_02 extends from HW41 (MP 255) to HW99 (MP 243) for a total reach length of 24.5 river miles.

The mesh for each subreach generally consisted of rectangular cells to represent the main channel and most side channels and triangular cells to represent the floodplain. Within the channel, rectangular cell sizes ranged between 5-10 ft laterally and 20-30 ft longitudinally. The final grids were comprised of approximately 117,000 cells within the Reach 1A_01 model and 138,000 cells within the Reach 1A_02 model. Terrain data for Reach 1A are a compilation of ground-based survey points and photogrammetry collected in 1998, combined with in-channel bathymetry collected by boat using SONAR in 2009. The final topographic models for each subreach were created in State Plane CA III, NAVD88 ft. Flows modeled to date were based upon the availability of calibration data and range from 270 cfs to 7,650 cfs. Rating curves developed from measured flows and water surface elevations at HW 41 and HW 99 served as the downstream boundary conditions for each model.

Hydraulic roughness (Manning's *n*) is defined at each cell in a computational mesh. Initial roughness values were delineated based on zones of vegetation density and land use from 2007 aerial photographs (MEI, 2000; DWR, 2010). Roughness zones were modified in some areas to better reflect current conditions based upon 2011 aerial photos and to improve calibration with initial model results. Final computational meshes for model Reach 1A_01 and Reach 1A_02 consist of 8 roughness categories (table 2).

Model calibration was conducted for both subreaches using available water surface elevation and flow measurements. In-channel calibration was performed first to define roughness within the channel, and then a subsequent calibration effort was conducted to define roughness within the floodplain. Calibration was performed by varying roughness in model simulations to determine the best match to measured water surface elevations (table 2). The goal of the model calibration was to predict water surface elevations with a root mean squared error (RMSE) of less than 0.5 ft.

Table 2 Calibrated roughness values for SRH-2D hydraulic simulations.

Land Use Type	**Reach1A_01**	**Reach1A_02**
Channel Bed	0.04	0.04
Off-Channel Open Water	0.04	0.045
In-channel Riffles/Rough areas	0.065	0.065
Open /Bare Ground/ Scattered Brush	0.045	0.068
Scattered Trees	0.06	0.09
Medium Density Trees/Brush	0.08	0.12
Dense Trees/ Brush	0.1	0.15
Agriculture	0.045	0.055

Depth and velocity data were processed for 350 cfs in each reach to determine areas meeting spawning habitat hydraulic criteria. This discharge was selected as representative of the flow present during Spring-run and Fall-run Chinook spawning based upon the flow release schedule from Friant Dam into Reach 1A as specified in the Stipulation of Settlement (NRDC v. Rodgers, 2006). The spawning habitat hydraulic criteria were provided by the San Joaquin River Spawning and Incubation Subgroup and represent the depth and velocity ranges considered suitable on the Stanislaus River. Areas meeting the criteria for depths ranging between 0.7 and 3.7 feet and velocities ranging between 0.8 and 3.4 ft/s were delineated as polygons within GIS and determined as potentially suitable for spawning based on hydraulic conditions.

Bed Material Characterization: Bed material sampling has been conducted throughout Reach 1A of the San Joaquin River numerous times over the last 20 years using multiple sampling techniques to meet a variety of project goals. To most efficiently evaluate bed material for spawning habitat, a spatially continuous map of bed material was necessary. Facies maps provide an opportunity to capture spatial variability of the sediment comprising a channel bed through delineation of boundaries between notably different areas of bed material. Facies mapping was initially completed within Reach 1A in 2002, but only encompassed the first 12.3 miles downstream from Friant Dam (Stillwater Sciences, 2003), and several locations may have experienced local areas of change within the last 10 years. As such, during the summer of 2013, an effort was undertaken to update and expand upon the initial facies mapping to reflect current conditions of the river bed and to help characterize areas with suitable bed material for Chinook spawning.

In both the 2002 and 2013 mapping efforts, the Buffington and Montgomery (1999) mapping technique was adapted with slight variations between the two years. This is a hierarchical classification system of each facies according to the three most prevalent gain classes (i.e. silt, sand, gravel, cobble, and boulder) and sub-divided according to a classification based on phi-size class (very fine, fine, medium, coarse, very coarse). For example, 'sandy gravel' indicates that the most prevalent grain class is gravel but there are significant amounts of sand. Facies mapping was conducted by floating the river by kayak, delineating areas of bed material change, and visually identifying the facies classification. Simultaneously, pebble counts were performed in areas where no previous volumetric or pebble count samples had been collected. The maps and all sediment data were transferred to GIS.

An analysis was completed to associate a range of gradations with each facies category based upon pebble count data collected over the last 20 years. However, the results indicated that the pebble count data alone were not sufficient to differentiate between the coarse-scale facies categories. In addition, the pebble count data alone were incapable of differentiating between spawnable and non-spawnable facies categories because the resulting range of gradations for each facies where pebble counts were performed covered the preferred range of diameters for spawning. In other words, the results suggested that every facies category with one or multiple pebble counts contained suitable substrate for spawning. Another complication was that many facies categories, such as those over bedrock or in silt, contained no pebble count data.

Surface Water Temperature: The SJRRP has determined that water temperature is likely a limiting factor for each life history stage of Chinook salmon in the San Joaquin River, particularly in the warmest and driest years

(CDFW, 2012). As part of the SJRRP, a water temperature monitoring system was developed to better understand the longitudinal distribution of water temperature and aid in successful management of flow releases during critical salmon life-stages. With respect to salmon spawning, surface water temperature is a key factor influencing adult salmon behavior and survival during late summer and fall (August through December). Twenty water temperature monitoring locations are present within Reach 1 to help identify the spatial distribution of the potential spawning areas based upon known temperature limitations for Chinook salmon. Data collected at these sites within the last several years suggest that in general, the closer the site is to Friant Dam, the more suitable the water temperatures are during the critical spawning period. In 2011 it was observed that the closer the site was to the dam, the greater the number of days temperatures were below critical (14.4 ℃) and lethal (15.6 ℃) temperature thresholds for spawning and incubation; however, due to releases from the dam (>13℃) being greater than the optimal temperature (13℃) and cooler air temperature in late fall, more days met optimal temperature conditions further downstream than just below the dam (figure 2).

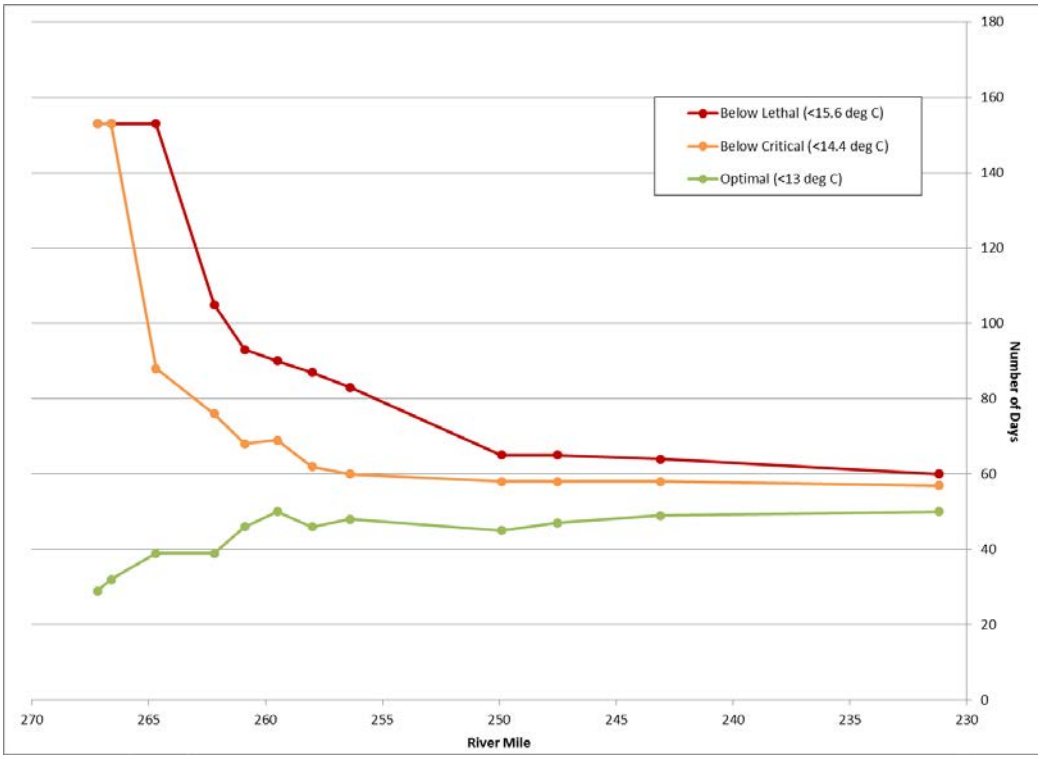

Figure 2 Number of days during expected spawning and incubation period (August through December, 2011) that water temperature was below objectives for incubation and emergence (SJRRP, 2010c).

Spring-run Chinook historically spawned in the San Joaquin River between late August and October, and Fall-run Chinook still spawn within tributaries to the San Joaquin River from October through December, peaking in early to mid-November. Based on this timing, water temperature monitoring indicates that Fall-run Chinook may not be limited by surface water temperatures during spawning within Reach 1A (figure 3). However, Spring-run spawning may be restricted to the first 10 miles downstream from Friant Dam.

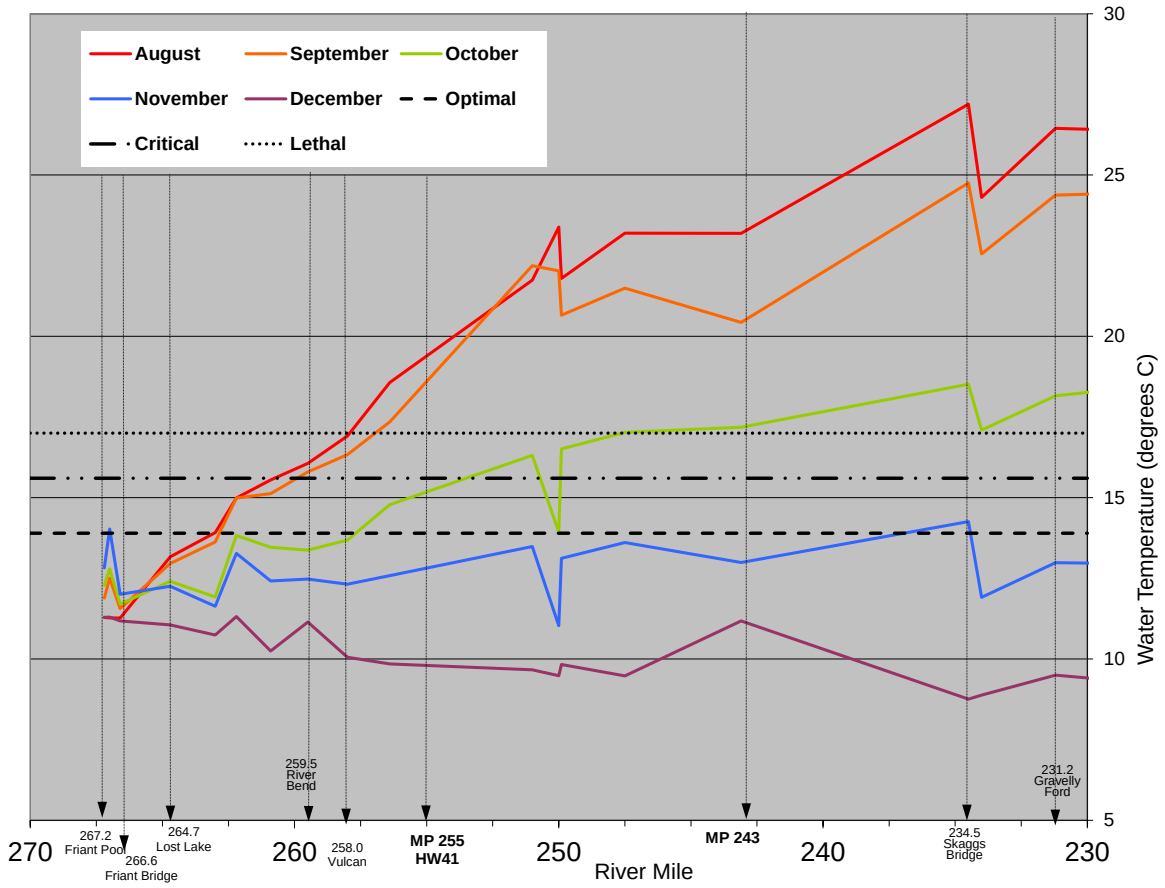

Figure 3 Monthly average stream temperatures for the period of record along with the optimal, critical, and lethal temperature ranges for spawning. The period of record differs slightly for each gage and therefore some points may represent longer time frames than others.

RESULTS OF ANALYSIS

The total modeled area encompassed over 12,000 acres (ac) (table 3). At a discharge of 350 cfs, 1,090 ac of the channel were inundated with depths greater than 0.1 feet. However, only 80 ac were determined to be potentially suitable for spawning based upon hydraulic conditions (0.7 to 3.7 ft depth and 0.8 and 3.4 ft/s velocities), indicating that only 7.4% of the total inundated area was determined to be suitable for spawning based upon hydraulic conditions alone. Inundated areas and areas of suitable hydraulic conditions were also compared with facies mapping to determine the existence of correlations between hydraulics and substrate. An example illustration of the delineation of mapped features is shown in figure 4. Inundated areas with facies designations were evaluated by dominant substrate type (figure 5). The majority of inundated area (excluding gravel pits, side channels, overbank areas, and channel margins) was comprised of sand (59%), while gravel and cobble represented a combined 36% of inundated area. The area deemed suitable based upon hydraulic conditions within each dominant substrate type is depicted in figure 6. Hydraulically suitable conditions were most common in gravel and cobble-dominated substrate, representing a total of 78% of the area (58.3 acres) identified as suitable. Twenty percent of the area with suitable hydraulic conditions was within substrate dominated by sand based upon the facies mapping.

Table 3 Modeled and inundated areas based on two-dimensional modeling results compared with the area meeting the depth and velocity criteria for spawning for each reach and also combined. Results presented are in acres.

	Area (Acres)		
	Reach1A_01	**Reach 1A_02**	**Total Combined**
Modeled Area	5,375	6,627	12,002
Inundated Area	293	797	1,090
Area Meeting Depth and Velocity Criteria for Spawning	44	36	80

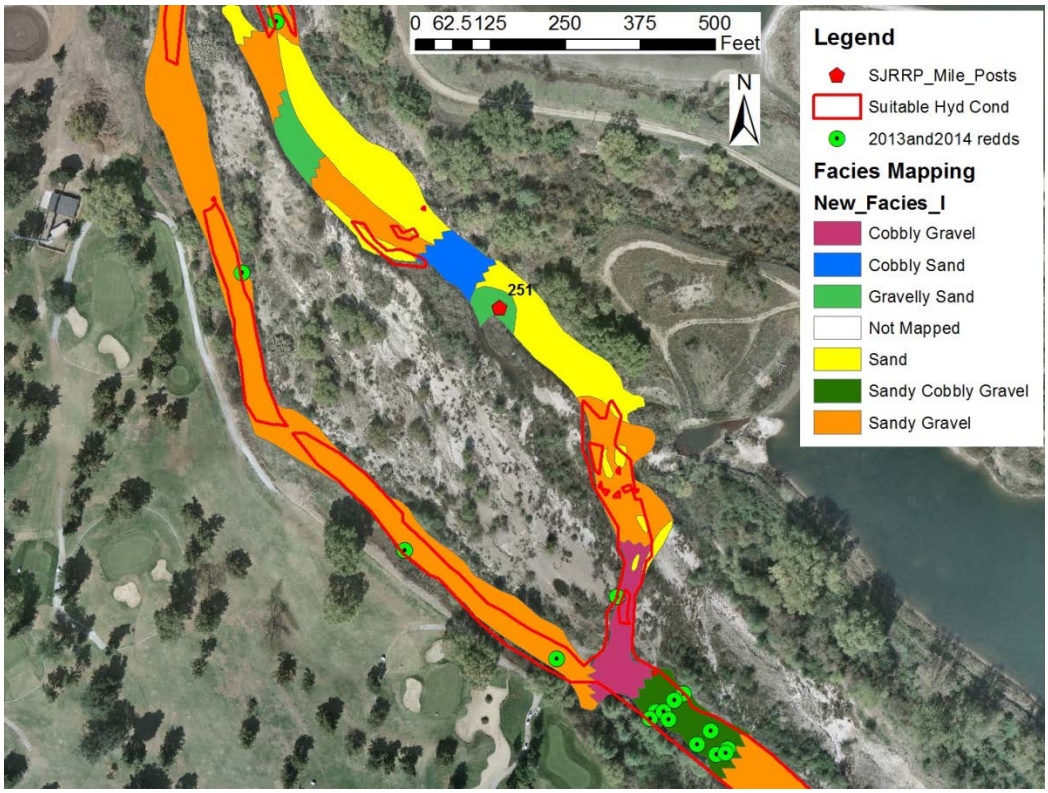

Figure 4 Example map of the delineation of redd locations, suitable hydraulic condition polygons, and facies categories near MP 251.

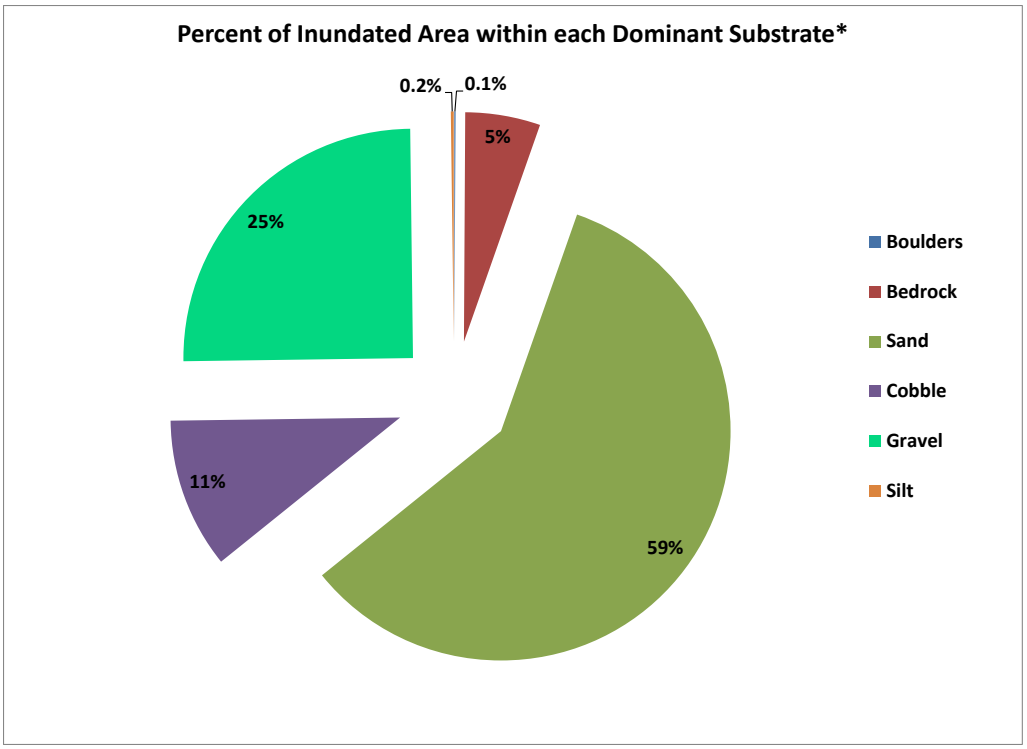

Figure 5 Percent of inundated area within each dominant substrate. *This analysis excludes inundated areas that did not have facies characterization, such as gravel pits, side channels, and channel margins.

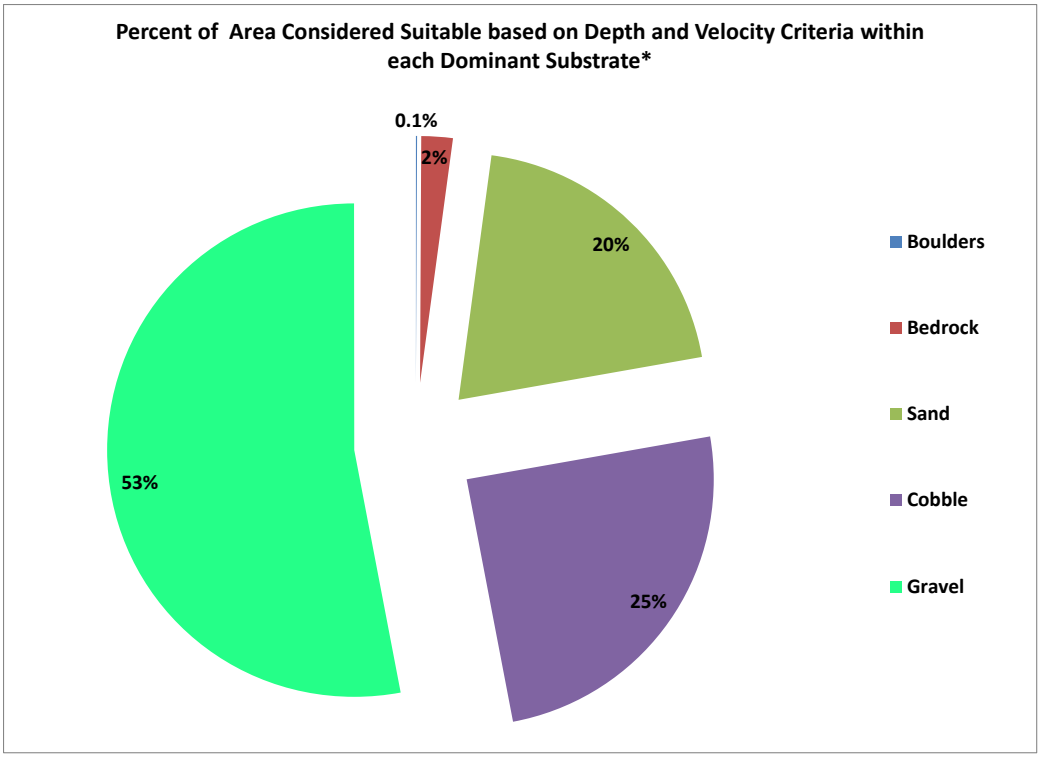

Figure 6 Percent of area with suitable hydraulic conditions within each dominant substrate type. *This analysis excludes suitable areas that did not overlap with facies characterizations, such as those in side channels and along channel margins.

There were 130 redds surveyed within the reach between Friant Dam and HW99 (figure 1) during 2013 and 2014 combined. There were an additional 22 redds surveyed just at or downstream from HW99 that were not included in the analysis because they were not located within the longitudinal extent of the mapped facies and two-dimensional modeling boundary. An analysis was done to identify which type of substrate the fish selected to spawn in based upon the facies mapping. The distribution of spawning within dominant substrate is shown in figure 7. Ten of the 130 redds were located outside of the mapped facies areas in areas identified as islands or channel margins above the low flow channel. Of the remaining 120 redds, the salmon overwhelmingly selected to spawn in facies with a gravel- (84 redds, 70%) or cobble-dominated (23 redds, 19%) substrate. However, several still chose to spawn in facies mapped as being dominated by sand or bedrock. This could be due to the presence of patches of gravel and cobble within larger generalized areas of mapped substrate.

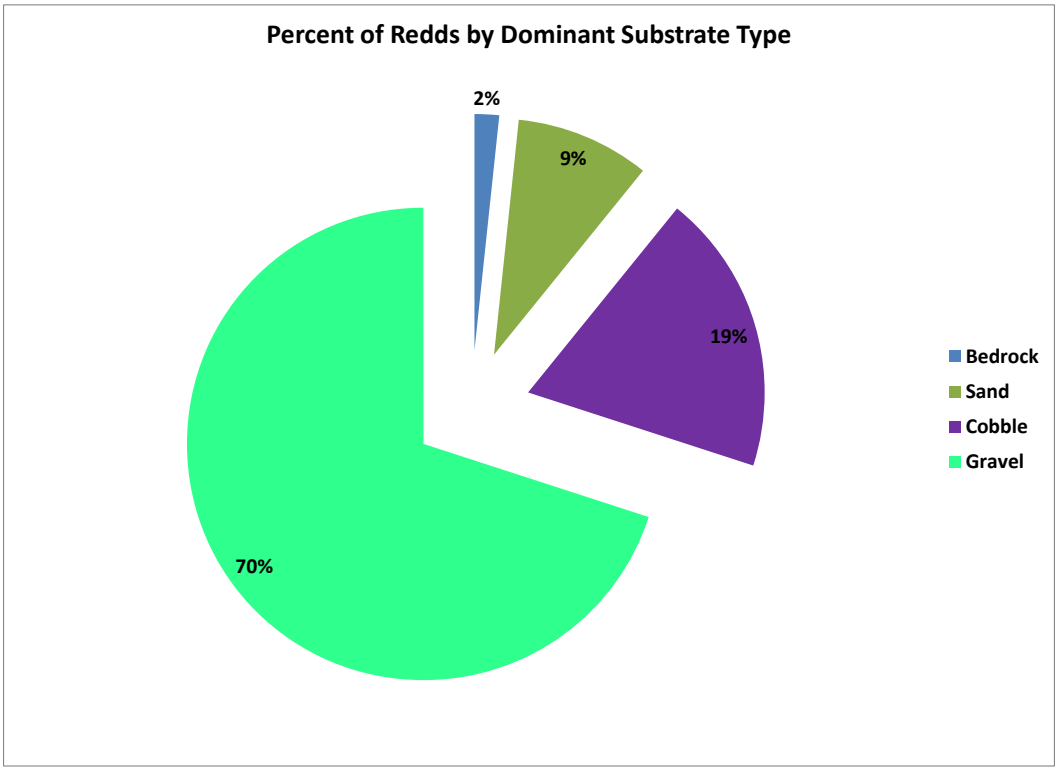

Figure 7 Percent of the occurrence of redds by dominant substrate type out of 120 redds.

Of the 130 redds within the reach, 96 of them (74%) were located within an area with suitable hydraulic conditions based upon two-dimensional modeling results; 123 (95%) were located within 15 feet of an area with suitable hydraulic conditions. It should be recalled that the numerical model grid within the channel was typically comprised of quadrilaterals ranging in size between 5-10 ft by 20-30 ft.

An investigation was completed to determine the association between those 96 redds within suitable hydraulic conditions and the dominant substrate type. Three of the redds were not located in a mapped facies as they were all constructed at the very edge of the low flow channel boundary. The results show little variation from the results of all 130 redds illustrated in figure 7, which is expected because most all the redds were located within the area defined as hydraulically suitable. A final statistical evaluation was performed using Jacob's electivity analysis to determine the preference of salmon to place redds within each dominant substrate type and within hydraulically suitable areas. Jacob's index was measured using the following formula:

$$D = (r - p)/(r + p - 2rp)$$

Where r represents the proportion of habitat used; p represents the proportion of habitat available, and D varies from -1 to 1, indicating a degree of preference for each habitat type (Hamann et al., 2014). A value of -1 indicates strong avoidance; a value of +1 indicates strong preference, and values approaching 0 suggest that the habitat is used in

proportion to its availability in the environment. The results and interpretation of the analysis are presented in table 4 and table 5.

Table 4 Results of electivity analysis indicating the degree of association of redds with hydraulic conditions.

	Jacob's Index	Interpretation
Hydraulically Suitable Area	0.9	Strong Preference
Non-hydraulically Suitable Area	-0.9	Strong Avoidance

Table 5 Results of electivity analysis indicating the degree of association of redds with dominant substrate type.

Dominant Substrate	Jacob's Index in total inundated area with mapped facies	Jacob's Index in hydraulically suitable area	Jacob's Index in non-hydraulically suitable area	Interpretation
Boulders	-1.0	-1.0	-1.0	Strong Avoidance
Bedrock	-0.5	-0.7	-0.2	Avoidance
Sand	-0.9	-0.9	-0.9	Strong Avoidance
Cobble	0.3	0.4	0.2	Mild Preference
Gravel	0.7	0.7	0.8	Preference
Silt	-1.0	-1.0	-1.0	Strong Avoidance
Cobble and Gravel	0.9	0.9	0.9	Strong Preference

CONCLUSIONS

Results of this effort provide supportive evidence for characterizing spawning habitat using hydraulic information gained from two-dimensional modeling and from substrate characterization. Based upon the hydraulic modeling effort, only 7.4% of the total inundated area was determined to be suitable for spawning. However, 74% of the redds surveyed within the last 2 years were located within these areas, and 95% were within 15 feet of these areas. These data suggest a strong correlation between the hydraulic conditions determined to be suitable for spawning using depth and velocity and between locations selected by salmon for redd construction. The results may also indicate that the current grid resolution captures the preferred spawning locations to within +/- 15 feet because the cell sizes within the channel were typically 5-10 ft wide by 20-30 ft long to limit model simulation time. A refined model at select locations may assist in further refining localized spawning preferences. However, the results also point towards the possible use of a buffer zone of approximately 15 feet around areas deemed suitable when a coarser-scale model is necessary to capture long reaches.

Redd data analyses reveal that salmon tend to spawn in gravel and cobble more frequently than other substrate. However, some fish selected to spawn in facies dominated by sand substrate. This may be partially attributed to the detail of the facies mapping. A benefit of the facies mapping is the ability to map long reaches of channel within a relatively short time frame. Patches of gravel and cobble are often present along channel margins or locally within the channel and may not be captured in the facies mapping. Refined mapping within mapped facies dominated by sands may improve the correlation between large substrate and redd construction location. Another possible explanation may be that salmon are less concerned with substrate than other factors when searching for a location to spawn, and the substrate is more important to defining incubation habitat and egg survival. Data from this effort could be used to develop preference curves for substrate for spawning salmon, in which sand and boulder substrate receive lower values than cobble and gravel substrates.

Examination of the dominant substrate within areas determined to be suitable for spawning based upon hydraulic conditions shows that even though gravel and cobble only represent a combined 36% of the total inundated area with mapped facies, 78% of the suitable hydraulic conditions are within gravel- and cobble- dominated substrate.

Similarly, the 96 redds within suitable hydraulic conditions were located in gravel- and cobble-dominated substrate 89% of the time. These data along with Jacob's electivity analysis results demonstrate a strong preference for redd sites to be located in suitable hydraulic conditions and in gravel- and cobble- dominated substrates. Clear correlations exists between substrate and suitable conditions for spawning, between redd sites and hydraulically suitable conditions, and between redd sites and gravel- and cobble-dominated substrate. From a common understanding of physical processes with the respect to the influence of hydraulic conditions on sediment transport and resultant substrate, the data from this exercise suggest that both hydraulic conditions and substrate are important in redd sites selection.

Finally, water temperature was also reviewed in this study to evaluate how it may limit the area considered suitable for spawning. Results suggest that water temperature may not limit spawning for Fall-run Chinook in most years because the temperatures, while not optimal, are below lethal in October, November, and December from Friant Dam downstream to HW 99 (~MP 243). However, the water temperatures may limit Spring-run Chinook spawning to the first 10 miles downstream from Friant Dam. These first 10 miles of the entire 24.5 mile reach encompasses 36.2 acres of suitable spawning habitat based upon depth and velocity, which represents 45% of the total suitable spawning area within Reach 1A.

STUDY DIRECTION

This current study presents a small fraction of the analysis necessary to eventually define the availability and quality of spawning and incubation habitat within Reach 1A. However, this step is important in determining that two-dimensional modeling results and substrate can indeed be used to help quantify available suitable spawning habitat. Additional analyses are planned to determine the applicability of mesohabitat maps in delineating potentially suitable spawning habitat. In addition to the reach-scale two-dimensional hydraulic modeling, finer-scale modeling of several riffles within Reach 1A is planned to identify the sensitivity of model results to refined topographic information and mesh resolution.

The quality of spawning and incubation habitat will be further distinguished through incorporation of findings from studies characterizing the hyporheic environment (DO, toxicity, temperature), vegetation and cover mapping, sediment mobility, substrate permeability, fine sediment accumulation within redds, egg survival, and escapement. One of the greatest challenges anticipated from this effort is the extrapolation of localized findings within one or several redds or riffle to the entire Reach 1A.

The ultimate goal of the larger-scale endeavor is the capability to predict the quantity and location of habitat meeting the needs of Chinook salmon to successfully complete their life cycle through spawning and incubation. Once the abundance or scarcity of suitable spawning and incubation habitat is determined based upon the anticipated fish use of the system, the limiting factors can be identified, and any means necessary to improve those conditions and the locations in need of improvement will be definable.

ACKNOWLEDGEMENTS

The authors of the paper express gratitude to all SJRRP members for their efforts in collecting and analyzing data related to spawning and incubation habitat that was used for this study. Erica Meyers was responsible for maintaining and evaluating the water temperature data as it relates to spawning and incubation, and Andy Shriver significantly contributed to the collection and GIS translation of the facies characterization. We are grateful to the SJRRP for continuing to support spawning habitat investigations, and appreciate the continued input by members of the Spawning and Incubation Subgroup.

REFERENCES

Aceituno, M. (1990). Habitat Preference Criteria for Fall-run Chinook Salmon Holding, Spawning, and Rearing in the Stanislaus River, California, U.S. Fish and Wildlife Service, Fish and Wildlife Enhancement, 27pp.

Aceituno, M. (1993). The Relationship between Instream Flow and Physical Habitat Availability for Chinook Salmon in The Stanislaus River, California, U.S. Fish and Wildlife Service, Sacramento, CA.

Buffington, J. M., and D. R. Montgomery (1999), A Procedure for classifying textural facies in gravel-bed rivers, Water Resour. Res., 35(6), 1903–1914

California Department of Fish and Wildlife (CDFW; 2012). San Joaquin River Restoration Program Stream Temperature Monitoring Study Water Year 2012 Annual Report.

California Department of Water Resources (DWR; 2010) DRAFT Two-dimensional hydraulic model of the San Joaquin River: Reach 1A, March 2010.

Elliott, J.M. (1981). Some aspects of thermal stress on freshwater teleosts. Chapter 10, in A.D. Pickering, ed. Fish and Stress. Freshwater Biological Association. Cumbria, England. Academic Press, London.

Gard, M. (1997). Technique for adjusting spawning depth habitat utilization curves for salmon, US Fish and Wildlife Service, Rivers 6(2):94-102.

Graham Matthews and Associates (2011). "San Joaquin near Ledger Island Water Year 2011 Bedload Sampling, Technical Memorandum dated June 13,2011. In Appendix D Sediment of 2011 Final Annual Technical Report San Joaquin River Restoration Program.

Hamann, E.J., Kennnedy, B.P., Whited, D.C, and J.A. Stanford (2014). Spatial variability in spawning habitat selection by Chinook salmon (*Oncorhynchus Tshawytscha*) in a wilderness river. River Res.Applic. 30:1099-1109.

MEI (2000). Hydraulic and Sediment Continuity Modeling of the San Joaquin River from Friant Dam to Mendota Dam, California.

Moir, H. J. and Pasternack, G. B. (2010). Substrate requirements of spawning Chinook salmon (Oncorhynchus tshawytscha) are dependent on local channel hydraulics. River Research and Applications 26:456-468.

NRDC v. Rodgers et al. (2006). Notice of Lodgment of Stipulation of Settlement, United States District Court, Eastern District of California, Sacramento Division, filed 09/13/2006.

Reclamation (2008). SRH-2D version 2: Theory and User's Manual, Sedimentation and River Hydraulics Group, Technical Service Center, Denver, CO. November, 2008.

Reclamation (2012a). Hyporheic water quality and salmonid egg survival in the San Joaquin River. Technical Memorandum No. 86-68220-12-03. Prepared for the San Joaquin River Restoration Project, Mid-Pacific Region, US Bureau of Reclamation.

Reclamation (2012b). Hydraulic Studies for Fish Habitat Analysis. Technical Report No. SRH-2012-15. Prepared for San Joaquin River Restoration Project, Mid-Pacific Region, US Bureau of Reclamation, Technical Service Center, Denver, CO.

Reclamation (2014a). Sediment Budget Analysis of the San Joaquin River for Water Years 2010 through 2012, Technical Report No. SRH-2015-18. Prepared for San Joaquin River Restoration Program, Mid-Pacific Region.

Reclamation (2014b). Two-dimensional modeling of Reach 1A of the San Joaquin River between Friant Dam and Highway 99. Technical Report No. SRH-2014-14, Prepared for the San Joaquin River Restoration Program, Mid-Pacific Region.

SJRRP (2010a). Final 2011 Agency Plan, Appendix A. November 2010.

SJRRP (2010b). Draft Annual Technical Report, Appendix G, Meso-Habitat Surveys. March 2010.

SJRRP (2010c). Fisheries Management Plan.

SJRRP (2011). Final 2011 Annual Technical Report. Appendix A. May, 2012.

SJRRP (2012). 2012 Mid-Year Technical Report, July 2012.

SJRRP (2013a). Final 2014 Monitoring and Analysis Plan. November 2013.

SJRRP (2013b). Artificial Redd Fine Sediment Accumulation Study, 2012 Final ATR Summary. Available online: http://restoresjr.net/flows/data-reporting/index.html

SJRRP (2013c). Fall-run Captive Rearing Study Update. February 2013. Available online: http://restoresjr.net/flows/data-reporting/index.html

SJRRP (2013d). Draft SJRRP Sediment Gradation Atlas - 1995 to 2012, version 2. July, 2013.

SJRRP (2013e). Effect of Altered Flow Regime on Channel Morphology in Reach 1A. August 2013.

SJRRP (2014a). 2014 Monitoring and Analysis Plan.

SJRRP (2014b). Draft 2013 Facies Mapping Geodatabase from Friant Dam to Highway 99. Last updated October 10, 2014.

Stillwater Sciences (2003). Draft Restoration Strategies for the San Joaquin River. Prepared by Stillwater Sciences, Berkeley, California for Natural Resources Defense Council, San Francisco, California and Friant Water Users Authority, Lindsay, California.

Tappel, Paul D. and Bjornn, Ted C. (1983). A new method of relating size of spawning gravel to salmonid embryo survival. North American Journal of Fisheries Management 3: 123-135.

TetraTech (2012a). San Joaquin River: Evaluation of sand supply, storage, and transport in reaches 1A and 1B.

TetraTech (2012b). 2011 San Joaquin River Sand Storage Evaluation.

EARLY WARNINGS AND LONG-TERM CHANGES: APPLICATION OF CONTINUOUS TURBIDITY MONITORING TO PROTECT AN ENDANGERED FISH SPECIES DURING CONSTRUCTION OF A LARGE-SCALE FLOOD-REDUCTION EFFORT

John D. Jastram, Hydrologist, US Geological Survey, Richmond, VA, jdjastra@usgs.gov;
Douglas L. Moyer, Hydrologist, US Geological Survey, Richmond, VA, dlmoyer@usgs.gov;
Kenneth E. Hyer, Hydrologist, US Geological Survey, Richmond, VA, kenhyer@usgs.gov

Flooding of the Roanoke River has caused substantial damage in the City of Roanoke, Virginia, over the past century. With over $1 billion worth of property at risk from potential flood damage, the City of Roanoke partnered with the U.S. Army Corps of Engineers (USACE) to construct the Roanoke River Flood Reduction Project (RRFRP) in an effort to reduce flooding impacts within the City. Construction of the RRFRP was complicated by concern that construction-related increases in sediment transport would potentially harm the endangered Roanoke logperch (*Percina rex*).

In early 2005, approximately coincident with the beginning of RRFRP construction, the U.S. Geological Survey (USGS) Virginia Water Science Center (VAWSC) partnered with the USACE to initiate a monitoring program using continuous turbidity monitoring stations and suspended-sediment sampling to assess changes in sediment transport through the affected reach and to provide a real-time warning system for potential impacts from sediment releases on logperch habitat. Specifically, the objectives were to:

a) Detect short- term changes in suspended-sediment transport during construction of the RRFRP in near real-time; and to
b) Assess spatial and temporal trends in suspended-sediment transport in the affected section of the Roanoke River.

This suspended-sediment monitoring program was conducted in synchrony with complementary monitoring programs focused on assessing geomorphological change and logperch community structure during construction of the RRFRP. These complementary programs were conducted by the VAWSC and the USGS Virginia Cooperative Fish and Wildlife Research Unit at Virginia Polytechnic and State University, respectively.

Continuous turbidity monitors were deployed at multiple locations along the construction reach for various time periods. These deployments were located, spatially and temporally, such that active construction reaches were closely bracketed with a monitor near the upstream and downstream extents of active construction to monitor flow into and out of the active construction reach – construction reaches were limited to 4,000 linear feet, progressing upstream. Continuous turbidity monitors also were deployed at the upstream and downstream extent of the RRFRP for the duration of the RRFRP, and suspended-sediment sampling was conducted at these benchmark stations throughout the period of study (2005-2012).

During the study, and particularly during active construction phases, differences between upstream and downstream turbidity measurements were tracked daily by construction managers

to identify potential inputs of sediment from construction activities. With instruments monitoring the water flowing into and out of active construction reaches, an input potentially attributed to the RRFRP would be expected to generate an increased turbidity response at the outflow location as compared to turbidity at the inflow location. In the event of such a pattern, further data exploration utilizing other measured water-quality parameters would be conducted, and, if warranted, a site visit would be conducted to rule out instrument fouling or other malfunction as the cause of the observed pattern. Upon completion of the construction activities, cumulative distribution frequencies (CDFs) were plotted by construction phase to evaluate discrepancies in turbidity between the inflow and outflow monitors to assess whether changes in the turbidity regime occurred that were indicative of RRFRP activities altering sediment transport.

The relation between turbidity and SSC was determined, and potential changes in this relation over time and/or space were explored, using multiple linear regression. Site-specific simple linear regression (SLR) models were developed using SSC and corresponding turbidity measurements from the discrete sampling activities at the two benchmark stations. Determination of change in the turbidity-SSC relation over time was accomplished by adding a time term to the turbidity-SSC model and evaluating the significance of time in the model. Evaluation of whether the turbidity-SSC relation varied between the benchmark stations was accomplished using Analysis of Covariance (ANCOVA), in which indicator variables were added to the turbidity-SSC SLR to determine significance of location within a pooled model calibrated using data from both stations.

Results of the analysis of turbidity distributions by construction phase indicated that turbidity generally increased in the downstream direction throughout the overall study reach and that turbidity was highly variable throughout the period of the study. No evidence of RRFRP induced sediment transport was apparent in the CDFs, though this analysis was limited at times because of the lack of pre-construction monitoring for some phases.

Turbidity was an effective surrogate for suspended sediment at the two benchmark sites, as indicated by the strong statistical significance of turbidity in the models ($p < 0.0001$) and high coefficients of variation ($R^2 = 0.95$) in each of the site-specific regressions. These regression models remained static over the period of study, as evidenced by the lack of significance of a time term in the regressions, indicating that the turbidity-sediment relation was not changing over time. Additionally, these models were static spatially, as no significant difference was detected between the two stations using the ANCOVA – a single model was statistically indistinguishable from site-specific models.

The results of the temporal and spatial analysis of the turbidity-SSC regressions provide further evidence that the RRFRP did not induce sediment transport within the study reach. Increases in local contributions to suspended-sediment transport would be expected to alter sediment characteristics such as color, organic content, and size-distributions, which would result in changes in the turbidity-SSC relation. Further, these changes would only be apparent at the downstream site receiving water from the construction reach, yet no significant difference between the two stations was detected.

The results of this monitoring and analysis program indicate that no detectable changes in suspended-sediment transport occurred in association with RRFRP construction, suggesting that the construction activities did not have deleterious effects on logperch habitat. These findings are consistent with findings of the complementary geomorphological and logperch community monitoring programs.

SHORTCOMINGS OF TWO-PARAMETER POWER FUNCTIONS FOR FITTING BEDLOAD RATING CURVES

David Gaeuman, Geomorphologist, Trinity River Restoration Program, Weaverville, CA, (530) 623-1813, dgaeuman@usbr.gov

INTRODUCTION

The capacity to estimate the sediment loads of streams is a key component of numerous types of geomorphic investigations (Andrews, 1986; Inman and Jenkins, 1999; Singer and Dunne, 2001; Syvitski et al., 2005; Klonsky and Vogel, 2011). Sediment loads at defined locations along a stream are frequently calculated with empirical sediment rating curves developed by statistically fitting the parameters of a transport model to a set of paired water discharge and sediment transport measurements.

Various transport models can be fit to sediment transport and stream flow data. Whether a particular model is appropriate depends on the purpose of the rating curve. Often, the purpose of fitting a rating relation is simply to estimate sediment loads. In cases where transport computations are confined to interpolated values within the range of observed discharges, the form of the fitted equation and the values of the fitted parameters may be of little importance. However, the use of incorrect functional models can lead to large errors when extrapolation beyond the observed range of discharges is required (Glysson, 1987). Moreover, sediment rating curve parameters are also sometimes used to investigate the transport process by inferring relationships between the fitted parameters and physical attributes of the system (Asselman, 2000; Barry et al., 2004; Gaeuman, 2010). Where extrapolation is required or when parameter values are to be assigned physical meaning, the use of appropriate fitting procedures and a functional form that accurately represents the transport process are critical.

Perhaps the most common transport model used for this purpose is a simple 2-parameter power function:

$$Q_s = aQ^b \qquad (1)$$

where Q_s is the sediment transport rate, Q is the water discharge, and a and b are parameters. This method may serve as a reasonable approximation for the relationship between flow and suspended sediment transport, but it provides an unrealistic representation of coarse bedload transport. The existence of a threshold for sediment entrainment below which coarse sediment is immobile is a fundamental concept in bedload transport theory. Such a threshold can be accommodated by fitting bedload transport data with a shifted power function in which a discharge threshold required for the initiation of sediment transport (Q_c) is subtracted from Q:

$$\begin{aligned} Q_s &= a(Q - Q_c)^b \qquad for\ Q_c > Q \\ Q_s &= 0 \qquad\qquad\quad otherwise \end{aligned} \qquad (2)$$

This 3-parameter transport model is analogous to numerous sediment transport equations (e.g. Meyer-Peter and Müller 1948) that express the sediment transport rate as a function of the excess

dimensionless shear stress exceeding a critical value defined by the Shields number. Inclusion of Q_c in the rating relation accounts for the behavior of coarse bedload fractions that remain motionless at small discharge levels. Where the data show that no such threshold exists, Q_c can take a value of zero, thereby reducing (2) to a standard two-parameter power function.
Although equation (2) offers a more flexible and realistic representation of the bedload transport process, a large proportion of investigators prefer to base their analyses on the simpler two-parameter model. Given the popularity of the simple power function for representing bedload transport, it is prudent to consider the effect arbitrarily forcing Q_c to zero has on the quality of the fitted rating curve. This paper presents a numerical experiment demonstrating that incorrectly ignoring non-zero values of Q_c can produce gross errors in the fitted values of both *a* and *b*. The significance of those errors for various rating curve applications is discussed and demonstrated using bedload measurements collected in the field.

EXAMPLE USING SYNTHETIC DATA

The potential impact of inappropriately imposing a two-parameter power function on a system where a non-zero entrainment threshold exists is demonstrated by fitting synthetic data drawn from a hypothetical rating curve defined by equation (2) with *a*, *b*, and Q_c set to 0.1, 2, and 1.5 m^3/s. Eleven paired Q-Q_s data points spanning a range of Q from 1.53 to 3 m^3/s were drawn from the curve. No error was added to the computed values of Q_s, so the 11 data points matched their parent curve exactly. Those data were then fit with a 2-parameter power function given by equation (1) using the linear regression functionality in Microsoft Excel, which implements linear least squares with log transformed data. As illustrated in Figure 1, that procedure results in a poor fit that deviates markedly from the actual parent curve used to generate the data. The value of the fitted exponent *b* of 9.31 is 4.66 times larger than the actual value of 2, and the value of the fitted coefficient is 5 orders of magnitude too small. These results are typical – in general, incorrectly forcing Q_c to zero invariably results in overestimation of *b* and, for datasets in which Q is predominantly greater than unity, underestimation of *a*.

The magnitude of the errors depends to a large extent on how much greater the values of Q in the dataset are than Q_c. For the example of Figure 1, the data used to fit the power function spans a range of Q between 1.02 times Q_c and $2Q_c$. If the range of Q used to fit the curve is limited to $1.02Q_c$ to $1.9Q_c$ while holding all other conditions constant, the estimated value of *b* increases to 9.86, or 4.93 times the correct value, and the estimated value of *a* is further reduced to 0.000013.

These errors in the parameter estimates can produce substantial errors in sediment loads computed with equation (1), although the nature and magnitude of the errors will depend on the characteristics of the hydrograph the rating curve is applied to. It is clear from Figure 1 that the 2-parameter fit to the data will under-predict transport rates associated with discharges near the center of the data range (e.g., the transport rate computed for 2 m^3/s with the 2-parameter curve is just 44 percent of the correct value). The potential for overestimation of transport rate at discharges beyond the range of the sample data, however, is a more significant problem. Although sediment rating curves should, in principle, be based on sample data spanning the full range of the flows they will be applied to, that is not always possible. Sampling at the highest discharges may be impractical for numerous reasons, including safety considerations, equipment limitations, lack of funds, or time constraints. Large flow events often remain unsampled, such

that load estimates for those events must be based on measurements obtained at relatively small discharges.

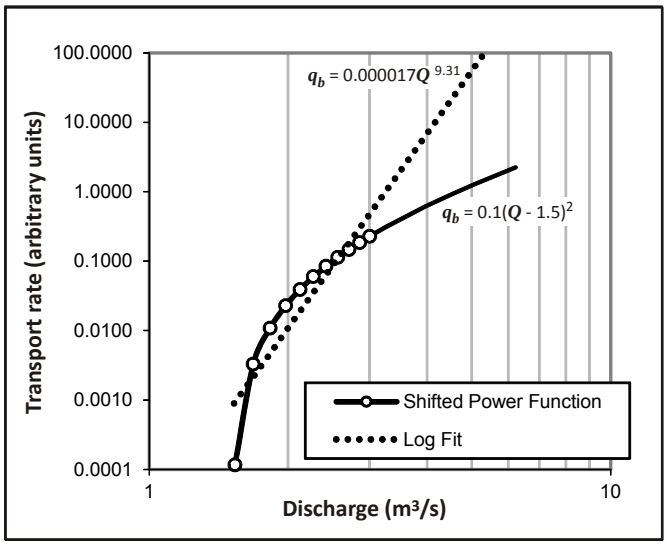

Figure 1 Comparison between a shifted power function [equation (2)] with known parameters and a fitted curve based on a 2-parameter power function [equation (1)] with parameters fit by ordinary least squares. The data points drawn from the shifted power function used in the fitting operations are indicated by the open circles.

The magnitude of the potential errors caused by extrapolating a 2-parameter rating curve beyond the range of the data is illustrated using the synthetic hydrograph shown in Figure 2. That hydrograph starts at 1.5 m^3/s (equal to Q_c) and rises at a steady rate of 0.15 m^3/s per day for 20 days to a peak of 4.5 m^3/s ($3Q_c$). The peak is maintained for 3 days, after which flow recedes at an exponential rate of 1.5 percent per day for 71 days.

At $3Q_c$ and 3 days, neither the magnitude nor the duration of the peak is extraordinary, and the mean discharge over the full hydrograph (2.8 m^3/s) is within the range of the transport data. Nonetheless, greatly overestimated transport rates at the higher discharges produces large errors in the total computed load. The 2-parameter rating curve based on data spanning 1 to 2 times Q_c (Figure 1) produces an estimated transport rate for 4.5 m^3/s that is 23 times larger than the correct value and a total load for the full hydrograph that is 10.2 times too large. If the 2-parameter rating curve based on transport data spanning 1 to 1.9 times Q_c is used, the maximum transport rate is 40 times too large and the total load is overestimated by a factor of 17.

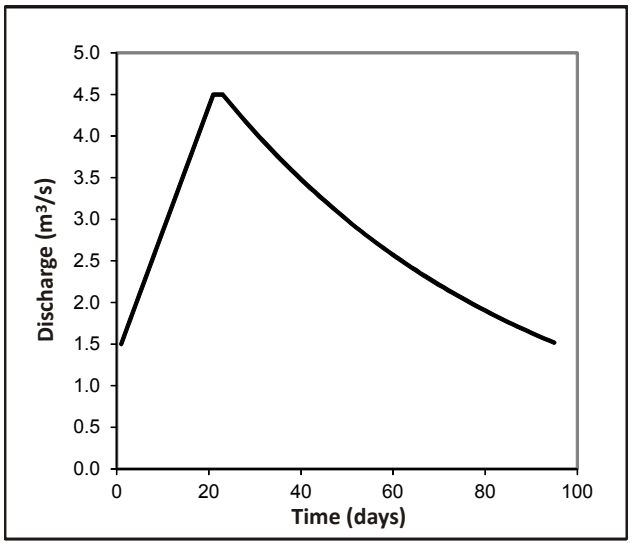

Figure 2 Synthetic hydrograph used to demonstrate the effect of extrapolating a 2-parameter rating curve to higher discharges when estimating total sediment loads.

EXAMPLE USING FIELD DATA

The data presented in this section consists of 18 bedload transport samples collected in Rush Creek, a tributary to the Trinity River in northern California, in water years 2004 and 2005 (Figure 3). These bedload samples were obtained at discharges ranging from 3.4 to 13.4 m^3/s, which slightly exceeds the stream's mean annual daily maximum flow of 11.6 m^3/s, based on 10 years of available record (water years 2004-2013, USGS 11525530 Rush Creek near Lewiston, CA). The annual mean flow in the creek over the same 10-year period is 1.2 m^3/s.

When fitted with a rating curve of the form given by equation (2), these data yielded estimates of a, b, and Q_c of 1.243, 2.415, and 1.8 m^3/s, respectively, whereas fitting these same measurements with a 2-parameter power function produced estimates of a and b of 0.0798 and 3.422. As with the previous example, forcing Q_c to equal zero by imposing equation (1) substantially increased the estimated value of b (by 42 percent in this example) and decreased the estimated value of a by orders of magnitude.

Elevations in the Rush Creek watershed range from about 540 m above sea level at the confluence with the Trinity River to more than 2200 m at the creek's headwaters in the Trinity Alps. Consequently, relatively long-duration flood events can occur during the spring snowmelt, but the largest floods tend to be brief events associated with intense winter storms that produce heavy rain in the lower elevations and rain-on-snow higher in the mountains. Acquiring sediment transport samples over the full range of flows therefore requires the ability to quickly mobilize a sampling crew during the relatively sudden and short-duration peaks that occur during winter storms.

In the case of the 2004 and 2005 Rush Creek data presented here, neither the instantaneous peak discharge nor a discharge equaling the maximum daily mean were sampled. Both maxima were attained during a storm on February 17, 2004 when the instantaneous peak flow reached 54.9

m^3/s and the daily mean flow was determined to be 25.7 m^3/s. Although an attempt was made to collect bedload samples during that storm, none were obtained until the following day (February 18) when discharge was between 13.4 and 10.7 m^3/s (Figure 4). Thus, computing the total sediment load for any time period that includes water year 2004 requires extrapolation beyond the range of the measured data.

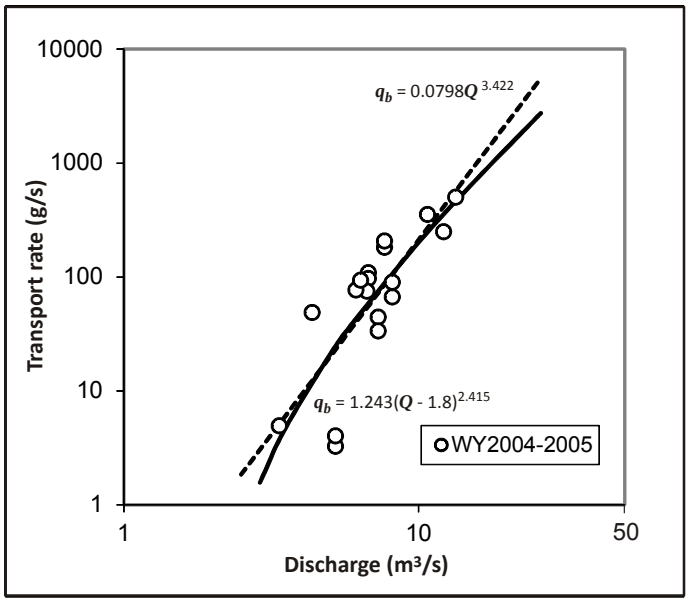

Figure 3 Comparison between a 3-parameter rating relation incorporating an entrainment threshold and a 2-parameter power function fit to bedload data collected in Rush Creek.

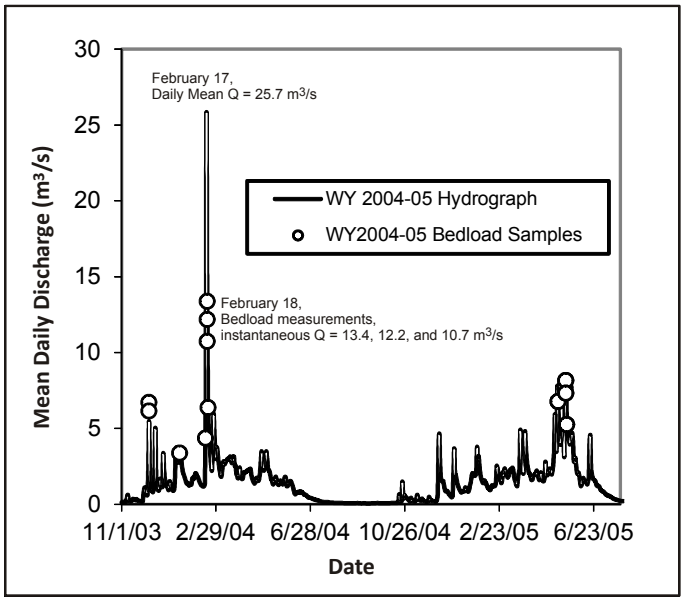

Figure 4 Daily mean discharge in Rush Creek in water years 2004 and 2005. Open circles indicate days on which bedload samples were acquired and the corresponding discharges.

Application of the 3-parameter rating relation based on equation (2) to the daily mean flows recorded for Rush Creek in water year 2004 results in a total bed sediment load of 305 metric tons, whereas application of the 2-parameter curve fit the same data yield a total load of 560 metric tons. Thus, omission of Q_c from the rating relations developed from Rush Creek bedload samples increases the total estimated bed sediment load for the year by a factor of more than 1.8. The increase would be even larger if the instantaneous peak, which was more than twice as large as the daily mean, had been considered in the analysis. It is also worth pointing out that the nearly 2-fold overestimation of the load described here arises from a hydrological record containing just one day on which the daily mean flow exceeded the range of measurements. It seems reasonable to suppose that, in some instances, it may be necessary to compute loads from hydrological records that exceed the range of sediment transport measurements on multiple days.

IMPLICATIONS FOR INTERPRETING TRANSPORT PROCESSES

Several previous authors have attempted to link variability in bedload rating curve parameters to differences in site conditions and the physical processes involved in bedload transport (Emmett and Wolman, 2001; Barry et al., 2004; Bunte et al., 2006). According to Barry et al. (2004), variations in b at different stream locations are inversely proportional to q^*, the measure of relative substrate armoring introduced by Dietrich et al. (1989). Similarly, Bunte et al. (2006) reported an inverse correlation of b with armoring as expressed by the ratio of the surface to subsurface median particle sizes, as well as a positive correlation with stream width.

Given that both of these studies used 2-parameter rating curves, it seems likely that the reported variations in b are related to differences in the relative magnitudes of Q_c at the various sampling locations as much as any other factor. That is, use of a 2-parameter rating curve should be expected to produce larger values of the exponent b for sample data sets associated with smaller values of Q_U/Q_c, where Q_U represents the upper limit of the range of the discharges sampled. The reported correlations between b and measures of substrate armoring and channel geometry may arise simply because those measures co-vary with Q_c. This interpretation is consistent with the observations of Emmett and Wolman (2001), who noted a positive correlation between b and the median and 90^{th}-percentile bed surface particle sizes and suggested that delayed onset of bedload mobility (i.e., a larger Q_c) due to the presence of a coarse armor layer on the streambed causes the rating relation to steepen (i.e., increase in b). If correct, the interpretation offered here implies that the value of b obtained from equation (1) may depend on attributes of the sampling effort, such as the range of discharges over which bedload samples were obtained, as much as any physical attributes of the stream.

Statistical relationships have also been reported between values of the coefficient a and certain physical parameters. Barry et al. (2004) observed an inverse correlation between a and drainage basin area, and attributed it to a proportionality between a and the ratio of sediment transport rate and stream discharge. Of five statistical relationships between a and physical parameters related to stream substrate or geometry reported by Bunte et al. (2006), three (bankfull width, basin area, and bankfull discharge) involve inverse relationships with alternative measures of stream scale. Similarly, Syvitski et al. (2000) found an inverse correlation between a and long-term mean discharge, although that study considered fine suspended sediment transport rather than bedload.

The tendency for a to decrease with increasing stream size, however, requires no geomorphic interpretation. It is simply a mathematical consequence of using a power function to model the rating relation. A generic power function equivalent to equation (1) can be written:

$$Y = aX^{b} \qquad (3)$$

Here, the substitution of X and Y for Q and Q_c is intended to emphasize the fact that the mathematical properties of the equation are independent of any geomorphic considerations. Solving for a yields:

$$a = Y/X^{b} \qquad (4)$$

It is clear from equation (4) that a is inversely proportional to X^b, such that, for constant Y, a must decrease whenever X increases, regardless of what X represents. It can also be seen that the magnitude of the decrease in a for a given change is X is greatly magnified by an increase in b, provided X is greater than unity. In general, any increase in b will cause a disproportionately large change in a, and will amplify the effect of increasing or decreasing X.

CONCLUSIONS

Sediment rating curves are commonly developed by fitting transport data to a simple 2-parameter power function that implicitly incorporates an assumption that sediment transport persists at all discharge levels. This assumption may be valid for the transport of fine suspended sediment, but is an unrealistic representation of coarse bedload transport, which generally ceases at discharges below a non-zero threshold (Q_c). The existence of such a threshold can be accommodated by fitting the transport data to a 3-parameter power function in which an entrainment threshold is subtracted from the measured water discharge.

Numerical experiments demonstrate that inappropriately fitting sediment transport data with a 2-parameter power function can result in large errors in both parameter estimates. Fitting the 2-parameters model to synthetic data with discharges ranging from Q_c to $2Q_c$ produced estimates of the exponent, b, between 4 and 5 time larger than the correct value, and estimates of the coefficient, a, that are orders of magnitude too small. Application of the resulting rating curves to a hypothetical hydrograph showed that these parameter errors can propagate to large errors in estimated sediment loads, particularly if extrapolation beyond the range of the measured data is required. In a similar analysis of bedload transport and stream flow data collected in a California stream, the value of b determined with a 2-parameter rating curve exceeded the value of b determined with a 3-parameter transport model by 42 percent. The estimated annual load based on the 2-parameter model and daily stream flow data is 80 percent larger than the annual load estimated with the 3-parameter model.

In general, forcing Q_c to zero by fitting bedload data with a 2-parameter power function exaggerates the value of the b. The degree to which b is exaggerated increases as the ratio of Q_c to the range of discharges sampled increases. The value of a scales in proportion to $1/Q^b$. Consequently, errors in b can lead to disproportionately large errors in a, depending on the range of discharges in the sample data. Overall, distortion of these parameter values caused by

improperly forcing Q_c to zero undermine efforts to interpret the physical meaning of variability in rating curve parameter values. Statistical relationships between rating curve parameters and various physical attributes of streams described in the literature may actually reflect spurious correlations related to the selection of physical metrics that co-vary with Q_c or to mathematical properties of the power function model.

REFERENCES

Andrews, E.D. (1986). "Downstream effects of Flaming Gorge Reservoir on the Green River, Colorado and Utah," Geological Society of America Bulletin 97(8):1012-1023.

Asselman, N.E.M. (2000). "Fitting and interpretation of sediment rating curves," Journal of Hydrology 234(3-4):228-248.

Barry, J.J., Buffington, J.M., and King, J.G. (2004). "A general power equation for predicting bed load transport in gravel bed rivers," Water Resources Research 40, W10401, doi:10.1029/2004WR003190.

Bunte, K., Abt, S.R., and Swingle, K.W. (2006). "Predictability of bedload rating and flow competence curves from bed armoring, stream width and basin area", Proceedings of the 8th Federal Interagency Sedimentation Conference, April 2 – 6, 2006, Reno, NV.

Dietrich, W.E., Kirchner, J.W., Ikeda, H., and Iseya, F. (1989). "Sediment supply and the development of the coarse surface layer in gravel-bedded rivers," Nature, 340:215-217.

Emmett, W.W. and Wolman, M.G. (2001). "Effective discharge and gravel-bed rivers," Earth Surface Processes and Landforms, 26:1369-1380.

Gaeuman, D. (2010). "Mechanics of bedload rating curve shifts and bedload hysteresis in the Trinity River, California." Proceedings of the 9th Federal Interagency Sedimentation Conference, June 27 – July 1, 2010, Las Vegas, NV.

Glysson, G.D. (1987). "Sediment-transport curves," U.S. Geological Survey Open-File Report 87-218. U.S. Geological Survey, Reston VA.

Inman, D.L. and Jenkins, S.A. (1999). "Climate change and the episodicity of sediment flux of small California rivers," The Journal of Geology 107:251-270.

Klonsky, L. and Vogel, R.M. (2011). "Effective measures of 'effective' discharge," Journal of Geology, 119:1-14.

Meyer-Peter, E. and Müller, R. (1948). "Formulas for bed-load transport," In Proceedings of the 2nd Meeting of the International Association for Hydraulic Structures Research, pp. 39-64, Int. Assoc. for Hydraul. Struct. Res., Stockholm, Sweden.

Singer, M.B. and Dunne, T. (2001). "Identifying eroding and depositional reaches of valley by analysis of suspended sediment transport in the Sacramento River, California," Water Resources Research 37(12):3371-3381.

Syvitski, J.P.M., Morehead, M.D., Bahr, D.B., and Mulder, T. (2000). "Estimating fluvial sediment transport: The rating parameters," Water Resources Research 36(9):2747-2760.

Syvitski, J.P.M., Vorosmarty, C.J., Kettner, A.J., and Green, P. (2005). "Impact of humans on the flux of terrestrial sediment to the global coastal ocean," Science 308:376-380.

A DEFINITIVE METHOD FOR THE SELECTION OF SEDIMENT TRANSPORT RELATIONS

David T. Williams, Ph.D., PE, PH, CFM, CPESC, F.ASCE
President, David T. Williams and Associates, Engineers, LLC, David@dtwassoc.com
1112 Oakridge Drive, #104, PMB 236, Fort Collins, Colorado 80525

EXTENDED ABSTRACT

The emphasis of this paper is a methodology for the selection of total bed material sediment transport relations and although only 4 transport functions are presented, it is applicable for analysis of any sediment transport function. Based upon analysis of over 8,000 measurements from flumes and rivers, the data are partitioned into dimensionless grain size intervals. The methodology then requires the development of a weighting function by taking the ratio of the measured versus the predicted sediment transport concentrations and determining the accuracy and precision of the ratio within the dimensionless grain size interval for each sediment transport function. Within each dimensionless grain size interval, four dimensionless parameters, dimensionless grain size, relative depth, grain Froude number, and dimensionless Stream Power, are computed based upon the data and dimensionless number that produces the best overall statistical results for the four transport functions is selected. The statistical results for each transport function, using the best dimensionless number within the dimensionless grain size interval, are used to select the best function.

The methodology determines not only the ranking of sediment transport methods for a given river situation, but also indicates if the methods have high to low applicability. This method can then be used to select an appropriate sediment transport method dynamically in a sediment transport model over time and space. However, to illustrate the methodology, four total bed material sand transport relations are used in this presentation. The transport relations are: Ackers and White (1973), Brownlie (1981a), Engelund and Hansen (1967), and Yang (1973).

TWO-DIMENSIONAL POISSONIAN HOMOGENEOUS MODEL FOR SUSPENDED SEDIMENT AND POLLUTANT MOVEMENTS IN OPEN-CHANNEL FLOW

Geraldo Wilson Júnior, Docteur d'Etat, COPPE/Federal University of Rio de Janeiro-UFRJ, Rio de Janeiro, Brazil, jrwilsong@gmail.com

Cid da Silva Garcia Monteiro, D.Sc., Modelling Methods and Geophysic Computational Laboratory-LAMEMO/UFRJ, Rio de Janeiro, Brazil, csgm25@yahoo.com.br

Abstract: When classic equations are used to study the sediment movements in open-channel flows, some problems appear, relating to: (i) the non-linearity of the equations, (ii) the complexity of the liquid and solid interactions and (iii) the unawareness of the liquid and solid movement's changes. The Random Theory avoids such problems and proposes a kinematic analysis of the flow and solid particles movements, exploiting, simultaneously, the open flux turbulent characteristics. The two-dimensional suspended sediment or pollutant trajectories $\omega(x,z,t)$ result from the combination of two 1-D chronological displacements series in the *i = 1, 3* senses, intercalated with periods of time when the grain does not move in these senses. These two series are interdependent. When the one-dimensional series are described by Homogeneous Poissonian Random Process, the resultant two-dimensional model is also Homogeneous Poissonian, defined by four mobility density functions, which characterize the particles' movement. The objectives of this work are: (i) to present the longitudinal and vertical two-dimensional Random Process Model; (ii) to calibrate and validate it, using radiotracers data from laboratory channels experiments; (iii) to show that the Random Theory may be applied to evaluate the 2-D sediment and pollutant movements in open-channel flows, for instantaneous and continuous injections conditions. To validate the model, data obtained from radioactive applications in a prismatic channel 12.0 m long, 0.40 m width and 0.60 m height of the *Central Hydraulic Laboratory of France – LCHF* were used. They have showed that the 2-D Random Process may describe, with precision, the suspended movement of fine sediment particles and/or contaminants in open channel flows, whatever kind of immersion may be.

INTRODUCTION

The bed and suspended load movements of sediments and contaminant particles in open channel flows characterize stochastic process, where the elementary events are the single grains' trajectories. They are dependent of the liquid phase turbulent structure, or in other words, of the hydrodynamic process. The trajectories or achievements of the single particle or of the group of particles can be analyzed by Lagrangean or Spatial and Eulerian or Temporal Descriptions and by the Random Processes Theory. Two stochastic processes are considered:

$$\vec{R}(t,\omega)=\left[X(t,\omega),Y(t,\omega),Z(t,\omega)\right]=X_{ti}(\omega);\ i=1,2,3 \tag{1}$$

that characterizes the evolution of the particle's position vector as a function of time, which longitudinal, lateral and vertical components are $X(t,\omega)$, $Y(t,\omega)$ and $Z(t,\omega)$, respectively. The second 3D stochastic process:

$$T(x,y,z,\omega)=\left[T(x,\omega),T(y,\omega),T(z,\omega)\right]=T_{xi}(\omega);\ i=1,2,3 \tag{2}$$

characterizes the particle's passing time by the point of coordinates (x,y,z).

$T(x,\omega)$, $T(y,\omega)$ and $T(z,\omega)$ represent the times spent by the particle to travel the distances *0x*, *0y* and *0z*, respectively. ω represents the trajectory or the sediment particle achievements, as presented in Figure 1, following. $X_{ti}(\omega)$ and $T_{xi}(\omega)$ processes can be defined by their Probability Distribution Functions:

$$F_t(x_i)=P\left\{X_i(t,\omega)\le x_i\right\};\ x_i\ge 0;\ i=1,2,3 \tag{3}$$

$$Q_{xi}(t)=P\left\{T(x_i,\omega)\le t\right\};\ t\ge 0;\ i=1,2,3 \tag{4}$$

which are related to each other by Todorovic´'s Equation (5) (Todorovic´ *et al.*, 1966; Wilson-Jr., 1987):

$$F_t(x_i) = 1 - Q_{xi}(t); \quad i=1,2,3 \tag{5}$$

They had shown that the Probability Distribution Function of these random processes can be expressed in terms of two pairs of Approximate Functions $F_{t1}(x_i)$ and $F_{t2}(x_i)$; $Q_{x1i}(t)$ and $Q_{x2i}(t)$; $i = 1,2,3$, respectively, such that:

$$0 \le F_{t1i}(x_i) \le F_{ti}(x_i) \le F_{t2i}(x_i) \le 1; \quad i=1,2,3 \tag{6}$$

$$0 \le Q_{x2i}(t) \le Q_{xi}(t) \le Q_{x1i}(t) \le 1; \quad i=1,2,3 \tag{7}$$

In each direction, e. g. in the longitudinal direction $0x_{i=1}$, where $x_i = x_1 = x$, the Approximate Distribution Functions $F_{tj}(x)$ and $Q_{xj}(t)$, $j = 1,2$ can be explained as functions of two new stochastic processes $G_n^{0,x}$ and $E_n^{0,t}$ from the same elementary events ω:

$$G_n^{0,x} = \{\mu_{0,x} = n\} \tag{8}$$

which represents the medium number of grain displacements, $\mu_{0,x}$ over the distance $[0, x]$, and,

$$E_n^{0,t} = \{\eta_{0,t} = n\} \tag{9}$$

the medium number of grain displacements, $\eta_{0,t}$ over the time period $[0, t]$.

$G_n^{0,x}$ and $E_n^{0,t}$ are Markovian Processes with similar properties. So, for the set $G_n^{0,x}$, it has:

$$\left\{\begin{array}{l} P\{G_1^{x,x+\Delta x} | G_k^{0,x}\} = \lambda_2(x,k)\Delta x + \vartheta(\Delta x) \\ P\{G_\nu^{x,x+\Delta x} | G_k^{0,x}\} = \vartheta(\Delta x) \quad \nu \ge 2 \\ P\{G_0^{x,x+\Delta x} | G_k^{0,x}\} = 1 - \lambda_2(x,k)\Delta x + \vartheta(\Delta x) \\ P\{G_0^{0,0}\} = 1 \end{array}\right\} \qquad \Delta x \to 0 \tag{10}$$

where $\vartheta(\Delta x)$ is a grain first order infinitesimal displacement distance.

The $G_n^{0,x}$ and $E_n^{0,t}$ occurrence probabilities are solutions of the system of equations derived from these properties:

$$\left\{\begin{array}{l} \dfrac{\partial}{\partial x} P\{G_k^{0,x}\} = \lambda_2(x,k-1) P\{G_{k-1}^{0,x}\} - \lambda_2(x,k) P\{G_k^{0,x}\} \\ \dfrac{\partial}{\partial x} P\{G_0^{0,x}\} = -\lambda_2(x,0) P\{G_0^{0,x}\} \end{array}\right. \tag{11}$$

with the following initial conditions:

$$x = 0 \begin{cases} P\{G_0^{0,x}\} = 1 \\ P\{G_k^{0,x}\} = 0; \; k \ge 1 \end{cases} \tag{12}$$

Similar analytical expressions to the Equations (10), (11) and (12) are obtained for the $E_n^{0,t}$ process. The solution of these differential equations yields the probability laws for the numbers of displacements in time and spatial intervals.

Two functions $\lambda_1(t,n)$ and $\lambda_2(x,n)$ appear, which describe the sediment particle mobility, in time and in that particular direction $x_{i=1} = x_1 \approx x$. Considering the three directions of the orthogonal axes $0xi$, $i = 1, 2, 3$, three pairs of Mobility Functions $\lambda_{1i}(t,n)$ and $\lambda_{2i}(x_i,n)$ are obtained, which describe the sediment grains 3D movements, in time and space. In each x_i direction it has been:

$$\begin{cases} \lambda_{1i}(t,n_i) = \lim_{\Delta t \to 0} \dfrac{P\left\{E_{1i}^{t,t+\Delta t} \middle| E_{n_i}^{0,t}\right\}}{\Delta t} \\ \lambda_{2i}(x_i,n_i) = \lim_{\Delta x_i \to 0} \dfrac{P\left\{G_{1i}^{x_i,x_i+\Delta x_i} \middle| G_{n_i}^{0,x_i}\right\}}{\Delta t} \end{cases} \qquad i = 1,2,3 \qquad (13)$$

PARTICLES' RANDOM TRAJECTORIES

The particle's trajectory ω results from the combination of three chronological displacement series: (i) an alternate series of longitudinal displacements in the direction of the flow, with intercalated periods of time when the particle ceases to progress in this sense; (ii) an alternate series of vertical displacements in the direction of gravity , with intercalated periods when the particle ceases to decant; (iii) a series of lateral displacements, with intercalated periods when the particle ceases to move laterally, as shown in Figures 1 and 2 (Wilson-Jr., 2004). One can observe that: (1) when the particle ceases to progress in the direction of flow, it can be decanting or moving laterally, (2) when it ceases to decant, it can be moving in the longitudinal or lateral directions, (3) when it ceases to progress towards one of the walls, it can be decanting or moving in the longitudinal direction. In this manner, the three series are interdependent and should be considered together.

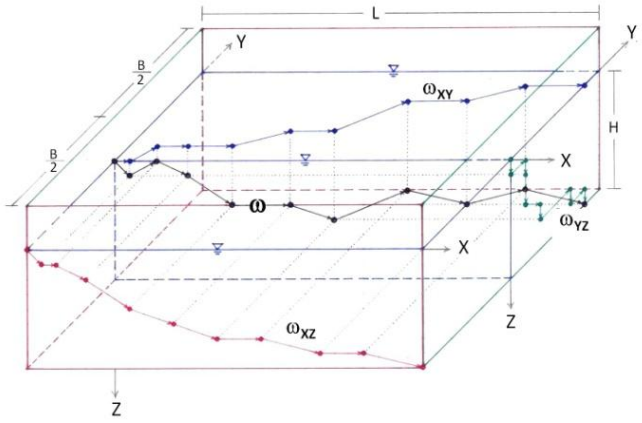

Figure 1. Sediment particle trajectory and its components in open channel flow (Wilson-Jr., 2004)

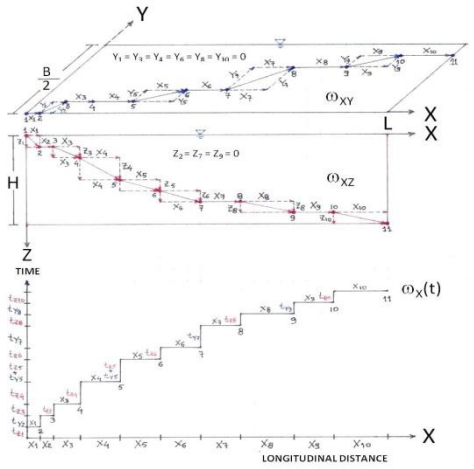

Figure 2. Particle trajectories on the horizontal ω_{XY} and vertical ω_{XZ} plans and longitudinal chronological series ω_X (*t*) (Wilson-Jr., 2004)

As positive longitudinal and vertical displacements are predominant these random series are more appropriate to describe the particle movements than the series of lateral displacements, where the negative movement (opposite to the direction of one of the walls) no can be neglected. Thus, the 2D resulting Random Processes that characterize the Lagrangean and Eulerian Descriptions, become respectively equal to:

$$\vec{R}(t,\omega) = \left[X(t,\omega), Z(t,\omega)\right] = X_{ti}(\omega); \qquad i=1,3 \qquad (14)$$

$$T(x,z,\omega) = \left[T(x,\omega), T(z,\omega)\right] = T_{xi}(\omega); \qquad i=1,3 \qquad (15)$$

OBJECTIVES

General Objectives

The general purpose of this work includes the study of Lagrangean and Eulerian Descriptions of bed and in suspension sediments and contaminants particles' movements and cases of instantaneous and continuous immersion of these particles in open channel flows, using the Theory of Random Process.

Specific Objectives

In particular, it is intended: (i) show that the Theory of Random Process accurately describe the 2D movements,

longitudinal and vertical, of sediment and pollutants in open channel flows; (ii) present the 2-D Poissonian models of sediments and contaminants in longitudinal and vertical suspension movements; (iii) highlight the importance of Temporal and Spatial Intensity Mobility Functions in the definition of random models, as well as in calibration and validation of 2D models, with data obtained in laboratory channels and nature.

3-D LAGRANGEAN RANDOM PROCESS

To better illustrate the ω trajectories of the particles, it will adopt Lagrangean Description of the Random Processes $X_{ti}(\omega)$, $i = 1,2,3$; shown in Figure 2.

Probability Density Function $f_t(x, y, z)$

Conceding the mutual independence of the Random Processes $X_{ti}(\omega)$, $i = 1,2,3$; the Probability Distribution Function of the particles' position with respect to time can be simplified, and be described by the general equation (Sayre and Conover, 1967; Wilson-Jr., 1987, 2004):

$$F_t(x,y,z) = \sum_{n=0}^{\infty} P\left\{ \sum_{j=0}^{N(t)} X_j \le x,\ \sum_{j=0}^{N(t)} Y_j \le y,\ \sum_{j=0}^{N(t)} Z_j \le z,\ N(t) = n \right\} \tag{16}$$

where $N(t)$ represents the number of particle displacements in time interval $[0,t]$. Thus, the Probability Density Function of the position of the particle in time t, is given by:

$$f_t(x,y,z) = \frac{\partial^3 F_t(x,y,z)}{\partial x \partial y \partial z} = f_t(x)\, f_t(y) f_t(z) P\left\{ \sum_{n=0}^{\infty} N(t) = n \right\} = f_t(x)\, f_t(y) f_t(z) \tag{17}$$

The pairs of Mobility Functions $\lambda_{1i}(t,n)$ and $\lambda_{2i}(x_i,n)$, $i = 1,2,3$; also called Particle Kinematic Change Functions, characterize the particles temporal and spatial movements, respectively (Wilson-Jr., 1987; Monteiro, 2004; Wilson-Jr. and Monteiro, 2013). When the probability of the grains' displacements, in time and distance intervals $[t,\ t+\Delta t]$ and $[x,\ x+\Delta x]$, Δt and Δx tending to zero, are independents of time, particle position and previous displacements, i.e., independents of the sediment particle history, the particle movement is called <u>*out of memory*</u>. In this case, the Mobility Functions are positive constants and the Density Probability Functions $f_t(x_i)$, $i = 1, 2, 3$ are described by Homogeneous Poissonian Random Processes (Wilson-Jr., 1987). For the 3D model results:

$$0.0 \le f_{t1}(x_i) \le f_t(x_i) \le f_{t2}(x_i) \le 1.0 \tag{18}$$

$$\begin{cases} f_{t1}(x_i) = \lambda_{2i}\, e^{-\lambda_{1i} t - \lambda_{2i} x_i} \displaystyle\sum_{k=0}^{\infty} \frac{(\lambda_{1i} t)^k}{k!} \frac{(\lambda_{2i} x)^k}{k!} \\ f_{t2}(x_i) = \lambda_{2i}\, e^{-\lambda_{1i} t - \lambda_{2i} x_i} \displaystyle\sum_{k=0}^{\infty} \frac{(\lambda_{1i} t)^{k+1}}{(k+1)!} \frac{(\lambda_{2i} x)^k}{k!} \end{cases} \qquad i = 1, 2, 3 \tag{19}$$

For any kind of sediment and/or pollutant immersion, if there is no loss or gain of particles in the course of time and distance, the total volume occupied by the particles is preserved after immersion time t_d. That is, it has been:

$$M_t = \int_{x=0}^{\infty} \int_{y=0}^{\infty} \int_{z=0}^{\infty} f_t(x,y,z)\, dx\, dy\, dz = 1; \quad t \ge t_d \ge 0 \tag{20}$$

To illustrate the performance of the 3D model components, plots of the probability density functions for some values of the mobility functions λ_{1i} and λ_{2i}, $i = 1,2,3$, are presented in Figures 3, 4 and 5 (Wilson-Jr., 2004). The mobility values are obtained by comparing the experimental and theoretical variations of the particles' position moments as function of time, and/or of the particles' passing time moments through cross sections. T^{-1} and L^{-1} in the figures correspond to the units of λ_{1i} and λ_{2i}, $i = 1,2,3$, that is, the inverse of time and length units, respectively.

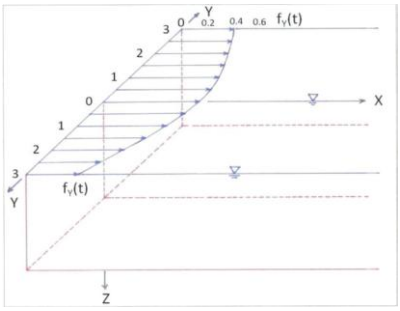

Figure 3. Probability density function of lateral displacements in time. ($\lambda_{1y} = 0.07T^{-1}$; $\lambda_{2y} = 0.90L^{-1}$)

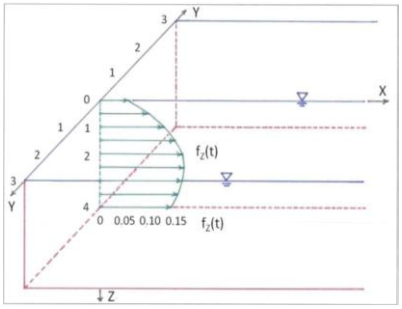

Figure 4. Probability density function of vertical displacements in time. ($\lambda_{1z} = 0.15T^{-1}$; $\lambda_{2z} = 1.15L^{-1}$)

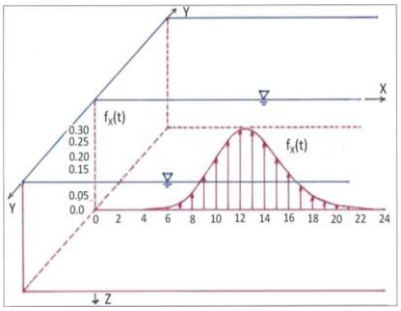

Figure 5. Probability density function of longitudinal displacements in time. ($\lambda_{1x} = 0.15T^{-1}$; $\lambda_{2x} = 3.50L^{-1}$)

To determine Probability Density Functions $f_t(x)$, $f_t(y)$ and $f_t(z)$, the software PAICON (***P**rocessos **A**leatórios com Injeção **I**nstantânea e **CON**tínua*) was used, implemented in *Delphi language* from *Inprise Corporation* (Monteiro and Wilson-Jr., 2002; Monteiro, 2004). These curves are fitted to the experimental results of projects on sediment and pollutants' transport and dispersion with the use of tracers: radioactive, fluorescents or chemicals, among others. In the Figure 6 is shown the points of the Rhodamine-B transit curve through a River *Loire*'s cross section and the upper and lower theoretical probability density approximate curves $q_{xj}(t), j = 1,2$, adjusted with the use of the PAICON Program (Monteiro and Wilson-Jr., 2003). The tracer application technique known as Double Labelling Method (*Méthode de Double Marquage*) was used. Simultaneous labelings and injections of water and fine sediments (special type named *schlam*) with Rhodamine-B and Au^{198}, respectively, allowed a comparative study of sediment and fluid transfer properties, in the segment between *Grangent* and *Villerest* Dams, on the River *Loire* (Tola *et al.*, 1981; Wilson-Jr., 1987).

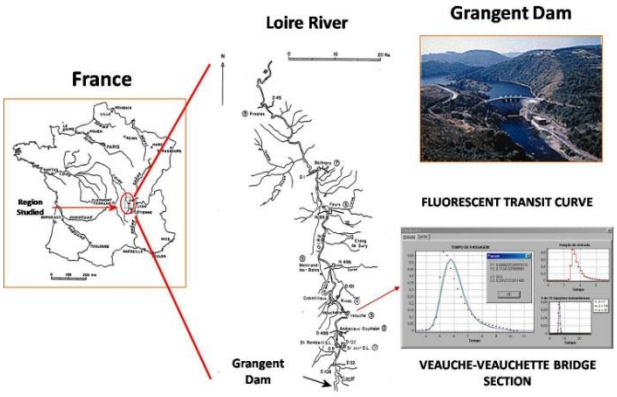

Figure 6. Rhodamine-B transit curve through the *Veauche-Veauchette* Bridge section, on the River *Loire* (Tola *et al*., 1981; Monteiro and Wilson-Jr., 2003)

Intensity of Particle Mobility Functions

The Mobility Functions λ_{1i} and λ_{2i}, $i = 1,2,3$, defined by Equations (13) appeared from the analytical development of Random Processes $X_{ti}(\omega)$ and $T_{xi}(\omega)$ to explain sediment mobility in each direction i and on the instant t. Different models can be obtained from the mathematical expressions that define these mobility functions, which should consider the sediment and/or contaminant particle characteristics, as well the hydrodynamic properties. The general expressions for λ_{1i} and λ_{2i}, $i = 1,2,3$, obtained by Vukmirovic´(1975) and Wilson-Jr. (1987, 2012) consider the mobility of the particles as a function of time, of the distances traveled in one direction and of its past performance in time (n) and distance (k), in each direction (i):

$$\begin{cases} \lambda_{1i}(t,n) = \lambda_{1i}(t)\,\lambda_{2i}(n) \\ \lambda_{2i}(x_i,k) = \lambda_{2i}(x_i)\,\lambda_{2i}(k) \end{cases} \qquad i = 1, 2, 3 \qquad (21)$$

$$\begin{cases} \lambda_{1i}(t,n) = \lambda_{1i} = const. \\ \lambda_{2i}(x_i,k) = \lambda_{2i} = const. \end{cases} \qquad i = 1, 2, 3 \qquad (22)$$

where: λ_{1i} is the particle mobility factor in a given time t in the direction i; and
λ_{2i} the particle mobility factor in a certain position x_i in the direction i.

2-D HOMOGENEOUS LAGRANGEAN RANDOM POISSONIAN PROCESSES

For these cases the grain mobility functions in the longitudinal and vertical directions assume constant values in accordance with Equation (22), or simply:

$$\text{for } i = 1 = x \Rightarrow \begin{cases} \lambda_{11} = \lambda_{1x} = const_{11} \\ \lambda_{21} = \lambda_{2x} = const_{21} \end{cases} \tag{23}$$

$$\text{for } i = 3 = z \Rightarrow \begin{cases} \lambda_{13} = \lambda_{1z} = const_{13} \\ \lambda_{23} = \lambda_{2z} = const_{23} \end{cases} \tag{24}$$

Some of the main statistical properties that characterize the 2-D Homogeneous Lagrangean Random Process $X_t(x,z)$, for cases of **instantaneous** and **continuous immersions**, are analytically described by the following equations (Monteiro, 2004; Wilson-Jr. and Monteiro, 2004):

Instantaneous Immersion Case

Probability density function $f_t(x,z)$

$$0.0 \le f_{t1}(x,z) \le f_t(x,z) \le f_{t2}(x,z) \le 1.0 \tag{25}$$

$$\begin{cases} f_{t1}(x,z) = \lambda_{21}\,\lambda_{23}\, e^{-\lambda_{11}t-\lambda_{21}x}\, e^{-\lambda_{13}t-\lambda_{23}z} \sum_{n=0}^{\infty}\sum_{k=0}^{\infty} \dfrac{(\lambda_{11}t)^n}{n!}\dfrac{(\lambda_{21}x)^n}{n!}\dfrac{(\lambda_{13}t)^k}{k!}\dfrac{(\lambda_{23}z)^k}{k!} \\ f_{t2}(x,z) = \lambda_{21}\,\lambda_{23}\, e^{-\lambda_{11}t-\lambda_{21}x}\, e^{-\lambda_{13}t-\lambda_{23}z} \sum_{n=0}^{\infty}\sum_{k=0}^{\infty} \dfrac{(\lambda_{11}t)^{n+1}}{(n+1)!}\dfrac{(\lambda_{21}x)^n}{n!}\dfrac{(\lambda_{13}t)^{k+1}}{(k+1)!}\dfrac{(\lambda_{23}z)^k}{k!} \end{cases} \tag{26}$$

Probability distribution function $F_t(x,z)$

$$0.0 \le F_{t1}(x,z) \le F_t(x,z) \le F_{t2}(x,z) \le 1.0 \tag{27}$$

$$\begin{cases} F_{t1}(x,z) = e^{-\lambda_{11}t-\lambda_{21}x}\, e^{-\lambda_{13}t-\lambda_{23}z} \sum_{n=0}^{\infty}\sum_{k=n}^{\infty} \dfrac{(\lambda_{11}t)^n}{n!}\dfrac{(\lambda_{21}x)^k}{k!} \sum_{m=0}^{\infty}\sum_{p=m}^{\infty} \dfrac{(\lambda_{13}t)^m}{m!}\dfrac{(\lambda_{23}z)^p}{p!} \\ F_{t2}(x,z) = e^{-\lambda_{11}t-\lambda_{21}x}\, e^{-\lambda_{13}t-\lambda_{23}z} \sum_{n=0}^{\infty}\sum_{k=n}^{\infty} \dfrac{(\lambda_{11}t)^{n+1}}{(n+1)!}\dfrac{(\lambda_{21}x)^k}{k!} \sum_{m=0}^{\infty}\sum_{p=m}^{\infty} \dfrac{(\lambda_{13}t)^{m+1}}{(m+1)!}\dfrac{(\lambda_{23}z)^p}{p!} \end{cases} \tag{28}$$

Median position of particles $M_t(x,z)$

$$M_{t1}(x,z)_{Inst.} \le M_t(x,z)_{Inst.} \le M_{t2}(x,z)_{Inst.} \tag{29}$$

$$\begin{cases} M_{xz1}(t)_{Inst.} = E\left[F_{t1}(x,z)\right] = \dfrac{1}{\lambda_{21}\,\lambda_{23}}\left[\lambda_{11}\,\lambda_{13}\,t^2 + (\lambda_{11}+\lambda_{13})t + 1\right] \\ M_{xz2}(t)_{Inst.} = E\left[F_{t2}(x,z)\right] = \dfrac{\lambda_{11}\,\lambda_{13}}{\lambda_{21}\,\lambda_{23}}\,t \end{cases} \tag{30}$$

Variance of the particles' positions $\left[S^2_{xzj}(t)\right]_{Inst.}$

$$\left[S^2_{xz1}(t)\right]_{Inst.} \le \left[S^2_{xz}(t)\right]_{Inst.} \le \left[S^2_{xz2}(t)\right]_{Inst.} \tag{31}$$

$$\begin{cases} \left[S^2_{xz1}(t)\right]_{Inst.} = \dfrac{2\lambda_{11}\lambda_{13}(\lambda_{11}+\lambda_{13})t^3+\left[(\lambda_{11}+\lambda_{13})^2+10\,\lambda_{11}\lambda_{13}\right]t^2+6(\lambda_{11}+\lambda_{13})t+3}{(\lambda_{21})^2(\lambda_{23})^2} \\ \left[S^2_{xz2}(t)\right]_{Inst.} = \dfrac{2\lambda_{11}\lambda_{13}(\lambda_{11}+\lambda_{13})t^3+2\lambda_{11}\lambda_{13}t^2}{(\lambda_{21})^2(\lambda_{23})^2} \end{cases} \tag{32}$$

Continuous Immersion Case

This case consists of a uniform injection, laterally distributed in the free surface at the channel's upstream extremity during a period of time t_d, as illustrated in Figures 7 and 8. In the experiments conducted at the LCHF (*Laboratoire Central d'Hydraulique de France*), t_d varied from 7.0 to 13.0 minutes (Wilson-Jr., 1987).

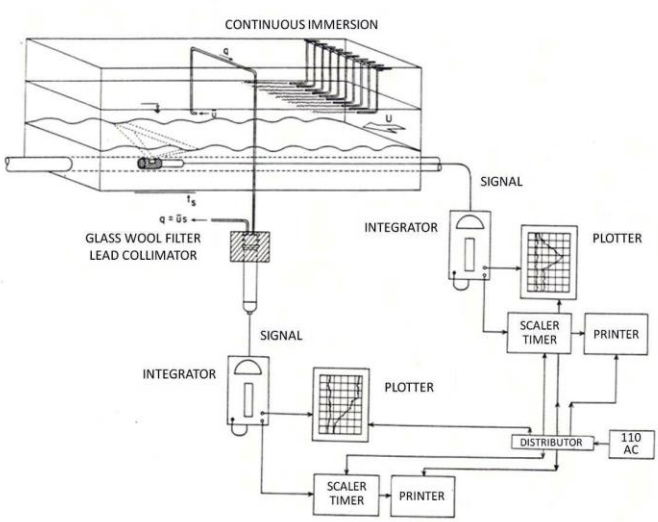

Figure 7. Immersion and detection system of bed and suspended movements of fine sediments in laboratory channel (Wilson-Jr., 1987)

Figure 8. Continuous immersion of fine sediments on the free surface of LCHF's channel

In the following equations $t_o \geq t_d$ represents the period of time of continuous recording of tracer's passage by the sampling points. To shorten the text, only the statistical properties related to the upper approximate probability density function of the 2-D Homogeneous Lagrangean Random Processes $X_{ti}(\omega)$, $i = 1,3$ will be presented.

Probability density function $h_{to}(x,z)$

$$h_{to}(x,z) = \frac{1}{t_d}\int_0^{t_d} f_{t_o-\tau}(x)\, f_{t_o-\tau}(z)\, d\tau \tag{33}$$

For the 2-D Poissonian Random Process, the upper approximate probability density function $h_{to2}(x,z)$ becomes:

$$h_{to2}(x,z) = \frac{1}{t_d}\int_0^{t_d} \lambda_{21}\, e^{-\lambda_{21}x}\, e^{-\lambda_{11}(t_o-\tau)} \sum_{n=0}^{\infty}\left\{\frac{\left[\lambda_{11}(t_o-\tau)\right]^{n+1}}{(n+1)!}\frac{(\lambda_{21}x)^n}{n!}\right\}\times \lambda_{23}\, e^{-\lambda_{23}z}\, e^{-\lambda_{13}(t_o-\tau)} \sum_{n=0}^{\infty}\left\{\frac{\left[\lambda_{13}(t_o-\tau)\right]^{n+1}}{(n+1)!}\frac{(\lambda_{23}x)^n}{n!}\right\} d\tau \tag{34}$$

Probability distribution function $H_{to}(x,z)$

$$H_{to}(x,z) = \frac{1}{t_d}\int_0^{t_d} F_{t_o-\tau}(x)\, F_{t_o-\tau}(z)\, d\tau \tag{35}$$

The distribution functions $F_{to\text{-}\tau}(x)$ and $F_{to\text{-}\tau}(z)$ are obtained from the 1-D models approximate equations in the longitudinal and vertical directions, respectively, that is, from the 1-D Homogeneous Poissonian equations system, in the *i = 1, 3* directions, with instantaneous immersions (Monteiro, 2004):

$$0.0 \le F_{t1}(x_i) \le F_t(x_i) \le F_{t2}(x_i) \le 1.0 \tag{36}$$

$$\begin{cases} F_{t1}(x_i) = e^{-\lambda_{1i} t - \lambda_{2i} x_i} \sum_{\nu=0}^{\infty} \sum_{k=\nu+1}^{\infty} \frac{(\lambda_{1i} t)^{\nu}}{\nu!} \frac{(\lambda_{2i} x_i)^{k}}{k!} \\ F_{t2}(x_i) = e^{-\lambda_{1i} t - \lambda_{2i} x_i} \sum_{\nu=0}^{\infty} \sum_{k=\nu}^{\infty} \frac{(\lambda_{1i} t)^{\nu}}{\nu!} \frac{(\lambda_{2i} x_i)^{k}}{k!} \end{cases} \tag{37}$$

Thus, for the Upper Approximate Probability Distribution Function $F_{(to\text{-}\tau)2}(x_i)$, *i = 1,3*, it has been:

$$F_{(t_o-\tau)2}(x_i) = e^{-\lambda_{1i}(t_o-\tau) - \lambda_{2i} x_i} \sum_{\nu=0}^{\infty} \sum_{k=\nu}^{\infty} \frac{[\lambda_{1i}(t_o-\tau)]^{\nu}}{\nu!} \frac{(\lambda_{2i} x_i)^{k}}{k!} \qquad i = 1,3 \tag{38}$$

Average position of the particles

The average position of the particles is given by the first-order moment, defined by:

$$\left[M^1_{xz}(t_o)\right]_{Cont.} = \frac{1}{t_d} \int_0^{t_d} M^1_x(t_o-\tau)\, M^1_z(t_o-\tau)\, d\tau \tag{39}$$

which can be estimated by two approximate first order moments, such that:

$$\left[M^1_{xz1}(t_o)\right]_{Cont.} \le \left[M^1_{xz}(t_o)\right]_{Cont.} \le \left[M^1_{xz2}(t_o)\right]_{Cont.} \tag{40}$$

Combining Equations 28, 29, 30, 39 and 40, one obtains the approximate expressions of the average position of the particles. The upper approximation is given by:

$$\left[M^1_{xz2}(t_o)\right]_{Cont.} = \frac{\lambda_{11}\,\lambda_{13}}{\lambda_{21}\,\lambda_{23}} \left(t_o^2 - t_o\, t_d + \frac{t_d^2}{3} \right) \tag{41}$$

Variance of the particles' position

Similarly, one can obtain the approximate expressions of the second order moment and of the Variance from the following definitions:

$$\left[M^2_{xz}(t_o)\right]_{Cont.} = \frac{1}{t_d} \int_0^{t_d} M^2_x(t_o-\tau)\, M^2_z(t_o-\tau)\, d\tau \tag{42}$$

$$\left[S^2_{xz}(t_o)\right]_{Cont.} = \left[M^2_{xz}(t_o)\right]_{Cont.} - \left[M^1_{xz}(t_o)\right]^2_{Cont.} \tag{43}$$

SUSPENDED SEDIMENT MOVEMENTS IN LABORATORY OPEN CHANNEL

An original experimental device was developed for the study of bed and suspended load with vertical transfers in a LCHF's channel 12.0 m long having a rectangular cross section 0.40 m wide by 0.60 m deep (Wilson-Jr., 1987). The lateral walls are made of glass, allowing for visual observations of bed configurations evolutions and the following of injections of sediments labeled with tracers. The channel was adapted, as schematized in Figure 7, such that hydraulic and sedimentologic measurements could be performed simultaneously with conventional methods.

Among several hydraulic and sedimentologic measurements performed, the following are highlighted: (i) the 3-D liquid velocities field; (ii) transport and dispersion of bed load particles; (iii) the vertical and transversal concentration profiles of suspended sediments continuously injected in the open surface of the channel, during time intervals; and (iv) the temporal and specific evolutions of the sediments deposited in the channel bed.

Examples of vertical profiles of cohesive and non-cohesive sediment concentration obtained in cross sections of the channel are presented in Figures 9 and 10, while examples of similar theoretical curves obtained from the probability density functions $f_t(x,z)$ are shown in Figure 11.

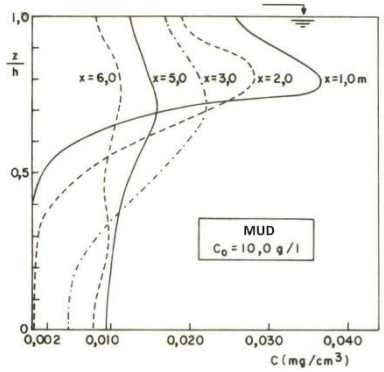

Figure 9. Vertical profiles of suspended cohesive sediment concentration across fixed section (Wilson-Jr., 1987)

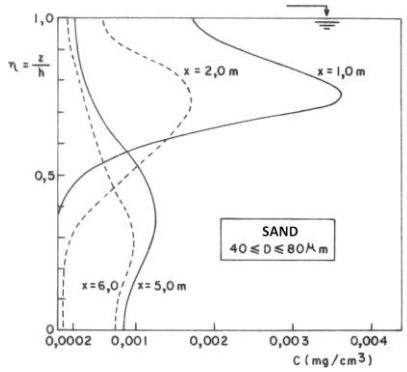

Figure 10. Vertical profiles of suspended non cohesive sediment concentration across fixed section (Wilson-Jr., 1987)

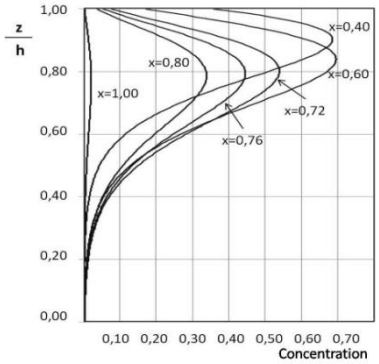

Figure 11. Theoretical vertical profiles of suspended cohesive sediment concentration across fixed section.

The comparison of these theoretical and experimental curves indicate that the 2D Random Models are so promising as the 1D models that the authors have been applied in laboratory channels and nature, in projects and investigations of Civil and Environmental Engineering.

SUSPENDED SEDIMENT MOVEMENTS RESULTS

Mendes and Wilson-Jr. (1998), Wilson-Jr. and Monteiro (2004) showed that the Homogeneous One-dimensional Poissonian Models described precisely the sediment and pollutant passage time through open channel cross sections. Data from experiments performed in Brazil and France consisting on the instantaneous immersion of tracers in suspension an upstream section and on the determination of the transit time's curves through some downstream cross sections were used for the 1-D applications using the PAICON-1D software. Some of these applications are highlighted in Wilson-Jr. and Monteiro (2004, 2013).

For the implementation of 2-D Poissonian models, the PAICON program was restructured to include the two-dimensional case and modern techniques of graphic outputs. This PAICON-2D version calculates the values of the approximate probability density and distribution functions of the Lagrangean and Eulerian descriptions, to estimated or experimentally obtained values of the λ_{11}; λ_{13}; λ_{21} and λ_{23} Mobility Functions.

To calibrate and validate the 2D Random Models is necessary to determine the values of these functions in the directions: longitudinal (λ_{11} and λ_{21}) and vertical (λ_{13} and λ_{23}). They are determined by the probability density functions moments of first and second order in each direction and by the longitudinal and vertical mean velocity of the particles, namely by Equations (44) to (47), following (Wilson-Jr. and Monteiro, 2013).

Temporal and spatial mobility of the particles in the x_i; i=1,3 directions

$$\begin{cases} \lambda_{1x_i} = \lim_{\Delta t \to 0} \dfrac{P\left\{E_{1x_i}^{t,t+\Delta t}\right\}}{\Delta t} \\ \lambda_{2x_i} = \lim_{\Delta x_i \to 0} \dfrac{P\left\{G_{1x}^{x_i,x_i+\Delta x_i}\right\}}{\Delta x_i} \end{cases} \qquad i = 1,3 \tag{44}$$

Longitudinal and vertical mean positions of a group of particles

$$\begin{cases} X_m(t) = \dfrac{\lambda_{1x}}{\lambda_{2x}} t = \dfrac{\lambda_{11}}{\lambda_{21}} t \\ Z_m(t) = \dfrac{\lambda_{1z}}{\lambda_{2z}} t = \dfrac{\lambda_{13}}{\lambda_{23}} t \end{cases} \tag{45}$$

Variances of the longitudinal and vertical positions of a group of particles

$$S_j^2(t) = 2\frac{\lambda_{1j}}{\lambda_{2j}^2}t \qquad j = x, z \text{ ou } j = 1, 3 \qquad (46)$$

Longitudinal and vertical mean velocities of a group of particles

$$U_j = \frac{\lambda_{1j}}{\lambda_{2j}} \qquad j = x, z \text{ ou } j = 1, 3 \qquad (47)$$

Each pair of values of the Mobility Functions describes the sediment grain movement in one direction. The results of the evolution in time of their approximate superior probability density function are shown in Figures 12 and 13.

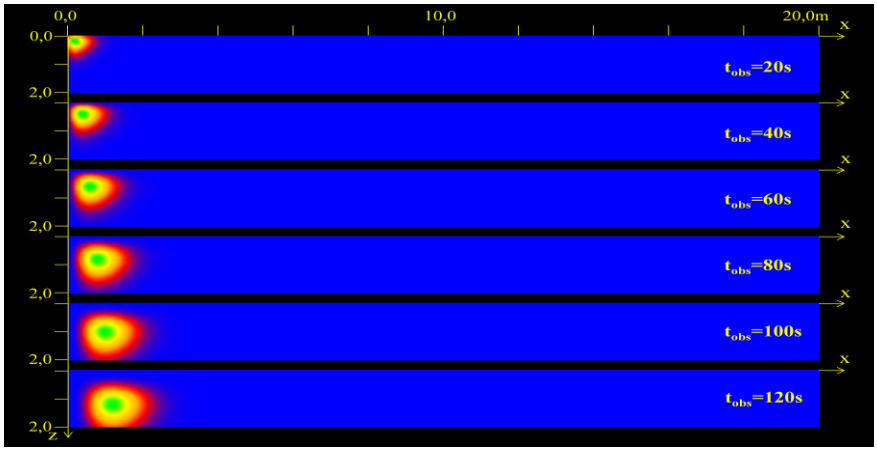

Figure 12. Cloud of sediments due to an instantaneous immersion at the free surface: case of equal longitudinal and vertical mobility.
($\lambda_{1x} = \lambda_{1z} = 0.10\ s^{-1}$; $\lambda_{2x} = \lambda_{2z} = 10.0\ m^{-1}$; $U_x = U_z = 0.01\ m\ s^{-1}$)

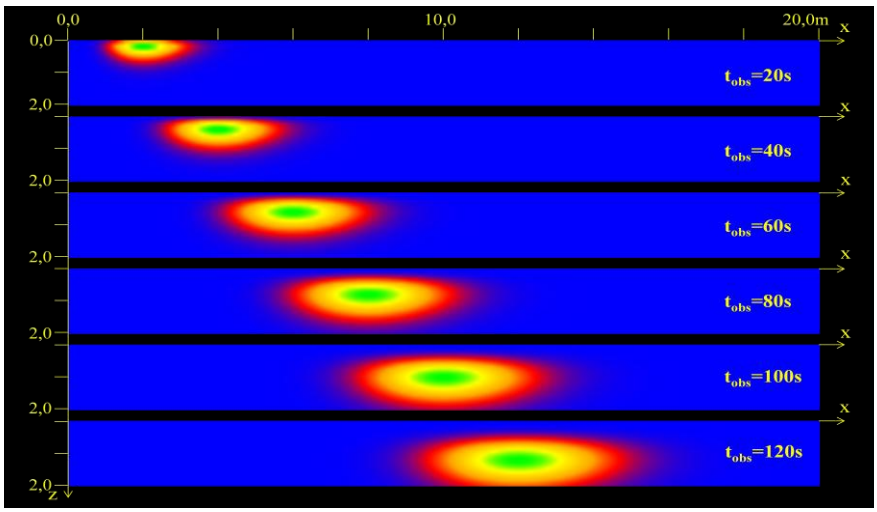

Figure 13. Cloud of sediments due to an instantaneous immersion at the free surface: in which case longitudinal mobility is greater than the vertical.
($\lambda_{1x} = 1.0\ s^{-1}$; $\lambda_{1z} = 0.10\ s^{-1}$; $\lambda_{2x} = \lambda_{2z} = 10.0\ m^{-1}$; $U_x = 0.10\ m\ s^{-1}$; $U_z = 0.01\ m\ s^{-1}$)

Their values are proportional to the concentration of sediment in suspension injected instantly to the free surface of a section located at the upstream extremity of the flow, for the cases where: (i) longitudinal and vertical mobility are equal; (ii) in the case of fine sediment which longitudinal mobility is about one order of magnitude higher than its vertical mobility or settling velocity. Similar studies were considered in the case of a continuous immersion for a time $[0, t_d]$ for t_d equal to 120 seconds. They are shown in Figures 14 and 15.

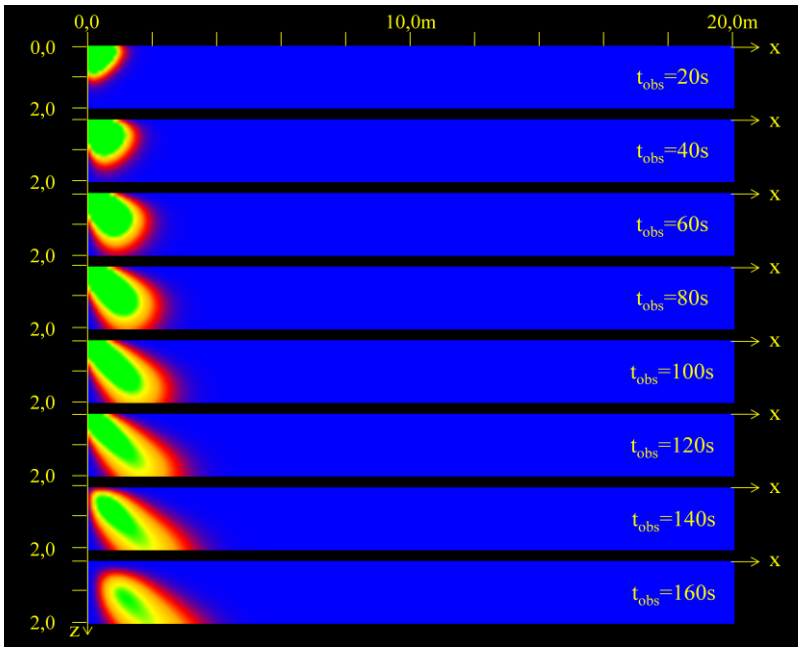

Figure 14. Plume of sediments due to continuous immersion at the free surface during the time interval $[0, t_d]$: case of equal longitudinal and vertical mobility. ($\lambda_{1x} = \lambda_{1z} = 0.20$ s^{-1}; $\lambda_{2x} = \lambda_{2z} = 10.0$ m^{-1}; $t_d = 120$ s; $U_x = U_z = 0.02$ m s^{-1})

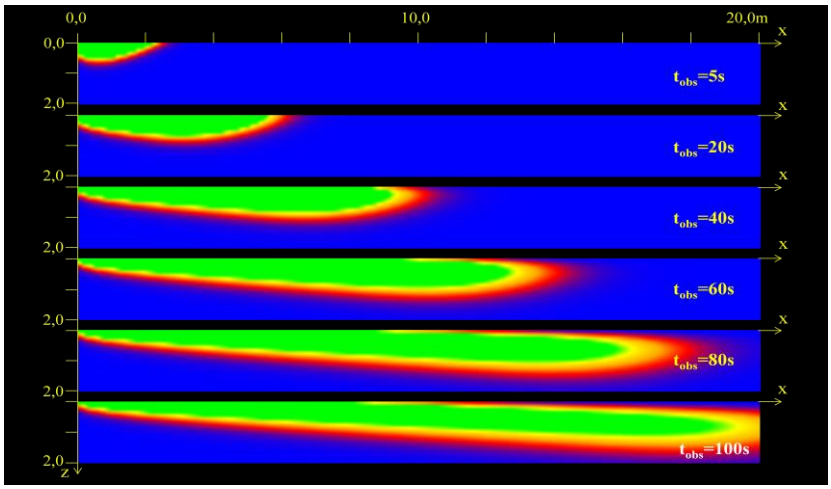

Figure 15. Plume of sediments due to continuous immersion at the free surface during the time interval $[0, t_d]$: in which longitudinal mobility is greater than the vertical. ($\lambda_{1x} = 2.0$ s^{-1}; $\lambda_{1z} = 0.10$ s^{-1}; $\lambda_{2x} = \lambda_{2z} = 10.0$ m^{-1}; $U_x = 0.20$, $U_z = 0.01$ m s^{-1})

CONCLUSIONS AND RECOMMENDATIONS

The Random Theory has shown that the trajectory ω of the particle results from the combination of two chronologic series of movement periods: (i) an alternate series of longitudinal downstream steps intercalated by time periods when the particle does not move in this sense, and (ii) an alternate series of fall vertical steps intercalated by time periods when the grain does not move vertically. These series are defined by the Mobility Functions: $\lambda_{x1}(t,n)$, $\lambda_{z1}(t,n)$, $\lambda_{t2}(x,n)$ and $\lambda_{t2}(z,n)$, which analytical expressions characterize the particles random movements.

It has been shown that the Random Process Theory is very enveloping, in such way that the diffusion dispersion Fickian classical equations of suspended sediment and pollutant movements are particular random process cases, characterized by constant values of the mobility functions, or in other words, by Homogeneous Poissonian Models.

When the sizes and concentrations of the sediment grains are reduced (fine sand, clays, and mud mixtures with concentrations lower than 150 mg/l), the solid particles behave as those of the fluid and the 1-D suspended movement can be described by 1-D Homogeneous Poissonian Models. This results is not surprising, since for large values of x and t, the Poissonian Model approaches the Gaussian Model, classical solution of the Diffusion-Dispersion equation.

When the grain mobility is not constant, more complexes models are generated, combining longitudinal and vertical non-homogeneous Poissonian and non-Poissonian models. Mobility Functions obtained in open channel flows, with grain of sediment labeled with radiotracers, permit the determination of the Mobility Functions and to adjust and validate the resultant random models.

Two research lines are opened: (i) the study of sediment and/or pollutant movement described by Mobility Functions that vary with time, distance and number of displacements performed in time and space, that is, performed by particles *with memory*; (ii) a description of the sediment movement by 2-D and 3-D processes. For these courses, a collection of data on sediment and pollutant movement obtained in laboratory channel and in nature with use of radioactive, dyes and chemical tracers is available for the use of this powerful Theory of Random Processes.

REFERENCES

Mendes, M.F.A.; Wilson-Jr., G. (1998). Homogeneous one-dimensional Poissonian model applied to the suspended movement of pollutant and fine sediments in open channel flow. *VII Intern. Symp. on River Sedimentation*, Hong Kong, China.

Monteiro, C.S.G. (2004). *Processos Aleatórios com Injeções Instantânea e Contínua, Aplicados ao Movimento de Sedimentos e Poluentes em Escoamentos com Superfície Livre.* M. Sc. Thesis. COPPE/UFRJ. 294 p., Brazil.

Monteiro, C.S.G.; Wilson-Jr., G. (2001). PAICON 4.0: Um Software Descritivo do Movimento de Sedimentos e Poluentes com Uso da Teoria dos Processos Aleatórios. *XIV Simp. Bras. Rec. Hídr., ABRH.* Aracaju, Brazil.

Monteiro, C.S.G.; Wilson-Jr., G. (2002). Descrição do movimento de sedimentos e de poluentes, com uso de microcomputadores e da teoria dos Processos Aleatórios. *XIX Congr. Nac. del Água*, Córdoba, Argentina.

Monteiro, C.S.G.; Wilson-Jr., G. (2003). Estudo Comparativo do Movimento de Sedimentos em Suspensão e de Poluentes Líquidos no Rio Loire com o Uso da Teoria dos Processos Aleatórios. *XV Simp. Bras. Rec. Hídri., ABRH*. Curitiba, PR, Brazil.

Sayre, W.W.; Conover, W.J., (1967). General Two-Dimension Stochastic Model for the Transport and Dispersion of Bed Material Sediment Particles. *Proceedings of 12th Congress of International Association for Hydraulic Research.* Fort Collins, Colorado, USA.

Tola, F. *et al.* (1981). *Etude des Propriétés de Transport en Suspension et Dispersion de Sédiments Fins en Aval du Barrage de Grangent, au Moyen de Traceurs Radioactifs et Colorés*. Rapport ORIS/SAR/S/81-18/T16/FT.

Todorovic', P.; Vukmirovic', V.; Vukotic', R.; Filip, A. (1966). A Contribution to the Kinetic Theory of Bed-Material Discharge. In: *Symp. on the Use of Isotopes in Hydrology.* IAEA, SM-83/19, p 271-290. Vienna.

Vukmirovic', V. (1975). *Analiza Kretanja Vucenog Nanosa Pomucu Slucajnih Procesa.* D. Sc. Thesis. Civil Engineering College. University of Belgrade. Yugoslavia.

Wilson-Jr., G. (1987). *Etude du Transport et de la Dispersion des Sédiments en tant que Processus Aléatoires.* Thèse de Doctorat d'Etat ès Sciences Physiques. Université Paris VI, France.

Wilson-Jr., G., (2004). Modelo Poissoniano homogêneo tridimensional do movimento de sedimentos em suspensão em escoamentos com superfície livre. *VI Enc. Nac. de Eng. de Sedimentos.* Vitória, ES, Brazil.

Wilson-Jr., G., (2012). Funciones de intensidad de mudanza del estado cinemático del movimiento de los sedimentos en los cursos de agua. *XXV Cong. Latinoam. de Hidr. San José, Costa Rica.*

Wilson-Jr., G.; Monteiro, C.S.G. (2004). Sediment and pollutant movements in open channel flows as stochastic processes. *6th International Conference on Hydro-informatics*, World Scientific Ed., p. 494-501. Singapore.

Wilson-Jr., G.; Monteiro, C.S.G. (2013). Modelo Poissoniano 2D del Movimiento en Suspensión de los Sedimentos y Contaminantes en Escurrimientos con Superfície Libre. *XXV Cong. Latinoam. Hidr. Santiago, Chile.*

ACKNOWLEDGEMENTS

The authors express their sincere gratitude to PENO/COPPE/UFRJ, CAPES, FAPERJ and CNPq for the institutional support received, without which, the realization of this work would not have been possible.

ESTIMATION OF SUSPENDED-SEDIMENT AND NUTRIENT FLUXES AND ASSOCIATED TRENDS ACROSS THE CHESAPEAKE BAY WATERSHED

EXTENDED ABSTRACT

Douglas L. Moyer, Hydrologist, U.S. Geological Survey, Richmond, Virginia, dlmoyer@usgs.gov; Jeffrey G. Chanat, Hydrologist, U.S. Geological Survey, Richmond, Virginia, jchanat@usgs.gov; Kenneth E. Hyer, Hydrologist, U.S. Geological Survey, Richmond, Virginia, kenhyer@usgs.gov; Michael J. Langland, Hydrologist, U.S. Geological Survey, New Cumberland, Pennsylvania, langland@usgs.gov; Joel D. Blomquist, Hydrologist, U.S. Geological Survey, Baltimore, Maryland, jdblomqu@usgs.gov

Chesapeake Bay is the largest of the Nation's estuaries and one of the most ecologically productive in the world. Excessive transport of suspended sediment and nutrients from the Chesapeake Bay watershed has had a detrimental effect on the habitat available to the living resources throughout the entire bay. Considerable effort has been taken by the Chesapeake Bay Program (CBP), comprised of Federal, State, and local governments, academic institutions, and non-profit organizations to reduce the amount of suspended-sediment and nutrients delivered annually to the bay. In 2010, the Environmental Protection Agency mandated the development of a total maximum daily load for the bay watershed as part of continued effort to reduce suspended-sediment and nutrient delivery to the bay. Improvement is expected in bay habitat as measured by improvements in water clarity, submerged aquatic vegetation, and dissolved oxygen. The CBP supports the operation of the CBP Nontidal Monitoring Network, which is a 120-station monitoring network, in the bay watershed. Data from this network are used to monitor current water-quality (suspended sediment and nutrients) conditions and track how these conditions change over time. Suspended-sediment and nutrient fluxes and changes in fluxes over time are key indicators that water resource managers use to assess the progress being made towards improving the structure and function of the bay ecosystem.

The U.S. Geological Survey (USGS), as a partner of the CBP, is responsible for the estimation of suspended-sediment and nutrient fluxes at all CBP Nontidal Monitoring Network stations as well as quantifying long- and short-term changes in suspended-sediment and nutrient fluxes. This flux and trend information is essential to the CBP to (1) assess progress made towards meeting water-quality goals, (2) efficiently allocate resources to areas of the watershed with degrading water-quality conditions, and (3) forecast conditions in the estuary for upcoming critical periods. The USGS ensures the integrity of the observed suspended-sediment and nutrient flux results by meeting three objectives:

1) Provide training for and evaluation of agencies monitoring water-quality conditions across the 120-station CBP Nontidal Monitoring Network to verify that all agencies are monitoring the full range of hydrologic conditions, while utilizing depth- and width-integrating isokinetic sampling techniques;

2) Evaluate and improve the statistical tools used to estimate fluxes and trends; and

3) Assess the quality of the observed water-quality data used to drive the statistical analyses to ensure that the flux and trend results are as accurate and defensible as possible.

The U.S. Geological Survey serves as the technical lead for the collection of suspended-sediment and nutrient data, across the CBP Nontidal Monitoring Network. They are responsible for ultimately ensuring that monitoring data are comparable from station-to-station and are appropriate for generating representative observed suspended-sediment and nutrient fluxes. Historically, our CBP monitoring partners (i.e. State agencies and River Basin Commissions) collected suspended-sediment and nutrient samples on a monthly basis by collecting a single grab sample from the centroid of flow. These samples were typically part of a larger ambient water-quality monitoring program. However, these monitoring techniques are not sufficient for the determination of suspended-sediment and nutrient fluxes because they do not capture the vertical and/or horizontal heterogeneity that often exists during high-flow conditions. The USGS, working with each of the CBP monitoring partners, added two critical sampling elements required for a monitoring station to be included in the CBP Nontidal Monitoring Network: targeted storm-flow monitoring and sample collection using isokinetically collected width- and depth-integrating techniques. The USGS annually evaluates how well each monitoring partner has represented water-quality conditions across the full range of each site's flow regime. Additionally, routine field audits are performed of all CBP monitoring agencies to ensure that monitoring is being performed consistently.

The U.S. Geological Survey annually estimates the total monthly and annual fluxes of suspended sediment and nutrients at each nontidal monitoring station as well as estimates the extent to which these fluxes are changing over time. Historically, USGS utilized a multiple-regression approach (ESTIMATOR) (Cohn and others, 1989) to estimate daily suspended-sediment and nutrient concentrations based on daily streamflow, time, and season. Two shortcomings of this historical approach were (1) the functional form of the ESTIMATOR model forces the relation between concentration and discharge to be linear or quadratic which makes ESTIMATOR susceptible to considerable over- or under- prediction of flux at stations that exhibit sigmoidal (s- shape) relations between concentration and discharge; and (2) the inability of ESTIMATOR to determine trends in flux estimates which the CBP require to directly measure progress towards reducing suspended-sediment and nutrient delivery to the bay.

The U.S. Geological Survey recently completed an evaluation of a new approach used to estimate suspended-sediment and nutrient fluxes and associated trends in fluxes, to address the shortcomings of the ESTIMATOR model. This new approach, Weighted Regression on Time, Discharge, and Season (WRTDS) is similar to ESTIMATOR in that it estimates daily concentrations based on daily streamflow, time, and season; however, instead of predefining the relation between concentration and flow as only linear or quadratic, WRTDS allows the relation between concentration and streamflow to be more flexible (Hirsch and others, 2010). The greatest effect of using WRTDS for flux estimates is an overall reduction in flux bias (the tendency to over- or under-predict observed flux) compared to flux estimates from ESTIMATOR (Moyer and others, 2012; Hirsch, 2014). Additionally, WRTDS allows for direct determination of trends in monthly and annual fluxes which provides CBP managers

more relevant information regarding how much annual fluxes of suspended-sediment and nutrients have changed (Moyer and others, 2012).

The U.S. Geological Survey routinely reviews the water-quality record, for each nontidal monitoring station, for the presence of non-environmental heterogeneities that may bias resulting flux and trend estimates. Causes for these heterogeneities typically fall into three categories, which are: (1) inconsistent storm sampling whereby targeted storm sample collection is added to a fixed-frequency monitoring record (2) changes in analytical laboratory censoring levels, and (3) changing analytical laboratory procedures (e.g. switching from total suspended solids to suspended-sediment concentration analysis). Using subsampling experiments on densely- sampled records, the USGS is characterizing the potential effects of the first of these heterogeneities in water-quality records. Preliminary experiments indicate that inconsistent storm sampling can result in deviations in estimated annual fluxes on the order of +/- 10 percent for dissolved inorganic nitrogen, +/- 15 percent for total phosphorus, and +/- 30 percent for suspended sediment, relative to a temporally homogenous baseline dataset containing both monthly and targeted storm samples. The USGS has developed simple screening-level indicators to identify which records may have been collected using inconsistent storm sampling methods. The analysis of the potential effects of inconsistent storm sampling can serve as a model for quantifying the effects of the other methodological heterogeneities listed above, and help to assure the quality of USGS and CBP monitoring partners' water-quality records, and the resulting flux and trend estimates provided to the CBP.

The U.S. Geological Survey is currently pursuing future enhancements to implemented data-collection and data- analysis techniques that will continue to reduce uncertainty in and improve the accuracy of each nontidal monitoring station's suspended-sediment and nutrient flux estimates and associated trends in estimated fluxes. Data-collection enhancements include: (1) continuous *in situ* monitoring of water-quality field parameters including pH, specific conductance, dissolved oxygen, turbidity, and water temperature; (2) use of those continuous water-quality parameters as surrogates for estimating suspended-sediment and/or nutrient fluxes, and (3) continuous *in situ* monitoring of dissolved nutrients (i.e. nitrate and orthophosphorus). Jastram and others (2009) demonstrated that suspended-sediment and nutrient fluxes, estimated using continuous *in situ* water-quality field parameters, exhibited reduced uncertainty when compared to suspended- sediment and nutrient fluxes estimated using streamflow. Data-analysis enhancements include: (1) utilization of continuous observed water-quality field parameters, for the estimation of suspended-sediment and nutrient fluxes, and (2) development of a weighted-regression approach similar to WRTDS that allows for the estimation of concentrations and fluxes at sub- daily time intervals, which is essential for small (~ less than 100 square miles) flashy watersheds.

These steps taken by the U.S. Geological Survey help to ensure that the most appropriate monitoring and analysis techniques are being used to support the determination of suspended-sediment and nutrient fluxes and associated trends in flux across the bay watershed. These steps also serve to distinguish the CBP Nontidal Monitoring Network as one of the most robust water-quality monitoring networks in the Nation.

REFERENCES

Cohn, T.A., DeLong, L.L., Gilroy, E.J., Hirsch, R.M., and Wells, R.M. (1989). Estimating constituent loads: Water Resources Research, v. 25, no. 5, p. 937–942.

Hirsch, R.M. (2014). Large biases in regression-based constituent flux estimates: causes and diagnostic tools: Journal of the American Water Resources Association, v. 50, no. 6, p. 1401-1424.

Hirsch, R.M., Moyer, D.L., and Archfield, S.A. (2010). Weighted regression on time, discharge, and season (WRTDS), with an application to Chesapeake Bay river inputs: Journal of American Water Resources Association, v. 46, no. 5, p. 857–1064.

Jastram, J.D., Moyer, D.L. and Hyer, K.E. (2009). A comparison of turbidity-based and streamflow-based estimates of suspended-sediment concentrations in three Chesapeake Bay tributaries: U.S. Geological Survey Scientific Investigations Report 2009-5165, 37 p.

Moyer, D.L., Hirsch, R.M., and Hyer, K.E. (2012). Comparison of two regression-based approaches for determining nutrient and sediment fluxes and trends in the Chesapeake Bay watershed: U.S. Geological Survey Scientific Investigations Report 2012-5244, 118 p.

FORMULATING GUIDELINES FOR RESERVOIR SUSTAINABILITY PLANS

Sean Kimbrel, Hydraulic Engineer, Bureau of Reclamation, Denver, CO, (303)445-2539, skimbrel@usbr.gov,
Kent Collins, Hydraulic Engineer, Bureau of Reclamation, Denver, CO, (303)445-2549, kcollins@usbr.gov,
and Tim Randle, Supervisory Hydraulic Engineer, Bureau of Reclamation, Denver, CO, (303)445-2557,
trandle@usbr.gov

INTRODUCTION

As time passes, reservoirs storing water also continue to fill with sediment, causing storage loss, reducing water supply reliability, and impacting infrastructure, particularly marinas, boat ramps, outlet works, turbines, and water intakes. In addition, reservoir deltas may extend upstream from the full reservoir pool and increase the frequency of flooding. The release of clear water downstream from the dam can lead to channel degradation. Sedimentation will also reduce the surface area available for recreation. The rate of reservoir sedimentation varies across the world and is very site specific, ranging from an average annual storage loss of 2.3 percent in China to 0.2 percent in North America (Garcia et al., 2008). The traditional approach in the design of federal dams in the United States was to construct the outlet works intake structure to be above the predicted reservoir sediment level at the dam during the first 50 to 100 years of operation, thereby allocating space in the bottom of the reservoir for sediment. However, reservoir sediment accumulation affects all levels of the reservoir (Utah Division of Water Resources, 2010), affecting all storage allocations by use (e.g. Conservation, Multi-Use, or Flood Pool). Under traditional dam building approaches, future generations will have to take some action after the sediment design life is reached, which could include dredging, sediment flushing, or dam decommissioning. However, the cost or feasibility of these measures was not determined.

In the field of natural resources management in the United States, there is recently more attention on reservoir sedimentation by managers, engineers, and scientists. For example, there is the recent resolution proposed by the Subcommittee on Sedimentation (SOS) to the Advisory Committee on Water Information (ACWI), who represents the interests of water-information users and professionals in advising the Federal Government on Federal water-information programs and their effectiveness in meeting the Nation's water-information needs (www.acwi.org):

> "Continued sedimentation threatens the project benefits for many of the Nation's reservoirs. The SOS encourages all Federal agencies to develop long-term reservoir sediment-management plans for the reservoirs that they own or manage by 2030. These management plans should include either the implementation of sustainable sediment-management practices or eventual retirement of the reservoir. Sustainable reservoir sediment-management practices are practices that enable continued reservoir function by reducing reservoir sedimentation and/or removing sediments through mechanisms that are functionally, environmentally, and economically feasible. The costs for implementing either sustainable sediment management practices or retirement plans are likely to be substantial, and sustainable methods to pay for these activities should also be identified.
>
> Federal agencies are encouraged to start developing sustainable reservoir sediment-management plans now for one or two reservoirs per year on a pilot basis. From this experience, interagency technical guidelines will be developed for preparing sustainable reservoir-sedimentation plans."

This technical report provides information beginning the development of guidelines for the formulation of reservoir sustainability plans for the effective management of inflowing sediment loads and in-situ deposits.

METHODS

This technical document summarizes key information from a Reclamation Science and Technology (S&T) Program research report (Reclamation, 2015), which provides addition details in the development of guidelines for the formulation of reservoir sustainability plans. Two key questions were set at the beginning of the research process, along with further pertinent information as the research progressed:

1. What is the process for developing a plan and strategy for the managing sediment inflow and deposition in Reclamation reservoirs? Sedimentation occurs at all reservoirs at various rates and sedimentation eventually impacts reservoir facilities and storage capacity. Taking a proactive approach to managing reservoir sediment provides the best chance for extending the useful life of any reservoir.

A sediment management plan must address the social, environmental, technical, economic, and legal challenges. With guidance adapted from Utah Division of Water Resources (2010) and Garcia et al. (2008), the following broad and general steps are provided to develop a reservoir sustainability plan. Not all steps are mandatory and some steps can occur concurrently:

   a. Determine the magnitude of the sediment problem
   b. Define preliminary sediment management options
   c. Define stakeholders and constraints
   d. Assess feasibility and economic viability of options
   e. Develop and implement a sediment management plan
   f. Monitor and revise plan if necessary

2. What is the best method for identifying which Reclamation reservoirs present the highest risk for experiencing adverse operational impacts and pose the greatest need for implementing an appropriate sustainability plan? Many Reclamation reservoirs in multiple Regions have experienced operational challenges due to sedimentation. Early identification of sediment related problems and proactive implementation of a customized sustainability plan are vital components in the preservation of a dam or reservoir's ability to meet Reclamation's mission.

The best way to determine the rate and extent of the reservoir sedimentation begin with direct surveys. However, the vast majority of Reclamation's reservoirs haven't even been surveyed since dam closure. Other indirect methods are available to estimate the amount of storage loss and determine which reservoirs have the greatest sedimentation problems.

Further guidance on the steps in developing a reservoir sustainability (or any other sediment sustainability) management plan and methods on quantifying reservoir impacts are detailed in further sections. This document details the preliminary steps in terms of what sustainable reservoir sediment management options are available in formulating a reservoir sustainability plan.

There is a wealth of knowledge giving detailed options available in addressing the problems of reservoir sedimentation. Garcia et al (2008) provides a good general discussion on reservoir sedimentation and sediment management options. Morris and Fan (1998) and Basson and Rooseboom (1997) both provide the most comprehensive information on sediment management in reservoirs. This research is intended to only reference the options as part of the guidelines for formulating reservoir sustainability plans.

a. Determine the Magnitude of the Problem:

The second question asked in the research effort was: what is the best method for identifying which Reclamation reservoirs present the highest risk for experiencing adverse operational impacts and pose the greatest need for implementing an appropriate sustainability plan?

As the saying goes, "one cannot manage what they cannot measure." The best method, or in this case methods, of determining the magnitude of the problem are direct measurements. As mentioned in the summary, there are two direct ways to measure storage loss and the potential of sediment problems in a reservoir:

1. Performing a repeat hydrographic survey of the reservoir, and;
2. Sediment flux measurements upstream and downstream of the reservoir.

Chapter 9 in Reclamation's Erosion and Sedimentation Manual (Reclamation, 2006) provides guidance on the performance of reservoir surveys. Prior to the development of modern measurement techniques with Global Positioning System (GPS) and acoustic depth sounding equipment, early reservoir surveys were performed along range lines (cross sections), where the station and depth were directly measured from a boat. With modern techniques, the entire reservoir can be surveyed and contour maps can be developed. The comparison of reservoir

survey data collected using entirely different methods can result in high uncertainty. Therefore, to reduce uncertainty in the estimate and distribution of reservoir storage loss, more frequent reservoir surveys are needed to accurately measure the rate of reservoir sedimentation.

Sediment flux measurements entail the continuous or repeated measurement of suspended sediment loads and bed load sediments both upstream and downstream of a reservoir, where then by conservation of mass, the amount of sediment depositing in the reservoir, or the storage lost, is estimated. Flux measurements, however, give only a storage loss estimate, and do not provide a measurement of sedimentation near important features (e.g. marinas, boat ramps, outlet works and water intakes).

Sediment flux measurements generally require more continuous monitoring and therefore more resources than periodic reservoir surveys. However, in combination, both provide a robust estimation of the timing and rate of reservoir sedimentation, including the properties of incoming and outgoing sediments (e.g. particle size).

Chapter 9 in Reclamation (2006) notes that the frequency of reservoir surveys should depend on the estimated rate of reservoir sediment accumulation, along with the current operation and maintenance plan.

Generally, the availability of funding limits the performance of direct measurements by reservoir survey and/or sediment flux measurements. At a lesser cost, the potential impacts of reservoir sediment to important features (e.g. outlet works, water intakes, boat ramps) can be evaluated with a reconnaissance survey, where a profile of the reservoir is rapidly surveyed to determine priorities.

At lesser cost but with greater uncertainty, there are several indirect methods are available to estimate the amount of storage loss and determine which reservoirs pose the greatest of impacts. Prior to the implementation of using indirect methods to determine sedimentation rate, one can define reservoirs that are offstream and possibly those in a series that have may have reduced sedimentation rates. These reservoirs generally have a low likelihood of impacts due to reservoir sedimentation.

On the other end of the spectrum, according to Basson and Rooseboom (1997) and Dendy et al. (1973), reservoirs with small storage/runoff ratios in relatively small catchments in semi-arid areas with high sediment yield ratios are highly vulnerable to reservoir sedimentation.

As far as indirect computations, the simplest method to determine reservoir storage loss and potential impacts at a given reservoir is to extrapolate storage loss or sediment yield rates from other nearby surveyed reservoirs in RESSED which are in similar hydrologic/geologic areas.

Next, a more detailed and process intensive way to estimate reservoir storage loss rates is the use of Geographic Information System (GIS) analyses. Several methods are listed, from least to most detailed:

1. Compute the regional rate of storage loss, for example by applying a regional regression equation. For example, extrapolate from other nearby reservoirs or by Hydrologic Unit Code (HUC). Another example is the 3W Model (Minear and Kondolf, 2009), which is a reservoir sedimentation prediction model that accounts for regional sediment yields, changing trap efficiencies over time in reservoirs, and the passing of sediment between a series of reservoirs.
2. Perform detailed watershed sediment yield estimates with GIS information. Several models/methods are available, such as the Watershed Erosion Prediction Project (WEPP) model (http://www.ars.usda.gov/News/docs.htm?docid=10621)

Additional Site Specific Data:

For a given site, once preliminary information is gained and there are potential sediment impacts that confirm the need for development of a sustainable sediment management plan, additional site-specific data should be collected. A reservoir survey should be performed if one was not recently collected. Next, a study should be performed of the composition of sediments that are flowing into and possibly out of the reservoir, and of sediments that may have already deposited in the reservoir. This study would include fluvial sediment sampling of the river above and below the reservoir, and in-situ sediment sampling of reservoir deposits.

In some cases, the presence of any contaminants above background concentrations will need to be determined prior to the implementation of any sediment management options. An inventory of upstream and downstream infrastructure in and near the reservoir which may be impacted by sediments and/or any changes to the reservoir and dam is necessary.

Depending on the availability of data, a more detailed hydrologic study may be necessary to better understand the timing and volume of inflows into the reservoir as part of developing any further sediment management options. In addition, data describing the operations of the reservoir is necessary.

Once preliminary information and rates of sedimentation are identified for a reservoir, the next step is to determine when sedimentation will impact key features.

Estimating Reservoir Life:
Once storage loss rates are calculated, various methods are available to determine the amount of time until reservoir sedimentation affects the design function of a reservoir. One traditional way is estimating the reservoir life, or the time until the usable storage pool completely fills with sediment, presumably followed by the abandonment of the structure (Garcia et al., 2008). However, sediment problems will arise well before the reservoir completely fills with sediment (Garcia et al, 2008) and reservoir life should not be viewed in such a manner. Some reservoirs experience problems with storage loss as little as 6% (Loehlein, 1999; Garcia et al.,2008). Reservoir sedimentation will become a serious problem when an important structure or key feature (e.g. outlet works, water intake, and boat marina) are buried, clogged, or abraded by sediments. An empirical method to estimate when sediment levels reach key features is to spatially estimate the sediment distribution in a reservoir based on methods from Reclamation (1982) and Reclamation (1962). Without direct measurement of sedimentation patterns, the spatial distribution of sediment may have high uncertainty.

According to Garcia et al. (2008), the "life" of a reservoir is better described based on the three distinct stages:

1. Continuous Sediment Trapping
2. Partial Sediment Balance
3. Full Sediment Balance

Most large reservoirs worldwide are operated in Stage 1, continuously trapping sediment. Only a few reservoirs worldwide have been designed to achieve Stage 3, which is the ultimate goal in formulating a sediment management plan for a reservoir. By achieving a Full Sediment Balance between upstream and downstream points of the reservoir, additional reservoir storage is no longer lost.

The time when sediment will reach key structures can be estimated by extrapolation from measurements, numerical modeling, or physical modeling. In addition, GIS analyses can be used to evaluate the complex bathymetry of reservoirs (e.g. Reclamation, 2012). Generally, analyzing profiles of repeat surveys, and estimating either the rate of delta progression for an upstream feature, such as a marina, or estimating the rate of bottomset delta growth near dam intakes are means to estimating when sediment problems will affect these particular facilities.

One useful way to determine the relative impact of the arrival of sediments to infrastructure at a dam is comparing the hydrologic size (Reservoir Capacity/Mean Annual Runoff), K_w, and the reservoir capacity to sediment inflow (Reservoir Capacity/Mean Annual Sediment Yield), K_t, of a particular facility to other facilities in an inventory.

Figure 1 presents this empirical diagram, derived from Basson and Rooseboom (1997), which is also a means to understand ways to manage reservoir sedimentation. The larger the hydrologic size (K_w) of the reservoir, the more important carry over storage into multiple years becomes for the facility. Data needs for this method are:

1. Total Reservoir Capacity
2. Mean Annual Sediment Yield
3. Mean Annual Runoff

In general, the farther a particular reservoir is toward the bottom left quadrant of Figure 1, the sooner that reservoir sediments will impact infrastructure located near the dam. For example, in Reclamation's inventory of dams, Black

Canyon, Guernsey, Paonia, and Lake Sumner are reservoirs near the bottom and left of the diagram. Currently, all these facilities pass measurable amounts of sediment through their respective outlet works facilities. The former Lake McMillan was nearly filled with sediment and replaced with the larger Brantley Dam, inundating the structure. An important feature to Figure 1 is that as time passes and reservoirs fill with sediment (decrease in storage), their plotting position moves toward the bottom left quadrant.

Figure 1 also presents three potential sediment management options: flushing, sluicing, and storage/dredging. The ranges of these preliminary options are taken from Basson and Rooseboom (1997), and are based on empirical data from Chinese and South African reservoirs. At the most bottom-left, flushing, is defined as drawing down the water level to re-entrain previously deposited sediments and to remove these sediments from the reservoir through bottom outlets. In the middle, sluicing, is defined as an operation technique whereby sediment-laden inflows are passed through the reservoir before the sediment particles can settle, thereby reducing the sediment trap efficiency of the reservoir, and maintaining reservoir storage capacity. The storage or "dredging" option is defined as inflowing sediment is stored in the reservoir and mechanical means are necessary to maintain or possibly regain storage, with the exception that the venting of turbid density currents is a possible sediment management option for reservoirs in this category. The majority of Reclamation reservoirs in RESSED fall into the "dredging" category. These potential sediment management options, along with several others, are presented in more detail in the following section.

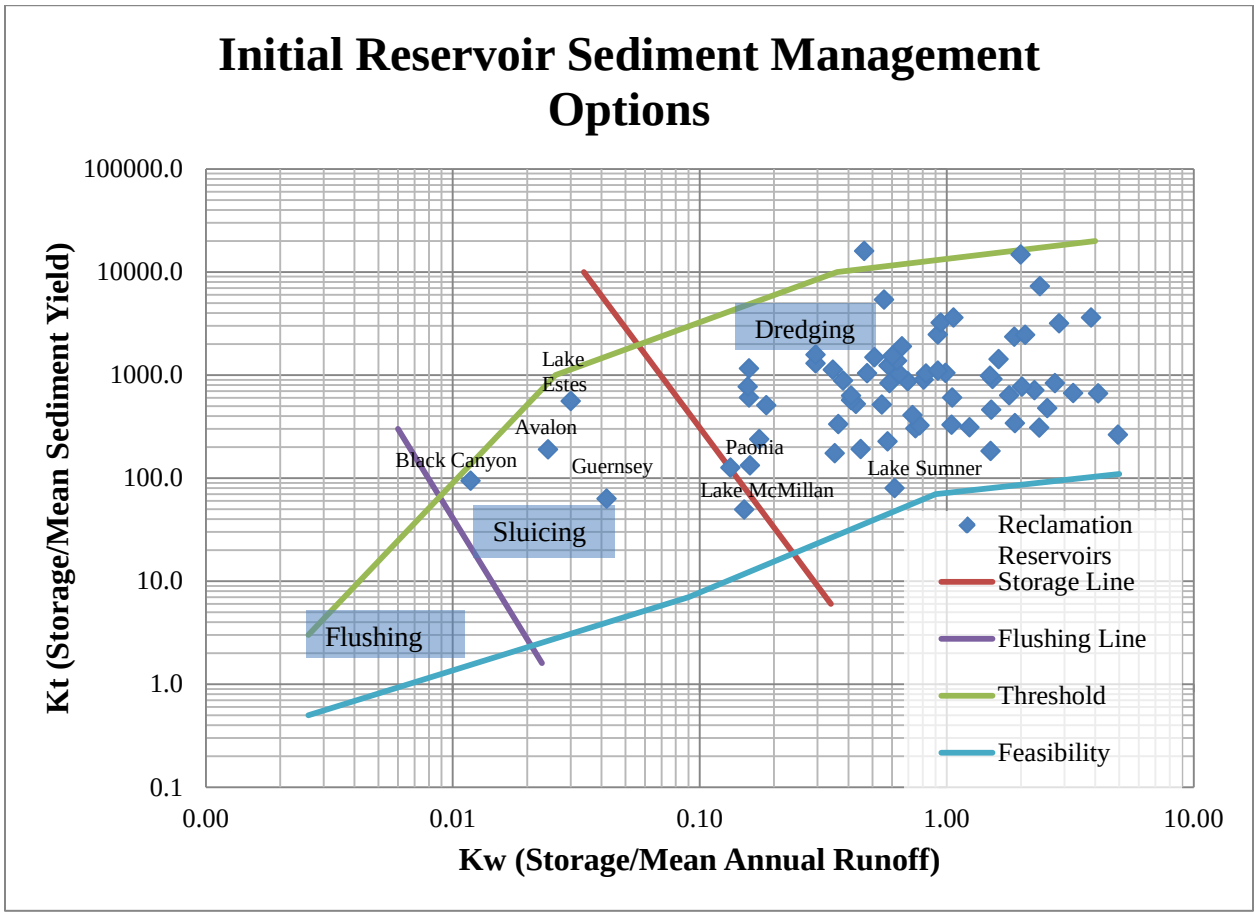

Figure 1. Diagram Adapted from Basson and Rooseboom (1997) for Determining Relative Reservoir Impact and Preliminary Reservoir Sediment Management Options

Necessity of a Sediment Management Plan:
Sediment management plans for achieving reservoir sustainability at Reclamation facilities are currently developed on a reactive basis for reservoirs which are already experiencing impacts from reservoir sedimentation. Currently, no programmatic-level allocation of resources is in place at Reclamation for proactive, comprehensive, sustainable sediment management of facilities. However, in addition to the SOS resolution promoting the development of sediment management plans, there is the push within other organizations at International (e.g. China and South Africa), Federal (e.g. U.S. Army Corps of Engineers), and State (e.g. California, Utah, Kansas, and Texas) levels that are in the process of systematically developing and implementing reservoir sustainability plans for reservoirs.

Whether sediment management planning of reservoirs is performed programmatically or at an ad-hoc basis, in the likeliest case of limited funding, prioritization is necessary to determine the reservoirs that may need to implement a sustainable sediment management plan.

Basson and Rooseboom (1997) provided general guidance for South African reservoirs relative to other reservoirs quantified using the index presented in Figure 1. According to their guidance, if the relative storage loss rate, K_t is less than 50, the reservoir sedimentation problem is considered serious, meaning sediment management actions need to be taken.

Comparing Reclamation's surveyed inventory, only the former Lake McMillan falls below a K_t value of 50. It is important to note that this inventory does not include any reservoirs which have not been surveyed. If the criterion were set to a value K_t less than 300, this would encompass most reservoirs with already known sediment issues, which are 13 of the 83 surveyed Reclamation reservoirs (16%) in RESSED. These facilities would have initial priority in following the guidelines developed in this document to formulate a sustainable sediment management plan. Other prioritization schemes to determine the necessity of a sediment management plan or dam decommissioning may involve the quantification of the time until sediments reach key features, and the quantification of the loss of benefits as a result of plugging, burial, and/or abrasion of pertinent features which provide benefits.

Eventually, all reservoirs need to be managed sustainably to provide benefits for future generations or decommissioned. The process is envisioned that a continued development of sustainable sediment management plans would occur for most Reclamation reservoirs that have inflowing sediments or a decommissioning plan would be put in place.

b. <u>Define Preliminary Sediment Management Options:</u>
With the development of relative reservoir impact and the unveiling of preliminary potential sediment management options presented in Figure 1, this section provides more detail of potential sustainable reservoir sediment management options/methods that have been applied to other reservoirs worldwide. All reservoir sediment management methods can be put into three different categories (Garcia et al, 2008; Kondolf et al, 2014):

1. Reduce Sediment Delivery (Watershed Management)
2. Prevent Sediment Deposition (Route Sediments through or around Storage)
3. Increase or Recover Volume (Removal of Deposited Sediments)

Figure 2 shows a variety of sediment management techniques placed into the three above categories by Kondolf et al. (2014). The exception within the three categories is raising a dam to increase storage, which does not fully deal with the management of incoming sediments, but extends the reservoir life by the creation of more storage.
There can be instances where a combination of methods from the above categories is necessary to maintain reservoir capacity and achieve reservoir sustainability.

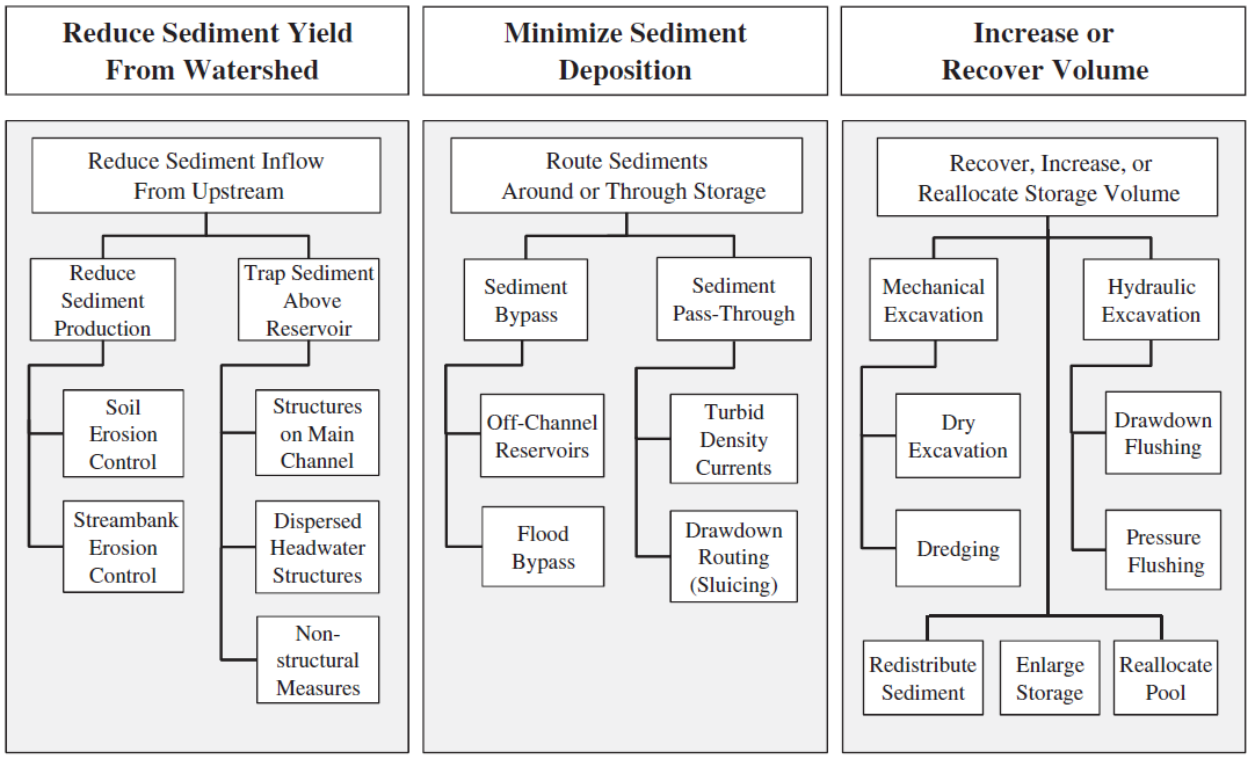

Figure 2. Diagram of Sediment Management Options for Reservoir Sustainability (taken from Kondolf et al. 2014)

The majority of sustainable sediment management options which are applicable to Reclamation's Mission are focused within the second and third categories presented in Figure 2. The first category, watershed management, is to reduce the amount of sediments entering there reservoir (thereby reducing sediment yield) would require involvement with other federal agencies, such as the U.S. Forest Service, Bureau of Land Management, State, County, and City resource managers, and private landowners.

Watershed management options include the control of land use practices; such as grazing, mining, logging, and land development. Other structural options include the development of land terracing, check dams, erosion control structures, and sediment basins in tributaries. A unique method is warping, which is the release of sediment laden flows on agricultural land to filter out sediments and return clearer flows back to the river.

The second category involves reducing sediment deposition of sediments flowing into a reservoir. This would either entail designing features to bypass sediment either through or around the reservoir. Included is the construction of bypass features in the reservoir, which may be an open channel, tunnel, or pipeline to divert sediment-laden flows from upstream end of the reservoir and discharge the flows downstream of the dam. Other means of reducing sediment deposition is to allow sediment-laden flows to pass-through the reservoir, either by allowing turbid density currents to pass through outlet works structures while the reservoir is full, or by drawing down the reservoir before the arrival of sediment-laden flows to keep flow velocities high enough through the reservoir and outlet works to pass sediment. Another option is this category includes the development of offstream reservoirs, where sediment-laden flows pass downstream, and clear water flows are diverted from the river to the reservoir.

The third category involves methods to remove deposited sediments. The first subcategory is hydraulic removal, where either the reservoir is drawn down, allowing flow velocities to increase near outlet works structures in order to erode previously deposited sediments (drawdown flushing), or by opening the outlet works gates and to not allow the reservoir to completely draw down, but rely on velocities near the structure to flush sediments through the gates (pressure flushing). The second subcategory is mechanical removal of sediments, which is by either dredging deposited sediments while storage remains near full in the reservoir or by dry excavation with construction equipment when the reservoir is drawn down.

Dredging is the most common sediment management method for reservoirs located in regions where carry over storage through multi-year droughts is paramount, and the reservoir cannot be drawn down. Dredging is typically more expensive than operational sediment management techniques (flushing or sluicing) to pass sediment downstream of the dam, and typically only occurs locally around structures due to the expense. Basson and Rooseboom (1997) noted that dredging is generally more expensive than creating new storage (e.g. dam raise), but that technology has narrowed the gap in cost. The most typical type of dredgers are cutter-suction and bucket-wheel types for reservoir depths less than 30 meters. If the reservoir is short enough in distance (e.g. less than 4km), a hydrosuction type of dredge is the most economical dredging option. Electric powered dredging is cheaper than diesel-powered when electricity is readily available nearby. The disposal cost of sediment is a major factor when estimating the cost of dredging as a sediment management option for reservoir sustainability. The dredging of reservoirs to maintain storage capacity is less expensive than dredging for navigation because the shape of the excavation area is not nearly as important and there is less movement and downtime with reservoir dredging.

Basson and Rooseboom (1997) and Morris and Fan (1998) both provide comprehensive information on the dredging of reservoirs for sediment management.

Timing of Methods:
Recovering decades of storage lost to sedimentation may be cost prohibitive. However, long-term dredging of the average annual sediment load may be economically viable, especially when compared to the long-term costs of no action and reservoir retirement.

The timing of reservoir sediment management methods is generally determined on a site-specific basis. For example, the method of sluicing requires drawdown of the reservoir before the arrival of the snowmelt or flood season in order to pass the initial sediment-laden flows and then capture the clear water flows at the end of the flood season for storage and use during drier periods of the year. Dredging may need to occur while the reservoir is or nearly at full pool for the dredger to access and remove deposited sediments. Nonetheless, dredging could occur at different locations depending on the reservoir level, where depths ranging from 30 to 50 feet are targeted. Over the longer term, sediment management methods may occur annually or periodically (e.g. biennial, decadal), depending on the rate of inflowing sediments and other site constraints.

c. Define Stakeholders and Constraints:

The majority of dams and reservoirs will have a unique combination of site specific constraints. Critical to the identification of site constraints is the involvement of all stakeholders that benefit or may be impacted by the implementation of sediment management methods for reservoir sustainability. The determination of unique and potentially conflicting requirements on a given reservoir or set of reservoirs is necessary prior to further development and implementation of any reservoir sediment management methods within a plan. The general types of constraints to identify as part of developing a sustainable reservoir sediment management plan are:

a. Physical Constraints
    a. Dam Height
    b. Storage Volume
    c. Reservoir Length and Width
    d. Hydrology
    e. Geology
    f. Spatial sediment distribution
    g. Sediment grain size
b. Operational Constraints
    a. Allocation of Use
    b. Carryover Storage
c. Economic Constraints
    a. Loss of Revenue
    b. Reduction of Benefits

c. Costs of retirement under the no action alternative

d. Environmental Constraints
   i. Downstream Impacts
      1. Infrastructure
      2. Water Quality
      3. Reversal of channel degradation
      4. Permitting
      5. Other reservoirs
   ii. Upstream Impacts
      1. Reversal of channel aggradation
   iii. Contaminants

e. Other Constraints

In most cases, the implementation of a reservoir sustainability plan will cause a reduction in benefits in the short-term, with the tradeoff that the reduced benefits will be available on a sustainable basis. Some stakeholders will potentially lose some short term benefits in order to sustainably manage a reservoir. Ultimately, however, all benefits would be lost to all stakeholders if the reservoir fills with sediment and the dam must be decommissioned at great expense to future generations.

d. <u>Assess Feasibility and Economic Viability of Options:</u>

The economics, or in other words, the associated costs relative to the associated benefits over the life of the reservoir, ultimately drive whether to finance sediment management methods to manage a reservoir sustainably. Traditional design and economic analyses do not appropriately take into account the long-term costs or benefits to achieve reservoir sustainability (Garcia et al., 2008). The long-term loss of benefits for agricultural, municipal, industrial, recreational, and other uses due to the loss in reservoir storage due to reservoir sedimentation must be accounted for in comparison to the long-term costs of maintaining the associated benefits the facility provides, in addition to the cost of decommissioning the dam or the creation of additional storage once reservoir sedimentation problems have become too severe.

The goal of making a resource, in this case the water storage a reservoir provides, sustainable or renewable requires a change from the traditional economic concept of time discounting a reservoir's value, which ignores the potential loss of benefits to future generations. A life cycle approach must be developed, where either the reservoir is managed as an exhaustible resource with a sinking fund to pay for the decommissioning of the dam and the development of new storage, or to manage the resource sustainably, such as using the RESCON (REServoir CONServation) approach (Palmieri et al, 2003).

As best stated in Garcia et al. (2008), the RESCON methodology proceeds in three stages:

1. Determine which methods of sediment management are technically feasible;
2. Determine which alternatives are more desirable based on an economic analysis;
3. Incorporate environmental and social factors to select the best course of action for sediment management.

The RESCON approach is applicable to proposed or existing dams and reservoirs to develop a preliminary assessment of sustainable sediment management alternatives, and to compare the alternatives to the alternative of allowing the reservoir to fill up with sediment and the ensuing course of dam decommissioning (Garcia et al., 2008). The RESCON approach accounts for major benefits and costs over the complete project life-cycle and, in particular, acknowledges the concept of *intergenerational equity*, which is the concept of taking into account the economic, social, and environmental cost and benefits of all future generations. Making a reservoir a sustainable, rather than an exhaustible resource, promotes intergenerational equity (Annandale, 2013). Additional information regarding the performance of the RESCON approach as part of determining sustainable sediment management options for a reservoir can be referenced in Palmieri et al (2003).

Environmental Considerations:
In order to achieve reservoir sustainability, a change in the operation and maintenance of the reservoir may be required. It is then necessary to consider the environmental consequences, and to minimize any impacts that are potentially detrimental. For example, some sediment management methods require the passing of sediments downstream of the reservoir. The release of high sediment concentrations from a reservoir can pose serious impacts to downstream aquatic environments, infrastructure, and recreation (Utah Division of Water Resources, 2010). However, high sediment concentrations could be of benefit to fisheries and geomorphic features reliant on higher sediment concentrations (e.g. cover and sandbar development), such as the case in many Southwestern United States Rivers (e.g. Colorado River in the Grand Canyon). Federal laws and agencies are in place to enforce the law of the land where, in the case of the United States, relatively strict water quality standards are in place to protect environmental resources. Determination of water quality impacts from reservoir sediments and any potential contaminants must be analyzed to minimize adverse environmental impacts and to comply with various laws, such as the National Environmental Protection Act, Clean Water Act, and the Endangered Species Act (Utah Division of Water Resources, 2010). Sources providing more information on sediment impacts and regulatory requirements include Sedimentation Engineering (Garcia et al., 2008) and Managing Sediment in Utah's Reservoirs (Utah Division of Water Resources, 2010).

e. Develop and Implement a Sediment Management Plan:

Based on the potential feasible sustainable sediment management methods that are determined in combination with the RESCON approach, water quality requirements, and any other unique site-specific constraints, a detailed consensus-based reservoir sustainability plan can be developed and implemented for the reservoir. The reservoir sustainability plan itself would detail any changes involving the dam and reservoir, which would include a combination of a monitoring plan of incoming, depositing, and passing sediments, the change in operational and maintenance procedures, the design and construction of new infrastructure to pass sediments, a periodic dredging plan, agreements of funding, and coordination with other stakeholders public and private.

f. Monitor and Revise Plan if Necessary:

As with the management of any resource, continued monitoring of reservoir sediments is necessary to track whether the implemented sediment management options are performing as predicted or not. If a particular sediment management method is not sustainably maintaining the storage of a reservoir, the plan may need to be revised to meet the criteria of sustainability. This revision of the plan may require one or more of the previous steps outlined in this document.

CONCLUSION AND SUMMARY

This technical paper details the general steps and guidance that could be followed in developing a reservoir sustainability plan (Reclamation, 2015). The dam owner and investigator(s) should not only follow these general guidelines, but should refer to other guidelines and case studies that are widely available and referenced throughout this document, such as Utah Division of Water Resources (2010), Garcia et al. (2008), Morris and Fan (1998), and Basson and Rooseboom (1997). Development of reservoir sustainability plans for reservoirs will be no less site-specific and unique as the site conditions and operations that each dam and reservoir inherently encompasses. The reservoir sustainability guidelines outlined in this document are:

a. Determine the magnitude of the sediment problem
b. Define preliminary sediment management options
c. Define stakeholders and constraints
d. Assess feasibility and economic viability of options
e. Develop and implement a sediment management plan
f. Monitor and revise plan if necessary

Findings from the research in Reclamation (2015), pertinent to Reclamation's inventory of dams and reservoirs, recommends the development of additional Geographic Information System (GIS) data that includes the storage capacity, drainage area, mean annual inflow, and mean annual sediment yield for all Reclamation reservoirs. This data would be valuable in further determining the relative impact of reservoir sedimentation in all Reclamation reservoirs, short of a comprehensive reservoir survey program for all Reclamation reservoirs. Additional reservoir sedimentation distribution tools can be refined and developed to estimate the spatial and temporal impacts of reservoir sedimentation to important features. Other prioritization schemes to determine the necessity of a sediment management plan or dam decommissioning may be necessary. These decision-making schemes may involve the quantification of the time until sediments reach key features, and the quantification of the loss of benefits as a result of plugging, burial, and/or abrasion of pertinent features which provide benefits.

REFERENCES

Annandale, G.W. (2013). Quenching the Thirst: Sustainable Water Supply and Climate Change, CreateSpace, North Charleston, S.C.

Basson, G.R., and Rooseboom, A. (1997). Dealing with Reservoir Sedimentation. Water Research Commission Report No. TT 91/97, Pretoria, xxxiii+395 pp.

Brown, T. C. (2006), "Trends in water market activity and price in the western United States" Water Resour. Res., 42, W09402, doi:10.1029/2005WR004180.

Bureau of Reclamation (1992). Statistical Compilation of Engineering Features of Bureau of Reclamation Projects. United States Department of Interior. Bureau of Reclamation. Denver, CO.

Dendy, F.E., Champion, W. A., and Wilson, R. B. (1973). Reservoir sedimentation surveys in the United States. American Geophysical Union, Washington D.C.. 17: 5-7. doi: 10.1029/GM017p0349.

García, M. H. (2008). Sedimentation Engineering, Manual 110, Chapter 12, ASCE, Reston, Va.

Gray, J.R., Bernard, J.M., Stewart, D.W., McFaul, E.J., Laurent, K.W., Schwarz, G.E., Stinson, J.T, Jonas, M.R., Randle, Timothy, and Webb, J.W., 2010, "Development of a National, Dynamic Reservoir Sedimentation Database". Proc. 9th Federal Interagency Sedimentation Conference, June 27–July 1, Las Vegas, Nevada, 12 p.

Kondolf, G.M. et al. (2014). "Sustainable Sediment Management in Reservoirs and Regulated Rivers: Experiences from Five Continents". *Earth's Future, 2,* 256-280, doi:10.1002/2013EF000184.

Minear, J. T., and G. M. Kondolf (2009), "Estimating reservoir sedimentation rates at large spatial and temporal scales: A case study of California", Water Resour. Res., 45, W12502, doi:10.1029/2007WR006703.

Morris, G.L., and Fan, Jiahua. (1997). Reservoir Sedimentation Handbook. McGraw-Hill. New York.

Murthy, B. N. (1977). *Life of reservoir,* Central Board of Irrigation and Power, New Delhi.

Palmieri, A., Farhed, S., Annandale, G. W., and Dinar, A. (2003). "The RESCON Approach: Economic and Engineering Evaluation of Alternatives Strategies for Managing Sedimentation in Storage Reservoirs." The World Bank, Washington, D.C.

Reclamation (2015). Formulating Guidelines for Reservoir Sustainability: Submitted to the Reclamation Science and Technology Program. U.S. Department of the Interior. Bureau of Reclamation. Technical Service Center Sedimentation and River Hydraulics Group. Denver, CO.

Reclamation (2012). 3D Visual Reservoir Sedimentation Model and Sediment Manual, Bighorn Lake, WY/MT, Pick-Sloan Missouri Basin Project, Great Plains Region. Bureau of Reclamation.

Reclamation DataSpace Version 10.0.0.0. (2006-2011). U.S. Bureau of Reclamation\The Michael Thomas Group Inc. Accessed Aug 15, 2014.

Reclamation (2006). Erosion and Sedimentation Manual. U.S. Department of the Interior. Bureau of Reclamation. Technical Service Center Sedimentation and River Hydraulics Group. Denver, CO.

Reclamation (1962). Revision of the Procedure to Compute Sediment Distribution in Large Reservoirs, Sedimentation Section, Bureau of Reclamation, Denver, CO.

Reclamation (1982). Reservoir Sedimentation, Technical guideline for Bureau of Reclamation, Sedimentation and River Hydraulics Section, Bureau of Reclamation, Denver, CO.

Utah Division of Water Resources (2010). Managing Sediment in Utah's Reservoirs: Utah State Water Plan.

AN INVENTORY OF SEDIMENTATION IN HAWAII'S RESERVOIRS USING MIXED METHODS

Kim Falinski, Research Assistant, University of Hawaii at Manoa, Water Resources Research Center, Honolulu, HI 96822, falinski@hawaii.edu; David Penn, Project Coordinator, Pacific Cooperative Studies Unit, University of Hawaii at Manoa, Honolulu HI 96822, dpenn@hawaii.edu

Abstract: Hawaii's reservoirs face increasing scrutiny due to heightened dam safety and flood control concerns, growing water demands, and uncertain water pollution effects. In order to promote long term reservoir sustainability, it is vital that we improve our understanding of reservoir capacity loss due to sedimentation. We collected, organized, and analyzed existing physical data about reservoirs located on the main Hawaiian Islands, and interviewed reservoir managers throughout the state about storage capacity and sedimentation processes. Results showed that although sedimentation of Hawaii's reservoirs is rarely measured and poorly documented, it is a serious concern and the accurate measurement of reservoir sedimentation is a challenge for proper reservoir management. We grouped reservoirs into five different management types —federal, state, county, private agriculture and private development – and found that management practices and reservoir maintenance differed significantly between these groups. Sedimentation, in some cases, was significant enough to lead to dry reservoirs conditions. However, unlike in other parts of the world where reservoir sedimentation can be directly correlated with watershed erosion practices, most reservoirs in Hawaii are off-stream impoundments, fed by stream diversions and irrigation systems that are far from the watersheds above the reservoir. Existing engineering surveys focus on the structural integrity and safety of dams, few surveys address capacity loss. We suggest that the use of dual-frequency bathymetric surveying equipment would provide accurate assessments of reservoir depths, and recommend a cooperative effort to systematically conduct statewide surveys. Reservoirs in Hawaii are a significant resource for adaptive and sustainable water supply, conservation, and flood control, and as such the maintenance, including assessment and removal of sediments, is an important consideration for water use and development on each island.

INTRODUCTION

Worldwide, sedimentation is a leading causes of reduced capacity in small reservoirs (Wang and Hu, 2009). Global water use is rising with population and development, while long-term water availability is declining, posing challenges for resource managers. Water needs and constraints in Hawaii follow this pattern (Water Resources Associates, 2003; Bassiouni and Oki, 2013). With a rapidly growing population, increasing development, and the forecasted establishment of a diversified agricultural sector, Hawaiian resource planners and managers must carefully consider how to meet growing water demand while balancing human welfare, economic impact, and ecological sustainability. Reduced reservoir storage capacity has real economic costs, including less available water, higher maintenance costs (i.e. dredging), greater risk of dam breach, less capacity to reduce flooding and capture sediments, and lower potential for electricity generation (Hawaii Department of Agriculture, 2010; Randle et al., 2013).

In addition to providing water capacity, small reservoirs are also effective sediment retention basins that positively impact downstream water quality (Liu et al., 2014). Small reservoirs also increase water availability and reduce the peak flow of storm runoff (Deitch et al., 2013). Aquatic ecosystems can benefit from small dams that reduce the amount of sediment and nutrients carried in surface runoff (Verstraeten and Prosser, 2008). The ability to retain sediment is especially important for Hawaii where very small watersheds (often < 20 km^2) are directly connected to coastal waters that are highly valued for their coral reef systems and recreation use capacity. Sedimentation on the reef is considered to be a primarily driver of the ecosystem's decline in Hawaii (Jokiel et al., 2014).

Reservoir sedimentation data is used widely to better understand the relative contribution of watershed characteristics to sediment and nutrient export (Verstraeten et al., 2003). Modeling approaches that calculate annual sediment yield based on land use, such as InVEST and N-SPECT, are limited by a lack of validation data. For Pacific high islands such as Hawaii and Guam, the particular watershed physical characteristics and land use and management actions that dominate sediment export remain unclear (Nakama, 1992; Hoover and Mackenzie, 2009; Storlazzi et al., 2009). Additional sediment export data would help to calibrate and validate sediment export models for developing watershed-scale conclusions. Reservoir accumulation provides data that integrates physical and human processes over longer periods of time than most in-situ sampling efforts can achieve.

Regardless of whether reservoir sedimentation data are used to describe changes in water storage capacity or to better understand watershed processes that contribute to sediment export, an understanding of reservoir sedimentation processes is critical to surface water management (Angulo et al., 2011; Ignatius and Jones, 2014). The United States Geological Survey (USGS) maintains nation-wide information about reservoir sedimentation for the Reservoir Sedimentation Database (RESSED, http://water.usgs.gov/osw/ressed/). However, the RESSED database currently does not currently contain any records for Hawaii reservoirs.

Therefore, the objectives of our research were to (1) analyze existing Hawaii reservoir data for trends that could be related to reservoir sedimentation, and to (2) conduct semi-structured interviews with the reservoir managers and owners to augment and explain archival information and available reservoir records.

BACKGROUND

The Hawaiian island chain, located in the north central Pacific Ocean, has a total land area of 16,636 km^2. The formation of the volcanic islands created high, steep, rain-catching ridges and dikes that confine freshwater in basal and high level aquifers. The islands have few natural freshwater lakes, 376 perennial streams (providing more than half the irrigation water statewide), and nearly all water for domestic and industrial use is obtained from groundwater supplies (Tribble, 2008). Flashy streams in short watersheds prevent streams from storing sediment in floodplains. Streams supply more than 50% of irrigation water in Hawaii, which is often stored in reservoirs (Oki, 2003).

The sugar industry was a major driver of Hawaii's economy from the mid-1800s until the mid-1900s. The first successful sugarcane plantation began on Kauai in 1835. As the forests were cut down to create more land for sugar, records indicate that the amount of rainfall decreased, as well (MacLennan, 2007). Ambitious irrigation ditch systems were created to bring water from higher elevations to the plantations, and reservoirs were used to store that water. The major irrigation systems include the Pioneer Mill irrigation system in west Maui, the Waimea irrigation system on Hawaii Island, and the East Kauai irrigation system in Kauai (Wilcox, 1996). The sugar industry began to falter in the 1930s, and continued to decline into the 1940s and 1950s, when pineapple rose in prominence as a cash crop. Pineapple was farmed commercially in the islands until the late 1990s to early 2000s, when industrial farms stopped production. Land use changes (urbanization) in the last century led to decreases in overall water demand but increases in potable water demand. Climate change impacts may create conditions that are drier in some areas, and wetter in others, that could change vegetation patterns and the frequency and intensity of large storm events leading to more erosion into reservoirs (Timm and Diaz, 2009).

Agriculture in many parts of the islands depends on a steady irrigation supply, yet Hawaii's 140 largest reservoirs that store water for irrigation are currently being breached and decommissioned at a rapid rate. This is due to a variety of factors, including (1) tighter dam safety regulations that took effect following the 2006 Kaloko dam break, (2) the risk of structural instability due to age, construction, and deferred maintenance, (3) the loss of storage and operational capacity caused by sedimentation, debris accumulation, and clogging of inlet and outlet structures; and (4) the lack of paying customers for reservoir-based water service. Figure 1 shows the location, size and use type for DLNR-regulated reservoirs in Hawaii. Reservoir water use was valued at $436 million by the US Department of Agriculture in 2003. The Hawaii Dam Safety Act, which determined that the landowner was responsible for the maintenance of reservoirs on their land, was passed in 1987. On March 16, 2006, the Kaloko reservoir on northeastern Kauai broke during heavy rains, killing seven people (Godbey, 2007). The Dam Safety Act was updated in 2007 to more closely supervise the safety of the remaining reservoirs (Hawaii State Legislature, 2007).

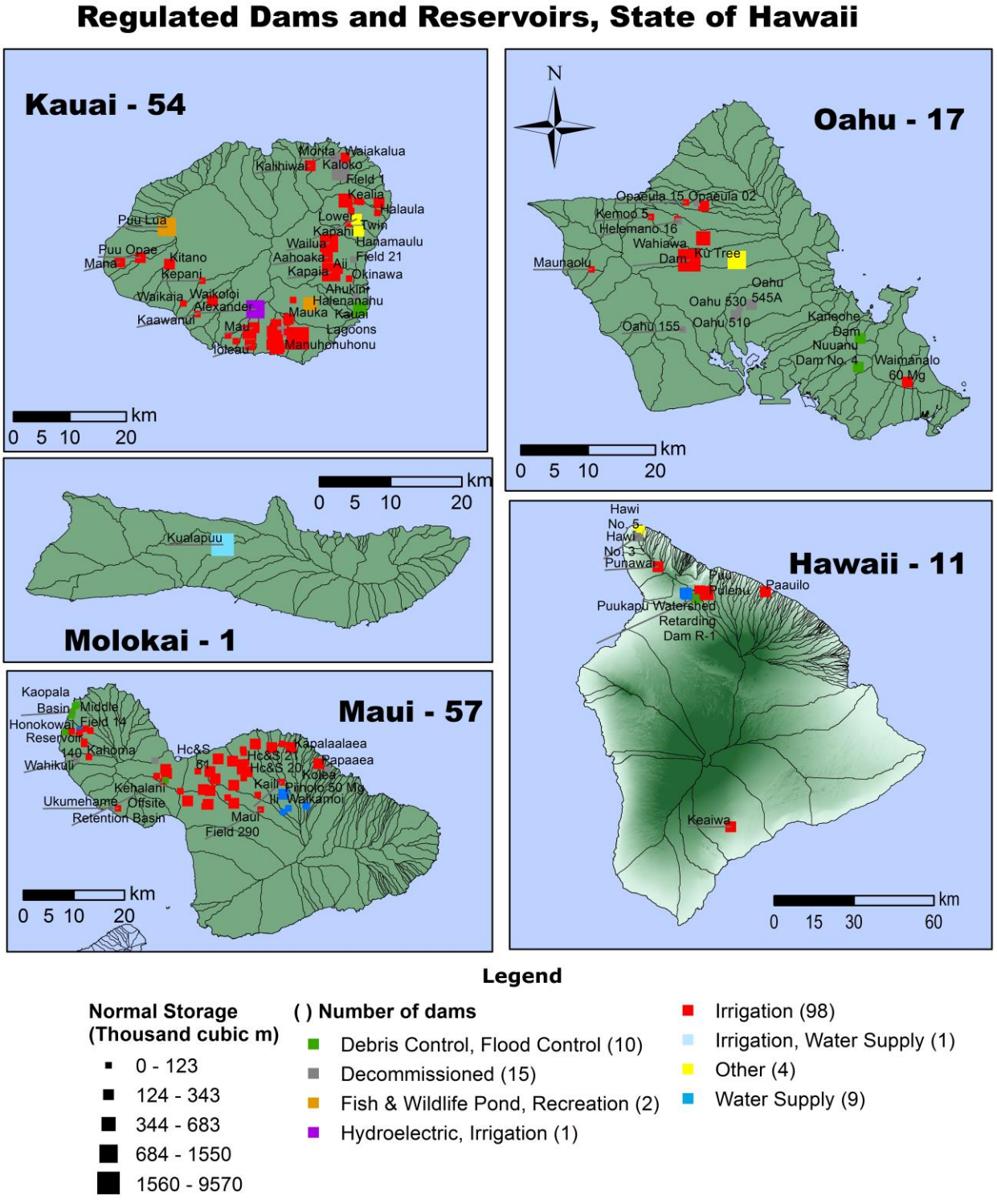

Figure 1 Reservoirs classified by use type. The total number of reservoirs in the Hawaii Dam Safety database (as of March 2013) is listed next to the island name. Some reservoirs have since been decommissioned. GIS data made available from the State of Hawaii Office of Planning, the Coastal Geology group at University of Hawaii at Manoa and the Department of Land and Natural Resource Dam Safety program.

METHODOLOGY

Data Acquisition

We obtained permission from the U.S. Army Corps of Engineers to access the National Inventory of Dams (NID) via its secure online portal. At an initial meeting with the staff of the State of Hawaii Dam Safety Program (HDSP), we obtained similar permission to access the HDSP inventory. The NID and HDSP contain about the size, capacity, spillway characteristics, year built, and ownership of most of the 140 regulated reservoirs in Hawaii. Management types in the databases were further classified by owner into five categories: Federal, State, Local, Private-Agriculture and Private-Development (defined as private owners who manage three reservoirs or less by a single private owner).

With the federal and state inventories as our foundation, we conducted literature searches and gathered references that document reservoir-specific physical characteristics (e.g., geotechnical investigations, dam safety inspections, emergency action plans, and environmental assessments). We collected the HDSP reports to the legislature from 2007 to 2015 describing changes in the dam status (Dam and Reservoir Safety Program, 2011) and private reports on selected reservoirs, obtained with the permission of reservoir owners and the cooperation of reservoir authors. Additionally, we used remote sensing products including 2011 World View 2 (1m resolution) to determine whether a reservoir was being maintained dry or not dry, and compared these results to other sources.

To house this information, we created a database in Microsoft Access that mimics the structure of the national RESSED database for data input, and combined and cross-checked the data from both the NID and HDSP databases with the RESSED fields. Lastly, we added fields that are not part of the official RESSED structure, yet allow for more detailed analysis of the dataset, including operational water level, excavation history, and level of sedimentation.

Interviews with Reservoir Owners

Using the HDSP inventory, we contacted the 42 dam owners and operators, covering the 140 reservoirs in the HDSP inventory, to participate in our project. The survey instrument used in the follow-up phone and on-site interviews is presented in Table 1. The survey was designed to locate and acquire existing information, and to provide a semi-structured opportunity for reservoir managers to describe possible problems related to sediment accretion and mitigation efforts. After the interview was conducted, we summarized open-ended responses into themes (Wengraf, 2001). Interviewees are not identified by name in this report, and information provided about specific reservoirs was acquired through public records.

Table 1. Survey instrument for Hawaii's regulated reservoir owners and managers.

	Question	Answer format
1	When was the last time your reservoir(s) was (have been) surveyed/measured?	Year
2	Original plans available?	Yes/no
3	As-built drawings available?	Yes/no
4	How many times has it been surveyed?	Number
4a	Who did the survey?	Name
4b	What method?	Acoustic, bathymetric survey, sediment sampling,
4c	How much did it cost?	Number
5	Why did you do it?	Open
6	What will you do with the results?	Open
7	Are you willing to share those results with us?	Yes/no
8	What is your level of interest in conducting new surveys/measurements in order to find out how much the reservoir has filled in with sediment? (1–5)	Scale (1–5)
9	Is sedimentation a significant issue in the reservoirs you manage?	Open
10	What mitigation efforts have you used to prevent additional sediment?	Open

	build-up?	
11	What are your incentives for continuing to use/maintain the reservoir?	Open
12	Would you like to continue to talk with us and help us gather more information on reservoir sedimentation in Hawaii?	Yes/No

Between April and August 2013 we visited publicly and privately owned reservoirs on the islands of Oahu, Maui, and Hawaii, and gathered other information through email and phone calls. The primary purpose of the site visits was to visually survey and assess the extent of reservoir sedimentation and to gather otherwise unavailable copies of documents describing sedimentation. Through extensive collaboration with the Hawaii Department of Agriculture we obtained particularly significant information about a number of reservoirs.

RESULTS

Although there were 140 regulated reservoirs in the state of Hawaii as of 2013, only one is documented sufficiently to populate the record fields required by the national RESSED database: Kaneohe reservoir, Oahu (see Wong (2001)). Of the 25 regulated dams removed statewide since the program began, most of the removals were initiated after the 2006 Kaloko dam disaster and the 2007 regulatory response (11 on Oahu, 3 on Maui, 5 on Hawaii and 4 on Kauai). Seven reservoirs that were local or state owned had partial information that could be provided to the RESSED database, including Nuuanu Dam and Kalihiwai Reservoir (Aqua Technex, 2009) have bathymetric surveys. We identified recent engineering studies for 34 reservoirs that were conducted for dam safety compliance purposes, many involving dam breach, removal or undersizing. Our research indicated that each reservoir has a unique history of maintenance, sediment build-up and water use, and that to acquire sedimentation data for specific reservoirs requires a detailed, recorded history of how it was managed and operated in the past. Evidence is mostly anecdotal, and the types of documents typically did not include formal sedimentation surveys. The most complete datasets are associated with public works reservoirs and reservoirs owned by large corporations. During this investigation, we found that many irrigation systems are spatially disconnected from the watersheds that provide the system water.

Data Analysis of Reservoirs in Hawaii

Hawaii's reservoirs have the capacity to store 44.6 million cubic meters (11,800 Mgal) of water at normal levels, with the majority of the capacity (43%) located on Kauai (Table 1). Statewide, most reservoirs are used for irrigation purposes (80%), as seen in Table 2, and only 10 reservoirs are purposed for municipal water supply. Categorical analysis made some calculations difficult, especially when reservoirs were listed with multiple uses (this occurred in 26 out of 140 dams). An example is Alexander reservoir in Kauai, used for both hydroelectric power generation and for irrigation. Multiple uses of reservoir water allow for multiple benefits to the hydrologic systems.

Table 1 Storage capacity by island.

	Normal Storage (thousand m^3)	Maximum Storage (thousand m^3)	Percent of total capacity
Hawaii	1532	3681	3%
Kauai	19184	33872	43%
Maui	5362	8349	12%
Molokai	5261	6269	12%
Oahu	13325	25655	30%
Total	44665	77825	57

Compared to other worldwide locations where significant information for watershed sedimentation processes are collected from sediment deposition rates, 80% of the reservoirs used for irrigation in Hawaii often have water delivered far from the reservoir, or only a portion of the stream is used to supply the reservoir. These off-stream, and sometimes off-ditch reservoirs do not offer enough information to be able to discern larger watershed processes, but are still relevant to understanding the loss of capacity due to sedimentation.

Only Kualapu'u reservoir on Molokai is used for both irrigation and water supply, and its normal operating level is kept close to capacity. In general, we found that the reservoirs were only kept close to capacity when used for water supply (80% of max) or for fish and wildlife ponds (97% of max) (Table 2). The operating level for irrigation reservoirs, which represent 80% of all reservoir use averages at 67% capacity. The one hydroelectric dam that is currently regulated in Hawaii operates at 42% maximum storage capacity. However, conversations with the owner indicate that sediments are problematic and contribute to reduced storage level. Although 64% of the reservoirs are considered small in size, 74% of the capacity is provided by intermediate sized reservoirs (n = 49)[1].

Table 2 Data for reservoirs use type across the Hawaiian Islands.

Reservoir Type	Normal Storage (thousand m^3)	Max Storage (thousand m^3)	Number of Reservoirs	Percent of Total	Percent Capacity	High or Proposed High (%)+
Debris control	191	773	5	4	25	100
Flood control	1298	13791	11	8	9	91
Fish and wildlife pond	1771	1826	3	2	97	67
Recreation	2456	12184	7	5	20	100
Hydroelectric	1320	3133	1	1	42	100
Irrigation	38957	58164	112	80	67	88
Water supply	6297	7876	10	7	80	80
Other	4188	5653	17	12	74	82

+ Hazard classification refers to the design of the dam spillway relative to the probable maximum inflow flood

The majority (by number) (70%) are reservoirs are owned in part by private owners, including large farms (56%) and a diverse array of owners, including small farms, housing developments and recreation and tourism facilities (14%) (Figure 2). The Private-Development group is more likely to be using the reservoirs for development or other urban reservoir uses, including for aesthetic reasons. Unlike the private and agriculture owners, smaller private owners are less likely to have the resources to repair or excavate reservoirs.

[1] The National Inventory of Dams specifies small reservoirs as less than 1,000 ac-ft (1,233,481 m^3) and greater than 50 ac-ft (61,674 m^3); intermediate reservoirs are between 1,000 ac-ft (1,233,481 m^3) and 50,000 ac-ft, (61,674,092 m^3) and large reservoirs are greater than 50,000 ac-ft. Academic literature generally considers small reservoirs to be less than 100,000 m^3.

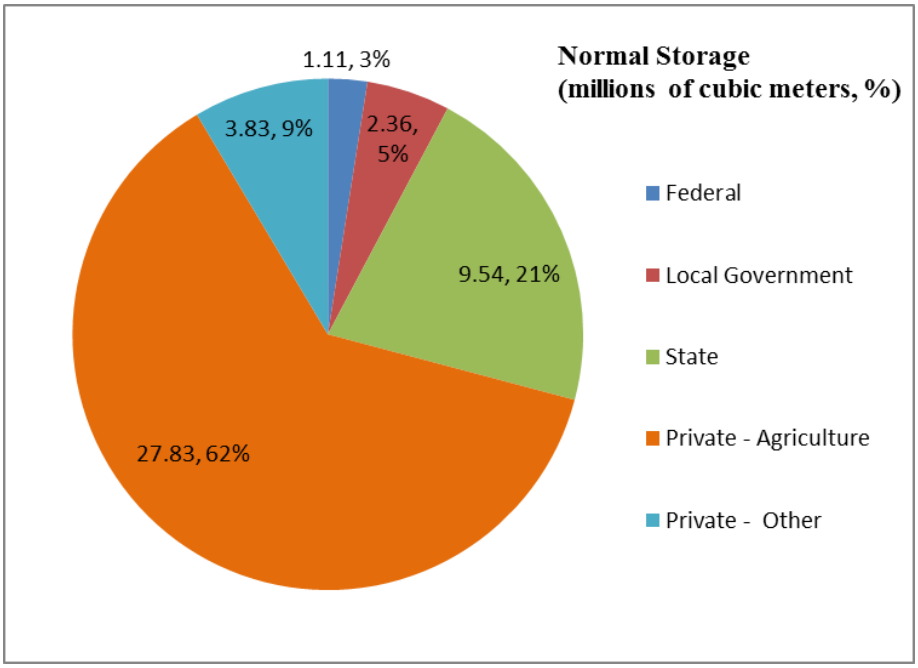

Figure 2: Storage capacity of Hawaii's reservoir by management type

Figure 3 presents the cumulative age of reservoirs for the four counties of Hawaii. Many of Hawaii's reservoirs are approaching 100 years old. The rate of reservoir building slowed considerably after 1920, and no new reservoirs were built before and after World War II (1935-1951), or between 1958 and 1965. With the exception of Kualapu'u on Molokai, finished in 1969, reservoir size too declined over time, by about 4800 m^3 per year, on average. Kualapu'u, as a large reservoir, was created during the water engineering boom post-1950 that was seen nationwide. The results are more striking if you consider the many reservoirs that were built and decommissioned from use before the Hawaii Dam Safety Program was established in 1987, known today only through archival records.

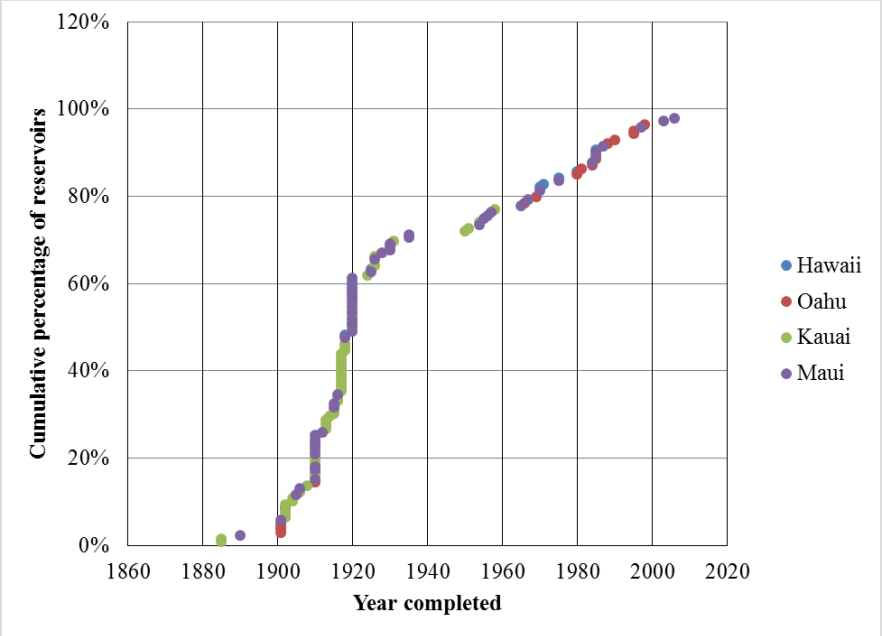

Figure 3. Age distribution of reservoirs by county, State of of Hawaii. Note that nearly 60% of the reservoirs were completed by 1920. The most recent dams have been constructed for flood prevention and sediment retention.

Interviews with Reservoir Owners

Table 3 indicates that most reservoir managers have experienced some level of sedimentation issue with their reservoir, and that others have developed methods to mitigate the effects of sediment build-up.

Table 3 Summary of survey responses by owner type.

	Federal	State	Local Government	Private-Agriculture	Private-Other	Total
Number of owners	1	4	6	9	15	35
Number responded to survey	1	3	3	5	10	22
Mean interest level (1-5)	5	4	5	5	3.4	

Interviews and field visits suggest that sedimentation is not the primary issue for compliance with safety regulations; dams are vulnerable to aging infrastructure. As a result of the new regulations after the Kaloko reservoir breach, many owners are shifting towards decommissioning their reservoirs. Historically, Private-Agriculture reservoirs were maintained through public-private partnerships, but lack of finances and demand combined with a more robust dam safety regulatory structure led to their disuse. Individuals, trusts, and smaller business associations that generally managed only one or two reservoirs (private/other) are facing greater struggles to understand and comply with the new dam safety regulations, and some have made significant investments in engineering studies to substantiate their position with dam safety regulators (see for instance Kalihiwai homeowners, County of Honolulu Board of Water Supply).

Notably, many former and current large agricultural land owners with multiple reservoirs employed a single point person to manage all the reservoirs. These managers made few written records available, but shared their institutional knowledge and expertise. Larger agriculture owners acknowledged sedimentation as a fact of life, actively used reservoirs as detention basins, and implemented schedules for dredging accumulated sediments. It appears that this group may be an important source of formal records, and represents some of the most useful sites for field surveys of sedimentation rates.

Another theme that emerged from the conversations was that there are at least 300–400 unregulated dams with no reporting requirements that would otherwise provide information to facilitate the achievement of watershed research objectives. Not surprisingly, there is a trend towards taking a regulated reservoir and converting it to a smaller non-regulated reservoir. Increasingly, watershed management plans are suggesting that smaller dams (often smaller than the regulated limit), including gabion dams, be used as retention basins to mitigate sedimentation into coastal waters (for instance, the Ala Wai Watershed Management Plan (2013) and the Lanai Community Plan (2014)). The longevity of these structures and their ability to withstand flood events remains unclear.

Many of the interviewees perceived that there is an ideal method for removing sediment from a reservoir. Current practice is to drain the reservoir, which may take several weeks, and then manually remove sediment using backhoes and other mechanical equipment. If the reservoir was not originally designed to allow access for these types of vehicles, then the sediment must be removed manually. This was done recently at Waikoloa Reservoir No. 2 on Hawaii Island, which suffered earthquake damage in 2006. Private agricultural companies have the heavy earth moving and forming equipment available, and can also divert water to allow the reservoir to be dredged. The dredge spoils can be then placed on land. If the landowner does not have a use for the excavated sediment, transport and disposal pose additional challenges. Material including sediment-sorbed contaminants may prevent movement of the sediments to other properties or landfills.

Reservoirs that are operated and maintained for public water use consider sediment in their maintenance costs. For instance at the Waikoloa reservoirs, sediments are removed through flocculation processes (requiring flocculant additives), and the water is treated in sedimentation basins. The sediments must periodically be dredged and treated per Department of Health requirements.

The interviews and government document research found that many owners and operators conduct new investigations to support dam removal and compliance with newly revised dam safety regulations. These investigations (often by consulting companies) typically do not include measurement of reservoir bathymetry and determination of base elevation and changes in bed elevation over time, thereby neglecting possible capacity loss to sedimentation. Investigations consist primarily performing of structural analyses and presenting recommendations for maintaining the reservoir in a safe condition.

Interviewees suggested that while the sugarcane plantations frequently dredged out small reservoirs to retain full capacity, large reservoirs were not usually dredged unless sediment and debris blocked the reservoir inlets. In most case, sedimentation is not the only limitation to water capacity. Most of the aging reservoirs require the installation of new-HDPE style liners (or equivalent) to prevent seepage, as well as vegetation removal and structural improvements for earthen embankments that have degraded over time. Maintenance of dilapidated spillway, pump systems and removing vegetation are the primary modifications that need permits.

Another theme that emerged from the interviews, specifically with larger agricultural managers, was the use of reservoirs (both regulated and non-regulated) for fire mitigation. . It is estimated that 0.5% of the total state land area burns each year (Hawaii Wildfire Management Organization 2014), and fire is recognized as a major threat to native species in remaining forest lands (Conry, 2010). Interviewees, especially managers of agricultural lands that had gone fallow, indicated that reservoirs were often used by local and state agencies to combat wildfire. Previously, plantation and ranch personnel served as fire wardens, but changing land use practices reduced the amount of people willing and knowledgeable to serve in this role. In combination with the reduction of reservoirs operating at capacity, reduced capacity from sedimentation presents a significant threat.

Erosion of irrigation channels is a concern that is separate from normally modeled hillslope processes, yet one that was mentioned by participants. The ditch system that once fed reservoirs today diverts water directly into streams, including Honokowai and Wahikuli Streams on Maui (Department of Land and Natural Resources, 2011) and streams in the Upper Kapaa region on Kauai. In other subtropical islands, many off-stream reservoirs that are fed by irrigation ditches, sedimentation is not a significant issue (Morris, 2010). Others, such as the Lower Hamakua ditch, reported an approximate one-foot depth of sediment build-up when it was refurbished in 2004. For the Maunawili ditch system on Oahu leading to Waimanalo Reservoir, interviews revealed that hired workers manually clean the ditches of silt and debris on a daily basis. Because many of the reservoirs are off-stream, they are often disconnected from the watershed-scale hydrologic processes. Sedimentation in the reservoir is still evident, although minimal, from the degradation of the channel leading into the reservoir.

Many reservoir managers (n=14) reported that the use of their reservoirs changed over time. For some managers, reducing the size of the reservoir below the regulatory limit was a solution more amenable than creating a new reservoir or maintaining the old reservoir at regulatory size. Other managers maintain their reservoir in a dry state, yet keep the reservoir in the system for possible future use or until it can be breached (for example, Manuhonuhonu reservoir, Kauai). Private-Development managers consider the reservoir that is now amongst homes and golf courses as an aesthetic asset, and the homeowners association or builder adopts the responsibility of maintaining the reservoir and the safety documents (for example, Kauai Lagoons, Kauai). These reservoirs are often still considered for irrigation use, flood control or other use in the database, but are providing a new ecosystem service to residents within their viewshed.

Two reservoirs on Oahu are notable for providing different uses than originally intended. Wahiawa reservoir, otherwise known as Lake Wilson, is a state recreation area known for its bass fishing. It also provides the important function of flood mitigation of the Kaukonaua streams leading to populated Haleiwa. As one of the largest reservoirs, no study has ascertained its current bathymetry, although it is assumed that sedimentation has reduced its capacity. Nuuanu Dam No 4, also used for flood protection, is currently being dredged (R.M. Towill Corporation, 2013). A bathymetry was completed in 2010, acknowledging that sediments had reduced capacity. Neither reservoir was originally designed for flood control. Similarly, the reservoirs build in west Maui in the 1980s for debris control (Honokowai Structure #8, Mahinahina, Kahana, and more) today are being used to capture sediment, yet their design does not permit efficient trapping of sediments during larger storms.

DISCUSSION

The level of information available for bed elevation and other sediment-related reservoir characteristics varies widely. It would take considerable effort (beyond the resources of the current project) to track down reasonably complete information about each reservoir. We determined that bed elevation is not routinely included in reservoir inventories, databases, and documents. In some cases, bed elevation may be derived from existing inventory data about dam height, site elevation, and reservoir depth (which by itself must generally be derived from reservoir surface area and storage capacity). However, initial estimates of original bed elevation are available for reservoirs national program investigations in the 1970s, which include area-capacity curves that indicate a base elevation at which storage capacity is zero (Harding-Lawson Associates, 1978).

No new reservoirs have been built since 2006, and a majority of the reservoirs built in the last three decades were built on Maui for a distinctly different purpose: to prevent debris from getting to the coral reef ecosystem offshore. Figure 3 represents only the ages of the reservoirs that are currently in the database; archival research indicates that many more reservoirs existed pre-1950 that were removed from use before the Dam Safety program was created. Similar with the responses of larger agricultural managers today, sugarcane-era documents support that reservoir building and maintenance occupied a significant amount of workers time. Lacking this maintenance, sedimentation of reservoir and degradation of irrigation ditches will continue to be a problem. Future research is needed to identify and employ efficient sediment removal methods that meet environmental protection requirements.

Funding is a critical issue for all aspects of reservoir sustainability. In 2014, Hawaii voters approved a legislatively referred amendment to the state constitution that authorizes the state to issue special purpose revenue bonds and use the proceeds from the bonds to offer loans to qualifying dam and reservoir owners to improve their facilities to protect public safety and provide significant benefits to the general public as important water resources (Hawaii State Legislature, 2014d). In addition, the state budget typically includes line items for generic reservoir safety improvements in state-owned irrigation systems and for specified capital improvements particular public reservoirs.

For example, the current biennium budget (July 2013-June 2015) includes $9 million for land acquisition, design, and construction for statewide reservoir safety improvements (deemed necessary to qualify for federal aid financing and/or reimbursement) and $7 million for compliance-related improvements to three specific reservoirs (Hawaii State Legislature, 2014a). However, the legislature did not approve separate measures that proposed to spend an additional $1.8 million for dam rehabilitation and remediation at a different public reservoir (Hawaii State Legislature, 2014b), and to require that a state agency prepare all studies to determine the safe removal or retirement of a dam or reservoir upon the request of a homeowner association or homeowner of property where a dam or reservoir is situated (Hawaii State Legislature, 2014c).

Re-developing agriculture in Hawaii will require reliable access to water for irrigation. Yet, the overall number of reservoirs in the state of Hawaii is in a steady decline. Irrigation reservoirs, which make up a majority of the reservoirs, have been decommissioned in the last five years at a disproportionately high rate, yet it was determined that sedimentation is not the highest concern of reservoir managers. Many reservoirs act like sediment retention basins, and prevent sediments from delivery and transport to coastal waters, thereby preventing possible water quality problems. The State of Hawaii may not have sufficient resources and interest to support the development and implementation of extensive reservoir sustainability measures. It remains to be seen how many more dams will be removed due to safety concerns and economic constraints. However, sediment deposition in reservoirs is an ongoing problem, and leaving issues unaddressed until problems become acute leads to costly, ineffective solutions.

CONCLUSION

The reservoirs of Hawaii serve multiple purposes – they are essential for irrigation, provide a safety net for water supply, offer possible provide habitat for aquatic ecosystems and perform as fire mitigation, flood and sediment controls. Our findings indicate that many reservoir managers consider sedimentation an operational concern, and that the current bathymetric data available does not allow for reliable estimates of watershed-scale sediment export processes. The database information analyzed here presents only part of the story, as there are many smaller reservoirs that are not regulated that serve important water capacity, fire prevention, flood regulation and sediment retention services. Quantifying actual reservoir storage capacity and the costs of restoring capacity lost to sedimentation are important considerations for water supply planning, as are detailed assessments of relationships

between stream diversions, ditch flows, reservoir storage, stream baseflows, and the achievement of instream flow objectives.

ACKNOWLEDGEMENTS

We would like to thank the USGS for providing support for this study under project number 2012HI370B. We are also grateful to the DLNR Dam Safety office, the Hawaii DOA, the Honolulu Board of Water Supply, and all of the interviewees for providing opportunities for collaboration.

REFERENCES

Angulo, J., A. Jenkins, et al. (2011). "Assessing the Lifespans of Reservoirs in Region 2 of Puerto Rico," pp.

Aqua Technex, L. (2009). "Kalihiwai Reservoir Bathymetry Study." from http://ww.kalihiwaireservoir.info/mapping_study.html.

Bassiouni, M. and D. S. Oki (2013). "Trends and Shifts in Streamflow in Hawai'i, 1913-2008," Hydrological Processes, 27(10), pp 1484-1500.

Conry, P. J. (2010). "Hawaii Statewide Assessment of Forest Conditions and Trends: 2010," Department of Land and Natural Resources, Division of Forestry and Wildlife, Honolulu, HI, 277p.

Dam and Reservoir Safety Program (2011). "Report on the Hawaii Dam and Reservoir Safety Program," Department of Land and Natural Resources, State of Hawaii, EN12-Dam-Safety-Report-FY11, 15p.

Deitch, M., A. Merenlender, et al. (2013). "Cumulative Effects of Small Reservoirs on Streamflow in Northern Coastal California Catchments," Water Resources Management, pp 1-18.

Department of Land and Natural Resources (2011). "Application for a Dlnr Dam Safety Contruction/Alteration Permit, Permit No. 48, Wahikuli Reservoir," Engineering Division, Hawaii Department of Land and Natural Resources, Honolulu, HI, Agenda Item L-1, July 11, p.

Godbey, R. C. (2007). "Report of the Independent Civil Investigation of Teh March 14, 2006 Breach of Ka Loko Dam: Volume 1," State of Hawaii, Special Deputy Attorney General, Honolulu, HI, 222p.

Harding-Lawson Associates (1978). "Phase I Report: National Dam Safety Program, Wahikuli Dam, I.D. No. 55." Department of the Army, Pacific Ocean Division, Corps of Engineers,. Honolulu, HI, p.

Hawaii Department of Agriculture (2010). "Economic Impacts of Agricultural Reservoir Closurers in Hawaii: A Report to the Hawaii State Legislature Per Act 118, Slh 2006," Honolulu, HI, 28p.

Hawaii State Legislature (2007). "Relating to Dam Safety," State of Hawaii, Honolulu, HI, SB1946 SD2 HD2 CD1, p.

Hawaii State Legislature (2014a). "Hb1700 Hd1 Sd1 Cd1, Relating to the State Budget," State of Hawaii, Honolulu, HI, p.

Hawaii State Legislature (2014b). "Sb1362, Relating to Capital Improvement Projects for the Benefit of the Fourth Senatorial District," State of Hawaii, Honolulu, HI, p.

Hawaii State Legislature (2014c). "Sb2332 and Hb1729, Relating to Dam and Reservoir Safety," State of Hawaii, Honolulu, HI, p.

Hawaii State Legislature (2014d). "Sb2876 Sd2 Hd2, Proposing an Amendment to Article Vii, Section 12 of the Hawaii State Constitution to Assist Dam and Reservoir Owners," State of Hawaii, Honolulu, HI, p.

Hoover, D. J. and F. T. Mackenzie (2009). "Fluvial Fluxes of Water, Suspended Particulate Matter, and Nutrients and Potential Impacts on Tropical Coastal Water Biogeochemistry: Oahu, Hawai'i," Aquatic Geochemistry, 15(4), pp 547-570.

Ignatius, A. R. and J. W. Jones (2014). "Small Reservoir Distribution, Rate of Construction, and Uses in the Upper and Middle Chattahoochee Basins of the Georgia Piedmont, USA, 1950–2010," ISPRS International Journal of Geo-Information, 3(2), pp 460-480.

Jokiel, P. L., K. S. Rodgers, et al. (2014). "Response of Reef Corals on a Fringing Reef Flat to Elevated Suspended-Sediment Concentrations: Moloka'i, Hawai'i," PeerJ, 2, pp e699.

Lanai Planning Commission (2014). "Lanai Community Plan Update, Final Draft," County of Maui, Long Range Planning Division, 196p.

Liu, Y., W. Yang, et al. (2014). "Assessing the Effects of Small Dams on Stream Flow and Water Quality in an Agricultural Watershed," Journal of Hydrologic Engineering, 19(10), pp 1-14.

MacLennan, C. (2007). "Kilauea Sugar Plantation in 1912: A Snapshot," Hawaiian Journal of History, 41, pp 1-34.

Morris, G. L. (2010). "Offstream Reservoirs for Sustainable Water Supply in Puerto Rico". AWRA 2010 Summer Specialty Conference, San Juan, Puerto Rico, AWRA.

Nakama, L. Y. (1992). "Storage Capacity of Fena Valley Reservoir, Guam, Mariana Islands, 1990," United States Geological Survey, Books and Open-File Reports Section, 92-4114, 17p.
Oki, D. S. (2003). "Surface Water in Hawaii," U.S. Geological Survey, State of Hawaii Commission on Water Resource Management, Honolulu, HI, Fact Sheet 045-03, 6p.
R.M. Towill Corporation (2013). "Nuuanu Dam No 4 Final Environmental Assessment," Board of Water Supply, City and County of Honolulu, Honolulu, HI, 486p.
Randle, T. J., K. L. Collins, et al. (2013). "Avoiding the Inevitable? Capacity Loss from Reservoir Sedimentation," Eos, Transactions American Geophysical Union, 94(1), pp 4-4.
Storlazzi, C. D., M. E. Field, et al. (2009). "Sedimentation Processes in a Coral Reef Embayment: Hanalei Bay, Kauai," Marine Geology, 264(3-4), pp 140-151.
Takayama, K. H. (2001). "Hawaii Administrative Rules Directory," Legislative Information Systems Bureau, Honolulu, Hawaii, State of Hawaii, 147p.
Timm, O. and H. F. Diaz (2009). "Synoptic-Statistical Approach to Regional Downscaling of Ipcc Twenty-First-Century Climate Projections: Seasonal Rainfall over the Hawaiian Islands*," Journal of Climate, 22(16), pp 4261-4280.
Tribble, G. W. (2008). "Ground Water on Tropical Pacific Islands--Understanding a Vital Resource," U.S. Geological Survey, Honolulu, HI, 1312-35, 35p.
U.S. Army Corps of Engineers, Honolulu District (2013). "Review Plan: Ala Wai Canal Project, Island of Oahu, Hawaii, Feasibility Report," Honolulu, HI, 38p.
Verstraeten, G., J. Poesen, et al. (2003). "Sediment Yield Variability in Spain: A Quantitative and Semiqualitative Analysis Using Reservoir Sedimentation Rates," Geomorphology, 50(4), pp 327-348.
Verstraeten, G. and I. P. Prosser (2008). "Modelling the Impact of Land-Use Change and Farm Dam Construction on Hillslope Sediment Delivery to Rivers at the Regional Scale," Geomorphology, 98(3-4), pp 199-212.
Wang, Z. Y. and C. H. Hu (2009). "Strategies for Managing Reservoir Sedimentation," International Journal of Sediment Research, 24(4), pp 369-384.
Water Resources Associates (2003). "Agricultural Water Use and Development Plan," Hawaii Department of Agriculture, Honolulu, HI, 154p.
Wengraf, T. (2001). Qualitative Research Interviewing: Biographic Narrative and Semi-Structured Methods. Sage Publications, Ltd, London.
Wilcox, C. (1996). Sugar Water: Hawaii's Plantation Ditches. University of Hawai'i Press, Honolulu, HI.
Wong, M. F. (2001). "Sedimentation History of Waimaluhia Reservoir During Highway Construction, Oahu, Hawaii, 1983-98," US Geological Survey, 02-4005, 55p.

Simulations of Lakes Mills Drawdown Experiment Using SRH2D Model

Jennifer G. Duan[1], Lei Liu[2], Chunshui Yu[3]

[1] Associate Professor, Dept. of Civil Engineering and Engineering Mechanics, University of Arizona, Tucson, Arizona. Email: gduan@email.arizona.edu. (Corresponding Author)

[2]Visiting Student, Dept. of Civil Engineering and Engineering Mechanics, University of Arizona, Tucson, Arizona. Email : leiliull@gmail.com.

[3]Post-doc Research Associate, Dept. of Civil Engineering and Engineering Mechanics, University of Arizona, Tucson, Arizona. Email : chunshui@email.arizona.edu.

Abstract

The removal of Elwha Dam and Glines Canyon Dam in Washington State has caused considerable sediment release to the lower reach of Elwha River. A reliable sediment transport model is needed for predicting post-dam removal sediment transport. This presentation reports the verification of SRH2D model for simulating fluvial sediment transport processes during the 1994 Lake Mills drawdown experiment on the Elwha River. SRH2D model is a depth-averaged two-dimensional model for flow and sediment transport in alluvial rivers developed by the Bureau of Reclamation. The experiment drawdown was performed in April 1994 by gradually lowering the Lake level by 18 feet over one week period. Flow discharge, cross sectional data, and sediment size distributions were collected at the reservoir reach during the experiment. This study simulated flow hydrodynamic and sediment transport during the experimental drawdown. The simulation used surveyed cross section data to reconstruct the lake bathymetry. Surveyed flow discharge and sediment load are used as the upstream boundary conditions for flow and sediment. Observed lake level in the reservoir was the downstream boundary condition. Multiple simulation runs using different sediment transport formulas, computational meshes, and various Manning's roughness are compared with field surveyed data. Results showed the importance of initial channel bathymetry, non-equilibrium sediment transport, locally induced turbulence, and bank erosion for simulating the morphodynamic processes of reservoir sedimentation delta. Additionally, the simulation results also demonstrated the applicability of SRH2D model in simulating complex sediment transport processes.

1 Introduction

The objective of this study is to simulate fluvial processes during the 1994 Lake Mills drawdown experiment in the Elwha River, Washington. The experiment drawdown was performed in April 1994 by gradually lowering the Lake level by 18 feet over one week period. Flow

discharge, cross sectional data, and sediment size distribution were collected at the reservoir reach during the drawdown experiment (Childers *et al.* 2000). This study simulated the experimental drawdown using SRH2D model and compared the simulated results of cross sectional changes with measurements. SRH-2D, Sedimentation and River Hydraulics – Two Dimensional model, is two-dimensional hydraulic, sediment, temperature, and vegetation model for river systems developed at the Bureau of Reclamation (BOR 2008). We conducted two series of simulations: one is to use the measured data to extract cross sections, and then test the sensitivities of modeling results to meshes, roughness coefficient, various sediment transport formulas, and different methods of adaptive lengths; the other is to use a refined mesh with many breaklines to pre-define the channel flow.

2 Model Set-up

2.1 Computational Grid

The simulation domain is the Lake Mills reservoir reach covering the reservoir delta from Section 3 to Section 17 as shown in Fig.1 and 2. The simulation boundary including the left and right banks is obtained from the boundaries of measured cross sections. The bathymetry in the simulated reach is interpolated using the surveyed bed elevation at each cross sections in 1994.

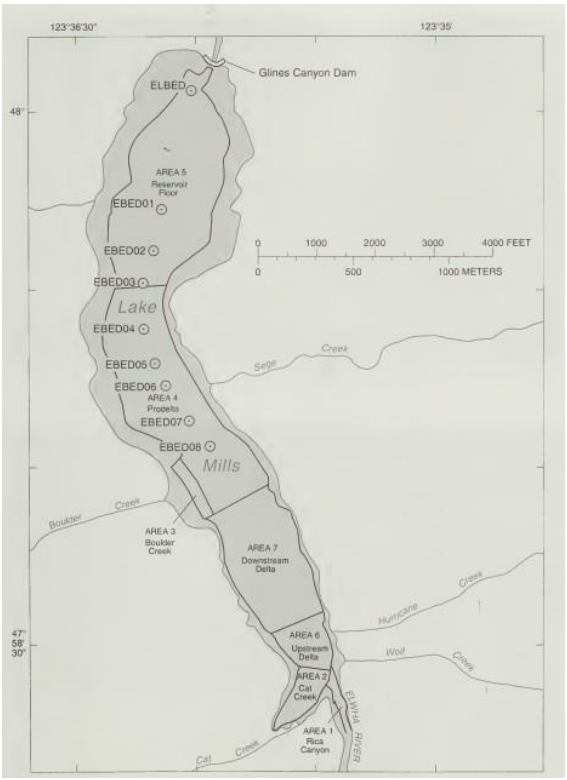

Fig.1 Location of the simulation reach.

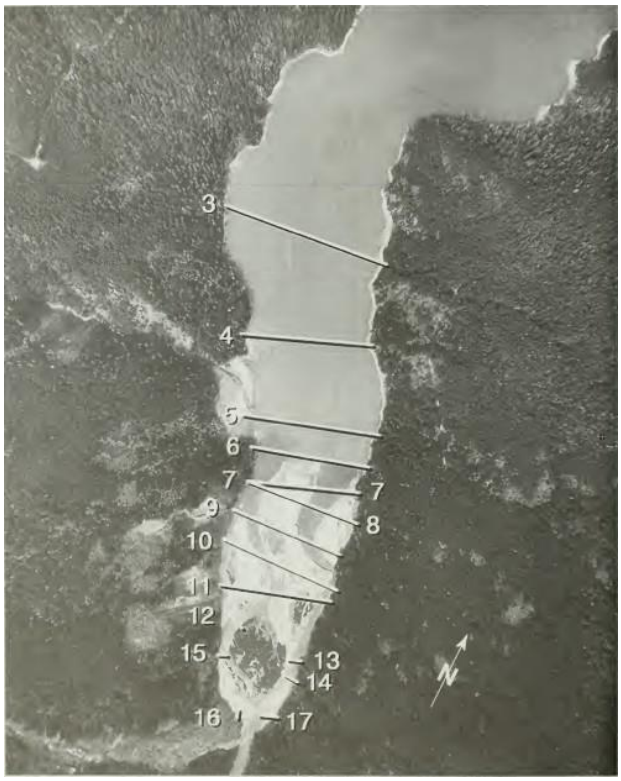

Fig.2 Location of surveyed cross sections

The simulation domain is the Lake Mills reservoir reach covering the reservoir delta from Section 3 to Section 17 as shown in Fig.2. The simulation boundary including left and right banks

is obtained from the boundaries of measured cross sections at April 8th. All other measured data points on the delta from USGS GIS shape files are also used (Fig.3a). The bathymetry in the simulated reach is interpolated using the surveyed cross sections and all other measured points on the delta. The measured data points in the tables of USGS report is based on the local coordinates. Conversions are needed to change the elevations to the NAD88 datum. The local elevation was added 0.9 ft to the NGVD29 system, and added 3.625 ft to the NAD88 datum. Therefore, the recorded elevations in the USGS report were added 4.525 ft to the NAD88 datum. The initial bed bathymetry showed two small side channels near both banks (Fig.3b). Cross sections, 16 and 17, are used as the inlets. This study used an improved quadrilateral mesh, shown in Fig.3c, to accommodate the complex geometry of the delta channels at the beginning of the drawdown experiment.

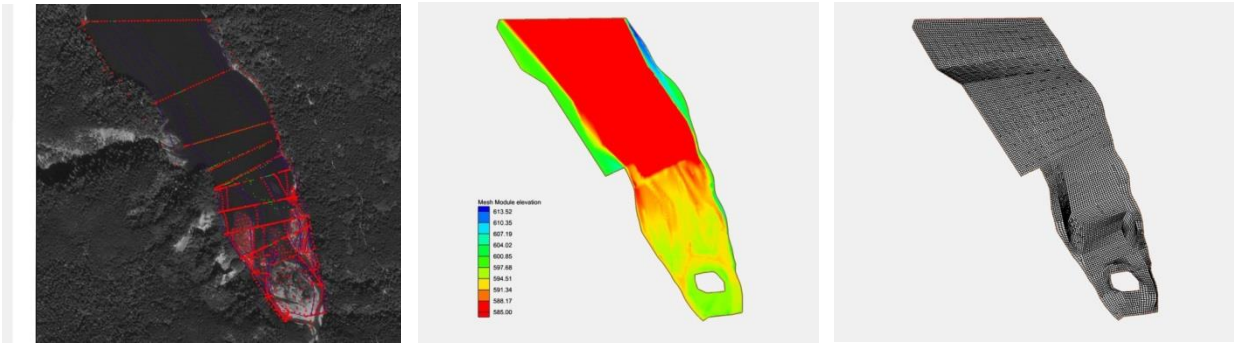

(a) **(b)** **(c)**

Fig.3 Scatter data points, initial bed elevations, and computational grid

2.2 Simulation Data

Stream flow data were collected at five sites. Stream flow data were collected at five sites. Daily flows at ELWW, a gaging station that was established just a few weeks prior to the beginning of the drawdown experiment. The stream flow discharge (Fig.4a) at ELWW gauge is used. The measured discharge is divided into two parts: one part is 40% of the total discharge at the cross section #16, and the rest is at the cross section #17. Both suspended and bed load sediment discharges measured at ELWW gauge (Fig.4b) are used as sediment upstream boundary condition.

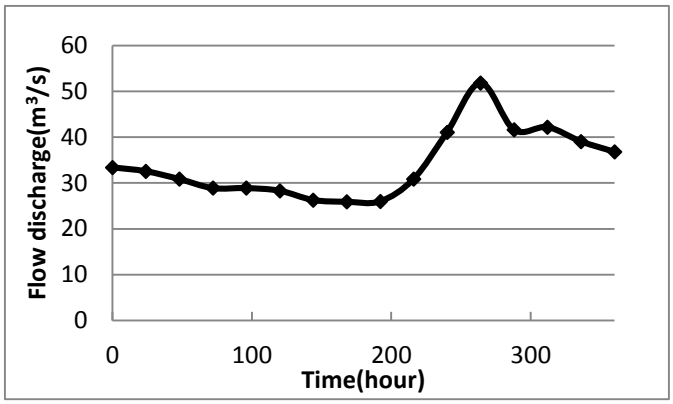

(a)

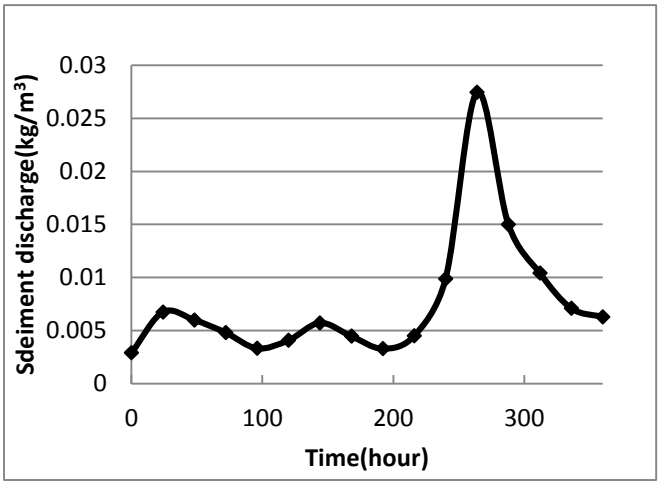

(b)

Fig.4 Stream flow and sediment discharge

The lake drawdown began with a full lake at 8:00 am on April 9, 1994. During the experiment, the lake's water level was lowered 18 feet over a 1-week period from April 9 to 16. Drawdown rates were about 3 feet per day for the first 5 days, for a total of 15 feet. The lake was drawn down 2 feet between April 14 and 15 and 1 foot between April 15 and 16. A drawn down of 18 feet was reached 8:00 am on April 16, and then held at constant elevation for a week. The changes of lake level are shown in Fig.5, and were used as the downstream boundary condition. The particle-size distribution collected at ELD1 station was used. The distribution curve is shown in Fig.6.

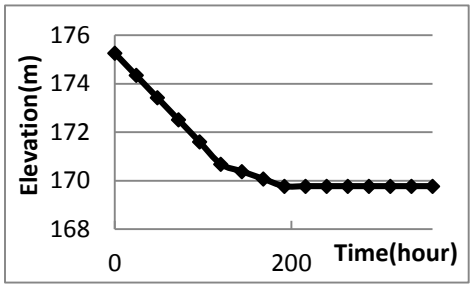

Fig.5 Downstream boundary conditions

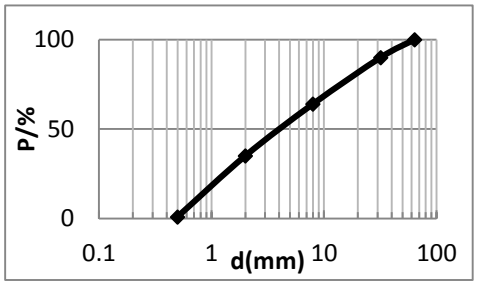

Fig.6 Particle-size distribution

The time step used for the three computational meshes is 5.0 s. The total simulation time is 360 hours. When the mesh size is decreased to 8 m, the SRH2D doesn't converge even reducing the time step to 0.01 s.

3 Simulation Results

The simulated bed elevations using the new mesh were compared with the measurements on April 23th, and shown in Fig.7. Only Yang's equation was used in this calculation in order to compare with the previous results by using only measured cross sections on April 8th, 1994. The final results at Section 3, 4, and 5 showed no erosion or deposition, the same as the measurements. At Section 6, the simulated results underestimated the deposition. From Section 7 to 11, two large channels are formed at both sides of the delta, while the simulated results also showed two channels formed on the delta, but the channel sizes cannot match the observed ones. The sizes of both channels are smaller than the observed ones. From Section 12 to 15, the simulated results considerably over-estimated the deposition comparing to observed bed elevation.

7a. Cross-section 3.

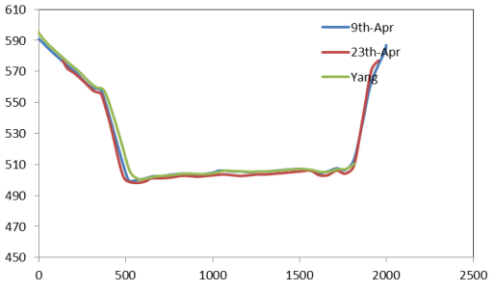

7b. Cross-section 4

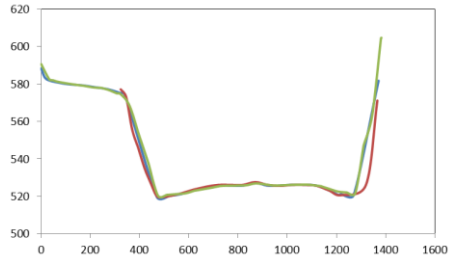

7c. Cross-section 5.

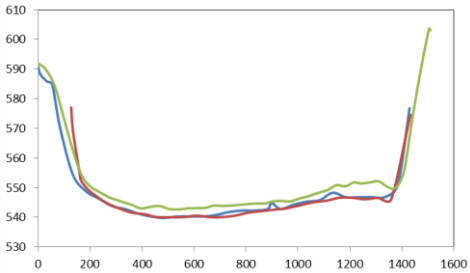

7d. Cross-section 6.

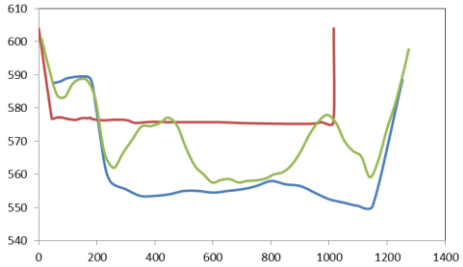

7e. Cross-section 7.

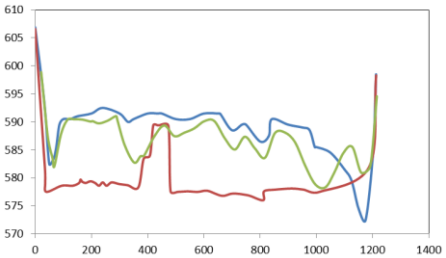

7f. Cross-section 8.

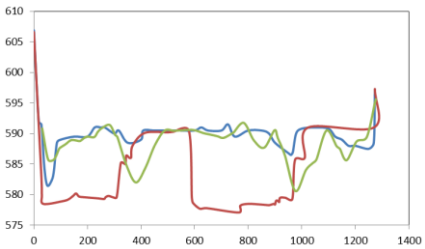

7g. Cross-section 9.

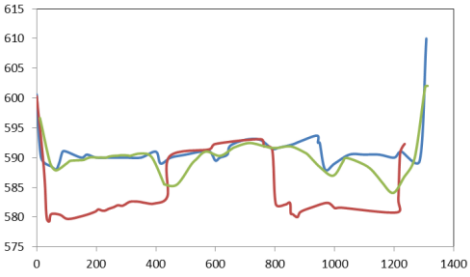

7h. Cross-section 10.

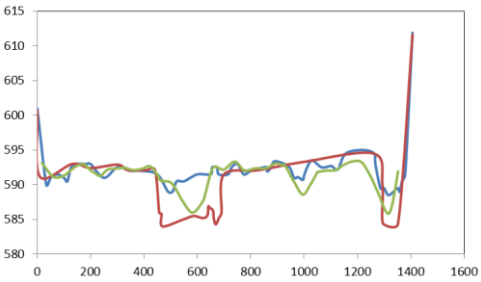

7i. Cross-section 11.

7j. Cross-section 12.

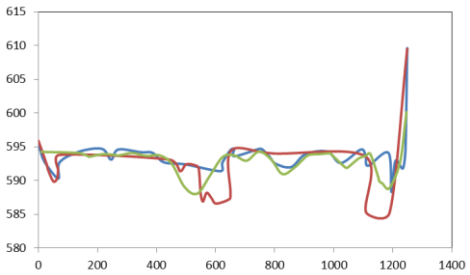

7k. Cross-section 13.

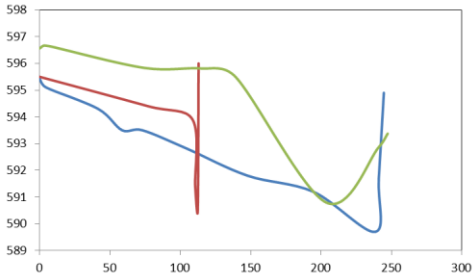

7l. Cross-section 14.

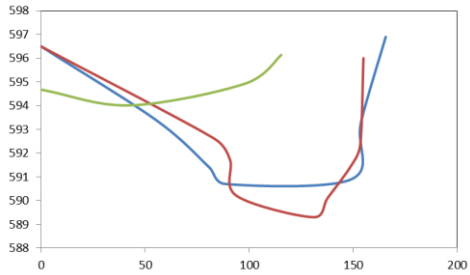

7m. Cross-section 15.

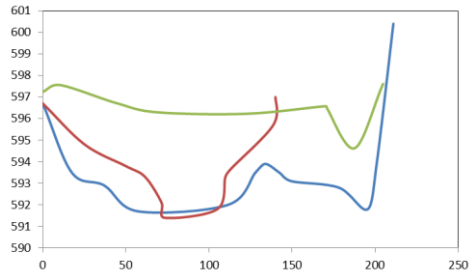

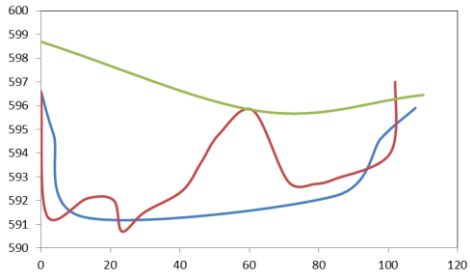

Fig.7 Simulated and measured bed elevation changes

The errors of simulated bed elevation changes may due to 1) local turbulence due to woody debris; 2) bank erosion induced channel changes have not been simulated; 3) avulsion or bifurcation processes may also need to be considered.

4. Conclusion

This study first applies the SRH2D model to simulate the experimental drawdown of Lake Mills in 1994. The simulated results showed no erosion or deposition within the reservoir at Section 3, 4, and 5, the same as the measurements. At the edge of exposed delta (Section 6), the simulated results underestimated the deposition. From Section 7 to 11 where delta is scoured by the drawdown flow, the simulated results showed two channels formed on the delta, but underestimated erosion occurred in the channels. At the delta upstream (Section 12 to 15), the simulated results considerably over-estimated the deposition comparing to observed bed elevation changes.

To test the sensitivities of modeling results to selected parameters, we chose three different mesh sizes using pure triangular, pure quadrilateral, and mixed triangular and quadrilateral meshes,

six different sediment transport equations, three different adaptation lengths, six combinations of roughness coefficients ranging from 0.02-0.06. The results showed that the modeling results are sensitive to sediment equations. Among selected equations, Yang (1973) relation yielded the maximum sedimentation and erosion at sections upstream of the delta, and the results are also sensitive to roughness coefficients. As roughness is increased, more erosion is predicted. However, the maximum roughness value in the simulation reach cannot exceed 0.06 according to field observations. The calibration of roughness coefficients will not lead to accurate results that match the observations. The modeling results are not sensitive to the selection of adaptation length, mesh types, and sizes.

In summary, SRH2D model approximately predicted the erosion in the delta front, in particularly, two side channels formed on the delta. However, the results of SRH2D underestimated the erosion due to water level drawdown that makes the simulated channel erosion much less than the observed.

5. Discussion

As seen from the simulated results, both SRH2D cannot accurately predicted the observed erosion due to lake level drawdown. As water withdraws from a lake, sediment erosion at channel bottom and bank collapse are visible. The model only predicted very small sediment transport rate due to very small bed shear stresses on the streamwise direction. Bed shear stress relates to both mean and near-bed turbulence flow (Biron *et al.* 2004, 2005; Huthnance *et al*. 2002, Kim et al., 2000). At present, we cannot tell if the under-predicted bed shear stress is due to the hydrodynamic model because there is no measured flow field that can verify the simulated flow velocity and water surface elevations. Whether or not the simulated flow fields, especially shear stress field, are accurate requires further experimental or field data verification. Therefore, we strongly recommend to verify SRH2D using a laboratory experimental case with measured flow field.

Secondly, currently sediment transport equations may not be able to predict sediment transport rate due to water surface drawn down. Water surface is down vertically that will cause an acceleration of vertical flow (Stelling 1984, Stelling and van Kester 1994). This vertical accelerated flow either directly entrains sediment from bottom or generates drag force that cause sediment transport. The erosion due to the vertical accelerated flow is the major erosion mechanism in lake level drawdown scenario. However, this mechanism was not considered in any sediment transport formula. The sediment transport rate in the model is determined by the horizontal shear stress, which is a function of depth-averaged horizontal velocity. Therefore, the model under-predicts or is unable to predict observed erosion.

Therefore, we recommend to verify the flow simulation of SRH2D model using a well-

defined laboratory experiment of lake level drawdown. If there is an existing laboratory experiment, it will be ideal. The physical experiment conducted at University of Minnesota can be a good choice, but needs to check if flow field measurements are available. After the simulated flow field is verified, we recommend modifications to sediment transport equations to account for the effect of vertical accelerated flow on sediment transport.

References

Biron, P. M., Robson, C., Lapointe, M. F., and Gaskin, S. J. (2004). "Comparing different methods of bed shear stress estimates in simple and complex flow fields." *Earth Surf. Process. Landforms, 29*, 1403-1415.

Biron, P. M., Robson, C., LaPointe, M. F., and Gaskin, S. J. (2005). "Three-dimensional flow dynamics around deflectors." *River Research and Applications*, 21, 961–975.

BOR (Bureau of Reclamation) (2008). "SRH-2D version 2: Theory and User's Manual, Sedimentation and River Hydraulics – Two-dimensional River Flow Modeling". Technical Report, Denver Technical Service Center, Bureau of Reclamation, Denver, Colorado. 109 pages.

Childers, D., Kresch, D. L., Gustafson, S. A., Randle, T. J., Melena, J. T., and Cluer, B. (2000). "Hydrologic Data Collected During the 1994 Lake Mills Drawdown Experiment, Elwha River, Washington." USGS, Water-Resources Investigations Report 99-4215.

Huthnance, J. M., Humphery, J. D., Knight, P. J., Chatwin, P. G, Thomsen, L., and White, M. (2002). "Near-bed turbulence measurements, stress estimates, and sediment mobility at the continental shelf edge." *Progress in Oceanography*, 52, 17 –194.

Kim, S. C., Friedrichs, C.T., Maa, J. P.-Y., and Wright, L. D. (2000). "Estimating bottom stress in tidal boundary layer from acoustic Doppler velocimeter data." *J. Hydraul. Eng*., 126(6), 399–406.

Pope, N. D., Widdows, J., and Brinsley, M. D. (2006). "Estimation of bed shear stress using turbulent kinetic energy approach – a comparison of annular flume and field data." *Cont. Shelf Res*., 26, 959–970.

Stelling, G. S. (1984). On the construction of computational methods for shallow water flow problems. *Tech. Rep. 35*., USGS Professional Paper.

Stelling, G. S., van Kester, J. A. T. M. (1994). On the approximation of horizontal gradients in sigma co-ordinates for bathymetry with steep bottom slopes. *Intern. J. Num. Meth. in Flu.* 18, 915-955

NUMERICAL MODELING OF ISLETA DIVERSION DAM GATE OPERATION HYDRAULICS TO MINIMIZE SEDIMENT EFFECTS

Drew C. Baird, Hydraulic Engineer, U.S. Bureau of Reclamation, Denver, Colorado, dbaird@usbr.gov; Michael Sixta, Hydraulic Engineer, U.S. Bureau of Reclamation, Denver, Colorado, msixta@usbr.gov.

INTRODUCTION

Isleta Diversion Dam was constructed in 1934 by the Middle Rio Grande Conservancy District (MRGCD) as part of their irrigation system, and is located on the Rio Grande about 10 miles south of Albuquerque, New Mexico, immediately downstream from the Highway 147 Bridge (Figure 1). The diversion dam was rehabilitated by Reclamation in 1955 as part of the Middle Rio Grande Project, authorized by Congress in the 1948 and 1950 Flood Control Acts. The Middle Rio Grande (MRG) has long been recognized for its characteristics of high sediment loads and dynamic channel conditions (Happ, 1948; Lagasse, 1980; Makar, 2010). The Isleta Diversion Dam consists of 30 river gates, three headworks gates on the Peralta Main canal (east side), and four headworks gates on the Belen Highline canal (west side) of the dam (Figure 2). The headworks gates are located in a sluiceway with a downstream gate used to maintain a maximum diversion head. Gate operations are used to provide water to downstream irrigators, meet downstream flow requirements of the 2003 Endangered Species Biological Opinion (USFWS, 2003), and manage sediment. Within the context of these multiple water use needs, a one-dimensional (1D) and two-dimensional (2D) fixed bed hydraulic models, sluiceway hydraulics, and sediment incipient motion analysis has been completed to provide recommendations on gate operations that would help reduce sediment impacts. The objectives of these recommendations are to reduce sediment diversion through the headworks gates into the irrigation system, reduce the potential for downstream formation of vegetated islands, maintain an open channel as much as possible along the right bank of the river downstream of the diversion dam, and minimize upstream sediment accumulation. This analysis does not evaluate the effects of sediment supply and sediment transport capacity. Documentation of historical channel characteristics and changes, local knowledge and observation by the staff of the Isleta Pueblo, and the MRGCD is coupled with modeling and incipient motion analysis to interpret results.

CHANNEL DESCRIPTION

The MRG has historically had a high sediment load, causing the channel to fill, especially during hydrograph recession periods, resulting in over bank flooding during subsequent high flow events and avulsing to lower areas of the valley, leading to aggradation (raising of the river bed and floodplain due to sediment accumulation) across the floodplain (Scurlock, 1998; Lagasse, 1980; Happ, 1948). This condition is believed to have existed prior to the 1500s (Scurlock, 1998). The resulting river channel was wide and shallow and generally sand bedded with small pockets of gravel (Scurlock, 1998; Lagasse, 1980). The MRG has changed significantly over the last century as a result of human activities such as irrigation diversions, levee and riverside drain construction, channel rehabilitation (channelization) and maintenance, upstream sediment and flood control reservoirs, trans-mountain diversion, and urbanization. There have also been diminished flood peaks and sediment supply from large tributaries to the Rio Grande since the 1940s (Lagasse, 1980). The following reach descriptions are summarized from Makar (2010), and Baird and Strand (2013) and provide a context of channel conditions and sediment supply into Isleta Diversion Dam. The Albuquerque Reach, extending from Angostura Diversion Dam downstream to the Isleta Diversion Dam (see Figure 1) narrowed from about 600 feet wide in 1972 to about 390 feet in 2002, and the plan form is transitioning from a wide, low-flow braided channel to a single thread channel with vegetated bank-attached bars. Bed material is changing from sand to areas of gravel bed. It is expected that the existing trends of incision, narrowing, and bed coarsening will most likely continue. The suspended sediment load has reduced by about 75 percent. The Belen Reach extends from Isleta Diversion Dam to the mouth of the Rio Puerco (Figure 1) and was about 550 feet wide prior to 1972. This reach currently averages about 350 feet wide, and the channel is continuing to narrow through island and bar development and is transitioning to a single thread channel. The historic sand bed is coarsening to areas of gravel bed. Both the Albuquerque and Belen Reaches appear to have a sediment transport capacity greater than the amount of sediment being supplied, whereas historically the sediment transport capacity appeared to be less than supply. These reaches will likely continue to experience channel slope reduction, through bed degradation and lateral migration. This means there is less sediment being supplied to Isleta Diversion Dam by the river than historically.

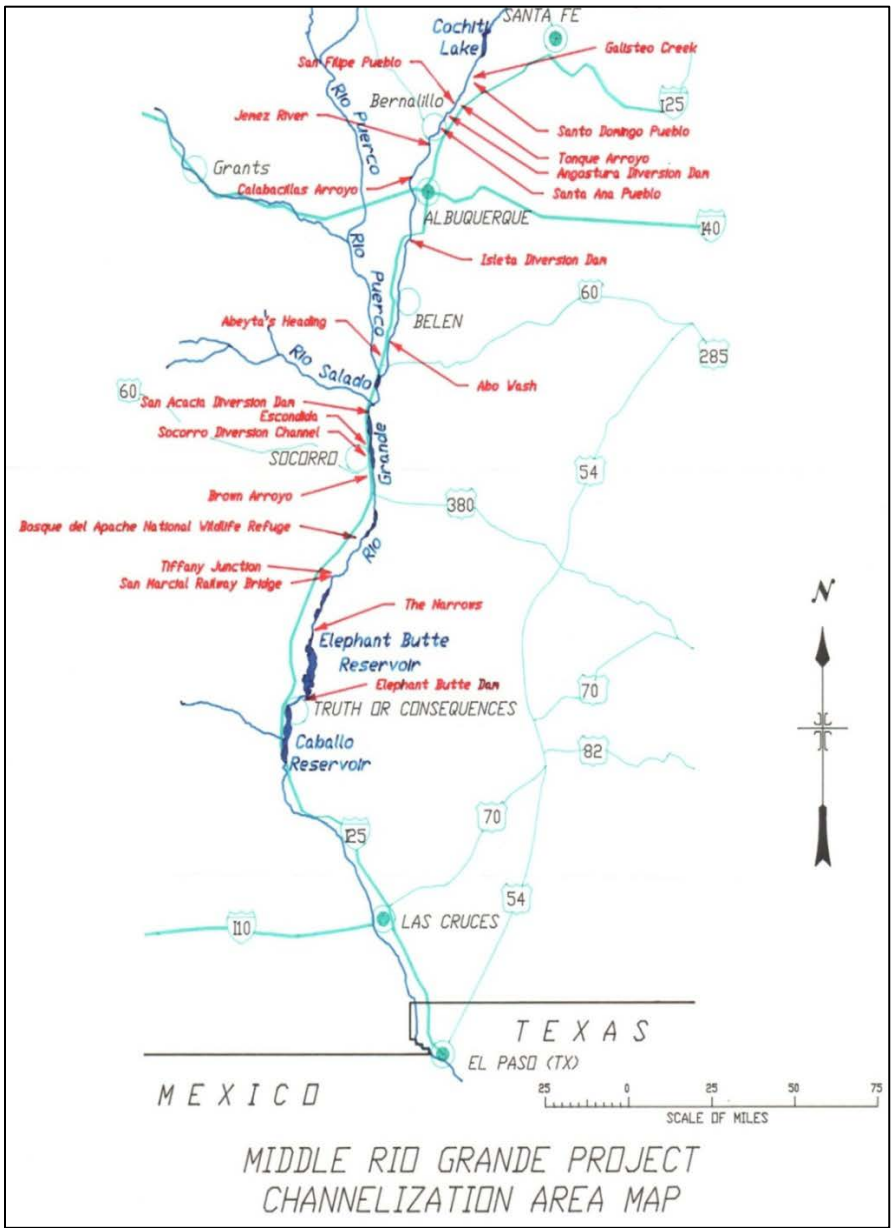

Figure 1. Location map.

MODEL SELECTION AND APPLICATIONS

The numerical models utilized for this study were HEC-RAS (v 4.1.0) and SRH-2D (v 3.0). HEC-RAS is a one-dimensional (1D) backwater step hydraulic model developed by the U.S. Army Corps of Engineers (USACE, 2008). This model simulated cross section averaged river hydraulics for a series of steady, gradually varied flows. The SRH-2D model utilized for this study is a two-dimensional (2D) fixed-bed hydraulic model specifically focused on the flow hydraulics of river systems (Lai, 2008). SRH-2D solves the depth-averaged dynamic wave equations with a depth-averaged parabolic turbulence model using a finite-volume numerical scheme. The model adopts a zonal approach for coupled modeling of channels and floodplains; a river system is broken down into modeling zones (delineated based on natural features such as topography, vegetation, and bed roughness), each with unique parameters such as flow resistance. One of the major features of SRH-2D is the adoption of an unstructured hybrid

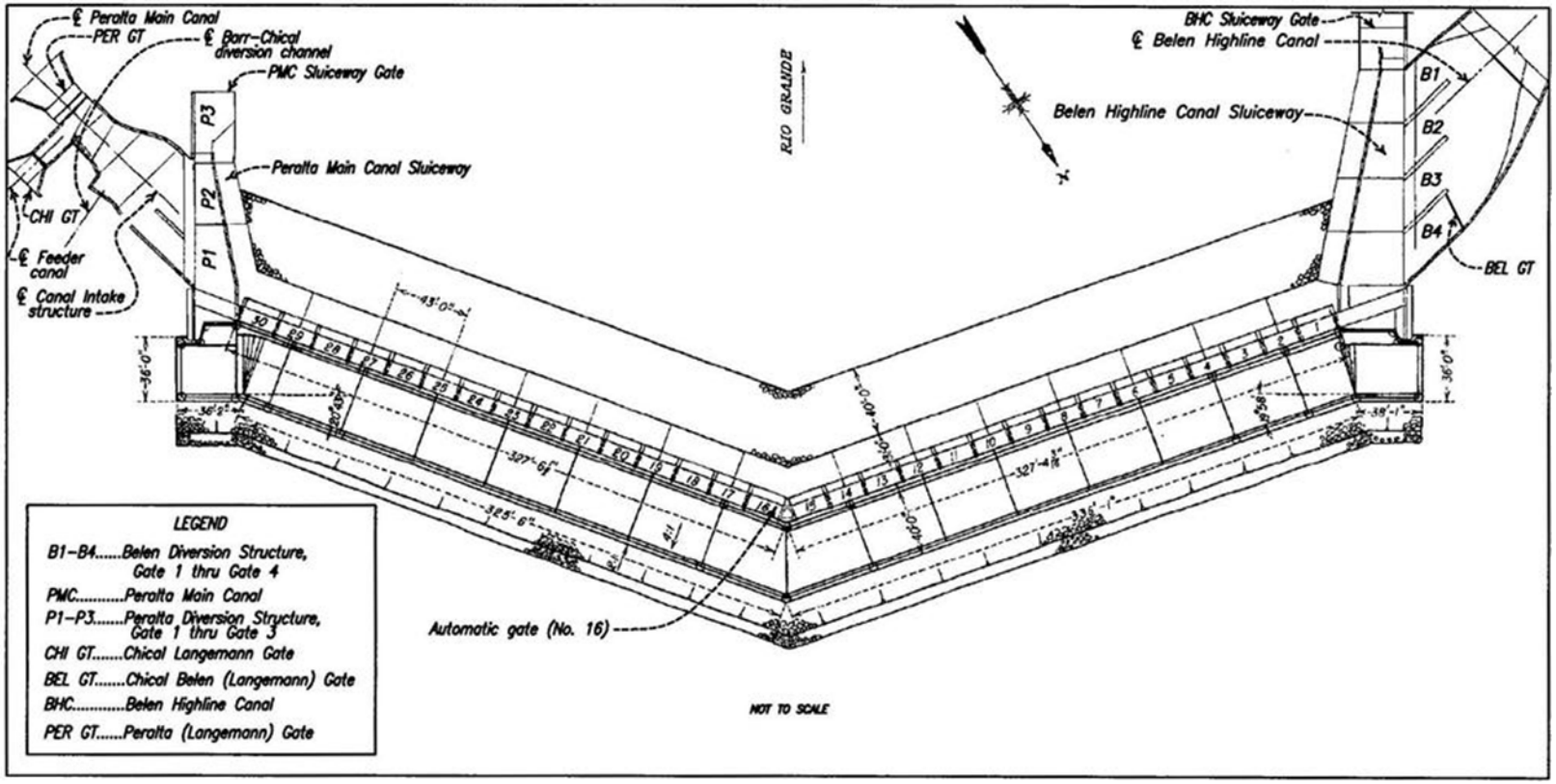

Figure 2. Isleta Diversion Dam plan view.

mixed element mesh, which is based on the arbitrarily shaped element method of Lai (2000) for geometric representation. This meshing strategy is flexible enough to facilitate the implementation of the zonal modeling concept; it allows for greater modeling detail in areas of interest, and ultimately leads to increased modeling efficiency through a compromise between solution accuracy and computing demand. HEC-RAS was utilized to set the downstream boundary in the SRH-2D model simulations, which consisted of a water surface elevation. At the time of this study, SRH-2D did not have the ability to model gates, while HEC-RAS did, so the HEC-RAS model was also utilized to formulate gate operations that made up a set of scenarios modeled in SRH-2D.

Topography Development: A combination of several data sets was utilized to construct the existing conditions topography of the study area. In-channel ground survey data were collected upstream and downstream of the diversion dam in 2005 and 2012 (exact dates are unknown) and supplemented with a more recent data set collected immediately upstream of the dam in June, 2013. These data were primarily used to represent the wetted portion of the channel (bathymetry). To supplement the survey data in the floodplain areas, a Digital Terrain Model (DTM) generated from Light Detection and Ranging (LiDAR) data collected in 2012 was utilized. By combining the interpolated survey data with the LiDAR data, a representative topographic surface was created in ArcGIS using a Triangulated Irregular Network (TIN) methodology. It is important to note that the channel bed near/around the diversion dam is extremely dynamic and based on river flows and operational strategy of the diversion dam gates; comparison of the 2012 and 2013 survey data showed that gate operations have a significant influence on the bed elevation upstream of the dam. During the data collection period in June 2013 all diversions were through the Peralta Main side of the dam, and sediment deposition was observed upstream of the Belen Highline headworks. The 2012 survey data upstream of the Belen Highline side was several feet lower than the 2013 data. Most likely during high flows, with both sluiceways open, both sides of the dam would have a lower bed elevation than when no diversion of flow through the gates adjoining the sluiceways is occurring. The lowest measured bed elevation on each side of the diversion dam was used in this study. A project was implemented to remove islands and widen the channel downstream of Isleta Diversion Dam. The topography downstream was based on the project design while the upstream topography remained the same for both the pre-project and post-project cases. The existing and post-island removal project topographic surfaces are shown in Figures 3 and 4.

Modeling to Establish and Evaluate Effects of Gate Operations: The HEC-RAS model was used to establish gate operations and resulting water stage at Isleta Diversion Dam. The diversion dam was represented through a series of radial gates. The sluiceway and accompanying canal diversions were not represented in the model. The 1D downstream boundary condition was set to a normal depth slope determined by the average bed slope near the lower end of the model domain dictated by the 2012 survey data. The 1Dupstream boundary condition consisted of various discharges related to the gate operational scenarios that were evaluated.

A SRH-2D fixed bed model was used to evaluate channel hydraulics for selected gate operations. Surface-water Modeling System (SMS) software was used to generate the 2D mesh which contains finer mesh cells near areas of interest, such as the diversion dam, and coarser mesh cells elsewhere. The mesh stores bed elevation information based on the topographic surface and consists of quadrilateral and triangular shaped elements. SMS was also utilized to delineate model roughness areas and assign model boundary conditions. Hydraulic roughness is the primary calibration parameter for hydraulic modeling assuming the channel and floodplain geometry is accurate. Roughness assignments included ‘main channel’, ‘vegetated overbanks-islands’, and ‘concrete’ (diversion dam and sluiceways). Lacking any new data to calibrate to the main channel and overbank roughness in the HEC-RAS model were set at 0.028 and 0.045, respectively based on prior modeling effort (Tetra Tech, 2012). The ‘concrete’ roughness value was assigned to be 0.015 according to values found in literature for a float finish (Sturn, 2001). Roughness values in a 2D model are often lower than those in a 1D model because the 2D model solves for eddy losses independently, as opposed to these losses being lumped into the roughness value or expansion/contraction loss coefficients. Therefore, roughness values were set slightly lower in the 2D model at 0.025, 0.045, and 0.015 for ‘main channel’, ‘vegetated overbanks/islands’, and ‘concrete’, respectively.

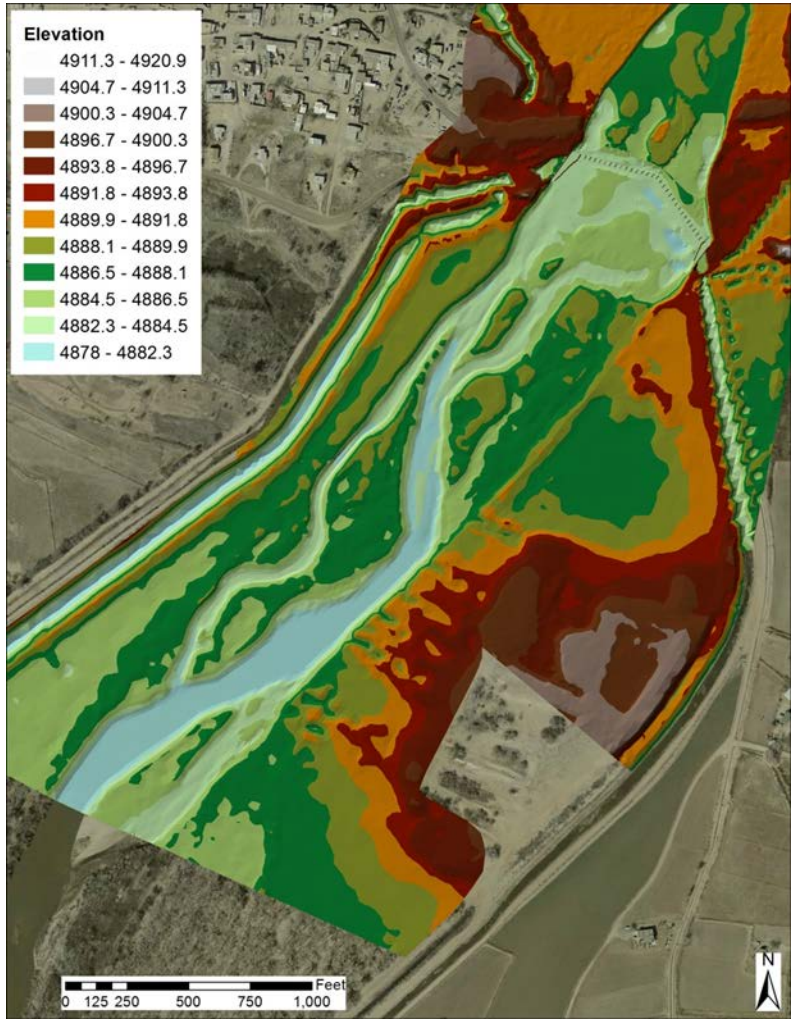

Figure 3. Existing conditions digital topographic surface.

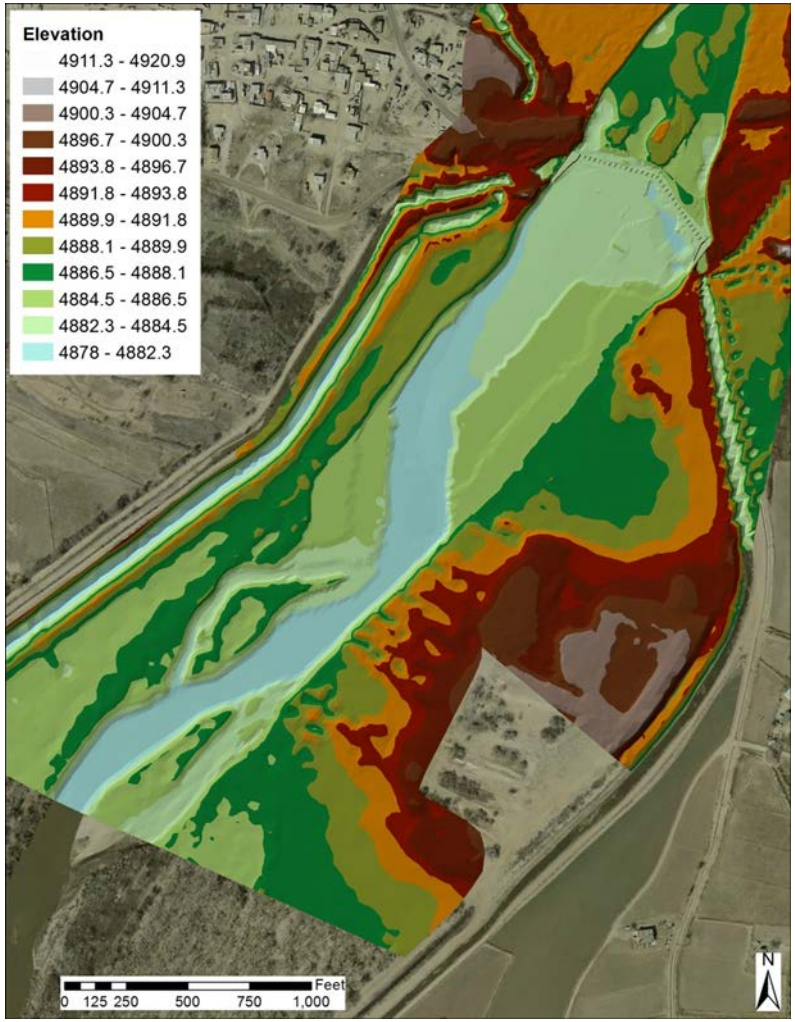

Figure 4. Post-project conditions digital topographic surface.

The 2D upstream boundary condition was specified as a steady flow input rate ranging from 500 to 5,000 cfs. The 2D downstream boundary condition was set to a corresponding water surface elevation based on output from the 1D model. Internal boundary conditions were also used to represent flow through each diversion dam and sluiceway gate as well as the sluiceway diversions. Maximum sluiceway diversions were 250 and 300 cfs down the Belen Highline and Peralta Main Canals, respectively. To ensure flow continuity, there were also a set of internal boundary conditions set up at the entrance to each sluiceway that controlled how much flow passed through each structure.

Sluiceway Hydraulics Methodology: The water surface elevation in both sluiceways predicted by SRH-2D for many of the flow scenarios was lower than required for full diversion head because the 2D model does not include hydraulic computations for pressurized flow through gates. Instead, local sluiceway velocity was evaluated using flow cross sectional area and discharge to solve the continuity equation (discharge= cross sectional area multiplied by the mean cross sectional velocity). For the Peralta Main sluiceway, diversions were equally divided for each headworks gate or bay (see Figure 2). For the Belen Highline sluiceway, all flows were diverted through the first and fourth headworks gate. The first headworks radial gate has been replaced by an automated Langaman gate which is used for all diversions (pers. communication David Gensler, 2013).

Sediment Incipient Motion Methodology: Incipient motion of sediment was computed to analyze the areas of potential sediment deposition, and sediment mobility. Incipient motion occurs when the shear stress (critical shear stress) acting on a particle of sediment overcomes the stabilizing force due to particle weight and size and the particle begins to move. The Shields Diagram (Shields, 1936) was used in this study to determine the critical shear which initiates sediment particle motion. Vanoni (1977) criterion was used to illustrate the velocity at which particles begin to move based upon extensive field and laboratory surveys. Bed sediment sizes upstream and downstream of Isleta Diversion Dam have coarsened from predominantly medium sand to coarse sand with some fine gravel, over time since about 1975 (Bauer, 2009). The most recent bed sediment sizes from the decade of the 2000s are shown in Table 1 which illustrates the median bed material size in the reach containing Isleta Diversion Dam is 0.6 mm (Bauer, 2009). Visual estimates from a recent field visit in 2013 validate similar sand sizes are present near Isleta Dam. One of the bed material measurements in Table 1 can be classified as fine gravel (4-8 mm). Visual observations of the downstream river bed indicate that gravel transport through the diversion dam delta is not likely at present. The upstream channel has degraded (bed lowered) but the delta length of about 2 miles has remained approximately the same between 1936 and 2002 (Baird and Strand, 2013). Because this study focus is mainly on sediment mobility in the island removal and channel widening area downstream of the Isleta Diversion Dam, only sand sizes were considered in this assessment.

Table 1 Median Bed Material Sizes (Bauer, 2009), Critical Velocity and Shear Stress for Incipient Motion Upstream and Downstream of Isleta Diversion Dam.

Direction from Isleta Diversion Dam	Distance from Isleta Diversion Dam (Miles)	Median Bed Material Size (mm)	Critical Velocity Hjulstrom (1935) ft/s	Critical Velocity (Vanoni, 1977) ft/s	Critical Shear Stress (Shields, 1936) lb/ft^2
Upstream	6.23	0.63	0.15	0.50	0.047
Upstream	3.54	5.72	N/A	N/A	N/A
Upstream	3.52	0.40	0.10	0.47	0.047
Upstream	3.53	0.40	0.10	0.47	0.047
Downstream	3.22	0.58	0.14	0.50	0.047
Downstream	3.23	0.80	0.20	0.55	0.047
Average		0.575 (Excluding Upstream Gravel Sizes)	0.14	0.50	0.05

Flow Scenario Gate Operations: Many different combinations of dam, sluiceway and headworks gate operations are used to meet water user, and Rio Grande Silvery Minnow flow requirements. Having 10-15 percent of the diverted flow pass through each sluiceway gate creates enough velocity and shear stress to nearly always eliminate sediment deposition in the Peralta Main and Belen Highline Canal headworks sluiceways. In this paper "sluicing" refers to having 10-15 percent of the diverted flow amount pass through each sluiceway gate (sluiceway outflow) and be released into the downstream river channel. Maximum sluiceway flows has been observed to maintain an open channel along the banks, especially the west (Belen Highline Canal) side. Opening every other gate has also been observed to minimize the propensity for downstream sediment bar deposition. Flow scenarios were selected to include representative peak diversions with maximum sluicing, representative minimum diversions with minimum sluicing (less than 10 percent), spring runoff peak river flows with maximum diversion, an inflow resulting in opening about ½ of the river gates, and maximum flows in each sluiceway. A summary of the above scenarios showing the magnitude of flows modeled in each scenario is shown in Table 2 followed by an example schematic of scenario #1 (Figure 5).

Table 2 Summary of modeled flow scenario gate operations.

Scenario ID	Scenario summary	Total flow upstream of the dam (cfs)	River gates flow (cfs)	Sluiceways	Sluiceway inflow (cfs)	Sluiceway diversion (cfs)	Sluiceway outflow (cfs)	Total flow downstream of the dam (cfs)
1	Maximum diversion with maximum sluicing	680	30 (Gate #16)	Peralta Main	345	300	45	130
				Belen Highline	305	250	55	
2	Minimum diversion (summer) with minimum sluicing	529	91 (Gate #16)	Peralta Main	235	220	15	124
				Belen Highline	203	185	18	
3	Typical spring runoff peak (non-drought) - all open gates	5,000	variable (all open)	Peralta Main	400	300	100	4,450
				Belen Highline	350	250	100	
4	Typical spring runoff peak (non-drought) - select open gates	2,820	1780 (10 gates at 178 each)	Peralta Main	520	300	220	2,270
				Belen Highline	520	250	270	
5	Maximum diversion - no open gates	1,565	0 (all gates closed)	Peralta Main	760	300	460	1,015
				Belen Highline	805	250	555	

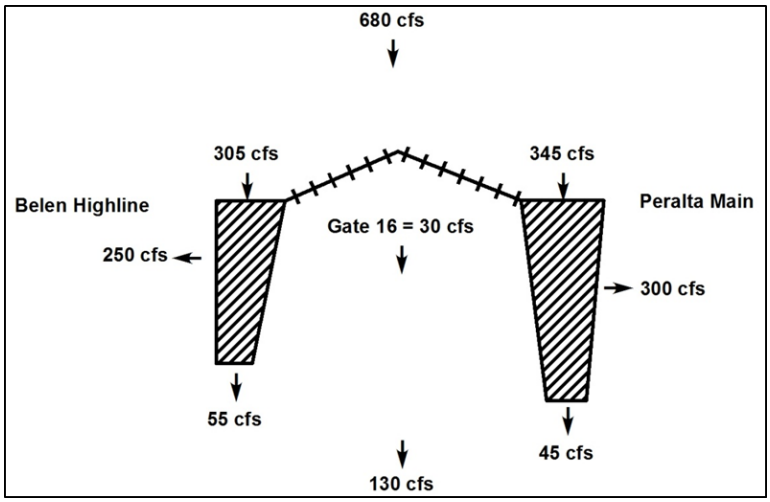

Figure 5 Schematic of scenario #1.

RESULTS AND DISCUSSION

This section compares and contrasts differences between each scenario for project topography. Also presented are sluiceway velocity and sediment incipient motion results for each scenario and the smallest sluiceway outflow volume which minimizes sediment deposition for all operations. Results and discussion for each scenario are presented first for scenarios with low likelihood, and second with high likelihood of bed change due to sediment deposition or transport. A qualitative evaluation of potential channel response to the island/attached bar lowering and channel widening project is also provided.

Potential for Deposition in Sluiceways: Flow velocity in the Peralta Main sluiceway is less than critical velocity, for median (0.6 mm) and larger sediment sizes, downstream of the third gate (P3 in Figure 2) in scenario #2, and in the Belen Highline sluiceway in front of gate #2 (B3 in Figure 2) and downstream of the fourth gate (B1 in Figure 2) for scenario #2. These results indicate a high likelihood of sediment deposition in both sluiceways when the operation has minimum summer diversions with minimum flow to pass through the sluiceway. The velocities were evaluated as being sufficient to transport sediment through the sluiceway in all other scenarios. For any diversion operation, the minimum sluiceway outflow discharge most likely to prevent sediment deposition in the Belen Highline sluiceway is 35 cfs, and 30 cfs in the Peralta Main sluiceway..

Gate Operation Effects on Potential Sediment Deposition and Erosion: This section provides results from the 2D model to evaluate the potential for sediment deposition versus erosion downstream of the dam for the proposed case where islands were removed and the channel widened (see Figures 3 and 4). The modeled water surface upstream of the diversion dam for all but scenario #3 was lower than needed to provide full diversion head. This resulted in larger velocities in the model results than actual field velocity. Therefore, this paper describes and uses model results downstream of the diversion dam for all scenarios except scenario #3. For scenario #3, all of the gates are open and upstream water surface elevations are accurate and consistent with field observations and HEC-RAS model results, and both upstream and downstream results are described. Model and incipient motion results are divided into two categories. Category 1 has a low likelihood for sediment erosion or deposition except in the immediate downstream vicinity of open gates. Category 1 includes scenario #1 and 2. Category 2 includes scenarios #3, 4, and 5 which have a high likelihood for sediment erosion or deposition. The proposed project topography results are shown and discussed for scenarios in each category with a qualitative discussion of likely channel response.

Category 1, scenarios #1 and 2 have a low likelihood of appreciable sediment deposition, due to the upstream sediment supply being low for this discharge. While there is low likelihood of erosion or deposition, if there was sediment supply from upstream tributaries this section describes potential areas change. Since scenario #1 and #2 have very similar hydraulic results, scenario #1 model results are used to represent both scenarios. The dark blue color in Figure 6 represents flow velocities which are up to the critical velocity of 0.5 ft/s for scenario #1 with the proposed channel widening downstream of the dam, and shows areas of potential sediment deposition. Zones of

potential sediment deposition are found in the first 400 ft. downstream of the dam between gates 16 and the Peralta left bank looking downstream of the left sluiceway (Figure 6). In the widened channel area there is a potential zone of deposition between about 1,000 ft. to about 1,900 ft. downstream of the dam apex, indicating a likelihood of sediment deposition which would potentially result in channel narrowing or areas where sediment would need to be excavated to maintain the channel width. Likely zones with small scour potential would be downstream of gate 16, downstream of the left sluiceway, between the right sluiceway and in the channel downstream of the right side sluiceway, and in the downstream channel center until the second bend (Figure 6).

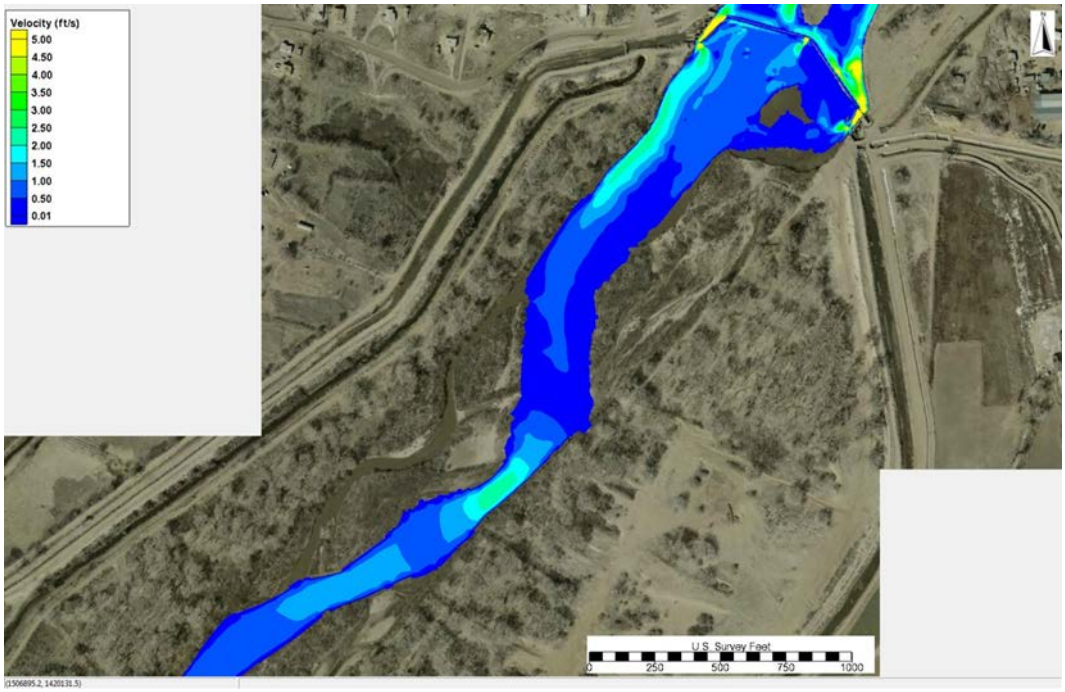

Figure 6 Proposed topography depth-averaged velocity contours for scenario #1.

Category 2 scenarios, #3, 4 and 5, each have a high likelihood of sediment deposition due to the sediment supply being relatively higher than for inflows to the diversion dam ranging from 1,565 to 5,000 cfs. Each of these scenarios has very different inflows and gate operations and results will be summarized separately. For Scenario #3, all river gates are open with 100 cfs flowing through each sluiceway; 4,450 cfs passes through the dam. Potential erosional areas would be around the upstream island (Figure 4). Flows near 4,450 cfs would provide the maximum opportunity for the widened channel to remain near the design width according to the SRH-2D model results and incipient motion criteria. The bank attached bars between 400 and 1500 ft. downstream of the Peralta Main sluiceway were lowered (Figures 3 and 4), and have velocities indicating potential for sediment deposition.

Scenario #4 has 1,780 cfs passing through 10 open river gates, and 220 cfs and 270 cfs flowing out the Peralta Main and Belen Highline sluiceways, respectively. One-to-three gates are closed between each open gate. The open gates are clearly shown in the velocity results (Figures 7 and 8). Flow velocity accelerates through the open gate contractions. Between open gates there are zones of low velocity and eddies (Figure 8). Deposition between open gates has been observed in the field. Downstream of each open gate there is high velocity with the potential for erosion. Zones of high velocity are found downstream of each sluicegate, and along the right main channel. The inundated portion of the east side bank attached lowered bar shows potential for sediment deposition. Flows near 1,780 cfs would provide opportunity for the widened channel to remain near the design width according to SRH-2D model results and incipient motion criteria. But not as much opportunity as 4,450 cfs flows in scenario #3. The bank attached bar on the left side between 400 and 1500 ft. downstream of the Peralta Main sluiceway was lowered (Figure 7 and 8) and made into two surfaces. These lowered surfaces are inundated at 1,780 cfs, and have velocities indicating potential for sediment deposition.

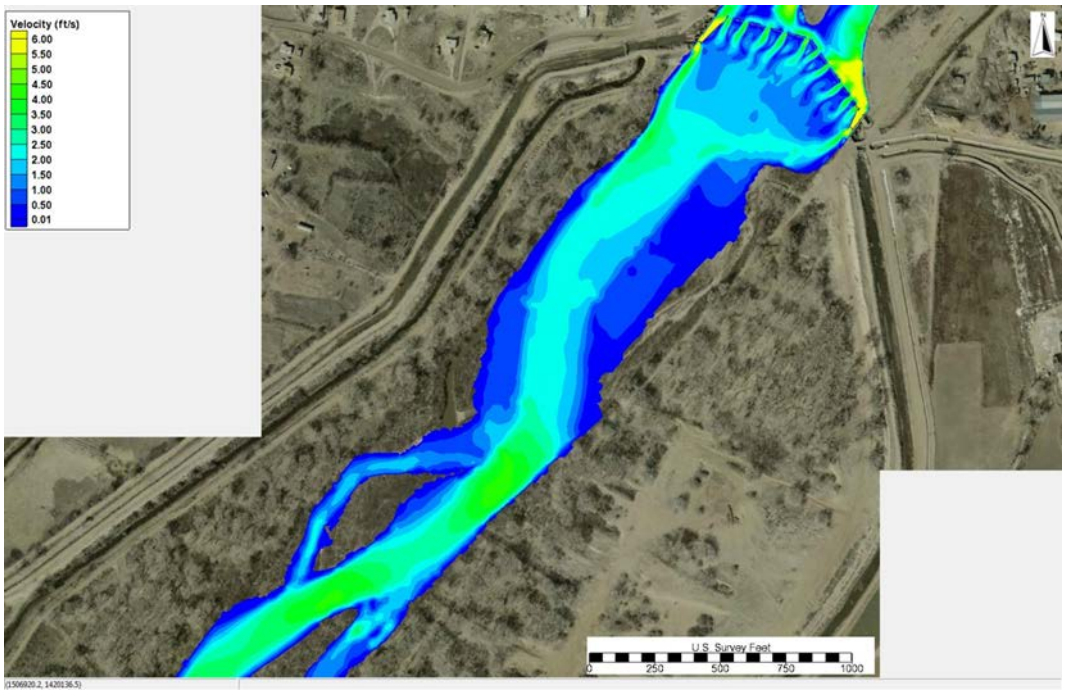

Figure 7 Project design topography depth-averaged velocity contours for scenario #4.

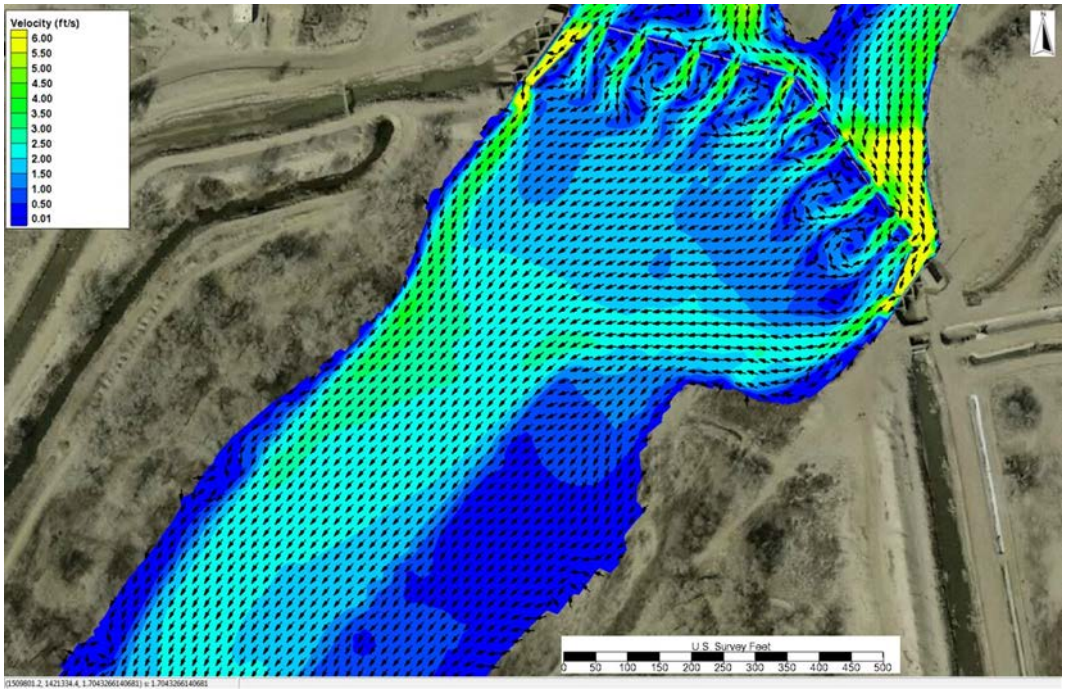

Figure 8 Project design topography depth-averaged velocity contours and vectors for scenario #4.

All river gates are closed in Scenario #5. Flow is maximized through each sluiceway in the amount of 460 cfs in the Peralta Main canal sluiceway, and 555 cfs in the Belen highline canal sluiceway. Maximum flow discharging through each sluiceway results in very high shear stress and velocity downstream of each sluiceway, especially the Belen Highline sluiceway. Downstream of the Belen Highline sluiceway the high velocity zone extends downstream about 600 ft. The majority of the zone downstream of the diversion dam between the sluiceways is depositional as a result of the formation of a slow velocity zone until the flow paths reconnect into the relatively

narrower downstream channel. Flow on the east abutment downstream of the sluiceway has the potential to cause scour extending across the east third of the distance across the channel below the dam. Scouring velocities also occur along the west bank downstream of the Belen Highline sluiceway downstream through the widened proposed topography reach. Flow in the left channel around the island shows potential for scour, while flow around the right side channel path shows potential for deposition and slight erosional tendencies.

These results are based upon the median sand sediment size of 0.6 mm requiring a velocity of 0.5 ft/s or larger to limit deposition (Table 1). Larger sediment particles could deposit in areas where velocity is between 0.5 and 1.0 ft/s, resulting in more areas of sediment deposition than described above. Results are also based upon fixed bed topography without potential bed elevation changes which would develop when considering sediment supply and sediment transport capacity.

SUMMARY AND CONCLUSIONS

A fixed bed two-dimensional hydraulic model was developed for Isleta Diversion Dam and the upstream and downstream channel. In addition a sluiceway hydraulic analysis was completed for the Belen Highline and Peralta Main canal sluiceways. Using the upstream and downstream median sand bed sediment sizes, the velocity which initiates sediment transport was estimated using the Vanoni, (1977) method. These results provide a quantitative basis for recommending gate operations to reduce sedimentation impacts.

Headworks sluiceway hydraulics and critical velocity analysis results indicate which scenario's result in sediment deposition or transportation through both headworks sluiceways. When the sluiceway outflow in the Peralta Main Canal is less than 30 cfs there is potential for sediment deposition. The Belen Highline Canal sluiceway velocity shows potential for sediment transport when sluiceway flows are 35 cfs or larger.

The SRH-2D model results and incipient motion analysis provided results to show velocity patterns and potential zones of sediment deposition or erosion for five flow scenarios ranging from 124 to 4,450 cfs river flows downstream of the diversion dam. In general maximizing flow volume in each sluiceway provides for potential erosion and high velocity flow along each bank downstream of each sluiceway and particularly along the west bank (Scenario #5). Opening every other or every third gate results in eddy currents and zones of potential deposition between gates. Operating only the sluiceways causes eddy currents near the downstream apex of the dam between sluiceways which indicates a potential for sediment deposition. The flow scenarios with river discharges equal to or greater than 1,780 cfs show potential for maintaining the widened channel. All flows inundating the lowered bank attached bars and islands showed potential for sediment deposition. Given the variable nature of Rio Grande hydrology, it is likely that the widened channel can be partially maintained with river flows, but supplemental mechanical widening may be needed to maintain the excavated hydraulic geometry.

ACKNOWLEDGEMENTS

The Albuquerque Office of the U.S. Bureau of Reclamation (Reclamation) contributed the 2012 LiDAR data of the overbank areas. Vincient Benoit and Nathan Holste assisted with topography measurements upstream of the diversion dam. Tetra Tech Inc. (Walt Kuhn, of the Tetra Tech Inc. Albuquerque, NM Office) provided cross section data, design topography for the downstream island lowering and channel widening and their HEC-RAS model. Yong Lai, of the Sedimentation and River Hydraulics group (Reclamation) provided technical support for the use of the SRH-2D model. Cody Walker of the Isleta Pueblo, and David Gensler, Kevin Lente, and Jim Russell of the Middle Rio Grande Conservancy District provided their observations of flow patterns for various historic gate operations. Jennifer Bountry of the Sedimentation and River Hydraulics group (Reclamation) provided helpful experience for project planning and reviewed this manuscript. These contributions are gratefully acknowledged.

REFERENCES

Baird, D.C., and Strand, R.I., (2013). "Channel Characteristics of the Middle Rio Grande, near Isleta Diversion Dam and Sediment Management Gate Operations," U.S. Department of the Interior, Bureau of Reclamation, Technical Service Center, Sedimentation and River Hydraulics Group, Denver, CO. Report No. SRH-2013-10.

Bauer, T. (2009). "Draft Sediment Effects on the Middle Rio Grande, NM," U.S. Department of the Interior, Bureau of Reclamation, Technical Service Center, Sedimentation and River Hydraulics Group, Denver, CO.

Happ, S.C. (1948). "Sedimentation in the Middle Rio Grande Valley, NM," Geological Society of America Bulletin 59(12):1191-1216.

Gensler, D. 2013. Hydrologist, Middle Rio Grande Conservancy District, Albuquerque, New Mexico.

Lagasse, P.F. (1980). "An Assessment of the Response of the Rio Grande to Dam Construction-Cochiti to Isleta Reach," Technical Report for United States Army Corps of Engineers, Albuquerque District, Albuquerque, NM.

Lai, Y.G. (2000). "Unstructured Grid Arbitrarily Shaped Element Method for Fluid Flow Simulation,) *AIAA Journal*. 38(12), 2246-2252.

Lai, Y.G. (2008), "SRH-2D version 2: Theory and User's Manual," U.S. Department of the Interior, Bureau of Reclamation, Technical Service Center, Sedimentation and River Hydraulics Group, Denver, CO.

Makar, P.W. (2010). "Channel Characteristics of the Middle Rio Grande, NM," U.S. Department of the Interior, Bureau of Reclamation, Technical Service Center, Sedimentation and River Hydraulics Group, Denver, CO. Report No. SRH-2011-05.

Scurlock, D. (1998). "From the Rio to the Sierra: An Environmental History of the Middle Rio Grande Basin," General Technical Report RMRS-GTR-5. : U.S. Department of Agriculture, U.S. Forest Service, Rocky Mountain Research Station, Fort Collins, CO.

Shields, A, 1936, Anwendung der Aehnlichkeitsmechanik und der Turbulenzforschung auf die Geschiebebewegung, Mitt. Preuss. Versuchsanst.

Sturm, T.W. (2001). Open Channel Hydraulics. McGraw-Hill Series in Water Resources and Environmental Engineering. New York, NY. 493 pp.

Tetra Tech Inc., (2012), HEC-RAS model of the Rio Grande, Albuquerque, NM.

U.S. Army Corps of Engineers (USACE), (2008), "HEC-RAS River Analysis System User's Manual," Version 4.0, Hydrologic Engineering Center, Davis CA.

U.S. Fish and Wildlife Service (USFWS), (2003). "Programmatic Biological Assessment of Bureau of Reclamation's Water and River Maintenance Operations, Army Corps of Engineers' Flood Control Operation, and Non-Federal Actions on the Middle Rio Grande, New Mexico March 1, 2003-February 28, 2013," *U.S.* Department of the Interior, Fish and Wildlife Service, New Mexico Ecological Services Office, Albuquerque NM.

Vanoni, V.*A.*, ed., (1975). Sedimentation Engineering. ASEC Task Committee for the Preparation of the Manual on Sedimentation of the Sedimentation Committee of the Hydraulics Division (reprinted 1977) Manual 54, American Society of Civil Engineers.

GEOMORPHIC CHANGE IN THE LIMITROPHE REACH OF THE COLORADO RIVER IN RESPONSE TO THE 2014 DELTA PULSE FLOW, UNITED STATES AND MEXICO

Erich R. Mueller, Research Hydrologist, U.S. Geological Survey, Southwest Biological Science Center, Grand Canyon Monitoring and Research Center, Flagstaff, Arizona, emueller@usgs.gov
John C. Schmidt, Professor, Department of Watershed Sciences, Utah State University, Logan, Utah, jack.schmidt@usu.edu
David J. Topping, Research Hydrologist, U.S. Geological Survey, Southwest Biological Science Center, Grand Canyon Monitoring and Research Center, Flagstaff, Arizona, dtopping@usgs.gov
Paul E. Grams, Research Hydrologist, U.S. Geological Survey, Southwest Biological Science Center, Grand Canyon Monitoring and Research Center, Flagstaff, Arizona, pgrams@usgs.gov

Abstract A pulse of water was released from Morelos Dam into the dry streambed of the Colorado River in its former delta on March 23, 2014. Although small in relation to delta floods of a century ago, this was the first flow to reach the sea in nearly two decades. The pulse flow was significant in that it resulted from an international agreement, Minute 319, which allowed Colorado River water to be used for environmental restoration. Here we present a historical perspective of channel change and the results of geomorphic and sediment transport monitoring during the pulse flow between Yuma, Arizona and San Luis Rio Colorado, Sonora. This reach is known as the Limitrophe, because the river channel is the legal border between the United States and Mexico. Peak discharge of the pulse flow was 120 m^3/s at Morelos Dam, but decreased to 71 m^3/s at the southern border because of infiltration losses to the dry streambed. In contrast, flood flows in the 1980s and 1990s peaked above 600 m^3/s at the southern border, and high flows above 200 m^3/s were common. The sustained high flows in the 1980s caused widening and reworking of the river channel downstream through the delta. In the Limitrophe, flooding in 1993 from the Gila River basin dissected the 1980s flood surfaces, and smaller floods in the late 1990s incised the modern "active" channel within these higher surfaces. Field observations show that most geomorphic change during the pulse flow was confined to this pre-pulse, active channel. Relatively little bank erosion was evident, particularly in upstream reaches where vegetation is most dense, but new sandbars formed in areas of flow expansion. Farther downstream, localized bed scour and deposition ranged from 10s of centimeters to more than a meter, and fluvial dunes aggraded the bed in several locations. Measurable suspended-sediment transport occurred throughout the Limitrophe. Sediment concentrations peaked during the rising limb, and suspended sand concentrations suggest deposition in the lower 7 km of the Limitrophe as the channel gradient decreases by an order of magnitude. The pulse flow was small compared to historic floods, and flood magnitudes greater than the 2014 pulse flow are therefore necessary to significantly rework stable geomorphic surfaces or induce channel widening.

INTRODUCTION

The Colorado River delta is a completely transformed landscape. The Colorado River in much of its former delta is now an intermittent stream and includes long segments that are persistently

dry. Historically, the delta extended from a point approximately 21 km upstream from the Gila River confluence near Yuma, Arizona, downstream to the Gulf of California, and includes the closed basins of the Salton Sink in the United States and Laguna Salada in Mexico. Sykes (1937) estimated the delta covered approximately 8600 km^2. Prior to the construction of large dams and diversions, the flow of the Colorado River in its delta fluctuated annually with high flows from snowmelt in the Rocky Mountains and periodic widespread rain or rain-on-snow events in the lower basin. Discharge recorded at the Yuma stream gage exceeded 5000 m^3/s several times in the early 20^{th} century, and, occasionally, during periods of extended low flow, no water reached the estuary in the pre-dam period (Sykes, 1937). In its natural state, the Colorado River delta was characterized by shifting channels and high sand, silt, and clay loads. Meade et al. (1980) estimated that the Colorado River delivered more than 10^8 tons of sediment per year to the delta prior to significant human activity in the watershed. The completion of diversions to the Imperial and Mexicali valleys in the early 1900s initiated the period of major regulation of streamflow and sediment to the delta, which became increasingly dramatic following the construction of large dams such as Hoover Dam (1935) and Glen Canyon Dam (1963). Today, the Colorado River is normally dry throughout the year along large segments of its former delta in the United States and Mexico and essentially no sediment reaches the Gulf of California.

High flows of the 1980s and 1990s rejuvenated portions of the riparian and wetland ecosystems of the delta that had been lost during the filling of upstream reservoirs. The ecological impact of these flows created significant bi-national interest in using intentional flow releases to rehabilitate parts of the delta ecosystem (Tiegs et al., 2005; Glenn et al., 2008; Flessa et al., 2013). Following more than a decade of international negotiations, Minute 319 of the International Boundary and Water Commission (IBWC) established the political foundation for one experimental flow release. The release of intentional flows into the delta is extremely controversial in a fully utilized river system faced with protracted drought. Thus, the science that underlies this pulse flow and the monitoring of its consequences is crucial to deciding if future environmental flows will occur. Here we present an overview of historical geomorphic change and effects of the spring 2014 pulse flow release in the Limitrophe. The Limitrophe, or border, reach of the river lies between Morelos Dam, the last dam on the river, and the Southern International Boundary (SIB) (Fig. 1). The Limitrophe is a critical segment of the Colorado River in the delta because it is the only segment that is a shared border of the U.S. and Mexico, it is relatively rich in native riparian and marsh habitat in its upstream half (Glenn et al., 2008), and it is almost always dry in its downstream half. This zone was potentially an area of significant loss of flow into the bed and ground water system, and the losses here may greatly decrease the magnitude of flows in Mexico where the potential for rehabilitation is greater.

POST-DAM HYDROLOGY OF THE COLORADO RIVER DELTA The construction of Hoover and Glen Canyon Dams, and the subsequent filling of the reservoirs they impound, resulted in progressively decreasing flows and drastically reduced sediment loads to the lower Colorado River. Stream gaging at SIB serves as a measure of flows to the Mexican portion of the delta from 1950 to the present, and represents the minimum discharge in the Limitrophe because of infiltration losses to the streambed in the downstream half of the Limitrophe. We present the following hydrologic analysis based solely on this stream gage. From 1950 to 1963, Hoover Dam modulated flood flows from the upper Colorado River basin, but the river often flowed to the

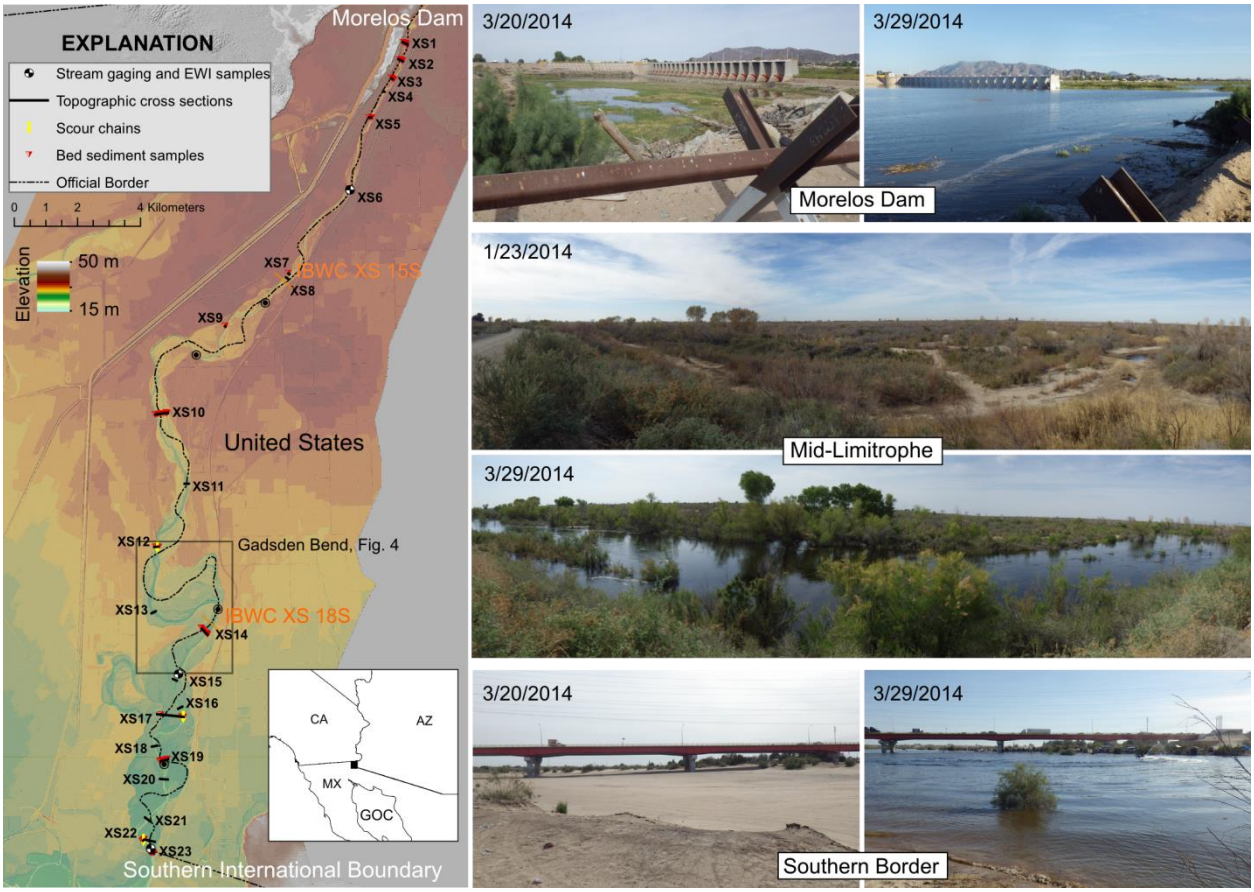

Figure 1 The Limitrophe reach study area (left); inset map shows the location of the Limitrophe as a black square; GOC: Gulf of California. Photos before and during the pulse flow (right).

Gulf of California. During that time the peak daily discharge was 581 m^3/s, the average daily discharge was 93 m^3/s, and zero flow was recorded on only 14 days. From 1963 to 1981, the filling of Lake Powell upstream from Glen Canyon Dam and other reservoirs in the upper basin greatly reduced flows; the peak daily discharge was 268 m^3/s, the average daily discharge was 15 m^3/s, and no flow was recorded 18 percent of the time.

POST-DAM DELTA FLOODS In the 1980s, successive years of extremely high snowmelt runoff from the upper Colorado River basin resulted in a period of high flow releases from Glen Canyon and Hoover Dams (Fig. 2). As a result, flood flows in the delta region were the greatest since the completion of Hoover Dam and caused considerable channel adjustment (McCleary, 1986; Tiegs and Pohl, 2005). Peak daily discharge at SIB reached 934 m^3/s on August 20, 1983, andremained above 500 m^3/s for more than 250 consecutive days. From 1983 to 1987, mean daily discharge remained above 150 m^3/s for nearly four consecutive years. Since that time, flows with magnitudes of 150 m^3/s have occurred less than 3% of the time (Fig. 2). Following the 1980s floods, periods of zero discharge at SIB became increasingly common. From 1989 to 1992, there was no flow recorded at SIB 92% of the time. This dry period was punctuated by flood flows from the Gila River in 1993 that peaked at 646 m^3/s on March 7th and 8th (Fig. 2). The 1993 flooding was caused by a series of winter storms that produced widespread rain and

rain-on- snow in the upper Gila River watershed (House and Hirschboeck, 1997). Discharge at SIB remained relatively high throughout much of 1993 because of continued upstream water releases from reservoirs on the Gila River. Following extended periods of zero discharge in the middle 1990s, a series of moderately high flows occurred in the late 1990s. These high flows peaked above 200 m^3/s and followed releases from Hoover Dam that resulted in over-deliveries to Mexico. Progressively decreasing flows have been recorded at SIB since 2000 (Fig. 2).

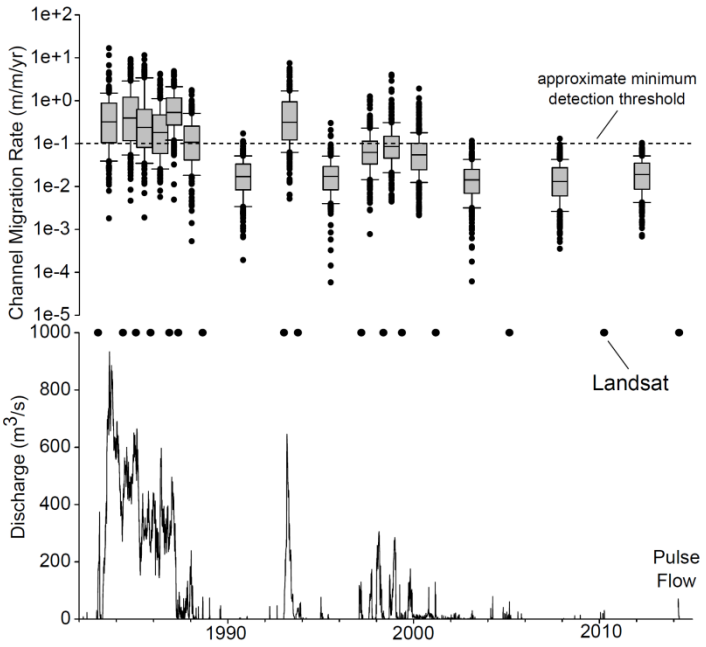

Figure 2 Box plots (top) showing channel migration rates of the Colorado River in the 50 km reach downstream from Morelos Dam; rates are bracketed by the Landsat imagery dates shown. Boxes represent the 25th, 50th, and 75th percentiles; whiskers represent the 5th and 95th percentiles, with outliers as dots. Daily mean discharge (bottom) recorded at SIB, 1980 to present.

THE PULSE FLOW The periodic floods of the 1980s and 1990s created bare sediment surfaces for native seedling recruitment, and made water more available to maturing trees during subsequent periods of low or no flow. But since 2000, drought conditions in much of the Colorado River basin have greatly reduced flows past Morelos Dam. Typically, the upstream half of the Limitrophe has some baseflow because of a higher water table and irrigation return flows. Periods of no flow at SIB have occurred more than 60% of the time since 2000, and the channel bed is usually dry in most of the downstream half of the Limitrophe where the groundwater table is meters below the streambed. This contributed to losses of native riparian vegetation, such as cottonwood and willow, which had established in the prior two decades. The maximum daily discharge measured at SIB since 2000 was 129 m^3/s (on March 1st, 2001). The last measured discharge at SIB prior to the pulse flow peaked at 30.5 m^3/s (in April, 2010) following several winter and spring storms in the lower basin (Ramírez-Hernández et al., 2013).

On March 23rd, 2014, an experimental pulse of water bypassed Morelos Dam and flowed into the dry river channel. The maximum peak discharge released past Morelos Dam was 120 m^3/s on March 29th, which decreased to 71 m^3/s at SIB (Fig. 2) because of infiltration losses to the dry

streambed (discussed further in the results). The peak release occurred during a three-day period, and the flow was reduced to zero during a period of approximately three weeks after which flow from Morelos Dam ceased. Additional water was supplied to the river from irrigation canals downstream from SIB in order to supplement the losing flow of the river. The pulse flow reached the Gulf of California on May 15th, by which time the discharge was approximately 0.6 m^3/s.

GEOMORPHOLOGY In the Limitrophe, the Colorado River follows approximately the same path as reported in some of the earliest accounts of river navigation (Sykes, 1937). The river delta was essentially natural until 1900, when large-scale diversions and levees began to be constructed. The period 1900-1930 saw the river channel avulse several times in the delta, with most of the sediment load deposited internally downstream from the Limitrophe, but not flowing to the sea (Sykes, 1937). Closure of Hoover Dam muted flood peaks and greatly decreased the sediment load. Nevertheless, aerial photographs from 1949 show the Colorado River as a dynamic meandering channel with many active bars and bounded by floodplains and terraces that show evidence of recent occupation (Fig. 3). Olmstead and others (1973) report that the Colorado River incised from 3-6 meters from north of Yuma to SIB following the construction of Hoover Dam, but they provide no supporting data. Cross-sections surveyed by the IBWC, spaced approximately 2-3 km apart in the Limitrophe, show 2 to 3 m of bed incision during high flows in the early 1940s. Following this degradation, the bed remained vertically stable or aggraded slightly until the early 1980s (IBWC data, unpublished). There was significant channel widening in the 1980s (Tiegs and Pohl, 2005), and bed elevations in 1989 remained similar to those in 1982, but were still lower than those observed in the early 1940s (Tetra Tech, 2004; NCD/FPC, 2006). The flood of 1993 reworked much of the river corridor that was inundated in the 1980s, and dissected finer channel threads into the 1980s deposits (Tiegs and Pohl, 2005). By 1999, vegetation encroachment, dominated by tamarisk, had created a narrower channel (Tiegs and Pohl, 2005; Tiegs et al., 2005), and the thalweg of most of the IBWC cross-sections reached their minimum elevations (Tetra Tech, 2004; NCD/FPC, 2006).

THE MODERN COLORADO RIVER IN THE LIMITROPHE The Limitrophe can be divided into two major geomorphic segments that have a gradational boundary. The river channel in the upstream segment is more confined within levees, and irrigation return flow results in a wetted channel with dense bank vegetation. In the downstream segment, the river channel is dry, bank vegetation is less dense, and the channel is less confined by levees (Fig. 1). The width of the alluvial corridor between the levees ranges from approximately 0.5 km immediately downstream from Morelos Dam, to more than 4 km in the downstream part of the Limitrophe. The average channel gradient is 0.00022 m/m along the modern thalweg, but reach-scale (5-10 km) gradient ranges from 0.000044 to 0.00040. Sediments range in grain size from silt and clay to gravel, with the active channel composed dominantly of fine to medium sand and finer sediments on higher abandoned surfaces.

METHODS

In this paper, we present results from two related elements to characterize the geomorphic response of the Colorado River in the Limitrophe to the 2014 pulse flow. First, we build on the analysis of historic channel changes from 1983 to 2014 that shaped the configuration of the pre-pulse channel and set the boundary conditions for surface water flow and sediment transport

during the pulse. Second, we report results from geomorphologic and sediment transport monitoring of the pulse flow.

CHANGES IN CHANNEL MORPHOLOGY, 1983-2014 We used 30 m Landsat imagery to map changes in the channel thalweg or centerline using 16 image sets that bracketed major flow events. We purposefully chose periods of relatively low flow to more accurately digitize the channel thalweg. During the periods of sustained high discharge in the 1980s, flows were often too high to define the thalweg, and we used the channel centerline instead. After digitizing the channel thalweg/centerline, we used the Planform Statistics Toolbox from the National Center for Earth Surface Dynamics (Lauer, 2006) to calculate channel migration in 100-300 m segments. The exact length of individual segments depended on the degree of channel sinuosity, and thus point spacing, in the digitizing process. In order to account for different segment distances and time intervals, we report the results in meters of lateral change per meter of streamwise distance per year. We approximate the error in thalweg location as plus or minus 30 m, or one pixel width, as a conservative estimate of a minimum detection threshold. Our analysis builds on that of Tiegs and Pohl (2005), extending it through 2014, and establishes the magnitude of those flows that are sufficient to cause significant lateral channel migration.

We also developed a geomorphic base map of portions of the Limitrophe reach to better understand the spatial and temporal evolution of geomorphic change. We used high-resolution aerial photography and a 1-m bare earth lidar digital elevation model acquired from an airborne scanner in March 2014 prior to the pulse flow. Aerial photography dating back to 1949 was available for the entire Limitrophe reach (earthexplorer.usgs.gov). Imagery from 1949 and 1963 is sub-meter resolution, imagery from 1976, 1981, and 1989 has a resolution ranging from 5 to 6 m per pixel, and data sets from 1992 to present (1992, 1996, 2003, 2007, and 2013) are 1-m resolution. These aerial photo dates include images of the river corridor prior to construction of Glen Canyon Dam, which caused major reductions in flow as discussed above. These photo dates also bracket the major floods of the 1980s and 1990s, allowing for documentation of channel change in response to these events. In addition to these aerial photos, we compared historic IBWC cross-sections to the pre-pulse flow lidar to document changes since 1999, and to provide a quantification of changes in bed elevation. Here we present data for two IBWC cross-sections that we could most reliably match to the lidar data (Fig 1).

GEOMORPHOLOGY AND SEDIMENT TRANSPORT DURING THE PULSE FLOW We used repeat cross-sections, scour chains, and suspended sediment transport measurements at multiple locations to document the geomorphic response to the pulse flow. We established 23 cross-sections within the Limitrophe reach (Fig. 1) to document changes in bed elevation and installed scour chains at three of these cross-sections (12, 17, and 22, Fig. 1) to analyze scour and fill. We spaced cross-sections 1 to 4 km apart and focused on areas likely to be inundated by the flood. Cross-sections were more concentrated immediately downstream from Morelos Dam, and in the dry reach in the downstream portion of the Limitrophe (Fig. 1). We collected 3 to 15 sediment samples on representative surfaces at 14 of the cross-sections before and after the pulse flow. Lidar data were obtained for the entire Colorado River delta in March and August 2014, and will be used to provide a broader spatial picture of channel change resulting from the pulse flow (as of the time of writing, the second lidar data set was still being processed). Suspended sediment measurements were made at three locations in the Limitrophe to provide a record of

sand and silt and clay concentrations. Daily equal width increment (EWI) samples were collected on six occasions at three sites during the period of peak discharge of the pulse flow. Here we report results from the two downstream sites located near cross section 15 (Colorado River near Gadsden, Arizona) and at SIB (Colorado River at the Southern International Boundary) (Fig. 1).

RESULTS AND DISCUSSION

CHANGES IN CHANNEL MORPHOLOGY, 1983-2014 Channel migration rates during the three decades since 1983 were greatest during the large floods of the 1980s. Landsat imagery bracketing individual hydrograph peaks during this time shows that between 50 and 75% of the channel had migration rates above the minimum detection threshold, and as much as 25% of the river channel migrated at rates exceeding 1 m/m/yr (Fig. 2). Channel change was particularly pronounced in the downstream portion of the Limitrophe, and substantial portions of higher pre-dam terraces eroded 500 to 1000 m laterally, effectively increasing the size of the lower elevation channel (Fig. 3). There was little channel activity in the late 1980s and early 1990s during a period of very little flow (Fig. 2). The Gila River floods of 1993 caused a similar proportion of the channel to migrate as during floods in the 1980s (Fig. 2). Yet most geomorphic change was confined to the part of the channel affected by the 1980s floods, rather than eroding older and higher terraces (Fig. 3). The 1993 flood dissected much of the 1980s flood surfaces, resulting in a braided appearance on many of these surfaces (Tiegs and Pohl, 2005). Measureable channel migration occurred along approximately 25% of the channel for three periods analyzed during moderately high flows in the late 1990s and early 2000s (Fig. 2). Channel migration rates were 2-10 times less than during the larger 1980s and 1993 floods, and confined to a narrower zone in the river corridor. No measureable channel migration, within the resolution of the Landsat data, has occurred since 2001 (Fig. 2).

Our analysis of aerial photography and the historic IBWC cross-sections suggest that bed incision occurred during high flows in the late 1990s that peaked above 200 m^3/s. While the exact positioning of cross-sections has changed over time, decreasing confidence in smaller scale changes, it is clear that the modern cross-sections derived from lidar are similar to the form measured in 1999 (Fig. 4). The 1980s floods caused significant channel change between 1982 and 1989, but relatively little change in bed elevation (Fig. 4; Tetra Tech, 2004; NCD/FPC 2006). By 1999, the thalweg of the channel had incised below the 1989 thalweg, and the 2014 lidar indicates that the channel configuration is very similar to that observed in 1999. Prior to the 1980s floods, the IBWC data suggest that the most significant channel changes occurred in the early 1940s when there was roughly 2 and 3 m of bed degradation (IBWC unpublished data). The resulting geomorphology of the river corridor in the Limitrophe thus benches down from higher terraces that were active in the pre-dam period, to intermediate terraces representing portions of the active channel and floodplain in 1949 that were largely stable by 1963, and finally to more recent surfaces of the 1980s and 1990s (Fig. 3). Aerial photos and lidar suggest that, in the downstream part of the Limitrophe, the floods of the early 1980s deposited a higher alluvial surface (Fig. 3), and smaller flood peaks in the late 1980s formed an inset channel within this surface (Fig. 3). The 1993 flood reworked this lower 1980s surface considerably, but also caused a more defined thalweg to become incised. The floods in the late 1990s mostly modified this inset channel, which became further incised, and forms the modern "active" channel (Fig. 3). The bed of this inset active channel is 2 to 3 m below those surfaces reworked in 1993, and has a

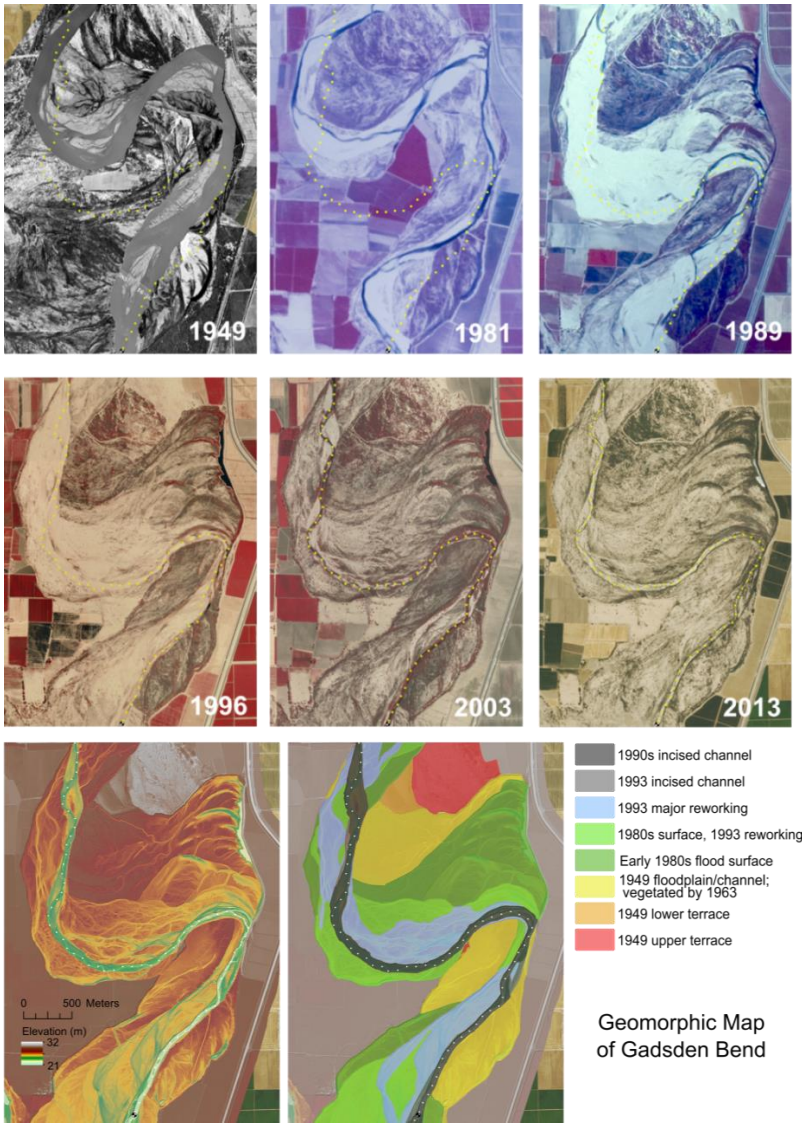

Figure 3 Aerial photos showing geomorphic change for six years from 1949 to 2013; yellow dots indicate modern thalweg. Pre-pulse flow lidar (bottom left) and geomorphic surfaces (bottom center), showing modern thalweg in modern "active" channel incised in the late 1990s.

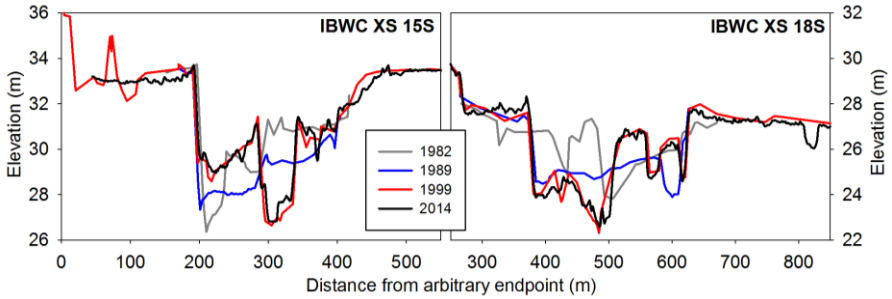

Figure 4 Historic cross-section changes at two locations shown in Figure 1 in the Limitrophe from 1982 to present. 1982, 1989, and 1999 surveys from the U.S. IBWC (data from TetraTech, 2004 and provided by NCD/FPC, 2006), and 2014 data from pre-pulse flow lidar.

typical width of 50-200 m in the Limitrophe. This incised part of the channel contained the majority of the pulse flow, but it did inundate higher surfaces with shallow, low-velocity flow.

GEOMORPHOLOGY AND SEDIMENT TRANSPORT DURING THE PULSE FLOW

The hydrograph of daily flow from Morelos Dam shows a 3-day period of maximum releases, a second discharge spike three days after the peak, and several other fluctuations during the falling limb (Fig. 5). Attributes of the hydrograph observed in the Morelos Dam releases are preserved downstream, but discharge decreased by 30 to 40% because of flood attenuation and, primarily, by infiltration losses to the dry streambed. Further, because of increased groundwater levels during the preceding week, the second peak was of similar magnitude to the first peak in the downstream reaches that were initially dry. The pulse flow tended to inundate a wider area upstream, resulting from a combination of higher discharge upstream and greater channel roughness from dense bank vegetation (Fig. 6).

Suspended sediment concentrations were somewhat greater at the beginning of the pulse and decreased over time, and there is evidence of discharge-concentration hysteresis as measured at our two sampling locations in the downstream part of the Limitrophe (Fig. 5). The decrease in sand concentration at SIB during the pulse may coincide with the formation of dunes that increased drag, because both the grain size and concentration of suspended sand decreased as flow increased. Alternatively, suspended sand coarsened slightly with discharge at our measurement site 7 km upstream (near Gadsden). Sand concentrations were two to three times greater at this upstream site, but silt and clay concentrations were similar between the two sites. Thus, silt and clay likely behaved as wash load and moved downstream to Mexico, whereas sand deposition is likely to have occurred in the downstream 7 km of the reach. Channel gradient is an order of magnitude less between the Gadsden gage and SIB, compared to the reach immediately upstream, and may be a factor in decreasing downstream sand concentrations.

Geomorphic change in response to the pulse flow was limited to the incised active channel that formed during the progressively decreasing flows of the late 1990s and early 2000s. Cross-sections show that the pulse flow inundated most areas to an elevation equal to or slightly greater than the bank top elevation of the previously incised active channel (Fig. 5). In the upstream part of the Limitrophe, thick bank vegetation focused channel change on the narrow, ~20 to 50 m wide, part of the channel that was within, or immediately adjacent to, the wetted portion of the pre-pulse channel. There was little evidence of bank erosion, but sandbars locally buried vegetation and the main channel bed was reworked (Fig. 6, top photo). Because of the negligible upstream sediment contributions and the confined nature of the active channel, we expected that bed incision would occur in these upstream reaches (XS1-XS6, Fig. 1). Instead, our repeat surveys show little evidence of bed incision in these reaches, and, in fact, slight (~0.25 m) aggradation at several cross-sections. A potential sediment source immediately downstream of Morelos Dam was the erosion of dredged material composed of sand and gravel along the Mexican side of the river corridor, but outside of the primary active channel. Much of the channel bed that had been composed of sand overlain by finer sediments bound by an organic mud was composed of sand and gravels following the pulse. Sandbars formed in zones of flow expansion, and the bed of the river developed pool-riffle topography in several locations. Riffles were characterized by coarser bed material and active bed load transport at baseflow discharges (~1-2 m^3/s) following the pulse flow.

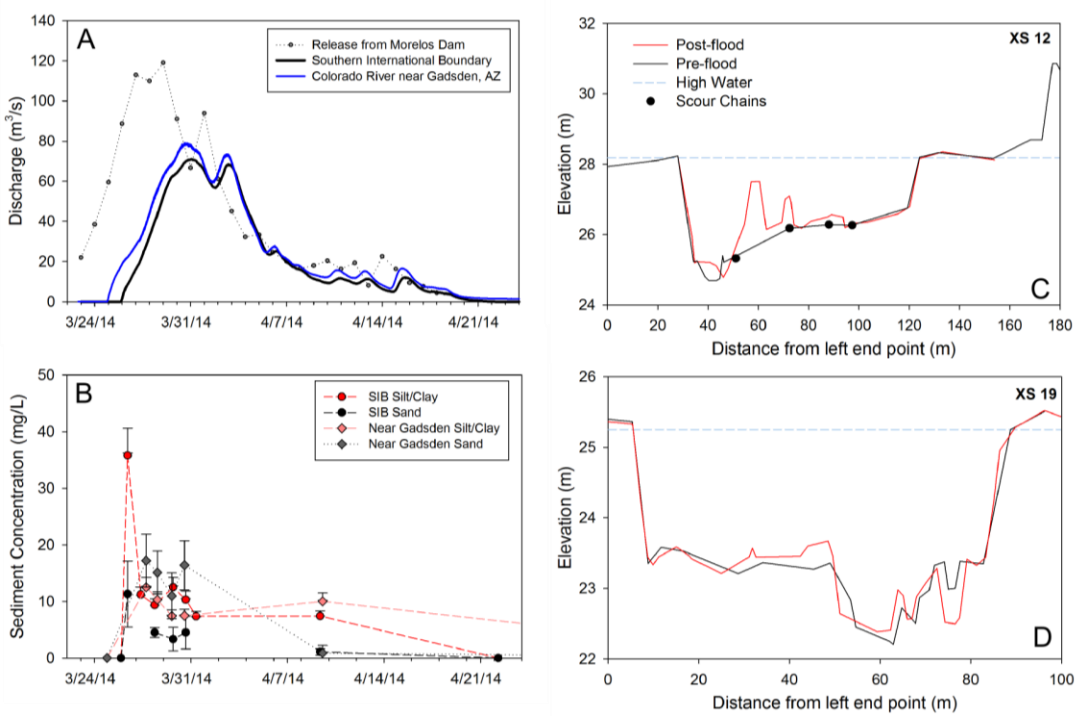

Figure 5 Hydrograph of the pulse flow released at Morelos Dam and measured near Gadsden, Arizona and at SIB (A). Measured sediment concentrations at the Gadsden and SIB gages (B). Two example cross-sections showing topographic change during the pulse flow (C and D).

Downstream where the channel widens, areas of localized bed scour and deposition ranged from tenths of meters to more than a meter and fluvial dunes provided evidence of widespread bed mobilization (Figs. 5 and 6). In the middle portion of the Limitrophe, the main thalweg usually has some baseflow that has allowed dense riparian vegetation to flourish, which protected the stream banks from erosion during the pulse flow. However, there are also remnants of the old 1990s channel that are dry and barren of vegetation. These open sand areas (tens of meters by hundreds of meters) were zones of active dune transport despite relatively shallow flow. The dunes had wavelengths of order 5-15 m, and amplitudes of 0.2 to 0.4 m. Alternatively, the wetted part of the channel in the middle Limitrophe generally showed bedforms associated with topographic steering in a more confined and sinuous channel. Five scour chains placed across the active channel in the mid-Limitrophe show no evidence of bed scour, but as much as a meter of deposition (XS-12, Fig. 5). Immediately upstream from the scour chains there was obvious bed scour and the repeat cross-section shows areas of erosion and deposition in the thalweg.

In the farthest downstream section of the Limitrophe, where the channel was dry and the channel bed was largely devoid of vegetation, evidence of dune migration was obvious throughout the reach. Localized lobate forms (1-10 m) and larger-scale dune fields (>100 m) were common in many places (Fig. 6). Cross-sections in this reach show evidence of both scour and deposition (XS-19, Fig. 5), with little change in grain size. Of our scour chains, and those of our Mexican colleagues, only two locations show evidence of significant scour (>0.1 m) prior to deposition, whereas most show simply scour or deposition. Scour chains at our site just upstream of SIB did show 0.05-0.15 m of scour followed by up to 0.3 m of deposition. Dunes are clearly visible from

Figure 6 Landsat image from 3/31/2014 during the peak of the pulse flow and examples of sediment deposition and bed forms because of the pulse flow. Backpack (circled), 2 m rod in foreground, and person (circled) for scale. Width of channel is approximately 300 m in the Worldview panchromatic image at right.

aerial photos at this site during the waning stage of the pulse flow (Fig. 5). As stated above, the lower 7 km of the Limitrophe was likely a depositional reach, and the short duration of the pulse likely limited downstream transport distances. Any sediment transported past the border must have been deposited on the channel bed far upstream from the estuary as flow rapidly decreased.

Sediment transport and geomorphic change in the Limitrophe during the pulse flow was concentrated in the recent active channel where flow depths were several meters. Higher surfaces were only marginally inundated, and there was no noticeable geomorphic change. Thus, these surfaces served as a pseudo-floodplain for flows similar to the 2014 pulse flow, which flowed through a channel roughly sized to convey that discharge. Ongoing studies will provide quantification of sediment concentrations in the upstream part of the Limitrophe measured at XS-6 (Fig. 1), and allow us to construct sediment budgets between the three gaging stations. We also anticipate that our future analysis of repeat lidar measurements will provide a more spatially robust link between the flux-based sediment budgets and morphologic change, and document the fate of sediment transported to reaches farther downstream in Mexico.

CONCLUSIONS

The Colorado River in its delta is now an intermittent sand-bedded stream for much of its course. Decreasing peak flows during the last two decades shaped the active channel in the Limitrophe reach, and the active channel is sized to convey flows of roughly 100 m^3/s. Terraces formed during the 1980s floods and dissected by the 1993 flood served as a pseudo-floodplain during the 2014 pulse flow. Geomorphic change and sediment redistribution during the pulse flow was limited to reworking of the channel bed and topographic changes of order 1 m or less within the active channel. Channel widening or widespread scouring or burial of vegetation that may affect

native vegetation recruitment is only likely to occur with higher discharges. This presents a dilemma for future planning of environmental flows to the delta, because higher river flows correspond to a greater cost in terms of volume of water lost to the subsurface and may cause further channel incision. Furthermore, long-term restoration outcomes will also be contingent on larger floods that will occur periodically from widespread and persistent precipitation in the Gila River basin, and monitoring strategies should consider these unplanned floods.

REFERENCES

Flessa, K.W., Glenn, E.P., Hinojosa-Huerta, O., de la Parra-Rentería, C.A., Ramírez-Hernández, J., Schmidt, J.C., and Zamora-Arroyo, F.A. (2013) "Flooding the Colorado River delta: A landscape-scale experiment," Eos Trans. AGU, 94(50), pp. 485.

Glenn, E.P., Hucklebridge, K., Hinojosa-Huerta, O., Nagler, P.L., and Pitt, J. (2008) "Reconciling environmental and flood control goals on an arid-zone river: case study of the Limitrophe Region of the Lower Colorado River in the United States and Mexico," Environmental Management, 41(3), pp. 322-335.

House, P.K., and Hirschboeck, K.K. (1997) "Hydroclimatological and paleohydrological context of extreme winter flooding in Arizona, 1993," Reviews in Engineering Geol., 11, pp. 1-24.

Lauer, J.W. (2006) "Channel planform statistics, NCED Stream Restoration Toolbox," http://www.nced.umn.edu/content/stream-restoration-toolbox.

McCleary, D.P. (1986) "Channel adjustments of the lower Colorado River," Fourth FISC Conference, Las Vegas, NV, pp. 5-103-5-112.

Meade, R.H., Yuzyk, T.R., and Day, T.J. (1990) "Movement and storage of sediment in rivers of the United States and Canada," in Wolman, M.G. and Riggs, H.C. (eds), Surface Water Hydrology – The Geology of North America, Geological Society of America, pp. 255-280.

NCD/FPC, Natural Channel Design/Fred Phillips Consulting (2006) "Restoration strategy: a preliminary design for enhancement of native riparian habitats, lower Colorado River, limitrophe reach, U.S.-Mexico," Final report to Environmental Defense, 122 pp.

Olmstead, F.H., Loeltz, O.J., and Irelan, B. (1973) "Geohydrology of the Yuma area, Arizona and California," USGS Professional Paper, 486-H, 226 pp.

Ramírez-Hernández, J., Hinojosa-Huerta, O., Peregrina-Llanes, M., Calvo-Fonseca, A., and Carrera-Villa, E. (2013) "Groundwater responses to controlled water releases in the limitrophe region of the Colorado River: Implications for management and restoration," Ecological Engineering, 59, pp. 93-103.

Sykes, G. (1937). The Colorado Delta. American Geographical Society Special Publication No. 19, 193 pp.

Tetra Tech. (2004) " Lower Colorado River, proposed pilot channel analysis." Final report to U.S. Army Corps of Engineers, Memorandum of Understanding IBM 92-21, 98 pp.

Tiegs, S.D. and Pohl, M. (2005) "Planform channel dynamics of the lower Colorado River: 1976-2000," Geomorphology, 69, pp. 14-27.

Tiegs, S.D., O'Leary, J.F., Pohl, M.M., and Munill, C.L. (2005) "Flood disturbance and riparian species diversity on the Colorado River Delta," Biodiversity and Conservation, 14(5), pp. 1175-1194.

Any use of trade, product, or firm names is for descriptive purposes only and does not imply endorsement by the U.S. Government.

BASIN-SCALE GEOMORPHOLOGY AND SEDIMENT TRANSPORT ANALYSIS FOR THE MOUSE/SOURIS RIVER ENHANCED FLOOD PROTECTION PLAN

Peter Hinck, PE, Barr Engineering Company, Minneapolis, MN, phinck@barr.com; Benjamin Sheets, PhD, Barr Engineering Company, Minneapolis, MN, bsheets@barr.com; Miguel Wong, PhD, PE, Barr Engineering Company, Minneapolis, MN, mwong@barr.com; Amy Anderson, PE, Barr Engineering Company, Minneapolis, MN, aanderson@barr.com

INTRODUCTION

Understanding the basin-scale geomorphology and dominant sediment transport processes active in any river system is an important first step when evaluating the potential impacts of large civil works projects. This paper focuses on the study of the Mouse/Souris River watershed in north-central North Dakota, conducted as part of the Mouse River Enhanced Flood Protection Plan. The work was conducted following the Mouse/Souris River flood of record in 2011 when the peak flow was more than five times the estimated 100-year peak flow for which existing channels and levees (constructed by USACE in the 1970's and 1990's) had been designed. In response to this catastrophic event, a plan to reduce the risk of flooding and flood-related damages was developed, including 21.6 miles of levees, 2.8 miles of floodwalls, two high-flow diversions, several transportation closure structures, and stormwater pump stations, among other measures.

This paper presents a framework for understanding how sediment is mobilized through the watershed and riverine system that is based on relating the geologic history of the basin to key present-day watershed (e.g., topography, soils, land use) and river (e.g., channel cross section, stream slope, planform) characteristics. The present day characteristics of the Mouse/Souris River are highly constrained by the area's glacial history, resulting in distinct river segments delineated by major geomorphologic features. Stream classification using basin-scale data affords a foundational understanding of the natural tendencies of the river that is essential in order to adequately evaluate the potential impacts on the morphodynamics (erosion and/or sedimentation) of the Mouse/Souris River associated with the proposed project.

GEOLOGIC SETTING

The configuration of today's Mouse/Souris River Basin is the result of the area's glacial history. The basin's origins can be traced to a catastrophic outburst of glacial melt water in Canada about 11,000 years ago (Lord (1991), Kehew and Teller (1994)). Floodwaters from this outburst carved what are now known as the Des Lacs and Mouse/Souris River valleys (Figure 1, Kehew and Clayton (1983)). The meltwater eventually flowed into glacial Lake Souris, which extended from Verendrye to the Canadian border, creating two distinct Mouse/Souris River reaches in North Dakota (upstream and downstream of Verendrye), each with its own behavior and structure.

Geologic events shaped not only the landscape but the paths the Mouse/Souris River now takes, affecting in particular its ability to convey water and sediment during extreme flood events. Signatures of the ancient glacial flood, such as shape and size of the Des Lacs and Mouse/Souris

River valleys and the lack of a confining valley downstream of Verendrye, still influence certain aspects of water and sediment movement (Figure 2). Of note for this study is that the highest potential for erosion will continue to exist in the river reaches upstream of Verendrye, while the downstream reaches will be more likely to experience sediment deposition in future floods.

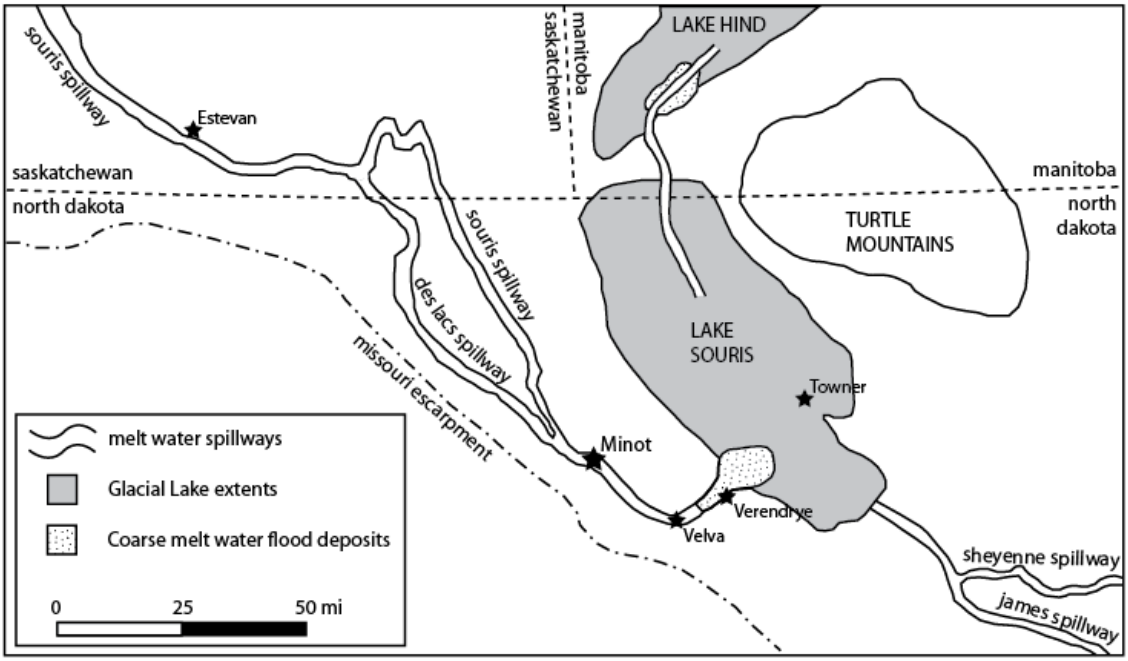

Figure 1 Schematic map of significant glacial landforms in the Mouse/Souris River watershed, after Kehew and Clayton (1983).

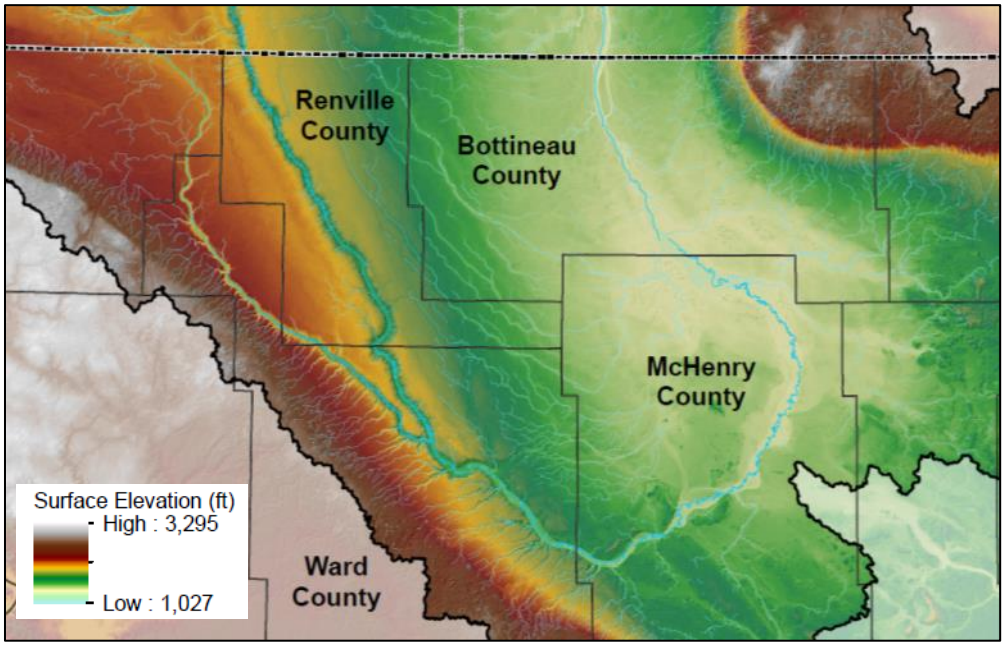

Figure 2 Mouse/Souris River watershed topography.

VALLEY AND STREAM CHARACTERISTICS AND CLASSIFICATION

The overall goal of stream classification is to organize and describe stream reaches based on shared attributes. The methods, metrics, and spatial and temporal scales used in stream classification systems vary widely, but such systems frequently use common characteristics such as river width, valley width, slope, sinuosity, and amplitude or radius of curvature (see for example Leopold et al. (1964), Montgomery and Buffington (1993), and Rosgen and Silvey (1996)). Grouping stream reaches based on quantitative characteristics presents the ability to look for patterns, identify commonalities and differences, and make inferences about the future behavior of the stream system. The emphasis of the analysis presented here is on developing an understanding of the processes at work in the Mouse River and its history rather than to take a point-in-time snapshot of the river under current conditions. For this study, streams were classified according to features of both the valley and the river channel.

Characteristics used in stream classification

- Valley width
- Valley slope (in direction of river flow)
- Valley sediment types (represented by % sand)
- Land use
- Channel width
- Channel cross-sectional area
- Channel slope (in direction of river flow)
- Channel length per unit valley length (sinuosity)
- Channel planform

The project team classified the Mouse/Souris River into nine reaches that vary in length and have been grouped according to similar valley, channel, and sediment characteristics (Figure 3). The nine reaches defined for the Mouse/Souris River can be broadly considered as three separate groups: upstream of Burlington (reaches G-H-I), between Burlington and Verendrye (reaches D-E-F), and downstream of Verendrye (reaches A-B-C). This grouping corresponds to the major geologic shifts along the Mouse/Souris River: the confluence with the Des Lacs River at Burlington and the entrance to the bed of glacial Lake Souris at Verendrye.

The reaches of the Mouse/Souris River between Burlington and Verendrye (reaches D-E-F) received the most attention in the study because 1) they are the areas with the steepest river gradient and contain soils most likely to be mobilized; 2) have been most affected by changes in the last several decades; and 3) will be the most directly affected by the proposed project. This section of the river is the most susceptible to erosion.

The reaches downstream of Verendrye (reaches A-B-C) may also be influenced by the proposed project because they lie downstream of the project features and receive sediment carried from upstream reaches. These reaches represent the portions of the river that have 1) the lowest river gradients; 2) soils typically finer than those in upstream reaches; 3) the most open water and wetlands; and 4) the lowest channel banks. This section of the river is the most likely to experience sediment deposition.

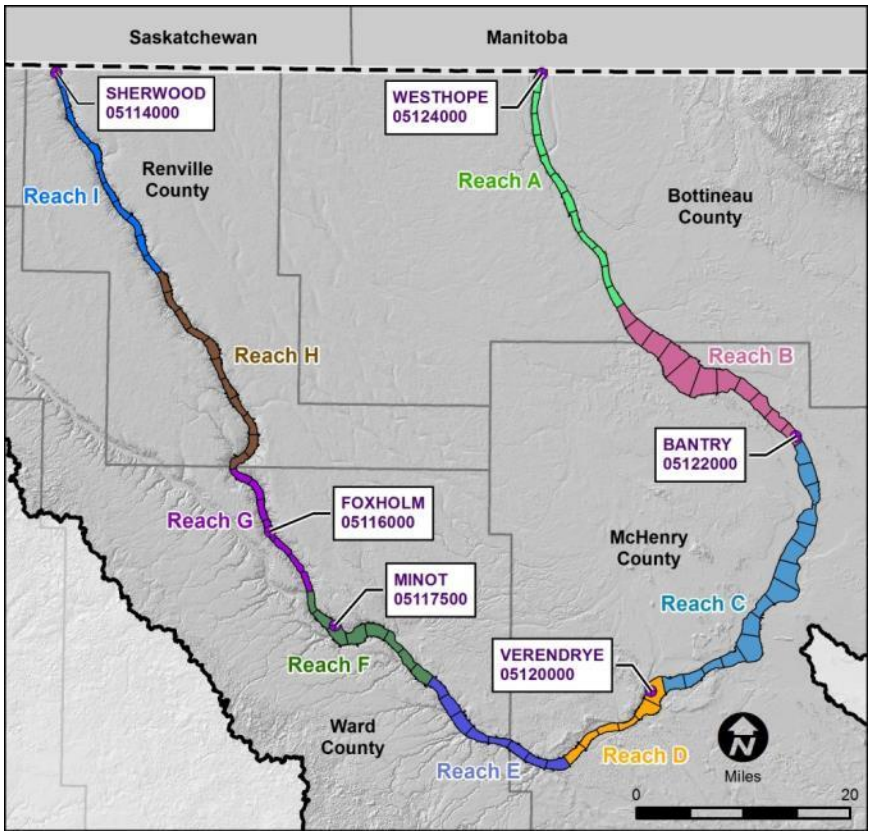

Figure 3 Mouse/Souris River valley geomorphic reaches.

The reaches upstream of Burlington (reaches G-H-I) will be less affected by the project partly because Lake Darling controls sediment movement in the system.

CHANGES IN RIVER SHAPE OVER TIME

The Mouse/Souris River valley has undergone significant anthropogenic changes in the past 150 years, including shifts in land use, increasing population, and construction of several federal flood-risk-reduction projects. The historical changes in the valley suggest how the river may adapt to future modifications of the channel and/or floodplain.

A key source of historic information about the Mouse/Souris River is aerial photography. The consulting team compared aerial photos taken in 1946 and 1969 with 2010 images and assessed the changes in the river's centerline. The 1969 photos show the river as it existed before the addition of flood-risk-reduction measures between Burlington and Velva. The 1946 images, although taken after the construction of Lake Darling, constitute the area's earliest full set of aerial photographs.

Comparing the images revealed that in areas not located near flood-risk-reduction works, changes in river alignment and in the river length (or sinuosity) over the past several decades have been minimal. While the Mouse/Souris River actively meanders, the observed rate of

channel migration—the slow but constant reshaping of a sinuous river—is not high for a river with its characteristics.

In contrast, pronounced changes in river length have occurred in reaches subject to the channel straightening and cutoff of bends that were part of federal projects (Figure 4). For the 10-mile-long section of river valley near Minot, these projects caused a reduction in stream length of more than 40% (9 river miles) between 1969 and 2010. The sinuosity (ratio of river length to valley length) for this section of the valley is now markedly different from that in the rest of the Mouse/Souris River valley, a condition that can cause excessive erosion and "unraveling" as the river attempts to compensate for the imposed reduction in length. Although no observable major changes in other river characteristics have occurred since the federal projects were completed, there is a limit to how much straightening can be performed without increasing erosion.

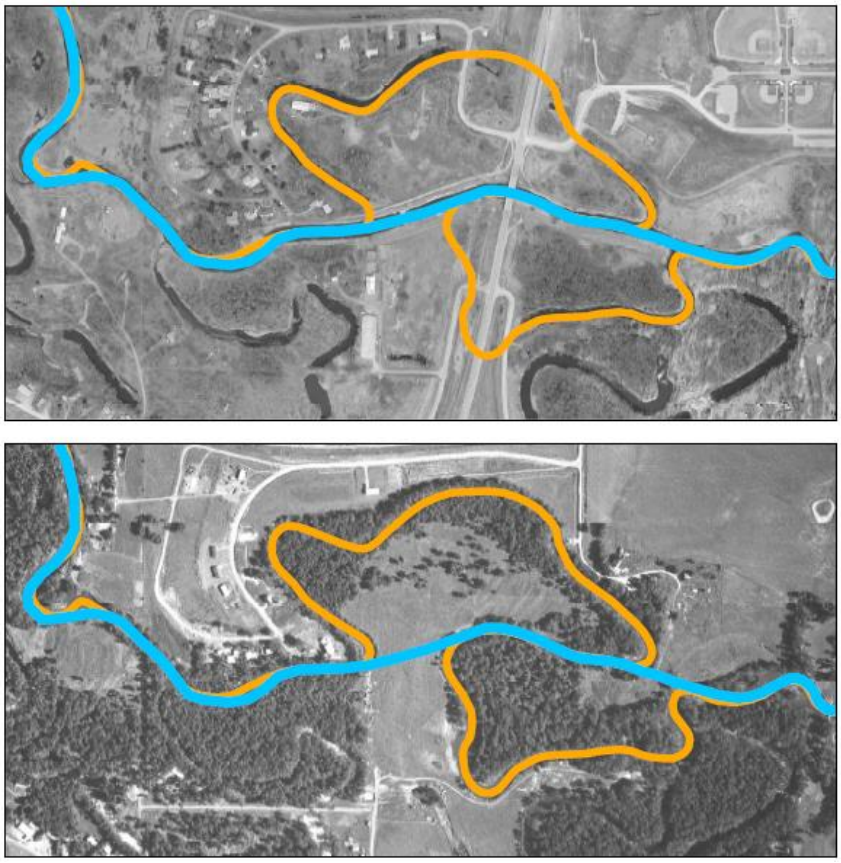

Figure 4 Aerial photographs from 1969 (bottom) and 2010 (top) showing a meander cut off by a federal flood risk reduction project.

SEDIMENT CHARACTERISTICS

Another important source of historic information is sediment transport data, including measurements of the type and quantity of sediment that is transported in the river system. Measurements of the channel-bed material size are especially important, because different types of soil particles interact differently with flowing water.

The available sediment-transport data for the Mouse/Souris River was collected mostly by the U.S. Geological Survey in the 1970s. Because the data is very limited in the most sensitive Burlington-to-Verendrye reach (especially with respect to channel-bed material and to sediment transport rates for a wide range of flows), the team could not quantify erosion or sedimentation potential. Based on the available data, the Mouse/Souris River in the vicinity of Minot appears to have bed material of primarily fine sand and relatively low suspended sediment concentrations (Figure 5).

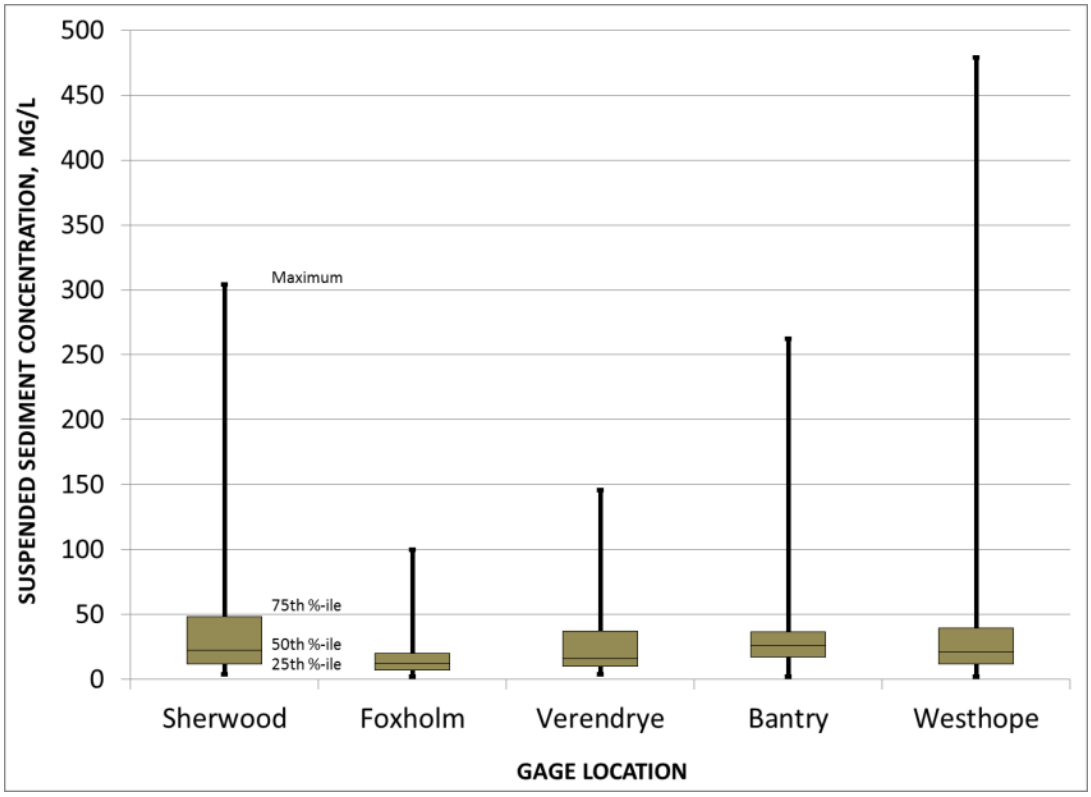

Figure 5 Mouse/Souris River suspended sediment concentration ranges.

PRELIMINARY EVALUATION OF POTENTIAL PROJECT IMPACTS

Based on the initial characterization of the processes of erosion, transport, and deposition of river sediment in the study area, it is possible to offer a preliminary qualitative assessment of erosion and sedimentation impacts that may occur in the Mouse/Souris River if the proposed flood-risk-reduction project is implemented.

As discussed above, the reaches of the Mouse/Souris River between Burlington and Verendrye are naturally more susceptible to erosion. Because the project will increase flow velocities in some locations during very high flow conditions, the project's most likely local impact is an increased risk of erosion. The design considerations of the preliminary project alignment are intended to reduce the potential for erosion by including areas of overbank excavation and widening many of the bridge openings and by providing scour protection near diversion

structures. However, current plans call for some bridge crossings to significantly constrict flood flows—a situation that may lead to erosion in extreme flood events.

In addition, there is a risk of increased erosion (both bank erosion and channel scour) where the river channel is constricted by levees occupying a significant portion of the floodplain. This is particularly true in areas where the river is restricted to a very narrow region between a levee on one side and a valley wall on the other. At these locations, flow convergence may result in increased erosion (Figure 6).

Figure 6 Significant erosion and channel migration after the 2011 flood opposite the existing levee at Velva.

The Souris Valley Golf Course in Minot (Figure 7) will continue to be an area within the proposed project limits that is subject to sediment deposition. In the preliminary alignment created for this project, the golf course is the only area within Minot where the river has an appreciable floodplain, which reduces flow velocity even during very large floods and allows sediment deposition to occur. Similar deposition is also likely just downstream of Minot where the river will leave the protected area and return to its natural floodplain.

Judging by the characteristics of the Mouse/Souris River's valley and channel and by observations from the 2011 flood, it is unlikely that erosion and sedimentation impacts from the project will extend beyond the most sensitive reaches between Burlington and Verendrye. However, additional field investigations and numerical modeling are warranted to validate this

initial conclusion, particularly as it relates to the development of river management alternatives in the rural areas.

Figure 7 Sand deposition after the 2011 flood at the Souris Valley Golf Course.

There is not sufficient information available (especially for sediment characteristics) to numerically quantify the magnitude of the erosion and sedimentation impacts discussed above. These impacts can be quantified by modeling the most sensitive reaches of the river—modeling that accounts for driving forces (e.g., shear stress) and sediment characteristics (especially of the bed material) and sediment loading.

CONCLUSIONS

Present day characteristics of the Mouse/Souris River are highly constrained by the area's glacial history, resulting in distinct river segments delineated by major geomorphologic features. Stream classification using basin-scale data affords a foundational understanding of the natural tendencies of the river that is essential in order to adequately evaluate the potential impacts on the morphodynamics (erosion and/or sedimentation) of the Mouse/Souris River associated with the proposed project.

The primary objective of this study was to characterize the river morphology and sediment transport processes in the study area and to use this characterization to conduct a preliminary evaluation of the proposed project's potential to result in undesirable erosion and sedimentation

impacts. The evaluation was qualitative due to the limited available historic information on sediment-related variables. The qualitative evaluation has served the purpose of identifying data gaps and additional analyses that will be required to determine the magnitude of the impacts and propose measures to lessen these impacts.

One of the preliminary conclusions of this study is that despite the significant existing alteration of some Mouse/Souris River reaches (such as channel straightening and levee construction), only isolated erosion and sedimentation impacts were observed in a very extreme event (the 2011 flood of record). Additional river alignment alterations associated with the proposed project or alterations in the rural areas could translate into a different outcome.

The main outstanding questions in this report that may be addressed in a future phase of study are 1) how will the project change sediment transport upstream and downstream of project features, and 2) what will be the magnitude of the associated erosion or sedimentation responses to such changes?

REFERENCES

Kehew, A.E., and Clayton, L. (1983). "Late Wisconsinan floods and development of the Souris-Pembina spillway system," in Glacial Lake Agassiz, Teller, J.T. and Clayton, L. (eds), Geological Association of Canada Special Paper 26, pp. 187-210.

Kehew, A.E., and Teller, J. (1994). "History of late glacial runoff along the southwestern margin of the Laurentide ice sheet," Quaternary Science Reviews, vol. 13, pp. 859-877.

Leopold, L. B., Wolman, M. G., and Miller, J. P. (1964). Fluvial Processes in Geomorphology. Dover Publications, New York.

Lord, M. (1991). "Depositional record of a glacial-lake outburst: Glacial Lake Souris, North Dakota," Geological Society of America Bulletin, vol. 103, pp. 290-299.

Montgomery, D. R., and Buffington, J. M. (1993). Channel classification, prediction of channel response, and assessment of channel condition. Washington State Timber, Fish and Wildlife.

Rosgen, D., and Silvey, H. (1996). Applied River Morphology, Wildland Hydrology, Pagosa Springs, Colorado.

SUSPENDED-SEDIMENT TRANSPORT THROUGH A LARGE FLUVIAL-TIDAL CHANNEL NETWORK

Scott A. Wright, Research Hydrologist, U.S. Geological Survey, Sacramento, CA, sawright@usgs.gov; Tara L. Morgan, Hydrologist, U.S. Geological Survey, Sacramento, CA, tamorgan@usgs.gov

INTRODUCTION

The Sacramento – San Joaquin River Delta (the Delta) is formed at the confluence of the Sacramento River and San Joaquin River, the two main watersheds draining California's Central Valley (Figure 1). Once an extensive tidal marsh system, the Delta has been subject to an array of changes since the discovery of gold and subsequent development of California in the mid-1800s. These changes include the following: construction of channel levees and draining of tidal marshes for agriculture; hardening (rip-rap) of existing channels and construction of new channels/canals to support water conveyance; hydraulic gold mining activities which introduced large quantities of fine sediment to the Delta in the late 1800s; construction of large dams in the watershed in the mid-1900s that trap sediment and reduce sediment loads to the Delta; construction and ongoing dredging to maintain shipping channels through the Sacramento River (upstream to Sacramento) and San Joaquin River (upstream to Stockton); and the construction of large pumping facilities in the south Delta that export water to the San Joaquin valley and southern California for agricultural and urban uses. These physical modifications have affected the hydrodynamics and sediment transport characteristics of the Delta (Lund et al., 2007, Whipple et al., 2012), which have in turn affected the aquatic ecosystem. In addition to the physical modifications, the ecosystem has been affected by direct biological modifications, in particular the introduction of non-native species.

Delta smelt, a fish species endemic to the Delta currently listed as Threatened under the Federal Endangered Species Act and Endangered under the California Endangered Species Act, is currently a major regulatory, management and scientific focus in the Delta. The Delta smelt, along with other native and non-native species, experienced abrupt population declines in the early 2000s, referred to locally as the Pelagic Organism Decline., or POD. While the POD is generally thought to be the result of multiple stressors, Delta smelt habitat and migration patterns have been linked with turbidity and temporal changes in turbidity such as "first flush" river runoff events (for a review of Delta smelt habitat studies refer to Sommer and Mejia, 2013). First flush refers to the first major runoff event in the watershed that produces substantial sediment loads and increases in turbidity in the Delta. Increases in turbidity in the southern Delta in the vicinity of the State Water Project and Central Valley Project pumping facilities (near Clifton Court Forebay, see Figure 1) have been linked to high entrainment of Delta smelt at the facilities (Grimaldo et al., 2009), which can lead to severe curtailments of water deliveries south of the

Delta on which 25 million people depend for at least part of their drinking water supply. Because turbidity in the Delta is caused by suspended sediments, studies of sediment transport dynamics are important for understanding Delta smelt habitat and informing Delta smelt management decisions.

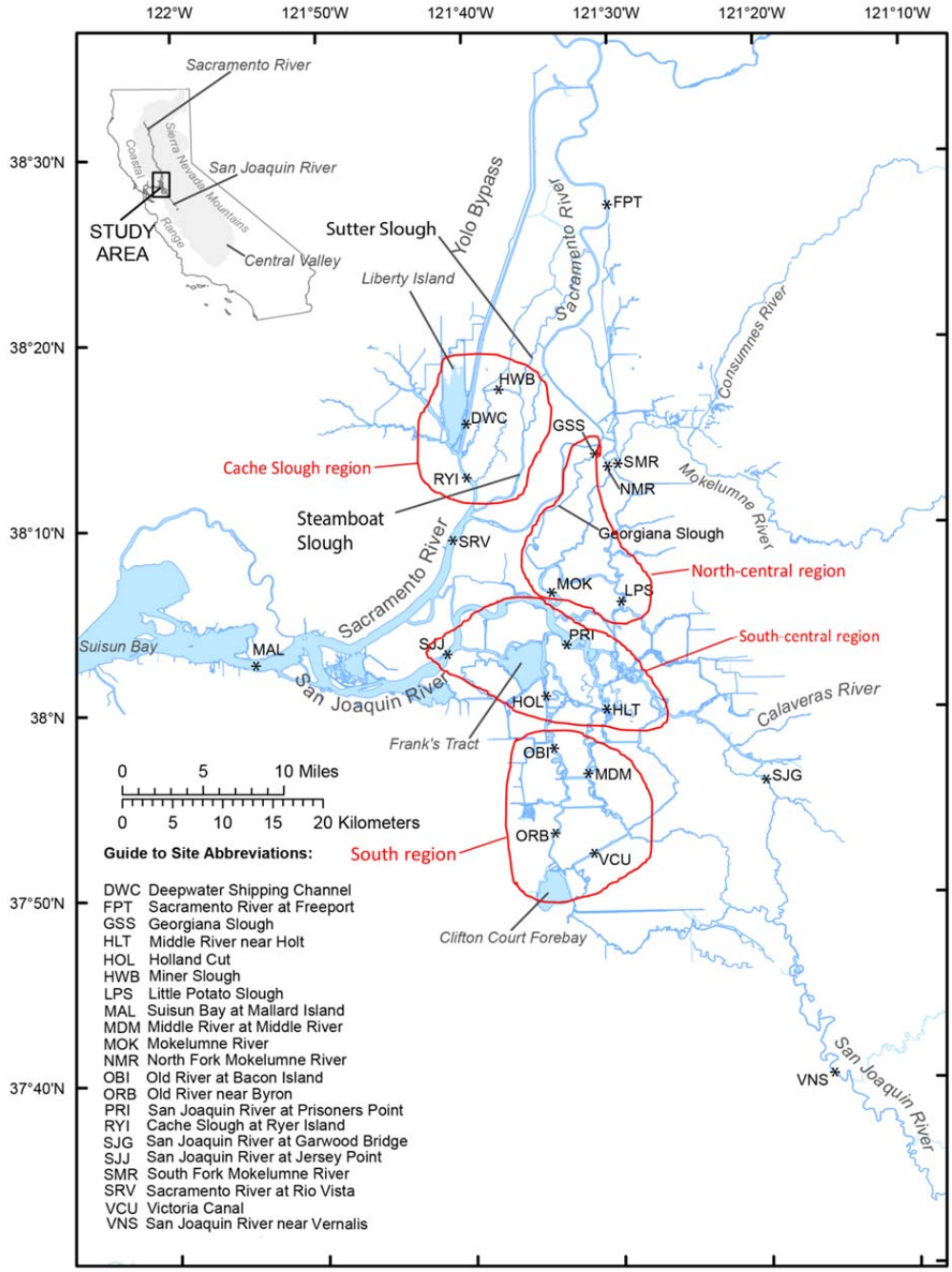

Figure 1 – Site map showing locations of gages and region outlines used in this study.

The objective of this paper is to describe the advection and dispersion of a first flush sediment pulse through the Delta. We focus on a single event that occurred in December 2012 (Figure 2, first pulse beginning around 1-Dec-2012) to illustrate these processes, because this event provided a very clean signal from the Sacramento River and throughout the Delta due to relatively low sediment flux from the San Joaquin and Mokelumne rivers (Figure 2). The Sacramento River is the dominant source of water and sediment to the Delta (Wright and Schoellhamer, 2005), such that events like the December 2012 first flush can be considered fairly typically in terms of influencing Delta turbidity. In addition, these first flush events are known to be a cue for Delta smelt migration upstream into the Delta (Sommer et al., 2011, Bennett and Burau, 2014) and potentially into the zone of influence of the south Delta export facilities, where they are subsequently salvaged at the export facility fish screens and ultimately resulting in export curtailments.

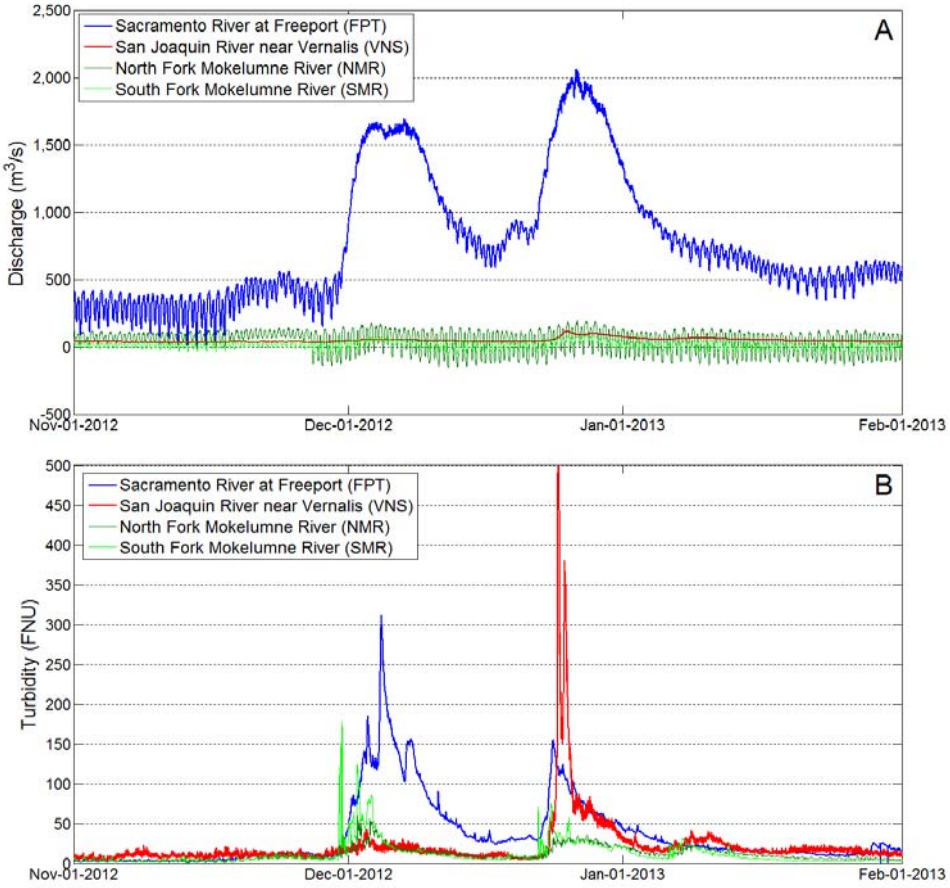

Figure 2 – Discharge (A) and turbidity (B) at upstream Delta boundaries.

METHODS

The U.S. Geological Survey (USGS), California Department of Water Resources (DWR), and Bureau of Reclamation (BoR) maintain an extensive flow and water quality monitoring network

in the Delta. Flow monitoring (USGS) is conducted using index velocity methods (Ruhl and Simpson, 2005, Levesque and Oberg, 2012). *In situ* continuous monitoring of turbidity, temperature, and conductivity (USGS, DWR, and BoR) is accomplished using multi-parameter sondes (Wagner et al., 2006). Suspended-sediment concentration (SSC) time series are generated through calibration of turbidity sensors (Rasmussen et al., 2009). In the analysis presented herein, we rely directly on the turbidity data (instead of SSC) because 1) turbidity is monitored at more sites than suspended sediment, and 2) the basic results of the analysis are the same whether turbidity or suspended sediment are used (we do not present sediment flux or sediment budgets). Figure 1 shows the gaging stations that were used in this study. Flow and velocity data were accessed from the USGS NWISweb database (http://waterdata.usgs.gov/ca/nwis/); turbidity data were accessed from NWISweb (for USGS data) and the California Data Exchange Center database (http://cdec.water.ca.gov/index.html) (for DWR and BoR data). The discharge at Mallard Island (downstream boundary of the Delta) and the discharge from the south Delta pumping facilities (daily water project exports from the vicinity of Clifton Court Forebay, Figure 1) were obtained from the DAYFLOW program (http://www.water.ca.gov/dayflow/).

Several metrics were computed from the time series data and used to evaluate transport processes during the event: 1) the pre-flood (base) and peak turbidity at each site; 2) the travel time of the turbidity peak to each gage from the upstream boundary (Sacramento River at Freeport); 3) the duration of the rising limb in turbidity at each site; and 4) the distance to each gage (along the most direct channel route) from the upstream boundary. These metrics were used to evaluate the transport pathways of the sediment pulse as well as the mechanisms controlling transport between sites.

RESULTS AND DISCUSSION

Time series of turbidity (panel A), tidally-averaged discharge (instantaneous discharge averaged over a tidal period, approximately 25 hours, panel B), and velocity (panel C) for all sites are shown in Figures 3-7. Each figure presents the conditions in a different region of the Delta, in the downstream direction from the source of the sediment pulse (the Sacramento River): Figure 3 shows conditions along the mainstem Sacramento River; Figure 4 shows conditions in the Cache Slough area; Figure 5 shows conditions in the north-central Delta; Figure 6 shows conditions in the south-central Delta; and Figure 7 shows conditions in the south Delta region. In each figure, the legend is organized from upstream to downstream. The conditions at the upstream boundary (Sacramento at Freeport) are shown in all figures; the y-axis scales are the same for Figures 3-5 but are condensed in Figures 6-7 (south-central and south Delta) in order to illustrate the dispersion of the sediment pulse as it moves southerly through the Delta. Refer to Figure 1 for the locations of the gaging stations identified in the time series figures.

The evolution of the sediment pulse as it travels down the mainstem Sacramento River (Figure 3) illustrates the processes of advection and tidal dispersion. At the upstream boundary (Freeport), flows are typically unidirectional (with some tidal influence) under low Sacramento River inflows (e.g. most of the year), but during the runoff event the tidal influence was washed out and the signal was entirely fluvial (Figure 3C). Further downstream at Rio Vista, the turbidity peak was reduced and the tidal signal is evident. At Mallard Island (downstream boundary of the Delta), the turbidity peak was further reduced and the signal was substantially broadened (increased time to peak). These features are the basic elements seen throughout the Delta as the sediment pulse moves through the fluvial-tidal transition.

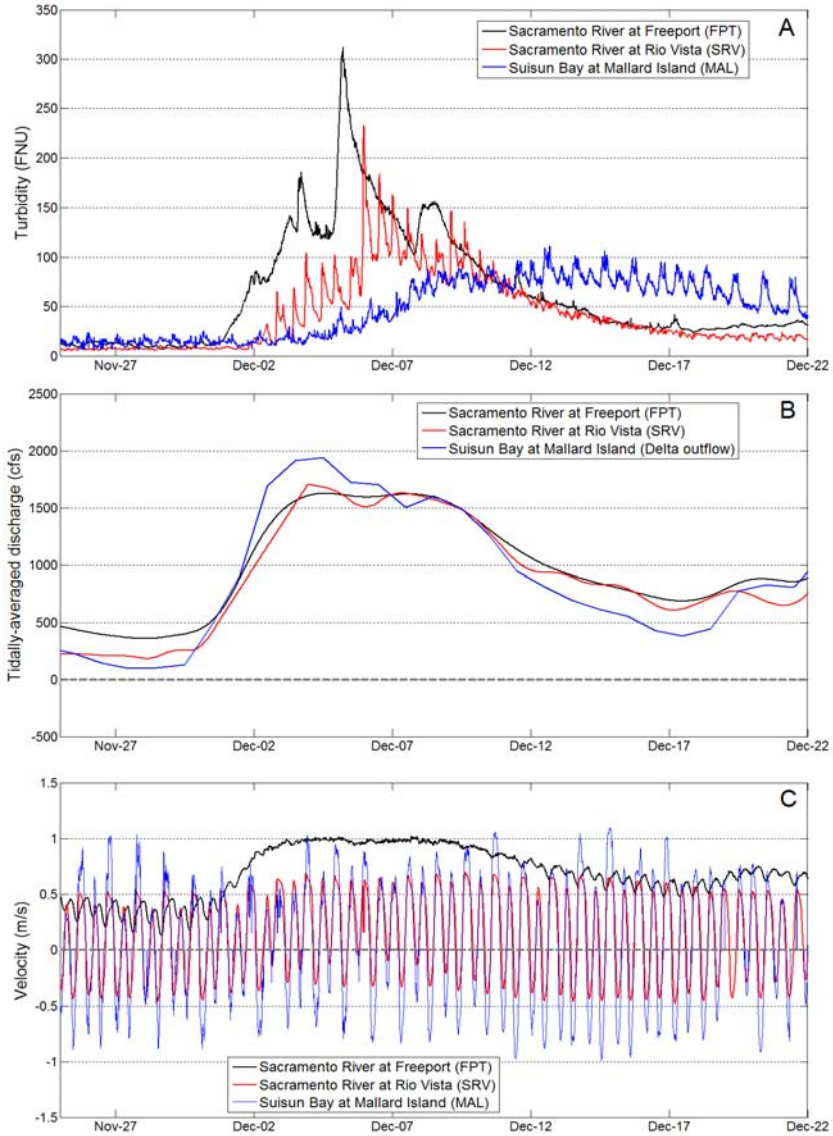

Figure 3 – Turbidity (A), tidally-averaged discharge (B), and velocity (C) along the mainstem Sacramento River.

Conditions in the Cache Slough and north-central Delta regions are shown in Figures 4 and 5, respectively, and illustrate the influence of the Sacramento River distributary channels. As the Sacramento River encounters tidal influence (around Freeport), it splits into several distributary channels (in downstream order: Sutter Slough, Steamboat Slough, Georgiana Slough, see Figure 1). During low flow, each of these distributary channels typically carries 10-20% of the upstream Sacramento River flow; during high flow, a combination of Sutter and Steamboat Sloughs can carry about 40% of the flow upstream at Freeport.

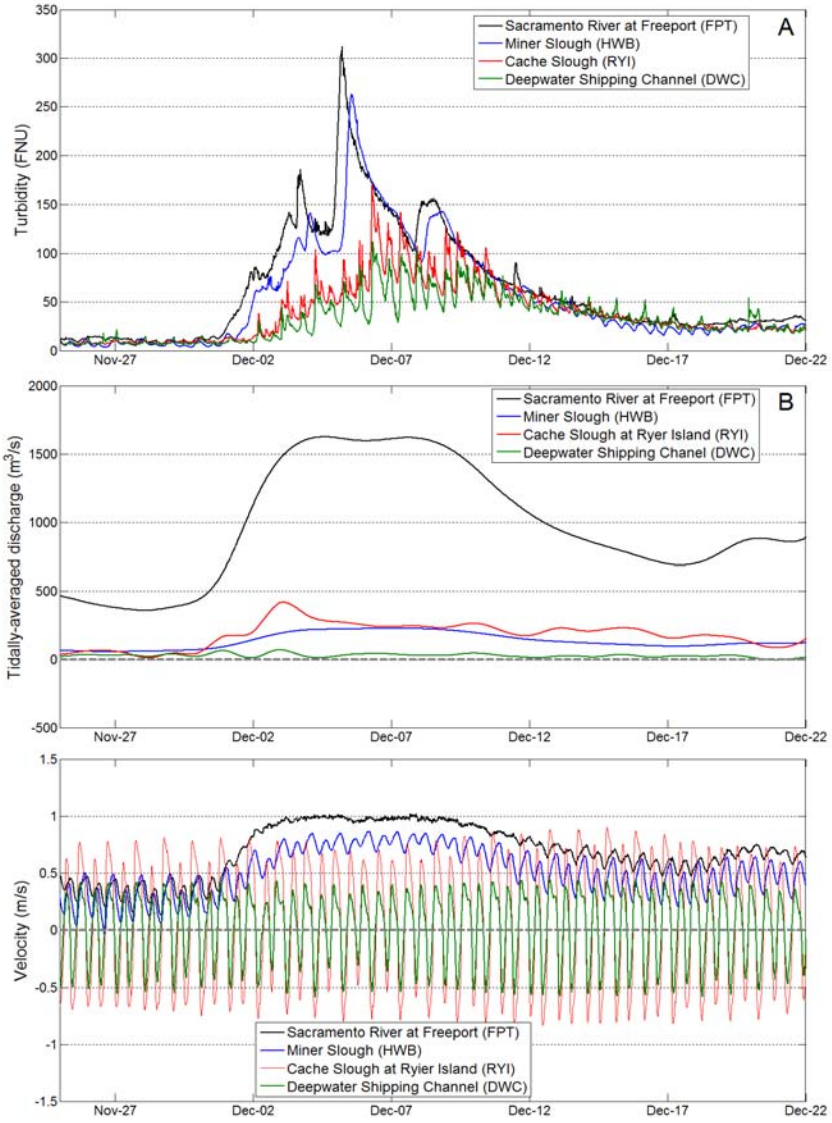

Figure 4 – Turbidity (A), tidally-averaged discharge (B), and velocity (C) in the Cache Slough region of the Delta.

Figure 4 shows that, based on the sampling stations we analyzed, Miner Slough is the primary pathway for sediment to reach the Cache Slough area; the turbidity signal in Miner Slough is nearly identical to that on the Sacramento at Freeport and the sites further downstream in the

Cache Slough area illustrate the effects of tidal dispersion and deposition (reduced turbidity peaks, increased tidal variability). Similarly, Figure 5 shows that Georgiana Slough is the pathway for sediment to reach the north-central Delta (the Delta Cross Channel is closed during high flow events); the turbidity signal in Georgiana is nearly identical to the Sacramento River at Freeport and the sites further downstream (Mokelumne River, Little Potato Slough) demonstrate the effects of tidal dispersion and deposition. This pathway also has particular importance for transport to the south Delta, as discussed below.

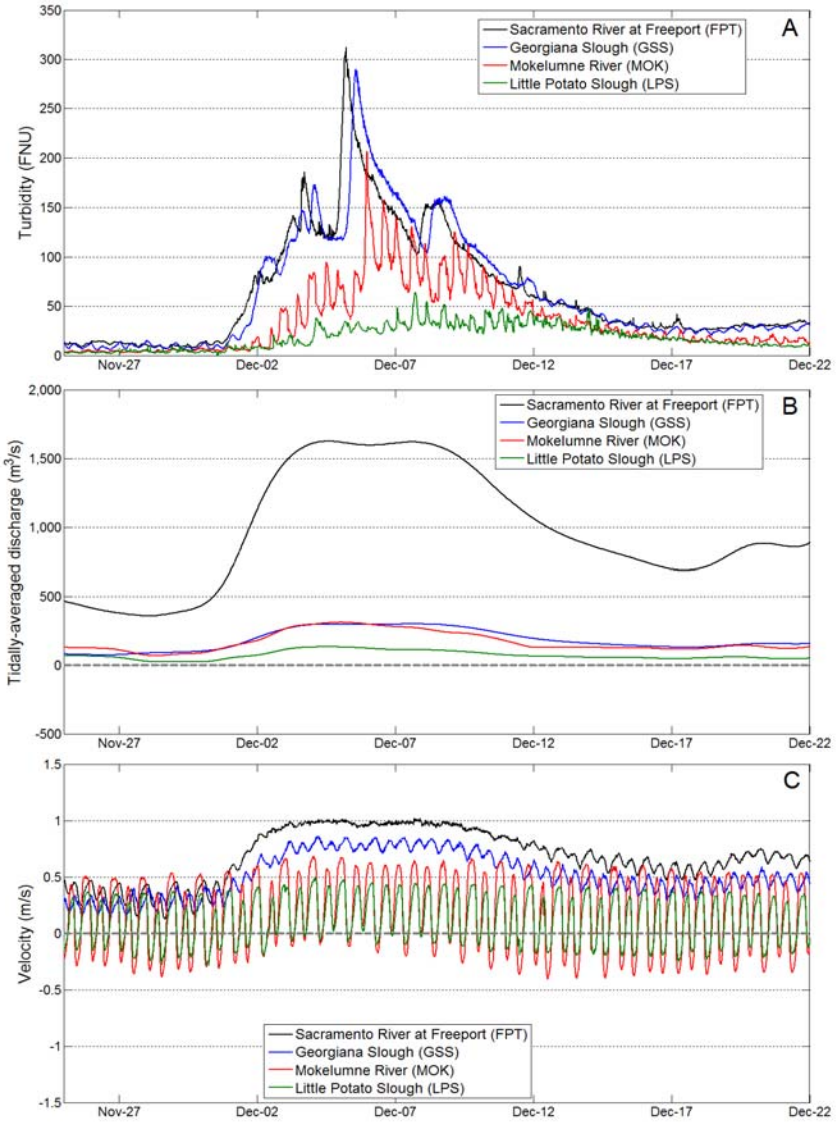

Figure 5 – Turbidity (A), tidally-averaged discharge (B), and velocity (C) in the north-central region of the Delta.

Conditions in the south-central Delta and south Delta regions are shown in Figures 6 and 7, respectively. The y-scale in the turbidity panels was reduced in order to better illustrate the signals, but the signal at Freeport was included for illustrative purposes. The sites in the south-

central Delta (Figure 6) include several along the San Joaquin River and have turbidity signals similar to other downstream tidal sites (such as Mallard Island), with reduced turbidity peaks and broader distributions. The sites in the south Delta (Figure 7) have even lower turbidity peaks and broader distributions due to tidal dispersion and deposition. An important aspect of transport processes in these regions is the direction of the tidally-averaged (net) flows (panel B) and the influence of the water export facilities. Negative net flows in these regions indicate "reverse" (landward) flows to the south toward the export facilities. In the absence of water exports, the net flows in these regions would be seaward and the mechanism for sediment transport into the south Delta (advection with the landward net flow) would not exist. Thus, the water export facilities play a key role in elevating turbidity in the south Delta during Sacramento River runoff events.

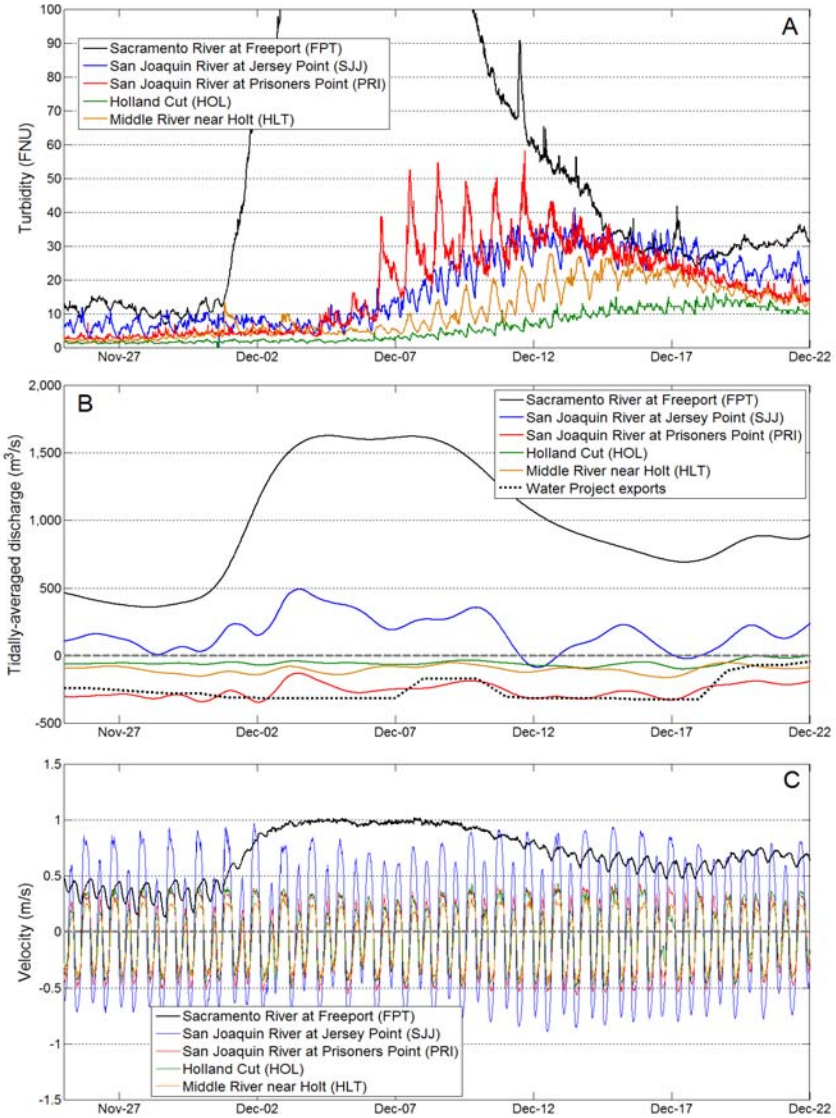

Figure 6 – Turbidity (A), tidally-averaged discharge (B), and velocity (C) in the south-central region of the Delta.

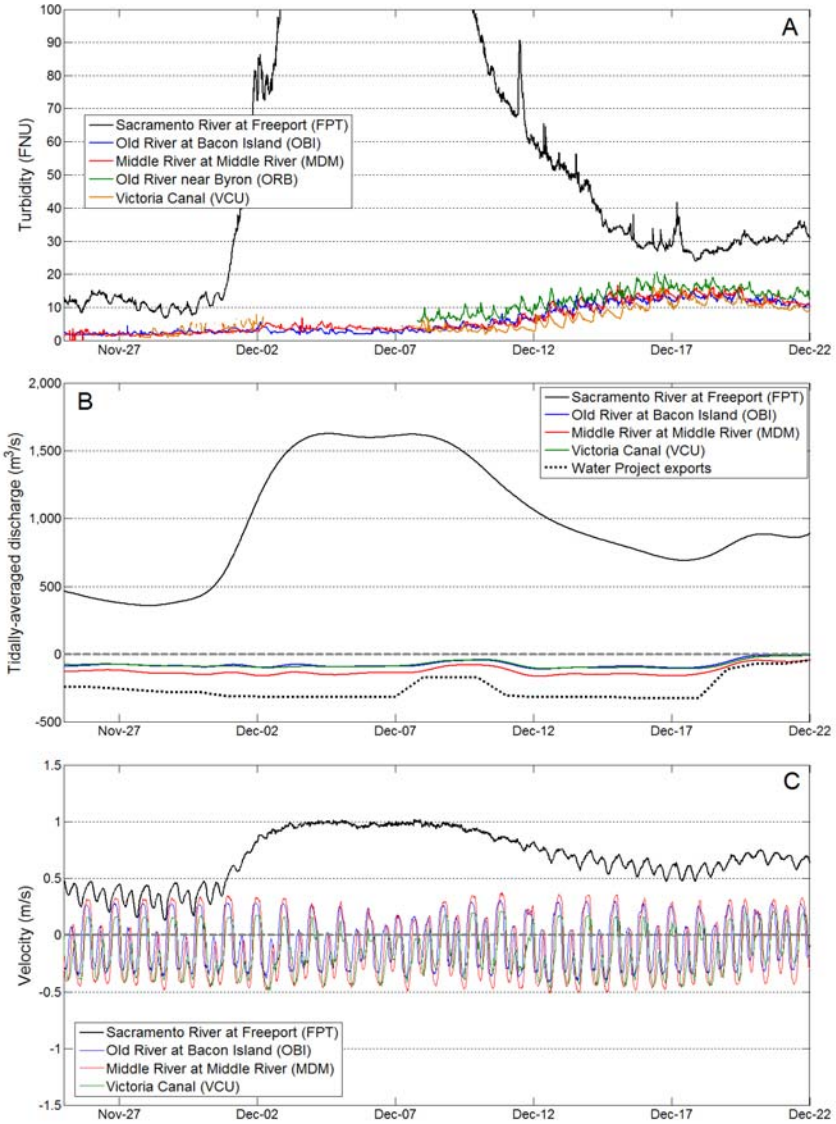

Figure 7 – Turbidity (A), tidally-averaged discharge (B), and velocity (C) in the south region of the Delta.

Figure 8 summarizes the pre-flood and peak turbidities for all of the sites, organized by region and in a downstream direction within each region. The decreases in peak turbidity in the downstream direction illustrate the processes of tidal dispersion and deposition that occurs through the fluvial-tidal transition. Figure 8 also shows the order of magnitude decrease in peak turbidity that occurs from the upstream boundary to the furthest downstream sites (south Delta).

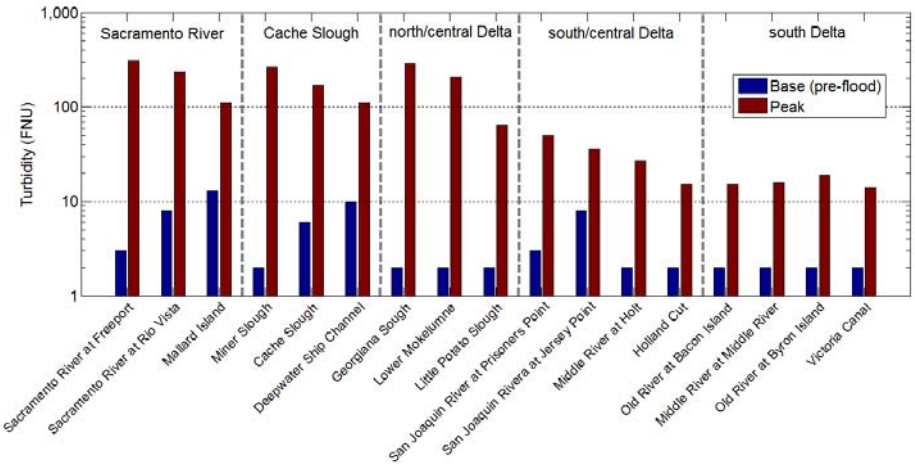

Figure 8 – Pre-flood (base) and peak turbidity at the sites identified in figure 1.

The change in several metrics of the sediment pulse as it moves through the Delta and the fluvial-tidal transition is shown in Figure 9. Three metrics were used: the peak turbidity (panel A); the travel time of the turbidity peak (measured from the Sacramento River at Freeport, panel B); and the duration of the rising limb of the turbidity signal (panel C). These metrics are indicative of the advection and dispersion processes between a given site and the source of the sediment pulse, and are plotted in Figure 9 as a function of distance downstream from the Sacramento River at Freeport. For all metrics, a relatively abrupt transition is apparent at 50-60 km downstream from Freeport. This is roughly the distance along the north Delta distributary channels to Cache Slough, as well as the distance along the Georgiana/Mokelumne pathway to the San Joaquin River. At these locations, there is an abrupt increase in the channel capacity and therefore an increase in tidal forcing and concomitant reduction in the net flow velocity. Thus, sites upstream of these junctions illustrate primarily fluvial responses with a weaker tidal influence, and sites downstream illustrate reduced fluvial influence with much greater tidal influence. Figure 9B demonstrates an order of magnitude reduction in the velocity of the sediment pulse through this transition, from about 0.6 m/s in the fluvial region to about 0.04 m/s in the tidal region. This is accompanied by about a two-fold increase in the duration of the rising limb of the pulse (Figure 9C), from about 4 days in the fluvial region to about 8-10 days in the tidal region. Finally, elevated pre-flood (base) turbidities at Mallard Island, Rio Vista and the Deepwater Ship Channel are given as one of the reasons Delta smelt are found at these location under pre-first-flush conditions (Sommer and Mejia, 2013).

SUMMARY OF MAIN FINDINGS

Herein we have examined the evolution of a sediment pulse, originating from the Sacramento River, as it moved through the fluvial-tidal transition in the Sacramento-San Joaquin Delta. This examination revealed the following main findings related to transport processes:

- Sacramento River distributary channels convey sediment to different regions of the Delta, resulting in elevated turbidity in these regions. In particular, Georgiana Slough is the primary pathway for sediment from the Sacramento River to the south Delta region.
- Sediment transport in the northern region of the Delta, near the upstream source, is dominated by fluvial processes. Tidal influence increases dramatically at about 50-60 km from the Sacramento River at Freeport, where the north Delta distributary channels encounter Cache Slough and the Mokelumne River system encounters the San Joaquin River
- Water export facilities in the south Delta result in negative (landward) net flows in this region and contribute to the landward transport of sediment and elevated turbidity in the south Delta.

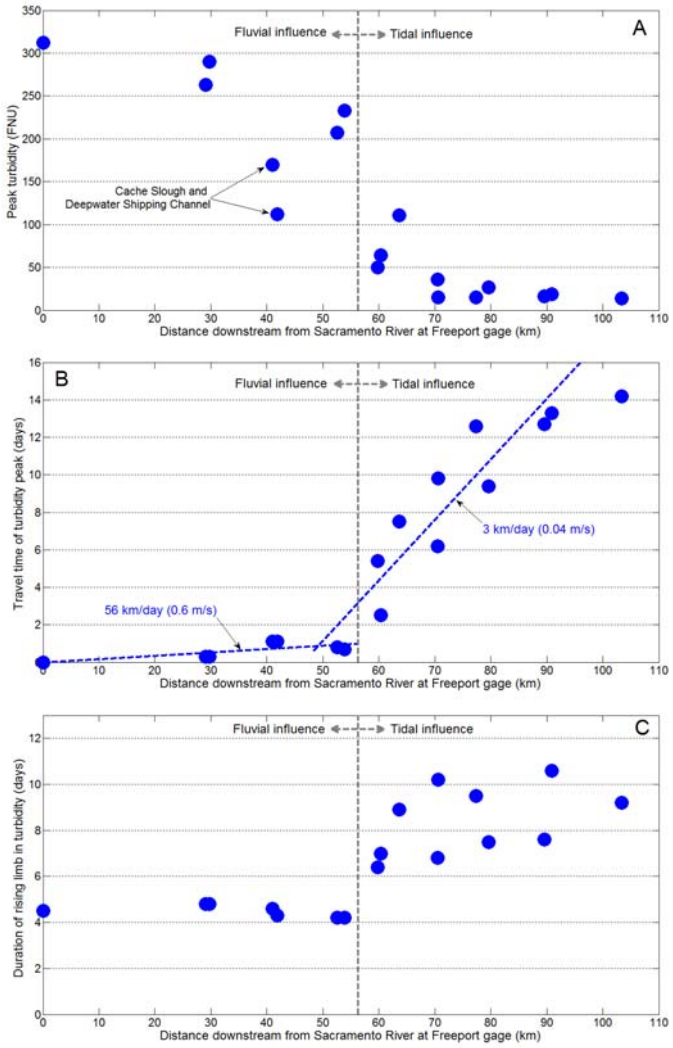

Figure 9 – Peak turbidity (A), travel time of turbidity peak (B), and duration of the rising limb in turbidity (C) versus distance downstream from the upstream sediment pulse source.

REFERENCES

Grimaldo, L. F., Sommer, T., Van Ark, N., Jones, G., Holland, E., Moyle, P. B., and Smith, P. (2009). Factors affecting fish entrainment into massive water diversions in a tidal freshwater estuary: can fish losses be managed?. North American Journal of Fisheries Management, 29(5), 1253-1270.

Levesque, V.A., and Oberg, K.A., 2012, Computing discharge using the index velocity method: U.S. Geological Survey Techniques and Methods 3–A23, 148 p., http://pubs.usgs.gov/tm/3a23/

Rasmussen, P.P., Gray, J.R., Glysson, G.D., and Ziegler, A.C., 2009, Guidelines and procedures for computing time-series suspended-sediment concentrations and loads from in-stream turbidity-sensor and streamflow data: U.S. Geological Survey Techniques and Methods, book 3, chap. C4, 52 p.

Ruhl, C.A., and Simpson, M.R., 2005, Computation of discharge using the index-velocity method in tidally affected areas: U.S. Geological Survey Scientific Investigations Report 2005-5004, 31 p.

Sommer T, Mejia F, Nobriga M, Feyrer F, Grimaldo L. 2011. The Spawning Migration of Delta Smelt in the Upper San Francisco Estuary. San Francisco Estuary and Watershed Science (2011) 9 (2), 16 pages.

Sommer, T., and Mejia, F., 2013, A Place to Call Home: A Synthesis of Delta Smelt Habitatin the Upper San Francisco Estuary, San Francisco Estuary and Watershed Science 11(2), 27 p.

Wagner, R.J., Boulger, R.W., Jr., Oblinger, C.J., and Smith, B.A., 2006, Guidelines and standard procedures for continuous water-quality monitors—Station operation, record computation, and data reporting: U.S. Geological Survey Techniques and Methods 1–D3, 51 p. + 8 attachments; accessed April 10, 2006, at http://pubs.water.usgs.gov/tm1d3

Whipple, A., Grossinger, R., Rankin, D., Standford, B. & Askevold, R. (2012) Sacramento-San Joaquin Delta Historical Ecology Investigation: Exploring Pattern and Process. San Francisco Estuary Institute.

Wright, S. A., and D. H. Schoellhamer, 2005, Estimating sediment budgets at the interface between rivers and estuaries with application to the Sacramento–San Joaquin River Delta, Water Resour. Res., 41, W09428, doi:10.1029/2004WR003753.

BEDLOAD DATABASE AND PREDICTION PERFORMANCE

Rollin H. Hotchkiss, Ph.D., P.E., D.WRE, F.ASCE., Professor, Dept. of Civ. & Env. Eng., 368 Clyde Building, Brigham Young University, Provo, UT 84602, Phone: (801) 422-6234, Email: rhh@byu.edu

Darren D. Hinton, P.E., Ph.D., Northwest Hydraulic Consultants, 835 S. 192nd Street, Bldg C, Ste 1300, Seatac, WA 98148, Phone: (206) 241-6000, Email: DHinton@nhcweb.com

Abstract: This topic will be of interest for two reasons: (1) we make available to all interested parties thousands of high-quality bedload transport measurements that can be used in research and applications, and (2) we tested two empirical bedload transport equations using data from the database. We compiled the most comprehensive database to date containing high quality and well-documented bedload sediment transport measurements. We used a subset of the database to test the performance of the Barry et. al 2004 formula and Rosgen's Pagosa Good/Fair (FlowSed) formula. Each method used a single measurement at or near bankfull to calibrate the formula. The ability of each method to predict bedload transport was determined using the Root Mean Square Error of the logarithms of predicted and measured values of bedload. The Pagosa curve provided the greatest accuracy. The varying exponent of the Barry formula approximated the static exponent of the Pagosa formula. By improving bedload transport prediction, stream restoration professionals will have greater confidence in the competency of restored streams and reduce the potential for aggradation or degradation through improved channel design.

INTRODUCTION

Bedload transport formulae for gravel bed streams are used for stream restoration and urban stream design, sediment budget calculations, fish habitat assessment, and mitigating downstream effects of dams [Wilcock et al., 2009]. Unfortunately, despite widespread use, these formulae fail to consistently and accurately predict bedload transport across a wide range of natural conditions [Gomez and Church, 1989; Wong and Parker, 2006]. Due partly to inaccuracies and uncertainties, field measurements are often collected to calibrate formulae. However, bedload sampling is both expensive and difficult, which leads some practitioners to simply apply bedload formulae without calibration [Doyle et al., 2007]. While calibration of bedload formulae is known to improve accuracy [Wilcock, 2001], previous studies have not compared the relative performance of calibrated formulae. Additionally, previous studies have only focused on semi-empirical formulae, which are based on theoretical considerations and then adjusted using flume or field data.

Therefore, the objective of this research was to evaluate and compare the performance of two calibrated bedload transport formulae. Both of the selected formulae were empirical, essentially created by fitting a best-fit curve to large quantities of data. This research employed more measurements than previous comparison studies and used one field measurement near bankfull discharge for calibration. This analysis evaluates the advantage of calibrating a formula with a single measurement. It also evaluates the predictive performance of two formulae not previously examined.

LITERATURE REVIEW

The comparison of bedload transport formulae is not a new idea. Numerous comparison studies of total sediment load (including suspended load and bedload) have been conducted. While many studies

studies favor sand bed channels, some also include elements pertinent to coarse bed channels [Karamisheva et al., 2006; Molinas and Wu, 2001; Pacheco-Ceballos, 1989; Wu et al., 2000]. For example, Yang and Huang [2001] used a large flume data to test a series of formulae that included mostly total load equations with a few interspersed bedload transport equations. They also referenced an additional twelve total load comparison studies largely dealing with total load formulae and sand bed channels.

McLean [1980] reported that very little effort had been made to test bedload predictive formulae on gravel bed streams up until that time. Since that time, a number of comparisons of bedload transport formulae have been conducted. McLean used field data from five rivers (Vedder River near Yarrow, Canada; Elbow River near Bragg Creek, Canada; North Saskatchewan River at Nordegg, Canada; Snake River near Anatone, WA; and Clearwater River near Spalding, FL) to compare bedload predictive formulae. Gomez and Church [1989] used 358 measurements, 90 of which came from flume experiments and the rest from field sampling, to test twelve predictive equations on gravel bed streams. Reid et al. [1996] used data from Nahal Yatir, an ephemeral stream located within the Negev Desert, Israel, to perform a comparison study of six equations. Almadeij & Diplas [2003] used 174 measurements from three gravel-bed streams to test four equations. Bravo-Espinosa et al. [2003] used 1,020 measurements from 22 gravel-bed streams to test seven equations. Martin [2003] used data from the Vedder River in Canada to test four formulae. Barry et al. [2004] used 2,104 measurements from 24 gravel bed rivers in Idaho to test eight different variations of four bed load transport equations. In addition to the equations evaluated in this study, they proposed a new empirical formula calibrated using sub-basin characteristics. Duan et al. [2006] using three formulae tested 14 bedload samples on the Las Vegas Wash, a desert, gravel-bed stream in Las Vegas that conveys effluent wastewater and drainage.

In summary, although there have been many tests evaluating bedload formulae, this present study is warranted for several reasons. First, there are still a significant number of formulae that have not been tested; this study includes two such equations which, uniquely, are empirical. Second, testing of bedload equations has been performed often in the past using increasing numbers of observations with each iteration. The present study improves on past efforts in that it uses a sub-set of a database with more than 8,000 high-quality observations from 160 field sampling datasets (Hinton, 2012).

BEDLOAD TRANSPORT FORMULAE

This study compared the Barry and Pagos bedload transport formulae as summarized in Table 1. The Barry formulae was selected because, first, it is an empirical formula and, second, because of a reference outlining the calibration process [Barry et al., 2004]. The Pagosa formula was selected because it is perhaps the most well-known empirical bedload predictive formula [Lave, 2008; Rosgen et al., 2006; Simon et al., 2007; Simon et al., 2005]. Both formulae used the same sampling methodology for data collection. The following section describes each formula in greater detail.

Table 1 Summary of selected bedload transport formulae

Formula Name	D_{50} Range for Formula Development	Collection Location	Collection Method	Stream Slope
Barry	23 mm – 204 mm	Idaho Streams	Helley-Smith	0.0005 < S < 0.0718
Pagosa	~76 mm[1]	Colorado Streams	Helley-Smith	0.0117

Barry et al. [2004] developed an empirical power relationship between flow and bedload transport derived from Snake River Adjudication data. The Barry et al. general power formula (Barry) was derived for channels with coarse-grained surfaces and takes the form (refer to Table 2 for formula notation):

$$q_b = 257\, A^{-3.41} Q^{(-2.45q^* + 3.56)} \quad (1)$$

$$q^* = \left(\frac{\tau_{Q_2} - \tau_{D_{50S}}}{\tau_{Q_2} - \tau_{D_{50ss}}}\right)^{\frac{3}{2}} \quad (2)$$

The Barry formula is essentially a rating curve in which the coefficient is related to the tributary drainage area and the exponent is related to the channel armoring of the site relative to its transport capacity and sediment supply. As such, it may be considered an "off-the-shelf" formula that does not require direct calibration. However, the drainage area coefficient may be calibrated to match measured bedload data. The exponent is not adjusted and is calculated using the average cross-sectional shear stress at bankfull with the critical shear stress required to mobilize the surface and subsurface layers.

Barry et al. [2004] reported there were three streams in their study for which the exponent could not be calculated. This is due to a weakness in how the relative armoring coefficient is calculated. If the total cross-sectional average shear stress at the 2-year return discharge is less than the critical shear stress required to mobilize the D_{50} of either the surface or subsurface, the exponent becomes undefined and can no longer be calculated. It should also be noted that this formula is unable to predict sediment transport by sediment size class or the effects of changing velocity and shear stress.

The Pagosa Good/Fair and Poor (Pagosa) methods were developed by David Rosgen with Helley-Smith data collected from six streams near Pagosa Springs in Colorado [Rosgen et al., 2006]. The data were non-dimensionalized using a measurement of discharge and bedload transport at bankfull and then fit with a power relationship for each stability class [Rosgen et al., 2006]. The two power fit relationships are (refer to Table 2 for formula notation):

$$G_* = -0.0113 + 1.0139 Q_*^{2.1929} \quad \text{[Good/Fair]} \quad (3)$$

$$G_* = 0.07176 + 1.0217 Q_*^{2.3772} \quad \text{[Poor]} \quad (4)$$

The Good/Fair curve represented three streams exhibiting good/fair stabilities while the Poor curve represented three streams with significant degradation or aggradation. Only the Good/Fair curve is used in this analysis. A disadvantage of the Pagosa formula is that it must always be calibrated using field measurements at bankfull discharge that are difficult to obtain or may not occur during the study period. It also is unable to directly predict sediment transport by sediment size class or the effects of changing velocity and shear stress.

Table 2 Formula notation

Notation	Description	Units
A	drainage area	km^2
G*	bedload transport term equal to the ratio of the given transport rate with the transport rate at bankfull	-
Q	discharge	m^3/s
q_b	unit bedload transport rate	kg/s/m
Q_b	bedload transport rate	kg/s
q*	relative armoring term	-
Q*	discharge term equal to the ratio of the given discharge with bankfull discharge	-
$\tau_{D_{50s}}$	critical shear stress required to mobilize the surface layer	N/m^2
$\tau_{D_{50ss}}$	critical shear stress for the subsurface layer	N/m^2

STUDY METHODOLOGY

The study first commenced with collecting the necessary data. Prior to the bedload comparison effort, a bedload database of more than 8,000 bedload field measurements was compiled as described in Hinton [2012]. Quality bedload measurements from around the world were gathered from sources including published journal articles, direct physical measurements of bedload by the authors, and other researchers' unpublished data. Following data selection, the formulae were calibrated and then statistically analyzed. These three phases are described in more detail in the following paragraphs.

Data selection

Data were selected based on appropriateness and availability of information required to solve the formulae. Sites that produced negative or unrealistic exponents for the Barry formula were not selected. All bedload data selected for the study were collected with Helley-Smith pressure differential samplers.

Nearly 2,300 distinct bedload measurements obtained from 23 sites were included in this comparison. The data represent varying geologic compositions and drainage areas ranging from 3 to 360 square kilometers. Because very few sites included measurements of the bottom channel width, the top width was used instead. Some sites reported bankfull discharge derived from field-based parameters while others approximated bankfull using the 1.5-year discharge calculated using a Log-Pearson Type III analysis of historical stream gage data.

The sites included in this study were coarse bed channels with surface median diameters ranging from 10 to 160 mm. Surface grain size distributions were measured using standard pebble count methodology while subsurface grain size distributions were measured by collecting bulk core

samples on site and then analyzing the composition in the laboratory. Water surface slopes ranged from 0.001 to 0.055. Additional information regarding the sites can be found in the references provided in Table .

Table 3 General information for study sites

Site #	Data Set	State	Number of Samples	Drainage Area (km^2)	Source
1	East St. Louis Creek	CO	109	8	*St. Louis Creek Dataset*[1,2]
2	Fool Creek	CO	95	3	
3	St. Louis Creek Site 1	CO	98	56	
4	St. Louis Creek Site 2	CO	117	54	
5	St. Louis Creek Site 3	CO	107	54	
6	St. Louis Creek Site 4	CO	208	34	
7	St. Louis Creek Site 4A	CO	185	34	
8	St. Louis Creek Site 5	CO	93	21	
9	Little Granite Creek	WY	69	55	*Little Granite Creek Dataset*[2,3]
10	Fivemile Creek	OR	12	91	*Klamath Dataset*[4]
11	South Fork Sprague River	OR	11	161	
12	Sycan River above Marsh	OR	17	256	
13	Annie Creek	OR	20	73	
14	Big Wood River near Ketchum	ID	92	356	*Idaho Dataset*[5,6]
15	Little Slate Creek	ID	134	162	
16	Lolo Creek Data	ID	82	106	
17	Main Fork Red River	ID	174	129	
18	Rapid River	ID	166	280	
19	South Fork Red River	ID	170	99	
20	Trapper Creek	ID	156	21	
21	Fall Creek	CO	81	12	*Rosgen Dataset*[7]
22	Wolf Creek at Bridge	CO	72	47	

[1] *[S E Ryan et al., 2002]*

[2] *Personal Communication. Sandra Ryan-Burkett. 22 Nov. 2010.*

[3] *[S E Ryan and Emmett, 2002]*

[4] *Personal Communication. Walt Lucas. 8 Jun. 2011*

[5] *[Barry et al., 2004]*

[6] *Online content: http://www.fs.fed.us/rm/boise/research/watershed/BAT/index.shtml Access: 21 Oct 2010.*

[7] *Personal Communication. David Rosgen. 13 Jan. 2012.*

Formulae Calibration

Using the methods listed earlier within the Bedload Transport Formulae section, two formulae calibrated with one bedload measurement were compared. The calibration point was used to match predicted values to measured values by adjusting the leading coefficient of the Barry power relationship. The predicted rates were then compared with the actual measurements of transport rate. The Idaho data was used to derive the Barry formulae; however, the calibration process adjusted the coefficient from its standard "off-the-shelf" form.

Statistical Analyses

The root means square error (RMSE) has previously been used [Gomez and Church, 1989] as a statistical comparison between predicted and measured values of bedload transport. The root mean square error can be computed according to Equation 5:

$$RMSE = \sqrt{\frac{\sum_{i=1}^{n}\left(x_{p,i}-x_{m,i}\right)^2}{n}} \qquad (5)$$

where:

x_p = predicted bedload transport (kg/s)
x_m = measured bedload transport (kg/s)
n = number of samples

Because the RMSE accounts for the differences between predicted and measured values, errors associated with higher discharges will be emphasized. In other words, the same percent difference will produce much higher errors for high discharges than for low discharges. To remove this bias, a log transformation was applied to the predicted and measured values by adding 1 to each value and then calculating the base-10 logarithm. The RMSE was then calculated for the transformed values. The transformation and resulting RMSE equation is summarized in Equation 6, referred to as the root mean square error of the logarithmic values (RMSEL).

$$\mathrm{RMSEL} = \sqrt{\frac{\sum_{i=1}^{n}\left(\log_{10} x_{p,i}-\log_{10} x_{m,i}\right)^2}{n}} \qquad (6)$$

RESULTS AND ANALYSIS

The RMSEL values comparing the logarithms of the predicted and measured rates are reported in Table 4 which include errors for each individual stream. Also included in Table 4 was the exponent calculated for the Barry formula. Figure Figure 1 shows the predicted versus measured transport rate and includes a 1:1 relationship line for comparison. If the predicted values perfectly matched the measured values, they would match the 1:1 relationship line. Both the Barry and Pagosa formulae shown in Figure Figure 1 approximate a 1:1 correlation between measured and predicted values.

The Pagosa formula was most successful at predicting bedload transport with RMSEL values ranging from 0.002 to 0.114. The Barry provided slightly less accurate results with RMSEL values ranging from 0.002 to 0.228. However, both results were comparable as shown in Figure 1. During the data selection process it became evident that the Pagosa formula was easier to apply to various sites because the exponent of the Barry formula becomes undefined if the critical shear stress calculated for the surface and subsurface D_{50} grain size is greater than the average shear stress at the predicted bankfull discharge. On the other hand, it was noted that for very small measured bedload rates the Pagosa formula occasionally erroneously predicted negative transport rates.

As was mentioned previously, the exponent for the Barry formula was calculated using bankfull characteristic and gradations of the channel surface and subsurface. In this analysis, the calculated exponent ranged from 1.24 to 3.53 with a weighted average of 2.47. A rating curve

relating bedload transport to discharge for any given site has been shown to vary between 2 and 5 for Helley-Smith sampling data [Pitlick et al., 2004].

In comparison, the Pagosa formula exponent remains at a static value of 2.19. The Pagosa formula differs from typical rating curves as it relates bedload transport rate to the percent of bankfull discharge, not discharge itself.

Table 4 Bedload transport formulae root mean square error of the logarithms

Data Set	Number of Samples	RMSE (log)		Barry Calculated Exponent
		Barry	Pagosa	
East St. Louis Creek	109	0.005	0.005	1.53
Fool Creek	95	0.002	0.002	1.61
St. Louis Creek Site 1	98	0.026	0.023	2.72
St. Louis Creek Site 2	117	0.024	0.023	2.99
St. Louis Creek Site 3	107	0.023	0.024	2.79
St. Louis Creek Site 4	208	0.014	0.014	2.92
St. Louis Creek Site 4A	185	0.013	0.013	2.78
St. Louis Creek Site 5	93	0.009	0.009	2.30
Little Granite Creek	69	0.031	0.046	2.59
Fivemile Creek	12	0.006	0.005	2.19
South Fork Sprague River	11	0.043	0.002	3.44
Sycan River above Marsh	17	0.077	0.035	2.83
Annie Creek	20	0.056	0.066	1.92
Big Wood River near Ketchum	92	0.099	0.114	3.53
Little Slate Creek	134	0.022	0.015	1.99
Lolo Creek Data	82	0.026	0.007	2.03
Main Fork Red River	174	0.126	0.016	2.99
Rapid River	166	0.228	0.073	2.55
South Fork Red River	170	0.025	0.011	2.60
Trapper Creek	156	0.009	0.009	1.77
Fall Creek	81	0.005	0.005	2.37
Wolf Creek at Bridge	72	0.025	0.022	1.24
All Data	2,268	0.045	0.023	2.47

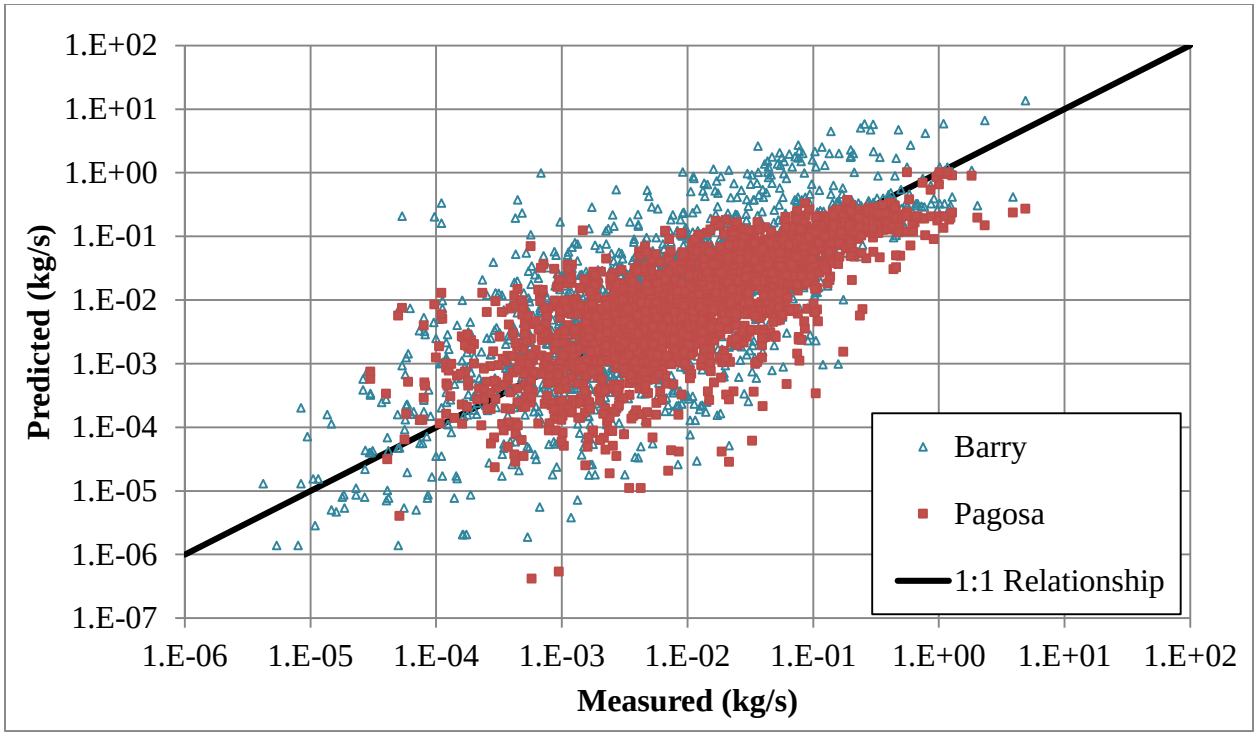

Figure 1 Barry and Pagosa predicted versus measured bedload transport values

CONCLUSION AND RECOMMENDATIONS

Two bedload transport prediction formulae were compared using nearly 2,300 Helley-Smith measurements from 22 different streams in the western United States using calculated RMSEL values. The sites included in this study had water surface slopes, median diameters, and drainage areas between 0.001 and 0.055, 10 and 160 mm, and 3 and 360 km^2, respectively. The performance of these formulae in this study have not previously been compared. Of the formulae compared, the Pagosa Good/Fair equation was the best predictor of bedload transport rates.

The exponent calculated for the Barry formula for the 22 sites varied between 1.2 and 3.5; however, the average value for all data was 2.5. This is compared to the 2.2 exponent of the Pagosa formula.

REFERENCES

Almedeij, J. H., and P. Diplas (2003), "Bedload transport in gravel-bed streams with unimodal sediment," *Journal of Hydraulic Engineering*, *129*(11), 896-904.

Barry, J. J., J. M. Buffington, and J. G. King (2004), "A general power equation for predicting bedload transport rates in gravel bed rivers," *Water Resources Research*, *40*(10), W10401.

Bravo-Espinosa, M., W. Osterkamp, and V. L. Lopes (2003), "Bedload transport in alluvial channels," *Journal of Hydraulic Engineering*, *129*, 783.

Doyle, M. W., D. Shields, K. F. Boyd, P. B. Skidmore, and D. W. Dominick (2007), "Channel-forming discharge selection in river restoration design," *Journal of Hydraulic Engineering*, *133*, 831.

Duan, J. G., L. Chen, and S. Scott (2006), "Application of surface-based bedload transport equations to a desert gravel-bed stream," *Journal of Hydraulic Research*, *44*(5), 624-630.

Gomez, B., and M. Church (1989), "An assessment of bedload sediment transport formulae for gravel bed rivers," *Water Resources Research*, *25*(6), 1161-1186.

Hinton, D. (2012). Complexity of Bedload Transport in Gravel Bed Streams: Data Collection, Prediction, and Analysis. Dissertation, Brigham Young University, Provo, Utah.

Karamisheva, R. D., J. F. Lyness, W. R. C. Myers, and J. O'Sullivan (2006), "Sediment discharge prediction in meandering compound channels," *Journal of Hydraulic Research*, *44*(5), 603-613.

Lave, R. A. (2008), The Rosgen Wars and the Shifting Political Economy of Expertise, Dissertation thesis, 251 pp, University of California, Berkeley, Berkeley, California.

Martin, Y. (2003), "Evaluation of bedload transport formulae using field evidence from the Vedder River, British Columbia," *Geomorphology*, *53*(1), 75-95.

McLean, D. G. (1980), Flood Control and Sediment Transport Study of the Vedder River, Thesis, University of British Columbia, Vancouver.

Molinas, A., and B. Wu (2001), "Transport of sediment in large sand-bed rivers," *Journal of Hydraulic Research*, *39*(2), 135-146.

Pacheco-Ceballos, R. (1989), "Transport of sediments: analytical solution," *Journal of Hydraulic Research*, *27*(4), 501-518.

Pitlick, J., Y. Cui, P. R. Wilcock, and R. M. R. Station (2009), *Manual for Computing Bedload Transport Using BAGS (Bedload Assessment for Gravel-bed Streams) Software*, United States Dept. of Agriculture, Forest Service, Rocky Mountain Research Station.

Reid, I., D. M. Powell, and J. B. Laronne (1996), "Prediction of bed-load transport by desert flash floods," *Journal of Hydraulic Engineering*, *122*(3), 170-173.

Rosgen, D. L., H. L. Silvey, and D. Frantila (2006), *Watershed Assessment of River Stability and Sediment Supply (WARSSS)*, Wildland Hydrology.

Ryan, S. E., and W. W. Emmett (2002), *The Nature of Flow and Sediment Movement in Little Granite Creek Near Bondurant, Wyoming*, US Department of Agriculture, Forest Service, Rocky Mountain Research Station.

Ryan, S. E., L. S. Porth, and C. Troendle (2002), "Defining phases of bedload transport using piecewise regression," *Earth Surface Processes and Landforms*, *27*(9), 971-990.

Simon, A., M. Doyle, M. Kondolf, F. Shields Jr, B. Rhoads, and M. McPhillips (2007), "Critical evaluation of how the Rosgen Classification and associated “Natural Channel Design” Methods fail to integrate and quantify fluvial processes and channel response," *Journal of the American Water Resources Association*, *43*(5), 1117-1131.

Simon, A., M. Doyle, M. Kondolf, F. Shields Jr, B. Rhoads, G. Grant, F. Fitzpatrick, K. Juracek, M. McPhillips, and J. MacBroom (2005), "How well do the Rosgen Classification and associated "Natural Channel Design" Methods integrate and quantify fluvial processes and channel response," *Proc. American Society of Civil Engineers, May*, 15-19.

Wilcock, P. R. (2001), "Toward a practical method for estimating sediment transport rates in gravel bed rivers," *Earth Surface Processes and Landforms*, *26*(13), 1395-1408.

Wilcock, P. R., J. Pitlick, Y. Cui, and R. M. R. Station (2009), *Sediment Transport Primer: Estimating Bed-Material Transport in Gravel-Bed Rivers*, US Dept. of Agriculture, Forest Service, Rocky Mountain Research Station.

Wong, M., and G. Parker (2006), "Reanalysis and correction of bedload relation of Meyer-Peter Muller using their own database," *Journal of Hydraulic Engineering, 132*, 1159.

Wu, W., S. WANG, and Y. Jia (2000), "Nonuniform sediment transport in alluvial rivers," *Journal of Hydraulic Research, 38*(6), 427.

Yang, C. T., and C. Huang (2001), "Applicability of sediment transport formulas," *International Journal of Sediment Research, 16*(3), 335-353.

THE ANALYSIS OF MODELED AND SATELLITE GREAT LAKES SNOW WATER EQUIVALENT DATA AND INCORPORATING NEAR REAL-TIME ESTIMATES INTO WATER LEVEL FORECASTING

James W. Lewis, Research Hydraulic Engineer, U.S. Army Engineer Research and Development Center, Coastal and Hydraulics Laboratory, 3909 Halls Ferry Road, Vicksburg, MS 39180, James.W.Lewis@usace.army.mil, (601)634-3895;
Carrie M. Vuyovich, Research Civil Engineer, U.S. Army Engineer Research and Development Center, Cold Regions Research and Engineering Laboratory, 72 Lyme Road, Hanover, NH 03755, Carrie.M.Vuyovich@usace.army.mil, (603)646-4251;
Steven F. Daly, Research Hydraulic Engineer, U.S. Army Engineer Research and Development Center, Cold Regions Research and Engineering Laboratory, 72 Lyme Road, Hanover, NH 03755, Steven.F.Daly@usace.army.mil, (603)646-4218

Abstract: Snow water equivalent (SWE) is an important quantity contributing to the spring water level rise on each of the Great Lakes. This study analyzed modeled and satellite SWE data available for the Great Lakes basin from three primary sources: (1) the SNOw Data Assimilation System (SNODAS) created by NWS National Operational Hydrologic Remote Sensing Center (NOHRSC), (2) the Defense Meteorological Satellite Program (DMSP) Special Sensor Microwave/Imager (SSM/I), and (3) the Large Basin Runoff Model (LBRM) developed by NOAA Great Lakes Environmental Research Laboratory (GLERL). SWE data were evaluated for ability to estimate the absolute and relative magnitudes of annual SWE as well as the timing of snow accumulation and melt. The comparison shows that the satellite SSM/I data severely underestimates Great Lakes SWE and seems to be heavily affected by vegetation cover. Although the SNODAS SWE estimates appear reasonable, it has limited availability for the Great Lakes, with complete binational coverage dating back only to 2011. One challenge for the U.S. Army Corps of Engineers is incorporating near real-time SWE estimates into the water level forecasts for the coming months. In particular, when SWE estimates are very high or very low, the magnitude of influence on the lake's forecasted water level is poorly understood given that the water level is also influenced by other hydrologic components. Since SWE primarily enters the lake through runoff, historical runoff estimates based on measured stream discharges are also analyzed along with historical precipitation data. A useful relationship is found between observed runoff to Lake Superior and the combined total of precipitation and melted SWE across the Lake Superior watershed. A methodology is presented for how current SWE can be used to improve forecasted runoff and forecasted water levels.

INTRODUCTION

Mission: The Detroit District (LRE) of the U.S. Army Corps of Engineers (USACE) under the auspices of the International Joint Commission (IJC) and the Coordinating Committee on Basic Great Lakes Hydraulic and Hydrologic Data (CCBGLHHD) has a crucial role in water management decisions on the Great Lakes. Hydrologists and others interested in the hydrologic budget of the Great Lakes require estimates of snow water equivalent (SWE), and knowledge of the SWE statistics at various times throughout the winter. USACE has been forecasting the Great Lakes water levels as part of its operational mission since 1952. Near the beginning of each month, LRE releases the "Monthly Bulletin of Water Levels for the Great Lakes" which

includes the six-month forecast of Great Lakes water levels. An improved knowledge of SWE would enable the forecasters to determine whether the current values are above or below normal and improve the accuracy of the water level forecasts. The objective of this study is to improve Great Lakes water level forecasting based on an analysis of the available modeled and satellite SWE data for the Great Lakes Basin.

Background: The seasonal snowfall of the Great Lakes Basin is an important feature of the hydrometeorology of the region and snowmelt an important contribution to the runoff entering the Great Lakes (Norton and Bolsenga, 1993). Snowfall occurs in the Great Lakes watershed as a result of the northern latitude and "continental" climate. The Great Lakes themselves also create "lake-effect zones" where air and water temperature differentials drive enhanced snowfall downwind of the lakes. Figure 1 shows the Great Lakes and their respective basin delineations by country.

Figure 1 Binational delineation of the Great Lakes basins

The volume of water stored in the seasonal snow cover can be a significant fraction of the total annual runoff entering the lakes. For example, the volume of the annual maximum SWE in the Lake Superior watershed for the period 1979-2004 (Daly et al., 2007) ranged from 28% to 58% of the total estimated annual runoff entering the lake. The ability to estimate the volume of SWE contained in the Great Lakes watershed can lead to improvements in the forecasts of the Great Lakes water surface elevations. However, estimation of SWE volume contained in the watersheds of the Great Lakes in real or near real time is fraught with difficulties. There are three basic approaches: using ground-based and aerial observations, modeling, and satellite remote sensing.

Ground and aerial observations (CRREL): Geospatial interpolation of ground and aerial observations of SWE can be used to estimate the SWE volume contained in the entire watershed. Daly et al. (2007) used ground observations to estimate the time series of SWE volume for the Lake Superior basin for the period 1979-2004. This study, referred to as CRREL data from this point forward, relied exclusively on National Weather Service (NWS) first-order and cooperative stations for data in the United States and daily and weekly snow depth observations taken by the Meteorological Service of Canada and 20 other agencies for Canada. Unfortunately, the NWS changed its observation procedure in the 1990's through deployment of the Automated Surface Observing System (ASOS) at most first-order stations. ASOS does not measure snowfall or snow depth and remains ineffective for measuring SWE (Doeskin and McKee, 2000). Almost all cooperative stations snow observations are limited to snow depth. The result is that at the present time there are almost no regular observations made of SWE by the NWS throughout the Great Lakes Basin. The number of Canadian SWE observations made each winter has declined continuously starting in the 1980's (Daly et al 2007).

Satellite-based observations (SSM/I): Satellite observations of SWE are based on measuring the passive microwave signal naturally emitted from the Earth. Passive microwave signals at frequencies greater than 25 GHz are scattered as they pass through the snowpack; lower frequencies are not scattered to the same degree. The estimated SWE is proportional to the difference between the emitted signals at a low frequency that is not scattered by snow and a high frequency that is scattered. A singular advantage of satellite observations of emitted passive microwave signals is that they can be observed through cloud cover and at night.

In practice, the accuracy of SWE estimation using passive microwave signals is limited by factors that impact the emitted passive microwave signal. Sources of error in microwave SWE retrievals stem from the dynamic nature of snow and the static assumptions made in the empirical formulations concerning snow properties. Several studies have shown a significant impact of vegetation on the passive microwave signal (Chang et al 1996, Foster et al 2005, Derksen et al. 2005). Other factors that can cause errors include excessive snow depth (Dong et al., 2005, Foster et al., 2005, Clifford, 2010), liquid water in the snowpack (Matzler, 1987, Hallikainen et al., 1986, Walker and Goodison, 1993), changes in snow density and grain size (Foster et al., 1999, Hall et al., 1986; Josberger and Mognard, 2002) and topology of the ground (Matzler and Standley 2000, Dong et al., 2005, Vuyovich and Jacobs, 2011). Ongoing research, which has attempted to account for these errors and to improve results regionally and seasonally, has had varied success (Farmer et al. 2010, Tedesco and Narvekar 2010, Mizukami and Perica 2012).

Daily passive microwave SWE data from the Special Sensor Microwave/Imager (SSM/I) were used for this investigation. The SSM/I sensor was launched in 1987 on board the Defense Meteorological Satellite Program (DMSP) satellites. These data are available near real-time and have the advantage of a relatively long historical record. SWE estimates are derived from the SSM/I brightness temperatures measured at wavelengths 19 and 37 GHz, and have a spatial resolution of 69x43km (19.4 GHz) and 37x29km (37 GHz) (Armstrong and Brodzik 1995). Data are available from the National Snow and Ice Data Center (NSIDC) in an Equal-Area Scalable Earth Grid (EASE-Grid) projection at a 25 km resolution. To avoid gaps at the basin boundaries,

the passive microwave data were re-sampled to 1 km^2 grid cells using the nearest neighbor method which assigns the same value to the pixel as the data layer in that location without any interpolation. SSM/I SWE products are available twice daily; ascending passes which occur in the afternoon and descending passes which occur in the early morning. For this study, only descending SWE data was used to reduce the potential wet snow impacts in the afternoon. A gap in the satellite swath coverage can occur every 3 to 4 days, depending on the latitude of the region.

SNODAS Model: Modeled estimates of SWE throughout the Great Lakes watershed are provided by the NWS National Operational Hydrologic Remote Sensing Center (NOHRSC). It offers a near real-time estimate of SWE and other snow properties for the U.S. through its SNOw Data Assimilation System (SNODAS). SNODAS is physically based, spatially distributed, energy-balance and mass-balance snow accumulation and ablation model run at a 1-km^2 resolution. SNODAS ingests data from the Rapid Update Cycle numerical weather prediction model and downscales it from 13 to 1 km^2. Multiple sources of available satellite, airborne, and ground-based snow observations are assimilated into the model and used to adjust model output by using a Newtonian nudging technique. The objective of using all of the available snow data is to produce a 'best estimate' of near real-time snow conditions for the conterminous USA and to minimize error associated with any individual method (Carroll et al., 2006). Though these data are also subject to errors, this product provides the best spatially distributed estimate of snowpack conditions throughout the U.S. and is used operationally in a number of locations. The snow model within SNODAS has been evaluated and generally shown to provide good results at a point scale (Rutter et al., 2008, Frankenstein et al., 2008, Clow et al., 2012), though over a larger scale, particularly where ground observations are sparse, additional error is introduced. The SNODAS model provides 1-km^2 estimates of snow cover and associated parameters near real-time on a 3-hourly and daily basis. SNODAS data are available from 01 October 2003 through the present from the National Snow and Ice Data Center (NSIDC). The data for Canada begins in approximately 2011. Due to this discrepancy in period of record, this study analyzed the SWE estimates of the US portion with the respective historical results, along with the watershed totals for the recent period.

Large Basin Runoff Model: Developed by NOAA's Great Lakes Environmental Research Laboratory (GLERL), the Large Basin Runoff Model (LBRM) is a lumped-parameter model of runoff for the Great Lakes Basin (Croley and He 2002). Within the LBRM framework, the daily snow pack is calculated from the previous day's snow pack, precipitation, air temperature, and a snowmelt rate parameter. In general, it is more simplified than the SNODAS model, since it only computes daily time steps and does not include any observational SWE data. However, it has the advantage of being able to simulate daily snow pack as far back as 1950, which is the available range of reliable meteorological data.

METHODOLOGY

This study analyzed time series for each of the Great Lakes watersheds of the SSM/I, SNODAS, and LBRM data over their periods of record. The evaluation compared the SSM/I and SNODAS data sets for each watershed using the estimated annual maximum SWE and the weekly maximum SWE values. The results for the Lake Superior watershed were compared to the

results of an independent study that was conducted earlier (Daly et al. 2007). The SWE statistics for each day of the year were determined.

Average basin SWE estimates from passive microwave and SNODAS SWE products were compared over the contributing watersheds to each of the Great Lakes in the north-central U.S. (Figure 1). Weekly time series of SWE and annual maximum values were evaluated over 10 years from 2004 through 2013. SNODAS data is available in the Canadian portion of the Great Lakes basins only since 2011, so the historical comparison was done only in the U.S. portions of the basins.

In order to improve the understanding of how SWE influences Great Lakes water levels, the historical record of LBRM SWE estimates were analyzed, beginning with the Lake Superior basin. Other basins could be analyzed in the future using the framework presented in this study. Statistics for the monthly LBRM SWE data were computed and compared with other historical hydrologic datasets. For the runoff component of the hydrologic cycle, the GLERL Area Ratio Method (ARM) is the most reliable historical data set. ARM includes stream flow observations within the basin, extrapolating from gauged areas to ungauged areas using an area-weighted approach. For precipitation data, the internationally coordinated over-basin precipitation data set is used. This precipitation data set begins with NOAA GLERL's Thiessen Method, is reviewed by NOAA Center for Operational Oceanographic Products and Services (CO-OPS), and is agreed upon between USACE and Environment Canada. Currently, the coordinated precipitation data set spans 1900 through 2010.

RESULTS

Gridded daily SWE data from SSM/I and SNODAS were obtained for ten water years when both datasets were available, 2004 – 2013. For both datasets, the gridded data were aggregated by basin region to produce a daily time series of average-basin SWE. Weekly time series were also developed for each basin using the maximum weekly values in order to accommodate the satellite overpass cycle which results in some days without satellite observations. Annual maximum SWE values for each of the ten water years were extracted from the weekly time series. Daily maximums, minimums, and averages were calculated from the daily time series. Data for the Superior, Michigan, Erie, and Ontario basins are shown in Figure 2 through Figure 5.

The SSM/I data is clearly underestimating the SWE in the Great Lakes. The passive microwave results seem to be heavily affected by the significant vegetation in the region considering the U.S. portion of the Lake Erie basin has a 14.9% forest fraction while the Superior, Michigan, Huron, and Ontario basins all have greater than 30% forest fraction according to the Vegetation Continuous Field collection from the University of Maryland (Hansen et al. 2006). Azar et al (2008) evaluated the SSM/I SWE products in the Great Lakes region using the SNODAS data and found poor results using the original passive microwave algorithm. They were able to improve the SSM/I results around the Great Lakes by developing an algorithm that uses a Normalized Difference Vegetation Index (NDVI) to classify the mixed use forest in the region. Figure 6 shows the SWE for the U.S. portion of the Lake Superior basin during the winter of 2003-2004, the only winter in common between the SSM/I, SNODAS, and CRREL data sets. In

the winter of 2003-2004, the SNODAS and CRREL data are well correlated ($R^2 = 0.91$) as might be expected since both the SNODAS and CRREL estimates likely use the same ground observations. This provides some confidence in the SNODAS SWE.

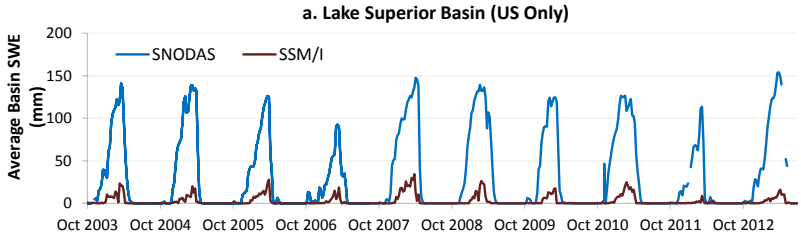

Figure 2 Lake Superior basin (US only) SWE estimates since 2003

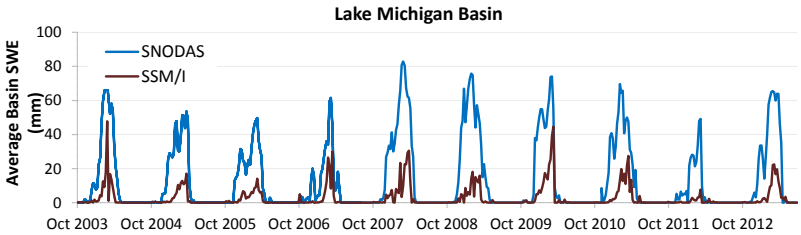

Figure 3 Lake Michigan basin SWE estimates since 2003

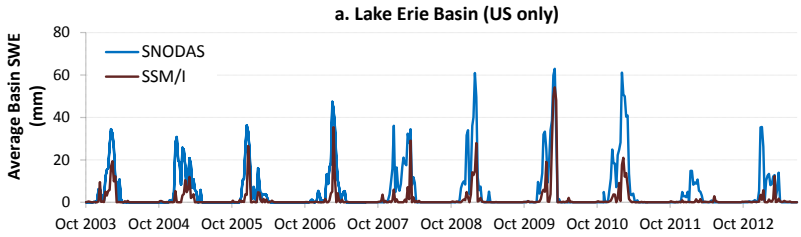

Figure 4 Lake Erie basin (US only) SWE estimates since 2003

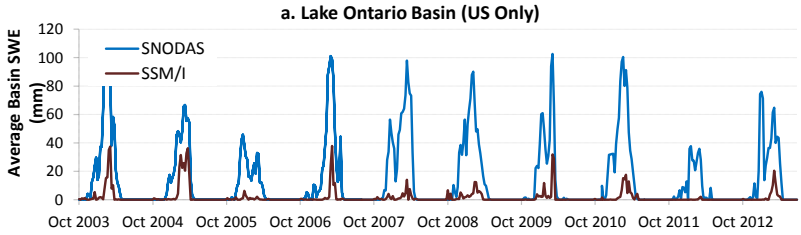

Figure 5 Lake Ontario basin (US only) SWE estimates since 2003

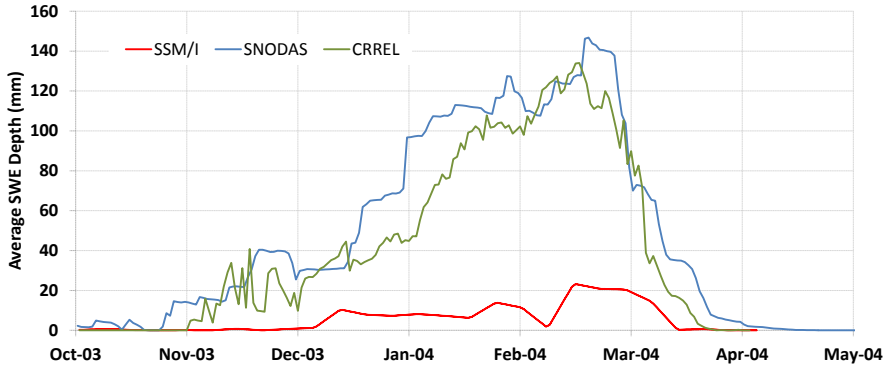

Figure 6 CRREL (daily), SNODAS (daily), and SSM/I (weekly) SWE estimation for Lake Superior (US only) for the winter of 2003-04

The LBRM Lake Superior SWE statistics were calculated using end-of-month data and are shown in the box and whisker plot of Figure 7. For Lake Superior, the snow pack generally begins to develop in November, peaks in March, and lasts until May. A further analysis is to look at the decline of SWE through each month, as shown in Figure 8, which shows the amount of water which is made available to runoff (when positive) or the amount of precipitation which enters snow pack (when negative). This figure clearly shows that SWE typically gives a boost to runoff, and hence the Lake Superior water level, during the months of April and May.

To further understand the influence of SWE within Lake Superior's hydrology, the statistics for historical runoff and historical precipitation were also analyzed, as shown in Figure 9 and Figure 10, respectively. The runoff component has been converted to depth units of mm over land, in order to match the units of SWE. The precipitation data set represents units of mm averaged over the entire basin, and this study will assume that the depth is constant over each part (land area and lake area). When comparing Figure 8 with Figure 9, one can clearly see an influence of SWE on runoff. However, Figure 10 shows that there is also an increase in precipitation at this time of the year as well.

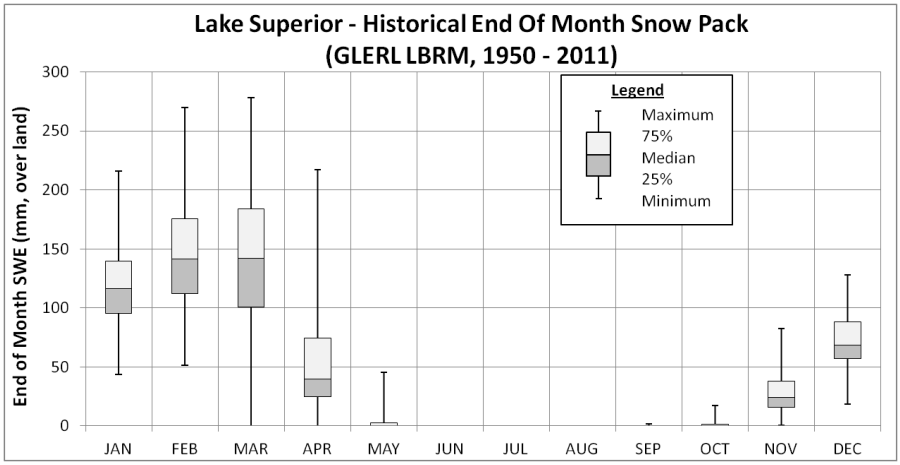

Figure 7 Lake Superior LBRM historical snow pack

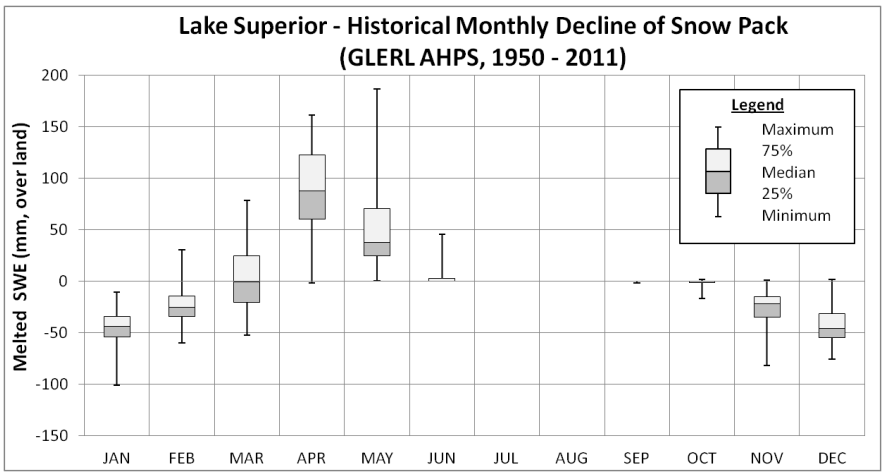

Figure 8 Lake Superior LBRM historical average decline of snow pack

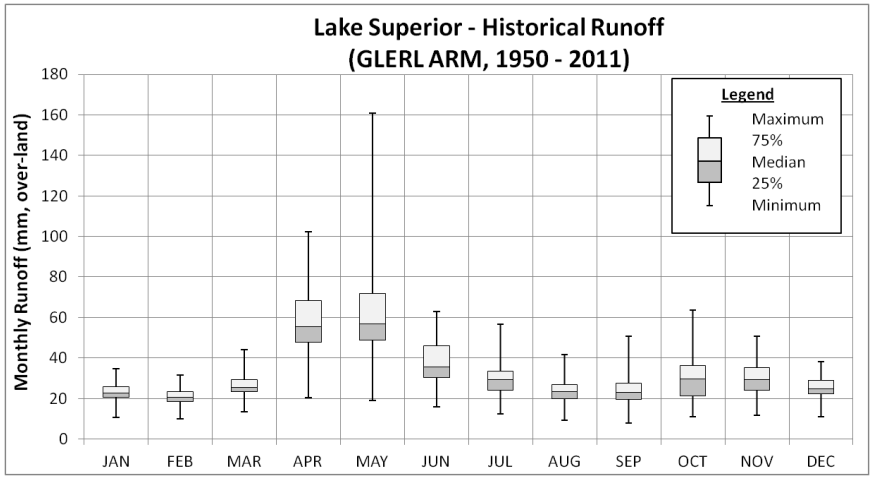

Figure 9 Lake Superior ARM historical runoff

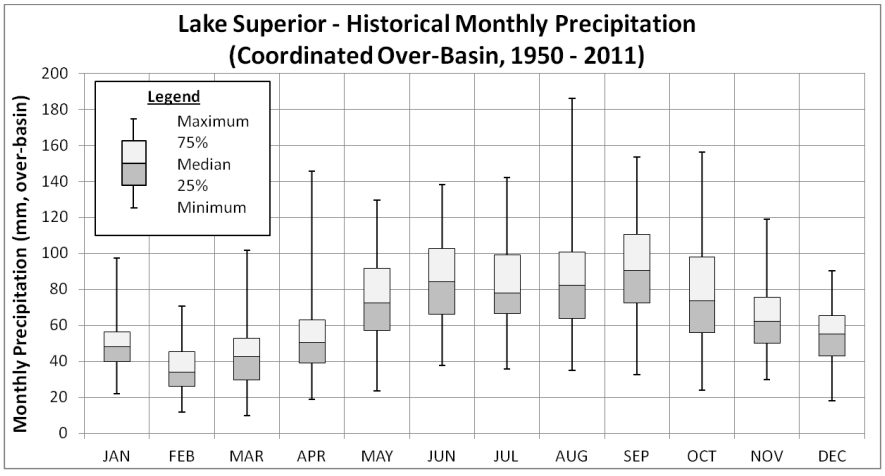

Figure 10 Lake Superior historical coordinated precipitation

Water which is available for spring's seasonal runoff to Lake Superior comes from two sources: melted SWE and spring over-land precipitation. This study found that developing a relationship

between only one of these components and runoff was not as strong as including both components. Figure 11a shows the historical data for Lake Superior during April of runoff on the vertical axis and the combined total of melted SWE and over-land precipitation on the horizontal axis. Figure 11b shows the historical data for the month of May. Other months exhibited much weaker relationships.

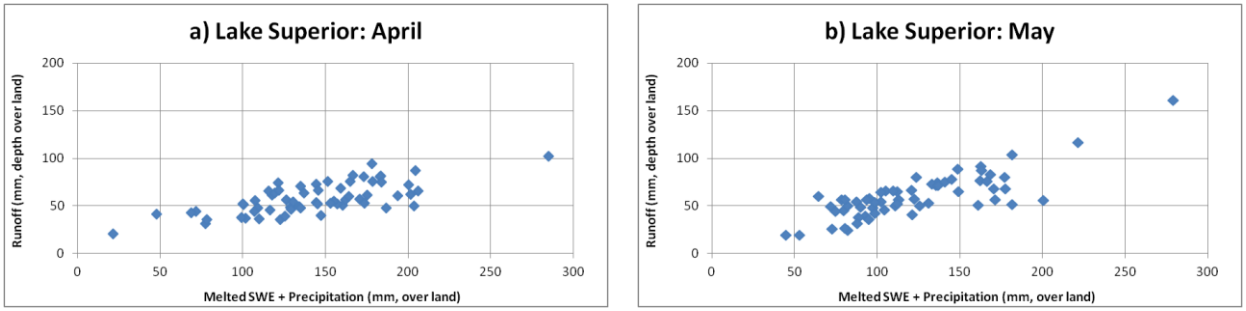

Figure 11 Relationship between Lake Superior runoff and the combined total of melted SWE and over-land precipitation for the months of (a) April and (b) May

As shown in the above figures, the total amount of available water is significantly greater than what arrives to the lake since much of the water infiltrates into the ground or is taken up by vegetation. For example, during the month of April the historical average amount of melted SWE in the Lake Superior drainage basin is 11.24 km^3 and the average over-land precipitation is 6.91 km^3 for a total of 18.15 km^3, while the average runoff during April is only 7.41 km^3. Assuming the two sources of water behave equally, 62% of Lake Superior's April runoff typically comes from melted SWE and 38% comes from over-land precipitation. For the month of May, 39% of Lake Superior's runoff typically comes from melted SWE while 61% comes from over-land precipitation.

APPLICATION: WATER LEVEL FORECASTING

A challenge in forecasting the Great Lakes water levels is determining how much of an adjustment to implement in the predicted water supply when viewing the near real-time SWE estimates within the basin. The analysis in the previous section demonstrated a clear relationship between the April and May runoff and the available water from melted SWE and over-land precipitation during each month. These relationships can be used in the water level forecast for the months of April and May.

Implementing the relationships of Figure 11 into operational forecasting is suggested in two basic steps: assess the current SWE and then adjust the forecasted runoff. First, the near real-time SWE estimates are compared with the average SWE for that time of the year. For example, a current end-of-March SNODAS SWE estimate is divided by the historical average end-of-March LBRM SWE. At the current time, this comparison has uncertainty since the best SWE estimates are from the SNODAS model while the relationships developed in the previous section used the LBRM data set. The SNODAS model only has full basin coverage since 2011, and although the two model results seem to agree relatively well in the recent overlapping years, this method should improve as more years of data become available.

Once the current relative SWE is determined, as a percentage of the typical SWE, the forecasted runoff can be adjusted using the typical proportion of melted SWE for that month. For the month of April, the average runoff volume for Lake Superior is 7.41 km^3, 62% of which (or 4.59 km^3) comes from melted SWE and the rest (2.82 km^3) from over-land precipitation. Since the relationship between runoff and available water was linear in Figure 11, the runoff adjustment is made by directly multiplying the SWE portion of runoff (4.59 km^3) by the current relative SWE. This text explained the connection in terms of water volume, but in general the USACE forecasts use units of flow rate for the runoff component. For runoff in units of flow rate, the same logic can apply by calculating the proportion (62%) of the flow coming from melted SWE and adjusting it based on the current relative SWE. As an example, if the current end-of-March SWE was 150% of average and the typical runoff for April was 2,560 m^3/s, the adjusted runoff for the forecast would be 3,350 m^3/s. An improvement to the forecasted runoff will also improve the Great Lakes water level forecast.

CONCLUSION

Available historic SWE data from passive microwave SSM/I and NOAA NOHRSC SNODAS were compared for the Great Lakes basin. Since the Canadian coverage of the SNODAS model is only available since 2011, figures present the 10 available years (since 2003) of U.S. coverage of SWE. Results indicate that SSM/I data severely underestimates Great Lakes SWE, likely due to the significant forest fraction within the basin. Historical LBRM snow pack, ARM runoff, and coordinated precipitation were analyzed for the Lake Superior basin in order to quantify the influence of SWE on the Lake Superior water level. A linear relationship was found between runoff and the combined total of melted SWE and over-land precipitation during the months of April and May. A method of adjusting the forecasted April and May runoff is suggested which uses near real-time SWE and the historical proportions of runoff which originate from melted SWE and over-land precipitation. As more years of SNODAS become available, the understanding of SWE behavior and its incorporation into the Great Lakes water level forecasts will continue to improve, as will the uncertainty in the proposed method.

LIST OF ABBREVIATIONS

ARM:	Area Ratio Method (of GLERL)
ASOS:	Automated Surface Observing System
CCBGLHHD:	Coordinating Committee on Basic Great Lakes Hydraulic and Hydrologic Data
CO-OPS:	Center for Operational Oceanographic Products and Services (of NOAA)
CRREL:	Cold Regions Research and Engineering Laboratory (of USACE)
DMSP:	Defense Meteorological Satellite Program
EASE-Grid:	Equal-Area Scalable Earth Grid
ERDC:	Engineer Research and Development Center (of USACE)
GLERL:	Great Lakes Environmental Research Laboratory (of NOAA)
IJC:	International Joint Commission
LBRM:	Large Basin Runoff Model (of GLERL)
LRE:	Detroit District (of USACE)
NDVI:	Normalized Difference Vegetation Index
NOAA:	National Oceanic and Atmospheric Administration

NOHRSC: National Operational Remote Sensing Center (of NOAA)
NSIDC: National Snow and Ice Data Center
NWS: National Weather Service (of NOAA)
SNODAS: SNOw Data Assimilation System (of NOHRSC)
SSM/I: Special Sensor Microwave/Imager (of DMSP)
SWE: Snow-water equivalent (usually units of depth over the land surface)
USACE: U.S. Army Corps of Engineers

REFERENCES

Armstrong, R. L., and M. J. Brodzik. 1995. An earth-gridded SSM/I data set for cryospheric studies and global change monitoring. Advances in Space Research 16: 155-163.

Azar, E. A., H. Ghedira, P Romanov, S. Mahani, M. Tedesco and R. Khanbilvardi. 2008. Application of satellite microwave images in estimating snow water equivalent. Journal of the American Water Resources Association 44(6) : 1347-1362.

Carroll, T., D. Cline, C. Olheiser, A. Rost, A. Nilsson, G. Fall, C. Bovitz and L. Li. 2006. NOAA's National Snow Analyses. Proceeding of the 74th Annual Meeting of the Western Snow Conference 74:13.

Chang, A., J. Foster, and D. Hall. 1996. Effects of forest on the snow parameters derived from microwave measurements during the boreas winter field campaign. Hydrological Processes 10 : 1565-1574.

Clifford, D. 2010. Global estimates of snow water equivalent from passive microwave: history, challenges and future developments, International Journal of Remote Sensing 31(14) : 3707-3726.

Clow, D. W., L. Nanus, K. L. Verdin. and J. Schmidt (2012) Evaluation of SNODAS snow depth and snow water equivalent estimates for the Colorado Rocky Mountains, USA Hydrol. Process. DOI: 10.1002/hyp.9385

Croley II, T.E. and C. He (2002) Great Lakes Large Basin Runoff Model. Proceedings, Second Federal Interagency Hydrologic Modeling Conference, Subcommittee on Hydrology of the Interagency Advisory Committee on Water Data, Las Vegas, NV, 2002, 12 pp.

Daly, S. F., T. B. Baldwin, P. Weyrick (2007) Analysis of the Lake Superior Watershed Seasonal Snow Cover, Cold Regions Research and Engineering Laboratory, ERDC/CRREL TR-07-5, May 2007.

Derksen, C., A. E. Walker, B. E. Goodison, and J. W. Strapp. 2005. Integrating in situ and multiscale passive microwave data for estimation of subgrid scale snow water equivalent distribution and variability. IEEE Transactions on Geoscience and Remote Sensing 43: 960-972.

Doesken, N. J. and T. B. McKee (2000) Life after ASOS (Automated Surface Observing System) -- Progress in National Weather Service snow measurement Proceedings of the 68th Annual Western Snow Conference. April 2000 sites/westernsnowconference.org/PDFs/2000Doeskin.pdf

Dong, J., J. Walker, and P. Houser. 2005. Factors affecting remotely sensed snow water equivalent uncertainty. Remote Sensing of the Environment 97 : 68-82.

Farmer, C.J.Q, T.A. Nelson, M.A. Wulder, C. Derksen. 2010. Identification of snow cover regimes through spatial and temporal clustering of satellite microwave brightness temperatures. Remote Sensing of Environment 114 : 199-210.

Foster, J. L., D. K. Hall, A. T. C. Chang, A. Rango, W. Wergin, and E. Erbe. 1999. Effects of snow crystal shape on the scattering of passive microwave radiation. IEEE Transactions on Geoscience and Remote Sensing 37: 1165-1168.

Foster, J. L., C. J. Sun, J. P. Walker, R. Kelly, A. Chang, J. R. Dong, and H. Powell. 2005. Quantifying the uncertainty in passive microwave snow water equivalent observations.Remote Sensing of Environment 94: 187-203.

Frankenstein, S., A. Sawyer, and J. Koeberle. 2008. Comparison of FASST and SNTHERM in three snow accumulation regimes. Journal of Hydrometeorology 9: 1443-1463.

Hall, D. K., A. T. C. Chang, and J. L. Foster. 1986. Detection of the depth-hoar layer in the snowpack of the Arctic Coastal-Plain of Alaska, USA, using satellite data. Journal of Glaciology 32: 87-94.

Hallikainen, M. T., F. T. Ulaby, and M. Abdelrazik. 1986. Dielectric-properties of snow in the 3 to 37 ghz range. IEEE Transactions on Antennas and Propagation 34: 1329-1340.

Hansen, M., R. DeFries, J.R. Townshend, M. Carroll, C. Dimiceli, and R. Sohlberg. 2006. Vegetation Continuous Fields MOD44B, 2001 Percent Tree Cover, Collection 4, University of Maryland, College Park, Maryland, 2001.

Josberger, E. G., and N. M. Mognard. 2002. A passive microwave snow depth algorithm with a proxy for snow metamorphism. Hydrological Processes 16: 1557-1568.

Matzler, C. 1987. Application of the interaction of microwaves with the natural snow cover. Remote Sensing 2 (2) : 259-287.

Matzler, C., and A. Standley. 2000. Relief effects for passive microwave remote sensing. International Journal of Remote Sensing 21: 2403-2412.

Mizukami, N. and S. Perica. 2012. Towards improved snow water equivalent retrieval algorithms for satellite passive microwave data over the mountainous basins of western USA. Hydrological Processes 26(13): 1991-2002.

Norton, D. C., S. J. Bolsenga, 1993: Spatiotemporal Trends in Lake Effect and Continental Snowfall in the Laurentian Great Lakes, 1951–1980. J. Climate, 6, 1943–1956. doi: http://dx.doi.org/10.1175/1520-0442(1993)006<1943:STILEA>2.0.CO;2

Rutter, N., D. Cline and L. Li. 2008. Evalutation of the NOHRSC Snow Model (NSM) in a One-Dimensional Mode. Journal of Hydrometeorology, 9(4) : 695-711.

Tedesco, M. and P. S. Narvekar. 2010. Assessment of the NASA AMSR-E SWE product. IEEE Journal of Selected Topics in Applied Earth Observations and Remote Sensing 3(1) : 141-159.

Vuyovich, C. and J. Jacobs (2011) Snowpack and runoff generation using AMSR-E passive microwave observations in the Upper Helmand Watershed, Afghanistan, Remote Sensing of the Environment, Vol. 115, pp. 3313 – 3321.

Walker, A. and B. Goodison (1993) Discrimination of a wet snow cover using passive microwave satellite data, Annals of Glaciology, Vol. 17, pp. 307 – 311.

HYDRAULIC MODELING AND MAPPING OF THE YELLOWSTONE RIVER TO SUPPORT CUMULATIVE EFFECTS ASSESSMENT

Laurel J. Hamilton, E.I., Hydraulic Engineer, U.S. Army Corps of Engineers, Omaha, NE, laurel.j.hamilton@usace.army.mil; Kevin K. Adams, P.E., Hydraulic Engineer, U.S. Army Corps of Engineers, Omaha, NE, kevin.k.adams@usace.army.mil; Megan A. Splattstoesser, Geographer, U.S. Army Corps of Engineers, Omaha, NE, megan.a.splattstoesser@usace.army.mil; Roger L. Kay, P.E., Hydraulic Engineer, U.S. Army Corps of Engineers, Omaha, NE, roger.l.kay@usace.army.mil

Abstract: Hydraulic modeling was performed in support of the Yellowstone River Corridor Cumulative Effects Assessment (CEA). The CEA is a joint effort of the Yellowstone River Conservation Districts Council and the U.S. Army Corps of Engineers, Omaha District (Omaha District). The interdisciplinary study examines hydrologic, hydraulic, geomorphic, biologic and socioeconomic characteristics of and impacts on the Yellowstone River and adjacent floodplain in a 565-mile reach from Gardiner, Montana, to the confluence with the Missouri River in western North Dakota. The purpose of the study is to perform an assessment of the cumulative impacts for the entire river corridor and develop a comprehensive plan that provides for sustainable use of the river and its floodplain for both economic and environmental needs.

The hydraulic analysis is intended to detect changes associated with two potential drivers of cumulative effects: altered (regulated) hydrology due to water resources development within the Yellowstone River basin and physical alteration (development) of the Yellowstone River floodplain. One facet of the cumulative impacts assessment is to characterize the impacts of human development including man-made structures, encroachments, storage, diversions, and depletions on the Yellowstone River hydraulic profiles and flood boundaries, by comparing current and “pre-historic” conditions.

The hydraulic analysis utilized the modeling software HEC-RAS and geospatial software ArcGIS and the Geo-RAS extension for model geometry development and floodplain mapping. Flow information was obtained from an intensive hydrology study of the basin performed jointly by Montana U.S. Geological Survey (USGS) and Omaha District. The hydraulic model was developed to evaluate human impacts by generating two geometry files and two flow files. The geometry files include “Developed” conditions (i.e., the file represents current conditions with existing bridges, embankments, diversion dams, etc.) and “Undeveloped” conditions (i.e., human made structures are manually removed from the geometry file.) The flow files include “Regulated” conditions (i.e., hydrologic discharges representing current conditions resulting from human-controlled reservoirs, irrigation canals, etc.) and “Unregulated” conditions (i.e., hydrologic discharges represent natural conditions). Four scenarios were modeled using these input files.

Comparison of the results from modeling and mapping the combinations of the geometric and hydrologic conditions provided valuable information for a range of flow frequencies that will

assist the CEA and restoration planning process. Results critical to the cumulative effects assessment include the extent of inundated floodplain under differing scenarios, hydraulic characteristics (e.g., river stages, velocities, flow depths) and the differences between each scenario. Of particular interest to cumulative effects assessment and restoration planning is the frequency of side channel and floodplain inundation and how that frequency may have changed over time due to channel modifications and water resourcing.

INTRODUCTION

The Yellowstone River is one of the longest free-flowing rivers in the lower 48 states (USGS, 2013). The river corridor provides for various sized communities; supports agricultural (range and crop), industrial, commercial and recreational uses; and is home to abundant wildlife. The river crossings in the study reach are limited to bridges and low-head weirs, and channel modifications consist of bank stabilization, flow deflectors and side channel cutoffs. Floodplain development includes urbanization; transportation routes; Federal, community and agricultural levees; and irrigated and dryland farming. The width of the 100-yr floodplain ranges from 0.12-miles to 2-miles within the study reach. Narrow floodplain widths are due to both natural and man-made flow constrictions.

The study area for the Yellowstone River hydraulic analysis extends from the Park-Sweet Grass County line at River Mile 478.2 to the confluence of the Missouri River floodplain at River Mile 2.8 (Figure 1). Within the study reach, the Yellowstone River and its corridor are described by its alluvial system characterized by its meandering flow path, anabranching side channels, vegetated islands and dynamic gravel bars (DTM Consulting, 2009).

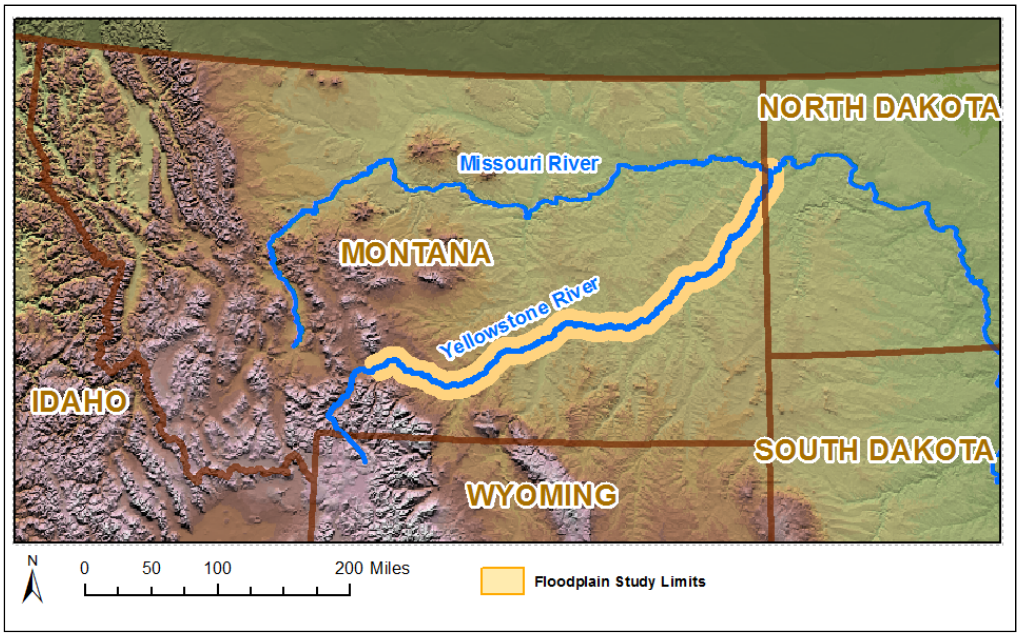

Figure 1 Hydraulic Study Location and Extents

MODELING APPROACH

Water surface profile models of the Yellowstone River were developed using the U.S. Army Corps of Engineers Hydrologic Engineering Center-River Analysis System (HEC-RAS) backwater computer program Version 4.1 (USACE, 2010) utilizing steady-state and subcritical flow computations to calculate water surface profiles and associated hydraulic parameters. The main computational procedure, generally known as the standard step method, is based on the solution of the one-dimensional energy equation with energy loss from friction evaluated with Manning's equation and from flow constrictions and expansions. The model requires terrain and flow inputs to characterize the floodplain and hydrology, respectively.

Hydrologic Data: The hydrologic analysis was conducted as two studies. The hydrology for the reach upstream of the Big Horn River was conducted by the Omaha District (USACE, 2011). The study downstream of the Big Horn River was conducted by the USGS (USGS, 2013). The same methodology was utilized to develop the Regulated and Unregulated discharges in both studies. Daily stream flow data were collected from gauging stations throughout the Yellowstone River Basin for the 1928-2002 study period. Missing periods were synthesized from monthly mean flows. Once an entire dataset of observed flows was developed for the period of record, historical depletions (including reservoir holdouts) recorded by the Bureau of Reclamation were added to the observed flow dataset, and Bulletin 17B methodology was used to generate the Unregulated peak-flow frequency data. Then, the depletions recorded in 2002 were subtracted from the Unregulated dataset to generate the Regulated peak-flow data. The discharges selected for the hydraulic analysis include the 67-, 50-, 20-, 10-, 5-, 2-, 1-, 0.5- and 0.2-% annual chance exceedance (ACE) events and the 5% by duration event. These discharges were identified as beneficial for the cumulative effects assessment, and hydraulic results are intended to support concurrent studies including aquatic, riparian, avian, socioeconomics and water quality.

Topographic Data: Topographic data was collected in 2004 and in 2007 as Light Detection and Ranging (LiDaR) data and supplied as Triangulated Irregular Network (TIN) data file. The data were provided in Montana State Plane Coordinates, NAD83, suitable for generation of 1-meter contours. Accuracy was evaluated with ground truthing and surveyed spot elevations, meeting National Map Accuracy Standards. Bathymetric data was collected in 2004 for select study reaches. Floodplain and bathymetric data were merged and provided in TIN format and 2.5-meter Digital Elevation Models (DEMs). All elevations are referenced to the North American Vertical Datum of 1988 (NAVD88) unit meters. Aerial imagery was collected in 2004 and 2007.

Hydraulic Model: Nine individual HEC-RAS projects were created covering the ten counties included within the study. The hydraulic model geometry was created utilizing the ESRI ArcGIS software and HEC-GeoRAS, a GIS extension specifically designed to process geospatial data for use with HEC-RAS. The HEC-GeoRAS extension allows the creation of an HEC-RAS import file containing geometric attribute data from an existing digital terrain and complementary data sets. The corresponding ArcGIS software extensions 3D Analyst and Spatial Analyst were also utilized for geometry development.

In HEC-GeoRAS, an import file was created containing river, reach and station identifiers by generating GeoRAS layers consisting of a stream centerline, cross-sectional cut lines, bank

stations, overbank flowpaths, and cross-sectional roughness coefficients. These GeoRAS layers were combined with the terrain elevation files, and the software calculated the downstream reach lengths for overbanks and channel, extracted cross-sectional station and elevations points, and generated the HEC-RAS input file.

Cross sectional cutlines were spaced approximately 500 to 1000 feet apart, with closer spacing near structures and areas of specific interest to adequately represent the hydraulic impacts of the structure. Spacing exceeded 1000 feet in areas of sharp channel bends to prevent the cutlines from overlapping in the overbanks and in areas of inadequate survey data. Cutlines were drawn perpendicular to both channel and overbank flow and often dog-legged to adequately represent the overbanks and sinuous channel as a one-dimensional system. Cross sections were extended to high ground to ensure capture of elevation data for the 0.2% ACE.

Additional GeoRAS layers were incorporated. A vegetative cover shapefile was provided by the Montana Natural Resource Conservation Service (NRCS) for the entire study area as a 2006 vegetative cover map. Corresponding Manning's Roughness Values were assigned based on available reference data and engineering judgment. The overbank flow paths were drawn based on the anticipated flow path of the 1% ACE. Once the GeoRAS layers were compiled, the HEC-RAS import file was generated and brought into the program.

In HEC-RAS, the structures such as bridges, levees and diversion dams were characterized, channel bank locations were edited and river mileage was included. The roughness values imported from GeoRAS were verified for the channel and overbanks and adjusted where appropriate. Expansion and contraction coefficients were 0.3 and 0.1, respectively, for typical channel cross sections. The coefficients of 0.5 and 0.3, respectively, were used to characterize all bridges and the diversion dam. Bank stations were placed at locations defining the main channel and typically assigned elevations between the 67% ACE and 0.2% ACE profiles.

In areas where bathymetric data was not collected, a low-flow trapezoidal channel was incorporated into the model geometry. The channel flows at the time the LiDaR surveys and aerial photographs were collected were used to approximate the channel width and depth and applied to the entire county reach. The modeled low flow water surface was compared and calibrated to the LiDaR water surface and the wetted channel shown in the aerials. Adjustments to the low flow channel dimensions were made to individual cross sections. The calibration of the low-flow channel was generally within one foot of the LiDaR surveyed water surface.

Developed Model Geometry: The developed model geometry represents current conditions and includes terrain alterations due to human development. Structures incorporated into the model include transportation embankments, Federal and agricultural levees, canals and ditches, wastewater treatment lagoons, and designed depressions and pilings (e.g., quarries and electrical tower pilings). Yellowstone River structures requiring manually-entered descriptions in HEC-RAS include bridges and low head dams. Bridge surveys were performed by the Montana USGS between 2005 and 2009 and included bridge dimensions, chord elevations, and pier and channel descriptions. A total of 39 bridges were modeled, and one low head dam was modeled at Intake, MT in Dawson County. Surveys of Intake Diversion Dam were obtained from the Intake Fish Passage Study (USACE, 2009).

Ineffective flow areas and levees were coded into the HEC-RAS model by inspecting cross sections, contours, aerial photographs and structure descriptions to determine applicability, location and elevation. The locations of Federal levees were verified and natural and agricultural levees were identified based on the terrain elevation and flow characteristics between adjacent cross sections. Ineffective flow restraints were also added manually to the geometry to follow conveyance expansion and contraction guidelines. The ineffective flow area and levee options were set with the attempt to represent all stream flows; however the 1% ACE was used as the basis for calibration.

An in-depth Physical Feature Inventory was generated as part of the CEA study. This database includes locations and descriptions of various structures including bridges, embankments, low-head dams, canals, irrigation returns, and bank stabilization. The inventory and geo-database was useful in determining structures location, type and applicability to the hydraulic modeling.

Undeveloped Model Geometry: The Developed model geometry was used as a base for the Undeveloped model geometry. The Undeveloped geometry was generated by manually adjusting each cross section's station elevation points from the Developed geometry file that represent man-made features such as railroad embankments, levees, elevated roads, etc. Elevations of natural land adjacent to the structures were used to estimate natural elevations at the structure. Bridges and inline structures and the immediate downstream bounding cross section were also removed within the HEC-RAS model. Manning's Roughness Values for urban areas, decreased expansion and contraction coefficients which define bridges, ineffective flow areas representing flow restriction due to man-made structures, and other associated geometric components attributed to human impacts were also adjusted or eliminated to reflect natural conditions.

Figure 2 shows a cross section in Billings, MT at River Mile 366.2. The cross section, high-lighted in red on the top image, is depicted in the bottom image. The station elevation points shown in pink represent the man-made structures captured in the LiDAR surveys. These points were manually removed and the final undeveloped geometry is shown in black. Similarly, the ineffective flow areas were widened due to the removal of the man-made structures allowing more of the overbanks to convey flow.

The channel geometry, including the approximated low flow channel, was not adjusted as part of the Undeveloped geometry characterization. Although locations of bank stabilization (e.g., riprap protection, flow deflectors, etc.) have been identified through the CEA, it is difficult to predict the spatial and vertical degradation and aggradation potential and the extent of channel migration under completely natural terrain and flow conditions.

Flowpaths were not adjusted as part of the Undeveloped geometry adjustments. The 1% ACE flowpath was used to describe channel and overbank flow distances between cross sections for the Developed geometry. Structures such as embankments and levees may cause significant flow restrictions and affect the flow path and distance. Removing a flow-restricting structure would widen the conveyance area resulting in a shorter flowpath.

Most structures are apparent on the recent aerial photographs and terrain surveys and were listed in the physical feature inventory. In some areas with significant or questionable development, the 1950 historic aerial photographs (DTM Consulting, 2006) were used as a guide to estimate the extent and contours of the natural system. However, significant engineering judgment was used to create the Undeveloped geometry files due to the limited historic information and the use of current terrain data to estimate undeveloped terrain.

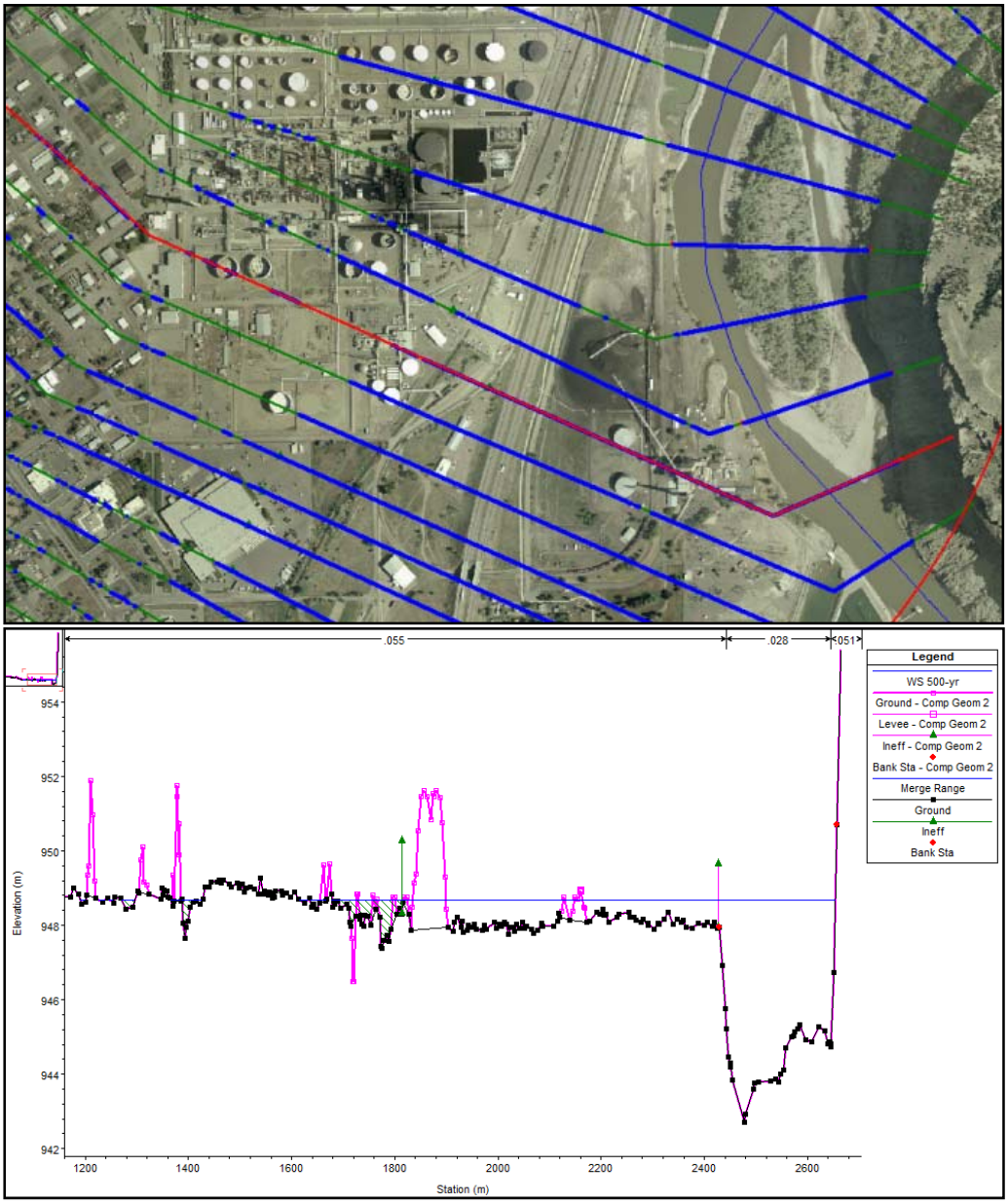

Figure 2 Removed Man-Made Structures in Undeveloped Geometry File, Billings, MT

In several instances, human modification was apparent, but the level and extent was uncertain as comparison of adjacent terrain and current and historic aerials did not always offer an indication of historic conditions. For example, much of the floodplain consists of irrigated cropland that has

been terraced and sloped in an effort to maximize irrigation efforts. However, it is difficult to discern if soil was added, removed, or both, in order to obtain the gentle slope. A potential example of this is shown in Figure 3 and highlighted in green for River Mile 68.1 in Dawson County. In areas of uncertainty, the Undeveloped terrain was not adjusted, and the Developed geometry obtained from the LiDAR surveys was used.

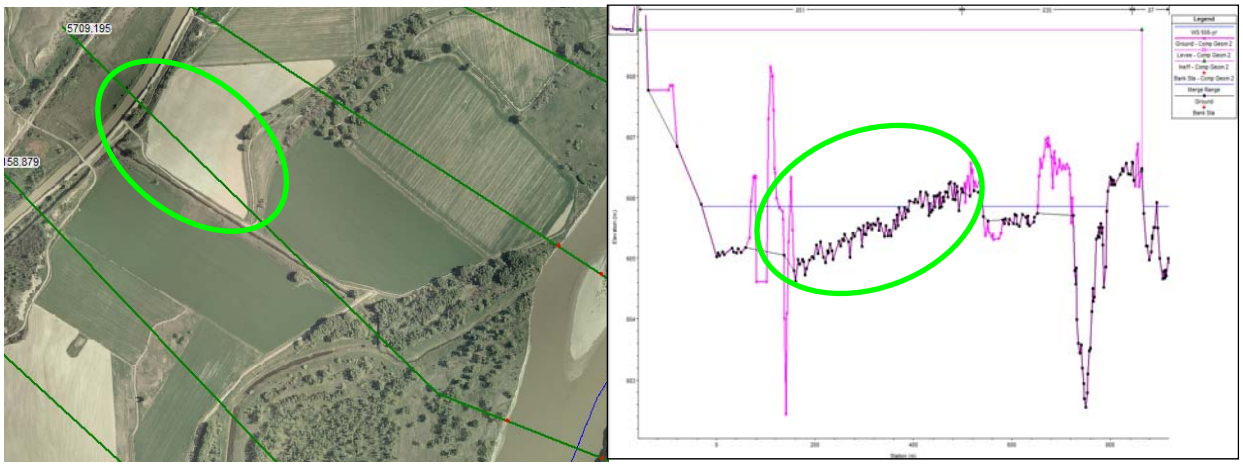

Figure 3 Undeveloped Terrain Uncertainty

Model Plans: A starting water surface for each profile was either computed by HEC-RAS using the normal depth calculation based on the energy slope for subcritical flow or was defined by water surface results from adjacent models. Results were incorporated between adjacent models to ensure continuity throughout the study reach.

Four modeling scenarios were executed as individual HEC-RAS plans for each model. By modeling a combination of the Developed and Undeveloped geometries with the Regulated and Unregulated flows, the individual components of human impacts on the terrain and flow regulations, can be evaluated. The scenarios modeled are listed in Table 1.

Table 1 Scenarios Modeled

Scenario	Geometry File	Flow File	Characterization Intent
Developed Floodplain Conditions A	Developed	Regulated	Current conditions
Developed Floodplain Conditions B	Developed	Unregulated	Storage reservoirs and irrigation diversions impacts
Undeveloped Floodplain Conditions A	Undeveloped	Regulated	Man-made structures impacts
Undeveloped Floodplain Conditions B	Undeveloped	Unregulated	Natural conditions

By comparing results from the four modeled scenarios, it is possible to characterize the impacts of human influence on the system. Table 2 lists the water surface elevation computed for the 5% ACE

at selected locations upstream and downstream of structures. By comparing the resulting elevations of the four scenarios, the impacts of the structures and flow regulations on the river stages are apparent. Similarly, Figure 4 depicts the resulting water surface profiles for the four scenarios at the railroad bridge in Glendive, MT.

Table 2 Water Surface Results (elevation meters), 5% ACE (20-yr), Dawson County

Location	River Mile	Develop A	Develop B	Undevelop A	Undevelop B
Five miles upstream of Glendive	99.68	632.77	633.13	632.77	633.13
Upstream of the BNSF RR Bridge in Glendive	94.57	628.46	628.90	628.07	628.38
Upstream of the I-90 Bridge in Glendive	92.18	625.62	626.03	625.35	625.70
Five miles downstream of Glendive	87.17	620.65	620.99	620.65	620.99
Upstream of the Intake Diversion	73.07	609.25	609.52	608.94	609.23
Downstream of the Intake Diversion	72.83	608.60	608.92	608.60	608.92

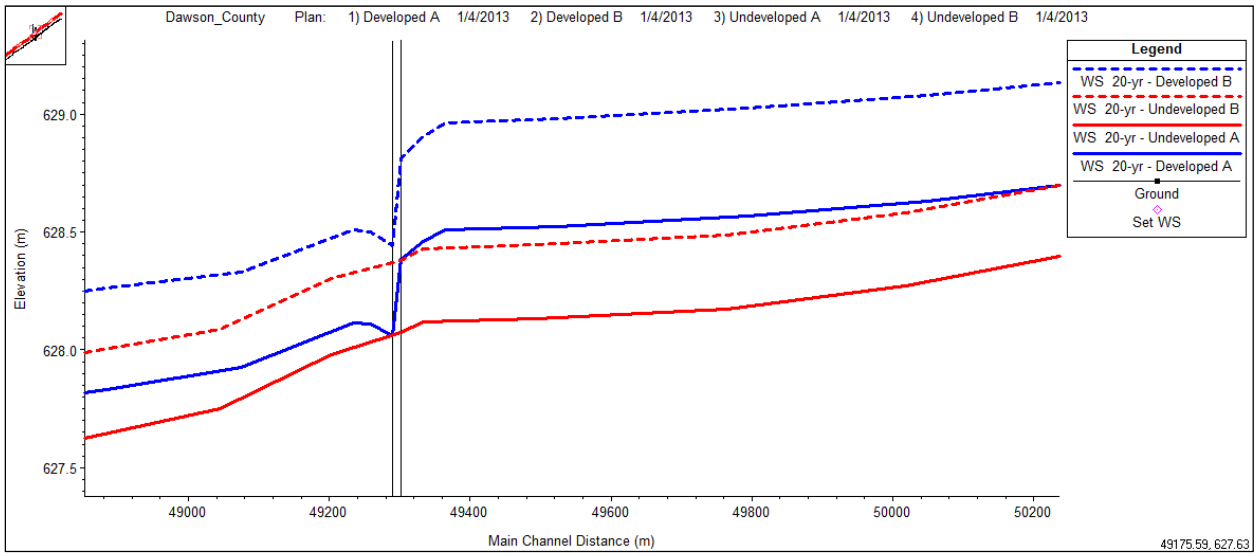

Figure 4 Water Surface Profiles at the BNSF Railroad Bridge in Glendive, MT

MAPPING APPROACH

Inundation maps were generated for select water surface profiles and scenarios to the extent of the survey data and as shapefile polygons, depth grids and 0.2-meter depth interval polygons. All mapping products have a projection of NAD 1983 Montana State Plane and NAVD 88 datum, unit meters. Due to ArcMap constraints, all inundation mapping was performed utilizing the 2.5-meter DEMs generated from the LiDaR surveys.

Mapping was performed for each county model utilizing the HEC-GeoRAS ArcMap extension, and inundations extend to the county lines to ensure continuity within the study reach. Once initially mapped, backwater areas were identified. Backwater areas connect to the inundated system at one location resulting in a single water surface elevation for the backwater area. Since

HEC-GeoRAS mapping is performed using a sloping water surface TIN for the entire river reach, proper mapping of backwater areas required additional efforts. For Undeveloped conditions, only backwater areas that occurred due to the natural terrain were remapped. Due to the additional level of effort, only backwater areas that affect large areas and several flood profiles were considered and remapped.

Backwater modeling efforts included one of two approaches, depending on the number and locations of backwater areas. If several backwater locations were identified in a county reach, a new water surface TIN was generated that incorporated the sloping profile of the main channel and the single elevation of each backwater, and the entire reach was remapped with the GeoRAS extension. If only a couple backwater areas were identified, these locations were remapped individually. The original, sloping backwater was clipped out and the revised backwater elevation was merged with the main channel. This was done for both the inundation shapefiles and the inundation depth grids.

An example of the backwater mapping result is shown in Figure 5. The image shows the right bank of the Yellowstone River just downstream of the Highway 310 Bridge in Laurel, MT at the Clarks Fork confluence for the Developed Floodplain Conditions A 1% ACE. Traditional GeoRAS mapping extends the calculated water surface profile from the main channel across the entire cross sections (shown as green lines) and results in an inundation boundary shown in orange. Upon close examination, the inundated area only connects to the main channel at one downstream location. The elevation at the connecting point was used to reprocess the water surface and the resulting main channel and backwater inundation area is shown in blue. Tributaries to the Yellowstone River were not part of this study; therefore the final backwater inundation only represents the impacts from the Yellowstone River flood event.

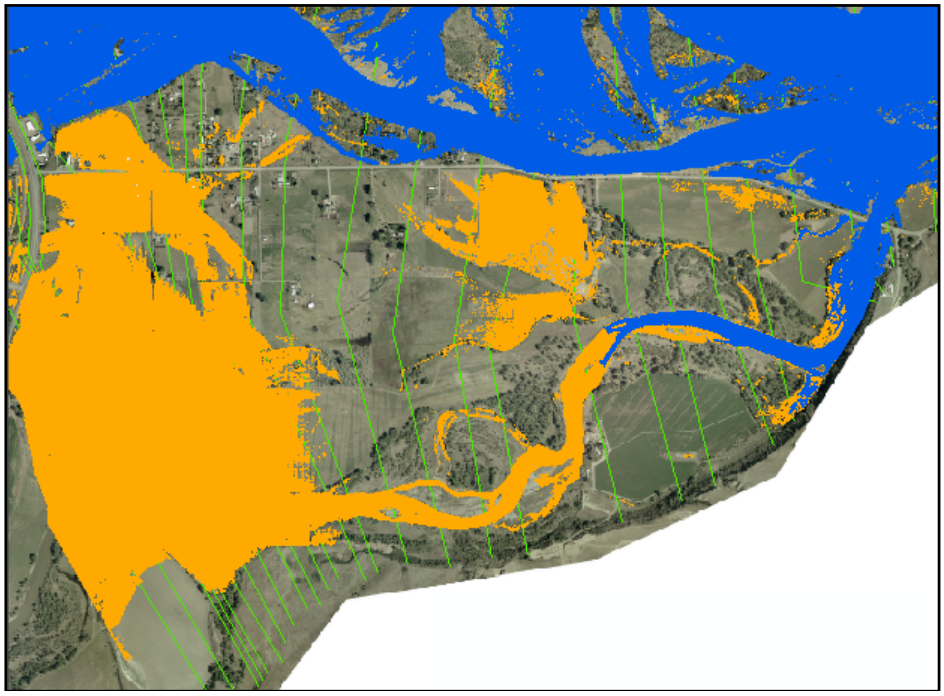

Figure 5 Backwater Inundation Remapped at Clarks Fork Confluence

During mapping editing, excess ponding areas and disconnected floodplains were removed if they were not directly connected to the main channel. Some areas appeared connected through a culvert or a bridge that was not removed in the survey data. If a culvert, bridge or other connection point is evident in the aerials or survey data then the area was considered connected and mapped as inundated. If a connection was uncertain, then the inundated area was considered disconnected and removed.

Undeveloped geometry mapping required additional efforts. Although the structures and station-elevation points were removed in the HEC-RAS models, the man-made features were not modified in the terrain data files. Therefore, manual adjustments were made to the inundation shapefiles in areas where man-made structures are present. For example, the presence of a road embankment may detach an inundated area of the floodplain from the main channel, and these areas were manually connected to reflect the Undeveloped inundation extent. Only disconnected areas or backwater locations due to the natural terrain were removed or remapped, respectively. Similarly, inundations boundaries were smoothed where any structure (e.g., bridge embankment, fishing access point, etc.) causes an unnatural boundary. Although the inundation shapefiles were edited, the depth grids reflect the depths with respect to structures since they were generated from the DEMs.

Figure 6 shows the mapping results for the Undeveloped conditions at Forsyth, MT. The image on the left compares the edited inundation boundary of the Developed condition in blue to the Undeveloped condition in orange for the 1% ACE Regulated flow. The Federal Levee is located on the south overbank and significantly restricts floodplain conveyance, apparent in the image on the left. The image on the right depicts the same area as a depth grid for the Undeveloped condition. The structures captured in the LiDAR survey are apparent and were not adjusted for the final depth grid. However, these features were edited for the inundation shapefile to show the areas spanning the structures as flooded.

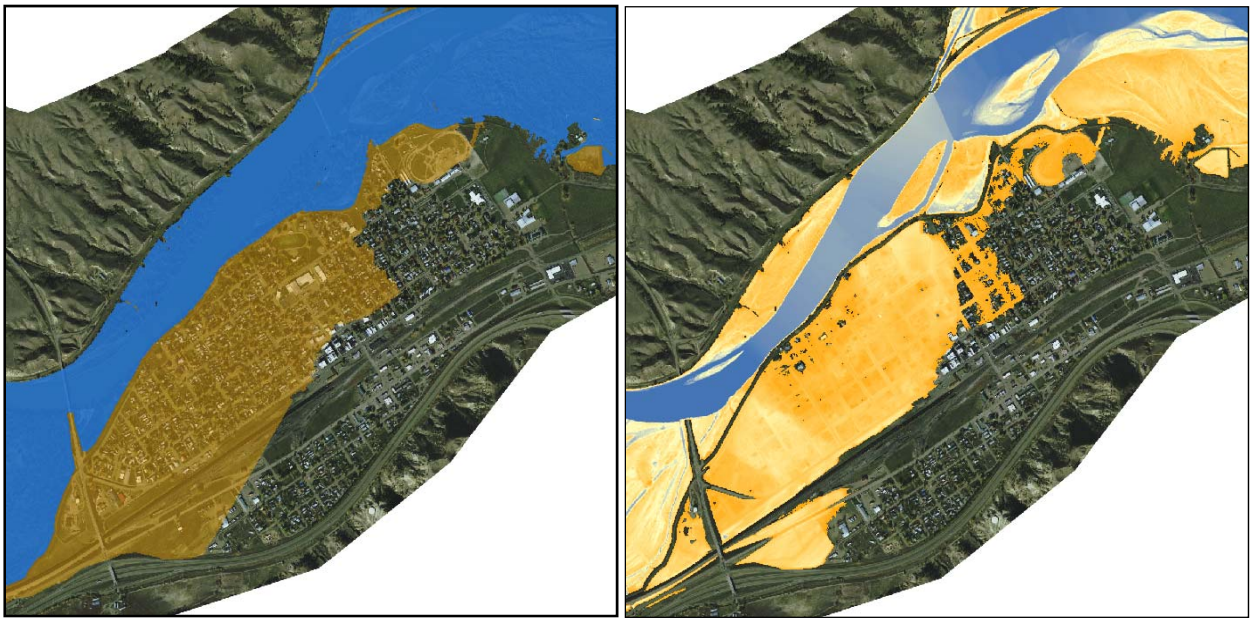

Figure 6 Undeveloped Conditions Shapefile and Depth Grid

DIFFICULTIES AND ASSUMPTIONS

Topographic data was provided as TINs and DEMs. When performing the hydraulic analyses, utilization of the TINs are preferred due to the slight increased level of accuracy over the generated DEMs. However, several of the TINs supplied contained errors and could not be read by the ArcMap software. For consistency throughout the study, the DEMs were used for the majority of the modeling and all of the mapping products. The DEMs were created using 2.5-meter pixels. This high resolution resulted in minimal added error.

Portions of the floodplain terrain were not fully captured or were incomplete. In areas of incomplete data, cross sections were spaced further than the desired 1,000 feet, were modeled by manual adjustments within HEC-RAS using USGS topology maps, or the DEMs were patched with USGS digital terrain data.

In some mapping products, the edges of the floodplain shapefiles and depth grids do not line up exactly with the source DEMs. This was observed between the shapefiles and corresponding depth grids, between individual profiles and between scenarios. The error varies between products and is less than one pixel (2.5-meter). The source of the error appears to occur during the extraction of the shapefiles and depth grids from the HEC-GeoRAS geodatabase. Although the error is small, caution should be used when comparing mapping products.

The HEC-RAS program is a one-dimensional model that was used to represent a wide floodplain and a range of stream flows. The one-dimensional computations assume a constant water surface elevation across the entire cross section. In reaches with large islands, this assumption may not be accurate and would warrant a split flow analyses. Similarly, ineffective flow area locations may be unique to each stream flow based on water surface elevations and terrain conditions. Therefore, the single or dual geometry files used in this analysis may not accurately characterize all flow conditions and results should be considered a general representation of the system.

The Undeveloped geometry created for this study is a generalized representation of the natural topography of the floodplain. The use of the developed terrain to generate the undeveloped conditions is a significant limitation to the hydraulic analysis. Although manmade structures were removed within the model and maps, some components such as inhibited channel migration and floodplain aggradation and degradation, which may have occurred extensively under natural conditions, could not be represented without significant further analysis and was beyond the scope of this study.

CUMULATIVE EFFECTS ASSESSMENT

Comparison of the results from modeling and mapping the combinations of the geometric and hydrologic conditions will provide valuable information for a range of flow frequencies that will assist the cumulative effects assessment and restoration planning process. Results critical to the cumulative effects assessment include the extent of inundated floodplain under differing scenarios, resulting hydraulic characteristics (e.g., river stages, velocities, flow depths) and the differences between each scenario. Of particular interest to cumulative effects assessment and

restoration planning is the frequency of side channel and floodplain inundation and how that frequency may have changed due to channel modifications and water resourcing.

Inundation shapefiles have been generated for select locations, scenarios and profiles. From these mapping results, comparisons can be made to characterize the impacts that man-made structures, flow regulation, or both have on the Yellowstone River Corridor. Isolated floodplains due to 1) flow regulation, 2) physical structures, and 3) both flow regulation and physical structures were evaluated as part of the CEA to characterize the impacts humans have had on the floodplain for the 50%-, 20%- and 1%-ACE. An example of Historic Floodplain Isolation is depicted in Figure 7 at the Rosebud-Custer County Line for the 1% ACE. The orange polygon represents the area of natural floodplain that is no longer inundated due to human development and flow regulation, and the blue polygon represents the current floodplain inundation.

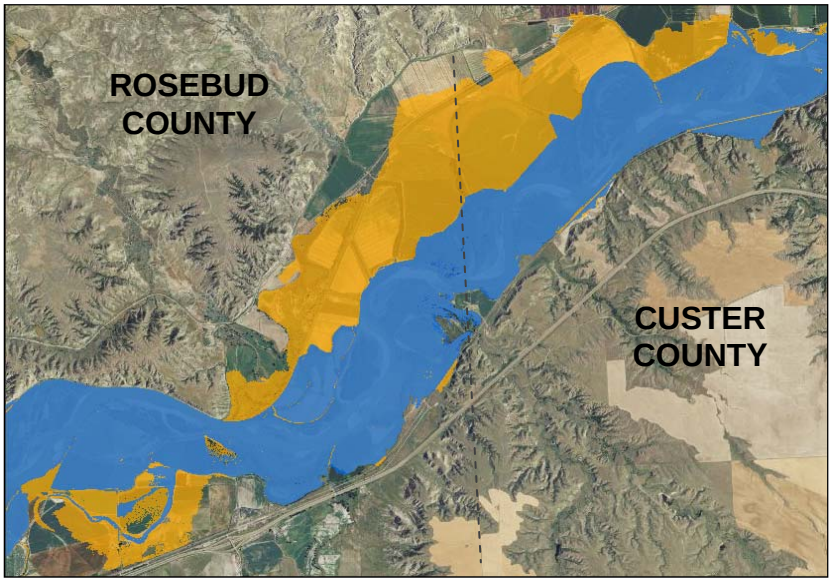

Figure 7 Historic 1% ACE Floodplain Isolation Example at the Rosebud-Custer County Line

REFEERENCES

U.S. Geologic Survey. (2013). Streamflow Statistics for Unregulated and Regulated Conditions for Selected Locations on the Yellowstone, Tongue, and Powder Rivers, Montana, 1928-2002.

DTM Consulting, Inc. (2006). U.S. Geologic Survey Circa 1950s Aerials, Developed and Geo-referenced as part of the Yellowstone River Cumulative Effects Study.

DTM Consulting, Inc. and Applied Geomorphology, Inc. (2009). Yellowstone River Channel Migration Zone Mapping Report.

U.S. Army Corps of Engineers, Hydrologic Engineering Center. (2010). HEC-RAS River Analysis System User's Manual, Version 4.1.

U.S. Army Corps of Engineers, Omaha District. (2009). Lower Yellowstone Project Fish Passage and Screening, Preliminary Design Report, Draft.

U.S. Army Corps of Engineers, Omaha District. (2011). Yellowstone River Corridor Study, Upper Yellowstone River Hydrology.

THE COLORADO RIVER BASIN WATER SUPPLY AND DEMAND STUDY: MODELING TO SUPPORT A ROBUST PLANNING FRAMEWORK

Alan Butler, Hydrologic Engineer, Bureau of Reclamation, Lower Colorado Region, rabutler@usbr.gov; Carly Jerla, Operations Research Analyst, Bureau of Reclamation, Lower Colorado Region, cjerla@usbr.gov; Ken Nowak, Hydrologic Engineer, Bureau of Reclamation, Lower Colorado Region, knowak@usbr.gov; Jim Prairie, Hydraulic Engineer, Bureau of Reclamation, Upper Colorado Region, jprairie@usbr.gov; Bill Oakley, Software Engineer, Center for Advanced Decision Support for Water and Environmental Systems, University of Colorado-Boulder, billo@colorado.edu; Neil Wilson, Software Engineer, Center for Advanced Decision Support for Water and Environmental Systems, University of Colorado-Boulder, nwilson@colorado.edu; Edie Zagona, Director, Center for Advanced Decision Support for Water and Environmental Systems, University of Colorado-Boulder, zagona@colorado.edu

BACKGROUND

The Colorado River provides drinking water to nearly 40 million people and supplies water to irrigate over five million acres of farmland across seven western states and is vital to agricultural and municipal needs within the United Mexican States. The Colorado River also supports numerous ecological and recreational resources, provides water for hydropower generation, and is the lifeblood for 22 federally recognized tribes within the Colorado River Basin (Basin) (Bureau of Reclamation, 2012). The Basin is depicted in Figure 1.

As part of the Bureau of Reclamation's (Reclamation) WaterSMART program, the Colorado River Basin Water Supply and Demand Study (Basin Study) was conducted by Reclamation and the seven Colorado River Basin States in collaboration with stakeholders throughout the Basin. The Study's objectives were to assess future water supply and demand imbalances in the Basin over the next 50 years and develop and evaluate options and strategies to resolve the imbalances. To address the considerable amount of uncertainty in projecting the future state of the Colorado River system, the Study adopted a scenario planning approach that resulted in four water supply scenarios (each with over 100 future realizations), six water demand scenarios, and two reservoir operation scenarios. The combination of all of these scenarios is referred to as the baseline in the Basin Study. The Basin Study shows that by 2060, the median supply and demand imbalance in the baseline is approximately 3.2 million acre-ft, though it can range from 0 to over 7 million acre-ft. Though these estimates ignore both the effectiveness of using reservoirs to help meet demands in times of drought and the geographic disparity of supply and demand, it indicates that in the absence of any actions, there is potential for large imbalances in the future (Bureau of Reclamation, 2012).

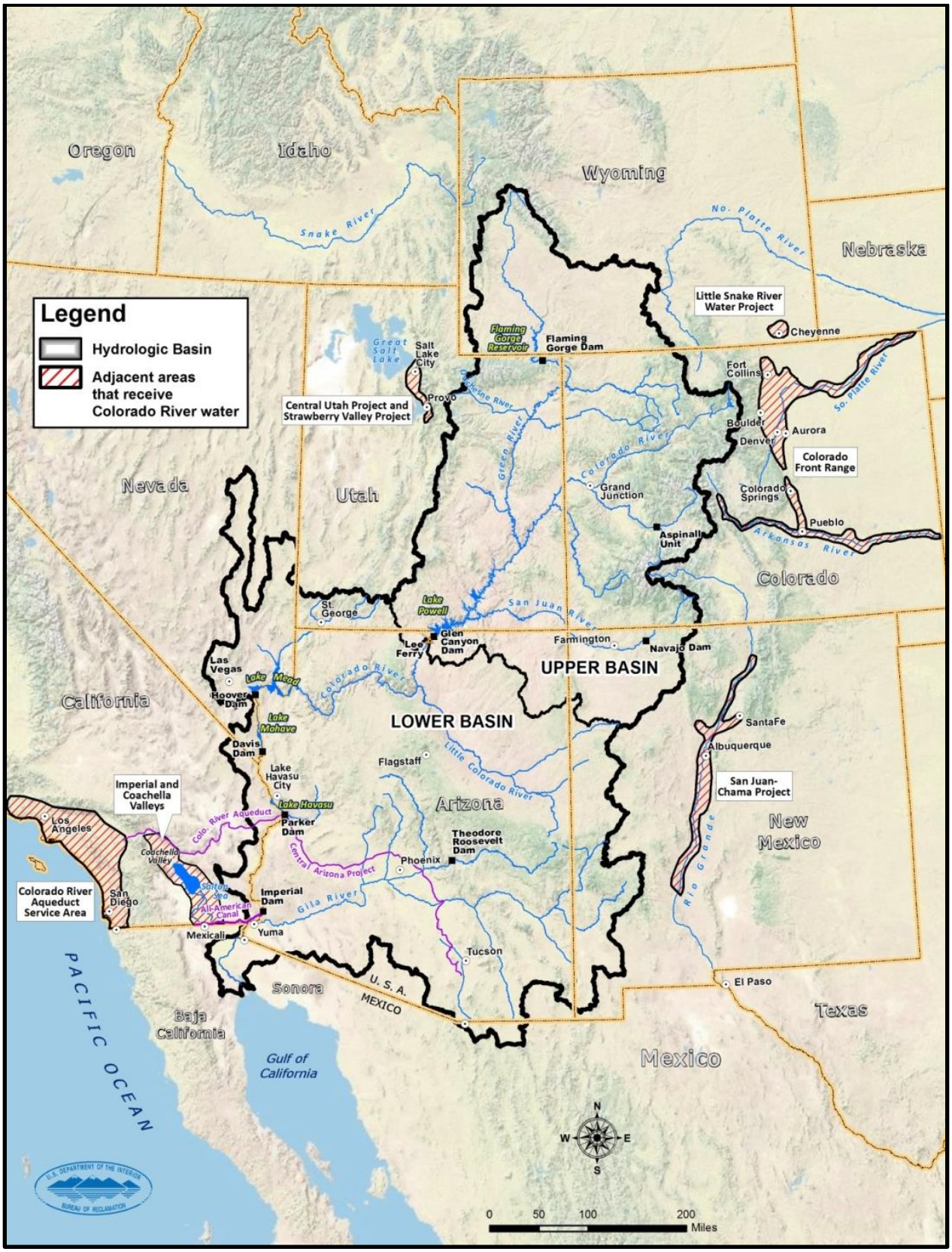

Figure 1 The Colorado River Basin

Options to help address the projected imbalances were solicited from the public. 160 options ranging from increasing the supply through importations or desalination to decreasing demand through various conservation efforts were submitted during the Study. Four unique portfolios, or strategies combining various options, were then developed from the many options as examples of different strategies for resolving system imbalances. The combination of each portfolio combined with all baseline scenarios to analyze the performance of the portfolios across a wide range of plausible future scenarios. The tradeoffs between price, yield, and ability to improve system performance were compared across portfolios using a robust decision making framework. System performance was indicated through reliability metrics that were developed for water delivery, electrical power, water quality, flood control, recreational, and ecological resource categories. The metrics were evaluated to understand how resource vulnerabilities changed through time, geography, and across resources, and the extent to which vulnerabilities could be mitigated through actions.

The Study concluded that the Basin faces an uncertain future with a range of potential imbalances between supply and demand, and that all resources within the Basin are increasingly vulnerable through time, due to both increasing demands and the potential for decreasing supply due to climate change. However, the Basin Study's portfolios demonstrated that actions do help meet the imbalances and reduce vulnerabilities. Actions and diligent planning are necessary at the local, state, regional, and Basin-wide levels, as there is no single solution. Rather, as demonstrated by the many options comprising the portfolios, a wide-range of solutions are necessary and it is imperative to begin work to further some of the concepts in the near future. Though there was no decision made in the Basin Study, the modeling tools and methods employed during the Study provide a common technical foundation for future actions. A suite of modeling tools forms the basis of this technical foundation and was necessary to conduct the Basin Study.

MODELING TOOLS

In order to carry out the scenario planning approach employed by the Basin Study, a suite of modeling tools was necessary. The foundation of the suite was an existing model, though some enhancements were necessary, and several new tools were developed to both help meet the needs of the Study and provide for generalized tools with application beyond the Basin Study.

The Colorado River Simulation System (CRSS): The Colorado River Simulation System (CRSS) has been Reclamation's long-term planning model since the 1980's. Originally developed in Fortran, CRSS was converted to RiverWare®, a generalized reservoir operations modeling platform (Zagona et al., 2001), in 1996. CRSS models the entire Basin, from headwaters in the Upper Basin, e.g., Green, San Juan, and Gunnison, down to the northerly international boundary with Mexico. The operations of nine Upper Basin Reservoirs and three Lower Basin reservoirs, including Lakes Powell and Mead, are represented in CRSS while deliveries are simulated to hundreds of users throughout the Basin. The basis of the simulation is a mass balance (or water budget) calculation that accounts for water entering the system, water leaving the system (e.g., from consumptive use of water, trans-basin diversions, evaporation),

and water moving through the system (i.e., either stored in reservoirs or flowing in river reaches). The model is used to simulate the future conditions of the Colorado River system on a monthly time-step for decades into the future (2012-2060 in the Basin Study). See Reclamation (2012) for more details on CRSS.

CRSS was used as the modeling tool in the Basin Study to simulate all 240 scenarios (the combination of all four supply scenarios, six demand scenarios, two reservoir operating options, and four portfolios). As each scenario contains over 100 future realizations, all together over 110,000 unique 50-year simulations were made. Studies such as the Basin Study or the modeling to support the Colorado River Interim Guidelines for Lower Basin Shortages and Coordinated Operations for Lake Powell and Lake Mead EIS (Reclamation, 2007) that utilize CRSS take advantage of RiverWare's features and policy language to perform efficient "what-if" analysis. Features in RiverWare make it easy to import different data to perform such analyses; however, until recent development, this was a manual step. In the case of the Basin Study, which simulated 240 total scenarios, this would require many human hours to complete. Additionally, manually launching each scenario increases the total run time for such an effort.

RiverSMART: To help alleviate these issues while supporting the Basin Study and other similar scale studies, development of the RiverWare Study Manager and Research Tool (RiverSMART) was undertaken. The RiverSMART facilitates the creation, execution and archiving of planning studies that compare the results of many scenarios, all steps one must manually take when using RiverWare to simulate multiple scenarios. RiverSMART provides a user friendly interface as shown in Figure 2. For construction of a study, this also provides a graphical representation of the study to help conceptualize all of the components and their interactions.

RiverSMART is built on a plug-in architecture and provides the framework for communication amongst the various plugins. In general, the plugins generate hydrologic ensembles, specify alternative input data to the RiverWare model, define alternative model configurations and policy, and post process desired outputs. Each individual instance of a plugin is called an event. Each event has settings that are configured by the user. Following is a description of some of the plugins available in RiverSMART (input side) and utilized in the Basin Study:

- Hydrology Simulator and Disaggregation Plugins: The Hydrology Simulator plugin synthesizes an ensemble of streamflows from reference values, usually observed historical or paleo reconstructed values. There are various methodologies available including K Nearest Neighbor resampling, Paleo Conditioned Homogenous Markov Chains, and Paleo Conditioned Non-homogenous Markov Chains. There is also a Spatial Disagg plugin to disaggregate the flows from one site to a number of sites according to correlations of the reference data. The Temporal Disagg plugin disaggregates annual ensemble data to a monthly timestep.
- RiverWare Model: The RiverWare Model plugin instructs which RiverWare model to use. This allows the user to develop alternative facilities or model configuration as a component in the study.
- RiverWare DMI: The Data Management Interface (DMI) plugin instructs which RiverWare DMIs in the model should be run to bring in alternative data. DMI events are grouped into user-named categories that contain input alternatives. For example there might be a category of DMI events named "Supplies" that contains several ensembles of

hydrologic inflows, and a category of DMI events named "Demands" that includes different demand schedules. DMI events instruct RiverWare to bring in data from specified sources such as a database, text files, or excel spreadsheet. In addition, the Demand Input Tool (DIT) can be used to develop the sets of demands. This Excel-based tool generates the detailed demands for water in the entire basin and allows easy modification of demand projections and automatic loading of the new demands into a RiverWare model. The DIT enables users to enter baseline demand data, create and enter alternative demand scenarios and plot the baseline and scenario data to visualize changes.

- RiverWare Policy: The RiverWare Policy plugin specifies the RiverWare ruleset to use. This allows the user to develop alternative operations as one of the scenario components.

Once the study network has been defined and all of the events have been configured, the user instructs RiverSMART to generate the list of scenarios. Scenarios are specific combinations of input data, policy sets, models, and run configurations. RiverSMART first creates a list of all possible combinations of alternatives and then the user can then look through the list of scenarios and deactivate those that are not of interest. Figure 2 illustrates the different supply and demand scenarios in the Basin Study organized in RiverSMART.

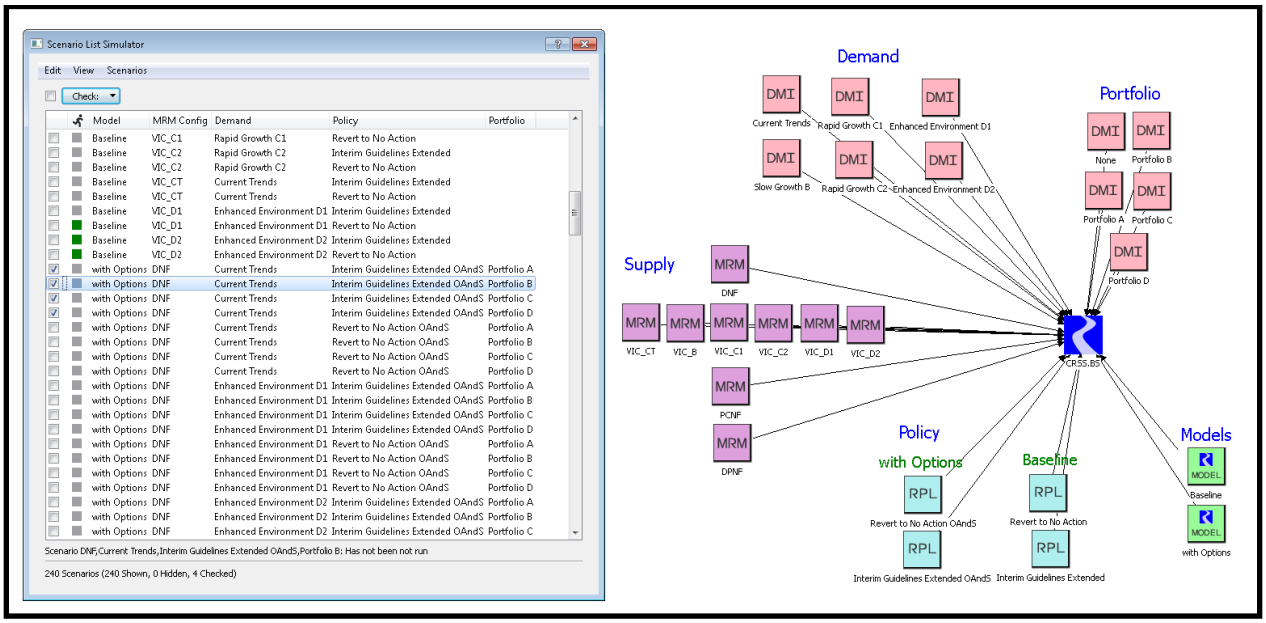

Figure 2 Screenshot of Basin Study in RiverSMART

The user then runs the specified scenarios with RiverSMART managing the data archiving, importing data for new scenarios, and starting the next scenario. The runs utilize RiverWare's distributed Multiple Run Management where individual runs are spread over available computer processors.

Once the scenarios are simulated, the user instructs RiverSMART to post process the scenarios by executing events that act on each scenario or on sets of scenarios. The plugins for post processing scenarios include plugins to convert files from RiverWare's Data Format (RDF) to Excel and annualize monthly data to an annual timestep. Plugins can generate plots using an R

Script plugin or generate graphs in Excel using the Graphical Policy Analysis tool, GPAT. This Excel tool allows users to visualize and analyze RiverWare model outputs as well as other data sets. This tool is designed to allow statistical comparisons and graphing of multiple modeling runs that may vary with respect to hydrology, operational policy, or other parameters.

The Basin Study utilized the R programming language to process results from all scenarios simultaneously, evaluate the reliability metrics, and prepare the data for plotting. For the Basin Study, the post-processing step was critical to distill the results of 240 scenarios into understandable and meaningful figures. R was used to process the data and prepare it for use within Tableau, software for interactive data visualization and analytics. Figure 3 is taken from the Basin Study and shows the percent of future simulations in which Lake Mead drops below 1,000 feet, a critical elevation for water deliveries to Las Vegas. This figure distills the results from over 20,000 simulations and 48 scenarios into 144 points. This type of visualization allows one to understand how the results for the particular variable vary with supply scenario, demand scenario, operational option, and through time. Additionally, Tableau helped the modelers understand and verify model results during the Basin Study by utilizing its interactive features, a step that is critical in any modeling exercise.

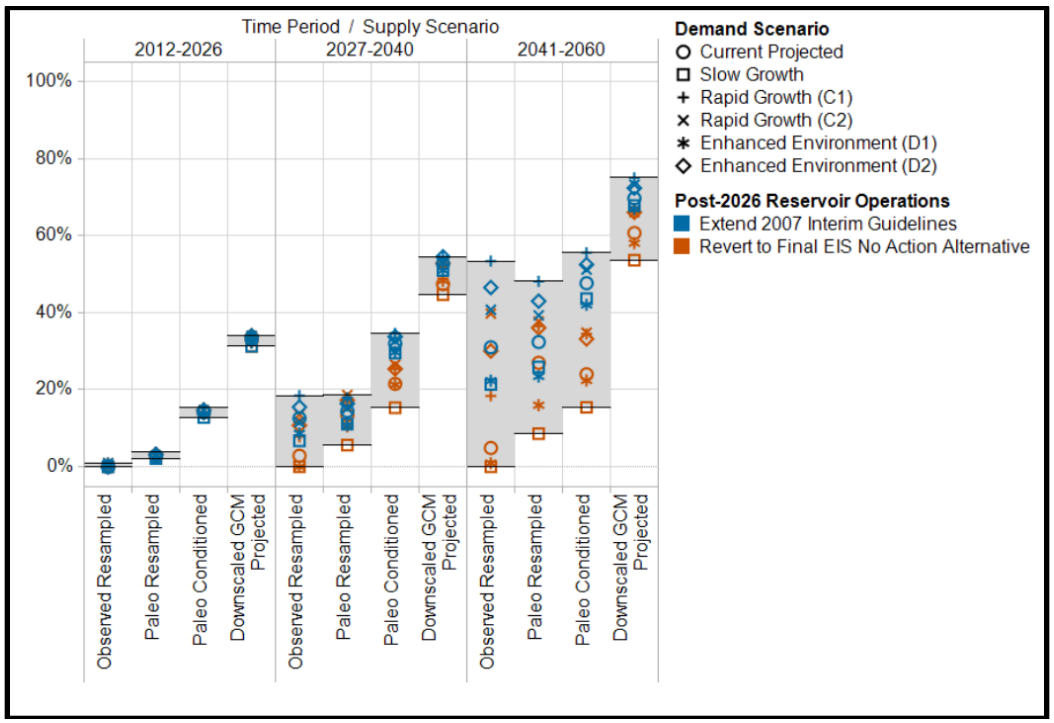

Figure 3 Percent of Baseline Future Simulations Resulting in Lake Mead Less than 1,000 feet

Even with the efficiency of RiverWare, RiverSMART and R, the total computing time for simulating and processing the scenarios was on the order of 4-6 weeks. To help decrease the computing time and based on other lessons learned during the Basin Study, Reclamation has continued to support targeted development for RiverWare and RiverSMART components. An R plugin was added to RiverSMART and RiverWare now supports exporting data in a format directly readable by Tableau, which will expedite the analysis process and cutout one of the post-

processing steps. Additional work is underway to support exporting data from RiverWare to NetCDF files; a step that could help make modeling results machine readable, and could decrease the total storage size of results. The RiverSMART tool has also become part of Reclamation's widely relied upon modeling tools utilized in many different studies. As RiverWare helped CRSS evolve in 1996, RiverSMART is the next step in this evolution of Reclamation's modeling tools.

SUMMARY

The Basin Study helped quantify the potential supply and demand imbalance on the Colorado River Basin over the next 50 years, while analyzing potential options for alleviating such imbalances. A scenario planning approach led the Basin Study to use many scenarios to quantify a wide range of plausible future outcomes. All together 240 scenarios were simulated using CRSS—the Basin-wide model developed in RiverWare.

The suite of tools employed in the Basin Study, i.e., RiverWare, RiverSMART, R, and Tableau, was critical to the development and management of the numerous simulations necessary for the robust decision making framework utilized in the Basin Study. This suite of tools can be used to support any planning study or "what-if" analyses that require many iterations of input or assumptions. Since the completion of the Basin Study, the tools have become part of Reclamation's standard suite of modeling tools, and development has continued to enhance their capabilities.

REFERENCES

Bureau of Reclamation (Reclamation). 2007. Colorado River Interim Guidelines for Lower Basin Shortages and Coordinated Operations for Lake Powell and Lake Mead Final Environmental Impact Statement.

Bureau of Reclamation (Reclamation). 2012. Colorado River Basin Water Supply and Demand Study.

Zagona, E. A., T. J. Fulp, R. Shane, T. Magee, and H. M. Goranflo (2001), RiverWare: A generalized tool for complex reservoir system modeling, Journal Of The American Water Resources Association, 37(4), 913 – 929.

TRUCKEE-CARSON RIVERWARE© PLANNING MODEL DESCRIPTION AND APPLICATIONS

Heather Gacek, Project Manager, Precision Water Resources Engineering, Loveland, CO, heather@precisionwre.com; Thomas Scott, Hydrologic Engineer, Bureau of Reclamation, Carson City, NV, tscott@usbr.gov; Shane Coors, Principal, Precision Water Resources Engineering, Loveland, CO shane@precisionwre.com

Abstract: The Bureau of Reclamation's (Reclamation) Lahontan Basin Area Office has developed a long-term RiverWare© model of the Truckee River Basin (Basin) including the Newlands Project area. The Truckee River basin contains seven upstream storage reservoirs, including Lake Tahoe, and terminates in the Great Basin at Pyramid Lake. The basin's seven upstream storage reservoirs are operated to meet the demands of downstream agricultural, environmental, industrial, and municipal water users along the Truckee River, as well as the agricultural demands of the Newlands Project in the Carson River Basin. Supplying the Newlands Project requires an inter-basin diversion from the Truckee River to the Carson Basin through the Truckee Canal.

The RiverWare© model, known as the Truckee-Carson Planning Model (Planning Model), was developed through a collaborative effort between several of the significant basin stakeholders, often with competing interests. Participating entities include the Bureau of Reclamation, Federal Watermaster, Truckee Meadows Water Authority, Pyramid Lake Paiute Tribe, the state of California, and the state of Nevada. The model represents the entire river system, and simulates each of the stakeholders' current operational policy. The model also allows users to adjust many operational criteria and variables to analyze proposed policy, hydrology, and water use changes for up to 100 years.

This unique collaboration has both facilitated wide acceptance of the model and driven the model development to be amenable to a wide range of applications. The model is designed to assist water managers and stakeholders in making long-term planning and management decisions. Applications include the Newlands Project Planning Study, the Truckee Basin Study, and policy revision studies.

An overview of the collaborative development process, a review of the primary model components, and a description of past, current, and proposed applications of the model will be presented.

INTRODUCTION

The Truckee River system is approximately 100 miles long, flowing from Lake Tahoe in the Sierra Nevada mountain range to Pyramid Lake in Nevada. There are seven upstream reservoirs, including Lake Tahoe, that regulate approximately 70% of the basin's water supply. The majority of the Basin water supply originates in California, while the majority of the water usage takes place along the Truckee River in Nevada.

In addition to water users along the Truckee River, water is diverted through the Truckee Canal as part of an inter-basin water transfer to supplement supply to agricultural water users in the Newlands Project within the Carson River Basin. The inter-basin diversion takes place at Derby Dam and delivers water to water users along the Truckee Canal and supplements the storage at

Lahontan Reservoir. Construction of the Truckee Canal was the first Reclamation project in 1903. A map displaying the combined Truckee and Carson River basin is shown in figure 1.

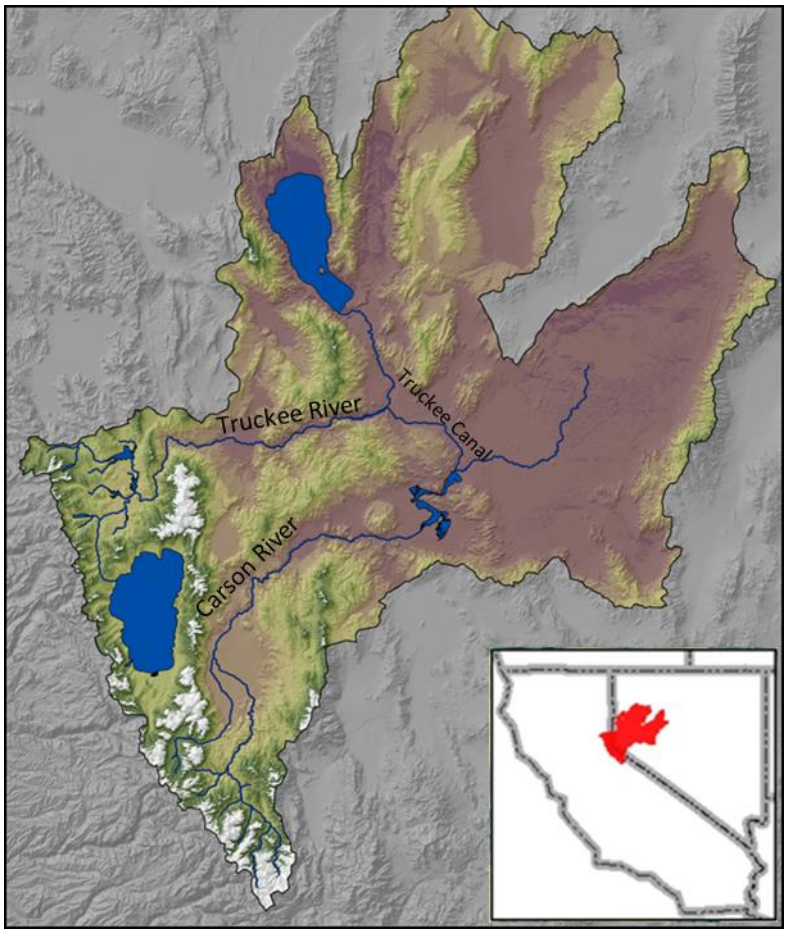

Figure 1 Map of the Truckee and Carson River Systems

A daily timestep RiverWare model has been developed by Reclamation to simulate the Truckee River System, including the Truckee Canal, for up to 100-year model runs. The Planning Model simulates the entire system's operations and performs complete daily water accounting of the water rights within the system. The model, its development process, and its uses are discussed in more detail in the following sections.

MODEL DEVELOPMENT PROCESS

The Truckee River Basin has a suite of modeling tools developed and maintained by Reclamation and the Federal Watermaster. This paper discusses the long-term Planning Model tools which were developed as part of a collaborative effort by many of the key basin stakeholders and government agencies.

Model Development Team: The Planning model was developed by a collaborative effort among many of the significant basin stakeholders, often with competing interests. Participating entities include the Bureau of Reclamation, Federal Watermaster, Truckee Meadows Water Authority, Pyramid Lake Paiute Tribe, the state of California, and the state of Nevada. In late 2009, the

formation of the Planning Model development group and the start of the development of the Planning Model began. Participating parties have met every 6 to 10 weeks in-person and/or video conference meetings to discuss development of the model and review the progress.

Pre-TROA Planning Model: At the start of the Planning Model development effort, the Truckee River Operating Agreement (TROA) had been approved and signed by the parties, but was still being contested in the courts. The existing basin policies, now known as the Pre-TROA operating policies, were still in effect. The model was therefore initially constructed to model the current, Pre-TROA, operating policy.

In addition to simulating the current operating policy, the model is designed to be a long-term planning and management tool. Unlike the existing and more mature Operations model, the Planning model cannot be overly dependent upon the user to control operations on a daily or even an annual time frame. This required an increased level of detail and more comprehensive operational logic than in the short-term daily operations model, which was already being used within the basin. The participating members of the Planning Model development team were tasked with providing detailed operational polices for their individual systems sufficient enough to allow the model to operate under all operational and hydrologic conditions without requiring additional input from the user.

Although the Planning Model will continue to be developed as basin policies change and stakeholders' operational policies evolve, the Pre-TROA version of the Planning Model was largely completed in 2014. The Pre-TROA version of the model was the foundation for the TROA Planning Model.

TROA Planning Model: Under the 1990 Settlement Act, the Secretary of the Interior was directed to negotiate an operating agreement for the Truckee River Reservoirs. The purpose of the policy is to improve operational flexibility and efficiency of Truckee River Reservoirs while satisfying water rights in conformance with existing decrees. TROA was officially signed into law in 2008, but court challenges have delayed its implementation. TROA is currently expected to be implemented in 2015.

As the TROA operating policy came closer to being implemented, the Planning Model development group began the process of incorporating the new operating policy within the framework of the existing Planning Model. In 2013 the Planning Model development team began the implementation of TROA within the Planning Model with the goal of using the model to support the Truckee River Basin Study in 2014. The Truckee River Basin Study was a Bureau of Reclamation study that identified and quantified potential impacts to the Truckee Basin due to climate change. An updated version of the Planning Model referred to as TROA-Lite was completed in mid-2014 for use in the Truckee Basin Study. This model simulated the most fundamental elements of TROA for water and supply. Model development work is ongoing to incorporate additional, more flexible operating policies such as complex water exchanges

involving instream flows below reservoirs in California, and voluntary exchanges between parties under a variety of conditions.

TROA operating policy allows parties to hold back unneeded, but entitled flows to establish credit water in the reservoirs. It also allows for a multitude of possible exchanges between the water right holders. Along with the increased flexibility and efficiency, TROA adds a lot of complexity to the system which needs to be captured by the modeling tools. The basin stakeholders are continuing to refine policies for their individual operations under the operating agreement as part of the model development

MODEL COMPONENTS

A RiverWare model workspace consists of objects, each representing a specific component of the modeled system, linked together to simulate the storage, flow, diversion and consumption of water in a system. The primary model components in the Planning Model include the seven upper Truckee River reservoirs, the Truckee Meadows section of the river between Farad gage and Derby Dam, the Truckee Canal and Lahontan Reservoir, and the lower Truckee River below Derby Dam and including Pyramid Lake. These four sections are each discussed in more detail below. A schematic diagram of the model components is provided as Figure 2.

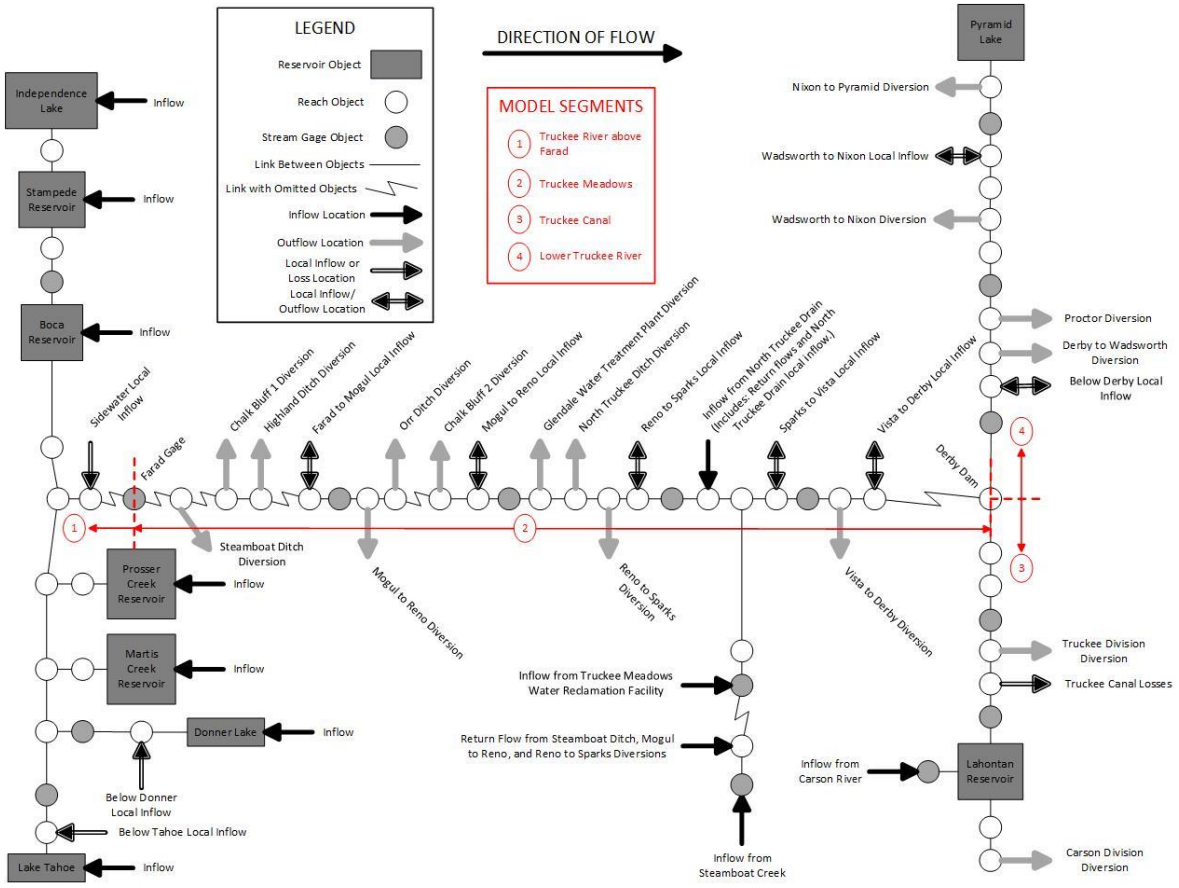

Figure 2 Schematic showing the reservoirs, reaches, outflows, and inflows for the Pre-TROA Truckee-Carson RiverWare Planning Model

Truckee River above Farad (1): The Truckee River above Farad section of the model is everything upstream of the gage at Farad. This section contains seven reservoirs: Lake Tahoe, Donner Lake, Martis Creek Reservoir, Prosser Creek Reservoir, Boca Reservoir, Stampede Reservoir, and Independence Lake. The majority of the water in the Basin originates within this section of the basin. The reservoirs regulate the flow of the water in the river. The system is operated to meet flow targets at Farad Gage, referred to as the Floriston Rate target flows.

Truckee Meadows (2): The Truckee Meadows represents the reach of the Truckee River between the gage at Farad and Derby Dam. This portion of the model contains: agricultural diversions, municipal diversions, industrial diversions, return flows from the Truckee Meadows Water Reclamation Facility, inflows from tributaries, and system losses.

Truckee Canal (3): The Truckee Canal portion of the model represents diversions at Derby Dam through the Truckee Canal to Lahontan Reservoir and its downstream water users. This portion of the model also includes an inflow point representing the inflow to Lahontan Reservoir from the Carson River. This portion of the model represents the entire Newlands Project. The Newlands Project includes agricultural diversions taken directly from the Truckee Canal as well as agricultural diversions taken downstream of Lahontan Reservoir.

Lower Truckee River (4): The lower Truckee River represents everything below Derby Dam flowing to the terminus at Pyramid Lake. For this reach of the river the model currently contains: agricultural diversions, environmental flow targets, and system losses. In the future, conditions in this reach are expected to include municipal diversions as well as the before mentioned demands.

MODEL APPLICATIONS

The following section includes descriptions of past and future model uses. The Planning model is intended for use by system operators to analyze existing Basin policies and to develop future operational strategies and Basin policies. It is also intended for use by individual stakeholders to develop their own operational strategies and perform reliability testing on their water supply and current policies. The following examples are just a handful of the possible applications of the Planning Model tools.

Newlands Project Planning Study: The Newlands Project Planning Study (Study) was conducted by Reclamation to formulate, develop, and evaluate a range of alternatives to reliably deliver water to Newlands Project water rights holders while also reducing risk to local communities from operating the Truckee Canal. Reclamation describes the impetus for and purpose of the Study in the report, *Newlands Project Planning Study Special Report,* as:

> The Newlands Project is one of Reclamation's first irrigation projects and nearly as old as the agency itself. Reclamation began the Project in 1903 to provide irrigation water to the Lahontan Valley, near Fallon, Nevada, and to lands in the Truckee Basin near Fernley, Nevada.

In the early morning of January 5, 2008, a 50-foot portion of the Truckee Canal embankment failed about 12 miles downstream from Derby Dam, releasing water that inundated a residential development in the City of Fernley, flooding 590 properties. No fatalities occurred, but more than $1 billion in tort claims were filed against the Federal government, local governments, and the Truckee-Carson Irrigation District (TCID), and have now been consolidated into class action lawsuits.

Although the damaged portion of the canal embankment was soon repaired, evaluations of the canal revealed a high potential for future failure. In response, Reclamation imposed restrictions on the water surface elevation allowed in the canal and the amount of water allowed to flow through the canal. The flow restrictions were reinforced by the Federal District Court for Nevada. If not lifted, these restrictions could complicate the long-term ability of Reclamation to provide Newlands Project water rights holders with reliable supplies.

Federal authorization for the Study was provided in the Omnibus Appropriations Act of 2009 (Public Law 111-8, 123 Statute 609), which directed Reclamation to determine the actions necessary to rehabilitate the Truckee Canal so restrictions on its operation can be removed.

The modeling effort for the Newlands Project Planning Study included the modeling of 24 preliminary alternatives, a no action alternative, and a desired reliability alternative. After thorough review of the modeling results, environmental and regulatory review, engineering and cost estimates, and financial and benefits analysis were performed, seven final alternatives were identified. These seven alternatives were then modeled using the Planning Model and reviewed to develop the study's key findings.

Truckee River Basin Study: The Truckee River Basin Study (Basin Study) is a part of Reclamation's response to the Department of the Interior's WaterSMART Program to enact the SECURE Water Act of 2009. The Basin Study was kicked off in late 2012. The RiverWare modeling effort was performed in 2014. The Basin Study is part of a program "to evaluate and report on risks and impacts from a changing climate and identify appropriate adaptation and mitigation strategies in conjunction with stakeholders." (Bureau of Reclamation Mid-Pacific Region Lahontan Basin Area Office, October 2013)

The Basin Study Team worked with key Basin stakeholders as part of the Project Steering Team and Technical Advisory Group to develop the study components and analyze the potential impacts of the Basin Study's hydrology and demand scenarios on the Truckee Basin water users and environment. The Basin Study Team engaged the community at multiple public meetings throughout the process.

The Basin Study Team developed a broad range of potential climate change hydrology scenarios to capture the possible effects of climate change on the region. The Team also developed three

demand scenarios to encompass possible future development within the Basin. The Planning Model was used to perform model runs combining these various hydrology and demand scenarios. The results from these model runs were analyzed collectively to identify system vulnerabilities due to climate and demand changes. Once the vulnerabilities in the system were identified, the Basin Study team were able to evaluate tradeoffs between different mitigation strategies and develop robust operational strategies for the future. These strategies were modeled using the Planning Model and the improvements were quantified and reported in the Basin Study.

Boca Reservoir Study: As part of a larger study, an alternative was performed to analyze the impacts of introducing a reduced water surface elevation limit on Boca Reservoir. Six runs of the Planning Model were performed to model three reservoir storage limit scenarios with two different demand scenarios. The purpose of the study was to determine the impacts on the remainder of the Truckee Basin as a result of altering the storage limits at Boca. The demand scenarios were meant to provide a range for the impacts given that basin demand levels remain near current levels or demand levels are increased to represent future water use.

Future Model Uses: Future use of the Planning Model will include the Truckee Canal Environment Impact Statement, and subsequent policy revision studies. Additionally, it is expected that individual Basin stakeholders will use the model to perform their own private studies. The implementation of TROA will necessitate these private studies as parties work to determine the most efficient and robust operating policies with the framework of the new flexible operating system.

SUMMARY

The Truckee-Carson Planning Model was developed through a collaborative effort between several of the significant basin stakeholders. Currently there are two versions of the Planning Model, one containing only the Pre-TROA operating policies and one under development which contains both the Pre-TROA and TROA operating policies. The Planning Model has been used by several federally funding planning studies to date, including the Newlands Project Planning Study and the Truckee River Basin Study. The model is slated for use in future federally funded planning studies as well as private studies to be performed by individual Basin stakeholders.

REFERENCES

Bureau of Reclamation Mid-Pacific Region Lahontan Basin Area Office. (April 2013). "Newlands Project Planning Study Special Report," Carson City, NV.

Bureau of Reclamation Mid-Pacific Region Lahontan Basin Area Office, (October 2013). "Truckee River Basin Study, Current Water Supply Report," Carson City, NV.

Precision Water Resources Engineering. (January 2015). "Boca Project Modeling Report," Loveland, CO.

UTILIZING PROBABILISTIC FORECASTS FOR COLORADO RIVER RESERVOIR OPERATIONS USING A MID-TERM PROBABILISTIC OPERATIONS MODEL FOR DECISION MAKING AND RISK MANAGEMENT

Anthony Powell, Project Engineer, Precision Water Resources Engineering, Loveland, CO, tony@precisionwre.com; Daniel Bunk, Bureau of Reclamation, River Operations Group, Boulder City, NV, DBunk@usbr.gov; Shana Tighi, Bureau of Reclamation, River Operations Group, Boulder City, NV, STighi@usbr.gov; Katrina Grantz, Hydrologic Engineer, Bureau of Reclamation, Salt Lake City, UT, KGrantz@usbr.gov; Shane Coors, Principal, Precision Water Resources Engineering, Loveland, CO shane@precisionwre.com

Abstract: The Bureau of Reclamation (Reclamation) manages reservoirs on the Colorado River Basin (Basin) from the headwater sub-basins down to the border with Mexico. Ensemble inflow forecasts are utilized to develop probabilistic information that supports decision-making at various temporal scales, from daily operations and spring runoff routing to annual operations and multi-year planning. The Upper Basin reservoirs, from the headwaters to Lake Powell, are supply driven and their operations depend heavily on forecasted inflows. Risk management in the Upper Basin balances water supply, hydropower, flood control, endangered species, fish and wildlife, and recreation. Operations of Lower Basin reservoirs, from Lake Mead to the border with Mexico, utilize Upper Basin probabilistic operational scenarios to manage risk by identifying a range of future Lake Mead elevations and potential impacts on water delivery in the Lower Basin. Probabilistic risk management helps to inform decision making for Basin stakeholders concerned with flood control, hydropower, recreation, environment, water supply, and water delivery in the Lower Basin.

Reclamation has developed a suite of RiverWare™ operations and planning models to aid with different aspects of decision making and risk management in both the Lower and Upper Basins. The Mid-Term Probabilistic Operations Model (MTOM) is the newest model utilized by both basins to support decision making by Reclamation and other Basin stakeholders. The MTOM System provides 5-year probabilistic projections for the Basin's major reservoirs and critical reaches at a monthly time step. The MTOM system is comprised of several components that include an ensemble forecast from the Colorado Basin River Forecast Center, a RiverWare™ operations model of the major reservoirs of the Colorado River System, and probabilistic output with an analysis and visualization tool. The system is currently being used to generate a 5-year probabilistic operational outlook for the Basin that is distributed monthly to stakeholders and decision makers.

This paper will present an overview of key components of the MTOM System and also highlight sample results and applications of the system for particular Basin operations.

INTRODUCTION

Current climate and hydrologic conditions in the Southwestern United States and predictions of increased climatic variability in the future give rise to the need for improved predictive tools for managing water resources in the region. The Bureau of Reclamation (Reclamation) is responsible for the operation of the infrastructure that provides water, hydropower, and flood control to the Colorado River Basin (Basin) states of Arizona, California, Colorado, Nevada,

New Mexico, Utah, and Wyoming. Historically, Reclamation has used two primary Basin-wide modeling and decision support tools. These are (1) the 24-Month Study and (2) the Colorado River Simulation System (CRSS). The 24-Month Study, which is used in the Annual Operating Plan (AOP) process, is an operational model with a 2-year outlook that uses most a probable inflow forecast (updated monthly) provided by the National Weather Service's Colorado Basin River Forecast Center (CBRFC). The 24-Month Study is limited in its ability to incorporate hydrologic uncertainty because it is designed to simulate only one hydrologic and operational scenario and future reservoir operations must be input manually. CRSS, which is used in long-term planning studies (e.g., the Colorado River Basin Water Supply and Demand Study and development of the 2007 Interim Guidelines for the Coordinated Operations of Lake Powell and Lake Mead), is a planning model that simulates Basin conditions decades into the future. Although CRSS accounts for hydrologic uncertainty in its ability to simulate hundreds of future hydrologic scenarios, it is limited in its ability to incorporate real-time forecasts and operations. Reclamation and Basin stakeholders have desired a decision support tool that blends the probabilistic strength of CRSS with the operational knowledge of the 24-Month Study. The Mid-Term Probabilistic Operations Model (MTOM) System was developed to meet this need. It provides probabilistic information about risk and uncertainty associated with Basin reservoir operations in the 1- to 5-year timeframe. The MTOM System consists of a RiverWare™ model and supporting components that enable the model to access input and produce output in an efficient manner. The MTOM System uses an ensemble of hydrologic forecasts to produce probabilistic 5-year operational projections for the major reservoirs in the Basin. The model results are then analyzed collectively to quantify the likelihood of significant future system conditions.

ENSEMBLE FORECASTS

The primary input, and main driver of operations, for the MTOM System is an ensemble of unregulated inflow forecasts at various forecast points in the Upper Basin. Unregulated flow is the forecasted flow that would arrive at a specific point if there were no dams located upstream of that point. The CBRFC provides thirty 60-month traces for 12 forecast points in the Upper Basin (locations of Upper Basin inflow points are provided in Figure 1). Each inflow forecast is derived from historical sequential climatology (temperature and precipitation based on the period from 1981 to 2010) that is applied to the current Basin conditions (e.g. soil moisture, antecedent streamflow, snowpack). The CBRFC utilizes the data to develop 30 traces of hydrologic inflow forecasts.

The CBRFC methods of producing the forecasts involve the use of the Ensemble Streamflow Prediction (ESP) System which is part of the National Weather Service Forecast System (NWSFS). A continuous hydrologic model comprised of two main sub models, the Sacramento Soil Moisture Accounting Model (SAC-SMA) and the SNOW-17 snow model, are used to simulate the soil moisture and snow states throughout the Basin, which determine the initial conditions for the ESP System, Brandon (2005).

The ESP System then generates multiple scenarios of forecast streamflow time series from which probability functions for water supply volume can be computed. The future scenarios are based on a combination of the current soil moisture and snow states mentioned above and the historical sequences of precipitation and temperature to produce the ensemble of streamflow forecasts. Each year of historical climatology data is assumed to be a possible representation of future

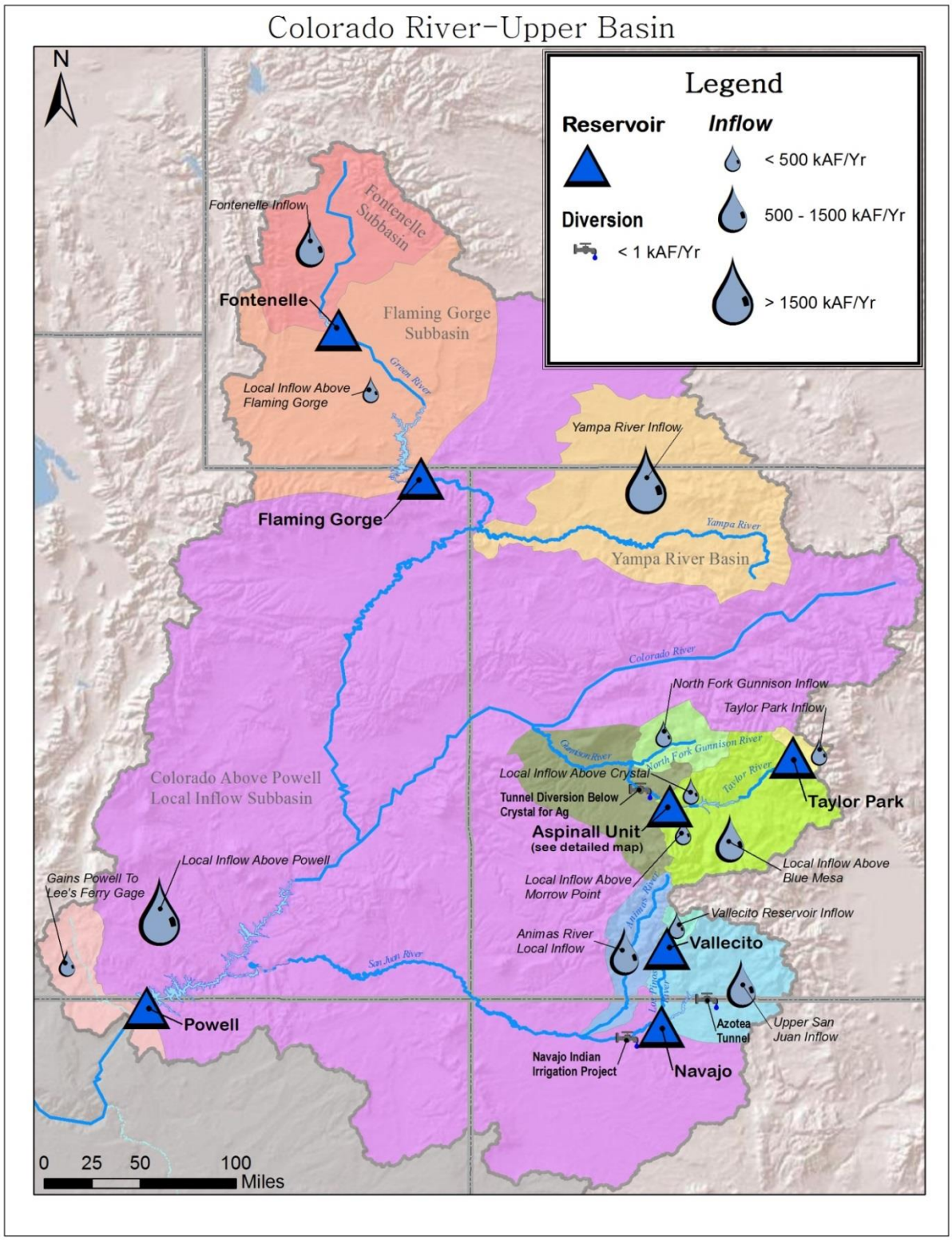

Figure 1 Upper Colorado River Basin as Represented in the MTOM System Model

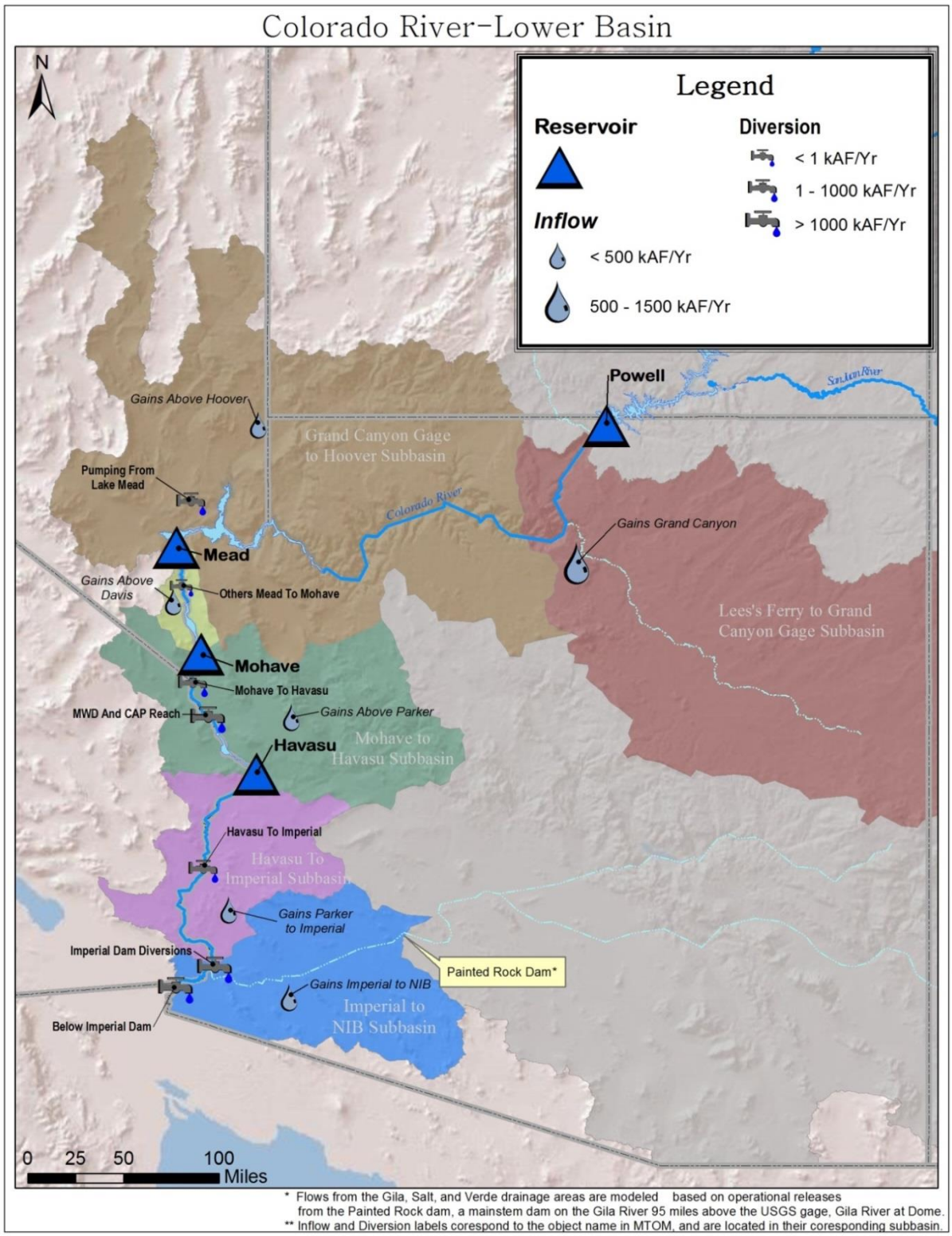

Figure 2 Lower Colorado River Basin as Represented in the MTOM System Model

streamflows in the Basin and each forecast trace produced by the ESP System is treated as equally likely to occur

The ensemble of 30 equally likely unregulated inflow forecasts is run through MTOM to produce an ensemble of potential operations and system conditions. The results can then be analyzed collectively to project potential future conditions within the Basin, and quantify the uncertainty in those projections.

Lower Basin intervening inflow projections are based on a resampling of historical data over the period from 1981 through 2010 in the reaches above Lake Mead and on statistics (median, 10th percentile, and 90th percentile) from the same 30-year period for reaches below Lake Mead (locations of Lower Basin inflow points are provided in Figure 2).

MID-TERM PROBABILISTIC OPERATIONS MODELING SYSTEM

The MTOM System consists of a RiverWare™ model and supporting components that enable the model to access input and produce output in an efficient manner. The modeling system as a whole is comprised of six components that allow for MTOM to function either as (1) a single run (deterministic) simulation model, which allows the users to compare the results of the MTOM run to those from the 24-Month Study model; or (2) as an ensemble, or probabilistic, modeling tool that can be used to estimate the probability of outcomes given an ensemble of inflow forecasts as demonstrated in Figure 3. This paper focuses on MTOM's strength as a probabilistic operations modeling system.

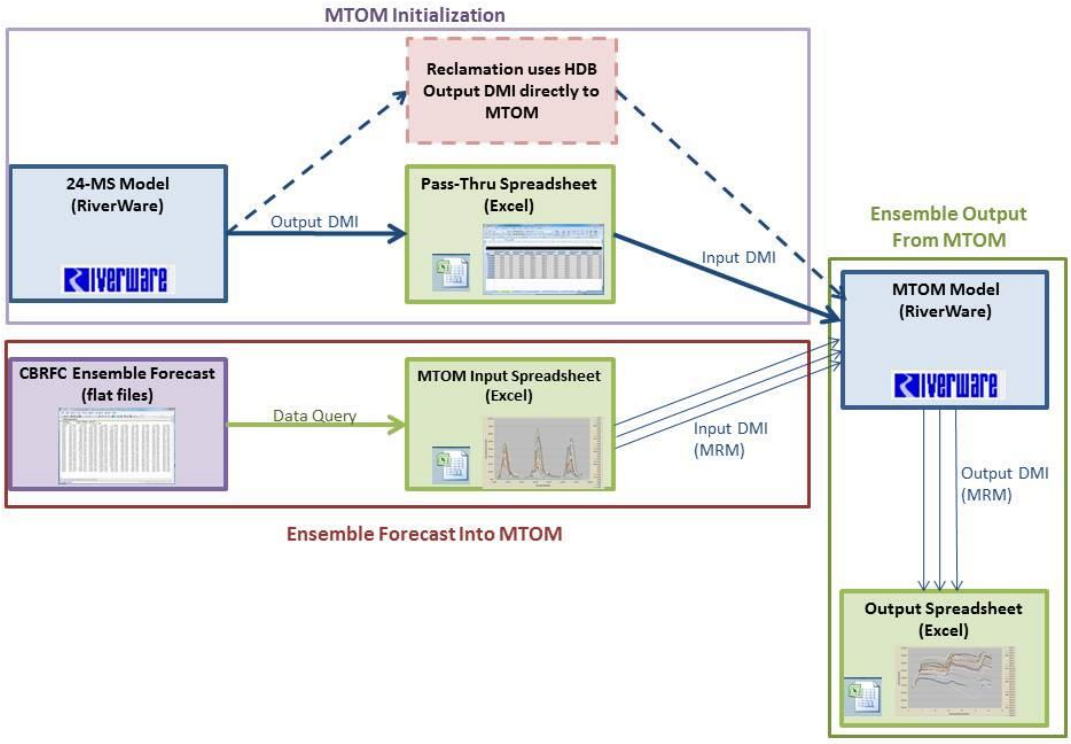

Figure 3 MTOM System Schematic

The MTOM Input Spreadsheet is a Microsoft Excel spreadsheet application designed to import the CBRFC forecast ensembles from data files and provide a platform for MTOM to access those data. The spreadsheet includes forecasts for each of the 12 forecast points in the Upper Basin as well as intervening flows (derived from the historical record) for reaches between Glen Canyon Dam and Hoover Dam. The spreadsheet provides users the capability to view the ensemble of forecasts for each forecast point, and formats the data for import into the RiverWare™ model.

MTOM is a basin-wide RiverWare™ model which simulates reservoir operations at a monthly time step. MTOM uses two RiverWare™ components to correctly model the Basin. The first is a workspace which represents Basin. This allows for the setup of reservoirs, reaches, diversions, and data objects to describe the physical characteristics of the Basin.

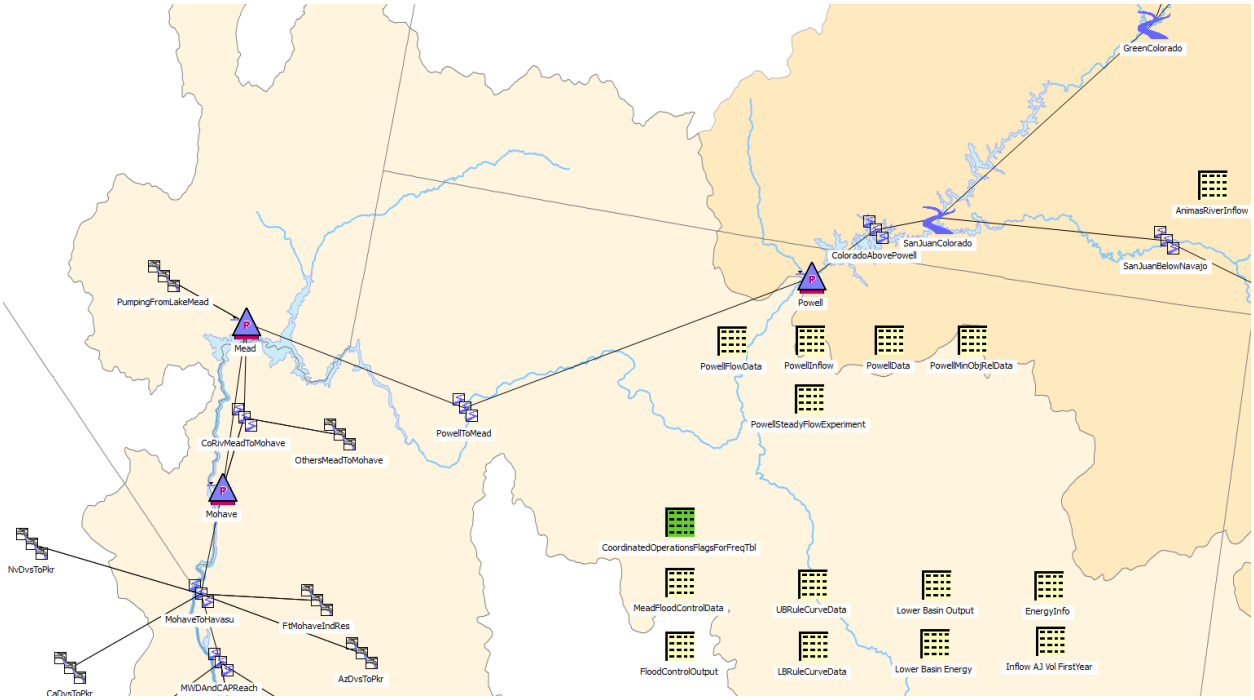

Figure 4 MTOM Workspace above Lake Powell to Below Davis Dam

The second component is a unique programming language known as the RiverWare™ Policy Language or RPL. This language allows users to code operational policy into MTOM. RiverWare™ then uses this policy to determine the various physical components within the model to solve the mass balance equations in place of user inputs for operations in MTOM. The RPL policy is developed in separate components called rules. Rules are written to contain a specific piece of policy language, such as a guide curve for simulating releases from a reservoir, or implementation of flood control operations under high inflow conditions. The individual rule format, as opposed to a single script containing all of the policy coding, is used to order policy components by priority. The rules guide the simulation of the Basin and are based on the law that governs the operations of the reservoirs in the Basin as well as operational guidance provided by reservoir operators.

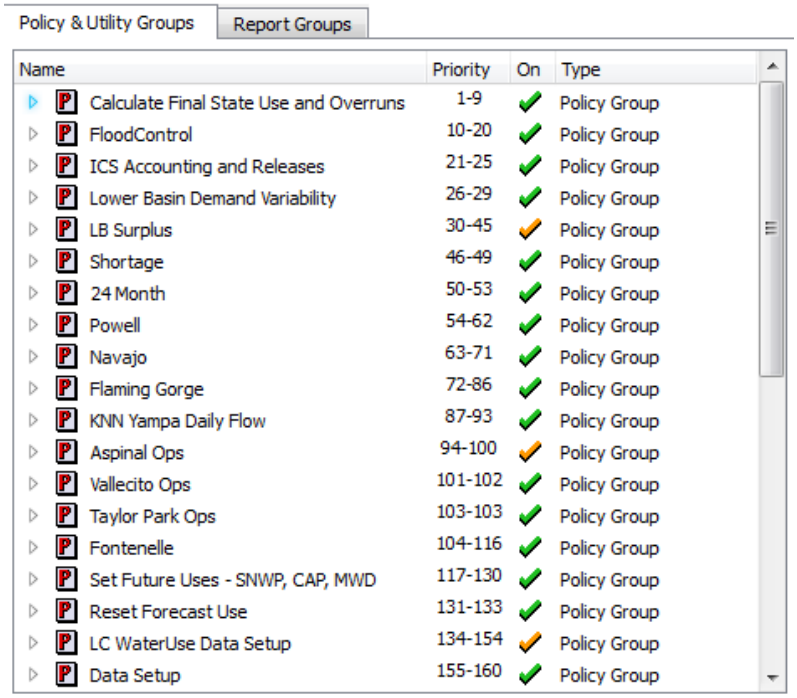

Figure 5 MTOM RiverWare™ Policy Language Interface

In addition to the physical workspace and the rules that that drive reservoir operations in the model, MTOM uses a unique capability in RiverWare™ called run cycles. Run cycles allow the model to solve the entire system in pieces using select portions of RPL logic to solve a portion of the system in each run cycle. This is useful because it allows the model to provide needed information from one piece of the reservoir system to the next. In MTOM, once operations are set for the most upstream reservoirs, operations for the next downstream reservoirs can be simulated. Information about upstream reservoir operations is required before operations can be set for the downstream reservoirs because a full year of projected inflow is required for planning reservoir releases at those downstream reservoirs (in accordance with the distinct RODs that govern operations of those reservoirs). Additionally, operations for Lake Powell and Lake Mead are frequently set in an iterative manner, as Lake Powell and Lake Mead operations are coordinated based on their respective releases and resulting elevations. Four run cycles are utilized in the MTOM RiverWare™ model. The upstream reservoirs in the headwaters of the system (Fontenelle Reservoir, Vallecito Reservoir, and Taylor Park Reservoir) are solved in the first run cycle, the remainder of the Upper Basin reservoirs (Flaming Gorge Reservoir, Navajo Reservoir, and the Aspinall Unit) down to Lake Powell are solved in the second run cycle, Lake Powell and the Lower Basin are solved in the third run cycle, and any operations at Lake Powell or Lake Mead that need to be fine-tuned in an iterative manner solve in the fourth run cycle. The run cycles allow the MTOM model to solve the basin according to the Law of the River and various operational guidelines throughout the Basin.

The Output Spreadsheet is a Microsoft Excel spreadsheet application that stores and processes the results of each simulation of a multi-trace model run. The spreadsheet is used to process the model's output so that information can be disseminated in a way that is useful for stakeholders and decision makers within the Basin. Data can be viewed in the raw output form for a given

output variable of interest, or data can be viewed post-processing to give an in-depth look at the frequency of occurrence for certain conditions within the Basin. The Output Spreadsheet is a tool that summarizes the probabilistic analysis and risk assessment that is provided through the MTOM System.

OUTPUT FOR DECISION MAKING AND RISK MANAGEMENT

The output from the MTOM System model is an ensemble of results throughout the Basin that includes inflow, outflow, and content for reservoirs; diversions for water users; and indicators of specific operational conditions such as lower Basin shortage, surplus and flood control. The Output Spreadsheet compiles the output data into useful plots and tables that can be used by Reclamation to disseminate information to stakeholders throughout the Basin. Using an ensemble of equally likely forecasts to drive multiple runs of the model and then collecting and analyzing the ensemble of results provides stakeholders and water managers with an estimate of uncertainty at any point in the time range of the model run. Because the MTOM System provides a more complete characterization of what the future condition of the Colorado River Basin might be, it enables decision-makers to more effectively manage their water supplies.

The most informative and standard product of the MTOM System process is a table that gives the percent of traces showing the occurrence of system conditions at Lake Mead and Lake Powell. Table 1 displays a template of this frequency table, where the system conditions are defined in the Interim Guidelines for Lower Basin Shortages and the Coordinated Operations of Lake Powell and Lake Mead (2007). Events that are categorized in this table include the annual release tier at Lake Powell and the annual release volume (if the volume is categorized further). In the Lower Basin the water supply conditions Shortage, Surplus, or Normal are categorized.

Table 1 Example of Percent of Occurrence of System Conditions Produced by the MTOM System

	Event or System Condition	WY1	WY2	WY3	WY4	WY5
Upper Basin - Lake Powell	**Equalization Tier**					
	Equalization - annual release > 8.23 maf					
	Equalization - annual release = 8.23 maf					
	Upper Elevation Balancing Tier					
	Upper Elevation Balancing - annual release > 8.23 maf					
	Upper Elevation Balancing - annual release = 8.23 maf					
	Upper Elevation Balancing - annual release < 8.23 maf					
	Mid-Elevation Release Tier					
	Mid-Elevation Balancing - annual release = 8.23 maf					
	Mid-Elevation Balancing - annual release = 7.48 maf					
	Lower Elevation Balancing Tier					
	Lower Elevation Balancing - annual release > 8.23 maf					
	Lower Elevation Balancing - annual release = 8.23 maf					
	Lower Elevation Balancing - annual release < 8.23 maf					
Lower Basin - Lake Mead	**Shortage Condition - any amount (Mead <= 1,075 ft)**					
	Shortage - 1st level (Mead<= 1,075 and >= 1,050)					
	Shortage - 2nd level (Mead<1,050 and >= 1,025)					
	Shortage - 3rd level (Mead< 1,025)					
	Surplus Condition - any amount (Mead >= 1,145 ft)					
	Surplus - Flood Control					
	Normal or ICS Surplus Condition					

The output spreadsheet also provides a tool to view any number of the output traces for any of the mass balance components of the reservoirs included in MTOM. The graphics produced from this tool, sometimes referred to as spaghetti plots, give a visual representation of the probabilistic outcome of an MTOM System run. Figure 6 shows an example of results for the Lake Mead pool elevation.

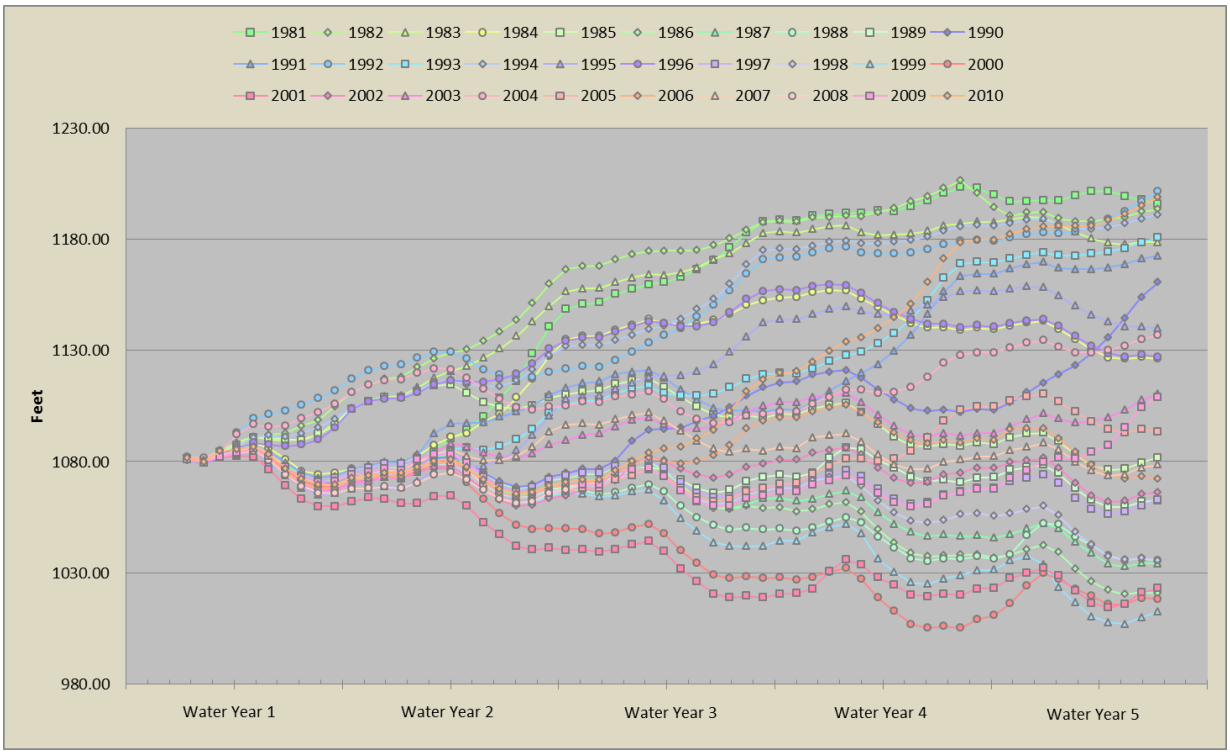

Figure 6 Example of Raw Lake Mead Pool Elevation Output from the MTOM System

The raw output traces are further processed using a month by month exceedance algorithm that can provide further analysis of the ensemble output. This month by month exceedance analysis can provide a possibly more informative view of the MTOM System output as demonstrated in Figure 7. It is important to note, however, that the exceedance algorithm produces traces that could be outside of the bounds of any given ensemble forecast; meaning that the driest (90 percent) trace may be drier than any one of the 30 output traces and the wettest (10 percent) trace may be wetter than any one of the 30 traces. This is due to the monthly exceedance analysis performed on the data which calculates an exceedance value for each month based on the raw data. The exceedance analysis is performed month-by-month such that the 90 percent trace is the 90 percent value for each individual month appended together into a single trace. Each exceedance trace is actually a compilation of the driest 90 percent value of each month in the run. This makes a very dry trace and this effect is more pronounced at the extremes than the raw ensemble output. The month by month exceedance value calculation is demonstrated with Table 2 and Equation 1 to obtain the 35 percent exceedance value for Lake Mead Pool Elevation using linear interpolation; which solves to a value of 1,081.50 feet for Month 1.

Table 2 Ranking of Lake Mead Pool Elevation (PE) for Exceedance Calculation Algorithm

Rank	8	9	10	11	12	13
Rank/n observations	25.81%	29.03%	32.26%	35.48%	38.71%	41.94%
Month 1 Ranked Mead PE Values	1,081.51	1,081.51	1,081.48	1,081.43	1,081.41	1,081.36
Month 2 Ranked Mead PE Values	1,080.49	1,080.48	1,080.46	1,080.41	1,080.30	1,080.23
Month 3 Ranked Mead PE Values	1,083.44	1,083.40	1,083.29	1,083.19	1,083.14	1,083.06

$$LakeMeadPE_{30\%,Month1} = \mathrm{PE}_9 + (\mathrm{PE}_{10} - \mathrm{PE}_9) * \frac{(30\% - \%_9)}{(\%_{10} - \%_9)} \quad (1)$$

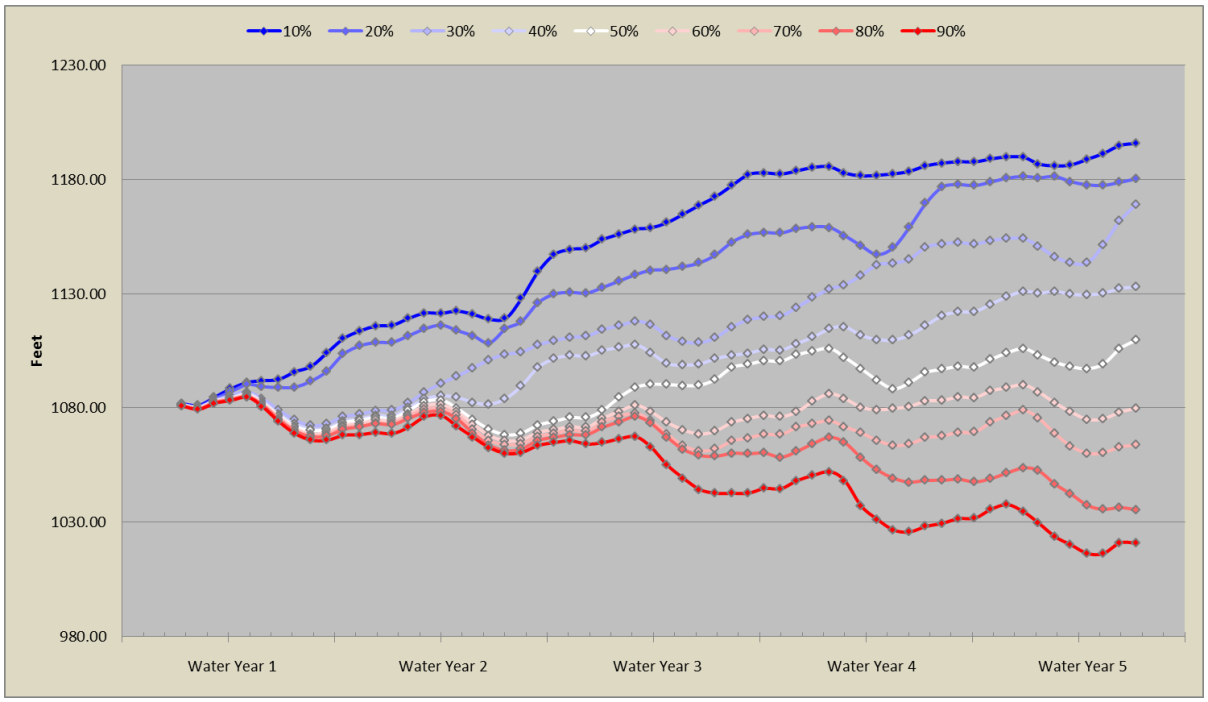

Figure 7 Example of Monthly Exceedance Processing of Lake Mead Pool Elevation Output

SUMMARY

MTOM has been developed to compliment two established and well-used models of the Colorado River Basin. It builds on the operations-specific strength of the 24-Month Study and the probabilistic strength of the Colorado River Simulation System to provide a probabilistic 60-month outlook for reservoir operations throughout the Basin. MTOM is a RiverWare™ model that uses RiverWare™ Policy Language and run cycles so that the specific operational policy and guidelines in the Basin can be modeled correctly at a monthly time step. The MTOM System includes the use of Colorado Basin River Forecast Center ensemble forecasts as the probabilistic input for the model. The System includes input and output spreadsheets as components that allow users to interact with the input and output data easily. The MTOM System outputs probabilistic data for reservoir operations and specific Basin conditions that aid in the understanding of risk and uncertainty in future conditions within the Basin. With MTOM

and the other modeling tools used in the Basin, Reclamation and Basin stakeholders obtain greater information for decision-making through ensemble forecasting and probabilistic analysis.

REFERENCES

Brandon, David G., (2005) Using NWSRFS ESP for Making Early Outlooks of Seasonal Runoff Volumes into Lake Powell, National Weather Service – Colorado Basin River Forecast Center (CBRFC). Web October 15, 2014 <http://www.cbrfc.noaa.gov/papers/forecastpaper.pdf>

U.S. Department of the Interior, Bureau of Reclamation. Record of Decision Colorado River Interim Guidelines for Lower Basin Shortages and the Coordinated Operations for Lake Powell and Lake Mead. USBR, December 2007. Web September 20, 2013 <http://www.usbr.gov/lc/region/programs/strategies/RecordofDecision.pdf>

Zagona, Edith A., Terrance J. Fulp, Richard Shane, Timothy Magee, and H. Morgan Goranflo (2001), RiverWare: A Generalized Tool for Complex Reservoir Systems Modeling, Journal of the American Water Resources Association, AWRA 37(4):913-929.

PIPELINE STREAM CROSSINGS – A RISK-BASED APPROACH TO MINIMIZE AQUATIC IMPACTS

Janine Castro, Geomorphologist, US Fish & Wildlife Service, Portland, Oregon, Janine_M_Castro@fws.gov; Anne MacDonald, Principal, Rivergrove Environmental Consulting, Lake Oswego, Oregon, rivergrove.environmental@frontier.com; Erin Lynch, Hydrogeologist, Ecology & Environment, Portland, Oregon, elynch@ene.com; Colin Thorne, Professor, University of Nottingham, Nottingham, UK, colin.thorne@nottingham.ac.uk.

INTRODUCTION

The global increase in the supply and demand of natural gas and oil has resulted in many new proposals for pipeline delivery systems throughout North America, which will result in thousands of new stream crossings if constructed. These pipes will cross a wide spectrum of stream, floodplains, and aquatic ecosystems – from arid, headwater streams, to perennial, mainstem channels – that vary greatly in their response to natural and anthropogenic disturbance. Even without additional new pipelines, the current distribution of pipelines throughout North America is quite extensive (Figure 1), and poses varying levels of risk to ecosystems.

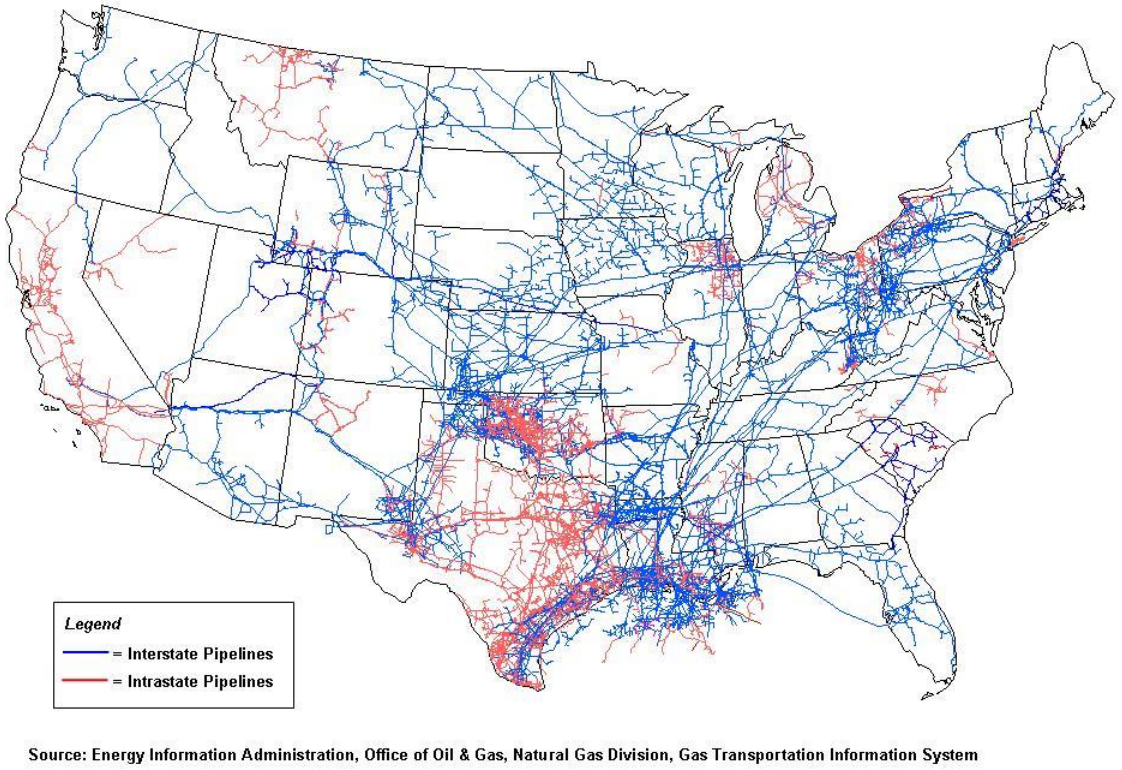

Figure 1 US natural gas pipeline network in 2009, not including the recently completed Ruby Pipeline from: http://www.eia.gov/pub/oil_gas/natural_gas/analysis_publications/ngpipeline/ngpipelines_map.html.

RISK ASSESSMENT

Because of the static nature of pipes and the dynamic nature of many streams, there are inherent risks at many of these crossing locations to aquatic species and habitats. To assess these risks, the US Fish and Wildlife Service in collaboration with the Ruby Pipeline, LLC, have developed a pipeline crossing framework (Figure 2) and linked risk assessment screening matrix (Figure 3) for project applicants and reviewers.

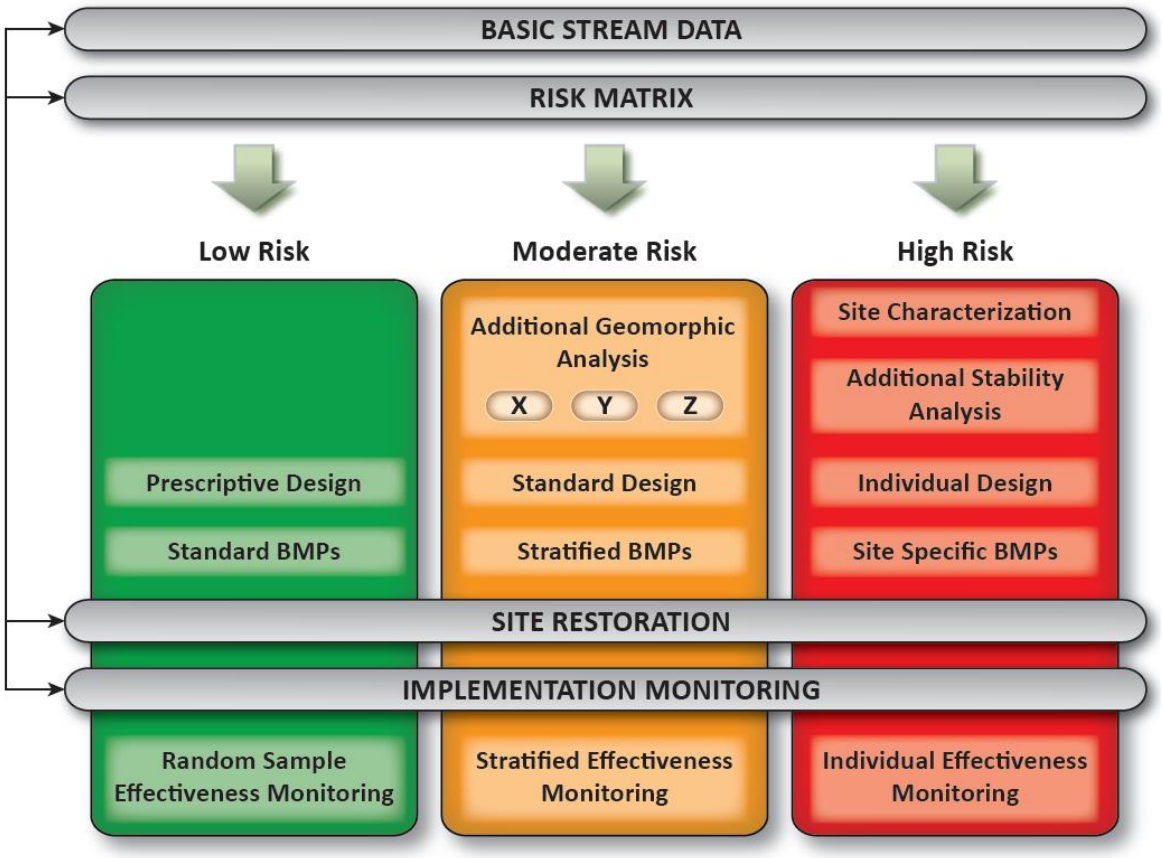

Figure 2 Generic waterbody crossing framework developed by the FWS

The crossing framework provides a robust justification for baseline data collection that is linked to a risk analysis, project design, site restoration, and implementation and effectiveness monitoring. Baseline data include floodplain and stream characteristics, such as valley width, riparian corridor, floodplain dimensions, stream type, stream slope, sinuosity, and bed and bank materials that allow application of the risk screening matrix.

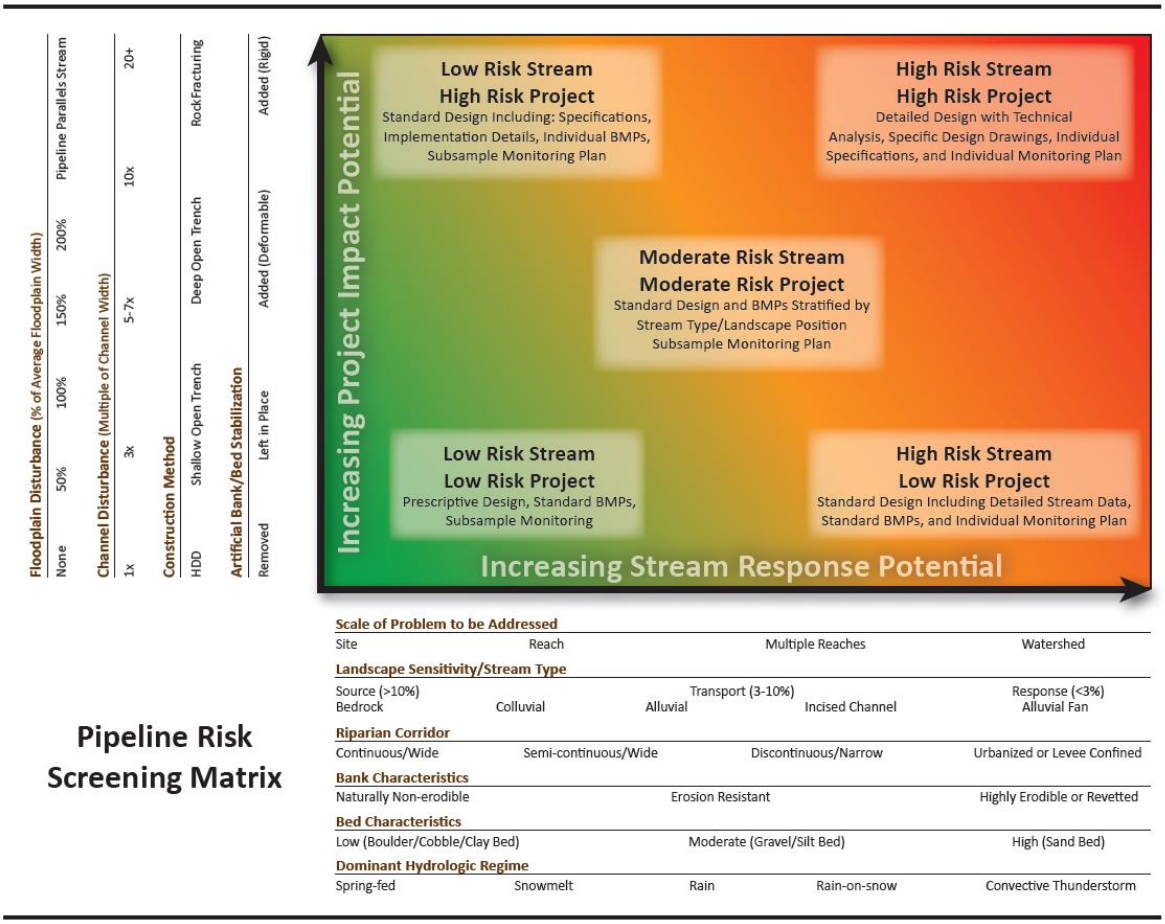

Figure 3 Pipeline Risk Screening Matrix

The risk matrix, embedded within the framework, is based on potential stream responsiveness to disturbance utilizing physical characteristics of the stream system. Because the x-axis relates to physical characteristics, reduction of risk generally requires relocation of the stream crossing. The y-axis describes potential impacts due to the degree of disturbance, construction methods, and extent of artificial stabilization, so risk on this axis can be reduced through both design and relocation. Using this geomorphology baseline, combined with the qualitative evaluation of relative risk, potential effects to aquatic habitat and species can be inferred.

CASE STUDY

The framework and matrix were tested on the Ruby Pipeline which traverses Wyoming, Utah, Nevada, and Oregon and crosses 1200 water bodies (Figure 4).

Figure 4 Ruby Pipeline Route

The process was highly effective in screening out low risk crossings, which received prescriptive designs and standard Best Management Practices, from higher risk crossings that were individually designed and monitored. This framework and risk matrix approach allows project developers and reviewers to focus resources and monitoring on the crossings that present the highest risks to aquatic habitat and species, while expediting design and construction, and minimizing the monitoring of low risk crossings.

SUMMARY

While primarily intended for new pipeline projects, the framework and matrix are also well-suited to the evaluation of existing pipelines to identify crossings that are at a high risk of pipeline exposure and rupture. The framework and risk matrix are easily adaptable to any linear transmission and/or transportation projects, such as power lines and highways.

The approach described in this extended abstract is provided in detail in the following publication:

Castro, J., A. MacDonald, E. Lynch, and C.R. Thorne. 2014. Risk-based approach to designing and reviewing pipeline stream crossings to minimize impacts to aquatic habitats and species. *River Research and Applications*. Published online in Wiley Online Library (wileyonlinelibrary.com) DOI: 10.1002/rra.2770.

MULTI-OBJECTIVE MODELING IN RIVERWARE FOR USACE-SWD

John Daylor, Hydraulic Engineer, USACE, Tulsa, OK, John.Daylor@usace.army.mil; David Neumann, Water Resource Engineer, Center for Advanced Decision Support for Water and Environmental Systems, University of Colorado, Boulder, CO, David.Neumann@Colorado.edu; Edith Zagona, Director, Center for Advanced Decision Support for Water and Environmental Systems, University of Colorado, Boulder, CO. Edith.Zagona@Colorado.edu; Jennifer Steffen, Hydraulic Engineer, USACE, Tulsa, OK, Jennifer.Steffen@usace.army.mil

Abstract: The U.S. Army Corps of Engineers Southwestern Division (USACE-SWD) and associated Districts operate numerous multipurpose reservoirs for flood control, water supply, hydropower, navigation, recreation, and water quality. They have developed several models in RiverWare for planning studies. This paper describes the methods and functions in RiverWare, how they are applied in the context of the rulebased simulation solver to perform these studies, and some additional utilities in RiverWare developed in collaboration with SWD to strengthen their usability and analysis capabilities. The SWD methods include: surcharge release from reservoirs, regulation discharge computations to determine the available space at downstream control points, system-wide flood control algorithm that computes flood control releases at all reservoirs while maintaining balanced storages and releasing flood storage over a forecast period without flooding downstream control points, water supply and stream diversions, minimum flow releases to meet targets while balancing reservoir storage, and hydropower releases to meet system load. The integration of the SWD algorithms brings together RiverWare's object-oriented modeling features and the power and flexibility of the priority rulebased simulation. The algorithms are thus implemented in modular, object-specific contexts for ease of maintenance and extension, as well as flexibility of use through user-selectable methods. In addition to these multi-objective planning studies, the capability to perform single or multiple reservoir yield studies was developed by enhancing RiverWare's Multiple Run Manager using a user-define logic to make iterative runs that converge on the demand that empties the conservation pool during a specified hydrologic sequence. RiverWare includes statistical post-processing and a direct data connection to the Corps' Data Storage System (DSS). Numerous studies arise that involve requests for proposed reservoir and system operational changes and associated affects to the existing operating plan. Typical studies include reallocation of authorized purposes, dam safety concerns, navigation enhancement, dependable yield determination, changes in target pool elevations, and downstream channel constraints. Period of record modeling with RiverWare provides tools for evaluating these proposed alternative operating management plans. This paper will also present examples of RiverWare modeling of case studies in SWD Tulsa District. RiverWare was developed by the University of Colorado Center for Advanced Decision Support for Water and Environmental Systems (CU-CADSWES) under sponsorship of the Tennessee Valley Authority (TVA), the U.S. Bureau of Reclamation (USBR), and the USACE.

INTRODUCTION

The Corps of Engineers, Tulsa District is responsible for managing 45 multipurpose reservoirs plus five run of river lock and dams. Major river systems in Tulsa District include the Arkansas and Red Rivers with contributing runoff areas extending from central Kansas, southwest

Missouri, all of Oklahoma, northern Texas, Texas panhandle, and western Arkansas, as shown in Figure 1. These reservoirs and river systems have series and tandem configurations with common downstream focus points for operational management, as well as individual reservoir requirements. Management follows existing reservoir and system operating guidance that has been adopted and accepted by the Corps, other Federal and state agencies, and numerous stakeholders. An authorized operating management plan is in place, however public and political interests exist that often conflict with the authorized plan. Examples of authorized purposes for the reservoirs include flood storage, navigation, water supply, water quality, irrigation, recreation, and hydropower. On a regular basis, there are requests for the Corps to investigate proposed changes to the authorized reservoir and system management plan. Some examples include different seasonal guide curves, additional water withdrawals, water quality variations, hydropower loading, and navigation enhancements. Due to the complexity of the reservoir and river system, a modeling approach is needed to investigate impacts of these requested operational changes. The RiverWare program provides a modeling tool for such analyses.

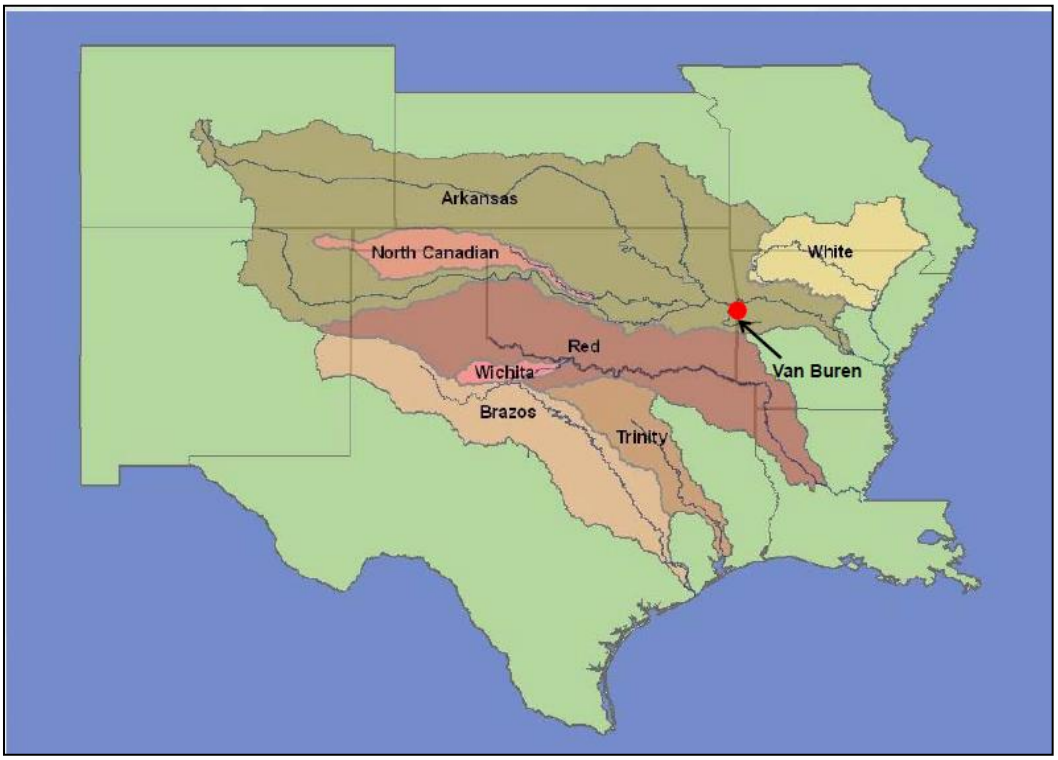

Figure 1 Corps of Engineers SWD-Districts RiverWare modeled basins.

RIVERWARE PROGRAM: TULSA DISTRICT APPLICATION

The reservoirs in Tulsa District were constructed and became operational over a period of time spanning from the late 1930's into mid-1980's. To investigate proposed changes in the reservoir and river system, a period of record planning model with rulebased simulation in RiverWare is used. The RiverWare model configuration for the Arkansas River, as shown in Figure 2 has 21 reservoirs, 48 regulation stream control points, and numerous routing reaches. All reservoirs are

configured in the model as being operational during the entire period of record simulation time frame, thus depicting a present day system condition analysis approach. For the Arkansas River model the period of record spans from January 1, 1940 through December 31, 2008 with daily time step computations. Historic surface water hydrology records are used to obtain local intervening area flow into headwater reservoirs and downstream control points. Historic precipitation and evaporation are applied to reservoir surface areas. During this 69-year timeframe of daily historic hydrology, significant extremes have occurred that provide wide variation of basin hydrologic conditions. Therefore, flood, drought, and average operations can reasonably be investigated.

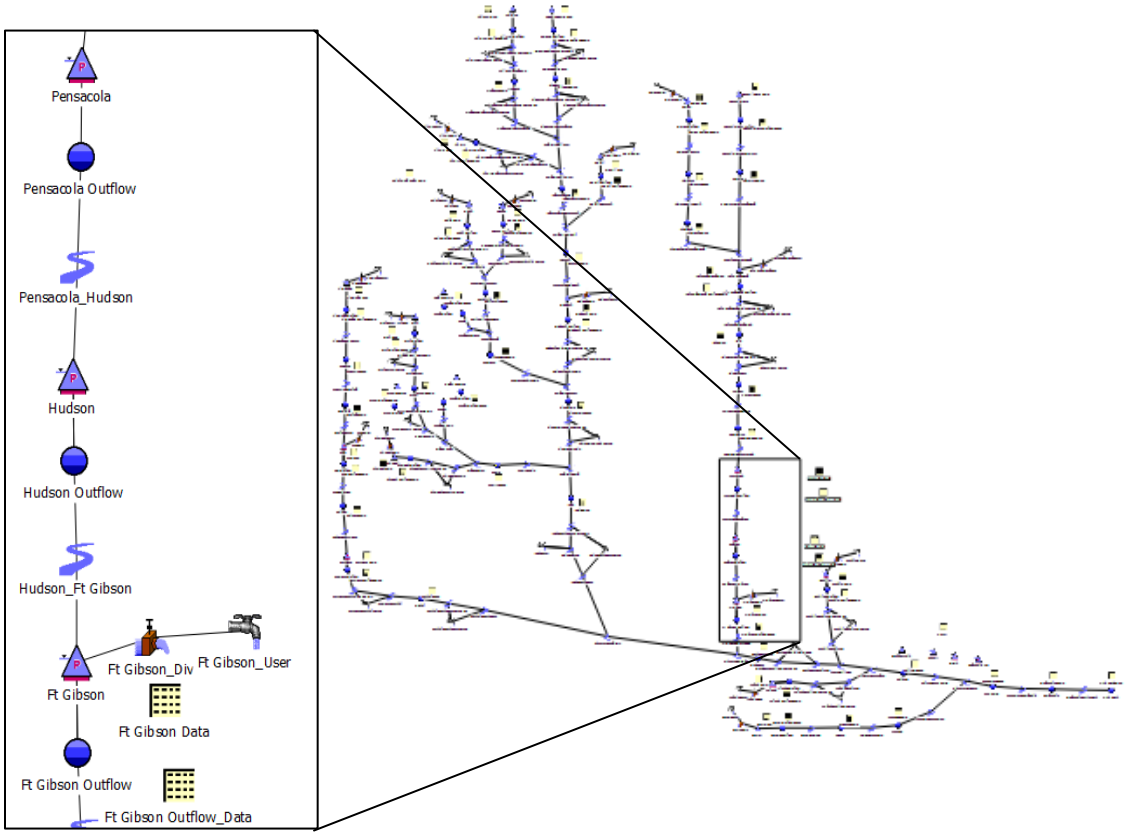

Figure 2 Arkansas River RiverWare model object configuration.

RiverWare's rulebased simulation approach is used by Tulsa District to replicate the reservoir and river system operating criteria. RiverWare is rich with rule development potential, both with pre-configured functions and user developed logic. One of the pre-configured sets of logic involves the Corps of Engineers Southwestern Division (SWD) flood control method which is a system approach to flood storage evacuation. This approach includes predefined functions, user selectable methods on individual objects, and methods that apply across a group of objects called a subbasin. The rules typically execute the methods or do the computation on the objects and subbasin. Data and user configuration options on the objects allow the different calculation approaches for different objects. The results of the computations are values for the decision

variables, usually reservoir releases and/or diversions. A sample ruleset that includes the SWD method for the Arkansas River model is shown in Figure 3.

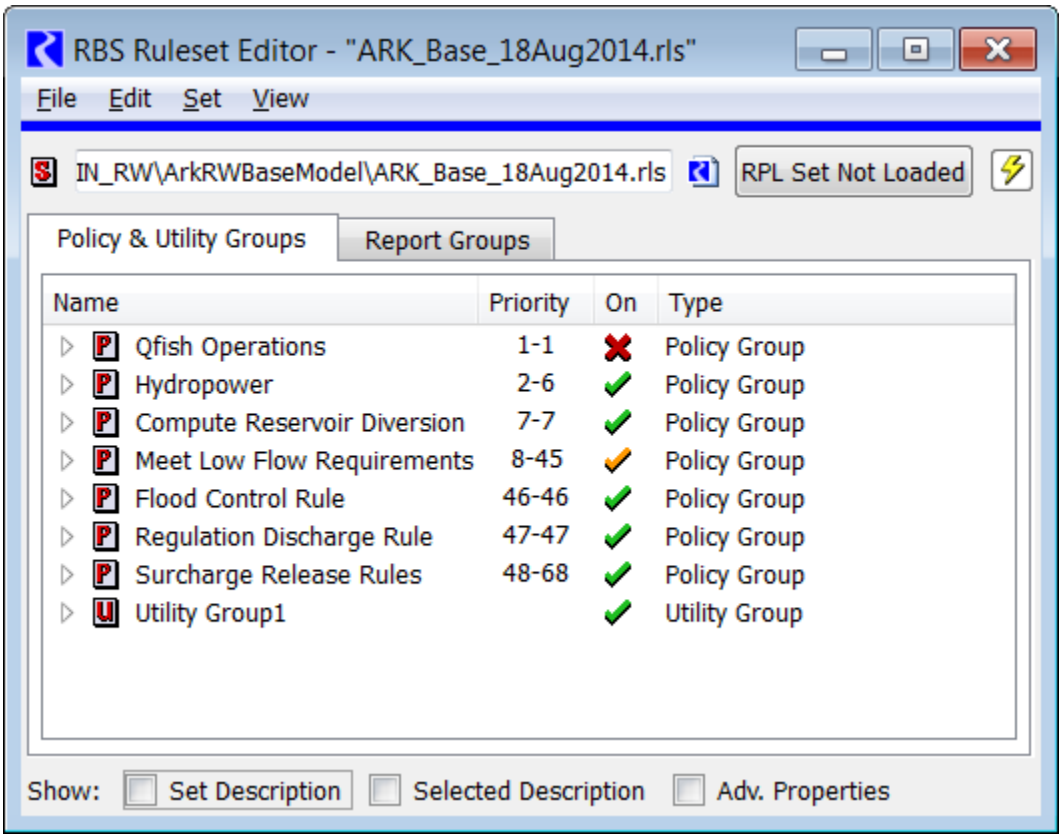

Figure 3 RiverWare ruleset for the Arkansas River basin.

Surcharge Release Rule: The surcharge release rule evaluates if inflow into each reservoir is sufficient to exceed flood storage and enter into surcharge conditions. If so, a release schedule is determined regardless of downstream conditions. The headwater reservoirs are evaluated first, such that any upstream reservoirs' surcharge release becomes part of a downstream reservoir's inflow. All reservoirs are evaluated in this upstream to downstream order to determine these mandatory surcharge releases.

Regulation Discharge Rule: The regulation discharge rule considers available channel space at each downstream regulation control point. The space hydrograph is the difference between the flow limit and actual flow that is a combination of local intervening area runoff flow plus prior time steps routed flow from upstream reservoirs releases. For each control point, a multi-time step space hydrograph is computed for upstream reservoir release potential. There are four general methods for configuring a control point's regulation criteria as used by the SWD:

- channel maximum flow method: The channel method usually involves a single maximum flow limit.
- current level regulation method: The current level regulation method considers an upstream reservoir's fullness at current time.

- future regulation method: The future level regulation method considers an upstream reservoir's fullness over the next several time steps.
- system method: The system percent method considers several upstream reservoirs' collective fullness. A key control point configuration and designation is used in the SWD flood control method to identify those control points that usually govern reservoir releases over other control points.

In the Arkansas River model, the main constraint for reservoir releases on the Arkansas River is Van Buren, Arkansas regulation control point. This location, as shown in Figure 1, has flow limitations based on the fullness of 13 reservoirs that have influence on this location. Flood damage flow is a consideration as well as flow benches for navigation. Flood storage evacuation must also follow a tapering plan for navigation. The Van Buren control point is designated as a key control Point.

Flood Control Rule: The flood control rule evaluates if any reservoir is in the flood storage zone; if so, a multi-day release schedule is developed based on downstream control points' available space as well as its fullness compared to other reservoirs in the system. If several reservoirs are competing for channel space, a priority scheme is used in the SWD flood control method. Each reservoir is configured with a balance level verses percent full of flood storage, Figure 4, which is used to determine priorities for flood storage releases as per the system manual operating criteria. In this way, the flood control logic computes reservoir releases to prevent downstream flooding. When the inflows to the system are reduced, the reservoir releases are computed to recover the flood control space in a balanced manner while not exceeding the downstream flow targets.

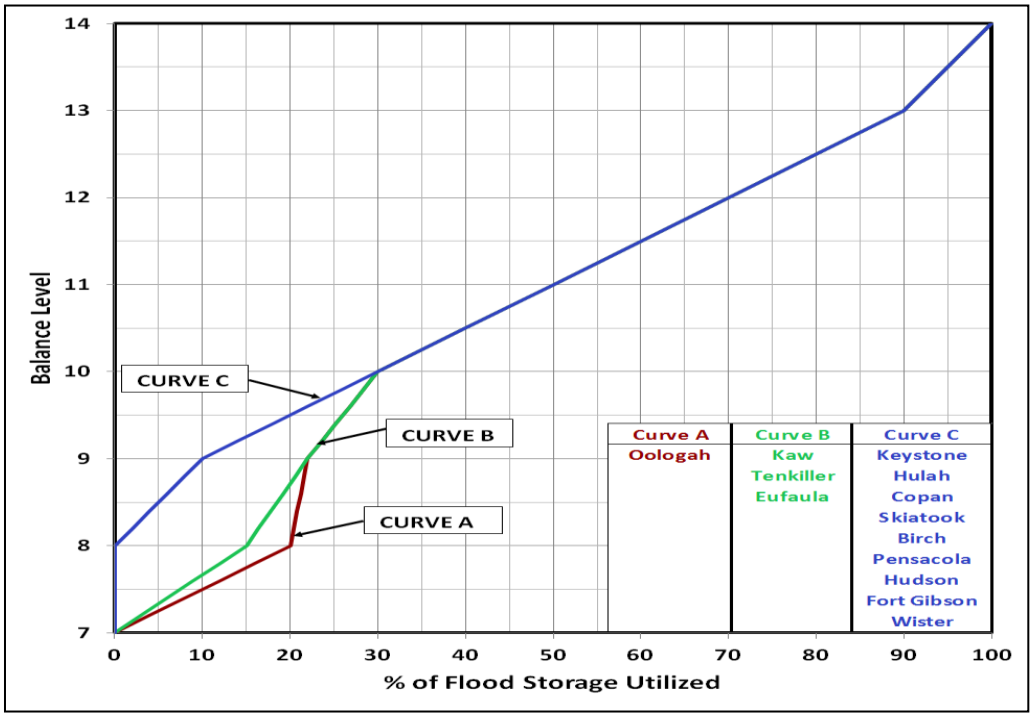

Figure 4 Balance level vs. percent of flood storage for reservoirs.

Low Flow Rule: The meet low flow requirements rule tries to meet low flow targets at several downstream locations from one or more upstream reservoirs. Low flow requirements can be a constant rate or can vary by season, as well as a function of the supplying reservoir's fullness. For example, as the providing reservoir's conservation storage is being depleted, the downstream minimum flow requirement can be reduced. The rules compute the releases to meet the low target based on the fullness of the supplying reservoirs. Releases are made from the fullest reservoir first up to its maximum specified release and then releases are made from the next fullest reservoir, and so on until either the low flow requirement is met or there is no more water to meet low flows.

Reservoir Diversion Rule: The compute reservoir diversions rule evaluates reservoir withdrawals, typically for municipal and industrial (M&I) demands. A monthly request for diversion is input and can be configured with return fraction. Actual withdrawals are based on the reservoir's available storage and the withdrawal can be reduced with depleting storage. The rules compute the available water and compute the flow necessary to meet the demand. Stream withdrawal points can also be configured with dependencies on reservoir conditions in the system.

Hydropower Rule: Any releases made for other purposes are automatically sent through the turbines to the extent possible, but additional power demands may exist that require additional turbine releases. The hydropower rule computes the power load requirements and then makes releases to meet that load. The load can be input several ways in RiverWare. Examples include period of record firm loadings, reservoir guide curve, and system energy in storage. Weekday and weekend loading ratios are available. Downstream channel space availability is considered when making hydropower. A hydropower release is proposed and then the system is solved downstream to ensure that the proposed release does not cause additional downstream flooding. If it does, the hydropower release is cut back. Thermal purchase (power deficiency) and dump energy (power surplus) computations are made in conjunction to input firm power requirements. RiverWare period of record modeling computations for Tulsa District is a daily time step and the computed daily average turbine release for the day may meet a required low flow release for the day on a daily average basis. In reality there are a few hours during the day where this low flow requirement is not being met with turbine release, therefore RiverWare includes functions to consider and account for the partial day of turbine release and resultant low flow release needed for the remaining hours of the day.

Post-Run Analysis: RiverWare has many tools for viewing and analyzing post simulation results. RiverWare's statistical functions on the data object are a common use for Tulsa District, as well as graphical and tabular features. Unique computations of interests can be developed with the expression slot tool. The output manager provides features for configuring and saving outputs. RiverWare's model report tool can be used to develop HTML report files with user selected input for study specific areas of interests. RiverWare's data management interface (DMI) can be used to transfer datasets into and out of the RiverWare interface, such as the Corps of Engineers' DSS file format, commonly used by Tulsa District. An example of the output manager's graphical capabilities is the pie chart shown in Figure 5. This pie chart shows the percentage of flood control storage for a single example time step at 10 reservoirs in the lower

Arkansas River basin. Each wedge represents that reservoir's fraction of the total flood control space. The colored portion of the wedge represents the flood control storage percentage at that time step. Labels and numeric data provide specific information on the flood storage volume and percentage. RiverWare's pie chart function has animation capability that allows viewing over several time steps.

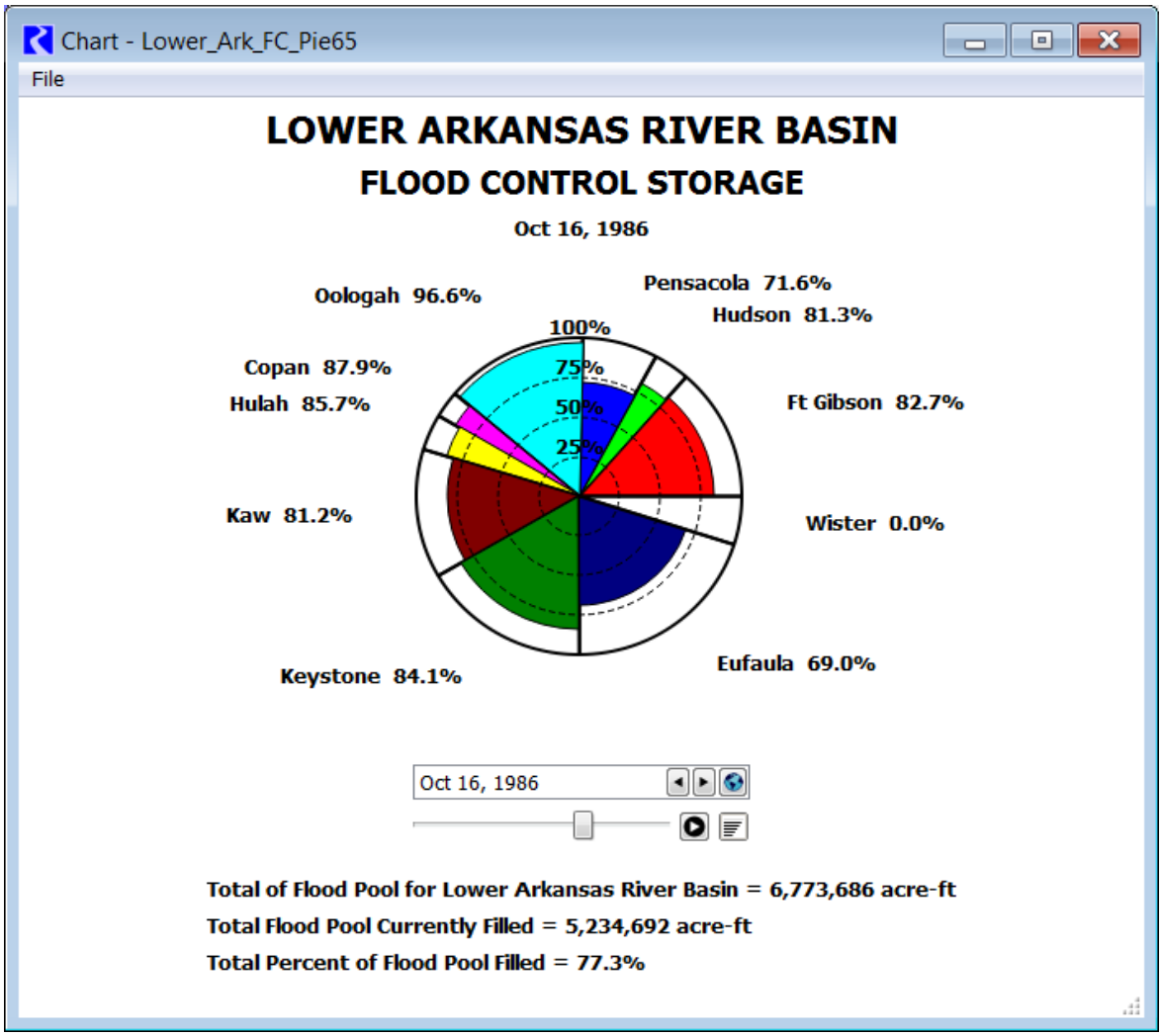

Figure 5 Pie Chart for reservoirs with flood storage.

CASE STUDY: FIRM YIELD ANALYSIS

Tulsa District Corps determines dependable reservoir yield by examining the period of record hydrology and determining the reservoir withdrawal that can be sustained during the most severe drought of record. In other words, what yield (firm yield) can be maintained while exhausting the conservation pool storage without going below the bottom of conservation pool zone. To accomplish this analysis, Tulsa District uses RiverWare's iterative multiple run manager tool to cycle through the period of record to converge on this firm yield value. The iterative MRM makes a run through the period of record and then executes logic to determine if another run is

needed and if so, the variables that should be changed. Using this tool, the period of record can be run many, many times with different inputs to search for the desired solution. For the yield study, an initial estimate for yield is either input or the program uses average annual inflow on the first passes to get bounding conditions. The iterative MRM rules then converge on the yield using a modified bisection algorithm to find the withdrawals that exactly exhausts the storage at some point in the period. The user specifies a tolerance target for convergence limits. RiverWare's system control table (SCT) is used to show the iterative and final values, as shown in Figure 6. This example provides results from a single reservoir yield determination in the Red River multi-reservoir system. This firm yield analysis approach with RiverWare's MRM can also be configured sequentially to compute firm yield for several or all reservoirs in the system.

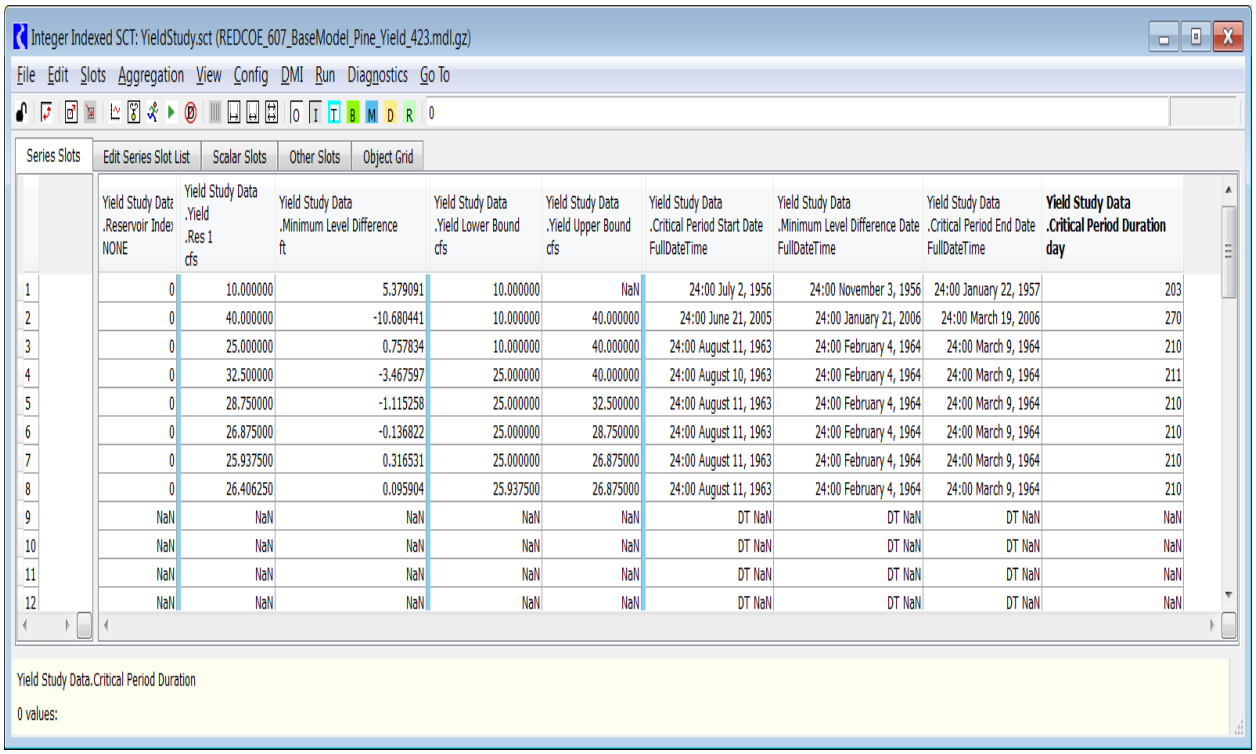

Figure 6 System Control Table with Iterative Multiple Run Manager for firm yield analysis.

CASE STUDY: PINE CREEK LAKE DAM SAFETY

Pine Creek Lake is a headwater reservoir on the Little River in southeastern Oklahoma that is a major tributary to the Red River. Embankment seepage around the gated conduit has been discovered at Pine Creek Dam. The Corps' dam safety team is currently evaluating corrective measures. For precautionary measures the dam safety team has requested a lower operating level for the top of conservation pool elevation. Pine Creek is a multipurpose reservoir with flood control storage, water supply and low flow requirements, and recreation interests. Pine Creek is one of 15 reservoirs in the Red River system that collectively operate for the common downstream regulation point at Shreveport, LA. A RiverWare model was used to investigate various proposed alternative operating levels for Pine Creek in conjunction with the Red River system operating plan. Impacts of reducing the conservation storage needed to be investigated

and mitigated. Figure 7 shows the elevation duration relationship of the normal operating level at elevation 438.0 ft and the reduced operating level at elevation 433.0 ft. The selected interim operating level provides minimal impacts to the system while providing reduced risk of embankment concerns.

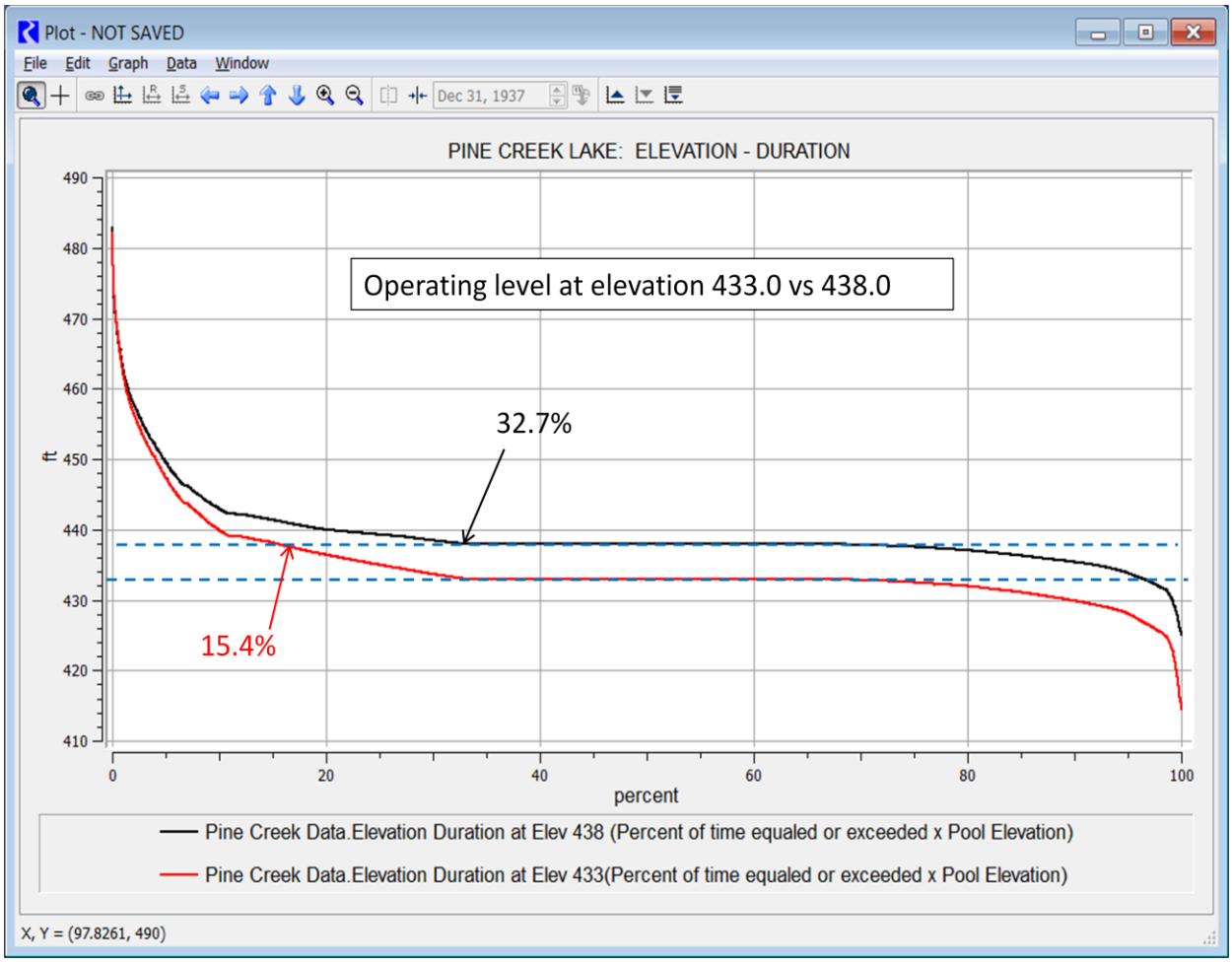

Figure 7 Pine Creek Lake elevation - duration for alternative top of conservation pools.

TYPICAL MISCELLANEOUS APPLICATIONS BY TULSA DISTRICT

On a periodic basis the District's Reservoir Operating Manuals and System Manuals are updated. The period of record hydrology and any operating changes are updated in RiverWare to provide simulated data for these manual updates. The Corps is currently involved with dam safety evaluations, periodic assessments of structures, and levee certifications, hence numerous requests are made of RiverWare's reservoir and system modeling output. RiverWare modeling provides for a rapid and easy tool to investigate potential deviations to operational management. The impoundments in Tulsa District are aging and experiencing depleting storage due to sediment deposition. Figure 8 showing Keystone Lake on the Arkansas River main stem provides an example of reduced storage as measured with periodic resurveys. The effects of depleted capacities can be investigated.

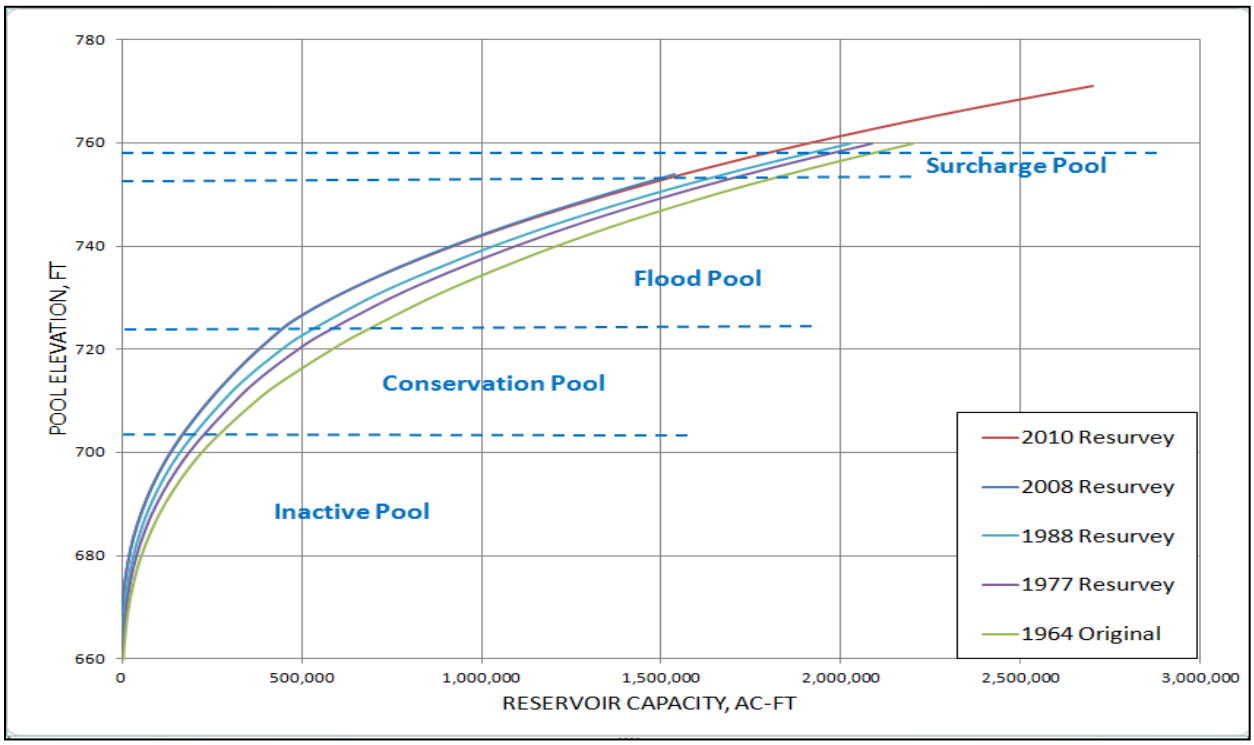

Figure 8 Capacity reduction with sediment deposition for Keystone Lake.

CLIMATE CHANGE ANALYSIS

RiverWare modeling has potential to investigate climate change concerns. In Tulsa District's period of record rulebased modeling, the historic surface water hydrology, precipitation, and evaporation can be adjusted for climate change scenarios. Operational rule logic can be configured to analyze responses to basin conditions and trends. In Tulsa District watershed, most precipitation and resultant runoff typically occurs in the spring months and another inflow season in the fall. Summer and winter seasons typically have less experienced runoff. One example of conditional operation with RiverWare rule simulation that can be applied for climate change effects involves evaluating the inflow into a reservoir during a specified time frame, say the spring months and comparing to a selected threshold. If the threshold is not met an alternative reservoir target operational guide curve is used in an attempt to maintain some additional pool storage in late spring for upcoming dry summer months. In the future, the RiverWare models of the basins will be used to perform this type of studies.

CONCLUSION

Tulsa and other Districts in the Southwestern Division of the Corps have numerous reservoirs that must be operated individually and as a system for existing authorized purposes as well as the many interests competing for finite resources. RiverWare's rulebased simulation modeling provides a study approach for evaluation and decision tools to manage the system as well as compare the effects of proposed alternative operating scenarios.

REFERENCES

Center for Advanced Decision Support for Water and Environmental Systems (CADSWES). RiverWare User's Guide. http://www.riverware.org/PDF/RiverWare/documentation.

U.S. Army Corps of Engineers Tulsa and Little Rock Districts. (1980). "Arkansas River Basin: Water Control Master Manual."

CHANNEL AND BANK STABILITY OF THE BURNETT RIVER IN THE AFTERMATH OF THE 2011 AND 2013 FLOODS: IMPLICATIONS FOR SEDIMENT DELIVERY TO THE GREAT BARRIER REEF

Andrew Simon, Senior Consultant/Geomorphologist, Cardno, P.O. Box 1236, Oxford, Mississippi 38655, USA, andrew.simon@cardno.com; Natasha Bankhead, Senior Project Scientist, Cardno, P.O. Box 1236, Oxford, Mississippi 38655, USA, natasha.bankhead@cardno.com and Peter Wilson, Soil Scientist, Burnett-Mary Regional Group, Bundaberg, QLD, Australia, peter.wilson@bmrg.org.au

Abstract The Burnett River, QLD Australia, experienced severe flooding in early 2011 and 2013, with the latter flood breaking all historical records. As a result, damage to infrastructure and the loss of agricultural land from bank erosion was considerable. Exacerbated by the floods is concern about sediment delivered to downstream locations including dams/weirs, and ultimately to the Coral Sea and the Great Barrier Reef (GBR). The primary objectives of this work were to: (1) provide strategies for cost-effective protection of local assets and (2) determine the relative contributions of bank sediment (particularly fine-grained material) to overall sediment loads to the GBR.

Analysis of aerial imagery between 2009 and 2013 revealed that a total of about 27.8 million m^3 (47.3 Mt) of materials were eroded from the banks of the lower 300 km of the Burnett River main stem (about 6.1 million m^3/y or 10.4 Mt/y). An equal volume is not delivered to the Coral Sea, as an unknown proportion is deposited on low-bank surfaces, beds, bars and floodplains. It can be assumed that the majority of the fine-grained materials is transported through the system Approximately 21 million m^3 (35.6 Mt) or about two thirds of these sediments were eroded from banks downstream of Paradise Dam while much of the hydraulically-controlled bank sediment eroded from reaches upstream of rkm 170 was trapped behind the dam (7.0 million m^3).

Long-term simulations (42 years) were conducted using the Bank Stability and Toe Erosion Model (BSTEM), to compare longer term averages with the 2009-2013 rates calculated from aerial imagery. Over this longer time period, annual bank-erosion rates are about 3.1 million Mt/y; about 18 times greater than the value predicted by the catchment model SedNet. Bank-erosion rates below Paradise Dam (rkm 131) are 2.4 million t/y. Assuming 100 years of simulation and using an empirical relation between the period of BSTEM simulations and calculated erosion rates, a conservative value for the average, annual rate of bank erosion is 2.0 Mt/y. Bank erosion, instead of being a minor source of sediment representing 8% of the total, was found to be the single largest contributor of sediment in the Burnett River Catchment, representing at least 44% of the total, annual sediment budget.

The implications of these findings are considered in the context of erosion sources and rates in Brodie et al., (2003) who report that on average, 2.75 Mt/y are eroded from the catchment. By replacing their 0.175 Mt/y from the banks with the 2.0 Mt/y calculated in this study, a new total of 4.6 Mt/y is obtained. Given these significant differences in both the relative importance and absolute rates of bank erosion than was earlier reported, sediment management should be re-focused to include this important source. Doing so would not only protect local assets by limiting land loss and bank retreat, but would help maintain reservoir and harbour capacity, minimize downstream flooding, and protect marine resources.

INTRODUCTION AND BACKGROUND

The Burnett River is one of the Reef Catchments flowing through the city of Bundaberg in its downstream reaches before exiting to the Coral Sea. The Burnett River experienced severe flooding in early 2011 and 2013, with the latter flood breaking all historical records. As a result of these floods, damage to assets, infrastructure and the loss of agricultural land from bank erosion was considerable. Massive amounts of sediment were transported to the Coral Sea (Figure 1). In an effort to develop a strategy for prioritizing and determining resilient and cost-effective protection measures, an understanding of both site-specific and system-wide stability conditions is essential. For site- and reach-specific solutions, this is accomplished by quantifying the driving (flow and gravitational) forces and resisting (shear strength) forces operating on the channel banks, and testing how alternative stabilization measures would perform over a range of flows. System-wide analysis then provides the spatial and temporal context of

channel instability to determine the suitability of conducting various types of channel works (i.e. energy dissipation, bank stabilization, etc.) to protect assets and to aid in prioritization of those works.

The geographic scope of this study extends from the mouth of the Burnett River east of Bundaberg, upstream about 300 km to Eidsvold (Figure 2). Results of this study will also be germane to managing sediment delivery from the catchment to the Coral Sea and the Great Barrier Reef by providing data on sediment contributions from streambank erosion.

Figure 1 Sediment plume from the Burnett River entering the Coral Sea, January 2013. Image provided by D. Honor (Bundaberg Regional Council; 2013).

FLOWS

This study was undertaken in the context of flood recovery following the record flows of January 2013. It is important, therefore, to put the magnitude and frequency of these kinds of devastating events in the perspective of the long-term flow record. Fortunately, the Burnett River has flow records extending back for more than a century. Annual-maximum peak flows from 1910 to present are shown in Figure 3 for the gauge at Walla Weir (136001A). Over the period, the flow of January 2013 represents the maximum recorded peak since 1910 and by definition, has a return period of at least 104 years. When viewed over the period of record, the 2013 peak is significantly greater (46%) than the previous maximum of 10,780 m^3/s recorded in 1942. In comparison, the 2013 peak was 157% greater than the peak flow in 2011. However, when the peak flows of 1890 and 1893 are considered, a slightly different picture emerges. Discharges for the large floods in 1890 and 1893 were estimated from stage data provided by Department of Natural Resources and Mines (DNRM; R. Maynard, written comm, 2013) and included in the peak-flow series. These flows represent the second and third largest flows since 1890, respectively, and demonstrate that the flood of January 2013 was (1) not that uncommon, and (2) only 17% greater than the estimated 1890 peak. By also considering the flood of February 1875 which had a peak 0.9 m below that of the 2013 peak at Bundaberg (DNRM, 2013), the return period for the 2013 flood reaches 139 years.

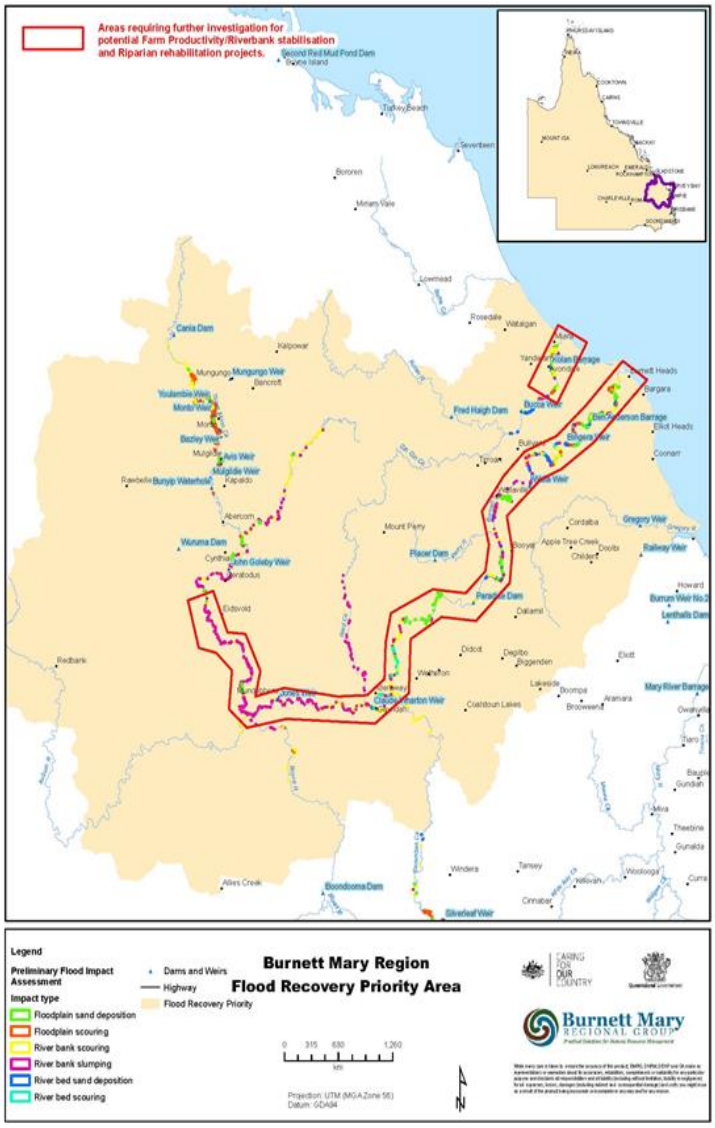

Figure 2 Geographic scope of the study along the Burnett River.

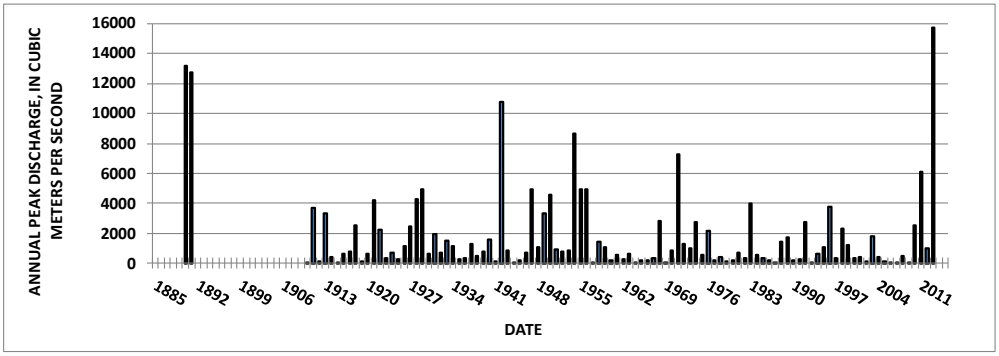

Figure 3 Annual maximum peak flows for the Burnett River at Walla Weir.

SYSTEM-WIDE STABILITY CONDITIONS

Analysis of current geomorphic conditions and dominant channel processes along the study reaches were conducted, in part through the use of Rapid Geomorphic Assessments (RGAs). RGAs utilize diagnostic criteria of channel form to infer dominant channel processes and the magnitude of channel instabilities through a series of nine, channel criteria. Inclusion of each criterion in the ranking scheme is founded on 30 years of research on the controlling forces and processes in unstable channels (Simon and Hupp, 1986; Simon, 1989; Simon and Downs 1995).

For each RGA, the dominant processes occurring along a reach were recorded using a Channel-Stability Ranking Scheme. Scoring for each criterion is such that a higher value indicates greater potential for erosion and instability. A maximum value of four (4) can be assigned to each, preventing subjective assumptions on the relative importance of each criterion. The nine criteria are directed at determining trends of recent channel adjustments through identification of the stage of channel evolution as impaired streams undergo a systematic adjustment (stages of channel evolution) as processes migrate through a channel network with time. To provide detail, the 2013 post-flood, aerial imagery of the reaches was analyzed over adjacent 2-km reaches to obtain information needed for the RGAs. The result is an almost continuous evaluation of channel conditions and dominant processes over 300 km of the Burnett River.

As hypothesized at the inception of this study, the effects of the impoundments on channel stability can be dramatic. The channel-stability index shows wave-like longitudinal variations, with peak values just downstream from the impoundments and other river-crossing structures. These effects attenuate (decrease) with distance downstream from each of the structures (Figure 4). The most unstable reaches are included in the orange fill (scores of 20-30) and are indicative of an incised channel with actively failing banks and limited vegetative cover over much of each of those 2-km reaches. Conversely, those reaches within the green fill (scores of 0-10) are generally stable with no active bank failures and generally good vegetative cover. The reaches with the most severe instabilities are located just downstream of Walla Weir and Paradise Dam where values of the channel-stability index are typically greater than 20 (Figure 4). Conversely, stable conditions extend upstream from these two impoundments; for 39 km above Paradise Dam (to rkm 170) and, for about 16 km above Walla Weir (to rkm 90). The stability imparted through the hydraulic effects of the dam extends about 20 km upstream of the head of the impoundment at rkm 150.

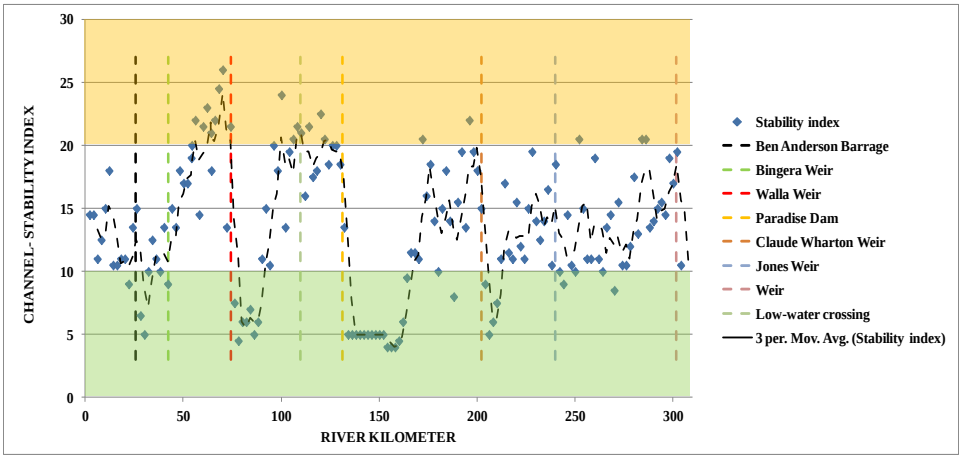

Figure 4 Longitudinal variation in the channel-stability index along the Burnett River main stem showing the effects of dams. Orange fill denotes very unstable conditions (20-30) while the green fill denotes very stable conditions (0-10).

Data on system-wide channel geometry (bank height, width, and slope) were obtained at 2-km increments from analysis of LiDAR data in those reaches where available. LiDAR coverages are not all from the same time, ranging from 2009 to early 2011. For the purposes of this study, it was assumed that they are all from one data set, representing the pre-flood condition of the channel. To determine the magnitude and extent of recent bank erosion, an analysis of the 2010 pre-flood and the 2013 post-flood, aerial photography was conducted. Fixed points on each bank were identified at 2-km increments in each paired image (2010 and 2013) to determine the distance from the

point to the top-bank edge. A comparison of the difference in these distances produced the amount of lateral retreat of the particular bank over the time period. Multiplying this value by the height of the bank provided the amount of material eroded per unit length of channel (in m^2/m). To then obtain an estimated value of the volume of sediment delivered to the channel by bank erosion, the average value between two adjacent reaches was then multiplied by the reach length (2,000 m).

BANK-DERIVED SEDIMENT LOADINGS

Unit bank-erosion rates provided information of the average amount of land lost to the river per unit length (m) of channel, but did not assume that each meter of a specific 2-km reach retreated at the same rate. This would only be the case if "percent reach failing" values obtained from the RGA analysis were 100%. Unit bank-erosion rates shown in Figure 5 again display the typical wave-like functions with peaks on the downstream sides of the impoundments.

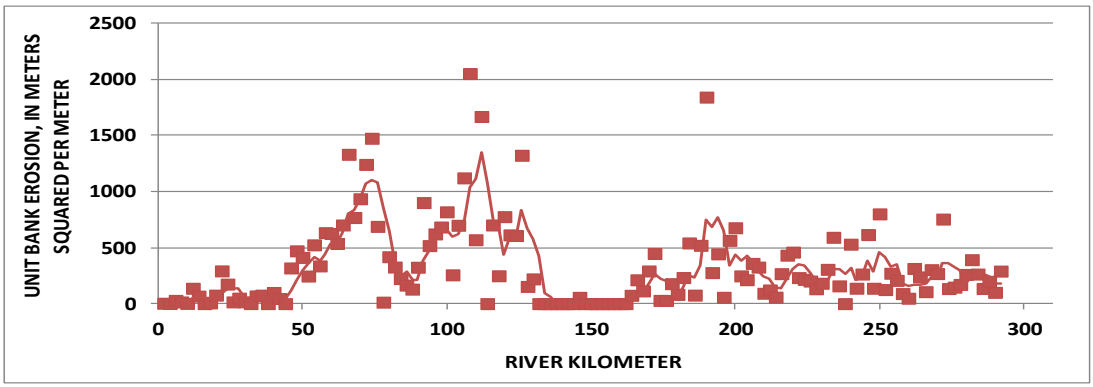

Figure 5 Unit bank-erosion rates, representing land loss (in m2/m) along the Burnett River main stem

To calculate total volumes of bank material eroded from the margins of the Burnett River, the unit bank-erosion rates for each bank, along each 2 km reach were multiplied by the "percent reach failing" (from the RGA data set) and by the reach length (2,000 m) (Figure 6).

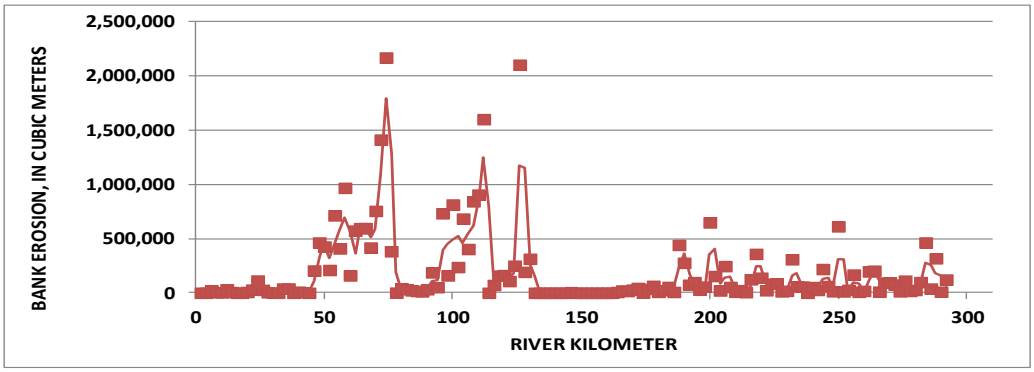

Figure 6 Volume of bank material eroded from floodplains and terraces along the Burnett River mainstem.

Summing the eroded-volume data along the entire 292 km reach of the Burnett River main stem gives a total volume of material eroded by bank processes of about 27.8 million m^3 (47.3 million t) or, about 6.1 million m^3/y (10.4 million t/y) over the 4.58-year modelling period. Erosion of these bank materials does not equate to an equal volume being delivered to the river mouth and the Coral Sea, as an unknown proportion is deposited on low-bank surfaces, beds, bars and floodplains. It can be assumed, however, that the majority of the fine-grained materials (silts and clays) are transported through the system and out to sea. Approximately 21 million m^3 (35.6 million t) or about two thirds of these sediments were eroded from banks downstream of Paradise Dam. One can assume that much of the

hydraulically-controlled bank sediment (less than 7 million m^3) eroded from reaches upstream of rkm 170 was trapped behind Paradise Dam. Erosion volumes are shown mapped in Figure 7.

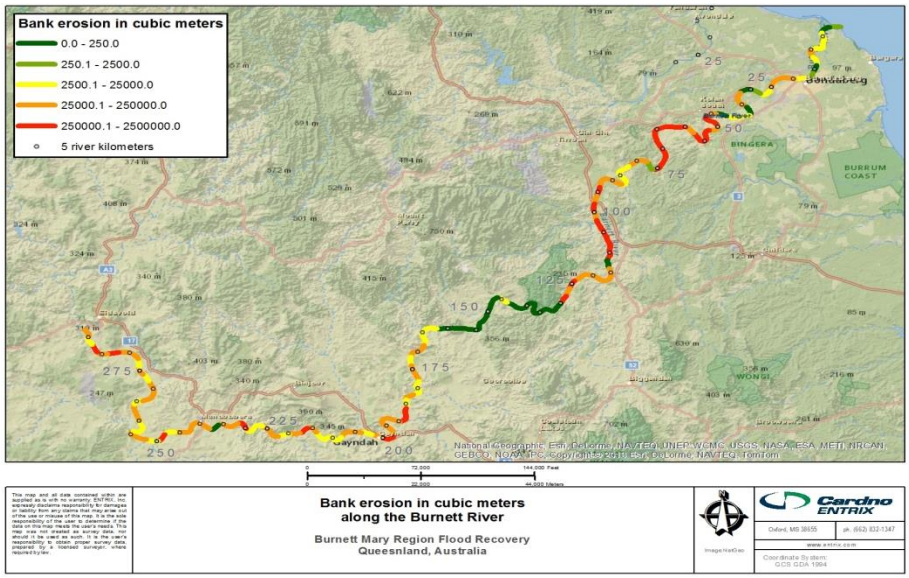

Figure 7 - Volumes of bank erosion over the period 2010-2013 along the Burnett River main stem.

Given these very high rates of bank erosion over the 2009-2013 period, it is important to place them in the context of longer-termed erosion rates and their implications for the management of sediment being delivered to the Coral Sea and the Great Barrier Reef (GBR). This is particularly germane to: (1) the Reef Rescue Program where conservation measures to reduce sediment delivery to the GBR are presently focused on upland and agricultural sources of sediment and not on streambanks, and (2) plans to dredge the lower Burnett River to reduce flood risks in Bundaberg.

Results of SedNet modelling in the Burnett River Catchment predict that on average, 175,000 t/y of sediment are eroded from banks of the Burnett River and its tributaries (Brodie et al., 2003). This represents about 8% of the predicted total amount of sediment erosion, with hillslope (1.6 million t/y) and gully (0.93 million t/y) sources making up the bulk of the total. Although it is unclear as to the length of the SedNet simulation period, we assumed that mean-annual flow was used to generate results expressed as "average annual" values. As a result of this large discrepancy between the SedNet results and those provided above, and its implications for sediment management, average, annual bank-erosion data were required for purposes of comparison.

AVERAGE ANNUAL RATES OF BANK EROSION: BSTEM MODELING

To obtain average, annual rates of bank erosion, values over a sufficiently long period of time were required. This was accomplished using numerical modelling. Geotechnical and hydraulic resistance of the bank and bank-toe materials were determined *in situ* at eight sites using conventional techniques (Iowa Borehole Shear Tester: Lohnes and Handy, 1968; Lutenegger and Hallberg, 1981, and the Submerged Jet-Test Device, Hanson, 1990; Hanson and Cook, 1997). Bank surveys and observations of stratigraphic layering for the tested banks were also obtained in the field. The field data were used with mean-daily flow data from gauges along the Burnett River to populate the Bank Stability and Toe Erosion Model (BSTEM-Dynamic 2.0; Simon et al., 2000) for the purpose of simulating bank-erosion rates over time periods ranging from about 4.5 to 42.5 years.

To obtain erosion results in units similar to those reported in Brodie et al., (2003), an average bulk unit weight of 1.7 kN/m^3 was used to convert m^3 to tonnes (t), resulting in a value of 47.3 million t of eroded bank sediment over the 2009-2013 period. This gives an average-annual rate of 10.3 million t over the 4.58-year simulation period. It is important to recall that this value represents 292 km of the Burnett River main stem and does not include bank erosion in the tributaries. Of course, it is unrealistic to use this average bank-erosion value because it represents a

short time period and a period of high and record flows. In order to make more direct and robust comparisons to the SedNet bank-erosion estimates, two steps were required.

First, bank erosion was calculated for the 292 km of main-stem channel using the BSTEM results from the mainstem sites over the 2009 to 2013 period. This necessitated the interpolation of erosion rates at the simulated sites to adjacent reaches and then summing them for the entire river. We then compared these results to the 47.3 million t that was calculated empirically to provide confidence in the methodology. Second, BSTEM was used again at the six sites to predict bank erosion over a longer time period. These results were then used to interpolate bank-erosion rates to adjacent reaches and to sum the values again. An average, annual bank-erosion rate was then obtained by dividing the result by the number of years used in the simulations. The resulting value was then compared directly with the results from SedNet. Unit bank-erosion rates were obtained for each of the six main-stem sites by modelling daily bank erosion over three periods:

- Calibration period (2009-2013) using 2009 as the starting geometry;
- Existing period (2003-2013) using 2013 as the starting geometry; and
- Long-term period (1971-2013) using 2013 as the starting geometry.

Overall, unit-erosion volumes for the 2009-2013 calibration period (in m^3 per length of channel) ranged from 40.5 m^3/m at the Gayndah (BMRG-06) site, to a maximum of 360 m^3/m at the Shalom College (BMRG-03) site. Bank-top retreat in the BSTEM calibration runs ranged from 4.70 m at the Eidsvold (BMRG-08) site, to 23.9 m at the Shalom College (BMRG-03) site (Table 1). It should be noted here that unit-erosion volumes are a function not only of bank-top retreat, but also of bank height.

In general, modeled bank retreat in the calibration runs corresponded reasonably well with the aerial- photography analysis and site-specific notes made in the field. Modeled rates of retreat during the calibration period were between -29% and 114% of those measured from the aerial photographs, with an average difference of 12%. In the case of BMRG-05, where the percent difference between measured and modeled bank retreat showed the highest percent difference (114 %). When the actual retreat values are compared, it can be seen that we are comparing bank retreat values of 2.94 and 6.29 m. Comparison of the aerial photographs from 2009 and 2013 for the entire reach showed however, that there is considerable variation in bank erosion along the reach, and a four meter difference between the two values could simply be a slight variation in field testing location versus digital measurement on the photographs. This percent difference at BMRG-05 is, therefore, not considered to be of concern and the calibration run is within a reasonable range for the reach.

Table 1 Unit erosion volumes for each site from BSTEM 2009-2013 simulations, and comparison with bank retreat measured from aerial photography.

Site	Unit Erosion Volumes from BSTEM (2009 to 2013) (m^3/m)	Bank Retreat from Aerial Photography (2009 to 2013) (m)	Bank Retreat from BSTEM (2009 to 2013) (m)	% Difference Between Measured and Modeled Bank Retreat
BMRG-02- Rubyanna	161	18.0	20.2	12.0
BMRG-03- Shalom	360	23.0	23.9	3.96
BMRG-04- Kolan	110	13.9	11.7	-15.8
BMRG-05- Wallaville	213	2.94	6.29	114
BMRG-06- Gayndah	40.5	6.01	6.19	3.00
BMRG-07-Munduberra	345	8.67	6.17	-28.8

BMRG-08- Eidsvold	81.9	4.89	4.70	-3.89

BSTEM results for each time period are shown in Table 2 and were then multiplied by the "percent reach failing" (obtained from the RGA analysis of each 2- km segment of the channel) and the reach length to obtain a volume of material eroded in each 2-km reach. Summing these values over the entire 292 km provided the volume of eroded material over 292 km of the Burnett River main stem. Unit-erosion values obtained for each of the sites were assigned over a reach extending halfway upstream and downstream to the next modelled site (Table 3). Values for the downstream-most site (BMRG-02; Rubyanna) at rkm 20 were extended to the mouth. Values for the upstream-most site (BMRG-08; Eidsvold) were extended to the top of the reach at rkm 292.

Table 2 Results of BSTEM-Dynamic 2.0 simulations for the calibration, existing and long-term periods.

Simulation period	Calibration	Existing	Longterm
Days	1673	3865	15529
Years	4.58	10.6	42.5
Site	**Eroded Volume (m^3/m)**		
BMRG-02	161	135	158
BMRG-03	360	783	1390
BMRG-05	213	252	625
BMRG-06	40.5	57.7	75.4
BMRG-07	345	528	665
BMRG-08	81.9	63.7	550

Simulation period	Calibration	Existing	Longterm
Days	1673	3865	15529
Years	4.58	10.6	42.5
Site	**Average Eroded Volume (m^3/m/y)**		
BMRG-02	35.2	12.8	3.72
BMRG-03	78.6	74.0	32.7
BMRG-05	46.5	23.8	14.7
BMRG-06	8.84	5.45	1.77
BMRG-07	75.3	49.9	15.6
BMRG-08	17.9	6.02	12.9

Table 3 Interpolation of unit-erosion rates calculated by BSTEM-Dynamic 2.0 at the main stem sites to adjacent reaches of the Burnett River main stem for the three simulation periods.

Site	River kilometer	Unit erosion (m^3/m)	Reach (rkm)
Calibration Period			
BMRG-02	12	161	0-32
BMRG-03	54	360	34-72
BMRG-05	91	213	74-146
BMRG-06	202	40.5	148-220
BMRG-07	239	345	222-260
BMRG-08	279	81.9	262-308
10-Year Period			
BMRG-02	12	135	0-32
BMRG-03	54	783	34-72
BMRG-05	91	252	74-146
BMRG-06	202	57.7	148-220
BMRG-07	239	528	222-260
BMRG-08	279	63.7	262-308
Long term Period			
BMRG-02	12	158	0-32
BMRG-03	54	1390	34-72
BMRG-05	91	625	74-146
BMRG-06	202	75.4	148-220
BMRG-07	239	665	222-260
BMRG-08	279	550	262-308

Results for the calibration period using interpolation of the BSTEM results showed that 25.1 million m^3 (42.7 million t) of bank erosion occurred over the 292 km-long reach. This value is about 10% less than the value obtained from the detailed empirical analysis of each 2 km segment and, therefore, provides sufficient confidence in the approach to utilize the 10-year and 42-year simulation periods to interpret long-term rates of bank erosion.

As one might expect, the empirical analysis showed greater longitudinal variability owing to data analysis of topographic data every 2 km (Figure 8). Average, annual bank-erosion over this 4.58-year period comes to about 5.5 million m^3/y (9.3 million t/y). The 10-year simulations, used to determine future erosion rates under "existing" (no action) and mitigated conditions represent a relatively short timeframe by which to compute long-term erosion rates. In this case, interpolation of the 10-year simulations at the six sites over the 292 km reach resulted in 39.5 million m^3 (67.2 million t) of bank erosion, with an average, annual value of 3.7 million m^3/y (6.3 million t/y). Details of these simulations (which include an analysis of the relative contributions from equal durations (5 years) of "wet" and "dry" periods) are included in the discussions of modelling results for each site. The bulk (about 90%) of the bank-derived sediment is delivered to the channel during the wet periods. However, it is important to note that the dry periods can still be effective at hydraulically eroding bank-toe sediments, thus making the bank more susceptible to further undercutting and collapse both during and after high-flow events.

The long-term simulations were conducted using a period slightly greater than 42 years (January 21, 1971 to July 31, 2013). This period was selected because it represented a timeframe covered by all of the gauges that were ultimately used to generate daily-flow data along the main stem. In our view, this was a sufficiently long period to determine average, annual bank-erosion rates. BSTEM simulations were again conducted for the six sites using daily time steps for this period. Results for the individual sites are shown in Table 3. Summing these results for each 2-km reach gives a total volume of bank erosion of 77.1 million m^3 (131million t). Dividing by 42.52 years gives an average, annual bank-erosion rate of 1.8 million m^3/y. Converting to tonnes produces a long-term rate of 3.1 million t/y over the 42 years of simulation, almost 18 times greater than the value predicted by SedNet. A value of 2.4 million t/y is calculated by summing just those reaches below Paradise Dam.

With all of the simulation periods including the peak flows of 2011 and 2013, it is not surprising that the calculated average, annual erosion rates decrease with increasing length of the simulation period. Plotting the calculated erosion rates against the length of the simulation period (Figure 9) shows this tendency. Because episodes of accelerated erosion are closely linked to high-flow years, it is essential, therefore, to use as along a simulation period as possible to accurately determine long-term, average-annual rates. Extrapolating the regression shown in Figure 9 to assume a 100-year simulation period gives an average, annual bank-erosion rate of 2.0 million t/y (from just the main stem channel), still more than an order of magnitude greater than the previous catchment-wide estimates from this source.

Brodie et al., (2003) reports that on average, 2.75 Mt/y are eroded from the catchment. By replacing the 0.175 Mt/y from the banks with the 2.0 Mt/y calculated in this study, a new total of 4.6 Mt/y is obtained. Assuming that the estimates from gully (0.93 Mt/y) and hillslope (1.65 Mt/y) sources are accurate, bank erosion becomes the single largest contributor, delivering 44% of the total sediment load; and once again, this does not include contributions from the tributaries. Brodie et al., (2003) further reports that average, annual total export of sediment from the Burnett River to the Coral Sea is 0.47 Mt/y, implying that 83% of all eroded sediment is deposited behind dams and on floodplain surfaces. Although this is a critically important parameter in estimating sediment export, it is beyond the scope of this investigation to verify that only 17% of the sediment eroded in the Burnett River Catchment reaches the Coral Sea and the GBR. Comparison of capacity surveys beyond structures such as Paradise Dam and additional LiDAR information with which to calculate floodplain-deposition would be valuable data used to validate and refine this parameter value. If however, we use a sediment-delivery rate of 17% with the improved predictions of bank erosion calculated in this study, a 66% increase in the export of sediment (0.79 Mt/y) is obtained. We assume that if erosion of bank sediments from tributaries were included in this analysis, that this figure would be even higher.

Bank erosion, instead of being a minor source of sediment representing 8% of the total (Brodie et al., 2003), has been shown to be the single largest contributor of sediment in the Burnett River Catchment, representing at least 44% of the total, annual sediment budget. In absolute terms, this is an increase in the average, annual rate of bank erosion from 0.175 Mt/y to 2.0 Mt/y. Given these significant differences in both the relative importance and absolute

rates of bank erosion than was reported earlier, sediment management should be re-focused to include this important source. Doing so would not only protect local assets by limiting land loss and bank retreat, but would help maintain reservoir capacity, minimize downstream flooding, reduce dredging costs, and protect marine resources.

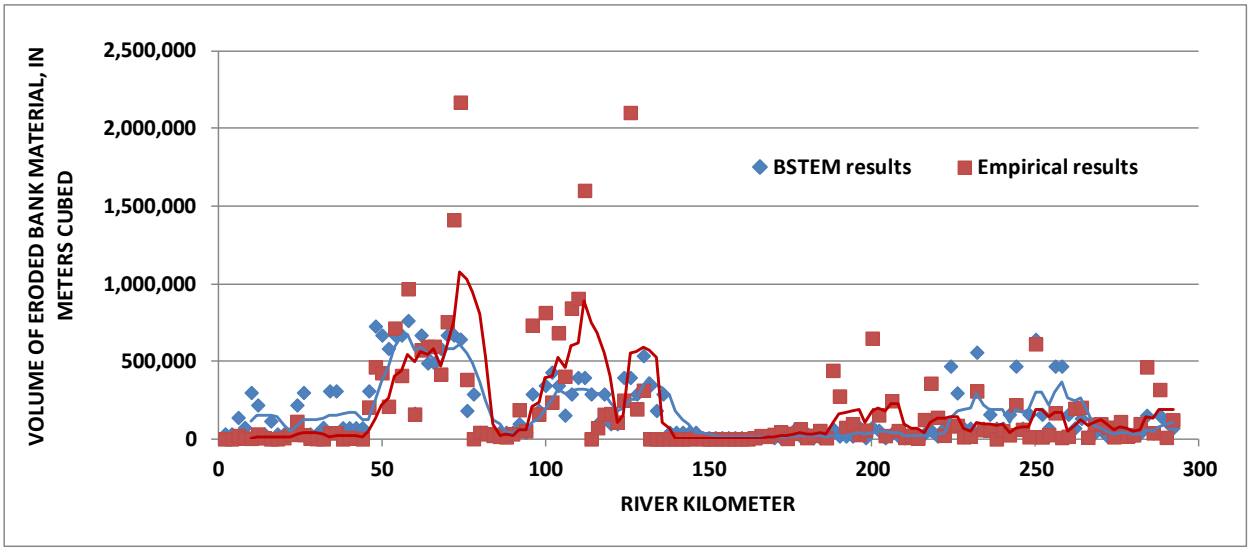

Figure 8 Comparison of bank-erosion volumes for each 2-km section of the Burnett River main stem as calculated from interpolation of BSTEM results and from analysis of LiDAR and air photo data over the 2009-2013 period.

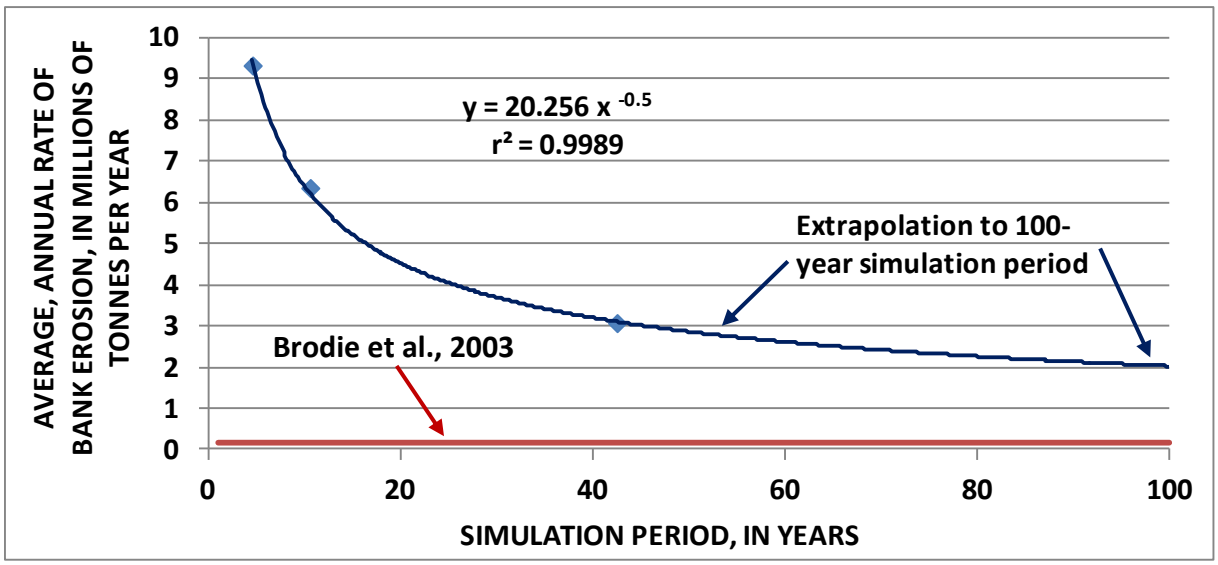

Figure 9 Comparison of average, annual bank-erosion rates (in millions of tonnes per year) for the Burnett River main stem derived from SedNet modelling (Brodie et al., 2003) and by interpolation of BSTEM results using different simulation periods.

SUMMARY AND CONCLUSIONS

Between 2009 and 2013 a total of about 27.8 million m^3 (47.3 Mt) of land were eroded from the banks of the lower 300 km of the Burnett River main stem. This translates into about 6.1 million m^3/y (10.4 Mt/y). Erosion of these bank materials does not equate to an equal volume being delivered to the river mouth and the Coral Sea, as an unknown proportion is deposited on low-bank surfaces, beds, bars and floodplains. It can be assumed, however, that the majority of the fine-grained materials (silts and clays) are transported through the system and out to sea.

Approximately 21 million m^3 (35.6 million t) or about two thirds of these sediments were eroded from banks downstream of Paradise Dam. One can assume that much of the hydraulically-controlled bank sediment eroded from reaches upstream of rkm 170 was trapped behind Paradise Dam (7.0 million m^3).
Long-term simulations (42 years) were conducted to determine average, annual rates of bank erosion. By again summing the results for each 2 km reach gives a total volume of bank erosion of 77.1 million m^3 (131 million t). Dividing by 42.52 years gives an average, annual bank-erosion rate of 3.1 million Mt/y, about 18 times greater than the value of 0.175 Mt/y predicted by SedNet. Bank-erosion rates below Paradise Dam are 2.4 million t/y. Assuming 100 years of simulation and using an empirical relation between the length of BSTEM simulations and calculated erosion rates, a conservative value for the average, annual rate of bank erosion is 2.0 Mt/y, and this does not include tributary contributions.

The implications of these findings are considered in the context of erosion sources and rates in Brodie et al. (2003) who report that on average, 2.75 Mt/y are eroded from the catchment. By replacing their 0.175 Mt/y from the banks with the 2.0 Mt/y calculated in this study, a new total of 4.6 Mt/y is obtained. Assuming that the estimates from gully (0.93 Mt/y) and hillslope (1.65 Mt/y) sources are accurate, bank erosion becomes the single largest contributor, delivering 44% of the total sediment load. Even using the 17% sediment-delivery rate reported in Brodie et al (2013), with the predictions of bank erosion calculated in this study, a 66% increase in the export of sediment (0.79 Mt/y) is obtained. We assume that if erosion of bank sediments from tributaries were included in this analysis, this figure would be even higher. Given these significant differences in both the relative importance and absolute rates of bank erosion then was earlier reported, sediment management should be re-focused to include this important source. Doing so would not only protect local assets by limiting land loss and bank retreat, but would help maintain reservoir and harbour capacity, minimize downstream flooding, reduce dredging costs, and protect marine resources.

REFERENCES

ASTM (1995). Annual Book of ASTM Standards: Section 4, Construction, v. 04-09. American Society for Testing and Materials, West Conshohocken, PA.

Brodie, J., McKergow, L.A., Prosser, I.P., Furnas, M., Hughes, A.O., and Hunter, H. (2003). Sources of Sediment and Nutrient Exports to the Great Barrier Reef World Heritage Area. Australian Centre for Freshwater Tropical Research Report Number 03/11, 192 p.

Hanson, G.J. (1990). "Surface erodibility of earthen channels at high stress, Part II - Developing an in situ testing device", Transactions ASAE, 33(1), pp.132–137.

Hanson, G.J., and Cook, K.R. (1997). "Development of excess shear stress parameters for circular jet testing", American Society of Agricultural Engineers Paper No. 97-2227. American Society of Agricultural Engineers, St. Joseph, MO.

Lohnes, R. A. and Handy, R. L., (1968). Slope Angles in Friable Loess. Journal of Geology. 76(3), 247-258.

Lutenegger, J. A. and Hallberg, B. R., (1981). Borehole Shear Test in Geotechnical Investigations. ASTM Special Publications 740, 566-578 p.

Simon, A., (1989). A model of channel response in disturbed alluvial channels. Earth Surface Processes and Landforms, 14(1): 11-26.

Simon, A., A. Curini, S. A. Darby, and E. J. Langendoen. (2000). Bank and near-bank processes in an incised stream. Geomorphology, 35: 193–217.

Simon, A. and Downs, P.W. (1995). An interdisciplinary approach to evaluation of potential instability in alluvial channels, Geomorphology, 12(3): 215-232,

Simon, A., and Hupp, C. R., (1986). Channel evolution in modified Tennessee channels, Proceedings of the *Fourth Federal Interagency Sedimentation Conference*, March 1986, Las Vegas, Nevada, v. 2, Section 5, 5-71 to 5-82.

Thorne, C. R., Murphey, J. B. and Little, W. C., (1981). Stream Channel Stability, Appendix D, Bank Stability and Bank Material Properties in the Bluffline Streams of Northwest Mississippi. U.S. Department of Agriculture, Agricultural Research Service, National Sedimentation Laboratory. Oxford, MS. 227 p.

SEDIMENT DIVERSION EFFICIENCY, LESSONS LEARNED FROM MISSISSIPPI RIVER MODELS

Ronnie Heath, Ronald.E.Heath@usace.army.mil, Gary Brown, Gary.L.Brown@usace.army.mil, and Jeremy Sharp, Jeremy.A.Sharp@usace.army.mil, Research Civil Engineers, U. S. Army Corps of Engineers, Engineer Research and Development Center, Coastal and Hydraulics Laboratory, Vicksburg, Mississippi.

ABSTRACT

Large scale diversions of sediment and water from the Mississippi River have been proposed as a means to restore valuable wetlands along the Louisiana coast (CRPA 2012). Successful design and operation of diversions requires that diverted water volumes and sediment loads be carefully balanced to maintain channel stability and to achieve restoration goals. In general, diversions reduce sediment transport capacity in the river downstream of the withdrawal, and disproportionally large diversions of bed material are required to balance this reduction. In the Mississippi River, deposition induced by insufficient sediment diversions may impact other authorized project purposes such as navigation and flood control.

Sediment diversions are defined in the HEC-6 one-dimensional sedimentation model by coefficients defining the fractions of water and sediment diverted from the river (USACE, 1993). The sediment diversion coefficient, k_{SD}, the ratio of the diverted sediment concentration, C, to the ambient concentration in the river (equation 1), describes the efficiency of the sediment diversion and is proposed as the basis for metrics suitable for comparing diversion alternatives and informing design and operation planning.[1] For computational purposes, the coefficient also may be defined in terms of water discharge, Q, and sediment load, Q_S. While the sediment diversion coefficient is conceptually simple, its application and estimation can be complex and challenging.

$$k_{SD} = \frac{C_{Diversion}}{C_{River}} = \frac{\left(Q_S/Q\right)_{Diversion}}{\left(Q_S/Q\right)_{River}} \quad (1)$$

The U. S. Army Engineer Research and Development Center's (ERDC) Coastal and Hydraulics Laboratory (CHL) has conducted model studies ranging from analytical models (Letter et al. 2008 and Brown et al. 2013) to estimate equilibrium sediment diversion efficiencies to multi-dimensional model studies of the West Bay Sediment Diversion (Sharp et al. 2013) and the Old River Control Complex to gain insight into the behavior and impacts of existing diversions. The CHL is currently working with the U. S. Army Corps of Engineers New Orleans District and the

[1] Closely related variations on the sediment diversion coefficient appearing in the literature include the water-sediment ratio, concentration ratio, and sediment diversion ratio.

State of Louisiana to conduct a comprehensive evaluation of proposed sediment diversions from the Mississippi River to restore coastal wetlands.

REFERENCES

Brown, G. L., Letter, J. V., Heath, R. E., McAdory, R. T., Wehmeyer, L. L., and Gunkel, B. L. (2013). "A Simplified Analytical Investigation of the Riverside Effects of Sediment Diversions," ERDC/CHL CHETN-VII-13, Vicksburg, Mississippi. http://acwc.sdp.sirsi.net/client/search/asset/1030340

CRPA (2012). Louisiana's Comprehensive Master Plan for a Sustainable Coast. Coastal Protection and Restoration Authority (CRPA) of Louisiana, Baton Rouge, Louisiana. http://coastal.la.gov/a-common-vision/2012-coastal-master-plan/

Letter Jr., J.V., Pinkard Jr., C. F,, and Raphelt, N. K. (2008). "River Diversions and Shoaling," ERDC/CHL CHETN-VII-9, Vicksburg, Mississippi. http://chl.erdc.usace.army.mil/library/publications/chetn/pdf/chetn-vii-9.pdf

Sharp, J., Little, C., Brown, G., Pratt, T., Heath, R., Hubbard, L., Pinkard, F., Martin, K., Clifton, N., Perky, D., and Ganesh, N. (2013). West Bay Sediment Diversion Effects, ERDC/CHL Technical Report 13-15, Vicksburg, Mississippi. http://acwc.sdp.sirsi.net/client/en_US/search/asset/1032362

U. S. Army Corps of Engineers (1993). HEC-6, Scour and Deposition in Rivers and Reservoirs, User's Manual, Hydrologic Engineering Center, Davis, California. http://www.hec.usace.army.mil/software/legacysoftware/hec6/hec6-documentation.htm

VEGETATION CANOPY COVER EFFECTS ON SEDIMENT AND SALT LOADING IN THE UPPER COLORADO RIVER BASIN MANCOS SHALE, PRICE AND FERRON, UTAH

Erik Cadaret, Graduate Program of Hydrologic Sciences, Desert Research Institute, Division of Earth and Ecosystem Sciences, Reno, Nevada Erik.Cadaret@dri.edu; Robert Blank, Research Soil Scientist, United States Department of Agriculture, Agricultural Research Service, Reno, Nevada bob.blank@ars.usda.gov; Kenneth McGwire, Associate Research Professor, Desert Research Institute, Division of Earth and Ecosystem Sciences, Reno, Nevada Ken.McGwire@dri.edu; Sayjro K. Nouwakpo, Research Professor, University of Nevada Reno, Department of Natural Resources and Environmental Science, Reno, Nevada snouwakpo@cabnr.unr.edu; Colleen G. Rossi, Water Quality Salinity Specialist, Bureau of Land Management, Salt Lake City, Utah crossi@blm.gov; Mark Weltz, Rangeland Hydrologist and Research Leader, United States Department of Agriculture, Agricultural Research Service, Reno, Nevada mark.weltz@ars.usda.gov; Todd Adams, Rangeland Ecologist, University of Nevada Reno, Department of Natural Resources and Environmental Science, Reno, Nevada todd.adams@ars.usda.gov; Alice Boizet, University of Nevada Reno Summer 2014 Environmental Science Scholar, Montpellier SupAgro, Montpellier, France; Sandra Li, Biological Science Lab Technician, United States Department of Agriculture, Agricultural Research Service, Reno, Nevada sandra.li@ars.usda.gov; Tye Morgan, Biological Science Lab Technician (Soils), United States Department of Agriculture, Agricultural Research Service, Reno, Nevada tye.morgan@ars.usda.gov; Jacob Phillips, Biological Science Lab Technician (Soils), United States Department of Agriculture, Agricultural Research Service, Reno, Nevada

ABSTRACT: The Price River contributes only one percent of the water but three percent of the total dissolved solids in the Colorado River. To investigate mechanisms driving salinity loads in the Price River Basin we are focusing on saline and sodic soils associated with the Mancos Shale formation. Rainfall simulations have been performed at study areas across a variety of slope angle and rainfall intensity to evaluate the effects vegetation has on salinity and sediment concentration in runoff. A 6x2 meter, computer-controlled Walnut Gulch rainfall simulator was ran with rainfall event intensities derived from the NOAA ATLAS 14 precipitation database: 2 year (5.08 cm/hour), 10 year (8.89 cm//hour), 25 year (11.43 cm/hour), and 50 year (13.97 cm/hour) and each intensity was replicated three times at each site. For each simulated rainfall event, we measured the time-varying concentration of major cations (Calcium, Magnesium, Sodium, Potassium, and Ammonium) and anions (Chlorine, Sulfate, Nitrite, and Nitrate) in runoff. We also compare depth-varying soil chemistry in soil cores at vegetated and un-vegetated areas to identify the effects of plants on soil chemistry distribution. Results of these simulations will be used to parameterize the dynamic Rangeland Hydrology and Erosion Model (RHEM) for saline and sodic soils of the Price rangeland areas and to assess the feasibility of mitigation strategies for reducing salinity loads to the Colorado River.

INTRODUCTION

The Bureau of Land Management, USDA Agricultural Research Service, Bureau of Reclamation, and Desert Research Institute are investigating salinity contributions to the

Colorado River from saline and sodic soils of rangelands in the Colorado Plateau. Field sites in Price and Ferron, Utah were selected to perform rainfall simulations to measure the response of salinity and sediment loads with respect to vegetation canopy cover (Figure 1). It is suspected that vegetation canopy cover has a large effect on water erosion and runoff processes primarily because of rainfall interception (Wischmeier and Smith, 1978). Interception of rainfall by vegetation is a function of precipitation and canopy characteristics (Hamilton and Row, 1949; Slatyer, 1965; Navar and Bryan, 1990; Domingo et al., 1994). Vegetation interception reduces runoff volumes, and stemflow may promote deep infiltration in the soil directly beneath the canopy (Branson et al., 1972). At the beginning of a rainfall event, canopies efficiently intercept almost all rainfall within the area they project over the ground until a maximum is reached when the cumulative interception (through-fall, foliar drip, and stemflow) is equal to the amount of precipitation. The amount of time to reach maximum cumulative interception is dependent upon the type of plant and the rainfall intensity (Wood et al., 1998). Proportionally, rainfall lost to vegetation interception is most prominent under conditions of lower rainfall intensities and may strongly influence erosion rates under such conditions (Simanton et al., 1991). Vegetation-driven spatial heterogeneity (VDSH) explains the relationship between soil development and evolution processes between vegetation and interspace areas (Puigdefabregas, 2005). VDSH influences sheet runoff and concentrated flow processes that in turn influence rill and channel development, and thereby affect salinity and sediment loading along those flow paths (Wilcox et al., 1996; Davenport et al., 1998; Urgeghe et al., 2010). Rills and gullies are considered erodible sediment conveyors, transporting detached sediment downslope depending on VDSH and the detachment and conveyance hydraulic factors (Puigdefabregas, 2005; Al-Hamdan et al., 2012).

There are two goals for this project: (1) improve the understanding of sources and transport mechanisms of salinity and sediment loads into streams from rainfall induced runoff within the Upper Colorado River Basin (UCRB) and specifically in the Price River Basin and (2) parameterize our findings for vegetation canopy cover so they can be implemented into the Rangeland Hydrology Erosion Model (RHEM). We hypothesize that the amount of vegetation canopy cover has a strong influence on the salinity and sediment loading in runoff during a rainfall event due to reduced splash erosion, increased infiltration, and reduced flow velocity. To accomplish these goals and test our hypotheses, we conducted rainfall experiments with the Walnut Gulch rainfall simulator (WGRS) (Paige et al., 2004) using four rainfall intensities replicated three times at two different field sites differing in slope, geology, and vegetation canopy cover. This rainfall simulator was chosen to perform these experiments because of the long history of successful use to measure how rainfall affects runoff and erosion, transportability, and its computer controlled interface. Using the WGRS, we may conduct experiments that accurately simulate specified rainfall intensities, and in turn, measure representative runoff and erosion processes occurring at the plot scale (6x2 m). Ultimately, our experiments will produce meaningful data to incorporate into the RHEM model so it can be used as a management tool by determining how vegetation affects the surface hydrology and controls salinity in the UCRB.

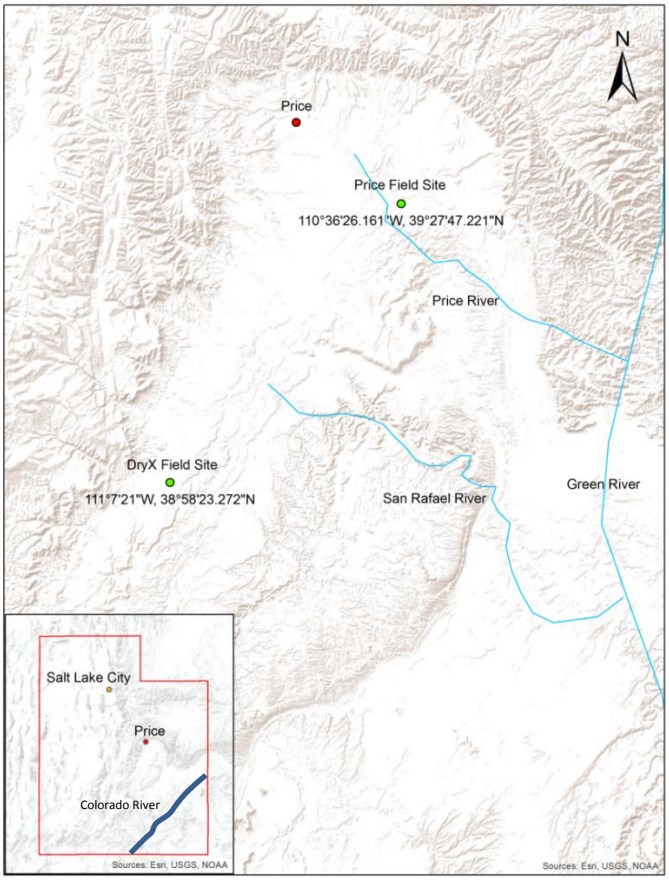

Figure 1 Map of field area in Price, Utah

MATERIALS AND METHODS

Location, Field Site Characteristics, and Experimental Design: The experimental sites were at Price (-110° 36' W, 39° 27' N) and Dry-X Ranch (-111° 7' 21" W, 38° 58' N) located in Utah. The Price field site contains well developed, light gray soil crusts surrounded by sparse vegetation on shallow grade slopes (0.6% - 10%). The vegetation at the site is comprised of halophytes that include a mixture of four shrubs (*Krascheninnikovia lanata*, *Chrysothamnus nauseosus, Atriplex gardneri, Ephedra viridis*), two subshrubs (*Eriogonum microthecum* & *Helianthella microcephala*), and three grass species (*Achnatherum hymenoides, Hilaria jamesii, Elymus elymoides*). The most predominant plant species were *Ephedra viridis, Atriplex gardneri*, and *Achnatherum hymenoides*. The Dry-X field site contains poorly developed, light-medium gray soil crusts surrounded by dense vegetation on steep grade slopes (11.4% - 24.5%). The vegetation at the site is solely comprised of salt tolerant shrub species *Atriplex Corrugata*. Both sites contained a marginal amount of cattle and antelope hoof impressions as they were a part of the natural landscape.

At both Price and Dry-X, 6x2 m rainfall simulation plots were installed and placed on the hillsides representative and NEPA approved for this study. The locations of each plot on the hillside were based upon where rills were already developed and would carry water down-gradient. Once the locations of each plot were determined, a Nikon NPR 352 total station was

used to make the borders square to one another. Metal stakes and construction string where then used to indicate where the 2x0.2 m steel plates are installed on the top and side borders. At the bottom of the plot, a flume was installed to channel runoff from the plot into the runoff collection pit. At each site, there were 5 types of plots: (1) control (no rainfall), (2) 2 year storm, (3) 10 year storm, (4) 25 year storm, and (5) 50 year storm. Each intensity, except for the controls, was replicated three times (Figure 2) resulting in 12 rainfall plots per site and 4 control plots per site.

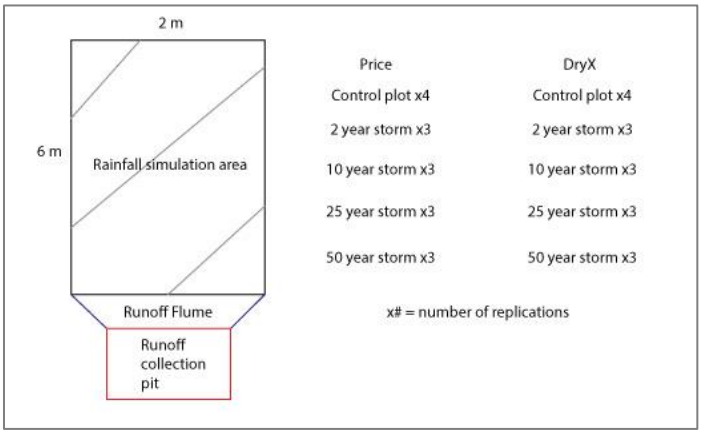

Figure 2 Rainfall plot design and types

Rainfall Simulations and Sampling Protocol: In this study, we used the WGRS that covers the 6x2 m plots. The WGRS was connected to a Husky 3785 L self-supporting onion tank using a series of water hoses and pumps. Intensities for our rainfall simulations were determined from 5 minute rainfall amounts reported in the NOAA Atlas14 point precipitation frequency estimates for the Price area.

Runoff was collected during each simulation using two different collection containers. The source water supply and runoff water quality samples were collected using VWR 50 mL centrifuge tubes. Runoff sediment samples were collected using 1 liter Nalgene bottles. Neither type of bottle was pretreated. The source water supply was sampled before each rainfall simulation was initiated. The same runoff sampling protocol was applied to each field site with the exception of the timing intervals. At Price, runoff was collected every 30 seconds for the first nine minutes and after the ninth minute, runoff was collected every minute until the end of the rainfall simulation. At Dry-X, runoff was collected every 30 seconds for the first three minutes and after the third minute, runoff was collected every 3 minutes until the end of the rainfall simulation. The timing interval was different at the two field sites because of the difference in vegetation cover and slope which influence runoff response timing. The runoff sediment samples were labeled and stored without refrigeration in plastic crates. The runoff water quality samples were para-filmed to reduce the chance of leakage and placed in large plastic Ziploc bags that were pre-labeled and stored inside coolers with dry ice in order to reduce subsequent bacterial reactions.

Samples of pre-rainfall soils were collected on the control plots using a standard hand shovel due to the lack of soil adhesion. Separate control plots were used to provide information on pre-simulation soil characteristics, since sampling in the rainfall plots prior to simulation would affect the flow and erosion. After rainfall simulations, soil samples were collected using an AMS

split soil core sampler with a 5 cm inside diameter. At each plot, soils were collected at three locations under the vegetation canopy and three interspace locations. Soil sample locations were quasi-randomly chosen by the field technician (Figure 3) in an area towards the middle portion of the plot to minimize the lateral flow affects that may occur near the plot borders. Soil samples were separated by depth increments into the surface crust (~0 cm), depth increment 1 (0-5 cm), and depth increment 2 (5-10 cm) (Figure 4). Finally, soil samples from each plot were aggregated by vegetation versus interspace for each depth increment, resulting in 6 composite samples per plot. The number of depth increments and the total depth to be collected was based on the wetting front from a test soil core taken from the first plot of each intensity. It was determined that two 5 cm depth increments were sufficient to capture the changes in soil moisture status during a rainfall event. We collected a total of 192 soil samples; 96 from Price and 96 from Dry-X.

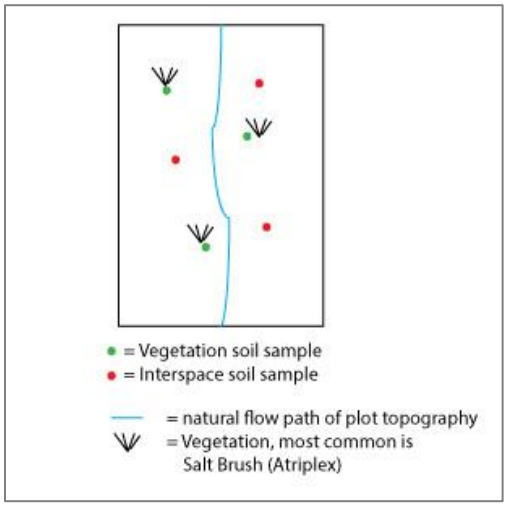

Figure 3 Aerial view of plot

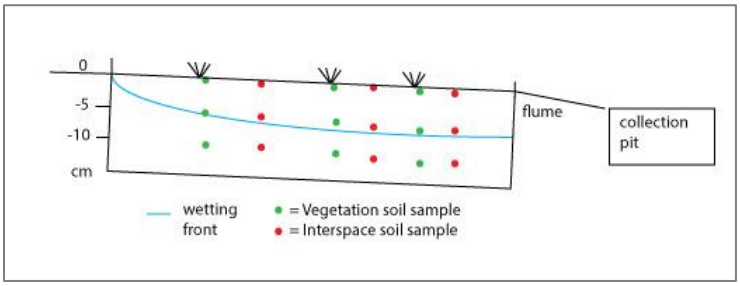

Figure 4 Profile view of plot

Vegetation Canopy Cover: A field technician took digital photographs spaced approximately 1 m apart all around the plot before and after the simulation. These digital images will be processed to planimetrically accurate orthophotographs and we will measure the distribution of canopy, litter, and bare soil. There was minimal detached litter, likely due to grazing on the site.

Laboratory Processing:

Water Chemistry

Runoff water quality samples were processed and measured at the USDA-ARS soils laboratory in Reno, NV. Price samples were centrifuged at 2000 rpm for three minutes to settle sediments and DryX samples were centrifuged at 5000 rpm for 5 minutes to settle sediments due to suspected high sodium concentrations. We measured the ions directly from the sample VWR 50 mL centrifuge tube. Major cations (Ca^{2+}, Mg^{2+}, K^{+}, Na^{+}) were measured using a Perkin Elmer Atomic Absorption (AA) Spectrometer. Ammonium ($NH4^{+}$) was measured using a Lachat Quickchem FIA+ instrument. Major anions (NO_2^{-}, NO_3^{-}, SO_4^{2-}, Cl^{-}) were measured using a Dionex Ion Chromatograph (IC). Water pH and EC were measured in the lab using an Oakton pH Meter 510 Series and VWR Scientific EC Meter Model 2052, respectively.

Soil Chemical Content and Texture

Soil samples were processed using several different methods. The total pool of soluble phase ions from the soils was processed by performing immiscible displacement (ID) (Mubarak and Olsen, 1977). To get the total pool of available exchangeable cations from the soils (mineral phase cations), we performed ammonium acetate ($NH_4C_2H_3O_2$) extractions (Thomas, 1982). Ammonium and nitrate were processed from the soils by performing KCl extractions (Bundy and Meisinger, 1994). Cation exchange capacity (CEC) was measured according to methods of Bower et al. (1952). Major cations were measured on the AA; major anions were measured on the IC, and ammonium and CEC on the Lachat. Soil soluble phase ion solution produced by ID was measured for pH and EC using an Oakton pH Meter 510 Series and VWR Scientific EC Meter Model 2052, respectively. Soil texture was measured using methods of Jackson and Barak (2005).

Data Analysis:

Principal Component Analysis, T-tests, and Regression Analysis

Data analysis is currently underway. Principal Component Analysis will be used as a data exploration tool that will aid us to determine sources of variability across different categories of interest. Data distributions will be normalized to correct for severe skewness and substantial outliers will be investigated. Two-sample T-tests with unequal variances will be performed on the runoff and soil data to ascertain whether or not the following hypotheses are true:

1. Is there a significant difference between Price soils (μ1) and DryX soils (μ2)?

    i. H_o: The Price and DryX soils mean difference = 0

    b. Is there a significant difference between Price soils SAR (μ1) and DryX soils SAR (μ2) (SAR = sodium absorption ratio)?

    i. H_o: The Price and DryX soils SAR mean difference = 0

    c. Is there a significant difference between Price soils CEC (μ1) and DryX soils CEC (μ2) (CEC = cation exchange capacity)?

    i. H_o: The Price and DryX soils CEC mean difference = 0

2. Is there a significant difference between Price runoff (μ1) and DryX runoff (μ2)?

    a. Is there a significant difference between Price sediment load in Runoff (μ1) and DryX sediment load in Runoff (μ2) (Sediment load units = g/L)?

    i. H_o: The Price and DryX soils sediment load mean difference = 0

    b. Is there a significant difference between Price salinity load in runoff (μ1) and DryX salinity load in runoff (μ2) (Salinity load = total dissolved solids (mg/L))?

    i. H_o: The Price and DryX soils Salinity Load mean difference = 0

3. Is there a significant difference between vegetation soils (μ1) and interspace soils (μ2) at each site?

   a. Is there a significant difference between vegetation soils sum of ions (μ1) and interspace soils sum of ions (μ2) at each site (Sum of ions (mg/L))?

      i. H_o: The vegetation and interspace soils sum of ions mean difference = 0

4. Is there a significant difference between vegetation (μ1) and interspace soils sum of ions (μ2) with depth at each site (Sum of ions (mg/L))?

   a. H_o: The vegetation and interspace soils mean difference = 0 at depth 1; 2; 3

We will conduct regression analyses of salinity concentration versus sediment concentration in runoff in order to evaluate if sediment concentration can be used as a proxy for salinity (TDS) when using the RHEM model.

1. By using sediment load (g/L) data, can sediment load be used as a proxy to reasonably estimate salinity load represented by TDS (mg/L)?

   a. H_o: Slope of salinity load against sediment load is zero; m = 0

PRELIMINARY RESULTS

Figures 5-7 present the mean sodium absorption ratio (SAR) values at Price and Dry-X for the pre- and post-rainfall soil samples and the mean runoff sediment load.

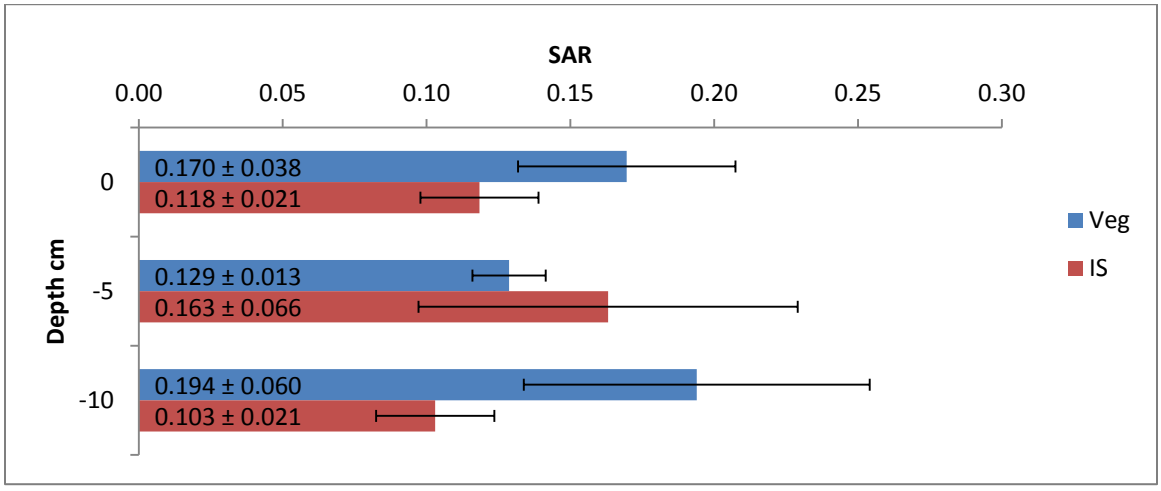

Figure 5 Price mean SAR ± standard error values with depth

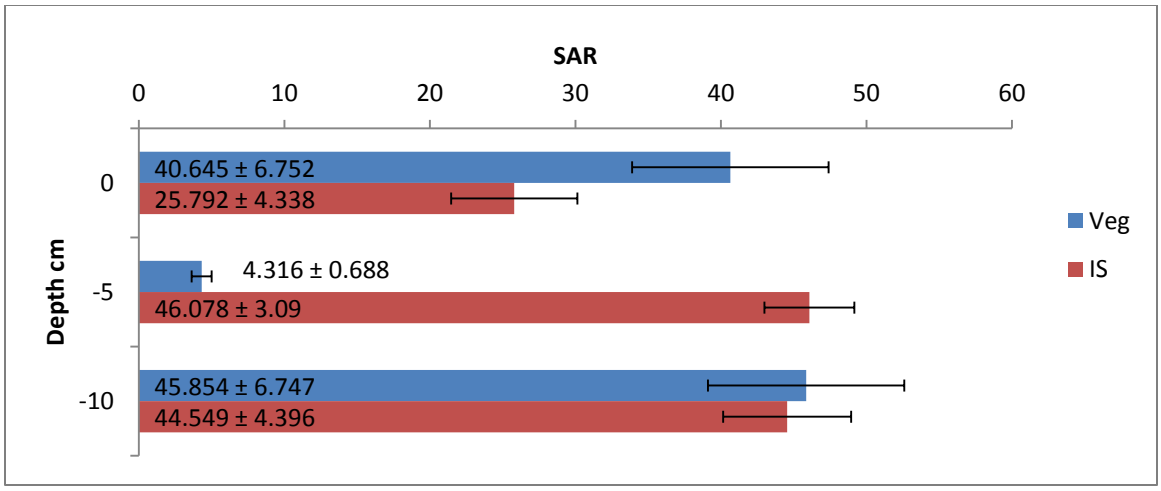

Figure 6 Dry-X mean SAR ± standard error values with depth

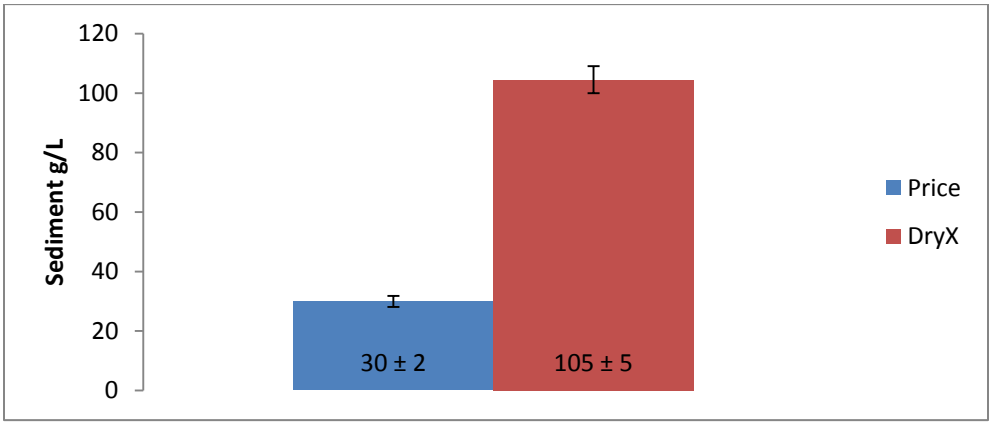

Figure 7 Mean sediment load ± standard error values at Price and Dry-X

The mean EC values at Price and Dry-X for the applied rainwater and runoff (Figure 8).

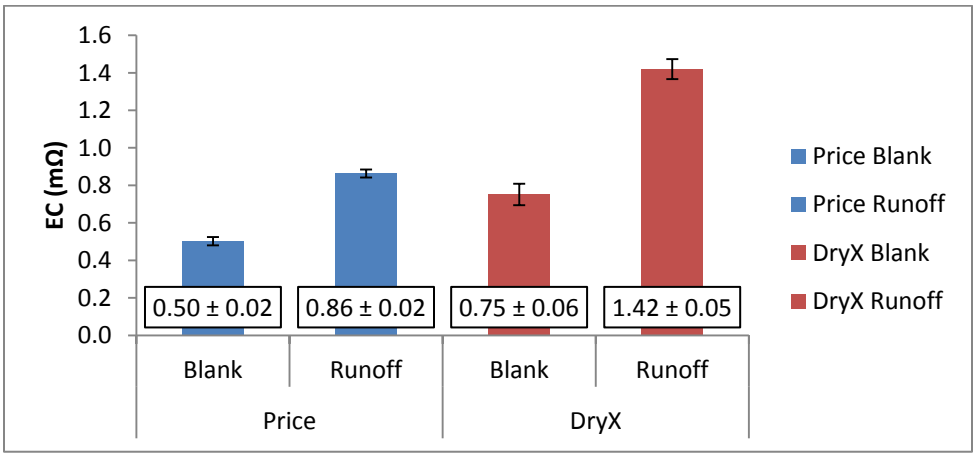

Figure 8 Mean EC ± standard error values for both Price and Dry-X

Price mean SAR values are < 1.0, indicating the soils have low dispersion (Figure 5). Almost all the Dry-X mean SAR values are substantially greater than 15.0 indicating the soils have high dispersion which indicates high erodibility (Figure 6). Price soils have substantially lower mean SAR values than Dry-X and indicate variation with depth, but there is no major difference between soil samples collected under the vegetation canopy (Veg) and those from the interspace soil (IS). Dry-X soils have substantially greater mean SAR values than Price and clearly present a decrease with depth at -5 cm for Veg. Dry-X mean sediment load and EC are much greater than Price (Figures 7 and 8). This may be a result of the level of soil dispersion and slope.

CONCLUSIONS

This study investigates vegetation canopy cover effects on salinity and sediment loading in runoff. Vegetation canopy cover may control salinity and sediment loads by rainfall interception and VDSH. Our data analysis will evaluate the complexity of interactions within our system and determine: 1) if sediment load may be used as a proxy for salinity load, 2) the sensitivity of vegetation canopy cover in RHEM, 3) the role of VSDH on salinity and sediment loading. Studies at these two sites which have substantial differences despite being from the same Mancos Shale formation will inform our understanding of the difficulties in applying the RHEM model to saline-sodic soils with variable vegetation canopy cover. Future results will help to prioritize improvements to the RHEM model and ultimately be used to assess mitigation strategies to reduce salinity loads into the Colorado River Basin.

REFERENCES

Al-Hamdan, O.Z., Pierson, F.B., Nearing, M.A., Williams, C.J., Stone, J.J., Kormos, P.R., Boll J., and Weltz, M.A. (2012). "Concentrated flow erodibility for physically based erosion models: temporal variability in disturbed and undisturbed rangelands". Water Resources Research 48. Doi: 10.1029/2011wr011464.

Branson, F.A., Gifford, G.F., and Owen, J.R. (1972). Rangeland hydrology society for range management Denver, Colorado.

Bower, C.A., Reitemeier, R.F., and Fireman, M. (1952). "Exchangeable cation analysis of saline and alkali soils". Soil Sci., 73, 251-261.

Bundy, L.G., and Meisinger, J.J. (1994). Nitrogen availability indices. In: Weaver, R.W., Angle, S., Bottomley, P., Bezdicek, D., Smith, S., Tabatabai, A., Wollum, A. (Eds.), Methods of Soil Analysis. Part 2. Microbiological and Biochemical Properties, Soil Science Society of America, Madison, WI, pp. 951–984.

Davenport, D.W., Breshears, D.D., Wilcox, B.P., and Allen, C.D. (1998). "Viewpoint: Sustainability of pinon-juniper ecosystems: A unifying perspective of soil erosion thresholds". Journal of Range Management 51:231-240.

Domingo, F., Puigdefabregas, J., Moro, M.J., and Bellot, J. (1994). "Role of vegetation cover in the biogeochemical balances of a small afforested catchment in southeastern Spain". Journal of Hydrology 159:275-289

Hamilton, E.L., and Row, P.B. (1949). "Rainfall interception by chaparral in California"

Jackson, M.L., and Barak, P. (2005). Soil chemical analysis: advanced course. UW-Madison Libraries Parallel Press.

Mubarak, A., and Olsen, R.A. (1977). A laboratory technique for appraising in situ salinity of soil. Soil Sci Soc Am J 41:1018–1020.

Navar, J., and Bryan, R. (1990). "Interception loss and rainfall redistribution by three semi-arid growing shrubs in northeastern Mexico". Journal of Hydrology 115:51-63.

Paige, G.B., Stone, J.J., Smith, J.R., and Kennedy, J.R. (2004). "The walnut gulch rainfall simulator: a computer-controlled variable intensity rainfall simulator". American society of agricultural engineers, 20(1), 25-31.

Puigdefabregas, J. (2005). "The role of vegetation patterns in structuring runoff and sediment fluxes in drylands". Earth surface processes and landforms 30:133-147. Doi: 10.1002/esp.1181.

Simanton, J. R., Weltz, M. A., and Larsen, H. D. (1991). "Rangeland experiments to parameterize the water erosion prediction project model: vegetation canopy cover effects". Journal of Range Management, 276-282.

Slatyer R. (1965). "Measurements of Precipitation Interception by an Arid Zone Plant Community (Acacia Aneura F. Muell)", Unesco Arid Zone Research, Vol. 25, pp 181-192, 1956, 7 Fig, 2 Tab, 13 Ref, Disc.

Thomas, G.W. (1982). Exchangeable cations. In A.L. Page, R. H. Miller, and D. R. Keeney (eds.). Methods of soil analysis. Part 2. Chemical and microbiological properties. 2nd ed., Agron. Monogr. 9, ASA and SSSA, Madison, WI. p. 159-165.

Wilcox, B., Davenport, D., Pitlick, J., and Allen, C. (1996). "Runoff and erosion from a rapidly eroding pinyon-juniper hillslope", Los Alamos National Lab., NM (United States).

Wischmeier, W. H., and Smith, D. D. (1978). "Predicting rainfall erosion losses-A guide to conservation planning". Predicting rainfall erosion losses-A guide to conservation planning.

Wood, M. K., and Blackburn, W. H. (1981). "Grazing systems: their influence on infiltration rates in the Rolling Plains of Texas". Journal of Range Management, 331-335.

Urgeghe, A.M., Breshears, D.D., Martens, S.N., and Beeson, P.C. (2010). "Redistribution of runoff among vegetation patch types: on ecohydrological optimality of herbaceous capture of run-on". Rangeland ecology & management 63:497-504.

CONTINUOUS VERTICAL SORTING MODEL IN SRH-1D

Sean Kimbrel, Hydraulic Engineer, Bureau of Reclamation, Denver, CO, skimbrel@usbr.gov; Blair Greimann, Hydraulic Engineer, Bureau of Reclamation, Denver, CO, bgreimann@usbr.gov; Victor Huang, Hydraulic Engineer, Bureau of Reclamation, Denver, CO, vhuang@usbr.gov

ABSTRACT

Reclamation's one-dimensional numerical hydraulics and sediment transport model, SRH-1D (Huang and Greimann, 2012), is used within Reclamation for its extensive capabilities, including the prediction of the routing of reservoir sediments as a result of dam removal. The development of SRH-1D over the past 15+ years has been important to the predictions of sediment-related impacts for several of Reclamation involved projects, which includes dam removal assessments for the Klamath River and Matilija Dam Removal studies, and continued monitoring of the removal of Glines Canyon and Elwha Dams on the Elwha River. Other studies include erosion downstream of Taiwan Dams, the Rio Grande River, and the San Joaquin River Restoration Project.

The current bed-material mixing algorithm in SRH-1D relies upon the active layer concept and this methodology has been observed to have difficulties simulating the change of the bed-material composition from a coarse, armored bed to a mixed bed of sand and gravel sized sediments. The current bed-material mixing algorithm requires the user-specified number of N layers, in which the bed is composed of one active layer and N-1 inactive layers. Most sediment models using the active layer concept simulating the release of finer sediments over a coarse armor layer are 'tricked' by making the initial armor immobile and giving the initial active layer an averaged grain size distribution of the reservoir sediments. This workaround keeps the pre- and post-dam release bed layers separate, thereby accurately simulating the transport of finer grained sediments, but neglects the potential mobility of the armor layer after finer-grained sediments are transported through the system.

Current research is developing and applying a continuous vertical sorting model in SRH-1D, with potential of incorporation into Reclamation's two-dimensional hydraulics and sediment transport model, SRH-2D (Lai, 2008). A continuous vertical sorting model was most recently proposed in Merkel and Kopmann (2012). This continuous vertical sorting model (or algorithm) has the ability to account for multiple sediment layers of varied thickness and gradation that are continuously depositing and eroding through time, thereby yielding a temporally and spatially varied stratigraphy of sediment layers. This method automatically keeps the coarse pre-dam removal armor layer separate from the finer sediment layers deposited and eroded from the channel. The research model is being tested against field and laboratory data.

REFERENCES

Huang, V.H. and Greimann, B. (2012). Sedimentation and River Hydraulics – One Dimension, Version 3.0. Sedimentation and River Hydraulics Group, Technical Service Center. Bureau of Reclamation. Denver, CO.

Lai, Y.G. (2008). SRH-2D version 2: Theory and User's Manual. Sedimentation and River Hydraulics – Two-Dimensional River Flow Modeling. U.S. Department of the Interior, Bureau of Reclamation, Technical Service Center, Denver, CO.

Merkel, U.H. and Kopmann, R. (2012). "A continuous vertical grain sorting model for Telemac & Sisyphe". Proceedings from the River Flow 2012 Conference. San Jose, Costa Rica. pp. 457-463.

BANKFULL WIDTH CONTROLS ON RIFFLE-POOL MORPHOLOGY UNDER CONDITIONS OF INCREASED SEDIMENT SUPPLY: FIELD OBSERVATIONS DURING THE ELWHA RIVER DAM REMOVAL PROJECT

Andrew K. Brew, River Engineer, Anchor QEA, Bellingham, WA, abrew@anchorqea.com; Jacob A. Morgan, PhD Student, Colorado State University, Fort Collins, CO, jamorgan@rams.colostate.edu; Peter A. Nelson, Assistant Professor, Colorado State University, Fort Collins, CO, peter.nelson@colostate.edu;

Abstract: Many gravel-bed rivers feature quasi-regular alternations of shallow and deep areas known as riffle-pool sequences, which in straight reaches are often forced by variations in channel width. The mechanisms responsible for the formation and maintenance of riffle-pool sequences are still poorly understood. There is also much uncertainty in the basic understanding of how fluvial systems respond and readjust to large sediment fluxes through time, as may occur during and after dam removal. Field observations have been made during a natural experiment on the Elwha River in Washington State, where the largest dam-removal project in history is providing riffle-pool sequences with greatly increased sediment supply. Analysis of aerial imagery and repeat bathymetric measurements indicate that prior to dam removal, pools on the Elwha were co-located with local decreases in bankfull width. During dam removal, a pulse of sediment temporarily filled in the pools, but eventually most of the pools reemerged at their prior location. During this time, the river did not experience large overbank flows. The persistence of the location of riffles and pools, even with large changes in sediment supply, suggests that channel width imposes an important local control on bed morphology and riffle-pool dynamics.

INTRODUCTION

Alternating vertical undulations in bed elevation, referred to as riffles and pools, are characteristic of both straight and meandering gravel-bed rivers with slopes less than 0.02 (Knighton, 1998). Areas of higher relative elevation with a symmetrical cross-section and coarser bed material are termed riffles. Conversely, pools have relatively low topography and characteristically have finer bed material (Richards, 1976). The diverse range of flows associated with riffle-pool sequences makes these features important for aquatic ecology and overall stream health (Allan and Castillo, 1995). Consequently, the creation or regeneration of riffles and pools is often a component of stream restoration projects (e.g. Pasternack and Brown, 2013).

The genesis and persistence of riffle-pool sequences is still not fully understood (Wohl, 2014). The velocity reversal hypothesis, first proposed by Keller (1971) and subsequently explored in numerous studies (e.g. Lisle, 1979; Keller and Florsheim, 1993; Clifford and Richards, 1992; Thompson et al., 1999; Thompson, 2011), suggests that at low discharge, flow velocities, and consequently sediment transport rates, are higher in riffles than in pools, but at high discharge this pattern reverses so that velocities and transport rates in pools exceed those in riffles. More recently, flow convergence routing (e.g., MacWilliams et al., 2006) has suggested that convergence of flow through constrictions is more important for riffle-pool maintenance than velocity reversal, an idea supported by Sawyer et al.'s (2010) observations and modeling of the Yuba River in California.

Downstream variations in valley and channel width have been shown to be important influences on the development and persistence of riffle-pool sequences. White et al. (2010) examined a rapidly incising, laterally-confined reach on the Yuba River and found that riffles were persistently located in areas of greatest valley width. One-dimensional numerical modeling by de Almeida and Rodríguez (2012) also suggests that riffles and pools can spontaneously emerge at wide and narrow locations in the channel, respectively, and that the relative grain size sorting between riffles and pools is dependent on unsteady flow. These studies have been valuable in demonstrating the importance of downstream width variations on the development and maintenance of riffle-pool morphology, but how riffle-pool sequences might respond to large changes in sediment supply remains poorly understood.

The Elwha River restoration project provides an opportunity to explore how dramatic changes in sediment supply interact with downstream variations in channel width to influence riffle-pool morphology. In this paper, we present field observations of river width and bathymetry collected during the first two years of the removal of Glines Canyon Dam. The objectives of this study are to characterize downstream patterns of bankfull width and to document changes in channel bed morphology in a relatively straight reach of the middle Elwha River before and after the release of a large amount of reservoir sediment. Our observations suggest that channel width can be an important control on the persistence of riffles and pools, even under conditions of large changes in sediment supply.

METHODS

Study Site: The Elwha River is located on the Olympic Peninsula in Washington State. It flows from its headwaters in Olympic National Park 45 miles to the Strait of Juan de Fuca in the Pacific Ocean. Historically, the Elwha river network has been very productive salmon system with typical annual spawning runs of 400,000 fish (Smillie, 2014). The Elwha was once a member of a select few Pacific Northwestern rivers that supported all five Pacific salmon species (Chinook, chum, coho, pink, sockeye) in addition to four species of anadromous trout (Steelhead, coastal cutthroat, bull, and Dolly Varden char). Beginning in 1910, Elwha Dam, the first of a series of two dams, was constructed at river mile 4.9 in the lower reaches of the river. The dam was poorly constructed and subsequently failed in 1912. However the dam was rebuilt and completed by 1913 (Crane, 2011). Twelve miles upstream, Glines Canyon dam was constructed at river mile 17 and completed by 1926. The dams provided the neighboring town of Port Angeles and its paper mill with inexpensive hydropower. The dams lacked fish passage, however, and it has been estimated that spawning returns were reduced to fewer than 3,000 fish annually (Smillie, 2014).

As decades passed it became clear that the dams were inefficient at generating power and it appeared that their costs to the ecosystem exceeded their economic benefits. In 1992, President George H. W. Bush signed the Elwha River Ecosystem and Fisheries Restoration Act into law. This transferred ownership of the dams to the federal government and allocated funds for dam mitigation. Following reservoir sedimentation modeling and laboratory experiments by Bromley et al. (2011), it was determined that the sedimentation issues could be managed by removing the dams in a controlled manner. It has been estimated that up to 34 million yd^3 of sediment had been trapped in the reservoirs with the majority (~28 million yd^3) behind Glines Canyon Dam in

Lake Mills (Draut and Ritchie, 2015). Beginning with Elwha Dam in Fall of 2011, both dams have gone through a stepped down removal process and periods of holding to allow reservoir sediments to stabilize and anadromous fish to move through the Elwha main stem and into tributaries. Elwha Dam was completely removed in March of 2012 and the final 30 ft. of Glines Canyon Dam was blasted away in August of 2014 completing the removal project. Turbidity issues due to increased reservoir sediment have occurred at a downstream water treatment plant, but overall the project has gone to plan and is viewed as a major success among large-scale dam removal projects.

The field site used for this study is a reach of the middle Elwha River located between the two former dams (Figure 1). This site has a relatively low sinuosity of 1.06, is close to the USGS stream gage at McDonald Bridge, and is far enough away from both dam sites that the local hydrologic regime is probably not significantly altered from backwater effects created by the former Elwha Dam. During the time period we are examining (from before dam removal until November 2013), approximately 7.8 million yd^3 of sediment was released from the former Lake Mills (East et al., 2015).

Bathymetric Boat Surveys: Throughout the Elwha restoration project, the U.S. Bureau of Reclamation (USBR) and National Park Service (NPS) have collected bathymetric data as part of their sediment management monitoring program, documenting the morphological evolution of the Elwha River (Bountry, 2014). Data sets are available from July 2011, before the dam removal, through their most recent survey in November 2013. Boat survey data has been refined to reduce the data set to points most representative of the channel thalweg (J. Bountry, personal communication, 2013). The reach we are using is located between river stations 50+000 and 53+000 (Figure 1). This stationing corresponds to the distance in feet upstream from the river mouth at the Strait of Juan de Fuca, with the "+" stationing analogous to a comma. In this analysis, we use bathymetric datasets collected by the USBR on July 20, 2011, May 9, 2013 and August 1, 2013.

Bankfull Width Mapping: To obtain an understanding of how channel width might interact with riffle-pool morphology in the Elwha system, a series of aerial images available on Google Earth were used to characterize downstream patterns of bankfull width in the study reach. Aerial photos from June 6, 2009, September 3, 2012 and July 5, 2013 were selected because of their temporal proximity to the bathymetric surveys of interest. For each aerial photo, bank lines corresponding to the bankfull discharge were estimated and digitized. Indicators such as sand bars, dense vegetation, and terraces were used to visually estimate bank locations. The channel centerline was also digitized by estimating the current thalweg under normal flow conditions. These geometric data were exported as KML files and converted to shape files in ArcGIS. The banks were used to develop a polygon containing both banks and the extents of the river reach. Cross-sections perpendicular to the centerline were created at 1-ft intervals and trimmed within the boundaries of this polygon.

Hydrologic Analysis: Flows in the study reach during the period of interest were characterized using streamflow data from USGS gage 12045500 at McDonald Bridge. Both daily average values and daily maximum 15 minute instantaneous peaks were gathered over the period of interest in this study (September 10, 2011 to June 28, 2014). These values were plotted against

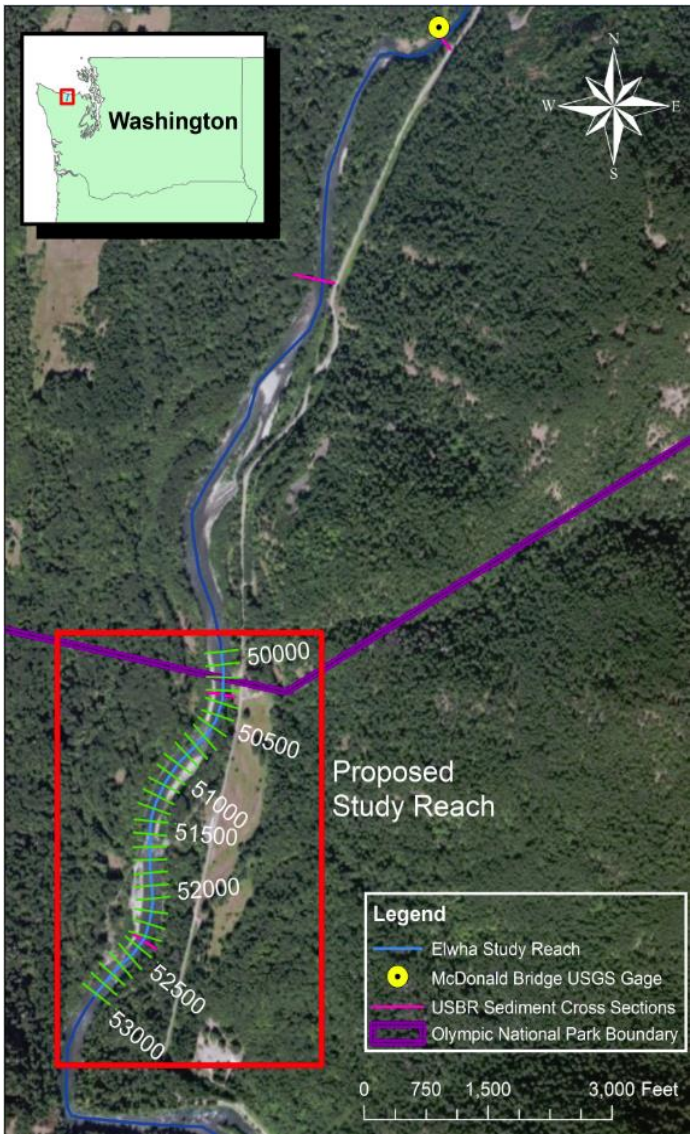

Figure 1 Elwha study reach between river stations 50+000 – 53+000 between former dam sites.

time to generate a hydrograph for the Elwha River below Glines Canyon Dam during dam removal. Annual peak flow values were collected as well, with hydrologic data available beginning in 1897. These data were then ranked from highest to lowest discharge. The recurrence interval for each flow in the annual maximum series were calculated using a Weibull plotting position technique

$$T = \frac{R}{n+1} \tag{1}$$

where R is the overall rank of that discharge in the annual maximum series, n is the number of peak flow values, and T is the return period of that particular flow in years.

RESULTS AND DISCUSSION

Sequential Pool Filling and Evacuation on the Elwha: Figures 2-4 show the evolution of the bed and water surface profiles in the study reach over the period of interest. The baseline dataset from July 20, 2011 (before dam removal) shows three clearly defined riffle-pool sequences within this reach as depicted with the brown line in Figure 2. At the time of the survey, the discharge was 2,340 cfs and the reach displayed a typical riffle-pool backwater profile. The average bed slope across the reach at this time was 0.0063.

By the May 9, 2013 survey, the pools had aggraded significantly, and the morphology approached a plane bed condition with a similar average slope of 0.0063 (Figure 3). At that time, Glines Canyon Dam had been partially removed and fine reservoir sediment was readily available to be transported. During the survey, the discharge was 3,390 cfs and the water surface profile was relatively flat and shallow, as would occur under quasi-normal flow conditions. This reduction of backwater effects induced by reduced riffle-pool relief suggests an increase in sediment transport capacity.

The August 1, 2013 profile has an average slope of 0.0064 and shows the reemergence of pools in their former locations (Figure 4). Up to 5 feet of incision took place between the May and August 2013 surveys. The water surface profile shown in Figure 4 indicates that the redeveloped riffles and pools produced locally-strong backwater effects under the summer low flow discharge of 851 cfs at the time of the survey. This morphodynamic adjustment suggests that there was a sharp reduction in upstream supply and the fine sediment that had filled the pools was evacuated.

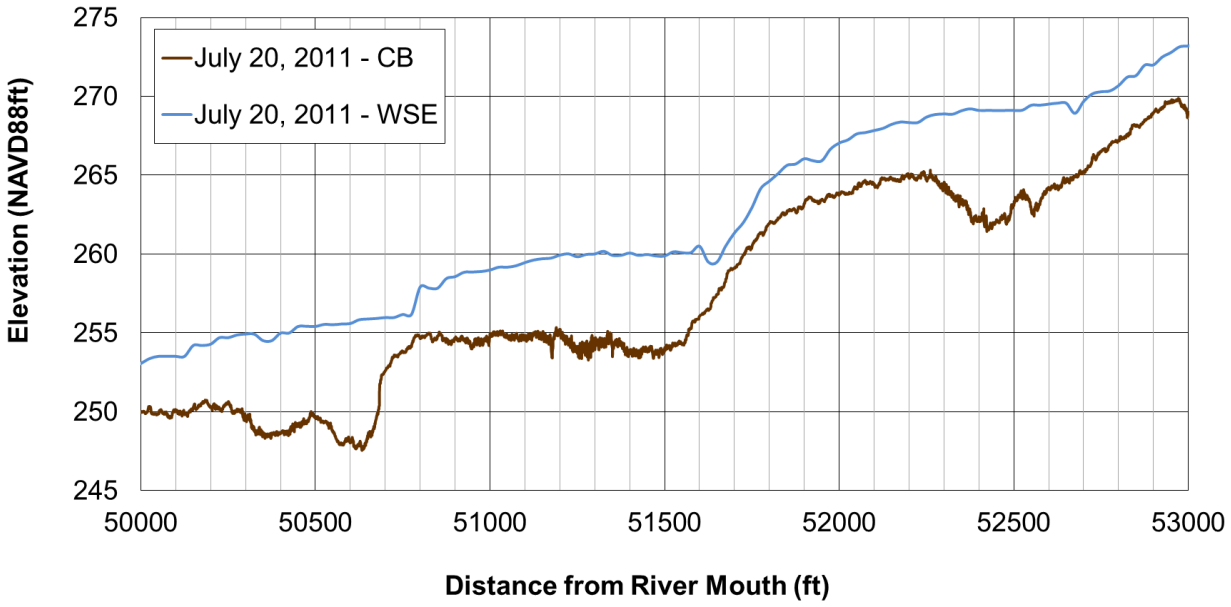

Figure 2 July 2011 channel bed and water surface profiles of the study reach before dam removal showing well developed riffle-pool morphology inducing a backwater profile (where CB is channel bed and WSE is water surface elevation).

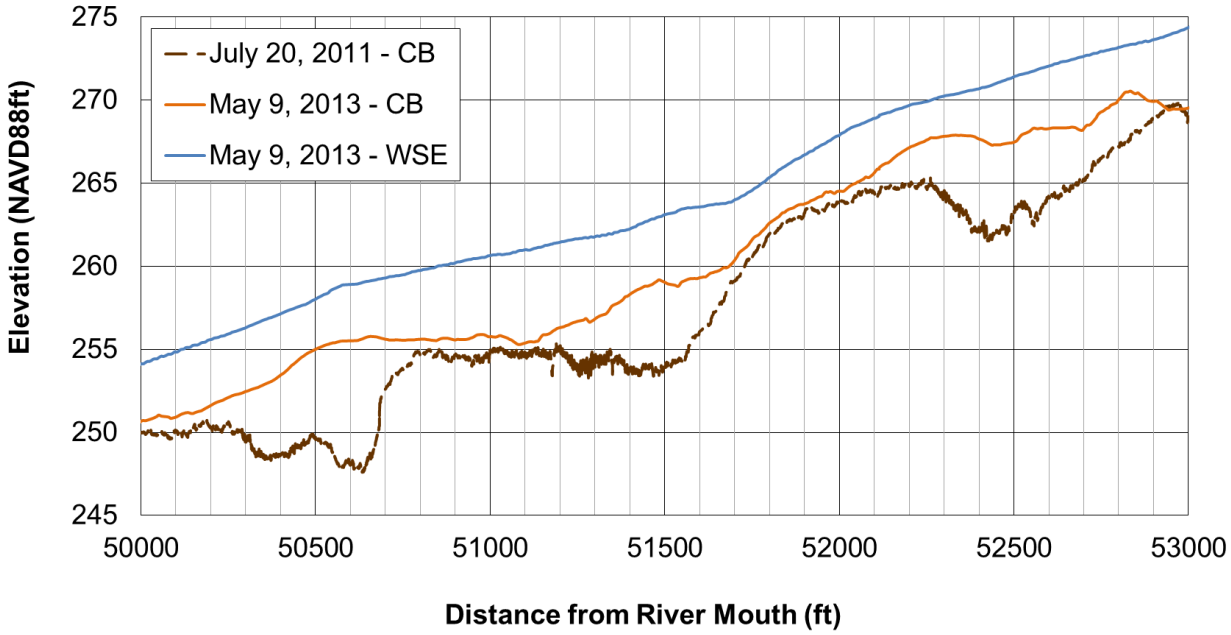

Figure 3 May 2013 channel bed and water surface profiles of the study reach during dam removal depicting temporary pool filling and a flattened water surface (where CB is channel bed and WSE is water surface elevation).

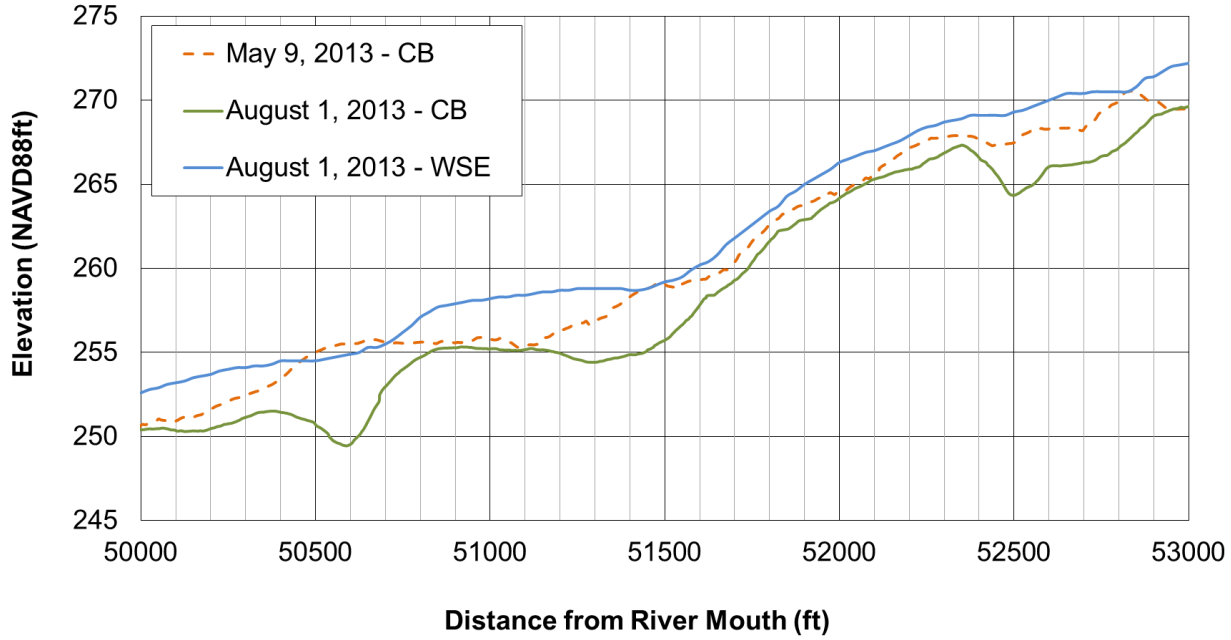

Figure 4 August 2013 channel bed and water surface profiles of the study reach during low flow conditions showing pool evacuation and the reemergence of riffle-pool morphology with reduced sediment supply (where CB is channel bed and WSE is water surface elevation).

Downstream patterns of bankfull width: The bankfull channel width of the study reach identified with Google Earth and spatially aligned with bed topography surveys is presented in Figure 5. The channel width ranged from about 100 to about 275 feet, with an average of approximately 180 ft. For each dataset, the channel showed a distinct downstream pattern of narrowing and widening with a wavelength of about 1000 ft, or 5-6 average bankfull widths. This pattern was consistent between 2009 and 2013, with relatively little change in bankfull width occurring during that time period.

The bathymetric survey data shows the three pools coinciding with the most constricted portions of the channel and riffles forming in the widest locations (Figure 5). Although the pools filled in temporarily, their reemergence at the same location suggests that channel width provides an important local control on pool persistence over a short time frame under conditions of dynamically changing sediment supply.

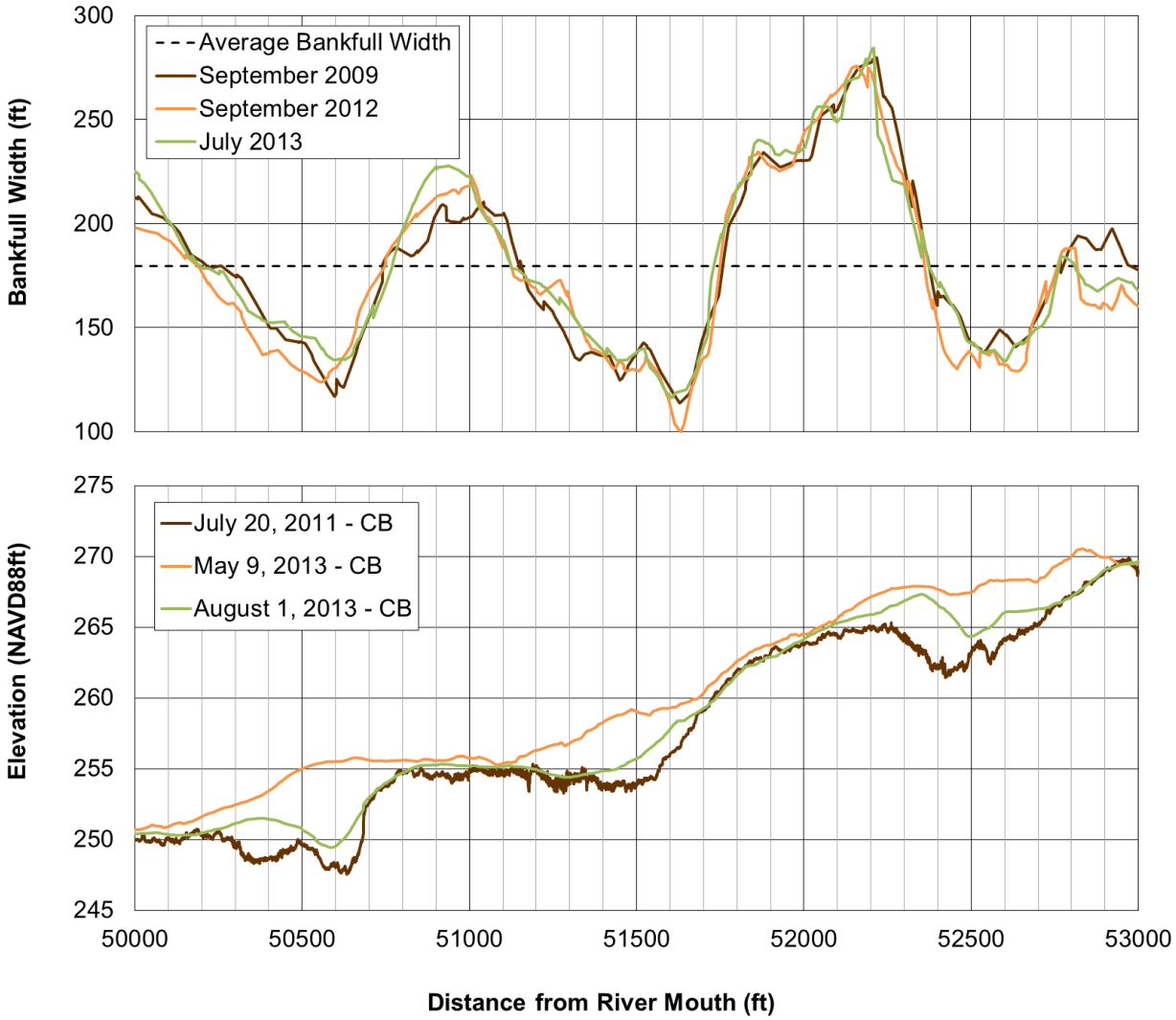

Figure 5 Coupling of bankfull channel width from Google Earth and bathymetry from in the Elwha Study Reach (where CB is channel bed).

Hydrologic Regime during Dam Removal: The flow record from the USGS gage at McDonald Bridge from September 10, 2011 to June 26, 2014 (Figure 6) shows a rain and snowmelt driven hydrologic regime typical of Pacific Northwestern watersheds at moderate elevations **(**Climate Impacts Group, 2014**)**. In a typical water year there is a peak due to winter storms, a recession and then another peak in late spring or early summer due to snowmelt runoff and "rain on snow events". In addition, the overall magnitude of peak flows showed the lack of a major channel-forming flow event exceeding bankfull conditions (Figure 6). A bankfull flow is typically defined as the discharge that fills the main channel and begins to spill onto the floodplain **(**Leopold, 1994**)**. It is considered very influential on geomorphic processes and often characterized as the discharge that has a recurrence interval of 1.5-2 years **(**Leopold, 1968; Williams, 1978; Andrews, 1980**)**. Table 1 shows the computed 1-, 1.5-, and 2-year recurrence interval flows for the Elwha River at the McDonald Bridge gage. During the time period of interest only three instantaneous peaks reached the 1.5-year value and none exceeded the 2-year flow. This period of relatively mild hydrology suggests that there were likely no overbank flows and major channel forming discharges probably did not occur. Therefore, the channel width may have acted as an important driver in the geomorphic processes that did occur, such as the observed pool filling and evacuation.

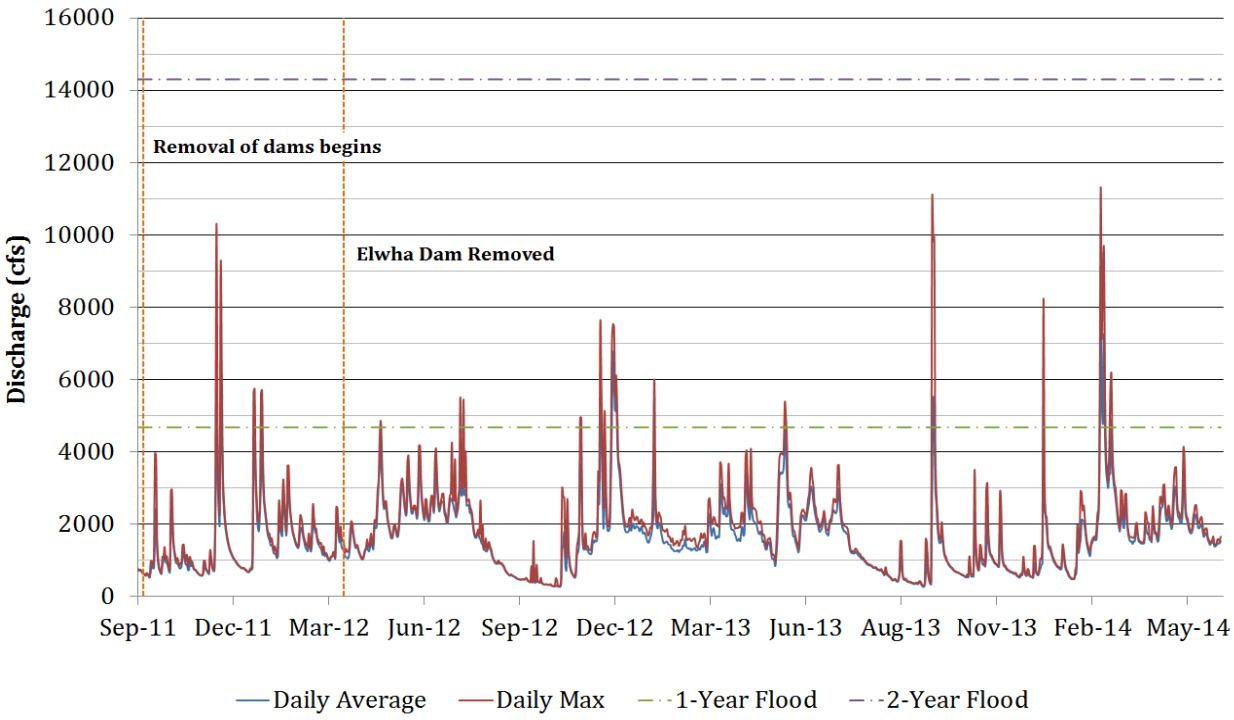

Figure 6 Hydrologic Record of the Elwha during the dam removal time period at the USGS stream gage at McDonald Bridge (Station 12045500).

Table 1 Discharge recurrence intervals on the Elwha River

Peak Flow Recurrence Interval (yrs)	Peak Flow (cfs)
1	4,680
1.5	10,300
2	13,848

CONCLUSIONS

Channel width has been shown to exert a local control on the development of riffle-pool morphology in certain environments (de Almeida and Rodriguez, 2012) and lead to pool maintenance through flow convergence routing (MacWilliams et al., 2006). Riffle-pool systems such as the Elwha develop and maintain riffle-pool topography due to this variable width condition. From the perspective of fluid momentum and sediment continuity, these expansions and contractions create variations in shear stress that induce preferential scour in pools and deposition across riffles.

Field results from the Elwha show that bankfull channel width imposed a local control on the locations of riffles and pools from 2011-2013, even when the system is undergoing dramatic changes associated with the removal of a large dam. The transient pool-filling apparent in the repeat longitudinal profiles and the re-emergence of the pools at the same locations, combined with the lack of large, channel-forming hydrologic events, suggests that the downstream changes in channel width provided an important control on the location and persistence of riffles and pools.

Understanding how and why pool filling after dam removal occurs will be important to salmon recovery efforts in coastal river systems. Pools provide critical holding locations for migrating fish to rest in as they navigate upstream to spawning grounds. If we can understand why temporary pool filling takes place and limit its occurrence during critical migratory time periods, this could enhance salmon recovery efforts.

ACKNOWLEDGEMENTS

We are grateful to Tim Randle and Jennifer Bountry at the USBR for providing access to their bathymetry data and valuable discussions. This work was partially supported by the National Science Foundation grant EAR-1425067.

REFERENCES

Allan, J. D., and Castillo, M. M. (1995). *Stream Ecology*. London: Chapman & Hall. 388 p.

Andrews, E. D. (1980). Effective and bankfull discharges of streams in the Yampa River basin, Colorado and Wyoming. *Journal of Hydrology*, 46(3): 311-330.

Bountry, J. (2014). Elwha river restoration sediment effects first two years of dam removal. RRNW 2014. Retrieved May 2, 2014, from http://archive.rrnw.org/docs/2014/11-2_Elwha%20Sediment%20Mgmt%20RRNW2014_Bountry.pdf

Clifford, N. J., and Richards, K. S. (1992). The reversal hypothesis and the maintenance of riffle-pool sequences: a review and field appraisal. In *Lowland Floodplain Rivers: Geomorphological Perspectives* (Carling and Petts, eds.). Chichester: John Wiley & Sons. 43-70.

Climate Impacts Group. (2014). Climate Impacts Group. Retrieved June 11, 2014, from http://cses.washington.edu/cig/pnwc/deadend_rivertypes.shtml

Crane, J. (2011). *Finding the River: An Environmental History of the Elwha*. Corvallis: Oregon State University Press. 256 p.

de Almeida, G. A. M., and Rodríguez, J. F. (2012). Spontaneous formation and degradation of pool-riffle morphology and sediment sorting using a simple fractional transport model. *Geophysical Research Letters*, 39(6).

Draut, A. E., and Ritchie, A. C. (2015). Sedimentology of new fluvial deposits on the Elwha River, Washington, USA, formed during large-scale dam removal. *River Research and Applications*, 31(1): 42-61.

East, A. E., Pess, G. R., Bountry, J. A., Magirl, C. S., Ritchie, A. C., Logan, J. B., Randle, T. J., Mastin, M. C., Minear, J. T., Duda, J. J., Liermann, M. C., McHenry, M. L., Beechie, T. J., and Shafroth, P. B. (2015). Large-scale dam removal on the Elwha River, Washington, USA: River channel and floodplain geomorphic change. *Geomorphology*, 228: 765-786.

Keller. E. A. (1971). Areal sorting of bed-load material: the hypothesis of velocity reversal. *Geological Society of America Bulletin*, 82: 753-756.

Keller, E. A., and Florsheim, J. L. (1993). Velocity-reversal hypothesis: a model approach. *Earth Surface Processes and Landforms*, 18: 733-740.

Knighton, D. (1998). *Fluvial Forms and Processes: A New Perspective* (2nd ed.). London: Arnold. 383 p.

Leopold, L. B. (1968). Hydrology for urban land planning: A guidebook on the hydrologic effects of urban land use. *Geological Survey Circular 554*. 18 p.

Leopold, L. B. (1994). *A View of the River*. Cambridge: Harvard University Press. 290 p.

Lisle, T. E. (1979). A sorting mechanism for a riffle-pool sequence. *Geological Society of America Bulletin*, 90: 1142-1157.

MacWilliams, M. L., Wheaton, J. M., Pasternack, G. B., Street, R. L., and Kitanidis, P. K. (2006). Flow convergence routing hypothesis for pool-riffle maintenance in alluvial rivers. *Water Resources Research*, 42(10).

Pasternack, G. B., and Brown, R. A. (2013). Ecohydraulic design of riffle-pool relief and morphological unit geometry in support of regulated gravel-bed river rehabilitation. In *Ecohydraulics: An Integrated Approach* (Maddock et al., eds.). Chichester: John Wiley & Sons. 337-355.

Richards, K. S. (1976). The morphology of riffle-pool sequences. *Earth Surface Processes*, 1(1): 71-88.

Sawyer, A. M., Pasternack, G. B., Moir, H. J., and Fulton, A. A. (2010). Riffle-pool maintenance and flow convergence routing confirmed on a large gravel bed river. *Geomorphology*, 114: 143-160.

Smillie, J. (2014, March 30). Federal judge sides with wild-fish advocates on hatchery issue in Elwha River's restoration. *Peninsula Daily News*. Retrieved June 4, 2014, from http://www.peninsuladailynews.com/article/20140330/news/303309972/federa l-judge-sides-with-wild-fish-advocates-on-hatchery-issue-in.

Thompson, D. M. (2011). The velocity-reversal hypothesis revisited. *Progress in Physical Geography*, 35(1): 123-132.

Thompson, D. M., Wohl, E. E., and Jarrett, R. D. (1999). Velocity reversals and sediment sorting in pools and riffles controlled by channel constrictions. *Geomorphology*, 27: 229-241.

White, J. Q., Pasternack, G. B., and Moir, H. J. (2010). Valley width variation influences riffle–pool location and persistence on a rapidly incising gravel-bed river. *Geomorphology*, 121(3): 26-221.

Wohl, E. (2014). *Rivers in the Landscape: Science and Management*. Chichester: John Wiley & Sons. 318 p.

Williams, G. P. (1978). Bank-full discharge of rivers. *Water resources research*,14(6): 1141-1154.

SCOUR AND SUBSEQUENT REPAIR AT LOCK & DAM 25

Timothy Lauth, P.E., Hydraulic Engineer, US Army Corps of Engineers – St. Louis District, St. Louis, MO, Timothy.J.Lauth@usace.army.mil; David Gordon, P.E., Chief, Hydraulic Design Section, US Army Corps of Engineers – St. Louis District, St. Louis, MO, David.Gordon@usace.army.mil; Matthew Rector, P.E., Hydraulic Engineer, US Army Corps of Engineers – St. Louis District, St. Louis, MO, Matthew.A.Rector@usmc.mil; William Moeller, P.E., Structural Engineer, US Army Corps of Engineers – St. Louis District, St. Louis, MO, William.J.Moeller@usace.army.mil;

INTRODUCTION

Lock and Dam 25 is a U.S. Army Corps of Engineers navigation structure located at Upper Mississippi River mile 241.4 on the Mississippi River near Winfield, MO. Events in early 2011 led to a sustained necessary deviation from the normal operations practices for the roller and tainter gates, forcing the majority of the flow of the Mississippi River through gates 12 through 17 (the gates closest to the Illinois bank) for almost five months. This sustained deviation led to significant scour in the river bed downstream of the dam and adjacent to the lock, requiring repairs underneath the intermediate wall and downstream slab, removal and replacement of a portion of the downstream slab, and placement of rock for downstream slope protection and global stability of the structure. The following will outline the change in conditions at the structure and the subsequent necessary repairs.

DEVIATION, RESULTS, AND REPAIRS

The Operations Deviation: On March 6, 2011, at approximately 3 PM, operations of Lock and Dam 25 (L&D25) underwent a change that would lead to a necessary deviation from normal dam operation practices for nearly five months. The initiating change is outside of the scope of this paper; this paper is intended to focus on the deviation and its effects. The deviation consisted of routing the majority of the flow that would normally flow through a combination of all of the gates primarily thru Gates 12 to 17 (a plan view is presented in figure 1). From March 6 to July 26, the flow rate varied from approximately 107,000 cfs to 317,000 cfs for an average of approximately 216,000 cfs. Normal operations resumed at the lock and dam on July 26, 2011. As necessary for repairs, gates were closed by compensating with corresponding openings of other gates.

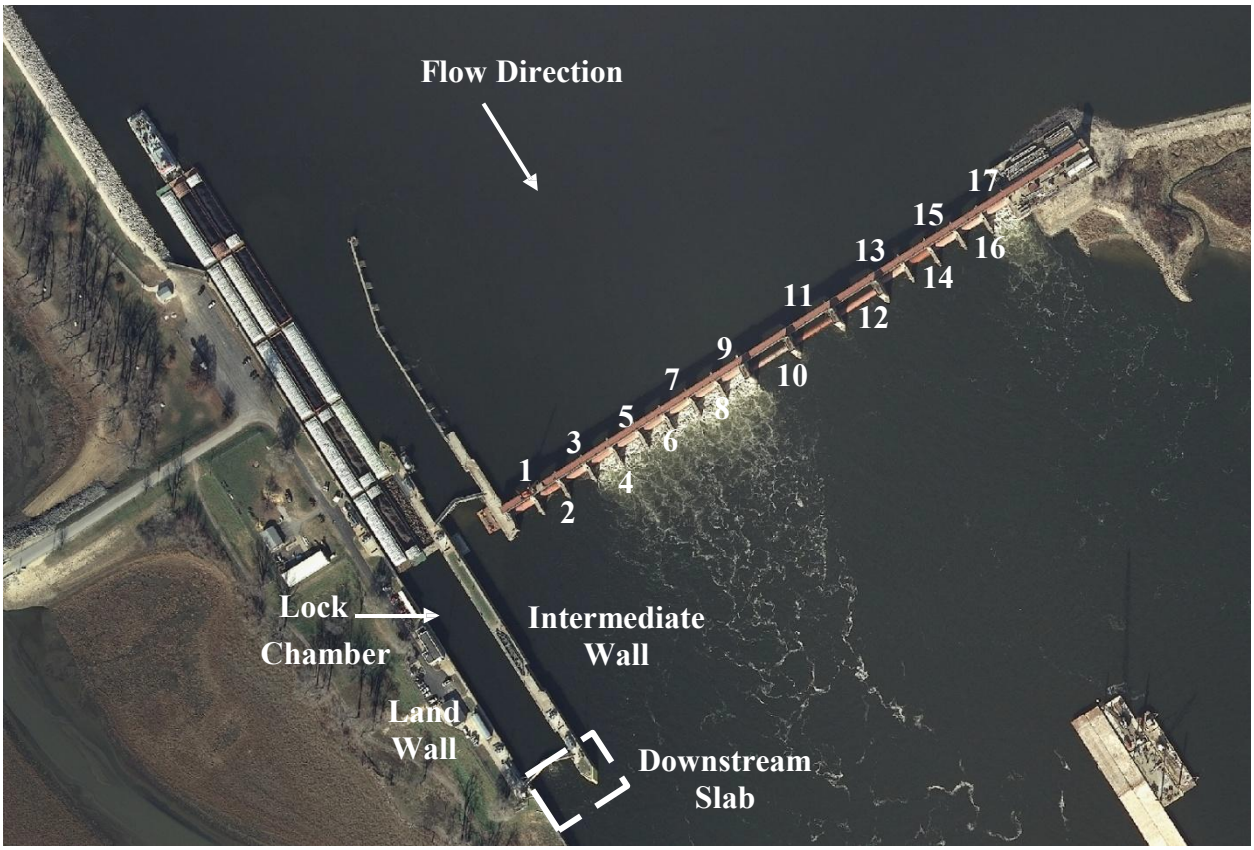

Figure 1 Plan view of L&D25 during late fall 2012, releasing approximately 48,000 cfs during normal operations.

Video taken March 17, 2011 (flow of approx. 127,000 cfs, figure 2) showed standing waves downstream of the open gates suggesting that supercritical flow was present outside of the stilling basin. This contrasts with normal flow conditions at the same approximate flow rate (figure 3), where energy dissipation is more three-dimensional and contained within the stilling basin. Additionally, anecdotal evidence from the surveying crew and other boats involved with the repair noted strong surface currents to the point that many areas downstream were deemed unsafe to survey until normal operations resumed. The hypothesis that energy dissipation was no longer contained in the stilling basin is further supported by looking at the head before and after the deviation (figure 4). The data shows that from approximately 120,000 cfs to 220,000 cfs, a head of up to 2.5 feet higher than normal was otherwise measured. For typical open river conditions (gates out of the water), flow is not forced under a gate, leading to a head of approximately 1 ft or less. When the flow is greater than 1foot, it is typically due to a regulated pool condition forcing the flow underneath the Tainter and roller gates, downward towards the stilling basin. In this case, a head representative of a regulated pool condition existed during what would normally be an open river condition. The higher head suggests flow was not passing through the structure as intended, with the possible result that energy dissipation that would normally occur in the stilling basin as designed was potentially happening downstream through the scour of downstream sediments.

Figure 2 Downstream view of L&D25 on March 17, 2011 showing large standing waves

Figure 3 Downstream view of L&D25 on May 23, 2012 showing similar flow conditions

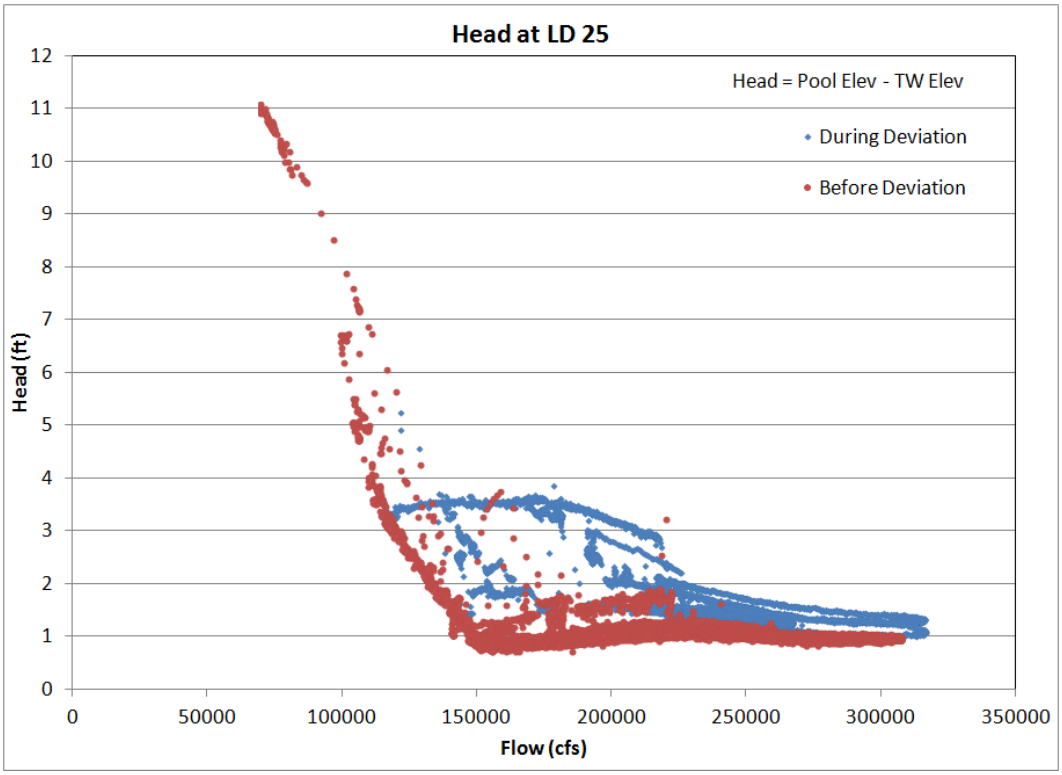

Figure 4 Head for different flows before and during deviation

The Results of the Deviation: The St. Louis District took a number of multibeam hydrographic surveys upstream and downstream of the dam for monitoring purposes. These surveys showed fluctuating deposition and erosion upstream and downstream of the dam as sediment waves moved through the system. The first comprehensive hydrographic survey following the deviation was taken on August 2,2011. The survey revealed significant downstream scour, well outside of the normal fluctuations. The four scour holes downstream of the lock and dam before the deviation had transformed into two deeper holes. The two primary interest areas for scour were downstream of Gates 12 to 16 and along the Intermediate Wall (I-Wall). The scour downstream of Gates 12 to 16 scoured over 55 ft of material in the worst scour locations, and over 30 ft at the deepest location (figure 5). Reports of shallow areas downstream of the lock and dam from the navigation industry prompted the collection of a pre-dredge hydrographic survey. The survey revealed excess material downstream of the lock and further downstream in the navigation channel that was not present the year before; assumedly, this was partially the material that had scoured out downstream of the dam and rock used as protection near the slab. The material further downstream in the navigation channel was removed with St. Louis District's Dredge Potter; the material immediately downstream of the lock could not be dredged due to the large rock mixed with the sand.

In the immediate vicinity of the I-Wall, loss of material along and downstream of the I-Wall (over 45 ft at the worst location) led to a partial failure of the downstream slab (figure 6). This slab serves to prevent undermining of the I-Wall due to the lock's discharge ports and tows entering and leaving the lock. Due to the slab failure, the lock was instructed to halt usage of the I-Wall's discharge ports, increasing the time required for lockages and leaving the lock with no redundancy for emptying the lock chamber.

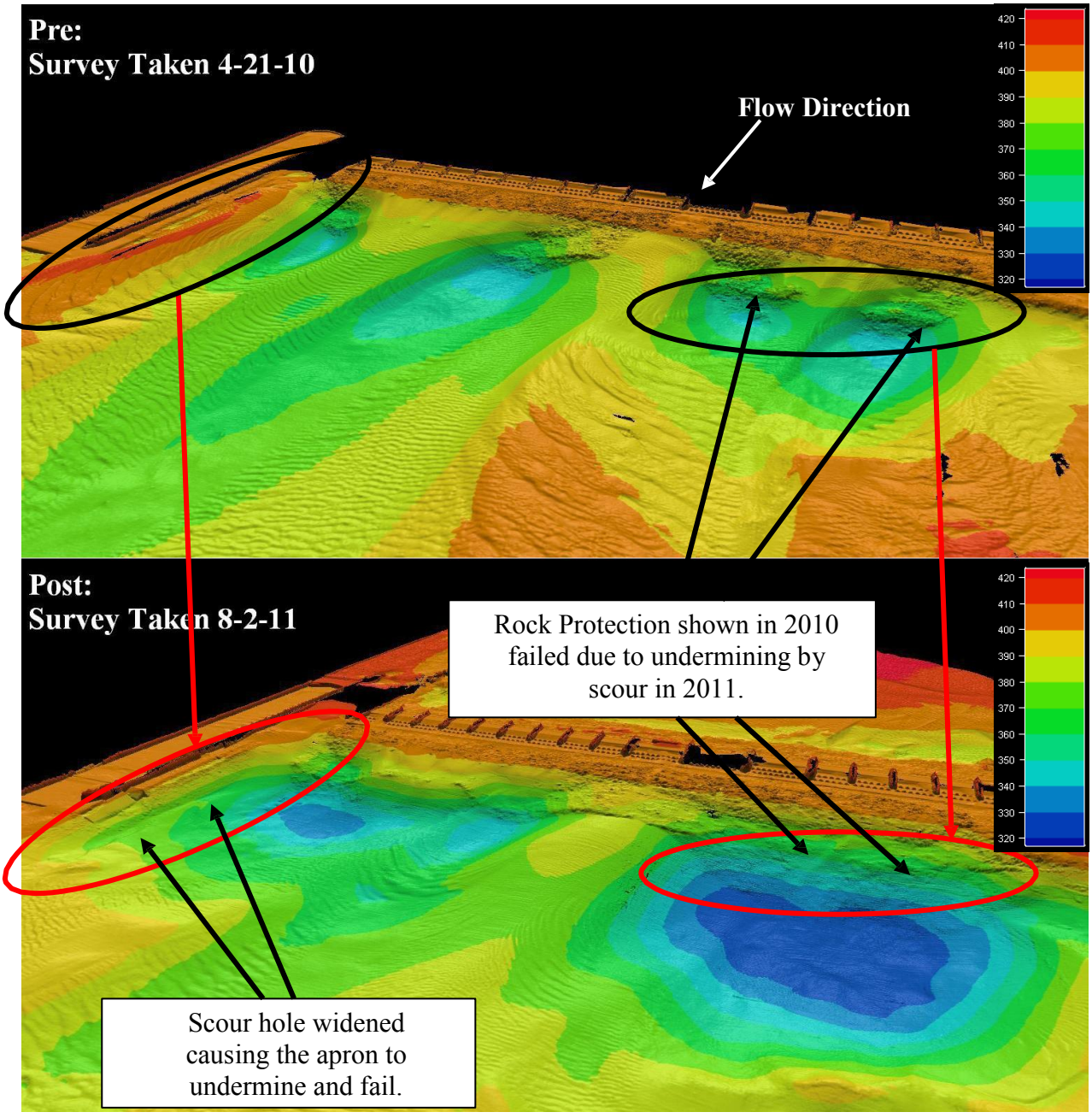

Figure 5 Before and after hydrographic surveys downstream of L&D25

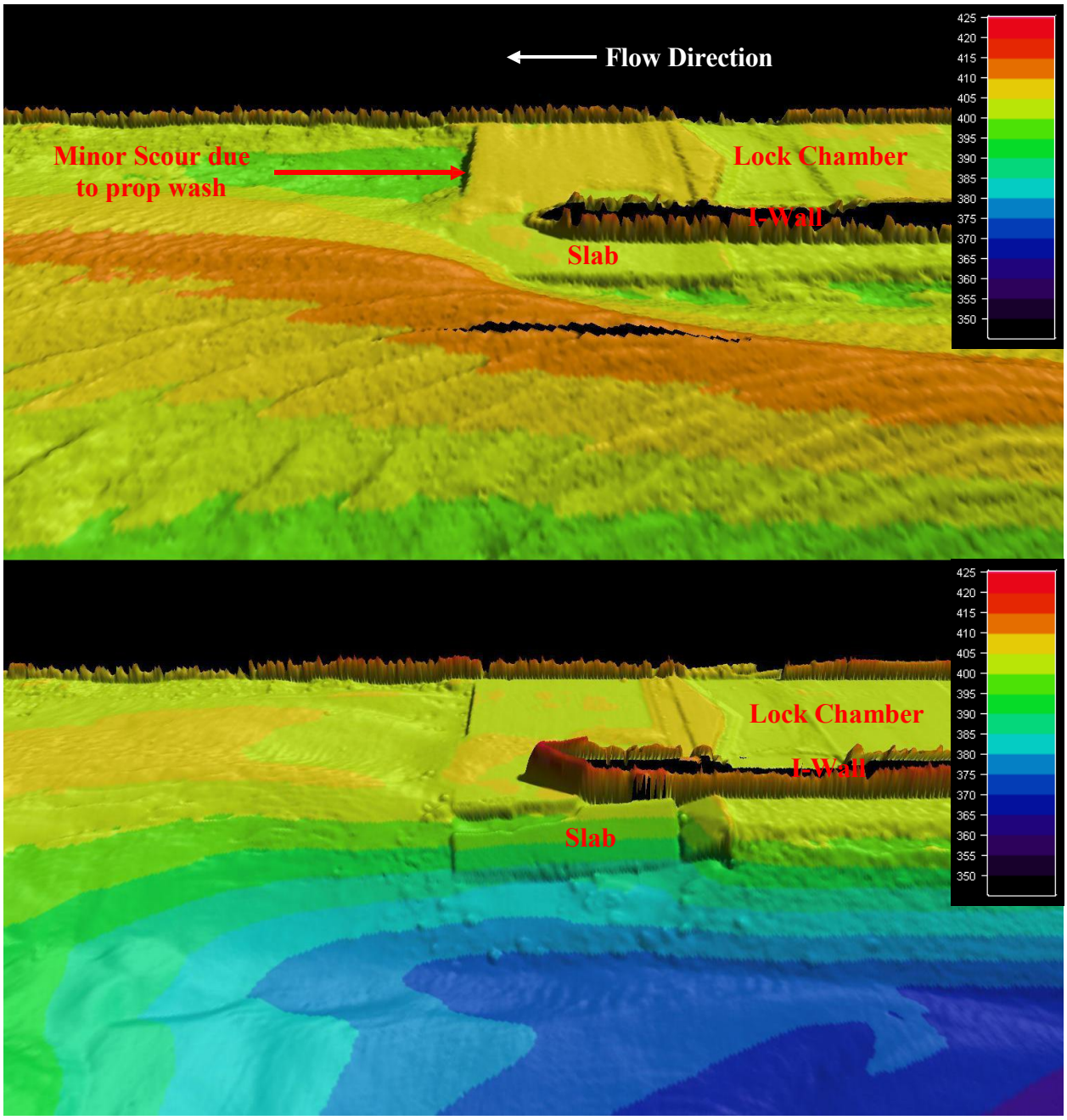

Figure 6 Before and after hydrographic surveys of downstream slab

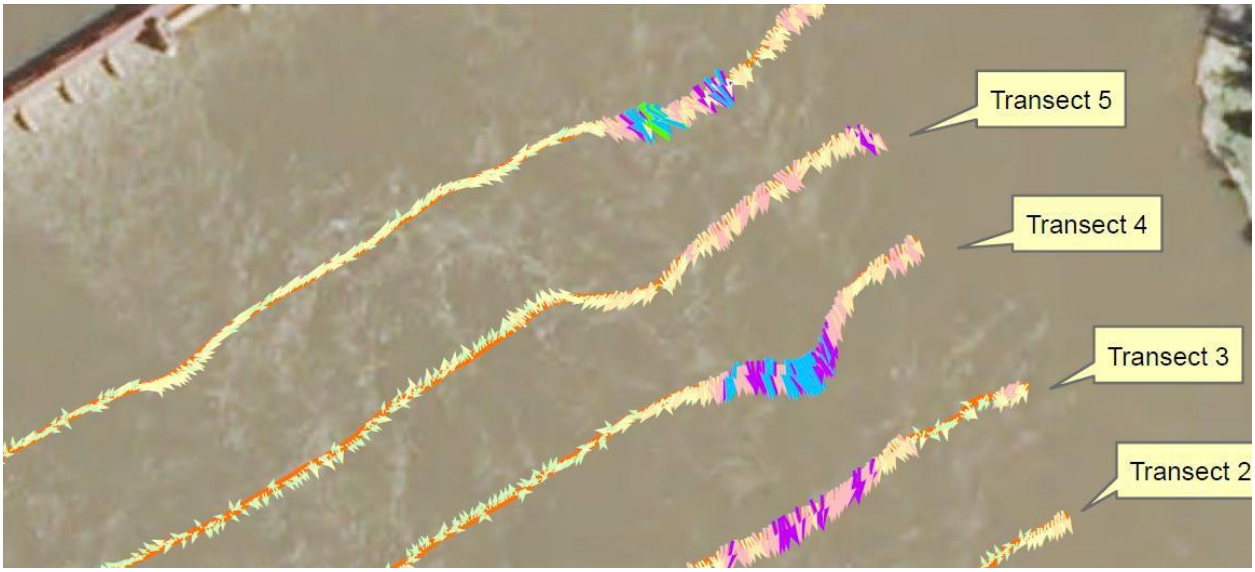

Figure 7 Velocity magnitudes and directions processed from ADCP data collected

It was suggested that scour adjacent to the I-Wall was partially caused by a significant eddy back towards the I-Wall that developed downstream of the dam due to the reliance on Gates 12 to 17 to pass flow. Anecdotally, the eddy was mentioned by pilots of survey and contractor repair boats. To test to see if an eddy back towards the I-Wall did in fact occur during releases through principally Gates 12-17, this condition was simulated. Unfortunately, the same flows passing through the dam during the deviation could not be simulated due to the time of year (measurements were taken around approximately 53,000 cfs, figure 7). The results of the ADCP collection showed some transects, particularly Transect 5, demonstrated flow vectors back towards the dam, supporting the eddy hypothesis.

Initial analysis after identifying the scour determined that there were two significant problems: 1) the potential of a global stability failure of the I-Wall due to loss of adjacent material, and 2) the potential for undermining of I-Wall and additional undermining of the slab surrounding the intermediate wall beyond what had already failed. Calculations were run to determine the stability of the lock and dam, particularly the I-Wall. The global stability of the I-Wall was found to be an issue, and plans were made to support the slope adjacent to the I-Wall with material in the repairs. Multiple boat-based multibeam surveys were used to monitor the location of the broken slab pieces, as the slab began to slide into the adjacent scour hole.

Multiple dive inspections were undertaken in the vicinity of the I-Wall, slab, downstream of the lock chamber, and land wall. The dive inspections revealed scour underneath the slab adjacent to the broken off section of the slab, downstream of the lock, and underneath the I-Wall. Verbal descriptions were used to characterize the scour occurring in each location. To better improve the knowledge of the undermining of the intact slab and position of the failed slab portion, an in-situ multibeam sonar device was used. A company was contacted and a demonstration was scheduled with a corresponding dive. The multibeam device was mounted on both a tripod and metal plate on the bottom of the river for different scans, and scans were taken from multiple placements around the area of interest (figure 8). From the scans, a better picture of the broken slab was

developed and the extent of intact slab undermining was better determined, allowing for better quantities estimates for the repair design.

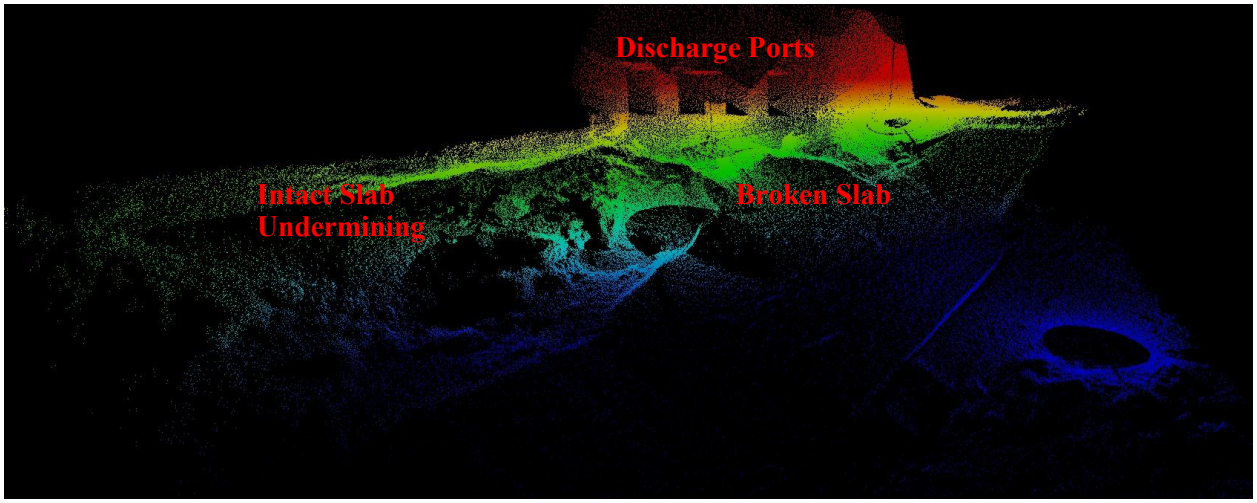

Figure 8 In-situ multibeam survey results

The Repairs: Phase I of the repair contract was awarded on February 8, 2012. Phase I consisted of filling in voids beneath the downstream edge of the slab. Holes were cored through the slab to fill the void. To contain the grout, a sheet pile wall was constructed along the edge of the slab from the landside wall to the eastern edge of the I-Wall. To prevent further downstream scour due to tows entering and exiting the lock chamber, the bed downstream of the slab and sheet pile wall was protected with 40 ft of 2,200 lb riprap.

An emergency repair was required to address undermining of the I-Wall itself. An initial dive inspection on September 24, 2011 identified an undermined area of approximately 6 ft long 1 ft below the base of the lock wall concrete extending at least 3 ft under the lock wall. At the time, the diver could feel that the timber piles that support the wall were exposed. Subsequent dive inspections identified the scour as both lengthening the width of the scour hole and its extents under the I-Wall. To repair this undermining, a 35 ft long, leave-in-place form was designed to cover the mouth of the scour hole. This form was designed with two holes, one at the bottom and top, so that grout could be pumped in the bottom hole until it filled the hole enough to run out the top, so that excess grout was not pumped under the I-Wall leading to a stability issue.

Phase II of the repair contract was awarded on May 25, 2012 for approximately $5.1 million dollars. The Phase II repair consisted of: 1) removing the failed slab, 2) construction of the remainder of the sheet pile wall along the slab edge including the dimensions desired to rebuild the slab, 2) grouting to re-establish the slab and fill voids underneath the intact slab section, 4) placement of rock to support the slope adjacent to the I-Wall, and 5) placement of stone downstream of Gates 11-16 to maintain the slope to the toe of the scour hole. The stone placed on the slope adjacent the I-Wall was constructed in two phases, the first to support the slope before the driving of the sheet pile and slab repair, and the second filling out the slope adjacent to the slab repair. During the design phase for the second phase of the repair, there had been discussion about the potential need for a thicker layer of additional rock downstream of Gates

11-16 to more completely rebuild the slope, including a supporting berm. This idea was rejected as it was thought normal operations would re-establish an approximation of the prior sediment deposition patterns downstream; this has since proven to be the case.

The project was completed in January 2013. Since the project was completed, as mentioned above briefly, the bed has begun to re-establish its pre-deviation form – a sediment deposition has developed adjacent to the I-Wall, two scour holes of less depth have formed downstream of Gates 1-9, and deposition has occurred in the scour hole downstream of gates 11-16 (figure 9). Monitoring of the I-Wall instrumentation has revealed no significant movement. Since project completion, the St. Louis District has returned to taking yearly hydrographic surveys upstream and downstream of the lock for monitoring purposes.

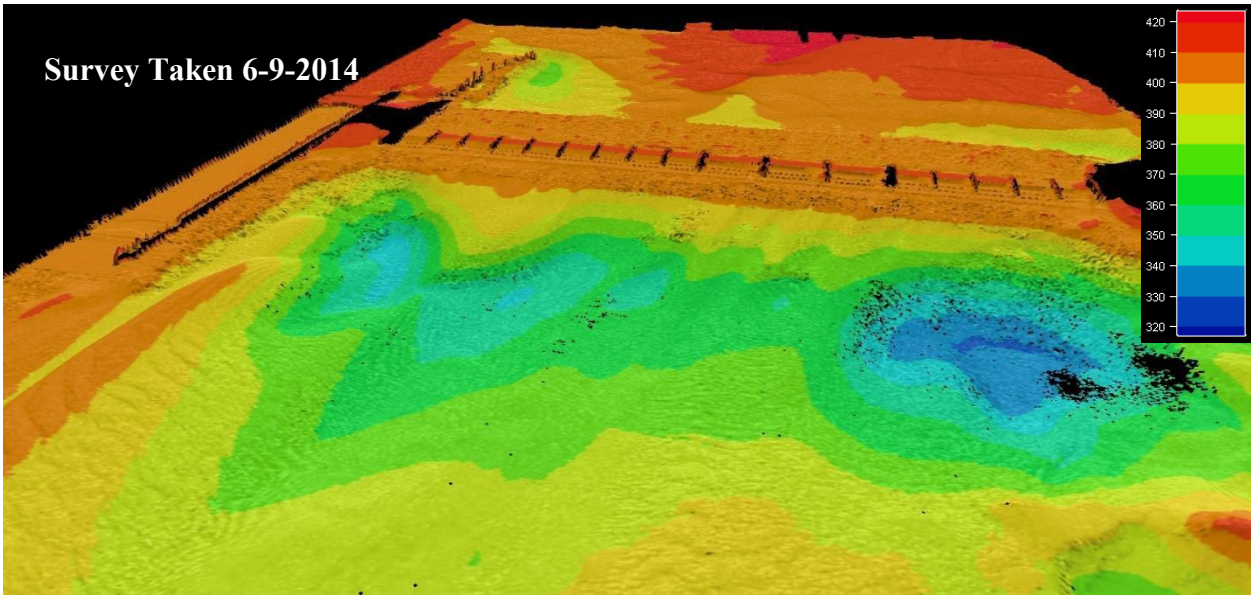

Figure 9 Most recent hydrographic survey

CONCLUSIONS

In March 2011, circumstances necessitated a deviation from normal operations at Lock and Dam 25 for nearly five months, with the large majority of flow being passed through Gates 12-17. Surveys and dive inspections after normal operations resumed revealed significant scour downstream of Gates 12-16 and adjacent to the Intermediate Wall. The scour adjacent to the I-Wall had led to the failure of a portion of the slab downstream of the lock, undermining of a portion of the I-Wall, and a global stability issue. Over the next roughly 1.5 years, repairs were done to return the lock to normal operations.

There were multiple lessons from the scour and subsequent repair from a hydraulics/sedimentation standpoint. The initial interest at the onset of the deviation from a hydraulics standpoint put a smaller emphasis on downstream scour, although this would later be the primary concern. Coupled with this, the potential that the hydraulics should change so drastically that energy dissipation may not have been largely confined to the stilling basin was

not the primary consideration during the deviation itself. Once the scour was identified after the deviation ended, the availability of multibeam surveys, both boat-based and for the first time in the St. Louis District in-situ, allowed for detailed monitoring of the site conditions, alternative development, and later, construction progress. The need for detailed monitoring extended to dive inspections, which revealed the critical I-Wall undermining. Lastly, the bed downstream of the dam has shown that, without any outside drivers, a riverbed will work to re-establish its equilibrium condition.

GEOMORPHIC ADJUSTMENTS ON THE UPPER MISSOURI RIVER IN RESPONSE TO DAM MANAGEMENT AND FLOODING

Katherine Skalak, Research Hydrologist, U.S. Geological Survey, 430 National Center, Reston, VA 20192, Ph: 703-648-5435, email: kskalak@usgs.gov; **Edward Schenk**, Research Ecologist, U.S. Geological Survey, 430 National Center, Reston, VA 20192; **Adam Benthem**, Hydrologist, U.S. Geological Survey, 430 National Center, Reston, VA 20192; **Cliff Hupp**, Research Ecologist, U.S. Geological Survey, 430 National Center, Reston, VA 20192; **Joel Galloway**, Investigations Chief, U.S. Geological Survey, 821 East Interstate Avenue, Bismarck, ND, 58501; **Rochelle Nustad**, Hydrologist, U.S. Geological Survey, 102 North 4th Street, Grand Forks, ND, 58201, US

ABSTRACT

The Missouri River has had a long history of anthropogenic modification with considerable impacts on riparian ecology, form, and function. During the 19th and 20th century, the Missouri River basin experienced several massive dam-building efforts for irrigation, flood control and the generation of hydroelectric power. The river today has over 1/3 of its length inundated by reservoirs, and another 1/3 channelized with the flow managed for recreational use, fisheries, and habitat maintenance. In this study we examine how massive flooding in 2011 affected the geomorphic adjustments related to river management.

Our study is conducted along the 70-mile free flowing Upper Missouri River reach bounded upstream by the Garrison Dam (1953) and downstream by Lake Oahe Reservoir (1959) around the City of Bismarck ND. The Upper Missouri River has had its hydroperiod greatly reduced and stabilized by the presence of these dams. Typical discharges prior to the dam ranged from 10,000- 100,000 cubic feet per second (cfs) and fell to 30,000-45,000 cfs afterwards. In response, sedimentation rates and patterns along the river have had over 50 yrs to adjust to this new regime. The largest flood since dam regulation occurred in 2011 following an abnormally high snow pack season and a week-long rain event in the headwaters. Flood releases from the Garrison Dam began in May 2011 and peaked in June with a flow of approximately 150,000 cfs, more than triple that of normal peak loads for two weeks. The 2011 flood has highlighted the critical need for quantifying the complex interaction between the regional geomorphology and human activities.

The dam releases have had a discernible impact on the Missouri River throughout this section, such as reduction in sediment loads and channel bed degradation. A quantitative investigation of the historical impacts of the dams on channel planform, morphology, and sediment dynamics is necessary to provide a baseline to assess the impact of the 2011 flood. We have created a spatial-temporal conceptual model of the governing fluvial and deltaic processes for the reach. Ecological and geomorphic effects of dams and reservoirs have been well documented at specific sites, however relatively little attention has been paid to their interaction along a river corridor. We examine the morphological and sedimentation changes in the Upper Missouri River between the Garrison Dam and Oahe Dam. Through the use of historical aerial photography, stream gauge data, and cross sectional surveys we demonstrate that the impacts of the upstream dam do not completely attenuate to natural conditions before the backwater effects of the downstream

reservoir begin. Analysis of historic cross-sections and channel planform resulted in a series of geomorphic classifications along river.

The segment between the Garrison and Oahe dams was divided into five geomorphic reaches termed: *Dam Proximal, Dam-Attenuating, River-Dominated Interaction, Reservoir-Dominated Interaction, and Reservoir*. The Dam Proximal reach of the river is located immediately downstream of the dam and extends 50 km downstream and contained 22 cross-section sites. The cross-sectional data and aerial images suggest that the Dam Proximal reach of the river is eroding the bed, banks, and islands. All sites experienced an increase in cross-sectional area. The areal extent of islands in the Dam Proximal Reach in 1999 was 43% of what is was in 1950. The Dam-Attenuating reach extends from 50 to 100 km downstream of the dam and contained 14 cross-section sites. The islands in this reach are essentially metastable (adjusting spatially but with little net increase or decrease in areal extent). The reach itself has experienced net erosion with respect to the bed and banks, but to a lesser extent than the Dam Proximal reach. Twelve cross sections in the Dam-Attenuating reach show an increase in cross-sectional area. The reach gained 16% in island area from 1950 to 1999. All major islands present in 1950 were still present in 1999 with mostly similar geometries and distribution. The River-Dominated Interaction reach extends from 100 to 140 km downstream of the dam and contains 11 cross-sections. This reach is characterized by an increase in islands and sand bars and minimal change in channel cross-sectional area. Four of the sites have erosion and 5 of the sites are depositional (2 show no change). The areal extent of island area in this reach in 1999 was 150% greater in 1950. The Reservoir-Dominated Interaction reach is located 140– 190 km downstream from the Garrison Dam and contains 11 cross-sections. Reservoir effects vary both annually and seasonally due to changing reservoir levels creating a recognizable deltaic morphology. The Reservoir- Dominated Interaction reach is characterized by aggrading islands, sand bars, and the flooded meander bends (former meanders that have been flooded by the reservoir). Nine sites indicate deposition. The active extent of this reach can migrate drastically from year to year depending on the reservoir level. The Reservoir reach (Lake Oahe) is depositional but the channel morphology is stable. This reach extends from approximately 190 km to just upstream of the Oahe Dam; 512 km downstream from Garrison Dam. Cross-sections in this section extend into the first 100 km into this reach. All 12 cross sections in the Oahe reach shows deposition. It should be noted that because the lower floodplain is impounded (unlike other sections of the river), the deposition that occurs is spread out laterally rather than vertically. Thus, even though the cross-sectional area for the surveyed sample transect in this reach has changed, the overall change in channel capacity is only 2.5%. General channel morphology remains stable and all pre-dam islands in this reach are submerged under several meters of water.

Results show that the 512 km between the Garrison and Oahe Dam is not enough distance to isolate their influence on the river and therefore requires that they are not considered separately in impact investigations. The conditions which created the current morphology of the Upper Missouri river are likely found in many other rivers across the US. Most major rivers in the US have dams which are proximal longitudinally and are likely interacting in a similar way as the Garrison and Oahe Dams. In a GIS analysis of 66 major rivers within the contiguous United States, 73% of 404 dams surveyed are separated by less than 100 km. Dams were identified using USACE National Inventory. For each river, only the main river stem was considered and river distance was delineated in ArcGIS to the nearest km. We propose a conceptual model of how a sequence of interacting dams might impact river geomorphology (Figure 1) based on our

results. We call this morphologic sequence the Inter-Dam Sequence, and we present a simplified model based on the Upper Missouri River that could be easily adapted to other river reaches. Although the morphologic sequence is a useful conceptualization, there are clear limitations to these results. This model likely only applies to large dams on alluvial rivers. Dams on rivers that are controlled by bedrock or where morphologic adjustment is limited by vegetation or cohesive banks may respond differently than the model presented here. Similarly, the downstream effects of small dams will likely attenuate over much shorter distances. However, this framework is a helpful advancement in our understanding of longitudinal responses to multiple dams.

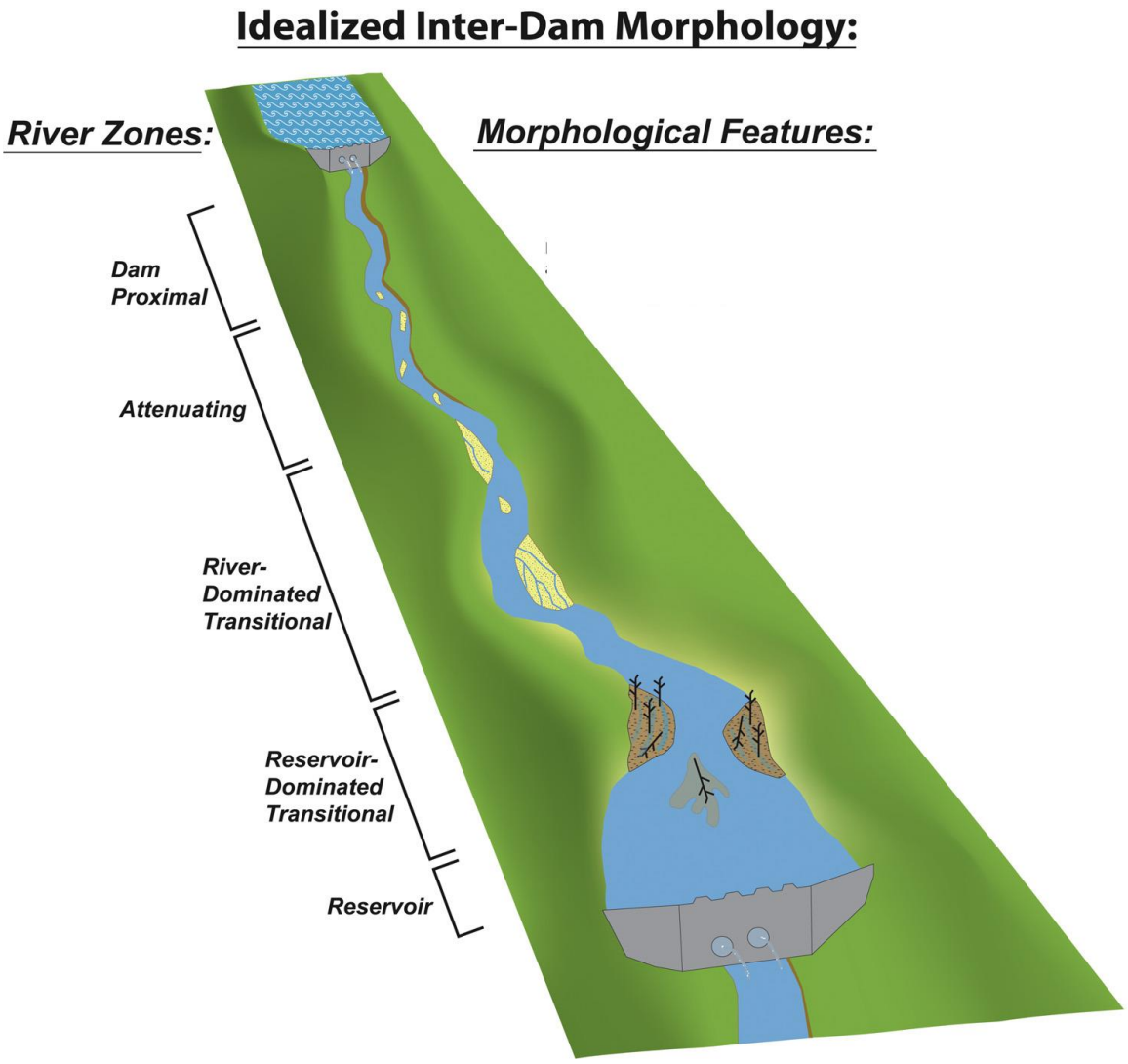

Figure 1 Idealized inter-dam morphology based on the geomorphic classification of the Missouri River.

ELWHA PLANECAM: AFFORDABLE NEAR-REAL-TIME ORTHOIMAGERY AND DIGITAL ELEVATION MODELS IN SUPPORT OF ADAPTIVE SEDIMENT MANAGEMENT AND MODELING DURING ELWHA AND GLINES CANYON DAM REMOVAL.

Andy Ritchie, Project Hydrologist/Geomorphologist, National Park Service, Port Angeles, Washington, andrew_ritchie@nps.gov.

Jennifer A Bountry, Hydraulic Engineer, U.S. Bureau of Reclamation, Denver, Colorado, jbountry@usbr.gov.

Timothy J. Randle, Supervisory Hydraulic Engineer, U.S. Bureau of Reclamation, Denver, Colorado, trandle@usbr.gov.

Topic Area: [Remote sensing]; Dam Removal/Rehabilitation; sediment yield and transport modeling, Fluvial Geomorphology

Subthemes: Innovation in measurement, management, and prediction of sediment in water and watersheds; dam removal, dam rehabilitation, and stream restoration; adaptive management

Elwha and Glines Canyon dams impounded about 28 million yd^3 ± 4 million yd^3 of sediment in Lake Mills and Lake Aldwell. Removal of these dams represents the largest dam removal and managed sediment release in U.S. history, with roughly a 20 year supply of coarse sediment and a 5 year supply of fine sediment released from October 2012 to March 2013 alone. Monitoring changes during dam removal presents a significant challenge due to limited monitoring resources, the large area affected by dam removal (approximately 16.5 river miles with an average valley width of about 3000 ft) and the near-real-time need for data from both reservoir and river reaches for adaptive project management decisions.

A rapid-deployment, low-cost method was developed to collect aerial imagery and generate orthoimagery and digital elevation models (DEMs) of the Elwha River during removal of Elwha and Glines Canyon dams. Imagery is collected with a firmware-modified consumer-grade camera and processed using structure from motion algorithms to produce a spatially accurate DEM with sub-foot resolution and orthoimagery with ~5 inch ground sample distance. A network of RTK GNSS surveyed ground control points (GCPs) with aerial targets are used to reference the DEM and orthoimagery to a geographic coordinate system and enable surface comparison using GIS tools. Flights are conducted on a weekly to monthly basis depending on hydrology and project progress, at a cost of roughly $300/flight. Imagery can be processed to produce DEMs and orthophotos of a specific reach in as little as 24 hours if needed.

Orthoimage resolution allows identification and measurement of features such as individual logs and sediment texture differences. Data are used to determine maximum inundation/erosion width, map banklines and evolution of depositional and erosional features such as midchannel bars and logjams, and to evaluate significant features affecting river morphology such as logjams and channel braidedness. The temporal frequency of flights makes it possible to compute bank erosion rates, meander migration rates, and the evolution of potential hazards.

DEMs are produced at 0.5 meter resolution. Features such as terraces, small channels, and individual logs can be identified. DEMs are used to calculate erosion volumes by comparing DEMs between flights, as well as comparing DEMs to LiDAR data, profile and cross-section surveys, and the pre-project surface model. DEMs also provide a measure of erosion slope along the reservoirs, and are used to calibrate the reservoir erosion model guiding dam removal. Comparison with LiDAR and RTK GNSS survey data indicate that DEMs provide an accurate tool with quantifiable error estimates and can be used to measure slopes and make volume calculations.

Elwha PlaneCam data have proven instrumental in monitoring difficult-to-reach areas, providing near-real-time updates to sediment erosion volumes during the project, and providing a high resolution spatial and temporal record of changes throughout the area affected by the removal of Elwha and Glines Canyon dams. Data from this survey method will produce a record of the project that is detailed enough to be mined for future research, yet rapid enough to provide feedback to calibrate models and guide project managers during dam removal.

COLLECTION AND INTERPRETATION OF RESERVOIR DATA TO SUPPORT SUSTAINABLE USE

Gregory L. Morris, GLM Engineering COOP, San Juan, Puerto Rico
gmorris@glmengineers.com

Abstract. Sustainable reservoir management seeks to retard sedimentation and reduce its adverse impacts, ultimately achieving an equilibrium between sediment inflow and outflow while sustaining storage capacity to maximize project benefits.

Sedimentation data has traditionally been collected with the objective of simply documenting the timewise decline in reservoir capacity and computation of reservoir "useful life." However, if the decision is made to manage the reservoir in a sustainable manner the available data needs to be analyzed differently, and additional data will be required to better understand sedimentation processes and develop management alternatives. This paper outlines some of the shortcomings of existing datasets and identifies data interpretation strategies and additional data types that can support sustainable reservoir management.

INTRODUCTION

Data on reservoir sedimentation has traditionally been collected with the objective of documenting the decline in storage capacity over time and accounting for its impact on the various reservoir pools. Most sedimentation datasets consist of periodic bathymetric surveys, presenting survey results as a change in volume over time, updating the elevation-volume curve and perhaps plotting representative cross-sections. Many reservoirs have never been surveyed at all.

When the decision is made to manage a reservoir for sustainable use instead of simply documenting its demise, it becomes necessary to: (1) re-process existing data to extract additional information, and (2) obtain additional and different types of data needed to better understand the sedimentation process, how it is changing over time, and to assess strategies for sustainable management. Sustainable management strategies are described by Morris and Fan (1997) and have been categorized in Figure 1.

RESERVOIR BATHYMETRIC DATA

Limitations of Bathymetric Datasets

Bathymetric data are used to document the change in reservoir volume over time, which is essential information for extrapolating future reservoir volume, discerning changes in sediment yield with time, and calibrating sediment transport models used to evaluate management alternatives. It is necessary to understand the limitations and potential problems with these datasets to interpret them properly and to plan a data collection program that supports sustainable management.

Bathymetric data are, for the most part, assumed to be accurate. However, many US and international datasets reveal significant error. When there are very few survey data, errors may go unrecognized. Consider, for example, reservoir volume data shown in Table 1.

Data from 5 of the 13 reservoirs are highlighted in bold red because they show that either total reservoir volume or the conservation pool volume has increased since reservoir construction. This is obviously an impossible result and therefore the affected data are deemed in error. However, the data for all the reservoirs are affected by error, but the potential for error is not noticed in the other reservoirs because the error is not as large or occurs in the opposite direction, thereby indicating an erroneously high rate of volume loss instead of a volume increase. However, because data for the other reservoirs have passed the "test of impossible results" they are tacitly accepted as accurate.

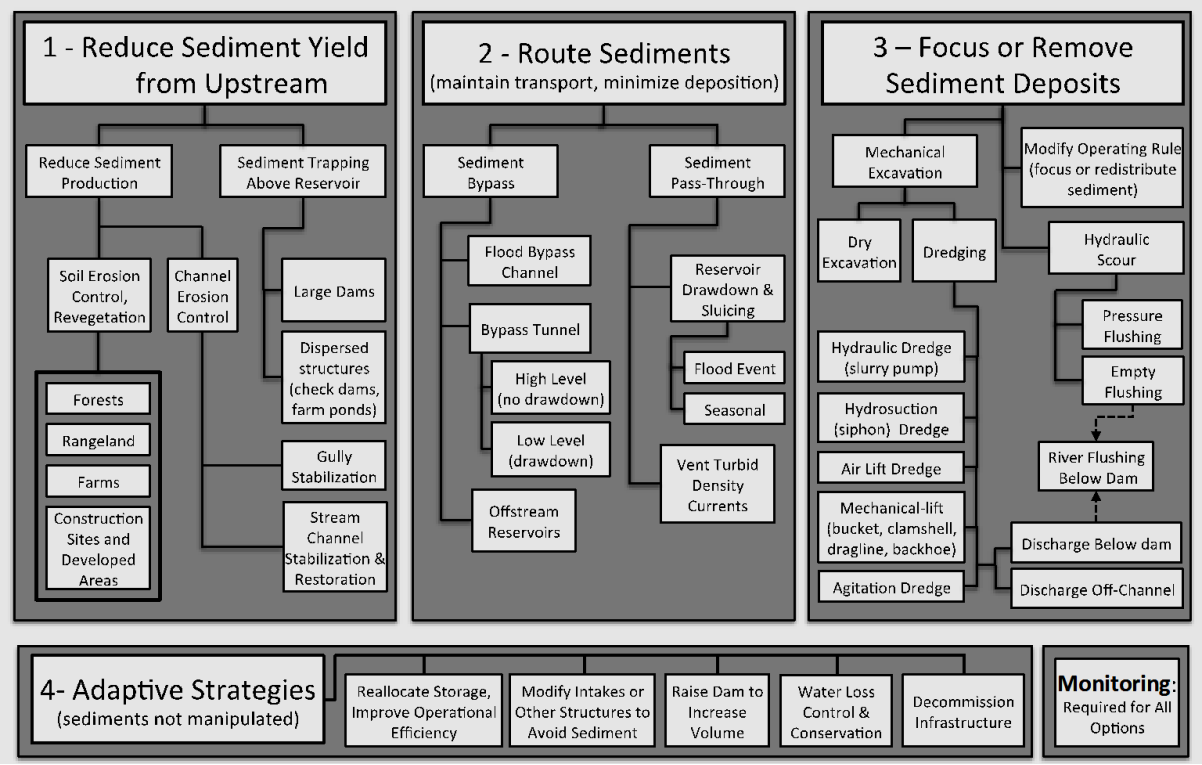

Figure 1 Strategies for sustainable reservoir management (after Morris, 2014).

Bathymetric errors can originate from a variety of sources. The original pre-impoundment reservoir volume is often not of high accuracy. It may have been determined by conventional ground survey, by photogrammetric methods, or computed from published topographic mapping. Post-impoundment volume surveys necessarily use different techniques. The ***range-line*** method has been used conventionally, but since the 1990s the ***contour method*** has come into widespread use. A contour survey collects a high-density of position and depth data points measured by GPS and sonar, from which the sediment surface is mapped and the volume computed by mapping or survey software. Survey methodologies are summarized by Ferrari and Collins (2009) and Ferrari (2006a).

All surveys incorporate errors, and these errors are not necessarily easy to detect since the bathymetric data collection process is typically open-ended without the check that occurs, for example, in a conventional topographic survey which may close back to the point of origin. As an example, consider the reservoir survey data presented in Figure 2. The data were collected on different days with the boat running track lines oriented perpendicular to each other on each day. The resulting checkerboard pattern, with both high and low survey lines, was the result of not

having the bathymetric equipment properly calibrated; different days produced track lines having different elevations for the same area. Because bathymetric track paths are typically parallel and do not repeat the same area, this type of error would not normally be detected.

Table 1 Reservoir Capacities for Corps of Engineer Reservoirs, Baltimore District.

Basin and Reservoir	Watershed (km^2)	Dam Closure Year	Last Survey Year	Storage Loss (%)	
				Below Top of Conservation Pool	Below Top of Flood Pool
North Branch Potomac River Basin					
Jennings Randolph	681	1981	1997	-6.8	-6.3
Savage	272	1952	1996	-3.3	-3.0
East Sidney	264	1950	2000	-15.2	-2.4
Whitney Point	660	1942	1997	-6.5	-2.6
Almond	145	1949	1997	-48.8	-8.5
Tioga	725	1978	1999	**+4.7**	**+0.5**
Hammond	316	1978	1999	-2.5	**+0.8**
Cowanesque	772	1980	1997	-7.8	-4.6
Bush	585	1962	1999	**+7.1**	-0.1
Sayers	878	1969	1997	-1.4	**+1.5**
Curwensville	945	1965	1997	-19.9	-3.7
Main Stem Susquehanna River Basin					
Stillwater	96	1960	2000	-28.0	-3.7
Aylesworth	16	1970	2000	-3.1	**+4.4**

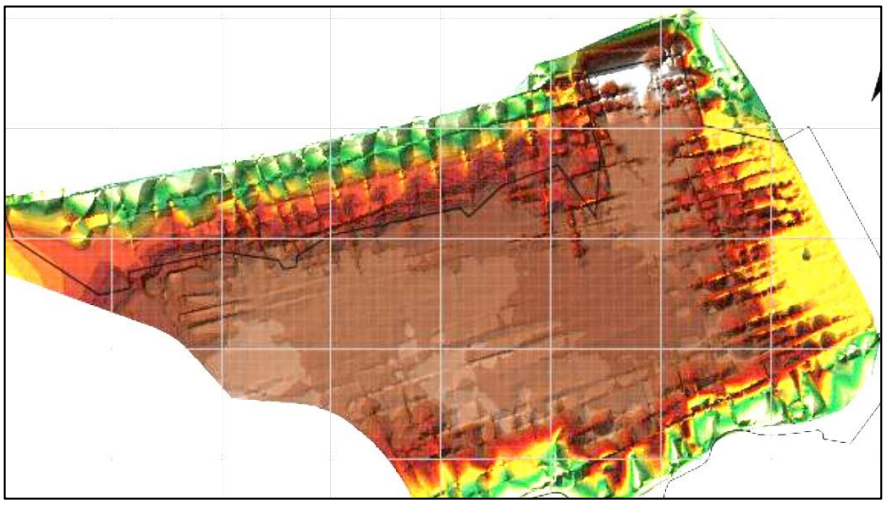

Figure 2: Bathymetric survey showing irregular gridded lines in the reservoir.

A potentially large source of error is associated with changes in methodology, such as changing from pre-impoundment to post-impoundment surveys, or from range-line to contour surveys. Given the differences in field measurement methods, together with the variety of computational techniques available for making volume computations, a change in methodology can generate a significant change in the measured volume, independent of sedimentation. Even contour survey

computational algorithms represent a potential source of error of some significance. For example, Ortt et al. (2000) analyzed digital datasets from Loch Raven and Prettyboy reservoirs in Maryland using two different software algorithms, resulting in volume differences of 1.4% and 2.2% respectively due to software differences alone.

Consider the data for John Redmond Reservoir in Figure 4, showing a recent increase in reservoir volume. The last survey was performed by the contour method, the prior surveys by range-line. The volume shift coinciding with the changed methodology makes the sedimentation trend unclear.

For sustainable management, the principal objective of repeated surveys is to calculate the rate of sedimentation, and not to simply achieve a more accurate measure of the current reservoir volume. For this reason, when changing survey methodologies it is always appropriate to compute the new volume measurement by both the old and the new methodologies. To support this dual-computation, the new survey track lines should be planned to insure that each of the original range lines is replicated to provide the necessary data needed for volume computation by the old method. By comparing the survey volume by the two methods, the difference in apparent volume due to the changed methodology may be separated from the physical volume change due to sedimentation.

Changing Sedimentation Rate

Data from U.S. reservoirs frequently show that the rate of volume loss is not constant, but tends to decline over time (see Figure 3 and Figure 4). The most important factors that probably contribute to this result are: (1) sediment compaction, and (2) declining sediment yield due to erosion control or upstream dams. Reduced trap efficiency due to volume loss is probably not an important consideration in reservoirs which still retain much of their original volume (Brune, 1953). Changes in measurement methodology would probably not introduce a uni-directional bias, and at many sites the measurement methodology is unchanged.

A timewise change in sedimentation rate will not be observable absent data from multiple surveys. Drawing a trend line from the pre-impoundment volume through a single bathymetric survey data point 20 or 30 years following impoundment may provide a poor estimate of the long-term sedimentation rate. For example, if only the pre-impoundment (1949) and the 1981 survey data were available for Harry Strunk Reservoir, the projection of capacity loss based on these two data points alone would be remarkably different from the situation revealed with more complete data, as illustrated by the difference in the trend lines drawn in Figure 3.

For many federal reservoirs the datasets needed to detect changing in rates of volume loss do not exist. For example, 70% of the Bureau of Reclamation's 400+ storage facilities have not been surveyed since initial impounding, and another 20% have only been surveyed once (Ferrari and Collins 2006).

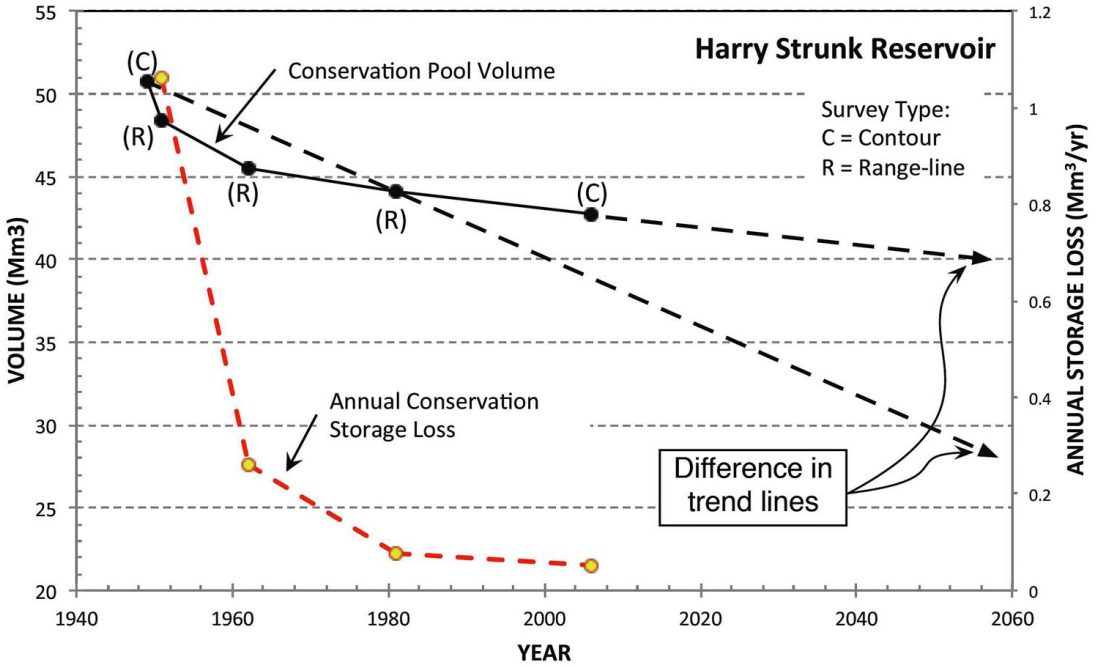

Figure 3 Timewise decline in reservoir volume and rate of storage loss at the Bureau of Reclamation's Harry Strunk Reservoir with trend lines superimposed (historical data from Ferrari 2006b).

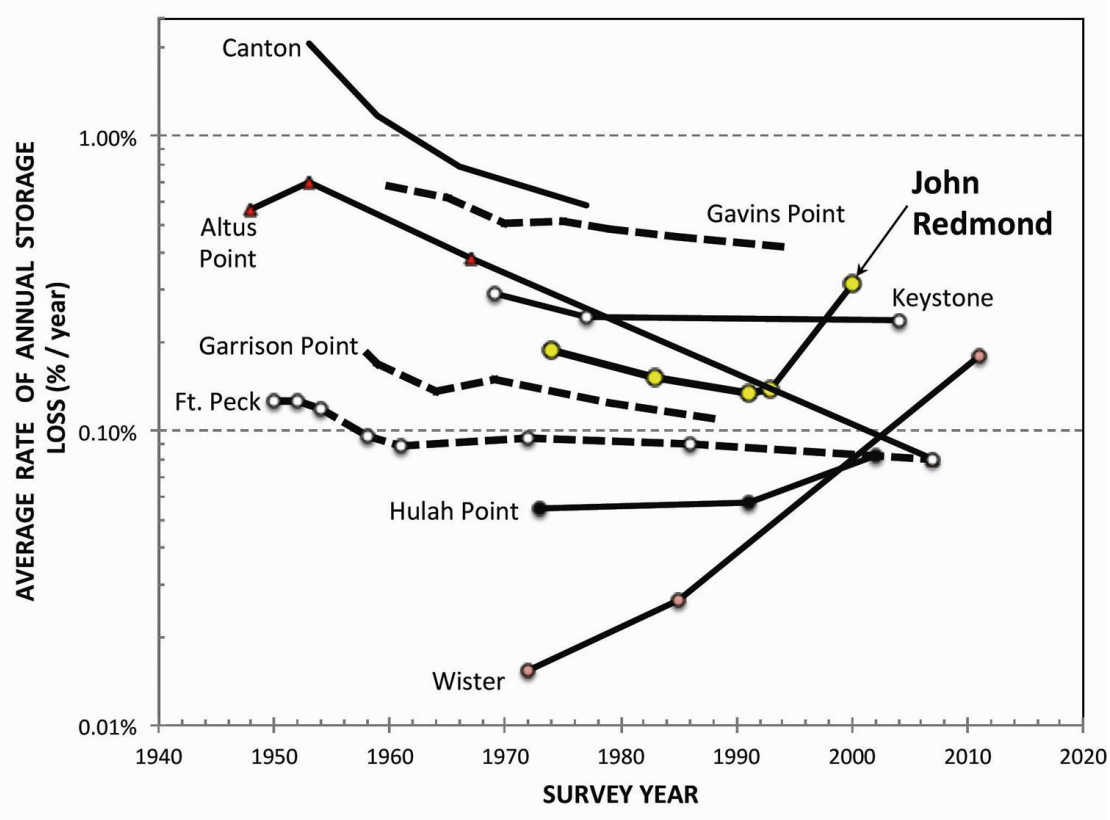

Figure 4 Change in rate of storage loss at several Corps of Engineers reservoirs in the Tulsa and Omaha districts.

Longitudinal Reservoir Profiles

Insight into the sedimentation process can be gained by plotting the timewise change in the reservoir's longitudinal bottom profiles. Profiles revealing horizontally-bedded sediment at the dam indicate that turbid density currents are transporting significant volumes of sediment to the dam which is not being released (Figure 5). Longitudinal profiles can also be used to monitor the pattern of delta advance (Figure 6) as influenced by the reservoir operational levels. It is quite difficult to deduce these patterns by examining changes in the elevation-volume curves over time (Figure 7). Although simple to construct and highly instructive of the sedimentation process, longitudinal profiles are not normally plotted in sedimentation studies. It can also be useful to prepare a graph showing a longitudinal plot of cumulative sediment volume. Existing datasets may be reprocessed to display this information.

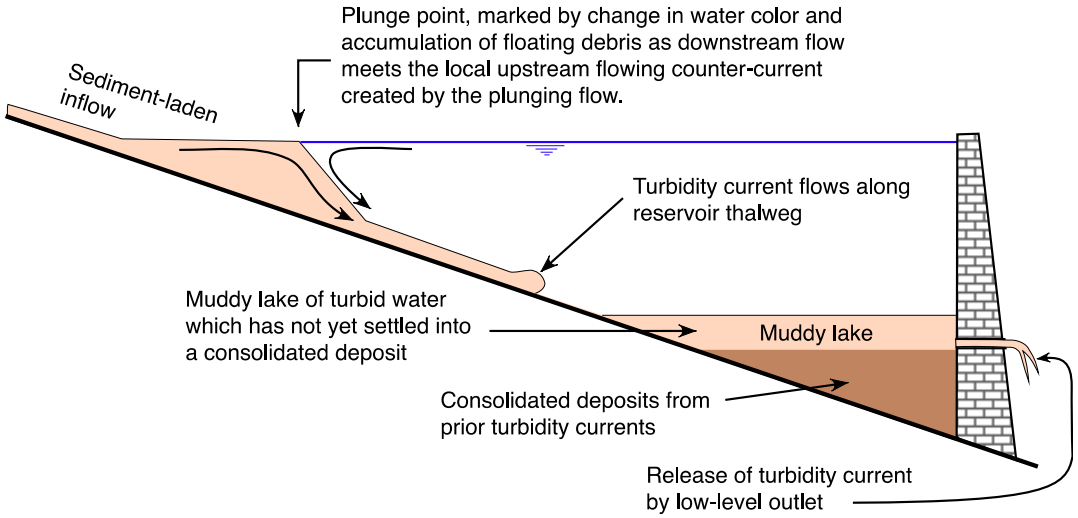

Figure 5 Longitudinal profiles can reveal the presence of turbidity current deposits at the dam.

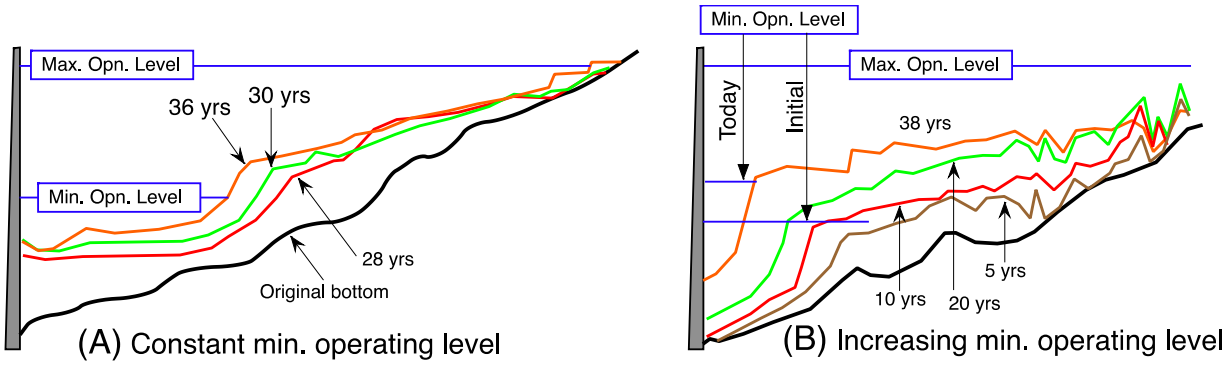

Figure 6 Longitudinal profiles showing different patterns of delta advance.

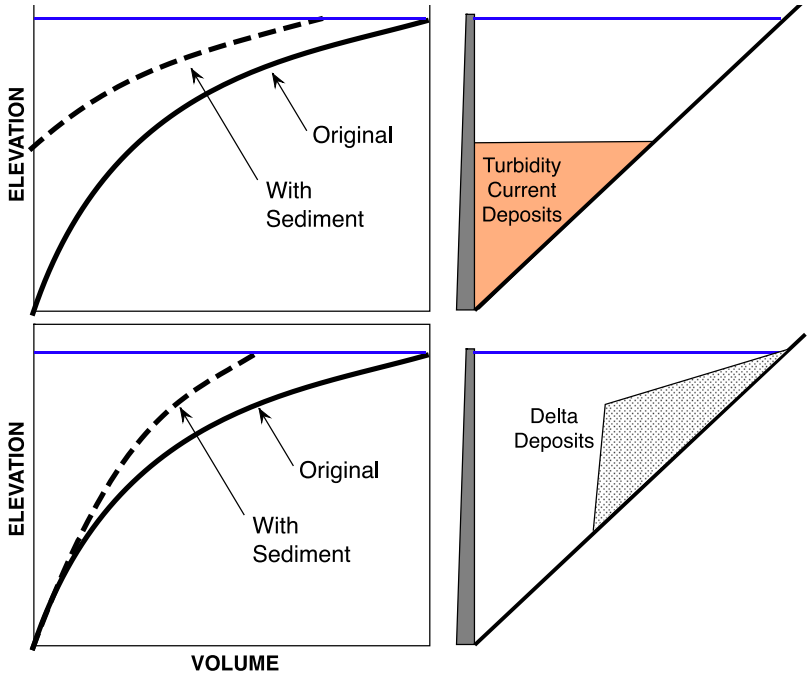

Figure 7 Change in shape of elevation-volume curve over time as influenced by the predominant pattern of sediment deposition in a reservoir.

SEDIMENT CORES

Sediment cores may be obtained from the bottom of a reservoir by conventional geotechnical boring equipment working from a floating platform. For example, at Tarbela Reservoir, Pakistan, ten cores penetrating up to 60 m of sediment thickness to reach the original reservoir bottom were obtained operating from a barge during 56 working days. This did not include time consumed by weather delay when the water was too rough to work (SMS Consultants, 2013). This is a costly and time-consuming sampling alternative. In contrast, for core lengths not exceeding about 3 to 4 m, low-cost vibracore equipment may be used for rapidly sampling multiple locations each day. Vibracore sampling and analysis protocols are described by Bennett et al. (2013). Portable vibracore equipment used to sample in water up to 60 m deep in a hydropower reservoir in Colombia is illustrated in Figure 8. The objective was to obtain bulk samples to determine how far sand was being transported in the direction of the power intake during reservoir drawdown, when the sandy delta is subject to scour and sediment remobilization.

Sediment cores are not routinely collected in reservoirs but can be important aids in understanding and managing the sedimentation processes. Because sediments deposit in an episodic nature, the sediments in a reservoir will be layered, and samples from the top of the deposits will not provide representative information. Sample cores are required to obtain a more representative characterization of the deposit characteristics for determining representative values for parameters such as grain size, bulk density, organic content, and sediment chemistry. Because sandy delta sediments will advance and prograde over previously deposited fines, the composition of the top part of the bed may be different from the bottom. Depending on the management strategy, the composition of the deeper sediment may or may not be a concern.

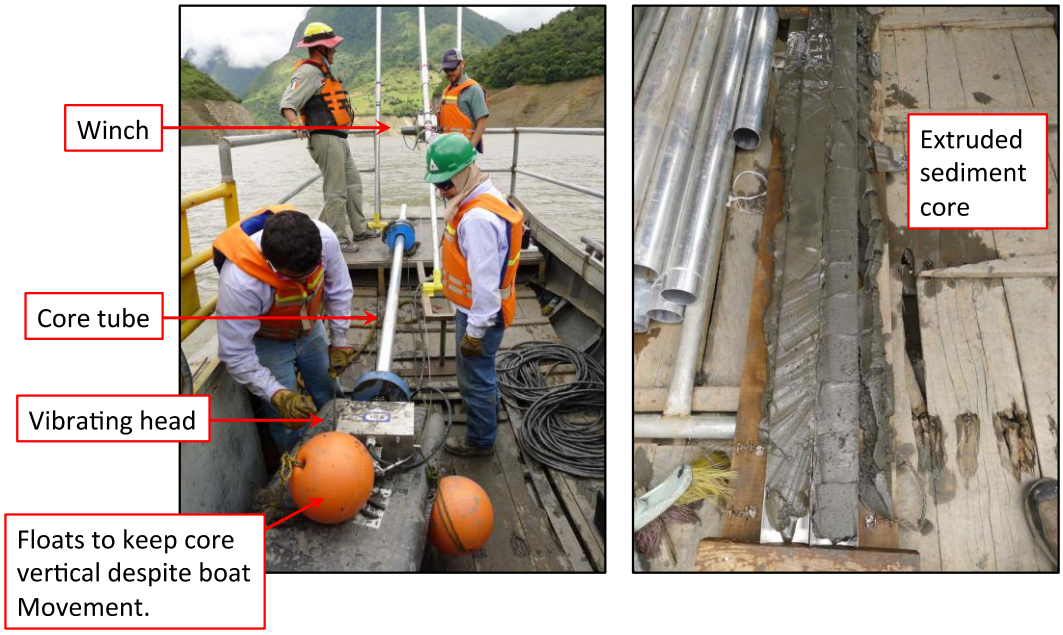

Figure 8 Battery operated vibracore used for sampling sand concentration near a hydropower intake.

Computing Sedimentation Rate

When the original volume of a reservoir is unavailable or uncertain, fully penetrating cores in combination with a dual-frequency bathymetric survey (sub-bottom profiler) can map both the top and bottom of sediment deposits. Cores are useful to confirm the bulk density of the deposits and to confirm the depth to original ground (sediment thickness) as identified by the sonar data. This approach will not work if reservoir sediments contain methane gas from organic decomposition, since the sonar signal is strongly reflected by the air-water interface created by bubbles in the sediment.

If there is a datable stratigraphic horizon within the sediment that can be identified in the cores, this can also provide additional information on relative rates of sedimentation on either side of the event horizon. Horizons may be created by a large wildfire, volcanic eruption, contaminant discharge, and the cesium-137 layers from atmospheric testing of thermonuclear weapons that started in 1952 and peaked in 1963 (Cox et al., 2002).

Determining Bulk Density

To determine sediment yield from sediment volume requires knowledge of the dry bulk density of the sediment deposits. Bulk density varies with sediment grain size, and generally decreases moving downstream in a reservoir. Higher bulk densities occur in coarse delta sediment and lower bulk densities in fine grained sediments near the dam. The bulk density of fine sediment is not static but increases over time (and with depth) due to the weight of overlying sediment. Because sediment is not uniformly deposited, in some areas of the reservoir (and particularly near the delta face), bulk density will also vary with depth due to sediment layers of different

grain sizes. Sediment cores can provide direct measurements of bulk density. Juracek (2006) provides information on sampling strategies for bulk density determinations.

Sediment Characteristics

Particle-size distribution data for different areas of the reservoir can provide useful information for calibrating sediment transport models. In hydropower plants, sand more than about 0.2 mm in diameter is generally considered to be highly abrasive, making it essential that is be excluded from the power intake. Sediment cores extending upstream from the intake can provide information on the grain size and percentage of sand, and can monitor its rate of advance toward the power intake. Knowledge of organic content, potential contaminants, and other parameters may be needed prior to excavating and discharging sediment, and samples required for this analysis are also normally obtained by cores.

DAILY SEDIMENT BALANCE

Sediment routing strategies (Figure 1) are based on the tendency for sediment discharge to be highly concentrated in time. Routing techniques reduce the rate of sediment accumulation by maintaining sediment-laden flood flows in motion, either passing them around the storage zone (sediment bypass) using offstream reservoirs or sediment bypass tunnels, or by passing sediment-laden flow though the storage zone with the minimum detention time or by releasing submerged turbid density currents. Given the episodic nature of sediment inflow events, daily discharge and concentration datasets are required to analyze these strategies, and depending on the site continuous (e.g., 15 minute) data may be required for refinement of the analysis and for subsequent operational purposes.

Aside from the difficulty and cost of acquiring reliable suspended sediment data, a significant disadvantage lies in the potentially high variability of sediment yield over time, particularly in mountainous watersheds. Large floods will frequently deliver sediment volumes that exceed several years of “normal” hydrology. Capturing data from these events, which may have a large impact on long-term sediment yield and the degree of success of a sediment routing strategy, requires a data collection platform that can withstand extreme floods and hurricanes, plus the good fortune to have the gage’s funding period coincide with an extreme event.

CONCLUSIONS

Today’s inventory of reservoirs cannot be managed in a sustainable manner without substantially expanded data collection and improved data analysis. The most critical issue at this point is to survey reservoirs at regular intervals to better determine the long term rates of storage loss, and document the timewise variability in these rates. These data can help identify reservoirs with the highest priority for management.

Many reservoirs in which capacity was previously determined by the range-line method will next be surveyed by the contour method. When changing methodologies it is essential to perform the new survey using both the old and the new methodologies, so that the volume change attributable to the change in methodology can be differentiated from the actual change in reservoir volume due to sedimentation.

While gage stations and daily data collection are essential for understanding sediment transport dynamics and developing workable management strategies, they do not substitute for good bathymetric datasets.

REFERENCES

Bennett, S.J., Dunbar, J.A., Rhoton, F.E., Allen, P.M., Bigham, J.M., Davidson, G.R., and Wren, D.G. (2013). "Assessing Sedimentation Issues within Aging Flood-Control Reservoirs." In ***The Challenges of Dam Removal and River Restoration***, Reviews in Engineering Geology, Geological Society of America, 25–44.

Brune, Gunnar M. (1953) "Trap Efficiency of Reservoirs." Trans. American Geophysical Union 34 (3): 407–18.

Cox, S.E., Bell, P.R., Lowther, J.S., and VanMetre, P.C. (2005) "Vertical Distribution of Trace-Element Concentrations and Occurrence of Metallurgical Slag Particles in Accumulated Bed Sediments of Lake Roosevelt, Washington, September, 2002." U.S. Geological Survey Scientific Investigations Report 2004-5090, Reston, VA.

Ferrari, R.L. (2006a) "Reconnaissance Techniques for Reservoir Surveys." U.S. Department of Interior, Bureau of Reclamation, Denver.

Ferrari, R.L. (2006b) "Harry Strunk Lake 2006 Sedimentation Survey." U.S. Department of Interior, Bureau of Reclamation, Denver, CO.

Ferrari, R., and Collins, K. (2006). "Reservoir Survey and Data Analysis." In: Yang, C.T. ed. ***Erosion and Sedimentation Manual***, US Dept. of Interior, Bureau of Reclamation, Denver, CO.

Juracek, K. (2006). "A Comparison of Approaches for Estimating Bottom-Sediment Mass in Large Reservoirs." USGS Scientific Investigations Report 2006-5168, 13p.

Lee, C., and Foster, G. (2013). "Assessing the Potential of Reservoir Outflow Management to Reduce Sedimentation Using Continuous Turbidity Monitoring and Reservoir Modeling." Hydrological Processes, 27(10), 1426–1439.

Morris, Gregory L. (2014) "Sediment Management and Sustainable Use of Reservoirs." In ***Modern Water Resources Engineering***, edited by Lawrence K. Wang and Chih Ted Yang, p 279–337.

Morris, G.L. and Fan, J. (1998) ***Reservoir Sedimentation Handbook***. McGraw-Hill Book Co., New York. (www.reservoirsedimentation.com)

Ortt, R.A., Jr, Kerhin, R.T., Wells, D., and Cornwell, J. (2000). "Bathymetric survey and sedimentation analysis of Loch Raven and Prettyboy reservoirs." Coastal and Estuarine Geology File Report 99-4, Maryland Geological Survey.

SMS Consultants Joint Venture (2013) "Sediment Management Study of Tarbela Reservoir, Vol. 4, Sediment Data Report". Report to WAPDA, Lahore, Pakistan.

UNSTEADY FLOW AND SEDIMENT MODELING IN A LARGE RESERVOIR USING HEC-RAS 5.0

John Shelley, Ph.D., P.E., U.S. Army Corps of Engineers, Kansas City District, john.shelley@usace.army.mil; Stanford Gibson, Ph.D., U.S. Army Corps of Engineers, Hydrologic Engineering Center, stanford.gibson@usace.army.mil; Aaron Williams, E.I.T., U.S. Army Corps of Engineers, Kansas City District, aaron.r.williams@usace.army.mil.

ABSTRACT

Sediment accumulation is a problem in many large reservoirs in the United States and around the world, including Tuttle Creek Lake in the Kansas River basin. A one-dimensional unsteady flow and sediment model was built for Tuttle Creek Lake using the Hydraulic Engineering Center – River Analysis System (HEC-RAS) Version 5.0 Beta. This paper provides an overview of Tuttle Creek Lake, describes the model setup, highlights how features new to HEC-RAS 5.0 operated in the modeling effort, and provides model results from a proof-of-concept model run. This model will be used to evaluate the technical feasibility and effectiveness of altering the reservoir operations to decrease sediment trapping efficiency.

INTRODUCTION

Sediment accumulation is a problem in many large reservoirs in the United States and around the world. Available storage is decreasing while demand for water is increasing. Downstream, channels degrade and reduced sediment supply threatens sediment-dependent aquatic species (Haslouer et al., 2005). Removal of accumulated sediment from large reservoirs tends to be prohibitively expensive. This underscores the need to optimally operate large reservoirs to decrease sediment deposition in the first place.

Tuttle Creek Lake is a large, Corps of Engineers reservoir in the Kansas River basin that provides flood control, water supply, recreation, and environmental benefits. Tuttle Creek Lake provides water supply to Manhattan, Kansas and provides releases to the Kansas River that benefit water users in Topeka, Lawrence, and Kansas City, Kansas. In addition, Tuttle Creek Lake releases water when necessary to provide navigation flows on the Missouri River.

As of 2009, the total storage up to the multipurpose pool level and flood control pool level were approximately 252,000 ac-ft and 2,118,000 ac-ft, respectively (USACE, 2012). The pre-construction estimate for the sedimentation rate in the multi-purpose pool was 4,151 ac-ft/yr

ac-ft/year. Based on repeated bathymetric surveys, the average sediment accumulation is estimated at 3,594 ac-ft/year (KWO, 2012). Since completion of the dam in 1962, 43% of the original multi-purpose storage volume has been lost to sediment accumulation. The current operational procedure for Tuttle Creek Lake traps 98% of all sediment, including fine silts and clays (Juracek, 2011). Dredging with upland disposal of the dredged material is prohibitively expensive, given the large quantity of incoming sediment load.

A one-dimensional unsteady flow and sediment model was built for this project using the Hydraulic Engineering Center – River Analysis System (HEC-RAS) Version 5.0 Beta (USACE, 2015, Gibson et al., 2006) to evaluate the technical feasibility and effectiveness of altering the reservoir operations to decrease sediment trapping efficiency. This model uses features that are new to HEC-RAS 5.0, including unsteady sediment modeling and customized RULES to calibrate ungaged inflows.

The model will assess trap efficiency response to alternate management strategies, assuring that they also meet current flood control reservoir functions. Operational changes within existing constraints may only decrease trapping efficiency slightly (Lee and Foster, 2013), but even a slight decrease in sediment trapping can save significant money compared to maintenance dredging. Small decreases in trapping efficiency over time can form a part of larger sediment management strategy.

MODEL SET-UP

Model cross-sections extend from the Big Blue River upstream of the reservoir, down through the reservoir to the confluence with the Kansas River, and on the Kansas River from Fort Riley to Wamego. Two additional major tributaries to Tuttle Creek Lake, the Little Blue River and the Black Vermillion River are included as point loads rather than modeled cross-sections. Figure 1 provides a general vicinity map of the project area including major components of the HEC-RAS model.

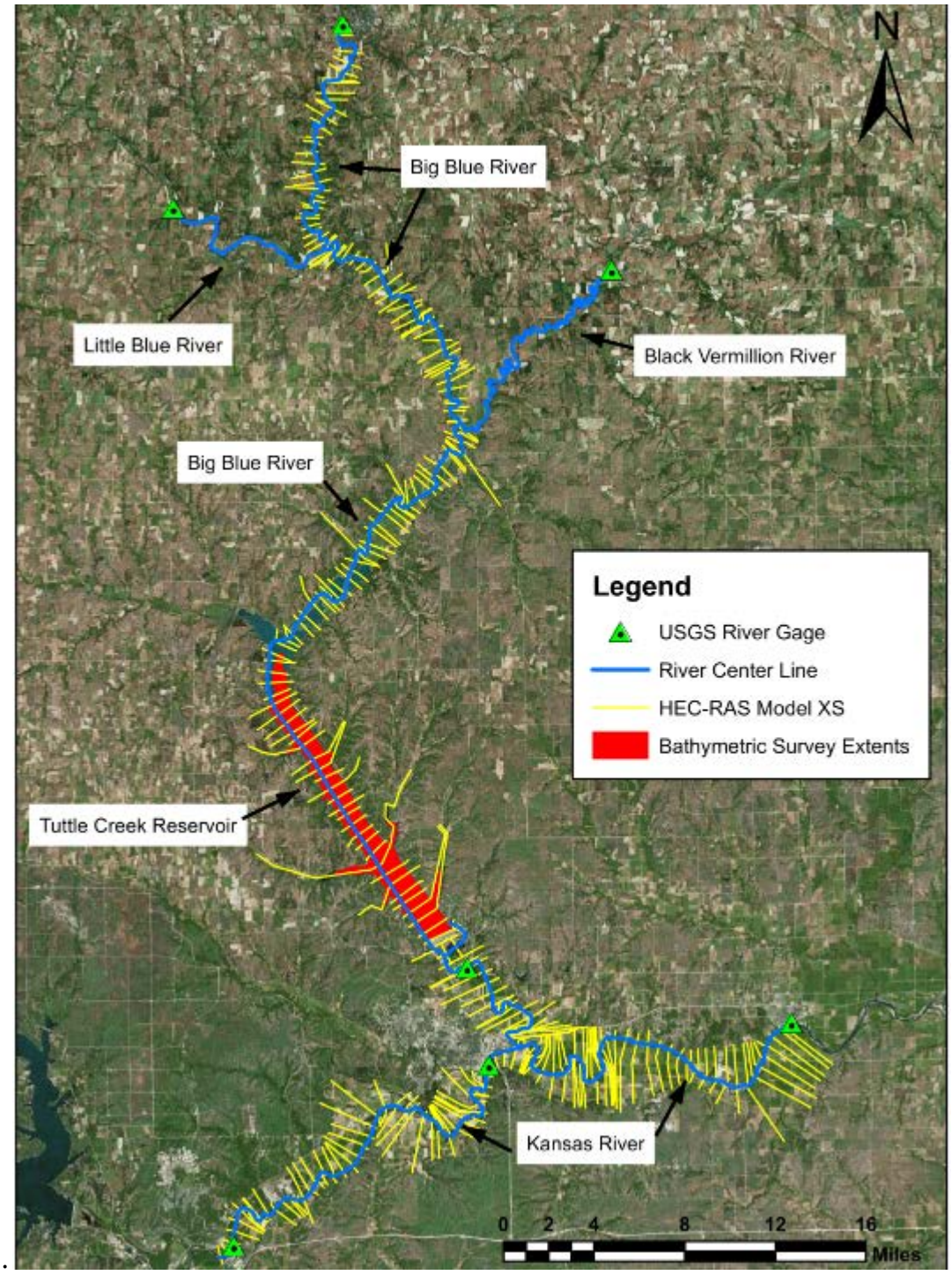

Figure 1. Model Schematic

DEVELOPMENT OF INITIAL BATHYMETRIC SURFACE

Model creation and calibration require a baseline survey to build model geometry and a final survey to compare to model output. Two recent bathymetric surveys were available, in 2000 and 2009 (Figure 2). The 2000 bathymetric survey had low point density (1.6 points per acre) and produced a surface with interpolation errors and insufficient channel detail. The 2009 survey had a much higher point density (25.8 points per acre) which provided excellent definition of the reservoir and channel bottom.

The following procedure compensated for insufficiencies in the 2000 data. First, a surface was interpolated from the 2009 survey points. The vertical change from 2000 to 2009 was computed at each 2000 bathymetric point using the 2009 surface. Then, these individual point changes were interpolated to create a surface of bed change from 2000 to 2009. Finally, this bed change surface was subtracted from the 2009 surface to create a more representative 2000 surface. Figure 3 illustrates model cross-section 18.17 cut from the original 2000 surface and from the 2000 surface created using the using the bed change method described above. As seen in Figure 3, the bed change method produced a more reasonable cross-section shape and a physically justifiable deposition pattern. Accordingly, the model cross-sections were derived using the 2000 bathymetric surface developed using the bed change method.

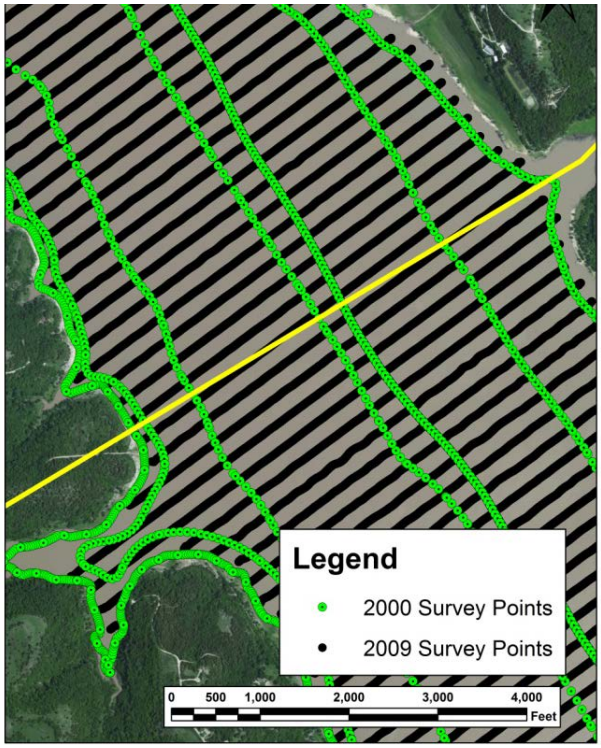

Figure 2. Comparison of 2000 and 2009 Bathymetric Survey Points, Model RS 18.17

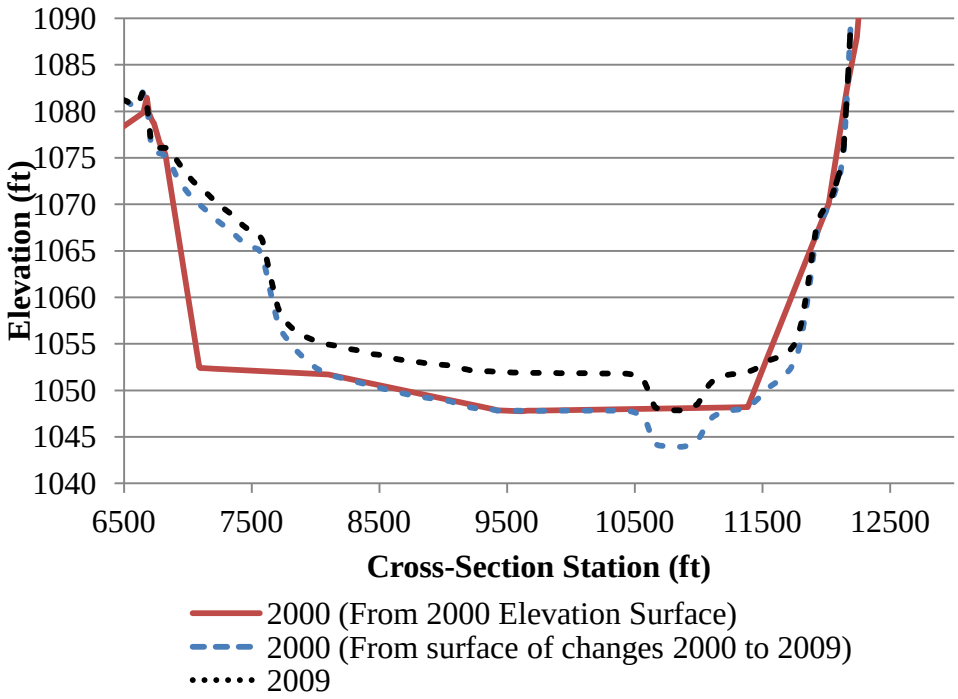

Figure 3. Cross-section Comparison of Surface Interpolation Methods, Model RS 18.17

FLOW AND SEDIMENT BOUNDARY CONDITIONS

Data from USGS gaging stations produced the relationships between flow and suspended sediment load at the three major tributaries to Tuttle Creek Lake seen in Figure 4. Daily suspended sediment loads were associated with daily inflows to the reservoir. Bed load data was not available and values were estimated as a percentage of suspended sediment loads.

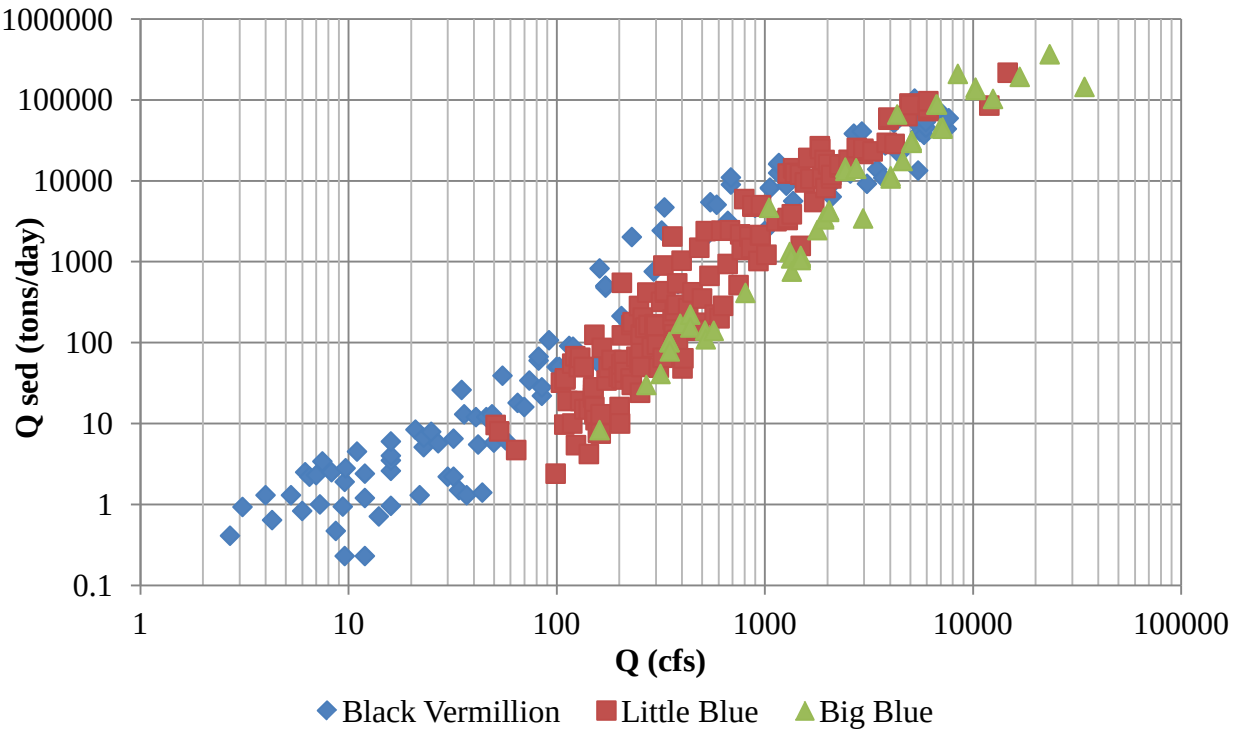

Figure 4. Suspended Sediment Loads on Three Major Rivers Flowing into Tuttle Creek Lake

Boundary load gradations were inferred from detailed gradation data collected by USGS from 2008 – 2010 (Juracek 2011). As seen in Figure 5, the sediment size composition on the Big Blue River and Little Blue River depend on the flow rate, while the Black Vermillion River load gradations are independent of flow. In Figure 5, solid lines represent gradations developed from measurements, while dashed lines represent extrapolation included for modeling purposes.

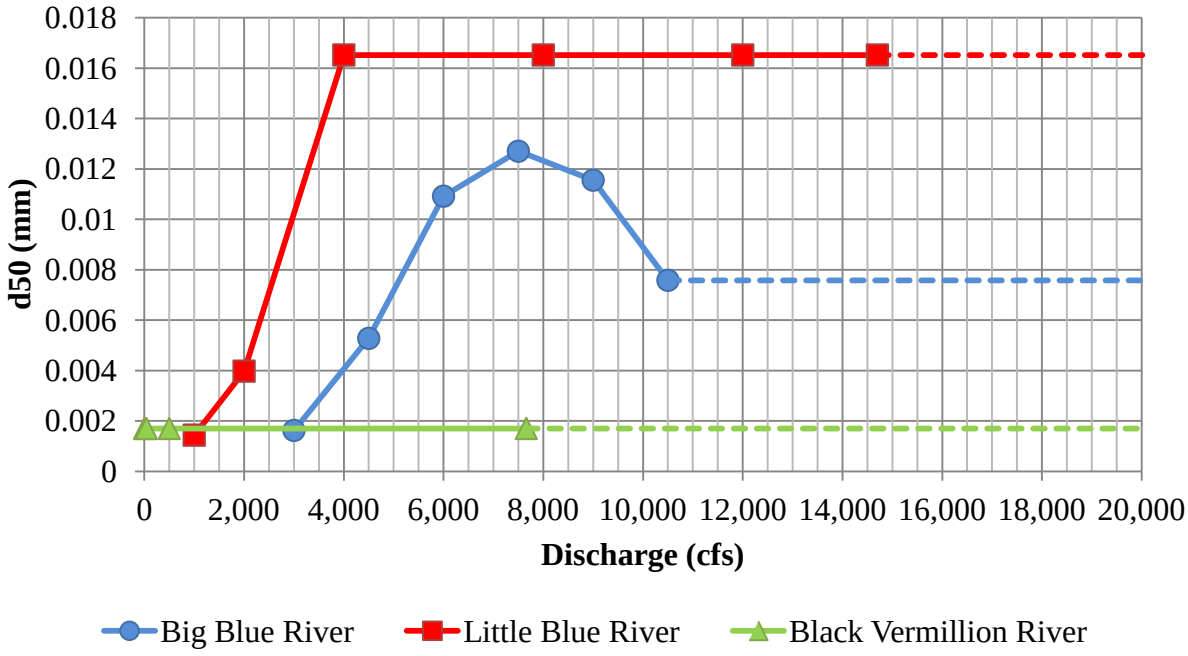

Figure 5. Suspended Sediment Median Grain Size (D50) on Major Tuttle Creek Tributaries.

NEW HEC-RAS FEATURES

UNSTEADY SEDIMENT

HEC-RAS 4.1 included a quasi-unsteady flow model for use in sediment modeling, simulating hydrodynamics with a series of steady flows. This simplification adequately describes many hydraulic systems because sediment-response time scales are so much longer than hydraulic-response time scales. However, reservoir scenarios are inherently unsteady, requiring explicit volume tracking and mass conservation to simulate system behavior. HEC-RAS 5.0 integrates sediment transport features with the unsteady flow module. This not conserves volume by coupling sediment transport with the Saint-Venant equations, but also makes a suite of reservoir modeling tools native to the unsteady flow modeling environment available in the context of sediment transport simulations.

RULES FOR CALIBRATION OF UNGAGED FLOW

HEC-RAS 4.1 included the RULES editor, a simple scripting language for building operational procedures for reservoir gates in unsteady flow. With the inclusion of sediment modeling in the unsteady flow environment, the RULES scripting language is available for reservoir sediment models (Gibson and Boyd, 2014). In this model, custom RULES allowed the solution to a

hydraulic calibration challenge. Inflow from the three gaged tributaries systematically summed to less than the recorded flow downstream of the reservoir, suggesting ungaged inflow contributions. However, reservoir storage effects prevented a straight-forward calculation of the daily ungaged inflows. Rather, custom code in the rules editor computed the daily series of ungaged inflows based on historic daily reservoir stages.

PROOF-OF-CONCEPT SEDIMENT MODEL

Sediment transport was added to the unsteady flow model for the calibration period (20 July 2000 to 14 September 2009). As a proof-of-concept, loads and gradations were significantly adjusted to approximate total volume and longitudinal distribution of reservoir deposits (Gibson and Pridal, 2015). Figures 6 and 7 plot model and measured values for the local and longitudinally-summed cumulative volume of bed change. These results will change as hydraulics and operations are refined. As seen in Figures 6 and 7, HEC-RAS 5.0 can model sediment transport during complicated unsteady reservoir operations and can approximate historic sedimentation.

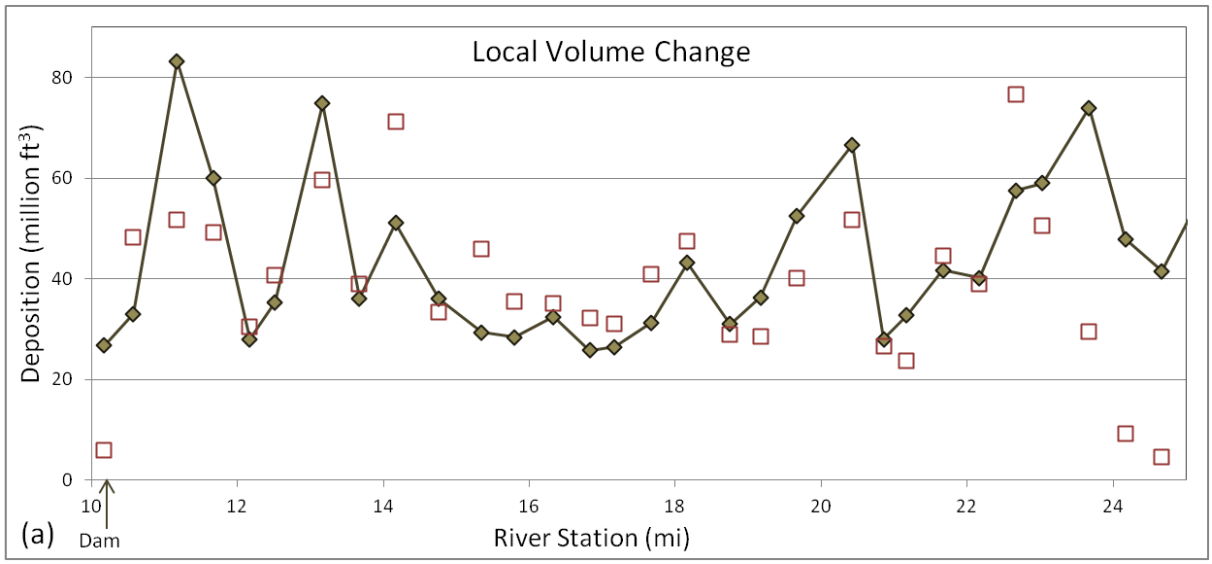

Figure 6. Model results compared to measured local deposition volume change from July 20, 2000 to Sept 14, 2009

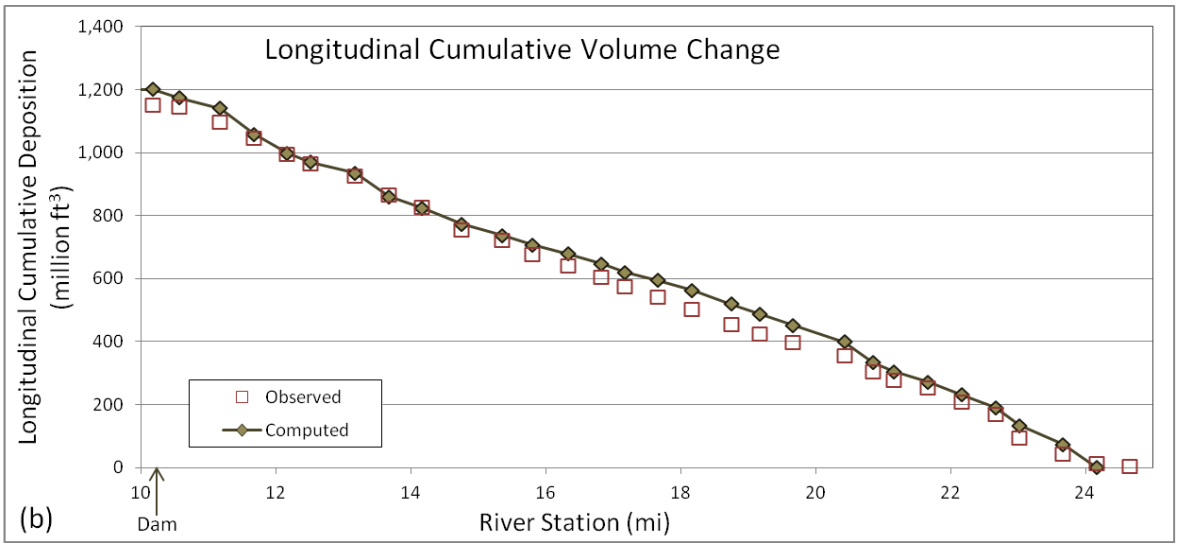

Figure 7. Model results compared to measured to longitudinal cumulative (summed from upstream to downstream) deposition volume change from July 20, 2000 to Sept 14, 2009

The addition of sediment to the stable unsteady flow model introduced numerous model instabilities, which required additional troubleshooting. The sediment model required a smaller time step, interpolated cross sections, and other stabilizing measures to run, which translated to longer run times. However, once the model achieved stability, the unsteady hydrodynamics and operational rules provided computational fidelity and alternative flexibility beyond what is possible in a quasi-unsteady approach.

CONCLUSION/NEXT STEPS

This paper described the initial development of a one-dimensional HEC-RAS 5.0 mobile-bed model for modeling and predicting sediment accumulation in Tuttle Creek Lake. This model utilizes new features in HEC-RAS 5.0 including Unsteady Sediment and new features in the RULES editor. Additional measures to ensure model stability were required beyond those necessary to produce a stable hydraulic model. As of this writing, calibration is in the early stages and all results are preliminary. This model demonstrates the utility of HEC-RAS 5.0 for sedimentation analysis of large reservoirs. Future work will quantify the reduction in sediment accumulation possible at Tuttle Creek Lake through changes to reservoir operational procedures.

REFERENCES

Gibson, S., Brunner, G., Piper, S., and Jensen, M., (2006). "Sediment Transport Computations in HEC-RAS." Eighth Federal Interagency Sedimentation Conference (8th FISC), Reno, NV, 57-64.

Gibson, S. and Boyd, P. (2014) "Modeling Long Term Alternatives for Sustainable Sediment Management Using Operational Sediment Transport Rules," *Reservoir Sedimentation* – Scheiss et al. (eds), 229-236.

Gibson, S. and Pridal, D. (2015) "Negotiating Hydrologic Uncertainty in Long Term Reservoir Sediment Models: Simulating Arghandab Reservoir Deposition with HEC-RAS," *SEDHyd: 10th Interagency Federal Sedimentation Conference*.

Haslouer, S.G.; Eberle, M.E.; Edds, D.R.; Gido, K.B.; Mammoliti, C.S.; Triplett, J.R.; Collins, J.T.; Distler, D.A.; Huggins, D.G. and Stark, W.J.; (2005). *Transactions of the Kansas Academy of Science* (1903-), Vol. 108, No. 1/2, pp. 32-46.

Juracek, K.E., (2011). Suspended-sediment loads, reservoir sediment trap efficiency, and upstream and downstream channel stability for Kanopolis and Tuttle Creek Lakes, Kansas, 2008-10: U.S. Geological Survey Scientific Investigations Report 2011-5187, 35 p. http://pubs.usgs.gov/sir/2011/5187/

Kansas Water Office, (2012). Tuttle Creek Reservoir Information Sheet, available at http://www.kwo.org/reservoirs/ReservoirFactSheets/Rpt_TuttleCreek_2011.pdf .

USACE, (2012). Kansas River Basin Reservoir Sedimentation Analysis. Submitted by HNTB to U.S. Army Corps of Engineers, Kansas City District.

USACE, (2015). HEC-RAS River Analysis System, Version 5.0, Hydrologic Engineering Center User Manual. U.S. Army Corps of Engineers.

DEVELOPING A SEDIMENT MANAGEMENT PLAN FOR PAONIA RESERVOIR

Kent Collins, Hydraulic Engineer, Bureau of Reclamation, Denver, Colorado, kcollins@usbr.gov,
Sean Kimbrel, Hydraulic Engineer, Bureau of Reclamation, Denver, Colorado, skimbrel@usbr.gov

INTRODUCTION/BACKGROUND

Paonia Dam and Reservoir are located on Muddy Creek, a tributary of the North Fork Gunnison River in western Colorado (Figure 1). Based on the most recent bathymetric survey of the entire reservoir, conducted in June 2013, the estimated average annual rate of sedimentation has been 101 acre-feet per year (Collins, 2014). Since dam closure in 1962, nearly 25% of the reservoir's original 20,950 acre-foot capacity has been lost to sediment deposition. At that rate the reservoir would be completely filled with sediment in another 150 years, gradually reducing the available pool over time. Long before sediment levels reach the full pool elevation however, reservoir intakes and outlet works are affected, adversely impacting project operations. In 2010, the outlet works became plugged with sediment and debris, emphasizing the urgency of formulating an effective sediment management plan for the impending deposition problem.

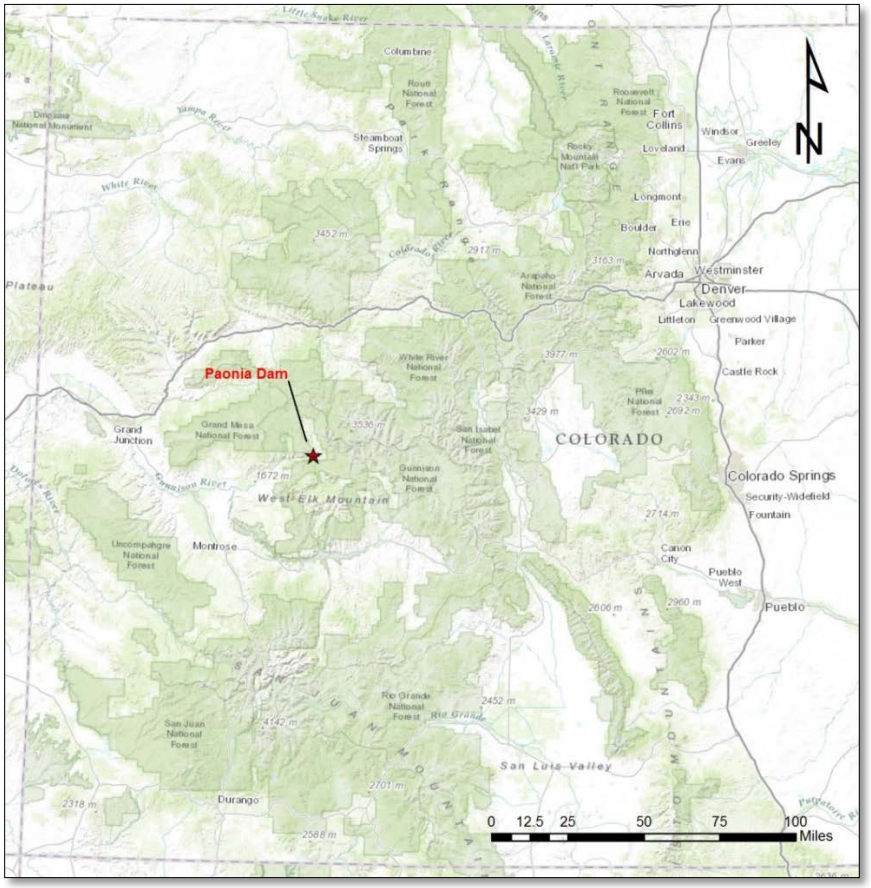

Figure 1 Paonia Dam and Reservoir on Colorado's western slope approximately 150 miles southwest of Denver

Although occasional sediment flushing was performed as early as 1997, starting in 2010-2011, annual operations were changed to include keeping the reservoir low and flushing sediment through the outlet works in early spring before filling the pool for irrigation (Denison, 2015). Until fall 2014 the flushing strategy through the long, narrow reservoir (pool is approximately 3 miles long and 0.2 miles wide) successfully maintained the outlet works, preventing them from becoming plugged. Reservoir drawdown in late-October revealed the reservoir dead pool had completely filled with sediment and the outlet works were plugged with cohesive sediment and submerged debris. Due to the recent discovery of accelerated sediment deposition rates, the original study objectives of developing a long-term plan to manage inflowing and deposited sediment more efficiently were altered to include short-term strategies for water delivery during the upcoming 2015 irrigation season.

Figure 2 Sediment deposition at Paonia Reservoir outlet works intake tower, October 2014

The Sedimentation and River Hydraulics Group of Reclamation's Technical Service Center in Denver, Colorado is leading an effort to study the past and current sediment issues at Paonia Dam and Reservoir, evaluate feasible sediment management alternatives, and formulate a plan for future operations and monitoring. The original study was built on historical and recently collected data, and the existing knowledge base to develop a comprehensive, sustainable sediment management plan. The initial study plan was executed in three phases:

- **Phase 1** consisted of an initial site visit to map and sample existing reservoir bottom sediments, a preliminary site evaluation upstream and downstream of the dam, establishment of time-lapse photo sites, and taking initial ground-based photos. Pebble counts were collected in Muddy Creek upstream of the reservoir and ground surveys were conducted for a limited distance upstream of the reservoir and downstream of the dam;
- **Phase 2** included a bathymetric survey of the entire underwater portion of Paonia Reservoir (June 2013) and 7 miles of the river downstream of the dam (May 2013), and collection of underwater core samples of reservoir bottom sediments. The bathymetric survey was used to generate a current area-capacity relationship for the reservoir and establish a baseline for comparing future data and other monitoring tasks; and
- **Phase 3** involved the evaluation of current and past operations and sediment management practices, investigation of feasible sediment management methods, focusing on those best suited for Paonia Dam and Reservoir, and providing recommendations for future sediment management operations and project monitoring. Survey and sediment data collected during previous phases were used to construct a one-dimensional mobile bed model to numerically simulate sediment transport for evaluating past, present, and potential future sediment management options.

The 2014 sediment deposition occurred during the execution of Phase 3 of the original study plan. Phase 3 analyses and tasks were modified to accommodate the new information. A reconnaissance visit/visual site inspection and GPS topographic survey were performed in November 2014. The new topography data was used for determining the additional volume of sediment and for numerical model calibration and validation. The immediate focus of the numerical model changed from simulating typical hydrographs for evaluation of long-term sediment management operations to mimicking likely spring runoff scenarios and dam operations for formulating potential short-term water delivery solutions. Once a short-term fix is identified and implemented, the numerical modeling efforts will be redirected towards the formulation and evaluation of possible long-term sediment management solutions.

2014 SEDIMENT DEPOSITION ISSUES

Beginning in 2011, Paonia Reservoir has been drawn down each year in late fall for outlet inspection, then again in early spring for sediment flushing prior to irrigation season. Reservoir drawdown in October 2014 revealed approximately 10 feet of sediment had deposited at the intake tower since June 2013, raising the lake bottom 6 feet above the sill of the outlet works (Figure 3). The June 2013 bathymetric survey measured the reservoir bottom elevation 4 feet below the outlet works sill. Figure 3 shows the steady loss of storage capacity along with the consistent increase in reservoir bed elevation at the outlet works (Western Engineers, Inc., 2006). While effective for flushing sediment through the dam outlet, yearly drawdown of the reservoir likely increased deposition rates in the dead pool.

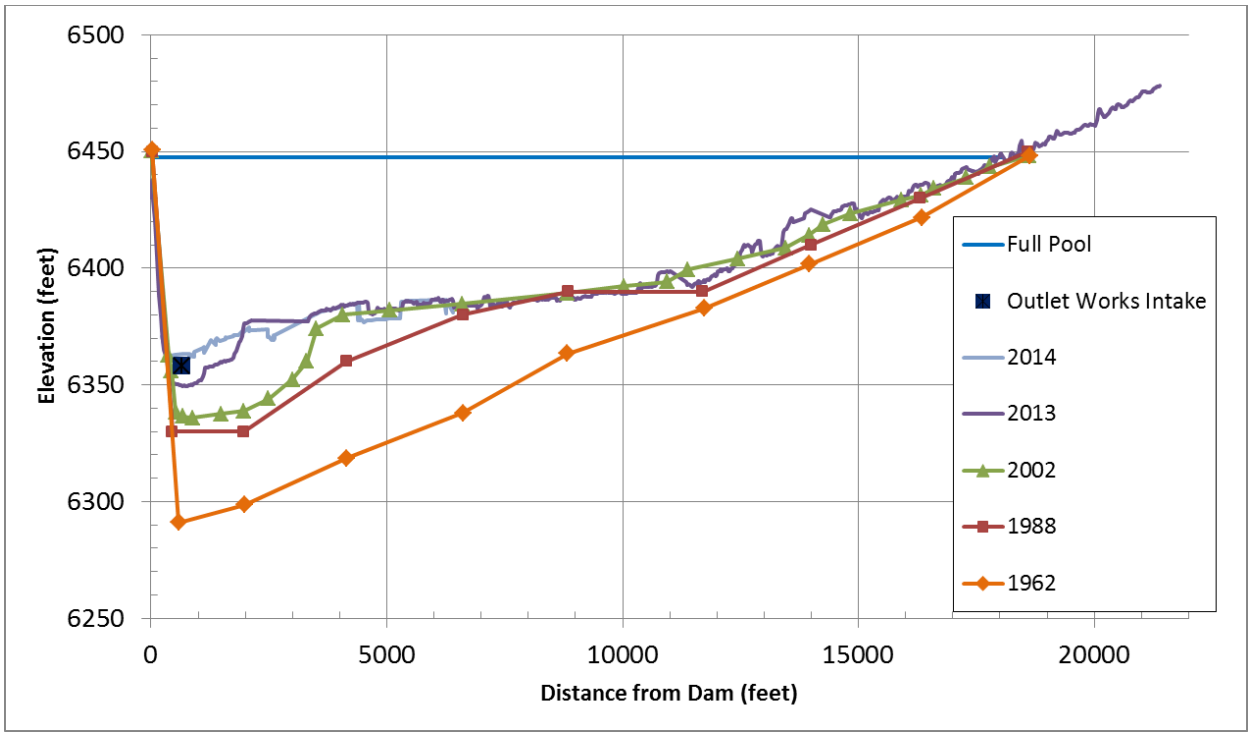

Figure 3 Paonia Reservoir survey profiles since dam closure in 1962

In 2014, increased sediment inflows resulting from high spring runoff caused the delta front to migrate more than 1,200 feet downstream towards the dam, over-filling the dead pool and partially burying the outlet works intake tower (Figure 4). Fire Mountain Canal Company and Northern Water Conservancy District crews immediately began 10-hour daily shifts removing the sediment and debris around the inlet tower using a long-reach excavator while clearing the trash racks by hand (Figures 5 and 6). Even at low flows, constant excavation and clearing were required to maintain an open outlet. Each morning when maintenance crews returned to the site, submerged debris and fine, cohesive sediments had blocked the intake tower trash racks as much as 6 feet above the sill elevation, backing water upstream.

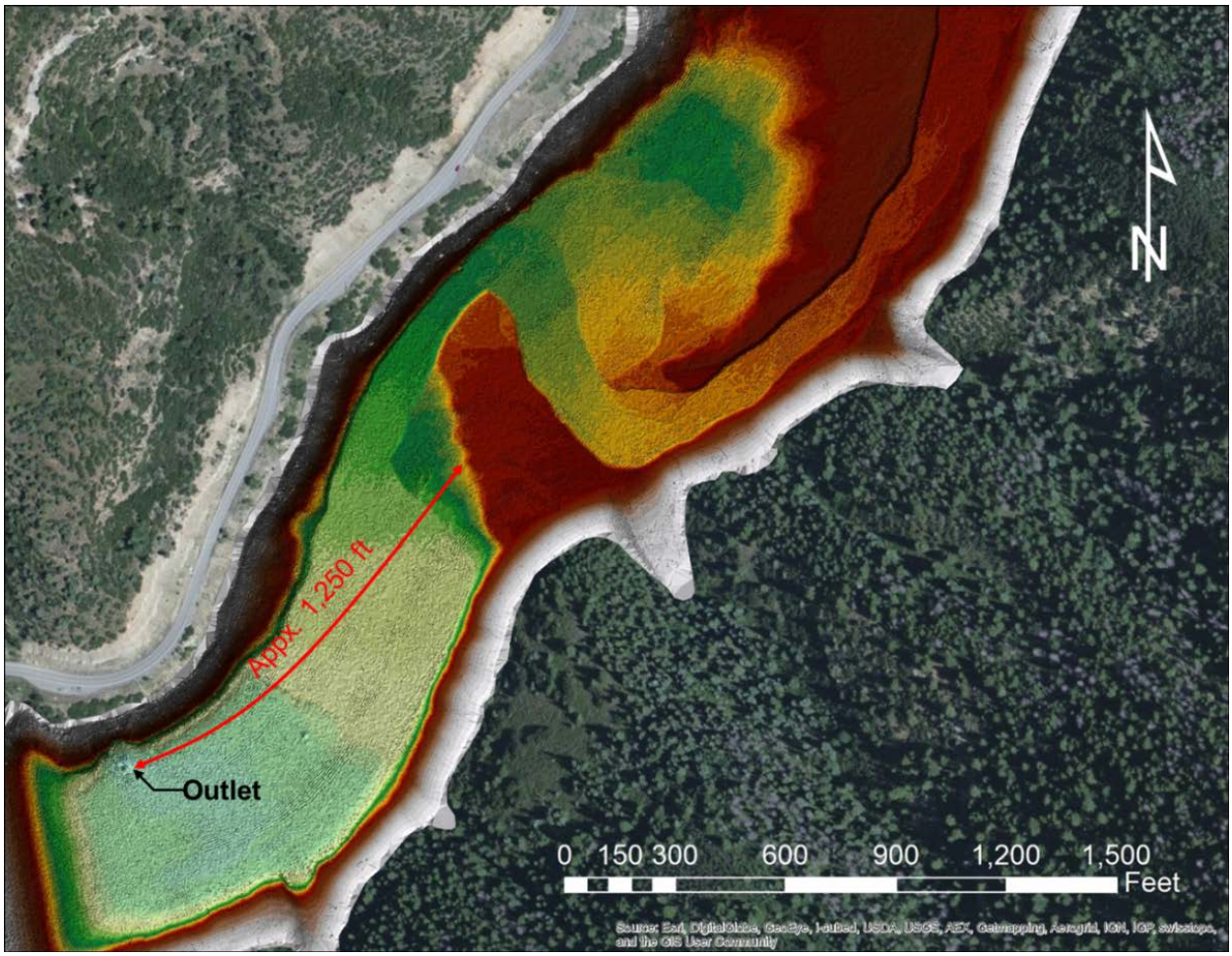

Figure 4. Plan view map of lower Paonia Reservoir showing the delta front in June 2013 and the migration distance required to partially bury the intake tower of the outlet works

Figure 5 Long-reach excavator removing sediment and debris from intake tower at Paonia Reservoir, November 2014

Figure 6 Manual clearing of intake tower trash racks to maintain open outlet works at Paonia Reservoir, November 2014

Manual clearing of debris and sediment around the outlet works occurred for over two weeks until sediment levels near the outlet works intake remained at or near sill level overnight and until ice began forming in the low flow channel near the tower. The outlet works high pressure gates were then closed and the water surface elevation of the reservoir returned to normal winter operation levels, several feet above the top of the intake tower, to avoid any issues with ice.

FUTURE SEDIMENT MANAGEMENT ENDEAVORS

For Spring 2015 dam operations, and for the future of Paonia Reservoir, several short- and long-term reservoir sediment management options are currently being investigated:

- Proposed Short-Term Management Analyses/Options:
    - Debris Management
    - Minimum Pool Level to Force Deposition at Upstream Delta
    - Temporary Siphon System to Maintain Irrigation Releases
- Proposed Long-Term Management Analyses/Options:
    - Outlet Works Modification/Replacement for Sediment Sluicing
    - Sediment Sluicing Efficiency with Numerical Sediment Transport Modeling
- Analyses of Downstream Impacts (e.g. Fisheries, Infrastructure)
- **GOAL**: **Sustainable Management of Reservoir Sediments**

REFERENCES

Collins, Kent L. (2014). 2013-2013 Data Collection on Paonia Reservoir, Muddy Creek, an North Fork Gunnison River. Sedimentation and River Hydraulics Group, Technical Service Center, US Bureau of Reclamation, Denver, CO.

Denison, Trey. (2015). February 4, 2015 Personal communication. Trey Denison, North Fork Water Conservation District, Paonia, CO.

Western Engineers, Inc. (2006). Technical Memorandum: Evaluation of Bureau of Reclamation Paonia Sediment Surveys. Submitted to the North Fork Water Conservation District on May 16, 2006.

RIO GRANDE AND COCHITI RESERVOIR SEDIMENTATION ISSUES: ARE THERE SUSTAINABLE SOLUTIONS?

C. M. Davis, Senior Hydraulic Engineer, WEST Consultants, Inc., Tempe, Arizona, Phone (480) 345-2155, Fax (480) 345-2156, cdavis@westconsultants.com;
C. Bahner, Senior Hydraulic Engineer, WEST Consultants, Inc., Salem, Oregon, Phone (503) 485-5490, Fax (503) 485-5491, cbahner@westconsultants.com;
D. Eidson, Regional Technical Specialist, U.S. Army Corps of Engineers, Walla Walla, Washington, CENWW-EC-H, Phone (509) 527-7291, Darrell.E.Eidson@usace.army.mil;
S. Gibson, Senior Hydraulic Engineer, Hydrologic Engineering Center, Davis, California, Phone (530) 756-1104, Stanford.Gibson@usace.army.mil

Abstract: The Pueblo de Cochiti (Pueblo), in cooperation with the U.S. Army Corps of Engineers, Albuquerque District (USACE-SPA), conducted a program of studies, known as the Cochiti Baseline Study, to define existing and historical environmental conditions of the Cochiti Dam and Lake located on tribal lands of the Pueblo de Cochiti, New Mexico. These included numerical sediment transport modeling of the Rio Grande upstream and downstream of Cochiti Dam completed by WEST Consultants. The purpose of this study was to better understand the impacts of reservoir sedimentation on the sediment processes in the study reach over time, to provide a tool to better manage the project within the Tribe's resource objectives and to help evaluate potential sedimentation effects on Tribal resources that could result from possible future changes in dam operations.

Cochiti Dam, closed in 1973, was constructed primarily for flood control and sediment retention. The dam traps sediment, reducing the suspended sediment loads downstream between 87% and 98%, and has created a lacustrine delta in the reservoir headwaters. The reach below Cochiti Dam responded to dam closure in typical ways including: thalweg degradation, bed armoring, and channel narrowing. The study reach is a highly complex system from a sediment transport perspective due to the two primary sediment inflows: the Rio Grande contributing primarily coarse-grained, non-cohesive sediment to Cochiti Lake, and the Rio Chama contributing primarily fine-grained, cohesive sediment.

This study applied the mobile-bed module of the USACE Hydrologic Engineering Center's River Analysis System (HEC-RAS) software to model sediment erosion, entrainment, transport, and deposition processes of cohesive and non-cohesive sediments. Cohesive sediment erosion/deposition parameters were estimated based on measured responses of samples collected in the lacustrine deposits in Cochiti Lake. Sample responses were measured using the Engineering Research Development Center's SEDflume mobile laboratory (erosion rates) and the Particle Imaging Camera System (PICS) developed by Smith and Friedrichs (settling properties). The numerical model utilized a volumetric limiter on the continuity routing for sediment deposition in the reservoir. Working with HEC and USACE-SPA, WEST developed a well-calibrated HEC-RAS model considering the system's complex cohesive aggregation processes. This base conditions model replicated the deltaic profile evolution spatially and temporally. The calibrated model was robust to wide ranges of sediment input parameters. Finally, this calibrated model was used to predict prototype response to a limited range of

representative theoretical future reservoir operation scenarios and to qualitatively assess long-term reservoir sustainability associated with these scenarios.

This effort determined that, while sediment could be redistributed higher in the reservoir and upstream canyon using increased pool elevations, operational constraints imposed by the dam infrastructure (e.g., minimum pool elevation) will make it difficult to pass significant sediment downstream with drawdown scenarios. The model predicted virtually no change in the downstream virtual river reach in response to the reservoir scenario modeling. These models are being used to help assess sustainability in a responsible and proactive manner. The models support the evaluation of a wider range of future operation scenarios by the Pueblo and USACE-SPA, within a virtual environment, thereby avoiding harmful effects to the actual environment, and permitting evaluation of (fully-reversible) impacts from alternative mitigation strategies.

INTRODUCTION

The Pueblo de Cochiti (Pueblo), in cooperation with the U.S. Army Corps of Engineers, Albuquerque District (USACE-SPA), conducted the Cochiti Baseline Assessment, a series of studies to define the existing and historical environmental conditions of the area surrounding Cochiti Dam and Lake on and near the Pueblo de Cochiti Reservation, New Mexico. The purposes of these studies were two-fold: first, to define existing conditions of the system, and second, to investigate and characterize impacts that have occurred to resources on Pueblo de Cochiti lands from operation and maintenance of Cochiti Dam and Lake. This information is being used to evaluate the potential effects on Tribal resources resulting from possible future changes in operations at Cochiti Dam and Lake. One of the studies within the Cochiti Baseline Assessment was a sediment modeling study of the Rio Grande upstream and downstream of the dam and reservoir, which is documented in this paper. Cochiti Dam, which began operation in 1973, was constructed primarily for flood control and sediment retention; many secondary uses exist for this reservoir as well, such as recreation.

Worldwide, the rate at which reservoir storage volume was added outpaced population growth from 1950 through about 1980. The rate of dam construction began to decrease in the 1980s, as it has continued to do to this day (Annandale, 2013). Even with increasingly efficient use of water resources, for an increasing world population to continue to beneficially utilize a much slower-growing amount of storage, the need to sustainably manage reservoir storage is paramount. The impact of reservoir sedimentation further complicates this need, as do the uncertainties imposed by climate change.

Morris and Fan (1998) summarized reservoir sustainability into three key parameters: water quantity, quality, and diversity. Sustainable use maintains all three of these parameters at a level equal to or higher than current conditions (or historic conditions, considering the system in question). All three of these issues have been impacted in the Rio Grande due to the closure of Cochiti Dam. As Morris and Fan (1998) point out,

> *Reservoirs also require unique natural components (dam sites having appropriate topography, hydrology, geology) and engineered components (dam, delivery canals, etc.). Replacement of the engineered components has no purpose if the storage volume is lost to sediment accumulation… A number of factors indicate that reservoirs should be*

> *considered as irreplaceable resources, no less important than [groundwater] aquifers, and should be designed and operated in accordance with the objective of sustained long-term utilization.*

These principles can readily be applied to the case study of Cochiti Dam. Drought and water scarcity issues of the western United States are often highlighted in popular media (*e.g.*, Bryan, 2014). Population growth, increasing dependence on irrigated agriculture, climate variability, and others factors threaten water quantity, in this region and worldwide (Morris and Fan, 1998). Dam closure already impacted water quality in the Rio Grande and impacted critical habitat of some endangered species with less turbid, cooler water being released from the reservoir. Changes in bed substrate particle size distribution and channel geometries downstream of the dam have also impacted aquatic and riparian habitat (USACE, 2007). Finally, the dam impacted both ecological and cultural diversity (Sallenave et al., 2010). Therefore, stakeholders must reach a consensus on future sustainable use of this reservoir. This definition may not be a fixed target, but a moving one. For example, if a continued future drought were to threaten downstream water supplies, would the impacted stakeholders possibly repurpose Cochiti Reservoir for water supply use? Annandale (2013) points out that prudent water resource planning should consider the ways that climate change might affect water supply reliability and sustainability. While water supply was not an objective in the design and construction of Cochiti Dam, its primary flood control purpose shares the requirement of excess water storage capacity with that of water supply projects. How might the sediment that depletes this available storage capacity be more effectively managed to preserve or prolong the useful benefits of the project while lessening impacts to the surrounding environment? Questions like these lie at the heart of reservoir sustainability, and the problems facing each new generation for sustainable water resources can only be solved through continuing study and communication of issues that arise.

Due to these concepts of sustainable use and oftentimes conflicting definitions of sustainability for different stakeholders, governmental agencies and other private entities have studied sedimentation problems along the Rio Grande for several decades. Several of these studies proposed projects to reduce bed aggradation while maintaining water quality, quantity, and diversity for downstream use. Channel modifications, levees, and dams were constructed to reduce flooding in Albuquerque and other areas, control sediment concentrations in the river, and increase sediment transport capacity.

Cochiti Dam reduces peak flows in the Rio Grande River below the dam to less than 10,000 cfs compared to common peak flows greater than 10,000 at the Otowi gage (the nearest gage upstream of the dam) and some flows in excess of 20,000 cfs throughout the period of record. The dam reduces the suspended sediment loading in the flows downstream of the dam between 87% and 98% (USACE, 2007; Novak, 2006). MEI (2002) estimated that Cochiti Dam traps approximately 1,100 acre-feet of sediment annually, releasing clear water with very low sediment concentrations, subjecting the downstream reach of the Rio Grande to highly erodible flows. As a result, there has been significant thalweg degradation downstream of the dam as well as some slight channel narrowing. The median bed sediment sizes have increased from an average of 0.1 mm in 1962 to an average of 24 mm in 1998 (Novak, 2006), armoring the bed downstream of the dam. Dam effects diminish downstream because of tributary sediment delivery and in-channel sources of sediment.

The purpose of this study for the Pueblo was to analyze present and historic geomorphic processes of Cochiti Lake and the Rio Grande River in the reservoir influence area with emphasis on landforms, erosion, sediment transport, and deposition. This study analyzed historical and new landscape-scale topographic, geomorphic, and sediment data, and developed two sediment transport models. Modeling objectives included:

- Identify past and current geologic and geomorphic conditions of the Rio Grande River channel and floodplain in the Cochiti Lake influence area;
- Assess sediment erosion, transport, deposition, and routing into, through, and downstream of Cochiti Lake; and
- Evaluate the influence on sediment mobilization, transport, and deposition for select reservoir operations scenarios to better understand prototype behavior.

The sediment transport models provided to the Pueblo and USACE-SPA were a tool for assessing long-term reservoir sustainability, especially in the event that alternative dam operations are proposed. This study explicitly considered water quantity impacts of reservoir storage losses to reservoir sedimentation. The models assessed changes in location and magnitude of erosion and deposition upstream and downstream of the dam. The models also support future ecological and human health risk assessments (water quality), and diversity analyses. This paper will focus on reservoir sustainability considerations in light of water quantity issues.

A model was developed for each of the two study areas: from below the Otowi gage to Cochiti Dam, and from below Cochiti Dam to Angostura Diversion Dam (located just upstream of the confluence of the Jemez River with the Rio Grande). WEST analyzed topographic, geomorphic, and sediment data, built the sediment transport models, and ran the models for the various proposed operational scenarios.

STUDY SITE

The Rio Grande River drains approximately 11,695 square miles above Cochiti Dam including portions of northern New Mexico and southern Colorado. The Rio Grande River enters the Cochiti Reservoir just downstream of White Rock Canyon, which has a slope of 10 ft/mile. Cochiti Dam is the upper limit of the "Middle Rio Grande Valley." This reach of the Rio Grande stretches from Cochiti Dam to the Elephant Butte Reservoir approximately 190 miles downstream. In the portion of the study reach below Cochiti Dam, the Rio Grande has cut an alluvial valley in the semiarid desert 100 to 300 feet deep and 1 and 3 miles wide. The elevation of the study reach drops from approximately 5,480 feet (NGVD 1929) at the thalweg of the Rio Grande near Otowi Bridge to approximately 5,100 feet (NGVD 1929) near the crest of the Angostura Diversion Dam, approximately 20 miles downstream of Cochiti Dam.

Important tributaries that feed the Rio Grande near the study reach include (from upstream to downstream) the Rio Chama, Santa Cruz River, and Santa Fe River above Cochiti Dam; and the Galisteo Creek and Jemez River below Cochiti Dam. Several smaller streams also feed the Rio Grande within the study reach. Although the water supply from these tributaries do not typically deliver most of the total volume of water transported in the study reach, these tributaries can provide major sources of water and sediment during certain hydrologic conditions.

GEOMORPHIC ASSESSMENT OF THE STUDY REACH

Two primary factors affect the geomorphology and sediment conditions of the upper study reach (i.e., above Cochiti Dam): the geologic control of White Rock Canyon and the water level in Cochiti Lake. Horizontal restrictions imposed by the canyon limit the Rio Grande planform in this reach. It cannot migrate laterally more than a few hundred feet at any location (i.e., approximately 2-3 times the typical top width of the river flow). The meander paths are constantly shifting and adjusting locally in the lateral direction (i.e., bend growth or bend decay) and longitudinally (i.e., down-valley migration) in response to hydrologic and sediment loading, but the general river path is confined to a meander band defined by the canyon walls.

The upstream sediment loads contain substantial fine materials. The main stem of the Rio Grande usually delivers mostly coarse-grained sediment (i.e., >62.5 μm), while the Rio Chama load can be dominated by fine-grained sediment (i.e., ≤62.5 μm). The load diversity generates alluvial "stratigraphy," alternating "layers" of coarse and fine sediment deposited along the banks of the Rio Grande and in the reservoir delta depending on the primary sediment source during the event represented. The material along the river subsequently erodes through bank failure and mass wasting processes delivering highly graded (poorly sorted) non-cohesive suspended sediment and bedload including fine sands to boulders.

The geomorphology and planform of the study reach shift to a much more depositional system above Cochiti Dam, immediately below the confluence of the Frijoles Canyon Creek and the Rio Grande River, because of the effects of the reservoir backwater. In 1992, the thalweg elevation near Frijoles Canyon Creek was 5,359.8 feet NGVD29. During the period from 1975-1996, the reservoir exceeded 5,350 feet NGVD29 several times (primarily between 1985 and 1988). Therefore, backwater frequently affects the area downstream of Frijoles Canyon and influences the geomorphic transition in this reach. This backwater effect created a significant headwater delta in the reservoir (see Figure 1).

Many studies and reports have characterized the geomorphology of the Middle Rio Grande downstream of Cochiti Dam and upstream of Angostura Diversion Dam (Novak, 2006; Sixta, 2004; Porter and Massong, 2004; MEI, 2002; Richard, 2001; Leon, 1998). These reports generally identify two primary geomorphic changes occurring in this reach as a response to the closure of Cochiti Dam: (1) streambed degradation throughout this reach and the bed armoring; and (2) a change in planform of the river from a braided, flat-bottom river in the early 1900's to a single-thread, meandering, deeper river. Additionally, most of these reports conclude that this reach is approaching a state of dynamic equilibrium. The rate of vertical (i.e., bed elevation) or horizontal (i.e., lateral migration, stream narrowing, and avulsion) change has reduced significantly since the period immediately following dam closure and are not expected to increase significantly in the near future. Anthropomorphic modifications have also reduced the rate of vertical and lateral erosion. The channel has been armored to mitigate stream bed degradation, and 115,000 Kellner jetty jacks were installed in the overbanks of the Middle Rio Grande between 1954 and 1962 (Grassel, 2002) to address lateral migration.

NUMERICAL SEDIMENT TRANSPORT MODELING

Calibrated fixed-bed hydraulic models built in HEC-RAS were used to develop HEC-RAS sediment transport models (USACE, 2011). Fixed-bed hydraulic model development followed standard procedures including: spatially georeferenced cross sections derived from digital elevation data, downstream reach lengths, bank stations, Manning's roughness coefficients, and ineffective flow areas. Each of these items was determined with the requisite engineering judgment and standard of practice. While the development of an accurate fixed-bed hydraulic model is an essential pre-requisite developing a mobile-bed sediment transport model (HEC, 1993; Thomas and Chang, 2008), this paper will focus on sediment transport modeling, methods and results.

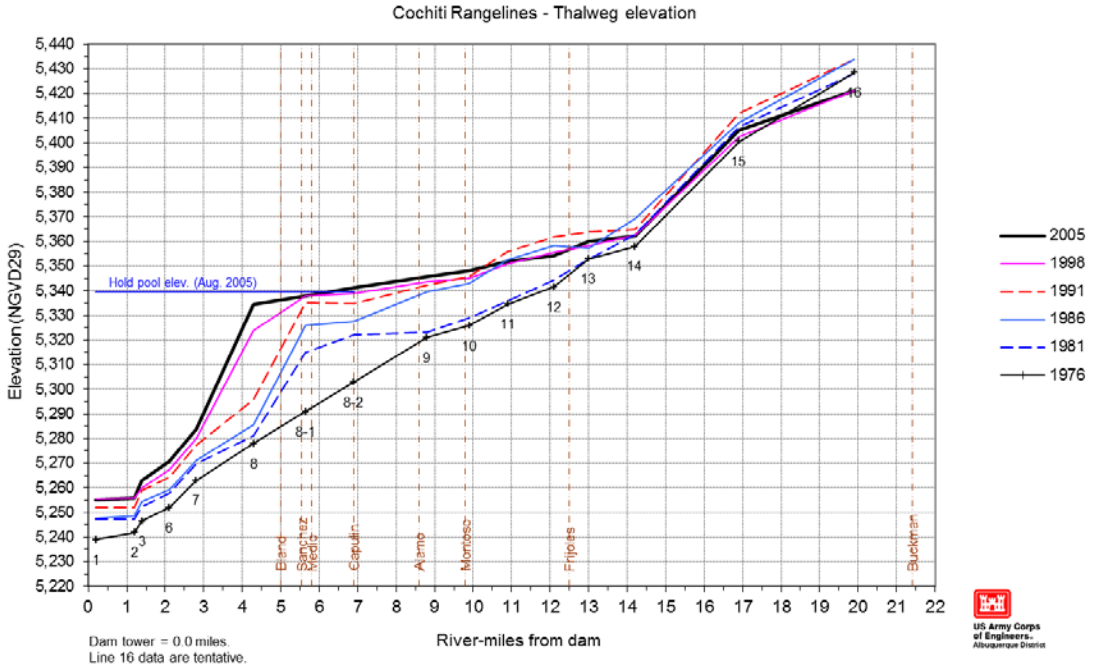

Figure 1. Growth of Cochiti Reservoir headwater delta based on Range Line surveys provided by USACE-SPA for survey years 1976, 1981, 1986, 1991, 1998, and 2005.

The base condition sediment transport models required input data (e.g., inflowing sediment loads, bed sediment gradations, suspended sediment gradations, and cohesive sediment parameters); calibration and verification. The different hydraulic and sediment conditions of the study reach upstream and downstream of Cochiti Dam, and the limitations of the quasi-unsteady hydrodynamic model in HEC-RAS when this study was conducted, the two reaches were modeled and discussed separately.

The base condition sediment transport models upstream and downstream of the dam included hydrology from shortly after dam closure in 1975 to present. The average bed elevation, (ABE) for each cross section at the end of each calibration period was compared to the average bed elevation of the measured cross section at the end of the same calibration period. Adjustments were made to the base conditions model such that the computed ABEs would reasonably

approximate the measured ones. Upstream of the dam, these adjustments included primarily changes to calibrated gradations and volumes of inflowing sediment load. Downstream of the dam, these adjustments included primarily changes to calibrated bed sediment gradations. Once the base conditions models were calibrated and verified, they were executed to predict future conditions for operational evaluation scenarios, as described in the next section.

The sediment transport module in HEC-RAS (USACE, 2011; Gibson et al., 2006) is a one-dimensional, movable boundary, open channel flow model designed to simulate stream bed profile changes over fairly long time periods. One dimensional sediment modeling can be very effective in reservoir scenarios, but there are some limitations inherent to the 1D framework. For example, it cannot simulate meander development or compute a lateral distribution of sediment load across a cross section. Finally, sediment transport results are strongly dependent on which transport function is selected and whether it was developed for the range of hydraulic conditions and sediment grain sizes representative of the study reach. It is paramount that an experienced modeler assesses the model results in light of these limitations.

Sediment Transport Model Upstream of Cochiti Dam: The quasi-unsteady flow model used for sediment transport in HEC-RAS 4.1 (the version available at the time of this study) approximates a hydrograph with a series of steady flows. Mean daily flow at the Otowi USGS Gage (USGS Gage ID 08313000) and mean daily water surface elevation at Cochiti Dam were provided by the USACE-SPA for the calibration period from 1975-2009 for the model upstream of Cochiti Dam. A maximum computational time step of one half of an hour was used for the computations. The hydrology used in the model consisted of a condensed record of mean daily flow values for the Rio Grande River at Otowi Bridge for flows greater than 1,000 cfs.

The Rio Grande River is the major sediment source, delivering most of the inflowing sediment to the study reach upstream of Cochiti Dam. Sediment loads from tributaries upstream of Cochiti Dam and downstream of the Otowi Gage are minor. The upstream load (inflowing sediment load and gradation from the Rio Grande) was developed from a combination bedload from the Española Sediment Transport Study (MEI, 2009) and the suspended sediment load data collected by the USGS. The D50 was approximately 0.07 millimeters indicating that inflowing load included both coarse-grained, non-cohesive sediment and fine-grained, cohesive sediment.

Sediment loads from tributaries upstream of Cochiti Dam were estimated based on the report completed by Resources Technology, Inc. (1994) for the USACE-SPA. This report developed regression equations for sediment loading based on drainage area. An additional correction based on a later study (Tetra Tech, 2005) was also applied to this methodology.

WEST used several bed sediment gradations collected by the USGS at gages in the study reach, including the Rio Grande at Otowi Bridge and the Rio Grande near White Rock, to define model bed gradations. The D50 of these samples were generally between 0.5 and 1.0 millimeter. Also, the USACE Engineering Research and Development Center (ERDC) collected core samples in the reservoir for this study. The D50 were all in the fine-grained, cohesive soils range (i.e., particle diameters less than 62.5 micrometers). ERDC also performed SEDFLUME analyses to parameterize the shear threshold, erosion rate, mass wasting threshold, and mass wasting rate for the Krone (1962) and Parthenaides (1962) algorithms used for cohesive sediment deposition and

erosion, respectively, in HEC-RAS. The τ_c of these samples varied from 0.79 Pa (1.65×10^{-2} lb/ft^2) to 0.12 Pa (2.51×10^{-3} lb/ft^2) and the erodibilities from 5.88×10^{-2} kg/m^2/sec (43.4 lb/ft^2/hr) to 3.78×10^{-3} kg/m^2/sec (2.8 lb/ft^2/hr), generally increasing with depth, but also influenced by the stratigraphy, alternating fine and coarse lenses from localized events in the main source tributaries.

A sediment transport function was selected based on a comparison of hydraulic and sediment parameters in the study reach with the range of data used to develop the transport functions. Copeland's (1989) modification of Laursen's (1958) relationship was used for this reach due to the significant contribution of fine sediments to the inflowing load. The model also limited sediment velocity to the water velocity to compute fine sediment deposition based on realistic residence times, which the Exner equation underpredicts without physical limiters.

WEST calibrated the model to twenty-three years (1975-1998) of bed change. After completing the calibration, a verification run was performed from 1998 to 2005 to demonstrate that the selected algorithms and parameters were robust. The results of the final verification run after model calibration are included in Figure 2. Additionally, the model replicated downstream bed fining (approaching the dam) (Figure 3). Corresponding sensitivity analyses were performed on this data to determine the sensitivity of the results to the variation in modeling parameters including sediment transport function, Manning's roughness, cohesive parameters, and others.

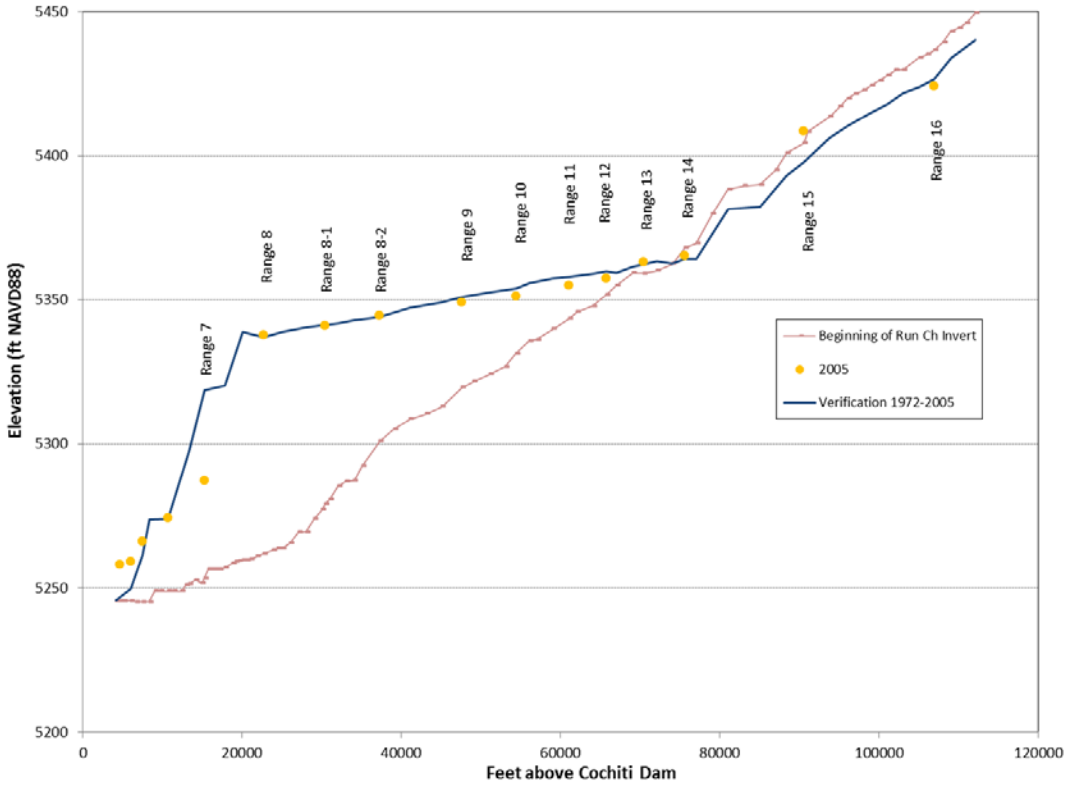

Figure 2. Bed profile results from the calibrated HEC-RAS model for the verification period (1975 – 2005) compared to measured data (points) in 2005.

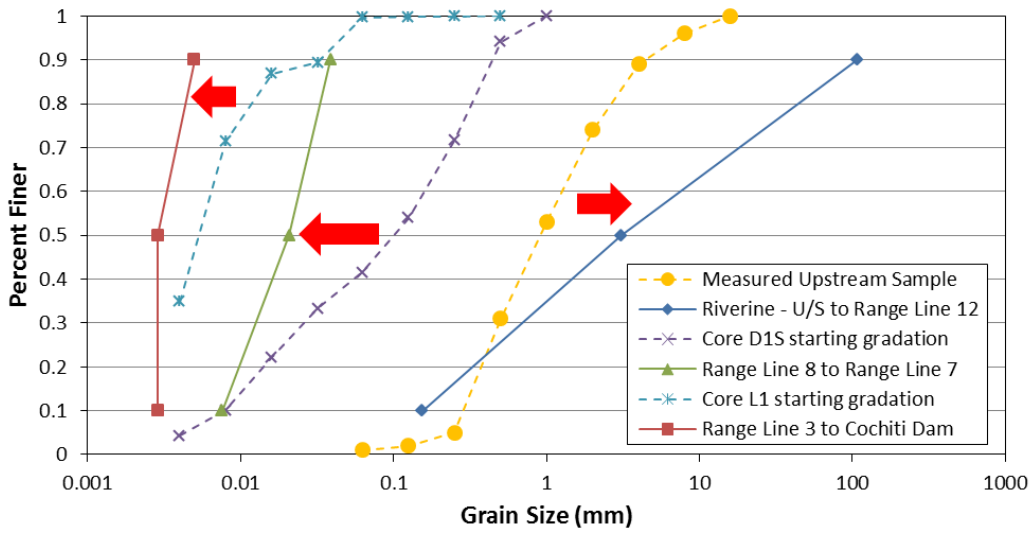

Figure 3. Reach-averaged bed gradation results from the calibrated HEC-RAS model for the verification period (1975-2005) shown in solid lines compared to the initial conditions data used in the sediment transport model shown in dashed lines; arrows indicate the direction of coarsening or fining of the bed.

Sediment Transport Model Downstream of Cochiti Dam: Mean daily flow at the USGS Gage below Cochiti Dam (USGS Gage ID 08317400) and a normal depth downstream boundary condition at Angostura Diversion Dam were used for the calibration and verification period from 1975-2009 for the model downstream of Cochiti Dam. A maximum time step of 0.5 hours was used as the computational time step with a condensed record of mean daily flow values for the Rio Grande River below Cochiti Dam for flows greater than 1,000 cfs.

Unlike the study reach above Cochiti Dam, the Rio Grande does not supply a significant source of sediment to the study reach below Cochiti Dam due to the trapping efficiency of the dam itself. Therefore, the primary sediment sources to the reach downstream of the dam are the local tributaries: Peralta Canyon, Borrego Canyon, Galisteo Creek, Arroyo de la Vega de los Tanos, Arroyo Tonque, and others. Sediment loads from tributaries downstream of Cochiti Dam were estimated based on the report completed by Resources Technology, Inc. (1994) for the USACE-SPA. This report developed regression equations for sediment loading based on drainage area. An additional correction based on a later study (Tetra Tech, 2005) was also applied to this methodology. Gradations for the tributary inflowing sediment loads were derived from sampling routines and estimates from these two studies.

Bed gradations downstream of Cochiti Dam were based on samples collected by the USGS at gaging stations in the study reach, including Rio Grande below Cochiti Dam and the Rio Grande at San Felipe. The D50 of these samples before dam closure were between 0.5 and 1.0 millimeter. Time series sampling at these locations showed bed coarsening over time, increasing the D50 at these locations by more than an order of magnitude. The final calibrated HEC-RAS sediment transport model reflected this bed coarsening over time.

A sediment transport function was selected based on a comparison of hydraulic and sediment parameters in the study reach with the range of data used to develop the individual sediment

transport functions available in HEC-RAS. Yang's equation (1973, 1984) was used for this reach due to the inclusion of both sands and gravels in the transported sediment load.

The model was run for a period of twenty-three years (1975-1998) as a calibration period. After completing the calibration, a verification run was performed from 1998 to 2009 to verify the modeling output, and results matched closely with observed values. Sensitivity analyses were performed for this model as well.

OPERATIONAL EVALUATION SCENARIO MODELING

This study also evaluated the influence of reservoir operation scenarios on sediment mobilization, transport, and deposition to evaluate scenarios outside of normal operations, providing a tool to assess conceptual alternate dam operations. The models can assess the relative location and magnitude of erosion and deposition upstream and downstream of the dam for operational alternatives evaluation, and support future ecological and human health risk assessments. It should be noted that this study only developed modeling tools for future operational alternative evaluations; no approved operational alternatives were developed herein.

USACE-SPA and WEST engineers computed reservoir boundary conditions (elevations and outflows) to model the three possible operational evaluation scenarios in the HEC-RAS quasi-unsteady flow model. These three operational alternatives were then implemented in the numerical sediment transport models, beginning with the final conditions of the calibrated base conditions model and run into the run into the future for 50 additional years.

Under current operations, the only permanent storage in Cochiti Reservoir is the 1,200-acre surface area pool that is used for recreation. During non-flood flows, the lake must be kept at a constant elevation to maintain this surface area requirement. There is no sediment management strategy based on the congressional authorization of this dam (USACE, 1996).

The first scenario increased reservoir elevations, raising the operational elevation approximately 50 feet (5,340 to 5,390 feet NGVD29). This scenario stored water for other possible uses (e.g., water supply for irrigation, additional recreational uses, etc.) recruiting sediment deposition further upstream in the reservoir headwater.

The second scenario drew the reservoir pool down for extended periods to erode the large headwater reservoir delta. The alternative was constrained by a minimum drawdown elevation of 5,322 feet NGVD29 to avoid unfavorable conditions at the reservoir outlet intake. However, the model was "stressed" to the operational constraints, dropping the reservoir level to 5,323 feet NGVD29 for the whole drawdown to evaluate the maximum possible response to this operational technique.

The third scenario lowered the reservoir seasonally (in the winter) to 5,323 feet NGVD29, then refilled the reservoir to the current operating elevation of 5,340 feet NGVD29 in the summer. The model drew down the reservoir gradually at the end of the Middle Rio Grande Valley irrigation season, to an elevation of 5,323 feet NGVD29, and the reservoir level stayed at this lowered pool for one month. The reservoir was then refilled in the spring back to an elevation of

5,340 feet NGVD29. This operation was designed to flush sediment from the reservoir and maximize the benefit of bypassing inflowing sediment load through the reservoir, while maintaining the standard pool for summer recreation. The cycle was repeated annually for the entire 50-year simulation period.

Results of the three scenarios compared to continuing normal operations in the reservoir for 50 years into the figure are included in Figure 4. The model did not compute significant sediment transported through the reservoir because of the physical characteristics of the reservoir itself and infrastructure limitations prohibiting further drawdown at this time. It did, however, indicate significant influence on the upstream deposition distribution was possible.

DISCUSSION

This paper attempts to answer questions regarding reservoir sustainability in terms of water storage capacity. In terms of usable reservoir life, defined by Morris and Fan (1998) as "*the period during which the reservoir may be operated for either its original or a modified purpose*," Cochiti Dam appears to be able to meet its originally intended purpose and a broad range of modified purposes for at least the next 50 years despite reservoir sedimentation.

The design philosophy when Cochiti Dam was conceived was based on an implied consideration of reservoir storage as an exhaustible resource. Annandale (2013) presents a convincing argument for the consideration of reservoir storage as a potentially sustainable resource. Because of the economics of dam construction, most prime sites for reservoir storage creation have largely been exhausted, with only less desirable and more-costly locations remaining. Thus, adding more reservoir capacity becomes more costly, and the need to preserve existing storage becomes more important in the hierarchy of approaches. Couple this with the uncertainties of watershed sedimentation from climate change, and the capacity issue becomes more complex. Understanding the sedimentation behavior of the project becomes an important planning and management tool in this respect.

The final calibrated sediment transport models also provide tools for the Pueblo and the USACE-SPA to further assess water quality and diversity issues in the study reach towards holistic reservoir sustainability analyses. Unsteady sediment transport in HEC-RAS 5.0, released after this work was complete, simplified the process of defining future operational alternatives for reservoir sediment management (Gibson and Boyd, 2014, Shelley et al., 2015), which will make additional alternative evaluation easier.

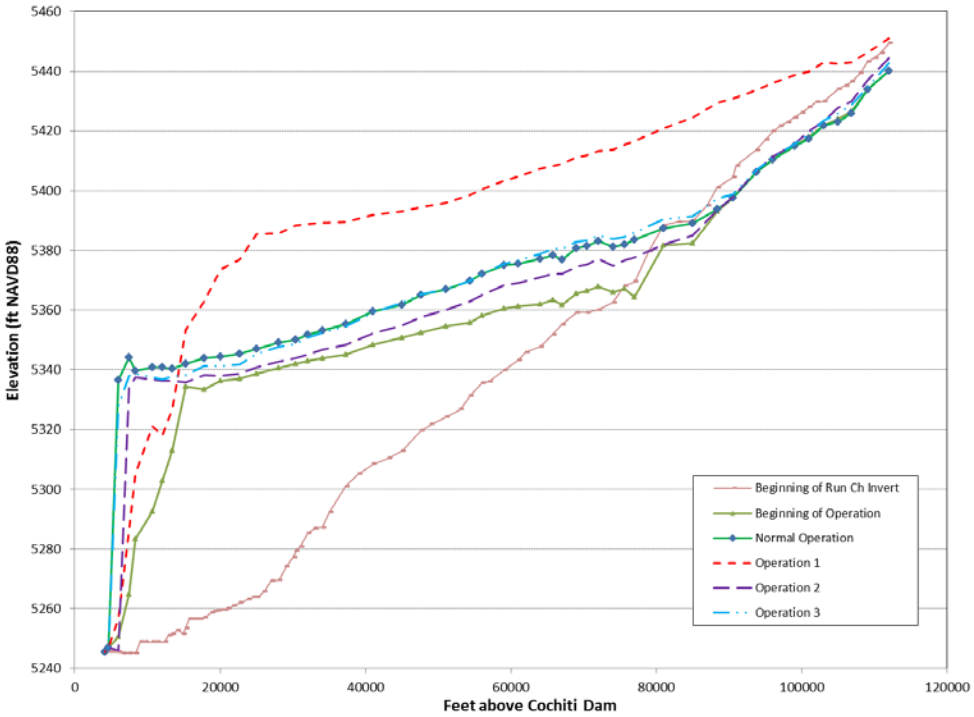

Figure 4. Bed profile results from various operational evaluation scenario HEC-RAS sediment transport models for the 50 year simulation window (2010-2059).

Limitations of this study include density current effects that probably affect Cochiti Reservoir (i.e. a "muddy lake effect" appears in range line profile plots) and remobilization of compacted alternating "layers" of cohesive and non-cohesive sediments in a lacustrine headwater delta, which will be explicitly modeled with future versions of HEC-RAS. The implications of climate change, and the associated response of watershed soils and vegetation, were also excluded from the current study, but are planned for future studies. As our knowledge improves regarding changes that might affect sediment supply to reservoirs, the ability to model and test reservoir responses will become more important. Sustainable solutions to reservoir sedimentation issues require a strong toolbox of continuously updating knowledge and information. In the case of Cochiti Reservoir, as in many other reservoirs, we must tackle the problem one step at a time.

REFERENCES

Annandale, George. (2013). *Quenching the Thirst, Sustainable Water Supply and Climate Change*. North Charleston, SC.

Boyd, P. M. and S. Gibson. (2013). Regional Sediment Management (RSM) Modeling Tools: Integration of Advanced Sediment Transport Tools into HEC-RAS. Coastal and Hydraulics Engineering Technical Note ERDC/CHL CHETN-XIV-36. Vicksburg, MS: U.S. Army Engineer Research and Development Center, Coastal and Hydraulics Laboratory.

Bryan, Susan Montoya. (2014). "Task force: New Mexico water supplies at risk." In the Albuquerque Journal, December 13, 2014. Retrieved online December 26, 2014.

Copeland, Ronald R., and Thomas, W.A. (1989). Corte Madera Creek Sedimentation Study, Technical Report HL 89-6, USACE, Waterways Experiment Station, Vicksburg, MS, April.

Gibson, S., Brunner, G., Piper, S., and Jensen, M. (2006) "Sediment Transport Computations in HEC-RAS." Eighth Federal Interagency Sedimentation Conference (8thFISC), Reno, NV, 57-64.

Grassel, K. (2002). “Issues of Jetty Jack Removal in Bosque and River Restoration Planning,” University of New Mexico Water Resources Program.

Hydrologic Engineering Center (1993) *Guidelines for the Calibration and Application of HEC-6*, Training Document 13, Davis, CA.

Krone, R.B. (1962). Flume Studies of the Transport of Sediment in Estuarial Shoaling Processes, Hydrologic Engineering Laboratory, University of California Berkeley.

Laursen, E. M. (1958). "The total sediment load of streams," Journal of the Hydraulics Division, ASCE, Vol. 84, No. HY1, p. 1530-1 to 1530-36, February 1958.

Leon, C. (1998). Morphology of the Middle Rio Grande from Cochiti Dam to Bernalillo Bridge, New Mexico. M.S. Thesis, Colorado State University, Fort Collins, CO.

Morris, G.L., and Fan, J. (1998). Reservoir Sedimentation Handbook, McGraw-Hill, New York, N.Y.

Mussetter Engineering, Inc. (2002). “Geomorphic and Sedimentologic Investigations of the Middle Rio Grande between Cochiti Dam and Elephant Butte Reservoir,” prepared for the New Mexico Interstate Stream Commission, Albuquerque, NM.

Mussetter Engineering, Inc. (2009). “Española Valley, Rio Grande and Tributaries, New Mexico Detailed Feasibility Study,” prepared for the USACE-SPA.

Novak, S.J. (2006). Hydraulic modeling analysis of the Middle Rio Grande River from Cochiti Dam to Galisteo Creek, New Mexico. M.S. Thesis, Colorado State University, Fort Collins, CO.

Partheniades, E. (1962). “A study of erosion and deposition of cohesive soils in salt water,” PhD Dissertation, University of California, Berkeley.

Porter, M.D., and T.M. Massong. (2004). “Analyzing changes in river channel morphology using GIS for Rio Grande silvery minnow habitat assessment.” In *Proceedings of the Second International Symposium on GIS/Spatial Analysis in Fishery and Aquatic Science*, September 3-6, 2002, University of Sussex, Brighton, U.K. Nishida, T., Kailola, P.J., Hollingworth, C.E. (Editors): 435-448.

Resource Technology, Inc. (1994). “Analysis of possible channel improvements to the Rio Grande from Albuquerque to Elephant Butte Lake: Phase I A, sediment yield analysis from the Rio Grande tributary basins,” prepared for the U.S. Army Corps of Engineers, Albuquerque District, Albuquerque, NM.

Richard, G.A. (2001). Quantification and prediction of lateral channel adjustments downstream from Cochiti Dam, Rio Grande, NM. Ph.D. Dissertation, Colorado State University, Fort Collins, CO.

Sallenave, R., Carrasco, C., and Cowley, D. (2010). “Fishes in the Middle and Lower Rio Grande Irrigation Systems of New Mexico,” New Mexico State University Circular 653, Cooperative Extension Service, College of Agricultural, Consumer and Environmental Sciences.

Shelley, J., Gibson, S., and Williams, A. (2015) “Unsteady Flow and Sediment Modeling in a Large Reservoir Using HEC-RAS 5.0” *Federal Interagency Sediment Conference.*

Sixta, M.J. (2004). Hydraulic modeling and meander migration of the Middle Rio Grande, New Mexico. M.S. Thesis, Colorado State University, Fort Collins, CO.

Tetra Tech, Inc. (2005). “FLO-2D Model Development Below Caballo Dam URGWOM: Final Report on FLO-2D Model Development,” prepared for U.S. Army Corps of Engineers, Albuquerque Dist., Albuquerque, NM.

Thomas, W.A. and Chang, H. (2008) “Computational Modeling of Sedimentation Processes,” *Sediment Engineering: Processes, Measurements, Modeling and Practice*, ASCE Manual of Practice 110, 649-680.

U.S. Army Corps of Engineers, Albuquerque District. (1996). “Cochiti Lake Water Control Manual: Appendix C to Rio Grande Basin Master Water Control Manual.”

U.S. Army Corps of Engineers, U.S. Bureau of Reclamation, and the New Mexico Interstate Stream Commission. (2007). “Upper Rio Grande Basin Water Operations Review: Final Environmental Impact Statement.”

US Army Corps of Engineers. (2011). “HEC-RAS River Analysis System, Hydraulic Reference Manual, Version 4.2 Beta.” Hydrologic Engineering Center, Davis, CA.

Yang, C.T. (1973). "Incipient motion and sediment transport," Journal of Hydraulic Division, ASCE, Vol. 99(10), 1679-1704.

Yang, C.T. (1984). "Unit stream power equation for gravel," Journal of Hydraulic Division, ASCE, Vol. 110(12)1783-1797.

A REVIEW OF THE LOWER MISSISSIPPI RIVER POTAMOLOGY PROGRAM

David S. Biedenharn, Biedenharn Group, Vicksburg MS, biedenharngroup@yahoo.com; John H. Brooks, Vicksburg MS, brooksjohnh@bellsouth.net; Roger A, Gaines, USACE MVM, Memphis TN, roger.a.gaines@usace.army.mil; Barbara A. Kleiss, USACE MVD, Vicksburg MS, barbara.a.kleiss@usace.army.mil; Charles F. Pinkard MVK, USACE Vicksburg MS, Freddie.pinkard@usace.army.mil; Wayne A. Stroupe, Vicksburg MS, sally.l.yost@usace.army.mil.

Abstract: The Mississippi River and Tributaries (MR&T) Project is a comprehensive water resources project for flood damage reduction and navigation improvement on the Mississippi River. MR&T elements include levees, floodways, diversion structures, tributary basin improvements, and channel improvements such as meander cutoffs, bank stabilization, dikes and dredging. Understanding how these elements, combined with natural factors, such as floods and droughts, impact the historical, current, and future river morphology is a complex challenge for those tasked with managing the Mississippi River for floods, navigation, environmental restoration, and coastal wetland loss.

Mississippi River potamology (the science of rivers) studies advance understanding of how natural and man-made factors combine to impact river morphology regarding present and future flood damage reduction, navigation, environmental restoration, and coastal wetland projects. The US Army Corps of Engineers (USACE) has conducted numerous potamology studies dating from the 1800s to modern times. Major studies were often the result of floods and follow-on beneficial projects. The epic 1927 flood fostered the first official USACE *Potamology Investigations* that resulted in more than 70 reports. The 1973 flood drove additional USACE potamology studies (T-1 and P-1 reports). However, funding, staffing, and interest in potamology studies waned, becoming almost nonexistent in recent times. Lessons learned and projects implemented from USACE's 1940s–1980s potamology studies helped pass the record-setting 2011 flows. The 2011 Mississippi River flood renewed interest in potamology, resulting in the creation of the USACE Mississippi Valley Division's (MVD) new Mississippi River Geomorphology and Potamology (MRG&P) Program. The first report of the MRG&P was a review of the Lower Mississippi River Potamology Program, including a comprehensive bibliography of potamology reports (Biedenharn et al., 2014). This paper provides a short review of USACE Mississippi River potamology studies.

INTRODUCTION

The Mississippi River and Tributaries (MR&T) Project is a complex, comprehensive water resources project, that provides flood control within the alluvial valley and navigation improvement of the Lower Mississippi River (LMR). The LMR extends from Cairo, IL, to the Gulf of Mexico, a distance of almost 1000 miles. The primary elements of the MR&T Project include levees, floodways and diversion structures, tributary basin improvements and channel improvement features such as meander cutoffs, bank stabilization, dikes, and dredging. The historical, present-day, and future morphology of the LMR reflects an integration of all these

features combined with natural factors such as floods and droughts, hurricanes, tectonic activity, geologic outcrops, climatic variability, and sea level rise. Understanding how these various factors affect the short- and long- term morphology of the LMR is a complex challenge for the river engineers and scientists responsible for managing this system for flood control, navigation, habitat restoration and reducing the loss of coastal marshes and wetlands in Louisiana. Much of the knowledge about the morphologic character of the LMR was gained through the U.S. Army Corps of Engineers (USACE) Potamology Program, which began in the early 1930s in recognition of the need to develop a better understanding of the underlying principles responsible for the behavior of the river.

HISTORICAL POTAMOLOGY PROGRAM

The word "potamology" has its root in the Greek word "potamas" and is defined as the scientific study of rivers or the science of rivers. Over the years, the focus of the program evolved as new demands and challenges arose. However, by the early to mid- 1980s, the program basically ceased to exist. In this section, the history of the Potamology Program is described.

Pre-Potamology Studies. The Mississippi River is the third largest river system in the world; it is the largest navigable river system in the world; and it is an incredible economic engine and economic advantage for the United States. Industry and agriculture depend on its transportation infrastructure; it is a source of water and recreation for millions of citizens; it is a vital ecosystem and environmental treasure. And at times, it can show the brute force of nature through devastating floods. The Mississippi River was used throughout history by Native Americans for transportation. The first river structures were levees constructed by European settlers above New Orleans in the early 1700s.

The U.S. Army Corps of Topographic Engineers became involved early on in river operations - there are discharge records of the river dating back to 1817. Other information documents were produced through the 1800s, including the seminal "Physics and Hydraulics of the Mississippi River" report by Capt. A.A. Humphreys and Lt. H.L. Abbot, which is considered as the "*beginning"* of hydraulic engineering on the river (Humphreys and Abott, 1861). At the time, it was also widely considered as the "*final*" report on river engineering. Since then, the Mississippi River has shown that any potamology or river engineering studies should only be considered "*interim*" as the river is constantly changing, forcing USACE efforts to advance understanding and knowledge of river processes. A comprehensive discussion of the management and engineering philosophy during this early period is presented in Elliott (1932).

The beginning of official USACE potamology studies is directly tied to the decision by Mississippi River Commission (MRC) president Brig. Gen. Harley B. Ferguson in the early 1930s to implement a cutoff program on the Mississippi River. These initial efforts focused on the study of the alluvial processes and their application to the management of the river system. The first MRC studies were conducted at the U.S. Army Engineer Waterways Experiment Station (WES) during the period of 1932-1935. These studies focused on determining the most favorable alignment to stabilize the Mississippi River in connection with the initiation of the cutoff program.

Subsequent studies examined bed materials in the system, materials in transport, and meandering of alluvial channels. This work included model studies and field sampling and surveys. The efforts were conducted in the late 1930s to the mid-1940s.

MRC Potamology Investigations. The first official MRC "Potamology Investigations" were initiated in the fall of 1946. These were the most extensive and comprehensive such studies conducted at the time. The program examined meandering tendencies to develop modeling for future river projects, the causes of revetment failures to prevent future occurrences, means of channel stabilization other than revetment, and development and testing of comprehensive plans to improve specific troublesome river reaches.

The majority of the early investigations were conducted by WES (which was under MRC control until 1949) with field assistance by the USACE Memphis, Vicksburg, and New Orleans Districts. The work included extensive field observations at several points on the Mississippi River, large-scale laboratory projects, soils studies, and instrumentation development and evaluation.

The MRC Potamology Board was established in 1957 that consisted of representatives from the MRC; the Memphis, Vicksburg and New Orleans Districts; and WES. It was active until 1961 and helped foster completion of additional potamology investigations. The Board was re-established in 1963 and expanded to include the entire Lower Mississippi Valley Division; a representative from the St. Louis District was added to the Board. In 1963, the MRC also established a Potamology Research Branch in the Engineering Division to coordinate studies recommended by the Potamology Board. The Board and the Branch were instrumental in completing several investigations. Over the next two decades, the Board and Branch were active, but over time and reorganizations, they had ceased to be active functioning elements by the mid- to late- 1970s. The USACE Committee on Channel Stabilization, established by the Chief of Engineers in 1962, was also instrumental in completing several studies impacting Mississippi River channel problems in the 1960s to early 1970s.

Potamology Early Years. Over the course of the mid-to-late-1900s, potamology studies and programs evolved to meet new demands and challenges. In the 1930s and 1940s the focus was on man-made cutoffs and their impact on the channel system. The spotlight moved to revetment failures and improved revetment construction and materials from the late 1940s to the early 1960s. From the 1960s to 1972, the focus shifted yet again as the MRC worked to develop the best ways to manage troublesome reaches of the river. Research and investigative studies were spawned by these activities, providing much needed information that advanced the understanding of the complex processes that nature and man-made structures combined to shape the river and how the river adjusted over time.

Crisis situations focus attention on problems. On the Mississippi River, the 1927 flood was such an event. The 1927 flood not only was the catalyst for the MR&T, it also drove efforts such as cutoffs and channel stabilization. Funding was made available to advance potamology knowledge as a result. The potamology studies of the 1930s through the late 1960s were accomplished due to this investment and the efforts of dedicated staff.

As with any crisis situation, knowledge and training prior to the event help provide the best response. Such was the case in 1927 when decades of preliminary work and research led to the

MR&T – the policy, direction, and framework in this landmark legislation were not developed overnight. The same can be said for potamology studies over the years. These studies provided USACE knowledge and also a generation of expert staff with the engineering expertise needed to help manage the river.

As is human nature, once we experienced a "comfortable" period in river conditions (fewer major floods and somewhat stable average flows), many leaders believed that our understanding of river behavior was sufficient for the current state. As such, interest, and more importantly, funding in potamology related studies waned.

1973 Flood & T-1/P-1. The 1973 Mississippi River flood was a "wake up" call for river science and engineering. The spring flood produced river stages that were higher (up to approximately 5 feet higher in some locations) than expected. These higher stages made it apparent that the stage-discharge relationships were several feet higher than the previous stage-discharge relationships used to establish levee grades and other flood control features. Therefore, the potential existed for a significant reduction in the flood capacity over a major portion of the LMR. To help address this critical issue, the President of the MRC - Division Engineer, LMVD implemented two new potamology study programs.

The "LMVD Potamology Study (T-1)" was initiated on August 7, 1974. This study was basically a data assembly effort that provided a current "snapshot" of conditions and information that focused on the nine major factors that impact river behavior. Each factor was covered by a separate T-1 Work Package:

Work Package 1 – Review of the Cutoff Program

Work Package 2 – Inventory of Revetment and Dike Systems

Work Package 3 – Geological Inventory

Work Package 4 – Hydrology Factors

Work Package 5 – Hydraulic Factors

Work Package 6 – Inventory of Physical Characteristics

Work Package 7 - Inventory of Levees

Work Package 8 - Inventory of Dredging Activities

Work Package 9 - Inventory of Sediment Data

Work packages 1 and 5 were conducted by the USACE Vicksburg District; 2, 3, 4, 6, and 7 were done by the University of Missouri at Rolla for the USACE St. Louis District; 8 was compiled by the USACE Memphis District; and 9 was completed by WES for the USACE New Orleans District. This effort assembled a large mass of data to feed follow-on studies to determine primary cause and effect relationships related to the Mississippi River.

Building off the T-1 work packages, the LMVD Potamology Program (P-1) was developed. The P-1 Program focused on defining the cause-and-effect relationships that resulted in short- and

long-term changes in the stage-discharge relationships in the LMR and developing improved design concepts and construction criteria for channel stabilization. The program continued the advancement of the level of knowledge and understanding of the Mississippi River behavior, allowing USACE to develop the most efficient and cost effective flood risk reduction and navigation channel possible.

This program also expanded the USACE view of potamology with investigations of four major parameters: hydrology (highly variable stages), sedimentation (sediments on or near the channel bed scoured from one location and deposited downstream), channel geometry (variable alignment impacting flow and sediment transport), and man-made modifications (levees, cutoffs, revetments, and dikes).

In the mid-1990s, the USACE Mississippi Division (MVD) formed the River Engineering Study Team (REST) in an effort to revitalize potamology studies. The REST consisted of river engineers and scientists from the division and district offices. The first meetings of the REST occurred on board the *MV Mississippi* during the May 1995 Channel Improvement trip. The purpose of the REST was to recommend, set priorities, plan, direct, and publish results from river engineering investigations on the LMR, with an aim towards developing an understanding of the short- and long term cause and effect relationships between the observed channel morphology and the channel improvement features. The REST proposed four broad study areas: (1) analysis of hydraulic slope and vertical adjustments; (2) channel geometry studies; (3) sediment studies; and (4) short- and long term numerical modeling of channel morphology. Each of these study areas would consist of a number of individual sub-areas. Unfortunately, only a few REST studies were initiated, and within a few years, the REST team disbanded.

Although the REST no longer existed, the USACE districts did continue to conduct river engineering studies, generally aimed at specific troublesome reaches of the river. In 1995, the St Louis District Hydraulics Branch established the Applied River Engineering Center (AREC) with the aim to conduct applied river engineering studies on the Mississippi River in an office/laboratory environment. A key component of the AREC is the Hydraulic Sediment Response (HSR) model, which is a small-scale, physical sediment transport model used to replicate the mechanics of an actual river on an area the size of a normal table top. Since its conception, numerous river engineering studies have been conducted on the Mississippi.

Historical Potamology Data and Unpublished Reports. As discussed above, the publication of technical reports was a major accomplishment of the Potamology Program. However, perhaps equally important is the vast amount of historical data and unpublished studies that were conducted as part of the program. Typical types of data that were collected included detailed hydrographic surveys, sediment sampling (both suspended and bed material), velocity and current direction measurements, boring data, divided flow data, bed form data, geologic information, water surface slopes, and geomorphic assessments. Unfortunately, some of this information has already been lost, and most of the data and studies exist only in hard copy form in somewhat obscure locations in various offices and archive areas at the USACE district and division offices. This is a massive set of data that represents an extremely valuable resource, which not only provides an historical perspective of the river, but more importantly, could be used to inform present-day efforts to understand the river system. One goal of the MRG&P is to gather and organize this historical data so that it will be of use for future studies.

FUTURE CONSIDERATIONS

The record setting 2011 Mississippi River flood again stirred interest in potamology related studies. This time interest was not driven by problems or failures; it was how successful the system safely passed the record flows of this epic event. Just as the 1973 flood was a wakeup call, the 2011 flood should be an equally important benchmark for us to understand the reasons for the difference in river response to the two floods. The lessons learned from the potamology studies of the late 1940s to the 1980s, and implemented in the river since the 1973 flood, worked fantastically when put to the ultimate test. But USACE realized it had basically lost a generation of continued potamology advancement along with the experienced staff with that important knowledge.

While Mississippi River flood damage reduction and navigation issues continue to be a major emphasis of USACE activities, especially on the lower river, there are new demands, interests, and economic focus areas championed by the public, river users, and stakeholders in the vitality of this national asset. Environmental restoration, conservation, recreation, coastal land loss and erosion, water quality and supply (surface and aquifer) and other basin-wide and localized issues are requiring attention in today's society.

Environmental factors, such as habitat development, fisheries enhancement, recreation, threatened and endangered species, invasive species, water quality, etc. are all now major considerations in USACE site specific projects and system-wide management strategies. Many new, and probably future, Mississippi River studies are being funded and driven based on environmental challenges.

In the last several decades, there has been an increased environmental activity concerning habitat development related to USACE dikes in the river. Notches have been installed on the bankside of dikes to increase habitat development that have provided additional recreational opportunities as well. During the MRC Low Water Inspection stop in Vicksburg, Miss., on August 21, 2013, the President of the MRC conducted a ceremonial signing of MVD/ERDC report "Conservation Plan for the Interior Least Tern, Pallid Sturgeon, and Fat Pocketbook Mussel in the Lower Mississippi River," with representatives of the U.S. Fish and Wildlife Service (USF&WS) and ERDC (Killgore et al., 2014). Besides featuring amazing interagency cooperation between USACE and USF&WS, the report featured a major potamology/geomorphology element.

The USACE has also lost a generation of experienced staff with potamology skills and expertise. This is due to various impacts including hiring reductions, funding constraints, and changes in mission focus. This staff expertise cannot be imported overnight, but must be fostered and grown by hiring and supporting capable engineers and scientists, providing training and mentoring, supporting intra- and interagency cooperation, and other innovative practices. There should always be a cadre of skilled professionals to pass corporate knowledge and ideas to those following, and also to those leading as well. A revitalized Potamology Program will keep USACE staff immersed, and interested, in understanding the morphologic processes that drive the important Mississippi River system.

This effort will have both short-term (less than 20 years) and long-term (20 to 200 years) implications and emphasis. Some river projects could use potamology knowledge

implementation today. On the other hand, the river is still responding to the cutoffs initiated 75+ years ago. Decisions made and implemented in the near future could have positive (or adverse) impacts for centuries. The re-establishment of a "Potamology" type program for the Mississippi River is needed to ensure incorporation of the best science and management practices from an engineering and environmental perspective for the complex and diverse demands of the 21st century and beyond.

REFERENCES

Biedenharn, D.S., Stroupe, W.A., and Brooks, J.H., (2014). "A Review of the Lower Mississippi River Potamology Program" USACE, MRG&P Report No. 1. Vicksburg MS. URL http://acwc.sdp.sirsi.net/client/search/asset/1035268.

Elliott, D. O., (1932). "Improvement of the Lower Mississippi River for Flood Control and Navigation" U.S. Corps of Engineers, Waterways Experiment Station, Vicksburg MS, May 1932.

Humphreys, A.A, and Abbot, H.L., (1861). "Report Upon the Physics and Hydraulics of the Mississippi River" Professional Paper No. 13, 1861, U.S. Army Corps of Topographic Engineers, Washington D.C.

Killgore, K.J., Slack, T., Fischer, R., Hoover, J., Harrison, A., Hartfield, P., Biedenharn, D., and Kleiss, B., (2014). "Conservation Plan for the Interior Least Tern, Pallid Sturgeon, and Fat Pocketbook Mussel in the Lower Mississippi River, (Endangered Species Act, Section 7(a)(1)" USACE MVD, MRG&P Report No. 4, November 2014, URL: http://acwc.sdp.sirsi.net/client/search/asset/1040663

GRAVEL DEPOSITS ON LOWER MISSISSIPPI RIVER SANDBARS

Richie McComas, **Hydraulic Engineer, USACE Vicksburg District, Vicksburg, MS, Richie.McComas@usace.army.mil; C. Fred Pinkard Jr., Hydraulic Engineer, USACE, Vicksburg District, Vicksburg, MS, Freddie.Pinkard@usace.army.mil;**

Abstract: The Mississippi River is known for its large sandbars that appear on the inside of bends during times of low stage. These sandbars on the lower Mississippi River are predominantly a medium to fine grained sand. The flood of 2011 and the drought of 2012 showed near record stages on both ends of the staff gage. Gravel deposits were observed on sandbars throughout the lower Mississippi during the low water inspections in the summer of 2012. These gravel deposits are not normally seen on the lower Mississippi River.

In the summer of 2012 gravel was identified on several sandbars during waterborne and aerial inspections. The distributions of gravel deposits were not consistent along the length or width of the river. Deposits also seemed randomly placed on each sandbar. A sampling plan was under development when the stage of the Mississippi River started to rise rapidly. Samples were taken from five sandbars with observed gravel near Vicksburg, MS before the deposits were covered with water; three above and two below the Yazoo River confluence. Several stations were sampled at each sandbar. Wolman pebble counts were done at sandbars with large gravel and grab samples were taken at multiple depths for lab analysis.

Gravel deposits on the lower Mississippi River are of interest for environmental and engineering reasons. If the gravel beds are an armoring layer and always part of the sandbar, then they could possibly be fish spawning spots. Gravel armoring a sandbar is an important process to know when calculating sediment transport rates and for calibration of sediment models. This paper will look at the location, distribution, and size of the gravel beds along the U.S. Army Corps of Engineers, Vicksburg District's section of the Mississippi River. A hypothesis of the transport mode (flood of 2011 or bar armoring) and the source of the gravel will be discussed.

SEDIMENT AND CARBON SEQUESTRATION IN THE LOWER ATCHAFALAYA BASIN, LOUISIANA

EXTENDED ABSTRACT

Cliff R. Hupp, Research Botanist, U.S. Geological Survey, Reston, Virginia, crhupp@usgs.gov; Daniel E. Kroes, Research Ecologist, U.S. Geological Survey, Baton Rouge, Louisiana, dkroes@usgs.gov; Edward R. Schenk, Research Ecologist, U.S. Geological Survey, Reston, Virginia, eschenk@usgs.gov; and Gregory B. Noe, Research Ecologist, U.S. Geological Survey, Reston, Virginia, gnoe@usgs.gov

Background: Sediment and organic material sequestration are important ecosystem functions of forested bottomlands along river systems. This is particularly true along Coastal Plain streams in the southeastern United States as they approach tide dominated estuaries (Hupp, 2000; Ensign et al., 2014). Floodplains along these low gradient systems are among the last places for significant trapping and storage of sediment and associated material, including carbon rich organic material, before they reach highly valued, ecologically and economically critical estuarine systems (Hupp, 2000).

The Atchafalaya River Basin (a distributary of the Mississippi River, Fig. 1) contains the largest relatively intact, functioning riparian area in the lower Mississippi Valley. Approximately 25% of the Mississippi River (drainage area about 3,200,000 km^2) and all of the Red River (drainage area about 233,000 km^2) flows through the Basin on an annual basis. The entire suspended- and bed-sediment load of the Red River and as much as 35% of the suspended and 60% of the bed sediment load of the Mississippi River (Mossa and Roberts, 1990) are now diverted through the Atchafalaya Basin. As a result, the Basin experiences exceptionally high sedimentation rates at sites with high connectivity to the main river (Hupp et al., 2008).

Recent studies have shown that temperate coastal lowlands may be an important sink for carbon (Ludwig, 2001; Raymond and Bauer, 2001; Noe and Hupp, 2005; 2009; Bridgham et al., 2006; Aufdenkampe et al., 2011) and associated nutrients (Hupp et al., 2008; Noe and Hupp, 2009), which may be stored in these systems as organic rich sediment. Initial results (Hupp et al., 2008) suggest that the central Atchafalaya Basin may conservatively trap 6.7 Tg of sediment annually (approximately 15% of total load entering the Basin), of which over 820,000 Mg are organic material. The temperate lowland trapping function or global service has largely been untested and ignored by many models of global carbon flux (Battin et al., 2008; 2009). Studies of lowland fluvial systems such as the Atchafalaya Basin may be critical towards our understanding of global carbon cycling, which in turn has direct implications for nutrient processing and global climate change. Following initial sediment trapping studies by Hupp et al. (2008), we began a spatially expanded (Fig. 1), ongoing study with the objectives to quantify sediment trapping in range of environments including areas of high deposition rates, which may subsequently allow for quantitative estimates of annual carbon sequestration in the Atchafalaya Basin.

Approach: Sediment deposition rates, in both studies, are determined using artificial markers, feldspar clay pads at stations along transects positioned near waterways/bayous. These pads were/are measured annually for deposit thickness above the clay. We monitored 20 transects located in the central part of the Basin in the 2008 study (Fig. 1). We established an additional 16 transects in the lower (downstream) part of the Basin in 2010 (Fig. 1). Like the earlier study,

transects are located in a range of depositional environments from sites where new land is accreting in previously open river water (exceptionally high deposition rates) to areas identified as potentially low depositional, hypoxic backswamps with poor connectivity to sediment laden river water. Deposition rates were converted to sediment mass trapping rates using bulk density information from sediment samples collected along the transects. Additionally, the samples were analyzed for loss on ignition (LOI) to determine organic content. In the ongoing study, samples are analyzed for carbon, nitrogen, and phosphorus content, including the determination of the amount of carbon isotopes and ratios ^{12}C: ^{13}C and ^{13}C: N to infer general carbon sources.

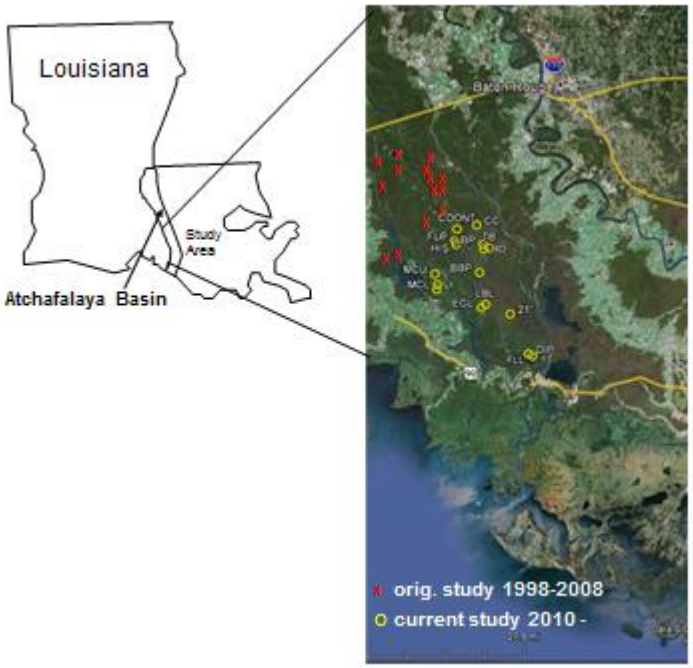

Figure 1 Location of study area in Louisiana. Transect locations in the central (red x's) and southern Atchafalaya Basin (yellow circles) for original and current studies, respectively, are shown.

Sediment and Carbon Trapping: The Atchafalaya Basin traps substantial amounts of suspended sediment annually; many areas have some of the highest documented sedimentation rates in forested wetlands of the United States (Hupp, 2000; Aust et al., 2012). Mean sedimentation rates ranged from about 2 to 40 mm y^{-1} in the central part of the Basin (Fig. 2A). Highest sedimentation rates occur in low elevations that receive sediment-laden water (high connectivity) from two or more sources, which may create slow velocities through hydraulic damming (D, E, and F transects, Fig 2A, Hupp et al., 2008). Mean sedimentation rates ranged from about 7 to greater than 150 mm y^{-1} in the actively aggrading lower part of the Basin (Fig. 2B). The highest sedimentation rates in this area are associated with island building in the main waterways and areas that receive water heavily laden with sediment from nearby channel cuts/canals and other hydrologic diversions (LI, HIS, and FLP, Fig. 2B). Low sedimentation rates throughout the Basin may occur on high levees or on low backswamps, both where there is little connection to river water because of high elevation or stagnant, sediment-depleted flow, respectively.

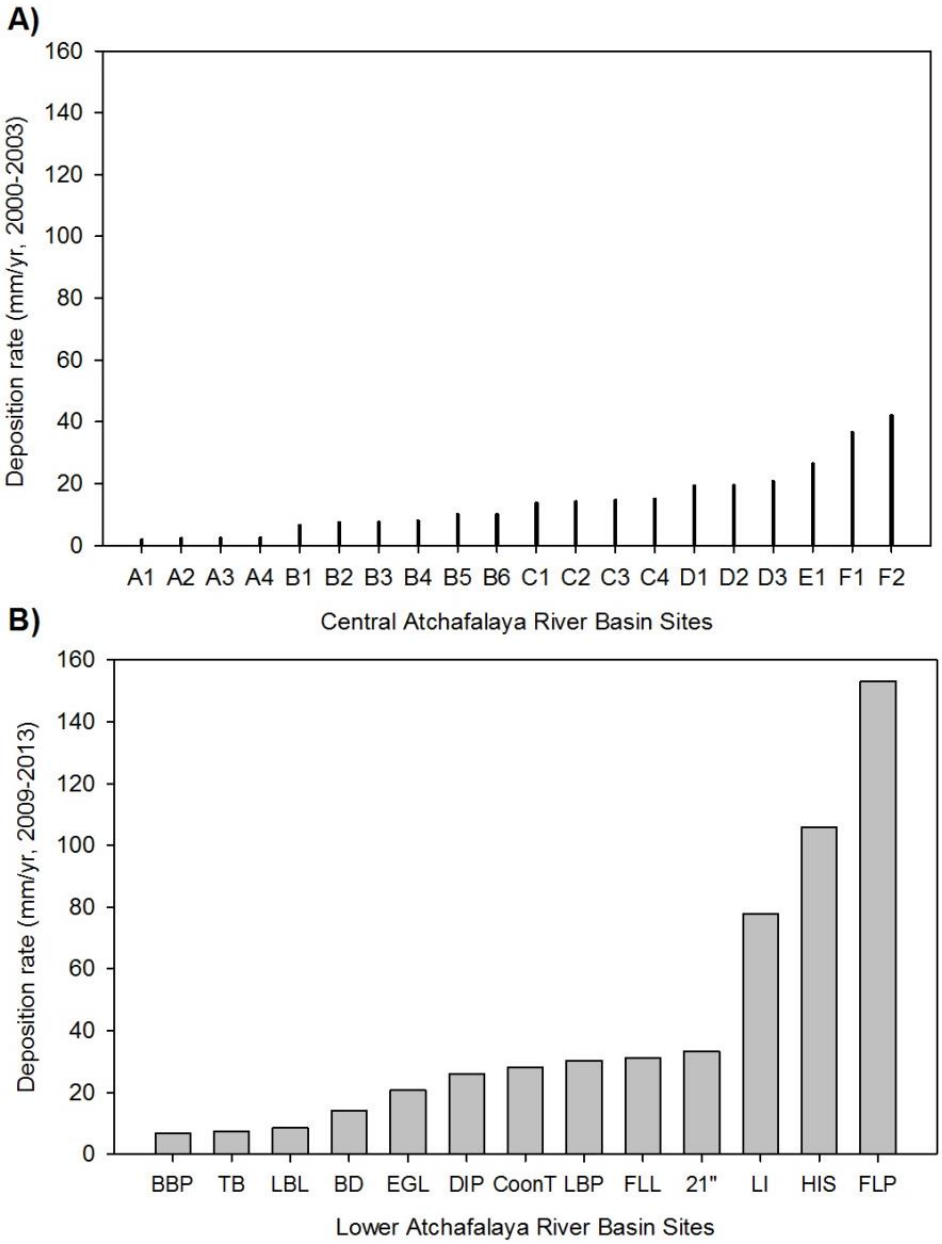

Figure 2 Sediment deposition rates in A, the central Atchafalaya Basin and B, the lower Atchafalaya Basin. Each bar represents the mean rate for named sites (indicated in Fig. 1).

Organic content in recent deposits is influenced by detrital inputs from on-site (in situ) sources (autochthonous) and from off-site material delivered by stream flow (allochthonous) that may be trapped as deposited sediment. Mean percentage organic material (LOI) was just over 10% and 16% in the central and lower parts of the Basin, respectively. This suggests that the Basin is an important area for organic material trapping (>800k Mg organic sediment of which 40% may be carbon) annually in the central Basin alone, Hupp, et al. 2008). The lower part of the Basin, with a higher mean organic content and order-of-magnitude higher maximum deposition rates than the central part of the Basin, undoubtedly traps substantially more organic material (mass estimates

have not yet been calculated). Studies using stable isotope measurements ($\delta^{13}C$, $\delta^{15}N$) have shown that the source of organic material maybe identified (Hackney and Haines, 1980; Craft et al., 1988) based on variance in vegetation utilization of C_3 versus C_4 photosynthetic pathways (forest vegetation-C_3, marsh/grass vegetation-C_4) and algal uptake of dissolved inorganic C. Carbon isotope values ($\delta^{13}C$) in the lower part of the Basin suggest that a range of carbon sources exist (Fig. 3). A large portion of Basin deposited carbon is probably allochthonous as 60% of samples have $\delta^{13}C$ values that are closer to that of river suspended sediment compared to forest leaf litterfall values. Thus, our results strongly suggest that the Atchafalaya Basin sequesters substantial amounts of allochthonous carbon (from the watershed) in addition to that produced in the Basin and that lowland alluvial areas (e.g. Lower Mississippi Valley) may be important sinks that should be considered in estimates and models of global carbon cycling.

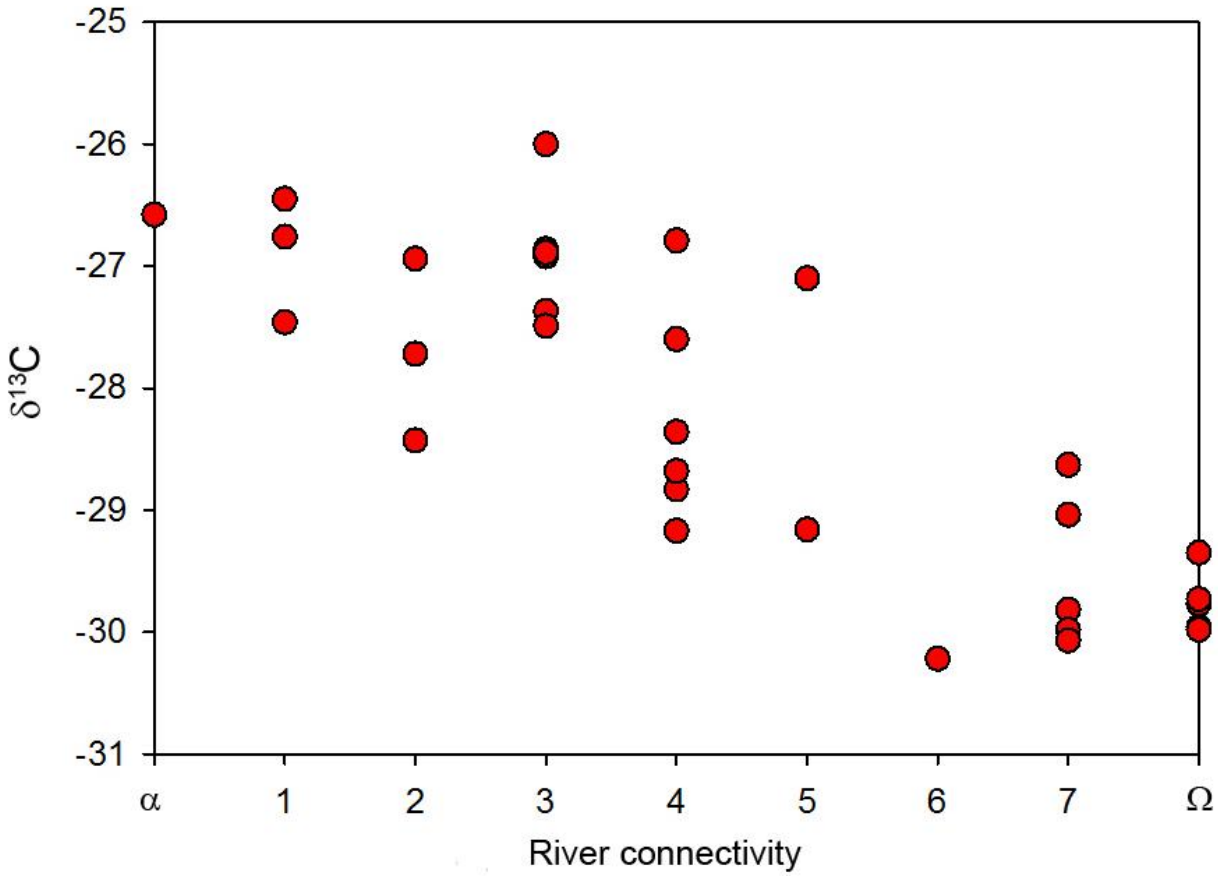

Figure 3 $\delta^{13}C$ values of deposited sediment along a gradient of river-water connectivity to floodplain in the southern Atchafalaya Basin. Sites were categorized into seven classes of connectivity, from high (1) to low (7) with connectivity decreasing from left to right along the x-axis. $\delta^{13}C$ of allocthonous, riverine suspended sediment (α) and autochthonous forest leaf litterfall (Ω) are included as potential end-members of organic sediment sources

REFERENCES

Aufdenkampe, A.K., Mayorga, E., Raymond, P.A., Melack, J.M., Doney, S.C., Alin, S.R., Aalto, R.E., and Yoo, K. (2011) Riverine coupling of biogeochemical cycles between land, oceans, and atmosphere. Frontiers in Ecology and the Environment 9, pp. 53-60.

Aust, W.M., McKee, S.E., Seller, J.R., Strahm, B.D., and Schilling, E.B. (2012). Long-term sediment accretion in bottomland hardwoods following timber harvest disturbances in the Mobile-Tensaw River Delta, Alabama, USA. Wetlands 32, pp. 871-884.

Battin, J.J., Kaplan, L.A., Findlay, S., Hopkinson, C.S., Marti, E., Packman, A.I., Newbold, J.D., and Sabater, F. (2008) Biophysical controls on organic carbon fluxes in fluvial networks. Nature, Geoscience 1, pp. 95-100.

Battin, J.J., Luyssaert, S., Kaplan, L.A., Aufdenkampe, A.K., Richter, A., and Tranvik, L.J. (2009) The boundless carbon cycle. Nature, Geoscience 2, pp. 598-600.

Bridgham, S.D., Megonigal, J.P., Keller, J.K., Bliss, N.B., and Trettin, C. (2006) The carbon balance of North American wetlands. Wetlands 26, pp. 889-916.

Craft, C.B., Broome, S.W., Seneca, E.D. and Showers, W.J. (1988) Estimating sources of soil organic matter in natural and transplanted esturarine marshes using stable isotopes of carbon and nitrogen. Estuarine, Coastal and Shelf Sciences 26, pp. 633-641.

Ensign, S.H., Noe, G.B., and Hupp, C.R. (2014) Linking channel hydrology with riparian wetland accretion in tidal rivers. Journal of Geophysical Research: Earth Surface 119, pp. 1-17.

Hackney, C.T. and Haines, E.B. (1980) Stable carbon isotope composition of fauna and organic matter collected in a Mississippi estuary. Estuarine and Coastal Marine Sciences 10, pp. 703-708.

Hupp, C.R. (2000) Hydrology, geomorphology, and vegetation of Coastal Plain rivers in the southeastern United States. Hydrological Processes 14, pp. 2991-3010.

Hupp, C.R., Demas, C.R., Kroes, D.E., Day, R.H., and Doyle, T.W. (2008) Recent sedimentation patterns within the central Atchafalaya Basin, Louisiana. Wetlands 28, pp. 125-140.

Ludwig, W. (2001) The age of river carbon. Nature 409, pp. 466–467.

Mossa, J. and Roberts, H.H. (1990) Synergism of riverine and winter storm-related sediment transport processes in Louisiana's coastal wetlands. Gulf Coast Association of Geological Societies Transactions 40, pp. 635–642.

Noe, G.B. and Hupp, C.R. (2005) Carbon, nitrogen, and phosphorus accumulation in floodplains of Atlantic Coastal Plain rivers, USA. Ecological Applications 15, pp. 1178-1190.

Noe, G.B. and Hupp, C.R. (2009) Retention of riverine sediment and nutrient loads by Coastal Plain floodplains. Ecosystems 12, pp. 728-746.

Raymond, P. A. and Bauer, J.E. (2001) Riverine export of aged terrestrial organic matter to the North Atlantic Ocean. Nature 409, pp. 497–500.

.

MISSISSIPPI RIVER MODEL

Edmund M. Howe, P.E., Senior Hydraulic Engineer, United States Army Corps of Engineers, Memphis, TN, edmund.howe@usace.army.mil, 901-544-0876

INTRODUCTION

Project Background: The Great Mississippi River Flood of 2011 was the catalyst behind the creation of detailed, unsteady flow, hydraulic models of the Mississippi River and Tributaries (MR&T). The MR&T system was tested to new levels during the 2011 event, and the hydraulic models provide a means of evaluating the system performance. The Memphis, Vicksburg, and New Orleans Districts of the Corps of Engineers worked in parallel to create separate models of their systems. The 2011 Post-Flood Assessment and the National System Performance Evaluation were two studies that utilized the first iteration of these hydraulic models. A limited timeline to complete those two projects did not allow for a detailed calibration to a wide range of flows, and the scope of the studies only concerned relative differences to the 2011 event. For the Mississippi River Flow Line and Geomorphology Study, a more detailed calibration of the models was necessary. Each district collected more data and updated its individual models in order to resolve major issues unique to their locations and calibrate to a range of flows before attempting to combine them into one model. This report provides a brief description of the background of the development of the Memphis District model, examples of novel methodologies and assumptions involved in calibrating this large, one-dimensional HEC-RAS model, and some of the methodologies and results from the coupled one-dimensional and two-dimensional HEC-RAS model.

Model Background: The Memphis District portion of the HEC-RAS model originated from the Ohio River Community Model (ORCM). A Mini-Model version of the ORCM was used during the 2011 Flood by the National Weather Service (NWS) with the aid of the Hydrologic Engineering Center (HEC) in an attempt to forecast river stages and the activation of the Bird's Point-New Madrid Floodway (BPNM). The Mini-Model had upstream extents of Chester, Illinois on the Mississippi River and Smithland, Kentucky on the Ohio River. The downstream boundary was Caruthersville, Missouri which is located approximately 110 river miles downstream of the confluence of the Mississippi and Ohio Rivers. The "Mini-Model" was updated significantly by the Memphis District and extended downstream to Vicksburg, Mississippi to include the major tributaries that either contribute significant flow or experience a considerable backwater effect during high flood events. Inflows due to precipitation within the Memphis District model limits were estimated using NWS hydrologic models and further routed by the Memphis District hydraulic model.

Two-dimensional RAS models of the BPNM and the confluence of the Arkansas, White, and Mississippi Rivers were constructed for this effort due to the complexity of those sites. These models were calibrated and refined using the most advanced features available in RAS. RAS2D was being developed during the initial calibration and not all the current software features were available as the work progressed.

DATA

Flow and Stage Data: An unsteady HEC-RAS model is based on a series of assumptions to represent open channel flow in one-dimension, upstream to downstream. It is a robust and flexible model, but like all models it is limited to the accuracy of the input data in addition to its one-dimensionality. The best, most accurate data reasonably obtainable was used for the model development.

For the external and internal boundaries of the Memphis District, flow and stage data needed to be obtained from the United States Geological Survey (USGS), the St. Louis District, the Lakes and Rivers Division, the Little Rock District, the Memphis District, the Vicksburg District, and the NWS. The NWS computes data in Coordinated Universal Time (UTC) while many of the district offices report in their respective time zones, typically Central Standard Time (CST). This data was compiled, converted, and stored in databases using HEC-DSS in both UTC and CST. By switching the databases, the model has the capability of reading data in either UTC or CST.

The vertical datum used for the model is the North American Vertical Datum of 1988 (NAVD88). Many of the gage zeros have been tied to the NAVD88 datum by surveying– that conversion was applied directly to obtain elevation in NAVD88. Other gages have not been surveyed and Corpscon6 software was used to convert the gage zero in the National Geodetic Vertical Datum of 1929 (NGVD29) to NAVD88.

Many points within the model with a significant contribution of flow are monitored by gages by either the USACE or the USGS. Most are real-time stage gages, and flow measurements are taken periodically to develop the stage-flow relationship, but some are merely staff gages read daily. Because the 2011 flood produced some of the highest stages in recent decades, the number of flow measurements at these high stages for available for comparison was limited, which contributed to uncertainty in the model. All stage and flow data was checked to permit accurate calibration.

GIS Data: GIS data was necessary for the creation of the hydraulic model. The HEC Geo-RAS tools for ArcGIS were used to translate the vector and raster data into an HEC-RAS geometry. The projection and datum for the terrain model were USGS Albers Equal Area and NAVD88 (ft), respectively. The terrain model associated with the Memphis District geometry was created from sets of bathymetric data and Laser Imaging, Detection and Ranging (LIDAR) or Digital Elevation Model (DEM) datasets obtained during different years. The use of data obtained in various years was unavoidable due to the model boundaries extending into other districts. However, all the data for the terrain model were obtained no earlier than 2001

Post-2001 Flood surveys and After-Action Reports (AAR) were used to help determine final breach sizes or areas of overtopping and to gain a general knowledge of the flood history. Levees and floodwalls in the National Levee Database (NLD) essential to calibration were included in the model.

METHODOLOGY AND ASSUMPTIONS

General Assumptions: HEC-RAS is a one-dimensional modeling software that has the capability to model split flows, to calculate water surface profiles for gradually varied flows, and to model a single stream reach or a full network of interconnecting channels. It has the ability to model subcritical, supercritical, and mixed-flow profiles. The basic computation routine solves the one-dimension energy equation, taking into consideration energy losses due to channel and overbank friction in the longitudinal direction, and expansion and contraction losses at bridges, culverts, and natural constrictions. HEC-RAS neglects variables such as density and temperature. Because RAS is a one-dimensional model, all input must be assignable to a longitudinal coordinate. The modeling of large, elaborate river systems in one-dimension involves mathematical assumptions, requiring creative use of RAS features to approximate the three-dimensional hydraulics that exist in the field.

As the initial calibration was underway, a two-dimensional modeling capability in HEC-RAS was under development (HEC-RAS 5.0 Beta). Therefore, complex sites such as BPNM and the confluence of the Arkansas, White, and Mississippi Rivers were developed in HEC-RAS 5.0 Beta to obtain a more realistic model. HEC-RAS 5.0 Beta contains a 2-D finite-volume model that solves either the full 2-D Saint Venant equations or the 2-D Diffusion Wave equations. The software has the ability to perform combined 1-D Rivers and Storage areas with 2-D Flow Areas. The combined 1-D/2-D computations are performed together on a time step by time step basis, making the connections from 1-D areas to 2-D Flow Areas more accurate than modeling them separately. The grids for the 2-D areas created are discretized, and an elevation-volume relationship is computed for each cell based on the underlying terrain and bathymetry. The effort to refine and calibrate these 2-D areas was limited, partly because the software was only in a Beta version during the time of the initial calibration. However, the major limitation in the software for this initial calibration was that only one Manning N-value could be assigned to the cells at one site. Once the model was set up and stable, there were few variables available to change to calibrate the 2-D areas. The general expectation was that the application of a RAS 2-D model at a complex site would be more accurate than a 1-D model, regardless of the limitations of the 2-D feature available then. The areas modeled in 2-D were delineated in such a way to represent overbank flow – which is in better agreement with the single Manning's N-value limitation of the software.

In addition to the theoretical assumptions of the software code, assumptions are inherent in the input data before the model is ever created. Regarding the use of surveys from multiple years, the general assumption was that the overall volume for the system has not changed significantly in the past 10 years. Local differences in geometry from the use of older data were not quantified but were rectified by weighting the calibration of the model to the more recent events. The typical error of the published flow data for calibration is considered to range from plus or minus 2 to 8 percent, or more. . The USGS publishes the results of flow measurements taken and estimated accuracy. That accuracy is based on a number of variables such as weather conditions, turbidity, and temperature. Overall, the published flow data was considered the most accurate available.

Methodology for Calibration (1-D): Gaining an understanding how the flow data and geometric data functions in the model for a variety of flood events is a daunting task. Correcting

flow data or modifying the geometric data was considered part of the calibration process. Determining the locations and elevations of lateral structures and corresponding weir coefficients, the storage area volumes and layouts, ineffective flow areas, levee points, and Manning's N-values were the other key tasks in calibrating the Memphis District model.

After the quality check on the published flow data, the calibration to a range of flows began initially by changing Manning's N-values, working upstream to downstream. The 2002, 2008, and 2011 events were the target events used to calibrate the model. Although the 2011 event was the most recent and highest event, 2008 was used for calibration of some of the areas of great complexity. For example, in 2011 there were four major breaches between Cairo and Caruthersville (three of the breaches were intentional, for operation of the BPNM floodway). The unintentional breach was not a breach of a project levee. Since none of those four breaches occurred during the 2008 event ,the 2008 event was used to help isolate variables unique to the cross section geometry. In general, comprehensive data from 2002 to 2011 was used to determine elevation trends for the different levels of flow, with emphasis on the more recent events. Modifying the Manning's N-values was an iterative process conducted by analyzing the trends of flow versus the difference between computed elevations and observed elevations (residuals).

Because of the complex nature of the Mississippi River, adoption of a single Manning's N-value representing the channel for all levels of flow was not prudent. A 0.03 value for the channel was the initial trial Manning's N-value. The initial value was changed on cross sections considered local to a particular gage to obtain a close approximation to in-channel flows. These modified values were then varied with flow by a series of multipliers. For example, if the model residuals were showing that computed elevations were too low for flow ranges of 200,000 to 300,000 cfs, a multiplier greater than 1.0 was used on the Manning's N-values for a series of cross sections delineated for a particular gage during that flow range. This process is tedious, and an automated roughness feature within HEC-RAS was used to help determine reasonable multipliers to correct a high or low trend at the various flow rates.

The Automated Roughness Calibration feature within HEC-RAS was used as a guide for the lower flows. It was used as a time saving feature and not used exclusively in all locations. The automated roughness feature determines the trends of the residuals with flow rates and iteratively determines the multiplier needed to minimize the difference between the computed and observed elevations. The output of this feature was a series of multipliers for the different reaches for the range of flows. This data was adjusted by the modeler to provide smoother transitions. After the in-channel flows at the gages were reasonably calibrated, calibration to higher, out-of-bank flows began. The automated roughness feature did not work as well for higher flows as the geometric features, breaches, and hydrodynamics become more complex, but Manning's N-values were still varied at higher flow rates by the modeler. At higher flow rates, more effort was necessary to represent the conveyance in the cross sections. This became apparent as the computed elevations began to slip in time and peak too late. To represent the conveyance in a given cross section, the cross section had to be delineated horizontally by Manning's n values and schematic changes to the model were necessary.

The larger geometric or schematic changes to the model as a part of the calibration process generally were related to storage areas and lateral structures within the MR&T levee system that

represented breaches that occurred or areas where large overbanks existed in the original cross sections. Storage areas within the MR&T levee system were only used if an obvious high elevation restriction existed. Most of these areas are partially bound by spur levees jutting out almost perpendicular to the path of overbank flow. In the majority of circumstances, water backs up into these areas and does not actively convey downstream; therefore, storage areas were deemed appropriate. The profiles of the lateral structures that control the flow of water into the storage areas were often cut from elevations with little difference in elevation on either side of the structure. The weir coefficients were set to low values (0.1 to 0.7 typically). These lower values not only best represent the flow into or out of these areas, but also tend to be more numerically stable. Ideally, a stage-stage boundary condition between the cross sections and the storage areas would best represent the flow into or out of the storage areas for a range of events, but this capability was not available in HEC-RAS at that time. Other areas of large overbank distance that could not be delineated by obvious elevation restrictions were represented using other tools and methods available in the HEC-RAS interface.

When a long, flat overbank distance (this can be many miles for the Mississippi River) is present in a cross section, issues can arise when attempting to calibrate the model temporally and spatially. When water begins to flood the overbanks, the one-dimensional assumptions in HEC-RAS are not realistic. Specifically, when the computed water levels exceed elevations of the overbanks, RAS assumes that all the water in the overbanks is at an equal elevation to that of the river. In actuality, the water surface elevations near the levees are not the same as that for the channel. A drop in the calculated water surface can be seen as water levels begin to exceed elevation in the flat overbanks of the cross sections, due to the generally flat overbanks. For overbanks with side channels or more depth in the overbanks, too much increase in elevation is seen as these areas begin to compute as conveyance in the model. In some cases, water in the overbanks is essentially stored until water levels in the river drop – at which point that volume begins to return to the channel. These areas were handled with ineffective area points. There are other cases where the water in the overbanks does convey, but slowly. If these areas are treated as strictly ineffective areas, the model will compute too much storage. This subtracts too much volume on the rising side of the hydrograph and returns the overestimated volume on the falling side of the hydrograph. These areas instead were delineated horizontally with associated Manning's N- values. Large Manning's N-values such as 0.2 or 0.3 were used at the fringes of the cross sections to reduce the conveyance of this volume downstream. N-values this high are not listed in any hydraulic textbook strictly for describing roughness, but the complex hydrodynamics actually taking place cannot be modeled otherwise in a one-dimensional model. The energy losses occurring transversely and vertically have to be accounted for, in addition to the standard longitudinal losses, to obtain the correct timing of calculated elevations at the main stem gages. Using these high Manning's N-values, as well as varying the Manning's N-value with flow rates, most of the events could be calibrated satisfactorily. For cases of unusually high flow or events that had a long duration at levels which caused water to oscillate in and out of channel, additional levee points and ineffective areas were necessary for the model to compute accurate elevations without significantly delaying the timing of the peaks. Due to the one-dimensionality of HEC-RAS, the superelevation of the water surface cannot be modeled; however, the conveyances within the cross sections were reasonably modified to compute a close approximation to the observed elevations near the time they occurred. Much effort was spent attempting to calibrate to the events temporally and spatially, but in a one-dimensional model of this magnitude trade-offs have to be made. Aerial photography and the terrain model helped

tremendously in determining how to handle the overbank conveyances. Figures 1 and 2 show prime examples of overbank flow during the 2011 flood and a few of the different methods used by the Memphis District for modeling.

Figure 1 is aerial photography obtained during the 2011 flood. At the top right corner of the photograph a breach occurred in a spur levee. A storage area was used to model the volume shortcutting the Mississippi River. On the right descending bank, a large area is inundated and labeled Storage. This area is partially bound by a levee on the upstream side that did not fail during the flood. Water tends to back up into this area rather than convey in a downstream direction. The bottom right corner of the photograph shows overbank flow modeled with cross sections. The overbank area was considered to be low conveyance instead of storage, as it was not confined by high ground. The sections extended across the overbank approximately 3 to 4 miles. The profile for section A-A in Figure 1 is shown in Figure 2.

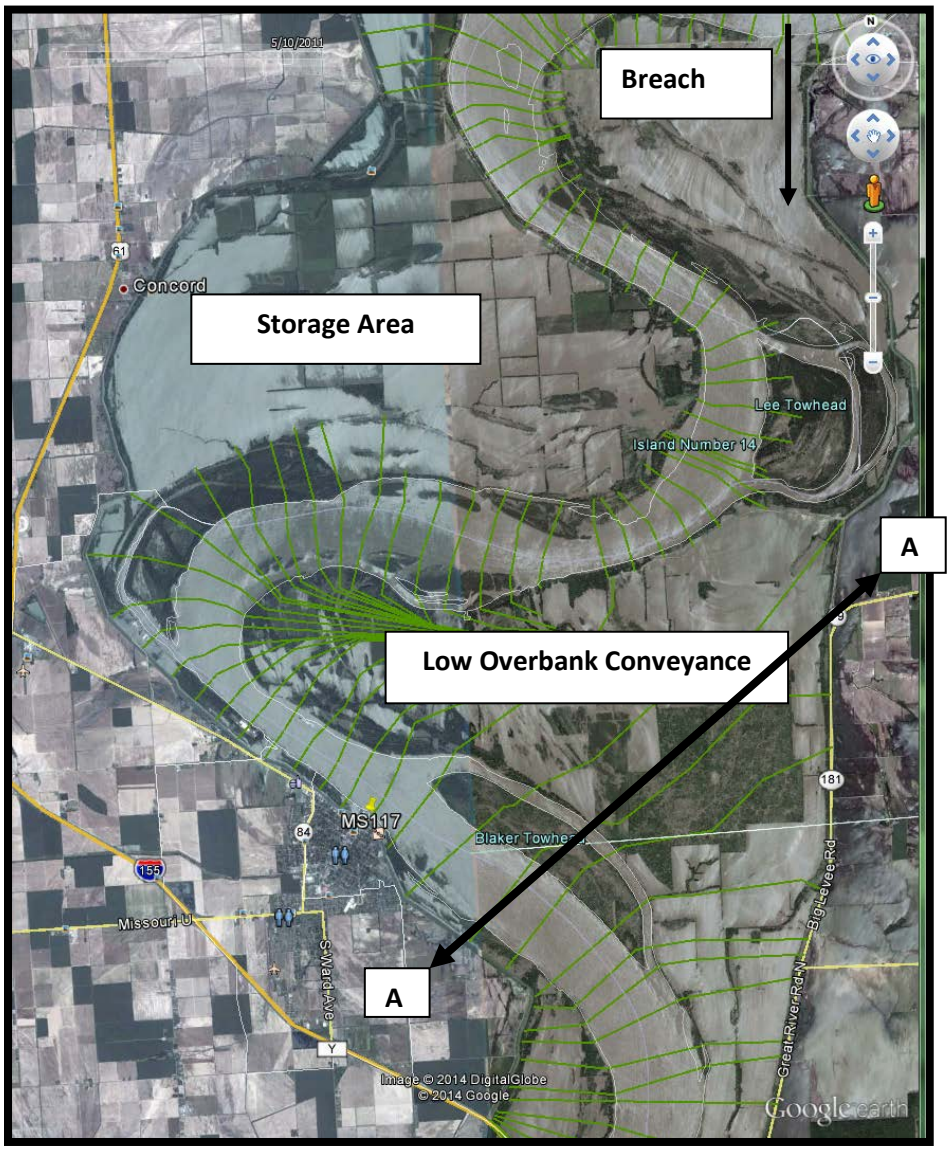

Figure 1 Photograph of Overbank Flow, May 2011

Figure 2 shows the profile for section A-A. The bars across the top indicate the Manning's N-value, as well as its conveyance delineation along the stationing of the profile. The two channels had clearly identifiable banks and were assigned N-values of 0.032. The overbank between the two channels was assigned an N-value of 0.11. The left side of the profile corresponds to the large overbank that has water which conveys downstream slowly. The Manning's N-value there was raised to a 0.17 in order to allow little conveyance downstream. From the plan view in Figure 1, it is clear that the flow in the overbank for this area was not stored, rather it moves slowly through the overbanks downstream. Also in Figure 2, a levee point is present at approximately 22,000 feet from the left overbank. However, this point does not represent a real levee; instead, the point limits flow from being computed in the first 22,000 feet of the cross section until that point is overtopped. Use of such levee points helps to transition the model transversely to fully out of bank flow.

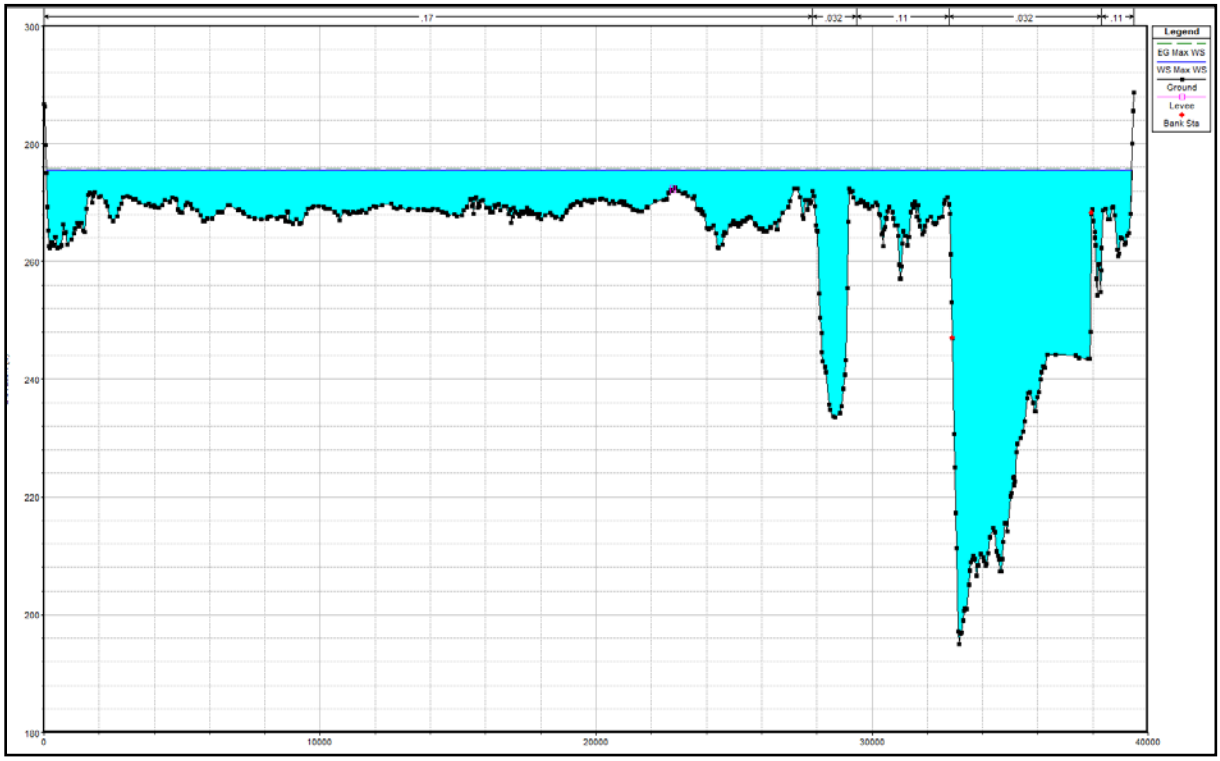

Figure 2 Section A-A – Example of Low Conveyance Overbank Flow

RESULTS AND CONCLUSIONS

Calibration Results: The calibration of the Memphis District hydraulic model focused on the 2002, 2008, and 2011 events primarily, but continuous data from 2002 through 2011 was run through the model as well. In general, gages that recorded hourly stage data were used for a detailed calibration analysis, but intermediate gages with daily data, high water marks, or staff gages with intermittent data were also used for refinement of the model. Table 1 shows results for each of the 3 primary events, and Table 2 shows results from the 10 year simulation from 2002 to 2008. In Table 1, results are listed for locations along the Mississippi River from Chester, Illinois downstream to Arkansas City, Arkansas. For each event and location, the accuracy of the model is described by listing the percent of calculated stages within 0.5 and 1.0 feet of the observed data and the average error. Also, the difference in peak elevations between calculated and observed stages is listed. For all three events the general tendency is for the model to more accurate at the upstream end than at the downstream end. Average errors and differences at peaks are less than 2.0 feet and typically less than 1.0 feet.

Table 1 Memphis District Calibration Results for 2002, 2008, and 2011

	2002 Event				2008 Event				2011 Event			
Gage	% within 0.5 ft	% within 1.0 ft	Average Error	Difference at Peak	% within 0.5 ft	% within 1.0 ft	Average Error	Difference at Peak	% within 0.5 ft	% within 1.0 ft	Average Error	Difference at Peak
Chester	82%	99%	0.29	0.32	81%	94%	0.32	-0.1	77%	99%	0.35	0.03
Red Rock	52%	93%	0.50	-0.05	63%	88%	0.49	-0.2	46%	86%	0.56	0.04
GrandTower	76%	88%	0.41	-1.25	70%	93%	0.39	0.45	73%	98%	0.39	-0.01
Moccasin Springs	22%	77%	0.81	-1.21	37%	50%	1.30	0.7	N/A	N/A	N/A	N/A
Cape Girardeau	54%	93%	0.52	-1	57%	92%	0.53	0.19	65%	99%	0.37	-0.08
Thebes	32%	82%	0.68	-1	74%	92%	0.39	-0.04	75%	96%	0.35	-0.22
Commerce	42%	85%	0.62	-1.05	N/A	N/A	N/A	N/A	N/A	N/A	N/A	N/A
Price Landing	26%	75%	0.73	-0.05	51%	88%	0.56	-0.42	60%	91%	0.43	0.37
Thompson Landing	56%	81%	0.57	-0.29	54%	83%	0.62	-0.95	N/A	N/A	N/A	N/A
Bird's Point	61%	89%	0.49	-0.68	47%	78%	0.66	-0.56	60%	84%	0.49	-0.32
Smithland	39%	65%	0.90	0.03	30%	59%	1.03	0.01	34%	56%	1.05	-0.99
Paducah	38%	66%	0.86	0.09	38%	56%	1.06	0.22	32%	61%	1.00	-0.46
Metropolis	N/A	N/A	N/A	N/A	N/A	N/A	N/A	N/A	34%	61%	0.97	0.31
Grand Chain	43%	64%	1.25	0.03	28%	42%	1.84	0.19	44%	69%	0.76	0.02
Cairo	58%	88%	0.52	-0.37	31%	56%	0.97	0.07	38%	71%	0.68	0
Hickman	30%	68%	0.81	-0.96	58%	87%	0.52	-0.32	60%	87%	0.48	-0.62
New Madrid	49%	84%	0.61	-0.83	58%	90%	0.50	-0.23	51%	84%	0.60	0.36
Tiptonville	53%	86%	0.57	-1.03	51%	83%	0.60	-0.46	60%	81%	0.55	1.01
Caruthersville	59%	91%	0.48	-1.1	65%	92%	0.47	-0.67	64%	90%	0.48	0.06
Osceola	59%	80%	0.61	-0.55	58%	81%	0.57	-0.11	34%	74%	0.76	0.14
Memphis	24%	54%	0.96	-0.55	50%	84%	0.59	-0.34	54%	78%	0.65	0.08
Helena	24%	54%	1.06	-0.57	41%	72%	0.81	-0.74	40%	69%	0.89	0.01
Montgomery Point	N/A	N/A	N/A	N/A	21%	38%	1.63	0.19	15%	35%	1.64	-0.64
Arkansas City	32%	60%	1.10	0.91	25%	51%	1.30	1.19	20%	44%	1.18	0.13

In Table 2, results are listed for locations along the Mississippi River from Chester, Illinois downstream to Arkansas City, Arkansas. The percentage of the availability of observed data for the 2002-2011 simulation period is listed. For each event and location, the accuracy of the model is described by listing the percent of calculated stages within 0.5 and 1.0 feet of the observed data and the average error. For the continuous simulation, the general tendency is for the model to more accurate at the upstream end than at the downstream end. Average errors are less than 2.0 feet and typically less than 1.0 feet.

Table 2 Memphis District Calibration Results – 2002-2011 Continuous Simulation

	2002 - 2011 Hourly Simulation			
Gage	Percentage of Observed Data Available	% within 0.5 ft	% within 1.0 ft	Average Error
Chester	100%	83%	98%	0.31
Red Rock	64%	69%	93%	0.47
GrandTower	89%	75%	95%	0.39
Moccasin Springs	69%	59%	84%	0.71
Cape Girardeau	100%	74%	95%	0.44
Thebes	97%	61%	89%	0.48
Commerce	60%	54%	80%	0.85
Price Landing	98%	51%	83%	0.57
Thompson Landing	74%	51%	77%	0.48
Bird's Point	97%	47%	75%	0.58
Smithland	98%	39%	64%	0.97
Paducah	100%	41%	68%	0.94
Metropolis	23%	66%	87%	0.32
Grand Chain	99%	39%	60%	1.24
Cairo	100%	36%	61%	0.77
Hickman	100%	56%	84%	0.58
New Madrid	100%	60%	89%	0.54
Tiptonville	98%	56%	85%	0.56
Caruthersville	100%	63%	91%	0.47
Osceola	96%	60%	86%	0.61
Memphis	78%	52%	81%	0.69
Helena	83%	41%	74%	0.87
Montgomery Point	72%	19%	34%	1.09
Arkansas City	83%	33%	61%	1.13

REFERENCES

Brunner, W., Gary. (January 2010), "HEC-RAS, River Analysis System Hydraulic Reference Manual."

Brunner, W., Gary. (January 2010), "HEC-RAS River Analysis System User's Manual Version 4.1."

Brunner, W., Gary. (June 2014), "Combined 1D and 2D Modeling with HEC-RAS."

RECENT AND HISTORICAL SEDIMENT LOADS IN THE LOWER MISSISSIPPI RIVER

Colin Thorne, University of Nottingham, Nottingham, UK, Colin.Thorne@nottingham.ac.uk; Kevin Knuuti, USACE Cold Regions Research and Engineering Laboratory, Hanover, NH, Kevin.Knuuti@usace.army.mil; Oliver Harmar, Environment Agency, Leeds, UK, Oliver.Harmer@environment-agency.gov.uk; Chester Watson, Biedenharn Group, Fort Collins, CO, Chester@ChesterWatson.com; Nick Clifford, Kings College, University of London, London, UK, Nicholas.Clifford@kcl.ac.uk; David Biedenharn, Biedenharn Group, Vicksburg, MS, Biedenharngroup@yahoo.com

Abstract: This paper reports the results of a study initiated by the USACE Engineer Research and Development Center (ERDC) and funded by the USACE New Orleans District that assembled available data on sediment loads in the Lower Mississippi River (LMR) and assessed its reliability and temporal variability. The database that resulted includes modern data collected by USACE New Orleans and Vicksburg Districts and historical measurements extending as far back as the mid-19th Century. In using the database, it is important to recognize variability and uncertainty in the records and a preliminary assessment was performed using the record for Tarbert Landing. The average annual measured load at Tarbert Landing between 1963 and 2005 was ~150 million tons, varying between 70 and 230 million tons. The median annual coarse suspended-sediment load over the same period was highly variable, varying from 5 to 80 million tons. The trend apparent in 19th and late-20th Century average loads suggests that, as widely perceived, there has been a long-term decline in the average annual suspended sediment load. This simple statement must, however, be treated with an appropriate degree of caution because: (i) robust statistical treatment of the data is hampered by gaps in the available records; (ii) data are sourced from multiple locations; (iii) there are high but unquantified uncertainties associated with early measurements of sediment load; and (iv) calculated measured loads underestimate the coarser fractions of the suspended load, and do not include sediment transported as bed load at all. Regression analyses for data from Tarbert Landing during the period 1959 to 2005 indicate that on-going, declining trends in suspended-sediment concentrations may have been partially offset by an increasing trend in water discharge, resulting in there being no significant trend in the annual sediment load. The database is available free and may be obtained on request from any of the authors, making the data easily accessible both in the USA and globally.

OVERVIEW

This paper reports the results of a project performed by Nottingham University, Halcrow (now part of CH2MHill) and the Biedenharn Group, in collaboration with the Army Corps of Engineers' Engineer Research and Development Center (ERDC), Vicksburg, Mississippi. The project assembled available data on sediment loads in the Lower Mississippi River, assessed its reliability, demonstrated its variability and performed a preliminary examination of historical trends.

The Lower Mississippi River extends from Cairo, Illinois to the Gulf of Mexico and currently transports approximately 150 million tons of sediment annually. Historically, the quantity and caliber of sediment derived from catchment erosion have been affected by changes in land-use and river management; increasing in the 19th and early-20th Centuries, before decreasing due to soil conservation and improved land management. The supply of sediment from tributaries is also believed to have decreased markedly as a result of river engineering and management. Specifically, the construction of large dams as part of the Mississippi River and Tributaries (MR&T) Project has trapped sediment that would otherwise have been supplied to the Mississippi, particularly by the Missouri River. Marked changes have also occurred in the extent of eroding banklines along the Mississippi and these must have reduced the input of sediment derived from that source. For example, during the last 3 decades, a sustained construction program of bank revetments and dikes has produced a stable planform alignment that has almost eliminated the input of sediment due to bank erosion. Finally, extensive dike fields installed in the Lower Mississippi River for navigation have trapped substantial quantities of sediment that might otherwise have been transferred downstream.

The Mississippi River Basin has been subjected to numerous alterations in the past century that have affected sediment loads in the river. The resulting decline in sediment loads in the lower river has been documented by several investigators. However, there is no consensus on the degree of reduction as a proportion of the previous 'natural' or undisturbed load, the time profile of that reduction or how current trends may change in the future. For example, based on the record for Tarbert Landing, Keown *et al.* (1981) suggest that the total annual suspended-

sediment load declined from 427 million tons prior to 1963 to 251 million tons by 1981. Robbins (1977) compared measured suspended-sediment records for the periods 1921 to 1931 and 1967 to 1974 and found that total suspended-sediment loads had decreased by roughly 40% since 1931 at both Arkansas City and Vicksburg. Extending the historical analysis further by using data from the Humphreys and Abbot (1861) report, Kesel (1988, 1989) suggested that total suspended-sediment loads in the Lower Mississippi River declined by approximately 80% in the period 1851 to 1982. These large reductions may not be unreasonable given the magnitude of the dams, length of revetments, and effectiveness of soil conservation programs in the basin.

Questions concerning past, present, and future temporal trends in the sediment load of the Lower Mississippi River are pertinent because the redistribution of available Lower Mississippi River sediment is vital to on-going efforts to reduce land loss and restore coastal marshes and wetlands in the Mississippi Delta. Cumulative land loss in Louisiana over a 50-yr period represents on the order of 80% of the coastal land loss in the United States. The Louisiana Coastal Area (LCA) was released by the United States Army Corps of Engineers (USACE) in 2004 and included consideration of approximately twenty-three diversions of water and sediment from the Mississippi River, with a total diversion capacity in the range of 150,000 to 200,000 cfs. This does not include the Third Delta diversion, with a proposed capacity of 120,000 to 240,000 cfs. The proposed LCA diversions pose significant management and engineering challenges and will require detailed modeling to support their design. The availability of reliable data on flows and associated sediment loads to support modeling would seem to be a prerequisite for meeting these challenges successfully.

Research to make available reliable sediment-transport data focused on compiling a database of measured suspended-sediment loads. Building this involved: (i) accessing recent measurements collected by the USACE New Orleans and Vicksburg Districts; and (ii) assembling available historical measurements extending as far back as the earliest available records, from the mid-19th Century.

Variability and historical trends in the sediment load are of great importance to plans to redistribute Lower Mississippi River sediments to restore coastal marshes and wetlands. Preliminary analysis focused on sediment load measurements at Tarbert Landing, which was selected because it is located in the upper part of the Mississippi Delta and, therefore, can be considered to be representative of the load available to the coastal region; and because it has the longest record of routine monitoring.

The average annual load at Tarbert Landing between 1963 and 2005 was approximately 150 million tons, varying between a minimum of 70 million tons and a maximum of 230 million tons. The median annual coarse load over the same period is highly variable, varying from 5 to 80 million tons.

Examination of historical measurements from the 19th and 20th Centuries suggests that there has been a long-term decline in the average annual load. This simple conclusion must, however, be treated with caution because:

(i) robust statistical treatment of the data is hampered by large gaps in the record;
(ii) data are sourced from multiple locations;
(iii) there are high but unquantified uncertainties associated with early measurements of sediment load; and
(iv) calculated measured loads will underestimate the coarser fractions of suspended load, and do not include sediment moving as bed load at all.

Linear regression analyses for data from Tarbert Landing during the period 1959 to 2005 indicate that on-going, declining trends in suspended-sediment concentrations may have been partially offset by an increasing trend in water discharge, resulting in there being no significant trend in the annual sediment load.

The analyses reported below are preliminary. It is proposed that further analyses be performed by researchers with Federal, state, and local agencies, as well as interested parties in the academic and private sectors. This study has facilitated further analyses by compiling a comprehensive database of available measured sediment-load data for the Lower Mississippi River and making it freely available and easily accessible. Copies of the database may be obtained from any of the authors of this paper.

Definition of sediment-transport terms: To avoid confusion in the interpretation and analysis of the database, the definitions of different types of sediment load referred to in this report are defined below.

Total Sediment Load: total mass of granular sediment transported by the river. This can be broken down by source, transport mechanism or measurement status.

Measured Load: portion of the total load measured by conventional suspended-load samplers. It includes a large proportion of the suspended load but excludes that portion of the suspended load moving very near the bed (that is, below the sample nozzle) and the entire bed load.

Unmeasured Load: portion of the total load that passes beneath the nozzle of a conventional suspended-load sampler, by near-bed suspension and as bed load.

Bed Load: component of total load made up of particles moving in frequent, successive contact with the bed. Transport occurs at or near the bed, with the submerged weight of particles supported by the bed. Bed load movement takes place by processes of rolling, sliding or saltation.

Suspended Load: component of the total load made up of sediment particles moving in continuous suspension within the water column. Transport occurs above the bed, with the submerged weight of particles supported by anisotropic turbulence within the body of the flowing water.

Bed-material Load: portion of the total load composed of grain sizes found in appreciable quantities in the stream bed. The bed-material load is the bed load plus the portion of the suspended load composed of particles of a size that are found in significant quantity in the bed (often taken to be coarser than D_{10} of the bed material).

Wash Load: portion of the total load composed of grain sizes finer than those found in appreciable quantities in the stream bed (often taken to be finer than D_{10} of the bed material).

Coarse Load: portion of the total load composed of grains coarser than 0.063 mm. The coarse load of the Mississippi River consists almost entirely of sand finer than 2 mm.

Fine Load: portion of the total load composed of grains finer than 0.063 mm. The fine load of the Mississippi River consists of silt and clay.

DATA ANALYSIS

Data sources: The project built on a previous database of suspended-sediment and bed-material measurements compiled by Thorne *et al*. (2001), which assembled sediment measurements made in the Lower Mississippi, Atchafalaya, Red, and Old Rivers since the 1970s. This project extended the existing database by compiling all available historic measurements made within the USACE Vicksburg District and New Orleans District (*i.e.* downstream from Arkansas City). Data were compiled from a variety of sources including: USACE Vicksburg District, USACE New Orleans District, US Geological Survey and a wide range of historical records by multiple organizations, extending back to the 1850s.

Data were obtained in a variety of formats and with differing amounts and types of post-collection processing of the original field measurements. The project report (which is available from the US Army Engineer Research and Development Center or the authors) provides a summary of post-1930 data sets including the location of sampling, the organization undertaking data collection, the time period covered, and a brief description of information contained within each data set. Data include measurements of some, or all, of the following variables: suspended-sediment concentration and particle size, discharge, suspended-sediment discharge, and flow velocity. Available metadata information describing the types of sampling, sampling strategy, and laboratory procedures are provided in the project report. The sediment sampling stations from which sediment data were collected and included within the database are listed in Table 1.

Seasonal variability: Seasonal variability in measured sediment concentrations and loads was investigated using the record for Tarbert Landing between 1963 and 2005. When analyzing variations in sediment concentration and

load, it is important to consider variations in discharge; seasonal flow exceedance curves for Tarbert Landing are shown in Figure 1. As a very general rule, during periods of peak flow in the spring, discharge is approximately double that during periods of peak flow in the fall. Discharge is, however, highly variable in any season, with 5% exceedance flows being typically three times higher than 95% exceedance flows.

Table 1 Sediment gauging stations included in the database.

River	Station Name	River Mile (RM) (above Head of Passes, LA)
Mississippi River	St. Louis, MO	179.8*
	Chester, IL	110*
	Thebes, IL	43.8*
	Memphis, TN	735
	Arkansas City, AK	554
	Lake Providence	487
	Vicksburg, MS	436
	Natchez, MS	363
	Coochie, LA	317
	Tarbert Landing, LA	306
	Red River Landing	302
	St. Francisville, LA	266
	Baton Rouge	228
	Donaldsville	175
	Carollton	103
	Belle Chasse	76
	Venice	11
	South Pass	0
Red River	Alexandria, LA	105†
	Madame Lee Revetment, LA	35†
Atchafalaya River	Simmesport	6‡
	Melville	30‡
	Morgan City	115‡
Old River	Knox Landing	312
	Low Sill Outflow	314

*Above the confluence of the Mississippi and Ohio Rivers
†Above the confluence of Red and Atchafalaya Rivers
‡Below the confluence of Red and Atchafalaya Rivers

Variations in coarse and fine sediment concentrations between 1963 and 2005 are shown using box and whisker plots in 2(a) and 2(b), respectively. In these plots, the 25th and 75th percentiles define the box, the minimum and maximum values define the whiskers, and the monthly median is indicated by the central bar. Concentrations of coarse suspended-sediment vary from 350 to less than 50 ppm, being both higher and more highly variable during winter and spring (Figure 2(a)).

Fine suspended-sediment concentrations range between 150 and 250 ppm and though they are less variable seasonally, intra-month variability can be extreme: for example concentrations measured in April varied from around 60 to close to 1,000 ppm. 3(a) and 3(b) illustrate variation in measured coarse and fine suspended-sediment loads at Tarbert Landing, respectively. Monthly loads have been calculated by summing daily loads estimated using the concentration interpolation method.

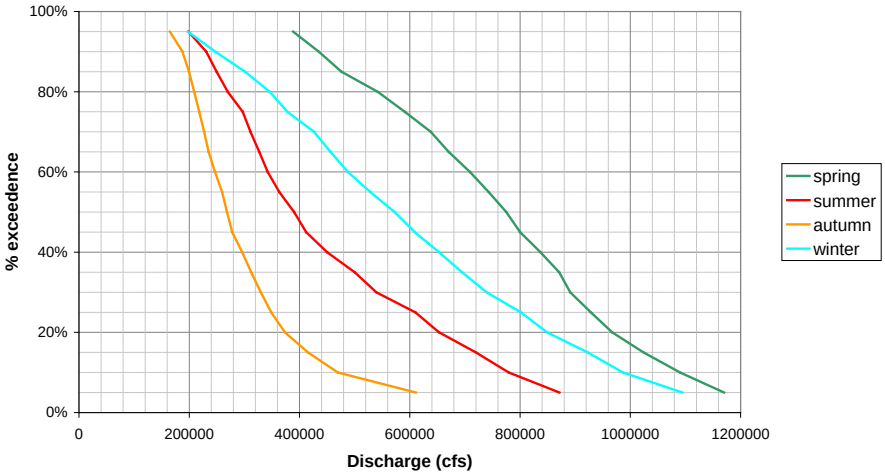

Figure 1 Seasonal flow-duration curves at Tarbert Landing (1963 to 2005).

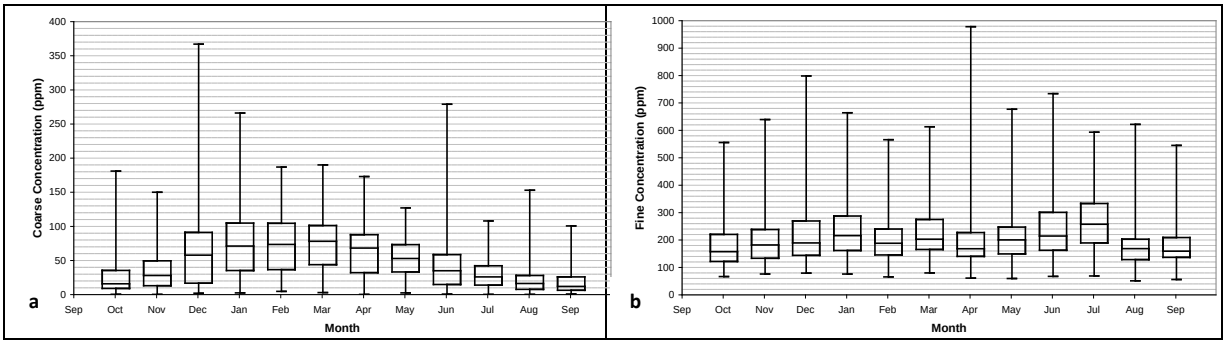

Figure 2 (a) Coarse suspended-sediment concentrations at Tarbert Landing (1963 to 2005).
(b) Fine suspended-sediment concentrations at Tarbert Landing (1963 to 2005).

High seasonal variability in monthly coarse suspended-sediment loads is evident in 3(a). For example, the median coarse load during Spring is approximately fifteen times that in the Fall. The same pattern is present for monthly total loads (Figure 3(b)), although the range of variation is smaller. Intra-month variability is also greater during the spring, particularly for the coarse load.

To further investigate the seasonal variations in the grade of sediment in transport, the cross-section-averaged D_{50} (median) and D_{90} (90th percentile) grain sizes were calculated and these are plotted in
Figure and 4(b). It should be noted that size gradations are not available for the clay fraction (sediment finer than 0.0039 mm).

The median (D_{50}) grain size at Tarbert Landing is overwhelmingly silt-sized though it does coarsen slightly during the winter and spring. The D_{90} is generally coarse silt during summer and fall, but coarsens to very fine sand during winter and spring, when discharges are higher. This indicates that suspended-sediment in the Lower Mississippi River is composed predominately of sediment smaller than fine sand, which differentiates it from the bed material, which is typically coarser than fine sand. As the bulk of the measured suspended load comprises sediment that is finer than that found in appreciable quantities in the bed, the load of the river can be said to be dominated by wash load.

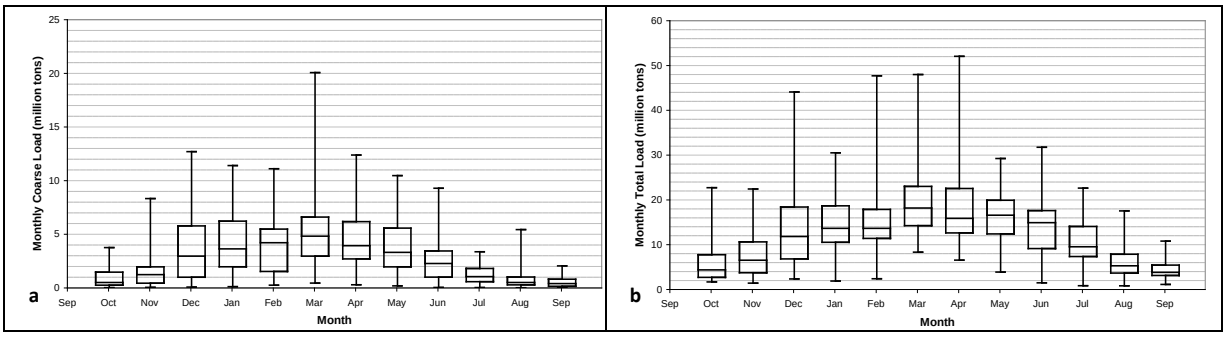

Figure 3 (a) Variation in monthly coarse suspended-sediment loads at Tarbert Landing (1963 to 2005). (b) Variation in monthly total suspended-sediment loads at Tarbert Landing (1963 to 2005).

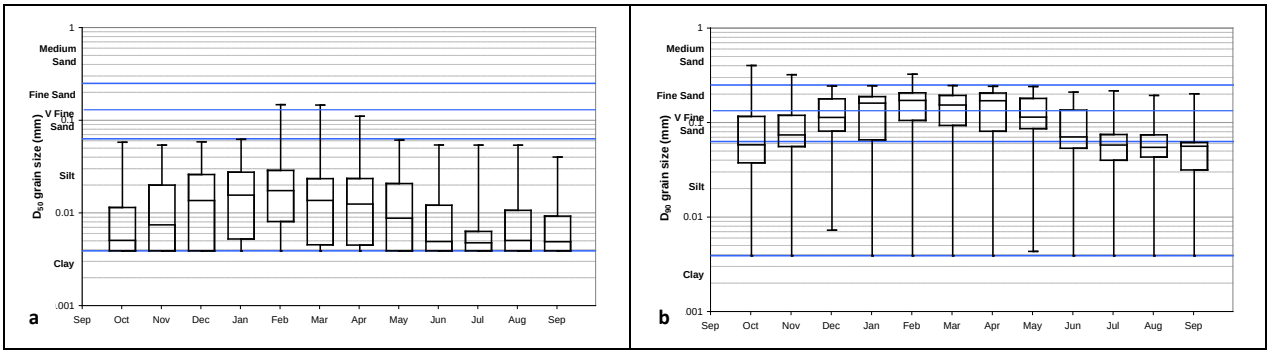

Figure 4 (a) Monthly variation in D_{50} at Tarbert Landing (1963 to 2005). (b) Monthly variation in D_{90} at Tarbert Landing (1963 to 2005).

Trend Analysis:

Historical trends: Historical trends in sediment load were investigated by plotting calculated annual loads for Tarbert Landing alongside historical loads based on older records that either reported annual loads, or included measurements from which annual loads could be calculated (Table 2). The results are plotted in Figures 5 and 6, which support the existence of a marked decline in sediment loads. However, in estimating how much loads and concentrations have decreased, caution must be exercised for four reasons. First, pre-1963 data were obtained from four different locations (Carollton, Baton Rouge, Red River Landing, and South Pass) and loads estimated from records at different gauging stations can vary considerably. Second, there are large gaps in the data during the first half of the 20th Century. Third, comparisons of loads between the 19th and late-20th centuries are limited by the high uncertainty concerning the early estimates of annual load. While the early data provide valuable insights, they are not sufficient to support statistical comparison to later data. Fourth, annual loads are based on measured suspended-sediment loads that almost certainly under-represent the coarser fraction of the suspended-sediment load, and do not account for bed load at all.

Recent trends: To assess whether loads in the Lower Mississippi River are continuing to decrease, a preliminary analysis of the Tarbert Landing data was conducted and Figures 7, 8 and 9 illustrate recent trends in annual sediment concentrations, suspended loads, and water discharges between 1959 and 2005. While scatter is present in data representing fine and total concentrations in Figure 7, P-values for the regression lines fitted to these data indicate downward trends that are statistically significant. Conversely, there is no significant trend in concentrations of coarse sediment. With respect to the annual sediment loads plotted in Figure 8, a slight, but statistically insignificant increasing trend is apparent in the coarse sediment loads. Fine and total loads appear to have slight downward trends, but these are also not statistically significant. Thus, while there may have been a slight decline in fine and total sediment concentrations between 1959 and 2005, the change in annual load is statistically insignificant. Lack of significant trends in sediment loads is unexpected given the decreasing trends identified in fine and total sediment concentrations. This apparent paradox may be explained at least in part by a slight, though statistically insignificant,

increasing trend in annual water discharges in Figure 9. The decline in sediment concentrations may have been partially offset by increasing water discharges, resulting in there being no significant change in the annual sediment loads.

It is important to note that this analysis is preliminary and it is recommended that full assessment be undertaken to investigate the complex behavior represented in the historical and recent records (*e.g.*, temporal periodicity, periods of no change, periods of slow change, periods of short-term, rapid change) employing the appropriate statistical techniques in time-series and trend analyses.

Table 2 Sediment records used in assessing historical trends.

Dates	Sampling Station	Source Organization	Available Data Types	Key Uncertainties
1964-2005	Tarbert Landing, RM 306	USACE New Orleans District	Coarse, fine, and total suspended-sediment concentrations at 2- to 4-week intervals	Frequent changes in sampling strategy, especially in period 1990 to 1994.
1959-1963	Red River Landing, RM 302	USACE New Orleans District, obtained from Old River Hydroelectric Study archives	Coarse, fine, and total suspended-sediment concentrations at 2- to 4-week intervals	This record is labeled as Tarbert Landing although measurements in the period 1959 to 1963 were taken 4 mi downstream at Red River Landing. Discharge measurements from the Tarbert Landing record have been used in sediment-load calculations.
1956-1958	Baton Rouge, RM 230	USACE New Orleans District, obtained from Old River Hydroelectric Study archives	Daily records for coarse, fine, and total concentrations	Unknown how daily record has been calculated. Discharge from Tarbert Landing record has been used in sediment-load calculations.
1949-1969	Baton Rouge, Red River Landing, and Tarbert Landing	USACE New Orleans District, reported in Old River Hydroelectric Study	Annual loads	Only available as calculated annual loads. Therefore, was not possible to estimate uncertainty from sampling strategy and annual load calculation.
1931	Red River Landing, RM 302	USACE, obtained from Paper U (1931)	Discharge and average concentration for surface, mid and near bottom samples, taken every 2 to 7 days over a 6-mo period	Annual load calculated by using a rating-curve approach to extend the 6 mo of data. Indicative error bars have been used in Figures 8 and 9 to show the high uncertainties associated with this approach.
1879-1893	South Pass, below Head of Passes	Quinn Survey, reported by Kesel (1995)	Annual loads	Large indicative error arrows have been used in Figures 8 and 9 to indicate high uncertainty in using this data to represent sediment loads in the main Lower Mississippi River.
1851-1853	Carollton, RM 103	Forshey – obtained from USACE Paper H (Vogel, 1930)	Approximately weekly measurements of discharge and average total concentration over a 2-yr period	In Figures 8 and 9, arrows have been used to indicate possible additional uncertainty due to location transfer.

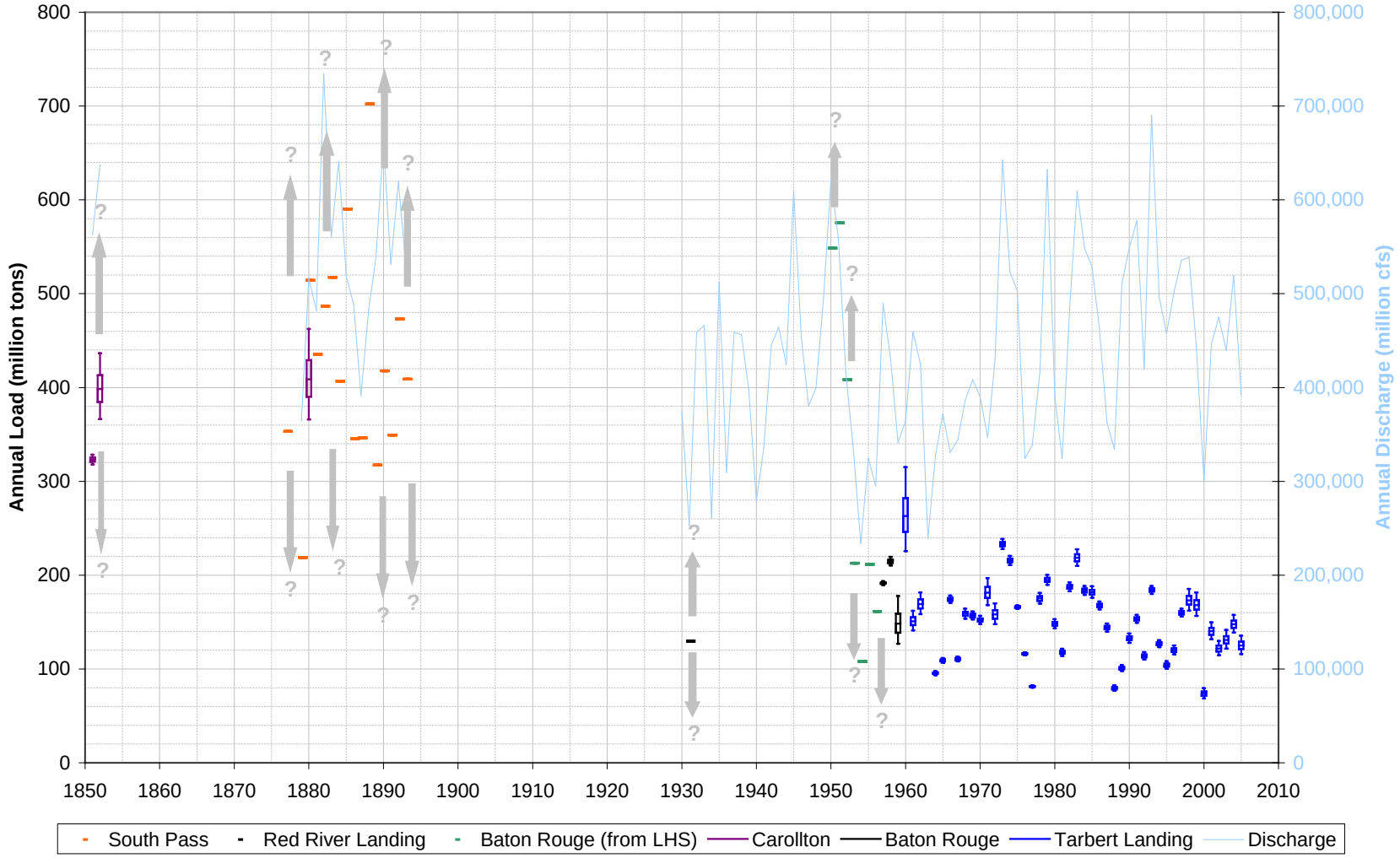

Figure 5 Long-term changes in the annual sediment load on the Mississippi River from multiple stations.

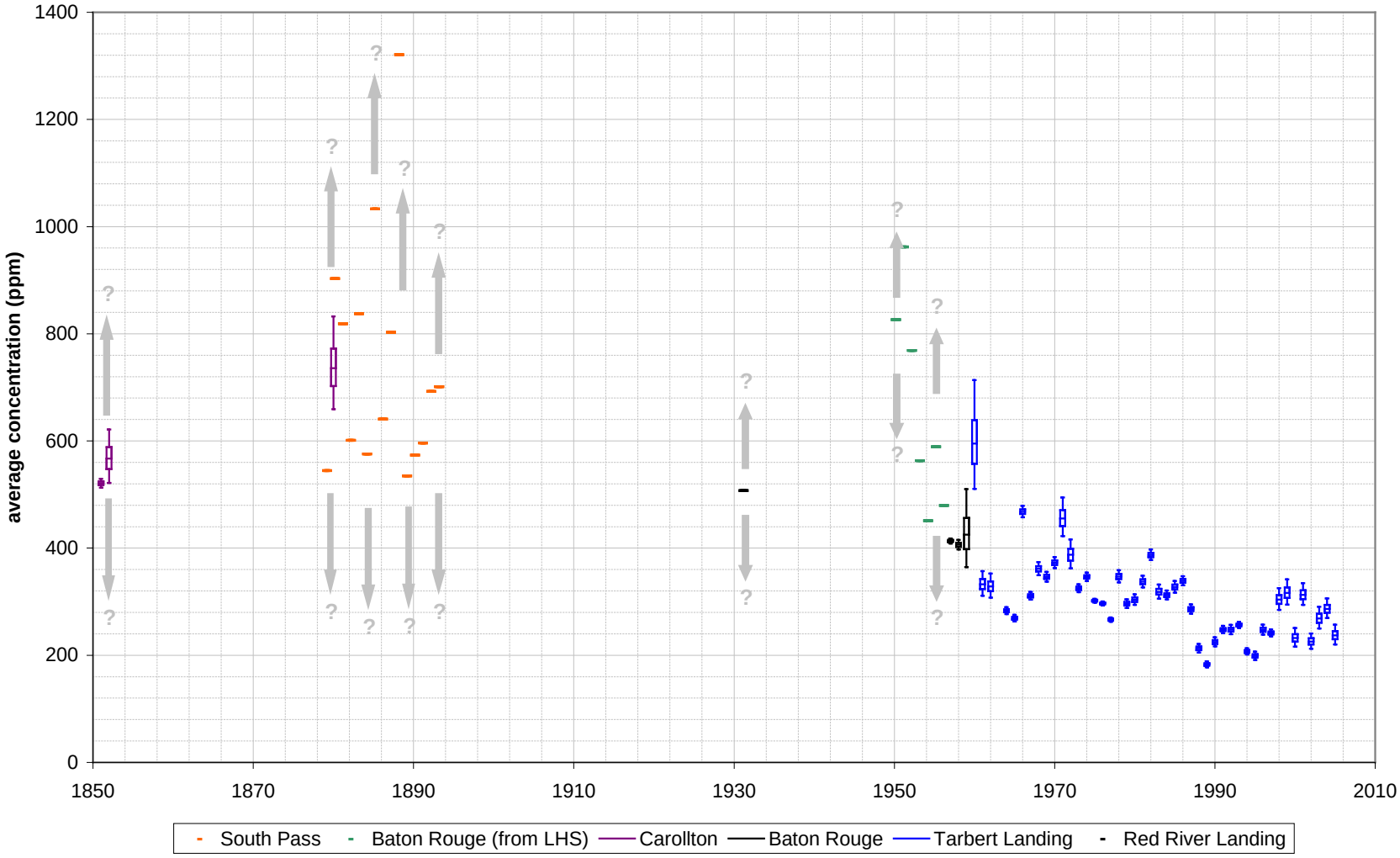

Figure 6 Long-term changes in annual average suspended-sediment concentration in the Mississippi River from multiple stations.

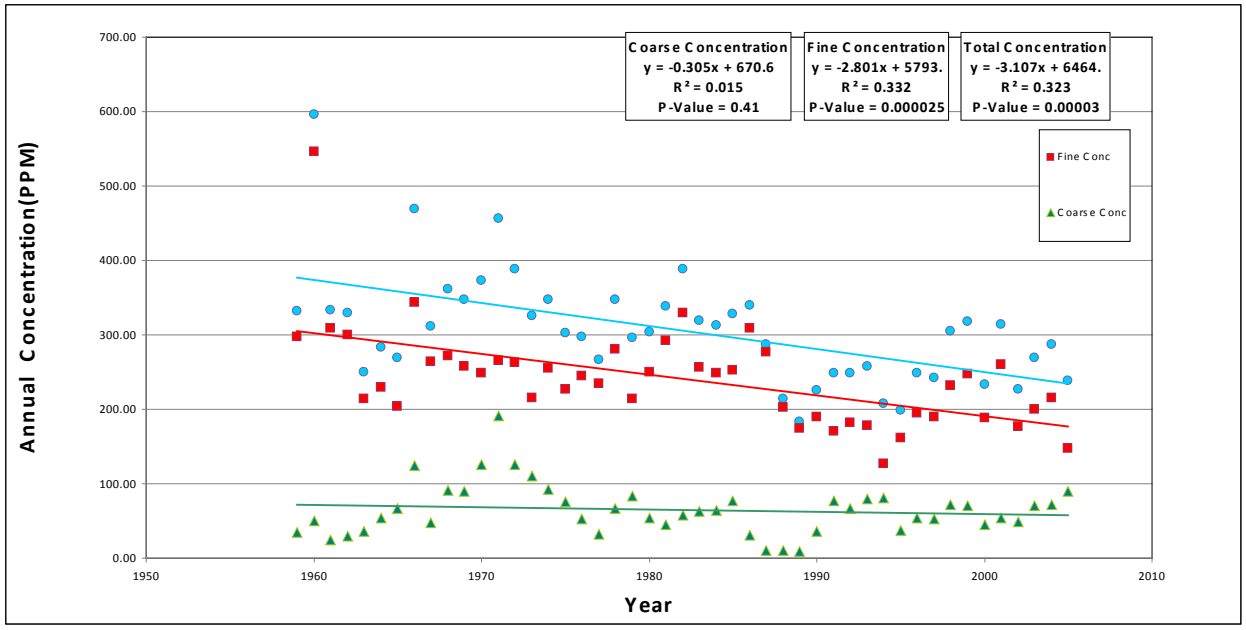

Figure 7 Tarbert Landing sediment concentrations, 1959 to 2005.

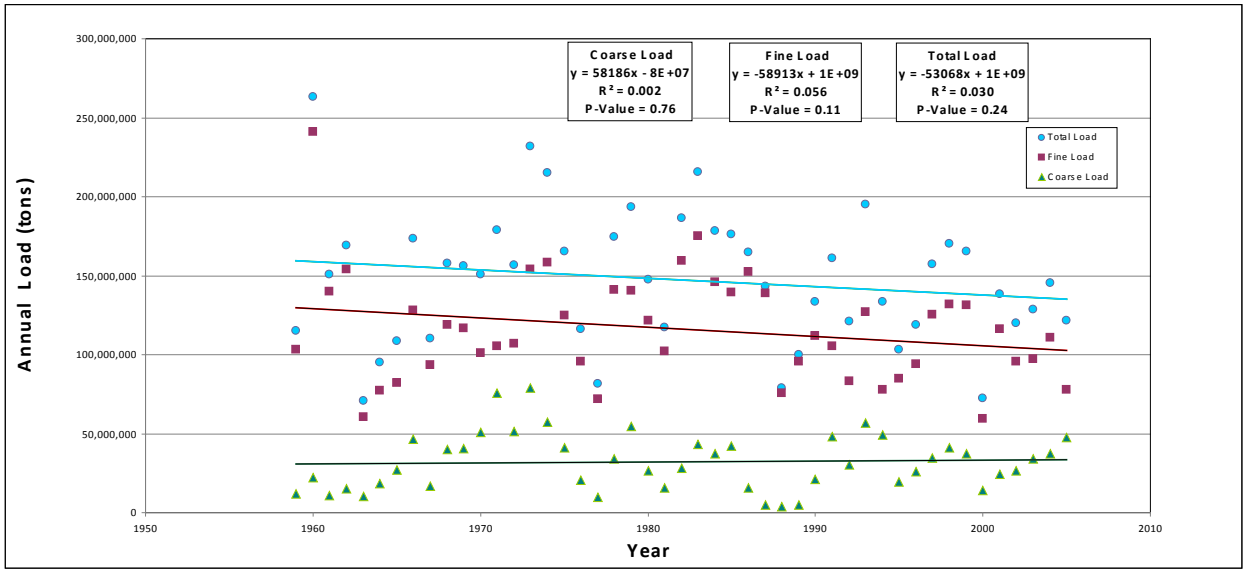

Figure 8 Tarbert Landing sediment loads, 1959 to 2005.

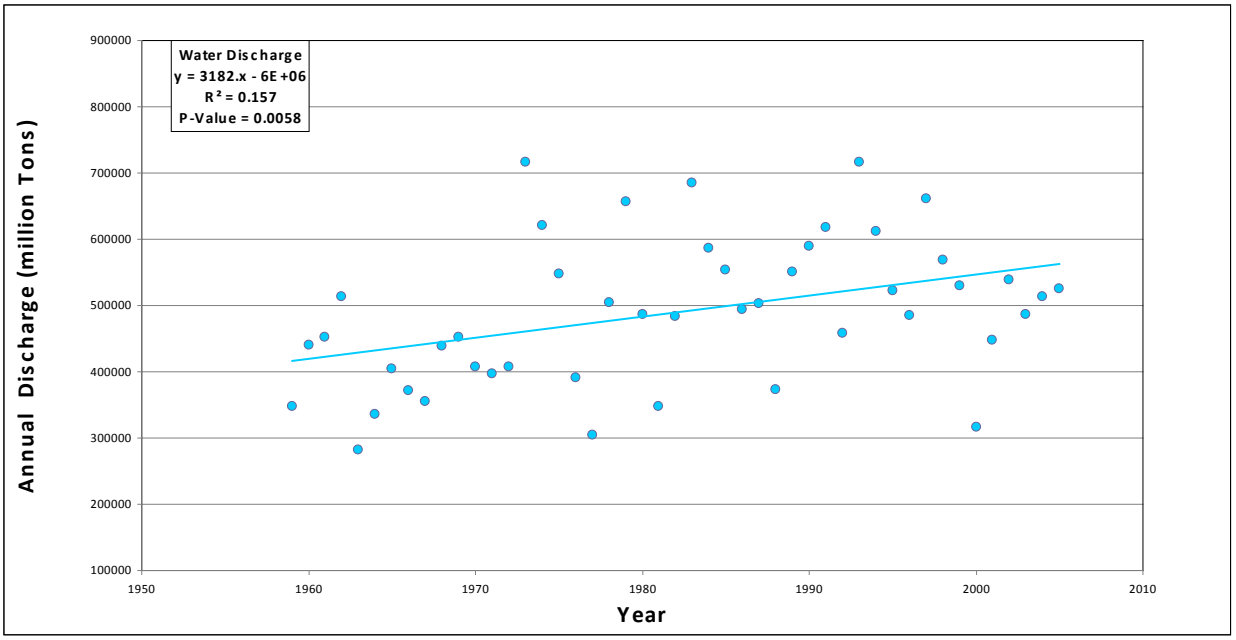

Figure 9 Annual water discharges at Tarbert Landing, 1959 to 2005.

ACKNOWLDEGEMENTS

The database described in this paper was compiled by the authors through a project funded by the U.S. Army Corps of Engineers New Orleans District, under contract number 1106-EN-01, which was awarded to the University of Nottingham, UK and facilitated by the U.S. Army's International Research Office in London, England. In compiling the database created in this project, considerable assistance was provided by the USACE ERDC, USACE Vicksburg District, USACE New Orleans District, USACE Mississippi Valley Division, and the United States Geological Survey (USGS). The authors thank these organizations for their collaboration and cooperation.

REFERENCES

Humphreys, A. A. and Abbot, H. L. (1876). Report on the physics and hydraulics of the Mississippi River. Professional Paper, Government Printing Office, Washington, DC.

Keown, M. P., Dardeau, E. A., and Causey, E. M. (1981). Characterization of the suspended-sediment regime and bed-material gradation of the Mississippi River Basin. United States Army Corps of Engineers Potamology Program (P-1) Report, Vicksburg, MS, 44 pp.

Kesel, R. H. (1988). The decline in the suspended load of the Lower Mississippi River and its influence on adjacent wetlands. Environmental Geology and Water Sciences, 11 (3), 271-281.

Kesel, R. H. (1989). The role of the Mississippi River in wetland loss in southeastern Louisiana, USA. Environmental Geology and Water Sciences, 13 (3), 183-193.

Kesel, R. H. (1995). Historical sediment discharge trends for the lower Mississippi River.

Robbins, L. G. (1977). Suspended sediment and bed material studies on the Lower Mississippi River. Potamology Investigations, Report 300-1, United States Army Corps of Engineers Vicksburg District, Vicksburg, MS.

Thorne, C. R., Harmar, O. P., and Wallerstein, N. (2001). Morphodynamics of the Lower Mississippi River. United States Army Research, Development and Standardisation Group-U.K., London.

USACE. (2004). Louisiana Coastal Area (LCA), Louisiana – Ecosystem Restoration Study. Volume 1: LCA Study – Main Report, United States Army Corps of Engineers, New Orleans District, November, 34p.

USACE. (1931). Sediment investigations on the lower Mississippi River and its tributaries 1930-31. Paper U of the United States Army Engineer Waterways Experiment Station.

Vogel, H.D. (1930). Sediment investigations on the Lower Mississippi River and its tributaries prior to 1930. Paper H of the United States Army Engineer Waterways Experiment Station.

SAINT-VENANT MODELING FOR LARGE RIVER BASINS – CHALLENGES AND DATA NEEDS

Ben R. Hodges, Assoc. Professor, Department of Civil, Architectural, and Environmental Engineering, University of Texas at Austin, hodges@utexas.edu; Frank Liu, Research Scientist, IBM Research Austin, frankliu@us.ibm.com; Alfredo Hijar, Graduate Student, University of Texas at Austin, ahijar@utexas.edu

INTRODUCTION

River networks in continental-scale river basins – e.g. the $O(10^6)$ river miles in the Mississippi basin – to date have used only with reduced-physics models. These models cannot represent the momentum dynamics and water depth evolution available with the full Saint- Venant (SV) equations derived by cross-section integration of the Navier-Stokes equations. Momentum and water depth are valuable for mechanistic sediment modeling, and hence their neglect in reduced-physics models is a severe limitation. Reduced-physics models are generally justified with the argument that SV models are too computationally expensive for large networks (Hodges, 2013). However, recent advances in computational methods have made SV equations a practical option (Hodges and Liu, 2014; Liu and Hodges, 2014), but challenges remain in developing large-scale applications. In this presentation we discuss the problems, challenges, and some possible solutions for creating data sets combining surveyed and estimated channel geometry over large river basins. The key open question is with regard to data requirements: *what is the level of cross-sectional detail that is actually needed for SV solutions, vice the data detail that is typically obtained in surveys?* Ideas from hydraulic geometry combined with historical stage-discharge data can be used to develop estimated cross-sectional data, which are useful where surveyed data are unavailable. Although it is likely that for the foreseeable future we will not have comprehensive survey data for entire river basins, we can use available data to estimate geometry for dynamic equation solutions rather than a priori reducing the physical processes represented.

SPRNT MODEL

The Simulation Program for River Networks (SPRNT) was developed by Liu and Hodges (2014) to demonstrate that the SV equations can be solved efficiently for large river networks without linearization. This initial work showed that $O(10^5)$ computational elements in a river network could be solved for an unsteady SV solution $330\times$ faster than real time using an ordinary desktop workstation without any parallel processing. As is the case for any SV solution method, SPRNT input data includes: (i) the river network topology, (ii) the channel slope (S_0) of each element in the network, (iii) representative channel cross-sections for each element, and (iv) the channel roughness. SPRNT uses the conventional Manning's n and a SV formulation with flow rate (Q), and cross-sectional area (A) as solution variables:

$$\frac{\partial Q}{\partial t}+\frac{\partial}{\partial x}\left(\frac{Q^2}{A}\right)+gA\frac{\partial h}{\partial x}=gA\left(S_0-S_f\right) \tag{1}$$

$$\frac{\partial A}{\partial t} + \frac{\partial Q}{\partial x} + q_\ell = 0 \tag{2}$$

where S_f is the friction slope and q_ℓ is the lateral flux from the landscape. The local water depth (h) is an auxiliary function that depends on the cross-section geometry i.e. $h = h(A)$. Using the Chezy-Manning equation for S_f allows one to write $AS_f = n^2Q^2F$, where $F = P^{4/3}A^{-7/3}$ is an equivalent friction geometry with P as the wetted perimeter of the cross-section. Note that $F^{-1} = AR_h^{4/3}$, where R_h is the traditional hydraulic radius that appears in the Chezy-Manning equation:

$$Q = \frac{1}{n} AR_h^{2/3} S_f^{1/2} \tag{3}$$

Thus F is simply a convenient approach to wrapping the cross-sectional dimensional relationships of Chezy-Manning into a single term. In SPRNT the full nonlinear discrete equations are solved with an iterative Newton-Raphson method using acceleration methods that have previously been applied in microprocessor design.

DATA NEEDS FOR SAINT-VENANT MODELING

The critical data needed for SPRNT are not detailed x:y surveys of every cross-section, but instead for auxiliary functions for $h = h(A)$ and $F = F(A)$ that are abstractions of the cross section. Obviously, given discrete x:y survey data it is straightforward to compute discrete h:A and F:A for each element. However, in the absence of comprehensive surveys: how can we approximate the auxiliary functions from other data? As a further issue, the discrete h:A and F:A functions for a survey will generally have significant discontinuities such that naive application of raw data provides jacobians for the Newton-Raphson solution in SPRNT that are insufficiently smooth. That is, the Saint-Venant partial differential equations can only approximate a smooth system, which a priori requires $h(A)$ and $F(A)$ be smooth functions, which in turn requires $A(h)$ and $\partial A / dh$ must be smooth. Turning this idea on its head, if we have some approximation of $A(h)$ that is smooth, we can easily obtain a smooth wetted perimeter $P(h)$ that is consistent with $A(h)$, and hence compute $F(A)$ and $h(A)$ functions for a SV solution. Thus, the critical question for SV modeling is not the precise, detailed survey shape of the cross-section, but what is a smooth approximation of $A(h)$ that can be estimated from available data? We are investigating several avenues for this approximation, which will be discussed in the presentation.

REFERENCES

Hodges, B.R. (2013). Challenges in continental river dynamics. *Environmental Modelling & Software*, 50:16-20.

Hodges, B.R., and Liu, F. (2014). River and electrical networks: Crossing disciplines in modeling and simulation. *Foundations and Trends in Electronic Design Automation,* 8(1):1-116.

Liu, F. and Hodges, B.R. (2014). Applying microprocessor analysis methods to river network modeling. *Environmental Modelling & Software*, 52:234:252.

SYNTHETIC BATHYMETRY METHOD DEVELOPMENT, VALIDATION AND APPLICATION TO FIVE PACIFIC NORTHWEST RIVERS

Zachary P. Corum, PE, Hydraulic Engineer, USACE Seattle District, Seattle, WA, zachary.p.corum@usace.army.mil; Travis D. Ball, Hydraulic Engineer, PE, CFM, USACE Seattle District, Seattle, WA travis.d.ball@usace.army.mil; Matthew J. Hubbard, Engineer 1, Brown and Caldwell, Tacoma, WA, mhubbard@brwncald.com

Abstract: This paper presents a simple, robust, and relatively efficient workflow to create and "burn in" high resolution synthetic river bathymetry data into existing LiDAR datasets. The Synthetic Bathymetry (SB) method uses widely available GIS and hydraulic modeling techniques to create physically-based synthetic bed elevation data without introducing significant error in computed water surface elevations and average channel velocities, under conditions where discharge at time of DEM data acquisition is known. The SB method was applied and validated on a small, steep, braided cobble bed river, large and small cobble bed wandering rivers with wide floodplains, and a small, entrenched, low gradient river with tidal influence all in Washington State – as well as a very large, flat gradient reservoir reach in Montana. As a test of the validity of the approach the results of models based on SB data were compared against models based on traditional survey methods, and against models based on LiDAR alone. For low (base) flows, bankfull (2-year) and 100-year flood flows the differences in computed water surface elevations, inundation area, and velocity were small (MAE in water surface elevation of less than 1 foot for all 5 study reaches under low flow, and less than 1 foot for all but the reservoir reach under 2 year and 100-year flood flows). At lesser flood flows to bankfull flows, the MAE in stage is modestly higher, as compared with the baseline models. For the reservoir reach, the model results were generally poor during 100-year flood flows as compared with the other rivers, however the error reduction in water surface elevation (from use of an unadjusted DEM alone) was nearly 30 feet. The good to excellent agreement of the SB models to the baseline in four of the five study reaches is attributed to the ability of the SB method to create the flow area needed to convey flood flows at comparable stages and velocities as survey based models. The SB method holds promise for speeding up and reducing the cost of 1-D and 2-D hydraulic modeling efforts where multiple decimal place accuracy is not required. The SB method can significantly reduce error in cases where only a DEM is available, and reduce the need for tedious, subjective terrain data manipulation commonly associated with interpolation between widely spaced cross sections. The SB method could improve the quality of models in cases where site conditions (unstable channel, remoteness, turbidity, safety) prevent bathymetric data collection but otherwise allow for above-water aerial survey techniques (photogrammetry, satellite, LiDAR, Structure from Motion). Other potential uses include estimation of bed elevations to track sediment movement under rapidly changing conditions, such as below a dam removal.

INTRODUCTION

This paper presents a relatively simple technique for creating physically based riverine bathymetric data from digital elevation models (DEMs) and discharge data using GIS and the US Army Corps of Engineers software HEC-RAS (USACE 2014). For the purposes of this paper DEM pertains to topographic datasets derived from photogrammetry or Light Detection And Ranging (LiDAR) techniques. The method described in this paper results in a “burned in” or “eroded” (synthetic) river bottom within a digital terrain model that otherwise lacks bathymetric data. In shallow rivers the method has shown promise at preserving riffle crest elevations, side channels, and large in-channel roughness elements. The technique can be used for any case where flow is nominally unidirectional, confined within banks, and is either known or can be estimated at time of topographic survey. Virtually any 1-D or 2-D modeling package that allows for computation of inundation maps can use this method.

The method, termed herein as the synthetic bathymetry (SB) method, has several potential applications in the fields of hydrology, hydraulics and fluvial geomorphology and is best suited for determining reasonably accurate water surface elevations in situations where data is scarce and/or where projects do not require stringent accuracy. The method also allows for filling in gaps between surveyed cross sections without interpolation, which helps preserve the near bank, and mid channel topography (large roughness elements) that may be important for 2-dimensional model studies. It also allows for a physically based estimate of riverbed elevations below the water surface which can be valuable for estimating long term geomorphic change over large areas.

This paper investigates the relative accuracy of one dimensional hydraulic models constructed from surveyed cross sections, from DEM data alone, and from DEM data blended with SB data. Published flood insurance study data or recently calibrated survey-grade hydraulic models are used as benchmarks to test the validity of the results using SB data.

BACKGROUND

LiDAR data sets are becoming widespread and have quickly become some of the most valuable data for hydrologic, hydraulic and geomorphic studies. The LiDAR data is usually extracted and processed for inclusion in a numerical model of hydrologic processes. Due to technical limitations many LiDAR datasets lack elevation information below the water surface (bathymetry), requiring collection of channel data with other methods. Alternately, models are used without this data due to cost constraints, reducing the quality of the results. As survey and post processing technologies improve, terrestrial floodplain topography can be acquired for large study areas in the time it takes to fly along the river in a helicopter or airplane. Despite their high resolution, most available LiDAR data sets used to create DEMs do not include bathymetric LiDAR data (now possible with certain sensors and shallow, clear water conditions – see River Bathymetry Tool Kit (McKean et al, 2009)). Other recent innovative methods to remotely survey the channel bottom, which also require clear water conditions, include correlation of aerial imagery based DEMs to physical measurements of depth (Javernick et al, 2014). Currently, several technologies are available to acquire high resolution topographic and bathymetric data to support floodplain studies (Bangen et al, 2014). Many of these technologies are complex and costly to use. Considerable effort and skill are necessary to check, verify, and blend available data to create a seamless riverine terrain model. Also, due to the high equipment costs associated with some technologies and large data sets created by modern equipment, considerable effort and expense are necessary to acquire, maintain, and post-process these data. But as two dimensional modeling moves to the forefront of hydraulic engineering practice, the demands for bathymetric data will continue to increase.

Thus, the current state of the practice is one where engineers and scientists have a plethora of terrestrial data sets to choose from, from which any number of cross sections can be created. Below-water bathymetric data, however, remain sparse and difficult to acquire in many settings. Use of interpolated or "best guess" bathymetry in hydraulic models introduces unknown errors that add uncertainty and risk to project findings and decisions resulting from the modeling. Fortunately, many of the issues resulting from missing bathymetry can be partly overcome by applying first principles and combining off-the-shelf GIS and hydraulic modeling software. This paper presents and validates one such method, termed the Synthetic Bathymetry (SB) method that allows for automatic manipulation of terrain data to "burn in" SB data under the LiDAR water surface to address circumstances where underwater survey data is lacking but improved model accuracy is desired.

SYNTHETIC BATHYMETRY METHODOLOGY

Commonly used open channel flow numerical models allow for computation of fluid depth based on first principles of open channel flow (conservation of energy, continuity of flow, conservation of momentum). If a numerical backwater model is used, such as HEC-RAS (USACE 2014), to perform a standard step backwater calculation, the energy losses due to cumulative expansion, contraction, and roughness losses can be accounted for in estimating the local variation in hydraulic conditions, such as velocity, depth, and stage. As with most open channel flow models, the quality of the hydraulic output depends on the quality of the input, namely survey data and how well the modeler captures the characteristics of the terrain.

For purposes of floodplain modeling and mapping, the goal is typically to first compute the losses in energy (expressed as fluid head) using standard step backwater computations, then to map the resulting water surface elevations across the terrain data used to construct the model. All major changes in cross section, planform, slope, and roughness need to be represented in the model to yield good estimates of local and cumulative energy losses. If a river model is constructed accounting for local changes in slope, width and roughness, then the depths and velocities can still be computed even if the bed elevations are not known with high accuracy. In this situation the accuracy of the results will be biased by the initial error in the bed elevations. Recognizing that LiDAR provides an extensive and detailed record of the water elevation at time of survey (calibration data), we can write the following equation for the LiDAR surveyed water surface elevation (WSE_{Survey}) resulting from a hydraulic simulation of the flow elevation at time of the LiDAR flight:

$$\mathbf{WSE}_{\mathbf{Survey}} = \mathbf{WSE}_{\mathbf{initial}} - \mathbf{E}_{\mathbf{initial}} \quad (1)$$

Where E represents error, the difference between the computed elevation ($WSE_{initial}$).and the "true" elevation and If the water level in the LiDAR is treated as terra firma in the model cross sections (as a false river bottom), all flow will then occur above the "correct" elevation. Thus the depth of flow above the initial "false bed" is the error in equation 1.

$$\mathbf{E}_{\mathbf{initial}} = \mathbf{WSE}_{\mathbf{initial}} - \mathbf{Z}_{\mathbf{false\ bed}} = \mathbf{Y}_{\mathbf{initial}} \quad (2)$$

Where:

$\mathbf{Z}_{\mathbf{false\ bed}}$ = **Bare earth LiDAR elev** = $\mathbf{WSE}_{\mathbf{Survey}}$

$\mathbf{Y}_{\mathbf{initial}}$ = **initially computed flow depth (above raw DEM)**

Expressed spatially, across a raster grid, at all locations within a raster cell,

$$\mathbf{E}_{\mathbf{initial\ (ij)}} = \mathbf{Y}_{\mathbf{initial\ (ij)}} \quad (3)$$

Where i and j denotes the spatial location of a given raster cell of a given dimension. It is then proposed that,

$$\mathbf{Z}_{\mathbf{SB\ (ij)}} = \mathbf{Z}_{\mathbf{false\ bed\ (ij)}} - \mathbf{Y}_{\mathbf{initial\ (ij)}} \quad (4)$$

Where $Z_{SB\ (ij)}$ represents a synthetic river bottom elevation at a given raster cell. By subtracting the initially computed flow depth ($Y_{initial\ (ij)}$) from the false bed ($Z_{false\ bed\ (ij)}$) at every raster cell, the synthetic river bottom is "burned" or "eroded" into the DEM, creating the SB data set ($Z_{SB\ (ij)}$). Note that the error is specific to each location in the modeled space, and that modern versions of both open channel flow and GIS software are needed to perform the above calculations. In this paper, Arc GIS version 10.1 and HEC-RAS version 5.0 were used. This version of HEC-RAS allows for simulation of 1- or 2-dimensional flows and rapid computation of inundation depth rasters (Geotiff format) at all points in the model domain. SB data creation requires low flow inundation depth rasters to be created at the same resolution as the underlying terrain raster (Figure 1).

Figure 1 below illustrates a short a portion of two Dungeness River low flow hydraulic models created to test the effects of the different bathymetric data sources on model accuracy (see low flow calibration and high flow calibration sections of this paper for more discussion). Figure 1 shows how the raw, LiDAR Only (LO) DEM compares with a SB based DEM, and how the approach uses GIS raster math to calculate the elevation of the SB raster data at the grid cell scale. Note the greater area of inundation present in the LO low flow model results – which is due to the effects of the artificially high false bed in the DEM. Also note the planar contours of the channel bed present in the LO DEM as compared with the SB DEM.

Once the "burned" or "eroded" DEM is created the quality of the resulting data needs to be checked by running the low flow hydraulic model extracted from the SB data. The low flow model should include reasonable flow resistance parameters and the best estimate for discharge available throughout the model domain. Using the water surface profile plot options and comparing the initial DEM-based plan to the SB-based plan in HEC-RAS allows for verification that the results are reasonable (Figure 2). Our experience is that minimal tuning of n-values is necessary to provide good fit between the computed and surveyed low flow water surface elevations. Figure 2 is representative of the quality of fit that results when low flow data is known with confidence and high quality LiDAR is used.

In application of the SB workflow (described during talk) we found that there are common difficulties when calibrating to low flow surveyed water elevations extracted from the DEM. These typically occur at the downstream end of the model (if the starting water surface is assumed to equal the surveyed water surface). Our initial experiences suggest that starting the model at normal depth will overcome most downstream boundary problems. Increasing n values locally can be used to force the river to deeper depths where pools are known to be present. If calibration difficulties are encountered throughout the model, this is most likely an indication of poor discharge estimates in the model. Even if available survey data is outdated, it should be used as a check of the SB DEM. If the SB data is suspect, it should be replaced with traditional survey data.

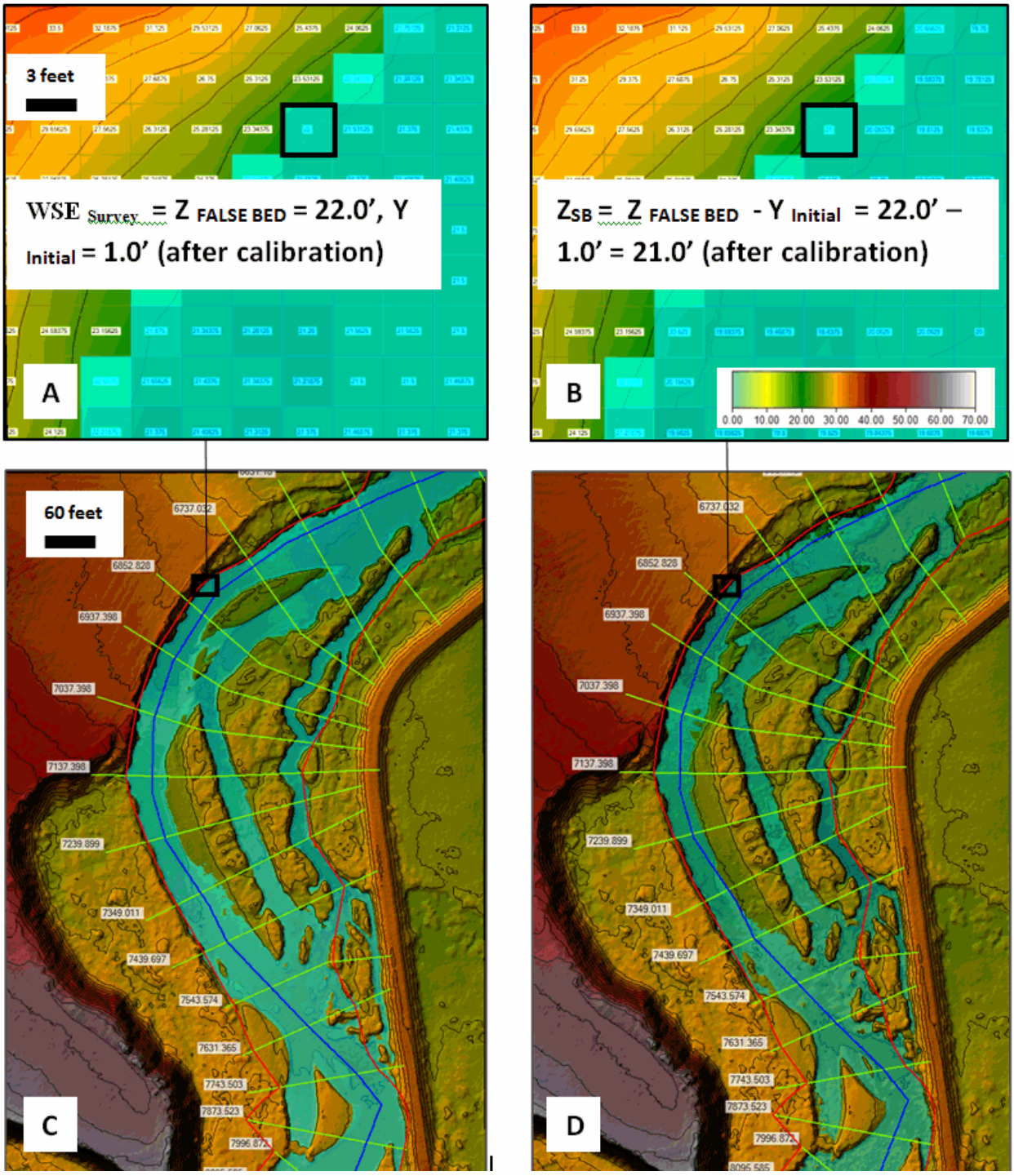

Figure 1: Dungeness River, WA (RM 1.3 to RM 1.6). (A) Close up showing initial LiDAR terrain grid cell center elevations ($Z_{FALSE\ BED}$). Each grid cell is 3 feet x 3 feet. Blue shaded numbers are cells that are wetted. Discharge at time of survey is 340 cfs. (B) Close up showing SB terrain computed grid cell center elevations (Z_{SB}), and how Z_{SB} is computed. (C) LiDAR terrain data overlaid with low flow hydraulic model cross sections, river centerline, banks, and resulting initial estimate of inundation area for flow at time of the LiDAR flight. Contour interval is 2 feet. Flow direction is south to north. (D) Synthetic bathymetry terrain data overlaid with low flow hydraulic model and computed inundation area. Note that all major geomorphic landforms with exception of deep pools are captured.

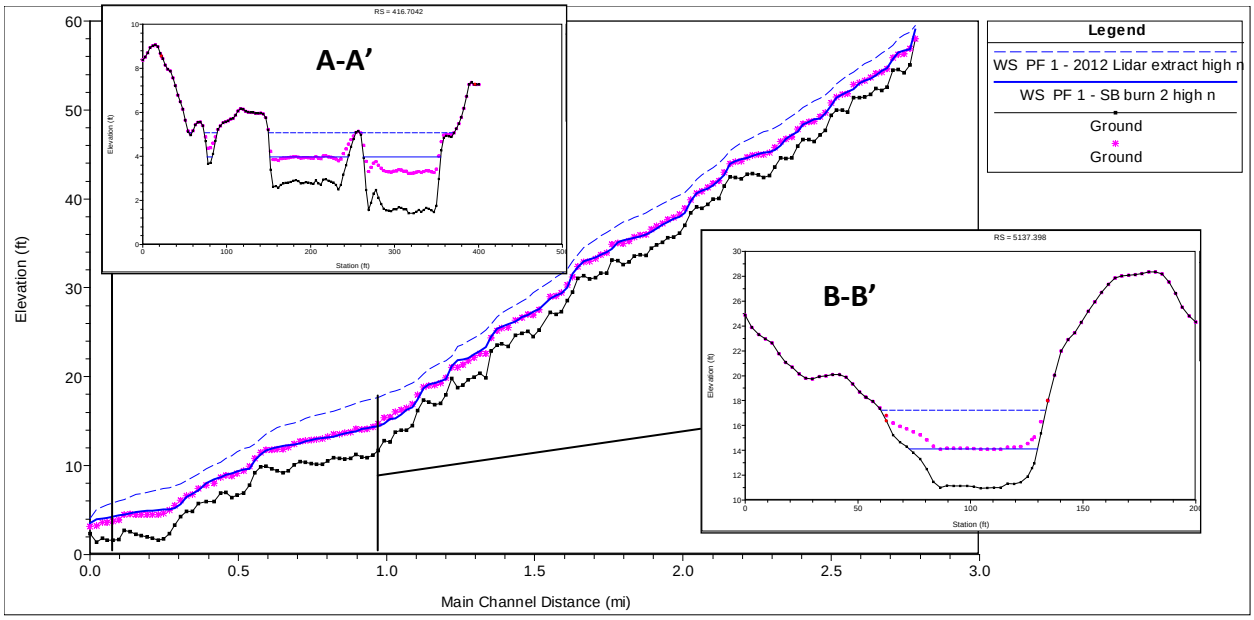

Figure 2 –Dungeness River, WA. Low flow hydraulic model verification against LiDAR surveyed water surface. In the water surface profile and cross sections the dashed blue line is initial estimate of water surface profile using LiDAR false bed elevation. Blue solid line is water surface computed after burning the initial depths into the LiDAR to create synthetic bathymetry (SB) data. Pink * is initial LiDAR surveyed water surface elevation (assumed to equal lowest point on cross section extracted from bare earth LiDAR) used to validate SB low flow model. Cross section A-A' shows how the method is able to burn side channels and main channels simultaneously while preserving large scale geomorphic features. The error in the depth is partly attributable to uncertainties about how much flow was in the main channel vs. the side channel. If the side channel was assumed dry, the main channel would have been stamped to a deeper elevation, which may have resulted in a better match. These errors are unavoidable without aerial photos to aid decisions on where to set limits of the channel in the model. Cross section B-B' is representative of how the method works in an ideal setting. The water surface matches the LiDAR survey, with minimal alteration of the cross section shape.

Note that the SB DEM is created after one or more calibration attempts to match low flow water elevations. This ensures that the low flow model and DEM have adequate conveyance to match low flow water surface elevations. In real rivers, as well as in numerical models, it is widely known that riffles are a primary control on flood elevations and that at high flows water surface elevations tend to follow a smoother longitudinal profile that drowns out bed elevation undulations more prominent at low flows. A fundamental assumption embedded in this approach is that as long as the SB DEM is the result of a well calibrated numerical model that captures riffle elevations (as shown in Figure 2 above), error in thalweg elevations between riffles will not significantly impact estimates of flood elevations. A primary goal of the high flow validation section of this paper is to test the validity of this assumption.

STUDY REACH DATA

Hydraulic models developed by others were acquired to establish baseline conditions for investigating the effects on the results of hydraulic models derived from ground survey based methods, from LiDAR alone, and from LiDAR blended with SB data. All baseline models used for validation purposes were developed by others. The Green River models were acquired from King County, prepared as part of a Preliminary Revised Flood Insurance Study (2007). The Skykomish River model was obtained from Snohomish County and was developed as part of a Revised Flood Insurance Study (2010). The Dungeness River model was developed by USACE Seattle District as part of a Feasibility Study (2014). The Clark Fork model was developed by USACE Northwest Division as part of the Columbia River Treaty Flood Risk Assessment (2012). All baseline models were used as-is, reflect real-world conditions and are based on modern modeling and mapping standards.

The Dungeness, Skykomish, and Green River in western Washington State, and the Clark Fork River, a tributary to the Columbia in Idaho and Montana were used for this study (Figure 3). For ease of comparison the Green River model was subdivided into the Middle and Lower Green Rivers based on a geologic reach break near river mile (RM) 32. All study reaches in Washington State are glacially modified alluvial floodplains, draining heavily forested mountains that have hydrology typical of the Puget Sound lowlands (high intensity fall and winter rains, spring snowmelt runoff). A flood control dam on the Green River caps flood flows at the pre-dam 2-year recurrence interval discharge, while the Skykomish and Dungeness are free flowing. In contrast, the Clark Fork River study reach is wholly contained by a bedrock gorge and is heavily influenced by hydroelectric dams located at both ends of the study reach, which causes the river to behave like a reservoir under all but the highest discharges.

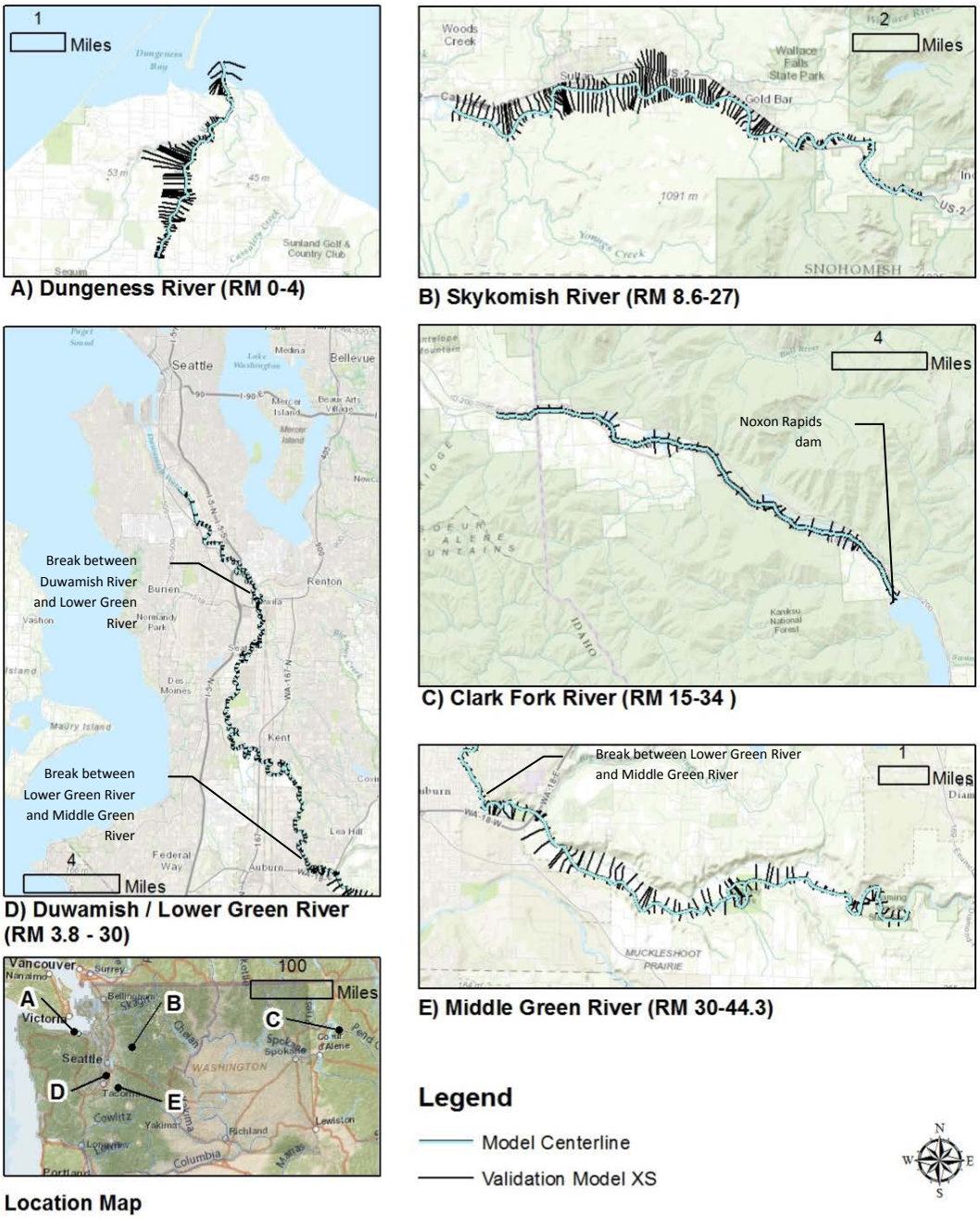

Figure 3: Location and vicinity maps of SB low flow and validation model reaches

The Dungeness River is the shortest and steepest of the study reaches, with the lowest 100-year discharge, while the Lower Green River is the longest and narrowest of the study reaches (Table 1). The flattest and most confined reach is the Clark Fork River – however the flat gradient is the result of a downstream dam. The natural valley gradient is much steeper given the canyon setting. The Dungeness, Skykomish, and Middle Green River are gravel/cobble bedded with boulders in places. The Skykomish River is the largest of the alluvial rivers studied, with large amplitude migrating meanders and wide floodplain All alluvial rivers studied are artificially confined by road embankments, revetments and levees near developed areas, the lower half of the Dungeness River and Lower Green River being the most confined. Hydrologic data available is of relatively high quality, with more than 80% of the study reaches gauged for all but the lower half of the Skykomish River. Flows at time of survey were about 10% of the 2 year discharge for the Dungeness and Green River, about 4% for the Skykomish, and about 22% for the Clark Fork, indicating that the discharge at time of survey was well below bankfull conditions.

Table 1: Study Reach Low Flow and Baseline Model Data

				Reach Average (Std Dev)		Discharge Estimates (cfs)		
Study Reach	**Length (miles)**	**Minimum % gaged in reach**	**Drainage Area (square miles)**	**EGL Slope & (EGL Stdev) (ft/ft) (1)**	**BFW/ BFD & (BFW/BFD Stdev) (ft/ft) (2)**	**@ time of survey**	**50% AEP (2-yr)**	**1% AEP (100-yr)**
A. Dungeness River, WA	2.8	95%	198	0.0044 (0.0024)	67 (95)	340	3,000	9,100
B. Skykomish River, WA	20.1	60%	563	0.0034 (0.0027)	42 (28)	1,040 to 2,400	37,800 to 51,700	118,000 to 156,900
C. Clark Fork River (ID, MT)	18.6	99%	22,067	0.000045 (0.0001)	23 (21)	17,000 to 19,400	78,000	140,000
D. Lower Green River, WA	26.1	91%	462	0.0004 (0.0002)	7 (4)	1,090 to 1,210	9,200	12,810 to 13,410
E. Middle Green River, WA	14.3	81%	390	0.0025 (0.0016)	18 (9)	660 to 1,090	9,200	12,250 to 12,810

(1) From 2-year discharge energy grade line computed from baseline (ground surveyed) model
(2) Bankfull Width (BFW) and Depth (BFD) computed from 2-yr discharge max depth and width (survey model)

SB LOW FLOW MODEL CALIBRATION

The key issues affecting the quality of the results of the SB method are determining the extent of low flow model cross sections, estimating the amount of flow present within the model at time of survey, and deciding how much to refine the model to achieve good match to the surveyed water surface elevations.

Table 2 below summarizes the error in the SB and LiDAR Only (LO) computed water surface elevations – in low flow conditions – for the five study reaches with respect to surveyed water surface elevations at each transect location in the model, after one or two calibration attempts. Calibration consisted of adjusting Manning's n values in the channel for the low flow model to better match the LiDAR surveyed water surface. In cases where significant amounts of flow was diverted at different elevations into side channels we either isolated all the flow into the dominant channel by limiting the cross section width, or constructed a connected side channel reach. The results were compared with the surveyed water elevations, which are extracted from the low point on each model cross section. Alternatively one could have used a 2-D model to estimate water elevations in the main and side channels at low flow.

The results for all five study reaches provide excellent-to-good matches of the surveyed water elevations during low flow conditions (average difference in computed low flow elevation is less than 0.1 to 0.5 feet from surveyed

elevation). In contrast the average error using only the LiDAR data ranges from 1.8 to 5.6 feet (and more than 25 feet in the Clark Fork reservoir reach). Note that in all cases additional refinements of the SB data to better match surveyed elevations were possible, however we viewed the low flow results as favorable enough to proceed to high flow validation.

Table 2: Low flow SB derived hydraulic model results after calibration vs. LO hydraulic model results as compared with low-flow surveyed water surface elevations

Study Reach	A. Dungeness, WA		B. Skykomish, WA		C. Clark Fork ID, MT		D. Lower Green, WA		E. Middle Green, WA	
Absolute Error in Computed WSE vs. Surveyed WSE	**SB** (ft)	**LO** (ft)	**SB** (ft)	**LO** (ft)	**SB** (ft)	**LO** (ft)	**SB** (ft)	**LO** (ft)	**SB** (ft)	**LO** (ft)
Median	0.03	1.81	0.46	3.12	0.66	25.84	0.07	5.61	0.22	2.12
Average	0.03	1.86	0.43	3.21	0.30	25.56	0.07	5.52	0.18	2.20
Stdev	0.29	0.48	0.47	0.91	0.62	1.63	0.41	2.05	0.36	0.79
Min	-0.7	0.9	-0.7	1.3	-0.9	17.2	-1.0	0.7	-1.5	0.6
Max	1.0	3.4	2.2	6.9	0.8	26.7	1.1	9.0	1.0	6.1
N=	145		222		42		292		185	
Reach length (mi)	2.8		20.1		18.9		26.1		14.3	

The excellent results on the 26-mile long Lower Green River reach were surprising given the tidal influence, however the survey at low tide and trapezoidal channel shape helped ensure that much of the channel conveyance area was captured in the initial terrain data. The higher-than-average errors in the Skykomish model are attributed to large uncertainties in flow at time of survey, effects of split flows around gravel bars, and errors and artifacts in the older vintage LiDAR data (trees, etc.). The excellent results for the Dungeness are partly attributed to the modern techniques used to acquire and post process the LiDAR data and the presence of a stream gage within the reach. The Clark Fork River reach – which is a backwatered canyon upstream of a dam – actually fairs better in the low flow than high flow model run (discussed in next section) because the known water surface at the downstream pool drives the water surface profile throughout the reach.

The good to excellent results over a wide range of channel sizes, slopes, and geomorphic types suggests that the SB method is capable of creating low flow hydraulic models that closely match surveyed water elevations, while preserving major geomorphic features of the channel (Figure 1D, Figure 2). Additionally, use of LiDAR data without adjustment may result in errors (under low flows) that exceed tolerances for most types of engineering studies. The effects of using unadjusted bare earth LiDAR data or SB terrain data without further parameter adjustment for flood conditions are presented in the next section.

SB HIGH FLOW MODEL VALIDATION

To validate the SB (and LO) DEMs, baseline hydraulic models developed by others to estimate floodplain depths and elevations were modified by re-cutting all cross sections from the original LO DEM and from the SB DEM. The steady flow step backwater models were then run with the new cross section data but without any further parameter or boundary condition adjustments to determine how the errors in the underlying terrain data affected the model results for the “bankfull” 2-year (50% annual exceedance probability) and “base” 100-year (1% annual exceedance probability) flood events.

Table 3 below summarizes the error in computed water surface elevation, flow area, average channel velocity, and average channel shear stress for the five study reaches from SB-based model and LO-based model with respect to results computed from the baseline models. The error statistics shown in Table 4 represent reach averages of the cross sectional difference between the results for the SB model or LO model and the baseline model. The percent change in error in Table 3 represents the reduction in error resulting from use of the SB model vs. the LiDAR only model.

Table 3: Study Reach Average Absolute Error Residuals in Computed WSE, flow area, velocity, and shear stress for SB and LiDAR Models with respect to Baseline Model

Study reach		A. Dungeness		B. Skykomish		C. Clark Fork		D. Lower Green		E. Middle Green		Study Average % Change	
		SB	**LO**	**SB**	**LO**	**SB**	**LO**	**SB**	**LO**	**SB**	**LO**	**Note 1**	**Note 2**
Δ 2-Yr WSE (ft)	Med	-0.2	1.2	0.4	1.1	0.7	25.8	-0.4	3.6	0.1	1.1	95%	96%
	Avg	-0.1	1.2	0.6	1.5	0.3	25.6	-0.2	3.5	0.1	1.3	92%	93%
	SD	0.3	0.5	1.0	1.2	0.6	1.6	0.6	0.8	0.5	0.9	29%	35%
	Min	-0.9	0.1	-1.4	-0.2	-0.9	17.2	-1.2	0.1	-0.9	0.1	1182%	967%
	Max	0.7	2.0	4.2	5.6	0.8	26.7	1.8	4.7	1.4	3.8	53%	62%
		SB	**LO**	**SB**	**LO**	**SB**	**LO**	**SB**	**LO**	**SB**	**LO**	**Note 1**	**Note 2**
Δ 100-Yr WSE (ft)	Med	0.0	0.9	0.3	0.7	4.9	30.2	-0.3	3.2	0.1	1.0	90%	89%
	Avg	0.0	0.9	0.5	1.2	4.7	29.9	-0.1	3.2	0.1	1.2	87%	87%
	SD	0.3	0.4	0.9	1.2	2.0	0.8	0.6	0.7	0.4	0.9	25%	-12%
	Min	-0.6	0.1	-1.2	-0.5	0.0	26.9	-1.0	0.1	-0.8	-0.6	332%	286%
	Max	1.3	1.8	5.8	7.0	7.3	30.6	1.7	4.3	1.3	3.4	42%	49%
		SB	**LO**	**SB**	**LO**	**SB**	**LO**	**SB**	**LO**	**SB**	**LO**	**Note 1**	**Note 2**
Δ 2-Yr Flow Area (ft^2)	Med	8	74	97	480	1617	-3465	13	64	46	551	85%	97%
	Avg	0	78	210	684	-333	-6521	-31	-15	75	863	39%	50%
	SD	77	121	879	1113	20411	19031	399	708	470	1183	40%	31%
		SB	**LO**	**SB**	**LO**	**SB**	**LO**	**SB**	**LO**	**SB**	**LO**	**Note 1**	**Note 2**
Δ 100-Yr Area (ft^2)	Med	21	122	92	535	6240	-2988	12	225	33	647	89%	133%
	Avg	8	421	145	762	8950	-3256	-36	334	134	1057	94%	150%
	SD	147	2124	1174	1205	25690	7542	411	960	543	1453	54%	-5%
		SB	**LO**	**SB**	**LO**	**SB**	**LO**	**SB**	**LO**	**SB**	**LO**	**Note 1**	**Note 2**
Δ 2-Yr Velocity (ft/s)	Med	-0.1	-0.3	-0.1	-0.3	-0.1	0.2	0.0	0.1	-0.1	-0.4	80%	90%
	Avg	0.0	-0.2	-0.2	-0.4	-0.1	0.6	0.0	0.2	0.0	-0.2	90%	95%
	SD	0.7	0.7	1.2	1.1	0.9	1.9	0.4	0.6	0.9	1.1	11%	19%
		SB	**LO**	**SB**	**LO**	**SB**	**LO**	**SB**	**LO**	**SB**	**LO**	**Note 1**	**Note 2**
Δ 100-Yr Velocity (ft/s)	Med	-0.1	-0.4	-0.1	-0.3	-0.7	0.3	-0.1	0.0	-0.2	-0.5	224%	243%
	Avg	-0.1	-0.3	-0.2	-0.4	-0.2	0.4	0.0	0.1	-0.1	-0.3	81%	95%
	SD	0.8	0.7	1.1	1.0	2.4	0.4	0.4	0.7	0.9	1.3	13%	-94%
		SB	**LO**	**SB**	**LO**	**SB**	**LO**	**SB**	**LO**	**SB**	**LO**	**Note 1**	**Note 2**
Δ 2-Yr Shear (lb/ft^2)	Med	0.0	0.0	0.0	0.0	0.0	0.0	0.0	0.0	0.0	0.0	50%	60%
	Avg	0.0	0.0	0.0	0.0	0.0	0.0	0.0	0.0	0.1	0.0	6%	35%
	SD	0.3	0.3	0.7	0.7	0.1	0.1	0.1	0.1	0.4	0.4	4%	9%
		SB	**LO**	**SB**	**LO**	**SB**	**LO**	**SB**	**LO**	**SB**	**LO**	**Note 1**	**Note 2**
Δ 100-Yr Shear (lb/ft^2)	Med	0.0	-0.1	0.0	-0.1	-0.1	0.0	0.0	0.0	0.0	-0.1	73%	121%
	Avg	0.0	0.0	0.0	0.0	0.0	0.1	0.0	0.0	0.1	0.0	8%	32%
	SD	0.4	0.4	0.8	0.6	0.4	0.1	0.1	0.1	0.4	0.5	2%	-73%

Note 1 – Study average % change is the difference in the LO reach average error statistic and SB reach average error statistic divided by the reach average LO error statistic, then averaged for all reaches (excluding Clark Fork).
Note 2 – Study average % change includes Clark Fork.

From Table 3 we can see that the study reach median error in SB model computed water surface elevation (WSE) ranged from -0.4 feet (Lower Green River) to 0.7 feet (Clark Fork) for the 2-year event, and ranged from -0.3 feet to 4.9 feet for the 100-year event (same reaches). The Dungeness and Middle Green models have the best overall match of the baseline WSEs, with 0.2 feet or less error on average for both the 2 year and 100-year events. Figure 5 provides a representative comparison of computed water surface profiles for all study reaches. The improvement in results from use of the SB method is most pronounced for the Lower Green, Clark Fork and Dungeness, which are all highly channelized or confined. The unconfined Middle Green and Skykomish have overbank floodplains that convey much of the flood flow, causing the results to be less sensitive to use of SB data.

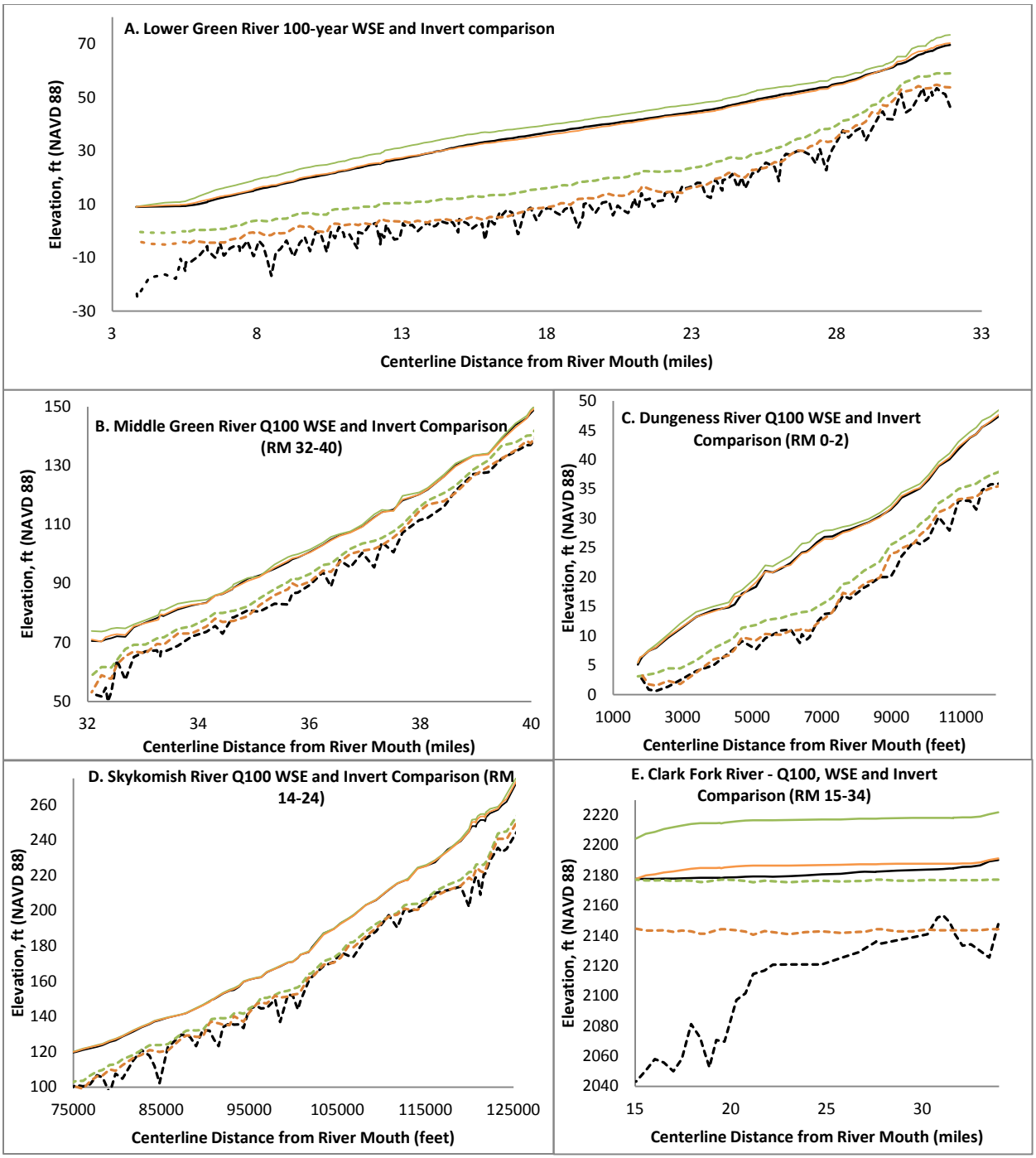

Figure 5. Computed 100-year flood water surface profiles and invert elevations for A) Lower Green (RM 3-32), B) Middle Green (RM 32-40), C) Dungeness (RM 0-2), D) Skykomish (RM 14-24), E) Clark Fork (RM 15-34). Green lines reflect initial bed elevation and computed WSE from original LO data, orange lines reflect SB bed elevation and computed WSE from SB data, black lines reflect surveyed bed elevation and computed WSE from baseline RAS model. Solid lines are computed WSEs, dashed lines are invert elevations.

The limitations and benefits of the SB method are seen from inspection of the Clark Fork results. Clearly the method cannot reproduce the river invert elevations submerged under the dam backwater, however the model still reduces average error in stage by more than 25 feet if one had used the LiDAR alone. For all but the Clark Fork the SB channel invert tracks the elevation of existing riffles quite closely, and results in hydraulic models that closely match

those of the baseline model in terms of WSE, flow area, velocity, and shear stress. Compared with models based on use of LiDAR alone, results are significantly improved for all study reaches.

The slight upward bias in flood stage resulting from the SB approach (under normal conditions) and more pronounced upward bias from use of LiDAR data without adjustment is when comparing total inundation area. Inundation area error is 0-5% in all reaches using the SB method, compared to 2-50% using the LO model. The error for the 2-year event is higher than that of the 100-year event for all but the channelized (trapezoidal) Lower Green. At higher stages the other reaches use more floodplain conveyance – which is not affected by the bathymetric data collection method.

SUMMARY

The SB method allows for creation of reasonable synthetic channel bathymetry data from LiDAR data, flow information, and widely available GIS and hydraulic software. The quality of the results can be easily demonstrated by comparing computed water elevations and velocities to the DEM water surface elevation at time of survey and to baseline model results or to high water marks. For this study the SB method results (comparison of computed flood stage to baseline) were excellent for a short steep sediment laden river with recent LiDAR and a gage within the reach, and poor for a reach upstream of a dam where true channel depths were many times that estimated using the SB approach. For a low gradient tidal river and medium gradient gravel bed river the results were very good. On a medium gradient wandering gravel bedded river with older LiDAR and higher uncertainty over low flow discharge the data were generally good to poor in isolated areas near bridges.

For all five study reaches the SB method significantly reduces the errors resulting from use of cross sectional data derived from LiDAR alone but does not eliminate the errors. This trend of reduced error is observed for all the flows analyzed and all the hydraulic parameters analyzed, other than depth. The median and average error when compared to baseline hydraulic models was typically less than 1 foot at bankfull stages, and under ideal conditions was less than 0.5 ft at 100-year flood stages. A river reach that is significantly affected by downstream backwater caused by a dam was used to check the quality of the method under non-ideal conditions. While the stage errors at low flow were less than 1 foot, the SB method was not able to create enough conveyance to pass 100-year flood flows with less than 4.7 feet of error (reach average). While this result at first glance is poor compared with the other reaches studied, the relative reduction in error compared with using a DEM without bathymetry is about six-fold. The location within a bedrock canyon suggests the error may not be significant with respect to adjacent development.

DISCUSSION

Under low and 2-year flood conditions we observed good to excellent matches of baseline and SB water surface elevations for all five study reaches, with the MAE of less than 1 foot for all but the Clark Fork reservoir reach. (Note that the results presented in this paper are not being compared to observed conditions at high flows which means that while the SB model results may provide a good match to the baseline model, the quality of the SB model with respect to real world conditions has only been evaluated for low flows and not under flood conditions). For nearly all flows and reaches, the results of the validation effort were surprisingly good (for the parameters that are typically meaningful for analysis and design, with the exception of maximum depth) considering that the SB based models lacked below-water survey data. This suggests that in similar conditions we would expect to have similar results, provided the quality of datasets and approach used to derive the SB data are similar.

To understand why the SB data results in a model that agrees well with the baseline, consider the significant error in maximum depth associated with models that still provided good to excellent estimates of flood stages (Figure 5) and inundation area. Concurrently, the good results of flow area, velocity, and stage shown in Table 3 (resulting from a 1-D step backwater model) suggest only reasonable estimates of cross sectional area, slope, and roughness are required. Because we are simulating physics of flow in one dimension, using open channel flow equations, all flow is assumed to be down valley, contained within banks, steady and uniform. During low flows, when LiDAR is typically acquired, these conditions are satisfied more often than not. We are simply using physical equations in the SB method (hydraulic model) to tell us how much space (area or volume) flow “takes up” at a given location. Then we are using GIS to create that space below the surface of a DEM for the river so it can pass the surveyed flow at the surveyed elevation. These results appear to confirm our primary assumption that as long as riffles are captured in the SB DEM that errors in flood stage will be small.

The quality of the results in this study are likely related to the setting and quality of the underlying data used to create the SB data. Reaches where the river was confined (Dungeness, Lower Green) with a trapezoidal cross section had the best agreement with the baseline models. The effort to create and apply SB data is significantly less than that needed to perform channel surveys. In less than one day we were able to use the technique to create a 40 mile long model that matched the baseline model computed 100-year flood elevations by less than 0.5 ft on average. While reach average hydraulic conditions computed from 1-D SB based models tracked closely with the baseline models, errors were higher at bankfull stages than at flood flows when the floodplain is active. Other difficulties were encountered where significant backwater was present, at hydraulic constrictions, and abrupt changes in grade or bed elevation. While no effort was made to calibrate the SB models to historical high water marks, we are confident that the close agreement with the baseline model results (with the exception of the Clark Fork) would allow for good calibration with reasonable parameters.

While the SB method will typically result in a DEM that includes a wider and shallower river than exists, it avoids the creation of artifacts common with using educated guesses or automated techniques to "burn" channels into DEMs from sparse survey data. For example all features above the water surface are preserved rather than "averaged out" as occurs when topography is created from widely spaced cross sections. This preserves side channels and bars that may be important for capturing flow paths or effects of macro roughness elements, however it will not capture deep pools or submerged features that may be important for habitat studies. This implies that a potential benefit of the SB approach is to improve the accuracy of a DEM (and model) between surveyed sections.

THE NEED FOR DUE DILLEGENCE AND REFINEMENT

This paper presents the promising results of a validation study of a method to create synthetic bathymetry for five rivers in the Pacific Northwest of varying size and geomorphic character. Until such time that the method has been validated for a wider range of channel types and rivers by other practitioners, we must recommend against applying it in cases where higher resolution survey grade data is warranted (i.e. life safety is of concern). In cases where flow data at time of DEM survey is lacking or uncertain, the SB approach will not provide reliable results, and could result in under-estimation of flood risk. Field data (discharge-elevation rating curves) may be needed to ensure the results are reasonable or to improve results. The potential cost savings of this method, while attractive, implore practitioners to collect detailed calibration and verification datasets to demonstrate the quality of the underlying SB data and model results. Models developed with this approach should be flagged as such, and a calibration and verification write-up should be included with model documentation. Before applying the SB method to a reach lacking a baseline model it is strongly recommended that one first independently validate the approach on a reach with a survey grade calibrated model to ensure that the approach is providing reasonable results. Further validation studies of the SB method with 1-D and 2-D unsteady state models are also recommended.

AKNOWLEDGMENTS

The authors appreciate the support of Seattle District staff and management and Clallam County, King County, and Snohomish County that provided baseline hydraulic models and data used to conduct the study. The authors wish to thank an anonymous reviewer that significantly improved the quality of the final manuscript.

REFERENCES

Bangen, S.J., Wheaton, J. M., Bouwes, N., Bouwes, B., Jordan, C. (2014) "A methodological intercomparison of topographic survey techniques for characterizing wadeable streams and rivers", Geomorphology, Volume 206, 1 February 2014, Pages 343-361

Javernick, L., Brasington, J., Caruso, B. (2014) "Modeling the topography of shallow braided rivers using Structure-from-Motion photogrammetry", Geomorphology, Volume 213, 15 May 2014, Pages 166-182

McKean, J. , Nagel, D., Tonina, D., Bailey, P., Wright, C.W., Bohn C., and Nayegandhi, A. (2009). "Remote Sensing of Channels and Riparian Zones with a Narrow-Beam Aquatic-Terrestrial LiDAR", Remote Sens. 2009, 1, November 2009, pages 1065-1096

USACE (2014). Combined 1D and 2D modeling with HEC-RAS. USACE Hydrologic Engineering Center.

PROBLEMS AND PROSPECTS OF SWAT MODEL APPLICATION ON AN ARID/SEMIARID WATERSHED IN ARIZONA

Yongping Yuan, Research Hydrologist, USEPA-Office of Research and Development; Las Vegas, NV 89119; phone: 702-798-2112; E-mail: yuan.yongping@epa.gov.
Wenming Nie & Emily Sanders, Former Student Services Contractor, USEPA-Office of Research and Development; Las Vegas, NV 89119

Abstract: Hydrological characteristics in the arid/semiarid southwest create unique challenges to watershed modelers. Streamflow in these regions is largely dependent on seasonal, short term, and high intensity rainfall events. The objectives of this study are: 1) to analyze the unique hydrology of a watershed located in the southwestern USA; and 2) to evaluate the Soil and Water Assessment Tool (SWAT) applicability on this watershed. USGS historical precipitation and stream discharge patterns were analyzed to determine the hydrological characteristics of the upper San Pedro watershed. It was found that runoff was decreased in downstream gauging locations because of transmission loss due to low groundwater level. Based on this analysis, the SWAT model was calibrated to reflect the unique hydrological characteristics of the watershed. After calibration, the Nash-Sutcliff efficiency (NSE) coefficient and coefficient of determination (R^2) values were above 0.5 (except the NSE coefficient for annual calibration at Redington gauge), and percent bias (PBIAS) were in the range of ±25% (except annual calibration at Charleston gauge), suggesting satisfactory model performance. The SWAT model, set up with the optimal parameters, generally reflected the hydrological characteristics of this arid/semiarid watershed.

Keywords: Arid/semiarid watershed; hydrology; San Pedro River Watershed; SWAT model; transmission loss

INTRODUCTION

Given the growing demand for water due to urban growth and the likelihood of decreasing precipitation due to climate change, water sustainability has become a dominant issue in the arid/semiarid regions such as the Southwestern USA. To address a nation's or a region's water-related sustainability problems, one of the key elements is to characterize and quantify water resources for different future scenarios including different Landuse and Landcover (LULC) and climate in order to develop better management practices. In the arid/semiarid areas, it has been a great challenge to quantify the water resources due to limited access and monitoring systems on the land and limited capability of hydrological and water quality models to handle the unique hydrology associated with these regions (Baillie et al. 2007, Yu et al. 2011). To accurately model a watershed, the basic hydrology of the region must first be understood.

Streamflow formation after rainfall storm events and interactions with groundwater and vegetation must be properly represented in the model. In arid/semiarid regions, peak discharge and the overall flow regime are mostly produced by extremely variable, high intensity, and short duration rainfall (Syed et al. 2003, Goodrich et al. 1997, Hernandez et al. 2000, Ouessar et al. 2009, Pilgrim et al. 2009, Ghaffari et al. 2010). The processes of streamflow generation and interactions with groundwater and vegetation may be different from humid regions (Pilgrim et al. 2009). For example, transmission loss to the aquifer was found to be a major component of the hydrological processes in the arid/semiarid region.

Models, such as the Soil and Water Assessment Tool (SWAT), are commonly used for future projection and alternative scenario assessment. Using spatially variable data of elevation, soil, and LULC, the model is capable of simulating major hydrological processes including evapotranspiration (ET), surface runoff, percolation, lateral flow, groundwater flow (return flow), transmission losses, and ponds (Arnold et al. 1998) and keeping track of water balance components and crop yields of different land units at various temporal scales. Input data and model outputs are processed through a GIS interface. The model utilizes an interface that is very user friendly and allows users to develop modifications using model documentation and source code (Ouessar et al. 2009, Neitsch et al. 2005). Although SWAT was designed to evaluate the impact of LULC change on watershed hydrology and water quality and has been widely applied for watershed scenario analysis, its application in the arid/semiarid regions has been few but increasing in recent years (Ghaffari et al. 2010, Ouessar et al. 2009, Veith et al. 2010, Gassman PW 2007). Therefore, the objectives of this study are: 1) to analyze the unique hydrology of a watershed located in the southwest of the US, and 2) evaluate SWAT applicability on this arid/semiarid watershed.

METHODS AND PROCEDURES

Study Area and Its Background Information: The upper San Pedro Watershed originates in Sonora, Mexico near Cananea and flows north into southeastern Arizona, USA (Figure 1). In this study, the investigation area is composed of the upper San Pedro Basin and a part of the lower San Pedro Basin to the Redington USGS gauge (Figure 1). For convenience, the entire study area is referred as upper San Pedro in the text.

The upper San Pedro Watershed has a drainage area of about 7,400 km^2, and lies between latitude 30°54′ and 32°30′ N and longitude -110°48′ to -109°45′ W. Elevations in the watershed range from 900 to 2900 m, and annual rainfall ranges from 300 to 750 mm (Biggs 2009). As shown in Table 1, the LULC classes in the watershed mainly include woodland (oak and mesquite together make up 14%), desertscrub (32%), grassland (35%), agriculture crops (2%), urban (2%) (Saleh et al. 2009). Most soils in the San Pedro watershed are gravelly, medium and moderately coarse-textured (USDA). They are nearly level to very steep soils on dissected alluvial fan surfaces. Major soil series include Sierravista (Loamy-skeletal, mixed, superactive, thermic Petronodic Calciargids), Diaspar (Coarse-loamy, mixed, superactive, thermic Ustic Haplargids), Libby (Fine, mixed, superactive, thermic Petronodic Ustic Paleargids), and Forest (Fine, mixed, superactive, thermic Ustic Calciargids). These soils are characterized as well-drained soils with moderately high to high permeability. Major municipal areas along the San Pedro River from south to north are Cananea (Mexico), Hereford, Sierra Vista, Ft. Huachuca, Charleston, Tombstone, St. David, Benson, and Redington (Figure 1).

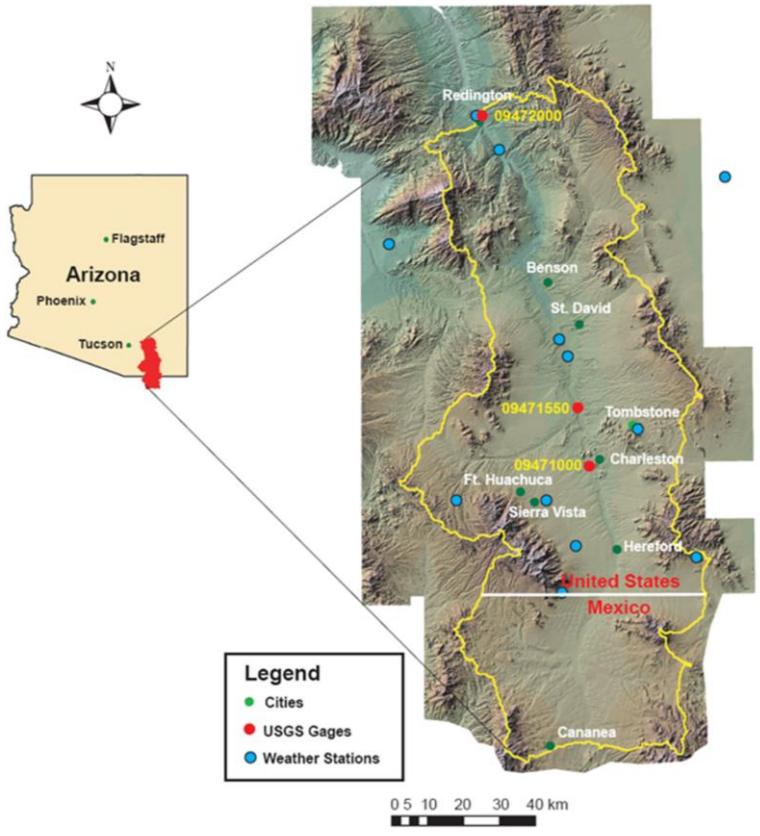

Figure 1 Locations of rural and municipal areas, USGS monitoring gauges, and weather stations in the upper San Pedro watershed (modified from (Kepner et al. 2000)).

The San Pedro River is the last remaining river in southern Arizona that has long perennial reaches (Kennedy and Gungle 2010). The San Pedro River headwaters flow north from Sonora, Mexico into Arizona where the river merges with the Gila River which flow into the Colorado River and finally empties into the Gulf of California. The Upper San Pedro River Basin is noted as a highly diverse ecosystem and important migratory bird habitat and is often studied for its vulnerability to landscape changes due to over development and lowering of the groundwater table (Steinitz 2003, Stromberg et al. 1996, Stromberg et al. 2005, Orr and Colby 2004, Arias 2000, Webb and Leake 2006, Steiner et al. 2000). Trend analysis of the San Pedro River at Charleston, Arizona shows a more than 50 percent decrease in annual streamflow during the 20th century (Thomas and Pool 2006). Efforts to conserve the Upper San Pedro basin are confounded by water rights, international mining

operations, conservation of protected riparian zones, and economic considerations (Steiner et al. 2000, Steinitz 2003). Historical trends show decreases in riparian vegetation and baseflow and storm runoff volumes since the 1900s caused by human induced changes to the landscape and climate changes (Webb and Leake 2006).

Streamflow Data Collection and Analysis: Streamflow data from the USGS stream gauge stations 09471000 San Pedro River at Charleston (31°37′33″ N and 110°10′26″ W), 09471550 San Pedro River near Tombstone (31°45′03″ and 110°12′02″), and 09472000 San Pedro River at Redington (32°22′50″ N and 110°26′45″ W) were downloaded from the USGS website (http://waterdata.usgs.gov) for flow analysis, model calibration and validation.

Locations of those USGS gauges stations are displayed in Figure 1. The Redington gauge station (09472000) is located downstream (north) of the other stations and drains the entire watershed area, which is about 7493 square kilometers. The other two gauge stations Charleston (09471000) and Tombstone (09471550) drains approximately 3159 and 4454 square kilometers, respectively.

To effectively calibrate the model, streamflow trends at three stations were analyzed first to understand the hydrological characteristics of the watershed. Since concurrent streamflow data for all three stations were only available from 1967 to 1985, a streamflow hydrograph (Figure 2) was plotted for the year 1985 to analyze and compare daily discharge characteristics at the three gauge locations. Annual runoff (Figure 3), the sum of monthly runoff downloaded from the three USGS gauge stations, for each location was plotted from1967 to 1985 to analyze annual runoff differences at three sites. The Redington gauge station (09472000) has the largest drainage area (7493 square kilometres), followed by the Tombstone (09471550). The Charleston gauge station (09471000) has the least drainage area (3159 square kilometres).

SWAT Model Description: The Soil and Water Assessment Tool (SWAT) model is a continuous, long-term, physically based semi-distributed model developed to assess impacts of climate and land management on hydrological processes, sediment loading, and pollution transport in watersheds (Arnold et al. 1998). In the SWAT model, a watershed is divided into subwatersheds or subbasins, which are further partitioned into a series of hydrological response units (HRUs). HRUs are uniform units that share unique combinations of soil and land use. Hydrological components, sediment yield, and nutrient cycles are simulated for each HRU and then aggregated for the subbasins.

The hydrological cycle simulated in SWAT is based on the water balance equation:

$$SW_t = SW_0 + \sum_{i-1}^{t} (R_{day} - Q_{surf} - E_a - w_{seep} - Q_{gw})$$

where, SW_t and SW_0 are the final and initial soil water content on day i (mm H_2O), t the time steps on day i, R_{day} the rainfall that reaches the soil surface on day i (mm), Q_{surf} the surface runoff on day i (mm), E_a the evapotranspiration on day i (mm), w_{seep} the interflow on day i (mm), and Q_{gw} is the baseflow on day i (mm) (Neitsch et al. 2005).

The simulated hydrological components include evapotranspiration (ET), surface runoff, percolation, lateral flow, groundwater flow (return flow), transmission losses, ponds, and water yield (Arnold et al. 1998). Evaporation and transpiration are simulated separately in SWAT: evaporation is computed using exponential functions of soil depth and water content and transpiration is estimated using a linear function of potential evapotranspiration (PET) and leaf area index. Three methods can be used to estimate PET: Hargreaves (Hargreaves et al. 1985), Priestley-Taylor (Priestley and Taylor 1972), and Penman-Monteith (Monteith 1965). The Pennman-Monteith method was used to calculate PET in this study. Surface runoff is simulated using a modification of the Soil Conservation Service (now the Natural Resources Conservation Service) Curve Number (SCS-CN) method (USDA, 2004) with daily rainfall. Curve number values used for runoff estimation are based on soil type, LULC, and land management conditions (Rallison and Miller 1981) and are adjusted according to soil moisture conditions (Arnold et al. 1993). Percolation is estimated using the combination of a storage routing technique and a crack-flow model (Arnold et al. 1998). The lateral flow is estimated simultaneously with percolation using a kinematic storage model (Solan et al. 1983). The groundwater flow (baseflow) into a channel is calculated based on the hydraulic conductivity of the shallow aquifer, distance from subbasin to main channel, and water table height (Hooghoudt 1940). Transmission loss, amount of water removed from tributary channels by transmission, is calculated using procedures described in the SCS Hydrology Handbook (USDA, 2007). The canopy interception is estimated based on the canopy storage which is a function of vegetation type.

Water yield, total amount of water leaving the HRU and entering main channel, is equal to surface runoff plus lateral flow and baseflow, and minus transmission loss and pond abstractions (Neitsch et al. 2005).

Model Input Preparation: The basic SWAT model inputs include a digital elevation model (DEM), soil data, LULC data, and meteorological data. The DEM was derived from the National Elevation Dataset (NED) of USGS with 1 arc-second resolution (Gesch et al. 2002), and the soil data was from the State Soil Geographic (STATSGO) database. The LULC data of 1992 and 1997 used for this study was from the NALC project (Landsat Multi-Spectral Scanner) and Landsat Thematic Mapper (Kepner et al. 2002, USEPA 1993). For climate information, daily maximum and minimum temperature, precipitation, solar radiation, relative humidity and wind speed are needed to account for temporal variations in weather. This data can be historically measured, generated using the SWAT built in WXGEN weather generator model (Sharpley and William 1990), or supplied to SWAT using a combination of the two methods. For this study, daily precipitation and minimum-maximum temperature from Jan. 1960 to Apr. 2008 were acquired from the National Climatic Data Center (NCDC). Twelve meteorological stations were found within or nearby the upper San Pedro watershed (Fig. 1). Missing records of daily observations of precipitation and minimum-maximum temperature were interpolated from weather data within a radius of 25 miles using the method developed by Di Luzio et al. (2008). The rest of the weather information (solar radiation, relative humidity and wind speed) used in SWAT simulation were generated by the WXGEN weather generator model (Sharpley and William 1990).

The area for stream definition was set as 3500 Ha, upon which the upper San Pedro River basin was divided into 116 subbasins. The divided subbasins matched 12-digit Hydrologic Unit Codes in the upper San Pedro watershed. The subbasins were further divided into HRUs based on the land use, soil, and slope types (0.1%, 1%, and 5%). The number of HRUs differs when using different LULC maps. As an example, the numbers of HRUs for 1992 and 1997 LULC are 2146 and 2225, respectively. There are 10 classes of LULC and 23 soil types in the upper San Pedro watershed. Watershed parameterization includes the calculation of subbasin geometry parameters from DEM and the assigning values to HRUs through inner database. The database of the SWAT model includes parameter values for crops, urban, and soils, such as CN2 values (SCS runoff curve number for moisture condition II), SOL_AWC (Available water capacity of the soil layer), LAI (leaf area index), and other soil physical and hydraulic properties. Values were assigned to each HRU based on its LULC class and soil type during the parameterization process. The simulation was initialized by setting default values of each parameter, a five year warm up period was applied to erase the impact of initial condition for the model calibration and validation.

SWAT Model Sensitivity Analysis, Calibration and Validation: A sensitivity analysis was first performed on parameters affecting streamflow using Latin hypercube (10 intervals) and one at a time (OAT) analysis with a ±5% parameter change (van Griensven et al., 2006). The analysis was done using the model set up with 1992 NALC LULC data and average streamflow response at the watershed outlet (subbasin 1) for five years from 1990 to 1994.

After sensitivity analysis, the model was calibrated by manually editing sensitive parameters for hydrological components (surface runoff, baseflow, lateral flow, ET, and channel transmission loss). Sensitive parameters on hydrological components were also reviewed from past sensitive studies of the model (Veith et al. 2010) and hydrological studies of the arid/semiarid areas (Hernandez et al. 2000, Goodrich et al. 1997). In this study, the lateral flow was assumed to be zero, because no obviously impervious layers in soil profiles, such as black shales, which were pre-required for the lateral flow to be generated, were observed in the watershed. The lateral flow was reduced to a very low level (close to zero) by changing the adjust factor for lateral flow (Adjf_latq) from the default value of 1 into 0.02 during SWAT simulations. Baseflow should be a very small portion recharging back to the stream because very large portions of the upper San Pedro River are ephemeral. At the Redington gauge (down- stream), the river only contains water during and immediately after a storm event and is dry the rest of the year. At the Tombstone and Charleston gauges (upper-stream), although the river flows intermittently, the water supply may not be from baseflow for the relatively higher elevation (corresponding to deeper groundwater table level values) than down-stream. Thus the baseflow was eliminated from simulations by reducing threshold water level in shallow aquifer for re-evaporation (REVAPMN) and enhancing the re-evaporation coefficient and threshold water level in shallow aquifer for baseflow (GWQMN).

Due to the availability of LULC (1992 and 1997) and the USGS data, simulations for model calibration were performed using the model set up of 1992 NALC LULC data which was also used for the sensitivity analysis. Annual (water year) and monthly streamflow from Oct. 1986 to Sept. 1995 at two USGS gauges (Redington and Charleston, Fig. 1) were used for model calibration. After model calibration, simulations for model validation were set up using 1997 Landsat Thematic Mapper LULC data; and annual (water year) and monthly streamflow

at Tombstone (10/1996 – 09/2005) and Charleston (10/1995 – 09/2005) were used for model validation. Validation was not performed at the Redington gauge station because monitoring data were not available after 1995. Three commonly used criteria were used to evaluate the model's performance on calibration and validation: Nash-Sutcliff efficiency (NSE) coefficient, coefficient of determination (R^2), and percent bias (PBIAS).

RESULTS AND DISCUSSION

Unique Hydrological Characteristics of the San Pedro River Watershed: Precipitation within the San Pedro Basin is generally characterized by a bimodal trend with a majority (about 70%) of the rainfall falling during the summer monsoon season (approximately mid-June to mid-October) and a minority (about 20%) during the winter wet season (early December to April) with the remaining throughout the rest of the year (Baillie et al. 2007). The Upper San Pedro watershed is characterized as semiarid conditions, and the sources of flow are attributed to intermittent precipitation governed by monsoon type rainfall events. As shown in Figure 2, the bimodal precipitation trend is reflected by the daily discharge data for 1985 plotted for each gaging station (Charleston, Tombstone, and Redington). In most channel locations (Figure 2) in the San Pedro River, low or intermittent baseflow with ephemeral peak discharge occuring during sporadic storm events was observed.

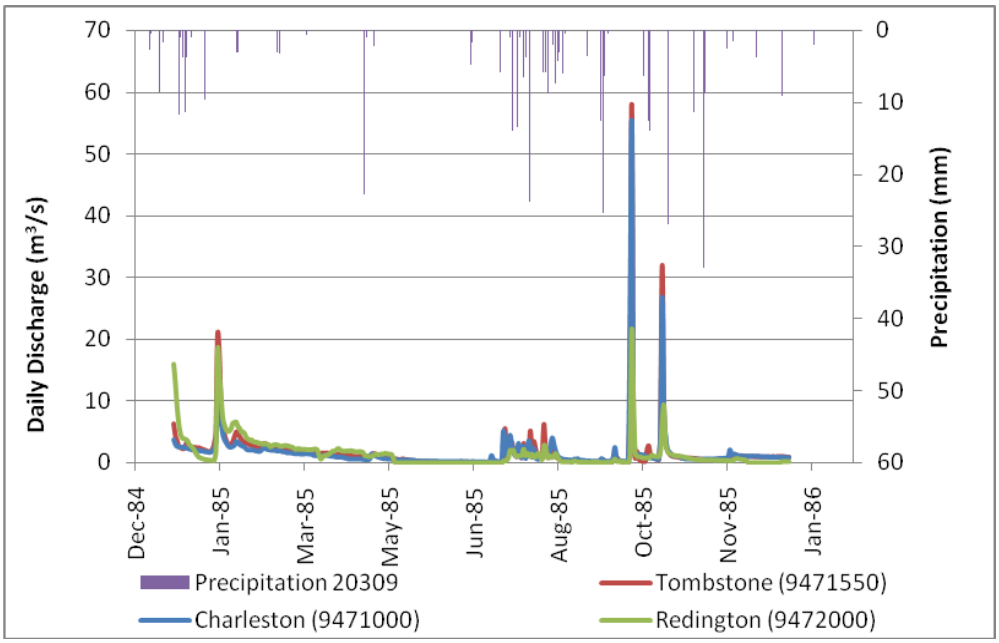

Figure 2 Daily Discharge (m^3/s) for from Jan. 1985 to Dec. 1985

Streamflow in gaining portions of the river is generally perennial; however, several sections of the upper San Pedro River can be classified as both gaining and losing reaches where streamflow is intermittent and associated with a mixture of monsoon water sources and aquifer sources stored in the alluvial groundwater. According to a USGS report released in 2010 (USGS, 2010), both gaining and losing reaches exist upstream from the gaging station near Tombstone. At the Tombstone gaging station, upstream groundwater flow to the vicinity of the stream is less than the volume of water removed by ET during the growing season; therefore, during the summer there is generally no base flow. The reach between the Charleston gauge and the Tombstone gauge is primarily losing (Kennedy and Gungle 2010). Following the summer monsoon, the water stored in near stream sediments must remain saturated for perennial flow to exist; however as shown in Figure 2 (1985 hydrograph), the summer flow is often insufficient to maintain flow in the fall, and thus, the upstream influent flow must re-saturate these sediments resulting in increased transmission loss and decreased to nonexistent streamflow conditions. The Redington station is the furthest downstream from the San Pedro River headwaters yet overall has the smallest response to rainfall events compared to the upstream stations. Transmission losses in the stream channel are likely responsible for this trend and must be considered accordingly when using a distributed model to simulate hydrologic conditions in this watershed. This trend is also noted in Figure 3 which depicts the annual runoff at each station from 1967 to 1985 (streamflow data is only available during 1967 to 1985 for all three gauge stations). Though the Redington station is hydrologically a larger stream order than the upstream gauge station locations, flow at Redington is characterized by containing the least amount of storm runoff and little baseflow

conditions. Larger order streams typically have greater baseflow and steadier flow conditions; however, this phenomena is not observed in this semiarid stream systems due to transmission losses and other factors, such as increased ET. Goodrich et al. (1997) found that the role of channel processes in semiarid watersheds becomes more critical in describing the peak runoff response as the size of drainage area increases. Transmission loss due to channel infiltration, evapotranspiration processes, and limited spatial uniformity of rainfall become dominant factors which limit the linearity of basin response to storm events in semiarid regions. Therefore, the accuracy of using a unit hydrograph, which assumes linearity in the response, in determining watershed runoff response in semiarid watersheds is not reliable due to the nonlinearity of the system.

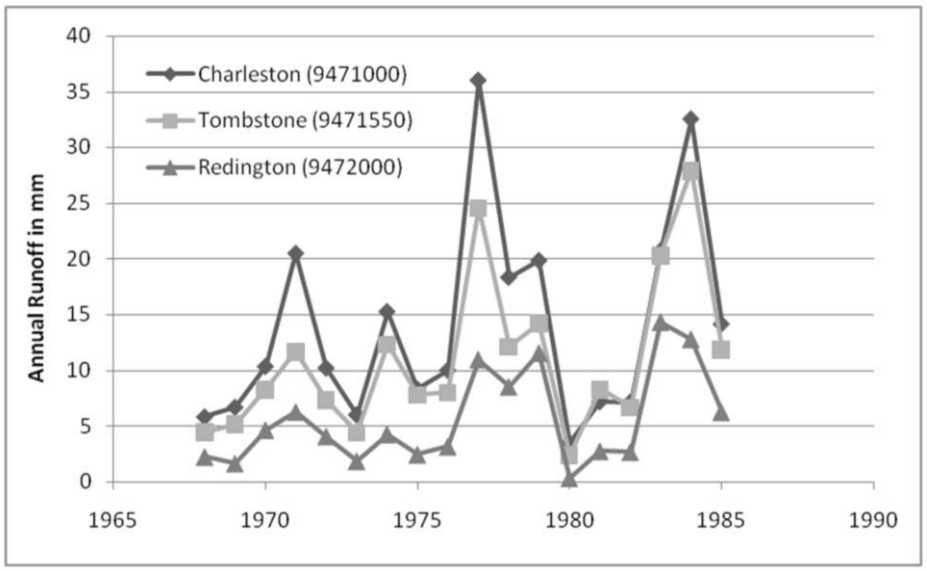

Figure 3 Annual Runoff at three gauges stations from 1967 to 1985

A recent USGS study statistically accounted for streamflow variations due to fluctuations in precipitation and found that predominant factors for the decrease in annual streamflow beyond fluctuations in precipitation and air temperature include changes in watershed characteristics, human activities, or changes in seasonal distribution of bank storage (Thomas and Pool 2006). Possible changes in watershed characteristics that may have influenced streamflow trends are changes in riparian vegetation, changes in landcover (mesquite invasion), and changes in stream-channel geomorphology. Human activities that may have influenced streamflow trends are ground-water pumping, construction of runoff-detention structures, urbanization, and cattle grazing. Seasonal pumping from wells near the river for irrigation in the spring and summer were a significant factor affecting streamflow; however, year-round pumping from wells in the regional aquifer away from the river did not significantly impact streamflow in the river (Thomas and Pool 2006).

Sensitivity Analysis and Calibration/Validation Results: The most sensitive input parameters are shown in Table 1. Those parameters are consistent with other SWAT parameter uncertainty and sensitivity analysis done for arid/semiarid conditions. The SWAT model is highly sensitive to surface runoff parameters (CN2, ESCO, SOL_AWC) and basin parameters (CH-K2) when the watershed is characterized by the intense and inconsistent precipitation events (Veith et al. 2010). High ratios of evaporation to precipitation may overwhelm the SWAT subsurface parameters (Veith et al. 2010); as does increased transmission loss due to stream bed geology and channel condition (gaining or losing) (Cataldo et al. 2010, Baillie et al. 2007). Since there is no persistent snowpack in the mountains of the San Pedro River Watershed, snowmelt and snowfall parameters were not shown to be sensitive for this watershed.

Surface runoff is the major water supply for the stream. Whereas, we noticed that streamflows were often under-estimated for light rainfall events and over-estimated for large rainfall events. Woodward et al. (2002) found that runoff estimates could be enhanced for relatively light rainfalls and be reduced for relative large rainfalls by changing the initial abstraction ratio to be 0.05 from its originally defined value of 0.2. Thus, to calibrate surface runoff, we set the initial abstraction ratio to be 0.05 and edited the CN2 (SCS runoff curve number) to a relatively low value to match the change of initial abstraction ratio. Channel transmission loss is a large portion (4% - 100%) of the water balance in the Walnut Gulch Experimental Watershed, a sub-watershed of the upper San Pedro River basin (Cataldo et al. 2010). USGS records show that monthly streamflow (in volume) at

downstream locations (Redington gauge) is not always larger than in upperstream (Tombstone and Charleston gauges), indicating that transmission loss exists for the major channel (stream order 4 and 5). However, it's hard to quantify the ratio of channel transmission loss to total water recharge. To calibrate the transmission loss, we set the TRNSRCH (Fraction of transmission loss partitioned into deep aquifer) to be 1 and manually edited the effective hydraulic conductivity of channel (CH_K2). The optimal values for SWAT calibration were listed in Table 1.

Table 1 Top ranking sensitive parameters (in the order of ranking) and their description, default and calibrated values that were used in the model calibration/validation (*, the multiple sign, indicates that default parameter values are multiplied by the number shown).

Parameter	Default	Description	Calibrated Value
Adjf_latq	1	Adjust factor for lateral flow	0.02
λ	0.2	Initial Abstraction Ratio	0.05
CN2	30-92	SCS runoff curve number for moisture condition II	*0.58
ESCO	0.95	Soil evaporation compensation factor	0.05
Revapmn	1	Threshold water level in shallow aquifer for revap	0
SOL_AWC	0.01-0.19	Available water capacity of the soil layer	*1.4
Sol_K		Saturated hydraulic conductivity of first layer	
CH_K2	0	Effective hydraulic conductivity of channel	0.6
GW_Revap	0.02	Revaporation coefficient	0.2
GWQMN	0	Threshold water level in shallow aquifer for baseflow	100
TRNSRCH	0	Fraction of transmission loss partitioned into deep aquifer	1

The comparison between simulated and observed annual (in water year) and monthly streamflow for the periods of calibration (Oct. 1986 – Sept. 1995) and validation (Oct. 1996 – Sept. 2005) are shown in Figures 4 and 5, respectively. Overall, a good match can be seen between simulated and observed values. The NS and R^2 values for the annual (in water year) and monthly calibration and validation are listed in Table 2. All NS and R^2 values are above 0.5 (except NS coefficient for annual calibration at the Redington gauge), and PBIAS are in the range of ± 25% (except annual calibration at the Charleston gauge), suggesting satisfactory model performance (Moriasi et al. 2007). Although the overall performance of the model is satisfactory as shown in Figures 4 and 5, and Table 2, a large difference was observed for the water year of 1992 at the Redington gauge and in 1993 at both the Redington and Charleston gauges. Intuitively, the simulated values seem more reasonable because they match the rainfall patterns as shown in Figure 4. Possible reasons for the discrepancies are the limitation of the curve number method. First, high uncertainties could be generated by using daily total rainfall depth as SWAT input. As an example, a large amount of streamflow (4.21 mm) at the Redington gauge on Aug. 1992 simulated in the SWAT model was mainly attributed to a daily rainfall of 127.8 mm on Aug. 24, 1992 in the downstream of the watershed close to the Redington gauge. Whereas, the rainfall depth at that day could be the combination of several relatively small rainfall events, which may not be able to generate significant runoff (recorded streamflow in Aug. 1992 is 0.58 mm). Second, the curve number method fails to consider the effects of duration and intensity of precipitation. For instance, runoff could be generated by some high-intensity, short-duration, limited areal extent summer thunderstorms (Simanton et al. 1996) near the observation gauges. Whereas, those limited areal extent summer thunderstorms may not be simulated by the SWAT model for a large extent.

Another reason for simulated streamflow peaks not fully matching with observations is due to the high heterogeneity of rainfall across the watershed. Rainfall events in the upper San Pedro watershed were mainly composed of high-intensity, short-duration, limited areal extent summer thunderstorms (Thomas and Pool 2006, Kennedy and Gungle 2010). The high heterogeneity of rainfall may not be fully represented by weather stations used in SWAT simulations in this study. Syed et al. (2003) used interpolated values from raingauges and found that the storm event's areal coverage, location within the watershed, and intensity are factors that impact runoff generation, which vary greatly as catchment size increases. SWAT has been shown to adequately simulate streamflow using sparse raingauge data over large arid basin areas, especially when combined with precipitation data estimated from radar predictions (Yu et al. 2011).

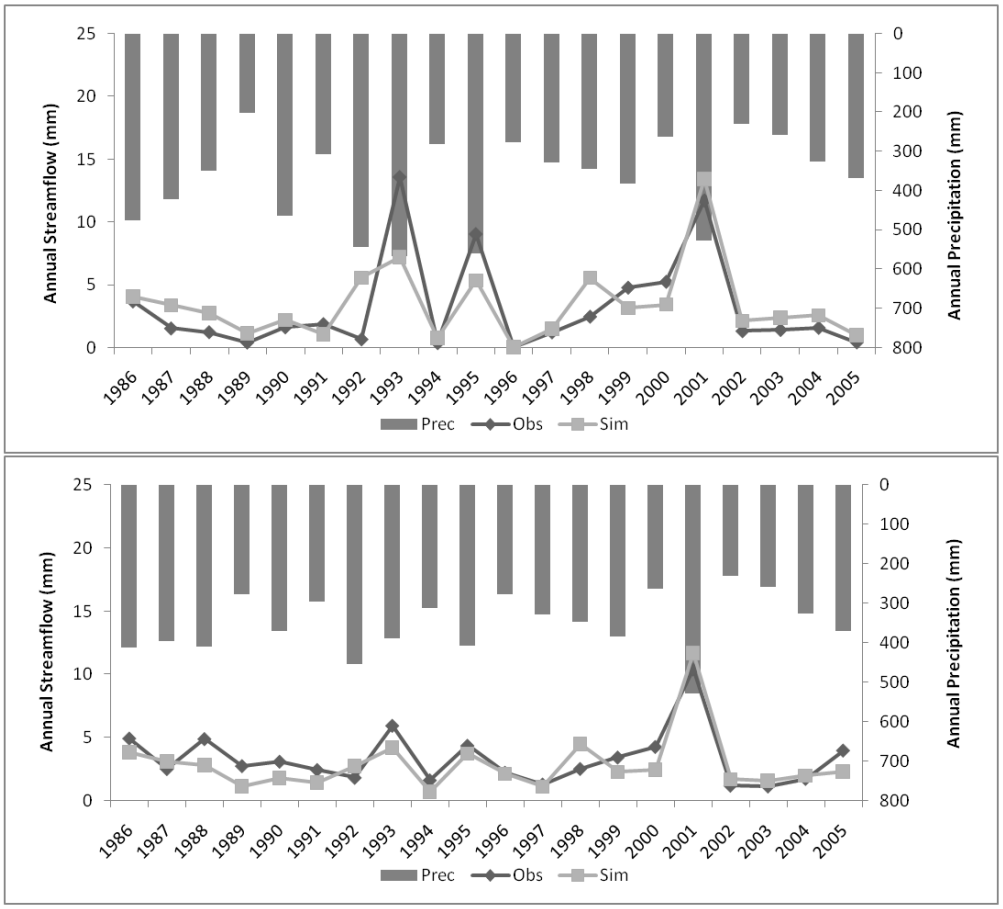

Figure 4 Annual (in water year) precipitation and simulated and observed streamflow in the upper San Pedro Watershed. Upper: Redington (1986 – 1995) and Tombstone (1997 – 2005) gauges; Lower: Charleston gauge (1986 – 2005).

A calibrated and validated SWAT model can be used to assess current conditions in the watershed, and then be used to evaluate alternative management scenarios. SWAT provided good correlation of simulated streamflow conditions, which have been applied to scenario analysis of management practices aimed to evaluate the effects of landuse changes on hydrological response (Ouessar et al. 2009, Ghaffari et al. 2010, Hernandez et al. 2000). Arid/semiarid watersheds are often coupled with issues of data availability. SWAT simulations using remote sensing input data have adequately simulated overland flow, channel flow, and transmission losses in watersheds where streamflow and climatic data are lacking (Al-Dousari et al. 2010, Hernandez-Guzman et al. 2008). The SWAT model has been found useful in arid/semiarid watershed analysis of the effect of landuse changes on hydrological properties and changes of water balance components due to crop management (Ghaffari et al. 2010, Hernandez et al. 2000).

Table 2 Criteria for examining the accuracy of calibration and validation (the validation period at Tombstone gauge is from Oct. 1996 to Sept. 2005).

Index	Calibration (10/1985 - 09/1995)				Validation (10/1995 - 09/2005)			
	Redington		Charleston		Tombstone		Charleston	
	Yearly	Monthly	Yearly	Monthly	Yearly	Monthly	Yearly	Monthly
NS Coefficient	0.45	0.56	0.82	0.52	0.94	0.57	0.93	0.55
R^2	0.66	0.57	0.66	0.55	0.84	0.70	0.82	0.70
PBIAS	1.94	-1.29	25.46	24.63	-16.27	-9.23	1.38	3.00

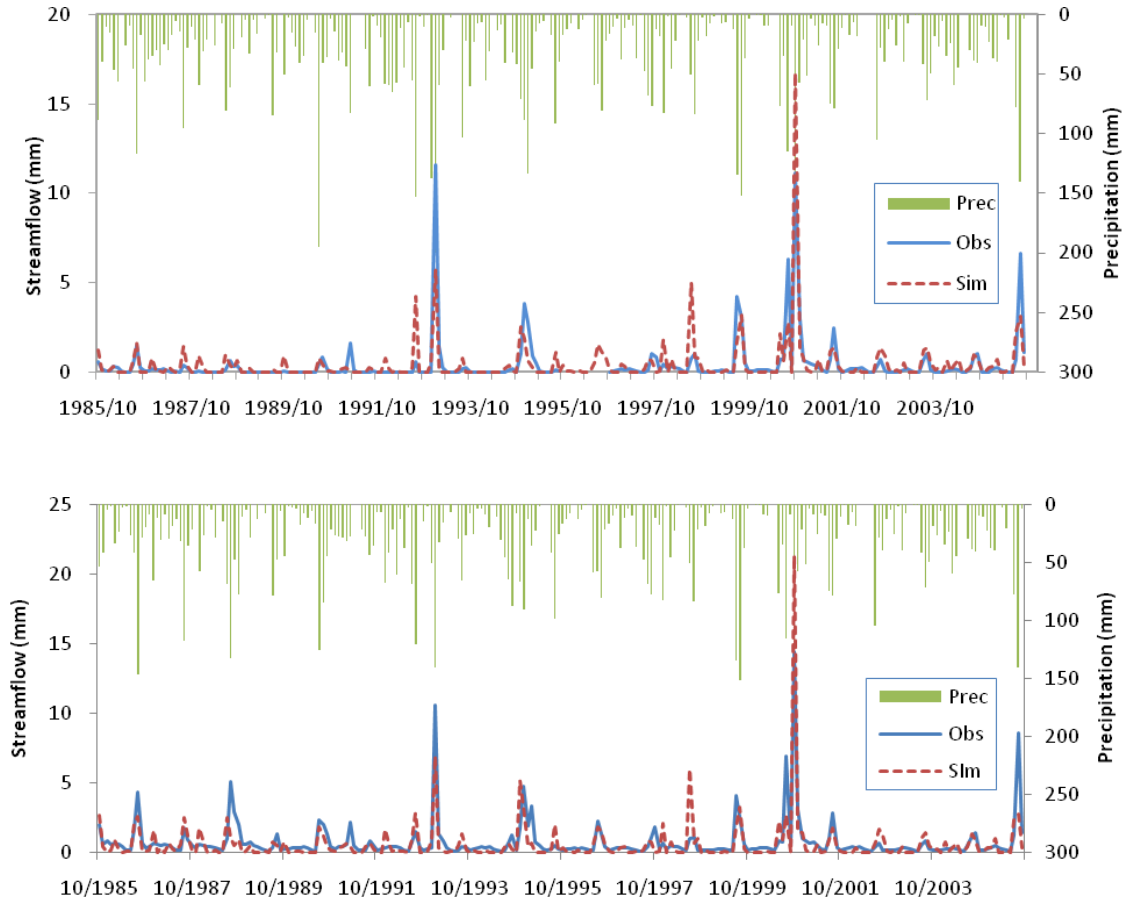

Figure 5 Monthly precipitation and simulated and observed streamflow in the upper San Pedro watershed. Upper: Redington (10/1985-09/1995) and Tombstone (10/1996-09/2005) gauges; Lower: Charleston gauge (10/1985-09/2005).

CONCLUSIONS

Identifying the impacts of LULC changes on hydrologic processes is the basis for watershed management and ecological restoration efforts. Semiarid regions of the southwest United States have unique hydrologic characteristics that create challenges for watershed modelers. Streamflow in these regions is largely dependent on short term, high intensity rainfall events during the summer monsoon season. In this study, the hydrology of the upper San Pedro watershed was assessed based on review of USGS trend analysis reports, historical precipitation and stream discharge patterns. Based on the hydrological characteristics of the region, SWAT sensitivity analysis for this watershed and findings from other studies performed under similar watershed conditions, sensitive SWAT model parameters were determined and calibrated to achieve suitable simulations of the watershed hydrologic processes. The SWAT model input parameters were modified to simulate the limited baseflow conditions, increased ET and transmission loss, and decreased runoff in downstream gauge stations observed in the watershed. All NS and R2 values were above 0.5 (except NS coefficient for annual calibration at the Redington gauge), and PBIAS were in the range of ± 25% (except annual calibration at the Charleston gauge), suggesting satisfactory model performance. Thus, the SWAT model, set up with the optimal parameters obtained through model calibration, generally reflects the hydrological characteristics of this arid/semiarid watershed. A calibrated and validated SWAT model can assess current conditions in the watershed, and then be used to evaluate alternative management scenarios.

ACKNOWLEDGEMENTS

The authors are grateful for the valuable comments and suggestions provided by reviewers.

Notice: Although this work was reviewed by the USEPA, and approved for publication, it may not necessarily reflect official Agency policy. Mention of trade names or commercial products does not constitute endorsement

or recommendation for use.

REFERENCES

Al-Dousari, A., Milewski, A., Din, S.U., and Ahmed, M. 2010. Remote Sensing Inputs to SWAT Model for Groundwater Recharge Estimates in Kuwait. *Advances in Natural and Applied Sciences,* 4(1), 71-77.

Arias, H. 2000. International groundwaters: The Upper San Pedro River Basin case. *Natural Resources Journal,* 40(2), 199-221.

Arnold, J.G., Allen, P.M., and Bernhardt, G. 1993. A Comprehensive Surface-Groundwater Flow Model. *Journal of Hydrology,* 142(1-4), 47-69.

Arnold, J.G., Srinivasan R, Muttiah R.S., and Williams J.R. 1998. Large area hydrologic modeling and assessment - Part 1: Model development. *Journal of the American Water Resources Association,* 34(1), 73-89.

Baillie, M.N., Hogan, J.F., Ekwurzel, B., Wahi, A.K., and Eastoe, C.J. 2007. Quantifying water sources to a semiarid riparian ecosystem, San pedro river, Arizona. *Journal of Geophysical Research-Biogeosciences,* 112(G3), 1-13.

Biggs, J.B., 2009. *Continuation of stage I drought response for Tucson water service area.*

Cataldo, J.C., Behr, C., Montalto, F.A., and Pierce, R.J. 2010. Prediction of Transmission Losses in Ephemeral Streams, Western U.S.A. . *The Open Hydrology Journal,* 4, 19-34.

Di Luzio, M., Johnson, G.L., Daly, C., Eischeid, J.K., and Arnold, J.G. 2008. Constructing retrospective gridded daily precipitation and temperature datasets for the conterminous United States. *Journal of Applied Meteorology and Climatology,* 47, 475-497.

Gassman P.W, Reyes, R.M., Green C.H., and Arnold J.G. 2007. The soil and water assessment tool: Historical development, applications, and future research directions. *Transactions of the Asabe,* 50, 1211-1250.

Gesch, D., Oimoen, M., Greenlee, S., Nelson, C., Steuck, M., and Tyler, D. 2002. The National Elevation Dataset. *Photogrammetric Engineering and Remote Sensing,* 68(1), 829-840.

Ghaffari, G., Keesstra, S., Ghodousi, J., and Ahmadi, H. 2010. SWAT-simulated hydrological impact of land-use change in the Zanjanrood Basin, Northwest Iran. *Hydrological Processes,* 24(7), 892-903.

Goodrich, D.C., Lane, L.J., Shillito, R.M., Miller, S.N., Syed, K.H., Woolhiser, D.A.1997. Linearity of basin response as a function of scale in a semiarid watershed. *Water Resources Research,* 33, 2951-2965.

Gupta, H.V., Sorooshian, S., and Yapo, P.O. 1999. Status of Automatic Calibration for Hydrologic Models: Comparison with Multilevel Expert Calibration. *Journal of Hydrologic Engineering,* 4(2), 135-143.

Hargreaves, G.L., Hargreaves, G.H., and Riley, J. P. 1985. Agricultural Benefits for Senegal River Basin. *Journal of Irrigation and Drainage Engineering-Asce,* 111(2), 113-124.

Hernandez-Guzman, R., Ruiz-Luna, A. and Berlanga-Robles, C. A. 2008. Assessment of runoff response to landscape changes in the San Pedro subbasin (Nayarit, Mexico) using remote sensing data and GIS. *Journal of Environmental Science and Health Part a-Toxic/Hazardous Substances & Environmental Engineering,* 43(12), 1471-1482.

Hernandez, M., Miller, S.N., Goodrich, D.C., Goff, B.F., Kepner, W.G., Edmonds, C.M., and Jones, K.G. 2000. Modeling Runoff Response to Land Cover and Rainfall Spatial Variability in Semi-Arid Watersheds. *Environmental Monitoring and Assessment,* 64(1), 285-298.

Hooghoudt, S.B. 1940. Bijdrage tot de kennis van enige natuurkundige grootheden van de grond. *Versl. Landbouwkd. Onderz.,* 46, 515-707.

Kennedy, J.R., and Gungle, B. 2010. *Quantity and Sources of Base Flow in the San Pedro River near Tombstone, Arizona.* U.S. Geological Survey Scientific Investigations Report 2010–5200, Scientific Investigations Report 2010–5200.

Kepner, W., Edmonds, C.M., and Watts, C.J. 2002. Remote Sensing and Geographic Information Systems for Decision Analysis in Public Resource Administration: A Case Study of 25 Years of Landscape Change in a Southwestern Watershed., 31.

Kepner, W., Watts, C.J., Edmonds, C.M., Maingi, J.K., Marsh, S.E., and Luna, G. 2000. A Landscape Approach for Detecting and Evaluating Change in a Semi-Arid Environment. *Environmental Monitoring and Assessment,* 64(1), 179-195.

Monteith, J.L., 1965. Evaporation and environment. *19th Symposia of the Society for Experimental Biology.* London, U.K.: Cambridge University, 205-234.

Moriasi D.N., Arnold J.G., Van Liew M.W., Bingner R.L., Harmel R.D., Veith T.L. 2007. Model evaluation guidelines for systematic quantification of accuracy in watershed simulations. *Transactions of the Asabe,* 50(3), 885-900.

Nash, J. E. and Sutcliffe, J. V. 1970. River flow forecasting through conceptual models part I - A discussion of principles. *Journal of Hydrology and Hydromechanics,* 10(3), 282-290.

Neitsch S.L., Arnold J.G., Kiniry J.R., and Williams J.R. 2005. *Soil and Water Assessment Tool. Theoretical Documentation. Version 2005*. Temple, TX.

Orr, P. and Colby, B. 2004. Groundwater management institutions to protect riparian habitat. *Water Resources Research*, 40(12), 1-9.

M. Ouessar, M., Bruggeman, A., Abdelli, F., Mohtar, R.H., Gabriels, D., and Cornelis, W.M. 2009. Modelling water-harvesting systems in the arid south of Tunisia using SWAT. *Hydrology and Earth System Sciences*, 13(10), 2003-2021.

Pilgrim, D.H., Chapman, T.G., and Doran, D.G. 2009. Problems of rainfall-runoff modelling in arid and semiarid regions. *Hydrological Sciences Journal*, 33(4), 379-400.

Priestley, C., and Taylor, R.J. 1972. Assessment of Surface Heat-Flux and Evaporation Using Large-Scale Parameters. *Monthly Weather Review*, 100(2), 81-82.

Rallison, R.E., and Miller, N., 1981. *Past, Present and future SCS runoff procedure.* Littleton, CO: Water Resources Publication.

Sharpley, A.N., and William, J.R. 1990. *EPIC-Erosion/Productivity Impact Calculator: I -- model documentation.* U.S. Department of Agriculture Tech. Bull.

Simanton, J.R., Hawkins, R.H., MohseniSaravi, M., and Renard, K.G. 1996. Runoff Curve Number Variation with Drainage Area, Walnut Gulch, Arizona. 39(4), 1391-1394.

Solan, P.G., Morre, I.D., Coltharp, G.B., and Eigel, J.D. 1983. *Modeling surface and subsurface stormflow on steeply-sloping forested watersheds. Water Resource Inst. Report 142.* Lexington: University of Kentucky.

Steiner, F., Blair, J., McSherry, L., Guhathakurta, S., Marruffo, J., and Holm, M. 2000. A watershed at a watershed: the potential for environmentally sensitive area protection in the upper San Pedro Drainage Basin (Mexico and USA). *Landscape and Urban Planning*, 49(3-4), 129-148.

Steinitz, C. 2003. Chapter 2: The Upper San Pedro River Basin. *Alternative Futures for Changing Landscapes: The Upper San Pedro River Basin in Arizona and Sonora.* Washington, DC: Island Press, 9-12.

Stromberg, J.C., Bagstad, K.J., Leenhouse, J.M., Lite, S.J., and Makings, E. 2005. Effects of stream flow intermittency on riparian vegetation of a semiarid region river (San Pedro River, Arizona). *River Research and Applications*, 21(8), 925-938.

Stromberg, J.C., Tiller, R. and Richter, B. 1996. Effects of groundwater decline on riparian vegetation of semiarid regions: The San Pedro, Arizona. *Ecological Applications*, 6(1), 113-131.

Syed K.H., Goodrich, D.C., Myers, D.E., and Sorooshian, S. 2003. Spatial characteristics of thunderstorm rainfall fields and their relation to runoff. *Journal of Hydrology* 271: 1-21.

Thomas, B.E., and Pool, D.R. 2006. *Trends in Streamflow of the San Pedro River, Southeastern Arizona, and Regional Trends in Precipitation and Streamflow in Southeastern Arizona and Southwestern New Mexico.* U.S. Geological Survey Professional Paper 1712.

USDA, NRCS, 2004. National Engineering Handbook, Part 630, Hydrology. Chapter 8, Land Use and Treatment Classes.

USDA, NRCS, 2004. National Engineering Handbook, Part 630, Hydrology. Chapter 9, Hydrologic Soil-Cover Complexes.

USDA, NRCS, 2004. National Engineering Handbook, Part 630, Hydrology. Chapter 10, Estimation of Direct Runoff from Storm Rainfall.

USDA, NRCS, 2007. National Engineering Handbook, Part 630, Hydrology. Chapter 19, Transmission Losses.

USEPA, 1993. *North American Landscape Characterization (NALC) Research Brief. EPA/600/S-93/0005.* Washington, D.C.: Office of Research and Development.

USGS, 2010. Quantity and Sources of Base Flow in the San Pedro River near Tombstone, Arizona. Available at http://pubs.usgs.gov/sir/2010/5200/. Accessed on Dec. 20. 2014.

Veith, T.L., Van Liew, M.W., Bosch, D.D., and Arnold, J.G. 2010. Parameter Sensitivity and Uncertainty in SWAT: A Comparison Across Five USDA-ARS Watersheds. *Transactions of the Asabe*, 53(5), 1477-1486.

Webb, R.H., and Leake, S.A. 2006. Ground-water surface-water interactions and long-term change in riverine riparian vegetation in the southwestern United States. *Journal of Hydrology*, 320(3-4), 302-323.

Woodward, D.E., Hawkins, R.H., Jiang, R, Hjelmfelt, A.T., Van Mullem, J.A., and Quan, Q.D. 2004. Runoff Curve Number Method: Examination of the Initial Abstraction Ratio. ed. *Proceedings of the Second Federal Interagency Hydrological Modeling Conference*, 2002 Las Vegas, NV.

Yu, M., Chen, X., Li, L., and Bao, A. 2011. Streamflow Simulation by SWAT Using Different Precipitation Sources in Large Arid Basins with Scarce Raingauges. *Water Resources Management*, 25(11), 2669-2681.

THE KINEROS2 – AGWA SUITE OF MODELING TOOLS

David C. Goodrich, Research Hydraulic Engineer, USDA-ARS, Tucson, AZ, dave.goodrich@ars.usda.gov; Carl L. Unkrich, Hydrologist, USDA-ARS, Tucson, AZ, carl.unkrich@ars.usda.gov; Yoganand Korgaonkar, Graduate Student, University of Arizona, Tucson, AZ, yoganandk@email.arizona.edu; Shea Burns, Senior Research Specialist, University of Arizona, Tucson, AZ, shea.burns@ars.usda.gov; Jeff Kennedy, USGS, Tucson, AZ, Hydrologist, USGS, Tucson, AZ, jkennedy@usgs.gov; Gabriel Sidman, GIS Analyst, Winrock International, Washington, D.C., gabriel.sidman@winrock.org; Brian Scott Sheppard, Graduate Student, University of Arizona, Tucson, AZ, bss1@email.arizona.edu; Mariano Hernandez, Associate Research Scientist, University of Arizona, Tucson, AZ, mariano.hernandez@ars.usda.gov; Phil Guertin, Professor, University of Arizona, Tucson, AZ, dpg@email.arizona.edu; Scott N. Miller, Professor, University of Wyoming, snmiller@uwyo.edu; William Kepner, Research Ecologist, EPA-LEB, Las Vegas, NV, kepner.william@epa.gov; Phil Heilman, Research Leader, USDA-ARS, Tucson, AZ, phil.heilman@ars.usda.gov; Mark Nearing, Research Agricultural Engineer, USDA-ARS, Tucson, AZ, mark.nearing@ars.usda.gov

INTRODUCTION

KINEROS2 (K2) originated in the 1960s as a distributed event-based rainfall-runoff erosion model abstracting the watershed as a cascade of overland flow elements contributing to channel model elements. Development and improvement of K2 has continued for a variety of projects and purposes resulting in an informal suite of K2-based modeling tools. Like any detailed, distributed watershed modeling tool, the K2 suite of tools can require considerable time to delineate watersheds, discretize them into modeling elements and then parameterize these elements. These requirements motivated the development of the Automated Geospatial Watershed Assessment (AGWA) tool. This ESRI ArcGIS-based tool uses nationally available, GIS data layers to parameterize, execute, and visualize results from the SWAT and KINEROS2 models. By employing these two models, AGWA can conduct watershed modeling and assessments at multiple time and space scales. The objectives of this paper are to: 1) Provide background in the development of K2 and AGWA; 2) Provide an overview of new features; 3) Briefly describe recent novel applications; and 4) Discuss plans for future model improvements.

KINEROS2 / (K2) – History: The USDA-Agricultural Research Service (ARS) initiated development of KINEROS2 (KINematic runoff and EROSion), or K2 in the late 1960s as a distributed event-based rainfall-runoff model. Conceptualization of the watershed in this form enables solution of the flow-routing partial differential equations in one dimension. Rovey (1974) coupled interactive infiltration to this model and released it as KINGEN. After substantial validation using experimental data, KINGEN was modified to include erosion and sediment transport as well as a number of additional enhancements, resulting in KINEROS, which was released in 1990 (Woolhiser et al., 1990; Smith et al., 1995).

KINEROS has been applied over a wide range of scales, from plot (<10 m^2) to large watersheds on the order of a thousand square kilometers. However, it has only been thoroughly validated for watersheds on the order of a hundred square kilometers where sufficient observations exist in

experimental watersheds (Goodrich et al., 2004). It was originally developed as an event-based model. Simulation times can vary from tens of minutes for small plots to more than a day for larger watersheds depending on the respective runoff response time. Computational time scales are dictated by adherence to the Courant condition (Roberts, 2003). Computational time intervals are automatically adjusted in the current model implementation, and the user can select the time interval at which simulation output is reported. Subsequent research with and application of KINEROS has led to additional model enhancements and a more robust model structure, which have been incorporated into the latest version of the model: KINEROS2 (K2).

Specialized versions of the event-based KINEROS2 model range from a flash-flood forecasting tool and the continuous KINEROS-OPUS biogeochemistry tool. The K2 flash flood forecasting tool is being tested with the National Weather Service (NWS) to provide timing and magnitude of peak flows from rapidly responding flash flood storms, that is useful information currently not available using NOAA/NWS flash flood forecasting methodologies at NWS offices. It assimilates the NWS Digital Hybrid Reflectivity (DHR) radar product in near-real time and can simultaneously run ensembles using multiple radar-reflectivity relationships (Unkrich et al., 2010). In addition to simulation of runoff and sediment transport, KINEROS-OPUS (K2-O2) can simulate management, plant growth, nutrient cycling (nitrogen, phosphorus and carbon), water quality and chemical runoff (Massart et al., 2010). K2 has also been coupled with a continuous energy-balance snow model and lateral saturated subsurface transport (K2-SM-hsB; Broxton et al., 2014). In addition, K2 has been used as the engine for runoff generation and routing for the overland transport of manure-borne pathogens and indicator organisms (K2-STWIR). STWIR was released as a separate software package (Guber et al. 2010) followed by sensitivity and uncertainty analysis (Guber et al., 2014). A relatively thorough overview of the theoretical background of K2, including several applications, is presented by Semmens et al. (2008). More recently, Goodrich et al. (2012) provided further details on K2 and included a discussion of model limitations, expectations, and strategies and approaches for K2 calibration and validation. K2 is open-source software that is distributed freely, along with associated model documentation and example input files (www.tucson.ars.ag.gov/kineros).

AGWA History and Overview: The Automated Geospatial Watershed Assessment (AGWA) tool was initially released in 2002 (Miller et al., 2002) to support the parameterization and execution of K2/KINEROS2 and the Soil Water Assessment Tool (SWAT; Arnold and Fohrer, 2005). AGWA parallels other efforts (ArcSWAT, BASINS, MWSWAT, HEC-GeoHMS, ArcAPEX) that use Geographic Information Systems (GIS) to support the application of hydrologic models, but distinguishes itself by offering models that allow it to be used on a continuum of spatial and temporal scales, ranging from hillslopes (~hectares) to large watersheds (>1000 km^2) and from individual storm events (minute time steps) to continuous simulation (daily time steps over multiple years). Like K2, AGWA is open-source software available from the AGWA website (Miller et al., 2007; www.tucson.ars.ag.gov/agwa). This site also contains documentation, supporting references, tutorials, and a user forum. Support for K2 and AGWA is typically accomplished via the user forum, e-mail, and phone communication. We also welcome visitors to the USDA-ARS Southwest Watershed Research Center to work with model developers on application projects and/or model improvements.

The development of AGWA has been a joint effort with the USDA-ARS SWRC, US EPA LEB, University of Arizona, and University of Wyoming. It has been under continual development to incorporate new features and functionality and has seen multiple major and minor releases, including but not limited to: AGWA 1.3 for ArcView 3.x in 2002 (initial AGWA release); AGWA 2.0 for ArcGIS 9.x in 2007 (initial ArcGIS/ArcMap 9.x release); AGWA 2.4 for ArcGIS 10.x in 2011 (initial ArcGIS/ArcMap 10.x release); and AGWA 3.x for ArcGIS 10.x in 2013 (current major release for ArcGIS/ArcMap 10.x).

The guiding principles for the development of AGWA include: 1) that it provides simple, direct, transparent, and repeatable parameterization routines through an automated, intuitive interface; 2) that it is applicable to ungauged watersheds at multiple scales; 3) that it evaluates the impacts of management and be useful for scenario development; and 4) that it uses free and commonly available GIS data layers. From the very first release in 2002 to the most current release in 2015, AGWA has followed these guidelines to ensure it can be used by the widest possible audience, which, to name a few, includes multiple EPA regions (Burns et al., 2013a; Barlow et al., 2014; and Korgaonkar et al., 2014), land use impact studies on water resources in Africa (Baker and Miller, 2013), predictive modeling of oil and gas development impacts (Miller et al., 2012), and numerous Federal Agencies working collaboratively on Dept. of Interior National Interagency BAER (Burned Area Emergency Response) teams modeling hydrological impacts of wildfire (EPA, 2014; Goodrich et al., 2012) and for the Natural Resources Conservation Service (NRCS) Conservation Effects Assessment Project (CEAP).

AGWA has been integrated into the EPA Council for Regulatory Environmental Modeling (CREM) Models Knowledge Base[1] as well as the Registry of EPA Applications, Models and Databases (READ)[2]. All versions of AGWA have been included in the Downloadable GIS Tools section of the EPA EnviroAtlas[3]. In addition a Certificate of Networthiness (CoN) has been obtained for AGWA that enables its use on U.S. Army cyber infrastructure. Additional information and details on AGWA are presented in the following section as there has not been a recent detailed publication on AGWA unlike K2 (Goodrich et al., 2012).

AGWA Data Requirements and Process: **AGWA supports watershed modeling efforts by including functionality that steps through all stages of a watershed assessment, including: watershed delineation; watershed discretization into discrete model elements; watershed parameterization; precipitation definition; model simulation creation; model execution; and model results visualization. Various data are required to support this functionality, including: a raster-based DEM (digital elevation model); a polygon soil map (NRCS SSURGO, NRCS STATSGO, or FAO soil maps are supported); and a classified, raster-based land cover (NLCD, NALC, and SWGAP datasets are supported via provided look-up tables, however other datasets may also be used if accompanied with a respective look-up table). AGWA does not require observed precipitation or runoff to drive the models when used for relative assessment/differencing between scenarios, and can use user-defined**

[1] http://cfpub.epa.gov/crem/knowledge_base/crem_report.cfm?deid=75821
[2] http://ofmpub.epa.gov/sor_internet/registry/systmreg/resourcedetail/general/description/description.do?infoResourcePkId=11982
[3] http://enviroatlas.epa.gov/enviroatlas/tools/agwa.html

depths and durations, user-defined hyetographs, or design storms to drive K2, and included weather station-based generated, daily precipitation (U.S. only) to drive SWAT. However, high-quality rainfall-runoff observations are required for calibration and confidence in quantitative model predictions (Goodrich et al., 2012). The AGWA process is described in more detail below and in Figure 1.

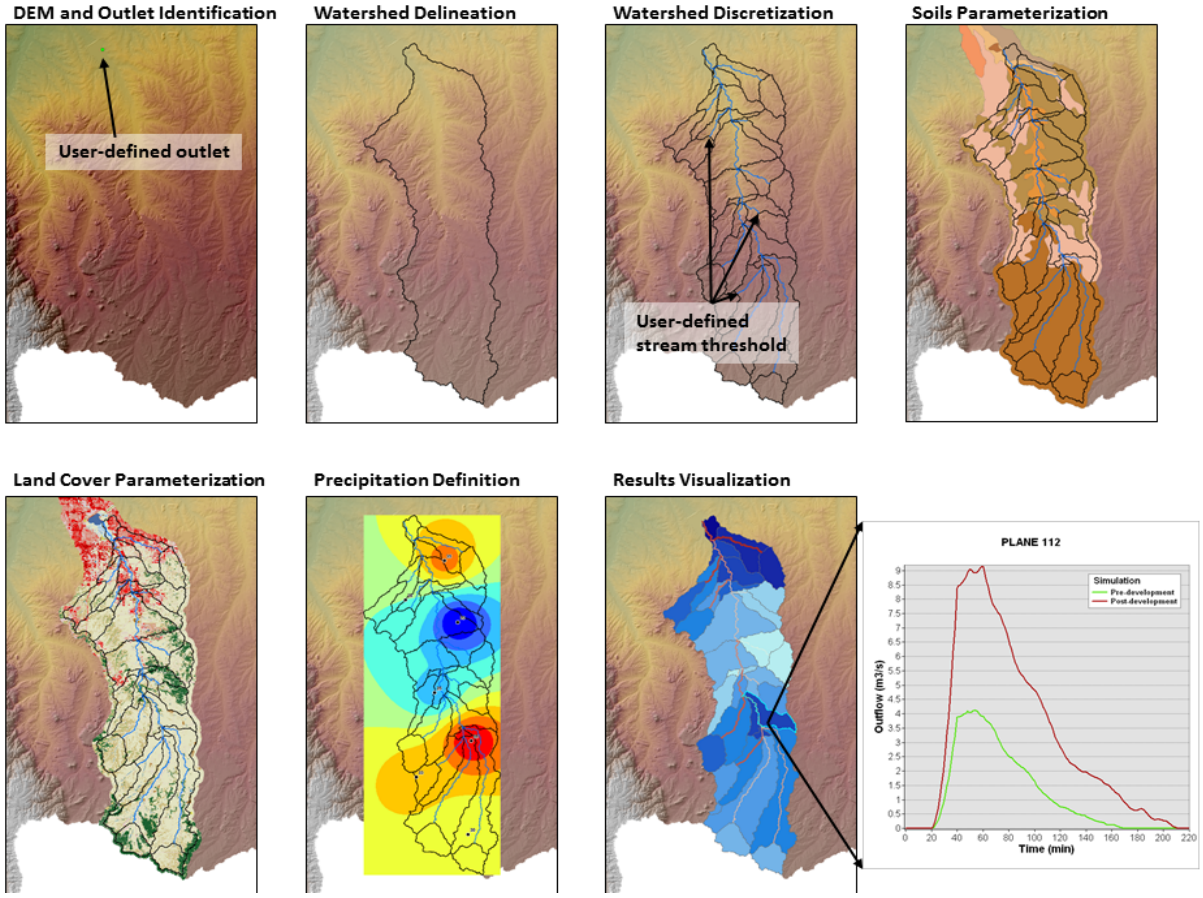

Figure 1 The required steps in AGWA to perform a watershed assessment. A DEM is used to delineate the watershed, subdivide it into model elements, and parameterize the elements in conjunction with the soils and land cover layers. Precipitation drives the model and model results are imported and visualized in the GIS. For any model element selected hydrographs and sedigraphs can be displayed (lower right).

Watershed Delineation: Watersheds delineation is performed by, at a minimum, selecting a workspace location, delineation name, DEM, and watershed outlet. If the DEM has not been filled to ensure proper drainage, AGWA will fill it. Likewise, if a flow direction raster and a flow accumulation raster have not been selected, AGWA will create them in the delineation process. Selecting a watershed outlet entails selecting a pre-existing outlet point or by defining an outlet and snapping it to the highest flow accumulation value within a user-defined search radius. Alternatively, the user can delineate a group of watersheds using multiple pre-existing outlet points or by selecting an area of interest (such as a political, management, or administrative

boundary) and defining a maximum extent for the group of watersheds. Watershed delineations are stored as feature classes within a geodatabase created during this step.

Watershed Discretization: Watershed discretization is performed by defining a stream network for the watershed delineation and subdividing the watershed based on the stream network. Various methods exist for creating the stream network, including: a minimum accumulated area required for stream definition (contributing source area, or CSA, approach); a minimum accumulated flow length required for stream definition (flow length approach); or a pre-existing stream network approach where stream initiation is defined by the upstream most points of a user-selected, existing stream network snapped to the underlying stream network of the DEM (the upstream most points are snapped to the highest flow accumulation or highest flow length within a user-defined snapping distance). Model selection is also defined during the watershed discretization step because the models have non-compatible watershed representations. Watershed discretizations are stored as feature datasets containing single polygon, polyline, and nodes feature classes within the geodatabase created in the watershed delineation.

Watershed Parameterization: Watershed parameterization is performed by intersecting the model elements from the watershed discretization with the DEM, a DEM-derived slope raster, a soils polygon, and a land cover raster. The model elements are then characterized using the topographic, soil, and land cover properties from the layers they intersect and these parameters are stored in related tables (with a parameterization name to identify it) within the geodatabase created in the watershed delineation.

Precipitation Definition: Precipitation definition is performed differently for each model because of the difference between event-based precipitation versus continuous daily precipitation. For K2, precipitation is created using user-defined hyetographs, user-defined depths and durations, pre-defined design storms, or raster-based precipitation surfaces representing return period-duration depths. For non-user-defined hyetographs, K2 precipitation events can be represented with a uniform intensity or with an intensity derived from the SCS Type II distribution. For SWAT, precipitation is created by selecting one or more rain gages and providing a continuous, daily rainfall record for each gage. If more than one rain gage is selected, AGWA will create Thiessen polygons to intersect with the watershed discretization to area-weight the depth assigned to each subwatershed. For all models, precipitation is stored as flat text files in a (precip) directory that is nested in the workspace location defined in the watershed delineation step under subdirectories named for the watershed delineation and watershed discretization.

Model Simulation Creation: Model simulations may be created following the precipitation definition step for K2, or after the watershed parameterization step for SWAT if the model will be driven by weather station generated daily rainfall values. Creating K2 simulations requires defining a simulation name, and selecting a watershed discretization, a parameterization of that discretization, and a precipitation file created for that discretization. Optionally, parameter multipliers may also be defined for K2. For SWAT, similar steps are required, but additional selections must also be made. The user may elect to forgo selecting a precipitation file (and also a daily temperature file) and instead generate daily precipitation (and temperature) using a user-selected weather station. The user must also define the start and end date of the simulation as

SWAT is a continuous model. Optionally, the user may define subbasin adjustment factors, groundwater parameters, crop types, and a results output timestep (the model runs on a daily timestep regardless of the results output timestep). For both models, simulations are stored as flat files in a directory named for the simulation name that are nested in the workspace location defined in the watershed delineation step under subdirectories named for the watershed delineation and watershed discretization.

Model Execution: Model execution is performed by selecting a watershed discretization and a simulation already created for that discretization. Model execution is separated from model simulation creation to provide the user the ability to edit model input files following simulation creation but prior to model execution. This capability allows the user to rerun existing simulations limitlessly if changes are made to the simulation outside of AGWA.

Model Results Visualization: Model results visualization is performed by selecting a watershed discretization, importing/re-importing completed simulations, and selecting model outputs to map onto the watershed discretization. A variety of outputs can be displayed for any upland or channel model element including major water balance components and fluxes. K2 can also display hydrographs for simulations. Both models can calculate differences between two simulations as either an absolute difference or a percent difference.

NEW FEATURES

AGWA: AGWA 3.x, the current major release cycle (i.e. the left-most number of the version number) of AGWA was released in 2013 (Burns et al., 2013b). It incorporates new functionality, new models, user interface changes, usability improvements, and bug fixes. With the move to ArcGIS 10.x, deploying AGWA offered the opportunity to switch from a custom installation program that registered the AGWA components so that they could be recognized by ArcMap to using ESRI ArcGIS add-in functionality. The add-in deployment process is both faster and more user-friendly. The move to AGWA 3.x also saw the opportunity to support more raster and vector input types in AGWA, also resulting in a more user-oriented experience.

The upgrade from AGWA 2.x to AGWA 3.x entailed refactoring of the look-up tables used to store parameterizations so that they are more relational. This rivals the upgrade from AGWA 1.x to AGWA 2.x, when delineations and discretizations moved from a GRID and shapefiles into feature classes within a geodatabase. The significance of this upgrade in AGWA 3.x is the flexibility it allows to create and store countless parameterizations without needing to create simulations for each parameterization to store the parameterization information. With the ability to create and store multiple parameterizations in place, AGWA 3.x built on this new functionality to allow users to perform batch parameterizations. This can be of great assistance if the user has multiple, lengthy scenarios/parameterizations to run that would otherwise require user interaction at in-opportune times. Batch simulation functionality was also added to further enhance the ability to work with multiple scenarios/parameterizations.

The release of AGWA 3.x also included the Rangeland Hydrology and Erosion Model (RHEM; Hernandez et al., 2015) in a desktop application. The inclusion of RHEM required changes to both the stream definition methodology in the discretization step and also the slope definition

processing in the parameterization step. To try and better define complex hillslopes shapes, a stream definition methodology based on flow length instead of flow accumulation was added to the discretization process. Additionally, support for using an existing stream network like National Hydrologic Dataset (NHD) to define the stream network and starting points of first order channels was also added to take the guesswork out of picking an appropriate flow length or flow accumulation threshold. RHEM also supports complex slope profiles, so the slope definition process was enhanced to include a complex slope weighting process versus the existing uniform slope weighting for overland flow planes contributing laterally to channels. The complex slope weighting process uses a methodology derived from Flanagan et al. (2011) where the representative slope profile is derived by weighting slope values along flowpaths at certain distances away from the channel by their flow length and flow accumulation. This weighting process assumes longer flow paths and flow paths with greater flow accumulation contribute proportionally more to the slope profile (and associated processes) than shorter flow paths with less flow accumulation.

KINEROS2 / K2: The erosion and sediment transport models from the RHEM (Wei et al., 2007; Hernandez et al., 2015) were incorporated into K2 and linked to the overland flow model. The overland flow model in K2, which represented a uniform slope, was extended to duplicate the original RHEM's ability to represent complex hillslope profiles (as well as uniform slopes). The RHEM hydrology model used the Green-Ampt infiltration equation, and while there is a parameter in the K2 infiltration equation that controls the transition of water content across the wetting front, it can approach but not duplicate piston-flow behavior. Consequently, the K2 infiltration model was extended to include an explicit Green-Ampt option.

The K2 urban element is a composite element consisting of up to six overland flow areas representing various combinations of pervious and impervious surfaces contributing to a paved crowned street. It represents an abstraction of one half of an urban/suburban street, and was validated and used successfully by Kennedy et al. (2013) in a highly instrumented suburban catchment. It has been modified to incorporate features representing LID/GI practices, including water harvesting, retention/infiltration basins, and pervious pavement (see Korgaonkar et al., 2015).

The K2 model was developed with a tree structure, where upstream elements can only contribute to a single downstream element, which is typical of natural watersheds. To address partial diversion of flow such as for irrigation, into constructed wetlands, etc. a diversion element has been introduced. This element can divert water and sediment from a single upstream element to as many as 10 downstream elements. Diversion rates are determined from a user-supplied tabular relationship between the inflow rate from the upstream element and the rates diverted into each downstream element.

The version of K2 that was designed to run as a forecast tool in National Weather Service Forecast Offices (K2-NWS) using real time weather radar data (Unkrich et al., 2010) can now utilize data from the National Weather Service Radar Product Central Collection Dissemination Service FTP server. The data typically appears on the server within 1-2 minutes of acquisition by the radar and allows K2-NWS to run in real time outside of a NWS Weather Forecast Office. The radar file decoder used by K2-NWS has also been upgraded to ingest the new dual

polarization Digital Precipitation Rate (DPR) product. The new product uses a finer resolution, 1-degree by 250 meter polar grid, but the decoder can also down-sample the data to the legacy 1-degree by 1 km grid.

NOVEL APPLICATIONS

KINEROS2 / K2: K2-NWS was successfully applied to the 128 km^2 semi-arid Fish Creek basin located in the Anza Borrego State Park near Borrego Springs, California (Schaffner et al., 2014a). As there is no stream gage at the forecast point, the model calibration was based on categorical flood magnitudes (minor flood, moderate flood, major flood, etc.) rather than estimated discharge values. The calibration included seven rainfall events representing a full range of conditions from below flood stage up to the record flood event. Two sets of parameters were identified; one set optimized for below the major flood level and the other for larger flood levels. Calibration was successful in reproducing both the category and estimated time of peak flood. In forecast mode, the model provided an average lead time of 98 minutes to the initial flood stage, and 63, 50 and 48 minutes for minor, moderate and major flood stages respectively.

The calibration from Fish Creek was subsequently tested at nearby Borrego Palm Canyon, 70 km northwest of Fish Creek (Schaffner et al., 2014b). The goal was to evaluate whether the Fish Creek parameters could be used as a regional calibration, which would reduce the resources needed to set up the model at similar locations. The 56 km^2 Borrego Palm Canyon watershed was instrumented with a USGS stream gage from 1950 until September 10, 2004 when the gage was destroyed by a large flow. In 2002 the watershed was burned by a wildfire, with about a third suffering moderate burn severity and the rest low severity or unburned. Four test events were selected, one from 2003 with rainfall mostly over the lightly burned area, and the rest from 2013. Peak flows from simulations of the four events using the Fish Creek parameters fell within or close to the observed flood categories, suggesting that regional calibrations could be a viable option when resources are limited or when calibration data is unavailable.

AGWA: In studies by Burns et al. (2013a) and Barlow et al. (2014) a methodology was developed to characterize the hydrologic impacts of future urban growth through time. Future growth is represented by housing density maps generated in decadal intervals from 2010 to 2100, produced by the US-EPA Integrated Climate and Land-Use Scenarios (ICLUS; Bierwagen et al., 2010) project. ICLUS developed future housing density maps by adapting the Intergovernmental Panel on Climate Change (IPCC) social, economic, and demographic storylines to the conterminous United States. To characterize the hydrologic impacts of future growth, the housing density maps were reclassified to National Land Cover Database 2006 land cover classes and used to parameterize the SWAT model using AGWA. Burns et al., (2013) conducted this effort in the international San Pedro Basin in southeast Arizona and did not find a substantial impact on average surface runoff or on sediment yield at the watershed outlet for all scenarios. However, over smaller subwatersheds where development was concentrated the hydrologic changes are more significant. Barlow et al. (2014) found similar results in the South Platte Basin that contains the greater Denver, Colorado metro region.

AGWA was used by the Department of Interior National Burn Area Emergency Response (BAER) team for rapid post-fire watershed assessments on the Elk Wildfire Complex that burned

over 130,000 acres east of Boise, Idaho in August of 2013. Initially, the BAER team identified ~16,000 treatable acres within the burned watersheds that consisted of high burn severity and steep slopes. AGWA was used to simulate the watershed response for pre-fire and post-fire conditions to identify areas of high-risk for runoff and erosion. The interdisciplinary BAER team used spatially explicit AGWA results in an interactive process to locate polygons across the burned area that posed the greatest threat to downstream values-at-risk. The group combined the treatable area, field observations, professional judgment, and AGWA output to target seed and mulch treatments that most effectively reduced the threat. Using this process, the BAER Team reduced the treatable acres from the original 16,000 acres to between 2,000 and 4,000 acres depending on the selected alternative. The final awarded contract for post-fire mulch treatments cost roughly $600/acre, therefore, BAER/AGWA targeted treatment applications resulted in a total savings of ~$7.2 to $8.4 million by only treating the reduced acreage (EPA, 2014).

Since wildfire severity impacts post-fire hydrological response, fuel treatments can be a useful tool for land managers to moderate this response. Sidman et al. (2015) conducted a spatial modeling approach that couples three models used sequentially to allow managers to model the effects of fuel treatments on post-fire hydrological impacts. Case studies involving a planned prescribed fire at Zion National Park and a planned mechanical thinning at Bryce Canyon National Park were used to demonstrate the approach. Fuel treatments were modeled using FuelCalc and FlamMap within the Wildland Fire Assessment Tool (WFAT). The First Order Fire Effects Model (FOFEM) was then used to evaluate the effectiveness of the fuel treatments by modeling wildfires on both treated and untreated landscapes. Post-wildfire hydrological response was then modeled using KINEROS2 within AGWA. This approach provides a viable option for landscape scientists, watershed hydrologists, and land managers hoping to predict the impact of fuel treatments on post-wildfire runoff and erosion and compare various fuel treatment scenarios to optimize resources and maximize mitigation results.

FUTURE PLANS AND MODEL DEVELOPMENT

The AGWA GI (Green Infrastructure) tool (Korgaonkar et al., 2015) will undergo further testing and be released with a future version of AGWA. Eventually the K2-O2 continuous biogeochemical model will be coupled with the AGWA GI tool to provide capabilities to simulate plant growth, evapotranspiration, and nutrient transformations to address water quality. For post-fire watershed assessments an effort is underway by Sheppard et al. (2015) to locate high quality pre- and post-fire rainfall, and runoff data to improve procedures for adjusting post-fire infiltration, roughness, and cover parameters as a function of burn severity, pre-fire cover type, and time from fire to track recovery. A need has also been identified for post-fire flood inundation modeling on a reach scale near values of interest (e.g. structures, camp grounds, etc.). A tool is under development to take peak post-fire discharge generated from AGWA from either a design storm or observed historical storm and compute inundation in cases where significant backwater effects are absent. LIDAR or ground acquired channel cross-section data collected by BAER field crews assist in making this a viable tool. An automated channel cross-section extraction tools is also under development where LIDAR topographic data is available.

At present AGWA uses nationally available land cover maps that are static and only provide information on the type of cover but not its condition (an average condition is assumed in

AGWA). The ready availability of time varying remotely sensed vegetation products from satellites like MODIS provides an opportunity to ingest time varying measures of cover into AGWA. An AGWA tool to automatically ingest remotely sensed cover measures is under development. Initial results indicate that relatively large changes in cover condition (e.g. fires) are required to have a substantial impact on watershed response.

Small impoundments such as stock ponds are ubiquitous in much of the west and serve as a common management practice to provide water for cattle and wildlife. In addition they can be highly effective in trapping sediment and contaminants tightly bound to sediment. An AGWA pond tool is under development to allow the user to select a variety of pond types and geometries to rapidly place them within the channel network parameter file so scenarios for the type and number of ponds to reduce peak runoff rates or achieve load reductions can be made. Finally an internet version of AGWA is under development. Key issues for this project include where and how large geospatial and remotely sensed data sets will be stored and served.

REFERENCES

Arnold, J.G., and Fohrer, N., (2005). SWAT2000: current capabilities and research opportunities in applied watershed modeling. Hydrological Processes 19(3), 563-572.

Baker, T.J., and Miller, S.N. (2013). Using the Soil and Water Assessment Tool (SWAT) to assess land use impact on water resources in an East African watershed. Journal of Hydrology. 486: 100-111. http://dx.doi.org/10.1016/j.jhydrol.2013.01.041.

Barlow, J.E., Burns, I.S., Kepner, W.G., Sidman, G.S., Goodrich, D.C., Guertin, D.P., and McCarthy, J.M. (2014). Assessing hydrologic impacts of future land cover change scenarios in the South Platte River Basin (CO, WY, & NE). EPA/600/R-14/328 and ARS/309194.

Bierwagen, B.G., Theobald, D.M., Pyke, C.R., Choate, A., Groth, P., Thomas, J.V., and Morefield, P. (2010). National Housing and Impervious Surface Scenarios for Integrated Climate Impact Assessments. Proceedings of the National Academy of Sciences of the United States of America. Vol. 107, No. 49 20887-20892.

Broxton, P., Troch, P., Schaffner, M., Unkrich, C., Goodrich, D. (2014). Coupling the Kinematic Erosion and Runoff (KINEROS) and hillslope-storage Boussinesq Soil Moisture (hsB-SM) Models for all-season operational flash flood forecasting, Bulletin of the American Meteorological Society, 95(3), 399-407.

Burns, I.S., Kepner, W.G., Sidman, G.S., Goodrich, D.C., Guertin, D.P., Levick, L.R., Yee, W.W.S., Scianni, M.M.A., Meek, C.S., and Vollmer, J.B. (2013a). Assessing hydrologic impacts of future land cover change scenarios in the San Pedro River (U.S./Mexico). EPA/600/R-13/074 and ARS/294076.

Burns, I.S., Korgaonkar Y., Guertin, D.P., Goodrich, D.C., Kepner, W.A., Miller, and S.N., Semmens, D.J. (2013b) Automated Geospatial Watershed Assessment (AGWA) 3.0 Software Tool. USDA Agricultural Research Service and U.S. EPA, Washington, DC (http://www.tucson.ars.ag.gov/agwa/).

EPA. (2014). Tool saves millions of dollars after wildfire. http://blog.epa.gov/science/2014/06/tool-saves-millions-of-dollars-after-wildfire/. Accessed January 2015.

Flanagan, D.C., Frankenberger, J.R., Cochrane, T.A., Renschler, C.S., and Elliot, W.J. (2011). Geospatial application of the Water Erosion Prediction Project (WEPP) model. Trans. ASABE 56.2, pp. 591-601.

Goodrich, D.C., Williams, D.G., Unkrich, C.L., Hogan, J.F., Scott, R.L., Hultine, K.R., Pool, D., Coes, A.L., and Miller, S.N. (2004). Comparison of methods to estimate ephemeral channel recharge, Walnut Gulch, San Pedro River basin, Arizona. In *Recharge and Vadose Zone Processes: Alluvial Basins of the Southwestern United States*, 77-99. F. M. Phillips, J. F. Hogan, and B. Scanlon, eds. Water Science and Application, vol. 9. Washington, D.C.: American Geophysical Union.

Goodrich, D.C., Burns, I.S., Unkrich, C.L., Semmens, D.J., Guertin D.P., Hernandez, M., Yatheendradas, S. Kennedy, J.R., and Levick, L.R. (2012). KINEROS2/AGWA: Model use, calibration, and validation, Trans. of the ASABE. 55(4): 1561-1574.

Guber, A.K., Pachepsky, Y.A., Yakirevich, A.M., Shelton, D.R., Sadeghi, A.M., Goodrich D.C., and Unkrich, C.L. (2010). STWIR, a microorganism transport with infiltration and runoff add-on module for the KINEROS2 runoff and erosion model: documentation and user manual. U.S. Department of Agriculture Technical Bulletin. (http://www.ars.usda.gov/ba/anri/emfsl/code)

Guber, A.K., Pachepsky, Y.A., Yakirevich, A.M., Shelton, D.R., Whelan, G., Goodrich, D.C., and Unkrich, C.L. (2014). Modeling runoff and microbial overland transport with KINEROS2/STWIR model: Accuracy and uncertainty as affected by source of infiltration parameters. *Journal of Hydrology*, *519*, 644-655.

Hernandez, M., Nearing, M., Stone, J., Armendariz, G., Pierson, F., Al-Hamdan, O., Williams, C.J., Spaeth, K., Weltz, M., Wei, H., Heilman, P., and Goodrich, D. (2015). Web-based Rangeland Hydrology and Erosion Model. SEDHYD Conf. April 19-23, 2015, Reno, NV.

Kennedy, J., Goodrich, D., and Unkrich, C. (2013). Using the KINEROS2 Modeling Framework to Evaluate the Increase in Storm Runoff from Residential Development in a Semi-Arid Environment. *J. Hydrol. Eng.*, 2013.18:698-706.

Korgaonkar, Y., Burns, I.S., Guertin, D.P., Goodrich, D.C., Unkrich, C.L., Barlow, J.E., and Kepner, W.G. (2014). Representing green infrastructure management techniques in arid and semi-arid regions: software implementation and demonstration using the AGWA/KINEROS2 watershed model. EPA/600/R-14/329 and ARS/309819.

Korgaonkar, Y., Burns, I.S., Barlow, J.E., Guertin, D.P., Unkrich, C.L., Goodrich, D.C., and Kepner, W.G. (2015). Representing green infrastructure management techniques in arid and semi-arid regions: software implementation and demonstration using the AGWA/KINEROS2 watershed model. SEDHYD Conf. April 19-23, 2015, Reno, NV

Massart, J., Guertin, D.P., Smith, R.E., Goodrich, D.C., Unkrich, C.L., and Levick, L., 2010. K2-O2 (KINEROS-Opus) spatially based watershed hydrologic and biogeochemical model. Proc. 2nd Joint Federal Interagency Conference, Las Vegas, NV, June 27 - July 1, 2010, 12 p. http://acwi.gov/sos/pubs/2ndJFIC/

Miller, S.N., Semmens, D.J., Miller, R.C., Hernandez, M., Goodrich, D.C., Miller, W.P., Kepner, W.G., and Ebert, D.W. (2002). GIS-based Hydrologic Modeling: The Automated Geospatial Watershed Assessment Tool. In: Proceedings, Second Federal Interagency Hydrologic Modeling Conference, Las Vegas, Nevada, July 28 - August 1, 2002.

Miller, S.N., Semmens, D.J., Goodrich, D.C., Hernandez, M., Miller, R.C., Kepner, W.G., and Guertin, D.P. (2007). The Automated Geospatial Watershed Assessment Tool. J. Environmental Modeling and Software. 22:365-377.

Miller, S.N., Caffrey, P.A., and Berendsen, M. (2012). Spatially explicit predictive hydrologic modeling in advance of oil and gas development. Oral presentation and abstract to AWRA's

2012 Spring Specialty Conference Geographic Information Systems (GIS) and Water Resources VII, New Orleans, LA, March 26-28, 2012.

Roberts, A.J. (2003). A holistic finite difference approach models linear dynamics consistently. *Math. of Computation* 72(241): 247-262.

Rovey, E.W. (1974). A kinematic model for upland watersheds. MS thesis. Fort Collins, Colo.: Colorado State University.

Schaffner, M., Unkrich C., Goodrich, D., Tardy, A., and Laber, J. (2014a). Modeling flash flood events in an ungaged semi-arid basin using a real-time distributed model: Fish Creek near Anza Borrego, California. National Weather Service, Western Region Technical Attachment 14-02, 42 p. (http://www.wrh.noaa.gov/media/wrh/online_publications/TAs/TA1402.pdf)

Schaffner, M., Unkrich C., Goodrich, D., Tardy, A., Laber, J., and Sheppard, B. (2014b). Evaluation of regional calibration parameters using a distributed rainfall-runoff model: Borrego Palm Canyon near Borrego Springs, California. National Weather Service, Western Regional Technical Attachment 14-04, 38 p., (http://www.wrh.noaa.gov/media/wrh/online_publications/TAs/TA1404.pdf)

Semmens, D.J., Goodrich, D.C., Unkrich, C.L., Smith, R.E., Woolhiser, D.A., and Miller, S.N. (2008). KINEROS2 and the AGWA modeling framework. Chapter 5: In Hydrological Modelling in Arid and Semi-Arid Areas (H. Wheater, S. Sorooshian, and K. D. Sharma, Eds.). Cambridge University Press, London. Pp. 49-69.

Sheppard, B.S., Sidman, G., Guertin, D.P., Goodrich, D.C., Burns, I.S., Falk, D., Thoma, D., Canfield, E., Korgaonkar, Y., and Kepner, W.G. (2015). Automated Geospatial Watershed Assessment Tool (AGWA): Applications for fire management and assessment, SEDHYD Conf. April 19-23, 2015, Reno, NV.

Sidman, G., Guertin, D.P., Goodrich, D.C., Thoma, D., Falk, D., and Burns, I.S. (2015). A coupled modeling approach to assess the impact of fuel treatments on post-wildfire runoff and erosion, International Journal of Wildland Fire, (*in press)*.

Smith, R.E., Goodrich, D.C., Woolhiser, D.A., and Unkrich, C.L. (1995). KINEROS - A kinematic runoff and erosion model, Chap. 20 of Computer Models of Watershed Hydrology, (Ed. by Singh, V. J.) Water Resour. Pub., Highlands Ranch, Colo., pp. 697-732.

Unkrich, C.L., Schaffner, M., Kahler, C., Goodrich, D., Troch, P., Gupta, H., Wagener, T., and Yatheendradas, S. (2010). Real-time flash flood forecasting using weather radar and a distributed rainfall-runoff model. Proceedings, Federal Interagency Hydrologic Modeling Conf., Las Vegas, NV, June 27 - July 1, 2010, 11 p. http://acwi.gov/sos/pubs/2ndJFIC/.

Wei, H., Nearing, M.A., and Stone, J.J. (2007). A new sensitivity analysis framework for model evaluation and improvement using a case study of the Rangeland Hydrology and Erosion Model. Trans. Am. Soc. Agric. Bio. Eng. 50(3): 945-953.

Woolhiser, D.A., Smith, R.E., and Goodrich, D.C. (1990). *KINEROS, A Kinematic Runoff and Erosion Model: Documentation and User Manual*. ARS-77. Tucson, Ariz.: USDA-ARS Southwest Watershed Research Center. Available at: www.tucson.ars.ag.gov/kineros.

REPRESENTING GREEN INFRASTRUCTURE MANAGEMENT TECHNIQUES IN ARID AND SEMI-ARID REGIONS: SOFTWARE IMPLEMENTATION AND DEMONSTRATION USING THE AGWA/KINEROS2 WATERSHED MODEL

Yoganand Korgaonkar, Graduate Student, University of Arizona, Tucson, AZ, yoganandk@email.arizona.edu; I. Shea Burns, Senior Research Specialist, University of Arizona, Tucson, AZ, shea.burns@ars.usda.gov; Jane Barlow, Graduate Student, University of Arizona, Tucson, AZ, jbarlow@email.arizona.edu; D. Phillip Guertin, Professor, University of Arizona, Tucson, AZ, dpg@email.arizona.edu; Carl Unkrich, Hydrologist, USDA-ARS, Tucson, AZ, carl.unkrich@ars.usda.gov; David C. Goodrich, Research Hydraulic Engineer, USDA-ARS, Tucson, AZ, dave.goodrich@ars.usda.gov; William Kepner, Research Ecologist, EPA/ORD/NERL, Las Vegas, NV, kepner.william@epa.gov.

Abstract: Increasing urban development in the arid and semi-arid regions of the southwestern United States has led to greater demand for water in a region with limited water resources and has fundamentally altered the hydrologic response of developed watersheds. Green Infrastructure (GI) practices are being widely adopted to mitigate the impacts of development on water quantity and quality. However, Geographic Information System (GIS) based watershed tools for rapid GI planning and assessment that operate from the lot-to-subdivision-to-watershed level are lacking. The Automated Geospatial Watershed Assessment (AGWA) tool was modified to allow the design and placement of a small set of GI practices in order to simulate urban hydrology with and without GI features. This software development effort was undertaken to take advantage of the advanced, physically-based infiltration algorithms and geometric flexibility of the Kinematic Runoff and Erosion (KINEROS2) watershed model. The resulting software provides an up-to-date GIS GI assessment framework that automatically derives model parameters from widely available spatial data. The software is also capable of manipulating GI features and simulating at the lot-scale within a graphical interface to conveniently view and compare simulation results with and without GI features. The AGWA GI software was tested at the lot level with and without GI features to validate the water balance and to verify steady state runoff rates. Testing was also conducted at the subdivision level, without GI features, as high-resolution rainfall-runoff observations were available from a subdivision in Sierra Vista, Arizona. Testing at both these scales confirmed programming integrity and the capability to realistically simulate urban hydrology, indicating that the software can realistically represent and simulate storm runoff responses for the selected GI features. The AGWA GI tool offers a foundation for the incorporation of a broader array of GI features.

INTRODUCTION

Urbanization has numerous effects on a watershed as it replaces vegetation and pervious open areas with impervious surfaces such as roofs, driveways, parking lots, and roads. The introduction of impervious surfaces has significant impacts on watershed hydrology, especially in regard to drastic reductions in infiltration of rainfall, resulting in increased runoff volumes, peak discharges, and higher energy releases. Increased runoff results in lower groundwater recharge and base flows in humid regions (Leopold, 1968)

Traditional storm water management techniques involve transporting the water away from urban areas as quickly as possible; reducing lag times, and increasing runoff volume and peak flows (Hood et al., 2007; Leopold, 1968). The Department of Environmental Resources of Prince George's County, Maryland, pioneered Green Infrastructure (GI, also referred to as Low Impact Development or LID) to mitigate the urbanization impact of increasing impervious surfaces (County and June, 1999). As opposed to traditional storm water management practices, GI aims to preserve the pre-development hydrology using a variety of cost effective on-site design techniques that store, infiltrate, evaporate, and detain runoff. Prince George's County introduced a new concept of Integrated Management Practices (IMP), that include many GI practices such as bioretention cells or basins, dry wells, filter strips, vegetated buffers, level spreaders, grassed swales, rain barrels, cisterns, and infiltration trenches. GI practices help reduce the need for more traditional storm water management techniques such as curb-and-gutter systems or large detention basins.

GI practices have been implemented and evaluated all around the world. Much effort has been put into the modeling of these practices to aid in decision making with respect to design, cost, efficiency, and effectiveness (Ahiablame et al., 2012a; Elliott and Trowsdale, 2007). Models that simulate GI practices include the Storm Water Management Model (SWMM) (Rossman and Supply, 2010), Long-Term Hydrologic Impact Assessment – Low Impact Development (L-THIA-LID) model (Ahiablame et al., 2012b), System for Urban Storm Water Treatment and Analysis Integration (SUSTAIN) (Lee et al., 2012), Hydrologic Simulation Program – Fortran (HSPF) (Bicknell et al., 2001), and BMP Decision Support System (BMPDSS) (Cheng et al., 2009).

This paper demonstrates the use of the Automated Geospatial Watershed Assessment (AGWA) tool to design and model GI practices in urban environments. The AGWA GI software serves as a decision support tool, applicable at the lot-, subdivision-, and small watershed-scales. It utilizes several of the features of the KINEROS2 rainfall-runoff and erosion model that are well suited to arid and semi-arid watersheds (Goodrich et al. 2012).

GREEN INFRASTRUCTURE PRACTICES

A small subset of GI practices, commonly used in arid and semi-arid regions, was selected for incorporation into the modeling tool. These include bioretention systems, permeable pavements and rainwater harvesting systems.

Bioretention systems are depressions filled with highly permeable soil, and planted with vegetation. These systems allow storm water to pond and infiltrate, thereby supporting vegetation growth while achieving storm water retention, pollutant removal, and groundwater recharge. Smaller-scale bioretention systems are also referred to as rain gardens and their design and effectiveness are more dependent on lot sizes and placement within the watershed.

Permeable pavements are paved surfaces that reduce runoff by allowing infiltration. These are usually designed as a matrix of concrete paver blocks with voids filled with sand, gravel, or soil. These voids encourage infiltration of storm water into the underlying soil layer.

Rainwater harvesting includes the use of rain barrels and cisterns to retain rooftop runoff for future use. Rain barrels tend to have a storage capacity of less than 0.38 cubic meters (100 gallons) and are usually placed above the ground. Cisterns have a capacity of more than 0.38 cubic meters and can be self-contained, above-ground, or below-ground systems.

AGWA AND KINEROS2

The AGWA tool provides a GIS user interface for two hydrologic models - the Kinematic Runoff and Erosion model (KINEROS2) and the Soil and Water Assessment Tool (SWAT) (Daniel et al., 2011, Miller et al., 2007). AGWA is a customized toolbar in ESRI ArcMap that uses existing spatial datasets in the form of digital elevation models, land cover maps, soil maps, and weather data as inputs (figure 1). These inputs are processed to prepare input parameters for hydrologic models. The simulation results are quantified and imported back into AGWA for spatial display and analysis. The interoperability of KINEROS2 and AGWA is described in Goodrich et al. (2012).

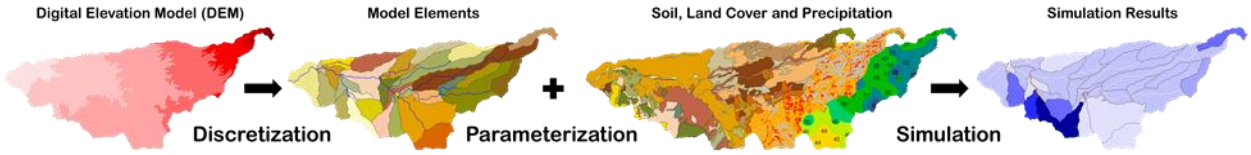

Figure 1 AGWA Workflow

KINEROS2 is a distributed, physically based model that simulates runoff and erosion for small watersheds. It utilizes kinematic equations to simulate overland flow, over rectangular planar or curvilinear hillslopes, and channelized flows, through open trapezoidal channels (figure 2) (Woolhiser, et al., 1990; Goodrich et al., 2012). KINEROS2 has dynamic infiltration in which the infiltration is coupled with the routing, and flow depth is computed with a finite difference solution of the kinematic wave equations and the Smith-Parlange infiltration equation at each finite difference node. This makes the model particularly well suited to simulate runoff-runon conditions over surfaces with distinctly different infiltration or cover characteristics. In addition to the standard overland flow (planar or curvilinear) and channel modeling elements, KINEROS2 also has an Urban modeling element (figure 2) that consists of up to six overland flow areas that contribute to one-half of a paved, crowned street with the following configurations: (1) directly connected pervious area, (2) directly connected impervious area, (3) indirectly connected pervious area, (4) indirectly connected impervious area, (5) connecting pervious area, and (6) connecting impervious area. The Urban modeling element represents an abstraction of a typical subdivision. Kennedy et al. (2013) evaluated the urban element and concluded that KINEROS2 could successfully model urban residential watersheds with this abstract representation of different surface types and runoff-runon combinations.

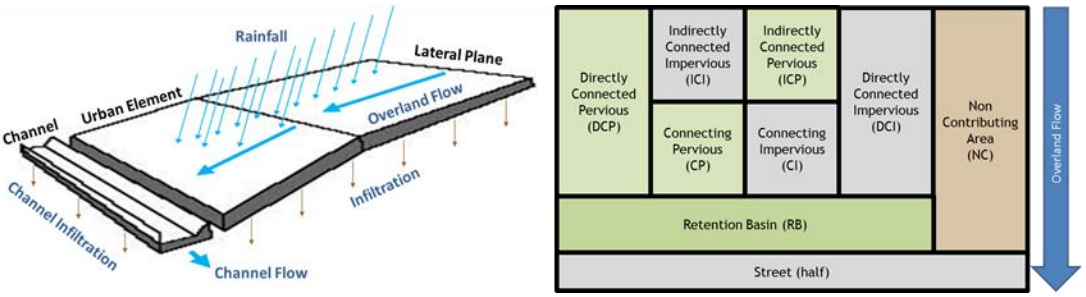

Figure 2 KINEROS2 element and Urban element components.

Very few software packages exist that can provide a decision-support system with spatial, robust, and accurate modeling capabilities. Popular models lack the physical routing of water through the watershed, provisions for erosion modeling, or the use of a spatial tool. The robustness of KINEROS2 and the GIS interface provided by AGWA creates the option to use these in unison to provide a powerful modeling platform for GI practices in urban development scenarios.

WORKFLOW

Based on the existing AGWA functionality, a modified workflow was designed to utilize KINEROS2 to simulate urban environments and GI practices. The modified workflow was developed in the .NET Framework using Microsoft Visual Studio 2010. C# and VB.NET were the programming languages used. ESRI provides an ArcObjects software development kit for the .NET Framework to build Windows applications with GIS functionalities. With the help of ArcObjects, Windows-based forms were developed which could use existing GIS functionalities in ESRI ArcMap. The description for each step in the workflow is given below.

Setup Urban Geodatabase: The Setup Urban Geodatabase form allows the user to provide a location and a name for a geodatabase, which becomes the workspace for feature classes and tables that are created in subsequent processes. The user also provides the subdivision parcels and a corresponding road layer in the form of polygon feature classes.

Flow Routing: Flow routing is an important step in simulating an urban subdivision as post construction flow paths are typically different from pre-development topography. KINEROS2 requires the path that water will follow from the lot to the basin outlet. The Urban element in KINEROS2 assumes all of the rainfall flows from the lot towards the street. The street is assumed to be crowned to allow the routing of water along the streets. With the help of the Flow Routing form, the user draws flow paths on the parcel feature class using built-in drawing tools in ESRI ArcMap. Once saved, the flow paths are checked by the software to ensure that all parcels are associated with a flow path, and that they fall within the boundaries of the parcels. Using these flow paths, a conceptual flow map (figure 3) draining towards the outlet is created.

Parameterization: The Parameterization step defines KINEROS2 input parameters based on geometry, land cover, and soils properties for each parcel. The user provides inputs to the Element Parameterization form and the Land Cover and Soils form. The first form defines element parameters, including the parcel width field, house area, driveway area, slope, street width, cross slope, and grade, all of which can also be defined using fields from the feature

classes or with user-defined values. The second form defines land cover and soils parameters, including: canopy cover fractions; impervious, pervious, and street roughness; and impervious and pervious interception values. A Soil Survey Geographic (SSURGO) soil map is required along with the corresponding database to prepare soil parameters. For each soil mapping unit in SSURGO soil map, AGWA applies these parameters uniformly to all the parcels in the subdivision that intersect that soil mapping unit, and spatially, averages the parameters when parcels intersect multiple soil mapping units. Additionally, AGWA stores all of these parameters in tables, which allows the user to modify these values using data from field surveys or other sources.

Figure 3 Flow routes drawn by the user on the La Terraza subdivision in Sierra Vista, AZ.

Green Infrastructure Design and Placement: The Green Infrastructure Design and Placement tool allows users to design and place retention basins, permeable pavements, or rainwater harvesting systems on one or more parcels in a subdivision. Each design can be saved in the Geodatabase with a unique name. A combination of these designs can be saved as a "Placement Plan".

Retention Basins: A retention basin design requires the width, length, and depth of the retention basin in order to calculate the area and volume associated with it. In addition to the above dimensions, KINEROS2 requires the soil saturated hydraulic conductivity of the retention basin. Water from the lot is assumed to flow into the retention basin before flowing on to the street half.

Permeable Pavements: Design parameters for permeable pavements can be provided in the form of length and width, or selecting the "Same as driveway area" option. Using this option,

AGWA calculates the permeable pavement area based upon the driveway area defined in the Element Parameterization step. A soil saturated hydraulic conductivity value is also required. The permeable pavement driveways allow infiltration of water based on the hydraulic conductivity provided by the user.

Rainwater Harvesting: For the design of a rainwater harvesting system, the volume of the rain barrel (or cistern) can be provided, or can be calculated using the height and diameter of the rain barrel. Rainwater falling on the roof of the house is captured by this rainwater harvesting system.

Precipitation: KINEROS2 accepts rainfall data in the form of time-intensity pairs or time-depth (where depth represents accumulated depth) pairs. AGWA allows the user to provide rainfall data in the form of precipitation frequency grids, design storm tables, user-defined depths, or user-defined hyetographs. Rainfall is assumed to be applied uniformly over the entire subdivision area. If observed rainfall is available from more than one rain gauge, KINEROS2 employs a piece-wise planar space-time interpolation scheme that can also accommodate radar-rainfall estimates. This functionality remains unchanged from the original AGWA implementation. More information can be found in the AGWA Documentation on the AGWA website (www.tucson.ars.ag.gov/agwa/ or http://www.epa.gov/esd/land-sci/agwa/).

Write Input Files: In the Write Input Files step, AGWA aggregates all the inputs that were provided in the preceding steps and prepares input files required by the KINEROS2 model. The user selects the flow routing table, parameterization, placement plan table, and precipitation file, and provides a unique name for the simulation.

Execute KINEROS2 Model: In the Execute KINEROS2 Model step, the user selects a simulation and runs the KINEROS2 model. A command prompt displays the progress of the simulation and whether it was successful or if it encountered any errors. The output file (.out), which summarizes the hydrology for each urban element, is created in the simulations directory by the model. AGWA imports these values in the next step.

View Results: The View Results form allows the user to visualize the results of the KINEROS2 simulation. AGWA allows the user to visualize the output for each parcel in the form of infiltration, runoff, and accumulated runoff volumes, as well as absolute and percent differences between two simulations. Infiltration and runoff volumes (figure 4) results are visualized for each individual parcel. Accumulated runoff (figure 5), which is comprised of the runoff from each parcel along with the runoff from the upland parcel, can be visualized along the street.

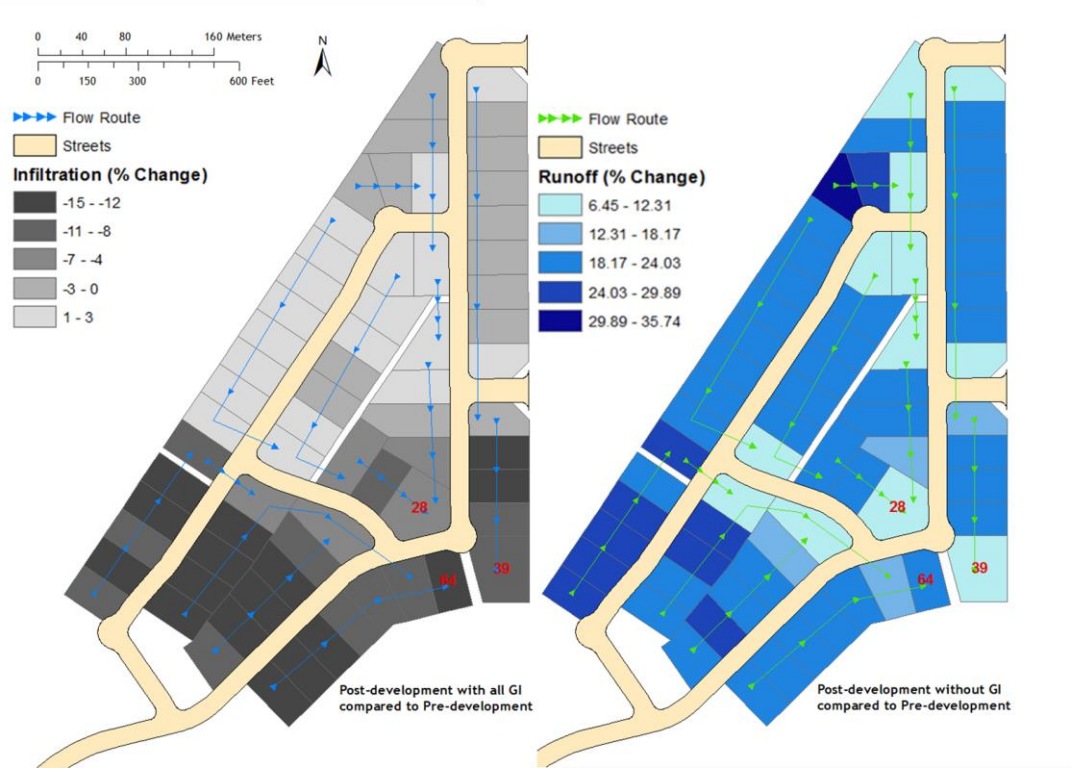

Figure 4 Visualization of the AGWA GI infiltration and runoff results for parcels.

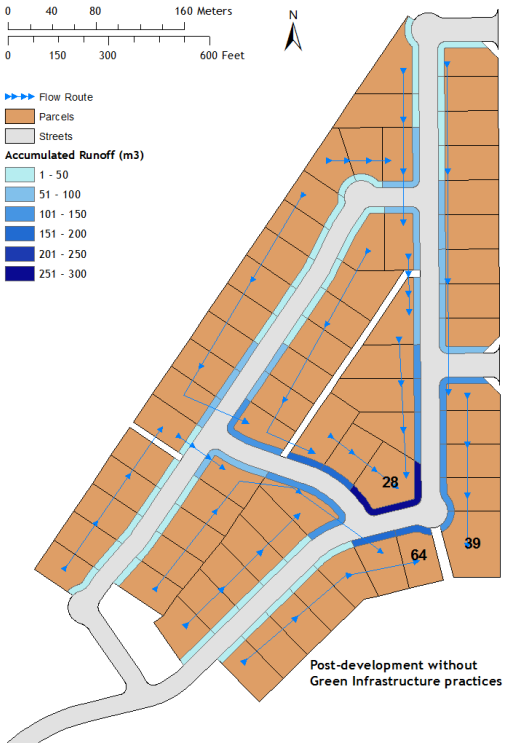

Figure 5 Visualization of the AGWA GI flow accumulation results on the roads.

TESTING

Lot Level: Verification of the Urban element at the lot-scale was approached by confirming the following: 1) Event volumes of hydrologic components are balanced properly; and, 2) Steady-state runoff rates based on a constant rainfall intensity with a configuration of areas with known infiltration rates. To test both, an element was created representing a typical lot in the La Terraza subdivision and was used in six scenarios (Table 1): pre-development; post-development without GI; retention basins; permeable pavements; rainwater harvesting; and all GI practices.

Table 1 Description of the lot-scale verification scenarios.

Pre-development	Empty lot with a street and soils attributes obtained from the NRCS SSURGO soils spatial database
Post-development (without GI)	Lot with a house area of 2500 square feet and a ~12 feet by 19.5 feet impermeable driveway (21.76 square meters)
Retention Basin	Post-development parameters with the addition of a retention basin with a hydraulic conductivity of 8.3 in/hr (~210 mm/hr) and sized with a surface area of approximately 72 square feet and a depth of ~10 inches, yielding a retention capacity of ~60 cubic feet (~444 gallons)
Permeable Pavement	Post-development parameters with a permeable driveway with a hydraulic conductivity of 8.3 in/hr (~210 mm/hr)
Rainwater Harvesting	Post-development parameters with a rainwater harvesting feature with a capacity of ~500 gallons (1.9 cubic meters)
All GI practices	Post-development parameters along with all of the above GI practices

Verifying the water balance is a basic accounting exercise that ensures model inputs equal model outputs plus any change in storage. In this exercise, a 12.5 mm/hr rainfall event was applied for a duration of two-hours onto a lot size of 0.1933 hectares, yielding a total rainfall volume of 96.66m^3; this rainfall volume is the model input. Model outputs include interception, infiltration, storage, and outflow in cubic meters. For all scenarios, the error for the water balance was less than 1 percent.

Effective hydraulic conductivity is defined as the rainfall minus outflow rate at steady-state (figure 6). Because each scenario reached steady-state outflow rates, the effective hydraulic conductivity could be compared to the expected steady-state weighted saturated hydraulic conductivity calculated from the different overland flow areas of the Urban element. The weighted hydraulic conductivity is calculated by converting the infiltration capacity in mm/hr to cubic meters for each of the overland flow areas of the element. Conversion to a volumetric rate is necessary so that contributing volumes can be subtracted out when overland flow areas that receive input from upslope have higher infiltration capacities than the rainfall rate.

Subdivision Level: Verification of the model for the La Terraza subdivision (figure 3) was conducted using observed rainfall and runoff data collected from July 2005 through September 2006 (Kennedy, 2007). Rainfall was measured by four recording rain gauges, with areal average rainfall event totals ranging from 2 to 35 mm (events less than 2 mm were not used). Runoff,

both into and out of the La Terraza subdivision, was measured by v-notch weirs. Runoff events that overtopped the outlet weir were excluded, giving a high-quality data set of 47 events.

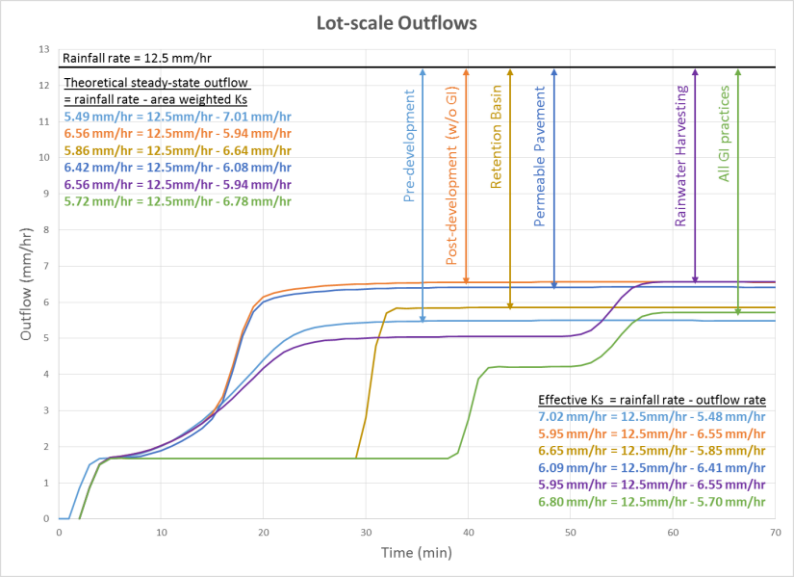

Figure 6 Hydrographs illustrating effective hydraulic conductivities for lot-scale testing.

The parameter file created by AGWA was modified to incorporate some of the parameters used by Kennedy (2007) as well as the measured inflows from the adjacent undeveloped watershed. The altered parameters included the interception and Manning n values, and street slopes were reduced from 0.02 to 0.01 to better reflect the values measured by Kennedy (2007). Initial soil saturation values for each event were also obtained from Kennedy (2007).

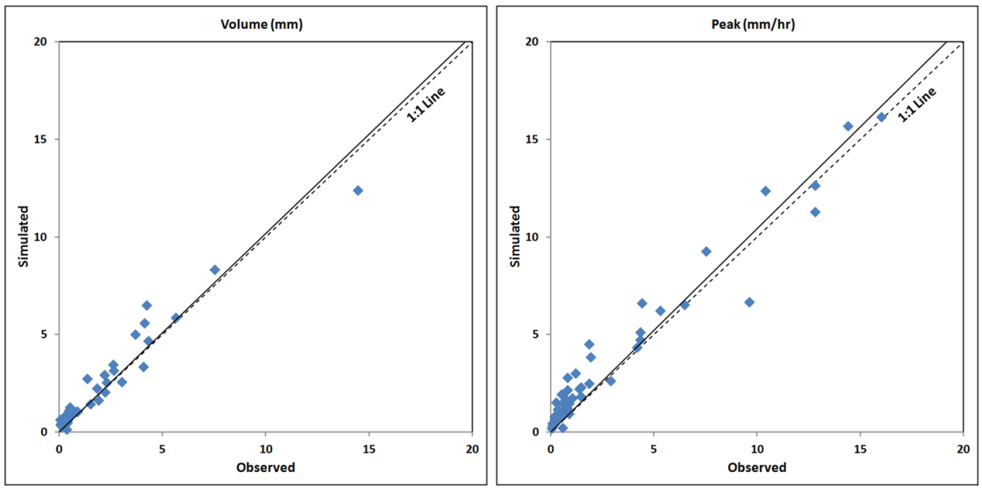

Figure 7 Simulated versus observed event runoff volume (mm) and peak flows mm/hr (n = 47) for July 2015 through September 2006 for the La Terraza subdivision.

The total event runoff volumes and peak flow rates for the 47 simulated events compared to measured values are shown in figure 7. Both volumes and peaks yielded Nash-Sutcliffe

efficiencies (coefficients of determination) greater than 0.9, with very little tendency to over or under predict the observed values. This test provides assurances that with high-quality rainfall-runoff observations, the AGWA GI tool can realistically simulate the effects of subdivision-scale development for multiple lots and streets within a larger watershed with upslope contributions from a natural, undeveloped sub-catchment. Ideally, a development containing GI features with high-quality rainfall-runoff observations could be located to provide real world testing of the AGWA GI tool. Until such data becomes available, this test coupled with the successful lot level testing described in the prior section, provides a measure of confidence in the ability of the AGWA GI tool to simulate the selected GI features in arid and semiarid areas at the lot-, subdivision-, and small catchment-scale.

LIMITATIONS AND ISSUES

Limitations of the KINEROS2 model are discussed in Goodrich et al. (2012). KINEROS2 is currently an event-based model and will not simulate plant water use, soil water movement between events, or track snow accumulation and melt, or subsurface flow. Before simulating an event, it requires an initial estimate of soil moisture. The event-based version precludes modeling of the changes in soil moisture due to drainage, evaporation, and plant water use. This could have an impact when attempting to realistically simulate how water captured by rain harvesting GI practices is drawn down for watering through different weather scenarios. The representation of two-soil layer infiltration available in KINEROS2 has not been implemented within the AGWA GI tool. Unless site specific post-development soils and infiltration data is available this limitation is not viewed as a major shortcoming for the AGWA GI tool.

While KINEROS2 can compute infiltration and route runoff on planar or curvilinear overland flow elements, the Urban GI element is restricted to a planar surface with one slope designated for the non-street components and another slope for the one-half street component. The urban element assumes water flows directly to the street, and the street is assumed to be crowned to allow independent routing of water on each side of the street. Flow from one lot will not cross the mid-line of the street to the other half, so street runoff is uniquely associated with one lot. The Urban GI element in KINEROS2 assumes all of the runoff generated will flow from the back of the lot towards the street. In reality, lot-generated runoff could flow onto adjacent lots. KINEROS2 provides a representation for dead storage, such as a swimming pool or walled yard that effectively traps and holds runoff, however, the AGWA GI tool currently lacks the ability to incorporate this.

If high-quality post construction topographic data from LIDAR were available, it would be possible to further sub-divide a lot into more than one overland flow element coupled with an Urban GI element in these cases. Currently, this is most easily done by altering the KINEROS2 parameter file outside of the AGWA GIS environment, but tools to subdivide elements will be supported in AGWA in the future. This limitation is not seen as a major shortcoming as the primary application envisioned for the AGWA GI tool is for rapid relative change assessments to evaluate the hydrologic response effects of GI features where minor flow path deviations should not have a major effect on the overall assessment of the value of adding GI features.

CONCLUSIONS

The AGWA GI tool was designed and developed to represent retention basins, permeable pavements, and rainwater harvesting systems within the AGWA/KINEROS2 modeling environment. The Urban element in KINEROS2 was modified to provide a realistic representation of individual housing lots and the placement of the GI features noted above. Two new GI tools were developed to spatially prepare parameters for the KINEROS2 Urban GI model element. The Flow Routing tool allows the user to draw flow paths on the map, guiding storm water along platted or post-development drainage paths and to the outlet. This is important as analysis of pre-development topography from nationally or locally available digital elevation model (DEM) data will not typically result in flow paths similar to post-development. Even in urbanized areas with high-resolution DEM data on the scale needed to construct 0.3 m (1 foot) contour intervals, accurate flow paths can often be difficult to discern with automated drainage analysis due to small drainage control features such as curbs and gutters. The GI Design and Placement tool allows the design and placement of retention basins, permeable pavements, and rainwater harvesting systems at each lot in a subdivision. Additionally, various combinations of GI placements can be designed and simulated for an entire subdivision. Three output types are provided by the AGWA GI tool, i.e. infiltration, runoff, and accumulated runoff. Comparisons using these outputs can be made between pre-development and post-development with or without GI practices.

The hydrologic behavior of GI practices was tested at the lot level by verifying: 1) that event volumes of hydrologic components were balanced properly; and 2) the steady-state runoff rate reflected the independently computed effective hydraulic conductivity. Verification of the model at the subdivision-scale was conducted on the La Terraza subdivision using a high-quality set of observed rainfall and runoff data. Simulated runoff volumes and peak flow rates yielded high Nash-Sutcliffe efficiencies (>0.9) and very little bias compared to the observed data. Based on these tests, the AGWA GI tool performed as expected.

At present the AGWA GI tool only focuses on hydrology. Some limitations mentioned related to KINEROS2 will be addressed when the continuous version is available, which includes plant growth functionality and biogeochemistry (K2-O2; Massart et al., 2010). Once integrated into AGWA, the continuous version of KINEROS2 will enable simulation of numerous water quality effects of GI practices. The AGWA GI tool can be a used to inform planning decisions related to urban development and storm water management on lot-, subdivision-, and small catchment-scales. This information will be useful in understanding the expected differences in storm water runoff between neighboring developments or natural environments. In traditional post-development urban environments, the increase in storm water runoff can negatively impact downstream natural resources. GI features have the potential to mitigate those effects by achieving pre-development runoff volumes.

REFERENCES

Ahiablame, L. M., Engel, B. A., and Chaubey, I. (2012a). “Effectiveness of low impact development practices: Literature review and suggestions for future research,” Water, Air, and Soil Pollution, 223(7), pp 4253-4273.

Ahiablame, L. M., Engel, B. A., and Chaubey, I. (2012b). "Representation and evaluation of low impact development practices with L-THIA-LID: An example for site planning," Environment and Pollution, 1(2), p1.

Bicknell, B. R., Imhoff, J. C., Kittle, J., Jobes, T. H., and Donigian, A. (2001). HSPF version 12 user's manual. National Exposure Research Laboratory. Office of Research and Development US Environmental Protection Agency.

Cheng, M., Zhen, J. X., and Shoemaker, L. (2009). "BMP decision support system for evaluating stormwater management alternatives," Frontiers of Environmental Science and Engineering in China, 3(4), pp 453-463.

County, P. G. S. and June, M. D. (1999). Low-impact development design strategies: An integrated design approach. Department of Environmental Resources, Programs and Planning Division, Prince George's County, Maryland.

Elliott, A., and Trowsdale, S. (2007). "A review of models for low impact urban stormwater drainage," Environmental Modelling and Software, 22(3), pp 394-405.

Goodrich, D. C., Burns I. S., Unkrich C. L., Semmens D. J., Guertin D. P., Hernandez M., Yatheendradas S., Kennedy J. R., and Levick L. R. (2012)."KINEROS2/AGWA: Model Use, Calibration, and Validation," Transactions of the ASABE, 55(4), pp 1561-1574.

Hood, M. J., Clausen, J. C., and Warner, G. S. (2007). "Comparison of stormwater lag times for low impact and traditional residential development," Journal of the American Water Resources Association, 43(4), pp 1036-1046.

Kennedy, J.R. (2007). "Changes in storm runoff with urbanization: The role of pervious areas in a semi-arid environment." M.S. thesis, University of Arizona, Tucson, AZ.

Kennedy, J., Goodrich, D., and Unkrich, C. (2013). "Using the KINEROS2 modeling framework to evaluate the increase in storm runoff from residential development in a semiarid environment," Journal of Hydrologic Engineering, 18(6), pp 698-706.

Lee, J. G., Selvakumar, A., Alvi, K., Riverson, J., Zhen, J. X., Shoemaker, L., and Lai, F. (2012). "A watershed-scale design optimization model for stormwater best management practices," Environmental Modelling and Software, 37(0), pp 6-18.

Leopold, L. B. (1968). Hydrology for urban land planning: A guidebook on the hydrologic effects of urban land use. Washington (DC): US Geological Survey.

Massart, J., Guertin, D.P., Smith, R.E., Goodrich, D.C., Unkrich, C.L., Levick, L. (2010). "K2-O2 (KINEROS-Opus) spatially based watershed hydrologic and biogeochemical model," Proc. 2nd Joint Federal Interagency Conference, Las Vegas, NV, June 27 - July 1, 2010, pp 12.

Miller, S. N., Semmens, D. J., Goodrich, D. C., Hernandez, M., Miller, R. C., Kepner, W. G., and Guertin, D. P. (2007). "The automated geospatial watershed assessment tool," Environmental Modelling and Software, 22(3), pp 365-377.

Rossman, L. A, and Supply, W. (2010). Storm water management model user's manual, version 5.0. National Risk Management Research Laboratory, Office of Research and Development, US Environmental Protection Agency.

Woolhiser, D. A., Smith, R., and Goodrich, D. C. (1990). KINEROS: A kinematic runoff and erosion model: Documentation and user manual US Department of Agriculture, Agricultural Research Service.

INTEGRATED MODELING APPROACH FOR FATE AND TRANSPORT OF SUBMERGED OIL AND OIL-PARTICLE AGGREGATES IN A FRESHWATER RIVERINE ENVIRONMENT

Faith A. Fitzpatrick, U.S. Geological Survey; Rex Johnson, Global Remediation Technologies, Inc.; Zhenduo Zhu, University of Illinois Ven Te Chow Hydrosystems Laboratory; David Waterman, University of Illinois Ven Te Chow Hydrosystems Laboratory, Richard D. McCulloch, LimnoTech, Inc., Earl J. Hayter, U.S. Army Corps of Engineers; Marcelo H. Garcia, University of Illinois Ven Te Chow Hydrosystems Laboratory; Michel Boufadel, New Jersey Institute of Technology; Timothy Dekker, LimnoTech, Inc.; Jacob S. Hassan, U.S. Environmental Protection Agency; David T. Soong, U.S. Geological Survey; Christopher J. Hoard, U.S. Geological Survey; and Kenneth Lee, Fisheries and Oceans (Canada) and the Australian Commonwealth Scientific and Industrial Research Organisation

Abstract The Enbridge Line 6B pipeline release of diluted bitumen into the Kalamazoo River downstream of Marshall, Michigan, U.S.A., in July 2010 was one of the largest oil spills into freshwater in North American history. A portion of the oil interacted with river sediment and submerged requiring the development and implementation of new approaches for detection and recovery of oil mixed with river sediment. Hydrodynamic and sediment transport modeling became an integral part of containment and recovery operations for decision support about the potential fate and migration of submerged oil and oiled sediment. Three models were developed for the U.S. Environmental Protection Agency to cover a range of spatial scales of interest to onsite operations. Two-dimensional (2D) hydrodynamic and sediment transport models from the Environmental Fluid Dynamics Code and the sediment bed model SEDZLJ[1] were used to simulate potential resuspension, migration, and deposition of submerged oil and oiled sediment along a 38-mile reach of the Kalamazoo River affected by the oil from Marshall to Kalamazoo. An algorithm was added to SEDZLJ to represent three additional particle size classes of oil-particle aggregates (OPAs) with a range of sizes, specific gravities, and settling velocities. Field and laboratory experiments and flume tests were done to support the numerical modeling of OPAs. A three-dimensional hydrodynamic model was developed to simulate hydrodynamics and OPA tracking through Morrow Lake, the most downstream impoundment. This model incorporated wind and dam operations into high and low flow, lake drawdown, and containment simulations. Finally, a 2D unstructured grid model, HydroSed2D, was used to simulate flows and sediment transport along 1- to 2-mile segments of the Kalamazoo River around islands and through side channels and backwater areas that are particularly prone to submerged oil deposition.

Integrated models could be developed quickly due to the availability of information and services combined with spill response operations that included: bathymetry and topography data, field-based geomorphic mapping of submerged oil, and discharge measured at U.S. Geological Survey streamflow gauges. Modeling results were included in a multiple-lines-of-evidence approach that was used by the Federal On-Scene Coordinator and operations staff for decision-making related to assessment and recovery of submerged oil, as well as net environmental benefit analysis. Similar modeling approaches will likely be useful for future oil spills in riverine environments.

BACKGROUND

The Enbridge Line 6B pipeline release of diluted bitumen (dilbit) into the Kalamazoo River downstream of Marshall, Michigan in July 2010 was one of the largest freshwater oil spills in North American history (Fig. 1). Only the 2004 Delaware River (Philadelphia) spill of about 265,000 gallons of heavy crude oil (U.S. Coast Guard, 2005) and the nearly 800,000 gallon spill of diesel fuel into the Monongahela River, near Pittsburgh in 1988 (Clark and others, 1990) are comparable in size to the 843,000 gallon release reported by Enbridge from Line 6B (http://www.epa.gov/enbridgespill/). The spill happened during a flood with a 4 percent exceedance probability (Hoard et al., 2010). Much of the floating oil was recovered quickly following the spill using conventional methods such as surface containment, absorbent boom, vacuum trucks, and drum skimmers (Dollhopf et al., 2014). However, the remaining oil mixed with river sediment, submerged, and deposited along 38 miles of the river, requiring the development and implementation of new approaches for detection and recovery of submerged oil and oiled sediment (Dollhopf et al., 2014). These approaches included the development of integrated hydrodynamic models to better understand and predict the fate and transport of the residual oil and its association with sediments over the range of environmental conditions encountered as a consequence of changes in river flow and spill response operations.

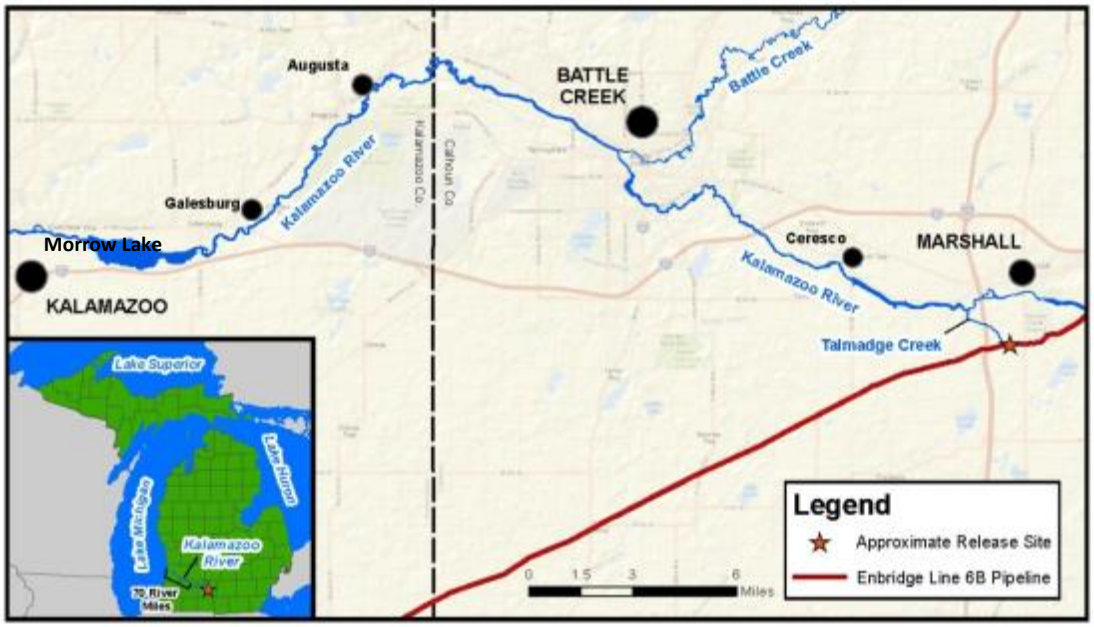

Figure 1 Location map of the Kalamazoo River affected by the July 2010 Enbridge Line 6B oil spill.

Hydrodynamic modeling originated with Enbridge in 2011 to help answer operational questions about the resuspension and downstream deposition of remaining submerged oil under different river flows scenarios and whether the oil could migrate past the most downstream impoundment, Morrow Lake (Enbridge Energy, L.P., 2012a, b). River flows in the Kalamazoo River can quickly increase by an order of magnitude, ranging from summer low flows of about 300 ft^3/s to rainfall or rain-snowmelt related runoff flows of greater than 3,000 ft^3/s. A set of hydrodynamic and sediment transport models using the 2-dimensional (2D) Environmental Fluid Dynamics Code (EFDC) was developed by Tetra Tech for Enbridge in 2011-12 to simulate river water levels, flows, velocities, shear stresses, sediment loads, and erosion and deposition patterns and rates along the 38 miles of the oil-affected Kalamazoo River (Enbridge Energy, L.P., 2012a, b).

A main assumption of the Enbridge modeling was that the transport characteristics of silt-sized sediment could be used as a surrogate for submerged oil. This assumption was based on the consistent spatial association of the remaining submerged oil with fine-grained soft sediment in slow-moving depositional areas of the river (Dollhopf et al., 2014) (Fig. 2). The Enbridge models were rapidly developed (within 3 months) using available data including topography from light detection and ranging (lidar) flown along the oil affected river corridor in 2011, and bathymetry from thousands of elevations associated with sediment poling assessments (agitation of river sediment using an aluminum pole with an 8-in diameter metal disc) for submerged oil (Enbridge Energy, L.P., 2012a). Data sets from two recently constructed HEC-RAS models for the upper and lower portions of the oil affected reach (Hoard et al., 2010; AECOM, 2011a, b; U.S. Army Corps of Engineers, Hydrologic Engineering Center, 2002, 2010) also were used for model setup and calibration. Discharge data from U.S. Geological Survey (USGS) gauging stations provided upstream and downstream boundary conditions as well as model calibration and validation comparisons. Water levels and oil marks collected by Enbridge and the U.S. Environmental Protection Agency (EPA) provided additional validation data.

Figure 2 Photos from the Kalamazoo River: (A) Oiled soft sediment in the vicinity of the Ceresco impoundment in 2012 and (B) typical oil sheen and globs on the water surface near soft sediment deposits in the Battle Creek Millponds in 2013.

Starting in 2013, a team of scientists and modelers continued the hydrodynamic and sediment transport modeling for EPA by updating the Enbridge models with additional data. Efforts were focused on expanding simulations using additional spatial scales and operational considerations including containment and water-level drawdowns in impoundments. The physical properties of the oiled sediment, including its persistence in the environment, were also reassessed in terms of the original representation of submerged oil as being transported with silt particles in the models. Repeated visual observations of spontaneously releasing globs from agitation of sediment during poling assessments, observations of oil globs in sediment cores, and ultraviolet epi-fluorescence microscopy of oil and sediment mixtures indicated that the oiled sediment was likely in the form of oil-mineral aggregates, similar to those that readily form in marine environments (Lee, 2002; Lee et al., 2011; Lee et al., 2012; Dollhopf et al., 2014). Aggregates were renamed oil-particle aggregates (OPAs) for the Kalamazoo River in recognition that a portion of the particulate matter is composed of organic as well as mineral particles. With the addition of the new field and laboratory data, a new set of sediment classes representing typical OPAs for dilbit in the Kalamazoo River were added to an existing sediment transport model. Updated and new models were developed to help answer operational considerations for continued recovery of submerged oil in the Kalamazoo River through the 2014 dredging efforts (Dollhopf et al, 2014).

The objectives of the 2013-14 EPA models are summarized in the following questions:

- Where and under what streamflow conditions will the remaining submerged oil and oiled sediment resuspend, transport, and settle along the river?
- What will happen to the remaining submerged oil and oiled sediment after dredging the impoundments and sediment traps?
- Will more submerged oil migrate into Morrow Lake and what conditions will allow it to pass through Morrow Dam?
- What are the effects of containment and recovery strategies on the migration potential of remaining Line 6B submerged oil?

This paper describes the design and framework of EPA's integrated modeling approach for simulating the fate and transport of submerged oil and OPAs in the Kalamazoo River following the 2010 Enbridge Line 6B release of dilbit. Whereas the final results of the modeling effort were not available for release at the time of this writing (October 2014),updated and new model results were used as they became available, during the decision-making process for remaining oil in the river in the Fall of 2012 through 2014.

THE KALAMAZOO RIVER

The Line 6B pipeline release happened in a wetland adjacent to Talmadge Creek 2 miles upstream of its confluence with the Kalamazoo River near Marshall, in Calhoun County Michigan (Figure 1). The drainage area of the Kalamazoo River near Marshall is 449 mi^2 and more than doubles in size at the downstream end of the oil-affected reach near Comstock with a drainage area of 1,010 mi^2 in large part because of the addition of Battle Creek, a tributary with a drainage area of 241 mi^2. The downstream end of the oil-affected reach is approximately 70 miles upstream of the river's confluence with Lake Michigan. The Kalamazoo River experiences a continental climate with about 32 in. of precipitation and over 40 in. of snowfall annually. Average July temperatures are 72^o F and January temperatures are 24^o F. Surficial geology mainly consists of glacial outwash composed of sand and gravel, as well as medium to coarse textured glacial till (Monaghan and Larson, 1984). Soils have mainly sandy loam textures (U.S. Department of Agriculture, 1994).

The oil-affected reach between Marshall and Kalamazoo has three impoundments – Ceresco, the Mill Ponds near the City of Battle Creek, and Morrow Lake. Flows are minimally affected by power plant releases at Marshall, on Battle Creek, and at Morrow Dam. The width of river varies between about 75 and 200 ft and is generally wide with a width/depth ratio of 40 and a gentle slope of 0.06 percent (3.14 feet/mile) (Tetra Tech, 2011). Water depths range from about 1 to 4 ft. The bottom is composed of gravel, cobble and boulders in the main channel in riffles and thick deposits of organic-rich muck in impoundments. Aquatic vegetation is abundant in summer months. The floodplain of the river is almost completely forested wetland which gives the suspended and bottom sediment a relatively high organic matter content, on the order of 20 percent or more. The river contains many islands, bars, and oxbows. Deposition of submerged oil associated with the Line 6B release occurred along channel margins, backwaters, side channels, oxbows, and in impoundments. Resuspension of submerged oil and settling downstream was evident in repeated poling assessments following floods (Dollhopf et al., 2014).

MODELING DESIGN AND FRAMEWORK

The updated modeling efforts encompassed three main modeling types for simulating submerged oil and oiled sediment transport resuspension, migration, and settling in areas of the river with continued issues with submerged oil: (1) a 2D EFDC model (Hamrick, 1992) of the 38-mile oil-affected reach of the Kalamazoo River; (2) a 3D EFDC model (Hamrick, 1992) for Morrow Lake that accounted for wind and subsurface withdrawals at Morrow Dam; and (3) nested sub-models of enhanced sediment traps using HydroSed2D (Zhu, 2011). These three models, with updated sediment transport algorithms and sediment properties, were needed to address questions at the appropriate spatial scales being asked by operational response staff. It was necessary to have a multidisciplinary modeling team for this work including expertise in heavy oil and sediment transport to be able to develop new algorithms for OPA resuspension, migration, and settling. The USGS, GRTusa, and Weston, Inc. provided coordination, oversight, and direction for the new models, as well as direct and rapid communication with operations staff and the Federal On-Scene Coordinators (FOSCs). They also worked with Tetra Tech and reviewed the 2012 Enbridge model. LimnoTech, Inc. updated the 2D EFDC model. The U.S. Army Corps of Engineers (USACE) developed the OPA algorithm that was coupled to SEDZLJ and conducted onsite SEDFLUME tests (Perkey et al., 2014). The University of Illinois Ven Te Chow Hydrosystems Laboratory (VTCHL) developed the 3D EFDC model, the HydroSed2D model, and conducted *in situ* flume tests and laboratory experiments for OPA. Oil experts from the New Jersey Institute of Technology, and the Canada Offshore Oil, Gas and Energy Research Centre at the Bedford Institute of Oceanography (COOGER) guided laboratory experiments and flume tests and overall modeling approaches.

The modeled flows encompassed a range of flow conditions (Table 1). The updated 2D EFDC models overlapped with two flow simulations included in the Enbridge model for comparison purposes. For the floods, the peak flow associated with the July 2010 flood during the oil spill had a 4-percent probability of the event being equaled or exceeded in any given year for the Marshall USGS streamflow gauge and a 20-percent probability downstream of the Battle Creek confluence (Hoard et al., 2010). The April 2013 high flow also had an exceedance probability of 20 percent, and had corresponding velocity measurements and suspended sediment samples. For the October-November 2011 high base flow period, these flows were equaled or exceeded 20 percent of the time over the period of record and the time period was chosen that overlapped with velocity measurements. The July 2013 low flow was included to represent depositional conditions in the river with flows being equaled or exceeded 50 percent of the time over the period of record. The July 2013 low flow also was chosen to examine the potentially erosional effects in Morrow Lake during low flow from the bottom draw turbines at Morrow Dam. The August 2012 low flow period was used to simulate containment effects on flows when there were corresponding velocity measurements. Lastly, mean daily flows from July-October and November-January from the Kalamazoo River near Battle Creek streamflow gauge were used for simulations of water level drawdowns in Morrow Lake to assist in decision making on whether to dredge oiled sediment in Morrow Lake delta or excavate in the dry.

Table 1 Types of models and in-common flow scenarios for 2D EFDC, 3D EFDC, and HydroSed2D. [H, hydrodynamic; S, sediment transport; PT, particle tracking; O, Oil-particle aggregate transport]

Model Description	Jul 2010 Oil spill flood	Oct-Nov 2011 High base flow	Aug 2012 Low flow	Apr-May 2013 flood	Jul 2013 Low flow	Flood 1-percent exceedance probability	Mean daily Jul-Oct, Nov-Jan
2D EFDC	H[1]	H[1], S[1], O		H	H, S		H[2]
3D EFDC			H[3]	H, PT	H, PT		H[2]
HydroSed2D				H	H	H, S	

[1]Updated simulations for comparison with the Enbridge model.
[2]Simulated Morrow Lake drawdown.
[3]Containment added in Morrow Lake delta.

The Enbridge 2D EFDC model was assembled from new and existing bathymetric and topographic data collected up through the fall 2011 (Enbridge Energy, L.P., 2012a, b). Boundary conditions were established using available streamflow data at five USGS gauges along the Kalamazoo River and its tributaries between Marshall and Comstock. Suspended sediment concentration and particle size data were not available for the streamflow gauges in the modeled reach and had to be assembled from a larger geographic area of representative locations on upstream and downstream streamflow gauges on the Kalamazoo River and on adjacent streams. Some sediment transport parameters were estimated from existing published literature. Bathymetry data were generated from poling assessment data points, combined with surveyed longitudinal profile points, single beam survey of Morrow lake bathymetry conducted in September 2010, channel cross sections measured for the HEC-RAS modeling, and flood inundation mapping. For floodplain topography, 1-ft contours were generated from the 2011 Enbridge lidar data used in the HEC-RAS modeling and flood inundation mapping for the entire area within the 100-yr floodplain boundary (AECOM, 2011a, b). Banklines for the riverine grid were drawn in a geographic information system (GIS) from November 2011 aerial imagery raster files at a scale of 1:100. Streambed characteristics for particle sizes were applied to the grids from 2011 surficial core data assigned to specific geomorphic mapping units and supplemented with substrate types recorded in poling assessments.

The updated 2D EFDC hydrodynamic-sediment transport model was compared with the Enbridge model, as well as used to run new simulations for 2013 high and low flows. The updated model was run with the Sandia National Labs version of EFDC (SNL-EFDC), which incorporates the sediment transport algorithms of SEDZLJ (Jones and Lick, 2001) instead of the standard sediment transport module included in the Enbridge model. Similar to the Enbridge model, the updated model had a domain of the entire oil-affected reach of the Kalamazoo River and consisted of two base grids, one for in-channel flows, called the riverine grid, with a boundary fitted curvilinear-orthogonal horizontal grid network, and another for out-of-bank flows, called the floodplain grid, with a finer-scaled Cartesian grid network with cells of approximately 15 x 15 m. The Cartesian grid network was needed for simulating overland flood flows beyond the sinuous channel. The sediment transport and OPA simulations were run only using the riverine grid. The updated 2D EFDC hydrodynamic model provided flow inputs and

checks for the HydroSed2D models and overall checks with the 3D EFDC model for the upstream delta portion of Morrow Lake.

The domain of the 3D EFDC model (Hamrick, 1992) was Morrow Lake and its dam (Fig. 1). The model incorporated wind data and a 3D view of the gates and turbines at Morrow Dam. This was important to consider because the turbines withdraw a substantial amount of flow, especially during low flow conditions. It was thought originally that outflows from the updated 2D EFDC model would serve as inflows for the 3D EFDC model at the upstream end of Morrow Lake; however, measured water levels at the upstream end of Morrow Lake were used instead because it was thought that measured water elevations were more quantitative for upstream boundary conditions than simulated flows. The 3D EFDC hydrodynamic model provided simulations of the effects of a water level drawdown in Morrow Lake on velocity and bed shear stresses in the upstream delta area. A simplistic design of subsurface containment curtains in Morrow Lake delta were also explored for a July 2012 low flow period that had corresponding velocity measurements along the containment curtains.

The HydroSed2 model code was previously developed at the VTCHL (Liu et al., 2008; Zhu, 2011). The model was chosen to run simulations at a subset of enhanced sediment traps at mileposts (MP) along the spill-affected reach of MP 10.4, MP 10.5, MP 14.75, and MP 21.5 because its unstructured triangular mesh could be detailed enough to represent complex river geomorphology of backwaters (MP 10.4, 10.5), side channels and islands (MP 14.75), and meander cutoffs and oxbows (MP 21.5). An example sediment transport run was included for MP 14.75 and part of the Mill Ponds impoundment.

Common outputs for all models included maps of velocity magnitudes and bed shear stress for the hydrodynamic models. Results from the hydrodynamic models were felt to be the most robust because of the relative wealth of water level, velocity, and discharge data available for calibrations and validation. Initially, velocities of less than 30 cm/s were associated with submerged oil depositional areas and a critical bed shear stress for erosion of 0.4 Pa was used as a conservative estimate of areas where erosion was likely.

Sediment transport runs were more time consuming and had less validation data. Keeping this in mind, fewer runs were done for the 2D EFDC and HydroSed2D models. Typical output included maps of net erosion and deposition. For the 3D EFDC model, less time was spent on sediment transport and instead a Lagrangian particle-tracking model was developed for OPAs.

At the time of this writing (October 2014), documentation for the individual models (2D EFDC, 3D EFDC, HydroSed2D, OPA algorithm) were in the technical review stage. By the time of the SEDHYD 2015 conference, the documents should be available to the public. Some of the datasets that made these models possible to develop relatively quickly for submerged oil and OPAs are highlighted below.

UPDATED DATA SOURCES

The Enbridge models were calibrated in the Spring 2012 to discharge, water surface elevation, and velocity using USGS data from streamflow gauges and other measurements collected by Enbridge and the USGS in 2010-2011 (Enbridge Energy, L.P., 2012a, b). Erosion and sedimentation rates and sediment loads could not be calibrated or validated because no sediment data were available; however, historical suspended sediment data were used from an upstream streamflow gauge at Albion, Michigan and outputs were visually checked against depositional

areas mapped in the geomorphic surfaces unit maps. Model sensitivity analyses were performed on several input parameters to assess how small variations might affect model outputs. Results from these analyses indicate that the models were most influenced by flow and bathymetry and that more data were needed for these and for sediment transport characteristics.

The three new sets of models included major updates of bathymetry, floodplain topography, tributary flow inputs, dam configurations and ratings, channel roughness, and suspended sediment characteristics from data collected in 2012-14 (Table 2). Inclusion of wind data in the 3-D model was important because the majority of Morrow Lake is less than 6 ft deep, which allows for wind to establish strong vertical circulation cells with upwellings and downwellings. The stage/discharge curve was developed for Morrow Dam with the help and experience of the dam operators.

Table 2 Selected major updates in data inputs and calibration for the U.S. Environmental Protection Agency updated 2D EFDC, 3D EFDC, and HydroSed2D models.

Data Type	**Description**
Grids	2D EFDC grids same as Enbridge model, new grids for 3D EFDC and HydroSed2D
Bathymetry and HEC-RAS	Based on multiple sources – poling assessments, surveyed elevations and cross sections, acoustic surveys. Updated with additional data collected in 2012-13, including new HEC-RAS cross sections. Redeveloped bathymetry raster melded with topography at banklines.
Floodplain topography	New county lidar. Redeveloped topography raster.
Tributary flow inputs	Tributary flows redistributed based on drainage area
Dam configurations	Configurations for all dams updated, including dam geometry. Headwater elevations and 3-part stage/discharge rating curve were need for the powerplant operations at Morrow Dam.
Channel roughness	Roughness recalibrated using additional stage and velocity data
Suspended sediment concentration and particle size	Concentration/discharge curves updated with suspended sediment data collected at five U.S. Geological Survey streamflow gauges during six events 2012-14.

Even though there were major data gaps and the Enbridge 2D EFDC model had to be constructed quickly, preliminary model results for flow, water levels, velocity, and shear stress were carefully considered by operations staff. The models helped to verify areas of the river that likely changed from depositional during lows to erosional during high flows. The models also were used for prioritizing and verifying the depositional characteristics of enhanced sediment traps during a range of flows (Mahajan et al., 2013).

Recent developments in remote sensing made it possible to construct detailed, complex hydrodynamic models for a long stretch of the river relatively quickly. High-resolution lidar data were available for constructing detailed topography of the floodplain. High-resolution survey-grade global positioning systems were used to collect the geospatial coordinates of several thousand poling assessment points, which could be used for bathymetry. Powerful and organized onsite GIS capabilities made it possible to construct detailed and complex maps on a daily basis. Acoustic/sonar methods, combined with survey-grade GPS, were used to collect reliable and detailed velocity (e.g., stationary and transect data) and discharge measurements.

SEDFLUME AND IN SITU FLUME TESTS

In 2012, there was a lack of quantitative data that could be used for sediment transport model calibration and validation including oiled sediment and OPAs. River bed substrate was represented in the Enbridge model with selected sediment core data from 2011 applied to mapped geomorphic surface units with simplified sediment types (Enbridge Energy, L.P., 2012a). For the updated models, the Enbridge database was supplemented with additional data derived from sediment cores collected in 2012, onsite SEDFLUME tests of nine cores by the USACE (Perkey et al, 2014), and onsite *in situ* flume tests at five sites by the VTCHL (report in draft at time of this writing) in 2013.

The onsite flume-style erodibility tests were done in three general areas—the Mill Ponds, the downstream end of Morrow Lake (SEDFLUME only), and the upstream delta area of Morrow Lake (Perkey et al., 2014). Most of the tests were done to represent the cohesive layered organic-rich silt and fine sand deposits in Morrow Lake delta with moderate to heavy oiling conditions. *In situ* flume tests were done at a subset of the SEDFLUME core locations.

The two flumes measure potential erosion in different ways, making the results complimentary. The mobile SEDFLUME measures gross erosion rates with depth in a core at various shear stresses, as well as physical properties specific to vertical layering. The *in situ* flume tests measured erodibility of the near-surface sediment over a larger area than that of a single core. The *in situ* flume estimates bed shear stress and net erosion rates based on the mass of sediment eroded at a range of discharges which complements the SEDFLUME test results.

These tests were also done in areas that had repeated agitation toolbox techniques done as part of 2011 submerged oil recovery efforts (Dollhopf et al., 2014). Using a combination of results from these tests, literature values, and hydrodynamic results, bed layer properties of particle size, wet bulk density, critical shear stress for erosion, and erosion rates were generated for the updated 2D EFDC SEDZLJ model.

LABORATORY PROPERTIES OF OIL-PARTICLE AGGREGATES

Laboratory experiments and flume tests were done by VTCHL in 2013-14 to specifically characterize and quantify the weathering characteristics of Cold Lake Blend dilbit and the properties of OPAs formed by its subsequent mixing in the presence of Kalamazoo River sediment. The properties of interest for OPAs included the shape and arrangement (Fig. 3), oil droplet size, oil density, number of oil droplets in an OPA, size of OPA, density of OPA, settling velocity, and critical shear stress to entrain OPAs. The first laboratory tests were to weather the diluent from the bitumen while tracking oil mass loss and oil density and viscosity over a range of temperatures found in the Kalamazoo River. The results from these tests confirmed that weathered Cold Lake Blend remained positively buoyant at room temperature, similar to test results by Belore (2010).

The size distributions of oil globules within OPAs and the OPAs themselves were tested with an orbital shaker run at a range of mixing energies while held at room temperature. The globule size is a function of mainly the viscosity of the oil and amount of turbulence, which is commonly characterized with the turbulent kinetic energy dissipation rate. To form OPAs, the weathered bitumen was mixed in the shaker with Kalamazoo River sediment, and the mixing energy, time, sediment type, and sediment concentration were varied. Photography was used to capture the

size of the large globules and a Laser In-Situ Scattering and Transmissiometry (LISST) instrument was used for the small globules.

The OPA also was examined under an ultraviolet epi-fluorescence microscope using similar techniques as those used by Lee et al. (2012) and Ma et al. (2009). Preliminary results from these tests indicate that the OPAs generated in the laboratory tests were composed of complexly shaped aggregates of oil globules ranging from about 10 to 100 μm with attached particles of about 10 μm or smaller. The most common OPA type observed in the photomicrographs were the single and multiple droplet aggregates as illustrated in Figure 3A; solid-type aggregates were observed when unconventional mixing conditions were implemented.

Annular flume experiments were run to determine the critical bed shear stresses associated with re-entrainment of the OPA from the bed into the water column. In addition, a settling column was used to measure OPA settling velocities.

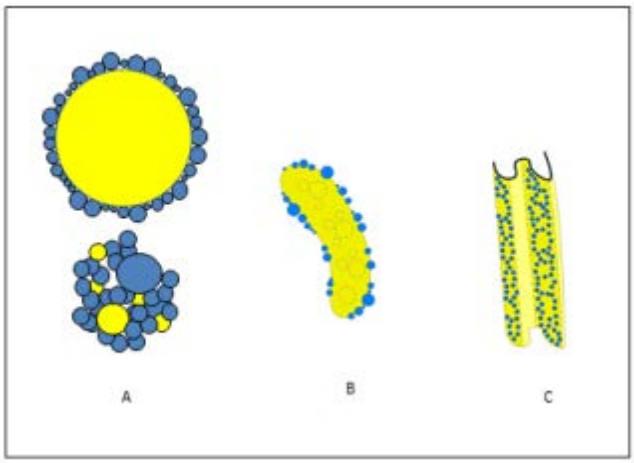

Figure 3 Types of oil-particle aggregates: (A) single and multiple droplet aggregate, (B) solid aggregate of large, usually elongated mass of oil with interior particles (dashed blue circles), and (C) flake aggregate of thin membranes of clay aggregates that incorporate oil and fold up (modified from Stoffyn-Egli and Lee, 2002). Blue color represents particles and yellow represents oil.

Results from these tests were used, along with other field data, for characterizing OPA properties in SEDZLJ and 3D EFDC particle tracking models. Within these models, the OPA maintains a stable form. Future models could be developed from these data to simulate the mechanisms responsible for the formation and breakup of OPAs in freshwater riverine environments.

DEVELOPMENT OF AN OIL-PARTICLE AGGREGATE ALGORITHM

A preliminary simple algorithm for OPAs was developed by the USACE for inclusion in the Kalamazoo River SEDZLJ model. The algorithm represents oiling conditions in the river in 2012, after formation of OPAs. The algorithm uses existing data from other studies of OPAs (Lee et al., 2012), onsite observations from poling assessments and cores, and preliminary results from VTCHL experiments and flume tests. Three groups of OPAs have been included in the model, in recognition that there are likely multiple sizes and densities of oil globules and OPAs in the riverbed. The groups, which are considered substrate classes in SEDZLJ, range from a large 2-mm single oil globule with a 10-μm silt coating to more complex OPAs with multiple smaller globules and diameters of 31 μm and 100 μm. Densities range from just greater than the density of freshwater for the large oil globule with silt coating (1.034 g/cm^3) to somewhat

heavier and close to the density of organic matter for the OPAs (1.511 g/cm^3). Settling velocities range from 0.2 to 20+ mm/s, depending on the amount of oil relative to the size of the aggregate. A major assumption is that the OPAs stay intact, i.e., they do not breakup or disaggregate, during model runs. The bed layering in SEDZLJ required data on the mass fraction of OPA and its size, the density of the OPA, and erosion rate of each layer. The Kalamazoo River streambed from the 2012 Enbridge model was updated with SEDFLUME core data to obtain layer properties, and then further overlaid with 2012 oiled areas of the river to estimate properties of OPAs. The simplified transport algorithm for OPAs is a start for future modeling of OPA formation, transport, and deposition.

SUMMARY AND CONCLUSIONS

Multiple-scale hydrodynamic and sediment transport models were successfully developed in a rapid fashion to address operational questions regarding the fate and transport of submerged oil associated with the July 2010 Enbridge Line 6B spill. Preliminary hydrodynamic models covering several miles of river could be constructed quickly because of the relatively large amount of quickly collected bathymetry and topographic data during response operations and available discharge data at existing USGS streamflow gauges. An organized geographic information system allowed the daily addition of data that was made available immediately across a common platform for sharing inputs and results among models. Due to the length of the cleanup time, the 2012 Enbridge model was updated with more data on bathymetry, velocity, water levels, dam operations, suspended sediment, and streambed conditions. Results from the 2012 and updated models were part of a multiple-lines-of-evidence approach that was used by the Federal On-Scene Coordinator for decision-making related to assessment and recovery of submerged oil, as well as net environmental benefit analysis.

The updated models fill a niche in simulating submerged oil transport and fate, in that they are the first of their kind to model oil-particle aggregates (OPAs) in a riverine freshwater environment. It is hoped that the modeling approach used for the Kalamazoo River will be useful if future oil spills occur in similar freshwater environments and that characteristics of OPAs can be applied to lacustrine hydrodynamic models as well. Rivers in the Midwestern U.S. have characteristics conducive to formation, deposition, and resuspension of OPAs including suspended sediment in the water column (especially during floods), shallow depths, wide channels, relatively low gradient, abundant impoundments, and turbulent flows. These characteristics will likely result in the need for submerged oil recovery and oiled-sediment cleanup for both light and heavy crude oil spills, and a closer look at the ecological risks and potential benefits of physical oil dispersion mediated by the presence and availability of suspended particles.

REFERENCES

AECOM (2011a). “Kalamazoo River Flood Inundation Mapping—Hydraulics,” AECOM Technical Memorandum, June 2011.

AECOM (2011b). “Kalamazoo River Flood Inundation Mapping—Hydrology,” AECOM Technical Memorandum, June 2011.

Belore, R. (2010). “Properties and fate of hydrocarbons associated with the hypothetical spills at the marine terminal and in the confined channel assessment area,” Enbridge Northern Gateway Project, SL Ross Environmental Research LTD., Ottawa, Ontario, variable pagination.

Clark, R.M., Vicory, A.H., Goodrich, J.A. (1990). The Ohio River Oil Spill: A Case Study: Journal of American Water Works Association, 82(3), pp 39-44.

Dollhopf, R.H., Fitzpatrick, F.A., Kimble, J.W., Capone, D.M., Graan, T.P., Zelt, R.B., Johnson, R. (2014). "Response to heavy, non-floating oil spilled in a Great Lakes river environment: a multiple-lines-of-evidence approach for submerged oil assessment and recovery," Proceedings, 2014 International Oil Spill Conference, Savannah, GA, pp 434-448.

Enbridge Energy, L.P. (2012a). Kalamazoo River Hydrodynamic and Sediment Transport Model. Enbridge, 70 p., Attachments. Submitted April 20, 2012.

Enbridge Energy, L.P. (2012b). Kalamazoo River Hydrodynamic and Sediment Transport Model Report Addendum. Enbridge, 4 p., Attachments. Submitted May 8, 2012.

García, M.H. (Editor-in-Chief) (2008). Manual of Engineering Practice 110, "Sedimentation engineering," Environmental and Water Resources Institute (EWRI), American Society of Civil Engineers (ASCE), 1150 p.

Hamrick, J.M. (1992). "A three-dimensional Environmental Fluid Dynamics Computer Code: Theoretical and Computational Aspects," *Special Report No. 317* in Applied Marine Science and Ocean Engineering, Virginia Institute of Marine Science, Gloucester Point, VA., pp 1-64.

Hoard, C.J., Fowler, K.K., Kim, M.H., Menke, C.D., Morlock, S.E., Peppler, M.C., Rachol, C.M., Whitehead, M.T. (2010). "Flood-inundation maps for a 15-mile reach of the Kalamazoo River from Marshall to Battle Creek, Michigan," U.S. Geological Survey Scientific Investigations Map 3135: pamphlet, 6 sheets, scale 1:100,000.

Jones, C., Lick, W. (2001). SEDZLJ: A Sediment Transport Model. Dept. of Mech. and Env. Eng., University of California, Santa Barbara.

Lee, K. (2002). "Oil-particle interactions in aquatic environments: influence on the transport, fate, effect, and remediation of oil spills," Spill Science and Technology Bulletin, 8(1), pp 3-8.

Lee, K., Boudreau, M., Bugden, J., Burridge, L., Cobanli, S.E., Courtenay, S., Grenon, S., Hollebone, B., Kepkay, P. Li, Z., Lyons, M. Niu, H. King, T.L., MacDonald, S., McIntyre, E.C., Robinson, B., Ryan S.A., Wohlgeschaffen, G. (2011). State of Knowledge Review of Fate and Effect of Oil in the Arctic Marine Environment: Report for the National Energy Board of Canada, Arctic Roundtable: State-of-Knowledge Review of Fate and Effects of Oil in Arctic Offshore. Fisheries and Oceans Canada. 259 p.

Lee, K., Bugden, J., Cobanli, S., King, T., McIntyre, C., Robinson, B., Ryan, S., Wohlgeschaffen, G. (2012). UV-Epifluorescence microscopy analysis of sediments recovered from the Kalamazoo River: Dartmouth, Nova Scotia, Centre for Offshore Oil, Gas and Energy Research (COOGER) Report, October 24, 2012.

Liu, X., Landry, B., García, M.H. (2008). Two-dimensional scour simulations based on coupled model of shallow water equations and sediment transport on unstructured meshes," Coastal Engineering, 55(10), pp 800-810.

Ma, X., Cogswell, A., Li, Z., Lee, K. (2009). "Particle size analysis of dispersed oil and oil-mineral aggregates with an automated ultraviolet epi-fluorescence microscopy system," Environmental Technology, 29(7), pp 739-748.

Mahajan, R., Rodriguez, H., Plis, M., Hamrick, J., and Davie, S. (2013). "Use of sediment transport model to support remediation in river oil spills," Environmental and Water Resources Institute, American Society of Civil Engineers Annual Conference Proceedings.

Monaghan, G.W., Larson, G.J. (1984). Glacial Geology of Kalamazoo County, Michigan. East Lansing, Mich., Michigan State University, Department of Geology, 35 p.

Perkey, D.W., Smith, S.J., Kirklin, T. (2014). "Cohesive sediment erosion field study: Kalamazoo River, Kalamazoo, Michigan," U.S. Army Corps of Engineers Research and Development Center, Coastal and Hydraulics Laboratory, Vicksburg, MS, Letter Report, 16 p. + appendixes.

Stoffyn-Egli, P. Lee, K. (2002). "Characterization of oil-mineral aggregates," Spill Science and Technology Bulletin, 8(1), pp 31-44.

Tetra Tech, Inc. (2011). Oil Mark Survey Technical Memorandum. Marshall, MI, March 18, 2011.

Thibodeaux, L.J., MacKay, D. (Editors) (2011). Handbook of Chemical Mass Transport in the Environment. CRC Press, Boca Raton, FL, 614 p.

U.S. Army Corps of Engineers Hydrologic Engineering Center (2002). HEC-RAS River Analysis System, Hydraulic Reference Manual, version 3.1, [variously paged].

U.S. Army Corps of Engineers Hydrologic Engineering Center (2010). HEC-RAS, River Analysis System Version 4.1.0. Davis, CA.

U.S. Coast Guard, 2005, T/S ATHOS I Evaluation Report: U.S. Coast Guard National Strike Force Coordination Center, Elizabeth City, NC, 57 p.

U.S. Department of Agriculture Soil Conservation Service (1994). State Soil Geographic (STATSGO) Data Base. Fort Worth, Tex., 113 p.

Zhu, Z. (2011). Simulation of Suspended Sediment and Contaminant Transport in Shallow Water Using Two-Dimensional Depth-Averaged Model with Unstructured Meshes. Master Thesis, University of Illinois at Urbana-Champaign.

DEMONSTRATION OF THE CAPABILITIES OF THE KINEROS2 – AGWA 3.0 SUITE OF MODELING TOOLS

Shea Burns, Senior Research Specialist, University of Arizona, Tucson, AZ, shea.burns@ars.usda.gov; Carl L. Unkrich, Hydrologist, USDA-ARS, Tucson, AZ, carl.unkrich@ars.usda.gov; David C. Goodrich, Research Hydraulic Engineer, USDA-ARS, Tucson, AZ, dave.goodrich@ars.usda.gov; Yoganand Korgaonkar, Graduate Student, University of Arizona, Tucson, AZ, yoganandk@email.arizona.edu; Jeff Kennedy, USGS, Tucson, AZ, Hydrologist, USGS, Tucson, AZ, jkennedy@usgs.gov; Gabriel Sidman, GIS Analyst, Winrock International, Washington, D.C., gabriel.sidman@winrock.org; Brian Scott Sheppard, Graduate Student, University of Arizona, Tucson, AZ, bss1@email.arizona.edu; Mariano Hernandez, Associate Research Scientist, University of Arizona, Tucson, AZ, mariano.hernandez@ars.usda.gov; Phil Guertin, Professor, University of Arizona, Tucson, AZ, dpg@email.arizona.edu; William Kepner, Research Ecologist, EPA-LEB, Las Vegas, NV, kepner.william@epa.gov; Phil Heilman, Research Leader, USDA-ARS, Tucson, AZ, phil.heilman@ars.usda.gov; Mark Nearing, Research Agricultural Engineer, USDA-ARS, Tucson, AZ, mark.nearing@ars.usda.gov

Abstract: The Automated Geospatial Watershed Assessment tool (AGWA) is a watershed modeling tool that supports the parameterization and execution of several distributed hydrologic models, KINEROS2, RHEM (Rangeland Hydrology and Erosion Model), and SWAT (Soil & Water Assessment Tool version 2000 and version 2005) in the following GIS environments: ESRI ArcView 3.x, ESRI ArcMap 9.x, and ESRI ArcMap 10.x. KINEROS2 is an event-based rainfall-runoff model that is physically-based, representing interception, infiltration, surface runoff, sediment detachment, sediment transport, and sediment deposition processes for overland and channel flow. For a more detailed description of AGWA and KINEROS2, including their histories, see Goodrich et al. (2015; these proceedings) and their respective websites (www.tucson.ars.ag.gov/agwa and www.tucson.ars.ag.gov/kineros). This demonstration will showcase the capabilities of both AGWA and KINEROS2 in a variety of applications, scenarios, and use-cases.

AGWA supports the parameterization and execution of hydrologic models for watershed modeling efforts by performing the following tasks: watershed delineation; watershed discretization into discrete model elements; watershed parameterization; precipitation definition; model simulation creation; model execution; and model results visualization (Figure 1). Watershed delineation uses a filled, hydrologically correct DEM and derived flow direction and flow accumulation with a user-defined outlet to create a watershed boundary. Watershed discretization subdivides the watershed into model specific elements based on the user's model selection and stream network definition choice. Watershed parameterization assigns area-weighted topographic, soils, and land cover parameter estimates to the model elements. Precipitation definition creates individual storm event files for KINEROS2 or continuous, daily precipitation aggregates for SWAT that drive the models. Model simulation creation creates the model input files required to execute a simulation. Model execution runs the model in a command prompt window. Finally, model results visualization imports the model results into tabular format that can be associated with and displayed on the model elements in the GIS.

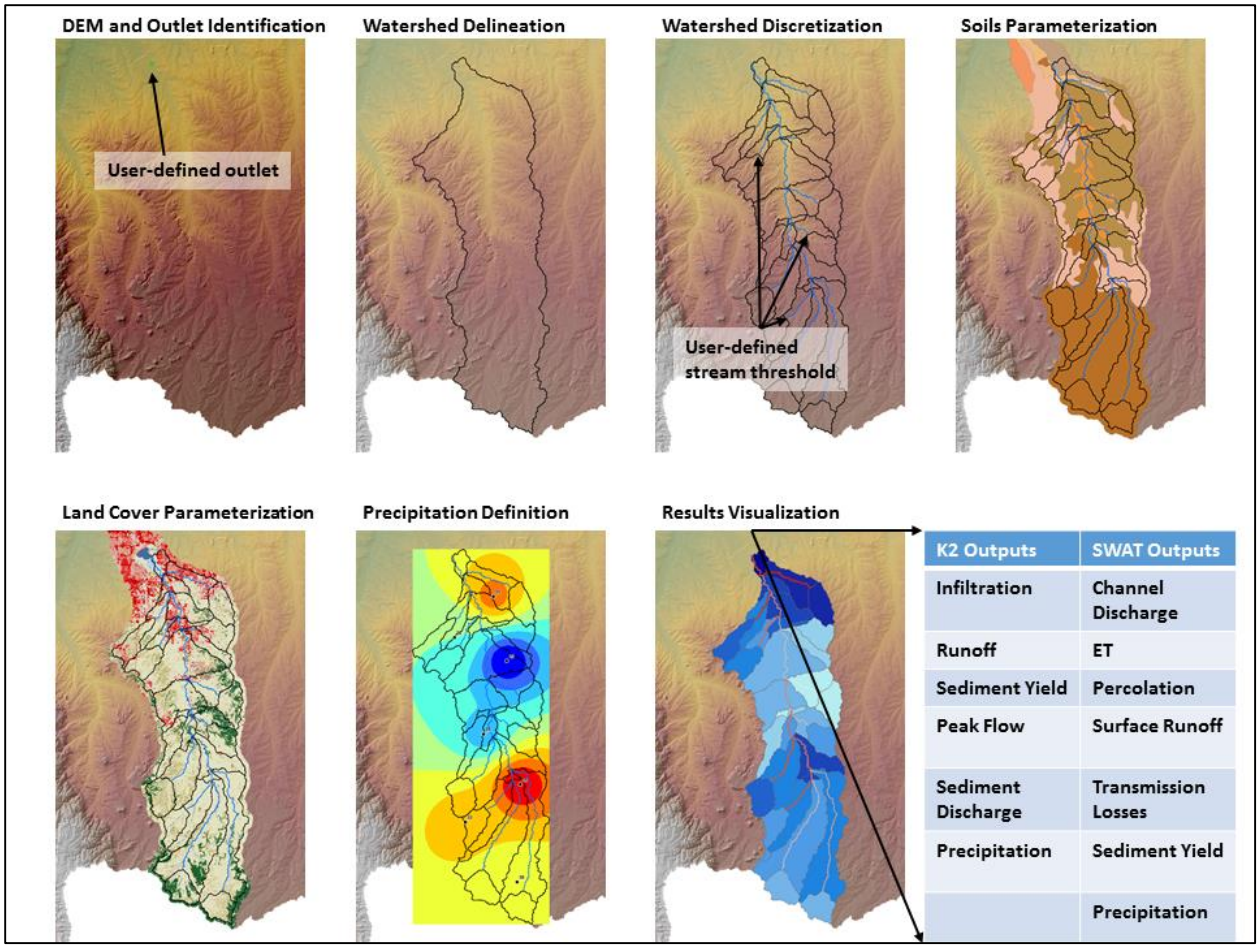

Figure 1 The required steps in AGWA to perform a watershed assessment. A DEM is used to delineate the watershed, subdivide it into model elements, and parameterize the elements in conjunction with the soils and land cover layers. Precipitation drives the model and model results are imported and visualized in the GIS.

The AGWA demonstration will feature the seven general AGWA steps. In addition, it will highlight some advanced features/functionality recently added to AGWA, including: an area-of-interest group delineation tool for delineating watersheds within a defined boundary (political, management, administrative, etc.); batch simulations; batch parameterizations; hillslope sub-discretizations; additional stream network definition methodologies utilizing a flow length threshold, flow accumulation threshold, or an existing stream network; rapid-post fire watershed assessments and report generation; use of dynamic erosion formulations in the RHEM (Rangeland Hydrology and Erosion Model) model; and incorporation of Low Impact Development (LID) features in the KINEROS2 model.

DEMONSTRATION OF THE WATER EROSION PREDICTION PROJECT (WEPP) INTERNET INTERFACE AND WEB SERVICES EXTENDED ABSTRACT

Jim Frankenberger, Computer Specialist, USDA-ARS, West Lafayette, IN, Jim.Frankenberger@ars.usda.gov
Dennis Flanagan, Research Agricultural Engineer, USDA-ARS, West Lafayette, IN, Dennis.Flanagan@ars.usda.gov
Bill Elliot, Research Engineer, USDA Forest Service, Moscow, ID, welliot@fs.fed.us
Eric Theller, Computer Science Intern, USDA-ARS, West Lafayette, IN, etheller@purdue.edu

Abstract: The Water Erosion Prediction Project (WEPP) model is a process-based FORTRAN computer simulation program for prediction of runoff and soil erosion by water at hillslope profile, field, and small watershed scales. To effectively run the WEPP model and interpret results additional software has been developed. Software external to WEPP includes user interfaces, databases of model parameters and software to provide translation to WEPP input formats along with spatial mapping and graphical software to present modeling results. Recent WEPP projects at the USDA-ARS National Soil Erosion Research Laboratory (NSERL) have included web-based user interface development. Providing access to the WEPP modeling resources using a web browser allows easy access for users and a central point for any model or data updates. In addition to web browser interfaces WEPP model services are made available through representational state transfer (REST) web services. The WEPP REST software services allow additional web sites or applications to be developed that make use of the WEPP technology.

This presentation will demonstrate the current WEPP internet GIS and hillslope interfaces available from servers at the NSERL. How to use the WEPP REST web services will also be demonstrated.

INTRODUCTION

The Water Erosion Prediction Project (WEPP) model is a process-based FORTRAN computer simulation program for prediction of runoff and soil erosion by water at hillslope profile, field, and small watershed scales. The inputs to the WEPP model consist of text files with parameters for climate, soils, topography/slope and land use management. Watershed simulations also include input files that describe the channel parameters and connectivity. Creating the WEPP input files and presenting model results are handled by separate user interface programs. When WEPP was first released in 1995 the intent was that DOS file building interface programs would be replaced with more user-friendly interfaces. Additional desktop interfaces have included support for Microsoft Windows (Flanagan, et al. 1998) and the GeoWEPP extensions to ArcGIS (Renschler, 2003).

Web-based applications of the WEPP hillslope and watershed models are available from the WEPP NSERL website at: http://milford.nserl.purdue.edu/. The US Forest Service has also developed specialized web-based applications of WEPP for forest conditions available at: http://forest.moscowfsl.wsu.edu/fswepp/ (Elliot, 2004). Web-based interfaces allow the model to be used by groups with different expertise levels by simplifying the user interfaces. For full access to all model inputs for research purposes the desktop version of WEPP and interface are still available. In addition to the WEPP interfaces available through browsers, web services have been developed. These allow additional interfaces to be developed while still taking advantage of having the model simulations and data centrally located. The WEPP web services have been designed to be REST compatible. This allows the most number of client application types to use the services since information is transferred in common formats such as XML or JSON using HTTP methods (Rodriguez 2008).

This extended abstract describes three web-based technologies that have been developed to make complex science within the WEPP model more usable by managers, scientists, students and the general public.

WEPP INTERNET HILLSLOPE MODEL

The WEPP hillslope model requires four types of input files to be setup to run a simulation. These include the climate input, slope characteristics, soil information and management input (Flanagan and Livingston,1995). The online WEPP interfaces use the CLIGEN model to generate daily climate data required by the model (Nicks and Gander, 1994). In the simple hillslope interface the slope inputs are entered directly on the web page. Soil data are read from local WEPP soil files stored on the server or can be accessed using the NRCS soil data access for SSURGO data (NRCS, 2011). The management data can be read from local WEPP management files stored on the server or converted from RUSLE2 (Revised Universal Soil Loss Equation version 2) management data.

WEPP produces extensive outputs that include spatial soil loss down the profile and also daily outputs of model variables. This information can be shown graphically in model output pages. Figure 1 shows a hillslope simulation page with inputs on the left panel and a brief summary of the model outputs on the right panel.

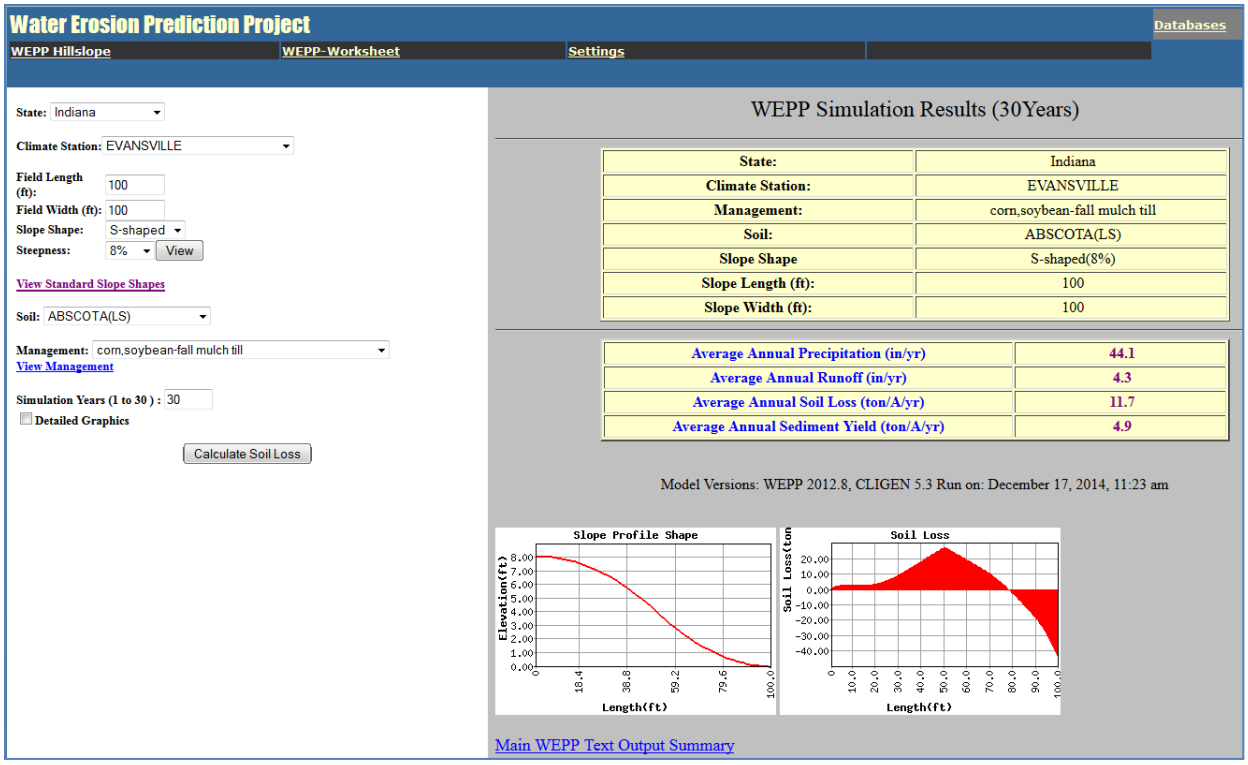

Figure 1 WEPP hillslope model simulation. Inputs are chosen from simple choice lists.

The web server is comprised of a Ubuntu Linux system running the Apache 2 web server. The server side software includes PHP scripts and custom C++ programs to setup, run and process outputs from the WEPP model.

WEPP INTERNET WATERSHED MODEL

The WEPP watershed model internet interfaces use a DEM to determine a channel network and watershed subcatchments. The TOPAZ model is used to delineate the channel network and subcatchment areas within a watershed (Garbrecht and Martz, 1997). The interface uses Google Maps for base map images and overlays modeling results from TOPAZ or WEPP as additional layers. Figure 2 shows an area with the TOPAZ calculated channel network overlaid on the Google Maps Physical layer.

Figure 3 shows the same area after an outlet point has been selected and the watershed delineated from that location. The input files for WEPP simulations are prepared using the area delineated by TOPAZ, and involves extracting WEPP soil parameters from the SSURGO soils data, using the USGS National Landcover data to determine management inputs and using the USGS DEM to determine the slope profile inputs to WEPP. Climate inputs can be adjusted by using the PRISM gridded data (PRISM Climate Group, 2004) if the area of interest has different weather characteristics than the nearest station in the Cligen database.

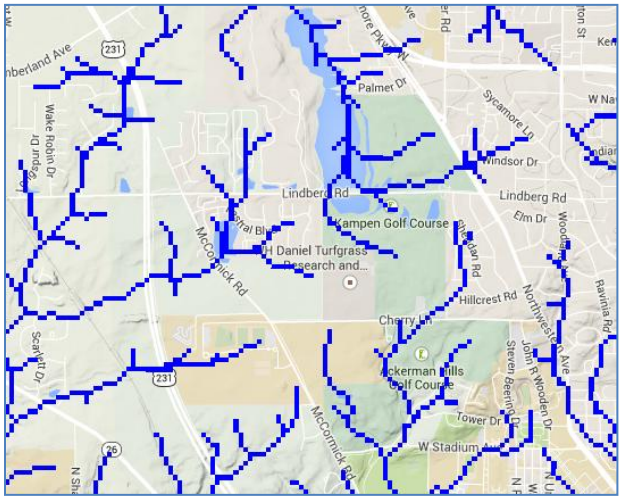

Figure 2 Channel delineation from TOPAZ model.

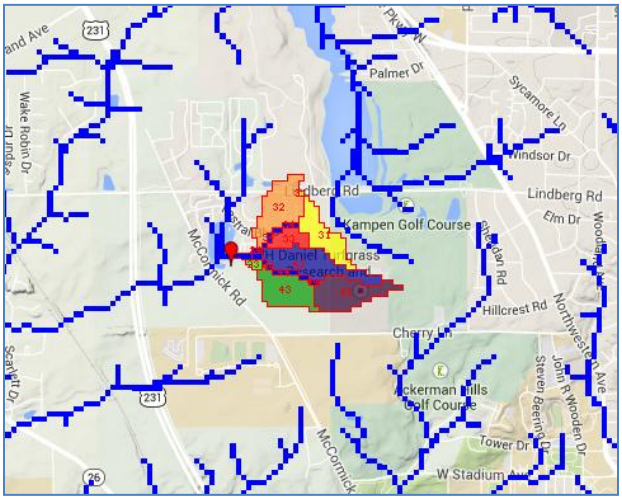

Figure 3 Watershed delineation using the TOPAZ model.

The online WEPP watershed interface supports two types of simulations: flowpath and representative hillslope (Cochrane and Flanagan, 1999; Flanagan et al., 2013). In the flowpath method each flowpath in the watershed is simulated as a WEPP hillslope profile. The spatial soil loss determined on each flowpath can be output as a GIS layer as shown in Figure 4. Flowpath simulations may take hundreds or thousands of WEPP simulation runs to cover a watershed. No channel routing is currently performed when applying the flowpath method.

The representative hillslope method simulates one hillslope per subcatchment and includes channel routing. This method takes much less computing resources than the flowpath method, however the results are not as detailed at the subcatchment scale. The watershed simulation does include channel processes so that offsite effects of runoff and sediment leaving the watershed can be evaluated. Figure 5 shows the GIS output layer for a representative hillslope run. Color shading indicates areas of higher erosion above the tolerable soil loss in red, 3 t/ha/yr in this example, to areas below the tolerable soil loss in shades of green, while areas of deposition are shown in yellow in Figures 4 and 5.

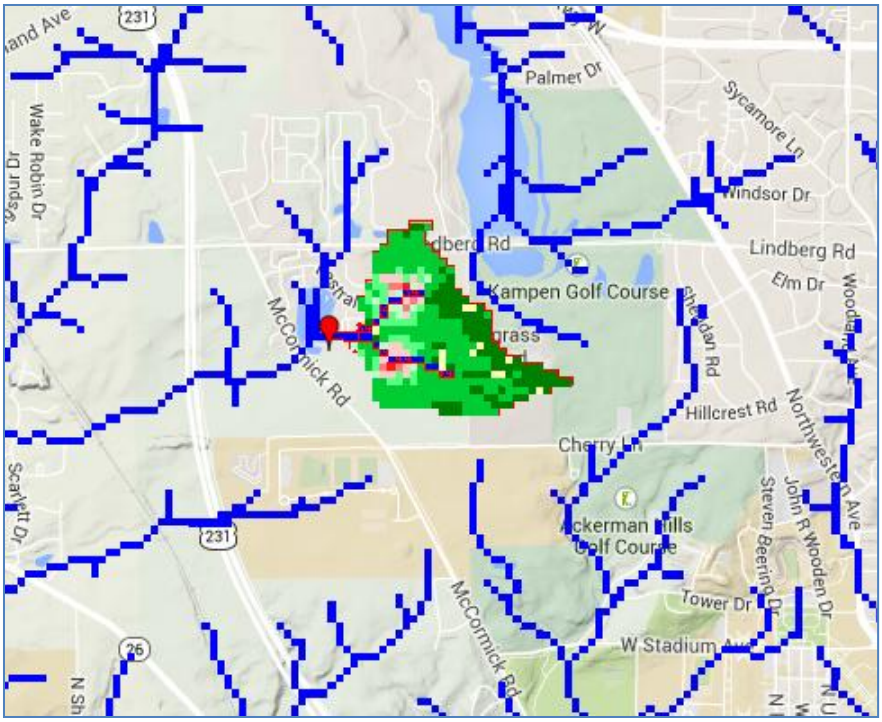

Figure 4 Flowpath output

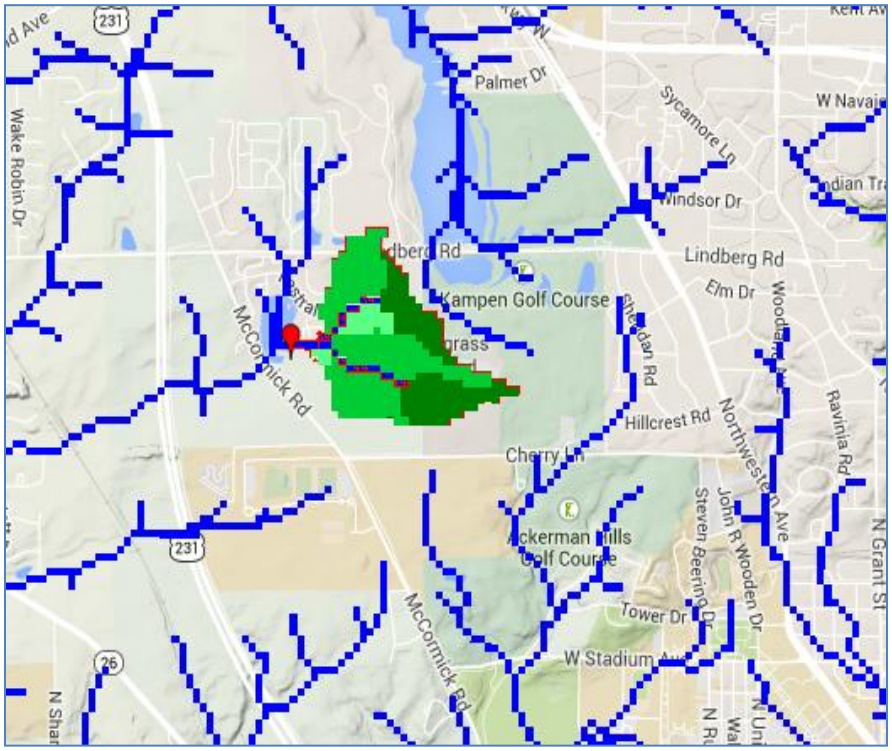

Figure 5 Representative hillslope output

Similar to the WEPP hillslope interface the web server is comprised of a Ubuntu Linux system running the Apache 2 web server. The server side software consists of PHP scripts and custom C++ programs to setup, run and process outputs from the WEPP model (Frankenberger et al., 2011). In addition, the OpenLayers JavaScript library is used to display GIS data on the client machine. Google Maps background images are used in the application. The server also uses the MapServer application to provide GIS functions for raster and vector data.

WEPP REST WEB SERVICES

Although the existing web-based interfaces are useful they are limited by what interfaces are available on the web servers. Changes to the interfaces require coordination with developers, or rehosting the WEPP model, data and web pages on a different server. This makes it difficult to develop specialized interfaces or integrate the model with other web-based tools. RESTful web services allow communication with software services using the standard HTTP protocol. This allows the data and modeling processing to reside in one server environment and the user interface to reside on a different server website, Windows application or mobile app. The WEPP web service categories are summarized in Table 1.

Table1 WEPP REST services

Climate Data for CLIGEN	WEPP Model Runs
WEPP soils from SSURGO	TOPAZ Model Runs
Management Data, local or RUSLE2	DEM Grids for WEPP Watershed Runs
CLIGEN Model Runs	TOPAZ outputs for WEPP Watershed Runs

The client application that uses the services can be written in any language. Below is an example using the command line curl program to request all the Cligen stations in Indiana. The URL can also be entered into a browser.

```
curl -i -H "Accept: application/json" -X GET
http://milford.nserl.purdue.edu:8080/wepprest/d/climate/cligen/IN
```

The return information is in JSON format:

```
[
    {
        "id": "IN120177.PAR",
        "lon": -85.6800003,
        "name": "ANDERSON QUARTZ PLT",
        "lat": 40.0999985
    },
    {
        "id": "IN120676.PAR",
        "lon": -84.9499969,
        "name": "BERNE",
```

```
        "lat": 40.6699982
    }...
```

The following example makes a 10 year Cligen run for a station in Indiana. This request is slightly different from the previous request. The URL includes the Cligen version to run along with the station id and output file. An extra file is also passed that includes additional Cligen parameters.

```
curl -H "Content-Type: application/json" -X POST -d
@runcligen.txt
"http://milford.nserl.purdue.edu:8080/wepprest/m/climate/cligen/4
.3/IN122660/test123"

# contents of runcligen.txt:
{
  "years" : 10,
  "type" : "continuous",
  "interp" : "None"
}
```

The next request reads the model output from the Cligen run. In this URL the run identifier and particular output file are included.

```
curl -i -H "Accept: application/octet-stream" -X GET
http://milford.nserl.purdue.edu:8080/wepprest/m/climate/cligen/te
st123/output.cli
```

An example Windows WEPP hillslope application was developed in C# to test the WEPP web services. This application runs on the Windows desktop but does not install any WEPP related programs or files. Instead it uses the WEPP web services to setup and run simulations. Figure 7 shows the climate selection panel which uses the Cligen services data to plot locations in Bing maps.

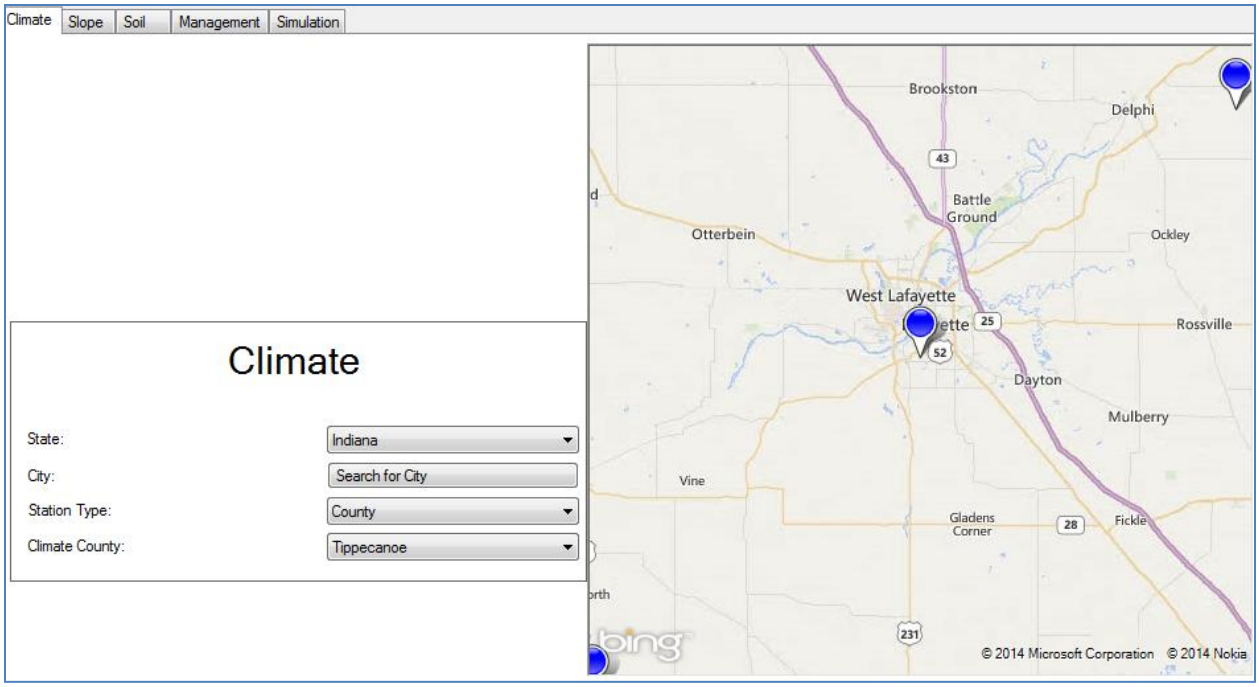

Figure 7 Climate location selection for a WEPP run.

Figure 8 shows the soil window which formats data returned from requesting WEPP soil data from the web service. By requesting SSURGO data the web server is also communicating with the NRCS soil data access web services to get the requested WEPP soil parameters.

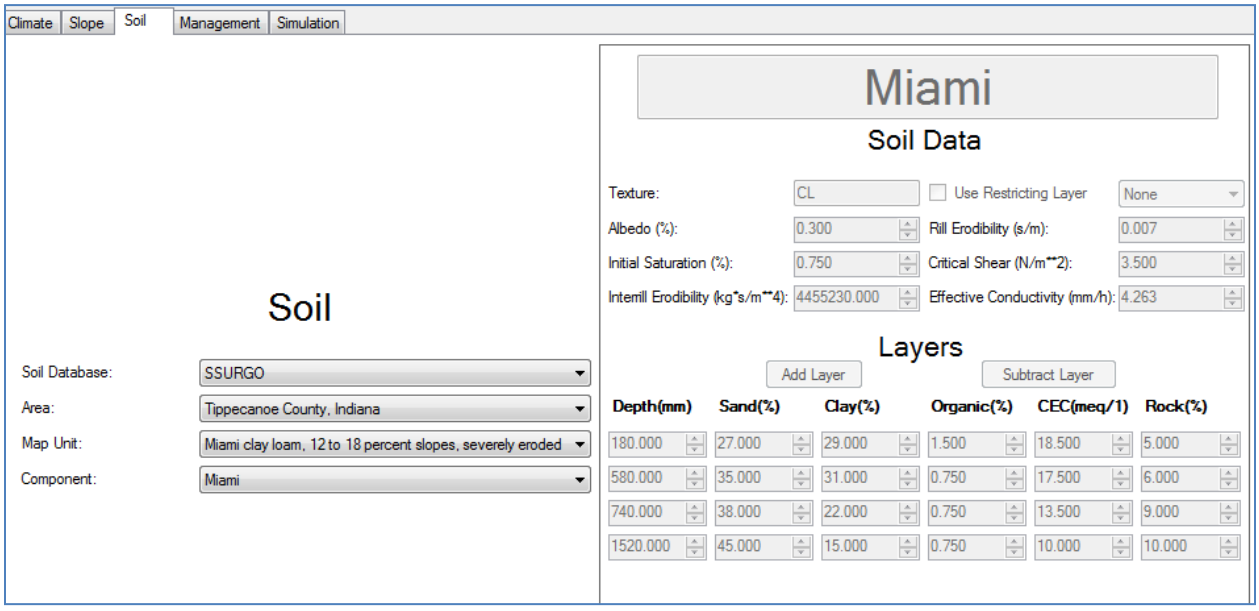

Figure 8 Soil selection for a WEPP run.

The management selection is made by first requesting a list of managements that apply to the area of simulation. A default list of WEPP managements along with a list of RUSLE2

managements is returned and displayed. The RUSLE2 management database has over 20,000 records. If a RUSLE2 management is selected the data are translated to WEPP format. Figure 9 shows the list of managements for Indiana.

After the management is selected the number of years is input and the WEPP hillslope model run. A brief output is displayed. The input files for the run are displayed on the right with additional output data and graphs available. Figure 10 shows the WEPP output page.

Future work involving WEPP internet applications involves expanding the web services application programming interface (API) to allow more of the model functionality to be available. Other data sources relevant to WEPP modeling, such as NASS land cover and more detailed DEM's will be included. In addition, the NRCS Cloud Services Innovation Platform (CSIP) implements a set of web services for NRCS models and data (David et al., 2013). WEPP is being integrated into the CSIP platform. Having WEPP compatible with CSIP will allow WEPP to be used for NRCS conservation planning. The expanding CSIP infrastructure will also allow more WEPP model simulations than the current server environment.

Figure 9 Management selection for a WEPP run.

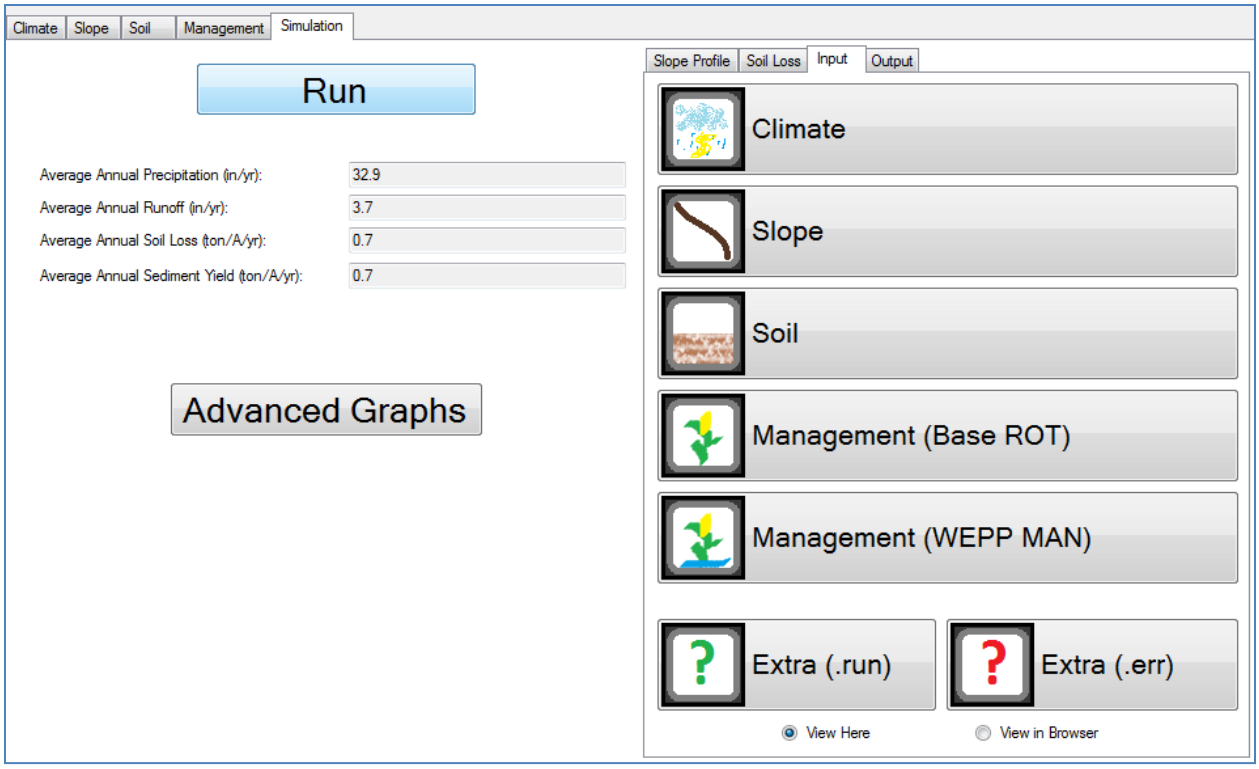

Figure 10 WEPP model results and links to input files used in the simulation.

SUMMARY

The WEPP web-based interfaces allow users to more easily apply the model to single hillslope and watershed simulations. Although the existing web-based interfaces are useful they are limited by what interfaces are available on the web servers. Changes to the interfaces require coordination with developers, or rehosting the WEPP model, data and web pages on a different server. The REST services for WEPP allow the model to be integrated into new internet, desktop or mobile applications without having to include model programs and databases since the model and data reside on servers. Accessing the model through the web services allows for more flexible development of WEPP related applications.

REFERENCES

Cochrane, T.A., and Flanagan, D.C. (1999). “Assessing water erosion in small watersheds using WEPP with GIS and digital elevation models”. J. Soil and Water Cons. 54(4): 678-685.

David, O., Ascough, J.C. II, Lloyd, W., Green, T.R., Rojas, K.W., Leavesley, G.H., and Ahuja, L.R. (2013). “A software engineering perspective on environmental modeling framework design: The Object Modeling System”. Environmental Modelling & Software. Vol 39 pp 201-213.

Elliot, W.J. (2004). "WEPP internet interfaces for forest erosion prediction". J. American Water Resour. Assoc. 40(2): 299-309.

Flanagan, D.C., and Livingston, S.J. eds. (1995). USDA—Water Erosion Prediction Project User Summary. USDA ARS NSERL Rep. 11. USDA ARS, West Lafayette, IN.

Flanagan, D.C., Fu, H., Frankenberger, J.R., Livingston, S.J., and Meyer, C.R. (1998). "A Windows interface for the WEPP erosion model". ASAE Paper No. 98-2135. ASAE, St. Joseph, Mich.

Flanagan, D.C., Frankenberger, J.R., Cochrane, T.A., Renschler, C.S., and Elliot,W. J. (2013) "Geospatial application of the Water Erosion Prediction Project (WEPP) Model". Transactions of the ASABE 56(2):591-601.

Frankenberger, J.R., Dun, S., Flanagan, D.C., Wu, J., Elliot, W. (2011) "Development of a GIS interface for WEPP model application to Great Lakes forested watersheds". Proceedings of the International Symposium on Erosion and Landscape Evolution (ISELE), Anchorage, AK, ISELE Paper No. 11139. ASABE, St. Joseph, Mich.

Garbrecht, J., and Martz, L.W. (1997). TOPAZ: An Automated Digital Landscape Analysis Tool for Topographic Evaluation, Drainage Identification, Watershed Segmentation and Subcatchment Parameterization; TOPAZ User Manual. U.S. Department of Agriculture, Agricultural Research Service, Grazinglands Research Laboratory, El Reno, Oklahoma, USA, ARS Publication No. GRL 97-4, 119 pp., April 1997

Nicks, A.D., and Gander, G.A. (1994). "CLIGEN: A weather generator for climate inputs to water resource and other models". In: Proc. 5th Intl. Conf. on Computers in Agriculture, publication 3-94, ASAE, St. Joseph, Mich.

NRCS. (2011). Soil Data Access Web Services. Available at: http://sdmdataaccess.nrcs.usda.gov Accessed 17-Dec-2014.

PRISM Climate Group (2004). Oregon State University, http://prism.oregonstate.edu. Accessed 21-Jan-2015.

Renschler, C.S. (2003) "Designing geo-spatial interfaces to scale process models: The GeoWEPP approach". Hydrological Processes 17:1005–1017.

Rodriguez, A. (2008). "RESTful Web services: The Basics". IBM DevelopWorks Technical Library. Available at http://www.ibm.com/developerworks/library/ws-restful/ws-restful-pdf.pdf Accessed 17-Dec-2014.

MODELING OF A NON-PHYSICAL FISH BARRIER

Marcela Politano, Research Engineer, IIHR – Hydroscience & Engineering, The University of Iowa, Iowa City, IA, marcela-politano@uiowa.edu; Ezequiel Martin, Assist. Research Scientist, IIHR – Hydroscience & Engineering, The University of Iowa, Iowa City, IA, juan-martin@uiowa.edu; Yong Lai, Hydraulic Engineer, Technical Service Center, Bureau of Reclamation, Denver, CO, ylai@usbr.gov; Merlynn Bender, Hydraulic Engineer, Technical Service Center, Bureau of Reclamation, Denver, CO, mbender@usbr.gov; Dave Smith, Research Ecologist, US Army Corps of Engineers, Vicksburg, MS.

Abstract: Non-physical barriers (NPBs) are used to deter fish from entering an undesirable pathway without restricting flow. NPBs are commonly comprised of a bubble curtain, low-frequency sound, and hi-intensity light-emitting diode (LED) Modulated Intense Lights (MILs). In this study a 3D numerical model was developed to predict bubble, sound and light fields in the vicinity of an NPB. A Boussinesq approach was used to account for the reduction of density in the zones where bubbles are present. A simplified diffusive model for the sound intensity was developed. Two methods are proposed for light, one for high attenuation/scattering conditions based on P-N models and the other for low scattering conditions based on the superposition of analytical solutions for elementary one-dimensional cases. To validate the solvers, several experiments were simulated. A sample model application to a simplified NPB located in Georgiana Slough in the Sacramento River is presented and discussed.

INTRODUCTION

Non-physical barriers (NPBs) use behavioral stimuli such as bubbles, low-frequency sound, and high-intensity light-emitting diode (LED) Modulated Intense Lights (MILs) to deter fish from entering undesirable locations. The sound is concentrated within the bubble curtain due to the difference in the velocity of sound of water and air to prevent sound saturation. Lights projected onto the bubble curtain improve visibility for fish swimming in the direction of the curtain. This NPB arrangement is typically referred to as a Bioacoustic Fish Fence (BAFF).

The migration of juvenile salmonids in the San Joaquin and Sacramento Rivers is of great environmental interest due to decline of native species. Fish diversion into the Delta may result in delayed migration, elevated risk of predation, exposure to poor water quality conditions, and mortality in pumping facilities. The California Department of Water Resources (CDWR) and the U.S. Bureau of Reclamation (Reclamation) proposed to use a NPB to reduce the diversion of juvenile salmonids from the Sacramento River into the interior and south Delta. The effectiveness of NPBs in deterring fish is variable, depending on the location, barrier geometry, and river flows. NPB can also have unintended effects, such as increased predation upstream and downstream of the barrier. All the above increase the environmental risk requiring site specific study and evaluation. In this study a numerical model for a NPB was developed to better understand the effect of the barrier on the Sacramento River hydrodynamics and support the design and operation of a NPB to deter and direct fish movement.

NUMERICAL MODEL

In this study, we first developed the model equations to simulate the bubbles, sound and light fields. The model equations were then implemented into the open source code OpenFoam (Weller et al. 1998). OpenFoam is a collection of C++ libraries, based on object oriented programming, designed for continuum mechanics applications. A new solver, pisoFoamBLS, which includes simplified models for predicting bubbles, sound and light fields near a non-physical fish barrier, was developed based on the code pisoFoam using a modular approach. Several studies related to implementation of different solvers in OpenFoam may be found in the literature (Hussein 2009, Kassem et al. 2011, Flores et al. 2013, among others) and repeated herein.

MODELING OF BUBBLES

Mathematical Modeling: A bubbly flow, i.e., a discrete gas phase in a continuous fluid, is formed in bubble curtains. As illustrated in Figure 1, bubbles injected in an initially quiescent medium induce a motion in the liquid similar to that observed in buoyancy-induced flows. Three distinct zones can be observed in a bubble curtain:

1. The primary bubble zone: where bubbles accelerate as they detach from the nozzle
2. The plume zone: where bubble breakup and coalescence prevail to form the plume

3. The free bubble zone: where the dynamic process of breakup and coalescence have reached an equilibrium and bubbles rise without significant size change

Measurements of gas volume fraction, bubble frequency and chord length by Castillejos and Brimacombe (1987) indicate that bubble breakup in the plume zone predominantly occurs near the injection location. Close to the free surface, the bubble velocity decreases as liquid moves tangent to the free surface, which enhances coalescence and promotes larger bubble sizes.

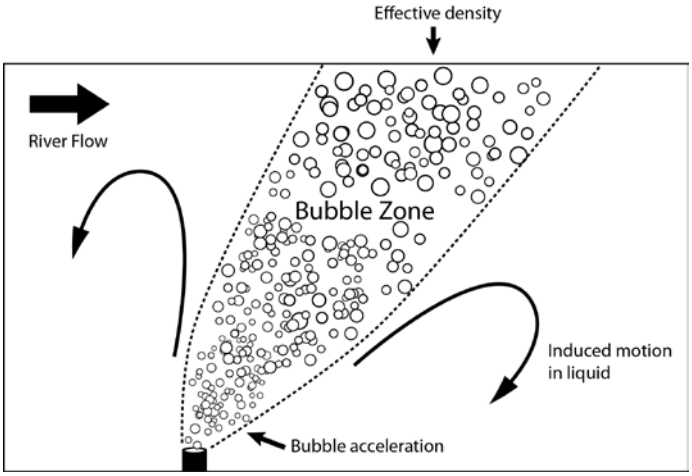

Figure 1 Induced liquid motion for a bubble curtain in a river

Most of bubble plume models found in the literature are intended for the free bubble zone region. The current modeling effort is based on the model presented by Buscaglia et al. (2002). The authors used a two-fluid approach assuming an incompressible mixture gas-liquid phase. In this approach, the Navier-Stokes equations are restored, significantly simplifying the formulation. The main advantage of this model is that an equation for the gas phase is included and therefore the shape of the bubble zone can be predicted. Future model improvements such as inclusion of a bubble size distribution, breakup and coalescence, bubble dissolution, bubble compression, bubble induced turbulence, etc., can easily be incorporated into the model using this formulation. Following Buscaglia et al. (2002), density differences are neglected except where they appear in the term multiplied by the acceleration due to gravity resulting in:

$$\nabla \cdot \vec{u}_m = 0 \tag{1}$$

$$\rho_l \frac{\partial}{\partial t}\vec{u}_m + \rho_l \nabla \cdot \left(\vec{u}_m \vec{u}_m\right) = -\nabla P + \nabla \cdot \left[\tau_m^{\mathrm{Re}} + \tau_m\right] + \rho_m \vec{g} \tag{2}$$

Equations (1) and (2) can be solved to compute pressure and velocity of the mixture phase with any single-phase CFD solver adding a source term in the momentum equation $\vec{S}_m = -(\rho_l - \rho_g)\alpha \vec{g}$. In this study an isotropic turbulence model $k-\varepsilon$ was used for turbulence closure. The gas velocity was obtained from the momentum equation for the gas phase. Inertia, gravity force and viscous shear stresses are significantly smaller than liquid-gas interfacial forces due to the small density and viscosity of the gas phase and are usually neglected. In this particular application, drag is the most important interfacial force and lift and virtual mass can be neglected resulting in:

$$-\nabla\left(P + \frac{2}{3}k\right) + \frac{3}{8}\frac{C_g^D}{R}\vec{u}_r\left|\vec{u}_r\right| = 0 \tag{3}$$

In a bubble curtain, bubble size can change due to breakup, coalescence, mass transfer and pressure variations. In this study, an equation for the bubble number density was used:

$$\frac{\partial N}{\partial t} + \nabla \cdot \left[\vec{u}_g N\right] = \frac{\nu^t}{Sc}\nabla^2 N_g \tag{4}$$

The bubble volume at a given position can be calculated from $v_b = \frac{P_c}{P}\frac{4}{3}\pi R_c^3$, where P_c and R_c are the pressure and radius at the injection point. The bubble zone can be determined using the gas volume fraction, which can be obtained from the mass conservation equation for the gas phase $\alpha = \frac{4}{3}\pi R^3 N$.

Model Comparison with Experiments: The model was used to simulate an experiment by Grevet et al. (1982) in which a water-filled cylindrical tank was agitated by a gas bubble stream, and compared against velocity data measured inside the tank. The modeled tank radius, R, was 0.3 m and the water height, H, 0.6 m. Bubbles were injected into the quiescent liquid through an orifice of 0.0127 m (0.5 inch) at a flowrate of 205 cm3/s. Only one fourth of the tank was simulated to reduce grid size and computational time. Symmetry boundary conditions were used on the sides. Grid size was approximately 105 nodes. Since bubble velocities were not measured, it is assumed that bubbles enter the domain at their terminal velocity. Reasonable agreement was found between model predictions and experimental data for three axial positions (Figure 2). As rising bubbles leave the injector, they generate an inward flow at the left bottom side of the tank. The bubble stream then generates an upward flow in the center of the tank and a large clockwise vortical structure at the upper right side, with negligible radial velocities. The rising bubble velocity is terminated at the free surface and the liquid vertical moment is converted to horizontal flow. The horizontal flow is blocked by the tank wall and is redirected downward along the side wall. The model is considerably less accurate near the walls, but since wall interaction is not important in a bubble curtain, grid refinement was not performed to capture the velocity profile near the walls. The proposed model assumes one variable bubble size. Implementation of a bubble size distribution is expected to improve model accuracy. Figure 3 shows the gas volume fraction distribution in the tank. For the low gas volume fraction injected, bubbles concentrated in the core of the tank, rise almost uniformly in a nearly straight line. Near the injector, bubble velocity increases due to the upward liquid flow in the center of the tank. This local increase of the liquid velocity causes a reduction of the gas volume fraction. Conversely, bubble velocities are reduced near the free surface resulting in a local increase of the gas volume fraction.

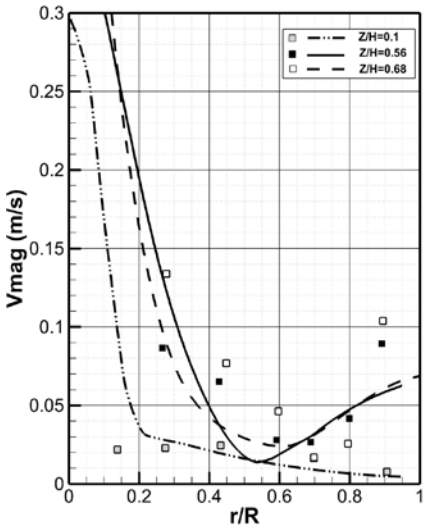

Figure 2 Comparison between predicted and measured velocity magnitude. Symbols: experiments by Grevet et al. (1982) and lines: model results

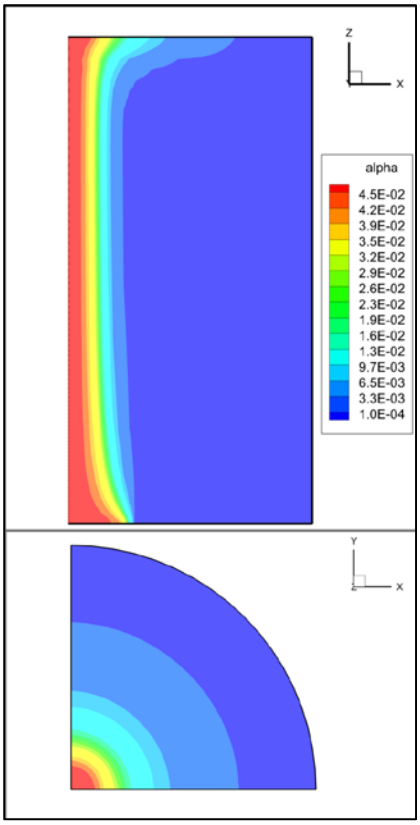

Figure 3 Gas volume fraction contours

MODELING OF SOUND

Mathematical Modeling: The acoustic field in a domain can be represented by an equation of acoustic energy conservation:

$$\frac{\partial W}{\partial t} = -\nabla \cdot \boldsymbol{I} - D \tag{5}$$

where W is the acoustic energy and $\boldsymbol{I}$ the acoustic energy flux. The last term in the RHS represents dissipation effects. In this study a method was developed to deal with the strong changes in fluid properties introduced by the presence of the bubble barrier as well as the multiple surfaces that partially absorb the sound signals at the boundaries. The diffusive equation used in architectural acoustics was identified as a viable candidate to fulfill these requirements. A Fick's law-type relation is postulated between the energy flux and the energy density, $\boldsymbol{I} = -\boldsymbol{D_W}\nabla W$, which adapted to give a dependence of the dissipation on W rather than $\boldsymbol{I}$, transforms the conservation equation for sound energy to:

$$\frac{\partial W}{\partial t} = -\nabla \cdot (\boldsymbol{D_W}\nabla W) - \alpha_W^2 |\boldsymbol{D_W}| W + S_W \tag{6}$$

where a general distributed source term S_W has also been included. A new parameter, an anisotropic diffusion coefficient $\boldsymbol{D_W}$, has been introduced, for which modeling is required. The expression for the dissipation term is such that the exponential decay of a plane wave in an isotropic media is recovered. Following Picaut (2002), absorption is modeled as a boundary condition. Picaut et al. (1999) proposed a diagonal tensor related to length-scale of domain for the diffusion coefficient:

$$\frac{D_{xx}}{\ell_x} = \frac{D_{yy}}{\ell_y} = \frac{D_{zz}}{\ell_z} = D_{3D} \tag{7}$$

with the diffusion proportional to sound speed ($D_{3D} \sim c$). Eq. (6) is a standard diffusion equation for which solution methods are well established and can be readily implemented in OpenFoam. Certain features of the sound field are lost by using this approach, such as the appearance of interference patterns and the rapid evolution of the sound field that can be found with the ray tracing method. However, it is questionable that those features are of significant importance for the current application, as it is expected that the cases of interest will be quasi-steady in both bubble-encapsulated and non-encapsulated sound fields as the fluid velocity is much smaller than the speed of sound, and the sound source are non-pulsating in time.

A set of linear attenuation coefficients and speed of sound data for bubbly flows presented by Silberman (1957) were used in this study.

Model Comparison with Experiments: The data presented by Würsig et al. (2000) represent one of the few reported field experiments with useful, albeit scarce, data for model validation. Sound levels produced by a pile-driving hammer in shallow waters were measured with and without a bubble curtain designed to mitigate the sound. Measurements of background noise are also available, but there is no measurement of sound levels near the source or inside the bubble curtain area. A slab geometry with an average depth of 8 meters was simulated. In Figure 4, the measured data on April 26, 1996 is shown along with the simulated results. The authors reported an overall sound level for frequencies spanning 100 Hz to 25.6 kHz, as well as results for the different one-octave bands. Notable differences in attenuation by the bubble curtain occur for the different frequencies, but it was found that the reported average trend for all frequencies is consistent with the results for low frequencies (as the sound intensity is largest for the 400 Hz octaves), and a representative frequency of 400Hz was chosen to perform the simulations. A uniform source for the background noise and an additional source near the coordinates' origin were obtained. The relationship between the wall attenuation coefficient and the diffusion parameter was established using the expression proposed by Silberman (1957). An extremely low value of Dyy /Drr = 1.6x10-4 was found from the experimental data, and as shown in Figure 4, the predicted decay matches well with the data. Finally, a mean gas volume fraction was estimated from the reported flow rate, assuming a terminal bubble velocity and a corresponding plume spreading angle. The resulting bubbly region is a ring, 25 m in diameter and 0.5 meter in thickness, with an estimated gas volume fraction of 0.02. It is reported that the resulting attenuation by the bubble barrier is about 3 to 5 dB, which agrees well with the estimated attenuation. The simulations required a smaller value of gas volume fraction to match the data of 0.003. When experimental data become available, further simulations and analyses should be performed to identify the reason for this discrepancy.

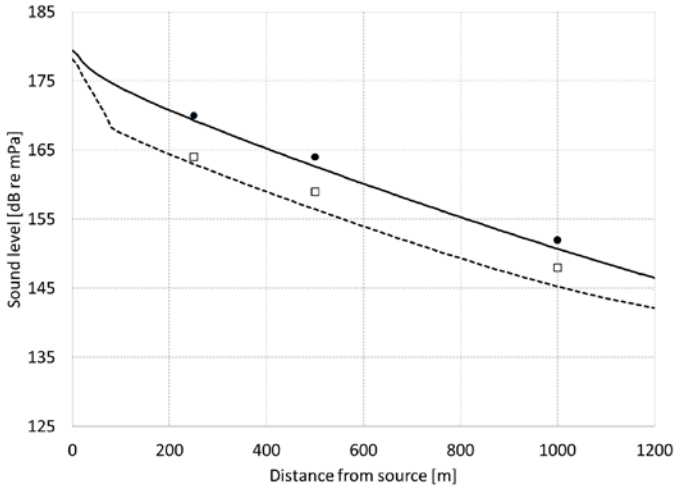

Figure 4 Sound levels in a slab. Symbols: Würsig et al. (2000) experimental data (black circles: bubble curtain off; white squares: bubble curtain on) and lines: simulation results

MODELING OF LIGHT

Mathematical Modeling: Calculations of light intensity can be extremely resource-intensive and are typically done using Monte Carlo simulations; or are based on semi-analytical approximations to an integro-differential equation. The latter approach was used in this study. The fundamental equation describing the light field in a continuous media is called the radiative transfer (RT) equation. The RT conservation equation balances the changes of spectral radiance (L) in a given direction with the processes that can modify it: absorption, scattering and emission. The attenuation of the beam is given by the absorption, defined by the absorption coefficient $a_{\mathrm{E}}(x,\lambda)$ times the radiance and all the scattering out of the beam direction that can be approximated as $-b_{\mathrm{E}}(x,\lambda)L$, with bE the average of the volume scattering function. The elastic (i.e., without a change of wavelength) scattering for other directions into a given direction constitutes a source and is represented as an integral that accounts for all the contributions over all possible 4π solid angle directions to a given one. Finally, emission may correspond to an actual source or due to inelastic scattering from other wavelengths, and can be expressed as a general source sE, per steradian. The complete RT equation can be written as (Mobley, 2001):

$$\Omega\nabla L(\boldsymbol{x},\theta,\varphi,\lambda) = -c_{\mathrm{E}}(\boldsymbol{x},\lambda)L(\boldsymbol{x},\theta,\varphi,\lambda) + \int_{4\pi} L(\boldsymbol{x},\theta',\varphi',\lambda)\beta_s(\boldsymbol{x},\theta',\varphi',\theta,\varphi,\lambda)d\Omega' + s_{\mathrm{E}}(\boldsymbol{x},\theta,\varphi,\lambda) \quad (8)$$

with β_s is the angle dependent volume scattering function and c_{E} the sum of a_{E} and b_{E}. Eq. (8) contains both an integral on the solid angle and spatial derivatives which can be very difficult to solve explicitly. In this study, the scalar irradiance, *E*, obtained by integration of *L*, was used. Extensive literature exists on different methods implemented to solve Eq. (8). In this study, two methods were implemented. A superposition of elementary solutions is proposed when scattering effects are not important and a P-1 model for high attenuation and/or scattering.

Certain apparent optical properties such as the diffuse attenuation coefficient can be approximated as a function of intrinsic properties for certain simple cases (Kirk, 2003; Kirk, 2006). Two simple solutions for the scalar irradiance can be found for planar and point sources by simple integration of Eq. (10):

$$E(z) = E_0\exp(-Kz) \quad (9)$$

$$E(r) = \frac{r_0^2}{r^2}E_0\exp(-Kr) \quad (10)$$

In the superposition of elementary solutions method, multiple elementary solutions are automatically combined to produce a light field that approximates the solution of RTE:

$$\nabla\cdot(\mathbf{u_E}E) = S_{\mathrm{E}} - KE \quad (11)$$

where $S_{\mathrm{E}} = 4\pi s_{\mathrm{E}}$, and *K* is the diffuse attenuation coefficient. To recover the solutions presented before (Eqs. 9 and 10), a dimensionless vector field is defined as $\mathbf{u_E}$ = (0,0,-1) for a plane source emitting in the z negative direction and $\mathbf{u_E} = \mathbf{e_r}$ the radial unit vector for the point source case. By presenting the solution as a result of a numerical integration it is possible to introduce more complex geometries and also variability of the attenuation factor, which can be calculated independently of the solution. With this simple scheme it is possible to reproduce background illumination due to natural daylight as a plane source, as well as including the stroboscopic lights of the barrier as point sources.

P-N models use a diffusive representation of the RTE, and as such its range of validity is for conditions with high attenuation and/or scattering (Sazhin et al., 1996). In general, P-N models are based on the expansion of the solution to RTE in orthogonal series of spherical harmonics. For the P-1 model only the first and third terms of the series are kept resulting in:

$$-\sum_{i=1}^{3}\frac{\partial}{\partial x_i}\frac{1}{3(a_{\mathrm{E}}+b_{\mathrm{E}})}\frac{\partial L^{(0)}}{\partial x_i} = 4\pi s_{\mathrm{E}} - a_{\mathrm{E}}L^{(0)} \quad (12)$$

Attenuation and absorption coefficients available in USEPA (2000) and Mobley (2001) as a function of water molecules, chlorophyll, inorganic matter and colored dissolved organic matter were used.

For a bubbly flow, the effect of the bubbles in the attenuation of light must also be considered. For most cases, it can be assumed than the bubble's radius R is much larger than the wavelength of the incident light. This condition is known as the geometric optic limit, for which both the geometric approximation and the Mie theory of scattering will predict the same far-field solution for the interaction of a plane wave and a single large sphere (Randrianalisoa and Baillis, 2014). It is a good assumption to neglect the absorption within the bubble and only consider the scattering contribution (Shamoun et al., 1999). For multiple scatters, the interaction between particles can be neglected if the characteristic spacing between particles is large compared to both the wavelength and the particle radius. In that case, the scattering characteristics can be obtained as a summation of the individual contributions. The resulting extinction coefficient due to bubbles is $c_{\mathrm{b}} = \frac{3}{4}\frac{\alpha}{R}$:

In this study reflections at the boundaries from the original sources were implemented using a cosine emission law.

Model validation: Some simple geometries were run to validate the implemented models and to highlight the differences between the two models. Unfortunately, no data for controlled bubbly flows were identified that could be simulated, other than some information on attenuation coefficients that was already included in the modelling process. The dimensionless irradiance field for two point sources in a closed cavity were simulated. First reflections are possible in the bottom boundary only. The model predicts the irradiance reduction with the radial distance shown in Eq. (10) (Figure 5). Total irradiance shown on the left frames is the summation of incidente (middle frame) and reflected (right frame) irradiances. This case shows the feasibility of representing the modulated intense lights (MILs) for the fish barrier as the solution of superimposed single point sources.

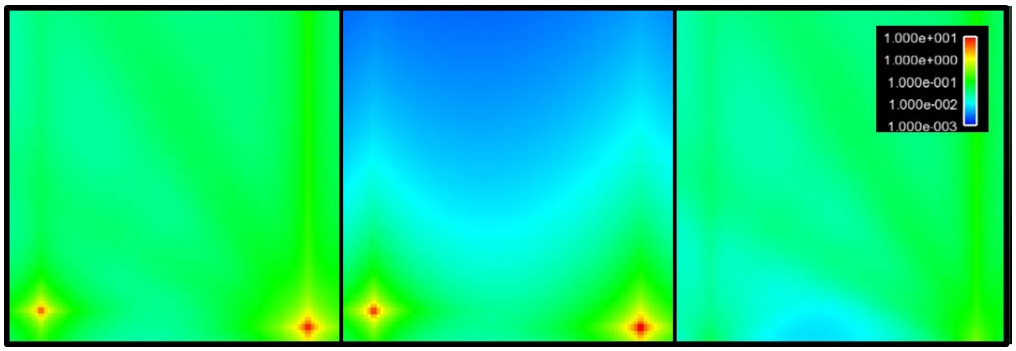

Figure 5 Total irradiance (left), incidente (middle) and reflected (right) from two point sources near the bottom of a cavity

The focus of the validation of the P-1 model was to demonstrate the effect of bubbles on the distribution of the irradiance. Figure 6 shows the basic profile for the case where no bubbles are present. As expected, the irradiance decays radially from the source with an equivalent diffuse attenuation coefficient $K = (3a_{\mathrm{E}}c_{\mathrm{E}})^{1/2}$. Two possible boundary conditions are shown in Figure 6 for the boundary closest to the source, the partial reflective condition (left frame) and full reflective conditions (right frame). As expected, the latter results in larger values for E, but given the rapid decay of the irradiance most differences between the two cases are localized to the region immediate to the source and very close to the boundary.

The deformation of the radial pattern due to the presence of a bubble curtain is shown in Figure 7. The extension of the curtain is shown with dashed lines. Several values of gas volume fraction with fully reflecting boundary were considered. The main effect of the bubbles is to concentrate the light field into a smaller region and with a larger maximum value for E. The distribution of the light field varies radically depending on whether the light source is contained in the bubble curtain, in which case very little illumination escapes the curtain, or whether the source is placed near the curtain, in which case bubbles act as a reflector.

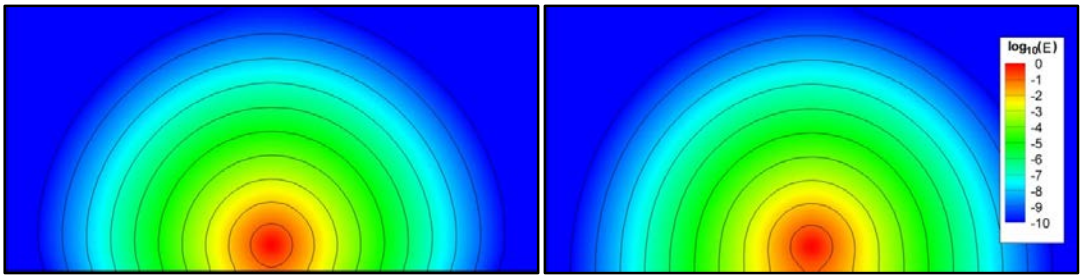

Figure 6 Unit irradiance source near a boundary. Left, lower boundary correspond to a water-air interface; right, fully reflecting boundary

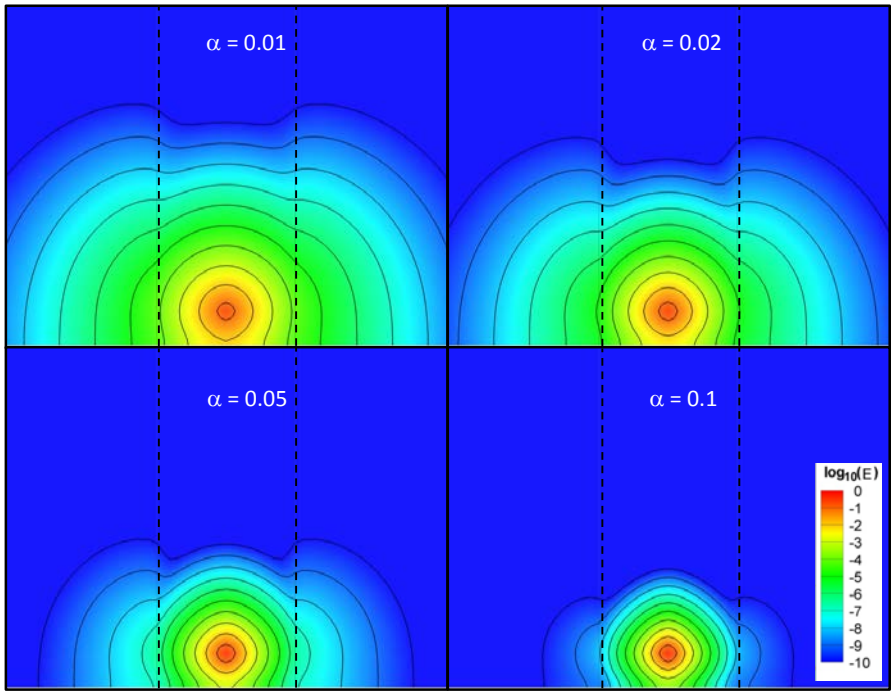

Figure 7 Unit irradiance source within a bubble curtain near a boundary

SIMULATION OF A NON-PHYSICAL FISH BARRIER

Simplified Georgiana Slough: A main channel with two bifurcations and a non-physical fish barrier upstream of the smallest stream was simulated to test the capability of the proposed model to predict the flow field and bubble, sound and light fields in the vicinity of a fish barrier (Figure 8). The geometry of the Georgiana Slough in the Sacramento River was used (McQuirk and Reeves, 2012). Since bathymetric information was not available a constant water depth of 9.1 m was used. This value was selected based on information of underwater sound measurements that were taken between 2.9 m to 14.6 m (McQuirk and Reeves 2012). In this paper a simulation using typical conditions in the Sacramento River upstream of the Georgiana Slough is presented. Flowrates upstream and downstream of the curtain were 334 m3/s and 132 m3/s, respectively. Small bubbles of 0.8 mm (0.03 inch) diameter were injected at the bottom of the river at a pressure of 1.91 105 Pa and at 25 oC. The diffusion coefficient was set using Eq. (12), with constant D3D = 0.1cwater, lz=10 m and lx=ly=200 m, a mixed boundary condition was imposed on the bottom and the side walls, and release conditions at the surface. Sound sources operating in the range 5-600 Hz with a mean sound level of 152 dB re 1□Pa were installed in the field near Georgiana Slough (McQuirk and Reeves, 2012). A far field value (~200 m) of about 110 dB re 1□Pa was reported. In this study, nineteen sound projectors were located immediately downstream of the bubble barrier and each projector was modeled as a constant source of acoustic energy density of 0.01 W/m. Four lights sources of 10 W/m3 were included upstream of the bubble barrier.

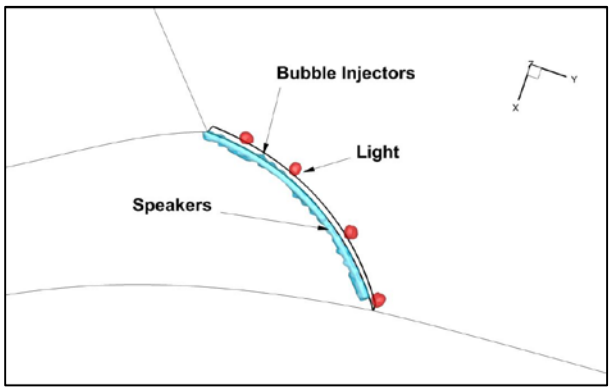

Figure 8 Simulated fish barrier

Figure 9 shows slices near the river bed (a), in the mid plane (b) and at the free surface (c). Vectors were interpolated in an equally-spaced structured mesh to enhance visualization. Bubbles significantly modify the flow pattern near the curtain. Two phenomena affect the gas volume fraction distribution; the most important is the buoyancy that drives bubbles toward the free surface and the other is the downstream convective transport by the river. The latter is significant at high river velocities and can be noted downstream of the curtain where the plume is directed towards the left bank. Upstream of the curtain and at small depths, the liquid velocity reverses direction due to the horizontal surface flow created when the plume reaches the free surface.

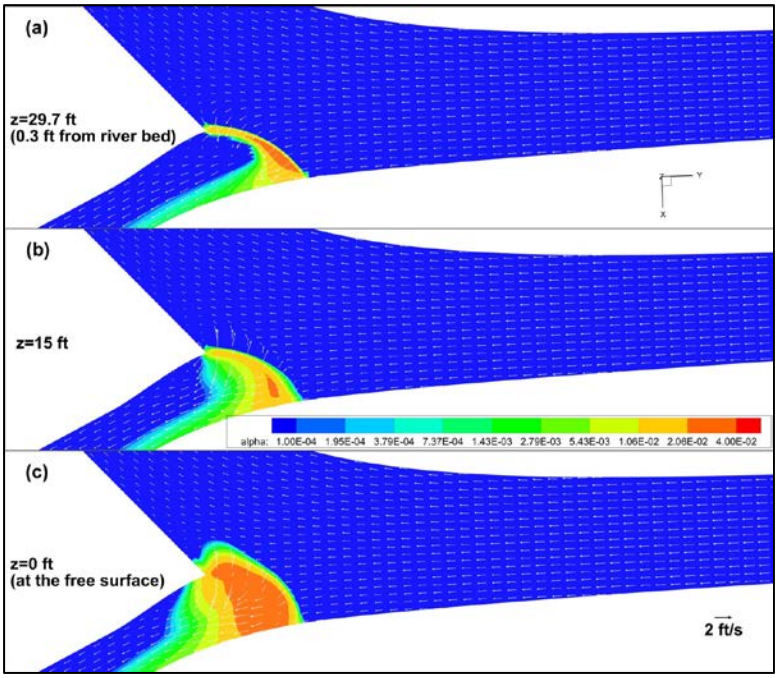

Figure 9 Gas volume fraction and velocity vectors at (a) 9 m (29.7 ft), (b) 4.5 m (15 ft) and (c) 0 m (0 ft)

Figure 10 shows flow characteristics near the bubble curtain. The frames in the top and middle show gas volume fraction isosurfaces and distribution of gas volume fraction at slices through the middle of the channels, respectively. Bubbles are transported away from the plume center by the strong surface current induced by the gas phase. The gas distribution and flow pattern are not symmetric relative to the bubble plume center due to the geometry and convective transport by the river flow. Streamlines colored by velocity magnitude in the bottom frame show back flow near the inner wall of the larger branch towards the bubble curtain.

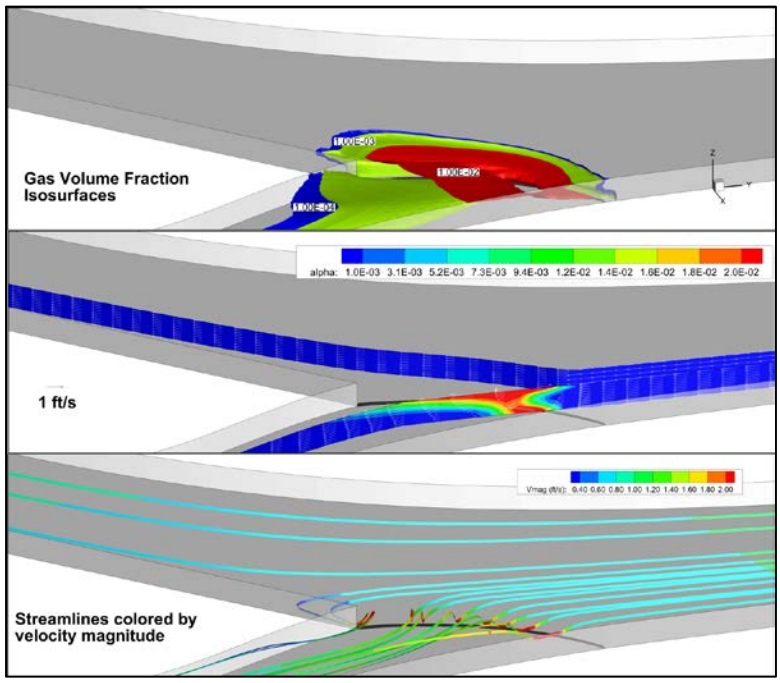

Figure 10 Gas volume fraction isosurfaces (top), gas volume fraction distribution in each river branch (middle), and streamlines colored by velocity magnitude (bottom)

Figure 11 shows the gas distribution and recirculation zones generated by the bubble curtain. As the bubble plume rises through the water column it entrains ambient water inducing two recirculating zones. Near the injector, the gas volume fraction is reduced as bubble velocity increases due to entrained liquid into the plume. On the other hand, near the free surface, the gas volume fraction increases for two phenomena, one is the increment in bubble volume due to decompression and the other is the reduction of liquid vertical velocity near the free surface. Note that since slip velocity increases with bubble size, a larger relative velocity is expected near the free surface. However, this effect is less important than the reduction of liquid velocity by the free surface.

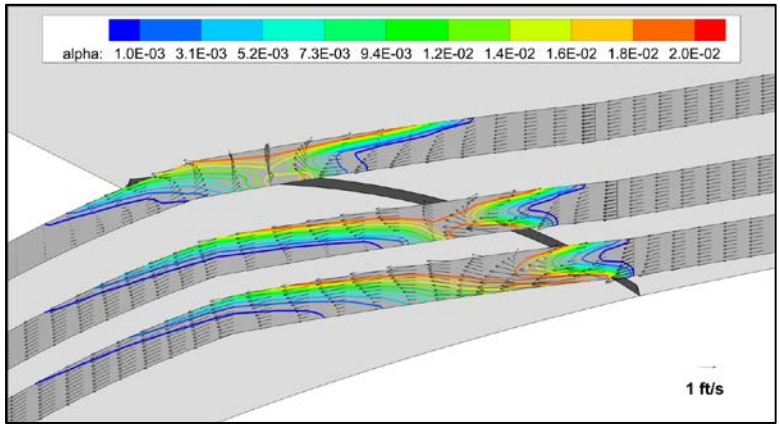

Figure 11 Gas volume fraction and velocity vectors near the bubble curtain

Figure 12 shows isosurfaces of sound energy. Bubbles encapsulate the sound within the fish barrier. However, some differences in the level of sound are observed due to increased sound attenuation by bubbles transported near the outer wall along the smaller channel.

Figure 13 shows the irradiance generated by the high-intensity LED MILs predicted with the superposition of elementary solution method (a) and P1 model (b). Light scattering and absorption by the bubbles results in an appreciable concentration of light within the fish barrier.

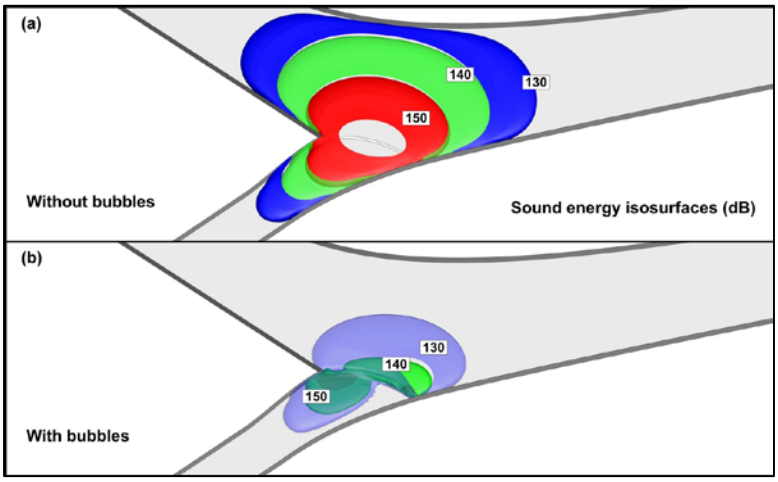

Figure 12 Isosurfaces of sound energy. Before bubble injection (a) and with bubble curtain (b)

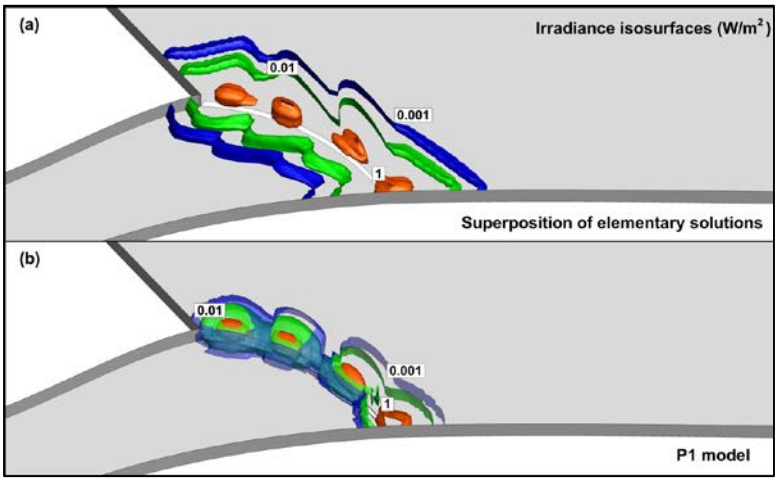

Figure 13 Isosurfaces of irradiance. Before bubble injection (a) and model P-1with bubble curtain (b)

CONCLUSIONS AND FUTURE DIRECTIONS

Numerical models for predicting the hydrodynamics, bubble, sound, and light distributions near a non-physical fish barrier were developed. The models were implemented using a modular approach in the open source code openFoam. A Boussinesq approach was used to account for the reduction of density in the zones where bubbles are present. The effect of the bubbles on the sound and light fields were considered through attenuation coefficient models found in the literature. Simple geometries were simulated to validate the implementation of the models. Model results for a non-physical fish barrier located in a bifurcation similar to Georgiana Slough indicate that the bubble plume has a strong effect on the flow pattern near the barrier. The resulting large-scale recirculations and increased accelerations near the barrier are expected to influence fish migration route. Sound and light are strongly coupled with the bubble plume. Bubbles effectively encapsulate both sound and light within the barrier region. According to the model, the effectiveness of bubbles to attenuate sound depends on the position of the speakers relative to the bubble plume. Since the bubble plume location depends on the induced liquid movement as well as downstream transport by the river, optimal location of speakers is a function of the river flowrate and gas injection rate through the diffusers.

Additional research needs to include a full set of experimental data and monitoring near a fish barrier, at several river and barrier operational conditions, for better quantification of important variables. Examples include measurements of gas volume fraction, bubble size, river depth, liquid velocities, and sound and light fields. The complex three-dimensional nature of the problem will require measurement stations at several transects near the barrier. This is essential to fully validate and improve the developed numerical tool and identify areas where future modeling effort should focus.

REFERENCES

Buscaglia, G.C., Bombardelli F.A. and Garcia, M.H. (2002). "Numerical modeling of large-scale bubble plumes accounting for mass transfer effects". *Int. J. Multiphase Flow*, 28, pp 1763-1785.

Castillejos, A.H. and Brimacombe, J.K. (1987). "Measurement of physical characteristics of bubbles in gas-liquid plumes: Part II. local properties of turbulent air-water plumes in vertically injected jets". *Metallurgical Transactions B*, 18B, pp 659-671.

Flores, F., Garreaud, R. and Muñoz, R. (2013). "CFD simulations of turbulent buoyant atmospheric flows over complex geometry: solver development in OpenFoam". *Computers and Fluids*, 82, pp 1-13.

Grevet, J.H., Szekely, J. and El-Kaddah, N. (1982). "An experimental and theoretical study of gas bubble driven circulation systems". *Int. Journal of Heat Mass Transfer*, 25(4), pp 487-497.

Hussein, A.S. and El-Shishiny, H. (2009). "Influences of wind flow over heritage sites: a case study of the wind environment over the Giza Plateau in Egypt". *Environ Modell Software*, 24, 389–410.

Kassem, H., Saqr, K., Aly, H.S., Sies, M.M. and Wahid, M. (2011). "Implementation of the eddy dissipation model for turbulent non-premixed combustion in OpenFOAM". *Int. Communications in Heat and Mass Transfer*, 38, pp 363-367.

Kirk, J.T.O. (2003). "The vertical attenuation of irradiance as a function of the optical properties of the water". *Limnol. Oceanogr.*, 48, pp 9–17.

Kirk, J.T.O. (2006). "Light field around a point light source in the ocean". *Journal of Geophys. Res.*, 111, C07008.

McQuirk, J. and Reeves, R. (2012). "2011 Georgiana Slough Non-Physical Barrier performance evaluation project report". California Department of Water Resources, Sacramento, CA.

Mobley, C.D. (2001). "Radiative transfer in the ocean". in *Encyclopedia of Ocean Sciences*, edited by J. H. Steele, S. Thorpe, and K. Turekian, pp. 2321–2330, Elsevier, New York.

Picaut, J., Hardy, J. and Simon, L. (1999). "Sound propagation in urban areas: a periodic disposition of buildings". *Physical Review E*, 60, pp 4851-4859.

Picaut J. (2002). "Numerical modeling of urban sound fields by a diffusion process". *Applied Acoustics*, 63, pp 965-991.

Randrianalisoa, J. and Baillis, D. (2014). "Analytical model of radiative properties of packed beds and dispersed media". *Int. J. of Heat and Mass Transfer*, 70, pp 264-275.

Sazhin, S.S., Sazhina, E.M., Faltsi-Saravelou, O. and Wild P. (1996). "The P-1 model for thermal radiation transfer: advantages and limitations". *Fuel*, 75, pp 289-294.

Shamoun, B., Beshbeeshy, M.E.and Bonazza, R. (1999). "Light extinction technique for void fraction measurements in bubbly flow". *Exp. in Fluids*, 26, pp 16-26

Silberman E. (1957). "Sound velocity and attenuation in bubbly mixtures measured in standing wave tubes". *The Journal of the Acoustical Society of America*, 29, pp 925-933.

USEPA (2000). "Chesapeake Bay submerged aquatic vegetation water quality and habitat-based requirements and restoration targets: a second technical synthesis". http://archive.chesapeakebay.net/pubs/sav/savreport.pdf.

Weller, H., Tabor, G., Jasak, H. and Fureby, C. (1998). "A tensorial approach to computational continuum mechanics using object-oriented techniques". Comp. Phys. 12(6), pp 620–31.

Würsig, B., Greene, C.R. and Jefferson, T.A. (2000). "Development of an air bubble curtain to reduce underwater noise of percussive piling". *Marine Environmental Research*, 49, pp 79-93.

RIVERWARE DEMONSTRATION

EXTENDED ABSTRACT

David Neumann, Senior Research Assistant, Center for Advanced Decision Support for Water and Environmental Systems, University of Colorado, Boulder, CO, david.neumann@colorado.edu
Edie Zagona, Director, Center for Advanced Decision Support for Water and Environmental Systems, University of Colorado, Boulder, CO, zagona@cadswes.colorado.edu;

RiverWare is a river and reservoir modeling tool used by water managers, planners, consultants, utilities, researchers and stakeholders for forecasting and scheduling reservoir and hydropower operations, water rights and water accounting, developing and evaluating alternative operating policies and planning new projects. Developed by the University of Colorado Center for Advanced Decision Support for Water and Environmental Systems (CADSWES) with sponsorship of the Tennessee Valley Authority, the Bureau of Reclamation and the U.S. Army Corp of Engineers, RiverWare simulates the hydrologic response of a river/reservoir system given inflows and multi-objective operating policies. This demonstration will show how the object-oriented models are constructed from the palette of objects and linked together to form a river system network as shown in Figure 1.

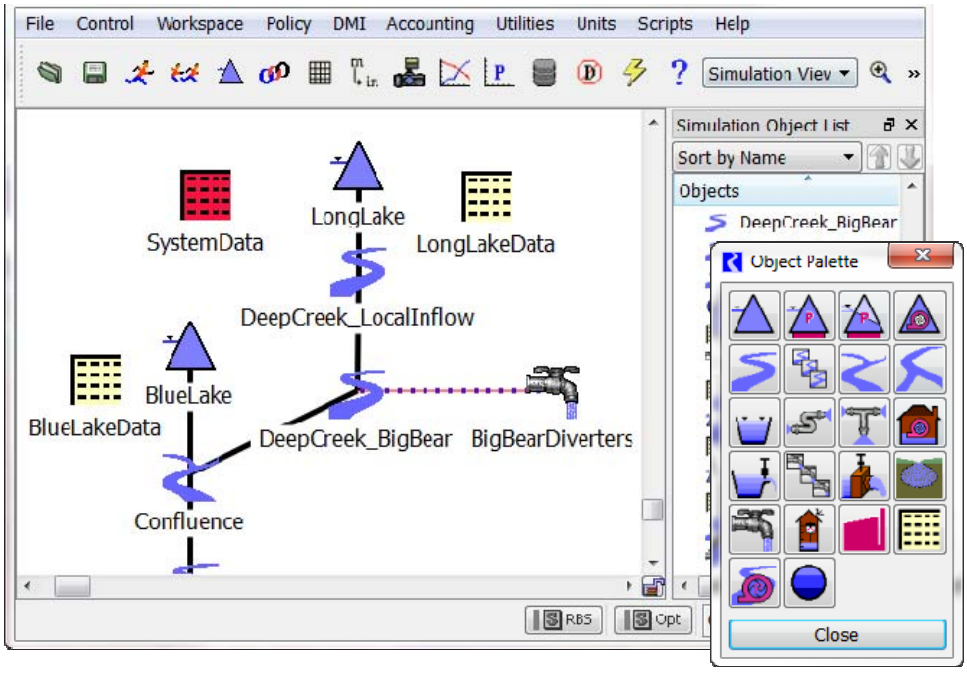

Figure 1 RiverWare Workspace and Object Palette

Simulation demonstrations will include hydrologic processes in rivers and reservoir, consumptive uses and return flows, distribution canals, groundwater interaction and pumping, pipe flows, hydropower and pumped storage, inline pumping and hydropower plants. A water quality module tracks salinity, temperature and dissolved oxygen throughout the system using

ether a simple well-mixed or layered/discretized approach. In the demonstration, we will show how to model the salinity and flow interaction of the surface water with groundwater including inflows from surface water (including point sources), pumping, deep aquifer brine inputs, evaporation, and evapotranspiration.

The rulebased simulation solution is driven by prioritized, logical rules that represent the multi-objective operating policies such as flood control, water supply, environmental flows and hydropower production. We'll show how to create and execute these policies, using them to produce operating schedules, manage flood events or evaluate alternatives for EIS analysis. RiverWare also models water ownership and can perform water accounting calculations – we'll demonstrate how agencies use RiverWare for prioritized water allocation, to operate with rules based on water ownership, and to perform after-the-fact legal accounting.

The optimization solution is driven by prioritized goals that represent policy constraints and objectives. We'll demonstrate how utilities use RiverWare's pre-emptive linear goal programming to optimize hydropower production while meeting water management constraints.

We'll show how data can be easily loaded into RiverWare from various sources using the input Data Management Interface (DMI) which allows data to be automatically loaded from text files, Excel spreadsheets, HEC DSS files, HDB database or any other database.

We will demonstrate RiverWare's many utilities for viewing, analyzing and visualizing data including a fully featured plotting utility, outputs to HTML model reports and tabular series slot reports, pie charts, and tea cup diagrams. There are many options for exporting data from RiverWare including the output DMIs to any database, direct export to Excel, HEC DSS, and HDB. We'll show how to export RiverWare results to netCDF files and files that can be used directly in the Tableau Software for data processing, analysis, and visualization.

RiverWare's multiple run management utilities can be used to automate thousands of runs, and produce probabilistic outputs, or to perform yield studies. This concept of running many runs can be further structured using the RiverWare Study Manager and Research Tools (RiverSMART). This tool automates a planning study by organizing and running scenarios of hydrologic inputs, demand inputs and policy sets and then provides utilities to analyze and compare the results from these scenarios. Using this approach, water managers can run proposed operating policy changes through climate change hydrologies to analyze impacts and compare alternatives. We'll show how to define a RiverSMART study, generate scenarios, simulate the scenarios and then post process the results of either scenarios or sets of scenarios. We'll describe and show the various plugins that can be used within RiverSMART including the R plugin, the GPAT graphs plugin, and the Hydrology Simulator plugins.

RiverWare's script utility can be used to automate many of the processes that are performed on a day to day basis. Scripts contain actions which execute a process in RiverWare. For example, a script that load a ruleset, import observed data from a database, configure initial conditions, make a run, and generates output plots. Scripts are run from a configurable Script Dashboard, as shown in Figure 2, in which model operators can also view and change key decision variables. We will demonstrate how scripts and dashboards can be used to simplify modeling processes.

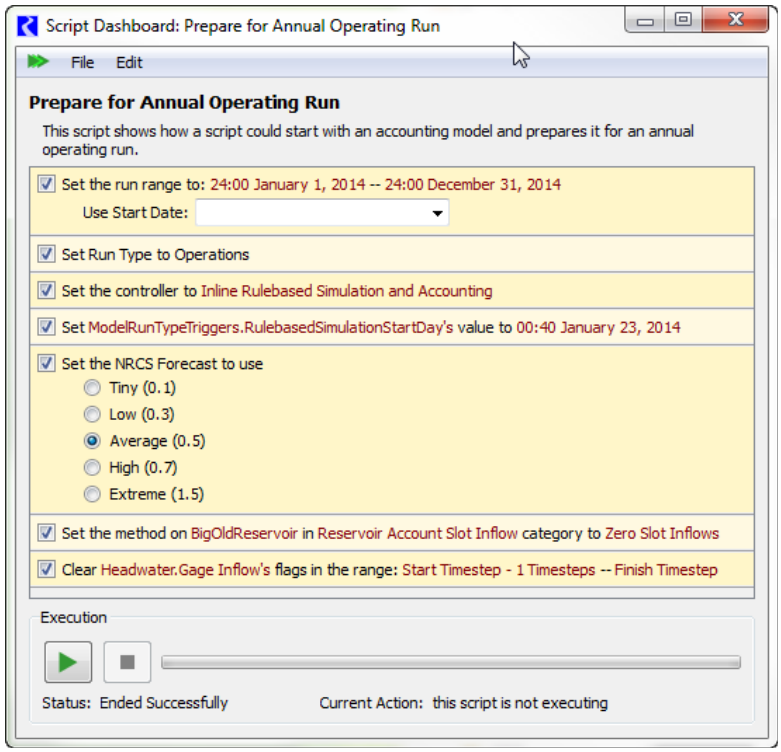

Figure 2 RiverWare Script Dashboard

RiverWare is integrated into the U.S. Army Corp of Engineers Corp Water Management System (CWMS). Further, it is integrated as a component of multiple Flood Early Warning Systems (FEWS) developed by Deltares. This integration allows for tighter coupling of RiverWare with other modeling tools for real time operations and management.

RiverWare's easy-to-use graphical user interface, statistical post-processing, script management, spreadsheet-view of data, direct database connection configurations, and powerful diagnostic and analysis utilities will complement as we show examples of the application of RiverWare to numerous river basins. Free evaluation versions of the software with demo models will be given to interested visitors.

RVR MEANDER – A TOOLBOX FOR RIVER MEANDER PLANFORM DESIGN AND EVALUATION

Eddy J. Langendoen, U.S. Department of Agriculture, Agricultural Research Service, National Sedimentation Laboratory, Oxford, MS, eddy.langendoen@ars.usda.gov; Davide Motta, AMEC, Philadelphia, PA, davide.motta3@gmail.com; Jorge D. Abad, Department of Civil and Environmental Engineering, University of Pittsburgh, jabad@pitt.edu; Marcelo H. Garcia, Ven Te Chow Hydrosystems Laboratory, Department of Civil and Environmental Engineering, University of Illinois at Urbana-Champaign, mhgarcia@illinois.edu; Roberto Fernandez, Ven Te Chow Hydrosystems Laboratory, Department of Civil and Environmental Engineering, University of Illinois at Urbana-Champaign, fernan25@illinois.edu; Nils Oberg, Ven Te Chow Hydrosystems Laboratory, Department of Civil and Environmental Engineering, University of Illinois at Urbana-Champaign, noberg@illinois.edu;

Abstract: Restoring the meandering planform or spatial variability of historically meandering streams that have been channelized or highly disturbed is one of the most difficult aspects in river restoration. River planform and cross-sectional geometry are the result of complex interactions between flow, boundary materials, and channel morphology. Hence, simple methods based on the reference-reach concept or hydraulic geometry relationships have often failed to produce long-term, stable meander reaches without additional bank protection. More sophisticated river meander models use empirical relations to calculate rate of channel migration, limiting their applicability as they do not explicitly account for the physical properties of the floodplain soils. The RVR Meander platform merges the functionalities of: the first version of RVR Meander developed by the University of Illinois, which is based on the classical meander migration model of Ikeda, Parker and Sawai; and the streambank erosion algorithms of the channel evolution computer model CONCEPTS developed by the US Department of Agriculture. It is written in C++ language and is composed of different libraries for preprocessing, hydrodynamics, bank erosion, migration, filtering, plotting, and I/O. It runs as a stand-alone application on Windows and Linux operating systems or as a plugin for ESRI's ArcMap software. RVR Meander has been used to model the migration of various rivers in the US and abroad.

INTRODUCTION

The ongoing modification and resulting reduction in water quality of U.S. rivers have led to a significant increase in river restoration projects over the last two decades (Bernhardt et al., 2005). The increased interest in restoring degraded streams, however, has not necessarily led to improved stream function. Palmer and Allan (2005) found that many restoration projects fail to achieve their objectives due to the lack of policies to support restoration standards, to promote proven methods and to provide basic data needed for planning and implementation. Proven models of in-stream and riparian processes could be used not only to guide the design of restoration projects but also to assess both pre- and post-project indicators of ecological integrity.

One of the most difficult types of river restoration projects concern reconstructing a new channel, often with an alignment and channel form different from those of the degraded pre-

project channel. Recreating a meandering planform to provide longitudinal and lateral variability of flow and bed morphology to improve in-stream aquatic habitat is often desired. Channel meander planform is controlled by a multitude of variables, for example channel width to depth ratio, radius of curvature to channel width ratio, bankfull discharge, roughness, bed-material physical characteristics, bed material transport, resistance to erosion of the floodplain soils, riparian vegetation, etc. Therefore, current practices that use simple, empirically based relationships or reference reaches have led to failure in several instances, for example a washing out of meander bends or a highly unstable planform, because they fail to address the site-specific conditions (e.g., Kondolf, 2006).

Recently, progress has been made to enhance a physically- and process-based model, RVR Meander, for rapid analysis of meandering river morphodynamics with reduced empiricism. For example, lateral migration is based on measurable physical properties of the floodplain soils and riparian vegetation versus the driving forces of the river hydrodynamics. The model can also be used in a Monte Carlo framework to statistically describe the long-term evolution of the meander planform. RVR Meander has been used to evaluate migration rates of restored meandering streams and bends on the Big Sioux River, SD and Trout Creek, CA at engineering time scales. It has also been used to assess the uncertainty and risk associated with the alignment of the meandering low-flow channel of the planned diversion of the Red River of the North around the metropolitan area of Fargo, ND and Moorhead, MN. The RVR Meander model and example applications are presented in the below sections.

RVR MEANDER

The current RVR Meander platform (Motta et al., 2012; http://rvrmeander.org/) extends the capabilities of the original version of RVR Meander (Abad and Garcia, 2006) by merging it with the stream-bank erosion submodel of CONCEPTS (Langendoen and Simon, 2008). The original version employed the classical migration approach (CMA) of Ikeda et al. (1981), who linearly related the local rate of meander migration to the near-bank velocity using a migration coefficient. RVR Meander is composed of modules to simulate hydrodynamics, bed topography, bank erosion, and migration of meandering rivers. It is available as a plugin for ArcGis versions 9.3.x and 10.x.

Hydrodynamics and Bed Topography: The model for hydrodynamics and bed topography implemented in RVR Meander is analytical and obtained from linearization of the two-dimensional depth-averaged Saint Venant equations. It follows the approach first developed by Ikeda et al. (1981) and adopts the secondary flow correction derived by Johannesson and Parker (1989), who introduced an "effective centerline curvature" that lags behind the local channel curvature and determines the transverse bed slope through a coefficient of proportionality named scour factor. Important model assumptions are: spatially- and temporally-constant channel width; bed topography is only a function of channel planform; and spatially-constant friction coefficient.

Bank Erosion and Meander Migration: In the physically-based meander-migration approach (PMA) in RVR Meander developed by Motta et al. (2012), simulated bank retreat is controlled

by the resistance to hydraulic erosion and the occurrence of cantilever and planar failures (Langendoen and Simon, 2008).

Hydraulic erosion requires that the local boundary shear stress exceeds the critical value to detach bank material, and is modeled with an excess shear stress relation. An average erosion distance is computed for each layer comprising the composite bank material. The shear stress acting on each of the bank material layers is obtained by scaling the shear stress at the toe, which is the bed shear stress at the bank computed with the linear hydrodynamic model, using the hydraulic radius of the flow area impinging on the layer.

Cantilever failure is the collapse of an overhanging slab of bank material formed by preferential retreat of more erodible underlying layers or simply by the erosion of the bank below the water level with respect to its upper, unsaturated portion. The occurrence of cantilever failure, for the case of shear collapse mechanism (Thorne and Tovey, 1981) considered here, is simply determined from geometrical considerations, once an undercut threshold is exceeded. The undercut threshold is defined as the ratio of bank material cohesion to unit weight. Mass failures along planar slip surfaces are analyzed using a limit equilibrium method in combination with a search algorithm to find the failure block configuration with the smallest factor of safety (Langendoen and Simon, 2008). Factor of safety is the ratio of available shear strength to mobilized shear strength, and when smaller than one the bank is unstable. The method accounts for the effects of pore-water pressure on bank material shear strength, confining hydrostatic pressure provided by the water in the channel, and can automatically insert tension cracks if the upper portion of the failure block is under tension.

Input Data Requirements: Because RVR Meander is intentionally a simplified 2D model it inputs are limited. The main physical input parameters are: (1) design or bankfull discharge; (2) channel dimensions such as width, depth, and slope; (3) channel centerline to determine channel curvature; (4) valley slope; (5) channel boundary roughness; (6) scour factor; (7) bank profiles; and (8) resistance to erosion properties of the bank soils, i.e. erodibility and shear-strength parameters.

Software: The RVR Meander model can be executed in two modes (Figure 1): (1) as a stand-alone version from the command line in MS Windows or Linux; and (2) through a graphical user interface that is a plugin for ESRI's ArcMap 9.3.x or 10.x software. The compute engine is the same for both modes. The software, its manuals, and tutorial files can be downloaded at the URL http://rvrmeander.org.

The stand-alone version requires four input files: (1) "testdata.txt," pairs of easting and northing coordinates of the initial channel centerline; (2) "valley.txt," pairs of easting and northing coordinates of the valley centerline; (3) "prototype.cfg," general parameters for simulation; and (4) "InitialSectionProperties.dat," initial configuration of channel banks (shape and bank-material properties) for physically-based approach for meander migration. The ArcMap plugin uses the same input files, which are however prepared within ArcMap. The output files for the standalone version are designed to be post-processed using such software as Tecplot and MS Excel. The ArcMap plugin generated files can be directly viewed inside ArcMap with the

exception that the current version does not support "Bank geometry output," and needs plotting software such as MS Excel to view this output.

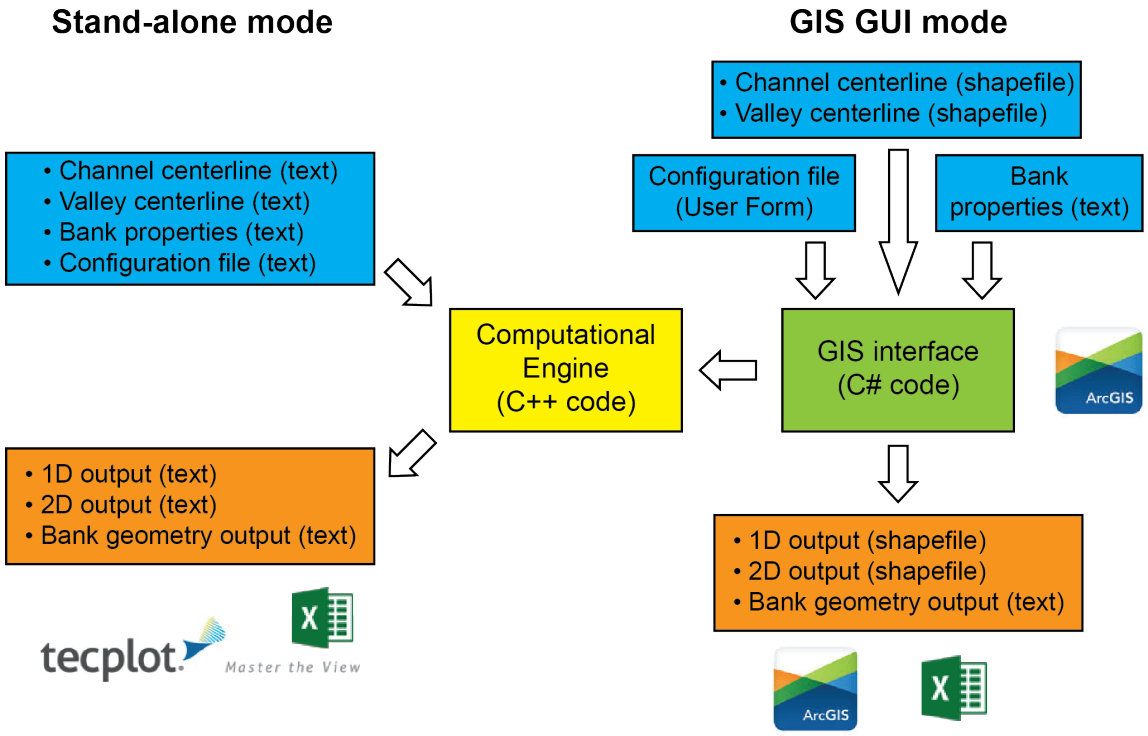

Figure 1 RVR Meander software is available as a stand-alone program for MS Windows and Linux operating systems and as a plugin for ESRI's ArcMap.

APPLICATIONS

Mackinaw River, Illinois: The performance of the proposed approach was tested for a reach on the Mackinaw River in Tazewell County between the towns of South Pekin and Green Valley, Illinois. The average width of the study reach is 38 m, valley slope is 0.47 m/km, and effective discharge is 62 m^3/s. The migration of the centerline between 1951 and 1988 was simulated with RVR Meander using both CMA (migration coefficient calibrated as $3.3x10^{-7}$) and PMA. Bank retreat in the physically-based method was assumed to be caused by hydraulic erosion only, and the critical shear stress τ_c =9 Pa (measured critical shear stress is approximately 8 Pa).

Figure 2 compares the centerline migration obtained with the classical migration-based and the physically-based approaches. The channel centerline simulated using PBA agrees well with that observed away from the boundaries of the model reach. The channel centerline simulated using CMA is similar to that obtained by PMA for the upstream part of the study reach. However, CMA significantly overestimates the channel centerline migration, both in terms of meander amplitude and downstream translation, along the downstream part of the study reach.

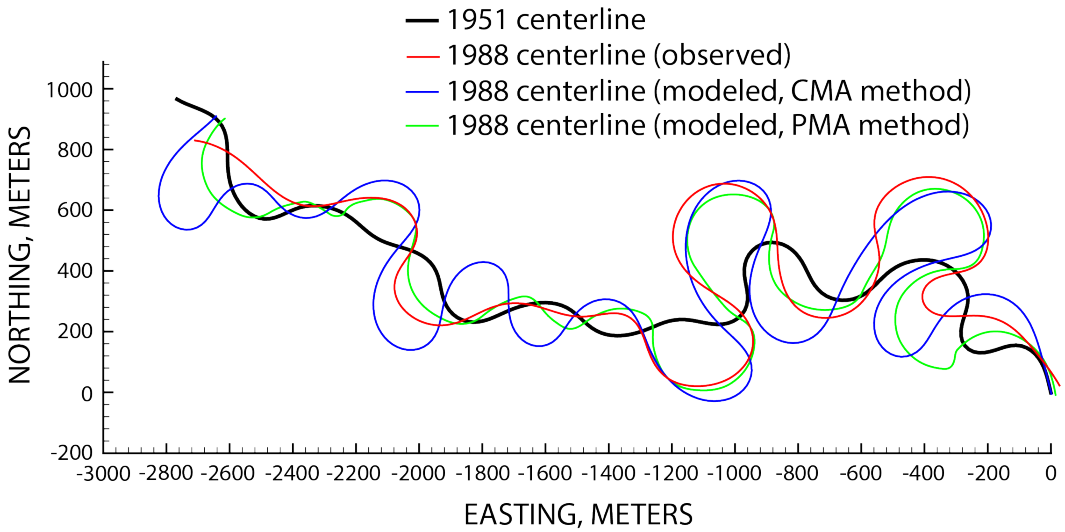

Figure 2 Comparison of observed and modeled centerline migration between 1951 and 1988 of a reach on the Mackinaw River, Illinois, USA. Flow is from right to left.

Big Sioux River, South Dakota: RVR Meander was used to assess potential erosion zones for a 34-km long reach on the Big Sioux River between Dell Rapids and Sioux Falls, South Dakota. The reach is fairly sinuous with an average sinuosity (ratio of channel length over valley length) of 1.6. The average channel top width and depth are 40.5 m and 2.2 m, respectively. The average channel slope is 0.4 m/km, and valley slope is 0.66 m/km. The 1.5-year return period discharge is 57.5 m^3/s, which is assumed to represent the bankfull discharge. The Manning *n* roughness coefficient is 0.052. A scour factor of 7 produced a transverse bed slope similar to that observed. The bed material is sand dominated with the median bed material grain size along the study reach varying between 0.03 and 7.0 mm with a mean value of 1.4 mm. Bank material is cohesive except for the sediments/soils at depth, which consist of sands and gravels. The upper cohesive layer primarily comprises erodible loam and sandy loam soils, but percent clay is found as high as 55%.

Figure 3 shows an example 11 meander bends with large simulated shear stresses near the outer bank. The plotted shear stress distributions were normalized by the reach-averaged shear stress representing uniform flow conditions. RVR Meander simulated high shear stresses at 45 unprotected bends that may potentially lead to enhanced migration rates. Sixteen of these bends have exhibited significant migration between 1991 and 2012, and should be targeted for construction of bank protection works. Eleven of these bends are located along a section of the Big Sioux River where several meander bends were cutoff between 1937 and 1991, which has resulted in increased bank erosion rates due to the channel adjustment caused by the local channel shortening and consequent increased gradient.

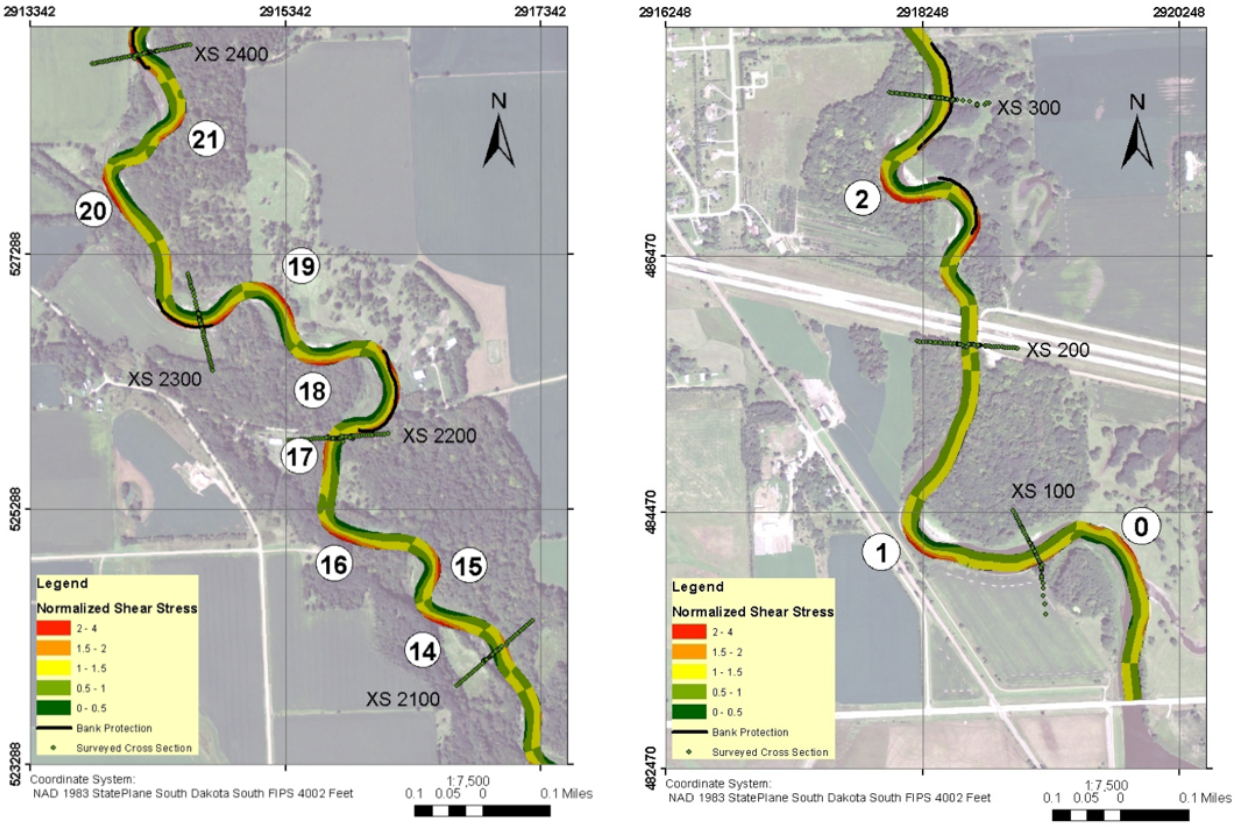

Figure 3 Example locations of large near-bank bed shear stresses simulated by RVR Meander along selected reaches of the Big Sioux River between Dell Rapids and Sioux Falls, South Dakota. Flow is from top to Bottom

Meander Belt Width Analysis, Red River Diversion, North Dakota: The Fargo-Moorhead Metropolitan Area Flood Risk Management Project seeks to prevent flooding of the cities of Fargo, North Dakota, and Moorhead, Minnesota by constructing a 36-mile diversion channel to the west of the metropolitan area. Included in the project plans is a low-flow channel (LFC) with a meandering planform (initial target sinuosity was 1.5) to provide enhanced aquatic habitat to mitigate the loss of approximately 5.5 miles of Lower Rush and Rush River reaches cut off by the diversion. An analysis of flow and sediment conveyance determined the LFC top width at 100 feet. The bottom width of the main diversion channel was set at 300 feet.

RVR Meander was used to determine if a meandering planform of the LFC was feasible given these widths. A Monte Carlo approach was followed, which facilitates risk analysis—in this case, calculating the probability that the meander belt will expand beyond the constraints of the diversion channel, given different conditions (e.g., planform configurations, resistance-to-erosion of boundary materials, channel aspect ratios, construction sequence). For example, only a limited number of soil samples could be collected along the planned course of the diversion (samples from more readily accessible locations were used as substitutions). For each design, a 1000 simulations were conducted over 50- or 100-year periods. The planform was generally sine-generated, and the cross-sectional shape was trapezoidal. We used the 1.5-yr return

discharge as the design discharge. Planform width, sinuosity, and dominant wavelength were the parameters that were assessed (see Figure 4).

The Monte Carlo simulations indicated that the LFC meander belt would generally have a tendency to narrow over time. Of factors considered, the initial wavelength had the largest impact on LFC migration; initial amplitude was also seen to be important. Other parameters such as the channel side slopes and bottom width, however, did not appear to significantly impact meander belt width over the life of the project. Also of note were simulation results for a phased construction scenario — assuming that construction of the diversion channel downstream of the Lower Rush River was completed first. These results suggested that in the first 10 years following phased construction, the change in meander belt width would be very small.

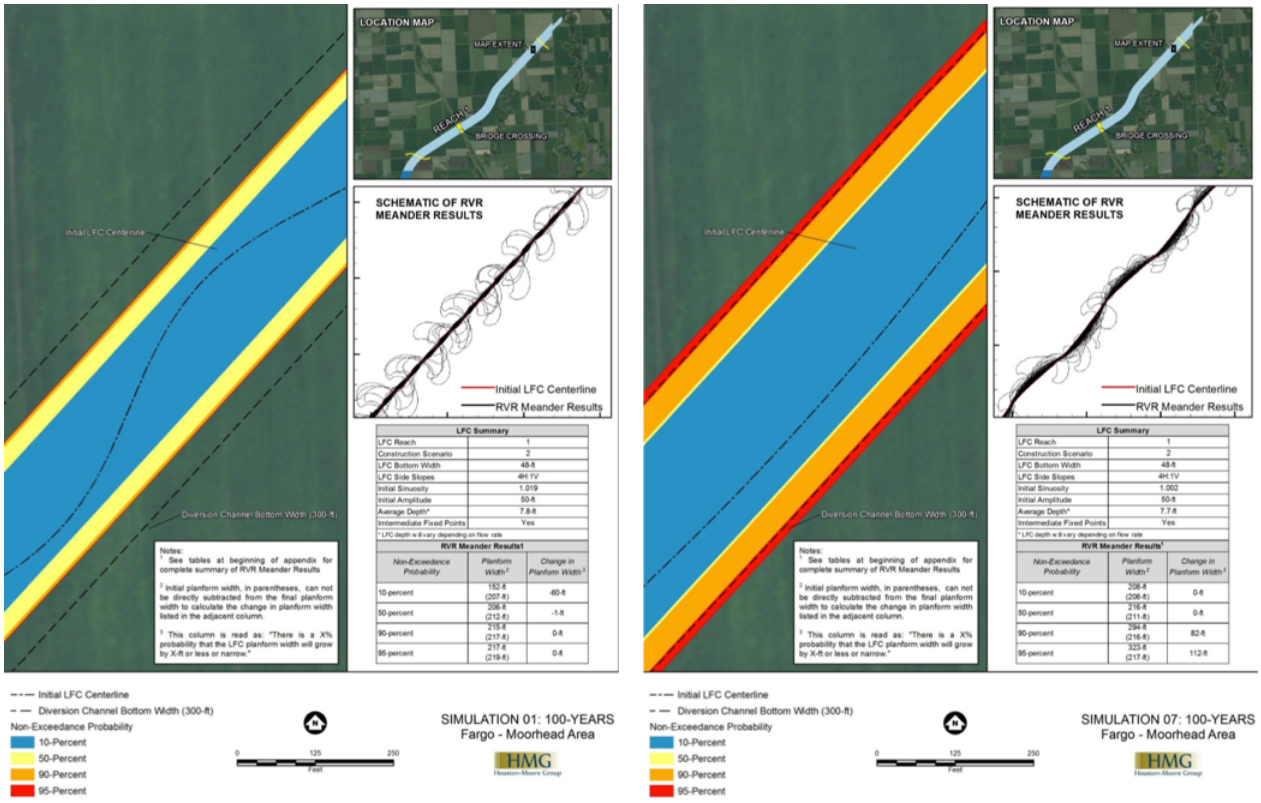

Figure 4 Example results of probabilistic meander belt width analysis of the LFC of the Red River, North Dakota, are presented using non-exceedance contours. (Left) meander planform with an initial sinuosity of 1.02 that tends to straighten. (Right) meander planform with an initial sinuosity of 1.002 that tends to increase its sinuosity and planform width; there is a 10% probability that the LFC will migrate into the diversion sidewall.

REFERENCES

Abad, J.D., and Garcia, M.H. (2006). "RVR Meander: A toolbox for re-meandering of channelized streams," Computer & Geosciences, 32(1), pp 92-101.

Bernhardt, E.S., Palmer, M.A., Allan, J.D., Alexander, G., Barnas, K., Brooks, S., Carr, J., Clayton, S., Dahm, C., Follstad-Shah, J., Galat, D., Gloss, S., Goodwin, P., Hart, D.,

Hassett, B., Jenkinson, R., Katz, S., Kondolf, G.M., Lake, P.S., Lave, R., Meyer, J.L., O'Donnell, T.K., Pa- gano, L., Powell, and B., Sudduth, E. (2005). "Synthesizing U.S. river restoration efforts," Science, 308, pp 636-637.

Ikeda, S., Parker, G., and Sawai, K. (1981). "Bend theory of river meanders. Part 1. Linear development," J. Fluid Mech., 112, pp 363-377.

Johannesson, H., and Parker, G. (1989). "Velocity redistribution in meandering rivers," Journal of Hydraulic Engineering, 115(8), pp 1019-1039.

Kondolf, G.M. (2006) "River restoration and meanders," Ecology and Society, 11(2), pp 42.

Langendoen, E.J., and Simon, A. (2008). "Modeling the evolution of incised streams. II: Streambank erosion," Journal of Hydraulic Engineering, 134(7), pp 905-915.

Motta, D., Abad, J.D., Langendoen, E.J., and Garcia, M.H. (2012). "A simplified 2D model for meander migration with physically-based bank evolution," Geomorphology, 163-164, pp 10-25.

Palmer, M.A., and Allan, J.D. (2005). "Restoring rivers," Issues in Science and Technology, National Academy of Sciences, 22, pp 40–48.

Thorne, C.R., and Tovey, N.K. (1981). Stability of composite river banks. Earth Surface Processes and Landforms, 6(5), pp 469-484.

WINDAM C EARTHEN EMBANKMENT

INTERNAL EROSION ANALYSIS SOFTWARE

Karl Visser, PE; Hydraulic Engineer; USDA-NRCS; National Design, Construction, and Soil Mechanics Center; Fort Worth, Texas; karl.visser@ftw.usda.gov;
Ronald D. Tejral, PE; Agricultural Engineer; USDA-ARS; Hydraulic Engineering Research Unit; Stillwater, Oklahoma; ronald.tejral@ars.usda.gov;
Mitchell L. Neilsen, PhD, Professor of Computing and Information Sciences, Kansas State University; Manhattan, Kansas; neilsen@k-state.edu

Abstract: Two primary causes of dam failure are overtopping and internal erosion. For the purpose of evaluating dam safety for existing earthen embankment dams and proposed earthen embankment dams, Windows Dam Analysis Modules C (WinDAM C) software will simulate either internal erosion or erosion resulting from an overtopping event. WinDAM C models erosion failure of a homogeneous embankment. Future expansion includes non-homogeneous embankments, and embankment protection analysis.

The four essential functions of the software are:

1. Hydraulically routes one input hydrograph through, around, and over a single earthen dam.
2. Estimates internal erosion and potential breaching of an earthen embankment dam.
3. Estimates erosion of the earthen embankment caused by overtopping of the dam embankment.
4. Estimates auxiliary spillway erosion in up to three earthen or vegetated auxiliary spillways.

The user imports an inflow hydrograph into WinDAM C and selects either internal erosion analysis or overtopping analysis.

Regarding internal erosion within the earthen embankment, the user sets the elevation and initial size of the internal erosion conduit. WinDAM C initially assumes a horizontal, rectangular conduit shape. The internal erosion conduit grows larger as flow erodes embankment material. The erosion may breach the embankment and drain the reservoir.

Since the research has been completed, United States Department of Agriculture (USDA) and Kansas State University (KSU) are currently verifying and validating a working version of WinDAM C, which should be released for external evaluation and testing in 2015.

INTRODUCTION

Windows Dam Analysis Modules (WinDAM) is a modular software application to analyze earthen embankments during internal erosion and overtopping. Recently released for testing and evaluation by the dam safety community, WinDAM B (USDA, et al. 2012) includes erosional failure of a homogeneous embankment through overtopping and release of stored water. The alpha version of WinDAM C, currently under development, includes analysis of internal erosion. Future planned development includes non-homogeneous embankments. The US Department of Agriculture – Agricultural Research Service (USDA-ARS), US Department of Agriculture – Natural Resources Conservation Service (USDA-NRCS), and Kansas State University (KSU) are working jointly to develop this software.

For nearly seventy years, the USDA-NRCS has partnered with landowners, municipalities, conservation districts and other sponsors to construct more than 11,000 rural flood control dams. These structures provide $1.5B in annual benefits by providing flood control, municipal and rural water supplies, irrigation water, wetland habitat, and recreation among others. Many of these aging dams were designed with a 50-year service life, and time takes a toll on these structures. Sediment pools fill and encroach upon the flood detention volume. Structure components deteriorate, and hazard creep occurs in urbanizing areas that were once rural cropland areas. As a result, the consequences of dam failure must be considered when evaluating and prioritizing these structures for rehabilitation since the structures may no longer meet NRCS design criteria (USDA, 2005).

Overtopping and internal erosion are the primary causes of dam failures, with each mode attributed to a roughly equal number of failures (Foster, Fell and Spannagle 1998). For a given dam, one (or neither) mode may be more likely. For example, many of the storage reservoirs in arid West have large volumes relative to inflow and are managed such that overtopping is very unlikely. The US Bureau of Reclamation (USBR, 2011) names internal erosion of embankments (or their foundations) as the number one cause of dam failures in the western US. WinDAM C, when completed, will estimate breach erosion of an earthen dam through one of two modes: internal erosion through the embankment or overtopping the embankment. This document describes the WinDAM model currently being developed to examine internal erosion. The model is currently at the alpha stage of development undergoing verification and validation testing by the developers. It is anticipated that additional testing by the dam safety user community will also be required.

WINDAM C CAPABILITIES

Purpose of Software: The essential functions of WinDAM C software are threefold:

- Hydraulically route (level pool routing) one inflow hydrograph through, around, and over a single earthen dam.
- Estimate auxiliary spillway erosion in up to three earthen or vegetated auxiliary spillways.
- Estimate erosion of the earthen embankment caused by internal erosion or by overtopping of the dam embankment.

Since WinDAM C does not include any hydrology component, the user must create the reservoir inflow hydrograph in other software, such as WinTR-20 (USDA-NRCS, 2009) or SITES (USDA-NRCS, 2015). The user can import the hydrograph or paste the hydrograph points into the user interface. The user has the flexibility to choose the hydrologic software most suitable for analysis of site conditions.

Internal Erosion of Homogenous Earthen Embankment: WinDAM C models the dam embankment as a homogenous earthen material. Many USDA-NRCS dams are homogenous earthfill, so the WinDAM C model applies. If applied to zoned embankments, the suggested approach is to consider material and geometry that will dominate the process. For computational purposes, the earthen embankment fits into a simplified, rectangular-shaped valley (Figure 1) with vertical abutments and level valley floor.

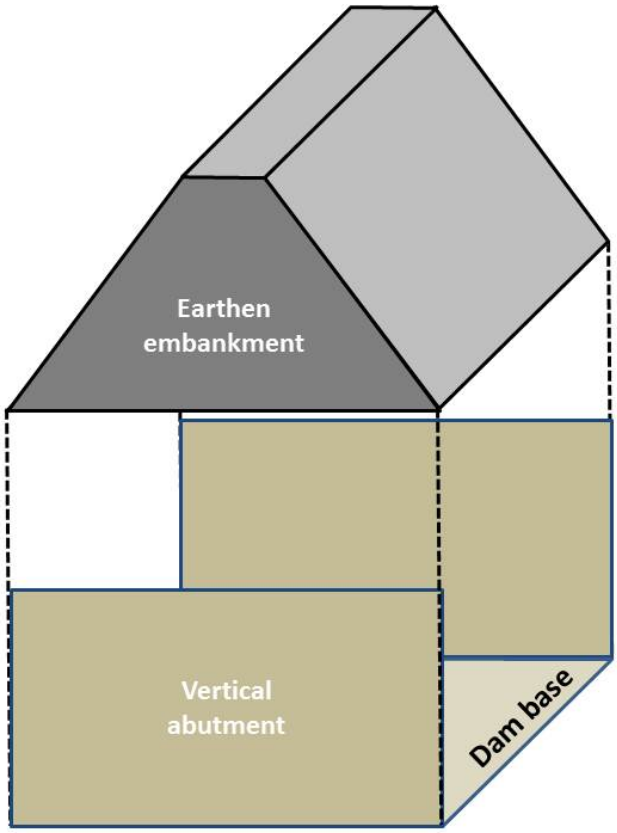

Figure 1 Homogenous earthen embankment in rectangular-shaped valley

Initial Internal Erosion Conduit: For a WinDAM C internal erosion analysis, the user specifies the initial size and location of the internal erosion conduit. To simplify the analysis, the conduit is horizontal—there is no slope in the upstream-downstream direction through the embankment, as shown in Figure 2. The conduit is assumed to be rectangular. The user must specify the

initial conduit dimensions—width and height. The user must input the initial elevation of the conduit invert, as well as the lateral stationing between the left and right abutment.

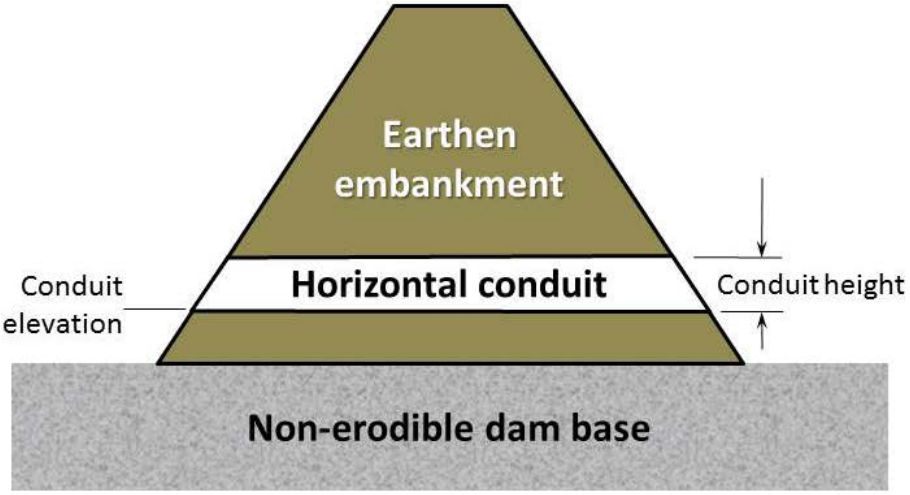

Figure 2 WinDAM C internal erosion horizontal conduit profile

In WinDAM C the left and right abutments are considered to be non-erodible and vertical, as shown in Figure 3. The embankment foundation, or dam base, is non-erodible and level. The dam crest profile is defined as a series of user-entered points (Figure 3).

The internal conduit erodes laterally until it reaches an abutment, as shown in Figure 3. The conduit also erodes vertically between the dam crest profile and the dam base. As long as some portion of the conduit is flowing full and the shear stress is sufficient to erode the embankment material, the conduit expands in all four directions equally. Once conduit erosion reaches one of the embankment boundaries (abutment, dam base, or dam crest), expansion/erosion in that direction stops.

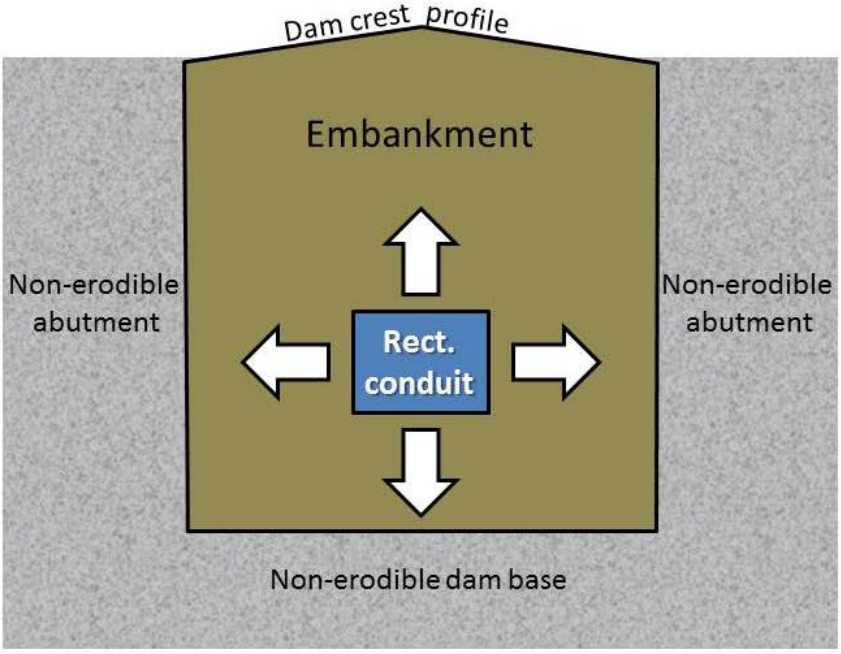

Figure 3 WinDAM C conduit cross-section looking upstream

Erosion Processes: Two erosion processes are simulated. The conduit enlarges concentrically due to shear detachment (laterally and vertically in a conduit simplified as having a rectangular cross section); classically this is the only process associated with internal erosion. However, development of a headcut at the outlet and subsequent advance of that headcut also play an important role in breach by internal erosion in some instances, so this process is also modeled.

At the beginning of each time step, the model computes the shear stress produced by flow passing through the rectangular internal erosion conduit. In instances where conduit is full for less than entire length, a backwater curve and resulting average shear stress along conduit length are computed. If the average shear stress is greater than the user-specified critical shear stress, then the amount of erosion is estimated and the conduit expanded accordingly for the next time step.

In addition to simply expanding the internal conduit laterally and vertically, WinDAM C also checks to see if a headcut will form at the downstream invert of the conduit (Figure 4). After this headcut has formed, headcut advance and deepening is computed for each time step using the user-prescribed erosion model (Table 3). This process is simulated much like that of a headcut formed in overtopping with important distinction that width is controlled by the conduit.

Transition from Internal Conduit Erosion to Breach Erosion: Once this headcut reaches the upstream face of the embankment the internal conduit has become an open breach and flow

transitions to breach flow. At this point, lateral expansion of the breach is the same as with overtopping flow conditions.

In the early stages of internal erosion, the conduit is usually stable regardless of support by hydrostatic water pressure. As the conduit enlarges, the support provided by water becomes critical. There are three cases when the roof of the conduit is considered to be stable:

1. The conduit is flowing full over the entire length of the conduit.
2. The conduit is flowing full over some part of the conduit length.
3. When flow transitions to free surface flow along the entire length of the conduit and the conduit width is less than twice the overburden height (vertical distance from the dam crest to conduit roof).

As the breach progresses and reservoir drains the roof of the internal erosion conduit will collapse. WinDAM C considers the conduit roof collapsed for these two cases:

1. Erosion of the roof reaches the dam crest profile
2. Free surface flow along the entire conduit length and the conduit width is more than twice the vertical distance from the dam crest to the roof.

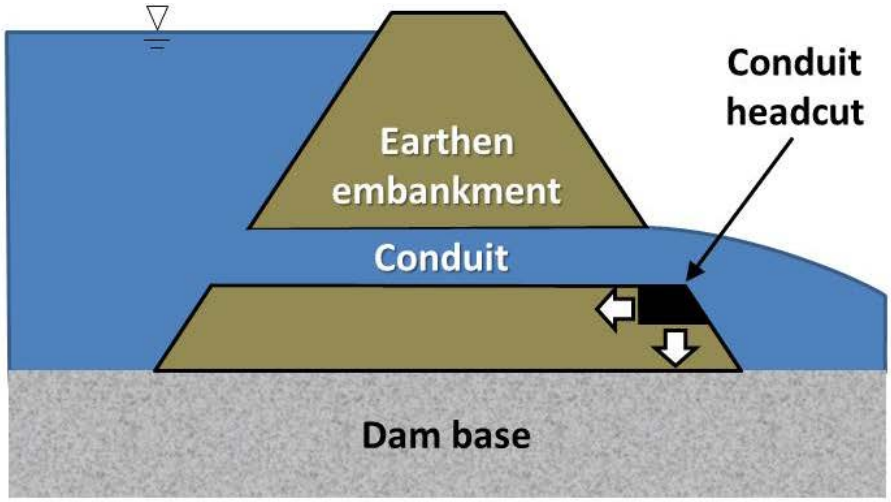

Figure 4 Conduit headcut

Negligible Internal Conduit Erosion Cases: There are cases where the resulting internal erosion is negligible. These possible cases include:

- Elevation of internal erosion conduit is above maximum water surface in the reservoir, which results in no flow in internal erosion conduit.
- Insufficient time or flow to produce meaningful erosion because the generated stress does not exceed the soil critical stress by sufficient time or amount.

- Highly erosion-resistant embankment materials may not generate shear stresses greater than the soil critical stress.

Overtopping Breach Erosion: If the user selects overtopping erosion analysis in WinDAM C, flow through the breach depends on the eroded breach area and the driving head based on the reservoir water surface, breach elevation, and any downstream tailwater. The four stages of the overtopping breach are described in Table 1.

Table 1 Four stages of WinDAM overtopping breach

Stage 1	Surface protection on downstream embankment slope fails. Headcut forms on downstream face of dam at low point in the crest profile.
Stage 2	Headcut advances through the crest to upstream embankment slope. Breach is initiated when the headcut enters the upstream crest and begins to lower the hydraulic control.
Stage 3	Headcut continues to advance into the reservoir pool releasing stored water.
Stage 4	Headcut continues to widen as reservoir drains following local removal of the embankment in the breach area.

Modeling Flow Through Embankment Cracks: Earthen embankments are susceptible to cracking from seismic activity or from desiccation in arid regions. As an overtopping erosion event, the only way to evaluate a crack is to input the crack in the dam crest profile. WinDAM overtopping erosion analysis was not developed for such evaluation and is not appropriate for several reasons. First, crest width in WinDAM is a constant and WinDAM evaluates both stress and erosion strictly from a depth perspective rather than considering the extremely steep profile segments as walls. Second, overtopping is considered on a one-dimensional, unit-discharge basis.

However, analyzing a crack, even one that extends to the dam crest, as an internal erosion event may be appropriate if the user develops a thorough understanding of the computational model and interprets inputs and results accordingly. Cracks have been associated with internal erosion (Bonelli et al., 2006) (Fell et al., 2003). The geometry of a crack can be more correctly approximated in an internal erosion simulation in WinDAM C. However, the research program and software were not undertaken to address the early stages of breach development represented by narrow cracks. Users should recognize model constraints and interpret results accordingly, e.g.

- WinDAM C assumes turbulent flow through the internal conduit, whereas flow through narrow cracks may be laminar flow.

- WinDAM C embankment materials properties do not change during the analysis. Over a sufficiently long period of time, flow within small cracks may saturate portions of the embankment and alter its resistance to erosion.

Interaction Of Erosion And Hydraulics: The hydraulics and erosion are coupled for the embankment breach analysis. In other words, a larger breach in the embankment lets more flow pass through the embankment breach during the next time step. Erosion prediction is relatively straightforward in the homogeneous earth embankment.

Erosion prediction in the auxiliary spillway, however, is much more complex than in the homogenous earth embankment. Hydraulics and erosion are not coupled in the auxiliary spillway because the erosion model only includes information on the weakest unit width subsurface materials in the auxiliary spillway. As a result, WinDAM C does not have the data to estimate the lateral expansion in the auxiliary spillway. Erosion computations in the auxiliary spillway stop when the headcut reaches the upstream edge of the level crest of the auxiliary spillway.

WINDAM VERSIONING

Research is ongoing for future enhancements to WinDAM software, as shown in Table 2. USDA and KSU are currently verifying and validating a working version of WinDAM C, which should be released for evaluation and testing in 2015.

Table 2 WinDAM Versioning

Version	Existing Capabilities or Future Enhancements
WinDAM A+ (2008)	Embankment overtopping analysis (Slope protection evaluation: no embankment erosion analysis)
WinDAM B (2011)	Homogenous fill embankment overtopping and erosion analysis
WinDAM C (2015)	Internal erosion prediction through homogenous fill embankment
WinDAM D (proposed)	Potential failure initiation at toe, berms, and groins. Alternative embankment slope protection materials (i.e. blocks, reinforced vegetation)
WinDAM E (proposed)	Zoned fill embankment overtopping erosion prediction

INPUT DATA

The auxiliary spillway materials in WinDAM C are described with the same data inputs as in SITES (USDA-NRCS, 2015).

WinDAM C requires the user to input one flow hydrograph. This hydrograph input is similar to the SITES input procedure. SITES gives the user the option to input hydrology through a watershed model, but WinDAM C only allows hydrology input through a single hydrograph. Various design hydrographs will require a different WinDAM C run for each hydrograph.

WinDAM C may be run with or without embankment breach evaluation. When breach evaluation is desired, the earthen embankment must be described so WinDAM C can model either internal erosion or overtopping erosion. The user specifies the embankment slope protection: vegetation, rock riprap, or no cover. The dam embankment crest and slope dimensions are also input.

For the breach analysis option, the user selects one of two headcut models: Temple/Hanson Energy model or Hanson/Robinson Stress Model (Hanson, et al. 2011). The WinDAM C erosion prediction models are designed for estimating erosion of typical NRCS earthen embankments composed of fine-grained, cohesive materials, where the dominant erosion process is the formation, advance, and deepening of a headcut. The soil parameter inputs for each model are listed in Table 3.

Table 3 WinDAM C Erosion Model Soil Inputs

Model	Hanson/Robinson Stress Model	Temple/Hanson Energy Model
Input Parameter *(Units)*	Erodibility (ft/hr)/(lb/ft^2)	Erodibility - (ft/hr)/(lb/ft^2)
	Critical Shear Stress (*lb/ft^2)*	Critical Shear Stress – (*lb/ft^2)*
	Undrained Shear Strength (*lb/ft^2)*	Advance coefficient - *(ft/hr)/(ft/s^3)*
	Total Unit Weight (*lb/ft^3)*	

All four input parameters in the Hanson/Robinson stress model can be measured. In addition this model is recommended for tall dams (> 50 ft high). Since the advance coefficient parameter in the Temple/Hanson cannot be measured directly, most users select the Hanson/Robinson stress model.

A WinDAM C internal erosion analysis covers a few hours or days. The WinDAM model does not account for wetting or drainage of embankment soils during the erosion analysis. Therefore, the material properties of the embankment soil do not change over the period of the breach analysis.

Generally, the outflow from dams is controlled primarily by the hydraulic features of the dam—principal spillway and auxiliary spillway. For these dams where backwater effects are not significant, a single downstream tailwater elevation is sufficient. However, some dams have downstream hydraulic features such as levee or road embankments that impose significant and dynamic backwater effects. WinDAM C incorporates a tailwater rating table to simulate how the outflow from the dam varies with downstream capacity. This backwater is used when analyzing the auxiliary spillway flow, but is not yet utilized when computing the auxiliary spillway erosion.

OUTPUT

WinDAM C has three forms of output; the initial summary screen the user sees upon completion of a valid run, ASCII text output files, and numerous graphical plots. WinDAM C has multiple text output files to describe the expected performance of the embankment and multiple auxiliary spillways. The current list of available output plots in WinDAM C are listed below.

- Conduit/Breach Width
- Dam Cross-section
- Dam Crest Profile
- Conduit Width/Height
- Headcut Advance
- Headcut Position
- Hydrographs

- Reservoir Surface Area
- Reservoir Storage Volume
- Reservoir Water Surface
- Maximum Overtopping / Breach Discharge
- Maximum Overtopping Head
- Overtopping Stress
- All Discharge Ratings
- Auxiliary Spillway Ratings
- Principal Spillway Rating
- Tailwater Elevation
- Tailwater Rating

A sample of the Headcut Advance plot is shown in Figure 5.

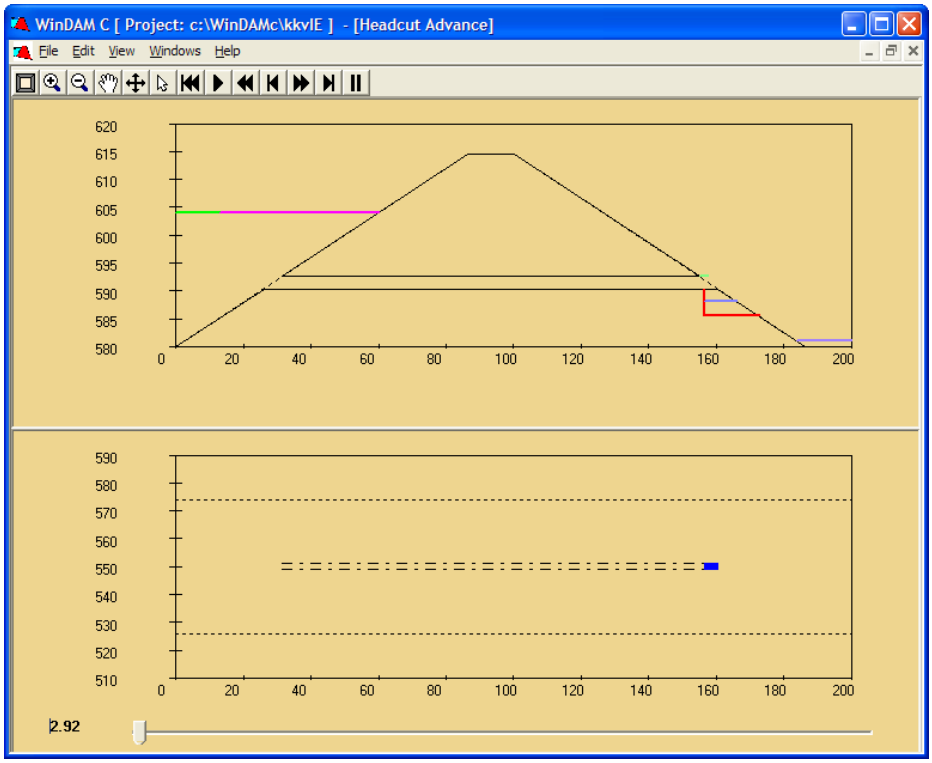

Figure 5 Sample WinDAM C headcut advance plot. Top half is dam cross-section. Bottom half is plan view.

INITIAL MODEL VALIDATION

Four different internal erosion tests on earthen embankments have been conducted at the ARS Hydraulic Engineering Research Unit in Stillwater, OK. Qualitatively, the WinDAM C predicted erosion matches the prototype erosion. The tests indicate that critical shear stress is a key parameter for initiation of erosion and particle detachment, especially for low-head dams (R. Tejral, personal communication, 2014).

CONCLUDING REMARKS

This report contains a preview of the internal erosion modeling capability being developed for WinDAM C. In addition, attention was given to capabilities already available to WinDAM B users—analysis of auxiliary spillways and overtopping breach. WinDAM software download and answers to frequently asked questions can be found at http://go.usa.gov/8Oq.

REFERENCES

Bonelli, S., Olivier, B., Borghi, R., and Benahmed, N. (2006). On the modelling of piping erosion. Comptes Rendus Mecanique , 555-559.

Fell, R., Wan, C.F., Cyganiewicz, J., and Foster, M. (2003). Time for Development of Internal Erosion of Piping in Embankment Dams. Journal of Geotechnical and Geoenvironmental Engineering , 129 (4).

Foster, M.A., Fell, R., & Spannagle, M. (1998). *Analysis of Embankment Incidents.* Sydney, Australia: The University of New South Wales.

Hanson, G.J., D.M. Temple, S.L. Hunt, and R.D. Tejral. (2011). Development and Characterization of soil material parameters for embankment breach. ASABE, Applied Engineering in Agriculture. Vol. 24(7):587-595.

USDA-NRCS. (2005). Earth Dams and Reservoirs. Technical Release TR-60 Washington D.C.: USDA Natural Resources Conservation Service.

[USBR] US Bureau of Reclamation. (2011). Best Practices and Risk Methodology Chapter 24 – Internal Erosion and Piping Risks for Embankments.

USDA-ARS and –NRCS and Kansas State University: WinDAM B. (2012). WinDAM-B, Version 1.1, Computer Program Release. http://go.usa.gov/8Oq.

USDA-NRCS. (2009). WinTR-20 Watershed Hydrology. Version 1.11. http://www.nrcs.usda.gov/wps/portal/nrcs/detailfull/null/?cid=stelprdb1042793.

USDA-NRCS: SITES. (2015). SITES 2005, Water Resource Site Analysis Computer Program, Version 2005.1.8, and User Documentation. Washington D.C. http://go.usa.gov/83z

WINTR-20 VERSION 3.10.00 PROJECT FORMULATION HYDROLOGY SOFTWARE COMPUTER DEMONSTRATION

Quan D. Quan, Hydraulic Engineer, USDA-NRCS, Beltsville, Maryland, quan.quan@wdc.usda.gov
William H. Merkel, Hydraulic Engineer, USDA-NRCS, Beltsville, Maryland, william.merkel@wdc.usda.gov
Helen Fox Moody, Hydraulic Engineer, USDA-NRCS, Beltsville, Maryland, helen.moody@wdc.usda.gov

INTRODUCTION

WinTR-20 model is a storm event surface water hydrologic model applied at a watershed scale. The model assists in hydrologic evaluation of flood events for use in the analysis of water resource projects. It can be used to analyze current watershed conditions as well as assess the impact of proposed changes made within the watershed. Multiple storms (or rainfall frequencies) can be analyzed within one model run. A summary table for all storms within the run can be produced. Direct runoff is computed from watershed land areas resulting from synthetic or natural rain events. The runoff is routed through channels and/or impoundments to the watershed outlet.

WINTR-20 CAPABILITIES

Primary Purposes of Software:

- The WinTR-20 model is the heart of the system and performs the rainfall-runoff and watershed routing calculations.
- The Data Converter transforms oldTR-20 input data to the new input format accepted by the WinTR-20 model.
- The HEC-RAS Reformatter transforms HEC-RAS output profile data to WinTR-20 Stream Cross section data.
- The National Oceanic and Atmospheric Administration (NOAA) Atlas 14 rainfall data converter import NOAA data into WinTR-20 (csv or text files).
- The Northeast Regional Climate Center (NRCC) rainfall data converter imports NRCC data to WinTR-20 (text files).
- WinTR-20 generates inflow hydrographs to import into WinDAM software (filename.hyd) based on NRCS Technical Release 60 (TR-60) criteria.

WinTR-20 version 3.10.00 has been released and is available for download.

COMPUTER DEMONSTRATION

A computer will be set up with WinTR-20 version 3.10.00 to demonstrate use of the software. Experts will be available to answer questions.

SOFTWARE AVAILABILITY

The WinTR-20 system, documentation, and training material may be downloaded at no expense from http://go.usa.gov/KoZ . Questions may be directed to the WinTR-20 support team e-mail address: NRCS-TR20@usda.gov .

2011 MORGANZA CONTROL STRUCTURE TAILBAY SCOUR DEVELOPMENT & SEDIMENT DISTRIBUTION

T. (Jerry) Shih, Ph.D., P.E., U.S. Army Corps of Engineers, New Orleans, Louisiana,
Tzenge-Huey.Shih@usace.army.mil
Suchen Chien, U.S. Army Corps of Engineers, New Orleans, Louisiana,
Suchen.Chien@usace.army.mil

Abstract Completed in February 1954, the Morganza Control Structure (MCS) is a very unique Mississippi River flow diversion structure. When the forebay stage reaches 56.0 feet design height, the MCS is capable of diverting 600,000 cubic feet per section (cfs) water. Since completion, the MCS has been used to divert the flood water twice.

The first operation was started on April 17, 1973. The 1973 diversion caused significant scour at the MCS tailbay. As a remedy to protect the MCS tailbay from future scour, a reinforced concrete plunge pool was built in 1977. The second operation was started on May 15, 2011, but significant scour occurred again and promulgated even further downstream.

Six multi-beam surveys were performed between May 17 and June 6, 2011 to monitor the scour development. Each survey showed new scour holes and the development of original findings. The most severe scour holes were approximately 30 feet lower than their original elevations. Scour holes were un-watered in April 2012 and a Terrestrial LiDAR survey was performed on June 23, 2012. According to the survey results scour holes continued to develop after June 6, 2011, but they were not as severe as those in the early operation.

In May 2011, USGS performed a preliminary sediment deposition survey. Daniel Kroes et al. found that an estimated 326,000 cubic yards of dense soil were scoured away immediately downstream of the structure. The scoured soil became approximately 571,000 cubic yards of loose sediment and was deposited at least 30 miles from the MCS. If sediment that was deposited in the forebay and the sediment that came through the structure are included, the deposited sediment could be as high as 2 million cubic yards.

USACE's Engineering & Research Development Center (ERDC) was asked to perform an investigational study using a physical model as it is better than the numerical model for this type of rehabilitation experiment. After 18 months of repair and construction, successfully completed in March 2014, the MCS is now ready and capable of passing the project flood.

Based on ERDC's modeled results, three principle reasons caused the 2011 MCS tailbay scouring: (1) little to no tailwater immediately behind the structure (2) benchmarked headwater stage had been increased since the structure was constructed in 1954 and (3) only some of the 125 gates were used to pass the flood waters.

Lessons learned from both 1973 and 2011 operations and ERDC's physical model experiment are that tailwater conditions are critical for the stilling basin design and energy dissipation calculation, operation needs to be maintained no more than the maximum headwater design stage, and gate operations are extremely important to minimize and prevent tailbay scour.

INTRODUCTION

Completed in February 1954, the Morganza Control Structure (MCS) is a very unique Mississippi River flow diversion structure. The MCS forebay and the Mississippi River are separated by a three-mile long potato ridge. The waters of the Mississippi River can flood the MCS forebay when the stage is above elevation 43.0 feet NGVD29. When the forebay stage reaches 56.0 feet design height, the MCS is capable of diverting 600,000 cfs water.

The structure has 125 gate bays and is 3,906 feet long. Each gate bay has a crest weir with a top elevation of 37.5 feet NGVD29, and on top of the crest weir is a two-leaf (upper and lower panel) gate. According to the current MCS water control manual, a gate shall be either fully opened or closed to divert sufficient floodwater from the Mississippi River to avoid unacceptable stress along the main stem of the Mississippi River. At the toe of the weir's downfall, there are two rows of baffle blocks installed on the stilling basin floor to dissipate the energy of the floodwaters passing through the structure. The floor and end-sill wall of the 86 feet long stilling basin is at elevation 29.0 and 32.0 feet NAVD29, respectively. Behind the end-sill wall, there is an 80 feet long extended derrick stone apron installed parallel to the structure as shown in Figure 1.

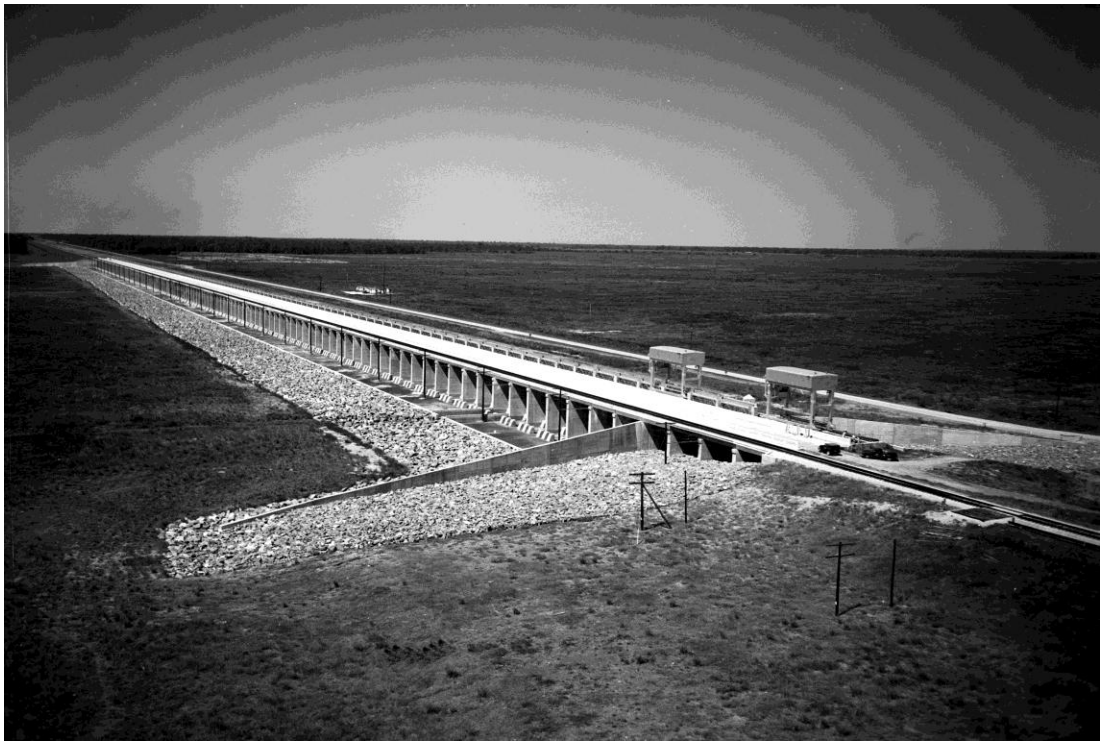

Figure 1 The Morganza Control Structure (MCS) in 1954

The operation of the MCS is based on a Mississippi River and Tributaries flood damage risk reduction feature called "Project Flood" to prevent riverine flood stages from (1) exceeding the approved flow line, i.e. encroachment on freeboard requirements, (2) limiting flows to design discharge of 1,500,000 cfs between MCS and Bonnet Carre Spillway, and (3) limiting flow below the Bonnet Carre Spillway to the design flow of 1,250,000 cfs.

1973 OPERATION

Since completion, the MCS has been used to divert the flood water twice. The first operation was started on April 17, 1973. The operation was not triggered by the Mississippi River flow rate, but by the vulnerability of the Atchafalaya River primary diversion facility, the Old River Control Structure. At the peak stage, 46.0 feet, approximately 210,000 cfs were diverted by the MCS. The 1973 diversion caused significant scour at the MCS tailbay. As a remedy to protect the MCS tailbay from future scour, a reinforced concrete plunge pool was built in 1977 as shown in Figure 2.

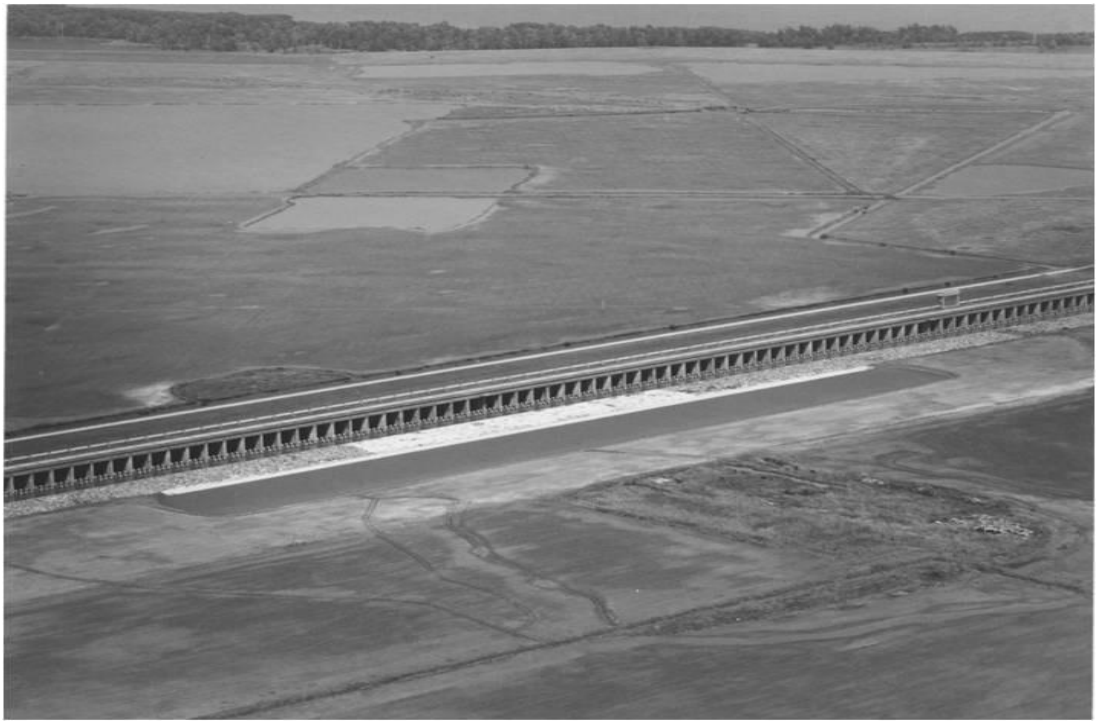

Figure 2 The MCS with Plunge Pool in 1976

The pool is located downstream of the derrick stone apron, between Gates 42 and 86, which had a Vertical (V)/Horizontal (H) =1/10 concrete paved front slope and a V/H=1/4 back slope. The plunge pool bottom was partially lined with concrete and riprap with a bottom elevation of 19.0 feet NGVD29. The horizontal distances of concrete and riprap varied from 90 feet to 110 feet and 10 feet to 30 feet, respectively. The front and back slopes met with ground elevations at 31.0 feet and 32.0 feet NGVD29, respectively. The repair made in 1977 was believed to be sufficient in preventing future scour.

2011 SCOUR DAMAGES

The second operation was started on May 15, 2011. While the operation in 2011 was successful, significant scour occurred which promulgated even further downstream. During the 2011 flood

fight, even though the highest forebay stage was 59.6 feet, the maximum diversion flow rate was only 185,000 cfs because fewer gates were used in 2011 than in 1977.

Severe scour located downstream of the MCS was observed by the operation manager on May 16, 2011 because scour indicators embedded five feet below the ground were missing. Since the MCS could be vulnerable if scour holes extended back toward the structure, a survey was immediately ordered to investigate the scour development at the MCS tailbay.

Six multi-beam surveys were performed between May 17 and June 6, 2011 to monitor the scour development. They were May 17, 2011; May 18, 2011 (plunge pool south only); May 19, 2011 (plunge pool only); May 20, 2011, May 26, 2011 (no plunge pool); and June 6, 2011. Each survey showed new scour holes and the development of original findings. The most severe areas were at the vicinity of the plunge pool downstream, which were approximately 30 feet lower than their original elevations. The scour development was obtained by using the "Fledermaus" program to compute and plot ground elevation changes between surveys. Scour damage that developed between June 6, 2011 & May 17, 2011 is presented in Figure 3. Major scour that developed between two referenced dates were downstream of the plunge pool, especially at areas located at two extruded corners, which were close to 27.5 feet in difference.

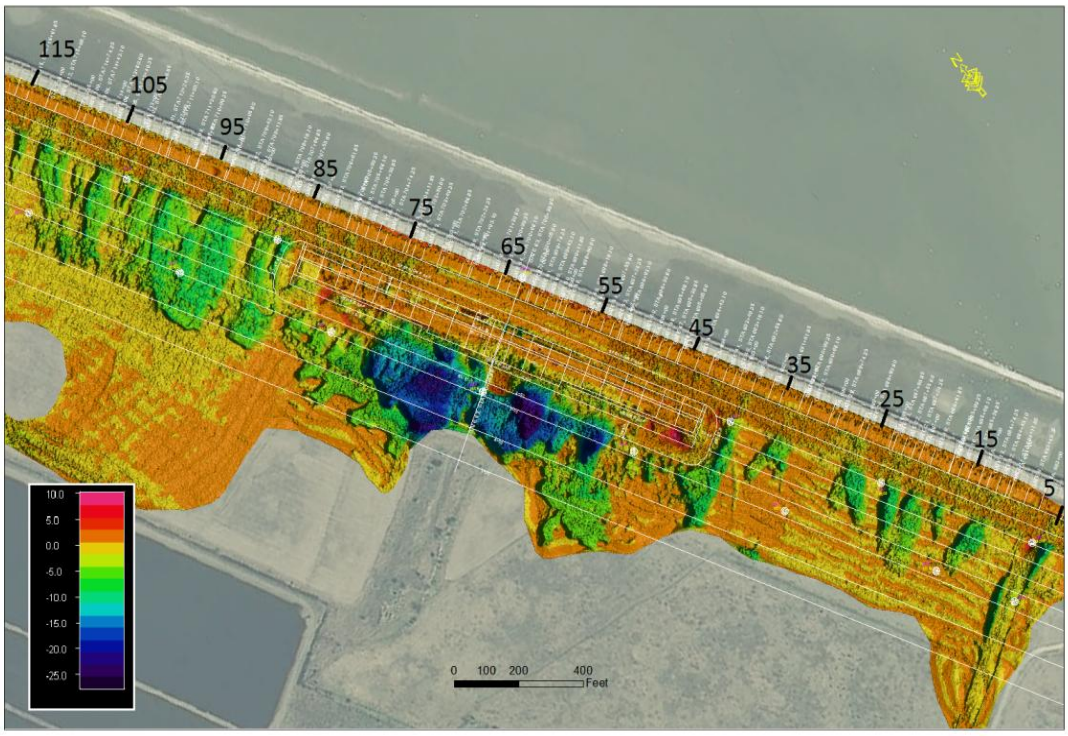

Figure 3 Scour Damage Developed between June 6, 2011 & May 17, 2011

Scour damage that developed between June 6, 2011 & May 18, 2011 (south plunge pool only) are presented in Figure 4. Major scours developed between two referenced dates remained downstream of the plunge pool, especially at areas located at two extruded corners. It seems like there was not much scour development from May 17, 2011 to May 18, 2011.

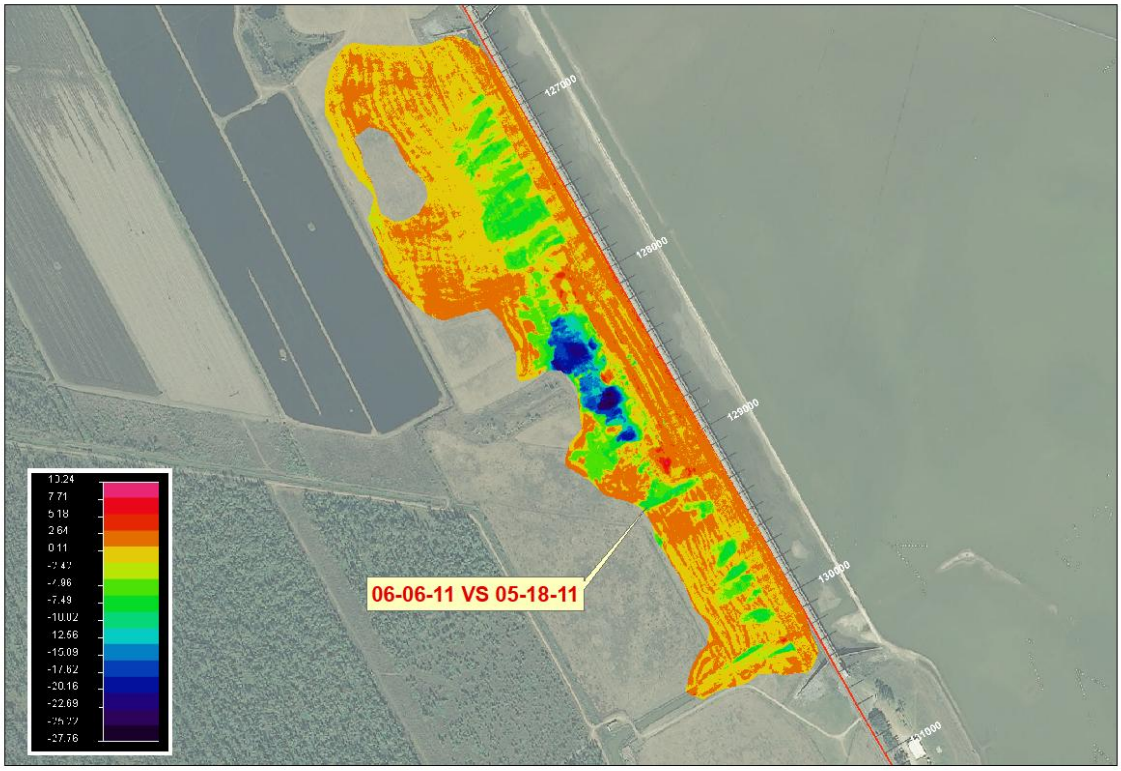

Figure 4 Scour Damage Developed between June 6, 2011 & May 18, 2011

Contours plotted according to May 17, 2011 survey, and scour (elevation difference) contours that developed between May 20, 2011 and May 17, 2011; May 26, 2011 and May 20, 2011; as well as June 06, 2011 and May 26, 2011 are presented in Figure 5. Survey results concluded that the tailbay terrain was changing continuously while the MCS was in operation. All surveys showed that major scour areas were downstream of the plunge pool, especially at areas located near two extruded corners.

The multibeam survey performed on June 6, 2011 showed that scour holes were created at almost all of the tailbay for a distance as far as 600 feet away from the structure. The worst scour area was at the immediate downstream of the plunge pool, which had elevations lower than 10 feet NAVD88. At the plunge pool's two extruded corners, elevations were close to 3 feet NAVD88, which mean approximately 30 feet of ground earth was scoured away from its location. Presented in Figure 6 is the survey performed on June 6, 2011.

The generated scour maps helped tremendously with gate operation exercise during the 2011 operation. Since the MCS middle gates faced plunge pool, the 2011 flood fight used middle gates more frequently. The MCS gate opening frequencies during the 2011 flood fight are presented in Figure 7.

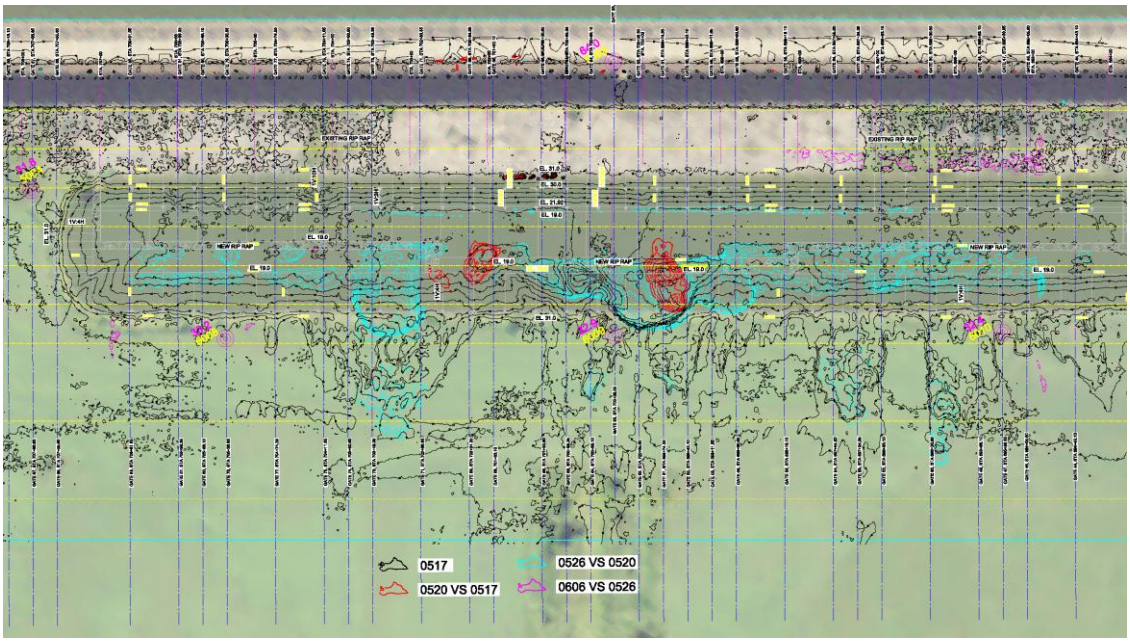

Figure 5 Scour Damage Developed between Two Adjacent Surveys

Figure 6 Multibeam Survey Performed on June 6, 2011

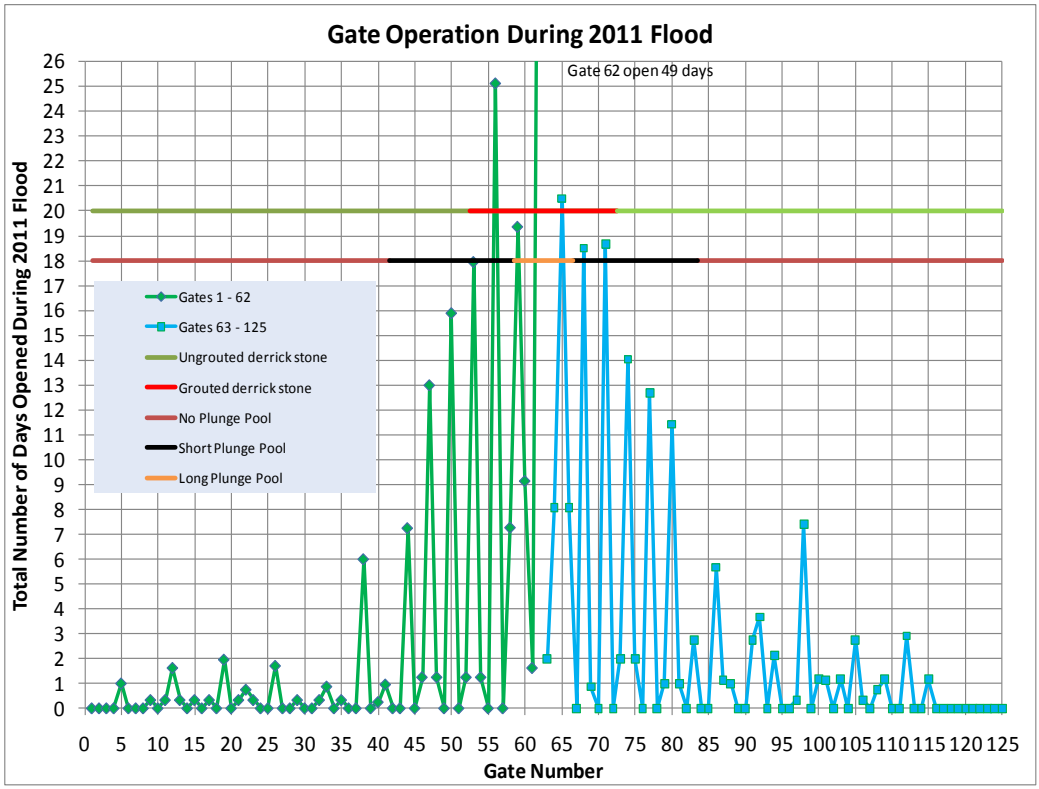

Figure 7 MCS Gate Opening Frequencies during the 2011 Flood Fight

2012 TERRESTRIAL LIDAR SURVEY

In April 2012, the U.S. Army Corps of Engineers (USACE) New Orleans District (MVN) un-watered the scour holes to inspect the undermining damage to the concrete slab at the bottom of the plunge pool and to perform a topographic survey. Figure 8 depicts the scour profile plotted downstream of each operated gate bay. Assuming no further development after the last dated 2011 operation, July 7, 2011, the tailbay contour should be the same as a June 23, 2012 Terrestrial LiDAR survey. The MCS tailbay scour development from June 6, 2011 to the last date of operation is presented at Figure 9. After June 6, 2001 operation scour damages were 2 feet or less, with the exception of a few small areas.

After the plunge pool was un-watered, scour damages can be found as shown in Figures 10 and 11. Several rocks as heavy as 6,000 pounds were carried away from the derrick stone apron. Some were carried away as far as 600 feet downstream on top of a rising hill. Nine out of 15 MCS tailbay buoys were missing after the 2011 operation.

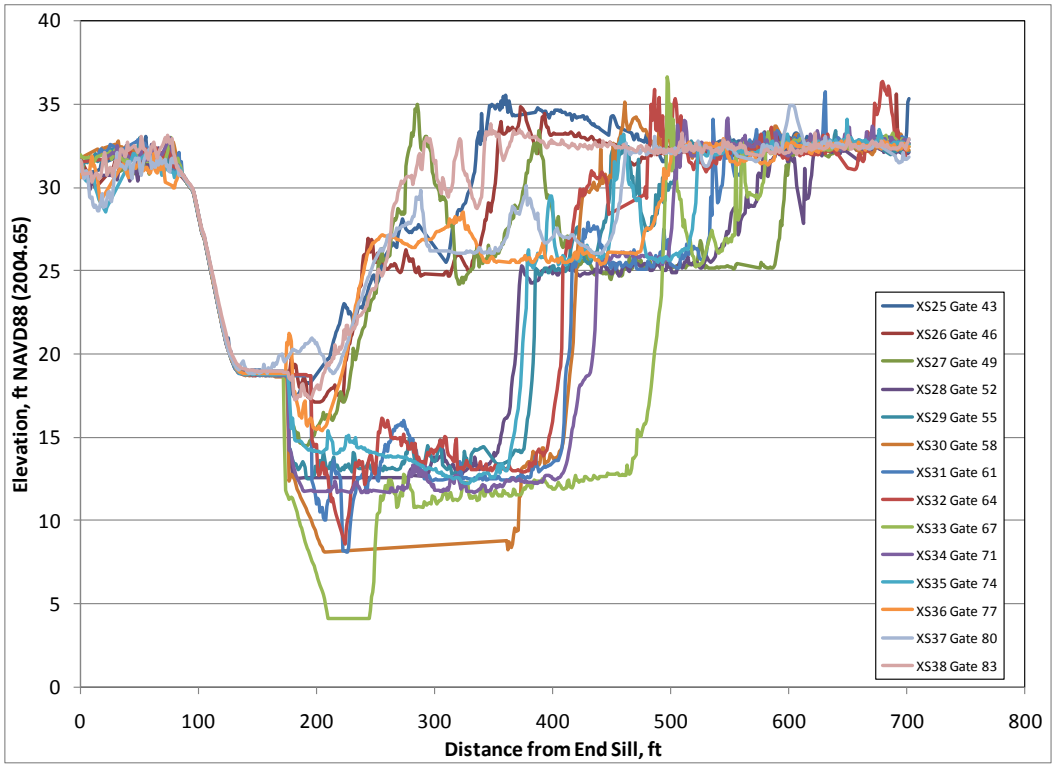

Figure 8 Scour Profile Downstream of Each Operated Gate Bay

Figure 9 Scour Damage Developed between June 6, 2011 & End of Operation

Figure 10 Scoured MCS Tailbay after 2011 Operation

Figure 11 Scour Holes Downstream of the Plunge Pool's Extruded Corners

MCS TAILBAY REPAIR

USACE's Engineering & Research Development Center (ERDC) was asked to perform an investigational study using a physical model as it is better than the numerical model for this type of rehabilitation experiment. The investigation had four specific purposes: (1) to develop a scour protection plan for the plunge pool gate bays (2) to develop a scour protection plan for the non-plunge pool gate bays (3) to update the 1951 discharge rating curve to include a higher headwater, actual crest design, and actual pier design information and (4) to use the study findings to update the MCS gate operation sequence to reduce/eliminate the scour damage seen in 1973 and 2011.

To meet the primary project goal of having the MCS fully repaired by the 2014 flood season, the construction phase of the repair work was executed by the New Orleans District (MVN) in three consecutive phases, each occurring upon completion of its respective physical model experiment. The repair and construction materials (mainly riprap stone) were hauled from pre-approved quarries along the upper Mississippi River via barges to an off loading site along the west bank of the Mississippi River near the town of Morganza. The material strength, stability, slopes and protection of critical sections replicated the conditions tested by the model. After 18 months of repair and construction, successfully completed in March 2014, the MCS is now ready and capable of passing the project flood.

Presented in Figure 12 is a MCS physical model in 1:22 scale. A MCS physical model with plunge pool experiment is presented in Figure 13.

Figure 12 MCS Physical Model in 1:22 Scale

Figure 13 MCS Physical Model with Plunge Pool Experiment

SEDIMENT DEPOSITION AFTER 2011 OPERATION

In May 2011, USGS performed a preliminary sediment deposition survey. Daniel Kroes et al. (2014) found that an estimated 326,000 cubic yards of dense soil were scoured away immediately downstream of the structure. The scoured soil became approximately 571,000 cubic yards of loose sediment and was deposited at least 30 miles from the MCS. If sediment that was deposited in the forebay and the sediment that came through the structure are included, the deposited sediment could be as high as 2 million cubic yards.

An estimated sediment distribution caused by the 2011 operation is presented in Figure 14.

CONCLUSIONS

Based on ERDC's modeled results, three principle reasons caused the 2011 MCS tailbay scouring: (1) little to no tailwater immediately behind the structure (2) benchmarked headwater stage had been increased since the structure was constructed in 1954 and (3) only some of the 125 gates were used to pass the flood waters.

Lessons learned from both 1973 and 2011 operations and ERDC's physical model experiment are that tailwater conditions are critical for the stilling basin design and energy dissipation calculation, operation needs to be maintained no more than the maximum headwater design stage, and gate operations are extremely important to minimize and prevent tailbay scour.

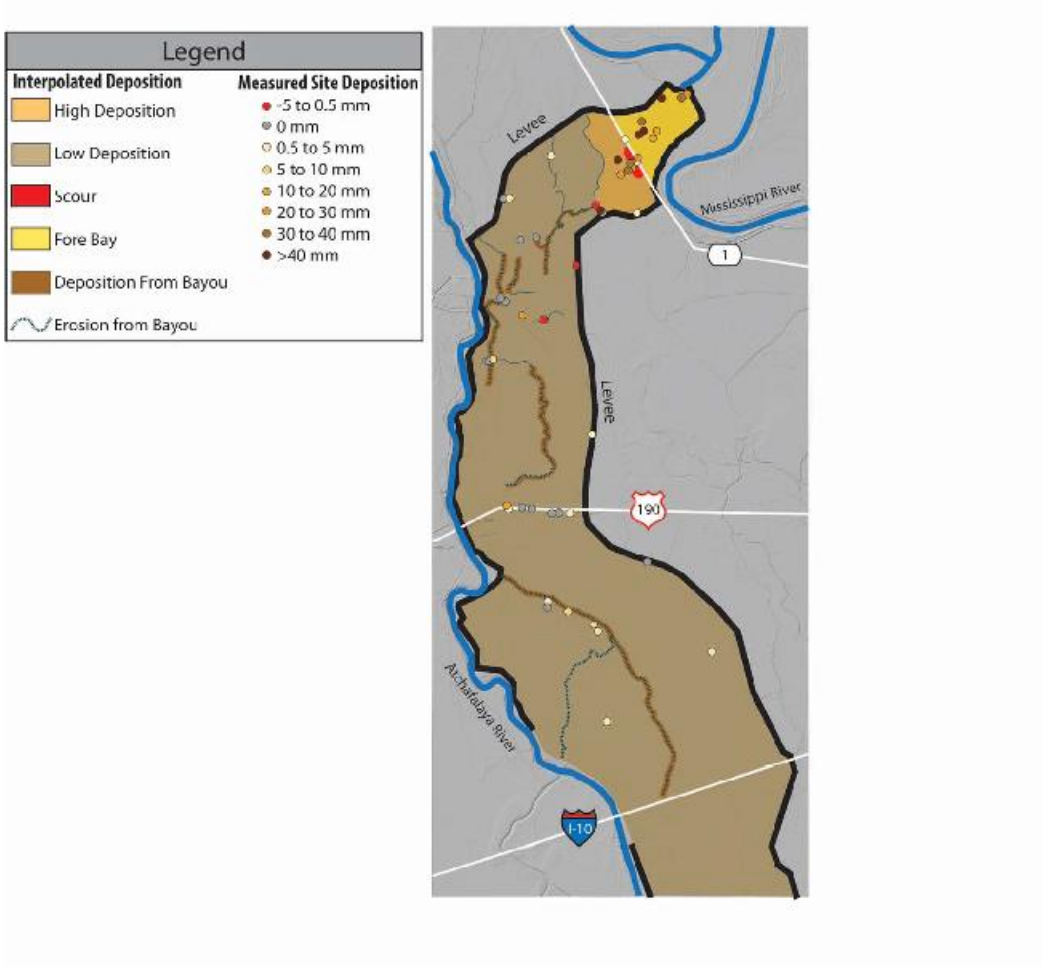

Figure 14 Estimated Sediment Depositions after 2011 Operation (by Daniel Kroes of USGS)

ACKNOWLEDGMENTS

Authors want to acknowledge the following agencies and people who encouraged and supported the scour investigation, making the MCS floodway rehabilitation possible: HQUSACE, MRC, MVD, MVN, MVK, ERDC (especially Dr. Steve Maynord), USGS, MCS Tailbay Rehabilitation project PDT members, and many others.

REFERENCES

Kroes, D., and Schenk, E., et al. (2014). Sediment and Nutrient Trapping as a Result of a Mississippi River Diversion: the Morganza Spillway during the 2011 Mississippi River Flood (Article Submitted to Ecological Engineering for Peer Review). U.S. Geological Survey. Baton Rouge, Louisiana.

AN APPROXIMATION OF THE SEDIMENT BUDGET FOR THE TOMBIGBEE RIVER AND THE MOBILE RIVER BASINS

John J. Ramírez-Avila, Assistant Research Professor, Civil and Environmental Engineering Department, Mississippi State University, Mississippi State, MS, jjr149@cee.msstate.edu; William McAnally, Emeritus Professor, Mississippi State University, Mississippi State, MS, McAnally@ngi.msstate.edu; Sandra L. Ortega-Achury, Research Associate, Civil and Environmental Engineering Department, Mississippi State University, Mississippi State, MS, sandraortega@cee.msstate.edu

ABSTRACT

A sediment budget is an accounting of the sources and disposition of sediment as it travels from its point of origin to its eventual exit from a drainage basin. Sediment budgets are important in defining the dynamic behavior of a river system. The Mobile River Basin covers two thirds of the state of Alabama and portions of Mississippi, Georgia, and Tennessee. It is the fourth largest basin in the United States in terms of flow volume and is the sixth largest river system in the U.S. in terms of area. The lower Mobile Bay is a designated national estuary under the EPA's National Estuary Program. The Mobile Bay and the rivers draining into it support major uses with national implications which include the Tennessee-Tombigbee Waterway, the Port of Alabama, various commercial fisheries, large industry, tourism and recreation, and abundant development. Surface water in the Tombigbee River and Mobile River Basins generally meet Federal and State drinking water standards and guidelines for protection of aquatic life. However, water quality conditions along both river basins have been reported to be adversely affected by urban and agricultural activities, as indicated by elevated concentrations of sediments, nutrients, pesticides, and other organic compounds and biological communities commonly exhibit signs of environmental stress. A study was performed to develop a sediment budget for the Tombigbee River Basin and the Mobile River Basin. A two tier analysis was developed to determine the annual sediment changes along the Tombigbee River Basin and the Mobile River Basin. Results indicate that important sedimentation processes are occurring on the impoundments distributed along the Tombigbee River Basin and the Alabama River Basin, which receives waters from the Cahaba River, Coosa River, and Tallapoosa River. Higher rates of sediment along the lower part of the Tombigbee River Basin could be related to the occurrence of river bank instability processes between the Demopolis and the Coffeeville Dams on the Tennessee-Tombigbee Waterway. Total sediment loads at the entrance of the Mobile River ranged from 0.8 to 18.75 Mg yr^{-1}. Changes on morphological and hydrodynamic processes below the diversion of the Mobile River in two distributaries can be favoring sedimentation processes along the lower part of the basin and the Mobile Bay. Assessment of a sediment budget in the Mobile River Basin is important to increase the scientific understanding of sediment behavior and distribution within the basin, as important factors that influence water quality trough the basin itself, the Mobile Bay and the Gulf of Mexico.

INTRODUCTION

A sediment budget is an accounting of the sources and disposition of sediment as it travels from its point of origin to its eventual exit from a drainage basin (Stream Systems Technology Center, 2004). Sediment budgets are important in defining the dynamic behavior of a river system (Sharp, 2007). Knowledge of stream and watershed characteristics is important for understanding natural processes and problems associated with watershed management and stream restoration. Sediment production and deposition have been linked to variations in fluvial sediment transport. In many lowland rivers, a major part of sediment is transported in suspension.

The Mobile River is the sixth largest river basin in the United States and the fourth largest in terms of flow (Figure 1). The water resources on the Mobile River Basin (MRB) are influenced by an array of

natural and cultural factors, which impart unique and variable qualities to the streams, rivers, and aquifers and provide abundant habitat to sustain the diverse aquatic life in the basin (McPherson et al., 2003). Surface water in the Mobile River Basin generally meets Federal and State drinking water standards and guidelines for protection of aquatic life. However, water quality conditions are adversely affected by urban and agricultural activities, as indicated by elevated concentrations of nutrients, pesticides, and other organic compounds, and biological communities commonly exhibit signs of environmental stress (Atkins et al., 2004). Approximately 70% of the MRB is covered by forest and silviculture is the largest industry. Logging and other silviculture activities can significantly contribute high rates of sediment from erosion and runoff.

Assessment of a sediment budget in the MRB is important to increase the scientific understanding of sediment behavior and distribution within the basin as important factors that influence water quality trough the basin itself, the Mobile Bay and the Gulf of Mexico. A study was conducted to provide an estimate of sediment inflows, outflows and deposition along different sites within the Tombigbee River Basin (TRB) and the Mobile River Basin (MRB). Results from the two tier analysis approach considered to determine the annual sediment changes along the Tombigbee River Basin and the Mobile River Basin are reported.

Description of the Study Area

The MRB encompasses 113,185 km^2 along the states of Mississippi, Alabama, Tennessee and Georgia (Figure 1A). The western part of this basin, which is the sixth largest river basin in the United States, is comprised of the TRB (35,674 km^2) and the Black Warrior River (BWR - 16,280 km^2). The eastern MRB is drained by the Alabama River (ARB- 58,726 km^2) which receives waters from the Cahaba River, Coosa River, and Tallapoosa River. The Mobile River is formed by the confluence of the Alabama and Tombigbee Rivers, near Vermont, AL. Downstream from the confluence, the Mobile River flows about 48 km to the south before splitting into several distributaries (Johnson et al., 2002). After flowing across a deltaic plain, these distributaries discharge into the Mobile Bay, which discharges into the Gulf of Mexico (Figure 1B).

The mean annual flow in the MRB is about 1760 $m^3 s^{-1}$. The Alabama and Tombigbee Rivers contribute about 52 and 48% of the flow, respectively (Atkins et al., 2004). Mean annual runoff and precipitation generally are uniform throughout the MRB, with a highest precipitation amount typically occurring in the northeast part and southern area of the basin. Streamflow in the MRB is highly regulated by upstream impoundments. Around 1,020 km^2 of impoundments are extended along the entire basin, some of them constructed for hydroelectric generation and flood control purposes; other series of navigable impoundments were created by completion of the Tennessee Tombigbee Waterway to connect the MRB with the Tennessee River drainage in northeast Mississippi. As a result of this regulation, natural season flow patterns in these tributaries have been altered, with moderated peaks and low flows downstream from the impoundments. Water quality is affected by sediment and nutrients that are trapped in the impoundments and contribute to eutrophication, algal blooms, low oxygen levels and fish killing (Atkins et al., 2004).

Water quality agencies have identified numerous causes and sources of surface water impairment in the MRB. The complex combination of natural (e.g. physiography, geology, soils, climate, hydrology and ecology) and human factors (e.g. built impoundments, land use changes, mining) within the MRB are considered the principal influences on water quality (Johnson et al., 2002).

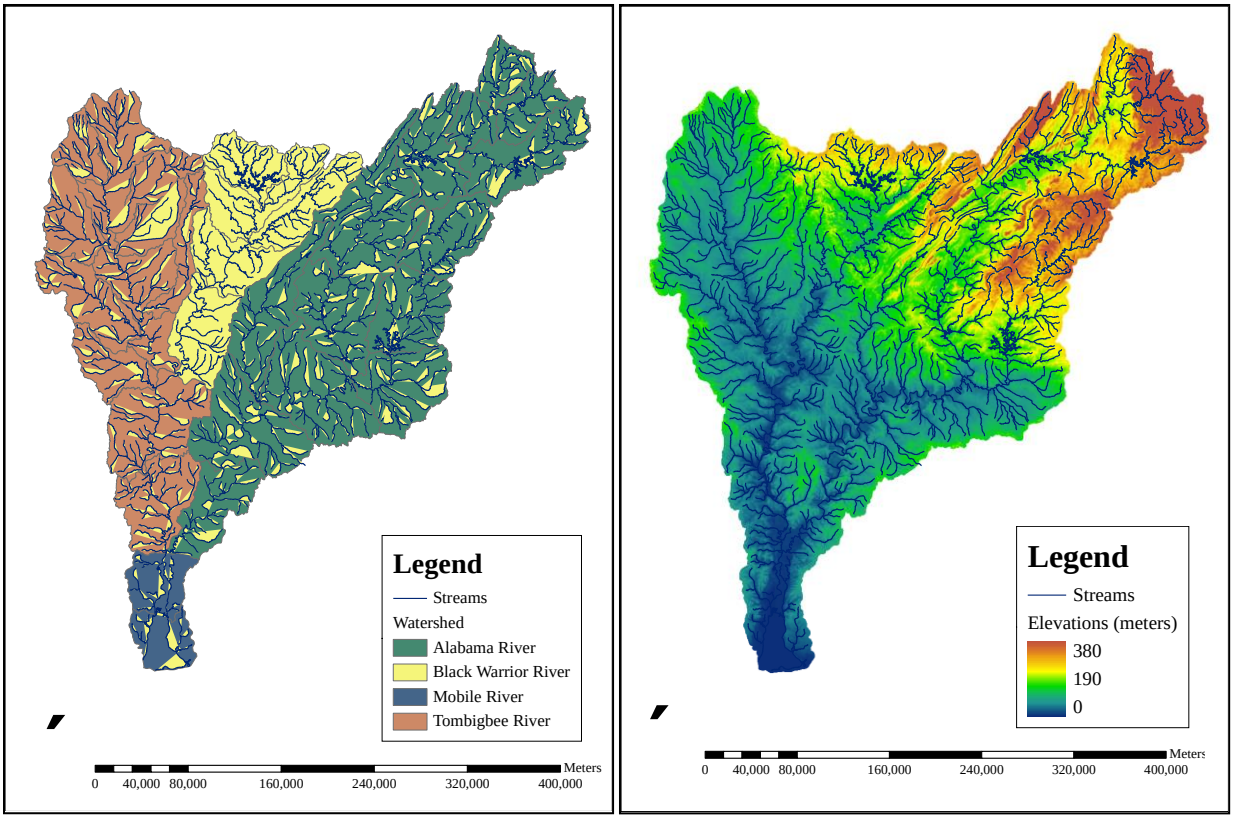

Figure 1. A) Mobile River Basin and principal Subbasins B) Topography in the Mobile River Basin.

METHODS

The development of the sediment budget for the TRB and the MRB included the application of a two tiered analysis, based on the proposed sediment budget template developed by Sharp (2007). Initially, data from USGS stations within the MRB in the form of suspended sediment concentrations, suspended sediment loads, instantaneous flow, daily average flow and peak flow were collected. All available data from 1975 to 2010 for all the USGS gauging stations involved in the present study were used. Table 1 presents the USGS stations where data were collected.

All the USGS stations within the Upper Tombigbee River (HUC 03160101), the Middle Tombigbee River (HUC 03160106) and the Middle Tombigbee River-Chickasaw (HUC 03160201) subbasins were evaluated to provide an estimate of sediment inflows, outflows and deposition in the TRB (Figure 2). Results of the sediment budget developed by Sharp (2007) for the Aberdeen Pool were setup as the initial sediment load input for the upper subbasin (HUC 03160101). The sediment load at the outlet of each subbasin was considered as the total sediment load entering the next segment downstream. USGS stations within the same subbasin but not located on the Tombigbee River were used to determine the contribution of flow and sediment loads from tributary watersheds. The entire sediment load of a tributary watershed considered both, accounted and unaccounted areas. The upstream section within a watershed or subbasin contributing at the location of a USGS station was part of the accounted area. The section between the location of a USGS station and the mouth of the watershed, the outlet of a subbasin or a specific location within a subbasin (e.g. entrance of a lake) was considered as the unaccounted area. The sediment load of the accounted area of a watershed or subbasin was divided by its extension providing calculations of mean daily (Mg d^{-1} km^2) or mean annual (Mg yr^{-1} km^2) sediment yield for Tier 1 and Tier 2, respectively.

The unaccounted area of a subbasin or a tributary watershed was considered to have similar sediment yield than the sediment yield observed at the upstream area contributing to a USGS station.

A sediment rating curve (expressed as Equation 1), which represents the relationship between suspended sediment discharges (Q_s) and the stream or river flow (Q), was developed for the entire dataset within a specific subbasin. The development of the sediment rating curves were the base of both of the tiered analyses, and were used to determine the sediment load generated by each tributary watershed, subbasin or upstream area contributing to a lake.

$$\mathbf{Q_s = aQ^b} \qquad \text{Equation 1}$$

where
Q_s is the suspended sediment discharge (Mg d^{-1}), Q is the observed instantaneous flow (m^3 s^{-1}), and *a* and *b* are regression parameters.

The Tier 1 analysis implements basic principles to create an initial sediment budget by determining suspended sediment (SS) loads and yields at the magnitude of the effective discharge, also known as bankfull discharge ($Q_{1.5}$). A flow frequency distribution was generated from the annual maximum peak flow series at each USGS station by using the model PKFQWin (Version 5.2). The $Q_{1.5}$ was calculated from the generated flow frequency distribution (Figure 3, annual exceedance probability=0.6667).

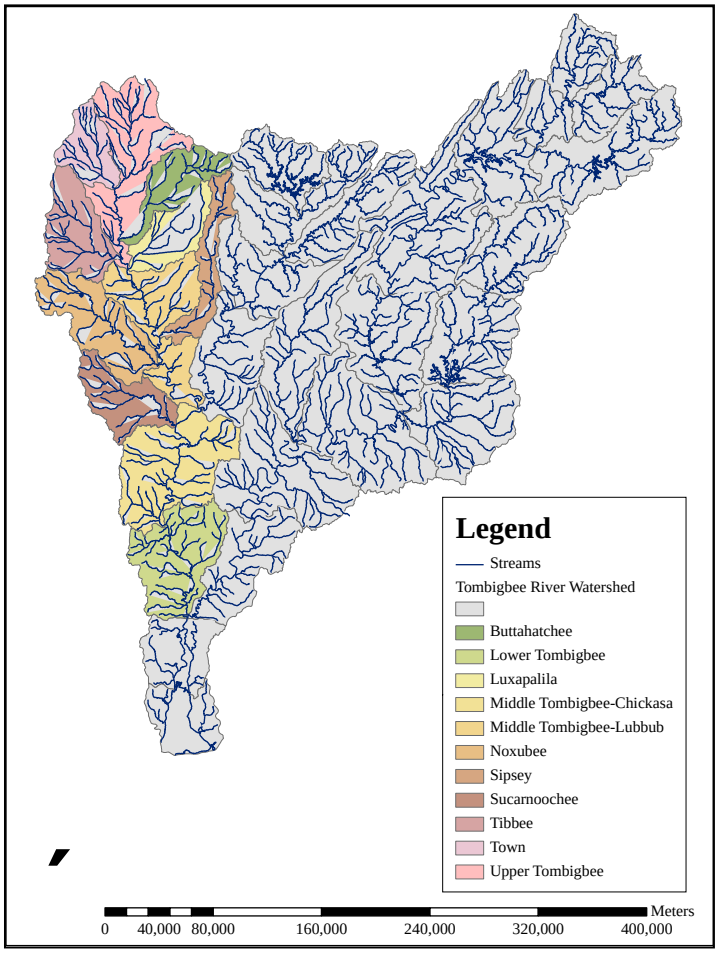

Figure 2. Tombigbee River Basin and subbasins

The SS load and daily SS yield at the $Q_{1.5}$ was obtained for each USGS station by using the sediment rating curve developed for each subbasin. Changes on sediment load (erosion or deposition) caused by the presence of an impoundment (e.g. lake) were evaluated by determining a sediment mass balance, which determines amounts of sediment entering the lake, dredging and sediment loadings from the lake.

Tier 2 analysis is a second stage where annual sediment discharges for each station are estimated using its mean daily flow data series. For this study, flow data series ranged from 1974 to 2010, when available. The sediment rating equation of each site was used to calculate mean daily SS load values (Mg d^{-1}) from the mean daily flow (m^3 s^{-1}). The mean daily SS loads were added for each complete calendar year to provide an annual SS load (Mg yr^{-1}). A mean annual SS load was generated by averaging annual sediment loads from 1974 to 2010. Once each station has a calculated annual SS load, a SS yield (Mg yr^{-1} km^2) was estimated for the contributing area where each station was located. Ungaged areas located downstream of a USGS station were considered to have similar sediment yield that gaged areas, when both areas were located within the same hydrologic unit (watershed) and flow was not routed through a downstream impoundment (dam).

The Tier 2 considers bed load as a percentage of the SS load. The bed load can be estimated as the 20% of the SS load for locations without the presence of an impoundment, or locations representing the influent of an impoundment. A lower value of 5% can be considered to calculate effluent flows from any impoundment in this study.

More extended and detailed information about the conceptualization and methodology used to develop a tiered sediment budget analysis is described by Sharp (2007) and Ramirez-Avila (2011).

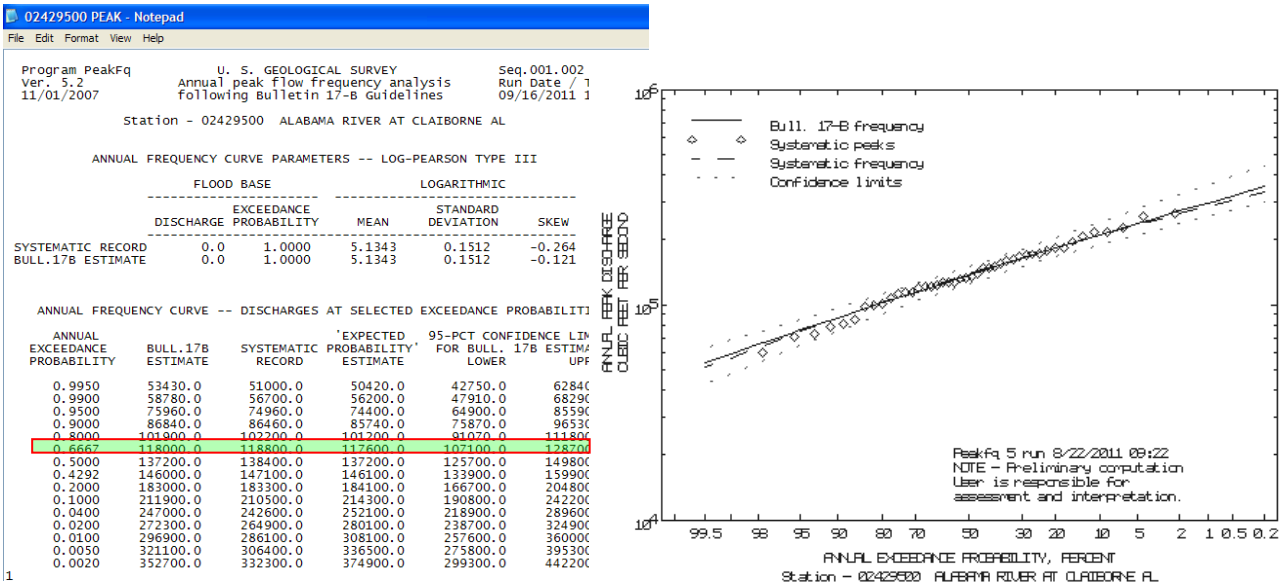

Figure 3. Output file and plot of a flow frequency distribution generated by PKQWin (Ver. 5.2) for USGS stations

Table 1. USGS stations used to determine the sediment budget for the Tombigbee River Basin and the Mobile River Basin

River	Station	Type	Information
Tombigbee River	02437100 & 02437500	M	Tombigbee River at Aberdeen, MS
	02439400	T	Buttahatchee River nr Aberdeen, MS
	02441000	T	Tibbee Creek nr Tibbee, MS
	02443500	T	Luxapallila Creek nr Columbus, MS
	02444160 & 02444161	M	Tombigbee River below Bevil L&D nr Pickensville, AL.
	02444490	T	Bogue Chitto Creek near Memphis, AL
	02444500	M	Tombigbee River nr Cochrane, AL
	02446500	T	Sipsey River nr Elrod, AL
	02447025 & 02447026	M	Tombigbee River below Heflin L&D nr Gainesville, AL
	02448000	T	Noxubee River at Macon, MS
	02467000		Tombigbee River at Demopolis L&D nr Coatopa, AL
	02467500[1]	T	Sucarnoochee River at Livingston, AL
	02469525	M	Tombigbee River nr Nanafalia, AL
	02469761	M	Tombigbee River below Coffeeville L&D nr Coffeeville, AL
Black Warrior River	02462501	M	Black Warrior River below Bankhead L&D nr Bessemer, AL
	02465000	M	Black Warrior River at Northport, AL
	02466030 & 02466031	M	Black Warrior River at Selden L&D nr Eutaw, AL
Coosawattee River	02380500	T	Coosawattee River nr Ellijay, GA
	02383500	T	Coosawattee River nr Pine Chapel, GA
	02387500	M	Oostanaula River at Resaca, GA
Alabama River	02420000	M	Alabama River nr Montgomery, AL
	02423000	M	Alabama River at Selma, AL
	02428400, 02428401 & 02429500	M	Alabama River at Claiborne, AL
Mobile River	02470500[2]	M	Mobile River at Mt Vernon, AL
	02470629	D	Mobile River at River Mile 31.0 at Bucks, AL
	02471019	D	Tensaw River nr Mt Vernon, AL

RESULTS

Annual sediment loads and yields were calculated based on a two tiered analysis for each USGS station within the TRB, the BWR and the lower Alabama-Coosa-Tallapoosa River Basin (ACT) with enough available sediment and flow dataset. The annual SS load estimations based on the Tier 1 and Tier 2 analyses for four subbasins within the TRB and for the outlets of the BWR and the lower ARB are presented in Tables 2 and 3.

Calculated deposition rates at the Columbus Lake were 10.2 and 3.4 millions Mg yr^{-1} of sediment using the Tier 1 and Tier 2, respectively. The Tier 1 deposition rate for the Aliceville Lake was 407,200 Mg yr^{-1} while the Tier 2 estimation described that the system is balanced when no dredging is performed. For the mass balance estimations reported dredging rates of 100,000 Mg yr^{-1} and 127,000 Mg yr^{-1} (McAnally et al., 2004) were considered for the Columbus and Aliceville Lake, respectively.

The sediment load from the BWR, a mixed land use basin, represented only 9% of the sediment load entering to the Mobile River. The relatively low sediment load from this area reflected the influence of impoundments upstream of the subbasin's outlet. Similar observations in the reduction of sediment loads from this subbasin were reported by McPherson et al. (2003).

For both methods of analysis, the Middle Tombigbee River-Chickasaw was the subbasin with the higher annual sediment yield (Mg km^{-2} yr^{-1}) within the TRB. Two important structures (Demopolis and Coffeeville Locks and Dams) are located within this subbasin, which could be the key to explain the significant increase in sediment loads occurred between the inlet and the outlet of this area. According to Bankhead et al., (2008) a considerable amount of widening (up to 85 m between 1974 and 2003) has occurred along the length of the Tombigbee River within this subbasin. During their research, areas of high bank erosion were more commonly observed in certain locations with a spatial trend being seen between the dams established in this subbasin. Downstream of Demopolis Dam bank erosion rates were low, but increased up to 3 m yr^{-1} along the following 48 km from the dam. Downstream of this length, trends of bank erosion decreased towards Coffeeville Dam, with bank erosion increasing again a few kilometers upstream of the dam. Below Coffeeville Dam, bank erosion rates were high, and then decreased downstream along the following 64 km.

The annual SS load entering the Mobile River after the junction of the Tombigbee/Warrior system with the Alabama River just north of the city of Mobile, AL was estimated as 34 million of Mg and 5.4 million of Mg for the Tier 1 analysis and Tier 2 analysis, respectively. Downstream from the confluence, the Mobile River flows about 48 km to the south before splitting into the Tensaw River and the Mobile River. A USGS station is located on each branch few kilometers after the diversion. The observed reduction in the cumulated magnitude of the SS load for both Tier analyses (Tables 2 and 3) was evidenced after estimating the individual load on each station. This reduction (deposition) can be caused by the individual occurrence or the combination of three factors: i) the changes on flow velocity caused by the diversion of the Mobile River; ii) the minimum change of channel slope and the meandering path of the branches from the diversion to their outlet into the Mobile Bay; and iii) the probable deposition on areas along the deltaic plain during high flow events.

The extension of the entire ACT represented the 53.1% of the total area contributing to the Mobile River; however, in both analyses the SS load contribution from this basin was 1.8 times smaller than the SS loaded by the Tombigbee/Warrior system. The observed lower sediment loads along the ACT could be attributed to the presence of a significant number of highly regulated impoundments constructed for hydroelectric generation and flood control processes.

For each tiered analysis, a linear relationship between the area of the watersheds and subbasins within the TRB and the BWR and the estimated SS load was determined (Figures 4 and 5). The best fitting observed when using the Tier 1 for estimations can be explained because the SS load variability depends only from the magnitude of the bankfull discharge ($Q_{1.5}$) after being determined a unique rating curve for each subbasin. For sediment load estimations based on the Tier 2, the change in the mean daily flow on each station along the different years the rating curve was routed (generally from 1974 to 2010) was the factor that affected the reduction in the linear fitting of the dataset.

Although the Tier 2 analysis used the same USGS flow gages that the Tier 1 analysis, the use of daily flow events provides a closer approximation to the natural flow conditions (Sharp, 2007). The occurrence of flows similar to or higher than the bankfull discharge is different for each watershed and subbasin. In the performance of an ongoing study, the same authors of this study found that flows with magnitude similar to, or above the bankfull discharge represented only the 15% of the entire flow records for the Buttahatchie River in Mississippi. This condition determines that the application of the Tier 1 generates a significant overprediction of the rate of sediment yield by a specific watershed and/or sediment deposited on specific locations (e.g. Columbus Lake on this study), and further analysis is necessary to perform a more accurate estimation of sediment loads when limited flow data is available.

Considering the application of the Tier 2 as the more accurate method to determine the sediment flux along the different watersheds and subbasins into the MRB, a total sediment load ranging from 0.8 to 18.75 million Mg yr^{-1} is expected to enter the Mobile River after the junction of the Alabama and the Tombigbee Rivers (Table 4). Further analysis is needed to determine the rate of reduction of the SS load and the total load of sediment along the distributaries below the Mobile River diversion. When comparing the similar range of dates (2004 to 2010) between the loads at the entrance of the Mobile River and the distributaries the trend to reduce the magnitude of the loads is consistent.

Table 2. Estimation of annual suspended sediment load for different subbasins within the Mobile River Basin based on Tier 1

Subbasin	Drainage Area* (km^2)	Area Contribution (%)	Annual Suspended Sediment Load at $Q_{1.5}$ (Mg yr^{-1})	Suspended Sediment Load Contribution+ (%)
Upper Tombigbee River (03160101)	11,575	10.5	3,928,845	12
Middle Tombigbee River (03160106)	23,588	21.3	7,049,007	21
Lower Black Warrior River (03160113)	16,280	14.7	3,014,198	9
Middle Tombigbee River Chickasaw (03160201)	47,774	43.2	20,001,609	59
Lower Tombigbee River (03160203)	51,954	46.9	21,751,656	64
Lower Alabama River (03150204)	58,726	53.1	12,242,934	36
Suspended Sediment Load entering the Mobile River	110,680	100	33,994,591	100
Suspended Sediment load at distributaries			31,201,756	

* Including all upstream subbasin's area

+ Ratio of total suspended sediment load entering to the Mobile River in AL.

Table 3. Estimation of annual suspended sediment load for different subbasins within the Mobile River Basin based on Tier 2

Subbasin	Drainage Area* (km^2)	Area Contribution (%)	Mean Annual Suspended Sediment Load ($Mg\ yr^{-1}$)	Suspended Sediment Load Contribution+ (%)	Mean Annual Bed Load ($Mg\ yr^{-1}$)	Mean Annual Total Load ($Mg\ yr^{-1}$)
Upper Tombigbee River (03160101)	11,575	10.5	732,223	14	146,445	878,668
Middle Tombigbee River (03160106)	23,588	21.3	3,701,669	69	740,334	4,442,002
Lower Black Warrior River (03160113)	16,280	14.7	348,827	7	69,765	418,593
Middle Tombigbee River Chickasaw (03160201)	47,774	43.2	3,168,627	59	633,725	3,802,353
Lower Tombigbee River (03160203)	51,954	46.9	3,445,867	64	689,173	4,135,041
Lower Alabama River (03150204)	58,726	53.1	1,915,331	36	383,066	2,298,398
Suspended Sediment Load entering the Mobile River	110,680	100	5,361,199	100	1,072,240	6,433,438
Suspended Sediment load at distributaries			3,098,150		619,630^	1,691,870

* Including all upstream subbasin's area

+ Ratio of total suspended sediment load entering to the Mobile River in AL

^Percentage of sediment load assumed as bed load could be different due to the change on morphological and hydraulic conditions after the diversion

Table 4. Range of sediment loads for the lower subbasins of the Mobile River Basin

Subbasin	Tombigbee River Output	Alabama River Output	Entering Mobile River	Distributaries*
Maximum SS Load ($Mg\ yr^{-1}$)	11,526,200	4,091,100	15,617,350 8,197,719*	5,831,500
Minimum Load ($Mg\ yr^{-1}$)	548,350	251,700	800,000	587,500
Maximum Bed Load ($Mg\ yr^{-1}$)	2,305,250	818,200	3,123,500 1,639,544*	1,166,200
Minimum Bed Load ($Mg\ yr^{-1}$)	109,650	50,300	16,000	117,500
Maximum Total Load ($Mg\ yr^{-1}$)	13,831,450	4,909,300	18,740,850 9,837,300*	6,997,700
Minimum Total Load ($Mg\ yr^{-1}$)	658,000	302,000	816,000	705,000

*Values determined only between 2004 and 2010 due to availability of data in one of the USGS stations.

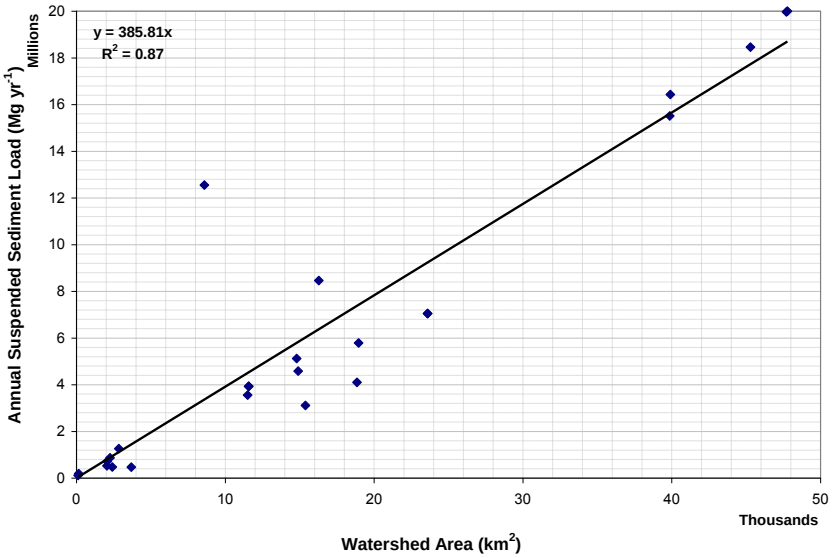

Figure 4. Relation between watershed area and Tier 1 estimated annual suspended sediment load.

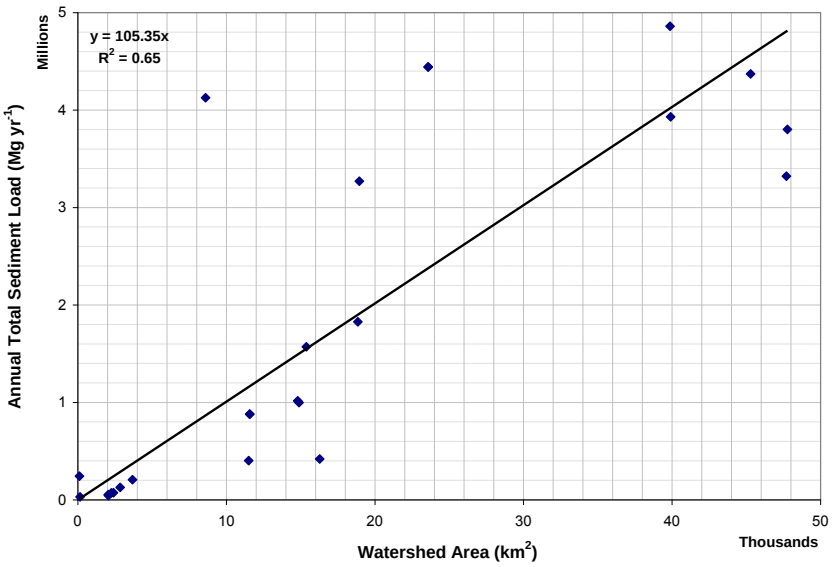

Figure 5. Relation between watershed area and Tier 2 estimated annual suspended sediment load.

CONCLUSION AND RECOMMENDATION

Results from the sediment budget analysis of TRB and the MRB evidenced that the system is contributing significant amounts of sediment to the impoundments. It was also observed that the system is experiencing an important process of sediment deposition along the lower part of the MRB. Based on sediment contributions from the upstream basin, which could range between 0.8 and 18.75 millions Mg yr^{-1}, the sediment deposition along the lower part of the MRB ranges between 0.1 and 2.85 millions Mg yr^{-1}. Since the availability of data is limited for the lower part of the Basin and the Bay, where sediment concentration is different due to changes in morphological and hydrodynamic processes, further analysis is needed and the collection of data would be an initial step to facilitate the process. As discussed in the analysis of sediment trends along the upstream basins and the changes on sediments behavior below the Mobile River diversion, the Tier 2 appears to be a reasonable procedure to determine the loads and the

trends of sediment processes along the entire watershed. The authors expect to develop a more detailed analysis along the Alabama River Basin to generate more important insights in the behavior of sedimentation processes along the Mobile River Basin.

REFERENCES

Atkins, B. J. 2004. Water quality in the Mobile River Basin, Alabama, Georgia, and Mississippi, 1999-2001. USGS, Reston VA. Circular 1231. 34 pp.

Avendaño, J. A., J.J. Ramírez-Avila, E.A. Rodriguez. 2012. Application of the models CONCEPTS and BSTEM to optimize and evaluate streambank stabilization designs (In Spanish). Proceedings of the XX National Seminary of Hydraulic and Hydrology and 1st International Seminar of River and Coastal Restoration, Barranquilla, Colombia, August 8-10, 2012.10 pp.

Bankhead, N., Simon, A., and Klimetz, D. (2008). Analysis of streambank erosion along the Lower Tombigbee River, Alabama. USDA-ARS National Laboratory Technical Report No. 62.

Johnson, G., R. E. Kidd, C. A. Journey, H. Zappia, and J. B. Atkins. 2002. Environmental Setting and Water-Quality Issues of the Mobile River Basin, Alabama, Georgia, Mississippi, and Tennessee. U.S. Geological Survey Water-Resources Investigations Report 02-4162, 120 pp.

McAnally, W. H., J. F. Haydel, and G. Savant. 2004. Port Sedimentation Solutions for the Tennessee-Tombigbee Waterway in Mississippi. Civil and Environmental Engineering Department. Mississippi State University.

McPherson, A. K., R. S. Moreland and B. Atkins. 2003. Occurrence and distribution of nutrients, suspended sediment, and pesticides in the Mobile River basin, Alabama, Georgia, Mississippi. Montgomery, Ala.: U.S. Dept. of the Interior, U.S. Geological Survey ; Denver, CO : U.S. Geological Survey, Branch of Information Services. 110 pp.

Sharp, J. 2007. Sediment Budget Template Applied to Aberdeen Pool. Master Thesis. Civil and Environmental Engineering Department. Mississippi State University. MS. 95 pp.

Stream Systems Technology Center. 2004. Rapid Evaluation of Sediment Budgets. In: Stream Notes. Stream Systems Technology Center, Rocky Mountain Research Station,

Fort Collins, Colorado. John Potyondy, Program Manager. http://www.stream.fs.fed.us/news/streamnt/pdf/apr04.pdf (accessed September 12, 2011).

CONTINUOUS TURBIDITY MONITORING AS A TOOL FOR EVALUATING SUSPENDED SEDIMENT LOADING IN THE MIDDLE TRUCKEE RIVER AND TRIBUTARIES, PLACER AND NEVADA COUNTIES, CALIFORNIA

Brian Hastings, PG, Geomorphologist, Balance Hydrologics, Inc., P.O. Box 1077, Truckee, California 96161, bhastings@balancehydro.com
David Shaw, PG, Principal Hydrologist/Geologist, Balance Hydrologics, Inc. P.O. Box 1077, Truckee, California 96161, dshaw@balancehydro.com
Stefan Schuster, PE, CPESC, Principal, CDM Smith, 12313 Soaring Way, Truckee, California 96161, schustersl@cdmsmith.com
Beth Christman, Restoration Director, Truckee River Watershed Council, 10418 Donner Pass Road, Truckee, California 96161, bchristman@truckeeriverwc.org

Abstract

The Middle Truckee River is currently listed by the California State Water Resources Control Board as being impaired by excessive sediment. Water quality is of particular concern because the river is habitat for two federally-listed fish species, cui-ui (*Chasmistes cujus*) and Lahontan cutthroat trout (*Oncorhynchus clarki henshawi*). The Lahontan Regional Water Quality Control Board (Lahontan Water Board) has developed a Total Maximum Daily Load (TMDL) for suspended-sediment concentration to attain sediment-related water quality objectives in the Middle Truckee River, the segment of the Truckee River extending from the outflow of Lake Tahoe at Tahoe City to the California-Nevada state line near Farad, California. A four year study (WY 2011–WY 2014) was conducted to: a) document suspended-sediment loads; b) evaluate the relationship between streamflow, suspended-sediment concentration, turbidity, and suspended-sediment transport rates, and; c) evaluate changes in these relationships over time in response to land management, sediment control strategies, and other implementation measures outlined in the TMDL. Note that The Water Year (WY) begins on October 1 and ends on September 30 of the named year. Water year 2014 began on October 1, 2013 and ended on September 30, 2014.

Cold Creek, Donner Creek, and Trout Creek were monitored in the Town of Truckee, California. Cold Creek is largely undeveloped with a history of logging, road-building, and railroad infrastructure, Donner Creek is heavily urbanized, and Trout Creek is a mix of open space with lightly developed suburban/recreational land uses. Additional monitoring was initiated on the mainstem of the Middle Truckee River across two years (WY 2013 and WY 2014) at two stations located upstream and downstream of the tributaries and used to evaluate significance of these tributaries in delivering suspended sediment to the Truckee River.

Monitoring, analysis and computations have been used to characterize suspended-sediment production and delivery (i.e. yields and loads) at each of the six stations and compare suspended-sediment loads between watersheds and across all years and calculate contributions from each tributary to the mainstem. We also have compared suspended-sediment loads and load durations to a regulatory target set forth in the Middle Truckee River TMDL.

At four of the six stations, we calculated suspended-sediment loads using two methods: 1) establishing relationships between instantaneous suspended-sediment transport rates and

instantaneous streamflow ("streamflow-suspended sediment rating curve"), then applying that relationship to the near-continuous streamflow record, and; 2) establishing relationships between instantaneous suspended-sediment concentration and turbidity ("turbidity-suspended sediment rating curve"), and applying that relationship to the near-continuous turbidity and streamflow records. In the absence of a continuous-logging turbidity meter at the remaining two stations, loading was calculated using only the streamflow-based rating curve method.

The initial year of monitoring (WY 2011) was much wetter than average, with significantly above average snowpack and a longer than normal runoff period. The following three years constituted one of the driest three-year periods on record. A range of runoff and sediment-delivery events occurred during the period, and can generally be classified as rain-on-snow, rain-on-ground, summer thunderstorms, or spring snowmelt. Our conclusions can be summarized as follows:

- Comparison of results between two computational methods suggests that a continuous record of turbidity is better able to capture discrete events or more accurately assess changes in loading during an event, thereby providing more accurate estimates of daily and annual suspended-sediment loading.
- Suspended-sediment load duration curves for turbidity-based loads (15-minute data) can be used to evaluate if streams met regulatory targets or water quality guidelines for the watershed.
- Comparisons of streamflow-based sediment rating curves to historical data were used to evaluate improvements or further degradation; these data currently do not indicate reductions in loading to the Middle Truckee River over time.
- In WY 2013 and WY 2014, Cold Creek, Donner Creek, and Trout Creek delivered 27 and 19 percent of the total suspended-sediment load in the Middle Truckee River, respectively. These subwatersheds only represent 5 percent of the total watershed below Lake Tahoe.
- In all years, Donner Creek delivers higher loads and yields (loads normalized by watershed area) when compared to Cold Creek and Trout Creek. These results appear to reflect the urban nature of the subwatershed, with high hydrologic connectivity between impervious surfaces and the stream.

EFFECTS OF BEDLOAD SAMPLER NETTING PROPERTIES ON HYDRAULIC AND SAMPLING EFFICIENCY

Kristin Bunte, Research Scientist, Colorado State University, Engineering Research Center, 1320 Campus Delivery, Fort Collins, CO 80523, kbunte@engr.colostate.edu; Kurt W. Swingle, Environmental Scientist; 630 Iris Ave., Boulder, CO 80304, kskb@ix.netcom.com; Steven R. Abt, Professor emer., Colorado State University, Engineering Research Center, 1320 Campus Delivery, Fort Collins, CO 80523, sabt@engr.colostate.edu; Daniel A. Cenderelli, Fluvial Geomorphologist/Hydrologist, USDA Forest Service, National Stream and Aquatic Ecology Center, 2150 Centre Ave., Fort Collins, CO 80526, dcenderelli@fs.fed.us.

Abstract Bedload samplers with coarse nets let small particles pass through the net, while samplers with fine nets have various problems capturing fine and coarse gravel bedload. Using samplers with nets of different mesh sizes may facilitate capture of a wider range of bedload particle sizes. However, preliminary evidence suggests that sampled transport rates are influenced by mesh size as well as by other net properties that tend to change with mesh size. Hence, a user would need to know and adjust for those differences before combining transport rates sampled with different mesh-width nets. To further investigate effects of netting properties on flow hydraulics and sampled transport rates, this study compares water throughflow and gravel transport sampled with two different mesh-size nets attached to non-flared bedload traps. One bag is a flexible, non-precision net with a 3.6 mm mesh width, the other bag is a stiff 1.18 mm precision mesh. The 1.18 mm net had a slightly better throughflow as long as the net remained empty, attributable to its slightly larger percent open area. Adding a substantial—but not uncommon—volume of 10 liters of organic material to the 1.18 mm net retarded and ponded the approach flow considerably because the organic material accumulated at the end of the cylindrical net where it blocked throughflow from exiting. The funnel-shape taken by the 3.6 mm net let most of flow exit shortly behind the bedload traps entrance, while captured solids traveled along the net bottom towards the bag end. The segregation of exiting flow from the accumulated material avoided major blockage of flow. In the 1.18 mm precision net, two hydraulic effects combined: higher through-flow for empty nets and compromised throughflow as organic material starts to accumulate at higher flow and transport. As a result, the 1.18 mm net sampled higher transport rates than the 3.6 mm net at low flow, while the 3.6 mm net sampled higher rates at higher flow.

INTRODUCTION

Coarse-bedded mountain streams transport a wide range of bedload particle sizes from sand to cobbles, but most bedload samplers can capture only a limited range of particle sizes. The sampler opening sets the upper limit of collectable particles, while the mesh width sets the lower limit. Large opening samplers with a large volume collection bag or basket and a coarse mesh of 4 to 25 mm collect only coarse particles, such as basket (Nanson 1974) or net-frame samplers (Bunte 1996, Whitacker and Potts 2007a,b), bedload traps (Bunte et al. 2004, 2007, 2008, 2010 a and b) or hanging baskets (Rickenmann et al. 2012). Those samplers provide satisfactory measurements of medium and coarse gravel or cobble transport rates but yield no information on transport of sediment finer than the mesh width. Samplers intended to capture coarse sand and

fine gravel typically have 0.2 to 0.5 mm mesh width bags. However, sand and fine organic particles quickly clog those bags, and the approximately 5-liter volume bag attached to small pressure difference samplers fill quickly when transport rates are high. Clogging and filling limit a sampler bag's water through-flow rates and sampling efficiency (Druffel et al. 1976; Johnson et al. 1977; Beschta 1981, 1983). Sampling times are typically kept to 2 minutes or less to avoid mesh clogging and bag overfilling, but if sampling times are too short to integrate over the natural fluctuations of bedload transport rates (Gomez et al. 1989; Turowski 2011) transport rates are overestimated when transport is low and underestimated when transport is high (Bunte and Abt 2005, Singh et al. 2009). Increasing both mesh and bag size alleviates the fast clogging and bag filling (Beschta 1981, 1983; O'Leary and Beschta 1981), and the subsequently higher throughflow rates increase sampled bedload rates. However, for a flared sampler body that is designed to have a hydraulic efficiency > 1 to compensate for the retardation of flow velocity in the fine-mesh and small-volume bag, increasing hydraulic and sampling efficiency via a coarser and larger bag to mitigate clogging might overcompensate.

Considering the limited range of particle sizes that can be representatively captured with a specified sampler body and bag, capturing a wider range of bedload particle sizes seems to require combining samples collected with nets of different mesh diameters. However, transport rates sampled using nets with different mesh widths differ (Beschta 1981, 1983; O'Leary and Beschta 1981). Furthermore, differences in mesh width are tied to changes in other net properties such as thread width, mesh shapes, and net stiffness, all of which can further affect hydraulic efficiency. An example of how the relation between mesh width and thread width affects a net's throughflow capacity is given below.

The percent open area A_o is a measure that relates the mesh opening width w to the thread width d in woven nets, or to the width of the knitted strands surrounding mesh openings in knitted nets, respectively (Figure 1a). Bunte and Swingle (2009) attached various nets with opening sizes of 0.5 to 3.6 mm to bedload traps, measured flow depth at the entrance of bedload traps deployed in a gravel/cobble bed stream, and showed that ponding of the approach flow increased with

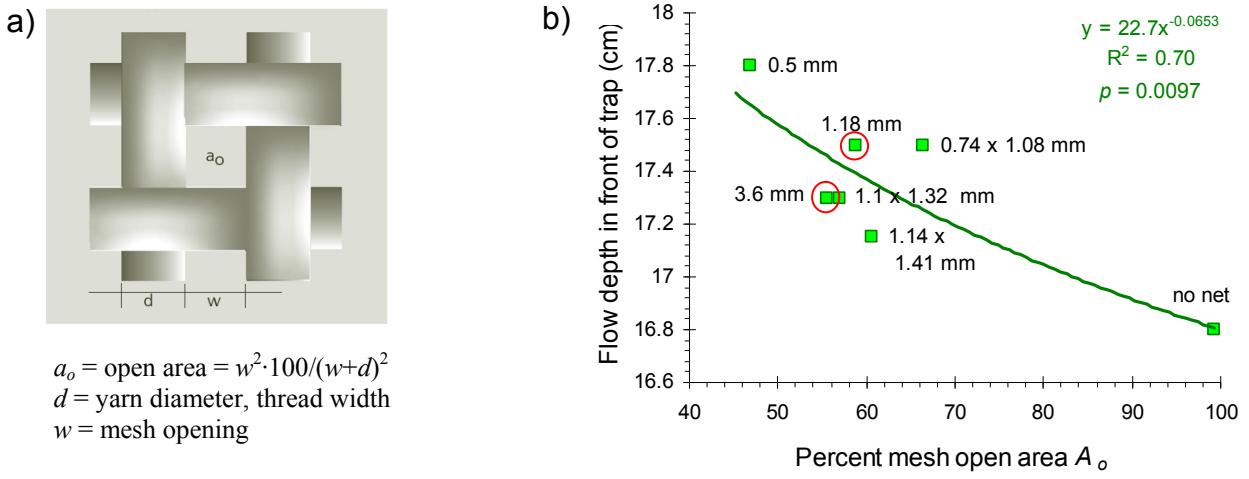

Figure 1: Schematic diagram of netting dimensions (from www.Sefar.com; slightly altered) (a). Negative relation between upstream ponding of flow and a net's percent open area A_o. Numbers next to data points indicate the mesh opening width w; note that not all meshes are square. The two circled nets were used in this study (a).

deceasing percent mesh open area A_o (Figure 1b). Scatter in the relation of ponding vs. A_o is attributed to concomitant netting properties such as being knitted vs. woven which determines mesh shapes and netting stiffness and whether mesh and net shapes change with increasing flow.

If throughflow rates, and hence sampled transport rates, differ between nets, then samples from different nets cannot be combined without first quantifying how those nets affect the sample outcome. However, systematic studies on how different nets affect sampled transport rates are rare. In this study we compare upstream flow hydraulics and sampled bedload rates between a 3.6 mm and a 1.18 mm mesh-width net attached to bedload traps with non-flared openings. Of the nets tested by Bunte and Swingle (2009), the 1.18 mm net was attractive because it would extend the size range collectible in bedload traps to coarse sand and pea gravel, while the square and precise mesh shape should give a precise lower limit of sampled particle size, and the sturdy nylon material suggested durability. The 0.5 mm nylon precision net was not included in this study because of its known propensity for immediate clogging and ponding (Bunte and Swingle 2003).

METHODS

Properties of the two study nets The 3.6 mm mesh-width net is knitted in a hole-pattern from thin, lightly twisted nylon yarn and is the original netting with which bedload traps were designed. This non-precision netting—called knotless Raschel (www.deltanetandtwine. com) and used for catfish farming—is very stretchable (and hence handles well). Mesh holes have a parallelogram shape when being gently stretched at low flows but become almost square when being fully stretched at moderate flows (Figure 2a). The bag, sewn as a cylinder, stretches to a funnel shape when subjected to flow (Figure 2b). The 1.18 mm mesh-width net is precision netting woven from 0.36 mm diameter nylon monofilament thread (www.Sefar.com). This netting is relatively stiff and unstretchable (Figure 2c), and the square mesh shape and the sewn cylindrical net shape are retained at all flows (Figure 2d). Both nets are about 1.2 m long. Properties of the two nets are summarized in Table 1.

Table 1: Characteristics of the two netting materials tested with bedload traps.

Netting material	Formal description	Open mesh width w (mm)	Width of thread or strand d (mm)	Ratio w/d	Open area A_o (%)	Smallest collectable 0.5 phi size class (mm)
hole-pattern knitted from thin, twisted nylon yarn, non-precision	Raschel 210d/9	3.6 - 5 based on stretching	1.23	2.9	56	4
Square mesh woven from nylon monofilament, precision	Sefar 06-1180/59	1.18	0.36	3.3	59	1.41

Field site The field comparison was carried out during snowmelt runoff at Fool Creek, a small step-pool mountain stream near Fraser in central CO. The reach-averaged gradient is 0.044 m/m, channel width is 1.3 m. The surface D_{16}, D_{50}, and D_{84} particle sizes are 12, 52, and 122 mm; 2% of the surface particles are smaller 2 mm and 11% and smaller 8 mm. The channel has a plane-bed morphology with low steps at the site, but turns to step-pool morphology about 10 m upstream. In the step-pool reach, the stream has carved a tortuous path around numerous large woody debris (LWD) pieces and created miniature forced bars. Storage and release of sediment around those semipermeable LWD dams causes highly variable transport rates.

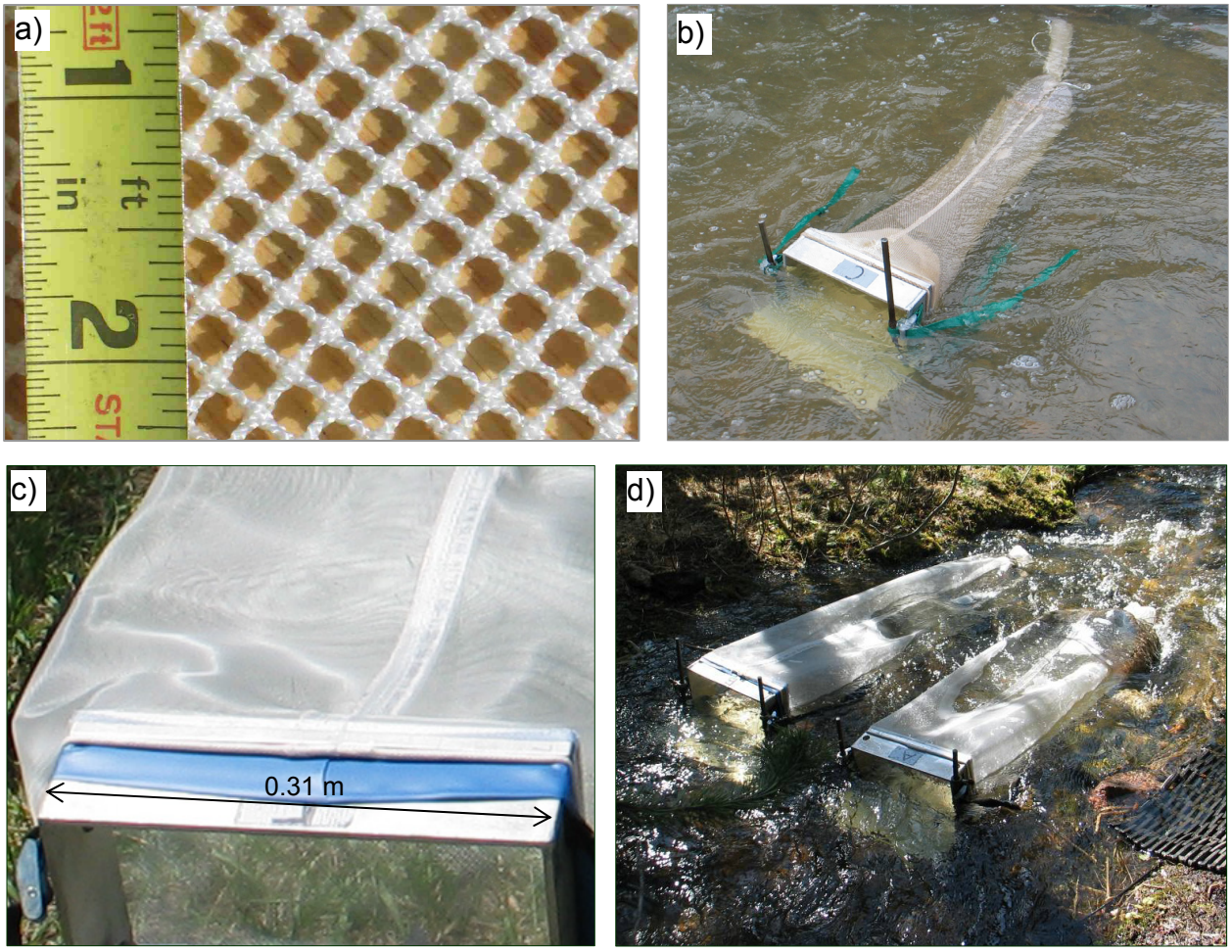

Figure 2: Detail of the 3.6 mm knitted nylon Raschel non-precision netting as the material is stretched to pull the meshes open into almost square shapes (a). The net—attached to a bedload trap—stretches to a funnel shape when subjected to flow (b). Detail of the 1.18 mm precision net woven from monofilament thread (c). The unstretchable 1.18 m nets—attached to bedload traps—retain a square mesh and cylindrical bag shape in all flows (d).

Bedload sampling Bedload traps have a 0.2 by 0.3 m frame to which a sampling net is attached. To cover the lateral variability of bedload transport, two bedload traps were installed next to each other on the channel bed, which resulted in a 0.2 m trap spacing, much tighter than the 0.8 to 1.2 m distance typically kept between neighboring bedload traps in wider streams. A set of two bedload traps with either the 3.6 mm (Figure 3a) or the 1.18 mm netting attached (Figure 3b) was alternately deployed for one-hour sampling times. When the 1.18 mm net visibly started to bulge at about 50% bankfull flow, sampling time was reduced to 30-40 minutes. Bedload samples were collected in flows of 20 to 80% of bankfull.

Data pairing To compare transport rates between the two netting materials, samples from both nets were sorted into data pairs collected no more than an hour apart. On some occasions, transport rates from two consecutive samples collected with the same net were averaged before pairing. In order to plot samples with zero transport, they were assigned a transport rate of 1E-6 g/s which is more than an order of magnitude less than the smallest sampled rate.

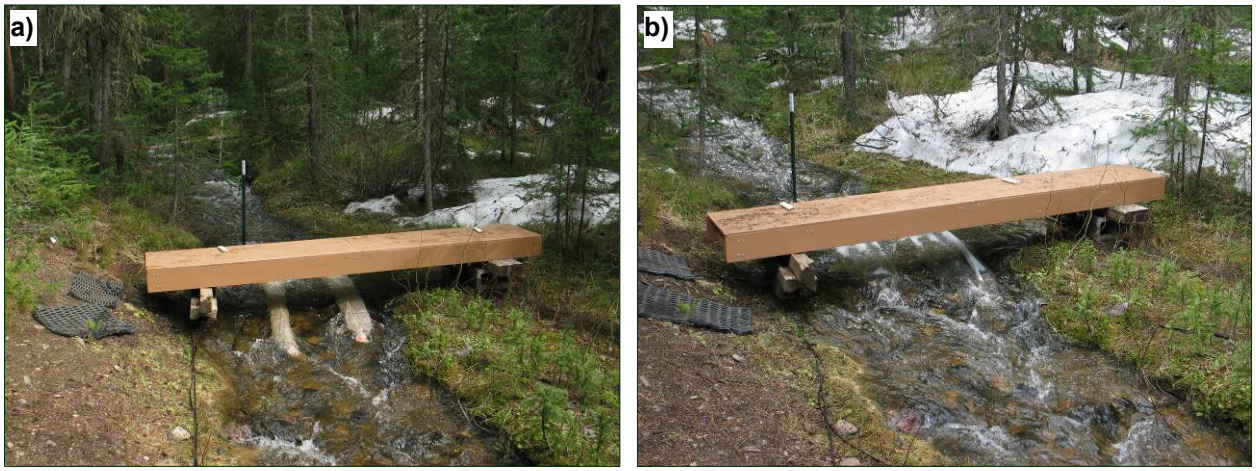

Figure 3: Fool Creek bedload sampling cross-section with footbridge and two bedload traps installed: the original 3.6 mm mesh width nets (a) and 1.18 mm precision nets (b).

Measurements of flow depth and velocity Flow depth as well as the mean vertical flow velocity at 0.6 of the flow depth was measured at distances of 0, 0.15, 0.305, and 0.61 m in front of the ground plates along the center line of the two traps with either the 3.6 mm or the 1.18 mm net attached. Flow depth was measured with a ruler and flow velocity with a Marsh-McBirney electromagnetic current meter. Depth measurements have an error of approximately 5 mm; the error in the velocity measurements was not estimated. The operator moved on a footbridge and a wooden plank placed across the stream in order not to disturb the flow. Pieces of tape on the upstream and downstream sides of the plank marked the measuring locations of 0.305 and 0.61 m in front of the traps. Flow depth and velocity were measured for three conditions: 1) at the bare ground plates with no trap installed, 2) with traps installed but empty, and 3) with traps to which 10 liters of organic material (mostly scales of conifer tree cones) had been added. The amount of organic material typically collected in Rocky Mountain streams in 1-hr bedload trap samples ranges from less than 0.1 to more than 20 l over a highflow season (Bunte et al. 2015, poster session, this volume). A 10-l volume—substantial, though not uncommon—fills about 20% of the net's volume. The measurements were repeated on two different days with flows of 0.17 and 0.20 m^3/s (57 and 67% Q_{bf}) and resulted in 48 individual measurements of flow depth and of flow velocity per net and day, a total of 192 measurements. At a discharge of 0.17 m^3/s, flow depth approached the upper rim of the sampling frame at the right trap and reached to about 75% of the frame height on the left trap. At a discharge of 0.2 m^3/s, flow started to overtop the upper rim of the right trap and reached to about 80% of the frame height on the left trap.

RESULTS AND DISCUSSION

Analysis of flow hydraulics in front of bedload traps

Effect of bedload trap presence on upstream flow hydraulics Compared to a bare ground plate, presence of a bedload trap generally caused ponding which increased the upstream flow depth and reduced the vertical mean flow velocity. The addition of organic material to the net further increased ponding, and retarded flow as shown in all plots of Figure 4. However, the degree of ponding and retardation, and the upstream extent of these effects, are determined not only by the netting properties, but also by the local flow hydraulics.

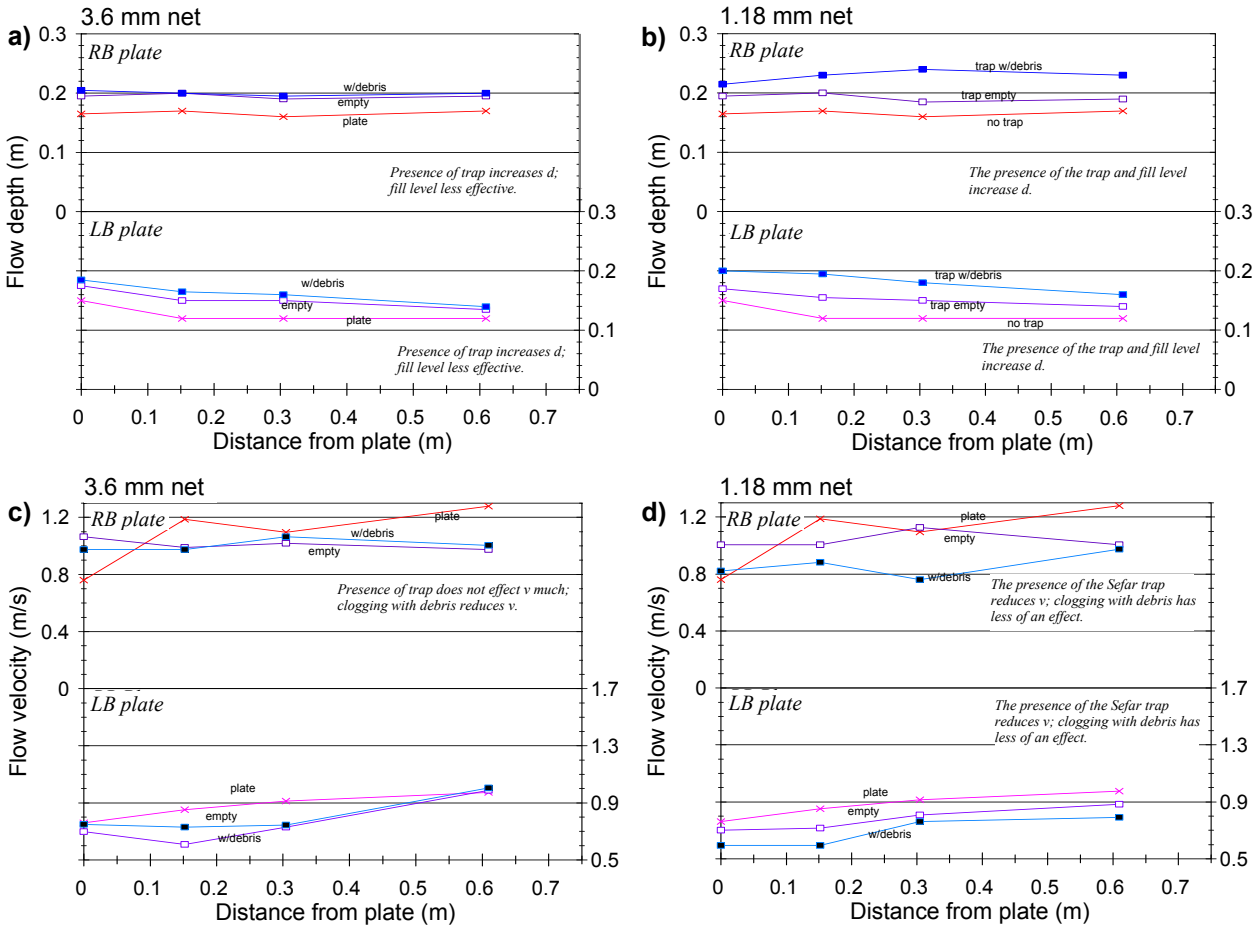

Figure 4: Flow depth (a, b) and mean flow velocity at 0.6 *h* (c, d) measured at a discharge of 0.17 m^3/s at four locations in front of the right and left bedload traps fitted with the 3.6 mm net (a, c) and the 1.18 mm net (b, d). Reddish lines refer to bare ground plates with traps removed. Purple lines refer to empty traps, and bluish lines to traps filled with 10 liters of organic debris.

For example, flow was deeper and faster at the RB plate and overtopped the RB trap, while 25% of the LB trap height protrudes through flow. There may also be hydraulic interference be-tween the two traps due to their close spacing. In order to integrate over local effects and focus on the general effects exerted by the netting properties, this study averaged the measurements of flow depth and flow velocity over all four longitudinal locations and over the left and right traps.

Average ponding and reduction in mean flow velocity For the two sampled flows of 0.17 m^3/s (Figure 4) and 0.20 m^3/s (not shown because patterns are very similar to those at 0.17 m^3/s), empty traps fitted with the original 3.6 mm net increased flow depth in front of the traps by about 18% and 20%, respectively, compared to the flow depth measured over the bare ground plates. The addition of 10 liters of organic material produced only a minor increase in flow depth for the 3.6 mm net (Table 2). Compared to flow depth on the bare plates, bedload traps with organics raised flow depth by 23%. Traps with empty 1.18 mm nets increased flow depth similarly by 18% for the lower flow and to slightly more (22%) at the higher flow. In contrast to the 3.6 mm traps, the 10 liter of organics added to the 1.18 mm nets increased flow depth by an additional 19 and 15% such that compared to the bare plates, traps with organics increased flow depth by 40%.

The response of retardation of flow velocity is similar to that of ponding (Table 2). Again, compared to the bare ground plate, an empty trap with a 3.6 mm mesh reduced the mean flow velocity by 10 and 13% at the two flows, and adding the organic material retarded the flow just slightly more. Empty traps with 1.18 mm nets reduced mean flow velocity a few percent less than empty 3.6 mm nets (about 7 and 10%), possibly due to the slightly higher open area of the 1.18 mm net (59%) compared to the 3.6 mm nets (56%). However, the added organic material reduced flow velocity in the 1.18 mm nets by another 15% in both flows, while the effect of organic material in the 3.6 mm nets was again minor.

Table 2: Average effect of empty and filled bedload traps fitted with the original 3.6 mm and the 1.18 mm nets on upstream flow depth and mean flow velocity at two discharges Q.

	Empty trap *vs*. no trap		Added 10 l of org. mat. *vs*. empty trap		Trap with 10 l of org. material vs. no trap	
	Q = 0.17 m^3/s	Q = 0.2 m^3/s	Q =0.17 m^3/s	Q = 0.2 m^3/s	Q = 0.17 m^3/s	Q = 0.2 m^3/s
Percent increase in flow depth						
Orig. 3.6 mm nets	18.3	20.7	4.3	1.6	23.4	22.7
1.18 mm nets	17.9	22.4	19.1	14.8	40.4	40.6
Percent decrease in flow velocity						
Orig. 3.6 mm nets	- 9.5	- 12.9	2.4	- 3.2	-7.4	-15.7
1.18 mm nets	- 7.4	- 10.3	- 14.7	- 15.0	-21.0	-23.7

The pronounced effect of captured organic material on flow ponding and retardation in the 1.18 mm precision nets is caused by the stiffness of the net material which makes the net retain its cylindrical shape at all flows. Organic material that enters the net accumulates along the upper back part of the bag, where most of the water would otherwise exit, and obstructs water through-flow (Figure 5a, c). A similar response was observed at a 0.5 mm precision net that bulged and ponded flow within minutes of deployment in low to moderate flow (Bunte and Swingle 2003), suggesting that fine-meshed, stiff precision nets should not be used when organic material is in motion. The original 3.6 mm bedload trap net, by contrast, stretches to a funnel shape, and most of the flow exits the net just shortly behind the trap frame (Figure 5b). Organic material and bedload is directed to travel along the bottom of the net, and both accumulate in the narrow net end (Figure 5d) where solids do not have much effect on flow hydraulics near the trap entrance.

Comparison of fractional transport rates At the lowest transporting flows when small gravel particles were just starting to move, the non-precision 3.6 mm net collected either no particles or lower rates of the 4 - 5.6 mm size class than the 1.18 mm net (Figure 6a). The nominal 3.6 mm mesh size probably lets flat particles of the 4-5.6 mm size class pass when meshes still have a parallelogram shape before they are fully stretched by flow. Adding to the particle escape is the fact that the first 4 – 5.6 mm bedload particles in motion also tend to be the flatter and less voluminous specimens of the size class. At higher flows when meshes are fully stretched and almost square, the 3.6 mm net is believed to capture particles of the 4-5.6 mm size class representatively.

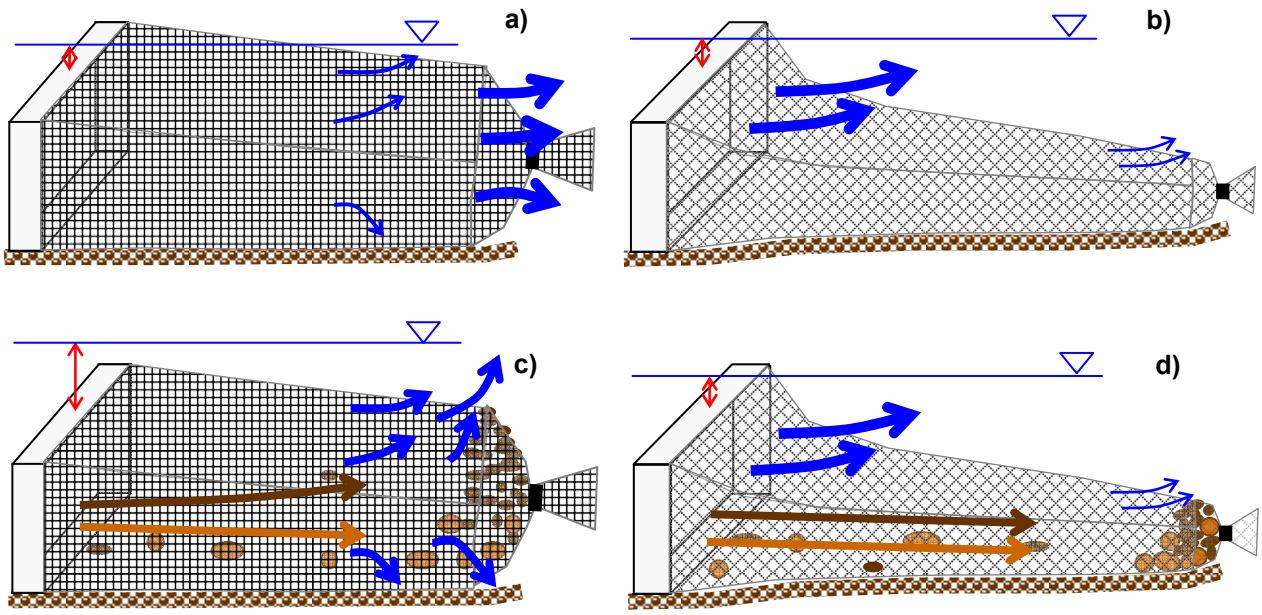

Figure 5: Sketches of flow and solid transport through the 1.18 mm precision net (a) and through the stretchable 3.6 mm Rachel (b) in the absence of organic material. Organic material added to the nets accumulated in the net end and blocked the exit of flow in the stiff 1.18 mm net (c) but not in the flexible, funnel-shaped 3.6 mm net (d). Blue arrows indicate water through-flow, dark brown arrows indicate the path of organic material, beige arrows indicates the bedload path.

At low transport, the 3.6 mm net often contained no 5.6 - 8 mm particles (Figure 6b), while the 1.18 nets had captured one or several. Similar observations held for the 8 - 11.2 (Figure 6c) and the 11.2 - 16 mm size class (Figure 6d). As suggested by the measured flow velocity, the 1.18 mm net with a 59% open area retarded throughflow less at very low flows than the 3.6 mm net with a slightly lower open area of 56%. Thus, absent high organic concentrations, the 1.18 mm net performed better at lower flows. At moderate transport rates, both nets collected all size bed-load fractions at similar rates, i.e., within a factor of about ±4 of each other, given Fool Creek's fluctuating transport. At the highest sampled transport rates, the 3.6 mm net tended to collect higher transport rates than the 1.18 mm net in all size fractions.

Ratios of transport rates collected with the two nets

Ratios of transport rates collected in the 3.6 mm vs. the 1.18 mm net for fractional and total bed-load transport (excluding zero samples) plotted vs. discharge (Figure 7a) show that the 1.18 mm net yields higher transport rates than the 3.6 mm net at the lowest flows, which is expected because the 1.18 mm net has a slightly higher percent open area and retards flow slightly less than the 3.6 mm net (Table 2). As discharge exceeds about 0.21 m^3/s (70% of bankfull flow), the 3.6 mm net started collecting higher rates than the 1.18 mm net for all particle size classes. The switch is attributed to the capture of organic material typically transported in Rocky Mountain streams during snowmelt runoff, and with increasing flow those organics comprise increasingly larger proportions of the solid transport (Bunte et al. 2015, this volume). Captured organic material accumulates in the bag ends where it blocks flow from exiting the 1.18 mm nets. As a consequence, the 1.18 mm nets start to bulge at their downstream ends (Figure 7b), pond, and retard flow at the net entrance, and decrease sampling efficiency.

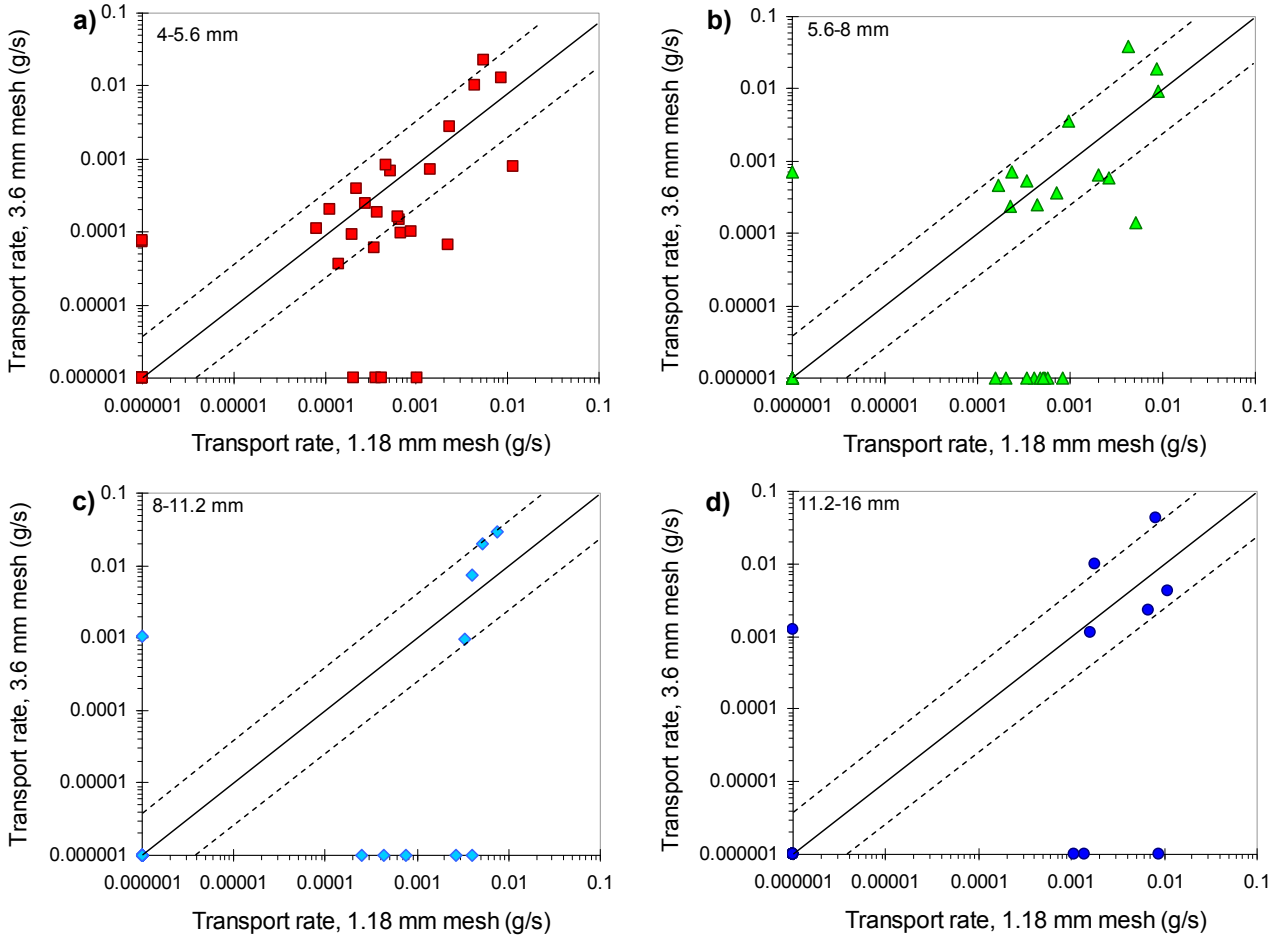

Figure 6: Pair-wise comparison of fractional transport rates collected with the two bedload trap nets. Samples that do not contain a particle were assigned the transport rate of 0.000001 g/s and plotted along the x- and y-axes. The solid diagonal line is the 1:1 line. Stippled lines indicate a factor 4 range above and below the 1:1 line.

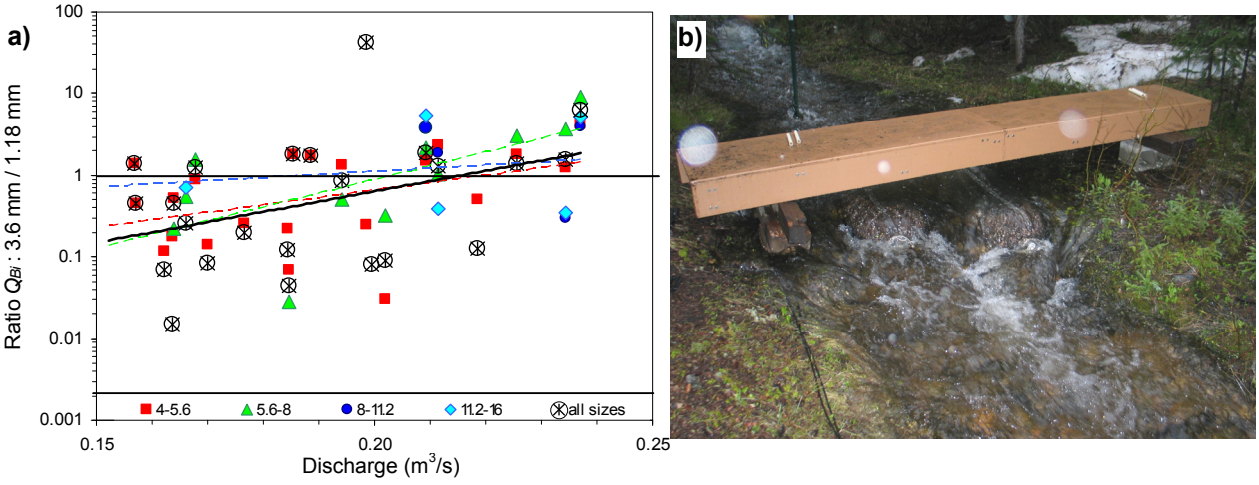

Figure 7: Ratios of transport rates collected in the 3.6 mm vs. the 1.18 mm net for fractional and total bedload transport (a). The 1.18 mm precision nets bulge when the start capturing organic material and pond water upstream (b).

SUMMARY AND CONCLUSION

- The study shows interactions between different netting properties and how they affect flow ponding and retardation, throughflow, and sampled transport rates.

- Hydraulic and sampling efficiency differs between nets of different mesh width even though both netting materials have percent open areas that are not very different.

- Netting stiffness affects hydraulic and sampling efficiency. Stiff nets that retain a near-cylindrical bag shape at all flows are prone to throughflow blockage by organic material, and respond with bulging, ponding, and retardation of flow, as well as with a reduction in sampled transport rates. Flexible nets segregate the paths of water throughflow and solid transport in the net such that solids accumulate where they have much less effect on hydraulic and sampling efficiency.

- At low flows, the 1.18 mm net measured higher transport rates of fine gravel particles with fewer zero samples than the 3.6 mm net. Both nets approach similar transport rates in moderately high flows (70% of bankfull), but in higher flows, the 3.6 mm yields higher rates than the 1.18 mm net. This switch in sampling efficiency between the two nets has implications on sampled gravel transport relations which increase more steeply with flow (i.e. the bedload rating curve slope) if the 3.6 mm net is used rather than the 1.18 mm net.

- The study showed that responses of hydraulic and sampling efficiency to netting properties are complex. Hydraulic efficiency is a response to the combined effects of the percent open area of the mesh, increasing flow, the shape taken by the net in flowing water, and net clogging and blockage which typically intensify with higher flow, higher transport rates of organic material, and longer sampling time.

Acknowledgements We are grateful to Rico Thueler, the executive vice president of the Sefar company who sent us free of charge 10 yards of the Sefar netting material (06-1180/59) when the desired netting (06-1140/66) was not available. We thank Mark Dixon, Lucas Herman, Laurie Porth, Sandra Ryan and Kelly Elder (USDA Forest Service, Rocky Mountain Research Station) for project support. Field experience by Gustavo Merten (Univ. of Minnesota) who successfully used bedload traps with a mosquito net attached initiated this study and encouraged us to analyze the effects of a net with a 1 to 2 mm mesh width for sampling coarse sand and pea gravel. We are grateful to John Potyondy (USFS ret.) and the USFS Stream Team who provided us with the opportunity for further field testing of bedload traps.

REFERENCES

Beschta, R.L. (1981). "Increased bag size improves Helley-Smith bed load sampler for use in streams with high sand and organic matter transport," In: Erosion and Sediment Transport Measurement. IAHS Publ. no. 133, pp 17-25.

Beschta, R.L., 1983. "Sediment and organic matter transport in mountain streams of the Pacific Northwest," In: *Proceedings of the D.B. Simons Symposium on Erosion and Sedimentation*, R.-M. Li (ed.), Simons, Li & Associates, Ft. Collins, Colorado, pp 1.69-1.89.

Bunte, K. (1996). Analyses of the temporal variation of coarse bedload transport and its grain size distribution (Squaw Creek, Montana, USA). U.S.D.A., Forest Service, Rocky Mountain Forest and Range Experiment Station, General Technical Report RM-GTR-288, 123 pp.

Bunte, K., and K. Swingle (2003). Results from testing the bedload traps at Little Granite Creek, 2002: effect of sampling duration and sampler type on bedload transport rates and systematic variability of rating curves with basin area and stream bed parameters. Report submitted to the Stream Systems Technology Center, USDA Forest Service, Rocky Mountain Research Station, Fort Collins, CO, 110 pp.

Bunte, K., Abt, S.R., Potyondy, J.P., and S.E. Ryan (2004). "Measurement of coarse gravel and cobble transport using a portable bedload trap," J. Hydraul. Eng., 130(9), pp. 879-893.

Bunte, K., and Abt, S.R. (2005). "Effect of sampling time on measured gravel bed load transport rates in a coarse-bedded stream," Water Resour. Res., 41, W11405, doi:10.1029/2004WR003880.

Bunte, K., Swingle, K., and S.R. Abt (2007). Guidelines for using bedload traps in coarse-bedded mountain streams: Construction, installation, operation and sample processing. General Technical Report RMRS-GTR-191, Fort Collins, CO, U.S. Department of Agriculture, Forest Service, Rocky Mountain Research Station, 91 pp. http://www.fs.fed.us/rm/pubs/rmrs_gtr191.pdf

Bunte, K., Abt, S.R., Potyondy J.P., and K.W. Swingle (2008). "A comparison of coarse bedload transport measured with bedload traps and Helley-Smith samplers," Geodinamica Acta 21(1/2), pp. 53-66 http://www.treesearch.fs.fed.us/pubs/30814

Bunte, K., and K. Swingle (2009). Testing bedload traps with a 1.18 mm mesh width netting. Report submitted to Stream Systems Technology Center, USDA Forest Service, Rocky Mountain Research Station, Fort Collins, CO, 32 pp.

Bunte, K., K.W. Swingle and S.R. Abt (2010b). "Necessity and difficulties of field calibration of signals from surrogate techniques in gravel-bed streams: possibilities for bedload trap samples," In: Gray, J.R., Laronne, J.B., and Marr, J.D.G, Bedload-surrogate monitoring technologies: U.S. Geological Survey Scientific Investigations Report 2010-5091, 17 p., available online at: http://pubs/usgs.gov/sir/2010/5091.

Bunte, K., S.R. Abt, K.W. Swingle, and J.P. Potyondy (2010a). "Functions to adjust transport rates from a Helley-Smith sampler to bedload traps in coarse gravel-bed streams (rating curve approach)," In: Proceedings, 9th Federal Interagency Sedimentation and 4th Federal Interagency Hydrologic Modeling Conference in Las Vegas, NV, Session: Fluvial Geomorphology, CD-ROM ISBN 978-0-9779007-3-2. http://acwi.gov/sos/pubs/2ndJFIC/Contents/10D_Bunte_03_01_10.pdf

Bunte, K., Swingle, K.W., Turowski, J., Abt S.R., and Cenderelli, D.A. (2015). "Coarse Particulate Organic Matter Transport in two Rocky Mountain Streams," In: Proceedings of SEDHYD 2015, 10th Federal Interagency Sedimentation and 5th Interagency Hydrologic Modeling Conference, Reno, NV, Session 5C, Physical measurement and monitoring.

Druffel, L., Emmett, W.W., Schneider, V.R., and Skinner, J.V. (1976). Laboratory hydraulic calibration of the Helley-Smith bedload sediment sampler. U.S. Geological Survey Open-File Report 76-752, 63 pp.

Gomez, B., Naff, R.L., and Hubbell, D.W. (1989). "Temporal variation in bedload transport rates associated with the migration of bedforms," Earth Surface Process. Landforms, 14 pp 135-156.

Johnson, C.W., Engleman, R.L., Smith J.P., and Hansen, C.L. (1977). "Helley-Smith bed load samplers," J. Hydraul. Div., ASCE, 103 (HY10), pp 1217-1221.

Nanson, G.C. (1974). "Bedload and suspended-load transport in a small, steep, mountain stream," Am. J. Science 274, pp 471-486.

O'Leary, S.J., and Beschta, R.L. (1981). "Bed load transport in an Oregon Coast Range stream," Water Resourc. Bull. 17(5), pp 886-894.

Rickenmann, D., Turowski, J.M., Fritschi, B., Klaiber A., and Andreas L. (2012). "Bedload transport measurements at the Erlenbach stream with geophones and automated basket samplers," Earth Surf. Process. Landforms, 37(9) pp 1000-1011, DOI: 10.1002/esp.3225

Singh, A., Fienberg, K., Jerolmack, D.J., Marr, J., and Foufoula-Georgiou, E. (2009). "Experimental evidence for statistical scaling and intermittency in sediment transport rates," J. Geophys. Res. 114, F01025,doi:10.1029/2007JF000963.

Turowski, J.M. (2011). "Probability distributions for bed form–dominated bed load transport: The Hamamori distribution revisited," J. Geophys. Res., 116, F02017, doi:10.1029/2010JF001803.

Whitaker, A.C., and Potts D.F. (2007a). "Coarse bed load transport in an alluvial gravel bed stream, Dupuyer Creek, Montana," Earth Surface Process. Landforms 32, pp 1984-2004. DOI: 10.1002/esp.1512.

Whitaker, A.C., and Potts D.F. (2007b). "Analysis of flow competence in an alluvial gravel bed stream, Dupuyer Creek, Montana," Water Resour. Res., 43, W07433, doi:10.1029/2006WR005289.

MEASURES OF SEDIMENT IN MINNESOTA

Greg Johnson, Hydrologist
Minnesota Pollution Control Agency
520 Lafayette Road
St. Paul, MN 55155
651-757-2471
gregory.johnson@state.mn.us
Bill Thompson, Research Scientist
Minnesota Pollution Control Agency
18 Wood Lake Drive SE
Rochester, MN 55904
507-206-2627
bill.thompson@state.mn.us

Abstract: Sediment is one of the most significant pollutants to lakes and streams in Minnesota. Various measures have been used to represent sediment as an impairment of water quality. The Minnesota Pollution Control Agency and its partners have completed many Total Maximum Daily Loads for turbidity given the numeric criteria for turbidity in Minnesota's water quality standards (WQS). Much effort was expended in dealing with the variability in the measurement of turbidity and the development of total suspended solids (TSS) surrogates for the turbidity standards. The MPCA has recently adopted regional TSS water quality standards to replace the turbidity water quality standards to lessen the uncertainty present in the measurement of turbidity. TSS criteria were developed given the extensive dataset present for TSS even though we know that TSS is an incomplete measure of sediment in streams and rivers. A partnership with United States Geological Survey (USGS) has given Minnesota resource agencies the opportunity to evaluate the relationships between TSS and suspended sediment concentrations as well as to explore the use of surrogate technologies for SSC, conduct bedload monitoring, and evaluate dimensionless sediment rating curves in stream geomorphology assessments. While these evaluations have provided a more robust approach, on-going efforts will be required to fully characterize sediment in Minnesota's rivers and streams.

INTRODUCTION

Various parameters have been used to describe sediment suspended in water. The MPCA has traditionally used total suspended solids as a measure of the sediment suspended in water. It has also used turbidity and Secchi tube depths as measures of sediment in water. The USGS typically uses SSC as their measure of suspended sediment. The following text describes how the four parameters are being used in Minnesota.

TURBIDITY

Minnesota was one of only a few states that adopted numeric criteria for turbidity in its water quality standards. The turbidity WQS for warm and cold water streams were 25 and 10 NTU, respectively. The basis for the numeric criteria is not clear based on a review of the primary documents used in the development of early state water quality standards (Appendix B, MPCA,

2007). The lack of clarity in the development of the standard along with changes in the technology used to measure turbidity over time and variable responses of material in water to light passage made for many uncertainties in the application of the turbidity water quality standard (WQS) in assessing streams for impairment and completing TMDLs.

Sadar (1998) describes the development of turbidity measurement technologies with their similarities and differences. For a period of time around the development of the WQ criteria guidelines, various turbidity units, including JTU, ppm, NTU and even 'turbidity units' or no units, were used in the literature. Federal Water Pollution Control Administration (1968) and U.S. Environmental Protection Agency (1976) contained references to many of these units. The resulting documentation for Minnesota's numeric criteria for turbidity was silent on the method and units used in establishing the criteria.

As MPCA staff began evaluating data for TMDLs, differences in the data became evident. An initial comparison of turbidity measurements grew out of overlapping temporal data sets obtained from Hach 2100A and Hach 2100P meters in two monitoring programs at sites near Lock and Dam #3 on the Mississippi River. Definite differences in the data were apparent over similar monitoring periods (Figure 1) even though the sampling was not completed on the same days. A second comparison of turbidity data came from turbidity measurements made by two laboratories on split samples for a river remote sensing project in 2004. Samples were collected at several sites spread across the southern half of Minnesota. A plot of the data (Figure 2) shows the difference between NTU and NTRU values as measured by Hach 2100A and Hach 2100AN meters, respectively. Based on a regression analysis of the data, a surrogate value for the water quality standard for turbidity of 25 NTU was estimated to be 39 NTRU. The variability in turbidity data lead to extended discussions about the appropriate measure of turbidity to apply to the numeric criteria, differences in turbidity data resulting from the use of different meters, and differences in the relationships of turbidity and suspended solids across Minnesota.

TOTAL SUSPENDED SOLIDS

As the state water quality agency, the MPCA has traditionally used total suspended solids as its measure of sediment suspended in water. The development of this use is likely the result of the focus of the USEPA and state water quality agencies on point source pollution and wastewater treatment. Gray et al. (2000) presents information from various editions of standard laboratory methods published by the American Public Health Association, American Water Works Association, and Water Pollution Control Federation (1946, 1971, 1976, and 1985) that describes the application of TSS through the years with the transition to its application to natural waters in the 1976 edition.

TSS is a water quality parameter that is widely used as a measure of the suspended particles in rivers. It is often used as a measure of the amount of inorganic sediment suspended in water, although it also includes the organic suspended material present in water. As a measure of suspended sediment, TSS concentrations provide an indication of water quality condition for use in evaluating aquatic life use support. The TSS methods in Minnesota most often involve a simple grab sample from the stream, followed by lab analysis where a subsample is used to determine a concentration.

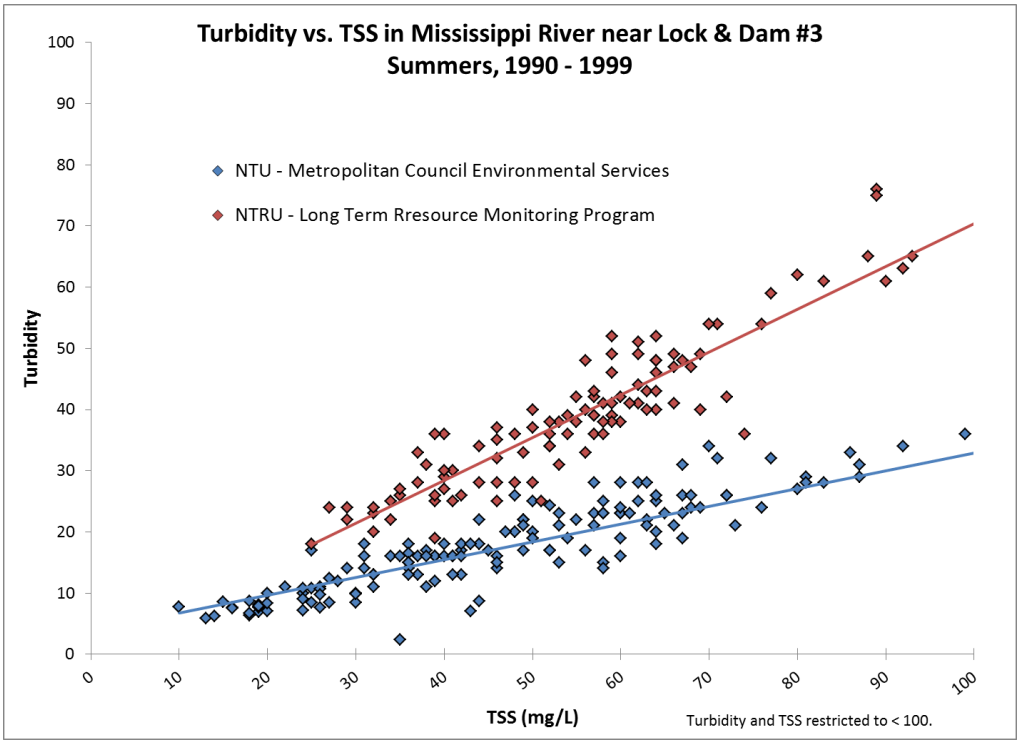

Figure 1 Comparison of turbidity data from different meters versus TSS concentrations.

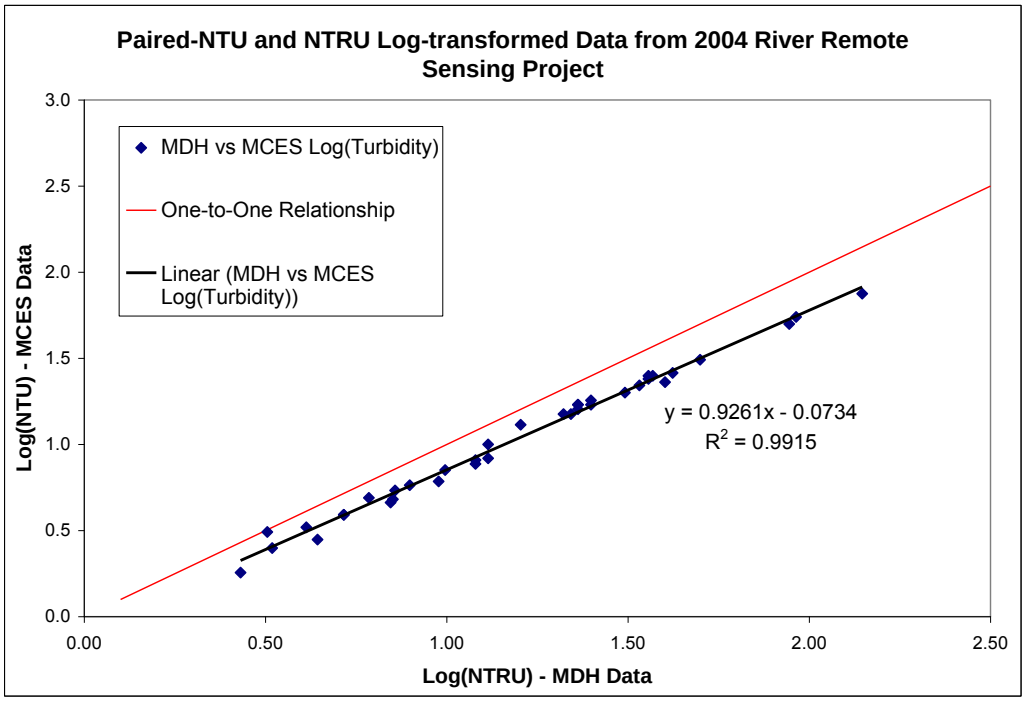

Figure 2 Relationship between paired turbidity data from different meters.

The use of TSS relative to water quality standards and TMDLs in Minnesota developed with the need to complete TMDLs for the turbidity WQS. Given that turbidity is not a measure of mass in a volume of water (concentration), a concentration surrogate had to be established in order to calculate loads for TMDLs. The use of TSS as the state's measure of particulates suspended in water and the correlation of TSS to turbidity lead to the primary use of TSS in turbidity TMDLs (MPCA 2007). The TMDL protocol (MPCA 2007) provided guidance for the development of the surrogate concentrations using simple linear regression. It noted that individual relationships should be developed for each impaired stream reach unless data analysis demonstrated that a whole stream, watershed, or region provided an equivalent result.

As the recognition of the variability in turbidity measurements and the factors causing that variability grew, the MPCA began evaluating the potential for replacing the turbidity WQS. Using two data analysis efforts, the MPCA developed proposed amendments to Minnesota water quality standards (Minn. Rule 7050) that included regional and time components for TSS (MPCA 2014). Relationships between fish and macroinvertebrate data and TSS concentrations were evaluated using quantile regression and changepoint analysis. The statistical methods are relatively new tools being used to identify threshold concentrations and establish numeric criteria to protect aquatic life. The second analysis effort involved the development of TSS frequency curves for "reference" or "least-impacted" streams in the state (Markus 2011).

Proposed TSS criteria were developed for three regions of the state for warm water aquatic life use based on a combination of major watershed and aquatic ecoregions and statewide for cold water aquatic life use. The criteria also provide temporal considerations of elevated TSS concentrations during snowmelt and storm events by indicating that the standards are not to be exceeded more than 10 percent of the water samples collected in the period, April through September. In addition, site specific water quality standards were developed for the mainstems of the Red and lower Mississippi Rivers. The statement of need and reasonableness (SONAR) required in Minnesota's rulemaking process noted that the TSS criteria would provide a transition from a statewide turbidity standard to regional standards, better connection of the water quality variable to biotic response, and more direct TMDL load calculations (MPCA 2014a). The TSS criteria were adopted following the state's rulemaking process in June 2014; however, final review and approval by EPA is still pending as of mid-January 2015.

The MPCA established the Watershed Pollutant Load Monitoring Network (WPLMN) to provide a long-term network of monitoring sites across the state to obtain spatial and temporal pollutant load information from Minnesota's rivers and streams. The WPLMN uses TSS as its measure of the sediment suspended in water. Annual and average pollutant loads, yields, and flow weighted mean concentrations are computed for each site using FLUX32 software (MPCA 2014b). Figure 3 shows the flow weighted mean concentrations for TSS for the major watershed sites in Minnesota from 2007 – 2011.

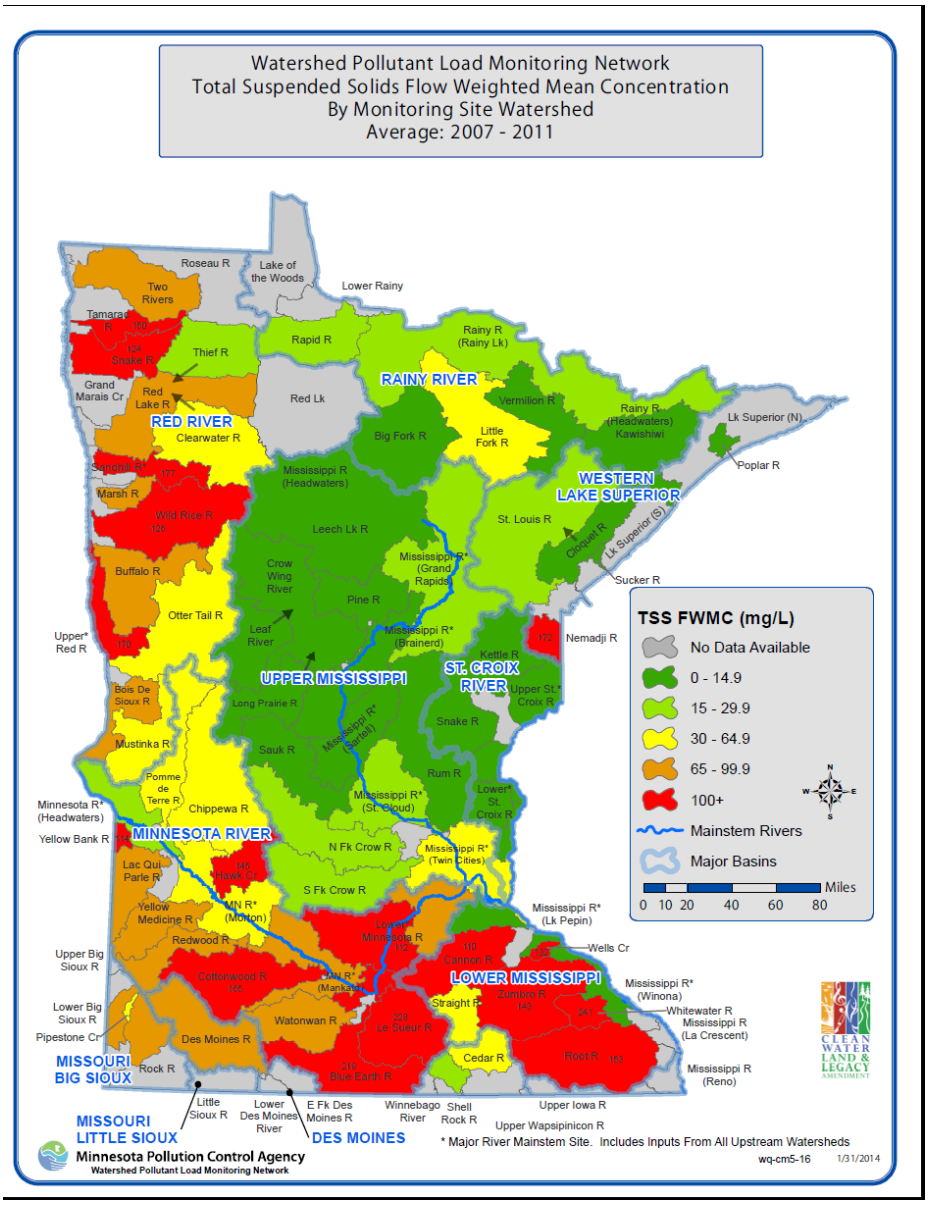

Figure 3 Flow-weighted mean concentrations of TSS by major watershed in Minnesota.

SUSPENDED SEDIMENT CONCENTRATION

Suspended sediment has been sampled by USGS at various times and locations in Minnesota. The first SSC data in Minnesota dates back to the late 1800s. Suspended-sediment concentration (SSC) samples were collected at several sites in the 1970s and 1980s as part of a focus on developing a national dataset for use in evaluating suspended sediment. Tornes (1986) compiled and analyzed the suspended sediment data in Minnesota from 1960 to 1981. SSC sampling decreased in Minnesota after the 1980s paralleling decreases at a national level. With a few exceptions, SSC monitoring was reduced to a single daily sediment station on the Minnesota River at Mankato.

A cooperative effort between the MPCA and USGS renewed a SSC monitoring effort in 2007. The monitoring network was designed to improve the understanding of fluvial sediment transport relations through systematic sampling of SSC, TSS, and turbidity in selected Minnesota rivers. SSC monitoring was deemed important given that TSS concentrations have often been found to be significantly different from corresponding SSC (Gray et al. 2000). With these differences and the great influence of sediment on water quality impairments, MPCA staff believed that it was important to characterize differences between TSS and SSC in identifying the sediment processes affecting aquatic life.

The establishment of the sediment monitoring network provided the opportunity to continue the state's progress in addressing sediment-related impairments. Although the MPCA has moved toward establishing a water quality standard for TSS, a more complete understanding of the whole amount of sediment moving in streams and rivers is needed. The results of the current study through 2011 showed that the average TSS concentration was significantly different from the corresponding SSC for each of the seven rivers sampled (Figure 4). The overall average for the seven sites combined indicated a 50 percent difference in concentration (Ellison et al. 2014). Characterization of the differences between TSS and SSC is needed to provide estimates of the total suspended sediment being transported in Minnesota's rivers in addition to the total suspended solids load provided through the use of TSS in the MPCA's statewide load monitoring program. The data and relationships established will allow better calibration of the sediment component of the HSPF watershed models being completed for each 8-digit HUC watershed in Minnesota, improved identification and characterization of the sediment stressors affecting fish and macroinvertebrates in the MPCA's stressor identification process, the incorporation of the unmeasured sediment component in TSS in sediment transport studies, and identification of best management practices needed to control excess sediment. SSC and bedload data have also been collected in a related project to evaluate the use of dimensionless sediment rating curves in stream geomorphology assessments.

The current monitoring effort has transitioned from evaluating the differences between TSS and SSC to developing hydroacoustic techniques for continuous SSC following the work of USGS and others. The use of hydroacoutics as a surrogate for SSC present an opportunity to provide sediment data that is more accurate and less costly than traditional sampling and analysis techniques (Landers 2010). The study will work to incorporate the latest developments by USGS and others in the work to develop standard procedures for the use of hydroacoustic technology.

SECCHI TUBE

Secchi tube measurements through Minnesota's volunteer stream monitoring program provide a fourth measure of sediment in water. It is an indirect measure of the amount of dissolved and suspended material in water. The Secchi tube forms the foundation of the MPCA Citizen Stream-Monitoring Program (CSMP). The CSMP is part of the volunteer water-monitoring program in Minnesota. The CSMP began in 1998 with the goal to provide individuals an opportunity to get involved in a simple, yet meaningful stream monitoring program. The Secchi tube is a modified transparency tube that is designed to function like a traditional Secchi disk used in lake monitoring (MPCA 2011). 358 CSMP volunteers monitored almost 500 sites in 2013. The transparency data are entered into the MPCA's water quality database and is used in conjunction

with turbidity and TSS data in assessing the water quality condition of Minnesota's streams (MPCA 2013).

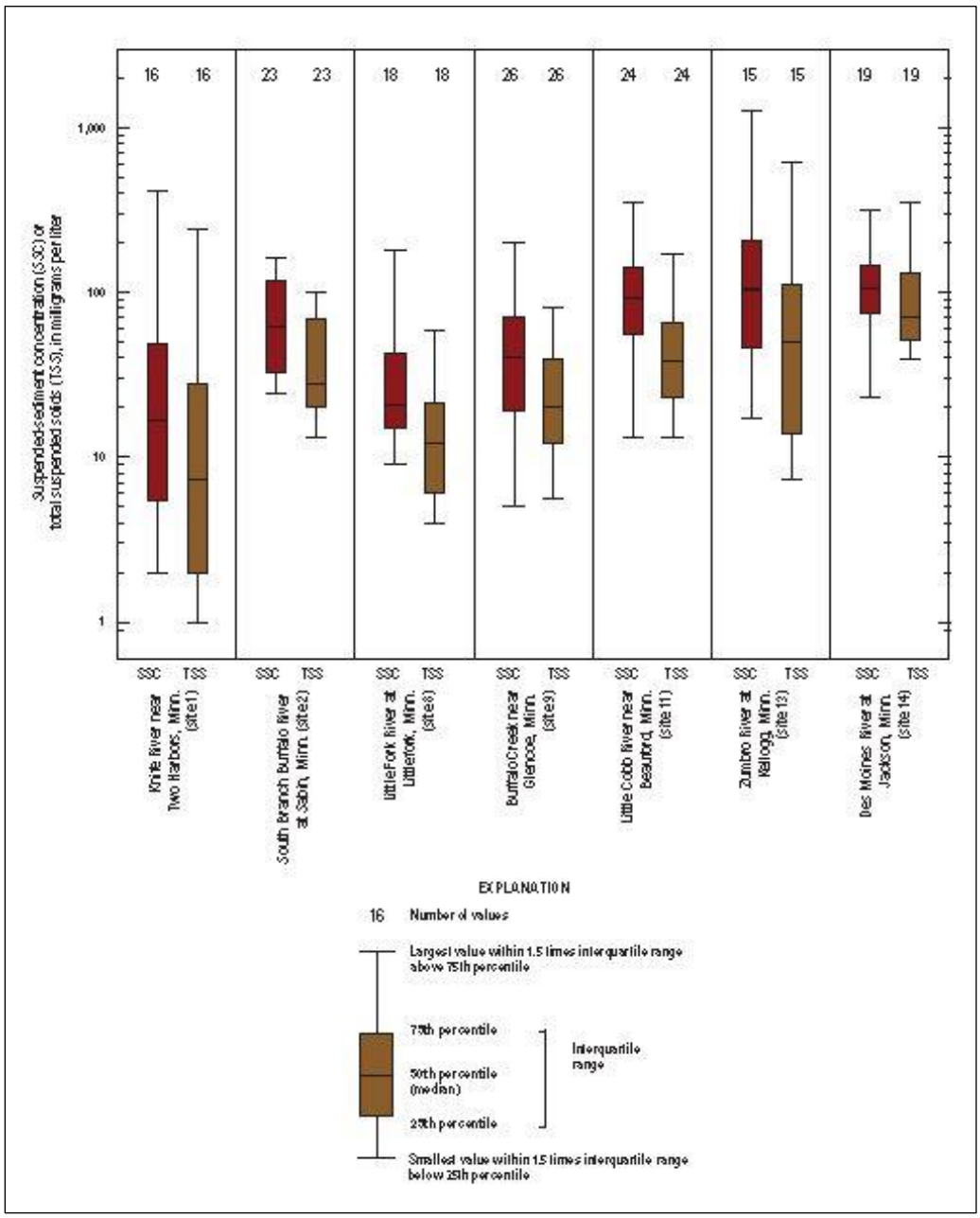

Figure 4 Suspended-sediment concentrations and total suspended solids for selected sites in Minnesota, 2007 through 2011 (from Ellison et al. 2014).

DATA APPLICATIONS

Various measures of sediment have been used in Minnesota. The use of each has its own positive and negative aspects. The use of turbidity will switch from being a numeric water quality standard to more of a surrogate for sediment issues. TSS will provide an improvement to

Minnesota's water quality standards by providing a parameter with units of concentration and mass, incorporating an explicit exceedance interval, and shifting to a direct measure of sediment. Watershed models are being developed for each major watershed in Minnesota using the Hydrological Simulation Program – FORTRAN (HSPF) computer model. The models will simulate the surface hydrology and water quality of Minnesota's 81 major watersheds. Calibration of the model requires the use of available water quality data. The model calibration for sediment relies primarily on TSS data. HSPF predicts sediment output as concentrations of clay, silt, and sand. Calibration requires that assumptions be made regarding the particle sizes of the sediment in the water and that sampled by TSS.

Sediment budgets provide an accounting method for sediment entering, leaving, and stored in a landscape unit, accounting for the sediment sources and disposition (Phillips, 1986; Reid and Dunne, 1996). Sediment budgets have been developed using various types and amounts of data. Early sediment budgets were completed by Beach (1994) and NRCS (1994, 1996, and 1997). Barr Engineering Company (2004) completed a project for the MPCA evaluating the sediment data available for the Lower Mississippi River Basin in Minnesota. Wilcock (2010) describes the most recent sediment budget work done to identify and quantify the sources of fine sediment in the Minnesota River Basin. An integrated sediment budget for the Le Sueur River Basin was completed as part of this work (Gran et al. 2011). A similar project for the Greater Blue Earth River Basin is scheduled for completion in 2015. With the exception of limited SSC and bedload data, the sediment budgets have had to rely on TSS data.

The addition of SSC and bedload monitoring through the cooperative agreement with USGS provides the opportunity to provide a more direct calibration of the watershed models, complete more comprehensive sediment budgets, and identify specific stressors affecting aquatic life. The best approach, which to date has not been fully implemented, would be to utilize a sediment budget approach incorporating improved monitoring techniques for suspended and bedload materials and to concurrently assess both stream geomorphology and the biotic community. Such an effort cannot be done for every watershed in the State, but it would be beneficial to have it in selected watersheds. Knowledge about the sand-sized particles along with the fines in suspended sediment is especially important in making connections between impaired aquatic life, habitat, and sediment sources and transport processes.

REFERENCES

American Public Health Association and American Water Works Association. (1946). Standard Methods for the Examination of Water and Sewage (9th ed.): New York, American Public Health Association, 286 pp.

American Public Health Association, American Water Works Association, and Water Pollution Control Federation. (1971). Standard Methods for the Examination of Water and Wastewater (13th ed.): Washington, D.C., American Public Health Association, 874 pp.

American Public Health Association, American Water Works Association, and Water Pollution Control Federation. (1976). Standard Methods for the Examination of Water and Wastewater (14th ed.): Washington, D.C., American Public Health Association, 1193 pp.

American Public Health Association, American Water Works Association, and Water Pollution Control Federation. (1985). Standard Methods for the Examination of Water and Wastewater (16th ed.): Washington, D.C., American Public Health Association, 1268 pp.

Anderson, C.W. (2005). Turbidity (version 2.1), U.S. Geological Survey Techniques of Water-Resources Investigations, book 9, chap. A6, section 6.7.

Barr Engineering Company, (2004), Lower Mississippi River Basin Sediment Evaluation Project, Minnesota Pollution Control Agency, 142 pp

Beach, Timothy. (1994). "The fate of eroded soil: sediment sinks and sediment budgets of agrarian landscapes in Southern Minnesota, 1851-1988," Annals of the Assoc. of American Geographers, 84(1):5-28.

Ellison, C.A., Savage, B.E., and Johnson, G.D. (2014). Suspended-sediment concentrations, loads, total suspended solids, turbidity, and particle-size fractions for selected rivers in Minnesota, 2007 through 2011: U.S. Geological Survey Scientific Investigations Report 2013–5205, 43 pp.

Federal Water Pollution Control Administration. (1968). 1968 *Report of the Committee on Water Quality Criteria.* U.S. Department of the Interior. April, 1968.

Gran, K., P. Belmont, S. Day, C. Jennings, J.W. Lauer, E. Viparelli, P. Wilcock, and G. Parker, (2011). An Integrated Sediment Budget for the Le Sueur River Basin Final Report, Minnesota Pollution Control Agency, 128 pp.

Gray, J.R, Glysson, G.D., Turcios, L.M., and Schwaz, G.E. (2000). Comparability of suspended-sediment concentration and total suspended solids data, USGS Water-Resources Investigations Report 00-4191, 14 pp.

Landers, M.N. (2010). "Review of methods to estimate fluvial suspended sediment characteristics from acoustic surrogate metrics," 2nd Joint Federal Interagency Conference, Las Vegas, NV, June 27 - July 1, 2010.

Markus, H.D. (2011). Aquatic Life Water Quality Standards Draft Technical Support Document for Total Suspended Solids (Turbidity), Minnesota Pollution Control Agency, 50 pp.

MPCA. (2007). Turbidity TMDL Protocols and Submittal Requirements, Minnesota Pollution Control Agency, 95 pp.

MPCA. (2011). Citizen Stream Monitoring Program Instruction Manual, Minnesota Pollution Control Agency, 34 pp.

MPCA. (2013). Annual Summary of the Citizen Monitoring Program, Minnesota Pollution Control Agency.

MPCAa. (2014). Book 3: Total Suspended Solids (TSS), Minnesota Pollution Control Agency Environmental Analysis and Outcomes Division Statement of Need and Reasonableness: In the Matter of Proposed Revisions of Minn. R. Ch. 7050, Relating to the Classification and Standards for Waters of the State; and 7053 Relating to Effluent Limits and Treatment Requirements for Discharges to Waters of the State, Minnesota Pollution Control Agency, 33 pp.

MPCAb. (2014). Watershed Pollutant Load Monitoring Network, Minnesota Pollution Control Agency, http://www.pca.state.mn.us/pyrieeb, accessed January 20, 2015.

NRCS. (1994). Sediment Budget for the Nemadji River Wateshed, Minnesota and Wisconsin, USDA NRCS, St. Paul, Minnesota.

NRCS. (1996). Erosion – Sedimentation – Sediment Yield Report, Thief and Red Lake Rivers Basin, Minnesota, USDA NRCS, St. Paul, Minnesota.

NRCS. (1997). Sediment Budget, Whitewater River Watershed, USDA NRCS, St. Paul, Minnesota.

Phillips, J.D.(1986). "The utility of the sediment budget concept in sediment pollution control," Professional Geographer, 38(3):246-252.

Reid, L. M. and Dunne, T. (1996). Rapid Evaluation of Sediment Budgets, Catenna Verlag GMBH, Reiskirchen, Germany, 164 pp.

Sadar, M.J. (1998), Turbidity Science, Technical Information Series - Booklet No. 11, Hach Company, Loveland, CO, 26 pp.

Tornes, L.H., (1986), Suspended Sediment in Minnesota Streams, U.S. Geological Survey Water-Resources Investigations Report 85-4312, 33 p.

U.S. Environmental Protection Agency. 1976. *Quality Criteria for Water 1976.* Office of Water, Regulations and Standards, Washington, DC. July 1976.

USGS. (2004). USGS Water Quality Technical Memorandum 2004.03, http://water.usgs.gov/admin/memo/QW/qw04.03.html, accessed January 13, 2015.

Wilcock, PR, on behalf of the Minnesota River Sediment Colloquium Committee. (2009). Identifying sediment sources in the Minnesota River Basin, Minnesota Pollution Control Agency, 16 pp.

ONLINE MODELING TOOLS ASSIST IN EVALUATING POSTFIRE FLOODING AND EROSION RISK

Peter Robichaud, Research Engineer, USDA Forest Service, Rocky Mountain Research Station, Moscow, Idaho, probichaud@fs.fed.us; William Elliot, Research Engineer, USDA Forest Service, Rocky Mountain Research Station, Moscow, Idaho, welliot@fs.fed.us; Erin Brooks, Assistant Professor, University of Idaho, Moscow, Idaho, ebrooks@uidaho.edu; Marianna Dobre, Post-doctoral Fellow, University of Idaho, Moscow, Idaho, mdobre@uidaho.edu; Dennis Flanagan, Research Agricultural Engineer, USDA Agricultural Research Service, National Soil Erosion Laboratory, West Lafayette, Indiana, Dennis.Flanagan@ars.usda.gov; James Frankenburger, Information Technology Specialist, USDA Agricultural Research Service, National Soil Erosion Laboratory, West Lafayette, Indiana, James.Frankenburger@ars.usda.gov

Abstract: Postfire assessment teams need erosion modeling tools to quickly assess the risks of elevated runoff and sediment delivery to infrastructure and water resources. Major advancements in our knowledge of postfire assessments, risk analysis and erosion control treatment effectiveness have improved our ability to understand the consequences and outcomes that occur in the postfire environment. Disturbed areas often increase overland flow connectivity degrading water quality and water resource. We have developed accessible and easy-to-use Water Erosion Prediction Project (WEPP) based online models to help forest land managers predict postfire runoff, soil erosion and sediment delivery from disturbed forests and rangelands. These models, the Erosion Risk Management Tool (ERMiT), Disturbed WEPP and the Peak Flow Calculator allow users to vary climate, soil texture, local topography, vegetation, and surface cover (burn severity, management activities, etc.). ERMiT is more appropriately used by land managers to predict the probability of postfire sediment delivery for a given storm for hillslopes left untreated and hillslopes treated mulch, seeding, or erosion barriers. The latter model aids in decisions of where, when, and how to apply postfire mitigation treatments. Disturbed WEPP predicts annual runoff and sediment yields from young and old forests, following wildfire, grazing, and timber harvest disturbances. These tools are also available as ERMiT Batch and Disturbed WEPP Batch allowing users to vary input parameters and efficiently compare results in simple spreadsheet output tables. The Peak Flow Calculator allows users to quickly determine peak discharge rates for small watersheds. Online GIS-WEPP BAER Interface is the most recent addition to our suite of user-friendly model platforms. Local topographic, soils, fire effects and climatic variables are seamlessly incorporated into the WEPP Watershed model with point-and-click area selection using online mapping services. These easy to access and easy to use tools assist in making the best use of limited rehabilitation resources and assessing fire effects on soils in conjunction with local climate and watershed characteristics.

INTRODUCTION

Land management issues related to wildfires and postfire response have become more prominent as the frequency of large wildfires has increased. Resource managers are concerned with both the direct effects of the flame front and the postfire consequences. Postfire peak runoff and erosion can be orders-of-magnitude larger than prefire values due to the loss of surface cover and fire-induced changes in soil properties (Moody et al. 2013). Direct and indirect fire effects impact

larger numbers of people as source water for municipal water supplies and community developments are encompassed by areas increasingly at risk for wildfire (Miller et al. 2011).

ONLINE MODELING TOOLS

Many of our postfire erosion models (http://forest.moscowfsl.wsu.edu/fswepp/; Figure 1) were developed as part of a suite of tools (http://forest.moscowfsl.wsu.edu/BAERTOOLS/) for use by Burned Area Emergency Response (BAER) teams. The models are fully open to the public and there are no costs associated with their use allowing both public and private specialists access to the same tools. Behind the interfaces, the Water Erosion Prediction Project (WEPP) Model, a distributed physically-based hydrology and erosion model (Flanagan and Nearing 1995; Laflen et al. 1997), is the server-based "engine" that processes inputs and creates outputs based on the Forest Service WEPP interfaces.

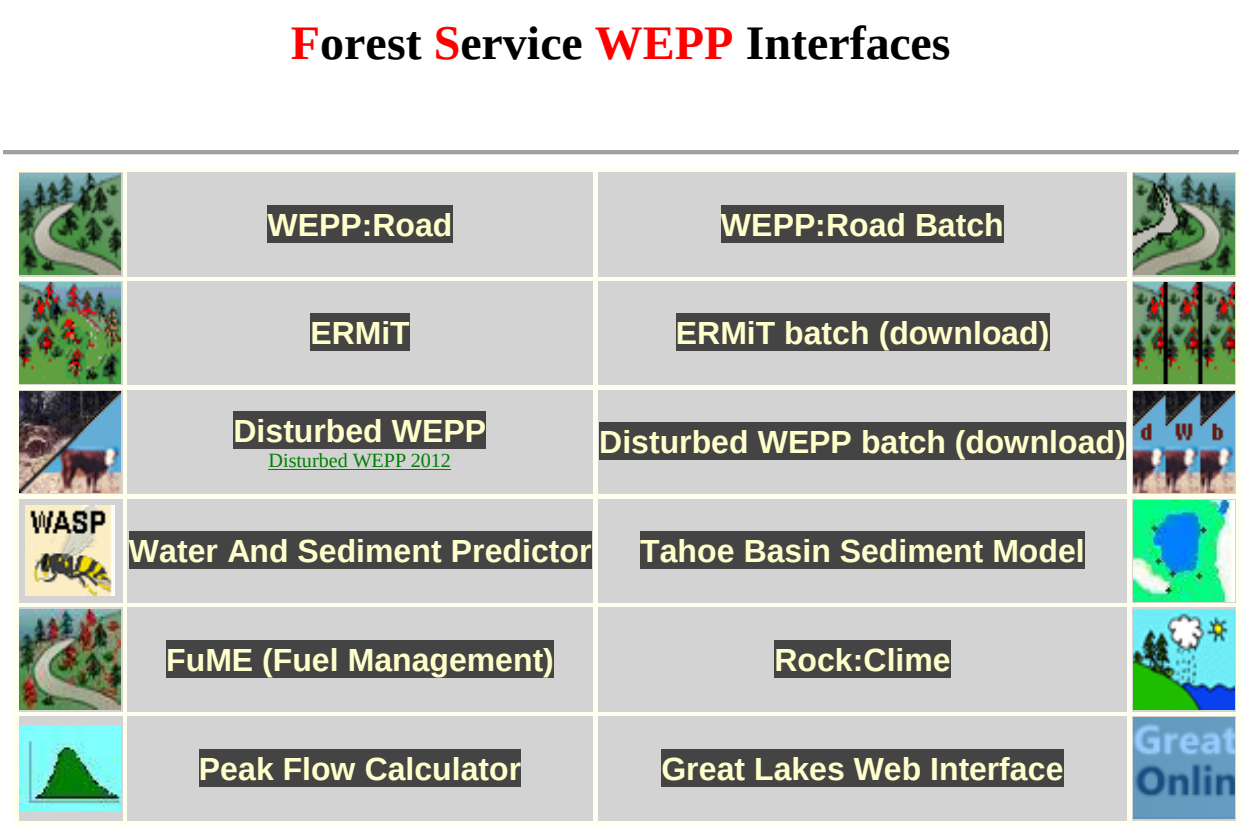

Figure 1. Online web page for accessing Forest Service WEPP models (http://forest.moscowfsl.wsu.edu/fswepp).

ERMiT: The Erosion Risk Management Tool (ERMiT) predicts the probability of a given depth of runoff and sediment yield from a single rainfall or snowmelt event on unburned, burned, and recovering forest, range, and chaparral hillslopes (Robichaud et al. 2007a; b). ERMiT provides a distribution of single event erosion rates with the likelihood of their occurrence. ERMiT also predicts the sediment yields following mulching, seeding, and installing of log erosion barriers (Figure 2).

Sediment Delivery					
Probability that sediment yield will be exceeded 35 % go	Event sediment delivery (ton ac^{-1})				
	Year following fire				
	1st year	2nd year	3rd year	4th year	5th year
Untreated	10.63	4.73	2.1	1.06	0.25
Seeding	10.63	2.87	1.82	1	0.25
Mulch (0.5 ton ac^{-1})	2.97	2.22	2.1	1.06	0.25
Mulch (1 ton ac^{-1})	2.06	1.83	2.1	1.06	0.25
Mulch (1.5 ton ac^{-1})	2.02	1.75	2.1	1.06	0.25
Mulch (2 ton ac^{-1})	1.97	1.73	2.1	1.06	0.25
Erosion Barriers: Diameter 0.7 ft Spacing 65 ft go ?					
Logs & Wattles	7.75	4.21	1.71	0.84	0.15

Figure 2. ERMiT output screen showing various treatment effect on sediment delivery.

Disturbed WEPP: Disturbed WEPP predicts annual erosion rates for forest and rangeland hillslopes (Elliot 2013). Disturbed WEPP can simulate a variety of management scenarios, including the effects of wildfire, fuel treatments, timber harvest, and regeneration. The output includes mean annual runoff, erosion rate, sediment yield, and the probability of these occurring.

Peak Flow Calculator: Our online interface to the Natural Resource Conservation Service (USDA-NRCS) Curve Number method is used to estimate stream peak flow from small burned watersheds. The rainfall and runoff amounts predicted by ERMiT, other computer programs, or reported in the literature can be used to estimate a curve number for a selected land use condition, which in the case of fire is generally related to the soil burn severity.

ERMiT and Disturbed WEPP Batch Spreadsheet Tools: Downloadable batch spreadsheet tools for the ERMiT and Disturbed WEPP interfaces are available (http://forest.moscowfsl.wsu.edu/fswepp/batch/bERMiT.html; http://forest.moscowfsl.wsu.edu/fswepp/batch/dWb.html). The model runs are carried out on our server, but input scenarios and processing of results are done on the user's computer with spreadsheet software. These spreadsheets allow users to run ERMiT or Disturbed WEPP for multiple hillslopes simultaneously. Drop down menus and copy/paste features facilitate the process of filling out the input worksheet(s).

Online GIS-WEPP BAER: We have developed new beta-release tool that uses the open-source MapServer© online GIS in conjunction with WEPP spatial analysis procedures to allows users to conduct watershed analysis without the need to have a GIS program on their computer or the need to reformat data sets (Frankenberger et al. 2011). The interface uses Google Map images and TOPAZ analysis to define a watershed for simulation with WEPP, based on the USGS seamless DEM. The post-fire burn severity map is the primary input to define the spatial extent

of the fire which is used in conjunction with the soil layer, the vegetation layer, and DEMs (Frankenberger et al. 2011; Flanagan et al. 2013). These interfaces do not require advanced GIS skills, such as the downloading and preprocessing of topography, soils, or land cover databases.

REFERENCES

Elliot, W.J. (2013). Erosion processes and prediction with WEPP technology in forests in the Northwestern U.S. Transactions of the ASABE 56(2), 563–579.

Flanagan, D.C., and Nearing, M.A. (1995). USDA-Water Erosion Prediction Project: Hillslope profile and watershed model documentation. US Department of Agriculture, National Soil Erosion Research Laboratory, NSERL Report No. 10. West Lafayette, IN.

Flanagan, D.C., Frankenberger, J.R., Cochrane, T.A., Renschler, C.S., and Elliot, W.J. (2013). Geospatial application of the Water Erosion Prediction Project (WEPP). Transactions of the ASABE 56(2), 591–601.

Frankenberger, J.R., Dun, S., Flanagan, D.C., Wu, J., and Elliot, W.J. (2011) Development of a GIS interface for WEPP model application to Great Lakes forested watersheds. Presented at International Symposium on Erosion and Landscape Evolution, 18–21 September 2011, Anchorage, AK. Paper No. 11139. American Society of Agricultural and Biological Engineering: St. Joseph, MI.

Laflen, J.M., Elliot, W.J., Flanagan, D.C., Meyer, C.R., and Nearing. M.A. (1997). WEPP—Predicting water erosion using a process-based model. Journal of Soil and Water Conservation 52(2), 96–102.

Miller, M.E., MacDonald, L.H., Robichaud, P.R., and Elliot, W.J. (2011). Predicting post-fire hillslope erosion in forest lands of the western United States. International Journal of Wildland Fire 20(8), 982–999.

Moody, J.A., Shakesby, R.A., Robichaud, P.R., Cannon, S.H., and Martin. D.A. (2013). Current research issues related to post-wildfire runoff and erosion processes. Earth-Science Reviews 122, 10–37.

Robichaud, P.R., Elliot, W.J., Pierson, F.B., Hall, D.E., Moffet, C.A., and Ashmun, L.E. (2007a). Erosion risk management tool (ERMiT) user manual, version 2006.01.18. US Department of Agriculture, Forest Service, Rocky Mountain Research Station, General Technical Report RMRS-GTR-188. Fort Collins, CO.

Robichaud, P.R., Elliot, W.J., Pierson, F.B., Hall, D.E., Moffet, C.A., and Ashmun, L.E. (2007b). Predicting postfire erosion and mitigation effectiveness with a web-based probabilistic erosion model. Catena 71, 229–241.

Robichaud, P.R., and Ashmun, L.E. (2013). Tools to aid post-wildfire assessment and erosion-mitigation treatment decisions. International Journal of Wildland Fire 22, 95–105.

POTAMOD – MOBILE-BED SEDIMENT-TRANSPORT MODELING APPLICATION FOR USE WITH SIAM AND HEC-RAS

Amanda L. Cox, Assistant Professor, Parks College of Engineering, Aviation and Technology, Saint Louis University, St. Louis, MO, coxal@slu.edu; David S. Biedenharn, Hydraulic Engineer, Biedenharn Group, LLC, Vicksburg, MS, biedenharngroup@yahoo.com; Chester C. Watson, Hydraulic Engineer, Biedenharn Group, LLC, Vicksburg, MS, chester@chestercwatson.com; Michelle Martin, Hydraulic Engineer, Anderson Consulting Engineers, Inc., Fort Collins, CO, mlmartin@acewater.com

Abstract: The Potamology Model (PotaMod) was developed for mobile-bed modeling using the Sediment Impact and Analysis Methods (SIAM) model within HEC-RAS. PotaMod allows for updating of hydraulics in response to erosion and sedimentation. The SIAM component of HEC-RAS is a sediment budget tool that compares annualized sediment reach transport capacities to supplied sediment and identifies reaches of overall sediment surplus or deficit. SIAM uses a reach-averaged approach; thus, PotaMod follows with bed-elevation and grain-size distribution adjustments on a per-reach basis in response to sediment transport. PotaMod uses SIAM sediment-transport output data for a given series of hydrologic events to update grain-size distributions and HEC-RAS cross-section elevations for each reach. Specifically, PotaMod uses the local sediment balance output of SIAM to determine depths of aggradation or degradation for each reach, and it uses the sediment balance by grain size output to determine adjustments to grain-size distributions for each reach. PotaMod was used to simulate 100 years of sediment transport in the Long Creek Watershed located in Mississippi. The watershed includes a seven-mile reach of the Long Creek and five miles of the Caney Creek tributary. Thalweg profiles and reach-based changes in bed elevation, local balance by grain size, and grain size distributions were computed for each year.

INTRODUCTION

For projects that implement modifications to reduce watershed-sediment loads, analyzing system-wide sediment process linkages is imperative to ensure there are no negative impacts in other parts of the watershed. The Sediment Impact and Analysis Methods (SIAM) model was developed to evaluate watershed- and reach-scale sediment processes through integration of watershed-scale sediment continuity concepts and stream rehabilitation and management. SIAM is a reach-based 1-D continuity model that compares annualized sediment transport capacities to supplied sediment and identifies reaches of overall sediment surplus or deficit. SIAM results can be mapped to illustrate potential imbalances in a channel network to help identify design or remediation needs. (Little and Jonas, 2010)

In 1985, the Delta Headwaters Project (DHP), formerly the Demonstration Erosion Control (DEC) Project, was initiated with the primary objective of providing channel stability and reducing delivery of sediments to downstream reservoirs, flood-control channels, and wetlands (Hudson, 1997 and Watson et. al., 1997). SIAM was originally developed as part of the DHP and is currently embedded in the Army Corps Hydrologic Engineering Center River Analysis System (HEC-RAS) as a hydraulic design function. SIAM can be used as a screening tool for

assessing multiple rehabilitation alternatives during the reconnaissance and feasibility phases of a project (Martin et al., 2010).

The Potamology Model (PotaMod) application was developed for mobile-bed modeling using the SIAM hydraulic design function in HEC-RAS. PotaMod allows for updating of hydraulics in response to erosion and sedimentation. SIAM uses a reach-averaged approach; thus, PotaMod follows with bed-elevation and grain-size distribution adjustments on a per-reach basis in response to sediment transport. PotaMod uses SIAM sediment-transport output data for a given series of hydrologic events to update grain-size distributions and HEC-RAS cross-section elevations for each reach. Specifically, PotaMod uses the *local sediment balance* output of SIAM to determine depths of aggradation or degradation for each reach, and it uses the *sediment balance by grain size* output to determine adjustments to grain-size distributions for each reach.

As a reach-based mobile-boundary model, PotaMod has a critical advantage compared to cross-section based mobile-boundary sediment-transport models. It has the capability to simulate several years of mobile-bed sediment transport in a relatively short time period. Simulation computations are significantly shorter than cross-section based models due to reach-based sediment transport calculations and adjustments. Also, bed elevation and grain-size distribution adjustments are made after simulating a full hydrograph with varying flows and flow durations. As a point of comparison, for the Long Creek model discussed near the end of this paper, the 100-year simulation with 13 reaches and 139 cross sections completed in 10.1 minutes.

PotaMod can be used to evaluate the impacts of rehabilitation and management alternatives over a long period of time with updated hydraulic conditions allowing insight into potential changes in channel stability. Along with the benefits, PotaMod has the following limitations:

- computations are based on reach-averaged properties;
- adjustments to cross-section elevations and grain size distributions are made at the reach scale;
- adjustments to cross-section elevations and grain size distributions are made after a simulated duration of the input hydrograph;
- model assumes no limitation on bed-material supply; and
- computations are steady state and one-dimensional.

MODEL INPUTS

PotaMod works with an existing HEC-RAS SIAM model. Therefore, all inputs for a HEC-RAS and SIAM project are required to use the application. Additional required inputs include:

1. Calibration data for each reach
    a. *Local Balance Calibration Criteria*
        i. *Calibration adjustment factor* – a multiplier applied to SIAM computed sediment transport.
        ii. *Max aggradation or degradation value* – a maximum value given as a rate in ft/yr.
        iii. *Negligible aggradation or degradation value* – given in units of ft.

b. *Representative flow depths*– used for computing adjustments to grain-size distributions. Three options are provided: reach-averaged hydraulic depth, reach-averaged maximum cross-sectional flow depth, and a user-defined depth. All depths are given in ft.
c. *Minimum wash load criteria* – user can choose a criterion from a list of grain-size categories or user may choose to have no minimum wash load criterion.

2. Number of iterations to perform – program uses the duration curve provided in the SIAM input to determine simulation period.

MODEL CALCULATIONS

Once a simulation is initiated, PotaMod executes HEC-RAS and then SIAM. Subsequently, PotaMod uses the *local sediment balance* and *balance by grain size* data from the SIAM output and updates both cross-section elevations and grain-size distributions for each SIAM reach. This section details how the model calculates changes in cross-section elevations and grain-size distributions.

Cross-Section Elevation Adjustments for SAIM Reaches: Using the *local sediment balance* SIAM output for each reach, HEC-RAS cross sections are adjusted on a per-reach basis. The following provides an outline of how the program computes changes in cross-section elevations and how those changes are applied to a series of cross sections within a SIAM reach:

1. *Local sediment balance* output from SIAM is adjusted using the *local balance calibration factor.*

2. Adjusted local balance is converted from tons to volume of bed material using a unit weight of 95 lbs/ft^3 for the bed material.

3. The volume of bed material is divided by the reach length and the reach-averaged channel bankfull width to obtain a channel-elevation adjustment for the entire reach: depth of aggradation, d_A or depth of degradation, d_D. Reach lengths are determined as the difference between the upstream-most and downstream-most river stations within a defined SIAM reach *plus* one-half of the distance between the upstream-most cross section within the reach and the adjacent cross section upstream of the reach *and* one-half of the distance between the downstream-most cross section within the reach and the adjacent cross section downstream of the reach. Eq. 1 provides the mathematical expression used for computing reach lengths:

$$L = (Sta_{US} - Sta_{DS}) + 0.5(Sta_{Ad-US} - Sta_{US}) + 0.5(Sta_{DS} - Sta_{Ad-DS}) \quad \text{Eq. 1}$$

where L is the reach length (ft); Sta_{US} is the upstream-most river station within a SIAM reach (ft); Sta_{DS} is the downstream-most river station within a SIAM reach (ft); Sta_{Ad-US} is the river station adjacent to the SIAM reach on the upstream end (ft); and Sta_{Ad-DS} is the river station adjacent to the SIAM reach on the downstream end (ft).

For SIAM reaches that have only one cross-section, the reach length is computed using Eq. 2:

$$L = 0.5\left(Sta_{Ad-US} - Sta_{US}\right) + 0.5\left(Sta_{DS} - Sta_{Ad-DS}\right) \qquad \text{Eq. 2}$$

Further, for computing reach-averaged channel bankfull widths, individual cross-section bankfull widths are determined as the distance between the defined left-bank station and right-bank station within each HEC-RAS cross section.

If the depth of degradation or aggradation is less than the user-defined negligible tolerance, no adjustment is made to the cross-section elevations within that reach. Otherwise, computed reach elevation adjustments are converted to a degradation or aggradation rate by dividing by the simulation period (units of ft/time). If the degradation or aggradation rate is greater than the user input limiting rate, the depth of degradation or aggradation is set to the limiting value for that reach.

4. Cross-section elevation data points within the bankfull width are identified for each cross section using the defined left-bank and right-bank stations from HEC-RAS data.

5. Identified cross-section points within the bankfull width are adjusted by the computed depth of aggradation or degradation.

Grain-Size Distribution Adjustments for SIAM Reaches: Using the SIAM output for *local sediment balance by grain size*, grain-size distributions (GSD) are adjusted for each SIAM reach. Initially, PotaMod develops a GSD for aggradation or degradation from the *local sediment balance by grain size* SIAM output data for each reach. Subsequently, PotaMod determines whether aggradation or degradation occurred from the *local balance*. For aggradation, an aggradation GSD is developed from the aggraded particle sizes and any degraded particle sizes are neglected. For degradation, a degradation GSD is developed from the degraded particles sizes and any aggraded particles sizes are neglected.

Case of Aggradation If the depth of aggradation is greater than the user-defined negligible depth of aggradation for a given reach, a new bed-material GSD is computed using a weighted average with the computed aggradation GSD and the previous bed-material GSD. A volume-based averaging method is used where the aggradation GSD is weighted by the depth of aggradation and the previous GSD is weighted by 10% of the representative flow depth. The averaging method is presented in Eq. 3:

$$GSD_N = \left(\frac{d_A}{d_A + (10\%)y}\right) GSD_A + \left(\frac{(10\%)y}{d_A + (10\%)y}\right) GSD_P \qquad \text{Eq. 3}$$

where GSD_N is the bed-material percent-finer value for a given particle-size classification (GSD) for next time-step simulation; d_A is the depth of aggradation determined from *local sediment balance* [L]; y is the representative flow depth assigned as either the reach-averaged

hydraulic depth or maximum reach hydraulic depth[L]; GSD_A is the aggradation GSD determined from *local sediment balance by grain size*; and GSD_P is the GSD for previous simulation. If the depth of aggradation is less than the user-defined negligible depth of aggradation, then no adjustment to the GSD is made for that reach ($GSD_N = GSD_P$).

Case of Degradation If the computed depth of degradation, d_D, is less than the computed mixing depth (10% of the representative flow depth) and is greater than the negligible degradation depth, a new bed-material GSD is computed using a weighted average with the computed degradation GSD and the previous bed-material GSD. A volume-based averaging method is used where the armor layer GSD is weighted by the depth of the armor layer and the previous bed-material GSD is weighted by 10% of the representative flow depth. The averaging method is presented in Eq. 4:

$$GSD_N = \left(\frac{d_{AL}}{d_{AL} + (10\%)y}\right) GSD_{AL} + \left(\frac{(10\%)y}{d_{AL} + (10\%)y}\right) GSD_P \qquad \text{Eq. 4}$$

where GSD_{AL} is the armor layer GSD as determined by Eq. 5; and d_{AL} is the depth of armor layer as determined by Eq. 6 [L].

$$GSD_{AL} = \frac{GSD_P(d_T) - GSD_D(d_D)}{d_{AL}} \qquad \text{Eq. 5}$$

where d_T is the total depth of previous bed material altered ($d_T = d_{AL} + d_D$) as determined by Eq. 7 [L]; GSD_D is the degradation GSD determined from *local sediment balance by grain size*; and d_D is the depth of degradation determined from local sediment balance [L].

$$d_{AL} = d_T - d_D \qquad \text{Eq. 6}$$

$$d_T = d_D Max\left(GSD_D / GSD_P\right) \qquad \text{Eq. 7}$$

If the depth of degradation, d_D, is greater than the computed mixing depth (10% of the representative flow depth), then no adjustment to the GSD is made for that reach ($GSD_N = GSD_P$). Also, if the depth of degradation, d_D, is less than the user-defined negligible depth of degradation, then no adjustment to the GSD is made for that reach ($GSD_N = GSD_P$).

Wash Load Criteria Adjustments for SIAM Reaches: If the *Minimum Wash Load Criterion* is set to "0, None" in the calibration input for a given SIAM reach, the *Wash Load Maximum Class Diameter* for SIAM calculations is adjusted based solely on the updated grain-size distributions. Specifically, the grain-size classification with the largest grain-size diameter where less than 10% of the particles by weight are finer is set as the new *Wash Load Maximum Class Diameter* for the next iteration. If the *Minimum Wash Load Criterion* is set to one of the twenty grain-size classifications in the calibration input, the grain-size classification with the

largest grain-size diameter where less than 10% of the particles by weight are finer is compared to the *Minimum Wash Load Criterion* and whichever is largest is set as the new *Wash Load Maximum Class Diameter* for the next iteration.

MODEL OUTPUTS

PotaMod provides output data for: 1) bed elevations and changes for each iteration; 2) local balance by grain size; 3) reach grain-size distributions; and 4) thalweg profiles for each iteration. The following sections provide details for each type of output data.

Bed-Elevation Data: Bed-elevation output data contain information on changes in bed elevations for each SIAM reach and each iteration. Specifically, the following data are provided: *Reach ID*, *Reach Name*, *Iteration Number*, *Time* (yrs), *Local Balance* (tons), *Bed Elevation Change* (ft), *Cumulative Bed Elevation Change* (ft), *Average Bankfull Flow Depth* (ft), and *Maximum Bankfull Flow Depth* (ft).

Local Balance by Grain Size Data: Local balance by grain size output data contain information on the local balance by grain size for each SIAM reach and each iteration. Specifically, the following data are provided: *Reach ID*, *Reach Name*, *Iteration Number*, *Total Local Balance* (tons), and *Local Balance by Grain Size* (tons). The grain-size classifications are consistent with those used within SIAM, in which there are twenty classifications ranging from Clay to LB (large boulder).

Reach Grain Size Distribution Data: Reach GSD output data contain information regarding the grain-size distribution and wash load index for each SIAM reach and each iteration. Specifically, the following data are provided: *Reach ID, Reach Name, Iteration Number, Wash Load Index,* and *Grain-Size Distribution*. Similar to the *local balance by grain size*, *grain-size distributions* are reported using the grain-size classification system within SIAM. Further, the *Wash Load Index* is given as an integer value between 1 and 20 and directly correlates to the grain-size classifications.

Thalweg Profiles: Thalweg profile output data contain information regarding thalweg elevations for each river station and iteration. Specifically, the following data are provided: *River Reach Name*, *SIAM Reach Name*, *River Station* (ft), *Initial Thalweg Elevation* (ft), and *Thalweg Elevation* for a given iteration (ft).

APPLICATION TO LONG CREEK WATERSHED

Martin et al. (2010) presented SIAM analyses conducted for three of the DHP watersheds: Hickahala Creek, Long and Caney Creeks, and Harland Creek. The baseline SIAM model for the Long Creek Watershed was used as input for PotaMod to evaluate 100 years of sediment transport. The Long Creek Watershed is located in Mississippi and has an area of 39.7 mi^2 (Figure 1). The watershed includes a seven-mile reach of Long Creek and five miles of the Caney Creek tributary. For the SIAM and PotaMod analyses, the watershed was divided into 13 SIAM reaches (Figure 2).

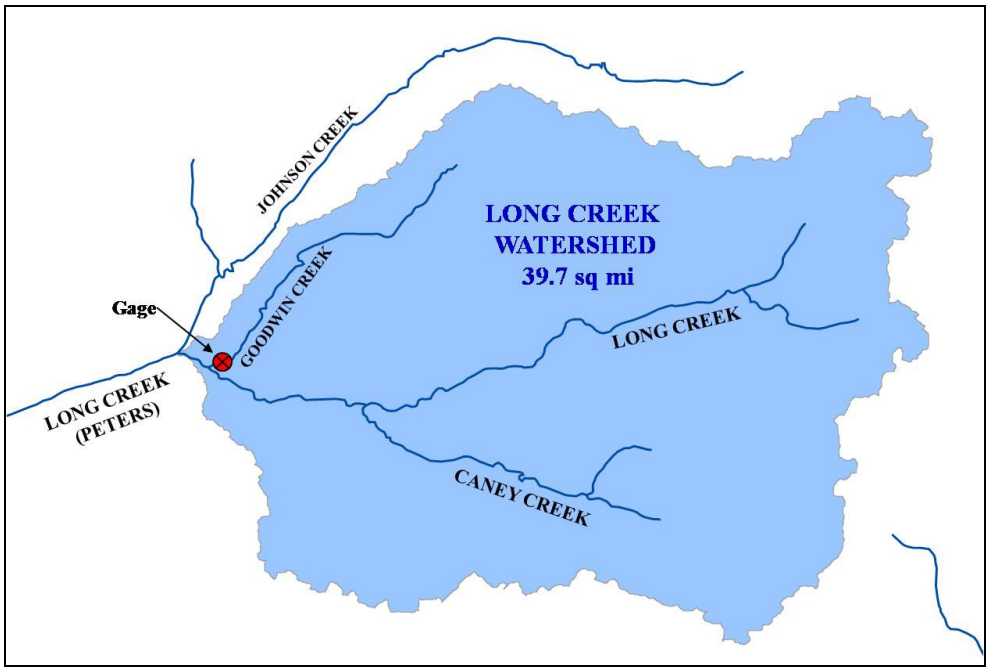

Figure 1. Long and Caney Creek Watershed (Martin et al., 2010)

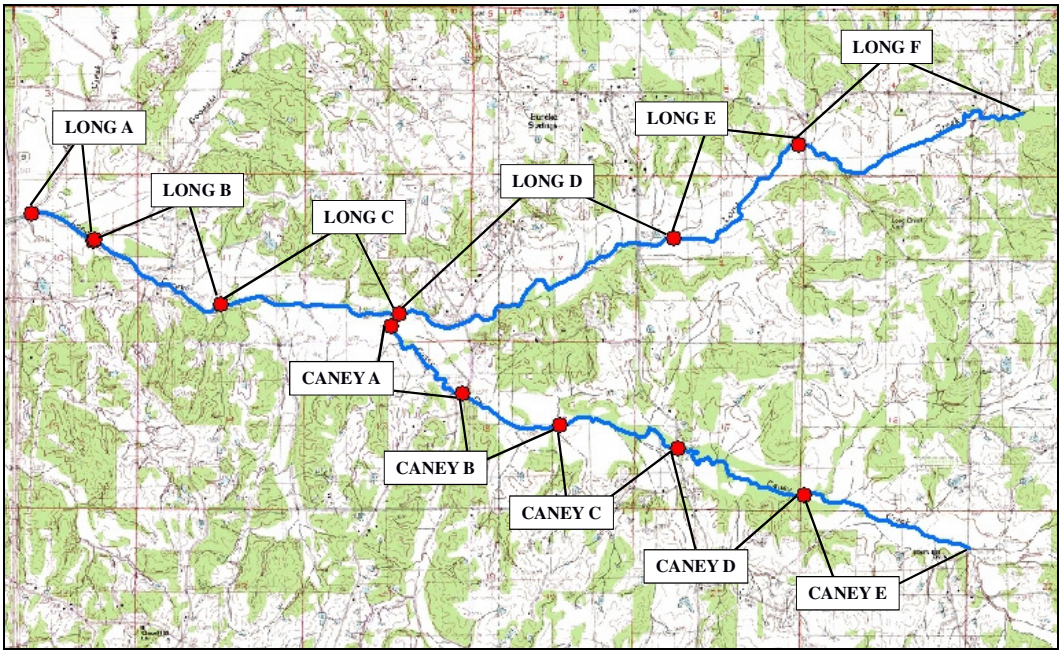

Figure 2. Long Creek and Caney Creek SIAM reaches (Martin et al., 2010)

Results of the Martin et al. (2010) SIAM analysis indicated that the DHP reduced fine sediments delivered from the Long Creek Watershed by 44%. Figure 3 shows pre- and post-project fine-sediment supply (determined from SIAM models) for the Long Creek Watershed resulting from implementing DHP features (bank stabilization and grade control structures).

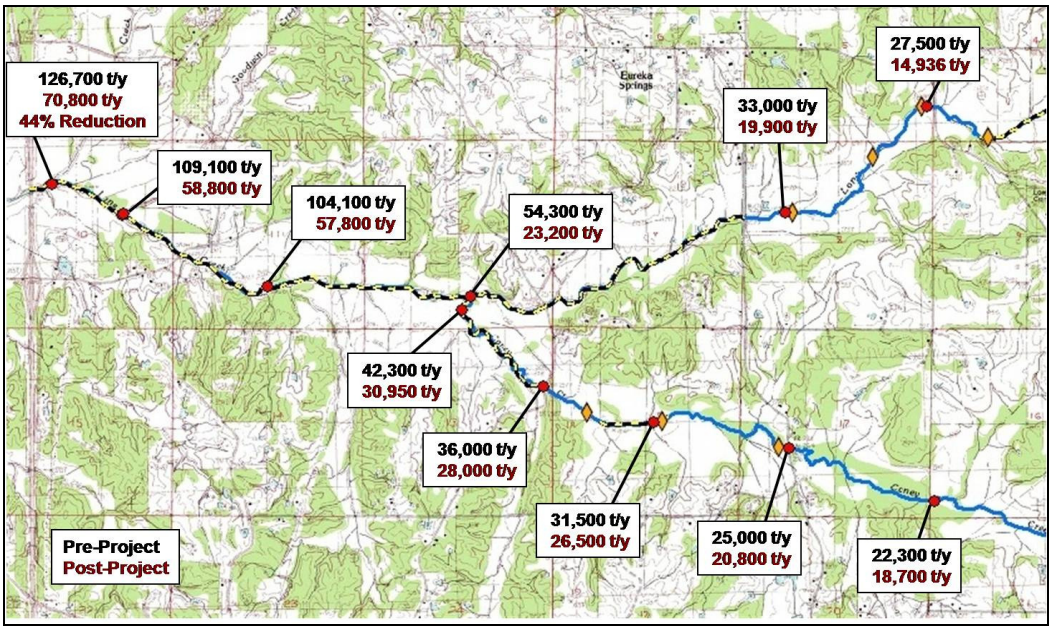

Figure 3. Reductions in fine-sediment supply along Long and Caney Creeks as a result of the DHP features determined from SIAM analysis (Martin et al., 2010)

Model Inputs Reach-based model input parameters are provided in Table 1 The Laursen (Copeland) SIAM transport function was specified for sediment transport computations and a calibration coefficient of 0.01 was used for all reaches. Maximum scour or aggradation rates were set to 0.5 ft/hr for all reaches except for the reaches at the model boundaries. The downstream boundary reach had a limiting aggradation and degradation rate of 0.01 ft/yr and both upstream boundary cross sections had a limiting rate of 0.25 ft/hr. The wash load criteria threshold was set at very fine sand (VFS) meaning that the wash load particle size was not allowed to be less than 0.125 mm. The input parameters were varied to assess the sensitivity of each parameter and the values in Table 1 were used for the model results presented within this paper. The input parameters were not calibrated using field data, as the purpose of this project was to illustrate the model utility of the program and long-term aggradation and degradation data were not available for calibration.

Table 1. Reach-based input parameters

SIAM Sediment Reach Name	Sediment Transport Calibration	Limiting Rate of Agg/Deg (ft/yr)	Mixing Depth Criteria	Initial Representative Depth (ft)	Min Wash Load Criteria
Long A	0.01	0.01	Average	17.6	6, VFS
Long B	0.01	0.5	Average	14.17	6, VFS
Long C	0.01	0.5	Average	13.11	6, VFS
Long D	0.01	0.5	Average	10.56	6, VFS
Long E	0.01	0.5	Average	10.08	6, VFS

SIAM Sediment Reach Name	Sediment Transport Calibration	Limiting Rate of Agg/Deg (ft/yr)	Mixing Depth Criteria	Initial Representative Depth (ft)	Min Wash Load Criteria
Long F	0.01	0.5	Average	9.75	6, VFS
Long USBC	0.01	0.25	Average	8.54	6, VFS
Caney A	0.01	0.5	Average	13.6	6, VFS
Caney B	0.01	0.5	Average	13.17	6, VFS
Caney C	0.01	0.5	Average	9.83	6, VFS
Caney D	0.01	0.5	Average	6.2	6, VFS
Caney E	0.01	0.5	Average	5.44	6, VFS
Caney USBC	0.01	0.25	Average	5.38	6, VFS

USBC = upstream boundary condition.

The one-year hydrograph data used in the model are shown in Table 2. The model computed sediment-transport budgets for the one-year hydrograph using SIAM, then updated bed elevations and grain-size distributions in the HEC-RAS model based on SIAM output data. PotaMod repeated this process 100 times for a total simulation time of 100 years.

Table 2. One-year hydrograph for SIAM calculations

Duration (days)	Discharge (cfs)
104.52	11
28.51	22
26.91	44
26.64	88
35.85	179
40.01	362
42.23	733
35.11	1485
20.94	3007
4.53	6086

Model Results Cumulative bed-elevation changes for reaches in Long Creek and Caney Creek are shown in Figure 4 and Figure 5, respectively. The maximum degradation depth for Long Creek was approximately five feet and it occurred in Long F Reach at the end of the 100-year simulation. The maximum aggradation depth in Long Creek was about one foot and it occurred in Long C Reach after 23 years of simulation. Gradual degradation was the general trend for Long Creek over the 100 years with an average degradation rate of approximately 0.01 ft/yr.

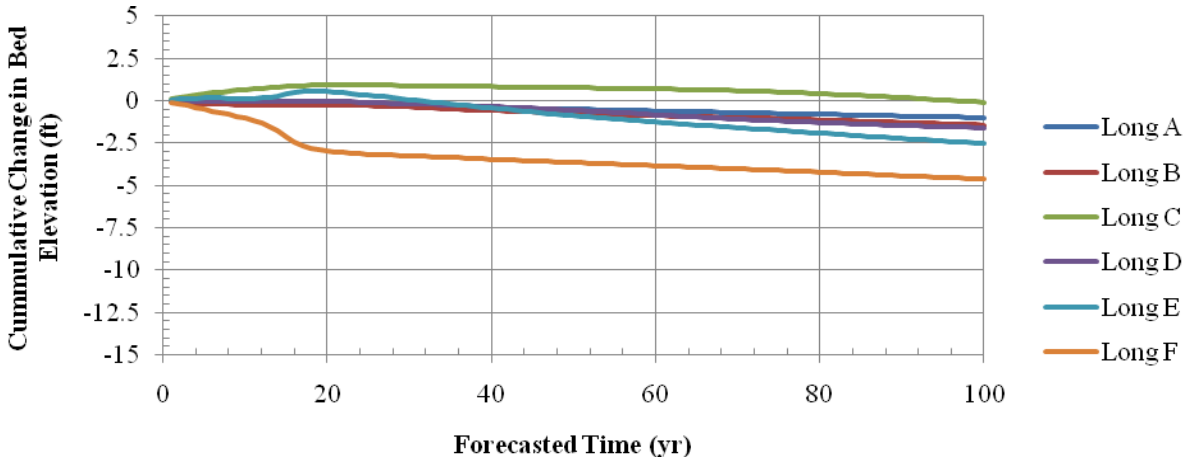

Figure 4. Cumulative bed-elevation change versus model forecasted time for Long Creek reaches

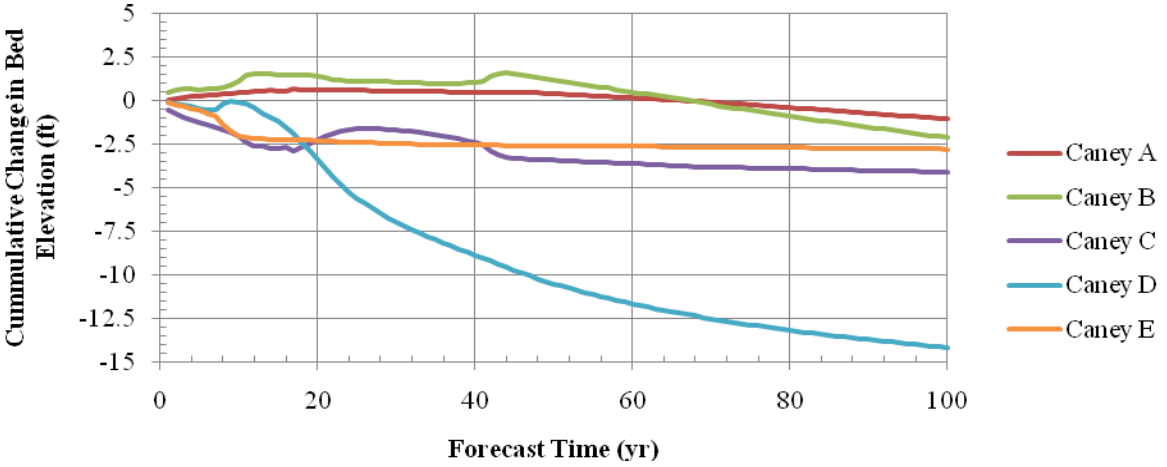

Figure 5. Cumulative bed-elevation change versus model forecasted time for Long Creek reaches

Caney Creek output indicated an overall general trend of degradation; however, the magnitudes were much larger compared to those observed in Long Creek. The maximum degradation depth for Caney Creek was approximately 14 feet and it occurred in Caney D Reach at the end of the 100-year simulation. The maximum aggradation depth in Long Creek was about 1.6 feet and it occurred in Caney B Reach after 44 years of simulation. For Caney Creek, there were significant differences between rates of bed-elevation changes between reaches. Caney D which had the largest projected degradation depth was bound by two reaches that had significantly lower rates of degradation and degradation depths.

Reach-Specific Output Data Modeling results for Long C Reach and Caney C Reach are presented in this section to illustrate the other types of information that are provided in the model output. These two reaches were chosen because they generally encompass the ranges of trends observed in the reaches where there were minimal changes over time in Long C Reach and larger, more pronounced changes for the Caney C Reach. Total local sediment balance versus

time for the two reaches are shown in Figure 6, and grain-size distributions for Long C Reach and Caney C Reach for 1, 25, 50 and 100 years are shown in Figures 7 and 8, respectively.

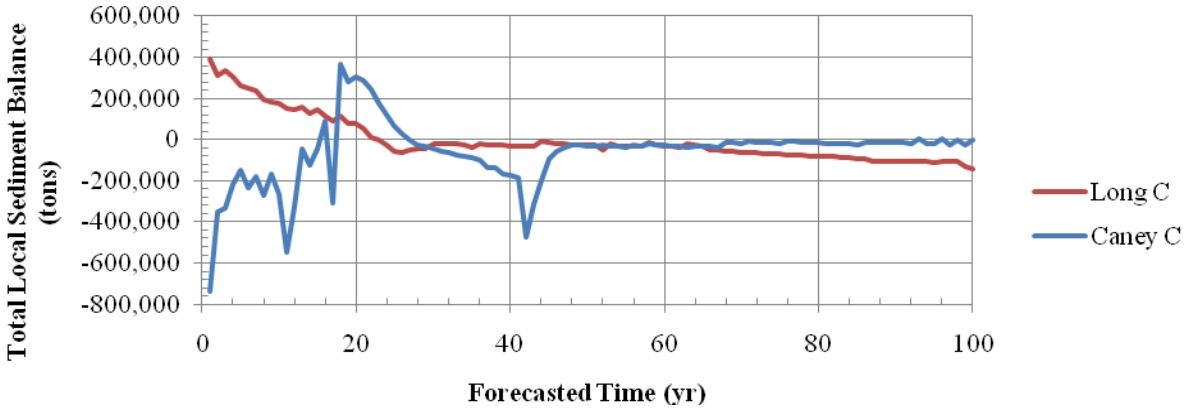

Figure 6. Total local sediment balance for Long C and Caney C reaches.

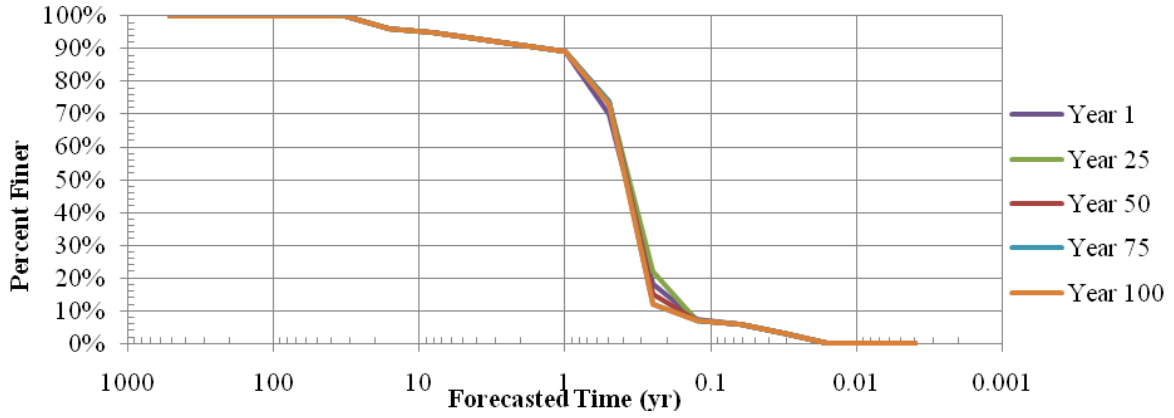

Figure 7. Grain-size distributions for Long C Reach for 1, 25, 50 and 100 years

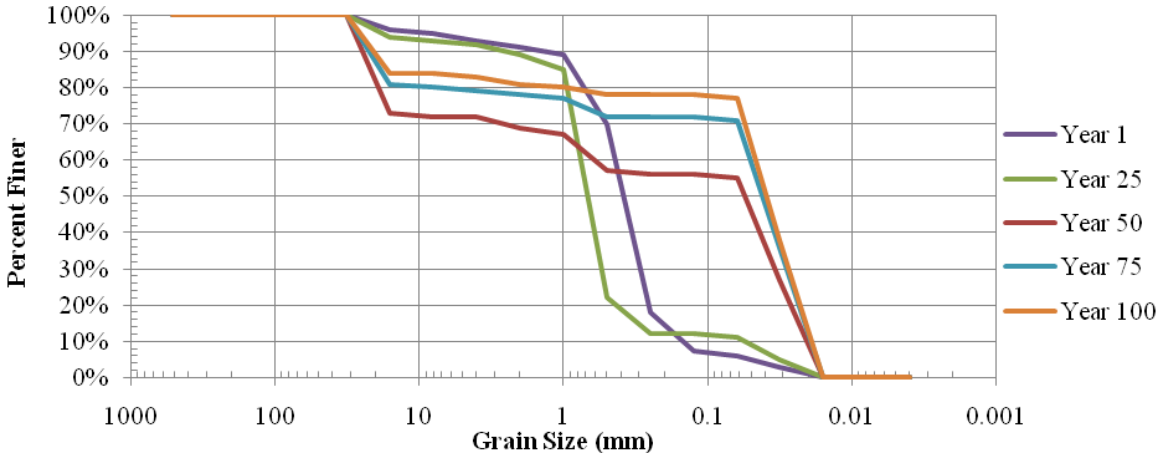

Figure 8. Grain-size distributions for Caney C Reach for 1, 25, 50 and 100 years

SUMMARY

The PotaMod computer application was developed for 1-D mobile-bed modeling using output from the SIAM hydraulic design function within HEC-RAS. PotaMod updates cross-section elevations and grain-size distributions on a per-reach basis to allow updating of hydraulics in response to computed erosion and sedimentation. Specifically, PotaMod uses the *local sediment balance* output of SIAM to determine depths of aggradation or degradation for each reach, and it uses *sediment balance by grain size* to determine adjustments to grain-size distributions for each reach. The PotaMod application has an advantage over other 1-D sediment transport models because it can simulate several years in a relatively short time period. The model can be used to evaluate the impacts of different rehabilitation and management alternatives over a long period of time with updated hydraulic conditions allowing insight into potential changes in channel stability.

PotaMod was used to evaluate 100 years of sediment transport and channel stability in the Long Creek Watershed. The model included 13 SIAM reaches with a total of 139 cross sections. The 100-year simulation required 10.1 minutes to complete. The purpose of this project was to illustrate the utility of the PotaMod application and model results were not calibrated to known bed-elevation changes as those data were not available. Ideally, sediment-transport input parameters would be calibrated with measured field data; however, a relative comparison of model results can be conducted between a baseline condition and different rehabilitation and management alternatives to identify general aggradation and degradation trends within a watershed over time.

REFERENCES

Hudson, F.E. (1997). "Project Formulation of the Demonstration Erosion Control Project," Proceedings of the Conference on Management of Landscapes Disturbed by Channel Incision, pp 120-124, The University of Mississippi, Oxford, MS.

Little, C.D., and Jonas, M. (2010). "Sediment Impact Analysis Method (SIAM): Overview of Model Capabilities, Applications, and Limitations," 2nd Joint Federal Interagency Conference on Sedimentation and Hydrologic Modeling, Riviera Hotel, Las Vegas, NV.

Martin, M., Biedenharn, D.S., Little, C., Smith, K, and Watson, C.C. (2010). "Analysis of Three Delta Headwaters Project (DHP) Streams Using the Sediment Impact Analysis Method (SIAM) Model." 2nd Joint Federal Interagency Conference on Sedimentation and Hydrologic Modeling, Riviera Hotel, Las Vegas, NV.

Watson, C.C., Raphelt, N.K., and Biedenharn, D.S. (1997). "Historical Background of Erosion Problems in the Yazoo Basin." Proceedings of the Conference on Management of Landscapes Disturbed by Channel Incision, S.S.Y. Wang, E.J. Langendoen, and F.D. Shields, Jr. (eds), The University of Mississippi, University, MS.

QUANTIFYING AND MODELING SEDIMENT LOADS FROM STREAMBANK EROSION ALONG THE HEADWATERS OF TOWN CREEK IN MISSISSIPPI

John J. Ramírez-Avila, Assistant Research Professor, Civil and Environmental Engineering Department, Mississippi State University, Mississippi State, MS, jjr149@cee.msstate.edu; Eddy J. Langendoen, Research Hydraulic Engineer, National Sedimentation Laboratory, US Dept of Agriculture, Agricultural Research Service, Oxford, MS, Eddy.Langendoen@ars.usda.gov; William McAnally, Emeritus Professor, Mississippi State University, Mississippi State, MS, McAnally@ngi.msstate.edu; James L. Martin, Porfessor, Civil and Environmental Engineering Department, Mississippi State University, Mississippi State, MS, jlmartin@cee.msstate.edu; Sandra L. Ortega-Achury, Research Associate, Civil and Environmental Engineering Department, Mississippi State University, Mississippi State, MS, sandraortega@cee.msstate.edu; Ron Bingner. Agricultural Engineer. National Sedimentation Laboratory, US Dept of Agriculture, Agricultural Research Service, Oxford, MS, Ron.Bingner@ars.usda.gov

ABSTRACT

The prediction of erosion is an important component in the development of land management strategies, particularly where sediment is identified as the cause of water quality impairment. Computational models that predict streambank erosion allow the user not only to quantify the streambank erosion rates and processes along a stream, but also to take subsequent decisions regarding sediment loads reduction, especially when those decisions need to pay special attention to stream channel processes and stabilization of eroding reaches. Streambank erosion processes were hypothesized to be an important mechanism driving sediment supply from the Town Creek Watershed in Mississippi. Field monitoring observations along the main channel of the Town Creek and several of its tributaries have indicated that the incised headwaters can contribute up to 70% of the suspended sediment loads exported by the watershed. Observations also evidenced that annual streambank retreat rates and loads in the Town Creek headwaters could be as high as 2.67 m and 28.5 Mg per meter of stream length, respectively. Thus, streambanks were a significant source of sediments loads to the Tombigbee River and the Aberdeen Pool on the Tennessee-Tombigbee Waterway. The ability of the Conservational Channel Evolution and Pollutant Transport System (CONCEPTS) computer model to predict streambank erosion along the Town Creek Watershed in MS was tested through its application to a 270-m long headwater incised reach. Model predictions over a 13 month period were compared with cross section surveys at 8 transects along the modeling reach. Results showed that CONCEPTS accurately predicted top width retreat and streambank failures in time and magnitude. Results from field monitoring and computational modeling offer important insights into the relative effects of land and streambank erosion on the stream water quality and sediment budget for Town Creek Watershed. Reduction of suspended sediment loads should focus on the attenuation of geomorphic processes and stabilization of reaches and agricultural lands near streambanks at the headwaters within the watershed.

INTRODUCTION

Research along the Town Creek Watershed, MS (TCW) provided evidence that gravitational failure of the incised streambanks located along the northern and western headwaters channels of this watershed was the primary source of sediment loads to the system (Ramirez-Avila, 2011). Monitoring of streambank erosion processes and rates along these unstable channels has documented the occurrence of channel changes, loss of valuable agricultural land, and degradation of stream habitat for fish and other aquatic organisms (Ramirez-Avila, 2010; Ortega-Achury et al., 2009).

Prediction of erosion processes (upland, gully and streambank) is an important component of the development of land management strategies in areas where sediment is identified as the cause of impairment (Staley et al., 2006). Computational models to predict streambank erosion allow the user not only to quantify the streambank erosion rates and processes along a stream, but also to guide subsequent decisions regarding sediment loadings reductions, especially when those decisions need to pay special attention to stream channel processes and stabilization of eroding reaches.

The CONservational Channel Evolution and Pollutant Transport System (CONCEPTS) computer model is a product of continuing research at the US Department of Agriculture, Agricultural Research Service (ARS) National Sedimentation laboratory (NSL) to predict channel adjustment and evolution of incised stream systems. Various studies have been carried out to compare CONCEPTS model predictions of streambed and streambank degradation to field measurements in different areas under diverse scenarios, including studies in the Yalobusha River, MS, Goodwin Creek, MS, Kalamazoo River, MI, Shades Creek, AL, Stroubles Creek, VA and James Creek, MS (Simon et al., 2002; Thomas and Langendoen, 2002; Wells et al., 2007; Simon et al., 2004; Staley et al., 2006; Langendoen and Simon, 2008; Langendoen and Alonso, 2008). Only one of these studies has been carried out within the Ecoregion 65. The study in TCW was the first developed within that Ecoregion that involves comparison of assessed and predicted sediment streambank erosion processes and yields in a short term scenario. The field monitoring dataset includes information on stormflow events, changes in streambank morphology, and characterization of streambank soils and streambed.

Results are presented from the application of the CONCEPTS model to simulate and predict streambank erosion rates along an incised section of a 270 m long reach on the Yonaba Creek, MS, a representative stream segment located at the northern headwaters area of the TCW. The general objective of the study was to assess the performance and capability of the CONCEPTS model to simulate temporal and spatial streambanks changes along the modeled reach. The model evaluation includes: 1) calibration of the CONCEPTS model against existing data detailing streambank changes over the entire reach from February 2009 to July 2009; 2) validation of the model application over the entire reach from August 2009 to March 2010; and 3) development of a sensitivity analysis for CONCEPTS parameters directly related with the prediction of streambank top width retreat, planar failures and fluvial erosion. This paper includes final results from the first two components of evaluation, only.

CONCEPTS Model

The CONservational Channel Evolution and Pollutant Transport System (CONCEPTS) is a computer model developed by the US Department of Agriculture (USDA), Agricultural Research Service (ARS) at the National Sedimentation Laboratory (NSL) in Oxford, MS. The model simulates unsteady one-dimensional flow, graded-sediment transport, streambank erosion and failure processes to predict the dynamic response of flow, and sediment transport to in-stream hydraulic structures (Langendoen, 2000). The CONCEPTS model is a tool designed for the assessment of stream corridor restoration projects. CONCEPTS is composed of three physical processes simulation components: 1) hydrodynamics for unsteady flow hydraulics, 2) mobile streambed dynamics for sediment transport and streambed adjustment, and 3) streambank erosion and channel widening from both hydraulic and geotechnical mechanisms. CONCEPTS is capable of assessing the long term effectiveness of restoration efforts when combined with watershed scale modeling programs as AGNPS or SWAT (Staley et al., 2006).

CONCEPTS simulates open channel hydraulics by numerically integrating the St. Venant equations representing open channel flow. The model uses the generalized Preissman method of

discretization, a forward time finite difference numerical method to approximate the Saint Venant equations. CONCEPTS predicts sediment transport capacity and streambed adjustment through sediment scour and aggradation dynamics by solving the sediment mass conservation equation. A modification of the SEDTRA (Sediment Transport Capacity Predictor) model (Garbrecht et al., 1996) is included into the CONCEPTS model to calculate the total sediment transport by size fraction for a total of 17 pre-defined size classes with a specific sediment transport equation for each one. Channel width adjustments are modeled by CONCEPTS by incorporating the physical process for streambank retreat through hydraulic erosion and gravitational failure. Hydraulic erosion of bank material is calculated by CONCEPTS using an excess shear stress approach for cohesive soils. CONCEPTS also simulates the two most frequent types of streambank failure observed for incised streams with steep banks: 1) planar failure and 2) cantilever failure for heterogeneous cohesive streambank materials (Langendoen, 2000). Based on the shear strength of the streambank soils, a Factor of Safety (FS) is determined for the geometry and the soil properties of the streambank. For the cantilever failure, CONCEPTS determines a FS based on the weight of the overhanging streambank and the shear strength of the streambank soil. Detailed information about the model can be found in Langendoen (2000),

A Java-based Graphical User Iinterface facilitates the model input for CONCEPTS (Figure 1). Three main elements are observed when the interface is opened: the physical data, the channel models, and the run data elements. Detailed information about the model components and the use of the interface to enter information to develop a simulation is found in Ramirez-Avila (2011).

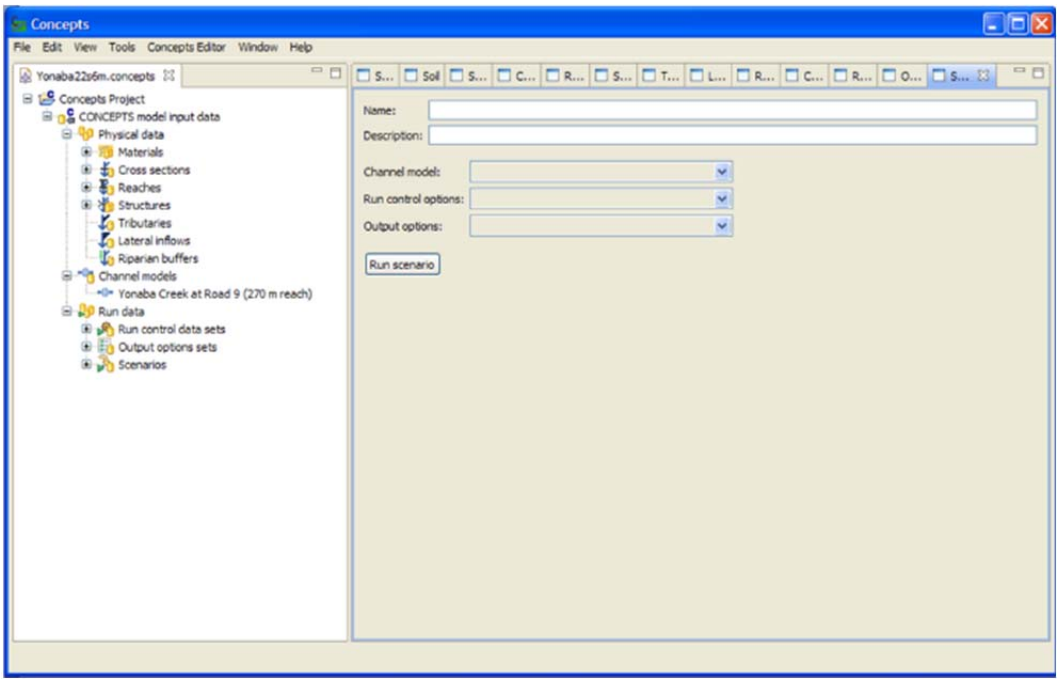

Figure 1. View of the Java Graphical User Interface for the CONCEPTS model

METHODS

Model Setup

The Yonaba Creek reach is a principal tributary of Town Creek located in the northern area of the TCW. The geometry of the 270-m long modeling reach is represented by 8 cross sections (Figure 2). Although the modeling reach is intersected by a bridge along the State Road 9 approximately 50 m below the first cross section, under visual observations its substructure did not contract streamflow or induce deposition or scour so was not included in simualtions. Along the modeling reach, three regions with differing characteristics were identified. First, two cross sections along the upstream sub-reach, which is a straight segment including an 85 m long section with rip rap protection along its entire streambank height.

This segment intersects the State Road 9 bridge. Second, four cross sections along the bendway sub-reach, which evidenced the most significant amounts of streambank erosion and streambank instability. Third, two sections along the downstream sub-reach, which is a straight segment evidencing some streambank gully erosion events, although its geomorphical characteristics did not favor streambank instability processes because of the presence of a berm along its entire length.

Channel Geometry

The eight transects (at river stations 0, 20, 135, 140, 165, 210, and 270 m) along the 270 m modeling reach were periodically surveyed from February 2009 to March 2010. Initial cross sections were surveyed between left to right streambank looking upstream by using a Total Station Positioning System (Leica TSP 1100 Professional Series) in February 13 and 20, 2009. A Real Time Kinematic (RTK) GPS system (TOPCON Hiperlite Plus) was used for the next surveys from May 19, 2009 to March 19 2010. A more detailed description about the cross section surveying performed at this reach was provided in Ramirez-Avila (2011).

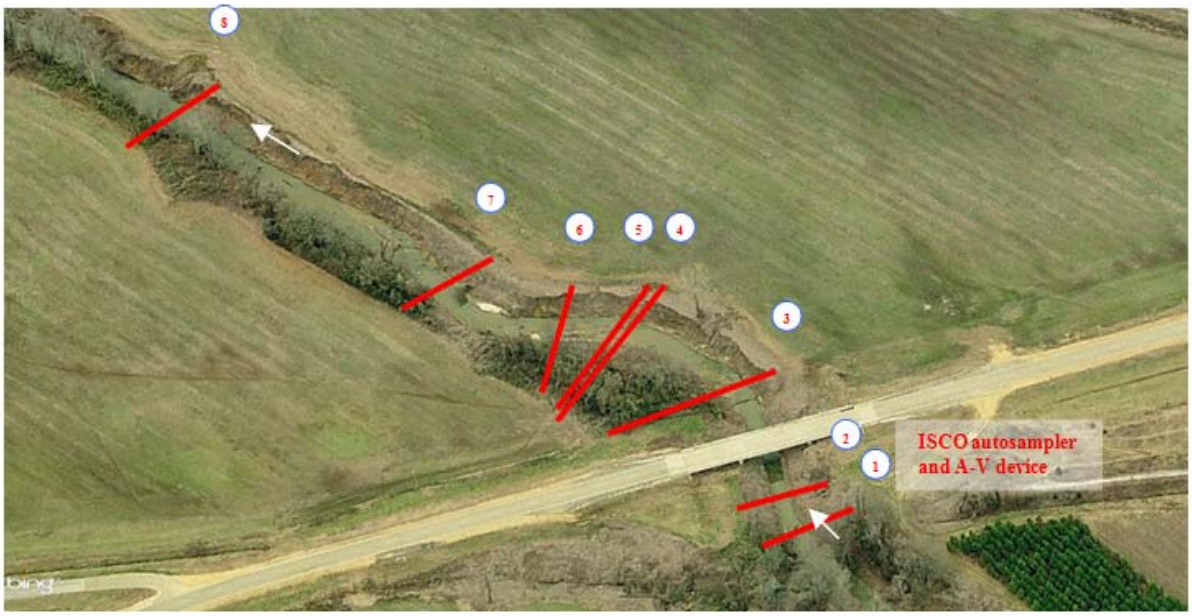

Figure 2. Yonaba Creek study site. Plan view showing the location of surveyed cross sections

Streambank Material Physical Properties

Sampling and testing of streambed and streambank materials for textural composition and geotechnical properties was conducted at the Environmental Laboratory of the Civil and Environmental Engineering Department of Mississippi State University and at the National Sedimentation Laboratory in Oxford, MS. Streambank and streambed materials were analyzed to determine particle size distribution by sieve-hydrometer and by the sieve-pipet method, respectively. Streambed sampling did not show a significant difference in textural composition along the length of the modeling reach. The field observation and particle size analysis results for the streambanks material allows defining representative streambank profiles, including the 85 m segment with rip rap protection.

The modeling reach formed into the spatial distribution of the Jena soil series. The streambank profile along the entire modeling reach is very homogenous. Particle size analysis characterized the entire layers of soils as very fine sandy loam. The soil series description for a typical pedon presents one main layer below the top soil (0.1 m) to a depth of 1.2 m and a second main layer from this depth going deeper than 2 m. Field observations showed an apparently less permeable third soil layer (approximately 5.5 to 6 m depth) and a subsequent gray bottom layer, usually covered by loose material located at the toe of the

streambank produced by streambank failures (Figure 3). Particle size analysis for the deposited material showed a significant reduction in the contents of silt and clay of about 58%.

Streambanks along the modeling reach are very steep. The streambanks at the outer margin (left) of the bendway segment are eroded to near vertical profiles until a failure event produces deposition of loose material at the streambank toe (Figure 3). The angle of the first planar failure of the streambanks (β) was directly related to the friction angle of the streambank material (ϕ') and the initial streambank slope (α) (Equation 1), which was considered homogeneous along the streambank height. Considering the homogeneity of the textural composition along the streambanks height in the modeling reach, the friction angle (ϕ') was determined by evaluating the change in the streambank slope observed after consecutive failure events in the streambanks where it occurred. Initial values for the suction angle (ϕ_b) for each soil were assumed based on their corresponding textural characterization from values suggested by Selby (1993) and Nieber et al. (2008). The cohesion (c') of the streambank soil was considered negligible due to the textural composition of the streambank material, based on the typical values for different materials suggested by Selby (1993) and Nieber et al. (2008).

$$\beta = \left(\frac{\alpha}{2} + \frac{\phi'}{2} \right) \qquad \text{Eq. 1}$$

Figure 3. Representative streambank soil profiles observed along the modeling reach at Yonaba Creek in Blue Springs, MS

The submerged jet test device was used to determine the streambank material soil resistance to hydraulic erosion (Figure 4). The average value of three jet tests conducted at each streambank layer was used for input of τ_c and k_d into the CONCEPTS model. Critical shear stress and erodibility of the streambank material ranged from 0.14 to 11.84 Pa and from 0.76 to 35.8 $cm^3\ N^{-1}\ s^{-1}$, respectively. Coarse grain loose material deposited on the streambank toes presented an average value of 1.12 Pa and 99.41 $cm^3\ N^{-1}\ s^{-1}$ for τ_c and k_d, respectively.

Roughness values (Manning n) were assigned to streambed and streambank sections of each cross section based on in-situ characteristics of the channel (e.g. rip rap protection of streambank, woody vegetation, etc), using the guidelines proposed by Langendoen (2000) and Chow (1959). In general, roughness values for the channel streambed ranged from 0.02 to 0.1 and streambanks from 0.03 to 0.17.

Figure 4. View of the a) jet test device setup, b) jet of water applied on the streambank material, and c) scour generated on the streambank material after a test

Discharge

Hydraulic conditions at the upstream and downstream boundaries of the simulated reach were obtained from observed discharge and stage. A monitoring station consisting of an automatic sampler (ISCO Model 6712) and area velocity flow module (ISCO-750) was setup at the upstream location of the modeling reach from early February 2009 to April 1, 2010. The continuous 15-min hydrographs of all runoff events between February 27, 2009 and April 1, 2010 were used to simulate the hydraulics and morphology of the model reach.

A rating curve (Equation 2) was developed as the downstream boundary condition based on stream velocity and depth profiles measured using a Son Tek flow tracker at cross section #8 (X=270 m) on different dates between August 2008 and June 2009.

$$Q = 3.25 * h^{1.95} \qquad \text{Eq. 2}$$

where Q=Discharge in m^3s^{-1} and h=flow depth in m.

Modeling Assumptions, Calibration and Validation

Although the major amount of the boundary physical properties to evaluate the prediction of streambank erosion processes and rates by using the CONCEPTS model were determined or measured *in situ*, some assumptions had to be made about the data assigned to materials and cross sections within the modeling reach. These assumptions concern sediment loadings, the streambed material resistance parameters, the effective cohesion and the suction angle of the streambanks. CONCEPTS is unable to predict the increased hydraulic forces acting on the left streambank side caused by the helical streamflow pattern in the bendway. Following Langendoen and Simon (2008), the increased shear stresses along the bendway were represented by a reduction in the resistance to erosion of the streambank material in the left streambanks of the sections #3 and #6. Similarly, the presence of a pipe on the lower part of left streambank at the section #5 was represented by a modification in the magnitude of its critical shear stress. Sediment inflows into the study reach were assumed equal to the transport capacity of the streamflow at the section #1 (wash load size class <0.025 mm). No downstream control was established. Processes related with the streambank stability analysis for this simulation included positive pore water pressures, matric suction, confining pressures, and groundwater table dynamics. A number of 5 shear emergences and a block retention time (time needed by flow to remove failed material deposited on the streambank toe) of 15 days were selected. From field observations, the maximum tension crack depth in the streambank stability analyses was determined as 1.7 m.

The calibration scenario included the analysis of hydraulics and streambank stability processes for the entire modeling reach from February 22, 2009 to June 30, 2009. The validation scenario was setup from July 1, 2009 and ended in March 19, 2010. A sensitivity analysis was performed to evaluate the effect of the critical shear stress, erodibility, friction angle and cohesion of the streambank material, streambank roughness and block retention time on the sediment loads and streambank failure events. Results from the sensitivity analysis are reported in Ramirez-Avila (2011).

RESULTS

The 15-min time series of modeled and observed streamflow values at the downstream end of a 270 m long reach along the Yonaba Creek in Blue Spring, MS, are shown in Figure 5. The calibrated modeled time series agreed very well with the observed streamflow time series. A minimum rational change in the initial input value of the determined friction angle (ϕ') for the streambank material was necessary to improve the model accuracy during the calibration phase.

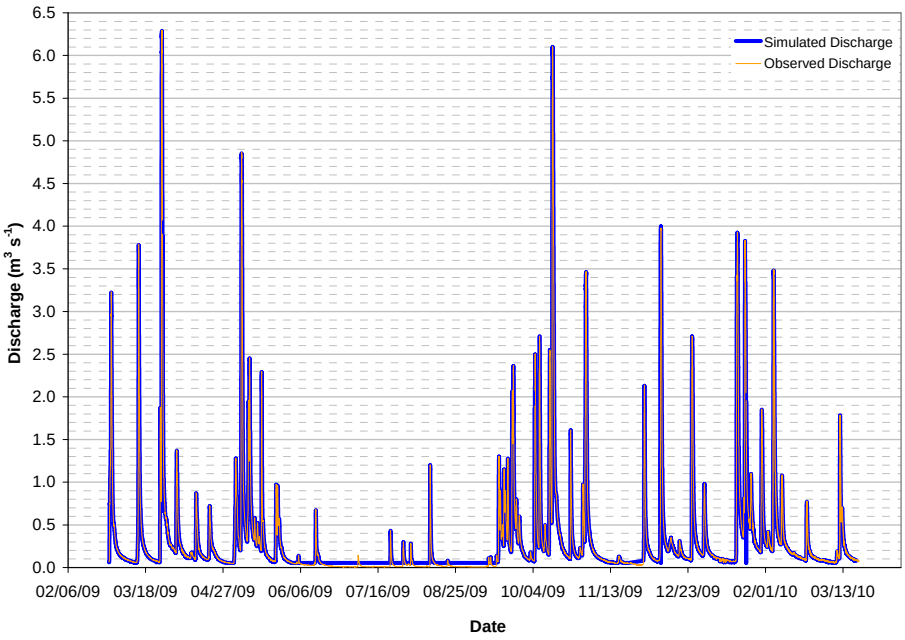

Figure 5. Observed and simulated streamflow discharge for a 270 m long modeling reach along the Yonaba Creek in Blue Springs, MS

Factor of Safety and Streambank Instability

The time series of the computed Factor of Safety (Figure 6) allows visualizing the time of occurrence of a planar or a cantilever failure event during continuous changes in streamflow depths. Along the FS time series, a FS=0.987 during the stormflow event that started in February 26, 2009, and a FS=0.975 during the successive stormflow events that started in March 25, 2009, were observed for sections #3 and #6, respectively. In both cases, the streambank presented a planar failure. The stormflow event that induced the planar failure of section #6 did not induce a planar failure on section #3, probably due to the presence of remaining streambank material deposited on the streambank toe after the previous streambank failure. It also could be because only a cantilever failure of streambank material at the streambank toe height occurred.

Figure 6 shows how the factor of safety (FS) for sections #3, #4, #5 and #6 was reduced after the occurrence of the stormflow peak observed in March 26, 2009. The reduction in the FS indicated two processes: 1) the steepening of the streambank caused by the scour of the streambank material from the streambank itself or from deposited loose material near the streambank by fluvial erosion (Langendoen, 2000); and 2) the loss of matric suction relative to the increase in confining pressure along the streambank height caused by the rising stormflow level. When the FS was smaller than 1, a planar failure on the streambank occurred.

Although the FS for Section #6 was reduced below the critical value of 1 just after the occurrence of the stormflow peak, the planar failure occurred only until the stormflow depth felt to a depth where the forces reducing the strength on the saturated streambank were not higher than the confining pressure exerted by the stormflow (for this specific condition h=2.14 m). Once the failure occurred, the FS was increased due to reduction in streambank angle.

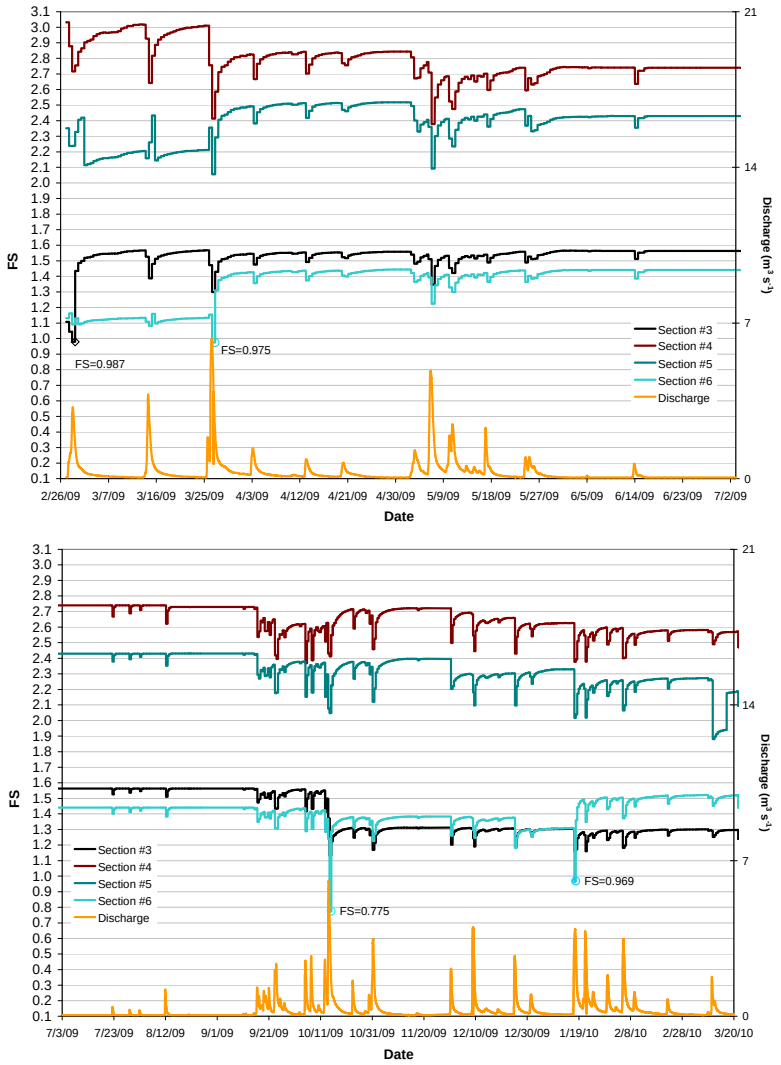

Figure 6. Predicted Factor of Safety (FS) for the left streambanks on a bendway along a 270 m long reach on the Yonaba Creek, MS, between February 22, 2009, and March 18, 2010

Streambank Top Width Retreat

Figures 7 and 8 compare simulated and surveyed cross section changes along the modeling reach obtained during the phases of calibration and validation. The changes in sections #3 and #6 were observed from the surveys performed in May 12, 2009, November 3, 2009, and March 18, 2010, and notes and pictures from field observations confirmed dates when the failures occurred. During the entire simulation, CONCEPTS accurately predicted the stability of the sections upstream and downstream of the bendway segment (Sections #1 #2, #7 and #8). The model adequately predicted in time and magnitude the 1.53 m of streambank top width retreat caused by the planar failure event that occurred on February 28, 2009, on the left streambank of section #3. In general, the simulation of individual planar failures in section #6 was well predicted in time, but the magnitude of the retreat was over-predicted. The 0.89 m of change in the streambank top width observed in March 27, 2009, was slightly over-predicted by 4.5%, but the 0.76 m retreat occurred in January 17, 2010, was over-predicted by 88.2% (Table 1). CONCEPTS predicted a change in FS that reflected a planar failure along the left streambank of section #6 in October 15, 2009, but the model under-predicted by 40.6% the 1.97 m of the top width retreat observed in the survey dated

in November 3, 2009. Overall, the total top width retreats induced by planar failures on section #3 and section #6 were well predicted by CONCEPTS with a difference of 0.02 m and 0.09 m, respectively.

Sections #1, #2 and #7 did not reflect any erosive process from these streambanks, whereas CONCEPTS overestimated the observed streambank erosion in section #8. Both conditions differed from the actual observations due to the inability of CONCEPTS to simulate sediment deposition on the streambank surface. The deposition of sediment on the streambanks surfaces represented at least a 3.5% of difference in the total amount of the actual sediment amount contributed by the streambanks.

Table 1. Observed and simulated changes in top width at the left streambank of two sections along the Yonaba Creek between February and July 2009

Failure Date	Simulated	Observed	Absolute error	Relative Error
Section #3				
Feb 28, 2009[c]	1.54 m	1.53 m	0.01m	0.7%
Total	1.54 m	1.53 m	0.01m	0.7%
Section #6				
March 27, 2009[c]	0.93 m	0.89	0.04 m	4.5 %
October 15, 2009[v]	1.17 m	1.97 m	-0.80 m	-40.6 %
January 17, 2010[v]	1.43 m	0.76 m	0.67 m	88.2 %
Total	3.53 m	3.62 m	-0.09 m	-2.5 %
Segment (Section #3 + Section #6)				
Total	5.07 m	5.15 m	-0.08 m	-1.6 %

[c] Results obtained during model calibration [v] Results obtained during model validation

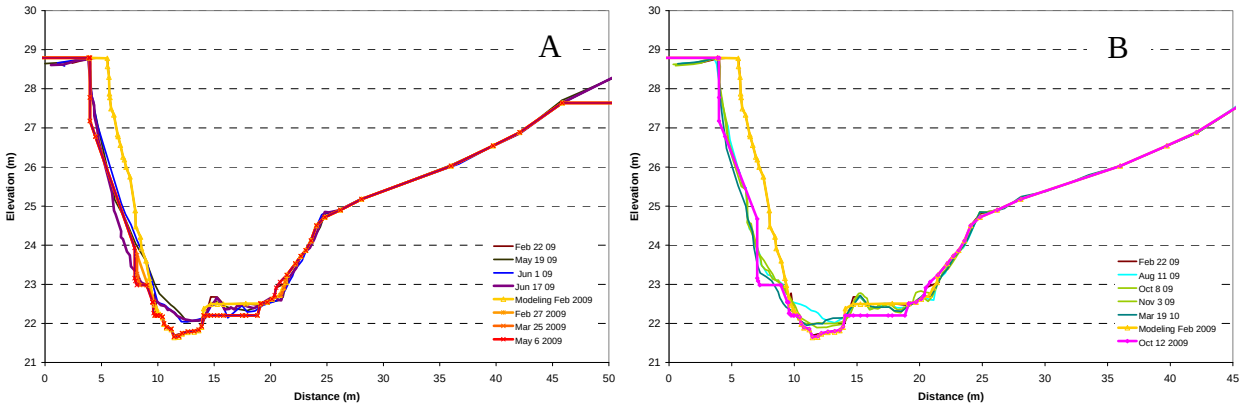

Figure 7. Comparison between simulated and observed cross-sectional changes of section #3 between February 2009 and June 2009 (A), and between July 2009 and March 2010 (B).

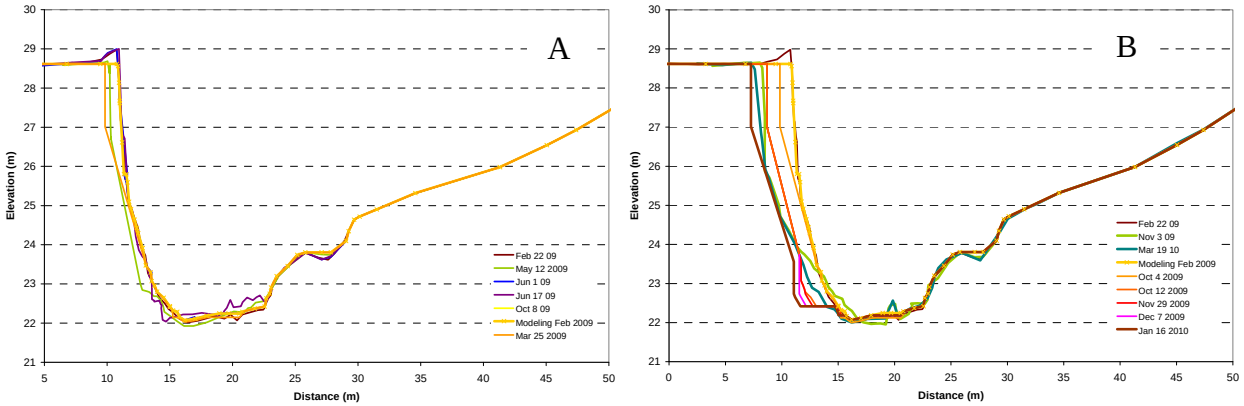

Figure 8. Comparison between simulated and observed cross-sectional changes of section #6 between February 2009 and June 2009 (A), and between July 2009 and March 2010 (B)

Table 2. Observed and simulated streambank erosion yield along a 270 m long reach on the Yonaba Creek in Blue Springs, MS between February 22, 2009 and March 18, 2010

Section	Distance (m)	Simulated		Observed	
		Streambank Erosion⁻ (Mg)	Contribution~ (%)	Net Streambank Erosion⁺ (Mg)	Contribution (%)
#1	0	0.0	0.0%	3.7	-0.2
#2	20	0.0	0.0%	-54.8*	3.2
#3	90	-892.2	44.5%	-506.4	29.3
#4	135	-49.4	2.5%	-49.3	2.8
#5	140	-56.8	2.8%	-289.3	16.7
#6	165	-996.3	49.7%	-827.6	47.8
#7	210	0.0	0.0%	-7.8	0.5
#8	270	-5.2	0.3%	0.8'	-0.1
Total		**-1999.9**		**-1,730.7**	

Positive values = Deposition Negative values (-) = Erosion

-Simulated streambank erosion yield did not include sediment deposited on streambanks surfaces

~Overall cumulated sediment yield ratio across the total amount of gross streambank erosion

+Observed streambank erosion yield included sediment deposited on streambanks surfaces

*Erosion and deposition on section #2 was merely related to exchange of loose material carried by the stormflow events. A net contribution of streambank material was not expected because the streambank was revetted with rip rap

' Estimated only for the cross section

CONCEPTS was able to simulate fluvial erosion and cantilever failures acting at the height of the left toe streambank at section #5, but was not able to replicate the different events of mass wasting which occurred above this height. Total contributions from this section represented around 16.7% of the total streambank erosion observed along the modeling reach. Mass wasting events at section #5 were induced by the scouring effect caused by the streamflow around a 0.75 m diameter corrugated pipe, which collected the concentrated runoff flow from upland. One of these observed events also included pop-out failures that occurred above the pipe height.

It was previously documented that CONCEPTS was very accurate when simulating the total magnitude of planar failures occurring sections #3 and #6. However, simulated total streambank erosion yield and contributions from both sections was overestimated by 1.8 and 1.2 times the observed results, respectively (Table 2). This condition could be caused by the difference in the actual block retention time and the 15-days value used by the model (a higher value for block retention time could not be assigned to the model due to an interruption during the running process attributed to a bug in the block retention routine, which has since been corrected). The block retention time represents the time that the failed loose material stayed on the streambank toe, protecting the streambank from fluvial erosion and streambank

failures, and reducing the amount of sediment yield directly contributed to the streambed and the streamflow after a planar failure. Figure 9 shows how after the first planar failure at section #3, the failed material could stay on the streambank toe during at least 4 more months before being removed by fluvial erosion. It also shows how the streambed received direct contribution from the failed streambank material, changing, among other conditions, the geometry of the cross section and the streambed elevation. The actual change in the streambed was not simulated by CONCEPTS after the first streambank planar failure, and in general during the entire simulation. This condition could also be an important factor affecting the net contribution of the streambank at section #3, as well as the sediment transport analysis along the entire reach. Another factor that could be affecting the total amount of sediment yield by the streambanks could be the magnitude of the soil erodibility parameter determined *in-situ* by jet testing.

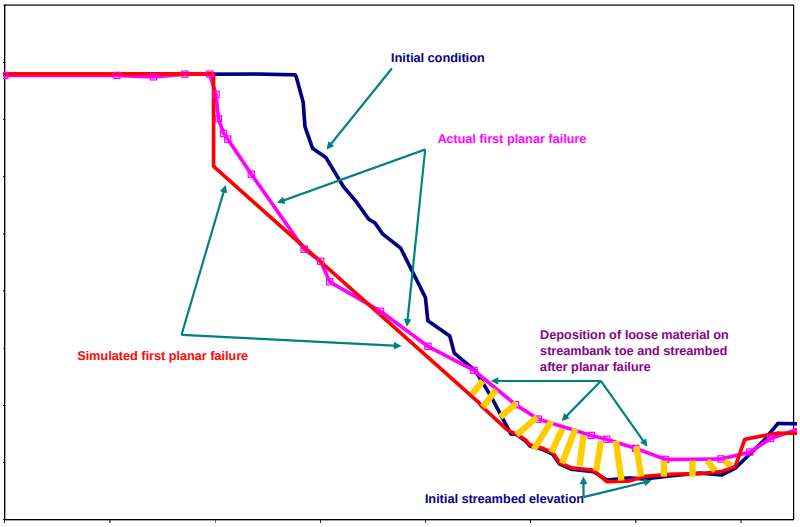

Figure 9. Comparison between actual and simulated planar failure, streambed deposition and erosion of deposited material on the streambank toe at section #3 on Yonaba Creek, MS.

CONCLUSIONS

The ability of CONCEPTS to predict streambank erosion was tested through its application to a 270 m long reach along the Yonaba Creek in Blue Springs, MS. Model predictions between February 2009 and March 2010 were compared with cross section surveys on 8 transects along the modeling reach. Results showed that CONCEPTS very accurately predicted top width retreat and streambank failures in time and magnitude. CONCEPTS simulation yielded streambank degradation predictions comparable to those observed during the studied period. An annual rate of about 2,000 Mg of streambank retreat was assessed by both methods; field measurements and CONCEPTS modeling. However, CONCEPTS did not account for sediment deposition that occurred on the streambank, a condition that slightly reduced the observed net amount of sediment yield contributed by streambank processes. Streambank gravitational failure was the dominant mechanism inducing streambank erosion for the studied reach. CONCEPTS is unable to simulate tangential flows through the bendway section. Moderate changes in the critical shear stress of streambanks for the cross sections along the bendway represent the increased shear stress generated by stormflows along this section. The presence of a pipe on the lower part of left streambank at the section #5 was represented by a modification in the magnitude of its critical shear stress. However, the model was unable to simulate local streambank retreat caused above the pipe. Although it was not observed or studied in detail, the influence of subaerial erosion processes could be significant in accounting for the total retreat amount during winter.

REFERENCES

Chow V.T. 1959. Open channel hydraulics. McGraw-Hill, New York, pp. 680.

Garbrecht J., R.A. Kuhnle, and C.V. Alonso. 1996. A sediment transport capacity formulation for application to large channel network. Journal of Soil and Water Conservation, 50, 5, pp. 527-529.

Langendoen E.J. 2000. CONCEPTS-CONservational Channel Evolution and Pollutant Transport System: Stream Corridor Version 1. Research Report No. 16. US Department of Agriculture, Agricultural Research Service, National Sedimentation Laboratory: Oxford, MS, pp. 160.

Langendoen E.J. and A. Simon. 2008. Modeling the Evolution of Incised Streams: II. Streambank Erosion. Journal of Hydraulic Engineering ASCE. 134, 7, pp. 905-915.

Langendoen E.J. and C.V. Alonso. 2008. Modeling the Evolution of Incised Streams: I. Model Formulation and Validation of Flow and Streambed Evolution Components. Journal of Hydraulic Engineering ASCE 134, 6, pp. 749-762.

Nieber J.L., B.N. Wilson, J.S. Ulrich, B.J. Hansen, and D.J. Canelon. 2008. Assessment of streambank and bluff erosion in the knife river watershed. Final report submitted to Minnesota pollution control agency, Department of Bioproducts and Biosystems Engineering University of Minnesota, pp. 58.

Ortega-Achury S.L., J. J. Ramirez-Avila, W. H. McAnally, J. L. Martin, and T. E. Davis. 2009. Nutrient and Sediment Production, Watershed Characteristics, and Land Use in the Town Creek Watershed, Mississippi. Proceeding Publication in the American Society of Biological and Biological Engineering, ASABE Annual International Meeting, Reno, Nevada, June 2009.

Ramírez-Avila J. J. 2010. Suspended Sediment Transport in a Southeastern Plains Watershed. ASCE-EWRI Environmental and Water Resources Engineering Student Technical Paper Contest. 1st Place.

Ramírez-Avila J.J. 2011. Assessment and prediction of streambank erosion rates in a Sotheastern Plains Ecoregion watershed in Mississippi. Mississippi State University. Bagley College of Engineering. Civil and Environmental Engineering Dept. Ph.D. Dissertation. 332 pp.

Selby M.J. 1993. Hillslope Materials and Processes. Oxford University Press, Oxford, pp. 480.

Simon, A., Bingner, R. L., Langendoen, E. J. and Alonso, C. V. 2002. Actual and reference sediment yields for the James Creek Watershed - Mississippi. U.S Department of Agriculture-Agricultural Research Service, National Sedimentation Laboratory Research Report. No. 31.

Simon A., E. Langendoen, R. Bingner, R. Wells, Y. Yuan, and C. Alonso. 2004. Suspended-Sediment Transport and Bed-Material Characteristics of Shades Creek, Alabama and Ecoregion 67: Developing Water-Quality Criteria for Suspended and Bed-Material Sediment. U.S Department of Agriculture-Agricultural Research Service, National Sedimentation Laboratory Technical Report 43.

Staley N.A., T. Wynn, B. Benham, and G. Yagow. 2006. Modeling channel erosion at the watershed scale: Model review and case study. Center for TMDL and watershed studies, Biological Systems Engineering, Virginia Tech, pp. 123.

Thomas R.E. and E.J. Langendoen. 2002. Numerical simulation of post-disturbance stream channel evolution: the Yalobusha River, Mississippi, USA. United States Departmanet of Agriculture, Research report No. 29, pp. 42.

Wells R.R., E.J. Langendoen, and A. Simon. 2007. “Modeling pre- and post-dam removal sediment dynamics: The Kalamazoo River, Michigan,” Journal of the American Water Resources Association, 43, 3, pp. 773–785.

SEDIMENT AND NUTRIENT TRAPPING ON THE MORGANZA SPILLWAY DURING THE 2011 MISSISSIPPI RIVER FLOOD.

Daniel E. Kroes, Research Ecologist U.S. Geological Survey, dkroes@usgs.gov; Edward R Schenk; Gregory B Noe; Adam J Benthem

The 2011 Mississippi River Flood resulted in the opening of the Morganza Spillway for the second time since its construction in 1954. The opening of the Spillway structure released 7.6 km^3 of water through agricultural and forested lands into the Morganza Floodway and the Atchafalaya River Basin (the Basin). This volume represented 5.5 % of the Mississippi River (MR) discharge and 14% of the total discharge through the Basin during the Spillway operation and 1.1 % of the MR and 3.3% of the Basin 2011 water year discharge. During the release there was a net sediment deposition of 0.77 Tg over the 500 km^2 Morganza Spillway and 0.26 Tg was eroded from behind the Spillway structure. The majority of deposition (63 %) occurred in the Forebay (upstream of the structure) and within 4 km downstream of the Spillway structure with minor deposition on the rest of the Floodway. There was a net deposition of 2,600 Mg of nitrogen (N) and 536 Mg of phosphorous (P), during the diversion and was equivalent to 0.17% N and 0.33% P of the 2011 annual MR load. Deposited sediment (84%) was composed of particles that were finer than 50 μm. Median deposited sediment grain size at the start of the Forebay was 13 μm and decreased to 2 μm 15 km downstream of the Spillway structure. Deposition on the Morganza Spillway was limited by a lack of hydraulic connectivity. There was one source of water whose sediment and nutrient content were rapidly deposited. The reconnection of floodplains via flood control spillways can be an effective means to reduce nutrient loading to eutrophied water bodies, like the Gulf of Mexico.

SEDIMENT CHARACTERISTICS AND SEDIMENT TRANSPORT MODELING FOR THE SAGINAW RIVER NAVIGATION CHANNEL

John Barkach, Great Lakes Environmental Center, Inc., Farmington Hills, MI, jbarkach@glec.com
Carol J. Miller, Professor, Wayne State University, Department of Civil and Environmental Engineering, Urban Watershed Environmental Research Group, Detroit, MI, ab1421@wayne.edu
James Selegean, US Army Corps of Engineers, Detroit, MI and Seattle, WA
Fatemeh Babakhani, Wayne State University, Department of Civil and Environmental Engineering

The Saginaw River is a 22.4-mile-long (36.0 km)[2] river located in mid-Michigan and is formed by the confluence of the Tittabawassee and Shiawassee rivers southwest of Saginaw. It flows northward into the Saginaw Bay of Lake Huron. The watershed area is 6,132 square miles (15,881 km^2) and contains 315 dams. The Saginaw River is an important shipping route for mid-Michigan, passing through the cities of Saginaw and Bay City and is one of Michigan's few inland navigable rivers. To maintain the depth of the navigation channels, the Saginaw River is subject to frequent dredging. Since 1963, the Saginaw River navigation channel has been dredged 81times. A total of 22,967,252 cubic yards of sediment were removed at a cost of $65,721,086.

Prior to removal of sediment, the dredged material is subject to a pre-dredge sediment quality assessment. Since 1967, 15 sediment quality assessments have been conducted by the U.S. Army Corps of Engineers; these sediment samples were collected and tested for a variety of physical and chemical characteristics. In this paper, the sediment quality of the Upper and Lower Saginaw River, as well as Saginaw Bay are presented and discussed in conjunction with sediment transport model assumptions.

In addition, an overview of the extensive sediment transport modeling that has been conducted by the U.S. Army Corps of Engineers is discussed in relationship to the total sediment load that is transported from the Saginaw River to Saginaw Bay. These USACE studies have determined that the total sediment load from the Saginaw River to Saginaw Bay ranges from 238,099 to 280,525 tons/year. Sediment flux to the Saginaw Bay was also estimated using the BQART equation that was developed by Syvitski and Milliman (2007). Using the BQART equation, the total sediment load for the Saginaw River was calculated to be 298,724 tons/year at a mean flow (8,320 cubic feet per second) and is similar to the estimates developed by the USACE. Lastly, during the preparation of this paper, it is apparent that the GIS resources that have been developed the MDEQ and State of Michigan can potentially be used to develop a new equation that can be used for smaller streams (<30 m^3/sec) that dominate the Great Lakes region. These areas of further research are presented in this paper.

SEDIMENT CORE CHEMISTRY IN THE ESCALANTE AND SAN JUAN RIVER DELTAS IN LAKE POWELL, UT, IN 2010-2011

POSTER PRESENTATION

Nancy Hornewer, Hydrologist, USGS, Arizona Water Science Center, Flagstaff Programs, njhornew@usgs.gov.

Robert (Bob) J. Hart, Supervisory Hydrologist, USGS, Arizona Water Science Center, Flagstaff Programs, bhart@usgs.gov.

Recent studies by the U.S. Geological Survey, have documented the presence of trace elements, organic compounds including polycyclic aromatic hydrocarbons, and radionuclides in sediment from the Colorado River delta in Lake Powell, UT and from sediment in some side canyons in Lake Powell, Utah and Arizona (Hart and others, 2004 and 2005). The fate of many of these contaminants is of significant concern to the resource managers of the National Park Service at Glen Canyon National Recreation Area because of potential health impacts to humans and aquatic and terrestrial species. The U.S. Geological Survey completed sediment-core sampling in 2010, in the San Juan River and Escalante River deltas in Lake Powell, Utah, to help the National Park Service further document the presence or absence of contaminants in deltaic sediment (Hornewer, 2014).

Three sediment cores were collected from the San Juan River delta in August 2010 and three sediment cores were collected from the Escalante River delta in September 2011. Sediment from the cores was subsampled and composited for analysis of major and trace elements. Fifty-five major and trace elements were analyzed in 116 subsamples and 7 composited samples for the San Juan River delta cores, and in 75 subsamples and 9 composited samples for the Escalante River delta cores. Six composited sediment samples from the San Juan River delta cores and eight from the Escalante River delta cores also were analyzed for 55 low-level organochlorine pesticides and polychlorinated biphenyls, 61 polycyclic aromatic hydrocarbon compounds, gross alpha and gross beta radionuclides, and sediment-particle size. Additionally, water samples were collected from the sediment-water interface overlying each of the three cores collected from the San Juan River and Escalante River deltas. Each water sample was analyzed for 57 major and trace elements.

Most of the major and trace elements analyzed were detected at concentrations greater than reporting levels for the sediment-core subsamples and composited samples. For the San Juan River delta, all elements were detected in each subsample except for rhenium, sulphur, selenium, and tellurium; and all elements were detected in each composited sample except for copper, rhenium, selenium, and tellurium. For the Escalante River delta, all elements were detected in each subsample except for boron, bismuth, molybdenum, rhenium, sulphur, selenium, tin, tellurium, and zinc; and all elements were detected in each composited sample except for rhenium, selenium, and tellurium.

Low-level organochlorine pesticides and polychlorinated biphenyls were not detected in any of the samples. Low-level concentrations of several polycyclic aromatic hydrocarbons were detected in the San Juan and Escalante River deltas but were below reporting levels.

Gross alpha and gross beta radionuclides were detected in both river deltas at concentrations greater than reporting levels for all samples ranging from 8 to 32 pCi/g for gross alpha radioactivity and from 17.1 to 34 pCi/g for gross beta radioactivity. Most of the major and trace elements analyzed were detected at concentrations greater than reporting levels for water samples.

For the water samples, most of the 57 major and trace elements analyzed were detected at concentrations greater than reporting levels in the San Juan and Escalante Rivers. For the San Juan, however, cobalt, cesium, europium, nickel, and thorium were not detected in any of the samples and cadmium, phosphorus, and tin were not detected in 67 percent of the samples. For the Escalante, cobalt, chromium, phosphorus, and tin were not detected in any of the samples and tellurium was not detected in
67 percent of the samples.

REFERENCES CITED

Hart, R.J., Taylor, H.E., Antweiler, R.C., Graham, D.D., Fisk, G.G., Riggins, S.G., and Flynn, M.E., 2005, Sediment Chemistry of the Colorado River Delta of Lake Powell, Utah, 2001, U.S. GEOLOGICAL SURVEY Open-File Report 2005-1178, 33 p.

Hart, R.J., Taylor, H.E., Antweiler, R.C., Fisk, G.G., Anderson, G.M., Roth, D.A., Flynn, M.E., Peart, D.B., Truini, M., and Barber, L.B., 2004, Physical and Chemical Characteristics of Knowles, Forgotten, and Moqui Canyons, and Effects of Recreational Use on Water Quality, Lake Powell, Arizona and Utah, U.S. GEOLOGICAL SURVEY Scientific Investigations Report 2004-5120, 43 p.

Hornewer, N.J., 2014, Sediment and water chemistry of the San Juan River and Escalante River deltas of Lake Powell, Utah, 2010–2011: U.S. Geological Survey Open-File Report 2014-1096, 7 p., http://dx.doi.org/10.3133/ofr20141096.

SEDIMENT FINGERPRINTING TO DELINEATE SOURCES OF SEDIMENT IN AN URBAN SUB-WATERSHED WITHIN THE CHESAPEAKE BAY WATERSHED

POSTER PRESENTATION

Baker, A.C., Gellis, A.C., Sanisaca, L.G., and Noe, G.B.

The Chesapeake Bay is the nation's largest estuary, its watershed covering 165,800 square kilometers and six states. The Chesapeake Bay is designated under the Clean Water Act as an impaired water body due to degradation by excess sediment and nutrients. Eroded upland sediment contributes to the degradation of the Bay and its tributaries by transporting nutrients and toxic contaminants, burying habitat, and reducing water clarity which diminishes light penetration and subsequently affects submerged aquatic vegetation.

Land management practices are being implemented throughout the Bay watershed to reduce and control sediment erosion and transport. The identification and understanding of sediment sources to fluvial systems and a differentiation between in-stream and upland sources of erosion are important to selecting and implementing the most appropriate management actions. Sediment fingerprinting offers a method for identifying fine sediment sources and their contributions to suspended sediment flux within a watershed. This approach entails the establishment of a minimal set of environmental tracers based on physical and chemical properties that can be used to uniquely define each source in the watershed. Suspended sediment collected under different flow conditions exhibits a composite or fingerprint of these properties that allows them to be traced back to their respective sources.

The sediment fingerprinting approach is being used to help identify sources of suspended sediment to Difficult Run, a tributary to the Potomac River and to the Chesapeake Bay. Difficult Run is located in Fairfax County, VA, in the Piedmont Physiographic Province of the Mid-Atlantic Region of the United States (drainage area of 14.2 km2) (NWIS web). The Difficult Run watershed is an urban watershed crossed by several major highways, and is characterized by forested, urban, and mixed residential and commercial land cover. Potential upland sources of sediment including roads, road-cuts, lawns, and forested areas, and in-stream sources (stream banks) will be evaluated in conjunction with suspended sediment collected from Difficult Run. Preliminary results of this sediment fingerprinting analysis will be presented.

SIMULATING SALINITY CONCENTRATION AT THE COLORADO RIVER BASIN SCALE

POSTER ABSTRACT

James Prairie, Hydrologic Engineer, Bureau of Reclamation, Upper Colorado Region, jprairie@usbr.gov
David Neumann, Water Resource Engineer, Center for Advanced Decision Support for Water and Environmental Systems, University of Colorado, Boulder, david.neumann@colorado.edu
Nicholas Williams, Environmental Engineer, Bureau of Reclamation, Upper Colorado Region, nwilliams@usbr.gov
Edith Zagona, Director, Center for Advanced Decision Support for Water and Environmental Systems, University of Colorado, Boulder, zagona@colorado.edu

The U.S. Environmental Protection Agency (EPA) suggested the development of water quality criteria for salinity in the Basin following passage of the Federal Water Pollution Control Act (Clean Water Act) of 1972. In response, the Basin States formed the Colorado River Basin Salinity Control Forum (Forum) to develop numeric salinity criteria and an implementation plan to ensure compliance while allowing the Basin States to continue to develop their Compact-allocated water. The Forum recommends, the States adopt, and EPA approves the flow-weighted average annual salinity criteria for three locations on the lower Colorado River. The criteria, first established in 1975, are reviewed every 3 years; the latest review was completed in 2014.

Reclamation's long-term planning model, the Colorado River Simulation System (CRSS) implemented in RiverWare, supports the Triennial Review of the flow-weighted average annual salinity criteria in the lower Colorado River and development of a salinity control implementation plan. The framework supporting salinity modeling within CRSS begins with a nonparametric regression model to simulate the natural flow and salt mass relationship coupled with a nonparametric temporal disaggregation model to transfer from an annual to the monthly time step required for the planning model. The planning model integrates the projected natural salt mass with salinity contributed by irrigated agriculture and removed by trans-basin diversion and salinity control projects thereby simulating projected salinity concentrations throughout the Colorado River basin. This framework supports the stochastic methods required to model projected supply variability and determine the associated variability in salinity concentration that is consistent with projected supply variability. This framework is presented and its use in the 2014 Triennial Review is demonstrated.

STATE OF THE PRACTICE OF SEDIMENT MANAGEMENT IN RESERVOIRS: MINIMIZING SEDIMENTATION AND REMOVING DEPOSITS

Kathleen M. Healy, Research Assistant; Parks College of Engineering, Aviation and Technology, Saint Louis University, St. Louis, MO, khealy2@slu.edu; Amanda L. Cox, Assistant Professor, Parks College of Engineering, Aviation and Technology, Saint Louis University, St. Louis, MO, coxal@slu.edu; Daniel M. Hanes, Professor, Department of Earth and Atmospheric Science, Saint Louis University, dhanes@slu.edu; Lisa G. Chambers, Assistant Professor, Department of Earth and Atmospheric Science, Saint Louis University, chamberslg@slu.edu

Abstract: Sedimentation in reservoirs is becoming more problematic as water storage and supply become increasingly endangered with the aging American infrastructure. Three general strategies for addressing reservoir sedimentation are currently utilized: reduction of incoming sediment yield, minimization of sediment deposition, and removal of sediment from reservoirs. This paper addresses the latter two strategies and their associated management methods. The main management methods associated with minimizing sediment deposition are construction of sediment bypass structures, sediment pass-through (or sluicing), and venting of a sediment-laden density current. The main overall advantage of sediment bypass structures is that they do not interfere with regular reservoir operation; however, the method is difficult to apply, requires careful planning, and cannot be utilized in arid climates where the need for water is high. Sluicing is one of the more often used sediment-management techniques, but depends upon the existing structure of the dam and can cause adverse impacts to the downstream environment if not carefully monitored. Density current venting is seldom-used due to its reliance on the existence and surveying of a density current; however, it has been shown to be effective under certain circumstances. The main management methods associated with removing sediment from reservoirs nearing critical storage loss are flushing and dredging. Drawdown flushing has been studied extensively and has been found to work optimally on narrow, gorge-shaped reservoirs where the water can be fully drawn down. Pressurized flushing is not implemented as often as drawdown flushing as its main purpose is in clearing the area immediately surrounding the bottom outlets of the dam. Flushing generally has more noticeable effects on the downstream ecosystem than sluicing. Dredging, the most often used sedimentation management technique, is also a highly expensive and time-consuming practice, although efficacious when complimented by other methods, particularly for settling basins at the inlet of the reservoir.

INTRODUCTION

America is aging, and its reservoirs are no exception. A report published in 1968 determined that the average annual storage loss of U.S. reservoirs was slightly more than 0.2 percent of the total initial capacity (Dendy, 1968). Though this statistic was not alarming in 1968, after nearly 50 years, about ten percent of the total initial capacity will have been lost due to sedimentation. In fact, the life expectancy of most reservoirs is only 100 to 200 years, and at least 200 of the largest United States reservoirs were more than 40 years old as of 2008 (Baker, et. al, 2008). Figure 1 is a photograph of a dam for floodwater storage in northwest Iowa that was completely silted in from years of soil erosion from land in its watershed.

Figure 1. Dam in northwest Iowa completely silted in and no longer functioning to store floodwaters (Photo by Tim McCabe; Photo courtesy of USDA Natural Resources Conservation Service; Photo by USDA NRCS).

Sediment management is now more than ever a challenge for the current generation (Morris and Fan, 1998). The predicament is further complicated with environmental concerns related to sediment capture and release. Already the effect of dams on American rivers has been so great from an ecologic or hydrologic standpoint that even the predictions of future global climate change impacts are in no way comparable (Graf, 1999). Perhaps the largest problem, however, is the lack of data for the majority of U.S. reservoirs. A report on Kansas reservoirs stated that most of the nearly 6,000 regulated reservoirs do not have bathymetric data, which is essential information for any sediment-management project (Baker, et. al, 2008). This review of the state of the practice of sediment management aims to inventory the feasibility, efficiency, and environmental impacts of various techniques currently in use.

Three main strategies exist for dealing with reservoir sedimentation: reducing incoming sediment yield, minimizing siltation, and removing deposited sediment from reservoirs. Within each of these strategies various techniques present themselves for certain situations. This review will focus on techniques from the latter two of the three aforementioned strategies. Sediment bypass structures, sluicing, and density current venting aim to minimize siltation in reservoirs; and flushing and dredging remove sediment that has settled on the bottom of reservoirs. These techniques battle the issue of sedimentation in reservoirs so that situations such as the one shown in Figure 2 of Lake Red Rock in central Iowa can be prevented or resolved.

Figure 2. Sediment filling Lake Red Rock in central Iowa at rates much faster than anticipated. (Photo by unknown photographer; Photo courtesy of USDA Natural Resources Conservation Service; Photo by USDA NRCS).

MINIMIZING SILTATION

Many effective means of preventing storage loss in United States reservoirs focus on the upstream environment and the transport of sediment entering the low-velocity area where particles settle out; however, minimizing settling inside reservoirs also serves an important purpose in regions where flood events carry the majority of sediment, and reservoirs serve only as water supply. The main management methods associated with this particular strategy are construction of sediment bypass structures, sediment pass-through (or sluicing), and venting of the density current.

Sediment Bypass Sediment bypass structures route high-sediment flows, generally resulting from floods, around the reservoir using canals, pressurized pipelines, or tunnels. Construction of canals is an expensive practice with its viability depending upon local topography, reservoir size and shape, and hydraulics of the river system. Pressurized pipelines for bypassing sediment are also rarely used and not often mentioned in literature due to the specific conditions necessary for its successful implementation and the high cost of construction (Batuca and Jordaan, 2000). Bypass tunnels are more common than canals or pressurized pipelines, but also suffer from high investment and management costs. A majority of these structures are operated in Switzerland and Japan where slopes are high (1% - 4%) due to mountainous topography and reservoirs are small (Sumi et al., 2004). The effectiveness of this management method is seen in the Nunobiki Dam in Japan whose tunnel has allowed the reservoir to maintain a constant storage volume since 1908 (Annandale, 2013).

Abrasion at the inlet due to high sediment concentrations is the main challenge with bypass tunnels. A design suggestion to combat the degradation of the inlet involves utilizing high strength concrete (30 N/mm^2 or more) and allowing for deep abrasion protection (10 – 35 mm); however, more research is necessary on the topic (Sumi et al., 2004).

From an ecological standpoint, sediment bypassing boasts a lesser impact on the downstream environment when compared to sluicing, flushing, or no management strategy at all. During flood events, sediment from the upper reaches of the river, which would naturally flow downstream without the existence of a reservoir, remains in suspension at approximately the same concentration (Auel and Boes, 2011). The suspended sediment concentration is neither higher from scouring of the reservoir bottom nor lower from releasing the clear water at the top of the reservoir.

The main overall advantage of sediment bypass structures, however, is that they do not interfere with regular reservoir operation, as no drawdown of the water level is needed. However, the method is difficult to apply, requires careful planning, and cannot be utilized in arid climates where the need for water is high (Tigrek and Aras, 2011). In addition, regions with flood control concerns will find that sediment bypassing undermines the original intent of the reservoir (Annandale, 2013).

Sluicing Sediment pass-through, also known as sluicing, is another way of abating sediment deposition in reservoirs. For this method, the reservoir level is drawn down during the flood season and allowed to flow through the sluice gates to maintain the incoming sediment in suspension (Tigrek and Aras, 2011). When particles enter the low-velocity area of a reservoir, they settle and form a delta consisting first of the heavier coarse sediments, then further on a more shallow layer of fine sediment. This phenomenon can be seen in the illustration in Figure 3. A depiction of the sluicing technique to reduce the development of this delta is shown in Figure 4. A 1996 study of the North Fork Feather River in Northern California determined that using sluicing as a sediment-management technique viably maintained the equilibrium of sediment between the reservoir and downstream environment over an extended operating period (Chang et al., 1996). The study also showed that sluicing would not result in adverse impacts on the fish habitat downstream as long as it followed the suggested operating rules.

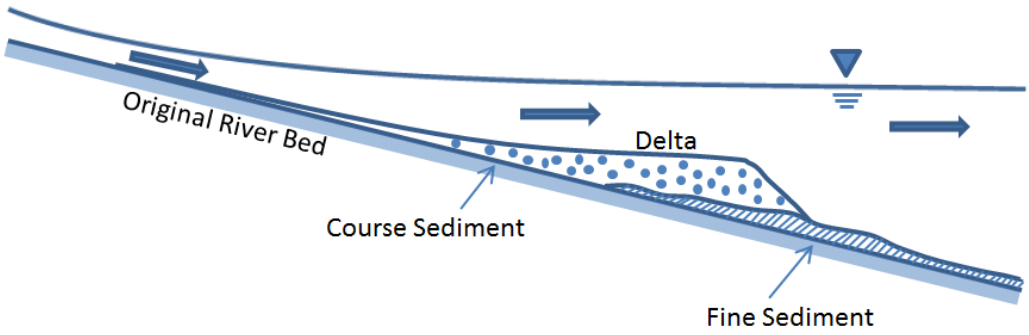

Figure 3. Longitudinal reservoir profile with delta formation.

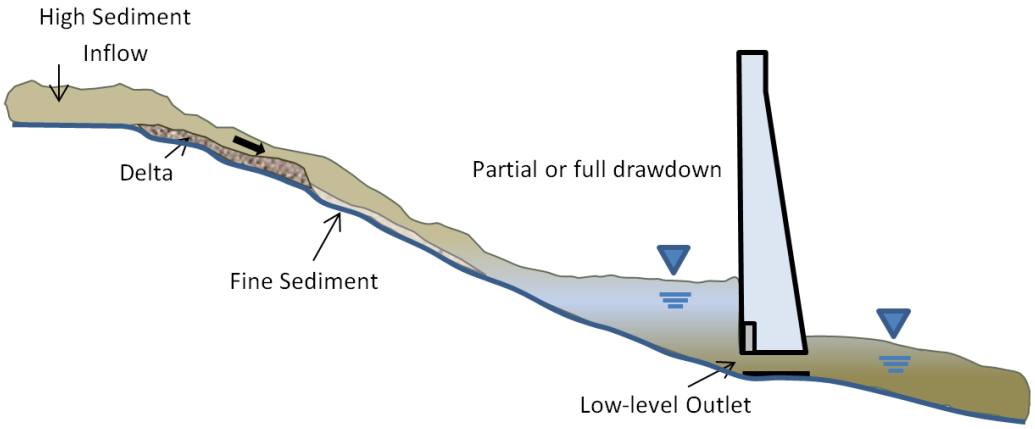

Figure 4. Longitudinal reservoir profile with sediment sluicing.

One restriction of sluicing is its dependence upon the existing structure of the dam, as sluice gates must be positioned appropriately along the bottom for the sediment to flow through efficiently. A 1988 assessment of several countries' sluicing techniques recommended that the sluice gates be at a height of 1.5 to 2.5 meters with an area determined from design curves presented in their paper (Paul and Dhillon, 1988). They also advised that only the width of the gate should be changed to increase effectiveness. In addition, Bogardi (1974) suggested that the sluicing technique is most effective when: 1) water depths are low and discharge is high; 2) sluice gates are wide and located near the bottom of the dam; 3) the original stream bed is steep and the reservoir has a short, straight bottom; 4) and the reservoir is in an advanced stage of siltation and the deposits consist of fine grained, recently settled material. With these specifications met, sluicing has been found effective in many instances, especially in China, where it is practiced routinely due to high sediment loads (Hotchkiss, 1990).

Density Current Venting Density current venting, a seldom-used technique, involves the discharge of turbid sediment-laden water from a low-level outlet (like a sluice gate) while the surface waters remain clear or unchanged. Turbidity currents develop when water with a high sediment load enters a reservoir and immediately plunges to the bottom, travelling through the original channel until settling near the dam in what is called a "muddy pool" (Morris and Fan, 1998). Management of these currents can drastically reduce sediment build-up at the base of a dam. However, density currents form only under certain conditions and can be difficult to detect. Under optimal conditions, approximately 50% of the total sediment can be vented, though the average is closer to 20% since early detection methods are lacking (Utah Division of Water Resources, 2010). One innovative way of managing density currents was developed in Japan at the Katagiri Dam where a curtain wall permitted only the sediment laden density current at the bottom of the reservoir to spill over the top of the dam (Annandale, 2013). A depiction of the standard density current venting method is shown in Figure 5.

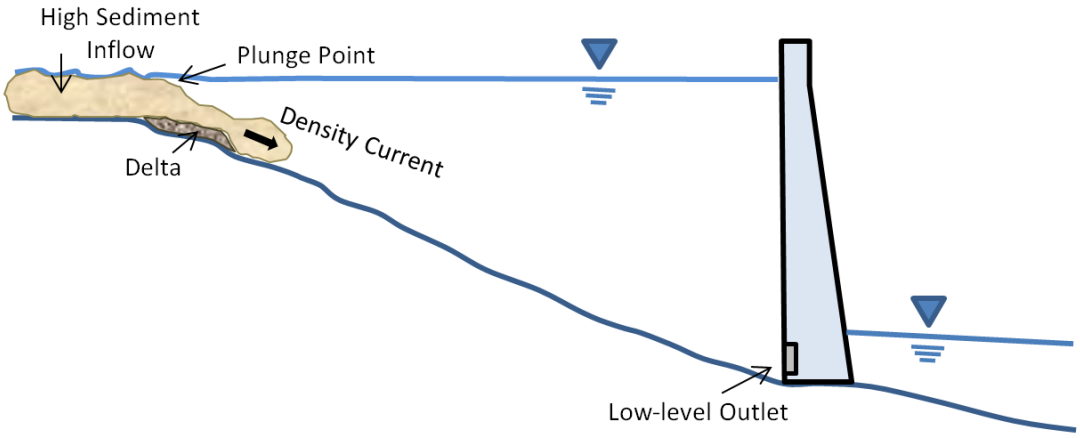

Figure 5. Density current along longitudinal reservoir profile.

A recent study of this method conducted on the Tsengwen Reservoir in Taiwan using 3D numerical models as well as measured and simulated typhoon flood events proposed the following formula for estimating the outflow concentration and venting efficiency of an outlet (Lee et al., 2014):

$$C_O = KC_L\left[\frac{(s-1)gh_L^{\ 5}}{Q_O}\right]^{1/5} \qquad \text{Eq. 1}$$

where C_o is the outflow concentration [ML^{-3}]; K is the venting coefficient calibrated based on the outlet structure [ML^{-3}]; C_L is the layer averaged concentration of the density current [ML^{-3}], s is the specific weight of the suspended solid [$ML^{-2}T^{-2}$], g is gravitational acceleration, h_L is the distance between the outlet center and the interface of clear water and dense layer [L], and Q_o is the outflow discharge [L^3T^{-1}].

REMOVING DEPOSITS

Removing sediment is quickly becoming an issue of great concern as reservoirs which were constructed decades ago without any consideration of sediment management have slowly built up enormous deposits of silt and sand and now are reaching levels which impede recreation and impact water supply. The main management methods associated with removing sediment from submerged reservoirs are flushing and dredging. Flushing can be further characterized as either drawdown or pressurized.

Drawdown Flushing Drawdown flushing is highly similar to sluicing; however, it is not executed during flood season. Rather, it is done when the river is at low-flow conditions so that drawing down the water level takes less effort and does not affect the water supply (Annandale, 2013). The operationally-favorable conditions for drawdown flushing generally occur before the flood season or at the end of the dry season (Batuca and Jordaan, 2000). A depiction of drawdown flushing is shown in Figure 6.

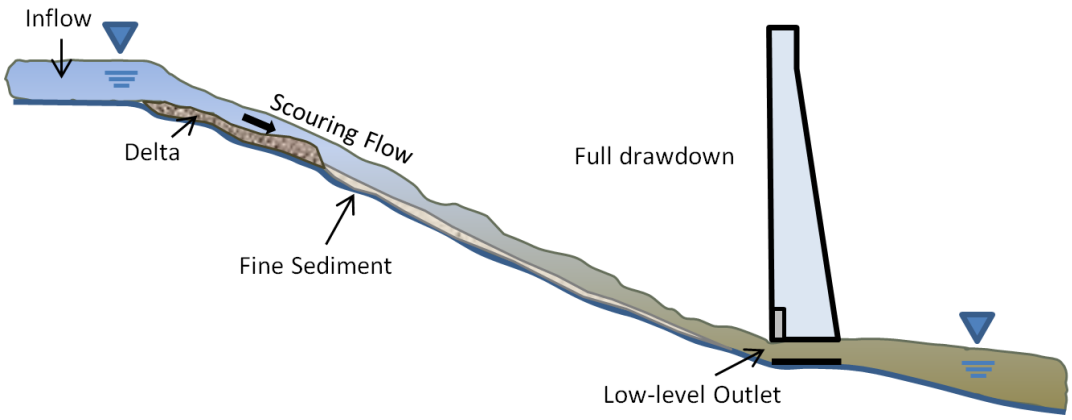

Figure 6. Longitudinal reservoir profile with sediment flushing.

A study of the Tapu reservoir in Taiwan used optimization of operational-rule curves to increase flushing efficiency, with a final recommendation that the particular reservoir be flushed every two to four years in the months of May or June (Chang et al., 2003). A more recent study on the Kali Gandaki hydropower reservoir used a three-dimensional numerical modelling program called Sediment Simulation in Intakes with Multiblock Option (SSIIM) to prove that this could be a practical alternative to the difficult task of planning and optimizing the flushing process for complex reservoir geometries (Haun and Olsen, 2012). The study also identified limitations of physical modeling of reservoir flushing, stating that the magnitude of bed forms is challenging to properly scale in a physical model.

Drawdown flushing is generally most effective in narrow, gorge-shaped reservoirs like the Gebidem reservoir in Switzerland, and water must be allowed to be fully drawn down, making it near impossible to implement in hydropower dams (Tigrek and Aras, 2011). This technique is also impossible to implement in reservoirs without low-level outlets, such as sluice gates.

Pressurized Flushing Pressurized flushing removes only a fraction of the amount of sediment when compared to drawdown flushing. This method is rarely used and its main purpose is to clear the area immediately surrounding the bottom outlets (Annandale, 2013). As the sediment is flushed out, the area around the outlet forms a funnel-shaped crater, known as a "flushing cone" (Emamgholizadeh et al., 2006). Meshkati et al. (2009) addressed the development of the flushing cone and identified a set of non-dimensional relationships which could be used to estimate the development of the cone and, therefore, increase efficiency and sediment output. Despite this progress, keeping the bottom outlets clear of sediment will likely continue to be the only valuable use of pressurized flushing.

The impact on the ecosystem downstream of the reservoir is an important consideration with either drawdown or pressurized flushing as a sediment-management method. A study of the Valgrosina reservoir in northern Italy where free-flow flushing was utilized to maintain reservoir capacity found that fish densities decreased up to 73 percent while biomass decreased up to 66 percent after a flushing event (Crosa et al., 2010). To avoid spikes in suspended solid concentration and to manage scouring effects, they recommended that a yearly flushing occur in that particular reservoir. An earlier study of regulated rivers in California suggested that flushing could help clean fine sediment deposits from downstream gravel to encourage fish spawning

(Kondolf and Matthews, 1991). However, it also observed that flushing could be counterproductive as potential high flow velocities might end up carrying some of this ecologically important bed load away with the fine sediment.

In addition to the effect on the downstream ecosystem, the associated high sediment concentrations also affect downstream infrastructure. Sediment can clog irrigation canals and heat exchangers for industrial cooling systems, wear down hydropower turbines, and cause issues at water purification plants with low capacities for suspended solids (Morris and Fan, 1998).

Dredging An expensive but effective solution to extreme storage loss in reservoirs, dredging is perhaps the most often used sediment-management technique. Dredging removes deposited sediment from the bottom of reservoirs using pumps, hydraulic suction, or clamshell buckets (Utah Division of Water Resources, 2010). A photograph of sediment-laden water being pumped as part of a dredging operation at Lake Panorama in central Iowa is shown in Figure 7. In 2010, the average cost of dredging reservoirs was estimated to be \$8.70/m^3, a serious investment for any small city operating on a budget (Smith et al., 2013). According to a 2008 study of Kansas reservoirs, dredging one of the larger reservoirs in the state could cost more than 100 times the original amount invested in constructing the reservoir (Baker, et. al, 2008).

Figure 7. Sediment-laden water pumped as part of a dredging operation at Lake Panorama in central Iowa (Photo by Lynn Betts; Photo courtesy of USDA Natural Resources Conservation Service; Photo by USDA NRCS).

One main issue with dredging is the environmental impact of disturbing several years of settled sediment. Closed buckets are recommended for areas with contaminated silts since they minimize the seepage of polluted water into the environment (Utah Division of Water Resources,

2010). However, it has also been proven that dredging can reduce eutrophication in shallow lakes and reservoirs. The 2009 report on the dredging of Lake Yuehu in central Wuhan, China, showed that internal nutrient loads were reduced and the zooplankton community had progressed toward a less eutrophic balance post-dredging (Zhang et al., 2009).

Dredging is often chosen over employing conventional best management practices (BMPs) concerning croplands. This can be attributed to the limited effect of these BMPs in comparison to the cost of implementation. It was determined in a 2013 economic study that BMP enactment should be carefully planned to optimize cost-effectiveness, and even the most effective practices may not preclude the need for future dredging (Smith et al., 2013).

SUMMARY

Sediment management in reservoirs is a complex and expensive undertaking no matter which technique is used. A perfectly sustainable solution for every situation does not exist, but efforts can be optimized for the particulars of each reservoir. Methods concerned with preventing the deposition of sediment such as sediment bypass structures, sluicing, and density current venting can be most effective in regions where high sediment loads occur often and in a predictable manner. Methods concerned with removing sediment deposits such as flushing or dredging are often used as a result of non-sustainable reservoir design in an effort to reclaim lost storage. With the aging of America's infrastructure, more attention must be focused on the upkeep of the nation's reservoirs before sedimentation renders them useless.

REFERENCES

Annandale, G. (2013). *Quenching the Thirst: Sustainable Water Supply and Climate Change*, CreateSpace Independent Publishing Platform, North Charleston, SC.

Auel, C., and Boes, R.M. (2011). "Sediment bypass tunnel design – review and outlook," *Dams and Reservoirs under Changing Challenges*, Taylor & Francis Group, London, England, pp 403-412.

Batuca, D. G., and Jordaan, J. M. (2000). *Silting and Desilting of Reservoirs*, A.A.Balkema, Rotterdam, The Netherlands.

Bogardi, J. (1974). *Sediment Transport in Alluvial Streams*, Budapest, Hungary.

Chang, H. H., Harrison, L. L., Lee, W., and Tu, S. (1996). "Numerical Modeling for Sediment-Pass-Through Reservoirs," *Journal of Hydraulic Engineering*, 122(7), pp 381-388.

Change, F., Lai, J., and Kao, L. (2003). "Optimization of operation rule curves and flushing schedule in a reservoir," *Hydrological Processes*, 17(8), pp 1623-1640.

Crosa, G., Castelli, E., Gentili, G., and Espa, P. (2010). "Effects of suspended sediments from reservoir flushing on fish and macroinvertebrates in an alpine stream," *Aquatic Sciences*, 72(1), pp 85-95.

Dendy, F.E. (1968). "Sedimentation in the Nation's Reservoirs," *Journal of Soil and Water Conservation*, 23(4), pp 135-137.

Emamgholizadeh, S., Bina, M., Fathi-Moghadam, M., and Ghomeyshi, M. (2006). "Investigation and Evaluation of the Pressure Flushing through Storage Reservoir," *ARPN Journal of Engineering and Applied Sciences*, 1(4), pp 7-16.

Graf, W. L. (1999). "Dam nation: A geographic census of American dams and their large-scale hydrologic impacts," *Water Resources Research*, 35(4), pp 1305-1311.

Haun, S., and Olsen, N. R. B. (2012). "Three-dimensional numerical modelling of the flushing process of the Kali Gandaki hydropower reservoir," *Lakes & Reservoirs: Research & Management*, 17(1), pp 25-33.

Hotchkiss, R. H. (1990). "Reservoir Sedimentation and Sediment Sluicing: Experimental and Numerical Analysis," St. Anthony Falls Hydraulic Laboratory, Minneapolis, Minnesota.

Baker, D., and deNoyelles, F. (2008). "Can Reservoir Management Reduce Sediment Deposition?," *Sedimentation in Our Reservoirs: Causes and Solutions*, pp 57-71.

Kondolf, G. M., and Matthews, W. V. G. (1991). "Management of Coarse Sediment in Regulated Rivers of California," *University of California Water Resources Center*, Berkeley, California.

Lee, F., Lai, J., Tan, Y., and Sung, C. (2014). "Turbid Density Current Venting through Reservoir Outlets," *KSCE Journal of Civil Engineering*, 18(2), pp 694-705.

Meshkati, M. E., Dehghani, A. A., Naser, G., Emamgholizadeh, S., and Mosaedi, A. (2009). "Evolution of Developing Flushing Cone during the Pressurized Flushing in Reservoir Storage," World Academy of Science, Engineering and Technology, 3(10), pp 1088-1092.

Morris, G. L., and Fan, J. (1998). *Reservoir Sedimentation Handbook: Design and Management of Dams, Reservoirs, and Watersheds for Sustainable Use*, McGraw-Hill Book Co., New York, New York.

Paul, T. C., and Dhillon, G. S., (1998). "Sluice dimensioning for desilting reservoirs," *International Water Power & Dam Construction*, 40(5), pp 40-44.

Smith, C., Williams, J., Nejadhashemi, A. P., Woznicki, S., and Leatherman, J. (2013). "Cropland management versus dredging: An economic analysis of reservoir sediment management," *Lake and Reservoir Management*, 29(3), pp 151-164.

Sumi, T., Okano, M., and Takata, Y. (2004). "Reservoir Sedimentation Management with Bypass Tunnels in Japan," Proceedings of the Ninth International Symposium on River Sedimentation, Yichang, China, pp 1036-1043.

Tigrek, S., and Aras, T. (2011). *Reservoir Sediment Management*, CRC Press, Leiden, The Netherlands, pp 41-60.

Utah Division of Water Resources, (2010). "Managing Sediment in Utah's Reservoirs," *Utah State Water Plan*, Salt Lake City, UT.

Zhang, S., Zhou, Q., Xu, D., Lin, J., Cheng, S., and Wu, Z. (2009). "Effects of sediment dredging on water quality and zooplankton community structure in a shallow of eutrophic lake," *Journal of Environmental Sciences*, 22(2), pp 218-224.

SURROGATE ANALYSIS AND INDEX DEVELOPER (SAID) TOOL AND REAL-TIME DATA DISSEMINATION UTILITIES

Marian Domanski, Hydrologist, USGS, mdomanski@usgs.gov, 217-328-9758
Timothy Straub, Hydrologist, USGS, tdstraub@usgs.gov, 217-621-9587
Molly Wood, Hydrologist, USGS, mswood@usgs.gov, 208-387-1320
Mark Landers, Hydrologist, USGS, landers@usgs.gov, 678-924-6616
Gary Wall, Hydrologist, USGS, grwall@usgs.gov, 518-285-5621
Steven Brady, Computer Scientist, USGS, sbrady@usgs.gov, 785-832-3518

Abstract: The use of acoustic and other parameters as surrogates for suspended-sediment concentrations (SSC) in rivers has been successful in multiple applications across the Nation. Critical to advancing the operational use of surrogates are tools to process and evaluate the data along with the subsequent development of regression models from which real-time sediment concentrations can be made available to the public. Recent developments in both areas are having an immediate impact on surrogate research, and on surrogate monitoring sites currently in operation.

The Surrogate Analysis and Index Developer (SAID) standalone tool, under development by the U.S. Geological Survey (USGS), assists in the creation of regression models that relate response and explanatory variables by providing visual and quantitative diagnostics to the user. SAID also processes acoustic parameters to be used as explanatory variables for suspended-sediment concentrations. The sediment acoustic method utilizes acoustic parameters from fixed-mount stationary equipment. The background theory and method used by the tool have been described in recent publications, and the tool also serves to support sediment-acoustic-index methods being drafted by the multi-agency Sediment Acoustic Leadership Team (SALT), and other surrogate guidelines like USGS Techniques and Methods 3-C4 for turbidity and SSC.

The regression models in SAID can be used in utilities that have been developed to work with the USGS National Water Information System (NWIS) and for the USGS National Real-Time Water Quality (NRTWQ) Web site. The real-time dissemination of predicted SSC and prediction intervals for each time step has substantial potential to improve understanding of sediment-related water-quality and associated engineering and ecological management decisions.

INTRODUCTION

Streamflow, sediment, and water-quality data are needed to establish baseline information for water-resource managers to evaluate historical and current conditions and plan management alternatives. Real-time, continuous SSC data can be useful for monitoring river response downstream of areas affected by recent wildfires, construction or remediation activities, levee failures, or changing land uses. Additionally, real-time data can provide an early warning for operators of municipal water supply and hydroelectric facilities concerned with avoiding damage to infrastructure from sediment. Surrogates are becoming widely used to better understand physical and chemical processes in natural systems (Rasmussen and others, 2009). Acoustic technology is becoming increasingly used for velocity measurements and is also being used as a surrogate for sediment concentrations.

The Surrogate Analysis and Index Developer (SAID) tool is a standalone tool to assist in the development of ordinary least squares (OLS) regression models that relate response and predictor variables (Helsel and Hirsch, 2002) by providing visual and quantitative diagnostics to the user (figure 1). The tool is written in the Matlab® programming language. There is no limit on the number of explanatory variables to be used in the linear model and no requirement of which explanatory variables to use. SAID is under beta development and is not yet formally released as a USGS software product.

SAID has applications for relating surrogate-technology parameters such as turbidity, acoustics, and others. SAID can be used for processing acoustic parameters to be used as predictor variables for suspended-sediment concentrations (SSC).The sediment-acoustic method, which assumes a constant spatial suspended-sediment concentration and grain size distribution with respect to range along the acoustic axis of the beam, utilizes acoustic data from fixed-mount stationary acoustic Doppler velocity meters (ADVM). Some of the earliest USGS applications and research were done by Topping and others (2004, 2006, 2007), Wright and others (2010), Landers

(2012), and Wood and Teasdale (2013). The sediment-acoustic method, as described in these references, is used in SAID to compute the sediment attenuation coefficient and sediment corrected backscatter from ADVM acoustic parameters. SAID allows for quick adjustment of complex ADVM data-processing options, changes in the variables used in the regression, and evaluation of the created model. The tool also enables the user to transform loaded variables, build linear regression models, view linear model diagnostic statistics and plots, export the model information, and generate a predicted time series.

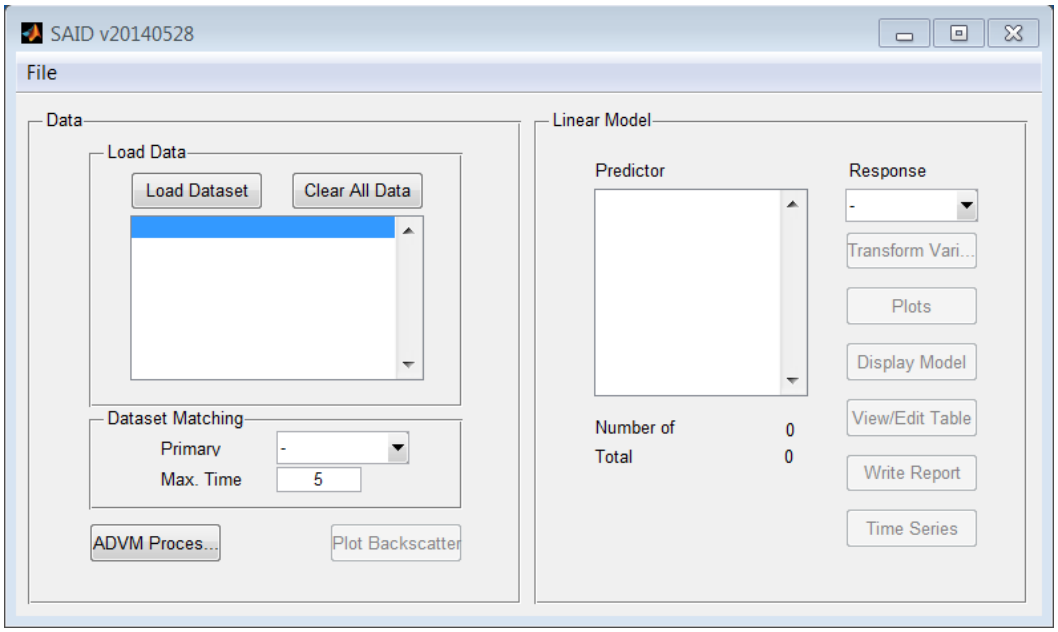

Figure 1 Main SAID window for beta version 20140528

This paper provides an overview on processing and loading data into SAID for developing regression models among surrogate data and measured constituents. In addition, this paper discusses the ADVM configuration parameters that are used in the calculation of acoustic surrogate parameters. Lastly, the paper gives an overview of how the regression models developed in SAID can be used in utilities that have been developed to disseminate predicted SSC in real-time.

SURROGATE ANALYSIS AND INDEX DEVELOPMENT

In the development of linear regression models, explanatory and response variables must be selected. These variables are contained in time series dataset files stored on disk. Because surrogate observations are continuous, and constituent observations occur at irregular time intervals, it is typical to store surrogate and constituent time series in separate dataset files. In order to choose observation sets of variables to develop a linear regression model, observations from the surrogate and constituent time series must be matched. Once a linear regression model is created from a set of matched observations, it must be evaluated for validity and appropriateness. SAID provides the ability to load and match datasets, select the response and predictor variables, and evaluate the created linear regression model. An overview of the dataset workflow is briefly described below and the following sections describe the process to develop regression models in more detail.

- ***Loading datasets***
  - Data that are stored on disk in ASCII files are loaded into memory by SAID.
- ***Choose primary datasets***
  - A dataset is selected that serves as the primary time series to synchronize observations. The selected dataset is known as the primary dataset and other loaded datasets become secondary datasets.
  - Adjusting the maximum time difference value (Max. Time) changes the upper limit of the time difference to which observations are synchronized.

- ***Choose linear model variables***
  - Available variables will be displayed in the Predictor Variables list box and the Response Variable drop-down list. SAID creates a linear model after a valid set of predictor and response variables are selected.
- ***Evaluate linear model***
  - SAID provides several diagnostic plots to determine if the created linear model created fits the assumptions of the OLS method.

Datasets: SAID is capable of loading two types of data. The term "loaded datasets" refers to datasets that have been loaded from disk. The data can be stored as tab delimited ASCII files or a collection of Argonaut ASCII files. Loaded datasets are not necessarily stored in separate files because of a constituent/surrogate relationship. Having dissimilar time steps is a typical reason for storing and loading datasets separately.

Variables with names that match the patterns CellXXAmpY and CellXXSNRY (where XX is the cell number, from 00 to 99, and Y the beam number, either 1 or 2) are dedicated variables for backscatter counts (Amp) and signal-to-noise ratio (SNR) and are used in the computation of the sediment attenuation coefficient and mean sediment corrected backscatter. These variables are not available for use in the creation of a linear model but are necessary in the computation of the ADVM acoustic surrogate metrics.

Variables named ADVMTemp and Vbeam also are dedicated variables used for the temperature and water depth. The temperature must be in units of degrees Celsius and is directly used in computing the ADVM parameters and is therefore necessary. The water depth is used to determine if the cell is out of water when the vertical orientation is selected in the ADVM Processing dialog box. A minimum Vbeam value also is set by the user in order to exclude samples taken when the water is below a certain depth.

During the time a dataset is being loaded, the program checks for variable names that are already loaded. If a variable that is in the dataset that is to be loaded exists in an already loaded dataset, then the selected dataset will not be loaded. Once the datasets are loaded, the data are then available for matching.

Matching Time-Series Observations: In order to build a linear model, it is necessary that a dataset with observations of predictor (surrogate) and response (water-quality) variables exist. Matching occurs in order to synchronize observations from the loaded datasets. The result of matching is the creation of a single dataset containing the matched data, which is then used to develop the linear model.

The primary dataset is the loaded dataset that contains the observations whose date and time of observation form the basis for matching in the secondary datasets. In a typical application for SAID, the primary dataset is the dataset that contains the constituent observations. The primary dataset is chosen by selecting it from the Primary Dataset drop-down list (figure 1). A linear model will not be created until a primary dataset is selected.

Secondary datasets are loaded datasets that contain observations that are matched to primary dataset observations. The term secondary dataset refers to all of the datasets that are not the primary dataset. Observations from the secondary datasets are only copied to the synchronized dataset if they have a date-time that matches a primary dataset observation within the user specified time interval allowance (Max. Time).

Selecting a primary dataset initiates the matching algorithm. For each observation in the primary dataset, SAID calculates the minimum absolute time difference between the observation date and time variables and the date and time variables of the secondary dataset being compared. If the minimum absolute time difference is less than or equal to the user specified value for the maximum time difference, the observations from the secondary dataset being compared are matched with the observations of the primary dataset and the values are copied to the matched dataset. If the minimum absolute time difference is greater than the user specified maximum time difference (Max. Time), then the corresponding variables in the observation in the matched dataset are set to an invalid value. In other words, the observation in the primary dataset will not be matched to an observation in the dataset being compared.

After a primary dataset is selected, the program will indicate that it is matching datasets and will remain unresponsive until the matching is complete. The time it takes for the program to create a matched dataset depends on the number of loaded datasets and the number of observations in each dataset. When the program has completed the matching algorithm, the variables available for use in the linear model are shown in the Predictor Variables and Response Variable lists.

Processing and Viewing Acoustic Backscatter Data (optional in SAID): The following ADVM-related parameters are required by SAID before the acoustic backscatter data are processed and acoustic surrogate parameters are computed:

- ADVM Configuration - Frequency, Effective Transducer Diameter, Slant Angle, Blanking Distance, Cell Size, Number of Cells
- ADVM Processing - Intensity Scale Factor (if Amp is selected for Backscatter Values), Minimum Mid-Point Cell Distance, Maximum Mid-Point Cell Distance, Minimum Vbeam

The configuration parameters are taken from a configuration record file that is saved by the ADVM with each ADVM data file. Once the required parameters in the ADVM Processing window have valid values, the ADVM parameters with at least one valid observation will be available in the Predictor Variables list. By clicking on the ADVM Processing button (figure 1), the ADVM configuration and processing options used in the calculation of the ADVM parameters can be changed (figure 2). ADVM configurations needed for input to SAID can be found in the setup parameters section of the ADVM software.

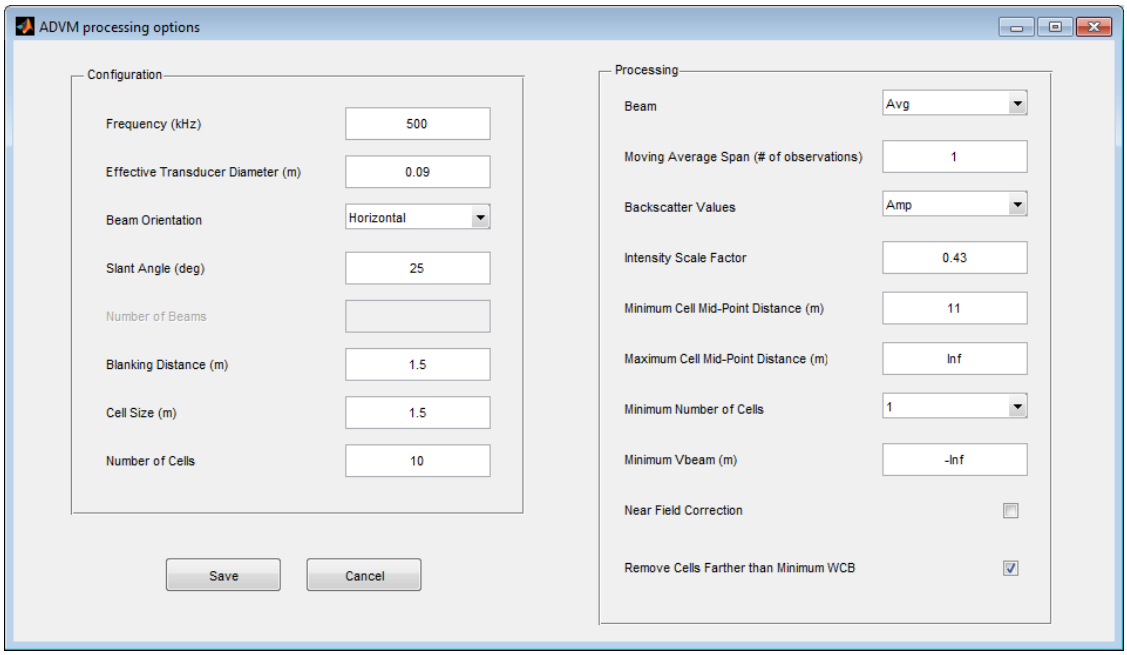

Figure 2 ADVM deployment configuration and acoustic parameter options window

Configuration Parameters: The following parameters indicate the ADVM type and setup and are necessary to compute the acoustic surrogate parameters (figure 2).

- ***Frequency*** – The frequency of the ADVM acoustic signal.
- ***Effective Transducer Diameter*** – The effective diameter in meters of the ADVM transducer. The effective transducer diameter is only used when the Near Field Correction option is selected in the Processing section.
- ***Beam Orientation*** – The orientation of the acoustic beams of the ADVM. If 'Vertical' is selected for this field, then the Vbeam for each observation is compared to the cell edges, and each cell that is out of water is marked as invalid.
- ***Slant Angle*** – The angle of the acoustic beam with respect to the vector that represents the cell distance from the instrument. This angle, along with the blanking distance, cell size, and number of cells, is used to find the mid-point distance of each cell along the acoustic beam.

- ***Number of Beams*** – The number of acoustic beams on the instrument. This value is not used. SAID assumes that the instrument has two beams.
- ***Blanking Distance*** – The distance in meters from the instrument to the beginning of the first cell. This value is used in the computation of the mid-point distance of each cell along the acoustic beam.
- ***Cell Size*** – The length of each cell in meters. This value is used in the computation of the mid-point distance along the acoustic beam of each cell.
- ***Number of Cells*** – The number of cells in the configuration of the ADVM under analysis. The number of cells directly affects the values displayed in the Minimum Number of Cells drop down list.

Processing Parameters: The following parameters control how ADVM backscatter data are screened and processed (figure 2).

- ***Beam*** – The beam number from which the backscatter values are taken. When 'Avg' is selected for this field, the average cell backscatter values are used.
- ***Moving Average Span*** – The span, in number of observations, used in a centered moving averaging of the backscatter time series. The span must be an odd positive integer.
- ***Backscatter Values*** – The backscatter values used in the computation of the ADVM parameters. When 'Amp' is selected, the backscatter values are multiplied by the value in the Intensity Scale Factor field. The Intensity Scale Factor field is made available only when 'Amp' is selected. (Caution: the model developed will be specifically for SNR or Amp units and cannot be switched without building a new model. All empirical testing for best model using SNR or Amp should be evaluated.)
- ***Intensity Scale Factor*** – The scaling factor to convert backscatter counts to decibels. This field is only available when 'Amp' is selected in the Backscatter Values drop-down list. The factor defaults to 0.43 (typical for SonTek® instruments); but should be taken from manufacturer literature for specific ADVMs.
- ***Minimum Cell Mid-Point Distance*** – The minimum distance in meters from the transducer that the mid-point of a cell has to be in order for it to be used in the computation of the ADVM parameters.
- ***Maximum Cell Mid-Point Distance*** – The maximum distance in meters from the transducer that the mid-point of a cell can be in order for it to be used in the computation of the ADVM parameters.
- ***Minimum Number of Cells*** – The required minimum number of valid cells that an ADVM sample has to have in order for its computed parameter to be included as an observation in the linear model.
- ***Minimum Vbeam*** – The minimum value for Vbeam that a sample must have in order for it to be used as an observation. Vbeam is the water height in meters that the ADVM reports.
- ***Near Field Correction*** – When the box is checked, a near field correction to the backscatter values is made (Downing and others, 1995). When the box is not checked, no near field correction is applied. In general, data from the near field should be avoided by setting the blanking distance and/or Minimum Cell Point distance greater than the near field for a given instrument.
- ***Water Corrected Backscatter (WCB) Profile Adjustment*** – When this box is checked, the range of cells that include and are beyond the cell with the minimum water corrected backscatter (minWCB) are not included in the calculation, unless the cell with the minWCB is the last or first cell in the range considered.
    - If the cell with the minWCB is the last cell, the value is retained and all cells are used to calculate the sediment corrected backscatter and attenuation coefficient.
    - If the cell with the minWCB is the first cell, all other cells are not considered, and the water corrected backscatter value in the first cell is used as the sediment corrected backscatter value for the observation, and no attenuation coefficient is calculated.

Viewing acoustic backscatter profiles: When a valid response variable is matched with valid predictor variables, the Plot Backscatter button will be made available. When this button is clicked, a window with three sets of axes is displayed. From the top, the axes show Sediment Corrected Backscatter (SCB), Water Corrected Backscatter (WCB), and Measured Backscatter (MB), all in decibels, versus the cell mid-point distance along the acoustic beam (figure 3). Also shown in the window is a list of observation numbers and times from the model. The observation times are taken from the primary dataset. Only the backscatter samples that correspond to observations in the linear model are shown. Selecting sample times in the list displays the plots of the backscatter values on the axes. Multiple observations can be selected and plotted.

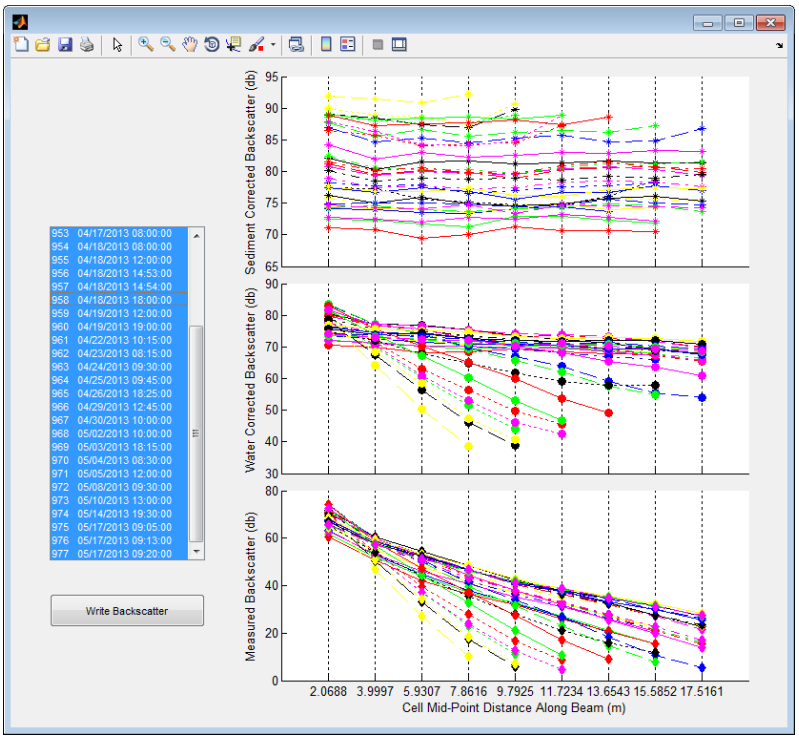

Figure 3 Backscatter profile plotting window

Development of Linear Regression Models: The available variables for use in the development of linear regression models in SAID appear in the Predictor Variable list and Response Variable in the Linear Model screen (Figure 4). There is no limit on the number of variables used in the creation of an Ordinary Least Squares (OLS) linear regression model, and there are no restrictions regarding which variables must be used. The Transform Variable button provides the option to transform a loaded variable using a transform function. When transformed, the variable will be available as a selection in the Predictor Variable list and the Response Variable drop down list.

As datasets are loaded, and if the Match Variable is a valid selection, the variables that are available for use in developing the linear model are shown in the Predictor Variables list and the Response Variable drop-down list. Selecting a variable in the Predictor Variables list, then one from the Response Variable drop-down list, will result in the generation of a model. Selecting the variable that is used for the Response Variable in the Predictor Variables list deselects the predictor variables and resets the response variable selection to the first in the list.

After a model is successfully created by selecting variables, a user can begin to evaluate the model results. This program includes tools to assist in model evaluation, available using the Plot Backscatter, View/Edit Table, Display Model, Write Report, Plots, and Time Series buttons. The number of observations used in the model is shown next to the Number of Observations label.

If a valid linear model exists within the program, the Number of Observations field will show the number of samples used in the development of the linear model. This corresponds to the number of valid observation values for the selected variables within the primary dataset. The Total Samples field shows the total number of samples in the loaded dataset. This number corresponds to the number of samples in the dataset that is selected in the Match Variable drop-down list.

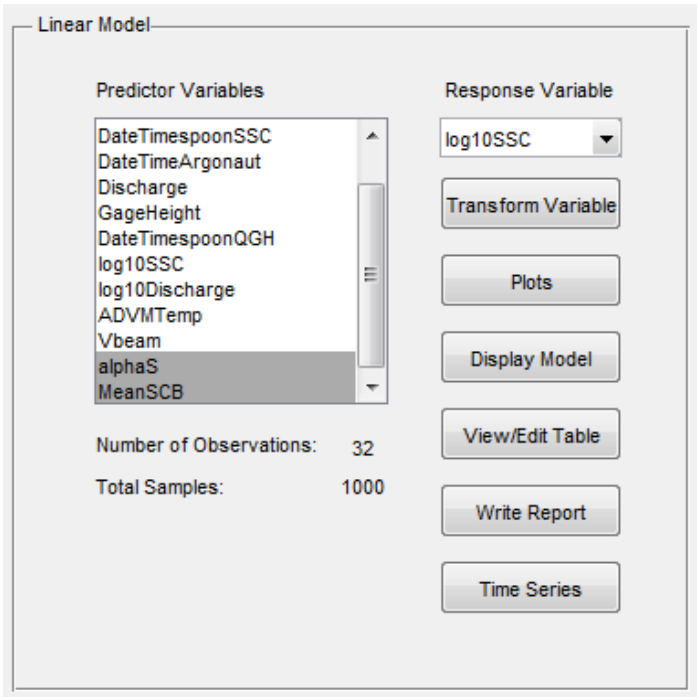

Figure 4 Linear Model options on the main SAID window

Evaluation of Regression Models: SAID provides several ways to graphically evaluate the linear model. Clicking on the Plots button within the main SAID window will display another window that provides several plotting options. In any plot figure, if Data Cursor Mode is enabled, any observation data point can be selected and the corresponding observation number will be shown along with the values plotted. The Model button will show different figures depending on if the linear model is a simple linear regression (SLR) or a multiple linear regression (MLR) or if the response variable is transformed. If the existing linear model is an SLR model, then a figure with the response observations plotted against the explanatory observed values will be shown (figure 5). When the existing model is an MLR, a partial residual plot for each variable in the model will be shown. If the response variable is transformed, then a linear-space plot will be shown with a smeared estimate fit line and confidence bounds.

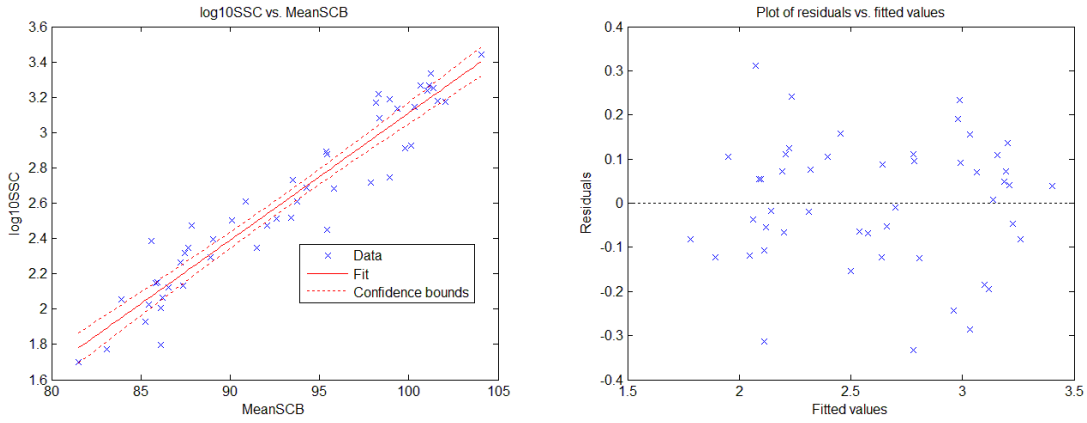

Figure 5 Linear model scatter plot and residual plot for a SLR model

Predicted versus observed plots can be selected to display the predicted response variable with the observed response variable. Also plotted is a one-to-one data line for comparison. If the response variable is transformed, then an additional figure will show the predicted versus observed values in linear space. Additionally the following residual plots can be selected:

- ***Raw Vs. Fitted***—Illustrates a plot of the raw residuals against the fitted response values.
- ***Probability***—Normal probability plot of raw residuals.
- ***Stan. Ser. Corr.***—Standard serial correlation plot of the residuals shown with a LOWESS fit line to detect autocorrelation. If the LOWESS fit line shows a trend that deviates far from 0, serial correlation may be present.
- ***Vs. Time***—Raw residuals plotted against time to see if a time dependent trend exists with the residuals.

The Display Model button will provide a window that displays the model results and statistics (figure 6). The information includes the linear equation, coefficient estimates, estimated confidence intervals, R^2 values for the model, and root mean squared error. This information also is written to a report with the Write Report button on the main SAID window.

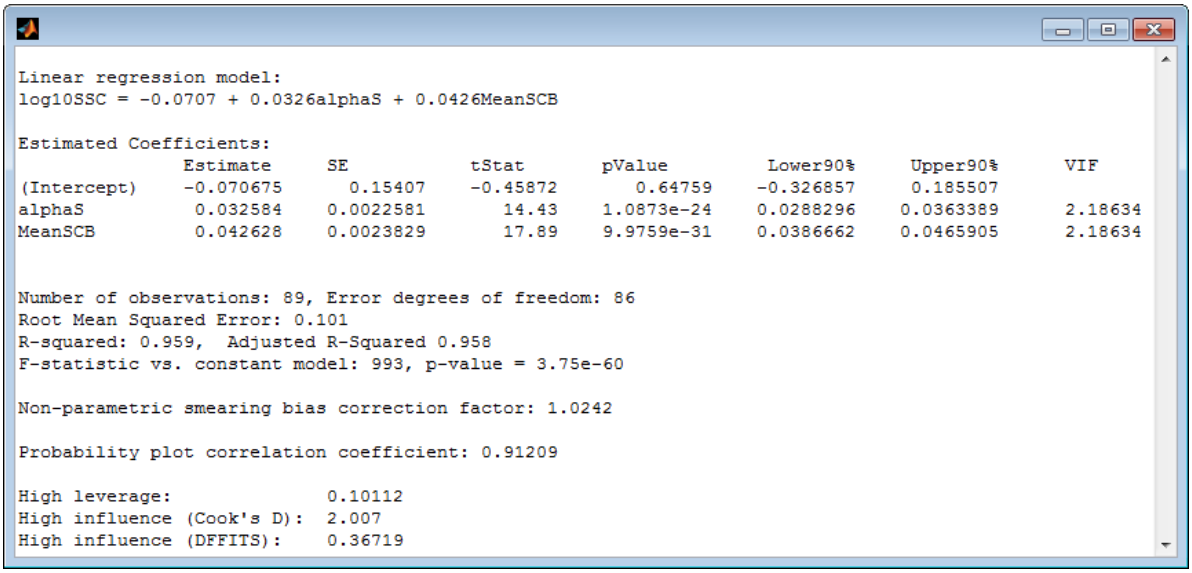

```
Linear regression model:
log10SSC = -0.0707 + 0.0326alphaS + 0.0426MeanSCB

Estimated Coefficients:
               Estimate      SE           tStat       pValue          Lower90%      Upper90%      VIF
(Intercept)    -0.070675      0.15407    -0.45872       0.64759     -0.326857      0.185507
alphaS          0.032584    0.0022581       14.43    1.0873e-24     0.0288296     0.0363389      2.18634
MeanSCB         0.042628    0.0023829       17.89    9.9759e-31     0.0386662     0.0465905      2.18634


Number of observations: 89, Error degrees of freedom: 86
Root Mean Squared Error: 0.101
R-squared: 0.959,  Adjusted R-Squared 0.958
F-statistic vs. constant model: 993, p-value = 3.75e-60

Non-parametric smearing bias correction factor: 1.0242

Probability plot correlation coefficient: 0.91209

High leverage:              0.10112
High influence (Cook's D):  2.007
High influence (DFFITS):    0.36719
```

Figure 6 Linear model regression model statistics window

Clicking on the View/Edit Table button will display a window that contains the observation information used in the model. The information shown is the observation number, the corresponding primary date and time variable, the response variable, and the predictor variables. Also shown are diagnostic statistics for each observation for outlier detection (Helsel and Hirsch, 2002). Calculated indicator values that exceed the corresponding critical values for the model are highlighted in red.

Observations can be removed by checking the boxes in the far left column and clicking the Remove Observation button. This action flags the date and time within the program and sets the variables that correspond to the date and time to an invalid value. Once a date and time is flagged as removed, any future variables that are used in the model will have the corresponding values set as invalid. This will continue until the Restore All Observations button is clicked, which clears the date and times flagged.

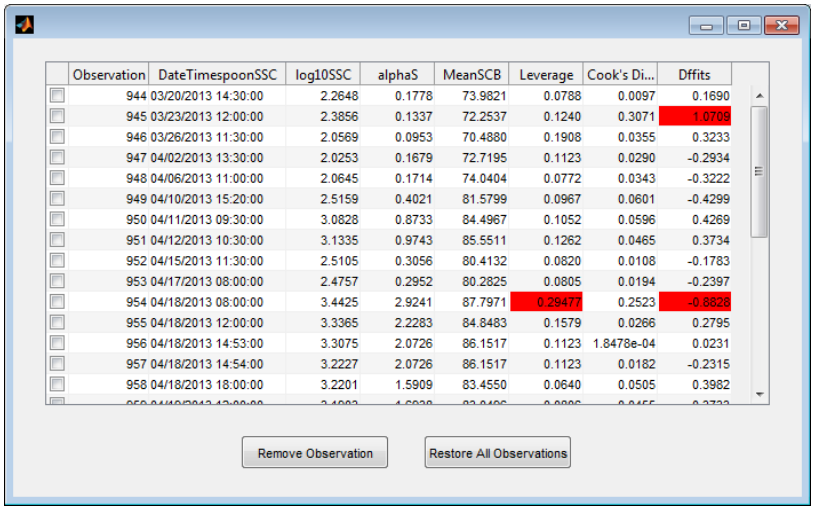

Figure 7 Observation table window used to view and remove observations from the model dataset

Generation of Report Output: To write a full summary report for the linear model, click on the Write Report button within the main SAID window. The user will be prompted for a location and name of a comma separated value file to write the report to. Selecting and entering a valid location and file name will write the report. The contents of the report include:

- ADVM configuration and processing options
- Dataset file names and locations
- Linear model summary and statistics
- Critical outlier indicator values
- The dataset observations that were used in the creation of the model along with Observation number, fitted response variable values, raw residuals, an estimate of the non-transformed variable with bias correction applied (if the response variable is transformed), and calculated outlier indicator values
- The observations that were removed from the model dataset

REAL-TIME DATA DISSEMINATION UTILITIES

After a surrogate regression model is developed and approved, the model can be used to generate continuous, real-time SSC estimates. The USGS has two utilities that make use of the computational algorithms in SAID to continuously estimate and display real-time sediment data:

- Real-time Acoustic Sediment Surrogate DAta Transfer (RASSDAT) program
- National Real-Time Water Quality (NRTWQ) program

RASSDAT is a Visual Basic Graphical User Interface (GUI) wrapped around a Python™ script that runs on a Windows® computer (figure 8), interfaces with the USGS National Water Information System (NWIS), and displays computed SSC on the NWIS Web Interface (http://waterdata.usgs.gov/nwis). NRTWQ is run from a centralized server and displays computed SSC on the NRTWQ Web site (http://nrtwq.usgs.gov/; figure 9). RASSDAT is under beta development and is not yet formally released as a USGS software product. Questions about RASSDAT development can be directed to the authors.

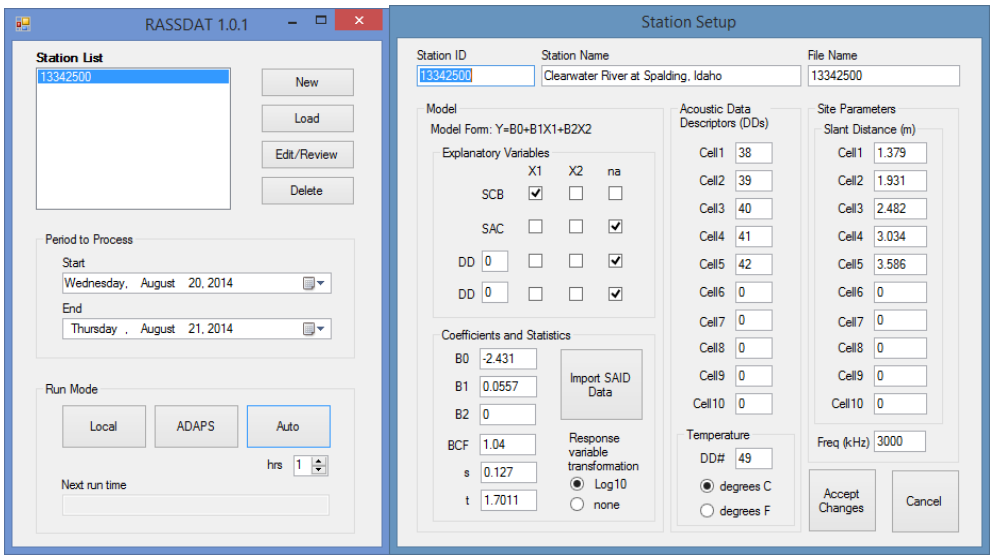

Figure 8 Screen captures of main processing (left) and station setup (right) windows from the USGS RASSDAT program, beta test version 1.0.1.

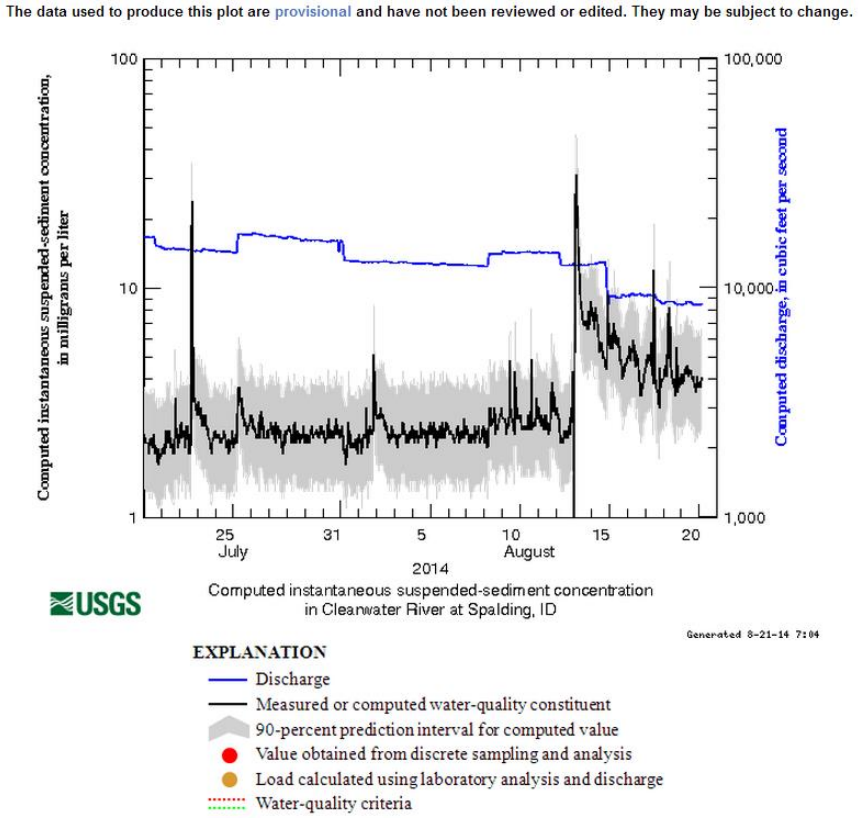

Figure 9 Screen capture from NRTWQ Web site showing example of SSC and SSC prediction intervals computed by using a sediment acoustic surrogate model developed for the Clearwater River at Spalding, Idaho (USGS Identification number 13342500).

SUMMARY

The use of continuous parameters as surrogates for water quality constituents has been successful in multiple applications across the Nation. Critical to advancing the operational use of surrogates are tools to process and evaluate the data along with the subsequent development of regression models from which real-time sediment concentrations can be made available to the public. Recent developments of these tools are having an immediate impact on surrogate research, and on surrogate technologies for monitoring, assessment, rapid decision making, and adaptive management. The Surrogate Analysis and Index Developer (SAID) standalone tool processes complex datasets and creates regression models that related surrogate to constituent data by providing visual and quantitative diagnostics to the user. SAID is currently under development and beta testing at the U.S. Geological Survey.

SAID can be used to create regression models between surrogate data and constituent measurements. Additionally, SAID is a standalone tool to assist in the development of ordinary least squares (OLS) regression models with any response and predictor variables by providing visual and quantitative diagnostics to the user. There is no limit on the number of variables that can be used in the linear model, and there are no restrictions regarding which variables must be used. The sediment acoustic method utilizes acoustic parameters from fixed-mount stationary equipment with the assumption that the sediment concentration along the acoustic beam path is constant for a given time period. Within SAID, the user can set ADVM configuration and processing options, transform a loaded variable, build linear regression models, view linear model diagnostic statistics and plots, export the model information, and generate a predicted time series.

After a surrogate regression model has been developed and approved, the model can be used to generate continuous, real-time SSC estimates. Results from SAID provide direct inputs to two USGS utilities: the Real-time Acoustic Sediment Surrogate DAta Transfer (RASSDAT) program and the National Real-Time Water Quality (NRTWQ) program. The output from these utilities are displayed on USGS Web sites as real-time continuously computed sediment data. RASSDAT, currently under development and in beta testing at USGS, is a Visual Basic Graphical User Interface (GUI) wrapped around a Python™ script that runs on a Windows® computer, interfaces with the USGS National Water Information System (NWIS), and displays computed SSC on the NWIS Web Interface (http://waterdata.usgs.gov/nwis). NRTWQ is run from a centralized server and displays computed SSC on the NRTWQ Web site. The real-time dissemination of predicted SSC and prediction intervals for each time step has substantial potential to improve understanding of sediment-related water-quality and associated engineering and ecological management decisions.

ACKNOWLEDGEMENTS

The USGS Midwest Region and the Federal Interagency Sediment Project supported the development of these utilities. The Midwest Region support was through the River Sediment and Nutrient Investigations Initiative. We thank the many beta testers for their thorough testing and comments. Any use of trade, firm, or product names is for descriptive purposes only and does not imply endorsement by the U.S. Geological Survey.

REFERENCES

Helsel, D.R., and Hirsch, R.M., 2002, Statistical methods in water resources—hydrologic analysis and interpretation: U.S. Geological Survey Techniques of Water-Resources Investigations, book 4, chap. A3, 510 p.

Landers, M.N., 2012, Fluvial suspended sediment characteristics by high-resolution, surrogate metrics of turbidity, laser-diffraction, acoustic backscatter, and acoustic attenuation. Ph.D. Dissertation, Georgia Institute of Technology. Available at http:hdl.handle.net/1853/43747 (accessed on 14 June 2012).

Rasmussen, P.P., Gray, J.R., Glysson, G.D., and Ziegler, A.C., 2009, Guidelines and procedures for computing time-series suspended-sediment concentrations and loads from in-stream turbidity-sensor and streamflow data: U.S. Geological Survey Techniques and Methods book 3, chap. C4, 53 p.

Topping, D. J., Melis, T. S., Rubin, D. M. and Wright, S. A. (2004), High-resolution monitoring of suspended-sediment concentration and grain size in the Colorado River in Grand Canyon using a laser acoustic system, in Proceedings of the 9th International Symposium on River Sedimentation, Yichang, China, 18-21 October, Tsinghua University Press, 2507-2514.

Topping, D. J., Wright, S. A., Melis, T. S., and Rubin, D. M. (2006), High-resolution monitoring of suspended-sediment concentration and grain size in the Colorado River using laser-diffraction instruments and a three-frequency acoustic system. Proceedings of the 8th Federal Inter-Agency Sedimentation Conference, Reno, NV, April 2–6, 2006, 555–559

Topping, D. J., Wright, S. A., Melis, T. S. and Rubin, D. M. (2007), High-resolution measurement of suspended-sediment concentrations and grain size in the Colorado River in Grand Canyon using a multi-frequency acoustic system, in Proceedings of the 10th International Symposium on River Sedimentation, Moscow, Russia, 1-4 August, 330-339

Wood, M.S., and Teasdale, G.N., 2013, Use of surrogate technologies to estimate suspended sediment in the Clearwater River, Idaho, and Snake River, Washington, 2008–10: U.S. Geological Survey Scientific Investigations Report 2013-5052, 30 p.

Wright, S. A., Topping, D. J., & Williams, C. A. (2010). Discriminating silt-and-clay from suspended-sand in rivers using side-looking acoustic profilers. 2nd Joint Federal Interagency Conference. Las Vegas, NV.

THE INFLUENCE OF SAMPLING TECHNIQUE ON BEDLOAD PREDICTION

Darren D. Hinton, P.E., Ph.D., Northwest Hydraulic Consultants, 835 S. 192nd Street, Bldg C, Ste 1300, Seatac, WA 98148 | Phone: (206) 241-6000 | Email: DHinton@nhcweb.com

Rollin H. Hotchkiss, Ph.D., P.E., D.WRE, F.ASCE., Professor, Dept. of Civ. & Env. Eng., 368 Clyde Building, Brigham Young University, Provo, UT 84602 | Phone: (801) 422-6234 | Email: rhh@byu.edu

Abstract: The difficult task of predicting the quantity and timing of bedload motion in gravel bed streams is complicated by limitations in sampling technique. This work illustrates a specific example where two common direct sampling techniques (Helley-Smith and net trap sampler) failed during flood flows and describes a new low cost technique that was able to successfully collect bedload samples at high discharges.

Early in the spring of 2013 net trap samplers were set up at three sites along Hobble Creek, a coarse-bed stream that flows through Springville City, Utah into Utah Lake. Then exceptionally unusual weather patterns produced a series of flood events that exceeded bankfull discharge by as much as four times. The net traps were no longer accessible and the back-up method, hand-held Helley-Smith samplers, were unusable. Attaching net trap samplers to the end of a pole and securing the pole against the flow with a tether to both banks, bedload samples were able to be collected during the highest flows of the season. This new technique was referred to as a Stanley sampler, or pole-mounted net trap.

Forty-one samples were collected on a Central Utah stream using this new technique and are used to illustrate the influence of sampling technique on bedload transport rate prediction. Four bedload formulae are compared to the data to show how predictive success of any given formula is related to the sampling technique used to collect the data from which it was derived. In other words, a formula derived from Helley-Smith data will perform better predicting against other Helley-Smith data than a formula derived from net trap data, and vice-versa. This work also provides evidence that the Helley-Smith and net trap samplers collect two very different sampling populations that must be considered when selecting a predictive formula.

WEB-BASED RANGELAND HYDROLOGY AND EROSION MODEL

Mariano Hernandez, Associate Research Scientist, University of Arizona, Tucson, AZ, Mariano.Hernandez@ars.usda.gov
Mark Nearing, Research Agricultural Engineer, USDA-ARS, Tucson, AZ, Mark.Nearing@ars.usda.gov
Jeffry Stone, Retired, USDA-ARS, Tucson, AZ
Gerardo Armendariz, IT Specialists, USDA-ARS, Tucson, AZ, Gerardo.Armendariz@ars.usda.gov
Fred Pierson, Research Leader, USDA-ARS, Boise, ID, Fred.Pierson@ars.usda.gov
Osama Al-Hamdan, Research Associate, University of Idaho, Moscow, ID, Osama.Al-Hamdan@ars.usda.gov
C. Jason Williams, Hydrologist, USDA-ARS, Boise, ID, Jason.Williams@ars.usda.gov
Ken Spaeth, Rangeland Management Specialist, USDA-NRCS, Dallas, TX, Ken.Spaeth@ftw.usda.gov
Mark Weltz, Research Leader; USDA-ARS, Reno, NV, Mark.Weltz@ars.usda.gov
Haiyan Wei, Associate Research Scientist, University of Arizona, Tucson, AZ, Haiyan.Wei@ars.usda.gov
Phil Heilman, Research Leader, USDA-ARS, Tucson, AZ, Phil.Heilman@ars.usda.gov
Dave Goodrich, Research Hydraulic Engineer, USDA-ARS, Tucson, AZ, Dave.Goodrich@ars.usda.gov

Abstract: The Rangeland Hydrology and Erosion Model (RHEM) is a newly conceptualized model that was adapted from relevant portions of the Water Erosion Prediction Project (WEPP) Model and modified specifically to address rangelands conditions. RHEM is an event-based model that estimates runoff, erosion, and sediment delivery rates and volumes at the spatial scale of the hillslope and the temporal scale of a single rainfall event. It represents erosion processes under normal and fire-impacted rangeland conditions. Moreover, it adopts a new splash erosion and thin sheet-flow transport equation developed from rangeland data, and it links the model's hydrologic and erosion parameters with rangeland plant community by providing a new system of parameter estimation equations based on diverse rangeland datasets for predicting runoff and erosion responses on rangeland sites distributed across 15 western U. S. states. A dynamic partial differential sediment continuity equation is used to route sediment along the hillslope, with sediment source terms to represent the detachment rate of concentrated flow and rain splash and sheet flow. Recent work on the model is focused on representing intra-storm dynamics, using stream-power as the driver for detachment by flow, and deriving parameters for after fire conditions. Additional work to the model is continuing on the RHEM system: a new component has been developed to estimate erosion in probabilistic terms for risk-based management decisions; it will be improved to allow for orographic effects on precipitation by incorporating existing technology based on PRISM and CLIGEN; the model will be improved for application to both undisturbed and disturbed conditions across the western US. The purpose of this paper is to present the Web-based RHEM system and demonstrate the tool for assessing annual runoff and erosion changes for each community phase of the Limy Upland 12-16" p.z. Ecological Site (ES) within Major Land Resource Area 41 (MLRA 41), southeastern Arizona, USA.

INTRODUCTION

Rangelands are estimated to cover approximately 31% of the United States (Havstad *et al.*, 2009), and developing tools for assessment of those lands is a critical resource management need. Predicting soil erosion is common practice in rangeland management for assessing the effects of management practices and control techniques on soil productivity, sediment delivery and offset water quality. Effective decision-making requires the integration of knowledge, data, simulation models and expert judgment to solve practical problems, and to provide a scientific basis for decision-making at the hillslope or watershed scale (National Research Council, 1999). Over the last 50 years the federal government has spent millions of dollars on the creation of spatial datasets and model development. While these simulation models are used extensively in research settings, they are infrequently incorporated into the decision-making process. One aspect of erosion modeling is the continued use of simpler, empirically-based erosion models (e.g. USLE, MUSLE, and RUSLE) instead of more complex, physically-based models (e.g. WEPP, DWEPP, EUROSEM). Reasons for the exclusion include: data requirements are usually only attained in research settings; deriving model input parameters is extremely time consuming and difficult; and the models are difficult to use with the current interfaces.

This problem can be addressed with improvement to model interfaces, lookup tables for model parameters, and internal file management. However, as erosion models continue to become more complex and integrate with other technologies, users will be required to have experience in GIS, computer operating systems, remote sensing, Internet

search engines for data gathering, and graphics, as well as good foundation of erosion processes knowledge. One solution to this problem is the development of Internet-based applications (Kingston *et al.*, 2000; Elliot, 2004; Flanagan *et al.*, 2004).

A Web-based interface for the Rangeland Hydrology and Erosion Model has been developed by the USDA-Agricultural Research Service, Southwest Watershed Research Center in Tucson, Arizona to assist different professional or stakeholder groups to develop, understand and evaluate alternative soil conservation strategies. It was built with the following goals in mind: 1) simplify the use of RHEM; 2) manage users sessions; 3) centralize scenario results (model runs); 4) compare scenario results; and 5) provide tabular and graphical results.

This paper describes the current status of the RHEM Web-based interface, and provides an example application of the software.

MODEL DESCRIPTION

Rangeland Hydrology and Erosion Model Concepts: RHEM computes soil loss along a slope and sediment yield at the end of a hillslope (Nearing *et al.*, 2011). Splash and sheet erosion is described as a process of soil detachment by raindrop impact and surface water flow, transport by shallow sheet flow and small rills, and sediment delivery to larger concentrated flow areas such as arroyos. Sediment delivery rate from hillslopes is computed by using an improved equation developed by Wei *et al.* (2009) using rangeland runoff and erosion data from rainfall simulation experiments. Concentrated flow erosion is conceptualized as a function of the flow's ability to detach sediment, sediment transport capacity, and the existing sediment load in the flow. The appropriate scale of application is for hillslope profiles. Details of the model have been published (Nearing *et al.*, 2011; Al-Hamdan *et al.*, 2012a, 2012b, 2013, 2014).

RHEM has been applied successfully to illustrate the influence of plant and soil characteristics on soil erosion and hydrologic function in MLRA 41 located in the Southeastern Basin and Range region of the southern U. S. (Hernandez *et al.*, 2013); assess non-federal western rangeland soil loss rates at the national scale for determining areas of vulnerability for accelerated soil loss using USDA Natural Resources Conservation Services (NRCS) National Resources Inventory (NRI) data (Weltz *et al.*, 2014); predict runoff and erosion rates for refinement and development of Ecological Site Descriptions (Williams *et al.*, 2014).

Model Parameter Estimation: The RHEM model requires 13 input parameters grouped in three categories: rainfall, soils, and slope profile. An important aspect of the model relative to rangeland application by rangeland managers is that RHEM is parameterized based on four plant lifeform classification groups (annual grass and forbs, bunchgrass, shrubs, and sodgrass) (Nearing *et al.*, 2011). RHEM is continuing to evolve and improve, in RHEM V [2.2], a new set of parameter estimation equations were developed based on the regression equations of Rawls *et al.* (1982), as a function of soil texture, litter percent cover and basal percent cover to estimate effective hydraulic conductivity for the Smith-Parlange infiltration equation. The link http://apps.tucson.ars.ag.gov/rhem/ provides further details about the equations to estimate effective hydraulic conductivity for the Smith-Parlange infiltration equation.

WEB-BASED RHEM INTERFACE

In this section, we describe the Web-based interface for RHEM and its components for assessing runoff and erosion changes under several land management alternatives. It was designed as a shared application to assist in the decision-making processes and to offset the software and data requirement typically required in a desktop application.

Software Architecture: The RHEM Web-based tool has been developed based on the Model-View-Controller* (MVC) software architectural pattern which promotes the separation between the application logic and the presentation or user interface. This software architecture style allows for future application modifications and updates to be more flexible, encouraging code modularity, code reuse, and data integrity. CodeIgniter* was the web application framework selected to implement MVC in the RHEM Web Tool. CodeIgniter* is a lightweight and high-performance web application framework written in PHP with a rich set of libraries that facilitate the

implementation of user authentication, web page caching, data persistence, session management, and application security. These features added agility to the development of the RHEM Web Tool.

Hardware Architecture: The RHEM Web Tool has been created based on a well-established three-tier architecture which is a client-server architecture in which the application presentation, processing, and data management functionalities are physically separated. The three tiers are: 1) the presentation tier, 2) the application logic tier, and 3) the data tier. For the RHEM Web Tool, the presentation tier is the user or client's PC whereas the application logic tier is powered by a Dell Xeon* 3GHz Windows* 2008 Server running IIS7. The data tier is powered by a Dell Xeon 3GHz Windows 2008 Server machine running MySQL* 5.1

*Trade names and company names, included for the reader's benefit, do not imply endorsement or preferential treatment of the product listed by the USDA or The University of Arizona.

Overview of the Web-based system: Figure 1 illustrates the operations performed within the system and the numbers on the inside of the circle show the sequence in which they are performed. First the user accesses the application through an Internet browser interface, and must register to use the application and to be notified of any major updates, and to allow the user to save and edit scenarios that they create. The following steps describe the sequence of actions to run the model: 1) create a new scenario, 2) select a climate weather station, 3) select a soil texture class, 4) provide a description of slope and topography characteristics, 5) provide estimates of foliar canopy cover and ground cover characteristics, 6) run new scenario, and 7) perform comparison of scenarios.

Once the user has logged in, they can create a new scenario within the Define Scenario Panel (1 in Figure 1) by typing a name that identifies the new scenario and providing a short description of the project on the Name and Description dialog boxes, respectively. A scenario is defined as a unique set of input parameters needed to run RHEM. It can be saved to view results, compared with other scenarios, or modified to create a new scenario. The user can select the units to be used for the current scenario's input and output values.

The second step involves entering the climate data to parameterize the simulation model. In the Climate Station Panel (2 in Figure 1) two dialog boxes are available, in the State dialog box select the state of the project location and in the Name dialog box select the name of the climate station that is close to the location being analyzed or a station with similar elevation to the study area. Climate data is obtained via the CLIGEN climate generator [Zhang and Garbrecht, 2003]. RHEM uses the CLIGEN model to generate daily rainfall statistics for a 300-year weather sequence that is representative of a time-stationary climate and used by the rainfall disaggregation component of RHEM. The disaggregation component uses rainfall amount, duration, ratio of time of peak intensity to duration, and the ratio of peak intensity to average intensity to compute a time-intensity distribution of a rainfall event. The CLIGEN database consists of 2600 weather stations across the continental US.

In the Soil Texture Panel (3 in Figure 1), the user defines the soil texture of the upper 4 cm (1.57 in.) of the soil profile. It is input as a class name from the USDA soil textural triangle. The RHEM database contains a list of soil hydraulic properties to parameterize the Smith-Parlange infiltration equation and look-up tables with percent of sand, silt and clay to estimate the Darcy-Weisbach friction factor (Al-Hamdan *et al*., 2013), and the maximum initial concentrated flow erodibility coefficient (Al-Hamdan *et al*., 2014).

To characterize the topography of the hillslope profile, the Hillslope Profile Panel (4 in Figure 1) presents three dialog boxes to enter the slope length, slope shape, and slope steepness. In regard with the estimation of the slope length in RHEM, we define slope length as the length of the path that water flows down a slope as sheet and rill flow until it reaches an area where flow begins to concentrate in a channel, or to the point where the slope flattens out causing deposition of the sediment load. Slope length up to 120 m (394 ft.) are supported. A distance greater than 120 m (394 ft.) is considered to be a very long slope length. In addition, RHEM provides four hillslope shapes for different topographic scenarios as follows: uniform, convex, concave, and S-shaped. In order to assess sediment delivery from a hillslope to a channel, the user must designate the shape of the hillslope either as a concave or S-shaped. These are the slope shapes that will experience toe-slope deposition. The slope steepness is the slope of the hillslope area rather than the average land slope.

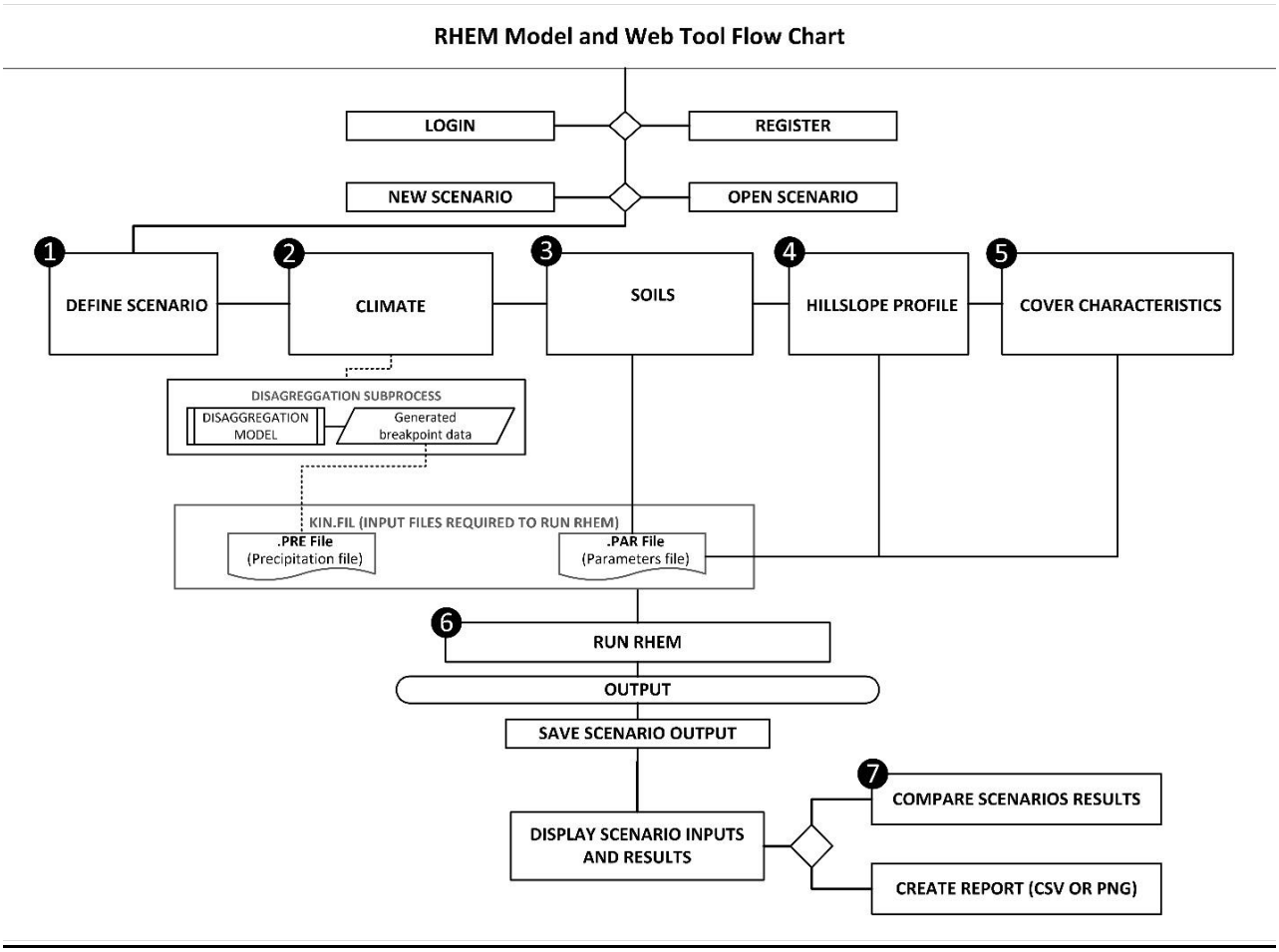

Figure 1. RHEM Web-based system schematic.

The Cover Characteristics Panel (5 in Figure 1) presents nine Dialog Boxes to enter information on vegetative foliar canopy cover and surface ground cover. RHEM's system of parameter estimation equations and procedure reflects the concept that hydrology and erosion processes are affected by plant growth forms and surface ground cover. Thus, the user can enter percent foliar canopy for four rangeland plant communities: bunchgrass, shrub, sodgrass, and annual grass and forbs. In regard with surface ground cover input parameters, RHEM was designed to require minimal inputs that are readily available for most rangeland ecological sites. Percent ground cover by component are defined as follows: rocks, plant litter, plant basal area, and biological soil crust.

The Run Panel (6 in Figure 1) is used to generate output from: a new scenario, an edited scenario, and re-named scenario. The web-based interface generates a summary report, input parameter file, and the storm file.

The Comparison Panel (7 in Figure 1) allows the user to compare up to five existing scenarios.

MODEL APPLICATION

The reminder of this paper will be comprised of an example application of the RHEM Web-based interface, and examining how it can be used to evaluate the hydrologic response of plant communities to management and disturbances as conceptualized within a State-Transition Model (STM) of an Ecological Site Description (ESD).

Experimental Site: We illustrate the use of the RHEM Web-based interface at the Kendall Grassland site ($109^{O}56'28"W$, $31^{O}44'10"N$), 1526 m asl), located in the Walnut Gulch Experimental Watershed (WGEW), *ca*. 11 km east of Tombstone, AZ. The mapping unit consisting of a complex of Loamy Upland and Limy Slopes covers much of the northeastern portion of the watershed, including the grass-dominated study area known as Kendall.

According to Skirvin et al. (2008), the Kendall Grassland is a desert grassland, historically dominated by black grama (*Bouteloua eripoda*), side-oats (*B. curtipendula*), hairy grama (*B. hirsute*), tangle-head (*Heteropogon contortus*), curly mesquite (*Hilaria berlangeri*), and the exotic South African bunchgrass, Lehmann lovegrass (*Eragrostis lehmanniana*). Soils at the Kendall site are in the Elgin-Stronghold complex and are dominated by Stronghold series, which are gravelly fine sandy loams, classified as coarse-loamy, mixed, superactive thermic Ustic Haplocalcids (Breckenfeld *et al.*, 1995). The climate of the area is semiarid with annual precipitation of 345 mm and a highly spatially and temporally varying precipitation pattern dominated by the North American Monsoon. Monsoon storms are typically characterized as short-duration, high intensity, localized rainfall events. Mean annual temperature is 17.7^{O}C.

Potential problems with Limy Slopes include invasion by Lehman lovegrass (*Eragrostis lehmanniana*) or the shrub species dominant on Limy Upland. With long-term erosion, Limy Slopes can lose their mollic cap and degrade to a Limy Upland site with calcic material at the surface (Robinett, 1992). Loamy Upland, found on 1 to 15 % slopes, is very prone to invasion by Lehmann lovegrass, as well as mesquite (*Prosopis sp*). Both Limy Slopes and Loamy Upland have a much greater natural potential to produce grass than Limy Upland, with up to 85% of the annual production on undisturbed sites coming from grass and grasslike species (Robinett, 1992).

A STM for the Limy Slopes ecological site is shown in Figure 2. The model for this site includes 4 states. The ecological states are outlined by bold black rectangles. Plant community phases are shown by light gray rectangles. Within the Historic Climax Plant Community (HCPC) state, fire and drought could cause temporary shifts between the two plant communities shown. The Eroded state is considered so degraded by soil erosion that it has crossed a threshold and now has a different, less productive, potential plant community.

By 2006, seed sources for the both shrub and Lehmann lovegrass (Transition 1a) had appeared in the upland areas around Kendall study area (Heilman *et al.*, 2010). The vegetation was beginning to transition from the HCPC state toward the Lehmann state as small shrub trees were getting established. Prolonged drought resulted in high perennial grass mortality prior to the 2006 summer monsoon (Robinett, 1992), and 2006 saw a significant shift toward the Exotic grass and the Shrub invaded states, which impacted the hydrological and sediment response of the system for a period of time (Polyakov *et al.*, 2010).

If the principal management objective is to minimize runoff and erosion, one might favor the Lehmann state, as this exotic grass can produce up to a third more biomass than native grasses, once established (Robinett, 1992).

Hydrology and Erosion Model: The RHEM model was applied to estimate annual runoff and erosion for each plant community phase of the Limy Slopes 12-16" p.z. ES. We applied the methodology developed by Williams *et al*. (2014) for integrating eco-hydrologic information into the ESD, therefore, key information was extracted from the approved NRCS ESD for the Limy Slopes 12-16" p.z. ES (USDA-NRCS 2014) and from the rainfall simulator study conducted by Hamerlynck *et al*. (2012) at the Kendall site. The study by Hamerlynck *et al*. (2012) was carried out on four 2 x 6 m plots that took place from 21 June to 24 July 2008 at the Kendall Grassland site, they recorded and classified canopy cover as grass, shrub, or forb. The relative dominance (% of plant canopy) of the invasive Lehmann lovegrass, all native bunch grasses, and broad-leaved forbs was estimated by dividing the sum of hits for each plant by the total number of plants hits for each plot. Ground cover was recorded as rock + gravel (> 2mm), litter, basal, and bare soil and was measured both under and between canopy cover. They defined litter as dead plant material in contact with the soil surface. Total vegetative canopy cover was 20-26% in low-cover plots and 43-56% in high-cover plots, however, with the former dominated by the invasive South African bunchgrass, Lehmann's lovegrass. Ground cover was similar in terms of litter and basal area.

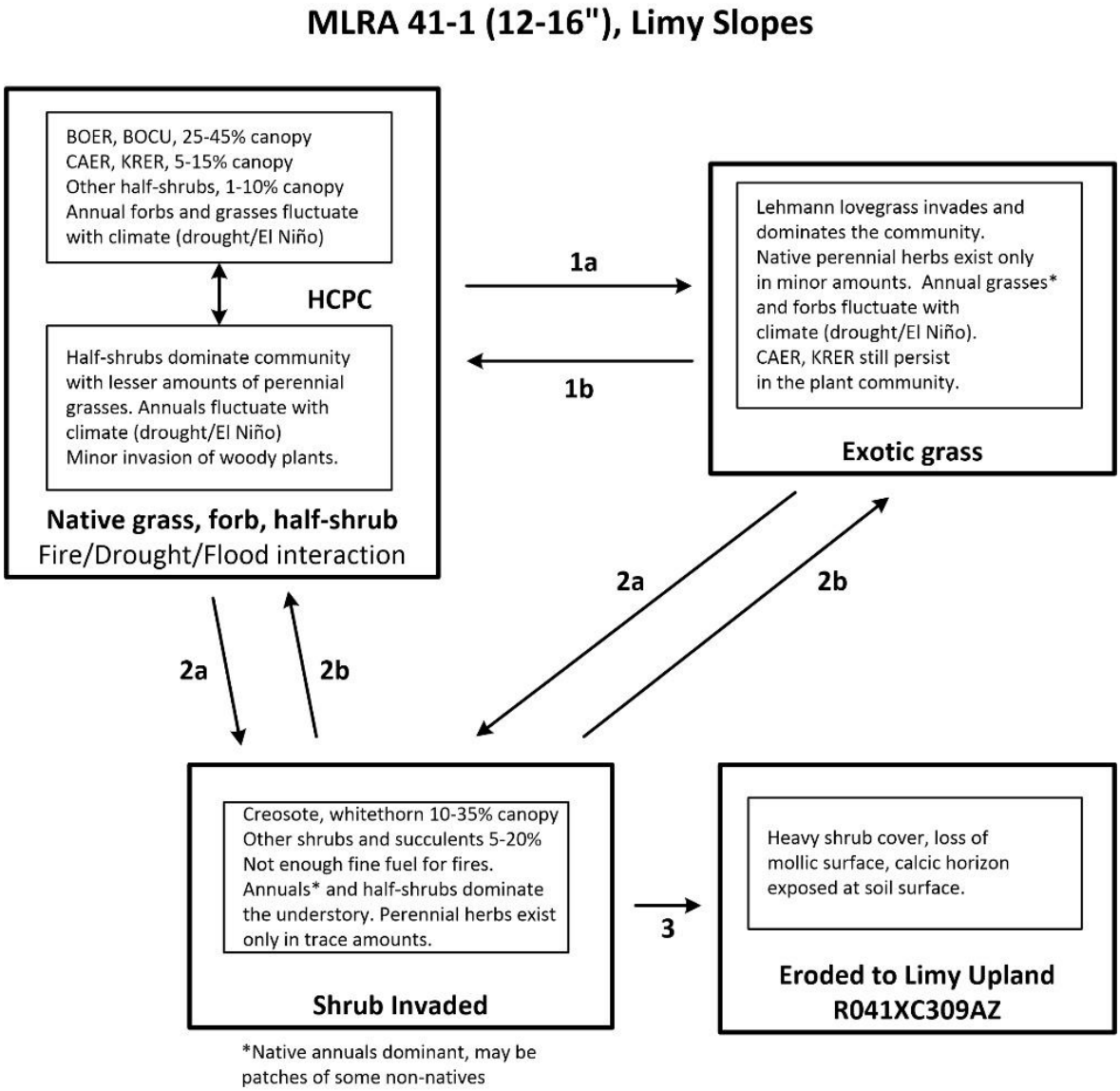

Figure 2. The State and Transition Model for the Limy Slopes 12-16" p.z. ES.

A baseline RHEM model scenario was configured to represent community phases using a CLIGEN station for rainfall inputs (Tombstone, AZ; Station ID: 0222, 1396 m elevation, 335 mm annual precipitation), sandy loam surface soil texture (46% sand, 39% silt, 15% clay), 50-m hillslope length, S-shape slope topography, and 12.5% slope gradient representative of the climate, soil, and topography attributes for the study site. In addition, the ESD provided a basis for foliar canopy and ground cover parameter estimation of the HCPC baseline scenario. Our baseline RHEM model scenario was applied to each plant community phase by adjusting cover characteristics (retaining the baseline climate, soil, and topography data) to reflect changes in the community composition. Foliar canopy cover information on the transition from native grass to Lehmann lovegrass in the STM was obtained from the 2 low-cover plots described in Hamerlynck *et al*. (2012), they pointed out that these plots were dominated by Lehmann lovegrass. Furthermore, foliar canopy cover for the shrub-invaded state was obtained from data presented in the STM. In addition, ground cover information was obtained from rainfall simulator studies on shrub-dominated plots at WGEW (Stone, unpublished data). Based on the description of the Eroded state in the STM (Figure 2), the site potential changes to something resembling to Limy Upland 12-16" p.z. ES, which includes the shrub-dominated Lucky Hills watersheds in the WGEW. Hence, canopy cover data was obtained from shrub-dominated rainfall simulator plots at this site. Ground cover remained similar in terms of rock cover across all states. Table 1 presents a summary of the input parameters of the Kendall Grassland site.

Runoff and erosion rates predicted by RHEM were consistent with published literature on the "Limy Slopes 12-16 p.z." (Nearing *et al.*, 2007; Polyakov *et al.*, 2010). Simulation results for each scenario are shown in Table 2. In the study by Polyakov *et al.* (2010), they analyzed 58 successfully sampled sediment events during 19 years of observation. Annual sediment yield for different periods varied from 1.64 t ha^{-1} to 0.01 t ha^{-1}. Hernandez *et al.* (2013) applied the RHEM tool on 134 of the National Resource Inventory (NRI) rangeland field locations with data collected between 2003 and 2006 in MLRA 41. The average annual soil erosion rates varied from 0.20 t ha^{-1} to 0.5 t ha^{-1} on the "Limy Slopes 12-16" p.z. Nearing *et al.* (2007) estimated average annual sediment yield for the Kendall watershed in WGEW (0.07 t ha^{-1}).

Table 1. Summary of input parameters of the Kendall Grassland "Limy Slopes 12-16 p.z." Ecological Site (NRCS 2014).

SCENARIO INPUTS

	BASELINE SCENARIO HCPC	SCENARIO 1 ERODED	SCENARIO 2 SHRUB_INVADED	SCENARIO 3 EXOTIC_GRASS
Version				
State ID	AZ	AZ	AZ	AZ
Climate Station	Tombstone	Tombstone	Tombstone	Tombstone
Soil Texture	Sandy Loam	Sandy Loam	Sandy Loam	Sandy Loam
Soil Water Saturation %	25	25	25	25
Slope Length (meters)	50	50	50	50
Slope Shape	S-Shaped	S-Shaped	S-Shaped	S-Shaped
Slope Steepness %	12.5	12.5	12.5	12.5
Bunch Grass Foliar Cover %	50	0	1	26
Forbs and/or Annual Grasses Foliar Cover %	1	0	2	2
Shrubs Foliar Cover %	10	35	35	10
Sod Grass Foliar Cover %	0	0	0	0
Total Foliar Cover %	61	35	38	38
Basal Cover %	8	0	3	3
Rock Cover %	16	16	16	16
Litter Cover %	45	9	10	35
Cryptogam Cover %	1	0	0	0
Total Ground Cover %	70	25	29	54

Table 2. Summary of predicted annual average runoff, sediment yield, and soil loss on the Kendall Grassland site "Limy Slopes 12-16 p.z." ES

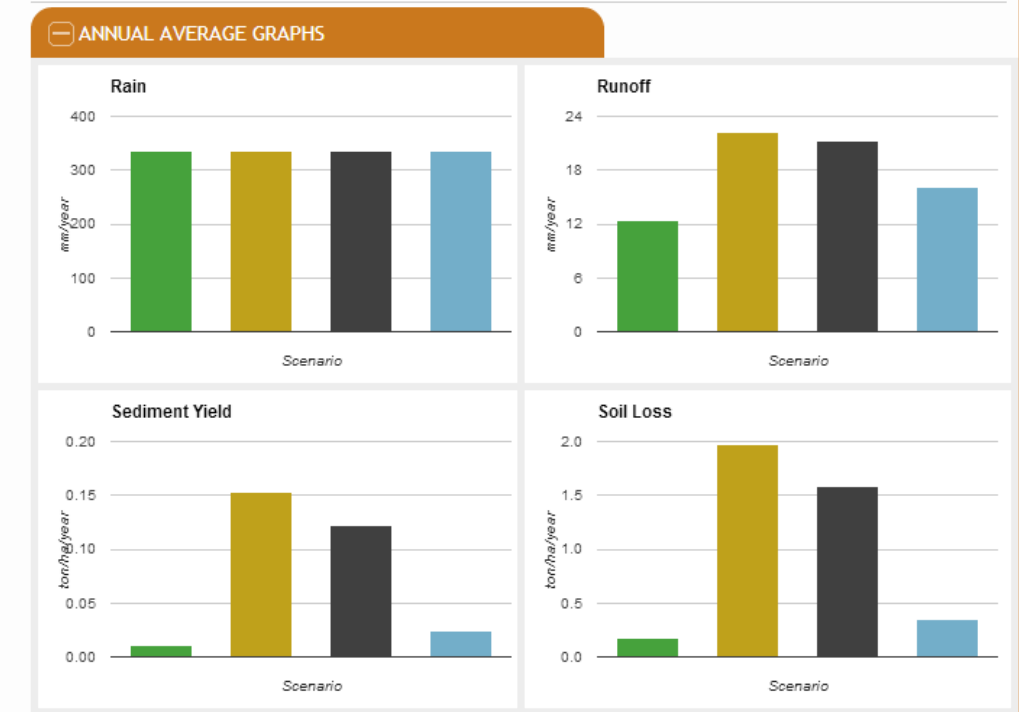

ANNUAL AVERAGES

	HCPC	ERODED	SHRUB_INVADED	EXOTIC_GRASS
Avg. Precipitation (mm/year)	335.330	335.330	335.330	335.330
Avg. Runoff (mm/year)	12.417	22.223	21.201	16.187
Avg. Sediment Yield (ton/ha/year)	0.011	0.153	0.122	0.025
Avg. Soil Loss (ton/ha/year)	0.171	1.969	1.584	0.347

Analysis of the RHEM simulation runs on the "Limy Slopes 12-16 p.z." ES provides a basis for interpreting the impacts of vegetative canopy cover, surface ground cover, and topography on dominant processes in controlling infiltration and runoff as well as sediment detachment, transport and deposition in overland flow at each state. Our results suggest that RHEM can predict runoff and erosion according with vegetation structure and behavior of different plant community phases. That is, an explanation for the difference in runoff and erosion in the HCPC and Lehmann states can be related to the increased water storage on the native bunchgrasses due to the formation of litter dams. The grass cover and litter on the baseline state cause water to pond behind small litter and debris dams as it moves downslope, which has the effect of backing up water and allowing more time for infiltration (Mitchel and Humphreys, 1987; Nearing *et al.*, 2007). According to Polyakov *et al*. (2010), before the Lehmann lovegrass invasion, the microtopgraphy characteristic for the Kendall site where small terraces formed upslope of large clumps of vegetation. With die-out of native grasses and greater spread of Lehmann lovegrass, there were fewer obstructions, which allowed water to move down the slope more rapidly, increasing runoff and sediment yield. The erosion rate in both Shrub-dominated and Eroded scenarios is only slightly different as shown in Table 2.

FUTURE WORK

Additional work is continuing on the RHEM Web-based interface system, which is currently fully functional for estimating erosion rates on relatively non-disturbed (e.g., fire impacted) scenarios, and a fully functional product including risk assessment and fire impact is expected to be completed by the end of 2015.

RHEM will be improved for application to both undisturbed and disturbed conditions across the western US. This work is intended to allow it to represent disturbed conditions, develop parameter estimation procedures for disturbed conditions. Initial analysis of data from fire-disturbed rangeland sites illustrate the importance of intra-storm dynamics on soil erodibility and the dominance of detachment by small concentrated flow channels as opposed to broad sheet flow. A new component has been developed to estimate erosion, in probabilistic terms, for potential varying management scenarios. Based on a 300-year CLIGEN run, RHEM produces average annual soil loss rates with a probability of occurrence for each RHEM management scenario. In addition, because of the strong orographic effects that dominate spatial precipitation patterns in the western U.S, the model will be improved to allow for orographic effects on precipitation by incorporating existing technology based on PRISM and CLIGEN into the RHEM model system. This capability will also allow for assessing climate change scenarios with the model, building on previous work by the investigators on soil erosion and climate change (Zhang *et al.*, 2012; Nearing *et al.*, 2004).

CONCLUSIONS

RHEM, as applied in this study with input values reported in the literature, can be a valuable tool for predicting relative measures of runoff and erosion within the ESD framework. However, we caution against interpretation of RHEM results as absolute measures of runoff and erosion given the potential variability in soil loss across widely variable conditions within an individual ecological state or community phase and with increasing spatial scale. It is not possible to parameterize the model for all possible vegetation conditions of a given state or community phase. Rather, we suggest applying the model for average vegetation conditions and utilizing the results to interpret relative hydrologic and erosion function.

The framework of the RHEM tool facilitates the inclusion of new capabilities. Current research includes the integration of new equations for the application of RHEM in disturbed rangelands such as fire to predict surface erosion from postfire hillslopes, and to evaluate the potential effectiveness of various erosion mitigation practices. The RHEM probabilistic approach will be meaningful for land managers when they want to apply RHEM to risk-based management decisions.

REFERENCES

Al-Hamdan, O. Z., Pierson, F. B., Nearing, M. A., Stone, J. J., Williams, C. J., Moffet, C. A., Kormos, P. R., Boll, J., & Weltz, M. A. (2012a). “Characteristics of concentrated flow hydraulics for rangeland ecosystems: Implications for hydrologic modeling”, *Earth Surface Processes and Landforms*, 37:157-168.

Al-Hamdan, O.Z., Pierson, F.B., Nearing, M.A.,Williams, C.J., Stone, J.J., Kormos, P.R., Boll, J., & Weltz, M.A. (2012b). “Concentrated flow erodibility for physically based erosion models: Temporal variability in disturbed and undisturbed rangelands”, *Water Resources Research*, 48:W07504.

Al-Hamdan, O.Z., Pierson, F.B., Nearing, M.A., Williams, C.J., Stone, J.J., Kormos, P.R., Boll, J., & Weltz, M.A. (2013). “Risk assessment of erosion from concentrated flow on rangelands using overland flow distribution and shear stress partitioning”, *Transactions of the ASABE*, 56:539-548.

Al-Hamdan, O.Z., Hernandez, M., Pierson, F.B., Nearing, M.A., Williams, C.J., Stone, J.J., Boll, J., & Weltz, M. A. (2014). “Rangeland Hydrology and Erosion Model (RHEM) enhancements for applications on disturbed rangelands”, *Hydrological Processes*, DOI: 10.1002/hyp.10167

Breckenfield, D.J., Svetlik, W.A., & McGuire, C.E. (1995). Soil survey of Walnut Gulch Experimental Watershed, Tucson, AZ: USDA Soil Conservation Service.

Elliot, W. J. (2004) "WEPP internet interfaces for forest erosion prediction", *Journal of the American Water Resources Association*, 40:299-309.

Flanagan, D.C., Frankenberger, J. R., & Engel, B. A. (2004). "Web-based GIS application of the WEPP Model", ASAE/CSAE Meeting Paper No. 04-2024. ASAE, St. Joseph, Michigan.

Kington, R., Carver, S., Evans, A., & Turton, I. (2000). "Web-based public participation geographic information systems: an aid to local environmental decision-making", *Computers, Environment and Urban System* 24:109-25.

Hamerlynck, E.P., Scott, R. L., & Stone, J.J. (2012) "Soil moisture and ecosystem function responses of desert grassland varying in vegetation cover to a saturating precipitation pulse", *Ecohydrology* (5): 297-305.

Havastad, K.M., Peters, D.C., Allen-Diaz, B., Bartolome, J., Bestelmeyer, B.T., Briske, D., Brown, J., Brunson, M., Herrick, J.E., Huntsinger, L., Johnson, P., Joyce, L., Pieper, R., Svejcar, A.J., & Yao, J. (2009. "The western United States rangelands, a major resource", In Grassland Quietness and Strength for a New American Agriculture, eds. W.E. Wedin, and S.L. Fales, 7575-93. Madison, WI: American Society of Agronomy Inc., and Soil Science Society of America Inc.

Heilman, P., Stone, J.J., & Robinett, D. (2010). "Ecological sites of the Walnut Gulch Experimental Watershed", American Water Resources Association Specialty Conference, Orlando, FL March 29-31, 2010.

Hernandez, M., Nearing, M.A., Stone, J.J., Pierson, F.B., Wei, H., Spaeth, K.E., Heilman, P.H., Weltz, M.A., & Goodrich, D.C. (2013). "Application of a rangeland soil erosion model using National Resources Inventory data in the southeastern Arizona", *J. Soil Water Cons*., 68(6), 512-525.

Mitchell, P.B., & Humphreys, G.S. (1987). "Litter dams and microterraces formed on hillslopes subject to rainwash in the Sydney Basin, Australia", *Geoderma*, (39):331-357.

National Research Council (1999). New Strategies for America's Watersheds. National Academy Press, Washington.

Nearing, M.A., F.F. Pruski, and M.R. O'Neal. (2004). "Expected climate changes impacts on soil erosion: A Review", *Journal of Soil and Water Conservation*, Vol.59, Number 1.

Nearing, M.A., Nichols, M. H., Stone, J.J., Renard, K.G., & Simanton, J. R. (2007). "Sediment yields from unit-source semiarid watersheds at Walnut Gulch", *Water Resources Research*, Vol. 43, doi:10.1029/2006WR005692

Nearing, M.A., Wei, H., Stone, J.J., Pierson, F.B., Spaeth, K.E., Weltz, M.A., Flanagan, D.C., & Hernandez, M. (2011). "A Rangeland Hydrology and Erosion Model", *Trans. ASABE* 54(3):1-8.

Polyakov, V. O., Nearing, M.A., Stone, J.J., Hamerlynck, E.P., Nichols, M.H., Holifield Collins, C.D., & Scott, R.L. (2010). "Runoff and erosional responses to a drought-induced shift in a desert grassland community composition", *Journal of Geophysical Research* Vol. 115, G04027, doi:10.1029/2010JG001386.

Rawls, W.J., Brakensiek, D.L., & Saxton, K.E. (1982). "Estimation of soil water properties", *Trans. ASAE* 25(5):1316-1320, 1328.

Robinett, D. (1992). "Lehmann lovegrass and drought in southern Arizona", *Rangelands* 14:100-103.

Skirvin, S., Kidwell, M., Biedenbender, S.H., Henley, F.P., King, D. M., Holifield Collins, C.D., Moran, M.S., & Weltz, M.A. (2008). "Vegetation data Walnut Gulch Experimental Watershed, Arizona, United Sates", *Water Resources Research*, Vol. 44 W05S08, doi:101029/2006WR005724.

Wei, H., Nearing, M.A., Stone, J.J., Guertin, D.P., Spaeth, K.E., Pierson, F.B., Nichols, M.H., & Moffet, C.A. (2009). "A new splash and sheet erosion equation for rangelands", *Soil Science* Society of America 73:1386-1392

Weltz, M.A., Jolley, L.W., Hernandez, M., Spaeth, K.E., Rossi, C., Talbot, C., Nearing, M.A., Stone, J.J., Goodrich, D.C., Pierson, F.B., Wei, H., & Morris, C. (2014). "National Assessment of Soil Loss on Non- Federal Rangelands", *Journal of Soil and Water Conservation* 66(5):154A-162A.

USDA-NRCS (United States Department of Agriculture-Natural Resources Conservation Service, 2014). Interagency Ecological Site Description Handbook for Rangelands. Washington DC, USA: United States Department of Agriculture. 109 p.

Williams, C. J., Pierson, F.B., Spaeth, K.E., Brown, J.R., Al-Hamdan, O.Z., Weltz, M.A., Nearing, M.A., Herrick, J. E., Boll, J., Robichaud, P. R., Goodrich, D.C., Heilman, P., Guertin, D. P., Hernandez, M., Wei, H., Hardegree, S.P., Strand, E.K., & Metz, L.J. (2014). "Ecohydrology in the Ecological Site Description Concept", *Rangeland Ecology & Management*, in press.

Zhang, X. C., & Garbrecht, J. D. (2003). "Evaluation of CLIGEN precipitation parameters and their implication on WEPP runoff and erosion", *Trans. ASAE*, 46(2), 311-320.

Zhang, Y., Hernandez, M., Anson, E., Nearing, M.A., Wei, H., Stone, J.J. and Heilman, P. (2012). "Modeling climate change effects on runoff and soil erosion in southeastern Arizona rangelands and implications for mitigation with conservation practices", *Journal of Soil and Water Conservation* 67(5): 290-405, doi:10.2489/jswc.67.5.390.

NUMERICAL MODELING OF LABORATORY FLUME EXPERIMENTS FOR TRACKING UNSTEADY SEDIMENT TRANSPORT USING COLORED PARTICLES

Mustafa S. Altinakar, Director and Research Professor, The University of Mississippi, Oxford, MS, altinakar@ncche.olemiss.edu; Reza Marsooli, Post-doc Research Associate, The University of Mississippi, Oxford, Mississippi, reza@ncche.olemiss.edu; Zhaosong Qu, President, SINFOTEK, Haidan District, Beijing, China, qsl188@126.com

Abstract: Developed at the National Center for Computational Hydroscience and Engineering, CCHE1D is a one dimensional numerical model for simulating unsteady flow hydrodynamics and sediment transport in natural dendritic channel systems, such as the drainage network of a watershed. CCHE1D has an Arc-GIS based user interface and can be run in coupled mode with AnnAGNPS and SWAT watershed models. The unsteady flow hydrodynamics uses a hybrid approach that solves full dynamic Saint-Venant equations when the flow is subcritical and reverts to a diffusive wave equation when the flow locally becomes transcritical or supercritical. The sediment transport and fluvial morphodynamics module calculates unsteady fractional sediment transport using a non-equilibrium sediment transport approach. The channel bed is modeled in three layers with the topmost layer being the mixing layer. The CCHE1D model calculates bed area change for each size class and tracks the percentage of each size class of sediment in the water column and in the upper two layers of the bed.

The CCHE1D model was used to model two laboratory experiments of sediment transport under unsteady flow conditions, which were carried out at the Hydraulic Research Laboratory of the Federal Institute of Technology in Lausanne, Switzerland. The experiments were performed in a 17.8m-long and 0.60m-wide tilting laboratory flume using symmetric triangular hydrographs with the same nominal base and peak discharge, but varying base widths. The mobile bed was made of gravel in the size range of 3−8mm, with a d_{50} of 5.8mm. During the experiments, the discharge in the supply pipe, the water-surface elevation at eight stations, and the velocity profiles at three stations were measured. In addition, the submerged weight of the sediment particles falling into a sediment trap located near the downstream end of the flume was also continuously measured and recorded. To track the length of travel of sediment particles, the bed upstream of the sediment trap was prepared by laying eight strips of sediments with different colors. Each strip had a length of 0.7m and the total length of the reach with colored sediments was 5.6m. The colored sediments were used as tracers to track the movement during the passage of the triangular hydrograph. After an experiment with a triangular hydrograph, each colored sediment strip was divided into four strips of equal length. The sediment particles in each 0.175m-long strip were separated by hand into color groups and the groups were weighed. Similarly, the sediments collected in the sediment trap were also separated into color groups and weighed. The experimental results show that the length of travel is related to the width of the base of the hydrograph.

To be able to track the travel distances and locations of sediments of different color and size class in numerical simulations a total of 27 size classes were defined. This corresponds to nine colors, including the natural uncolored sediments, and the same three size classes for each color. The paper presents the results of two experiments, CM01 and CM02, and the corresponding numerical models. The computed results are compared with experimental measurements.

DESCRIPTION OF THE EXPERIMENTAL STUDY

The unsteady flow experiments over a movable bed were performed in a 17.75 m long tilting flume. The channel has a rectangular section which is 0.60m wide and 0.80m high. The side walls are made of transparent glass. The flume can be tilted to any slope from -1% to +9%. All the experiments described in the paper, were performed with the same bed slope of $S_o = 0.3\%$.

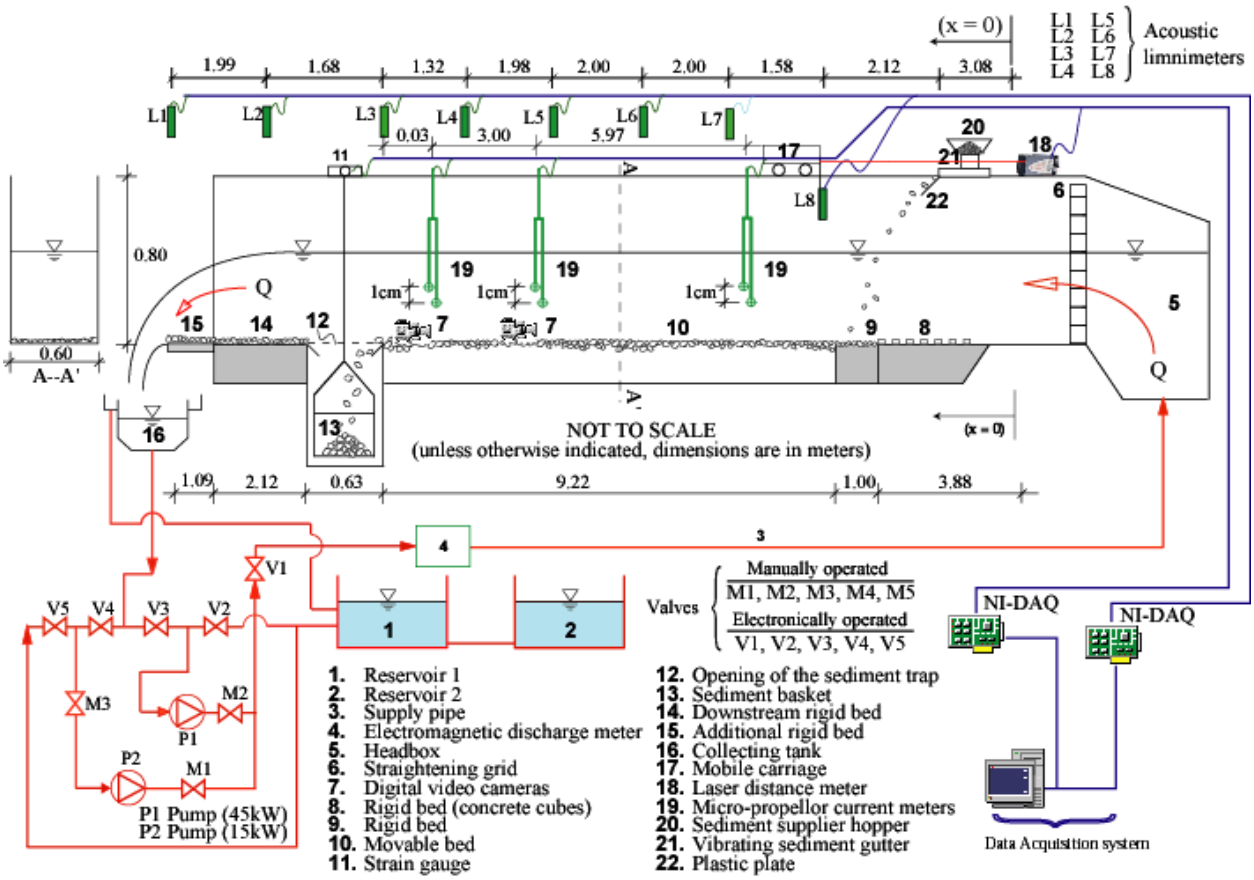

Figure 1 General view of the experimental installation and the measuring equipment.

Figure 1 shows the general view of the experimental installation and the locations of the measuring instruments. The flume was operated in a closed circuit mode. A pump controlled by a computer pumps the water stored in tanks 1 and 2 into the head tank of the flume according to a prescribed triangular hydrograph. The pumped discharge is measured continuously by the electromagnetic current meter mounted on the supply pipe. Water entering the flume through a flow straightener flows over a 4.88m-long fixed-bed reach roughened by gluing artificial elements to the first 3.88m and fine gravel particles to the remaining 1.00m. Downstream of the fixed-bed section, there is a 9.22m-long and 10cm-deep movable-bed section filled with compacted fine gravel. A sediment trap is located at the downstream end of the movable-bed section. The perforated basket inside the sediment trap hangs from a force transducer, which continuously measures and records the cumulative weight of the sediment particles falling into the basket in order to determine the sediment discharge. The section of the flume downstream of the sediment trap has a fixed bed on

which the fine gravel particles are glued. At the downstream end of the flume, the flow freely falls into a collector and returns to storage tanks 1 and 2 to complete the circuit.

The movable bed is filled with fine gravel having a specific density of 2.65. Figure 2 shows the grain-size distribution curve obtained continuously using a video imaging technique. A few representative sizes are listed on the same figure. Considering that $d_{95}/d_5 = 2.54 < 4$ and $\sigma_g = \sqrt{d_{84.1}/d_{15.9}} = 1.33 < 1.35$, the bed material can be considered as uniform (Raudkivi 1988). Before each experiment the bed was raked, leveled, and compacted. Attention was paid to keep the grain-size distribution of the sediment the same for all experiments. The bed elevation along the flume centerline was measured and recorded before and after each experiment using an ultrasonic limnimeter mounted on a carriage (L8 in Figure 1). There was no sediment feed at the upstream of the movable bed. The bed-load transport rate during the experiment was low and the maximum bed level change at the end of experiments was found to be about d_{50}.

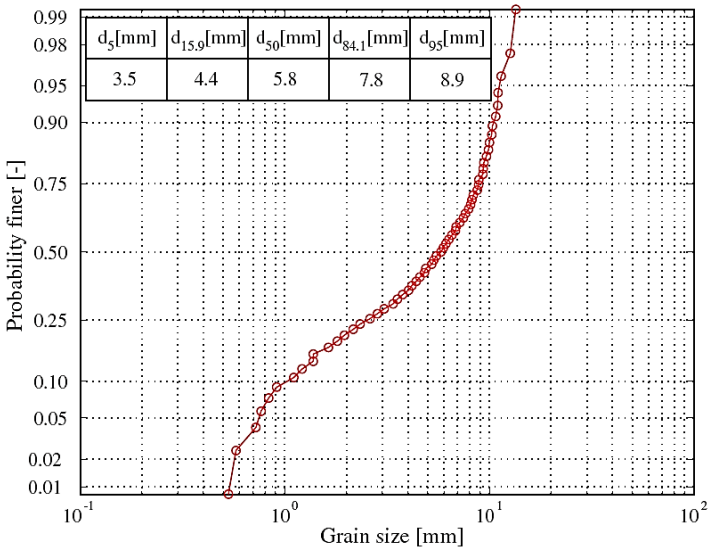

Figure 2 Grain size distribution curve of the fine gravel.

Figure 3 shows the longitudinal profile of the flume with the locations of the measuring stations and the layout of colored sediments used for bed-load tracking. The following variables were measured and recorded as a function of time:

- Discharge in the supply pipe was measured using an electromagnetic discharge meter.
- The flow depth were measured at eight locations along the flume length using ultrasonic limnimeters (L1 to L8 in Figure 3).
- Velocity profiles were measured at three locations along the flume (1, 2 and 3 in Figure 3) using six propeller current meters. At each measuring station two propeller current meters were positioned at prescribed elevations from the bed to measure the time varying local velocity. The same experiment was repeated 8 to 12 times by changing position of the propeller current meters. Time varying velocity profile over the entire flow depth was reconstituted from these point measurements. The velocity profiles were also then used to evaluate the time variation of shear stress, discharge and other useful flow parameters.

- The cumulative weight of the sediment particles falling into the basket in the sediment trap was recorded during the experiment. The bed-load transport rate at the end of the movable bed section was obtained from the cumulative weight curve. Given that the same experiment was repeated 8 to 12 times to obtain the complete velocity profile, it was possible to obtain a highly accurate measurement of time-varying bed-load rate by calculating the ensemble average.

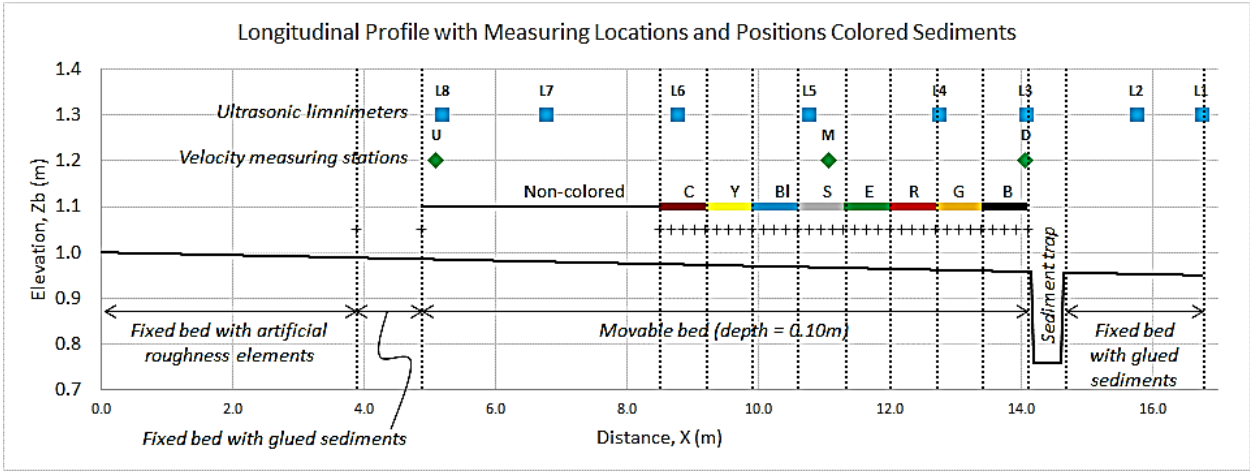

Figure 3 Longitudinal profile of the flume showing locations of the measuring instruments and the layout of colored sediments used for tracking bed-load movement.

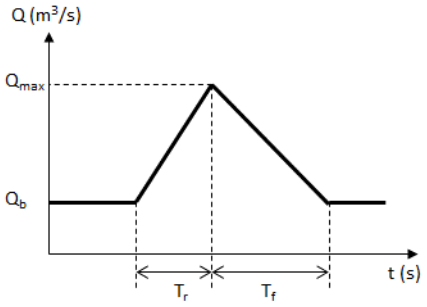

Colored-Gravel Exp.	Corresponding TM series Experiment	T_r (s)	T_f (s)	Q_b (m³/s)	Q_m (m³/s)	Ω (-)
CM01	TM01	150	150	0.050	0.140	0.41
CM02	TM03	50	50	0.040	0.160	1.64
CM03	TM06	10	10	0.040	0.140	7.45
	TM09	10	10	0.040	0.140	6.50
	TM10	10	10	0.040	0.140	6.80

Figure 4 Definition sketch for the triangular hydrographs and the list of experiments.

Figure 4 shows the definition sketch for the triangular hydrograph and provides a list of the experiments considered in this paper. As it can be seen the experiments were performed with three different symmetric hydrographs ($T_r = T_f$) with different base times: 300s (TM01), 100s (TM03), and 20s (TM06, TM09 and TM10). The base and the maximum discharges for the hydrographs are nominally same to each other. The unsteadiness parameter, $\Omega = (h/{u_*}^2)\,(\Delta Q/\Delta t)$, for the experiments is also listed on the last column of the table in Figure 4. After the experiments with three hydrographs were completed, one additional experiment was performed with each hydrograph using colored sediments for tracking the bed load. These experiments are listed in Figure 4 as CM01 (300s), CM02 (100s), and CM03 (20s).

The colored sediments were produced by painting the fine gravel used as bed material and have the grain-size distribution shown in Figure 2. The gravel was immersed in paint and then dried on plastic sheets. Attention was paid to keep the paint thin in order not to change the characteristics of the particles. Eight different colors were used Black (B), Golden (G), Red (R), Green (E), Argent (A), Blue (U), Yellow (Y), and Copper (C). Natural, uncolored sediments are denoted by "N". Before each bed-load tracking experiment, the colored sediments were carefully laid on top of the natural colored sediments in 0.70m-long stripes along the 5.6m reach immediately upstream of the sediment trap as shown in Figure 3. The thickness of the bed layer was about 3 cm (~5×d_{50}).

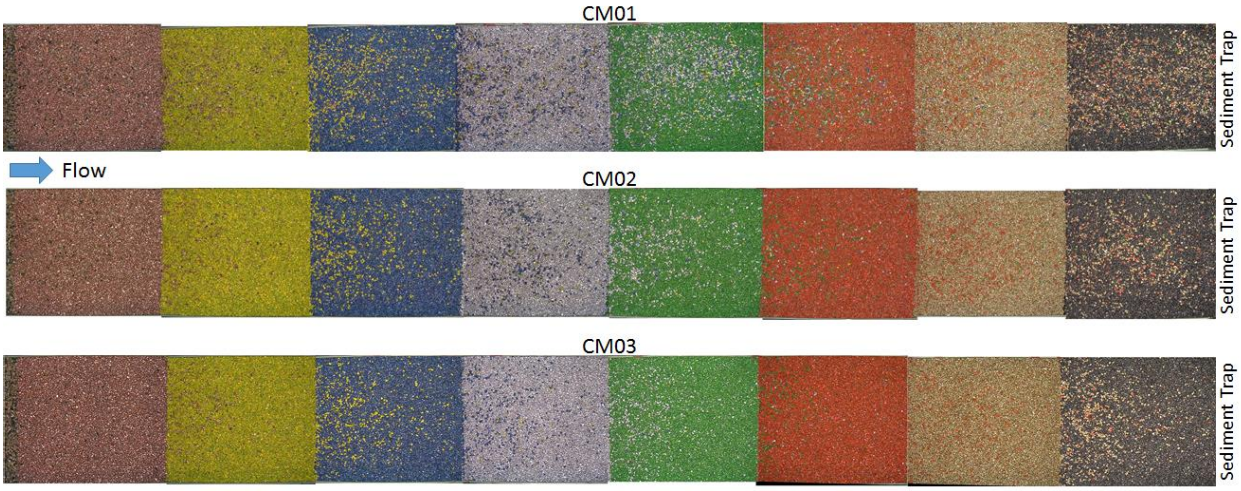

Figure 5 Appearance of the bed with colored sediments at the end of the experiments.

There is no sediment transport during the base flow. As the discharge increases, the bed shear increases above the critical shear stress to initiate the movement. The sediments are transported downstream as bed-load. The general appearances of the bed at the end of experiments CM01, CM02 and CM03 are shown in Figure 5. In order to determine how far the sediments traveled during the passage of the hydrograph, each color reach was divided into four equal length stripes of 17.5cm. The sediment particles in the 3cm-deep surface layer were collected carefully. The sediments collected from each stripe were then manually separated into different colors, including the natural sediments that were transported from upstream. Dry weight of sediments in each color were then measured and recorded.

The unsteady flow experiments discussed in this paper are part of an extensive experimental study performed at the Laboratory of Environmental Hydraulics of the Federal Institute of Technology, Lausanne, Switzerland. Detailed information on the complete set of experiments can be found in Qu (2002). A short presentation of the experimental study can be found in Qu et al. (2004). A preliminary analysis of the experiment with colored sediments is presented in Altinakar et al. (2014).

BRIEF DESCRIPTION OF THE CCHE1D NUMERICAL MODEL

The experiments CM01 and CM02 with colored sediments were simulated using the CCHE1D software, which was developed at the National Center for Computational Hydroscience and

Engineering, The University of Mississippi. CCHE1D is a software package to simulate one-dimensional unsteady free-surface hydrodynamics with unsteady non-equilibrium transport of non-uniform sediments and the resulting morphodynamic changes in dendritic channel networks. Modules are also available for modeling of contaminant transport and fate, and water quality, which includes nitrogen, phosphorous, and phytoplankton cycles. The CCHE1D can be run in coupled mode with AnnAGNPS and SWAT watershed models.

CCHE1D computes unsteady flows by solving the Saint-Venant equations given as:

$$\frac{\partial A}{\partial t} + \frac{\partial Q}{\partial x} = q \tag{1}$$

$$\frac{\partial}{\partial t}\left(\frac{Q}{A}\right) + \frac{\partial}{\partial x}\left(\frac{\beta Q^2}{2A^2}\right) + g\frac{\partial h}{\partial x} + g\left(S_f - S_o\right) = 0 \tag{2}$$

where *x* and *t* are the spatial and temporal axes; *A* is the flow area; *Q* is the flow discharge; *h* is the flow depth; S_0 is the bed slope; β is a correction coefficient for the momentum due to the non-uniformity of velocity distribution at the cross section; *g* is the gravitational acceleration; and *q* is the side discharge per unit channel length. S_f is the friction slope, defined as:

$$S_f = Q|Q|/K^2 \quad \text{with} \quad K = \sum_{l=1}^{3} \frac{1}{n_l} A_l {R_l}^{2/3} = \sum_{l=1}^{3} \frac{1}{n_l} {A_l}^{5/3} {P_l}^{-2/3} \tag{3}$$

where A_l is the flow area of subsection *l*; R_l is the hydraulic radius; P_l is the wetted perimeter; and n_l is the Manning's roughness coefficient. *l* is the index for subsections 1, 2 and 3 (left flood plain, main channel and right flood plain, respectively). CCHE1D employs an improved version of the implicit four-point finite difference scheme proposed by Preissmann (1961) to discretize the Saint-Venant equations. The solution scheme uses the increments in water depth Δh and flow discharge ΔQ as dependent variables. The resulting system of equations form a pentadiagonal matrix, whose solution is obtained with the help of the Thomas Algorithm, also called the Double-Sweep Method. CCHE1D adopts a hybrid dynamic/diffusive wave model. The dynamic wave model is solved when the Froude number is less than 0.9. For higher Froude numbers, CCHE1D solves the diffusive wave model.

The governing equations for the 1D non-equilibrium transport of non-uniform sediment and the resulting bed area change are given by the following expressions, respectively

$$\frac{\partial (AC_{tk})}{\partial t} + \frac{\partial Q_{tk}}{\partial x} + \frac{1}{L_b}(Q_{tk} - Q_{t^*k}) = q_{lk} \tag{4}$$

$$(1 - p')\,\frac{\partial A_{bk}}{\partial t} = \frac{1}{L_b}(Q_{tk} - Q_{t^*k}) \tag{5}$$

where C_{tk} is the section-averaged sediment concentration of size class k; Q_{tk} is the actual sediment transport rate of size class k; Q_{t^*k} is the sediment transport capacity of size class k; L_b is the

adaptation length of non-equilibrium sediment transport; and q_{lk} is the side inflow or outflow sediment discharge from bank boundaries or tributary streams per unit channel length, p' is the porosity of the bed material, and $\partial A_{bk}/\partial t$ represents the rate of change of bed area for the size class k. The first term on the left-hand side of Eq. (4) accounts for sediment storage, while the last term on the left-hand side represents the exchanges between the moving sediment and the bed material. The transport capacity for size class k can be expressed as:

$$Q_{t^*k} = p_{bk}\, Q^*_{tk} \tag{6}$$

where p_{bk} is the percentage of sediments of size class k in the bed material. The potential equilibrium transport rate for sediments of size, Q^*_{tk}, can be determined using a suitable empirical sediment transport formula. To take into account the variation of the vertical gradation of sediment size due to erosion and deposition processes, the bed is represented in three layers. The topmost layer is the mixing layer. All sediment particles in the mixing layer are subject to exchange with the water column. The second layer is the subsurface layer. The subsurface layer exchanges sediments only with the mixing layer. There is no sediment exchange between the subsurface layer and the bottommost third layer. The temporal variation of the bed-material gradation in the mixing and subsurface layers is determined using the following relationships, respectively:

$$\frac{\partial(A_m p_{bk})}{\partial t} = \frac{\partial A_{bk}}{\partial t} + p^*_{bk}\left(\frac{\partial A_m}{\partial t} - \frac{\partial A_b}{\partial t}\right) \tag{7}$$

$$\frac{\partial(A_s p_{sbk})}{\partial t} = -p^*_{bk}\left(\frac{\partial A_m}{\partial t} - \frac{\partial A_b}{\partial t}\right) \tag{8}$$

where A_m and A_s are the bed areas for the mixing and subsurface layers, respectively, A_b is the total bed area. The total bed deformation rate is the sum of bed deformation rates of all size classes, i.e. $\partial A_b/\partial t = \sum_{k=1}^{N} \partial A_{bk}/\partial t$ in which N is the number of size classes used. When $(\partial A_m/\partial t - \partial A_b/\partial t) \leq 0$ one has $p^*_{bk} = p_{bk}$, otherwise $p^*_{bk} = p_{sbk}$. This system of equations is closed by introducing semi-empirical expressions for various parameters, such as non-equilibrium adaptation length, L_b, thickness of mixing layer, sediment porosity, settling velocity of grains, etc. The system of equations is also discretized and solved using Preissmann's (1961) method.

SIMULATION OF EXPERIMENTS USING CCHE1D AND RESULTS

CCHE1D was used to simulate the experimental test cases CM01 and CM02 by dividing the grain size distribution curve shown in Figure 2 into three size classes: 1) coarse and very coarse sand (0.5mm<d<2mm); 2) fine and very fine gravel (2mm<d<8mm); and 3) medium gravel (8mm<d<16mm) where d is the sediment diameter. Furthermore, in order to be able to track the sediments with different colors during the simulation, the same size distributions were repeated for each of the eight colors as well as the natural sediments. This resulted in 27 size classes as shown in Table 1. All size classes have a dry specific density of 2.65.

The computational mesh comprises 336 grid nodes with a fixed grid spacing equal to 5 cm. The Manning roughness is calibrated as 0.016 $m^{-1/3}s$ and the time step is 0.5 second. The thickness of mixing layer is assumed to be twice the mean grain size. Wu et al. (2000) formula is used to

compute the transport capacity. The characteristics of the triangular hydrograph imposed at the upstream end of the model for CM01 and CM02 simulations are summarized in Figure 4.

Table 1 Sediment size classes used for tagging the sediments of different color. All sediments have a dry specific density of 2.65.

ID	d_{rep} (mm)	D_{LL} (mm)	D_{UL} (mm)	Color	ID	d_{rep} (mm)	D_{LL} (mm)	D_{UL} (mm)	Color
1	1.00	0.50	2.00	Natural (N)	16	1.00	0.50	2.00	Green (E)
2	4.00	2.00	8.00		17	4.00	2.00	8.00	
3	11.31	8.00	16.00		18	11.31	8.00	16.00	
4	1.00	0.50	2.00	Copper (C)	19	1.00	0.50	2.00	Red (R)
5	4.00	2.00	8.00		20	4.00	2.00	8.00	
6	11.31	8.00	16.00		21	11.31	8.00	16.00	
7	1.00	0.50	2.00	Yellow (Y)	22	1.00	0.50	2.00	Golden (G)
8	4.00	2.00	8.00		23	4.00	2.00	8.00	
9	11.31	8.00	16.00		24	11.31	8.00	16.00	
10	1.00	0.50	2.00	Blue (U)	25	1.00	0.50	2.00	Black (B)
11	4.00	2.00	8.00		26	4.00	2.00	8.00	
12	11.31	8.00	16.00		27	11.31	8.00	16.00	
13	1.00	0.50	2.00	Silver (S)					
14	4.00	2.00	8.00						
15	11.31	8.00	16.00						

d_{rep}= representative diameter of a size class; d_{LL}= lower limit of a size class; d_{UL}= upper limit of a size class.

In Figure 6 and Figure 7, the water surface elevations computed at the locations of the eight acoustic limnimeters (L1 to L8 in Figure 3) are compared with the measurements for experiments CM01 and CM02, respectively. The agreement is relatively good although the computed hydrographs have systematically higher peaks. Since the travel distance of the wave over the length of the flume is short, the attenuation is not important and the wave keeps its shape. In Figure 8 and Figure 9, the discharge, velocity and flow depth computed at the three measuring stations, "D" (x=14.07m), "M" (x=11.07m), and "U" (x=5.10m), are compared with the measurements for experiments CM01, and CM02, respectively. For the experiment CM01 with slower rising and falling hydrograph, the computed discharge and depth shown in Figure 8 agree well with the measurements at all three stations. The computed velocity, however, is larger than the measured one for the stations "D" and "M". In Figure 9, similar plots are provided for the experiment CM02 with a faster rising and falling hydrograph. The measurements at the station "U" were not recorded due to a faulty cable. Although the computed flow depths agree well with the measurements at stations "D" and "M", the computed discharge and velocity are under predicted. This may be due to the secondary effects introduced by the faster hydrograph that are not well modeled with the Saint-Venant equations.

The CCHE1D continuously tracks the percentage of each size class in the bed. Since the ID numbers of three size classes representing each color, including the natural color, are known, it was possible to calculate the weight of each color as a function of the distance. This in turn gives the information about the travel distance of each size class during the passage of the triangular hydrograph.

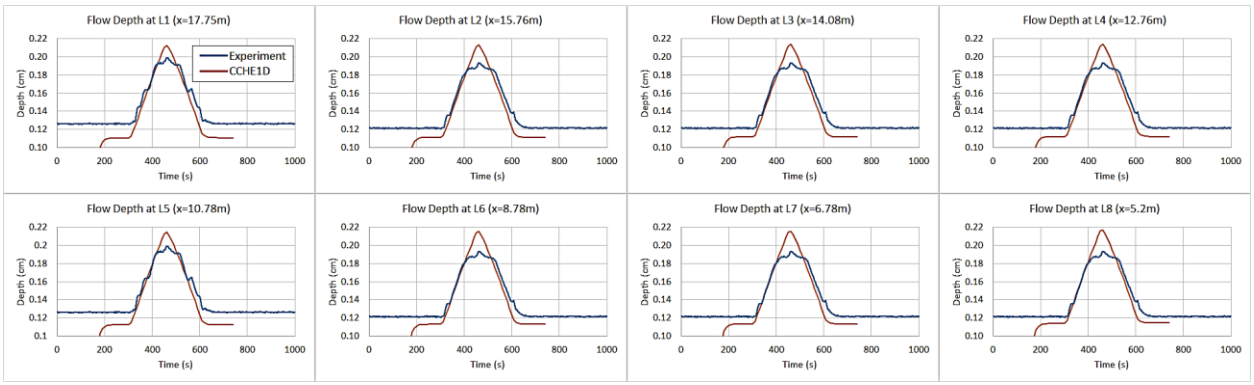

Figure 6 Comparison of measured and computed water depths for the experiment CM01.

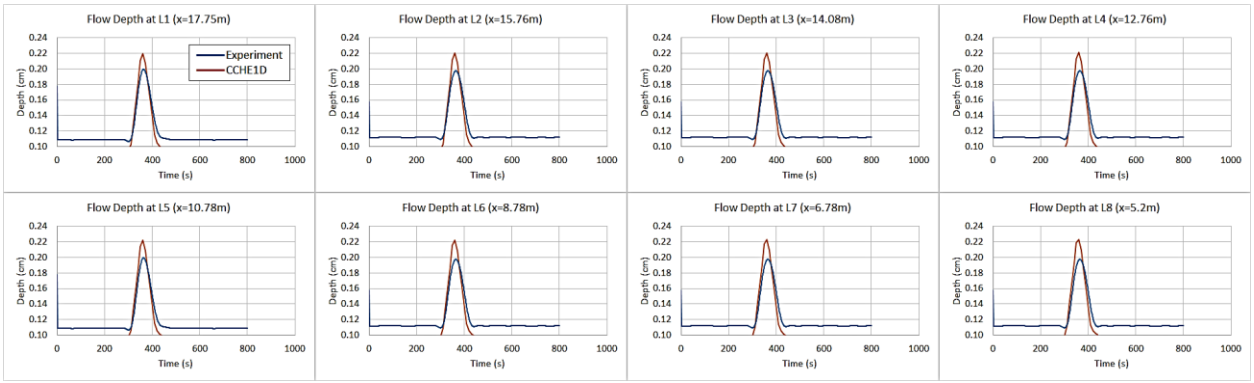

Figure 7 Comparison of measured and computed water depths for the experiment CM02.

The computed mass of the sediments of different colors composing the bed after the passage of the triangular hydrographs in CM01 and CM02 are plotted in Figure 10 and Figure 11, respectively. The experimental data are superposed on the computed weights. Since the black sediments are falling immediately into the basket of the sediment trap, the rightmost plot at the bottom row shows a histogram of the mass of the sediment of different colors accumulated in the basket. The agreement between the computed and measured sediment weights as a function of the distance is satisfactory despite some differences that are probably well within the uncertainty to be expected in comparison with a single sediment transport experiment. For the experiment CM01, the computed mass of the sediment accumulated in the basket is 1,609gr. A series of 12 experiments repeated with the same hydrograph as in CM01 yielded the average mass of the sediments as 1190.63gr±216.60gr. The computed value is about 200gr higher than the upper limit of experiments. Similarly, the computed mass of sediments falling into the basket is 698.65gr, whereas the experimental results a series of 12 experiments with the same hydrograph as in CM02 yields and average mass of 832.31gr±216.87gr. The computed value is well within the experimental range. Based on these results it can be concluded that the simulations of experiments with CCHE1D produce results that are comparable to those measured in the experiments.

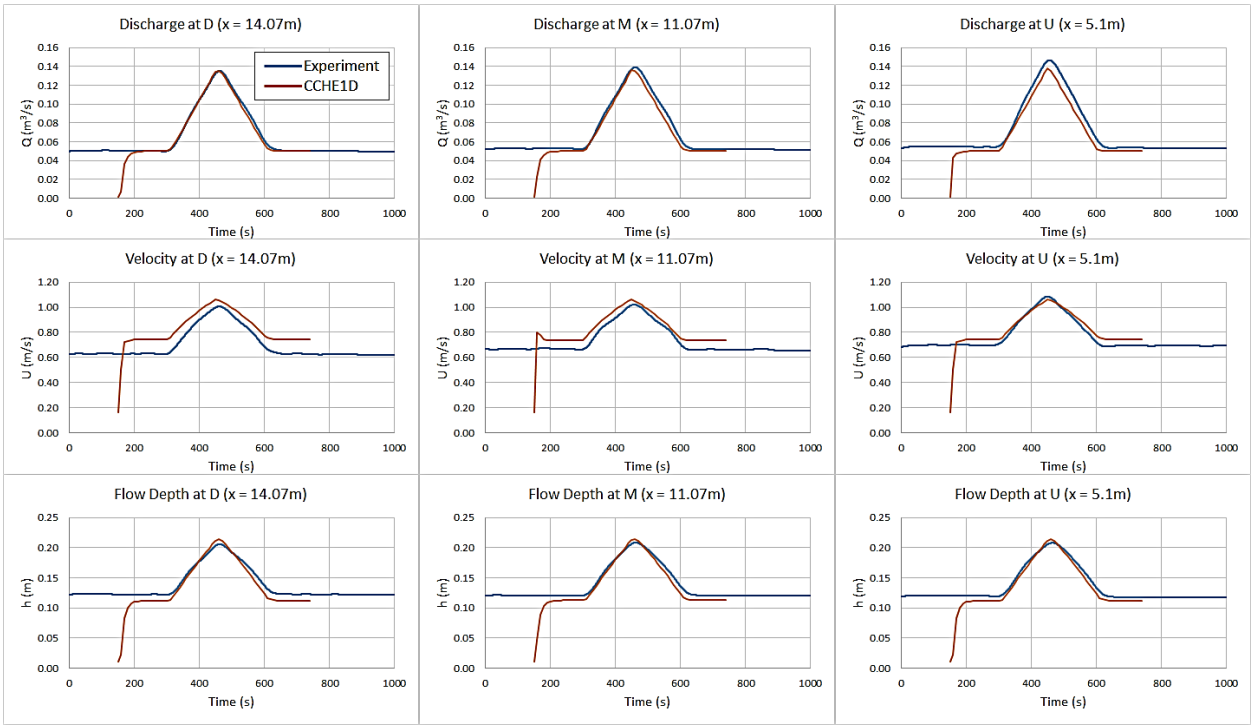

Figure 8 Comparison of measured and computed discharge, velocity and flow depth at three measuring stations D (x=14.07m), M (x=11.07m), and U (x=5.10m) for the experiment CM01.

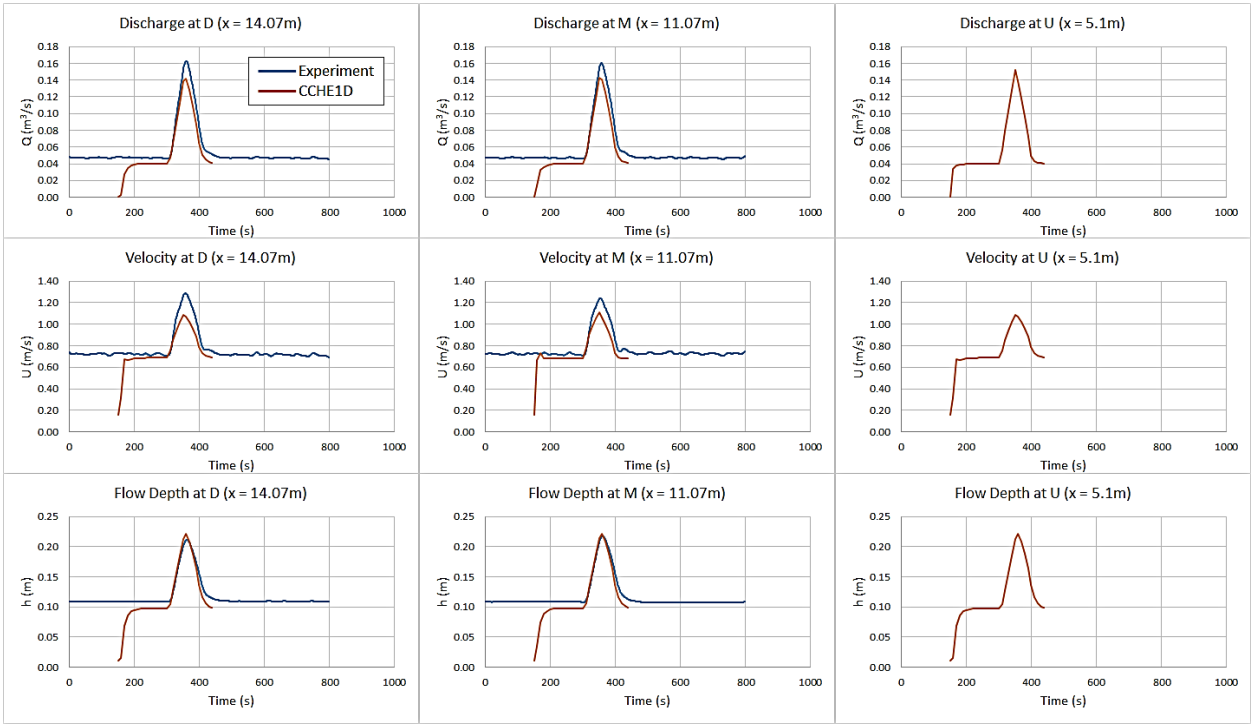

Figure 9 Comparison of measured and computed discharge, velocity and flow depth at three measuring stations D (x=14.07m), M (x=11.07m), and U (x=5.10m) for the experiment CM02.

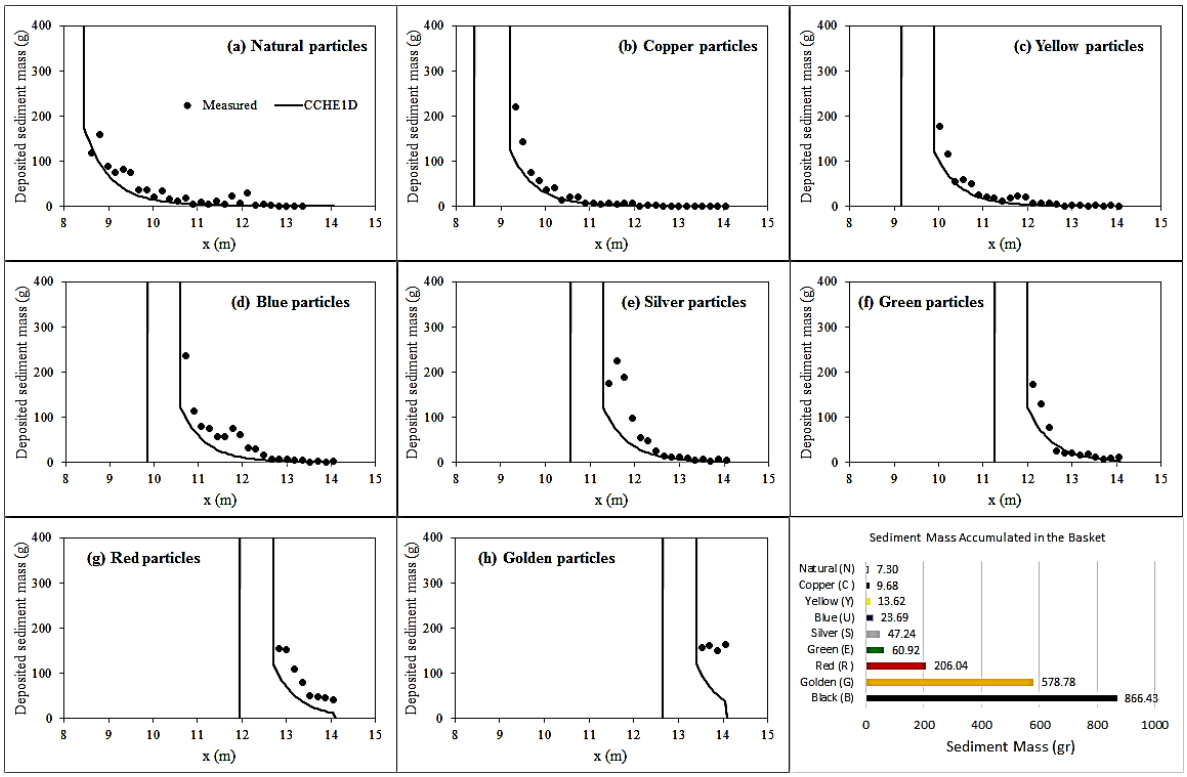

Figure 10 Comparison of computed and measured travel distances of the sediments for CM01.

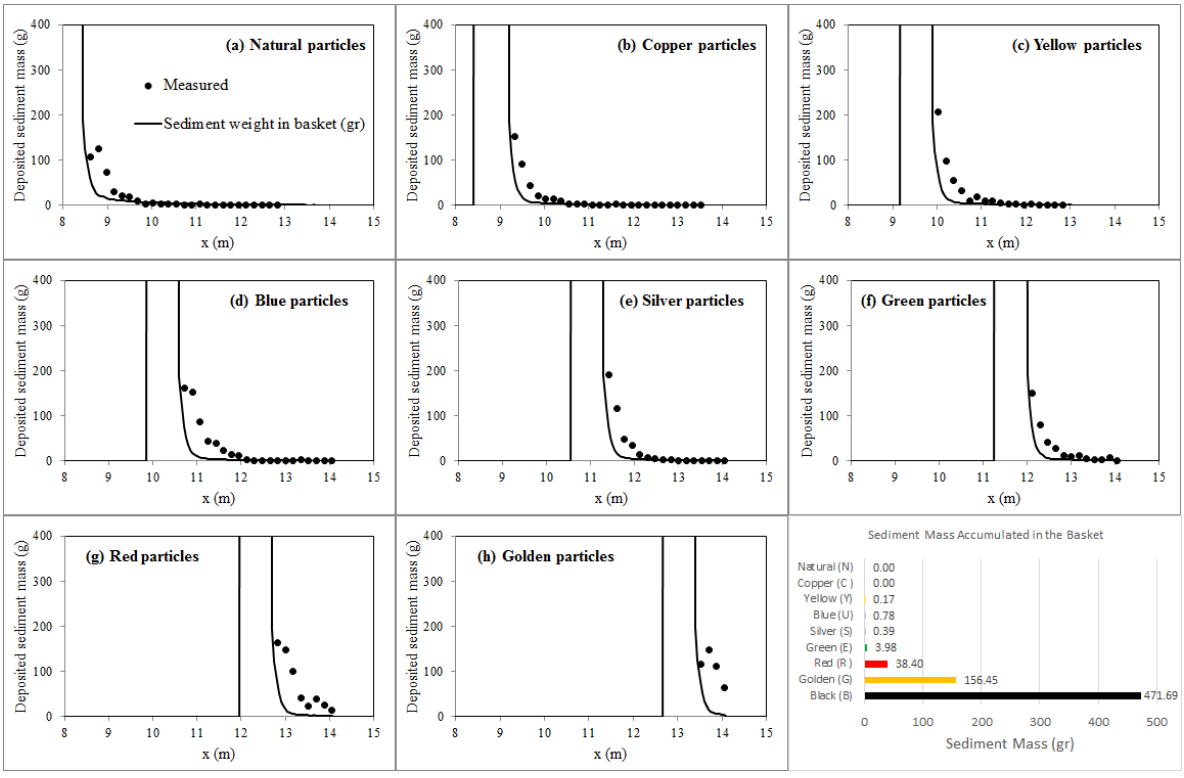

Figure 11 Comparison of computed and measured travel distances of the sediments for CM02.

CONCLUSIONS

The CCHE1D model developed at the national Center for Computational Hydroscience and Engineering was used to simulate two out of three experiments carried out at the Laboratory of Environmental Hydraulics of the Federal Institute of Technology, Lausanne, Switzerland, for tracking the movement of colored sediments during the passage of a triangular hydrograph. The hydrograph for CM01 rises from 50 m^3/s to 140 m^3/s in 150s and falls back to same base discharge in 150s. The hydrograph for CM02 rises from 40 m^3/s to 160 m^3/s in 50s and falls back to same base discharge in 50s. CM02 has a faster rising and falling hydrograph than CM01 for the same nominal base and peak discharges. The unsteadiness parameter, $\Omega = (h/{u_*}^2)(\Delta Q/\Delta t)$, where u_* is the shear velocity and $\Delta Q = Q_m - Q_b$, is 0.41 for CM01 and 1.64 for CM02. Comparison of computed results with the experimental results show that the computed water surface elevations, discharges and velocities agree well with the measurements. For the experiment CM02, the velocities are under predicted although discharge and flow depth show better agreement. This may be due to secondary effects that are not well represented by the Saint-Venant equations. The computed distances traveled by each color agree well with the experimental results. The computed mass of the sediments accumulated in the basket of the sediment trap located at the downstream end of the movable bed section also agree well with the experimental data. Additional simulations by varying various parameters such as the adaptation length and the mixing length thickness, are currently under way. Moreover, the simulations are also being carried out for the third colored experiment, which rises from 40 m^3/s to 140 m^3/s in only 10s and falls back to same base discharge again in 10s. This experiment has the fastest hydrograph and the unsteadiness parameter is about 6.9, which is significantly higher than those for CM01 and CM02. The results of the ongoing simulations will be reported during the conference.

ACKNOWLEDGMENTS

The authors gratefully acknowledge that the funds for this research were provided by the U.S. Department of Agriculture (USDA), Agricultural Research Service (ARS), through the Cooperative Agreement No. 58-6408-1-609.

REFERENCES

Altinakar, M.S., Franca, M.J., Hassan, M., and Qu, Z. (2014). "Gravel Particles Entrainment and Deposition under Unsteady Flow Conditions," AGU Fall Meeting, ePoster https://agu.confex.com/data/handout/agu/fm14/Paper_28868_handout_1613_0.pdf, San Fransisco, Dec 15-19, 2014.

Preissmann, A. (1961). "Propagation des intumescences dans les canaux et les rivières", 1er Congres de l'Association Francaise de Calcule, Grenoble, France.

Qu, Z., Altinakar, M.S., and Lyn, D. (2004). "Laboratory Investigation of Unsteady Flows over Fixed and Mobile Beds," Proceedings of the 6th International Conference on Hydroscience and Engineering, May 31 – June 3, 2004, Brisbane, Australia

Qu, Z. (2002). Unsteady Open-Channel Flow over a Mobile Bed, Doctoral Dissertation No 2688, Laboratory of Environmental Hydraulics, Federal Institute of Technology, Lausanne, Switzerland.

Raudkiwi, A.J. (1998). Loose Boundary Hydraulics, A.A. Balkema Publishers, The Netherlands.

SCALING RELATIONS FOR EXPONENTS AND COEFFICIENTS OF BEDLOAD TRANSPORT AND FLOW COMPETENCE CURVES IN COARSE-BEDDED STREAMS WITH CHANNEL GRADIENT, RUNOFF YIELD, BASIN AREA AND SUBSURFACE FINES

Kristin Bunte, Research Scientist, Colorado State University, Engineering Research Center, 1320 Campus Delivery, Fort Collins, Colorado 80523, kbunte@engr.colostate.edu; Steven R. Abt, Professor emeritus, Colorado State University, Engineering Research Center, 1320 Campus Delivery, Fort Collins, Colorado 80523, sabt@engr.colostate.edu; Kurt W. Swingle, Environmental Scientist; 630 Iris Ave., Boulder, Colorado 80304, kskb@ix.netcom.com; Daniel A. Cenderelli, Fluvial Geomorphologist/Hydrologist, USDA Forest Service, National Stream and Aquatic Ecology Center, 2150 Centre Ave., Fort Collins, Colorado 80526, dcenderelli@fs.fed.us; Dieter Rickenmann, Research Scientist, Swiss Federal Research Institute WSL, Mountain Hydrology and Mass Movements, Zürcherstrasse 111, 8903 Birmensdorf, Switzerland; dieter.rickenmann@wsl.ch; Dave Gaeuman, Research Scientist, Trinity River Restoration Program, Weaverville, California, dgaeuman@usbr.gov.

Abstract Relations of bedload transport (Q_B) and flow competence ($D_{max,QB}$) with water discharge Q are difficult to measure or to accurately estimate in steep mountain streams. To further the understanding of how gravel transport and flow competence curves differ among streams, this empirical study relates exponents and coefficients of power functions fitted to gravel transport ($Q_B = aQ^b$) and flow competence curves ($D_{max,QB} = fQ^g$) to watershed, channel, and bed material parameters. Exponents b and g are found to systematically increase with basin area, the bankfull width/depth ratio and stream width, and to decrease with the bankfull unit runoff yield per basin area as well as the percentage of subsurface fines. The exponents are non-monotonically (convexly) related to stream gradient, unit stream power, relative bankfull depth, and roughness. A tight linear relation between the b- and g-exponents reveals that steep Q_B curves result when increasing flows find increasingly larger particles to transport, a feature best expressed in steep plane-bed streams. Coefficients a and f are inversely related to the b and g exponents, respectively, hence scaling relations positive for exponents are negative for coefficients and vice versa. Overall, r^2-values of scaling relations are within 0.3 to 0.6 and significant, sufficient to determine the range of expected exponents and coefficients, but not tight enough to predict them with certainty. Scaling relations are tightened, and their practical applicability for predicting Q_B and $D_{max,QB}$ curves enhanced, when stream types are segregated based stream gradient and basin area.

INTRODUCTION

Particle entrainment and subsequent bedload transport is difficult to predict in steep mountain streams because entrainment and transport are caused by complex interactions between flow hydraulics and sediment transport dynamics. Flow hydraulics, including turbulence, scour jets, wake eddies, and secondary circulation, exert fluctuating and variable forces on coarse channel beds. Coarse beds are typically comprised of not only a wide mix of particle sizes ranging from sand to boulders, but also contain a variety of structural characteristics that develop in response to the interactions between flow hydraulics and sediment supply (Church et al., 1998). Particles may be exposed on top of the bed, embedded firmly in the bed, integrated in steps, particle clusters or stone structures, or anchored to other particles, tree roots, or bedrock. Hence, bed particle entrainability ranges from highly mobile to very stable (e.g., Bunte et al., 2013). The variability of flow hydraulics, sediment supply, and channel bed characteristics between streams controls the rate at which the quantity and size of gravel in motion increases as discharge increases. As a result, each stream has a specific bedload transport and flow competence relation. The variability of transport and flow competence curves is evident in studies that bring together observations from numerous streams (Barry et al., 2004; Bunte et al., 2008, 2013, 2014; Bathurst, 2013; Schneider et al., 2014). Case studies also show that bedload transport and flow competence curves can vary for a given stream in response to changes in sediment supply which alter bed material conditions and particle transportability within or between events (e.g., Beschta, 1987; Lenzi, et al., Mao et al., 2012; Yu et al., 2009; Hassan et al., 2014). The complexities of flow hydraulics, sediment supply, and bed structure—all of which are difficult to quantify—cannot be accounted for in bedload transport equations typically used for estimating transport rates or incipient motion. To be simple enough for practical application, transport equations must be limited to a few parameters (typically flow depth, stream gradient, and the median size of bed surface particles). Those bedload equations therefore cannot capture the processes that determine how gravel transport rates and flow competence relate to flow in a specific stream, and computed transport rates can deviate from measured gravel transport rates by several orders of magnitude (e.g., Bathurst, 2007; Barry et al., 2008; Schneider et al., 2015).

Numerous applications in fluvial geomorphology and channel management would benefit from a method to quickly and accurately estimate the steepness (exponent) and *y*-axis intercept (coefficient) of gravel transport and flow competence relations from simple field-measured parameters, or more conveniently from parameters quantified from maps and areal photographs. This study uses an empirical approach similar to that used for quantifying suspended sediment transport relations (e.g., Asselmann, 1999, 2000; Syvitski et al., 2000; Dodov and Foufoula-Georgiou, 2005; Yang et al., 2006) and provides a comparison and prediction of exponents and coefficients of bedload transport and flow competence curves. Earlier studies that empirically predicted exponents and coefficients of bedload transport curves from watershed, flow, channel, and bed material parameters were based on a narrow range of *b*-exponents (Barry and Buffington, 2002; Barry et al., 2004), an artifact of the Helley-Smith samplers used (Bunte et al., 2004, 2008), or the empirical studies lacked robustness due to data paucity (Bunte and Swingle, 2003; Bunte and Abt, 2003; Bunte et al., 2006). For this study, we gathered a large dataset from a wide range of coarse-bedded mountain streams where gravel transport was measured with samplers suitable for gravel bedload to 1) show how watershed, flow, channel, and bed material parameters affect exponents and coefficients of bedload transport and flow competence curves; 2) to assess which parameters best capture the characteristics of the flow- and bed material interactions; and 3) to explore the potential for improving the prediction of bedload transport. While simple watershed, flow, channel morphometry, and bed material parameters are obviously not the direct factors entraining or restraining bed particles, this study proposes that those parameters have either provided conditions for actual channel processes or been influenced by them and hence serve as easily quantifiable proxies for actual gravel transport processes, especially when streams are segregated according to gradient and size.

METHODS

Compilation of datasets Of the 45 datasets of gravel bedload transport relations (Q_B curves) from wadeable, steep gravel- and cobble-bed streams worldwide compiled in this study, 29 datasets also include flow competence relations ($D_{max,QB}$ curves). Forty percent of the datasets are derived from gravel transport and flow competence measured mainly in the Rocky Mountain streams with snowmelt regimes. (Bunte et al., 2004, 2008, 2010a; Potyondy et al., 2010). The other datasets include streams in alpine and arctic pro-glacial environments, densely forested watersheds, and high desert environments. Sediment supply ranges from very high to very low with bankfull unit transport rates that extend over ten orders of magnitude from 1E-4 to 1E6 g/m·s. Study sites span a wide range of basin areas (1-260 km^2), bankfull stream widths (1-20 m), stream gradients (0.007-0.136 m/m), and bed surface sizes (D_{50} of 20 - 200 mm, D_{84} of 33-360 mm). Gravel transported in the study streams was collected either with bedload traps, vortex, net-frame, basket, and pit samplers (see references in Ryan et al. (2005a) and Bunte et al. (2013) for those samplers), as well as with hanging baskets, including those that deploy automatically (Rickenmann et al., 2012), or was quantified from continuous, automated surveys of an accumulating debris pile volume (Lenzi et al., (1999, 2004, 2006). Bedload data from pressure difference samplers were not included in this compilation because they yield Q_B and $D_{max,QB}$ curves that are significantly flatter that those from bedload traps (Bunte et al., 2004, 2008, 2010b) and are not thought to accurately represent the transport-discharge relation. Also not included are steep streams in which wedges of fine-grained sediment build up low-gradient sections between log steps (Green et al., 2014). Most of the gravel bedload datasets used in this study are described in Bunte et al. (2014), and many of the flow competence data are summarized in Bunte et al. (2013).

Fitted bedload transport and flow competence curves The increase of transport rates Q_B with water discharge Q (Q_B curves) is typically (and admittedly somewhat simplistically) described by power functions in the form $Q_B = a Q^b$, where a and b are empirically determined (e.g., Barry et al., 2004; Bunte et al., 2008, 2014). Exponents b, which refer to flow quantified by Q in this study, are lower than exponents of bedload transport curves obtained when water flow is quantified by flow depth d (or shear stress). Exponents b are independent of the units used to quantify Q_B and Q, while a-coefficients are unit-dependent. All the a-coefficients in this study are based on Q_B units of g/s and discharge in units of m^3/s. Flow competence relations ($D_{max,QB}$ curves) are also described by power functions as $D_{max,QB} = f Q^g$ (e.g., Mao, 2012; Bunte et al., 2013), where $D_{max,QB}$ is the largest bedload particle size collected in a sample, and f and g are empirically determined; Q is quantified in units of m^3/s, while $D_{max,QB}$ (often measured in 0.5 phi increments) is expressed in units of mm. For some of the study streams, sediment supply changed between the rising and falling limbs of flow during a highflow season, or between individually sampled years. When this caused notable differences, two separate Q_B and/or $D_{max,QB}$ curves were fitted. Mathematically complex function types may describe gravel transport or flow competence relations more accurately (e.g., Gaeuman et al., 2014), but simple power functions described all of the authors' Q_B and $D_{max,QB}$ curves. Power functions are

commonly reported for Q_B and $D_{max,QB}$ curves in other studies, and the empirically quantified exponents and coefficients are fully adequate to describe the scaling relations developed in this study.

Stream parameters Four stream parameters were quantified for the study datasets:

- basin area (A),
- bankfull unit runoff yield (q_{bf}/A) where bankfull flow Q_{bf} was field-determined or based on the 1.5-year recurrence interval flood (Castro and Jackson 2001), and bankfull unit flow is $q_{bf} = Q_{bf}/w_{bf}$,
- stream gradient (S), and
- the percentage of subsurface sediment < 8 mm ($\%D_{sub<8}$) (not available for all the bedload dataset in this study).

Study stream grouping The progression from step-pool to plane-bed morphology in mountain streams is generally concomitant with an increase in basin area. However, the lower gradient plane-bed streams with occasional riffle-pool sequences occur in small drainages <10 km^2 as well as in large drainages of 60 - 260 km^2. Similarly, some step-pool streams in this study have small basin areas of only a few km^2, while others have areas up to 27 km^2. To reflect the different sizes of streams with similar gradients, study reaches were first categorized into three stream gradient classes to denote the basic channel morphology (Montgomery and Buffington, 1997):

- step-pool,
- steep plane-bed with low, narrow steps but no pools, and
- low gradient plane-bed with occasional pool-riffle sequences, especially forced around sharp channel bends.

The three channel types were then segregated into those with small and large basin areas along a cutoff value of 15 km^2 (Table 1) which is slightly less than the dataset's geometric mean drainage size. Those group thresholds are somewhat arbitrary and are reflective of conditions encountered among the study streams and could shift if more data sets become available for this line of analyses.

Table 1 Stream type grouping based on basin area size and stream gradient.

Stream type	Drainage area (km^2)	Gradient range (mm)	Secondary morphological features	Abbreviation
Small step-pool	< 15	0.040 – 0.136	rare, short plane-bed reaches	small s-p
Large step-pool	> 15			large s-p
Small steep plane-bed [1)]	< 15	0.016 – 0.038	some low, narrow steps, no plunge pools	small steep p-b
Large steep plane-bed	> 15			large steep p-b
Small plane-bed	< 15	0.007 – 0.014	forced or occasional pool-riffle sequences	small p-b w/p-r
Large plane-bed	> 15			large p-b w/p-r

[1)] not encountered among the study streams

Regression analyses Exponents b and g as well as coefficients a and f from all datasets and for the stream groups delineated in Table 1 were regressed against the various watershed, channel, and bed material parameters. Power functions in the form of $b = \alpha_1 \cdot X^{\gamma 1}$, $a = \alpha_2 \cdot X^{\gamma 2}$, $g = \alpha_3 \cdot X^{\gamma 3}$, and $f = \alpha_4 \cdot X^{\gamma 4}$ generally obtained the best fit, where X denotes a watershed or streambed parameter; α and γ are empirically determined.

RESULTS AND DISCUSSION

Scaling relations of exponents from Q_B and $D_{max,QB}$ curves with watershed, channel, flow, and bed material parameters The steepness of the Q_B and $D_{max,QB}$ curves compiled in this study differed widely between streams. Exponents b covered a seven-fold range from 2.6 to 18.2, while exponents g spanned a 20-fold range from 0.27 to 5.5. These exponents vary systematically with watershed, flow, channel, and bed material parameters. Exponents b and g are both positively, moderately, but nevertheless significantly related to basin area size A with r^2-values of 0.32 and 0.40 (Figure 1a). Exponents b and g decrease with unit bankfull runoff yield (q_{bf}/A) (Figure 1b), a parameter that indicates the flow per drainage area available to supply and transport bedload. Scaling relations are likewise negative with $\%D_{sub<8}$ (Figure 1c). An abundance of subsurface fine gravel and a well-developed armor in coarse bedded streams typically suggest that a large supply of fine gravel is transported. The negative scaling relations (Figure 1b and c) are moderately well-defined (r^2 of 0.20 to 0.43) and likewise significant, and they confirm that Q_B (and $D_{max,QB}$) curves are flatter in streams with higher sediment supply and more bed mobility (Dietrich et al., 1989; Laronne and Reid, 1993; Lisle, 1995; Reid and Laronne, 1995; Laronne et al., 2001; Hayes et al., 2002; Lisle and

Church, 2002; Barry et al., 2004; Ryan et al., 2005b; Bunte et al., 2006; Gran et al., 2006; Hassan et al., 2008; Diplas and Shaheen, 2008).

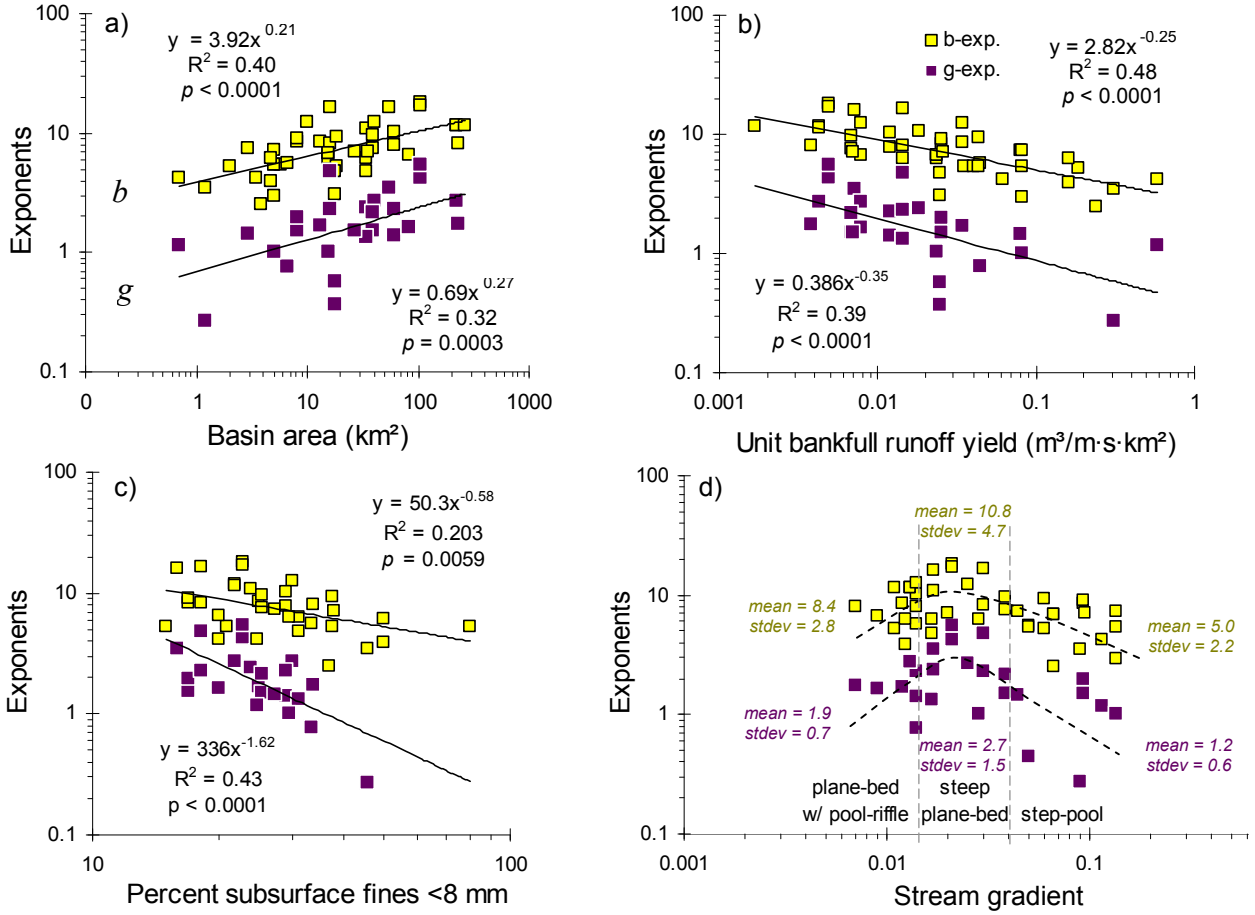

Figure 1 Scaling relation of *b*- and *g*-exponents with the four stream parameters from the 44 datasets show a positive trend with A (a), negative trends with q_{bf}/A and $\%D_{sub<8}$ (b, c), and a non-monotonic, convex trend with S (d). Yellow symbols denote *b*-exponents of Q_B curves and purple symbols denote *g*-exponents of $D_{max,QB}$ curves. All relations are significant.

Exponents non-monotonically related to stream type Among the study streams, the highest exponents coincide with streams that are moderately steep (S of 0.016 to 0.039 m/m), moderately rough (D_{84}/d_{bf} of 0.03 to 0.04), moderately deep (d_{bf}/D_{50} 6 to 8) and moderately powerful (ω_{bf} of 7 to 11 kg/m·s) (Figure 1d). Those reaches have steep plane-bed channels with occasional low, narrow steps, but no plunge pools. Exponents are lower in the lower gradient study reaches where $S \leq 0.014$ m/m, $D_{84}/d_{bf} < 0.03$, $d_{bf}/D_{50} > 8$, and stream power <7 kg/m·s. Those conditions are typical of the lower gradient plane-beds with occasional or forced riffle-pool sequences. The trend of rating curve flattening for lower gradient streams is attributed to higher sediment supply with less transport capacity and competence (see above). This study identifies a second, opposing trend: Compared to the steep plane-bed reaches, exponents are about half as large in the steepest streams where $S > 0.04$ m/m. These channels are coarse, rough, and shallow; they have high stream power, and exhibit step-pool morphology. As a result of two opposing trends, exponents *b* and *g* have non-monotonic (convex) relations with S (Figure 1d).

Occurrence of the steepest Q_B curves in steep plane-bed streams is attributed to the combination of two bed material conditions: The inundated bed surface harbors minimal fine gravels, and their scarcity keeps transport very low early in the highflow season. Transport is still relatively low at moderate flows, but at flows above bankfull, coarse gravel and cobbles on the upper surface of bar deposits—inaccessible at moderate flows—become available for transport. The large difference between very low transport rates of small gravels early in a highflow season and cobble transport at above bankfull flow may span 7-8 orders of magnitude and causes steeply increasing Q_B and $D_{max,QB}$ curves

in steep plane-bed streams. By contrast, flat Q_B curves result in step-pool streams where small gravel pockets provide ample bedload supply early in the highflow season, but flows above bankfull do not produce cobble transport because bar deposits are scarce and bed particles are restrained by structural bed stability. Low gradient plane-bed streams take an intermediate position. The low flow sediment supply is moderate, and an increase in Q_B and $D_{max,QB}$ at the highest flows may be slowed if moderate flows have already transported all but the very largest bed particles.

Scatter around the scaling relations Scaling relations in Figure 1 provide suitable estimates of the range of exponents to be expected for Q_B and $D_{max,QB}$ curves for a given parameter value. However, even for the best-developed scaling relations, measured *b*- and *g*-exponents vary by a factor of about ±2 around the predicted value. Much of this variability is attributed to natural inter-annual variability in Q_B and $D_{max,QB}$ curves that is not related to or not yet reflected in watershed, channel, runoff, or bed material parameters. Variability in exponents also arises from less than optimally measured Q_B and $D_{max,QB}$ relations due to sampling errors which may include a low number of field samples, a narrow range of measured flows, poor quantification of the lowest or highest Q_B, unfortunate timing of samples within the high-flow season, or a poor fit of measured data to a power function. The remainder of the variability reflects the suitability of a watershed, channel, flow or bed material parameter to serve as a proxy for processes that cause gravel transport, and the parameter's ability to provide or respond to the specific conditions that supply, entrain, or restrain particles and determine gravel transport.

Scaling relations for exponents segregated by stream type and stream size Prediction of *b*- and *g*-exponents is improved when scaling relations in Figure 1 are segregated by stream type. The discussion here is limited to *b*-exponents because the effects of stream-type segregation are very similar for *b*- and *g*-exponents, but *b*-exponents have richer datasets.

For scaling relations of *b* with *A* (Figure 2a), step-pool and steep plane-bed streams follow the same positive trend, irrespective of stream gradient. However, a secondary stratification by *S* occurs in the low-gradient plane-bed

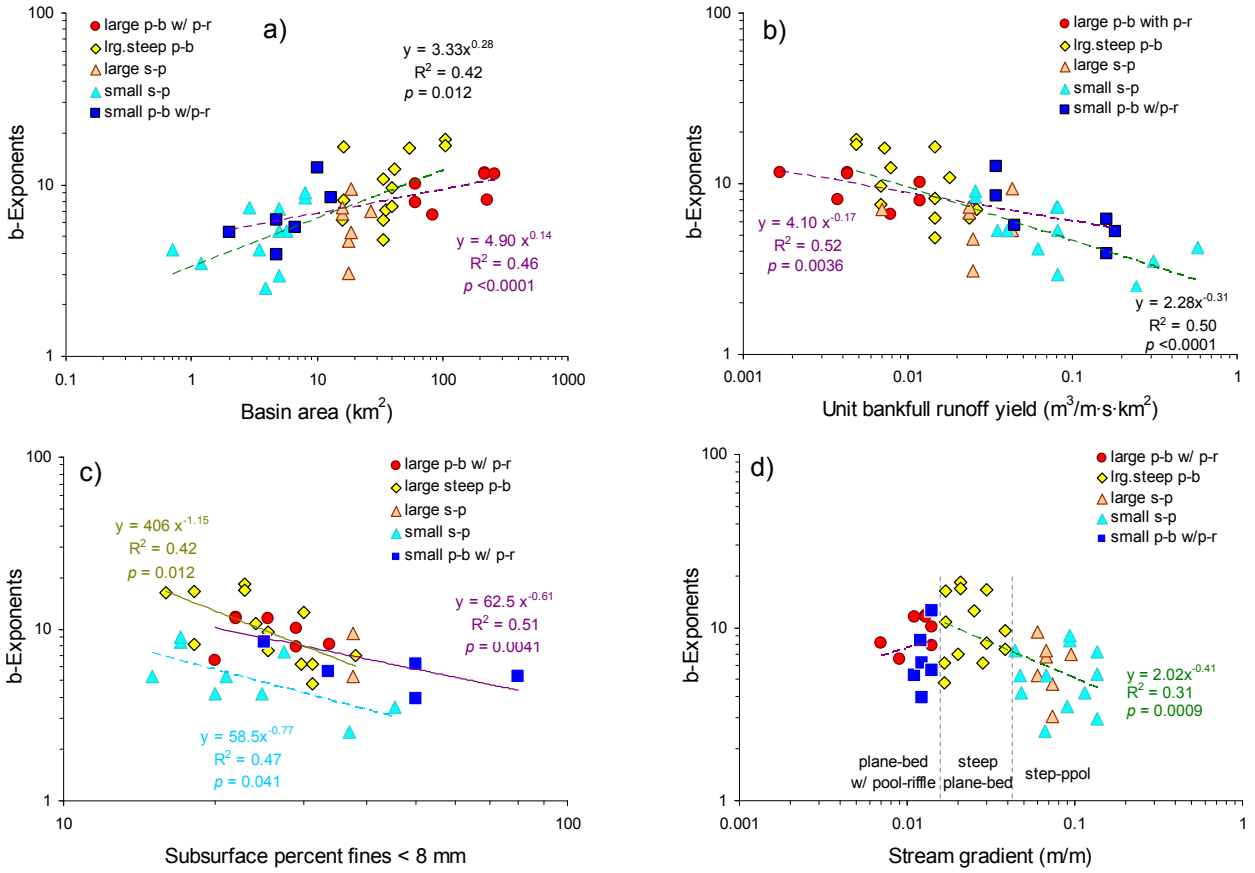

Figure 2 Scaling relations for *b*-exponents shown in Figure 1 segregated by stream type.

streams and describes a scaling relation with a flatter trend. The same segregation patterns hold true for scaling relations of b with q_{bf}/A (Figure 2b), which are better defined than for A and make q_{bf}/A a better predictor of b. The non-monotonic trend of b-exponents vs. S (Figure 2d) is not further segregated by basin area. However, gradient and basin area act together and define three distinct scaling relations for b with the $\%D_{sub<8}$ (Figure 2c). The b-exponents for step-pool and steep plane-bed streams are clearly differentiated by stream size, such that large, steep plane-bed and step-pool stream define a scaling relation of b with subsurface fines that is notably higher than that for small step-pool streams. The low-gradient plane-bed streams follow a flatter scaling relation, but again with higher exponents for larger, and slightly lower exponents for smaller streams. Segregation by stream type is especially effective for the parameter $\%D_{sub<8}$ as it narrows the range of b-exponents to a factor of about 2 for a given $\%D_{sub<8}$ and stream type, rendering $\%D_{sub<8}$ a parameter suitable for the prediction of b.

Interrelatedness of steepness and coefficients of Q_B and $D_{max,QB}$ curves

Exponents with exponents and coefficients with coefficients The a-coefficients and b-exponents of Q_B curves as well as the f-coefficients and g-exponents of $D_{max,QB}$ curves are strongly related. Exponents b and g increase in direct proportion with a well defined linear relation ($r^2 = 0.91$) as shown in Figure 3a. This proportionality explains the almost parallel trend of the scaling relations for b- and g-exponents shown in Figure 1 and lets g be computed from b and vice versa. The tight, positive relation between b- and g-exponents is not segregated by stream types and clearly shows that the steepness of Q_B curves depends on whether increasing flows find increasingly larger particles to entrain and transport. If that is the case, $D_{max,QB}$ and Q_B curves steepen.

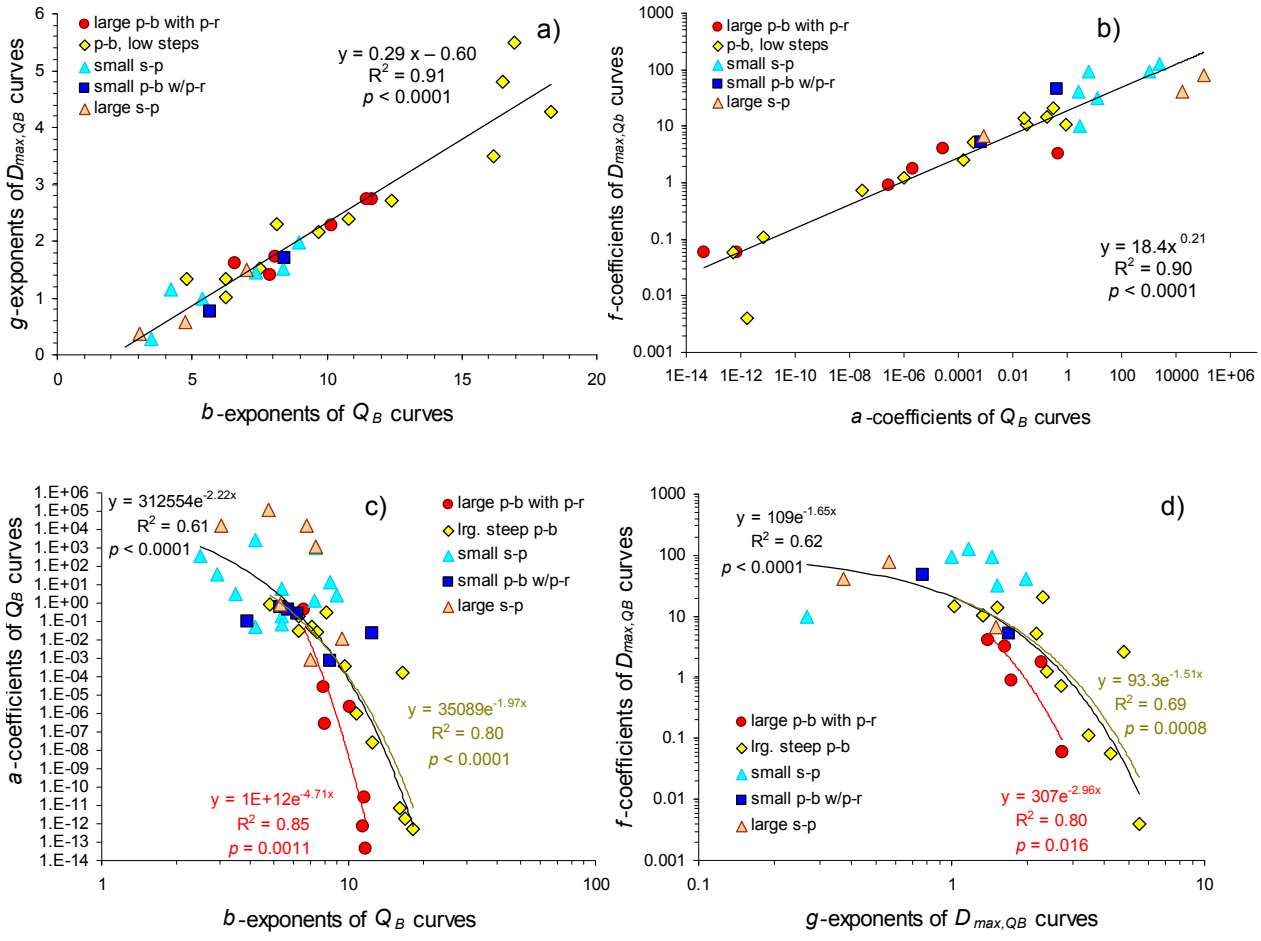

Figure 3 Interrelatedness of Q_B and $D_{max,QB}$ curves: among the two exponents (a), among the two coefficients (b), and among coefficients and exponents (c and d).

Inherent inverse relations between exponents and coefficients Power function coefficients represent not only the *y*-axis intercept for $x = 1$ but are also inversely related to the function's steepness. Negative relations between exponents and coefficients are a general feature of power functions. Consequently, all positive scaling relations for exponents (Figure 1) become negative for coefficients and vice versa. For the study stream Q_B curves, an increase of *b*-exponents by 1 is met by a 1 to 2 order of magnitude decrease in *a*-coefficients (Figure 3c); *f*-coefficients of $D_{max,QB}$ curves decrease less, by about half an order of magnitude as *g*-exponents increase by 1 (Figure 3d). Coefficients are also directly controlled by the magnitude of bedload transport rates. For example, a doubling in transport rates for all Q doubles the coefficient. The two-fold control of coefficients (by exponent steepness and by transport rates) complicates a comparison of coefficients among streams: A Q_B curve with a coefficient 10 times larger than that of another Q_B curve at a specified parameter *x*-value does not mean that transport rates of the two curves differ by a factor of 10.

Values of *a*- and *f*-coefficients from fitted Q_B and $D_{max,QB}$ curves extend over about 10 and over 4 orders of magnitude, respectively. Nevertheless, the negative relation between *a*-coefficients and *b*-exponents is fairly well and significantly described by an exponential function (r^2 of 0.61) (Figure 3c), as observed for suspended sediment (Syvitski et al. 2000; Yang et al. 2007). The relation between *a*-coefficients and *b*-exponents is clearly affected by stream type. Segregation by stream gradient raises the correlation for large, steep, plane-bed streams to an r^2 of 0.80 and to an r^2 of 0.85 for large, low-gradient plane-bed streams with occasional riffles and pools (Figure 3c). Hence for the large study streams, segregation by *S* narrows the range of *a*-coefficients for a given *b*-exponent from 10 to about 6 orders of magnitude. Stream size segregates the *a*-*b* relation for step-pool streams; large step-pool streams have a steep relation, while small step-pool streams have a flatter one. Stream gradient segregates the *a*-*b* relation between small streams with higher *a*-coefficient for small step-pool streams than for small, more gently sloped plane-bed streams.

For $D_{max,QB}$ curves, the trend between *f*-coefficients with *g*-exponents is likewise fairly well and significantly described by a negative exponential function (r^2 of 0.62) (Figure 3d). Segregation by stream gradient improves r^2 from 0.62 for all data to 0.69 for large steep plane-beds, and to 0.80 for large low-gradient plane-bed streams with occasional riffles and pools. However, a further segregation of step-pool streams by size or small streams by gradient is not evident.

Scaling relations of Q_B and $D_{max,QB}$ curve coefficients with watershed, channel, flow, and bed material parameters Coefficients of the Q_B and $D_{max,QB}$ curves are negatively related to basin area A (Figure 4a). A negative relation of *a* with A was also reported by Barry et al. (2004) for streams in Idaho. Following the inherent inverse relation between exponents and coefficients, coefficients are positively related to q_{bf}/A (Figure 4b). A positive scaling relation had also been expected for the bed material parameters $\%D_{sub<8}$ (Figure 4c) but is not revealed by the data. Similarly, the convex non-monotonic scaling relations observed for exponents with stream gradient does not turn into concave a non-monotonic relation for coefficients. Instead, coefficients display poorly to moderately well-developed positive trends with S (Figure 4d).

Predictability of coefficients Scaling relations for coefficients with the parameters A and q_{bf}/A (Figure 4a, b) are significant and tend to yield higher r^2-values than scaling relations for exponents (Figure 1a-b), but that does not render coefficients more predictable. Scatter around the fitted regression function is large, about ± 1 order of magnitude for coefficients of the $D_{max,QB}$ curves and ± 4 to 5 orders of magnitude for Q_B curves, which might preclude a meaningful prediction of Q_B coefficients from watershed and channel parameters.

Fitting Q_B and $D_{max,QB}$ curves with unit discharge $q = Q/w$ instead of total Q does not narrow the scatter in the scaling relations for coefficients. Compared to *a*, the range of a_q-coefficients obtained from Q_B curves with q instead of Q extend over a range about one order of magnitude wider than *a*, and neither the general trends of scaling relations (Figure 4), nor the patterns observed for individual stream groups change in a significant way between *a* and a_q.

Coefficients *a* of Q_B and *f* of $D_{max,QB}$ curves, like exponents, show a strong positive correlation ($r^2 = 0.90$) (Figure 3b), corroborating that gravel transport and flow competence increase in unison. The relation of *f*- vs. *a*-coefficients is not differentiated by stream type.

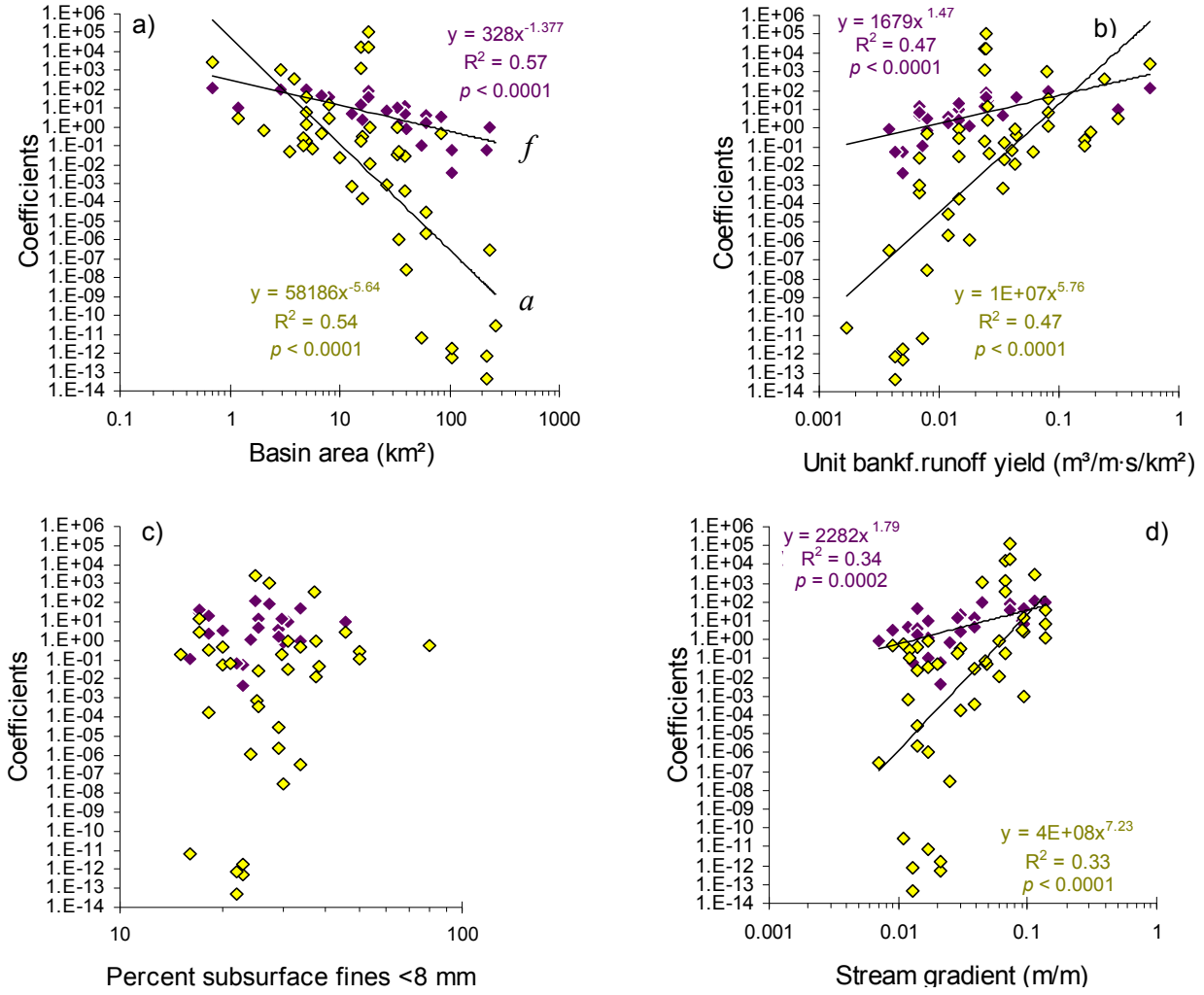

Figure 4 Scaling relations for *a*- and *f*-coefficients with the four stream parameters showing a negative trend with A (a), a positive trend with q_{bf}/A (b), a poorly defined positive trend with $\%D_{sub<8}$ (c) and a non-monotonic trend with S (d). Yellow symbols denote *a*-coefficients and purple symbols *f*-coefficients of $D_{max,QB}$ curves.

Differentiation of coefficients by stream type and stream size

The prediction of *a*- and *f*-coefficients from basin area, runoff yield, stream gradient, and the percentage of subsurface fines < 8 mm is improved when scaling relations are segregated by stream type; the discussion here is limited to *a*-coefficients for which datasets are richer than for *f*-coefficients. Segregation of the data scatter is primarily by stream size and indicates steep scaling relations for *a*-coefficients with all parameters for large streams, and flatter scaling for small streams. The resulting intersection of the two scaling relations for *a*-coefficients with A (Figure 5a) reflects two opposing segregation effects by stream gradient; among small streams, *a*-coefficients are clearly lower for plane-bed streams than for step-pool streams. The effect of gradient is reversed among large plane-bed streams; those with low-gradients have higher coefficients than those that are steeper. These segregation trends are not evident for all parameters. Trends for scaling relations of *a*-coefficients with A are reversed for the parameter q_{bf}/A (Figure 5b) except for the differentiation among gentle and steep-gradient plan-bed streams. Secondary stratification by stream gradient is consistent only among small streams and for all four parameters (Figure 5 a-d), with higher coefficients for the steeper streams. Being stratified by stream type in multiple ways makes A a better suited parameter for predicting *a*-coefficients.

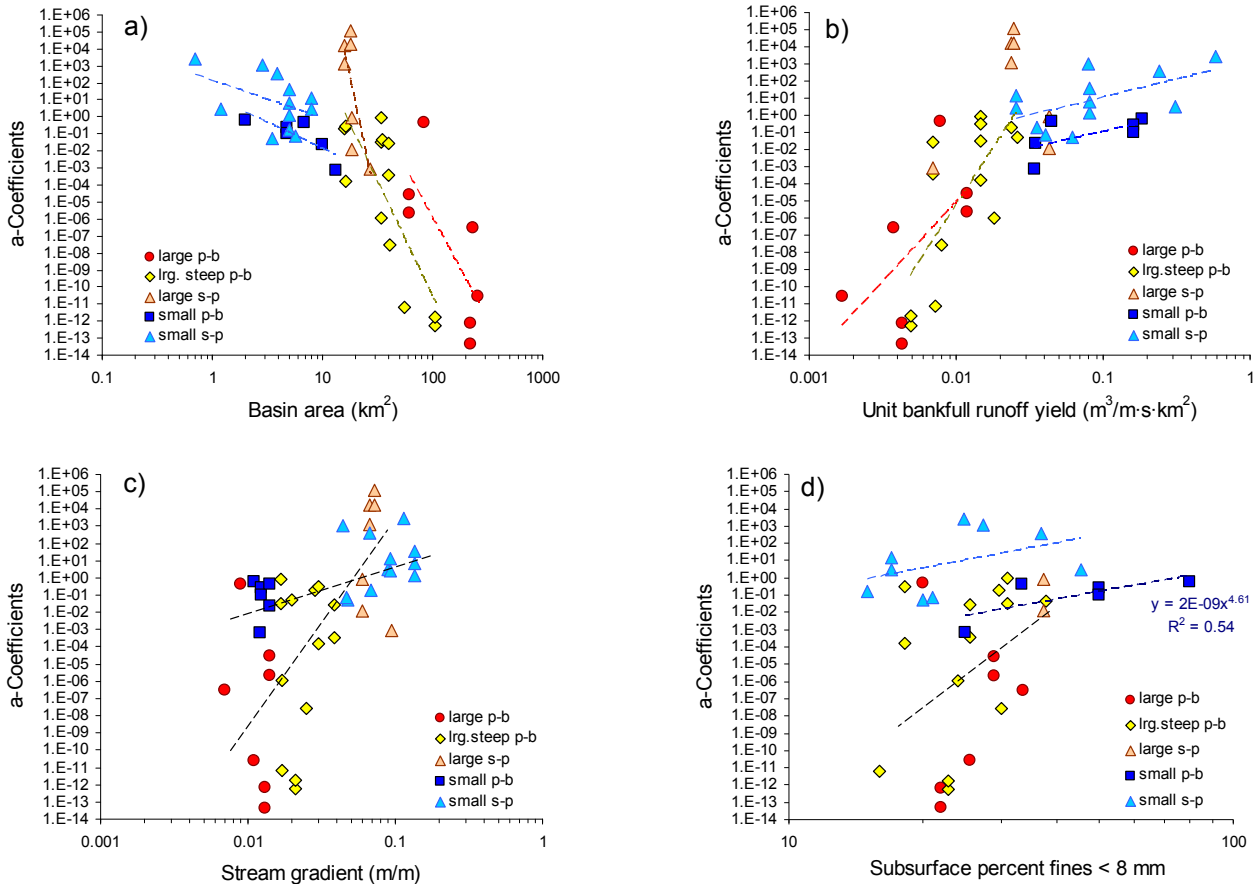

Figure 5 Scaling relations for *a*-coefficients shown in Figure 4 segregated by stream type. Dotted lines indicate possible trends.

SUMMARY AND CONCLUSION

- Study results demonstrate that exponents and coefficients of Q_B and $D_{max,QB}$ curves are systematically and significantly related to four parameters: basin area, runoff yield, stream gradient, and the percentage of subsurface fines < 8 mm. This finding is not reflected in current bedload transport equations and may serve to improve their application to gravel-bed rivers in mountain areas.
- Even though the data scatter is wide and the r^2-values are only moderate, the fairly large sample size of the study ensures significance and robustness of the scaling relations.
- The scaling relations of exponents with basin area, unit runoff yield, stream gradient, and percent subsurface fines scatter widely; hence a user can confidently determine the range of expected exponents but not accurately predict its value. Scaling relations of coefficients with those four parameters are slightly better correlated and likewise significant, but the wide scatter that extends over several orders of magnitude (especially for Q_B curves) appears to preclude any practical prediction of coefficients.
- Scatter can be narrowed when scaling relations for exponents and coefficients are differentiated by stream types.
- The specific effects of segregation by stream type on scaling relations differ among stream parameters as well as between exponents and coefficients, but segregation is primarily by basin area, and secondarily by stream gradient.
- At this stage of research, an iterative approach is suggested to estimate exponents and coefficients from scaling relations; the estimate is initially based on a parameter's *x*-value, and then narrowed based on stream type group. After repeating the process for all parameters, estimates are either averaged or weighted based on the parameter considered most relevant or reliable.

- Segregation by stream type can improve the r^2 of a scaling relation but decreases its significance. However, the lower sample size in data sets segregated by stream type lets an individual data point have influence on a scaling relation, hence a larger data base to increase certainty would be desirable.

Acknowledgment We thank all researchers who shared their hard-won bedload data with us: Gustavo Merten (Univ. of Minnesota, Duluth, USA) for data from Arvorezinha Creek, Francesco Comiti (Free University of Bolzano/Bozen, Italy) for Saldurbach data, and Luca Mao (Pontificia Universidad Catolica de Chile, Santiago, Chile) for Estero Morales data; Johannes Schneider and Jens Turowski (Swiss Federal Research Institute, WSL, Birmensdorf, Switzerland; Jens also at Helmholtz Centre Potsdam, GFZ, Potsdam, Germany) for data from the Riedbach and the Erlenbach. The National Stream and Aquatic Ecology Center (formerly Stream Systems Technology Center) of the USDA Forest Service, Fort Collins, Colorado, USA funded this study and the many years of field data collection that provided the basis for the analyses. We are indebted to John Potyondy (retired, Forest Service) for his vision and long-term support of our data collection efforts without which this study could not have been done.

REFERENCES

Barry, J.J. and Buffington, J.M. (2002). "A general power function for predicting bedload transport rates," Eos, Transactions, AGU, 83 (47), Fall Meeting Supplement, Abstract H21C-0817.

Barry, J.J., Buffington, J.M., and King, J.G. (2004). "A general power equation for predicting bed load transport rates in gravel bed rivers," Water Resources Research, 40, W10401, doi:10.1029/2004WR003190.

Barry, J.J., Buffington, J.M., Goodwin, P., King, J.G., and Emmett, W.W. (2008). "Performance of bed-load transport equations relative to geomorphic significance: Predicting effective discharge and its transport rate," Journal of Hydraulic Engineering, 134 (5), pp 601-615.

Bathurst, J.C. (2007). "Effect of coarse surface layer on bed-load transport," Journal of Hydraulic Engineering, 133 (11), pp 1192-1205. DOI: 10.1061/ASCE0733-9429(2007) 133:11(1192).

Bathurst, J.C. (2013). "Critical conditions for particle motion in coarse bed materials of non-uniform size distribution," Geomorphology, 197, pp 170–184; http://dx.doi.org/10.1016/j.geomorph.2013.05.008.

Bunte, K. and Abt, S.R. (2003). "Bedload rating and flow competence curves vary with watershed and bed material parameters," EOS, Trans. AGU, 84 (46) Fall Meeting Supplement, Abstract H32I-01. http://www.agu.org/meetings/fm03/waisfm03.html

Bunte, K. and Swingle, K. (2003). Results from testing the bedload traps at Little Granite Creek, 2002: effect of sampling duration and sampler type on bedload transport rates and systematic variability of rating curves with basin area and stream bed parameters. Report submitted to the Stream Systems Technology Center, USDA Forest Service, Rocky Mountain Research Station, Fort Collins, Colorado, 110 pp.

Bunte, K., Abt, S.R., Swingle, K.W., Cenderelli, D.A., Schneider, J.M. (2013). "Critical Shields values in coarse-bedded steep streams," Water Resources Research, 49(11), pp 7427-7447. http://dx.doi:10.1002/2012WR012672, 2013

Bunte, K., Abt, S.R. and Swingle, K.W. (2006). "Predictability of bedload rating and flow competence curves from bed armoring, stream width and basin area," In: Proceedings of the 8th Federal Interagency Sedimentation Conference, April 2-6, 2006 in Reno, Nevada., Session 4A-2, 9 pp. [CD ROM]. http://pubs.usgs.gov/misc_reports/FISC_1947-2006/html/pdf.html

Bunte, K., Swingle, K. and Abt, S.R. (2007). Guidelines for Using Bedload Traps in Coarse-bedded Mountain Streams: Construction, Installation, Operation and Sample Processing. General Technical Report RMRS-GTR-191, USDA, Forest Service, Rocky Mountain. Research Station, 91 pp, Fort Collins, Colordo. http://www.fs.fed.us/rm/pubs/rmrs_gtr191.pdf

Bunte, K., Swingle, K.W. and Abt, S.R. (2010a). "Necessity and difficulties of field calibration of signals from surrogate techniques in gravel-bed streams: possibilities for bedload trap samples," In: Bedload-surrogate monitoring technologies, Gray, J.R., Laronne, J.B., and Marr, J.D.G (eds.), USGS Scientific Investigation Report 2010-5091, 17 pp. http://pubs/usgs.gov/sir/2010/5091

Bunte, K., Abt, S.R., Potyondy, J.P., and Swingle, K.W. (2008). "A comparison of coarse bedload transport measured with bedload traps and Helley-Smith samplers," Geodinamica Acta, 21(1/2), pp 53-66.

Bunte, K., Abt, S.R., Potyondy, J.P., and Ryan, S.E. (2004). "Measurement of coarse gravel and cobble transport using a portable bedload trap," Journal of Hydraulic Engineering, 130(9), pp 879-893.

Bunte, K., Abt, S.R., Swingle, K.W., and Cenderelli, D.A. (2014). "Effective discharge in Rocky Mountain headwater streams", Journal of Hydrology, 519, pp 2136-2147, http://dx.doi.org/10.1016/j.jhydrol.2014.09.080

Bunte, K., Abt, S.R., Swingle, K.W., and Potyondy, J.P. (2010b). "Functions to adjust transport rates from a Helley-Smith sampler to bedload traps in coarse gravel-bed streams (rating curve approach)," In: Proceedings 9th Federal Interagency Sedimentation and 4th Federal Interagency Hydrologic Modeling Conference, Las Vegas, NV, June 27 – July 1, 2010, Session: Fluvial Geomorphology, CD-ROM ISBN 978-0-9779007-3-2. http://acwi.gov/sos/pubs/2ndJFIC/Contents/10D_Bunte_03_01_10.pdf

Bunte, K., Abt, S.R., Swingle, K.W., and Potyondy, J.P. (2009). "Comparison of three pebble count protocols (EMAP, PIBO, and SFT) in two mountain gravel-bed streams," Journal of the American Water Resources Association, 45(5), pp 1209-1227. DOI: 10.1111/j.1752-1688.2009.00355.x http://www.stream.fs.fed.us/publications/PDFs/Bunte_others_2009.pdf

Castro J.M., and Jackson, P.L. (2001). "Bankfull discharge recurrence intervals and regional hydraulic geometry relationships: patterns in the Pacific Northwest, USA", Journal of the American Water Resources Association, 37 (5), pp 1249-1262.

Church, M., Hassan, M.A., and Wolcott, J.F. (1998). "Stabilizing self-organized structures in gravel-bed stream channels: field and experimental observations," Water Resources Research, 34(11), pp 3169-3179.

Dietrich, W.E., Kirchner, J.W., Ikeda, H., Iseya, F. (1989). "Sediment supply and the development of the coarse surface layer in gravel-bedload rivers," Nature, 340, pp 215-217.

Diplas, P., and Shaheen, H. (2008). "Bed load transport and streambed structure in gravel streams," in: Gravel-Bed Rivers VI: From Process Understanding to River Restoration. H. Habersack, H. Piegay, and M. Rinaldi (eds.), Elsevier, Amsterdam, pp 291-312.

Dodov, B., and Foufoula-Georgiou, E. (2005). "Fluvial processes and streamflow variability: Interplay in the scale-frequency continuum and implications for scaling," Water Resources Research, 41, W05005, doi:10.1029/2004WR003408.

Gaeuman, D., Holt, C.R., and Bunte, K. (2014). "Maximum Likelihood Parameter Estimation for Fitting Bedload Rating Curves," Water Resources Research , 51, doi:10.1002/2014WR015872.

Gran, K.B., Montgomery D.R., and Sutherland, D.G. (2006). "Channel bed evolution and sediment transport under declining sand inputs," Water Resources, Research, 42, W10407, doi:10.1029/2005WR004306.

Hassan, M.A., Smith, B.J., Hogan, D.L., Luzi, D.S., Zimmermann, A.E., and Eaton, B.C. (2008). "Sediment storage and transport in coarse bed streams: scale considerations," in: Gravel-Bed Rivers VI: From Process Understanding to River Restoration. H. Habersack, H. Piegay, and M. Rinaldi (eds.). Elsevier, Amsterdam, pp 473-497.

Hayes, S.K., Montgomery, D.R., Newhall, C.G. (2002). "Fluvial sediment transport and deposition following the 1991 eruption of Mount Pinatubo," Geomorphology, 45, pp 211– 224.

Laronne, J.B., Garcia C., and Reid, I. (2001). "Mobility of patch sediment in gravel bed rivers: Patch character and its implications for bedload," in: Gravel-Bed Rivers V, M.P. Mosley (ed.), New Zealand Hydrological Society, Wellington, New Zealand, pp 249-290.

Laronne, J.B., and Reid, I. (1993). "Very high rates of bedload sediment transport by ephemeral desert rivers," Nature 366, pp 148-150.

Lenzi, M. A., Mao, L., and Comiti, F. (2004). "Magnitude-frequency analysis of bed load data in an Alpine boulder bed stream," Water Resources Research, 40, W07201, doi:10.1029/2003WR002961.

Lenzi, M.A., Agostino, V.D., Billi, P. (1999). "Bedload transport in the instrumented catchment of the Rip Cordon. Part I: Analysis of bedload records, conditions and threshold of bedload entrainment," Catena, 36, pp 171-190.

Lenzi, M.A., Mao, L., and Comiti, F. (2006). "Effective discharge for sediment transport in a mountain river: Computational approaches and geomorphic effectiveness," Journal of Hydrology, 326, pp 257–276, doi:10.1016/j.jhydrol.2005.10.031

Lisle, T.E., 1995. "Particle size variations between bed load and bed material in natural gravel bed channels," Water Resources Research, 31(4), pp 1107-1118.

Lisle, T.E., and Church, M. (2002). "Sediment transport-storage relations for degrading, gravel bed channels," Water Resources Research, 38 (11), 1219, doi:10.1029/2001WR0001086, 2002.

Montgomery, D.R., and Buffington, J.M. (1997). "Channel-reach morphology in mountain drainage basins.," Geol. Soc. Am. Bull., 109 (5), pp 596-611.

Potyondy, J.P., Bunte, K., Abt, S.R., and Swingle, K.W. (2010). Bedload movement in mountain channels: insights gained from use of portable bedload traps. Proc. 4th Fed. Interagency Hydrologic Modeling Conference and 9th Fed. Interagency Sedimentation Conference, Las Vegas, NV, 2010. CD-ROM ISBN 978-0-9779007-3-2. http://acwi.gov/sos/pubs/2ndJFIC/Contents/10D_Potyondy_03_01_10.pdf

Reid, I., and Laronne, J.B. (1995). "Bed load sediment transport in an ephemeral stream and a comparison with seasonal and perennial counterparts," Water Resources Research, 31(3), pp 773-781.

Rickenmann, D., Turowski, J.M., Fritschi, B., Klaiber A., and Andreas, L. (2012). "Bedload transport measurements at the Erlenbach stream with geophones and automated basket samplers," Earth Surface Processes and Landforms, 37(9), pp 1000-1011, DOI: 10.1002/esp.3225

Ryan, S.E., Bunte, K., and Potyondy, J.P. (2005a). Breakout Session II: Bedload Transport Measurements, Data Uncertainty, and New Technologies. Proceedings of the Federal Interagency Sedimentation Monitoring Instrument and Analysis Workshop, September 9-11, 2003, Flagstaff, Arizona, J.R. Gray (ed.). USGS Survey Circular 1276, pp 16-28. http://water.usgs.gov/pubs/circ/2005/circ1276/

Ryan S.E., Porth, L.S., and Troendle, C.A. (2005b). "Coarse sediment transport in mountain streams in Colorado and Wyoming, USA," Earth Surface Processes and Landforms, 30(3), pp 269-288. DOI: 10.1002/esp.1128

Schneider, J.M., Rickenmann, D., Turowski, J.M., Bunte, K., Kirchner, J.W. (2015). "Applicability of bedload transport models for mixed size sediments in steep streams considering macro-roughness," Water Resources Research, in revision.

Schoklitsch, A. (1962). Handbuch des Wasserbaus. [Handbook of Hydraulic Engineering.]. Springer Verlag, Wien.

Yang, G., Chen, Z., Yu, F., Wang, Z., Zhao, Y., and Wang Z. (2007). "Sediment rating parameters and their implication: Yangtze River, China," Geomorphology, 85, pp 166-175.

Yu, G., Wang, Z., Zhang, K., Chang T., and Liu, H. (2009). "Effect of incoming sediment on the transport rate of bed load in mountain streams," International Journal of Sediment Research, 24(3), pp 260–273.

IDENTIFYING SEDIMENT SOURCES IN THE SEDIMENT TMDL PROCESS

Gellis, A.C., Research Geomorphologist, U.S. Geological Survey, Maryland-Delaware-DC, Water Science Center, agellis@usgs.gov; Fitzpatrick, F.A., Research Hydrologist, U.S. Geological Survey, Wisconsin Water Science Center, fafitzpa@usgs.gov; Schubauer-Berigan, J.P., Chief, Environmental Stressors Management Branch, National Risk Management Research Laboratory, EPA, Cincinnati, Ohio, Schubauer-Berigan.Joseph@epa.gov; Landy, R.B., ORD Regional Science Liaison to Region III, EPA Region III Environmental Science Center, Fort Meade, Maryland, Landy.Ronald@epa.gov; and Gorman-Sanisaca, L., Physical Scientist, U.S. Geological Survey, Maryland-Delaware-DC Water Science Center, gormansanisaca@usgs.gov

ABSTRACT

Sediment is an important pollutant contributing to aquatic-habitat degradation in many waterways of the United States. This paper discusses the application of sediment budgets in conjunction with sediment fingerprinting as tools to determine the sources of sediment in impaired waterways. These approaches complement monitoring, assessment, and modeling of sediment erosion, transport, and storage in watersheds. Combining the sediment fingerprinting and sediment budget approaches can help determine specific adaptive management plans and techniques applied to targeting hot spots or areas of high erosion.

INTRODUCTION

In 2014, both sediment and turbidity were the second leading cause, after pathogens, of impairment of U.S. waterways (EPA, 2014). Typically, the sediment size class of concern is fine-grained silts and clays, which can degrade habitat, affect water supply intakes and reservoirs, and often carry pollutants of concern (Larsen et al., 2010).

When a stream is identified as impaired by sediment, the Clean Water Act requires states to develop numeric targets that describe the maximum amount of pollutants that a water body can receive over time, known as the "total maximum daily load" (TMDL). As part of the sediment TMDL protocol, the EPA requires that the sources of the sediment be determined (EPA, 1999). Many of the approaches used by states to identify sediment sources involve the use of models (EPA, 2008) or assessment tools such as the Watershed Assessment of River Stability and Sediment Supply (WARSSS) (Rosgen, 2006) and the Generalized Watershed Loading Functions (GWLF) (Haith et al., 1992). The TMDL Technical Advisory Group (TAG) was formed, consisting of scientists from universities, Federal and State agencies, and non-governmental organizations, to provide guidance.

In a 2002 review of sediment TMDLs in Georgia (EPA Region IV) 2 by the TAG (Keyes and Radcliffe, 2002), the following recommendations were made:

- A carefully crafted inventory of the potential sediment sources and pathways by which sediment enters the water body should be developed.
- To the greatest extent possible, problem identification should be based on currently available information, including water-quality monitoring data, watershed analyses, information from the public, and any existing watershed studies.

- It is also critical to have a thorough understanding of the relative contribution from various sediment sources. It is highly recommended that thorough onsite watershed surveys be conducted.
- Follow-up monitoring is a key component of the TMDL process and should be emphasized in the Phase 1 TMDLs.

Sediment is considered a nonpoint source pollutant when it originates from diffuse sources such as construction sites, crop and forest lands, and eroding streambanks (EPA, 2012). In a review of TMDL implementation, which included sediment, the U.S. Government Accountability Office (USGAO, 2013) reported that long-established TMDLs were not helpful for attaining reductions in nonpoint source pollution. In Pennsylvania, of the nearly 1,000 parts of water bodies identified as impaired by sediment, only two have been restored (USGAO, 2013).

These reviews clearly indicate a need for effective sediment-source identification in the TMDL process. In this paper, we describe combining sediment budgets and sediment fingerprinting, and present findings from a case study to demonstrate the effectiveness of sediment-source identification. The approaches we discuss are field efforts that may accompany modeling efforts to identify sediment sources supporting the TMDL process. These methods are part of a larger protocol for identifying sediment sources that is under development by the authors for EPA Regions III and V.

SEDIMENT-SOURCE INVENTORY

Sediment sources in any given watershed vary with location and time. In general, sediment sources can be divided into two broad categories: (1) upland sediment sources, and (2) channel sediment sources. Upland sediment sources include various land-use and land-cover types: forest, cropland, pasture, construction sites, roads, etc. Channel sediment sources can include the streambanks, beds, flood plain, and gullies. It is important to apportion sediment derived from uplands versus channels because sediment reduction strategies differ by source and require different management approaches. For example, reducing sediment loads from agricultural sources might require soil conservation and tilling practices, whereas channel sources might require streambank stabilization.

Erosion on upland surfaces can occur though sheetwash, rilling, gullying, and mass movements. Periods of heavy rain that lead to saturation excess overland flow or infiltration excess overland flow can mobilize and erode upland sediment. Streambanks erode during high flows, from mass wasting, and as a result of freeze and thaw activity in cold climates. The channel bed can be a source of sediment in incising channels. However, fine-grained sediment from channel beds has not traditionally been considered a sediment source, since in the absence of significant channel incision, sediment mobilized from the channel bed is typically thought to represent temporary storage of sediment originating from upstream sources (Gellis et al., 2009).

SEDIMENT BUDGET

The sediment budget approach quantifies the erosion, deposition, and storage of upland and channel elements in a watershed. A sediment budget can be presented as an equation:

$$I + \Delta S = O \quad (1)$$

Where I is the sediment input, ΔS is the change in sediment storage, and O is the sediment output.

The steps to generate a sediment budget for a given watershed are:

1. Choose the watershed scale of interest for the sediment budget.
2. Distinguish a time period of interest for the sediment budget.
3. Determine the geomorphic elements contributing to (I) or storing sediment (ΔS).
4. Ascertain what size sediment class is to be budgeted.
5. Determine approaches to quantify steps 1 through 4 (Table 1)
6. Define the watershed output (O) point and approaches to quantify sediment transported out of the watershed (Table 1).
7. Estimate or measure I, ΔS, and O over desired time period.
8. Extrapolate measurements of I and ΔS to the entire watershed to obtain a volume.
9. Using the density of soil or sediment representative of each geomorphic element, convert volume measurements from step 8 to a mass per unit time.
10. Sum mass per unit time values from step 9 for each geomorphic element and compare the results to the output (O).
11. Communicate results and provide error analysis.

In the first two steps of sediment budgeting, initial decisions on spatial and temporal scales of interest are made that will influence the design of the sediment budget. These scales will be determined by the management questions of interest. The watershed scale for the sediment budget can range from hillslopes (m^2) to major river basins (>100,000's km^2) (i.e. the Mississippi River). For this paper, it is assumed that small to medium watershed scales of up to hundreds of kilometers are of interest.

Time periods for which the sediment budget is developed can also vary, from single storm events to thousands of years (Reid and Trustrum, 2002). In regions that have had widespread land clearing from agriculture or clearcut logging, long-term time scales are of interest in order to compare
pre- and post-disturbance differences (Knox, 2001; Fitzpatrick and Knox, 2000). Budgets that include flood-plain sedimentation are useful for time scales of decades to centuries (Knox, 2001; Trimble, 1999; Fitzpatrick et al., 2009). For modern sediment budgets that cover a few years, sediment loads are typically measured at the watershed outlet (Gellis and Walling, 2011).

In step 3 of the sediment budget approach, potential sources of sediment can be identified in a watershed using a geographic information system (GIS) analysis, reconnaissance of the entire basin, "riverwalks" or reconnaissance along channels, field experiments, monitoring, and photogrammetric analysis using aerial photographs. Sources of sediment are then defined as a combination of geomorphic elements and human uses (i.e. streambanks, upland cropland, pastured gullies, and forests). Next, the outlet of the watershed is defined and appropriate techniques are used to quantify the sediment transported out of the watershed over a specified period of time (Mg/yr) (Table 1). The sediment size of interest is also decided initially (step 4) and can include all sediment sizes or individual size classes. If both fine and coarse sediment are of interest, watershed outlet measurements need to consider both suspended- sediment load and bedload (Edwards and Glysson, 1999).

Table 1 Examples of approaches and methods used in sediment budgets

Sediment budget element (I = input, S= storage, O=output)	Method	Method is used to quantify	Measurement dimension	Time scale of measurements
Channels (I,S)	Aerial photography airborne light detection and ranging (Lidar)	Channel morphologic changes in channel width, sinuosity, bar formation, and channel patterns (Thoma et al., 2005; Kessler et al., 2013)	m	Years, decades
Channels (I,S)	Surveys	Changes in channel width, depth, and slope (Gellis et al., 2012)	m	Per storm (days) to years
Channels (I,S)	Bank pins; Terrestrial LiDAR	Bank erosion and deposition (Hupp et al., 2009; O'Neal and Pizzuto, 2011; Schenk et al., 2012)	cm, m	Per storm (days) to years
Channels	Rapid geomorphic assessments	Qualitative condition of the erosional/depositional characteristic of the streambanks (Simon and Downs, 1995)	NA	NA
Channels (S)	Stratigraphy	Identification of time horizons (anthropogenic, geologic, radionuclides) to estimate changes in deposition rates (Allmendinger et al., 2007; Trimble, 1983)	cm	Years, decades, millennia
Channels (I,S)	Scour chains	Quantify change on the channel bed (Leopold et al., 1966)	cm	Days to years
Flood-plain Deposition (S)	Feldspar Pads	Flood-plain deposition rates (Hupp et al., 2008)	mm	Per storm (days) to years
Uplands (I,S,O)	Lake/Pond surveys using ^{137}Cs	Sediment loads and sediment yields, and changes in sedimentation over time (Gellis et al., 2006)	kg/m^2	Years, decades
Uplands (I,S)	^{137}Cs	Upland erosion and deposition rates (Gellis et al., 2009; Walling and He, 1999)	tons/hectare	Decades (50 yrs)
Uplands (I)	Sediment traps	Sediment yield (Gellis et al., 2012)	kg/m^2	Per storm (days) to years
Uplands (I,S)	Pins (nails)	Land-surface erosion (Gellis et al., 2012)	cm	Per storm (days) to years
Uplands (I)	Nets, silt fences	Erosion and sediment yield (Robichaud and Brown, 2002)	kg/m^2	Days to years
Uplands (I)	Aerial photographs	Qualitative description of areas that may contribute sediment (agriculture, mining, landslides, roads, etc.) (Reid and Dunne, 1996)	NA	NA
Uplands (I,S)	Dendro-chronology	Coring trees and counting rings to determine deposition and erosion rates (Hupp and Bazemore, 1993; Allmendinger et al., 2007)	cm	Decades
Uplands (I)	Eolian traps	Quantify eolian deposition (Gellis et al., 2012)	g	Years
Uplands (I) and Channels (I)	Multiple geochemical fingerprints	Quantify the contribution of sediment from source areas (Walling et al., 2008; Gellis and Walling, 2011)	%	Days to years
Sediment transport (O)	Collection of suspended sediment and bedload	Sediment loads (Gellis et al., 2006, 2012)	kg	Per storm (days), years to decades

The erosion and storage of sediment is determined for each geomorphic element (step 7) over the measurement period using the approaches outlined in Table 1. Most of the measurements in Table 1 produce linear (cm) or cross sectional area (cm^2) rates of change that are extrapolated

for each geomorphic element (step 8) over the entire watershed to obtain a volume (m^3) which is then converted to mass (kg) using the density (g/cm^3) of eroded/deposited sediment. Extrapolation can be performed using different independent variables, including, but not limited to, stream order, stream type, landscape feature, geomorphic landform, and geologic areas (Fitzpatrick and Knox, 2000; Fitzpatrick et al., 2009; Gellis et al., 2012). For example, bank pins might be used to measure erosion or deposition in centimeters. Erosion and deposition are then averaged for a bank face (cm) to obtain an area of bank change (cm^2). This value is extrapolated to a channel length (m) representative of that bank (i.e. stream order) to obtain a volume of bank change (m^3). Finally, mass (kg) is obtained by multiplying the density of the bank sediment (g/cm^3) by the volumetric change (m^3). Density can be measured by inserting core samplers of known volumes into the streambank.

For 30- to 50-m high valley bluff failures along tributaries to Lake Superior, aerial photograph analyses of bluff retreat rates, along with field measurements of bluff retreat, length, height, and stratigraphy, were used to determine that the bluffs were a major source of the eroded sediment that was causing burial and scouring of spawning gravels downstream (Fitzpatrick and Knox, 2000; Fitzpatrick et al., 2014). Flood-plain cores and interpreted sedimentation rates were extrapolated over appropriate areas based on geomorphic landform and cultural features such as bridges, railroads, and levees that influence the distribution of sediment deposition during floods (Fitzpatrick et al., 2009).

The erosion and deposition of each geomorphic element is summed and values are compared to the sediment measured at the outlet (step 10). Theoretically, all sediment inputs and storage terms should balance to the output (Eq. 1), however, this rarely happens (Kondolf and Matthews, 1991). Kondolf and Matthews (1991) reported imbalances > 100% of the total sediment output. The error represents the cumulative uncertainty of measurements and estimates over the range of both spatial and temporal scales. Error analysis can be performed by displaying the range of sediment budget results on each geomorphic element as confidence intervals around the mean (i.e. 10^{th} and 90^{th} percentiles).

Results from a sediment budget analysis can be presented as maps, diagrams, and tables (Fitzpatrick et al., 2009). Areas of high erosion, defined using the sediment-budget approach, can be portrayed in these ways to improve communication of the results and, subsequently, inform targeted management actions.

SEDIMENT FINGERPRINTING

Sediment fingerprinting identifies the source contribution of sediment delivered to a point in the watershed. The approach entails the identification of specific sources of sediment through the establishment of a minimal set of physical and/or chemical properties, i.e. fingerprints or tracers that uniquely define each source in the watershed. Tracers that have successfully been used as fingerprints include mineralogy (Motha et al., 2003), radionuclides (Walling and Woodward, 1992; Collins et al., 1997), trace elements (Devereux et al., 2010), magnetic properties (Slattery et al., 2000), and stable isotope ratios ($^{13}C/^{12}C$ and $^{15}N/^{14}N$) (Papanicolaou et al., 2003).

By comparing the tracers of the target sediment to the tracers of the source samples, and using a statistical "unmixing" model, the sources of the target sediment can be apportioned (Gellis and Walling, 2011). Target sediment can be deposited (bed sediment or flood-plain sediment) or transported (suspended sediment). Because tracer activity is largely found on fine sediment,

sediment fingerprinting is typically conducted on sediment less than 63 microns in diameter (Gellis and Walling, 2011).

Sediment sources in sediment fingerprinting are typically the same sources accessed in the sediment budget. In sediment fingerprinting, sediment samples from upland areas (i.e. agriculture, forests, and construction sites) are collected from the top 1.0 cm of the soil surface with a plastic hand shovel. A plastic shovel is used to protect the sample from metal contamination. To account for variability in tracer properties, sediment is collected across transects and composited. A representative sample of the streambank is collected 1 cm into the vertical bank and along the entire bank. Three to five transects spaced 10 m apart along the stream reach are sampled and composited into one sample.

Several statistical procedures are used to identify the optimum set of properties that will be used in the final composite fingerprint to distinguish the potential sources and establish their relative contribution to the sediment flux at the watershed outlet (Figure 1). The goal is to determine those properties that clearly identify the potential sources and to select a small subset that optimizes the discrimination provided by the composite fingerprint. The statistical steps outlined in Figure 1 were run using the free software statistical package R (R Core Team, 2013) from a Microsoft Access database platform*. Field data are entered into the database and the program guides the user through the necessary statistical procedures to produce relative source contribution results and an error analysis.

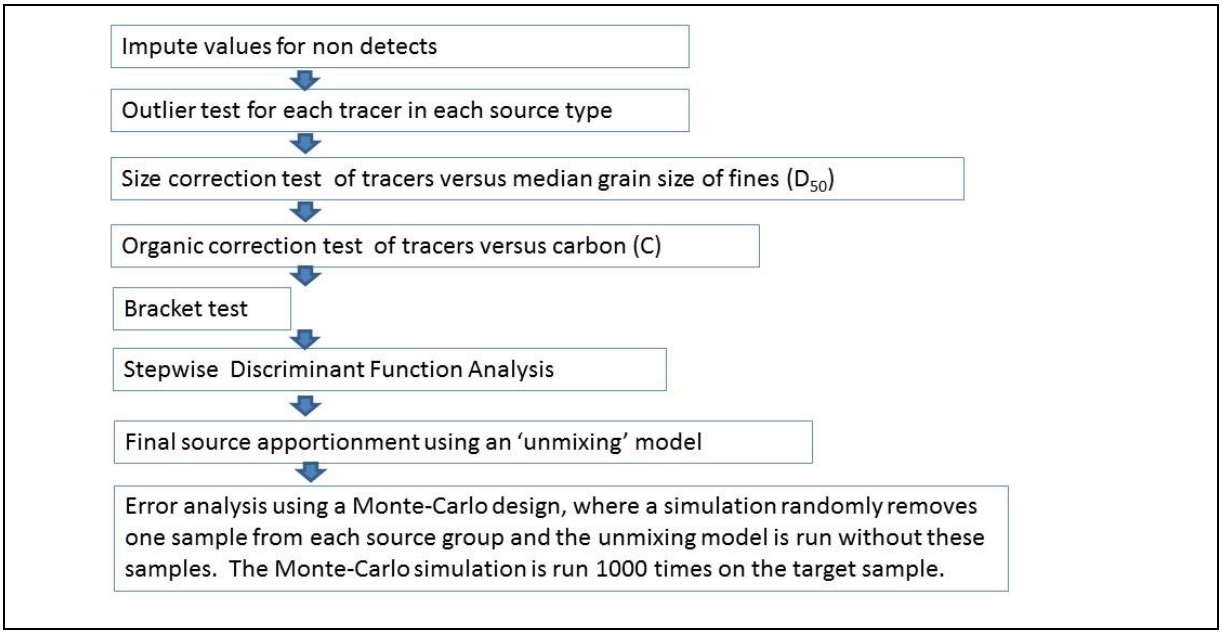

Figure 1 Statistical steps used to apportion sediment in the sediment-fingerprinting approach (From Gellis and Noe, 2013).

* Any use of trade, firm, or product names is for descriptive purposes only and does not imply endorsement by the U.S. Government.

The sediment-fingerprinting approach provides an apportionment of the sources of sediment but it does not provide quantification of the rate of erosion, overall mass of delivered sediment, or target "hotspots" of erosion. For example, sediment fingerprinting may indicate that the streambanks are a major source of sediment in a watershed, but areas with the highest rates of bank erosion cannot be identified using the sediment fingerprinting approach. The sediment budget approach, however, can help target prominent sources of erosion. Erosion and deposition results from the sediment budget can be combined with the sediment fingerprinting results and provide information on sediment delivery ratios (SDRs; the amount of delivered sediment to the amount of eroded sediment) (Gellis and Walling, 2011).

CASE STUDY – Linganore Creek, Maryland

Linganore Creek, Maryland is an example of a source-identification study where both the sediment budget and sediment fingerprinting approaches were used to determine the significant sources of fine-grained sediment between 2008 and 2010 (Figure 2) (Gellis and Noe, 2013; Gellis et al., 2014). Linganore Creek drains 147 km^2 of agricultural (62%) and forested (27%) land in the Piedmont Physiographic Province of the Chesapeake Bay watershed. Sediment budget results indicated that the greatest mass of sediment was eroded from agricultural lands, followed by streambanks and forests. Sediment storage areas included flood plains and farm ponds. The final sediment budget for Linganore Creek expressed as equation 1 is shown in Table 2.

During the period of study, 194 suspended-sediment samples were collected over 36 storm events and were used to determine their sources using the sediment fingerprinting approach. Samples were collected from 40 streambanks, 24 agricultural areas (cropland and pasture), and 19 forested sites. According to the sediment fingerprinting results, agricultural lands contributed 45% of the total fine-grained sediment transported out of the watershed, streambanks contributed 52% and forests contributed 3%. Combining the sediment fingerprinting results with the sediment budget approach indicated that 96% of the eroded agricultural sediment went into storage resulting in a SDR of 4%; 56% of the eroded streambanks went into storage with a SDR of 44% ; and 92 percent of eroded forest sediment went into storage with a SDR of 8 percent. Important storage sites of sediment included ponds, which stored 15 percent and flood plains, which stored 8 percent of all eroded sediment (6.33 x 10^7 kg/yr).

Management Implications

The sediment fingerprinting results indicated that the two main sources of fine-grained sediment delivered out of the Linganore Creek watershed were streambanks (52 %) and agricultural land (45 %). With a higher SDR for streambanks (44 %) compared to agricultural land (4 %), management actions implemented to reduce fine-grained sediment export out of the Linganore Creek watershed may be more effective if they are directed at stabilizing eroding streambanks. In addition, it would be informative to determine the geomorphic agent responsible for the erosion, such as increased runoff. These additional geomorphic insights can help to guide specific treatments for bank erosion within a broader adaptive management plan.

Table 2 Final annual fine-grained (<0.063 mm) sediment budget for Linganore Creek, Maryland, 2008-10. [Negative values in the sediment budget indicate erosion and positive numbers indicate deposition. The output of sediment was determined from the average annual suspended-sediment load computed for Linganore Creek near Libertytown, Maryland, 2008-2010 (USGS Station ID 01642438).]

	***I* (Mg)**	**ΔS (Mg)**	***O* (Mg)**
Agriculture (pasture + cropland)	-54,800		
Forest	-2,030		
Streambanks	-6,440	1,040	
Channel Bed	80	780	
Flood Plains		5,180	
Farm Ponds		9,320	
Unaccounted for sediment in budget		41,600	
Suspended sediment export at sediment station			-5,450

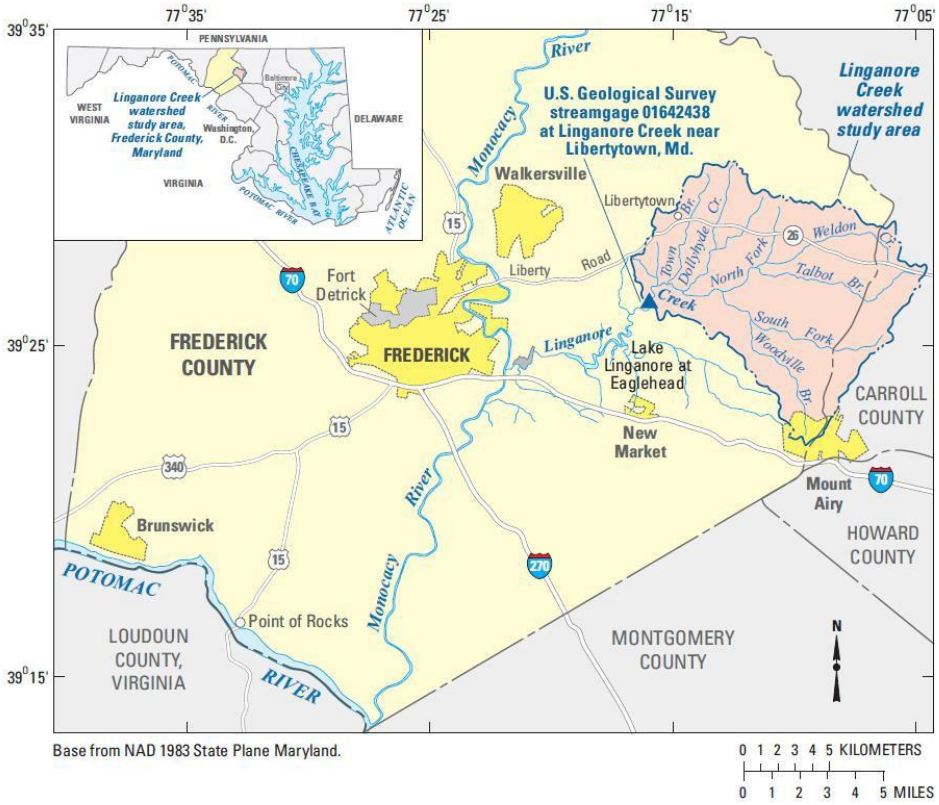

Figure 2 Location of Linganore Creek study area, Maryland.

Understanding sediment storage can be just as important as knowing where the erosion is occurring because sediment deposition influences the delivery and transport of fine-grained sediment to the measured outlet. Impoundments and flood plains were important sites of sediment storage in Linganore Creek. The ponds were estimated to store 9,320 Mg/yr of fine-grained sediment, which was 15 percent of the total eroded sediment. The estimated amount of sediment deposited on flood plains was 5,180 Mg/yr, or 8 percent of the total eroded sediment.

SUMMARY

Sediment is one of the leading causes of surface-water impairment in the United States. Two complementary approaches, sediment fingerprinting and sediment budgets, can be integrated to identify significant sources and sinks of fine-grained sediment in the sediment TMDL assessment process. These approaches can be used in addition to monitoring and assessment, as well as modeling of sediment erosion, transport, and storage in watersheds. Sediment fingerprinting determines the relative source contributions of fine-grained suspended sediment delivered out of a watershed, whereas the sediment budget approach utilizes measurements and estimates to quantify the erosion and deposition of sediment on various geomorphic elements throughout the watershed (streambanks, flood plains, channel beds, specific tributaries or land uses, and upland areas). In combination, these two approaches can help develop adaptive management plans and techniques that target specified hot spots.

REFERENCES

Allmendinger, N.E., Pizzuto, J.E., Moglen, G.E., and Lewicki, M. (2007). A sediment budget for an urbanizing watershed, 1951-1996, Montgomery County, Maryland, U.S.A.: Journal of the American Watershed Association, v. 43, no. 6, p. 1483-1498, doi: 10.1111/j.1752-1688.2007.00122.x

Collins, A.L., Walling, D.E., and Leeks, G.J.L. (1997). Sediment sources in the Upper Severn catchment -- a fingerprinting approach: Hydrology and Earth System Sciences, v. 1, no. 3, p. 509–521.

Devereux, O.H., Prestegaard, K.L., Needelman, B.A., and Gellis, A.C. (2010). Suspended-sediment sources in an urban watershed, Northeast Branch Anacostia River, Maryland: Hydrological Processes, v. 24, no. 11, p. 1391-1403.

Edwards, T.K., and Glysson, G.D. (1999). Field methods for measurement of fluvial sediment: U.S. Geological Survey Techniques of Water-Resources Investigations, Book 3, Chapter C2, 89 p.

Fitzpatrick, F.A., and Knox, J.C. (2000). Spatial and temporal sensitivity of hydrogeomorphic response and recover to deforestation, agriculture, and floods: Physical Geography, v. 21, no. 2, p. 89–108.

Fitzpatrick, F.A., Knox, J.C., Schubauer-Berigan, J.P. (2009). Channel, floodplain, and wetland responses to floods and overbank sedimentation, 1846–2006, Halfway Creek Marsh, Upper Mississippi Valley, Wisconsin: in James, L.A., Rathburn, S.L., and Whittecar, G.R., eds., Management and Restoration of Fluvial Systems with Broad Historical Changes and Human Impacts, Geological Society of America Special Paper 451, p. 23–42.

Fitzpatrick, F.A., Peppler, M.C., Saad, D.A., Pratt, D.M., and Lenz, B.N. (2014). Geomorphic, flood, and groundwater-flow characteristics of Bayfield Peninsula streams, Wisconsin, and implications for brook-trout habitat: U.S. Geological Survey Scientific Investigations Report 2014-5007, 79 p.

Gellis, A.C., and Walling, D.E. (2011). Sediment-source fingerprinting (tracing) and sediment budgets as tools in targeting river and watershed restoration programs: Simon, A., Bennett, S.., Castro, J.M., eds., Stream Restoration in Dynamic Fluvial Systems: Scientific Approaches, Analyses, and Tools, American Geophysical Union Monograph Series 194, p. 263-291.

Gellis, A.C., and Noe, G.B. (2013). Sediment source analysis in the Linganore Creek watershed, Maryland, USA, using the sediment fingerprinting approach: 2008 to 2010: In Mukundan, R., and Gellis, A.C., (eds.), Watershed Sediment Source Identification: Tools, Approaches, and Case Studies, Special issue of the Journal of Soils and Sediments, v. 13, p.1735-1753.

Gellis, A.C., Webb, R.M.T., Wolfe, W.J., and McIntyre, S.C.I. (2006). Changes in Land Use and Reservoir Sedimentation: A Case Study in the Lago Loiza Basin, Puerto Rico: Physical Geography, v. 27, no. 1, p. 39-69.

Gellis, A.C., Hupp, C.R., Pavich, M.J., Landwehr, J.M., Banks, W.S.L., Hubbard, B.E., Langland, M.J., Ritchie, J.C., and Reuter, J.M. (2009). Sources, Transport, and Storage of Sediment at Selected Sites in the Chesapeake Bay Watershed: Scientific Investigations Report 2008-5186, 95 p.

Gellis, A.C., Pavich, M.J., Ellwein, A.L., Aby, S., Clark, I., Wieczorek, M.E., and Viger, R. (2012). Erosion, Storage, and Transport of Sediment in Two Subbasins of the Rio Puerco, New Mexico: Geological Society of America Bulletin, v. 124; no. 5/6; p. 817–841.

Gellis, A.C., Noe, G.B., Clune, J.W., Myers, M.K., Hupp, C.R., Schenk, E.R., and Schwarz, G.E. (in press). Sources of Fine-Grained Sediment in the Linganore Creek Watershed, Frederick and Carroll Counties Maryland, 2008-10: U.S. Geological Survey Scientific Investigations Report 2014-5147.

Haith, D. A., Mandel, R., and Wu, R. S. (1992). Generalized Watershed Loading Functions Version 2.0 User's Manual, Department of Agricultural and Biological Engineering, Cornell University, Cornell University, Ithaca, New York, 62 p. (http://www.mapshed.psu.edu/Downloads/GWLFManual.pdf; last accessed Dec 16, 2014).

Hupp, C.R., and Bazemore, D.E. (1993). Temporal and Spatial Patterns of Wetland Sedimentation—West Tennessee: Journal of Hydrology, v. 14, p. 179-196.

Hupp, C. R., Demas, C. R., Kroes, D. E., Day, R. H., and Doyle, T. W. (2008). Recent sedimentation patterns within the central Atchafalaya Basin, Louisiana: Wetlands, v. 28, p. 125–140.

Hupp, C. R., Schenk, E. R., Richter, J. M., Peet, R. K., and Townsend, P. A. (2009). Bank erosion along the dam-regulated lower Roanoke River, North Carolina: In Management and Restoration of Fluvial Systems with Broad Historical Changes and Human Impacts, Geological Society of America Special Papers 451, James, L. A., Rathburn, S. L., and Whittecar, G. R., eds., p. 97–108, Geological Society of America, Boulder, Colorado. doi:10.1130/2009.2451(06).

Kessler, A.C., Gupta, S.C., and Brown, M.K. (2013). Assessment of river bank erosion in Southern Minnesota rivers post European settlement: Geomorphology, http://dx.doi.org/10.1016/j.geomorph.2013.07.006.

Keyes, A. M., and Radcliffe, D. (2002). A protocol for establishing sediment TMDLs: Prepared for the Georgia Conservancy and the University of Georgia Institute of Ecology, Athens and Atlanta, Georgia, found at http://soilphysics.uga.edu/media/ProtocolForEstablishingSedimentTMDLs.pdf; accessed December 12, 2014.

Knox, J.C. (2001). Agricultural influence on landscape sensitivity in the Upper Mississippi River Valley: Catena 42:193-224.

Kondolf, G.M., and Matthews, W.V.G. (1991). Unmeasured residuals in sediment budgets: A cautionary note: Water Resources Research, v. 27, p. 2483-2486.

Larsen, M.C., Gellis, A.C., Glysson, G.D., Gray, J.R., and Horowitz, A.J. (2010). Fluvial sediment in the environment: a national problem: in Proceedings, 2nd Joint Federal Interagency Conference, Las Vegas, Nevada, June 27 – July 1, 2010, available at http://acwi.gov/sos/pubs/2ndJFIC/Contents/OS_Larsen_9fisc_sediment_vision_3_4_2010.pdf, 15p.

Leopold, L.B., Emmett, W.W., and Myrick, R. M. (1966). Channel and hillslope processes in a semiarid area, New Mexico, U.S. Geological Survey Professional Paper 352G, 243 p.

Motha, J.A., Wallbrink, P.J., Hairsine, P.B., Grayson, R.B. (2003). Determining the sources of suspended sediment in a forested catchment in southwestern Australia: Water Resources Research, v. 39, p. 1056.

O'Neal, M.A., and Pizzuto, J.E. (2011). The Rates and Spatial Patterns of Annual Riverbank Erosion Revealed Through Terrestrial Laser Scanner Surveys of the South River, VA: Earth Surface Processes and Landforms, v. 36, no. 5, p 695-701.

Papanicolaou, A.N., Fox, J.F., and Marshall, J. (2003). Soil fingerprinting in the Palouse Basin, USA using stable carbon and nitrogen isotopes: International Journal of Sediment Research, v. 18, no.2, p. 291–297.

R Core Team (2013). R -- A language and environment for statistical computing: R Foundation for Statistical Computing, Vienna, Austria, http://www.R-project.org/, last accessed October 28, 2014.

Reid, L., and Dunne, T. (1996). Rapid evaluation of sediment budgets: Catena Verlag GMBH. Reiskirchen, Germany, 164 p.

Reid, L.M., and Trustrum, N.A. (2002). Facilitating sediment budget construction for land management applications: Journal of Environmental Planning and Management, v. 45, no. 6, p. 865–887.

Robichaud, P.R., and Brown, R.E. (2002). Silt fences-- an economical technique for measuring hillslope soil erosion: U.S. Department of Agriculture, General Technical Report RMRS-GTR-94, Forest Service, Rocky Mountain Research Station, Fort Collins, CO., 24 p.

Rosgen, D. (2006). Watershed assessment of river stability and sediment supply (WARSS): Wildland Hydrology, Fort Collins, CO, 648 p.

Schenk, E. R., Hupp, C. R., Gellis, A., and Noe, G. (2012). Developing a new stream metric for comparing stream function using a bank–floodplain sediment budget: a case study of three Piedmont streams: Earth Surface Processes and Landforms, v. 38, no. 8, p. 771-784.

Simon, A., and Downs, P.W. (1995). An interdisciplinary approach to evaluation of potential instability in alluvial channels: Geomorphology, v. 12, no. 3, p. 215-232.

Slattery, M.C., Walden, J., and Burt, T.P. (2000). Fingerprinting suspended sediment sources using mineral magnetic measurements—A quantitative approach: In: Foster, I., ed., Tracers in geomorphology, John Wiley and Sons, New York, p 309–322.

Thoma, D.P., Gupta, S.C., Bauer, M.E., Kircjhoff, C.E. (2005). Airborne laser scanning for riverbank erosion assessment: Remote Sensing of Environment, v. 95, p. 493–501.

Trimble, S. W. (1983). A Sediment Budget for Coon Creek Basin in the Driftless Area, Wisconsin, 1853-1977: American Journal of Science, v. 283, no. 5, p. 454-474.

Trimble, S.W. (1999). Decreased rates of alluvial sediment storage in the Coon Creek Basin, Wisconsin, 1975-93: Science, v. 285, no. 5431, p. 1244–1246.

United States Environmental Protection Agency (EPA) (1999). Protocol of developing sediment TMDLs: United States: Environmental Protection Agency, EPA-841-B-99-004.

United States Environmental Protection Agency (EPA) (2008). Handbook for Developing Watershed Plans to Restore and Protect Our Waters: United States Environmental Protection Agency, Office of Water Nonpoint Source Control Branch, Report EPA 841-B-08-002, 13 chapters.

United States Environmental Protection Agency (EPA) (2012). What is Nonpoint Source Pollution?: US EPA, Pollution Prevention and Control, Polluted Runoff, found at http://water.epa.gov/polwaste/nps/whatis.cfm, last accessed October 25, 2014.

United States Environmental Protection Agency (EPA) (2014) National Summary of Impaired Waters and TMDL Information: EPA, Water Quality Assessment and TMDL Information, Watershed Assessment, Tracking and Environmental Results, found at http://iaspub.epa.gov/tmdl_waters10/attains_nation_cy.control?p_report_type=T, last accessed October 25, 2014.

United States Government Accountability Office (USGAO) (2013). Clean Water Act Changes Needed If Key EPA Program Is to Help Fulfill the Nation's Water Quality Goals Report to Congressional Requesters: GAP Report GAO-14-80, 103 p. Available at http://www.gao.gov/assets/660/659496.pdf; last accessed October 25, 2014.

Walling, D. E., and He, Q. (1999). Improved models for estimating soil erosion rates from 137 Cs measurements: Journal of Environmental Quality, v. 28, p. 611–622.

Walling D.E., and Woodward J.C. (1992). Use of radiometric fingerprints to derive information on suspended sediment sources, in erosion and sediment transport monitoring programmes in river basins: Proceedings of the Oslo Symposium, August 1992: IAHS Publication Number 210, p.153–164.

Walling, D. E., Collins, A.L., and Stroud, R. W. (2008). Tracing suspended sediment sources and particulate phosphorous sources in catchments: Journal of Hydrology, v. 350, no. 3–4, p. 274–289.

PROGRESS ON DAM REMOVAL ANALYSIS GUIDELINES FOR SEDIMENT

Timothy J. Randle, Supervisory Hydraulic Engineer, Bureau of Reclamation, Denver, Colorado, trandle@usbr.gov and Jennifer A. Bountry, Hydraulic Engineer, Bureau of Reclamation, Denver, Colorado, jbountry@usbr.gov

INTRODUCTION

The Subcommittee on Sedimentation (SOS) recognizes that dam removal has become somewhat common in the United States as dams age and environmental values increase. American Rivers estimates that nearly 1,150 dams that have been removed in the United States between 1912 and 2013 (http://www.americanrivers.org/initiatives/dams/faqs/), with most dam removals occurring after 1980. Sediment management can be an important component of some dam removals, but there are no commonly accepted methods to assess the level of risk to river-related resources associated with the sediment stored behind dams. Therefore, SOS began sponsoring an effort in 2008 to develop the Dam Removal Analysis Guidelines for Sediment. This project only provides technical guidance and makes no endorsement on the merits of dam removal.

The process began by convening two technical workshops of invited experts from Federal agencies, universities, consultants and non-governmental organizations: October 14–16, 2008 in Portland, Oregon and October 27–29, 2009 in State College, Pennsylvania. The second workshop tested the guidelines on actual case studies. Preliminary results from this effort were presented at the 9th Federal Interagency Sedimentation Conference (Randle et al., 2010). At the time of this preliminary work, available literature was sparse and nearly all of the removed dams were small with just three notable exceptions:

- The 12-foot high Stronach Dam on the Pine River in Michigan, USA was removed between 1997 and 2003 and the reservoir contained 1 million yd^3 of sediment (Burroughs et al., 2009).
- The 50-foot high Marmot Dam on the Sandy River in Oregon, USA was removed in 2007 and the reservoir contained 0.95 million yd^3 of sediment (Major et al., 2012).
- The 28-foot high Milltown Dam on the Clark Fork River in western Montana, USA was removed in 2008 and the reservoir contained 6.6 million yd^3 of sediment (Wilcox et al., 2008).

Since 2010, two other large dam removal projects were completed:

- The Elwha River Restoration Project on the Elwha River, Washington, USA included the concurrent removal of the 105-foot high Elwha Dam and 210-foot high Glines Canyon Dam between September 2011 and August 2014 (Bountry et al., 2015). The combined reservoir sediment volume of 27-million yd^3 was the largest ever associated with a dam removal project.
- The 125-foot high Condit Dam on the White Salmon River, Washington, USA, was suddenly breached on 26 October 2011 and the reservoir contained 2.4 million yd^3 of sediment (Wilcox et al., 2014).

A great deal more was learned from these large projects and associated recent literature about phased dam removal, cases where there is still a significant reservoir pool, timing of dam

removal relative to seasonal hydrology, channel evolution in the reservoir sediments, and downstream transport (Wildman and MacBroom, 2005; Cannatelli and Curran, 2012; Sawaske and Freyberg 2012; Ferrer-Boix, 2014; East et al., 2015; Gelfenbaum et al., 2015; Magirl et al., 2015; Randle et al., 2015; Warrick et al., 2015). For example, phased dam removal can have significant control on the rate and extent of reservoir sediment erosion downstream sediment release. The actual hydrology, during and after dam removal, can affect the amount, rate, and timing of reservoir sediment erosion. The Dam Removal Analysis Guidelines for Sediment will now be completed using this new and important information.

GUIDELINE APPLICATION

The primary theme of the guideline is to link the amount of recommended pre-project data collection, analysis, and modeling to the risk associated with potential impacts from the reservoir sedimentation. The risk is defined as the product of the probability of impact and the consequence of impact. The greater the risk, the greater the recommended level of data collection, analysis, and modeling. The risk is intended to be a qualitative analysis in collaboration with technical experts, stakeholders and resource managers. The risk may be evaluated within the reservoir landscape or along the river channel upstream and downstream from the reservoir. For the purposes of this guideline, the reservoir sediment volume, relative to the annual sediment load or transport capacity of the river, is used as a surrogate for the probability of impact from releasing sediment as a result of dam removal. If the reservoir sediment contains contaminants above background levels, then the consequence of the potential release of contaminants to the environment will likely determine the level of risk for the project and if reservoir sediment can be released downstream.

In the guideline, the probability of reservoir sediment release is classified as negligible, small, medium, or large depending on the ratio of the reservoir sediment mass (γV_{res}) to the mean annual load or capacity of the river (Q_s):

Negligible Probability $$\frac{\gamma(V_{res})}{Q_s} < 0.1 \quad (1)$$

Small Probability $$0.1 \leq \frac{\gamma(V_{res})}{Q_s} < 1 \quad (2)$$

Medium Probability $$1 \leq \frac{\gamma(V_{res})}{Q_s} < 10 \quad (3)$$

Large Probability $$10 \leq \frac{\gamma(V_{res})}{Q_s} \quad (4)$$

Where the reservoir sediment mass is the product of the unit weight of sediment (γ) and the reservoir sediment volume (V_{res}). The ratios can be computed separately for coarse and fine sediment. For cases of little or no reservoir sediment, the probability and risk are assumed to be negligible and very little data collection and analysis are recommended.

Risk could be calculated by complex numerical analysis, but a more qualitative approach is presented in this guideline where the consequence and risk are categorized as small, medium, or

large. A qualitative risk calculator is presented in Table 1. If the consequence to any of the resources of concern is considered high, then the risk will be either medium or high, depending on the relative reservoir sediment volume.

Table 1 Qualitative risk estimate based on the combination of probability and consequence.

	Consequence of resource impact		
Probability (Fine or Coarse sediment)	**Low**	**Medium**	**High**
Small	Low	Low	Medium
Medium	Low	Medium	High
Large	Medium	High	High +

For the qualitative analysis, a list of potential management concerns and associated sediment-related consequences is generated for the project. Each potential consequence is linked to whether consequence would occur from released coarse reservoir sediment, fine reservoir sediment, or both. For example, the release of an excessive amount of coarse sediment could aggrade the river bed resulting in burial of habitat features, increased flood stage and the potential for stream bank erosion. The release of fine sediment could affect water quality for the aquatic environment and downstream water users, or affect habitat by filling interstitial spaces in downstream riverbed gravels.

Examples of low consequence are where there is no infrastructure or property that could be impacted by the release of reservoir sediment, such as in a canyon reach of river. In addition, there are no threatened or endangered aquatic species that are sensitive to sediment and present at the time and location of impacts. Other examples of low consequence might include natural resources that would benefit from the release of reservoir sediment, such as spawning gravels, recovery of habitat beneath the reservoir, reconnection of the channel with adjacent wetlands and floodplains, or coastal beach restoration.

Medium consequence might include cases where sediment-related impacts would be localized or temporary and such impacts may require mitigation. A medium consequence might also include cases where the consequence is not necessarily low or high.

Examples of high consequences would include streambed aggradation, leading to flooding or erosion of property or infrastructure. High sediment concentrations that would make it very difficult or impossible for water users to obtain water for beneficial uses. Threatened or endangered species that would be irreversibly harmed.

The consequences of an impact depend on the potential effects, regulations, and the perception of stakeholders to resources of concern. The potential concerns of stakeholders needs to be identified to help determine the level of consequences from the release of reservoir sediment upon dam removal. A qualitative judgment may have to be used to estimate the level of

consequence. Public and regulatory perception of the types and magnitude of potential sediment impacts may be greater than the actual impacts. Public education and outreach on hydraulic and sediment processes may be a useful way to help the public understand what the actual sediment effects may be and a collaborative way of determining the level of potential consequences to resources and stakeholders. For example, a medium relative reservoir sediment volume (and medium probability) would have a high level of risk if the consequence(s) were high. Conversely, a medium relative reservoir sediment volume would have a low level of risk if the consequence(s) were low.

For a given dam removal project, there may be a wide range of potential consequences of concern that could range from low to high. For determining the level of data collection, analysis, and modeling, it is recommended to take the highest risk associated with coarse and fine sediment separately. However, it is important to limit the potential consequences to what may actually occur based on the available reservoir volume and particle size gradation (fine versus coarse percentages). For example, Savage Rapids Reservoir near Grants Pass, Oregon had 98% coarse sediment stored in the reservoir with only 2% fine sediment (Bountry et al., 2013). Initially, there was concern about the potential for water quality impacts and release of contaminants. However, for this example, the sediment analysis emphasis was focused on coarse sediment because no contaminants were found above background levels and the fine sediment volume was too small to cause any significant water quality impacts. The types of data collection, analysis, and modeling needed for a high level of risk from coarse reservoir sediment would be different than from fine sediment.

GUIDELINE PROCUDURES

Application of the sediment analysis guidelines is described in the following nine steps:

Reservoir Data Gathering Steps

1. Reconnaissance
2. Characterize reservoir sediment
3. Contaminant assessment

Significance of Reservoir Sediment Volume

4. Determine the relative reservoir sediment volume

Sediment and Dam Removal Alternatives

5. Selection of dam removal and sediment management plan alternatives

Sediment Analysis and Modeling

6. Reservoir and downstream effects analysis

Uncertainty, Monitoring, and Adaptive Management

7. Assess prediction confidence
8. Discussion on sediment effects
9. Develop monitoring and adaptive management plan

An overview of the general guideline steps are presented in Figure 1.

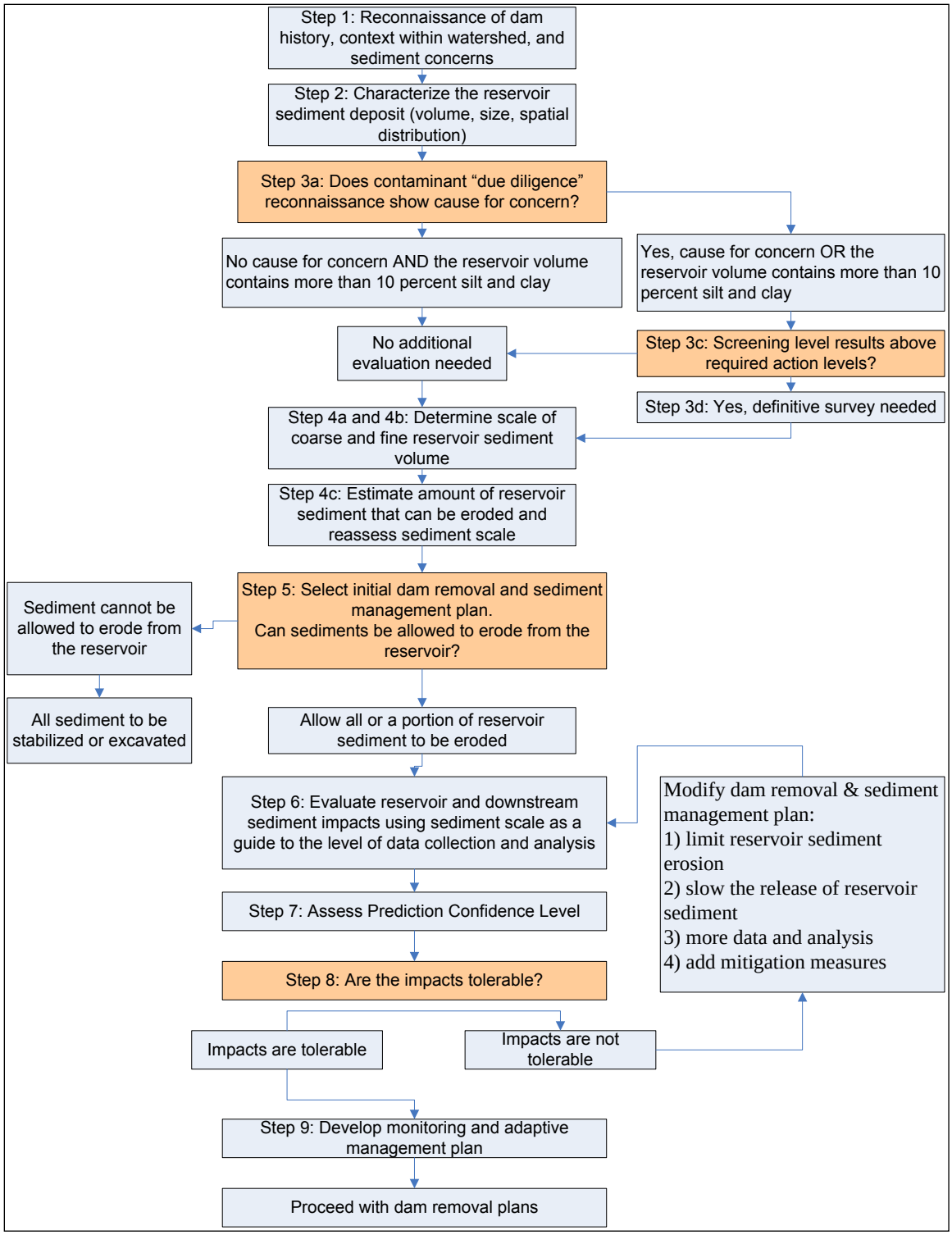

Figure 1 General sediment analysis steps are outlined in a flowchart.

TESTING OF ANALYSIS GUIDELINES

The dam removal sediment analysis guidelines will be tested with data from at least 20 actual dam removals case studies. These case studies will include dams from the eastern, Midwestern, and western United States and include reservoirs with negligible to very large relative sediment volumes.

CONCLUSIONS

The sediment-related impacts of dam removal fundamentally depend on the reservoir sediment characteristics (mass, size gradation, quality, and spatial distribution) and on the extent and rate of reservoir sediment erosion. The level of investigation for sediment impact predictions should be a function of the sediment risk, which is related to the relative reservoir sediment volume or mass.

The next steps to complete the guidelines are listed below:

- Include information from dam removals with large reservoir sediment volumes
- Synthesize results from tested case studies
- Obtain independent peer review
- Obtain approval from Subcommittee on Sedimentation
- Obtain approval from Federal Advisory Committee on Water Information
- Publish guidelines

REFERENCES

Bountry, J.A., Lai, Y.G., Randle, T.J., 2013. Sediment impacts from Savage Rapids Dam removal, Rogue River, Oregon. In: DeGraff, J.V., Evans, J.E. (Eds.), Reviews in Engineering Geology, 21. Geological Society of America, pp. 93–104.

Bountry, J.A.; Crain, P.; Chenoweth, J.; Randle, T.J.; Ritchie, A. (2015). Role of Adaptive Sediment Management in Elwha Dam Removal in Proceedings of the 10th Federal Interagency Sedimentation Conference, Reno, NV, April 20-23.

Burroughs, B.A., Hayes, D.B., Klomp, K.D., Hansen, J.F., Mistak, J. (2009). Effects of Stronach dam removal on fluvial geomorphology in the Pine River, Michigan, United States, Geomorphology 1010, 96-107.

Cannatelli, K.M., Curran, J.C. (2012). Importance of hydrology on channel evolution following dam removal: case study and conceptual model. Journal of Hydraulic Engineering 138(5), 377–390.

East, A.E., Pess, G.R., Bountry, J.A., Magirl, C.S., Ritchie, A.C., Logan, J.B., Randle, T.J., Mastin, M.C., Duda, J.J., Liermann, M.C., McHenry, M.L., Beechie, T.J., Shafroth, P.B., 2015, in press. Large-scale dam removal on the Elwha River, Washington, USA: River channel and floodplain geomorphic change. Geomorphology.

Ferrer-Boix, C., Martín-Vide, J.P., Parker, G., 2014. Channel evolution after dam removal in a poorly sorted sediment mixture: Experiments and numerical model. Water Resources Research 50, doi:10.1002/2014WR015550.

Gelfenbaum, G., Stevens, A.W., Miller, I.M., Warrick, J.A., Ogston, A.S., Eidam, E., 2015, in press. Large-scale dam removal on the Elwha River, Washington, USA: Coastal geomorphic change. Geomorphology.

Magirl C.S., Hilldale, R.C., Curran, C.A., Duda, J.J., Straub, T.D., Domanski, M., Foreman, J.R., 2015, in press. Large-scale dam removal on the Elwha River, Washington, USA: Fluxes of river sediment. Geomorphology.

Major, J.J., O'Connor, J.E., Podolak, C.J., Keith, M.K., Grant, G.E., Spicer, K.R., Pittman, S., Bragg, H.M., Wallick, J.R., Tanner, D.Q., Rhode, A., Wilcock, P.R., 2012. Geomorphic response of the Sandy River, Oregon, to removal of Marmot Dam. U.S. Geological Survey Professional Paper 1792. 64 pp.

Randle, T.J., Bountry, J.A., Blair P. Greimann, B.P. 2010. "Guidelines for Assessing Sediment-Related Effects of Dam Removal," in 9th Federal Interagency Sedimentation Conference, Las Vegas, Nevada, June 27 - July 1, 2010.

Randle, T.J., Bountry, J.A., Ritchie, A., Wille, K., 2015, in press. Large-scale Dam removal on the Elwha River, Washington, USA: Erosion of reservoir sediment. Geomorphology.

Sawaske, S.R., Freyberg, D.L., 2012. A comparison of past small dam removals in highly sediment-impacted systems in the US. Geomorphology 151, 50–58.

Wilcox, A. C., Brinkerhoff, D., & Woelfle-Erskine, C. (2008). Initial geomorphic responses to removal of Milltown Dam, Clark Fork River. In Montana, USA American Geophysical Union Fall Meeting.

Wilcox, A.C., O'Connor, J.E., Major, J.J., 2014. Rapid reservoir erosion, hyperconcentrated flow, and downstream deposition triggered by breaching of 38-m-tall Condit Dam, White Salmon River, Washington. Journal of Geophysical Research: Earth Science, 119, 1376–1394 .

Wildman, L.A.S., MacBroom, J.G., 2005. The evolution of gravel bed channels after dam removal: case study of the Anaconda and Union City dam removals. Journal of Geomorphology 71, 245–262.

Warrick, J.A., Bountry, J.A., East, A.E., Magirl C.S., Randle, T.J., Gelfenbaum, G., Ritchie, A.C., Pess, G.R., Leung, V., Duda, J.J., 2015, in press. Large-scale dam removal on the Elwha River, Washington, USA: Fluxes of river sediment. Geomorphology.

ROLE OF ADAPTIVE SEDIMENT MANAGEMENT IN ELWHA DAM REMOVAL

Jennifer Bountry, Hydraulic Engineer, Bureau of Reclamation, Denver, CO, jbountry@usbr.gov; Patrick Crain, Fisheries Biologist, National Park Service - Olympic National Park, Port Angeles, WA, patrick_crain@nps.gov; Josh Chenoweth, Restoration Botanist, National Park Service - Olympic National Park, Port Angeles, WA, joshua_chenoweth@nps.gov; Timothy Randle, Supervisory Hydraulic Engineer, Bureau of Reclamation, Denver, CO, trandle@usbr.gov; Andrew Ritchie, geomorphologist, National Park Service - Olympic National Park, Port Angeles, WA, andrew_ritchie@nps.gov

INTRODUCTION

Adaptive management is a structured, iterative process of robust decision making in the face of uncertainty, with an aim of reducing uncertainty over time via system monitoring (Williams and Brown, 2012). Adaptive management involves developing conceptual models, based on specific assumptions about the resource system, and identifying actions that might be used to resolve the problem. Testing of underlying model assumptions against monitoring data provides a foundation for learning and improvement of management actions based on what is learned. The Elwha River Restoration Project involved the largest and unprecedented sediment release associated with a phased dam removal. This three-year project provided an excellent opportunity for learning more about the benefits and challenges of adaptive management in a real-time environment.

The Elwha River flows north from the Olympic Mountains for about 70 km and enters the Strait of Juan de Fuca at Angeles Point, about 10 km west of Port Angeles, WA. In 1913, Elwha Dam was built 7.9 km upstream from the river mouth, and then removed between September 2011 and April 2012. This 32-m- high concrete gravity dam had 30 m of head and formed Lake Aldwell, which had a storage capacity of 10 million m^3 at the time of removal. Glines Canyon Dam was completed in 1927, 21 km upstream from the river mouth, and was removed between September 2011 and October 2014. This 64-m-high concrete arch dam had 59 m of head and formed Lake Mills, which had a storage capacity of 32 million m^3 at the time of removal (Bountry et al., 2011). Both dams were constructed to produce hydroelectric power. The dams virtually eliminated bed-material sediment supply to the river reaches downstream, forming large deltas at the upstream end of each reservoir. The deltas were composed of clay to cobble-sized sediment, while the lakebeds were composed of mostly silt with about 15 percent clay. The reservoir sediment also contained all sizes of wood and litterfall. In 1992, the United States (U.S.) Congress passed the Elwha River Ecosystem and Fisheries Restoration Act, which authorized the U.S. Department of the Interior to purchase and remove the privately constructed Elwha and Glines Canyon dams to restore fish passage. Rather than sediment excavation, a river erosion plan was selected for dam removal that utilized the natural stream power of the Elwha River to erode and redistribute reservoir sediment during phased dam removal and reservoir drawdowns (ONP, 1996). At the time of removal, Lake Aldwell contained 4.9 million m^3 of sediment and Lake Mills contained 16.1 million m^3 (Randle et al., 2015a).

Sediment Plan: The sediment management objective was to use phased reservoir drawdowns to erode as much of the sediment as possible during dam removal and to redistribute a portion of the eroded sediment along the valley margins to form a series of varying height sediment terraces (Randle et al., 2012). Based on a field drawdown experiment in 1994 (Childers et al., 2000), numerical modeling (Randle et al., 1996), and a physical model study of dam removal rates (Bromley, 2007), drawdown increments of 4.6 m were selected with 14-day hold periods in between (Randle and Bountry, 2010). The rate of dam removal was designed to be fast enough that sediment impacts would affect only a few brood years of fish, but slow enough that the rate of reservoir sediment erosion and redistribution kept pace with the rate of dam removal. Three additional reservoir hold periods (1½ to 2 months per period) were incorporated into the final dam removal plan to limit the release of reservoir sediments into the downstream river during critical fish usage periods referred to as fish windows. Modeling indicated elevated downstream sediment concentration loads would continue to occur for a few years post-removal, but reduce over time with the occurrence of large floods. The river erosion alternative required the construction of mitigation measures, prior to dam removal, to ensure adequate water supply and treatment for downstream users during the period of increased suspended sediment concentration and turbidity. Mitigation was also required to address potential impacts to downstream flood stages from the deposition of coarse sediment on the river bed (aggradation). The plan allowed for reservoir hold periods to be lengthened if monitoring data indicated the pace of reservoir sediment erosion was not keeping pace with the rate of dam removal, or there was risk of exceeding mitigation measures.

Vegetation Plan: An active plan to re-vegetate the reservoirs was designed to preempt invasive species colonization and to plant native forest species to initiate forest succession (Chenoweth et al., 2010). However, vegetation establishment on deep layers of inorganic sediment after dam removal was not well understood in 2011. Although over 1,000 dams had been removed in the United States before 2011, very little research had gone into documenting vegetation colonization of dewatered reservoirs (Heinz Center for Science, Economics and the Environment, 2002). It was clear that natural recolonization of the reservoirs would be dependent on distance from seed sources (Halpern and Harmon, 1983). One of the few surveys of vegetation development after the removal of several small dams in Wisconsin revealed a rapid colonization of the former reservoirs by invasive species such as reed canarygrass (Orr and Stanley, 2006). The Elwha reservoirs are large and inundated more than just the floodplain; upland terraces and valley walls were also inundated. The Elwha reservoirs were also unique in how sediment had accumulated over the last 80-100 years along with all sizes of wood and litterfall. Estimates prior to dam removal suggested the valley walls would be covered in 0.3-1.5 meters of fine sediment (silt and clay) and the valley bottom would be covered in 3-18 meters of sediment (upper 3-6 meters would be coarse sands and gravels) by the end of dam removal. Such deep layers of sediment were expected to be water stressed after the reservoirs were drained. It was also anticipated that sediment texture would influence successional trajectories. Several studies have demonstrated a relationship between substrate texture and plant species performance (Harper et al., 1965; Grubb 1986; Keddy and Constabel 1986; Smith et al., 1995; Leps et al., 2000; Walker and del Moral 2003; Naiman et al., 2005; Michel and Helfield, 2011). Leps et al. (2000) found that fine textured substrates favor colonization by graminoids over forbs or woody species. If the fine-textured sediments favor grasses and coarse sediments are substantially water stressed, rates of succession to forests and the return of ecosystem processes to pre-dam levels may be delayed due to the slow colonization of woody species into the basin. With so much uncertainty, the revegetation plan called for deliberate and gradual planting, combined with intensive monitoring over a 7-year period, to respond to vegetation growth and mortality and to respond to reservoir sediment erosion.

METHODS

Real-time monitoring of reservoir sediment erosion and export was accomplished through repeat topographic surveys that could be compared to pre-dam estimates of the valley bottom, and the pre-removal surveys completed in 2010. Surveys of channel slope and active channel width were accomplished using a real-time kinematic global position system (RTK GPS) during early dam removal, and later with more comprehensive methods such as LiDAR and photogrammetry. Changes in reservoir topography were tracked in a geographical information system relative to the 2010 surface (Bountry et al., 2011), which was represented by polygons of unique size gradation, aerial extent, and thickness (Gilbert and Link, 1995). Volumetric changes in fine (silt and clay) and coarse (sand, gravel, and cobble) sediment were computed between measurements. A sediment budget model, relying on empirical relationships of slope and channel width related to discharge, was used to predict future sediment erosion volumes and downstream concentrations throughout dam removal (Randle et al., 2015b). The empirical relationships were frequently updated using real-time monitoring information. Time-lapse cameras throughout the reservoirs provided documentation on the occurrence of daily channel change that could be correlated with discharge measurements made at the United States Geological Survey (USGS) McDonald Bridge gaging station. The USGS also measured turbidity and suspended sediment concentrations (SSC) upstream of (background) and downstream of the dam sites (Magirl et al., 2014). Downstream river aggradation as a result of released reservoir sediment was measured using photogrammetry for above water areas and RTK GPS and sonar for below water areas. Staff gages were also installed at about 20 river cross-sections to track discharge-stage rating curves that were used as a surrogate to infer periods of aggradation (East et al., 2014).

Monitoring of how fish populations responded to dam removal was accomplished using a variety of methods. Adult salmon abundance and distribution during dam removal was monitored through a combination of sonar observations (LEKT and Denton, 2014), spawning ground surveys (McMillan and Moses, 2013; McMillan et al., 2014), and an adult capture weir (Anderson, et al., in preparation). Juvenile abundance and distribution was evaluated through a combination of smolt traps (McHenry et al., 2014), snorkel surveys, and electrofishing.

The slow drawdown of the dams provided a unique opportunity to adaptively manage the vegetation development as the reservoirs receded. In the first two years of drawdown, experimental plantings were installed to determine native species performance in the deep layers of fine and coarse sediments covering the original forest soils. Permanent plots were established in both planted and unplanted areas to determine the effectiveness of treatments compared to natural patterns of recovery. Since random plot distribution does not always provide a complete picture of the

evolving patterns of natural vegetation development, the restoration ecologist frequently visited the newly exposed surfaces throughout each of the first three growing seasons. Areas within 50 meters of seed sources were left to naturally regenerate. To monitor the performance of planted native species, 860 plants representing 6 species were tagged in the first year and 675 plants representing 5 species were tagged in the second year. Water availability was monitored throughout the year in the sediments of the former Lake Mills reservoir using a tensiometer.

RESULTS

Reservoir Drawdown and Sediment Release: Elwha Dam was removed in the dry by periodically diverting the river, using cofferdams, through a spillway channel excavated in the left abutment. Lake Aldwell had one early drawdown in June 2011 followed by a 16 week hold period, and five additional drawdowns starting in September 2011 and ending in April 2012 when dam removal was completed. The hold periods after reservoir drawdown ranged from 2 to 8 weeks. During each reservoir drawdown, erosion of the reservoir delta occurred as a result of base-level lowering. The eroded sediment was re-deposited in the remaining lake, building new deltas that progressed downstream toward the dam site as the lake reduced in aerial extent and capacity. Downstream sediment releases were minor while sufficient trap efficiency remained in the lake, with a few minor peaks of sediment release during winter storms in November and December 2011 (Figure 1). By mid-March 2012, only 5% of the lake capacity was left and in April 2012 the sediment delta reached the dam site and bedload was released into the downstream channel. Suspended sediment levels in the downstream channel increased from mid-March to early July 2012, and then reduced to low levels as flows receded during late summer and fall. About 90 percent of the fine was transported to the sea, but some fine sediment deposited as thin coatings of mud along low-relief gravel bars and floodplain surfaces that were inundated during the spring 2012 snowmelt season (East et al., 2014). Sand and fine gravel released as bed-material load from Lake Aldwell resulted deposited in the larger downstream pools and eddies, but no aggradation of hydraulic controls (riffles and rapids) occurred.

The contractor completed the dam removal 4 months ahead of the government's estimated schedule (Figure 1). No large floods occurred during this initial dam removal period, and monitoring data indicated no problems with water quality. As expected, delta progradation kept pace with the rate of dam removal and reservoir. Therefore, no adaptive management changes were made to the dam removal schedule. There were issues with cofferdam breaches during winter high flows, but dam removal proceeded. A large portion of the pre-removal Lake Aldwell delta remained in place throughout dam removal. The river quickly incised along the far right side of the delta into cohesive sediment layers during the first two drawdowns; no large floods occurred during reservoir drawdowns that were capable of laterally eroding across the entire wide delta. Adaptive management actions were considered on the Lake Aldwell delta such as a reservoir drawdown one year prior to dam removal that would include a winter flood season. A center pilot channel was also considered during fall 2011 to encourage additional erosion of the Lake Aldwell delta during the dam removal period. Resource managers determined an early drawdown was not procedurally possible before June 2011, and no pilot channel was implemented because the amount of sediment remaining in the Lake Aldwell delta was small enough that impacts would be tolerable if erosion occurred after dam removal. Additionally, the Lake Mills sediment release was expected to be much larger and of greater focus for the adaptive management efforts. Monitoring data showed that small amounts of lateral erosion and channel incision did continue in Lake Aldwell during the two years following dam removal. The most extensive lateral erosion of the remaining delta occurred during a 3-year winter flood in December 2014.

On Lake Mills, a physical model (Bromley, 2007) predicted that excavation of a center pilot channel on the delta was necessary to prevent the river from incising on the valley margin and leaving tens of meters of delta sediment in place. Because of the larger delta size relative to Lake Aldwell, the first adaptive management action in September 2010 was to excavate a center pilot channel along the upstream portion of the delta, block off the main channel along the edge of the delta with a constructed log jam, and remove an existing log jam at the head of the delta to divert river flow into the pilot channel. A large flood followed in December 2010 that widened and deepened the pilot channel and refilled the reservoir. However, the pilot channel was successful in becoming the primary delta channel with a center alignment.

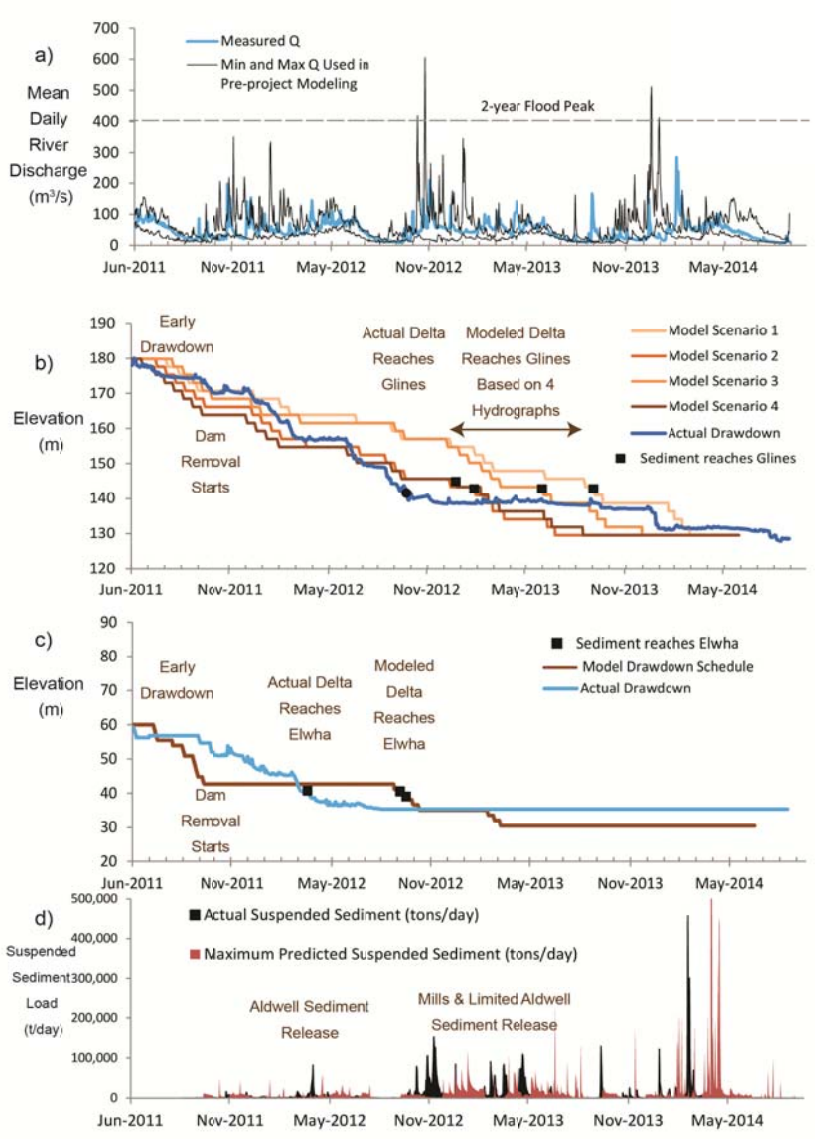

Figure 1 Monitoring results during June 2011 to September 2014 versus pre-project model assumptions for equivalent time periods using four different hydrograph assumptions: a) actual measured river discharge during dam removal compared with range of discharges assumed in model scenarios, b) Lake Mills actual drawdown compared with four model scenarios (differing rate dependent on hydrology), c) Lake Aldwell drawdown compared with model scenarios (same rate regardless of hydrograph), and d) actual suspended sediment load compared with maximum of four model scenario predictions.

An early reservoir drawdown of Lake Mills occurred during July 2011 followed by a 10 week hold period. Starting in September 2011 through April 2012, the first 21 m of Glines Canyon Dam was removed using a hoe ram sitting on a barge while flow was diverted through the gated spillway or through notches cut into the dam crest. The remaining 37 m of Glines Canyon Dam was removed using drill and blast techniques to cut notches on alternating left and right sides of the arch dam. Nine reservoir drawdown increments occurred following dam removal notches between October 2011 through October 2012 when the sediment delta reached the dam. The first hold period of 10 weeks occurred in November and December 2011. Although the first November-December fish window was not required, the hoe ram broke and dam removal had to be temporarily halted until new equipment could be brought to the site. After dam removal resumed in January 2012, hold periods ranged from 2 to 3 ½ weeks, except for the May-June fish window, which resulted in a 10-week hold period. The pace of Glines Canyon Dam removal began to

exceed original predictions in July 2012 because the blasting method was more efficient than the original plan to use a diamond-wire saw. Additionally, less than 10% of the reservoir capacity remained so the sediment was about to reach the dam site. A new round of predictions was made using the sediment budget model to evaluate varying rates of continued dam removal. The contractor was allowed to continue at a faster pace through October 2012, but adaptive management was used to reduce the total possible dam removal rate by one-third. The coarse sediment delta reached the dam after the last allowed blast in October 2012 (Figure 1). At that point, adaptive management was used to halt additional dam removal while new predictions and monitoring occurred to evaluate the first major sediment impacts to downstream water quality and river stage. Rates of sediment release were high until late December 2012 when flows reduced, but then increased with each set of subsequent high winter and spring snowmelt flows. Sediment released into the downstream river not only filled pools, but also aggraded the entire river bed causing the stage-discharge relationships to increase by up to 1 m as the sediment wave passed through. Although peak concentrations of fine sediment did not exceed predictions, the surface water intake designed prior to dam removal became overwhelmed in winter 2012 due to long duration and high volumes of silt, clay, sand, gravel, and organic material entering the plant. Dam removal had to be halted for one year until solutions could be implemented that reduced the amount of sediment entering the water treatment plant.

During the one year hold period, vertical incision up to 9 m and tens of meters of lateral erosion continued in Lake Mills despite the lack of additional base-level lowering at Glines Canyon Dam. The continued reservoir sediment erosion resulted in several years of average annual sediment load being released past the dam site during the one year hold period. Dam removal blasting resumed during fall 2013 with reservoir drawdowns during October 2013, January 2014, February 2014, and the final blast in August 2014. Adaptive management did not have to be used in the final year of dam removal because improvements to the water diversion and treatment plant were successful and river-bed aggradation had reduced. Channel aggradation did result in minor flooding of low relief campgrounds along with bank erosion in many locations along the river. Similar to Elwha Dam, large boulders were also present in the narrow canyon downstream of Glines Canyon Dam, possibly originating from construction activities in the late 1920s. These boulders created a new hydraulic control that increased river water surface upstream from the dam site after removal. Adaptive management was implemented to blast some of the boulders, but others continue to constrict the canyon and increase upstream water stage, possibly impacting fish passage.

At the end of the three year dam removal period, monitoring data indicated about half of the available 21 m^3 of Lake Aldwell and Lake Mills sediment had been eroded and released downstream. Actual river flows during the three year dam removal period never exceeded the 2-year flood for the Elwha River. The annual background suspended sediment load (fine sand, silt, and clay) was only 2 to 6% of the suspended sediment load released from the reservoirs. The largest background suspended sediment load occurred during a March 2014 storm, but was still only 3% of sediment load eroded from the reservoirs. Sediment erosion and release above background levels continued in the year following dam removal, particularly during the 3-year flood in December 2014.

Fisheries: The Elwha Project fisheries restoration plan assumed that mainstem water quality conditions below Glines Canyon Dam would be detrimental to natural fish production, particularly as there is very limited clean water refugium below Elwha Dam (Ward et al., 2008). Salmonids are sensitive to suspended sediment loading, and have been found to exhibit behavioral changes at concentrations as low as 100 ppm, while mortality directly related to turbidity has been seen at concentrations of 1000 ppm (Cook-Tabor, 1995). These effects are exacerbated by the duration of the exposure. Due to concerns regarding elevated turbidity loads during dam removal, the fish restoration plan relied on two fish hatcheries for protection of fish stocks during the sediment-impact period and to help initiate re-colonization following dam removal.

The intent of the fish windows were to provide extended periods of clean water (≤100 FNU) when salmonids (both hatchery and natural origin) could migrate into the river as adults or emigrate from the river as juveniles (Ward et al., 2008). The May-June fish window was specifically designed to accommodate emigration juveniles of all species, as well as the upstream migration of adult native steelhead. The August-September fish window was designed to accommodate the upstream migration of adult Chinook salmon and pink salmon, while the November-December fish window was designed to coincide with the upstream migration of adult Coho salmon, chum salmon, and hatchery origin steelhead (a program which was ultimately discontinued prior to the beginning of dam removal). Adult hatchery origin salmon were expected to recruit naturally to their hatchery of origin, although plans were also made to capture and relocate adults from the river to the hatcheries as necessary. Natural origin adults were expected to either migrate upstream to the best available habitat, or stray into the hatcheries as they sought out cleaner water.

Actual turbidity during the fish windows differed substantially from the modeled conditions (Figure 2; Table 1), being significantly higher than anticipated during the winter and spring periods, or lower than anticipated during the summer periods. More importantly, releases of hatchery fish were not consistently timed with the fish windows, due to either their age of release (yearling Chinook released in April vs fingerling Chinook released in June) or more rapid maturation in the hatchery than originally anticipated (Coho releases in April rather than May).

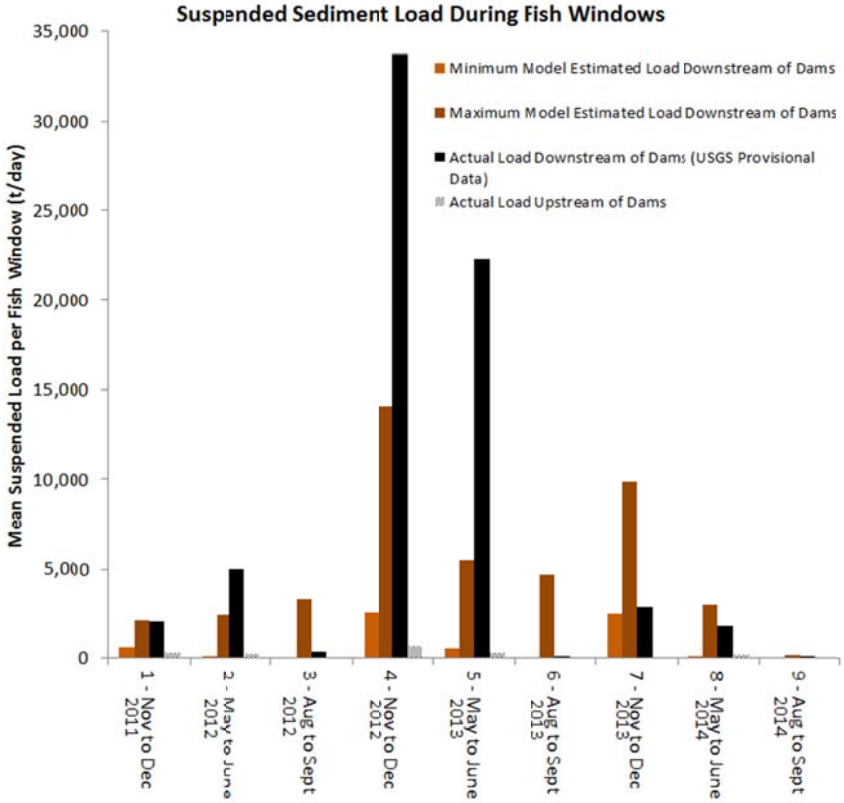

Figure 2 Predicted versus actual suspended sediment loads upstream of (background) and downstream of (actual SSC) the dam sites. Actual data is based on provisional USGS measurements (Magirl, 2014).

Table 1 Percent of time turbidity or discharge exceeded thresholds important to fish during fish windows.

	Mean of 4 model scenarios % Fish Window Exceeding			Actual Turbidity % Fish Window Exceeding			Actual Discharge Exceeded Mean Annual
Fish Window During 3 Year Dam Removal	>100 FNU	>500 FNU	>1000 FNU	>100 FNU	>500 FNU	>1000 FNU	
1 - Nov to Dec, 2011	45%	3%	1%	54%	2%	0%	28%
2 - May to June, 2012	22%	3%	3%	100%	2%	0%	100%
3 - Aug to Sept, 2012	74%	31%	19%	11%	0%	0%	2%
4 - Nov to Dec, 2012	66%	44%	30%	100%	97%	48%	87%
5 - May to June, 2013	7%	6%	3%	100%	77%	28%	90%
6 - Aug to Sept, 2013	11%	2%	1%	2%	0%	0%	0%
7 - Nov to Dec, 2013	17%	11%	5%	72%	36%	3%	7%
8 - May to June, 2014	6%	1%	1%	49%	3%	0%	92%
9 - Aug to Sept, 2014	0%	0%	0%	0%	0%	0%	0%

The largest mean-suspended sediment loading during any given fish window was nearly 35,000 tons/day, during the Nov-Dec window in 2012 (Figure 2). During this time, turbidity exceeded 100 FNU continuously and exceeded

1,000 FNU nearly 50% of the time (Table 1). The models had predicted that turbidity would exceed 100 FNU about 66% of the time and 1,000 FNU about 30% of the time. While turbidity and suspended sediment concentrations were substantially higher than projected, Coho and chum salmon moved into the river opportunistically, but tended to recruit primarily to the hatchery facilities. There was little indication that any Coho volitionally moved upstream of the Elwha Dam site (McMillan and Moses, 2013). Suspended sediment concentrations were also significantly higher than modeled during the May-June fish window of 2013. Although the mean concentrations were lower than those observed during the 2012 Nov-Dec window (~22,000 tons/day), turbidity greatly exceeded modeled conditions (Table 1). Turbidity exceed 100 FNU 100% of the time (modeled at 7%), exceeded 500 FNU 77% of the time (modeled at 6%), and 1,000 FNU 28% of the time (modeled at 3%).

While certain cohorts of hatchery fish were released during the spring fish windows (e.g. fingerling Chinook), other cohorts were released prior to the fish window (yearling Chinook, Coho). In April 2013, periods of high turbidity were associated with large scale observations of juvenile Chinook mortality following their release from the WDFW hatchery. Returns of Coho salmon in the fall of 2014 (originating from juveniles emigrating during the spring of 2013) were significantly lower than anticipated (PFMC, 2014). Conversely, turbidity and suspended sediment concentration during the summer fish windows was significantly lower than modeled; rarely exceeding 100 FNU and never exceeding 500 FNU (Table 1). This was conducive for Chinook and pink salmon upstream migration and spawning. Spawning ground surveys conducted in the mainstem channel and larger tributaries during the late summer of 2012, 2013, and 2014 observed 217, 765, and 1,310 redds respectively. Many of these redds were located in the mainstem channel above the Elwha Dam site (LEKT et al., In preparation). Unlike Coho salmon, very few Chinook recruited to either hatchery facility. The majority of adults needed for hatchery broodstock were collected from the river and transported to the WDFW hatchery.

Snapshot overview of vegetation establishment results on Mills and Aldwell: Phased dam removal and reservoir drawdown had a profound impact on the successful establishment of planted and natural vegetation; although sediment texture and distance from seed sources were important factors. The most likely explanation for the rapid colonization and high survival of planted species was the high water availability in the sediments due to the gradual reservoir drawdowns. The reservoirs left behind saturated sediments and a slowly-declining water table during the early phases of dam removal. In particular, the hold periods during the 2012 growing season (May, June, August, and early September) in the Lake Mills benefitted the establishing plants. High water availability proved critical to the germination and establishment of vegetation and to the performance of planted native species in both the fine textured surfaces and the coarse terraces.

However, over time, sediment texture has proven to impact vegetation. In general, vegetation establishment (tree species included) was rapid on fine-sediment surfaces and slow on coarse-textured terraces covering the valley bottom. The newly exposed valley slopes covered in fine sediments benefit from close proximity to seed sources. Natural regeneration was swift in most areas. Bare ground declined rapidly. In 2012, the first full growing season for most of the valley slopes; bare ground was 78%. Bare ground declined to 28% in 2013 and to 9% in 2014. The decline in bare ground is not exclusively the result of colonization by herbaceous species. Tree species were a significant component of the natural vegetation; with red alder (*Alnus rubra*) dominating many sites covered in fine sediments in both the former Lake Aldwell reservoir and the former Lake Mills reservoir. Woody species cover is increasing each year, from a low of 1% in 2012, 14% in 2013 to 57% in 2014. Planted sites also performed well on the valley slopes, with survival rates of 92% in 2012 and 96% in 2013 (Whisman, 2013; Calimpong, 2014).

Vegetation recovery on the coarse terraces has been slow. Most of the coarse terraces are not only water stressed, but are also far from seed sources. As a result, substantial natural regeneration has been limited. Bare ground on coarse terraces is declining slower than on fine sediment sites. In 2013, the first year of substantial exposure of coarse sediment in the former Lake Mills reservoir, bare ground was 90%. In 2014, bare ground declined to 77%, mostly as a result of planting and seeding efforts. Survival of planted species in the deep terraces of coarse sediment was high in 2012 and 2013 (88% and 90% respectively), most likely due to the water available during drawdown. In 2014, when the river had nearly dropped down to its pre-dam elevation, plant survival on the coarse sediments was extremely low, only 42%. This was due in part to unusually high summer temperatures (over 3 degrees Fahrenheit above average in July, August and September) and below average precipitation. However, some species performed surprisingly well. Black cottonwood and Nootka rose (*Rosa nutkana*) both had a 73% rate of survival on coarse terraces in 2014, demonstrating significant draught tolerance.

Natural vegetation colonization patterns were strongly influenced by the reservoir drawdown timing. The season of drawdown influenced the composition and rate of vegetation establishment. Drawdowns that occurred during the late fall and winter months were relatively slow to be colonized by vegetation. On fine sediment sites, red alder eventually colonized sites within 100 meters of mature trees. The most rapid and prolific establishment resulted from reservoir drawdowns that occurred during the seed dispersal of Salicaceae species. Willow (*Salix* species) and black cottonwood (*Populus balsamifera* ssp. *trichocarpa*) have very short-lived seed with very specific germination requirements tied directly to river discharge patterns in late spring (Naiman et al., 2005). Seeds are dispersed long distances by wind and water in May and June. Once seeds are saturated, they remain viable for only 2-3 days and must find appropriate sites to establish, usually newly exposed gravel bars in floodplains. Because reservoir drawdown was gradual over two years, there were two opportunities for substantial cottonwood and willow establishment during drawdown. The first opportunity was in 2011 when the first 4.5 to 5.5 meters of reservoir drawdown occurred in both reservoirs from June 2-11. The rate of drawdown created the perfect environment for seed germination and establishment. The wave action from the lake deposited saturated seed of cottonwoods and willows in perfect rows on the newly exposed shoreline (Figure 3a). In the former Lake Aldwell, mean sapling densities at these sites by the end of 2013 were 56,100 stems per acre and were over 2 meters tall. Most of the saplings were cottonwoods with a significant component of Sitka willow (*Salix sitchensis*). In 2012, a similar establishment event occurred in the former Lake Mills reservoir in both fine and coarse sediments. The most remarkable establishment was on a coarse-textured terrace that formed during drawdown in the former Lake Mills. Thousands of cottonwood seedlings successfully germinated and established on newly deposited sediments slowly drying during the summer of 2012. As dam removal progressed, the terraces became perched approximately 15 meters above the water table. Three years later the cottonwoods are thriving, having successfully established in xeric conditions (Figure 3b). The plants are small (less than 1 meter tall), but healthy and are one of the few woody species to naturally occur on the coarse terraces. On other coarse terraces not exposed during the late spring, cottonwood and willow establishment is limited to seasonal creeks meandering across the terraces.

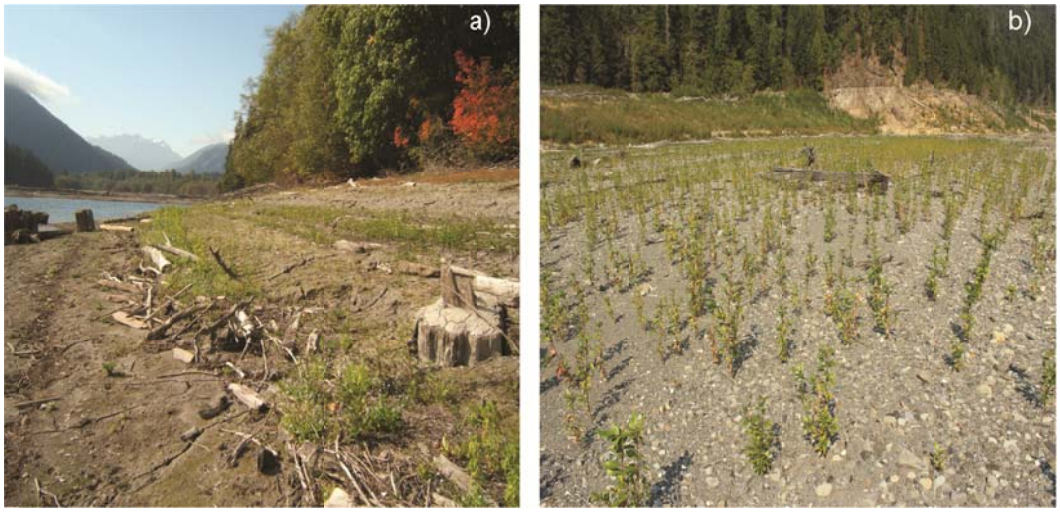

Figure 3 Vegetation growth in newly exposed reservoirs: a) Seedlings of cottonwoods and willows established during the June 2011 drawdown in the former Lake Aldwell reservoir - photograph taken September 12, 2011; b) three-year old cottonwood seedlings established in 2012 on a high terrace in the former Lake Mills reservoir - photograph taken September 16, 2014.

Many of the coarse textured terraces are not only water stressed, but are also far from seed sources. As a result, substantial natural regeneration has been limited and tends to be restricted to small seasonal creeks that are scattered across the landscape. The cover of bare ground at coarse sediment sites is much greater than on fine sediment sites. In 2013, the first year of substantial exposure of coarse sediment in the former Lake Mills reservoir, bare ground was 90% of the reservoir surface. In 2014, the bare ground declined to 77%, mostly as a result of planting and seeding efforts. Survival of planted species in the deep terraces of coarse sediment was high in 2012 and 2013 (88% and 90% respectively), clearly benefitting from the water still available during drawdown. In 2014, when the river was nearly down to its original elevation, plant survival on the coarse sediments was extremely low, only 42%. This was due in part to unusually high summer temperatures (over 3 degrees Fahrenheit above average in July, August

and September) and below average precipitation. However, some species performed surprisingly well. Black cottonwood and Nootka rose (*Rosa nutkana*) both had a 73% rate of survival in 2014, demonstrating significant draught tolerance.

DISCUSSION

Outcomes of phased dam removal were assessed for the Elwha River adaptive management program to evaluate how actual dam removal results compare to expectations from pre-project predictions. Differences in actual and expected results are investigated to identify which, if any, of the possible causes identified in adaptive management literature occurred: incorrect assumptions, poorly executed actions, changed environmental conditions, inadequate monitoring, or some combination of these causes (Williams and Brown, 2012).

Sediment Erosion during Early Drawdown and Dam Removal While a Lake Remained: Adaptive management is most successful when the ability to control the system with management decisions and actions is high. For the case of the Elwha Dam and Glines Canyon Dam removals, the greatest control on sediment release was both predicted and found through monitoring data to be prior to and during the phased-drawdown period while a lake still remained. Prior to dam removal, the early drawdowns on both lakes and pilot channel excavation on Lake Mills delta were effective at increasing the amount of sediment eroded and retained in the lake. This matched pre-project model assumptions of the benefit of early drawdown and starting delta channel along center alignment. However, we learned through monitoring that the effectiveness of early drawdown on sediment erosion rates and magnitude could have been increased by implementing the early drawdown prior to high flow periods, rather than at the after. Additionally, monitoring data indicated that reservoir sediment erosion tended to occurred when flows exceeded the mean-annual flow of 42 m^3/s and were not limited to occurrence of large floods (see Figure 1). Early drawdown was implemented after snowmelt recession. Dam removal started at both sites during the low flows of September 2011. Implementing the first drawdowns prior to the high flow period of the year (October through June) would have allowed more erosion to occur while the reservoirs still remained. This is consistent with other dam removal literature documenting that timing dam removal with hydrology of the river basin can be an effective tool (Cannatelli and Curran, 2012).

Sediment Impacts during Fish Windows after Lake Was Lost: More efficient construction methods at both dam sites resulted in a faster base level lowering and delta progradation to the dam sites than government estimates. For Lake Aldwell, the delta reached the dam just as the May-June snowmelt period and fish window was beginning. Discharge exceeded the mean-annual flow and was capable of eroding sediment 90-100% of the May-June fish windows, and a wider range of 7-87% during the November-December fish windows (see Table 1). The combination of faster reservoir drawdown and long duration flows effective at eroding and transporting sediment resulted in higher than anticipated sediment loads during the high flow fish windows and thus higher than expected impacts to fish. By adjusting the rate of dam removal, sediment impacts could have been shifted and potentially spread out to occur over the summer or following winter during high flows. The sediment delta reached Glines Canyon Dam just before the November-December fish window, 3 to 12 months ahead of the assumed schedule in pre-project model runs. The Lake Mills sediment volume released was large enough that the river needed several months during winter and snowmelt flows to transport the reservoir sediment through the downstream river channel. Given the large volume of reservoir sediment, it was not likely possible to minimize sediment impacts during the high-flow fish windows after the lake was lost in November-December or May-June. Monitoring data showed that despite the halting of dam removal after the lake was lost, higher than predicted sediment erosion volumes continued to occur and be released downstream even during a one-year long hold period. Channel incision was deeper, and knickpoint migration continued at a slower rate, than predicted during the year-long hold period. The incision was deeper because the reservoir-sediment grain size was finer with depth. The river in the middle of the reservoir incised as much as 9 m during the one-year hold period. The knickpoint migration tended to stall when river discharge was less than the mean-annual flow. Lateral erosion into the coarse and non-cohesive sediment terraces was much greater than predicted. A slower rate of dam removal would have reduced the sediment concentrations released downstream, but prolonged the duration of impact.

Vegetation Establishment versus Drawdown Timing: In general, vegetation establishment benefits tremendously from a gradual reservoir drawdown. Timing of drawdown also significantly impacts the rate of response and species composition and can lead to extensive establishment of Salicaceae species. The pattern of Salicaceae establishment,

related to the timing of drawdown, is not unique to the Elwha as it occurred during a 4-year drawdown of a large reservoir in Colorado (Auble et al., 2007). Black cottonwood is a particularly good species for early succession in a stressful environment because it is surprisingly draught tolerant, fast to grow, and is a critically important species for riparian restoration (Collins and Montgomery 2002). Residual moisture from the receding reservoirs may be the key to establishing woody species over graminoids on fine lacustrine sediments. Residual moisture also appears to create favorable conditions for planting on coarse sediments. For example, Douglas-fir (*Pseudotsuga menziesii*) had better rates of survival in coarse sediments in 2012 and 2013 (40% and 91% respectively) compared to after the sediments had dried out in 2014 (only 28%). The Douglas-firs established and tagged in 2012 and 2013 had very high survival in 2014 (100% and 89% respectively), showing the value of planting while moisture is high, allowing plants an opportunity to grow a root system capable of resisting future water stress. The moisture available to vegetation resulting from gradual reservoir drawdown creates a plant window, providing management a unique opportunity to establish desirable native species. This is particularly important for coarse-grained sediments that are slow to support natural vegetation.

Adaptive management of the vegetation during dam removal proved successful. The gradual planting plan in the first two years allowed the rapid pace of natural recolonization on most of the valley slopes to occur unhindered. The valley slope areas far from seed sources that were planted during drawdown had high rates of survival and continue to thrive after three years. Annually monitoring the changes to bare ground and species cover allows us to ensure our goal of accelerating forest development is being met. Our plots and the general observations from site visits have also showed us the need to focus management on coarse-sediment terraces and allow valley slopes to predominantly recover naturally. Tagging plants early in the project provided critical information that allowed us to shift our plant production to species best suited to plant into the coarse terraces.

Implementation Challenges of Adaptive Management for Dam Removal: A challenge of utilizing adaptive management during a real-time construction project was the need to incorporate new predictions with real-time monitoring data in a timely manner. The combined effect of implementing adaptive management that changed reservoir drawdown schedules with the lack of a large flood occurrence resulted in the need for more model iterations than planned to move forward with management decisions. Although the added model runs posed budget and time challenges, the adaptive management method of incorporating new knowledge from monitoring experience as the project moved forward was successfully utilized for each management decision on reservoir drawdown schedule. Another challenge was cross-coordination of multiple disciplines to help inform management decisions during dam removal. We formed an interdisciplinary team to discuss monitoring results and predictions so varying perspectives could be incorporated and used to get consensus on technical recommendations associated with dam removal. The most beneficial monitoring data that either confirmed or changed assumptions used for predictions was documentation of changing river width, elevation, and slope and corresponding river discharge hydrographs. Evolving monitoring methods from quarterly survey profiles and cross-sections to continuous and more frequent coverage with photogrammetry increased the accuracy of computations and better captured the non-uniform channel geometry. Time-lapse photography and collection of aerial photography was crucial to help with interpretations of complex and rapid changes in channel morphology that included super-imposed rounds of incision and lateral erosion from multiple drawdowns. Suspended sediment and bedload data (collected by partner agencies and Reclamation using research funds), along with staff gates and river profile surveys greatly improved monitoring information and our ability to analyze downstream sediment transport as part of the adaptive management program.

CONCLUSIONS

Through the use of key monitoring data and updated predictions, adaptive management was successfully implemented on the Elwha Dam removal project to control the rates of reservoir sediment erosion. Pre-project predictions were crucial to establishing mitigation measures, setting the initial pace of dam removal, and establishing the monitoring plan. We did not have to alter the type of real-time sediment monitoring data, but did benefit from improved methods that captured greater complexity at more frequent intervals than planned. The level of adaptive management control on downstream sediment release, and thus impacts to flooding, water quality, and fish, was highest while the reservoirs remained and eroded sediment was largely contained. Vegetation growth benefitted from the timing and rate of phased drawdown on both reservoirs, but was not planned to coincide with vegetation seed dispersal. While suspended sediment concentrations exceeded modeled expectations during a number of the fish windows, conditions during the May-June window of 2013 were of the greatest concern to hatchery and natural origin juveniles. This was exacerbated by the fact that releases of hatchery yearling Chinook,

hatchery Coho, and hatchery chum salmon occurred prior to the beginning of the fish window, as fish were smolting. Future adaptive management projects may benefit by analyzing what if implementation scenarios in pre-project planning that could result in increased or shifted timing of dam removal rates and associated sediment impacts, overlaid with vegetation growth seasons and fisheries considerations.

REFERENCES

Auble, G.T., Shafroth, P., Scott, M., and Roelle, M. (2007). "Early Vegetation Development on an Exposed Reservoir: Implications for Dam Removal," Environmental Management, 39, pp 806-818.

Anderson, J., Mizell, M., Ackley, M., Mayer, K. , Zimmerman, M. and Crain, P. (in preparation). Elwha River Adult Weir Project – 2013 Operations and Final Summary Report. WDFW Report # FP-XXX

Bountry, J., Ferrari, R., Wille, K., and Randle, T. (2011). 2010 Survey Report and Area-Capacity Tables for Lake Mills and Lake Aldwell on the Elwha River, Washington, Technical Service Center, Bureau of Reclamation, Denver, CO, 66 pages.

Bromley, J.C. (2007). "The morphodynamics of sediment movement through a reservoir during dam removal," Ph.D. thesis, the University of Nottingham.

Calimpong, C. (2014). "Elwha River Revegetation 2013: A Plant Performance Study. Master's thesis," University of Washington, School of Environmental and Forest Sciences, Seattle, WA.

Cannatelli, K.M., and Curran, J.C. (2012). "Importance of hydrology on channel evolution following dam removal: case study and conceptual model," Journal of Hydraulic Engineering 138(5), 377–390.

Chenoweth, J., Acker, S. A., and McHenry, M. (2010). "Revegetation and restoration plan for Lake Mills and Lake Aldwell. Elwha River ecosystem restoration project," Lower Elwha Klallam Tribe and the National Park Service, Port Angeles, WA.

Childers, D., Kresch, D.L., Gustafson, A.S., Randle, T.J., Melena, J.T., and Cluer, B. (2000). "Hydrologic Data Collected During the 1994 Lake Mills Drawdown Experiment, Elwha River, Washington," Water-Resources Investigations Report 99-4215, U.S. Geological Survey, Tacoma, Washington, 115 pages.

Collins, B.D. and Montgomery, D. R. (2002). "Forest Development, Wood Jams, and Restoration of Floodplain Rivers in the Puget Lowland, Washington," Restoration Ecology, 10, pp 237-247.

Cook-Tabor, C. (1995). "A literature review of the effects of suspended sediments on salmonids," U.S. Fish and Wildlife Service, Western Washington Resource Office, Olympia, WA.

East, A.E., Pess, G.R., Bountry, J.A., Magirl, C.S., Ritchie, A.C., Logan, J.B., Randle, T.J., Mastin, M.C., Minear, J.T., Duda, J.J., Liermann, M.C., McHenry, M.L., Beechie, T.J., and Shafroth, P.B. (2014). "Large-scale dam removal on the Elwha River, Washington, USA: River channel and floodplain geomorphic change," Geomorphology, v. 228, p. 765–786, doi:10.1016/j.geomorph.2014.08.028.

Gilbert, J. and Link, R. (1995). "Alluvium Distribution in Lake Mills, Glines Canyon Project and Lake Aldwell, Elwha Project, Washington," Elwha Technical Series PN-95-4, U.S. Bureau of Reclamation, Pacific Northwest Region, Boise, ID, 60 pages.

Grubb, P.J. (1986). "The ecology of establishment. In Ecology and Design in Landscape,". Ed. A.D. Bradshaw, D.A. Goode and E. Thorpe, pp. 83-98. Oxford: Blackwell.

Halpern, C.B. and Harmon, M.E. (1983). "Early Succession on the Muddy River Mudflow, Mount St. Helens, Washington," American Midland Naturalist, 110, 97-106.

Harper J.L., Williams, J.T. and Sagar, G.R. (1965). "The behavior of seeds in soil. Part I. The heterogeneity of soil surfaces and its role in determining the establishment of plants from seed," Journal of Ecology, 53, pp 273-286.

Heinz Center for Science, Economics and the Environment. (2002). Dam Removal: Science and Decision Making. Washington, D.C., 221 pp.

Keddy, P.A. and Constabel, P. (1986). "Germination of ten shoreline plants in relation to seed size, soil particle size and water level: an experimental study," Journal of Ecology, 74, pp 133-141.

Leps, J, Michalek, J., Rauch, O., and Uhlik, P. (2000). "Early succession on plots with the upper soil horizon removed," Journal of Vegetation Science, 11, pp 259-264.

Lower Elwha Klallam Tribe (LEKT) and Denton, K. (2014). Field Sampling Protocol and Data Uncertainty Analysis Plan for the Elwha Chinook (Oncorhynchus tshawytscha) SONAR Project.

Lower Elwha Kallam Tribe (LEKT), WDFW, ONP, and NOAA. (In Preparation). Spatial Spawning Distribution of Summer/fall Chinook Salmon (Oncorhynchus tshawytscha) in the Elwha River During Dam Deconstruction from 2012 to 2014.

Magirl, C.M., Hilldale, R.C., Curran, C.A., Duda, J.J., Straub, T.D., Domanski, M., and Foreman, J.R. (2014 in press). "Large-scale dam removal on the Elwha River, Washington: USA: Fluvial sediment load," Geomorphology, doi:10.1016/j.geomorph.2014.12.032.

Magirl, C.M. (2014). Provisional data of stream discharge, turbidity, and suspended sediment for the period October 2013 to September 2014. U.S. Geological Survey, Tacoma, Washington.

McHenry, M., Pess, G., Lehrman, M., and Peters, R. (2014). Field Sampling Protocol and Data Uncertainty Analysis Plan for the Elwha River Smolt Enumeration Project. Submitted to Olympic National Park In Fulfillment of Task 1, Contract #1443PC00296 with the Lower Elwha Klallam Tribe.

McMillan, J.R. and Moses, R.J. (2013). Summary of Coho Salmon Redd Surveys in Middle Elwha River 2012/2013. Annual report for NOAA and Lower Elwha Klallam Tribe. Provided to Olympic National Park by the Lower Elwha Klallam tribe and Keith Denton in fulfillment of Task 1 of Contract #144PCOO296.

McMillan, J.R., Moses, R.J., Pess, G., McHenry, M., Hugunin, H., and Crain, P. (2014). Summary of Coho Salmon Redd Surveys in Middle Elwha River 2013/2014. Annual report for NOAA and Lower Elwha Klallam Tribe.

Michel, J.T. and Helfield, J.M. (2011). "Seed Rain and Revegetation of Exposed Substrates Following Dam Removal on the Elwha River," Northwest Science, 85, pp 15-29.

Naiman,, R.J., H. Decamps, and McClain, M.E. (2005). Riparia: Ecology, Conservation, and Management of Streamside Communities. Elsevier Academic Press, Burlington, MA.

Olympic National Park (ONP). (1996). "Elwha River Ecosystem Restoration Implementation, Draft Environmental Impact Statement", National Park Service, Port Angeles, WA.

Orr, C.H. and Stanley, E.H. (2006). "Vegetation development and restoration potential of drained reservoirs following dam removal in Wisconsin," River Research and Applications, 22, 281-295.

Pacific Fisheries Management Council (PFMC). (2014). Preseason Report 1 – Stock Abundance Analysis and Environmental Assessment Part 1 for 2014 Ocean Fishery Regulations. Regulation Identifier # 0648-XD072.

Randle, T.J.; Young, C.A.; Melena, J.T.; Ouellette, E.M. (1996). "Sediment Analysis and Modeling of the River Erosion Alternative," Elwha Technical Series PN-95-9, U.S. Department of the Interior, Bureau of Reclamation, Boise, Idaho, 138 pages.

Randle, T.J., and Bountry, J.A. (2010). "Elwha River Restoration: Sediment Adaptive Management," 9th Federal Interagency Sedimentation Conference, Las Vegas, Nevada, June 27 - July 1, 2010.

Randle, T.J., Bountry, J.A., and Smillie, G. (2012). Technical Basis for Elwha Restoration Adaptive Sediment Management and Monitoring Plan. Department of Interior, Reclamation and NPS, Reclamation Report Number: SRH-2010-24, 69 pages.

Randle, T.J., Bountry, J.A., Ritchie, A., and Wille, K. (January 2015a). "Large-scale dam removal on the Elwha River, WA, USA: erosion of reservoir sediment," Geomorphology, doi:10.1016/j.geomorph.2014.12.045.

Randle, T.J., Bountry, J.A., and Wille, K. (2015b). "Elwha Reservoir Sediment Modeling in a GIS Framework," 10th Federal Interagency Sedimentation Conference, Reno, Nevada, April 19-23, 2015.

Smith, M, T. Brandt and Stone, J. (1995). "Effect of soil texture and microtopography on germination and seedling growth in *Boltonia decureens* (Asteraceae), a threatened floodplain species," Wetlands, 15(4), pp 392-396.

U.S. Department of Interior, Bureau of Reclamation. (1996). Removal of Elwha and Glines Canyon Dams, Elwha Technical Series PN-95-7, 86 pp.

Walker, L.R. and del Moral, R. (2003). Primary Succession and Ecosystem Rehabilitation. Cambridge, UK. Cambridge University Press.

Ward, L., Crain, P., Freymond, B., McHenry, M., Morrill, D., Pess, G., Peters, R., Shaffer, J.A., Winter, B., and Wunderlich, B. (2008). Elwha River Fish Restoration Plan–Developed pursuant to the Elwha River Ecosystem and Fisheries Restoration Act, Public Law 102-495. U.S. Department of Commerce, NOAA Technical. Memo. NMFS-NWFSC-90, 168 p.

Whisman, M. (2013). "Revegetation of Post-Dam Removal Riparian Sediments in the Lower Elwha River, WA," Master's thesis, Evergreen State College, Olympia, WA.

Williams, B.K., and Brown, E.D. (2012). Adaptive Management: The U.S. Department of the Interior Applications Guide. Adaptive Management Working Group, U.S. Department of the Interior, Washington D.C.

ELWHA RESERVOIR SEDIMENT MODELING IN A GIS FRAMEWORK

Timothy J. Randle, Supervisory Hydraulic Engineer, Bureau of Reclamation, Denver, Colorado, trandle@usbr.gov; Jennifer Bountry, Hydraulic Engineer, Bureau of Reclamation, Denver, Colorado, jbountry@usbr.gov; Kurt B. Wille, Supervisory Physical Scientist, Bureau of Reclamation, Denver, Colorado, kwille@usbr.gov

Abstract: An empirically based, sediment-budget model was developed in a geographic information system (GIS) framework to support an adaptive sediment management program for two dam removals on the Elwha River near Port Angeles, Washington State, USA. This numerical model had the advantages of being able to handle the complex three-dimensional topography of sediment layers in a reservoir, rapidly incorporate new monitoring data, and quickly simulate multiple future scenarios in response to changing conditions. Even though the model did not simulate the detailed hydraulics, it was able to simulate the most important aspects of channel evolution through reservoir sediments during dam removal.

Model simulations were used to aid the adaptive management program by predicting the channel evolution in the reservoir and forecast the coarse (sand and gravel) and fine (silt and clay) sediment release to the downstream river channel over time under various hydrologies and dam removal schedules. The simulated three-dimensional reservoir topography could easily be visualized in GIS. The model predictions helped to guide and focus the monitoring activities while the monitoring results helped to revise and calibrate the numerical model. This combined approach of hypotheses, incorporated into the numerical model, and monitoring results increased the rate of learning compared to singular approaches of only monitoring or modeling.

INTRODUCTION

This paper describes the development and application of an empirically based, sediment-budget model for the adaptive management program associated with a project to remove two large dams on the Elwha River near Port Angeles, Washington, USA. The model accounts for the primary geomorphic processes (e.g., channel incision, lateral erosion, aggradation, and new delta formation), but not the detailed hydraulics. The model was developed in a geographic information system (GIS) framework to account for the complex three-dimensional reservoir geometries and to facilitate the display of simulated reservoir topography.

The National Park Service, with technical support from the Bureau of Reclamation, removed Elwha and Glines Canyon Dams on the Elwha River to restore anadromous fish and the natural ecosystem (Figure 1). The Elwha River dams had blocked fish migration for a century. The two dams were the largest ever removed and together (before their removal) contained 27 million yd^3 of reservoir sediment (Randle et al., 2015). These dams were concurrently removed in controlled increments over a one and three-year period, which began in September 2011.

The 105-foot high Elwha Dam was completed in 1913 at river mile 5 and formed Lake Aldwell, which had an original storage capacity of 9,100 acre-feet (U.S. Department of the Interior and U.S. Department of Commerce, 1994). The 210-foot high Glines Canyon Dam was completed in 1927 at river mile 13 and formed Lake Mills, which had an original storage capacity of 40,500

acre-feet. Both dams were constructed to produce hydroelectric power and neither reservoir provided flood control or water supply storage.

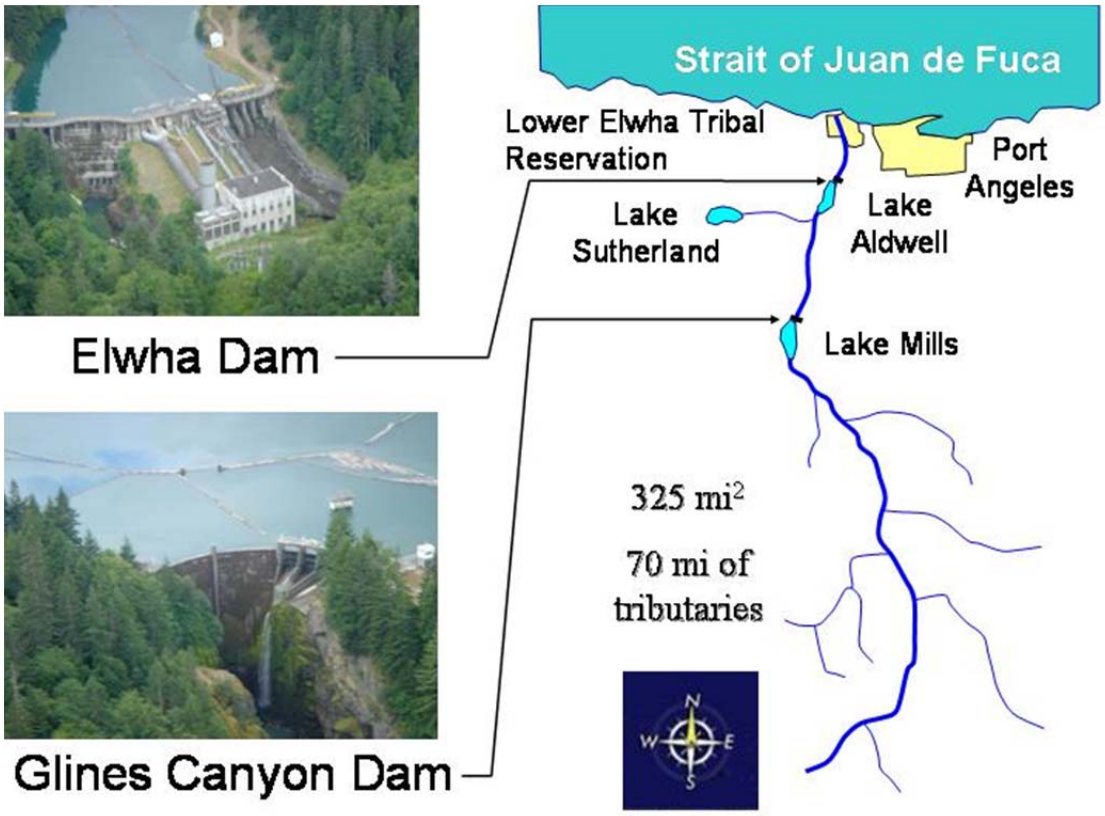

Figure 1. Elwha and Glines Canyon Dams are located on the Elwha River near Port Angeles, Washington, U.S.A.

In July 2010, reservoir sedimentation in both lakes was estimated to be 27 million yd^3 (Randle et al., 2015), which was 35 percent of the original storage capacity. Most of the coarse reservoir sediment (sand and gravel) had deposited as a large delta in Lake Mills (the upstream reservoir). The thickest delta deposit, measured from drill holes in 1999 and 1994, was 70.5 feet in Lake Mills and 42.6 feet in Lake Aldwell (Gilbert and Link, 1995).

In preparation for dam removal, new facilities were constructed for water quality and flood protection. The quantitative sediment effects of dam removal were initially predicted for an environmental impact statement (U.S. Department of the Interior, 1996) based on measured sediment erosion during the 1994 Lake Mills drawdown experiment (Childers et al., 2000), sediment and topographic surveys of the reservoir, a numerical sediment-budget model, and numerical modeling of the downstream river channel (Randle et al., 1996). Later, a laboratory model was utilized to evaluate the extent and rate of reservoir sediment erosion as a function of the dam removal rate (Bromley, 2007). Prior to the beginning of dam removal, the empirically-based sediment-budget model (initially developed by Randle et al., 1996) was updated and re-written in a GIS framework. The model described in this paper was used to provide up-to-date predictions based on dynamic reservoir sediment conditions, hydrology, and updated dam removal schedules. The model simulated the reservoir channel evolution, amount and timing of

coarse (sand and gravel) and fine (silt and clay) sediment erosion and release from both reservoirs and the volume and future topography of sediment remaining in the reservoirs.

An adaptive management program was designed to ensure that Elwha River Restoration Project management objectives were met and that sediment impacts were contained by mitigation facilities (Randle and Bountry, 2010 and Bountry, 2015 these proceedings). Key monitoring activities focused on the extent and rate of vertical and lateral erosion of the exposed reservoir sediment, downstream water quality impacts associated with release of fine sediment from the reservoirs, downstream aggradation from the release of coarse reservoir sediment, and forecasting the sediment release through the reservoirs with numerical modeling. Measured sediment effects were compared with predictions, so that adjustments in the dam removal schedule (or other corrective actions) could be taken when necessary.

The empirically-based, sediment-budget modeling approach was used, rather than a one- or two-dimensional (1D or 2D) sediment transport model. A 1D model could not simulate important lateral erosion and delta progradation processes. A 2D model would have required many days or weeks of computer time to simulate the necessary range of hydrologies and changing dam removal schedules and there would have been difficulty automatically adjusting the 2D model mesh with continued sediment terrace bank erosion. The sediment-budget model runs relatively fast and was able to track the complex three-dimensional topography of each reservoir over time.

DAM REMOVAL AND SEDIMENT MANAGEMENT PLAN

The dam removal and sediment management plan was to concurrently remove both dams in controlled increments and allow the Elwha River to incise and erode a portion of the reservoir sediments downstream to the Strait of Juan de Fuca (U.S. Department of the Interior, 1996). The model incorporated reservoir drawdown increments of 5 to 15 feet at a maximum allowable rate of 3 feet per 49 hours. After each reservoir drawdown increment, the remaining reservoir pool was held at relatively constant levels for two weeks to two months to induce lateral erosion of the exposed sediments. The longer reservoir hold periods were known as “fish windows” and corresponded to important fish migration periods: May 1 to June 30, Aug. 1 to Sep. 15, and Nov. 1 to Dec. 31.

Because of the anticipated large sediment release, several water quality and flood protection facilities were designed and constructed to mitigate impacts. Water treatment plants, new wells, and a new surface water intake were constructed to protect existing water users from high suspended sediment concentrations. Some new levees were constructed and the heights of existing levees were increased to protect property and infrastructure from possible increases in flood stage that could result from coarse sediment aggradation in the downstream river channel.

NUMERICAL MODEL OBJECTIVES AND OVERVIEW

The primary numerical model objectives are: (1) simulate the reservoir sediment erosion, re-deposition, and release of fine and coarse-sized sediment over time from both reservoirs; (2) predict the portion of sediment retained within the reservoir after dam removal; and (3) provide a framework to guide the collection and synthesis of monitoring data.

The empirical rules of the numerical sediment-budget model are based on geomorphic and sediment transport principals and field measurements. The model tracks fine sediment separately from coarse sediment. As the reservoir is drawn down, the river is assumed to erode a primary channel through the exposed reservoir sediments. The coarse sediment that is eroded during this process is assumed to redeposit in the receded reservoir so long as the reservoir exists. Fine sediment that is eroded during this process is assumed to become suspended in the receded reservoir. A portion of this fine suspended sediment is assumed to re-deposit on the lakebed while the remainder is assumed to transport past the dam. After the reservoir has been drained, eroding coarse and fine sediments are assumed to be transported past the dam.

The numerical sediment-budget model consists of three computer programs for each reservoir:

1. The pre-processing FORTRAN program determines the daily reservoir water and sediment inputs, the daily reservoir drawdown schedule, and the GIS model time steps. These GIS model time steps are variable, but typically range from one to two months and include a given reservoir drawdown increment and subsequent hold times, which may be extended due to high flows or fish windows.
2. The GIS model simulates the channel evolution through the complex topographic surfaces of the reservoir sediment terraces for each model time step.
3. The post-processing FORTRAN program computes the daily coarse and fine sediment loads and concentrations released past each dam based on the output from the GIS model.

MODEL BOUNDARY AND INITIAL CONDITIONS

The upstream model boundary conditions include hydrographs of water discharge and sediment load and the dam removal schedule. The initial conditions consist of the reservoir bathymetry and percentages of coarse and fine sediment for various sub-areas of the reservoir.

A range of historic discharge hydrographs (13-year periods) were used to simulate future conditions: (*i*) water years 1950 through 1963 (normal hydrology), (*ii*) water years 1969 through 1991(dry hydrology), (*iii*) water years 1971 through 1994 (normal hydrology), and (*iv*) water years 1999 through 2002 (wet hydrology). As dam removal progressed, each hydrology was updated with the measured discharge values. Discharge was measured at the McDonald Bridge stream gage (12045500), located between Glines Canyon Dam and Lake Aldwell. The fine and coarse sediment loads from the upstream watershed were computed from sediment-discharge rating curves (Randle et al., 1996).

The future reservoir drawdown schedules (a downstream boundary condition) were determined by the model based on the following information: (*i*) contractor's proposed construction schedule, (*ii*) reservoir inflow discharge, (*iii*) reservoir drawdown rate restrictions, (*iv*) reservoir drawdown increment limits, (*v*) overtopping flow work restrictions, and (*vi*) required reservoir hold periods, including fish windows.

Initial reservoir model conditions consisted of the reservoir bathymetry (measured in July 2010 by Bountry et al., 2011), coarse and fine sediment percentages, and initial alignment of river channels on the delta. A pilot channel was constructed on the Lake Mills delta during September

2010 and was incorporated into the initial topographic conditions. The predam reservoir topography was used by the model to represent the lower limit of reservoir sediment erosion. For Lake Mills, the predam topography was based on a 1921, 10-foot contour map. The Lake Aldwell predam topography had to be estimated from drill holes and thickness probes, and later by incorporating exposed pre-dam topography (Gilbert and Link, 1995; Randle et al, 2015). Percentages of coarse and fine sediment were specified for reservoir polygon areas defined by Gilbert and Link (1995). Single sediment layers were typically specified, but three vertical sediment layers were specified for the Lake Mills delta.

SIMULATION OF RESERVOIR CHANNEL EVOLUTION

For each model time step, the GIS spatial model computes a sediment balance between the upstream sediment-supply volume, the river-erosion volume of the exposed sediment, and the corresponding reservoir-deposition volume. The river-erosion volume is a function of the reservoir-drawdown increment, longitudinal erosion slope, peak discharge, and the river erosion width along the upstream portion of the delta and where the river meets the receded reservoir (Figure 2 and Figure 3). So long as a reservoir remains between the delta and the remaining dam, the coarse sediment fraction of the river erosion volume is assumed to re-deposit as a new delta in the receded reservoir on top of the fine lakebed sediment. The model is able to account for compaction of the underlying fine sediment. During each increment of reservoir drawdown, the delta front extends farther downstream into the receded reservoir causing some aggradation along the upstream erosion channel (Figure 2 profile view).

The fine sediment fraction of the river-erosion volume is assumed to enter the reservoir as suspended sediment. Using a sediment trap efficiency equation (Pemberton and Lara, 1971), the model calculates the portion of fine suspended sediment that will settle to the reservoir bottom and the portion that will be transported in suspension past the dam. Once the delta has prograded all the way downstream to the remaining dam, the reservoir pool no longer exists, and all eroded sediments are released past the dam.

For future simulations, the GIS spatial model uses the concepts illustrated in Figure 2 to simulate erosion and deposition of the complex topographic surfaces to ensure separate volume balances for coarse and fine sediments. The spatial model consists of a set of vector-based customizations and a series of raster-based analysis tools that are run at each time step according to the reservoir drawdown schedule. The vector-based customizations are used to determine potential erosion and deposition geometries. The vector geometries are fed into the raster-based analysis tools that update an input surface raster (10 ft × 10 ft) to reflect the sediment inflow, erosion, deposition, and downstream release.

The delta erosion, topset, and foreset slopes (S_T, S_T, and S_F) are specified by the model user while geometric dimensions of delta length, upstream channel width and channel width where it meets the lake (D_L, W_{min}, and W_L) are computed by the model. The volume calculations are linked where the river erosion channel meets the receded reservoir. At this location, the computed river erosion width equals the reservoir deposition width (W_{max}). Aggradation in the erosion channel is linked to the length of new delta deposition. Therefore, the model uses an iterative approach to achieve the volume balance for coarse sediment.

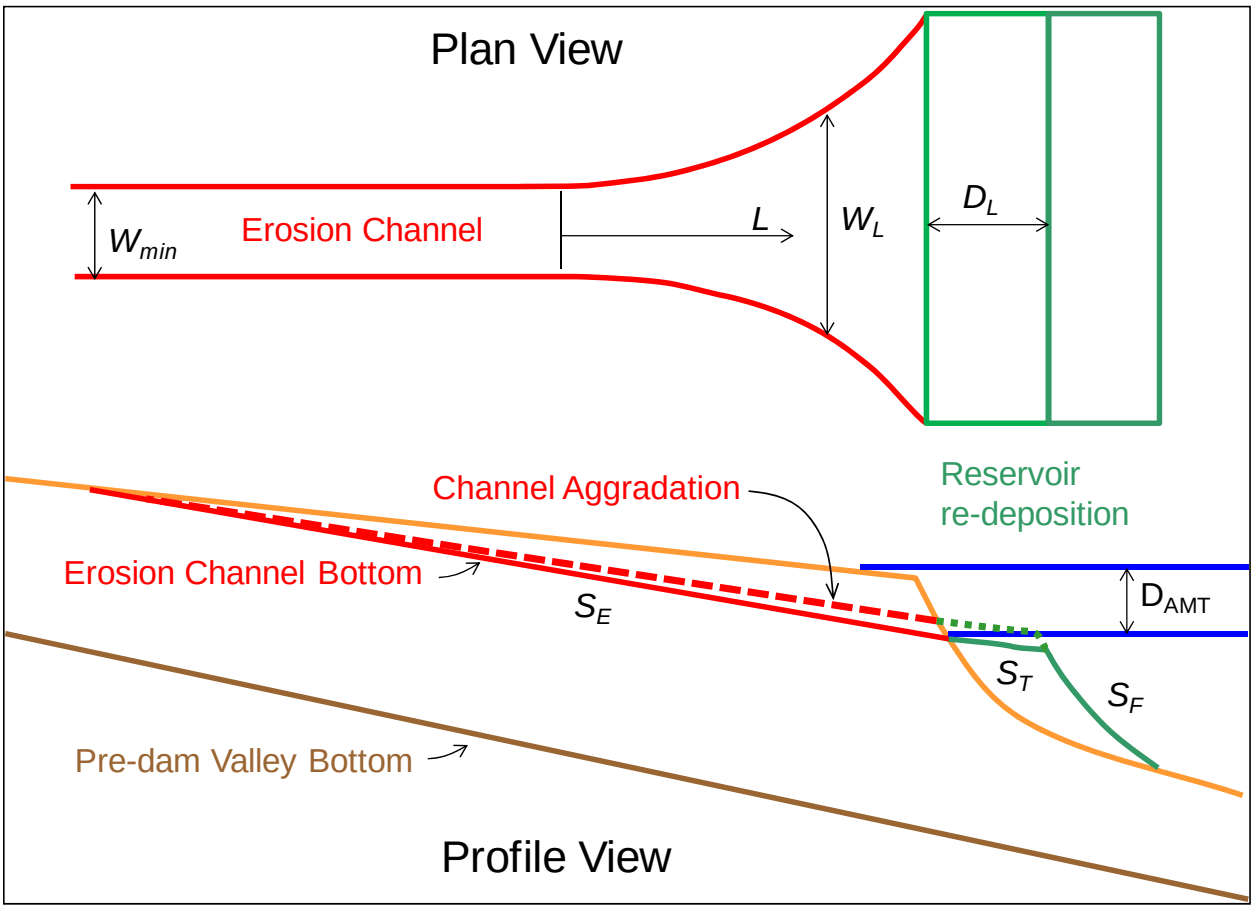

Figure 2. Plan and profile sketch of reservoir sediment erosion and re-deposition. The variables shown in the figure are described in the body of the paper.

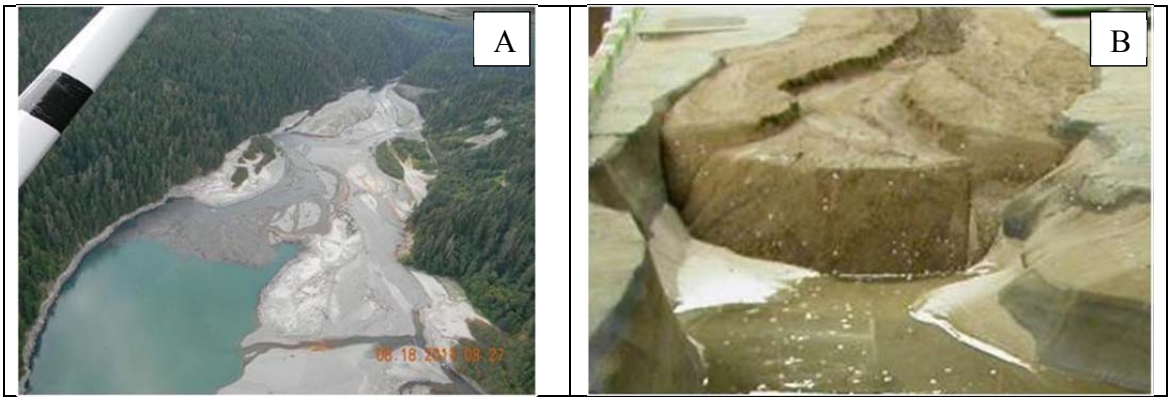

Figure 3. Photographs of sediment erosion and re-deposition at Lake Mills (A) as observed in August 2011 (16 feet of spillway drawdown prior to dam removal) and (B) in a laboratory model of Lake Mills conducted by Bromley (2007).

The model computes the sediment erosion volume using the topography at the beginning of the time step, the delta erosion slope (S_E) corrected for aggradation, and the channel erosion widths (Figure 2 plan view). The model computes the coarse, reservoir deposition volume using the delta topset slope (S_T) adjusted for aggradation, foreset slope (S_F), the deposition width across the receded reservoir (W_{max}), and the reservoir bathymetry at the beginning of the time step. After the Lake Mills delta prograded all the way to Glines Canyon Dam, there was a year-long hold period in order to reduce the rate of reservoir sediment erosion and downstream release. For this long hold period, the model exponentially decreased the channel erosion slope over time.

$$S_E(t_n) = S_E e^{(-7.57\text{E}-04\ T_Q)} \tag{1}$$

Where T_Q is the cumulative number of days since the delta reached the dam (10/23/2013) where the discharge was greater than a transport threshold (2,000 ft^3/s).

The reservoir drawdown increments in Lake Aldwell and Lake Mills nearly always eroded enough coarse sediment to deposit a new delta across the entire width of the receded reservoir. For this common case, the model computed the downstream length of the new delta topset (D_L). For the few cases where the erosion volume was not sufficient to deposit a new delta across the entire reservoir width, a default topset length wa9s specified and the model computed the delta deposition width (which is also equal to the maximum erosion width).

Sediment Erosion Volume Calculations For future simulations, the model computes the minimum erosion-channel width (W_{min}), for each time step, as a function of the peak discharge (Q_{max}) and a time-adjustment factor (T_A), which was developed from monitoring observations.

$$W_{min} = \left[aQ_{max}{}^{b}\right]T_A \tag{2}$$

The coefficient a is calibrated from measured erosion widths and the exponent b is chosen from literature (typically 0.5). The time-adjustment factor (T_A) is based on the number of days (N_D) (during the model time step) where the mean-daily discharge equals or exceeds the mean discharge (for the model time step) and is also above a user-specified threshold. An empirically determined coefficient (α) is also used in Eq. 3.

$$1 \le T_A = (\alpha N_D + 1) \qquad \alpha = \frac{2/3}{10} = 0.0667 \tag{3}$$

The minimum erosion width is assumed to increase as the river erosion channel approaches the receded reservoir where the channel laterally migrates to deposit sediments.

$$W_L = 2cL^2 + W_{min} \tag{4}$$

where W_L is the erosion width as the river approaches the receded reservoir, L is the longitudinal distance along the erosion channel centerline (Figure 2), and c is a coefficient computed by the model so that the erosion channel width equals the reservoir deposition width where the erosion channel meets the reservoir. The total length of channel (L_{max}) where the erosion width increases is specified by the model user as a function of the local reservoir width.

$$L_{max} = f\, W_{max} \tag{5}$$

Computation of the river-erosion volume begins with the reservoir drawdown increment. The downstream extent of the erosion channel is computed as the intersection of the erosion channel and the receded reservoir. Initially, the channel bottom elevation at the downstream end is assumed to equal the lowered reservoir-water surface elevation. From this elevation, the user specified longitudinal erosion slope is projected upstream to the intersection with the upstream sediment surface or the predam surface, whichever is encountered first. The aggradation volume in the sediment erosion channel is computed after the new delta length (D_L) is computed.

The erosion channel centerline is specified by the model user. The left and right banks of the river erosion channel are determined from the channel centerline and the computed erosion-channel widths. Alternatively, when measured bank-line data are available from the monitoring program, they can be used as an input feature in place of the computed erosion-channel widths in conjunction with the user-specified centerline. This was of particular value when the actual erosion width was non-uniform along substantial portions of the channel length.

Reservoir Sediment Trap Efficiency Calculations The reservoir sediment trap efficiency (P) is computed as a function of the sediment particle fall velocity (ω), inflow discharge (Q), and surface area of the remaining reservoir (A_s) (Pemberton and Lara, 1971). The sediment particle fall velocity (ω) is a function of the median fine sediment particle size (d, ft) and the water viscosity (ν, ft^2/s), which is a function of water temperature (T, ^{o}C).

$$P = \left(1 - \frac{1}{e^{\left(\frac{1.005\omega A_S}{Q}\right)}}\right) \tag{6}$$

$$\omega = \frac{\sqrt{36.064\, d^3 + (6\,\nu)^2} - 6\,\nu}{d} \tag{7}$$

$$\nu = \frac{0.00002}{(1.0334 + 0.03672\, T + 0.0002059\, T^2)} \tag{8}$$

Daily Reservoir Sediment Release Calculations The post-processing FORTRAN program uses the fine and coarse-sediment erosion volumes (computed by the GIS model for each simulation time period) to compute the daily fine and coarse sediment-release rates past each dam. A daily factor (D_F) is computed to distribute the sediment release volumes from the longer GIS model time step. Initially, each daily factor (D'_F) is computed as the weighted sum of the daily reservoir drawdown factor (R_F) and the daily discharge factor (Q_F) (Eq. 9). The daily factors within each GIS model time step are then adjusted to sum to 1 (Eq. 10). In the equations below, t_n indicates the value at day n and t_o indicates the value at the beginning of the time step. Model coefficients and exponents are described in Table 1, Table 2 and Table 3.

$$D'_F(t_n) = c_7 R_F + (1 - c_7) Q_F(t_n) \tag{9}$$

$$D_F(t_n) = \frac{D'_F(t_n)}{\sum_{n=1}^{m} D'_F(t_n)} \tag{10}$$

The computation of the daily reservoir drawdown factor (R_F) depends on whether the reservoir is drawing down, holding, or refilling. The daily reservoir drawdown increment (D_{INC}) (Eq. 11) and the cumulative drawdown increment since the beginning of the GIS model time step (D_{AMT}) (Eq. 12) are computed from the daily water surface elevations (WSE). The daily change in mean-daily discharge (ΔQ_w) (Eq. 13) is also computed to determine if the discharge is increasing.

$$D_{INC}(t_n) = WSE(t_n) - WSE(t_{n-1}) \tag{11}$$

$$D_{AMT}(t_n) = WSE(t_n) - WSE(t_o) \tag{12}$$

$$\Delta Q_w(t_n) = Q_w(t_n) - Q_w(t_{n-1}) \tag{13}$$

If the reservoir is drawing down, $D_{INC}(t_n) < c_3$, then

$$R_F(t_n) = 0.020\ c_1^{\left(\frac{-1\{D_{AMT}(t_n)\}}{1.5ft}\right)} \tag{14}$$

If the reservoir is holding, $D_{INC}(t_n) \geq c_3$, then

$$R_F(t_n) = c_2\ R_F(t_{n-1}); \tag{15}$$

If the reservoir inflow discharge is increasing, $\Delta Q_w(t_n) \geq 1{,}000$ ft^3/s, or the inflow is high, $Q_w(t_n) > 3{,}500$ ft^3/s, then

$$R_F(t_n) = 0.020\ c_1^{\left(\frac{Q_W(t_n)}{1{,}000ft^3/s}\right)} \tag{16}$$

Initially, the daily discharge factor (Q'_F) is computed as a function of the mean daily discharge (Eq. 17).

$$Q'_F(t_n) = (Q_w)^{c_4}(t_n) \tag{17}$$

$$Q_F(t_n) = \frac{Q'_F(t_n)}{\sum_{n=1}^{m} Q'_F(t_n)} \tag{19}$$

The model computes the concentration of fine sediment (ppm) being transported past the dam from the sediment trap efficiency (P), erosion volume (V_F), unit weight of sediment (γ), and the mean-daily river discharge (Q_w). A time lag is also applied to account for travel time through the reservoir.

$$Conc = \frac{(1-P)V_F\gamma}{Q_w}\left(\frac{2{,}000lbs/ton}{(62.4lbs/ft^3)(3{,}600s/hr)(24hrs/day)}\right)1{,}000{,}000 \tag{19}$$

Turbidity is computed from the concentration by use of a power equation, but the coefficient and exponent were found to vary over time under changing sediment conditions.

$$Turbidity = c_5\ (Conc)^{c_6} \tag{20}$$

MODEL CALIBRATION

Although there are many model calibration parameters, the coefficients and exponents appeared to be very reasonable. Compaction of fine reservoir sediment was considered, but not used. The median grain size for fine sediment was calibrated to a value of 0.01 mm, which represents fine silt. The delta channel erosion widths, lengths of delta erosion affected by deposition, and longitudinal erosion slopes were calibrated separately for Lake Mills and Lake Aldwell. The erosion channel centerline of the exposed delta is a user input. Measured past channel alignments were delineated in GIS. Future channel migration of the erosion channel alignment is based on past migration, geologic controls within the reservoir landscape, whether the channel was eroding into non-cohesive (coarse) or cohesive (fine) sediment, and professional judgment. Post processing model parameters were calibrated to match the pattern and magnitude of measured turbidity downstream from Elwha Dam. Summary lists of model input parameters are presented in Table 1 for river erosion, Table 2 for new delta deposition, and Table 3 for daily sediment release past the dam.

Table 1. Summary list of model input parameters for river erosion.

Variable	Description
a and b	Coefficient ($2.3 < a < 6$) and exponent (typically b = 0.5) used to compute the minimum erosion-channel width as a function of discharge (Eq. 2).
α	Coefficient used to compute the time-adjustment factor ($T_A = 0.0667$) (Eq. 3).
c	Coefficient used to compute the erosion-channel width near the receded reservoir. This coefficient is calculated by the model (Eq. 4).
f	Multiplier used to compute the maximum channel length (L_{max}) upstream from the receded reservoir where the erosion width is influenced by new delta deposition ($1 < f < 3$) (Eq. 5).
S_E	Longitudinal slope of the river erosion channel ($0.003 < S_E < 0.011$).

Table 2. Summary list of model input parameters for new delta deposition.

Variable	Description
D_L	Default topset length ($D_L = 200$ feet)
S_T	Topset slope ($S_T = 0.0009$ for Lake Aldwell and 0.0050 for Lake Mills)
S_F	Foreset slope ($S_F = 0.020$ for Lake Aldwell and 0.032 for Lake Mills)
Reservoir sediment trap efficiency parameters:	
d	Median particle size of fine sediment ($d = 0.010$ mm) (Eq. 7)
T	Water temperature ($T = 50$ degrees Fahrenheit) (Eq. 8)

Table 3. Summary list of model input parameters for daily sediment release.

Variable	Description
c_1	Sediment concentration time factor for continued reservoir drawdown ($c_1 = 1.10$) (Eq. 14 and 16)
c_2	Sediment concentration time factor for continued reservoir holding or refilling (if $t_n \leq 30$ days, then $c_2 = 0.97$; if $t_n > 30$ days, then $c_2 = 1$) (Eq. 15)
c_3	Threshold to distinguish between reservoir drawdown and holding or refilling ($c_3 = -0.50$ ft/day) (Eq. 14 and 15)
c_4	Exponent for weighting the discharge ($c_4 = 3.50$) (Eq. 17)
c_5	Coefficient to convert sediment concentration to turbidity ($c_5 = 0.992$) (Eq. 20)
c_6	Exponent to convert sediment concentration to turbidity ($c_6 = 1.0044$) (Eq. 20)
c_7	Weighting factor to compute the daily factor (D'_F) ($c_7 = 0.333$) (Eq. 9)

EXAMPLE MODEL RESULTS AND DISCUSSION

The reservoir sediment erosion model has been applied numerous times during concurrent dam removal to simulate a range of hydrologies and proposed dam removal schedules (Bountry et al., 2015 these proceedings). An example simulation, performed in April 2012, is provided using the historical flow records from water years 1950 through 1968, except that the actual flows were used for the period October 2010 through April 2012. Simulated hydro-graphs of reservoir water surface elevation, discharge, and turbidity are presented in Figure 4.

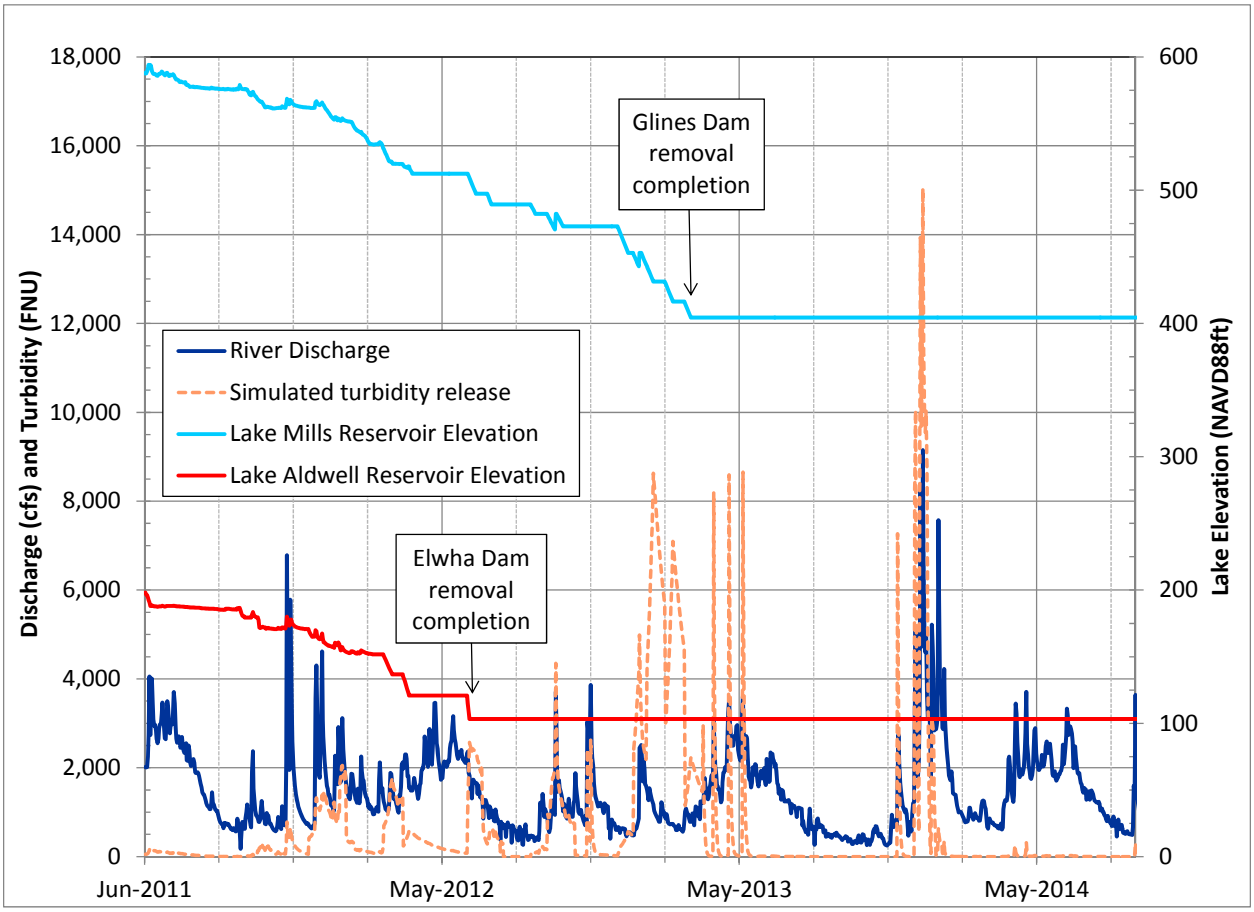

Figure 4. Example simulation of fine-sediment release from Lake Mills and Lake Aldwell.

The simulated reservoir sediment thickness before and after dam removal is presented in Figure 5 for Lake Mills and in Figure 6 for Lake Aldwell. Colored areas represent reservoir sediment terraces. The darker color red corresponds to the areas of thickest sediment while the gray areas represent areas where the sediments have been eroded down to the estimated predam surface.

For this example simulation, 50% of total reservoir sediment would be transported past the dam, 10 years after dam removal. About half of the sediment was measured to erode from the reservoirs by the end of 2014. The model correctly predicted the time when the eroding reservoir delta would reach the dam and the correct order of magnitude of downstream

turbidities. The model incorrectly assumed that the channel incision from a given reservoir drawdown increment would completely occur during a one- to two-month time step.

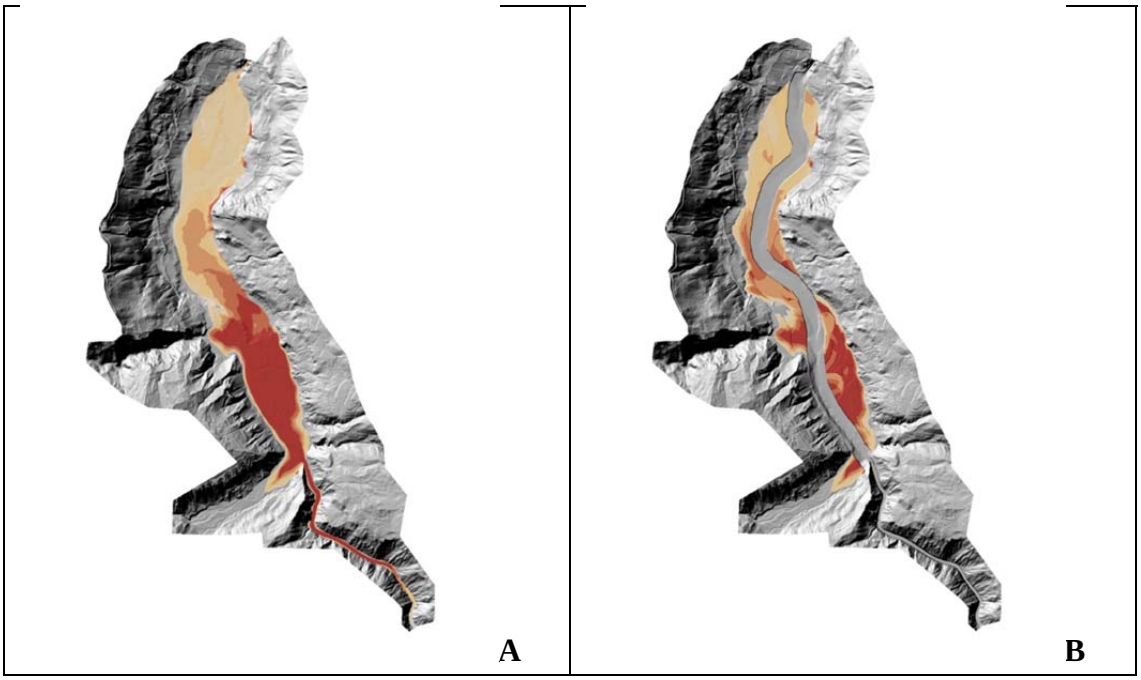

Figure 5. Example simulation of Lake Mills sediment thickness before (A) and after dam removal (B).

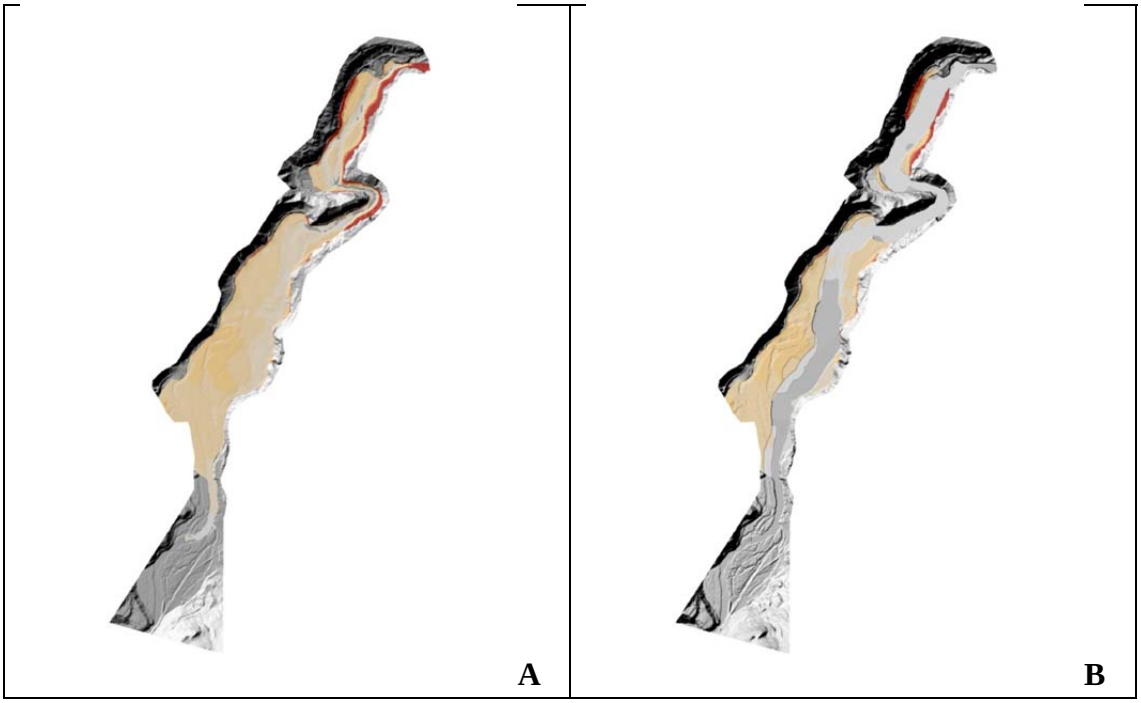

Figure 6. Example simulation of Lake Aldwell sediment thickness before (A) and after dam removal (B).

Actual knickpoint migration proved to be much slower, especially in Lake Mills. However, the actual reservoir erosion width, slope, and alignment could be updated as dam removal progressed, along with the hydrology and dam removal schedule, so that simulations of future scenarios were increasingly more accurate. The simulated volume of sediment erosion was most influenced by erosion channel width and slope. The daily patterns of sediment concentration and turbidity released downstream were most influenced by the coefficients c_1, c_2, c_3, c_4, and c_7.

Future model simulations were used in the decision to hold Glines Canyon Dam removal activities for the second year of project implementation. Actual river discharges were a bit different than the four historic hydrologies. Actual peak discharges were less than the 2-year flood peak during the first three years of project implementation, but mean discharge was above average. The dam removal contractor could work faster, and during higher river discharge, than assumed in the initial model simulations.

CONCLUSIONS

The reservoir sediment erosion model is able to simulate the channel incision, lateral erosion, and redeposition of sediment during phased dam removal. Model application requires the user to specify numerous parameters. All the physically-based model input variables are based on direct field measurements or calibrated using field measurements. Coefficients c_1 through c_7 (Table 3) are based on professional judgment, but are generally close to 1. The model was able to simulate the most important channel evolution processes and was able to simulate a large number of future scenarios of concurrent dam removal during project implementation.

In addition to the predictive capabilities, the numerical model represented a set of linked hypotheses that could be tested and updated based on monitoring data. The testing of these hypotheses with monitoring results increased the rate of learning compared to singular approaches of modeling or monitoring alone. The required model inputs and the outputs help focus and organize the monitoring data that were crucial for testing the hypotheses. The model was updated throughout the project as new information became available on dam removal schedules and monitoring on the rate and extent of sediment erosion.

REFERENCES

Bountry, J.A.; Ferrari, R.; Wille, K.; and Randle, T.J. (2011). 2010 Survey Report for Lake Mills and Lake Aldwell on the Elwha River, Washington, SRH-2010-23, U.S. Department of the Interior, Bureau of Reclamation, Denver, CO, June 2011.

Bountry, J.A.; Crain, P.; Chenoweth, J.; Randle, T.J.; Ritchie, A. (2015). Role of Adaptive Sediment Management in Elwha Dam Removal in Proceedings of the 10th Federal Interagency Sedimentation Conference, Reno, NV, April 20-23.

Bromley, C. (2007). The morphodynamics of sediment movement through a reservoir during dam removal. PhD Thesis, University of Nottingham, pp. 316.

Childers, D., Kresch, D. L., Gustafson, S. A., Randle, T. J., Melena, J. T., Cluer, B., 2000. Hydrologic data collected during the 1994 Lake Mills Drawdown Experiment, Elwha River, Washington. USGS Water-Resources Investigations Report: 99-4215.

Gilbert, J. and Link, R. (1995). "Alluvium Distribution in Lake Mills, Glines Canyon Project and Lake Aldwell, Elwha Project, Washington," *Elwha Technical Series PN-95-4*, U.S. Bureau of Reclamation, Pacific Northwest Region, Boise, ID, 60 pages.

Pemberton, E.L. and Lara, J.M. (1971). "A Procedure to Determine Sediment Deposition in a Settling Basin," U.S. Bureau of Reclamation, Sedimentation Investigations Technical Guide Series, Section E. Intake Works and Desilting Basins, Part 2. Setting Basins, Sedimentation Section, Denver, CO, 9 pages.

Randle, T.J.; Young, C.A.; Melena, J.T.; Ouellette, E.M. (1996). "Sediment Analysis and Modeling of the River Erosion Alternative," *Elwha Technical Series PN-95-9*, U.S. Department of the Interior, Bureau of Reclamation, Boise, Idaho, 139 pages.

Randle, T.J. and Bountry, J.A. (2010). "Elwha River Restoration: Sediment Adaptive Management," 9th Federal Interagency Sedimentation Conference, Las Vegas, Nevada, June 27 - July 1, 2010.

Randle, T.J.; Bountry, J.A.; Ritchie, A.; Wille K. (2015). "Large-scale dam removal on the Elwha River, Washington, USA: erosion of reservoir sediment," *Journal of Geomorphology*.

U.S. Department of the Interior and U.S. Department of Commerce. (1994). National Park Service, Bureau of Reclamation, Bureau of Indian Affairs, U.S. Fish and Wildlife Service; National Marine Fisheries Service; and Lower Elwha S'Klallam Tribe. *The Elwha Report — Restoration of the Elwha River Ecosystem and Native Anadromous Fisheries.* Olympic National Park, WA, January 1994.

U.S. Department of the Interior. (1996). *Elwha River Ecosystem Restoration Implementation, Draft Environmental Impact Statement*, National Park Service, Olympic National Park, Port Angeles, WA.

NEGOTIATING HYDROLOGIC UNCERTAINTY IN LONG TERM RESERVOIR SEDIMENT MODELS: SIMULATING ARGHANDAB RESERVOIR DEPOSITION WITH HEC-RAS

Gibson, S. PhD, Senior Hydraulic Engineer, Hydrologic Engineering Center, U.S. Army Corps of Engineers, Davis, CA. stanford.gibson@usace.army.mil
Pridal, D. PE, Senior Hydraulic Engineer, U.S. Army Corps of Engineers

Abstract: Water stored in the Arghandab Reservoir, in northeastern Afghanistan, supports subsistence agriculture in the Arghandab valley. The reservoir's contributing watershed is mountainous and mostly unvegetated, contributing unusually high sediment concentrations. Since its 1952 closure, sediment has filled about 45% of the reservoir volume. Lost reservoir capacity makes meeting downstream demand during low flow years difficult. The HEC-RAS sediment model was constructed and calibrated with a systematic, three step calibration process, targeting: 1) total volume, 2) longitudinal distribution and 3) gradation of sediment deposits. The calibrated model predicted reservoir stage-volume curves for four scenarios, including current conditions and three spillway raises. However, hydrologic uncertainty complicated prediction.

Gage flow records in this region are discontinuous, making hydrologic modeling challenging. Truncated time-series introduce uncertainty in sediment delivery and deposition simulations over standard, 50-year "project" time scales, longer simulations predicting reservoir lifespan. Therefore, stochastic scenarios of future hydrology included unobserved, low probability (1% to 0.1%) synthetic time series to quantify the uncertainty on long term (200 year) reservoir lifespan analyses associated with a brief measured flow record. This paper describes a systematic, three-stage method to calibrate 1D reservoir models, and an approach to hydrologic uncertainty in long-term sediment studies with short flow records.

Keywords: Sediment Modeling, Reservoir sedimentation, hydrologic uncertainty, sediment calibration, HEC-RAS

INTRODUCTION

The Arghandab River, and the irrigation systems built around it, made agriculture possible in arid southern Afghanistan, and are responsible for most of the region's economy (CID, 2008). The river supports subsistence agriculture in the Arghandab valley with water from mountain snow. Snow-melt hydrology is episodic, so converting it into reliable irrigation requires storage. The Arghandab reservoir, impounded by Dala -am, the second largest in Afghanistan, storing the episodic snow-melt regime and releasing predictable flows required for agriculture and irrigation. However, the mountainous, unvegetated watershed delivers unusually high sediment loads, filling 45% of the reservoir's capacity since the dam closure in 1952. As reservoirs fill with sediment, water storage is reduced and they lose the capacity to buffer communities against either floods or droughts. Storage lost to sediment increases the risk that water demand in dry years will not be met, which could have devastating social impacts on downstream agricultural communities.

The U.S. Army Corps of Engineers Omaha District and Hydrologic Engineering Center built hydrologic, hydraulic, and sediment models of this system to estimate the reservoir lifecycle and predict sedimentation effects on future drought vulnerability. The models also evaluated three spillway raise proposals and the influence these would have on reservoir life and future drought

risk on these estimates. The sediment modeling encountered two obstacles common in reservoir sediment transport modeling, equifinality and hydrologic uncertainty. The study documented approaches to:

1. Negotiate equifinality with a three-stage process of sediment calibration.
2. Quantify hydrologic uncertainty with stochastic analysis featuring hybrid time series including historical and synthetic hydrology.

These approaches to these common problems could inform and improve similar future work.

THREE-STAGE SEDIMENT CALIBRATION PROCESS

"Equifinality" - multiple parameter combinations can produce the same calibration results -is a challenge for any multi-parameter modeling problem (Beven, 1993; Pappenberger et al., 2005). Calibrating models with multiple, sensitive, uncertain parameters introduces non-unique solutions. Multiple parameter combinations can produce the same model result, reducing the confidence in the calibration and increasing the uncertainty of predictive results. Ordering free parameters by sensitivity and confidence can isolate the most important parameters (Ruark, 2011; USACE, 2014), those that are both sensitive and uncertain, but sediment models still often require multi-parameter calibration. Because sediment data are usually rare, sediment load magnitude and gradation are usually mostly uncertain. This is true in Western systems, but especially in regions of conflict like Afghanistan.

Evaluating a model against multiple, independent, calibration time windows (i.e. calibration-validation, though the terminology and methodology are controversial) is the classical approach to mitigate equifinality (e.g. Shelley and Gibson, 2015). However, in the absence of multiple calibration time-series, comparing results to several different prototype measurements over a single calibration window can help modelers negotiate non-unique calibration problems, converging on more robust models.

In an analogy of the n-equation solution to n-variable problems of more elegant mathematical systems, numerical calibration can mitigate equifinality with a multi-stage calibration approach, evaluating a multi- parameter calibration against multiple prototype measurements. In this case, two sensitive and uncertain parameters were estimated in a three-step calibration process.

Sediment calibration should always follow hydraulic calibration (HEC, 1993; Thomas and Cheng, 2007; e.g. Shelley and Gibson, 2014). Sediment models depend on good hydraulic calibration, as sediment results are highly sensitive to hydraulic parameters like bed roughness. Hydraulic calibration could be considered an additional stage to calibrate a third uncertain parameter (n-value). When possible the hydraulic calibration should be followed by a robustness analysis to test numerical stability, (HEC, 1993; Thomas and Cheng, 2007) though fundamentally non-equilibrium problems, like reservoir deposition, make the robustness concept difficult to apply.

After hydraulic calibration, the sediment calibration Arghandab Reservoir for the progressed through three stages, calibrating two free parameters by comparing model results to three

prototype measurements over a single calibration window (Table 1).

Table 1 Uncertain/sensitive model parameters and the prototype measurements used to estimate them.

Estimated Parameters	Evaluation Measurements
1. Load Magnitude	1. Total sediment volume
2. Load Gradation	2. Longitudinal sediment distribution
	3. Longitudinal bed gradation trend

1. Total Sediment Volume: Calibrating Load Magnitude

Most reservoir sediment models specify boundary sediment loads with flow-load rating curves. Even when the data to develop flow-load curves are available, scatter around a selected curve often span one- to-two orders of magnitude, making the flow load relationship a common calibration variable.

Mort et al. (1973) measured transects of the reservoir along historical, as-built cross sections, in 1971. A few years later data series end because of regional conflicts. These measurements created a 19-year calibration window that aligned with continuous upstream flow and reservoir stage data.

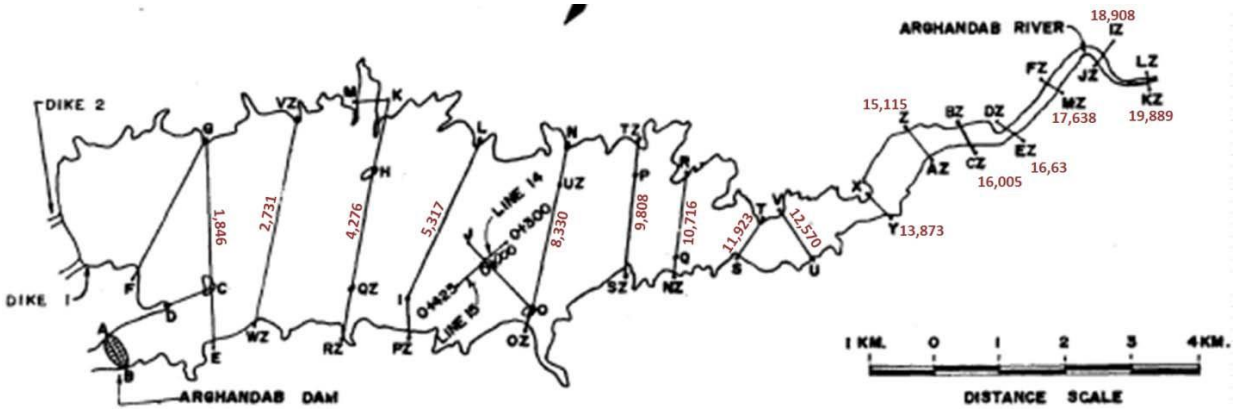

Figure 1 HEC-RAS cross section stations (red numbers) associated with the corresponding Mort et al. (1973) transects.

An as-built HEC-RAS model was constructed with the 1952 cross sections and run over the calibration period. Sediment volume change results were compared to the 89 million m3 deposition computed from the Mort et al. (1973) transects. The flow-load curve was adjusted until the model reproduced the total observed deposition volume. Results were compared to a few available load measurements and other regional flow-load curves.

2. Longitudinal Sediment Distribution: Calibrating Load Gradation

Most sediment transport models require sediment boundary conditions by grain class. Therefore, two uncertain parameters are wrapped up in the sediment load boundary: magnitude and

gradation. While load magnitude data are rare and noisy, load gradation data are usually even more uncertain, based on fewer and more erratic measurements.

In depositional environments however, load gradation can be calibrated to the longitudinal distribution of the deposits. Reservoirs sort sediment longitudinally by gradation and models use fall velocity to simulate that sorting relatively precisely (relative to the uncertainty in other transport algorithms). Therefore, once the total load is established with the flow-load curve, the gradational distribution of the inflowing loads can be adjusted to fit the longitudinal trend.

In the Arghandab model, load gradations were adjusted until the Arghandab HEC-RAS model re-created volume change at each location (Figure 2). This step sometimes requires feedback with the total volume analysis (Section 3.1), because moving mass to finer grain classes (e.g. clay or very fine silt) to induce deep pool deposition with trap efficiencies <100%, can reduce the total sediment mass deposited, requiring adjustments to the magnitude of inflowing loads. However the modeled trap efficiency and sediment releases through the dam should be checked against actual reservoir release concentrations, to verify that the estimated fine components are justified.

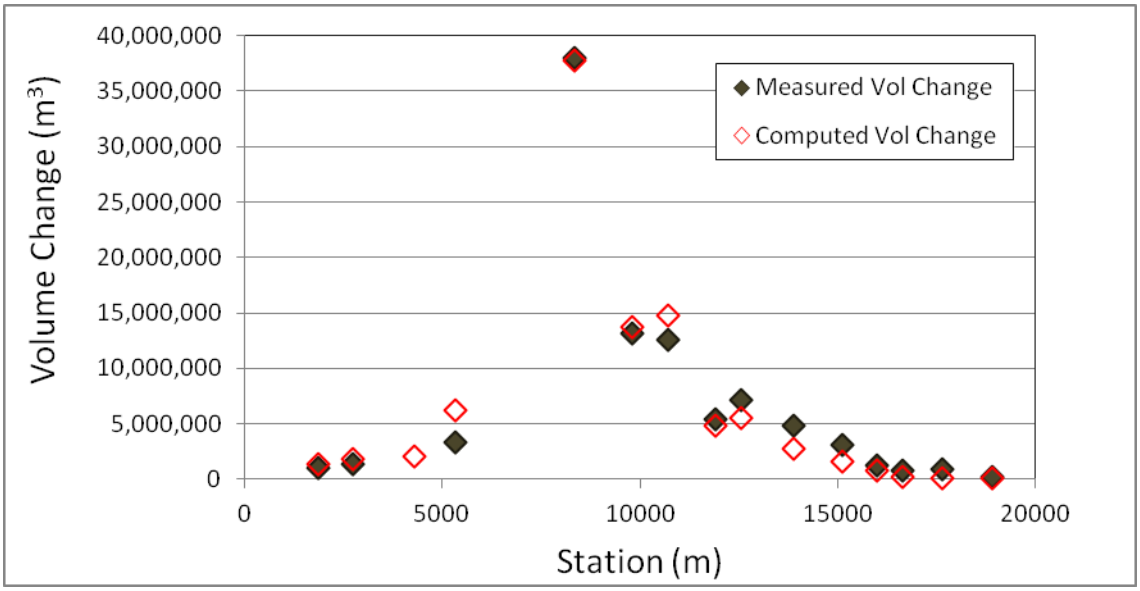

Figure 2 Computed and measured longitudinal volume change. Bed change at each cross section in the Arghandab reservoir between 1952 and 1971. The gradation of the upstream load boundary was adjusted to fit the computed result to the measurements.

3. Gradational Trend: Check and Update Load Gradations

Finally, the calibration was checked against bed gradations and updated accordingly. This could be considered a single-time-series analogy "verification," but verification terminology is controversial (Oreskes et al., 1994; Rykiel, 1996; Gibson, 2013), and production level models do not simply "fail" verification, but use the new data to update parameterization to produce the best final model possible.

Gradations were extracted from HEC-RAS calibration results and compared to a handful of 1973

bed gradations (Figure 3). Both the model and prototype gradation data must be interpreted carefully in this comparison. Computing gradational evolution results from active layer sediment models (like HEC- RAS) can be challenging. Cover layer gradations in HEC-RAS are a function of layer thickness, which are sometimes confounded by non-linear mixing dynamics. Especially detailed, multi-layer Lagrangian mixing methods like the Thomas and Copland methods (Exner 5 and 7 respectively in version 4.1) in HEC-RAS (which are required to develop and maintain the armor layers in the upper reach of the model), often reset cover gradations, making the surficial gradations at any time step stochastic, evolving non- monotonically.

Therefore, "computed gradations" were extracted from "total mass change" results, which develop more consistently. Because reservoir deposition is mainly monotonic, gradations can be computed from the depositional mass. This approach integrates vertical gradations in the deposit, extracting finer model gradations than the surficial prototype samples. As a reservoir delta progrades, finer material deposits deep in the reservoir, at the toe of the delta. Later, coarser deltaic deposits cover these deep, fine, materials. Reservoir sediment samples tend to collect the coarser, surface materials. The Arghandab model produced this result as the measured total-deposit gradations were coarser than the computed deposits (Figure 3).

Despite these complexities in comparing computed gradations of the active layer against surficial measurements, the comparison provided an independent evaluation of the model to mitigate equifinality uncertainty. Calibrating the model against three observations increased confidence and mitigated uncertainty in predictive results.

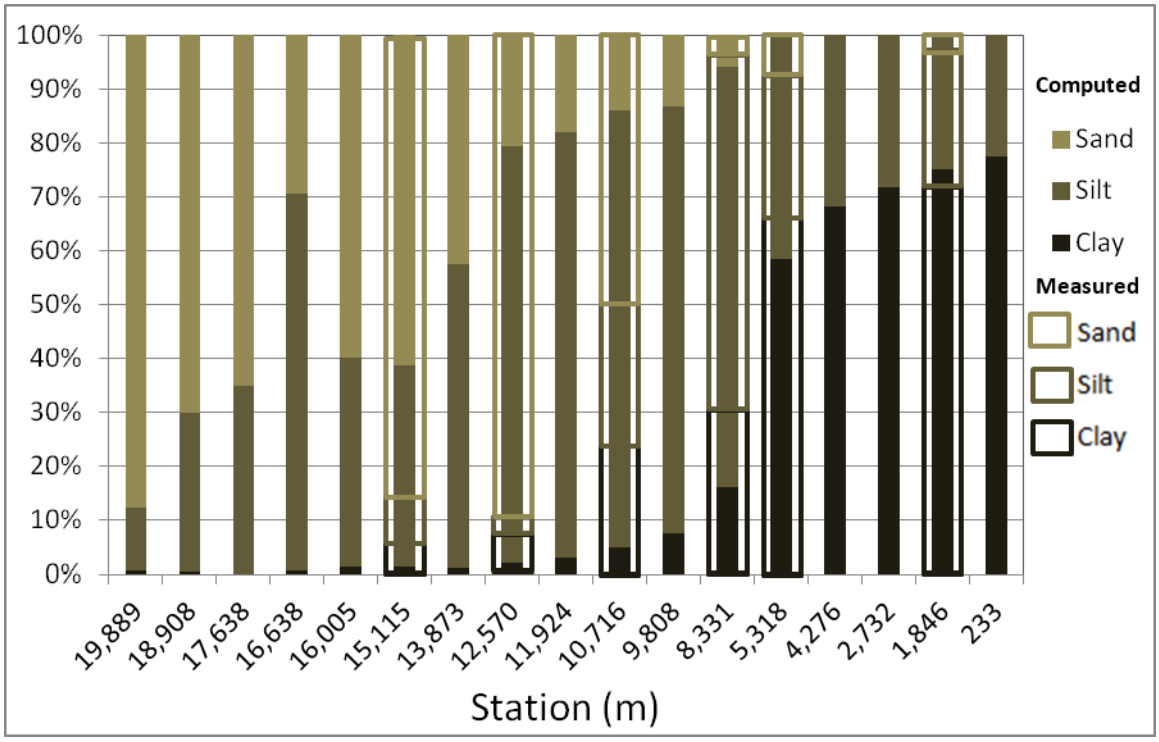

Figure 3 Computed and measured bed gradations for the 1952-1971 calibration of Arghandab reservoir deposition. Computed, vertically integrated, deposits are finer than the surficial measurements, as expected, but the trend "validates" load gradation calibration.

QUANTIFYING PREDICTIVE HYDROLOGIC UNCERTAINTY FOR SEDIMENT MODELS

Most reservoirs operate based on upstream and downstream flow gages, which provide good historic flow data for sediment models. Therefore sediment parameter uncertainty, confounded by limited data and scatter when data are available, usually overshadows historic flow uncertainty. However, when sediment analyses move from historic to predictive simulations, hydrologic uncertainty can dominate in a well-calibrated reservoir sediment model. Sediment transport is a non-linear function of flow, making projected deposition, reservoir life cycle, and future drought or flood protection heavily dependent on the flows in the following decades, particularly the frequency and timing of large events.

Historically, predictive sediment models have either ignored hydrologic uncertainty, by simply repeating historical records, or collapsed historical records into "representative years," sometimes augmented with probabilistic flows, that are repeated for every year of the simulation.

These approaches have limitations, however. Reservoir life cycles depend largely on the unknown time- series of future hydrology, so a repeated time-series will only predict the future (or even simulate a probable future) if it does not over or under predict flood frequency. Repeating the historical record can be particularly problematic in a system like Arghandab, where the regional history left a hydrologic record of only 28 years, and anecdotal evidence suggests that the ungaged records include much larger flows than those included in the measured time-series (Needham, 2006). Additionally, bed response to large events depends on their timing, sequence, and temporal relation to other events. A 1% event, five years into a simulation, may affect the system very differently than the same event in year 45.

Synthetic hydrographs of future conditions were developed to quantify hydrologic uncertainty in the Arghandab study. These stochastic hydrologic time-series were developed from a combination of 1) historical annual flow series and 2) synthetic flow years.

The HEC Statistical Software Package (HEC-SSP) (Brunner and Fleming, 2010) ordered the historic annual time-series and associated each with an exceedance probability based on peak seven-day flow volumes with a Log-Pearson III distribution (Figure 4). Each historical annual flow record was assigned a range of probabilities surrounding its plotting position. The ordered peaks had an "S-shaped" alignment, however, so the right half of the data (larger than average flows) had a prominent negative skew. Negative skew makes the log normal distribution (i.e. LPIII with zero skew) over predict high flows, so historical flow series were scaled to align with the flow at the corresponding position on the flow-frequency curve. For example, the 1954 flow record was assigned probabilities between 0.33 and 0.365 (based on where it plotted on the flow-frequency curve) and high flows were multiplied by a scaling factor of 0.94 to bring the seven-day volume in line with the log normal distribution.

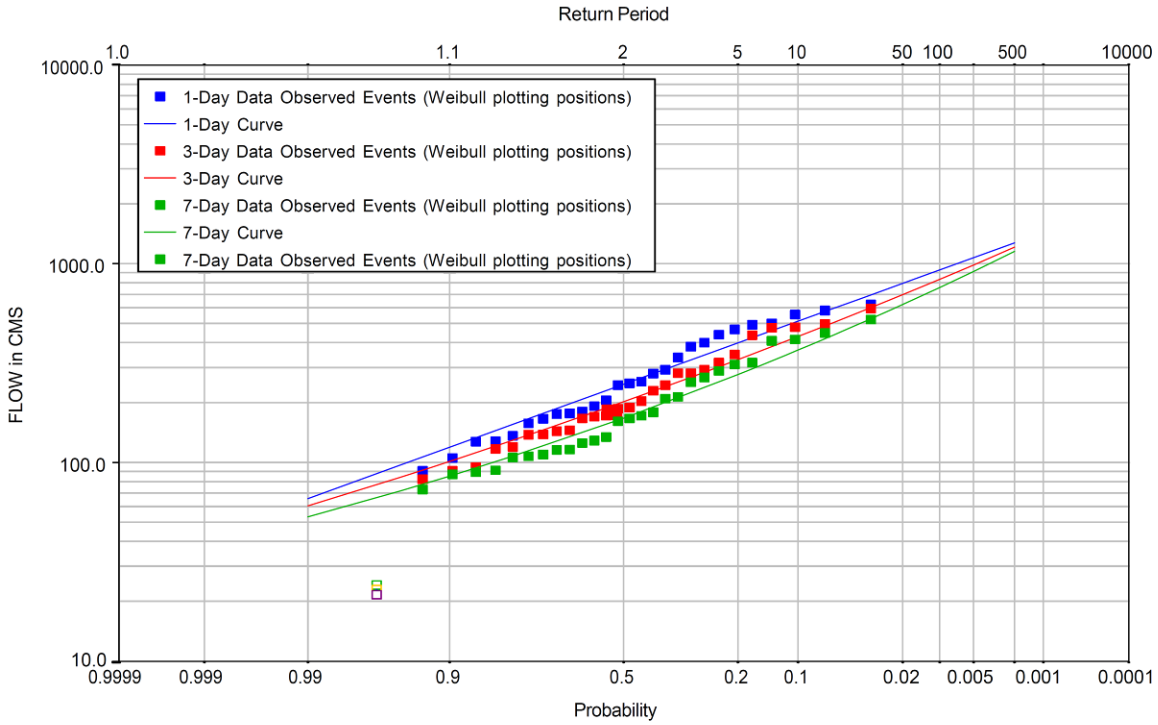

Figure 4 Volume frequency analysis for the gage upstream of Arghandab Reservoir (September 1951 to Mar 1979).

When using plotting positions, a 6% exceedance probability is assigned to the largest historical flow. Rarer events (5%, 2%, 1%, 0.5%, and 0.1%), were constructed by scaling a regularly shaped, single peak, historic "model" hydrograph (Water Year 1965) into synthetic, low-frequency flood events. The flood season flows of the model hydrograph were scaled by the ratio of the peak flow (computed in a separate HEC- SSP analysis) to the 1965 peak (Figure 5). Twenty, 50-year, synthetic flow series (1,000 total flow years) sampled these historic and synthetic annual time-series (Figure 6) with a random number generator, including nine 1% events, two 0.5% (200 year) events, and one 0.1% (1,000 year) event.

The HEC-RAS sediment model (with estimated contemporary bathymetry) simulated 50-year futures including a no-action alternative and three proposed spillway raises, by repeating the historic time-series and each of the twenty stochastic time-series for each of the four alternatives. Final bed elevation profiles for the three alternatives and no-action condition with the repeated historic record are plotted in Figure 7. However, the stochastic hydrologic analysis made it possible to compute and communicate the potential range of results hydrologic variability could produce. In Figure 8, the 50-year reservoir storage volume computed from the analyses in Figure 7 are plotted with results from the stochastic simulations, placing the repeated historic time-series results in the context of its hydrologic uncertainty.

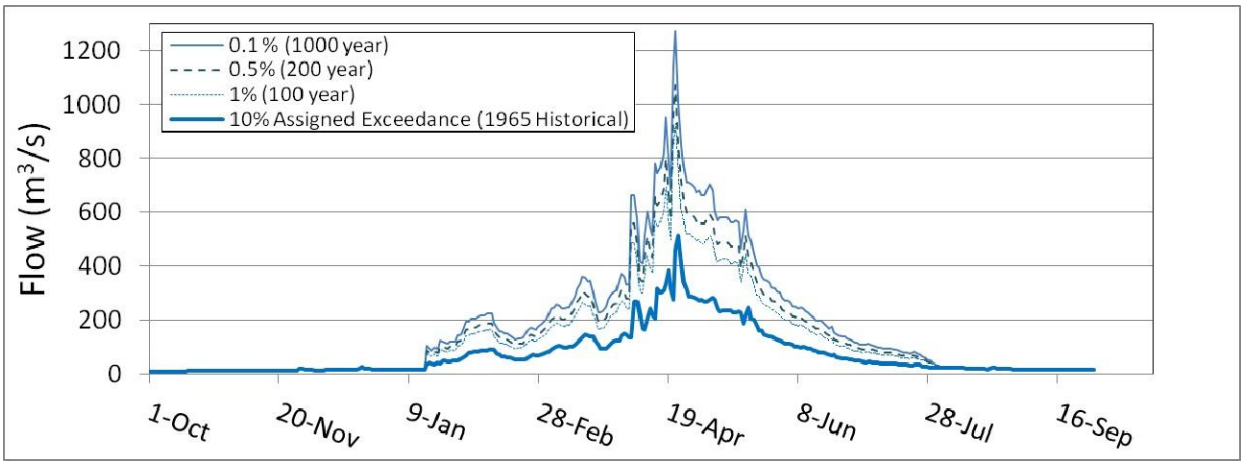

Figure 5 Synthetic annual flow series, low probability flows, larger than those observed during the 32 year flow record, constructed by scaling the 1965 event to the 7-day probabilistic volumes computed by HEC-SSP.

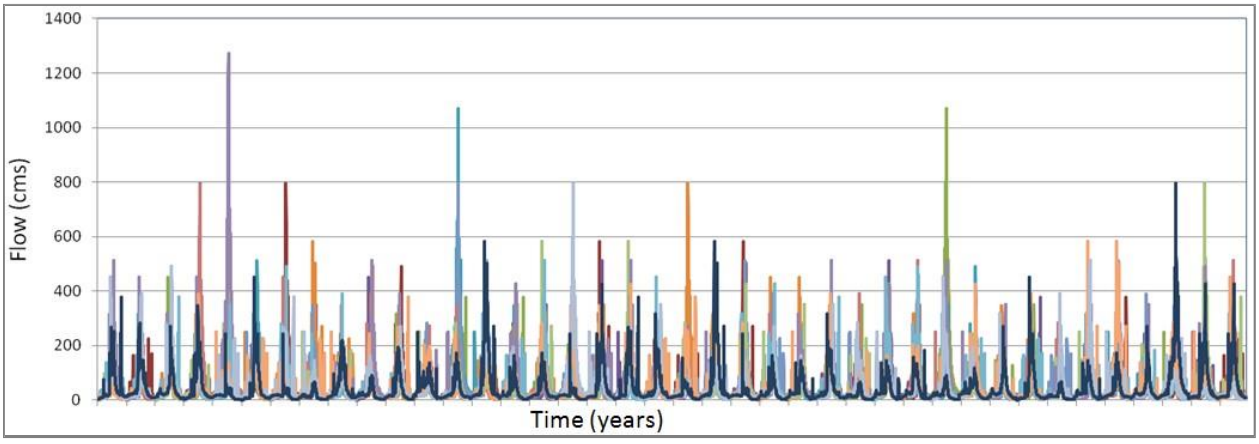

Figure 6 Twenty synthetic flow series used to quantify hydrologic uncertainty.

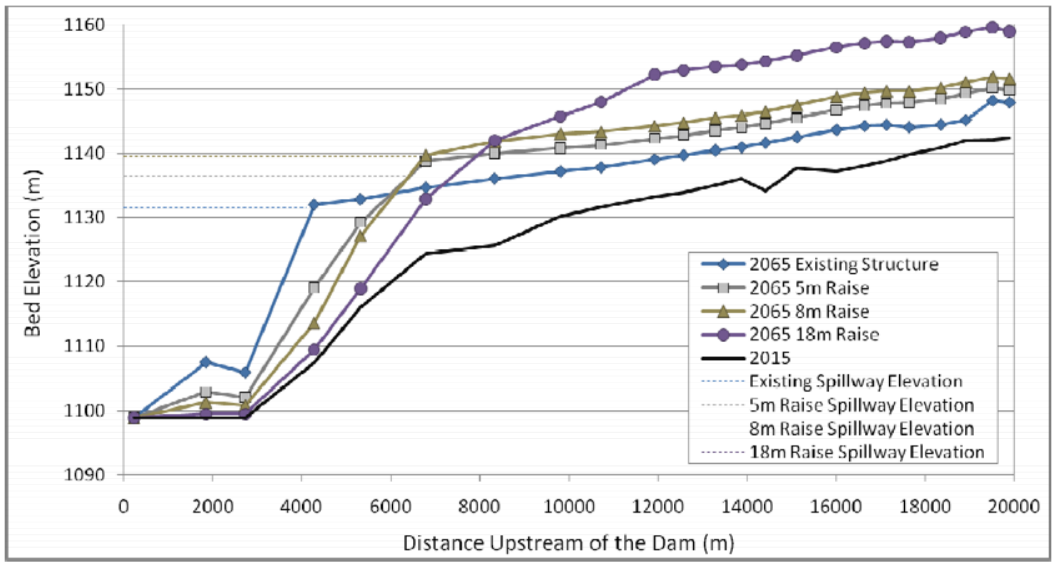

Figure 7 Predicted 2065 reservoir bed elevation (thalweg) for the existing structure and three alternatives, plotted with the initial (2015) profile.

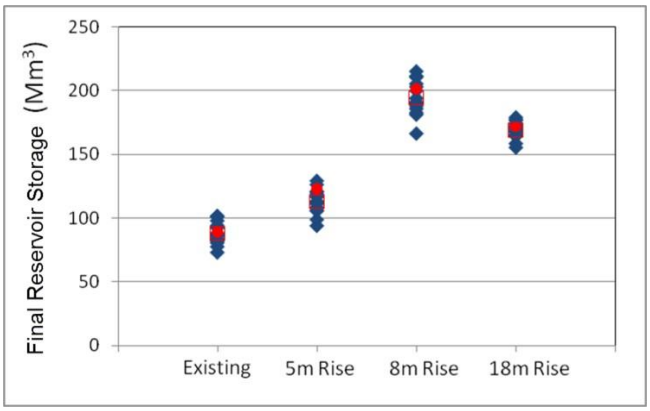

Figure 8 The final water volume (in 2065) beneath the original spillway elevation (1135.4 m) for the predictive simulation (red dot •), simulations based on random 50-year hydrologies (blue diamonds ◇) and the average of the random simulations (red square □).

RECENT DEVELOPMENTS

Customized code generated stochastic hydrologic time-series in this study. Since then, HEC has developed unsteady sediment transport capabilities in HEC-RAS (Gibson and Boyd, 2014; Shelley et al., 2015) and automated time-series sampling in the HEC-WAT (Dunn and Baker, 2010). Combining these capabilities automate sediment model hydrologic uncertainty analyses, like the one described above.

HEC-WAT creates time-series from historic and synthetic annual time-series like those depicted in Figures 5 and 6, and automatically launches HEC-RAS sediment simulations with each realization automatically. These developments will simplify hydrologic uncertainty for sediment models.

CONCLUSIONS

The uncertainty surrounding sediment models can reduce their utility and is sometimes cited as a reason to forgo modeling that could add value by reducing uncertainty. Good calibration against multiple time-series, or in their absence, against multiple measurements, can reduce model uncertainty to acceptable levels. However, the uncertainty associated with sediment transport model results is a fundamental characteristic of the analysis. Providing results with explicit uncertainty analyses puts results in the context of the project risk portfolio and provides the range of probable outcomes.

REFERENCES

Beven, K. (1993). Prophecy, reality and uncertainty in distributed hydrological modeling Advances in Water Resources, 16, 41- 51.

Brunner, G.W. and Fleming, M.J. (2010). HEC-SSP Statistical Software Package, Version 2.0, CPD-86, 313 p.

Canadian International Development Task Force (CID) (2008). Arghandab Irrigation Rehabilitation Project, Technical Appraisal Mission Report, 421 p.

Dunn, C., and Baker, P. (2010). "A Watershed Modeling Tool, HEC-WAT". Proceedings of the ASCE/EWRI Watershed Modeling Conference, Madison, Wisconsin.

Gibson, S. (2013) Comparing Depth and Velocity Grids Computed With One- and Two-Dimensional Models at Ecohydraulic Scales, UC Davis Thesis, 267 p.

Gibson, S. and Boyd, P. (2014) "Modeling Long Term Alternatives for Sustainable Sediment Management Using Operational Sediment Transport Rules," Reservoir Sedimentation – Scheiss et al. (eds), pp 229-236.

HEC (1993) "Guidelines for the Calibration and Application of HEC-6," Training Document No 13, The Hydrologic Engineering Center, Davis, California.

Mort, O.D., Ambayec, R.R., and Haase, R.J. (1973) Hydrographic and Sedimentation Survey of Arghandab Reservoir, U.S.

Bureau of Reclamation in Cooperation with the Helmand-Arghandab Valley Authority of the Royal Government of Afghanistan, 44p.

Needham, J. (2006). Design Review Memorandum: Comments on Kajaki Dam, 1976 Harza PMF Study.

Oreskes, N., Shrader-Frechette, K., and Belitz, K. (1994). Verification, Validation, and Confirmation of Numerical Models in the Earth Sciences, Science, 263(5147), pp 641-646.

Pappenberger, F., Beven, K., Horritt, M., and Blazkova, S. (2005), Uncertainty in the calibration of effective roughness parameters in HEC-RAS using inundation and downstream level observations, Journal of Hydrology, 302(1-4), 46-69.

Ruark, M.D., Niemann, J.D., Greimann, B.P., and Arabi, M. (2011). Method for Assessing Impacts of Parameter Uncertainty in Sediment Transport Modeling Applications, Journal of Hydraulic Engineering, 623-636.

Rykiel, E. (1996). Testing ecological models: the meaning of validation, Ecological Modeling, 90(229-244). Thomas, W. and Chang, H. (2007). "Computational Modeling of Sediment Processes, ASCE Manuals and Reports on

Engineering practices No. 110: Sedimentation Engineering – Processes, Modeling, and Practices, pp 649-681.

USACE (2014) Lewis and Clark Lake Sediment Management Study (LCLSMS) Phase II Part II: Sediment Transport and Flow Analysis through Lewis and Clark Lake Using the HEC-RAS Reservoir Model, 85p. Draft.

SEDIMENT MONITORING DURING SHORT-TERM DRAWDOWNS OF FALL CREEK LAKE, UPPER WILLAMETTE BASIN, OREGON

Liam Schenk, Hydrologist, USGS Oregon Water Science Center, Klamath Falls field office, lschenk@usgs.gov; Heather Bragg, Hydrologic Technician, USGS Oregon Water Science Center, hmbragg@usgs.gov;

INTRODUCTION

In December 2012 and December 2013, the U.S. Army Corps of Engineers (USACE) conducted operational drawdowns of Fall Creek Lake, Oregon, to enhance downstream passage of Endangered Species Act-listed juvenile spring Chinook salmon in response to requirements in the 2008 Biological Opinion on continued operations of the Willamette Valley Project (National Marine Fisheries Services, 2008). During these drawdowns the lake elevation was lowered from the normal winter low-pool elevation of 728 feet to approximately 690 feet, allowing inflowing water to pass freely through the regulating outlets of the Fall Creek Dam. The U.S. Geological Survey (USGS) monitored the resulting suspended sediment release and has estimated sediment loads transported during these events. Data generated from the monitoring efforts provides the USACE with important information regarding the amount of sediment transported during these operational drawdowns.

DATA COLLECTION

The USGS monitored turbidity and suspended sediment over a range of hydrologic and sediment transport conditions before, during, and after drawdown operations at Fall Creek Lake. Monitoring occurred from November 2012 through February 2013 during water year (WY) 2013 and November 2013 through March 2014 (during WY 2014). In WY 2013, six monitoring stations were established for the lake and at strategic locations downstream, including the two main inflows to Fall Creek Lake, Fall Creek below Fall Creek Dam (Fall Creek Outflow in Figure 1), Little Fall Creek (a tributary to Fall Creek), and two sites on the Middle Fork Willamette River (Dexter and Jasper, Figure 1). During WY 2014, only the station at Fall Creek Outflow was monitored. Turbidity sensors measuring in Formazin Nephelometric Units (FNUs) were deployed and Equal-Width-Increment (EWI) suspended-sediment concentration (SSC) samples were collected at all sites. Automatic pump samplers were installed at several sites to provide additional SSC data. Correction coefficients were calculated to adjust the pump sample concentrations to cross section EWI samples. All samples were analyzed for SSC (in milligrams per liter [mg/L]) and percent finer than 63 microns (percent fines) at the USGS Cascades Volcano Observatory sediment lab. Each discrete SSC sample was assigned an associated turbidity and streamflow (in cubic feet per second [cfs]) value from the continuously monitored instream data.

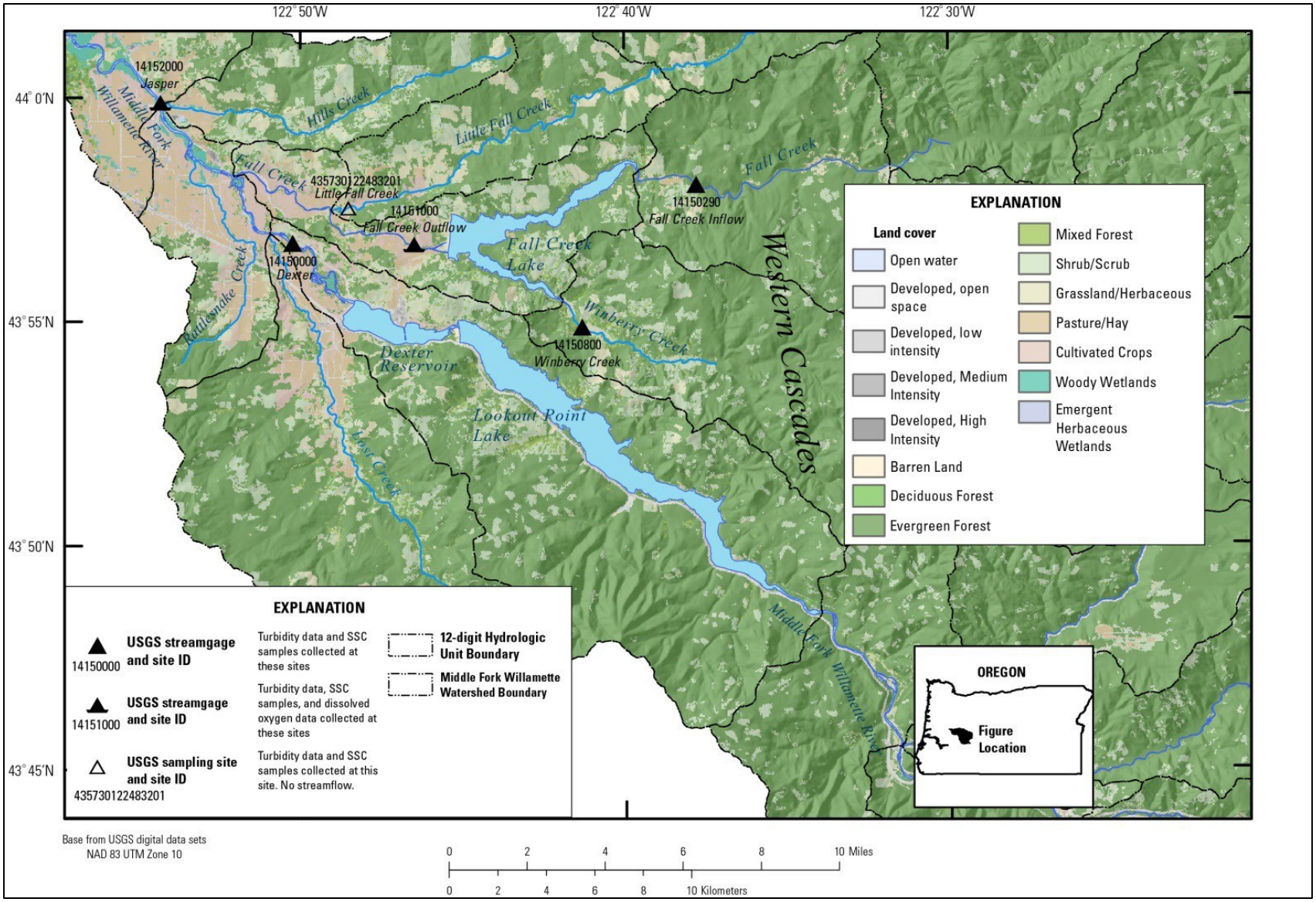

Figure 1 Location of study area and monitoring stations, Middle Fork Willamette Basin, Oregon (from Schenk and Bragg, 2014)

DATA ANALYSIS

Site-specific regression models were developed from discrete turbidity, streamflow, and SSC data. Sample data for sites downstream of the dam were divided into pre-drawdown, drawdown, and post-drawdown analysis periods. Log10-transformed and untransformed turbidity and streamflow data were used to create both simple and multiple linear regression models which were evaluated on residual plots and summary statistics. Model development followed USGS guidelines outlined in Rassumussen and others (2009). The preferred models were used to compute continuous SSC records for each of the sites. Continuous suspended-sediment loads were computed from the SSC and streamflow records. For WY 2013, suspended-sediment loads were computed for all six stations. For WY 2014, suspended-sediment loads were only computed for the single station (Fall Creek Outflow) before, during, and after the drawdown for comparison to the suspended sediment loads calculated in WY 2013.

RESULTS

The FY 2013 drawdown occurred for six days in December 2012 (Figure 2) and resulted in the net transport of approximately 50,300 tons of sediment from the lake, accounting for approximately 83% of the total suspended-sediment load delivered from Fall Creek Lake during the study period. The drawdown also resulted in approximately 16,300 tons of sediment deposited in the river reaches between Fall Creek Lake and a site on the Middle Fork Willamette River (Jasper), which was ten miles downstream of the lake (Schenk and Bragg, 2014).

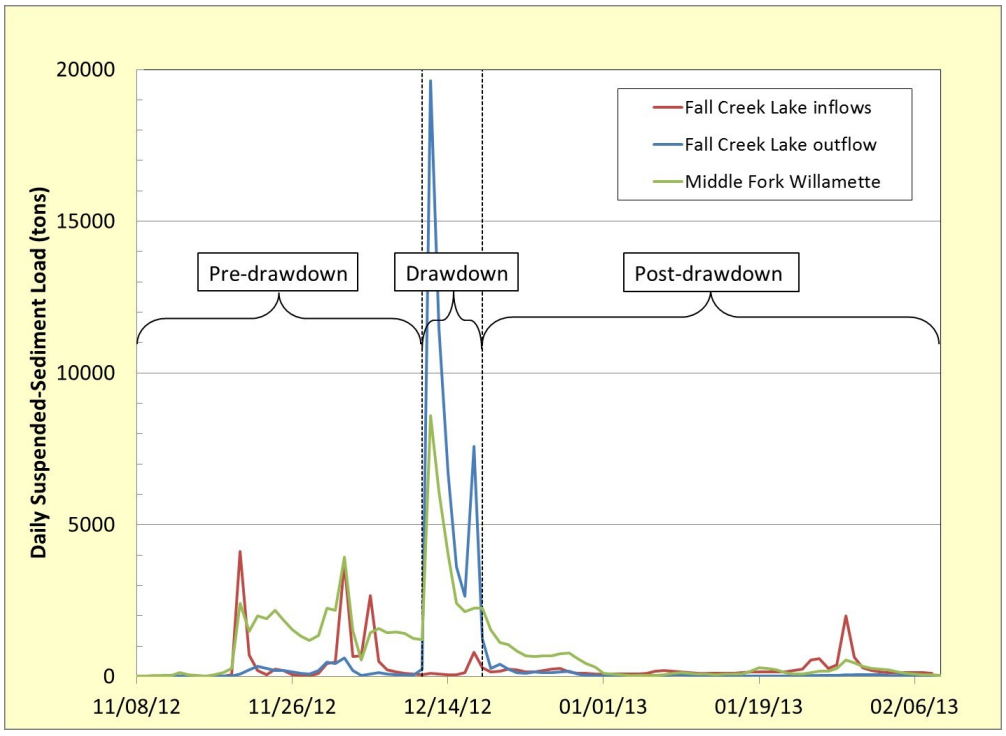

Figure 2 Water year 2013 daily suspended-sediment loads for Fall Creek Lake inflows, Fall Creek Lake outflow, and the monitoring site ten river miles downstream of Fall Creek Lake (Jasper) on the Middle Fork Willamette River.

Due to unseasonably cold weather, the suspended-sediment load during the WY 2014 drawdown was particularly low. The area received 8–10 inches of snow followed by air temperatures consistently below freezing for most of the drawdown period. The sediment exposed in the lakebed was frozen and unavailable for transport. During the first 5½ days of the ten-day drawdown in December 2013, only 3,300 tons of sediment was transported from the lake (Figure 3). Turbidity data were lost for the last 4½ days of the drawdown due to sensor fouling, and sediment loads were computed using daily mean values of SSC and streamflow, resulting in a total sediment load of approximately 5,220 tons during the ten-day drawdown period. This accounted for approximately 19% of the total sediment load during the study period and was 90% less than the previous drawdown in WY 2013.

Most of the sediment transport in WY 2014 occurred in February 2014, when the lake elevation dropped to approximately 700 feet, which was concurrent with extremely high streamflows (>3,500 cfs, peak streamflow of the WY). Monitoring was not conducted at the inflows to the lake in WY 2014, so how much of the suspended- sediment load came from upstream inflows compared to bank erosion or sediment re-suspension within the lake is unknown. However, given the limited contribution from the inflows in WY 2013 (approximately 2.5% of total sediment load) it is likely their contribution was similarly small in WY 2014. A preliminary analysis for the WY 2015 drawdown conducted in November 2014 suggests that approximately 20,000 to 35,000 tons of sediment was transported during a seven-day period, further highlighting the inter-annual variability in sediment transport during the operational drawdowns.

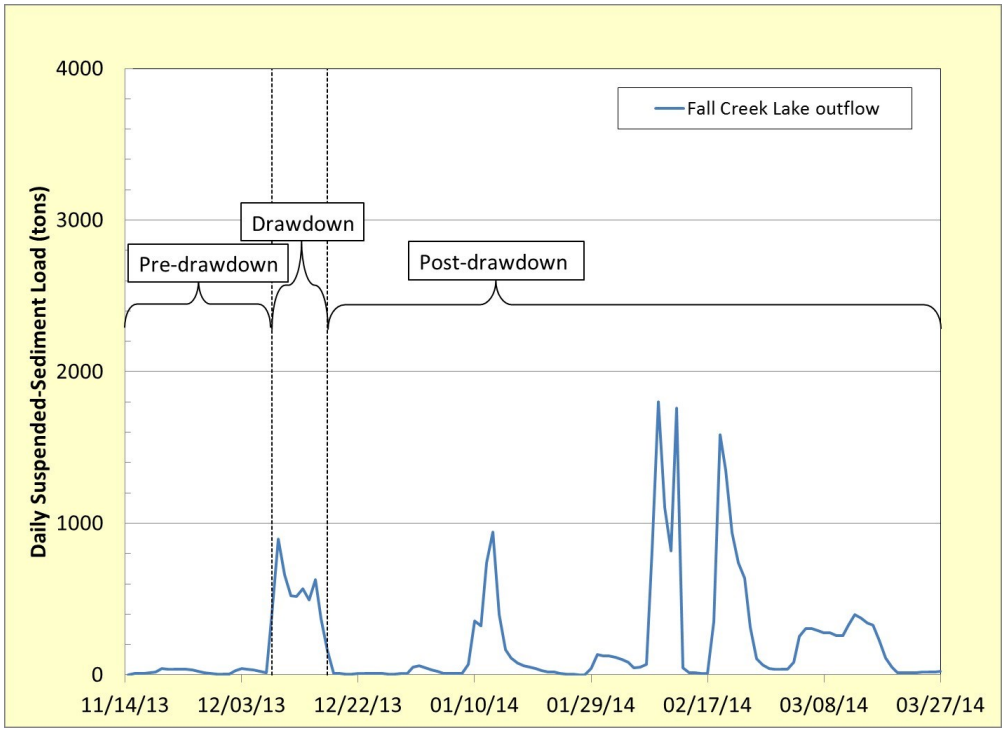

Figure 3 Water year 2014 daily suspended-sediment loads for Fall Creek Lake outflow.

SUMMARY

Results from suspended-sediment monitoring at Fall Creek Lake during two operational drawdowns suggest that variability in hydrologic and climatic conditions and lake elevation play an important role in sediment transport and supply. This is highlighted by the difference in sediment load estimates from the December 2012 and 2013 drawdown operations. Monitoring results suggest a 90% reduction in sediment loads from the 2012 to 2013 drawdown operations, but this decrease in loads was likely forced by weather conditions rather than a reduction in sediment supply after the previous drawdown. Ongoing monitoring and data collection efforts will continue to investigate inter-annual variability in sediment transport during these operational drawdowns, and provide useful information about changes in reservoir storage capacity that is beneficial for future flood control efforts.

REFERENCES

National Marine Fisheries Service. (2008). "PCTS consultation summary – Continued operation of 13 dams and maintenance of 43 miles of revetments in the Willamette basin, Oregon", National Oceanographic and Atmospheric Administration Web page, accessed March 31, 2014 at: *https://pcts.nmfs.noaa.gov/pcts-web/dispatcher/trackable/NWR-2000-2117?overrideUserGroup=PUBLIC&referer=/pcts-web/publicAdvancedQuery.pcts?searchAction=SESSION_SEARCH*

Rasmussen, P.P., Gray, J.R., Glysson, G.D., and Ziegler, A.C. (2009). "Guidelines and procedures for computing time-series suspended sediment concentrations and loads from in-stream turbidity-sensor and streamflow data," U.S. Geological Survey Techniques and Methods, book 3, chap. C4, 52 p.

Schenk, L.N., Bragg, H.M. (2014). "Assessment of suspended-sediment transport, bedload, and dissolved oxygen during a short-term drawdown of Fall Creek Lake, Oregon, winter 2012-13," U.S. Geological Survey Open-File Report 2014-1114, 80 p., *http://dx.doi.org/10.3133/ofr20141114*.

TIME SERIES AND GEOSPATIAL DATA INTEGRATION FOR RESERVOIR SEDIMENTATION STUDY THAT INCORPORATES MULTIPLE SEDIMENTATION MODELS AND RATES FOR CONVERGENT VALIDATION

Nathaniel Todea, USDA Natural Resources Conservation Service Hydraulic Engineer, 125 South State Street, Room 4010, Salt Lake City, Utah 84106, 801.524.4573
Nathaniel.Todea@ut.usda.gov

Abstract: As part of the Tibble Fork Dam Rehabilitation Environmental Assessment, a sedimentation study was undertaken to determine the current and future storage needed to provide at least 50 to 100 years of dam life. Tibble Fork Reservoir, located in American Fork Canyon in Utah County, Utah, is a small, 259 acre-foot reservoir fed by a 35 square-mile watershed, with an average elevation of 8,600 feet above mean sea level. Multiple analyses were used to determine erosion rates from the Van Dugway landslide and watershed sediment yields that directly contribute sediment into Tibble Fork Reservoir. Tibble Fork Reservoir was constructed with assistance from the U.S. Department of Agriculture, Soil Conservation Service, now the Natural Resources Conservation Service (NRCS), in 1966. Construction of the dam was accomplished through the authority of the Watershed Protection and Flood Protection Act, Public Law 566 (PL-566). NRCS is developing a dam rehabilitation plan for the dam that includes an auxiliary spillway analysis, sedimentation volume calculations, and seismic/geotechnical analyses to meet current dam safety criteria.

In 2012, Todea and Hasenyager made a sedimentation study of the Tibble Fork (Todea and Hasenyager, 2012). The results of that study were compared to new calculations as part of the dam rehabilitation environmental assessment study. Bedload measurements were taken during the 2011 spring runoff and were modeled using the U.S. Army Corps of Engineers (USACE) Hydrologic Engineering Centers River Analysis System (HEC-RAS) sediment transport model to estimate the sediment contribution (USACE, 2010). The RiverMorph and FlowSed/PowerSed (RIVERMorph, 2008) models were used to determine annual average bedload and suspended sediment loads from the 2011 spring runoff event. The Automated Geospatial Watershed Assessment (AGWA) (Burns et al., 2007) software, and the Soil and Water Assessment Tool (SWAT) (Arnold et al., 1994) were evaluated to estimate the watershed sedimentation rates that contribute to the reservoir. As part of the 2012 study, the Bridges 1973 sedimentation map was reviewed and correlated to the above studies. The following models resources were also considered:

1) The "*Managing Sediment in Utah's Reservoirs*" Utah State Water Plan produced by the Utah Division of Water Resources (UDWR) in 2010. Four reservoir sedimentation rates were filtered and compared due to the elevation and location of the reservoirs.
2) The Rangeland Hydrology Erosion Model (RHEM) (Nearing et al., 2011) is a slope-based program, not applicable for high alpine watershed erosion scenarios, but the model was used as part of this study.
3) Slaymaker (1977) reported on eleven relevant basins in the report "*Estimation of sediment yield in temperate alpine environments*."

Trap efficiency of the reservoir was considered and calculated using the USDA SCS (1975, revised) procedure titled "*Procedure-Sediment Storage Requirements for Reservoirs – Technical Release No. 12*" (TR 12).Finally, all methods were compared to bathymetric surveys that were conducted in 2010 and 2014.

The results of the 2012 study by Todea and Hasenyager estimated that an average 2.02 acre-

feet per year of material is deposited in Tibble Fork Reservoir. The compilation of sediment rates from the nine evaluations in the 2012 study ranged from 0.02 to 0.76 acre-feet per square mile, with most values ranging near or below 0.10 acre-feet per square mile. The 2014 bathymetric survey estimated an average annual sedimentation rate of 2.92 acre-feet (or 0.08 acre-feet/square mile) in the pool. This assumes that the original pool was accurately measured at 259 acre-feet of storage for the original design. The 1964 design sediment rate was calculated to be 3.32 acre-feet per year on average, this includes considering trap efficiency. Bridge's 1973 map is a good tool for providing initial estimates. Pairing of results from Rivermorph PowerSed/FlowSed with bedload and suspended sediment, HEC-RAS bedload with RiverMorph PowerSed/FlowSed suspended sediment, and AGWA SWAT with HEC-RAS bedload provided useful results. The RHEM is not optimally suited for these environmental conditions, but provides supporting documentation. Trap efficiencies in TR 12 (USDA SCS, 1975) are relevant.

INTRODUCTION

This study is a continuation of a sedimentation study performed by Todea and Hasenyager in 2012 for the Tibble Fork Reservoir. Todea and Hasenyager (2012) contains the following introduction: *"As part of a dam rehabilitation plan for a constructed Watershed Protection and Flood Prevention Public Law 566 (PL-566) dam, a sedimentation study was undertaken for Tibble Fork dam. Tibble Fork Reservoir, constructed in 1966, is located in American Fork Canyon in the Wasatch Mountains of Utah (Figure 1). To meet United States Department of Agriculture (USDA), Natural Resources Conservation Service (NRCS) Watershed Rehabilitation Program objectives, the dam rehabilitation outcome must have a design life of no less than 50 years* [and no more than 100 years]. *As part of the rehabilitation plan, alternatives that include decommissioning of the dam were analyzed. Sedimentation accrual within a dam and the effects on the design life must be considered when a dam is being rehabilitated. The original project in 1966 estimated a sediment storage capacity of 3.32 acre-feet/year (USDA SCS, 1964). The Van Dugway landslide located approximately 6,400 feet upstream has been actively contributing additional sediment to the reservoir since 1966. Multiple analyses were conducted to determine bedload gradation and suspended sediment material that is being deposited in Tibble Fork Reservoir*".

The components of the Todea and Hasenyager 2012 study were compared to a 2014 bathymetric survey. As part of this study the following were reviewed, modeled, or calculated:

- The Utah State Water Plan – "*Managing Sediment in Utah Reservoirs"* was reviewed and four dams that meet comparative requirements were reviewed.
- The Rangeland Hydrology Erosion Model (RHEM (Nearing et al., 2011) was calculated for a hillslope.
- Measured data from Slaymaker (1977), a sediment yield in temperate alpine environments study, were used.The Bridges 1973 sedimentation map was reviewed and sediment yield was determined for the Tibble Fork watershed study area.
- Trap efficiency (USDA SCS, 1975) was calculated and applied to the comparative sedimentation analysis.

The Todea and Hasenyager 2012 study used sedimentation techniques that include components from AGWA SWAT (Burn et al., 2007, and Arnold et al., 1994); bedload and sediment transport models from HEC-RAS; and Rivermorph FlowSed/PowerSed models

with bedload from the 2011 spring runoff measured upstream of the reservoir.

Figure 1 Tibble Fork Watershed Location Map (Todea and Hasenyager, 2012)

BACKGROUND

The Tibble Fork watershed is 35 square miles in area, at an elevation of 8,600 feet above mean sea level. The Van Dugway Landslide has contributed large amounts of sediment to the American Fork River for a reach length of 1,500 feet. The actively eroding portion of the landslide is located on the north, or right bank (looking downstream) of the American Fork River. The highest section of the landslide on the right bank of American Fork River is approximately 50 feet tall (Figure 2).

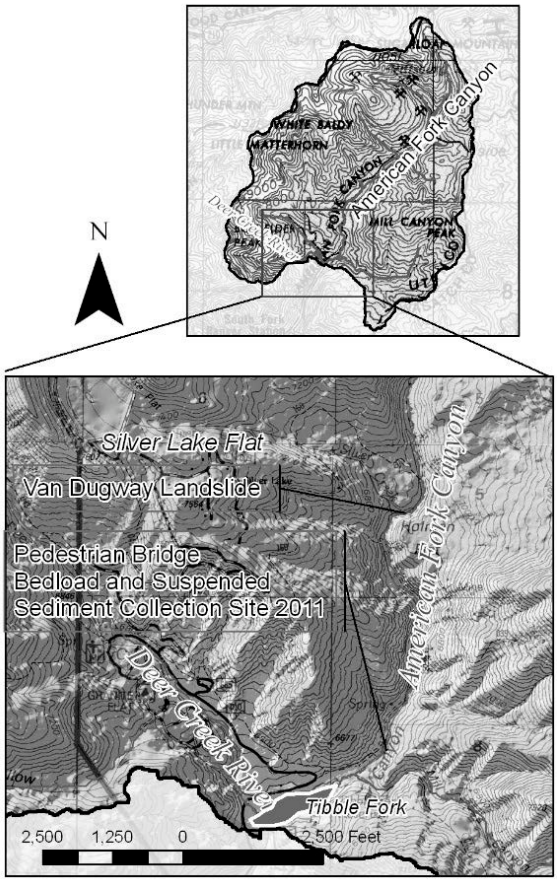

Figure 2 Tibble Fork Reference Map (Todea and Hasenyager, 2012)

The American Fork Canyon has a drainage area of approximately 26 square miles, and the adjacent Deer Creek has a 9.5-square-mile drainage area. They interconnect at the Tibble Fork Reservoir, providing a total watershed contribution area of 35.5 square miles (Figure 2). The American Fork Canyon drainage area contains the Van Dugway landslide. Below Van Dugway landslide, the American Fork River is characterized as a steep, confined valley with a Rosgen channel type B (Rosgen, 2006), that provides transport of large bedload material. Bedload samples were collected as part of Todea and Hasenyager (2012) study at a pedestrian bridge that crosses the river 2,700 feet upstream of Tibble Fork Reservoir, where the valley opens slightly and the channel is a Rosgen type C, which allows for transport of large cobbles at larger flows. Downstream from the pedestrian bridge to the Tibble Fork Reservoir the channel is a braided, Rosgen type D, where cobbles and gravels are deposited. The braided channel has distinct deposits of bed materials where the upper portion contains cobbles and the lower portion contains sand and fine gravels. Light Detection and Ranging (LiDAR) data were collected by Aero-Metric, Inc. (2010) as part of the Todea and Hasenyager (2012) study and was used for the hydraulic analysis.

Bathymetric data was collected by AMEC under contract with the NRCS in 2010 (AMEC, 2010). The bathymetric data and NRCS as-built drawings at ten-foot contours were analyzed by the Utah Division of Water Resources in 2011 to determine the volume of sediment contributed to the Tibble Fork Reservoir. It was determined that the sediment contributed to Tibble Fork Reservoir was between 84 and 142 acre-feet from 1966 to 2010 (UDWR, 2011), at an average rate of 1.91 to 3.23 acre-feet/year. This is approximately 1.41 to 0.09 acre-feet/year lower than the original estimate of 3.32 acre-feet/year. HDR Engineering, Inc. (2011) provided a study that resulted in a sedimentation rate of 2.21-2.82 acre-feet/year.

During the 2011 spring runoff, bedload and suspended sediment was measured. The Elwha bedload sampler was used to collect bedload material. A total of four samples was collected that included the rising and falling limb of the hydrograph of the spring runoff. Both the bedload and suspended- sediment samples were collected using guidance from USGS Field Measurements for Measurement of Fluvial Sediment (Edwards and Glysson, 1999). Suspended sediment was collected using a US DH-48 sampler. It is noted in the 2012 Todea and Haseyanger study *"Although the bedload is at a lower rate on the falling limb than the rising limb, the suspended sediment has the largest concentration of material captured on the falling limb of the hydrograph"*. This could have had an effect on the results that is artificially increasing the bedload and decreasing the suspended sediment, if only the rising limb values were used, resulting in higher bedload and lower suspended sediment values.

The purpose of the 2012 Todea and Hasenyager 2012 study was to obtain a more accurate estimate of sedimentation rates and provide information to determine the validity of mitigating the Van Dugway landslide. In 2011, NRCS conducted a bedload and suspended-sediment sampling program during the spring runoff on the American Fork River, below the Van Dugway landslide and above Tibble Fork Reservoir at the pedestrian bridge.

The Todea and Hasenyager study used multiple software programs and computations from collected bedload and suspended sediment approximations to narrow the range of estimates of sediment transported to Tibble Fork Reservoir. The Automated Geospatial Watershed Assessment (AGWA) (Burns et al., 2007) that uses Soil and Water Assessment Tool (SWAT) (Arnold et al, 1994) was evaluated to estimate watershed sediment yields. The RiverMorph (2008) FlowSed/PowerSed model was used with measured bedload to estimate the annual average bedload that passes through the sampling site. The AGWA SWAT model for the American Fork River (using 26 square miles of contributing area) calculated that 2,196 tons of material, on annual average, is transported into Tibble Fork Reservoir.

The Todea and Hasenyager study also used the HEC-RAS sediment transport model to estimate bedload contributions from the Van Dugway landslide and American Fork Canyon, and to determine the amount and gradation of bedload material being deposited into Tibble Fork Reservoir. The bedload data was collected during the one-percent recurrence interval from the spring runoff of 2011. The bedload material collected during the spring runoff was modeled by HEC-RAS as an estimate, until it mimicked observed and measured bed material from below the pedestrian bridge to Tibble Fork Reservoir. Four 100-pebble counts of the bed material were conducted from the pedestrian bridge to Tibble Fork Reservoir and used in the HEC-RAS model. The Yang (1972) transport function, Exner 5 (USACE, 2010) sorting method, and Rubey (1933) fall velocity method were used for sediment transport functions within HEC-RAS. USGS stream gage 10164500 15-minute discharge data was reduced by ten percent and used in the HEC-RAS model. Finally, United States Geological Survey (USGS) gage peak flow data (USGS, 2011), and flow frequency bedload curves were used to estimate bedload transport to the reservoir in Microsoft Excel, and to analyze the gradation of the material deposited as estimated from the HEC-RAS sediment transport model. The HEC-RAS sediment transport model calculated that of the 5,086 tons of material that passed below the pedestrian bridge in 2011, only 2,059 tons were actually deposited in the Tibble Fork Reservoir. The material that was deposited in Tibble Fork included fine gravel, very-fine gravel, and coarse sand.

Todea and Hasenyager (2012) used RiverMorph FlowSed/PowerSed to estimate annual

average bedload using a defined period within the stream gage records. Bedload measurements and estimated suspended sediment from the 2011 survey were used to calculate user-defined bedload and suspended sediment curves to be input into the RiverMorph model. Flow durations curves were generated in RiverMorph using records from the USGS stream gage 10164500 (USGS, 2011). RiverMorph FlowSed/PowerSed model and user-defined bedload and suspended sediment curves estimate an annual average bedload transport rate of 3,624 tons/year and a suspended sediment rate of 5,748 tons/year that passes under the pedestrian bridge at the collection site.

METHODS

The 2012 Todea and Hasenyager study (i.e. the 2010 bathymetry; bedload study from the Van Dugway landslide; HEC-RAS sediment transport model to Tibble Fork Reservoir; the RiverMorph FlowSed/PowerSed model calculations of material moving through the system annually) were compared to the 1973 USDA sedimentation maps, selected dams in the Utah Divisions of Water Resources (UDWR) sediment study for reservoirs, the study on sediment yield in temperate alpine environments (Slaymaker, 1977), and the Rangeland Hydrology Erosion Model (Nearing et al., 2011). USDA SCS Technical Release TR 12 "*Procedure--Sediment Storage Requirements for Reservoirs* was also evaluated and applied to all sediment rates to determine the range and applicability of sedimentation applications. Finally, 2014 bathymetry measurements were taken with a Z-Boat to determine current volumes or capacity of the reservoir.

The Bridges 1973 map entitled "*Estimated Sediment Yield Rates for the State of Utah*" has many referenced data sources as part of the map, including:

- Great Basin Upper Colorado and Lower Colorado Regions, Comprehensive Framework Study, Appendices VIII, Water Management, June 1971, Pacific Southwest Inter-Agency Committee/Water Resources Council,
- Utah State soils map and soil descriptions,
- Reservoir surveys by NRCS and USBR,
- Suspended load measurements by USGS, USGR and NRCS,
- Watershed studies by SCS/NRCS, and
- General knowledge of the state from regular NRCS program work.

Bridges notes "*Do not use these rates to determine sediment yields at specific sites. Large variations in sediment rates may occur within the delineated areas*".

The 2010 UDWR sediment study for the reservoir provides reference to 18 Utah dams, and includes tables provided by the nationwide REServoir SEDimentation Database (RESSED). As stated by UDWR, *"Sedimentation data exist for only 18 of Utah's major reservoirs; that is, those larger than 1,000 acre-feet. Much of these data comes from reservoir surveys conducted between 1930 and 1975 by the U.S. Soil Conservation Service (now the Natural Resources Conservation Service, NRCS) and the U.S. Bureau of Reclamation. The data were collected and published in a national summary of reservoir sediment deposition surveys (Dendy and Champion, 1978). This nationwide database was revised in 2009 and is now the REServoir SEDimentation Database (RESSED) available online at http://ida.water.usgs.gov/ressed/ and http://pubs.usgs.gov/ds/ds434/. The database is a cumulative historical archive that includes data from 1755 to 1993. The 1,823 reservoirs included in the database range in size from farm ponds to the largest U.S. reservoirs. Results from 6,617 bathymetric surveys are available in the database,*" (UDWR, 2010).

Table 1 illustrates data from four dams in the UDWR (2010) study used in the Tibble Fork project. The elevation of the reservoirs were also taken into consideration.

Table 1 Utah Department of Water Resources, reported sediment in selected reservoirs

Reservoir	Date Built	Storage Capacity Initial Survey (AF)	Drainage Area, square miles	Period Assessed	Sedimentation Rate (percent annual capacity loss)	Estimated Annual Sediment Volume (acre-	Average Annual Sediment Volume per mi^2 of DA	Estimated Capacity Loss as of
Booby Hole	1895	607	5	1895-1940	0.03	0.2	0.024	3
Indian Creek #1	1898	318	12	1898-1940	0.14	0.45	0.038	16
Duck Fork	1942	718	3.4	1942-1962	0.07	0.5	0.14	5
Iliff Anrus	1949	20	1.1	1949-1966	4.1	0.82	0.76	100

The 1977 Slaymaker study, "*Estimation of sediment yield in temperate alpine environments*" was reviewed to compare measured sediment yield at specific sites. The purpose of the Slaymaker paper was to compare sediment yield data and measurements of geomorphic process. Out of five locations and eight river basins, the Rio Nambe in the Sangre de Cristo Mountains was selected as the most applicable comparative site, based on available data, elevation, and watershed size.

As described by the RHEM developers (Nearing et al., 2011), "*RHEM is an event-based derivation of the WEPP model made by removing relationships developed specifically for croplands and incorporating new equations derived from rangeland data. RHEM estimates runoff, erosion, and sediment delivery rates and volumes at the spatial scale of the hillslope and the temporal scale of a single rainfall event*". SSURGO data was used to characterize the types of surface texture of the soils to be entered into RHEM. Precipitation data were pulled from the RHEM list of available stations that best matched the upper American Fork watershed. The hillslope was considered uniform and represented only a few slopes. Shane Green, a Range Conservationist with the NRCS, was consulted on the foliar cover percent averages for the study area.

In addition to the methods described above, USDA SCS Technical Release TR 12 (1975), "*Procedure – Sediment Storage Requirements for Reservoirs*" was evaluated and compared to the Todea and Hasenyager (2012) results. This was done to provide a reference calculation for sediment yield to material deposited into the Tibble Fork Reservoir. TN 12 provides trap efficiencies of reservoirs using the watershed size, reservoir capacity, and runoff, which are calculated into a Capacity – Inflow ratio. A curve for trap efficiency of reservoirs is also used based on the capacity-inflow ratio. TN 12 contains three sediment curves that include: 1) bedload or coarse material (highly flocculated and coarse-grained sediments); 2) colloids, dispersed clays, and fine silts and; 3) sediment consisting of a wide distribution of various grain sizes. The curve associated with colloids, dispersed clays, and fine silts was used for this study.

A Z-boat was provided by the Wyoming NRCS State office, and the survey was completed in July, 2014. The Z-boat is a remotely-operated survey boat that uses both Global Positioning Systems and echo sounders to receive location and associated depths (OceanScience, 2014). The Z-boat data were correlated to LiDAR data that had been was gathered for this project. The combined data were used to define a continuous terrain and to determine current

sediment volumes within the reservoir.

RESULTS

The range of values derived from the above methods is 0.02 – 0.76 acre-feet per square mile. When considering trap efficiencies, the range is 0.67 – 21.28 acre-feet per year. Table 2 illustrates annual sediment rates calculated in associated tons, including reservoir trap efficiencies for final deposition into Tibble Fork Reservoir. Also included are the 2012 Todea and Hasenyager values with reservoir trap efficiencies.

Table 2 Sedimentation results based on sediment yield and deposited material into Tibble Fork Reservoir

Method/Location/ Study	tons/year	Area Sq. Mi.	Estimated Annual Sediment Volume (acre-feet)	Average Annual Sediment Volume per mi of DA ($AF/mi^2/yr$)	With 20% trap efficiency, final sediment value in Tibble Fork
Booby Hole (UDWR, 2010)		35**	0.84	0.02*	0.67
Indian Creek #1 (UDWR, 2010)		35**	1.33	0.04*	1.06
Duck Fork (UDWR, 2010)		35**	4.90	0.14*	***3.92***
Iliff Anrus (UDWR, 2010)		35**	26.60	0.76*	21.28
Yield Class 5, 0.1-0.2 Ac-ft/Sq.Mi./Yr (Bridges,1973)		18	3.60	0.20*	***2.88***
Yield Class 6, less than 0.1 Ac-ft/Sq.Mi./Yr (Bridges,1973)		17	1.70	0.10*	1.36
Yield Class 5 + 6 (Bridges, 1973) TOTAL		35	5.30	0.30*	***4.24***
Temperate Alpine -- Sangre de Cristo Mountains (Rio Nambe) – (Slaymaker, 1977)		35**	0.84	0.02*	0.67
AGWA SWAT (interpolated)	2928.0*	35	1.25	0.04	1.00
RiverMorph FlowSed/PowerSed (suspended)	5748.0*	35	2.46	0.07	1.97
RiverMorph FlowSed/PowerSed (bedload)	3624.0*	35	1.55	0.04	1.24
RiverMorph FlowSed/PowerSed (suspended+bedload) TOTAL	9372.0*	35	4.01	0.11	***3.21***
HEC RAS Sedimentation	1403.6*	35	0.60	0.02	0.48
RiverMorph FlowSed/PowerSed suspended + HEC-RAS Bedload TOTAL	7151.6*	35	3.06	0.09	***2.45***
RHEM	14995.2	35	6.41	0.18	5.13
Z-Boat bathymetry (2014)			3.65	0.08	***2.92*** *

*Denotes method and how the data were initially captured.
**Denotes that watershed is normalized and interpolated to have consistent units.

The UDWR reservoir study has the largest differences among its dataset. However, the Duck Fork Reservoir does fall within an acceptable range. Of the four dams reported in this study, this dam has the highest elevation above mean seal level. The Iliff Anrus Reservoir location is currently unknown. The mean elevation of the Duck Fork Reservoir is 9,300 feet above

mean sea level. The mean elevation of the Tibble Fork watershed is 8,600 feet. The elevation difference between the Duck Fork and Tibble Fork watersheds is significant enough for the UDWR reservoir study to provide a cursory approximation or provide ranges when conducting sedimentation studies.

Bridges' sediment map provided the best results with the easiest amount of effort. At first glance, this method appears to be a good verification tool. However, as suggested by Bridges (1973), this method should not be used to determine specific yields at specific sites.

Of the Slaymaker (1977) sites, the Rio Nambe in the San de Cristo Mountains provided the best- suited environmental setting range. However, it did not correlate well. Nor did the AGWA SWAT interpolated results. This is due to user unfamiliarity and the variation of values that could be applied within the software. The Rivermorph FlowSed/PowerSed (bedload and suspended sediment) did correlate well.

The known transported bedload to Tibble Fork was computed by HEC-RAS. The number could be nearly half of the 3,624 tons of material that moved through the measured site using RiverMorph FlowSed/PowerSed opposed to what was modeled in HEC-RAS. That is, the HEC-RAS model provides results of 1,403.6 tons that was computed to reach the Tibble Fork pool.

The RHEM numbers did correlate well and estimated high, since only one hillslope face was estimated for the entire watershed. Due to the limited data fields of the program, it is reasonable to believe that with more hillslope entries, the sediment yield may be more accurate. Note that RHEM is not applicable due the tolerance of hillslope lengths being exceeded.

The Z-boat calculations produced an annual sediment deposition rate of 2.92 acre-feet per year. With the trap efficiency of 20 percent, the sediment yield is expected to be 3.63 acre-feet per year.

CONCLUSION

Having actual measurements provided confidence in the modeled results. As previously mentioned, the Bridges map narrowed down values to get a realistic picture of the potential for sediment deposition. The Utah dams could be further analyzed to determine sediment yields and trap efficiencies. The author does not fully endorse the use of AGWA SWAT due to his limited use and knowledge of the software. The potential of using the software to accurately provide sediment yields may be promising.

Although a bathymetric survey was supplied, additional familiarity with sedimentation methods is required to predict future conditions. Data acquisition using historic flows, the stream gages, and SSURGO data are precursors to understanding the sedimentation within the system. As mentioned before, the Todea and Hasenyager bedload study provided insight that data on the rising limb of the hydrograph are the most critical, however, both the falling and rising limbs were considered in the sediment-discharge curves, and this artificially raised the amount of bedload being transported to Tibble Fork. Ideally, all possible sediment would be accounted for. Understanding the process of sedimentation is crucial for dam design, as it has an impact on dam size and the longevity of the structure. The system of averages may be too general, but using many methods may be validated due to the consequences of under- or over-estimating the sediment that is either being delivered or moved through the reservoir.

ACKNOWLEDGEMENTS

The authors appreciate the assistance, review, and support from the following: United States Department of Agriculture Natural Resources Conservation Service (Utah and Wyoming), Norm Evenstad, Shane Green, Chris Gauthier, Chuck Schmitt, and Bronson Smart.

REFERENCES

Aero-Metric, Inc. (2010). Light Detecting and Ranging (LiDAR) data for American Fork Watershed, Utah. Collected July 29 and 30.

AMEC, (2010). Report Memo Sediment Survey and Sampling for Tibble Fork Reservoir and Silver Lake Flat Reservoir, Utah County, Utah: Unpublished report transmitted as an e-mail on November 12, 2010 from Robin Kurz, Project Geologist, at AMEC to Ana Vargo, Geologist, USDA NRCS.

Arnold, J.G., Williams, J.R., Srinivasan, R., King, K.W., and Griggs, R.H. (1994). *SWAT-Soil Water Assessment Tool*, USDA, Agricultural Research Service, Grassland, Soil and Water Research Laboratory, Temple, Texas.

Bridges, B.L. (August, 1973). Map: Estimated sediment yield for the State of Utah. Erosion and Sedimentation, Western U.S. Water Plan, prepared by SCS.

Burns, I.S., Scott, S.N., Levick, L.R., Semmens, D.J., Miller, S.N., Hernandez, M., Goodrich, D.C., and Kepner, W.G. (2007). Automated Geospatial Watershed Assessment 2.0 (AGWA 2.0) – A GIS-Based Hydrologic Modeling Tool: Documentation and User Manual; U.S. Department of Agriculture, Agricultural Research Service.

Dendy, F.E., and Champion, W.A. (1978). *Sediment Deposition in U.S. Reservoirs: Summary of data reported through 1975.* Miscellaneous Publication No. 1362. Compiled by USDA Agricultural Research Service's Sedimentation Laboratory, Oxford, Mississippi.

Edwards, T. K., and Glysson, G.D. (1999). Field Methods for Measurement of Fluvial Sediment. U.S. Geological Survey, Techniques of Water-Resources Investigations, Book 3, Chapter C2. Reston, Virginia

HDR Engineering Inc. (2011). Van Dugway Landslide Erosion Investigation Report-Tibble Fork, PL-566 Dam Rehabilitation – Landslide Erosion Investigation. Salt Lake City, Utah. Prepared for the USDA NRCS.

Nearing M.A., Wei H., Stone J.J., Pierson F.B., Spaeth K.E., Weltz M.A., and Flanagan D.C. (2011). A rangeland hydrology and erosion model. Transaction of American Society of Agricultural and Biological Engineers 54:1-8.

OceanScience (2014). Z-boats. Available at **http://www.oceanscience.com/products/z-boat/home.aspx**. Accessed in November 2014.

RIVERMorph, LLC (2008). Rivermorph User's Manual Version 4.3. Louisville, Kentucky, 40223.

Rosgen, D.L. (2006). FlowSed/PowerSed – Prediction Models for Suspended and Bedload Transport, Proceeding from the 8th Joint Federal Interagency Conference, Reno, Nevada.

Rubey W. (1933). Settling Velocities of Gravel, Sand, and Silt Particles. American Journal of Science. Vol. 25.

Green, S. (2014). Personal communication. State Range Conservationist, Utah USDA-NRCS, Salt Lake City, Utah.

Slaymaker, O. (1977). Estimation of sediment yield in temperate alpine environments. International Association of Hydrological Sciences, Publication no. 122: 109-117.

Todea, N., and Hasenyager, C. (2012). Integration of Time Series data with Geospatial Data for Tibble Fork Reservoir Sedimentation Study. American Water Resources Association Spring Specialty Conference, Geographic Information System and Water Resources VII, New Orleans, Louisiana, March 26-28.

U.S. Army Corps of Engineers Institute for Water Resources (USACE) (2010). HEC-RAS: Hydrologic Engineering Centers River Analysis System Hydrologic Engineering Center, Davis, California.

United States Department of Agriculture Soil Conservation Service (USDA-SCS) (1964). American Fork-Dry Creek Watershed Protection and Flood Prevention Project, Utah County, Utah: Plans for the Construction of Tibble Fork Debris Basin. Salt Lake City, Utah.

United States Department of Agriculture Soil Conservation Service (USDA-SCS) (1975). Procedure, sediment storage requirements for reservoirs. Engineering Division Tech. Release No. 12.

United State Geological Survey (USGS) (2011). Stream gage data for Gage No. 10164500 American Fork above Upper Power plant, near American Fork, Utah.

http://waterdata.usgs.gov/ut/nwis/nwisman/?site_no=10164500. Accessed 2011.

Utah Division of Water Resources (UDWR) (2010). Managing Sediment in Utah's Reservoir - Utah State Water Plan. Salt Lake City, Utah.

Utah Division of Water Resources (UDWR) (2011). Tibble Fork Dam Phase II Evaluation and Analysis. May. Salt Lake City, Utah.

Yang, C.T. (1972). Unit Stream Power and Sediment Transport. Journal of Hydraulic Division, American Society of Civil Engineers, Vol 98 No. HY10, pp. 1805-1826.

ACCOUNTING FOR IMPERFECT RESERVOIR OPERATIONS IN THE TRUCKEE RIVER SYSTEM

Caleb Erkman, Project Engineer, Precision Water Resources Engineering, caleb@precisionwre.com; Shane Coors, Principal, Precision Water Resources Engineering, shane@precisionwre.com; Jeff Boyer, TROA Implementation Coordinator, TROA Planning Office, jtboyer@troa.net; Patrick E. Fritchel, P.E., Hydrologic Engineer, TROA Planning Office, pfritchel@uswatermaster.org

Abstract: The Truckee River System in California and Nevada contains seven reservoirs in its upper basin. Under the proposed Truckee River Operating Agreement (TROA), several parties are able to store and use their water supplies in new ways, consistent with their water rights. Prior to TROA and in TROA, all of the water that is impounded in the seven upper Truckee River basin reservoirs is allocated, and thus all storage and releases from reservoirs must be credited or charged to the appropriate account and owner. TROA provides new mechanisms for parties to establish credit waters, exchange water from one reservoir to another, and release water to meet their operational goals.

A RiverWare© model is used to determine the best operation of the reservoirs based on the TROA policy, the goals of the parties and the forecasted inflows to the system. Once operations are executed, the same RiverWare© model is then used to determine the final accounting of water in the system based on the measured release from each reservoir and the measured inflows. These measured outflows will differ from the intended or perfect operation of the system due to operational imperfections/imprecisions, inaccuracies in the forecast, and errors in gaging. It is necessary to account for these various imperfections so that the end-of-day accounting of the system correctly charges all of the water that was released to the appropriate accounts in the respective reservoirs.

An accounting method is under development that fully allocates the flow from each of the reservoirs, releases the desired amount of each party's water and closely matches the requests and availability to establish and exchange water throughout the system. Due to the complex and multi-objective nature of the releases a simple algorithm is not sufficient to provide an acceptable solution. Additional considerations must be taken when considering imperfections on reservoirs in series as opposed to reservoirs in parallel.

An overview of the RiverWare© model, the allocation process for imperfect operations, and an approach to testing the algorithm will be discussed in the following sections.

INTRODUCTION

Truckee River History: Water rights in the Truckee River Basin are well defined and fully appropriated. Original water rights from the Truckee River are mostly vested rights established by historic use for irrigation and power generation between 1861 and 1878. The vested rights were adjudicated between 1913 and 1926 and recorded in the Orr Ditch Decree (ODD), Orr Ditch Decree (1944).

Water management policy to satisfy ODD rights during the dry season and during more extended drought periods is established by the 1935 Truckee River Agreement (TRA), Truckee River Agreement (1935). The TRA provides for a simple-to-manage, supply driven system that specifies required rates of flow at the California/Nevada state line based on month of the year and the water surface level of Lake Tahoe. These specified flows are measured at the Farad Gage near the town of Floriston, California (see FaradGage in Figure 1) and are known as Floriston Rates (FR). The critical FR measurement point is down-stream from all Truckee Basin storage reservoirs. When the FR is met there is adequate water instream to satisfy all ODD water rights. During runoff season, water can be stored if the FR is met. FR storage is later released during the dry season to increase river flows up to the FR.

Water right markets (Nevada's water law that allows water right owners to apply to change manner and place of use) and a lengthy list of court rulings have accommodated the demand-shift for limited water resources from agricultural (Ag) to municipal and industrial (M&I) uses as well as for some newly recognized environmental purposes. However, the market transfers of ownership and use to date, have not been paired with suitable changes in reservoir operating policy. Specifically, M&I drought supplies have not been increased, because the FRs have not changed.

The proposed Truckee River Operating Agreement (TROA), Truckee River Operating Agreement (2008), system for river and reservoir management changes the operating system from one that is supply-driven and relatively simple to manage to one that is much more complex, but better meets separate, modern demands, Wilds (2010). TROA allows some water right owners to hold back a portion of their water right out of FR releases to establish Credit Waters to be released to directly meet their specific scheduled demands. The new TROA system is demand driven, adds many new Credit Water categories and sub-categories, responds to water right owners Scheduling requests and requires a very detailed, complex daily monitoring and accounting approach.

In October 2014, TROA was authorized, which will allow the parties to store and use their water more flexibly with much added complexity. A map of the Truckee River Basin is included in figure 1 for reference.

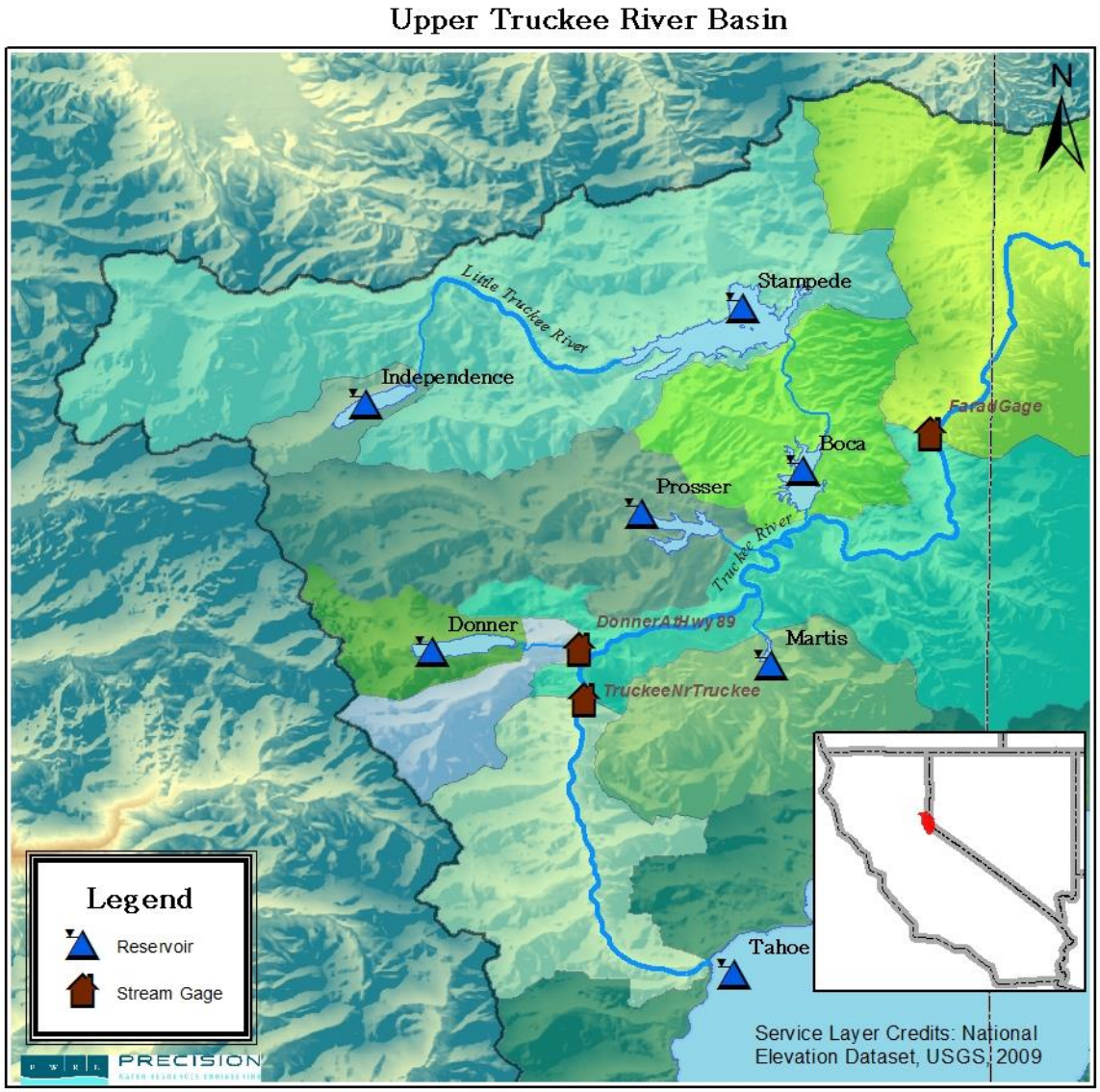

Figure 1 Map of the Truckee River Upper Basin Reservoirs

TROA Policy: TROA allows parties to establish credit water by holding back a portion of the FR release to establish credit water for later use at their scheduled request. A holdback can occur when FR water is being released from a reservoir to meet the Floriston Rate, as shown in the Pre-Holdback condition in Figure 2, the reservoir release is reduced and the amount that was held back is transferred from the FR account on the reservoir to the account of the party requesting the hold back on the reservoir. The net effect is that the outflow of the reservoir is reduced, the storage of a specific category of credit water in the reservoir is increased, credit water is established for Account B, and the storage of FR water in the reservoir is unaffected (i.e., FR Account is reduced by 150 cfs in both cases).

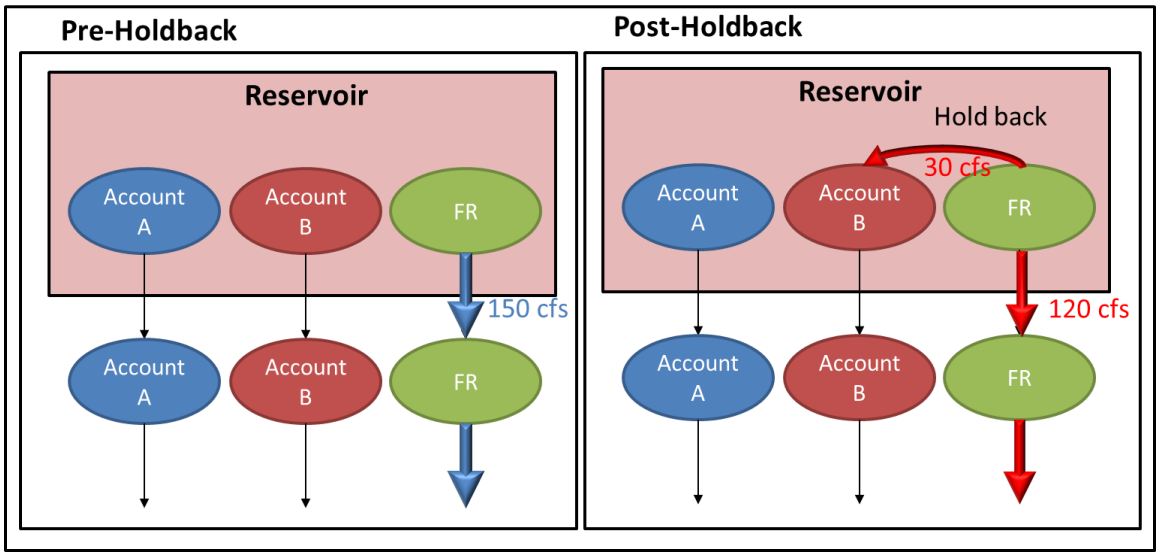

Figure 2 Typical Holdback of a FR Release on a Reservoir.

Once credit water is established TROA provides mechanisms for parties to move water between reservoirs, including trades and exchanges. For a trade, two parties with water in different reservoirs switch the location of an equal amount of water at the mutual consent of each party. If a party would like to move its credit water into a reservoir where a different party is releasing water then there is opportunity for an exchange. This process is best illustrated with the example shown in figure 3. The party that has a demand to release water, the FR Account, would be releasing 150 cfs of demanded water from Reservoir 2 as shown in the Pre-Exchange condition. The party that is moving its water, Account B, releases and transfers 30 cfs of its credit water from Reservoir 1 into the FR Account in the river. This is known as the Borrow as shown on Reservoir 1 in the Post-Exchange condition. Next the party releasing water for a demand (FR Account in Reservoir 2) reduces its release by 30 cfs and transfers 30 cfs of FR water into the account of the party that is moving water (Account B). This is known as the Payback as shown on Reservoir 2 in the Post-Exchange condition. Note that at the confluence below the two reservoirs, the river flow remains unchanged at 150 cfs. These processes give greater flexibility to the parties so that drought sources can be maintained in a secure location. Additionally, this same process can be used to increase streamflows in select reaches of the river to achieve other desirable goals set for recreation and the environment (e.g., rafting, fishing, and riparian habitat).

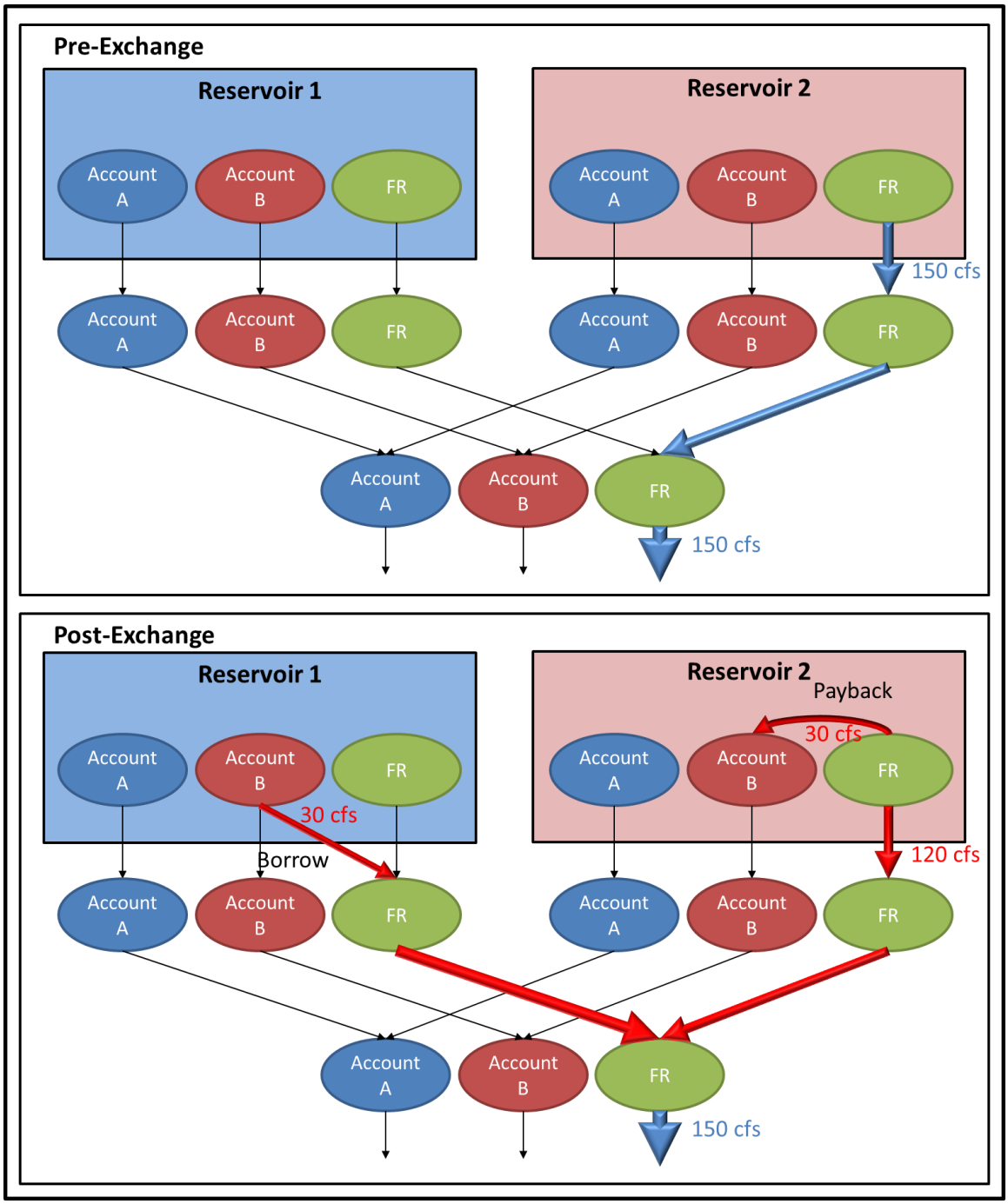

Figure 3 Typical FR exchange between two reservoirs showing the Pre-Exchange condition and the Post-Exchange condition.

Accounting Approach: A RiverWare© model is used to determine the best operation of the reservoirs based on the TROA policy, the goals of the parties and the forecasted inflows to the system. Once operations are executed the same RiverWare© model is then used to determine the final accounting of the system based on the actual release from each reservoir and the measured inflows. These measured outflows will differ from the intended or perfect operation of the system

for several reasons, including but not limited to: operational imperfections/imprecisions, inaccuracies in the forecast, and errors in gaging. It is necessary that the reservoir water accounting reflect these various imperfections so that the end-of-day accounting of the system charges all of the actually released water to the appropriate accounts in the respective reservoirs.

A method was developed to optimize allocations for the releases that fully allocates the flow from each of the reservoirs and releases the desired amount of flow from each party's storage account. Due to the complex and multi-objective nature of the releases, a simple algorithm is not sufficient to provide an acceptable solution. Additional considerations must be taken when considering imperfections on reservoirs in series as opposed to reservoirs in parallel. In the Truckee River system there are both reservoirs in series and reservoirs in parallel. To meet these objectives, a three step approach to reconciling imperfect accounting has been developed:

1. Determine Farad Process Allocation
2. Determine Main Truckee Reservoir Process Allocations
3. Determine Little Truckee Reservoir Process Allocations

Processes, as referred to in this paper, include the release, storage, establishment, or exchange of a specific category of water (e.g., M&I Credit Water Establishment). The three step approach is discussed in the following sections.

DETERMINE FARAD PROCESS ALLOCATION

In priority based systems such as the Truckee River Basin, it is desirable that the senior water rights be afforded higher protection than junior water rights. This is the practice when setting operations and it is desirable to approach accounting in a similar way such that the priority order is honored. With this approach we can use the imperfections as a way to perfect operations for the higher priority waters and their associated processes. Imperfections in the operations would be distributed to the lower priority waters. The advantage of a priority based system is that in most cases all processes achieve the desired allocation except for the lower priority process(es). A lower priority process, or floater, reconciles the imperfections to balance all or part of the system. By starting from the bottom of the system and working our way up we can use flexibility within the location of process releases to achieve the system goals. Setting a valid Farad allocation is the first step to ensure the success of the later steps in the imperfect operations accounting algorithm.

MAIN TRUCKEE ALLOCATION

Once the Farad allocation is set, the process allocation for the parallel reservoirs can be completed. These reservoirs include: Tahoe, Donner, Prosser, Martis, and the Little Truckee (LT) as shown in Figure 1. Because Boca is the outlet of the Little Truckee River and its release includes releases from Boca, Stampede and Independence, we will consider these three series reservoirs as a single reservoir, referred to as the LT, in this step.

This process has several goals:

1. Fully allocate the outflow of each reservoir.

2. The sum of the allocations on all main Truckee reservoirs for each process should match the Farad allocation for the respective process.
3. The allocation for each process on each reservoir should be as close as possible to the perfect operation.

The following loops outline the method that was found to give the best results in achieving the goals specified above, see Figure 4 for a flowchart that diagrams the steps below. These steps are meant to summarize the algorithm that has been developed and are therefore not comprehensive.

1. Loop over processes in order of increasing number of reservoirs involved (this is the loop in the upper left corner of Figure 4).
2. For each process, loop over the reservoirs that are releasing that process (this is the loop in the lower right corner of Figure 4). Each reservoir will fall into one of three categories (a-c) and will be allocated as specified below and in the respective part of Figure 4.
    a. If the current process is the floater process for the current reservoir, then set the reservoir process allocation to reconcile the reservoir while honoring the necessary limits and tolerances
    b. If the current reservoir is the last reservoir on the process list, reconcile the process while honoring the necessary limits and tolerances
    c. For all other cases allocate the theoretical perfect process allocation while honoring the necessary limits and tolerances.

The last allocation will reconcile the last process and the last reservoir at the same time, giving a reconciled system. This works because the sum of the Farad allocation for all processes is equal to the sum of the actual releases from the Main Truckee reservoirs.

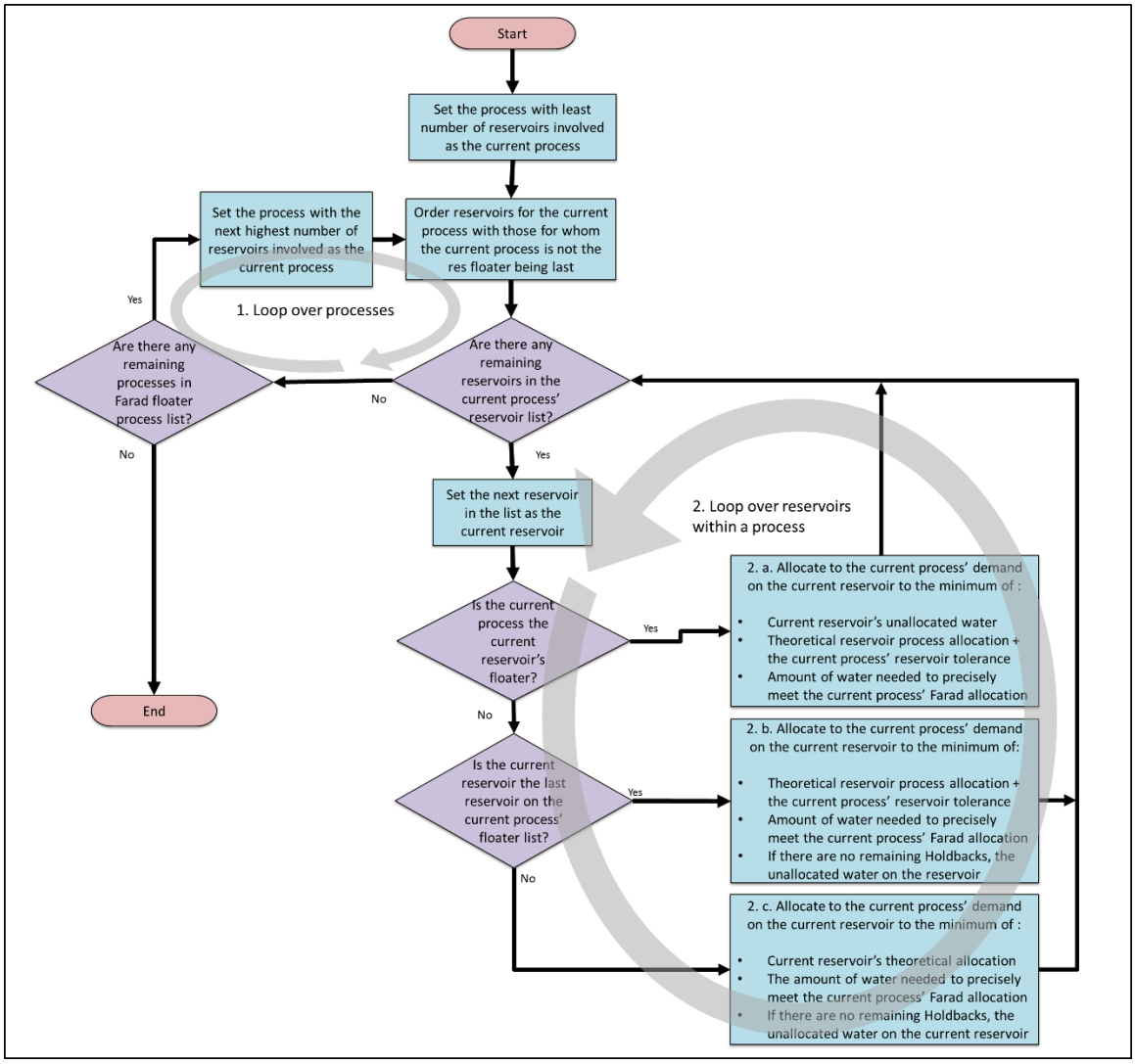

Figure 4 Flow chart for setting process allocations for the Main Truckee reservoirs**.**

LITTLE TRUCKEE ALLOCATION

Once the Main Truckee reservoirs are reconciled, the allocations for the LT aggregate reservoir can now be disaggregated into allocations for the three series reservoirs: Boca, Stampede and Independence.

Here, the remaining flow on a reservoir is difficult to determine until the flow from the upstream reservoir(s) are accounted for. Part of the release from a reservoir may be water being passed through from an upstream reservoir's release, and some of it may be a release from that reservoir. Another complication is that an upstream reservoir may release water with the intention of restoring it in a downstream reservoir. Considering these complications, it was determined that the best approach was to apportion releases to meet the LT allocation for each process letting the most downstream reservoir with each process float, if possible. Once this step is completed and the LT allocations set in the previous step are met, a check is made if the sum of the releases from

the reservoir and pass-through releases from upstream reservoir(s) is greater than the reservoir outflow. When this occurs it is necessary to re-label a process release on an upstream reservoir to a more downstream reservoir, if possible. If this is not a viable solution, an exchange can be created that moves credit water storage to a more upstream reservoir. The type of water moved is at the discretion of the TROA Administrator and may be used to meet standing requests of the parties. This allows reconciliation of the system even in dire scenarios. When the sum of the releases from storage for a reservoir and all pass-through releases from upstream reservoirs is less than the measured outflow from that reservoir, the remainder is labeled as a release to be restored in the next downstream reservoir. The account that is restored is prioritized based on the Administrator's discretion, and may meet a standing request of a party.

SYSTEM RELIABILITY AND TESTING

Because TROA has not been implemented, there is no measured data available to test the algorithm. Therefore, it is necessary to manufacture realistic synthetic data for testing purposes. Thorough testing of the algorithm discussed previously will provide for a smoother transition into administrating TROA when implementation begins.

In order to facilitate reasonable testing it is important that data be randomized to simulate the imperfections that will occur primarily from imprecise reservoir releases and imperfect knowledge of the system inflows. If data is randomized for too long of a period at once the perfect operation will diverge from the randomized operation due to changes in storage in the reservoirs. To avoid this and best simulate the day-to-day practice of setting releases and performing accounting of the measured flows the following day, it is important that the flows be randomized for each day and the operation for the next day be set based off of the storage from the accounting of the previous day's imperfect operations. This is done by coupling the RiverWare© operations and accounting model with a spreadsheet that randomizes the system flows and reservoir levels one day at a time. This process must be completed for each day in a water year which makes it a prime candidate for automation. To do this a RiverWare© batch mode script was written that simulates one day of reservoir operations based off of a forecast. The system operation is then sent to a spreadsheet via a RiverWare© Data Management Interface (DMI), where the reservoir outflows and system inflows are randomized. These randomized flows are then inputted to the RiverWare© model via another DMI as if they were measured in the field. The RiverWare© model is then run again and the newly randomized flows are accounted for using the accounting algorithm. The RiverWare© model then performs the best operation based off the supplied forecast and the process is repeated. This method allows for testing of a year of operations and accounting using the imperfect operations model by running a script overnight. In this way the RiverWare© accounting model can be tested for many hypothetical years with varying initialization and hydrological conditions. By analyzing the results of the hypothetical accounting years the accounting algorithm can be improved to address a wide variety of potentially difficult scenarios. This testing and development routine should provide a smoother transition once TROA is implemented.

PROVISIONS FOR NON-STANDARD OPERATIONS

Although it is desired to approach reservoir accounting in a systematic way it is understood that many obscure scenarios may occur where the systematic approach is insufficient to reconcile the

system. These scenarios may occur for a variety of reasons including maintenance, extreme natural phenomena, experimental reservoir operations, etc. Since many of these events are one time occurrence it is desired to have a method to complete the reservoir release accounting manually instead of developing special provisions in the RiverWare© accounting algorithm for these extra-ordinary scenarios. With this goal in mind, a method to review the daily results of the accounting algorithm was developed which provides the necessary information for the TROA Administrator to manually set the reservoir release allocation when deemed necessary.

SUMMARY

Considering the complexity that TROA introduces into Truckee River operations, it is necessary for the TROA Administrator to have a reliable and systematic method to perform the final reservoir accounting of the measured releases from the reservoirs. A three step priority based algorithm has been developed to perform the reservoir release accounting. These steps include:

1. Determine Farad Process Allocation,
2. Determine Main Truckee Reservoir Process Allocations, and
3. Determine Little Truckee Reservoir Process Allocations.

In order to provide a smooth transition into administering TROA, a method to generate realistic synthetic reservoir operations has been developed to test the reliability of the accounting algorithm.

REFERENCES

Orr Ditch Decree (1944), Final Decree, U.S.A. vs. Orr Ditch Company, et al., U.S. District Court in Nevada, Equity Docket No. A3. Web: http://www.troa.net/documents/OrrDitch_Decree/index.pdf.

Truckee River Agreement (1935). Web: http://www.troa.net/documents/TRA_1935/.

Truckee River Operating Agreement (2008). Web: http://www.troa.net/documents/TROA_Sep2008/troa_final_09-08_full.pdf.

Wilds, L. J. (2010). Water Politics in Northern Nevada: A Century of Struggle, Wilbur S. Shepperson Series in Nevada History, University of Nevada Press, Reno, Nevada, pp.64-66.

UNDERSTANDING DRIVERS OF SEDIMENT LOADS IN A MORPHOLOGICALLY ACTIVE WATERSHED: A MULTIDISCIPLINARY APPROACH TO WATERSHED MANAGEMENT

Amanda Stone, Water Resources Engineer, Boulder, CO, amanda.g.stone@gmail.com; James Selegean, Hydraulic Engineer, U.S. Army Corps of Engineers – Detroit District, Detroit, MI, james.p.selegean@usace.army.mil; Travis Dahl, Research Hydraulic Engineer, U.S. Army Corps of Engineers – Coastal and Hydraulics Laboratory, Vicksburg, MS, travis.a.dahl@usace.army.mil; Mark Riedel, TMDL Project Manager, Wisconsin Department of Natural Resources, marks.riedel@wisconsin.gov; Alex Brunton, Geomorphologist, Baird, Oakville, ON, abrunton@baird.com

Abstract: The Knife River is a tributary to Lake Superior in northern Minnesota draining 56,000 acres of mostly forested and wetland areas with minimal development. The river is home to the North Shore's only wild Steelhead population and is the only tributary with no barriers to upstream migration. Although development is minimal, the morphologically active and flashy nature of the watershed results in large sediment loads which impact the harbor downstream, aquatic invertebrate habitat, the trout fishery, and contribute large quantities of sediment to Lake Superior. Because of the morphologically active nature of the watershed, the river is sensitive to engineering modifications and large structural solutions may be ineffective. This places an emphasis for watershed management on understanding the sensitive hydrologic nature of the system and careful land use decisions. Our study took a multi-disciplinary approach focused on gaining an understanding of the watershed system by looking at causes, linkages, and relative contributions of different channel modifications and landuse changes within the watershed on sediment and hydrologic dynamics. We used a combination of desktop analyses, geomorphic assessments, modeling (river hydraulics, watershed modeling, and snowpack ripening), regional analyses, and sensitivity scenarios to understand relative importance of different drivers of the hydrologic system. As part of a sensitivity assessment, we examined the impacts of different forestry practices, beaver dam management, and conversion of wetlands. Our study identified areas within the watershed that that may be sensitive to land use conversion or logging. In addition, we provided a summary of how beaver dam activity and management might impact hydrology and aquatic habitats, how changes in landuse might change snowmelt characteristics, and how changes in climate patterns (snowpack dynamics and rainfall intensity) might change sediment loading patterns. With this multi-disciplinary approach, we were able to provide an overview framework for proactive watershed management in a complex and morphologically active system by understanding relative importance of many facets of the watershed hydrology.

INTRODUCTION

Watershed management for reduction of sediment loads often focuses on sediment loading from soil erosion; however, in watersheds with numerous natural and anthropogenic forces driving sediment loads, this approach may be inadequate. In systems that are geologically young and morphologically active, rivers are especially sensitive to engineering modifications and hard engineering solutions may fail. This places an emphasis for watershed management on a big-picture understanding of the sensitivity of morphologic drivers and relative contribution to

sediment load and erosion in order to make effective management and engineering decisions at the watershed scale.

The Knife River (Figure 1), a tributary to Lake Superior in northern Minnesota, is a prime example of a watershed with a very large sediment load causing impairments to aquatic life, yet land use change and development are minimal within the watershed. The watershed drains 56,000 acres of mostly forested and wetland areas (Figure 2). The river is home to the North Shore's only wild Steelhead (*Oncorhynchus mykiss*) population, and it is the only tributary with no barriers to upstream migration. Post-glacial rebound results in morphologically-active valleys in this region, and the naturally flashy nature of the watersheds creates large sediment loads which impact harbors and estuaries downstream, degrade aquatic invertebrate habitat and the trout fishery, and which contribute large quantities of sediment to Lake Superior (Riedel, et al, 2005).

Figure 1 Knife River under high flow conditions carrying large sediment load

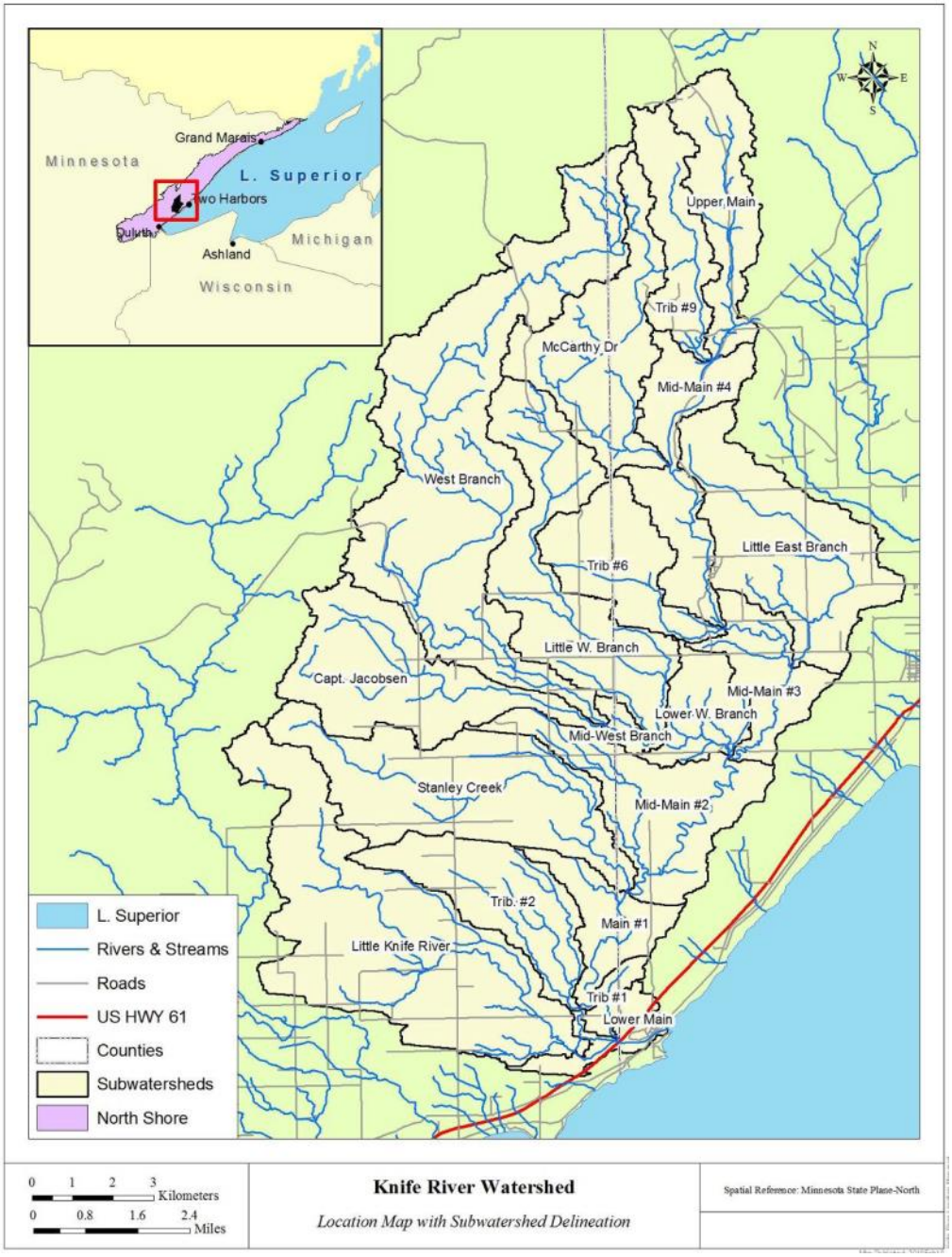

Figure 2 Knife River watershed location

While lacustrine clay and clay-dominated tills in the area under natural land cover are generally resistant to erosion (NRCS, 1998), activities within the watershed that expose soils or disturb banks can increase runoff resulting in fluvial erosion and destabilized channels (Riedel et al., 2005; Riedel et al., 2002). Our study took a multi-disciplinary approach focused on gaining an understanding of the Knife River watershed system by examining causes, linkages, and relative contributions of different channel modifications and land use changes within the watershed to hydrology and sediment loads. The knowledge gained from this multi-disciplinary approach can be used to support effective decision-making for watershed managers.

METHODOLOGY

We used a combination of desktop analyses, modeling, and sensitivity scenarios to determine the relative importance of different drivers of hydrology and sediment loading in the Knife River watershed. Four major factors driving sediment load in the watershed were examined by this study:

- Watershed physiography (climate, geology, soils, terrain, river network characteristics)
- Beaver *(Castor canadensis*) activity
- Watershed land use and disturbance
- Sediment loading relationship to hydrology

Literature and Data Review: The first step in the approach was to review available studies and data. This review included existing reports and studies as well as interviews with local and state resource managers. Data gathered for the study area included historic flow and sediment data as well as geospatial data to support desktop analyses and modeling (MPCA, 2009). Spatial data to support the study included elevation, landcover, soil, geology, canopy, and detailed wetland coverage. In addition, a comprehensive review of literature on beaver activity was conducted to understand how land use changes have resulted in dramatic changes in beaver habitat and resultant populations, density, and behavior (USDA, 2002).

Desktop analyses: The datasets collected during the literature and data review were used to complete desktop analyses to give further insight into the hydrology and morphology of the watershed. Elevation datasets were used to calculate fluvial power and pinpoint areas that may be susceptible to higher levels of erosion and mass wasting. These datasets were also used to develop longitudinal profiles of all streams within the watershed to identify potential areas of head-cut migration or river valley evolution associated with natural or anthropogenic causes.

Historic flow and sediment records from the USGS gage near the mouth of the river were reviewed to examine flow frequency, flashiness, seasonality, and historical changes in flow. Understanding the magnitude and frequency of both flood and low-flow events in the watershed from a historic perspective and existing conditions is key to understanding sediment loading patterns and the relative impact of land use changes on hydrology.

Modeling: A suite of hydrologic, hydraulic, and snowpack models were developed to understand existing conditions in the watershed and to support scenario analyses for different land management decisions. The modeling builds upon the analyses done in the literature and data review both for providing input data and context for what scenarios to assess for sensitivity analysis and management scenarios.

Beaver activity in the watershed has increased dramatically since pre-settlement conditions due to reductions in trapping (Butler and Malanson, 2005). Dam-building activity creates a step-pool structure in tributaries which disconnects riverine habitat for fish and changes thermal regime (Pollock et al., 2003), and may cause floods from cascading failures (Butler and Malanson, 2005). A 1-D HEC-RAS model of a representative reach in the watershed was developed to simulate the impacts of a variety of beaver-dam densities on the river. Pre-settlement dam density in this area was 3.0 dams/mile (Winchell and Upham, 1884), while current conditions are

much higher at 10.6 dams/mile (Verry, 2005). Results showed step-pool structures caused by high-density beaver activity with cascading dam failures under flood conditions (Figure 3).

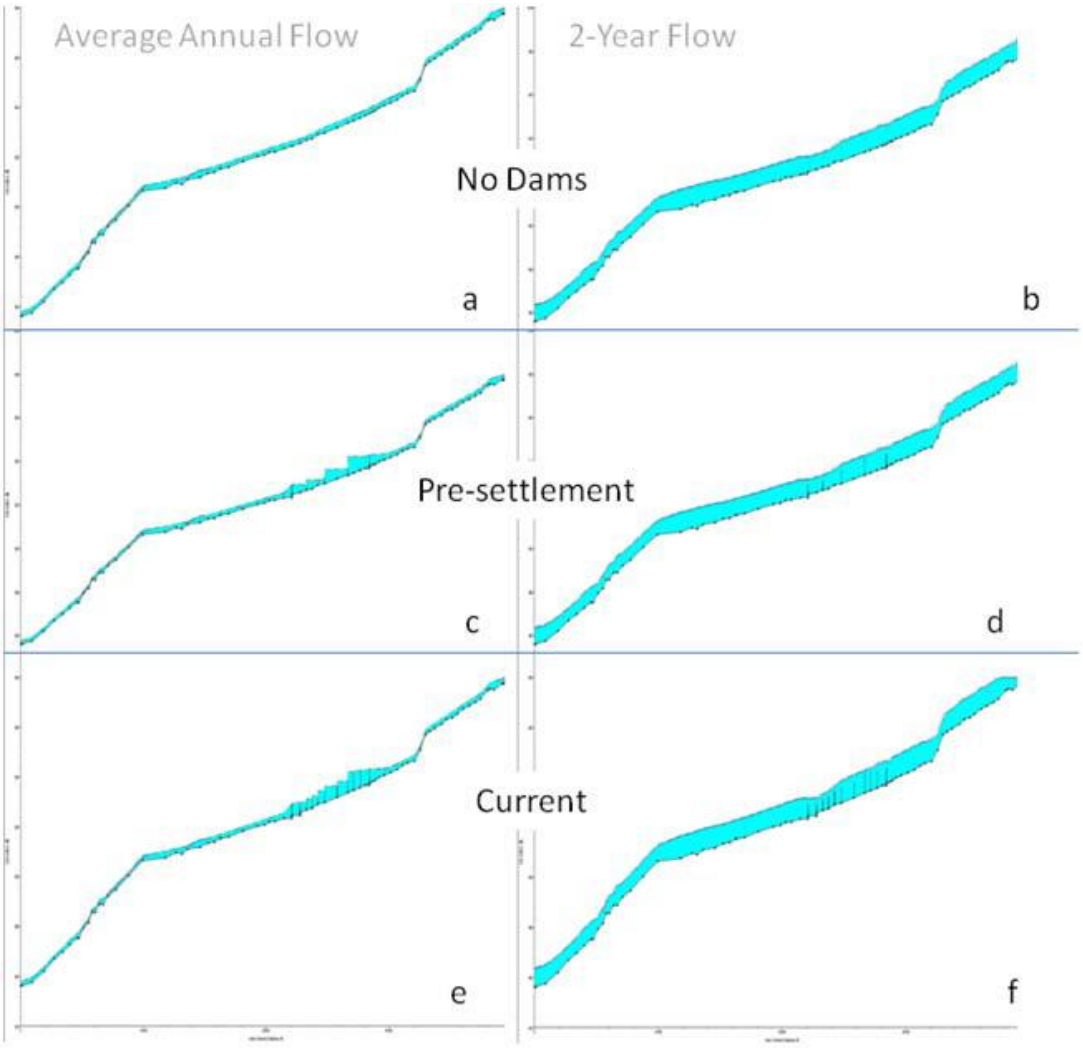

Figure 3 Beaver dam hydraulic modeling results. Beaver dams were represented under each scenario for typical spacing and density as reported in literature.

A watershed hydrology model was developed using HSPF (Hydrological Simulation Program – Fortran) to model existing conditions and simulate the hydrologic impact of potential land use changes. Several scenarios were simulated including pre-settlement conditions, various timber harvesting practices, forest restoration, and wetlands conversion. Results showed the watershed hydrology was most sensitive to conversion of wetlands relative to other land management scenarios. Wetlands play a key role in hydrologic response in the watershed, especially given the naturally low infiltration capacity of the clay soils in the watershed. Results of the existing conditions hydrology mode,l as well as the scenario applications, supported identification of areas susceptible to erosion under existing conditions as well as subwatersheds that may be sensitive to various land use changes in the future. An example of the sensitivity ranking results is shown in Figure 4.

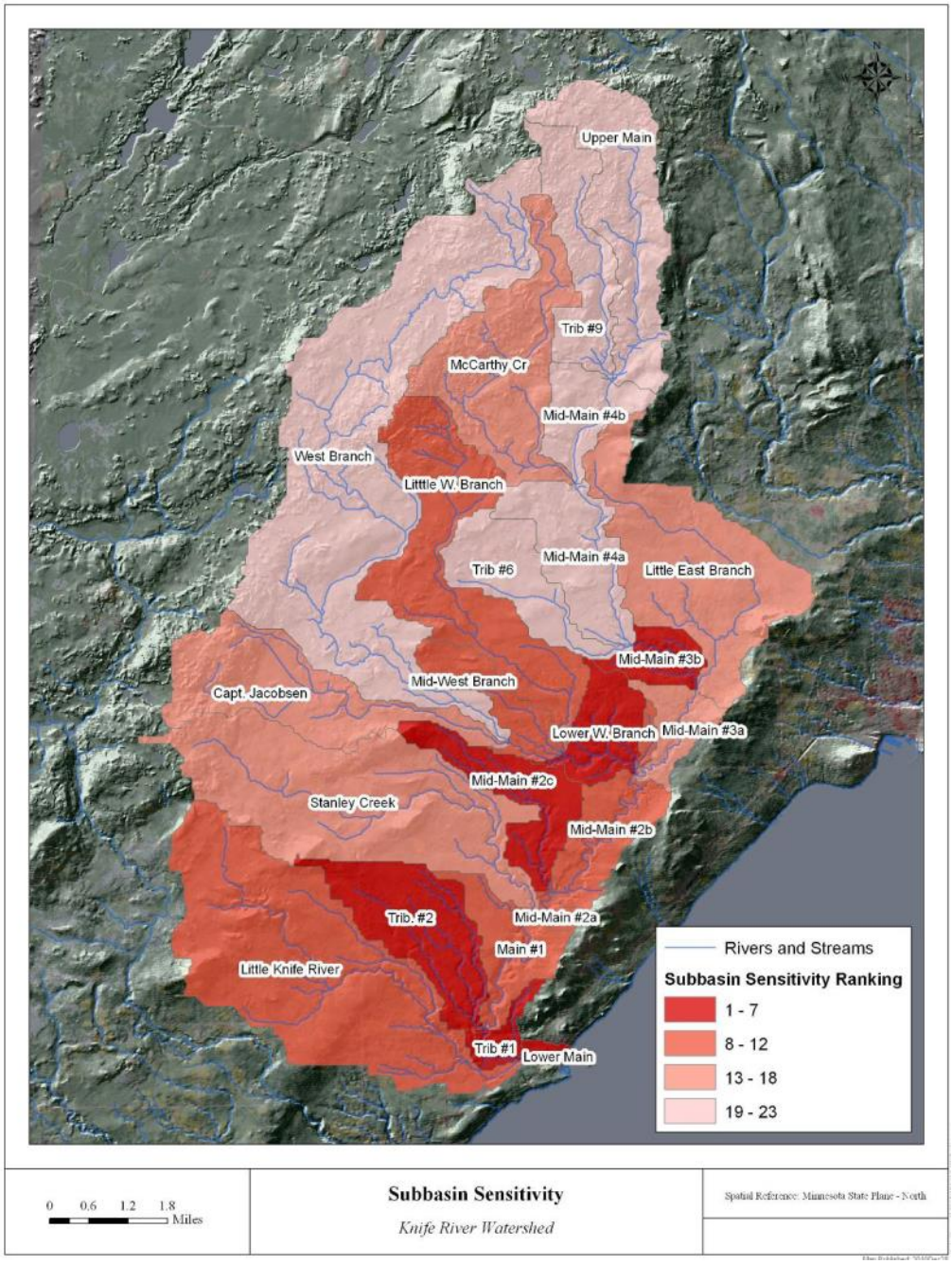

Figure 4 Example subbasin sensitive ranking

The snowmelt period plays a very important role in the hydrology of the watershed as 50 % of the runoff near the mouth occurs from mid-March through the end of May. Logging in the Midwest has been shown to have a potentially large impact on water yield and peak runoff during spring melt (Verry et al., 1983; Verry, 1986). Because of the relative importance of the melt runoff, a mechanistic snowpack model was developed to simulate the potential impacts of various land management practices on snowpack development and the corresponding melt. The HSPF model was also examined in detail during this period under several scenarios to compare results to the snowpack model.

Sediment budget analysis: Finally, a sediment budget analysis was conducted to develop a range of estimates for sediment yield for the watershed (Riedel et al., 2008). This included a variety of regional studies as well as detailed review of sediment data collected at the USGS gage. Estimates of sediment loads using a simple relationship between discharge and suspended sediment concentration fell within the expected range for yields for this region (Figure 5). The analyses indicated a strong positive relationship between discharge and sediment concentration. This observation is key in interpreting hydrologic and hydraulic analyses in relation to sediment load in the basin. Despite being predominantly forested and having extensive wetlands in its headwaters, the Knife River exhibited sediment yield results similar to watersheds with extensive agricultural land use conversion. This is because the geologic setting in this region is much more vulnerable to land disturbance and changes in climate compared to more geologically mature and evolved watersheds (Riedel et al., 2002).

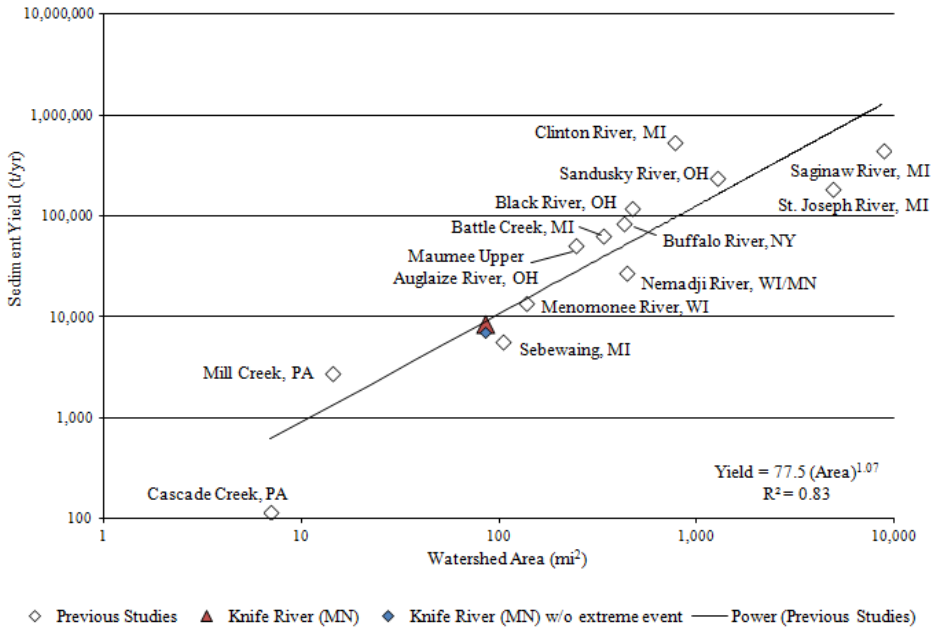

Figure 5 Regional sediment yields based on watershed area from other Great Lakes studies

Review of literature indicated that bank erosion and valley wall failure play a significant role in sediment loading in the watershed (Nieber et al., 2008). Using sediment data collected by the USGS in conjunction with local metrological data, multiple linear regression analysis was used to identify potential key weather drivers for large sediment loads. Results indicated that an interaction between rainfall intensity and cumulative rainfall (resulting in saturated soils) plays a significant role in watershed loading as well. Changes in rainfall patterns for the region may result in changes in sediment loads based on this analysis.

CONCLUSIONS

In a watershed where anthropogenic forces may not be the principal driver of sediment loads, understanding the existing conditions and sensitivity of the basin to different management practices is critical for watershed managers. Because of the morphologically active nature of the watershed and the river valleys due to post-glacial rebound, the sediment load is more sensitive

to changes in land use and changes in climate patterns than more mature watersheds. By taking a multi-disciplinary approach in the Knife River watershed, we were able to identify potentially sensitive regions within the watershed, assess the potential impact of various land management practices, provide a summary of the general impact of beaver dam activity and management, and examine how potential changes in climate patterns (snowpack and rainfall) might change sediment loading patterns. With this approach, we provide a framework for proactive watershed management in a complex and morphologically active system by understanding relative importance of many facets of the watershed hydrology.

ACKNOWLEDGEMENTS

This work was possible thanks to the funding provided by the Great Lakes Tributary Modeling Program – Section 516(e) of the Water Resources Development Act and the assistance of the stakeholder groups of the Knife River watershed.

REFERENCES

Butler, D.R., and Malanson, G.P. (2005). "The Geomorphic Influences of Beaver Dams and Failures of Beaver Dams." Geomorphology, 71(1-2), 48-60.

MPCA, Minnesota Pollution Control Agency, (2009). “Total Maximum Daily Load Study of the Turbidity on the Knife River Watershed.”

Nieber, J.L., Wilson, B.N., Ulrich, J.S., Hansen, B.J., and Canelon, D.J. (2008). “Assessment of Streambank and Bluff Erosion in the Knife River Watershed.” Report to the Minnesota Pollution Control Agency.

NRCS. (1998). Nemadji River Basin Project Report. USDA Natural Resources Conservation Service, St. Paul, MN.

Pollock, M.M., Heim, M., and Werner, D. (2003). "Hydrologic and Geomorphic Effects of Beaver Dams and Their Influence on Fishes." American Fisheries Society Symposium 37.

Riedel, M.S., Brooks, K.N., and Verry, E.S. (2005). “Impacts of Land Use Conversion on Bankfull Discharge and Mass Wasting”. Journal of Environmental Management, 76(2005)326–337.

Riedel, M.S., Verry, ES and Brooks, K.N. (2002). “Land use Impacts on Fluvial Processes in the Nemadji Watershed.” Hydrological Science and Technology, 18 (1-4): 197-205.

Riedel, M.S., Dahl, T.A., and Selegean, J.P. (2008). “Sediment Budget Development for the Great Lakes Region.” Great Lakes Tributary Monitoring Program 516(e). July 2008.

USDA. (2002). ″Reducing Beaver Damage Through and Integrated Wildlife Damage Management Program in the State of Minnesota.″ Final Environmental Assessment. U.S. Dept. of Agriculture, Animal and Plant Health Inspection Service, Wildlife Services, January. 59.

Verry, E.S. (1986). “Forest Harvesting and Water: The Lakes States Experience.” Water Resources Bulletin, 22(6), 1039-1047.

Verry, E. S. (2005). The Dark River opportunities for restoration. Ellen River Partners. Grand Rapids, MN. 49p.

Verry, E.S., Lewis, J.R., and Brooks, K.N. (1983). "Aspen Clearcutting increases snowmelt and storm flow peaks in north central Minnesota." Journal of the American Water Resources Association, 19(1), 59-67.

Winchell, N. H. and W. Upham. (1884). The geological and natural history survey of Minnesota 1872-1882. Vol. I of the final report. p5.

MIDDLE MISSISSIPPI RIVER SEDIMENTATION ANALYSIS AT TRIBUTARY JUNCTIONS

Lisa C. Andes, Graduate Research Assistant; Parks College of Engineering, Aviation and Technology, Saint Louis University, St. Louis, MO, andes@slu.edu; Amanda L. Cox, Assistant Professor, Parks College of Engineering, Aviation and Technology, Saint Louis University, St. Louis, MO, coxal@slu.edu

INTRODUCTION

The Mississippi River System (MRS) has a cumulative length of 6100 miles and connects 17 inland rivers. In 2012, MRS transported 1,402 million short tons of cargo through over 100 inland ports primarily through vessel traffic on federally-authorized navigation channels (U.S. Army Corps of Engineers (USACE), 2013). The Middle Mississippi River (MMR) is an integral piece of the MRS, beginning at the confluence of the Ohio River near Cario, IL and extending 300 miles upstream to just below Lock and Dam 22 as shown in Figure 1 (USACE, 2015).

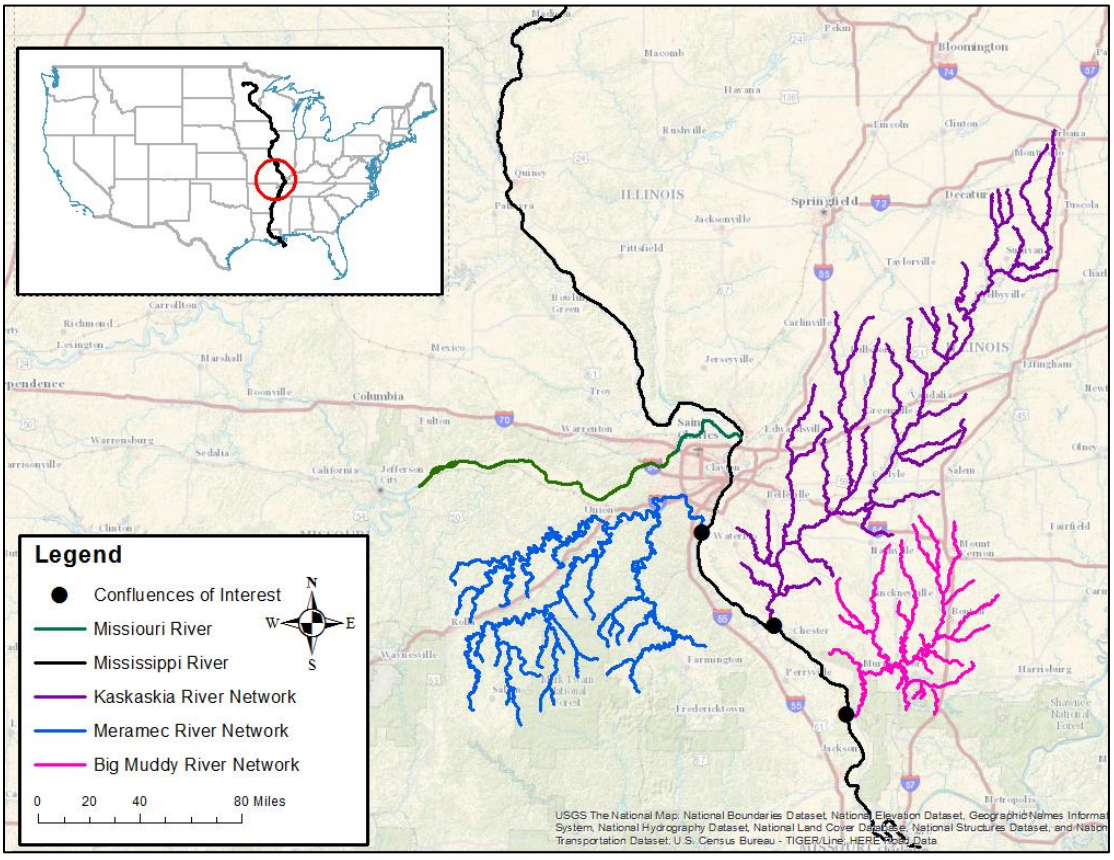

Figure 1 Middle Mississippi River study area

The MMR reach of the MRS marks a change in river management at the confluence of the Missouri River, where the Mississippi River transitions from an open river downstream to a slack-water navigation system upstream that continues through the Upper Mississippi River

(UMR). A slack-water navigation system requires construction of a series of Locks and Dams that create navigable pools to maintain channel depth. These operations may require routine maintenance dredging. The open river portion of the MMR maintains safe channel depths through routine maintenance dredging. Some characteristic descriptors of the open river portion of the MMR are crescent-shaped point bars, an atypically uniform width, and low to moderate sinuosity (Brauer et al., 2005).

Pinter et al. (2004) reviewed reported dredge volumes per river mile between 1964 and 1997, a 34-year record, of the UMR and MMR and noted that the open portion of the river had persistent sedimentation at tributary junctions. The MMR has four river confluences in the open channel reach, namely the Big Muddy River (BMR) confluence, Kaskaskia River (KR) confluence, Meramec River (MER) confluence, and Missouri River (MOR) confluence. Sedimentation rates and patterns described by Pinter et al. (2004) are briefly summarized here. Cumulative dredge volume near the BMR junction was 4.6 million cubic yards (mcy). Sedimentation occurred over a 3.1-mile reach of the MMR just downstream of the tributary junction. Dredge volumes and shoal formation size were along the downstream reach of the KR and not explicitly noted in the study; however, they were described as being a larger volume than both the MER and BMR. Pinter et al. (2004) also noted that sediment discharge from the KR is declining due to upstream Lock and Dam structures. Dredge volumes reported at MER totaled 4.8 mcy, occurring over a 4.1-mile distance of the MMR downstream of the junction. Dredge volumes reported at the MOR were an order of magnitude smaller (0.8 mcy covering 1.3 miles downstream of the junction). Pinter et al. (2004) speculated that the reduced sedimentation at the MOR was attributed to the upstream river training structures that may trap sediment. Due to the lack of similarity between MOR and BMR, KR and MER, the MOR was not included as part of this study.

The spatial distribution of cumulative dredge volumes per river mile provides essential insight into morphologic features of the MMR that continue to promote recurrent sedimentation and required routine maintenance to sustain navigable waters. An in-depth analysis of the temporal and spatial variability of these shoals as a function of the local hydraulic and sediment dynamics is needed to provide insight and yield innovative solutions to improve current dredge practices. Understanding the variability and physical mechanisms behind shoal development is a key step in developing science-based strategies that reduce routine dredge maintenance volumes.

There are two primary objectives of this study: (1) describe the temporal and spatial evolution of shoal formations downstream of tributary junctions using a collection of continuous hydrographic surveys of the navigation channel, and (2) examine the relationship between the morphologic evolution and variation in bulk hydrodynamic parameters.

CLASSICAL MODEL OF TRIBUTARY JUNCTION MORPHOLOGY

The classic morphologic model of asymmetric channel confluences has three main components: tributary mouth bars, a scour hole, and a sediment bar formed downstream of the junction (Best, 1986) (Figure 2). The tributary mouth bars develop at the entrance of one or both tributaries into the confluence. Tributary bars form primarily through bed load transport from the tributaries to the junction, and prograde and recede as a function of relative discharge of the tributaries (Biron,

1996). Presence of only one tributary bar is commonly observed when discharge from the main stream of the junction is highly dominant, typically due to a depth differential, i.e. discordant bed geometry, between both tributary mouths (Ashmore et al., 1983; Kennedy, 1984).

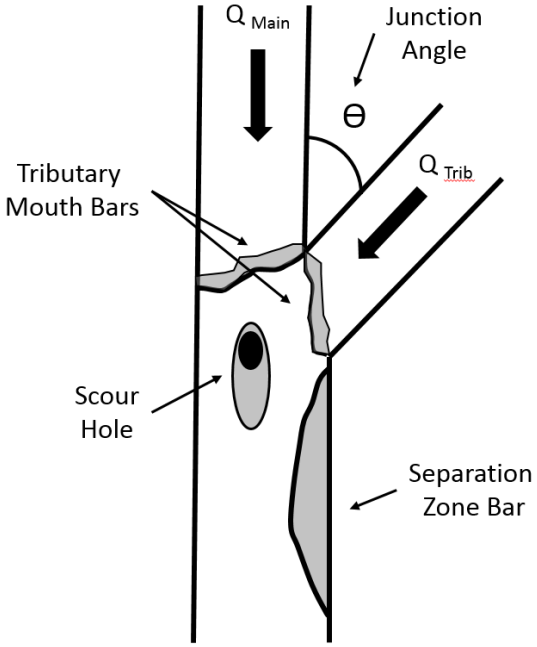

Figure 2 Asymmetrical confluence schematic

Scour holes form slightly downstream of the junction apex and typically bisect the junction angle where the two flows converge and there is downward directed momentum and increased turbulent kinetic energy from secondary circulation (Best, 1986; Rhoads and Kenworthy, 1998). Position of the scour hole can be inferred visually from the observed position of surficial flow convergence (Rhoads et al., 2009). However, in discordant systems such as the confluences of the MER, KR and BMR, scour hole morphology maybe not be easily observed (Biron et al., 1996; Biron et al., 1993; Bristow et al.,1993). One mechanism that could lead to the absence of a scour hole is a prograding tributary bar that has aggraded over the scour hole and essentially buried the hole.

A bank-attached sediment bar formation downstream of a tributary junction is often due to flow separation of the converging tributary flow around the downstream confluence junction. The confluence angle and its degree of confluence symmetry dictate the size and position of the downstream bar (Best, 1986). Confluence symmetry is defined by the confluence planform, where symmetric confluences are more "Y" shaped and asymmetrical confluences occur when the tributary channel joins the flow path of the main channel as shown in Figure 2 (Mosely, 1976). The bank-attached bar forms at the downstream junction corner of the tributary due to flow separation and is composed of fine sediment primarily from the tributary drainage network (Best, 1984; Best, 1986; Bristow et al., 1993). Bank-attached separation-zone bars increase in size when discharge of the tributary channel is comparable or greater than discharge of the main channel through creation a large low-flow, depositional zone and have the potential to deflect

flow from the main channel around the bar due to flow constriction around the bar (Best, 1986; Kenworth and Rhoads, 1995).

The tributary mouth bars, scour hole, and bank-attached tributary bar are dynamic in nature and migrate as a function of planform symmetry, junction angle (Figure 2), depth ratio, discharge ratio, and momentum flux ratio described in Equation 1 through Equation 3,

$$D_r = \frac{D_{Trib}}{D_{Main}} \tag{1}$$

$$Q_r = \frac{Q_{Trib}}{Q_{Main}} \tag{2}$$

$$M_r = \frac{\rho_{Trib} Q_{Trib} v_{Trib}}{\rho_{Trib} Q_{Trib} v_{Trib}} \tag{3}$$

where D_r is the dimensionless depth ratio; D_{main} and D_{trib} are the mean cross-sectional depths of the main and tributary channels [L]; Q_{main} and Q_{trib} are the discharges of the main and tributary channels [L^3T^{-1}]; ρ_{main} and ρ_{trib} are the density of the main and tributary channels [ML^{-3}]; and v_{main} and v_{trib} are the mean cross-sectional velocities of the main and tributary channels [LT^{-1}].

PRELIMINARY RESULTS AND SUMMARY

This study investigates the spatial and temporal variability of sedimentation downstream of the MER, KR and BMR confluences of the MMR. Preliminary results of sedimentation on the MMR downstream of the KR confluence are described in the following section. It is the intent of this effort to analyze a detailed record of hydrographic survey data for the BMR, KR, and MER to identify sedimentation near their confluences with the MMR. These efforts will be summarized in detail during the presentation. The presentation will also include an analysis of bulk hydraulic parameters in efforts to quantify the physical processes that yield sedimentation in these regions.

Preliminary Results – Kaskaskia River Confluence: The Kaskaskia River junction occurs at River Mile 161 along the MMR (Figure 1). Figure 3 compares a before and after dredge survey taken at the confluence (USACE, 2015). Both surveys were collected the USACE, Saint Louis District. Before-Dredge (BD) surveys are often conducted in regions that typically have recurrent sedimentation and are likely to require routine dredging to maintain navigation. The BD survey presented in Figure 3 was conducted on 5 August 2014. Qualitatively from the BD survey there appears to be notable sedimentation at two locations: (1) on the left bank (looking downstream) between the downstream junction corner of the KR and the first downstream weir, i.e. Weir 117.2(L), and (2) across the channel (right bank looking downstream) extending from Weir 117.5(R) downstream of Weir 117.1(R). Sedimentation occurring on the right bank appears to accumulate laterally into the navigation channel.

The After-Dredge (AD) survey was performed on 17 September 2014. AD surveys are used to ensure that after dredging occurs problematic sedimentation has been removed. From the AD

survey presented in Figure 3, it can be observed that the sediment accumulation on the right bank was removed and a wider channel was established. Sediment accumulation on the left bank downstream of the junction appears to have a slight accumulation, but does not appear to be impeding the navigation channel. The AD survey also shows sediment excavation from the KR channel allowing for deeper draft vessel traffic.

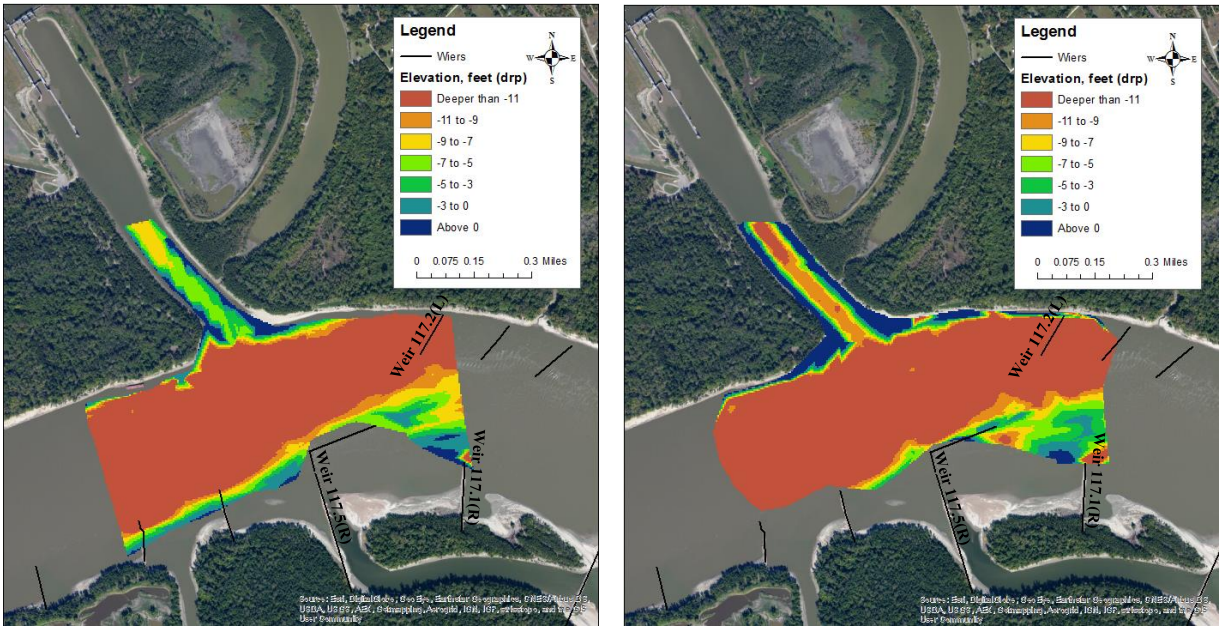

Figure 3 KR confluence showing a Before-Dredge Survey (left) and After-Dredge Survey (right)

REFERENCES

Ashmore, P. & Parker, G. (1983). Confluence scour in braded streams. Water Resources Research, 19(2), pp. 392-402.

Best, J. L. (1986). The morphology of river channel confluences. Progress in Physical Geography. 10: 157.

Best, J. L. 1987. Flow dynamics at river channel confluences: implications for sediment transport and bed morphology, in Ethridge, F. G., Flores, R. M. and Harvey, M. D. (Eds), *Recent* Developments in Fluvial Sedimentology, Society of Economic Paleontologists and Mineralogists, Special Publication, 39, Tulsa, Oklahoma, 7–35.

Biron, P., Roy, A.G., Best, J. L., & Boyer, C. J. (1993). Bed morphology and sedimentology at the confluence of unequal depth channels. Geomorphology, 8 pp. 115-129.

Biron, P., Best, J. L., & Roy, A. G. (1996). Effects of bed discordance on flow dynamics at open channel confluences. Journal of Hydraulic Engineering, 122, pp. 676-682.

Brauer, E. J., Busse, D. R., Strauser, C., Davinroy, R. D., Gordon, D. C., Brown, J. L., Myers, J. E., Rhoads, A. M., & Lamm, D. U.S. Army Corps of Engineers, Saint Louis District, (2005). Geomorphology Study of the Middle Mississippi River.

Bristow, C. S., Best, J. L., Roy, A. G. (1993). Morphology and facies models of channel confluences. Alluvial Sedimentation, Special Publication of the International Association of Sedimentologists, 17, pp. 91-100.

Gordon, D. (2015). Drought, Low Water, and Dredging of the Middle Mississippi River in 2012. 10th Federal Interagency Sedimentation Conference,

http://sedhyd.org/2015/openconf/modules/request.php?module=oc_program&action=summary.php&id=91.

Kenworhy, S. T. & Rhoads, B. L. (1995). Hydrologic control of spatial patterns of suspended sediment concentration at a stream confluence. Journal of Hydrology, 168, pp. 251-263.

Kennedy, B. A. (1984). On Playfair's Law of Accordant Junctions. Earth's Surface Processes and Landforms, 9, pp. 153-173.

Mosely, M. P. (1976). An experimental study of channel confluences. The Journal of Geology, 84 (5), pp. 535-562.

Pinter, N., Miller, K., Wlosinski, J. H., van der Ploeg, R. R. (2004). Recurrent shoaling and channel dredging, Middle and Upper Mississippi River, USA.

Rhoads, B.L. & Kenworthy, S. T. (1998). Time-averaged flow structure in the central region of a stream confluence. Earth Surface Processes and Landforms, 23, pp. 171-191.

Rhoads, B. L., Riley, J. D., Mayer, D. R. (2009). Response of bed morphology and bed material texture to hydrological condition at an asymmetrical stream confluence. Geomorphology, 109, pp. 161-173.

U.S. Army Corps of Engineers (USACE), Navigation and Civil Works Decision Support Center. (2013). Transportation Facts and Information, http://www.navigationdatacenter.us/factcard/factcard13.pdf.

U.S. Army Corps of Engineers (USACE), Saint Louis District. Navigation. Web. 30 January 2015.

INNOVATIVE SEDIMENT MANAGEMENT METHOD TO REDUCE DREDGING

Randall Tucker, President, Streamside Technology LLC., Findlay, OH, (419) 348-5167, rltucker@streamsidetechnologyllc.com; Tim Welp, Research Hydraulic Engineer, U.S. Army Corps Engineer Research and Development Center, Vicksburg, MS, (601) 634-2083, Timothy.L.Welp@usace.army.mil; Robert Thomas, Chief, Hydrology and Hydraulics/Water Management Branch, U.S. Army Corps of Engineers Galveston District, Galveston, TX, (409) 766-3975, Robert.C.Thomas@usace.army.mil

INTRODUCTION

An innovative sediment management method, a 30-ft wide, high capacity, Sediment Collector™, is currently installed in Fountain Creek, Pueblo, Colorado upstream of the confluence with the Arkansas River (location shown in Figure 1). This installation is intended to demonstrate a new technology available to reduce the need for dredging. This Sediment Collector™ was installed to demonstrate technology needed to alleviate the need for dredging by lowering the downstream grade to reduce flooding and ultimately reduce sediment deposition as far downstream as John Martin Reservoir, a U.S. Army Corps of Engineers (USACE) managed lake. The system operates on the principle that sediment in bedload can be trapped by gravity and removed at the natural rate of transport, instead of episodically. This technical paper describes the technology and installation at Fountain Creek, other possible applications, lists lessons learned, cost, and provides some general guidance for applying collector technology at other sites.

Figure 1 Location of Sediment Collector™.

SEDIMENT COLLECTOR™ INSTALLATION IN FOUNTAIN CREEK

A 30-ft wide, high capacity Sediment Collector™ was installed in Fountain Creek Pueblo, CO upstream of the confluence with the Arkansas River in July 2011 to demonstrate a one year long trial of the viability of this new technology. The Sediment Collector™ system, as installed in Fountain Creek, consists of 6 main parts:

1. Collector: 30 FT wide Bedload Collector
2. Pump: 50 HP, submersible variable frequency drive (VFD) pump
3. Controller: Electronic controls with internet access and remote interface
4. 6 inch discharge and 8 inch water return DR11 (160 pounds per square inch) high density polyethylene (HDPE) pipelines
5. Sediment separator: 100 tons/hr
6. Stacker: capable of storing approx. 1,000 cu yds.

The primary component of the collector is a steel hopper (Figure 2) placed on the bottom along a sediment transport pathway. A manifold system (see Figure 3) inside the hopper focuses flow across a small region within the hopper, providing high velocities needed to entrain sediment. A dredge pump, housed in the hull with the hopper, pumps water and sediment through the manifold to the placement area. The pump can also be mounted remotely on land, the preferred configuration for maintenance. Booster pumps can be added to increase the pumping distance, as required.

Figure 2 Sediment Collector™ installed in the dry in Fountain Creek.

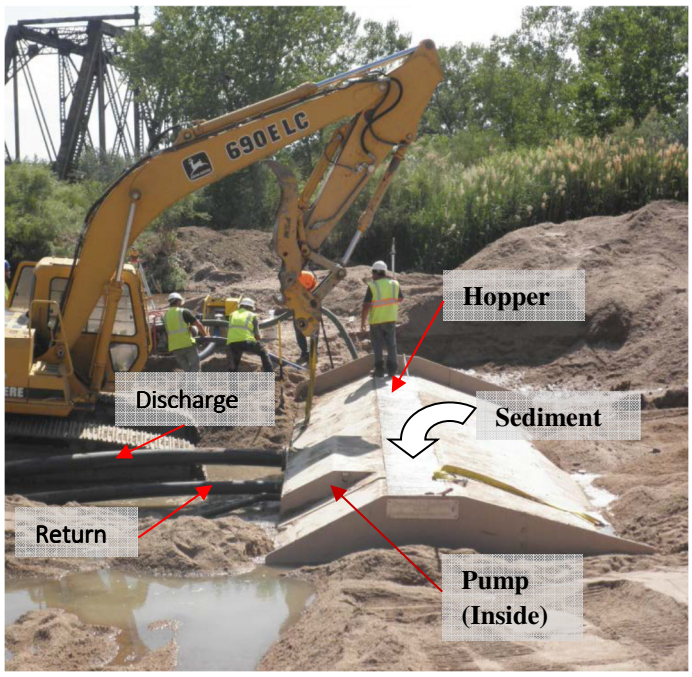

Figure 3 Sediment Collector™ at install.

The system can either be operated in an open or closed cycle. In the open cycle, water is drawn into the Collector manifold from across the screen, since the area of the screen openings is much greater than the area of the manifold orifices, velocity across the screen is very small (<1 ft/s), even though velocity at the manifold is large enough to transport sediment. In the closed cycle, the slurry is discharged into a holding tank and separated from the water, and then the water is returned to the collectors opposite side of the suction manifold, so that water is drawn from the holding tank instead of across the screen; advantages of the closed cycle include minimal impingement velocity (reducing potential for clogging) on the hopper screen, reduced risk of entrainment of aquatic organisms, and greatly reduced consumptive water loss. Sediment is discharged into a bin at the base of the screw separator (Figure 4 left), which separates and drops the coarse sediment onto the stacker (Figure 4 right). Sediment is stockpiled at the stacker until it can be trucked away.

Figure 4 Archimedes screw separator (left) and stacker (right).

Electronic controls (Figure 5) enable automatic or remote operation, reducing or eliminating the cost of labor to supervise operation. The system can be set to run at specified times, as a function of stream gage data, or as a function of hopper capacity (still in development). Dredge pumps, piping, separators, and stackers are all off the shelf technology used in dredging and other industries with documented performance metrics.

Figure 5 Electronic control panel and Archimedes screw separator.

Demonstration Project Cost: Component, installation, and total cost of the system installed at Fountain Creek is shown in Table 1. The project was championed by the City of Pueblo and funded through EPA 319 (Colorado Department of Pueblo Health and Environment, Non-Point Source Office), Pueblo County, Natural Resources Conservation Service (NRCS), and Colorado Water Conservation Board (CWCB) in collaboration with the equipment developer, Streamside Systems, LLC. Since the initiation of the project, the Fountain Creek Watershed, Flood Control, and Greenway District were created. Costs shown in Table 1 are approximate and not intended to represent the actual system cost. Various others have reported the cost to range from $600,000 to $1,000,000, although details associated with the higher estimates of cost are unavailable.

Table 1 Sediment Collector™ cost.

Collector (pumps, controllers, pipe, etc.)	$419,000
Sediment Stacker	$39,000
Installation	$110,000
Approx. Cost of Contract Documents	$50,000
Upgrades/Repairs	$10,000
Total	$628,000

Cost of operating the system has been minimal since it has been operated for short periods of time. The system is capable of being operated remotely; however, because of potential risk to human safety associated with the separator and stacker, the system was only operated under direct supervision. The system uses about 1,000 Watts per hour (1kWh) per minute of operation. If the system were run continuously for 1 year, electricity cost would be about $52,560 (based on cost of $0.10/kWh).

Minor repairs were required after the flood of September 2011. Record breaking rainfall resulted in extreme flooding and record creek flows, but did not damage the Collector. Damage to an exposed junction box required repairs totaling $1,765. The remaining cost for Upgrades/Repairs included a return flow pump and minor modification to the initial layout of the piping. A 1,800 gallon tank was added at the separator along with a pneumatically actuated valve that provides return prime water for the dredge pump at startup to ensure that the specific gravity of the slurry is managed.

Performance: Monitoring of the demonstration project has been underway since installation. Parameters that were planned for measurement included stream bed elevation within ½ mile of the collector, water level, sediment removed, electricity usage, maintenance required, and hours in operation. Specific performance data was collected at various flow rates over approximately 500 hours. Since the system was not operated continuously over many months and with the bedload transport continuing when the system was not in operation, short term stream bed elevation and coarsening impacts were overwhelmed. Therefore, stream bed elevation was not resurveyed at the end of the project.

Record breaking rainfall in September 2011 resulted in extreme flooding and record creek flows of 13,800 cu ft/s. High water damaged the junction box, causing total down time of about 2.5 months while City of Pueblo worked to get a repair contract executed. This flood demonstrated survivability of the system in an extreme event. Repair time was less than one day, once the repair contract was executed. Winterization (heat tracing and freeze protection) was not specified and the system was not operated for about 2 months during the winter months.

Production rate was the key performance parameter measured. Prior to installation of the 30-ft bedload collector, a 2-ft bedload collector (shown in Figure 7 right) was temporarily installed in Fountain Creek to estimate bedload transport extraction rates and assess optimal elevation for collector operation. The 2-ft collector pumped sediment into a drop box (Figure 7 left) that, in turn, allowed a 3 cu ft container to be filled with the subsequent fill time noted to calculate a production rate. Sediment was collected over a three day duration with extraction rates at respective stream flows listed in Table 2. Assuming a linear extraction rate function for a longer collector, respective production rates were estimated for a 30-ft long collector and listed in Table 2 as well.

Figure 7 2-ft collector (right) and drop box (left) used to estimate production rates.

Table 2 Measured 2-ft collector and estimated 30-ft collector extraction rates.

Stream Flow (cu ft/sec)	2-ft Collector Bedload Extraction Rates	Estimated 30-ft Collector Bedload Extraction Rate (cu yds/hr)
120	3 cu ft/26 min	2.8
100	3 cu ft/38 min	2.6
600	3 cu ft/6 min	16.7

Figure 8 plots maximum production rate vs. creek discharge for all data collected, with a second order polynomial trend line fit to the data. Excluding the September 2011 flood, the range of discharge rates captured represents the typical range expected at this site during any year. The figure shows the dependence of bed load on discharge. The estimated production rates in Table 2 (based on the 2-ft collector extraction rates) agree well with the production curve in Figure 8 at the lower flow rates of 100 and 120 cu ft/sec, but less so for the 600 cu ft/sec flow rate condition. Peak measured production rate for the 30 ft Collector is 100 cu yds/hour. At this rate, if sufficient bed load were available, the single 30 ft collector would move 876,000 cu yds/year. The high capacity of a single unit makes it possible to use structures in conjunction with collectors to maximize total capture with fewer collectors.

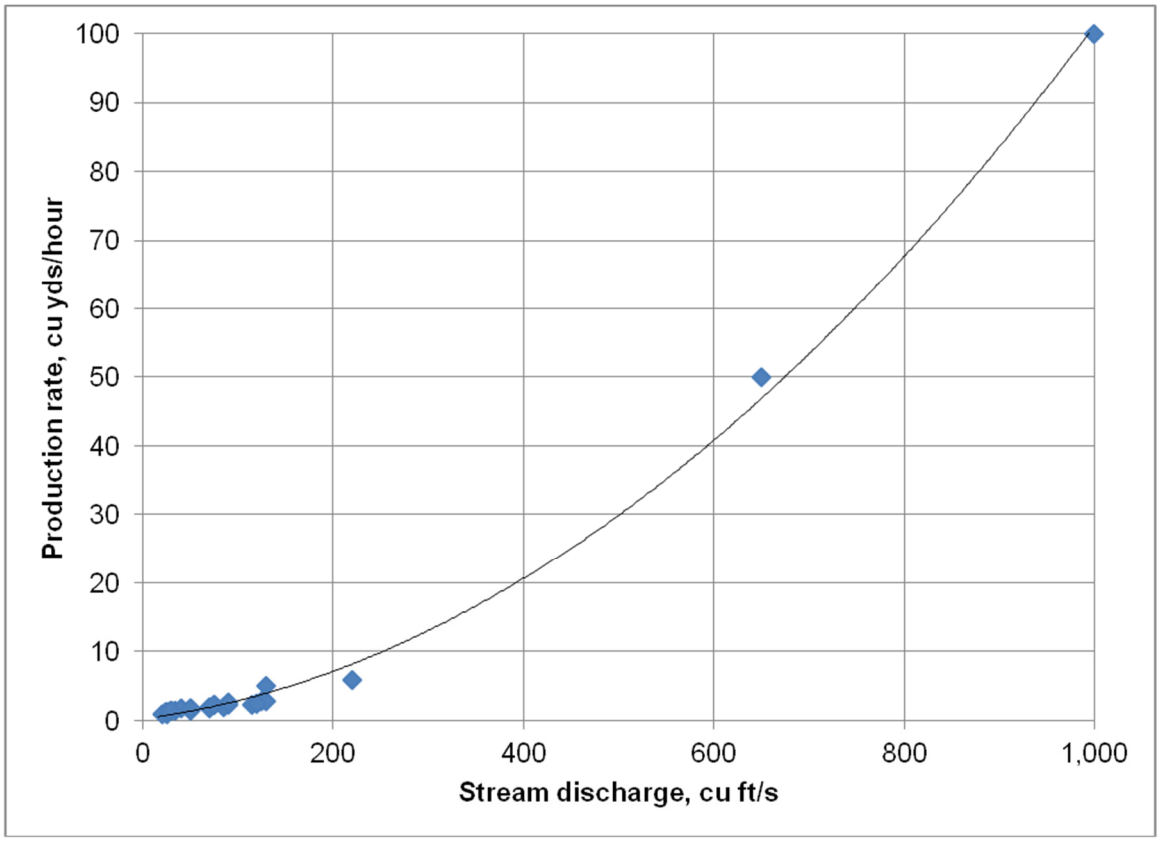

Figure 8 Sediment Collector™ production curve.

Visual inspection of the hopper and other system components were made at least monthly over the course of the year. No significant wear or corrosion is shown on any parts although the

urethane coating on the mild steel hull did sustain scouring and erosion. No repairs have been required other than those associated with initial system configuration, as a result of the flood in September 2011, and vandalism that damaged the power and control conduit leading to the dredge pump. Additional automation and instrumentation was added with the return water tank that included a variable level control and high-level switch that assists with balancing the system.

Lessons Learned: Initial deployment of new systems is an opportunity to inform design and improve installation procedures. The following list describes lessons learned during the demonstration project:

- All electrical components should be well above potential flood water levels.
- Pipelines should be as straight as possible, with no sharp turns; limiting the potential for air to be trapped in the lines.
- When operating the system with return flow, a sufficiently large water storage container should be available at the discharge point to prevent air intrusion during pump start up and to ensure that an acceptable slurry specific gravity is maintained.
- Experience at Fountain Creek suggests that the return flow pump is a worthwhile investment, reducing risk associated with grade control and that the return flow also prevented the Collector from being clogged from surges of sediment that accumulated in the hopper (i.e., the return flow re-fluidizes these sediment "slugs" in the hopper and meters it into the suction ports).
- Accurate survey for grade control during installation is essential both at the discharge point and hopper.
    - Elevation of the hopper directly controls elevation of the bed during operation.
    - Elevation of the pipeline discharge point (relative to the hopper) controls the size of the return flow pump or required head difference if attempting to run without a return flow pump.
- As with any industrial operation, measures must be taken to ensure that unauthorized personnel do not gain access to the material management equipment (Separator and Stacker). The six-foot tall fence around the demonstration project site was insufficient to prevent the curious from gaining access to the dangerous electrical and mechanical equipment. Yard lighting is recommended for night operations.
- Screen configuration and size should be based on the aggregate particle sizes in bedload. This demonstration project selected the standard coarse sand, stainless steel, round bar stock with a 3/8th inch spacing in lieu of recommended vibratory screens. During periods of low flow, larger aggregate can align in the screen apertures - resulting in bridging. Vibrating screens or jet systems could be added to offset this requirement.
- To ensure that stream flow and bedload are delivered across the collector screens, appropriate permanent or temporary cross-vane structures are recommended. Tangential interception of the stream flow by the collector screens can exacerbate the aforementioned screen bridging issues identified.

- Careful collaboration between the technology vendor (or other experts), engineer responsible for system/site design, and construction contractor is essential to avoid additional cost associated with field modifications during installation and initial testing. Design build may be the best procurement mechanism for initial full scale applications.

RECOMMENDED GENERAL APPROACH FOR COLLECTOR PROJECTS

Sediment Collector™ technology should be considered when substantial quantities of sediment selected for removal are being transported as bedload. Recommended key steps in scoping, design, construction, and operation of a Sediment Collector™ project are identified below:

Pre-Design Analysis: Appropriate analyses should be conducted to determine sediment transport processes and expert advice should be solicited to determine if a collector is feasible for each site. Key parameters that should be investigated to determine if a collector project is feasible include:

- Sediment transport (size and rate): typically measured through deployment of a 2' to 6' collector emplaced and operated during varying stream flow conditions (Lipscomb, Darrow and Thornton 2005).
- Transport processes and pathways: typically assessed through combination of expertise, field data and inspection, and application of numerical models.
- Sediment management: Identify potential placement locations and methods of conveyance.
- Operations plan: Identify who will be responsible for operating and maintaining the system after construction.
- Benefits analysis: Compare cost, both financial and environmental, to alternative methods to identify the least cost method of removal.

Design: After the decision to install a Collector has been made, design of the plant should be conducted by an experienced engineer consulting with the system developer or other expert in collector installation. Major components of design analyses include:

- Collector design: Based on data collected and analyses conducted in the Pre-Design phase; consult with the system developer to determine the appropriate configuration of the full scale collector system.
- Placement area design/plan: Design the placement area and plan operations to manage the sediment load anticipated. Contingencies for minimal oversight should be considered.
    - If not conducted during Pre-Design phase, it may be necessary to collect more data or conduct additional analyses to determine the rate of sediment that must be handled.

    - Placement area options range from direct discharge to a complete mechanical separation plant, like the one used at Fountain Creek.
- Pump and pipeline design: Pipeline layout should minimize head loss, prevent air from being trapped, and follow the shortest possible route. Pump size will be a function of sediments, collector size and configuration, placement area design, and pipeline configuration.
- Electronic control and electrical design: Electronic controls and electrical wiring for the collector system must be designed. The Control system should be designed with the collaboration of the system vendor.
- Final site design: Other design features typical of a civil project such as grading, drainage, roads, utilities, lighting, site safety etc.

Construction: The system should be installed by a qualified construction contractor with an expert in collector installation on staff. The demonstration project identified some issues to consider during construction, listed below:

- Construction quality control: Lessons learned during the pilot highlighted the importance of quality control (QC) during construction. Elevation tolerances, pipeline layout, and electrical wiring all had issues at Fountain Creek that could have been eliminated through QC during construction.
- Initial testing: Like any new system, initial testing should be conducted to determine if the system is operating as intended.

Operations and Maintenance: After construction, the system should be monitored to ensure that it is functioning as designed. Some topics for consideration after construction include:

- Monitoring: system components (collectors, pumps, electronics, etc.) and environmental factors (sediment size and transport rate, flow rate, etc.) should both be monitored to assess performance and to inform system maintenance or tuning.
- System tuning: Because of the uncertainty associated with modeling and measuring sediment transport, it is likely that actual production will be different than predicted. It may be possible to modify system configuration to optimize performance; plan to reevaluate system layout after monitoring data has been gathered and analyzed.

Length of monitoring duration necessary to make system tuning decisions will, of course, depend on which system design aspects are being evaluated. The decision to relocate the certain Fountain Creek electrical components well above potential flood water levels happened immediately after the components were flooded, whereas something like a system re-configuration may take longer to more accurately re-assess site specific conditions (e.g., optimum sediment transport volumes and patterns).

OTHER POTENTIAL APPLICATIONS

Collector technology adds two key improvements over other installed dredging systems. This technology can provide selective capture for both the size and quantity of sediment to be removed. Since the system operates with very low or no head across the screen into the hopper, only sediments coarse enough to be transported in bedload are trapped (fine sands to gravels), while finer sediments (silts and clays) remain in suspension. The top size of the sediment is limited by screen opening size. The total volume captured can be modified by controlling the duration of system operation, and by varying the width of the collector installed.

This technology also removes sediment at the natural transport rate. The collector is only capable of trapping sediments when they are supplied by natural forcing (currents or waves). Therefore, the system (when installed at grade) can never exceed natural transport processes. Removing sediment at the natural rate more closely mimics nature, reducing known and potential unforeseen environmental impacts. A permanent Collector serves as a grade-control structure. When installed above grade on a complete cross-section, the Collector will cause aggradation upstream to the desired new elevation. When installed below grade the Collector will initiate a controlled-depth head cut upstream.

The selective capture of bed load at the natural transport rate leads to some specific new capabilities. Although not exhaustive, some potential applications for collector technology are discussed below:

Watershed Management: By actively managing sediments at the watershed level it is possible to drastically reduce sediment load to the area or channel of interest. Managing sediments at many locations throughout the watershed may optimize habitat restoration and protection, and also be more cost effective and environmentally friendly than the traditional practice of dredging at the problem site. This also presents an opportunity to take advantage of flexibility in siting, helping to address issues with property ownership, road access, material handling and transportation, power availability, etc. Collectors are scalable to any stream width, and can be readily retrofitted to existing cross-vane or other structures. They also allow users to actively manage grades in the vicinity of the collector.

Reduce Quantity of Contaminated Sediment Dredging: Coarse sediments can be removed before being deposited in an area known to be contaminated, reducing the total volume of sediment that must be dredged and placed under more stringent requirements typical for removing contaminated sediments.

Sediment Bypassing: At inlets, in tidal systems, or other locations where there is a clearly defined sediment pathway crossing a navigation channel, a Collector could be installed as a sediment bypassing system, allowing sediment to be removed and pumped past the navigation channel, preventing deposition. The system would be installed at reaches where deposition is typical and the discharge located in an area with potential for scour or transport away from the channel.

Reservoir sedimentation can be reduced by capturing and removing bedload at tributary mouths, and either removing the material or reintroducing the sediment below the dam (at the natural transport rate, to offset channel and habitat degradation due to a sediment deficit caused by reservoir trap efficiency). Using collectors to design or retrofit sustainable reservoirs will not only reduce dredging requirements, but will help maintain reservoir storage capacity and related hydroelectric generating capacity, and reduce flood risks that would otherwise increase with a loss of storage.

Sediment Backpassing: On beach locations that experience accretion, the Collector could be installed as a sediment backpassing system allowing sediment to be removed from the accretion area and pumped back to beach erosional "hotspots" within practical pumping distance.

Application in Remote Locations: Since a collector system can be installed with standard truck able equipment, they offer the potential for application in remote locations, where there is a need to control grade in streams, to prevent downstream migration of excess or contaminated sediments, to maintain a navigable channel, or to supply coarse sediment with lower impact than traditional mining practices. In many headwater locations (e.g., first or second-order streams impacted by logging, agriculture, or road construction) stream gradient may allow for Collector clearing on a siphon basis, for continuous operation with no pump or power requirement.

In addition to the potential applications listed above, application of this new technology could result in other benefits not yet fully investigated. Since there is essentially no flow into the hopper (with a closed water cycle), there is little risk of ingesting wildlife or foreign material that might clog the pump. This may help to meet permit requirements or avoid the need for some permits. Closed cycle operations may also be used to address water rights issues by returning water to the hopper. Aesthetic impacts of dredging, and operational limits (e.g., due to Threatened and Endangered species (T&E), or spawning seasons) could be avoided, since there is very low or no flow into the system.

CONCLUSIONS

This paper presented application of Sediment Collector™ technology in Fountain Creek in Pueblo, CO and discusses how it might be applied to reduce USACE navigation dredging. The installation successfully demonstrated the technology; specifically that Collector Technology:

- Works with coarse sediments in a shallow unidirectional flow environment
- Has minimal maintenance costs over a 1-year deployment
- Survives record floods with minimal damage
- Is capable of producing up to 100 cu yds per hour with a single 30-ft collector
- Is relatively inexpensive and easy to deploy without specialized equipment

Further investigation of collector technology through larger scale demonstration at navigation projects is recommended. Future demonstrations should consider testing application in areas

with wave dominated transport, application with finer sediments, application in deeper water, and with different placement options.

REFERENCES

Lipscomb, C. M., Darrow, A., and Thornton, C. I., (2005). "Removal Efficiency Testing of Streamside Systems Bedload Monitoring Collector," Colorado State University Engineering Research Center Report.

Thomas, R. C., and Welp, T., (in press). "Sediment Management Methods to Reduce Dredging: Part 1, Sediment Minimization Concept and Demonstration Project Introduction and Overview," DOER Technical Notes Collection, U.S. Army Engineer Research and Development Center, Vicksburg, MS. www.wes.army.mil/el/dots/doer

HYDROLOGIC ANALYSIS OF MESCAL CANYON WATERSHED AND GEOMORPHIC ASSESSMENT OF LOWER MESCAL ARROYO CONFLUENCE

Vincent Benoit, Hydrologic Technician, Bureau of Reclamation, 555 Broadway NE Ste 100 Albuquerque NM, 8710, Office: 505-462-3628, Cell: 435-757-0936, Email: vbenoit@usbr.gov

INTRODUCTION

Mescal Arroyo empties into the Rio Grande roughly two miles downstream of Elephant Butte Dam. Mescal arroyo is fed by a watershed with a contributing area of roughly 14,000 acres. The vertical relief throughout the watershed ranges from 5,800 feet at the peak of Caballo Cone to an elevation of 4,250 feet at the mouth of the arroyo. The main channel of the Rio Grande above the confluence of the arroyo and river is constrained by natural features and influenced by Mescal Arroyo. Flanked on either side by steep mountainous terrain, the Rio Grande is constricted in width and its channel location is restricted. These constraints are primarily above the confluence of the river and the arroyo, and have a limited effect on the planform around the mouth of Mescal Arroyo. Anthropogenic constraints have a greater effect on the planform of the river channel around the arroyo mouth.

Flows on the Rio Grande in this reach have been controlled by the operation of Elephant Butte Dam since 1916. The channel downstream of Elephant Butte Dam has also been channelized to preserve the conveyance capacity of the channel for delivery of irrigation water downstream and to protect adjacent infrastructure from damage due to high flows. Continuous river maintenance work is performed through the channelized portion of the river downstream of Elephant Butte Dam to maintain the authorized 5,000 cfs channel capacity per the congressional Flood Control Acts of 1948 and 1950.

As is common in ephemeral channels, the slope of the arroyo is greater than that of the river channel. Figure 1 contains two profiles from surveyed data that illustrates the difference in slopes between the arroyo and the river channel, in this case they are an order of magnitude different.

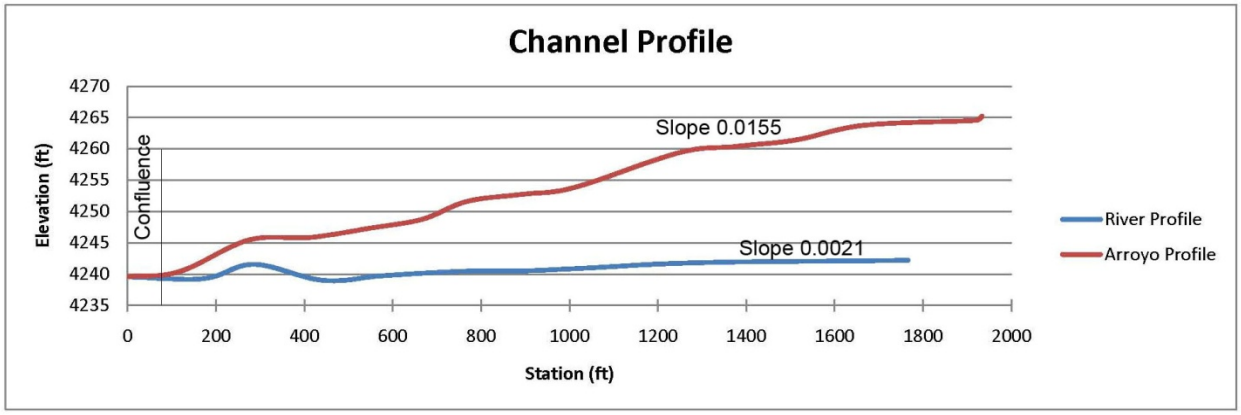

Figure 1 Comparison of Rio Grande Channel slope and Mescal Arroyo slope.

A combination of high runoff potential of the soils and sparse surface vegetation in the upper Mescal Arroyo watershed, high slope of the Arroyo, and a monsoon dominated hydrology, with its periods of intense rainfall result in high rates of sediment transport and deposition during these flashy events. High rates of sediment transport from Mescal Arroyo lead to alluvial fan deposition at the confluence with the Rio Grande that has on occasion both partially and fully blocked river flows, reducing the channel capacity of the Rio Grande below Elephant Butte Dam. The reduction of channel capacity reduces the ability of meeting downstream flow requirements. Deposition also creates a backwater area that impacts the operation of Elephant Butte Dam. Because of the importance of releasing and maintaining the flow downstream to Caballo Reservoir, an analysis of potential solutions to reduce the amount of sediment introduced to the Rio Grande from Mescal Arroyo or increase the sediment transport capacity of the Rio Grande in the vicinity of the arroyo needs to be pursued. Before potential solutions can be decided on it is important to have an understanding of the physical processes at work in the system and how they influence those problems. This geomorphic review presents an analysis of historic channel morphology of the Rio Grande at the confluence with Mescal Arroyo, and a rainfall runoff model to assess the morphological changes occurring in Mescal Arroyo and the effects of storms on the arroyo.

HISTORIC CHANNEL AND FLOODPLAIN ANALYSIS

Rio Grande Channel: The occurrence of high sediment runoff and deposition into the Rio Grande is not solely due to anthropogenic changes, this problem has existed prior to any man-made changes to the river channel. In the 1935 and 1957 aerial photographs shown in Figure 2, sediment deposition is evident at the arroyo's confluence with the river. The 1935 aerial photo was taken before the state road NM 51 was built on the north side of the river, in the photo the red arrow point toward an alluvial fan that has been created by flows from Mescal Arroyo. The blue arrow illustrates the response of the Rio Grande to the sediment influx, with the main channel shifting north. Because the channel is able to shift its location; as shown in the 1935 photo, the additional sediment from the arroyo doesn't impact water flow through the reach. In the 1957 photo, the road embankment and channelization constricted the river to the point where it could no longer alter its course in response to the sediment input from the arroyo. The red arrow on the 1957 aerial shows an alluvial fan that has constricted the channel further.

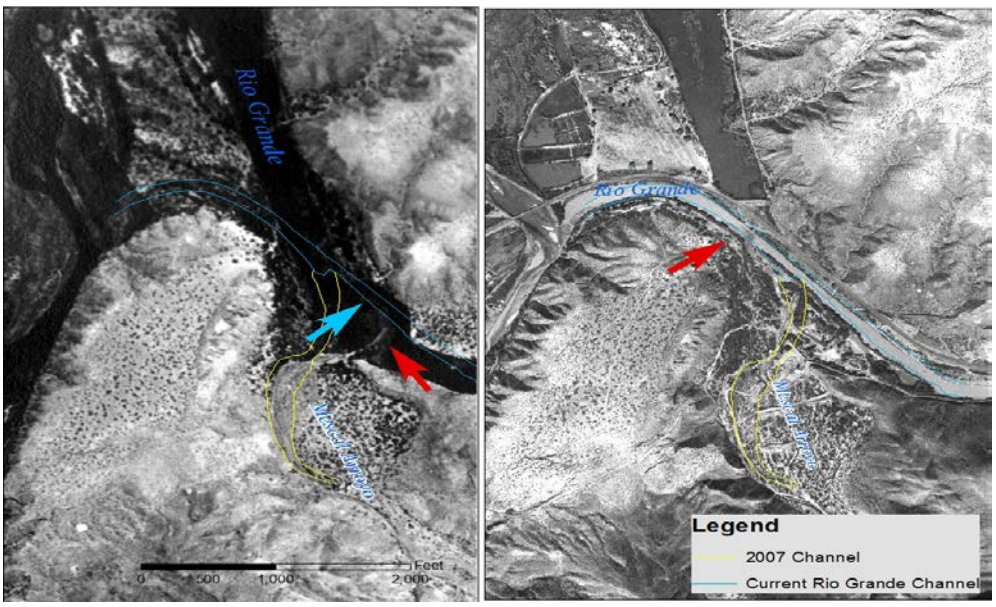

Figure 2 Left aerial photo 1935 and Right aerial photo 1957, blue line illustrates the river channel as of 2012 and yellow line illustrates the 2007 arroyo channel.

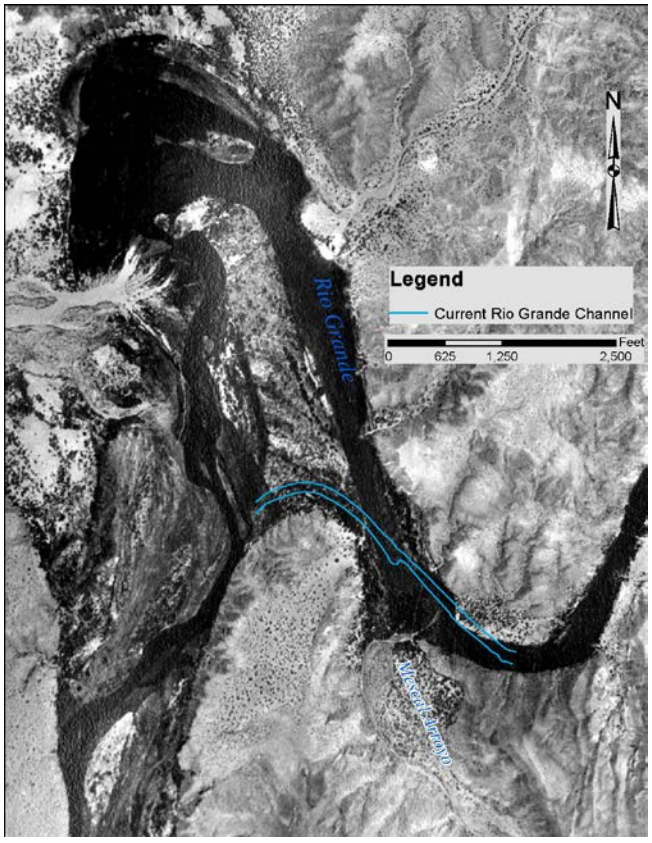

Figure 3 Channel morphology of the Rio Grande prior to anthropomorphic effects.

The Rio Grande was channelized to the location seen in the aerial photograph sometime between 1935 and 1956. Prior to channelization the Rio Grande was constrained by geologic formations to the sinuous planform seen in the 1935 aerial photography (Figure 3). The Rio Grande channel length; illustrated by the blue line in Figure 3 and measured from River Mile 25.2 to River Mile 24.5, was decreased from 8,700 feet in 1935 to 4,100 feet in 1956 through this reach. The active channel was also narrowed in width from an average of 169 feet in 1935 to an average of 98 feet in 1956. The river channel in 1935 also had a floodplain width of 402 feet, which is nonexistent in the 1956 channel. Channel length and widths were estimated using the georectified aerial photography from the corresponding years. The channelization resulted in an increase in the channel's slope by a factor of 1.9. A 1985 channel rehabilitation project was designed to meet the 5,000 cfs channel capacity requirement. The river channel was dredged and drop structures were installed downstream of Mescal Arroyo. (Drew Baird, pers. Comm.).

Post-channelization aerial photos from 1957 illustrate the sensitivity of the channel to the sediment input from Mescal Arroyo due to the loss of floodplain and channel areas for deposition; the red arrow seen on Figure 2 shows an alluvial fan created by the arroyo. Prior to channelization, the river had enough freedom to widen and shift in response to flow and sediment regimes. Both channelization and narrowing efforts led the channel to be more sensitive to sediment input from the arroyo by reducing the width of the river channel. The reduced channel width and the bank protection on the opposite bank has created a situation where the water from the arroyo is deflected and slowed by the highway embankment. The deflection of the western bankline and the river backwater effects on the sediment laden arroyo flow allows for the larger sediment to deposit creating an alluvial fan at the confluence of the river and arroyo. The highway embankment also prevents the river from shifting its course to the west to adjust to additional sediment. Any sediment introduced to the main channel needs to be mobilized by the flows of the Rio Grande, rather than the Rio Grande altering its course in response to the additional sediment.

Figure 4 Left photo taken 7/10/08 and right photo taken 9/10/08

The photos in Figure 4 were taken during one of the rainfall runoff events in the 2008 monsoon season. The line of bubbles; as shown by the red arrows, at the edge of the Rio Grande seen in the leftmost figure delineates the leading edge of the developing fan. The rightmost photo was taken at the same location on 9/10/08 after the monsoon season. Resulting alluvial fan

development has progressed further into the channel where it has constricted the mainstem Rio Grande flow, raising the water surface elevation and creating a backwater condition upstream.

Mescal Arroyo: Anthropomorphic changes at the lower portion of Mescal Arroyo to its confluence with the Rio Grande have altered the way runoff flows move through the arroyo affecting sediment deposition patterns at the confluence. Sometime between 1935 and 1957, the lower portion of Mescal Arroyo was channelized by sediment control embankments on both sides. Prior to the installation of these embankments, storm runoff flows flowed in more of the dendritic pattern exhibited by alluvial fans. These small migrating channels transport runoff water across the alluvial fan. The embankments were likely installed to reduce flow across the alluvial fan to protect the arroyo road crossing. As a result of channelization and flow regulation on the Rio Grande, the alluvial fan of the arroyo extended north (Figure 2) creating a larger alluvial area increasing the arroyo channel length and decreasing the arroyo slope; measured from the 2012 arroyo road crossing location to the river channel, the length of the arroyo increased from 542 ft in 1935 to 1626 ft in 1957. Some of that decrease in slope and increase in arroyo channel length can be attributed to the different location of the Rio Grande channel and the location of the confluence. From 1957 to 2012, the lower arroyo channel was shortened from the 1626 ft to 1199 ft in 2012, due to the relocation of the arroyo's confluence. The current spoil area west of the arroyo mouth existed as a vegetated bar prior to 1956. Currently, the arroyo is constricted near the upper end of the spoil location where rip-rap was installed in 2001 and has mostly been washed away by arroyo flows (Brent Tanzy, Pers. Comm.). Two Wolman pebble counts were performed across the channel in two locations, one cross section further into the arroyo and the second close to the spoil area. The D_{50} for the upstream location was in the range of 6mm or fine gravel and for the downstream location the D_{50} was in the range of 10mm or fine gravel. The coarser downstream size distribution is likely due to the location of the thalweg of the arroyo. At the upper cross section, the active channel was wider and less confined than the downstream cross section. The lower cross section is located below the road crossing and had a more defined active channel consisting of finer material. At the lower cross section there was a bar dominated by coarser sediments likely deposited at higher flows.

Elephant Butte Dam Operations: The operation of the dam and powerplant influences the discharge in the Rio Grande below the dam. Flow releases from the dam are established by the El Paso office in conjunction with the downstream irrigation district's demand (Ben Kalminson, pers. Comm.). Because dam releases are demand driven, there are times where there are no flow releases at all, at these times there is minimal seepage flows in the Rio Grande at the confluence with Mescal Arroyo.

Precipitation/Evaporation: Daily rainfall data from a National Climatic Data Center gauge in Truth or Consequences (35 year record) shows a mean annual rainfall amount of 9.43 inches. Most of the rainfall each year tends to come in the late summer months as short duration but high intensity monsoon storms. Figure 7 consists of average monthly rainfall data for the 35 years of record at the T or C gage and illustrates the meteorology of the monsoon storms. Plotted against the average monthly releases from Elephant Butte, the supply and demand dynamic can be seen. Demand for releases is reduced during monsoon season.

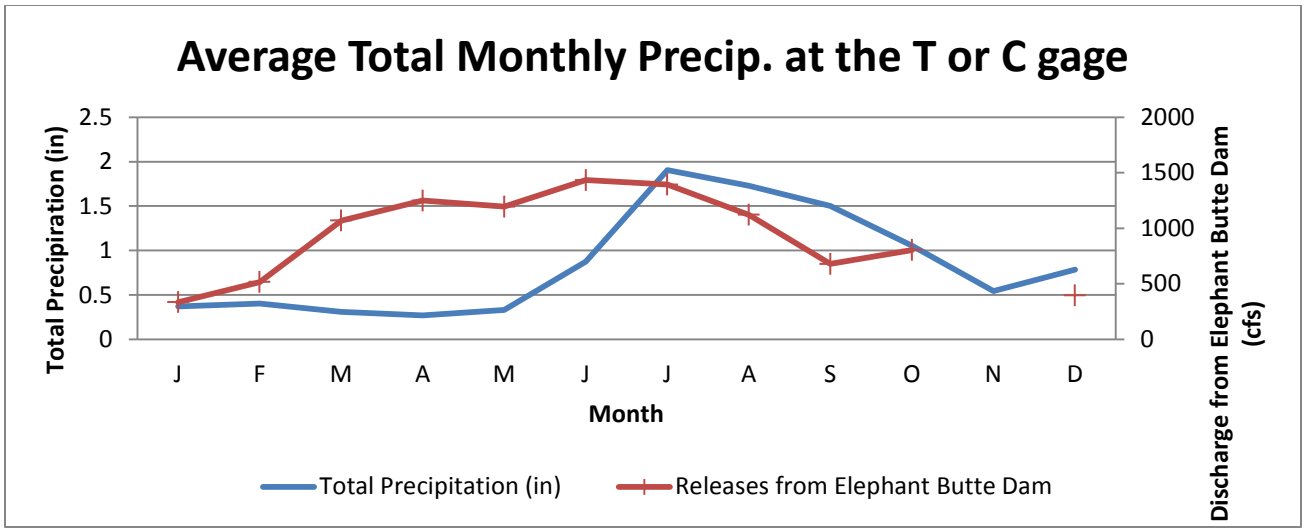

Figure 5 Average Total Monthly Precipitation for all years of record at the NCDC Truth or Consequences gauge compared to average monthly releases from Elephant Butte Dam.

HYDROLOGIC MODEL DEVELOPMENT

Data for the model was processed using the Hec-GeoHMS toolset for ArcGIS 9.3. This toolset aids in the development of model parameters by taking advantage of data published in GIS format. The HEC-GeoHMS toolset takes portions of GIS formatted data and creates model parameters from the data. This model used the 2005 New Mexico Geospatial Data Acquisition Coordination Committee (GDACC) 10 meter enhanced DEM to derive; sub-basin delineation, slopes within the sub-basin, basin centroid, flow path lengths, and channel slopes, for use in modeling the topography of the basin. Once the physical data has been processed through Hec-GeoHMS, the information can be exported to Hec-HMS where additional input values are chosen to describe and make assumptions about the basin model. The additional input values included in the model included soil data, geologic data, estimated evaporation rates and rainfall gage data for Mescal Arroyo. These include the type of basin and meteorologic model, and any specific precipitation gage data that may be available.

HYDROLOGIC MODELING RESULTS

The Mescal Arroyo Hec-HMS model was run for each of the six storm event models representing the different ARIs. Each of the resulting synthetic hydrographs seen in Figure 10 shows a sharp rise in runoff early in the simulation due to the nature of the NOAA precipitation estimates. The attenuation time and peak discharge from the simulations vary as a function of the data used and assumptions made in putting the model together.

Assumptions include:

- The DEM accurately represents the actual ground surface.
- The actual vegetation condition closely matches the assumptions made for the model.
- The precipitation estimates are accurate for the watershed.
- Runoff modeling accurately represents actual runoff in the watershed.

- The precipitation rate closely follows the rainfall curve used in the model.
- Precipitation is distributed equally across the entire watershed.
- Estimated evaporation loss rates are accurate for the watershed.

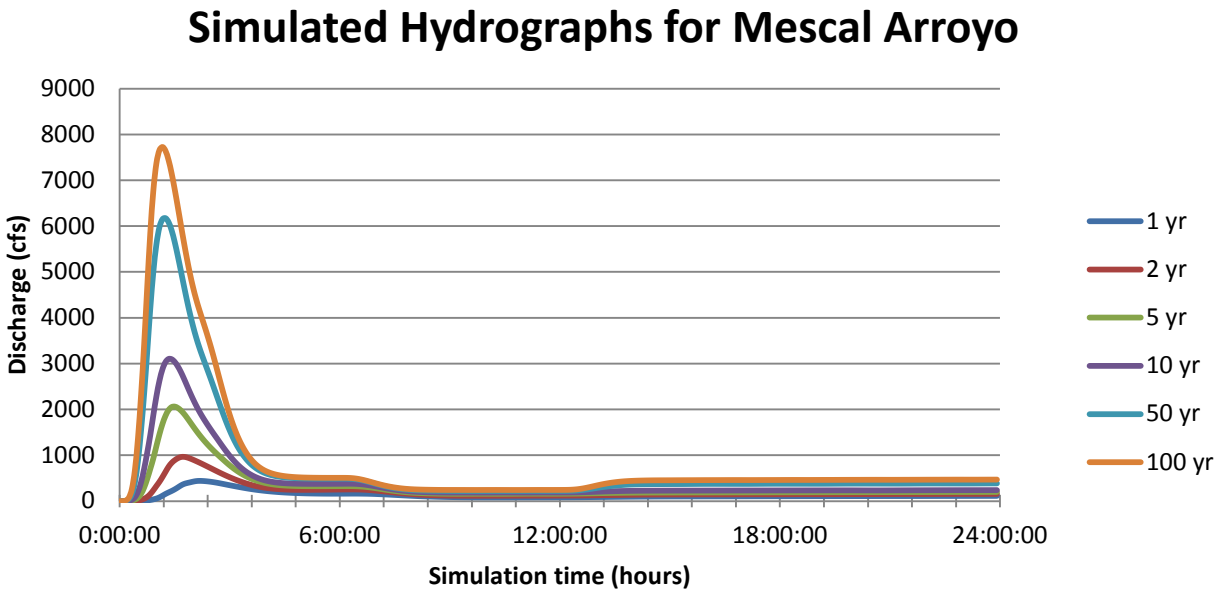

Figure 6 Simulated hydrograph results from the HEC-HMS model

Table 1 Estimated peak discharge and total event runoff for 24 hr return interval storm events.

Return Interval	Estimated Peak Discharge (cfs)	Estimated Event Runoff (ac-ft)
1 yr	450	263
2 yr	975	423
5 yr	2000	657
10 yr	3100	863
50 yr	6100	1458
100 yr	7700	1775

Model results presented in Figure 10 and Table 3, illustrate the high runoff potential in the Mescal Arroyo watershed. The high runoff and the soil types in the watershed have the potential to produce large amounts of sediment runoff. Table 4 provides visual quantity estimates and precipitation data showing the high sediment transport potential of the arroyo.

Table 2 Comparison of sediment removed from the mouth of the arroyo, rainfall through the monsoon season and yearly rainfall data from the Truth or Consequences gage over the yearly period

Estimated Sediment volume removed from Mescal Arroyo and Precipitation data from the T or C gage			
Year	Quantity Removed (cubic yards)	Total Precip for July through September	Total Yearly Precip
2001-2002	3500	3.65	5.48
2002-2003	2200	2.6	5.08
2003-2004	1000	2.85	5.38
2004-2005	5000	5.56	11.19
2005-2006	5000	0.53	3.81
2006-2007	15460	3.56	13.05
2007-2008	1200	3.98	5.42
2008-2009	8400	10.8	11.97
2009-2010	3000	5.44	9.86
2010-2011	3472	8.32	12.36

Table 4 lists an estimate of material removed at the confluence of the arroyo and the mainstem of the Rio Grande by the crew at Elephant Butte compared to the monsoon season precipitation and the total yearly precipitation for that year. Generally, the years with higher precipitation are also years with more sediment removed from the confluence. Aside from water years 2005 and 2006 where the majority of the precipitation occurred in the months January and February for 2005 and in October for 2006, most of the rainfall comes during monsoon season. These two outliers illustrate how variable weather in the arid southwest is. For the Mescal Arroyo model, the precipitation is distributed equally over the entire watershed, this assumption differs from storms in the real world that may be localized and only cover portions of the watershed. This may be one of the sources of poor correlation between yearly rainfall and sediment removed, since a storm of a certain magnitude focused higher in the watershed may yield less channel flow than a storm of the same magnitude closer to the confluence of the arroyo and river.

A PSIAC (Pacific Southwest Inter-Agency Committee) Sediment Yield calculation was performed to gain an idea of the amount of sediment that the arroyo is able to produce. The PSIAC method estimates yearly sediment discharge using a system to rate the arroyo conditions based on a number of parameters including; surface geology, soils, runoff, and land management types. For Mescal Arroyo, there were 9 ratings broken down by soil units. The calculations yielded an estimate of 3.4 ac-ft per square mile per year. Table 5 lists the PSIAC estimate of sediment volume produced by the corresponding geologic soil formation group.

Table 3 Estimates of sediment volume transported through Mescal Arroyo using the PSIAC method.

PSIAC Sediment Yield Estimates			
Unit number	Geomorphic association	Estimated sediment yield (yd^3/ sq-mi/yr)	Estmated sediment yield (AF/sq-mi/yr)
4	Akela	322.67	0.2
21	Bluepoint	387.20	0.24
28	Courthouse rock outcrop	968.00	0.60
30	Delnorte-Cave-Tencee complex	290.40	0.18
34	Albutte- Courthouse complex	806.67	0.50
37	Glendale-Gila complex	403.33	0.25
52	Lozier rock outcrop	371.07	0.23
64	Nickel-Tencee-Delnorte complex	451.73	0.28
71	Courthouse rock outcrop	1484.26	0.92
	Total estimated sediment yield	5485.32	3.4

CONCLUSIONS AND RECOMMENDATIONS

A historic geomorphic assessment of Mescal Arroyo and its confluence with the Rio Grande was done to provide information regarding its condition and history, as well as to illustrate the link between high-intensity rainfall events and the potential for sediment transport through the watershed. At times the arroyo sediment deposition tends to block or partially block flow in the mainstem Rio Grande, disrupting the continuity of flow downstream to Caballo Reservoir. The mainstem Rio Grande channel has been modified for flood control to effectively pass 5,000 cfs and also to meet delivery requirements downstream. Channel location has also been modified for the same reasons plus modification from road and embankment establishment. In addition, dam operations control the Rio Grande releases below Elephant Butte primarily for power and irrigation demand. The combination of these factors creates a situation where the Rio Grande is unable to adjust laterally to sediment input, nor is it able to mobilize most of the sediment deposits at the arroyo outfall with current flow releases.

This geomorphic review presents an analysis of historic channel morphology of the Rio Grande at the confluence with Mescal Arroyo, and a rainfall runoff model to assess the morphological changes occurring in Mescal Arroyo and the effects of storms on the arroyo. The results of the hydrologic analysis and the geomorphic assessment show:

- The alignment of the Rio Grande channel has been channelized to its current location, where it has been narrowed, channel length shortened and excavated to pass the required 5000 cfs. The channel is also restricted from meandering to adjust to sediment inputs.
- Flow regulation due to the dam has disrupted the natural flow regime of the Rio Grande.
- Anthropogenic modifications in the mouth of Mescal Arroyo have channelized the flow into a single channel coming out of the arroyo. The area chosen to spoil material excavated from the Rio Grande channel has further channelized and shortened the arroyo channel.

- The geology of the arroyo consists primarily of sedimentary formations, and geologic processes have left steep slopes within the watershed.
- Soils in the watershed are generally well drained and shallow, with a mostly impermeable substrate. Which have a high runoff potential.
- Monsoon storm meteorology dominates the yearly rainfall amounts in the arroyo. Monsoon storms drop large amounts of rainfall in a short period of time.
- The region is an arid region so vegetation consists of hardy drought tolerant plants.
- A rainfall runoff model was developed for the watershed using existing data for inputs. The results of the model provide an idea of the discharges that are possible from the watershed.
- PSIAC calculations were made to estimate the amount of sediment runoff that can be produced by the arroyo. Estimated total sediment yield is 74 ac-ft of sediment per year over the entire 14,000 acres of Mescal Arroyo.

Addressing the sediment transport problems associated with the arroyo and its confluence will be a continual maintenance concern. Because there are a number of land owners within the area of the arroyo any solution that requires work to be completed in the arroyo will have to consider land ownership issues. The arroyo is an extremely dynamic system any possible solution will have to be designed so that it can withstand the variable flows as well as minimize maintenance. Alternatives should be defined to be designed to withstand the 10 yr flow or about 3000 cfs. Finally, the design alternatives should have no impact on the delivery of water from Elephant Butte downstream. The following is a list of possible solutions to pursue related to sediment management of the arroyo:

- Alteration of dam operations – Operations of the dam could be altered to increase the amount of water in the Rio Grande below Elephant Butte Dam. The idea behind this is that increasing the water flow in the river in response to a rainfall event would be enough to keep the additional sediment mobile, helping to transport excess sediment downstream. This would require rapid response to rainfall events.
- Installation of sediment control structures in lower portion of Mescal Arroyo– Sediment control structures would decrease the amount of sediment introduced to the river. These structures would have to be robust enough that they can withstand the large variations in flow and would require periodic sediment removal. Control structures could include Gabion Baskets, Check Structures and grade control structures. It is important to note that any work in the arroyo is outside of Reclamation's authority under the Middle Rio Grande Project.
- Provide stable transition channel with continued need to remove sediment at confluence – Realignment of the arroyo channel would change the confluence of the arroyo and river to reduce the angle at which the arroyo meets the river. This concept assumes the reduced angle, the additional sediment would most likely be deposited in a location that wouldn't constrain the river channel as much. In addition to the new deposition location, the water velocities at the confluence should be high enough to keep the sediment mobile. Any structures associated with this would have to be robust and periodic removal of deposited sediment would be performed.

REFERENCES

Beven, Keith J., 2001 Rainfall-runoff Modeling: The Primer, New York NY: John Wiley & Sons, Inc,

Bonnin, Geoffrey M., Martin, Deborah, Lin, Bingzhang, Parzybok, Tye, Yekta, Michael, and Riley, David, 2006, Precipitation-Frequency Atlas of the United States: Volume 1 Version 4.0: Semiarid Southwest (Arizona, Southeast California, Nevada, New Mexico, Utah) , Silver Spring MA: US Department of Commerce.

Green, Gregory N. and Jones, Glen E.1997 The Digital Geologic Map of New Mexico in ARC/INFO Format, Open-File Report OF-97-52, http://greenwood.cr.usgs.gov/openf-file-reports/ofr-97-0052/1:500,000

Hornberger, George M, Raffensperger, Jeffrey P., Wiberg, Patricia L., and Eshleman, Keith N., 1998, Elements of Physical Hydrology, Baltimore MA: The Johns Hopkins University Press,

Institute for Transportation, 2009 Iowa Stormwater Management Manual, Iowa State University Institute for Transportation 2C-10

Lacy, Stephen, Geology and Pacific Southwest Inter-Agency Committee (PSIAC) Sediment Yield Evaluation for Mescal Canyon, Sierra County, New Mexico, NRCS Report 22 pgs.

_____ 1986, Urban Hydrology for Small Watersheds: Natural Resources Conservation Service Technical Release 55

United States Department of Agriculture Natural Resources Conservation Service 2011 Custom Soil Resource Report for Sierra County Area, New Mexico, NRCS Report http://websoilsurvey.nrcs.usda.gov/app/HomePage.htm

INTEGRATING GIS WITH ANNAGNPS WATERSHED MODEL FOR OPTIMAL PLACEMENT OF CONSERVATION PRACTICES IN AGRICULTURAL WATERSHEDS

Henrique G. Momm, Assistant Professor, Middle Tennessee State University, Murfreesboro, TN, 37130, henrique.momm@mtsu.edu; Ronald L. Bingner, Agricultural Engineer, USDA-ARS NSL, Oxford, MS, ron.bingner@ars.usda.gov; Leah Kraemer, Graduate Research Assistant, Middle Tennessee State University, Murfreesboro, TN, 37130, leah.kraemer@amecfw.com; and Robert R. Wells, Research Hydraulic Engineer, USDA-ARS NSL, Oxford, MS, robert.wells@ars.usda.gov

Abstract: The development of technology designed to maximize crop production while minimizing the impact to ecosystems services in agricultural watersheds is a complex undertaking. Integrated and multifaceted relationships exist between multiple systems controlling the transport of non-point source pollution from upstream croplands into downstream water bodies. Some of the known factors controlling non-point source production include: environmental conditions, type and location of sources, selection of farming practices, and implementation of efficient conservation measures. Existing watershed-scale modeling technology, such as the United States Department of Agriculture (USDA) Annualized Agricultural Non-Point Source pollutant loading model, AnnAGNPS, offers the necessary tools to describe existing conditions and even perform simulations of possible suggested scenarios. The challenge resides in the selection of conservation practices (or series of them), their key parameters, and their spatial allocation. This task is difficult due to the integrated nature between erosion sources and conservation systems. For example, implementation of a localized conservation practice upstream can have a positive effect locally; however, it could have a negative effect elsewhere in the watershed (clean water effect). To address this optimization task, a spatial decision support systems (SDSS) based on the AnnAGNPS model, GIS, and genetic algorithms, is being developed to support optimized spatial allocation of conservation practices in agricultural watersheds. In this study, we describe the developed foundational technology to link the optimization algorithm with the riparian filter strips component within the AGNPS system. The technology developed will be integrated with optimization algorithms and will support the long-term objective of determining an optimal alternative that would minimize soil erosion and maximize production area.

INTRODUCTION

In watershed systems, the transport of sediments from croplands to downstream water bodies is influenced by an integrated and multifaceted relationship between farming practices, sediment sources (sheet, rill, gully, and channel), and conservation measures. As the understanding of the impact of each of these factors upon sediment detachment and transport improves, new modeling technologies are being developed to support the decision making process of improving agricultural yield while reducing the ecosystem's pollution.

The Research Service (ARS) and the Natural Conservation Service (NRCS), both branches of the USDA, jointly developed the AnnAGNPS pollution modeling system (Bingner and Theurer, 2001). AnnAGNPS predicts the origin and movement of water, sediment, and chemicals at any

location within the watershed. The model was developed with multiple integrated components, to account for different sediment source areas and sinks, and considers the impacts of conservation practices upon the watershed. Pollutant and sediment tracking provides an important link to their sources enabling valuable insight into the effect and most effective placement of conservation practices. The model is capable of distinguishing between erosion processes (i.e., sheet and rill, tillage-induced ephemeral gullies, classical and edge-of-field gullies processes) and streambed and bank sources.

The challenge resides in the selection of conservation practices (or series of them), their key parameters, and their spatial allocation. Theoretically, there are infinite alternatives on how to implement conservation practices with varying cost and efficiency. However, there is a reduced number of alternatives that minimize sediment output through the implementation of conservation practices at the most critical locations within the watershed while maximizing crop yield through keeping production areas. This problem can be investigated using system-engineering concepts in the form of spatial decision support systems.

The utilization of SDSS can expedite the selection of the most appropriate solution. Our proposed technology integrates modeling (AnnAGNPS), database management, GIS, and optimization algorithms (genetic algorithms). The conservation practice selection and spatial allocation tool is still under development, however, the general linkage between the optimization algorithm, GIS, and the AnnAGNPS model is described in this text.

METHODS

The utilization of riparian vegetation in agricultural fields has been recognized as an effective conservation practice to reduce sediment/nutrients transport from croplands. A riparian buffer component (Momm et al., 2014) has been developed to estimate the influence of riparian vegetation on sediment loadings from sheet, rill, and ephemeral gully sources (Momm et al., 2012). Users can vary basic input parameters used to characterize riparian buffers through the development of a GIS raster grid layer describing the riparian zone spatial extent and vegetation type. This is usually a time consuming task which requires multiple iterations to select the appropriate riparian zone characteristics (width and vegetation type) as well as to spatially allocate riparian zones at the most efficient locations throughout the watershed.

The basic unit of the AnnAGNPS model is the sub-catchment (figure 1A). The entire watershed is sub-divided into sub-catchments and each of them is characterized based on a large number of parameters from multiple databases. To simplify the description of the proposed methods, only one sub-catchment is used (figure 1B). In the AnnAGNPS riparian buffer component (AGBUF), each sub-catchment is intersected with a user-provided riparian buffer layer (figure 1C) and key raster grid cells recorded (figure 1D). A candidate solution in AGBUF is represented as two raster grid layers: one defining the riparian zone extent (figure 1C) and another defining the riparian zone vegetation type.

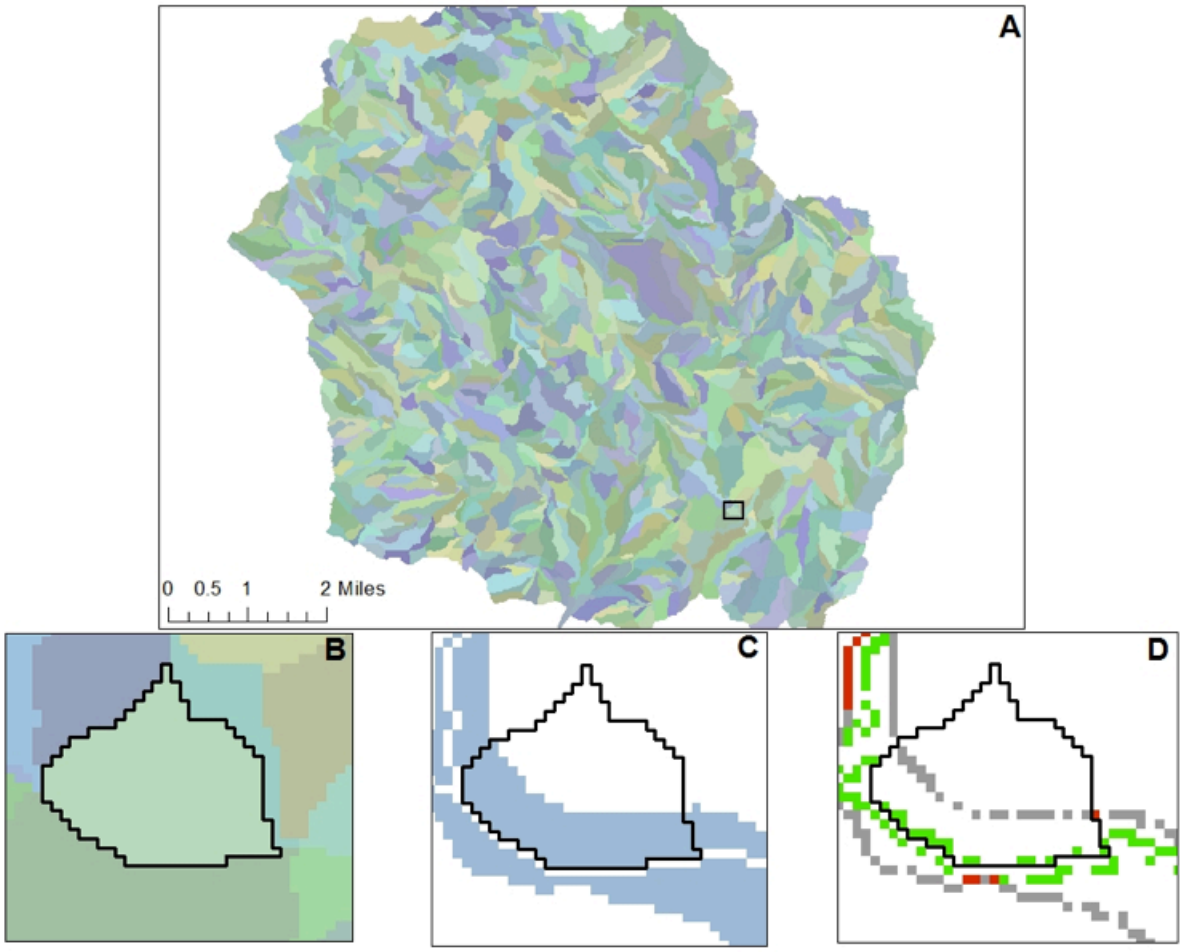

Figure 1 Watershed characterization into sub-catchments (A). Each individual sub-catchment (B) is spatially intersected with land cover layer containing riparian filter strip zone (blue layer in C). The raster grid cells receiving flow from outside the riparian zone (marked in gray in D) and having flow leaving the riparian zone (marked in green in D) are used as input information into the AnnAGNPS buffer GIS technology (AGBUF) described by Momm and others (2014).

The utilization of genetic algorithms (GA) as the optimization engine was sought to streamline the selection process. Genetic algorithms are computer programs inspired by the Darwinian theories of biological evolution, which states that individuals that best fit the environment that they live in will have a higher chance of survival and passing their genes to the next generation (survival of the fittest). During the evolutionary process, the program generates a set of candidate solutions randomly and sorts them based on user-defined fitness criteria. The top fit individuals are selected to form the new set of candidate solutions after crossover and mutation operations are performed. This iterative procedure is repeated until the stopping criteria are reached. For genetic algorithm, the set of candidate solutions is represented by a vector of bits (zeros and ones).

Our contribution was to develop an automated GIS procedure to translate candidate solutions from AGBUF representation (raster grid) into GA representation (vector of bits) and vice versa. The key component in this procedure is the generation of a list of rows and columns of the raster

grid cells marked as downstream edge locations (figure 2). These locations are marked within the grid with a value of 2 and describe raster grid cells located within the riparian zone and with flow exiting the riparian zone (green raster grid cells in figure 3A).

TYPE	2	2	2	2	2	2	2	2	2	2	2	2	2	2	2	2	2	2
ROW	1089	1090	1090	1091	1092	1092	1092	1093	1093	1093	1094	1094	1094	1095	1095	1095	1095	1095
COL	1050	1051	1052	1052	1053	1054	1055	1055	1056	1057	1057	1071	1074	1059	1060	1065	1066	1068
	1	1	1	1	1	1	1	1	1	1	1	1	1	1	1	1	1	1

Figure 2 The list of raster grid cells marked as upstream riparian zone edge. These vectors are translated into a single vector of bits representing a candidate solution and are understood by the optimization algorithm.

From AGBUF to GA: The user provides a raster grid layer containing the maximum extent of the desired riparian buffer zone throughout the watershed. This is something that would not be practical to implement due to limited resources of conservation agencies and the significant reduction of farming area. However, this layer representing the maximum extent is used to develop a database of row and column information of the raster grid cells marked as riparian downstream edges (green raster grid cells in figure 3A and first three rows in figure 2). The maximum extent raster grid is represented as a vector of ones with the same size (length) as the vectors recording rows and columns of key raster grid cells (fourth row has the same size as the first three rows in figure 2).

From GA to AGBUF: In this part, the program uses the following as input: (i) flow vector layer, (ii) watershed sub-catchment layer, (iii) database of downstream edge raster cells, and (iv) binary vector (GA candidate solution). The algorithm starts by comparing the binary vector with the database of downstream edge raster cells. Only the rows and columns paired with the value of one in the binary vector are marked in the new riparian buffer zone raster grid (green raster grid cells in figure 3). The algorithm then iterates to determine and mark all the raster grid cells flowing into the already marked cells (blue raster grid cells in figure3). Examples of iteration over each buffer raster grid cell labeled 2 (in green) once (A), twice (B), and three times (C) are illustrated in figure 3. The output from the last iteration represents the raster grid layer containing the riparian buffer zone information (used as input into AGBUF).

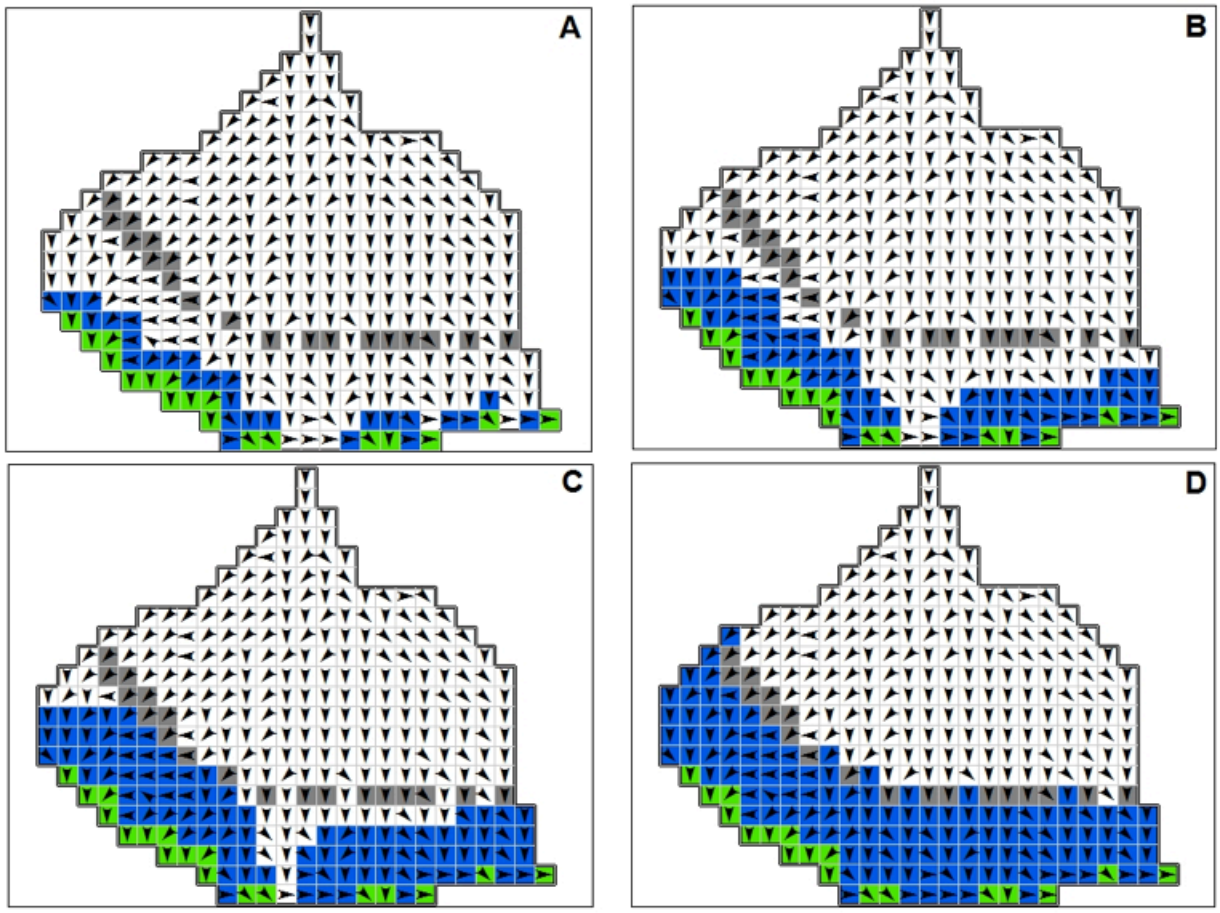

Figure 3 Iterative procedure to translate a candidate solution represented as a vector of bits into a raster grid file. Blue cells show the results of string to raster conversion after one (A), two (B), and three (C) cycles around each green raster grid cell. The final riparian buffer zone is obtained when the maximum width is reached (D).

Evolving Optimal Candidate Solutions: During the evolutionary process, GA generates and combines a large number of different candidate solutions. Different candidate solutions are generated by varying the zero and one values in each binary vector (figure 4). If a binary vector has only zeros, no riparian buffer is generated. A single value of one generates a riparian zone with the only one downstream edge raster grid cell; however its size varies depending upon the drainage pattern into the downstream edge raster grid cell (figure 4A). It is possible that a candidate solution would generate riparian filter strips off from the main concentrated flow paths (figure 4B and 4C), however they would receive poor scoring due to the estimated sediment trapping efficiency being low.

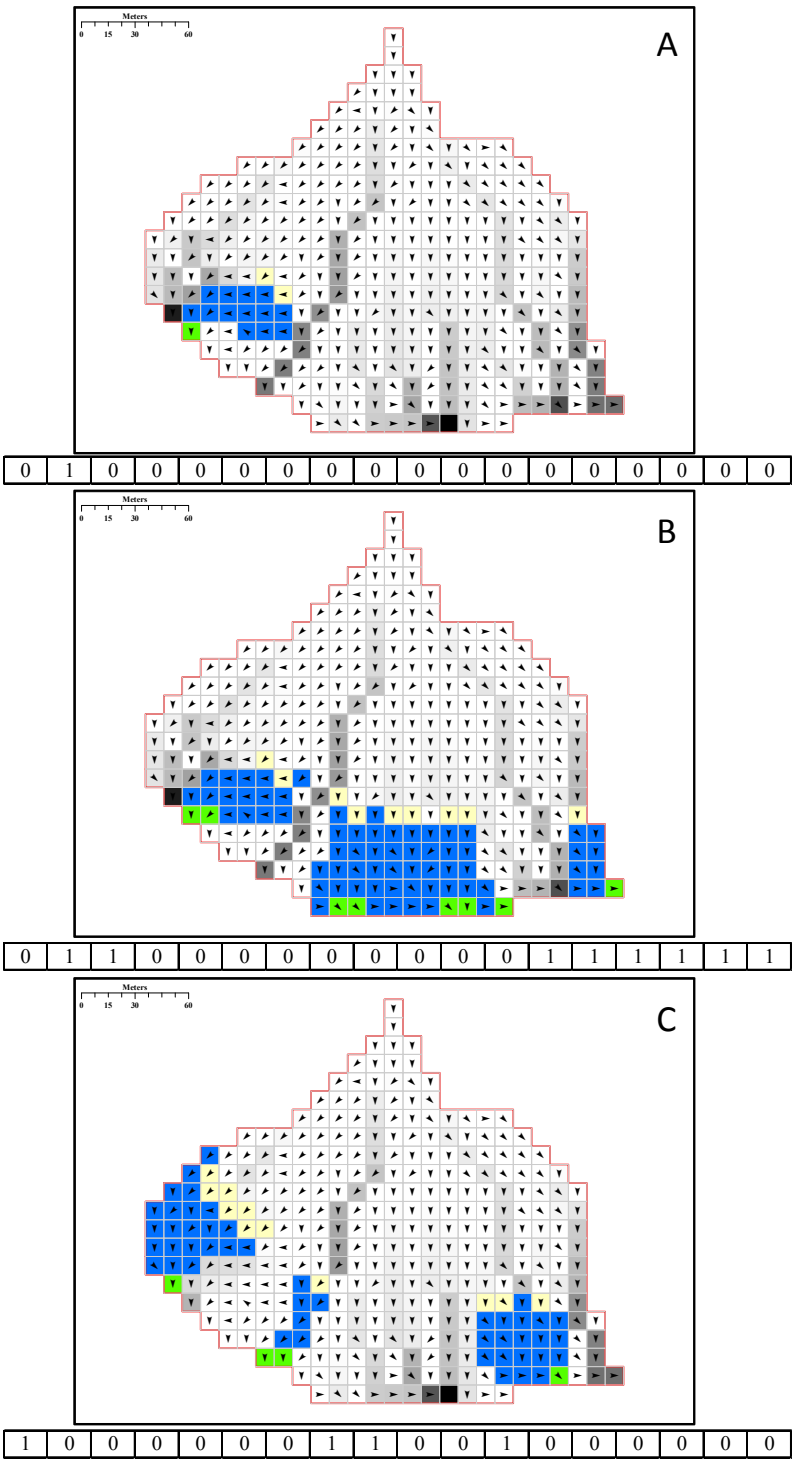

Figure 4 Examples of multiple scenarios in both representation formats: raster grid cell and vector of bits. Raster grid cells marked with gray scale symbology represent flow accumulation and indicate the presence of concentrated flow paths. Green represents downstream edge raster grid cells, yellow upstream raster grid cells, and blue riparian buffer zone raster grid cells. In the first scenario (A) only one of the downstream edge raster grid cells are activated. In the second (B) and third (C) scenarios (B) several downstream edge raster grid cells are activated, displaying the different configurations.

FINAL REMARKS

The described methods serve as the foundation to the development of a comprehensive SDSS integrating a well-established watershed modeling technology (AnnAGNPS), optimization algorithms (genetic algorithm), and GIS. Future developments will encompass the integration of these three components into a single system, with accompanying detailed documentation and easy-to-use graphical user interface.

Our long-term objective is to identify an optimal alternative that spatially locates conservation practices at the most critical locations throughout the watershed and determine their key design parameters. This optimal alternative should minimize nutrient-rich soil losses and, at the same time, maximize production area. Such technology represents an important step in understanding and accounting for the integrated effect of conservation practices and erosion sources by utilizing resources efficiently and promoting sustainable agricultural production.

REFERENCES

Bingner, Ronald L., and Theurer, Fred D. (2001). AGNPS 98: A suite of water quality models for watershed use. In: Proceedings of the Sedimentation: Monitoring, Modeling, and Managing, 7th Federal Interagency Sedimentation Conference, Reno, NV, 25–29 Mar. 2001. United States Dept. of the Interior, Bureau of Land Management, Washington, D.C. p. VII-1-VII-8.

Momm, Henrique G., Bingner, Ronald L., Wells, Robert R., and Wilcox, Darlene (2012). AGNPS GIS-based Tool for Watershed-Scale Identification and Mapping of Cropland Potential Ephemeral Gullies. *Applied Engineering in Agriculture Journal*, **28**(1), 1:13.

Momm, Henrique G., Bingner, Ronald L., Yuan, Yongping, Locke, Martin L., and Wells, Robert R. (2014). Spatial Characterization of Riparian Buffer Effects on Sediment Loads from Watershed Systems, *Journal of Environmental Quality*, **43**, 1736:1753.

USE OF ANNAGNPS AND REMOTELY-SENSED DATA IN WATERSHED CONSERVATION MANAGEMENT PLANNING

Ronald L. Bingner, Agricultural Engineer, National Sedimentation Laboratory, United States Department of Agriculture-Agricultural Research Service, Oxford, MS, Ron.Bingner@ars.usda.gov; Henrique G. Momm, Assistant Professor, Department of Geosciences, Middle Tennessee State University, Murfreesboro, TN, Henrique.Momm@mtsu.edu; Robert R. Wells, Research Hydraulic Engineer, National Sedimentation Laboratory, United States Department of Agriculture-Agricultural Research Service, Oxford, MS, Robert.Wells@ars.usda.gov; Roger A. Kuhnle, Research Hydraulic Engineer, National Sedimentation Laboratory, United States Department of Agriculture-Agricultural Research Service, Oxford, MS, Roger.Kuhnle@ars.usda.gov

Abstract: The development of watershed conservation management plans involves many decisions that affect various aspects of a watershed system, with consequences that are difficult to measure. In addition, the efficient placement of practices throughout a watershed as part of an integrated management plan can be difficult without the use of remote sensing data and technology. Watershed modeling technology can use remotely sensed data to evaluate the best placement of edge-of-field buffers and grassed waterways or drop-pipes for gully erosion control for efficient use of conservation resources. This study evaluated the capability of using remotely sensed data and technology for assessments with the USDA Annualized Agricultural Non-Point Source pollutant loading model, AnnAGNPS, in agricultural watersheds. Identification of ephemeral gully and riparian buffers locations and their characteristics were developed using remote sensing components developed as part of AnnAGNPS for comparison to actual locations and characteristics observed in the Goodwin Creek Watershed in North-Central Mississippi that is part of the USDA-ARS Benchmark CEAP-Watershed Assessment Study project. Simulations were performed with AnnAGNPS to assess various levels of conservation practice implementations identified with remotely sensed data and compared to measured loads.

Developing enhanced technology and research to assess conservation management plans is critical for planning and implementing conservation practices specifically designed for erosion and other pollutant control. This study describes the current state of using remote sensed data and research needs for assessing integrated conservation practices and management planning for controlling pollutant loads using the AnnAGNPS watershed model.

Real-Time Forecasting Using HEC-HMS and HEC-MetVue

EXTENDED ABSTRACT

Myles McManus, Hydraulic Engineer, U.S. Army Corps of Engineers, Tulsa District, Myles.B.McManus@usace.army.mil

The procedures and methods used in developing HEC-HMS models by the Corps of Engineers, Tulsa District provide the functionality to predict inflow volumes, rates, and elevations into the reservoirs of the district. This information is used by water managers to make key decisions on the operations of the reservoirs and the consequences of these actions resulting at downstream locations. Tulsa District has been actively pursuing and developing HEC-HMS models for several years to replace the legacy forecast tools with the CWMS (Corps Water Management System) suite of programs by the HEC (Hydrologic Engineering Center). The existing real time rainfall/runoff models are HEC-1 based, in conjunction with various utility programs used for data management.

In order to show how Tulsa District is performing real-time forecasting in lieu of having a complete CWMS package and database setup, a model demonstration using HEC-MetVue, HEC-DSSVue, and HEC-HMS will be shown. The demonstration shows how Tulsa District is extensively testing our HEC-HMS models in preparation for unplugging our legacy WCDS database, programs, and forecasting methods in the interim period while we complete the various tasks involved with completing our full CWMS initiative.

The HEC-HMS models are calibrated using three historical events for each HMS model. Selection of the historical event involves consideration of many factors, such as an isolated storm event, basin wide runoff, variations of rainfall magnitude, observed data availability, and availability of digital precipitation from radar. Archived digital stage III radar files are obtained from the National Weather Service Arkansas-Red River Forecast Center's (ABRFC) office. The program, HEC-MetVue, is used to develop subarea hyetograph data sets using watershed model subbasin shapefiles from the stage III radar files. The hyetographs are used in HEC-HMS to calculate the rainfall runoff volume.

The transform method used is a modified Tulsa regional Snyder's unit hydrograph method. Stream routing methods are primarily Modified Puls routing method for most reach elements. Where Modified Puls storage discharge relationship data is unavailable, the Muskingum routing method is used. Routing lags are also used in the models where there may be significant backwater effects that would cause timing issues with the flow when routing to downstream calibration points. Overall, the routing method chosen is based on available data as well as the most appropriate method for the routing reach.

The base flow method used is Initial Recession, where an initial flow, ratio to peak, and recession constant parameters are used. The reservoirs are modeled using pool routing elements. Paired data for uncontrolled spillway outflow potential is configured using elevation-discharge relationships. Other releases are configured using a user specified controlled release component of the total outflow. Some dams have totally controlled releases, while others have a combination of controlled and uncontrolled releases. This approach allows data for observed inflow, outflow, and elevation to be used in calibration of HEC-HMS models for both historic and real-time events.

Once a full CWMS package is developed and unrolled, we will have HEC-MetVue, HEC-HMS, HEC-ResSim, HEC-RAS, and HEC–FIA, and HEC–CAVI watershed models to use over our entire district. This will allow us to work within the HEC-CAVI program, using a native model implementation approach, to access all the modeling

programs within a single interface. Our current Water Control Data System (WCDS), a database for all our water information including gage and reservoir data, will be transferred onto a new Oracle database to be used with the CWMS system.

The following is a very brief rundown of each piece of software that will be used in CWMS. HEC-MetVue will provide the hyetograph data from radar precipitation data files. HEC-HMS will process the inflow hydrographs at reservoirs and gages, HEC-ResSim will provide reservoir simulation with release logic built for each dam. HEC-RAS will provide in depth flow analysis and inundation mapping. HEC-FIA will provide damage and risk economic assessments. All these programs will be run from inside the HEC-CAVI environment. Any refining or adjustments to observed data in the database will be performed in HEC-CWMSVue, which is very similar to HEC-DSSVue, but has the ability to connect to the CWMS Oracle database and edit that data as well as DSS data.

At this time, Tulsa District is in the model building phase. Recently, CWMS 3.0 was released and is currently being tested with the suite of CWMS models for one of our watersheds. This process is ongoing and will require extensive testing, debugging, time, and effort. Our CWMS Oracle database is also being built at this time. In order to ease the transition to CWMS and ensure we are maintaining all our current abilities to forecast and provide high quality flood control information to the water managers in Tulsa District, we are testing our HEC-HMS models with HEC-Metvue and HEC-DSSVue to compare these results to our legacy software results for the same events and observed data. This allows us to be testing the software and models that are critical to forecasting without having a full CWMS package developed. The current methods and procedures used for real-time forecasting using HEC-HMS models should provide insight on how the hydrological modeling is progressing and evolving within the Corps of Engineers, Tulsa District.

A NEW FRAMEWORK FOR MONITORING THE GREAT LAKES WATER BALANCE ERROR

James W. Lewis, Research Hydraulic Engineer, U.S. Army Engineer Research and Development Center, Coastal and Hydraulics Laboratory, 3909 Halls Ferry Road, Vicksburg, MS 39180, James.W.Lewis@usace.army.mil, (601)634-3895;
Rebecca Bolinger, Postdoctoral Fellow, NOAA Great Lakes Environmental Research Laboratory, 4840 South State Road, Ann Arbor, MI 48108, Becky.Bolinger@noaa.gov, (734)741-2248

Abstract: Agencies across multiple U.S. states and Canadian provinces seek to better understand the hydrologic cycle of the Great Lakes basin. Each estimated hydrologic component, whether based on models or observations, contributes an error to the Great Lakes water balance. A common goal among all agencies is to reduce the water balance error through improved modeling and measurement techniques such that the combined effect of the estimated components matches the water level behavior. Traditionally, different quantities for residual and component net basin supplies have been used to evaluate the Great Lakes water balance. However, these quantities add an unnecessary level of complexity and confusion when cooperating to target primary sources of error in the water balance. A relatively simple framework, based on conservation of mass, is presented in this study that calculates the water balance error for each lake. The primary outcome is a framework where different model estimates can be compared and large contributions to the water balance error can be cooperatively prioritized and targeted. General plots of each lake's error show a number of clear observations suggesting an oscillating seasonal error of precipitation, a potential bias in some connecting channel flow data, and what would happen to the water balance error with the hypothetical inclusion of thermal expansion and contraction. A cooperative reduction in the magnitude of the water balance error will improve Great Lakes water policy and management.

INTRODUCTION

The Great Lakes basin stretches internationally across eight states within the United States of America and two provinces within Canada, containing approximately 20% of the world's volume of fresh water. Water levels and the fluctuations of water levels have significant impact to a broad range of stakeholders, including economic and environmental impacts to both countries. The very important effort of monitoring the hydrologic system of the Great Lakes is cooperative between multiple agencies on each side of the border (Gronewold and Fortin 2012, Fry et al. 2014). There is a growing effort among the Great Lakes community to "close the water balance".

The U.S. Army Corps of Engineers (USACE), Detroit District has developed procedures for monitoring the Great Lakes' water balance and has implemented them as a Corps Division-level International Organization for Standardization (ISO) process. The process provides a standard for review and analysis of the Great Lakes hydrologic and hydraulic (H&H) data that the Division uses in operations and in support of the International Joint Commission (IJC) boards of control. There is a large amount of uncertainty in the current modeling and estimation techniques of each hydrologic component, and although a perfect estimate of each component is

impossible, there is room for improvement among the various techniques. Quantifying the uncertainty in each component as well as the uncertainty in the overall water balance will offer insight about which improvements would be most valuable.

The primary components of the water balance for each Great Lake can be represented by Equation 1. This equation, based on the law of conservation of mass, assumes that the density of water is constant, and is therefore presented as a conservation of volume relationship. In reality, the huge volumes of the lakes can allow for slight differences in density to have an impact, and the ΔS_T term accounts for this. Each term of the equation must have the same units; typically units of volumetric flow, such as m^3/s. The equation is typically used for a specific time period, such as one month or one year. Some terms may not apply to every lake (e.g. Lake Superior does not have a connecting channel inflow).

$$\Delta S = I + P + R - E - O + D + G - C + \Delta S_T \quad (1)$$

where:

ΔS	=	Change in volumetric storage of the lake
I	=	Connecting Channel Inflow
P	=	Precipitation falling directly on the lake surface
R	=	Runoff draining from the land surface to the lake
E	=	Evaporation of water from the lake surface
O	=	Connecting Channel Outflow
D	=	Diversion of water into (+) or out of (-) the lake
G	=	Groundwater flowing to the lake, arriving from below the land surface
C	=	Net effect of consumptive uses (withdrawn water minus returned water)
ΔS_T	=	Change in lake storage due to thermal expansion (+) or contraction (-)

A quantity known as the net basin supply (NBS) is useful for combining the effects of the hydrologic components into one value to represent the general basin conditions for each lake. There are two different ways to calculate the NBS, the residual method and the component method. The component method of calculating NBS is to add/subtract the estimates from each component, hence the name. In practice, the component method is equal to $P + R – E$. The other method is called the residual method, and in practice it is equal to $\Delta S + O – I +/– D$. The final three terms of Equation 1, G, C, and ΔS_T, are significantly smaller than the other terms and are often assumed to have a negligible influence. This assumption introduces some error, though it may be small, whenever it is implemented. Altogether, the residual and component methods of estimating NBS should be relatively similar.

Traditionally, the closure of the water balance has been measured by comparing residual net basin supplies with component net basin supplies (Lee 1992; Neff and Nicholas 2005; DeMarchi, et al. 2009; Deacu, et al. 2012). Although this comparison between component and residual net basin supplies can be informative, it also adds an extra level of explanation and potential confusion when evaluating uncertainty. The framework presented in this paper relates the individual terms directly to the overall water balance error. The analysis of just one overall equation for each lake will provide helpful information about the individual components and clear insight about how well they fit together. This proposed framework deviates from the

traditional analysis and eliminates the need for calculating or evaluating the net basin supplies when analyzing the uncertainty in each component.

Equation 1 can be rearranged such that everything is on the right side of the equation, and the water balance equation in theory should be equal to zero, as shown in Equation 2, for each lake. In reality the equation contains significant uncertainty, as shown by the rearranged Equation 3 representing the typical terms which are used in practice. There are numerous sources of the error in the water balance equation, and each term of Equation 3 contains uncertainty due to measurement errors, spatial and temporal variations, modeling errors, etc.

$$0 = -\Delta S + I + P + R - E - O + D + G - C + \Delta S_T \quad (2)$$

$$Error = -\Delta S_R + I_R + P_R + R_R - E_R - O_R + D_R \quad (3)$$

where:

$Error$	=	Overall error, or gap, in the lake's water balance equation
ΔS_R	=	Recorded/estimated change in volumetric storage of the lake
I_R	=	Recorded/estimated connecting channel inflow
O_R	=	Recorded/estimated connecting channel outflow
P_R	=	Recorded/estimated precipitation falling directly on the lake surface
R_R	=	Recorded/estimated runoff draining from the land surface to the lake
E_R	=	Recorded/estimated evaporation of water from the lake surface
D_R	=	Recorded/estimated diversion of water into (+) or out of (-) the lake

METHODOLOGY

An analysis of the *Error* for each lake was performed using Equation 3. Data sets were organized and converted into common units of m^3/s for each month, using the actual number of days in each month, so that the monthly *Error* could be calculated for each lake. Some of the terms in Equation 3 could be estimated using multiple methods which are available. This analysis chose one of the possible combinations based primarily on the historical availability of the data sets. The following list shows the data set which was used for each term in the water balance for this initial assessment:

Term	Data set used
ΔS_R	Calculated from coordinated beginning-of-month lake-wide average water levels
I_R	USACE records of connecting channel flows
O_R	USACE records of connecting channel flows
P_R	Coordinated over-basin precipitation (other data sets are also compared)
R_R	NOAA GLERL Area Ratio Method
E_R	NOAA GLERL Evaporation
D_R	USACE records of diversion flows

USACE and Environment Canada (EC) coordinate the official historical data set of Great Lakes beginning-of-month (BOM) lake-wide average water levels back to 1900. The network of water level gauges currently used for the lake-wide average levels is shown in Figure 1. Gauges in the United States are operated by the National Oceanic and Atmospheric Administration (NOAA) National Ocean Service (NOS) Center for Operational Oceanographic Products and Services

(CO-OPS). Gauges in Canada are operated by the Canadian Hydrographic Service (CHS). This network of gauges was chosen by the Coordinating Committee on Great Lakes Basic Hydraulic and Hydrology Data (Coordinating Committee), a group composed of representatives from United States and Canadian federal agencies that keep official records of water levels, flows in the connecting channels, and other data related to the Great Lakes hydrologic system for the last fifty years. The difference in BOM water levels from one month to the next is multiplied by the officially coordinated lake surface area (Coordinating Committee, 1977) to determine the change in volume for each lake. This volume is divided by the time duration using the actual number of days for each month to obtain the change in volumetric storage with units of a flow rate, such as m^3/s.

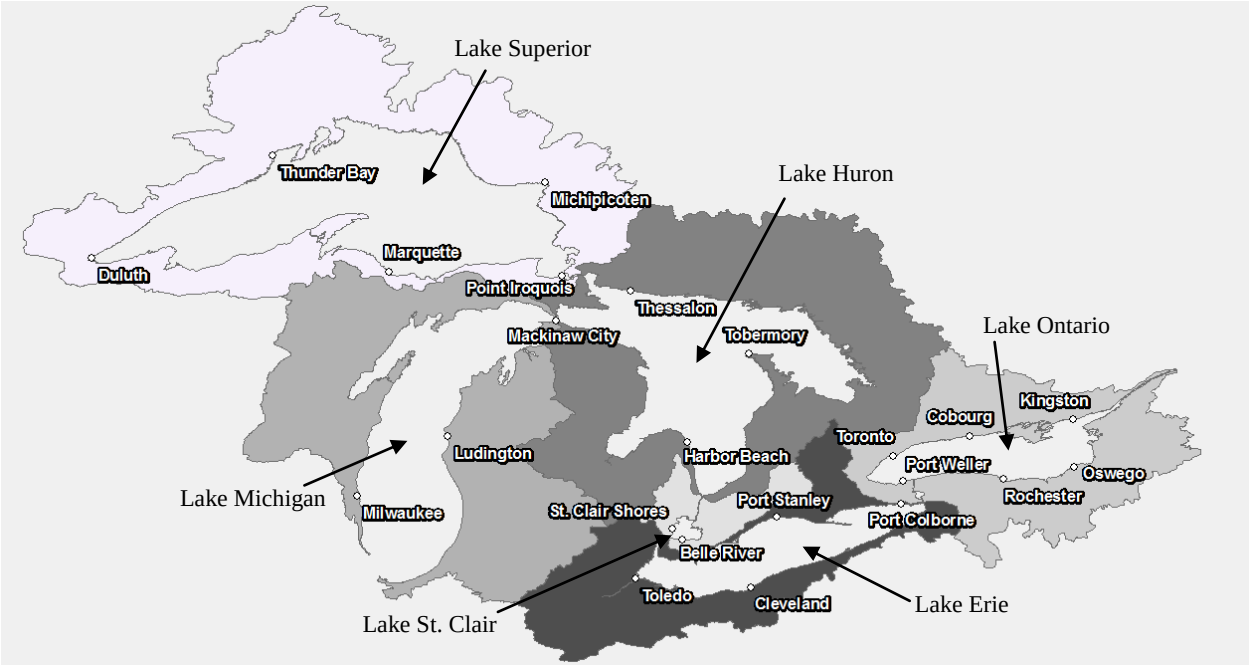

Figure 1 Location of water level gauges used in lake-wide average levels

USACE records of connecting channel flows consist of flows coordinated by the Coordinating Committee and preliminary flows. Preliminary flows are estimated by the Detroit District using a combination of the fall between the upstream and downstream lakes as well as information from NOAA and CHS water levels within the connecting channels. The officially coordinated records of connecting channel flows span 1900 to 2008, with the exception of St. Lawrence River which is coordinated through 2005. Similarly, flow through each of the five diversions (Long Lac, Ogoki, Chicago, the Welland Canal, and the New York State Canal System) is coordinated through the Coordinating Committee, with the official period of record varying for each diversion.

The coordinated over-basin precipitation data is first calculated by the NOAA Great Lakes Environmental Research Laboratory (GLERL) Thiessen Method for estimating precipitation. NOAA CO-OPS then reviews the data and compiles it to be passed on to USACE and EC for coordination. The Coordinating Committee has generally assumed that the over-lake precipitation is better estimated using the over-basin Thiessen method instead of the over-lake

Thiessen method. This assumption may have originated from Croley and Lee 1993, who explain that the Thiessen over-lake precipitation method relies on near-shore meteorology where the lake effects are significant. For this reason, Croley and Lee 1993 used all available meteorological stations throughout the basin to estimate over-lake precipitation, rather than using only near-shore stations. This assumption is investigated near the end of this report, where other data sets produced by the GLERL Thiessen Method were also evaluated; namely Thiessen over-lake and Thiessen over-land. The historical records of all GLERL Thiessen precipitation estimates span 1900 through 2010.

The most complete historical set of runoff data for each of the Great Lakes is the NOAA GLERL Area Ratio Method (ARM). This method extrapolates runoff from gauged drainage areas to un-gauged drainage areas using an area-weighted approach. The window of availability of runoff data varies, with beginning years ranging from 1900 to 1932 depending on the lake.

Evaporation data used in this study are calculated by NOAA GLERL, using their Large Lake Evaporation and Thermodynamics Model. The evaporation data set has the least amount of available data with a historic range going back to 1950.

Using the above data sets, the monthly error (units of m^3/s) is calculated for each lake as well as the annual error (units of m^3/s) from 1950 through 2010. Annual errors are calculated using the time duration of the entire year for each term in Equation 3. In order to perform useful lake-to-lake comparisons of the relative errors, the historical average of all flow into or out of each lake is used for normalizing the errors. This flow is calculated from $I + P + R$ ($+D$, if diversion flows into lake) and should be the same as $O + E$ ($+D$, if diversion flows out of lake) on average. The normalizing flow varies for each lake.

RESULTS

Table 1 shows the calculated annual and monthly average water balance errors for each lake using Equation 3. For interpretation, positive errors are generally caused by the overestimation of any term providing water to the lake or the underestimation of any term removing water from the lake. The converse is true for interpreting negative errors. Each lake's error was normalized by the total average flow into or out of the lake. These normalizing flows were 3700, 8000, 5500, 7000, and 7800 m^3/s for lakes Superior, Michigan-Huron, St. Clair, Erie, and Ontario, respectively, based on each lake's hydrology. Figure 2 shows the chart of average errors in units of m^3/s while Figure 3 shows the normalized percentages.

For more detail on the range of each lake's water balance error for each calendar month, the median, 25% quartile, 75% quartile, maximum and minimum were calculated. These statistical properties are shown in Figure 4 through Figure 8.

Table 1 Average Great Lakes water balance errors

Units of m^3/s													
	Annual	Jan	Feb	Mar	Apr	May	Jun	Jul	Aug	Sep	Oct	Nov	Dec
Superior	**120**	-20	340	-20	-570	100	210	510	710	790	300	-480	-380
Michigan-Huron	**400**	-410	100	-270	-360	300	370	880	1480	1970	1530	20	-810
St. Clair	**-10**	-30	-10	50	50	0	-60	-80	-50	-30	0	40	0
Erie	**-80**	150	-40	-140	-30	-30	0	130	-20	-150	-340	-240	-280
Ontario	**190**	20	110	130	230	160	100	180	320	390	400	240	20
Normalized (%)													
	Annual	Jan	Feb	Mar	Apr	May	Jun	Jul	Aug	Sep	Oct	Nov	Dec
Superior	**3.4**	-0.5	9.1	-0.6	-15.4	2.7	5.8	13.9	19.1	21.4	8.1	-13.1	-10.4
Michigan-Huron	**5.0**	-5.1	1.3	-3.4	-4.4	3.8	4.7	11.0	18.5	24.7	19.1	0.2	-10.1
St. Clair	**-0.2**	-0.6	-0.2	0.9	0.8	0.0	-1.1	-1.4	-0.9	-0.5	0.0	0.7	-0.1
Erie	**-1.2**	2.2	-0.5	-2.0	-0.4	-0.4	0.0	1.8	-0.3	-2.1	-4.9	-3.4	-4.0
Ontario	**2.5**	0.2	1.5	1.7	3.0	2.0	1.3	2.3	4.1	5.0	5.1	3.0	0.2

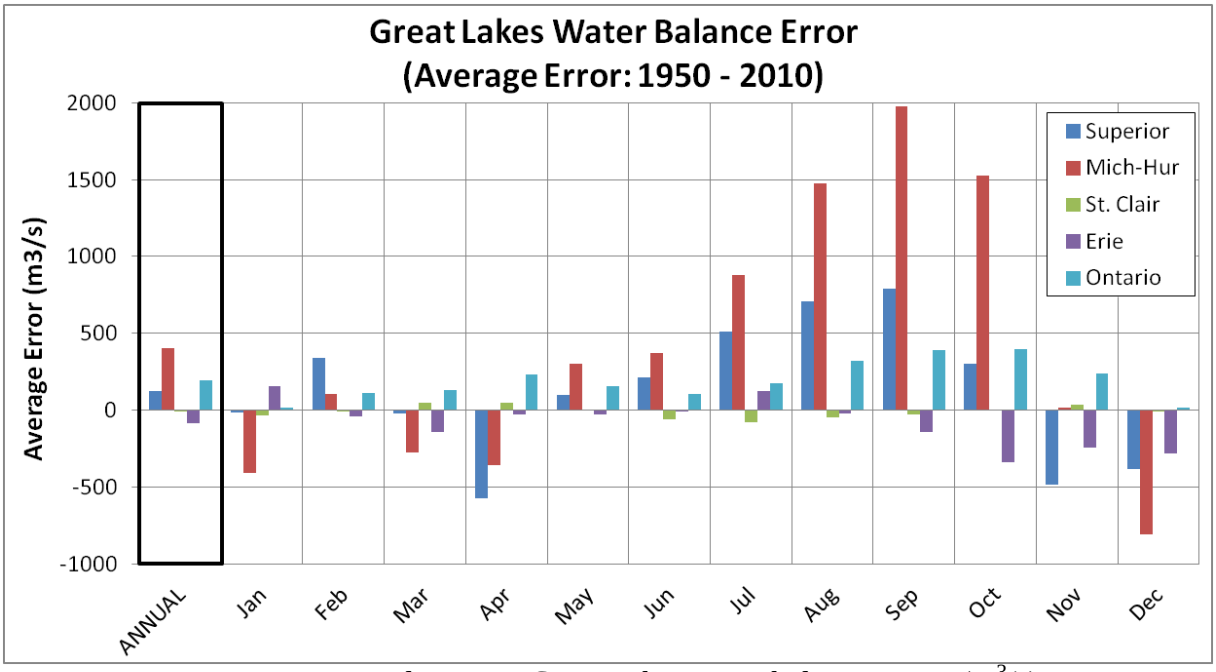

Figure 2 Historical average Great Lakes water balance errors (m^3/s)

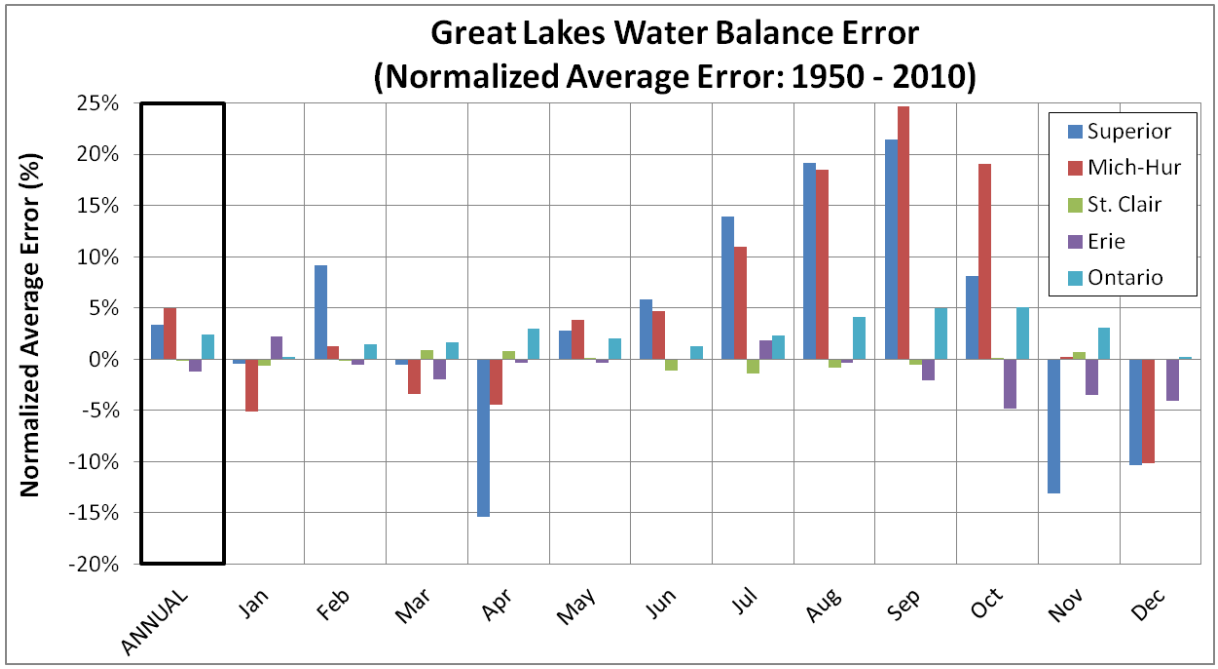

Figure 3 Historical average Great Lakes water balance errors (%)

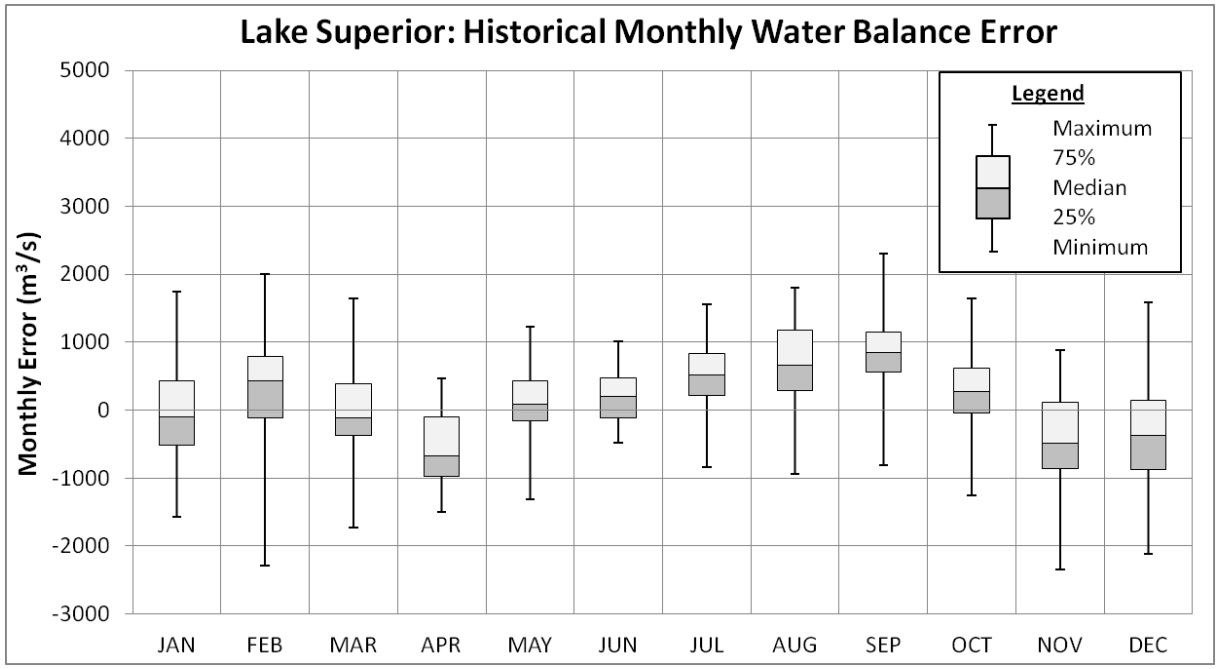

Figure 4 Lake Superior monthly water balance error statistics

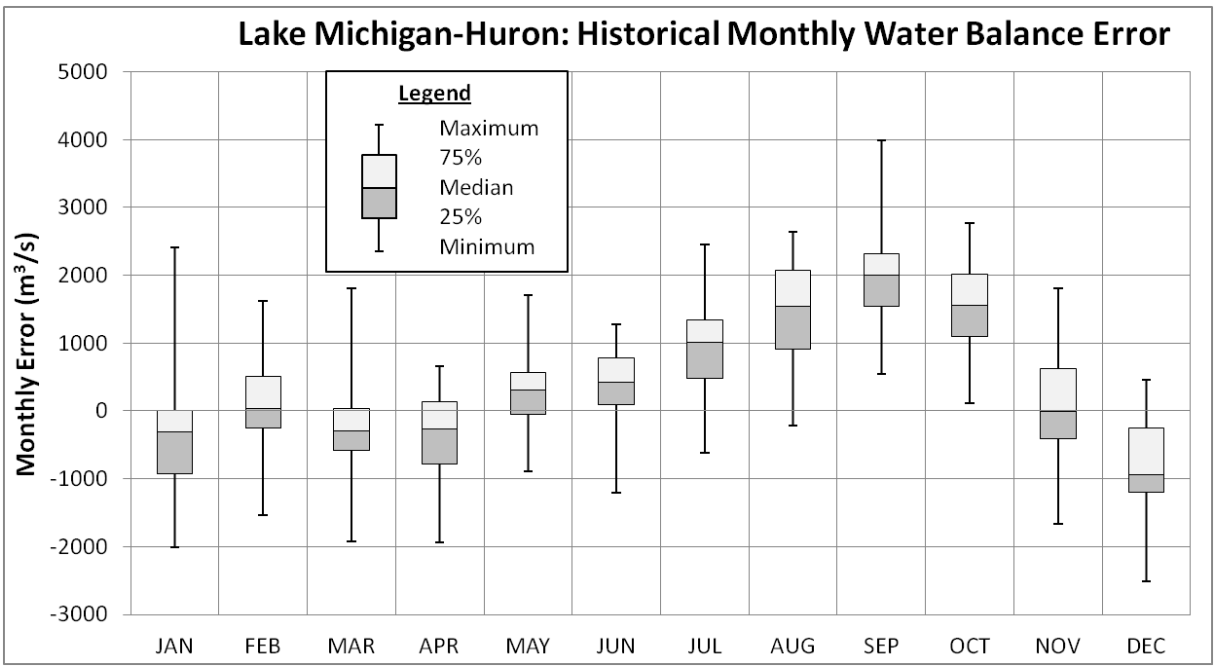

Figure 5 Lake Michigan-Huron monthly water balance error statistics

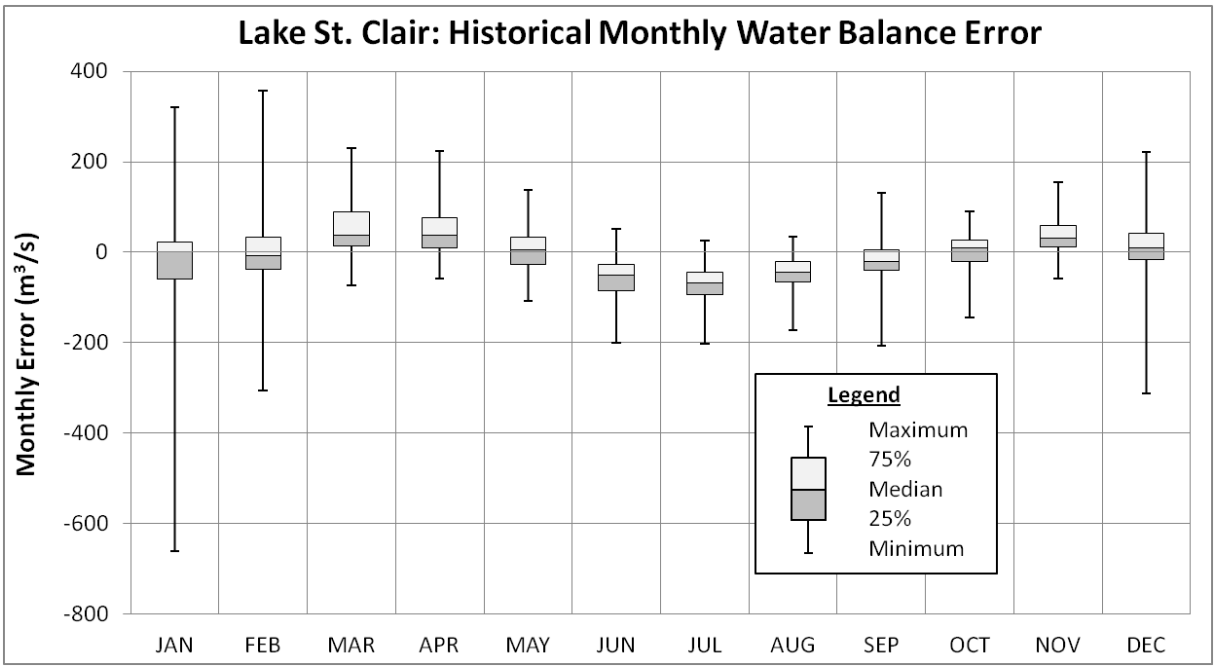

Figure 6 Lake St. Clair monthly water balance error statistics

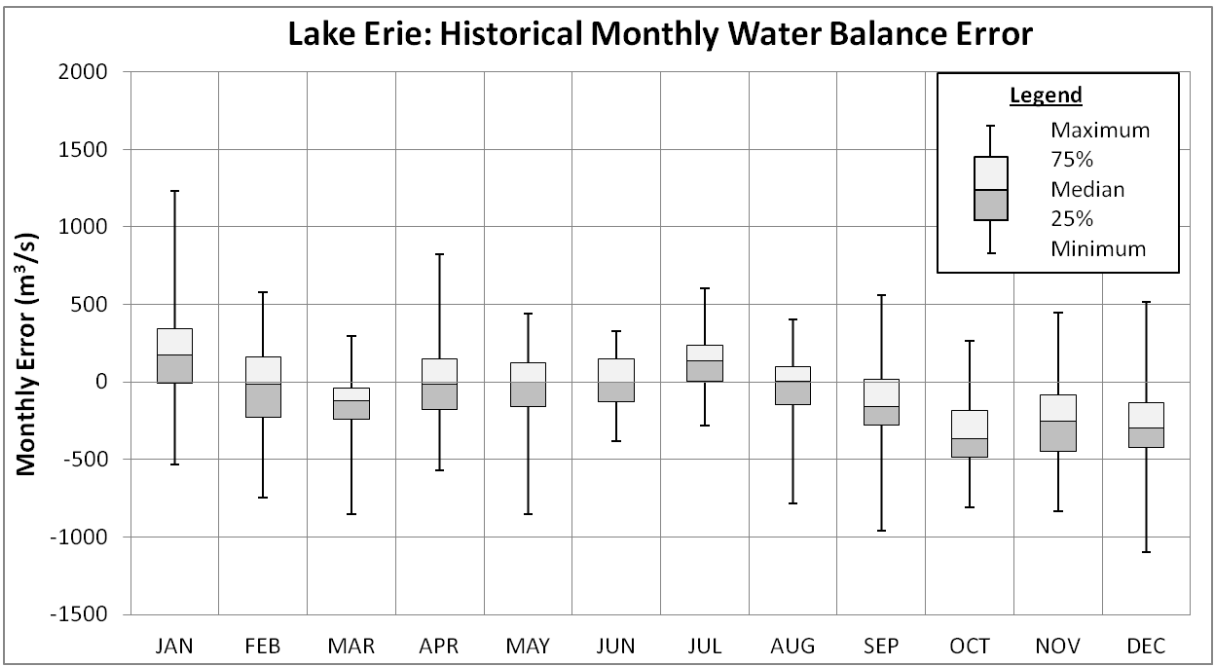

Figure 7 Lake Erie monthly water balance error statistics

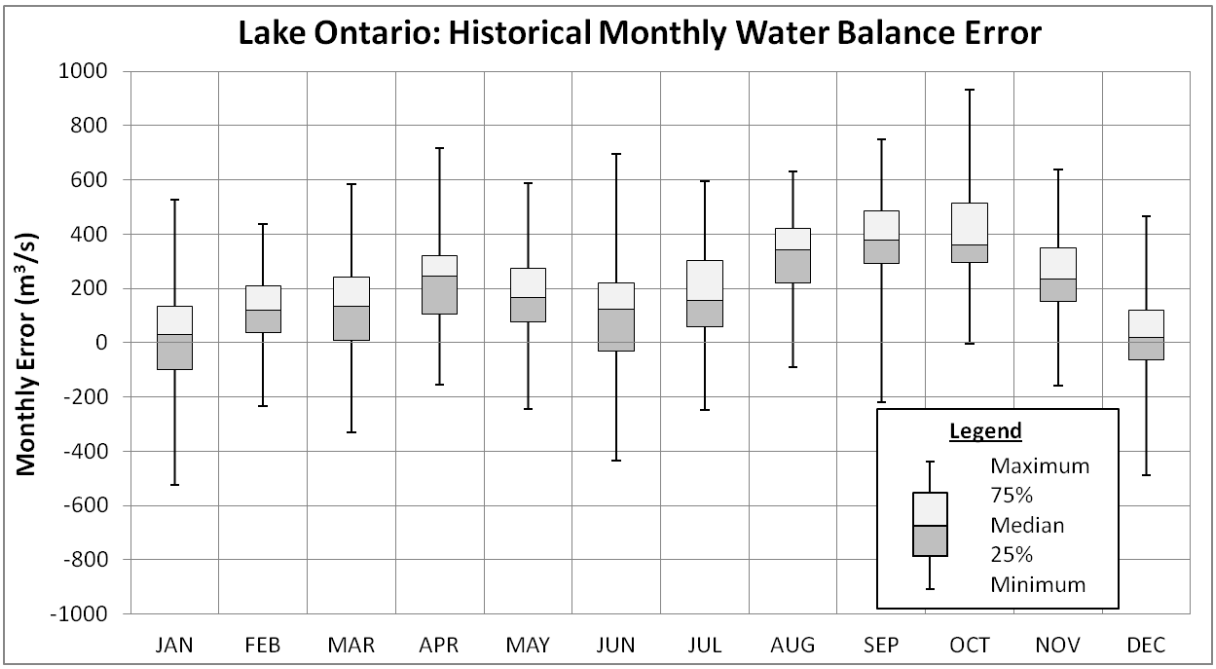

Figure 8 Lake Ontario monthly water balance error statistics

Drawing specific conclusions about errors in individual terms of the water balance requires caution, but these preliminary results reveal many interesting observations. Lakes Superior, Michigan-Huron, and Ontario each had a positive average annual error while lakes St. Clair and Erie had negative errors. In general, the Lake Michigan-Huron water balance errors are the largest while the Lake St. Clair errors are relatively small. This is apparently due to the lake surface area and drainage area of each lake. Since the area is small for Lake St. Clair, the components of *P*, *E*, and *R* are much smaller than the inflow through the St. Clair River and the

outflow through the Detroit River. For Lake Michigan-Huron, however, evaporation is approximately the same magnitude as the inflow from the St. Marys River and the combination of over-lake precipitation and runoff is larger than the outflow through the St. Clair River. A large error suggests that improving the estimates of over-lake precipitation, evaporation, and runoff, especially for Lake Michigan-Huron, should be a priority. A small water balance error for Lake St. Clair implies that the balance between connecting channel flows and water levels is relatively well estimated. However, it is possible that the St. Clair River and Detroit River could both have a bias error in the same direction which would not be detectable when looking at the Lake St. Clair error alone.

Interestingly, errors in the connecting channel flow estimates can influence both the lake upstream and downstream in an opposite manner. For example, decreasing the Niagara River flow estimates would cause both the Lake Erie and the Lake Ontario water balance errors to improve, i.e., move toward zero. Therefore, a re-evaluation of the Niagara River flow estimation method, and/or the investigation of any available hydraulic models, is suggested.

Another interesting observation can be made related to the thermal expansion and contraction of the lakes. In general, the summer water balance errors are positive for the Great Lakes, with the exceptions of lakes St. Clair and Erie. Lake St. Clair is generally below zero for June through August while Lake Erie is near zero for April through August. As the lake water warms in the summer time there is an increase in the lake's water volume due to thermal expansion, creating a positive contribution to the water balance error. Although this would be a more accurate representation of lake storage, it would generally move the Superior, Michigan-Huron, and Ontario errors further away from zero since the errors are already positive, and it would make Lake Erie's error worse as well since it is near zero during those months. This implies that the inclusion of thermal expansion and contraction alone would not perfectly solve the water balance. This is not to suggest that it should be purposefully ignored, but just that it may not be as high of a priority. A proper inclusion of thermal expansion and contraction should be included when available because the goal of monitoring is to have as good of an estimate for each term as possible.

Lakes Superior, Michigan-Huron, and Ontario exhibit some similar seasonal error patterns. The water balance error seems to increase through the summer and then drop significantly at the end of the fall season. This consistent error behavior across multiple lakes may indicate a bias in one or more of the methods used to estimate the components (P, E, or R). Relevant literature (Derecki 1976, Kresge et al. 1964, Holman et al. 2012, and Changnon 1961) acknowledges that the over-lake to over-land precipitation ratio is relatively low in the summer and relatively high in the winter. Since the Thiessen method precipitation estimates are based primarily on gauges over the land, it makes sense that the sign of the seasonal errors shown in the figures could be caused by the over-lake and over-land dynamics. A correction to account for the over-lake and over-land precipitation dynamics would seem to provide significant benefit to the water balance by decreasing the error in the summer months and increasing the error (from a negative value toward zero) in the winter months.

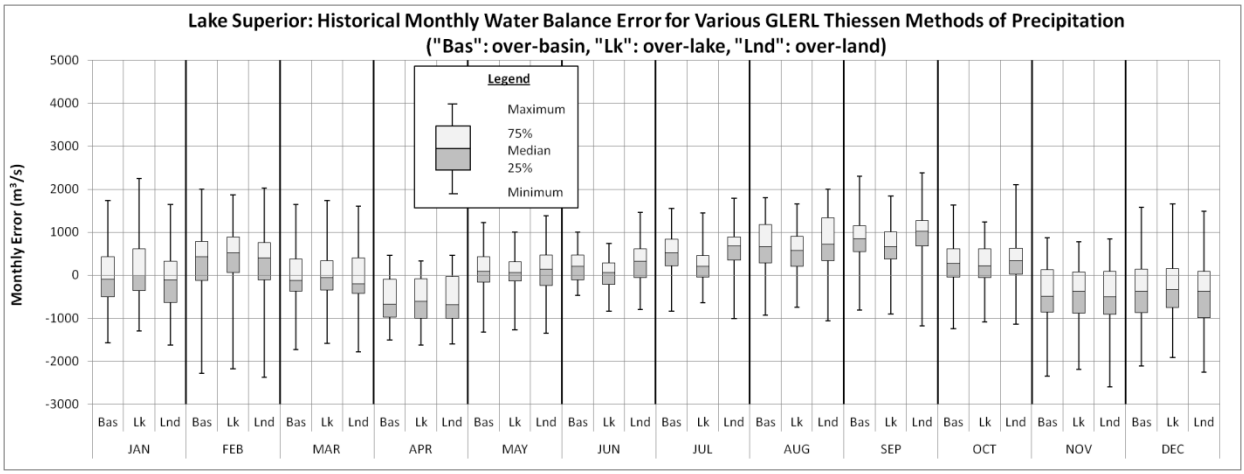

Figure 9 Comparison of GLERL Thiessen precipitation estimates within the framework of the Lake Superior water balance error

As mentioned above, the Thiessen over-basin method is typically used to estimate the over-lake precipitation component of the water balance. Figure 9 presents the side-by-side comparison of GLERL Thiessen Methods for over-basin, over-lake, and over-land precipitation in terms of their influence on the Lake Superior water balance error. In every month except for February, the median Lake Superior water balance error would be improved by using the Thiessen over-lake estimates instead of the over-basin estimates. The month of July is a clear example, where the Lake Superior median error would become 200 m^3/s instead of 500 m^3/s. This indicates that the assumption made by Croley and Lee 1993 appears to be incorrect. It is recommended that this type of comparison be made for each of the other lakes. The Coordinating Committee may wish to consider coordinating Thiessen over-lake precipitation estimates rather than Thiessen over-basin estimates. It is important to note that the Thiessen over-lake estimates are based on near-shore stations, and according to Holman et al. 2012, the seasonal differences between over-lake and over-land precipitation should be much greater than is calculated by the respective GLERL Thiessen methods.

DISCUSSION

The framework for computing the water balance error, presented in Equation 3, will be helpful for relating various sources of uncertainties to one another within the Great Lakes water balance. Comparisons using this basic conservation equation provide more readily apparent observations to a wide audience than the traditional comparisons between residual and component net basin supplies. From a preliminary analysis, which used only one method of estimation for each term of Equation 3, statistical properties were calculated for the monthly and annual water balance errors for each lake. One interesting observation is that the consistent error pattern across multiple lakes suggests that improving the historical precipitation estimates based on seasonal over-lake and over-land dynamics should be a high priority for moving toward "closing the water balance". On the other hand, these preliminary results seem to indicate that although the inclusion of thermal expansion and contraction could provide a more accurate estimate of lake storage, it would not resolve some of the largest magnitudes of water balance error and could even push them further away from zero. Going forward, a comparison using multiple estimation

methods for each term within this framework could provide further insight about individual modeling and estimation techniques.

REFERENCES

Changnon, S. A. (1961). Precipitation contrasts between the Chicago urban area and an offshore station in southern Lake Michigan. Bulletin of the American Meteorological Society, 42(1), 1-10.

Coordinating Committee on Great Lakes Basic Hydraulic and Hydrology Data (1977). Coordinated Great Lakes physical data. Detroit, Michigan and Burlington, Ontario, 12 p.

Croley II, T.E. and Lee, D.H. (1993). Evaluation of Great Lakes net basin supply forecasts. Water Resources Bulletin, 29(5), 267-282.

Deacu, D., Fortin, V., Klyszejko, E., Spence, C., and Blanken, P. D. (2012). Predicting the net basin supply to the Great Lakes with a hydrometeorological model. Journal of Hydrometeorology, 13(6), 1739-1759.

DeMarchi, C., Dai, Q., Mello, M. E., and Hunter, T. S. (2009). Estimation of overlake precipitation and basin runoff uncertainty. International Upper Great lakes Study.

Derecki, J. A. (1976). Hydrometeorology: Climate and hydrology of the Great Lakes. Great Lakes Basin Framework Study, Appendix, 4, 71-104.

Fry, L.M., Gronewold, A. D., Fortin, V., Buan, S., Clites, A. H., Luukkonen, C., Holtschlag, D., Diamond, L., Hunter, T., Seglenieks, F., Durnford, D., Dimitrijevic, M., Subich, C., Klyszejko, E., Kea, K., and Restrepo, P. (2014). The Great Lakes Runoff Intercomparison Project Phase 1: Lake Michigan (GRIP-M). Journal of Hydrology, in press.

Gronewold, A.D. and Fortin, V. (2012). Advancing Great Lakes hydrological science through targeted binational collaborative research. Bull. Amer. Meteor. Soc., 93, 1921–1925.

Holman, K. D., Gronewold, A., Notaro, M., & Zarrin, A. (2012). Improving historical precipitation estimates over the Lake Superior basin. Geophysical Research Letters, 39(3).

Kresge, R., Blust, F., and Ropes, G. (1964). A comparison of shore and lake precipitation observations for northern Lake Michigan. Int. Assoc. Sci. Hydrol, 5, 311.

Lee, D.H. (1992). Computation of net basin supplies – A comparison of two methods. International Joint Commission levels reference study, Final Report Subtask 19.1.2a.

Neff, B. P., and Nicholas, J. R. (2005). Uncertainty in the Great Lakes water balance. Date Posted: November 23, 2005: US Geological Survey Scientific Investigations Report 2004-5100, 42 p.

RIVER RESTORATION DECISION ANALYSIS - 2D HYDRODYNAMIC APPROACH TO PROJECT PRIORITIZATION

David J. Bandrowski, Trinity River Restoration Program, U.S. Bureau of Reclamation, Weaverville, CA, USA, dbandrowski@usbr.gov; Yong G. Lai, Technical Service Center, U.S. Bureau of Reclamation, Denver, CO, USA, ylai@usbr.gov; D. Nathan Bradley; Technical Service Center, U.S. Bureau of Reclamation, Denver, CO, USA, dnbradley@usbr.gov; Josh Murauskas, Anchor QEA LLC, Wenatchee, WA, USA; jmurauskas@anchorqea.com

Abstract: In the field of river restoration sciences there is a growing need for analytical modeling tools and quantitative processes to help identify and prioritize project sites. Two-dimensional (2D) hydraulic models have become more common in recent years and with the availability of robust data sets and computing technology, it is now possible to evaluate large river systems at the reach scale. The Trinity River Restoration Program (TRRP) – Bureau of Reclamation in Northern California is now analyzing a 40 mile segment of the Trinity River to determine priority and implementation sequencing for its Phase II channel rehabilitation projects. A comprehensive approach and quantitative tool has recently been developed to analyze this complex river system. The 2D-Hydrodynamic-Based Logic Modeling (2D-HBLM) tool utilizes various hydraulic output parameters combined with biological, ecological, and physical metrics at user-defined spatial scales and flow discharges to evaluate geomorphic characteristics, riverine processes, and habitat complexity. The habitat metrics are integrated into a comprehensive Logic Model framework to perform statistical analyses to assess project prioritization. The Logic Model will analyze various potential project sites within the 40 mile restoration reach by evaluating connectivity and key response variable drivers. The 2D-HBLM tool will help inform management and decision makers by using a quantitative process to optimize desired response variables with in determining the highest priority locations within the river corridor to implement restoration projects.

Keywords: 2D Hydraulic Modeling, Quantitative Prioritization, Evaluation Metrics, Logic Modeling, Statistical Analysis, and River Restoration

INTRODUCTION

Effective river restoration prioritization starts with well-crafted goals that identify the biological objectives, address underlying causes of habitat change, and recognize that social, economic, and land use issues may constrain restoration options (Beechie et. al. 2008). In addition, effective management actions need to be tied to a Structured Decision Making (SDM) process that connects decisions to objectives (Hammond et al. 1999, Clemen and Reilly 2001). Applying natural resources management actions to the SDM process, like restoration prioritization, is essential for successful project implementation (Conroy and Peterson, 2013; Evers, 2008). This paper describes a river restoration prioritization approach that integrates two-dimensional (2D) hydraulic modeling with desired response and limiting factor metrics into a statistical model framework. This river restoration tool, referred to as two-dimensional hydrodynamic-based logic modeling (2D-HBLM), will analyze and evaluate key biological, physical, and ecological desired responses in relation to various physical and social constraints that may limit restoration options. In this paper, we will demonstrate how this approach can be effectively applied to a large river restoration program to help prioritize projects systematically and objectively.

All too often restoration actions are site specific without considering and evaluating ecosystem scale processes, protection of existing high quality habitats, or an understanding of the effectiveness of specific restoration techniques (Roni et. all. 2002). With over two decades of scientific literature and applied practice, the restoration community has a thorough understanding of the role of channel morphology in the formation of physical habitats (Montgomery and Buffington 1998) and the relationship between flow depth and velocity and habitat quantity and quality (Singh 1989, Lamouroux 1998, Stewart et. al. 2005, Saraeva and Hardy 2009, Goodman et. al. 2014). The understanding of geomorphic processes and physical habitats have been integrated into models to assess hydraulic relationships quantitatively (Schweizer et. al. 2007, Dunbar et. al. 2012) and eco-hydraulic questions through prediction-based simulations (Bovee 1982, Gore et. al. 1998, Milhous et. al. 1989). Model utilization requires restoration science not only to embrace uncertainty (Darby and Sear 2008, Hillman et. al. 2008, Wheaton et. al. 2008), but to integrate bio-physical diversity, variability, and complexity into river management (Brierley and Fryirs 2008). Evaluating tradeoffs and examining alternatives to improve fish habitat through optimization modeling (Null and Lund, 2012) is not just a trend but rather the scientific strategy that management needs to embrace and apply in its decision framework.

The overall approach of this reach-based prioritization is to evaluate the river system through integration of 2D hydraulic modeling, quantitative metric evaluation, and statistical logic modeling within a broader adaptive management and SDM framework. The topics described below include: an overview of 2D hydraulic modeling, the application of the 2D model to the Trinity River, the development of the habitat module quantitative metrics, and the approach to the logic model framework.

OVERVIEW OF 2D HYDRAULIC MODELING

Stream flow modeling is one of the most widely used tools to understand how hydraulic conditions change between discharges and how they are related to fish habitat (Bovee, 1982; Milhous et al., 1989). Building on the early use of one-dimensional (1D) models, 2D hydrodynamic modeling has been widely used for evaluating hydraulic habitat data (e.g. water depth, water velocity, and substrate size). 2D models can be operated on a finer scale than 1D models and they can accurately predict hydraulics in near-shore habitat and across large-scale roughness features (Waddle et al., 2000). 2D models can more accurately predict water velocities and depths at local scales due to the ability to calculate both longitudinal and lateral velocity distributions (Crowder and Diplas, 2000). Sample applications of 2D hydrodynamic models for habitat evaluation include Tharme 2003), Wheaton et al. (2004), Stewart et al. (2005), Mingelbier et al. (2008), Yarnell et al. (2010), Waddle (2010), and Hatten et al. (2013).

In recent years, the trend has been to use a 2D model to represent the roughness elements at the individual boulder scale (e.g., Waddle, 2010), because riverine salmonid species are known to use flow obstructions as velocity shelters in order to minimize energy expenditure while foraging and resting (Bjornn and Reiser, 1991). Boulder placement and the use of large wood are techniques of river restoration commonly used to provide increased diversity of velocity patterns in generally uniform river channels. Accurate modeling of such areas can provide better information about the extent of habitat in rivers and tools for design of constructed habitats.

In this study, we use the U.S. Bureau of Reclamation's Sedimentation and River Hydraulics Two Dimensional depth averaged hydraulic model (SRH-2D). SRH-2D, documented by (Lai 2008; Lai 2010), has been widely used for evaluation of river projects. The robustness and accuracy of SRH-2D have been proven with a wide range of model verifications, as well as many project applications, at both Reclamation and external institutions. SRH-2D has a few unique features which make it ideal for river applications. First, SRH-2D uses a flexible mesh that adopts the arbitrarily shaped element method of Lai et al. (Lai, 2003) for geometric representation. In practice, a hybrid mesh normally uses quadrilaterals in the main stream and near structures and triangles in the floodplain and transition zones. The hybrid mesh achieves the best compromise between accuracy and computing efficiency and such a mesh is relatively easy to generate. Second, SRH-2D adopts very robust (stable) numerical schemes with a seamless wetting-drying algorithm. Reliable solutions may be obtained with the primary tuning parameter of Manning's n. Third, SRH-2D solves the 2D depth-averaged St. Venant dynamic-wave equations using an implicit solution scheme and unstructured meshes with arbitrary mesh cell shapes. It solves both steady and unsteady flows over all flow regimes (subcritical, supercritical or transcritical flows).

APPLICATION OF THE 2D MODEL ON THE TRINITY RIVER

The Trinity River is an ideal location for an applied scientific assessment of a reach based model due to the wealth of robust data sets that span large spatial and temporal scales. The Trinity has been monitored consistently for decades and has been surveyed at high resolution as required for two dimensional hydraulic modeling. A seamless Digital Terrain Model (DTM) that integrates terrestrial and bathymetric topography is the basis of the 40 mile hydraulic model. The DTM for the Trinity consists of airborne LiDAR topography and boat-based sonar bathymetry across the entire reach (Woolpert, 2013) that has been validated within 95% vertical confidence intervals using 0.320-foot RMSEz (Root Mean Square Error) for LiDAR and +/-0.686-foot RMSEz for sonar. This validated accuracy is based on extensive quality control field measurements consisting of 40 channel spanning cross-sections and 849 independent GPS-RTK check shots along the Trinity. The DTM has been certified by a professional licensed land surveyor and exceeds both National Map Accuracy and American Society of Photogrammetry and Remote Sensing (ASPRS) Standards.

In addition to topographic data sets, aerial imagery orthophotography has been collected in multiple years and serves as the foundation data set for geospatial mapping on many projects including the 2D hydraulic model mesh generation. Two model meshes were developed for this project: a coarse mesh to use for model calibration (the calibration mesh) and a denser mesh to use for the actual assessment (the habitat mesh). Both meshes are hybrid meshes that use rectangular elements in the main and side channels and triangular elements in areas that are dry at most flows. The calibration mesh contains one quarter the number of elements as the habitat mesh across the 40 mile reach on the Trinity River.

The calibration mesh was developed from channel bank lines digitized from the aerial imagery data set (Figure 1). The complexity and curvature of the channel dictated the length of elements in a reach. Long straight reaches contain longer elements, Tight bends and areas of complex morphology contain shorter elements.

The width of main channel mesh elements is 1/8 of the local channel width. Side channel

mesh elements are 1/3 of the local side channel width. Calibration mesh elements range from approximately 10 to 50 feet in length and 5 to 25 feet in width. The mean area of calibration mesh elements is 284 square feet.

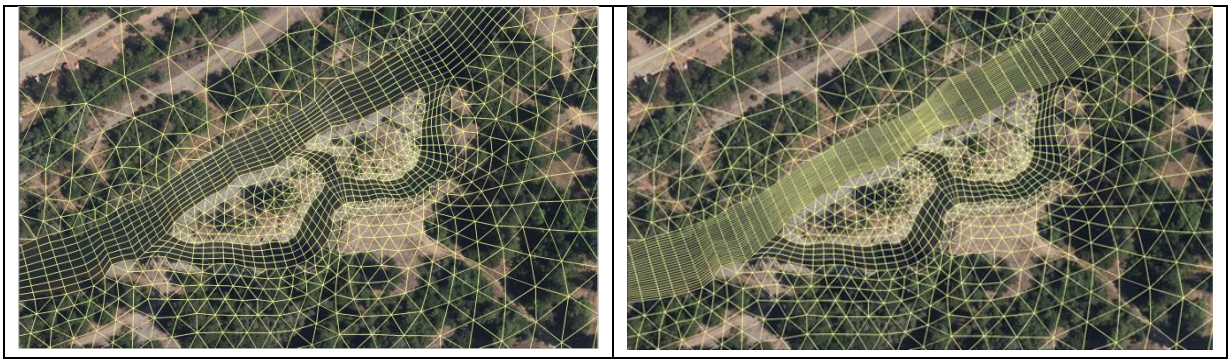

Figure 1 Comparison of the calibration mesh (left) and the habitat mesh (right)

The habitat mesh was developed by dividing each calibration mesh element into four elements. Channel elements in the habitat mesh range in width from approximately 1 foot to 10 feet. The mean area of habitat mesh channel elements is 71 square feet.

The sole calibration parameter available in SRH-2D is the channel roughness, represented by Manning's n. Increasing channel roughness by increasing the value of Manning's n has the effect of raising the water surface elevation and reducing the flow velocity. Decreasing channel roughness has the opposite effect. The calibration data we used are water surface elevations measured during the bathymetric survey at seven different discharges ranging from 500 cfs to 4500 cfs. About 91% of the model error (modelled elevation minus observed elevation) is within +/- 0.5 feet and the error is symmetrically distributed around zero. This error is similar to the error in the bathymetric data collection.

HABITAT MODULE QUANTITATIVE METRICS

The 2D hydraulic model was run for approximately 20 different discharge cases, ranging from 300 cfs to 14,000 cfs. The hydraulic output of the 2D model is used by a tool called the "Habitat Module to evaluate riverine characteristics using a series of biological, ecological, and physical criteria. The Habitat Module uses quantitative algorithms to calculate key hydraulic variables or "metrics" throughout the river. The metrics are grouped into three spatial output types: 1) Panel-Based "Panel"; 2) Cross-Sectional; and 3) Spatially Distributed - across the mesh elements. For this study, the Panel output was the primary type used. The Panels are 200 meter long and are based off a sampling protocol system currently being used on Trinity for system wide monitoring called Generalized Random Tessellation Stratification (GRTS). Across the entire 40 mile reach, there are 319 Panels from upstream to downstream. The Panel system was used to help organize the hydraulic output and metrics into a uniform system to which further statistical analyses can be applied.

The metrics calculated from the hydraulic model are categorized into three types: Biological, Ecological, and Physical. The other types of information used were field collected empirical data from the Trinity. Table 1 below shows all the available metrics calculated and empirical data that was field measured.

Table 1 Evaluation Metrics from SRH-2D Habitat Module

<table>
<tr><th colspan="3">Metrics calculated from the 2D Hydraulic Model (habitat module)</th><th>Empirical Data</th></tr>
<tr><th>Physical</th><th>Biological/Ecological</th><th>Ecological</th><th>Field Collected</th></tr>
<tr><td>Depth</td><td>Depth/Velocity (DV) -Fry Habitat</td><td rowspan="4">Suitable Area for Riparian Regeneration</td><td>Redd Locations</td></tr>
<tr><td>Velocity</td><td>Cover (C) -Fry Habitat</td><td rowspan="3">River Bed Topography Bed Elevation Data (Bathymetry)</td></tr>
<tr><td>Water Surface</td><td>Depth/Velocity -Pre Smolt Habitat</td></tr>
<tr><td>Wetted Edge Length</td><td>Cover -Pre Smolt Habitat</td><td rowspan="5">Elevation (Delta) Difference between Water Surface and Adjacent Topography</td></tr>
<tr><td>Shear Stress (avg, StD, etc.)</td><td rowspan="2">Depth/Velocity/Cover (DVC) for both Fry and Pre Smolt Habiat</td></tr>
<tr><td>Stream Power</td><td>Bedrock Features</td></tr>
<tr><td>Vorticity</td><td>Adult Holding Habitat</td><td>Tributaries</td></tr>
<tr><td>Flow Direction/Crossover</td><td rowspan="4">Weighted Usable Area (WUA) for Fry and Pre Smolt Habitat – Based on Above Habitat Suitability Criteria (HSC)</td><td>Land Ownership</td></tr>
<tr><td>Wetted Area/Wetted XS</td><td>Wetted Edge</td><td rowspan="3">Infrastructure: including roads, bridges, houses, etc</td></tr>
<tr><td>Sinousity and Thalwag</td><td>Wetted Area</td></tr>
<tr><td>Width/Depth Ratio</td><td></td></tr>
</table>

Physical Metrics: Restoration activities on the Trinity River include flow and sediment management intended to promote the dynamic fluvial processes that create diverse physical habitat and rejuvenate the aquatic ecosystem. The physical process metrics used in this study were developed to help quantify the existing geomorphic complexity within each Panel. The fluvial processes involved in the maintenance of high-quality habitat are tightly linked to sediment supply and sediment transport capacity. Scour and fill processes, in which the elevation of the steam bed or bar surface changes dynamically through time, create topographic complexity, maintain substrate quality, and rejuvenate riparian vegetation. Lateral erosion of the banks facilitates planform adjustment and contributes to the formation of alcoves, sloughs, and complex bar features. Although the habitat module cannot address questions about sediment supply, its output includes several metrics intended to assess the spatial variability of sediment transport capacity and geomporhic complexity within each Panel. Shear stress and stream power metrics within each Panel represents the rate of energy dissipation against the bed and banks of a river, which can be used as an indicator of local sediment transport capacity. Using the first derivative of the shear stress can provide an additional metric, which helps determine if the stress in the Panel is increasing or decreasing, providing an indication of where local scour or fill might be expected. The Vorticity metric calculates the angular velocity of a fluid particle and is a kinematic property of the flow field which as a measure of river complexity.

Additional physical metrics include: Flow Direction Change Hydraulic Cross-Over, Wetted Edge Length, Sinousity, Thalweg, etc. For example, Edge Length is the total length of wet-dry boundaries within a panel and reflects complexities of flows around islands, boulders, etc. Various physical metrics can be combined into one representative metric to compare and evaluate the system-wide geomorphic potential or its overall physical complexity at applicable flow discharges. Assessing these metrics in combination can be accomplished using a statistical approach called Principal Components Analysis (PCA). A PCA is used to model variation within a set of metrics to produce a smaller number of independent linear combinations (i.e., principal components; JMP ® 11, SAS Institute, Cary, North Carolina). The first principal component of variables related to geomorphic potential at 6,000 cfs—including velocity, average bed shear stress, average first derivative of shear stress, and stream power—was derived to show the most prominent direction of these metrics using a single variable.

Biological Metrics: A deficit of juvenile rearing habitat has been identified as the primary limiting factor of salmonid populations in the Trinity Rivr and many other rivers. Fry and Pre-smolt critical rearing habitat is computed from the hydraulic model output using Habitat Suitability Criteria (HSC) of derived Depth (D), Velocity (V), and Cover (C). These HSC values were developed for the Trinity River specific to the life stage and species (Goodman et al. 2014). The metric for rearing habitat is fry and Pre Smolt area is based on meeting the depth and velocity combinations (DV) and cover requirements determined by field validated HSC values. The cover criteria are based on field-derived values of suitable distance to vegetation, wood, or other escape cover. The HSC values serve as an index or value range to determine if the habitat is within suitable desirable criteria range for rearing habitat. (See Table 2 below)

Table 2 Trinity River binary habitat suitability criteria from Goodman et al. (2014)

Life stage	Depth	Velocity	Cover
Fry (< 50 mm fork length)	≤ 0.6 meter	≤ 0.15 meters/second	≤ 0.6 meters
Presmolt (50 to 100 mm fork length)	≤ 1.0 meter	≤ 0.24 meters/second	≤ 0.6 meters

The Weighted Useable Area (WUA) metric is a method of combining the scores from the above HSC data for depth, velocity, and cover to evaluate the quality of habitat at a range of values rather than using a binary approach of index cut-off values. WUA habitat values were the primary metric used for the evaluation of biological quality throughout the Trinity system.

APPROACH TO THE LOGIC MODEL FRAMEWORK

The objective of the Logic Model is to assimilate professional judgment, 2D modeling outputs, and empirical data to objectively prioritize restoration projects. Once the hydraulic variables and metrics are calculated within the habitat module and synthesized for each of the 319 Panels. The Logic Model is the component within the 2D-HBLM process that analyses the data statistically and links desired responses with limiting factors to prioritize areas of the river for restoration. Quantitative approaches have long been recognized as a key to improving processes (Box and Myer 1986). Modeling, hierarchical ordering of effects, and identifying key relationships and root causes for deficiency is commonplace in manufacturing (Harry and Schroeder 2006) and increasingly in biological sciences (Dassau et al. 2006; Huang et al. 2009). The Logic Model utilizes such approaches to assess key measures and relationships followed by integration of desired responses and limiting factors to inform prioritization.

Measures used in the Logic Model include physical, biological, and ecological based metrics, along with metrics from empirical data selected using professional judgment prior to analysis. Desired responses include improvements to the quality, connectivity, and complexity of salmonid habitat (Roni et al. 2002). Conversely, limiting factors constrain the ability to implement restoration projects (e.g., access or infrastructure). The distinction between desired responses and limiting factors is important in that the Logic Model is intended to prioritize restoration projects where the need, relative benefit, and practicality are optimized.

Data used in the Logic Model were examined prior to statistical modeling. Both desired responses and limiting factors were reduced to a set of uncorrelated variables using Principal Component Analysis (SAS Institute 2008). This step minimizes the issue of multi-collinearity

in further analyses, particularly with predictor variables (Saab 1999). Desired responses and limiting factors were further analyzed for spatial autocorrelation since standard statistical techniques assume independence among observations. For example, preliminary evaluations show that suitable fry habitat has a partial autocorrelation with at least the two preceding panels at 4500 cfs. Quantitative approaches used in the Logic Model compensate for the relationships among neighboring panels to ensure that parameter estimates and significance tests yield reliable results (Isaak et al. 2010).

Five metrics were ultimately chosen to be used in the Logic Model analysis to represent biological quality, connectivity, and river complexity, see Table 3 below. Biological quality was defined as the habitat calculated from the weighted usable area (WUA) at winter base flow (300cfs) and at a typical spring flow (1500cfs). Connectivity was defined by the total number of redds observed within each panel and three upstream panels (i.e., a running total of four panels). Complexity was defined by the standard deviation of bed elevation and the standard deviation of stream power at 8,500 cfs. Each panel was ranked relative to the remaining panels (1 to 319) for all five metrics, with ascending ranks for habitat quality and complexity and descending ranks for connectivity (redds). Thus, panels with low WUA values, low variation in complexity, and proximity to a large number of redds would receive lower rankings across the five metrics.

Table 3 Weighting of Metrics Used in the Logic Model in Panel Scoring

Metric	Category	Weight	Relative influence
Rearing Habitat at 300 cfs rank	Habitat Quality (Low Flow)	1.50	0.333
Rearing Habitat at 1,500 cfs rank	Habitat Quality (Mid Flow)	1.00	0.222
Total spawning redds (upstream 3 Panels) rank	Biological Connectivity	1.00	0.222
Standard Deviation of bed elevation (m) rank	Topographic Complexity	0.50	0.111
Standard Deviation of unit stream power (8,500 cfs) rank	Hydraulic Complexity	0.50	0.111

Panels were scored by summing the total ranks across the five metrics, with each metric weighted according to values shown in Table 3. For example, habitat rank at 300 cfs with median accretion has a weighting of 1.50 (33.3% influence), whereas the standard deviation of bed elevation has a weighting of 0.50 (11.1% influence). Each increase in habitat rank and standard deviation of bed elevation rank, therefore, represents a corresponding increase of 1.50 and 0.50 in the total score, respectively. Scores were then scaled relative to the least desirable candidate for a restoration action (i.e., highest score). Scores for each panel, therefore, represent existing habitat quality with the influence of connectivity to spawning habitat and measures of river channel complexity.

Scores across multiple panels were then analyzed to identify segments of the river most suitable for restoration action. First, a cluster analysis (performed by USFWS) was used to identify regions of similar scores that were spatially grouped based on statistical principles from Aldstadt and Getis (2006) and Ord and Getis (1995). The cluster analysis provides a mechanism to evaluate areas desirable for restoration irrespective of arbitrary ESL boundaries. A total of 150 spatially-related clusters of similar scores were identified. The top ten clusters of ascending desirability for restoration action are shown in Table 4 and in Figure 3 below. In addition, these results eliminate any clusters that have less than three adjacent Panels to remove any locations that contain areas that is not practical for restoration actions.

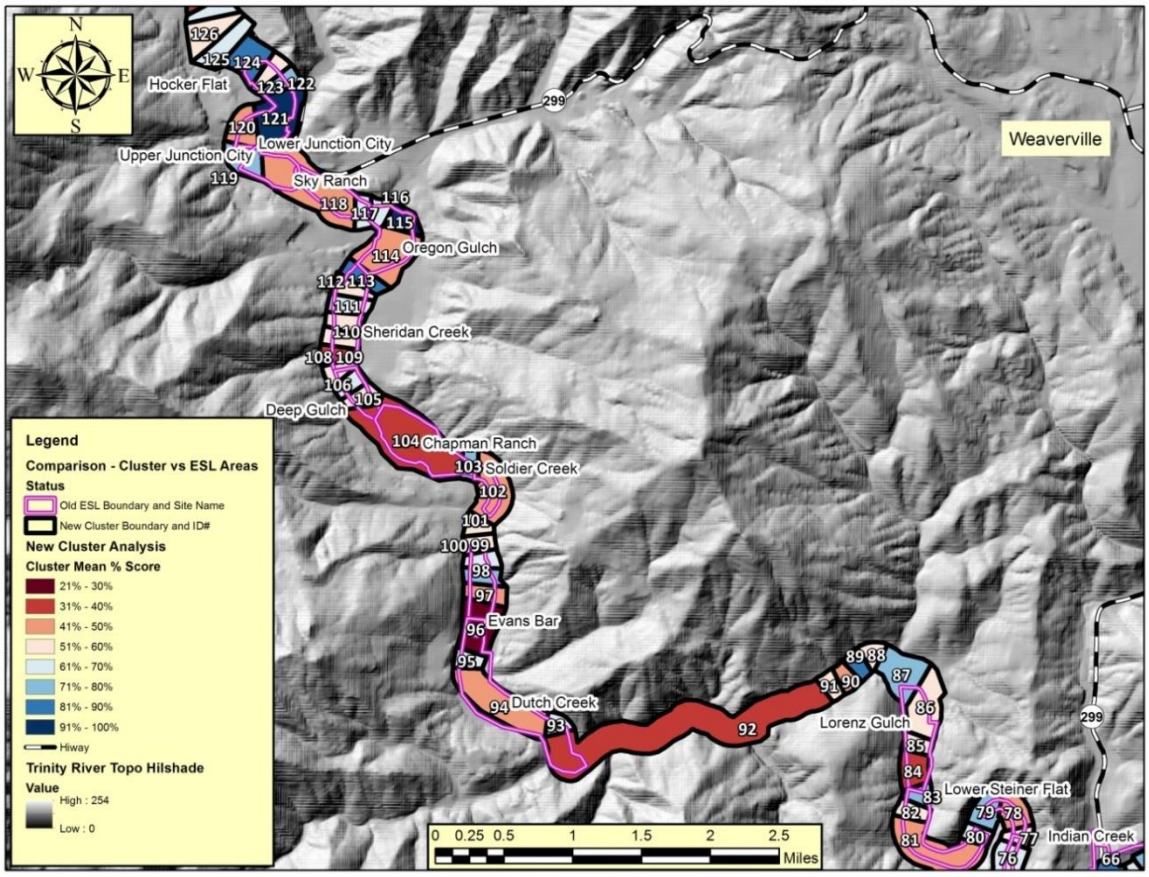

Note: The deeper the color is red the more desirable that location is for restoration; deeper the color is blue the less desirable that location is for restoration. Numbers represent cluster ID that is referenced in the tables below

Figure 2 Map of the new cluster analysis results compared with the old ESL boundaries.

Table 4 Trinity River ESL Segments Ranked by Ascending Desirability for Restoration

Geographic Location	**Evaluation Metric**					**Mean Panel Ranking**	**Additional Considerations for Ranking**				
ESL Name	Rearing Habitat (300cfs)	Rearing Habitat (1500 cfs)	Total Redds (Uprera 3 panels)	SD of Bed Elevation (m)	SD of Unit Stream Power (8,500 cfs)	**Mean Score**	Percent Public Ownership	Adjacent Road Length	Bedrock Area	Topographic Constraint	Geomorphic Potential
Chapman Ranch	85	77	154	69	125	**38.3%**	71%	2,570	0	4.52	-0.46
Below Lorenz (the canyon)	70	59	121	241	217	**43.2%**	58%	2,675	1,084	15.74	1.96
Dutch Creek	103	135	97	149	124	**44.0%**	72%	723	181	7.57	-0.38
Pear Tree Gulch	86	64	173	215	108	**44.2%**	100%	1,354	166	11.95	0.29
Soldier Creek	115	88	150	171	121	**47.0%**	87%	1,151	0	12.39	0.05
Indian Creek (Vitzthum Gulch)	111	115	182	196	103	**51.6%**	64%	2,201	0	7.87	-1.54
Sky Ranch	134	132	97	168	211	**52.2%**	55%	4,464	45	6.34	0.83
Tom Lang Gulch	124	104	176	138	188	**52.9%**	14%	4,426	0	14.59	-0.44
Oregon Gulch	179	177	105	96	114	**55.2%**	60%	3,182	0	3.80	-0.45

Table 4 above, also shows the mean Panel ranking for the five Logic Model metrics along with mean feasibility metrics shown for evaluation. Colors are shaded from red (low scores) to green (high scores) according to ranking scheme described in the approach.

In addition, mean scores were provided across project boundaries (ESLs) to provide context in how river segments used in past evaluations rank under this approach. Metrics judged to be important for assessing project feasibility were calculated based on both clusters and ESLs. These included percent public ownership, road length, bedrock area, topography, and geomorphic potential (the first principal component of velocity, average bed shear stress, average first derivative of shear stress, and stream power at 6,000 cfs). An example of mean feasibility metrics for the identified clusters is shown in Table 5. These metrics are intended to provide additional detail for management's consideration when making final decisions for selecting and prioritizing restoration sites.

Table 5 Top Ten Panel Clusters Ranked by Ascending Desirability for Restoration

Cluster ID	Number of Panels Included	Mean Score	Associated Upstream Project Area (ESL)
96	3	28.7%	Dutch Creek
92	19	35.2%	Below Lorenz (the canyon)
104	7	35.6%	Chapman Ranch
150	7	38.6%	Pear Tree Gulch
60	5	40.2%	Indian Creek (Vitzthum Gulch)
102	4	40.5%	Soldier Creek
114	3	41.3%	Oregon Gulch
94	6	42.7%	Dutch Creek
118	7	45.4%	Sky Ranch
31	4	46.8%	Tom Lang Gulch
Note: See Figure 2 Below for Geographical Representation of the information in this Table			

Table 6 Example of Mean Feasibility Metrics Associated with Clusters

Cluster ID	Associated upstream ESL	Percent Public Ownership	Road Length (ft)	Bedrock Area (ft^3)	Topography ($ft^3 \times 10^6$)	Geomorphic potential (PCA)
96	Dutch Creek	52%	3,719	0	4.6	-0.38
92	Below Lorenz (the canyon)	52%	2,871	1,332	15.8	1.30
104	Chapman Ranch	68%	2,335	0	5.8	-0.52
150	Pear Tree Gulch	100%	2,008	225	12.8	-0.26
60	Indian Creek (Vitzthum Gulch)	89%	1,746	0	7.9	-1.59
102	Soldier Creek	93%	1,052	0	13.3	0.18
114	Oregon Gulch	54%	2,232	0	3.8	-1.43
94	Dutch Creek	77%	-	11	6.3	-0.63
118	Sky Ranch	56%	4,864	153	6.3	0.71
31	Tom Lang Gulch	6%	5,326	0	14.5	-0.70

SUMMARY

The 2D-HBLM process of combining 2D hydraulic modeling output with evaluation metrics and statistical tools is helping bridge new gaps and provide more ways to inform river restoration practitioners and managers. Adaptive Management Processes and Decision Support Systems are often difficult to apply and don't provide the resolution needed for detailed management decisions. 2D-HBLM helps integrate the latest trends in river science and Structured Decision Making processes, allowing for a decision framework that is repeatable, transparent, and quantitative.

Of course, all models have their limitations and therefore the integration between model output and professional judgment is necessary to help validate and ground truth output results. On the Trinity, the entire 2D-HBLM process incorporated many partner organizations and agencies that helped foster a collaborative multi-disciplinary effort. The output results from the cluster analysis were informally validated by technical experts from various disciplines including: fishery biology, geomorphology, and hydraulic engineering with expert knowledge of the Trinity River system. The cluster analysis results matched closely with professional judgment and gave the technical team confidence in making final recommendations to management.

The results from the 2D-HBLM framework were applied to the Trinity River by re-defining the prioritization for channel rehabilitation project sites designs that were being scheduled for the 2015 calendar year. The final 2D-HBLM cluster analysis results were refined based on professional judgment from internal team members. The team members took into account other factors like constructability, site access logistics, as well as, relationship factors such as site interdependence and geographic affiliation. Contiguous projects could help increase design efficiency and create synergy among projects and design teams. Therefore out of the recommended clusters, the Trinity River Restoration Program – Design Team recommended to management to select clusters: 104 through 114 (Chapman Ranch through Oregon Gulch) and the top ranking cluster - 96 (Dutch Creek/Upper Evans Bar). Management agreed to adopt the technical recommendation and therefore the project sites are currently in the design process. This new approach to project prioritization was implemented successfully through the diverse stakeholder partnership of the TRRP and has provided improved technical transparency and decision making defensibility.

REFERENCES

Aldstadt, J., & Getis, A. (2006). Using AMOEBA to create a spatial weights matrix and identify spatial clusters. Geographical Analysis, 38(4), 327-343.

Beechie, T., et al. (2008). Setting river restoration priorities: a review of approaches and a general protocol for identifying and prioritizing actions. North American Journal of Fisheries Management 28.3: 891-905.

Bjornn, T.C. and Reiser, D.W. (1991). Habitat requirement of salmonids in streams. The American Fisheries Society Special Publication 19: 38-138. ISBN: 0913235687.

Bovee, K.D. (1982). A Guide to Stream Habitat Analysis using the Instream Flow Incremental Methodology. Instream Flow Information Paper No.12,Biological Report 86(7). U. S. Fish and Wildlife Service: Fort Collins, Colorado.

Box, G. E., Meyer, R. D., (1986). An analysis for unreplicated fractional factorials. Technometrics, 28(1), 11-18.

Brierley, Gary J., and Kirstie A. Fryirs (2008). Geomorphology and river management: applications of the river styles framework. John Wiley & Sons

Clemen, R. T., and T. Reilly. (2001). Making Hard Decisions with Decision Tools (Duxberry).

Conroy, M. J., & Peterson, J. T. (2013). Decision making in natural resource management: a structured, adaptive approach. John Wiley & Sons.

Crowder DW, Diplas P. (2000). Using two-dimensional hydrodynamic models at scales of ecological importance. Journal of Hydrology 230(3–4): 172–191.

Darby, Stephen, and David Sear, eds. (2008). River restoration: managing the uncertainty in restoring physical habitat. John Wiley & Sons, Dassau, E., Zadok, I., Lewin, D. R., (2006). Combining six-sigma with integrated design and control for yield enhancement in bioprocessing. Industrial & engineering chemistry research, 45(25), 8299-8309.

Dassau, E., Zadok, I., & Lewin, D. R. (2006). Combining six-sigma with integrated design and control for yield enhancement in bioprocessing. Industrial & engineering chemistry research, 45(25), 8299-8309.

Dunbar, M. J., Alfredsen, K. and Harby, A. (2012), Hydraulic-habitat modeling for setting environmental river flow needs for salmonids. Fisheries Management and Ecology, 19: 500–517. doi: 10.1111/j.1365-2400.2011.00825.

Evers, Mariele. (2008): An analysis of the requirements for DSS on integrated river basin management. Management of Environmental Quality: An International Journal 19.1 37-53.

Goodman, D. H., Som, N. A., Alvarez, J. and Martin, A. (2014): A mapping technique to evaluate age-0 salmon habitat response from restoration. Restoration Ecology. doi: 10.1111/rec.12148

Gore, James A., Dina J. Crawford, and David S. Addison. (1998). "An analysis of artificial riffles and enhancement of benthic community diversity by physical habitat simulation (PHABSIM) and direct observation." Regulated Rivers: Research & Management 14; 69-77.

Hammond, J. S., R. L. Keeney, and H. Raiffa. (1999). Smart choices: a practical guide to making better life decisions. Broadway Books, New York.

Harry, M. J., Schroeder, R., (2006). Six Sigma: The breakthrough management strategy revolutionizing the world's top corporations. Random House Digital, Inc.

Hatten, J.R., Batt, T.R., Scoppettone, G.G., and Dixon, C.J., (2013). An Ecohydraulic Model to Identify and Monitor Moapa Dace Habitat. PLoS ONE 8(2): e55551. doi:10.1371/journal.pone.0055551.

Harry, M. J., Schroeder, R., (2006). Six Sigma: The breakthrough management strategy revolutionizing the world's top corporations. Random House Digital, Inc.

Hermans, Caroline, et al., (2007). Collaborative environmental planning in river management: An application of multicriteria decision analysis in the White River Watershed in Vermont. Journal of Environmental Management 84.4 534-546.

Huang, J., Kaul, G., Cai, C., Chatlapalli, R., Hernandez-Abad, P., Ghosh, K., Nagi, A. (2009). Quality by design case study: an integrated multivariate approach to drug product and process development. International journal of pharmaceutics, 382(1), 23-32.

Huang, Ivy B., Jeffrey Keisler, and Igor Linkov., (2011) Multi-criteria decision analysis in environmental sciences: ten years of applications and trends. Science of the total environment 409.19: 3578-3594.

Hillman, Mick, and Gary J. Brierley. (2008). Restoring uncertainty: translating science into management practice." River futures: an integrative scientific approach to river repair, Island Press, Washington DC: 257-272.

Isaak, D.J., Luce, C.H., Rieman, B.E., Nagel, D.E., Peterson, E.E., Horan, D.L., Parkes, S., Chandler, G.L. (2010). Effects of climate change and wildfire on stream temperatures and salmonid thermal habitat in a mountain river network. Ecological Applications 20, 1350–1371. doi:10.1890/09-0822.1

Lai, Y.G., Weber, L.J., and Patel, V.C. (2003). "Non-hydrostatic three-dimensional method for hydraulic flow simulation - Part I: formulation and verification." J. Hydraulic Engineering, 129(3), 196-205.

Lai, Y.G. (2008). SRH-2D version 2: Theory and User's Manual, Technical Service Center, Bureau of Reclamation, Denver, CO 80225.

Lai, Y.G. (2010). Two-Dimensional Depth-Averaged Flow Modeling with an Unstructured Hybrid Mesh. J. Hydraulic Engineering, ASCE, 136(1), 12-23.

Lamouroux, Nicolas. (1998): Depth probability distributions in stream reaches. Journal of Hydraulic Engineering 124.2 224-227.

Montgomery, David R., and John M. Buffington. (1998): Channel processes, classification, and response. River ecology and management 112 1250-1263.

Milhous, R.T., Updike, M.A., and Schneider, D.M. (1989). Physical habitat simulation system reference manual – Version II. U.S. Fish and Wildlife Service Biological Report 89(16): 403.

Mingelbier, M., Brodur, P., and Morin, J. (2008). Spatially explicit model predicting the spawning habitat and early stage mortality of Northern pike in a large system: the St. Lawrence River between 1960 and 2000. Hydrobiologia 601: 55-569. DOI: 10.1007/s10750.007-9266-z

Null, Sarah E., and J. R. Lund. (2012). Fish habitat optimization to prioritize river restoration decisions." River Research and Applications 28.9 1378-1393.

Ord, J. K., & Getis, A. (1995). Local spatial autocorrelation statistics: distributional issues and an application. Geographical analysis, 27(4), 286-306.

Raleigh, R., Zuckerman, L.D., and Nelson, P.C. (1986). Habitat suitabilily index models and instream flow suitability curves: Brown trout. revised. U.S. Fish and Wildlife Service Biological Report 82(10.124): 65.

Roni, P., Beechie, T. J., Bilby, R. E., Leonetti, F. E., Pollock, M. M., Pess, G. R., (2002). A review of stream restoration techniques and a hierarchical strategy for prioritizing restoration in Pacific Northwest watersheds. North American Journal of Fisheries Management, 22(1), 1-20.

Saab, V., (1999). Importance of spatial scale to habitat use by breeding birds in riparian forests: a hierarchical analysis. Ecological Applications 9, 135–151

Saraeva, Ekaterina, and Thomas B. Hardy. (2009): Prediction of fisheries physical habitat values based on hydraulic geometry and frequency distributions of depth and velocity. International Journal of River Basin Management 7.1 31-41.

SAS Institute., (2008). Jmp Release 8 Statistics and Graphics Guide. SAS Institute.

Sear, David, et al. (2009). A method for applying fluvial geomorphology in support of catchment-scale river restoration planning. Aquatic conservation: Marine and freshwater ecosystems 19.5: 506-519.

Stewart, G., Anderson, R., and Wohl, E. (2005). Two-dimensional modeling of habitat suitability as a function of discharge in two Colorado Rivers. River Research and Applications 21: 1061-1074, DOI: 10.1002/RRA.868.

Schweizer, Steffen, et al. (2007). Predicting joint frequency distributions of depth and velocity for instream habitat assessment. River Research and Applications 23.3: 287-302.

Singh, Krishan P., and Sally McConkey Broeren. (1989). Hydraulic geometry of streams and stream habitat assessment. Journal of Water Resources Planning and Management 115.5: 583-597.

Tharme, R.E. (2003). A global perspective on environmental flow assessment: emerging trends in the development and application of environmental flow methodologies for rivers. River Research and Applications 19: 397-441. DOI: 10.1002/RRA.736.

Waddle T, Steffler P, Ghanem A, Katopodis C, Locke A. (2000). Comparison of one- and two-dimensional open channel flowmodels for a small habitat stream. Rivers 7: 205–220.

Waddle T. (2010). Field evaluation of a two-dimensional hydrodynamic model near boulders for habitat calculation. River Research and Applications 26:730-741. DOI: 10.1002/rra.1278

Wheaton, J.M., Pasternack, G.B., and Merz, J.E. (2004). User of habitat heterogeneity in salmonid spawning habitat rehabilitation design. Proceedings Fifth International Symposium on Ecohydraulics, Madrid; 792-796.

Wheaton, Joseph M., Stephen E. Darby, and David A. Sear. (2008). The scope of uncertainties in river restoration. River Restoration: Managing the Uncertainty in Restoring Physical Habitat, edited by SA Darby, and DA Sear: 21-39.

Woolpert Inc. (2013) Trinity River bathymetry, airborne laser data and photogrammetric DTM site specific update. Report to U.S. Bureau of Reclamation, Trinity River Restoration Program by Woolpert Inc, Englewood, CO.

Yarnell, Y.M., Lind, A.J., and Mount, J.F. (2010). Dynamic flow modeling of riverine amphibian habitat with application to regulated flow management, River Research and Applications, DOI: 10.1002/rra.1447.

TAPER - A REAL-TIME DECISION SUPPORT TOOL FOR BALANCED FLOOD OPERATION OF THE ARKANSAS RIVER IN TULSA DISTRICT

Jennifer Steffen, Hydraulic Engineer, USACE, Tulsa, OK, Jennifer.Steffen@usace.army.mil; Jody Stringer, Hydraulic Engineer, USACE, Tulsa, OK, Jody.Stringer@usace.army.mil; John Daylor, Hydraulic Engineer, Tulsa, OK, John.Daylor@usace.army.mil; David Neumann, University of Colorado Center for Advanced Decision Support for Water and Environmental Systems, david.neumann@Colorado.edu; and Edith Zagona University of Colorado Center for Advanced Decision Support for Water and Environmental Systems, Edith.Zagona@Colorado.edu

Abstract: The U.S. Corps of Engineers Tulsa district is responsible for water management of the Arkansas River as it flows through Kansas and Oklahoma including the operation of numerous flood storage reservoirs and five navigation locks. The goal is to minimize flooding throughout the network with the key regulation control location at Van Buren, Arkansas. Upstream of Van Buren are 13 major flood storage reservoirs (7.6 million acre-feet) with 7,200 sq miles of uncontrolled local runoff that are managed to minimize flooding. The system flood evacuation plan calls for releases that evacuate the flood storage as quickly as possible without causing flooding, while still balancing the system storage and tapering down the flow at Van Buren.

During flood operations, Corp staff use a real-time decision support system named TAPER, implemented in RiverWare, which simulates the river and reservoir network, including all of the reservoir operations. The RiverWare model imports observed and forecasted inflows and local runoff and then uses rulebased simulation to model mandatory surcharge releases, allowable flow at various control locations, and the releases to meet the allowable flow in a balanced manner. The regulation discharge at Van Buren is computed based on a seasonally varying guide curves representing the equivalent percent of basin storage utilized. This algorithm allows higher flows during flooding seasons and when the system is full to recover the flood storage space in the upstream projects. The targets also include a smooth tapered recession to bring the system down to normal operations while allowing for scouring and dredging for navigation.

Given this regulation discharge, the RiverWare model computes a set of proposed release to balance the relative reservoir storages while not exceeding the downstream flow targets. Routing is modeled using the step response routing algorithm. Water managers collectively review the proposed releases and river flows and modify releases based on event specific conditions. RiverWare System Control Tables, plots, and output tools provide a friendly user interface focusing on the key variables in the system. As water managers modify releases, the model is re-run to compute downstream flows and reservoir levels. This process repeats until the managers are satisfied. The final release schedule and other reports are sent to dam operators, other federal agencies, local water managers, power authorities and other interested stakeholders.

RiverWare is a river and reservoir modeling tool developed by the University of Colorado Center for Advanced Decision Support for Water and Environmental Systems (CADSWES) with sponsorship of the Tennessee Valley Authority, the Bureau of Reclamation and the U.S. Army Corp of Engineers.

INTRODUCTION

The Arkansas River originates in central Colorado and flows through Kansas, Oklahoma, and Arkansas to its confluence with the Mississippi River. The U.S. Army Corps of Engineers (USACE) Tulsa District is responsible for water management of the river through Kansas and Oklahoma (Figure 1). During flood events, the system is operated to reduce downstream flooding and then evacuate the flood pool storage as quickly as possible in a balanced manner while still meeting navigation objectives. The Tulsa District has developed a RiverWare operations model called TAPER which helps the District perform this operation on a day-to-day basis as needed. This paper describes the basin and its operations during these flood pool evacuation operations and presents information on the TAPER model.

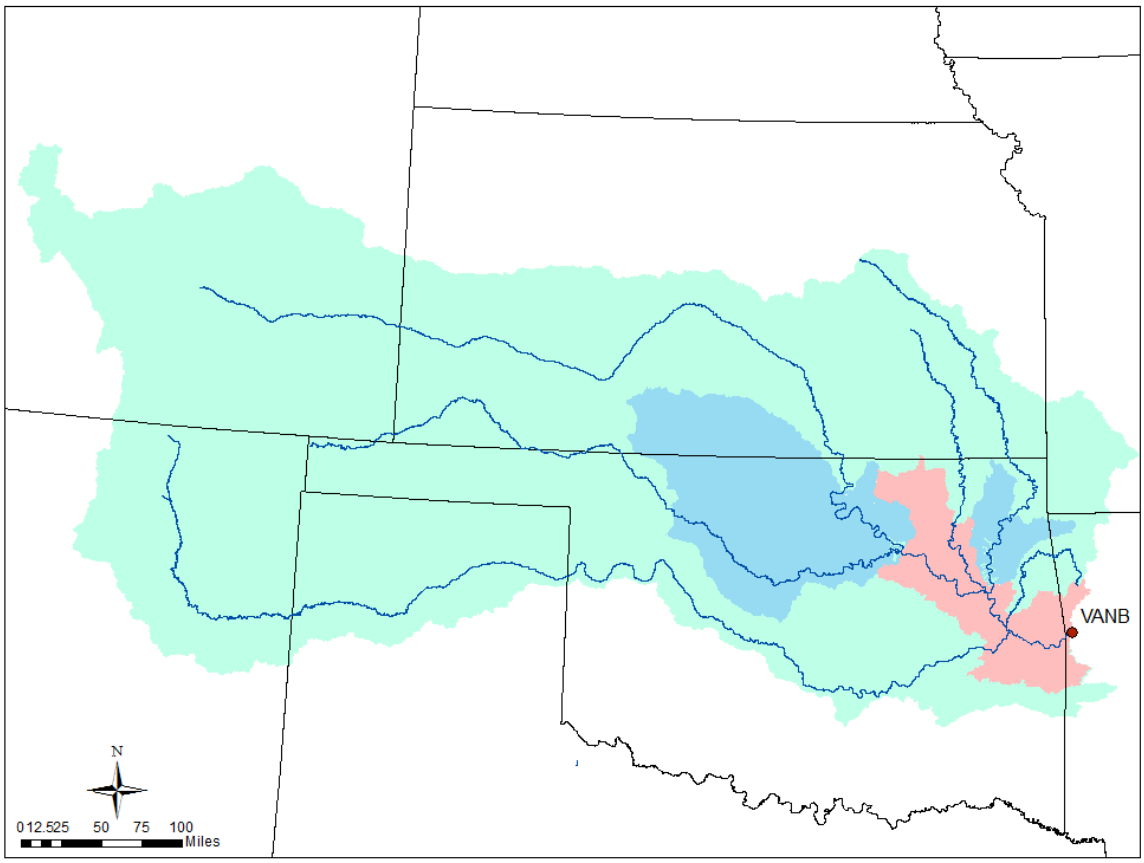

Figure 1 Drainage area (green) for the Arkansas River to Van Buren including locals (above reservoirs (blue), uncontrolled (pink)).

Basin Background: Thirty flood storage reservoirs exist on the Arkansas River and tributary system in Kansas and Oklahoma, including five navigation lock and dams. These reservoirs contribute to a common downstream control point for system regulation at Van Buren, Arkansas (VANB). Thirteen of these reservoirs (Copan, Hulah, Oologah, Birch, Skiatook, Kaw, Keystone, Pensacola, Hudson, Fort Gibson, Tenkiller, Eufaula, and Wister) are all in close proximity to VANB.

The Tulsa District manages the Arkansas River to VANB near Van Buren, Arkansas, and water management policies are specified in the Arkansas River Basin: Water Control Master Manual (USACE Tulsa and Little Rock District). The Arkansas River is managed to keep flows below regulation stage, evacuate flood storage in a timely manner, meet navigation needs, slowly taper flows down to allow for scouring, dredging of navigation channels, and provide for miscellaneous stakeholders needs. When upstream reservoirs are in the flood pools, the Corps is responsible for evacuating this pool. The combined flood pool storage of these lakes is 7.6 million acre-ft and the releases from all 13 reservoirs must be managed along with 7,200 sq miles of uncontrolled local runoff (Figure 2), to meet these multiple objectives, with a max regulation discharge of 150,000 cfs. Based on the percent of flood storage utilized, each reservoir is given an allocation and priority that guides in its releases to meet the flow hydrograph at VANB.

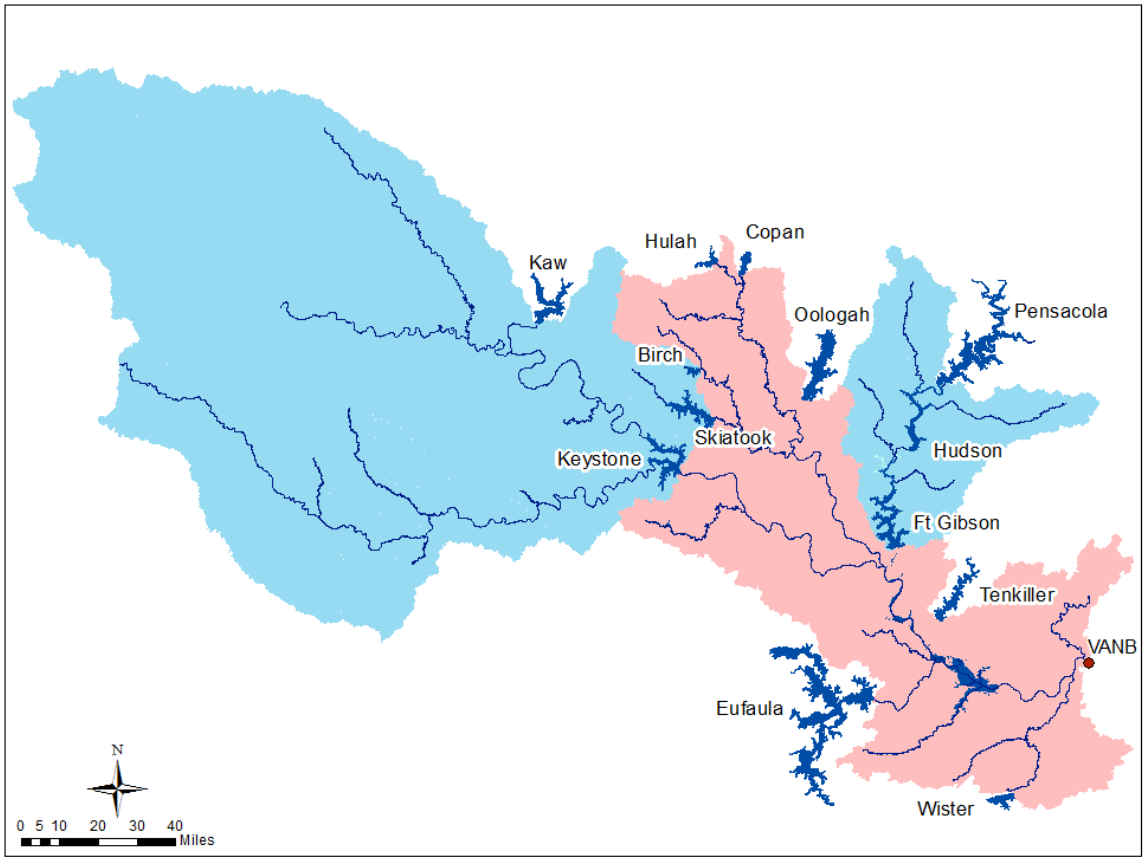

Figure 2 Thirteen reservoirs along Arkansas River and local areas (uncontrolled (pink), above reservoirs (blue))

Taper Operations: Tulsa District uses a procedure called TAPER to balance releases through the Arkansas River to Van Buren. The goal of TAPER is to determine releases using the system flood storage evacuation plan, which correlates system percent full with target flow. The target flow allowed at Van Buren consists of a series of stepped down benches set by a guide curve, which is based on the equivalent percent of basin storage utilized. The benches vary seasonally based on historical flood patterns. Flood water is released quicker during flooding seasons to

increase available flood storage in the upstream projects, and includes a tapered recession for navigation to allow for scour and dredging. A typical evacuation operation period is twenty-one days. To assist with the TAPER operations, Tulsa district uses simulation models to represent the system. The original TAPER program was a daily timestep model, with daily average releases and flows. This caused issues with high and low flow fluctuations in the navigation system. These fluctuations contribute to bank caving and shoaling issues in the system. In order to reduce fluctuations with the old TAPER program the gate changes are entered into a HEC-1 forecast model to route the flows through the Arkansas River. Then gate changes are manipulated to try and reduce fluctuations. This method of operating the system was very time consuming, and was not efficient. A new model was needed with 6-hr timesteps, better routing, and the ability to make a better initial suggestion at the release schedule. RiverWare was selected as the modeling tool in which to implement a new version of TAPER.

The RiverWare TAPER model is a real-time flood management model that imports forecast inflows and local runoff from forecast models. It then uses rulebased simulation to model water management strategies used by the USACE Southwest Division. These rules balance the system by allowing reservoirs to set releases based on priority curves and reservoir fullness, but also by allowing for a smooth flow transitions through reaches, and to not allow rivers to rise above flood stage. RiverWare TAPER produces a set of proposed releases for all reservoirs in the system. Water managers collectively look over proposed releases and modify based on event specific conditions. The final release schedule is sent to stakeholders who have an interest in the reservoirs and river system.

RIVERWARE TAPER MODEL

RiverWare is a river and reservoir modeling tool developed by the University of Colorado Center for Advanced Decision Support for Water and Environmental Systems (CADSWES) with sponsorship of the Tennessee Valley Authority, the Bureau of Reclamation and the U.S. Army Corp of Engineers. RiverWare models operations of the reservoirs and routes releases through routing reaches (CADSWES, 2014). The models consist of reservoirs, control points, confluence objects, routing reaches, and data objects (Figure 3).

Initial Conditions and Inflow Forecasts: To provide an effective evaluation of the river, 30 days of observed pre-simulation release and local inflows are provided to accurately prime the system. For the simulation period, initial elevations, reservoir inflows, and local uncontrolled runoff come from HEC-1 forecast models. HEC-1 is a rainfall runoff model developed by HEC (USACE Hydrologic Engineering Center, 1998). Forecast models are developed for each of the reservoirs and for the local areas. During flood operations, forecast models are calibrated for the specific storm events, using initial and constant loss, Snyder unit hydrograph, and baseflow recession. The corresponding reservoir inflows and local runoffs are imported into RiverWare using RiverWare's Data Management Interface (DMI) tool.

Rules: TAPER uses rules to determine releases that evacuate the flood pool in an efficient manner while not causing flooding downstream and limiting downstream flow for system benches. The goals of the rules are to keep flows at Van Buren below regulation levels determined using system evacuation guide curves, keep all control points below regulation

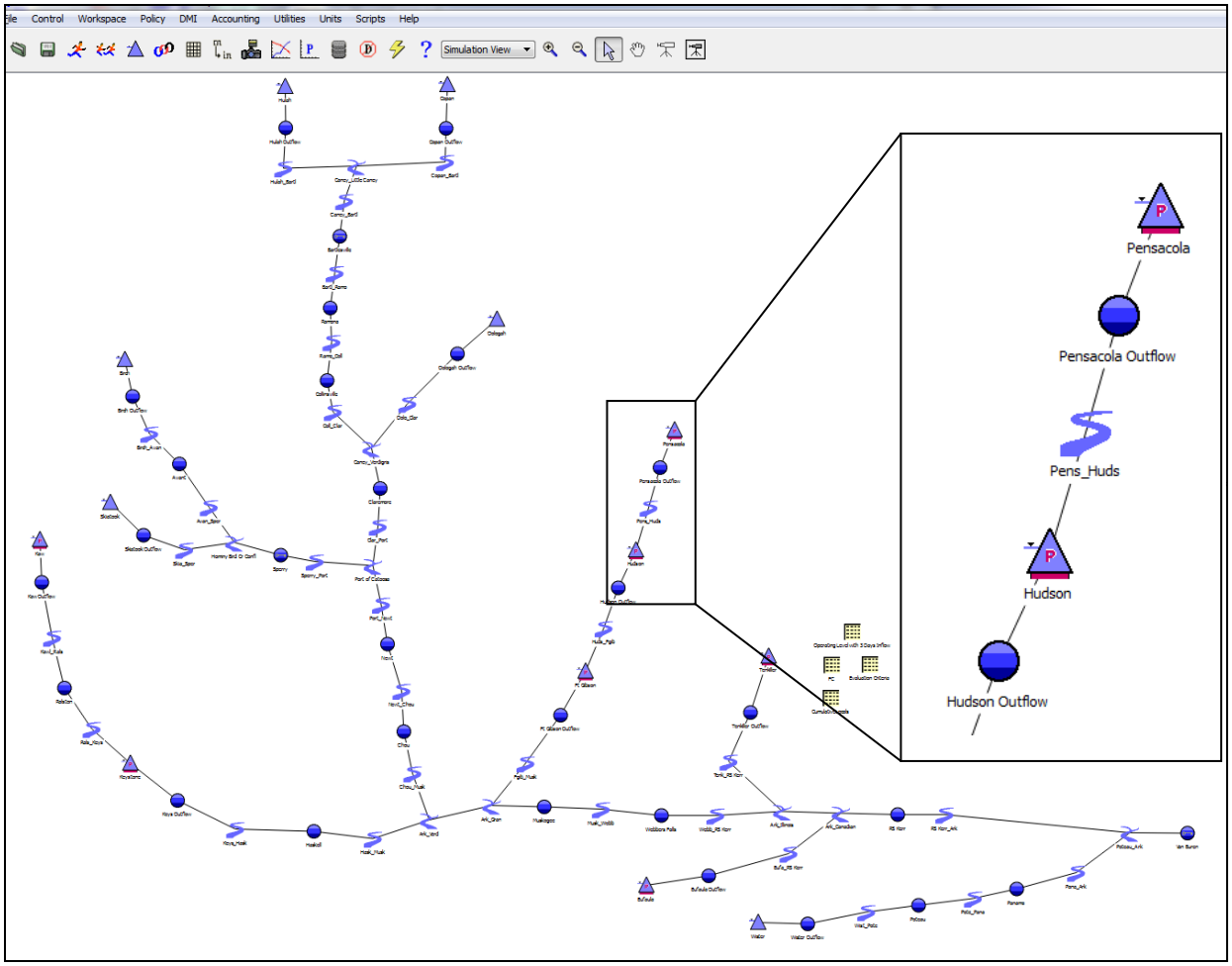

Figure 3 Schematic of RiverWare workspace

limits, and balance the system. The releases are determined using the surcharge, regulation discharge, and flood control rules developed for the USACE Southwest Division, based on the operating policies.

Surcharge: Surcharge occurs when flood water in the lake is above the flood pool and water must be released, regardless of downstream conditions. The surcharge releases are calculated for each reservoir one at a time starting with the most upstream reservoir. In the case where surcharge releases are necessary, they are routed through the system. If the upstream reservoir is above another reservoir, the releases are routed downstream to become inflows to the next reservoir. This reservoir then calculates its surcharge releases. This process continues until surcharge releases have been calculated for every reservoir.

Regulation Discharge: The regulation discharge, which is the maximum flow allowed at Van Buren, varies seasonally and with regard to the percent of basin storage utilized, summarized in the Van Buren Guide Curve (Figure 4).

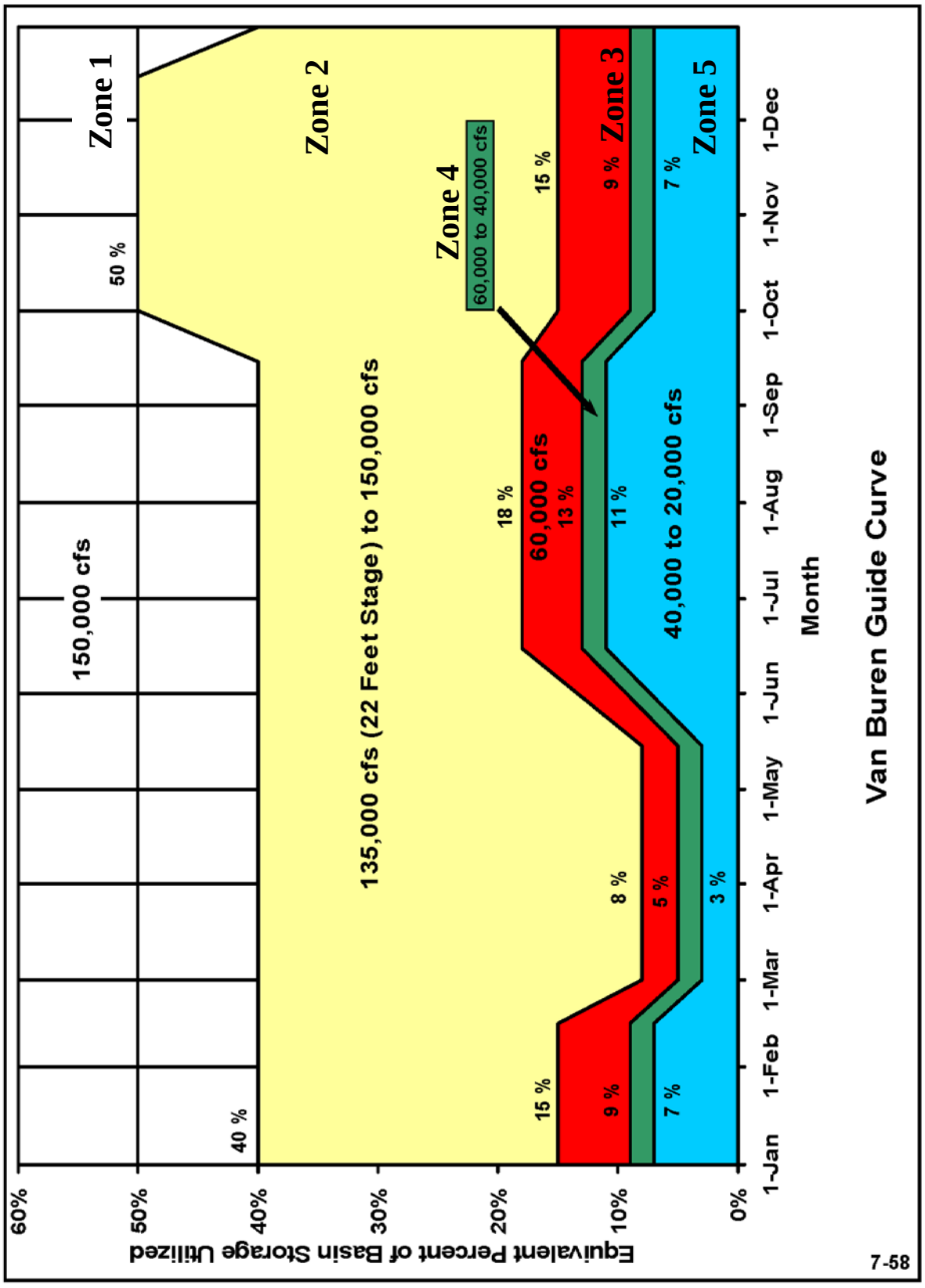

Figure 4 Van Buren Guide Curve with specified regulation discharge flows for five zones.

The Equivalent Percent of Basin Storage Utilized is calculated as

$$\frac{\sum_{@t} S + \left(\sum_{t}^{t+3} I - \sum_{t}^{t+3} O\right)}{\sum_{@t} S_{Total}} * 100 \quad (1)$$

where S is reservoir's flood pool storage utilized, I is reservoir inflow, O is reservoir releases, S_{Total} is the reservoir's total flood pool storage, and t is the current time in days. Depending on the time of year the equivalent percent of basin storage utilized correlates to a regulation discharge at Van Buren, ranging from a high of 150,000 cfs to a low range of 40,000 to 20,000 cfs. There are five zones and each has additional criteria that determines the flow and time period for the range of flows (Figure 4). Some of the zones represent maximum regulation discharge values, while others show a range of flows to transition between. For example Zone 5 requires a tapered recession from 40,000 to 20,000 cfs in 21 days (USACE Tulsa and Little Rock District, Chapter 7). There are also other regulation points in the system such as Bartlesville, Ramona, Collinsville, Claremore, and Muskogee. Each regulation point has a site specific regulation discharge.

Flood Control: The SWD Flood Control rules try to balance the system by reducing each lake to the same balance level/operating level. Tulsa District developed a correlation between percent flood pool storage with a balance level. This allows for a priority assignment for reservoir releases that are competing for downstream channel space. The balance level is based on the system flood storage balance level vs. storage curves (Figure 5). Curve C is the highest priority until the percent of flood storage utilized reaches thirty percent than all lakes have the same priority. Curve B is next in priority followed by Curve A. Each reservoir is assigned a release schedule that will bring all reservoirs to the same operating (balance) level without causing downstream flooding. This process is repeated for each timestep in the forecast time period. The RiverWare rules execute this logic through the use of the predefined Flood Control function which executes the system wide solution. The results are the outflows from each reservoir which are then routed through the system.

Iterative MRM: Since the equivalent percent full equation (1), uses the outflow from the reservoirs, this value will change based on the releases computed in the Flood Control rules. To perform this iteration, RiverWare's Iterative Multiple Run Manager (MRM) is used. This utility allows an entire simulation run to be made and then logic is executed to decide if another simulation is necessary. The logic sets values in the system and another run is executed. For the first pass, the Iterative MRM sets the outflow values in equation (1) to 180,000 acre-ft. For every other run it is set to the computed outflow from the reservoirs. The model runs through three different runs, until the results converge to a solution.

RESULTS

After three iterative runs are made the results are shown in RiverWare's System Control Table (SCT). For each reservoir, the inflow sum, outflow, operating level, pool elevation, percent of flood control pool, and operating level with three days inflow are summarized in a the table (Figure 6). The water managers then look at the model's suggested release schedule and make changes based on engineering experience not captured by the rules and special circumstances.

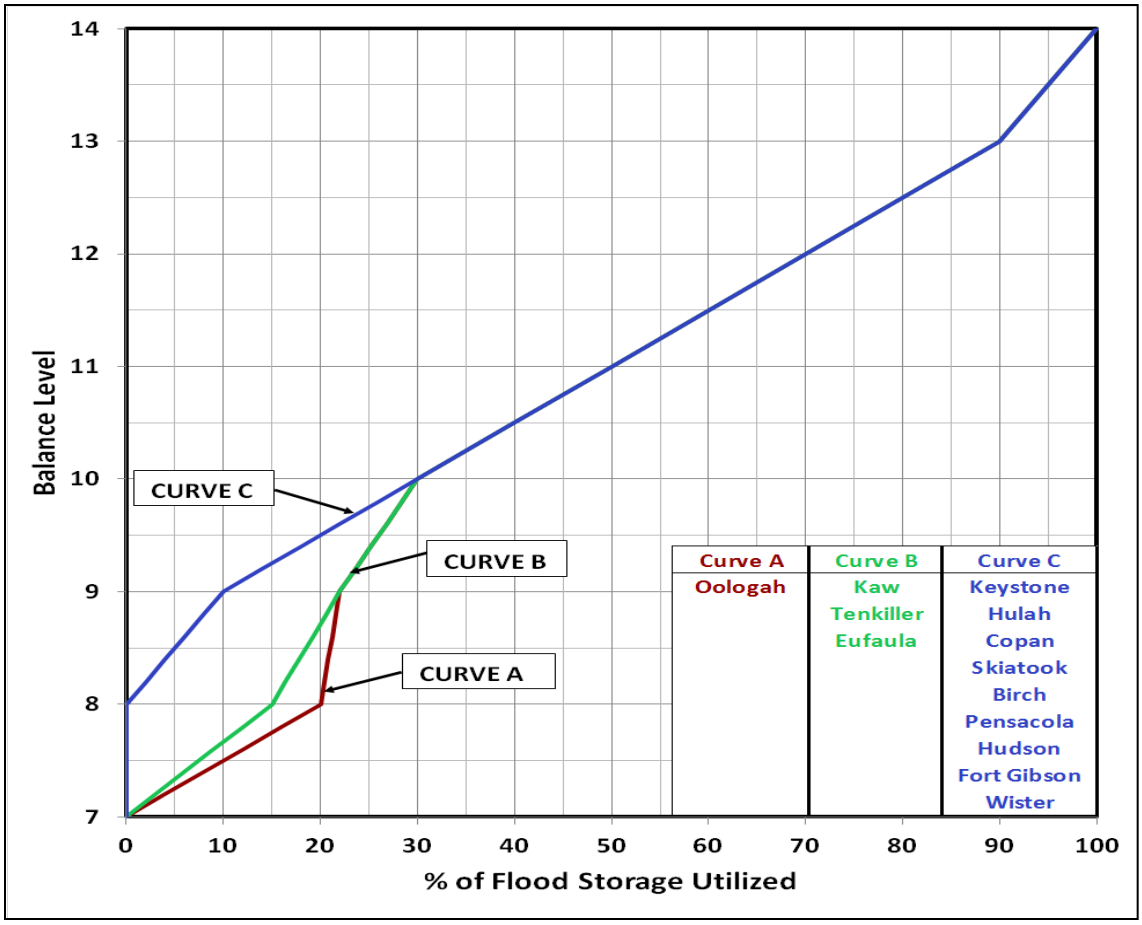

Figure 5 Balance level vs. percent of flood storage utilized curves.

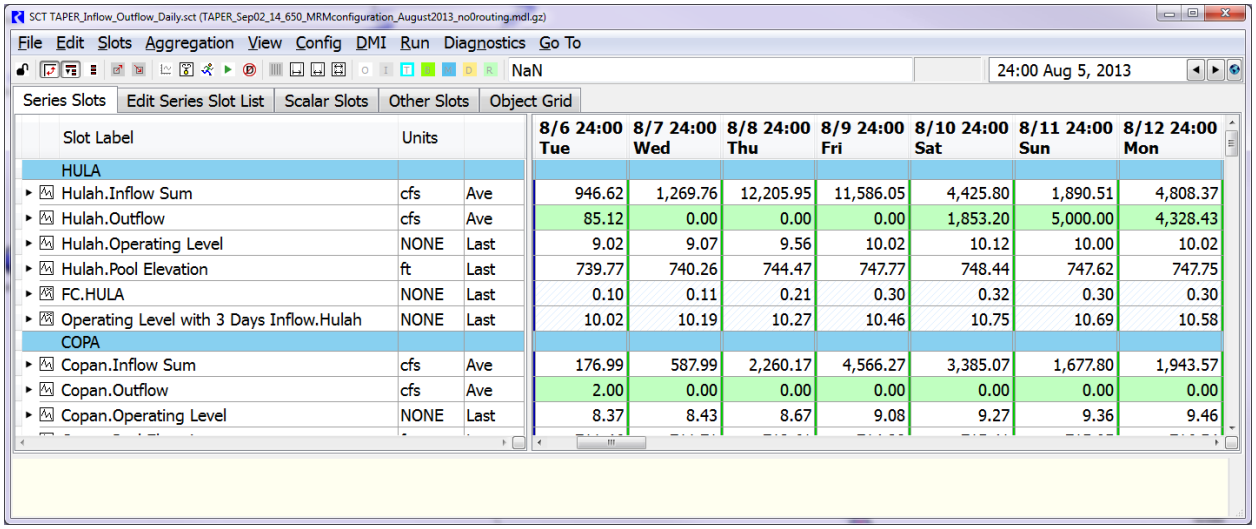

Slot Label	Units		8/6 24:00 Tue	8/7 24:00 Wed	8/8 24:00 Thu	8/9 24:00 Fri	8/10 24:00 Sat	8/11 24:00 Sun	8/12 24:00 Mon
HULA									
Hulah.Inflow Sum	cfs	Ave	946.62	1,269.76	12,205.95	11,586.05	4,425.80	1,890.51	4,808.37
Hulah.Outflow	cfs	Ave	85.12	0.00	0.00	0.00	1,853.20	5,000.00	4,328.43
Hulah.Operating Level	NONE	Last	9.02	9.07	9.56	10.02	10.12	10.00	10.02
Hulah.Pool Elevation	ft	Last	739.77	740.26	744.47	747.77	748.44	747.62	747.75
FC.HULA	NONE	Last	0.10	0.11	0.21	0.30	0.32	0.30	0.30
Operating Level with 3 Days Inflow.Hulah	NONE	Last	10.02	10.19	10.27	10.46	10.75	10.69	10.58
COPA									
Copan.Inflow Sum	cfs	Ave	176.99	587.99	2,260.17	4,566.27	3,385.07	1,677.80	1,943.57
Copan.Outflow	cfs	Ave	2.00	0.00	0.00	0.00	0.00	0.00	0.00
Copan.Operating Level	NONE	Last	8.37	8.43	8.67	9.08	9.27	9.36	9.46

Figure 6 System Control Table summarizing daily results for 6-hr timestep model

Once the water managers have set their releases, they are locked in as input values for a few days and the model is rerun for the rest of the simulation period. The model determines any unspecified release based on the modified release scenario. The water managers check that gages downstream stay below regulation discharge, and lock in several more days of releases. This process continues until the water managers are satisfied with the final release scenario. Once water managers are satisfied with the results, then html reports, plots (Figure 7), DSS files, and text files are developed for stakeholders. Water managers use the releases plan to make requested gate changes from the dam operators, and coordinate hydropower releases.

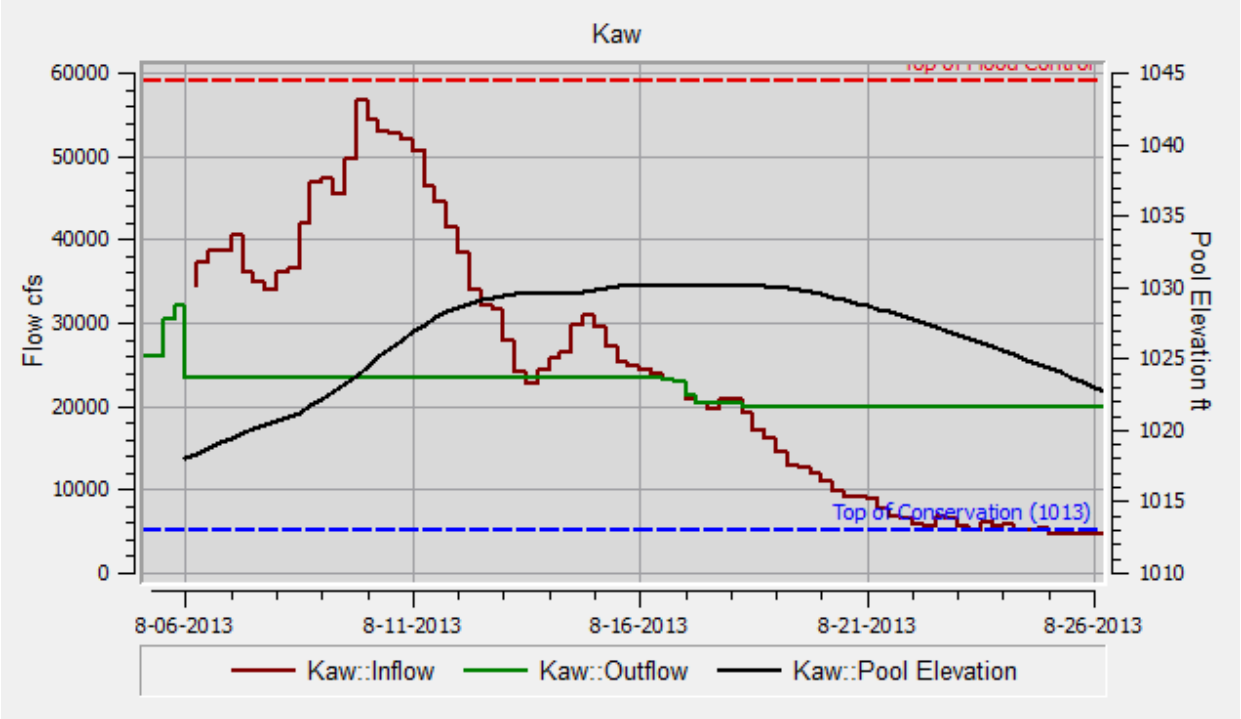

Figure 7 Example of plot sent to stakeholders

CONCLUSION

The U.S. Army Corps of Engineers, Tulsa District manages flows to Van Buren, Arkansas, using a RiverWare model to help with TAPER operations. The model uses operating curves and model constraints to create a recommended release plan that evacuates the flood pool in an efficient manner, while maintaining many stakeholder and navigation needs. The RiverWare model and user interface tools will save water managers time and create a more efficient process to create release plans. The 6-hr model will help to reduce flow fluctuations at the Arkansas River lock and dams, and will allow for one model to create and edit release plans reducing the amount of time spent by water managers.

REFERENCES

Center for Advanced Decision Support for Water and Environmental Systems (CADSWES). (2014) RiverWare User's Guides. http://www.riverware.org/PDF/RiverWare/documentation.

U.S. Army Corps of Engineers Tulsa and Little Rock Districts. Arkansas River Basin: Water Control Master Manual. Chapter 7.

U.S. Army Corps of Engineers Hydrologic Engineering Center. (1998) HEC-1 Flood Hydrograph Package User's Manual.

INTEGRATING HYDROLOGIC AND RIVER OPERATIONS MODELING WITH EXPLICIT SIMULATION OF GROUNDWATER AND SURFACE-WATER EXCHANGE

Eric D. Morway, Hydrologist, U.S. Geological Survey, Carson City, NV emorway@usgs.gov; Richard G. Niswonger, Hydrologist, U.S. Geological Survey, Carson City, NV rniswon@usgs.gov; Enrique Triana, Senior Water Resources Engineer, MWH Global, Fort Collins, CO enrique.triana@mwhglobal.com

Abstract: Existing hydrologic/river-operations model couplings found in the scientific literature adopt a feed-forward approach for updating groundwater surface-water (GW-SW) interactions in the operation component of the coupling, and likewise, for updating simulated diversions (including pumping) in the hydrologic model. In many western US river basins, where GW-SW is a significant component of the overall river budget, it is increasingly important to more accurately account for groundwater returns under increased climate variability and changes in groundwater and surface water management. Because standard functionality available in today's river operation models simulate GW-SW interaction using simplified one-dimensional equations or estimated stream-depletion factors, they do not accurately account for the spatially and temporally distributed influence of groundwater on operations, especially during periods of low-flow. To address this weakness, a generalized river basin Decision Support System and network flow model (MODSIM) is integrated with the modular three-dimensional groundwater flow model (MODFLOW). MODSIM is a river basin management decision support system capable of simulating complex administration of water rights and agreements in large-scale surface-water networks. MODFLOW is a physically-based distributed-parameter finite-difference model used for simulating groundwater systems. The strengths of each code compliment the current weaknesses of the other. That is, MODSIM's inability to simulate spatially-varying GW-SW interaction is a long-standing strength of MODFLOW through the use of the lake (LAK) and stream flow-routing (SFR2) packages. Conversely, MODSIM is well-equipped to administer available river flow and storage accounts among spatially distributed diversions and reservoirs while honoring the constraints of prior appropriation doctrine and in-stream flow requirements. Multiple attempts to inform river operations models with MODFLOW output have been found in the scientific literature, but the feed-forward nature of such attempts fails to synchronize their respective solutions. Recent efforts have focused on iteratively passing information (i.e., GW-SW exchanges, canal diversion amounts, reservoir releases) between MODSIM and MODFLOW in memory to achieve synchronization between the respective model solutions before advancing to the next time-step. To accomplish this goal, the Lake (LAK) and Streamflow-Routing (SFR2) packages available with MODFLOW were integrated with MODSIM. The newly developed code will provide water planners and managers in over-appropriated systems with a more robust decision making support tool than is possible with either model applied independently or run using a feed-forward implementation. A demonstration of third-party injuries (i.e., those not directly involved in the transfer of water use) resulting from proposed alternative management interventions during periods of low-flow is demonstrated with an example model.

WINDAM C EARTHEN EMBANKMENT

INTERNAL EROSION ANALYSIS SOFTWARE

Karl Visser, PE; Hydraulic Engineer; USDA-NRCS; National Design, Construction, and Soil Mechanics Center; Fort Worth, TX; karl.visser@ftw.usda.gov;
Ronald D. Tejral, PE; Agricultural Engineer; USDA-ARS; Hydraulic Engineering Research Unit; Stillwater, OK; ronald.tejral@ars.usda.gov;
Mitchell L. Neilsen, PhD, Professor of Computing and Information Sciences, Kansas State University; Manhattan, KS; neilsen@k-state.edu

ABSTRACT Two primary causes of dam failure are overtopping and internal erosion. For the purpose of evaluating dam safety for existing earthen embankment dams and proposed earthen embankment dams, WinDAM C software will simulate either internal erosion or erosion resulting from an overtopping event. WinDAM C models erosion failure of a homogeneous embankment. Future expansion includes non-homogeneous embankments, and embankment protection analysis.

The four essential functions of the software are:

1. Hydraulically routes one input hydrograph through, around, and over a single earthen dam.
2. Estimates internal erosion and potential breaching of an earthen embankment dam.
3. Estimates erosion of the earthen embankment caused by overtopping of the dam embankment.
4. Estimates auxiliary spillway erosion in up to three earthen or vegetated auxiliary spillways.

The user imports an inflow hydrograph into WinDAM C and selects either internal erosion analysis or overtopping analysis.

Regarding internal erosion within the earthen embankment, the user sets the elevation and initial size of the internal erosion conduit. WinDAM C initially assumes a horizontal, rectangular conduit shape. The internal erosion conduit grows larger as flow erodes embankment material. The erosion may breach the embankment and drain the reservoir.

Since the research has been completed, USDA and KSU are currently verifying and validating a working version of WinDAM C, which should be released for external evaluation and testing in 2015.

INTRODUCTION

Windows Dam Analysis Modules (WinDAM) is a modular software application to analyze earthen embankments during internal erosion and overtopping. Recently released for testing and evaluation by the dam safety community, WinDAM B (USDA, et al. 2012) includes erosional failure of a homogeneous embankment through overtopping and release of stored water. The alpha version of WinDAM C, currently under development, includes analysis of internal erosion. Future planned development includes non-homogeneous embankments. The US Department of Agriculture – Agricultural Research Service (USDA-ARS), US Department of Agriculture – Natural Resources Conservation Service (USDA-NRCS), and Kansas State University (KSU) are working jointly to develop this software.

For nearly seventy years, the USDA-NRCS has partnered with landowners, municipalities, conservation districts and other sponsors to construct more than 11,000 rural flood control dams. These structures provide $1.5B in annual benefits by providing flood control, municipal and rural water supplies, irrigation water, wetland habitat, and recreation among others. Many of these aging dams were designed with a 50-year service life, and time takes a toll on these structures. Sediment pools fill and encroach upon the flood detention volume. Structure components deteriorate, and hazard creep occurs in urbanizing areas that were once rural cropland areas. As a result, the consequences of dam failure must be considered when evaluating and prioritizing these structures for rehabilitation since the structures may no longer meet NRCS design criteria (USDA, 2005).

Overtopping and internal erosion are the primary causes of dam failures, with each mode attributed to a roughly equal number of failures (Foster, Fell and Spannagle 1998). For a given dam, one (or neither) mode may be more likely. For example, many of the storage reservoirs in arid West have large volumes relative to inflow and are managed such that overtopping is very unlikely. The US Bureau of Reclamation (USBR, 2011) names internal erosion of embankments (or their foundations) as the number one cause of dam failures in the western US. WinDAM C, when completed, will estimate breach erosion of an earthen dam through one of two modes: internal erosion through the embankment or overtopping the embankment. This document describes the WinDAM model currently being developed to examine internal erosion. The model is currently at the alpha stage of development undergoing verification and validation testing by the developers. It is anticipated that additional testing by the dam safety user community will also be required.

WINDAM C CAPABILITIES

PURPOSE OF SOFTWARE The essential functions of WinDAM C software are threefold:

- Hydraulically route (level pool routing) one inflow hydrograph through, around, and over a single earthen dam.
- Estimate auxiliary spillway erosion in up to three earthen or vegetated auxiliary spillways.

- Estimate erosion of the earthen embankment caused by internal erosion or by overtopping of the dam embankment.

Since WinDAM C does not include any hydrology component, the user must create the reservoir inflow hydrograph in other software, such as WinTR-20 (USDA-NRCS, 2009) or SITES (USDA-NRCS, 2012). The user can import the hydrograph or paste the hydrograph points into the user interface. The user has the flexibility to choose the hydrologic software most suitable for analysis of site conditions.

INTERNAL EROSION OF HOMOGENOUS EARTHEN EMBANKMENT WinDAM C models the dam embankment as a homogenous earthen material. Many USDA-NRCS dams are homogenous earthfill, so the WinDAM C model applies. If applied to zoned embankments, the suggested approach is to consider material and geometry that will dominate the process. For computational purposes, the earthen embankment fits into a simplified, rectangular-shaped valley (Figure 1) with vertical abutments and level valley floor.

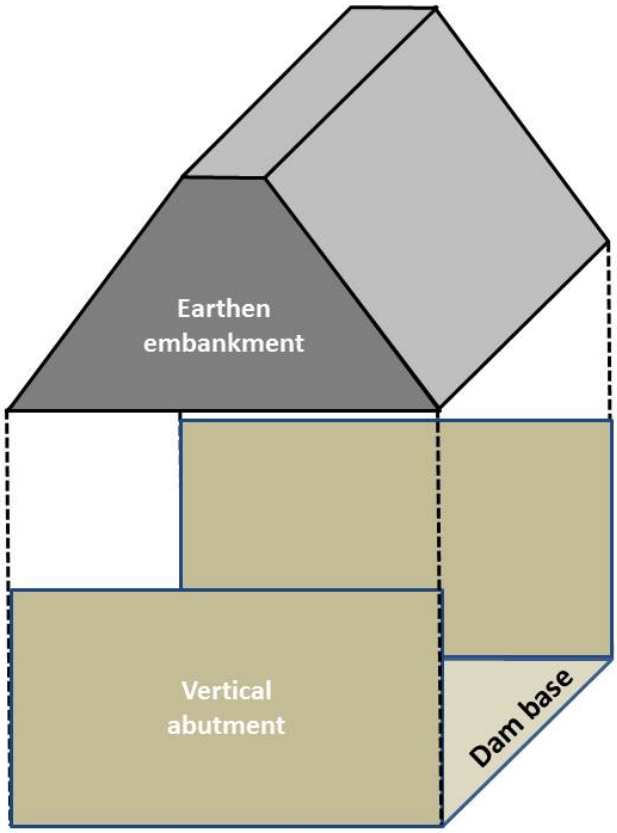

Figure 1 Homogenous earthen embankment in rectangular-shaped valley

INITIAL INTERNAL EROSION CONDUIT For a WinDAM C internal erosion analysis, the user specifies the initial size and location of the internal erosion conduit. To simplify the

analysis, the conduit is horizontal—there is no slope in the upstream-downstream direction through the embankment, as shown in Figure 2. The conduit is assumed to be rectangular. The user must specify the initial conduit dimensions—width and height. The user must input the initial elevation of the conduit invert, as well as the lateral stationing between the left and right abutment.

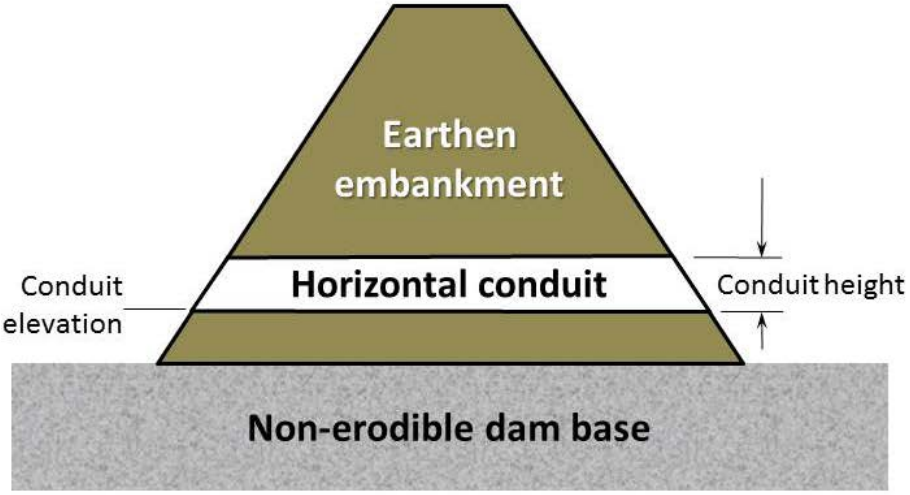

Figure 2 WinDAM C internal erosion horizontal conduit profile

In WinDAM C the left and right abutments are considered to be non-erodible and vertical, as shown in Figure 3. The embankment foundation, or dam base, is non-erodible and level. The dam crest profile is defined as a series of user-entered points (Figure 3).

The internal conduit erodes laterally until it reaches an abutment, as shown in Figure 3. The conduit also erodes vertically between the dam crest profile and the dam base. As long as some portion of the conduit is flowing full and the shear stress is sufficient to erode the embankment material, the conduit expands in all four directions equally. Once conduit erosion reaches one of the embankment boundaries (abutment, dam base, or dam crest), expansion/erosion in that direction stops.

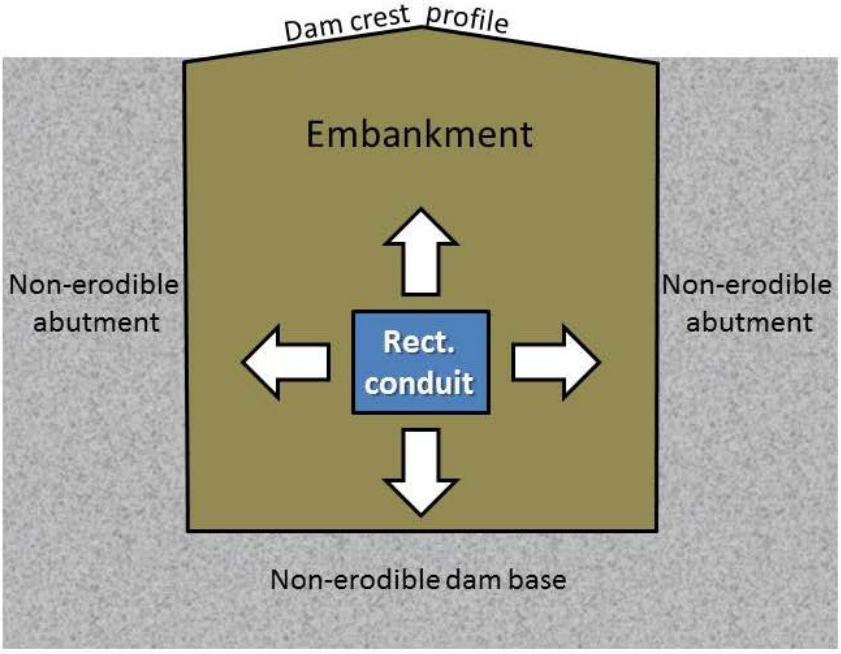

Figure 3 WinDAM C conduit cross-section looking upstream

EROSION PROCESSES Two erosion processes are simulated. The conduit enlarges concentrically due to shear detachment (laterally and vertically in a conduit simplified as having a rectangular cross section); classically this is the only process associated with internal erosion. However, development of a headcut at the outlet and subsequent advance of that headcut also play an important role in breach by internal erosion in some instances, so this process is also modeled.

At the beginning of each time step, the model computes the shear stress produced by flow passing through the rectangular internal erosion conduit. In instances where conduit is full for less than entire length, a backwater curve and resulting average shear stress along conduit length are computed. If the average shear stress is greater than the user-specified critical shear stress, then the amount of erosion is estimated and the conduit expanded accordingly for the next time step.

In addition to simply expanding the internal conduit laterally and vertically, WinDAM C also checks to see if a headcut will form at the downstream invert of the conduit (Figure 4). After this headcut has formed, headcut advance and deepening is computed for each time step using the user-prescribed erosion model (Table 3). This process is simulated much like that of a headcut formed in overtopping with important distinction that width is controlled by the conduit.

TRANSITION FROM INTERNAL CONDUIT EROSION TO BREACH EROSION Once this headcut reaches the upstream face of the embankment the internal conduit has become an

open breach and flow transitions to breach flow. At this point, lateral expansion of the breach is the same as with overtopping flow conditions.

In the early stages of internal erosion, the conduit is usually stable regardless of support by hydrostatic water pressure. As the conduit enlarges, the support provided by water becomes critical. There are three cases when the roof of the conduit is considered to be stable:

1. The conduit is flowing full over the entire length of the conduit.
2. The conduit is flowing full over some part of the conduit length.
3. When flow transitions to free surface flow along the entire length of the conduit and the conduit width is less than twice the overburden height (vertical distance from the dam crest to conduit roof).

As the breach progresses and reservoir drains the roof of the internal erosion conduit will collapse. WinDAM C considers the conduit roof collapsed for these two cases:

1. Erosion of the roof reaches the dam crest profile
2. Free surface flow along the entire conduit length and the conduit width is more than twice the vertical distance from the dam crest to the roof.

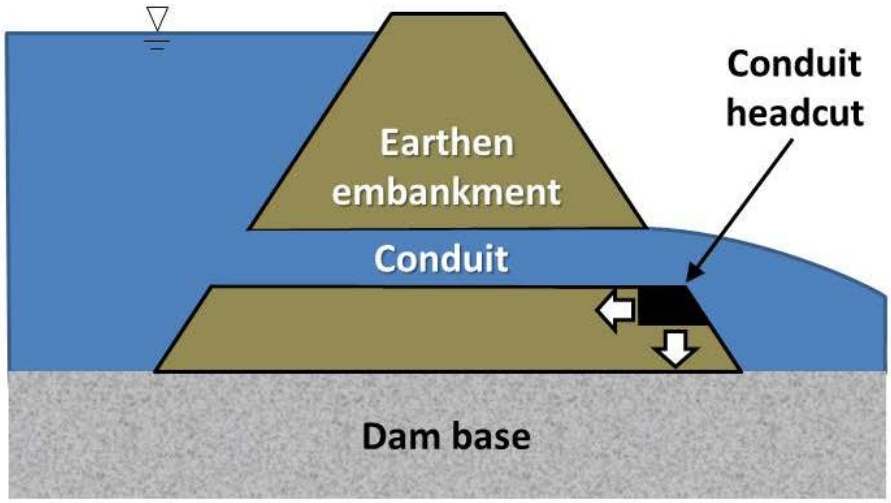

Figure 4 Conduit headcut

NEGLIGIBLE INTERNAL CONDUIT FLOW CASES There are cases where the resulting internal erosion is negligible. These possible cases include:

- Elevation of internal erosion conduit is above maximum water surface in the reservoir, which results in no flow in internal erosion conduit.
- Insufficient time or flow to produce meaningful erosion because the generated stress does not exceed the soil critical stress by sufficient time or amount.
- Highly erosion-resistant embankment materials may not generate shear stresses greater than the soil critical stress.

OVERTOPPING BREACH EROSION If the user selects overtopping erosion analysis in WinDAM C, flow through the breach depends on the eroded breach area and the driving head based on the reservoir water surface, breach elevation, and any downstream tailwater. The four stages of the overtopping breach are described in Table 1.

Table 1 Four stages of WinDAM overtopping breach

Stage 1	Surface protection on downstream embankment slope fails. Headcut forms on downstream face of dam at low point in the crest profile.
Stage 2	Headcut advances through the crest to upstream embankment slope. Breach is initiated when the headcut enters the upstream crest and begins to lower the hydraulic control.
Stage 3	Headcut continues to advance into the reservoir pool releasing stored water.
Stage 4	Headcut continues to widen as reservoir drains following local removal of the embankment in the breach area.

MODELING FLOW THROUGH EMBANKMENT CRACKS Earthen embankments are susceptible to cracking from seismic activity or from desiccation in arid regions. As an overtopping erosion event, the only way to evaluate a crack is to input the crack in the dam crest profile. WinDAM overtopping erosion analysis was not developed for such evaluation and is not appropriate for several reasons. First, crest width in WinDAM is a constant and WinDAM evaluates both stress and erosion strictly from a depth perspective rather than considering the extremely steep profile segments as walls. Second, overtopping is considered on a one-dimensional, unit-discharge basis.

However, analyzing a crack, even one that extends to the dam crest, as an internal erosion event may be appropriate if the user develops a thorough understanding of the computational model and interprets inputs and results accordingly. Cracks have been associated with internal erosion (Bonelli, et al. 2006) (Fell, et al. 2003). The geometry of a crack can be more correctly approximated in an internal erosion simulation in WinDAM C. However, the research program and software were not undertaken to address the early stages of breach development represented by narrow cracks. Users should recognize model constraints and interpret results accordingly, e.g.

- WinDAM C assumes turbulent flow through the internal conduit, whereas flow through narrow cracks may be laminar flow.

- WinDAM C embankment materials properties do not change during the analysis. Over a sufficiently long period of time, flow within small cracks may saturate portions of the embankment and alter its resistance to erosion.

INTERACTION OF EROSION AND HYDRAULICS The hydraulics and erosion are coupled for the embankment breach analysis. In other words, a larger breach in the embankment lets more flow pass through the embankment breach during the next time step. Erosion prediction is relatively straightforward in the homogeneous earth embankment.

Erosion prediction in the auxiliary spillway, however, is much more complex than in the homogenous earth embankment. Hydraulics and erosion are not coupled in the auxiliary spillway because the erosion model only includes information on the weakest unit width subsurface materials in the auxiliary spillway. As a result, WinDAM C does not have the data to estimate the lateral expansion in the auxiliary spillway. Erosion computations in the auxiliary spillway stop when the headcut reaches the upstream edge of the level crest of the auxiliary spillway.

WINDAM VERSIONING

Research is ongoing for future enhancements to WinDAM software, as shown in Table 2. USDA and KSU are currently verifying and validating a working version of WinDAM C, which should be released for evaluation and testing in 2015.

Table 2 WinDAM Versioning

Version	Existing Capabilities or Future Enhancements
WinDAM A+ (2008)	Embankment overtopping analysis (Slope protection evaluation: no embankment erosion analysis)
WinDAM B (2011)	Homogenous fill embankment overtopping and erosion analysis
WinDAM C (2015)	Internal erosion prediction through homogenous fill embankment
WinDAM D (proposed)	Potential failure initiation at toe, berms, and groins. Alternative embankment slope protection materials (i.e. blocks, reinforced vegetation)
WinDAM E (proposed)	Zoned fill embankment overtopping erosion prediction

INPUT DATA

The auxiliary spillway materials in WinDAM C are described with the same data inputs as in SITES (USDA-NRCS, 2012).

WinDAM C requires the user to input one flow hydrograph. This hydrograph input is similar to the SITES input procedure. SITES gives the user the option to input hydrology through a

watershed model, but WinDAM C only allows hydrology input through a single hydrograph. Various design hydrographs will require a different WinDAM C run for each hydrograph.

WinDAM C may be run with or without embankment breach evaluation. When breach evaluation is desired, the earthen embankment must be described so WinDAM C can model either internal erosion or overtopping erosion. The user specifies the embankment slope protection: vegetation, rock riprap, or no cover. The dam embankment crest and slope dimensions are also input.

For the breach analysis option, the user selects one of two headcut models: Temple/Hanson Energy model or Hanson/Robinson Stress Model (Hanson, et al. 2011). The WinDAM C erosion prediction models are designed for estimating erosion of typical NRCS earthen embankments composed of fine-grained, cohesive materials, where the dominant erosion process is the formation, advance, and deepening of a headcut. The soil parameter inputs for each model are listed in Table 3.

Table 3 WinDAM C Erosion Model Soil Inputs

Model	Hanson/Robinson Stress Model	Temple/Hanson Energy Model
Input Parameter *(Units)*	Erodibility (ft/hr)/(lb/ft^2)	Erodibility - (ft/hr)/(lb/ft^2)
	Critical Shear Stress (*lb/ft^2)*	Critical Shear Stress – (*lb/ft^2)*
	Undrained Shear Strength (*lb/ft^2)*	Advance coefficient - *(ft/hr)/(ft/s^3)*
	Total Unit Weight (*lb/ft^3)*	

All four input parameters in the Hanson/Robinson stress model can be measured. In addition this model is recommended for tall dams (> 50 ft high). Since the advance coefficient parameter in the Temple/Hanson cannot be measured directly, most users select the Hanson/Robinson stress model.

A WinDAM C internal erosion analysis covers a few hours or days. The WinDAM model does not account for wetting or drainage of embankment soils during the erosion analysis. Therefore, the material properties of the embankment soil do not change over the period of the breach analysis.

Generally, the outflow from dams is controlled primarily by the hydraulic features of the dam—principal spillway and auxiliary spillway. For these dams where backwater effects are not significant, a single downstream tailwater elevation is sufficient. However, some dams have downstream hydraulic features such as levee or road embankments that impose significant and dynamic backwater effects. WinDAM C incorporates a tailwater rating table to simulate how the outflow from the dam varies with downstream capacity. This backwater is used when analyzing the auxiliary spillway flow, but is not yet utilized when computing the auxiliary spillway erosion.

OUTPUT

WinDAM C has three forms of output; the initial summary screen the user sees upon completion of a valid run, ASCII text output files, and numerous graphical plots. WinDAM C has multiple text output files to describe the expected performance of the embankment and multiple auxiliary spillways. The current list of available output plots in WinDAM C are listed below.

- Conduit/Breach Width
- Dam Cross-section
- Dam Crest Profile
- Conduit Width/Height
- Headcut Advance
- Headcut Position
- Hydrographs
- Reservoir Surface Area
- Reservoir Storage Volume
- Reservoir Water Surface
- Maximum Overtopping / Breach Discharge
- Maximum Overtopping Head
- Overtopping Stress
- All Discharge Ratings
- Auxiliary Spillway Ratings
- Principal Spillway Rating
- Tailwater Elevation
- Tailwater Rating

A sample of the Headcut Advance plot is shown in Figure 5.

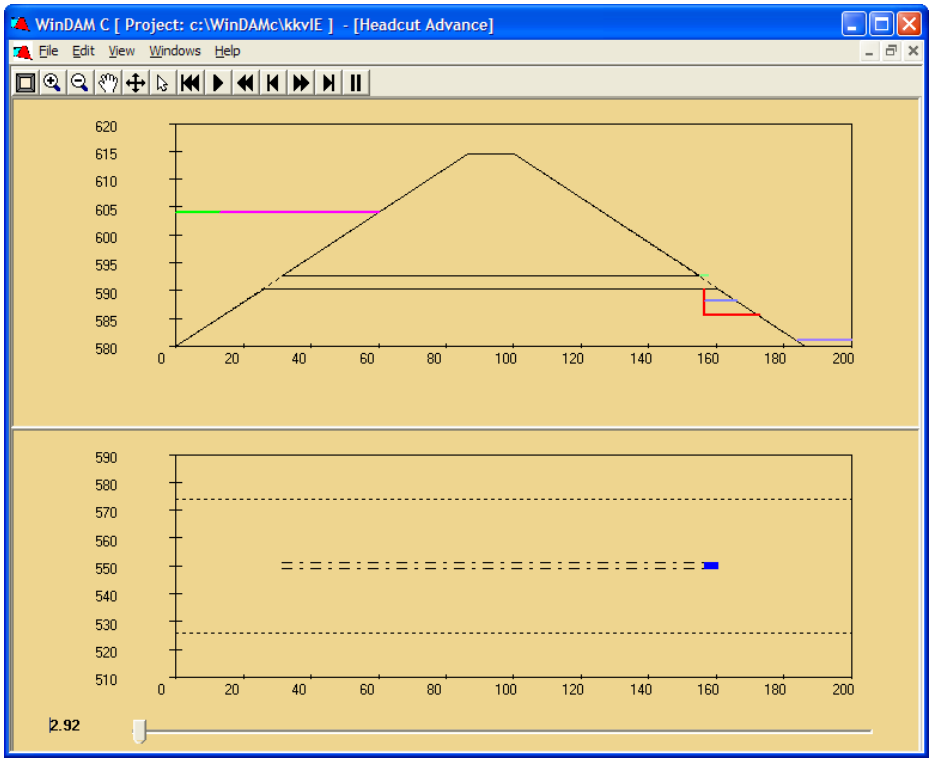

Figure 5 Sample WinDAM C headcut advance plot. Top half is dam cross-section. Bottom half is plan view.

INITIAL MODEL VALIDATION

Four different internal erosion tests on earthen embankments have been conducted at the ARS Hydraulic Engineering Research Unit in Stillwater, OK. Qualitatively, the WinDAM C predicted erosion matches the prototype erosion. The tests indicate that critical shear stress is a key parameter for initiation of erosion and particle detachment, especially for low-head dams. (Tejral, 2014)

CONCLUDING REMARKS

This report contains a preview of the internal erosion modeling capability being developed for WinDAM C. In addition, attention was given to capabilities already available to WinDAM B users—analysis of auxiliary spillways and overtopping breach. WinDAM software download and answers to frequently asked questions can be found at http://go.usa.gov/8Oq.

REFERENCES

Bonelli, S., Olivier, B., Borghi, R., & Benahmed, N. (2006). On the modelling of piping erosion. Comptes Rendus Mecanique , 555-559.

Fell, R., Wan, C. F., Cyganiewicz, J., & Foster, M. (2003). Time for Development of Internal Erosion of Piping in Embankment Dams. Journal of Geotechnical and Geoenvironmental Engineering , 129 (4).

Foster, M. A., Fell, R., & Spannagle, M. (1998). *Analysis of Embankment Incidents.* Sydney, Australia: The University of New South Wales.

Hanson, G. J., D. M. Temple, S. L. Hunt, and R. D. Tejral. (2011). Development and Characterization of soil material parameters for embankment breach. ASABE, Applied Engineering in Agriculture. Vol. 24(7):587-595.

USDA-NRCS. (2005). Earth Dams and Reservoirs. Technical Release TR-60 Washington D.C.: USDA Natural Resources Conservation Service.

[USBR] US Bureau of Reclamation. (2011). Best Practices and Risk Methodology Chapter 24 – Internal Erosion and Piping Risks for Embankments.

USDA-ARS and –NRCS and Kansas State University: WinDAM B. (2012). WinDAM-B, Version 1.1, Computer Program Release. http://go.usa.gov/8Oq.

USDA-NRCS. (2009). WinTR-20 Watershed Hydrology. Version 1.11. http://www.nrcs.usda.gov/wps/portal/nrcs/detailfull/null/?cid=stelprdb1042793.

USDA-NRCS: SITES. (2013). SITES 2005, Water Resource Site Analysis Computer Program, Version 2005.1.7, and User Documentation. Washington D.C. http://go.usa.gov/83z

CHANGES IN THE ACOUSTIC RESPONSE OF SOILS AS A FUNCTION OF GRASS COVER

Blake Armstrong, Graduate Student, National Center for Physical Acoustics The University of Mississippi, University, Mississippi, boarmstr@go.olemiss.edu
Dr. Craig Hickey, Associate Director for Applied Research National Center for Physical Acoustics & The University of Mississippi Research Associate Professor of Geological Engineering, University, Mississippi, chickey@olemiss.edu
Dr. Zhiqu Lu, Senior Research Scientist National Center for Physical Acoustics and The University of Mississippi Research Assistant Professor of Physics, University, Mississippi, zhiqulu@olemiss.edu

Abstract

Overtopping erosion accounts for 34 % of earthen dam failures. Grass cover has commonly been used to strengthen slopes and decrease the erodibility of embankment surfaces. Bermuda and Bahia are the most commonly used grasses on embankments and earthen dams due to their dense, deep root systems. A literature review of the acoustics of soils, soil erodibility, and traditional methods for the evaluation of soil surfaces was conducted. The review revealed an acoustic based apparatus capable of measuring mechanical and hydraulic properties that influence soil surface erodibility would be beneficial to soil scientists and engineers. In this study, we investigate the interaction of sound with the ground as a possible technique for assessing the erodibility of embankment surfaces. Physical properties common to both acoustic and erodibility behaviors of soils include: porosity, permeability, bulk density, moisture content, degree of compaction, and mechanical strength. An experiment is currently being conducted on soils with two different types of Bermuda grass, one type of Bahia grass, and one bare soil surface as a control. Acoustic transducers were placed at a depth of four inches to measure the changes in the acoustics behavior of the soil during the grass growth.

INTRODUCTION

In the last 50 years critical infrastructure has evolved to accommodate the steady increase of demand for freshwater and other natural resources. Dam infrastructure systems have assisted in providing an economic supply of freshwater, flood management, and soil conservation Richardson (2001). New technologies for monitoring the performance of the existing dam infrastructure systems must be developed to secure the continued availability of these resources.

Most traditional methods for characterizing erosion resistance involve invasive methods and lab tests. Flume tests have been used to study overtopping on grass covered dams by measuring water flow velocity and shear stress on the soil surface, Powledge et al. (1989). In 1991, a jet erosion test (JET) was developed to characterize erosion resistance on spillways, Hanson (1991).

Soil samples were subjected to varying jet velocities, and erosion was expressed as scour depth divided by time. This study showed that erosion in the site-specific submerged jet testing device may be related to the jet velocity, a time function, and a soil parameter (jet index). The jet index could then be used to provide a common method of expressing erosion resistance. The Erosion Function Apparatus (EFA) is another method to predict erosion rates as a function of shear stress in fine grained soils was designed for scour which could be closely related to the effect of overtopping erosion in earthen embankments. The EFA predicts these erosion rates in a lab by running water over a prepared soil sample at a certain velocity. Scour rate is measured as the height of the sample lost per time and is plotted against water velocity and shear stress on sample, Briaud et al. (2001).

Slot Erosion Test and Hole Erosion Test have been used to study internal soil erosion characteristics in embankment. The Hole Erosion test was used to estimate a priori a coefficient of piping erosion. The radius evolution of the pipe followed a scaling law between critical stress and time of piping erosion, which were a function of the initial hydraulic gradient and the coefficient of erosion. The time of failure and peak flow were related to the coefficient of erosion and the maximum pipe diameter before breaching, Bonelli. (2010). The rate of erosion is shown to be dependent on fines content, plasticity, dispersivity, compaction, water content, density, and saturation. Coarse-grained soils have lower critical shear stressed and erode more rapidly than fine-grained soils Wan et al. (2004).

In recent years acoustic methods have been developed to study soil wetting, compaction and other processes, Berkenhagen. (1998), Lu et al. (2004), Whalley et al. (2012). These acoustic methods utilize mechanical waves to measure soil properties. The acoustic approach has the benefits of being non-invasive and can be performed in the field. Besides the JET, the previously discussed tests require a prepared soil sample in a lab setting.

Acoustic waves traveling through soil interact with the soil particles and fluids. Acoustic parameters are constant-fabric characteristics and can be used to monitor ongoing internal changes of soil properties. Some of the properties that affect the acoustic response include moisture content, soil tension, density, effective stress, and porosity. The velocity of propagation of an acoustic wave can be modeled using

$$V_p = \sqrt{\frac{0.306a\sigma'^{\frac{1}{3}}Z}{\rho n b^{\frac{2}{3}}}} \quad (1)$$

This equation was proposed by Brutsaert et al. (1964) to model the compressional wave (acoustic) velocity in a media of randomly stacked spheres of different sizes as a function of

density (ρ), porosity (n), and effective stress (σ′). Z is a function of saturation, and a and b are adjustable parameters determined from fitting experimental data. Effective stress can then be broken down into 3 stresses. The first is total stress (σ) or overburden pressure which can be expressed as $\rho g h$ where g is the gravitational acceleration and h is the depth of the testing point. The second is the atmospheric pressure (σ_a) which is assumed to be zero. The last stress is soil tension (σ_c), also known as water potential or capillary pressure. This is weighted by saturation (S). These stressed are shown in the equation below.

$$\sigma' = \sigma - \sigma_a - S\sigma_c \quad (2)$$

For near surface areas of low saturation, soil tension is believed to be the main factor that affects sound speed Brutsart et al. (1964). This suction effect draws the soil particles together making the media more elastic which is indicated by increased wave velocities. At intermediate saturation, density and soil tension govern the acoustic behavior and decrease the sound speed. When approaching full saturation, sound speed is known to increase rapidly to the speed of sound in water. Acoustic response is also affected by overburden, but this is not a major parameter in near surface soils. Cohesion is also a factor affecting sound speed. The soil prepared in the current experiment is, for all practical purposes, homogeneous in soil type, so cohesive properties should not vary except due to soil tension. In this paper we discuss the feasibility of a method that estimates mechanical properties that influence soil surface erodibility by observing the changes in the acoustic wave velocity of the soil as a function of grass root growth.

METHODOLOGY

The experimental setup shown in Figure 1 includes a cast acrylic box divided into four quadrants, three quadrants having different grass types and one having a bare soil for control. Each soil quadrant is 1 ft (31 cm) deep with a surface area of 4 sf (0.37 m^2). The soil consists of 1% sand, 67% silt and 32% clay. This material is classified as a silty clay loam commonly used in the construction of earthen embankments. The soil was dried, grinded, and compacted into the box. Compaction was done in 1 inch (2.5 cm) layers with a metal plate. There were a total of 12 layers per quadrant to reach the depth of 1 foot (31 cm). The acoustic sensors consist of bimorph transducers built at The National Center for Physical Acoustics (NCPA) and placed at a depth of 4 inches (10 cm). Each quadrant has three transducers acting as one source and two receivers. This allows for two sets of time of flight measurements. With a known spacing of 6 inches (15 cm) and the travel time, the compressional wave velocity can be calculated.

Figure 1 Experimental setup

After the soil was compacted into the experimental box, time was allowed for relaxation of the initial effective stresses in the soil. The water was then slowly introduced from a drain in the bottom center of the box while the soil was under tension. The water level in an external reservoir was slowly raised to saturate the soil to the surface. Once saturated to the surface, the water in the reservoir was then lowered slowly back to a height of 1 inch (2.5 cm) above the bottom of the soil layer. The common Bermuda sod was donated by a commercial turf company, Tula Turf. The 007 Sumrall Bermuda grass was collected from pasture land, and the wild Bahia mix was collected from a slope covered in Bahia grass.

Grow lights were placed 1 ft (31 cm) above the top of the grass and left on for over 12 hr/day. The grass was cut weekly and fertilized twice a week with 15-30-15 fertilizer to boost root growth. Air temperature and pH of the soil was measured daily. Soil tension was measured at a depth of 6 inches (15 cm) with a tensiometer positioned in the middle of the quadrants. A HydraProbe II was used to measure the dielectric properties of the soil. These dielectric properties were then converted to volumetric moisture content and soil temperature. Figure 2 shows the grass just after the sod was placed on a) September 15, 2014 and later on b) January 16, 2015.

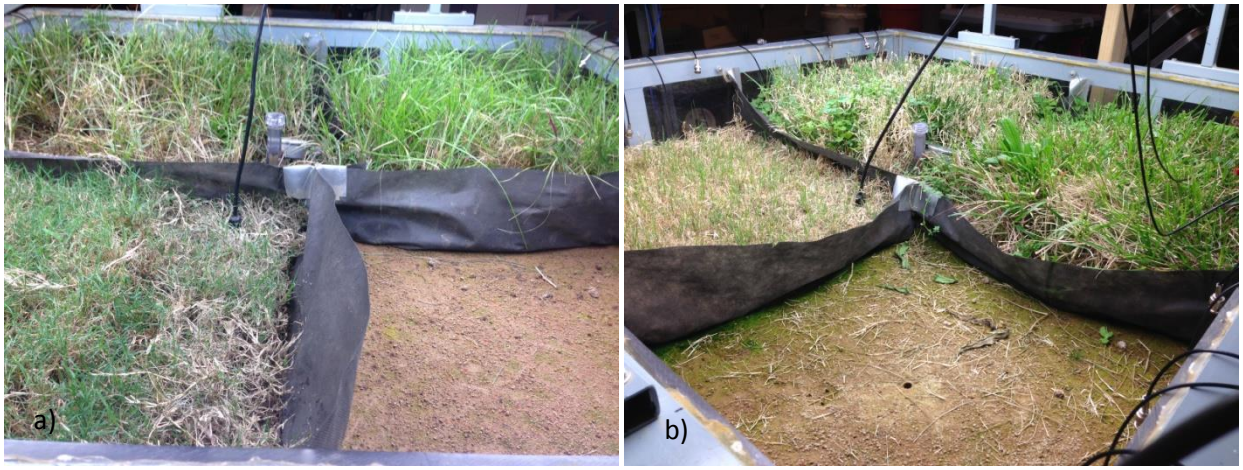

Figure 2 Grass cover on a) September 15, 2014 and b) January 16, 2015

RESULTS

The compressional wave velocities were calculated using Equation 3. The spacing of the transducer pairs (x) is constant at 15 cm (6 inches). The travel time of the sound denoted by Δt was measured using the receiving transducer. A picking routine detected the first arrival on the received waveform.

$$V_p = \frac{x}{\Delta t} \tag{3}$$

The control in this experiment was the bare soil velocities. The velocities in each grass type were compared to the bare soil velocities as a percent change as a function of time. The formula is given by Equation 4.

$$\Delta\% = \frac{V_i - V_b}{V_b} \times 100 \tag{4}$$

V_i is the velocity in the soil of the given grass. V_b is the velocity of the bare soil. The results of the experiment are presented below. Soil tension at the depth of 6 inches (15 cm) as a function of time is shown in Figure 3. The tension has remained very low around 1 – 2 kPa (0.15 – 0.3 psi). By October 4, 2014 the tension increased to 3 – 5 kPa (0.44 – 0.73 psi) before settling back around 1 - 2 kPa (0.15 – 0.3 psi) in November 1, 2014. The tension is moderately low and constant the next month and a half but started to vary more at the start of 2015. Such low tension is a consequence of the high degree of saturation. The soil tension averages about 2 kPa (0.3 psi) and varies ± 1 kPa (0.15 psi).

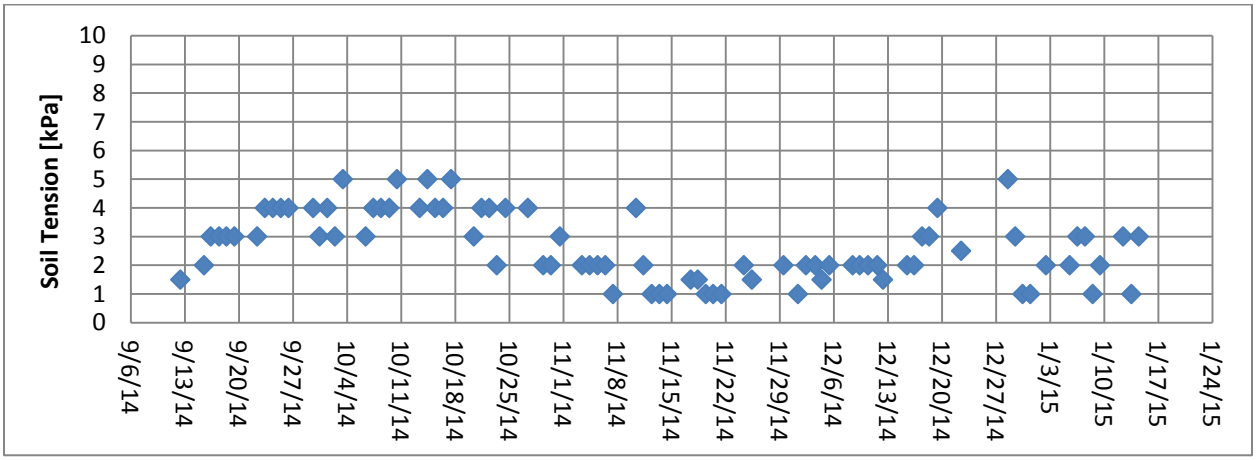

Figure 3 Soil tension since planting sod

The volumetric moisture content is shown as a function of time in Figure 4. It remains rather consistent from 0.51 – 0.54 m^3/m^3 (± 0.03 m^3/m^3). This is near fully saturated for this soil type. It is commonly believed that soil tension would increase with decrease in moisture content due to the soil's capillary rise when the water level is lower. This has not been observed for this experiment. The soil tension decreased with moisture content from October 25, 2014 to November 15, 2014. The accuracy of the HydraProbe II is ± 0.03 m^3/m^3, so this change in moisture content could be negligible. Volumetric moisture content has remained 0.51 m^3/m^3 (± 0.005 m^3/m^3) since December 9, 2014.

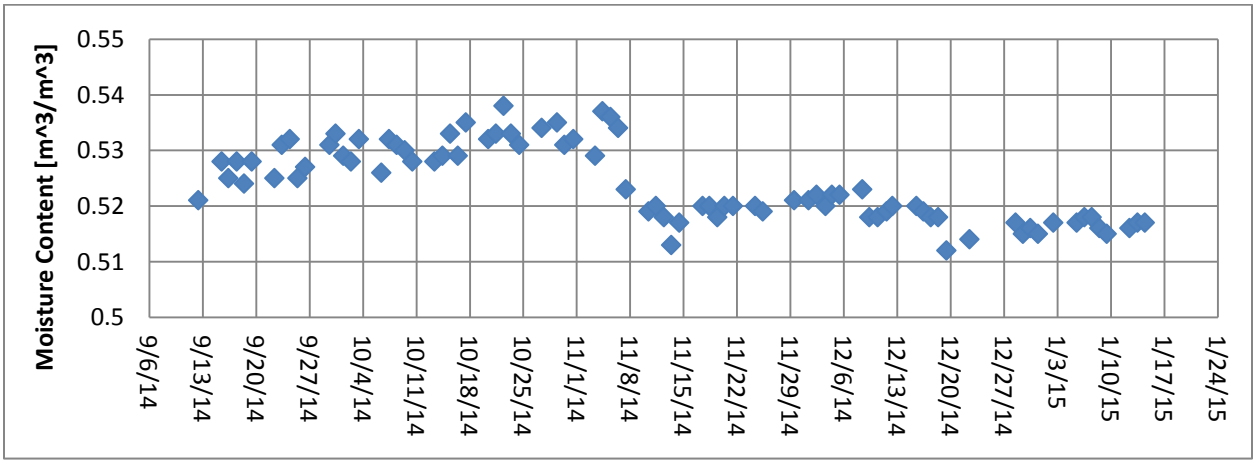

Figure 4 Volumetric moisture content since planting sod

The percent change in velocity with respect to the sound speed in the bare soil as a function of time is plotted in Figure 5. The range of sounds speeds has been from 150 – 260 m/s (492 – 853 ft/s). This is consistent with a soil tension <10 kPa (1.5 psi) and a moisture content around 0.50 m^3/m^3 Lu et al. (2009). Percent change seems to be greatest in the taller grasses. The velocities in the forage Bermuda and the Bahia mix increased approximately 20% compared to the bare soil. The sound speed in the common Bermuda, on the other hand, decreased around 10 – 15 % compared to the bare soil.

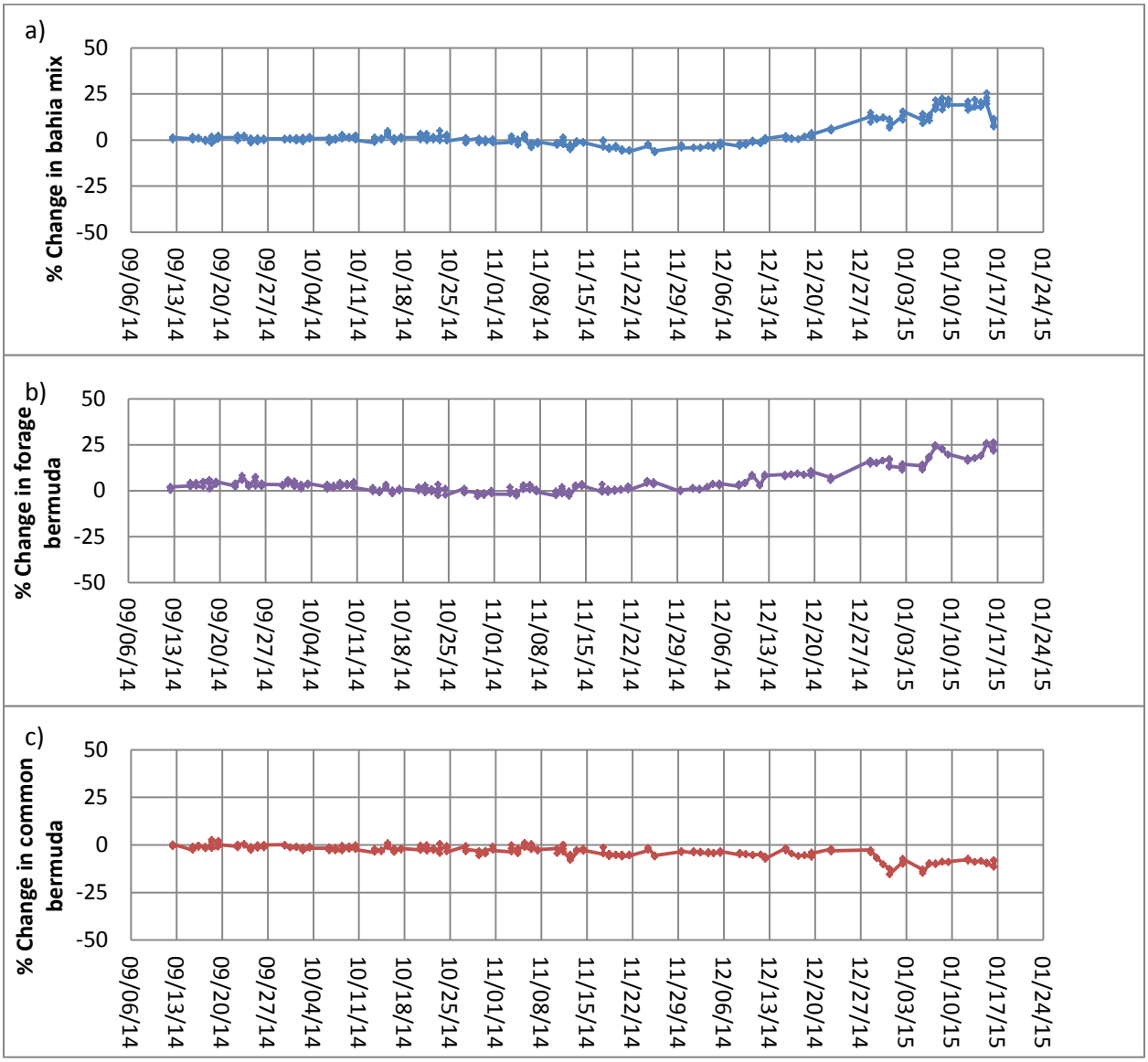

Figure 5 Percent change in sound speed with respect to bare soil for the a) wild Bahia mix, b) forage Bermuda, and c) common Bermuda grasses

The presented measurements to date aim to establish the sensitivity of acoustic measurements with the growth of different grass covers commonly used on earthen dams. In conclusion, an empirical relationship between root growth and sound speed has yet to be determined. More data will be collected over the next months as grass root matrixes become denser. If larger changes in acoustic velocity are observed with the further root growth, the project will be extended to measure the acoustic response as well as erodibility on controlled soil surfaces with several different types of grass covers and cross-plot acoustic, erodibility and grass cover properties to evaluate empirical relationships.

REFERENCES

Berkenhagen, J. H., Hickey, C. J., Prasad, S. N., & Römkens, M. J. M. (1998). "Acoustic Observation of a Clay during a Wetting-Drying Cycle." In Proceedings of the Bouyoucos Conference on Agroacoustics **Third Symp., Tishomingo, MS**: 77-89.

Bonelli, S., & Benahmed, N. (2010). "Piping flow erosion in water retaining structures: inferring erosion rates from hole erosion tests and quantifying the failure time." In IECS 2010, 8th ICOLD European Club Symposium Dam Safety-Sustainability in a Changing Environment.

Briaud, J. L., Ting, F. C. K., Chen, H. C., Cao, Y., Han, S. W., & Kwak, K. W. (2001). "Erosion function apparatus for scour rate predictions." Journal of Geotechnical and Geoenvironmental Engineering **127**(2): 105-113.

Brutsaert, W., and James N. Luthin (1964). "The velocity of sound in soils near the surface as a function of the moisture content." Journal of Geophysical Research **69**(4): 643-652.

Hanson, G. J. (1991). "Development of a jet index to characterize erosion resistance of soils in earthen spillways." Transactions of the ASAE **34**.

Hickey, C. J., Ekimov, A., Hanson, G. J., & Sabatier, J. M. (2009). "Time-lapse seismic measurements on a small earthen embankment during an internal erosion experiment." In 22nd EEGS Symposium on the Application of Geophysics to Engineering and Environmental Problems.

Howard, W., & Hickey, C. J. (2009). "Investigation of the near subsurface using acoustic to seismic coupling." Ecohydrology **2**(3): 263-269.

Lu, Z., Hickey, C. J., & Sabatier, J. M. (2004). "Effects of compaction on the acoustic velocity in soils." Soil Science Society of America Journal **68**(1): 7-16.

Powledge, G., Ralston, D., Miller, P., Chen, Y., Clopper, P., and Temple, D. (1989). "Mechanics of Overflow Erosion on Embankments. I: Research Activities." Journal of Hydraulic Engineering **115**(8): 1040-1055.

Richardson, C. (2001). Protecting Our Watersheds through Research and Management. Challenges and Opportunities. 2001.

Wan, C. F., & Fell, R. (2004). "Investigation of rate of erosion of soils in embankment dams." Journal of Geotechnical and Geoenvironmental Engineering **130**(4): 373-380.

Whalley, W. R., Jenkins, M., Attenborough, K. (2012). "The velocity of shear waves in unsaturated soil." Soil and Tillage Research **125**: 30-37.

COMPARING PROCESS-BASED BREACH MODELS FOR EARTHEN EMBANKMENTS SUBJECTED TO INTERNAL EROSION

Ronald D. Tejral, Agricultural Engineer, ronald.tejral@ars.usda.gov, and
Sherry L. Hunt, Research Leader and Research Civil Engineer, sherry.hunt@ars.usda.gov,
USDA Agricultural Research Service, Hydraulic Engineering Research Unit, Stillwater, OK

Abstract: A sustainable infrastructure is one for which the risks are understood. Part of understanding the risks for dams is considering the consequences of failure. Predicting the potential flooding from a dam site requires prediction of outflow resulting from breach. Conservative estimates from the assumption of instantaneous breach or from an upper envelope of historical cases are readily computed, but these estimates do not reflect the properties of a specific dam. If it is desired to understand the effects of soil materials, embankment construction, and reservoir characteristics, a process-based model is needed.

WinDAM C is the most recent module of the dam breach software under development by USDA-NRCS in cooperation with USDA-ARS and Kansas State University. It builds on the functionality of previous WinDAM releases (evaluation of embankment surface protection, breach by overtopping, and integrity of auxiliary spillways) by adding the ability to evaluate internal erosion. A process-based model of this type provides an additional tool for the engineer to evaluate the potential impact of site-specific characteristics including erosion process, embankment materials, reservoir storage, and embankment geometry. In addition, this tool may aid in the development of flood warning systems, emergency action plans, and prioritizing dams for rehabilitation.

In this study, results of WinDAM C are compared and contrasted to those obtained using BREACH. A set of hypothetical, synthetic dams was used to represent the range of USDA Small Watershed Structures by varying height and reservoir volume augmented by three variations of detachment/transport rate. Outcomes of historical failure cases and physical model studies were compared to the synthetic set. The work suggests that WinDAM is predicting in the correct order of magnitude and exhibiting appropriate sensitivity to material parameters.

INTRODUCTION

Dams are a component of infrastructure that play many critical roles: supplying municipal and rural water (i.e. for consumption, recreation, agricultural production, etc.), generating or even storing energy, and flood protection for not only populations of residents located downstream but also infrastructure like homes, utilities, and transportation routes. Take for example the subset of flood protection dams that were constructed through the assistance of the USDA Small Watershed Program. These dams were built in partnership with the USDA Natural Resources Conservation Service, formerly the Soil Conservation Service. Even in early projects, sustainability was considered. Careful consideration was given to assure cost was justified by the benefits. Furthermore, federal conservationists and private landowners laid out plans that reduced soil loss, thereby mitigating sediment delivery to the reservoir.

Another facet in the sustainability of dams is risk analysis. The essential questions revolve around 1) identifying incident types and their probabilities and 2) assessing the outcome of each incident type if it were to occur. This report is concerned with the latter, and for that purpose estimates from the assumption of instantaneous breach or from an envelope of historical cases are readily computed. However, the effect is that all dams sharing only the most basic parameters, e.g. height and storage, are predicted to behave identically. Even the limited number of failure cases illustrates this is not true. If it is desired to understand the effects of soil materials, embankment construction, and reservoir characteristics, a process-based model is needed.

Fread (1988) with the National Weather Service developed an early model (BREACH) for breach prediction. Modelers could examine breach by modes of overtopping and internal erosion, which was termed piping. Erosion was computed using the Meyer-Peter and Müller formula as adapted for steep channels by Smart (1984).

WinDAM C is the most recent module of the dam breach software under development by USDA-NRCS in cooperation with USDA-ARS and Kansas State University. Earlier modules supported evaluation of embankment surface protection, breach by overtopping, and integrity of auxiliary spillways. In contrast to BREACH, erosion is computed as detachment-limited and taking the form of a headcut. The headcut behavior is included in the modeling of breach by internal erosion.

To compare these models, a set of inputs was developed which represent the trends of the dams in the USDA Small Watershed Program. Outcomes of historical failure cases and physical model studies were compared to those for representative dams within the synthetic set. This is a part of a more comprehensive and ongoing effort to verify and validate WinDAM C.

METHODS

Because few high quality data sets exist, this exercise was conducted using a synthetic set of dams. This set is derived from existing trends in dams and physical modeling. To aid in assessing the models, other methods of peak breach discharge were used as comparators.

Synthetic Set: The synthetic set of dams consists of a realistic series of dam sizes to evaluate and compare model predictions. A comprehensive database of basic dam parameters is found in the National Inventory of Dams maintained by US Army Corps of Engineers (2007). This database was used to quantify a typical dam built under the USDA Small Watershed Program. Height was selected as the independent variable and median height was found to be 32 ft. A series of heights based on powers of two were selected to include the median and span the range within the USDA Small Watershed Program from 4 to 128 ft.

Reservoir Characteristics: The next step was to define a height to storage relationship. The median trace of maximum storage volumes through these heights with bin boundaries determined by midpoints in logarithmic space was constructed. For example, the representative reservoir storage for 32 ft dams was selected by finding median from within $2^{4.5} \leq h_d < 2^{5.5}$ ft, or $22.6 \leq h_d < 45.3$ ft. A second-degree polynomial was fit to the values:

$$V_{max} = 0.39h_d^2 - 2.5h_d + 220 \quad (1)$$

where V_{max} = maximum storage volume (assumed to correspond to top of dam), ac-ft, and
h_d = dam height, ft.

Storage relationship is plotted in Figure 1; reduced data are shown in Table 1.

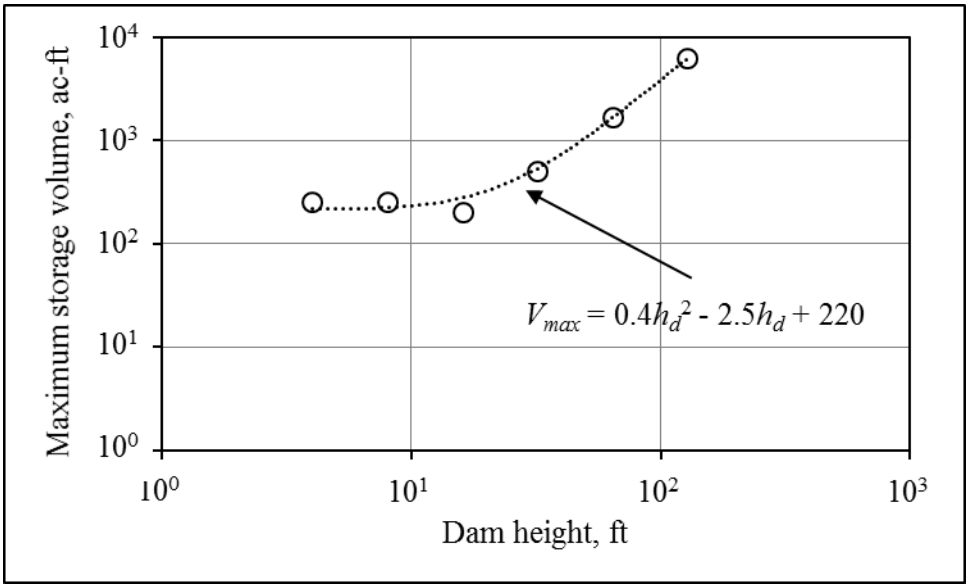

Figure 1 Dam height versus maximum storage volume.

The other reservoir characteristic is shape, which can be described by a hypsometric function. It is presented here similar to Walder and O'Connor (1997):

$$V = V_{max}\left(\frac{h}{h_d}\right)^m \quad (2)$$

Where V = volume of water in reservoir at h, ac-ft,
h = reservoir level, relative to base of dam, ft, and
m = shape parameter.
A fixed shape as defined by m = 3 was used throughout. This reservoir shape may be visualized as a cone as per Clarke (1982) or pyramid (of any base) with vertex at bottom and base defined by water surface.

While WinDAM accepts hypsometry data as height versus either volume or area, BREACH is restricted to area. Equation 2 was differentiated with respect to h to solve for area.

Dam Geometry: Embankment length is included in the NID. In finding the median length for each range of dam height, interesting behaviors are observed and reported in Table 1. Short dams (4 and 8 ft) tend to be long relative to their height. A plausible explanation are NID criteria, which would exclude all low hazard dams in this range unless they are both 6 ft high and store 50 ac-ft

or more; dams that meet inclusion on this criterion alone will tend to be long. From median heights of 16 to 64 ft, the trend is for length to increase linearly with height. This part of the data behaves as one might expect. These expectations are not unreasonable given this is the region in which bulk of data resides, and therefore has shaped our expectations. However, the trend does not continue into the bin with median height of 128 ft. Here, the explanation is likely a combination of topography and design criteria. The authors suspect that in general these dams are located in more steeply incised valleys, and were therefore taller to attain the storage necessary for flood control. This tendency toward a narrower valley led, in turn, to shorter lengths. Despite the lack of a clear trend, the overall variation in length was not extreme: median lengths do not even double (while dam height and maximum volume span one and nearly three orders of magnitude, respectively). For this reason, a single length of all dams was arrived at from average of the median lengths rounded to 1 significant figure: 900 ft.

While length was a field in the NID, other guidance was needed to select top width and slopes. A relationship for varying top width was defined using guidance on minimum top width by USDA-NRCS (2005). While actual top widths may be greater, it was assumed that these minimums were representative. The resulting top widths are reported in Table 1.

The final geometric considerations were upstream and downstream slopes. According to US Bureau of Reclamation (1987) upstream slopes are typically 2.5 or 3 (horizontal) to 1 (vertical). Similarly, Ralston (1987) stated that downstream slopes are usually 2.5:1 or 3:1. For the exercise, 3:1 was selected for both upstream and downstream slopes.

Table 1 Dam heights, medians of maximum storage volume, maximum storage volume of synthetic set, median crest lengths, and top widths.

Dam height, h_d, ft	Bin median of Maximum Storage Volume, ac-ft	Maximum Storage Volume as computed by eqn. 1, V_{max}, ac-ft	Median crest length, ft	Top Width, ft
4	254	220	1231	8
8	253	220	931	8
16	203	280	706	10
32	503	540	840	14
64	1687	1660	1018	14
128	4806	6300	855	16

Material Properties: Each model requires some quantification of the rate at which material comprising the dam will be eroded or transported. In WinDAM C, the notable parameters are erodibility (k_d) and critical shear stress (τ_c). They are obtainable by jet erosion test developed by

Hanson (1991) among other methods. The rate of headcut advance may be increased by slide of the headcut face principally as a function of undrained shear strength (c_u).

BREACH uses the Meyer-Peter and Müller equation as modified for steep slopes by Smart (1984) to model transport. This relation employs descriptors of the material's gradation: uniformity (D_{90}/D_{30}) and median particle size (D_{50}), being more sensitive to the latter. Additionally, the rate of failure can be increased by computations which rely on strength parameters, cohesion (C) and friction angle (ϕ) to predict slope failure. In contrast to WinDAM, these slope failures are of the channel sides.

Rather than arbitrarily varying any or all these parameters, three combinations of these were selected to correspond to physical tests conducted by ARS. The experiments from which they were taken presented a range of failure rates: Breach formation in less than 30 minutes to incomplete breach (initiation, but not formation) at 24 hours. Representative values of the soil test results and estimated parameters are presented in Table 2. For BREACH, gradation was available, but strength parameters were estimated from unconfined compression results.

Soils information also may be used by BREACH to estimate Manning-Strickler roughness. In an example Fread (1988) recommended use of Darcy friction factor and Moody diagram for a soil with median grain size diameter of 1 mm. As all soils represented here were of $D_{50} < 1$ mm, that was the method employed.

Table 2. Soils information.

Soil Property	Synthetic subset		
	High	Medium	Low
Unified Classification	SM	ML	CL
Plasticity Index	non	3	15
Erodibility, k_d, $ft^3\ lb^{-1}\ hr^{-1}$	70	1.3	0.3
Critical shear stress, τ_c, psf	0	0.2	0.2
Undrained shear strength, c_u, psi	300	700	1700
Cohesion, psf	150	400	1000
Friction angle, degrees	32	32	28
D_{50}, mm	0.14	0.04	0.02
Uniformity, D_{90}/D_{30}	4	50	130

Initial Conditions: Both models define the path of internal erosion very simplistically. The user specifies initial dimensions and invert elevation, and it is assumed to be horizontal and perpendicular to the crest. Longitudinally, BREACH models the path as located at center of dam relative to length, while WinDAM allows the station to be specified. For these simulations,

internal erosion was modeled as located at the centerline station and at elevation coinciding with $0.25h_d$ above base of dam base. The internal erosion was assumed to be initiated with a void square in cross section and having dimensions of 0.2 ft high and 0.2 ft wide.

A sunny-day failure is simulated with water surface elevation at $0.75h_d$ above dam base and little or no inflow. BREACH has been known not to run with a hydrograph having zero inflow as experienced by Tejral (2009), and therefore a constant inflow of 1 cfs was used.

Comparators: To provide context for the model results, USDA-NRCS peak discharge criteria and a subset of failure cases and experiments were used as comparators.

TR-60 Peak Breach Discharge: The peak breach discharge as predicted by the criteria in USDA-NRCS (2005) TR-60 was computed for each dam of the synthetic set. Because depth of water for all dams was less than 103 ft, the first equation that applied was

$$Q_{max} = (1{,}100)\left[\frac{(V_s)(H_w)}{A}\right]^{1.35} \quad (3)$$

where Q_{max} = peak discharge, ft^3/s
V_s = reservoir storage at time of failure, ac-ft
H_w = depth of water at time of failure, ft, and
A = cross-sectional area of embankment at breach location, ft^2.

Recall that short dams of the synthetic set had disproportionally large storage relative to population. This brought into play additional criteria that places an upper envelope on peak discharge (when $H_w \leq 103$ ft).

$$Q_{max} = (65){H_w}^{1.85} \quad (4)$$

The effect is that Q_{max} for the dam heights of 4 and 8 ft plot slightly above the trend established by higher dams.

TR-60 additionally considers effect of valley cross section. Here it was assumed that the valley did not constrain peak discharge.

Failure and Experimental Cases: The failed dams cases were selected from Wahl (1998) where piping was identified as the failure mode; rockfill embankments were excluded. There was no further screening of data to match synthetic set characteristics. Added to these failure cases were the three experiments conducted by ARS (and from which soils information was used to construct synthetic set). The testing conditions of these 4-ft high embankments closely matched the synthetic set criteria describe in *initial conditions*. The selected cases and their peak breach discharges are reported in Table 3.

Table 3 Peak breach discharges for earthen dam failures for which piping was mode from Wahl (1998) and experiments conducted by USDA-ARS.

Case	Dam Height, ft	Peak Breach Discharge, ft^3/s
Apishapa, Colo.	112	6850
Baldwin Hills, Calif.	233	1130
Bradfield, England	95	1150
Davis Reservoir, Calif.	39	510
Frankfurt, Germany	32	80
Fred Burr, Mont.	34	650
French Landing, Mich.	40	930
Frenchman Creek, Mont.	41	1420
Kelly Barnes, Ga.	38	680
Lake Avalon, N.M.	48	2320
Lake Latonka, Penn.	43	290
Lawn Lake, Colo.	26	510
Little Deer Creek, Utah	86	1330
Lower Two Medicine, Mont.	37	1800
Teton, Idaho	305	65120
ARS Piping 1	4	110
ARS Piping 2	4	100
ARS Piping 3	4	40

RESULTS AND DISCUSSION

Peak breach discharges were tabulated for the completed model runs. In Figure 2 all results of WinDAM are shown, while the results corresponding to only the medium erodibility dams were plotted for BREACH. This was done because the predictions were essentially identical, and separate series could not be readily perceived on log-log plot.

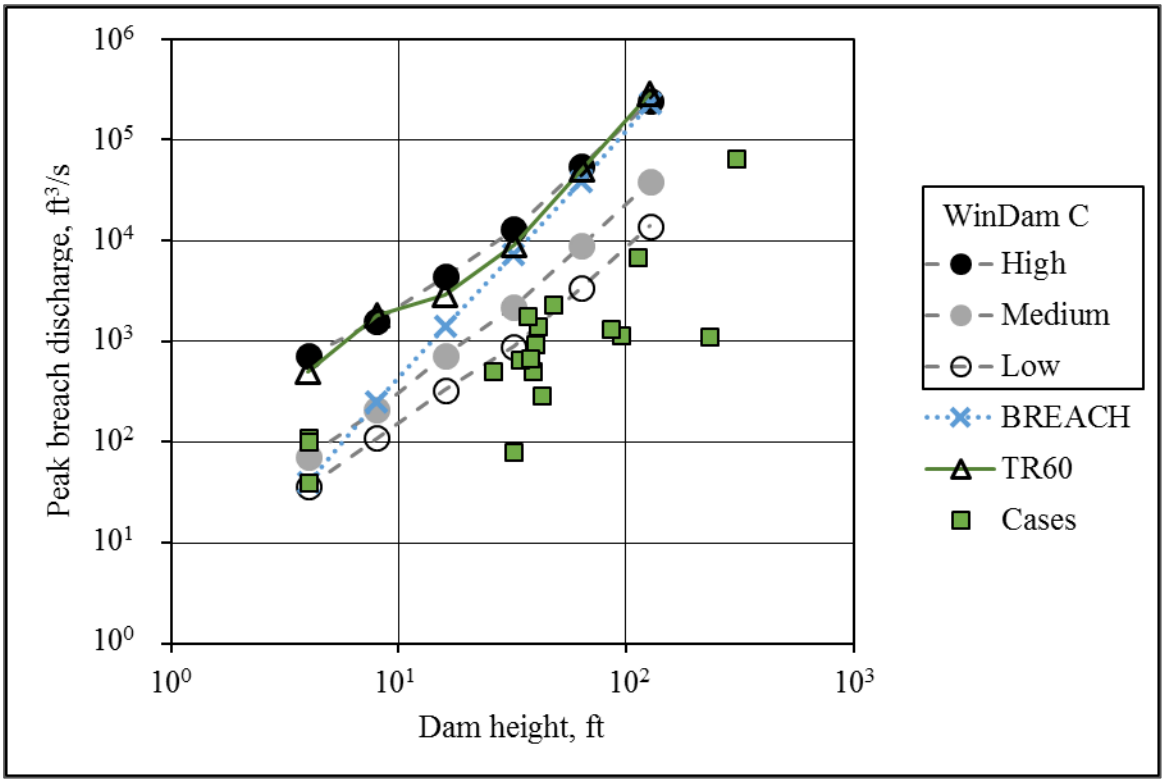

Figure 2 Peak breach discharge versus dam height for synthetic sets as predicted by WinDAM C and BREACH. For context also plotted are peak breach discharge for NRCS TR-60 and selected failure cases from Wahl (1998) and ARS research.

Relative to TR-60, BREACH arrives at very similar predictions for dams from 32 to 128 ft in height. WinDAM results for highly erodible dams track closely to the TR-60 relation throughout the full range of heights. Results for the more erosion resistant subsets (Medium and Low erodibility) roughly parallel the TR-60 series, but fall well below it, approximately an order of magnitude for the Low subset.

While plotted as points, there is often considerable uncertainty in the peak discharge. This uncertainty aside, note that none of the cases from Wahl plots above the Medium subset as predicted by WinDAM.

Times of peak discharge were also examined. While peak discharge exhibited little sensitivity in BREACH, there were discernible differences in time. The model tended to predict peak discharge of the highly erodible dams would occur in about twice the time as for low erodibility dams. For WinDAM, the time to peak was roughly 20 to 30 times greater for the low erodibility dams than the high erodibility dams. This was consistent with the behavior of physical models at USDA ARS.

CONCLUSIONS

Based on WinDAM results, for dams that are near the median storage, highly erodible material would be necessary for maximum discharge to approach that predicted by TR-60 equations. Conversely, if they were to breach under a similar scenario, most of the USDA Small Watershed Program structures would likely exhibit peak discharges well below TR-60.

The soils used to develop the synthetic sets exhibited considerably different erosion rates when tested. Note in the discussion that BREACH predicted the highly erodible dams would reach peak discharge *later* than more erosion resistant dams. For materials of higher plasticity, BREACH computes a critical shear stress similar to that found by jet erosion test. However, the representative diameter dominates the MPM-Smart equation. In BREACH, recall that roughness was estimated using soil gradation. This roughness was likely not representative of the form roughness that is more relevant to modeling flow rate. A user-selected roughness, however, further limits BREACH's sensitivity to a soil's characteristics. Because BREACH is unable to differentiate the behavior for these very different soils, this study further illustrates the difficulty in modeling detachment of cohesive materials as sediment transport.

The TR-60 equations and internal erosion cases suggest WinDAM is predicting in the correct order of magnitude. However, additional testing of the WinDAM model is needed to determine validity and bounds of application.

In closing, it is reiterated that the work presented here is part of the verification and validation testing by the developers. It is anticipated that WinDAM will be made available to a broader group for additional validation testing in the near future. As with any model, the results presented here require sound engineering judgment when applied.

ACKNOWLEDGEMENTS

The authors thank Mitch Neilsen, Don Hazlewood, and Darrel Temple for their support of WinDAM software.

REFERENCES

Clarke, G. K. (1982). Glacier outburst floods from "Hazard Lake," Yukon Territory. and the problem of flood magnitude prediction. *Journal of Glaciology, 28*(98), 3-21.

Fread, D. L. (1988). *Breach: An erosion model for earthen dam failures.* Silver Spring, Maryland, USA: National Weather Service, NOAA.

Hanson, G. J. (1991). Development of a jet Index to characterize erosion resistance of soils in earthen spillways. *Transactions of the ASAE, 34*(5), 2015-2020.

Ralston, D. (1987). Mechanics of embankment erosion during overflow. *1987 National Conference on Hydraulic Engineering* (pp. 733-738). Reston, Virginia: ASCE.

Smart, G. M. (1984). Sediment transport formula for steep channels. *Journal of Hydraulics Division, 110*(HY3), 267-276.

Tejral, R. D. (2009). *Impact of dam and reservoir parameters on peak breach discharge predictions.* Master Thesis, Oklahoma State University, Stillwater.

US Army Corps of Engineers. (2007). *National Inventory of Dams*. Retrieved from http://nid.usace.army.mil

US Bureau of Reclamation. (1987). *Design of Small Dams.* Washington, D.C.: U.S. Governement Printing Office.

USDA-Natural Resources Conservation Service. (2005). *Earth Dams and Reservoirs.* Washington, D.C.: United States Department of Agriculture.

Wahl, T. L. (1998). *Prediction of embankment dam breach parameters: A literature review and needs assessment. DSO-98-004.* Denver, Colorado: Dam Safety Office, Water Resources Laboratory, U.S. Bureau of Reclamation.

Walder, J. S., & O'Connor, J. E. (1997). Methods of predicting peak discharge of floods caused by failure of natural and constructed earth dams. *33*(10).

NONDISCRIMINATION STATEMENT

EFFECTIVENESS OF CHANNEL IMPROVEMENT WORK ON THE MISSISSIPPI RIVER

Richie McComas, Hydraulic Engineer, USACE Vicksburg District, Vicksburg, MS, Richie.McComas@usace.army.mil; and C. Fred Pinkard, Jr., Hydraulic Engineer, USACE, Vicksburg District, Vicksburg, MS, Freddie.Pinkard@usace.army.mil.

Abstract: The Mississippi River has long been a major contributor to the physical and economic development of our nation. However, at the time that the United States was first settled, the Mississippi River was a natural alluvial stream characterized by a wide, shallow channel, numerous shifting sandbars, and large fluctuations in stage. The river was active and freely meandered across its floodplain. In this natural state, the river could not provide a dependable channel to meet the nation's commercial navigation needs nor could it provide for the efficient passing of flood flows.

To meet both navigation and flood control needs, a dependable, low maintenance channel had to be developed. Initially, dredging was conducted to provide adequate depths for navigation and levees were constructed to ease flooding problems. However, these measures alone proved ineffective. Then in 1927, a great flood devastated the entire Mississippi River Valley. As a result of this flood, Congress passed the Flood Control Act of 1928. This legislation authorized the U. S. Army Corps of Engineers to develop a comprehensive system of flood control and navigation improvements for the Lower Mississippi River. To provide an efficient navigation channel and to provide protection for the flood damage reduction levees, the banks of the river had to be locked in place. In response to this need, the Corps of Engineers initiated a comprehensive bank stabilization program. The use of revetment consisting of articulated concrete mattress (ACM) on the lower bank in conjunction with stone paving on the upper bank has proved to be most effective in controlling the erosion of the river's banks. However, revetment alone was not sufficient to provide a low maintenance channel. During low water periods, substantial dredging was required to maintain adequate channel dimensions. As a result of this continued dredging, a system of stone dikes was developed to provide adequate channel dimensions through trouble reaches. Now approximately 85 percent complete, the dike program has greatly reduced the expensive dredging requirements. Dredging within the Vicksburg District is only occasionally required in a limited number of isolated problem reaches.

Even with the proven success of the channel improvement program, additional work is required. With continued construction of the remaining planned channel improvement structures and continued maintenance of existing structures, an efficient navigation channel will continue to be provided on the Lower Mississippi River. During 2001 a paper which summarized the effectiveness of channel improvement work on the Mississippi River was prepared for the 7th Federal Interagency Sedimentation Conference. This current paper provides an update and expands on the information provided in that paper, takes a more detailed look at the project's environmental conservation and enhancement features, and identifies the performance of the channel improvement features during both the historic flood of 2011 and subsequent extreme low water in 2012.

BASIN CHARACTERISTICS

The Mississippi River drainage basin is the third largest in the world, exceeded in size only by the Amazon River in South America and the Congo River in Africa. The Mississippi River drains 41 percent of the lower 48 states, including all or parts of 31 states, extending from New York in the east to Montana in the west. The Ohio, Missouri, Tennessee, Arkansas, and Red River basins are part of the Mississippi River basin. The Mississippi River flows some 2,350 miles from its source at Lake Itasca in Minnesota to the Gulf of Mexico. The Lower Mississippi River Valley extends from just below Cape Girardeau, Missouri for approximately 600 miles to the Gulf of Mexico. The lower valley ranges in width from 30 miles to 125 miles with an average width of 45 miles and includes parts of Missouri, Illinois, Kentucky, Tennessee, Arkansas, Mississippi, and Louisiana. Figure 1 is a map that identifies the boundaries of the Mississippi River basin.

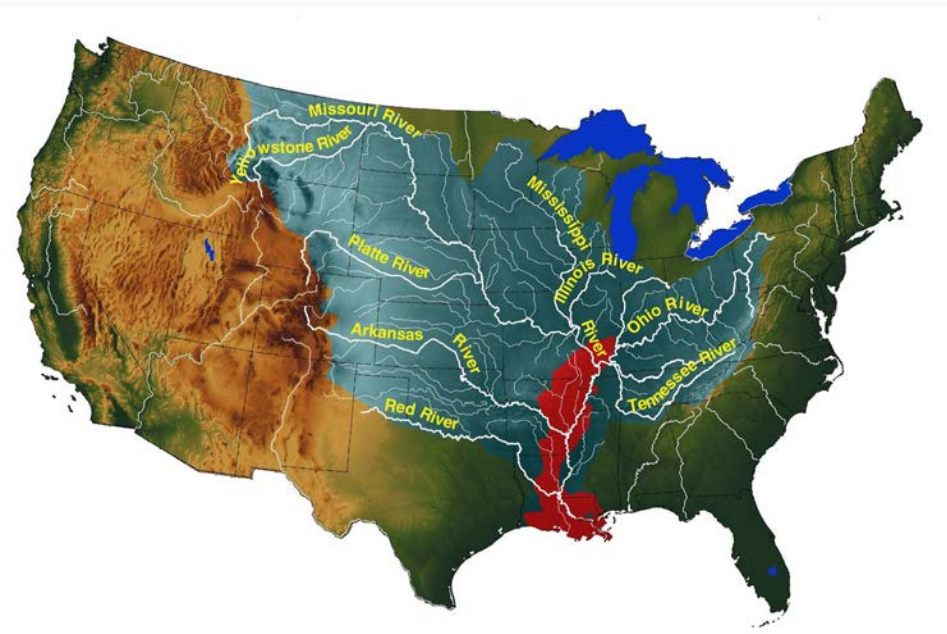

Figure 1. Mississippi River Drainage Basin

On the Mississippi River, flows, stages, and channel velocities vary over a wide range. During the 1943 through 2014 period, the average flow at Vicksburg, Mississippi was 625,000 cubic feet per second (cfs). The minimum recorded flow during this 71-year period was 126,000 cfs during January 1964 while the maximum recorded flow was approximately 2,300,000 during the 2011 flood. During that period, flows ranged on average from a low of around 305,000 cfs to a high of about 1,000,000 cfs. River stages also vary greatly. During the 1943 through 2014 period, the average annual low stage at Vicksburg was 54.1 feet, National Geodetic Vertical Datum (NGVD), the average stage was 66.3 feet, NGVD, and the average annual high stage was 78.4 feet, NGVD. Based on these averages, stages typically varied a little over 24 feet from annual highwater to low water. The lowest stage ever recorded at Vicksburg was 39.2 feet, NGVD during February 1940 while the highest stage recorded was 103.3 feet, NGVD during the 2011

flood. Channel velocities typically range from about 2 to 3 feet per second during low water to over 10 feet per second during highwater.

The Mississippi River is an alluvial river that carries a large and highly variable sediment load. Available data indicates that the annual suspended sediment load at Tarbert Landing, Mississippi (River Mile 306.3) has varied from about 70,000,000 tons to over 575,000,000 tons. Between 1963 and 2005, the average annual measured suspended sediment load was approximately 150,000,000 tons (Thorne et al., 2015). This sediment load equates to 133 tons per square mile of contributing drainage area per year. Sieve analyses indicate that on average, this suspended sediment load consists of about 20 percent sand and 80 percent fine material (silt and clay). Studies have indicated that over time, the measured suspended sediment load on the Mississippi River has significantly decreased primarily due to the construction of the channel improvement features, closure of multipurpose reservoirs, and improved land use management procedures. However, since the measured suspended sediment load is predominantly silt and clay, which are not found in large quantities in the bed, the total measured suspended sediment load could have decreased without any decrease in the bed material load, which is mostly unmeasured. In fact, as pointed out by Biedenharn (1995), the river through much of the Vicksburg and Memphis Districts has a steeper slope and larger stream power (QS) today than it did prior to the 1930's. Therefore, since studies (Nordin and Queen, 1992) show that the bed material size (D50) of the river has not changed significantly since the early 1930's, it is possible that the bed material load in these steeper reaches is higher today than it was prior to that time. This conclusion would suggest that more sediment of the size that deposits in the navigation channel and historically required removal by dredging is carried by the river today.

NAVIGATION DEVELOPMENT HISTORY

The Mississippi River has long been recognized as a valuable transportation benefit. Native Americans traveled the river by canoe for centuries before the European explorers arrived. The Europeans used the river for settlement expansion and small-scale commercial navigation to transport goods such as furs and supplies. The introduction of the steamboat during the early 19th century ignited an explosion of development along the river. However, the river was unpredictable and many steamboats fell victim to hazardous snags, shifting sandbars and high channel velocities. As early as 1820, the Federal Government recognized the importance of improving the Mississippi River for navigation. In that year, Congress appropriated funds for the preparation of a survey, maps, and charts of the Ohio and Mississippi Rivers. In 1824, the Corps of Engineers initiated channel improvement work by removing snags in the Mississippi River below the mouth of the Missouri River. For several years thereafter, channel improvement work was sporadic and limited to localized areas. All channel improvement work halted during the Civil War. As the country began to heal after the war, the need for more substantial Federal involvement in improvements of the river for navigation and flood control was generally recognized. In 1879, Congress established the Mississippi River Commission (MRC) to coordinate engineering operations within the Mississippi River Valley. The MRC was assigned the primary duties "…to take into consideration and mature a plan or plans and estimates as will correct and permanently locate, and deepen the channel and protect the banks of the Mississippi River; improve and give safety and ease to the navigation thereof; prevent destructive floods;

promote and facilitate commerce, trade, and the postal service…". In 1894, dredging began on the river. The success of these dredging operations prompted Congress in 1896 to authorize a 9-foot deep by 250- foot wide navigation channel from Cairo, Illinois to the Gulf of Mexico, to be maintained by dredging alone. However, dredging alone was not entirely effective in providing the required navigation channel and did not provide for the overall development needs of the valley. Then in 1927, the most disastrous flood in the history of the Lower Mississippi River Valley occurred. This flood inundated an area of about 26,000 square miles. During this flood, levees were breached, cities and towns were flooded, industry was paralyzed and crops were destroyed. Over 200 lives were lost and over 600,000 people were displaced. As a result of this flood, Congress passed the Flood Control Act of 1928, the nation's first comprehensive flood control and navigation act. This act increased the authorized navigation channel width to 300 feet and initiated a policy of river improvement and systematic construction of the channel improvement feature. The act also authorized the Mississippi River and Tributaries (MR&T) Project. Every year since the Flood Control Act of 1928 was passed, Congress has appropriated funds for the MR&T Project. The MR&T Project consists of four major components. These components include levees, floodways, tributary basin improvements, and channel improvement. Channel improvement includes stabilization to provide and maintain an efficient navigation alignment, increase the flood carrying capacity of the river, and protect the levee system. To provide for this component, an intense program of revetment and dike construction was initiated and is on-going today. The estimated total construction cost of the Vicksburg District's portion of the MR&T channel improvement program is $1,251,000,000. Through 2014, $1,083,708,129 (87%) has been expended. Maintenance is a critical part of the channel improvement program. Adequate funding must be provided in order to insure the continued functionality of the structures once they are constructed. The Vicksburg District currently receives maintenance funds annually. As more channel improvement works are completed and as existing works continue to age, more maintenance funds are required. However, the availability of funds for maintenance is not increasing resulting in maintenance requirements not being fully met.

Waterborne commerce on the Mississippi River has increased from 30 million tons in 1940 to nearly 500 million tons today. This tonnage includes such commodities as agricultural products including various grains, coal and coke, petroleum products, sand, gravel, and stone, salt, sulphur and other chemicals, among others. Without this valuable transportation system, the railways and highways would have to bear the burden of transporting these commodities. One standard barge that is 35 feet wide and 195 feet long has a capacity of 1,500 tons of cargo. One of these barges has the capacity of 15 railroad cars or 58 18-wheeler trucks. Therefore, it would require approximately 5,000,000 railroad cars or 19,230,000 18-wheeler trucks to transport the tonnage that moves on the Mississippi River today. The Mississippi River also provides an important link in the mobilization of our nation's defense forces. Therefore, the on-going development of the channel improvement program has resulted in the Mississippi River continuing to thrive as a crucial link for the country's economic development.

BANK STABILIAZTION

As is common on natural alluvial rivers, the Mississippi River has historically experienced bankline erosion and resulting migration. As evidenced by the numerous oxbow lakes and meander scars that exist today, the Mississippi River freely meandered across its floodplain. In

this natural state, the river was wide and shallow with numerous shifting sandbars. To provide a dependable navigation channel and to protect the flood damage reduction levees, the banks of the river had to be locked in place along the desired alignment. Therefore, an intense program of bank stabilization was initiated. In the past, several types of revetment have been used including willow, lumber, and asphalt mattresses. While these types of revetment proved somewhat successful, the most economical and effective means of protecting the banks continues to be a revetment composed of articulated concrete mattress (ACM) on the lower bank and stone paving on the upper bank. The current method of ACM placement is unique and is the result of years of research and development.

The use of ACM is restricted to large rivers due to the size of the floating plant required to place the mat. Therefore, in the Vicksburg District, ACM has only been used on the Mississippi River and on the lower Red River below the mouth of the Black River. The mat placement process includes several phases. The first phase involves clearing the bank. Many of the banks on the lower Mississippi River have vegetation that hinders the sinking process. Therefore, a narrow strip is cleared along the top bank to allow anchors to be provided during the sinking process. Caving banks are usually very steep. Therefore, to insure the stability of the revetment, the bank is graded to a flatter stable slope. The banks are graded by a large floating diesel-electric powered dragline. The clearing and grading of the banks are conducted on a schedule so that work is completed as close to the arrival of the mat-sinking unit as possible. This minimizes the potential for erosion of the freshly graded bank, reducing the overall cost of the operation and producing a better product. Natural vegetation re-establishes itself quickly along the stabilized top bank following completion of the revetment construction. Once the banks are graded, ACM is placed (or sunk) by the Mat Sinking Unit. The ACM consist of individual units of mat that are pre-cast and stored at strategically located casting fields along the river. Each unit contains 16 separate concrete blocks that are held together by corrosion-resistant wire embedded in the concrete. Each unit is 25 feet long by 4 feet wide by 3 inches thick and is commonly referred to as a square (100 square feet). Once the revetment season begins, the ACM squares are loaded onto barges and transported to the construction sites. Once on site, the squares are loaded on a specially designed mat-sinking barge. The squares are wired together into a mattress that is 140 feet wide and anchored to the bank with cables. As the mat is assembled, the sinking barge moves out into the river along the mooring barge. As the sinking barge moves, the ACM is launched off the barge and covers the river bottom. Placement of the mat continues to beyond the deepest part of the channel. The mat sinking plant is then moved upstream to lay the next section of mattress. This process continues with each succeeding mattress overlapping the previous mattress in a manner similar to shingles on a roof until the desired length of bank has been revetted. Once the ACM is sunk, placing stone riprap on the graded upper bank completes the revetment process.

ACM is typically placed during the low water season. On the lower Mississippi River, the revetment season usually extends from early September until all scheduled revetment placement is complete, usually in November. The location and amount of revetment placed each year is based on a prioritization of needed stabilization work and available funding. Through 2014, approximately 293 miles of revetment have been placed on the Mississippi River within the Vicksburg District with only 15 miles of revetment remaining to be constructed. Therefore, the revetment construction program is approximately 95 percent complete.

Figure 2. ACM Stacked on the Casting Field

Figure 3. Mat Sinking Unit

During 2011, the flood of record was experienced on much of the Lower Mississippi River with both record stage and discharge set at Vicksburg, Mississippi. During that event, the revetments were severely challenged. While damage did occur to some revetments, no catastrophic failures occurred to any of the revetments within the Vicksburg District. Therefore, during this historic event, the revetments continued to provide protection to the flood damage reduction levees by preventing channel migration due to eroding banks. Congress appropriated supplemental funds after the flood for damage repairs. As of late 2014, the Vicksburg District has completed all flood damage repairs to revetments.

CHANNEL CONTRACTION

The channel improvement feature that has had the greatest impact on dredging is dikes. Dikes are constructed on the Mississippi River to contract the width of the low water channel to provide and maintain adequate channel dimensions for navigation. Historically, dikes have been constructed of timber pile or stone or a combination of the two materials. Since stone is more permanent, this construction material is now used exclusively for dike construction. Dikes on the Mississippi River are constructed to a sufficient height to maintain an efficient low water channel but low enough so as not to hinder the passage of flood flows. Dikes within the

Vicksburg District are typically constructed so as to provide a 2,500-foot width between the riverward end of the dike and the opposite bank of the river. The Vicksburg District has been constructing channel control dikes on the Mississippi River since the early 1960's. As of 2014, 301 dikes totaling approximately 127 miles have been constructed. The dike construction program is approximately 85 percent complete with approximately 23 miles of dikes remaining to be constructed.

As previously mentioned, the Federal Government has been involved in dredging the Mississippi River since the 1890's. As the MR&T bank stabilization and channel control programs progressed, less dredging has been required to provide and maintain an efficient navigation channel. The Mississippi River is dynamic. As river conditions change, dredging is required in trouble reaches. As this occurs, dikes are designed and constructed to greatly reduce or eliminate required dredging.

Figure 4. Mississippi River Dike Field

Records indicate that required dredging within the Vicksburg District often well exceeded 10,000,000 cubic yards per year during the 1960's and the first half of the 1970's. However, during those years, the dike construction program was in its infancy. Figure 5 presents a graphical comparison of the annual dredging conducted on the Mississippi River within the Vicksburg District versus the cumulative amount of completed dike construction. This plot is for channel dredging only and does not include required dredging in the harbors. As the figure shows, in 1970 over 18,000,000 cubic yards were dredged. By that time, a total of less than 35 miles of dikes had been constructed. As the dike construction continued, the amount of dredging required to maintain a dependable low water navigation channel drastically decreased. In 1980, approximately 4,600,000 cubic yards of dredging was required and almost 65 miles of dikes were complete. In 1988, only 4,700,000 cubic yards were dredged even though the basin was experiencing a severe low water with river stages falling lower than had occurred in several decades. At Vicksburg, the low stage recorded in 1988 was the lowest in almost a quarter century. By 1988, just over 75 miles of dikes had been constructed. During the late 1990's and the early 2000's, less than 2,000,000 cubic yards were dredged annually. An increase in dredging was experienced during the later part of the 2000's. This can be primarily attributed to

changing channel conditions at Victoria Bend. The Vicksburg District designed and constructed additional dikes at Victoria Bend during recent years that has lead to a decrease in the need for dredging at this location. In fact, during 2011and 2013, no channel dredging was required in the Vicksburg District and only 282,000 cubic yards were dredged during 2014. Extreme low water occurred during 2012. That year, the lowest stage was recorded at Vicksburg, Mississippi since the extreme low water in 1988. In fact, 86 days with stages below 2 feet were recorded at Vicksburg from July through December 2012. This extreme, long duration low water severely challenged the effectiveness of the channel control dikes especially after many had been damaged during the historic flood experienced the previous year. A combined 6,400,000 cubic yards of channel dredging was required in 2012 at Victoria Bend plus an additional 5 different locations. Since that time, many of the dikes damaged during the 2011 flood have been repaired. However, repair work is still required at approximately 15 dikes. Repairs are being made as funding becomes available. Figure 5 shows the drastic reduction in required dredging as dike construction has progressed. Even during the extreme low water years of 1988 and 2012, channel dredging was limited to manageable amounts. The limited required dredging is a testament to the effectiveness of the channel improvement program.

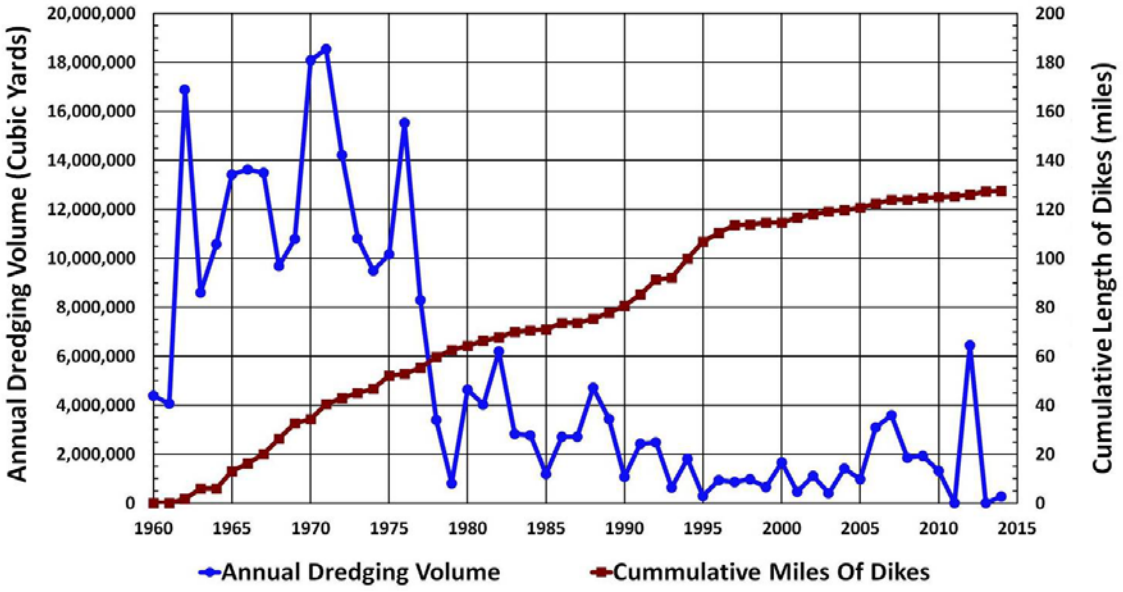

Figure 5. Mississippi River Channel Dredging Versus Cumulative Length of Dikes in Vicksburg District (1960 – 2014)

Environmental Conservation and Enhancement

Since the 1990's, the Vicksburg District has made a concerted effort to provide channel improvement features that not only provide for the authorized missions of flood damage reduction and navigation but also conserve or enhance the environment. For both revetments and dikes, a no work period is provided during April, May, and June for the pallid sturgeon spawning season. Also, restrictions are enforced on both revetment and dike work within set distances from known nesting least terns. Since the mid 1990's, environmental enhancement has

been provided by way of constructing grooves on the surface of the articulated concrete mat. The surface of the mat is grooved during the casting process by dragging a large wire brush type tool over the uncured concrete after it is placed into forms. Use of the grooved mat improves the aquatic habitat provided by the river by increasing the surface area for growth of macro-invertebrates which retain and recycle organic materials that would otherwise be lost from the system. This process provides a food source for fish with recreational, ecological, and economical value.

One of the environmental features currently used by the Corps of Engineers for dikes is the notched concept. By leaving a notch in selected dikes, the navigation channel can be maintained while at the same time provide diverse habitats for a variety of species including fish and the endangered least tern. The intended result is to insure that flow is maintained for longer durations in secondary channels than would otherwise be provided without the notches. The size and location of the notch in dikes is determined by the overall configuration of the river channel at each specific location. The Vicksburg District provides notches with varying widths and bottom elevations of the notch depending on the site. The District's current plan is to notch all future dikes that are constructed across secondary channels. All existing dikes extending across secondary channels that require raising in the future will also be notched at the time they are raised. The Vicksburg District first constructed notched dikes on the Mississippi River during the mid-1980's. Since that time, some 86 notched dikes have been constructed within the District. Figure 6 is an example of a notched dike.

Figure 6. Mississippi River Notched Dike

During 2011 and again in 2013, the Vicksburg District partnered with the U.S. Fish and Wildlife Service, Mississippi River Trust, and the Lower Mississippi River Conservation Committee (LMRCC) to improve habitat for species in the lower Mississippi River without compromising the vital navigation and flood risk reduction systems. The LMRCC is a coalition of 12 state natural resource conservation and environmental quality agencies in Arkansas, Kentucky,

Louisiana, Mississippi, Missouri, and Tennessee. The LMRCC was formed in 1994 and is dedicated to conserving the natural resources of the lower Mississippi River floodplain. This partnership involved the notching of 4 existing dikes at Island 70 and 2 existing dikes at Below Prentiss and another 2 existing dikes at Catfish Point for secondary channel restoration. Each partner agency has a clearly defined role in completing these projects. The Corps of Engineers provides engineering design and construction oversight. The LMRCC secures all necessary permits for regulatory compliance, coordinates all activities and procures the construction contract. Funding for the construction is provided by the USFWS through the Fish Passage Program (Prestwood and Rodgers, 2014). Figure 7 is a photograph of an existing dike at Island 70 being notched.

During July 2013, the Corps of Engineers Mississippi Valley Division in consultation with the U.S. Fish and Wildlife Service (USFWS) developed a conservation plan for three endangered

Figure 7, Dike Notching at Island 70

species on the Lower Mississippi River. Those species include the interior least tern, pallid sturgeon, and the fat pocketbook mussel. Specifically, the conservation plan is a programmatic mechanism by which the channel improvement program of the Mississippi River and Tributaries (MR&T) Project is being utilized to implement conservation measures that maintain and improve habitat values within the Lower Mississippi River for recovery of endangered and other trust species inhabiting the river channel. As a result of the information presented in the conservation plan, the USFWS issued a biological opinion on the channel improvement program on the Lower Mississippi River in December 2013. A biological opinion is required to determine if Federal action (channel improvement program) is likely to jeopardize the existence of a listed (threatened or endangered) species or result in the destruction or adverse modification of critical habitat. The conclusion of the biological opinion was stated by the USFWS as follows: "After reviewing the current status of the interior least tern, pallid sturgeon, and fat pocketbook mussel, the environmental baseline for the action area, the effects of continued operation and maintenance of the channel improvement program, it is the Service's biological opinion that the channel

improvement program is not likely to jeopardize the continued existence of the interior least tern, pallid sturgeon, and fat pocketbook mussel. No critical habitat has been designated for these species; therefore, none will be affected."

CONCLUSIONS

The Mississippi River has been and remains a major contributor to the physical and economic development of the nation. It carries the runoff from rainfall and snow melt for about 41 percent of the contiguous United States plus a small portion of Canada along with about 150,000,000 tons of sediment annually to the Gulf of Mexico. The river also supplies water for millions people and unnumbered industries and power plants. Currently, approximately 500,000,000 tons of commerce are transported on its navigation channel annually. Since their inception, the channel improvement works completed by the Corps of Engineers have contributed significantly to the efficient operation of this mighty river and its service to the nation. More recently, the systematic placement of channel training structures have significantly reduced the need for costly dredging to maintain a dependable navigation channel. The revetment program proved invaluable during the historic 2011 flood in maintaining channel alignment and protecting the flood damage reduction levees from channel migration. Also, the channel improvement program features being utilized to implement conservation measures have proved effective in maintaining and improving habitat values within the Lower Mississippi River for recovery of endangered species that inhabit the river channel.

REFERENCES

Biedenharn, David S., 1995, Lower Mississippi River Channel Response: Past, Present, and Future, Dissertation for Degree of Doctor of Philosophy, Colorado State University, 127.

Nordin, C. F. and Queen, B. S., 1992, Particle Size Distributions of Bed Sediments Along the Thalweg of the Mississippi River, Cairo, Illinois to Head of Passes, Potamology Program (P-1), Report 7, U.S. Army Corps of Engineers, Lower Mississippi Valley Division, Vicksburg, Mississippi.

Prestwood, Deanna. and Rodgers, Angeline, Summer 2014, "Engineering Ecosystem Restoration – A Partnership Approach", Our Mississippi, U.S. Army Corps of Engineers.

Robinson, Michael C., Ethridge, Loyde T., U.S. Army Corps of Engineers, Lower Mississippi Valley Division, Mississippi River Commission August 1984, History of Bank Protection Through The Use Of Revetments.

Thorne, Colin R., Knuuti, Kevin, Harmar, Oliver, Waston, Chester, and Biedenharn, David, April 2015, "Recent and Historical Sediment Loads in the Lower Mississippi River" SEDHYD Proceedings Paper, Reno, Nevada.

U.S. Army Corps of Engineers, Mississippi River Commission, September 1992, Lower Mississippi River Environmental Program, Report 19, Effects of Surface Texture of Articulated Concrete Mattress Blocks on Their Habitat Value.

U.S. Army Corps of Engineers, Mississippi River Commission and Lower Mississippi Valley Division, March 1976, Flood Control In The Lower Mississippi River Valley.

U.S. Army Corps of Engineers, Mississippi Valley Division and Engineer Research and Development Center, July 2013, Conservation Plan for the Interior Least Tern, Pallid Sturgeon, and Fat Pocketbook Mussel in the Lower Mississippi River (Endangered Species Act, Section 7(a)(1)).

U.S. Fish and Wildlife Service, Mississippi Field Office, December 2013, Biological Opinion, Channel Improvement Program, Mississippi River and Tributaries Project, Lower Mississippi River.

DEVELOPING A NEW STREAM METRIC FOR COMPARING STREAM FUNCTION USING A BANK-FLOODPLAIN SEDIMENT BUDGET: A CASE STUDY OF THREE PIEDMONT STREAMS

Edward R. Schenk, Research Ecologist, U.S. Geological Survey, 12201 Sunrise Valley Dr. Mail Stop 430, Reston, VA 20192 eschenk@usgs.gov;
Cliff R. Hupp, Research Botanist, U.S. Geological Survey, 12201 Sunrise Valley Dr. Mail Stop 430, Reston, VA 20192 crhupp@usgs.gov;
Allen Gellis Research Hydrologist, U.S. Geological Survey, 5522 Research Park Dr. Baltimore, MD 21228 agellis@usgs.gov;
Greg Noe Research Ecologist, U.S. Geological Survey, 12201 Sunrise Valley Dr. Mail Stop 430, Reston, VA 20192 gnoe@usgs.gov;

EXTENDED ABSTRACT

Suspended sediment is one of the most detrimental pollutants to the Chesapeake Bay.; Streams in the Piedmont Physiographic Province have the highest suspended sediment concentrations in the Bay watershed. The Piedmont region has been heavily impacted by historic land uses including land clearing for agriculture, colonial era riparian sedimentation, low-head dam construction, subsequent reforestation in the 20th century, and presently by urbanization including development near Washington, DC and Baltimore, MD. The Piedmont Physiographic Province is developing at a greater rate than any other portion of the Bay watershed while also contributing the highest sediment yield (Gellis et al. 2009).

One of the objectives of our study was to develop a metric for comparing stream function between basins through the quantification of floodplain and bank sediment storage and supply (see Schenk et al. 2013 for the full manuscript). In particular, we developed a floodplain trapping metric to compare streams with variable characteristics and determine the ability of a stream's floodplain to trap and retain sediment transported during flood events. This objective was accomplished by creating a bank and floodplain sediment budget (hereafter referred to as a "sediment budget") for three Piedmont streams tributary to the Chesapeake Bay and comparing these estimations to published sediment yields for the same streams. A second objective was to use this floodplain-bank sediment budget to better understand the processes that govern sediment dynamics within relatively small streams in the Piedmont region of the Chesapeake Bay.

The watersheds of each stream vary in land use from urban to agricultural but have similar catchment areas and annual stream discharges (Table 1). Linganore Creek (LIN) has the highest amount of agriculture in its watershed (Gellis et al. In Press). Little Conestoga Creek (LCC) is influenced by rapid urbanization from nearby Lancaster, PA as well as current and recent low-head dams that have influenced floodplain connectivity (Schenk and Hupp, 2009). Difficult Run (DR) has the highest amount of urbanization resulting in a flashier hydrograph than the other two streams (Hupp et al. 2013).

Table 1. Watershed characteristics of each studied stream. Sediment yield measurements from each stream are from their respective USGS streamgages except DR where an upstream streamgage collected sediment loads (USGS streamgage 01645704). Sediment loads were collected during Water Years 2008-2011, 2003, and 2009 for LIN, LCC, and DR respectively.

		Annual	Annual	Basin			
	USGS	mean discharge	sediment yield	Area	Land Use (%)		
Stream	streamgage	m^3/s (cfs)	$Mg/km^2/yr$	Km^2	Agriculture	Forested	Developed
Linganore Creek (LIN)	01642438	1.4 (50)	43.5	147	71	22	7
Little Conestoga Creek (LCC)	01576712	1.7 (61)	65.1	160	68	10	22
Difficult Run (DR)	01646000	1.8 (62)	163.9	141	6	40	54

Field measurements included cross-sectional surveys extending from the valley headwall to the opposite bank of the channel (one half of the total floodplain as well as the entire channel). Bank height, channel width, floodplain width, and changes in channel morphology were all noted. Three floodplain transects were established per site per stream. Each transect consisted of 1 to 13 artificial marker horizons (feldspar clay) to determine floodplain deposition rates over time. Five bank transects were established per site with 6 bank pins per transect (3 on each side of the channel at low, middle, and high locations on the bank). Catchment area above each study site, elevation, gradient, width-depth ratio, and sinuosity along the reach at each site were determined from LiDAR imagery (0.03m vertical accuracy), digital elevation models (DEMs), topographic maps, and channel cross sections. Relations between fluvial geomorphic variables and both floodplain deposition and bank erosion were tested for significant correlations using Pearson Product-Moments analysis. Within each watershed, site floodplain deposition and bank erosion rates were related to basin area, channel sinuosity, channel gradient, bank height, channel cross-sectional area, and the ratios of bank height to floodplain width, channel width to depth, channel cross-sectional area to floodplain width and channel width to floodplain width. Variables were transformed when necessary to meet the parametric assumptions of the analyses.

Net site sediment budgets were best explained by gradient at Difficult Run, floodplain width at Little Conestoga Creek, and the relation of channel cross-sectional area to floodplain width at Linganore Creek. A correlation for all streams indicated that net site sediment budget was best explained by relative floodplain width (ratio of channel width to floodplain width). A new geomorphic metric, the floodplain trapping factor, was used to compare sediment budgets between streams with differing suspended sediment yields. Site sediment budgets were normalized by floodplain area and divided by the stream's sediment yield to provide a unit-less measure of floodplain sediment trapping. A floodplain trapping factor represents the amount of upland sediment that a particular floodplain site can trap (e.g. a factor of 5 would indicate that a particular floodplain site traps the equivalent of 5 times that area in upland erosional source area). Using this factor we determined that (1) Linganore Creek had the highest gross and net (floodplain deposition minus bank erosion) floodplain trapping factor (107, 46 respectively), (2) that Difficult Run the lowest gross floodplain trapping factor (29), and (3) that Little Conestoga Creek had the lowest net floodplain trapping factor (-14, indicating that study sites were net contributors to the suspended sediment load; Figure 1). The trapping factor is a robust metric for comparing 3 streams of varied watershed and geomorphic character, it promises to be a useful tool for future stream assessments, especially on projects related to stream and floodplain restoration. The trapping factor metric, and the relative floodplain width correlation with net site sediment budgets, is currently being tested at 30 streams in the Piedmont and Valley and Ridge Physiographic Provinces to determine if the metric and geomorphic correlation can be confidently extrapolated to other streams in the Mid-Atlantic region.

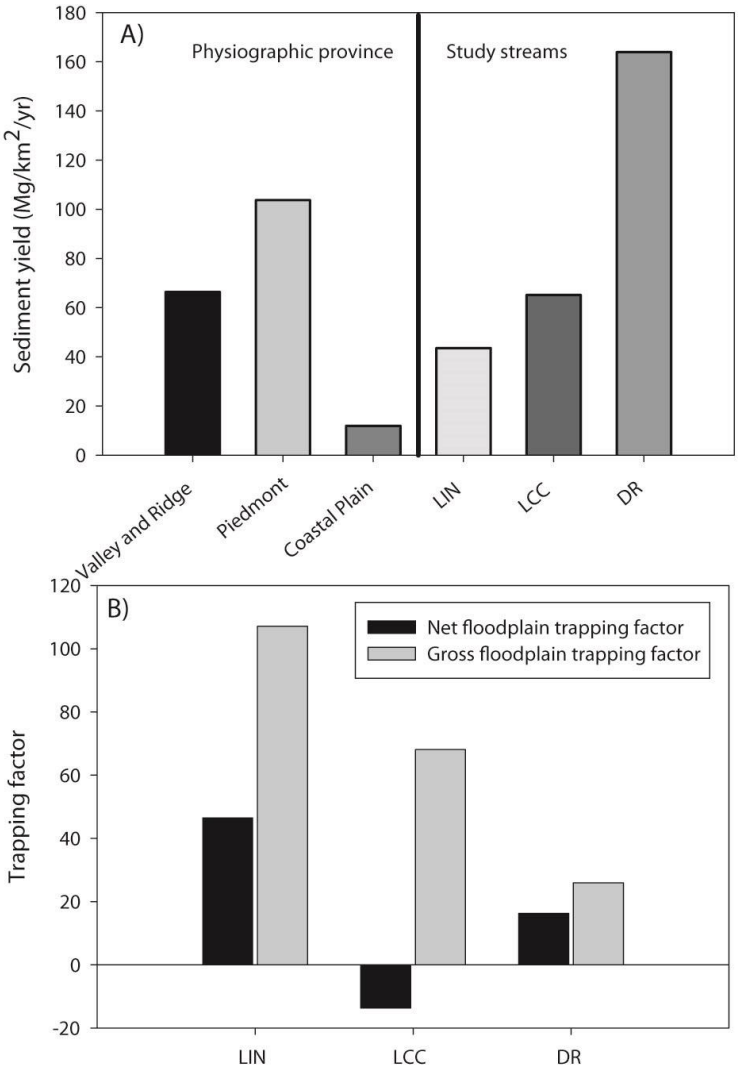

Figure 1. A) Mean sediment yields for select Physiographic provinces of the Chesapeake Bay (Gellis et al. 2009) and sediment yields for the study streams from Table 1. B) Mean gross and net floodplain trapping factor by study stream. LIN, LCC, and DR represent Linganore Creek, Little Conestoga Creek, and Difficult Run respectively.

REFERENCES

GELLIS AC, HUPP CR, PAVICH MJ, LANDWEHR JM, BANKS WSL, HUBBARD BE, LANGLAND MJ, RITCHIE JC, REUTER JM. (2009). SOURCES, TRANSPORT, AND STORAGE OF SEDIMENT AT SELECTED SITES IN THE CHESAPEAKE BAY WATERSHED: *U.S. GEOLOGICAL SURVEY SCIENTIFIC INVESTIGATIONS REPORT 2008-5186*, 95 PP.

GELLIS, A.C., G.B. NOE, J.B. CLUNE, M.K MYERS, C.R. HUPP, E. SCHENK, AND G. SCHWARZ. (IN PRESS). SOURCES OF FINE-GRAINED SEDIMENT IN LINGANORE CREEK WATERSHED, FREDERICK AND CARROLL COUNTIES, MARYLAND: 2008 TO 2011. USGS SCIENTIFIC INVESTIGATIONS REPORT 2014-5147.

HUPP, C.R., NOE, G.B., SCHENK, E.R., AND BENTHEM, A.J., (2013). RECENT AND HISTORIC SEDIMENT DYNAMICS ALONG DIFFICULT RUN, A SUBURBAN VIRGINIA PIEDMONT STREAM. GEOMORPHOLOGY 180-181:156-169.

SCHENK ER, HUPP CR. (2009). LEGACY EFFECTS OF COLONIAL MILLPONDS ON FLOODPLAIN SEDIMENTATION, BANK EROSION, AND CHANNEL MORPHOLOGY, MID-ATLANTIC, USA. *JOURNAL OF THE AMERICAN WATER RESOURCES ASSOCIATION* 45: 597-606. DOI: 10.1111/J.1752-1688.2009.00308.X

SCHENK, E. R., HUPP, C. R., GELLIS, A., AND NOE, G. (2013). DEVELOPING A NEW STREAM METRIC FOR COMPARING STREAM FUNCTION USING A BANK–FLOODPLAIN SEDIMENT BUDGET: A CASE STUDY OF THREE PIEDMONT STREAMS. *EARTH SURFACE PROCESSES AND LANDFORMS*, *38*(8), 771-784.

AUTOMATED UPDATES TO 2D HYDROLOGIC MODELS FOR OPEN-PIT MINING

Christopher Smemoe, PhD, PE, Aquaveo, 3210 N Canyon Rd, Suite 300, Provo UT, csmemoe@aquaveo.com; Clark Barlow, PE, CFM, Aquaveo, 3210 N Canyon Rd, Suite 300, Provo UT, cbarlow@aquaveo.com

Abstract Open-pit mines exhibit complicated hydrologic and sediment transport processes that impact the surrounding environment. Building and calibrating an initial hydrologic model that models these processes is a challenge, and updating this model poses further challenges. Hydrologic models of open-pit mines must be frequently updated because of constant changes to the topography, land use, pumping stations, and settling ponds surrounding the open-pit mine. The Gridded Surface Subsurface Hydrologic Analysis (GSSHA) 2D hydrologic model, developed by the US Army Corps of Engineers (USACE) Engineer Research and Development Center, can be used to analyze the complicated processes in an open-pit mine, among other things. The Watershed Modeling System (WMS) software, developed by Aquaveo, provides graphical tools to develop a GSSHA model and view the model output. We have developed an automated modeling wizard in the WMS that assists GSSHA modelers in updating the topography, land use, pumping stations, settling ponds, and associated model parameters for open-pit mine hydrologic models. This paper describes the procedures followed in automatically updating these model parameters using this wizard.

INTRODUCTION

Open-pit mines exhibit complicated hydrologic and sediment transport processes that impact the surrounding environment. Building and calibrating an initial hydrologic model that models these processes is a challenge, and updating this model poses further challenges. Hydrologic models of open-pit mines must be frequently updated because of constant changes to the topography, land use, pumping stations, and settling ponds surrounding the open-pit mine. This study included developing a semi-automated wizard-based approach for updating hydrologic models in watershed areas surrounding open-pit mines.

The Gridded Surface Subsurface Hydrologic Analysis (GSSHA) hydrologic model, developed by the USACE's Engineer Research and Development Center, was used to model the watershed areas surrounding the open-pit mines described in this study. GSSHA "is a physics-based, distributed, hydrologic, sediment and constituent fate and transport model. Features include two dimensional (2D) overland flow, 1D stream flow, 1D infiltration, 2D groundwater, and full coupling between the groundwater, shallow soils, streams, and overland flow" (Downer and Ogden, 2015). Because GSSHA offers so many processes that can be modeled, it offers an ideal solution for modeling the complex hydrologic processes surrounding open-pit mines.

The Watershed Modeling System (WMS) software, developed by Aquaveo, provides graphical tools to develop a GSSHA model and view the model output. We used WMS to

collect the necessary data and to build, run, and calibrate GSSHA models for this study. Then we read and view the GSSHA results in WMS. Aquaveo developed an automated modeling wizard in WMS that assists GSSHA modelers in updating the topography, land use, pumping stations, settling ponds, and associated model parameters for open-pit mine hydrologic models.

The model study area was the watershed areas surrounding three large open-pit coal mines in Indonesia. Several watersheds surround these mines, and water quality and erosion in the surrounding watersheds are a concern. Aquaveo built and calibrated separate GSSHA models for each of the watersheds surrounding the mines. Aquaveo then tested the wizard on each of these models to determine its usefulness in automatically updating the models of the watersheds surrounding the mines. This paper gives an overview of the model development and shows how the WMS wizard is used to automatically update the hydrologic models for the watersheds surrounding the open-pit mines. The techniques used in this wizard can be used to automatically update other types of hydrologic models and could possibly be used to auto-generate GSSHA hydrologic models sometime in the future.

METHODS

This section first gives an overview of the models that were developed and then describes the processing required to update the various types of data for each of the models in the WMS wizard.

Model Overview: 21 different GSSHA models were built and calibrated to represent the watershed areas surrounding 3 different yet closely-spaced open-pit coal mines. Techniques involved in setting up the initial GSSHA models using WMS are described elsewhere (see Nelson and Smemoe, 2015). A photo of one of the open-pit mines is shown in figure 1.

Ponded water, loose sediment, and drainage are a major problem in the areas surrounding these open-pit mines. Because of the impacts of the mine, there are some areas surrounding the mines where erosion is a major concern (figure 2).

The watershed models determined areas with large amounts of sediment erosion and deposition, areas with high channel velocities, and determined the impacts of sediment mitigation efforts, including adding sediment settling ponds (figure 3) at the downstream end of the watersheds.

Figure 1 One of the open-pit coal mines

Figure 2 An eroded culvert crossing close to one of the mines

Figure 3 A series of sediment settling ponds surrounding one of the open-pit mines.

A plan view of the GSSHA-computed water depths after a storm event is shown in figure 4.

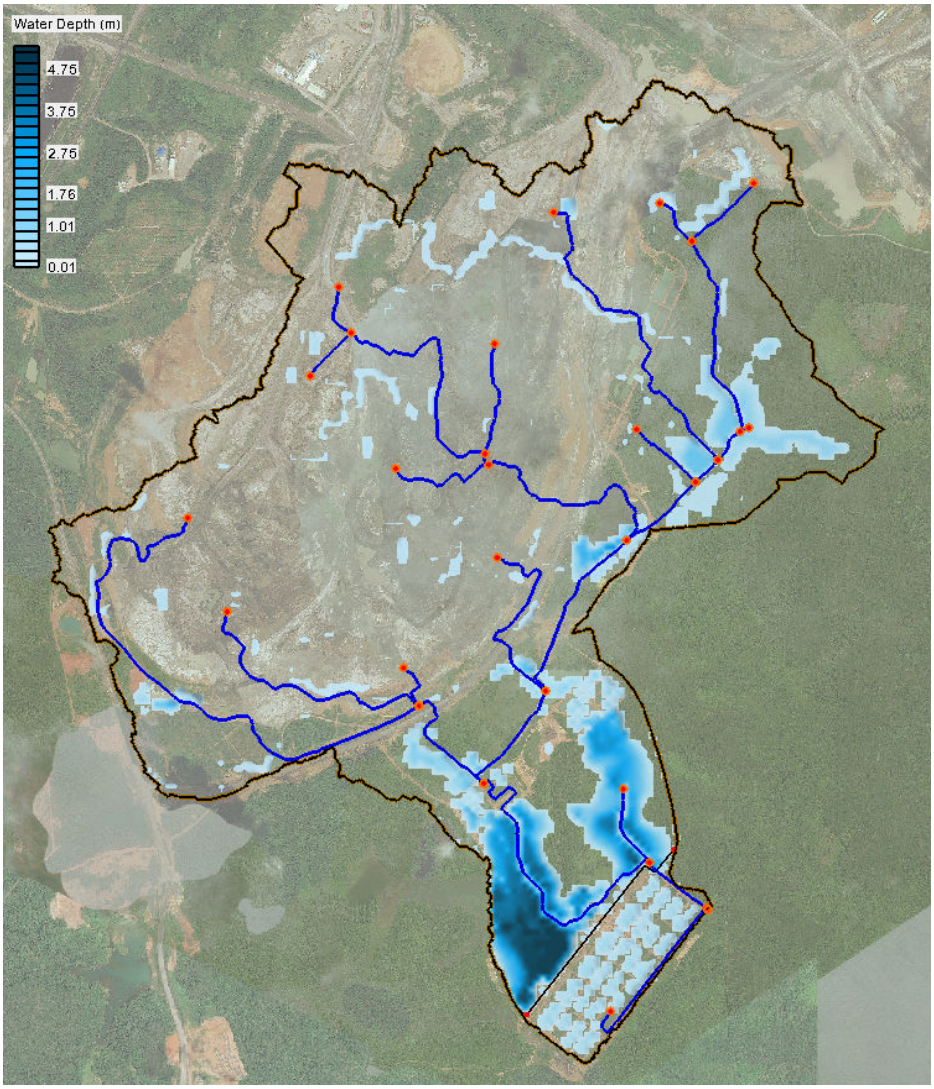

Figure 4 Computed water depths in one of the watersheds surrounding the open-pit mine.

A similar example of the GSSHA-computed erosion/deposition map is shown in figure 5.

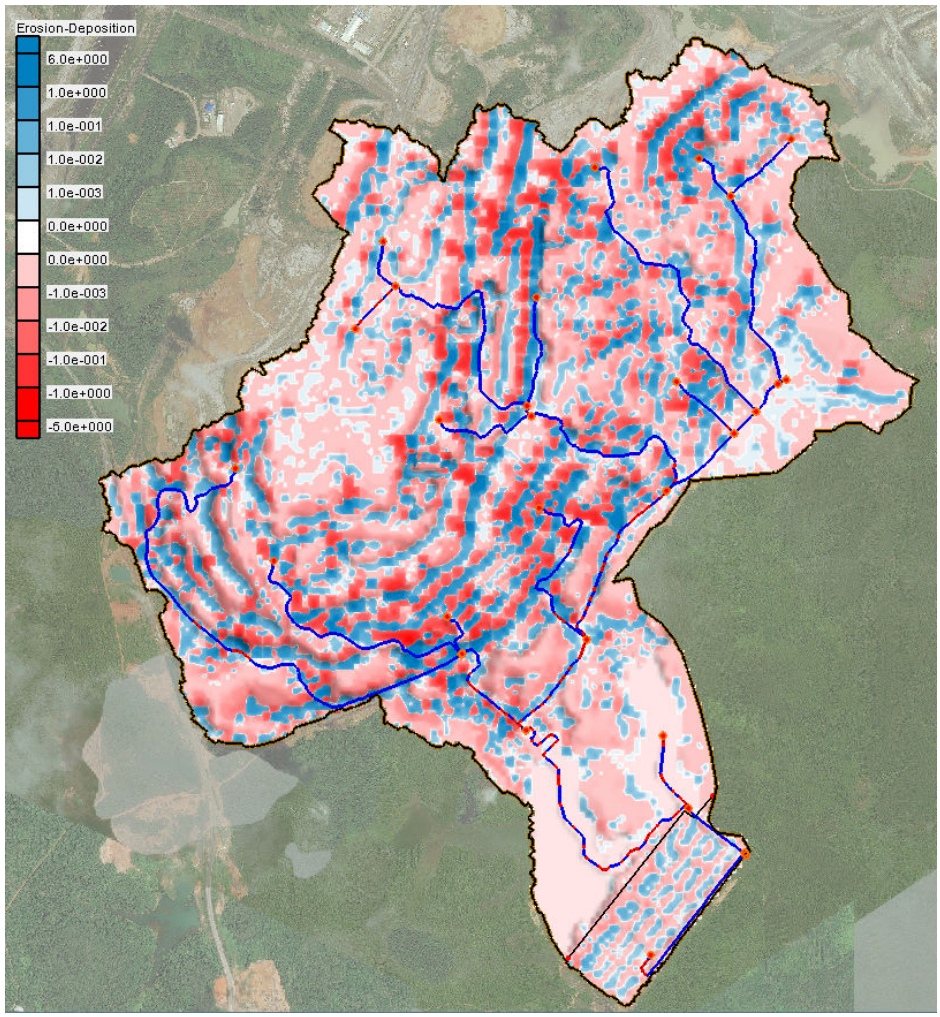

Figure 5 Aerial map showing computed sediment erosion (red-tinted areas) and deposition (blue-tinted areas) in one of the watersheds surrounding the open-pit mine.

The WMS mine wizard can be used to update changing model inputs for the 21 existing GSSHA models and outputs many useful model parameters that are described in the section on model output.

Update Elevation Data: An image showing the GSSHA model update wizard with each of its steps is shown in figure 6.

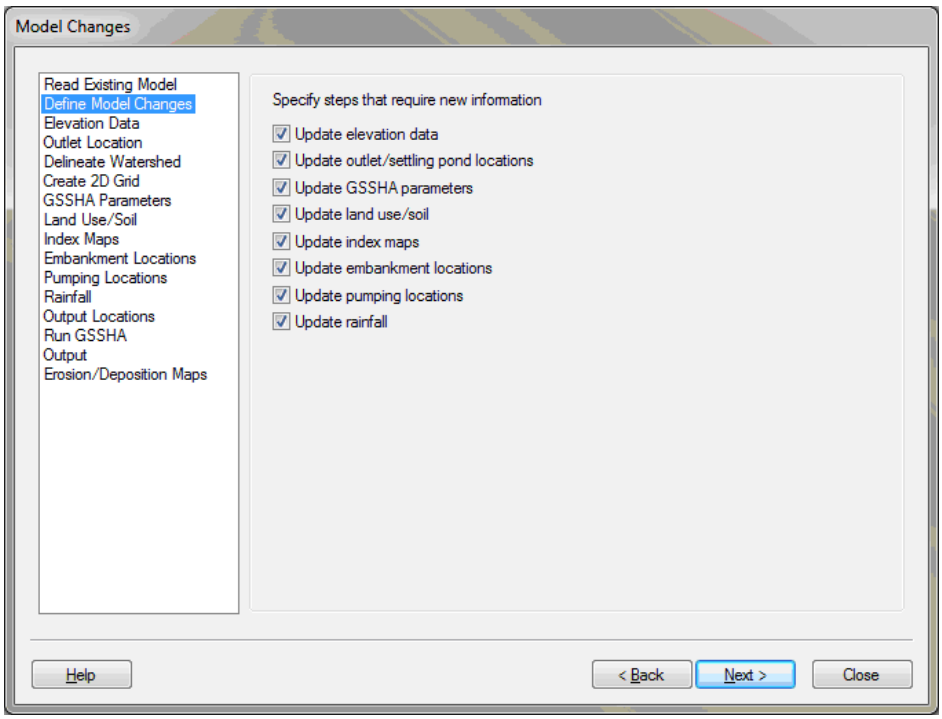

Figure 6 GSSHA mine model update wizard.

You can use the Update Elevation Data step of the wizard to read updated elevation data, if necessary. The updated elevation data is used to delineate the watershed and update the 2D Grid elevations in the GSSHA model. When delineating a watershed, it is important to determine flow directions and flow accumulation values from the elevation data, and this step includes an option to compute these grids from the elevation data.

Update Outlet/Settling Pond Locations: Sometimes, the locations of the settling ponds are changed or new settling ponds or embankments are added to the watershed that change the flow and may require the watershed outlet point and the watershed boundary to be changed. Because of this, we added a step to the wizard to assign a new outlet location. If a drainage coverage (layer) already exists in the model, WMS copies this coverage to a new drainage coverage. If no drainage coverage exists, WMS creates a new drainage coverage so the outlet can be added to that coverage. When assigning a new outlet location, WMS deletes all the geometric data in the coverage and the watershed boundary is re-computed when the watershed is delineated in the next step.

Watershed Delineation: This step determines the watershed boundary based on the flow directions and accumulations and the outlet point in the active drainage coverage.

Update 2D Grid: The Create 2D Grid step is used to update or create a 2D grid for running GSSHA from the delineated watershed boundary. In this step, you select a grid cell size or number of cells, assign an optional depression coverage, and assign an optional coverage containing GSSHA structures (such as detention basin outlets) and select a button to create a 2D grid and initialize your GSSHA model parameters.

WMS does the following when you select the Create 2D Grid button:

1. Convert the delineated drainage coverage to a GSSHA coverage.
2. Intersect the stream arcs (polylines) in the GSSHA coverage with the depression coverage (if this option is on) and split the stream arcs at the intersections.
3. Redistribute stream vertices so the vertex spacing matches the specified 2D grid cell size.
4. Smooth any stream arcs that are outside of depression coverage polygons. If no depression coverage exists, WMS removes all adverse slopes on the streams.
5. Combine the stream arcs so they are no longer split at the intersections of polygons in the depression coverage.
6. Assign default stream attributes to all the streams (Trapezoidal channel with the following attributes: Manning's n = 0.03, depth = 3 m, width = 4 m, and side slope = 0.5.
7. If the option to assign structures from an existing GSSHA coverage is selected, WMS copies the embankments, detention basin nodes, and pumps and their attributes from the selected GSSHA coverage to the new GSSHA coverage.
8. Creates a 2D grid filling the watershed boundary polygon at the specified cell size.
9. Initializes the GSSHA model data and copies the previously defined GSSHA model job control information over to the new GSSHA model.

Update GSSHA Parameters: This step of the wizard is used to specify the GSSHA land use and soil type parameters assigned to the land uses and soil types in WMS. These parameters are later assigned to the GSSHA model after updating the land use and soil data assigned to your model. Default parameter files can be read and used from other projects to parameterize values in the active GSSHA model.

Update Land Use/Soil Data: The define land use and soil data step converts GIS shapefiles to data in the WMS Map module. WMS uses the boundary of the watershed in the GSSHA coverage to clip the shapefile data for the selected files.

Update Index Maps: The index maps step is used to generate GSSHA index maps from the polygons in the WMS land use and soil type coverages. After WMS defines the GSSHA index maps, it generates GSSHA mapping tables from the index map ID's and the GSSHA land use and soil type parameters defined in the GSSHA Parameters step of the wizard.

Update Embankment Locations: The embankment locations step is used to layout or change the locations of GSSHA embankment arcs within a watershed. These embankment arcs could represent structures such as hauling roads, detention basin embankments, or settling pond embankments.

Update Pumping Stations: The pumping locations step of the wizard is used to delete or add pumping stations and to define the pumping rates. Pump stations are where water or sludge is transferred from the open-pit mine to the watershed. These pumping stations can be a major source of sediment load in each of the watersheds surrounding the mines.

Update Rainfall: The model rainfall occasionally needs to be updated to forecast future sediment loads and water depths in each of the watersheds surrounding the open-pit mines.

Output: Several output parameters that are useful for managing the watersheds surrounding the open-pit mine are exported from the model after running the model. Some of the parameters that are output include:

1. Simulation input parameters, such as pumping rates, model duration, and watershed area.
2. General simulation results at each user-specified output point, such as peak flow, runoff volume, volume of water pumped, and total infiltration.
3. Information about the settling ponds, such as their initial storage, volume of rainfall in the ponds, volume of runoff to the ponds, and the peak discharge from the ponds.
4. A sediment summary, including the maximum and average erosion rates, the total sediment eroded and deposited in various parts of the watershed, and sediment concentrations.
5. Discharge and runoff volume are also computed at each user-specified output location in the model.
6. An erosion/deposition plan view map is computed and displayed as part of the output.

DISCUSSION, CONCLUSION, AND FUTURE WORK

Open-pit mines can impact their surrounding watersheds in various ways. The GSSHA model can be used to model some of these impacts on the environment. Some of these impacts include sediment erosion, sediment deposition, and flooding from settling pond embankments and hauling roads. WMS can be used to develop GSSHA models, and the open-pit mine wizard in WMS allows you to update these GSSHA models in a semi-automated fashion.

This paper provided an overview of the GSSHA hydrologic models surrounding three open-pit coal mines and shows how the WMS wizard can automatically update the hydrologic models for the area surrounding the open-pit mine. We would like to extend the techniques used in this wizard to automatically update other types of GSSHA hydrologic models and perhaps to auto-generate hydrologic models for any watershed of interest.

REFERENCES

Downer, C., and Ogden, F. (2015). Gridded Surface Subsurface Hydrologic Analysis Web Reference. http://gsshawiki.com/

Nelson, E. J. and Smemoe, C. M. (2015). Watershed Modeling System Online Help. http://xmswiki.com/wiki/WMS:WMS

LOW WATER PLANNING IN THE COLUMBIA RIVER BASIN

Thomas Chisholm, Hydraulic Engineer, U. S. Army Corps of Engineers, Northwestern Division, Portland, OR, tom.a.chisholm@usace.army.mil

INTRODUCTION

Storage reservoirs even out variation in river flow. A chief benefit of this function is more reliable supplies of both hydropower and water. For reservoirs that supply power and water perhaps the most basic design question is: how much reservoir capacity is required given natural flow and demand.

In 1961 United States President Dwight Eisenhower and Canadian Prime Minister John Diefenbaker signed the Columbia River Treaty. The Treaty's preamble states: "Recognizing that the greatest benefit to each country can be secured by cooperative measures for hydroelectric power generation and flood control, which will make possible other benefits as well." Thus, the Treaty focuses on flood control and hydropower. During low water conditions attention focuses on hydropower over flood control. Although in many rivers water supply is the primary objective in the Columbia River Treaty it falls into "other benefits". However, attention to ecological processes, which value water supply, has increased since the signing of the Treaty.

The Treaty and its annexes provide guidelines for developing project operating plans and apportioning benefits. Both operating plans and benefit calculations use the critical period concept. Article I of the Treaty entitled Interpretation includes:

(d) "**critical stream flow period**" means the period, beginning with the initial release of stored water from full reservoir conditions and ending with the reservoirs empty, when the water available from reservoir releases plus the natural stream flow is capable of producing the least amount of hydroelectric power in meeting system load requirements.

CRITICAL PERIOD DEVELOPMENT

Critical Period Concept: Considering that Treaty ratification occurred in 1961, the Treaty used methods existing in 1961. In 1961 computers were in their infancy. The concept of critical period arose in water supply engineering. In the water supply context critical period has the same definition as in the Treaty but with water substituted for hydroelectric power. The critical period concept is applied when calculating reservoir capacity required to meet demand and also the demand that a reservoir of a given capacity can meet. The concept may have arisen before the name critical period. Oguz and Bayazit (1991) describe statistical properties of the water supply critical period. They credit Hall, Askew and Yeh (1969) with inventing the concept of critical period, clearly not the case. However, Hall, Askew and Yeh include a modest bibliography and do not cite papers that describe critical periods, but they imply the technique was in use. Like Oguz and Bayazit this author has not located literature with critical period in the title prior to Hall Askew and Yeh's paper. Also, all literature on critical period analysis located by this author treat water supply not hydropower.

Klemes' papers (1979 1984) expound on historical development of the reservoir sizing problem. The seminal paper in this field is Rippl (1883) who proposed the mass curve method. This technique plots a time series of cumulative inflow. The maximum deviations of the plot below a straight line with a slope at the demand for water allow calculation of reservoir size required to support the demand. The time period covered by the line used to size the reservoir is the critical period. The graphical nature of this method made it appealing prior to the advent of computers.

A similar method, which Klemes (1984) credits to Varlet (1923), requires plotting two mass curves separated by the reservoir capacity. This method is commonly called the stretched string method. The yield of the reservoir is the flattest line that extends from the bottom line to the top line. The extent of this line is the critical period. The intuitiveness and graphical nature of this method made it appealing prior to the advent of computers. The author is not aware of this method being applied to the power problem. However, it is conceivable that it was used in analysis leading to development of the Treaty.

Power: The hydropower generation equation is

$$P = e\rho ghQ \tag{1}$$

Where P denotes power, e nondimensional efficiency, ρ density of fluid, g acceleration of gravity, h hydraulic head, and Q volume flow rate. Metric units yield generation in Watts. Efficiency depends on dam and generator physical properties in addition to flow rate and head. Because operating conditions continually vary, long term planning uses average values.

Assuming head scales linearly with impounded volume, V, and generating flow is the sum of inflow, I, and change of impounded volume dV/dt yields

$$P = e\rho g\ aV\left(\frac{dV}{dt} + I\right) \tag{2}$$

This equation indicates that maximizing system generation when decreasing reservoir content primarily requires retaining maximum head in projects that have the highest Q. If two reservoirs, denoted by subscripts one and two, are in series with inflow to the upstream reservoir, generation as the reservoirs draft from full to empty is:

$$G = e\rho g \int_0^T aV_1\left(\frac{dV_1}{dt} + I\right) + bV_2\left(\frac{dV_1}{dt} + \frac{dV_2}{dt} + I\right) \mathrm{dt} \tag{3}$$

The critical period definition includes drafting reservoirs from full to empty. Its power interpretation requires retaining volume in projects that make the largest contribution to head. Note that in many cases inflow originates from an upstream project. Typically headwater projects have lower inflows so drafting them first maximizes generation. As equation 3 illustrates, the downstream project passes all the outflow from the upstream project plus draft

from the downstream project. As power demand continues to require draft, reduced head reduces generation per unit of water. This requires ever-increasing draft to meet generation targets.

Calculating power critical periods using current technology is an optimization problem. But when the Treaty was developed USACOE (1981) describes it as "trial and error." While the principles in the previous paragraph guide an operation, gradient solvers (Fletcher 1987) often struggle because in complex hydrosystems the problem is very nonlinear. Conditions where projects spill are particularly challenging because if discharge is greater than turbine capacity there is no gradient in generation until flow decreases below maximum turbine capability. However, a successfull solution describes a system operation that is useful for planning.

Treaty: The Treaty determines Columbia River Basin hydro operation using a procedure called the Treaty Storage Regulation (TSR). This calculates an operation which meets operational constraints and at least critical period power. Constraints include those described in the Flood Control Operating Plan (2003) along with physical ones. The wide variety of operational constraints serving fish and environmental concerns are not addressed by the TSR because they did not exist when the Treaty was signed. Some are addressed by supplemental agreements negotiated between the United States and Canadian Entities.

The TSR plans an operation which guarantees critical period generation unless water is unavailable. If reservoirs are empty generation becomes limited by inflow. The Treaty uses 30 years of water record from 1929 -1960 as its period of record. With the Treaty based on 30 years of record and Mica Dam completed in 1973 the dams have been in operation for longer than the period of record. Analysis performed by Hicks and Baldrica (1970) using synthetic records give a return period of 385 years for the 1929-1932 critical period. USACOE (1981) refers to a reanalysis performed by the University of Washington which reduces this return period to 164 years. One would think that the long return period of the critical period in the Treaty's period of record would avoid ever drafting reservoirs to empty. But the TSR called for drafting reservoirs to empty in 2001. However Treaty language that allows operation as agreed to by the parties allows ad hoc hedging, which is described in the next section, in actual operations.

Treaty Assumptions: The delivery vs. availability diagram has long been used to describe reservoir operation. Draper and Lund (2004) explain its use but did not invent it. The flat section of line in the unhedged case between 10 and 20 on the horizontal axis shows operations when the reservoir is between full and empty and meets demand for water. To the left, passing inflow plus drafting available water cannot meet demand so the reservoir drafts to empty then passes inflow. To the right of the flat line the reservoir is full so it passes inflow. Both the left and right are undesirable situations. To the left water demand is not met and to the right the reservoir cannot make any contribution to flood reduction.

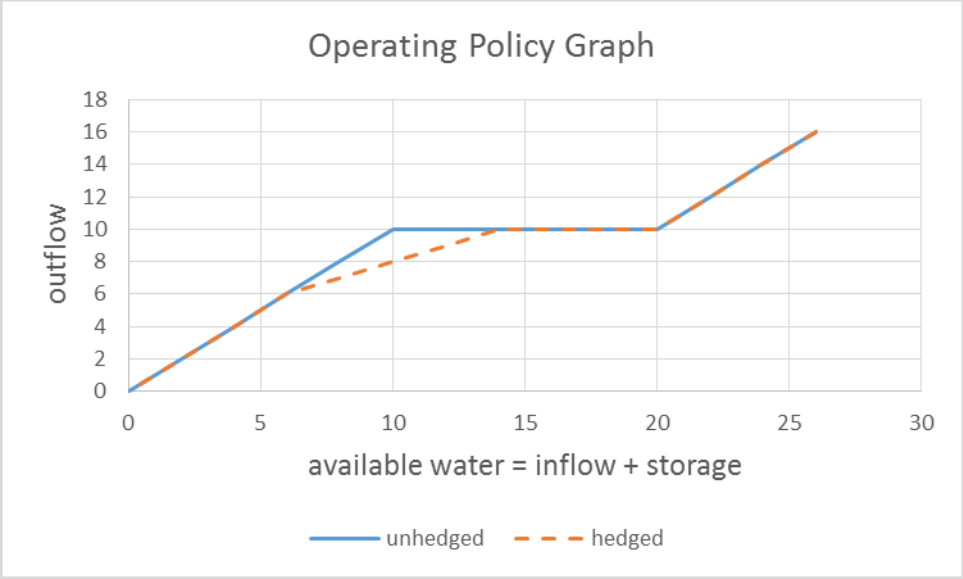

Figure 1 Effect of hedging on outflow.

The hedged line in Figure 1 shows water delivery curtailment before the reservoir drafts to empty. This increases probability of a curtailment but reduces probability of a very severe curtailment. The balance between avoiding curtailments and avoiding empty reservoirs has received attention in the literature recently. For example, Google Scholar indicates J. W. Labadie's (2004) article "Optimal Operation of Multireservior Systems State of the Art Review" has been cited 728 times. Many of these articles apply modern optimization techniques to optimizing reservoir operations. The Treaty makes no attempt to hedge. Hedging theory was developed prior to negotiation of the Treaty. One of the seminal works in optimization, Little (1954), applied dynamic programming to operation of the Columbia River dams. Perhaps the Treaty developers were aware that the unusually dry period in the period of record led to conservative operations.

COLUMBIA RIVER CRITICAL PERIOD

Low Water Periods: Calculating periods of lowest average unregulated inflow of various lengths provides insight. The unregulated flows used for planning in the Columbia River Basin are the modified flows published by the Bonneville Power Administration (2011). These modified flows are essentially flow that would exist if dams did not exist but irrigation withdrawals occurred at 2010 levels. Using modified flows and a spreadsheet one can calculate consecutive rolling averages of increasing lengths. For example, a column of three month averages contains averages of August through October, September through November, October through December and so on until all data are used. Columns going across contain progressively longer periods August through October, August through November, etc. Each column has a minimum value. These minimum values increase as longer periods are averaged. Figure 2 shows periods of lowest average unregulated flow at The Dalles for periods between one and 76

months. Most periods of lowest average flow add one month to the preceding shorter period. However, periods sometimes jump years away. For example the smallest ten month average extends from July 1936 to April 1937, the smallest 11 month average extends from July 1936 to May 1937, but the smallest 12 month average extends from December 1976 to November 1977.

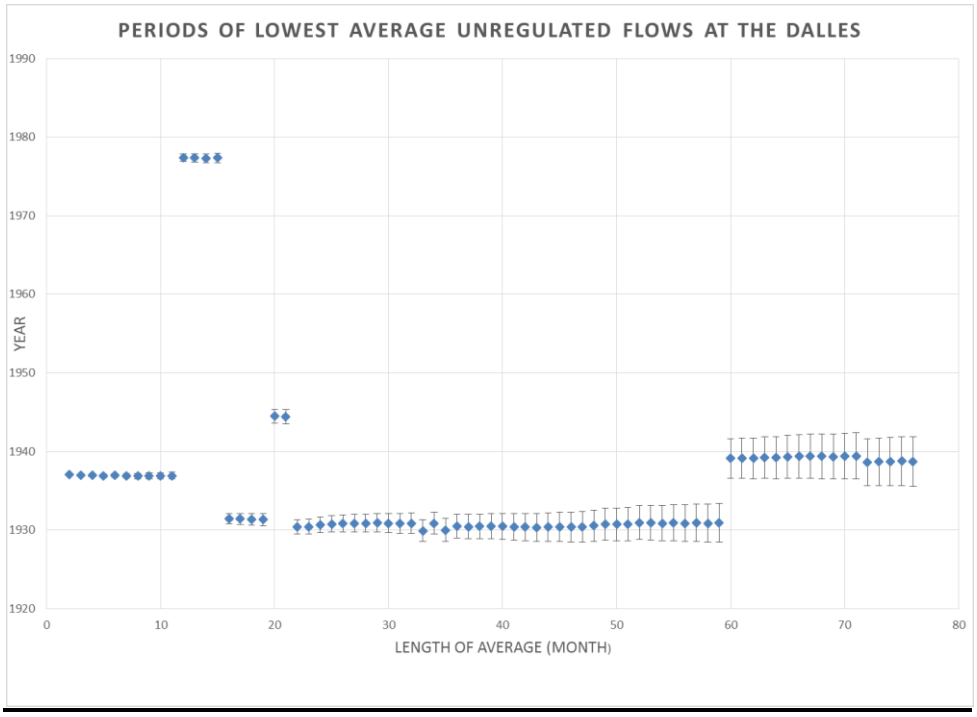

Figure 2 Periods of lowest unregulated flows at The Dalles

Water Supply Critical Period: To include effects of reservoir drafting in critical periods, reservoir content is divided by the number of months averaged and added to the average flow values described in the previous section. Longer periods have reservoir content divided by a larger period length yielding a smaller result. Smaller storage content also yields a smaller value. Over longer periods average reservoir contribution decreases but average stream flow increases. There exists a time where the sum of these two competing effects result in a minimum value. This is the critical period flow. Figure 3 shows average critical period flow with drafting for some storage levels. The periodicity of the plot arises from the seasonality of flow. Higher flow occurs during spring snow melt and lower flow occurs in fall and winter.

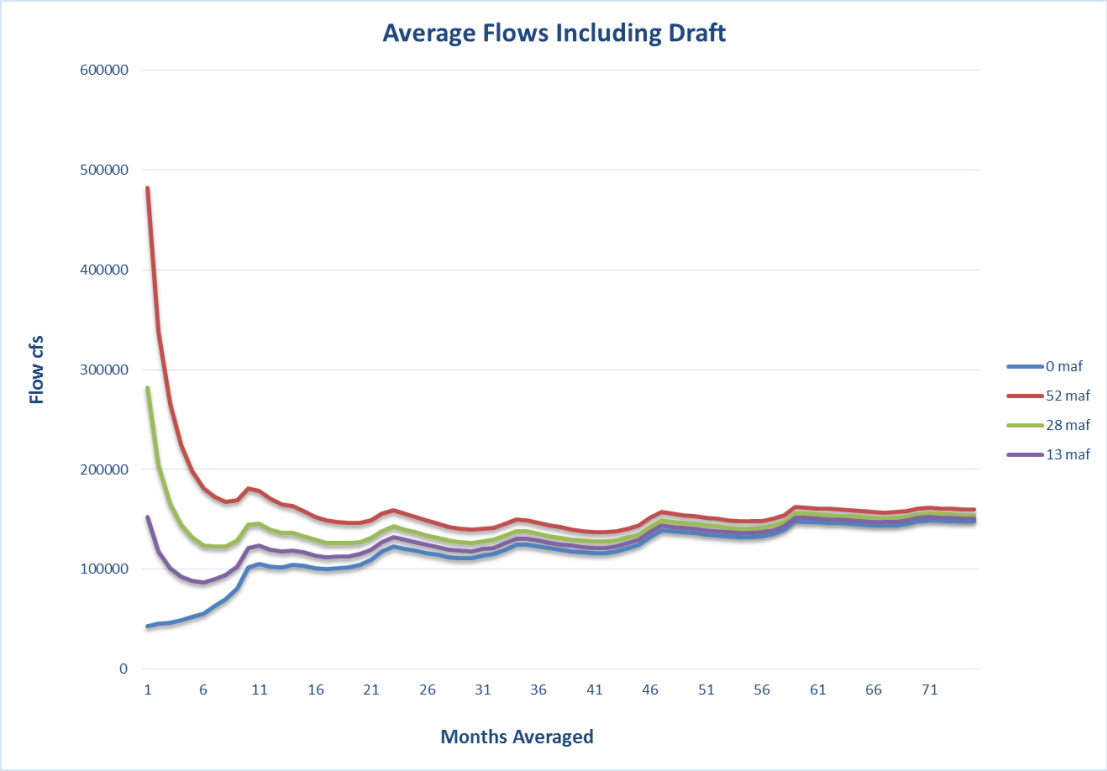

Figure 3 The Dalles average flows with drafting

Comparison of Water and Power Critical Periods: Given the complexity of calculating power critical period it is worth examining the difference between power critical periods and water supply critical periods. The power critical periods come from Columbia River Treaty Operating Committee (2013). Table 1 shows time periods are usually quite similar.

Table 1 Power and flow critical periods.

Storage	Power Critical Period	Water Critical Period
52 maf	Aug 1928 Feb 1932	Sept 1928 – Feb 1932
28 maf	Sept 1943 April 1945	Aug 1936 – March 1937
13 maf	Nov 1936 April 1937	Sept 1936 – March 1937

The power and water critical periods for the 28 maf case appear quite different. However, the two critical periods are eight and 20 months long, respectively. As discussed regarding Figure 3 critical periods with similar values may have lengths differing by 12 months due to the annual shape of flow variation. Figure 2 shows the 20 month flow minimum is near 1945 whereas the eight month minimum is near 1937. Figures 4 and 5 apply the stretched string method to these two periods. The line showing draft in 1945 just barely makes it between the upper and lower lines.

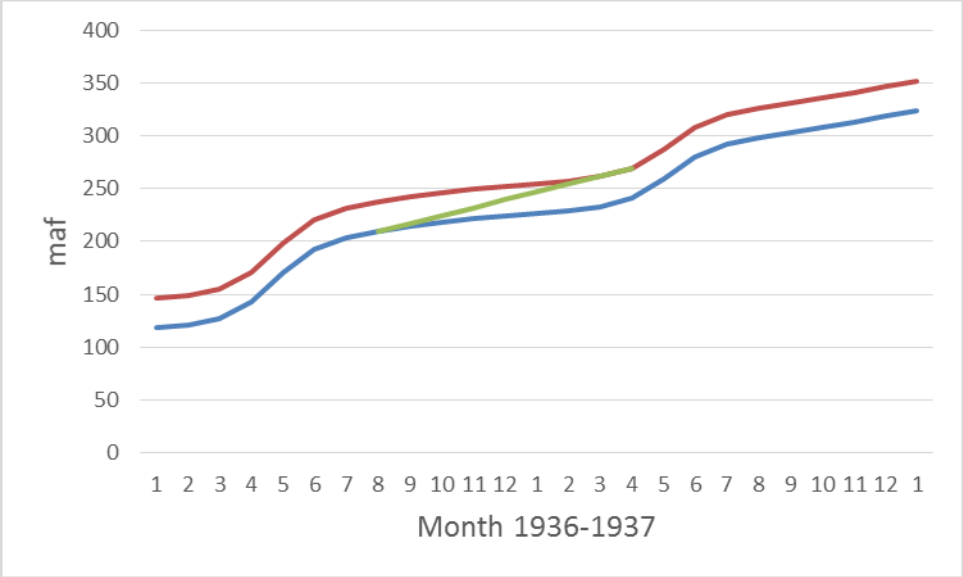

Figure 4 Stretched string approach applied to 1936-1937.

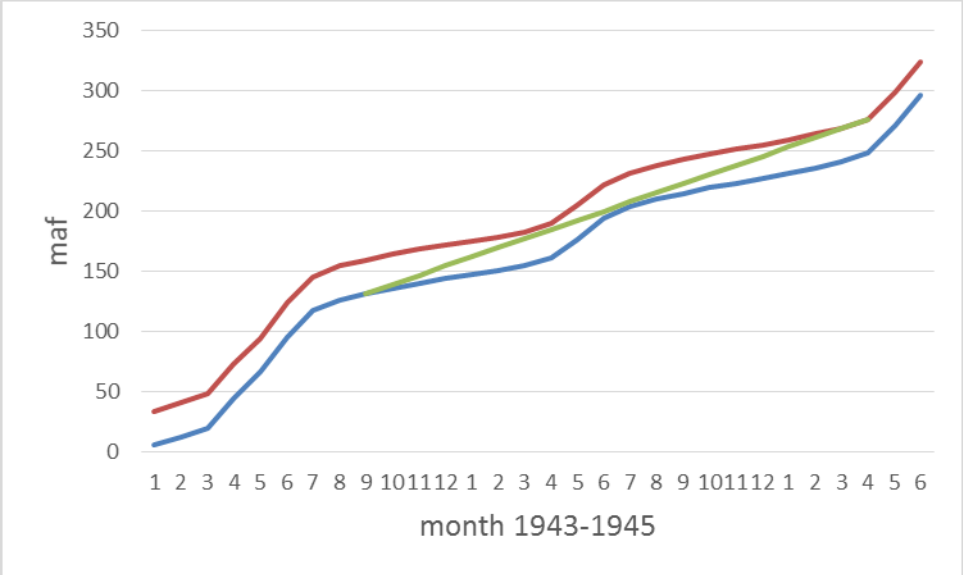

Figure 5 Stretched string approach applied to 1943-1945.

CONCLUSION

The concept of critical period, the period of minimum flow as a reservoir drafts from full to empty, has a long history in reservoir planning. However, critical period is often referred to by other names in the literature. It has been improved by using a stochastic approach to flows and hedging when low flow conditions exist. The Columbia River Treaty used a straight critical period without either of these improvements. However, the Treaty allows for supplemental agreements between parties, so in practice the United States and Canada often implement these improvements.

Power and water supply critical periods are similar. Power critical period calculations require calculating project operation making these calculations more complicated. Portions of a basins often have different critical periods than the basin as a whole. Consequently, power critical periods depend on where hydrogeneration is located in a basin.

REFERENCES

Bonneville Power Administration (2011) 2010 Modified Streamflows http://www.bpa.gov/power/streamflow/default.aspx

Columbia River Treaty Operating Committee (2013) Columbia River Treaty Assured Operating Plan and Determination of Downstream Power Benefits. http://www.nwd-wc.usace.army.mil/PB/PEB_08/docs/aop/19AOPddpb.pdf

Draper, A. J. and Lund, J. R. (2004). "Optimal Hedging and Carryover Storage Value," Journal of Water Resources Planning and Management, ASCE, pp.83-87.

Fletcher, R. (1987) Practical Methods of Optimization, Wiley Interscience, Cornwall, UK.

Hall, W. A., Askew A. J. and Yeh, W. W-G. (1969). "Use of the Critical Period in Reservoir Analysis," Water Resources Research, 5(6), pp. 1205-1215.

Hazen, A., (1914). "Storage to be Provided in Impounding Reservoirs for Municipal Water Supply," Trans. ASCE, 77, pp.1539-1640.

Hicks, R. H. and Baldrica, D. J. (1970) Preliminary Probability Study on the Occurrence of Adverse Streamflows, Memorandum Bonneville Power Administration.

Klemes, V. (1979). "Storage Mass-Curve Analysis in a Systems-Analytic Perspective," Water Resources Research, 15(2), pp. 359-370.

Klemes, V. (1987) "Extended Review: One Hundred Years of Applied Storage Reservoir Theory," Water Resources Management 1, D. Reidel Publishing Co., pp. 159-175.

Labadie, J. W. (2004) "Optimal Operation of Multireservoir Systems: State-of-the-Art Review," Journal of Water Resources Planning and Management, ASCE, 130(2), pp.93-111.

Little, J. D. C. (1954). "Use of Storage Water in a Hydroelectric System", PhD dissertation, Massachusetts Institute of Technology.

Oguz, B. and Bayazit, M. (1991) "Statistical Properties of the Critical Period," Journal of Hydrology, Elsevier Science Publishers, 126, pp.183-194.

Rippl, W. (1883). "The Capacity of Storage Reservoirs for Water-Supply," Minutes Proc. Inst. Civil Eng., 71, pp. 270-278.

Varlet, H. (1923). “Graphical Analysis of Operating Conditions of a Flow-Control Reservoir” (in French), Ann. Pants Chausstes Mem. Doc. Partie Tech. 93, pp 61-79.

U. S. Army Corps of Engineers (1981) Determination of Critical Period, Internal Memorandum.

U.S. Army Corps of Engineers, Northwestern Division (2003) “Columbia River Treaty Flood Control Operating Plan”, Portland, OR.

RIVER ENGINEERING RESEARCH NEEDS IN THE ARMY CORPS OF ENGINEERS

Meg Jonas, Senior Hydraulic Engineer, USACE Headquarters, Engineering & Construction, Washington, DC, meg.m.jonas@usace.army.mil; John Remus, Chief – Hydrologic Engineering Branch, USACE Omaha District, Omaha, Nebraska, john.i.remus@usace.army.mil

Abstract River engineering is one of the core competencies of the Army Corps of Engineers. As a cross-cutting topic, river engineering research falls under many separate topic areas: sediment transport modeling; ecosystem restoration; dam and levee safety; infrastructure; fluvial geomorphology; design of riverine structures; and others. The Corps expert Committee on Channel Stabilization has reviewed multiple submitted topics and has identified research topics that would advance the discipline of river engineering. Since the field of river engineering is so broad, and many topics cut across traditional program funding lines, it is easy for key needs to lose visibility. This presentation will discuss the priorities identified by the expert Committee.

INTRODUCTION

The importance of river engineering in USACE was described in an earlier paper (Remus and Jonas, 2010). Research was identified as a critical component, with a recommended first step of reviewing the research needs submitted by Corps field personnel. The collected statements form a valuable record of research needs.

In May 2014, the Corps expert Committee on Channel Stabilization reviewed a collated list of river engineering research needs and ranked them as high, medium or low. Ten needs received high rankings from a strong majority of committee members. These ten are listed below. The order does not reflect any priority.

The research needs were drawn from the Flood Risk Management (FRM) Gateway. Any Corps employee can submit an R&D Statement of Need (SON) for consideration for research funding. Submission guidelines and all previously submitted SONs are included at the FRM Gateway: **http://operations.usace.army.mil/flood.cfm**. Corps employees are strongly encouraged to submit SONs.

The Committee did not attempt to identify research needs not included in the list of SONs. Therefore, the rankings below are a preliminary effort to prioritize river engineering needs, based on the needs that were submitted. Additional work will be required to develop a comprehensive, prioritized list.

RIVER ENGINEERING RESEARCH NEEDS – HIGH PRIORITY

The needs below were all ranked high as the consensus of the Committee. The order does not reflect any relative priority. The descriptions are taken from the FRM Gateway website.

1. **Effects of Training Structures on River Stages**.
    a. **Tracking Number** 2008-F-46
    b. **Need that Drives Requirement**. For many years, various river training structures have been constructed on America's rivers to reduce bank caving and to develop and maintain adequate channel dimensions that support commercial navigation. These training structures include various types of bank stabilization techniques as well as various dikes schemes. These structures provide a more efficient channel by eliminating channel migration through the prevention of bank erosion, realigning a river reach, constricting a channel to increase depth, cutting off side channels and chutes, and concentrating braided rivers into single channels. During the recent floods on the Upper Mississippi River, some have purported that the presence of river training structures actually resulted in higher stages. Previous studies/investigations addressing the impacts of river training works on flood stages will serve to reevaluate and update those findings.
    c. **Extent of Need Across USACE**. Training structures are frequently used throughout the United States to develop rivers for storm damage reduction, navigation, water supply, environmental restoration, recreation, and hydropower. In many parts of the country, floods cause extensive damage even with current flood damage reduction projects in place. If training structures result in increased river levels, then the current level of protection provided by storm damage reduction measures (especially levees) is reduced during floods.
    d. **Requirement**. R&D requirement is to develop a methodology and guidance for evaluating river training structures, especially their impact on overall river stages. This effort will include the evaluation of available tools (including models) and the identification of the ones that are most applicable. An often complex combination of various factors influence channel morphology and thus, river stages. A critical step in determining impacts on river stages is to conduct a detailed geomorphic assessment that identifies these factors for a given river system and determines how these factors are integrated to produce channel morphology.
    e. **Consequences if Requirement Not Met**. The consequences of not meeting the requirement include the potential loss of current levels of protection for flood damage reduction measures on rivers that have been developed with channel training structures. A loss in the level of protection prevents the flood damage reduction measures from providing the benefits that the projects were designed to provide resulting in an increased risk of damage.
    f. **Product Recommendation.** A methodology and guidance for the evaluation of river training structures on river stages will be developed. The Upper and Middle Mississippi River will be used as a test case. Applicable data will be collected and the training works evaluated as to their impact on river stages.

2. **The WES Stream Investigation and Streambank Stabilization Handbook**
    a. **Tracking Number** 2014-F-24
    b. **Need that Drives Requirement**. The WES Stream Investigation and Streambank Stabilization Handbook was last updated in 1997. The handbook is widely used

by USACE field offices, other Federal agencies and the public to provide and outline templates for proper investigative, stabilization and restoration techniques.

c. **Extent of Need Across USACE**. The stream investigation, stabilization and restoration community of practice has greatly progressed in the past 15 plus years and practitioners need to have the most current information to address natural resource issues.

d. **Requirement**. Combine the current handbook with updated ERDC Tech Notes and Reports, Bulletins, EM updates, Hydraulic Design Criteria and additional pertinent information.

e. **Consequences if Requirement Not Met**. If the current WES Stream Investigation and Streambank Stabilization Handbook (1997) is not updated the USACE field offices, other Federal Resource Agencies and the public will not have the most current and up to date stream stabilization and restoration methods.

f. **Product Recommendation.** A methodology and guidance for the evaluation of river training structures on river stages will be developed. The Upper and Middle Mississippi River will be used as a test case. Applicable data will be collected and the training works evaluated as to their impact.

3. **Streambank Stabilization and Grade Control Techniques Suitable for Stream and Watershed Restoration Projects (Update of Section 32 Program)**

a. **Tracking Number** 2008-F-43

b. **Need that Drives Requirement**. Engineering design criteria for low-cost, environmentally relevant streambank protection and grade stabilization techniques suitable for stream and watershed restoration projects. The Corps has excellent design guidance for measures such as full bank riprap revetment, but no guidance for innovative and alternative measures increasingly requested by local stakeholders. Methods such as rootwads, Newbury rock riffles, stone barbs, J-hooks, W-weirs and many more are described in the gray literature, without reliable design criteria. Many have only limited design criteria or are emerging techniques. Reviewing the performance of completed projects is complicated by the lack of as-built plans, design computations, or monitoring, and by the use of unique designs, among other considerations. The Corps capability to include innovative stream stabilization measures in the engineering toolbox is critical to our success in stream and watershed restoration, as well as in regional sediment management.

c. **Extent of Need Across USACE**. This need exists through all Corps districts. It applies in particular to smaller watershed and stream restoration projects. It would also be useful in projects where watershed sediment reduction is a goal.

d. **Requirement**. The following R&D efforts would be effective in meeting this need: a. A major step would be an update of the Section 32 program to address stream stabilization measures (bed and bank) suitable for restoration projects. (The original Section 32 demonstration program constructed low-cost innovative streambank stabilization measures, and monitored their performance over time.) Like the original Section 32 program, an updated program should combine district expertise and ERDC and NRCS research capability. b. R&D to evaluate the performance of a wide range of ecologically relevant stabilization measures in

constructed projects, along with available design criteria. The goal would be to come up with relevant design recommendations. (R&D work has been done along these lines for bendway weirs and for stone toe protection, which are only two of numerous techniques in use. This work has been leveraged against work done by the US Bureau of Reclamation.) This work should be coordinated with the efforts of other agencies, such as the US Bureau of Reclamation. c. R&D to compile a comprehensive national list of methods used, with engineering and ecological limitations and benefits. This would be a joint effort with the USBR. It would take a USBR hydraulic engineering report for the Middle Rio Grande, and give it national application by addressing other methods and constraints. (Listings of methods and techniques have been performed in several references, but lack discussion of the engineering design criteria.) This national list of methods is probably the logical first step of the three listed here. It should be performed by ERDC-CHL in conjunction with IWR, ERDC-EL, district personnel, USBR, and NRCS.

e. Consequences if Requirement Not Met. The consequences of not meeting this need are: a. A lack of design guidance for streambank stabilization and grade control measures suitable for stream and watershed restoration projects. b. A lack of leadership in an arena where the Corps has traditionally provided guidance to both Corps districts and the wider community of practice c. A lack of a systems approach to restoration projects. The incorporation of sound engineering criteria for ecologically-friendly techniques is essential to project success.

f. Product Recommendation. This effort would build on several ongoing efforts by ERDC-CHL, USBR, NRCS, USDA, and the Desert Research Institute. The results should be incorporated into Corps guidance.

4. Full Integration of Hydraulic Engineering with Ecological Components of Project Planning and Design

a. Tracking Number 2008-F-49

b. Need that Drives Requirement. Since the Corps has added the mission of aquatic ecosystem restoration, an increasing percentage of projects include restoration goals. Although the restoration objectives are formulated by ecologists, their successful attainment relies on the support of hydraulic engineers (for hydrologic, hydraulic, and sedimentation aspects of design). There is a need for improvements in the planning and design process that would fully integrate Corps engineering and ecological components from the beginning of projects. The need is to ensure that hydrology, hydraulics, and most importantly, sedimentation, are not tacked on at the end of the planning process. The goal is a systems approach that would include all disciplines from start to finish, with a common vision of project goals and processes. The benefits include an improved capability to deliver viable and sustainable projects that meet goals and functions.

c. Extent of Need Across USACE. This need exists through all Corps districts, and covers a majority of projects.

d. Requirement. Extension and coordination of Planning and Engineering guidance and processes to address the gap that currently exists between ecologists and engineers. This should be based on R&D into a) the best engineering methods to

support ecosystem restoration projects, and b) the best metrics for ecologists to furnish to engineers to assure project success. This would focus on integrating design with habitat form, function, and maintenance, since these are physical processes that can be defined. A further step of tying species response to physical changes should not be included in this work unit, since the temporal and spatial variance is too great. This work unit should focus on fully integrating what is currently known in the engineering and ecological disciplines into a coherent approach.

e. **Consequences if Requirement Not Met**. The current consequences of not meeting this requirement include the following: a. Projects which cannot achieve goals in a sustainable manner b. Delays (or in some cases cancellation) of projects due to lack of coordination among disciplines. c. Increased projects costs due to delays, and to lost opportunities in shared data collection and information gathering. d. Decreased customer satisfaction.

f. **Product Recommendation.** This R&D should be conducted jointly by the Institute of Water Resources (IWR), Coastal & Hydraulics Laboratory, and Environmental Laboratory. The hydraulic engineering component should be overseen by a Project Development Team (PDT) using the expert Committee on Channel Stabilization as a nucleus. The results should be included in applicable guidance that is coordinated through both Planning and Engineering functions.

5. **Natural Channel Design Manual**
   a. **Tracking Number** 2008-F-79
   b. **Need that Drives Requirement**. The Corps is presently involved in river restoration projects throughout the country in which the goal is to restore habitat, improve fisheries and stabilize fluvial sediments. While the NRCS National Engineering Handbook does a thorough job of documenting Rosgen's methods for natural channel design, there is presently little Corps guidance for design and construction of river restoration projects using channel design methods that fully utilize our hydraulic engineering modeling capability in sediment transport, hydraulics, and hydrology. The Corps has designed and constructed many stream restoration projects using non-Rosgen methods, but has not documented the methodology in a comprehensive manner. Hydraulic and design engineers need this guidance to improve the likelihood of a stable and functional stream restoration project. (Note: the term "natural channel design" is normally associated with the methodology published by Dave Rosgen. It's used here to describe the design of a channel that has the appearance and function of a natural channel to the maximum extent possible.)
   c. **Extent of Need Across USACE**. This need exists through all Corps districts.
   d. **Requirement**. Perform literature review and critical evaluation of restoration channel design methodologies. Document experiences of field engineers with significant experience in successful natural channel designs. Document lessons learned from constructed stream restoration projects. The final product should be a design manual that has incorporates the results of these investigations into a step-by-step procedure for natural channel design that meets the highest hydraulic engineering standards of the Corps.

e. **Consequences if Requirement Not Met**. Not meeting this need will result in poorly designed and non-functioning river restoration projects. In many cases failure of the project will result in loss of habitat and the production of sediment that will ultimately have to be removed from federal navigation or flood control channels.
f. **Product Recommendation.** This R&D should result in a manual that hydraulic and design engineers can use to guide them though a river restoration project. The Corps expert Committee on Channel Stabilization should be involved in work unit oversight. Division technical experts in sedimentation should be included in the field review.

6. **Watershed Sediment Management: R&D to support engineering assessments**
   a. **Tracking Number** 2008-F-42
   b. **Need that Drives Requirement**. Corps districts need relevant and up-to-date methods for evaluating the technical effectiveness of sediment reduction measures. While these measures are proposed in an increasing number of watershed studies, their benefits (in decreased sediment yield) are not adequately estimated without overall guidance. The accurate technical estimation of the benefit (or impact) of various alternatives on sediment volumes and channel stability is critical to an appropriate plan formulation process. Existing guidance has not been updated to incorporate advances in the understanding and analysis of sedimentation, to address innovative practices, or to discuss current automation tools (such as GIS).
   c. **Extent of Need Across USACE**. This need exists through all Corps districts. An increasing number of studies include sediment reduction as a goal.
   d. **Requirement**. R&D to answer technical questions in several areas, with eventual incorporation in guidance. These areas include an evaluation of current sediment management techniques, recommended software and analysis methods , data collection, quantifying uncertainty in the data used - model selection and results, how to deal with data gaps and unknowns, impacts of region and land use on results, incorporation of current methods such as GIS, and others.
   e. **Consequences if Requirement Not Met**. The consequences of not meeting this need include: a. Delays in approval or requests for reformulation b. Watershed projects that do not deliver the intended benefits due to inaccurate technical estimates of sediment reduction. c. Increased study costs due to data and modeling unknowns.
   f. **Product Recommendation.** The final product should be cost-effective and available for use. It should take advantage of completed and ongoing R&D to the maximum extent possible. This would involve significant coordination with other federal agencies (USGS, NRCS, EPA, etc.), as well as state, local, and non-governmental organizations. The methods developed should be coordinated with field personnel, and should also be demonstrated to ensure utility. Three to five district studies should be selected as demonstration sites; the methods developed should be coordinated with the district personnel implementing these studies. The final products should be incorporated into Corps guidance. The R&D efforts

should be undertaken by ERDC-CHL (and coordinated with IWR through the Regional Sediment Management Program).

7. Evalutaion of Sediment Flushing and Other Means of Sediment Bypass for Reservoirs

a. Tracking Number 2008-F-40

b. Need that Drives Requirement. Sediment deposition reduces the useful life of reservoirs and often severely impacts authorized project purposes. Many USACE reservoirs are nearing the end or have exceeded their project lives and others are experiencing decreased project benefits due to sediment deposition. Flushing and other means of sediment bypass through reservoirs offer potential solutions for reducing the deposition of sediment thereby extending their useful lives. While flushing can be effective in reducing sediment deposition, the effects of sediment that is flushed must also be considered as it relates to water quality and downstream channel morphology. Also, the loss of coastal wetlands and freshwater marshes, particularly along the gulf coast region of the United States, is an ecological problem with far-reaching consequences and may be related to the reduction in available fine grain sediment load of the river system which feeds the wetlands. Fine grain sediment is required for the restoration of degraded wetland areas as well as the long term maintenance of healthy marsh. Reservoirs located along the main stem and tributaries of the upper river system may trap much of the fine grain sediment, preventing the material from ever reaching the coastal boundary. The re-entrainment of fine grain material deposited in reservoir pools through flushing operations, and the bypass of sediment through the reservoir by means of tunnels or conduits are potential solutions for addressing the deposition of fine grain sediment in the reservoirs. The feasibility of these methods to prevent deposition of material in the reservoirs and to supply the material to the river system for potential delivery to the coastal zone needs to be addressed.

c. Extent of Need Across USACE. The USACE maintains and operates more than 380 dams and reservoirs within the United States. Continued sediment deposition within these reservoirs results in the loss of storage allocated for project uses such as flood control, water supply, hydropower, recreation, and environmental purposes. With rising costs, as well as adverse environmental impacts of constructing new dams, the need for extending the useful life of existing reservoirs is becoming increasingly important. Research offers the benefit of developing more universal methods of increasing the useful life of reservoirs by reducing the amount of sediment that is being trapped in our reservoirs and possibly removing portions of the material already deposited, thus preventing additional depletion of storage or recovering storage lost due to sediment deposition. Also, USACE districts, as well as other federal agencies such as the U.S. Bureau of Reclamation, that own/operate reservoirs need effective ways to prevent the retention of fine grain sediment that could potentially be used for wetland restoration and maintenance farther downstream.

d. Requirement. R&D requirement is to develop methodology and necessary models for evaluating the potential for flushing and re-entraining sediment

through reservoir operational techniques/manipulation, and to develop models, physical and numerical, to determine hydraulic functionality and structure configuration of potential sediment bypass systems. Furthermore, analysis needs to be conducted to evaluate the intermediate impacts of bypassed sediment on the geomorphology of the river system between the reservoir and the ultimate destination of the sediment to ensure that no adverse impacts are created.

e. **Consequences if Requirement Not Met**. The consequences of not meeting the requirement include the continued reduction in the useful lives of existing reservoirs and the loss of project benefits due to storage volume depletion. Additional consequences include a lost potential opportunity to increase the available sediment concentrations which could be beneficial to slowing or halting the continued loss of coastal wetlands and marshes.
f. **Product Recommendation.** Methodology and guidance for analysis and design of sediment flushing procedures and sediment bypass systems. Increased understanding and modeling capabilities for assessment of both temporal and spatially varied morphological changes within the entire system.

8. **Sediment Modeling Tools**
   a. **Tracking Number** 2008-F-57
   b. **Need that Drives Requirement**. Watershed erosion and sediment transport modeling are crucial to the Corps' navigation mission and are finding increased application as the Corps takes on environmental rehabilitation work. Dredging of inland waterways, channel restoration, dam removal, bank stabilization, reservoir operation, Total Maximum Daily Load (TMDL) computations and water quality best management practices(BMPs) planning all require significant sediment analysis. Additionally, the Corps is beginning to consider the impact of bed change on levee risk (which can be the result of either erosion or deposition) and certification. Analyses of this type are notoriously complex yet nearly all of the technology available in Corps models is decades old and targeted to historical applications (e.g. dredging). There have been notable advancements in the last 20 years that should be incorporated in the Corps' sediment models. Additionally, there are and other problems require original, innovative R&D solutions. Finally, because of the significant uncertainty associated with sediment data and analysis, it is also imperative that Corps sediment models begin to incorporate stochastic principles in their simulations, allowing users to articulate results in terms of outcome uncertainty.
   c. **Extent of Need Across USACE**. Any Corps of Engineers District with dredging, levee certification, channel modification, river restoration, reservoir management, dam removal or watershed management missions needs to perform sediment transport analyses. Increasingly the Corps of Engineers is asked to perform detailed sediment studies to justify these efforts, select strategies or predict outcomes.
   d. **Requirement**. R&D products (main stream H&H models) that are heavily used in Corps planning studies need to be able to model the detailed aspects of water movement in urban areas. Most Corps of Engineers software products for H&H analyses have only recently added rudimentary sediment capabilities and still

require serious research and development before they are robust enough to answer the kinds of questions district engineers and biologists are likely to pose in the next decade.

e. **Consequences if Requirement Not Met**. The consequences for not meeting this requirement include the inability to perform detailed sediment analysis for Corps planning studies. Consequences of poorly planned sediment management include bank failure, levee risk (from toe scour and aggredation), unplanned or unnecessary dredging costs and habitat degradation.

f. **Product Recommendation.** Specific products to provide this capability should draw on methods and technology available from peer reviewed literature and other research institutions. Design and development of techniques and computer algorithms should be consistent with published standards for sediment transport modeling. However, wherever possible short-comings of existing techniques should be identified, and improved methodologies should be researched and developed wherever possible.

9. Web-based Storage and Retrieval System for Channel Cross-Section Data

a. **Tracking Number** 2014-F-4

b. **Need that Drives Requirement**. USGS gage data is readily accessible via the internet, and accordingly, academic and other research literature extensively utilizes gage data to draw broad conclusions about degradation or aggradation trends. The COE has invested hundreds of millions of dollars in regular bathymetric surveys which, if they were more easily accessible, could likewise be used by academic, Corps of Engineers, and other researchers to develop good science to improve management of our flood control channels. Unfortunately, the hassle involved in requesting data from the Corps of Engineers, plus the time it takes to meet such requests, severely limits the use of the data. The need for better management of large amounts of cross-section data has been so pressing in the Kansas City District that we contracted the development of a tool for querying, displaying, exporting, and generating useful geomorphic information.

c. **Extent of Need Across USACE**. Virtually all districts with flood control or navigation projects use cross-sections as a method for assessing channel degradation or aggradation over time. I know of no district that has made this data easily available for widespread benefit.

d. **Requirement**. The Kansas City District (NWK) has an especially robust dataset, which we have compiled into a single database with tens of thousands of cross-sections. We recently contracted with North Arrow Research to develop a tool for querying, displaying, exporting, and generating useful geomorphic information from the cross-sections. This tool has been developed as a desktop utility, but could easily be implemented on a web platform to allow easy access by researchers outside of the Corps. The architecture for storage, display, and information generation is already built. The tool would need to be adapted to operate in a web browser, the data stored on ERDC servers, and other districts made aware of how to format and upload their own data.

e. **Consequences if Requirement Not Met**. Business as usual means a continued under-utilization of hundreds of millions of dollars in excellent bathymetric data.

Adapting the NWK Cross-section Viewer/Analysis tool for web-based storage and retrieval will allow that data to be used more broadly and help the Corps to better understand and manage our projects.

f. Product Recommendation. An adaptation of the NWK Cross-section Analysis/Viewer tool to allow web-based storage and retrieval of information. Presentation of the tool at the 2015 sediment conference, through webinars, or other appropriate venues for technology transfer to other districts.

10. Sediment Data Collection Techniques and Model Applications

a. Tracking Number 2008-F-42

b. Need that Drives Requirement. Many Corps of Engineers projects have a component which must consider sedimentation effects. These investigations often involve the use of a suite of sediment models. The current and future generation of these sediment models will utilize 1, 2 and 3D hydrodynamics, and will potentially have the highest degree of uncertainty of any models used in H&H work. Successful, cost effective modeling requires the utilization of the correct balance of sediment and bathymetric data, field investigation, and experience. Sediment and bathymetric data are often scarce and expensive to acquire. Some of the newer techniques, such as particle tracking, are quite expensive and represent a substantial project investment. The purpose of this proposal is to develop guidance to assist Corps personnel in making decisions on the value of different data collection strategies, as well as the optimization of data collection and modeling efforts.

c. Extent of Need Across USACE. Most Corps offices require sediment impact assessments and modeling at various degrees of complexity.

d. Requirement. The R&D requirement for this need is to develop a coordinated approach for evaluating data requirements, data collection protocols, optimization of data, effective incorporation of data into sediment models, and value of data for a variety of sediment assessment and transport models utilized in large and small scale applications.

e. Consequences if Requirement Not Met. The consequences for not meeting the requirement are increased cost and uncertainty of results which impact project life cycle performance.

f. Product Recommendation. The products from this work are guidelines and methodologies that will help project managers and engineers make decisions on data collection efforts for a variety of applications, with the intent of optimizing model parameter input. This guidance will help reduce the uncertainty of model input data and therefore reduce the uncertainty of model results. A specific goal of the work should be the development of a PROSPECT course, along with workshops which will describe field data collection techniques, new technologies, and the selection and application of sediment assessment and transport models that are currently available.

OTHER CONSIDERATIONS

Research needs were discussed in both the 2014 conference call held by the Committee and in the 2009 workshop on river engineering capability (Remus and Jonas, 2010). Other considerations related to research are identified below.

- There is a continuing need for river engineering research: not all the work has been done.
- The river engineering community of practice should identify and articulate research needs.
- Training and technology transfer of research products is essential.
- In the past, river engineers at USACE Divisions and Headquarters played a critical role in maintaining the agency's focus on both research and training related to river engineering.

SUMMARY AND CONCLUSIONS

River engineering is one of the essential technical competencies of the Corps of Engineers. Ongoing research is required to answer critical questions and address current topics. This paper discusses submitted SONs in the field of river engineering, and the identification of high priority research needs by the expert committee. A logical next step would be the development of an overall strategic plan for river engineering research needs for the Corps. Ideally, this could be used to coordinate efforts with other federal agencies and entities.

ACKNOWLEDGEMENTS

The authors would also like to express their appreciation to the members of the Corps expert Committee on Channel Stabilization, and to the river engineering community within the Corps. Ms. Jonas would like to express her appreciation to Mr. Bill Curtis and Dr. Cary Talbot of ERDC Coastal and Hydraulics Laboratory, for her liaison assignment in support of the Flood Risk Management Research Area.

REFERENCES

Remus and Jonas (2010). "River Engineering – Past, Present and Future: A Comprehensive Systems Approach," FISC, Las Vegas, NV.

MODELING EXTREME FLOOD HYDROLOGY FOR GRAND COULEE DAM

Frank Dworak, Hydrologic Engineer, U.S. Bureau of Reclamation, Denver Federal Center, Bldg. 67, Rm. 580, PO Box 25007 (86-68250), Denver, CO 80225-0007, fdworak@usbr.gov; John England, Hydrologic Engineer, U.S. Bureau of Reclamation, Denver Federal Center, Bldg. 67, Rm. 580, PO Box 25007 (86-68250), Denver, CO 80225-0007, jengland@usbr.gov; Marketa Elsner, Hydrologic Engineer, U.S. Bureau of Reclamation, Denver Federal Center, Bldg. 67, Rm. 580, PO Box 25007 (86-68210), Denver, CO 80225-0007, melsner@usbr.gov; Ralph Klinger, Geologist, U.S. Bureau of Reclamation, Denver Federal Center, Bldg. 67, Rm. 580, PO Box 25007 (86-68330), Denver, CO 80225-0007, rklinger@usbr.gov

Abstract: The Bureau of Reclamation is conducting a Hydrologic Hazard Analysis (HHA) for Grand Coulee Dam to develop probabilistic flood frequency estimates for use in a dam safety risk analysis. The major challenges of this study include: 1) developing methodology capable of modeling hydrology for a 74,100 square mile international drainage basin, of which approximately 39,500 square miles are situated in the province of British Columbia, Canada, and 2) modeling a basin that is regulated by 76 major dams located within the Columbia River Basin (CRB) that are owned and operated by a mix of the U.S. federal, state, provincial, or local government, public utilities, and private entities. Following an extensive literature review and investigation into previous and current studies in the CRB, Reclamation is using a multiple methods approach, leveraging the modeling and data analysis completed by other agencies and universities for operations planning, climate change impacts assessments, and the Columbia River Treaty review. Two methods will be used to characterize hydrologic hazards at Grand Coulee Dam: the Expected Moments Algorithm (EMA) with streamflow and paleoflood data to estimate peak-flow statistics; and applying the Variable Infiltration Capacity (VIC) rainfall-runoff model and one-dimensional hydraulic models to develop flood peak and volume hazard curves. The two methods are used in order to: (1) ensure consistency between the rainfall-runoff model and streamflow data (including historical data and paleofloods); (2) provide data and models to estimate and extrapolate hydrologic hazard curves to annual exceedance probabilities (AEPs) of interest; and (3) include uncertainty estimates for the hydrologic hazard curves. The VIC hydrologic output will be used as input to the U.S. Army Corps of Engineers' (USACE) Hydrologic Engineering Center's Watershed Assessment Tool (HEC-WAT).

INTRODUCTION

The Bureau of Reclamation is conducting a Hydrologic Hazard Analysis (HHA) for Grand Coulee Dam to develop probabilistic flood frequency estimates for use in a dam safety risk analysis. Reclamation uses the most updated data and technology, as available and appropriate, to estimate hydrologic risk at dams. When dam loading estimates do not reflect the current information and technology available at one of its facilities, whether it is hydrologic, seismic, or static loading, it is common practice to perform an Issue Evaluation (IE) study to update the loading parameters. The hydrologic loadings for Grand Coulee Dam are being updated to Reclamation's current standard of practice.

The major challenges of this study include: 1) developing methodology capable of modeling hydrology for a 74,100 mi^2 international drainage basin, of which approximately 39,500 mi^2 are situated in the province of British Columbia, Canada, and 2) modeling a basin that is regulated by 76 major dams located within the Columbia River Basin (CRB) that are owned and operated by a mix of the U.S. federal, state, provincial, or local government, public utilities, and private entities. Most of the dams located within the CRB will not play a direct role in estimating hydrology for Grand Coulee Dam; however they will play an important role in estimating how the CRB will be operated as a system. Figure 1 shows the dams that were modeled in the USACE's Columbia River Treaty (CRT) review including Grand Coulee Dam. The project will rely on maximizing the use of previous and current flood studies for Grand Coulee Dam and the CRB.

Grand Coulee Dam is a concrete gravity structure located on the Columbia River in north-central Washington State, located approximately 75 miles west-northwest from Spokane, Washington. The towns of Grand Coulee and Coulee Dam are located immediately upstream and downstream, respectively, of the dam. The drainage basin is composed of mountainous terrain as well as large expanses of high desert plains in eastern Washington, eastern Oregon, and western Idaho. Elevations range from approximately 1,300 feet at the dam crest to over 13,000 feet in the mountains throughout the drainage basin. The CRB has large variations in mean annual precipitation. West of the Cascade Mountains, many regions receive over 30 inches of precipitation annually, while east of the Cascades precipitation is less than 20 inches, with some areas receiving as little as 7 inches (Climate Impacts Group, 2014). Annual precipitation in the Cascade Mountains can be as much as 100 inches. By several accounts, more than 70% of streamflow in the region originates as mountain snowpack (Hamlet et al. 2005; Elsner et al. 2010). Most of the drainage basin accumulates a snowpack throughout the winter followed by rainy periods in the spring and early summer. The high flow period for the Columbia River is driven by snowmelt during the spring and early summer from warming temperatures and rain.

There are two important large scale studies conducted in the CRB that will provide much of the data, modeling and methodology to conduct this study. The USACE has made a large effort to review the river operations, hydraulics, and hydrology involved in updating the 2014/2024 revision to the Columbia River Treaty between the U.S. and Canada (USACE, 2012). This effort has involved developing a detailed model of the Columbia River System, called the Watershed Assessment Tool (WAT), which includes updated terrain and bathymetry, river operations, routing scenarios, climate change, and potential updates to the Columbia River Treaty. The model is capable of estimating daily and flood control operations for the Columbia River system. The model is also capable of computing Monte Carlos simulations of river routings incorporating multiple forecast, operations and hydrology scenarios.

The northwest report of the Third U.S. National Climate Assessment (Snover et al., 2014) assesses the state of climate change in the northwest United States, including the CRB. This report primarily draws from recent studies, including the Washington State Climate Change Impacts Assessment (2009) and the Oregon Climate Assessment Report (2010). The report represents the key climate change issues in the growing body of regional research. The Washington State Climate Change Impacts Assessment (Miles et al. 2010) used climate projections from the Intergovernmental Panel on Climate Change (IPCC) Fourth Assessment

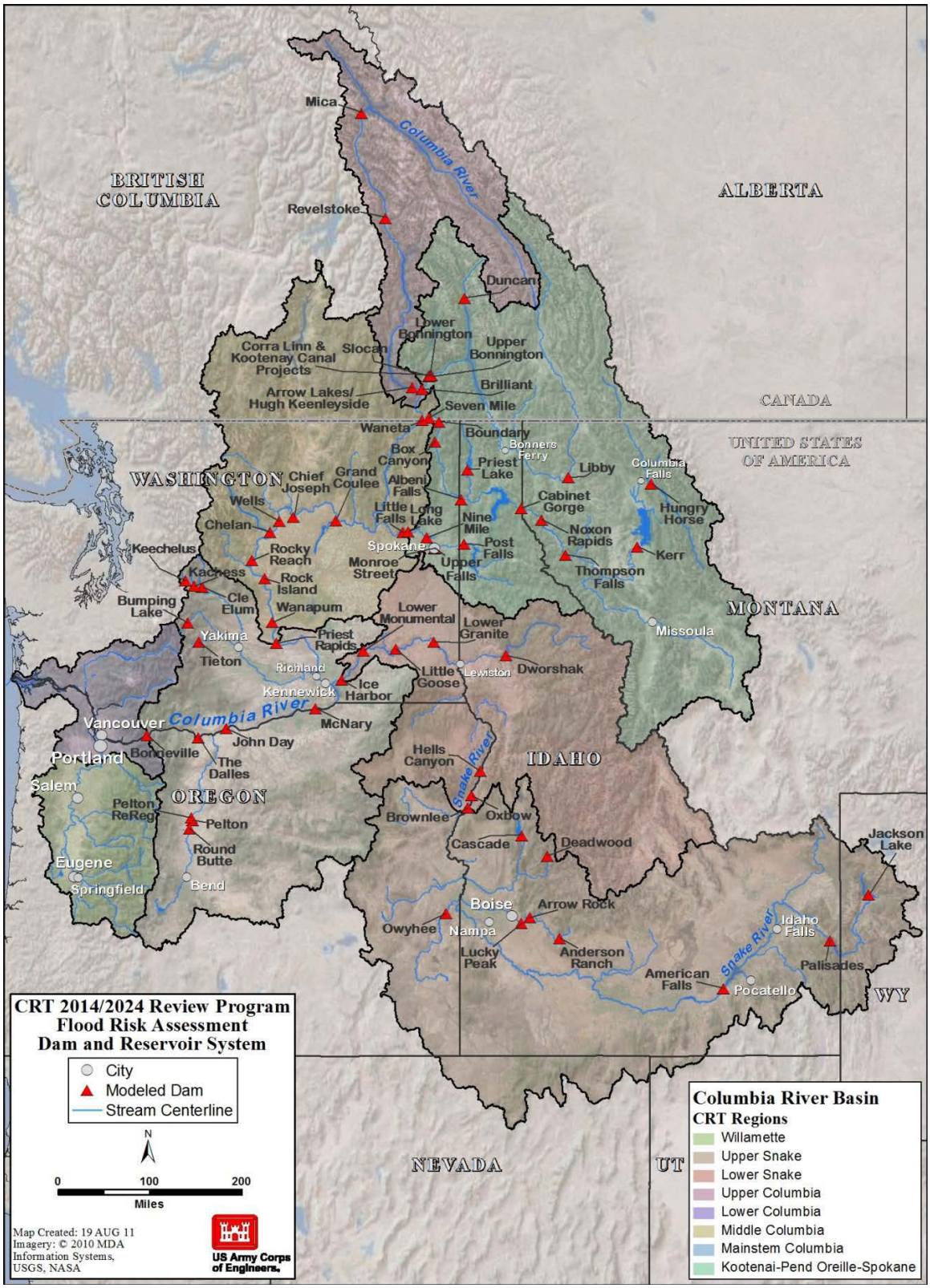

Figure 1 Image illustrating the dams that were modeled as part of the USACE CRT 2014/2024 Review Program, including Grand Coulee Dam (USACE, 2012).

Report (IPCC, 2007). Building on the modeling developed as part of the Washington State Climate Change Impacts Assessment, the Columbia Basin Climate Change Scenarios Project culminated in a comprehensive database of climate and hydrologic scenarios to support climate change analysis and adaptation planning. The intent of work is to provide a range of data for a variety of end users, including planning officials and research scientists. Some advances from this effort include hydrologic model calibration and development of additional climate change scenarios.

HYDROLOGIC HAZARD ANALYSIS

Reclamation uses a multiple methods approach to estimate hydrologic hazard for higher-level dam safety studies, including Issue Evaluations (IE) and Corrective Action Studies (CAS) at specific facilities (Reclamation, 2013). Multiple methods will be used to estimate the hydrologic hazard at Grand Coulee Dam. The approach uses two methods: 1) Expected Moments Algorithm (EMA) streamflow statistics and paleoflood data, and 2) rainfall statistics along with rainfall runoff and hydraulic modeling. The two methods are used in order to: (1) ensure consistency between the rainfall-runoff model and streamflow data (including historical data and paleofloods); (2) provide the data and models to estimate and extrapolate hydrologic hazard curves to AEPs of interest (Swain et al., 2006); and (3) include uncertainty estimates for the hydrologic hazard curves. Both methods will leverage and attempt to incorporate much of the past and ongoing work completed by Reclamation, University of Washington (UW), USACE, and Bonneville Power Administration (BPA).

Streamflow Statistics: EMA (Cohn et al., 1997) is a moments-based parameter estimation procedure that was designed to incorporate many different types of systematic, historical, and paleoflood data into flood frequency analysis. EMA assumes the LP-III distribution best represents the distribution for annual floods. EMA develops approximate confidence intervals using normal theory with and without an adjustment to correct for the correlation between the quantile estimate and its estimated standard deviation (Cohn et al., 2001). EMA has been documented in several journal articles (Cohn et al., 1997; England et al., 2003a; England et al., 2003b; Cohn et al., 2001) and provides a suitable flood frequency model. EMA has been applied by Reclamation at many sites for peak-flow frequency (England et al., 2003b; Swain et al., 2006; England, 2012).

Streamflow statistics will be calculated using EMA and will leverage the hydrology work completed by the USACE for the Columbia River Treaty Review (USACE, 2012). The EMA analysis will use the 2010 no regulation no irrigation (NRNI) dataset (BPA, 2014), synthetic floods developed by the USACE, and paleoflood data. The 2010 NRNI dataset (BPA, USACE, Reclamation) has a period of record (POR) daily from 1929-2008.

The EMA analysis will directly incorporate paleoflood and historic flood estimates into the LPIII analysis. The 1894 flood is the flood of record at most locations along the Columbia River and will be an important parameter in the study. Synthetic floods developed by the USACE may also be used in the EMA analysis or may be used to develop additional synthetic floods specific to flooding at Grand Coulee Dam.

The results of the EMA analysis are flood peak discharges, however the shape and volume of the hydrograph are needed. Flood hydrographs will be developed using several different methods and will then be scaled according to flood peak discharge to represent similar flood patterns. The USACE has developed balanced hydrographs from past large floods. Hydrographs have been developed in the past for historic large floods, such as the 1894 and 1948 floods. These hydrographs may be scaled according to flood peak discharge to represent similar flood patterns. Calibrated rainfall runoff and hydraulic models are part of this hydrologic hazard project and may be used to develop flood hydrographs representative of the runoff patterns for the drainage basin. For a hydrograph scaling approach it may be most appropriate to use a suite of hydrographs that represent historic floods and scale the hydrographs according to peak discharge. Representative hydrographs have been developed for historic large floods on the Columbia River.

Paleoflood Data: Paleoflood information will be used in this study to help extrapolate estimates of the flood frequency beyond the historical record. Paleofloods are past or ancient floods that were not observed by traditional means, but are often preserved in the sedimentary record (Figure 2). Most conventional estimates for the frequency of large floods are based on extrapolations from stream gaging records, and commonly utilize record lengths shorter than 100 years. Paleoflood hydrology ties together estimates associated to peak discharge and age developed from geomorphic and geologic evidence.

The Columbia River, as one of the largest river systems in the U.S. and one famously known as the avenue for the glacial Lake Missoula outburst floods, will require a substantial field effort to develop paleoflood data for this study. Four general locations have currently been proposed as sites to collect paleoflood information: two from the major tributaries that flow into Lake Roosevelt (the mainstem Columbia River and the Spokane River), one at a location downstream of Grand Coulee Dam on the mainstem Columbia River, and the last at a location near The Dalles, OR. The site at The Dalles, OR is intended to serve as a location where paleoflood data

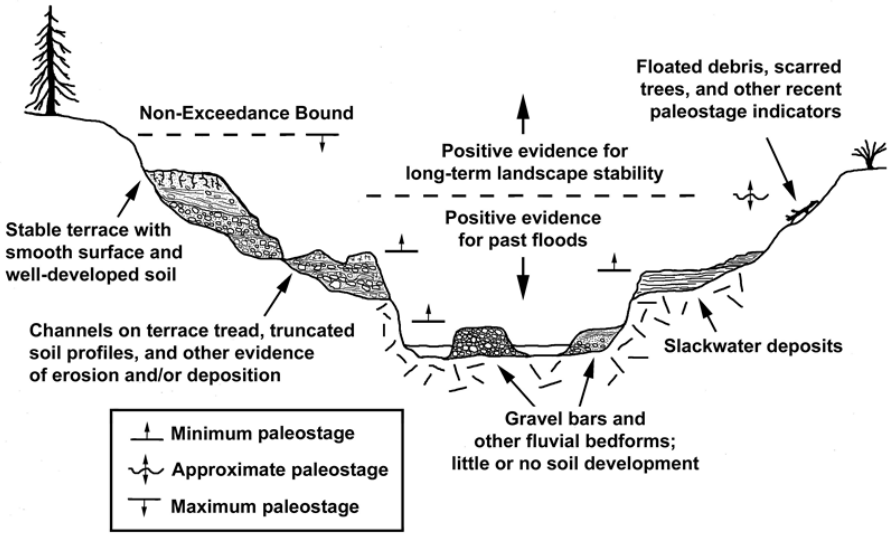

Figure 2 Idealized channel cross-section illustrating the concept of a non-exceedence bound and the fluvial landforms and related deposits associated with paleofloods.

can be developed downstream of the confluence with other major tributaries to the Columbia (i.e., the Yakima and Snake Rivers). The four sites outlined for the study are intended to collect data at key points within the basin that were considered vital and to keep overall study costs downs. A broader range of locations along the mainstem Columbia River upstream of Lake Roosevelt and an additional site on the Clarks Fork may be needed to reconcile the contributions to the reservoir.

Rainfall Statistics and Rainfall Runoff Modeling: The rainfall statistics and runoff modeling approach will use a combination of custom meteorological inputs, stochastic rainfall runoff modeling, hydraulic modeling, and paleoflood data to estimate a range of floods (peaks and volumes) with annual exceedance probabilities (AEPs) from 10^{-3} to 10^{-6}, or as needed for Reclamation dam safety risk-based decision-making. The general concepts that are proposed focus on leveraging the existing Variable Infiltration Capacity (VIC) rainfall-runoff model and the USACE Hydrologic Engineering Center's Watershed Assessment Tool (HEC-WAT) hydraulic model, and their ongoing applications within the Columbia River basin.

Extreme storm rainfall and snowpack data sets will be developed by Reclamation while leveraging the existing work. The custom meteorological inputs will be used as forcings in the VIC Model developed for the Columbia Basin Climate Change Scenarios Project. The VIC model and associated input datasets were developed at 1/16th degree latitude/longitude spatial resolution over the CRB as part of climate change studies. The VIC hydrologic output will be used as input to the HEC-WAT model. The Columbia River HEC-WAT model was developed by the USACE for the CRT Review and is capable of routing flows through the extensively regulated CRB to develop frequency flow estimates for Grand Coulee Dam. This approach will allow for the development of hydrologic hazard estimates at Grand Coulee Dam, and quantify associated uncertainties.

Meteorology: A major effort of this work is to develop custom extreme storm rainfall and snowpack data sets for use as meteorological forcings in the VIC rainfall-runoff model. Some key meteorological assumptions for this study are as follows.

1) Grand Coulee Dam is a major flood control dam with approximately 5.185 million acre-feet (MAF) of dedicated flood storage on the Columbia River system (USACE, 1991), that is operated on a very strong seasonal cycle (USACE, 1997; USACE, 1999; USACE, 2003; USACE, 2012). Meteorological inputs will primarily focus on the late spring and early summer April-May-June (AMJ) season in order to maximize potential CRB inflow volumes.
2) Combined flood control storage within the CRB upstream of Grand Coulee Dam is approximately 33.8 MAF (USACE, 1991; USACE, 2003), including storage at Mica, Arrow, Duncan, Libby, Hungry Horse, and Grand Coulee. In order to examine the potential effects of extreme floods on dam safety at Grand Coulee Dam, estimated extreme storm rainfalls in combination with snowmelt runoff are needed.
3) Snowpack depths and snowmelt runoff potential, in combination with extreme rainfall, are also key meteorological considerations, given the CRB flood storage. The application of season-specific or synoptic mechanism-specific frequency and extreme storm analyses may be investigated to confirm these assumptions are valid.

Meteorology will be developed by leveraging existing data and analyses that use historical and reanalysis data sets, as well as gathering and analyzing new data. It is anticipated that the analysis of 20 individual storm events, including spatial and temporal precipitation distributions, moisture fluxes, storm centering and orientation, will be performed. The main data sets initially include the following:

- the 1/16th degree precipitation and temperature gridded data (1915-2006) from Deems and Hamlet (2010) with consideration of recent updates (Livneh et al., 2013);
- observed point precipitation and temperature from the Global Daily Climatology Network (GDCN) and Global Historical Climatology Network (GHCN)
- daily precipitation, temperature, and related variables from the NRCS SNOTEL network;
- Climate Forecast System Reanalysis (CFSR) data (Saha et al., 2010);
- trajectory analyses and relevant meteorological fields from recent work by Alexander et al. (2013); and
- model runs of individual storms, historical events and ensembles over the CRB using the Weather Research and Forecasting (WRF) regional climate model by University of Washington and U.S. Army Corps of Engineers.

Specific precipitation and temperature perturbations and storm sequencing scenarios will be developed from these data sets. Climate change inputs and hybrid delta scenarios used in the CRB climate change studies commissioned by the State of Washington under House Bill 2860 (Hamlet et al., 2010) will also be considered. Meteorological scenarios may be added to investigate the potential influence of climate change.

Seasonality of extreme storm events will initially focus on analysis of April, May, June (AMJ) rainfall and snowmelt runoff sequences for specific flood years (Table 1). To date, detailed hydrometeorological analyses of the events listed in Table 1, including spatial and temporal patterns, depth-area-duration data, inflow moisture and associated analyses have not been completed. The initial data analysis of the extreme storm season may also be expanded to include warm-season events in summer (July-August) and fall (September-October) after investigation of storm hydrometeorology and snowmelt volume within this large region.

Table 1 Major spring storms in the CRB used for flood risk assessment (USACE, 2012)

Water Year	**Flood Dates**	**Comments**	**Key References**
1894	May 20 - June 15	May rain-on-snow; used as design event for the CRB system-wide flood control (USACE, 1991)	USGS (1949); USACE (1991); USACE (2009)
1948	May 19-23; May 26-29	May rain-on-snow; rainfall	USGS (1949); USACE (1991); USACE (2009)
1956	May 20 – June 6	predominately snowmelt	USACE (2012)
1971	May 31 (peak)	rain may have been predominant	USACE (2012)
1972	May 31 – June 14	snowmelt with some rain	USACE (2012)
1974	May and June	snowmelt	USACE (2012)
1997	May and June	snowmelt with some rain	USACE (2012)

The areal coverage of large precipitation events will be a main driver of extreme flooding. One objective is to develop storm centerings that are capable of producing extreme floods for the project area. The location of the storm centering will drive the possible areal extent of the storm as orographic effects from the Coastal and Cascade Mountains, as well as the aridity of eastern Washington and western Idaho will help to define the possible sizes and locations of storms.

Regional precipitation frequency analysis using L-Moments (Hosking and Wallis, 1997) will be used to estimate extreme storm rainfall point (10 mi^2) probabilities. The storm rainfall inputs will be developed for annual exceedance probabilities (AEPs) ranging from about 10^{-2} to 10^{-6}. Analyses will be done for several (two to three) regions to represent extreme storm rainfall sequences over various combinations of the CRB. The approach that will be developed for this study focuses on partial-area storm rainfall, and existing techniques that are adequate for smaller basins that will need to be modified because of the large CRB watershed.

One critical factor of this study is to couple the storm rainfall sequences in combination with snowmelt runoff. The largest runoff events (to date) have occurred in May and June (Table 1) and are extreme rainfalls in combination with a large snowpack. Spatial coverage of snowpack and snowpack depths are critical components. Scenarios using seasonal snowpack, temperatures, and melt sequences of individual events, such as the record May-June 1948 sequence, will be developed.

Many of the dams within the CRB, including Grand Coulee Dam, are operated for flood control. Seasonal snowmelt forecasting is an important component of flood control and will be examined for potential inclusion in this study. USACE (2012) indicates that forecast error (as well as operations) is a critical aspect to the CRB. The potential to include forecasts and associated forecast errors will be explored.

Rainfall-Runoff Modeling: The Variable Infiltration Capacity (VIC) model (Figure 3) developed for the Columbia Basin Climate Change Scenarios Project (CBCCSP) (Hamlet et al. 2013) will be used to estimate flows from extreme storms, in combination with other meteorological forcings. The CBCCSP came about through a collaboration of the Washington Department of Ecology, the Bonneville Power Administration, the Northwest Power and Conservation Council, the Oregon Water Resources Department and the British Columbia Ministry of the Environment. The project built upon hydrologic model development from the Washington State Climate Change Impacts Assessment (Miles et al. 2010). Specifically, the Variable Infiltration Capacity (VIC) model and associated input datasets were developed at $1/16^{th}$ degree latitude/longitude spatial resolution (approximately 30km^2 or 7400 acres per cell) over the Columbia Basin and coastal drainages within Washington and Oregon. The model was calibrated on a monthly timestep over 12 subbasins of the Columbia Basin. Hydrologic variables such as snowpack, runoff, soil moisture, and evapotranspiration were produced at the grid resolution of the VIC model, and simulated natural streamflow (absent any management effects) was generated at approximately 300 locations throughout the basin.

The VIC model will be used to evaluate the implications of extreme hydrometeorological conditions on the Columbia Basin with respect to flood risk and water management. Frequency precipitation estimates will be used in the historic rainfall database to model extreme floods that

take into account the large drainage basin and multiple sub-basins in the VIC model. A separate interface may be developed to run the perturbed meteorology in a stochastic format with a Monte Carlos method to randomly select the stochastic inputs to the VIC model, run the model, and post processes the results while keeping track of the model parameters for each run. Climate change, and its potential impacts on extreme floods, will also be included in this study. The meteorological forcings to VIC will include appropriate future climate scenarios.

Hydraulics and River Operations Modeling: The USACE developed the HEC-WAT model to integrate the multiple functions of a river system that contribute to flood risk management. The HEC-WAT modeling framework will be used to route flood flows downstream using realistic dam operations. Items such as river regulation, hydropower generation, and structural inventory are modeled and integrated into HEC-WAT to provide an automated approach to develop the metrics necessary to define flood consequences and risk.

High resolution terrain data were collected for both terrestrial and bathymetric conditions. Terrestrial data were collected using LiDAR, which was processed into digital elevation models. Bathymetric data were collected by hydrologic surveys, which resulted in a set of three-dimensional cross-sections. These data were integrated into a seamless terrain model representing elevations on the land and underwater, which was subsequently incorporated into the hydrologic and hydraulic models developed for this study.

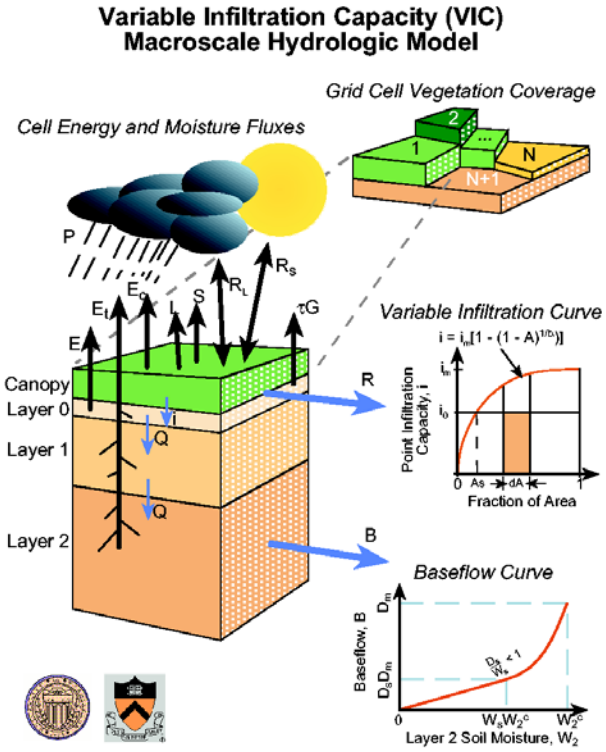

Figure 3 Overview schematic of Variable Infiltration Capacity (VIC) Model.

SUMMARY

Reclamation is performing a HHA for Grand Coulee Dam for use in a Dam Safety risk analysis. Due to the extraordinary large size of the Grand Coulee Dam drainage basin, Reclamation is taking a collaborative approach to the study that leverages the data collection, analyses, and modeling completed by other agencies and universities in both the United States and Canada. A multiple methods approach is being used, that is standard Reclamation practice for high level hydrologic studies, which combines streamflow and rainfall statistics with paleoflood data, hydrograph scaling, rainfall runoff and hydraulic modeling. A detailed HHA of this level has not been completed for Grand Coulee Dam in the past due to the expense and complicated nature of modeling. Leveraging the past and current work being completed in the CRB will allow Reclamation to complete an IE level HHA study for Grand Coulee Dam and help guide dam safety decisions for extreme floods.

REFERENCES

Alexander, M. et al. (2013). "Diagnosing the moisture sources for extreme precipitation events in the Intermountain West," NOAA/CIRES Project Report for Bureau of Reclamation Science and Technology Program, CIRES-Reclamation Project Agreement R11AC81334, November, 17 p.

BPA (2014). Website: http://www.bpa.gov/power/streamflow/default.aspx

Climate Impacts Group, (2014). http://cses.washington.edu/cig/pnwc/pnwc.shtml

Cohn, T.A., Lane, W.L, and Baier, W.G. (1997). "An algorithm for computing moments-based flood quantile estimates when historical information is available," Water Resour. Res. 33(9), pp. 2089-2096.

Cohn, T.A., Lane, W.L., and Stedinger, J.R. (2001). "Confidence intervals for EMA flood quantile estimates," Water Resour. Res. 37(6), pp. 1695-1706.

Deems, J. and Hamlet, A.F. (2010). "Historical Meteorological Driving Data Set," Chapter 3 in Final Report for the Columbia Basin Climate Change Scenarios Project. Climate Impact Group, University of Washington, http://warm.atmos.washington.edu/2860/report/

Elsner, M.M., L. Cuo, N. Voisin, J.S. Deems, A.F. Hamlet, J.A. Vano, K.E.B. Mickelson, S.Y. Lee, D.P. Lettenmaier, (2010). "Implications of 21st century climate change for the hydrology of Washington State", Climatic Change, doi: 10.1007/s10584-010-9855-0

England, J.F. Jr. (2012) Hydrologic Hazard Analysis. Section 7 in Dam Safety Risk Analysis Best Practices Training Manual, Bureau of Reclamation and US Army Corps of Engineers, Denver, CO, 12 p.

England, J.F. Jr., Salas, J.D., and Jarrett, R.D. (2003a). "Comparisons of two moments-based estimators that utilize historical and paleoflood data for the log-Pearson Type III distribution," Water Resour. Res., 39(9), 1243, doi:10.1029/2002WR001791.

England, J.F. Jr., Jarrett, R.D., and Salas, J.D. (2003b). "Data-based comparisons of moments estimators that use historical and paleoflood data," J. Hydrol., 278 (1-4), pp. 170-194.

Hamlet, A.F., Lettenmaier, D.P., (2005). "Producing temporally consistent daily precipitation and temperature fields for the continental," U.S., J. of Hydrometeorology, 6(3): 330-336

Hamlet, A.F., P. Carrasco, J. Deems, M.M. Elsner, T. Kamstra, C. Lee, S-Y Lee, G.S. Mauger, E.P. Salathé, I. Tohver, and L.W. Binder (2010). "Final Report for the Columbia Basin Climate Change Scenarios Project," Climate Impact Group, University of Washington

Hamlet, A.F., M.M. Elsner, G.S. Mauger, S-Y. Lee, I. Tohver, and R.A. Norheim. (2013). "An overview of the Columbia Basin Climate Change Scenarios Project: Approach, methods, and

summary of key results," Atmosphere-Ocean 51(4):392-415, doi: 10.1080/07055900.2013.819555.

Hosking, J.R.M. and Wallis, J.R. (1997). "Regional Frequency Analysis – An Approach Based on L-Moments," Cambridge University Press, 224 p.

IPCC (2007). "Summary for policymakers," In: Solomon S, Qin D, Manning M, Chen Z, Marquis M, Averyt KB, Tignor M, Miller HL (eds) Climate change 2007: the physical science basis. Contribution of working group I to the fourth assessment report of the intergovernmental panel on climate change. Cambridge University Press, Cambridge

Livneh, B., E. A. Rosenberg, C. Lin, B. Nijssen, V. Mishra, K. M. Andreadis, E. P. Maurer, and D. P. Lettenmaier, (2013). "A Long-Term Hydrologically Based Dataset of Land Surface Fluxes and States for the Conterminous United States,"Update and Extensions. *J . Climate*, 26.

Miles, E.L., M.M. Elsner, J.S. Littell, L.C. Whitely Binder, and D.P. Lettenmaier, (2010). "Assessing regional impacts and adaptation strategies for climate change: The Washington Climate Change Impacts Assessment," Climatic Change 102(1-2): 9-27, doi: 10.1007/s10584-010-9853-2.

Oregon Climate Change Research Institute (2010). "Oregon Climate Assessment Report," K.D. Dello and P.W. Mote (eds). College of Oceanic and Atmospheric Sciences, Oregon State University, Corvallis, OR

Reclamation (2013). "Design Standards 14, Appurtenant Structures for Dams (Spillways and Outlet Works), Chapter 2: Hydrologic Considerations, Final," Bureau of Reclamation, Denver, CO.

Saha, S., and Coauthors (2010). "The NCEP Climate Forecast System Reanalysis," Bull. Amer. Meteor. Soc., 91, 1015–1057, doi: http://dx.doi.org/10.1175/2010BAMS3001.1

Snover, Amy, (2014). "Climate Impacts on the Northwest, Key findings from the Third National Climate Assessment," Assistant Dean, Applied Research, Director, Climate Impacts Group, University of Washington, PNW Climate Science Conference, September 2014

Swain, R.E., England, J.F. Jr., Bullard, K.L. and Raff, D.A. (2006). "Guidelines for Evaluating Hydrologic Hazards," Bureau of Reclamation, Denver, CO, 83 p.

The Washington Climate Change Impacts Assessment, (2009). Website: http://www.ecy.wa.gov/climatechange/scientific_forecast2009.htm

U.S. Army Corps of Engineers (USACE) (1991). "Review of Flood Control, Columbia River Basin, Columbia River and Tributaries Study, CRT-63, Final Report," June 1991, Department of the Army, U.S. Army Corps of Engineers, North Pacific Divison, Portland, Oregon, 132 p. and appendix.

U.S. Army Corps of Engineers (USACE) (1997). "Columbia River Basin System Flood Control Review - Preliminary Analysis Report," February, 1997, Department of the Army, U.S. Army Corps of Engineers, North Pacific Divison, Portland, Oregon.

U.S. Army Corps of Engineers (USACE) (1999). "Kootenai River Flood Control Study, Analysis of Local Impacts of the Proposed VARQ Flood Control Plan. Status Report," Work to Date on the Development of the VARQ Flood Control Operation at Libby Dam and Hungry Horse Dam, January 1999, Department of the Army, U.S. Army Corps of Engineers, Seattle District, 83 p.

U.S. Army Corps of Engineers (USACE) (2003). "Columbia River Treaty Flood Control Operating Plan," May, 2003, Department of the Army, U.S. Army Corps of Engineers, Northwestern Division, Portland, Oregon, 42 p., tables, charts, and appendices.

U.S. Army Corps of Engineers (USACE) (2012). "DRAFT Columbia River Treaty 2014/2024 Review – Datasets and Models for Flood Risk Assessment Report," U.S. Army Corps of Engineers and Bonneville Power Administration, June, 2012.

DEVELOPMENT OF CCHE2D EMBANKMENT BREAK

Yafei Jia (primary author), National Center for Computational Hydroscience and Engineering, The University of Mississippi, University, Mississippi, jia@ncche.olemiss.edu; Sherry Hunt (co-author), USDA-ARS Hydraulic Engineering Research Unit (HERU) in Stillwater, OK, Sherry.Hunt@ars.usda.gov

Abstract: Flooding due to breaching of earthen embankments often results in detrimental impact on the people and their properties downstream in the flooded zone. The embankment breaching process is often caused by overtopping of excessive water in a reservoir or a river. The purpose of this study is to develop a practical numerical model for simulating overtopping and embankment breaching process. To achieve the goal, the key physical-empirical dam breaching mechanism of earthen embankment is adopted and implemented into CCHE2D surface flow model. A special function describing the shape of the breaching channel profile is introduced which significantly simplifies breach modeling. The developed model is validated using experiment data. The simulated flooding hydrograph, headcut migration, and breaching embankment profiles agree well with the observed data. Because this is a 2D model, the development makes it possible to simulate breaching in more complex conditions and study multiple embankment breaches at the same time. This broadens the applicability of the embankment break model significantly.

Keywords: Dam break, flooding, numerical simulation, two dimensional modeling, WinDAM, cohesive soil, overtopping

INTRODUCTION

Earthen embankments are effective infrastructures constructed across waterways or along rivers as dams or levees for flood protection. Due to aging or extreme hydrological events, embankments may fail and result in detrimental flooding. Embankment breaches have been studied by using physical experiments, numerical model simulations, and field observations. Most publications focus on dam breaching, but studies on the embankment erosion processes are relatively rare. Without considering the gradual breaching process of embankments, one may overestimate the dam break flood discharges. In this study, a numerical model to simulate embankment breaching is developed. Considering the complexity of the breaching process and the resulting flooding, a combination of a two dimensional flow model and a reliable dam break process model would have the potential for the best outcome. One can fully take the advantage of the capabilities of 2D models to accurately and reliably simulate embankment breaches in rivers and reservoirs.

Embankment breaching is often simplified as an instantaneous problem which can be simulated using only numerical flow models. There have been many developments in this area in recent years. Frazão and Zech (2002) measured flood waves in a channel bend and developed a finite volume model to simulate the flood. Aureli et al. (2008) simulated dam breach flooding using a finite volume code, the data were obtained by an imaging technique in a small scale experimental flume. Ying and Wang (2008) have developed a 1D finite volume model for flood wave simulation, where the HLL shock capturing scheme was used to solve the hydrodynamics implicitly. Zhou et al. (2004) validated a 2D model of dam breach flow using physical experiment data, with the complex channel geometry handled using cut-cell technique. Jia et al. (2010)

simulated the 2008 Midwest flood in Mississippi River using CCHE2D, a 2D flood model based on the finite element method. Multiple levee breaches and gradual breach processes have been considered, the simulation results are validated using satellite imagery.

Macchione and Sirangelo (1988) simulated the dam break process by solving 1D Saint Venant and sediment continuity equations. The breaching process was treated similar to that of non-cohesive sediment transport. This model was later applied to simulate multiple dam failures and had reasonable results (Macchione and Sirangelo, 1990). Wu and Wang (2006) simulated dam break processes with a 1D model, small-scaled experimental that considered dams constructed of loose materials. The density of sediment was accounted for in the flow modeling, and the non-equilibrium bed load sediment transport approach was applied. Ying and Wang (2010) have simulated the dam breaching process using a 2D model, simulating the flow using the 2D shallow water model based on the control volume method. The breaching process of an earthen dam composed of cohesive materials is simulated based on the linear model for cohesive soil erosion, which assumes that the erosion rate is proportional to the excessive shear stress acting on the soil surface. Wu (2013) proposed a method to simulate the erosional process causing dam breaching. The dam break slope, connecting the dam crest to the front toe, is assumed to be a straight line for non-cohesive sediment and a vertical drop for cohesive earth dams.

Embankment breaching processes have also been studied using physical experiments. Because embankments are constructed using cohesive materials, it takes extensive efforts to study and quantify the process using large scale physical experiments. Research engineers at the USDA-ARS Hydraulic Engineering Research Unit (HERU) constructed scale models of earthen embankments, and then breached them under controlled conditions. Hanson et al. (2005) conducted several outdoor experiments on large size models constructed of cohesive materials providing a unique set of data for dam breaching analyses and model validation. Their experiments have made significant contributions in collecting detailed observation data. Several other large scale dam break experiments have been carried out in Europe (Hassan, 2008; Vaskinn et al. 2001); in addition to homogeneous cohesive materials, breach processes with composite dam material were also tested.

The computer model Windows Dam Analysis Modules (WinDAM, Temple et al. 2006; Visser et al. 2012) has been developed for evaluation of dam breaching processes subjected to overtopping. It includes a reservoir routing model for the auxiliary spillway and the embankment. The model is capable of evaluating the ability of vegetation or riprap on the downstream face of the dam to withstand the overtopping flow. A homogeneous embankment constructed from cohesive soil materials of simple cross section is assumed.

The objective of this study is to develop an embankment breach model based on a two dimensional model of surface flow and the breach mechanism of the WinDAM model. Because the two–dimensional model is capable of simulating flows in both rivers and reservoirs, it will be applicable to both dam and levee breach cases with general flow conditions. In addition, two dimensional models can provide local flow solutions directly for the overtopping flow and the flow in the downstream flooding zone, the simulation results can be more accurate than one dimensional models. Two-dimensional models make it possible to simulate multiple breaches along a channel at multiple locations and under differing local flow conditions. The finite element method based model CCHE2D (Jia et al. 1999, 2002) has been used for this study.

NUMERICAL MODEL

CCHE2D is a depth-integrated model based on the finite element method for simulating free surface flows, sediment transport, bank erosion, vegetation effect, and water quality, and it is also applicable to coastal processes (Jia and Wang 1999, Jia et al. 2002, 2006, Ding et al. 2003, and Zhu et al. 2008). The model uses a collocation method and quadrilateral mesh system. Velocity-pressure coupling is achieved using a partially staggered grid arrangement. The velocity correction method is used to achieve momentum and mass conservation at each time steps. Temporal integration is of a second order Range-Kutta method. In order to increase computational efficiency, wet-dry capability was developed for handling moving boundary problems in areas with complex topography. It has been applied to a wide range of flow conditions from dam breaches of real scale reservoirs, large rivers such as the Mississippi, to small-scale experimental laminar flows.

EMBANKMENT BREACH MODEL

For cohesive earth embankments, the overtopping flow profile has two segments: a segment at the crest and a segment and the headcut. The conceptual evolution of the geometry of dam and levee breaches is depicted in figure 1.

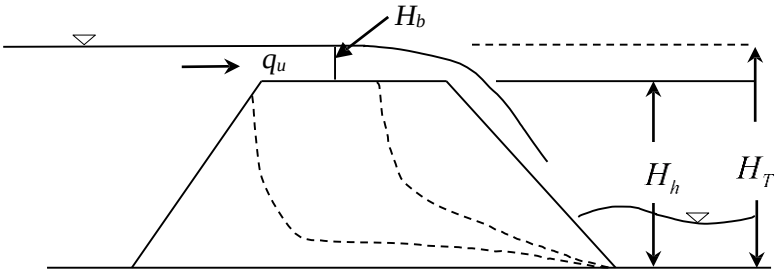

Figure 1 Dam break or levee breaching process sketch

Overtopping induced embankment breach process (figure 1) is normally recognized to have three stages:

1. Overtopping stage: the flow erodes the dam crest surface and front slope surface, these two surfaces lower their elevation almost uniformly. The discharge is relatively small, depending on how much higher the water surface in the reservoir is than that of the crest.
2. Headcut stage: The crest is continuously eroded. Headcut(s) are formed by soil erosion over the front slope and migrate upstream while incising deeper. In this stage the embankment is eroded significantly by the incised channel, but the flow discharge is relatively small because the crest elevation is still quite high. The headcut in the embankment widens due to both lateral erosion and soil mass failure.
3. Embankment breach stage: The headcut migrates to and intercepts with the back of the embankment (upstream slope), the flat dam crest disappeared. Because the remaining embankment is thin and has a sharp crest, its strength to resist flow erosion and water pressure is weakened. The headcut migration rate therefore increases significantly and the discharge increases quickly to the peak flood. The increasing discharge further erodes the remaining embankment crest, deepening and widening this incised channel. The breach

channel widens in this stage with a slower rate. Because the vertical erosion and lateral widening occur at the same time in numerical simulation, the third stage includes the III and IV stages suggested by Hanson (2005).

Because of the complexity of the breaching process, it is difficult to simulate by simply applying a numerical model for hydrodynamics, and sediment erosion and transport. A conceptual model similar to WinDAM was adopted in this study that considered with the following three major processes:

- Frictional erosion on embankment top segment
- Headcut erosion and migration
- Channel widening

Breaching Channel Profile: A simple power function is proposed to represent the headcut profile as indicated in figure 2. The elevation and length of the flat crest is lowered and shortened by top friction erosion and headcut migration. The friction erosion is controlled by the embankment soil property and the flow shear stress. Higher flow rate and more erodible soil would result in faster crest erosion and decrease in elevation. The headcut erosion is physically dominated by frictional erosion and flow plunging impact on soil surface, it is more intensive than crest erosion. One major headcut is considered. In figure 2, (x_T, z_T) is the location of the brink of the dam breach flow or headcut, it connects the two segments and moves in time. (x_b, z_b) is the location of the front toe of the embankment. (x_{tr}, Z_{tr}) and (x_{br}, Z_{br}) is back brink of the embankment crest and embankment back toe. The base line is considered non-erodible in this study.

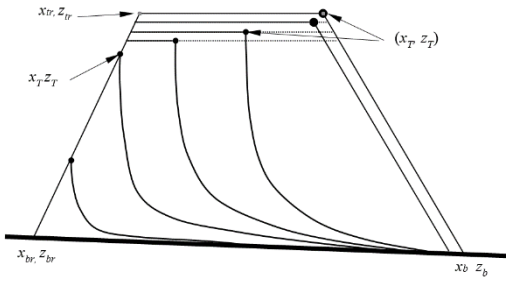

Figure 2 Side view of an overtopping induced dam-break process

It can be seen that the profile across the embankment is mainly represented by three segments:

$$\text{Crest segment}: \quad z = z_T \qquad x \le x_T \tag{1}$$

$$\text{Headcut segment}: \quad \left(\frac{z - z_b}{z_T - z_b}\right)^s = \frac{x - x_b}{x_T - x_b} \qquad x_T \le x \le x_b \tag{2}$$

$$\text{Back slope segment}: \quad \frac{z_T - z_{br}}{z_{tr} - z_{br}} = \frac{x_T - x_{br}}{x_{tr} - x_{br}} \qquad x_{br} < x_T < x_{tr} \tag{3}$$

The crest segment is the horizontal and flat top of the embankment. Its elevation is determined by surface friction erosion; its length can be shortened due to front slope erosion and head cut

migration. The headcut segment is approximated by a function combining the initial straight front slope and the head cut profiles. The shape parameter, *s*, defines a continuous transition from the first stage to second stage of headcuting:

s=1.0 : downstream slope at initial overtopping stage
s>1.0 : headcut stage

Figure 3 illustrates several headcut curves modeled using equation 2, in which *s* varies from 1 to 10.

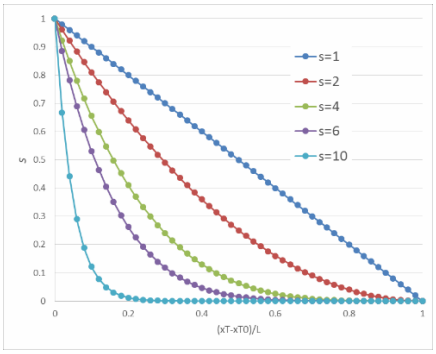

Figure 3 Non-dimensional headcut profile function

The exponent parameter *s* is formulated as a function of x_T and the width of the crest, L_T . It is assumed *s*=1 at the beginning, it increases to its maximum value (*s*=10) when the head cut advances to half of the crest width:

$$\begin{aligned} s &= 1 + 20\frac{(x_{T_0} - x_T)}{L_T}, && (x_T >= x_{T_0} - \tfrac{1}{2}L_T) \\ s &= 10 && (x_T < x_{T_0} - \tfrac{1}{2}L_T) \end{aligned} \quad (4)$$

Equation 4 is a model established to approximate the process of the changing headcut profile. Figure 4 shows this headcut profile parameter changing from the overtopping stage (*s*=1) to the fully advanced headcut stage (*s*=10). This equation assumes that after the headcut has reached a half of the dam crest (0.5L_T), *s* reaches its maximum value, and the headcut steepness remains unchanged in further process. The assumption would not affect the accuracy because the breach is dominated by the location of headcut $[x_T, z_T]$ and less by the shape of the profile.

Equation 3 represents the back slope segment of the embankment which intercepts with the headcut brink (x_T, z_T) when the headcut advance exceeds the back brink of the crest. At this time the remaining embankment becomes a sharp crest and the migration rate will be increased. By inserting x_T into equation 3, one can compute the crest elevation z_T. Inserting the new (x_T, z_T) into equation 2, a headcut profile for the breaching stage can be computed.

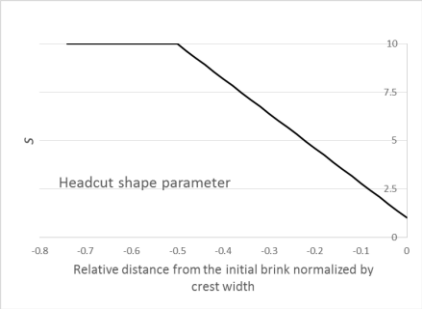

Figure 4 Headcut shape parameter *s*

Embankment Erosion Process: The headcut brink, (x_T, z_T), is the hydraulic control of the entire process. The downward movement of z_T is controlled by friction erosion of the crest. In this study, the crest erosion is governed (Hanson and Cook, 2004 and Hanson and Hunt, 2007) by

$$\frac{dz_T}{dt} = \varepsilon_r = k_d(\tau_e - \tau_c) \tag{5}$$

ε_r is the soil detachment rate in volume per unit time, k_d is the detachment rate coefficient which is an embankment material property parameter, τ_c soil critical shear stress, and τ_e the effective shear stress. Observed data indicate that k_d varies between 0.02~1000 depending on water content, compaction energy and texture of the soil (Henson et al. 2011).

The length of the crest segment will decrease because of the headcut migration. Computing headcut migration is to track the upstream movement of the brink point (x_T, z_T). Temple and Hanson's headcut advance rate model (Temple et al. 2005) is adopted for simulating this process:

$$\frac{dx_T}{dt} = C_h(q_u H_h)^{1/3} \tag{6}$$

where H_h is the headcut height (figure 1), C_h is a calibration parameter for headcut migration rate, q_u is the unit discharge of the overtopping flow. In this study q_u is directly computed by the 2D flow simulation model. The unit discharge would be a constant if the crest is resistant to erosion. In this case, the headcut will advance at a constant rate. If the headcut advances into the reservoir and intercepts the upstream slope of the dam, the brink point will lower its elevation while moving upstream, allowing for more flow to accelerate the breaching process. Experiments indicated that the migration rate would significantly increase when the upstream crest is reached (Hanson et al. 2005). As mentioned earlier, the speed-up is attributed to the weaker embankment condition, the coefficient C_h may have a larger value at the breaching stage. The C_h value is doubled in this study for the headcut migration during the breaching stage.

Widening of the Headcut Channel: In the process of breaching, the breaching channel incises into the embankment, the incision profiles can be computed as indicated in the previous section. However, the incised channel will also be widened due to lateral erosion and mass failure as its bed gets deeper and deeper. The lateral shear force of the flow will erode the materials from the embankment side walls and the steep side slope of the embankment may collapse due to gravity. The widening rate is correlated to the rate of deepening in WinDAM model (Temple et al. 2006): the rate of widening of the breaching channel is of 1.4 times of the rate of deepening. A side wall will therefore retreats 0.7 times of the mean depth erosion in a cross-section. This is equivalent to about 55 degrees along the wet toe of the side slope. In the case of two dimensional modeling, the incised breaching channel is represented by a number of mesh lines and the widening is dominated by the vertical toe erosion of the sidewalls. An effective angle of repose is used to model the channel widening: if the slope near a toe mesh point of the sidewall exceeds this angle due to toe erosion, the sidewall elevation at the higher node is "collapsed" to enforce the angle (figure 5). In the numerical tests, the effective angle of repose is adjusted slightly to fit the observed widening process (Tab. 1).

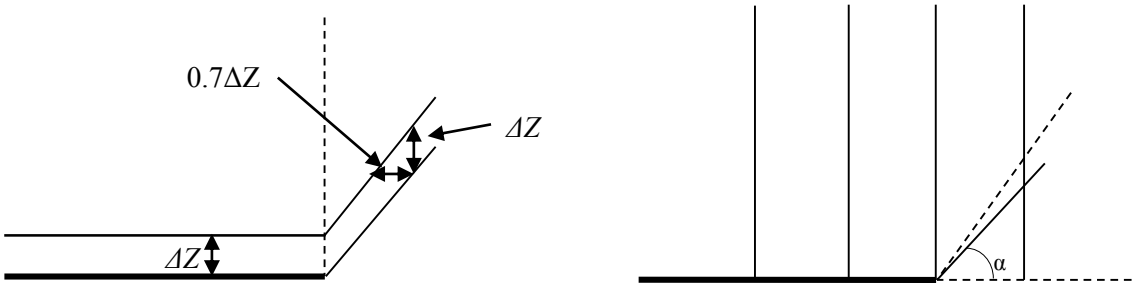

Figure 5 The width increases in time with the lower end being wider.

VALIDATION OF THE IMPLEMENTED CCHE2D DAMBREAK MODEL

Data from the experiment are required to validate the developed model. Large-scale overtopping breach tests on homogenous cohesive embankments conducted by Hanson et al. (2001, 2005) were selected for validation. Three sets of data from the experiments (E1S1, E1S2, and E1S3) were selected for testing. These three tests have the same shape and size of the embankment but built with three different soils. The embankment is 2.3 m high, 22 m long; a 0.46m deep by 1.83m wide notch was opened for the overtopping flow to develop. During the experiments, a flow of 1.0 m3/s is discharged into the reservoir.

Table 1 Parameters used for simulations

	Critical shear stress (Pa)	**Soil erodibility (cm^3/N-S)**	**Headcut coeff C_h**	**Effective angle of repose α(°)**	**Inflow discharge (m^3/s)**	**Soil**
E1S1	0.14	10.3	0.0035	62	1.0	1
E1S2	0.14	2.0	0.000288	50	1.0	2
E1S3	14	0.39	0.00004	55	1.0	3

It is generally recognized that the erosion to the embankment made of cohesive soil is related linearly to an erodibility parameter and the excessive shear stress (Hanson et al. 2001; Hanson, 1989a.) Parameters related to this approach have been calibrated using experimental data to obtain good agreements on comparing the simulated and observed flood process. Table 1 lists the

parameters for the experiments. C_h and α have been calibrated to obtain correct values for headcut advance and breach channel widening.

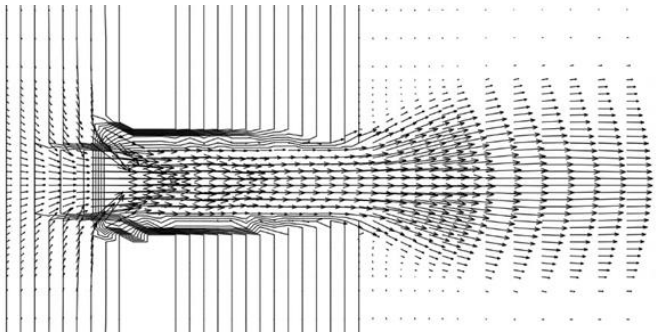

Figure 6 Simulated velocity distribution for E1S1 at t=38 min. Contours indicate the embankment

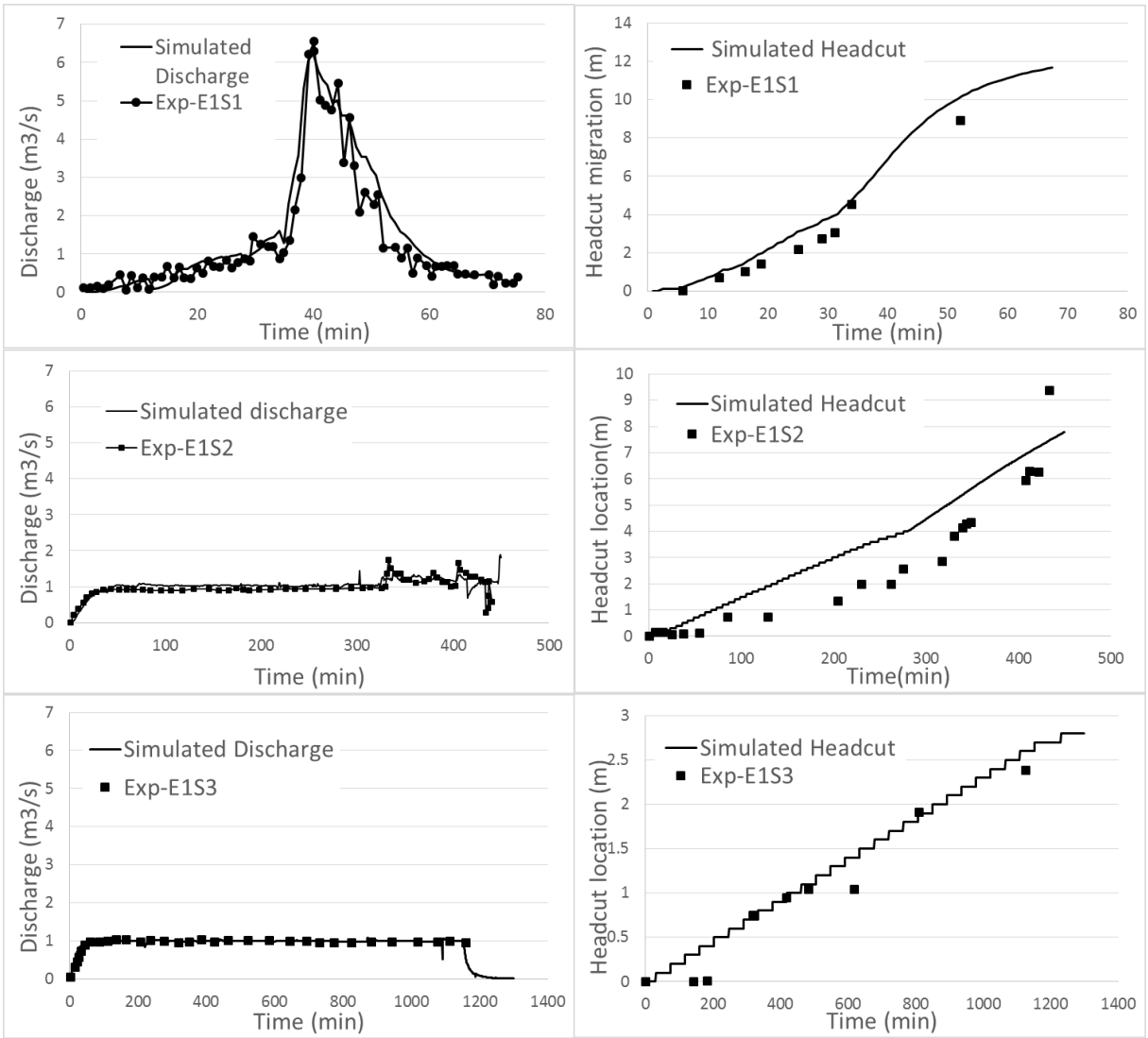

Figure 7 Comparisons of the computed and measured breaching flow discharge and headcut advancement

Figure 6 is a snap shot of the simulated flow field for the case E1S1. The headcut intercepts the back slope of the embankment at t=38 min approximately, the breaching stage starts and flow discharge is increasing rapidly. The vector field indicates the converging flow on the reservoir side and the diverging flow on the outside of the embankment. The variables in equation 5 and 6, τ_c, τ_e, H_h and q_u, are averaged from the simulated two dimensional flow in the friction erosion zone. It is seen the 2D model can represent the hydrodynamics of the breaching flow, the model predicted breaching flood can directly be used for inundation and mitigation analysis.

Figure 7 compares the computed and measured breaching flood discharge and headcut advance of all three test cases. The discharge hydrographs agreed very well including the peak of the flood and the shape of the hydrographs. The simulated headcut migrations also match those observed. Because the advance rate of the headcut is set to be doubled, the simulated migration speed up when the upstream brink of the embankment is reached by the headcut, as seen for E1S1 and E2S2. For the case E1S3, the experiment was terminated before breaching stage, both computed and observed migration are of a constant rate. One notes that the computed headcut location of the case E1S2 is a little ahead of the measured one, about 1 to 2 meters, and the two curves intercept at later time when the observed headcut migration suddenly accelerated.

Figure 8 shows the computed and measured breaching channel profiles of the case E1S2. The general agreement of the two sets of data is very good. The shape of the function-modeled headcut profile at different times are very similar to the measured ones. The 1 minute profile of the simulation has little movement from the initial profile; the measured counterpart has advanced about 1meter. The profiles of 19 minute and 85 minute agreed very well. The simulated profile of 203 minute and 314 minute advanced faster than the measured for about 1-1.5 meters. The agreements for the profiles of 342 minute and 407 minute become good again. These are consistent with headcut advance showing in Fig. 8, that the predicted and measured headcut locations are close at the beginning and near the end, but they have larger differences in the middle of the process.

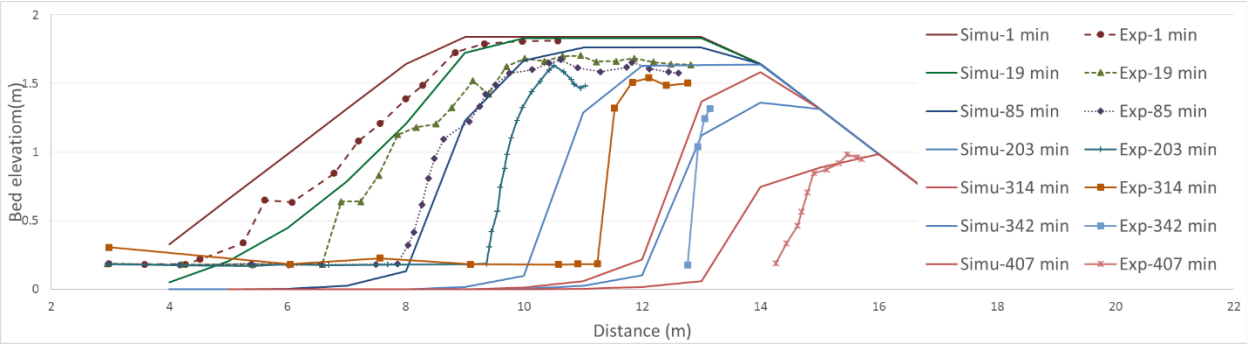

Figure 8. Comparisons of simulated and observed headcut profiles for case E1S2.

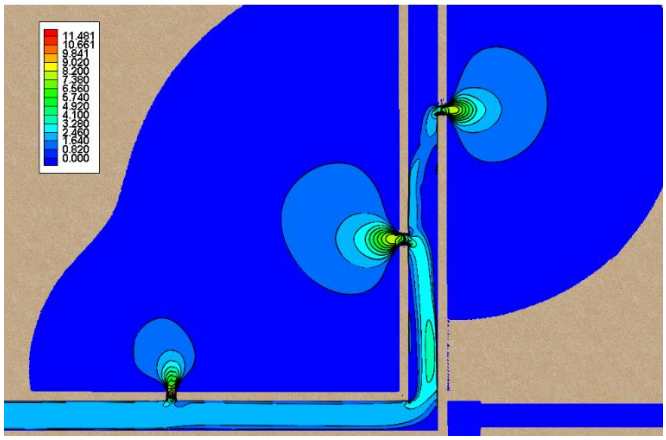

Figure 9 Simulated large scale test case with multiple levee breaching. The horizontal length of the figure is 2 km, the channel width is 100 m.

Figure 9 shows a hypothetical levee embankment breaching test. The flow velocity distribution of the simulated flooding results at about 14 hours is displayed. The maximum velocity exceeds 11m/s. The spatial scale of the simulation is quite large, the width of the domain is 2000 m, the width of the channel is about 100 m, the flow discharge is 1200m^3/s, and the relative levee height is about 7 m. A steady flow is established first, and three notches are made at the breach locations. A continuing run of the model resulted in three breaches along the channel. Because the parameters of the embankment at the three locations are set differently, the flow conditions along the channel and the simulated breach developments are different. This example demonstrates that a two dimensional model can significantly extend the application of the embankment breach model such as WinDAM.

CONCLUSIONS

A two-dimensional embankment breach model is developed by integrating the physical-empirical breach mechanism of the WinDAM model and the general surface flow model, CCHE2D. The new model is capable of simulating one or multiple embankment breaches at the same time in more complicated general surface water conditions. It therefore has a wider potential to be applied for flood prediction and disaster mitigation. A function is proposed to model the breach channel of the headcut which transitions the breach channel profile from the straight line at the beginning to the steep headcut at the end of the process. The function simplifies the computation because no erosion simulation is needed in the area from the headcut brink to the toe of the embankment. Validation tests using three sets of large scale experimental data have had good results indicating the developed model can really predict the physical process of dam breach or levee breaching. In particular, the modeled headcut profiles are very close to those measured. The developed model is embedded in the graphic user interface of the CCHE2D model, making applications of the model very easy.

ACKNOWLEDGEMENT

This research is supported in part by the USDA Agriculture Research Service under the Specific Research Agreement No. 58-6408-1-609, and monitored by the USDA-ARS National Sedimentation Laboratory (NSL) and The University of Mississippi (UM).

REFERENCES

Aureli, F., Maranzoni, A., Mignosa, P., and Ziveri, C., 2008, "Dam-break flows: acquisition of experimental data through an imaging technique and 2D numerical modeling". Journal of Hydraulic Engineering, Vol. 134, No. 8, August 1, 2008. ©ASCE, ISSN 0733-9429/2008/8-1089–1101/

Frazão, S.S., and Zech. Y., (2002), "Dam Break in Channels with 90° Bend", *Journal of Hydraulic Engineering*, Vol. 128, No. 11, November 1, 2002. ©ASCE, ISSN 0733-9429/2002/11- 956–968.

Hanson, G.J., Robinson, K.M., and Cook, K.R. 2001, "Prediction of headcut migration using a deterministic approach." *Trans. ASAE* 44(3): 525–531.

Hanson, G. J., Cook, K. R. and Hunt, S. L. (2005). "Physical modeling of overtopping erosion and breach formation of cohesive embankments." Trans. ASAE, 48(5), 1783 – 1794.

Hanson, G.J., D. M. Temple, S. L. Hunt, R. D. Tejral, 2011, "Development and characterization of soil material parameters for embankment breach." Applied Engineering in Agriculture, Vol. 27(4): 587-595, American Society of Agricultural and Biological Engineers ISSN 0883-8542.

Hassan, M., and Morris, M. W. (2008). "IMPACT project field tests data analysis." FloodSite Rep. T04-08-04, FLOODsite, European Community.

Jia, Y and Wang, S.S.Y. (1999). "Numerical model for channel flow and morphological change studies", *J. Hydraul. Eng.*, ASCE, 125(9), 924-933.

Jia, Y., Wang, S.Y.Y., and Xu, Y. (2002). "Validation and application of a 2D model to channels with complex geometry", *International Journal of Computational Engineering Science*, 3(1) (March 2002), 57-71.

Jia, Y., Hossain, A.K.M.A., Chao, X.B., (2010). "Computational Modeling of Midwest Flood 2008: Levee Breaching and Flood Propagation", Proceedings of World Environmental & Water Resources Congress 2010.

Jia, Y., Zhang, Y.X., and Wang, S.S.Y., 2006, "Numerical Simulations of Channel Response to Riverine Structures in Arkansas River", Published in the Proceedings of 7th Int'l Conference on Hydroscience and Engineering, Philadelphia, USA, September, 2006.

Macchione, F. & Sirangelo, B. (1988) "Study of earth dam erosion due to overtopping". Proc. Technical Conf. on Hydrology of Disasters, WM0, Geneva, 212-219.

Macchione, F. & Sirangelo, B. (1990) "Floods resulting from progressively breached dams", Hydrology in Mountainous Regions. II-Artificial Reservoirs, Water and Slopes, Proceedings of Two Lausanne Symposia, August 1990, IAHS Publ. No. 194, 325-332.

Temple, D. M., G. J. Hanson, M. L. Neilsen, and K. R. Cook. (2005). "Simplified breach analysis

for homogeneous embankments: Part1. Background and model components". In Proc. United States Society on Dams, Technologies to Enhance Dam Safety and the Environment, 151 - 161. Denver, Colo.: USSD.

Temple, D.M., Hanson, G.J., and Neilsen, M.L., 2006, "WINDAM – Analysis of Overtopped Earth Embankment Dams", Written presentation at 2006 ASABE Annual International Meeting, Portland Convention Center Portland, Oregon, 9 - 12 July 2006.

Visser, K., Hanson, G., Temple, D., and Neilsen, M., (2012), "Earthen Embankment Overtopping Analysis using the WinDAM B Software", Proceedings of ASDSO Dam Safety 2012, September 16-20, 2012 Colorado Convention Center, Denver, CO. (CDROM)

Wu, W. and Wang, S. (2006) "1-D Numerical Simulation of Morphodynamic Processes under Dam Break and Overtopping flows." World Environmental and Water Resource Congress 2006: pp. 1-10. doi: 10.1061/40856(200)67.

Wu, W., (2013). "Simplified Physically Based Model of Earthen Embankment Breaching", Journal of Hydraulic Engineering, Vol. 139, No. 8, August 1, 2013. © ASCE, ISSN 0733-9429/2013/8-837-851.

Ying, X.Y. and Wang, S.S.Y., (2008), "Improved implementation of the HLL approximate Riemann solver for one-dimensional open channel flows". Journal of Hydraulic Research Vol. 46, No. 1 (2008), pp. 21–34 © 2008 International Association of Hydraulic Engineering and Research.

Ying, X.Y., and Wang, S.S.Y., (2010), "2D Numerical Simulation of Breaching Process of Unlined Cohesive Earthen Dam." ASCE, World Environmental and Water Resources Congress 2010, 1317-1326.

Zhang, Y.X.(2008), "CCHE-GUI version 3.20— Graphical Users Interface for the NCCHE Model and Users Manual", *NCCHE-TR-2008-01,* April 2008

Zhou, J.G., Causon, D.M., Mingham, C.G.; and Ingram, D.M., 2004 "Numerical Prediction of Dam-Break Flows in General Geometries with Complex Bed Topography", *Journal of Hydraulic Engineering*, Vol. 130, No. 4, April 1, 2004. ©ASCE, ISSN 0733-9429/2004/4-332–340.

Zhu, T., Jia, Y., and Wang, S.S.Y. (2008). "CCHE2D Water quality and Chemical Model Capabilities", World Environmental and Water Resources Congress, 2008, Hawaii, (CD-ROM).

Vaskinn, K. A., Lovoll, A., Hoeg, K., Morris, M., Hanson, G. and Hossain, M. A.A.M., 2001, "Physical modeling of breach formation large scale field tests" IMPACT Project: Investigation of Extreme Flood Processes and Uncertainty. EC Contract No: EVG1-CT-2001-00037. www.impact-project.ne